Bergman's Comprehensive Encyclopedia of Human Anatomic Variation

Bergman's Comprehensive Encyclopedia of Human Anatomic Variation

R. Shane Tubbs, MS, PA-C, PhD

Professor and Chief Scientific Officer,
Seattle Science Foundation,
Seattle, Washington, United States
Professor of Anatomy
Department of Anatomical Sciences
St. George's University, Grenada
Centre of Anatomy and Human Identification
University of Dundee, Scotland, United Kingdom

Mohammadali M. Shoja, MD

Tuberculosis and Lung Disease Research Center
Tabriz University of Medical Sciences
Tabriz, Iran

Marios Loukas, MD, PhD

Professor and Chair
Department of Anatomical Sciences,
Dean of Research, School of Medicine
St. George's University, Grenada

WILEY Blackwell

Copyright © 2016 by John Wiley & Sons, Inc. All rights reserved

Published by John Wiley & Sons, Inc., Hoboken, New Jersey
Published simultaneously in Canada

No part of this publication may be reproduced, stored in a retrieval system, or transmitted in any form or by any means, electronic, mechanical, photocopying, recording, scanning, or otherwise, except as permitted under Section 107 or 108 of the 1976 United States Copyright Act, without either the prior written permission of the Publisher, or authorization through payment of the appropriate per-copy fee to the Copyright Clearance Center, Inc., 222 Rosewood Drive, Danvers, MA 01923, (978) 750-8400, fax (978) 750-4470, or on the web at www.copyright.com. Requests to the Publisher for permission should be addressed to the Permissions Department, John Wiley & Sons, Inc., 111 River Street, Hoboken, NJ 07030, (201) 748-6011, fax (201) 748-6008, or online at http://www.wiley.com/go/permission.

Limit of Liability/Disclaimer of Warranty: While the publisher and author have used their best efforts in preparing this book, they make no representations or warranties with respect to the accuracy or completeness of the contents of this book and specifically disclaim any implied warranties of merchantability or fitness for a particular purpose. No warranty may be created or extended by sales representatives or written sales materials. The advice and strategies contained herein may not be suitable for your situation. You should consult with a professional where appropriate. Neither the publisher nor author shall be liable for any loss of profit or any other commercial damages, including but not limited to special, incidental, consequential, or other damages.

For general information on our other products and services or for technical support, please contact our Customer Care Department within the United States at (800) 762-2974, outside the United States at (317) 572-3993 or fax (317) 572-4002.

Wiley also publishes its books in a variety of electronic formats. Some content that appears in print may not be available in electronic formats. For more information about Wiley products, visit our web site at www.wiley.com.

Library of Congress Cataloging-in-Publication Data

Names: Tubbs, R. Shane. | Shoja,
Mohammadali M. | Loukas, Marios.
Title: Bergman's comprehensive encyclopedia of human anatomic variation /
[edited by] R. Shane Tubbs, MS, PA-C, PhD, Professor and Chief Scientific Officer,
Seattle Science Foundation, Seattle, Washington, United States, Professor of
Anatomy, Department of Anatomical Sciences, St. George's University,
Grenada, Centre of Anatomy and Human Identification, University of Dundee,
Scotland, United Kingdom, Mohammadali M. Shoja, MD, Tuberculosis and Lung Disease Research Center,
Tabriz University of Medical Sciences, Tabriz, Iran, Marios Loukas,
MD, PhD, Professor and Chair, Department of Anatomical Sciences, Dean of
Research, School of Medicine, St. George's University, Grenada.
Other titles: Comprehensive encyclopedia of human anatomic variation |
Encyclopedia of human anatomic variation
Description: Hoboken, New Jersey : John Wiley & Sons, Inc., [2016] | Includes
index.
Identifiers: LCCN 2015039645 | ISBN 9781118430354 (cloth)
Subjects: LCSH: Human anatomy—Variation—Encyclopedias. | Human
anatomy—Encyclopedias.
Classification: LCC QM24 .C65 2016 | DDC 612.003—dc23 LC record available at http://lccn.loc.gov/2015039645

Set in 9.5/12pt Minion Pro by Aptara Inc., New Delhi, India

10 9 8 7 6 5 4 3 2 1

As the reader sees from the title of this textbook, it is dedicated to Dr. Ronald Bergman. Dr. Bergman was not the first to collect and publish on the variations of the human anatomy (e.g. Henle, Macalister, Adachi). However, he was the first to publish on this topic at such an in depth and comprehensive scale. My first introduction to Dr. Bergman's *Compendium of Human Anatomic Variation* was as a graduate student. As any dissector will eventually do, I came across something unusual in one of our cadavers during a routine dissection. I asked by my mentor, Dr. George Salter, about this who said, "You know there used to be a book in the lab office that focused on the anatomic variations of the body." After some digging, I was delighted to find this book, which I set out to memorize as best as I could. From that day on, Dr. Bergman's book and *Gray's Anatomy* were my main resources for studying anatomy. Therefore, this current text is not only an updated resource but also a tribute to the pioneering efforts of Dr. Ronald Bergman who reminded us that no two bodies are the same!

R. Shane Tubbs

I would like to dedicate my work on this enormous project to my son, Isaiah. Isaiah you are the light of my life! To my wife, Susan, you are the best. Many thanks to Drs. Rod Oskouian and Johnny Delashaw for their encouragement. Also, Dr. W. Jerry Oakes has supported this project and my other academic endeavors and I sincerely thank him. Lastly, I thank Dr. E. George Salter for persuading me to take on a career in anatomy and for first introducing me to the *Compendium of Human Anatomic Variation*!

R. Shane Tubbs

To Susan and Shane Tubbs, a very beautiful couple.

Mohammadali M. Shoja

To the love of my life, my wife Joanna Loukas

Marios Loukas

Contents

List of contributors, xi

Preface, xvii

Foreword by Stephen W. Carmichael, xix

Foreword by Ronald A. Bergman, xx

1 Skull, 1
Selcuk Tunali

2 Hyoid bone, 22
R. Shane Tubbs and Koichi Watanabe

3 Cervical vertebrae, 24
Joseph H. Miller, Michael C. Lysek and Mark N. Hadley

4 Thoracic vertebrae, 30
Benjamin J. Ditty, Nidal B. Omar and Mark N. Hadley

5 Lumbar vertebrae, 33
Ross Dawkins and Mark N. Hadley

6 Sacrococcygeal vertebrae, 37
R. Shane Tubbs and Marios Loukas

7 Scapula, 40
Peter Ward

8 Clavicle, 51
Z.J. Daruwalla, R. Malhotra, P. Courtis, C. Fitzpatrick, D. Fitzpatrick and H. Mullett

9 Humerus, 63
Peter Ward

10 Radius, ulna, carpals, metacarpals, and phalanges, 68
Munawar Hayat and Marios Loukas

11 Ribs and sternum, 76
R. Shane Tubbs and Koichi Watanabe

12 Pelvic bones, 82
Alper Cesmebasi and Marios Loukas

13 Bones of the lower limb, 89
Matthew Haffner and Michael Conklin

14 Temporomandibular joint, 116
Toral R. Patel and Jarrod A. Collins

15 Shoulder joint, 124
Brion Benninger

16 Elbow joint, 130
Giuseppe Giannicola, Federico Maria Sacchetti, David Polimanti, Gianluca Bullitta, Marco Scacchi and Pietro Sedati

17 Wrist and hand joints, 158
Benjamin Todd Raines and Jean Oakes

18 Sacroiliac joints, 165
Niladri Kumar Mahato

19 Hip joint, 176
Robert Ward

20 Knee joint, 181
Brion Benninger

21 Ankle and foot joints, 204
Takamitsu Arakawa

22 Orbital muscles, 207
Necdet Kocabiyik

23 Middle ear muscles, 212
José Francisco Rodríguez-Vázquez

24 Facial muscles and muscles of mastication, 217
Koichi Watanabe

25 Anterior neck muscles, 228
Hye Yeon Lee and Hee Jun Yang

26 Pharyngeal muscles, 236
Yujiro Sakamoto

27 Soft palate and tongue muscles, 240
Swetal Patel and Marios Loukas

28 Prevertebral and craniocervical junction muscles, 245
Yujiro Sakamoto

29 Laryngeal muscles, 254
Eva Maranillo and Jose Sanudo

30 Back muscles, 262
Barclay W. Bakkum and Nathan Miller

31 Scapulohumeral muscles, 289
Clare Lamb

32 Arm muscles, 293
Keiichi Akita and Akimoto Nimura

33 Forearm muscles, 298
Keiichi Akita and Akimoto Nimura

34 Hand intrinsic muscles, 315
Mirtha A. Gonzalez and David T. Netscher

35 Thoracic wall muscles, 335
Michael Snosek and Marios Loukas

36 Abdominal wall muscles, 369
Tsuyoshi Saga and Nagahiro Takahashi

37 Pelvic diaphragm and external anal sphincter, 381
Howe Liu and Yasser Salem

38 Perineal muscles, 384
R. Shane Tubbs and Koichi Watanabe

39 Gluteal muscles, 386
Helen Nicholson and Natasha Flack

40 Thigh muscles, 410
Maira du Plessis and Marios Loukas

41 Leg muscles, 421
H. Wayne Lambert

42 Intrinsic muscles of the foot, 438
Rene M. Kafka, Ian L. Aveytua, Regina C. Fiacco, Garen M. Ream, Anthony C. DiLandro and Anthony D'Antoni

43 Internal carotid artery and anterior cerebral circulation, 449
Paul Foreman, Christoph J. Griessenauer, John P. Deveikis and Mark Harrigan

44 Vertebrobasilar arteries, 461
R. Shane Tubbs and Marios Loukas

45 Persistent fetal intracranial arteries, 465
Soner Albay

46 Common carotid and cervical internal carotid arteries, 475
R. Shane Tubbs and Marios Loukas

47 External carotid artery, 477
Selcuk Tunali

48 Vertebral artery, 487
Bernard George and Michaël Bruneau

49 Thoracic aorta, 501
Veysel Akgun, Salih Hamcan, Yalcin Bozkurt and Bilal Battal

50 Coronary arteries, 530
Horia Muresian

51 Pulmonary arteries, 569
M. Cumhur Sivrikoz

52 Subclavian artery, 575
Selcuk Tunali

53 Upper limb arteries, 583
Anthony Olinger

54 Abdominal aorta, 619
Daisy Sahni, Anjali Aggarwal, Tulika Gupta, Harjeet Kaur, Richa Gupta, Kunal Chawla, Narbada Saini, Shallu Garg, Anjali Singla, Arpan Deep, Harsimran Jit Singh, Devendra Shekhawat and Megha Rapotra

55 Renal arteries, 682
Priti L. Mishall

56 Internal iliac arteries, 694
Richard Tunstall

57 Lower limb arteries, 741
Akshal Patel

58 Arteries of the spinal cord, 752
Marius C. Bosman and Albert van Schoor

59 Diploic veins, 770
Satoshi Tsutsumi

60 Dural venous sinuses, 775
Shamfa C. Joseph, Elias Rizk and R. Shane Tubbs

61 Cerebral veins, 800
Alireza Sadighi, Ulaş Cikla, Gregory C. Kujoth and Mustafa K. Başkaya

62 Emissary veins, 817
R. Shane Tubbs, Koichi Watanabe and Marios Loukas

63 Veins of the neck, 821
R. Shane Tubbs and Koichi Watanabe

64 Veins of the upper limb, 826
Teresa Vazquez and Jose Sanudo

65 Intrathoracic veins, 832
Jonathan D. Spratt

66 Cardiac veins, 854
Horia Muresian

67 Pulmonary veins, 871
Yutthaphan Wannasopha and Juntima Euathrongchit

68 Inferior vena cava, portal and hepatic venous systems, 877
Jonathan D. Spratt

69 Adrenal, renal, gonadal, azygos, hemiazygos, lumbar, and ascending lumbar veins, 890
Marios Loukas and R. Shane Tubbs

70 Iliac veins, 894
Deepali Onkar

71 Veins of the lower limb, 900
Santosh K. Sangari

72 Venous drainage of the spinal cord, 910
Joel Raborn, Christoph J. Griessenauer, Mohammadali M. Shoja and R. Shane Tubbs

73 Thymus, 914
Ivan Varga

74 Tonsils, 919
R. Shane Tubbs and Marios Loukas

75 Thoracic duct, chyle cistern, and right lymphatic duct, 921
Young-Bin Song

76 Lymphatics of the lower limb, 935
Shun Yamazaki, Hiroo Suami, Nobuaki Imanishi, Sadakazu Aiso, Minoru Yamada, Masahiro Jinzaki, Sachio Kuribayashi, David W. Chang and Kazuo Kishi

77 Forebrain, 939
R. Shane Tubbs, Mohammadali M. Shoja and Marios Loukas

78 Cerebral ventricles, 943
Martin M. Mortazavi, Nimer Adeeb, Mohammad Jaber and R. Shane Tubbs

79 Pons, medulla oblongata and cerebellum, 954
Dylan Goodrich, Jennifer Yang, Joseph H. Miller and W. Jerry Oakes

80 Subarachnoid space, 959
Martin M. Mortazavi, Nimer Adeeb, Fareed Rizq and R. Shane Tubbs

81 Meninges, 974
Nimer Adeeb, Martin M. Mortazavi and R. Shane Tubbs

82 Spinal cord and associated structures, 984
Shoko M. Yamada, Daniel J. Won, Pedro B. Nava, R. Shane Tubbs and Shokei Yamada

83 Cranial nerves *N*-VI, 989
Jenna R. Voirol, Kelley A. Strothmann, Anthony Zandian and Joel A. Vilensky

84 Facial nerve, 1005
Mohammadali M. Shoja and R. Shane Tubbs

85 Vestibulocochlear nerve, 1034
Mohammadali M. Shoja and R. Shane Tubbs

86 Glossopharyngeal nerve, 1036
Mohammadali M. Shoja, Marios Loukas and R. Shane Tubbs

87 Vagus, accessory, and hypoglossal nerves, 1041
Mohammadali M. Shoja, Christoph J. Griessenauer, Marios Loukas and R. Shane Tubbs

88 Autonomic nervous system, 1050
Paul Anthony Irwin, R. Isaiah Tubbs and R. Shane Tubbs

89 Spinal nerves, 1057
R. Shane Tubbs

90 Cervical plexus, 1062
Necdet Kocabiyik

91 Nerves of the upper extremity, 1068
Mark A. Mahan and Robert J. Spinner

92 Lumbosacral plexus, 1113
Nihal Apaydin

93 Facial asymmetry, 1130
Senem T. Ozdemir, Marios Loukas and R. Shane Tubbs

94 Eyelids, eyelashes, and eyebrows, 1133
Candace R. Wooten and Marios Loukas

95 Eye and lacrimal apparatus, 1145
Frederic J. Bertino

96 Lateral nasal wall and paranasal sinuses, 1158
Amr E. El-Shazly

97 Ear, 1167
Aman Deep, Martin M. Mortazavi and Nimer Adeeb

98 Salivary glands and ducts, 1182
Louise Wing and Tarik F. Massoud

99 Thyroid gland, 1189
Bulent Yalcin

100 Parathyroid glands, 1205
Bulent Yalcin

101 Laryngeal cartilages, 1209
Arán Pascual-Font and Jose Sanudo

102 Trachea, 1212
Koichi Watanabe

103 Lungs, 1217
Koichi Watanabe

104 Heart, 1234
Maira du Plessis and Marios Loukas

105 Esophagus, 1247
Koichi Watanabe

106 Stomach, 1253
Koichi Watanabe

107 Gallbladder and extrahepatic bile ducts, 1261
Mark D. Stringer

108 Liver, 1272
Koichi Watanabe

109 Pancreas, 1278
Koichi Watanabe

110 Spleen, 1282
Koichi Watanabe

111 Small intestines, appendix, and colon, 1285
Koichi Watanabe

112 Sigmoid colon, rectum, and anus, 1308
Thandinkosi E. Madiba and Mohammad R. Haffajee

113 Kidney, urinary bladder, and ureter, 1315
Mohammad Reza Ardalan

114 Adrenal gland, 1332
Gülnur Özgüner

115 Male genitourinary system, 1335
Courtney L. Shepard, Dustin T. Gayheart and David B. Joseph

116 Female genital system, 1364
Sedat Develi

117 Placenta and umbilical cord, 1387
Sedat Develi

118 Breast, 1390
Matthew Rubacha

Index, 1398

List of contributors

Nimer Adeeb
Children's of Alabama
Birmingham, Alabama, USA

Anjali Aggarwal
Postgraduate Institute of Medical Education & Research
Chandigarh, India

Sadakazu Aiso
Keio University
Tokyo, Japan

Veysel Akgun
Gulhane Military Medical Academy
Ankara, Turkey

Keiichi Akita
Tokyo Medical and Dental University
Tokyo, Japan

Soner Albay
Suleyman Demirel University Faculty of Medicine
Isparta, Turkey

Nihal Apaydin
Ankara University Faculty of Medicine
Ankara, Turkey

Takamitsu Arakawa
Kobe Graduate School of Health Sciences
Kobe, Japan

Mohammad Reza Ardalan
Tabriz University of Medical Sciences
Tabriz, Iran

Ian L. Aveytua
New York College of Podiatric Medicine
New York, New York, USA

Barclay W. Bakkum
Illinois College of Optometry
Chicago, Illinois, USA

Mustafa K. Başkaya
University of Wisconsin
Madison, Wisconsin, USA

Bilal Battal
Gulhane Military Medical Academy
Ankara, Turkey

Brion Benninger
Western University of Health Sciences
Portland, Oregon, USA

Frederic J. Bertino
St George's University, School of Medicine
St Georges, Grenada

Marius C. Bosman
University of Pretoria
Pretoria, South Africa

Yalcin Bozkurt
Golcuk Military Hospital
Kocaeli, Turkey

Michaël Bruneau
Hôpital Erasme
Brussels, Belgium

Gianluca Bullitta
"Sapienza" University of Rome
Rome, Italy

Alper Cesmebasi
St George's University, School of Medicine
St Georges, Grenada

David W. Chang
The University of Texas MD Anderson Cancer Center
Houston, Texas, USA

Kunal Chawla
Postgraduate Institute of Medical Education & Research
Chandigarh, India

Ulaş Cikla
University of Wisconsin
Madison, Wisconsin, USA

Jarrod A. Collins
Children's of Alabama
Birmingham, Alabama, USA

Michael Conklin
Children's of Alabama
Birmingham, Alabama, USA

Patrick Courtis
University College Dublin
Dublin, Ireland

Anthony D'Antoni
New York College of Podiatric Medicine
New York, New York, USA

Zubin J. Daruwalla
Beaumont Hospital
Dublin, Ireland

Ross Dawkins
University of Alabama at Birmingham
Birmingham, Alabama, USA

Aman Deep
Children's of Alabama
Birmingham, Alabama, USA

Arpan Deep
Postgraduate Institute of Medical Education & Research
Chandigarh, India

John P. Deveikis
University of Alabama at Birmingham
Birmingham, Alabama, USA

Sedat Develi
Gulhane Military Medical Academy
Ankara, Turkey

Anthony C. DiLandro
New York College of Podiatric Medicine
New York, New York, USA

Benjamin J. Ditty
University of Alabama at Birmingham
Birmingham, Alabama, USA

Maira du Plessis
St George's University
St Georges Grenada

Amr E. El-Shazly
Liège University Hospital
Liège, Belgium

Juntima Euathrongchit
Chiang Mai University
Chiang Mai, Thailand

Regina C. Fiacco
New York College of Podiatric Medicine
New York, New York, USA

David Fitzpatrick
University College Dublin
Dublin, Ireland

Clare Fitzpatrick
University College Dublin
Dublin, Ireland

Natasha Flack
University of Otago
Dunedin, New Zealand

Paul Foreman
University of Alabama at Birmingham
Birmingham, Alabama, USA

Shallu Garg
Postgraduate Institute of Medical Education & Research
Chandigarh, India

Dustin T. Gayheart
University of Alabama at Birmingham
Birmingham, Alabama, USA

Bernard George
Hôpital Lariboisière
Paris, France

Giuseppe Giannicola
"Sapienza" University of Rome
Rome, Italy

Mirtha A. Gonzalez
Baylor College of Medicine
Houston, Texas, USA

Dylan Goodrich
St George's University, School of Medicine
St Georges, Grenada

Christoph J. Griessenauer
University of Alabama at Birmingham
Birmingham, Alabama, USA

Richa Gupta
Postgraduate Institute of Medical Education & Research
Chandigarh, India

Tulika Gupta
Postgraduate Institute of Medical Education & Research
Chandigarh, India

Mark N. Hadley
University of Alabama at Birmingham
Birmingham, Alabama, USA

Mohammad R. Haffajee
University of KwaZulu-Natal
Durban, South Africa

Matthew Haffner
St George's University, School of Medicine
St Georges, Grenada

Salih Hamcan
Agri Military Hospital
Agri, Turkey

Mark Harrigan
University of Alabama at Birmingham
Birmingham, Alabama, USA

Munawar Hayat
St George's University, School of Medicine
St Georges, Grenada

Nobuaki Imanishi
Keio University
Tokyo, Japan

Paul Anthony Irwin
Children's of Alabama
Birmingham, Alabama, USA

Mohammad Jaber
Children's of Alabama
Birmingham, Alabama, USA

Masahiro Jinzaki
Keio University
Tokyo, Japan

David B. Joseph
Children's of Alabama
Birmingham, Alabama, USA

Shamfa C. Joseph
St George's University, School of Medicine
St Georges, Grenada

Rene M. Kafka
New York College of Podiatric Medicine
New York, New York, USA

Harjeet Kaur
Postgraduate Institute of Medical Education & Research
Chandigarh, India

Kazuo Kishi
Keio University
Tokyo, Japan

Necdet Kocabiyik
Gulhane Military Medical Academy
Ankara, Turkey

Gregory C. Kujoth
University of Wisconsin
Madison, Wisconsin, USA

Sachio Kuribayashi
Keio University
Tokyo, Japan

Clare Lamb
University of Dundee
Dundee, UK

H. Wayne Lambert
West Virginia University School of Medicine
Morgantown, West Virginia, USA

Hye Yeon Lee
Yonsei University College of Medicine
Seoul, Korea

Howe Liu
University of North Texas Health Science Center
Fort Worth, Texas, USA

Marios Loukas
St George's University, School of Medicine
St Georges, Grenada

Michael C. Lysek
University of Alabama at Birmingham
Birmingham, Alabama, USA

Thandinkosi E. Madiba
University of KwaZulu-Natal
Durban, South Africa

Mark A. Mahan
University of Utah
Salt Lake City, Utah, USA

Niladri Kumar Mahato
Ohio University
Athens, Ohio, USA

R. Malhotra
Beaumont Hospital
Dublin, Ireland

Eva Maranillo
Complutense University of Madrid
Madrid, Spain

Tarik F. Massoud
Stanford University School of Medicine
Stanford, California, USA

Joseph H. Miller
University of Alabama at Birmingham
Birmingham, Alabama, USA

Nathan Miller
National University of Health Sciences
Lombard, Illinois, USA

Priti L. Mishall
Albert Einstein College of Medicine
Bronx, New York, USA

Martin M. Mortazavi
University of Washington School of Medicine
Seattle, Washington, USA

Hannan Mullett
Beaumont Hospital
Dublin, Ireland

Horia Muresian
Cardiovascular Surgery
San Donato Milan, Italy
University Hospital of Bucharest
Bucharest, Romania

Pedro B. Nava
Loma Linda University School of Medicine
Riverside, California, USA

David T. Netscher
Baylor College of Medicine
Houston, Texas, USA
Weill Medical College, Cornell University
New York, New York, USA

Helen Nicholson
University of Otago
Dunedin, New Zealand

Akimoto Nimura
Tokyo Medical and Dental University
Tokyo, Japan

W. Jerry Oakes
Children's of Alabama
Birmingham, Alabama, USA

Jean Oakes
University of Alabama at Birmingham
Birmingham, Alabama, USA

Anthony Olinger
Kansas City University of Medicine and Biosciences
Kansas City, Missouri, USA

Nidal B. Omar
University of Alabama at Birmingham
Birmingham, Alabama, USA

Deepali Onkar
NKP Salve Institute of Medical Sciences and Research Centre
Nagpur, India

Gülnur Özgüner
Suleyman Demirel University
Isparta, Turkey

Arán Pascual-Font
Complutense University of Madrid
Madrid, Spain

Akshal Patel
Pennsylvania State University
Hershey, Pennsylvania, USA

Swetal Patel
St George's University, School of Medicine
St Georges, Grenada

Toral Patel
Children's of Alabama
Birmingham, Alabama, USA

David Polimanti
"Sapienza" University of Rome
Rome, Italy

Benjamin Todd Raines
University of Alabama at Birmingham
Birmingham, Alabama, USA

Megha Rapotra
Postgraduate Institute of Medical Education & Research
Chandigarh, India

Joel Raborn
University of Alabama at Birmingham
Birmingham, Alabama, USA

Garen M. Ream
New York College of Podiatric Medicine
New York, New York, USA

Elias Rizk
Pennsylvania State University
Hershey, Pennsylvania, USA

Fareed Rizq
Children's of Alabama
Birmingham, Alabama, USA

José Francisco Rodríguez-Vázquez
Complutense University of Madrid
Madrid, Spain

Matthew Rubacha
St George's University, School of Medicine
St Georges, Grenada

Federico Maria Sacchetti
"Sapienza" University of Rome
Rome, Italy

Alireza Sadighi
University of Wisconsin
Madison, Wisconsin, USA

Daisy Sahni
Postgraduate Institute of Medical Education & Research
Chandigarh, India

Tsuyoshi Saga
Kurume University School of Medicine
Fukuoka, Japan

Narbada Saini
Postgraduate Institute of Medical Education & Research
Chandigarh, India

Yujiro Sakamoto
Tokyo Medical and Dental University
Tokyo, Japan

Santosh Sangari
Weill Cornell Medical College
New York, New York, USA

Jose Sanudo
Complutense University of Madrid
Madrid, Spain

Marco Scacchi
"Sapienza" University of Rome
Rome, Italy

Albert van Schoor
University of Pretoria
Pretoria, South Africa

Pietro Sedati
"Sapienza" University of Rome
Rome, Italy

Harsimran Jit Singh
Postgraduate Institute of Medical Education & Research
Chandigarh, India

Anjali Singla
Postgraduate Institute of Medical Education & Research
Chandigarh, India

Devendra Shekhawat
Postgraduate Institute of Medical Education & Research
Chandigarh, India

Courtney L. Shepard
University of Alabama at Birmingham
Birmingham, Alabama, USA

Mohammadali M. Shoja
Tuberculosis and Lung Disease Research Center
Tabriz University of Medical Sciences
Tabriz, Iran

M. Cumhur Sivrikoz
Eskişehir Osmangazi University Medical Faculty
Eskişehir, Turkey

Michael Snosek
St George's University, School of Medicine
St Georges, Grenada

Young-Bin Song
Children's of Alabama
Birmingham, Alabama, USA

Robert J. Spinner
Mayo Clinic
Rochester, Minnesota, USA

Jonathan Spratt
University Hospital of North Durham
Durham, UK

Mark D. Stringer
Christchurch Hospital
University of Otago
Dunedin, New Zealand

Kelley A. Strothmann
Indiana University
Fort Wayne, Indiana, USA

Hiroo Suami
The University of Texas MD Anderson Cancer Center
Houston, Texas, USA

Nagahiro Takahashi
Kurume University School of Medicine
Fukuoka, Japan

Satoshi Tsutsumi
Juntendo University Urayasu Hospital
Chiba, Japan

R. Shane Tubbs
Seattle Science Foundation
Seattle, Washington, USA
St George's University, School of Medicine
St Georges, Grenada
University of Dundee
Dundee, UK

Richard Isaiah Tubbs
Children's of Alabama
Birmingham, Alabama, USA

Selcuk Tunali
TOBB University of Economics and Technology
Ankara, Turkey
University of Hawaii
Honolulu, Hawaii, USA

Richard Tunstall
The University of Warwick
Coventry, UK

Senem T. Ozdemir
Uludag University
Bursa, Turkey

Ivan Varga
Comenius University in Bratislava
Bratislava, Slovakia

Teresa Vazquez
Complutense University of Madrid
Madrid, Spain

Joel Vilensky
Indiana University
Fort Wayne, Indiana, USA

Jenna R. Voirol
Indiana University
Fort Wayne, Indiana, USA

Yutthaphan Wannasopha
Chiang Mai University
Chiang Mai, Thailand

Peter J. Ward
West Virginia School of Osteopathic Medicine
Lewisburg, West Virginia, USA

Robert Ward
Tufts Medical Center,
Boston, Massachusetts, USA

Koichi Watanabe
Kurume University School of Medicine
Fukuoka, Japan

Louise Wing
John Radcliffe Hospital
Oxford, UK

Stephanie Woodley
University of Otago
Dunedin, New Zealand

Candace R. Wooten
St George's University, School of Medicine
St Georges, Grenada

Daniel J. Won
Loma Linda University School of Medicine
Riverside, California, USA

Bulent Yalcin
Gulhane Military Medical Academy
Ankara, Turkey

Shoko M. Yamada
Loma Linda University School of Medicine
Riverside, California, USA

Shokei Yamada
Loma Linda University School of Medicine
Riverside, California, USA

Minoru Yamada
Keio University
Tokyo, Japan

Shun Yamazaki
Keio University
Tokyo, Japan

Jennifer Yang
University of Alabama at Birmingham
Birmingham, Alabama, USA

Hee Jun Yang
Gachon Graduate School of Medicine
Incheon, South Korea

Anthony Zandian
St George's University, School of Medicine
St Georges, Grenada

Preface

Since the beginning of time, differences between humans have made us identifiable to those around us. Some extreme forms of morphological variation have even resulted in individuals being either unique or outcasts. For example, dwarfs have been revered in various cultures and even represented in royal courts and some cultures have bestowed a god status on children born with multiple limbs. Other variations, however, have been viewed as "different" enough to warrant being ostracized. Children being born with a caudal appendage (tail) who were considered offspring of Satan exemplify this.

Human anatomic variation can be defined as human form that is outside of the normal. However, what is normal? This question is often very difficult to answer. For example, most would agree that having two breasts is normal but what about a woman with accessory breasts? Is this normal, abnormal or even pathologic? Is it a variant or an anomaly? Sometimes, the answer to these questions is based on cultural norms or societal acceptance.

Obviously, hair color is certainly varied among individuals with many having a color that doesn't fit into the classic brown, black, red, or blonde categories. But are various hair colors that one of these terms does not apply to have a variation or is this simply an issue of definition e.g. red in the broader sense would include auburn, strawberry, etc.? In other words, our definition of normal is the gauge by which an anatomic trait is considered a variation or not. Some have tried to shed light on this by using such words as "borderlands." Beyond the "border" a trait is thereby considered a variation. To confuse these issues, the term anomaly is and has been used interchangeably in regard to both variation and pathology. Herein, we have attempted to avoid pathologic anatomy but often, the line between an anatomic variation that is pathologic or predisposes one to pathology and one that is just a trait that is outside of what is considered normal is very gray. Moreover, as the term "anomaly" is often used to denote a variation that results in dysfunction or disease, we have tried to avoid this term when possible. However, the form of a structure may cause dysfunction in one person and not another. Therefore, "anomalies" do not always result in dysfunction or disease. The terms "abnormal" and "aberrant" have each been used loosely in the medical literature to describe anatomy that is non-pathologic or results in dysfunction.

Confoundedly, there are variations within variations. Where does one draw the line between a variation that is accepted as "normal" (the so-called normal variant) and a variation that is considered "abnormal"? In this text, we have attempted to be more inclusive than not. If the majority of individuals do not have an anatomic trait, then we have considered it a variation. With this however, the definition of majority has to be defined.

A quarter of a century ago, Dr. Ronald Bergman set forth to collect and publish a compendium of human variation. His textbook soon became the gold standard in human anatomic variation. As anatomists, we consulted this text almost daily. However, in the interim since its publication, radiologic technology and improved optics such as the surgical microscope have allowed us to see into the body with better accuracy than ever before. As a result, many more variations have come to the anatomist's and clinician's attention. Therefore, an updated textbook devoted to human anatomic variation seemed timely. However, as no single text on human anatomy can include all of the intricate details and structures of the body, so too can no single text on human anatomic variation capture all known or reported variants of the body, although we have tried. This tome will attempt to capture many of the known variants of the human form.

Nothing is pleasant that is not spiced with variety.
Francis Bacon

Through every rift of discovery some seeming anomaly drops out of the darkness, and falls, as a golden link into the great chain of order.
Edwin Hubbel Chapin

Variety's the very spice of life that gives it all its flavor.
William Cowper

The essence of the beautiful is unity in variety.
W. Somerset Maugham

I have called this principle, by which each slight variation, if useful, is preserved, by the term of Natural Selection.
Charles Darwin

Variety of mere nothings gives more pleasure than uniformity of something.
Jean Paul

The gifts of nature are infinite in their variety, and mind differs from mind almost as much as body from body.
Quintilian

To such an extent does nature delight and abound in variety that among her trees there is not one plant to be found which is exactly like another; and not only among the plants, but among the boughs, the leaves and the fruits, you will not find one which is exactly similar to another.

Leonardo DaVinci

The catalogue of forms is endless: until every shape has found its city, new cities will continue to be born. When the forms exhaust their variety and come apart, the end of cities begins.

Italo Calvino

R. Shane Tubbs

Foreword

With the possible exception of a few pairs of identical twins, the anatomy of every human being on this planet is unique. That means that there are as many anatomical variations as there are people! Obviously, only a small percentage of these variations are of clinical significance. There are subtle variations in facial anatomy that will allow a clinical anatomist to tell one person from another, but that is not the type of variation that this textbook is about. Instead, this textbook is a resource for the clinical anatomist who needs a single comprehensive source for all the variations that have been published in peer-reviewed journals or web sites.

This new text is the first of its kind since *Compendium of Human Anatomic Variation: Text, Atlas, and World Literature* by Ronald A. Bergman, Sue Ann Thompson, and Adel K. Afifi published in 1988. There have been many published accounts of variations since that time. In fact, this text contains thousands of published variations. This update is clinically important in view of recent advances in surgery and radiologic imaging. For a surgical example, endoscopic surgery makes what was previously an insignificant variation now necessary for the surgeon to recognize in order to perform a procedure safely. Improved resolution of radiologic images in all modalities makes it more important to be able to recognize what is pathologic and what is a normal variation.

Bergman's "Compendium" was the "gold standard" of its day. This text will soon become the new gold standard. Even Dr. Bergman would agree with that!

Respectfully submitted,
Stephen W. Carmichael, Ph.D., D.Sc.
Professor Emeritus of Anatomy and Orthopedic Surgery,
Mayo Clinic
Editor Emeritus, *Clinical Anatomy*

Foreword

This book, with great personal pride for me, provides elegant confirmation of the proven fact that the human body (as well as every living thing) is not created without variability. To paraphrase a profound statement by Sir William Osler, "variability is the rule of life"! The present book complements and extends a previous compendium, and an internet edition of human anatomic variation. Dr. Shane Tubbs conceived and developed this revision. He and his co-editors expand our knowledge and are to be very highly commended for keeping the concepts fresh in the minds of all who are interested in the structure and function of the human body.

Ronald A. Bergman, PhD
Emeritus Professor of Anatomy
The University of Iowa

1 Skull

Selcuk Tunali
TOBB University of Economics and Technology, Ankara, Turkey
University of Hawaii, Honolulu, Hawaii, United States

Frontal bone

The frontal sinus ostium is sometimes absent. In a cadaveric study, Ozgursoy et al. (2010) reported absence of right frontal sinus ostium in 3.6% of cases when there was a connection between the right and left frontal sinuses. They also noted that if one of the frontal sinus ostia cannot be found during sinus surgery, although this sinus and its recess can be seen on thick-sliced coronal computed tomographic scans, there could be an agenetic frontal sinus hidden by the extensive pneumatization of the contralateral sinus that crosses the midline (3.6%).

The frontal sinus itself can be absent. Computed tomographic scans in the axial and coronal planes of the frontal sinuses of 565 patients were examined. There was bilateral agenesis of the frontal sinus in 8.32% of these cases and unilateral absence of the frontal sinus in 5.66% (Danesh-Sani et al. 2011).

Another study investigated the prevalence of agenesis of the frontal sinuses using dental volumetric tomography (DVT) in Turkish individuals. The frontal sinuses of 410 patients were examined by DVT scans in the coronal plane. There was bilateral and unilateral absence of the frontal sinuses in 0.73% and 1.22% of cases, respectively (Çakur et al. 2011a). Aydinlioğlu et al. (2003) studied computed tomography (CT) scans of the paranasal sinuses in the axial and coronal planes from a series of 1200 cases. Bilateral and unilateral absences of the frontal sinuses were noted in 3.8% and 4.8%, respectively.

In a study on the septation of the frontal sinuses, Comer et al. (2013) concluded that frontal sinus septations appear to be significantly associated with and predictive of the presence of supraorbital ethmoid cells. Identifying frontal sinus septations on sinus CT could therefore imply a more complex anatomy of the frontal recess.

In a study by Bajwa et al. (2013), all patients older than 15 months and 23 days had completely fused metopic sutures. The estimated median age for the start of the fusion process was 4.96 months (95% confidence interval, 3.54–6.76 months), and the estimated median age for completion of fusion was 8.24 months (95% confidence interval, 7.37–9.22 months). The fusion process was complete between 2.05 and 14.43 months of age in 95% of the normal population. There was no significant difference between sexes. This study demonstrated wide variation in the timing of normal fusion, which can complete as early as two months of age (Bajwa et al. 2013).

Persistent metopic sutures can be misdiagnosed as vertical traumatic skull fractures extending down the midline in head trauma patients. The surgeon should therefore be aware of this anatomical variant during primary and secondary surveillance of the traumatized patient and during surgical intervention, especially including frontal craniotomy. A reconstructed tomography scan demonstrating sutural closuring status could provide useful additional information in the diagnostic sequence, superior to a plain X-ray in the emergency setting (Bademci et al. 2007). Nakatani et al. (1998) encountered a complete ectometopic suture in a 91-year-old Japanese male cadaver during a gross anatomy course. It was observed in 1 of 26 skulls aged 62–92 years and was about 13 cm long from the bregma to the nasion. A metopic suture is rare in a person of advanced age, as in their case.

In another study, 1276 adult Indian skulls were examined for the incidence of metopic sutures. There was metopism in 2.66% of the skulls and metopic sutures were present in 38.17% (35.27% in the lower part of the frontal bone in various shapes); the incidences in the upper, upper middle and lower middle parts of the frontal bone were 0.8% in each location. As well as the abovementioned findings, a peculiar shape (inverted Y) was seen in 0.63% and a radiating type in 0.31% of the skulls (Agarwal et al. 1979).

Hyperostosis frontalis interna is a condition of bony overgrowth of the frontal region of the endocranial surface, appearing in the scientific literature as early as 1719. During routine dissection of a donor's calvaria it was noted that she had significant bony overgrowth of the endocranium. Such overgrowth was diffuse throughout the frontal bone, extending slightly into the parietal region with midline sparing (Fig. 1.1). It ranged from 1.0 cm thickness in the temporal region to 1.3 cm adjacent to the midline in the frontal region. Large individual nodules were located along either side of the frontal crest at the intersection of the frontal and parietal bones. The largest nodules measured 2.08 cm in thickness on the right and 1.81 cm on the left (Fig. 1.2). As a result, the pathway of the middle meningeal artery was tortuous. In addition there was significant bilateral depression of the frontal lobes and surrounding neural tissues (Fig. 1.3) (Champion and Cope 2012).

Bergman's Comprehensive Encyclopedia of Human Anatomic Variation, First Edition. Edited by R. Shane Tubbs, Mohammadali M. Shoja and Marios Loukas.
© 2016 John Wiley & Sons, Inc. Published 2016 by John Wiley & Sons, Inc.

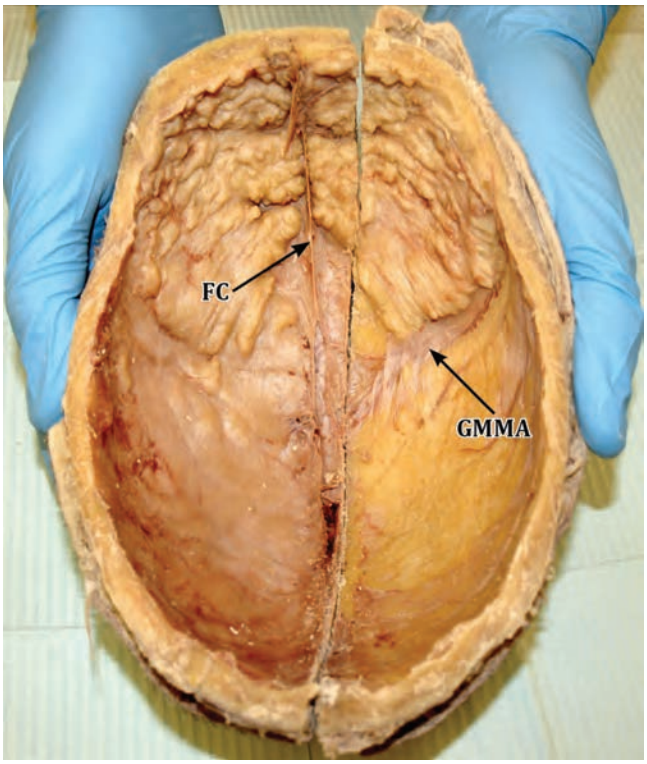

Figure 1.1 Severe case of hyperostosis frontalis interna with typical midline sparing along the frontal crest. Notice the tortuous pathway of the middle meningeal artery. FC: frontal crest; GMMA: groove for middle meningeal artery.

Source: Champion and Cope (2012). Reproduced with permission from International Journal of Anatomical Variations.

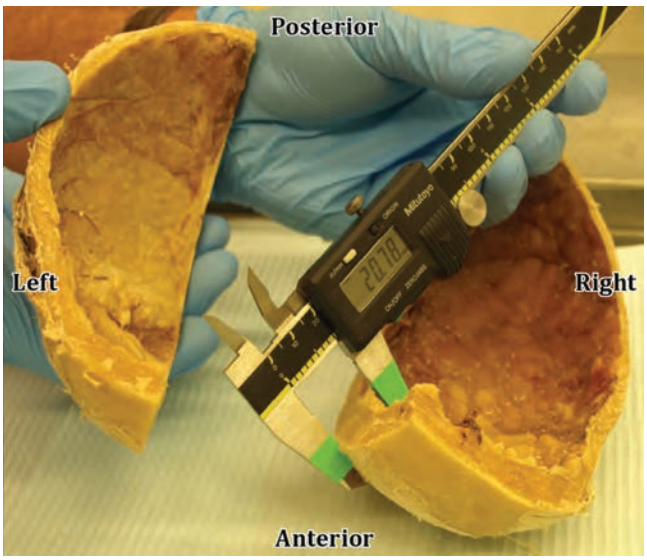

Figure 1.2 Picture shows the measurement of a large nodule (2.08 cm) located adjacent to the frontal crest at the juncture of the frontal and parietal bones.

Source: Champion and Cope (2012). Reproduced with permission from International Journal of Anatomical Variations.

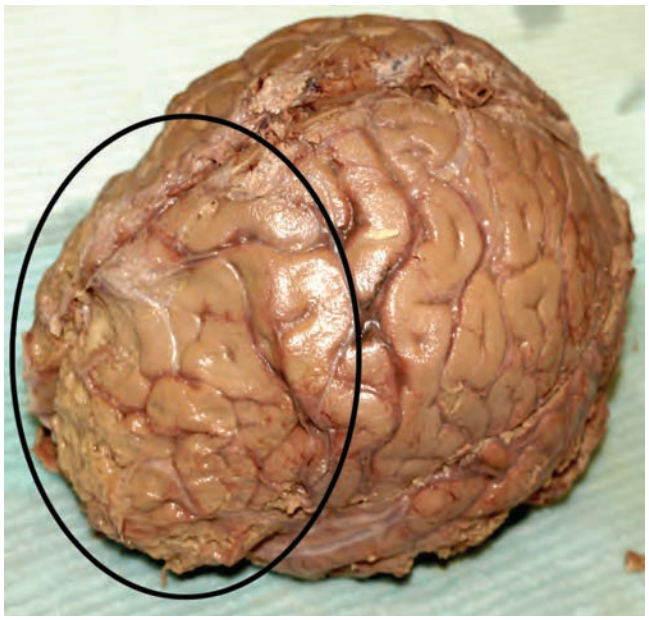

Figure 1.3 Notice the significant compression of the frontal lobes.

Source: Champion and Cope (2012). Reproduced with permission from International Journal of Anatomical Variations.

Nikolić et al. (2010) determined the rate of occurrence and appearance of hyperostosis frontalis interna (HFI) in females and correlated this phenomenon with aging. The sample included 248 deceased females, 45 with different types of HFI and 203 without HFI, average ages 68.3±15.4 (range 19–93) and 58.2±20.2 years (range 10–101), respectively. The rate of HFI was 18.14%. The older the woman, the higher the possibility of HFI (Pearson correlation 0.211, N=248, P=0.001), but the type of HFI did not correlate with age (Pearson correlation 0.229, N=45, P=0.131). The frontal and temporal bones were significantly thicker in women with HFI than in women without it (t=–10.490, DF=246, P=0.000, and t=–5.658, DF=246, P=0.000, respectively). These bones became thicker with aging (Pearson correlation 0.178, N=248, P=0.005 and 0.303, N=248, P=0.000, respectively). The best predictors of HFI were frontal bone thickness, temporal bone thickness, and age (respectively: Wald coefficient=35.487, P=0.000; Wald coefficient=3.288, P=0.070, and Wald coefficient=2.727, P=0.099). Diagnosis of HFI depends not only on frontal bone thickness but also on the waviness of the internal plate of the frontal bone and the involvement of the inner bone surface (Nikolić et al. 2010). May et al. (2011) studied two female populations separated by a period of 100 years: 992 historical and 568 present-day females. HFI was detected by direct observation or CT images. HFI was significantly more prevalent in the present-day than the historical females (P<0.05). The risk of developing it was approximately 2.5 times greater in present-day females than in those who lived 100 years ago (P<0.05). HFI tended to appear at a younger age in the present-day population. The last two decades have witnessed an increase in prevalence (from 55.6% to 75%); prevalence has also increased during the past century, especially among

young individuals, possibly indicating a profound change in human fertility patterns together with the introduction of various hormonal treatments and new dietary habits (May et al. 2011).

A accessory spine of the zygomatic process of the frontal bone is referred to as the spine of Broca.

Occipital bone

The occipital condyle can be oval, triangular, circular, or two-portioned in shape. Ozer et al. (2011) reported the most common type as oval or ovoid (59.67%), whereas the most unusual type was a two-portioned condyle (0.32%). In another study, occipital condyles were classified according to shape: type 1: oval-like; type 2: kidney-like; type 3: S-like; type 4: eight-like; type 5: triangular; type 6: ring-like; type 7: two-portioned; and type 8: deformed. The most common type was type 1 (50%) and the most unusual was type 7 (0.8%) (Naderi et al. 2005).

In some cases a median or third occipital condyle is present. This is occasionally located on the anterior margin of the foramen magnum. Some instances are expressed as a simple rounded tubercle, but in more developed cases an articular facet receives the tip of the odontoid process forming a true diarthrosis (Bergman et al. 1996; Figueiredo et al. 2008). The "condylus tertius" or "third occipital condyle" is an embryological remnant of the proatlas sclerotome. Anatomically, it is attached to the basion and often articulates with the anterior arch of the atlas and the odontoid apex; it is therefore also called the "median occipital condyle" (Udare et al. 2014). It varies in length (0.65 cm in this case); Hadley mentioned that a third condyle with a length of 13–14 mm had been reported in the literature (Rao 2002).

Various structures similar to parts of the atlas have been seen around the foramen magnum and have been described as occipital vertebrae ("manifestation of occipital vertebra"). The atlas can be fused in whole or in part with the occipital bone ("assimilation of the atlas"). This variation occurs in about 0.5–1% of skeletons and has been interpreted by some authors as a cranial shift in the regional grouping of vertebrae in the vertebral column. Signs believed to be associated with assimilated or occipital vertebrae around the foramen magnum include: (a) a massive paramastoid process; (b) an enlarged jugular process; (c) the anterior margin of the foramen magnum thickened and raised to form a bar of bone between the condyles; (d) the hypoglossal canal divided by a bony bridge; and (e) a tertiary condyle and a facet or other marking for the apex of the dens on the anterior margin of the foramen magnum (Bergman et al. 1996).

Bony elements extending towards the foramen magnum are partly attributable to occipital vertebrae. Prakash et al. (2011) reported a single median tubercle situated at the anterior margin of foramen magnum (basion), with the apex facing backwards into the foramen magnum. The tubercle measured 5 mm anteroposteriorly and 3 mm transversely (Fig. 1.4).

Occipitalization of the atlas can be detected incidentally at autopsies or during routine cadaveric dissections, or in dry skulls

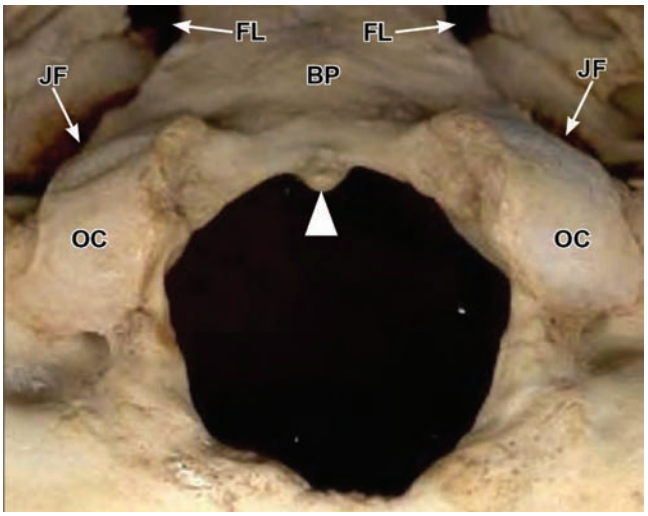

Figure 1.4 Photograph showing the tubercle at anterior margin of foramen magnum. BP: basilar part occipital bone; OC: occipital condyle; JF: jugular foramen; FL: foramen lacerum; white arrowhead: the tubercle.

Source: Prakash et al. (2011). Reproduced with permission from International Journal of Anatomical Variations.

in osteology classes. Fusion of the atlas with the occipital bone can result in compression of the vertebral artery and first cervical nerve. Occipitalization of the atlas (atlanto-occipital fusion, assimilation of the atlas) is a congenital osseous variation found in the craniovertebral junction. It is caused by assimilation of the first cervical vertebra (the atlas) to the basicranium (Bose and Shrivastava 2013).

Bose and Shrivastava (2013) reported a case where the atlas vertebra was almost completely fused with the occipital bone at the base of the skull, except at the transverse processes on both sides. The lateral masses had fused completely with the occipital condyles (Fig. 1.5).

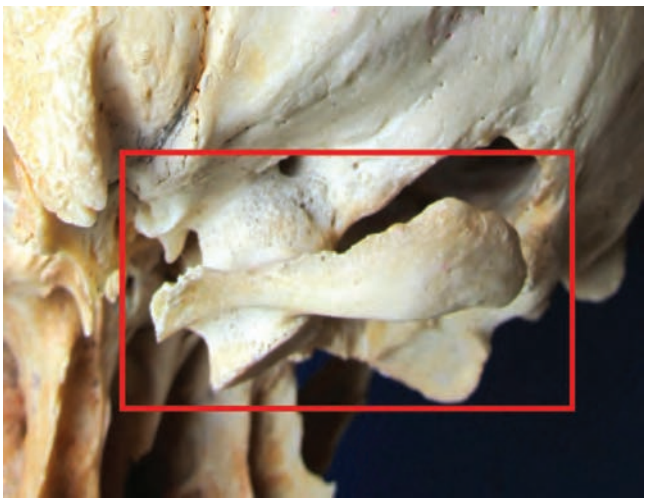

Figure 1.5 Illustration shows the side view of the skull to show the occipitalization of the atlas, shown in box.

Source: Bose and Shrivastava (2013). Reproduced with permission from International Journal of Anatomical Variations.

If there is duplication of the atlas, the condyles are of the occipitoatlantal type. In a series of 1246 skeletons, 13 (1.04%) exhibited two or more characteristics of manifestations of an occipital vertebra; 2 (0.16%) revealed assimilation of the atlas and were among 10 (0.80%) that manifested definite cranial shifting of the intersegmental boundaries of the vertebral column (Bergman et al. 1996).

Occipitalization is a congenital synostosis of the atlas to the occiput, which is a result of failure of segmentation and separation of the most caudal occipital sclerotome and the first cervical sclerotome during the first few weeks of fetal life. The degree of bony fusion between the atlas and occiput can vary; complete and partial assimilation have been described. In most cases assimilation occurs between the anterior arch of the atlas and the anterior rim of the foramen magnum, and is associated with other skeletal malformations such as basilar invagination, occipital vertebra, spina bifida of the atlas, or fusion of the second and third cervical vertebrae (Klippel-Feil syndrome). The incidence of atlanto-occipital fusion ranges from 0.14% to 0.75% of the population, both sexes being equally affected (Saini et al. 2009) (Fig. 1.6).

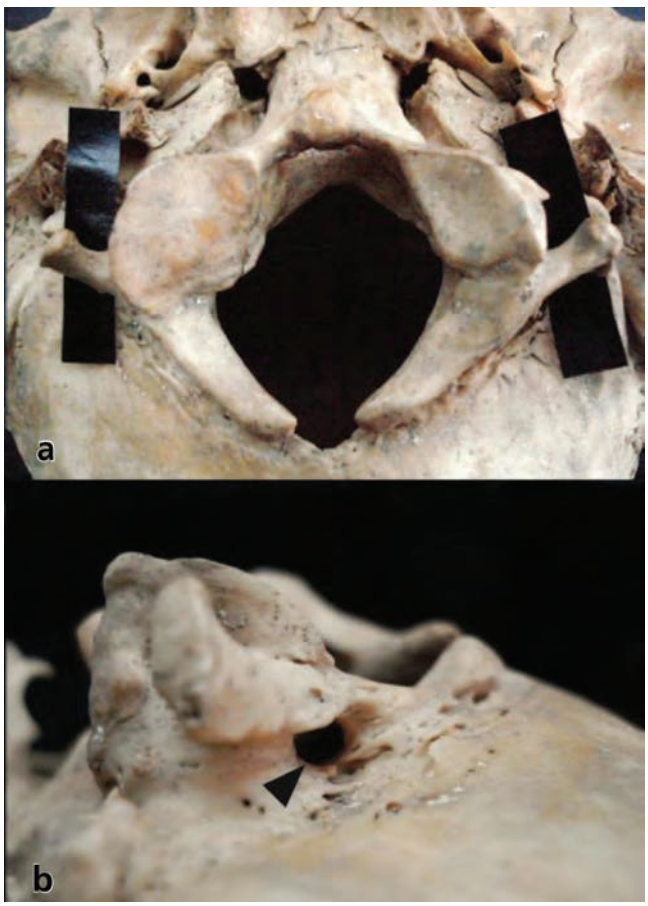

Figure 1.6 Total occipitalization of the atlas, with bifid posterior arch. (a) Incomplete foramen transversarium (black paper). (b) A foramen on the right side (arrowhead).

Source: Saini et al. (2009). Reproduced with permission from International Journal of Anatomical Variations.

Rarely, there is a bony canal in the clivus. This canal probably represents a persisting remnant of the notochord. Chauhan et al. (2010) reported a bony canal in the clivus traversing through the basilar part of the occipital bone from its superior to inferior surface. Considering the direction and location of the canal, they suggested two explanations for its formation: a connecting vein between the basilar plexus and pharyngeal venous plexus could pass through it, or it could have contained the remnant of the notochord (Fig. 1.7).

The hypoglossal canal exhibits variations. Five types can be distinguished: type 1, no evidence of division (typical single canal) (65.4%); type 2, one osseous spur located at either the inner or the outer orifice of the canal or inside it (16.1%); type 3, two or more osseous spurs along the canal (2.3%); type 4, complete osseous bridging in either the internal or external portion of the canal (13.1%); and type 5, complete osseous bridging occupying the entire extent of the canal (3.1%). Berry and Berry (1967) examined 585 skulls and discovered a double hypoglossal canal in 14.6%. The hypoglossal canal has been described as triple or quadruple in rare cases (Bergman et al. 1996; Paraskevas et al. 2009).

The jugular foramen can be divided into parts by intrajugular processes (Bergman et al. 1996). Six processes, arising from the petrous and the occipital bones, were identified and demonstrated in a study by Athavale (2010). The most prominent and common was the posterior petrous process toward the endocranial side, which has been described in the literature as an intrajugular process of the occipital bone and has formed the basis of previous classifications of the compartments of the jugular foramen. The tendency towards septation was more common near the endocranial side (Athavale 2010). Unusual bony projections can narrow the jugular foramen. Rastogi and Budhiraja (2010) reported a case in which a bony growth had converted the jugular foramen into a slit (Fig. 1.8). Such a narrow jugular foramen could cause neurovascular symptoms. Involvement of the ninth, tenth and eleventh cranial nerves at the jugular foramen is known as Vernet's syndrome, and could occur in such foramina (Rastogi and Budhiraja 2010). The right jugular foramen is usually larger than the left jugular foramen.

The grooving on the inner surface of the occipital bone is variable. In about 17% of cases the sagittal sulcus turns to join the left transverse sulcus. The sagittal sulcus can bifurcate, the larger groove turning to join the right transverse sulcus and the smaller one joining the left transverse sulcus (about 15% of cases). In rare cases, the larger groove joins the left and the smaller the right. In very rare cases, the right and left grooves appear equal in size (Bergman et al. 1996).

The shape of the foramen magnum varies in both children and adults. Lang (1990) classified the shapes into five groups: two semicircles (adults in 41.2% and children in 18.4%); elongated circle (adults in 22.4% and children in 20.4%); egg-shaped (adults in 17.6% and children in 25.5%); rhomboidal (adults in 11.8% and in children 31.6%); and rounded (adults

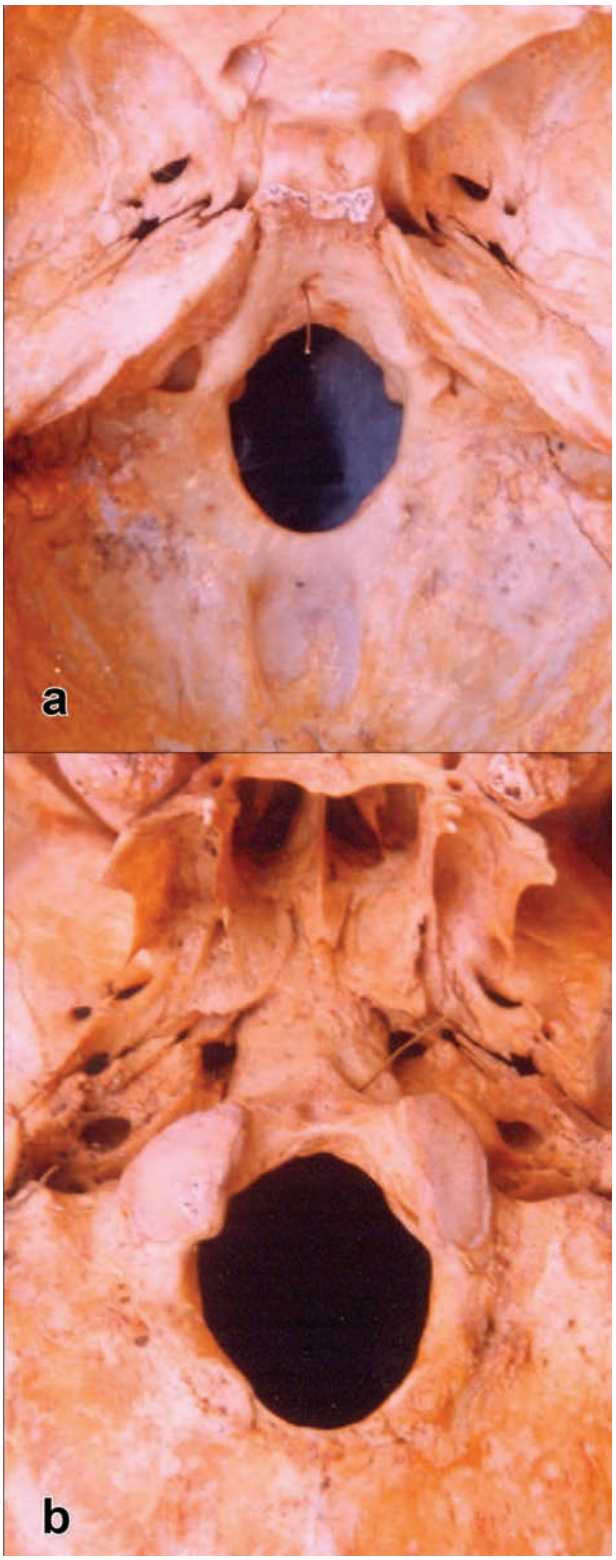

Figure 1.7 (a) Basis cranii interna showing inner opening of clival canal (wire in the canal). (b) Basis cranii externa showing outer opening of clival canal (wire in the canal).

Source: Chauhan et al. (2010). Reproduced with permission from International Journal of Anatomical Variations.

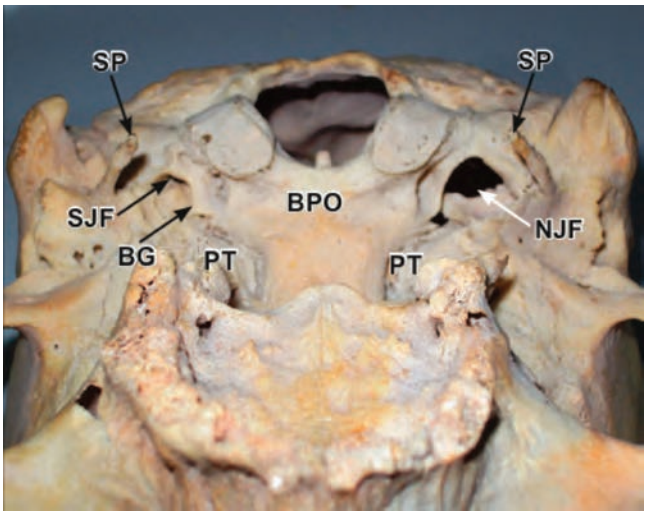

Figure 1.8 Skull base showing slit-like jugular foramen and the abnormal bone growth in the jugular fossa. NJF: normal jugular foramen; SJF: slit-like jugular foramen; BG: bone growth in jugular fossa; BPO: basilar part of the occipital bone; PT: petrous part of the temporal bone; SP: styloid process.

Source: Rastogi and Budhiraja (2010). Reproduced with permission from International Journal of Anatomical Variations.

in 7% and in children in 4%) (Bergman et al. 1996). Göçmez et al. (2014) determined the morphology of the foramen magnum using three-dimensional (3D) computed tomography and distinguished eight types of shape. In order of frequency, these were: round (18.8%); two semicircles (17.8%); egg-shaped (14.9%); hexagonal (13.9%); tetragonal (10.9%); oval (10.9%); pentagonal (8.9%); and irregular (4%). Burdan et al. (2012) examined Eastern European individuals using computed tomography. They found all the cranial and foramen measurements were significantly higher in individuals with the round type of foramen magnum. There was sexual dimorphism, related mainly to the linear diameters and area (not to the shape). There was a greater correlation between the examined parameters of the foramen and proper external cranial measurements in females than in males, which indicates more homogeneous growth in girls. Chethan et al. (2012) reported that in 20.7% of skulls the occipital condyle protruded into the foramen.

A Kerckring ossicle or pseudoforamen is sometimes seen. An accessory fontanelle can also be seen behind the foramen magnum and is known as the fontanelle of Hamy. A notch of the anterior rim of the foramen magnum is termed a keyhole foramen magnum.

Elevation of an area between the supreme and superior nuchal lines is termed a "torus occipitalis." Other names include "occipital spur." In these cases the inion can be greatly enlarged. It is the insertion site of the ligamentum nuchae (Bergman et al. 1996). The portion of the occipital bone between the superior and highest nuchal lines develops in membrane or in cartilage. This portion of the bone, which is denser, smoother, and

sometimes prominently bulged, is known as the torus occipitalis transversus; it forms a distinct projection in anthropoids and to a lesser extent in earlier races of man (Srivastava 1992).

Sutural bones are usually small, irregularly shaped ossicles, often found in the sutures of the cranium, especially in the parietal bones. When the lateral portions of the transverse occipital sutures persist, the situation is termed sutura mendosa. This starts from both lambdoidal sutures and represents the remnant of a transverse occipital suture. This suture forms an interparietal bone (Inca bone or intercalary bone or sutural bone). As many as 172 sutural or Wormian bones have been found in one skull (e.g., Bonthier D'Andernach's ossicle near the obelion). They are rarely found in the sutures of the face (Bergman et al. 1996). True interparietal bones or Inca bones are bounded by the lambdoid suture and sutura mendosa (transverse occipital suture). They were previously known as os Incae, os interparietale, or Goethe's ossicles. An Inca bone resembles the triangular architectural monument design of the Inca tribe; it is rare, ranging between 0.8% and 2.5%. Inca bones occur due to nonfusion of the multiple ossification centers in the membranous portion of the squamous part of the occipital bone (Udupi and Srinivasan 2011) (Fig. 1.9).

Other variants of the basiocciput include clefts, fissures, notochordal remnants, and intrasynchondrosal ossified bodies. Near the basioccipital junction, accessory ossicles known as the basiotic bone of Albrecht can sometimes be found. Accessory air cells of the jugular process of the occipital bone are known as the occipitojugular air cells of Mouret.

Figure 1.9 Photograph showing Inca (interparietal) bone.

Source: Udupi and Srinivasan (2011). Reproduced with permission from International Journal of Anatomical Variations.

Parietal bone

Accessory intraparietal or subsagittal sutures are rare but can be seen dividing the parietal bone. They can be explained on the basis of incomplete union of the two separate ossification centers. These are usually bilateral and fairly symmetrical, but can occasionally be unilateral. The pattern of development can give rise to numerous accessory sutures that could be mistaken for fractures, especially with plain film evaluation alone. A CT scan with 3D reconstruction is vital for further characterization of a questionable fracture (Sanchez et al. 2010).

In the anterior between the paired frontal and parietal bones there is sometimes an accessory ossicle, os bregmaticum, either free or fused with one of the frontals or parietals (Bergman et al. 1996). The anterior fonatanelle may remain open and the normal time to closure of this area is between 4 and 26 months of age (Tunnessen 1990).

A 14-week-old girl presented with characteristic signs of metopic craniosynostosis and frontal cranioplasty was recommended. Upon inspection of the cranium at the time of surgery, a large symmetrical bregmatic accessory bone (measuring 4.5 cm^2, pentagonal) was discovered. The cranium was broadly examined, including the area posterior to the region of the lambda and the area inferior to the squamosal sutures. No other unusual bones were present (Stotland et al. 2012).

Sutural or Wormian bones are small irregularly shaped bones found at the cranial sutures. Their size, shape, and number differ from skull to skull. A sutural bone is occasionally present at the pterion or junction of the parietal, frontal, greater wing of the sphenoid, and the squamous portion of the temporal bone. It is called "pterion ossicle," "epipteric bone," or Flower's bone. Nayak and Soumya (2008) reported a case of three sutural bones at the pterion (Figs 1.10, 1.11).

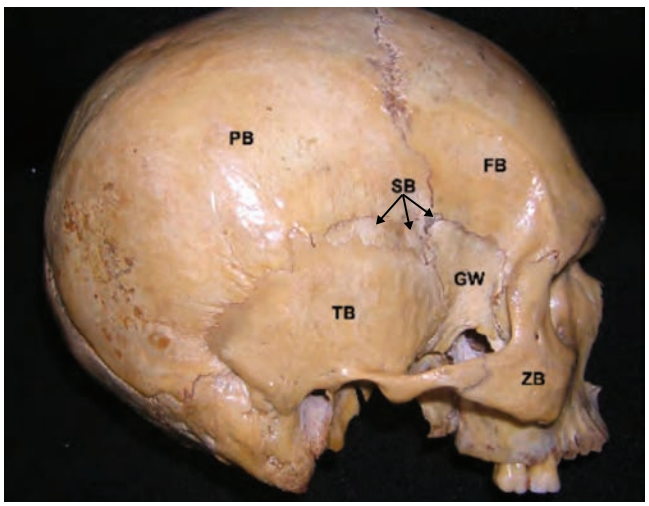

Figure 1.10 Lateral view of the skull showing sutural bones at the pterion. PB: parietal bone; FB: frontal bone; TB: temporal bone; GW: greater wing of sphenoid bone; SB: sutural bones; ZB: zygomatic bone.

Source: Nayak and Soumya (2008). Reproduced with permission from International Journal of Anatomical Variations.

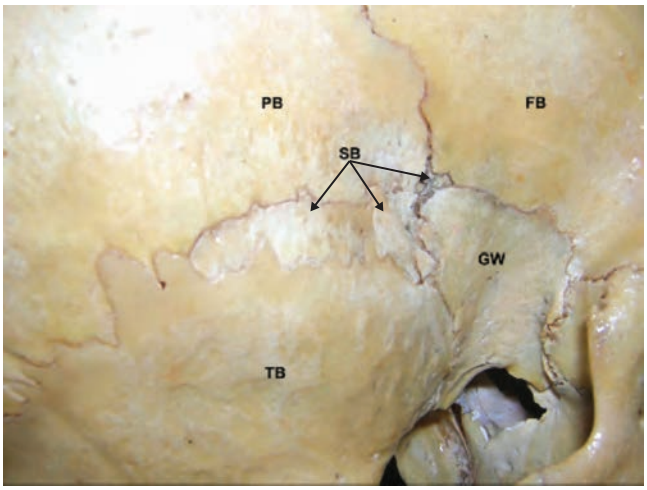

Figure 1.11 Closer view of the pterion with the sutural bones. PB: parietal bone; FB: frontal bone; TB: temporal bone; GW: greater wing of sphenoid bone; SB: sutural bones.

Source: Nayak and Soumya (2008). Reproduced with permission from International Journal of Anatomical Variations.

Sphenoid bone

The sphenoidal sinus varies in size, septation, and extensions. The dimensions of the average sinus are 20 mm (height), 18 mm (width), and 12 mm (length). The capacity of the sphenoidal sinus varies from 0.5 to 30 mL, averaging about 7.5 mL. The bony plate separating the sphenoidal sinus from the optic nerve, maxillary division of the trigeminal nerve, the nerve of the pterygoid canal, the cavernous sinus, the carotid artery, and the hypophysis is sometimes very thin or absent, rendering these structures vulnerable in chronic sinus infections (Bergman et al. 1996). Idowu et al. (2009) reported a main single intersphenoid septum in 95% of patients. Poirier et al. (2011) studied high-resolution computed tomographic scans of patients undergoing endoscopic trans-sphenoidal pituitary tumor resection. They reported a mean of 1.57 septations for each sphenoid sinus. Çakur et al. (2011a, b) investigated the prevalence of sphenoid sinus hypoplasia and agenesis using dental volumetric computed tomography in an adult population. They reported no bilateral agenesis of the sphenoid sinus, though there was unilateral agenesis in 0.26% of the sample and sphenoid sinus hypoplasia was seen in 0.52% (unilateral in 0.26%, bilateral in 0.26%).

A bony bridge sometimes connects the anterior and posterior clinoid processes, which are more usually connected by the fibrous interclinoid ligaments. If these ossify they give rise to the anatomical variation, which some authors consider rare. Its nomenclature in the literature is still vague; it has been variously named the interclinoid tenia, sella bridge, or interclinoid bony bridge. Its prevalence could be as high as 5% (Bergman et al. 1996; Aragão et al. 2013).

The sella turcica can be absent, hypoplastic, enlarged, and/or empty (i.e., empty sella syndrome). It has been reported to be duplicated or to have an intrasellar tubercle or spike.

The caroticoclinoid foramen is an inconstant structure located in the anterior cranial fossa. It is formed by the ossification of a fibrous ligament that begins on the anterior clinoid process and binds to the middle clinoid process. The caroticoclinoid foramen is a space through which the clinoidal segment of the internal carotid artery passes. It has an approximate diameter of 5.0–5.5 mm and causes morphological changes in the internal carotid artery in almost all cases, creating difficulty for neurosurgical techniques in the region (Freire et al. 2010) (Fig. 1.12).

Occasionally, ligaments near the foramen ovale – the pterygospinous (ligament of Civinini) and pterygoalar (ligament of Hyrtl) ligaments – ossify and form variant foramina. The pterygoalar bar is a bony bridge that stretches between the lateral pterygoid lamina and the greater wing of the sphenoid bone; the space under this bar is termed the pterygoalar foramen (Skrzat et al. 2005). Pterygospinous foramina occur in about 5% of cases. In another study, the pterygospinous foramen was found in 6.28% of 1544 skulls and in 5.46% of a second series of 2745 skulls in American whites and blacks; it was more frequent in the whites and in males (Bergman et al. 1996). Tubbs et al. (2009) analyzed 154 adult dry human skulls and reported one pterygospinous foramen (foramen of Civinini) and one pterygoalar foramen (foramen of Hyrtl). A study of 160 skulls revealed complete and incomplete pterygospinous foramina in 1.25% and 7.5%, respectively (Saran et al. 2013).

The foramen rotundum is 1–5 mm from the superior orbital fissure and has a lateral angulation of 3–20° (Sondheimer 1971).

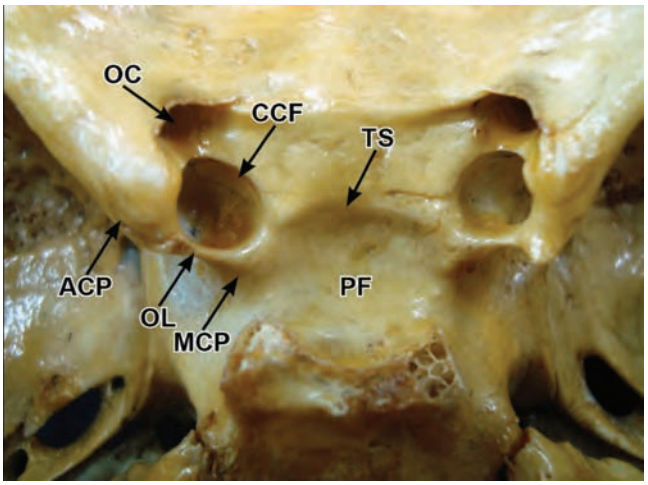

Figure 1.12 Internal view of skull with the caroticoclinoid foramen and adjacent structures. (CCF: caroticoclinoid foramen; ACP: anterior clinoid process; OL: ossified ligament; MCP: middle clinoid process; OC: optic canal; TS: tuberculum sellae; PF: pituitary fossa).

Source: Freire et al. (2010). Reproduced with permission from International Journal of Anatomical Variations.

Its length falls within the range 1–5 mm and average width is 1.5–4 mm. A small foramen within the foramen rotundum can sometimes be found in its inferomedial wall and might transmit an emissary vein (Sonheimer 1971). The foramen may be narrowed or missing.

Among several foramina on the greater wing of the sphenoid bone, the inconstant foramen of Vesalius connects the pterygoid plexus with the cavernous sinus and transmits a small emissary vein that drains the cavernous sinus. The importance of this foramen is that it offers a pathway for the spread of infection from an extracranial source to the cavernous sinus. The small foramen of Vesalius, if present, is generally situated posteromedially from the foramen rotundum and anteromedially from the foramen ovale, foramen spinosum, and carotid canal. In a study of 377 dry skulls, the foramen of Vesalius was present in 11.9% unilaterally and 4.2% bilaterally (Chaisuksunt et al. 2012). Vesalius was the first to describe and illustrate the foramen that bears his name (foramen Vesalii), which is 1–4 mm in diameter. It is also known as the sphenoid emissary foramen, foramen venosum (of Vesalius) and canaliculus sphenoidalis. When present, it is located between the foramen rotundum and the foramen ovale on its medial side. It is traversed by a vein (vein of Vesalius), a small emissary from the cavernous sinus to the pterygoid plexus. It is not uncommon: in 157 skulls it was found 26 times bilaterally (17%) and 20 times unilaterally (13%). One report suggests a frequency as high as 40% (unilateral or bilateral) (Bergman et al. 1996). In another study of 400 skulls, the foramen of Vesalius was identified in 135 (33.75%) and absent on both sides in 265 (66.25%). It was present bilaterally in 15.5%. Its incidence was 18.25%, 7.75% on the right side and 10.5% on the left (Shinohara et al. 2010). It is also variable in size, shape, and position.

An innominate canal of Arnold is sometimes found a few millimeters posterior to the foramen ovale and medial to the foramen spinosum. It is seen in about 20% of skulls. When present, the lesser petrosal nerve travels through this defect.

The foramen ovale occasionally exhibits variations. Its length ranges from 1 to 10 mm and the width from 3 to 10 mm (Sondheimer 1971). Ray et al. (2005) observed variant foramina ovale in 24.2% of the skulls they studied. Its venous segment can be separated from the remainder of its contents by a bony spur, resulting in a so-called doubled foramen ovale. Such spurs are present in 0.5% of subjects studied (Bergman et al. 1996). Reymond et al. (2005) found that the foramen ovale is divided into two or three components in 4.5% of cases. Moreover, the borders of the foramen ovale in some skulls were irregular and rough. On radiological images this could suggest morbid changes, possibly the sole anatomical variation. An accessory process behind the foramen ovale is termed the process of Weber. When the innominate foramen is not present, the lesser petrosal nerve exits the skull through the foramen ovale. The foramen ovale can be confluent with the foramen lacerum and/or the foramina spinosum and Vesalius.

The foramen spinosum is 2–4 mm long and may communicate with the innominate foramen. Bergman et al. (1996) reported the absence of the foramen spinosum in 0.64–4.57% of cases. Nikolova et al. (2012) reported its absence as 0.72% on the right side and 2.13% on the left in medieval female skulls. The absence of the foramen spinosum involves an unusual development and course of the middle meningeal artery and is usually accompanied by replacement of the conventional middle meningeal artery with one arising from the ophthalmic artery system. In these cases, the middle meningeal artery most often enters the middle cranial fossa through the superior orbital fissure and rarely through the meningo-orbital foramen (Nikolova et al. 2012). If the middle meningeal artery has its usual origin, it enters the cranial cavity via the foramen ovale in the absence of a foramen spinosum (Bergman et al. 1996). When the lacrimal artery arises from the middle meningeal artery, it enters the middle fossa through an accessory foramen in the floor of the sphenoid bone known as the foramen of Hyrtl.

The superior orbital fissure can be divided into three anatomical regions by the annulus of Zinn: lateral, central, and inferior regions. The lateral wall of the superior orbital fissure can also be divided into upper and lower segments; and the angle between them was found to be 144.27±20.03° (Shi et al. 2007). According to Govsa et al. (1999), nine different types of shape of the superior orbital fissure were observed based on the classification of Sharma et al. (1988) (Fig. 1.13, Table 1.1). The shape of the superior orbital fissure was first classified into six different types by Shapiro and Janzen (1960). Sharma et al. (1988) added three new types to this classification and Magden et al. (1995) added eight original types to Sharma's classification. Natori and Rhoton (1994) measured the distance from the superomedial to the superolateral edges of the superior orbital fissure as 15.9 mm (7.7–22.1 mm), the distance from the superolateral to the inferior edge as 17.6 mm (10–24.3 mm), and the distance from the superomedial to the inferior edge as 7.0 mm (5.6–8.2 mm) (Natori and Rhoton 1995). Govsa et al. (1999) found the distance from the superomedial edge to the superolateral edge to be 17.3±3.4 mm on the right side and

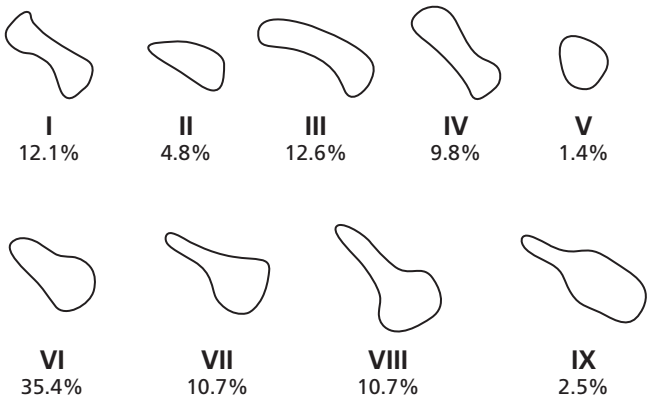

Figure 1.13 Variations in the shapes of the superior orbital fissure.

Source: Sharma et al. (1988).

Table 1.1 Comparative study of the types of shapes of the superior orbital fissure (percent).

Type	I	II	III	IV	V	VI	VII	VIII	IX	Other
Shapiro	40	16	12	12	11	9	—	—	—	—
Sharma	14	13	6.65	2.8	1.86	48.6	7.47	3.73	1.86	—
Magden	1.5	2.4	9.9	3.4	0.7	4.6	6	17.6	38.8	15.2
Govsa	12.1	4.8	12.6	9.8	1.4	35.4	10.7	10.7	2.5	—

Source: Govsa et al. (1999). Reproduced with permission from Wolters Kluwer Health.

16.9±2.9 mm on the left side, the distance from the superolateral to the inferior edge to be 20.8 ±3.9 mm on the right and 20.1±3.8 mm on the left side, and the distance from the superomedial to the inferior edge to be 9.5±2.2 mm on the right and 9.0±2.4 mm on the left side. Another study by Reymond et al. (2008) classified the morphology of the superior orbital fissure into nine types. Fissures A–E were grouped into one type and named type "a"; fissures F–I were grouped as morphological types "b." Type a occurred in 63% and type b in the remaining 37%. Type a had a mean length of 17.47 mm (SD=2.26) and a mean width of 7.31 mm (SD=2.34). Type b had a mean length of 12.48 mm (SD=3.15) and mean width of 7.86 mm (SD=2.45).

The inferior orbital fissure is medially narrower and laterally wider. Its anterolateral border in about 50% of individuals is formed by the zygomatic bone, while in the remaining 50% it is formed by the sphenoid and maxillary bones (Lang 2001). In rare cases, mainly in the older population, this part of the fissure may be thinned and orbital fat may protrude into the temporal fossa. Its length is approximately 20 mm long (Lang 2001). According to De Battista et al. (2012), the inferior orbital fissure length ranges from 25 to 35 mm (mean 29 mm). The length/width of the individual anterolateral, middle, and posteromedial segments averaged 6.46/5, 4.95/3.2, and 17.6/2.4 mm, respectively.

A study by Xu et al. (2004) classified the morphology of the inferior orbital fissure as either: (1) baseball bat shaped; or (2) V shaped.

The vomerobasilar canal lies between the sphenoid bone and the wings of the vomer. It is present in the majority of the cases. The palatovaginal canal is also present in the majority of the cases. The palatovaginal canal is formed by a longitudinal groove on the inferior surface of the vaginal process, which is converted into a canal anteriorly by the sphenoidal process of the palatine bone. Its anterior opening lies in the posterior wall of the pterygopalatine fossa. The posterior opening of the palatovaginal canal lies on the inferior surface of the vaginal process of the sphenoid bone. On that surface and posterior to the opening, a small groove is present in most cases. The vomerovaginal canal is bounded by the inferior surface of the sphenoid bone, the upper surface of the vaginal process of the pterygoid process. In 60% of the cases, the vomerovaginal canal originates posterior to the anterior opening of the pterygoid canal, with an average distance of 4.4 mm (Lang 1995). In the remaining 40%, the vomerovaginal canal originates within the pterygopalatine fossa medial to the anterior opening of the pterygoid canal. Tanaka (1932) found it arising from the anterior part of the pterygoid canal in 18.3% of his Japanese specimens. The overall mean length of the vomerovaginal canal was 7 mm.

Within the vomerovaginal canal there are on average three nerve fiber bundles with a thickness of 136 μm (55–370 μm) and also 1–3 arteries with an average lumen of 38 μm (74–814 μm). The median craniopharyngeal canal is present in 0.5% of the adult population. The lateral craniopharyngeal canal lies between the medial border of the superior orbital fissure and the vomerovaginal canal. It is usually seen in children of 6 years in age or less (Lang 2001).

The pterygoid canal travels below the level of the floor of the sphenoidal sinus in 38% of individuals (Lang 1989). The roof of the canal is dehiscent in 10% and the nerve runs at the same level in 18% (Lang 1989). The pterygoid canal (Vidian canal) is 11.5–23 mm long and, in 44% of cases, runs anteromedially. The posterior opening of the canal is 12.4–19.2 mm from the midline and the anterior opening is 5.5–17.5 mm from the midline (Lang 1989). In about one-third of skulls, the canal protrudes into the floor of the sphenoid sinus. In about 3% it is entirely within this sinus, and in 6% the roof of the canal is dehiscent (Sondheimer 1971).

The carotid canal is in the inferior aspect of the petrous part of the temporal bone; and is 5–6.5 mm wide and 3–4 cm long. It can be absent with associated agenesis of the internal carotid artery.

The basi-sphenoid can have a retro-orbital pseudoforamen.

The optic canal has variable dimensions as described by Maniscalco and Habal (1978) in their study of 83 cadavers, with a mean length of 9.22 mm (5.5–11.5 mm), mean horizontal canal width 7.18 mm (5–9.5 mm), mean medial canal wall proximal thickness 0.21 mm (0.1–0.31 mm), and mean optic ring thickness 0.57 mm (0.4–0.74 mm). In a study by Choudhry et al. (2005), the cranial openings of the optic canal viewed from the cranial aspect revealed a large number of recesses, fissures, and notches. In 229 sides (61.5%) of the 372 examined, the cranial opening of the optic canal was found to be associated with recesses on its lateral wall. These were bilateral in 224 sides (112 skulls) and unilateral in 7 sides. The recess was mostly accompanied by a fissure (42.4%) in the superior root of the lesser wing of the sphenoid bone. The upper slightly concave border of the roof had a small notch on 66 sides (17.7%).

A duplicated optic canal is a rare variation. Typically, the larger canal contains the optic nerve and the meninges and the smaller canal transmits the ophthalmic artery (Choudhry et al. 1988). Duplicated optic canals are separated by a septum of variable thickness dividing the posterior part of the canal into a large canal in the usual position and a smaller canal inferior to it or a bar forming the caroticoclinoid canal. Other duplicated canals may be divided by thin septae having a small slit (Choudhry et al. 1999). White (1923), Whitnall (1932),

Keyes (1935), and Choudhry et al. (1988, 1999) have reported duplicated optic canals. Bilaterally duplicated canals are very rare variations and are seldom reported in the literature (Zoja 1885; Le Double 1903; Warwick 1951; Choudhry et al. 1988; Magden and Kaynak 1996; Singh 2005).

Temporal bone

The styloid processes vary markedly in length and can comprise two–five osselets, articulating by synchondroses (Bergman et al. 1996); the stylohyoid ligament can calcify to make a rigid connection with the hyoid bone. A 75-mm-long styloid process has been reported but the usual length is 2–3 cm. When it is more than 3 cm it is called an elongated styloid process; and can cause pain in the throat, difficulty in swallowing, foreign body sensation, carotid artery compression syndrome, etc. This elongation was first described in 1652 by the Italian surgeon Pietro Marchetti. In 1937, Watt W. Eagle coined the term "stylalgia" to describe the pain associated with elongation of the styloid process. Kolagi et al. (2010) reported a case of bilaterally elongated styloid process with ossified stylohyoid ligament. The total length of the process was 8 cm and it was 1 cm thick at the base which is extremely rare. The styloid process proper was 5 cm long and the remaining 3 cm was ossified stylohyoid ligament, the junction between the two being marked by a bulge of bony mass (Fig. 1.14).

Mukherjee et al. (2011) reported a 24-year-old female who presented with a two-year history of foreign body sensation in her throat, more to the left side, along with dysphagia, excessive salivation, and vague pharyngeal pain radiating to the mastoid region aggravated by rotation of the head. Palpation of the tonsillar fossa revealed elongated styloid processes on both sides. Digital X-ray of the skull revealed asymmetrical ossification of bilateral stylohyoid chains. On the left side it comprised two components, with the long styloid process as proximal and calcified stylohyoid ligament as distal part, total length (approximately) 4.7 cm with prominent "pseudoarticulation." On the right side it was (approximately) 4.5 cm long, the distal portion being calcified stylohyoid ligament, but the proximal elongated styloid process was again divided into two parts representing its tympanohyal and stylohyal components (Fig. 1.15).

About 4% of the population has styloid processes more than 3 cm long; however, only 4.0–10.3% of these are symptomatic. Sasani et al. (2013) reported a case of bilateral elongated styloid processes that extended to the C3 vertebral level on the right side (78 mm) and C2 on the left (50 mm) (Fig. 1.16).

Embryologically, four different segments are present in the stylohyoid apparatus: the tympanohyal, stylohyal, ceratohyal, and hypohyal segments. The ligamentous part has its origin from the ceratohyal cartilage and extends from the stylohyal segment to the lesser horn of hyoid bone. There is a potential for ossification of the ligament, and when it is ossified there can be segmentation and pseudoarticulation (Sasani et al. 2013).

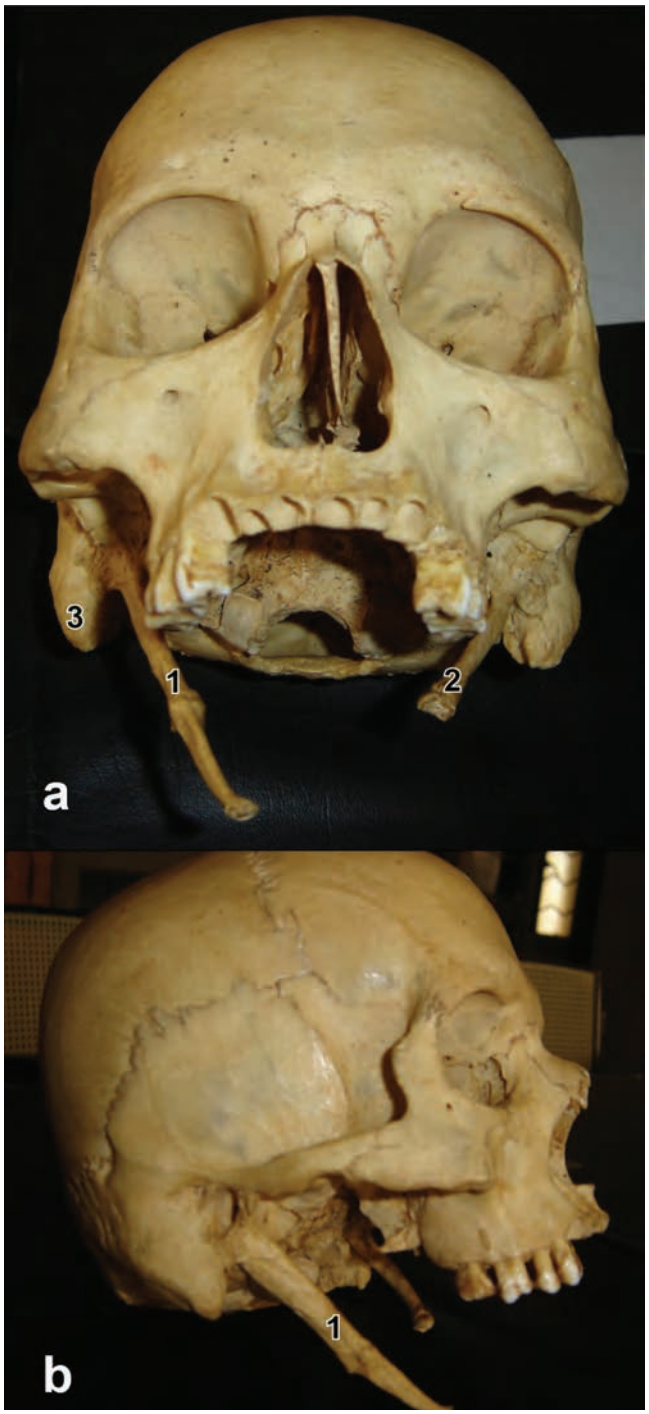

Figure 1.14 (a) Frontal view of skull showing bilateral elongated styloid processes. (b) Right elongated styloid process. 1: right styloid process; 2: left styloid process; 3: mastoid process.

Source: Kolagi et al. (2010). Reproduced with permission from International Journal of Anatomical Variations.

A canal or foramen (foramen of Hüschke) is found in the floor of the bony part of the external auditory meatus, near

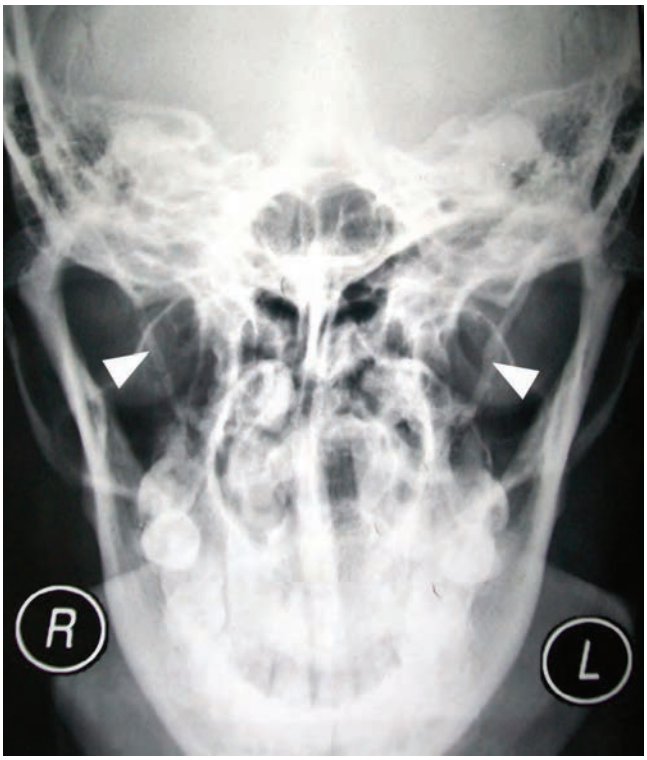

Figure 1.15 Photograph shows the bilateral asymmetrical ossification of the stylohyoid chain (white arrowheads).

Source: Mukherjee et al. (2011). Reproduced with permission from International Journal of Anatomical Variations.

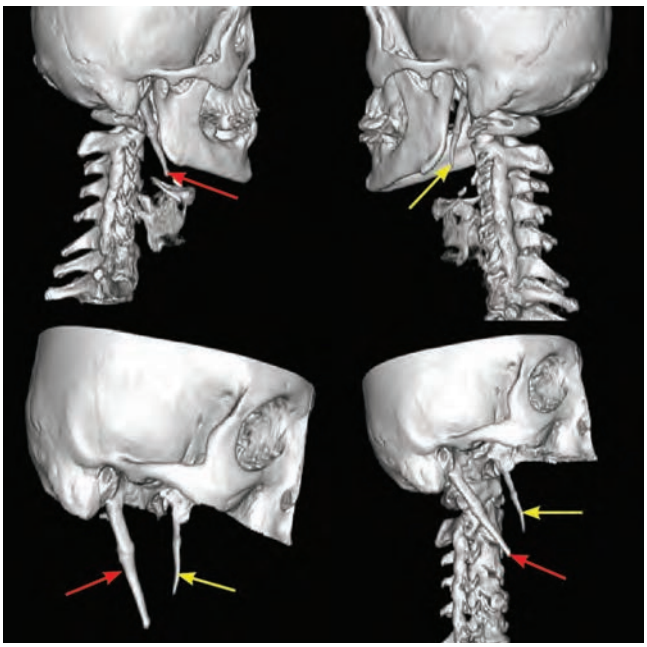

Figure 1.16 Bilateral elongated styloid processes are more prominent on the right side (red arrows) than the left side (yellow arrows), and extended to C3 vertebral level.

Source: Sasani et al. (2013). Reproduced with permission from International Journal of Anatomical Variations.

the tympanic ring, during the first five years of life. It can persist throughout life (Bergman et al. 1996). The German anatomist Hüschke (1797–1858) first described the probability of a deficiency in the development of the tympanic plate of the temporal bone, named the "foramen of Hüschke" or foramen tympanicum, which usually becomes apposed in adulthood. If it persists in adult life, complications can ensue such as herniation of the temporomandibular joint (TMJ), formation of salivary otorrhea, and spread of infection or tumor from the external acoustic meatus to the infratemporal fossa and vice versa. Srimani et al. (2013) identified seven cases of foramen of Hüschke among 53 skulls studied. The diameter of the foramen was 1–3 mm (Srimani et al. 2013) (Fig. 1.17). The external auditory meatus is sometimes duplicated (Vokurka 1989).

The mastoid process can have a doubled apex, the medial portion being divided from the lateral by a fissure. Usually, the medial lip of the groove forms a distinct ridge and provides the point of attachment of the digastric muscle; an enlarged paramastoid process can result from the development of air cells within the medial portion of the process. Air cells, usually confined to the mastoid process, can invade the horizontal or vertical part of the squama or even the pars petrosa (Bergman et al. 1996). In a study of 298 temporal bones, 6% of the mastoid processes exhibited variations. There was no statistically significant difference between genders (Manolis et al. 2008).

The petrosphenoid ligament may be ossified and result in a bony foramen for the abducens nerve to travel through. Acessory ossicles can be present in the foramen lacerum and are known as ossicles of Cortese and Riolan. An accessory tubercle

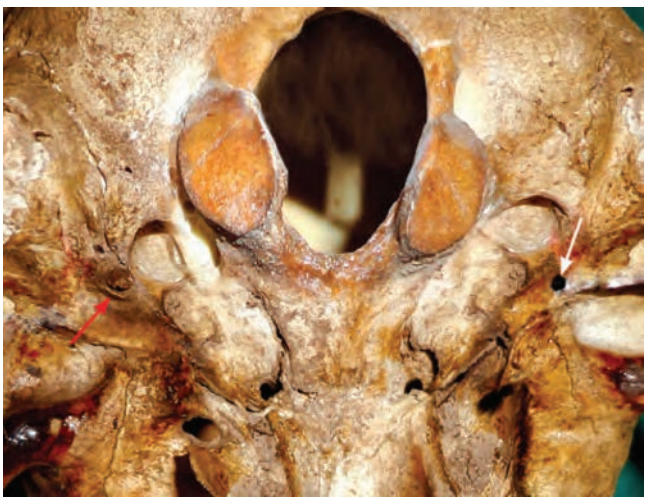

Figure 1.17 Figure showing a single oval-shaped foramen (red arrow) having transverse diameter of 0.2 cm and longitudinal diameter of 0.1 cm was noted on the left tympanic plate, and a single rounded foramen (white arrow) of 0.1 cm in diameter is present on the right side.

Source: Srimani et al. (2013). Reproduced with permission from International Journal of Anatomical Variations.

of the supramastoid crest is known as the tubercle of Waldeyer. The internal acoustic meatus can be narrowed, dehiscent, doubled, or tripled.

Ethmoid bone

The crista galli can be pneumatized (Bergman et al. 1996). Hajiioannou et al. (2010) reviewed computed tomography findings of the morphology of the crista galli in 99 patients. Pneumatization of the crista galli was noticed in 14.1% of the scans.

The superior nasal conchae can also be pneumatized. Ariyürek et al. (1996) evaluated CT scans of 52 patients who underwent CT examination prior to endoscopic sinus surgery and had normally aerated posterior ethmoidal cells and an unobscured nasal cavity. Pneumatization was evident in 48% of these patients. The superior turbinates seemed to be aerated through the posterior ethmoid cells.

There are sometimes accessory ethmoidal foramina. Takahashi et al. (2011) studied 54 orbits from 27 Japanese cadavers. Accessory ethmoidal foramina were detected in 18 orbits (33.3%) from 11 cadavers; one accessory foramen (middle ethmoidal foramen) was identified in 17 orbits, and two foramina (additional deep middle ethmoidal foramina) in one orbit (Takahashi et al. 2011). The textbook number of ethmoid foramina is two; Lang (1983) found them on the left side in 68.3% of skulls and on the right side in 67.4%. In the remainder there were three–five; there were three foramina in about 40% of skulls (Bergman et al. 1996).

The perpendicular plate may protrude outward between the nasal bones (Lang 1989).

Lacrimal bone

The lacrimal bone can be divided into two or more parts or fused with neighboring bones. This bone sometimes exhibits so many minute foramina that it takes the appearance of a bony net (Bergman et al. 1996). Its thickness is variable. Hartikainen et al. (1996) reported the mean thickness of the bone as 106 μm. In 67% of patients the mean thickness of individual lacrimal bones was less than 100 μm and in 4% it was more than 300 μm. The thinnest measured cross-section of the lacrimal bone sample was 11 μm and the thickest was 722 μm. The lacrimal bone is composed of a thin plate of lamellar bone. An accessory ossicle located deep to the lacrimal bone has been termed the ossicle of the lacrimal canal or the ossicle of Gruber.

Vomer

Isolated vomer aplasia is rarely reported in the literature. It is a genetic variant presenting with no significant medical problems (Verim et al. 2012). Recently, absence of the vomer during the first two trimesters of pregnancy was identified as a marker of trisomy 21 and trisomy 13. There was no single case of trisomy in which the vomer could be identified during the first or early second trimester. The diagnostic accuracy of the vomer as a marker for trisomy was 0.985 (Mihailovic et al. 2012).

The vomer can be separated from the perpendicular plate of the ethmoid by a strip of cartilage from the nasal septum (Bergman et al. 1996). Rarely, a recess of the sphenoid sinus can extend into the vomer (Lang 1989).

Inferior nasal concha

Lang and Kley (1981) reported absence of the conchae, the vomer, and perpendicular plate. Bony bridges may exist between the inferior and middle nasal conchae. The inferior concha may be notched or have a curved convex surface.

Maxilla

Two or more infraorbital foramina have been described. Gruber reported that the number can range from one to five. In 1970, Kadanoff, Mutafov and Jordanov tabulated and illustrated the variety of infraorbital foramina found in over 1400 skulls; they found it doubled in 9%, tripled in 0.5%, and more than tripled in 0.3% (Bergman et al. 1996). Boopathi et al. (2010) examined 80 dry adult South Indian human skulls of unknown age and gender. Accessory infraorbital foramina were found in 16.25%. Saylam et al. (1999) examined 119 crania and 229 maxillae (a total of 467 infraorbital foramina); they found a single accessory foramen in 11.5% of specimens and double accessory foramina in 1.28%. In 79.6% of those with a single accessory foramen, the accessory foramen was superior and medial to the main opening.

The infraorbital canal issues a small branch on its lateral face close to its midpoint to allow the anterior superior alveolar nerve to pass. This small canal, sometimes called the canalis sinuosus, runs forward and downward to the inferior wall of the orbit, lateral to the infraorbital canal and bent medially to the anterior wall of the maxillary sinus, passing below the infraorbital foramen (Neves et al. 2012).

Maxillary sinus hypoplasia is an uncommon condition. It can be misdiagnosed as an infection or a neoplasm of the maxillary sinuses. Variations of the other paranasal structures, especially the uncinate process associated with maxillary sinus hypoplasia, have been defined. Maxillary sinus hypoplasia shows three distinct patterns: type I, mild hypoplasia of the maxillary sinus, normal uncinate process and a well-developed infundibular passage; type II, significant hypoplasia of the maxillary sinus, hypoplastic or absent uncinate process and absent or pathological infundibular passage; and type III, absence of an uncinate process and cleft-like maxillary sinus hypoplasia (Erdem et al. 2002).

Bilateral maxillary sinus aplasia or severe hypoplasia with associated paranasal sinus variations is extremely rare. Tasar et al. (2007) reported two cases with severe maxillary sinus hypoplasia/aplasia, one of them associated with other paranasal sinus variants. Aydinlioğlu and Erdem (2004) examined CT scans in the axial and coronal planes of the paranasal sinuses of 1526 patients. They reported only one case of bilateral and only one case of unilateral maxillary sinus aplasia.

The maxillary sinus can be septated. These septa are barriers of cortical bone that arise from the floor or the walls of the sinus, and can even divide the sinus into two or more cavities. They can originate during maxillary development and tooth growth, in which case they are known as primary septa, or can be acquired structures resulting from the pneumatization of the maxillary sinus after tooth loss, in which case they are called secondary septa. Between 13% and 35.3% of maxillary sinuses have septa (Maestre-Ferrín et al. 2010).

Accessory ostia of the maxillary sinus are found in about 30% of skulls; as many as three in one skull have been reported (Bergman et al. 1996).

The incisive part of the alveolar process can be an independent bone, the os incisivum (Bergman et al. 1996). The discovery of the premaxillary bone (os incisivum, os intermaxillare, or premaxilla) in humans has been attributed to Goethe, so it has also been named "os Goethei". However, Broussonet and Vicq d'Azyr obtained the same result in 1779 and 1780, respectively, using different methods. Early anatomists described this medial part of the upper jaw as a separate bone in the vertebrate skull; Coiter was the first in 1573 to present an illustration of the sutura incisiva in the human (Barteczko and Jacob 2004). Sutural bones can sometimes be seen in the sutures of the hard palate.

Palatine bone

One study demonstrated that the sphenopalatine foramen can be single (61.5–87%), double (11.1–32.5%), triple (1.9–5.5%), or quadrupled (0.05%) (Lang 1995). It is located at the superior nasal meatus in 81.5% of cases, between the middle and superior nasal meatus in 14.8%, and in the middle nasal meatus in 1.9% (Scanavine et al. 2009).

The lesser palatine canal is frequently absent. It can also be located between the palatine bone and maxilla (Bergman et al. 1996).

The torus palatinus is an overgrowth of bone in the palatal region and represents an anatomical variation. Its prevalence varies with the population studied and its etiology is still unclear; however, it seems to be a multifactorial disorder with genetic and environmental involvement. Surgical removal of the torus palatinus is indicated under the following circumstances: (1) deglutition and speech impairment; (2) cancer phobia; (3) traumatized mucosa over the torus; and (4) prosthetic reasons (Nogueira et al. 2013). Palatal tori are seen in approximately 20–30% of the population and are more common in females than in males. Frequently, these bony outgrowths are incidental findings on routine oral examinations, and there is often considerable variation in clinical appearance (Bennet 2013). Simunković et al. (2011) studied 1679 subjects, 985 females and 694 males in the age range 9–99 years, who were subjected to clinical examination and analysis of plaster casts. The torus palatinus was found in 42.9%, 40.1% of females and 46.8% of males, indicating a significantly higher prevalence in the male population (P=0.006). Interestingly, Sisman et al. (2008) studied 2660 patients and reported the prevalence of the torus palatinus as low as 4.1%. Yildiz et al. (2005) examined a total of 1943 schoolchildren, 1056 males and 887 females ranging in age from 5 to 15 years. The prevalence of the torus palatinus in the study population was 30.9%, and was significantly more frequent in females than males (34.3 vs 28.1%, P<0.005). Most of the palatine tori were smaller than 2 cm (91.5%) and in molar location (62.9%).

The hard palate has been reported to be duplicated by Bruns (1947) and can have a cleft. Wormian bones can be seen in between the palatine bones or between this bone and the maxillary part of the hard palate.

Zygomatic bone

The zygomatic bone is sometimes divided into two parts by either a horizontal or a vertical suture. Such a bipartite bone has been called os Japonicum (os Ainoicum) as it has mostly been observed in Japanese subjects. A sutural bone may be seen between the zygomatic bone and temporal bones where they join to form the zygomatic arch. Anil et al. (2000) studied 1266 zygomatic bones in 633 dry Anatolian skulls and 1348 zygomatic bones in 674 plain cranium radiographs of adult patients. The os Japonicum was present in 2.2% of female and 1.7% of male specimens. All 24 multipartite bones observed in the study were bipartite except for one. In addition, 15 of 690 female (2.2%) and 12 of 658 male (1.8%) zygomatic bones examined radiologically were bipartite or tripartite; there was a total of 674 plain cranium radiographs. Jeyasingh et al. (1982) studied 500 crania in Uttar Pradesh and found the prevalence of os Japonicum to be 4%. Typical bipartite zygomatic bone was present in 40 instances. In only 6 bones, a horizontal groove was seen on the temporal surface. In one skull the zygomatic process of the maxilla and the zygomatic process of the temporal bone articulated directly on the temporal surface of the zygomatic bone. In another skull the maxilla and the temporal bone articulated with each other along the lower border of the zygomatic bone, giving the appearance of a tripartite condition.

Multiple zygomaticofacial and zygomaticotemporal canals can be observed; their detailed intrabony courses are unknown. Kim et al. (2013) scanned 14 sides of the zygomatic bones with micro-computed tomography, with 32 μm slice thickness. They

found that some zygomaticotemporal canals originated from the zygomaticofacial canal. In 71.4% of specimens the zygomaticotemporal canals divided from the intrabony canal along the course of the zygomaticofacial canals; 28.6% of zygomaticotemporal canals were opened through each corresponding zygomaticotemporal foramen. The zygomaticofacial canal originated from the zygomaticoorbital foramen, divided into some of the zygomaticotemporal canals, and finally opened as the zygomaticofacial foramen. Aksu et al. (2009) evaluated the number of foramina on the facial aspects of zygomatic bones. There were none in 15.6%, one in 44.4%, two in 28.1%, three in 6.3%, four in 4.4%, and five in 1.3% of sides. Loukas et al. (2008) studied 200 dry human skulls for zygomaticofacial (ZF), zygomaticoorbital (ZO) and zygomaticotemporal (ZT) foramina. All three foramina varied from absence to as many as four small openings. The authors classified each of these foramina as types I–V for single, double, triple, quadruple, and absent foramina, respectively. The relative frequencies were as follows: type I, ZO 50%, ZF 40%, ZT 30%; type II, ZO 20%, ZF 15%, ZT 15%; type III, ZO 10%, ZF 5%, ZT 5%; type IV, ZO 3%, ZF 1%, ZT 0%; and type V, ZO 17%, ZF 39%, ZT 50%.

Similarly, Mangal et al. (2004) studied these foramina in 165 dry human skulls. A single ZF foramen was seen in 148 (44.9%) sides. Two ZF foramina were found in 92 (27.9%) sides, out of which 29 (8.8%) sides had one ZO foramen, while 63 (19.1%) sides had two ZO foramina. Three ZF foramina, a relatively uncommon occurrence, were found in 17 (5.1%) sides, which included eight (2.4%) sides with one less and nine (2.7%) sides with the same number of ZO foramina. Four ZF foramina were seen in one (0.3%) side with three on the orbital aspect, a feature not reported before.

Govsa et al. (2009) reported that the angle between the ZT nerve and the ZF nerve within the orbit was approximately 42.21 degrees. The mean (SD) distance between the orbital opening of the ZT nerve and the meeting point of the ZT nerve was measured as 9.21 (5.18) mm. The mean (SD) distance between the orbital opening of the ZF nerve and the meeting point of the ZT nerve was calculated as 11.22 (4.25) mm. The mean (SD) distance between the orbital opening of the ZFN and the infraorbital margin of the orbit was 13.04 (3.21) mm. According to Tubbs et al. (2012), the zygomaticotemporal nerve penetrated the facial muscles at a mean of 2.3 cm superior to the zygomatic arch.

The orbital eminence (eminentia orbitalis) or marginal tubercle (of Whitnall) is located on the orbital surface of the frontal process of the zygomatic bone just within the orbital margin and about 1 cm inferior to the frontozygomatic suture (Didio 1962). The marginal tubercle serves as an attachment point for the lateral check ligament. According to Lang (1989), the marginal tubercle is present in 20% of the cases before puberty and in 95% of adults. The marginal process was present in 4% of the cases.

Other authors have also studied the incidence of the marginal tubercle and are presented in Table 1.2.

Table 1.2 Incidence of marginal tubercle.

Reference	No. samples	Incidence (%)
Whitnall (1911)	2000 skulls	>95
Buschkowitsch (1927)	419 skulls	63
Kangas (1928)	1,350 skulls	80.1
Ono (1928)	164 skulls	80
Tomita (1935)	476 skulls	49.15
Didio (1942)	285 skulls and 100 living	89.56
Didio (1962)	163 skulls	96.3

Mandible

The mandible varies extensively in size and weight during an individual's lifetime. The chin can protrude or recede, and there can be one rather than two mental tubercles (Bergman et al. 1996). A torus mandibularis can be present on one or both sides of the lingual aspect of the mandible.

The mental foramen is sometimes doubled or tripled. It can be located as far forward as the first premolar or as far back as the second. In very rare cases a median mental foramen is present, comparable with an arterial canal normally found in certain apes (Bergman et al. 1996). Sahin et al. (2010) reported a case with double mental nerve and foramina in a 44-year-old trauma patient. On the left side, below the level of the premolar teeth, two mental nerves emerged from two different mental foramina. The nerves had almost the same diameter. One of the mental foramina was located more anterior and superiorly (Fig. 1.18).

In contrast to other primates the mental foramen is usually single in humans, but accessory foramina have been recorded. It has been suggested that separation of the mental nerve into several fasciculi earlier than the formation of the mental foramen up to the 12th gestational week could explain why accessory mental foramina are formed (Hasan et al. 2010). Naitoh et al. (2011) analyzed

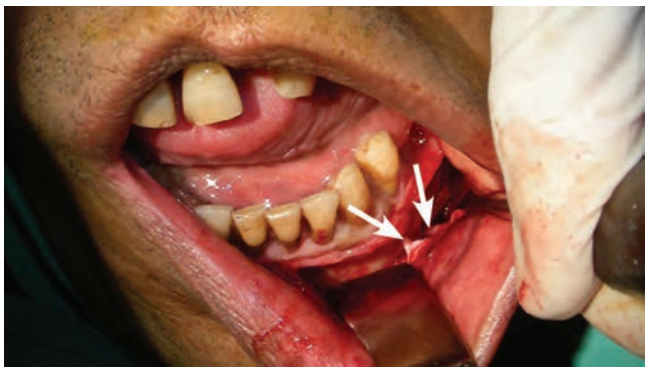

Figure 1.18 Intraoperative view of two mental nerves. (Arrows: mental nerves).

Source: Sahin et al. (2010). Reproduced with permission from International Journal of Anatomical Variations.

365 patients (130 males and 235 females). Para-panoramic images were reconstructed from cone-beam computed tomography (CBCT) images of the accessory mental foramen/foramina using 3D visualization and measurement software. A total of 37 accessory mental foramina were observed in 28 patients on CBCT images. Naitoh et al. (2009) studied CBCT images of 157 patients and found accessory mental foramina in 7%. The presence or absence of the accessory structure had no significant effect on the size of the mental foramen. The mean distance between the mental and accessory mental foramina was 6.3 mm (SD 1.5 mm). Toh et al. (1992) reported three cases with accessory mental foramina in which the distribution of the accessory mental nerve was different. These nerves communicated with the branches of the facial and buccal nerves.

In very rare cases the mental foramen is absent. The foramen was absent twice on the right side (0.06%) and once on the left side (0.03%) in a study of 1435 dry human mandibles (2870 sides) (de Freitas et al. 1979). The frequency of unilateral absence of the mental foramen ranges from less than 0.02% to 0.47%. No sexual or ethnic differences in absence of the mental foramen have been found (Hasan et al. 2010). Hasan et al. (2010) reported one case with bilateral absence of the mental foramina. The dry mandible (unspecified age and sex, and unknown ethnic background, average sized, and partially edentulous) was normal in all other aspects of gross morphology. The mandibular foramen was bilaterally symmetrical and the mandibular canal was patent to a distance of 3 cm on the right and 4.7 cm on the left side using a steel wire probe. Radiography established normal bone density with no evidence of age-related bone resorption or previous surgical or mechanical trauma, establishing that the case was one of congenital absence of the mental foramen (Fig. 1.19). An accessory foramen (of Dubreuil–Chambardel) has been described in the mandibular symphysis.

Figure 1.19 Dry human mandible with bilateral absence of mental foramen.

Source: Hasan et al. (2010). Reproduced with permission from International Journal of Anatomical Variations.

Figure 1.20 Mandible showing elongated coronoid processes, lateral view.

Source: Chauhan and Dixit (2011). Reproduced with permission from International Journal of Anatomical Variations.

Chauhan and Dixit (2011) reported a mandible with unusually long coronoid processes on both sides. It proved to be that of male in late adulthood. The length of the coronoid was taken from the line tangent to the deepest part of the mandibular notch to the apex; it measured 2.4 cm on the right and 2.6 cm on the left side (Fig. 1.20).

Coronoid processes project above the level of the condyles at the time of birth. As the neck of the mandible grows, it comes to lie at a lower level in adults. Unusual elongation of the coronoid process, formed of histologically normal bone with no synovial tissue around it, suggests hyperplasia. Bilateral hyperplasia of the coronoid processes of the mandible is quite infrequent and affects mostly males (male to female ratio 5:1) between the ages of 14 and 16. It leads to restricted mouth opening caused by impingement of the process on the medial and anterior surfaces of the zygomatic arch (Chauhan and Dixit 2011). Huang et al. (2013) studied mandibular morphology and dental anomalies to propose a relationship between mandibular/dental phenotypes and deficiency of CCAAT/enhancer-binding protein beta in mice. They concluded that CCAAT/enhancer-binding protein beta deficiency was related to elongation of the coronoid process and formation of supernumerary teeth.

A small accessory tubercle on the posterior border of the coronoid process is known as Delachapelle's tubercle. An accessory tubercle between the oblique line and anterior margin of the ramus of the mandible is termed the proeminentia lateralis of Rasche.

Nasal bone

There can be several nasal bones or only one (unpaired). Internasal bones have been found at the edges of the nasal bones in the upper corner of the piriform aperture, lying on the anterior tip of the perpendicular plate of the ethmoid (Fig. 1.21) (Bergman et al. 1996).

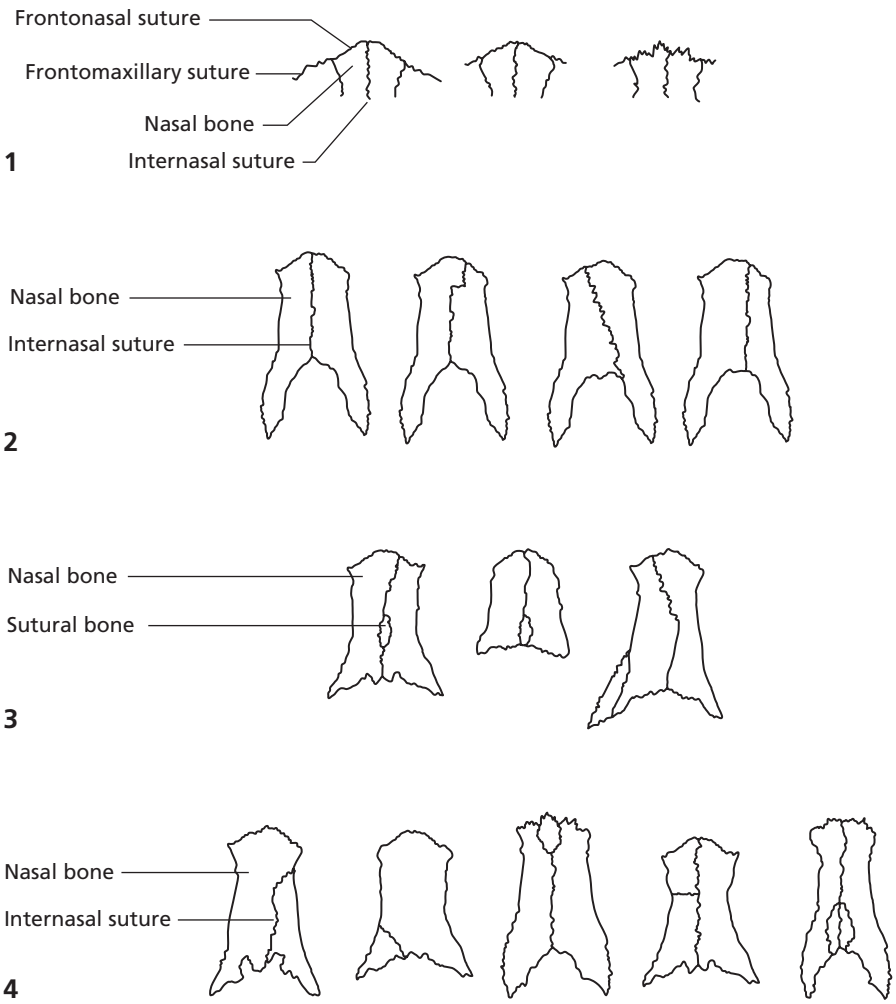

Figure 1.21 Variations in the sutures of the nasal bones. Redrawn after Krmpotić-Nemanić et al. (1988).

Teeth

It is common to find fewer (partial anodontia) than the normal complement of teeth, although complete absence (true anodontia) of the teeth has been reported (Woelfel and Scheid 1997). The upper lateral incisors are most often absent, then the second lower premolars, the wisdom teeth, and the medial incisors, in that order. The upper canines are rarely missing, the upper premolars and second molars even more rarely, and most rarely the first permanent molars (Bergman et al. 1996). The mandibular canine tooth and root can divide into labial and lingual parts or its lingual surface can be shovel-shaped. This rarely occurs with the maxillary canine (Woelfel and Scheid 1997).

Supernumerary teeth can appear in both deciduous and permanent dentitions, but usually in the permanent dentition, and occur in 0.3–3.8% of the population (Woelfel and Scheid 1997). The most common supernumerary tooth is a mesiodens, which is usually small and conical, between the maxillary incisors. This is generally followed by maxillary lateral incisor, maxillary fourth molar, and mandibular third premolar supernumeraries. Supernumerary maxillary premolar, canine, and mandibular fourth molar are the least common. The incidence in the mandibular anterior tooth area is about 0.01% (Rossi et al. 2010). Rossi et al. (2010) reported a supernumerary permanent lower incisor in the dry mandible of an adult Brazilian male. Owing to its location and morphology, the supernumerary tooth presented as a lower lateral incisor joined to the lower lateral incisor normal in the mandibular arch through their distal and mesial contact faces, respectively (Figs 1.22, 1.23).

Ozgul et al. (2013) evaluated 7551 non-syndromic patients aged 3–16 years who applied for routine check-up. Supernumerary teeth were detected in 74 (0.98%). Of these, 48 were male and 26 were female (male-to-female ratio: 1.84:1). A total of 84 supernumerary teeth were detected, 80 (95.2%) permanent and four (4.8%) deciduous (n=4). Most supernumerary teeth (n=59, 70.2%) were located in the maxillary arch. The most common supernumerary teeth were mesiodens (36.9%), followed by those located in the maxillary incisor region (33.3%), the mandibular

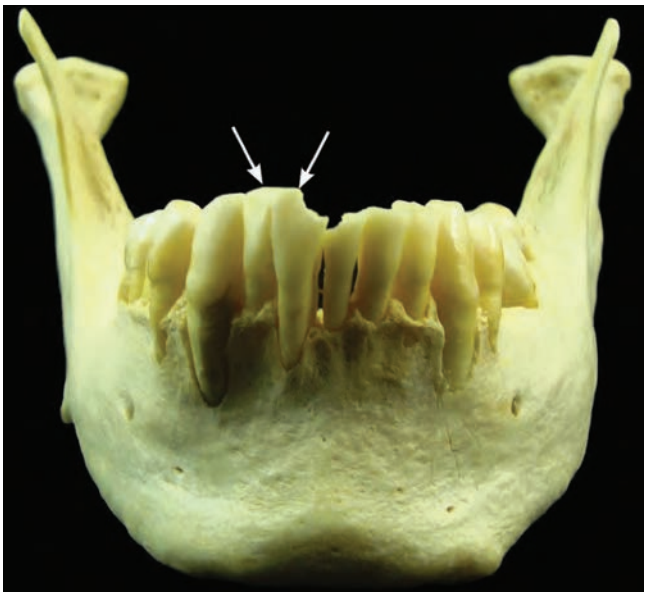

Figure 1.22 Frontal view of the mandible showing the two lateral incisors (arrows: lateral incisors).

Source: Rossi et al. (2010). Reproduced with permission from International Journal of Anatomical Variations.

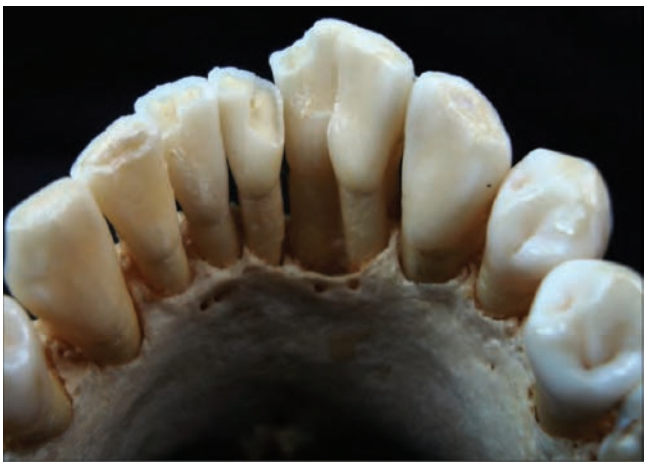

Figure 1.23 Occlusal view showing the union of the lateral incisors on the mesial surface.

Source: Rossi et al. (2010). Reproduced with permission from International Journal of Anatomical Variations.

premolar region (17.9%), the mandibular molar region (5.9%), the mandibular incisor region (4.8%), and the mandibular canine region (1.2%). Overall, the prevalence of supernumerary teeth was 0.98% and the mesiodens was the most common type. Mossaz et al. (2014) studied 82 patients with supernumerary teeth in the maxilla and mandible using cone-beam computed tomography. The study comprised a total of 101 supernumerary teeth. Most of the patients (80.5%) exhibited a single supernumerary tooth, while 15.8% had two and 3.7% had three. Males were affected more than females with a ratio of 1.65:1. Mesiodentes were the most frequently diagnosed type of supernumerary teeth (48.52%), followed by supernumerary premolars (23.76%) and lateral incisors (18.81%). Supernumeraries were most commonly conical in shape (42.6%) with a normal or inclined vertical position (61.4%).

Other oddities of the teeth include variable sizes, crown shape, peg-shaped lateral incisor or notched incisor or maxillary central incisors, fused teeth, multiple roots, accessory cusps or tubercles (e.g., cusp of Carabelli of the mesiopalatal upper first molar), shovel-shaped maxillary incisors, angled root, root fusion, segmented root, dwarfed (short) roots, unerupted teeth, transposition of the teeth, rotation of a tooth, and ectopic teeth (e.g., nasal septum) (Woelfel and Scheid 1997).

Middle ear bones

Stapes

The stapes exhibits marked variations. The head differs in the prominence of its margins, shape of the articular facet, and degree of inclination in relation to the crural arches. There is no correlation between the length of the stapes and its weight; the breadth and weight of the ossicle could be more closely related. In most cases the posterior crus was found to be thicker, larger, and more curved than the anterior crus. The junction of the anterior crus with the base is usually thinner than the junction of the posterior crus (Bergman et al. 1996).

Van de Maele et al. (1989) reported a columellaform stapes in an 18-year-old male patient with a conductive hearing loss. SEM and light microscopy demonstrated that the ossicle was smaller than normal. The head was linked to the base by a crural plate, probably formed by fusion of the material of the two crura. Microscopy demonstrated a slightly less interwoven structure of the fibrillar bone, mainly at the cranial aspect of the crural plate. Honeycomb-like bone was confined to the caudal part of the crural plate. Microscopy revealed a cavity in the center of the stapes at the transition between the base and the plate. During surgery, a bony structure was found to link the posterior side of the head of the stapes to the pyramidal eminence. The authors concluded that a columellaform stapes can occur without forming part of a syndrome.

Malleus

Arviso and Todd (2010) studied a total of 41 adult crania without clinical otitis. They measured: (1) the distance from the lateral process of the malleus to the umbo and to the annulus; and (2) the angles formed anteriorly and posteriorly at the umbo. The two metrics of malleus foreshortening did not correlate with one another; that is, the manubrium-length/tympanic-diameter ratio did not correlate with the posterior/anterior umbo angle ratio. Mastoid size did not correlate with either metric of malleus foreshortening. The authors concluded that a foreshortened malleus is an anatomical variant, not a sign of pathology.

Incus

Chien et al. (2009) studied the anatomy of the distal incus, including the lenticular process, in histological sections from 270 normal cadaveric human temporal bones covering an age range from less than 1 month to 100 years. All but nine of the sections exhibited signs of a bony connection between the long process of the incus and the flattened plate of the lenticular process, and in 108 specimens a complete bony attachment was observed in a single 20 μm section. In these 108 ears, the bony lenticular process consisted of a proximal narrow "pedicle" connected to a distal flattened "plate" that formed the incudal component of the incudo-stapedial joint. A fibrous joint capsule extended from the stapes head to the pedicle of the lenticular process on all sides, where it was considerably thickened.

References

Agarwal SK, Malhotra VK, Tewari SP. 1979. Incidence of the metopic suture in adult Indian crania. *Acta Anat (Basel)* 105: 469–474.

Aksu F, Ceri NG, Arman C, Zeybek FG, Tetik S. 2009. Location and incidence of the zygomaticofacial foramen: An anatomic study. *Clin Anat* 22: 559–562.

Anil A, Peker T, Turgut HB, Pelin C, Gülekon N. 2000. Incidence of os japonicum in Anatolian dry skulls and plain cranium radiographs of modern Anatolian population. *J Craniomaxillofac Surg* 28: 217–223.

Aragão JA, Fontes LM, Aragão JMR, Reis FP. 2013. Ossification of interclinoid ligaments and their clinical importance. *Int J Anat Var (IJAV)* 6: 201–202.

Ariyürek OM, Balkanci F, Aydingöz U, Onerci M. 1996. Pneumatised superior turbinate: a common anatomic variation? *Surg Radiol Anat* 18: 137–139.

Arviso LC, Todd NW Jr. 2010. The foreshortened malleus: Anatomic variant, not pathologic sign. *Otolaryngol Head Neck Surg* 143: 561–566.

Athavale SA. 2010. Morphology and compartmentation of the jugular foramen in adult Indian skulls. *Surg Radiol Anat* 32: 447–453.

Aydinlioğlu A, Erdem S. 2004. Maxillary and sphenoid sinus aplasia in Turkish individuals: a retrospective review using computed tomography. *Clin Anat* 17: 618–622.

Aydinlioğlu A, Kavakli A, Erdem S. 2003. Absence of frontal sinus in Turkish individuals. *Yonsei Med J* 44: 215–218.

Bademci G, Kendi T, Agalar F. 2007. Persistent metopic suture can mimic the skull fractures in the emergency setting? *Neurocirugia (Astur)* 18: 238–240.

Bajwa M, Srinivasan D, Nishikawa H, Rodrigues D, Solanki G, White N. 2013. Normal fusion of the metopic suture. *J Craniofac Surg* 24: 1201–1205.

Barteczko K, Jacob M. 2004. A re-evaluation of the premaxillary bone in humans. *Anat Embryol (Berl)* 207: 417–437.

Bennett WM. 2013. Images in clinical medicine. Torus palatinus. *N Engl J Med* 368: 1434.

Bergman RA, Afifi AK, Miyauchi R. 1996. Illustrated Encyclopedia of Human Anatomic Variation: Opus V: Skeletal Systems: Cranium. Available at http://www.anatomyatlases.org/AnatomicVariants/SkeletalSystem/Regions/Cranium.shtml (accessed 12 October 2015).

Berry AC, Berry RJ. 1967. Epigenetic variation in the human cranium. *J Anat* 101: 361–380.

Boopathi S, Chakravarthy Marx S, Dhalapathy SL, Anupa S. 2010. Anthropometric analysis of the infraorbital foramen in a South Indian population. *Singapore Med J* 51: 730–735.

Bose A, Shrivastava S. Partial occipitalization of atlas. 2013. *Int J Anat Var (IJAV)* 6: 81–84.

Bruns G. 1947. Über einen polygnathen Epignathus. *Virch Arch* 314: 125–136.

Burdan F, Szumiło J, Walocha J, Klepacz L, Madej B, Dworzański W, Klepacz R, Dworzańska A, Czekajska-Chehab E, Drop A. 2012. Morphology of the foramen magnum in young Eastern European adults. *Folia Morphol (Warsz)* 71: 205–216.

Buschkowitsch WJ. 1927. Ueber das "Tuberculum orbitale" des Jochbeins des Menschen. *Anat Anz* 63: 353–357.

Çakur B, Sumbullu MA, Durna NB. 2011a. Aplasia and agenesis of the frontal sinus in Turkish individuals: a retrospective study using dental volumetric tomography. *Int J Med Sci* 8: 278–282.

Çakur B, Sümbüllü MA, Yılmaz AB. 2011b. A retrospective analysis of sphenoid sinus hypoplasia and agenesis using dental volumetric CT in Turkish individuals. *Diagn Interv Radiol* 17: 205–208.

Chaisuksunt V, Kwathai L, Namonta K, Rungruang T, Apinhasmit W, Chompoopong S. 2012. Occurrence of the foramen of Vesalius and its morphometry relevant to clinical consideration. *Scientific World Journal* 2012: 817454.

Champion T, Cope JM. 2012. A severe case of hyperostosis frontalis interna and multiple comorbidities. *Int J Anat Var (IJAV)* 5: 76–78.

Chauhan NK, Chopra J, Rani A, Rani A, Srivastava AK. 2010. A bony canal in the basilar part of occipital bone. *Int J Anat Var (IJAV)* 3: 112–113.

Chauhan P, Dixit SG. 2011. Bilateral elongated coronoid processes of mandible. *Int J Anat Var (IJAV)* 4: 25–27.

Chethan P, Prakash KG, Murlimanju BV, Prashanth KU, Prabhu LV, Saralaya VV, Krishnamurthy A, Somesh MS, Kumar CG. 2012. Morphological analysis and morphometry of the foramen magnum: an anatomical investigation. *Turk Neurosurg* 22: 416–419.

Chien W, Northrop C, Levine S, Pilch BZ, Peake WT, Rosowski JJ, Merchant SN. 2009. Anatomy of the distal incus in humans. *J Assoc Res Otolaryngol* 10: 485–496.

Choudhry R, Choudhry S, Anand C. 1988. Duplication of optic canals in human skulls. *J Anat* 159: 113–116.

Choudhry R, Anand M, Choudhry S, Tuli A, Meenakshi A, Kalra A. 1999. Morphologic and imaging studies of duplicate optic canals in dry adult human skulls. *Surg Radiol Anat* 21: 201–205.

Choudhry S, Kalra S, Choudhry R, Choudhry R, Tuli A, Kalra N. 2005. Unusual features associated with cranial openings of optic canal in dry adult human skulls. *Surg Radiol Anat* 27: 455–458.

Comer BT, Kincaid NW, Smith NJ, Wallace JH, Kountakis SE. 2013. Frontal sinus septations predict the presence of supraorbital ethmoid cells. *Laryngoscope* 123: 2090–2093.

Danesh-Sani SA, Bavandi R, Esmaili M. 2011. Frontal sinus agenesis using computed tomography. *J Craniofac Surg* 22: e48–e51.

De Battista JC, Zimmer LA, Theodosopoulos PV, Froelich SC, Keller JT. 2012. Anatomy of the inferior orbital fissure: implications for endoscopic cranial base surgery. *J Neurol Surg B Skull Base* 73: 132–138.

de Freitas V, Madeira MC, Toledo Filho JL, Chagas CF. 1979. Absence of the mental foramen in dry human mandibles. *Acta Anat (Basel)* 104: 353–355.

Didio LJ. 1942. Observacoes sobre o "tuberculo orbitario" de Whitnall no osso zigomatico de homem (com pesquisas no vivo). *Anais Fac Med S Paulo* 18: 43–63.

Didio LJ. 1962. The presence of the eminentia orbitalis in the os zygomaticum of Hindu skulls. *Anat Rec* 142: 31–39.

Erdem T, Aktas D, Erdem G, Miman MC, Ozturan O. 2002. Maxillary sinus hypoplasia. *Rhinology* 40: 150–153.

Figueiredo N, Moraes LB, Serra A, Castelo S, Gonsales D, Medeiros RR. 2008. Median (third) occipital condyle causing atlantoaxial instability and myelopathy. *Arq Neuropsiquiatr* 66: 90–92.

Freire AR, Rossi AC, Prado FB, Caria PHF, Botacin PR. 2010. The caroticoclinoid foramen formation in the human skull and its clinical correlations. *Int J Anat Var (IJAV)* 3: 149–150.

Göçmez C, Göya C, Hamidi C, Kamaşak K, Yilmaz T, Turan Y, Uzar E, Ceviz A. 2014. Three-dimensional analysis of foramen magnum and its adjacent structures. *J Craniofac Surg* 25: 93–97.

Govsa F, Kayalioglu G, Erturk M, Ozgur T. 1999. The superior orbital fissure and its contents. *Surg Radiol Anat* 21: 181–185.

Govsa F, Celik S, Ozer MA. 2009. Orbital restoration surgery in the zygomaticotemporal and zygomaticofacial nerves and important anatomic landmarks. *J Craniofac Surg* 20: 540–544.

Hajiioannou J, Owens D, Whittet HB. 2010. Evaluation of anatomical variation of the crista galli using computed tomography. *Clin Anat* 23: 370–373.

Hartikainen J, Aho HJ, Seppä H, Grenman R. 1996. Lacrimal bone thickness at the lacrimal sac fossa. *Ophthalmic Surg Lasers* 27: 679–684.

Hasan T, Fauzi M, Hasan D. 2010. Bilateral absence of mental foramen — a rare variation. *Int J Anat Var (IJAV)* 3: 167–169.

Huang B, Takahashi K, Sakata-Goto T, Kiso H, Togo Y, Saito K, Tsukamoto H, Sugai M, Akira S, Shimizu A, Bessho K. 2013. Phenotypes of CCAAT/enhancer-binding protein beta deficiency: hyperdontia and elongated coronoid process. *Oral Dis* 19: 144–150.

Idowu OE, Balogun BO, Okoli CA. 2009. Dimensions, septation, and pattern of pneumatization of the sphenoidal sinus. *Folia Morphol (Warsz)* 68: 228–232.

Jeyasingh P, Gupta CD, Arora AK, Saxena SK. 1982. Study of Os japonicum in Uttar Pradesh crania. *Anat Anz* 152: 27–30.

Kadanoff D, Mutafov S, Jordanov J. 1970. The principle openings and incisures of the facial bones (incisura frontalis seu foramen frontale, foramen supraoriitale seu incisura supraorbitalis, foramen infraorbitale, foramen mentale). *Gegenbaurs Morphol Jahrb* 115(1): 102–118.

Kangas T. 1928. Das Vorkommen des "Tuberculum orbitale" in mensclichen Schaedel, insbesondere bei Finnen und Lappen. *Helsinki: Duodecim*, 68–74.

Keyes JEL. 1935. Observations on four thousand optic foramina. Albrecht v. *Graefes Archiv fur Ophthalmologie* 13: 538–568.

Kim HS, Oh JH, Choi DY, Lee JG, Choi JH, Hu KS, Kim HJ, Yang HM. 2013. Three-dimensional courses of zygomaticofacial and zygomaticotemporal canals using micro-computed tomography in Korean. *J Craniofac Surg* 24: 1565–1568.

Kolagi SI, Herur A, Mutalik A. 2010. Elongated styloid process – report of two rare cases. *Int J Anat Var (IJAV)* 3: 100–102.

Krmpotić-Nemanić J, Draf W, Helms J. 1988. *Surgical Anatomy of Head and Neck*. Berlin, Heidelberg: Springer-Verlag.

Lang J. 1983. *Clinical Anatomy of the Head, Neurocranium, Orbit and Craniocervical Region*. Berlin: Springer-Verlag.

Lang J. 1989. *Clinical Anatomy of the Nose, Nasal Cavity and Paranasal Sinuses*. New York: Thieme.

Lang J. 1990. *Clinical Anatomy of the Posterior Cranial Fossa and its Foramina*. Stuttgart, New York: Georg Thieme Verlag.

Lang J. 1995. *Clinical Anatomy of the Masticatory Apparatus and Peripharyngeal Spaces*. New York: Theime.

Lang J. 2001. *Skull Base and Related Structures, second edition*. New York: Thieme.

Lang J, Kley W. 1981. Über die agnesis und hypoplasie der concahe nasals und des septum nasi. *HNO* 29: 200–207.

Le Double AF. 1903. *Traite des Variations des Os du Crane de l'Homme p. 372*. Paris: Vigot Freres.

Loukas M, Owens DG, Tubbs RS, Spentzouris G, Elochukwu A, Jordan R. 2008. Zygomaticofacial, zygomaticoorbital and zygomaticotemporal foramina: anatomical study. *Anat Sci Int* 83: 77–82.

Maestre-Ferrín L, Galán-Gil S, Rubio-Serrano M, Peñarrocha-Diago M, Peñarrocha-Oltra D. 2010. Maxillary sinus septa: a systematic review. *Med Oral Patol Oral Cir Bucal* 15: e383–e386.

Magden AO, Kaynak S. 1996. Bilateral duplication of optic canals. *Ann Anat* 178: 61–64.

Magden O, Icke C, Arman C, Ozyurt D, Kaynak S. 1995. Fissura orbitalis superior: un original tipleri. *MN Oftalmoloji* 2: 130–135.

Mangal A, Choudhry R, Tuli A, Choudhry S, Choudhry R, Khera V. 2004. Incidence and morphological study of zygomaticofacial and zygomatico-orbital foramina in dry adult human skulls: the non-metrical variants. *Surg Radiol Anat* 26: 96–99.

Maniscalco JE, Habal MB. 1978. Microanatomy of the optic canal. *J Neurosurg* 48: 402–406.

Manolis E, Filippou D, Papadopoulos PV, Tsoumakas K, Katostaras T, Christianakis E, Fildisis G, Mompheratou E. 2008. Temporal bone and mastoid process morphology in Mediterranean population. *Ital J Anat Embryol* 113: 117–128.

May H, Peled N, Dar G, Abbas J, Hershkovitz I. 2011. Hyperostosis frontalis interna: what does it tell us about our health? *Am J Hum Biol* 23: 392–397.

Mihailovic T, Stimec BV, Terzic M, Dmitrovic A, Micic J. 2012. The absence of the vomer in the first and early second trimester of pregnancy – a new marker of trisomy 21 and trisomy 13. *Ultraschall Med* 33: E68–E74.

Mossaz J, Kloukos D, Pandis N, Suter VG, Katsaros C, Bornstein MM. 2014. Morphologic characteristics, location, and associated complications of maxillary and mandibular supernumerary teeth as evaluated using cone beam computed tomography. *Eur J Orthod* 36(6): 708–718.

Mukherjee P, Palit S, Tapadar A, Roy H. 2011. Asymmetrical bilateral ossification of stylohyoid chains — a case report with embryological review. *Int J Anat Var (IJAV)* 4: 134–136.

Naderi S, Korman E, Citak G, Güvençer M, Arman C, Senoğlu M, Tetik S, Arda MN. 2005. Morphometric analysis of human occipital condyle. *Clin Neurol Neurosurg* 107: 191–199.

Naitoh M, Hiraiwa Y, Aimiya H, Gotoh K, Ariji E. 2009. Accessory mental foramen assessment using cone-beam computed tomography. *Oral Surg Oral Med Oral Pathol Oral Radiol Endod* 107: 289–294.

Naitoh M, Yoshida K, Nakahara K, Gotoh K, Ariji E. 2011. Demonstration of the accessory mental foramen using rotational panoramic radiography compared with cone-beam computed tomography. *Clin Oral Implants Res* 22: 1415–1419.

Nakatani T, Tanaka S, Mizukami S. 1998. A metopic suture observed in a 91-year-old Japanese male. *Kaibogaku Zasshi* 73: 265–267.

Natori Y, Rhoton AL Jr. 1994. Transcranial approach to orbit: microsurgical anatomy. *J Neurosurg* 81: 78–86.

Natori Y, Rhoton AL Jr. 1995. Microsurgical anatomy of the superior orbital fissure. *Neurosurgery* 36: 762–775.

Nayak SB, Soumya KV. 2008. Unusual sutural bones at pterion. *Int J Anat Var (IJAV)* 1: 19–20.

Neves FS, Crusoé-Souza M, Franco LC, Caria PH, Bonfim-Almeida P, Crusoé-Rebello I. 2012. Canalis sinuosus: a rare anatomical variation. *Surg Radiol Anat* 34: 563–566.

Nikolić S, Djonić D, Zivković V, Babić D, Juković F, Djurić M. 2010. Rate of occurrence, gross appearance, and age relation of hyperostosis frontalis interna in females: a prospective autopsy study. *Am J Forensic Med Pathol* 31: 205–207.

Nikolova SY, Toneva DH, Yordanov YA, Lazarov NE. 2012. Absence of foramen spinosum and abnormal middle meningeal artery in cranial series. *Anthropol Anz* 69: 351–366.

Nogueira AS, Gonçales ES, Santos PS, Damante JH, Alencar PN, Sampaio FA, Garcia AS. 2013. Clinical, tomographic aspects and relevance of torus palatinus: case report of two sisters. *Surg Radiol Anat* 35: 867–871.

Ono R. 1928. Untersuchungen ueber die Orbita von Japaner. *Jap J Med Shi 1 Anatomy* 1: 307–308.

Ozer MA, Celik S, Govsa F, Ulusoy MO. 2011. Anatomical determination of a safe entry point for occipital condyle screw using three-dimensional landmarks. *Eur Spine J* 20: 1510–1517.

Ozgul BM, Arikan V, Oz FT. 2013. Prevalence and characterıstıcs of supernumerary teeth in a child population from central anatolıa — Turkey. *Oral Health Dent Manag* 12: 269–272.

Ozgursoy OB, Comert A, Yorulmaz I, Tekdemir I, Elhan A, Kucuk B. 2010. Hidden unilateral agenesis of the frontal sinus: human cadaver study of a potential surgical pitfall. *Am J Otolaryngol* 31: 231–234.

Paraskevas GK, Tsitsopoulos PP, Papaziogas B, Kitsoulis P, Spanidou S, Tsitsopoulos P. 2009. Osseous variations of the hypoglossal canal area. *Med Sci Monit* 15: BR75–BR83.

Poirier J, Duggal N, Lee D, Rotenberg B. 2011. Sphenoid sinus septations: unpredictable anatomic landmarks in endoscopic pituitary surgery. *J Otolaryngol Head Neck Surg* 40: 489–492.

Prakash BS, Latha PK, Menda JL, Ramesh BR. 2011. A tubercle at the anterior margin of foramen magnum. *Int J Anat Var (IJAV)* 4: 118–119.

Rao PV. 2002. Median (third) occipital condyle. *Clin Anat* 15: 148–151.

Rastogi R, Budhiraja V. 2010. Slit-like jugular foramen due to abnormal bone growth at jugular fossa. *Int J Anat Var (IJAV)* 3: 74–75.

Ray B, Gupta N, Ghose S. 2005. Anatomic variations of foramen ovale. *Kathmandu Univ Med J (KUMJ)* 3: 64–68.

Reymond J, Charuta A, Wysocki J. 2005. The morphology and morphometry of the foramina of the greater wing of the human sphenoid bone. *Folia Morphol (Warsz)* 64: 188–193.

Reymond J, Kwiatkowski J, Wysocki J. 2008. Clinical anatomy of the superior orbital fissure and the orbital apex. *J Craniomaxillofac Surg* 36: 346–353.

Rossi AC, Freire AR, Prado FB, Caria PHF, Botacin PR. 2010. Anatomical variation in a Brazilian human mandible: case report of a supernumerary permanent lower incisor. *Int J Anat Var (IJAV)* 3: 151–152.

Sahin B, Ozkan HS, Gorgu M. 2010. An anatomical variation of mental nerve and foramen in a trauma patient. *Int J Anat Var (IJAV)* 3: 165–166.

Saini V, Singh R, Bandopadhyay M, Tripathi SK, Shamal SN. 2009. Occipitalization of the atlas: its occurrence and embryological basis. *Int J Anat Var (IJAV)* 2: 65–68.

Sanchez T, Stewart D, Walvick M, Swischuk L. 2010. Skull fracture vs. accessory sutures: how can we tell the difference? *Emerg Radiol* 17: 413–418.

Saran RS, Ananthi KS, Subramaniam A, Balaji MT, Vinaitha D, Vaithianathan G. 2013. Foramen of civinini: a new anatomical guide for maxillofacial surgeons. *J Clin Diagn Res* 7: 1271–1275.

Sasani H, Ceyhan O, Sencer S, Sasani M. 2013. 3D reconstruction computerized tomography findings of an asymptomatic Eagle's Syndrome patient: a case report. *Int J Anat Var (IJAV)* 6: 176–178.

Saylam C, Özer MA, Bilge O, Ozek C, Alper M. 1999. Anatomic variations of the infraorbital foramen. *Ann Plast Surg* 43: 613–617.

Scanavine AB, Navarro JA, Megale SR, Anselmo-Lima WT. 2009. Anatomical study of the sphenopalatine foramen. *Braz J Otorhinolaryngol* 75: 37–41.

Shapiro R, Janzen AH. 1960. The Normal Skull. New York: Medical Division of Harper and Brothers.

Sharma PK, Malhotra VK, Tewari SP. 1988. Variations in the shape of the superior orbital fissure. *Anat Anz I65*: 55–56.

Shi X, Han H, Zhao J, Zhou C. 2007. Microsurgical anatomy of the superior orbital fissure. *Clin Anat* 20: 362–366.

Shinohara AL, de Souza Melo CG, Silveira EM, Lauris JR, Andreo JC, de Castro Rodrigues A. 2010. Incidence, morphology and morphometry of the foramen of Vesalius: complementary study for a safer planning and execution of the trigeminal rhizotomy technique. *Surg Radiol Anat* 32: 159–164.

Simunković SK, Bozić M, Alajbeg IZ, Dulcić N, Boras VV. 2011. Prevalence of torus palatinus and torus mandibularis in the Split-Dalmatian County, Croatia. *Coll Antropol* 35: 637–641.

Singh M. 2005. Duplication of optic canal in adult Japanese human skulls. *J Anat Soc India* 54(2): 1–9.

Sisman Y, Ertas ET, Gokce C, Akgunlu F. 2008. Prevalence of torus palatinus in cappadocia region population of Turkey. *Eur J Dent* 2: 269–275.

Skrzat J, Walocha J, Srodek R. 2005. An anatomical study of the pterygoalar bar and the pterygoalar foramen. *Folia Morphol (Warsz)* 64: 92–96.

Sondheimer FK.1971. Basal foramina and canals in Radiology of the Skull and Brain. *The Skull Vol 1*, Book 1 (Newton TH, Potts DG eds). Saint Louis: CV Mosby Co.

Srimani P, Mukherjee P, Ghosh E, Roy H. 2013. Variant presentations of "Foramen of Hüschke" in seven adult human crania. *Int J Anat Var (IJAV)* 6: 120–123.

Srivastava HC. 1992. Ossification of the membranous portion of the squamous part of the occipital bone in man. *J Anat* 180: 219–224.

Stotland MA, Do NK, Knapik TJ. 2012. Bregmatic wormian bone and metopic synostosis. *J Craniofac Surg* 23: 2015–2018.

Takahashi Y, Kakizaki H, Nakano T. 2011. Accessory ethmoidal foramina: an anatomical study. *Ophthal Plast Reconstr Surg* 27: 125–127.

Tanaka T. 1932. Ganglion sphenopalatinum des Menschen. *Arb. 3 Abt Anat Inst Kyoto* 3: 91–115.

Tasar M, Cankal F, Bozlar U, Hidir Y, Saglam M, Ors F. 2007. Bilateral maxillary sinus hypoplasia and aplasia: radiological and clinical findings. *Dentomaxillofac Radiol* 36: 412–415.

Toh H, Kodama J, Yanagisako M, Ohmori T. 1992. Anatomical study of the accessory mental foramen and the distribution of its nerve. *Okajimas Folia Anat Jpn* 69: 85–88.

Tomita S. 1935. On the tuberculum orbitale of the zygomatic bone in the Japanese (in Japanese). *Kanazawa daigaku igakubu kaibogaku kyoshitsu gyoseki* 20: 149–154.

Tubbs RS, May WR Jr, Apaydin N, Shoja MM, Shokouhi G, Loukas M, Cohen-Gadol AA. 2009. Ossification of ligaments near the foramen ovale: an anatomic study with potential clinical significance regarding transcutaneous approaches to the skull base. *Neurosurgery* 65: 60–64.

Tubbs RS, Mortazavi MM, Shoja MM, Loukas M, Cohen-Gadol AA. 2012. The zygomaticotemporal nerve and its relevance to neurosurgery. *World Neurosurg* 78: 515–518.

Tunnessen WW. 1990. Persistent open anterior fontanelle. *JAMA* 14: 2450.

Udare AS, Bansal D, Patel B, Mondel PK, Aiyer S. 2014. Condylus tertius with atlanto-axial rotatory fixation: an unreported association. *Skeletal Radiol* 43(4): 535–539.

Udupi S, Srinivasan JK. 2011. Interparietal (Inca) bone: a case report. *Int J Anat Var (IJAV)* 4: 90–92.

van de Maele C, Van Cauwenberge P, Kluyskens P, Vakaet L. 1989. Morphology of a columellaform stapes. *J Laryngol Otol* 103: 79–82.

Verim A, Faruk Çalım Ö, Yenigün A, Kocagöz GD, Kökten N, Özkul H. 2012. Hereditary characteristic of isolated congenital vomer aplasia. *J Craniomaxillofac Surg* 40: e392–e396.

Vokurka J. 1989. Congenital duplication of the external acoustic meatus. *Cesk Otolaryngol* 38: 314–317.

Warwick R. 1951. A juvenile skull exhibiting duplication of the optic canals and subdivision of the superior orbital fissure. *J Anat* 85: 289–291.

White LE. 1923. An anatomic and X-ray study of the optic canal in cases of optic nerve involvement. *Bos Med Surg J* 189: 741–748.

Whitnall SE. 1911. On a tubercle on the malar bone, and on the lateral attachments of the tarsal plaes. *Anat Physiol* 54: 426–432.

Whitnall SE. 1932. The Anatomy of the Hunan Orbit, second ed. London: Oxford University Press.

Woelfel JB, Scheid RC. 1997. Dental Anatomy: Its Relevance to Dentistry. Baltimore: Williams and Wilkins.

Xu LM, Zhang SZ, Xie XF. 2004. Inferior orbital fissure and groove: axial CT findings and their anatomic variation. *Fa Yi Xue Za Zhi* 20: 18–20.

Yildiz E, Deniz M, Ceyhan O. 2005. Prevalence of torus palatinus in Turkish schoolchildren. *Surg Radiol Anat* 27: 368–371.

Zoja G. 1885. Spora il foro ottico doppio. *Bollettino scientifico, Pavia*, 7, 65–69.

Further reading

Hauser G, De Stefano GF. 1989. Epigenetic Variants of the Human Skull. Stuttgart: E. Schweizerbart'sche Verlagsbuchhandlung.

Patil GV, Kolagi S, Padmavathi G, Rairam GB. 2011. The duplication of the optic canals in human skulls. J Clin Diag Res 5: 536–537.

Wolff E. 1976. Anatomy of the Eye and Orbit, seventh edition, vol. 15. London: HK Lewis.

2 Hyoid bone

R. Shane Tubbs[1] and Koichi Watanabe[2]
[1]Seattle Science Foundation, Seattle, Washington, USA
St George's University, School of Medicine, St Georges, Grenada
University of Dundee, Dundee, UK
[2]Kurume University School of Medicine, Fukuoka, Japan

The hyoid bone ossifies from six centers. The two centers that give rise to the lateral parts of the body are the basihyal and the two parts that give rise to the two centers of the greater horns are termed the thyrohyals. The two centers that give rise to the lesser horns are the ceratohyals (Evans 1940). The hyoid may be absent (Mendis and Moss 2007) or positioned more inferiorly than normal (Rajion et al. 2006). It may be located anterior to the thyroid cartilage (Kainz et al. 1990). The lesser horns may articulate with the greater horns (Porrath 1969) or be absent unilaterally or bilaterally (Fig. 2.1) (Gok et al. 2012). Parsons (1909) identified a synovial joint between the greater and lesser horns in 35 of 77 hyoid bones. This author also found that the lesser horn may fuse with the body of the hyoid and may do this without fusing to the lesser horn. In a radiographic study, Evans (1940) found lesser horns in only 20 cases. The lesser horns may persist into adulthood as partially or completely cartilaginous (Porrath 1969). The lesser horns may be elongated, especially when attached to a stylohyoid ossicular chain. Evans (1940) found that the lesser horn may be up to 12 mm in length. Janczak et al. (2012) described an adult male with syncope due to the carotid artery compression from an enlarged lesser horn of the hyoid bone. The hyoid may be connected to the styloid via a stylohyoid ossicular chain or continuous piece of bone (Krennmair and Piehslinger 1989). The greater horns may not fuse to the body of the hyoid (Porrath 1969), even in old age (Miller 1941). The greater horn of the hyoid may fuse to the greater horn of the thyroid cartilage or form a joint with the body of the hyoid bone. Ilankovan (1987) reported a 47-year-old male patient with an abnormal bone that articulated with the superior horn of the thyroid cartilage and the greater horn of the hyoid bone. Klinfelter (1952) reported a 39-year-old male who had suffered with pain in the right neck for 25 years. The pain came on with sudden rotation of the head to the right. Radiography identified a hyoid bone described as being 50% larger than usual. The right greater horn was 1.5 cm longer that the left greater horn. The right greater horn also consisted of a horizontal and vertical segment, which formed a number 7 shape. Additionally, the vertical segment formed a joint with the superior horn of the thyroid cartilage. The distal centimeter of the left greater horn was angulated 40 degrees posteroinferior. Puchowski (1933) reported a case where the thyrohyoid ligament was ossified. Di Nunno et al. (2004) found total fusion of the body of the hyoid bone with the greater horns in 10 (25%), partial fusion in 4 (10%), and evident articular rima between the body and the greater horns of the hyoid bone in 14 (35%). The lesser horns of the hyoid bone were symmetrical in 29 cases (72.5%), asymmetric in 11 (27.5), and absent in 1 (2.5%). A ridge may be found on the superior surface of the greater horn and mark the attachment of the middle pharyngeal constrictor muscle. The upward traction of the digastric and stylohyoid muscles on the greater horn may result in a slight notch.

Kanetaka et al. (2011) studied the structure of the joint between the body and the greater horn in the human hyoid bone in 259 cadavers (16–98 years). Joints were classified into three grades based on histological observations. Grade I showed fibrocartilage without degenerative change in the marginal region of the joint. Grade II showed prominent calcification or ossification on the outer margin of the joint without fusion. Grade III showed bony fusion. Evans (1940) described epihyal bones or ossification of parts of the stylohyoid ligament between the styloid process and hyoid bone. The hyoid may be pierced by the thyroglossal duct (Nathanson and Gough 1989). Kindschuh et al. (2012) found that the hyoid was broader in European versus African hyoids while the African hyoid was generally longer. The normally U-shaped hyoid may be horseshoe-shaped and may present with a midline superiorly projecting tubercle from the body termed the lingula (Ito et al. 2012). Kawar and Siplovich (2008) described a child with a bridge extending from the hyoid to the sternal notch.

Measurements (mm) of the hyoid bone (mean, SD, and range) for length, breadth, transverse diameter, medial height, anteroposterior thickness, maximum anteroposterior thickness, depth of the posterior surface, length of the greater horn, and width of the greater horn have been found to be: 36±4.1 (27.8–42.4); 40.7±5.2 (30.7–50.6); 23.4±2.5 (17.1–29.9); 10.6±1.2 (8–13.7); 5.1±1 (3.1–7.4); 5.1±1 (3.4–7.6); 2±0.7 (0.9–3.8); 28.1±3.8 (19.2–35.5); and 7±1.1 (5.2–9.3), respectively (Arsenburg et al. 1989). Papadopoulos et al. (1989) classified the hyoid bone into five types, in the following order of frequency: D-type, 29%; B-type, 26.5%; H-type, 21%; U-type, 18.5%; and V-type 5.0%. In 60% of the cases,

Bergman's Comprehensive Encyclopedia of Human Anatomic Variation, First Edition. Edited by R. Shane Tubbs, Mohammadali M. Shoja and Marios Loukas.
© 2016 John Wiley & Sons, Inc. Published 2016 by John Wiley & Sons, Inc.

Figure 2.1 Skeleton with absence of both lesser horns of the hyoid bone.

the shape of the hyoid bone did not belong to any of the shapes that are conventionally described. Almost half of the hyoid bones were asymmetric and/or anisometric. According to their width, the hyoid bones may be designated as narrow (45%), intermediate (34%), or wide (21%). There was no standard correlation of the distance between the tubercles of the greater horns to the distance between the lesser horns in the same hyoid bone.

The inferior aspect of the body of the hyoid may distinct knobs as identified in 6 of 108 hyoid specimens studied by Parsons (1909). He believed these to be outgrowths into the geniohyoid mucles. The mylohyoid often forms a slight ridge on the lower part of the anterior surface of the basihyal part of the hyoid (Parsons 1909).

References

Arensburg B, Tillier AM, Duday H, Schepartz LA, Rak Y.1989. A Middle Palaeolithic human hyoid bone. *Nature 338*: 758–760.

Di Nunno N, Lombardo S, Costantinides F, Di Nunno C. 2004. Anomalies and alterations of the hyoid-larynx complex in forensic radiographic studies. *Am J Forensic Med Pathol* 25: 14–19.

Evans WA. 1940. The epihyal bone; consideration of some small accessory bones of the neck. *Am J Roentgenol* 44: 714–715.

Gok E, Kafa IM, Fedakar R. 2012. Unusual variation of the hyoid bone: bilateral absence of lesser cornua and abnormal bone attachment to the corpus. *Surg Radiol Anat* 34: 567–579.

Ilankovan V. 1987. An anomaly of the thyro-hyoid articulation. *J Laryngol Otol* 101: 959–961.

Ito K, Ando S, Akiba N, Watanabe Y, Okuyama Y, Moriguchi H, Yoshikawa K, Takahashi T, Shimada M. 2012. Morphological study of the human hyoid bone with three-dimensional CT images: Gender difference and age-related changes. *Okajimas Folia Anat Jpn* 89: 83–92.

Janczak D, Skora J, Rucinski A, Szuba A. 2012. Recurrent syncope caused by compression of internal carotid artery by an anomalous hyoid bone. *Vasa* 41: 221–224.

Kainz J, Friedrich G, Anderhumber F. 1990. Two atavistic characteristics of the laryngeal skeleton. *Acta Anat (Basel)* 137: 103–108.

Kanetaka H, Shimizu Y, Kano M, Kikuchi M. 2011. Synostosis of the joint between the body and greater cornu of the hyoid bone. *Clin Anat* 24: 837–842.

Kawar B, Siplovich L. 2008. Congenital midline cervical skin bridge: a case report. *J Pediatr Surg* 43: 544–555.

Kindschuh SC, Dupras TL, Cowgill LW. 2012. Exploring ancestral variation of the hyoid. *J Forensic Sci* 57: 41–46.

Klinefelter EW.1952. The anomalous hyoid. Review of the literature and report of a case. *Radiology* 58: 224–227.

Krennmair G, Piehslinger E. 1999. The incidence and influence of abnormal styloid conditions on the etiology of craniomandibular functional disorders. *Cranio* 17: 247–253.

Mendis D, Moss AL. 2007. Case series: variations in the embryology of congenital midline cervical clefts. *Acta Chir Plast* 49: 71–74.

Miller RA. 1941. The laryngeal sacs of an infant and an adult gorilla. *Am J Anat* 69: 1–17.

Nathanson LK, Gough IR. 1989. Surgery for thyroglossal cysts: Sistrunk's operation remains the standard. *Aust N Z J Surg* 59: 873–875.

Papadopoulos N, Lykaki-Anastopoulou G, Alvanidou E. 1989. The shape and size of the human hyoid bone and a proposal for an alternative classification. *J Anat* 163: 249–260.

Parsons FG. 1909. Topography and morphology of the human hyoid bone. *J Anat Physiol* 43: 279–290.

Porrath S. 1969. Roentgenologic consideration of the hyoid apparatus. *AJR* 105: 63–73.

Puchowski B. 1933. Un cas d'anomalie de l'appareil hyoidien. *Acta-otolaryng* 18: 447–452.

Rajion ZA, Townsend GC, Netherway DJ, Anderson PJ, Hughes T, Shuaib IL, Halim AS, Samsudin AR, McLean NR, David DJ. 2006. The hyoid bone in Malay infants with cleft lip and palate. *Cleft Palate Craniofac J* 43: 532–538.

3 Cervical vertebrae

Joseph H. Miller, Michael C. Lysek and Mark N. Hadley
University of Alabama at Birmingham, Birmingham, Alabama, United States

The human cervical spine allows for a wide range of motion for the head while protecting the spinal cord, cervical nerve roots, and vertebral arteries. Variations in the bony anatomy of the cervical spinal column are common and fall on a continuum from near-normal to pathologic. The focus of this chapter is on variations of the cervical vertebrae and spinal column. These variants may have clinical significance and may present unique challenges in the operating room.

The cervical vertebrae are the most unique in the spine and exhibit a great deal of variability. The cervical spine supports the head and allows for a wide range of motion. The atlas (C1), axis (C2), and subaxial cervical spine are all unique bony structures with their own variations from what is seen in normal subjects.

Embryology

The developing fetal spine derives from the paraxial mesoderm that is located lateral to the neural tube. The paraxial mesoderm develops into paired somites that form the axial skeleton, associated ligaments, tendons, and paraspinal muscles (Dubrulle and Pourquié 2004; Mallo et al. 2009). The demarcation of individual vertebrae takes place through a process known as resegmentation in which the anterior and posterior portions of adjacent somites fuse (Bagnall et al. 1988; Christ et al. 1998; Dubrulle and Pourquié 2004). Each vertebral body is therefore formed from two sclerotomes. The intervertebral discs are formed at the boundary between the anterior and posterior sclerotomal portions of the somite (Mallo et al. 2009). The formation of the spine begins in utero and continues until early adulthood. Any variations in this process can result in congenital variants.

Ossification of the atlas and axis are unique compared with the remainder of the subaxial cervical vertebrae. The posterior atlantal arch ossifies by age 5 and the anterior arch of C1 is typically ossified by age 8 (Wang et al. 2001). The atlas achieves a normal adult radiographic appearance by the age of 7–8 (Fesmire and Luten 1989).

The axis is more complex in that there are a total of six ossification centers, unlike the typical four at other spinal levels. The two additional ossification centers are involved in the formation of the odontoid process. The odontoid process begins to fuse to the body of C2 between the ages of 3 and 6 (Fesmire and Luten 1989). This process is normally completed by age 11 (Fesmire and Luten 1989). The remaining four ossification centers are involved in the formation of the remainder of the vertebrae. During the tenth week of gestation, the four posterior vertebral arch chondrification centers unite to form paired ossification bilateral ossification centers. Each of the two ossification centers forms the ipsilateral pedicle, lateral mass, and half of the lamina. This process is normally completed by 2–3 years of age and any aberration in this process can produce a number of anatomic variants (Sakaura et al. 2013).

The subaxial cervical spine typically follows a similar ossification pattern from C3 inferiorly to C7. The ossification of the posterior arch follows the same pattern as C2 and is typically fused with the vertebral body by age 6. Complete ossification does not typically occur until age 25 (Fesmire and Luten 1989). Recognizing epiphyseal variants, incomplete ossification of synchondroses and apophyses, unique vertebral architecture, pseudosubluxation of C2 on C3, overriding of the anterior atlas in relation to the odontoid in extension, and varied atlantodental intervals (ADI) is central to understanding spinal radiographs, especially in children (Townsend and Rowe 1952; Dunlap et al. 1958; Cattell and Filtzer 1965; Shaw et al. 1999; Lustrin et al. 2003).

Atlas

The atlas of adults is a fused ring formed by multiple ossification centers (OC) (Junewick et al. 2011). These OC are quite varied. In a radiographic study of 298 children, Karwacki and Schnedier (2012) found singular (n=196, 66%), bipartite OC (n=86, 29%), and multiple OCs (n=16, 5%). The posterior arch

Bergman's Comprehensive Encyclopedia of Human Anatomic Variation, First Edition. Edited by R. Shane Tubbs, Mohammadali M. Shoja and Marios Loukas.
© 2016 John Wiley & Sons, Inc. Published 2016 by John Wiley & Sons, Inc.

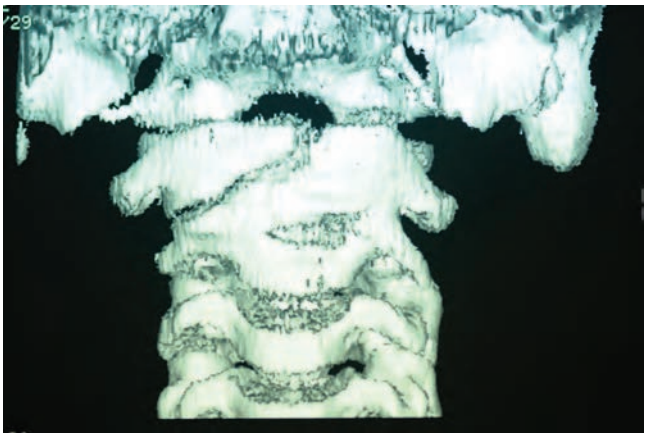

Figure 3.1 3D CT noting an oblique malfusion defect of the anterior arch of the atlas with simultaneous fusion anomaly.

usually fuses by 5 years of age and the anterior arch typically fuses before 8 years of age (Junewick et al. 2011). Incomplete fusion of the anterior or posterior part of the atlantal ring (Figs 3.1, 3.2) is considered a variant of normal when seen outside of the adolescent period. Both the anterior and posterior arches may have facets that articulate with the foramen magnum. Junewick's 13-part radiographic grading system of C1 ossification patterns is an indicator of the number of normal variants seen on routine imaging studies (Junewick et al. 2011) (Table 3.1). There are several cases in the literature that describe a congenital absence of the anterior portion of the ring of C1 (Thavarajah and McKenna 2012). This anomaly is quite rare and is estimated to occur in less than 0.1% of the population (Petraglia et al. 2012). The anterior arch may be enlarged and accessory ossicles may be found near it. Congenital malformation or non-union of the posterior ring is more common and is seen in approximately 4% of the population. Combined non-union of both the anterior and posterior rings is described as a bipartite atlas (Jans et al. 2009; Petraglia et al. 2012). A bipartite atlas is felt to be of little clinical significance, although there is a case report in the literature advocating cervical fusion in individuals with evidence of instability (Hu et al. 2009). The posterior arch may have two instead of one tubercle, which can also be bifid, and ossicles may be found in the posterior atlantooccipital membrane.

Table 3.1 Classification of C1 vertebra ossification patterns.

Classification	Description
Type 0	Completely cartilaginous anterior arch
Type 1	Single ossification center of the anterior arch; unfused neurocentral synchondroses
Type 2	Two symmetric ossification centers of the anterior arch; neurocentral synchondroses either unfused or fused
Type 3	Three ossification centers of the anterior arch; neurocentral synchondroses either unfused or fused
Type 3a	One large and one small ossification centers (type 3 morphology)
Type 4	Four symmetric ossification centers of the anterior arch; neurocentral synchondroses either unfused or fused
Type 4a	One large and two small ossification centers (type 4 morphology)
Type 5	Complete ossification of the anterior arch with fused neurocentral synchondroses
Type A	Unfused posterior synchondrosis
Type B	Bilateral paramedian clefts in posterior arch
Type C	Unilateral paramedian cleft in posterior arch
Type D	Posterior arch hypoplasia
Type E	Complete fusion of the posterior synchondrosis

Figure 3.2 Skull noting atlantooccipital fusion with simultaneous malfusion of the posterior arch of the atlas.

Spina bifida of the posterior arch of C1 is typically an incidental, asymptomatic variation of the atlas. However, Devi et al. (1997) described five male patients with symptomatic cervical stenosis secondary to C1 spina bifida. The pathologic distinction in these cases was that the bifid posterior arch was imbricated anteriorly. This latter pathologic variant should be differentiated from the more common congenital non-union of the posterior arch of the atlas.

The atlas articulates with the occipital condyles located at the base of the skull and there is considerable variation in this

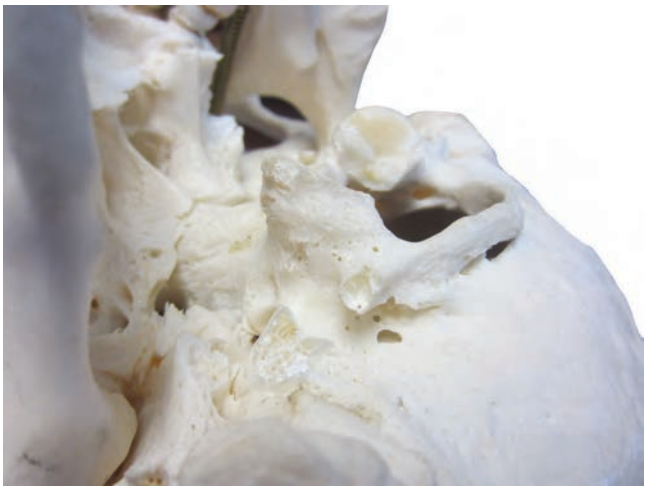

Figure 3.3 Lateral view of another skull with atlantooccipital fusion.

articulation. Interestingly, the atlas may rarely possess bipartite facets that articulate with projections from the occipital bone (Bergmann 1988; Billmann et al. 2007). The lateral mass of C1 where it articulates with the occipital condyles typically has a reniform or kidney-shaped appearance. Billmann et al. (2007) saw variation in the morphology of the lateral mass in 20.8% of specimens during a study of 500 atlases. Bipartition of the superior articular facets of C1 (foveae articulares craniales atlantis) were found both bilaterally (9.6%) and unilaterally (11.2%) (Billmann et al. 2007). The atlas may be fused with the skull base through the occipital condyles (assimilation of the atlas).

Assimilation of the atlas (Figs 3.2, 3.3) is felt to be a distinct variant from the presence of an occipital vertebrae. Another anomaly of the atlantooccipital region is the presence of paired ossicles within the atlantooccipital membrane that may represent a residual proatlas (Bergmann 1988).

The sulcus arteriae vertebralis is the sulcus created by the vertebral artery on the posterior arch of C1. These sulci may have varying levels of surrounding ossification. In as many as 13.8% of individuals there is a posterior bony spicule that projects from the superior articular process (Krishnamurthy et al. 2007). The atlas may even have a completely ossified arcuate foramen (Fig. 3.4a). In such cases, the vertebral artery exits the transverse foramen, passes through the arcuate foramen, and then travels through the foramen magnum (Fig. 3.4b). A laterally placed ponticulus may form a lateral arcuate foramen that can coexist with the more posteriorly located foramen resulting in a canal for the vertebral artery to travel through (Fig. 3.5).

An epitransverse process (Fig.3.6) can extend from the transverse process of the atlas superiorly and can even articulate with the paramastoid region of the occipital bone.

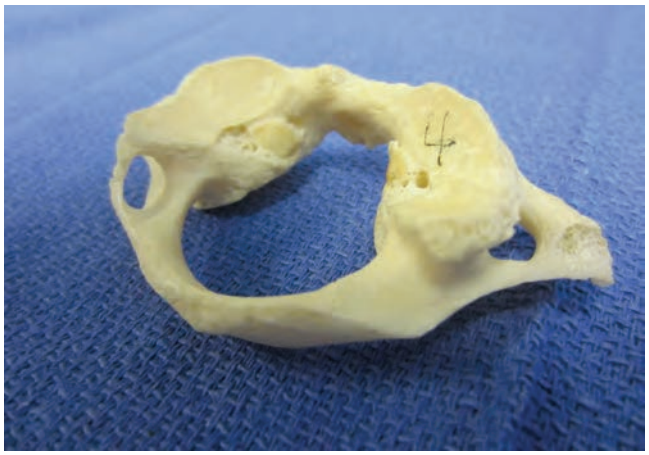

Figure 3.4 (a) Lateral view of the atlas with a left arcuate foramen; (b) 3D CT illustrating bilateral arcuate foramina with the vertebral artery traversing it. Courtesy of Dr Joel Curé.

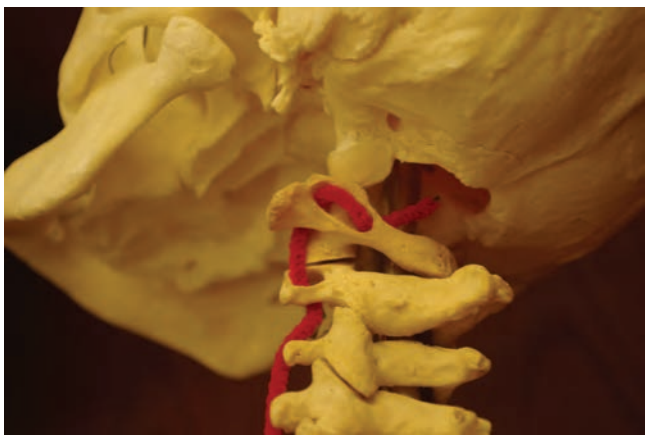

Figure 3.5 Lateral and posterior ponticles resulting in a bony canal for the vertebral artery.

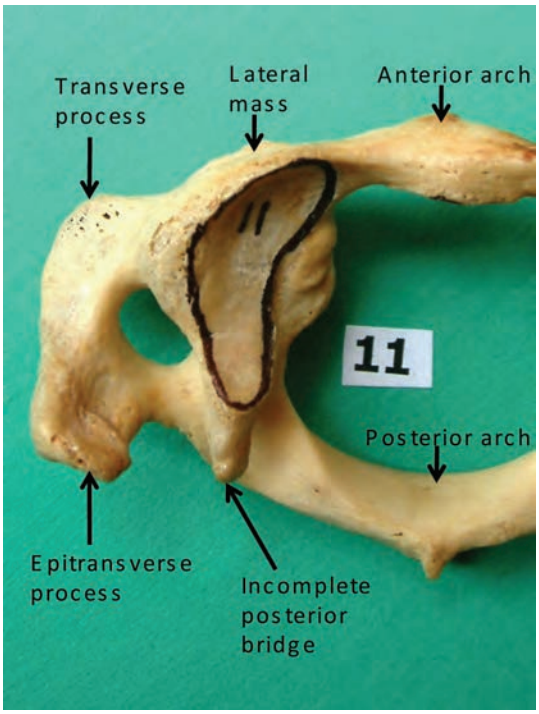

Figure 3.6 A left epitransverse process.

Source: Kaushal (2010). Reproduced with permission from International Journal of Anatomical Variations.

Axis

The axis (C2) is the most complex cervical vertebrae and allows for a tremendous degree of rotation. The odontoid process allows for this rotation and there is significant variation in this structure. Ossiculum terminale is a condition in which the secondary ossification center present at the apical portion of the odontoid does not fuse by the age of 12 (Gore et al. 2011). Ossiculum terminale is commonly identified on adult radiographs and usually carries no clinical significance. There are several case reports suggesting there may be an association with atlantoaxial instability (Liang et al. 2001).

Os odontoideum, a non-union of the synchrondosis of the odontoid process with pathologic instability, is a clinically distinct entity from ossiculum terminale. Radiographically the two can be differentiated by the location of non-union. The underlying etiology of non-union is likely embryologic as there is a known association between os odontoideum and failure of fusion of the atlas (Osti et al. 2006). Many authors consider os odontoideum to be inherently unstable regardless of findings on dynamic plain films. Klimo et al. (2008) described three patients with known os odontoideum that were followed non-operatively and experienced spinal cord injuries. Surgical management is often recommended in this pathologic variant to minimize risk of subsequent spinal cord injury.

Complete aplasia and hypoplasia of the odontoid process have been described (Clark and CSRSEC 2005). The most commonly described form of odontoid hypoplasia is a short, peg-like projection superior to the C1-2 facet articulation. The dens can be bifid, the so-called dens bicornis. A sulcus can sometimes be found at the base of the dens and represents the remnants of the synchondrosis found at this location. The length of the odontoid process ranges from 20 to 40 mm (Lang 1992). The odontoid process may be angulated posteriorly, referred to as a retroverted dens.

The C2 posterior arch fuses in the midline by the age of 3 years and with body of the axis between the ages of 3 and 6 (Gore et al. 2011). Failure of fusion of the posterior arch has been described. Additionally, there are case reports of laminar variants of the axis. Sakaura et al. (2013) described a bilaterally separated lamina that at age 68 resulted in cervical myelopathy (Fig. 3.2). Defects or spina bifida of the C2 is rare but may be clinically relevant.

An accessory bursa located above the odontoid process is known as the bursa of Trolard.

Uncinate process

The uncinate processes are superior projections from the C3 to C7 vertebral bodies that articulate with the superior vertebral body at its echancrure (anvil) (Tubbs et al. 2012). Tubbs et al. (2012) performed a morphometric analysis of 40 adult skeletons and classified the uncinate process based on three types of variants. A Type I uncinate process (80%) does not encroach on the adjacent intervertebral foramen. Type II processes (12%) project in a superior posterolateral direction to decrease the foraminal diameter, while Type III uncinate processes (8%) lack incline of projection but are sufficiently high-riding to create foraminal encroachment (Tubbs et al. 2012). The uncinate process may be underdeveloped or absent at the sixth and seventh cervical vertebrae.

Transverse foramen

The transverse foramina (TF) are paired and usually contain the vertebral artery. The vertebral artery typically enters the TF at C6 in 95.6% of individuals (Wakao et al. 2013). The actual morphology of the TF is dependent on the presence of a vertebral artery at that level. Wakao et al. (2013) found that in patients with a vertebral artery that enters at C7, the C7 TF will be wider and correspondingly the pedicle will be smaller. Instrumentation of the C7 pedicle therefore requires an appreciation of the variant anatomy that can occur in this region.

The morphology of the transverse foramen can be highly variable (Taitz et al. 1978). Taitz et al. (1978) developed a five-tiered grading system to quantify both the morphology and orientation of the TF. The atlas had the highest mean diameter of the TF while C7 had the lowest. Absent (0.8%), duplicate (5.2%),

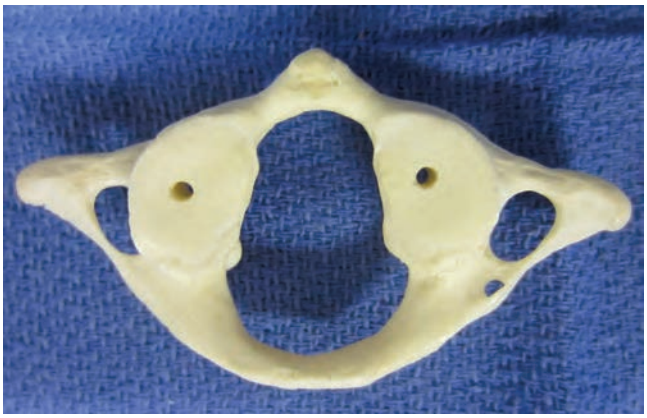

Figure 3.7 Accessory foramen of the transverse foramen. Note the defects in the central part of the articular processes are artifacts from postmortem articulation.

and triplicate (0.2%) foramina have also been observed (Taitz et al. 1978). Osteophytic encroachment of the TF is potentially a sequel of age-related spondylosis, but congenitally ossified TF have been described.

A posteriorly located accessory transverse foramen has a documented incidence of approximately 1% (Murlimanju et al. 2011). These foramen are typically smaller and they may be unilateral or bilateral. According to Murlimanju et al. (2011) only 0.3% of vertebrae exhibit three accessory transverse foramina (Fig. 3.7).

Spinous processes

The spinous processes of C2, C3, C4, and C5 are typically bifid. The C6 and C7 spinous process are occasionally bifid with two small lateral tubercles. Some individuals have cervical spines with nonbifid spinous processes. Only 9% of individuals have a nonbifid C2 spinous process while 1% have a bifid C7. Duray et al. (1999) performed a logistic regression analysis based on race and found that Caucasians have a statistically significant higher rate of bifid spinous processes, especially at C3 and C4 (Duray et al. 1999).

The vertebra prominens, the palpable prominence on the dorsum of the neck, is most commonly the C7 spinous process (70%). C6 (20%) and T1 (10%) may also be the most prominent spinous process.

Klippel–Feil syndrome

Neurologist Maurice Klippel and his resident Andre Feil described a case in which there was a congenital absence of cervical vertebrae. The thoracic cage was felt to be arising from the base of the cranium (Klippel and Feil 1975). The patient's autopsy revealed a fusion of cervical vertebrae that they labeled a cervicodorsal mass.

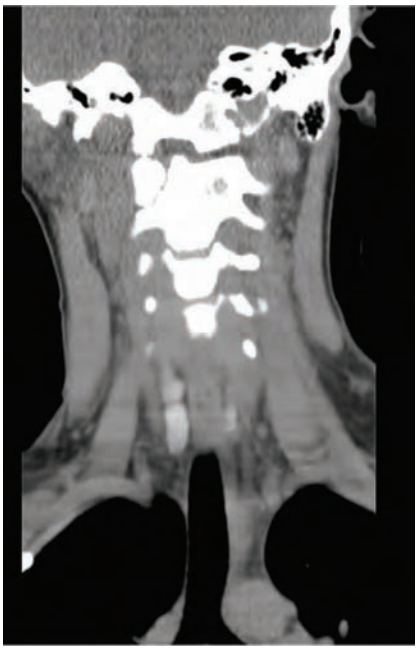

Figure 3.8 3D CT noting a fusion abnormality between C1 and C2. Also note the hemivertebra on the right side.

Congenital fusion of two or more cervical vertebrae is also commonly seen and is referred to as Klippel–Feil syndrome (Fig. 3.8). The classic triad of Klippel–Feil syndrome includes a short neck, low posterior hairline, and limited range of cervical motion. The majority of patients with a congenital fusion of the cervical vertebrae have a normal appearance and fewer than 50% exhibit this classic triad (Clark 2005).

Eight cervical vertebrae have been reported (Lane 1886). The laminae of the inferior cervical vertebrae frequently exhibit dorsally distinct tubercles from which fasciculi of the multifidus muscle arise. The nuchal ligament may have small ossicles associated with it. Segmentation anomalies of the cervical spine may result in the so-called butterfly vertebra.

Cervical ribs

Cervical ribs (discussed in more detail in Chapter 11) are present in approximately 2% of the population. These ribs are typically bilateral at the C7 vertebral level (40.3%). Demographically they occur more commonly in women (2.8%) and African-Americans (70.1%) (Viertel et al. 2012). Cervical ribs may represent a clinically insignificant anatomic variant although 10% of patients will develop or suffer from thoracic outlet syndrome.

The body of a cervical vertebra can be cleft in the sagittal or frontal plane. The pedicles may not be attached to bone anteriorly or posteriorly. The facet joints may be rotated.

References

Bagnall KM, Higgins SJ, Sanders EJ. 1988. The contribution made by a single somite to the vertebral column: experimental evidence in support of resegmentation using the chick-quail chimaera model. *Development* 103: 69–85.

Bergman RA. 1988. *Compendium of Human Anatomic Variation: Text, Atlas, and World Literature*. Baltimore: Urban & Schwarzenberg.

Billmann F, Le Minor JM, Steinwachs M. 2007. Bipartition of the superior articular facets of the first cervical vertebra (atlas or C1): A human variant probably specific among primates. *Anat Anz* 189: 79–85.

Cattell HS, Filtzer DL. 1965. Pseudosubluxation and other normal variations in the cervical spine in children. A study of one hundred and sixty children. *J Bone Joint Surg Am* 47: 1295–1309.

Christ B, Schmidt C, Huang R, Wilting J, Brand-Saberi B. 1998. Segmentation of the vertebrate body. *Anat Embryol (Berl)* 197: 1–8.

Clark CR, CSRSEC (eds) 2005. *The Cervical Spine, fourth edition*. Philadelphia: Lippincott Williams & Wilkins.

Devi BI, Shenoy SN, Panigrahi MK, Chandramouli BA, Das BS, Jayakumar PN. 1997. Anomaly of arch of atlas: A rare cause of symptomatic canal stenosis in children. *Pediatr Neurosurg* 26: 214–218.

Dubrulle J, Pourquié O. 2004. Coupling segmentation to axis formation. *Development* 131: 5783–5793.

Dunlap JP, Morris M, Thompson RG. 1958. Cervical-spine injuries in children. *J Bone Joint Surg Am* 40: 681–686.

Duray SM, Morter HB, Smith FJ. 1999. Morphological variation in cervical spinous processes: Potential applications in the forensic identification of race from the skeleton. *J Forensic Sci* 44: 937–944.

Fesmire FM, Luten RC. 1989. The pediatric cervical spine: Developmental anatomy and clinical aspects. *J Emerg Med* 7: 133–142.

Gore PA, Mortazavi M, Chang S, Tubbs RS, Theodore N. 2011. Pediatric cervical spine injuries: A comprehensive review. *Childs Nerv Syst* 27: 705–717.

Hu Y, Ma W, Xu R. 2009. Transoral osteosynthesis C1 as a function-preserving option in the treatment of bipartite atlas deformity: A case report. *Spine* 34: 418–421.

Jans C, Mahieu G, Van Riet R. 2009. Bipartite atlas mimicking traumatic atlantoaxial instability following a rugby tackle. *BMJ Case Reports* 2009.

Junewick JJ, Chin MS, Meesa IR, Ghori S, Boynton SJ, Luttenton CR. 2011. Ossification patterns of the atlas vertebra. *AJR Am J Roentgenol* 197: 1229–1234.

Karwacki GM, Schneider JF. 2012. Normal ossification patterns of atlas and axis: A CT study. *AJNR Am J Neuroradiol* 33: 1882–1887.

Kaushal P. 2010. Epitransverse process: A rare a rare outgrowth from atlas vertebra. *IJAV* 3: 108–109.

Klimo P Jr, Kan P, Rao G, Apfelbaum R, Brockmeyer D. 2008. Os odontoideum: Presentation, diagnosis, and treatment in a series of 78 patients. *J Neurosurg Spine* 9: 332–342.

Klippel M, Feil A. 1975. The classic: A case of absence of cervical vertebrae with the thoracic cage rising to the base of the cranium (cervical thoracic cage). *Clin Orthop* 109: 3–8.

Krishnamurthy A, Nayak SR, Khan S, Prabhu LV, Ramanathan LA, Ganesh Kumar C, Prasad Sinha A. 2007. Arcuate foramen of atlas: Incidence, phylogenetic and clinical significance. *Rom J Morphol Embryol* 48: 263–266.

Lane WA. 1886. Some variations in the human skeleton. *J Anat Physiol* 20: 388–404.

Lang J. 1992. Suboccipital Approach (and Other Approaches) to Aneurysms at the Craniocervical Junction. Stuttgart: Schattauer Verlagsgesellschaft.

Liang CL, Lui CC, Lu K, Lee TC, Chen HJ. 2001. Atlantoaxial stability in ossiculum terminale. Case report. *J Neurosurg* 95: 119–121.

Lustrin ES, Karakas SP, Ortiz AO, Cinnamon J, Castillo M, Vaheesan K, Brown JH, Diamond AS, Black K, Singh S. 2003. Pediatric cervical spine: Normal anatomy, variants, and trauma. *Radiographics* 23: 539–560.

Mallo M, Vinagre T, Carapuço M. 2009. The road to the vertebral formula. *Int J Dev Biol* 53: 1469–1481.

Murlimanju BV, Prabhu LV, Shilpa K, Rai R, Dhananjaya KVN, Jiji PJ. 2011. Accessory transverse foramina in the cervical spine: Incidence, embryological basis, morphology and surgical importance. *Turk Neurosurg* 21: 384–387.

Osti M, Philipp H, Meusburger B, Benedetto KP. 2006. Os odontoideum with bipartite atlas and segmental instability: A case report. *Eur Spine J* 15: 564–567.

Petraglia AL, Childs SM, Walker CT, Hogg J, Bailes JE, Lively MW. 2012. Bipartite atlas in a collegiate football player: Not necessarily a contraindication for return-to-play: A case report and review of the literature. *Surg Neurol Int* 3: 126.

Sakaura H, Yasui Y, Miwa T, Yamashita T, Ohzono K, Ohwada T. 2013. Cervical myelopathy caused by invagination of anomalous lamina of the axis: Case report. *J Neurosurg Spine* 19: 694–696.

Shaw M, Burnett H, Wilson A, Chan O. 1999. Pseudosubluxation of C2 on C3 in polytraumatized children: prevalence and significance. *Clin Radiol* 54: 377–380.

Taitz C, Nathan H, Arensburg B. 1978. Anatomical observations of the foramina transversaria. *J Neurol Neurosurg Psychiatry* 41: 170–176.

Thavarajah D, McKenna P. 2012. Congenital absence of the anterior arch of the atlas: A normal variant. *Ann R Coll Surg Engl* 94: 208–209.

Townsend EH Jr, Rowe ML. 1952. Mobility of the upper cervical spine in health and disease. *Pediatrics* 10: 567–574.

Tubbs RS, Rompala OJ, Verma K, Mortazavi MM, Benninger B, Loukas M, Chambers MR. 2012. Analysis of the uncinate processes of the cervical spine: An anatomical study. *J Neurosurg Spine* 16: 402–407.

Viertel VG, Intrapiromkul J, Maluf F, Patel NV, Zheng W, Alluwaimi F, Walden MJ, Belzberg A, Yousem DM. 2012. Cervical ribs: A common variant overlooked in CT imaging. *AJNR Am J Neuroradiol* 33: 2191–2194.

Wakao N, Takeuchi M, Kamiya M, Aoyama M, Hirasawa A, Sato K, Takayasu M. 2013. Variance of cervical vertebral artery measured by CT angiography and its influence on C7 pedicle anatomy. *Spine* 39: 228–232.

Wang JC, Nuccion SL, Feighan JE, Cohen B, Dorey FJ, Scoles PV. 2001. Growth and development of the pediatric cervical spine documented radiographically. *J Bone Joint Surg Am* 83: 1212–1218.

4 Thoracic vertebrae

Benjamin J. Ditty, Nidal B. Omar and Mark N. Hadley
University of Alabama at Birmingham, Birmingham, Alabama, United States

The thoracic spine comprises the longest segment of the human vertebral column. Unique to the thoracic spine are costovertebral articulations, which provide stability to thoracic vertebrae and are vital for the structural and functional integrity of the entire thorax. The tradeoff for the increased stability of the thoracic spinal column is that it affords less mobility than the cervical or lumbar spinal segments. However, it does play an important role in motions such as lateral flexion, axial rotation (more so in the upper thoracic vertebral segments), and flexion/extension (predominantly in lower thoracic vertebral segments) (Dvořák et al. 2008).

This chapter describes variations in the anatomy of human thoracic spinal vertebrae with differing degrees of clinical relevance. Although thoracic vertebrae tend to be relatively more uniform than cervical vertebrae, a number of morphologic variations have been characterized.

Embryology

Development of the thoracic spinal column begins with the formation of 12 pairs of thoracic somites derived from the paraxial mesoderm beginning at 20 days of gestation (Benzel and Stillerman 1999). The ventral aspect of each somite, known as the sclerotome, will condense around the notochord and neural tube to form a mesenchymal precursor to the spinal column that will later chondrify then ossify, with the exception of the cells in the caudal region of each sclerotome which contribute to the formation of the intervertebral discs (Benzel and Stillerman 1999). The notochord eventually regresses to form the nucleus pulposus of the intervertebral discs. It may persist as the persistent chorda dorsalis. Resegmentation of vertebrae occurs as the rostral aspect of each somite articulates with the caudal aspect of the somite above it (Benzel and Stillerman 1999).

In early embryonic development, all vertebrae possess primordial costal projections and consequently have the potential for rib formation (Benzel and Stillerman 1999; Herkowitz et al. 2006). Segmental expression of *Hox* genes is thought to be the determinant of completion of rib development from thoracic vertebrae (Benzel and Stillerman 1999). In cervical and sacral vertebrae, costal precursors fuse with the embryonic transverse processes; in lumbar vertebrae, costal precursors become the mature transverse processes, fusing with mammillary processes derived from the embryonic transverse processes (Herkowitz et al. 2006).

Spinal development is a dynamic process that continues long beyond the fetal period. Secondary ossification centers develop at puberty, and complete ossification of vertebrae is not achieved until around the age of 25 (Benzel and Stillerman 1999).

Vertebral bodies

Costal articulations

While the body of the first thoracic vertebra typically bears one entire facet for articulation with the head of the first rib it may bear, on one or both sides, two demi-facets as is typical in the 2–9th thoracic vertebra. If this is the case, the articulation of the first rib is with an inferior demi-facet from the seventh cervical vertebra and a superior demi-facet from the first thoracic vertebra (Cramer and Darby 2013).

In most specimens the ninth thoracic vertebra has only superior costal facets due to the 10–12th thoracic vertebrae each possessing a pair of full facets for articulation with their respective ribs. It is not abnormal for there to also be inferior demi-facets on the 9th thoracic vertebra for costal articulation with the 10th rib, in which case the facet on the 10th thoracic vertebra will assume a semilunar shape akin to a demi-facet (Cramer and Darby 2013).

Limbus vertebra

A limbus vertebra occurs when, in an immature skeleton, a fragment of the nucleus pulposus herniates through the ring hypophysis before fusion has occurred. This results in an ossified fragment, usually at the anterior superior edge of the vertebral body. This is commonly mistaken for a fracture of the superior endplate by less-experienced radiograph interpreters (McCarron 1987).

Failure of segmentation

The process of segmentation may fail to occur in the thoracic spine. When this occurs the intervertebral disc develops

Bergman's Comprehensive Encyclopedia of Human Anatomic Variation, First Edition. Edited by R. Shane Tubbs, Mohammadali M. Shoja and Marios Loukas.
© 2016 John Wiley & Sons, Inc. Published 2016 by John Wiley & Sons, Inc.

incompletely. The constellation of two partially fused adjacent thoracic vertebral bodies with a small, dysmorphic, incomplete disc space should not be confused with the appearance of inflammatory spondylodiscitis (Keats and Anderson 2012). Vertebral cleavage can occur in the sagittal or frontal planes.

Butterfly vertebra

Butterfly vertebra within the thoracic spinal column, also referred to as anterior rachischisis or somatoschisis, are caused by a congenital defect in which the notochord persists in the developing spine. When this occurs, the vertebral body exists in two (usually equal) triangular-shaped halves, which give the affected vertebra the appearance of a butterfly on a frontal radiograph. These halves may also be referred to as hemivertebrae (Garcia et al. 1993). Hemivertebrae consist of the triangular vertebral body, a pedicle and transverse process, superior and inferior articular processes, and half of a lamina with half of a spinous process (Kim et al. 2008). In most cases of butterfly vertebra, the two hemivertebrae are ankylosed to the adjacent superior and inferior thoracic vertebral bodies (Garcia et al. 1993).

The body of the vertebra may fail to form and the thoracic bodies, in general, vary greatly in their shape. The aortic impression on the anterior aspect of the thoracic vertebrae may be indemonstrable (Frazer 1933).

The body of the second thoracic vertebra usually exhibits an identifying tubercle marking the attachment of a fasciculus of the medial portion of the longus colli muscle.

Pedicles

There is significant variability in pedicle shape and size between individuals and between thoracic vertebral levels within individuals (Panjabi et al. 1997). The pedicles may not be fused to bone anteriorly or posteriorly or may be absent. The superior intervertebral notch may be very shallow or absent (Frazer 1933).

Upper

In one study, three out of five pairs of adult T2 vertebral pedicles viewed in cross-section perpendicular to the long axis were teardrop-shaped posteriorly transitioning to a kidney shape anteriorly, with the convexity oriented medially. Variations in upper thoracic pedicle morphology were identified in which the superior edges of the posterior portions of the pedicles formed a narrow ridge while the anterior portions were square. In yet another observed variation, the pedicles were oval to teardrop-shaped throughout (Panjabi et al. 1997).

Middle

Middle thoracic vertebral pedicles (levels T6 and T7) tended to demonstrate greater uniformity than upper thoracic vertebral pedicles with a narrow teardrop or hybrid kidney/teardrop shape. Again, the convexity of the pedicles was directed medially. At mid-thoracic vertebral levels, the only remarkable variant identified was asymmetric pedicle length in one specimen (Panjabi et al. 1997).

Lower

In the lower thoracic spine, at vertebral levels T10 and T11, the pedicles are shaped similarly to those in the middle thoracic spine. At these lower thoracic, more weight-bearing levels, thoracic pedicle shape differs most dramatically near the vertebral body where pedicles can be relatively rectangular, oval, teardrop, or kidney shaped. Lower thoracic pedicle size variations are common. Lower thoracic pedicles may have the largest pedicle diameter within the thoracic spine or may be so small that the medial and lateral cortical surfaces of the pedicles are in contact with one another without intervening cancellous bone. Posteriorly, nearly all the pedicles in the lower thoracic spine take on a teardrop- or kidney-shaped appearance (Panjabi et al. 1997).

Facets

In individuals for whom the 12th pair of ribs is absent, it is common for the 12th thoracic vertebra to assume a morphology similar to a lumbar vertebra, with its inferior articular facet surface oriented more in the sagittal plane (Singer et al. 1988). The transition from thoracic-type facet articular projections, in which the articular surfaces are coronally oriented, to the lumbar-type facet articular projections, in which they are oriented in the sagittal plane, typically occurs at the level of T11 (Cramer and Darby 2013). The 10th facet is usually small but may also be absent (Frazer 1933).

When lumbar-type facet articular projections occur in the thoracic spine, they may occur unilaterally rather than bilaterally, with resulting articular asymmetry. These anatomic variations may be clinically relevant in the event of potential thoracic pedicle screw fixation. Surgeons must assess for these potential anatomic discrepancies prior to proceeding with surgical internal fixation and fusion.

Transverse processes

A transverse foramen through T1 has been described by Turner (1883) and Duckworth (1911). The transverse processes of the thoracic vertebrae may fail to ossify, resulting in an appearance that could be confused with a fracture of the tip of the transverse process on a radiograph. This was initially described in 1913 by Rhys, who described six cases in which radiographic evidence of separation or displacement of the distal transverse process did not correlate with an injury mechanism or was not preceded by an injury at all (Rhys 1913). Infrequently, articulations may form between adjacent transverse processes within the thoracic spine as described by Keats and Anderson (2012).

At the T10 vertebral level the transverse process may not articulate with the 10th rib (Cunningham 1903; Gray and

Johnston 1938; Morris and Anson 1966; Gehweiler et al. 1980; Cramer and Darby 2013).

Variability in the morphology of the transverse processes of the T10, T11, and T12 vertebrae has been described. At these levels the transverse processes may possess superior, inferior, and lateral tubercles which correspond to the mammillary and accessory tubercles and transverse processes typical of a lumbar vertebra (Cramer and Darby 2013).

The body of the second thoracic vertebra usually exhibits an identifying tubercle marking the attachment of a fasciculus of the medial portion of the longus colli muscle.

Laminae and spinous processes

The apophysis at the tip of a thoracic vertebral spinous process may fail to unify. This anomaly has no structural or functional significance but could be mistaken for a fracture on thoracic spinal imaging (Keats and Anderson 2012). The spinous process can be absent with the laminae uniting across the midline.

Spina bifida occulta may occur at any level in the thoracic spinal column. It may result in a double spinous process. In other cases it may create the appearance of a double spinous process, which is not to be confused with a bifid spinous process (Keats and Anderson 2012).

The tip of an individual thoracic spinous process may be much larger than those adjacent to it. When this occurs it may suggest a mass on thoracic spinal imaging (Keats and Anderson 2012).

Although fusion of two or more vertebrae is most often seen in the cervical spine, the thoracic region can also be affected.

References

Benzel EC, Stillerman CB (eds). 1999. *The Thoracic Spine*. London: Taylor & Francis.

Cramer GD, Darby SA. 2013. *Clinical Anatomy of the Spine, Spinal Cord, and ANS*. St Louis: Elsevier Health Sciences.

Cunningham DJ. 1903. *Text-book of Anatomy*. New York: William Wood.

Duckworth WL. 1911. Report on an abnormal first thoracic vertebra. *J Anat Physiol* 45: 232–238.

Dvořák J, Dvořák V, Gilliar W, Schneider W, Spring H, Tritschler T. 2008. *Musculoskeletal Manual Medicine: Diagnosis and Treatment*. New York: Thieme.

Frazer JE. 1933. *The Anatomy of the Human Skeleton*. London: J & A Churchill.

Garcia F, Florez MT, Conejero JA. 1993. A butterfly vertebra or a wedge fracture? *Int Orthop* 17: 7–10.

Gehweiler JA, Osborne RL, Becker RF. 1980. *The Radiology of Vertebral Trauma*. Philadelphia: Saunders Elsevier.

Gray H, Johnston TB. 1938. *Gray's Anatomy: Descriptive and Applied*, 27th edition. London: Longmans, Green.

Herkowitz HN, Rothman RH, Simeone FA. 2006. *Rothman-Simeone: The Spine*, fifth edition. Philadelphia: Saunders Elsevier.

Keats TE, Anderson MW. 2012. *Atlas of Normal Roentgen Variants that May Simulate Disease*, ninth edition. Philadelphia: Saunders Elsevier.

Kim DH, Betz RR, Huhn SL, Newton PO 2008. *Surgery of the Pediatric Spine*. New York: Thieme.

McCarron RF. 1987. A case of mistaken identity, limbus annulare mimics fracture. *Orthop Rev* 16: 173–175.

Morris H, Anson BJ. 1966. Morris' Human Anatomy: A Complete Systematic Treatise, 12th edition. New York: McGraw-Hill.

Panjabi MM, O'Holleran JD, Crisco JJ, Kothe R. 1997. Complexity of the thoracic spine pedicle anatomy. *Eur Spine J* 6: 19–24.

Rhys OL. 1913. Pseudo-fractures of transverse processes. *Brit Med J* 1: 1103–1104.

Singer KP, Breidahl DP, Day RE. 1988. Variations in zygapophyseal joint orientation and level of transition at the thoracolumbar junction. Preliminary survey using computed tomography. *Surg Radiol Anat* 10: 291–295.

Turner W. 1883. A first dorsal vertebra, with a foramen at the root of the transverse process. *J Anat Physiol* 17: 255–256.

5 Lumbar vertebrae

Ross Dawkins and Mark N. Hadley
University of Alabama at Birmingham, Birmingham, Alabama, United States

Embryology

An educated discussion on the anatomic variations of the lumbar requires an understanding not only of the normal anatomy, but more importantly of how that anatomy came to exist. We therefore begin this chapter with a review of the embryological development of the human spine.

One might say that gastrulation is the starting point for formation of the nervous system. It is the stage at which a groove known as the primitive streak develops on the epiblast surface of the bilaminar disc. This streak establishes the basic anatomical concepts of the human body, including symmetry, rostral and caudal ends, and dorsal and ventral surfaces. Cells of the epiblast on either side of the primitive streak travel towards it, migrate through it, and end up between the epiblast above and the hypoblast below. These mobile cells give rise to the embryonic mesoderm and endoderm, while remaining cells of the epiblast form the ectoderm (Youmans and Winn 2011).

As the primitive streak extends forward, a collection of cells known as the primitive node, or Hensen's node, forms at one end of the streak. The primitive node defines the rostral end of the streak. A group of specialized cells migrate through the primitive node and give rise to the notochodal process. Certain cells of the notochordal process align to form the notochordal plate, which then folds to form the notochord with a central canal (Moore et al. 2013). Although our interest here focuses on the vertebral column, recall that just dorsal to the notochord is a developing neuraxis, which starts as an ectodermal invagination whose edges meet to form a neural tube. This neural tube lies directly above and runs in parallel with the notochord. Mesodermal cells migrating from the primitive streak begin to compact alongside the notochord and differentiate into three sections: paraxial, intermediate, and lateral mesoderm. The paraxial mesoderm, lying closest to the notochord on either side, segments into masses known as somites. The somites are paired and flank the notochord, developing in a craniocaudal direction. By the end of the fifth week, 42–44 pairs of somites will have formed: 4 occipital, 8 cervical, 12 thoracic, 5 lumbar, 5 sacral, and 8–10 coccygeal somite pairs (Moore et al. 2013).

Each somite differentiates into two parts: a sclerotome and a dermomyotome. The dermomyotomes will go on to form muscle cells and overlying dermis of the skin. The sclerotomes form the spinal column. During the fourth week of embryogenesis, they begin to surround both the notochord and the neural tube. As the sclerotomal mesoderm begins to condense about the notochord, the longitudinal mass of tissue begins to display segmentation. First, segmental arteries arising from the developing aorta cut bilaterally across the condensing sclerotome. Any given segmental artery will lie between two sclerotomes. A second segmentation process occurs within each sclerotome, essentially cutting the sclerotome in half. Here, the sclerotomal fissure separates a cranial portion, which is loosely packed with cells, from a caudal portion, which is densely packed. Some of the cells from the densely packed caudal portion migrate cranially towards the fissure. These cells will form the annulus fibrosus of the intervertebral disc. The nucleus pulposus develops from remnants of the notochord. As the intervertebral disc is forming, the cranial portion of the sclerotome is fusing with the caudal portion of the adjacent scleorotome to form the vertebral centrum, which further develops into the vertebral body. Vertebral bodies are therefore derived from adjacent pairs of sclerotomes, while discs are derived from within a single sclerotome (Moore et al. 2013). The vertebral centrum allows bone to continually develop around it.

Recall that some of the mesodermal cells migrate dorsally from somites and travel around the lateral and dorsal sides of the neural tube. The condensed arches of cells form the vertebral pedicles, laminae, and spinous processes. Lateral projections of the arches form transverse processes, which have been reported to have no contact with the body. Craniocaudal thickenings of the arches form the articular processes. These structures, like the vertebral bodies, receive contributions from adjacent sclerotomes. In order to complete the ring of a vertebra, the centrum and two arches must fuse together (Moore et al. 2013).

Chondrification of the mesenchymatous vertebrae begins during the sixth week of development. Signals from the notochord and neural tube induce this process (Moore et al. 2013). Ossification occurs following chondrification, after which the notochord disintegrates. There are three primary areas of

Bergman's Comprehensive Encyclopedia of Human Anatomic Variation, First Edition. Edited by R. Shane Tubbs, Mohammadali M. Shoja and Marios Loukas.
© 2016 John Wiley & Sons, Inc. Published 2016 by John Wiley & Sons, Inc.

ossification, one at the centrum and one on either side of the vertebral arch (Moore et al. 2013).

During the first two years of life, the neural arch halves unite dorsally. This union first occurs in the lumbar region shortly after birth and extends cranially, reaching the cervical regions by the second year. Fusion of the neural arch to the centrum begins first in the cervical region at three years of age. This process proceeds caudally and is completed in the sacrum around seven years of age.

Anatomic variations

The lumbar vertebrae, except for the fifth, probably show fewer variations of a congenital nature than any other vertebra. That being said, there exist a number of variations in vertebral anatomy that are not specific to, but can certainly be found in, the region of the lumbar vertebrae. We discuss these in addition to those variants more pertinent to the lumbar spine.

Vertebral body defects

Congenital block vertebra, or congenital synostosis, occurs as a result of a disturbance in segmentation of the somites during development of the vertebral column (Yochum 1987). This results in fusion of adjacent vertebral bodies, with fusion of the apophyseal joint in approximately 50% of cases. While this variant is more typical of the cervical spine, it is also known to occur in the lumbar spine. In some cases the two adjacent vertebrae fuse to form a solid block of bone. More often, a remnant of the intervening vertebral disc remains. A typical block vertebra has a decreased anterior/posterior diameter. As a result of the loss of the vertebral disc space the vertebral foramina are frequently narrowed with congenital block vertebrae, but can be normally sized or enlarged (Gehweiler et al. 1980; Taylor 2000).

Sagittal cleft vertebrae occur as a result of a failure of fusion of the two halves of the vertebral body. This is somehow associated with the embryologic extension of the notochord longitudinally through the vertebral column during ossification (Hollinshead 1982). Incomplete fusion of the two lateral chondral centers of the vertebral body results in a central sagittal constriction of the vertebral body (Taylor 2000). The sagittal cleft is created by the indentation of the endplate cortices (Yochum 1987). From the frontal view the body has the appearance of two triangular masses with opposing apices, hence the term butterfly vertebrae. The development of the ununited bodies is generally symmetrical (Yochum 1987). Furthermore, the cleft results in an increase in the interpediculate distance (Yochum 1987). The body may be cleft in the frontal plane. Enlarged fissures or Hahn's clefts may be seen. These are vascular channels within the vertebral body.

Lateral hemivertebrae appear as an absence of one lateral half of the vertebral body, and develop when one of the two lateral ossification centers of the vertebral body fails to grow. The apex of the lateral hemivertebra is directed medially. Normal disc spaces are usually present above and below the affected level (Yochum 1987). However, the endplates of the adjacent vertebrae are deformed, resulting in a trapezoid shape to those vertebrae. An isolated lateral hemivertebra will result in a scoliotic deformity, with the affected vertebra being located at the apex of the scoliotic curvature (Yochum 1987). It has been hypothesized that hemivertebrae can result from a lack of vascularization to the defective side (Hollinshead 1982).

Dorsal hemivertebrae appear as an absence of the anterior half of the vertebral body. The dorsal portion of the body tapers ventrally, and fibrous tissue replaces the absent ventral portion of the body. The adjacent vertebrae may demonstrate compensatory growth and come together in the defective area of the hemivertebra. Ventral hemivertebra is also a described anomaly. Dorsal and ventral hemivertebrae are much less frequent that lateral hemivertebrae (Taylor 2000).

The limbus bone is a small, triangular bony ossicle often adjacent to the anterior superior aspect of the vertebral body (Jaeger 1988). It is believed to result from a herniation of nuclear material through a secondary ossification center for the corner of the vertebral body. This results in nonunion of the secondary ossification center, and thus the presence of a bony fragment (Yochum 1987).

Nuclear impressions are invaginations in the vertebral endplates that result from notochordal remnants. They appear as broad curvilinear depressions of the endplate. They more commonly affect the inferior, rather than superior, endplate (Jaeger 1988; Taylor 2000). On a frontal view, the impressions create paramedian curvilinear indentations, creating the appearance of a double hump. This has been referred to as Cupid's bow contour (Yochum 1987; Taylor 2000).

Another vertebral disc variant, which can be confused with a nuclear impression, is a Schmorl's node. Vertical nucleus pulposus herniations, rather than notochordal remnants, are to blame for the endplate defects of Schmorl's nodes. Radiographically, a Schmorl's node appears as a squared-off, rectangular rim of sclerosis protruding through the endplate. It can be centrally or peripherally located. This is different from the defect of nuclear impressions, in which there is a smooth, wave-like cortical surface irregularity involving nearly all of the endplate (Yochum 1987).

Vertebral arch defects

Just as the notochord influences the development of the vertebral bodies, the neural tube produces signals integral to the regulation of vertebral arch development. Disruptions in arch formation can produce clefts in numerous parts of the vertebral arch. A retrosomatic cleft is found at the junction of the pedicle and vertebral body. It results as a failure of fusion between the ossifying neural arch and centrum. A cleft may also occur more posteriorly in the body of the pedicle itself. A retroisthmic cleft occurs on the lamina, behind the pars interarticularis.

One of the most-recognized neural arch cleft defects occurs in the area of the lamina or spinous process, and is known as spina bifida. Spina bifida occulta, or rachischisis, is a defect

in ossification at the spinous process or lamina (Hollinshead 1982; Jaeger 1988). The dorsal synchondrosis between the neural arches usually fuses during the first year of life. Failure of this fusion results in the formation of a dorsal cleft involving the spinous process or lamina. The size of cleft can vary from a small midline cleft to near absence of the vertebral arch. It is most commonly found in the lumbosacral region (Jaeger 1988).

When a spina bifida occulta defect occurs at the first sacral vertebra with an elongated spinous process of the fifth lumbar vertebra, this is known as a knife clasp deformity. The long spinous process may result from a fusion of the L5 spinous process with the first sacral tubercle (Jaeger 1988; Taylor 2000). An anterior/posterior radiographic view will demonstrate with spina bifida defect at S1 with a vertical enlargement of the L5 spinous process. A lateral view will show distal enlargement of the spinous process. This entity is so named due to the pain it induces when the patient extends the lumbar spine (Yochum 1987).

Spondylolysis is a vertebral arch cleft which occurs at the pars interarticularis. This disruption of the pars can be either unilateral or bilateral. There is debate as to whether a congenital etiology exists for this entity. Spondylolisthesis is defined as an anterior displacement of a vertebral body relative to the body immediately inferior. Approximately 90% of spondylolystheses involve the fifth lumbar vertebra (Yochum 1987). There are multiple types of spondylolisthesis. Those of interest here are the types that would result from a congenital deformity, as opposed to the acquired type. Dysplastic spondylolisthesis has a congenital implication with dysplasia in the neural arch of L5 or the sacrum, allowing anterior displacement of the former relative to the latter. If spondylolysis affects the bilateral pars interarticularis, the affected vertebra may become displaced. This is a subtype of isthmic spondylolisthesis. Some have stated that isthmic spondylolisthesis can result from poorly formed pars interarticularis (Youmans and Winn 2011). Again, given that a debate exists as to the possibility of a congenital etiology for sponylolysis, it is also unclear whether isthmic spondylolisthesis can be classified as a congenital variant. Of note, a higher incidence of spondylolysis and spondylolisthesis is associated with L5 spina bifida occulta (Taylor 2000).

Split cord malformation is a congenital anomaly where a longitudinal diastasis divides the spinal cord or cauda equina, depending on a thoracic or lumbar location. The division consists of either an osseous, cartilaginous, or fibrous band. Typically, there is an increased interpediculate distance. A total of 50% of cases are associated with other vertebral anomalies such as scoliosis, spina bifida occulta, and tethering of the spinal cord (Yochum 1987; Taylor 2000).

Agenesis of a vertebral pedicle is more likely to occur in the cervical spine, but has been documented in the lumbar region. Failure of development of the chondral center responsible for one side of the neural arch results in a unilaterally absent pedicle. The superior articular process and transverse process at the affected level may be dysplastic. In addition, the contralateral pedicle is often hyperplastic, which occurs more frequently in the lumbar spine opposed to the cervical spine (Yochum 1987).

If the chondral center responsible for the articular process fails to develop, then the rare entity of articular process agenesis occurs. The most common location is the inferior L5 articular process. In the place of the articular process is a nonossified, cartilaginous, or fibrous analogue (Jaeger 1988; Taylor 2000).

Nonfusion of secondary centers of ossification is known to occur in the lumbar vertebrae. One common site is the apophysis of the transverse process of the first lumbar vertebra. Another nonfusion site, which typically occurs in the lumbar region, is the inferior articular process apophysis. Found here are joint surfaces covered with cartilage. These often occur around the third lumbar vertebra. A triangular bony ossicle is found at the tip of the inferior articular process, referred to as Oppenheimer's ossicle (Jaeger 1988; Taylor 2000). A similar entity in the superior articular process is much less common (Jaeger 1988).

Variation in orientation of lumbosacral facet joints is known as tropism. The L1–2 to L4–5 facet joints are oriented in the sagittal plane. L5–S1 facet joints are oriented in the coronal plane. Tropism occurs when this convention is broken for either the right or left apophyseal joint at a given level. This most commonly occurs at the L4–5 and L5–S1 levels. On frontal radiographic views, normal lumbar spine facet joints are visible as linear radiolucencies between the superior and inferior facet. Tropism presents as an absence of the radiolucency on the affected side (Yochum 1987; Taylor 2000).

Rudimentary lumbar rib

The transverse processes in the lumbar spine are actually homologs of the ribs. Ribs of the lumbar ribs are actually more common that ribs of the cervical vertebrae (C7). The accessory process, a small tubercle projecting form the posterior surface of the transverse process medially, is the rudimentary true transverse process in that it serves as an attachment for spinal muscles along with the mammillary process on the superior and lateral aspect of the superior articular facet (Jinkins 2000). Rarely, an accessory process can be congenitally absent. This occurs more frequently in the fifth lumbar vertebra (Hollinshead 1982; Bergman et al. 1984). In contrast to an absent accessory process, a styloid process is defined as an elongated accessory process, exceeding a length of 3–5 mm. (Bergman et al. 1984). Occasionally, the mammillary and accessory processes are united by a bony bridge forming a foramen behind the transverse process. Variant supernumerary tubercles located lateral to the mammillary tubercle are known as the tubercle of Staurenghi.

A more common variation in this region of a lumbar vertebra is the presence of a rudimentary rib (gorilla rib) at the first lumbar vertebra, representing a congenital anomaly of the transverse process. The rib unites with the ventral surface of the transverse process or the tip of a short transverse process (Bergman et al. 1984). A transverse foramen may be present in the lumbar region, especially in L1 and L5.

Lumbosacral transitional vertebrae

Of all the vertebral transitional zones, the most commonly involved with anatomic variations is the lumbosacral. The typical human spine contains 24 presacral vertebrae. The 24th presacral vertebra, commonly identified as L5, may be partially or completely incorporated with the sacrum, either unilaterally or bilaterally. This is termed sacralization of L5 (Skinner 1927). Conversely, the first sacral vertebra, S1, can take on characteristics of a lumbar vertebra, including articulation rather than fusion with the remainder of the sacrum, lumbar-type facet joints, and a squared appearance in the sagittal plane. This is termed lumbarization of S1. Considered together, these variations are often referred to as a lumbosacral transitional vertebra (LSTV). The reported prevalence of LSTV falls within the range 4–30% (Konin and Walz 2010). There may be just four lumbar vertebrae in the absence of any fusion abnormalities.

There are varying degrees of sacralization of the fifth lumbar vertebra (O'Connor 1934). Castellvi et al. (1984) described a radiographic classification system identifying four types of LSTVs on the basis of morphologic characteristics as follows.

- Type I: unilateral (Ia) or bilateral (Ib) dysplastic transverse process, measuring at least 19 mm in width in the craniocaudad dimension.
- Type II: incomplete unilateral (IIa) or bilateral (IIb) lumbarization/sacralization with an enlarged transverse process that has a diarthrodial joint between itself and the sacrum.
- Type III: unilateral (IIIa) or bilateral (IIIb) lumbarization/sacralization with complete osseous fusion of the transverse process to the sacrum.
- Type IV: unilateral type II transition with a type III on the contralateral side (Castellvi et al. 1984).

Other characteristics of LSTV include a decreased disc height between the lumbar transitional vertebra and the sacrum as compared to a normal L5–S1 disc. In fact, this space may be completely devoid of any disc material. Conversely, when a lumbarized S1 is present, the S1–S2 disc height is greater than the typical rudimentary disc present in a normal spine (Nicholson et al. 1988). In addition to the disc space, the vertebral body displays morphologic changes with LSTV. With sacralization of L5, the lowest lumbar segment develops a wedged shaped. With lumbarization of S1, the highest sacral segment develops a squared appearance (Wigh and Anthony 1981). Finally, the facet joints of the transition point must be considered. With a sacralized L5 the facet joints are typically hypoplastic, if not all together nonexistent with complete fusion of L5–S1. With a lumbarized S1, S1–S2 facet joints can be identified, whereas a typical S1–S2 segment has osseous fusion (Konin and Walz 2010).

Transitional vertebrae often have enlarged transverse processes and may form a joint with the lateral mass of the sacrum. Such joints are termed assimilation joints.

References

Bergman RA, Thompson SA, Afifi AK. 1984. *Catalog of Human Variation*. Baltimore: Urban & Schwarzenberg.

Castellvi AE, Goldstein LA, Chan DP. 1984. Lumbosacral transitional vertebrae and their relationship with lumbar extradural defects. *Spine* 9: 493–495.

Gehweiler JA, Osborne RL, Becker RF. 1980. *The Radiology of Vertebral Trauma*. Philadelphia: Saunders Elsevier.

Hollinshead WH. 1982. *Anatomy for Surgeons*. Philadelphia: Harper & Row.

Jaeger SA. 1988. *Atlas of Radiographic Positioning: Normal Anatomy and Developmental Variants*. Norwalk: Appleton & Lange.

Jinkins JR. 2000. *Atlas of Neuroradiologic Embryology, Anatomy, and Variants*. Philadelphia: Lippincott Williams & Wilkins.

Konin GP, Walz DM. 2010. Lumbosacral transitional vertebrae: Classification, imaging findings, and clinical relevance. *Am J Neuroradiol* 31: 1778–1786.

Moore KL, Persaud TVN, Torchia MG. 2013. *The Developing Human: Clinically Oriented Embryology*. Philadelphia: Saunders.

Nicholson AA, Roberts GM, Williams LA. 1988. The measured height of the lumbosacral disc in patients with and without transitional vertebrae. *Brit J Radiol* 61: 454–455.

O'Connor DS. 1934. Anatomical variations in the fifth lumbar vertebra as factors in low-back pain. *Yale J Biol Med* 7: 147–150.

Skinner EH. 1927. Anatomical and postural variations of the lumbosacral spine. *Radiology* 9: 451–452.

Taylor JAM. 2000. *Skeletal Imaging: Atlas of the Spine and Extremities*. Philadelphia: Saunders.

Wigh RE, Anthony Jr RE. 1981. Transitional lumbosacral discs. Probability of herniation. *Spine* 6: 168–171.

Yochum TR. 1987. *Essentials of Skeletal Radiology*. Baltimore: Williams & Wilkins.

Youmans JR, Winn. 2011. *Youmans Neurological Surgery*. Philadelphia: Saunders Elsevier.

6 Sacrococcygeal vertebrae

R. Shane Tubbs[1] and Marios Loukas[2]
[1]Seattle Science Foundation, Seattle, Washington, USA
St George's University, School of Medicine, St Georges, Grenada
University of Dundee, Dundee, UK
[2]St. George's University, School of Medicine, St. Georges, Grenada

The sacrum and coccyx may be absent and the sacroccygeal intervertebral disc can be ossified (Zeligs 1940). Absence of the sacrum and coccyx, in part or complete, may be a part of the caudal regression syndrome. The coccyx may be duplicated (Mares and Bar-Ziv 1981).

The number of vertebrae in the sacrum may be increased by fusion of the first coccygeal, by (less often) addition of the last (fifth) lumbar (sacralization) (Fig. 6.1a, b), or by addition of both the last lumbar and first coccygeal vertebrae. The sacrum may be composed of six true sacral vertebrae. Although the cervical spine is the most consistent in having 7 vertebrae, the coccyx is the most variable. Ossification of the sacrococcygeal ligaments may result in a bony foramen of the fifth sacral nerves.

The number may be reduced to four by the "lumbarization" of the first sacral vertebra. In one study of 631 bodies, the sacrum was composed of five vertebrae in 77%, six in 21.7%, four in 1%, and seven in 0.2%. The lumbosacral junction is occasionally composed of a vertebra with characteristics of a lumbar vertebra on one side and a sacral on the other (so-called hemilumbarization or hemisacralization).

The articular surface of the sacrum may extend variably, over no more than the first two vertebrae or to the fourth sacral vertebra. Accessory articular facets may occur on the lateral sacral crest at the level of the first or second dorsal sacral foramen; these have been found to be unpaired or bilateral and to articulate with appropriate facets on the ilium. The sacrum may be malformed and take on the so-called scimitar appearance.

The sacral canal may be open dorsally because of failure of laminar fusion. Singh (2012) as did Smith (1902) (Fig. 6.2) reported a foramen through the ala and into the sacral canal. Fusion of the coccyx and sacrum occurs more often and earlier in males.

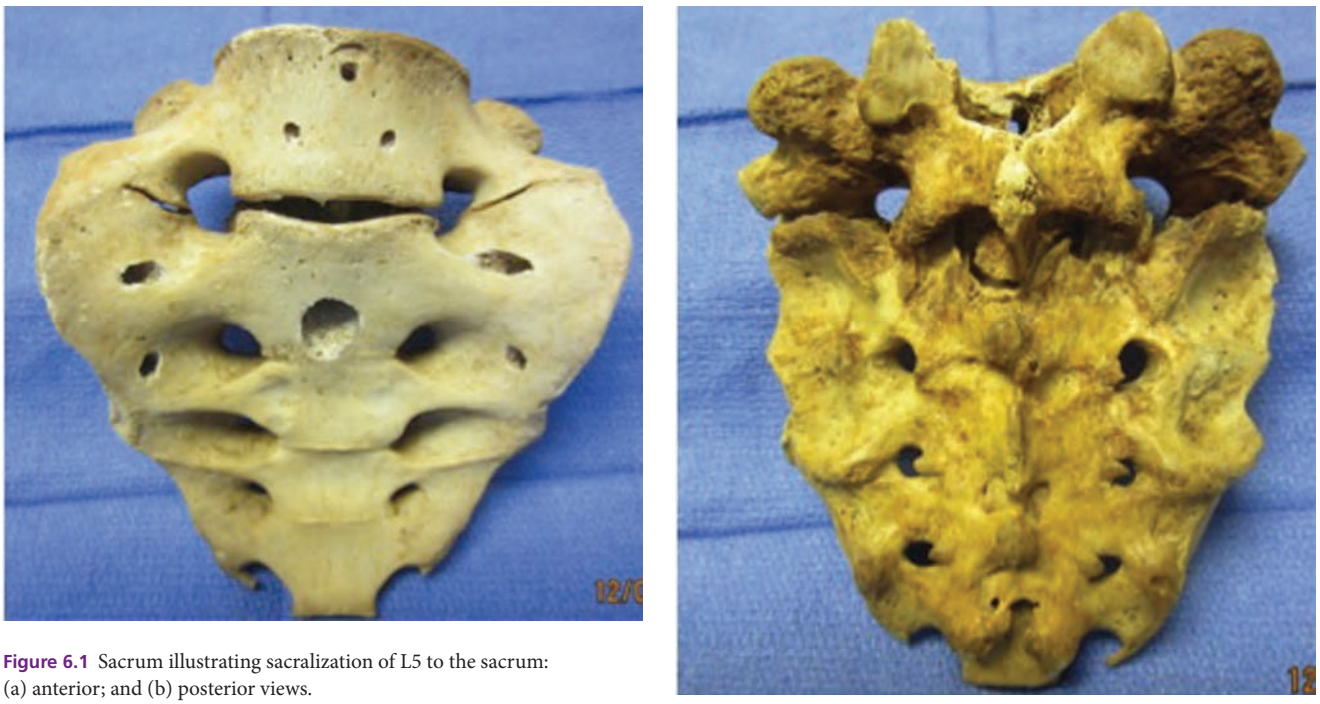

Figure 6.1 Sacrum illustrating sacralization of L5 to the sacrum: (a) anterior; and (b) posterior views.

Bergman's Comprehensive Encyclopedia of Human Anatomic Variation, First Edition. Edited by R. Shane Tubbs, Mohammadali M. Shoja and Marios Loukas.
© 2016 John Wiley & Sons, Inc. Published 2016 by John Wiley & Sons, Inc.

Figure 6.2 Variant foramen through the superior aspect of the right sacrum.

Source: Smith (1902). Reproduced with permission from John Wiley & Sons.

The subdural and subarachnoid spaces extend into the sacral canal as far as the middle third of the body of the second sacral vertebra; however, in 46% of 56 cadavers, these spaces extend caudal to this level.

The coccyx may be very short or elongated. If the coccyx is "sacralized" then five sacral foramina may be present (Singh 2011). Fusion of the coccyx and sacrum takes place less often and later in life in the female than in the male.

Ribs may be associated with the sacrum or coccyx (Mares and Bar-Ziv 1981; Pais et al. 1978; Rashid et al. 2008). The development of the ribs reaches their full development in the thoracic region, whereas normally in the other parts of the spine the costal elements fuse with the lateral or transverse processes during weeks 4–12 of development. Any defect in fusion may result in a supernumerary rib (Pais et al. 1978).

References

Mares AJ, Bar-Ziv J. 1981. Sacral (pelvic) "rib" or coccygeal duplication? *Z Kinderchir* 34: 72–76.

Pais MJ, Levine A, Pais SO. 1978. Coccygeal ribs: development and appearance in two cases. *Am J Roentgenol* 131: 164–166.

Rashid M, Khalid M, Malik N. 2008. Sacral rib: a rare congenital anomaly. *Acta Orthop Belg* 74: 429–431.

Singh R. 2011. Sacrum with five pairs of sacral foramina. *IJAV* 4: 139–141.

Singh R. 2012. A new foramen on posterior aspect of ala of first sacral vertebra. *IJAV* 5: 29–31.

Smith EB. 1902. Two rare vertebral anomalies. *J Anat Physiol* 36: 372–374.

Zeligs IM. 1940. Congenital absence of the sacrum. *Arch Surg* 41: 1220–1228.

Further reading

Anderson RJ. 1883. Observations on the diameters of human vertebrae in different regions. *J Anat Physiol* 17: 341–344.

Armstrong JR, Crisp EJ, Freedman B, Gillespie HW, Golding FC, Jackson H, Lloyd K. 1950. Discussion on the significance of congenital abnormalities of the lumbosacral region. *Proc R Soc Med* 43: 635–640.

Badgley CE. 1941. The articular facets in relation to low-back pain and sciatic radiation. *J Bone Joint Surg* 23: 481–496.

Barton PN. 1948 The significance of anatomical defects of the lower spine. *Industr Med* 17: 37–40.

Blumel J, Evans EB, Eggers GWN. 1959. Partial and complete agenesis or malformation of the sacrum with associated anomalies. *J Bone Joint Surg (Am)* 41: 497–518.

Boucher B. 1957. Sex differences in the foetal pelvis. *Am J Phys Anthropol NS* 15: 581–600.

Brailsford JF. 1928/29. Deformities of the lumbosacral region of the spine. *Brit J Surg* 16: 562–627.

Colcher AE, Hursh AMW. 1952. Pre-employment low-back x-ray survey. A review of 1,500 cases. *Indstr Med* 21: 319–321.

Danforth MS, Wilson PD. 1925. The anatomy of the lumbosacral region in relation to sciatic pain. *J Bone Joint Surg* 7: 109–160.

Dassel PM. 1961. Agenesis of the sacrum and coccyx. *Am J Roentgenol* 85: 697–700.

Del Duca V, Davis EV, Barroway JN. 1951. Congenital absence of the sacrum and coccyx. *J. Bone Joint Surg (Am)* 33: 248–253.

Derry DE. 1911. Note on accessory articular facets between the sacrum and Ilium, and their significance. *J Anat Physiol* 45: 202–210.

Ehara S, El-Khoury GY, Bergman RA. 1988. The accessory sacroiliac joint. A common variation. *Am J Roentgenol* 150: 857–859.

Fawcett E. 1907. On the complete ossification of the human sacrum. *Anat Anz* 30: 414–421.

Fawcett E. 1937/38. The sexing of the human sacrum. *J Anat* 72: 633.

Freedman B. 1949/50. Congenital absence of the sacrum and coccyx. Report of a case and review of the literature. *Brit J Surg* 37: 299–303.

Gillespie HW. 1949. The signifcance of congenital lumbo-sacral abnormalities. *Brit J Radiol* 22: 270–275.

Girard PM. 1935. Congenital absence of the sacrum. *J Bone Joint Surg* 17: 1062–1064.

Goldstein R. 1947. Agenesis of sacrum and coccyx. *Acta Med Orientalia* 6: 202–204.

Greulich WW, Thhoms H. 1938. The dimensions of the pelvic inlet of 789 white females. *Anat Rec* 72: 45–51.

Hadley LA. 1950. Accessory sacroiliac articulations with arthritic changes. *Radiology* 55: 403–409.

Hamsa WR. 1935. Congenital absence of the sacrum. *Arch Surg* 30: 657–666.

Harris HA. 1953. Ossification in the lumbo-sacral region. *Brit J Radiol* 6: 685–688.

Harrison RG. 1901. On the occurrence of tails in man, with a description of the case reported by Dr. Watson. *Johns Hopkins Hosp Bull* 12: 96–101.

Heyns OS, Kerrich JE. 1947. The number of vertebrae in the fetal Bantu sacrum. *Am J Phys Anthropol* 5: 67–78.

Katz JF. 1953. Congenital absence of the sacrum and coccyx. *J Bone Joint Surg (Am)* 35: 398–402.

Keith A. 1921. The disappearance and reappearance of the human tail. *Nature* 106: 845.

Lanier VS, McKnight HE, Trotter M. 1944. Caudal analgia: An experimental and anatomical study. *Am J Obst Gynec* 47: 633–641.

Letterman GS, Trotter M. 1944. Variations of the male sacrum. Their significance in caudal anesthesia. *Surg Gynecol Obstet* 78: 551–555.

Lewin T. 1968. Anatomical variations in lumbo-sacral synovial joints with particular references to subluxation. *Acta Anat* 71: 229–248.

Lichtor A. 1947. Sacral agenesis. *Arch Surg* 54: 430–433.
Mitchell GAG. 1936/37. The significance of lumbosacral transitional vertebrae. *Brit J Surg* 24: 147–158.
Nathan H, Arensburgh B. 1972. An unusual variation in the fifth lumbar and sacral vertebrae: A possible cause of vertebral canal narrowing. *Anat Anz* 132: 137–148.
Newell JL. 1934. A case of multiple congenital anomalies of the Müllerian and genito-urinary systems with absence of the coccyx. *New England J Med* 210: 1217–1218.
Phesant HC, Swenson PC. 1942. The lumbosacral region. A correlation of the roentgenographic and anatomical observations. *J Bone Joint Surg (Am)* 24: 299–306.
Piontek J. 1971. Variation of the level of closure of the sacral canal in man. *Folia Morphol (Warsaw)* 30: 460–464.
Pirkey EL, Purcell JH. 1957. Agenesis of lumbosacral vertebrae. A report of two cases in living infants. *Radiology* 69: 726–729.
Roller GT, Pribram HFW. 1965. Lumbosacral intradural lipoma and sacral agenesis. *Radiology* 84: 507–512.
Rowe GG. 1950. Anomalous vertebrae from the lumbo-sacral column of man. *Anat Rec* 107: 171–179.
Russell HE, Aitken GT. 1963. Congenital absence of the sacrum and lumbar vertebrae with prosthetic management. *J Bone Joint Surg (Am)* 45: 501–508.
Sinclair JG, Duren N, Rude JC. 1941. Congenital lumbosacral defect. *Arch Surg* 43: 473–478.
Smith ED. 1959. Congenital sacral anomalies in children. *Aust NZ J Surg* 29: 165–176.
Southworth JD, Bersack SR. 1950. Anomalies of the lumbosacral vertebrae in five hundred and fifty individuals without symptoms referable to the low back. *Am J Roentgenol* 64: 624–634.
Sugar 0. 1987. How the sacrum got its name. *JAMA* 257: 2061–2063.
Taylor RG. 1939. Anomalies of the lumbosacral articulations. *JAMA* 113: 463–465.
Trotter M. 1926. The sacrum and sex. *Am J Phys Anthropol* 9: 445–450.
Trotter M. 1937. Accessory sacroiliac articulations. *Am J Phys Anthropol* 22: 247–261.
Trotter M. 1940. A common anatomical variation in the sacro-iliac region. *J Bone Joint Surg* 22: 293–299.
Trotter M. 1947. Variations of the sacral canal: Their significance in the administration of caudal analgesia. *Curr Res Anaesth Analgesia* 26: 192–202.
Trotter M. 1964. Accessory sacroiliac articulations in East African skeletons. *Am J Phys Anthropol NS* 22: 137–142.
Trotter M, Letterman GS. 1944. Variations in the female sacrum. Their significance in continuous caudal anaesthesia. *Surg Gynecol Obstet* 78: 419–424.
Trotter M, Lanier PF. 1945. Hiatus canalis in American Whites and Negroes. *Human Biol* 17: 368–381.
Turner W. 1886a. The sacral index of the pelvic brim as a basis of classification. *J Anat Physiol* 20: 125–143.
Turner W. 1886b. The sacral index in various races of mankind. *J Anat Physiol* 20: 317–323.
Weisel H. 1954. The articular surfaces of the sacro-iliac joint and their relation to the movement of the sacrum. *Acta Anat* 22: 1–14.
Willis TA. 1923. The lumbo-sacral vertebral column in man, its stability of form and function. *Am J Anat* 32: 95–123.
Young M, Ince JGH. 1939/40. Transmutation of vertebrae in the lumbosacral region of the human spine. *J Anat* 74: 369–373.

7 Scapula

Peter J. Ward
West Virginia School of Osteopathic Medicine, Lewisburg, West Virginia, United States

Body of the scapula

The body of the scapula is typically triangular with distinct medial, superior, and lateral borders. The medial border meets the superior at the pointed superior angle of the scapula. The superior border meets the lateral border at the glenoid fossa, which articulates with the head of the humerus. The lateral border meets the medial border at the pointed inferior angle of the scapula.

The fossae for the supraspinatus and infraspinatus muscles are located on the scapula's posterior aspect and the bone in this region can become quite thin (Fig. 7.1a). Foramina through the body of the scapula, particularly in the infraspinatus fossa, have a reported incidence of between 0.9 and 3.4% (Vallois 1926; Gray 1942). These defects can be seen radiographically and remain unchanged over time. They are problematic if the resulting radiolucency is mistaken for a lesion of the lung (Citgay and Mascatello 1979; Prescher 2000; De Wilde et al. 2004).

An inconstant bone has been described residing immediately inferior to the inferior angle of the scapula (Fig. 7.2a). The presence of this bone simulated a radiopaque lung lesion leading to its discovery during a medical visit (Adler 1941; Kohler and Zimmer 1968; McClure and Raney 1975 quoting). Another unusual and incidental finding involving the body of the scapula was the case of a 42-year-old Chinese man whose scapula was shown radiographically to be missing its inferior one-quarter with a bifurcated inferior body (Fig. 7.2b). There was no history of injury or disability and the patient had presented for treatment of nausea, vomiting, and hiccups (Khoo and Kuo 1948).

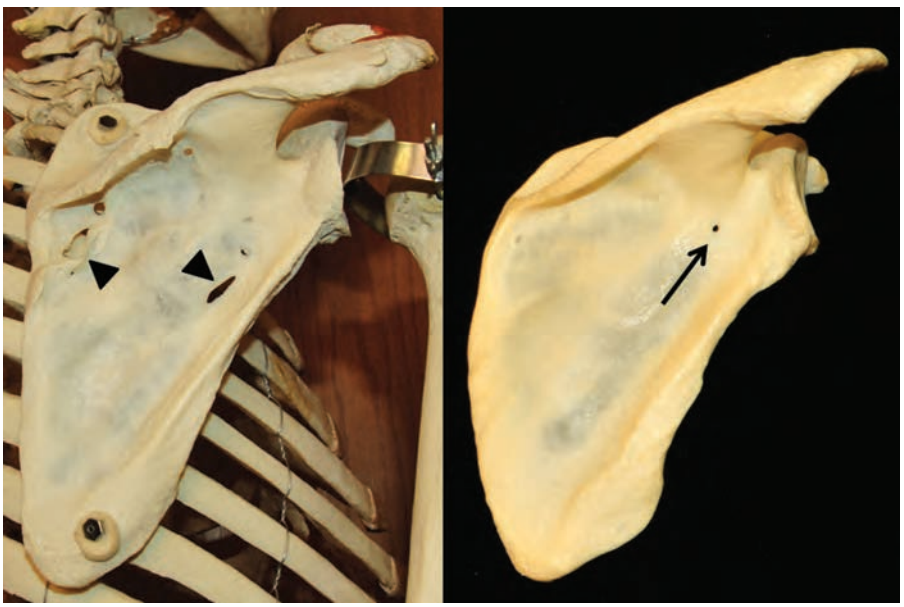

Figure 7.1 Defects of the body of the scapula. Abnormally large defects (arrowheads) are different from large nutrient foramina of the scapula (arrow).

Bergman's Comprehensive Encyclopedia of Human Anatomic Variation, First Edition. Edited by R. Shane Tubbs, Mohammadali M. Shoja and Marios Loukas.
© 2016 John Wiley & Sons, Inc. Published 2016 by John Wiley & Sons, Inc.

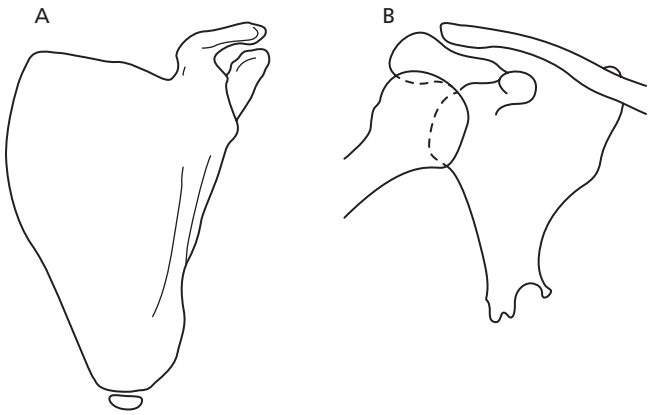

Figure 7.2 (a) Position of the infrascapular bone. (b) Rare dysplasia of the scapular body.

Source: McClure and Raney (1975). Reproduced with permission from Wolters Kluwer Health.

Scapular articulations with ribs

Typically the anterior surface of the scapula is smooth and articulates indirectly with the posterior thoracic wall via the scapulothoracic joint. The anterior surface of the scapula has sometimes been reported to have distinct synovial articulations with the ribs that restrict its motion. This has been reported occurring near the inferior angle, superior angle, and superior border of the scapula (Gruber 1864, 1872; Fontan 1912; Kajava 1924). The reported incidence of costal facets on scapulae has been reported as 5.6–7.2% (Vallois 1926; Gray 1942).

Curvature of the scapular body

The degree of concavity varies considerably and may impact the ease with which the scapula moves along the posterior thoracic wall (Dwight 1887). The angle formed by connecting the scapula's superior angle, base of the scapular spine, and inferior angle (Fig. 7.3) falls within the range 124–162° (Lehtinen et al. 2005; Aggarwal et al. 2011). The largest angle was associated with a tubercle of Luschka.

Figure 7.3 Different curvatures of the scapular body: (a) flat; (b) moderately curved; and (c) markedly curved.

Tubercle of Luschka

The tubercle of Luschka is an extension of bone from the superior angle of the scapula. It is not an osteochondroma or other bony tumor, but an extension of the scapula in the vicinity of the levator scapulae muscles (Lehtinen et al. 2005). A study of scapulae in the Huntington collection at the Smithsonian museum found 42/700 (6.0%) scapulae that displayed a prominent tubercle of Luschka (Edelson 1996). The authors also describe how the presence of the tubercle of Luschka may be associated with "snapping scapula." This condition causes a palpable and audible click as the scapula moves across the posterior ribcage (Parsons 1973; Percy et al. 1988).

Lateral border of scapula

The lateral border of the scapula is often a relatively direct line running from the inferior aspect of the glenoid to the inferior angle. However, there is variability associated with the prominence of the attachment site for the teres major muscle (Dwight 1887; Hrdlička 1942a–c). The prominence of this attachment site can vary from a slightly raised region of the lateral border to a "rhino-horn" projection. In one study a very prominent horn was seen in 22% of scapulae from the Huntington collection of the Smithsonian and 7/700 (1.0%) of those specimens had the projection veering medially and anteriorly towards the body, potentially restricting scapular motion (Edelson 1996). A sulcus for the circumflex scapular artery as it crosses the lateral border of the scapula has been reported as being absent in 14.5–40.0% of specimens (Kajava 1924; Vallois 1932; Bergman et al. 1988). The latissimus dorsi sometimes attaches to the dorsal surface of the inferior angle of the scapula.

Medial border of scapula

The medial border of the scapula can be convex (Fig. 7.4a), straight (Fig. 7.4b), or concave (Fig. 7.4c) (Graves 1910, 1921; Vallois 1928; Hrdlička 1942a, c). The reported variation of these features is fairly consistent: convex, 54.3–61.3%; straight, 20.8–27.0%; concave, 9.9–18.7%; and unclassifiable in 0.2% of the specimens studied (Graves 1921; Gray 1942).

Inferiorly, instead of a pointed inferior angle there may be a flat inferior border of the scapula (Fig. 7.4d). The medial border may also veer laterally (Fig. 7.4e) immediately superior to the scapular spine (Dwight 1887; Vallois 1928; Hrdlička 1942a). Medial angulation of the superior angle was seen superior to the spine of the scapula in 60/700 (8.5%) of scapulae from the Huntington collection of the Smithsonian (Edelson 1996).

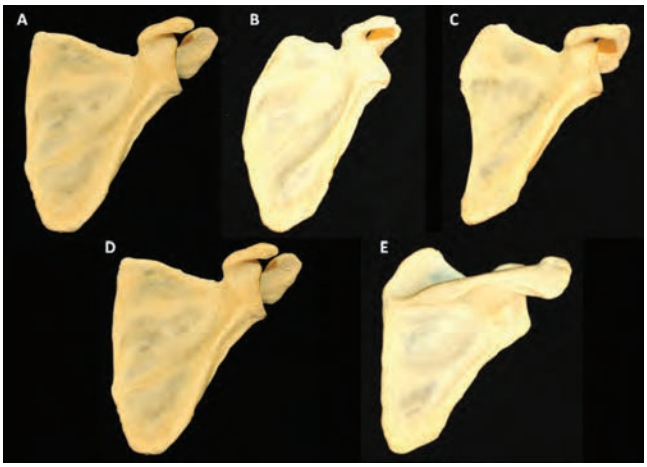

Figure 7.4 Medial and inferior borders of the scapula: (a) straight medial border; (b) convex medial border; (c) concave medial border; (d) distinct horizontal inferior border; and (e) sharp lateral inclination of medial border superior to spine of the scapula.

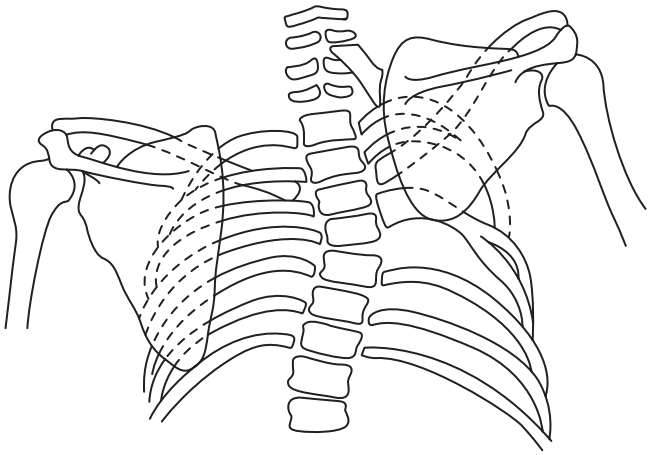

Figure 7.5 Undescended scapula with omovertebral bone.

Source: McClure and Raney (1975). Reproduced with permission from Wolters Kluwer Health.

Rarely, a bony bridge known as the omovertebral bone (Fig. 7.5) may exist between the medial border or the superior angle of the scapula and the spinous and transverse processes of the cervical vertebrae (McClure and Raney 1975; Bergman et al. 1988). This omovertebral bone was found in 54% of the subjects enrolled in a surgical study of Sprengel's deformity, congenital high scapula. Two cases demonstrated a synovial articulation between the omovertebral bone and scapula (Khairouni et al. 2002).

Superior border of scapula

The superior border is the most variable of the scapula's borders. The variations associated with the scapular notch and the coracoid process will be discussed separately. Aside from those two features the superior border can appear horizontal (Fig. 7.6a), moderately oblique (Fig. 7.6b), markedly oblique (Fig. 7.6c), deeply saddle-shaped (Fig. 7.6d), concave or semilunar (Fig. 7.6e), or wavy (Fig. 7.6f) (Hrdlička 1942a).

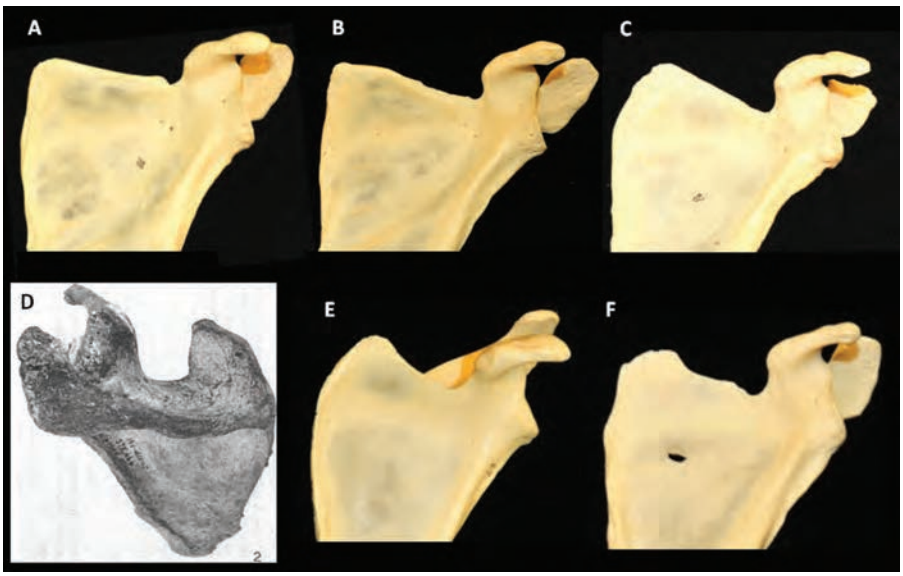

Figure 7.6 Types of superior scapular border: (a) horizontal; (b) moderately oblique; (c) markedly oblique; (d) saddle-shaped; (e) deeply concave; and (f) wavy.

Source (d): Hrdlička (1942c). Reproduced with permission from John Wiley & Sons.

Scapular notch

The differences in the appearance of the scapular notch contribute to the variability of the superior border of the scapula. Sometimes it is not present or only exists as a slight depression along the superior border (Fig. 7.7a). When present, it has been described as: J-shaped with the origin of medial border of notch notably inferior to origin of lateral border (Fig. 7.7b); deep U-shaped with the origins of medial and lateral borders of notch roughly equal (Fig. 7.7c); V-shaped with the inferior aspect of the notch forming an acute angle (Fig. 7.7d); the notch nearly surrounded by bone; or the notch wholly surrounded by bone (Fig. 7.7e) (Hrdlička 1942a). The frequency of each type of scapular notch varies widely between studies, which may be due to the subjective distinctions made by different authors. The reported variances are: J-shaped, 22%; deep U-shaped, 13.2–62.5%; V-shaped, 20–25%; slight indentation, 26.8%; and not present, 18% (Vallois 1926; Prescher 2000; Iqbal et al. 2010). An alternative set of terms (Type I = no notch; Type II = notch longest in transverse diameter; Type III = notch longest in vertical diameter; Type IV = bony foramen; and Type V = notch and a bony foramen) was proposed in a study by Natsis (2007a).

As noted above, the scapular notch is occasionally bridged by bone instead of the superior transverse scapular ligament (McClure and Raney 1975; Bergman et al. 1988; Osuagwu et al. 2005; Khan 2006). In these cases there is a circular suprascapular foramen that typically surrounds the suprascapular nerve. The reported rates of ossification of the superior transverse scapular ligament fall within the range 1.5–12.5% (Poirier and Charpy 1911; Kajava 1924; Vallois 1926, 1932; Gray 1942; Edelson 1995b; Prescher 2000; Bayramoğlu et al. 2003). One study in a Brazilian population had an unusually high incidence of 30.8% (Silva et al. 2007). The suprascapular foramen is more common in aged scapulae and in white males (Edelson 1995b).

In a study of 32 dissected scapulae, the superior transverse scapular ligament was described as bipartite (5/32), fan-shaped (17/32), or ossified (4/32), with the suprascapular nerve passing through the opening (Bayramoğlu et al. 2003).

Coracoid process

The coracoid process is located immediately lateral to the scapular notch on the superior border of the scapula. It forms from distinct centers of ossification that may fail to unite with the rest of the scapula. In this case it will exist as a separate bone (Bergman et al. 1988). The muscles associated with the coracoid process may also vary, giving it an unusual appearance. The pectoralis minor muscle, which typically inserts on the distal coracoid, may send muscle fibers superior to the coracoid process to insert on the scapular neck or humerus instead. In these cases, there is often a distinct groove on the superior aspect of the coracoid process (Seib 1938; Bergman et al. 1988).

The coracoclavicular ligaments that span the space between the superior aspect of the coracoid process and the inferior distal clavicle can sometimes ossify (Fig. 7.8a) to become a strut of bone (Nutter 1941; McClure and Raney 1975). One radiographic study of this condition found that in 12/1000 (1.2%) instances of this bony strut there was a distinct coracoclavicular joint (Fig. 7.8b) complete with cartilaginous articular surfaces (Nutter 1941). Other instances of this variation show either complete ossification between the coracoid and clavicle or a mix of fibrous and osseous material (McClure and Raney 1975).

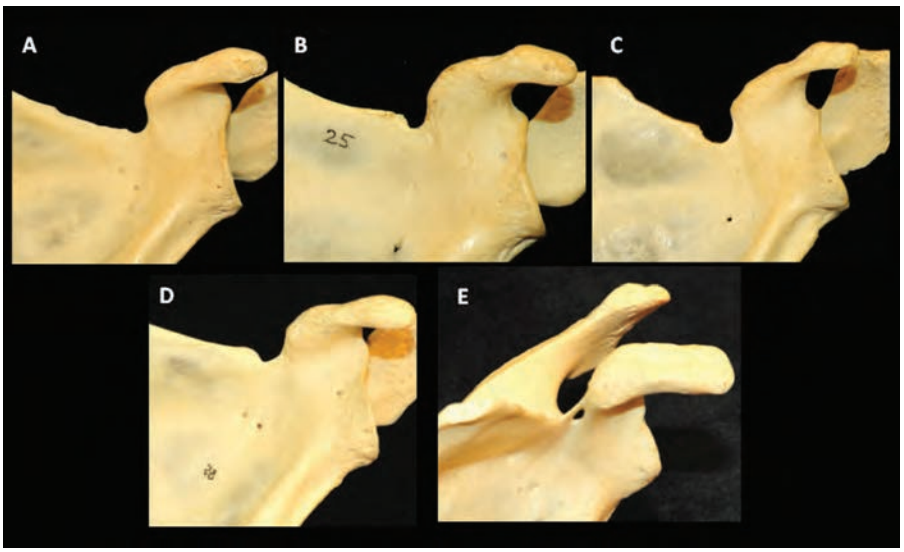

Figure 7.7 Variations of the scapular notch: (a) notch is almost wholly absent; (b) J-shaped; (c) deep U-shaped; (d) V-shaped; and (e) fully ossified superior transverse scapular ligament.

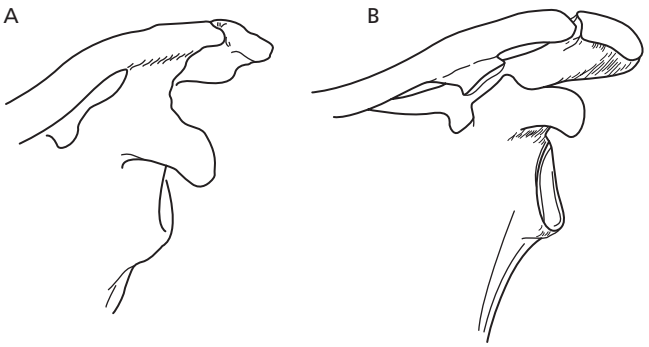

Figure 7.8 Osseous connections between the coracoid process of the scapula and the clavicle: (a) coracoclavicular bridge; and (b) coracoclavicular articulation.

Source (a): McClure and Raney (1975). Reproduced with permission from Wolters Kluwer Health.

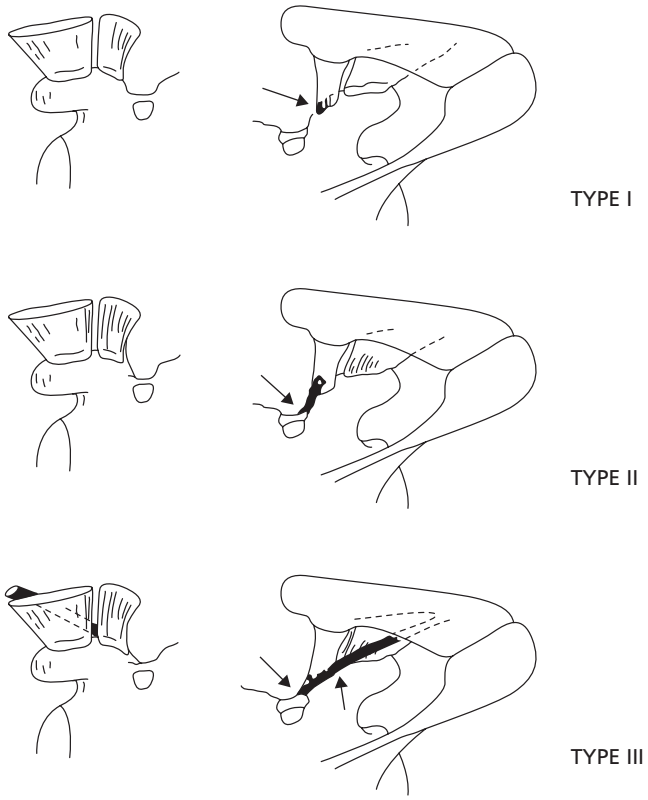

Figure 7.9 Proposed classification of the coracoclavicular ligament based on its variant scapular attachments. Type 1: conoid and trapezoid ligaments separate from superior transverse scapular ligament. Type II: ligamentous bridge between conoid and superior transverse scapular ligament. Type III: a ligamentous band extending from superior transverse scapular ligament across trapezoid ligament.

Source: Harris et al. (2001). Reproduced with permission from Elsevier.

An anterior coracoscapular ligament has been described spanning the medial side scapular notch to the medial aspect of the coracoid process (Avery et al. 2002; Bayramoğlu et al. 2003). It was seen in 16/27 cadavers (11/16 bilateral) that were examined and was distinct from the superior transverse scapular ligament in all cases. The suprascapular nerve passed inferiorly in all cases, the suprascapular artery passed superiorly in all cases, and the suprascapular vein passed superiorly in 81% of the cases. It was also possibly the ligament described in two case studies which described a split superior transverse scapular ligament in the vicinity of the medial coracoid base (Alon et al. 1998) and spanning the supraspinous fossa to the base of the coracoid process (Fabrizio 2012).

Three variations of the coracoclavicular ligaments have been reported. Type I coracoclavicular ligaments (9/18) had the conoid ligament originate from the posterior dorsal coronoid process and dorsal coronoid precipice (Fig. 7.9a). Type II ligaments (6/18) were similar but had fibers confluent with the superior transverse scapular ligament (Fig. 7.9b). Type III ligaments (3/18) had a fascicle running from the superior transverse scapular ligament to fuse with the trapezoid ligament (Fig. 7.9c) (Harris et al. 2001).

A bifid coracoid process was noted alongside a duplicated acromion in one case study (McClure and Raney 1974). A single case study has also described a feature referred to as the os coracosternale vestigale. In this instance, a 7-month-old boy presented with an elevated right shoulder that was rotated anteriorly across the superior shoulder. A bony connection between the coracoid process and the sternum was found, presumably a remnant of mesenchymal tissue that normally disappears during development (Finder 1936).

Shape of the glenoid fossa

The glenoid fossa is a concave depression where the scapula articulates with the round head of the humerus. The presence of a glenoid notch in the anterio-superior rim of the glenoid cavity gives the cavity an indented, piriform shape (Fig. 7.10a) instead of an oval appearance (Fig. 7.10b). The reported rates of these shapes vary widely, likely as a result of subjective distinctions made by different authors. In study of 1149 scapulae (Gray 1942) there were four types described: piriform with a glenoid notch (92.4%); round (0.4%); oval (6.8%); and unclassifiable (0.3%). Another study of 236 scapulae (Prescher and Klümpen 1997) found two shapes only: piriform (54.6%) and oval (45.4%). Yet another study of 90 scapulae (Coskun et al. 2006) strongly notched piriform shapes less frequently (28%) than oval (72%). The same authors showed some glenoid cavities exhibiting two notches (on the anterior and posterior aspects of the superior glenoid rim) but did not give a rate of incidence.

An unclassifiable or irregular glenoid fossa can be caused by dysplasia of the scapular neck. The inferior aspect of the glenoid cavity may be hypoplastic (Fig. 7.11a) with a dentate or notched

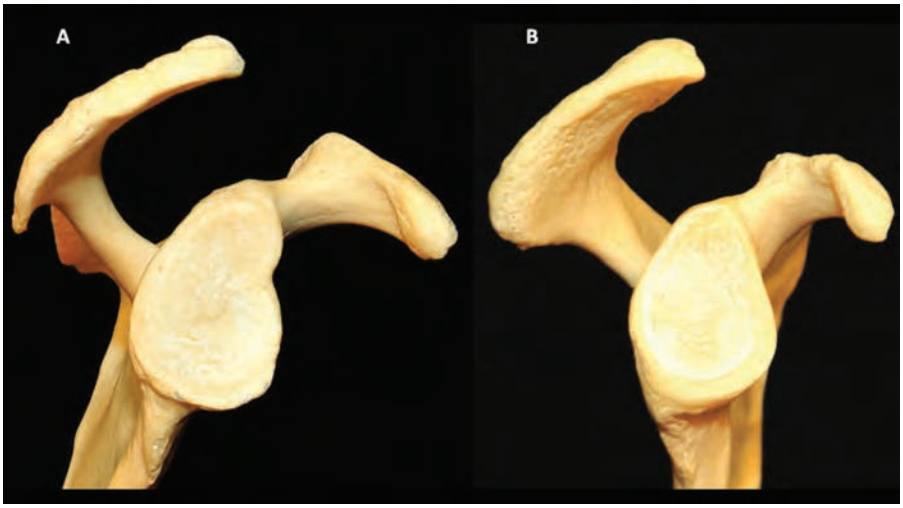

Figure 7.10 Different appearances of the glenoid fossa: (a) piriform with glenoid notch on anterior aspect of the fossa; and (b) oval without glenoid notch.

border (Brailsford 1953; Sutro 1967; McClure and Raney 1975). This occurs infrequently and is typically bilateral (Resnick et al. 1982). In very rare cases the glenoid cavity may be convex and the humeral head is slightly concave (Fig. 7.11b) (Brailsford 1953; McClure and Raney 1975).

The anterior superior aspect of the glenoid labrum is sometimes detached from the glenoid fossa, creating a small sublabral foramen (Cooper et al. 1992; Williams et al. 1994; Tirman et al. 1996). This variation may be mistaken for a lesion of the glenoid labrum, resulting in unnecessary surgery. In a retrospective study a sublabral foramen was seen in 24/200 (12%) of arthroscopic videos (Williams et al. 1994). These researchers found that 18/24 of these patients also had a cord-like middle glenohumeral ligament. They also noted the Buford complex in 3/200 (1.5%) of the subjects. The Buford complex is the combination of a cord-like middle glenohumeral ligament along with the absence of the anterosuperior glenoid labrum (Williams et al. 1994; Tirman et al. 1996).

The inferior transverse scapular ligament (sometimes called the spinoglenoid ligament) has been described as arising from the lateral scapular spine and inserting onto the rim of the glenoid fossa or glenohumeral joint capsule. It likely serves to keep the suprascapular neurovascular bundle intact as it crosses from the supraspinous fossa to the infraspinatus fossa (Prescher 2000; Demirkan et al. 2003; Plancher et al. 2005). However, one study set a very rigorous definition for what constituted a true ligament and found an unambiguous inferior transverse scapular ligament in only 2/75 shoulders examined (Demaio et al. 1991). A thickened aponeurosis was seen in its place in 10/75 specimens. Kharay and Sharma (2010) reported an ossified spinoglenoid ligament.

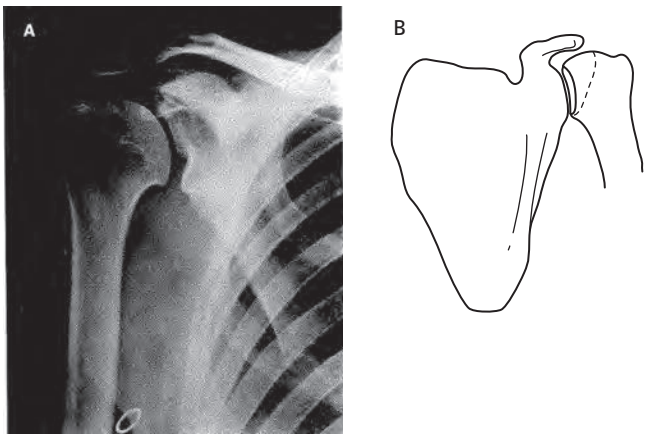

Figure 7.11 Irregular glenoid fossa and scapular neck dysplasia: (a) dentated/notched inferior glenoid fossa; and (b) hypoplasia of scapular neck, irregular notched glenoid articular surface, and widening of lower part of joint space.

Source (a): Sutro (1967). Reproduced with permission from J. Michael Ryan Publishing.

Shape of acromion

The spine of the scapula separates the supraspinous and infraspinous fossae and extends laterally to end in a bony strut that articulates with the distal clavicle. Viewed from above, the shape of the acromion has been described as falciform (Fig. 7.12d), triangular (Fig. 7.12c), quadrangular (Fig. 7.12a), or intermediate (Macalister 1893). Widely varying rates of occurrence have been reported: falciform (5.7–46.9%); triangular (8.3–61.3%); quadrangular (1.3–55.8%); and intermediate (5.1–61.2%). The wide variances in the percentage of scapulae in each category likely reflects a lack of agreement on what makes each type unique rather than pure morphologic variation (Kajava 1924; Vallois 1932; Gray 1942; Bergmann et al. 1988; Edelson 1995a). Other authors have described the superior aspect of the acromion as cobra-shaped, square, and intermediate (Edelson and Taitz 1992). One study using this nomenclature investigated 90 Turkish scapulae and found 31% cobra-shaped, 13% square, and 56% intermediate (Coskun et al. 2006).

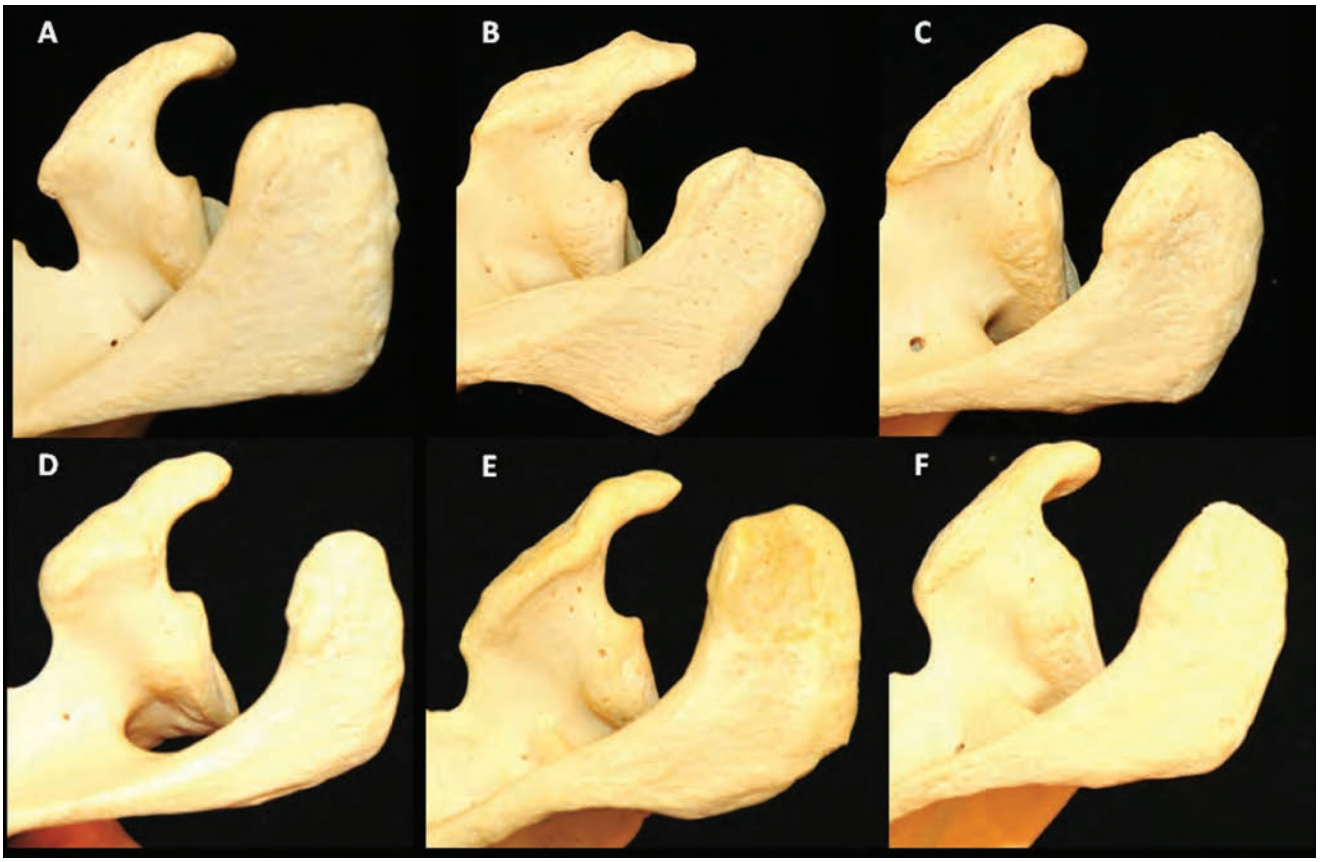

Figure 7.12 Shape of acromion from a superior view: (a) quadrangular; (b) quadrangular with prominent posterior angle; (c) triangular; (d) falciform (small posterior corner); (e) quadrangular (falciform tendency); and (f) triangular (falciform tendency).

When viewed laterally, the inclination of the acromion can vary significantly (Dwight 1887). This shape has been described as flat (Fig. 7.13a), curved (Fig. 7.13b), or hooked (Fig. 7.13c) (Bigliani et al. 1986). A fourth shape was later described wherein the acromion is curved with an inferiorly convex middle third (Fig. 7.13d) (Gagey et al. 1993; Natsis et al. 2007b). The reported incidence of each type of lateral acromial shape is tremendously variable: flat (10–43%); curved (25–89.8%); hooked (0–40%); and inferiorly convex (1.6–2.6%) (Bigliani et al. 1986; Epstein 1993; Gagey et al. 1993; Nicholson et al. 1996; Coskun et al. 2006; Natsis et al. 2007b). This variability may be due to differences in how each author viewed the scapulae as well as differences in terminology related to outgrowths from the distal acromion; these include such diverse terms as plaques, hooks, enthesophytes, beaks, osteophytes, spurs, etc. (Chambler and Emery 1997). One study of 394 scapulae (Getz et al. 1996) did apply a consistent quantitative algorithm of categorizing each acromial shape and found: flat (22.8%); curved (68.5%); and hooked (8.6%). While several studies did not find any connection between age and acromial shape (Getz et al. 1996; Nicholson et al. 1996), another study of 830 scapulae did find that hooked scapulae increased in proportion over time and that hooked acromia were present bilaterally in 73% of the specimens studied (Edelson 1995a). The author stated that the presence of an enlarged facet for the acromioclavicular joint may be what some authors have previously identified as a "hook."

The lateral shape of the acromion is of clinical interest primarily because of its potential role in rotator cuff dysfunction. Hooked acromia were found in much higher proportion in a population of patients with rotator cuff impingement or full-thickness tears of the supraspinatus tendon (Epstein et al. 1993). Likewise, lowering the coracoacromial arch by hooking of the acromion or inferior angulation of the coracoid process is associated with degenerative changes (Edelson and Taitz 1992). The coracoacromial ligament attaches to the acromion in four ways: on the inferior aspect of the acromion away from its apex (Fig. 7.14d) (22.2%); inferiorly at the apex (Fig. 7.14c) (21.6%); at the apex in line with the inferior aspect of the acromion (Fig. 7.14b) (49.5%); or at the apex but not in line with the inferior aspect (Fig. 7.14a) (8.7%). There were also hybrid types (Gagey et al. 1993). Curved or hooked acromia are also more likely to have enthesophytes near the location of the coracoacromial ligament (Gagey et al. 1993; Natsis et al. 2007b). The incidence of anterior acromial spurs increases from 7% in specimens under 50 years to 30% in specimens over 50 years (Nicholson et al. 1996).

Regarding very rare variations affecting the shape of the acromion, there is a case study of a German's miner who had an acromion that extended laterally and inferiorly to the level of the surgical neck of the humerus (Arens 1951; McClure and Raney 1975).

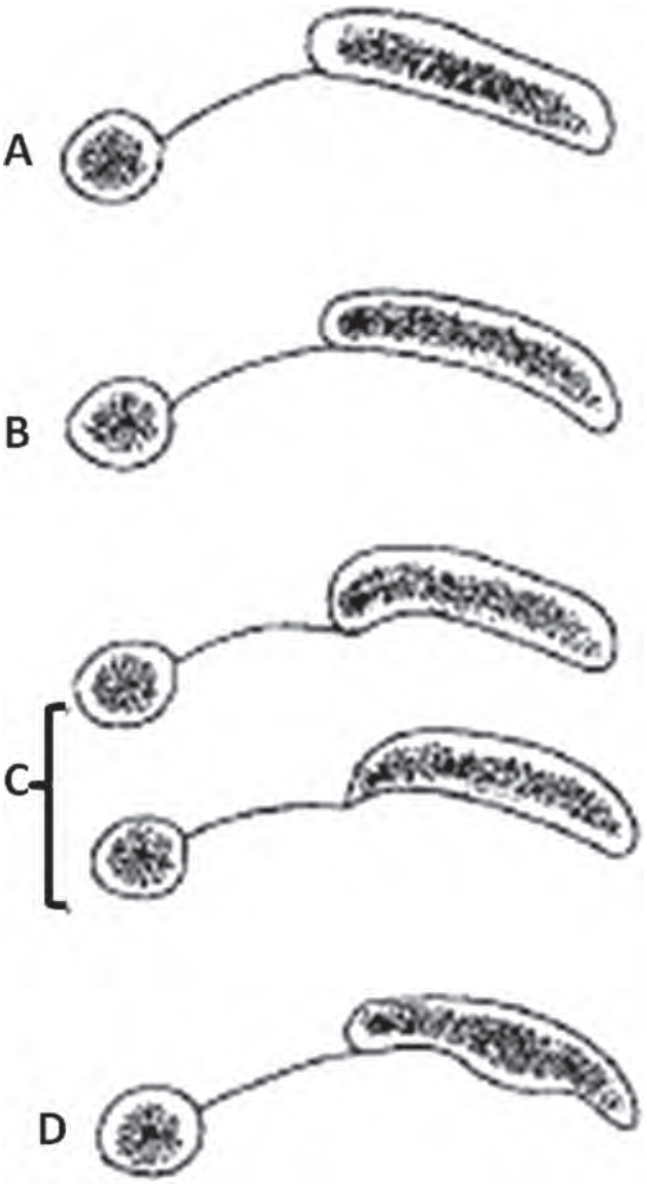

Figure 7.13 Diagram of the coracoacromial arch in the sagittal plane, showing the different types of acromion observed in MRI. These are classified in terms of appearance of their inferior aspect. (a) Type I, a flat plane (28.0% of cases); (b) type II concave inferiorly (59.5%); (c) type III, hooked with an inferior cavity (12.5%); and (d) type IV with an irregular inferior border.

Source: Gagey et al. (1993). Reproduced with permission from Springer Science and Business Media.

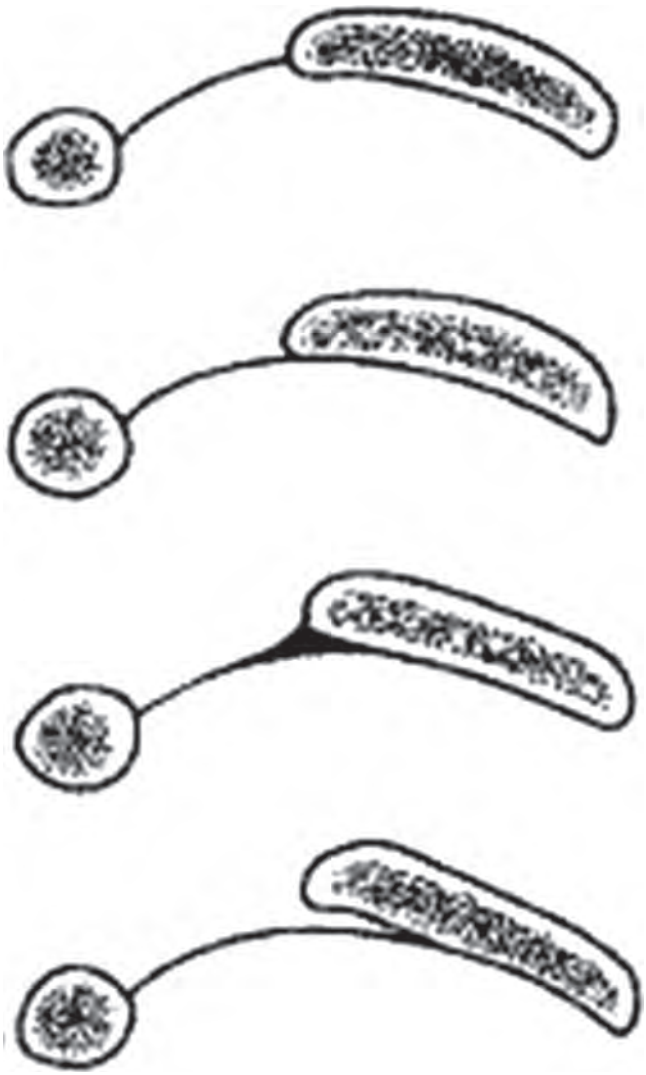

Figure 7.14 Coracoacromial arch in the sagittal plane showing the different modes of attachment of the coracoacromial ligament at the acromion as visualized by MRI: (a) attached to the apex of the acromion, giving an irregular appearance to the inferior aspect of the arch (8.7%); (b) to the apex of the acromion, giving a regular inferior aspect of the arch (49.5%); (c) to the apex and the inferior aspect of the acromion (21.6%); and (d) to the inferior aspect of the acromion only (22.2%).

Source: Gagey et al. (1993). Reproduced with permission from Springer Science and Business Media.

Os acromiale

The os acromiale (Fig. 7.15) is the term applied to the distal portion of the acromion when it exists as a separate bone between the scapular spine and the distal clavicle. It has been cited as occurring in 1.0–9.6% of specimens (Cruveilhier 1833; Pfitzner 1894; Symington 1900; Vallois 1926, 1932; Liberson 1937; Gray 1942; Grasso 1992; Edelson et al. 1993; Getz et al. 1996; Nicholson et al. 1996; Prescher 2000; Sammarco 2000).

The os acromiale occurs unilaterally more frequently than bilaterally (Vallois 1926; Gray 1942; Nicholson et al. 1996; Sammarco 2000) although one radiographic study found it unilateral in 8 specimens and bilateral in 13 (Liberson 1937). Os acromiale is more frequently seen on the right side (Bergman et al. 1988),

Figure 7.15 The os acromiale fragment, whether large or small, measures approximately one-third of the overall length of the acromion of which it is part.

Source: Edelson et al. (1993). Reproduced with permission from the British Editorial Society of Bone and Joint Surgery.

in males (Bergman et al. 1988; Sammarco 2000), and in African-American skeletons than whites (Sammarco 2000). In addition, an os acromiale will sometime fuse to the acromion later in life, leaving an indentation marking the former separation (Sammarco 2000).

In a meta-analysis of 23 studies, Yammine (2013) found: (a) a crude overall prevalence of 7.0%; (b) a crude cadaveric prevalence of 7.6%; (c) a crude archeological (skeletal) prevalence of 5.6%; (d) a crude radiological prevalence of 4.2%; (e) a true anatomical prevalence of 9.6%; (f) a significantly higher frequency in persons of black ancestry than in persons of white, Native American and Middle Eastern ancestries (OR ≈ 3); (g) significantly higher unilateral and bilateral frequencies in black ancestry (OR of 2 and 4, respectively); and (h) nonsignificant interactions of os acromiale frequency with gender and side. The commonest type of os acromiale was the meso-acromion type (76.6%). Degenerative changes were present in 66.6% of all os acromaiale.

The acromion forms from several small ossification centers that consolidate into the meta-, meso-, and pre-acromion during the first two decades of life (Macalister 1893; Liberson 1937; McClure and Raney 1975). All of these ossification centers are found along the lateral margin of the cartilage of the developing acromion (Macalister 1893; Edelson et al. 1993; Sammarco 2000) and are not stacked, as they have sometimes been represented (Liberson 1937; McClure and Raney 1975; Park et al. 1994; Coskun et al. 2006). The meta-acromion, which fuses to the scapular spine (basi-acromion), is prominent during acromial development. Os acromiale frequently results from the failure of the meso- and meta-acromion to fuse, leaving the cap-shaped os acromiale as a separate bone (Macalister 1893; Liberson 1937; Park et al. 1994; Sammarco 2000). The acromioclavicular joint facet most frequently exists on the os acromiale, but at other times the joint spans the distal acromion and os acromiale (Symington 1900; Edelson et al. 1993; Prescher 2000).

The os acromiale may be mistaken for a fractured acromion; however an os acromiale has smooth borders rather than the jagged edges associated with a fracture (McClure and Raney 1975). Degenerative changes have been noted at the site of nonunion, particularly on the proximal segment (Edelson et al. 1993; Park et al. 1994). Os acromiale should not be diagnosed until after age 25 due to possibility that ossification of the acromion is incomplete (Prescher 2000).

Studies of symptomatic shoulders may overestimate the occurrence of os acromiale while exclusively radiographic studies may underestimate its occurrence (Brailsford 1953; Edelson et al. 1993; Sammarco 2000). Computed tomography (CT) is more reliable in visualizing os acromiale than plain-film radiographs (Grasso 1992). Because the preacromion articulates with coracoacromial ligament and anterior deltoid and the mesoacromion anchors fibers of deltoid, a free os acromiale may be pulled inferiorly by deltoid contraction and impinge on the supraspinatus tendon, predisposing to rotator cuff problems (Sammarco 2000).

References

Adler KJ. 1941. Verwechslung der apopyse des angulus inferior scapulae mit einem Rudschatten. *Rontgenpraxis* 13: 188.

Aggarwal A, Wahee P, Harjeet, Aggarwal AK, Sahni D. 2011. Variable osseous anatomy of costal surface of scapula and its implications in relation to snapping scapula syndrome. *Surg Radiol Anat* 33: 135–140.

Alon M, Weiss S, Fishel B, Dekel S. 1988. Bilateral suprascapular nerve entrapment syndrome due to an anomalous transverse scapular ligament. *Clin Ortho Relat Res* 234: 31–33.

Arens W. 1951. Eine seltene angeborene mistbildung des schlterge lenkes. *Fortschr Geb Rontgenstrahlen* 75: 365.

Avery BW, Pilon FM, Barclay JK. 2002. Anterior coracoscapular ligament and suprascapular nerve entrapment. *Clin Anat* 15: 383–386.

Bayramoğlu A, Demiryürek D, Tüccar E, Erbil M, Aldur MM, Tetik O, Doral MN. 2003. Variations in anatomy at the suprascapular notch possibly causing suprascapular nerve entrapment: an anatomical study. *Knee Surg Sports Traumatol Arthrosc* 11: 393–398.

Bergman RA, Thompson SA, Afifi AK, Saadeh FA. 1988. *Compendium of Human Anatomic Variation*. Baltimore: Urban and Schwarzenberg.

Bigliani LU, Morrison DS, April EW. 1986. The morphology of the acromion and its relationship to rotator cuff tears. *Orthop Trans* 10: 216.

Brailsford JE. 1953. *The Radiology of Bones and Joints*, fifth edition. Baltimore: Williams & Wilkins Co.

Chambler AFW, Emery RJH. 1997. Acromial morphology: the enigma of terminology. *Knee Surg Sports Traumatol Arthrosc* 5: 268–272.

Cigtay OS, Mascatello VJ. 1979. Scapular defects: a normal variation. *Am J Roentgenol* 132: 239–241.

Cooper DR, Arnoczky SP, O'Brien SJ, Warren RF, DiCarlo E, Allen AA. 1992. Anatomy, histology, and vascularity of the glenoid labrum: an anatomical study. *J Bone Joint Surg (Am)* 74(1): 46–52.

Coskun N, Karaali K, Cevikol C, Demirel BM, Sindel M. 2006. Anatomical basics and variations of the scapula in Turkish adults. *Sudi Med J* 27(9): 1320–1325.

Cruveilhier J. 1833. *Traité d'Anatomie Descriptive*. Paris: JB Baillière.
Demaio M, Drez D Jr, Mullins RC. 1991. The inferior transverse scapular ligament as a possible cause of entrapment neuropathy of the nerve to the infraspinatus. *J Bone Joint Surg* 73A(7): 1061–1063.
Demirkan AF, Sargon MF, Erkula G, Kiter E. 2003. The spinoglenoid ligament: an anatomic study. *Clin Anat* 16: 511–513.
De Wilde V, De Maeseneer M, Lenchik L, Van Roy P, Beeckman P, Osteaux M. 2004. Normal osseous variants presenting as cystic or lucent areas on radiography and CT imaging: a pictorial overview. *Eur J Radiol* 51(1): 77–84.
Dwight T. 1887. The range of variation of the human shoulder-blade. *The American Naturalist* 21(7): 627–638.
Edelson JG. 1995a. The 'hooked' acromion revisited. *J Bone Joint Surg* 77B(2): 284–287.
Edelson JG. 1995b. Bony bridges and other variations of the suprascapular notch. *J Bone Joint Surg* 77B(3): 505–506.
Edelson JG. 1996. Variations in the anatomy of the scapula with reference to the snapping scapula. *Clin Orthop Relat Res* 322: 111–115.
Edelson JG, Taitz C. 1992. Anatomy of the coraco-acromial arch. *J Bone Joint Surg* 74B(4): 589–594.
Edelson JG, Zuckerman J, Hershkovitz I. 1993. Os acromiale: anatomy and surgical implications. *J Bone Joint Surg* 74B(4): 551–555.
Epstein RE, Schweitzer ME, Frieman BG, Fenlin JM, Mitchell DG. 1993. Hooked acromion: prevalence in MR images of painful shoulders. *Radiology* 187: 479–481.
Fabrizio PA. 2012. Unusual ligament of the scapula. *Int J Anat Var* 5: 54–55.
Finder JG. 1936. Congenital anomaly of the coracoid. *J Bone Joint Surg* 28(1): 148–152.
Fontan C. 1912. Articulations scapulocostales. *Bull Soc Anat (French)* 48: 182–192.
Gagey N, Ravaud E, Lassau JP. 1993. Anatomy of the acromial arch: correlation of anatomy and magnetic resonance imaging. *Surg Radiol Anat* 15: 63–70.
Getz JD, Recht MP, Piraino DW, Schils JP, Latimer BM, Jellema LM, Obuchowski NA. 1996. Acromial morphology: relation to sex, age, symmetry, and subacromial enthesphytes. *Radiology* 199: 737–742.
Grasso A. 1992. The incidence and role of the os acromiale in the acromiohumeral impingement syndrome. *Radiol Med* 84(5): 567–570.
Graves WW. 1910. The scaphoid scapula: a frequent anomaly in development of hereditary, clinical and functional significance. *Med Rec* 77(2): 861–873.
Graves WW. 1921. The types of scapulae. A comparative study of some correlated characters in human scapulae. *Am J Phys Anthropol* 4(2): 111–128.
Gray DJ. 1942. Variations in the human scapulae. *Am J Phys Anthropol* 29(1): 57–72.
Gruber W. 1864. Die bursae mucosae der inneren Achselhölenwand. *Arch F Anat Physop U Wissen Med* 1964: 358–366.
Gruber W. 1872. Über einen fortsatzartigen, cylindrischen Höcker an der Vorderfläsche de Angulus superior der Scapula. *Arch Pathol Anat Physiol Kiln Med* 69: 387–391.
Harris RI, Vu DH, Sonnabend DH, Goldberg JA, Walsh WR. 2001. Anatomic variance of the coracoclavicular ligaments. *J Shoulder Elbow Surg* 10(6): 585–588.
Hrdlička A. 1942a. The scapula: visual observations. *Am J Phys Anthropol* 29: 73–94.
Hrdlička A. 1942b. The juvenile scapula: further observations. *Am J Phys Anthropol* 29: 287–310.
Hrdlička A. 1942c. The adult scapula: additional observations and measurements. *Am J Phys Anthropol* 29: 363–415.
Iqbal K, Iqbal R, Khan SG. 2010. Anatomical variation in shape of suprascapular notch of scapula. *J Morphol Sci* 27(1): 1–2.
Kajava Y. 1924. Über den Schultergürtel der Finnen. *Ann Acad Sci Fenn Series A* 21(5): 1–69.
Khairouni A, Bensahel H, Csukonyi Z, Desgrippes Y, Pennecot GF. 2002. Congenital high scapula. *J Pediatr Orthop Part B* 11(1): 85–88.
Khan MA. 2006. Complete ossification of the superior transverse scapular ligament in an Indian male adult. *Int J Morphol* 24(2): 195–196.
Kharay SS, Sharma A. 2010. The spinoglenoid foramen. *Clin Anat* 23: 887–888.
Khoo FY, Kuo CL. 1948. An unusual anomaly of the inferior portion of the scapula. *J Bone Joint Surg* 30A(4): 1010–1011.
Kohler A, Zimmer EA. 1968. *Borderlands of the Normal and Early Pathologic in Skeletal Roentgenology*, eleventh edition. New York: Grune and Stratton, Inc.
Lehtinen JT, Tingart MJ, Apreleva M, Warner JJP. 2005. Quantitative morphology of the scapula: normal variation of the superomedial scapular angle, and superior and inferior pole thickness. *Orthopedics* 28(5): 481–486.
Liberson F. 1937. Os acromiale – a contested anomaly. *J Bone Joint Surg* 19(3): 683–689.
Macalister A. 1893. Notes on the acromion. *J Anat Physiol* 27: 498–509.
McClure JG, Raney RB. 1974. Double acromion and coracoid process. *J Bone Joint Surg* 56A(4): 830–832.
McClure JG, Raney RB. 1975. Anomalies of the scapula. *Clin Orthop Relat Res* 110: 22–31.
Natsis K, Totlis T, Tsikaras P, Appell HJ, Skandalakis P, Koebke J. 2007a. Proposal for classification of the suprascapular notch: a study of 423 dried scapulas and review of the literature. *Clin Anat* 20: 135–139.
Natsis K, Tsikaras P, Totlis T, Gigis I, Skandalakis P, Appell HJ, Koebke J. 2007b. Correlation between the four types of acromion and the existence of enthesophytes: a study of 423 dried scapulas and review of the literature. *Clin Anat* 20: 267–272.
Nicholson GP, Goodman DA, Flatow EL, Bigliani LU. 1996. The acromion: morphologic condition and age–related changes. A study of 420 scapulas. *J Shoulder Elbow Surg* 5(1): 1–11.
Nutter PD. 1941. Coracoclavicular articulations. *J Bone Joint Surg* 23(1): 177–179.
Osuagwu FC, Imosemi IO, Shokunbi MT. 2005. Complete ossification of the superior transverse scapular ligament in a Nigerian male adult. *Int J Morphol* 23(2): 121–122.
Park JG, Lee JK, Phelps CT. 1994. Os acromiale associated with rotator cuff impingement: MR imaging of the shoulder. *Radiology* 193(1): 255–257.
Parsons TA. 1973. The snapping scapula and subscapular exostoses. *J Bone Joint Surg* 55B(2): 345–349.
Percy EC, Birbrager D, Pitt MJ. 1988. Snapping scapula: a review of the literature and presentation of 14 patients. *Can J Surg* 31(4): 248–250.
Pfitzner W. 1894. Beitrange zur kenntnis des menschlichen extremitatenskelets. *Morphol Arb* 4: 347.
Plancher KD, Peterson RK, Johnston JC, Luke TA. 2005. The spinoglenoid ligament. *J Bone Joint Surg* 87A(2): 361–365.
Poirier P, Charpy A. 1911. *Traité d'Anatomie Humaine*, third edition. Paris: Masson.
Prescher A. 2000. Anatomical basics, variations, and degenerative changes of the shoulder joint and shoulder girdle. *Eur J Radiol* 35: 88–102.

Prescher A, Klümpen T. 1997. The glenoid notch and its relation to the shape of the glenoid cavity of the scapula. *J Anat* 190: 457–460.

Resnick D, Walter RD, Crudale AS. 1982. Bilateral dysplasia of the scapular neck. *AJR* 139: 387–389.

Sammarco VJ. 2000. Os acromiale: frequency, anatomy and clinical implications. *J Bone Joint Surg* 82A(3): 394–400.

Seib GA. 1938. The muscle pectoralis minor in American Whites and American Negroes. *Am J Phys Anthropol* 23(4): 389–419.

Silva JG, Abidu-Figueiredo M, Fernandes RMP, Aureliano-Rafael F, Sgrott EA, Silva SF, Babinski MA. 2007. High incidence of complete ossification of the superior transverse scapular ligament in Brazilians and its clinical implications. *Int J Morphol* 25(4): 855–859.

Sutro CJ. 1967. Dentated articular surface of the glenoid–an anomaly. *Bull Hosp Joint Dis* 27(2): 104–108.

Symington J. 1900. Separate acromion process. *J Anat Physiol* 34: 287–294.

Tirman PFJ, Feller JF, Palmer WE, Carroll KW, Steinbach LS, Cox I. 1996. The Buford complex: a variation of normal shoulder anatomy: MR arthrographic imaging features. *AJR* 166: 869–873.

Vallois HV. 1926. Les anomalies de l'omoplate chez l'homme. *Bulletins et Mémoires de la Société d'Anthropologie de Paris*, VII Série, tome 7 fascicule 1–3: 20–37.

Vallois HV. 1928. L'omoplate humaine, étude anatomique et anthropologique. *Bulletins et Mémoires de la Société d'Anthropologie de Paris*, VII Série, tome 9 fascicule 4–6: 129–168.

Vallois HV. 1932. L'omoplate humaine (suite). *Bulletins et Mémoires de la Société d'Anthropologie de Paris*, VIII Série, tome 3 fascicule 1–3: 3–153.

Williams MW, Snyder SJ, Buford D. 1994. The Buford complex – the "cord-like" middle glenohumeral ligament and absent anterosuperior labrum comlex: a normal anatomic capsulolabral variant. *J Arthroscop Rel Surg* 10(3): 241–247.

Yammine K. 2013. The prevalance of os acromiale: A systematic review and meta-analysis. *Clin Anat* 27(4): 610–621.

8 Clavicle

Z.J. Daruwalla[1], R. Malhotra[1], P. Courtis[2], C. Fitzpatrick[2], D. Fitzpatrick[2] and H. Mullett[1]
[1]Beaumont Hospital, Dublin, Ireland
[2]University College Dublin, Dublin, Ireland

The chief use of the clavicle is to hold the shoulder blade at the proper distance from the breastbone, since motion of the shoulder would be hindered if the two came close together, as seen in four-footed animals that can use their forefeet only for walking, and not in the way that men need their hands.

Therselben, 1790

Introduction

Although anthropometric work on the clavicle by Broca dates as far back as 1869 (Voisin 2008), the role of the clavicle was described more than 200 years ago in 1790 by Therselben (Andermahr et al. 2007). Specifically, its shape variation plays an important role in fractures of what is considered to be the shortest long bone in the human body. While one study stated that the clavicle is the most frequently fractured bone of the human skeleton (Andermahr et al. 2007), data collected in Malmö, Sweden between 1952 and 1987 showed that fractures of the clavicle only accounted for 4% of all fractures, although this represented 35% of all fractures in the shoulder region (Nordqvist and Petersson 1994). Other studies have shown similar results, estimating that clavicular fractures account for 5–10% of all fractures (Moore 1951; Rockwood and Green 1984) and 44% of all injuries to the shoulder girdle (Rowe 1968).

Numerous studies have verified that fractures to the middle third are the most common in adults and children, accounting for 80%, while fractures to the lateral third are seen in 15% with the remaining 5% affecting the medial third (Neer 1963; Eberle et al. 1973; Blomer et al. 1977; Pannicke 1982; Jager and Breitner 1984). This can be explained by a number of facts attributed to the clavicle's geometric and anatomic parameters. First, the narrowest part of the clavicle is at the meeting point of the sternal convexity and the acromial concavity, which is the location of the majority of clavicle fractures (Andermahr et al. 2007). Second, there is a significant decrease in bone density at the transition from middle to lateral thirds of the clavicle, explaining the increased frequency of fractures occurring in the middle and lateral thirds (Andermahr et al. 2007). It has also been previously shown that the mid-portion of the clavicle is the thinnest and narrowest part of the bone and represents a transitional region of the bone, both in curvature and cross-sectional anatomy, making it a mechanically weak area that is most likely to fracture (Harrington et al. 1993).

In terms of location, the sternoclavicular and acromioclavicular joints hold the clavicle in its anatomical position with the latter having been described as a "keystone" link between the scapula and clavicle (Fraser-Moodie et al. 2008). Its integrity plays an important role in the movement of the shoulder girdle. The construct of the acromioclavicular joint (ACJ) makes it a very strong joint able to tolerate a significant amount of force before disruption. This explains why, in comparison to clavicular fractures, injuries to the ACJ account for approximately only 12% of those to the shoulder girdle seen in clinical practice (Emery 1997). Much higher incidences are seen in contact sports. In rugby, ACJ injuries have been shown to account for 32% of shoulder injuries (Headey et al. 2007) and in American football they are the most common injury to the shoulder (Kaplan et al. 2005). Even in noncontact sports such as recreational skiing, about 20% of injuries to the shoulder girdle involve the ACJ (Kocher and Feagin 1996). With the majority of injuries to the ACJ seen in young males, the same applies to fractures of the clavicle (Robinson 1998).

Whenever a fixation implant is to be selected, several factors drive the decision. The fit on bone of any fixation plate has a direct impact on the strength of the construct, emphasizing the importance of understanding clavicular shape variation. However, many clavicular implants overlook the variations in geometry of the bone. A paper describing the anatomy of the clavicle stated that gender-specific anatomical features should be taken into consideration when performing intramedullary fixation of the clavicle (Andermahr et al. 2007). While the length, diameters and curvature of the clavicles measured were based on 196 embalmed specimens, cortical bone thickness and the medullary canal diameter were determined using only 10 fresh specimens. In a more recent article, it has been reported that cortical bone thickness and bone shape of the clavicle have large effects on bone responses until failure and on fracture location (Duprey et al. 2008). This study emphasized the need for geometrical per-

Bergman's Comprehensive Encyclopedia of Human Anatomic Variation, First Edition. Edited by R. Shane Tubbs, Mohammadali M. Shoja and Marios Loukas.
© 2016 John Wiley & Sons, Inc. Published 2016 by John Wiley & Sons, Inc.

sonalization of clavicle models in order to consider various age, gender, and shape discrepancies. However, the radiological aspect of this study was based only on six clavicles with the biomechanical testing based on 18 clavicles from 9 subjects with a mean age of 78.

While studies focusing on geometry do exist (Harrington et al. 1993; Kaur et al. 2002; Andermahr et al. 2007; Duprey et al. 2008), these studies have very small sample sizes. One recent study set out to characterize variations in clavicular anatomy and determine the clinical applicability of an anatomic precontoured clavicular plate designed for fracture fixation (Huang et al. 2007). However, the authors themselves stated that their main limitation was that it was a two-dimensional (2D) analysis of plate fit rather than a 3D analysis. By noting the shortcomings of the abovementioned studies, another study focused on the anatomy of the clavicle and the analysis and application of it to the design of currently available clavicle fixation plates in both a systematic and structured manner (Daruwalla et al. 2010a). However, before we look at the geometric and anatomic variations of the clavicle, it is vital to understand the terms "statistical shape analysis" and "principal component analysis."

Statistical shape analysis

Statistical shape analysis refers to geometrical analysis of shapes using statistics to define and calculate various parameters that describe the morphology of the shape in question. In turn, this allows us to gauge the variability of the shape within a sample group. Before proceeding, it is important to first define size and shape. While size refers to the scale of an object, shape refers to all the geometric features of it, excluding size, position, and orientation. If the size of an object is increased, so are its dimensions. However, the proportions of its dimensions remain unchanged. Hence, scaling, moving, and rotating an object do not change its shape. If two objects can be scaled, moved, and rotated such that they overlap each other and are a perfect match, they are said to have the same shape. If they cannot, they are deemed to have different shapes.

The purpose of statistical shape analysis and subsequent modeling in orthopedics is to construct a patient-specific model from incomplete or sparse data using knowledge of the actual population. By using an improved method of analysis known as geometric morphometrics, we are able to study variation in size and shape of objects or organisms. Initially, a set of ordered landmark coordinates are used to represent a subject. Coordinates from each subject are then superimposed upon each other and their distribution is analyzed in order to characterize shape variation within the sample. This can be achieved by employing Procrustes superimposition, where landmark configurations are scaled, translated, and rotated using least-squares fitting in order to register each set of points with one another.

However, before performing Procrustes superimposition, landmark data must be acquired. This may be achieved in a number of ways such as using cameras, x-rays, or any other form of imaging. With the advancements in technology today, high-resolution computerized tomography ensures the accurate capture of the abovementioned coordinates and provides us with images of the highest standard which can subsequently be analyzed with a very minimal loss of information. In turn, using this data allows a model to be produced that is an accurate anatomical representation of the population.

By using statistical shape analysis, statistical shape models of bones and joints can be built and have been used in conjunction with computer-assisted surgery in the past.

Principal component analysis

Invented more than a century ago (Pearson 1901), principal component analysis (PCA) is one of the main methods used for statistical shape analysis. The aim of PCA is to reduce the dimensionality of a multivariate dataset while retaining as much variation as possible. Using a mathematical procedure, a number of original and possibly correlated variables are transformed into a smaller number of uncorrelated variables known as principal components. These principal components (PCs) are linearly independent of one another. In simple terms, PCA helps us identify patterns in data. By reducing a high-dimension complex dataset to a low-dimension dataset that retains as much variation as possible, the underlying core structure can still be visualized.

By making the first PC (PC1) account for the maximum possible percentage of the entire variance seen in the sample population, it retains the most information about the original dataset and is a linear function of the variables that have maximum variance. All subsequent PCs are defined as being orthogonal to the PCs. It is important to remember that there is no correlation between any of the PCs, as mentioned earlier. Geometrically, if we had just two variables, they could be plotted on an x–y graph. A linear equation for x could be written in terms of y, and similarly a linear equation for y could be written in terms of x, but these two equations would be different as they are involved with reducing the distance from the points to the line in either the x- or the y-direction but not both. The first PC defines a best-fit line to the points, which reduces the perpendicular distance from the points to this line. The second PC is a line orthogonal to the first. If an ellipse was drawn around these points the major and minor axes of the ellipse would be the first and second PCs, respectively. The higher the correlation between x and y, the more variation there will be along the direction of the first PC and the less there will be along the direction of the second PC. This theory can be expanded for multiple variables. The number of variables is equal to the number of PCs. Each subsequent PC will be

orthogonal to the previous PC and will be responsible for less variation than it.

As all the PCs together account for 100% of variation within the sample population, this implies that no information is lost with the conversion of the original variables to principal components. However, selecting fewer PCs for analysis results in a loss of information. It is for this reason that deciding how many PCs should be retained is a difficult question to answer. On the one hand, you want to minimize the loss of information; on the other, you want to minimize the number of working variables to reduce the computational complexity. There are a number of rules that exist, stating how many PCs should be retained for analysis. One example is that of retaining the first few PCs that add up to 80% in terms of cumulative variance. While this is simple to follow, it must be noted that a variety of more complex rules also exist but are not described here.

Calculation of principal components is based on either the correlation or the covariance matrices. In either case, the principal components are the eigenvectors of the matrix with the signs of their coefficients usually being arbitrary. What is however important is the sign of a PC coefficient relative to the signs of the other coefficients in that PC. If PC coefficients have the same sign, it relates to the variability that the variables have in common. If PC coefficients have different signs it relates to differences in variability. For example, if a principal component had nearly equal coefficients of the same sign, the PC is a weighted average of all variables. An increase in one variable is matched by an increase in all the other variables and, similarly, a decrease will affect all variables equally. In terms of anatomic or biological measurements, this PC is usually associated with the size of the specimen. In other PCs there are usually two groups: one containing the positive coefficients and the other containing the negative coefficients of a non-negligible magnitude. An increase in the variables of one group is matched by a decrease in the proportions of the variables of the other. In anatomic terms, these PCs are thought of as describing the variations in shape of the specimen.

Rather than focusing on the similarity between variables, PCA concentrates on explaining the differences between them. By applying PCA successfully, is it possible to express the size and shape variation of the object in question in a concise manner and attribute it to fewer variables.

Geometric variation

The clavicle demonstrates a complex anatomy making its shape difficult to analyze. A variety of measures have been used to assess clavicular dimensions, including cadaveric samples and computerized tomography scans with the help of computer software. Several studies over the years have focused on shape variation. As these studies have used different methods, direct comparisons may be inaccurate but some clear trends are certainly notable. Using statistical shape and principal component analyses, we have reached the conclusions described in the following sections.

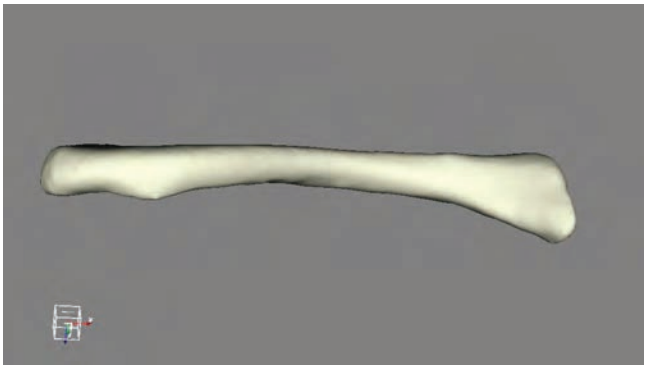

Figure 8.1 Type I clavicle from our study. Only an inferior curvature noted. Adapted from Daruwalla et al. (2010a) with permission from John Wiley & Sons.

Morphological groups

In dorsal view, modern human clavicles can be classified as one of three morphological groups based on Olivier's scheme (Voisin 2008), two of which were observed in our own study (Daruwalla et al. 2010a). Type I clavicles are the most common and only possess an inferior curvature (Fig. 8.1). While type II clavicles were described as having a superior curvature at the sternal end and inferior curvature at the acromial end (Fig. 8.2), type III have no curvature at the sternal end but a superior curvature at the acromial end. The latter are the least common.

Length

Adult clavicle length has been shown to fall within the range 100–180 mm (Haque et al. 2011; King et al. 2014) with other average clavicle lengths in studies falling within the range 140–155 mm (Terry 1932; Kaur 2002; Andermahr et al. 2007; Huang et al. 2007; Haque et al. 2011; King et al. 2014). The lengths of the clavicles in our study fell within the range

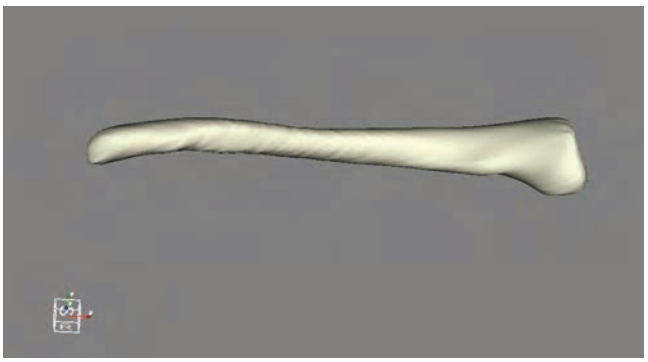

Figure 8.2 Type II clavicle from our study, demonstrating superior and inferior curvatures. Adapted from Daruwalla et al. (2010a) with permission from John Wiley & Sons.

Table 8.1 Mean geometric parameters. Adapted from Daruwalla et al. (2010a) with permission from John Wiley & Sons.

Mean	Length (S1) (mm)	Width 5 (50%) (S4) (mm)	Thickness 5 (50%) (mm)	Medial depth (S5) (mm)	Lateral depth (S6) (mm)	Sternal angle (°)	Acromial angle (°)
Male (*N*=9)	152.33[a] (156[1], 155[2])	12.78 (13[1], 13.5[2])	11.69	15.57 (17[1], 22.5[2])	12.81[f] (13[f], 13[2])	19.33[i]	22.06
Female (*N*=18)	140.34[a] (146[1], 143[2])	9.59 (11[1], 10[2])	9.34	15.84 (16[1], 17[2])	10.38[f] (11[1], 13.3[2])	22.72[i]	23.63
Left (*N*=15)	145.21 (152[1])	10.86 (12[1])	9.96	14.88[d] (16[1])	10.23[h] (12[1])	20.63	21.62
Right (*N*=12)	143.24 (149[1])	10.39 (12[1])	10.34	16.82[d] (17[1])	12.39[h] (13[1])	22.79	24.96
Male left (*N*=5)	153.25[b]	13.36	11.35	14.98	10.85[i]	18.55	20.21
Female left (*N*=10)	141.19[b]	9.62	9.26	14.83[e]	9.93	21.68	22.33
Male right (*N*=4)	151.19[c]	12.05	12.11	16.3	15.27[g, i]	20.31[k]	24.37
Female right (*N*=8)	139.27[c]	9.56	9.45	17.09[e]	10.94[g]	24.04[k]	25.25

[1]Andermahr et al. (2007); male (*N*=90), female (*N*=99), right (*N*=97)
[2]Duprey et al. (2008); male (*N*=90), female (*N*=99)
[a]M>F (P<0.002); [b]M L > F L (P<0.004); [c]M R > F R (P<0.025); [d]R > L (P=0.058); [e]F R > F L (P<0.05); [f]M > F (P<0.05); [g]M R > F R (P<0.03); [h]R > L (P = 0.07); [i]M R > M L (P=0.05); [j]F > M (P<0.05); [k]F R > M R (P=0.07).
The greater width and thickness in males compared to females was of statistical significance using all comparisons (M vs F, M L vs F L, M R vs F R).

129.41–161.2 mm (Daruwalla et al. 2010b). Clavicles in males were longer than in females. The male clavicle lengths ranged from 141.15 to 161.2 mm in comparison to 129.41–149.52 mm in females. Comparing the same sides between genders, this was found to be true regardless of side. It was also noted that the mean length was larger on the left than right. This was the case regardless of gender. In both males and females, left clavicles tended to be longer than those on the right. Table 8.1 summarizes these findings. In comparing six pairs of clavicles from the same persons however (Table 8.2), there was no significant difference between the mean lengths of the left and right sides even though the discrepancies between sides in the same patients ranged from 0.81 to 4.32 mm.

Depths and angles

The mean of the medial depths was significantly larger than the lateral depths (15.75 vs 11.19 mm). This was also evident independently across all subgroups. The opposite held true with regard to angles. The mean acromial angle was found to be larger than the sternal angle (23.1 vs 21.5 degrees). Again, this was noted independently across all subgroups.

Table 8.2 Comparison of clavicle lengths in same persons. Adapted from Daruwalla et al. (2010a) with permission from John Wiley & Sons.

	Age	Sex	Length left (mm)	Length right (mm)
JO	60	F	140.74	137.54
710018	83	F	141.03	143.98
801085	94	F	131.47	132.72
802093	74	F	135.69	134.88
90305	85	F	142.56	138.24
909020	73	F	145.89	149.52
Mean			139.56	139.48

Medial depth

Between genders, the average medial depth was larger in women. However, while this was true when comparing the right sides of men and women, the medial depth was larger in men when comparing left sides. When analyzing differences in sides, the average medial depth was larger on the right. This remained true when comparing right and left sides of males as well as right and left sides of females. Table 8.1 summarizes these findings.

Lateral depth

In terms of lateral depth, the opposite was noted. The mean lateral depth was larger in men. This remained a constant finding when comparing right sides of men and women as well as left sides. Between sides, the mean lateral depth was larger on the right. This remained true when comparing right and left sides of males as well as right and left sides of females. Table 8.1 summarizes these findings.

Sternal/medial angle

Between genders, the average sternal angle was larger in women. This remained a constant finding when comparing right sides of men and women as well as left sides. When analyzing differences in sides, the average sternal angle was larger on the right. This remained true when comparing right and left sides of males as well as right and left sides of females. Table 8.1 summarizes these findings.

Acromial/lateral angle

In terms of acromial angle, the mean was larger in women. This remained a constant finding when comparing right sides of men and women as well as left sides. Between sides, the mean angle was larger on the right. This remained true when comparing right and left sides of males as well as right and left sides of females. Table 8.1 summarizes these findings.

Width

The mean widths of the clavicles across their entire lengths at 10% intervals of total length were found to be significantly larger in males than in females at every interval. This remained a constant finding when comparing right sides of men and women as well as left sides. When comparing sides, left clavicles were found to be wider at every interval except the first and last where the widths were wider on the right. In comparing the width of left clavicles in males to right clavicles in males, the same was found except that the first interval from the acromial end was wider on the right. In comparing the width of left clavicles in females to right clavicles in females, left clavicles were wider at every interval except the first and second from the sternal end. Table 8.3 summarizes these results, which are depicted in a graphical representation of the change in width across the clavicle in Figure 8.3.

Thickness

The mean thicknesses of the clavicles across their entire lengths at 10% intervals of total length were found to be

Table 8.3 Clavicular width measured at 10% intervals of total length from sternal end. Adapted from Daruwalla et al. (2010a) with permission from John Wiley & Sons.

Mean	Sternal width (10%) (mm)	W2 (20%) (mm)	W3 (30%) (mm)	W4 (40%) (mm)	W5 (50%) (mm)	W6 (60%) (mm)	W7 (70%) (mm)	W8 (80%) (mm)	Acromial width (90%) (mm)
Male (*N*=9)	18.15	14.63	13.5	13.16	12.78	14.21	18.44	19.05	24.59
Female (*N*=18)	15.5	10.04	9.44	9.64	9.59	11.35	14.71	15.08	20.01
Left (*N*=15)	16.01	11.81	11.1	11.1	10.86	12.57	16.3	16.92	21.24
Right (*N*=12)	16.9	11.28	10.4	10.46	10.39	11.96	15.52	15.75	21.91
Male left (*N*=5)	18.64	15.83	14.43	13.92	13.36	14.72	19.1	20.02	22.84
Female left (*N*=10)	14.55	9.8	9.44	9.68	9.62	11.5	14.9	15.37	20.43
Male right (*N*=4)	17.33	13.13	12.34	12.22	12.05	13.57	17.61	17.83	26.77
Female right (*N*=8)	16.72	10.35	9.44	9.58	9.56	11.16	14.48	14.71	19.49

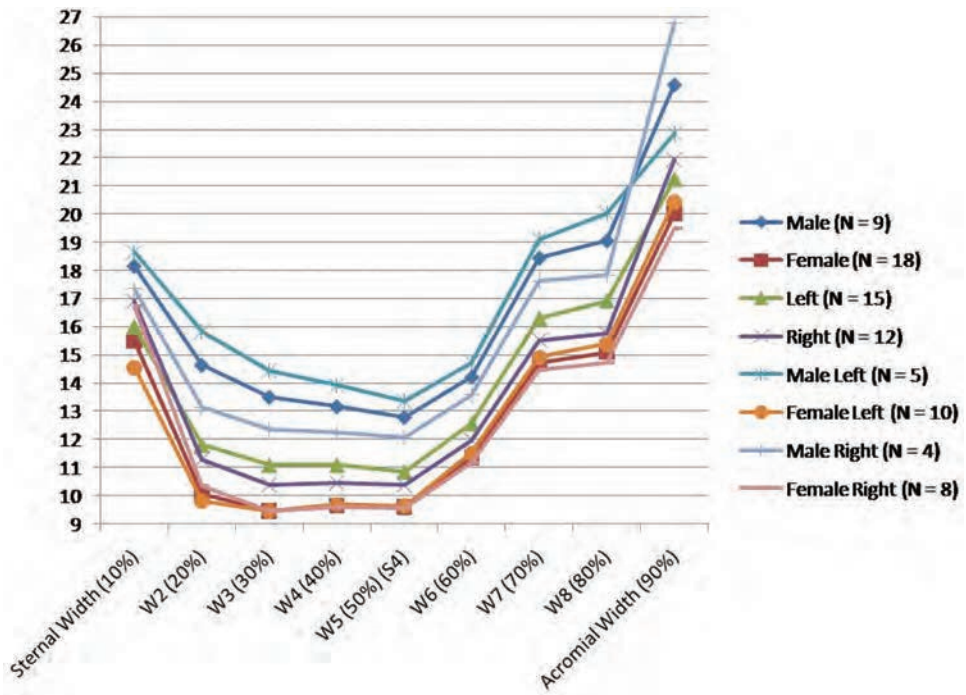

Figure 8.3 Clavicular width (mm) measured at 10% intervals of total length from sternal end. Adapted from Daruwalla et al. (2010a) with permission from John Wiley & Sons.

significantly larger in males than in females at every interval, except the first from the sternal end. This remained a constant finding when comparing right sides of men and women as well as left sides. When comparing sides, the right clavicles were thicker at the 10, 40, 50, 60, 70 and 90% intervals. The exact same applied in males, with the right clavicles being thicker at the 10, 40, 50, 60, 70 and 90% intervals. In females, the right clavicles were only thicker at the 40, 50, 60, 70 and 90% intervals but not the 10% interval. It was noted that they were also thicker at the 20 and 30% intervals. Table 8.4 summarizes these results, which are depicted in a graphical representation of the change in thickness across the clavicle in Figure 8.4.

Table 8.4 Clavicular thickness measured at 10% intervals of total length from sternal end. Adapted from Daruwalla et al. (2010a) with permission from John Wiley & Sons.

Mean	Sternal thickness (10%) (mm)	T2 (20%) (mm)	T3 (30%) (mm)	T4 (40%) (mm)	T5 (50%) (mm)	T6 (60%) (mm)	T7 (70%) (mm)	T8 (80%) (mm)	Acromial thickness (90%) (mm)
Male (*N*=9)	19.1	15.87	14.4	12.78	11.69	11.21	11.58	11.03	11.41
Female (*N*=18)	19.62	14.21	11.3	9.9	9.34	9.27	9.71	9.64	9.72
Left (*N*=15)	19.43	15.1	12.36	10.73	9.96	9.62	10.1	10.18	10.08
Right (*N*=12)	19.46	14.35	12.3	11.03	10.34	10.28	10.63	10.01	10.54
Male left (*N*=5)	18.98	17	14.71	12.59	11.35	10.71	11.3	11.25	11.34
Female left (*N*=10)	19.68	14.15	11.19	9.8	9.26	9.08	9.51	9.64	9.44
Male right (*N*=4)	19.28	14.47	14.02	13.02	12.11	11.85	11.94	10.76	11.49
Female right (*N*=8)	19.54	14.29	11.44	10.03	9.45	9.5	9.97	9.64	10.06

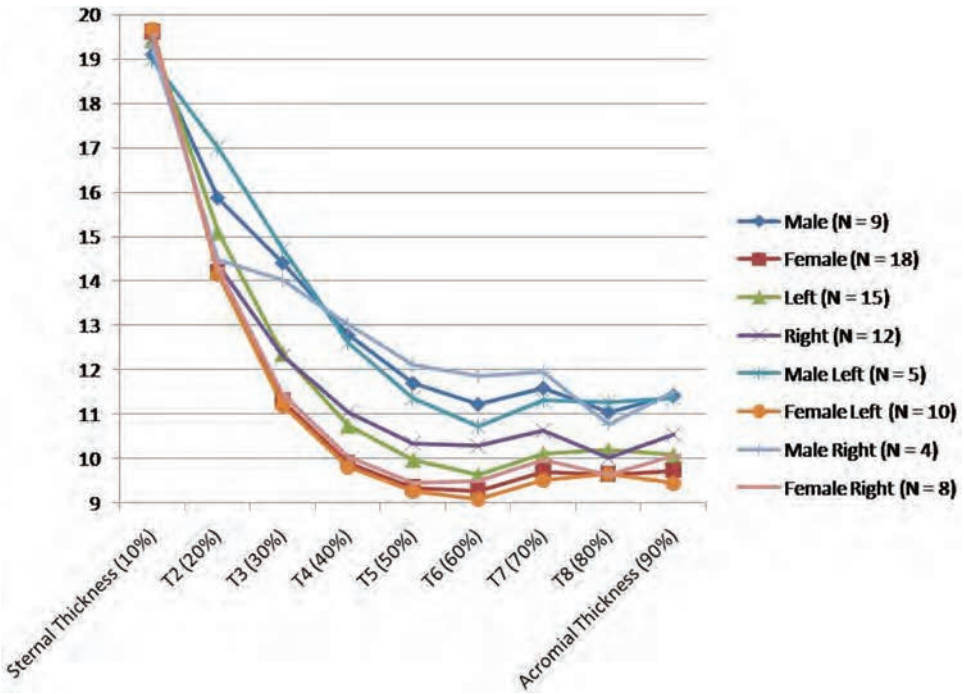

Figure 8.4 Clavicular thickness (mm) measured at 10% intervals of total length from sternal end. Adapted from Daruwalla et al. (2010a) with permission from John Wiley & Sons.

Anatomic variation

Other than variation in geometry, anatomic variants of the clavicle also exist and are briefly described in the following sections.

Clavicular absence

Hypoplasia, partial or complete absence of the clavicle, may be associated with a hereditary condition known as cleidocranial dysostosis (CCD), a rare congenital condition which can involve multiple bones resulting in aplastic or hypoplastic clavicles and/or abnormalities of dentition, facial bones, and/or thoracic and pelvic shape. Usually, the clavicle is hypoplastic to a varying degree and is absent in 10% of cases. As CCD has been extensively reviewed in the literature and is a result of a rare genetic mutation, it will not be discussed further (Candamourty et al. 2013).

Bifurcate/duplicate clavicle

Rare reports of clavicular bifurcation can be found in the literature. Authors have termed these as bifurcation (Rutherford 1921; Khanagwal et al. 2009), duplication (Golthamer 1957; Twigg and Rosenbaum 1981; Sharma 2003; Wilson 2006; Viard et al. 2013), bifid clavicle, or os subclaviculare (Golthamer 1957). There are little over ten case reports on this asymptomatic anatomical variant which has been incidentally picked up on radiographs and autopsies. Although these cases are too few to characterize in detail, some aspects are commonly noted.

Anatomy

The supernumary clavicle is developed on the lateral or distal aspect of the main clavicle, is inferiorly located, and smaller in size (Rutherford 1921; Golthamer 1957; Sharma 2003; Wilson 2006). The two clavicular masses may be fused medially (Rutherford 1921; Twigg and Rosenbaum 1981; Khanagwal et al. 2009) resulting in a forked appearance, or laterally (Sharma 2003) with both articulating with the acromion (Sharma 2003; Khanagwal et al. 2009). One report exists of the duplicate clavicle being medially free and laterally attached to the coracoid process (Golthamer 1957), although the reverse has also been described with a free lateral end and medial attachment to coracoid (Dwivedi et al. 2012). Interestingly, this anatomical variant has almost always been seen on the left, with one case of bilateral duplication more significant on the right (Reinhardt 1970).

Etiology

Several theories exist regarding the duplicate clavicle (Sharma 2003), including extra ossification centers or displacement or fragmentation of the ossification centers of the clavicle. It is thought to be congenital but has also been found to be "acquired" after trauma in skeletally immature patients (Ogden 1982; Wilson 2006).

Congenital pseudoarthrosis of the clavicle (CPC)

After first being noted in the early twentieth century (Fitzwilliams 1910), more than 200 cases of CPC have since been reported; it has become a well-recognized and unique entity (Figueiredo et al. 2012). Males and females are roughly equally affected (Persiani et al. 2008) in this rare, congenital defect of the middle third of the clavicle where two separate ends of the clavicle are adjoined by a cartilaginous joint (Alldred 1963).

Anatomy

Within the middle third of the clavicle, the pseudoarthrosis is located more towards the lateral end (Alldred 1963). Although there can be several variations (Currarino and Herring 2009), the classical description is that at the point of pseudoarthrosis, the proximal or sternal end of the clavicle is larger, superior, and anterior to the distal acromial end, that is, the sternal end overlies the acromial end (Alldred 1963; Adelaar and Urbaniak 1974; Ahmadi and Steel 1977; Manashil and Laufer 1979; Currarino and Herring 2009). There is variable mobility present at the pseudarthrosis (Alldred 1963; Gibson and Carroll 1970), and within the joint the lateral clavicle often has a bulbous appearance and the medial clavicle is rounded or beaked (Owen 1970; Currarino and Herring 2009). The resulting affected clavicle may be shortened, resulting in the shoulder being anteromedial, drooped, or hypermobile (Alldred 1963; Gibson and Carroll 1970; Owen 1970; Padua et al. 1999). It is almost always asymptomatic, nontender and does not usually affect shoulder function (Owen 1970; Wall 1970) but is usually associated with a palpable defect or visible bump depending on the angulation at the psuedoarthrosis (Gibson and Carroll 1970; Owen 1970; Wall 1970; Persiani et al. 2008). These bumps are usually first noticed at birth or early life (Alldred 1963; Gibson and Carroll 1970; Owen 1970; Adelaar and Urbaniak 1974; Padua et al. 1999; Sloan and Paton 2006; Persiani et al. 2008; Currarino and Herring 2009) and deformity tends to worsen with age (Alldred 1963).

Etiology

Failure of fusion of the two ossification centers at the middle third of the clavicle has been thought to be the cause (Lloyd-Roberts et al. 1975; Figueiredo et al. 2012). This anatomic variation is predominantly seen unilaterally on the right side, raising theories that the etiology involves the higher right subclavian artery at the middle third of the clavicle exerting pressure, resulting in failure of ossification at this point (Lloyd-Roberts et al. 1975). A familial link has also been noted (Alldred 1963; Gibson and Carroll 1970; Price and Price 1996; Akman et al. 2008) even when genetic testing was normal (Akman et al. 2008). It has therefore been noted that it can be associated with cervical ribs or abnormally vertical or elevated superior ribs (Lloyd-Roberts et al. 1975) which can increase the pressure of vasculature on the middle third of the developing clavicle. In support of this theory, the rarer left-sided unilateral pseudoarthrosis has been observed with dextrocardia (Gibson and Carroll 1970; Ahmadi and Steel 1977; Figueiredo et al. 2012); it has also been noted without dextrocardia, but in the presence of cervical ribs or a high left subclavian artery (Lloyd-Roberts et al. 1975).

Deltoid process

The roughened area on the superior surface of the clavicle known as the deltoid tubercle may be elongated to form a deltoid process.

Coracoclavicular syndesmosis

Coracoclavicular syndesmosis may be a diarthrosis or a cartilaginous symphysis rather than being bound to the inferior clavicle by the coracoclavicular ligament.

Radiographically visible costoclavicular ligament

The costoclavicular ligament may cause a deep impression in the clavicle and be mistakenly identified as a neoplastic lesion on radiographs.

Supraclavicular nerve canal

The clavicle has been noted to be traversed by a small canal filled in by one of the intermediate supraclavicular nerves, and has been reported to occur more commonly on the left.

Discussion and conclusions

Statistical shape analysis and subsequent modeling allow the construction of a patient-specific model using knowledge of the actual population, characterizing shape variation within the population. Geometric morphometrics is a method whereby a set of ordered landmark coordinates are used to represent a subject. Few studies have set out to define and measure geometric parameters and conclude whether or not the clavicle exhibits gender- or side-specific properties. In contrast to our study, none used clavicles from living persons. Further, statistical shape analysis did not form the basis of any studies.

Length

From a clinical point of view, restoration of clavicular length following a fracture of the clavicle is a determining factor for optimal restoration of function for the affected extremity (Andermahr et al. 2007) and prevents a higher nonunion rate and decreased patient satisfaction (Preston and Egol 2009). In order to achieve this, a correct definition and determination of length is vital. The length of the clavicle has been found to vary in terms of sex, age, and race (Terry 1932; Kaur et al. 2002; Haque et al. 2011). In terms of age, adults in their 20s have been noted to have slightly shorter clavicles on average than adults in their 30s. After a peak in the third decade, clavicle length gradually declines by 2–3 mm after the 60s. Racial differences have also been noted with the average Caucasian and African clavicle being 4–10 mm longer than the average Indian clavicle (Terry 1932; Kaur et al. 2002; Haque et al. 2011). Gender-related differences within races have also been observed. Male clavicles are longer than females by about 10–18 mm (Terry 1932; Kaur et al. 2002; Andermahr et al. 2007; Huang et al. 2007; King 2014). Several studies have also pointed out that, in both male and female adults, there may be a 2–4 mm difference between sides, the left clavicle being longer (Kaur et al. 2002; Haque et al. 2011; Cunningham et al. 2013; King et al. 2014). The average difference has been found to be 4.5 mm in men and 3.14 mm in women (King et al. 2014). A difference in clavicle length of 5 mm or more has also been shown in about 25% of cases, with a difference of 10 mm or more being far less common and seen in <10% of cases (Cunningham et al. 2013).

The average clavicle length in our study was 144.34 mm, but ranged widely between 129.41 and 161.2 mm. In males, the average length was 152.33 (range 141.15–161.2 mm) in comparison to 140.34 (range 129.41–149.52 mm) in females. This differed significantly in comparison to other studies, which described the mean clavicle length to be 159 mm (range 145–173 mm; Andermahr et al. 2007), 147 mm (range 143–165 mm; Duprey et al. 2008), 157 mm (range 145–176 mm; Harrington et al. 1993), and 149.4/151/135/136 mm (male right/male left/female right/female left; Kaur et al. 2002).

Two reasons may account for these differences. First, our study was based on American and Irish populations. Most of the other studies did not state their demographics. Perhaps variation in demographics accounted for these differences. Second, the definition and determination of length also varied between studies. By not defining a standardized and reproducible orientation, a small change in angle of imaging or clavicular placement may have caused a large difference in the measurement of this parameter. This can be understood by referring to the methods described by Andermahr et al. (2007). In this study, a conventional radiograph was taken of the clavicle placed over an aluminum ruler with the radiograph in craniocaudal projection. The fact that the image captured was dependent on the exact orientation of the radiograph as well as the exact position of the clavicle leaves much to chance and introduces error. This compromises accuracy, precision, and reproducibility. By performing 3D statistical shape analysis on reconstructed high-resolution images, we eliminated error and produced accurate, precise, and reproducible results.

While the methods used differed between studies, our study found that clavicle length is gender specific: clavicles in males are longer than in females. This corresponded to previously collected data (Kaur et al. 2002; Andermahr et al. 2007; Duprey et al. 2008). The possibility of being side specific also arose in our study. As observed in a previous study of 748 male and 252 female adults (Kaur et al. 2002), we also found left clavicles to be longer than the right but this was not statistically significant. Comparison of six left and six right clavicles from the same persons in our study noted no significant difference in mean lengths. We hypothesize that hand dominance is a determining factor in the length of a clavicle. As previously mentioned, the clavicle holds the scapula the proper distance from the sternum. Perhaps excessive motion on the dominant side plays a role in

wearing away both clavicular ends over time. Considering that the majority of people are right-handed, our hypothesis would explain the findings in a previous study (Kaur et al. 2002) as well as ours. Unfortunately, we were unable to correlate our findings with the handedness of our subjects as the latter data was unavailable.

Depths and angles

Curvature is difficult to define and refers to a variety of loosely related concepts in different areas of geometry. Simply, curvature is measured by the extent to which a geometric object bends or deviates from being flat at a specified point. However, this can vary as it is dependent on the point of view as well as context. The effect of the point of view can be explained by visualizing a rainbow. When looking at it from ground level, the arc formed can be seen. However, if looking down from directly above the rainbow, a straight line would be observed. To understand the dependence on context, picture a very small circle and a very large one. If you cut the circles in half and compare both, it seems that the smaller one has a greater curvature. This is solely because smaller circles bend more sharply.

While a previous study (Andermahr et al. 2007) used a measurement of the depth and radius on both the medial and lateral ends to determine the extent of curvature, we used the same depth measurements but also defined specific points and determined angles at these (Fig. 8.5). In our study, we found that medial depths were significantly larger than lateral depths in all groups. This finding was consistent with those of previous studies (Andermahr et al. 2007; Duprey 2008). The remaining two studies (Harrington et al. 1993; Kaur et al. 2002) did not use the same geometric parameters; it was therefore not possible to compare our results to theirs.

The medial depth was also noted to be larger on the right than the left, and statistically significantly so in females. These results contradicted a previous study (Andermahr et al. 2007). Between genders, the lateral depth was larger in men. A previous study also noted these findings, which were of statistical significance in that study (Andermahr et al. 2007). Interestingly, using sternal/medial and acromial/lateral angles to define and determine the curvatures proved to contradict our findings based on depth measurements. While the medial depth was found to be larger than the lateral depth in all subgroups, the acromial angle was larger than the sternal angle across all subgroups. However, correlating the sternal angle to the medial depth, results were similar with the sternal angle being larger in women than in men. The same did not apply when correlating the acromial angle to the lateral depth. While the former was found to be larger in women, the lateral depth was larger in men but this was not statistically significant.

The variation in results, depending on the use of depths or angles clearly illustrates how curvature is dependent on the point of view and context. In order to allow a fair comparison between medial and lateral depths as well as medial and lateral angles, a common reference point and plane must be defined for all four parameters. Using such a common reference point, it would be expected to find that not only are the medial and lateral depths comparable to each other but also to the medial and lateral angles, respectively. This should form the basis for any future studies of clavicular geometry.

Width and thickness

The clavicle tended to be wider and thicker at all points in males than in females except one for thickness. It also showed side-specific differences at various intervals along the length of the bone. However, the same trend in terms of the change in width and thickness across the clavicle was observed among all subgroups (Figs 8.3, 8.4). While the smallest width was noted at the mid-point of almost all the groups, the smallest thickness was at just after the mid-point at the 60% interval. These geometric findings explain why the middle third of the clavicle is the most commonly fractured.

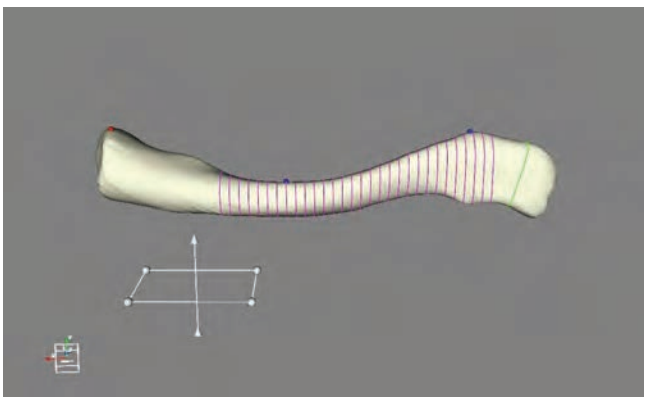

Figure 8.5 Depth defined as a measurement of a perpendicular line from the deepest point to the line joining the two lowest points.

Summary

Using principal component analysis, five groups of clavicles have been found to exist (Fig. 8.6) within a spectrum (Figs 8.7, 8.8). The clavicle demonstrates both gender- as well as side-specific geometric morphology as follows:

- clavicles in males are longer, wider and thicker than in females;
- right clavicles have a greater medial depth than left clavicles, especially in women;
- clavicles in males have a greater lateral depth than in females;
- the sternal angle in females is larger than in males; and
- left clavicles are wider than right clavicles at most intervals of length and left clavicles are longer than right clavicles, but a larger sample size is needed to show statistical significance.

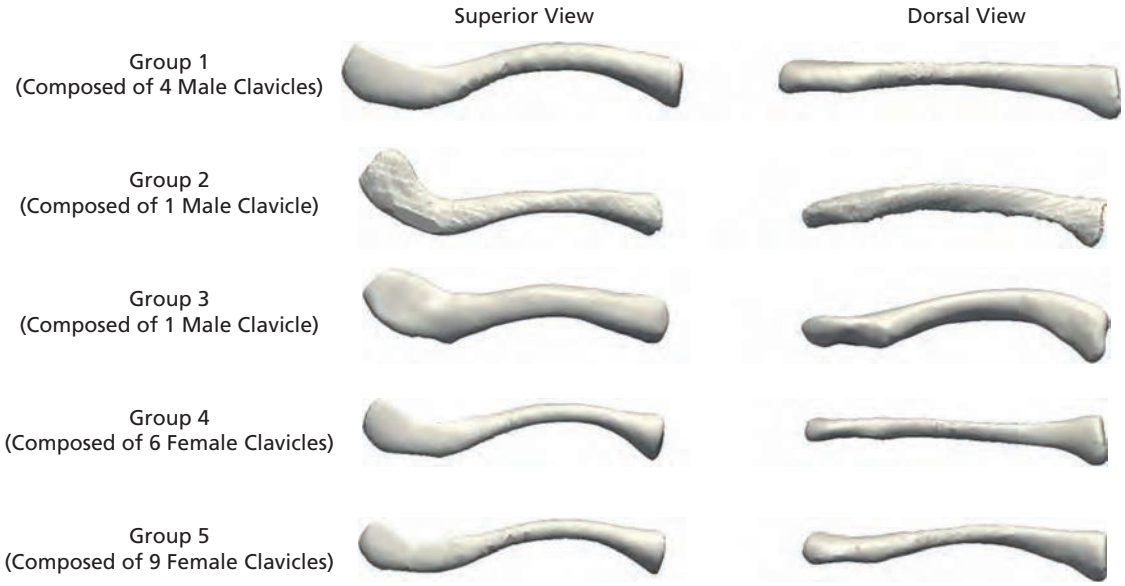

Figure 8.6 Mean shapes of the five morphological groups of clavicles. Adapted from Daruwalla et al. (2010b) under the terms of the Creative Commons CC-BY-2.0 licence.

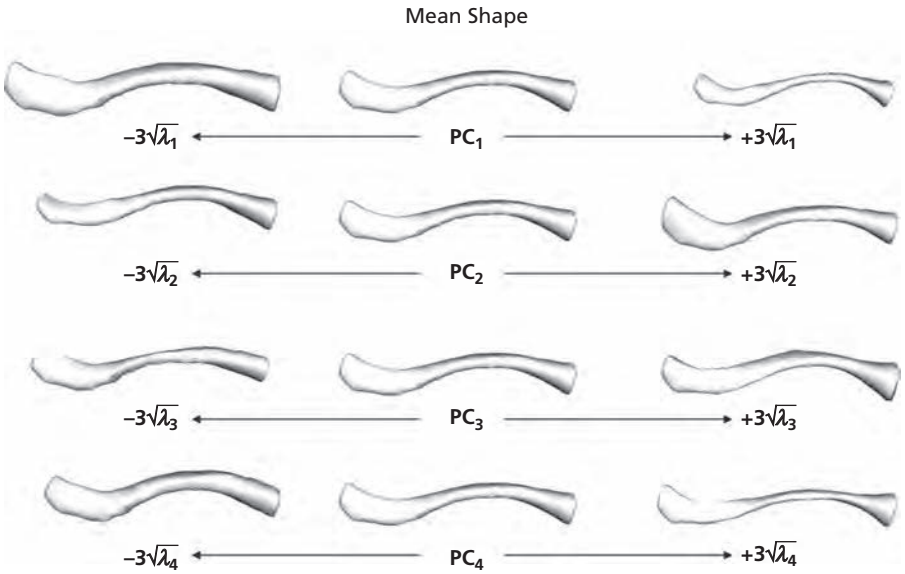

Figure 8.7 Superior view of effects of varying the first four principal components of the clavicle shape model individually. Adapted from Daruwalla et al. (2010b) under the terms of the Creative Commons CC-BY-2.0 licence.

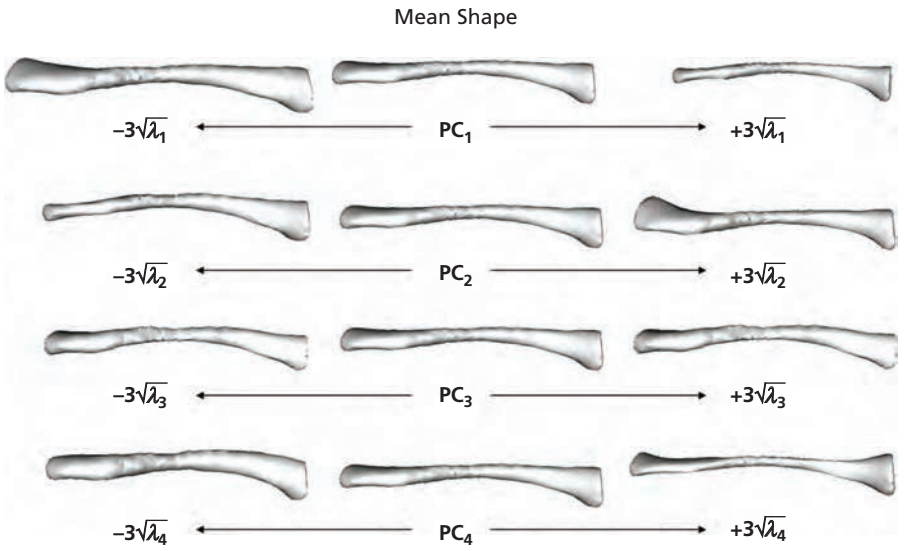

Figure 8.8 Dorsal view of effects of varying the first four principal components of the clavicle shape model individually. Adapted from Daruwalla et al. (2010b) under the terms of the Creative Commons CC-BY-2.0 licence.

References

Adelaar RS, Urbaniak JR. 1974. Congenital pseudarthrosis of the clavicle: a case presentation and review of the literature. *Interclin Information Bull* 11: 1–6.

Ahmadi B, Steel HH. 1977. Congenital pseudarthrosis of the clavicle. *Clin Orthop Relat Res* 126: 129–134.

Akman YE, Dogan A, Uzumcugil O, Azar N, Dalyaman E, Kabukcuoglu YS. 2008. Congenital pseudarthrosis of the clavicle in two siblings. *Acta Orthop Traumatol Turc* 42: 377–381.

Alldred AJ. 1963. Congenital pseudarthrosis of the clavicle. *J Bone Joint Surg Br* 45B: 312–319.

Andermahr J, Jubel A, Elsner A, Johann J, Prokop A, Rehm KE, Koebke J. 2007. Anatomy of the clavicle and the intramedullary nailing of midclavicular fractures. *Clin Anat* 20: 48–56.

Blomer J, Muhr G, Tscherne H. 1977. Ergebnisse konservativ und operativ behandelter Schlusselbeinbruche. *Unfallheilkunde* 80: 237–242.

Candamourty R, Venkatachalam S, Yuvaraj V, Kumar GS. 2013. Cleidocranial dysplasia with hearing loss. *J Nat Sci Bio Med* 4: 245–249.

Cunningham BP, McLaren A, Richardson M, McLemore R. 2013. Clavicular length: the assumption of symmetry. *Orthopedics* 36: 343–347.

Currarino G, Herring JA. 2009. Congenital pseudarthrosis of the clavicle. *Pediatr Radiol* 39: 1343–1349.

Daruwalla ZJ, Courtis P, Fitzpatrick C, Fitzpatrick D, Mullett H. 2010a. Anatomic variation of the clavicle: A novel three-dimensional study. *Clin Anat* 23: 199–209.

Daruwalla ZJ, Courtis P, Fitzpatrick C, Fitzpatrick D, Mullett H. 2010b. An application of principal component analysis to the clavicle and clavicle fixation devices. *J Orthop Surg Res* 5: 21.

Duprey S, Bruyere K, Verriest JP. 2008. Influence of geometrical personalization on the simulation of clavicle fractures. *J Biomech* 41: 200–207.

Dwivedi R, Ham-Ying L, Snape J. 2012. Problem based review: the patient presenting with an acutely swollen arm. *Acute Med* 11(2): 113–116.

Eberle H, Scholze H, Jonasch E, Mandl G, Florie-Albrecht G, Jekic M, Buff H, Meves H. 1973. Proceedings: 3. Claviculafrakturen. a. Klinik und behandlung der frischen fraktur. *Hefte Unfallheilkunde* 114: 165–179.

Emery R. 1997. Acromioclavicular and sternoclavicular joints. In: *Shoulder Surgery* (Copeland S, ed.) London: WB Saunders.

Figueiredo MJPSS, Braga SR, Akkari M, Prado JCL. 2012. Congenital pseudarthrosis of the clavicle. *Rev Bras Ortop* 47: 21–26.

Fitzwilliams DC. 1910. Hereditary craniocleido dysostosis. *Lancet* 176: 1466–1475.

Fraser-Moodie JA, Shortt NL, Robinson CM. 2008. Injuries to the acromioclavicular joint. *J Bone Joint Surg Br* 90B: 697–707.

Gibson DA, Carroll N. 1970. Congenital pseudarthrosis of the clavicle. *J Bone Joint Surg Br* 52: 629–643.

Golthamer CR. 1957. Duplication of the clavicle (os subclaviculare). *Radiology* 68: 576–578.

Haque MK, Mansur ID, Krishnamurthy A, Karki R, Sharma K, Shakya R. 2011. Morphometric analysis of clavicle in Nepalese population. *Kathmandu Univ Med J* 9: 193–197.

Harrington MA, Keller TS, Seiler JG, Weikert DR, Moeljanto E, Schwartz HS. 1993. Geometric properties and the predicted mechanical behaviour of adult human clavicles. *J Biomech* 26: 417–426.

Headey J, Brooks JHM, Kemp SPT. 2007. The epidemiology of shoulder injuries in English Professional Rugby Union. *Am J Sports Med* 35: 1537–1543.

Huang JI, Toogood P, Chen MR, Wilber JH, Cooperman DR. 2007. Clavicular anatomy and the applicability of precontoured plates. *J Bone Joint Surg (Am)* 89: 2260–2265.

Jager M, Breitner S. 1984. Therapiebezogene klassifikation der lateralen claviculafraktur. *Unfallheilkunde* 87: 467–473.

Kaplan LD, Flanigan DC, Norwig J, Jost P, Bradley J. 2005. Prevalence and variances of shoulder injuries in elite collegiate football players. *Am J Sports Med* 33: 1142–1146.

Kaur H, Harjeet, Sahni D, Jit I. 2002. Length and curves of the clavicle in Northwest Indians. *J Anat Soc India* 51: 199–209.

Khanagwal VP, Sharma L, Sirohiwal BL, Paliwal PK, Yadav RK, Yadav DR. 2009. A rare anomaly of the clavicle – bifurcation of the lateral one-third. *J Punjab Acad Forensic Med Toxicol* 9: 42–44.

King PR, Scheepers S, Ikram A. 2014. Anatomy of the clavicle and its medullary canal: a computed tomography study. *Eur J Orthop Surg Traumatol* 24(1): 37–42.

Kocher MS, Feagin JA Jr. 1996. Shoulder injuries during alpine skiing. *Am J Sports Med* 24: 665–669.

Lloyd-Roberts GC, Apley AG, Owen R. 1975. Reflections upon the aetiology of congenital pseudarthrosis of the clavicle. With a note on cranio-cleido dysostosis. *J Bone Joint Surg Br* 57: 24–29.

Manashil G, Laufer S. 1979. Congenital pseudarthrosis of the clavicle: report of three cases. *AJR Am J Roentgenol* 132: 678–679.

Moore TO. 1951. Internal pin fixation for fracture of the clavicle. *Am Surg* 17: 580–583.

Neer CS. 1963. Fracture of the distal clavicle with detachment of the coracoclavicular ligaments in adults. *J Trauma* 3: 99–110.

Nordqvist A, Petersson C. 1994. The incidence of fractures of the clavicle. *Clin Orthop Relat Res* 300: 127–132.

Ogden JA. 1982. Skeletal growth mechanism injury patterns. *J Pediatr Orthop* 2: 371–377.

Owen R. 1970. Congenital pseudarthrosis of the clavicle. *J Bone Joint Surg Br* 52: 644–652.

Padua R, Romanini E, Conti C, Padua L, Serra F. 1999. Bilateral congenital pseudarthrosis of the clavicle report of a case with clinical, radiological and neurophysiological evaluation. *Acta Orthop Belg* 65: 372–375.

Pannicke A. 1982. Claviculafrakturen: entstehung, einteilung, diagnose. In: *Hefte zur Unfallheilkunde* (von J. Rehn, LSchweiberer, eds). Berlin: Springer-Verlag, pp. 43–54.

Pearson K. 1901. On lines and planes of closest fit to systems of points in space. *Philosophical Magazine* 2: 559–72.

Persiani P, Molayem I, Villani C, Cadilhac C, Glorion C. 2008. Surgical treatment of congenital pseudarthrosis of the clavicle: a report on 17 cases. *Acta Orthop Belg* 74: 161–166.

Preston CF, Egol KA. 2009. Midshaft clavicle fractures in adults. *Bull NYU Hosp Jt Dis* 67: 52–57.

Price BD, Price CT. 1996. Familial congenital pseudoarthrosis of the clavicle: case report and literature review. *Iowa Orthop J* 16: 153–156.

Reinhardt K. 1970. A bilateral anomaly on the lateral third of the clavicula consisting of a curved duplication of the bone toward the coracoid and accessory bone elements. *Fortschr Geb Rontgenstr Nuklearmed* 113: 527–530.

Robinson CM. 1998. Fractures of the clavicle in the adult. *J Bone Joint Surg (Br)* 80B: 476–484.

Rockwood CA Jr, Green DP. 1984. *Fractures and Dislocations*. Philadelphia: JB Lippincott.

Rowe CR. 1968. An atlas of anatomy and treatment of midclavicular fractures. *Clin Orthop Relat Res* 58: 29–42.

Rutherford H. 1921. Bifurcate clavicle. *J Anat* 55: 286–287.

Sharma BG. 2003. Duplication of the clavicle with triplication of the coracoid process. *Skeletal Radiology* 32: 661–664.

Sloan A, Paton R. 2006. Congenital pseudarthrosis of the clavicle: the role of CT-scanning. *Acta Orthop Belg* 72: 356–358.

Terry RJ. 1932. The clavicle of the American Negro. *Am J Phys Anthrop* 16: 51–80.

Twigg HL, Rosenbaum RC. 1981. Duplication of the clavicle. *Skeletal Radiology* 6: 281.

Viard B, Karp JS, Tremlet J, Asali Z, Trouilloud P, Trost O. 2013. Unilateral duplication of the acromioclavicular joint: case report and literature review. *Surg Radiol Anat* 35: 973–977.

Voisin JL. 2008. The Omo I hominin clavicle: Archaic or modern? *J Hum Evol* 55: 438–443.

Wall JJ. 1970. Congenital pseudarthrosis of the clavicle. *J Bone Joint Surg Am* 52: 1003–1009.

Wilson TC. 2006. Duplication of the clavicle. *Orthopedics* 29: 79–80.

9 Humerus

Peter J. Ward
West Virginia School of Osteopathic Medicine, Lewisburg, West Virginia, United States

Retroversion of the humeral head

The humeral head is typically directed somewhat posteriorly as it sits in the glenoid fossa. However, the degree to which it faces posteriorly is quite variable (Fig. 9.1). In a study of 336 dry specimens of various ethnic groups, angles of retroversion ranged between –8° to +74°, with values ranging widely within each ethnic group. The authors examined 50 fetal skeletons and showed a mean angle of +78°, which is much greater than seen in adults (Edelson 1999). This shows that the retroversion of the humeral head becomes less pronounced over time.

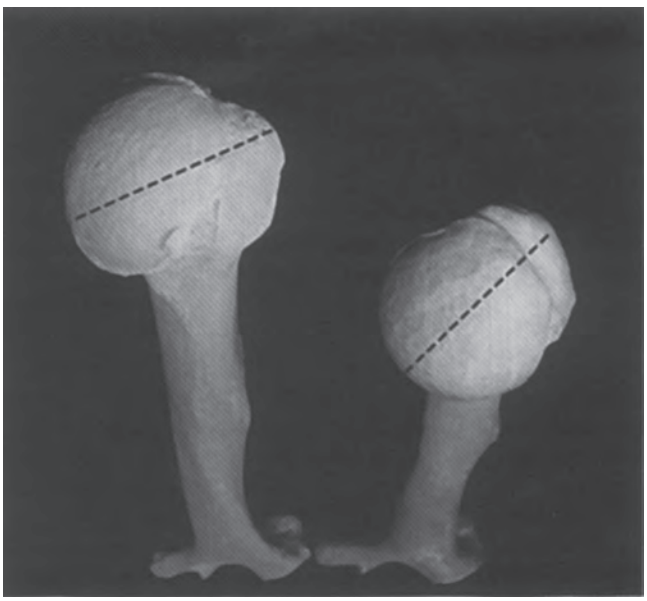

Figure 9.1 Right humeri of two Alaskan Eskimo specimens illustrating how line bisecting humeral head was drawn. Angles of retroversion are notably different between the two specimens.

Source: Edelson (1999). Reproduced with permission from Elsevier.

Intertubercular sulcus/bicipital groove

The tendon of the long head of the biceps brachii travels inferiorly from the supraglenoid tubercle and passes along the anterior aspect of the humerus. The intertubercular sulcus, also known as the bicipital groove, is an elongated depression in the bone that keeps the tendon in place. The intertubercular sulcus has an average depth of 3.7 mm but this mean depth is sex specific; one study found the average depth in males was 3.9 mm and in females 3.4 mm (Prescher 2000).

In addition to its depth, the angle of the intertubercular sulcus changes along its length (Fig. 9.2). One study examined the angle of the intertubercular sulcus relative to a line connecting the two humeral epicondyles. This angle varied between +22° to +89° and there was significant variation along the length of the humerus. At the anatomical neck of the humerus it measured +55.8±4.5°, while at the surgical neck of the humerus it measured +65.1±3.5° (Balg et al. 2006).

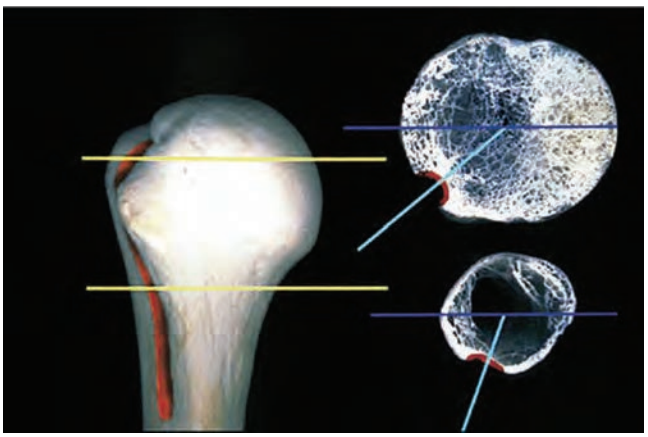

Figure 9.2 Humerus bone cuts demonstrate that the intertubercular sulcus is more retroverted distally than proximally (at the surgical neck level) due to its S-shape.

Source: Balg et al. (2006). Reproduced with permission from Elsevier.

Bergman's Comprehensive Encyclopedia of Human Anatomic Variation, First Edition. Edited by R. Shane Tubbs, Mohammadali M. Shoja and Marios Loukas.
© 2016 John Wiley & Sons, Inc. Published 2016 by John Wiley & Sons, Inc.

Supracondylar process and the ligament of Struthers

A supracondylar process (Fig. 9.3) is sometimes found extending inferiorly from the distal, medial aspect of the humerus. The supracondylar process has been variously called the supracondyloid, supraepitrochlear, supratrochlear, or supracondylar spur, or epicondylar or epicondylic process (Paraskevas et al. 2012). It was first described by Tiedmann in 1822 (Crotti et al. 1981; Talha et al. 1987; Ivins 1996). The associated ligament of Struthers extends from the inferior apex of the process and attaches to the distal, medial humerus; it was first noted in 1848 (Struthers 1849). The pronator teres can attach to the supracondylar process, the ligament of Struthers, or both (Aydinlioglu et al. 2000; Koshy et al. 2003; Jelev and Georgiev 2009).

The reported incidence of the supracodylar process falls within the range 0.1–2.7% (Gruber 1856; Testut 1889; Terry 1923 1930; Kumar 2008; Natsis 2008). It is most often unilateral (Natsis 2008) and originates 5–7 cm superior to the medial epicondyle (Finnegan 1978; Ay et al. 2002). The supracondylar process can be little more than a raised tubercle of the humerus connected to the ligament of Struthers (Rehak 2001; Natsis 2008) although its length from the shaft of the humerus falls within the range 2–20 mm. (Laha et al. 1977; Finnegan 1978; Ivins 1996; Natsis 2008).

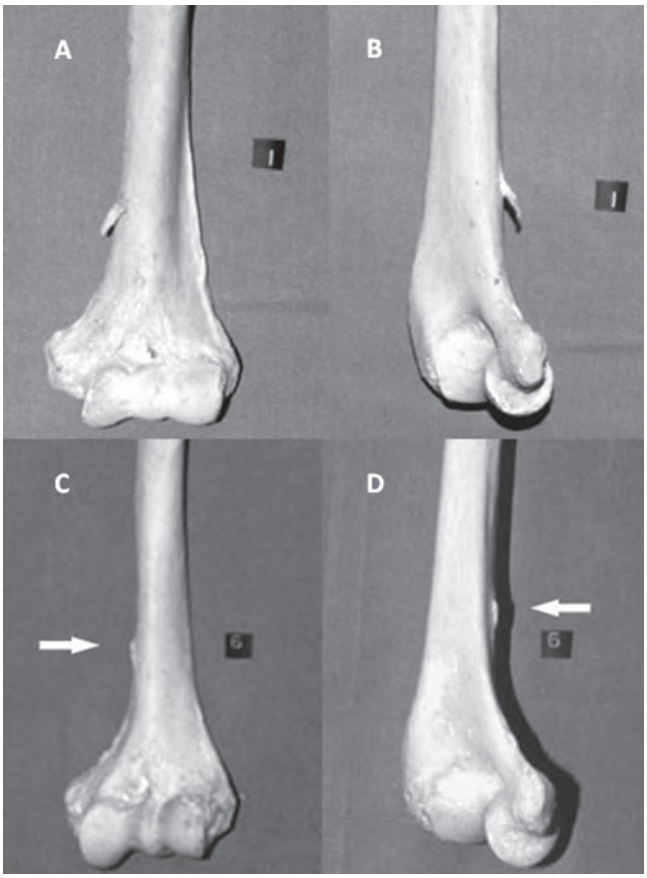

Figure 9.3 (a) Anterior and (b) lateral aspect of a left humerus having the supracondylar process shaped as a spine. (c) Anterior and (d) lateral aspects of a left humerus having the supracondylar process with tubercle form (arrow).

Source: Natsis (2008). Reproduced with permission from John Wiley & Sons.

The clinical relevance of the supracondylar process and ligament of Struthers is primarily due to the fibro-osseous channel they form. The space between the ligament of Struthers, the supracondylar process, and the humerus contains the median nerve and the brachial artery (or branches thereof). These structures can become compressed, causing signs of median nerve impingement. Symptoms typically manifest when the elbow is held in an extended and pronated position for a period of time (Barnard and McCoy 1946; Symeonides 1972; Smith and Fisher 1973; Engber et al. 1974; Laha et al. 1977; Talha et al. 1987; Bilge et al. 1990; Casadei et al. 1990; Eversmann 1992; Ivins 1996; Şener et al. 1998; Aydinlioglu et al. 2000; Rehak 2001; Ay et al. 2002; Pećina et al. 2002; Bilecenoglu et al. 2005; Lordan et al. 2005). There are case reports of the nerve and vessels passing superficial to the process and ligament (Ay et al. 2002) and of the vessels, but not the nerve, passing superficial to the process and ligament (Symeonides 1972).

On very rare occasions, instead of a supracondylar process and associated ligament of Struthers, the median nerve and brachial vessels may pass through a bony foramen (Fig. 9.4) that completely encloses them (Kazuki et al. 2004).

Fracture of the supracondylar process presents as painful swelling of the medial aspect of the distal arm (Lund 1930; Genner 1959; Kolb and Moore 1967; Newman 1969; Casadei et al. 1990; Spinner et al. 1994; Suresh 2008). A supracondylar process or a fracture fragment of it may be mistaken for a bony tumor or exostosis (Kolb and Moore 1967; Newman 1969). On the other hand, myositis ossificans involving the muscles of the anterior elbow might be mistaken for a non-pathologic supratrochlear process (Spinner et al. 1995) instead of a progressive pathological process. In studying patients with Cornelia de Lange syndrome, 50% (3/6) individuals in an admittedly small population were observed to have a supracondylar process (Curtis et al. 1977).

Supratrochlear foramen

Just proximal to the capitulum and trochlea of the distal humerus is a thin region of bone that is sometimes perforated, forming a foramen. The supratrochelar foramen, also known as a septal aperture, was first described in 1825 (Meckel 1825) and its reported incidence varies considerably (Fig. 9.5). Studies on humeri from India show an incidence of 23–34.3% (Singhal and Rao 2007; Nayak et al. 2009; Patel et al. 2013) while studies of other ethnic groups show a decreased incidence: Chinese 9.5% (Ming-Tzu 1935); Japanese 17%; Korean 11% (Akabori 1934); and European 6.9% (Mays 2008). The supratrochlear foramen is more frequently cited as occurring on the left side

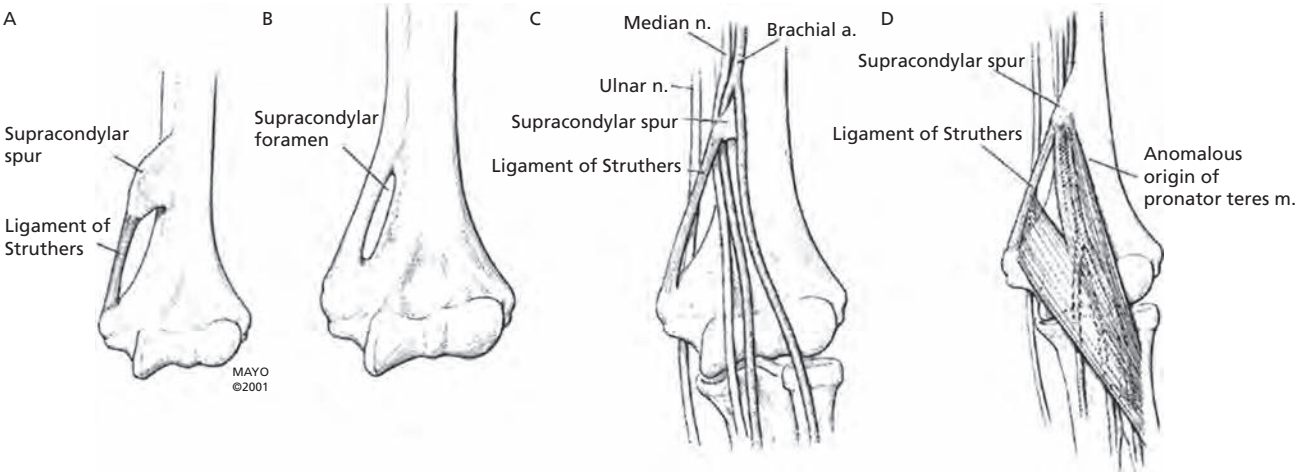

Figure 9.4 (a) The supracondylar spur and ligament of Struthers. (b) The supracondylar foramen represents the bony extreme of the ligament of Struthers complex and is homologous to a structure seen in certain mammals. (c) The relationships of the neurovascular structures to the supracondylar spur and the ligament of Struthers can be seen in this drawing. A high division of the brachial artery is demonstrated with the ulnar artery passing beneath the ligament. (d) A high takeoff of the pronator teres muscles from the supracondylar spur is illustrated.

Source: Lordan et al. (2005). Reproduced with permission from John Wiley & Sons.

Figure 9.5 Different appearances of the supratrochlear foramen: (a) no supratrochlear foramen; (b) large oval; (c) small oval; (d) round; and (e) triangular.

than the right, with a range of 53.3–56.0% on the left side (Akabori 1934; Ming-Tzu 1935; Mays 2008; Patel et al. 2013). However, two studies (Singhal and Roa 2007; Nayak et al. 2009) found slightly more supratrochlear formina on the right side (52.4–55.3%) than on the left (44.7–47.6%). The supratrochlear foramen is more frequently seen in women (Akabori 1934; Mays 2008).

The supratrochelear foramen has been described as having an oval (93.2–94.0%), round (4.5–5.3%), or triangular (1.5%) shape (Ming-Tzu 1935; Nayak et al. 2009; Patel et al. 2013). This foramen has not been observed during embryonic development (Hirsh 1927) and is presumed to develop during postnatal life.

The supratrochlear foramen is of clinical interest for several reasons. The presence of a supratrochlear foramen can predispose the distal humerus to fracture (Sahajpal and Pichora 2006) since there is simply less bone present in the region. Also, a supratrochlear foramen needs to be noted prior to

intramedullary fixation of a fractured humerus, as it decreases the available space for the surgical hardware (Singhal and Rao 2007; Nayak et al. 2009). In addition, bony fragments within the elbow joint may lodge in this space and mimic osteochondritis dessicans (Hirsh 1927; Millman 1945; Rowe 1951; Morgan 1953). Functionally, a large supratrochlear foramen may allow hyperextension of the elbow (De Wilde et al. 2004). Skeletal specimens with both a supratrochlear foramen and supracondlar process have been described (Varlam et al. 2005; Paraskevas et al. 2012).

References

Akabori E. 1934. Septal apertures in the humerus on Japanese, Ainu and Koreans. *Am J Phys Anthropol* 18: 395–400.

Ay S, Bektas U, Yilmaz C, Diren B. 2002. An unusual supracyondylar process syndrome. *J Hand Surg AM* 27A: 913–915.

Aydinlioglu A, Cirak B, Akpinar F, Tosun N, Dogan A. 2000. Bilatera median nerve compression at the level of Struthers' ligament. *J Neurosurg* 92: 693–696.

Balg F, Boulianne M, Boileau P. 2006. Bicipital groove orientation: considerations for the retroversion of a prosthesis in fractures of the proximal humerus. *J Shoulder Elbow Surg* 15: 195–198.

Barnard LB, McCoy SM. 1946. The supracondyloid process of the humerus. *J Bone Joint Surg* 28: 845–850.

Bilecenoglu B, Uz A, Karalezli N. 2005. Possible anatomic structures causing entrapment neuropathies of the median nerve: an anatomic study. *Acta Orthop Belg* 71: 169–176.

Bilge T, Yalaman O, Bilge S, Cokneşeli B, Barut S. 1990. Entrapment neuropathy of the median nerve at the level of the ligament of Stuthers. *Neurosurgery* 27: 787–789.

Casadei R, Ferraro A, Ferruzzi A, Innao V, Mercuri M. 1990. Supracondylar process of the humerus: four cases. *Chir Organi Mov* 75: 265–277.

Crotti FM, Mangiagalli EP, Rampini P. 1981. Supracondyloid process and anomalous insertion of pronator teres as sources of median nerve neuralgia. *J Neurosurg* 25: 41–44.

Curtis JA, O'Hara EO, Carpenter GC. 1977. Spurs of the mandible and supracondylar process of the humerus in Cornelia de Lange syndrome. *Am J Roentgenol* 129: 156–158.

De Wilde V, De Maeseneer M, Lenchik, L, Van Roy P, Beeckman P, Osteaux M. 2004. Normal osseous variants presenting as cystic or lucent areas on radiography and CT imaging: a pictorial overview. *Eur J Radiol* 51: 77–84.

Edelson G. 1999. Variations in the retroversion of the humeral head. *J Shoulder Elbow Surg* 8(2): 142–145.

Engber WD, McBeath AA, Cowle AE. 1974. The supracondylar process. *Clin Orthop Relat Res* 104: 228–231.

Eversmann WW. 1992. Proximal median nerve compression. *Hand Clinics* 8: 307–315.

Finnegan M. 1978. Non-metric variation of the infracranial skeleton. *J Anat* 125: 23–37.

Genner BA. 1959. Fracture of the supracondyloid process: a case report. *J Bone Joint Surg* 41A(7): 1333–1335.

Gruber WL. 1856. Monographie de canalis supracondyloidens humeri, und der processus supracondyloidei humeri et femoris der Sangethiere und des menschen. Thesis. St Petersburg.

Hirsh IS. 1927. The supratrochlear foramen: clinical and anthropological considerations. *Am J Surg* 11: 500–505.

Ivins GK. 1996. Supracondylar process syndrome: a case report. *J Hand Surg* 21A: 279–281.

Jelev L, Georgiev GP. 2009. Unusual high-origin of the pronator teres muscle from a Struthers' ligament coexisting with a veriatio of the musculocutaneous nerve. *Rom J Morphol Embryo* 50: 497–499.

Kazuki K, Egi T, Okada M, Takaoka K. 2004. Anatomic variation–a bony canal for the median nerve at the distal humerus: a case report. *J Hand Surg* 29A: 953–956.

Kolb LW, Moore RD. 1967. Fractures of the supracondylar process of the humerus. *J Bone Joint Surg* 49A: 532–534.

Koshy S, Rabi S, Indrasingh I, Vettivel S. 2003. Two anatomical variations associated with potential vascular entrapment in the upper limb. *Eur J Anat* 7: 97–100.

Kumar GR. 2008. A study of the incidence of supracondylar process of the humerus. *J Anat Soc India* 57: 111–115.

Laha RK, Dujovny M, DeCastro SC. 1977. Entrapment of median nerve by supracondylar process of the humerus. *J Neurosurg* 46: 252–255.

Lordan J, Rauh P, Spinner RJ. 2005. The clinical anatomy of the supracondylar spur and the ligament of Struthers. *Clin Anat* 18: 548–551.

Lund HJ. 1930. Fracture of the supracondyloid process of the humerus. *J Bone Joint Surg* 12: 925–928.

Mays S. 2008. Septal aperture of the humerus in a mediaeval human skeletal population. *Am J Phys Anthropol* 136: 432–440.

Meckel JH. 1825. A note on the septal apertures in the humerus of Central Indians. *Eastern Anthropologist* 33: 270–284.

Millman WS. 1945. Osteochondritis dissecans of the supratrochlear septum. *Can Med Assoc J* 53: 55–57.

Ming-Tzu P. 1935. Septal apertures in the humerus in the Chinese. *Am J Physical Anthropol* 20: 165–170.

Morgan PW. 1953. Osteochondritis dissecans of the supratrochlear septum. *Radiology* 60(2): 241–243.

Natsis K. 2008. Supracondylar process of the humerus: study of 375 Caucasian subjects in Cologne, Germany. *Clin Anat* 21: 138–141.

Nayak SR, Das S, Krishnamurthy A, Prabhu LV, Potu BK. 2009. Supratrochlear foramen of the humerus: an anatomico-radiological study with clinical implications. *Upsala J Med Sci* 114: 90–94

Newman A. 1969. The supracondylar process and its fracture. *Am J Roentgenol* 105: 844–849.

Paraskevas GK, Natsis K, Anastasopoulos N, Ioannidis O, Kitsoulis P. 2012. Humeral septal aperture associated with supracondylar process: a case report and review of the literature. *Ital J Anat and Embryo* 117: 135–141.

Patel SV, Sutaria LK, Nayak TV, Kanjiya DP, Patel BM, Aterkar SH. 2013. Morphometric study of supratrochlear foramen of humerus. *IJBAR* 4: 89–92.

Pećina M, Borić I, Anticević D. 2002. Intraoperatively proven anomalous Struthers' ligament diagnoses by MRI. *Skeletal Radiol* 31: 532–535.

Prescher A. 2000. Anatomical basics, variations, and degenerative changes of the shoulder joint and shoulder girdle. *Eur J Radiol* 35: 88–102.

Rehak DC. 2001. Pronator syndrome. *Clin Sports Med* 20: 531–540.

Rowe CA. 1951. Osteochondritis dissecans of the supratrochlear septum. *California Med* 75: 106–108.

Sahajpal DT, Pichora D. 2006. Septal aperture: an anatomic variant predisposing to bilateral low-energy fractures of the distal humerus. *Can J Surg* 49(5): 363–364.

Şener E, Takka S, Cila E. 1998. Supracondylar process syndrome. *Arch Orthop Trauma Surg* 117: 418–419.
Singhal S, Rao V. 2007. Supratrochlear foramen of the humerus. *Anat Sci Int* 82: 105–107.
Smith RV, Fisher RG. 1973. Struthers ligament: a source of median nerve compression above the elbow. *J Neurosurg* 38(6): 778–779.
Spinner RJ, Lins RE, Jacobson SR, Nunley JA. 1994. Fractures of the supracondylar process of the humerus. *J Hand Surg Am* 19: 1038–1041.
Spinner RJ, Jacobson SR, Nunley JA. 1995. Fracture of a supracondylar humeral myositis ossificans. *J Orthop Trauma* 9: 63–265.
Struthers J. 1849. On a peculiarity of the humerus and humeral artery. *Month J Med Sci* 9: 260–267.
Suresh SS. 2008. Fracture of supracondylar process of the humerus. *Sultan Qaboos Univ Med J* 8(2): 223–225.
Symeonides PP. 1972. The humerus supracondylar process syndrome. *Clin Orthop Relat Res* 82: 141–143.
Talha H, Enon B, Chevalier JM, L'Hoste PL, Pillet J. 1987. Brachial artery entrapment: compression by the supracondylar process. *Ann Vasc Surg* 1: 479–482.
Terry RJ. 1923. On the supracondyloid variation in the Negro. *Am J Phys Anthropl* 6: 401–403.
Terry RJ. 1930. On the racial distribution of the supracondyloid variation. *Am J Phys Anthropl* 14: 459–4623.
Testut L. 1889. L'apophyse sus-epitrochleenne chez l'homme. Internat Monatschr. *F Anat U Physiol* 6: 391.
Varlam H, St. Antohe D, Chistol R. 2005. Supracondylar process and supratrochlear foramen of the humerus (in French). *Morphologie: bulletin de l'Association des Anatomistes* 89: 121–125.

Further reading

Acton JD, McNally MA. 2001. Baumann's confusing legacy. *Injury, Int J Care Injured* 32: 41–43.
Auerbach BM, Raxter MH. 2008. Patterns of clavicular bilateral asymmetry in relation to the humerus: variation among humans. *J Hum Evol* 54: 663–674.
Camp J, Ishizue K, Gomez M, Gelberman R, Akeson W. 1993. Alteration of Baumann's angle by humeral position: implications for treatment of supracondylar humerus fractures. *J Pediatr Orthoped* 13: 521–525.
Keenan WN, Clegg J. 1996. Variation of Baumann's angle with age, sex, and side: implications for its use in radiological monitoring of supracondylar fracture of the humerus in children. *J Pediatr Orthop* 16: 97–98.
Krishnamurthy A, Reddy A, Takkalapalli A, Munishamappa V, Bovinndala B, Chandramohan M. 2011. Supratrochlear foramen of humerus–a morphometric study. *Int J Biol Med Res* 2: 829–831.
Laha RK, Lunsford LD, Dujovny M. 1978. Lacertus fibrosus compression of the median nerve. *J Neurosurg* 48: 838–841.

10 Radius, ulna, carpals, metacarpals, and phalanges

Munawar Hayat and Marios Loukas
St. George's University, School of Medicine, St. Georges, Grenada

Radius

There are several variations that affect the longitudinal growth of the radius. They are classified into four different types ranging from mild to more acute (Doyle and Bottle 2003) as follows.

- Type I: short radius. This is described with an abbreviated distal epiphysis with normal proximal epiphysis. There is typically mild shortening of the radius without bowing present. There will also be mild radial deviation of the hand present.
- Type II: hypoplastic radius. Presented with paucity in both distal and proximal epiphysis of the radius and a reduced-size radius. Here there will be moderate radial deviation of the hand.
- Type III: partial absence. There will partial absence of the proximal, middle, or the distal portion of the radius, resulting in severe radial deviation of the hand. Most commonly the distal portion is absent, resulting in a thickened and bowed ulna.
- Type IV: complete absence. This presents with complete lack of radius, resulting in a shortened and bowed ulna with severe radial deviation of the hand.

Radial dysplasia

Radial dysplasia is a congenital defect also known as radial clubhand or radial longitudinal deficiency, which results in a mildly to severely abbreviated forearm, typically associated with a deviated wrist (Netscher and Baumholtz 2007). This defect is usually seen as part of several systemic syndromes. Congenital absence (partial or complete) of the radius with normal hand development or with absence of the thumb has been reported (Bergman et al. 1988). The congenital bilateral absence of the radius has also been recorded (Bergman et al. 1988).

Radial–ulnar synthesis

This refers to an osseous fusion between the radius and ulna. The etiology can be either congenital or post-traumatic. This has been classified into four types by Cleary and Omer (1985):

- Type I: involves only fibrous synthesis;
- Type II: refers to bony synthesis;
- Type III: accompanied by posterior dislocation of the radius; or
- Type IV: involves anterior dislocation of the radius.

An accessory tubercle of the distal epiphysis of the radius is known as the lunar tubercle (of Mouchet and Jeanne).

Ulna

Ulnar variations are a result of abnormal growth of the epiphysis causing deficient ossification. This is classified into four groups according to their grade of aplasia (Doyle and Bottle 2003):

- Type I: hypoplasia of the ulna but with intact distal and proximal epiphysis and minute shortening of the ulna;
- Type II: partial aplasia with absence of the distal portion of the ulna;
- Type III: complete aplasia, presents with complete lack of the ulna; or
- Type IV: synthosis of the radius with the humerus.

Ulnar dysplasia

Also known as ulnar clubhand, ulnar deficiencies occur less frequently than radial defects. The majority of the cases that occur are unilateral. In most cases the ulna presents as shortened with radial bowing and defective digits. Congenital absence (partial or complete) of the ulna has also been reported (Bergman et al. 1988). A small tubercle can be found on the proximal ulna for attachment of the oblique cord.

Sesamoid bones of the forearm

Sesamoid bones are small nodular bones that are found within tendons. In the forearm, sesamoid bones may develop in the bicipital tendon over the radial tuberosity. Some sesamoid bones are occasionally found within the tendon of the triceps brachii muscle proximal to the olecranon. Another sesamoid (os coronoides) may also be found at the tip of the coronoid process. Sesamoid bones have been seen in the supinator tendon.

Variations of the hand

Skeletal variations of the hand are commonplace. Certain studies have reported that up to 31.3% of individuals have embryological derailment of the proper development of the carpal bones (Swanson 1976; Lister 1993; Freyschmidt et al. 2003).

Bergman's Comprehensive Encyclopedia of Human Anatomic Variation, First Edition. Edited by R. Shane Tubbs, Mohammadali M. Shoja and Marios Loukas.
© 2016 John Wiley & Sons, Inc. Published 2016 by John Wiley & Sons, Inc.

Epiphyses of the phalanx and metacarpal

Normally, the phalanx is a narrower structure than the adjacent metaphysis. However, the phalanx epiphyses can demonstrate an equal or greater width and is considered a normal variant. These variations in epiphyseal width may imply an abnormality in ossification process (Freyschmidt et al. 2003). One study concluded that a broader structure might imply an enhanced neurovascular supply (Smith 2000). Similarly, metaphyses may also be broader than normal and this is also considered a normal variation according to Freyschmidt et al. (2003). Finally, epiphyseal plates of the phalanges typically exemplify mild distal convexity compared to those in the metacarpals, which show slight proximal convexity (Freyschmidt et al. 2003).

Pseudoepiphyses

Pseudoepiphyses are additional epiphyses commonly found in the distal first metacarpal. These are considered to be normal variants that are commonly located in 65% and in 20–60% of the proximal second metacarpals of normal children. Unlike the normal epiphysis, pseudoepiphyses do not significantly assist in longitudinal growth bone. These pseudoepiphyses can be an incidental finding in healthy children, but may also be found with systemic defects involving skeletal growth, such as hypothyroidism or Down syndrome (Rochels and Schmidt 1980; Freyschmidt et al. 2003). They are most commonly found in children <10 years of age and often close earlier than normal epiphyses (Ogden et al. 1994; Freyschmidt et al. 2003). The frequency of pseudoepiphyses within the hand is greatest in the first metacarpal, followed by the second metacarpal then the fifth metacarpal; the least frequent is the fourth metacarpal and first proximal phalanx (Schafer 1952; Freyschmidt et al. 2003).

In a separate study by Ogden et al. (1994), three variations of pseudoepiphyses formation were described. In the first variation the central osseous bridge extends from the metaphysis to the epiphysis and subsequently grows to form a mushroom-like osseous structure (Ogden et al. 1994). In the second pattern the outer osseous bridge will initially form, creating either an osseous ring between the metaphysis and the epiphysis (Ogden et al. 1994). Finally, in the third pattern multiple bridges can occur (Ogden et al. 1994).

The cone-shaped epiphysis

The cone-shaped epiphysis is a rare variant that involves the hands of normal individuals (Giedion 1968; Freyschmidt et al. 2003). It is hypothesized to result from cessation of growth in the central region of the epiphysis, whereas the peripheral portion remains active. The condition is typically asymptomatic, but may present with symptoms when involving trophic disturbances (Freyschmidt et al. 2003). For example, in a study by Brenner et al. (2004) six individuals of a single family were found to have the same painful cone-shaped epiphysis along with several other skeletal anomalies. These anomalies were all associated with an identical genetic mutation found in all the affected family members (Brenner et al. 2004).

Brachymesophalangia

Brachymesophalangia is the most common skeletal variation of the middle phalanx, indentified as a shortened, and occasionally widened, middle phalanx. It frequently occurs involving the fifth digit, and affects about 20% of the Japanese and Native American populations (Williams et al. 2012) compared with 0.6–1% of Europeans. Further, cases of aplasia of the middle phalanx have been reported and occur in conjunction with an abbreviated, hypoplastic distal phalanx along with a compensatory long proximal phalanx (Dubost et al. 1960; Freyschmidt et al. 2003). There is a similar occurrence with brachymetacarpia, which is described as a shortened metacarpal bone and a compensated long proximal phalanx.

Brachyphalangia

Brachyphalangia is described as shortening of the phalanges, more commonly the proximal phalanx, and it is often accompanied by shortening of other osseous hand bones (Freyschmidt et al. 2003). Brachyphlangia is often seen as part of a syndrome, so is not referred to as a normal morphologic variant (Freyschmidt et al. 2003).

Symphalangia

This is a congenital form of dysplasia that results in an absent interphalangeal joint. The most commonly involved digits are the ulnar and medial digits, often bilateral, and are typically accompanied by other bony anomalies of the hand. A physical examination will reveal an absence of skin folds over normal joint locations. Radiological imaging shows a fusiform expansion where the phalanges have fused (Freyschmidt et al. 2003). Both the radiographic and clinical aspects are more apparent in adults, in comparison to pediatrics patients. In children, synchondrosis remains flexible on physical examination and becomes difficult to distinguish when compared to normal joints (Freyschmidt et al. 2003). It is also critical to identify congenital aplasia from acquired ankylosis; the latter is characterized by a transverse skin fold over the affected region (Freyschmidt et al. 2003).

Various studies have also associated symphalangia with proximal symphalangism, a congenital condition associated with gene mutation involving the human noggin (NOG) gene (Potti et al. 2011; Athanasakis et al. 2012; Usami et al. 2012; Liu et al. 2014). The NOG gene encodes noggin, a secreted polypeptide, which is critical factor in regulation of multiple signaling pathways during cartilage and bone development.

Syndactyly

This is a congenital defect resulting in the fusion of phalanges of separate digits (Freyschmidt et al. 2003). It is reported to occur in approximately one in 2500 births (Mandarano-Filho et al. 2013). It usually occurs bilaterally, primarily affecting

males, and is less common among blacks (Mandarano-Filho et al. 2013). Syndactyly occurs more commonly between the third and fourth digits, followed by the fourth and fifth, and then second and third digits (Mandarano-Filho et al. 2013). The cause of the defect is mainly sporadic mutations affecting differentiation of mesenchymal structures, although there are cases of autosomal dominant inheritance with variable expressivity (Flatt 1994; Mandarano-Filho et al. 2013).

Axial deviations of the phalanges

Axial deviations of the phalanges is a congenital variation that is also found with various syndromes, including achondroplasia, trisomies, or dysplasias (Freyschmidt et al. 2003). Regarding congenital, normal variants not associated with systemic disease or syndromes, camptodactyly and clinodactyly are the two most frequently occurring variations (Freyschmidt et al. 2003). Clinodactyly is described as ulnar or radial deviation of a distal phalanx secondary to a mis-shaped middle or delta phalanx (Freyschmidt et al. 2003). Any digit can be affected, but the most commonly affected digit is the fifth (Freyschmidt et al. 2003). One variant of clinodactyly is the Kirner deformity, where the distal phalanx of the fifth digit exhibits a dorsal convex deviation.

Camptodactyly is the second variation of axial deviation that is characterized by a hereditary contracture of individual phalangeal joints (Freyschmidt et al. 2003). This is likely due to a genetic mutation as both sporadic and autosomal dominant forms are present. Camptodactyly does not demonstrate any identifiable bone changes at its initial stages; however, the middle phalanx will develop a cleft in the neck of the first phalanx (Freyschmidt et al. 2003). This mainly involves the fifth digit and, less commonly, the fourth digit. The pathophysiology of the congenital contracture is due to an abnormal insertion of the lumbrical muscle or the superficial digital flexor muscles (Freyschmidt et al. 2003).

Polydactyly

Polydactyly is defined as having more than five digits on one hand, or greater than five tubular bones within the metacarpals. It is often associated with a variety of other anatomical variations of the hand (Freyschmidt et al. 2003). Bony complexes within supernumerary digits may exemplify normal development and organization, or may be elementary structures (Freyschmidt et al. 2003).

The classification of polydactyly is dependent on the location of the supernumerary digit or metacarpal bone: radial side (preaxial); ulnar (postaxial); or central (non-border) (Buck-Gramcko and Behrens 1989; Freyschmidt et al. 2003; Guo et al. 2013). Duplication of the thumb is the most common type of polydactyly, as reported by Guo et al. (2013). The incidence of preaxial polydactyly has been reported in up to 1 in 3000 births (Flatt et al. 1994; Jobe 2008). Postaxial polydactyly are defects that can range from a fully developed digit to skin tags. The prevalence is unknown because most skin tags are treated without surgical intervention (Guo et al. 2013). Finally, the central polydactyly is far less common; however, when it does occur, the most commonly seen duplication is that of the ring finger. It is also reported that central polydactyly is typically associated with syndactyly and this defect is referred to as synpolydactyly. The incidence of polydactyly associated with syndactyly was found to be 91% in one study (Wood 1971).

Polyphalangia

Polyphalangia, similar to polydactyly, is an uncommon duplication of one or more phalange within another digit (Freyschmidt et al. 2003). This differs from polydactyly as the duplicate phalange is within a digit; however, the total number of digits is not greater than five. Windle (1891) recorded a case of polyphalangia involving the human pollex. This condition is rarely seen as an isolated event; rather, it typically occurs as part of various syndromes (Almasi and Solgaard 2006).

Arachnodactyly

Arachnodactyly, also known as achromchia, is the development of asymmetrically long and slender digits. It is also accompanied by premature ossification, which is noted on imaging. Physical examination will reveal a positive Steinberg sign, which refers to the first digit extending past the ulnar border of the hand with a clenched fist (Freyschmidt et al. 2003). Arachnodactyly is typically diagnosed with numerous systemic syndromes, including Marfans syndrome, Elhers Danlos syndrome, and homocystinuria, and thus a comprehensive history and physical examination must be performed to identify any underlying pathology (Freyschmidt et al. 2003).

Carpometacarpal joint

The carpometacarpal (CMC) joint includes five joints within the wrist that articulate with carpal and metacarpal bones. There is much variation among the joints involving ligamentous and skeletal structures. The fourth metacarpal base shape is the most common cause of carpometacarpal joint variance (Viegas 2001; Phillips 2013). There have also been studies alluding to sexual dimorphism as being another cause of variation within the CMC joints; specifically, the joint surface area of the trapezium was found to be significantly smaller in females (Ateshian et al. 1992).

In a separate study, metacarpal base shapes have been classified into five types (Phillips 2013):

- Type I: includes a broad base for articulation with the hamate and one dorsal facet that is connected to the capitate;
- Type II: a broad base with articulation with the hamate and the dorsal and volar facets join with the capitate;
- Type III: a narrow-based articulation, where a small portion of the base is the only connection with the hamate;
- Type IV: a broader base which is attached to the hamate and includes a separate facet, which connects to the capitate; and
- Type V: a relatively broad base absent of any surfaces specifically for articulation; conjoins the hamate and the capitate.

Thumb

The thumb has shown great importance throughout the evolutionary history of mammals. The immense variations found anatomically and radiographically are clinically relevant. The variants of the thumb are quite diverse and usually accompanied by systemic syndromes. However, there are also normal variants that do exist with little association to pathological processes.

One normal benign variant of the thumb is called distal hyperextensibility of the thumb, also called hitchhiker's thumb, which is an extension of the distal interphalangeal joint of the thumb. In a study by Glass and Kistler (1953), the variation was found to have a recessive pattern of inheritance with 24.7% present in whites and 35.6% present in African Americans.

Another example is the triphalangial thumb (TPT), which can be due to a syndrome but can also be an incidental finding. Two studies found TPT to be common among the European population, occurring in 1 in every 25,000 births (Ferber 1952; Freyschmidt et al. 2003). TPT typically occurs in two functional types: opposable sporadic and unopposable (Qazi and Kassner 1988).

Hypoplastic thumb is another anomaly of the thumb where the osseous structures are hypoplastic, the thumb is shortened and malpositioned, and there is often a deficiency of the intrinsic and extrinsic muscles (Demirseren et al. 2007). This is also associated with systemic syndromes including Holt–Oram syndrome, Fanconi's anemia, Cornelia de Lange's syndrome, and diastrophic dwarfism.

Sesamoid bones of the hand

Typically there are five sesamoid bones located in the hand, which include the metacarpophalangeal (MCP) joint of the first, second and fifth digits and within the adductor pollicis and flexor pollicis brevis tendons. In a Turkish study by Kose et al. (2012), it was determined that the overall prevalence of sesamoid bones palmar to the MCP joint of the thumb was 100%, sesamoid bones in the first IP thumb 21.3%, in the second MCP 36.6%, in the third MCP 1.3%, in the fourth MCP 0.9%, and in the fifth MCP 53.2% (Kose et al. 2012).

Accessory ossicles of the wrist and hand

Accessory ossicles are secondary ossification centers which are separate from bone. Freyschmidt et al. (2003) reported the incidence of accessory ossicles to be 0.3–1.6% among the normal population. The accessory ossicles can be a result of congenital defect, post-traumatic, or degenerative disease affecting the joints. There have been numerous accessory ossicles of the wrist that have been reported in literature (Timins 1999; Freyschmidt et al. 2003). The pathophysiology of accessory ossicles involves a failure of fusion with the ossification centers, resulting in two separate bones. Accessory ossicles found in the wrist and hand are described in the following sections.

Os styloideum

The os styloideum is an accessory ossicle located in the wrist between the second and third metacarpal bones. The os styloideum can be mistaken for an accessory process of the trapezoid; sometimes this will replace the os styloideum, however. Patients with a history of degenerative joint disease such as osteoarthritis may experience pain over the region (Conway et al. 1985; Stein et al. 2011). The os styloideum can also be mistaken for a fracture; sagittal images should also be included in order to avoid such errors (Stein et al. 2011).

Os central

Os central is an additional bone located between the scaphoid, capitate, and trapezoid, or it can also be found between the lunate, triquetrum, and hamate towards the dorsal region of the hand. It is usually secondary to a failure of fusion between a small cartilaginous nodule and the scaphoid.

Lunula

Lunula is another accessory ossicle of the wrist, which is located within the triangular fibrocartilage complex between the ulna styloid process and triquetrum. It may be mistaken for an ulna styloid fracture (Doyle and Bottle 2003).

Os triangulare

Os triangulare, also referred to as os intermedium antebrachii or os triquetrum secundarium, is an accessory ossicle typically found between the ulna styloid, lunate, and triquetrum (Doyle and Bottle 2003). It can occur as a unilateral finding or bilaterally, and it is commonly confused with an ulna styloid process fracture.

Os hamuli proprium

Os hamuli proprium is an accessory ossicle found near the hamate. This ossicle forms when there is failure to fuse with the body of the hamate. On radiographic imaging, this can easily be interpreted as a fracture of the hook. However, it is unlikely a fracture if it is found bilaterally and if the patient is asymptomatic (Doyle and Bottle 2003).

Carpal boss

A carpal boss is described as a bony projection located on the dorsum aspect of the wrist. It is commonly found between the second and third metacarpal bones. The carpal boss may be derived from degenerative osteophytes or from an os styloideum, so it may be associated with pain or decreased mobility.

Os vesalianum

Another accessory bone that can be found between the hamate and the fifth metacarpal is called the os vesalianum, also found in the second and third metacarpals and between the trapezium and capitate bones. The os vesalianum carpus is an accessory bone found on the lateral region of the carpus close to the fifth metacarpal and hamate. It was first described by Vesalius in 1543, and was reported again 300 years later in 1870.

Lunate accessory ossicles

Accessory ossicles of the lunate include the os hypolunatum and os epilunatum. The os hypolunatum can be found proximal to the capitate, amid the lunate and scaphoid (Doyle and Bottle 2003; Freyschmidt et al. 2003). The os epilunatum is a spherical, bony protuberance on the dorsal aspect of the lunate (Freyschmidt et al. 2003).

Coalitions of the carpal bones

Carpal coalitions are osseous, fibrous, or cartilaginous fusions amidst two carpal bones that can be due to congenital or idiopathic etiologies (Freyschmidt et al. 2003). This is a result of incomplete segmentation of the cartilaginous precursors giving rise to fused portions of carpal bones. When contiguous carpal bones are fused, it is usually a result of idiopathic coalitions. According to Timins (1999), females and African Americans exhibit higher rates of idiopathic coalitions (Timins 1999; Stein et al. 2011). In a different study, 0.11% of Caucasians showed carpal coalitions, 1.6% of African Americans, and up to 8% of the Nigerian population (Drews and Gunther 1966; Freyschmidt et al. 2003;).

Lunotriquetral

The most common carpal fusion also occurs between the lunate and triquetrum, which is called the os lunatotriquetrum (Timins 1999). Lunotriquetral coalitions occur with a prevalence of 0.1% in the Caucasian population (Timins 1999; Stein et al. 2011; Phillips 2013). According to Timins, it is prevalent within females and is reported to occur bilaterally in 60% of cases (Timins 1999; Stein et al. 2011).

There are numerous variations of the lunotriquetral coalition, which include the site of fusion, distal and proximal fusion sites, as well as complete versus partial fusions (Freyschmidt et al. 2003). The Minaar classification (Timins 1999) of lunotriquetral coalitions includes four types of variations:

- Type I: proximal fibrous or cartilaginous coalition;
- Type II: incomplete osseous fusion with distal notch;
- Type III: complete osseous fusion; and
- Type IV: complete osseous fusion with other carpal anomalies.

Capitohamate

The next most frequent carpal coalition is capitohamate fusion, although incidence is significantly less frequent (Viegas 2001; Phillips 2013). This is the fusion between the trapezoid and capitate (Buysch et al. 1971). Leger reported a trapezoid coalition variant, which showed coalition with the second metacarpal base (Leger 1955; Seibert-Daiker 1975).

Specific variations in carpal bone

Bipartite carpals

A bipartite carpal is defined as a hand bone that has divided into two separate parts. It is considered a normal variant within the wrist. The frequency of bipartite carpals is as follows: scaphoid > triquetrum > pisiform > trapezium > trapezoid > capitate (Freyschmidt et al. 2003). A bipartite capitate and hamate bone have also been described (Ross 1954; Viehweger 1956; Kim et al. 2013). Pfitzner et al. (1885) reported a case of a bipartite trapezoid variant, where the two halves were split into dorsal and palmar aspects.

Lunate morphology

The lunate is one of the proximal carpal bones. The lunate may vary in its ossification and its morphology (Phillips 2013). Additionally, multiple ossification centers as well as a complete absence of the lunate have been described in previous studies (Postacchini and Ippoplito 1975; Poznanski 1984; Phillips 2013).

There are two main variations of the lunate, referred to as type I and II. Type I lunate is identified by a single facet on the midcarpal joint, where the capitate articulates. Type II lunate is distinguished by an additional facet located medially that joins the hamate (Viegas et al. 1990; Freyschmidt et al. 2003; Pfirrmann and Zanetti 2005; Stein et al. 2011; Phillips 2013). Types I and II have approximately equal prevalence rates, however some studies report type II lunates present in 65% of their cadavers (Viegas et al. 1990; Malik et al. 1999; Pfirrmann et al. 2002; Freyschmidt et al. 2003; Yazaki et al. 2008; Stein et al. 2011). Timins (1999) reported that the volar surface of the lunate in some instances may exhibit an irregular surface area; this is a result of an abundant vascular supply with multiple insertions sites for the blood vessels, however.

Hamate

The hamate is an asymmetrically shaped carpal bone of the wrist. Freyschmidt et al. (2003) described variants of the hamate, including atypical broadening of the hamate. This was thought to occur due to two reasons: (1) duplication of the fifth ray and (2) broadening and bifurcation of the accessory metacarpal bone. There have also been reports of variants of the hook of hamate, including bilateral hyperplasia of the hook (Viehweger 1957). In a study by Kim et al. (2013), the hook of hamate was studied in Korean patients which showed 9 cases of bipartite hooks, 30 cases of hypoplastic hooks, and 6 cases of aplastic hooks.

Scaphoid

The scaphoid is one of the largest carpal bones of the wrist that makes up the proximal row and the lateral (radial) aspect of the carpal tunnel. It also shows significant structural variations including biparitite, tripartite, or hypoplastic variations. Other variations have been described by Freyschmidt et al. (2003), including bilateral scaphoid and lunate aplasia. Freyschmidt et al. (2003) also reported scaphoid aplasia, both partial and complete, and with either partial lateral displacement of the lunate or bilateral fusion of the lunate and capitate. Freyschmidt et al. (2003) also reported abnormal positioning of the proximal carpal row with atypical articulations. There have also been reports of underdeveloped scaphoid with ulnar rearrangement of the lunate.

The scaphoid also has variations in bone density. Dwight (1907) showed that the proximal end of the scaphoid can be denser and have histological similarity to that of the femur. It was also noted that the greatest density was found in the radial half of the scaphoid.

Triquetrum

The triquetrum is another proximal carpal bone, located on the ulnar aspect of the wrist. Its variations commonly include involvement in carpal coalitions, with the triquetrum and hamate joint. Other uncommon variants have been described by Anderson and Bowers in 1985 with concomitant scapholunate dissociation and triquetral hypoplasia on the contralateral side (Anderson and Bowers 1985; Freyschmidt et al. 2003).

In a separate study by Mclean et al. (2006), the coalition between the hamate and triquetrum was studied and two types of variations were determined. The study also described two variations of the triquetrum. Type A has a broad proximal width and narrow distal width, and is double faceted at the triquetrum–hamate articulation. Type B is broad throughout the proximal and distal region, and has a concave hamate articulation region.

Pisiform

The pisiform is another carpal bone which comprises the ulnar portion of the carpal tunnel. The pisiform can typically have numerous ossification sites and a delayed onset of ossification, between 8 and 9 years of age (Freyschmidt et al. 2003). The pisiform is known to have a bipartite variant, along with an additional bony protrusion located in the distal region of the bone (Keats 1979; Freyschmidt et al. 2003).

Pisotriquetral lipping

Pisotriquetral lipping is a normal variant between the pisiform and the triquetrum articulation which can easily be mistaken for degenerative osteophyte formation in imaging (Timins 1999). In the latter there will be signs of osteophytes and calcification, as well as pain in the ulnar aspect of the hand.

References

Almasi A, Solgaard S. 2006. Polyphalangism – A rare anomaly. *Ugkr Lgr* 168: 2472–2473.

Anderson JW, Bowers WH. 1985. Congenital absence of the triquetrum: a case report. *J hand Surg* 10A: 620–622.

Ateshian GA1, Rosenwasser MP, Mow VC. 1992. Curvature characteristics and congruence of the thumb carpometacarpal joint: differences between female and male joints. *J Biomech* 6: 591–607.

Athanasakis E, Biarnes X, Bonati MT, Gasparini P, Faletra F. 2012. Identification of a new mutation (L46P) in human NOG gene in an Italian patient with symphalangism syndrome. *Mol Syndromol* 3: 21–24.

Bergman R. Thompson S. Afifi AK, Saadeh FA. 1988. *Compendium of Human Anatomic Variation: Catalog, Atlas and World Literature*. Baltimore and Munich: Urban & Schwarzenberg.

Brenner P, Hinkel GK, Krause-Bergmann A. 2004. Surgical therapy of cone-shaped epiphysis of the proximal interphalangeal joints in the tricho-rhino-phalangeal syndrome type I: a survey among three successive genereations of a single family. *Zentralbl Chir* 129: 460–469.

Buck-Gramcko D, Behrens P. 1989. Klassifikation der polydaktylie fur hand und foot. Handchir. *Mikrochir Plast Chir* 21195–204.

Buysch KH, Drewese J, Gunther D. 1971. Synostosen zwischen multangulum minus und capitatum. *Fortsch Rontgenstr* 115: 267–268.

Cleary JE, Omer GE. 1985. Congenital proximal radio-ulnar synostosis. Natural history and functional assessment. *J Bone Joint Surg Am* 67: 539–545.

Conway WF, Destouet JM, Gillula LA, Bellinghausen HW, Weeks PM. 1985. The carpal boss: an overview of radiographic evaluation. *Radiology* 156: 29–31.

Demirseren ME, Afandiyev K, Durgun M, Kilicarslan K, Yorubulut M. 2007. Congenital absence of flexor pollicis longus tendon without associated anomalies of thumb hypoplasia: A case report and review of the literature. *J Hand Surg* 2: 184–187.

Doyle JR, Bottle MJ. 2003. *Surgical anatomy of the hand and upper extremity*. Philadelphia: Lippincott, Williams and Wilkins.

Drews J, Gunther D. 1966. Uber angerborene synostosen im handwurzelberiech. *Radiologe* 6: 64–68.

Dubost E. Picard JM, Ecarlat B, Hernandez C. 1960. Trios forms d'anomalies congenitales des membres. *J Radiol Electrol* 41: 579–583.

Dwight T. 1907. *Clinical atlas variation of the hand and bones*. Philadelphia: JB Lippincott Company.

Ferber C. 1952. Ein beitrag zur dreigliedrigkeit des daumens. *Z Orthop* 83: 55–64.

Flatt AE. 1994. *The Care of Congenital Hand Anomalies*. St Louis: Mosby; Quality Medical Publishing.

Freyschmidt J, Brossmann J, Wiens J, Sternberg A. 2003. *Freyschmidt's "Koehler/Zimmer" Borderlands of Normal and Early Pathologic Findings in Skeletal Radiography*, fifth edition. New York: Thieme Verlag.

Giedion A. 1968. Zapfenepiphysen. Naturgeschichte und diagnostiche bedeutung einer storung des enchondralen wachstums. In *Ergebnisse der Medizinischen Radiologie* (Glauner R, Ruttimann A, Thurn P, Volger E, eds). Thieme, Stuttgart.

Glass B, Kistler JC. 1953. Distal hyper-extensibility of the thumbs. *Acta Genet Stat Med* 4(2–3): 192–206.

Guo B, Lee SK, Paksima N. 2013. Polydactyly, A Review. *Bull of the Hosp for Joint Dis* 71: 17–23.

Jobe M. 2008. Congenital anomalies of the hand. In *Campbell's Operative Orthopaedics*, Vol 11 pp. 4367–4449.

Keats TE. 1979. *An Atlas of Normal Roentgen Variants that may Simulate Disease*, third edition. Chicago: Year Book.

Kim JY, Lee LY, An KC, Kwon Y, Woo SH, Lee M. 2013. Anatomic variation of the hook of hamate in korea carpal tunnel syndrome patients. *International J Bio Science Bio Tech* 5: 99–106.

Kose O, Guler F, Turan A, Canbora K, Akalin S. 2012. Prevalance and distribution of sesamoid bones of the hand. A radiographic study of Turkish subjects. *Int J Morphol* 30: 1094–1099.

Leger Z. 1955. Beobachtung einer angeborenen synostose zwischen multangulum minus und metakarpale 2. *Z Orthop* 87: 70–76.

Lister G. 1993. *The Hand*, third edition. Edinburgh: Churchill Livingstone.

Liu F, Huang Y, Liu L, Liang B, Qu Z, Huang G, Li C, Tian R, Jiang Z, Liu X, Tang Z. 2014. Identification of novel NOG mutation in a Chinese family with proximal symphalangism. *Clin Chim Acta* 429: 129–33.

Malik AM, Schweitzer ME, Culp RW, Osterman LA, Manton G. 1999. MR imaging of the type II lunate bone: frequency, extent, and associated findings. *Am J Roentgenol* 173: 335–338.

Mandarano-Filho LG, Bezuti MT, Akita R, Mazzer N, Barbieri C. 2013. Congenital syndactyly: case by case analysis of 47 patients. *Acta Ortop Bras* 21: 333–335.

Mclean J, Bain G, Earnes M, Fogg Q, Pourgiezis N. 2006. An anatomic study of the triquetrum hamate joint. *J Hand Surg* 31: 601–607

Netscher DT, Baumholtz MA. 2007. Treatment of congenital upper extremity problems. *Plast Reconstr Surg* 119: 101e–129e.

Ogden JA, Ganey TM, Light TR, Besole RJ, Greene TL. 1994. Ossification and pseudoepiphysis formation in the 'nonepiphyseal' end of bones of the hands and feet. *Skeletal Radiol* 23: 3–13.

Pfirrmann CW, Zanetti M. 2005. Variants, pitfalls and asymptomatic findings in wrist and hand imaging. *European Journal of Radiology* 56: 286–295.

Pfirrmann CW, Theumann NH, Chung CB, Trudell DJ, Resnick D. 2002. The hamatolunate facet: characterization and association with cartilage lesions – magnetic resonance arthrography and anatomic correlation in cadaveric wrists. *Skeletal Radiol* 31: 451–456.

Pfitzner W. 1885. Beitrage zur kenntniss des menschlichen extremitatenskelts. VIII: Die morphologischen elemente des menschlichen handskeletts. *Zeit F Morphol U Anthrop* 2: 77.

Phillips BZ. 2013. Wrist joint anatomy. Available at: http://emedicine.medscape.com/article/1899456-overview (accessed 12 October 2015).

Postacchini F, Ippoplito E. 1975. Isolated absence of human carpal bones. *Teratology* 11: 267–71.

Potti TA, Petty EM, Lesperance MM. 2011. A comprehensive review of reportable heritable noggin-associated syndromes and proposed clinical utility of one broadly inclusive diagnostic term: NOG-related-symphalangism spectrum disorder (NOG-SSD). *Hum Mutat* 32: 877–886.

Poznanski AK. 1984. *Hand and Radiologic Diagnosis: With Gamuts and Pattern Profile*. Second edition. Philadelphia, Pa: WB Saunders.

Qazi Q, Kassner EG. 1988. Triphalangeal thumb, a review. *J Med Gen* 25: 505–520.

Rochels R, Schmid F. 1980. Morphologische und metrische abweichungen der handknochen beim Down-Syndrome – eine radiologischestudie. *Fortschr Roentgenstr* 133: 30–33.

Ross E. 1954. Os capitatum bipartitum. *Fortschr Rontgenstr* 81: 224–226.

Schafer H. 1952. Zur rontgenologischen und klinischen bedeutung der pseudoepiphysenbildung am kindlichen handskelett. *Kinderarztl Prax* 20: 77–86.

Seibert-Daiker FM. 1975. Anlage eines os hypolunatum beiderseits bei kongenitaler konkreszenz des scapoideum und trapezium. *Fortschr Rontgenstr* 122: 463–465.

Smith SL. 2000. Shape variation of the human pollical distal phalanx and metacarpal. *Am J of Phys Anthro* 113: 329–348.

Stein JM, Cook TS, Simonson S, Kim W. 2011. Normal and variant anatomy of the wrist and hand on MR imaging. *Magn Reson Imaging Clin N Am* 19: 595–608.

Swanson AB. 1976. A classification for congenital thumb formations. *J Hand Surg* 1: 8–22.

Timins ME. 1999. Osseous anatomic variants of the wrist: findings on MR imaging. *Am J Roentgenol* 173: 339–344.

Usami S, Abe S, Nishio S, Sakurai Y, Kojima H, Tono T, Suzuki N. 2012. Mutations in the NOG gene are commonly found in congenital stapes ankylosis with symphalangism, but not in otosclerosis. *Clin Genet* 82: 514–20.

Viegas SF. 2001. Variations in the skeletal morphologic features of the wrist. *Clin Orthop Relat Res* 383: 21–31.

Viegas SF, Wagner K, Patterson R, Peterson P. 1990. Medial (hamate) facet of the lunate. *J Hand Surg Am* 15: 564–571.

Viehweger G. 1956. Beitrag zur spaltbildung an den handwurzelknochen. *Fortschr Rontgenstr* 84: 376–377.

Viehweger G. 1957. Doppelseitige hyperplasie des os pisiforme und des hamulus ossis hamate. *Fortschr Rontgenstr* 86: 407.

Williams KD, Nahhas RW, Cottom CR, Lawrence S, Subedi J, Jha B, Czerwinski SA, Blangero J, Blangero SW, Towne B. 2012. Evaluation of qualitative methods for phenotyping brachymesophalangia-V from radiographs of children. *Am J Hum Biol* 24: 68–73.

Windle BCA. 1891. The occurrence of an additional phalanx in the human pollex. *J Anat Physiol* 26: 99–116.

Wood VE. 1971. Treatment of central polydactyly. *Clin Orthop Relat Res* 74: 196–205.

Yazaki N, Burns ST, Morris RP, Andersen CR, Patterson RM, Viegas SF. 2008. Variations of capitate morphology in the wrist. *J Hand Surg Am* 33: 660–666.

Further reading

Boyes JH (ed.) 1970. *Bunnell's Surgery of the Hand*, fifth edition. Philadelphia: J. B. Lippincott.

Burns JE, Tanaka T, Ueno T, Nakamura T, Yoshioka H. 2011. Pitfalls that may mimic injuries of the triangular fibrocartilage and proximal intrinsic wrist ligaments at MR imaging. *Radiographics* 31: 63–78.

Caffaratti E. 1950. Scafoide bipartito bilaterale del carpo di natura congenita. Quad Rad 13: 159 or Congenital bilateral bipartite carpal scaphoid. *G Batteriol Immunol* 41: 430.

Cerezal L, del Pinal F, Abascal Garcia-Valtuille R, Pereda T, Canga A. 2002. Imaging findings in ulnar-sided wrist impaction syndromes. *Radiographics* 22: 105–121.

Doman AN, Marcus NW. 1990. Congenital bipartite scaphoid. *J Hand Surg (Am)* 15A: 869–73.

Freyschmidt J. 2001. Melorheostosis: a review of 23 cases. *Eur Radiol* 11: 474–479.

Freyschmidt J, Freyschmidt G. 1996. *Haut-, Schleimhaut- und Skeletterkrankungen: SKIBO Disease*. Berlin: Springer.

Geyer E. 1962. Kritische betrachtung zur differentialdiagnose naviculare bipartitum-naviculare-pseudoarthrose. *Mschr Unfallheik* 65: 149–160.

Greene MH, Hadied AM. 1981. Bipartite hamulus with ulnar tunnel syndrome–case report and literature review. *J Hand Surg* 6: 605–609.

Helms CA, Major NM, Anderson MW et al. (eds) 2009. *Musculoskeletal MRI*, second edition. Philadelphia: Saunders Elsevier.

Kohler A, Zimmer E. 1993. *Borderlands of Normal and Early Pathologic Findings in Skeletal Radiography*, fourth edition. New York: Thieme Verlag.

Krause GP. 1949. Os naviculare bipartitum beider hande. *Fortschr Rontgenstr* 71: 359.

Krishna D, Chand S. 2013. Osteopoilioosis: A case report with review of literature. *J Orth Traum Rehab* 6: 84–86.

Metz VM, Schimmerl SM, Gilula LA, Viegas SF, Saffar P. 1993. Wide scapholunate joint space in lunotriquetral coalition: A normal variant? *Radiology* 188: 557–559.

Neiss A. 1955. Doppelseitige synostose zwischen demo s multangulum minus und demo s capitatum. *Fortschr Geb Rontgenstr* 82: 825.

O'Rahilly RJ. 1953. Survey of carpal and tarsal anomalies. *J Bone Jt Surg* 35A: 626–642.

Pfirrmann CW, Theumann NH, Chung CB, Botte MJ, Trudell DJ, Resnick D. 2001. What happens to the triangular fibrocartilage complex during pronation and supination of the forearm? Analysis of its morphology and diagnostic assessment with MR arthrography. *Skeletal Radiol* 30: 677–685.

Saccomanni B. 2009. Fracture of the proximal pole of the bipartite carpal scaphoid: a probable Holt–Oram-like syndrome. *Hand* 4: 140–144.

Schaaf J, Wagner A. 1962. Multiplizitat von handwurzelknochen bei drei geschweistern mit polytoper enchondraler dysostose. *Fortschr Rontgenstr* 97: 497–506.

Smith DK, Snearly WN. 1994. Lunotriquetral interosseous ligament of the wrist: MR appearance in asymptomatic volunteers and arthrographically normal wrists. *Radiology* 191: 199–202.

Totterman SM, Miller RJ. 1996. Scapholunate ligament: normal MR appearance on three-dimensional gradient-recalled-echo images. *Radiology* 200: 237–241.

Viegas SF, Ballantyne G. 1987. Attritional lesions of the wrist joint. *J Hand Surg Am* 12: 1025–1029.

Waugh RL, Sullivan RF. 1950. Anomalies of the carpus with particular reference to the bipartite scaphoid (navicular). *J Bone Jt Surg* 32-A: 682–686.

Yoshioka H, Tanaka T, Ueno T, Shindo M, Carrino JA, Lang P, Winalski CS. 2006. High-resolution MR imaging of the proximal zone of the lunotriquetral ligament with a microscopy coil. *Skeletal Radiol* 35: 288–294.

Yu HL, Chase RA, Strauch B. 2004. *Atlas of Hand Anatomy and Clinical Implications*. Maryland: Mosby.

Zanetti M, Linkous MD, Gilula LA, Hodler J. 2000. Characteristics of triangular fibrocartilage defects in symptomatic and contralateral asymptomatic wrists. *Radiology* 216: 840–845.

11 Ribs and sternum

R. Shane Tubbs[1] and Koichi Watanabe[2]
[1]Seattle Science Foundation, Seattle, Washington, USA
St George's University, School of Medicine, St Georges, Grenada
University of Dundee, Dundee, UK
[2]Kurume University School of Medicine, Fukuoka, Japan

Ribs

Variations include asymmetric ribs, cervical or lumbar ribs, fusion of ribs one and two, and the absence of ribs (Fig. 11.1). The first rib is occasionally absent. It may be absent unilaterally or bilaterally. The number of ribs may be increased by addition at either the cervical or lumbar end of the series. Eight true ribs have been observed (Cunningham 1889). The first rib may be shorter than usual, slender, and connected with the second costal cartilage. The number of ribs may also be decreased. The twelfth rib is variable in length and it may be markedly reduced in size. Asymmetric ribs are common and a variable number of costal cartilages may be absent (Colman and Bisgard 1934).

A bicipital rib is seen in relation to the first thoracic rib. It appears to be the result of the fusion of two ribs, either of a cervical and first thoracic or of the first two thoracic ribs. Unusual variations include the following. The costal cartilage and adjacent portions of the body of the rib are occasionally replaced by fibrous tissue. The first rib may be ossified at its extremities but fibrous between. The scapula may be fixed to the first rib by a short costocoracoid ligament. The ligament is a thickening of the clavipectoral fascia and is attached to the coracoid process of the scapula and inserted onto the conoid tubercle and trapezoid line of the clavicle. Two adjacent ribs may be completely fused (Fig. 11.2), or the bodies of two or more ribs may be joined by fusion due to small quadrilateral plates between the bones. Fusion of the first two ribs is common.

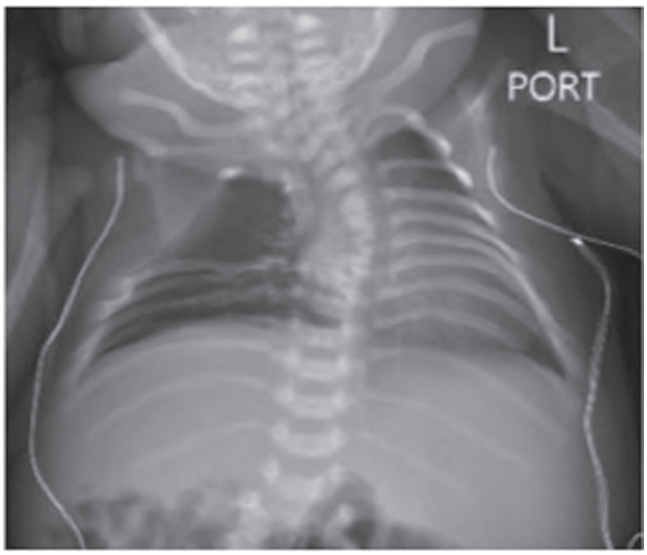

Figure 11.1 Anteroposterior thoracic radiograph noting absence of the upper right ribs in a neonate.

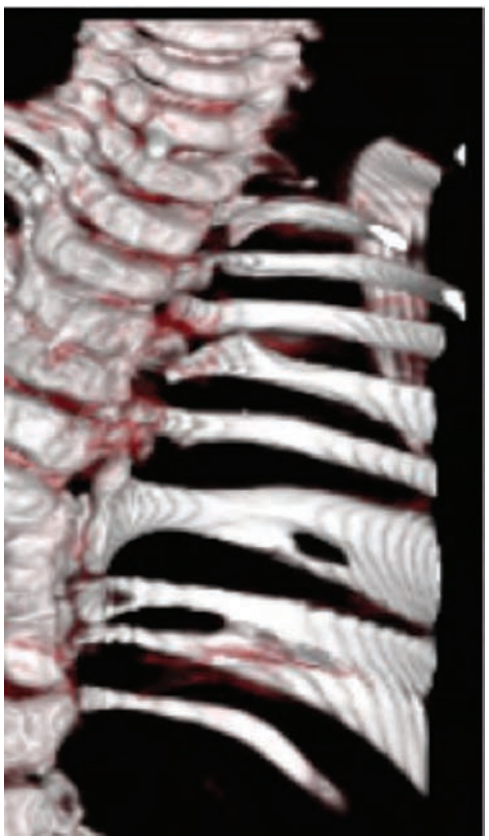

Figure 11.2 3D CT noting fused ribs on the left in a neonate.

Bergman's Comprehensive Encyclopedia of Human Anatomic Variation, First Edition. Edited by R. Shane Tubbs, Mohammadali M. Shoja and Marios Loukas.
© 2016 John Wiley & Sons, Inc. Published 2016 by John Wiley & Sons, Inc.

Ribs bifurcated at their sternal ends are occasionally observed, with the two extremities joined to a bifid costal cartilage. Bifurcated ribs occurred in 6 of 14,000 cases in one study. The tenth rib may be a floating rib. Two adjacent ribs, often five and six, and six and seven, sometimes articulate at their costal cartilages by a diarthrosis, synarthrosis, or syndesmosis. Unusual variants include fibrous tissue replacing costal cartilage.

The prevalence of rib variations has been reported to be 0.04–14%, with bifurcated ribs reported as the least common and cervical ribs as the most common. In another study of 47 patients with identified rib variations, the most common variant was fusion (72%), followed by bifurcation (28%) and hypoplastic ribs (26%) (Wattanasirichaigoon et al. 2003). Gupta et al. (2009) reported a synostosed first and second rib. This fusion created a bony tunnel with obliteration of the first intercostal space.

A bifid or bifurcated rib is generally found on one side and is not usually associated with symptoms. Bifurcation of a rib may result in a circular intercostal space (Kumar et al. 2013). Lim et al. (1982) found that bifid ribs were slightly more common on the right versus left side. Etter (1944) found that bifid ribs were more common in males versus females and occurred most commonly at the third and fourth ribs.

Thompson reported a first rib that was pierced by a branch of the first thoracic nerve. This foramen was located 1.25 inches external to the costochondral junction. After leaving the canal, the nerve was distributed to the axilla by joining the medial brachial cutaneous nerve of the arm.

Although rare, ribs that protrude into the thorax have been reported (Fig. 11.3) (Guimarães de Carvalho and Lopes 2012).

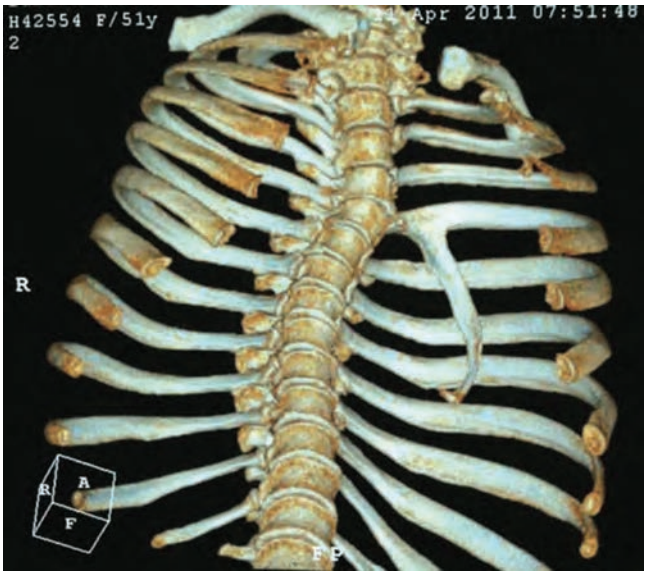

Figure 11.3 3D CT showing a left intrathoracic rib.

Source: Guimarães de Carvalho and Lopes (2012). Reproduced with permission from Brazilian Radiology.

Kamano et al. (2006) reviewed the world's literature and classified intrathoracic ribs as follows. Type I-a intrathoracic rib is a typical supernumerary intrathoracic rib, arising from an anterior-lateral portion of a vertebral body and extending laterally downwards, passing anterior to the origin of other ribs. Type I-b intrathoracic rib is also a supernumerary intrathoracic rib, arising from the posterior portion of a rib close to a vertebral body (proximal rib) and extending laterally downwards, passing anterior to the origin of other ribs. Cases of type I-a and I-b intrathoracic rib frequently exhibit attachment to the diaphragm, since the intrathoracic ribs run downwards. Type II intrathoracic rib is a so-called bifid intrathoracic rib; it is a rare variant of a bifid rib, with the bifurcation in a distal portion of the normal rib (distal rib). Type III intrathoracic rib is caused by local rib depression, in which one or more ribs is depressed into the thoracic cavity. Prados et al. (2013) identified four accessory intrathoracic ribs in a single case.

On radiographs, shadows around the rib cage (e.g., rib companion shadows, sharp lines along the lower margin of the ribs, rib overlying shadows) may mimic pleural and extrapleural disease on frontal chest radiographs (Kurihara et al. 1999).

A cervical rib (Fig. 11.4) is an anomaly that occurs when there is a development of a rib from the seventh cervical vertebra. This anomaly can also, but very rarely, arise from the sixth or fifth cervical vertebrae. The development of these structures has been

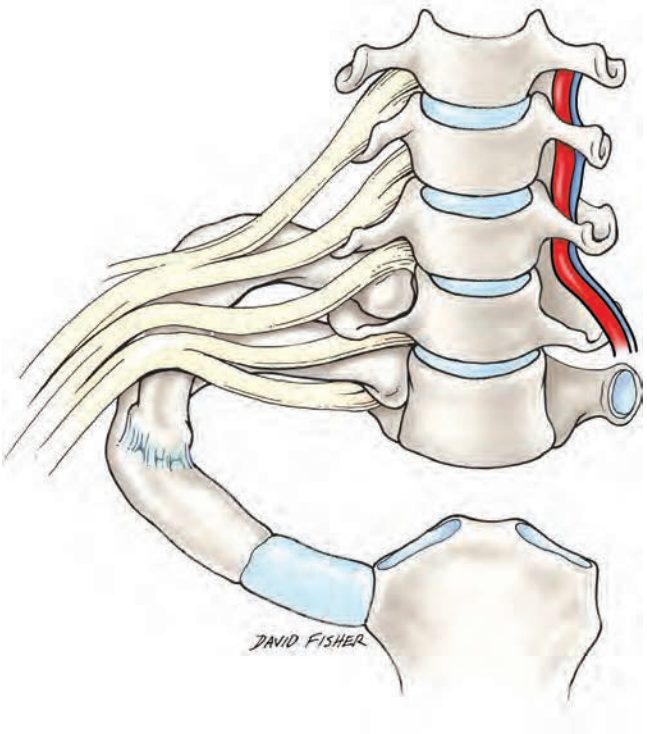

Figure 11.4 Schematic drawing of a right cervical rib with elevation of the lower trunk of the brachial plexus. Adapted from Tubbs et al. (2008) with permission from American Association of Neurological Surgeons.

attributed to hyperplasia of the secondary center of ossification of the transverse process. The cause of the hyperplasia has been linked to a Hox gene. With the development of a cervical rib, there is a change in the location for structures leaving the thoracic outlet (superior thoracic aperture). The change in the position of the thoracic outlet is moved cranially and the cervical rib then takes on the role of the first thoracic rib. The incidence of cervical ribs is 0.5–1%, and occurs twice as often in females. These supernumerary ribs have been reported to occur more often on the right side and are more often bilateral than unilateral. In some instances, there may be the presence of only a fibrous band or there may be a fully formed rib that connects with the manubrium or the first rib. The sizes of cervical ribs vary and there is no correlation between the size of the ribs and symptoms. For instance, a small cervical rib that has a fibrous connection to other structures may cause more symptoms than a larger cervical rib with no such connections. These fibrous bands travel from the cervical rib to the manubrium or first rib and may compress associated structures.

Cervical ribs most often arise from C7. However, cervical ribs from other ribs (e.g., C5 and C6) have also been reported (Applbaum et al. 1983). Double cervical ribs have been reported. They tend to be small but occasionally reach the sternum. The ventral extremity may: (a) lie free above or between the scalene muscles; (b) be connected to the sternum by a ligamentous prolongation; (c) articulate with the superior surface of the first thoracic rib; or (d) form a complete rib that articulates with the sternum. Because of their location, cervical ribs may cause a disturbance to the vascular or nerve supply to the upper limb. A cervical rib may pierce the middle scalene muscle.

Lumbar ribs (gorilla ribs) are usually quite small and seldom as complete as cervical ribs. Extra levator costae muscles may be associated with these ribs. Lumbar ribs have been reported to be more numerous than cervical ribs (8% of individuals).

Sacral ribs are very rare and have been reported as part of caudal regression syndrome (Shah et al. 2006). Coccygeal ribs may occur.

Sternum

Mall et al. (1991) analyzed 74 adult sternal specimens. Sex differences were confined mainly to the length, with males measuring 16.5 cm and females 15 cm. The width and thickness of the body (2.7–3.5 cm and 1.0–1.4 cm, respectively) showed relatively minor differences. Pectus excavatum and pectus carinatum are common sternal anomalies. Pectus excavatum is a depression of the anterior chest wall of variable severity that may be mild, moderate, or severe (Goretsky et al. 2004). All variations of depth, symmetry, and breadth of the deformity may be seen. The deformities may be small in diameter, deep, and cup-shaped, of large diameter and shallow, saucer-shaped, or eccentric. Pectus carinatum, or protrusion deformity of the chest, occurs less frequently than pectus excavatum (Goretsky et al. 2004).

Figure 11.5 Large sternal foramen.

Source: Kumarasamy and Agrawal (2011). Reproduced with permission from International Journal of Anatomical Variants.

It occurs in about 15% of patients with chest wall deformities. The prominence may involve the manubrium, which is called a chondromanubrial deformity or pigeon breast. The most common protrusion occurs in the lower or body of the sternum (the gladiolus), and is called chondrogladiolar or chicken breast. The protrusion may be unilateral, bilateral, or mixed.

The stenerbrae may be segmented into left and right parts as illustrated by Buchanan (1894).

In one radiographic study, sternal foramina were identified in 4.3% (Fig. 11.5) (Stark 1985). These may be located in the body or xiphoid process of the sternum (Kumarasamy and Agrawal 2011). The two lateral halves of the sternum may fail to unite and thereby form a cleft sternum (so-called fissura sterni) (Fig. 11.6) (Turner 1879). In other cases, the union of the two halves occurs in the manubrial region but fails distally although distal malfusion is extremely rare (Eijgelaar and Bijtel 1970). The cranial and caudal parts may be fused but the intermediate part remains separate. The failure to fuse can be very slight or very extensive. A more common variation in the sternum is asymmetry of the costal cartilages, which may articulate in an alternating pattern.

Episternal ossicles are retro- or supramanubrial accessory bones that result from supernumerary ossification centers and are usually embedded within the interclavicular ligament. Episternal ossicles may be unilateral or bilateral or pyramidal in shape, and have a diameter of 2–15 mm. The frequency of

Figure 11.6 Example of a cleft sternum.

Source: Turner (1879).

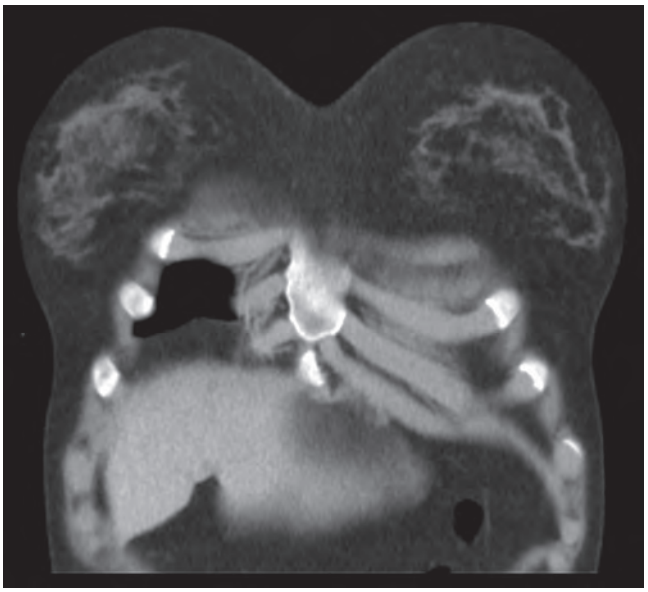

Figure 11.7 CT of the thorax, noting disarticulation between the body of the sternum and the xiphoid process.

occurrence is reported to be 6–7% of cadavers studied. By x-ray examination, Cobb found separate or fused suprasternal bones in 6.8% of adult whites and in 2.2% of adult blacks; the highest incidence of 7.6% was in white females.

The joint between the manubrium and the body of the sternum may become ossified. The manubrium sometimes extends to the insertion of the third costal cartilages. Han et al. (1999) observed photon-deficient regions in the lower sternum using SPECT in 31% of patients. These normal variants were in the area above the xiphoid process of the sternum and were oval in shape. The xiphoid process is typically variable in size and shape and may be absent. An abnormally long xiphoid, extending to a level of the umbilicus, has been reported. The xiphoid process may be perforated, more frequently than the body of the sternum. The xiphoid process may be bifid or doubled (Pansch 1875) or triplicated (Akin et al. 2011). The xiphoid process may be absent or disconnected from the rest of the sternum (Fig. 11.7).

In a detailed CT study of the xiphoid process in 500 patients, Akin et al. (2011) found the following xiphoid dimensions and findings: mean length 50 mm (range 20.6–81.5 mm); mean width 22 mm (range 6.5–46.7 mm); and mean thickness 7.3 mm (range 3.6–18.1 mm).

Positional variations

The xiphoid process was ventrally deviated in 65.4%. Ventral curving at the end of the xiphoid process resembling a hook accompanied ventral deviation in 2.2%. In 33.2%, the xiphoid process was aligned in the same or nearly the same axis as the sternal corpus. The tip of the xiphoid process was curved like a hook towards dorsal aspect in three patients (0.6%). In 0.8%, the xiphoid process was deviated dorsally in its proximal portion and ventrally in its distal portion exhibiting a reverse S-shape (Akin et al. 2011).

Xiphoid ending and ossification

Xiphoid endings had three different types: single in 62.6%; double in 32.8%; or triple in 4.6%. Ossification of the cartilaginous xiphoid process was fully completed in 50.8%. Partial ossification was detected in the one-third superior portion of the xiphoid process in 10.6%, in the two-thirds superior portion in 36.4%, one-third middle portion in 1%, one-third middle and inferior portion in 0.2%, and one-third superior and inferior portion in 0.6%. A xiphoid foramen was present in 43.2%; 34.2% had only one foramen, 6.2% had two, 1.4% had three, and 1.4% had four or more xiphoid foramina (Akin et al. 2011).

Sternoxiphoidal fusion and pseudoforamen

Sternoxiphoidal fusion was present in 214 patients (42.8%). Mean ages of the patients with and without sternoxiphoidal fusion were 53.1 and 50.7 years, respectively. Pseudoforamen due to the incomplete fusion of the sternoxiphoidal junction was observed in 1.2%. Yekeler et al. (2006) reported the frequency of the (complete or incomplete) sternoxiphoidal fusion as 62.7% in their study. These authors also found suprasternal bones were found in 41 (4.1%) subjects (22 bilateral, 18 unilateral, one midline). Suprasternal bones fused with each other

in the midline were seen in only one subject. A suprasternal tubercle was detected in 4% (27 bilateral and 13 unilateral) (Akin et al. 2011).

Manubriosternal and sternoxiphoidal fusions

Manubriosternal and sternoxiphoidal fusions were partial or complete. Manubriosternal fusion was partial in 10% subjects and complete in 19.6% subjects. Incomplete and complete sternoxiphoidal fusions were found in 32.4% and 30.3% subjects, respectively (Akin et al. 2011).

Sternal sclerotic band and cleft

Vertical sclerotic bands found by Akin et al. (2011) at the junction of the fused sternal pairs were highly frequent (37.1%; 11.1% in the manubrium, 17.8% in the body, and 8.2% in both the manubrium and body). Manubrial sclerotic bands were mostly (61.6%) located in the superior portion. The majority (77.3%) of the sternal bands of the body were located in the inferior part. Sclerotic band was not found in the xiphoid process. A manubrial cleft was depicted in 0.6%. All were in the superior portion of the manubrium and 83.3% were associated with a manubrial sclerotic band just inferior in relation to the cleft. Sternal clefts located in the body were detected in eight (0.8%) subjects (size range 5–26 mm; mean size 13 mm) and all were in the inferior part of the sternal body (Akin et al. 2011).

Sternal foramen

None of the subjects of Akin et al. (2011) had a foramen in the manubrium. A sternal foramen located in the body was found in 4.5%. All were present in the inferior part of the sternal body. The size of sternal foramina fell within the range 2–16 mm (mean 6.5 mm) (Akin et al. 2011).

Xiphoid process

In the study of Akin et al. (2011), the xiphoid process was absent in 1.1%. The xiphoid process was of three types: a single- (71%); double- (27.2%); or triple-ended (0.7%) xiphoid process. Xiphoid ossification was not seen in 2.3% (Akin et al. 2011). Xiphoid foramina were more frequent than those located in the sternal body. Xiphoid clefts were found in 1.9% (Akin et al. 2011).

Sternal clefts and foramina

Because of incomplete fusion at manubriosternal and sternoxiphoid junctions, one foramen at the manubriosternal junction and 3.3% clefts and 3.6% foramina at the sternoxiphoid junction were depicted. Asymmetric concavity of the sternal contours was depicted in only one subject. Nonfused superior and inferior sternal pairs were observed in nine subjects. The body of the male sternum is relatively longer than that of the female; in males it is more than twice the length of the manubrium whereas in females it is usually less than twice the length (Akin et al. 2011). Agenesis of the sternum is rare.

The term "tilted sternum" refers to a sternum that is not oriented in the horizontal left-to-right axis of the body but instead is oriented obliquely. The asymmetric orientation produces a unilateral irregularity of the chest wall (Restrepo et al. 2009). Yekeler et al. (2006) found such tilting of the sternum in 3.4% of subjects.

References

Akin K, Kosehan D, Topcu A, Koktener A. 2011. Anatomic evaluation of the xiphoid process with 64-row multidetector computed tomography. *Skeletal Radiol* 40: 447–452.

Applbaum Y, Gerard P, Bryk D. 1983. Elongation of the anterior tubercle of a cervical vertebral transverse process: an unusual variant. *Skeletal Radiol* 10: 265–267.

Buchanan AM. 1894. Abnormal sternum. *J Anat Physiol* 28: 313–314.

Colman JK, Bisgard JD. 1934. Congenital aplasia of costal cartilages. *Am J Surg* 25: 539–542.

Cunningham DJ. 1889. The occasional eighth true rib in man and its relation to right handedness. *J Anat Physiol* 24: 127–129.

Eijgelaar A, Bijtel JH. 1970. Congenital cleft sternum. *Thorax* 25: 490–498.

Etter LE. 1944. Osseous abnormalities of thoracic cage seen in forty thousand consecutive chest photo roentgenograms. *Am J Roentgenol* 51: 359–363.

Goretsky MJ, Kelly RE, Croitoru D, Nuss D. 2004. Chest wall anomalies: pectus excavatum and pectus carinatum. *Adolesc Med* 15: 455–471.

Guimaraes de Carvalho F, Lopes GP. 2012. Intrathoracic rib: a case report. *Radiol Bras* 45: 121–122.

Gupta V, Suri RK, Rath G, Loh H. 2009. Synostosis of first and second thoracic ribs. Anatomic and radiologic assessment. *IJAV* 2: 131–133.

Han JK, Shih WJ, Stipp V, Magoun S. 1999. Normal variants of photon-deficient area in the lower sternum demonstrated by bone SPECT. *Clin Nucl Med* 24: 248–251.

Kamano H, Ishihama T, Ishihama H, Kubota Y, Tanaka T, Satoh K. 2006. Bifid intrathoracic rib: a case report and classification of intrathoracic ribs. *Jap Soc Int Med* 45: 627–630.

Kumar N, Guru A, Patil J, Ravindra S, Badagabettu SN. 2013. Additional circular intercostal space created by bifurcation of the left 3rd rib and its costal cartilage: a case report. *J Med Case Reports* 7: 1–3.

Kumarasamy SA, Agrawal, R. 2011. A large sternal foramen. *IJAV* 4: 195–198.

Kurihara Y, Yakushiji YK, Matsumoto J, Ishikawa T, Hirata K. 1999. The ribs: anatomic and radiologic considerations. *Radiographics* 19: 105–119.

Lim CK, Lee KW, Bin JC, Rhee BC. 1982. Congenital anomalies of the ribs. *J Korean Soc Plast Reconstr Surg* 18: 487–495.

Mall G, Sprinzi G, Koebke J. 1991. Clinical morphology of the sternum. *Biomed Tech* 36: 288–289.

Pansch A. 1875. Über Anomalien am Thoraxskelette. *Arch Anat Physiol, Wissen Med* 1875: 552–564.

Prados J, Archilla F, Melguizo C, Aranega A. 2013. Four accessory (supernumerary) intrathoracic ribs: a case report. *Surg Radiol Anat* 35: 627–629.

Restrepo CS, Martinez S, Lemos DF, Washington L, McAdams HP, Vargas D, Lemos JA, Carrillo JA, Diethelm L. 2009. Imaging

appearances of the sternum and sternoclavicular joints. *Radiographics* 29: 839–859.
Shah JR, Sainani N, Patkar DP. 2006. Caudal regression syndrome with sacral rib: MRI features. *Acta Radiol* 47: 862–864.
Stark P. 1985. Midline sternal foramen. CT demonstration. *J Comput Assist Tomgr* 9: 489–490.
Tubbs RS, Louis RG Jr, Wartmann CT, Lott R, Chua GD, Kelly D, Palmer CA, Shoja MM, Loukas M, Oakes WJ. 2008. Histopathological basis for neurogenic thoracic outlet syndrome. Laboratory investigation. *J Neurosurg Spine* 8(4): 347–351.
Turner W. 1879. A description of a cleft sternum. *J Anat Physiol* 14: 103–106.
Wattanasirichaigoon D, Prasad C, Schneider G, Evans JA, Korf BR. 2003. Rib defects in patterns of multiple malformations: a retrospecitive review and phenotypic analysis of 47 cases. *Am J Med Gent A* 122A: 63–69.
Yekeler E, Tunaci M, Tunaci A, Dursun M, Acunas G. 2006. Frequency of sternal variations and anomalies evaluated by MDCT. *AJR Am J Roentgenol* 186: 956–960.

Further reading

Cohn BNE. 1944. Congenital absence of ribs. *Am J Roentgenol* 52: 495–499.
Hertslet LE, Keith A. 1896. Comparison of anomalous parts of two subjects, one with cervical rib, the other with a rudimentary first rib. *J Anat Physiol* 30: 562–567.
Jefferiss FB. 1900. A case of incomplete development of the third and fourth ribs. *Lancet* 1: 1437–1438.
Keating DR, Amberg JR. 1954. A source of potential error in the roentgen diagnosis of cervical ribs. *Radiology* 62: 688–694.
Krisch H. 1918. Rudimentäre halsrippen beiderseits und otosklerose. *Deutsch Med Wochenschr* 44: 670.
Lane WA. 1885. Supernumerary cervico-dorsal vertebra-bearing ribs, with vertebral asymmetry; abnormal articulation in a sternum. *J Anat Physiol* 19: 266–273.
Lanier RR. 1944. Length of first, twelfth, and accessory ribs in American Whites and Negroes: Their relationship to certain vertebral variations. *Am J Phys Anthropol NS* 2: 137–146.
Law AA. 1920 Adventitious ligaments simulating cervical ribs. *Ann Surg* 2: 497–499.
Lickley JD. 1904. On the relations of the seventh and eighth ribs to the sternum. *Anat Anz* 24: 326–331.
Low A. 1900. Description of a specimen in which there is a rudimentary first rib along with thirteen pairs of ribs and twenty-five presacral vertebrae. *J Anat Physiol* 34: 451–457.
Lucas MF. 1915. Two cases of cervical ribs. (2) An anomalous arrangement of the vagi. *J Anat Physiol* 69: 336–342.
Martin EJ. 1960. Incidence of bifidity and related rib abnormalities in Samoans. *Am J Phys Anthropol NS* 18: 179–187.
Michelson N. 1934. The calcification of the first costal cartilage among Whites and Negroes. *Human Biol* 6: 543–557.
Pancoast HK. 1901/02. Cervical rib. *Univer Penn Med Bull* 14: 394–398.
Purves RK, Wedin PH. 1950. Familial incidence of cervical ribs. *J Thorac Surg* 19: 952–956.
Riches EW. 1928/29. The anatomy of cervical rib: With a case report. *Brit J Surg* 16: 235–238.
Schafer EA, Symington J, Bryce TH. 1915. *Quain's Anatomy, 11th edition, vol. IV, Pt. I: Osteology and Arthrology*. London: Longman, Green, and Co.
Scott JH. 1879. Note of a case of articulation between two ribs. *J Anat Physiol* 13: 577.
Shimaguchi S. 1974. Tenth rib is floating in Japanese. *Anat Anz* 135: 72–82.
Steiner HA. 1943. Roentgenologic manifestations and clinical symptoms of rib abnormalities. *Radiology* 40: 175–178.
Stewart TD. 1934/35. Cervical intercostal articulation in a North American Indian. *J Anat* 69: 124–126.
Stickley CD, Tamura K, Labrash SJ, Lozanoff S. 2013. Bifurcation of the fourth rib as a possible indicator of Gorlin's syndrome in an 85-year-old female cadaver. *IJAV* 6: 86–89.
Struthers J. 1875. Variations of the vertebrae and ribs in man. *J Anat Physiol* 9: 17–96.
Sycamore LK. 1944. Common congenital anomalies of the bony thorax. *Am J Roentgenol* 51: 593–599.
Todd TW. 1912. Costal anomalies of the thoracic inlet, their interpretation and significance. *Anat Anz* 41: 257–271.
Todd TW. 1912. "Cervical rib": Factors controlling its presence and its size. Its bearing on the morphology and development of the shoulder. *J Anat* 46: 244–288.
Tredgold AF. 1897. Variations of ribs of primates, with especial reference to the number of sternal ribs in man. *J Anat Physiol* 31: 288–302.
Turner W. 1870. Supernumerary cervical ribs. *J Anat Physiol* 4: 130–139.
Wayburn E. 1946. Solitary pulmonary tumor. Cyst-like tumors associated with anomalies of ribs. *Am Rev Tuberc* 54: 413–417.
White JC, Poppel MH, Adams R. 1945. Congenital malformation of the first thoracic rib. *Surg Gynecol Obstet* 81: 643–659.
White JD. 1929. Abnormalities of the bony thorax. *Brit J Radiol* 2: 351–355.
Wilk E, Hüshoff T. 1957. Über eine seltene rippenanomalie. *Fortschr Röntgenstr* 86: 531–532.
Wood-Jones F. 1911. Variations of the first rib, associated with changes in the constitution of the brachial plexus. *J Anat Physiol* 45: 249–255.

12 Pelvic bones

Alper Cesmebasi and Marios Loukas
St. George's University, School of Medicine, St. Georges, Grenada

We discuss the anatomical variations of the skeletal structures that constitute the os coxae (coxal, hip, innominate bone).

The pelvic girdle is a basin-shaped configuration of skeletal structures, which serves as a conduit between the axial skeleton and lower appendicular skeleton. The bones that constitute the pelvic girdle are the two os coxae (which are created with the fusion of the ilium, ischium, and pubic bones) and sacrum. Prior to puberty, the three separate bones of the os coxae are connected to one another with the triradiate cartilage at the acetabulum, which is the cup-like depression on the lateral aspect of the pelvic girdle that allows articulation with the head of the femur. During puberty, the triradiate cartilage undergoes ossification to fuse the three bones. The two os coxae are connected anteriorly to each another at the pubic symphysis as a fibrocartilaginous joint; posteriorly, they articulate with the sacrum at the sacroiliac joints, which may be subject to different morphologies.

Sexual dimorphism of the os coxa

While the os coxa does not show much variation in the shape of its individual bones, there is notable sexual dimorphism when it comes to the pelvis. Male pelves exhibit a more narrow appearance with a lesser head:neck ratio of the pelvic inlet. Male pelves are labeled as android or anthropoid in type according to the Caldwell–Maloy classification system, where they are funnel-shaped with heart-shaped pelvic inlet appearance due to a more prominent sacral promontory projection. Female pelves tend to have a higher head:neck ratio as an adaption for child bearing. The ilia are less sloped and the distance between the anterior superior spines are noted to be greater in the female pelvis. These differences in the female pelvis make it larger and broader in comparison to the male pelvis. Additionally, the greater sciatic notches were found to be wider in females in comparison to males. Females were noted to have wider and shallower greater sciatic notches, but one study conducted by Davivongs (1963) found female sciatic notches also to be deeper in Australian aborigines. The greater sciatic angles were also noted to be more acute in males versus females, which may account for the increased sacral tilt backwards and larger anteroposterior pelvic diameter/inlet (Patriquin et al. 2005).

The male pelvis is also seen to be adapted for a more muscular build. The iliac crests are more rugged and increasingly medially inclined in the anterior portion in comparison to female iliac crests. Additionally, markings appear more pronounced with heavier architecture as an adaption to greater bulk of musculature. The male acetabulum is noted to have a larger diameter, while females have boarder sacral alae. The separation of the pubic tubercles is greater in females to allow a wider pubic width. The ischiopubic rami are more distinct in males to allow attachment of the penile crura, but are narrower and less built in females. Finally, the ischial spines are noted to be more inclined inward with a closer proximity to one another in males.

The pelvic inlet in females also has a more circular nature and is less shallow, making it more optimal for child birthing. According to the Caldwell–Moloy classification, this pelvis type is known as gynecoid due to its adaptation for parturition. However, not all females present with a gynecoid pelvis and may present with a more masculine pelvic type known as platypelloid.

It has been suggested in a few studies that the sexual variation in the human pelvic bones occurs during adolescent growth (LaVelle 1995). LaVelle (1995) states that at the age of 18, the pelvis demonstrates a posterior-to-anterior gradient of increasing dimorphism regarding the inlet and midplane of the pelvic canal. Males show an incremental growth of the acetabulum, while females show the widening of the pelvic cavity. Similarly, it was noted that gender differences in human pelves in children going through puberty do occur (Glorieux et al. 2000). In another study performed in South Africa, it was noted that ischial lengths and acetabular diameters presented as the most dimorphic features in South African whites and blacks, respectively, with males having the larger features in their pelves (Patriquin et al. 2005). In the same study, it was also noted that pubic length was found to be greater in females.

Bergman's Comprehensive Encyclopedia of Human Anatomic Variation, First Edition. Edited by R. Shane Tubbs, Mohammadali M. Shoja and Marios Loukas.
© 2016 John Wiley & Sons, Inc. Published 2016 by John Wiley & Sons, Inc.

Individual variations within the os coxa

The following section discusses topics with regards to individual variants seen with the bones that constitute the os coxa. These variations include unique observations with the foramina, spines, and joints in the pelvic girdle and are mostly normal anatomic variants rather than symptomatic pathology.

Variation in the iliac nutrient foramen

There have been noted variations in the nutrient foramen found on the ilium (Richardson and Montana 1985). On radiography, the nutrient foramina may present themselves and could be easily mistaken for stellate fractures. In a study conducted by Ebraheim et al. (1997), the foramen for the nutrient artery – a branch of the iliolumbar artery which supplies most of the intraosseous vascular supply to the acetabulum – on the internal surface of the ilium was found to have two different configurations of round and oval. The oval configuration was found to be three times more common than the round configuration. Additionally, some specimens showed small accessory foramina near the principal foramen, possibly for anastomoses (Ebraheim et al. 1997).

In a study performed by Beck et al. (2003), the nutrient artery has been noted to enter the bone at two possible locations with relation to the pelvic brim. It was noted in some specimens that the nutrient artery entered 1 cm lateral to the pelvic brim; in other specimens, it was found to enter the bone 1 cm medial to the pelvic brim. It is important to note these variations, especially when considering orthopedic procedures involving the acetabulum as damage to these arteries may cause avascular necrosis of the acetabulum. With the lateral entry-point it is simple to identify the artery, while the medial entry-point presents a difficulty in visualization (Beck et al. 2003).

Variations with the obturator foramen

The obturator foramen is also subject to variation in size, shape, location, and even number. There have been reported cases of double and triple obturator foramina found incidentally in patients (Karantanas et al. 2002; Das et al. 2006). An obturator foramen reported by Mudiraj and Jahagirdar (2011) appears to be a normal obturator foramen with a somewhat horizontal bony bridge separating the foramen into superior and inferior parts. These abnormalities likely occurred congenitally and have no known cause. Developmental disturbances in the ischial tuberosity may have occurred allowing for ossification into this variant. The variation in the shape of the obturator foramen has been noted to be related to both sex and height. In males, the obturator foramen was found to be large and oval, while females showed a smaller, triangular shape to their obturator foramen (Bierry et al. 2010). Additionally, it was noted that area of the obturator foramen also increased with height, and interobturator foramina length was greater in European women compared to African American women (Ridgeway et al. 2008). Bony spurs may also occur, projecting into the obturator foramina to give the appearance of a cyst. These exostoses are anatomical variants which may occur on either the pubis or ischium. However, they also pose risks with obturator nerve impingement, vascular impingement, and spasms of the obturator internus and externus muscles (Singh 2012). A bony canal may cover the obturator nerve prior to its emergence through the obturator foramen (Varricchio et al. 2013).

Ischiopubic synchondrosis

The ischiopubic synchondrosis is the temporary joint, occurring in childhood prior to the fusion of the ischial and pubic bones (Herneth et al. 2000). It is a normal anatomic finding on radiography of children and may appear as a tumor-like fusiform, radiolucent area in the ischiopubic zone (Herneth et al. 2000). This tumor-like appearance of the ischiopubic synchondrosis, when presenting unilaterally in a symptomatic patient, may be confused with neoplasia, stress fracture, osteolysis, or congenital disorders. The ossification of the cartilage is noted to be variable and asymmetric (Hardoff and Gips 1992). It has been noted that the ossification of the ischiopubic synchondrosis is not complete until between the ages of 4 and 12 (Cawley et al. 1983). However, cases of delayed or failed closure have been reported as incidental findings in asymptomatic patients. The ischiopubic synchondrosis may also become enlarged in children who participate in athletic activities, due to the mechanical forces exerted on the synchondrosis (Herneth et al. 2004). The exerted forces that cause the swelling of the ischiopubic synchondrosis may also delay its closure. Delayed or incomplete closure may lead to the presence of developmental notches in the ischiopubic junctions, which are asymptomatic and found incidentally on radiography. Finally, uneven mineralization of the synchondrosis may occur, yielding variant images on radiography (Cawley et al. 1983).

Iliac horns

Iliac horns are bony outgrowths that arise from the posterior ilium and are usually a protrusion of the posterior spines of the illum. Clinically, they may present as asymptomatic findings on radiologic studies (Wasserman 1976). However, the presence of iliac horns has been noted with high frequency in congenital disorders such as nail-patella syndrome, and can be considered pathognomonic of the disease. The iliac horns in nail-patella syndrome are bilateral, palpable, and have no effect on gait (Karabulut et al. 1996).

Paraglenoid sulci

Paraglenoid (preauricular) sulci are grooves frequently seen on the ilia parallel to the inferior surface of the sacroiliac joint (Gulekon and Turgut 2001). The sulci are occupied by fibers of the anterior sacroiliac ligaments (Zaaijer 1866). These sulci have been seen almost exclusively in female pelves in approximately 25% of women, and appear to be more distinctive in multiparous women (Dee 1981). The sulcus is absent in males, but when present it is underdeveloped, narrower, and shallower than in women (Hatfield 1971). It was also suggested

that, during pregnancy, the softening of other pelvic ligaments applies greater pressure on the anterior sacroiliac ligaments, which in turn cause pressure indentation on the sulcus making it more definitive (Hatfield 1971). The appearance of these sulci is a normal variant within females and should not be confused with destructive lesions.

Ischial spine projections

The ischial spine may project prominently toward the pelvic brim in acetabular retroversion, anatomic abnormalities of the hip causing head tilt deformities or pistol grip of the femoral head (Kalberer et al. 2008). The ischial spine is a process that extends from the posterior border of the superior part of the ischium at the same level of the lower border of the acetabulum. Normally, the projection of the ischial spine is lateral to the iliopectineal line, so is not noted on an anterior-posterior (A-P) radiograph of the pelvis. With acetabular retroversion however, it becomes more prominent with its projection as the acetabular opening is noted to be more posterolateral in direction (Kalberer et al. 2008). The presence of prominent ischial spine projections and acetabular retroversion is likely due to malrotation of the hip bones and it may lead to osteoarthritis. The ischial spine can be duplicated and thereby separate the greater sciatic foramen into two compartments.

Pelvic digit

The pelvic digit is a rare congenital anomaly usually seen on plain radiograph of the hip. This variation is described as bone tissue developing in a region of soft tissue adjacent to normal skeletal bone, which appears rib- or digit-like if there is an appearance with pseudoarticulations. The condition was first described by Sullivan and Cornwell in 1974, where a rib was noted radiologically in a teenage girl. Other case reports have shown pelvic digits at a variety of different locations in relation to the pelvic bones and may even possibly occur within the abdominal wall (Van Breuseghem 2006). However, most cases of pelvic digit variations occur with relation to the ilium.

The etiology behind the pelvic digit has yet to be established, but it is thought that it arises from the mesenchymal stage of bone growth during embryogenesis. In normal development, the independent cartilaginous costal primordium of the first coccygeal vertebra fuses into the vertebral column (Van Breuseghem 2006). If the fusion fails to occur, the cartilaginous center may develop on its own to form a rudimentary rib- or finger-like structure if pseudoarticulations occur (Goyen et al. 2000). Their presentation is usually asymptomatic and unilateral, though one case of bilateral pelvic digits has been reported (Hoeffel et al. 1993).

Pelvic digits must not be confused with myositis ossificans or avulsion injuries of the pelvis, which are conditions due to trauma (Granieri and Bacarini 1996). Myositis ossificans can be characterized as having a radiolucent core with a calcified periphery that is separate from the adjacent bones. Avulsion injuries of the pelvis are associated with trauma and seen to have a bony fragment with surrounding soft tissue hematoma. In either case, a lack of history of trauma can rule out these conditions and narrow the differential diagnosis to pelvic digit.

Bony islands

The presence of bony islands in the os coxa has been documented throughout the literature. Bone islands are described as the solitary focus of compact bone within cancellous bone and are most commonly found within the pelvis and upper femur, although they may occur in any skeletal bone (Smith 1973).They may be developmental and due to localized excess of bone formation in the spongiosa (Kim and Barry 1964). Bony islands may be confused with osteoblastic metastases or osteoid osteoma. However, they are usually well circumscribed and sharply delineated on radiography, frequently found in the absence of known neoplastic diseases, and are asymptomatic (Blank and Lieber 1965). They may appear unchanged in size over many years, but they do have a tendency for growth (Kim and Barry 1968). It was noted that changes within bony islands may be so slow that it may take many years to show growth on radiography (Kim and Barry 1968). They are termed giant bony islands after the lesion grows beyond 1 cm in diameter. Additionally, it is also noted that they may disappear over time, although this is very uncommon. Growing bone islands do not present with pain or symptoms in the patient; they are therefore found incidentally on radiography.

Hyperdense lines

Iliac hyperdense lines have been noted on anterior-posterior radiography of the pelvis. These lines may represent a normal variant of the crest on the posterior surface of the ilium, where the gluteus maximus and erector spinae muscle have their attachments (Keats and Anderson 2012). It may also represent a radiographic sign of gluteal muscle contracture (Cai et al. 2005). It was noted by Cai et al. (2005) that the iliac hyperdense line appeared only in patients with gluteal muscle contracture and not in controls. The etiology for this hyperdense lines is thought to result from long and persistent pulling by the gluteus maximus muscle, which causes the deformation of the posterior ilium (Cai et al. 2005). The origin of the iliacus muscle on the ilium may also cause a hyperdense line to appear on radiography. The hyperdense line associated with the iliacus muscle origin can be differentiated from lines caused by gluteal muscle contracture on CT scans as the corresponding spur-like ridge associated with the iliacus muscle origin is on the inner aspect of the ilium.

Ischial hyperdense lines have also been described on radiography (Keats and Anderson 2012). These hyperdense lines occur along the ischial tuberosity and may be caused by tension from the hamstring muscles: semitendinosus, semimembranosus, and biceps femoris.

Pelvic ears

Pelvic ears are normal variants described as benign lobular bony outgrowths at the anterior aspects of the iliac crests. They may appear symmetrical and bilaterally and are associated with long

caudad extensions of the iliac apophyses. They are noted incidentally on pelvic radiography.

Acetabular notches

A notch within the roof of the acetabulum has been noted on radiography of the hip. The presence of acetabular notches may be related to underlying pathology, but it can also be seen as a normal variant. The anatomic basis for normal variant acetabular notches, which appear in the acetabular roof, is an accessory fossa at the apex of the acetabulum (Johnstone et al. 1982). This accessory fossa may be formed due to improper fusion of the triradiate cartilage. Acetabular notches may be found in asymptomatic patients incidentally, but it has also been noted with acetabular retroversion and developmental hip dysplasia (Portinaro et al. 1994). Portinaro et al. (1994) suggests constitutional ligamentous laxity or malpositioning in utero causes altered loading of the acetabular ring, leading to the diminished growth in the cartilage and formation of the notch in the acetabulum.

Ossicles

The presence of ossicles is often a rare finding as an anatomic variant, but has been noted in the literature as occurring in children. Older literature may refer to these ossicles as Wormian bones, although Wormian bones are more commonly found associated with sutures in the cranium (Heidenblut 1963). Ossicles noted in the acetabuli are usually located in the superior portion of the acetabula, therefore referred to as os acetabuli marginalis superior. They usually present as unilateral, but bilateral cases have been reported. Most literature postulates the etiology of ossicles in the acetabular space as due to traumatic or degenerative conditions, as it presents symptomatic in the older population. However, the presence in children may be due to developmental changes with regards to the triradiate cartilage. Zander (1943) was the first author to comment on the persistence of an ossicle in the acetabular fossa, and Zimmer (1953) mentioned the presence of an additional bone in the acetabular fossa in children that eventually fused with the acetabulum by the second or third decade of life. Accessory ossification centers should be kept in mind when os acetabuli marginalis superior is found incidentally on radiograph, and further work in asymptomatic patients should be carried out for academic purposes (Hergan et al. 2000). An accessory ossification center of the anterior acetabulum is known as the central ossicle of Perna.

Asymptomatic ossicles may also appear near the symphysis pubis, if accessory ossification centers are present (Caffey and Madell 1956). Multiple ossification centers may occur in the pubic bone. On radiography of a newborn, these ossification centers may be noted as a normal variant. However, they may also lead to the formation of ossicles with the symphysis pubis.

Ligament ossification

Ossifications of ligaments with close relation to the individual bones of the os coxa have been noted on radiography. The two most common ligaments, which may undergo ossification and show as an anatomic variant on the os coxae, are the suprapubic and pectineal ligaments. On radiography, these ligaments may be found to be ossified rims with respect to their location. The ossified pectinal ligament is noted as a curved line paralleling the superior margin of the pubic bone, while the ossified suprapubic ligament may be seen as a bony bridge connecting the two pubic rami superiorly. Ossified ligaments may be mistaken for pathological or traumatic changes, though they appear as normal anatomic variants in older adults. Ossification of the suprapubic ligament may be noted postpartum in females due to the changes in the symphysis pubis that occur during pregnancy.

Malformations of the os coxae

Malformations of the individual bones that comprise the pelvic girdle are rare in isolation (Bergman et al. 1988). It should be noted any variations of the pelvic bones are related to underlying skeletal dysplasia caused by other conditions. In addition, the skeletal dysplasia will likely occur affecting multiple bones or joints including those of the pelvic girdle but not solely pelvic bones. Conditions associated with malformations of the hip bones may include achondroplasia, exstrophy of the bladder, Down syndrome, fibrochondrogenesis, and mucopolysaccharidosis.

The diagnoses of these abnormalities are usually noted incidentally on skeletal surveys for other conditions and/or dysplasias, due to their asymptomatic nature.

Absence of pubic rami

There have been reported cases of congenital absence of the pubic rami. In these reports it was noted that the pubic rami may be absent unilaterally or bilaterally, and is usually found with hip dysplasia and possible genitourinary anomalies. On a pelvic x-ray of a 44-year-old woman with history of incapacitating hip pain and uterine agenesis it was noted that her superior pubic rami were absent, there was acetabular dysplasia, and dysplasia of the iliac wings was present (Bashyal et al. 2011). In another case, a 2-year-old boy was noted to have a unilateral absence of his pubic rami, acetabular dysplasia, hypospadias, and cryptorchidism (Sarban et al. 2005). Another 2-year-old male was found to have bilateral pubic bone agenesis and bilateral undescended testes (Yildiz et al. 2008), while Sferopoulos and Tsitouridis (2003) reported two females with absences or hypoplasia of the pubic rami but no genitourinary abnormalities.

In all cases, the karyotyping screens were found to be normal, and no familial history was found. The aplasia of the pubic rami is likely due to failures in the ossification process of the ischiopubic regions. The ischiopubic region of the pelvis begins developing during the fifth and sixth month of fetal life from the ischial and pubic ossification centers. At birth, the ossification process is complete or near completion. However, if there are failures in these ossification centers, it is likely the causative factor which results in the pubic bone agenesis. It should be noted

that these abnormalities involving the pubic bones are similar to what may occur with bladder exstrophy, which is discussed in the "Exstrophy of bladder" section below.

Ischial absence/hypoplasia/duplication

There have been reports of congenital ischial absence/hypoplasia seen as an isolated anomaly and as part of a syndrome (Nishimura et al. 1998). In the reported cases, the patients were noted to have absent or decreased ossification of the ischial rami in mostly a symmetrical fashion, although one report states an asymmetrical ossification defect in the ischium (Nishimura et al. 1999). Another case mentions the hypoplasia of the ischial rami with broad ischial bodies. In the same case, it was noted there was a wide separation of the ischiopubic synchondrosis. In another case where hypoplastic ischial bones were noted, the iliac bones were described as narrow with a widened ischiopubic ramus. In this patient, it was also noted there was mildly hypoplastic ischial and pubic bones in the mother and brother, suggesting a possible familial inheritance (Kaissi et al. 2007). The ischium has been reported to be duplicated (Bergman et al. 1988). Further, the obturator foramen may not form properly if there is a failure of the ossification centers within the ischium and pubis that form the foramina.

Exstrophy of bladder

While this condition affects multiple organ systems, it should be noted that bony components of the pelvis are involved. The anterior aspects of the bony pelvis may not properly fuse during development, thus leading to bladder exstrophy. In addition to the symphysis pubis diastasis, there have been noted anomalies to the other structures that constitute the os coxae. Noted anomalies include obtuse iliac wing angles and widened sacroiliac joint angles (Anusionwu et al. 2012).

Down-syndrome-associated anomalies in the pelvis

Down syndrome has been noted to have an effect on the development of pelvic bones, which can begin to be noticed in utero during the early second trimester (Freed et al. 2000). While in utero, the iliac cartilage develops from a flattened state with an anterior and posterior surface. As embryologic growth progresses, the anterior iliac cartilage surfaces begins to turn medially due to lateral growth and attachment of abdominal musculature. Ossification begins to occur during the ninth week and articular surfaces develop. In Down syndrome the chromosomal abnormalities have an effect on these developmental processes, which result in a widened iliac angle due to poor anterior rotation of the ilium.

Radiologically, there are a number of distinct findings in the pelvis of newborns with Down syndrome. It is noted they have small acetabular angles, large ilia, and elongate ischia (Caffey and Ross 1956). The acetabular angles were found to be significantly smaller in Down syndrome infants compared to normal, healthy newborns. The angles may be up to half the normal values. Male infants with Down syndrome were noted to have smaller angles in comparison to female infants (Caffey and Ross 1956). This finding may suggest that Down syndrome seems to have a greater effect on the pelvic changes in males. The iliac bones in Down syndrome infants showed a typical appearance with the iliac image being wide and low, wings flared, and anterior superior iliac spine being low in position (Caffey and Ross 1956). The iliac angles were noted to be higher than normal, possibly lowering the position of the anterior superior iliac spine (ASIS) and giving the flared appearance. The ischium has also been noted to be elongated in shape, with the ASIS sometimes absent in the same studies. It has been proposed that widened iliac angles on prenatal sonography may be used as a marker for Down syndrome, although it has also been suggested to use anterior iliac separation due to less measurement variability (Kliewer et al. 2001).

Protrusio acetabuli

Protrusio acetabuli is a defect of the acetabulum where the acetabulum may be too deep and protrudes into the pelvis, causing a medial displacement of the femoral head beyond the ilioischial line. Protrusio acetabuli is divided into two types based on etiology: primary and secondary. Primary protrusio acetabula has been described as cases without explainable etiologies, while secondary protrusio acetabula are cases where there are known etiologies such as infection, inflammatory processes, metabolic, genetic, neoplastic, or trauma. Regardless of classification, the consequence of protrusio acetabula is secondary osteoarthritis with loss of medial joint space (Leunig et al. 2009). The mechanism has been explained by higher load transmission into the medial aspect of the joint, causing the femoral head to migrate medially over time.

The condition was first described in 1816 by Otto, while classification and etiologies were presented 100 years after that. Protrusio acetabuli have been noted to have a female predominance and with bilateral manifestations. Primary protrusio acetabuli is a diagnosis of exclusion next to mechanisms and etiologies that have been known to be associated with secondary protrusio acetabuli. It has been suggested that primary protrusio acetabula may be associated with accelerated epiphyseal growth and premature fusion of the triradiate cartilage, but these arguments have not yet been substantiated (Dunlop et al. 2005). Secondary protrusio acetabuli has been known to have a number of etiologies of underlying disease processes, which contribute to the progression of the hip protrusion if left untreated. The destructive processes of infection or inflammation can cause the femoral head to migrate medially within the joint, while metabolic conditions that affect the bone matrix will cause the femoral head to migrate superomedially. Genetic conditions, such as Marfan's or Ehler–Danlos syndromes, may cause acetabular protrusion by the mechanism of bone overgrowth due to weakened periosteum, which leads to less restriction of longitudinal growth.

Protrusio acetabuli can also be graded on deformity based on depth of protrusion (Sotelo-Garza and Charnley 1978). The

grading model took into account the distance between the projection of the upper margin of the superior pubic ramus and the acetabulum protruding into the pelvis. Three grades of protrusio were derived: Grade I (mild protrusio), measuring 1–5 mm; Grade II (moderate protrusio), measuring 6–15 mm; and Grade III (severe protrusio), measuring >15 mm.

References

Anusionwu I, Baradaran N, Trock BJ, Stec AA, Gearhart JP, Wright EJ. 2012. Is pelvic osteotomy associated with lower risk of pelvic organ prolapse in postpubertal females with classic bladder exstrophy? *J Urol* 188: 2343–2346.

Bashyal RK, Malchau H, Nimkin K, Holmes LB. 2012. The association of a dysmorphic pelvis, absence of pubic rami, hip dysplasia, and genitourinary anomalies. *Birth Defects Res A Clin Mol Teratol* 94: 57–60.

Beck M, Leunig M, Ellis T, Sledge JB, Ganz R. 2003. The acetabular blood supply: implications for periacetabular osteotomies. *Surg Radiol Anat* 25: 361–367.

Bergman RA, Thompson SA, Afifi AK. 1988. *Compendium of Human Anatomic Variation: Text, Atlas, and World Literature*. Baltimore: Urban & Schwarzenberg.

Bierry G, Le Minor JM, Schmittbuhl M. 2010. Oval in males and triangular in females? A quantitative evaluation of sexual dimorphism in human obturator foramen. *Am J Phys Anthropol* 141: 626–631.

Blank N, Lieber A. 1965. The significance of growing bone islands. *Radiology* 85: 508–511.

Caffey J, Madell SH. 1956. Ossification of the pubic bones at birth. *Radiology* 67: 346–350.

Caffey J, Ross S. 1956. Mongolism (Mongoloid deficiency) during early infancy: some newly recognized diagnostic changes in the pelvic bones. *Pediatrics* 17: 642–651.

Cai JH, Gan LF, Zheng HL, Li H. 2005. Iliac hyperdense line: a new radiographic sign of gluteal muscle contracture. *Pediatr Radiol* 35: 995–997.

Cawley KA, Dvorak AD, Wilmot MD. 1983. Normal anatomic variant: scintigraphy of the ischiopubic synchondrosis. *J Nucl Med* 24: 14–16.

Das S, Suri R, Kapur V. 2006. A triplicate obturator foramen. *Folia Morphol (Warsz)* 65: 164–106.

Davivongs V. 1963. The pelvic girdle of the Australian aborigine; sex differences and sex determination. *American Journal of Physical Anthropology* 21: 444–455.

Dee PM. 1981. The preauricular sulcus. *Radiology* 140: 354.

Dunlop CCR, Jones CW, Maffulli N. 2005. Protrusio acetabuli. *Bull Hosp Jt Dis* 62: 105–114.

Ebraheim NA, Lu J, Biyani A, Yang H. 1997. Anatomic considerations of the principal nutrient foramen artery on internal surface of the ilium. *Surg Radiol Anat* 19: 237–239.

Freed KS, Kliewer MA, Hertzberg BS, DeLong DM, Paulson EK, Nelson RC. 2000. Pelvic CT Morphometry in Down Syndrome: implications for prenatal US evaluation. *Radiology* 214: 205–208.

Glorieux FH, Travers R, Taylor A, Bowen JR, Rauch F, Norman M, Parfitt AM. 2000. Normative data for iliac bone histomorphometry in growing children. *Bone* 26: 103–109.

Goyen M, Barkhausen J, Markschies A, Debatin JF. 2000. The pelvic digit: a rare developmental anomaly. *Acta Radiologica* 41: 317–319.

Granieri GF, Bacarini L. 1996. The pelvic digit: five new examples of an unusual anomaly. *Skeletal Radiol* 25: 723–726.

Gulekon IN, Turgit HB. 2001. The preauricular suclus: its radiologic evidence and prevalence. *Kaibogaku Zasshi* 76: 533–535.

Hardoff R, Gips S. 1992. Ischiopubic synchondrosis. Normal findings, increased pubic uptake on bone scintigraphy. *Clin Nucl Med* 17: 139.

Hatfield, KD. 1971. The preauricular sulcus. *Austrasian Radiol* 15: 168–169.

Heidenblut A. 1963. Bilateral persistent Wormian bone on the posterior edge of the acetabulum (os acetabuli posterius bilaterale). *Fortschr Geb Rontgenstr Nuklearmed* 99: 109–111.

Hergan K, Oser W, Moriggl B. 2000. Acetabular Ossicles: normal variant or disease variant? *Eur Radiol* 10: 624–628.

Herneth AM, Trattnig S, Bader TR, Ba-Ssalamah A, Ponhold W, Wandl-Vergesslich K, Steinbach LS. 2000. MR imaging of the ischiopubic synchondrosis. *Magn Reson Imaging* 18: 519–524.

Herneth AM, Philipp MO, Pretterklieber ML, Balassy C, Winkelbauer FW, Beaulieu CF. 2004. Asymmetric closure of ischiopubic synchondrosis in pediatric patients: correlation with foot dominance. *AJR Am J Roentgenol* 182: 361–365.

Hoeffel C, Hoeffel JC, Got I. 1993. Bilateral pelvic digits. A case report and review of the literature. *Rofo* 158: 275–276.

Johnstone WH, Keats TE, Lee ME. 1982. The anatomic basis for the superior acetabular roof notch: "Superior acetabular notch." *Skeletal Radiol* 8: 25–27.

Kaissi AA, Chehida FB, Latos-Bielenska A, Gharbi H, Ghachem MB, Hendaoui, Kozlowski K. 2007. A novel form of ischio-vertebral syndrome. *Skeletal Radiol* 36: 77–81.

Kalberer F, Sierra RJ, Madan SS, Ganz R, Leunig M. 2008. Ischial spine projection into the pelvis. A new sign for acteabular retroversion. *Clin Orthop Relat Res* 466: 677–683.

Karabulut N, Ararurek M, Erol C, Tacal T, Balkanci F. 1996. Imaging of "iliac horns" in nail-patella syndrome. *J Comput Assist Tomogr* 20: 530–531.

Karantanas A, Velesiotou K, Sakellariou E. 2002. Double obturator foramen. *AJR Am J Roentgenol* 178: 245.

Keats TE, Anderson MW. 2012. The Pelvic Girdle. In *Atlas of Normal Roentgen Variants That May Simulate Disease*, ninth edition (KeatsTE, Anderson MW eds). Philadelphia: Saunders, pp. 257–284.

Kim SK, Barry WF. 1964. Bone island. *AJR Am J Roentgenol* 92: 1301–1306.

Kim SK, Barry WF. 1968. Bone islands. *Radiology* 90: 77–78.

Kliewer MA, Hertzberg BS, Freed KS, McNally PJ, DeLong DM. 2001. The anterior iliac sporation: alternative index for pelvic morphometry in fetuses with Down syndrome. *AJR Am J Roentgenol* 176: 1003–1007.

LaVelle M. 1995. Natural selection and developmental sexual variation in the human pelvis. *Am J Phys Anthropol* 98: 59–72.

Leunig M, Nho SJ, Turchetto L, Ganz R. 2009. Protrusio acetabuli: new insights and experience with joint preservation. *Clin Orthop Relat Res* 467: 2241–2250.

Mudiraj NR, Jahagirdar PL. 2011. A duplicate obturator foramen: a report of rare variation. *IJAV* 4: 155–156.

Nishimura G, Haga Y, Aoki K, Hasegawa T. 1998. Ischial hyoplasia, tibial hypoplasia, and facial abnormalities: a new syndrome? *Pediatr Radiol* 28: 975–977.

Nishimura G, Kimizuka M, Shiro R, Nii E, Nishiyama M, Kawano T, Kaku T, Kawada Y. 1999. Ischio-spinal dysostosis: a previously unrecognized combination of malformations. *Pediatr Radiol* 29: 212–217.

Otto AW. 1816. Ein Becken, mit kugelformig augedehnten Pfannen. In *Seltene Beobachtungen zur Anatomie, Physiologie und Pathologie gehorig. Vol IX*. (Heft E, ed.) Breslau: Verlag Willibald August Holaufer, pp. 19–20.

Patriquin ML, Steyn M, Loth SR. 2005. Metric analysis of sex differences in South African black and white pelves. *Forens Sci Int* 147: 119–127.

Portinaro NM, Matthews SJ, Benson MK. 1994. The acetabular notch in hip dysplasia. *J Bone Joint Surg Br* 76: 271–273.

Richardson ML, Montana MA. 1985. Nutrient canals of the ilium: A normal variant simulating disease on computed tomography. *Skeletal Radiol* 14: 117–120.

Ridgeway BM, Arias BE, Barber MD. 2008. Variation of the obturator foramen and pubic arch of the female bony pelvis. *Am J Obstet Gynecol* 198: 546e1–546e4.

Sarban S, Ozturk A, Isikan UE. 2005. Aplasia of the pubic bone in conjugation with hip dislocation. *J Pediatr Othop B* 14: 266–268.

Sferopoulos NK, Tsitouridis I. 2003. Ischiopubic hypoplasia: a rare constituent of congenital syndromes. *Acta Orthop Belg* 69: 29–34.

Singh R. 2012. Bony spurs projecting in the obturator foramen. *Folia Morphol (Warsz)* 71: 125–127.

Smith J. 1973. Giant bone islands. *Radiology* 107: 35–36.

Sotelo-Garza A, Charnley J. 1978. The results of Charnley arthroplasty of the hip performed for protrusio acetabuli. *Clin Orthop Relat Res* 132: 12–18.

Sullivan D, Cornwell WS. 1974. Pelvic rib: report of a case. *Radiology* 110: 355–357.

Varricchio P, Pinhal-Enfield G, Melovitz-Vasan C. 2013. Uncommon course of obturator nerve through an osseous tunnel: Clinical relevance. *IJAV* 6: 133–135.

Van Breuseghem I. 2006. The pelvic digit: a harmless "eleventh" finger. *Br J Radiol* 79: 106–107.

Wasserman D. 1976. Unilateral iliac horn (central posterior iliac process). Case report. *Radiology* 120: 562.

Yildiz C, Yurttas Y, Oto M, Kocaoglu M. 2008. Congenital agenesis of pubic bones: a case report. *J Pediatr Orthop B* 17: 299–300.

Zaaijer T. 1866. Untersuchungen uber die form des beckens javanischen frauen. *Natuurk Verhandel Holland Maatsch Wentesch Haarlem* 24: 1–42.

Zander G. 1943. Os acetabuli and other bone nuclei: periarticular calcification at the hip-joint. *Acta Radiol* 24: 317–327.

Zimmer EA. 1953. *Grenzen des Normalen und Anfange des Pathologischen im Roentgenbild des Skeletts*. Stuttgart: Thieme.

Further reading

Crowe JF, Mani VJ, Ranawat CS. 1979. Total hip replacement in congenital dislocation and dysplasia of the hip. *J Bone Joint Surg Am* 61: 15–23.

Demir M, Mavi A, Gumusburun E, Bayram M, Gursoy S, Nishio H. 2007. Anatomical variations with joint space measurements on CT. *Kobe J Med Sci* 53: 209–217.

Jusoh AR, Abd Rahman N, Abu Latiff A, Othman F, Das S, Abd Ghafar N, Haji Suhaimi F, Hussan F, Maatoq Sulaiman I. 2010. The anomalous origin and branches of the obturator artery with its clinical implications. *Rom J Morphol Embryol* 51: 163–166.

Kajbafzadeh AM, Tanhaeivash R, Elmi A, Shirazi M, Talab SS, Shabestari AA. 2010. Three-dimensional anatomy of the pelvic bone in bladder exstrophy: comparison between patients managed with osteotomy and pubic symphysis internal fixation using metal plates. *Urology* 76: 934–941.

Karachalios T, Hartofilakidis G. 2010. Congenital hip disease in adults: terminology, classification, pre-operative planning and management. *J Bone Joint Surg Br* 92: 914–921.

Kaufmann HJ, Tailard WF. 1961. Pelvic abnormalities in Mongols. *Br Med J* 5230: 948–949.

Kliewer MA, Hertzberg BS, Freed KS, DeLong DM, Kay HH, Jordan SG, Peters-Brown TL, McNally PJ. 1996. Dysmorphologic features of the fetal pelvis in Down syndrome: prenatal sonographic depiction and diagnostic implications of iliac angle. *Radiology* 201: 681–684.

Martin RJ, Fanaroff AA, Walsh MC. 2011. Neonatal orthopedics. In *Fanaroff and Martin's Neonatal-Perinatal Medicine: Diseases of the Fetus and Infant*, ninth edition (Martin RJ, Fanaroff AA, Walsh MC eds). St. Louis: Mosby, pp. 1771–1802.

McBride MT, Muldoon MP, Santore RF, Trousdale RT, Wenger DR. 2001. Protrusio acetabula: diagnosis and treatment. *J Am Acad Orthop Surg* 9: 79–88.

Moore KL, Dalley AF, Agur AMR. 2013. Pelvic Girdle. In *Clinically Oriented Anatomy*, seventh edition (Moore KL, Dalley AF, Agur AMR, eds). Philadelphia: Lippincott Williams & Wilkens, pp. 327–338.

Novacheck TF. 1996. Developmental dysplasia of the hip. *Pediatr Clin North Am* 43: 829–848.

Stevenson RE, Hall JG. 2006. Pectoral girdle, spine, ribs, and pelvic girdle. In *Human Malformations and Related Anomalies*, second edition (Stevenson RE, Hall JG, eds). New York: Oxford University Press, pp. 830–834.

Trotter M. 1937. Accessory sacroiliac articulation. *Am J Phys Anthropol* 22: 247–261.

13 Bones of the lower limb

Matthew Haffner[1] and Michael Conklin[2]
[1]St. George's University, School of Medicine, St. Georges, Grenada
[2]Children's of Alabama, Birmingham, Alabama, United States

In this chapter we discuss osteological variants of the lower limb. This will include true anatomic variants such as accessory ossicles and multipartite patellae, as well as variants of lower limb alignment (rotational and angular) and limb length. We also include some common radiographic variants, but for a complete discussion of these the reader is referred to other texts (Freyschmidt et al. 2003; Keats and Anderson 2013). In addition, whenever possible a brief discussion of findings that may assist in the differentiation between pathological conditions and anatomic variation is included.

Imaging considerations and normal variations

A few words on radiographic variants and advanced imaging are in order. In the clinical scenario, questions often arise as to findings noted on routine radiography or advanced imaging techniques such as magnetic resonance imaging (MRI). Throughout the chapter we discuss variations noted on radiography. Possible abnormalities are often noted when normal fossae or protuberances are caught at odd angles due to x-ray projection. Nutrient foramina can also cause confusion and may be mistaken for fracture. Care must be taken to correlate areas of radiographic concern with the clinical examination. If questions still exist regarding x-ray findings, then comparison views of the opposite extremity are helpful. CT imaging can further delineate bony detail.

MRI is a very sensitive tool for imaging bone and soft tissues. However, this increased sensitivity can lead to imaging findings that are mistaken for abnormalities. This is particularly true in the developing skeleton, due to the dynamic processes of bone growth and maturation.

Confusion can arise due to the normal transformation from hematopoietic to fatty marrow that occurs in a predictable pattern in the appendicular skeleton. At birth, the bones of the extremities are entirely hematopoietic and therefore of low signal intensity (SI) on T1-weighted images and high SI on T2-weighted images. During the first year of life, conversion from hematopoietic to fatty marrow begins (Vogler and Murphy 1988) which will appear as high signal intensity on T1-weighted imaging. Conversion starts in the distal aspect of the extremities (phalanges) and proceeds proximally towards the femora and humeri, concluding around skeletal maturity. Within a given bone, epiphyseal conversion occurs first within 6 months of appearance of the secondary ossification center (Jaramillo et al. 1991). Next, diaphyseal transformation occurs, proceeding lastly to the metaphysis (Vogler and Murphy 1988). The proximal femoral and proximal humeral metaphyses are therefore the last portions of the appendicular skeleton to convert. Unnecessary concern can arise from the appearance of "metaphyseal flames" (Babyn et al. 1998; Foster et al. 2004). These isolated foci of residual hematopoietic marrow can be seen as normal findings in the metaphyses. They appear as vertical elongated or flame-shaped foci based adjacent to the physis that are of low SI on T1 but still of SI greater than skeletal muscle.

Another normal MRI finding mimicking disease is the speckled marrow appearance that can be seen in the tarsal bones in children who have had a decreased weight-bearing status such as after fracture or immobilization (Laor and Jaramillo 2009).

The periosteum is a thick structure in children relative to adults. It is loosely adhered to the bone in the diaphysis and metaphysis but tightly bound down at the physis. In children, the periosteum is separated from the cortex by fibrovascular tissue, particularly at the level of the metaphysis. This tissue yields high SI on T2 imaging, the so-called "metaphyseal stripe," and can be confused with disease (Laor and Jaramillo 2009).

In the normal infant, the unossified epiphyses are of homogenous intermediate SI on T1 and low SI on T2. During epiphyseal ossification, patchy areas of high SI on T2 imaging are seen which are most apparent in the posterior aspect of the distal femoral epiphysis (Varich et al. 2000). Occasionally these areas can appear quite focal, mimicking disease.

Ossification begins in the center of the epiphysis and proceeds outward. Each epiphyseal ossification center abuts the physis on one end and is surrounded by a hemispherically shaped secondary physis. Enchondral ossification occurs in this secondary physis leading to enlargement of the secondary ossification center. During this ossification, radiographs may show multiple foci of ossification that eventually become incorporated into the secondary center of ossification. This irregularity can be confused

Bergman's Comprehensive Encyclopedia of Human Anatomic Variation, First Edition. Edited by R. Shane Tubbs, Mohammadali M. Shoja and Marios Loukas.
© 2016 John Wiley & Sons, Inc. Published 2016 by John Wiley & Sons, Inc.

with pathology, particularly in the posterior femoral condyles where it can simulate osteochondritis dessicans. Lack of adjacent bone marrow edema on MRI can differentiate this variant from osteochondritis dessicans (Gebarski and Hernandez 2005).

Femur

Proximal femur

The developing femur possesses three distinct epiphyses proximally: the greater trochanteric epiphysis; the femoral head epiphysis; and the lesser trochanteric epiphysis. The femoral head ossification center generally appears at 4–6 months of age, generally earlier in females than males. Differences in size and shape of the proximal femoral ossification center can be seen as normal variants within the first year of life (Freyschmidt et al. 2003). Ossification centers then appear fragmented, multifocal, or stippled, especially if found bilaterally, and without clinical complaints are considered a normal variant and should not be mistaken for Perthes disease (Freyschmidt et al. 2003; Keats and Anderson 2013). The proximal femoral physis is usually fully fused at 15–20 years of age (Cohn 1924; Freyschmidt et al. 2003). Persistence of the proximal femoral physeal plate as a visible line on radiographs is considered a normal variant and can be seen radiographically up to 25 years of age (Freyschmidt et al. 2003). Persistent radiographic appearance of the physeal scar can also be seen with the greater or lesser trochanteric epiphyses (Freyschmidt et al. 2003).

Another variant can be found on radiographs of children's hips just superior to the fovea. The "vertex notch" is a lucent area or notch in the ossification center noted on radiographs and located at the apex of the femoral head. It likely represents an area of unossified cartilage as arthrogram shows that it does not communicate with the hip joint. This notch is more common in boys, commonly appears after the age of 4 years and disappears gradually as the femur matures. It can be confused with pathology such as Legg–Calve–Perthes disease or epiphyseal dysplasia (Ozonoff and Ziter 1987). There have been reported incidences of double femoral notches present in a single femoral head (Keats and Anderson 2013). MRI can help differentiate, as in the normal variant "vertex notch" the overlying epiphyseal cartilage will be of uniform thickness and the epiphyseal marrow will be of normal SI.

The contour of the femoral head at its articulation with the acetabulum is smooth, except for the depression at the insertion of the ligamentum teres known as the fovea capitis. The shape of this depression has been found to be oval in 43%, triangular in 35%, and circular in 22% of studied femora (Piersol et al. 1919). A very large fovea capitis is a normal variant and may be mistaken for osteochondritis dissecans (Keats and Anderson 2013). The contour and size of the right and left fovea capitis may be asymmetric as a normal variant (Keats and Anderson 2013).

The greater trochanteric epiphysis is first seen between the ages of 2 and 5 years (Piersol et al. 1919; Cohn 1924; Freyschmidt et al. 2003) and becomes fully fused between the ages of 15 and 19 years (Piersol et al. 1919; Cohn 1924). This epiphyseal line bisects the quadrate tubercle (Sunderland 1938). An accessory ossification center may be present in the greater trochanter. This accessory ossification center is commonly found proximal to the superior aspect of the greater trochanteric ossification center (Keats and Anderson 2013). An accessory tubercle of the superior surface of the greater trochanter for attachment of some fibers of the gluteus medius is known as Mouchet's tubercle.

The lesser trochanteric epiphysis is the last to appear between the ages of 8 and 14 years, and is fully fused by 15–19 years (Piersol et al. 1919; Cohn 1924; Freyschmidt et al. 2003). A condition of the lesser trochanteric epiphysis that has been regarded both as a normal variant and an abnormality is duplication of the lesser trochanteric epiphysis (Freyschmidt et al. 2003).

A small tubercle on the femoral neck known as an epiphyseal spur can appear at the lateral edge of the femoral head epiphysis. If this epiphyseal spur persists after the femur is fully developed it is called a "developmental spur" of the femoral head. This "developmental spur" is found at the head/neck junction, projecting towards the greater trochanter running parallel to the femoral neck (Keats and Anderson 2013). Small tubercles can be seen midway down the medial femoral neck, especially in cases of coxa valga (Freyschmidt et al. 2003).

Another normal variant is the appearance of a notch in the femoral neck contour which can be found on the superior or inferior aspect of the femoral neck, or simultaneously on both. The femoral neck notch is similar to the notch found in the humeral neck and on other metaphyseal sites and commonly disappears with growth and maturation (Ozonoff and Ziter 1987; Keats and Anderson 2013). The "white line" of the femoral neck is also considered a normal variant. This is a radio-opaque line that probably represents the posterior insertion of the joint capsule on the femoral neck and should not be mistaken for a fracture (Keats and Anderson 2013). An accessory fossa of the femoral neck has been referred to as the fossa of Allen.

Another radiographic variant is seen in the proximal superior quadrant of the femoral neck in adults as a round or ovoid radiolucency. Although usually an incidental finding, its origin and relationship to hip pain and pathology have not been clearly delineated (Kim et al. 2011). It is felt to represent a herniation of soft tissue through the femoral neck cortex; it is therefore referred to as the "herniation pit" (Pitt et al. 1982).

Toogood et al. (2009) studied 375 femora and found that the femoral head tends to be anteverted and translated slightly anteriorly and inferiorly from the femoral neck axis. Femoral neck/shaft angles vary among individuals. Reported averages are: 129° (Toogood et al. 2009), 135° (Hoaglund and Low 1980), 124° (Humphry 1889), and 125° (Piersol et al. 1919). There is a wide-reported range for the neck/shaft angle (Humphry 1889; Anderson and Trinkaus 1998; Toogood et al. 2009), with a normal range varying from 110 to 150° (Anderson and Trinkaus 1998). Data support the claim of sexual dimorphism of the femoral neck angle though "sexual differences are small and

inconsistent" (Anderson and Trinkaus 1998). There is normally little to no difference between right and left femoral neck angles; however, Anderson and Trinkaus (1998) found that bilateral asymmetry of femoral neck angles of greater than or equal to 5° is not unusual. Additionally, it has also been shown that with an increasing sedentary existence there is a consistent pattern of increase of the femoral neck angle (Anderson and Trinkaus 1998).

Between the lesser and greater trochanter a radiographic appearance of speckled trabeculation can be seen, thought to be caused by reinforced trabeculae (Keats and Anderson 2013). This normal variant should not be confused with cartilaginous tumor matrix or bone infarction (Kerr et al. 1986). The proximal extent of the spiral line of the femur superior to the lesser trochanter is known as the anterior intertrochanteric ridge and is typically a distinct and rough line. Occasionally, the anterior intertrochanteric ridge is only faintly visible; rarely, a small hollow can be found in place of this line (Piersol et al. 1919). The posterior intertrochanteric ridge is more prominent and, at its junction with the greater trochanter, a vertical line or a prominence can be found: the quadrate line (*linea quadrati*) at the insertion of the quadratus femoris muscle (Piersol et al. 1919). A small bony outgrowth or ridge is occasionally found at the origin of the vastus lateralis muscle near the junction of the greater trochanter and the femoral shaft (Keats and Anderson 2013).

The lateral lip of the linea aspera ends proximally in the gluteal ridge, which receives fibers from the gluteus maximus. In muscular individuals, the gluteal ridge may be enlarged to form a rough knob, the spurious third trochanter, or a smooth rounded eminence, the true third trochanter. The true third trochanter can be found on a femur with no muscular ridges present, as in a "delicate female" (Piersol et al. 1919).

Femoral shaft

The strength of the femoral shaft is increased by a slight curvature. Normally, the anterior surface of the femur is curved by a mean angle of 22.2° (Stephenson and Seedhom 2001).

A normal radiographic variant of the femoral shaft that can be seen in the newborn is physiological periostitis appearing as periosteal new bone formation (Keats and Anderson 2013). This appears as a thin line of periosteal new bone often in the middle of the femoral shaft and commonly symmetric and bilateral (Shopfner 1966). The differential diagnoses includes abuse, syphilis, scurvy, and osteomyelitis. In adults, a normal variant of the femoral shaft is the presence of multiple transverse radioopaque lines, which may be present bilaterally (Keats and Anderson 2013).

The femur usually has a single nutrient foramen (47.7%) but may present with two foramina (44.2%), three foramina (3.5%), or absent nutrient foramen (4.6%) (Prashanth et al. 2011). The nutrient foramina are commonly found in the 2/5th and 3/5th section of the femur with a combined 93.9% incidence rate (Prashanth et al. 2011). Of all the nutrient foramina noted in their study Prashanth et al. (2011) found that c. 85% were associated with the linea aspera, either on the linea aspera (52%), medial lip (29%), or lateral lip (3.9%) of linea aspera. This is also supported by the findings of Collipal et al. (2007) (linea aspera 36.25%, lateral lip linea aspera 27.5%, medial lip linea aspera 21.25%). Piersol et al. (1919) found that there are usually two nutrient foramina with one present near the middle of the femur and the other between the converging line of the linea aspera. Gumusburun et al. (1994) found three nutrient foramina in 10.7% studied femora. An atypical nutrient foramen may be mistaken for a fracture. This can happen if the radiographic projection shows the foraminal lucency extending beyond the bone cortex into the bone medulla (Keats and Anderson 2013). These atypical nutrient foramen are more commonly found in the tibia and fibula than the femur, and will be discussed in that section below. Normally, the canals are directed away from the more actively growing ends of the bone but this can be reversed.

A prominent feature of the posterior aspect of the middle third of the femur is the linea aspera. This is the site of insertion for the large adductor and extensor muscles of the thigh. The lateral lip of the linea aspera extends proximally to end in the gluteal ridge or tuberosity. The medial lip divides proximally into the pectineal line and spiral line, coursing towards the lesser trochanter. Frequently in adults and occasionally in adolescents, the linea aspera is elevated by an underlying bony ridge known as the linea aspera-pilaster complex. This will appear on AP radiographs as two longitudinally oriented parallel radiodense lines in the middle third of the femur known as the "track sign" (Pitt 1982; Gheorghiu and Leinenkugel 2010). If the clinician is unaware of this normal variant, it could be confused with the "flame sign" of Paget's disease.

Commonly seen on radiographs of growing children are growth recovery lines, also known as growth arrest lines, Harris lines, or Park's lines. These occur when there is a temporary slowing of physeal growth due to systemic illness or trauma. This allows for continued deposition of bone at the zone of provisional calcification. When growth resumes, a sclerotic line is seen running parallel to the physis.

Distal femur

The distal femoral epiphysis is present in utero and can be detected sonographically at 28–35 weeks gestation (Mahony et al. 1985). It is important to understand normal variations in radiographic appearance of the distal femoral epiphyses in children. The distal femoral ossification centers can be multicentric or display irregular, frayed, and spiculated contours, especially during the ages of 2–6 years (Freyschmidt et al. 2003). These normal radiographic variants should not be confused with osteonecrosis, metabolic bone disease, or stippled epiphysis due to chondrodysplasia punctata (Freyschmidt et al. 2003). The corners of the distal femoral metaphysis can possess a crumpled appearance in children 2–3 years of age; this is normal and should not be confused with the metaphyseal corner fractures seen in abuse or the beak-like metaphyseal configuration seen in rickets and syphillis (Freyschmidt et al. 2003). Nutrient

foramen can also be seen in the distal femoral epiphysis, particularly during the ages of 7–11 years (Freyschmidt et al. 2003). When evaluating MR imaging of the distal femoral epiphysis in children, it is important to understand the age-related changes as described by Varich et al. (2000).

A number of variants can be seen in relation to the adductor tubercle on the medial distal femoral metaphysis. This tubercle is commonly found to have irregularities regarding its contour, occasionally presenting an indistinct or "fuzzy" cortical border that can be confused with the periosteal reaction seen in infection or malignant neoplasm (Keats and Anderson 2013). In adulthood, a prominent adductor tubercle can be seen. This tubercle can become particularly prominent in response to heavy mechanical stress or in cases of enthesiopathy (Freyschmidt et al. 2003). A small osteophyte-like outgrowth can be found proximal to the adductor tubercle at the insertion of the adductor magnus tendon, and has been termed a "tug lesion" (Keats and Anderson 2013). The "tug lesion" is in the same location and orientation as a larger osteophyte-like outgrowth known as the "coat-hook exostosis." The "coat-hook exostosis" is also a normal variant and is considered the femoral equivalent of the supracondylar process of the distal humerus (Freyschmidt et al. 2003). The marrow space of the "coat-hook exostosis" does not extend into the medulla of the femur, differentiating it from an osteochondroma. There are two main etiological theories regarding the "coat-hook exostosis:" (1) an insertional tendinopathy that has undergone extensive ossification; and (2) an early acquired or congenital prominence of a proximally displaced adductor tubercle of the femur (Freyschmidt et al. 2003). Given the location and orientation of these two normal variants, the "coat-hook exostosis" may be a more developed version of the "tug lesion."

On the distal femur proximal to the lateral femoral condyle there can also be a "tug lesion" in association with the vastus lateralis muscle (Keats and Anderson 2013). The lateral "tug lesion" commonly has a dome-like appearance while the "tug lesion" at the adductor magnus insertion is more pointed (Keats and Anderson 2013).

In a large 3D study of the distal femur, Mahfouz et al. (2012) classified 6 types of distal femoral shapes. Incidences were reported for six patient groups (male and female Caucasian, African American, Asian). Overall, there were significant differences between ethnic groups as well as between genders. This finding is supported by the studies of Saini et al. (2010), Gillespie et al. (2011), Leszko et al. (2011), and Terzidis et al. (2012).

The distal articulating surface of the femur may show grooves on the medial and lateral condyles. The groove on the lateral condyle is typically found extending anteriorly and laterally from the anterior aspect of the intracondylar fossa to expand into a triangular depression (Gray 1966). The anterior portion of the lateral meniscus rests in this depression when the knee is extended. The medial condylar groove is located on the medial aspect of the medial condyle; during full extension of the knee this groove receives the anterior portion of the medial meniscus. The lateral condylar groove is usually more defined than the medial condylar groove. These grooves are typically seen on an axial projection (sunrise) and lateral views and may simulate osteochondritis dissecans or compression fractures (Harrison et al. 1976; Keats and Anderson 2013). Contour irregularities of medial, lateral, or both femoral condylar articulating surfaces are considered normal variants while the distal femur is still maturing, and must be differentiated from osteochondritis (Keats and Anderson 2013). The lateral femoral condyle may possess a groove for the popliteus tendon (Keats and Anderson 2013).

The anatomy of the distal femur has been shown to be bilaterally symmetrical within individuals but show significant gender differences (Terzidis 2012). Males average 61 mm for both the lateral and medial femoral condylar depth, while females average 55 mm (Terzidis et al. 2012). The average intercondylar space in males is 21 mm (width) × 27.8 mm (depth), while this space in females averages 18.7 mm (width) × 23.7 mm (depth) (Terzidis et al. 2012). The bicondylar width also differs between males and females; in males it averages 88.6 mm while in females the average is 78.5 mm (Terzidis et al. 2012).

The trochlear groove separates the medial and lateral condyles of the distal femur and articulates with the patella. Wanner (1977) found the average angle of the trochlear groove created between the femoral condyles to be 147.93°. The trochlear groove is established long before weight bearing and Glard et al. (2005) determined that the angle is not correlated with age.

There are also some normal variants associated with the posterior aspects of the femur, particularly the popliteal fossa of the femur. The popliteal fossa is located between the divergent aspects of the linea aspera and transverse intercondylar line, producing a triangular fossa on the posterior aspect of the distal femur. This region of the femur can present with a variety of normal morphological and radiographic features: a "roughened" contour; a bony prominence found at the origin of the medial head of the gastrocnemius muscle (Keats and Anderson 2013); and new bone formation in response to mechanical stress (Freyschmidt et al. 2003).

Patella

The patella commonly arises from two different epiphyseal ossification centers and is usually fully ossified between 14 (Cohn 1924) and 18 years of age (Piersol et al. 1919). Initial ossification of the patella begins during 3–5 years (Ogden 1984). The second ossification center appears around the age of 12 years (Saupe 1921). Early in the ossification process irregularities in contour and ossification density (including asymmetric ossification) can be seen radiographically and should not be confused with fracture or osteochondritis dissecans (Keats and Anderson 2013). In children and adolescents, accessory ossification centers of the patella can be found distal to the inferior pole, proximal to the superior pole, or anterior to the patella. These ossification centers often have a "shell-like" or crenellated border abutting

the patella (Keats and Anderson 2013). In adults, it is common for the superior edge of the patella to possess jagged spines due to ossification of the quadriceps insertion (Piersol et al. 1919).

The average dimensions of the patella are: width 4.48±0.48 cm; thickness 2.24±0.23 cm; length 3.42±0.38 cm; and patellar ridge length 2.37±0.23 cm (Iranpour et al. 2008). In a patella unaffected by pathologies or erosion, the native thickness can be approximated as half its width (Iranpour et al. 2008). The patella and trochlear groove can manifest a variety of shapes, some of which are predisposed to patellar subluxation. There are commonly multiple nutrient foramina present on the anterior surface of the patella (Piersol et al. 1919).

A normal variant – the dorsal patellar defect – occurs with an incidence of 0.3–1%. This dorsal patellar defect commonly appears in the superolateral quadrant of the patella on the articulating surface in the second to third decade of life (Haswell et al. 1976). The etiological theory pertaining to this variant is that it develops due to a disturbance of ossification (Freyschmidt et al. 2003). This variant tends to spontaneously resolve, leaving behind an irregular sclerotic area. Differential diagnosis includes Brodie's abscess and osteochondritis dissecans (Freyschmidt et al. 2003; Keats and Anderson 2013). In the dorsal patellar defect the articular cartilage is generally intact, whereas it is damaged in cases of osteochondritis (Freyschmidt et al. 2003).

An additional normal variant of the articulating surface of the patella is known as "Haglund's groove." This variant presents as a deep concavity noted on the lateral radiograph tranversely orientated on the articular surface. The overlying cartilage may appear thickened on MRI (Freyschmidt et al. 2003).

Another normal variant of the patella is an osteophyte-like outgrowth on the anterior (non-articular) surface. This outgrowth is typically comma- or pencil-shaped and is usually directed distally off of the anterior patella. The etiology is unclear but may be linked to bone growth in response to stress induced at the insertion of the patellar tendon (Freyschmidt et al. 2003).

A double patella is considered a normal variant. In this condition, the patellae are typically of the same size and shape presenting as one located proximal to the other (Freyschmidt et al. 2003). Double patella differs from multipartite patella. Multipartite patella present as fragments that are located in the approximate position of a typical patella, while a double patella appears as two separate patellae arranged in a proximal-distal orientation. Another variant, patella emarginata, is defined as defects or irregularities in the contour of the patella with no history of trauma (Freyschmidt et al. 2003).

Multipartite patella can occur due to failure of fusion of the ossification centers. The incidence of bipartite patella is 1–2% (O'Brien et al. 2011). Bipartite patella has a higher incidence among males (Saupe 1921; Elias and White 2004) with male:female ratio around 3:1 (Bourne and Bianco 1990; Ogata 1994; Kavanagh et al. 2007; Oohashi et al. 2010), but the ratio has been reported to range from c. 2:1 (O'Brien et al. 2011) to >4:1 (Weaver 1977). Bilaterality rates of multipartite patella have been reported as: 25% (Oohashi et al. 2010); 43% (Weaver 1977); 50% (Saupe 1921); and 83% (Adams 1925).

There are currently two schemes for classifying the multipartite patella. One was developed from the seminal work of Saupe (1921) based upon the anatomic position of the fragments. The other was developed by Oohashi et al. (2010) and is based upon the location and number of fragments. The latter is a more complete classification of multipartite patella. This scheme presents four types of multipartite patella with various rates of incidence:

- superolateral bipartite: 83% (Saupe Type III);
- lateral bipartite: 12% (Saupe Type II);
- superolateral and lateral tripartite: 4%; and
- superolateral tripartite: 1%.

These rates of incidence are further supported by previous studies that found Saupe Type II has a 20% incidence and Saupe Type III has a 75% incidence rate (O'Brien et al. 2011). Additionally, a rare medial bipartite patella has been reported (Halpern and Hewitt 1978).

Multipartite patella may be symptomatic causing pain with strenuous activity and localized tenderness over the separated fragments upon physical examination (Oohashi et al. 2010). Patients may have pain while bending the knee, climbing stairs, walking, or in association with cold temperature. On physical examination, 50% of patients will have a bony prominence at the multipartite patella (Oohashi et al. 2010).

Another variant is congenital absence of the patella. This absence can present with little to no functional disability (Piersol et al. 1919). This can be differentiated from Nail-patella syndrome by the presence of a number of other features in the latter syndrome, including the presence of iliac horns. In Nail-patella syndrome the patella may be hypoplastic or completely absent. Additionally, the patellae when present in Nail-patella syndrome are often unstable or fixed in a dislocated position (Morrissy and Weinstein 2001).

Knee

Closely related to the knee joint is the common accessory ossicle of the fabella. There are two types of fabella: common fabella and the less common cyamella (*popliteal fabella*). In addition, another accessory ossicle of the knee joint is the meniscal ossicle.

Fabella

The fabella is a sesamoid bone located within the lateral head of the gastrocnemius muscle (Duncan and Dahm 2003; Freyschmidt et al. 2003) and is often found articulating with the posterior surface of the lateral femoral condyle (Phukubye and Oyedele 2011), usually in the inferolateral quadrant of that condyle (Tabira et al. 2012). It is generally not seen radiographically before 12–15 years of age (Freyschmidt et al. 2003) and can be either osseous or cartilaginous (Phukubye and Oyedele 2011; Tabira et al. 2012).

Reported incidence is 13–16% (Freyschmidt et al. 2003) or 10–30% (Duncan and Dahm 2003), but rates as high as 66% have been reported (Kawashima et al. 2007). Bilaterality falls within the range 63–85% (Freyschmidt et al. 2003). There is no difference in incidence between genders (Phukubye and Oyedele 2011; Tabira et al. 2012). The most common shape of the fabella is elliptical or circular. Average fabellar measurements are: 3.5–13.5 mm (length) × 2–9 mm (width) × 1.5–10 mm (depth) (Freyschmidt et al. 2003). Fabella have also presented as irregularly shaped, multipartite, or double (Keats and Anderson 2013).

Cyamella (popliteal fabella)

While uncommon in humans this accessory ossicle is present in many other primates and is found, like the fabella, articulating with the posterior surface of the lateral femoral condyle. However, the cyamella is a sesamoid bone found within the tendon or myotendinous junction of the popliteus muscle. Most commonly, this small accessory ossicle is found within the lateral femoral groove on radiographs (Munk et al. 2009). This accessory ossicle can be bipartite (Keats and Anderson 2013).

Meniscal ossicle

The composition of this ossicle is mature lamellar and cancellous bone, which contains fatty bone marrow surrounded by hyaline cartilage within the meniscus. Most commonly, these accessory ossicles are reported in the posterior horn of the medial meniscus (Conforty and Lotem 1979; Yu and Resnick 1994). MR imaging reveals a hypointense rim and isointensity to adjacent bone marrow (Rohilla et al. 2009). Lateral radiological investigations show that the ossicle moves with the tibia during knee rotation (Prabhudesai and Richards 2003).

Outside of these accessory ossicles there is rarely an unnamed ossicle found in the intercondylar notch of the tibial plateau (not located within either meniscus) (Keats and Anderson 2013).

Tibia and fibula

Proximal tibia and fibula

The proximal tibial ossification center usually appears in the last two months of fetal development (Freyschmidt et al. 2003) while the proximal fibular ossification center appears during the ages of 4–6 years (Piersol et al. 1919; Freyschmidt et al. 2003). The proximal fibular physis is fully fused by the ages of 20–25 years (Piersol et al. 1919; Freyschmidt et al. 2003). The proximal tibial physis typically fuses during the age 19–20 years (Piersol et al. 1919). The tibial tuberosity can develop from the proximal tibial epiphysis or from a separate ossification center. If a separate ossification center for the tibial tuberosity is present, it normally appears during 8–14 years and quickly fuses with the tibia (Piersol et al. 1919). A variant of the developing tibial tuberosity is an ununited and separate ossification center which can be confused with fracture (Keats and Anderson 2013). Occasionally a depression can be found radiographically in the anteromedial tibia of children before the tibial tuberosity ossification center develops. This depression commonly disappears with development of the tibial tuberosity ossification center (Keats and Anderson 2013). A variety of ossification patterns of the tibial tuberosity can be mistaken for Osgood–Schlatter's disease (Freyschmidt et al. 2003; Keats and Anderson 2013).

The proximal articulating aspect of the tibia (tibial plateau) commonly possesses two tibial spines (intercondylar eminences/tubercles) that are located centrally and are the anchoring points for the anterior and posterior cruciate ligaments and menisci. Occasionally, there are more than two intercondylar spines. If additional tibial spines are present they are labeled as follows: the third tibial spine is associated with the anterior aspect of the tibial plateau and the insertion of the ACL; and the fourth tibial spine is found on the posterior aspect of the tibial plateau and is associated with the insertion of the posterior cruciate ligament (PCL) (Keats and Anderson 2013). The third intercondylar tibial spine has a reported incidence of 3% and the fourth intercondylar tibial spine has a reported incidence of approximately 1% (Ravelli 1955). Approximately 50% of individuals with a fourth intercondylar tibial spine also possess a third intercondylar tibial spine (Freyschmidt et al. 2003).

The tibia and fibula are held in close contact with each other to form a syndesmosis (two bones linked by a strong membrane or ligament) (Hermans et al. 2010), which is best appreciated utilizing CT (Freyschmidt et al. 2003). At the apex of the syndesmosis (proximal to fibula) the lateral ridge (*crista interosseous tibiae*) of the tibia bifurcates into anterior and posterior ridges. There are some normal variants associated with the proximal articulation of the tibia and fibula. One of these normal variants is a prominent sulcus in the tibia for the articulation of the fibula (Keats and Anderson 2013). On the tibia, a spur-like projection near the articulating surface with the fibula can be seen (Keats and Anderson 2013).

The proximal fibula can show a number of configurations (Eichenblat and Nathan1983).

An accessory ossification center can be seen proximal to the fibular epiphysis (Freyschmidt et al. 2003; Keats and Anderson 2013). If this accessory ossification center fails to fuse it produces an unnamed accessory ossicle, found superior and proximal to the fibular head and distal to the tibial plateau (Keats and Anderson 2013).

A "tug lesion" can be found on the proximal fibula at the origin of the soleus muscle which, if prominent, can be labeled a fibular spur (Keats and Anderson 2013). If this "tug lesion" is present in an individual with an immature proximal fibula it can appear as an irregular contour of either the medial or lateral aspect of the fibular metaphysis (Keats and Anderson 2013). If the fibula is fully matured, the "tug lesion" can present as an osteophyte-like outgrowth projecting distal/medial and must be differentiated from an osteochondroma (Keats and Anderson 2013).

The soleus muscle can also cause the development of a "tug lesion" on the proximal tibia. The soleal line on the proximal

tibia can be exaggerated and quite prominent, and should be differentiated from periostitis (Levine et al. 1976).

Shaft of tibia and fibula

Anatomically, slight anterior bowing of the tibia is a normal finding in infants and small children. The thickness of the tibia is highly variable. A very thin tibia – a *platycnemic* tibia – can be seen and is commonly associated with a pilastered femur (Piersol et al. 1919).

In typical nutrient foramen the foraminal lucency is confined to the bone cortex, while in atypical nutrient foramen the radiolucency extends beyond the cortex into the medullary canal. These atypical nutrient foramen may simulate a fracture (Keats 1996). Lee et al. (2000) found that 14% of nutrient foramina in the fibula can present in this atypical manner. The fibula usually has one nutrient foramen (70% incidence) found most commonly on the posterior and medial surface within the middle third of the bone (71%), and is usually directed downward (87%). Atypical nutrient foramina were found more commonly when multiple foramina were present within the fibula (70%). These atypical foramina are found most commonly on the anterior surface significantly lower on the bone (79%) and, while a majority were directed downward (64%), a much higher proportion were directed upward (30%) than in the typical type (Lee et al. 2000). In the anatomic study by Prashanth et al. (2011), 90.2% of fibulae had one foramen while a nutrient foramen was absent in the other 9.8%. The foramen was usually found in the 3/5th area of the bone (60%). A single nutrient foramen was found in the tibia in 98.6% and was absent in 1.4% (Prashanth et al. 2011). The most common location for the nutrient foramen within the tibia was in the 2/5th region of the bone (98.3%) (Prashanth et al. 2011).

Distal tibia and fibula

The ossification center of the distal tibia appears during months 2–8 (Freyschmidt et al. 2003), but has been noted to appear as late as the second year of life (Cohn 1924). Distal tibial physeal fusion is complete during 16–20 years of age (Cohn 1924; Freyschmidt et al. 2003). The medial malleolus of the tibia occasionally has multiple centers of ossification which must be differentiated from fractures of the medial malleolus (Keats and Anderson 2013). An accessory malleolus (third malleolus of Destot) can be present. The distal tibial physis commonly appears irregular and wavy in nature (Freyschmidt et al. 2003) with a hump projecting proximally from its centromedial portion (Kump 1966; Freyschmidt et al. 2003).

The distal epiphysis of the fibula usually appears between month 13 and year 2 of life (Piersol et al. 1919; Cohn 1924) and full ossification has been reported to occur during the ages of: 18–21 years (Cohn 1924); 16–20 years of age (Freyschmidt et al. 2003); or 18–19 years (Piersol et al. 1919). The distal fibular epiphysis may show a slight medial offset in relation to its metaphysis (Freyschmidt et al. 2003). Occasionally, an additional ossification center appears at around 6 years, which is located lateral to the distal fibular metaphysis and proximal to the physeal plate. This ossification center will typically fuse with the fibula during puberty (Freyschmidt et al. 2003).

Separate ossification centers can be found at the tips of both the medial malleolus (30% incidence) and lateral malleolus (>30% incidence) (Freyschmidt et al. 2003). Selby (1961) reported that the separate ossification center found at the tip of the medial malleolus is more prevalent in females (47% incidence) than males (17% incidence) (Coughlin et al. 2006). It typically appears during the ages of 7–9 years, and is present bilaterally in females 90% of the time whereas males only present bilaterally in 27% (Selby 1961).

The anterior and posterior distal tibial margins enclose a concave triangular space known as the incisura fibularis tibiae (incisura tibialis, incisura fibulae, fibular incisure of the tibia, incisural notch, fibular notch of the tibia, peroneal groove of the tibia, syndesmotic notch). The depth of the incisura fibularis tibiae increases from proximal to distal and is an irregular rectangular shape. The depth of the incisura fibula tibiae is found to be either shallow (incidence of 25–40%) or more concave (60–75% incidence) (Hocker and Pachucki 1989; Elgafy et al. 2010). The incisura fibularis tibiae has depths of range 1.0–7.5 mm (Grass 2000; Sora et al. 2004) and is sexually dimorphic, with men possessing deeper incisura fibularis tibiae than women (Yildirim et al. 2003). The clinical implication of a more shallow incisura fibularis tibiae is that it may predispose towards syndesmotic injury (Ebraheim et al. 1998) as well as recurrent ankle sprains (Mavi et al. 2002).

Distally, the anterior tibial ridge ends as the anterior tibial tubercle (Chaput's tubercle) in the anterolateral aspect of the tibial plafond. At the same level there is a corresponding posterior tubercle. The anterior tubercle is more prominent, protruding further laterally and overlapping the medial 2/3rd of the fibula (Kelikian and Kelikian 1985). The anterior tibial tubercle prevents forward slippage of the distal fibula, whereas the posterior tibial tubercle, being less prominent, may allow posterior dislocation of the distal fibula (Hermans et al. 2010). Clinically, the overlap between the distal tibia and fibula on plain film is used to evaluate for syndesmotic injury. The horizontal distance between the medial fibular border and anterior tibial tubercle measured 1 cm proximal to the plafond should be greater than 1 mm of overlap on the mortise view (Pettrone et al. 1983; Pneumaticos et al. 2002; Nielson et al. 2005; Zalavras and Thordarson 2007). However, in a radiographic CT study of 324 patients, Sowman et al. (2012) found that 1.23% of the ankles viewed possessed no overlap; this variant can occur bilaterally (Hermans et al. 2010).

The fibular component of the syndesmosis is similar to the tibial component in some ways. The fibula possesses a ridge that bifurcates toward the syndesmosis. The medial ridge (*crista interosseous fibularis*) bifurcates into an anterior and posterior margin to form a concave triangular space distally, which is located above the articular surface of the lateral malleolus. The fibular anterior and posterior margins create tubercles distally. The anterior medial fibular ridge creates the anterior fibular

tubercle (Wagstaffe–Le Fort tubercle) and the posterior medial fibular ridge ends as the posterior fibular tubercle. As for the tibia, the anterior tubercle of the fibula is more prominent than the posterior tubercle (posterior tubercle is almost negligible in appearance) (Hermans et al. 2010). A normal variant is the presence of a prominent malleolar fossa within the fibula, and it is not uncommon to find accessory ossicles within this fossa (Freyschmidt et al. 2003).

There are a number of accessory ossicles associated with the distal tibia and fibula. These include os subtibiale, os subfibulare, and os retinaculi (*ossa retinaculi*). Due to their location and size, accessory ossicles can easily be mistaken for avulsion fracture. Radiographically, accessory ossicles show complete cortical boundaries while avulsion fracture fragments lack cortex at the site of avulsion (Freyschmidt et al. 2003).

Os subtibiale

This accessory ossicle can be found below the medial malleolar tip between the medial malleolus and the talus (Freyschmidt et al. 2003). Ossicles that are related to the anterior aspect of the medial malleolus tend to be smaller in size (Coughlin et al. 2006). The incidence varies from 0.2% (Leimbach 1938; Tsuruta et al. 1981a, b) to 2.1% (Coral 1987). Coral (1987) proposed criteria for an os subtibiale as being a rounded ossicle with a diameter of at least 4 mm.

When differentiating between an accessory ossification center of the medial malleolar tip and os subtibiale, location is key. Both appear as rounded in shape with well-defined margins; however, the os subtibiale will be closely related to the posterior colliculus of the medial malleolus while an accessory ossification center will be closely related to the anterior colliculus (Coral 1987; Coughlin et al. 2006).

Os subfibulare

The os subfibulare is between the lateral malleolus and the talus posterior to the tip of the lateral malleolus (Coughlin et al. 2006). Os subfibulare are typically found incidentally on AP radiographs (Coughlin et al. 2006), but oblique projections of the lateral malleolus may be necessary to detect small os subfibulare (Keats and Anderson 2013). The os subfibulare can be as large as 5–10 mm and usually presents as oval or elongated (Coughlin et al. 2006).

In a histoembryologic study, Trolle (1945, 1948) found the incidence of os subfibulare to be 0.2%. The incidence appears to have no correlation with age as rates of 0.2% have been reported in both children and adults (Leimbach 1938; Shands and Wentz 1953). Even though a single study of 300 ankle radiographs found the incidence of the os subfibulare to be as high as 6.67% (Bowlus et al. 1980), the consensus within the literature is that the os subfibulare is a very rare normal variant (Leimbach 1938; Trolle 1945, 1948; Shands and Wentz 1953; Maffulli et al. 1990).

Additional accessory ossicles may be found around the lateral malleolus. One of these is formed by an ununited apophysis of the lateral malleolus, which is located on the anterior aspect of the lateral malleolus. The os subfibulare is specifically found posterior to the tip of the lateral malleolus.

Os retinaculi (fibular ossicle)

Accessory ossicles that are paramalleolar and in direct contact with underlying bone are categorized as os retinaculi. The os retinaculi is usually flat in shape and can be seen on AP radiographs overlying the bursa of the lateral malleolus near the peroneal retinaculum. This bone does not have any incidence rates reported in the literature (Coughlin et al. 2006).

Foot

Calcaneus

The talus and calcaneus ossify by the third month of intrauterine life and are the first tarsi to ossify. The calcaneus may develop from two ossification centers with a fusion line occasionally visible in early childhood radiographs (Kumar et al. 1991; Freyschmidt et al. 2003; Keats and Anderson 2013). However, double ossification centers are seen more frequently in some bone dysplasias and Larsen's syndrome.

The posterior border of the calcaneal tuberosity typically appears jagged or wavy in children (Freyschmidt et al. 2003). Posterior to this, the apophysis of the calcaneal tuberosity will appear during the age of 6–10 years (Freyschmidt et al. 2003). This calcaneal tuberosity apophysis can show various patterns of ossification (density, fragmentation, irregular contour). This variable presentation should be considered normal and not indicative of pathological conditions (Freyschmidt et al. 2003; Keats and Anderson 2013). Fusion of the posterior border of the calcaneus to the calcaneal apophyseal ossification center occurs around the age of 17 years (Freyschmidt et al. 2003). If the ossification center for the calcaneal tuberosity does not fuse, this can simulate fractures (Keats and Anderson 2013). Variants of fusion of this ossification center can present as either a free unnamed ossicle with irregular shape or as a shelf-like indentation seen at the superoposterior aspect of the calcaneus, which can be mistaken for an erosive defect (Keats and Anderson 2013).

The nutrient foramen of the calcaneal tuberosity is commonly found on its plantar aspect and can be seen on oblique radiographs. The presence of a large nutrient foramen in this area should be considered normal (Keats and Anderson 2013).

A separate ossification center will form the peroneal trochlea (peroneal or trochlear process), which will separate the peroneus longus and brevis tendons. The peroneal trochlea may be very prominent in 30% (Freyschmidt et al. 2003; Keats and Anderson 2013). Rarely, the peroneal trochlea will be large enough to cause an impingement syndrome with the peroneus longus tendon (Boles et al. 1997). If the ossification center of the peroneal trochlea does not fuse with the calcaneus, an accessory ossicle – the os trochleare calcanei – results (discussed a few sections below).

On a lateral projection, in the adult calcaneus the sustentaculum tali can occasionally appear very prominent as a normal variant (Freyschmidt et al. 2003). The sustentaculum tali can give the appearance of a fracture line on lateral radiographic projections (Keats and Anderson 2013). A normal area of the calcaneus that can be confused as pathologic is located near the sulcus calcanei. In radiographs, there appears a lucent area (usually triangular in shape) below the sulcus calcanei. This is a normal area of sparse trabeculation with abundant fatty tissue present within (Freyschmidt et al. 2003). There is a variable presentation of this lucent area within the population: very pronounced (7.1%); moderately pronounced (22.1%); or faintly visible (70.8%) (Freyschmidt et al. 2003). This area can be misdiagnosed as a lipoma or as a unicameral bone cyst (due to lucency). A definitive differential of this area can be achieved using conventional radiographs if an oblique or end-on projection of a nutrient canal can be seen within the lucent area (Freyschmidt et al. 2003). With regards to MR imaging, this lucent area appears as a signal void on T1-weighted imaging and as high signal intensity on T2-weighted imaging.

In children before the age of 1 year, it is normal to see a bone spur on the plantar aspect of the calcaneus on lateral radiographs (Kumar et al. 1991; Keats and Anderson 2013). These bone spurs tend to present bilaterally and symmetrically and have a variable orientation projecting anterior, posterior, or inferior (Robinson 1976; van Wiechen 1987). These spurs commonly disappear by the first year of age (Kumar et al. 1991). In adults, there may be a "tug lesion" on the plantar aspect of the calcaneus at the origin of the long plantar ligament (connecting the cuboid and calcaneus) that is a projection oriented parallel with the course of this ligament; this is a normal variant (Keats and Anderson 2013).

Haglund's exostosis is a spur-like prominence on the posterosuperior border of the calcaneus. This exostosis is considered a normal variant but may impinge on the Achilles tendon, known as Haglund's heel or Haglund's syndrome, which is exacerbated by wearing high heels (Freyschmidt et al. 2003).

There may be a bony prominence arising from the superior talonavicular side of the calcaneal articulating surface, which is a normal variant. This prominence extends towards the navicular bone. It may even pseudoarticulate with the navicular, especially if the navicular possesses a prominent lateral projection. Additionally, the location of this variant bony prominence is the same location where an accessory ossicle of the foot (calcaneus secondarius) can occur. The locational correspondence between these two normal variants is indicative that the accessory ossicle os calcanei secundii may be an unfused apophysis of the bony process (Freyschmidt et al. 2003).

Accessory ossicles associated with the calcaneus include: os tuberis calcanei; os aponeurosis plantaris; os accessorium supracalcaneum; os trochleare calcanei; os sustentaculi; calcaneus secondarius; and calcaneus accessorius.

Melo (2012) has described a unique case of an adult with an osseous channel through the calcaneus in which the tendon of the flexor hallucis longus traveled.

Os tuberis calcanei (os subcalcis)

This accessory ossicle is located on the plantar aspect of the calcaneus, slightly posterior to the insertion of the plantar fascia. It can reach a diameter of 10 mm. Incidence rates are not reported (Coughlin et al. 2006).

Os aponeurosis plantaris

The os aponeurosis plantaris can be found entirely enclosed within the plantar aponeurosis. It varies in size and is usually oblong or flat. There are no reported incidence rates. This ossicle can be visualized on a lateral radiograph (Coughlin et al. 2006).

Os accessorium supracalcaneum

This accessory ossicle is located above the calcaneus some distance from the talus posterior to the location of the os trigonum (Freyschmidt et al. 2003). This accessory ossicle is separate from the posterior process of the talus and commonly articulates with the posterosuperior margin of the calcaneus (Milgrom et al. 1986).

Os trochleare calcanei

As stated earlier, this accessory ossicle may be the result of an unfused peroneal trochlea (Freyschmidt et al. 2003).

Os sustentaculi

This accessory ossicle is located adjacent or anterior to the sustentaculum tali. Occasionally, this accessory ossicle is psuedoarticulated via a fibrous or fibrocartilaginous synchondrosis with the sustentaculum tali, which can give the appearance of completing the sustentaculum tali (Freyschmidt et al. 2003). There have been reports of os sustentaculi fusing with the sustentaculum tali; this is referred to as an assimilated os sustentaculi (Bloom et al. 1986). Commonly, a joint between the assimilated os sustentaculi and the talus is formed and may be associated with a subtalar coalition (Harris and Beath 1948).

Os sustentaculi is found in >1% of the population (Bencardino et al. 1997). Reported incidences vary from 0.3% (Tsuruta et al. 1981a, b; Mellado et al. 2003) to 1.5% (Holle 1938). Gender preference has been noted with an incidence of 2–3% in adolescent males (Hoerr 1962).

The differential diagnosis for os sustentaculi includes calcaneus accessorius and tarsal coalition. The os sustentaculi presents on the medial aspect of the calcaneus, whereas the calcaneus accessorius is found on the lateral aspect of the talocalcaneal joint (Coughlin et al. 2006).

The os sustentaculi can produce a "double ankle" with a hard bony projection that can be palpated posterior to the medial malleolus. The differentiation between an os sustentaculi and os tibiale externum (discussed in more depth in the section on the navicular) must be made. The os tibiale externum is a bony projection that can be palpated more anteriorly than the os sustentculi (March and London 1993).

The clinical presentation of symptomatic os sustentaculi involves pain with prolonged walking. There is mild restriction

to passive inversion of the hindfoot and tenderness to palpation (Bencardino et al. 1997). The os sustentaculi is best evaluated by CT imaging, specifically axial and oblique coronal projections and 3D CT reconstructions (Mellado et al. 2002). T1- and T2-weighted coronal and axial MR imaging typically show a low signal intensity line transecting the sustentaculum tali (Bencardino et al. 1997).

Calcaneus secondarius (secondary os calcis)

This ossicle is the result of an unfused apophysis of an atypical bony process of the calcaneus. It is found in the space between the calcaneus, talus, cuboid, and navicular. It can be round but is most commonly triangular (Mellado et al. 2003). It ranges in size, but commonly presents as 3–4 mm in diameter (Coughlin et al. 2006). Pseudoarticulations can be found with any of the adjacent bones (Freyschmidt et al. 2003).

The reported incidence in adults varies, but is usually 0.4–7% (Pfitzner 1896; Leimbach 1938; Tsuruta et al. 1981a, b; Keats 1992; Sarrafian 1993). However, it appears more frequently within adolescents and with a gender bias: boys 7–11% and girls 6–7% incidence (Hoerr 1962). Some patients with this accessory ossicle have restricted subtalar motion (Coughlin et al. 2006).

Calcaneus accessorius

An alternative name for this ossicle is the os talocalcaneale laterale (O'Rahilly 1953). The calcaneus accessorius approximates the trochlear process of the calcaneus on the fibular aspect just distal to the fibular malleolus (Holland 1921; Mercer 1931; Hirschtick 1951).

In a histoembryological study, Trolle (1948) found the incidence of this accessory ossicle to be 0.6% (Coughlin et al. 2006). The size of this accessory ossicle can be as large as 5 mm in diameter, but it is rarely larger than the size of a pea (Trolle 1948).

Talus

At around the third month of intrauterine development, the ossification center of the talus becomes visible and occasionally two ossification centers are present. Additionally, the posterior process of the talus usually arises from its own ossification center. The lateral posterior talar process is also known as a trigonal or Stieda process. If this process is prominent it can lead to posterior ankle impingment syndrome, when repetitive or forceful plantarflexion occurs (Bureau et al. 2000).

In children and adolescents a deep notch, the subtalar sinus, may be found along the plantar border of the talus opposite a corresponding groove in the calcaneus. The adult talus has a total of seven cartilaginous surfaces. Due to the complex surface anatomy of the talus, certain projections can mimic fracture lines, most commonly on the lateral view. This effect usually occurs when the medial and lateral borders of the talar dome are projected separately (Freyschmidt et al. 2003). Irregular ossification of the talar dome can be seen radiographically as a normal variant (Keats and Anderson 2013).

If there are two ossification centers present there is a possibility that they will not fuse, resulting in a bipartite talus. This is usually asymptomatic, but can lead to decreased range of motion. Inversion and eversion are usually limited and may produce pain. Dorsiflexion is limited whereas plantarflexion is unaffected (Schreiber et al. 1985).

A normal variant of the posterior portion of the talus noted on MRI is a "pseudodefect;" caused by a groove for the posterior talofibular ligament, this can be confused with cartilage erosion if the clinician is unaware (Miller et al. 1997).

The inferomedial portion of the talus occasionally appears rarefied on AP radiographs, which can simulate pathological conditions. The normal process of cancellous bone being replaced by fatty tissue can cause this rarifaction, which is clearly demonstrated on CT imaging (Freyschmidt et al. 2003).

A saucer-like depression can be found on the dorsal/superior aspect of the talus distal to the talar dome and proximal to the articulating surface with the navicular (Keats and Anderson 2013). This normal saucer-like depression is in roughly the same location as the talar beak.

There are two similar variations pertaining to the talar neck: one is a normal variant and the other is indicative of pathological processes. Talar beaking occurs when the anterior superior aspect of the talar neck enlarges; this is associated with the pathological process of subtalar coalition. Alternatively, an enlargement more proximal on the dorsum of the talar neck is a normal variant called the talar nose. The talar nose is a physiological response to increased traction on the talus and is commonly found in persons who subject their ankles to heavy stress. The talar nose must also be differentiated from a marginal osteophyte seen in talonavicular osteoarthritis. This osteophyte is located on the superior articular margin of the talus. The talar nose is more proximal than the osteophyte (Freyschmidt et al. 2003).

The talus, like the calcaneus, has a number of accessory ossicles: os talotibiale; os supratalare; os talocalcaneare posterius; os trigonium; os accessorium supracalcaneum; and the talus accessorius.

Os talotibiale

This accessory ossicle is found inferoanterior to the anterior aspect of the medial malleolus and superior to the talus (Keats and Anderson 2013). Tsurata et al. (1981a, b) found the os talotibiale to be present in 0.5% of the population. There have been reports of gender bias, with an incidence of 0.6% in males and 0.3% in females (Tsuruta et al. 1981a, b). The etiology of this accessory bone has been theorized to be a vestige of the processus ascendens, which can be observed in immature birds (Teichert 1955).

This accessory ossicle must be differentiated from bony avulsion fragments of the anterior aspect of the distal tibia (Tsuruta et al. 1981a, b).

Os supratalare (os supertalare, astragalus secondarius)
This accessory ossicle can be found around the talar nose. The same forces that act upon the talar nose (increased traction upon the talus) may also lead to the metaplastic bone formation of this accessory ossicle. This bone has been associated with pain in some individuals, especially in combination with tight shoes and/or heavy loads.

Os supratalare has been incorrectly called "Pirie's bone," but this is more appropriately applied to the os supranaviculare (discussed in the section on navicular) (Freyschmidt et al. 2003). It must be differentiated from an avulsion fracture, which usually presents on projections as a bony shadow that has an irregular or shell-like appearance (Freyschmidt et al. 2003).

Os talocalcaneale posterius
This accessory ossicle can be found between the talus and calcaneus. It is best visualized on a projection similar to the oblique view of the ankle mortise (Anthonsen view). This bone is rarely noted either due to its rarity or the seldom utilization of this projection (Freyschmidt et al. 2003).

Os trigonum (talus secondarius, os intermedium tarsi)
Some misleading names that have been applied to this accessory bone include the talus secondarius, talus accessorius, and os intermedium tarsi (Freyschmidt et al. 2003). On the talus, the posterior process consists of a medial tubercle and the larger lateral tubercle with a groove between for the tendon of the flexor hallucis longus muscle. The os trigonum fits into a recess on the fibular side of the groove. Commonly, this ossicle is connected to the lateral tubercle via a fibrocartilaginous synchondrosis (Mellado et al. 2003). It has also been found to be fused with the lateral tubercle to form a singular process (Freyschmidt et al. 2003).

The os trigonum arises from a separate ossification center for the lateral tubercle of the posterior process of the talus that commonly appears during 8–11 years of age (McDougall 1955; Karasick and Schweitzer 1996). The reported incidence for this accessory ossicle is 1–25% (Bizarro 1921; Tsuruta et al. 1981a, b; Sarrafian 1993; Lawson 1994; Jones et al. 1999).

Due to the location of this accessory ossicle, it is frequently injured when placed under heavy mechanical loads (acute or repetitive). Os trigonum injury is most commonly seen in patient populations with repetitive forced plantar flexion (e.g., ballet dancers, soccer players, etc.). Posterior ankle impingement symptoms result (Freyschmidt et al. 2003). Multipartite os trigonum has been noted (Freyschmidt et al. 2003).

An os trigonum must be differentiated from a fracture of the lateral tubercle (Sheperd's fracture) or medial tubercle (Cedell's fracture) of the posterior process of the talus (Mellado et al. 2003). In avulsion fractures, the fragment is rarely displaced as far from the talus as the os trigonum (Mellado et al. 2003).

Os accessorium supracalcaneum
The os accessorium supracalcaneum is discussed previously in the section on the calcaneus.

Talus accessorius (os subtibiale)
The os subtibiale is discussed in the section on the tibia and fibula.

Navicular
The last ossification center of the tarsus to appear is that of the navicular which appears around 3–5 years of age, earlier in females than males. Most commonly, the navicular is a single ossification center but two centers can be seen. When two ossification centers appear, they are usually stacked dorsal/plantar rather than side-by-side. In rare cases the navicular possesses multiple ossification centers. In these cases, irregular mineralization of the bone is seen and the centers appear flattened (Freyschmidt et al. 2003).

Rarely, a bipartite or supranumary navicular can arise. In these situations, the navicular fragments are commonly divided into tibial and fibular segments of varying size (Mouchet and Moutier 1925; Paal 1933; Watkins 1937; Calausen 1944; Hohmann 1944; Mau 1960). Using CT imaging, a bipartite navicular and fracture can be easily differentiated (Shawdon et al. 1995).

Occasionally, nutrient canals of varying prominence can be seen in the navicular. If the nutrient foramen extends radiographically into the talonavicular joint a gap or defect can be seen, making differentiation from fracture difficult (Freyschmidt et al. 2003).

There are three accessory ossicles associated with the navicular: os supranaviculare, the much more common os tibiale externum, and the very rare os infranaviculare. The os tibiale externum also goes by other names: accessory navicular; os naviculare secondarium; os naviculare accessorium; os scaphoidea accesoria; and prehallux (Schweitzer and Karasick 2000).

Os tibiale externum (accessory navicular)
This ossicle is found proximal to the tuberosity of the navicular. It usually presents in adolescence with an incidence of 4–21% (Keats 1992; Romanowski and Barrington 1992; Sarrafian 1993; Miller et al. 1995; Perdikakis et al. 2011). The prevalence in females is higher (Pfitzner 1896; Mygind 1953; Lawson et al. 1984). A total of 50–90% of cases of os tibiale externum present bilaterally (Mygind 1953; Romanowski and Barrington 1992). Of those with os tibiale externum, 8.8% are bipartite and 5.9% are tripartite (Perdikakis et al. 2011).

This accessory ossicle can be subdivided into 3 types as follows (Freyschmidt et al. 2003).

- Type 1: A sesamoid bone within the tendon of the tibialis posterior. Approximately 2–3 mm in size with no cartilaginous connection to the navicular tuberosity. Most commonly asymptomatic.

- Type 2: This is the most frequent type with a reported incidence of 2–12% (Tsuruta et al. 1981a, b; Keats 1992; Sarrafian 1993; Lawson 1994; Bencardino and Rosenberg 2001; Miller 2002). This form may be an accessory ossification center within the cartilaginous anlage of the navicular. It is typically triangular or heart-shaped and approximately 9 mm × 12 mm in size (Choi et al. 2004). It connects via fibrocartilage or hyaline cartilage to the navicular tuberosity. This type of os tibiale externum is the most likely to be symptomatic. Patients with symptomatic type 2 os tibiale externum are commonly middle-aged women with pain and tenderness localized to the medial aspect of the foot (Coskun et al. 2009). Type 2 can be further subdivided into type 2A and type 2B, which are distinguished radiographically (Sella and Lawson 1987). In subtype 2A the accessory ossicle is connected to the navicular tuberosity by a less acute angle than in type 2B.
- Type 3: This designation is applied to prominent navicular tuberosities and is sometimes referred to as "cornuate navicular" or gorilloid naviuclar. It is considered a fused variant of type 2 (Lawson et al. 1984; Sella et al. 1986; Romanowski and Barrington 1992; Miller et al. 1995; Demeyere et al. 2001).

Of those presenting with os tibiale externum, type 1 represents 30%, type 2 represents 50–60%, and type 3 represents 10–20% (Freyschmidt et al. 2003).

Rarely, the tendon of the tibialis posterior muscle uses the accessory navicular as its primary insertion point, rather than the navicular tuberosity (Tax 1960).

Symptoms often present as tenderness over the medial aspect of the instep of the foot (Lawson 1994; Miller 2002; Fredrick et al. 2005; Coughlin et al. 2006). These symptoms are exaggerated during ambulation and exercise, and by direct pressure from shoes (Nakayama et al. 2005). Occasionally, the presence of this accessory ossicle is associated with flat feet (Coskun et al. 2009).

Os supranaviculare

Other names for this ossicle include dorsal astragaloscaphoid, intertaloscaphoid, Pirie's bone, and dorsal talonavicular ossicles.

This ossicle has the average dimensions of 6 mm × 5 mm × 6 mm (Freyschmidt et al. 2003) and is located on the dorsal aspect of the talonavicular joint, close to the midpoint of the joint. It can be seen on lateral radiographic projections of the ankle or foot as well as sagittal MR images (Mellado et al. 2003). The incidence is 0.5% (Freyschmidt et al. 2003) to 1% (Mellado et al. 2003). Os supranaviculare is reported more commonly in individuals with numerous foot deformities (Freyschmidt et al. 2003).

Eventually, this accessory ossicle may fuse with the rest of the navicular resulting in a bony prominence (Mellado et al. 2003). This ossicle must be differentiated from a detached osteophyte, especially if the patient has osteophytes on the adjacent talus and navicular articulating margins. The os supranaviculare must also be differentiated from cortical avulsion fracture of the navicular (Karasick 1994; Karasick and Schweitzer 1996).

Os infranaviculare

This rare accessory ossicle can be found in the space between the intermediate and medial cuneiform bones and the navicular. This ossicle is not found within the tendon of the tibialis anterior muscle, which would designate it an os paracuneiforme (discussed in cuneiform section). There is often a synfibrosis between this ossicle and the navicular. It is commonly found articulating with both the medial and intermediate cuneiform bones (Kim and Roh 2013). Due to the lack of articulation and the synfibrosis with the navicular, this strongly suggests that the os infranaviculare develops from a secondary ossification center of the navicular (Kim and Roh 2013).

It is possible that this accessory bone is a variant of the os intercuneiforme. This ossicle is also located in close proximity to the same bony structures as the os infranaviculare. The main difference between these two accessory ossicles is that the os infranaviculare articulates with the medial and intermediate cuneiform bones, whereas the os intercuneiforme has no articulations.

Os unci

This accessory ossicle is located on the plantar aspect of the foot between the navicular and cuneiforms 2 and 3 (Freyschmidt et al. 2003). The name of this ossicle may come from the nearby processus uncinatus (McCarthy and Drennan 2009). This accessory ossicle is rare and variable in location.

In addition to the above, there are also unnamed accessory ossicles found distal to the os tibiale externum as well as inferior to the plantar surface of the navicular (Keats 1992; Keats and Anderson 2013).

Cuboid

Ossification of the cuboid usually becomes apparent between the end of gestation and the first month of life. Multiple ossification centers are normally seen that usually unite quickly to form a single center (Freyschmidt et al. 2003).

In the adult cuboid the distal lateral aspect is relatively thin. The tuberosity can be found on the plantar aspect of the cuboid, which is relatively broad and strong. Located between the tuberosity and the distal articulating margin is a deep groove for the peroneus longus tendon which may appear as a notch on the oblique radiographic projection (Freyschmidt et al. 2003).

The proximal articulating surface of the cuboid can exhibit irregularity in contour (Keats and Anderson 2013). A normal variation of the proximal articulating surface of the cuboid, specifically the plantar aspect, is the appearance of a fossa, which can be mistaken for an erosion of the cuboid (Keats and Anderson 2013).

The cuboid has two accessory ossicles associated with it: the os peroneum and the os cuboideum secondarium.

Os peroneum (cuboid accessorium)

The os peroneum is an accessory sesamoid bone found within the tendon of the peroneus longus at the lateral plantar edge of

the cuboid in the groove for the tendon. It can be cartilaginous or osseous, exhibiting varying degrees of ossification (Le Minor 1987). Of those with os peroneum a fully ossified os peroneum occurs at a rate of 20%, whereas less than fully ossified os peroneum are found at a rate of 75% (Coughlin et al. 2006). The shape is round to oval with smooth margins that occasionally pseudoarticulate (synchondroses, fibrocartilaginous bridge) with the cuboid. Occasionally the os peroneum can be found further dorsal and more proximal; in these instances, it can form radiographic articulation with the calcaneus (Freyschmidt et al. 2003).

The incidence of os peroneum within the population varies over the range 10–30% (Siecke 1964; Mains and Sullivan 1973; Burton and Altman 1986; Le Minor 1987; Crain and el-Khoury 1989; Bessette and Hodge 1998; Sarin et al. 1999; Muehleman et al. 2009). In a histoembryologic study, the incidence was found to be 0.4% (Trolle 1948). Females present more frequently with an os peroneum than males.

The size, number, and incidence increases with age (Freyschmidt et al. 2003). Within the os peroneum population, the accessory ossicle is found to be multipartite in 25–30% of cases (Bianchi et al. 1991; Bessette and Hodge 1998).

Os cuboideum secondarium (secondary cuboid ossicle)

This ossicle is typically located between the calcaneus, talus, cuboid, and navicular (Dwight 1907, 1910; Holland 1921; Biermann 1922; Watkins 1937; Zimmer 1938; Trolle 1948; Jones 1949). There have been reported cases where this accessory bone is in different locations. In one case it was fused with the cuboid while in the other it was fused with the navicular; both fusions were found articulating with the talus (Pfitzner 1896). Also of note is that this accessory ossicle was found bisecting the flexor digitorum brevis tendon (Gaulke and Schmitz 2003). There is a 1–3% incidence in adolescents (Hoerr et al. 1962).

Coalitions of the foot

Tarsal coalitions

The tarsal bones can form coalitions that can be fibrous, cartilaginous, or bony (Bohne 2001). The currently accepted etiological theory on tarsal coalitions was posed by Leboucq in 1890. It is felt to be due to failure of segmentation of the mesenchyme of two or more of the bones of the hindfoot during embryological development (Bohne 2001). Tarsal coalitions appear to present with autosomal dominant inheritance (Wray 1963; Leonard 1974).

Tarsal coalitions are reported to occur with a total incidence of c. 1% (Leonard 1974; Snyder et al. 1981; Stormont and Peterson 1983; Nalaboff and Schweitzer 2008), however, there have been reports of incidence as high as 8.8% (Ruhli et al. 2003). It does not appear that tarsal coalitions present with a racial bias (Rankin and Baker 1974) and they are bilateral 50–80% of the time (Conway and Cowell 1969; Leonard 1974; Rankin and Baker 1974; Stormont and Peterson 1983; Mosier and Asher 1984). Calcaneonavicular coalitions have a higher rate of bilaterality than other coalitions (Conway and Cowell 1969; Leonard 1974; Rankin and Baker 1974; Stormont and Peterson 1983; Mosier and Asher 1984).

Some studies reveal a bias towards males (Wechsler et al. 1994), other studies show a bias towards females (Ruhli et al. 2003), and others have shown no gender bias (Pfitzner 1896; Leonard 1974).

The two most common tarsal coalitions are talocalcaneal and calcaneonavicular coalitions, while far more rarely encountered coalitions are the talonavicular, calcaneocuboid (Bohne 2001), and cubonavicular (Piqueres et al. 2002). There is differing opinion as to whether calcaneonavicular or talocalcaneal coalitions are more common. Some studies have found a higher incidence for calcaneonavicular coalitions (Stormont and Peterson 1983; Ruhli et al. 2003; Solomon et al. 2003; Nalaboff and Schweitzer 2008; Case and Burnett 2012). Other studies have found higher incidence rates for talocalcaneal coalitions (Mosier and Asher 1984) while there have been reports of comparable incidences for both coaltions (Kulik and Clanton 1996). Some patients may have more than one tarsal coalition (Clarke 1997).

Ossification within the tarsal coalition is age-dependent and leads to rigidity within the joint (Jayakumar and Cowell 1977). The usual presentation of tarsal coalition is pain around the ankle or hindfoot and frequent ankle sprains. Patients commonly present in the early to mid-teen years, but presentation has occurred after and has been reported within the 4th decade (Bohne 2001). Once a patient has reached their 20s it is common for the tarsal coalition to be asymptomatic (Cowell 1972); symptomatic patients after this age are infrequently encountered (Bohne 2001). Subtalar motion is decreased in hindfoot coalitions. Tenderness may be present upon palpation around the coalition.

MRI better depicts fibrocatilaginous coalitions while CT imaging yields good bony detail and suffices in most cases (Masciocchi et al. 1992; Wechsler et al. 1994).

Talocalcaneal (subtalar) coalition

This coalition generally occurs at the middle facet of the subtalar joint at the sustentaculum tali. If the coalition is large, the posterior facet can be altered presumably due to the decreased motion (Case 2012). True involvement of the posterior facet is less commonly seen (Conway and Cowell 1969; Masciocchi et al. 1992).

Even though all types of tarsal coalition are reported with a total incidence of c. 1%, there have been reported incidence rates of talocalcaneal coalitions as high as 4% (Sijbrandij et al. 2002). Talocalcaneal coalitions represent 22.8–25.7% of all tarsal coalitions (Nalaboff and Schweitzer 2008). The connection between the talus and the calcaneus is cartilaginous in 30.4%, fibrous in 30.4%, and osseous or partially osseous in 39.1% of cases (Nalaboff and Schweitzer 2008).

The talocalcaneal coalition tends to ossify and become symptomatic during the ages of 12–16 years (Jack 1954; Jayakumar

and Cowell 1977; Kulik and Clanton 1996). A prominence below the tip of the medial malleolus is a strong indication for this tarsal coalition (Bohne 2001).

Talocalcaneal coalition can be visualized on an axial x-ray of the subtalar joint, the Harris heel view, which can be difficult to obtain (Bohne 2001). The middle facet of the sustentaculum tali will show either an upward or downward tilt, the "drunken waiter sign" (Nalaboff and Schweitzer 2008). However, CT or MRI are better at delineating this coalition.

Calcaneonavicular coalition

Even though all types of tarsal coalition are reported with a total incidence of c. 1%, there have been reported incidence rates of calcaneonavicular coalitions as high as 5.6% (Lysack and Fenton 2004). This coalition was found to represent 71.4–77.2% of tarsal coalitions (Nalaboff and Schweitzer 2008).

The connection between the calcaneus and the navicular is cartilaginous in 42.3%, fibrous in 55.1%, and osseous in 2.6% of cases (Nalaboff and Schweitzer 2008). Calcaneonavicular coalitions tend to ossify and become symptomatic during the ages of 8–12 years (Jack 1954; Jayakumar and Cowell 1977; Kulik and Clanton 1996; Vincent 1998).

The calcaneonavicular coalition leads to alterations in the surface anatomy of the bones involved. The anterior process of the calcaneus is elongated yielding the "anteater sign" on lateral radiographs, while the navicular bone has significant alterations to its plantar surface (Case 2012). This coalition can be best seen on oblique radiographs (Bohne 2001).

Talonavicular coalition

Coalition between the talus and the navicular bones typically occurs at the articulating joint between the two bones and has been found to result in a large flattened square "talar head," often with some loss of the medial arch (Keats and Anderson 2013). This tarsal coalition is commonly symptomatic due to the central role of the talonavicular joint, which changes the foot from a rigid lever to a shock absorber during gait, and is the most important joint of the triple joint complex (talocalcaneonavicular joint) (Bordelon 1993; Astion et al. 1997; Bohne 2001). Excessive stresses are placed upon the other hindfoot joints when talonavicular motion is restricted. Talonavicular coalitions can be best seen on the lateral radiograph (Bohne 2001).

Cubonavicular coalition

This coalition can lead to substantial changes in the surface anatomy of the bones involved. The two bones typically connect between the navicular's plantar beak and the superomedial aspect of the cuboid, where the bones lie in closest proximity (Pfitzner 1896; Dwight 1907; Johnson et al. 2005; Case 2012). This represents 1% of all tarsal coalitions (Harris 1965). Cubonavicular coalition causes restriction of eversion and plantar flexion (Piqueres et al. 2002). Although oblique, anteroposterior, and axial projections can be used to visualize this tarsal coalition, CT is superior to plain radiographs (Piqueres et al. 2002).

Calcaneocuboid coalition

This tarsal coalition is rarely reported, rarely symptomatic, and usually does not cause dysfunction (Conway and Cowell 1969; Craig and Goldberg 1977). The coalition is located between the cuboid facet of the calcaneus and the calcaneal facet of the cuboid (Case 2012).

Naviculocuneiform coalition

This coalition can be found between the first cuneiform (plantar part of the navicular facet) and the navicular (plantar part of first cuneiform facet) (Case 2012). Incidence rates are low and coalition between the navicular and the other two cuneiform bones is even rarer (Burnett and Case 2005; Case 2012).

Studies have indicated a racial bias with South Africans and Japanese presenting more frequently than Europeans (Kumai, Takakura et al. 1998; Burnett and Case 2005).

Cuneocuboid coalitions

This rare coalition is typically between the plantar aspect of the cuboid and the lateral aspect of the third cuneiform (Case 2012).

Cuneiform bones

Of the three cuneiforms, the largest is the medial (first) cuneiform while the smallest is the middle (intermediate or second) cuneiform (Piersol et al. 1919).

Medial (first) cuneiform

The medial cuneiform develops from two separate ossification centers, a dorsal and plantar center. Normally these two ossification centers coalesce in late embryologic maturation into a single bone (Burnett and Case 2011). If the two ossification centers fail to fuse, a bipartite first cuneiform bone (*os cuneiforme I bipartitum*) results.

Bipartite medial cuneiform (os cuneiforme i bipartitum)

The reported incidence of bipartite medial cuneiform is between 0.33% (Gruber 1875) and 0.5% (Pfitzner 1896) in the adult population. Bipartite medial cuneiform showed an incidence of 2.4% in a histoembryologic study (Trolle 1948). Some authors note bipartite medial cuneiform to be common bilaterally (Dellacorte et al. 1992; Elias et al. 2008) while others report bilaterality rates of 27–33% (Gruber 1864, 1877; Pfitzner 1896; Barlow 1942).

The segmentation of the bipartite first cuneiform is usually horizontal and yields a large dorsal fragment (*os cuneiforme I dorsale)* and a smaller plantar fragment (*os cuneiforme I plantare*). When both fragments are amassed, their volume slightly exceeds that of an undivided medial cuneiform (Bizarro 1921; Biermann 1922; Friedl 1924; Mouchet and Moutier 1925; Barclay 1932; Boker 1936; Heidsieck 1936; Watkins 1937; Lichte 1941; Barlow 1942; Jones 1949; Smith et al. 1984; Dellacorte et al. 1992; O'Neal et al. 1995; Azurza and Sakellariou 2001). The dorsal segment articulates distally with the dorsal aspect of the first metatarsal base and proximally with the navicular. The

dorsal fragment's lateral surface articulates with the base of the second metatarsal and the middle cuneiform. The plantar fragment articulates proximally with the navicular and articulation varies with the intermediate cuneiform (Smith 1866; Gruber 1877; Bizarro 1921; Biermann 1922; Friedl 1924; Mouchet and Moutier 1925; Barclay 1932; Boker 1936; Heidsieck 1936; Watkins 1937; Lichte 1941; Barlow 1942; Jones 1949; Smith et al. 1984; Dellacorte et al. 1992; O'Neal et al. 1995; Azurza and Sakellariou 2001).

The bipartite medial cuneiform also differs with respect to vertical height. It has been found that in bipartite medial cuneiform both the dorsal and plantar aspects of the fragments show an increase of 5–8 mm in vertical height (Gruber 1877; Barlow 1942). While this amount may not appear great, it is equivalent to a vertical increase of 14–23% in the average adult American male (Harris 2009). The dorsal and plantar fragments are commonly held together by cartilaginous or fibrous tissue that may ossify with time (Anderson 1987; Burnett and Case 2011). With increasing age, the connection between the two fragments tends to be more fibrous with cartilaginous bridges being found in younger individuals (Kumai et al. 1998).

This variant can be visualized on an oblique X-ray, CT scan or MRI (Dellacorte et al. 1992; O'Neal et al. 1995; Azurza and Sakellariou 2001; Chiodo et al. 2002; Elias et al. 2008). Using a sagittal MR projection, a characteristic "E sign" has been described in cases of bipartite medial cuneiform by Elias et al. (2008) and Burnett and Case (2011).

Another normal variant of the medial cuneiform is an accessory ossification center. This commonly appears medial to the tip of the medial cuneiform (Keats and Anderson 2013). If this center fails to fuse with the medial cuneiform, it can give rise to an unnamed accessory ossicle (Keats and Anderson 2013). This unnamed accessory ossicle is distinct from an os paracuneiforme because it is not located within the tendon of the tibialis anterior muscle.

Intermediate (second) cuneiform

The intermediate cuneiform develops from a single ossification center that appears around the age of 4 years (Piersol et al. 1919). A normal variant pertaining to the intermediate cuneiform involves its lateral surface which articulates with the lateral cuneiform; rarely, a small facet can be found at the plantar distal angle of the bone (Piersol et al. 1919).

Lateral (third) cuneiform

This bone begins ossification within the first year of life (Piersol et al. 1919). At the distal dorsal angle of the bone, there may or may not be a facet for the fourth metatarsal (Piersol et al. 1919).

Cuneiform coalitions

There are two types of coalitions that can present between the cuneiform bones: between cuneiforms I and II and between cuneiforms II and III. These intercuneiform coalitions are extremely rare, with intercuneiform II–III being slightly more prevalent than intercuneiform I–II (Pfitzner 1896; Sarrafian 1993). Typical coalitions are located between the plantar 1/3 to 1/2 of the bones, although coalition locations have been found elsewhere (Case 2012).

Cuneiform accessory ossicles

The accessory ossicles associated with the cuneiforms include the os paracuneiforme, os intercuneiforme, os cuneo-I metatarsale-I plantare, os cuneo-I metarsale-II dorsale, and os intermetatarseum.

Os paracuneiforme

This sesamoid ossicle is partially or completely located within the anterior tibial tendon near the naviculocuneiform joint on the medial aspect of the foot (Morrison 1953). It has been reported to have a variable location. Some studies have found the os paracuneiforme to lie in a hollow on the medial side between the navicular and medial cuneiform bones (Dwight 1902; Cameron 1923; Holland 1928; Burman and Lapidus 1931). However, the os paracuneiforme has also been found lying against and articulating with the middle portion of the medial cuneiform (Carlier 1924; Morrison 1953). In a histoembryological study it was found with a prevalence of 13% (Trolle 1948).

Os intercuneiforme

The location of this ossicle is between the first and second cuneiforms just distal to the navicular on the dorsum of the midfoot (Coughlin et al. 2006). It typically presents as triangular in shape. Incidence rates as high as 1–2% have been reported (Geist 1914; Hoerr et al. 1962), whereas other studies have found lower incidence rates of 0.026–0.029% (Prescher 1997; Tsuruta et al. 1981a, b).

Os cuneo-I metatarsale-I plantare

This accessory ossicle occurs on the plantar aspect of the foot at the base of the first metatarsal (O'Rahilly 1953). Typically, it articulates with the first cuneiform and the plantar base of the first metatarsal. Estimates for the size of this rare ossicle are only cited as "the size of a cherry stone" (Trolle 1948). It can best be visualized on the lateral oblique projections, whereas in the dorsoplantar projection the ossicle is difficult to visualize (Coughlin et al. 2006).

Os cuneo-I metatarsale-II dorsal

This rare ossicle is located at the dorsal aspect of the articulation between the second metatarsal and intermediate cuneiform (Schoen 1935). It is usually wedge-shaped and the size has been described as being equivalent to a "peppercorn" (Trolle 1948).

Os intermetatarseum

This accessory ossicle is found lying dorsal to the tarsometatarsal border between the base of the first and second metatarsals and the dorsal distolateral corner of the first cuneiform (Case

et al. 1998). It is usually spindle shaped, with its base at the distal corner of the medial cuneiform and tapering distally to project between the first and second metatarsal (Coughlin et al. 2006). It can also be round (Mellado et al. 2003).

The reported incidences of os intermetatarseum differ depending upon the method of investigation. Radiographic studies report incidences of 0.2–6.8% (Miller 2002), whereas dissection studies have reported incidence rates of 1.2–12.5% (Dwight 1907; Shands and Wentz 1953; Miller 2002; Mellado et al. 2003). There have been reports of multipartite os intermetatarseum (Coughlin et al. 2006; Keats and Anderson 2013). Rates of bilaterality are 33% (Case et al. 1998).

This ossicle can be divided into three subtypes based upon its relationship to the surrounding bony structure: freestanding; articulating; and fused. Freestanding os intermetatarseum do not articulate with surrounding bones, nor do they form osseous connections. Articulating os intermetatarseum can be found articulating with any of the three surrounding bones (first metatarsal, second metatarsal, medial cuneiform). The fused ossicle is the rarest subtype of os intermetatarseum and presents with a variable fusion pattern to the surrounding bones. The fused subtype of os intermetatarseum is also referred to as first or second metatarsal bone spurs or first cuneiform bone spurs (Case et al. 1998).

Os intermetatarseum can be symptomatic. Tenderness can be elicited upon palpation of the dorsum of the midfoot at the first intermetatarsal space due to the compression of the superficial and deep peroneal nerves (Miller 2002). Studies have suggested that os intermetatarseum may be associated with hallux valgus deformity (Henderson 1963; Lawson 1994).

This accessory ossicle should be differentiated from fractures of the second metatarsal, specifically Lisfranc fracture/dislocations. This type of fracture occurs after violent forced plantar flexion and rotation, such as in motor vehicle accidents (Mellado et al. 2003). If significant soft tissue swelling is accompanied by bony malalignment then a Lisfranc injury is probable (Karasick 1994).

There have been reported cases of os intermetatarseum IV between the fourth and fifth metatarsal bones (Trolle 1948).

Metatarsals

During the third month of fetal development a primary ossification center appears within the shaft of each metatarsal. The epiphyseal ossification centers typically appear at 3 months of age. Fusion of the epiphysis with the shaft generally begins at 15 years of age (Freyschmidt et al. 2003). The metatarsals typically have one epiphysis. The epiphyses of metatarsals 2–5 are located at the distal end, whereas the first metatarsal epiphysis is proximal. It is considered a normal variant if metatarsal 1 demonstrates irregularity and notching at its distal end (Freyschmidt et al. 2003; Keats and Anderson 2013). This can give the appearance of a pseudoepiphysis of the metatarsal head. Accessory and multipartite epiphyseal centers of the metatarsals can be seen (Freyschmidt et al. 2003; Keats and Anderson 2013). This variant is common in cleidocranial dysostosis (Freyschmidt et al. 2003).

Occasionally, an accessory ossification center can be seen at the head of the first metatarsal (Keats and Anderson 2013). There are a couple of normal variants associated with the first metatarsal head. One of these variants is a small epiphyseal spur projecting lateral and proximal (Keats and Anderson 2013). Another is a dorsofibular process, an osteophyte-like bony outgrowth projecting distal and lateral from the head of the first metatarsal (Fischer 1988).

The apophysis at the tuberosity of the fifth metatarsal usually appears during ages 10–15 years (12–15 years in males, 10–14 years in females) (Freyschmidt et al. 2003). It can appear earlier during the ages of 6–8 years, but this is rare. This apophysis may have multiple ossification centers (Keats and Anderson 2013). It is normal for this apophysis to show irregular lucencies along the cartilaginous plate, radiographically (Freyschmidt et al. 2003) and irregular mineralization (Keats and Anderson 2013). This apophysis fuses around the age of 25 years (Freyschmidt et al. 2003). The tuberosity of the fifth metatarsal provides the attachment for the tendon of the peroneus brevis. Radiographically, the fifth metatarsal tuberosity possesses horizontally oriented trabeculae which can be mistaken for a fracture (Keats and Anderson 2013).

The metatarsals vary in size, the first metatarsal being the shortest and the second being the longest metatarsal. The fifth metatarsal has a slightly bowed shaft on both lateral and dorsal/plantar views. The shape and length of metatarsals 2–4 are basically the same, which can be helpful in the diagnosis of brachymetatarsia (Freyschmidt et al. 2003). On dorsoplantar radiographs the lateral contour of the first metatarsal can appear irregular due to superimposition of the dorsal and plantar aspects of its concave lateral wall (Freyschmidt et al. 2003).

In mature metatarsals there are notches present in the proximal lateral aspects (Keats and Anderson 2013), which are most prominent in metatarsals 2–4 (Freyschmidt et al. 2003). These notches are occupied by ligaments or are cartilage-covered surfaces. Additionally, both medial and lateral fossae at the base of metatarsals 2–4 are normal variants (Keats and Anderson 2013). Dorsoplantar radiographs of the metatarsals may give the appearance of false fracture lines due to Mach effects (Freyschmidt et al. 2003), which cause illusory dark or light bands found at abrupt changes in lucency (Wallis and Georgeson 2012). These false fracture lines are most prominent proximally on metatarsals 2–4 (Freyschmidt et al. 2003).

The metatarsal heads can manifest normal variants. The "great knob of Keats" is enlargement and knobbing of the head of the first metatarsal (Keats and Anderson 2013). The "lesser knob" is similar and found at the head of the fifth metatarsal (Keats and Anderson 2013). Another normal variant of the head of the fifth metatarsal is the presence of a lucency in the medial aspect, which should not be mistaken for an erosion (Keats and Anderson 2013). If the head of a metatarsal has a flat configuration and a resulting widening of the joint space, this is a normal variant and

should not be associated with aseptic necrosis of the metatarsals or Freiberg's disease; (Jensen and de Carvalho 1987). This normal variant can occur in a single metatarsal or simultaneously in multiple metatarsal heads (Keats and Anderson 2013).

Nutrient foramina of the metatarsals are typically located around midway along the shaft on the medial aspect of the bone and commonly course in a lateral and distal path. These nutrient foramina can mimic fractures (Freyschmidt et al. 2003).

There are several accessory ossicles that are associated with the metatarsals. These include os vesalianum pedis, os intermetatarseum, os cuneometatarsale I plantare, cuneometatarsale II dorsale, os unci, as well as persistent apophysis of the tuberosity of the fifth metatarsal.

Os vesalianum pedis

This small, rare ossicle can be found proximal or adjacent to the fifth metatarsal tuberosity within the peroneus brevis tendon at its insertion (Smith et al. 1984; Mellado et al. 2003; Freyschmidt et al. 2003). Reported incidence varies over the range 0.1–1% (Geist 1914; Heimerzheim 1924; Dameron 1975; Mellado et al. 2003). This accessory ossicle has been found to be as large "as an almond" (Trolle 1948). There are cases where the os vesalianum pedis is fused with the base of the fifth metatarsal (Harrison and Keats 1980).

The differential diagnosis includes the apophyseal ossification center, os peroneum, fracture, nonunion, and ununited apophysis of the fifth metatarsal base. The os vesalianum pedis is present just proximal to the tip of what would be a fully developed fifth metatarsal tuberosity (Coughlin et al. 2006).

Persistent apophysis of the tuberosity of the fifth metatarsal

This variant is an accessory ossicle that "completes" the shape of the tuberosity of the fifth metatarsal (Freyschmidt et al. 2003).

Sesamoid bones of the pedal phalanges/forefoot

Typically, there are four sesamoid bones found within the human foot (two found on the plantar aspect of the first metatarsal, and one each at the heads of the second and fifth metatarsals). It is not abnormal to find sesamoid bones below any of the metatarsal heads as well as the first and second distal interphalangeal joints (Freyschmidt et al. 2003; Keats and Anderson 2013). These sesamoid bones begin as cartilaginous centers that appear as early as the 12th week in utero. Ossification of these centers typically occurs after 8 years of age, with ossification completed around the age of 12 (Freyschmidt et al. 2003).

The appearance of the hallucal metatarsophalangeal (mtp) sesamoids is considered normal anatomy, while the fifth mtp sesamoids are considered normal variants. The medial fifth mtp sesamoid bone has an incidence of 5.5% while the lateral fifth mtp sesamoid has a reported incidence of 6.2% (Piersol et al. 1919).

Hallucal sesamoid bones

There are two sesamoid bones found in the first mtp joint which are important in the normal function of the hallux and are defined as either the medial (tibial) or the lateral (fibular) hallucal sesamoid (Coughlin et al. 2006). They are contained within the double tendon of the flexor hallicis brevis on the plantar aspect of the mtp joint (Coughlin et al. 2006). The dorsal aspect of the sesamoids articulates with the plantar aspect of the first metatarsal head. The sesamoids lie on the medial and lateral aspect of a crista or inter-sesamoid ridge on the plantar aspect of the first metatarsal (Coughlin et al. 2006; Freyschmidt et al. 2003). These sesamoid bones are stabilized via the plantar plate, the collateral ligament, sesamoid ligaments, joint capsule, and the plantar aponeurosis. The location of the sesamoids changes with changing position of the metatarsophalangeal joint. In a standing position the sesamoids are proximal to the metatarsal head, whereas when the hallux is dorsiflexed the sesamoids move distal (Coughlin et al. 2006).

The lateral sesamoid is located slightly more proximal while the medial sesamoid is larger in size (Kenwenter 1936; Freyschmidt et al. 2003). The medial sesamoid averages 9–11 mm wide × 12–15 mm long, while the lateral sesamoid has the average dimensions of 7–9 mm wide × 9–10 mm long (Coughlin et al. 2006). The lateral sesamoid can best be visualized on the lateral oblique view while the medial sesamoid is best seen on the medial oblique radiographs (Coughlin et al. 2006).

Ossification of these sesamoids typically occurs during the ages of 6–7 years. These sesamoid bones ossify from multiple centers, and multipartite sesamoids have been reported (Kenwenter 1936). The incidence of bipartite hallucal sesamoids is 6–33% (Burman and Lapidus 1931; Kenwenter 1936; Rowe 1963; Dobas and Silvers 1977; Munuera et al. 2007; Freyschmidt et al. 2003). The incidence of bipartite medial hallucal sesamoid is higher than for the lateral sesamoid (Burman and Lapidus 1931; Kenwenter 1936; Dobas and Silvers 1977; Jahss 1981). The reported incidence of bipartite medial (tibial) hallucal sesamoid falls within the range 7.2–30.6% (Burman and Lapidus 1931; Kenwenter 1936; Dobas and Silvers 1977). Bipartite lateral sesamoid has an incidence of 0.6% (Burman and Lapidus 1931) to 2.5% (Dobas and Silvers 1977). Bipartite hallucal sesamoids are more common in females than males (Freyschmidt et al. 2003). Multipartite hallucal sesamoids are bilateral in 13–34% of cases (Munuera et al. 2007; Freyschmidt et al. 2003).

The medial sesamoid is multipartite (2–4 fragments) much more commonly than the lateral sesamoid, which is rarely found other than bipartite (Coughlin et al. 2006). Inge and Ferguson (1933) found that bipartite hallucal sesamoids had articular cartilage between them. The presence of articular cartilage between the osseous fragments predisposes to fracture or disruption of the sesamoidal syndesmosis with minimal trauma (Coughlin et al. 2006). Kenwenter (1936) noted that bipartite sesamoids fractured with much less force than unipartite sesamoids under experimental conditions (Coughlin et al. 2006).

Differentiation between symptomatic bipartite hallucal sesamoid and fracture can be difficult. Partite sesamoid bones are normally larger than intact counterparts and reassembled fracture fragments (Freyschmidt et al. 2003). Additionally, axial

radiographs and CT scans have been shown to be helpful in differentiating between fracture and partite sesamoid. A bone scan can be helpful in the differentiating process, especially if chronic trauma is suspected (Richardson 1987; Freyschmidt et al. 2003), although there are mixed results within the literature regarding bipartite sesamoid behavior on bone scan (Van Hal et al. 1982; Klinmann et al. 1983). MRI can be of further use (Kulemann et al. 2010).

The bipartite sesamoid occupies a larger area than that occupied by the unipartite sesamoid (Freyschmidt et al. 2003). This tends to produce differences in orientation of the surrounding bone structure. Studies have found a higher prevalence of bipartite hallucal sesamoids in patients with hallux valgus (Weil and Hill 1992; Munuera et al. 2007). The presence of bipartite medial sesamoid was found significantly higher in hallux valgus deformity while bipartite lateral (fibular) hallucal sesamoid was not significantly different between feet with and without hallux valgus deformity (Munuera et al. 2007). These results indicate that a relationship exists between hallux valgus and bipartite medial sesamoid, although causality has not been established.

Congenital absence of hallucal sesamoid bone(s)

Congenital absence of both medial and lateral hallucal sesamoids is a rare occurrence (Jahss 1981; Leventen 1991; Le Minor 1999). Congenital absence of the medial sesamoid usually presents as an incidental finding in asymptomatic patients. However, congenital absence of the medial sesamoid can lead to clawing of the hallux and the development of hallux valgus deformity (Mann and Coughlin 1993). This is further supported by the fact that patients who have undergone a medial sesamoidectomy can develop clawing of the hallux or hallux valgus deformity (Zinsmeister and Edelman 1985; Goez and DeLauro 1995). Previous reports of congenital absence of hallucal sesamoid(s) have been linked to ossification errors (Zinsmeister and Edelman 1985; Jeng et al. 1998).

Pedal phalanges

The ossification of the distal phalanx of the hallux appears during the ninth week in utero. At around 11–12 weeks in utero the ossification centers of the distal phalanges of the lesser toes will appear. Ossification of the proximal phalanges occurs at around 14 weeks and the middle phalanges around the fourth month in utero. The epiphyses of the proximal phalanges appear between 5 months and 2 years of age. The middle phalangeal epiphyses appear between 9 months and 2 years of age. The epiphysis of the distal phalanx of the hallux appears in the first two years of life. The phalangeal physes will fuse earlier in females (15–17 years) than males (17–23 years) (Freyschmidt et al. 2003).

There are a number of normal variants associated with the pedal phalangeal epiphyses. Occasionally the epiphysis is broader along its medial or lateral aspect (Freyschmidt et al. 2003). In the proximal phalanges, dense and flat epiphyses can be seen as a normal variant (Freyschmidt et al. 2003; Keats and Anderson 2013). A longitudinal cleft may be seen radiographically, which may give the appearance of a bipartite epiphysis (Harrison and Keats 1980). True bipartite epiphysis is also seen (Freyschmidt et al. 2003). Epiphyseal ossification centers may be absent from the pedal phalanges, particularly in the middle phalanx of the fifth toe (Freyschmidt et al. 2003).

Another normal variant of the pedal phalangeal epiphyses is the presence of cone-shaped epiphyses. Cone-shaped epiphyses are typically found bilaterally and most commonly in the proximal phalanges of toes 2–4. They are rarely found in the middle phalangeal epiphyses or the fifth (Freyschmidt et al. 2003). These may be due to developmental disturbances of growth in the central portion of the epiphysis.

In the mature foot, the proximal phalanges show a more uniform shape than the middle and distal phalanges (Freyschmidt et al. 2003). Commonly, the proximal phalanx has a spindle-shaped configuration with a widening of the shaft near the base, which has been referred to as a "diaphyseal cuff" (Freyschmidt et al. 2003). The diaphyseal cuff presents with varying rates of incidence for each toe. Dihlmann et al. (1972) reports that "diaphyseal cuffing" occurs with an incidence of 80% within toe 5, 90% in toe 4, 85–95% in toe 3, 90% in toe 2, and 20% in the hallux (Freyschmidt et al. 2003).

There is also disparity between the size of the medial and lateral aspects within the base. The proximal phalanx of the hallux has a more prominent lateral base; however, this pattern is reversed for the proximal phalanges of the lesser toes. The basal expansion of the proximal phalanges can be mistaken for fracture callus or other pathologies (Freyschmidt et al. 2003).

The middle phalanges are much more variable in size and shape. Occasionally, the middle phalanges may be almost rectangular in shape due to lack of a waist. Additionally, the toes can have an angled appearance which is caused by the beveled ends of the shaft (Freyschmidt et al. 2003).

The distal phalanges can possess a pointed contour as a normal variant (Keats and Anderson 2013).

The middle and distal phalanges of the fifth will be fused in 25–33% of cases (Ellis et al. 1968; Freyschmidt et al. 2003; Keats and Anderson 2013). While synostosis of the middle and distal phalanges is common and considered normal in the fifth toe, it is considered anomalous in other toes (Freyschmidt et al. 2003).

The medial base of the distal phalanx of the hallux commonly possesses an exostosis-like bony prominence protruding from the medial and plantar aspect (Freyschmidt et al. 2003). Appearance occurs after closure of the physeal plate of the distal phalanx and is believed to be reactive to repetitive forces; incidence of this prominence is 88.5% (Lee et al. 1992). This normal variant can best be seen on dorsoplantar radiographs.

The normal variants of the pedal phalanges include two accessory ossicles: medial os paraarticulare and lateral os paraarticulare.

Hallucal interphalangeal sesamoid

The hallux may possess a sesamoid bone in the proximal interphalangeal joint. It is debatable as to whether this ossicle is

normal (Suwannahoy et al. 2012) or an accessory ossicle (Roukis and Hurless 1996; Davies and Dalal 2005).

This ossicle has two facets that articulate with the head of the proximal phalanx and a single facet that articulates with the base of the distal phalanx. Stabilization of this ossicle within the interphalangeal joint is accomplished by the plantar capsule with contributions from the flexor hallucis longus. The ossicle is separated from the flexor hallucis longus tendon via a clearly defined bursa (Davies and Dalal 2005).

The shape of this ossicle is pyramidal with an oval base plantarward. The average size is 3.4 mm (width) × 6 mm (length) × 2.5 mm (height) (Suwannahoy et al. 2012). The interphalangeal hallucal sesamoid has been found to be bipartite in 4–20% of cases (Davies and Dalal 2005; Suwannahoy et al. 2012).

The currently accepted etiological theory on the hallucal interphalangeal sesamoid was posed by Roukis and Hurless (1996). The proximal and distal hallucal phalanges develop between the 11th and 15th week in utero at the same time as the hallucal interphalangeal sesamoid (McCarthy et al. 1986; Moore 1988; Sarrafian 1993). It appears that the hallucal interphalangeal sesamoid arises from the rudiment of the lost middle phalanx of the hallux (Roukis and Hurless 1996).

There is a wide range (4.3–96%) of incidence reported (Piersol et al. 1919; Trolle 1948; Yanklowitz and Jaworek 1975; Masaki 1984). However, it has been proposed that this bone may present with a racial bias, with incidences of 91–96% in studied Japanese populations (Masaki 1984; Miki et al. 1988), 72.5% in studied British Caucasian populations (Davies and Dalal 2005), 88% in studied Thai populations (Suwannahoy et al. 2012), and 13% in studied American populations (Burman and Lapidus 1931; Suwannahoy et al. 2012). However, this wide range of incidences may be partly due to radiographic technique (Yanklowitz and Jaworek 1975; Davies et al. 2003). When present this ossicle is bilateral in 94.0% of individuals (Yanklowitz and Jaworek 1975).

This ossicle can cause hyperextension of the hallucal interphalangeal joint and commonly presents with a hyperkeratotic lesion on the plantar aspect of this joint (Sharon 1977; McCarthy et al. 1986; Valinsky et al. 1989; Genakos 1993).

Foot anomalies

Polydactyly

Polydactyly is defined as preaxial (along the tibial aspect of the foot), postaxial (fibular aspect), or central. It can occur as a result of autosomal dominant expression or as a manifestation of a syndrome with other congenital anomalies (Kapoor and Johnson 2011). Foot polydactyly is often associated with polydactyly in the hand. Reported incidences of polydactyly in both hands and feet are 0.03–0.1% (Woolf and Myrianthopoulos 1973), while isolated foot polydactyly has been reported to occur with an incidence of 0.003–0.105% (Woolf and Myrianthopoulos 1973). Preaxial polydactyly of the foot occurs with an incidence of 0.008% while postaxial polydactyly occurs in 0.124–1.353% of cases (Woolf and Myrianthopoulos 1973). Incidences of the three subtypes within the polydactyly population are 6% central, 84% postaxial, and 8% preaxial (Coppolelli, Ready et al. 1991). Although polydactyly shows no gender bias, it does show a bias for non-Caucasians (Woolf and Myrianthopoulos 1973). Polydactyly presents bilaterally with an incidence of 50% and, within the bilateral polydactyly population, 62% present symmetrically (Temtamy and McKusick 1969).

A succinct and straightforward pedal polydactyly classification system has been proposed by Seok et al. (2013) that encompasses syndactylism, angulation, and metatarsal involvement of the supranumerary digit (SAM classification). The SAM classification was developed specifically for pedal polydactyly and clarifies areas of ambiguity in previous pedal poldactyly classification systems (Wassel, Stelling and Turek, and Hirase classification schemes).

Syndactyly

The term syndactyly stems from the Greek words *syn* (together) and *dactyly* (digit), and the term is applied to conditions where the digits fail to fully separate. This condition is due to a failure of apoptosis of the interdigital mesenchyme during gestation (Kozin 2001; Canale and Beaty 2008).

Syndactyly is designated as complex or simple. Simple syndactyly has only soft tissue involvement while complex syndactyly is found to have both soft tissue and bony fusion. Syndactyly is also categorized as complete or incomplete. In complete syndactyly the fusion runs the entire length of the affected digits.

Syndactyly of the foot can be classified as one of two types: zygosyndactyly and polysyndactyly. Zygosyndactyly is defined as a cutaneous webbing (either complete or incomplete) between the toes, most commonly between the second and third toes. Zygosyndactyly is often an inherited trait and typically presents asymptomatically and bilaterally. Polysyndactyly is defined as a duplication (either complete or partial) of one or more toes where the duplicated toe is joined to the normal toe either through soft tissue (simple) or soft tissue and underlying bone (complex). Polysyndactyly is less common than zygosyndactyly (Morrissy and Weinstein 2001). Multiple syndactyly is a feature of the pathological condition Apert's syndrome.

Syndactyly of the hand has been studied far more extensively than syndactyly of the foot. Research has shown that various phenotypes of hand syndactyly have strong genetic linkages; some genetic studies have also shown a genetic linkage for types of foot syndactyly. Hand syndactyly is transmitted genetically in an autosomal dominant fashion with variable expression and penetrance (Burke et al. 1989; Eaton and Lister 1990; Green et al. 2005; Canale and Beaty 2008). It is reasonable to infer that syndactyly of the foot is caused by a similar genetic mechanism.

Limb deficiencies

Congenital absence of all or part of a bone in the lower extremities can occur due to errors in limb bud development. As such, they represent pathologic entities rather than normal variants, but a brief mention is appropriate. Older terminology could often be confusing with words such as phocomelia or hemimelia being insufficiently descriptive and ambiguous. A classification scheme for limb deficiency was therefore developed by the ISPO "Kay" committee in Dundee, Scotland in 1973 (Kay et al. 1975), and with minor modifications became accepted as an International Standard (8548-1 1989; Day 1991).

This scheme divides limb deficiencies into two types: transverse and longitudinal. In transverse deficiencies, all parts distal to the level of deficiency are absent. They are named according to the bones involved and the level. In longitudinal deficiencies (previously called hemimelia) there is an absence or reduction of skeletal elements in the long axis of the limb but there are skeletal elements present distal to the defect. The bones involved are named in a proximal to distal sequence and it is stated whether each affected bone is totally or partially absent.

Limb deficiencies can occur in isolation or in association with a variety of syndromes. Most, such as fibular longitudinal deficiency, are limb bud abnormalities that are not inheritable; some are inheritable however, such as tibial longitudinal deficiency. (autosomal dominant)

Leg length inequality

Differences in leg length between right and left side vary among humans. Understanding the normal range of leg length disparity is important in formulating treatment decisions. There are few anatomic studies on lower extremity leg length disparity. One of the classic studies on the subject utilized 1000 consecutive soldiers who underwent standardized radiographic exam due to low back symptoms. As such, there may be selection bias. It was found that only 23% had equal leg lengths. In 40.6% the right leg was shorter by an average of 7.47 mm, and in 36.4% the left leg was shorter by an average of 6.5 mm. Of the 770 cases with inequality, the inequality was 5 mm or less in 51.3%. Although all these patients presented with low back complaints, radiographic pathology of the lumbar spine was noted in 27.38% of those with equal lengths and 29.74% of those with unequal lengths (Rush and Steiner 1946).

Rotational variation

Lower extremity rotation varies among individuals and changes greatly during growth. Infants are born with significant femoral anterversion and internal tibial torsion that changes rapidly; most changes occur during the first 5 years of life. The foot progression angle (the angle the foot makes with the line of progression during gait) is determined by the femur (the angle of anterversion), the tibial torsion angle, and the morphology of the foot. In the clinical setting, when evaluating a patient with complaints related to rotation it is important to understand the change in rotation during growth and maturation and correlate this with the clinical exam. It is also important to understand the wide variation in normal ranges among individuals. The reader is referred to the classic work by Staheli in delineating the clinical exam findings and nomograms for the normal ranges (Staheli et al. 1985).

Femoral anteversion is the angle of forward inclination of the femoral neck relative to the femoral condyles in the transverse plane. Anteversion is greatest in infancy and decreases until skeletal maturity (Shands and Steele 1958; Crane 1959; Fabry et al. 1973). In a study of 1148 hips over 20 years it was noted that anteversion was 40° at birth decreasing to 16° by 16 years of age (Fabry et al. 1973). Patients with excessive anteversion usually present in early childhood with parents complaining of intoeing. Physical exam involves evaluation of hip internal and external rotation in a prone position. Treatment is generally parental reassurance.

Tibial torsion is defined as the angle between the bicondylar axis of the tibia at the knee joint and the bimalleolar axis in the tranverse plane. By convention, it is denoted as a positive number when the ankle is externally rotated relative to the knee. In fetal development the foot is internally rotated relative to the knee and the medial malleolus lies posterior to the lateral malleolus. By birth the medial and lateral malleoli are level and by walking age the lateral malleolus lies posterior (LeDamany 1909). Reported ranges for tibial torsion vary widely in the literature because of the variability in measurement techniques. Using the center of the malleoli to evaluate the transmalleolar axis on clinical exam, Staheli found the average tibial torsion to be 5° at birth and 15° by maturity (Staheli and Engel 1972; Staheli et al. 1985). Using CT imaging, Kristiansen et al. (2001) noted the average lateral tibial torsion at 4 years of age to be 28° (with a range of 20–37°). They noted an average increase of 1° per year until the age of 10 years with an additional 4° increase throughout the maturation process. The mean tibial torsion was 38° at adulthood (range 18–47°).

Whatever the measurement technique, there is a wide degree of normal variation and torsion changes over time. Variation is particularly great in the younger child and most deviations resolve spontaneously (Staheli and Engel 1972; Staheli et al. 1985; Staheli 1993). A thigh–foot angle that is 30° internally rotated (negative 30°) in the infant or toddler still falls within two standard deviations of normal (Staheli and Engel 1972; Staheli et al. 1985). Again, the nomograms depicting normal ranges are particularly useful in patient evaluation (Staheli et al. 1985). Patients with internal tibial torsion usually present as toddlers with the parents complaining of intoeing. The physical exam involves evaluation of the thigh–foot angle, transmalleolar axis, and foot progression angle. Once again, treatment is usually parental reassurance.

Genu varum and genu valgum

Lower extremity coronal plane alignment varies among individuals and changes with growth. Understanding this process is essential in differentiating between physiologic alignment and pathologic malalignment seen in rickets, bone dysplasias, or Blount's disease. Genu varum is normally greatest at birth, decreasing to neutral alignment by 1–2 years of age. Continued growth leads to genu valgum which peaks at 3–4 years of age and gradually decreases thereafter, reaching the normal adult alignment of slight valgus at 6–7 years of age (Salenius and Vankka 1975).

References

Adams JD. 1925. A developmental anomaly of the patella frequently diagnosed as fracture. *Surg Gynecol Obstet* 41: 601–604.

Anderson JY, Trinkaus E. 1998. Patterns of sexual, bilateral and interpopulational variation in human femoral neck-shaft angles. *J Anat* 192: 279–285.

Anderson T. 1987. A Medieval biparte cuneiform I with attempted unilateral fusion. *Ossa* 13: 39–48.

Astion DJ, Deland JT, Otis JC, Kenneally S. 1997. Motion of the hindfoot after simulated arthrodesis. *J Bone Joint Surg Am* 79: 241–246.

Azurza K, Sakellariou A. 2001. Ostoesynthesis of a symptomatic bipartite medial cuneiform. *Foot Ankle Int* 22: 499–501.

Babyn PS, Ranson M, McCarville ME. 1998. Normal bone marrow: signal characteristics and fatty conversion. *Magn Reson Imaging Clin N Am* 6(3): 473–495.

Barclay M. 1932. A case of duplication of the internal cuneiform bone of the foot (cuneiforme bipartitum). *J Anat* 67(Pt 1): 175–177.

Barlow TE. 1942. Os cuneiforme I bipartitum. *Am J Phys Anthropol* 29: 95–111.

Bencardino J, Rosenberg ZS. 2001. MR imaging and CT in the assessment of osseous abnormalities of the ankle and foot. *Magn Reson Imaging Clin N Am* 9(3): 567–578.

Bencardino J, Rosenberg ZS, Beltran J, Sheskier S. 1997. Os sustentaculi: depiction on MR images. *Skeletal Radiol* 26(8): 505–506.

Bessette BJ, Hodge JC. 1998. Diagnosis of the acute os peroneum fracture. *Singapore Med J* 39(7): 326–327.

Bianchi S, Abdelwahab IF, Tegaldo G. 1991. Fracture and posterior dislocation of the os peroneum associated with rupture of the peroneus longus tendon. *Can Assoc Radiol J* 42(5): 340–344.

Biermann MI. 1922. The supernumerary pedal bones. *Am J Roentgenol* 9: 404–411.

Bizarro AH. 1921. On sesamoid and supernumerary bones of the limbs. *J Anat* 55(Pt 4): 256–268.

Bloom RA, Libson E, Lax E, Pogrund H. 1986. The assimilated os sustentaculi. *Skeletal Radiol* 15(6): 455–457.

Bohne WH. 2001. Tarsal coalition. *Curr Opin Pediatr* 13(1): 29–35.

Boker WM. 1936. Das os cuneiform i bipartitum, eine fortschreitende umkonstruktion des quergewolbes im menschlichen fufs. *Anat Anz* 83: 193–204.

Boles MA, Lomasney LM, Demos TC, Sage RA. 1997. Enlarged peroneal process with peroneus longus tendon entrapment. *Skeletal Radiol* 26(5): 313–315.

Bordelon L. 1993. Heel pain. In: *Surgery of the Foot and Ankle* (Mann, MJ ed.). St Louis, Mosby, pp. 837–847.

Bourne MH, Bianco AJ Jr. 1990. Bipartite patella in the adolescent: results of surgical excision. *J Pediatr Orthop* 10(1): 69–73.

Bowlus TH, Korman SF, Desilvio M, Climo R. 1980. Accessory os fibulare avulsion secondary to the inversion ankle injury. *J Am Podiatry Assoc* 70(6): 302–303.

Bureau NJ, Cardinal E, Hobden R, Aubin B. 2000. Posterior ankle impingement syndrome: MR imaging findings in seven patients. *Radiology* 215(2): 497–503.

Burke FDM, McGrouther DA, Smith PJ. 1989. *Principles of Hand Surgery*. London: Churchill Livingstone.

Burman MSL, Lapidus PW. 1931. The functional disturbances caused by the inconstant bones and sesamoids of the foot. *Arch Surg* 22: 936–975.

Burnett SE, Case DT. 2005. Naviculo-cuneiform 1 coalition: Evidence of significant differences in tarsal coalition frequency. *The Foot* 15: 80–85.

Burnett SE, Case DT. 2011. Bipartite medial cuneiform: new frequencies from skeletal collections and a meta-analysis of previous cases. *Homo* 62(2): 109–125.

Burton SK, Altman MI. 1986. Degenerative arthritis of the os peroneum. A case report. *J Am Podiatr Med Assoc* 76(6): 343–345.

Calausen A. 1944. Os naviculare bipartitum pedis. *Nord Med* 23: 1802–1804.

Cameron PD. 1923. A hitherto undescribed bone in the tarsus. *Arch of Radiol and Electrotherapy* 27: 234.

Canale ST, Beaty JH. 2008. *Campbell's operative orthopaedic*. Philadelphia: Mosby Elsevier.

Carlier P. 1924. Os surnumeraire rare du tarse. Bulletins et Memoires de la Societe Anatomique de Paris et de Strasbourg. *6e serie*. 21: 272.

Case DT, Burnett SE. 2012. Identification of tarsal coalition and frequency estimates from skeletal samples. *Int J Osteoarchaeol* 22: 667–684.

Case DT, Ossenberg NS, Burnett SE. 1998. Os intermetatarseum: a heritable accessory bone of the human foot. *Am J Phys Anthropol* 107(2): 199–209.

Chiodo CP, Parentis MA, Myerson MS. 2002. Symptomatic bipartite medial cuneiform in an adult athlete: a case report. *Foot Ankle Int* 23(4): 348–351.

Choi YS, Lee KT, Kang HS, Kim EK. 2004. MR imaging findings of painful type II accessory navicular bone: correlation with surgical and pathologic studies. *Korean J Radiol* 5(4): 274–279.

Clarke DM. 1997. Multiple tarsal coalitions in the same foot. *J Pediatr Orthop* 17(6): 777–780.

Cohn I. 1924. Annals of Roentgenology Vol. IV: *Normal Bones & Joints*. New York: Paul B Hoeber.

Collipal E, Vargas R, Parra X, Silva H, Del Sol M. 2007. Diaphyseal nutrient foramina in the femur, tibia and fibula bones. *Int J Morphol* 25: 305–308.

Conforty B, Lotem M. 1979. Ossicles in human menisci: report of two cases. *Clin Orthop Relat Res*(144): 272–275.

Conway JJ, Cowell HR. 1969. Tarsal coalition: clinical significance and roentgenographic demonstration. *Radiology* 92(4): 799–811.

Coppolelli BG, Ready JE, Awbrey BJ, Smith LS. 1991. Polydactyly of the foot in adults: literature review and unusual case presentation with diagnostic and treatment recommendations. *J Foot Surg* 30(1): 12–18.

Coral A. 1987. The radiology of skeletal elements in the subtibial region: incidence and significance. *Skeletal Radiol* 16(4): 298–303.

Coskun N, Yuksel M, Cevener M, Arican RY, Ozdemir H, Bircan O, Sindel T, Ilgi S, Sindel M. 2009. Incidence of accessory ossicles and sesamoid bones in the feet: a radiographic study of the Turkish subjects. *Surg Radiol Anat* 31(1): 19–24.

Coughlin MJ, Mann RA, Saltzman CL. 2006. *Surgery of the Foot and Ankle*, eighth edition. Amsterdam: Elsevier.

Cowell HR. 1972. Talocalcaneal coalition and new causes of peroneal spastic flatfoot. *Clin Orthop Relat Res* 85: 16–22.

Craig CL, Goldberg MJ. 1977. Calcaneocuboid coalition in Crouzon's syndrome (craniofacial dysostosis): report of a case and review of the literature. *J Bone Joint Surg Am* 59(6): 826–827.

Crain MR, el-Khoury GY. 1989. Stress fracture of the os peroneum. *AJR Am J Roentgenol* 152(2): 430.

Crane L. 1959. Femoral torsion and its relation to toeing-in and toeing-out. *J Bone Joint Surg Am 41-a*(3): 421–428.

Dameron TB Jr. 1975. Fractures and anatomical variations of the proximal portion of the fifth metatarsal. *J Bone Joint Surg Am* 57(6): 788–792.

Davies MB, Dalal S. 2005. Gross anatomy of the interphalangeal joint of the great toe: implications for excision of plantar capsular accessory ossicles. *Clin Anat* 18(4): 239–244.

Davies MB, Abdlslam K, Gibson RJ. 2003. Interphalangeal sesamoid bones of the great toe: an anatomic variant demanding careful scrutiny of radiographs. *Clin Anat* 16(6): 520–521.

Day HJ. 1991. The ISO/ISPO classification of congenital limb deficiency. *Prosthet Orthot Int* 15(2): 67–69.

Dellacorte MP, Lin PJ, Grisafi PJ. 1992. Bilateral bipartite medial cuneiform. A case report. *J Am Podiatr Med Assoc* 82(9): 475–478.

Demeyere N, De Maeseneer M, Osteaux M. 2001. Quiz case. Symptomatic type II accessory navicular. *Eur J Radiol* 37(1): 60–63.

Dihlmann W, Cen M, Sturm W. 1972. Uber die Diaphysenmanschette an den Grundphalangen der Zehen. Fortschr. *Rontgenstr* 117: 350.

Dobas DC, Silvers MD. 1977. The frequency of partite sesamoids of the first metatarsophalangeal joint. *J Am Podiatry Assoc* 67(12): 880–882.

Duncan W, Dahm DL. 2003. Clinical anatomy of the fabella. *Clin Anat* 16(5): 448–449.

Dwight T. 1902. Os intercuneiforme tarsi: os paracuneiforme tarsi, calcaneus secundarius. *Anatomischer Anzieger* 20: 465.

Dwight T. 1907. Variations of the Bones of the Hands and Feet: A Clical Atlas. Philadelphia: JB Lippincott.

Dwight T. 1910. Description of a free cuboides secundarium, with remarks on that element and on the calcaneus secundarius. *Anat Anz* 37: 218–224.

Eaton CJ, Lister GD. 1990. *Syndactyly*. Hand Clin 6(4): 555–575.

Ebraheim NA, Lu J, Yang H, Rollins J. 1998. The fibular incisure of the tibia on CT scan: a cadaver study. *Foot Ankle Int* 19(5): 318–321.

Eichenblat M, Nathan H. 1983. The proximal tibio fibular joint. *Int Orthop* (SICOT 7: 31.

Elgafy H, Semaan HB, Blessinger B, Wassef A, Ebraheim NA. 2010. Computed tomography of normal distal tibiofibular syndesmosis. *Skeletal Radiol* 39(6): 559–564.

Elias DA, White LM. 2004. Imaging of patellofemoral disorders. *Clin Radiol* 59(7): 543–557.

Elias I, Dheer S, Zoga AC, Raikin SM, Morrison WB. 2008. Magnetic resonance imaging findings in bipartite medial cuneiform – a potential pitfall in diagnosis of midfoot injuries: a case series. *J Med Case Rep* 2: 272.

Ellis R, Short JG, Knepley DW. 1968. The two-phalanged fifth toe. *Jama* 206(11): 2526.

Fabry G, MacEwen GD, Shands AR Jr. 1973. Torsion of the femur. A follow-up study in normal and abnormal conditions. *J Bone Joint Surg Am* 55(8): 1726–1738.

Fischer E. 1988. Der dorsofibulare Fortsatz am Kopf des l Metatarsale, eine ossare variante. *Radiologe* 28: 45.

Foster K, Chapman S, Johnson K. 2004. MRI of the marrow in the paediatric skeleton. *Clin Radiol* 59(8): 651–673.

Fredrick LA, Beall DP, Ly JQ, Fish JR. 2005. The symptomatic accessory navicular bone: a report and discussion of the clinical presentation. *Curr Probl Diagn Radiol* 34(2): 47–50.

Freyschmidt J, Brossman J, Wiens J, Sternberg A. 2003. *Borderlands of Normal and Early Pathological Findings in Skeletal Radiography*. 5th Revised Edition. New York, Theime Medical Publishers, pp. 804–1103.

Friedl E. 1924. Das os intermetatarseum und die epiphysenbildung am processus trochlearis calcanei. *Dtsh Z Chir* 188: 150–160.

Gaulke R, Schmitz HG. 2003. Free os cuboideum secundarium: a case report. *J Foot Ankle Surg* 42(4): 230–234.

Gebarski K, Hernandez RJ. 2005. Stage-I osteochondritis dissecans versus normal variants of ossification in the knee in children. *Pediatr Radiol* 35(9): 880–886.

Geist ES. 1914. Supernumerary bones of the foot: A roentgen study of the feet of one hundred normal individuals. *Am J Orthop Surg* 12(403–414).

Genakos JJ. 1993. Clinical sign consistent with the hallucal interphalangeal sesamoid. *J Am Podiatr Med Assoc* 83(12): 696–697.

Gheorghiu D, Leinenkugel A. 2010. The linea aspera-pilaster complex as a possible cause of confusion with the 'flame sign': a case report. *Acta Orthop Traumatol Turc* 44(3): 254–256.

Gillespie RJ, Levine A, Fitzgerald SJ, Kolaczko J, DeMaio M, Marcus RE, Cooperman DR. 2011. Gender differences in the anatomy of the distal femur. *J Bone Joint Surg Br* 93(3): 357–363.

Glard Y, Jouve JL, Panuel M, Adalian P, Tardieu C, Bollini G. 2005. An anatomical and biometrical study of the femoral trochlear groove in the human fetus. *J Anat* 206(4): 411–413.

Goez J, DeLauro T. 1995. Congenital absence of the tibial sesamoid. *J Am Podiatr Med Assoc* 85(9): 509–510.

Grass R. 2000. Injuries of the inferior tibiofibular syndesmosis. *Unfallchirurg* 103(7): 519.

Gray H. 1966. Gray's Anatomy of the Human Body. 28th edition. Philadelphia, Lea & Febiger.

Green DP, Hotchkiss RN, Pederson WC, Wolfe SW. 2005. Green's Operative Hand Surgery, fifth edition. Philadelphia: Elvester.

Gruber W. 1864. *Vorlaufige mittheilung uber die sekundaren fusswurzelknochen des menschen*. Arch fur Anat Phys und wiss Med: 286–290.

Gruber W. 1875. Uber den fortsatz des seitenhockers-processus tuberositatis lateralis: des metatarsale v und sein auftreten als epiphyse. Arch Anat Physiol Wissenschaft Med: 48–58.

Gruber W. 1877. Monographie uber das zweigtheilte erste keibein beim menschen. *Mem d l'Acad Imp d Sci d St Petersbourg* 24: 1–35.

Gumusburun E, Yucel F, Ozkan Y, Akgun Z. 1994. A study of the nutrient foramina of lower limb long bones. *Surg Radiol Anat* 16(4): 409–412.

Halpern AA, Hewitt O. 1978. Painful medial bipartite patellae: a case report. *Clin Orthop Relat Res*(134): 180–181.

Harris RI. 1965. Retrospect: personeal spastic flat foot (rigid valgus foot). *J Bone Joint Surg Am* 47(8): 1657–1667.

Harris RI, Beath T. 1948. Etiology of peroneal spastic flat foot. *J Bone Joint Surg Br* 30b(4): 624–634.

Harris S. 2009. *Sexual Dimorphism in the Tarsals: Implications for Sex Determination*. Masters thesis, North Carolina State University.

Harrison RB, Keats TE. 1980. Epiphyseal clefts. *Skeletal Radiol* 5(1): 23–27.

Harrison RB, Wood MB, Keats TE. 1976. The grooves of the distal articular surface of the femur: a normal variant. *AJR Am J Roentgenol* 126(4): 751–754.

Haswell DM, Berne AS, Graham CB. 1976. The dorsal defect of the patella. *Pediatr Radiol* 4(4): 238–242.

Heidsieck E. 1936. Os cuneiforme I bipartitum. *Rontgenpraxis* 8: 712–715.

Heimerzheim A. 1924. Uber einen seltsamen knochenbefund am calcaneus. *Dtsch Z Chir* 187: 281–283.

Henderson RS. 1963. Os intermetatarseum and a possible relationship to hallux valgus. *J Bone Joint Surg Br* 45–b: 117–121.

Hermans JJ, Beumer A, de Jong TA, Kleinrensink GJ. 2010. Anatomy of the distal tibiofibular syndesmosis in adults: a pictorial essay with a multimodality approach. *J Anat* 217(6): 633–645.

Hirschtick AB. 1951. An anomalous tarsal bone. *J Bone Joint Surg Am* 33–a(4): 907–910.

Hoaglund FT, Low WD. 1980. Anatomy of the femoral neck and head, with comparative data from Caucasians and Hong Kong Chinese. *Clin Orthop Relat Res*(152): 10–16.

Hocker K, Pachucki A. 1989. The fibular incisure of the tibia. The cross-sectional position of the fibula in distal syndesmosis. *Unfallchirurg* 92(8): 401–406.

Hoerr NL, Pyell SI, Francis CC. 1962. Radiographic Atlas of Skeletal Development of the Foot and Ankle: *A Standard Reference*. Springfield Ill, Charles C. Thomas.

Hohmann G. 1944. Uber frakturen und andere traumatische storungen am os naviculare des fusses. *Arch Orthop Unfall Chir* 43: 12–19.

Holland CT. 1921. On rarer ossifications seen during x-ray examinations. *J Anat* 55(Pt 4): 235–248.

Holland CT. 1928. The accessory bones of the foot. *Robert Jones Birthday* Volume 157 (Milford H, ed.) London: Oxford University Press.

Holle F. 1938. Uber die inkonstanten Elemente am menschlichen Fussskelett. Innaugural dissertation. Munich.

Humphry FRS. 1889. The angle of the neck with the shaft of the femur at different periods of life and under different circumstances. *J Anat Physiol* 23(Pt 2): 273–282.

Inge, GA, Ferguson AB. 1933. Surgery of the sesamoid bones of the great toe. *Arch Surg* 27: 466–488.

Iranpour F, Merican AM, Amis AA, Cobb JP. 2008. The width: thickness ratio of the patella: an aid in knee arthroplasty. *Clin Orthop Relat Res* 466(5): 1198–1203.

Jack EA. 1954. Bone anomalies of the tarsus in relation to peroneal spastic flat foot. *J Bone Joint Surg Br* 36–b(4): 530–542.

Jahss MH. 1981. The sesamoids of the hallux. *Clin Orthop Relat Res*(157): 88–97.

Jaramillo D, Laor T, Hoffer FA, Zaleske DJ, Cleveland RH, Buchbinder BD, Egglin TK. 1991. Epiphyseal marrow in infancy: MR imaging. *Radiology* 180(3): 809–812.

Jayakumar S, Cowell HR. 1977. Rigid flatfoot. *Clin Orthop Relat Res*(122): 77–84.

Jeng CL, Maurer A, Mizel MS. 1998. Congenital absence of the hallux fibular sesamoid: a case report and review of the literature. *Foot Ankle Int* 19(5): 329–331.

Jensen EL, de Carvalho A. 1987. A normal variant simulating Freiberg's disease. *Acta Radiol* 28(1): 85–86.

Johnson TR, Mizel MS, Temple T. 2005. Cuboid-navicular tarsal coalition: presentation and treatment: a case report and review of the literature. *Foot Ankle Int* 26(3): 264–266.

Jones DM, Saltzman CL, El-Khoury G. 1999. The diagnosis of the os trigonum syndrome with a fluoroscopically controlled injection of local anesthetic. *Iowa Orthop J* 19: 122–126.

Jones FW. 1949. *Structure and Function as Seen in the Foot*, second edition. London: Bailliere, Tindall & Cox.

Kapoor R, Johnson RA. 2011. Polydactyly. *NEJM* 365: 2122.

Karasick D. 1994. Fractures and dislocations of the foot. *Semin Roentgenol* 29: 152–175.

Karasick D, Schweitzer ME. 1996. The os trigonum syndrome: imaging features. *AJR Am J Roentgenol* 166(1): 125–129.

Kavanagh EC, Zoga A, Omar I, Ford S, Schweitzer M, Eustace S. 2007. MRI findings in bipartite patella. *Skeletal Radiol* 36(3): 209–214.

Kawashima T, Takeishi H, Yoshitomi S, Ito M, Sasaki H. 2007. Anatomical study of the fabella, fabellar complex and its clinical implications. *Surg Radiol Anat* 29(8): 611–616.

Kay HW, Day HJ, Henkel HL, Kruger LM, Lamb DW, Marquardt E, Mitchell R, Swanson AB, Willert HG. 1975. The proposed international terminology for the classification of congenital limb deficiencies. *Dev Med Child Neurol Suppl*(34): 1–12.

Keats TE. 1992. *Atlas of Normal Roentgen Variants that may Simulate Disease*, fifth edition. St. Louis: Mosby, Year Book.

Keats TE. 1996. *Atlas of Normal Roentgen Variants that may Simulate Desease*, sixth edition. St Louis, CV: Mosby.

Keats TE, Anderson MW. 2013. *Atlas of Normal Roentgen Variants that may Simulate Disease*, ninth edition. Philadelphia: Elsevier Saunders, pp. 485–759.

Kelikian H, Kelikian S. 1985. *Disorders of the Ankle*. Philadelphia: W.B. Saunders Company.

Kenwenter Y. 1936. Die sesambeine des I metatarsophalangealgelenks des menschen. *Acta Orthop Scand Suppl* 2: 1–113.

Kerr R, Resnick D, Sartoris DJ, Kursunoglu S, Pineda C, Haghighi P, Greenway G, Guerra J Jr. 1986. Computerized tomography of proximal femoral trabecular patterns. *J Orthop Res* 4(1): 45–56.

Kim JA, Park JS, Jin W, Ryu K. 2011. Herniation pits in the femoral neck: a radiographic indicator of femoroacetabular impingement? *Skeletal Radiol* 40(2): 167–172.

Kim JK, Roh KJ. 2013. Symptomatic os infranaviculare. *Clin Orthop Surg* 5(2): 152–154.

Klinmann M, Gross A, Pritzkev K, Gretson N. 1983. Osteochondritis of the hallux sesamoid bones. *Foot Ankle* 3: 220–223.

Kozin SH. 2001. Syndactyly. *J Hand Surg Am* 1: 1.

Kristiansen LP, Gunderson RB, Steen H, Reikeras O. 2001. The normal development of tibial torsion. *Skeletal Radiol* 30(9): 519–522.

Kulemann V, Mayerhoefer M, Trnka HJ, Kristen KH, Steiner E. 2010. Abnormal findings in hallucal sesamoids on MR imaging–Associated with different pathologies of the forefoot? An observational study. *Eur J Radiol* 74(1): 226–230.

Kulik SA Jr, Clanton TO. 1996. Tarsal coalition. *Foot Ankle Int* 17(5): 286–296.

Kumai T, Takakura Y, Akiyama K, Higashiyama I, Tamai S. 1998. Histopathological study of nonosseous tarsal coalition. *Foot Ankle Int* 19(8): 525–531.

Kumar R, Matasar K, Stansberry S, Shirkhoda A, David R, Madewell JE, Swischuck LE. 1991. The calcaneus: normal and abnormal. *Radiographics* 11(3): 415–440.

Kump WL. 1966. Vertical fractures of the distal tibial epiphysis. *Am J Roentgenol Radium Ther NUcl Med* 97(3): 676–681.

Laor T, Jaramillo D. 2009. MR imaging insights into skeletal maturation: what is normal? *Radiology* 250(1): 28–38.

Lawson JP. 1994. International Skeletal Society Lecture in honor of Howard D. Dorfman. Clinically significant radiologic anatomic variants of the skeleton. *AJR Am J Roentgenol* 163(2): 249–255.

Lawson JP, Ogden JA, Sella E, Barwick KW. 1984. The painful accessory navicular. *Skeletal Radiol* 12(4): 250–262.

Le Minor JM. 1987. Comparative anatomy and significance of the sesamoid bone of the peroneus longus muscle (os peroneum). *J Anat* 151: 85–99.

Le Minor JM. 1999. Congenital absence of the lateral metatarsophalangeal sesamoid bone of the human hallux: a case report. *Surg Radiol Anat* 21(3): 225–227.

LeDamany P. 1909. La Torsion du tibia, normal, pathologique experimentale. *J Anat Physiol* 45: 598.

Lee JH, Ehara S, Tamakawa Y, Horiguchi M. 2000. Nutrient canal of the fibula. *Skeletal Radiol* 29(1): 22–26.

Lee M, Hodler J, Haghighi P, Resnick D. 1992. Bone excrescence at the medial base of the distal phalanx of the first toe: normal variant, reactive change, or neoplasia? *Skeletal Radiol* 21(3): 161–165.

Leimbach G. 1938. Bietrage zur kenntnis der inkonstanten skeletelemente des tarsus, (akzessorische fusswurzelknochen). *Arch Orthop Trauma Surg* 38: 431–448.

Leonard MA. 1974. The inheritance of tarsal coalition and its relationship to spastic flat foot. *J Bone Joint Surg Br* 56b(3): 520–526.

Leszko F, Hovinga KR, Lerner AL, Komistek RD, Mahfouz MR. 2011. In vivo normal knee kinematics: is ethnicity or gender an influencing factor? *Clin Orthop Relat Res* 469(1): 95–106.

Leventen EO. 1991. Sesamoid disorders and treatment. An update. *Clin Orthop Relat Res*(269): 236–240.

Levine AH, Pais MJ, Berinson H, Amenta PS. 1976. The soleal line: a cause of tibial pseudoperiostitis. *Radiology* 119(1): 79–81.

Lichte E. 1941. On bipartite os naviculare pedis. *Acta Radiol* 22: 377–382.

Lysack JT, Fenton PV. 2004. Variations in calcaneonavicular morphology demonstrated with radiography. *Radiology* 230(2): 493–497.

Maffulli N, Lepore L, Francobandiera C. 1990. Traumatic lesions of some accessory bones of the foot in sports activity. *J Am Podiatr Med Assoc* 80(2): 86–90.

Mahfouz M, Abdel Fatah EE, Bowers LS, Scuderi G. 2012. Three-dimensional morphology of the knee reveals ethnic differences. *Clin Orthop Relat Res* 470(1): 172–185.

Mahony BS, Callen PW, Filly RA. 1985. The distal femoral epiphyseal ossification center in the assessment of third-trimester menstrual age: sonographic identification and measurement. *Radiology* 155(1): 201–204.

Mains DB, Sullivan RC. 1973. Fracture of the os peroneum. A case report. *J Bone Joint Surg Am* 55(7): 1529–1530.

Mann RA, Coughlin MJ. 1993. *Surgery of the Foot and Ankle*, 6th edition. St Louis, CV: Mosby.

March HC, London RI. 1993. The os sustentaculi. *AJR Am J Roentgenol* 96: 1114–1118.

Masaki T. 1984. An anatomical study of the interphalangeal sesamoid bone of the hallux. *Nihon Seikeigeka Gakkai Zasshi* 58(4): 419–427.

Masciocchi C, D'Archivio C, Barile A, Fascetti E, Zobel BB, Gallucci M, Passariello R. 1992. Talocalcaneal coalition: computed tomography and magnetic resonance imaging diagnosis. *Eur J Radiol* 15(1): 22–25.

Mau H. 1960. Zur Kenntnis des Naviculare bipartitum pedis. *Z Orthop* 93: 404–411.

Mavi A, Yildirim H, Gunes H, Pestamalci T, Gumusburun E. 2002. The fibular incisura of the tibia with recurrent sprained ankle on magnetic resonance imaging. *Saudi Med J* 23(7): 845–849.

McCarthy DJ, Reed T, Abell N. 1986. The hallucal interphalangeal sesamoid. *J Am Podiatr Med Assoc* 76(6): 311–319.

McCarthy JJ, Drennan JC. 2009. *Drennan's The Child's Foot & Ankle*, second edition. Philadelphia: Lippincott Williams & Wilkins.

McDougall A. 1955. The os trigonum. *J Bone Joint Surg Br* 37–b(2): 257–265.

Mellado JM, Salvado E, Camins A, Ramos A, Sauri A. 2002. Painful os sustentaculi: imaging findings of another symptomatic skeletal variant. *Skeletal Radiol* 31(1): 53–56.

Mellado JM, Ramos A, Salvado A, Camins A, Danus M, Sauri A. 2003. Accessory ossicles and sesamoid bones of the ankle and foot: imaging findings, clinical significance and differential diagnosis. *Eur Radiol 13 Suppl* 6: L164–177.

Melo ELA. 2012. The calcaneus channel: apropos of a new anatomical variant. *Clin Anat* 25: 989–991.

Mercer J. 1931. The Secondary Os Calcis. *J Anat* 66(Pt 1): 84–97.

Miki T, Yamamuro T, Kitai T. 1988. An irreducible dislocation of the great toe. Report of two cases and review of the literature. *Clin Orthop Relat Res*(230): 200–206.

Milgrom C, Kaplan L, Lax E. 1986. Case report 341: Os accessorium supracalcaneum of the left hind foot (also present, but to a lesser extent, on the right). *Skeletal Radiol* 15(2): 150–153.

Miller TT. 2002. Painful accessory bones of the foot. *Semin Musculoskelet Radiol* 6(2): 153–161.

Miller TT, Staron RB, Feldman F, Parisien M, Glucksman WJ, Gandolfo LH. 1995. The symptomatic accessory tarsal navicular bone: assessment with MR imaging. *Radiology* 195(3): 849–853.

Miller TT, Bucchieri JS, Joshi A, Staron RB, Feldman F. 1997. Pseudodefect of the talar dome: an anatomic pitfall of ankle MR imaging. *Radiology* 203(3): 857–858.

Moore KL. 1988. *The Developing Human*, fourth edition. Philadelphia: W.B. Saunders.

Morrison AB. 1953. The os paracuneiforme; some observations on an example removed at operation. *J Bone Joint Surg Br* 35–b(2): 254–255.

Morrissy R, Weinstein SL. 2001. *Lovell and Winter's Pediatric Orthopaedics*, fifth edition. Philadelphia: Lippincott Williams & Wilkins.

Mosier KM, Asher M. 1984. Tarsal coalitions and peroneal spastic flat foot. A review. *J Bone Joint Surg Am* 66(7): 976–984.

Mouchet A, Moutier G. 1925. Osselets surnumeraires du tarse. *Presse Med* 23: 369–374.

Muehleman C, Williams J, Bareither ML. 2009. A radiologic and histologic study of the os peroneum: prevalence, morphology, and relationship to degenerative joint disease of the foot and ankle in a cadaveric sample. *Clin Anat* 22(6): 747–754.

Munk PL, Althathlol A, Rashid F, Malfair D. 2009. MR features of a giant cyamella in a patient with osteoarthritis: presentation, diagnosis and discussion. *Skeletal Radiol* 38(1): 69, 91–62.

Munuera PV, Dominguez G, Reina M, Trujillo P. 2007. Bipartite hallucal sesamoid bones: relationship with hallux valgus and metatarsal index. *Skeletal Radiol* 36(11): 1043–1050.

Mygind HB. 1953. The accessory tarsal scaphoid; clinical features and treatment. *Acta Orthop Scand* 23(2): 142–151.

Nakayama S, Sugimoto K, Takakura Y, Tanaka Y, Kasanami R. 2005. Percutaneous drilling of symptomatic accessory navicular in young athletes. *Am J Sports Med* 33(4): 531–535.

Nalaboff KM, Schweitzer ME. 2008. MRI of tarsal coalition: frequency, distribution, and innovative signs. *Bull NYU Hosp Jt Dis* 66(1): 14–21.

Nielson JH, Gardner MJ, Peterson MG, Sallis JG, Potter HG, Helfet DL, Lorich DG. 2005. Radiographic measurements do not predict syndesmotic injury in ankle fractures: an MRI study. *Clin Orthop Relat Res*(436): 216–221.

O'Brien J, Murphy C, Halpenny D, McNeill G, Torreggiani WG. 2011. Magnetic resonance imaging features of asymptomatic bipartite patella. *Eur J Radiol* 78(3): 425–429.

O'Neal ML, Ganey TM, Ogden JA. 1995. Fracture of a bipartite medial cuneiform synchondrosis. *Foot Ankle Int* 16(1): 37–40.

O'Rahilly R. 1953. A survey of carpal and tarsal anomalies. *J Bone Joint Surg Am* 35(3): 626–642.

Ogata K. 1994. Painful bipartite patella. A new approach to operative treatment. *J Bone Joint Surg Am* 76(4): 573–578.

Ogden JA. 1984. Radiology of postnatal skeletal development. X. Patella and tibial tuberosity. *Skeletal Radiol* 11(4): 246–257.

Oohashi Y, Koshino T, Oohashi Y. 2010. Clinical features and classification of bipartite or tripartite patella. *Knee Surg Sports Traumatol Arthrosc* 18(11): 1465–1469.

Ozonoff MB, Ziter FM Jr. 1987. The femoral head notch. *Skeletal Radiol* 16(1): 19–22.

Paal E. 1933. Fehlbeurteilungen bei Rontgenbildern. *Arch Orthop Unfall Chir* 33: 153–158.

Perdikakis E, Grigoraki E, Karantanas A. 2011. Os naviculare: the multi-ossicle configuration of a normal variant. *Skeletal Radiol* 40(1): 85–88.

Pettrone FA, Gail M, Pee D, Fitzpatrick T, Van Herpe LB. 1983. Quantitative criteria for prediction of the results after displaced fracture of the ankle. *J Bone Joint Surg Am* 65(5): 667–677.

Pfitzner W. 1896. *Beitrage zur kenntmiss des menschlichen Extremitatenskelets: VII. Die Variationen in Aufbau des Fusskelets*. Jena, Gustav Fischer.

Phukubye P, Oyedele O. 2011. The incidence and structure of the fabella in a South African cadaver sample. *Clin Anat* 24(1): 84–90.

Piersol GA, Dwight T, McMurrich CA, Hamann JW. 1919. *Human Anatomy: Including Structure and Development and Practical Considerations*, seventh edition. Philadelphia: J. B. Lippincott Company.

Piqueres X, de Zabala S, Torrens C, Marin M. 2002. Cubonavicular coalition: a case report and literature review. *Clin Orthop Relat Res* (396): 112–114.

Pitt MJ. 1982. Radiology of the femoral linea aspera-pilaster complex: the track sign. *Radiology* 142(1): 66.

Pitt MJ, Graham AR, Shipman JH, Birkby W. 1982. Herniation pit of the femoral neck. *AJR Am J Roentgenol* 138(6): 1115–1121.

Pneumaticos SG, Noble PC, Chatziioannou SN, Trevino SG. 2002. The effects of rotation on radiographic evaluation of the tibiofibular syndesmosis. *Foot Ankle Int* 23(2): 107–111.

Prabhudesai V, Richards PJ. 2003. Radiological appearance as a meniscal ossicle develops: a case report and review of literature. *Injury* 34(5): 378–382.

Prashanth K, Murlimanju B, Prabhu LV, Chettiar GK, Pai MM, Dhananjaya K. 2011. Morphological and topographical anatomy of nutrient foramina in the lower limb long bones and its clinical importance. *Australas Med J* 4(10): 530–537.

Prescher A. 1997. Some remarks on, and a new case of the rare os intercuneiforme (Dwight). *Ann Anat* 179(4): 317–320.

Rankin EA, Baker GI. 1974. Rigid flatfoot in the young adult. *Clin Orthop Relat Res*(104): 244–248.

Ravelli A. 1955. Zum Rontgenbild des proximalen Schienbiendrittels. Fortschr. *Rontgenstr* 82: 48.

Richardson EG. 1987. Injuries to the hallucal sesamoids in the athlete. *Foot Ankle* 7(4): 229–244.

Robinson HM. 1976. Symmetrical reversed plantar calcaneal spurs in children. A normal variant? *Radiology* 119(1): 187–188.

Rohilla S, Yadav RK, Singh R, Devgan A, Dhaulakhandi DB. 2009. Meniscal ossicle. *J Orthop Traumatol* 10(3): 143–145.

Romanowski CA, Barrington NA. 1992. The accessory navicular–an important cause of medial foot pain. *Clin Radiol* 46(4): 261–264.

Roukis TS, Hurless JS. 1996. The hallucal interphalangeal sesamoid. *J Foot Ankle Surg* 35(4): 303–308; discussion 372.

Rowe MM. 1963. Osteomyelitis of metatarsal sesamoid. *Br Med J* 1(5337): 1071–1072.

Ruhli FJ, Solomon LB, Henneberg M. 2003. High prevalence of tarsal coalitions and tarsal joint variants in a recent cadaver sample and its possible significance. *Clin Anat* 16(5): 411–415.

Rush WA, Steiner HA. 1946. A study of lower extremity length inequality. *Am J Roentgenol Radium Ther* 56(5): 616–623.

Saini UC, Bali K, Sheth B, Gahlot N, Gahlot A. 2010. Normal development of the knee angle in healthy Indian children: a clinical study of 215 children. *J Child Orthop* 4(6): 579–586.

Salenius P, Vankka E. 1975. The development of the tibiofemoral angle in children. *J Bone Joint Surg Am* 57(2): 259–261.

Sarin VK, Erickson GM, Giori NJ, Bergman AG, Carter DR. 1999. Coincident development of sesamoid bones and clues to their evolution. *Anat Rec* 257(5): 174–180.

Sarrafian SK. 1993. *Anatomy of the foot and ankle*. Philadelphia, Lippincott.

Saupe H. 1921. Beitrage zur patella bipartita. *Fortschr Geb Roentgenstr Nuklearmed Erganzungsbad* 28: 37–46.

Schoen W. 1935. Seltenere akzessorisch Knochen am Fussrucken. *Rontgenpraxis* 7: 775–776.

Schreiber A, Differding P, Zollinger H. 1985. Talus partitus. A case report. *J Bone Joint Surg Br* 67(3): 430–431.

Schweitzer ME, Karasick D. 2000. MR imaging of disorders of the posterior tibialis tendon. *AJR Am J Roentgenol* 175(3): 627–635.

Selby S. 1961. Separate centers of ossification of the tip of the internal malleolus. *Am J Roentgenol Radium Ther Nucl Med* 86: 496–501.

Sella EJ, Lawson JP. 1987. Biomechanics of the accessory navicular synchondrosis. *Foot Ankle* 8(3): 156–163.

Sella EJ, Lawson JP, Ogden JA. 1986. The accessory navicular synchondrosis. *Clin Orthop Relat Res* 209: 280–285.

Seok HH, Park JU, Kwon ST. 2013. New classification of polydactyly of the foot on the basis of syndactylism, axis deviation, and metatarsal extent of extra digit. *Arch Plast Surg* 40(3): 232–237.

Shands AR Jr, Wentz IJ. 1953. Congenital anomalies, accessory bones, and osteochondritis in the feet of 850 children. Surg Clin North Am: 1643–1666.

Shands AR Jr, Steele MK. 1958. Torsion of the femur; a follow-up report on the use of the Dunlap method for its determination. *J Bone Joint Surg Am* 40–a(4): 803–816.

Sharon SM. 1977. Interphalangeal joint hallux ossicle. *J Foot Surg* 16(2): 69–72.

Shawdon A, Kiss ZS, Fuller P. 1995. The bipartite tarsal navicular bone: radiographic and computed tomography findings. *Australas Radiol* 39(2): 192–194.

Shopfner CE. 1966. Periosteal bone growth in normal infants. A preliminary report. *Am J Roentgenol Radium Ther Nucl Med* 97(1): 154–163.

Siecke H. 1964. Beitrag zur Genese des Os peronaeum. *Z Orthop* 98: 358.

Sijbrandij ES, van Gils AP, de Lange EE, Sijbrandij S. 2002. Bone marrow ill-defined hyperintensities with tarsal coalition: MR imaging findings. *Eur J Radiol* 43(1): 61–65.

Smith AD, Carter JR, Marus RE. 1984. The os vesalinum: An unusual cause of lateral foot pain. *Orthopedics* 7: 86–89.

Smith T. 1866. A foot having four cuneiform bones. *Trans Path Soc London* 17: 222–223.

Snyder RB, Lipscomb AB, Johnston RK. 1981. The relationship of tarsal coalitions to ankle sprains in athletes. *Am J Sports Med* 9(5): 313–317.

Solomon LB, Ruhli FJ, Taylor J, Ferris L, Pope R, Henneberg M. 2003. A dissection and computer tomograph study of tarsal coalitions in 100 cadaver feet. *J Orthop Res* 21(2): 352–358.

Sora MC, Strobl B, Staykov D, Forster-Streffleur S. 2004. Evaluation of the ankle syndesmosis: a plastination slices study. *Clin Anat* 17(6): 513–517.

Sowman B, Radic R, Kuster M, Yates P, Breidiel B, Karamfilef S. 2012. Distal tibiofibular radiological overlap: Does it always exist? *Bone Joint Res* 1(2): 20–24.

Staheli LT. 1993. Rotational problems in children. *J Bone Joint Surg Am* 75: 939.

Staheli LT, Engel GM. 1972. Tibial torsion: a method of assessment and a survey of normal children. *Clin Orthop Relat Res* 86: 183–186.

Staheli LT, Corbett M, Wyss C, King H. 1985. Lower-extremity rotational problems in children. Normal values to guide management. *J Bone Joint Surg Am* 67(1): 39–47.

Stephenson P, Seedhom BB. 2001. Modelling femoral curvature in the sagittal plane: a cadaveric study. *Proc Inst Mech Eng H* 215(2): 221–228.

Stormont DM, Peterson HA. 1983. The relative incidence of tarsal coalition. *Clin Orthop Relat Res*(181): 28–36.

Sunderland S. 1938. The quadrate tubercle of the femur. *J Anat* 72(Pt 2): 309–312.

Suwannahoy P, Srisuwan T, Pattamapaspong N, Mahakkanukrauh P. 2012. Intra-articular ossicle in interphalangeal joint of the great toe and clinical implication. *Surg Radiol Anat* 34(1): 39–42.

Tabira Y, Saga T, Takahashi N, Watanabe K, Nakamura M, Yamaki KI. 2012. Influence of a fabella in the gastrocnemius muscle on the common fibular nerve in Japanese subjects. Clin Anat.

Tax HR. 1960. The accessory scaphoid. *Current Podiat* 9: 28–29.

Teichert G. 1955. Os talo-tibiale. *Fortschr. Rontgenstr.* 83: 734–736.

Temtamy S, McKusick V. 1969. Synopsis of hand malformations with particular emphasis on genetic factors. *Birth Defects* 5: 125.

Terzidis I, Totlis T, Papathanasiou E, Sideridis A, Vlasis K, Natsis K. 2012. Gender and side-to-side differences of femoral condyles morphology: osteometric data from 360 caucasian dried femori. *Anat Res Int* 2012: 679658.

Toogood PA, Skalak A, Cooperman DR. 2009. Proximal femoral anatomy in the normal human population. *Clin Orthop Relat Res* 467(4): 876–885.

Trolle D. 1945. De to accessoriske knogler: Os subtibiale og os subfibulare i relation til diagnosen af malleolarfracturer. *Nord Med* 25: 247–249.

Trolle D. 1948. *Accessory Bones of the Human Foot: A Radiological, Histoembryological, Comparative Anatomical and Genetic Study*. Copenhagen: Musksgaard.

Tsuruta T, Kato A, Atasumoto T, Yamazoe Y, Oike T, Sugiyama T, Saito M. 1981a. Radiological study of the accessory skeletal elements in the foot and ankle (abstract). *J Jap Orthop Assoc* 55: 357–370.

Tsuruta T, Shiokawa Y, Kato A, Matsumoto T, Yamazoe Y, Oike T, Sugiyama T, Saito M. 1981b. Radiological study of the accessory skeletal elements in the foot and ankle (author's transl). *Nihon Seikeigeka Gakkai Zasshi* 55(4): 357–370.

Valinsky MS, Hettinger DF, Mortvedt JK. 1989. Hallux interphalangeal joint sesamoidectomy using minimal incision technique. *J Am Podiatr Med Assoc* 79(2): 60–64.

Van Hal ME, Keene JS, Lange TA, Clancy WG Jr. 1982. Stress fractures of the great toe sesamoids. *Am J Sports Med* 10(2): 122–128.

van Wiechen PJ. 1987. Reversed calcaneal spurs in children. *Skeletal Radiol* 16(1): 17–18.

Varich LJ, Laor T, Jaramillo D. 2000. Normal maturation of the distal femoral epiphyseal cartilage: age-related changes at MR imaging. *Radiology* 214(3): 705–709.

Vincent KA. 1998. Tarsal coalition and painful flatfoot. *J Am Acad Orthop Surg* 6(5): 274–281.

Vogler JB 3rd, Murphy WA. 1988. Bone marrow imaging. *Radiology* 168(3): 679–693.

Wallis SA, Georgeson MA. 2012. Mach bands and multiscale models of spatial vision: the role of first, second, and third derivative operators in encoding bars and edges. *J Vis* 12(13): 18.

Wanner JA. 1977. Variations in the anterior patellar groove of the human femur. *Am J Phys Anthropol* 47(1): 99–102.

Watkins WW. 1937. Anomalous bones of the wrist and foot in relation to injury. *JAMA* 108: 270–274.

Weaver JK. 1977. Bipartite patellae as a cause of disability in the athlete. *Am J Sports Med* 5(4): 137–143.

Wechsler RJ, Schweitzer ME, Deely DM, Horn BD, Pizzutillo PD. 1994. Tarsal coalition: depiction and characterization with CT and MR imaging. *Radiology* 193(2): 447–452.

Weil LS, Hill M. 1992. Bipartite tibial sesamoid and hallux abducto valgus deformity: a previously unreported correlation. *J Foot Surg* 31(2): 104–111.

Woolf CM, Myrianthopoulos NC. 1973. Polydactyly in American negroes and whites. *Am J Hum Genet* 25(4): 397–404.

Wray JB. 1963. Hereditary transmission of congenital coalition of the calcaneus to the navicular. *J Bone Joint Surg Am* 45: 365–372.

Yanklowitz BA, Jaworek TA. 1975. The frequency of the interphalangeal sesamoid of the hallux. A retrospective roentgenographic study. *J Am Podiatry Assoc* 65(11): 1058–1063.

Yildirim H, Mavi A, Buyukbebeci O, Gumusburun E. 2003. Evaluation of the fibular incisura of the tibia with magnetic resonance imaging. *Foot Ankle Int* 24(5): 387–391.

Yu JS, Resnick D. 1994. Meniscal ossicle: MR imaging appearance in three patients. *Skeletal Radiol* 23(8): 637–639.

Zalavras C, Thordarson D. 2007. Ankle syndesmotic injury. *J Am Acad Orthop Surg* 15(6): 330–339.

Zimmer EA. 1938. Drankheiten, Verletzungen und Varietaten des Os naviculare pedis. *Arch Orthop Unfall Chir* 38: 396–411.

Zinsmeister BJ, Edelman R. 1985. Congenital absence of the tibial sesamoid: a report of two cases. *J Foot Surg* 24(4): 266–268.

Further reading

Aggarwal K, Gupta S, Jain VK, Mital A, Gupta S. 2008. Subungual exostosis. *Indian J Dermatol Venereol Leprol* 74: 173–174.

Carroll RE, Chance JT, Inan Y. 1992. Subungual exostosis in the hand. *J Hand Surg Br* 17(5): 569–574.

Dave S, Carounanidy U, Thappa DM, Jayanthi S. 2004. Subungual exostosis of the thumb. *Dermatol Online J* 10(1): 15.

Ilyas W, Geskin L, Joseph AK, Seraly MP. 2001. Subungual exostosis of the third toe. *J Am Acad Dermatol* 45(6 Suppl): S200–201.

Stanescu L, Popescu CF, Niculescu CE, Dumitrescu D, Mogoanta SS, Georgescu I. 2009. Subungual exostosis of the big toe. *Rom J Morphol Embryol* 50(3): 501–503.

14 Temporomandibular joint

Toral R. Patel and Jarrod A. Collins
Children's of Alabama, Birmingham, Alabama, United States

Introduction

The temporomandibular joint (TMJ) is a synovial joint that permits gliding, rotation, elevation, and depression. The normal function of the joint includes mastication, suckling, swallowing, yawning, speaking, and biting. The TMJ consists of bony articular surfaces of the mandibular fossa, the articular tubercle of the temporal bone, and the head of the mandible. The TMJ may be marked by a protuberance on the floor of the middle cranial fossa known as the eminentia mandibularis (Tubbs et al. 2008). The articular eminence (also known as the articular tubercle) is the convex bony elevation on the root of the zygomatic process representing the anterior-most boundary of the mandibular fossa. This is where the fibrous capsule and TM (lateral) ligament attach. The joint capsule attaches to the articular cartilage of the temporal bone and neck of the mandible. The TMJ is unusual in that its articular surfaces are lined by fibrocartilage (rather than hyaline cartilage) and its joint cavity is divided into two by an articular disc. The articular disc of the TMJ attaches to the capsule separating two synovial joint spaces lined by synovial membranes. The synovial membranes do not extend to cover the disc or the articular surfaces. The functions of the joint occur via the lateral ligament, stylomandibular ligament, and sphenomandibular ligament. The ligamentous muscles of the TMJ articulation are the temporalis, masseter, internal, and external pterygoids. The suprahyoid muscle group is also responsible for mandibular movement: digastric, mylohyoid, geniohyoid, and stylohyoid. The synovial joints are supplied by sensory nerve endings (mainly of proprioceptive variety), pain, and stretch receptors. The articular capsules and ligaments are highly vascularized, forming capillary networks over the synovial membranes.

Intra-articular disc

The intra-articular disc, also known as the meniscus, lies between the head of the mandible and mandibular fossa and is covered by fibrocartilage. The superficial part of the disc contains a large fibrous element while the deeper section contains cartilage. The disc is biconcave with a "bowtie" appearance on MRI. The lack of vascularity in the center of the disc is consistent with the middle portion of the disc acting as the force-accepting segment.

Mandibular condyle

The mandibular condyle sits in the glenoid fossa (also known as the mandibular fossa) of the temporal bone. The presence of fibrocartilage rather than hyaline cartilage is important, as fibrocartilage can repair and remodel.

Joint capsule

The joint capsule completely surrounds the TMJ from the articular margins of the mandibular fossa to the neck of the mandible. The joint capsule encloses the intra-articular disc at the inner aspect of the capsule. TMJ is supported by short capsular fibers running from the disc to the neck of the condyle, allowing the portion of the disc to be loose and the portion of the capsule below the disc to be tight. Sesamoid bones may be found in the TMJ (Lang 1995).

Synovial membrane

Two synovial membranes are associated with the TMJ, one above and one below the disc. Both the inferior and superior synovial membranes line the non-articular surfaces and fuse with the periphery of the disc.

Lateral, sphenomandibular, and stylomandibular ligaments

The TMJ consists of three ligaments, two of which are accessory and guide the movement of the mandible against the base of the skull. All of the ligaments are believed to be under the influence of muscular activity.

1. The lateral ligament is a thickened part of the joint capsule forming an intrinsic ligament that reinforces the lateral aspect of the joint capsule. The lateral ligament consists of two parts. The outer oblique part attaches to the neck of the condyle and the articular eminence. This ligament serves as a suspensory ligament and limits downward and posterior motion of the mandible and also limits rotation of the condyle during mouth opening, thus preventing posterior dislocation of the joint. The inner portion of the ligament is attached to the

Bergman's Comprehensive Encyclopedia of Human Anatomic Variation, First Edition. Edited by R. Shane Tubbs, Mohammadali M. Shoja and Marios Loukas.
© 2016 John Wiley & Sons, Inc. Published 2016 by John Wiley & Sons, Inc.

lateral pole of the condyle, posterior portion of the disc, and the articular eminence. It limits lateral displacement.

2. The sphenomandibular ligament presents on the medial side of the joint running from the spine of the sphenoid to the lingula or ramus of the mandible. This ligament is a primary passive support of the mandible.
3. The stylomandibular ligament is a thickening of the deep cervical fascia that separates the parotid and submandibular glands. Stylomandibular ligament runs from the styloid process of the temporal bone to the posterior border of the ramus of the mandible.

Arterial blood supply

The maxillary artery is the largest terminal branch of the external carotid artery, arising posterior to the neck of the mandible and running deep to the mandibular condyle and lateral to the stylomandibular ligament. The middle meningeal artery and anterior tympanic branches are the arterial blood supply to the TMJ.

The superficial temporal artery is the smaller terminal branch of the external carotid artery emerging onto the face between the TMJ and auricle. They run with the auriculotemporal nerve. The ascending pharyngeal artery arises as the first or second branch of the external carotid artery and ascends deep to the internal carotid artery. The ascending pharyngeal artery is the smallest branch of the external carotid artery.

The masseteric artery accompanies the masseteric nerve and supplies branches to the TMJ. The deep auricular artery also contributes a small branch to the TMJ.

Venous drainage

The retromandibular vein is a deep vessel of the face formed by the union of the superficial temporal vein and the maxillary vein. It runs posterior to the ramus of the mandible within the parotid gland and superficial to the external carotid artery to drain the TMJ.

The external jugular vein is formed by the retromandibular vein and the posterior auricular veins and drains the TMJ. The maxillary vein, from the pterygoid plexus, unites with the superficial temporal vein to form the retromandibular vein.

Lymph

The lymph from the lateral face, specifically the TMJ, drains to the deep parotid lymph nodes.

Nerve supply

The mandibular nerve (CN V3) arises from the trigeminal ganglion of cranial nerve V. The auriculotemporal and masseteric branches of the nerve supply the four muscles of mastication.

The auriculotemporal nerve encircles the middle meningeal artery and passes medial to the neck of the mandible and posterior to the TMJ sending sensory fibers to the TMJ. The articular branches of the auriculotemporal nerve enter the TMJ. The masseteric nerve also provides articular branches to the TMJ.

Variations in each component

Variations of the TMJ occur in size, shape, or compilation of the different components. The anomalies are a deviation of what is normally found with asymptomatic characteristics. Discrepancies in joint part sizes are usually proportional to the general skeletal size; however, structural anomalies asymmetrical to the skeleton may exist. Some examples include small condyles in large fossae, tight effective attachment of the disc to the condyle with loose attachment to the temporal bone or vice versa, strong joint ligaments, and steeply inclined glenoid eminences. In the region of the TMJ, studies have found a functional false joint anterior to the glenoid fossa, large and irregular articulating surfaces, false condyles with medial thickening, shallower glenoid fossa, and shorter postglenoid process. Rarely, the entire TMJ is absent; such a finding presents asymptomatically however, because the joint is non-load-bearing.

Disc

The disc size, shape, position, and presence can vary (Fig.14.1). The thickness falls within the range 2–3 mm posteriorly and 1–2 mm in the middle. The size and shape of the disc is determined by the shape of the articular surfaces and the condyle. The greater the steepness of the articular eminence, the greater the posterior thickness of the disc. Normally the disc intervenes between the head of the mandible and the mandibular fossa, and is thinnest at the posterior slope of the articular tubercle.

Disc displacement

A centric condyle position is regarded as the correct interposition of the disc; however, the disc can also be found to have significant anterior position or posterior position. The condyle

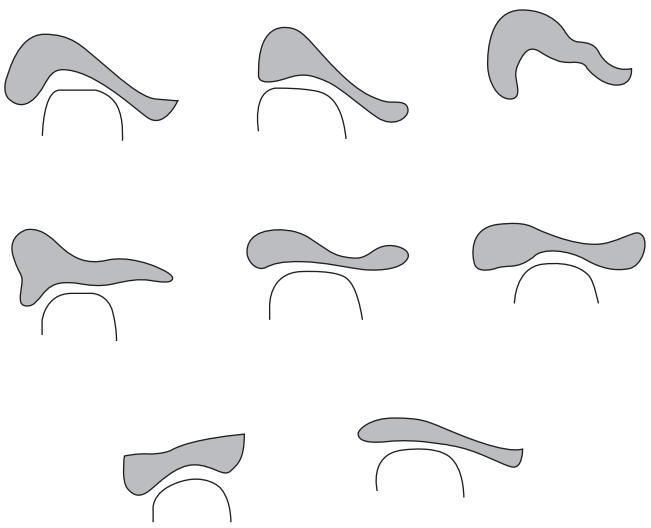

Figure 14.1 Variations in the shape of the articular disc.

Source: Hollinshead (1982). Produced with permission from LWW. Redrawn from Lubosch (1906).

can also be found to be anterior or posterior with regards to a normal disc position (Isberg 2001). If the anterior portion of the condyle and the inferior disc are >2 mm unaligned, the disc is displaced meaning that the anterior prominence of the condyle articulates against the posterior band of the disc or the side of the disc. The disc can be partially or completely displaced with the entire disc removed from normal position or partial amount of disc not found in the usual position. A displaced disc can be found oriented in any direction (anterior, posterior, anterolateral, anteromedial, posterolateral, posteromedial, lateral, and medial). Disc displacement in the medial direction can also present with the auriculotemporal nerve trunk coursing between the bony joint components in the articular fossa, instead of close to the condyle at the level of the temporal bone.

The width of the joint space (the distance between the condyle and its fossa) can vary. The joint space tends to be narrower with abnormally shaped condyles and hyperplasia and wider with hypoplasia of the condyle.

Internal derangement

Internal derangement, also known as disc displacement, is an abnormal disc position in relation to the articulating surfaces, specifically the condyle. In this case, the condyle is in contact with the retrodiscal tissue instead of the disc. There is a misalignment of the articular disc and condyle. Usual direction of displacement is anterior or anteromedial. It is assumed that the disc is permitted to be displaced by stretched ligaments that bind the disc to the condyle. An increased horizontal angle of the mandibular condyle has been associated with more advanced TMJ internal derangement. Moderate disc displacement is described as a condylar surface that is locally flattened or when there is none or <4 mm shortening of the condyle. Extensive disc displacement is when the condyle is small or shortened (>4 mm) with extensive flattening. This can also be due to a loss of disc contour and elongation of the discal collateral ligaments.

The disc can also be found to be detached from the superior retrodiscal lamina or be trapped anterior to the condyle with no superior disc space.

Mild dislocation, or subluxation, can be due to variations in disc tautness or looseness. This is more likely when the articular eminence is short and steep posteriorly with a longer and flatter anterior slope. Generalized joint laxity has been cited as a normal variant and has been shown to be significantly more prevalent in patients with internal derangements (Magnusson et al. 1994). Joint laxity can be due to lengthening of the anterior recess and a drag on the inferior surface of the disc during the rotation phase of early mouth opening or changes in ligament structure (Meunissier et al. 1993).

A study of asymptomatic subjects found prevalence of disc displacements in 33% of volunteers (Katzberg et al. 1996). A study of disc position in asymptomatic children found a rate of 6% in a population with a mean age of 11 years. Prevalence of disc displacement increased to 34% in a population with a median age of 16–19 years, suggesting that children begin to develop changes in disc position in their early teenage years (Tominaga et al. 2007).

Perforation

The disc can be perforated at the posterior slope of the articular tubercle with variations at the articular eminence. Mechanical breakdown in the articular disc such as perforation (instead of unusual disc position) can lead to chronic disc displacement and greater thickness of the disc (Wongwatana 1994). When no symptoms are present and only anomalies are visualized radiographically or postmortem, a perforation is labeled as an anatomic variant instead of a pathological disease process.

A study of perforations of the TMJs from 106 cadavers showed disc perforation within 28% of individuals of age range 53–90 years. Perforations occurred centrally, laterally, and posterior with equal presence of central and lateral perforations. Posterior perforations were least common. Central perforations were large, caused nearly complete destruction of the disc, and exhibited severe condylar remodeling under the perforation. Lateral perforations varied from small to large and associated condylar changes varied according to the size of the defect. Regardless of the amount of destruction, discs remained well attached to the periphery of the condyle (Barton and Ellenbecker 1987).

Disc–condyle adhesions

Fibrous adhesions within the TMJ, not caused by trauma or congenital deformities, are thought to occur mainly in the superior compartment of the TMJ, specifically between the disc and condyle. Bilateral adhesions can cause deepening of pre-angular notches (Bell 1990). Intra-articular disc adhesions often accompany thickening and flattening of the condylar head and narrowing of the joint space.

Detachment from lateral pterygoid muscle

Temporalis muscle fibers, masseter muscle fibers, and the lateral pterygoid upper head may occasionally attach to the articular disc. The masseter may attach to the anterolateral aspect of the articular disc and the lateral pterygoid may attach to the anterior or medial border of the articular disc. Occasionally, the lateral pterygoid muscles will not be attached to the disc of the joint capsule but will most commonly be attached to the triangular depression in front of the neck of the condyle. In other occasions, the lateral pterygoid may be attached more to the disc and less to the neck of the mandibular condyle.

Contour

Although variable, the disc is thickest behind the center at the deepest part of the mandibular fossa. Mediolateral variations are equally relevant. The disc is often incomplete and variably perforated (Standring 2009). Disc contour may additionally vary in orientation to posteriorly or anteriorly, or contour may not be present.

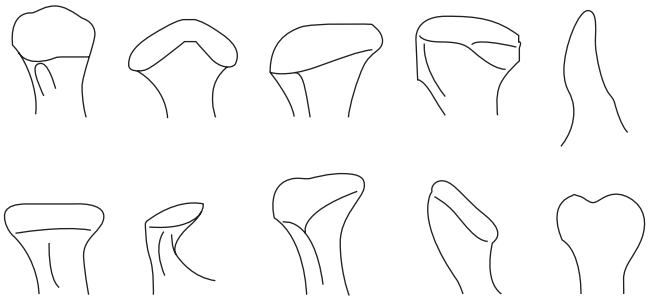

Figure 14.2 Variations in the shape of the mandibular condyle. Adapted from Mongini (1977) with permission from Elsevier.

Condyle

Individual variations do exist in the shape, form, position, presence, and size of the mandibular condyle. The prevalence of radiographic variation in condylar morphology has been reported to be 81.3% across persons (Mathew et al. 2011). The mandibular condyle has been documented to be 15–20 mm in length, 8–10 mm in width, and can protrude medially 15–20 mm. The shape of the condyle varies from flat or lancet-shaped to broad or narrow based (Fig.14.2). Rarely, the mandibular condyle can be superiorly convex.

The neck of the condyle can vary in length and width with a central ridge existing on the anterior surface of the neck. A fovea may exist on the anterior surface of the neck of the condyle, where the external pterygoid muscle can insert. The condyle can also have a backward or forward inclination with variations in the length of the neck. Some have a smooth continuation of the anterior neck into the convex articular surface while others have a narrow depression where the head of the condyle meets the neck, coexisting with a sharp anterior protrusion of the head (Zarb and Carlsson 1979). The condylar head can grow in the vertical direction, horizontally, or rotationally changing the position of the joint. The mandibular condyle can also be higher than the coronoid process and vary in angle relation to the ramus.

Hyperplasia

Hyperplasia can occur as a localized enlargement of the condyle or coronoid. Excessive size of the mandible with no abnormality of condylar size, shape, or function can also be found radiographically. The condyle sometimes appears falsely hyperplastic but is not enlarged and the neck of the condyle, body, and ramus of the mandible is elongated with no antegonial notching. Unilateral overgrowth of the condyle can cause facial asymmetry while bilateral hyperplasia results in mandibular prognathism. At times, the normal curvature is missing so that the width of the condylar neck is accentuated with an anterior projection giving an "L" deformity.

Hypoplasia

Hypoplasia is the incomplete development or underdevelopment of the mandible or cranial bones, and is less severe than aplasia. Unilateral condylar hypoplasia exhibits condylar deformity, short wide ramus, shortening of the body of the mandible, antegonial notching, and fullness of the face on the affected side. On the unaffected side, there can also be relative elongation of the mandibular body and flatness of the face. The vertical depth from the tip of the condyle to the inferior margin of the ramus can be shortened in hypoplasia, giving a "toadstool" appearance.

Aplasia and agenesis

Aplasia is incomplete development of the cranial bones or mandible. The most common developmental defect is the lack of growth of the condyle usually resulting from the incomplete development of the primordium of the condyle causing little or no articular fossa and a rudimentary or absent condylar eminence. The auditory apparatus is frequently affected and mandibular ramus is found to be shortened and wider with a missing condyle.

Complete absence (agenesis) of the mandible or maxilla is extremely rare bilaterally. If the condyle is absent or not in close approximation to the fossa, the fossa eminence loses it shape and presents as an anatomic variance.

Multilobular condyle

Also known as a double condyle, bifid condyles result in the replication of the head of the mandible, usually in the anteroposterior aspect. Although rare, many present asymptomatic. Bifid condyles may result from the separation of the lateral and medial aspects of the developing condyle by the vascular canals and their connective tissue septa that form in the human condyle (Moffett 1966). The splitting of the condyle may range from a shallow groove to two distinct condyles (Stefanou et al. 1998).

A medial and lateral head divided by an anteroposterior groove or an anterior and posterior head can be present. Multilobular condyle (Fig.14.3) is usually unilateral but may be found bilaterally. It is more likely to be diagnosed by radiological evidence than clinical evidence. A study of 1882 cadaveric skulls found the incidence of bifid mandibular condyle to be 0.48% (Szentpetery et al. 1990). Even rarer than bifid condyle, cases of trifid (three-lobed) and tetrafid (four-lobed) condyles have been reported in the literature (Sala-Perez et al. 2010; Sahman et al. 2011).

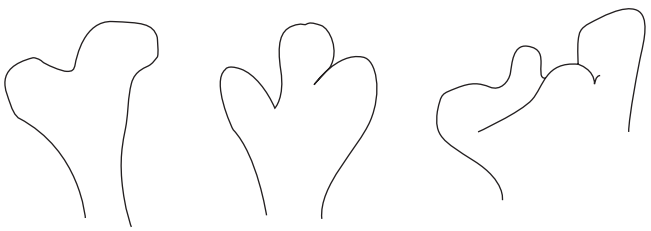

Figure 14.3 Multilobular condyles: bifid, trifid and tetrafid.

Condylar posterior surface concavity

Variations in shape are common radiographic findings in the posterior surface of the condyle. The bony surface of the condyle may be flattened or contain a bony protuberance which may cause an anatomical perforation in the disc. Although normally arched and concave, the condyle may present with a smooth depression in the superior articular surface or convex. This can be confused with a bifid condyle. The concavity can also vary in extent.

Capsule

The TMJ capsule can be stretched or the size can be variable. The variation in the capsule often presents with chronic dislocations of the disc.

Maxilla

Union of the coronoid process and maxilla

Bilateral union between the coronoid processes and the maxilla has been reported (Super and Cotton 1982).

Synostosis of mandible and maxilla

Hypertrophy of the coronoid process may interfere with jaw function; when bilateral, the interference is spontaneous. A patient has been reported with pseudoankylosis due to fusion between the lingula of the mandible and left pterygoid process (Super and Cotton 1986). Another case presented limited ability to open the mouth, caused by a fusion of the maxilla and mandible (Shams et al. 2006).

Mandible

The mandibular ramus could have a higher coronoid process, a shorter ramus, or no true sigmoid notch. The mandibular body could have a lesser angle, a shorter height, and an accentuated antegonial notch (Sarnat and Laskin 1962). The ramus and mandibular body can also be absent.

Coronoid process hyperplasia

Hyperplasia of the coronoid process is seen more in females and may be unilateral or bilateral. Bilateral cases are five times more common than unilateral cases (Neville et al. 2008). There may also be a nodular growth of the tipoff of the coronoid process.

Elongation of the coronoid process

Hyperplasia of the coronoid process is infrequent and may present with difficulty or limitation in opening the mouth. A case reported a geriatric male with lengths of the right and left coronoid process of 2.4 cm and 2.6 cm, respectively (Chauhan and Gupta 2011).

Absence of mandibular rami

Agenesis is partial to total absence of TMJ due to an absence of the mandibular condyle or rami. Congenital bilateral absence of the mandibular rami has also been noted (Kazanjian 1956). Persons with unilateral agenesis or any other form of unilateral mandibular growth arrest will exhibit a very characteristic appearance with a long face on one side and short face on the other side. The facial asymmetry includes mandibular deviation to the affected side during the open phase of the mouth.

Dysplasia

Dysplasia of the mandible and temporal bone are usually unilateral, asymmetric, and may occur with complete agenesis.

Hypoplasia

Hypoplastic deformities of the mandible do not usually affect articulation, but do affect the size or development of dentition. TMJ may become involved later as a result of functional disturbances due to a disparity in size between the mandible and maxilla, or to the absence of or severe disturbances in arrangement of dentition. Hypoplasia of the mandible can present with normal bicondylar widths.

Hyperplasia

Unilateral hyperplasia shows a longer ramus and mandibular body with normal TMJ functions.

Temporal bone

Variations along the articular eminence on the temporal bone may be due to developmental anomalies, but the joint forms normally.

Variation in articular surfaces

The articular eminence and articular surface are approximately 25° to the occlusal plane but the steepness is variable. The steepness of the articular eminence is indicated as a possible etiological factor in disc displacement and disc position. The articular eminence can be less prominent or absent from the TMJ. A widened disc space can also be seen with the loss of the articular eminence. The articular eminence is somewhat saddle-shaped, strongly convex from the side, and concave when viewed from the front or back. The degree of this convexity and concavity is highly variable. The medial and lateral borders of the articular eminence are often accentuated by fine bony ridges that are not secondary to a disease process or trauma.

The thinnest portion of the mandibular fossa may be lined with synovial membranes.

Blood supply

Ascending pharyngeal artery may branch from the common carotid instead of the external carotid artery (Standring 2009).

Variations in the superior temporal artery are largely in the relative sizes of the branches and their absence (Standring 2009). The superficial temporal artery and middle meningeal artery can also be superimposed.

The maxillary artery may pierce different aspects of the lateral pterygoid. Variations in the course of the maxillary artery include passage of the artery medial to the lateral pterygoid and to the lingual and inferior alveolar nerves, passage between the lingual and inferior alveolar nerves, passage through a loop formed by the inferior alveolar nerve, and branching of the middle meningeal artery distal to the inferior alveolar artery. The maxillary artery can also present superficial or deep to the lower head of the lateral pterygoid. The main stem of the maxillary artery may run superficial to both heads of the lateral pterygoid muscle, or may pass deep to the inferior head and emerge through the cleft between the two heads. Sometimes, the artery is found lateral to the lower head of the lateral pterygoid rather than medial to it. The maxillary artery has also been found to arise from a common stem with the facial artery allowing it to be parallel with the ramus of the mandible.

The middle meningeal artery may arise directly from the first part of the maxillary artery (most commonly when the maxillary artery lies superficial to the lateral pterygoid) or from a common trunk with the inferior alveolar artery. Variations in the origin of the middle meningeal artery in relation to the inferior alveolar artery have also been noted.

Penetrating vessels that supply the lateral pterygoid may also supply the mandibular condyle.

Vascular malformation is a rare entity in the temporomandibular joint as two-thirds of malformations of the jaws occur in the mandible, particularly the ramus or mandibular body. Most malformations are asymptomatic or have no distinct symptoms, and vary clinically, radiographically, and microscopically. This produces a major challenge to proper diagnoses (Abramowics et al. 2007).

Venous drainage

Often the retromandibular vein is not connected to the posterior auricular vein to form the external jugular vein, enlarging the anterior jugular vein.

Veins drain the anterior aspect of the joint and associated tissues into the plexus surrounding the lateral pterygoid; posteriorly, they drain into the vascular region that separates the two laminae of the bilaminar region of the disc.

Lymphatics

Lymphatics drain deeply to the upper cervical lymph nodes surrounding the internal jugular vein, specifically the deep parotid lymph nodes. Superficial parotid lymph nodes and cervical lymph nodes often drain the TMJ.

Nerve supply

The nerves to the temporal muscles (may present as one or three nerves, but usually there is an anterior and posterior deep temporal) may arise from the upper head of the lateral pterygoid muscle and the anterior bone forming the infratemporal fossa or both nerves may emerge between the two heads of the lateral pterygoid muscle. Studies have found three spurious jugular foramina located in the glenoid fossa of the temporomandibular joint and three in the zygomatic process (Angel 1948). The temporal nerves are usually accompanied by corresponding deep temporal arteries, but these again vary in number. The anterior deep temporal nerve may follow the masseteric above the upper border of the superior head of the lateral pterygoid muscle and the bone or emerge between the two heads of the lateral pterygoid.

The masseteric nerve and deep posterior temporal nerve can lie 2–5 mm posterior to the articulating eminence.

Muscles

Masticatory muscles attached to the TMJ and responsible for the TMJ functions can be hypertrophied or even absent due to congenital defects. A study of insertion of the pterygoid muscle into the disc-capsule complex of the TMJ found both two-headed and three-headed variants (Kilic et al. 2010). Additional investigations into the attachment of the pterygoid have found three types of variant attachments: the muscle inserting into the condyle and the disc-capsule complex (55%); the muscle only inserting into the condyle (27.8%); and the muscle inserting into only the disc-capsule complex (16.7%) (Antonopoulou et al. 2012).

Ligaments

Cases have shown an extra ligament – the mandibular-malleolar ligament or anterior malleolar ligament – connecting the neck and anterior process of the malleus to the superiormediposterior capsule, interarticular disc, and the sphenomandibular ligament (Pinto 1962).

A study has also confirmed the existence of variation in the lateral ligament in the TMJ. Macroscopic investigation found that 70% of 20 TMJ specimens exhibited an obvious ligament and the remaining 30% exhibited an indistinct structure. Of the obvious ligaments, 35.7% formed a cord-like structure with sharp borders (Nell et al. 1994).

Absence and hemiplasia

Due to the high variability of human anatomy, abnormalities of the TMJ may include the absence of virtually any of its components. For example, the complete absence of the left mandibular condyle was reported with no previous history of trauma or disease (Canger and Celenk 2012).

Hemi-, hyper-, or hypoplasias may also be present. In the case of a hemiplasia, a feature may exhibit partial enlargement or reduction in size locally with normal size throughout.

Congenital anomalies

Congenital anomalies of the TMJ include hyperplasia, hypoplasia, aplasia, and dysplasias. Familial traits of bilateral retrognathism or prognathism are not uncommon, while bilateral temporomandibular maldevelopment, such as Treacher Collins syndrome, are very rare.

Hyperplasia

Usually unilateral and resulting in movement disorders of the TMJ, hemihyperplasia syndromes inclde Beckwith–Weidemann syndrome, Klippel–Trenaunay–Weber sundrome, McCune Albright Syndrome, Langer Gledion syndrome, Maffuci syndrome, and Ollier syndrome.

Hypoplasia

Hyoplasia syndromes include mandibular sysostosis, oculoauriculovertebral syndrome (Goldenhar syndrome), and hemifacial microsomia. Hemifacial microsomnia, first and second branchial arch syndromes, or lateral facial dysplasias are commonly characterized as affecting the condyle and ramus of the mandible as well as the temporal bone. Hemifacial microsomia, or first arch syndrome, is characterized by mandibular growth with deficiency in soft tissue, hypoplasia of the first and second brachial arch muscles, and facial nerve palsy. This skeletal defect is classified by the mandibular ramus and TMJ. It can present with small sizes, hyoplastic anterior and medially displaced TMJ, or complete absence of the joint.

Treacher Collins syndrome, or mandibulofacial dysostosis, has bilateral facial microsomia and presents with hypoplastic TMJs with short mandibular rami. Treacher Collins syndrome includes craniofacial anomalies that include incomplete development of the cranial bones and the first and second brachial arches of the mandible. Within Treacher Collins syndrome, the mandible is smaller and the condyle will present smaller with posterior and inferior positioning in relation to the external acoustic meatus.

Hallermann–Streiff syndrome, oculomandibulodyscephaly, includes a small mandible, especially the condyles, and an anterior positioning of the condyle with a poorly formed fossa. It can be differentiated from Treacher Collins syndrome by the articulation of the condyles.

In both syndromes the condyles are hypoplastic; however, Treacher Collins syndrome presents with hypoplastic condyles that have a normal anteroposterior relationship to the fossa, while Hallermann–Streiff syndrome presents with hypoplastic condyles articulating with the articular eminence.

The Robin anomaly and the Piere–Robin syndrome feature hypoplasia of the mandible and maxilla.

Aplasia and agenesis

Aplasia and agenesis are most commonly unilateral, but asymmetry is common in bilateral cases. Goldenhar's syndrome exhibits partial or total absence of the TMJ. Nager–Reynier syndrome, or acrofacial dysostosis, is an abnormality of the TMJ which presents anomalies that closely resemble those found in facial microsomia, but maldevelopment is limited to the TMJ (which may be hypoplastic or absent) and the mandibular ramus.

Dysplasias

Fibrous dysplasia has slow benign swelling of the mandible or maxilla, where the fibrous connective tissue has a characteristic whorled pattern and contains trabeculae of immature nonlamellar bone. Fibrous dysplasia occurs in children and young adults, and usually becomes inactive when they reach skeletal maturity.

References

Abramowicz S, Marshall CJ, Dolwick MF, Cohen D. 2007. Vascular malformation of the temporomandibular joint: report of a case and review of the literature. *Oral Surg Oral Med Oral Path Oral Radiol* 103: 203–206.

Angel JL. 1948. Factors in temporomandibular joint format. *Am J Anat* 83: 223–246.

Antonopoulou M, Iatrou I, Paraschos A, Anagnostopoulou S. 2012. Variations of the attachment of the superior head of human lateral pterygoid muscle. *J Cranio Maxillo Facial Surg* 41: 1–7.

Barton JM, Ellenbecker MA. 1987. Anatomical variations in the articular disc of the human temporomanidbular joint. *Trans Nebraska Acad Sci* XV: 1–4.

Bell WE. 1990. Temporomandibular Disorders: *Classification, Diagnosis, Management*, third edition. Year Book Medical Publishers.

Canger EM, Celenk P. 2012. Aplasia of the mandibular condyle associated with some orthopaedic abnormalities: a case report. *Dentomaxillofacial Radiol* 31: 259–263.

Chauhan P, Gupta S. 2011. Bilateral elongated coronoid processes of mandible. *Int J Anat Variations* 4: 25–27.

Hollinshead WH. (ed.) 1982. *Anatomy for Surgeons: The Head and Neck. Vol. 1*. Third edition. Philadelphia: Harper and Row.

Isberg A. 2001. Temporomandibular Joint Dysfunction: *A Practitioner's Guide*. Informa Healthcare.

Katzberg RW, Westesson PL, Tallents RH, Drake CM. 1996. Anatomic disorders of the temporomandibular joint disc in asymptomatic subjects. *J Oral Maxillofacial Surg* 54: 147–153.

Kazanjian VH. 1956. Bilateral absence of the ascending rami of the mandible. *Brit J Plast Surg* 9: 77–82.

Kilic G, Dergin G, Yazar F, Kurt B, Kutoglu T, Ozan H, Balcioglu HA. 2010. Insertions of the lateral pterygoid muscle to the disc-capsule complex of the temporomandibular joint and condyle. *Turk J Med Sci* 40: 435–441.

Lang J. 1995. *Clinical Anatomy of the Masticatory Apparatus and Peripharyngeal Spaces*. New York: Thieme.

Lubosch W. 1906. Ueber den Meniscus im Kiefergelenk des Menschen. *Mit 5 Abbildungen Anat Anz* 29: 417–430.

Magnusson T, Carlsson GE, Egermark I. 1994. Changes in clinical signs of craniomandibular disorders from the age of 15 to 25 years. *J Orofacial Pain* 8: 207–215.

Mathew AL, Sholapurkar AA, Pai KM. 2011. Condylar changes and its association with age, TMD, and dentition status: a cross-sectional study. *Int J Dent 2011*: 1–7.

Meunissier M, Meunier A, Carpentier P, Marguelles-Bonnet R, Yung JP. 1993. Disc movements over the condylar head: radiographical study on autopsy materials. *J Orofacial Rehab* 20: 501–515.

Moffett B. 1966. The morphogenesis of the temporomandibular joint. *Am J Orthodontics* 52: 401–415.

Mongini F. 1977. Anatomic and clinical evaluation of the relationship between the temporomandibular joint and occlusion. *J Prosth Dent* 38(5): 539–551.

Nell A, Niebaurer G, Sperr W, Firbas W. 1994. Special variations of the lateral ligament of the human TMJ. *Clin Anat* 7: 267–270.

Neville BW, Damm DD, Allen C, Bouquot J. 2008. *Oral and Maxillofacial Pathology*, third edition. Saunders.

Pinto O. 1962. A new structure related to the temporomandibular joint and the middle ear. *J Prosthetic Dent* 12: 95–103.

Sahman H, Etoz OA, Sekerci AE, Etoz M, Sisman Y. 2011. Tetrafid mandibular condyle: a unique case report and review of the literature. *Dentomaxillofacial Radiol* 40: 524–530.

Sala-Perez S, Vazquez-Delgado E, Rodriguez-Baeza A, Gay-Escoda C. 2010. Bifid mandibular condyle: a disorder in its own right. *J Am Dent Assoc* 131: 1076–1085.

Sarnat BG, Laskin DM. 1962. Diagnosis and surgical management of disease of the temporomandibular joint. *Arthr Rheum* 6: 256–346.

Shams MG, Motamedi MHK, Abad HLD. 2006. Congenital fusion of the maxilla and mandible: brief case report. *Oral Surg Oral Med Oral Path Oral Radiol* 102: e1–e3.

Standring S. 2009. *Gray's Anatomy*, 40th edition. Churchill Livingstone.

Stefanou EP, Fanourakis IG, Vlastos K, Katerelou J. 1998. Bilateral bifid mandibular condyles: report of four cases. *Dentomaxillofacial Radiol* 27: 186–188.

Super S, Cotton JS Jr. 1982. Bilateral pseudoankylosis of the TMJ due to synostoses between the mandible and maxilla. *J Oral Maxillofacial Surg* 40: 590–592.

Super S, Cotton JS Jr. 1986. A case of pseudoankylosis between the pterygoid plate and mandible. *J Oral Maxillofacial Surg* 44: 467–468.

Szentpetery A, Gabor K, Marcsik A. 1990. The problem of the bifid mandibular condyle. *J Oral Maxillofacial Surg* 48: 1254–1257.

Tominaga K, Konoo T, Morimoto Y, Tanaka T, Habu M, Fukuda J. 2007. Changes in temporomandibular disc position during growth in young Japanese. *Dentomaxillofacial Rad* 36: 397–401.

Tubbs RS, Shoja MM, Loukas M. 2008. Letter to the Editor. *Clin Anat* 21:609.

Wongwatana S, Kronman JH, Clark RE, Kabani S, Mehta N. 1994. Anatomic basis of disc displacement in temporomandibular joint dysfunction. *Am J Orthodonics Dentofacial Orthopedics* 105: 257–264.

Zarb GA, Carlsson GE. (eds) 1979. Temporomandibular Joint: *Function and Dysfunction*. Missouri: Mosby.

15 Shoulder joint

Brion Benninger
Western University of Health Sciences, Portland, Oregon, United States

The term shoulder joint equates to the glenohumeral joint specifically (articulation between glenoid fossa and the humeral head) and in general is part of a shoulder complex involving five articulations, which are often described as the shoulder joint complex. These five articulations comprise three known synovial joints (glenohumeral, acromioclavicular, and sternoclavicular) and two clinically recognized articulations (scapulothoracic and acromiohumeral). The glenohumeral joint boasts the highest degree of movement of the joints in the human body. The humeral head to glenoid fossa ratio is approximately four to one, which provides its impressive degree of mobility. It relies on muscle tendon complexes, ligaments, and a relatively redundant reinforced capsule for its multiplanar extensive range of motion. There is a high degree of variation regarding structures associated with the shoulder joint complex because multiple structures are sharing relatively small and similar regions of attachment. The innervation of the glenohumeral joint and its intra-articular associated structures predominantly arise from C5,6,7 roots with some occasionally coming from C4. The nerves predominantly carrying the fibers are the axillary, suprascapular, and subscapular nerves. Contributions from the musculocutaneous nerve may be minimal or absent. Occasionally fibers may come from the posterior cord (Gardner 1948; DePalma 1983).

Humeral head and glenoid fossa positions

The humeral head is inclined at 130–150° in relation to the shaft. Retroversion of the humeral head can be highly variable both among persons and between sides (Evans and Krahl 1945). Boileau and Walsh (1997) reported a wide variation of retroversion ranging from −6.7° to 47.5°. Another team of investigators (Pearl and Volk 1995) reported a mean of 29.8° of retroversion with a range of 10–55°. The average vertical dimension of the articular region of the head is 48 mm with a 25 mm radius of curvature. The average transverse dimension is 45 mm with a 22 mm radius (Iannotti et al. 1992). The glenoid fossa is usually pear-shaped with an average vertical measurement of 35 mm and a transverse of 25 mm (DePalma et al. 1949). Saha (1961, 1971, 1983) reported that the glenoid fossa may either be anteverted or retroverted regarding the plane of the scapula. He noted that 75% of shoulders he analyzed had retroverted glenoid fossa averaging 7.4° and nearly 25% were anteverted 2–10°. The glenoid cavity may be concave inferiorly or concave superiorly. An area of thickened subchondral bone near the center of the glenoid fossa has been termed the tubercle of Ossaki (Fitzpatrick and Walz 2010). Full-thickness cartilage defects can also been seen of the glenoid fossa on imaging (Fitzpatrick and Walz 2010).

Labrum

The glenoid labrum is triangular-shaped in cross-section and attached to the glenoid fossa rim. It is known to vary in size from being a formidable structure within the articular joint to being absent. It is mistakenly compared to the fibrocartilage of the knee; however, Mosely and Overgaard (1962) demonstrated it was formed almost exclusively of dense fibrous tissue. The glenoid labrum can increase the depth of the fossa by 50% and accept attachment from the long heads of the biceps brachii and triceps brachii tendons and glenohumeral ligaments. Variations of the anterior superior labrum include the sublabral foramen seen in 8–25% of individuals (DePalma et al. 1949; Williams et al. 1994; Tuite and Orwin 1996; Park et al. 2000). Avulsions of the glenoid labrum can start at this foramen and can be mistaken for a Bankart lesion. An absent anterior superior labrum with an associated cord-like middle glenohumeral ligament, which is a unique variant termed "The Buford Complex," has been reported in 1.5–5% of cases. The middle glenohumeral ligament in these cases presents as a cord-like structure originating from the superior labrum at the base of the biceps tendon crossing the subscapularis tendon to insert on the humerus. "The Buford Complex" can be mistaken for a detached labrum. The labrum receives more arterial branches to its peripheral region than to its inner area from the suprascapular, circumflex scapular, and posterior circumflex humeral circumflex arteries (Cooper et al. 1992).

Bergman's Comprehensive Encyclopedia of Human Anatomic Variation, First Edition. Edited by R. Shane Tubbs, Mohammadali M. Shoja and Marios Loukas.
© 2016 John Wiley & Sons, Inc. Published 2016 by John Wiley & Sons, Inc.

Capsule

The articular capsule is approximately twice the surface area of the humeral head, allowing a comprehensive circular range of motion while enclosing the humeral head, glenoid cavity, tendon of the long head of biceps brachii, and the glenoid labrum. The capsule accepts 28–35 mL of fluid and females often hold more than males (Neviasev 1962). The capsule is variable in thickness, especially where it is reinforced by other structures, but is not known to be congenitally absent. It is generally thicker anteriorly. The capsule is reinforced from structures anteriorly and posteriorly, creating a capsular complex or mechanism. The anterior capsular mechanism includes the fibrous capsule, glenohumeral ligaments, synovial membrane and its recesses, glenoid labrum, subscapularis muscle tendon unit, and the scapular periosteum (Beltran et al. 2002). An area of the anterior capsule termed the rotator interval is composed of interacting fibers from the coracohumeral ligament, superior glenohumeral ligament, supraspinatus, and subscapularis tendons (Nobuhara and Ikeda 1987; Plancher et al. 2005). Insertion of the anterior capsule can be divided into three types depending on the proximity to the glenoid margin (Zlatkin et al. 1988).

The posterior capsular mechanism is formed by the posterior capsule, synovial membrane, glenoid labrum, periosteum, and the posterosuperior muscle tendon compressor (rotator) cuff structures (supraspinatus, infraspinatus, and teres minor). The long head of the biceps tendon merging into the superior aspect of the glenoid labrum and the long head of the triceps brachii tendon attaches to the infraglenoid tubercle and merges into the glenoid labrum inferiorly, providing additional supportive structures for the glenohumeral joint. The capsule receives its arterial supply from the suprascapular, circumflex scapular, and posterior circumflex humeral and anterior circumflex humeral vessels (Andary and Peterson 2002). The capsule may insert on the glenoid margin, glenoid neck, or more medially onto the scapula (Fitzpatrick and Walsh 2010).

Ligaments

The superior glenohumeral ligament (SGHL), which some refer to as Flood's ligament, is present in up to 97% of shoulders as reported by DePalma et al. (1949). Its dimensions can be cord-like, it can contain a few wispy fibers, or it can be absent (O'Brien et al. 1987). It arises from both the supraglenoid tubercle just anterior to the long head of the biceps brachii and the superior glenoid labrum. It then runs inferiorly and laterally to the posterior capsule, attaching on the humerus just superior to the lesser tuberosity. The SGHL along with the coracohumeral ligament is part of the rotator interval. Turkel et al. (1981) reported three common variations with its glenoid attachment (biceps tendon, glenoid labrum, and middle glenohumeral ligament).

The middle glenohumeral ligament is the most variable of the glenohumeral ligaments in both size and constancy (DePalma et al. 1949; Ferrari 1990; Beltran et al. 2002). It may be attenuated or absent in up to 30% of shoulders (Thomas and Matsen 1989) In a magnetic resonance imaging (MRI) study of asymptomatic volunteers, it was found in only 79% of patients (Park et al. 2000). The middle glenohumeral ligament (MGHL) usually arises from the neck of the glenoid just inferior to the origin of the SGHL. The MGHL may also originate with the SGHL and long head of the biceps brachii tendon, or with the long head of the biceps brachii tendon with an absent SGHL (Beltran et al. 2002). Its fibers then merge with the subscapularis tendon before attaching on the lesser tuberosity. The MGHL may be duplicated (Fitzpatrick and Walz 2010).

The inferior glenohumeral ligament (IGHL) is a complex structure that includes an anterior and posterior band with an axillary pouch sandwiched between them (O'Brien et al. 1990). In abduction and lateral rotation, the anterior band appears to broaden while the posterior band becomes cord-like. During medial rotation, the posterior band broadens while the anterior band appears cord-like. With the arm resting at the body's side, both anterior and posterior bands pass through a 90° arc and insert on the humerus. The anterior band of the IGHL arises from the glenoid. In most people, the anterior band of the IGHL has its origin from the labrum with some fibers extending to the glenoid neck. In some shoulders, the anterior band has its origin solely on the glenoid neck (Eberly et al. 2002).

The coracohumeral ligament is biomechanically not fully understood. It is a relatively strong band attaching from the lateral border of the coracoid process base as V-shaped and runs transversely to attach onto the greater tubercle. Its posterior border is intimate with the capsule. Some investigators (Williams and Warwick 1980) believe phylogenetically it represents a previous attachment of the pectoralis minor and has been reported in 15% of the population to have fibers of the pectoralis minor cross the coracoid process to attach on the humeral head. A region of the coracohumeral ligament is intimate with the articular surface of the supraspinatus tendon perpendicular to the tendon, thus forming a lateral arch which can be seen within the joint to the infraspinatus attachment.

An accessory ligament attached to the acromion and greater tubercle of the humerus is termed the accessory ligament of Malgaigne.

Tendons

The long head of biceps brachii provides minimal attachment to the supraglenoid tubercle and merges into the glenoid labrum allowing different fibers to reach the labrum; this results in four types of tendon labrum complexes, which can be differentiated (Vangsness et al. 1994; Huber and Putz 1997). The tendon lies in the bicipital groove, which is formed between the greater and lesser tuberosities. Anatomically, the bicipital groove has several variations. The depth of the groove, especially along its medial side, could predispose a person to tendonitis. Hitchcock

and Bechtol (1948) described six variations of the angle of the medial wall of the bicipital groove (type 1 grooves had an angle of the medial wall of 90°, type 2 grooves 75°, type 3 grooves 60°, type 4 grooves 45°, type 5 grooves 30°, and type 6 grooves 15°). The tendon and its relationship with the glenohumeral ligaments vary greatly. In most specimens, it blends with the superior glenohumeral ligament. In some, it blends with the middle glenohumeral ligament and, rarely, it remains continuous with all three glenohumeral ligaments. The tendon is generally described as having a partial intracapsular orientation. Anomalies can result in the tendon lying entirely intracapsular, form as a double structure or be absent (DePalma 1983). There have been four reported cases of congenital absence of the long head of the biceps brachii tendon (Smith et al. 2002; Glueck et al. 2003; Franco et al. 2005).

The long head of triceps brachii provides minimal attachment to the infraglenoid tubercle and merges into the glenoid labrum allowing fibers to reach the labrum, but remains extra articular.

Rotator cuff muscles

Relatively short muscles are referred to as rotator muscles, which more accurately behave as compressor muscles (supraspinatus, infraspinatus, teres minor, subscapularis). These tendons coalesce to create a muscle tendon complex, which compress the head of the humerus into the glenoid cavity (less accurately called the rotator cuff). This tendon complex lies over the posterior, superior, and anterior aspect of the glenohumeral joint, attaching at the greater and lesser tubercles. Rotham and Park (1965) and Fealy et al. (2006) describe six arteries that consistently provide arterial supply to the rotator cuff tendons: (1) suprascapular, 100%; (2) anterior circumflex humeral, 100%; (3) posterior circumflex humeral, 100%; (4) thoracoacromial, 76%; (5) suprahumeral, 59%; and (6) subscapular, 38%.

Bursae and recesses

Multiple bursae exist in the shoulder joint complex. There are two bursae that are present consistently and have importance clinically: subacromial and subscapular. The subacromial bursa is attached to the external surface of the greater tuberosity and compressor (rotator) cuff muscles, extending to adhere to the undersurface of the acromion and coracoacromial ligament. It essentially lies under the acromion, coracoid process, and deltoid muscle while remaining extracapsular. The subscapular bursa lies extracapsular between the tendon of the subscapularis muscle and neck of the scapula, and enters within the capsule between the superior and middle glenohumeral ligaments. Colas et al. (2004) revealed that a suspensory ligament attaches from the subscapularis bursae to the coracoid process. He demonstrated that, in 28% of the specimens studied, the subscapular bursa fused with the subcoracoid bursa to create a larger more unique bursa. The tendon of pectoralis minor may pass over the coracoid process to insert elsewhere. As a result, it may produce a characteristic groove on the superior part of the process. In these cases, a bursa intervening between the tendon and bone may communicate with the shoulder joint.

Numerous recesses are identified in the capsule between the glenohumeral ligaments and predominate along the anterior aspect of the capsule. DePalma et al. (1949) described six common variations or types of recesses in the anterior capsule, which are variations of the subscapularis bursae. Type 1 (30.2%) has one synovial recess above the middle glenohumeral ligament; type 2 (2.04%) has one synovial recess below the middle glenohumeral ligament; type 3 (40.6%) has one synovial recess above and below the middle glenohumeral ligament; type 4 (9.03%) has one large recess above the inferior glenohumeral ligament with the middle glenohumeral ligament being absent; type 5 (5.1%) the middle glenohumeral ligament has two small synovial folds; and type 6 (11.4%) has no synovial recesses.

Sprengel's deformity occurs when the scapula is formed near the cervical spine in the developing fetus. It causes a wide variety of shoulder dysfunction (Sprengel 1891). An omovertebral bone may connect the scapula to the cervical spine.

Glenoid hypoplasia results from failure of the inferior glenoid to develop (Gardner and Gray 1953).

Sternoclavicular

Tuscano et al. (2009) studied the sternoclavicular joint and found that the left and right SCJ space ranged from 0.2 to 1.37 cm. The difference (delta or asymmetry) between left SCJ space and right SCJ space ranged from 0 (symmetrical) to 0.57 cm in 104 cases. Left and right clavicular head diameters ranged from 1.2 to 3.7 cm with left/right asymmetry (delta) ranging from 0 cm (symmetrical) to 1 cm.

Acromioclavicular

The acromioclavicular joint may be duplicated (Viard 2013). The acromion may be straight, flat, curved, or hooked in shape. Gray (1942) reported 240 (22.12%) scapular facets in 1085 specimens. A total of 111 facets from 547 specimens were on left scapulae and 129 facets were on 538 right scapulae.

In a cadaveric study, Emura et al. (2014) classified the acromioclavicular joint into three major types according to the presence or absence of the articular disc.

Type 1 joints have an articular disc which completely divides the articular cavity; this was found in 3.8% of shoulders. The complete articular disc was entirely attached to the articular capsule at its periphery. The articular disc had two articular surfaces: the acromial surface and the clavicular surface. In these acromioclavicular joints, both articular surfaces were slightly convex; type 1 acromioclavicular joint is therefore classified

into the double ellipsoid joint. The articular disc was thick near the upper part of the attachment to the articular capsule and it became thinner at its lower part, forming a wedge shape in the coronal section. The upper part of the articular disc was made of fibrocartilage and the lower part of the disc comprised mostly dense connective tissue.

Type 2 joints are characterized by an incomplete articular disc, which incompletely divides the articular cavity of the acromioclavicular joint; this was found in 25.0% of shoulders. The incomplete articular disc originated from the upper part of the articular capsule, projected downward, and ended within the articular cavity instead of attaching to the capsule. This type is further subdivided into type 2a (13.5%) and type 2b (11.5%) according to the configurations of the articular surfaces. In type 2a, the acromial facet of the clavicle is convex both in the coronal and horizontal planes, and the clavicular facet of the acromion was flat. The incomplete articular disc of the type 2a acromioclavicular joint was coronally sectioned and histologically examined. The upper part of the incomplete articular disc was made of fibrocartilage. In type 2b, configurations of the articular surfaces of the clavicle and the acromion of the acromioclavicular joints are opposite to the counterparts of type 2a (11.5%). The acromial facet of the clavicle is flat, but the clavicular facet of the acromion is convex in both coronal and horizontal planes. The surface of the incomplete articular disc facing the clavicular facet of the acromion is concave.

Type 3 (71.2%) is characterized by the absence of the articular disc and is further subdivided into three types according to the configurations of the articular facets. In type 3a the clavicular facet of the acromion is concave in coronal and horizontal planes, suggesting an ellipsoid joint in 28.8%. In type 3b, configurations of the articular surfaces of the clavicle and acromion are opposite to those of type 3a (9.6%). The acromial facet of the clavicle is concave and the clavicular facet of the acromion is convex in both coronal and horizontal planes, suggesting that this type of the acromioclavicular joint be classified as an ellipsoid joint as in the case of type 3a. Both articular surfaces are flat in type 3c, forming a plane-type joint (32.7%).

Of 334 pairs, 29 left and 40 right scapulae showed facets on one side alone (Gray 1942). A total of 46 pairs showed facets on both the left and right sides. The facets on 22 pairs were identical to each other in size and other characteristics. Among 80 Indian scapulae, acromial facets were found in five cases (twice in 38 right scapulae and three times in 42 left scapulae).

Coracoclavicular joint

The coracoid process may be duplicated or even triplicated with any of these parts forming a joint with the overlying clavicle (Sharma 2003). The coracoclavicular joint is seen in up to 20% of the population. It may be more common in males and Asians, and some have opined that it is due to degenerative changes (Paraskevas et al. 2009). Nearby, the costoclavicular joint may have a bursa between its two layers. Additionally, accessory bursa may be found near the conoid or trapezoid ligaments (bursae of Poirier).

References

Andary JL, Peterson SA. 2002. The vascular anatomy of the glenohumeral capsule and ligaments: An anatomic study. *J Bone Joint Surg Am* 84: 2258–2265.

Beltran J, Bencardino J, Padron M, Shankman S, Beltran L, Ozkarahan G. 2002. The middle glenohumeral ligament: normal anatomy, variants and pathology. *Skeletal Radiol* 31: 253–262.

Boileau P, Walsh G. 1997. The three dimensional geometry of the proximal humerus. Implications for surgical technique and prosthetic design. *J Bone Surg Br* 79: 857–865.

Colas F, Nevoux J, Gagey O. 2004. The subscapular and subcoracoid bursae: Descriptive and functional anatomy. *J Shoulder Elbow Surg* 13: 454–458.

Cooper DE, Arnoczky SP, O'Brien SJ. 1992. Anatomy, histology and vascularity of the glenoid labrum. An anatomical study. *J Bone Joint Surg Am* 74: 46–52.

DePalma AF. 1983. *Surgery of the Shoulder*. Philadelphia: J. B. Lippincott.

DePalma AF, Callery G, Bennett GA. 1949. Variational anatomy and degenerative lesions of the shoulder joint. *Instr Course Lect* 6: 255–281.

Eberly VC, McMahon PJ, Lee TQ. 2002. Variation in the glenoid origin of the IGHL anterior band: implications for repair of the Bankart lesion. *Clin Orthop Rel Res* 400: 26–31.

Emura K, Arakawa T, Miki A, Terashima T. 2014. Anatomical observations of the human acromioclavicular joint. *Clin Anat* 27: 1046–1052.

Evans FG, Krahl VE. 1945. The torsion of the humerus. A phylogenetic survey from fish to man. *Am J Anat* 76: 303–337.

Fealy S, Adler RS, Drakos MC. 2006. Patterns of vascular and anatomical response after rotator cuff repair. *Am J Sports Med* 34: 120–127.

Ferrari DA. 1990. Capsular ligaments of the shoulder anatomical and functional study of the anterior superior capsule. *Am J Sport Med* 18: 20–24.

Fitzpatrick D, Walz DM. 2010. Shoulder MR imaging normal variants and imaging artifacts. In *Normal Variants and Pitfalls in Musculoskeletal MRI* (Morrison WB, Zoga AC, eds). Philadelphia: Elsevier.

Franco JC, Knapp TP, Mandelbaum BR. 2005. Congenital absence of the long head of the biceps tendon. *A case report. J Bone Joint Surg: Case Connector* 87: 1584–1586.

Gardner E. 1948. The innervation of the shoulder joint. *Anat Rec* 102: 1–18.

Gardner E, Gray DJ. 1953. Prenatal development of the human shoulder and acromioclavicular joint. *Am J Anat* 92: 219–276.

Glueck DA, Mair SD, Johnson DL. 2003. Shoulder instability with absence of the long head of the biceps tendon. Arthroscopy: *J Arthroscopic Related Surg* 19: 787–789.

Gray DJ. 1942. Variations in the human scapulae. *Am J Phys Anthropol* 29: 57–72.

Hitchcock HH, Bechtol CO. 1948. Painful shoulder. Observations on the role of the tendon of the long head of the biceps brachii in its causation. *J Bone Joint Surg Am* 30: 263–273.

Huber WP, Putz RV. 1997. Periarticular fiber system of the shoulder joint. *J Arthroscopic Rel Surg* 13: 680–691.

Iannotti JP, Gabriel JP, Schneck SL.1992. The normal glenohumeral relationships. An anatomical study of one-hundred and forty shoulders. *J Bone Joint Surg Am* 74: 491–500.

Moseley HF, Overgaard B. 1962. The anterior capsular mechanism in recurrent anterior dislocation of the shoulder. *J Bone Joint Surg Br* 44: 913–927.

Neviasev JS. 1962. Adhesive capsulitis of the shoulder (the frozen shoulder). *Med Times* 90: 783–807.

Nobuhara K, Ikeda H. 1987. Rotator interval lesion. *Clin Orthop Relat Res* 223: 44–50.

O'Brien SJ, Warren RF, Schwartz E. 1987. Anterior shoulder instability. *Orthop Clin North Am* 18: 395–408.

O'Brien SJ, Neves MC, Arnoczky, SP. 1990. The anatomy and histology of the inferior glenohumeral ligament complex of the shoulder. *Am J Sports Med* 18: 449–456.

Paraskevas G, Stavrakas ME, Stoltidou A. 2009. Coracoclavicular joint, an osteological study with clinical implications: a case report. *Cases J* 2: 8715.

Park YH, Lee JY, Moon SM, Mo JH, Yang BK, Hahn SH, Resnick D. 2000. MR arthrography of the labral capsular ligamentous complex in the shoulder imaging variations and pitfalls. *Am J Roentgenol* 175: 667–672.

Pearl ML, Volk AG. 1995. Retroversion of the proximal humerus in relationship to prosthetic replacement arthroplasty. *J Shoulder Elbow Surg* 4: 286–289.

Plancher KD, Johnson JC, Peteson RK, Hawkins RJ. 2005. The dimensions of the rotator interval. *J Shoulder Elbow Surg* 14: 620–625.

Rotham RH, Parke WW. 1965. The vascular anatomy of the rotator cuff. *Clin Orthop Relat Res* 41: 176–186.

Saha AK. 1961. *Theory of Shoulder Mechanism: Descriptive and Applied*. Springfield, Ill.: Charles C. Thomas.

Saha AK. 1971. Dynamc stability of glenohumeral joint. *Acta Orthop Scand* 42: 491–505.

Saha AK. 1983. The classic mechanism of shoulder movements and a plea for the recognition of "zero position" of glenohumeral joint. *Clin Orthop Relat Res* 173: 3–10.

Sharma BG. 2003. Duplication of the clavicle with triplication of the coracoid process. *Skeletal Radiol* 32: 661–664.

Smith EL, Matzkin EG, Kim DH, Harpstrite JK, Kan DM. 2002. Congenital absence of the long head of the biceps brachii tendon as a VATER association. *Am J Orthop* 31: 452–454.

Sprengel RD. 1891. Die angeborene verschiebung des schulterblattes nach. *Oben Arch Klin Chir* 42: 545–549.

Thomas SC, Matsen FA III. 1989. An approach to the repair of avulsion of the glenohumeral ligament in the management of traumatic anterior glenohumeral instability. *J Bone Jt Surg Am* 71: 506–513.

Tuite MJ, Orwin JF. 1996. Anterosuperior labral variants of the shoulder: appearance on gradient-recalled-echo and fast spin-echo MR images. *Radiology* 199: 537–540.

Turkel SJ, Panto MW, Marshal JL. 1981. Stabilizing mechanisms preventing anterior dislocation of the glenohumeral joint. *J Bone Joint Surg Am* 63: 1208–1217.

Tuscano D, Banerjee S, Terk MR. 2009. Variations in normal sternoclavicular joints: a retrospective study to quantify SCJ asymmetry. *Skeletal Radiol* 38: 997–1001.

Vangsness CT, Jorgenson SS, Watson T, Johnson DL. 1994. The origin of the long head of the biceps from the scapula and glenoid labrum. An anatomical study of 100 shoulders. *J Bone Joint Surg Br* 76: 951–954.

Viard B, Karp JS, Tremlet J, Asali Z, Trouilloud P, Trost O. 2013. Unilateral duplication of the acromioclavicular joint: case report and literature review. *Surg Radiol Anat* 35: 973–977.

Williams MM, Snyder SJ, Buford D Jr. 1994. The Buford complex: the "cord-like" middle glenohumeral ligament and absent anterosuperior labrum complex: A normal anatomic capsulolabral variant. *J Arthroscopic Rel Surg* 10: 241–247.

Williams PL, Warwick R. 1980. *Gray's Anatomy*. Philadelphia: W. B. Saunders.

Zlatkin MB, Bjorkengren AG, Gylys-Morin V. 1988. Cross-sectional imaging of the capsular mechanism of the glenohumeral joint. *AJR Am J Roentgenol* 150: 151–158.

Further reading

Beltran J, Bencardino J, Mellado J, Rosenberg ZS, Irish RD. 1997. MR arthrography of the shoulder: variants and pitfalls. *Radiographics* 17: 1403–1412.

Bencardino JT, Beltran J, Rosenberg ZS, Rokito A, Schmahmann S, Mota J, Mellado JM, Zuckerman J, Cuomo F, Rose D. 2000. Superior labrum anterior-posterior lesions: diagnosis with MR arthrography of the shoulder. *Radiology* 214: 267–271.

Carroll K, Helms C. 2002. Magnetic resonance imaging of the shoulder: A review of potential sources of diagnostic errors. *Skeletal Radiol* 31: 373–383.

Cash CJC, MacDonald KJ, Dixon AK, Bearcroft PWP, Constant CR. 2009. Variations in the MRI appearance of the insertion of the tendon of subscapularis. *Clin Anat* 22: 489–494.

Clark JM, Harryman DT. 1992. Tendons, ligaments, and capsule of the rotator cuff. *J Bone Joint Surg Am* 74: 713–725.

De Maeseneer M, Van Roy F, Lenchik L, Shahabpour M, Jacobson J, Ryu KN, Handelberg F, Osteaux M. 2000. CT and MR arthrography of the normal and pathologic anterosuperior labrum and labral-bicipital complex. *Radiographics* 20: S67–S81.

Farooki S, Seeger LL. 1999. Magnetic resonance imaging in the evaluation of ligament injuries. *Skeletal Radiol* 28: 61–74.

Fealy S, Rodeo SA, Dicarlo EF, O'Brien SJ. 2000. The developmental anatomy of the neonatal glenohumeral joint. *J Shoulder Elbow Surg* 9: 217–222.

Gardner E. 1968. The embryology of the clavicle. *Clin Orthop Relat Res* 58: 9–16.

Ide J, Maeda S, Takagi K. 2004. Normal variations of the glenohumeral ligament complex: An anatomic study for arthroscopic Bankart repair. *J Arthroscopic Rel Surg* 20: 164–168.

Ilahi OA, Labbe MR, Cosculluela P. 2002. Variants of the anterosuperior glenoid labrum and associated pathology. *J Arthroscopic Rel Surg* 18: 882–886.

Kreitner KF, Botchen K, Rude J, Bittinger F, Krummenauer F, Thelen M. 1999. Superior labrum and labral-bicipital complex: MR Imaging with pathologic-anatomic and histologic correlation. *AJR* 170: 599–605.

Kwak SM, Brown RR, Resnick D, Trudell D, Applegate GR, Haghighi P. 1998. Anatomy, anatomic variations, and pathology of the 11-to 3-O'clock position of the glenoid labrum: findings on MR arthrography and anatomic sections. *AJR* 171: 235–238.

Massengill AD, Seeger LL, Yao L, Gentili A, Shnier RC, Shapiro MS, Gold RH. 1994. Labrocapsular ligamentous complex of the shoulder:

Normal anatomy, anatomic variation, and pitfalls of MR Imaging and MR Arthrography. *Radiographics* 14: 1211–1223.

Matsen FA, Zuckerman JD. 1983. Anterior glenohumeral instability. *Clin Sport Med* 2: 319–338.

McCauley TR, Pope CF, Jokl P. 1992. Normal and abnormal glenoid labrum: assessment with multiplanar gradient-echo MR imaging. *Radiology* 183: 35–37.

Mohana-Borges AV, Chung CB, Resnick D. 2003. Superior labral anteroposterior tear: classification and diagnosis on MRI and MR Arthrography. *Am J Roentgenol* 181: 1449–1462.

Palmer WE, Caslowitz PL, Chew FS. 1995. MR arthrography of the shoulder: normal intraarticular structures and common abnormalities. *AJR Am J Roentgenol* 164: 141–146.

Pfirrmann CW, Zanetti M, Weishaupt D, Gerber C, Hodler J. 1999. Subscapularis tendon tears: detection and grading at MR Arthrography. *Radiology* 213: 709–714.

Prescher A. 2000. Anatomical basics, variations, and degenerative changes of the shoulder joint and shoulder girdle. *Europ J Radiol* 35: 88–102.

Rafii M, Minkoff J. 1998. Advanced arthrography of the shoulder with CT and MR imaging. *Radiol Clin N Am* 36: 609–633.

Rafii M, Firooznia H, Golimbu C. 1986. CT arthrography of capsular structures of the shoulder. *AJR Am J Roentgenol* 146: 361–367.

Rao AG, Kim TK, Chronopoulos E, McFarland EG. 2003. Anatomical variants in the anterosuperior aspect of the glenoid labrum a statistical analysis of seventy-three cases. *J Bone Joint Surg* 85: 653–659.

Robinson G, Ho Y, Finlay K, Friedman L, Harish S. 2006. Normal anatomy and common labral lesions at MR arthrography of the shoulder. *Clin Radiol* 61: 805–821.

Sanders TG, Morrison WB, Miller MD. 2000. Imaging techniques for the evaluation of glenohumeral instability. *Am J Sport Med* 28: 414–434.

Shankman S, Bencardino J, Beltran J. 1999. Glenohumeral instability: evaluation using MR arthrography of the shoulder. *Skeletal Radiol* 28: 365–382.

Steinbach LS. 2008. MRI of shoulder instability. *Eur J Radiol* 68: 57–71.

Tirman PF, Feller JF, Palmer WE, Carroll KW, Steinbach LS, Cox I. 1996. The Buford complex: a variation of normal shoulder anatomy: MR arthrographic imaging features. *AJR* 166: 869–873.

Waldt S, Metz S, Burkart A, Mueller D, Bruegel M, Rummeny EJ, Woertler K. 2006. Variants of the superior labrum and labor-bicipital complex: A comparative study of shoulder specimens using MR arthrography, multi-slice CT arthrography and anatomical dissection. *Europ Radiol* 16: 451–458.

Warner JP, Deng XH, Warren RF, Torzilli PA. 1992. Static capsuloligamentous restraints to superior-inferior translation of the glenohumeral joint. *Am J Sport Med* 20: 675–685.

Willemsen UF, Wiedemann E, Brunner U, Scheck R, Pfluger T, Kueffer G, Hahn K. 1998. Prospective evaluation of MR arthrography performed with high-volume intraarticular saline enhancement in patients with recurrent anterior dislocations of the shoulder. *AJR* 1: 79–84.

Zlatkin, MB. 2003. *MRI of the shoulder*. Wolters Kluwer Health.

16 Elbow joint

Giuseppe Giannicola, Federico Maria Sacchetti, David Polimanti, Gianluca Bullitta, Marco Scacchi and Pietro Sedati
"Sapienza" University of Rome, Rome, Italy

The function of the upper extremity depends largely on the efficiency of the elbow. This is considered a complex joint because it is composed of three closely connected articulations contained within a single capsule: the ulnohumeral joint; the radiohumeral joint; and the proximal radioulnar joint. The normal anatomy of the elbow is not yet fully known and few papers have described its anatomical variations. This chapter reviews the anatomical variations of the distal humerus, proximal radius, proximal ulna, and capsule–ligament structures of the elbow joint.

Distal humerus

The distal humerus is triangular, with an articular surface that represents its base and lateral and medial columns that represent the other two sides. The articular portion of the distal humerus comprises bony and cartilaginous structures within the joint capsule. The anterior capsule inserts proximally above the coronoid and radial fossae. Posteriorly, the capsule is attached just above the olecranon fossa, distally along the supracondylar bony columns. The articular surface of the distal humerus is divided into two parts by a slight ridge. The lateral portion of the surface consists of a smooth, rounded eminence, the humeral capitellum. Medially to the humeral capitellum lies the trochlea, which consists of a deep depression between two well-marked borders: the medial and the lateral ridges. The coronoid fossa, a small depression which receives the coronoid process of the ulna during flexion of the forearm, is found above the anterior part of the trochlea. The olecranon fossa, a deep depression which receives the top of the olecranon during extension of the forearm, is found above the posterior part of the trochlea. These fossæ are separated from one another by a thin, transparent lamina of bone named the supratrochlear septum (Fig. 16.1).

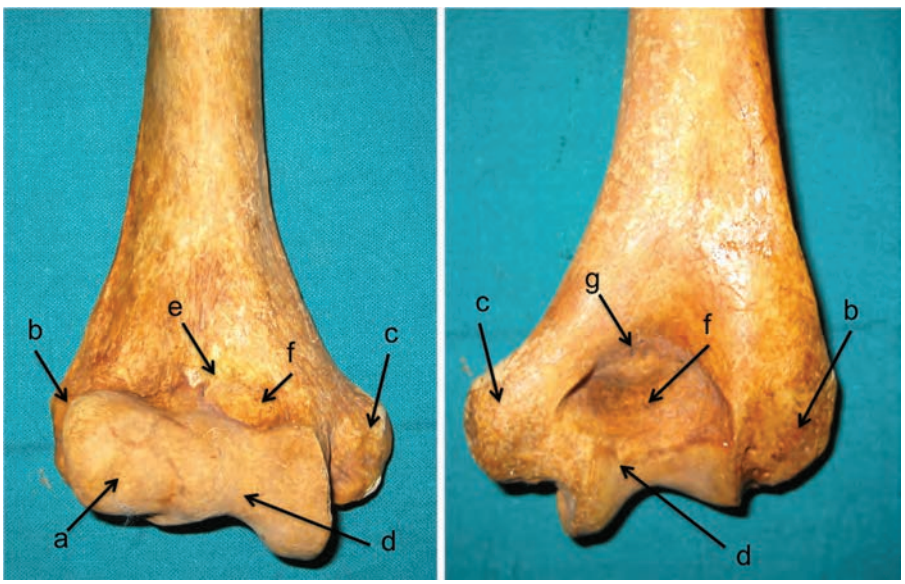

Figure 16.1 Anterior (left) and posterior (right) aspect of the distal humerus: a, capitellum of the humerus; b, lateral epycondile; c, medial epicondyle; d, trochlea; e, coronoid fossa; f, supratrochelar septum; g, olecranon fossa.

Bergman's Comprehensive Encyclopedia of Human Anatomic Variation, First Edition. Edited by R. Shane Tubbs, Mohammadali M. Shoja and Marios Loukas.
© 2016 John Wiley & Sons, Inc. Published 2016 by John Wiley & Sons, Inc.

The literature contains a very limited amount of information on the morphology of the distal humerus and, consequently, on its anatomical variations.

Capitulum humerus

The capitulum humerus was previously assumed to be spherical. However, Sabo et al. (2011) analyzed its morphology in 50 cadaveric human elbows using CT scanning, and considered its implications for implant design. Their study demonstrated that the capitellum is not completely spherical but somewhat ellipsoid, with a mean height of 23.2±2.8 mm (range 18.3–29.5 mm) and a mean width of 13.8±2.3 mm (range 9–19 mm). The sagittal radius of curvature is 11.6±1.4 mm (range 8.7–14.8 mm), while the transverse radius of curvature is 14.0±3.0 mm (range 9.6–20.9 mm). The authors demonstrated a moderate correlation between height and width and a good correlation between the sagittal and transverse radii of curvature. However, it was not possible to define a shape spectrum of the capitulum humerus or, consequently, its different morphotypes.

Trochlea

To our knowledge, only one previous study has investigated the characteristics of the articular surface of the trochlea. Goldfarb et al. (2012) studied the anatomy of the elbow using standard anteroposterior and lateral radiographs from a population of 125 adolescent (12–18 years) and 53 young adult (19–25 years) subjects, comprising 85 males and 93 females. The articular surface of the distal humerus was assessed using subjective and objective parameters to evaluate the size of the lateral trochlear ridge and the depths of the trochlear and trochleo-capitellar sulci.

The authors first subjectively evaluated the surface contour and identified three different patterns: a flat contour, defined as type 1; a small ridge with shallow adjacent sulci, defined as type 2; and a prominent ridge with deep sulci, defined as type 3 (Fig. 16.2). Analysis of the whole sample, regardless of age, revealed a frequency of 20.8% for type 1, 61.2% for type 2, and 18% for type 3. In the adolescent group, type 1 was observed in 23% of the sample, type 2 in 63%, and type 3 in 14%, whereas in the young adult group, type 1 was observed in 15%, type 2 in 57%, and type 3 in 28%. There was no gender difference in morphology.

The trochlear sulcus, the lateral trochlear ridge, the trochleo-capitellar sulcus, and the trochlear notch angle were then measured objectively. There were statistically significant differences between the three contour patterns for all the parameters with the exception of trochlear sulcus depth. The lateral ridge and the trochleo-capitellar sulcus were smaller and larger, respectively, in type 3. The trochlear notch angle was also lower in type 3 than in type 1. Furthermore, the statistical analysis revealed that young adult subjects had deeper trochlear and trochleo-capitellar sulci and a shallower lateral ridge than the adolescent group. In addition, males were found to have a deeper trochleo-capitellar sulcus.

In a recent study, Giannicola et al. (2015a) performed measurements on healthy volunteers using high-definition MRI scans (1.5 T; 8 channels dedicated array); patients with a clinical history of fracture of the humerus, elbow or forearm, lateral or medial epicondylitis or arthritis were excluded from the study. Thirty-nine skeletally mature subjects were then recruited, comprising 20 males and 19 females with mean age 28 years (range

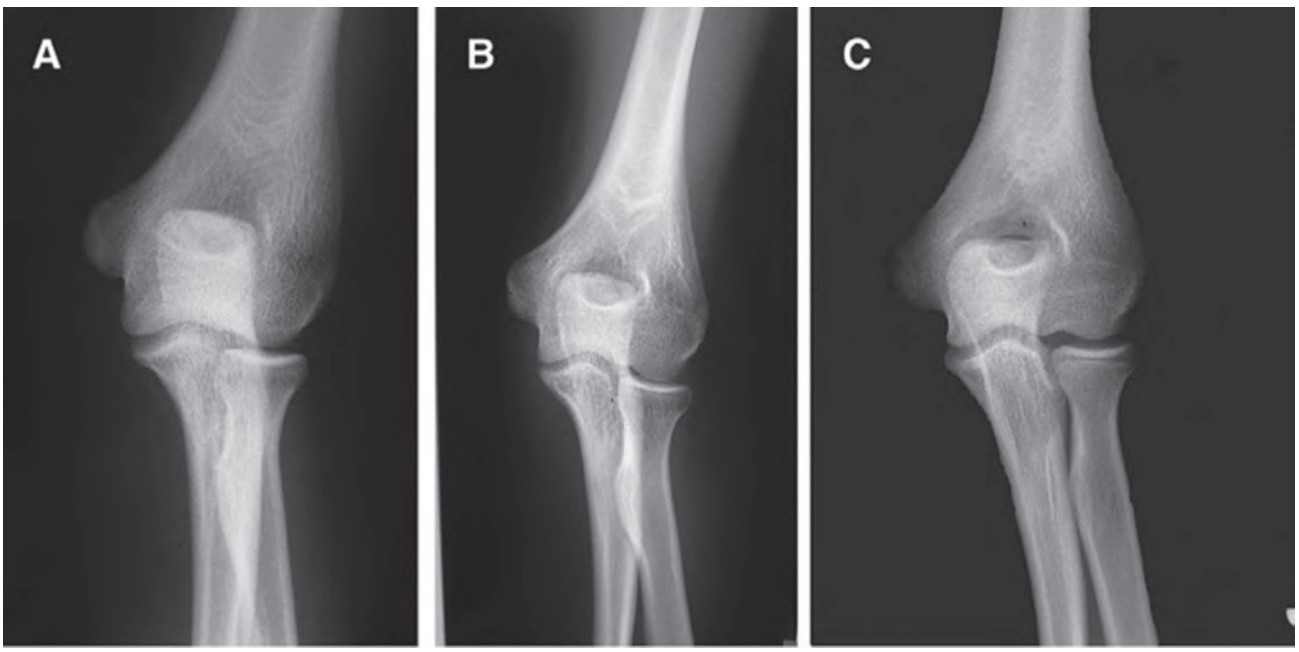

Figure 16.2 Examples of (a) Type I distal humerus contour; (b) Type II distal humerus contour; and (c) Type III distal humerus contour.

Source: Goldfarb et al. (2012). Reproduced with permission from Elsevier.

21–32 years), mean height 174.5 cm (range 191–160 cm) and mean weight 68.4 kg (range 92–52 kg). MRI scans were performed on the right and left elbows, images being acquired with the arm positioned in full extension and with the forearm in complete supination. Using these images, a range of anatomical characteristics were analyzed with the following body landmarks being adopted as reference points in the coronal view:

- the deepest point of the trochlear sulcus at the bony layer (a) and at the cartilage layer (A);
- the edge of the lateral trochlear ridge at the bony layer (b) and at the cartilage layer (B); and
- the edge of the medial trochlear ridge at the bony layer (c) and at the cartilage layer (C).

Using dedicated DICOM viewer software, these reference points were used to calculate the thickness of the cartilage at those levels and the trochlear notch angle at both the bony layer and the cartilage layer, which means the angle was formed between the reference points at the trochlear sulcus and the lateral and medial trochlear ridges (Fig. 16.3). The distance between the reference points defined the cartilage thickness at the trochlear sulcus and at the lateral and medial trochlear ridges: the mean cartilage thickness at the trochlear sulcus was 1.02 mm on the right side (range 1.43–0.72 mm) and 1.05 mm on the left (range 1.83–0.71 mm); at the lateral trochlear ridge, it was 1.04 mm on the right side (range 0.65–1.67 mm) and 1.03 mm on the left (range 0.67–1.71 mm); and at the medial trochlear ridge, it was 0.92 mm on the right side (range 0.62–1.39 mm) and 0.94 mm on the left (range 0.65–1.65 mm).

No significant differences were observed between the cartilage thickness at the level of the lateral trochlear ridge and at the sulcus, whereas a significant difference was found between these two points and the cartilage thickness at the medial trochlear ridge. These results demonstrate that cartilage thickness at the level of the trochlea is not homogeneous, with significant differences being observed between the values of cartilage thickness of the medial ridge and the other two points examined, which indicates that this layer may modify the shape of the bony trochlea. Moreover, statistical analysis revealed a good or moderate correlation ($p<0.05$) among the cartilage thicknesses at the landmarks previously described.

The trochlear notch angle at the bony layer and the cartilage layer was then calculated by connecting the reference points a, b, c and A, B, C, respectively, thereby defining two angles referred to as α and α′. The mean value of α was 142.2° (range 128.01–154.9°) for the right side and 141.8° (range 125.01–151.78°) for the left; the mean value of α′ was 142.6° (range 125.01–156°) for the right side and 142.16° (range 123.9–152.8°) for the left. There were no significant differences between α and α′ for either the right or the left elbow, and there was no significant difference between the two sides. These results demonstrate that the cartilaginous layer does not modify the shape of the trochlea at the level studied.

The width of the trochlea was also calculated (Fig. 16.4) with mean values of 2.25 cm (range 1.61–2.75 cm) and 2.24 cm (range 1.57–2.65 cm) for the right and the left sides, respectively. There was a significant correlation between patient height and the width of the trochlea (Fig. 16.5). Furthermore, males and females differed significantly, the former having a wider

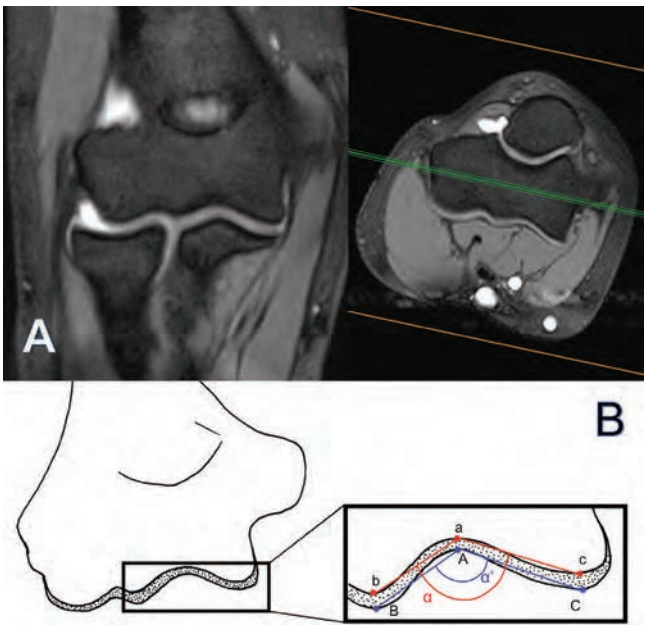

Figure 16.3 (a) Coronal and axial view of the elbow with MRI. Measurements were performed at the level of the flexion-extension axis on the coronal plane. (b) Details of the landmarks used for the measurements.

Figure 16.4 Coronal view showing the landmarks used to calculate the trochlear width.

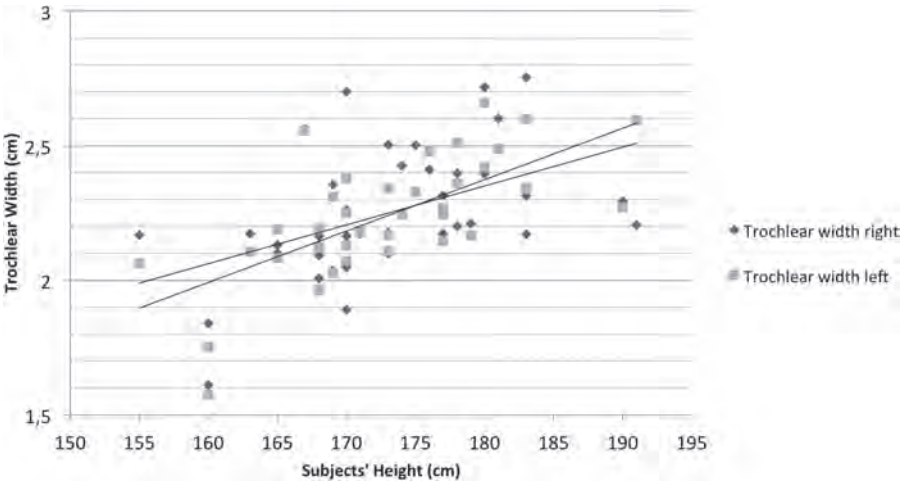

Figure 16.5 Positive correlation between patient height and trochlear width. A significant correlation was found between height and right trochlear width (Pearson= 0.475), height and left trochlear width (Pearson= 0.667).

trochlea than the latter. Moreover, no significant correlation emerged between the TNA at the bony or cartilage layers and subject height or trochlear width.

These results highlight that there exists a wide spectrum of shapes of the contour of the trochlea, ranging from flat to curved (Fig. 16.6), and that this variation is not correlated with bone sizes.

Morphology of distal humerus

Some authors have studied the morphology of the distal humerus and its effect on total elbow arthroplasty, focusing in particular on the anatomical congruence of the humeral component. Brownhill et al. (2007), who studied 40 freshly frozen cadaveric specimens using CT scanning, demonstrated that the distance between the center of the capitellum and the center of trochlear sulcus was greater in male than female specimens (22.5±1.1 mm and 19.2±1.5 mm, respectively), highlighting gender differences. The same author studied the anterior offset of the flexion-extension (FE) axis from the center of the medullary canal, which ranged from 6.6±3.2 mm at 42.6±4.6 mm of medullary canal length to 11.1±1.9 mm at 149.7±6.7 mm of medullary canal length, with a greater anterior offset of the FE axis in male than in female specimens (Fig. 16.7a). Moreover, McDonald et al. (2011), who measured the anterior offset of the

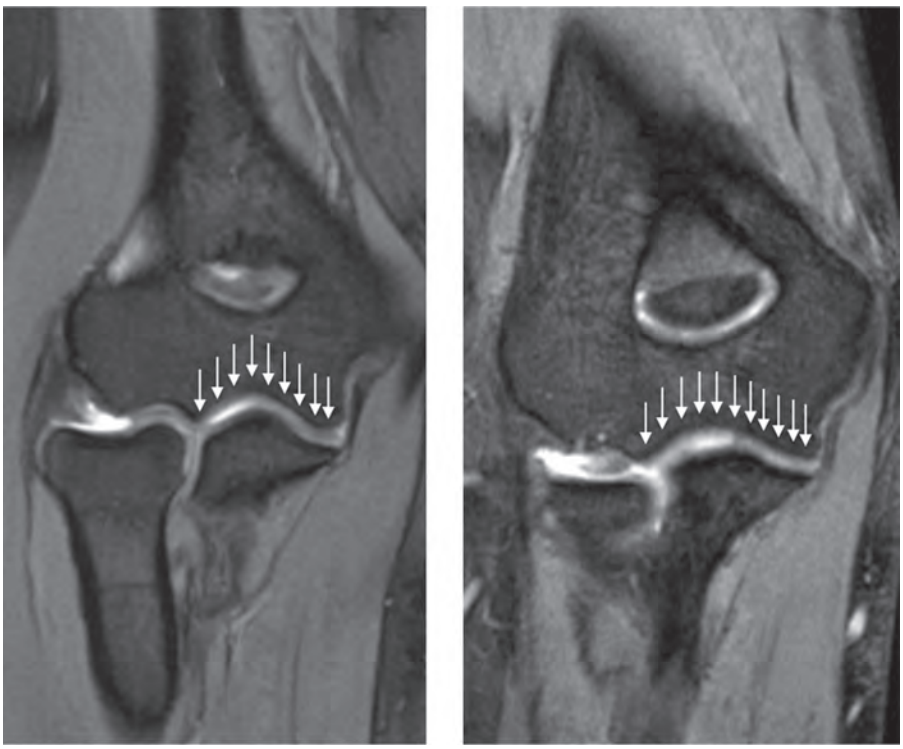

Figure 16.6 Two different morphotypes of contour of the trochlea: (left) curve-shaped trochlea and (right) flat-shaped trochlea.

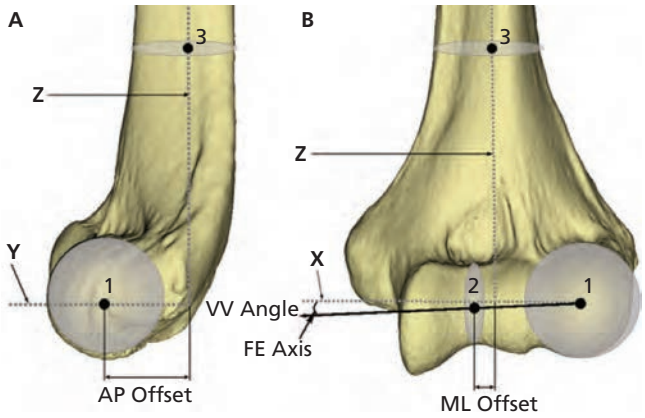

Figure 16.7 (a) The anteroposterior (AP) offset of the FE axis, defined as the offset of the trochlea from the *z*-axis in the sagittal plane. (b) The mediolateral (ML) offset of the FE axis, defined as the offset of the center of the trochlea from the *z*-axis in the coronal plane.

Source: McDonald et al. (2011). Reproduced with permission from Elsevier.

FE axis in 13 freshly frozen cadaveric specimens, reported values ranging from 9.1 to 14.5 mm, although it was not specified at what level of the axis of the medullary canal the offset was calculated. These studies suggest some variability between the position of the FE axis and that of the vertical axis of the humerus, yielding a shape spectrum of the distal humerus that is bowed to a greater or lesser extent on the sagittal plane (Fig. 16.8).

McDonald et al. (2011) also measured the varus-valgus angulation of the distal humerus, that is, the angle between the FE axis and the horizontal plane, yielding values ranging from –1° to 14.6°; these values point to varying degrees of inclination of the articular portion of the distal humerus. The medial-lateral offset, that is, the offset of the trochlea from the vertical axis in the coronal plane, was also calculated; values fell within the range 0.0–5.0 mm (Fig. 16.7b).

Figure 16.8 The different degrees of distal humerus bow, conditioning the anterior offset of the flexion-extension axis.

A deficit of the bony septum of the humerus that separates the coronoid from the olecranon fossa can determine the formation of a supratrochlear foramen, which was first reported by Meckel in 1825 (see Kate and Dubey 1970). Both genetic and environmental factors (e.g., nutrition and working conditions) that result in a marked impact pressure from the olecranon have been assumed to underlie the formation of these supratrochlear apertures (Glanville 1967). However, some authors have rejected this hypothesis on the grounds that repetitive pressure on the bony septum would cause hyperemia, thereby strengthening the bone instead of weakening it (Hrdlicka 1932).

The prevalence of the supratrochlear foramen varies among populations, ranging from 0.3% to 58%, and is usually more frequent in females than in males (Akabori 1934; Trotter 1934; Ming-Tzu 1935; Singhal and Rao 2007; Mays 2008; Nayak et al. 2009; Paraskevas et al. 2010; Christos et al. 2011; Mahajan 2011), although a higher incidence in males has been reported by some authors (Glanville 1967; Meier and Hunt 2006). Moreover, the supratrochlear foramen is more commonly found on the left side (Singhal and Rao 2007; Mahajan 2011). Several authors have measured the vertical and transverse diameters of the foramen and obtained values in the ranges 4.0–7.4 mm and 2.7–6.92 mm, respectively (Mahajan 2011; Bhanu and Sankar 2012; Ndou et al. 2013). They also categorized the apertures according to three shapes: round, oval, and triangular. The incidence of the oval supratrochlear foramen, which was the most frequent, fell within the range 53–93%, that of the round foramen 5.3–30%, and that of the triangular foramen 1.5–3.5%. A fourth, irregularly shaped supratrochlear foramen, with an incidence of 13.2%, has also been reported (Ndou et al. 2013).

Os supratrochleare dorsale

The os supratrochleare dorsale should also be included among the normal variants of the elbow. It was originally considered to be a loose body secondary to osteochondritis dissecans of the supratrochlear septum, but is now believed to represent an accessory ossification centre situated in the olecranon fossa (Obermann and Loose 1983; Gudmundsen and Ostensen 1987; Wood and Campbell 1994; Afshar 2011). The few case reports on the os supratrochleare dorsale available in the literature report values in the range 11–22 mm for the transverse diameter, 11–22 mm for the vertical diameter, and 7–20 mm for the anteroposterior diameter, with a shape sometimes described as discoid (Obermann and Loose 1983; Afshar 2011). The os supratrochlear dorsale should be distinguished from the so-called patella cubiti, which represents a sesamoid bone in the triceps tendon (Fig. 16.9). Although it is included within the normal anatomical variations of the elbow, it could be responsible for symptoms such as pain and limitation of motion, which often occur after minor trauma and can require surgery (Wood and Campbell 1994).

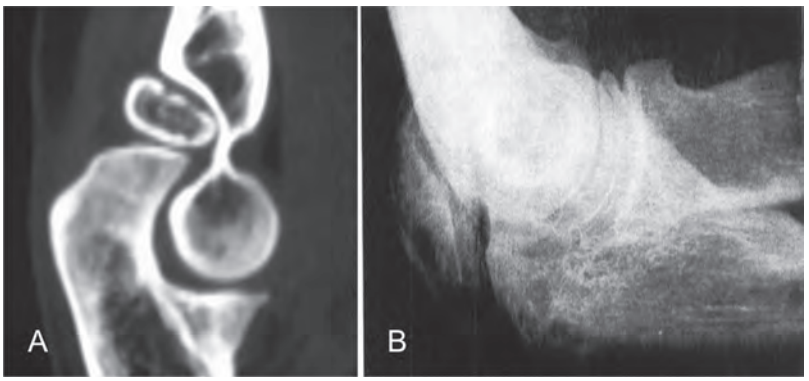

Figure 16.9 (a) Os supratrochleare dorsal. (b) Patella cubiti.

Source: (Afshar 2011). Reproduced with permission from Sage. and Ahlgren and Rydholm (1975). Reproduced with permission from A. Rydholm.

Proximal radius

The proximal radius consists of two main elements: the head and the neck. The radial head is cylindrical in shape with a depression in the mid-portion, defined as the fovea radialis, that accommodates the capitellum. Furthermore, its circumference has an articular surface for the sigmoid notch of the ulna. Distally, the radial head continues with the radial neck, which expands from the head–neck border to the proximal edge of the bicipital tuberosity (Fig. 16.10).

During the last decade, several anatomical studies have assessed the shape and size of the proximal radius using a range of methods including digital calipers, X-ray, CT scanning, magnetic resonance imaging, and coordinate measuring machines. These studies have been performed on various samples such as cadaveric dried bones without cartilage, cadaveric fresh bones, and healthy patients. Assessment of the exact geometry of the radial head and its possible anatomical variants has been aimed at improving the development of prosthesis designs for orthopedic surgery.

Radial head

Some studies have analyzed the shape and size of the radial head (King et al. 2001; Swieszkowsky et al. 2001; Captier et al. 2002; Van Riet et al. 2003; Mahaisavariya et al. 2004). Swieszkowsky et al. (2001), who analyzed 17 fresh radial heads with a coordinate measuring machine, demonstrated that the difference between diameters is small (mean 1.10 mm) and that the maximum and minimum diameters are correlated; he concluded that the articular surface of the radial head is therefore likely to be circular. Mahaisavariya et al. (2004) combined CT scanning with a reverse engineering technique on 40 Thai dry cadaveric bones and also found that the radial head is likely to be circular, with an average diameter of 20.5 mm (SD = 1.9).

In contrast, Captier et al. (2002), who studied a sample of 96 dry cadaveric bones, observed that 57% of the specimens were elliptical and 43% were circular. In particular, he found that when the shape was elliptical, the difference between the two diameters was significant (mean maximum diameter 22 mm; mean minimum diameter 20 mm); the difference in the circular group was not significant (mean maximum diameter 21.2 mm; mean minimum diameter 20.4 mm). Despite finding no significant difference between the two diameters, King et al. (2001) demonstrated that the radial head shape cannot be considered clearly circular, a conclusion subsequently confirmed by the authors of other studies (Van Riet et al. 2003; Kuhn et al. 2012) (Fig. 16.11).

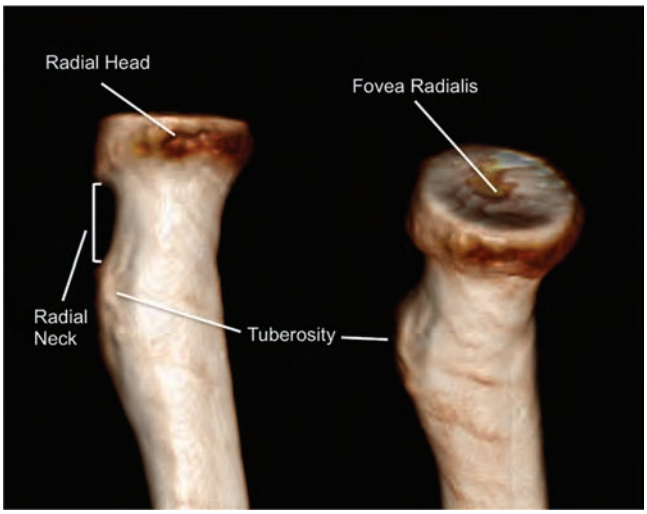

Figure 16.10 3D CT-scan images showing the proximal aspect of the radius.

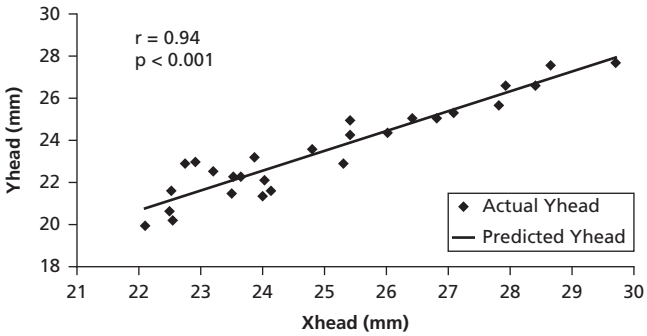

Figure 16.11 Actual *x* and *y* diameters of the outer diameters of the radial head. Predicted values of *y*-head for the corresponding *x*-head are shown as a continuous line. Predicted *y*-head = –0.53 + 0.96 *x*-head. The SD of measurements is shown as lines parallel to the predicted value of *y*. The correlation coefficient (*r*) and the significance of the correlation (*p*) also are shown.

Source: Van Riet et al. (2003). Reproduced with permission from Elsevier.

Figure 16.12 The optosil imprint was cut into 3 mm slices. The left side of the picture shows the optosil imprint cut in 3 mm horizontal slices. The right side of the picture shows optosil slices from 0 to 12 mm from the radiocapitular joint level. The position of the margo interosseous is marked on the slice in order to facilitate the imitation of different positions of rotation.

Source: Koslowsky et al. (2007). Reproduced with permission from Springer Science and Business Media.

Differences among the types of samples used and in the reference positions adopted during the acquisition of measurements of the radial head could explain the conflicting results from these studies. Indeed, Captier et al. (2002), King et al. (2001), and Van Riet et al. (2003) used, respectively, the neutral position, full supination, and the radioulnar bistyloid axis to perform their measurements. Koslowsky et al. (2007) instead measured the diameter using the imprints of the proximal radii in different positions of rotation per slice (0, 3, 6, 9, and 12 mm starting from the radiocapitellar articular surface), ranging from full supination to 60° of pronation (Fig. 16.12). That study revealed that the radial head diameter increased slightly from full supination to 30° of supination before decreasing to the minimum diameter at 60° of pronation. Furthermore, the maximum diameter of 24.13 mm (21.18–27.31 mm) and the minimum diameter of 22.67 mm (20.00–25.97 mm), which was perpendicular to the maximum, were measured 6 mm from the radiocapitellar joint surface.

In a recent study, Giannicola et al. (2015a) measured the cartilage thickness at the level of the minimum and maximum diameters of the radial head circumference of the left and right sides in 39 healthy volunteers (with no clinical history of elbow or forearm pathologies) using high-definition MRI scans (1.5 T; 8 channels dedicated array) in the axial view with the forearm in full supination. Using dedicated DICOM viewer software, this study evaluated the shape and size of the radial head with and without the cartilage surface just distal to the fovea radialis (Fig. 16.13). In the measurements without cartilage, the mean maximum and minimum bone diameters were 22.2 mm (range 18–26.4 mm) and 21.5 mm (range 17.7–25.3 mm),

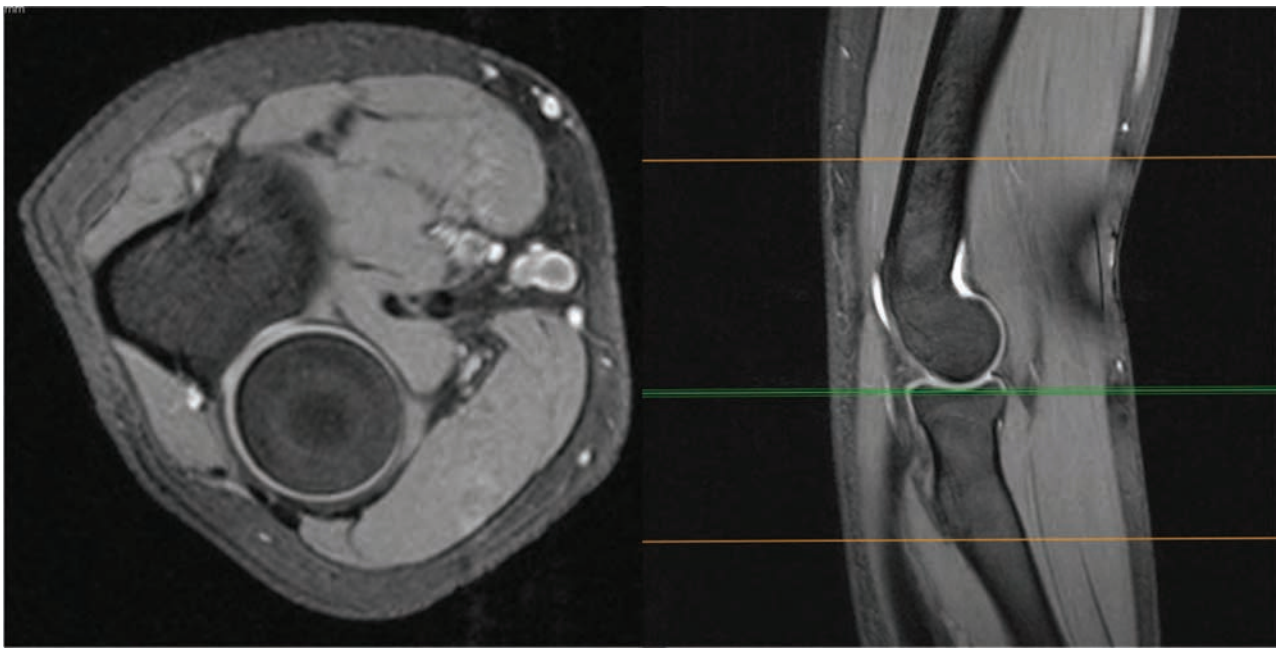

Figure 16.13 The MRI scans used to perform measurements.

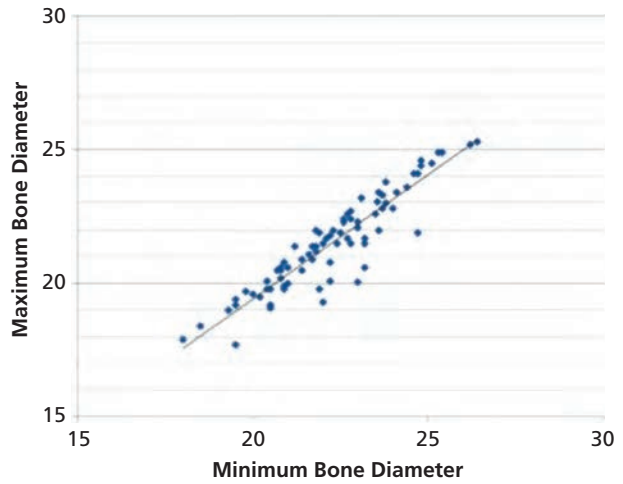

Figure 16.14 The correlation between the maximum and minimum bone diameters.

respectively; when cartilage thickness was included, the mean maximum and minimum total diameters were 24.0 mm (range 19.7–27.9 mm) and 23.2 mm (range 19.0–27.3 mm), respectively. There was no significant difference between the left and right radii of the same individual. A significant correlation was found between all radial head diameters (bone and total) and patient height. There were significant differences between the maximum and minimum bone diameters ($p<0.001$) and the maximum and minimum total diameters ($p<0.001$). Significant correlations also emerged between the maximum and minimum bone diameters and the maximum and minimum total diameters (Figs 16.14, 16.15). There were also correlations between the maximum bone and total diameters and the minimum bone and total diameters. In contrast, there was no significant correlation between maximum bone diameter and cartilage thickness, whereas a low negative correlation

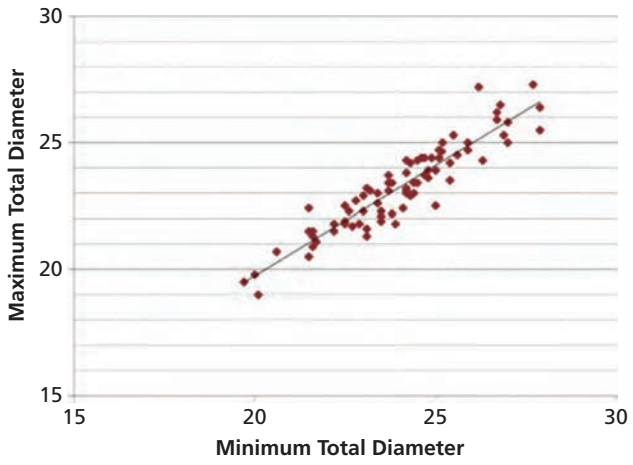

Figure 16.15 The correlation between the maximum and minimum total diameters.

Table 16.1 Measurement results of the radial head depth and fovea radialis diameter in comparable studies. (NA: not available.)

	Radial head depth (mm)	Fovea radialis diameter (mm)
Swieszkowsky et al. (2001)	1.92 (1.43–2.37)	Maximum 16.53 (14.61–18.05); minimum 14.95 (13.94–16.95)
King et al. (2001)	2.4 (1.1–3.5)	N/A
Captier et al. (2002)	N/A	12.1 (±1.6)
Van Riet et al. (2003)	2.4 (1.4–3.1)	17.7 (14.7–21.7)
Koslowsky et al. (2007)	1.95 (1.18–2.97)	16.7 (13.63–21.02)

emerged at the level of the minimum bone diameter. This study demonstrated that cartilage surface significantly increases the maximum and minimum bone diameters of the radial head and that it therefore modifies the shape of the proximal radius due to its uneven distribution. The study shows that cartilage thickness varies between subjects and does not correlate with bone radius size.

Other studies have assessed the diameter and the depth of the fovea radialis, yielding similar results with mean values of 15.56 mm and 2.17 mm, respectively; Table 16.1 lists these measurements in detail (King et al. 2001; Swieszkowsky et al. 2001; Captier et al. 2002; Van Riet et al. 2003; Koslowsky et al. 2007). However, it is not yet clear whether the shape of the fovea radialis, like that of the radial head circumference, is circular or elliptical. Captier et al. (2002) also demonstrated that the fovea was not in the center of the radial head circumference, but offset. The axial view revealed that the fovea radialis was backward eccentric in complete supination and forward eccentric in complete pronation (Fig. 16.16).

With regard to the articular height of the radial head circumference, no significant variation emerged from different studies. Captier et al. (2002) found that the mean ventral height (9.1 mm) and the mean dorsal height (9.2 mm) of the articular circumference were similar in the neutral position. Puchwein

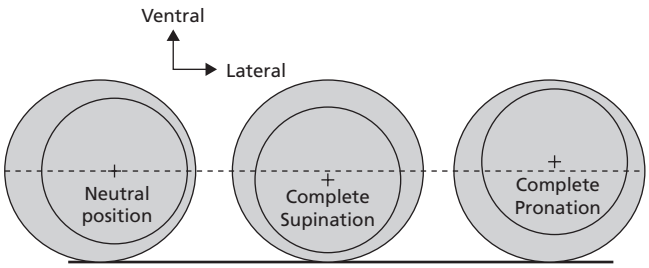

Figure 16.16 The radial head showing the fovea radialis offset. In complete supination the fovea radialis center is backward eccentric. In complete pronation the fovea radialis center is forward eccentric.

Source: Captier et al. (2002). Reproduced with permission from Springer Science and Business Media.

et al. (2013), who performed a CT scan in the supine position to evaluate the heights of the anterior, posterior, radial, and ulnar aspects of the radial head, demonstrated no significant differences, the mean value of these measurements being 11.80 mm. Other studies based on measurements of only the radial head height between the radial lip and the neck–head border near the radial tuberosity yielded similar findings, with mean values in the range 9.8–11.89 mm (Beredjiklian et al. 1999; Itamura et al. 2008; Giannicola et al. 2012). In contrast, Koslowsky et al. (2007) reported a significant difference in mean radial head height between the ulnar side (11.04 mm) and the radial side (10.02 mm).

Radial neck

Few authors have assessed the diameter and height of the radial neck (Beredjiklian et al. 1999; King et al. 2001; Popovic et al. 2005; Kuhn et al. 2012). Since such measurements are used above all for prosthesis design, most studies concentrate on the intramedullary diameter of the radial head and tend to neglect measurements of the outer diameter (Kuhn et al. 2012). For example, King et al. (2001) measured the minimum and maximum intramedullary diameters of the radial necks on radiographs on the AP and lateral view in 40 patients. He found that the mean diameter was 7.7 mm (range 5.5–10.9 mm) on the AP and 7.8 mm (range 5.0–12.4 mm) on the lateral view. Using CT scanning to assess the same parameters, Popovich et al. (2005) found that the mean minimum and maximum intramedullary diameters measured just above the bicipital tuberosity were 8.3 and 9.3 mm, respectively. Using MRI, Beredjiklian et al. (1999) found that the mean minimum diameter and mean maximum diameter were 9 and 10 mm at the narrowest point, respectively. He demonstrated that the narrowest part of the radial neck is at its end, proximal to the radial tuberosity, which suggests that the intramedullary canal is conical. Koslowsky et al. (2007) confirmed these results, finding a minimum diameter of 9.8 mm at the end of the neck.

Recently, Kuhn et al. (2012) analyzed the outer diameters of the radial neck and found that measurements decreased slightly from the proximal to the distal end. The maximum and minimum proximal radial neck diameters were 16.3 mm (range 12.4–22.7 mm) and 13.9 mm (range 10.8–19.3 mm), respectively, whereas the maximum and minimum distal radial neck diameters were 15.9 mm (range 11.8–21.6 mm) and 13.4 mm (range 9.6–18.2 mm), respectively. No studies have reported a correlation between the diameters of the radial neck and radial head (King et al. 2001; Popovic et al. 2005; Koslowsky et al. 2007).

The mean value of the radial neck height measured between the distal border of the radial head and proximal border of the radial tuberosity varies considerably among studies over the range 7.31–8.8 mm (Table 16.2). Giannicola et al. (2012) found a significant correlation between the radial neck height and the overall radial height (r=0.4397, p=0.003).

Table 16.2 Measurement results of the radial head height in comparable studies.

Reference	Radial neck height (mm)
Beredjiklian et al. (1999)	Male: 13 (8–18); female: 12 (10–18)
Van Riet et al. (2004)	13.0 (8.7–18.7)
Popovic et al. (2005)	12.3 (±2.81)
Koslowsky et al. (2007)	13.4 (8–20)
Itamura et al. (2008)	10.7
Kuhn et al. (2012)	11.9 (7.3–18.8)
Giannicola et al. (2012)	11.8 (7.2–14.6)
Puchwein et al. (2013)	Male 12.41 (±17); female 11.26 (±0.83)

Another aspect of the proximal radius that has been assessed by several authors is the posterolateral aspect of the radial head and neck, which does not articulate with the sigmoid notch during forearm rotation and is defined as a "safe zone" (Smith and Hotchkiss 1996; Caputo et al. 1998; Soyer et al. 1998; Kuhn et al. 2012) (Fig. 16.17). According to Smith and Hotchkiss (1996), this zone represents an arc of 110° included between two lines

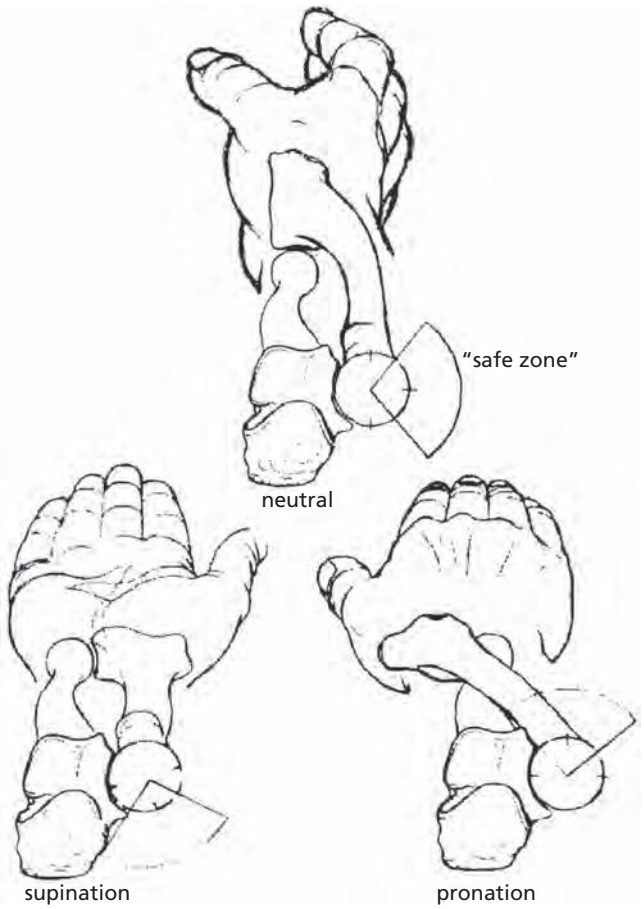

Figure 16.17 The "safe zone" seen with forearm in neutral, supinated, and pronated positions.

Source: Smith and Hotchkiss (1996). Reproduced with permission from Elsevier.

that bisect the radial head at 65° anterolaterally and 45° posterolaterally when the forearm is in a neutral position. Caputo et al. (1998) subsequently demonstrated that the safe zone corresponds to an arc of 90° between the projection of the radial styloid and the Lister tubercle on the radial head. In a preliminary cadaveric study using CT scanning to identify the safe zone, Kuhn et al. (2012) observed a safe zone arc of approximately 116°.

Giannicola et al. (2012) performed an anatomical study on 44 cadaveric dried radii and observed that the posterolateral aspect of the safe zone, in particular the bending radius of the neck–head curvature, exhibited marked morphological differences among specimens regardless of the radial dimensions. Upon gross inspection, three types of curvature of the safe zone were identified: type A, with a flat neck–head profile in which the depth of the curvature is markedly reduced or barely detectable; type B, with a low concave profile with a slight to moderate depth of curvature; and type C, with a clearly concave profile and a marked depth of curvature in the safe zone (Fig. 16.18). Types A, B and C were observed in 25%, 64%, and 11% of cases, respectively. The computed measurements of the bending radii of the head–neck zone in the three morphological types differed significantly, the mean values for types A, B, and C being 21.9°, 11.3°, and 7.4°, respectively.

Only one study has evaluated the angle formed between the head and neck of the proximal radius. This morphological study, performed using a coordinate measuring machine on fresh radius bone, revealed a mean head–neck angle of 2.5° (0.41° SD) in the front view and of 9.5° (0.52° SD) in the side view (Swieszkowski et al. 2001) (Fig. 16.19).

The angle formed by the diaphysis of the radius and the radial neck, which has also been studied by several authors, yielded a mean angle of 165° with values ranging widely among studies (134–178°) (Captier et al. 2002; Van Riet et al. 2004; Koslowsky et al. 2007; Puchwein et al. 2013). Captier et al. (2002) detected a correlation between the diaphysis–neck angle and the shape of the radial head, reporting that the angle of the elliptical radial head is greater (168.62°) than that of the circular radial head (166.75°).

Other studies have demonstrated that the radial head fovea is eccentric in relation to the neck, and that the offset varies. One of these studies, performed on 28 cadaveric upper extremities and 40 patients, revealed that the radial head fovea has an offset of 4.2 mm (±2.5 mm) from the neck axis (King et al. 2001). A second study on fresh cadaveric radii reported a mean medial offset of 1.71 mm (range 1.01–2.5 mm) in the front view (Swieszkowski et al. 2001) (Fig. 16.19).

In conclusion, all the studies considered that have analyzed the anatomy of the proximal radius demonstrate significant individual variability in each anatomical parameter examined. However, the same studies have demonstrated no significant differences between the left and right radii of the same individual, although this bone is shorter in women (King et al. 2001; Swieszkowski et al. 2001; Captier et al. 2002; Van Riet et al. 2003; Koslowsky et al. 2007). The lack of safe and reproducible reference points makes it extremely difficult to determine the exact morphology of the proximal radius; moreover, differences among the various samples examined (cadaveric dried bones without cartilage, cadaveric fresh bones, and healthy patients) and in the methods adopted (digital calipers, x-ray, CT scanning, MRI, and coordinate measuring machines) make it very difficult to compare different studies and define the exact anatomy of the proximal radius and, consequently, possible variants.

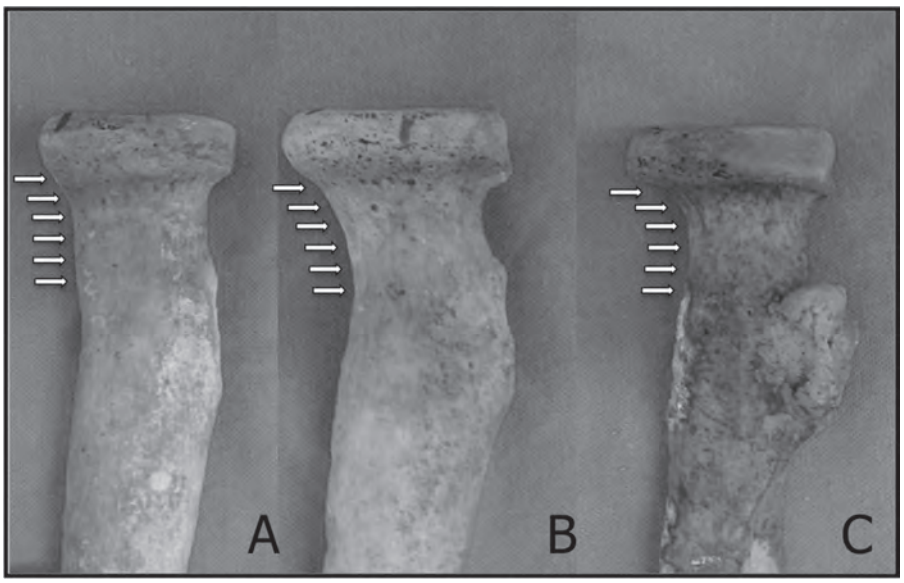

Figure 16.18 The three morphotypes of the safe zone: (a) type A, flat; (b) type B, low concave; and (c) type C, concave.

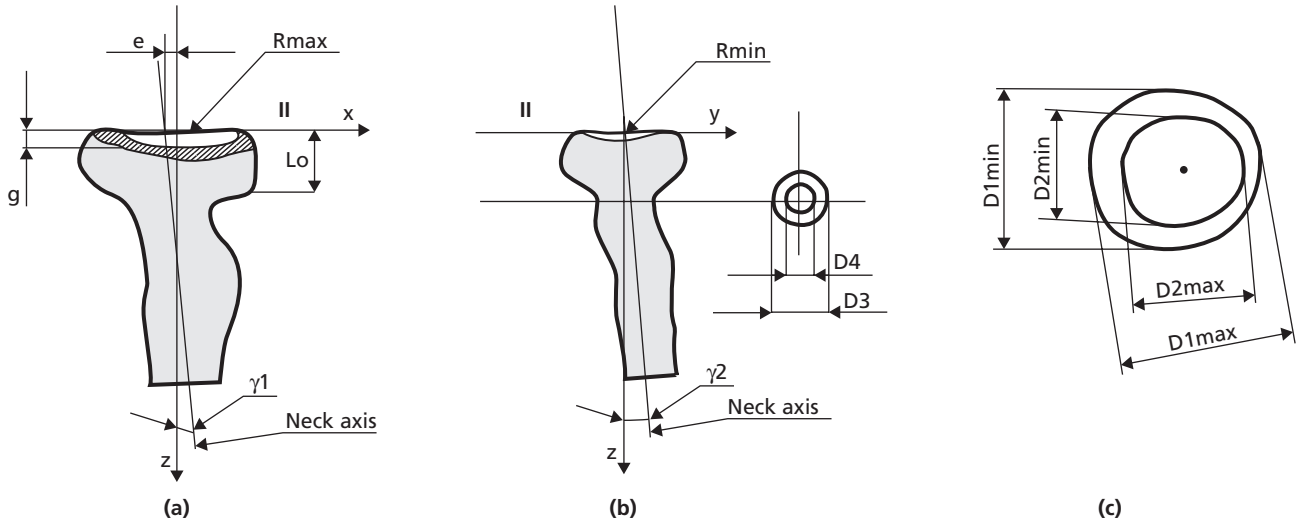

Figure 16.19 Radial head parameterization: (a) front view; (b) side view; and (c) top view where $D1_{max}$ and $D1_{min}$ are maximum and minimum diameters of the radial head; $D2_{max/min}$ are maximum and minimum diameters of the articular surface; $R_{max/min}$ are maximum and minimum radius of the articular surface; g is maximum depth of the articular surface; L_0 is maximum height of the radial head; γ1 and γ2 are angles at which the head is inclined relative to the neck: e is shift of the neck in relation to the head; D3 is minimum diameter of the neck; and D4 is minimum diameter of the marrow cavity.

Source: Swieskowski et al. (2001). Reproduced with permission from Elsevier.

Proximal ulna

The proximal ulna consists of two curved processes, the olecranon and the coronoid, which form the greater sigmoid notch (16.20). The greater sigmoid notch is joined to the humeral trochlea, thereby forming the main articulation of the elbow that provides its inherent stability. Despite the crucial role of the proximal ulna in the elbow joint, the literature contains few articles on its morphological variations. Most of the available information comes from forensic literature, which focuses mainly on size variations of the proximal ulna assessed to determine the gender of the subjects being investigated.

Cowal and Pastor (2008) assessed size variations of the proximal ulna in 223 European skeletal human ulnae from two separate osteological collections (eighteenth–nineteenth century), performing four different measurements: the notch length (NL) (Fig. 16.21); the width of the olecranon process (OW)

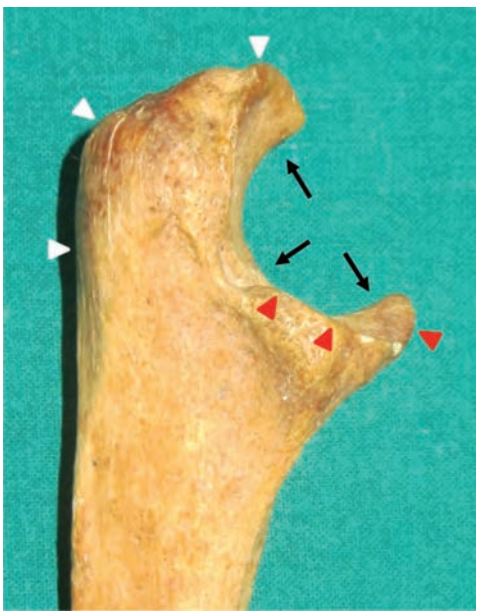

Figure 16.20 The olecranon (white arrowheads) and the coronoid processes (red arrowheads) of the proximal ulna form the greater sigmoid notch (black arrows).

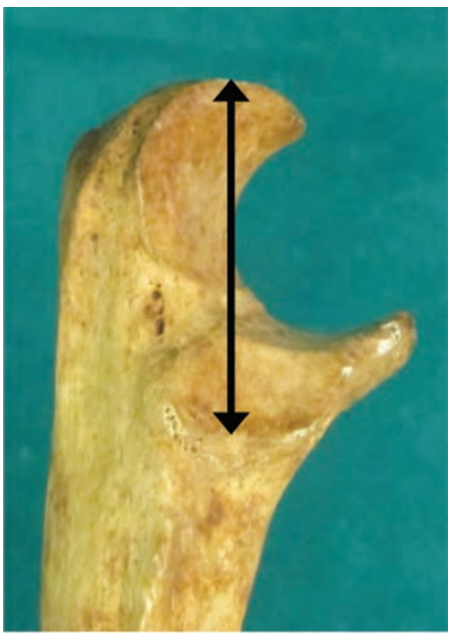

Figure 16.21 Ulnar notch length (NL) measurement (arrow), lateral view.

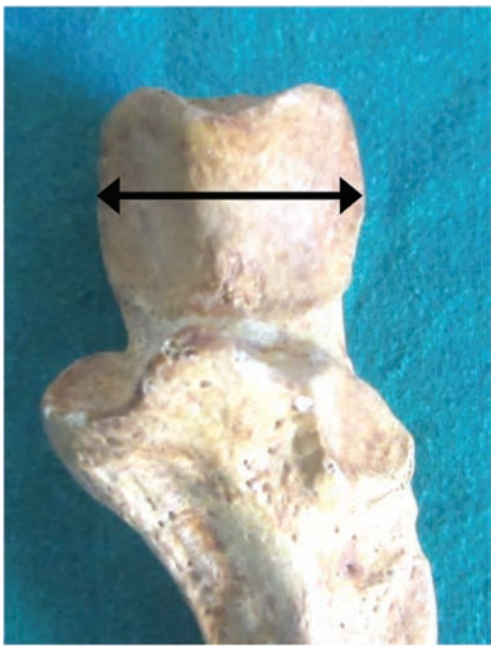

Figure 16.22 Ulnar olecranon width (OW) measurement (arrow), anterior view.

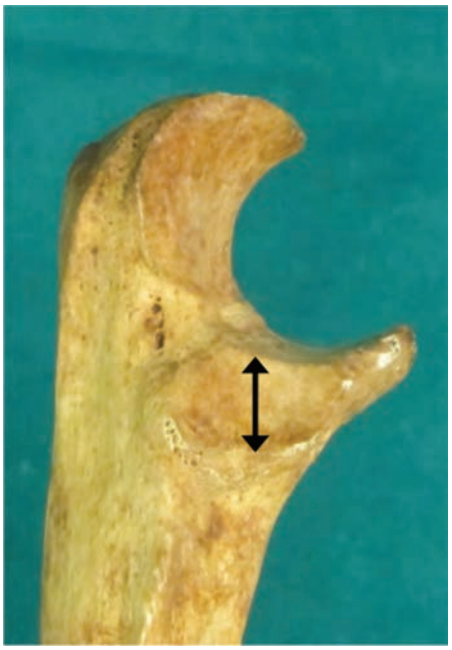

Figure 16.24 Ulnar radial notch height (RNH) measurement (arrow), lateral view.

(Fig. 16.22); the height of the coronoid process (CH) (Fig. 16.23); and the height of the radial notch (RNH) (Fig. 16.24). All the measurements were taken using a set of digital sliding calipers to the nearest tenth of a millimeter. In males, the mean NL was 36.05 mm (SD 2.97 mm), the mean OW was 25.08 mm (SD 2.04 mm), the mean CH was 36.50 mm (SD 2.68 mm), and the mean RNH was 11.29 mm (SD 1.34 mm). In females, the mean NL was 32.01 mm (SD 1.98 mm), the mean OW was 21.93 mm (SD 2.22 mm), the mean CH was 32.43 mm (SD 2.44 mm), and the mean NRH was 9.90 mm (SD 1.44 mm). The authors concluded that all the measurements of the proximal ulnae in males were significantly larger than those in females, indicating that the proximal ulna was sexually dimorphic in their European population.

Srivastava et al. (2013) subsequently measured NL, RNH, OW, CH, and radial notch width (RNW) (Fig. 16.25) in a total of 106 contemporary Indian skeletal ulnae, adopting the method

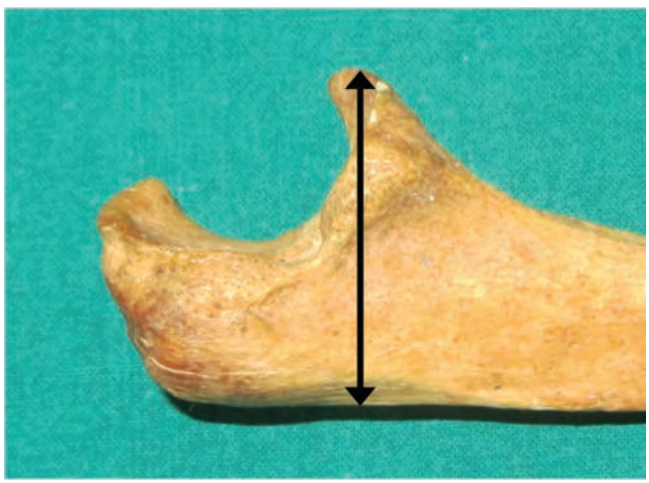

Figure 16.23 Ulnar coronoid height (CH) measurement (arrow), lateral view.

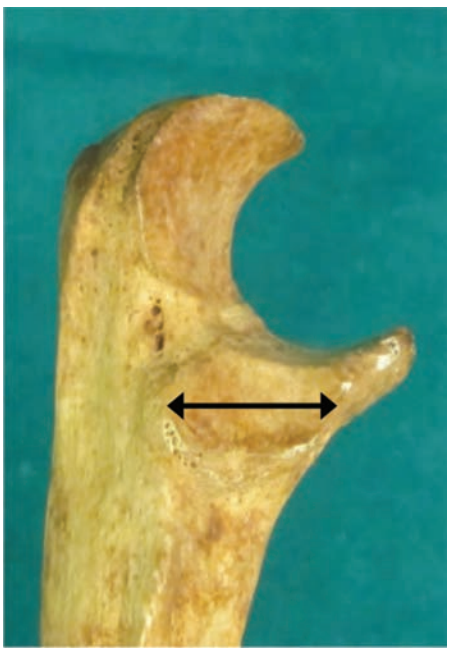

Figure 16.25 Ulnar radial notch width (RNW) measurement (arrow), lateral view.

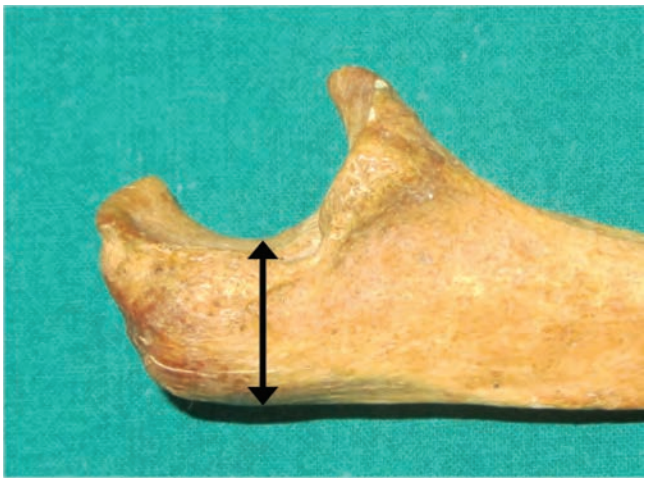

Figure 16.26 Olecranon anterior-posterior diameter (OAPD) measurement (arrow), lateral view.

of Cowal and Pastor (2008). The mean male and female values obtained were, respectively: 35 mm (SD 2.88 mm) and 31.4 mm (SD 2.64 mm) for the NL; 24.11 mm (SD 1.8 mm) and 21.21 mm (SD 1.87 mm) for the OW; 33.6 mm (SD 1.92 mm) and 31.2 mm (SD 2.14 mm) for the CH; 11.68 mm (SD 1.51 mm) and 9.61 mm (SD 1.49 mm) for the RNH; and 17.63 mm (SD 1.72 mm) and 13.86 mm (SD 2.35 mm) for the RNW. The data reported in their study are comparable to those obtained by Cowal and Pastor; the slight discrepancy between the two studies could be ascribed to body size differences between populations, varying degrees of sexual dimorphism, or changes over the centuries in the size and proportion of long bones. Mall et al. (2001) measured the "proximal ulna width" (PWD), which is very close in size to the OW, on 143 arm bones from a contemporary German autopsy sample. They reported mean values of 34 mm (SD 0.59 mm) and 29 mm (SD 0.36 mm) in males and females, respectively, which were significantly different.

Santoshkumar et al. (2011) measured the proximal ulna width (PWD), defined as the maximum breadth of the upper end of the ulna, in 193 adult Indian human ulnae. The mean PWD was 23.6 mm (SD 1.72 mm) in males and 20 mm (SD 1.97 mm) in females. The higher values that emerged from the study by Mall et al. (2001) could be ascribed to racial differences, as suggested by the fact that measurements by other Indian anatomists are consistent with those by Santoshkumar et al. (2011), or to the different measurement methods adopted. Santoshkumar et al. (2011) also measured the olecranon anterior-posterior diameter (OAPD), defined as the maximum distance perpendicular to the shaft between the anterior surface of the olecranon and the most posterior point distal to the middle of the trochlea (Fig. 16.26). The mean OAPD was 25 mm (SD 1.86 mm) in males and 22 mm (SD 1.25 mm) in females. No other studies have reported this measurement.

Purkait (2001) focused on the proximal ulna for the assessment of gender. Three measurements were taken from 160 bones in a contemporary Indian collection: the olecranon–coronoid angle (Fig. 16.27), formed by a line running parallel to the long axis of the ulna and a line connecting the tips of the olecranon and the coronoid; and the length and width of the inferior medial trochlear notch (Fig. 16.28). The author of that study reported mean olecranon–coronoid angles of 22.26° (SD 3.47°) and 14.73° (SD 4.46°) in males and females, respectively. The mean lengths of the coronoid in males and females were respectively 16.01 mm (SD 1.40 mm) and 14.39 mm (SD 0.98 mm), and the mean widths of the coronoid were respectively 14.10 mm (SD 1.24 mm) and 12.47 mm (SD 1.59 mm). The author found a highly significant difference between males and females in the olecranon–coronoid angle, which was 8.26° wider in the former. The lower coronoid height reported in this study than in the Cowal and Srivastava studies is ascribable to differences between measurement methods: coronoid height in this study was calculated from the coronoid tip to the trochlear notch, whereas in the previous studies it was calculated between the coronoid tip and the dorsal surface of the proximal ulna.

Using a three-dimensional (3D) digitizing system, Matzon et al. (2006) measured the coronoid height on 35 cadaveric bones from the tip of coronoid process and its base, defined as the line between two anatomical landmarks proximally (trough of the trochlear notch and the intersection between the guiding ridge and the transverse groove of the greater trochlear notch) and distally (coronoid

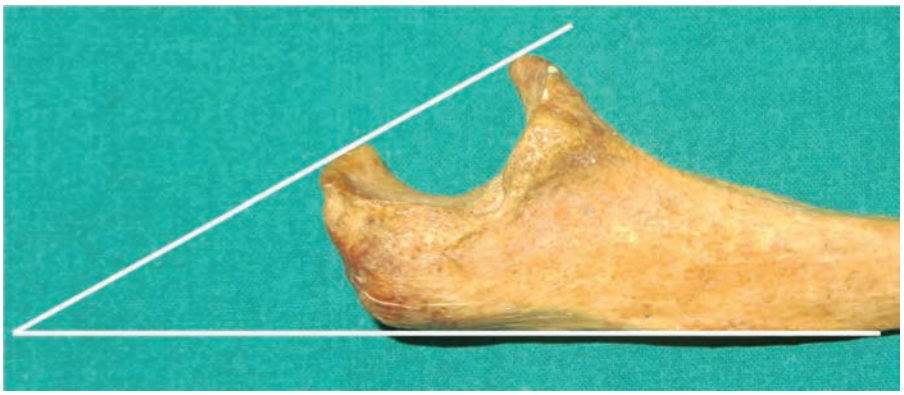

Figure 16.27 Olecranon–coronoid angle measurement, lateral view.

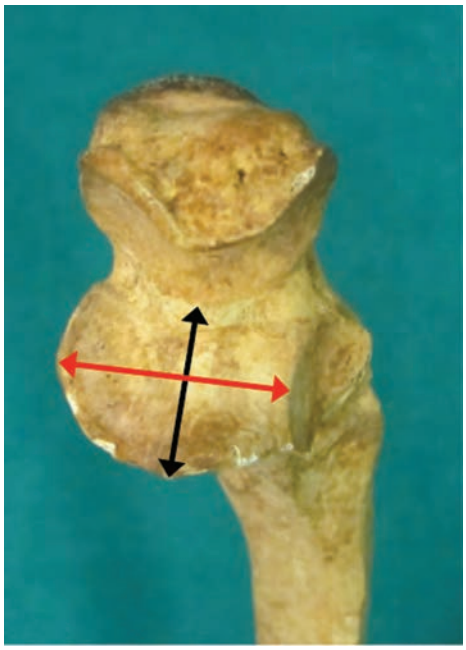

Figure 16.28 Length (black arrow) and width (red arrow) measurements of the inferior medial trochlear notch, anterior view.

process slope change and the distal-most aspect of the brachialis insertion), to the coronoid tip, yielding four different measurements (Fig. 16.29). The mean coronoid height values, as measured using the four different methods, were within the range 15–18 mm in males and 13–16 mm in females, thereby confirming that coronoid height was significantly greater in males. However, when the coronoid height was calculated as a percentage of either ulnar height or ulnar length, male and female specimens did not differ. In addition to the coronoid height, these authors also measured the olecranon–coronoid angle (Fig. 16.30) but not by the method used by Purkait (2001). This angle ranged from 33° to 38°, with a significant difference between males and females.

Figure 16.29 Coronoid height measurements with the base through the trough of the sigmoid notch to the slope change (dotted line) and to the brachialis insertion (solid line), lateral view.

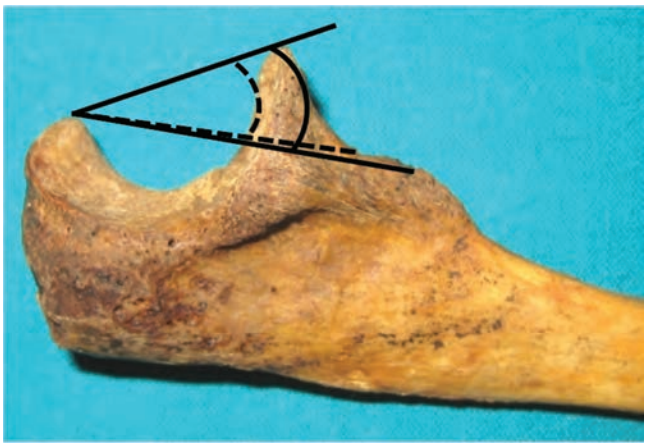

Figure 16.30 Olecranon coronoid angle at the anterior ulna distal to the coronoid process where the slope changes (dotted line) and at the distal insertion of the brachialis (solid line), lateral view.

The coronoid heights measured by other authors are similar. Ablove et al. (2006), who studied 10 cadavers, reported an average coronoid height of 16.98 mm (SD 2.5 mm). Using a series of 50 elbow CT scans, Guitton et al. (2011) measured the volume, the articular surface, and the height and width of the coronoid, finding significant differences between males and females. The authors of that study also found that total coronoid volume and total coronoid articular surface were significantly correlated with coronoid width, radial neck–head diameter and height, weight, and gender.

Rafehi et al. (2012) performed an anatomical study of coronoid cartilage thickness on 24 cadaveric ulnae using CT. They reported that the cartilage height at the coronoid tip was 3 mm (SD 0.9 mm) and cartilage thickness was 2.6 mm (SD 0.8 mm). No significant differences in cartilage thickness values emerged between the left and right paired specimens, whereas the cartilage was significantly thicker in males than females. Moreover, there was a strong inverse correlation between coronoid cartilage height/thickness at the tip and age, and a strong direct correlation between coronoid cartilage height/thickness at the tip and ulnar height and length.

To summarize, the data collected by various authors on variations in size of the proximal ulna confirm gender and racial dimorphisms. However, it is not clear whether these variations result from different morphological shapes of the proximal ulna or whether they depend exclusively on the overall size of the ulna, since most of the aforementioned studies did not address this topic (Mall et al. 2001; Purkait 2001; Ablove et al. 2006; Matzon et al. 2006; Cowal and Pastor 2008; Santoshkumar et al. 2011; Srivastava et al. 2013). The information available on the morphological variations of proximal ulna is therefore limited, the literature containing few articles on this topic.

Only one study reported morphological variations of the coronoid process. Weber et al. (2008) performed an anatomical study on 26 ulnae and observed that the anteromedial aspect of the coronoid had a smooth and regular surface without osseous irregularities or facets in 18 specimens (69.2%). In 10 of these 18 specimens (55.5%), the anteromedial aspect of the coronoid

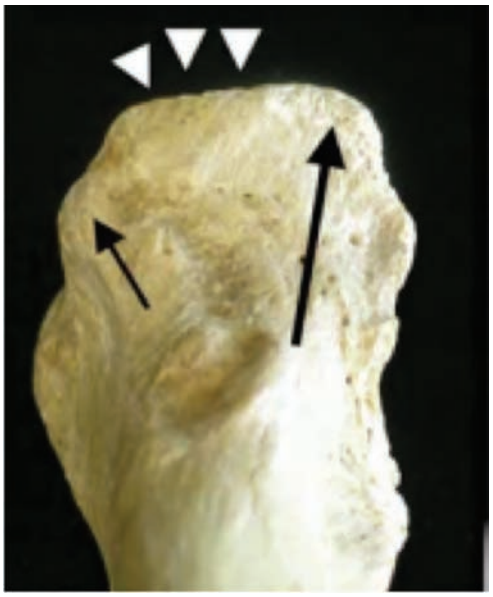

Figure 16.31 Anteromedial aspect (arrowheads) of coronoid process with a regular and flat morphology, located between the tip (large arrow) and sublime tubercle (small arrow).

Source: Weber et al. (2008). Reproduced with permission from Springer Science and Business Media.

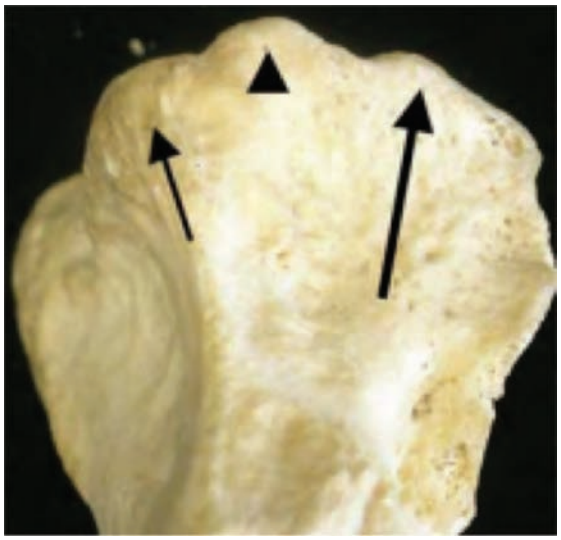

Figure 16.32 Anteromedial aspect of coronoid process with a ridge (arrowheads), located between the tip (large arrow) and sublime tubercle (small arrow).

Source: Weber et al. (2008). Reproduced with permission from Springer Science and Business Media.

process had a slightly convex morphology, whereas in the remaining eight specimens (44.5%) it had a flat regular surface (Fig. 16.31). The surface of the anteromedial aspect of the coronoid process was irregular in 8 of the 26 specimens (30.8%) with a small ridge being identified; the morphology of the coronoid process of the ulna in these 8 cases resembled the two humps on a camel's back, one hump being the tip and the other consisting of this small ridge (Fig. 16.32).

The anteromedial facet of the coronoid process was measured by Doornberg et al. (2007) on 21 elbow CT scans. These authors demonstrated the degree to which the anteromedial facet protrudes from the proximal ulnar metaphysis, revealing that, on average, 58% (range 26–82%) of this coronoid portion is unsupported by the proximal ulnar metaphysic. This marked variability suggests that the shape of the sublime tubercle varies considerably (Fig. 16.33).

Most of the information available on the orientation, angulation, and deviation of the proximal ulna derives from orthopedic literature regarding the treatment of ulnar fractures. Recently, Puchwein et al. (2012) studied 40 human elbow CT

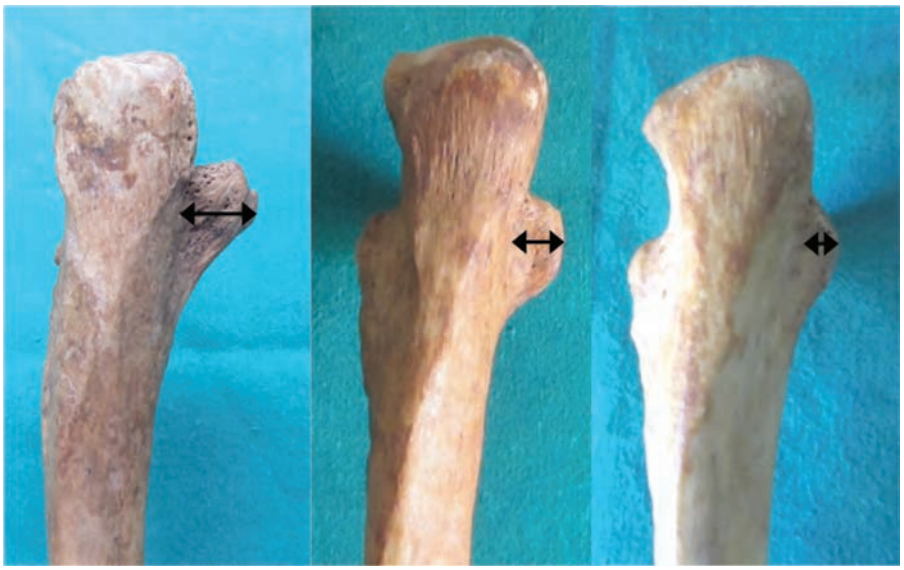

Figure 16.33 Posterior view of three different proximal ulna with different degree to which the anteromedial facet protrudes from the proximal ulnar metaphysic.

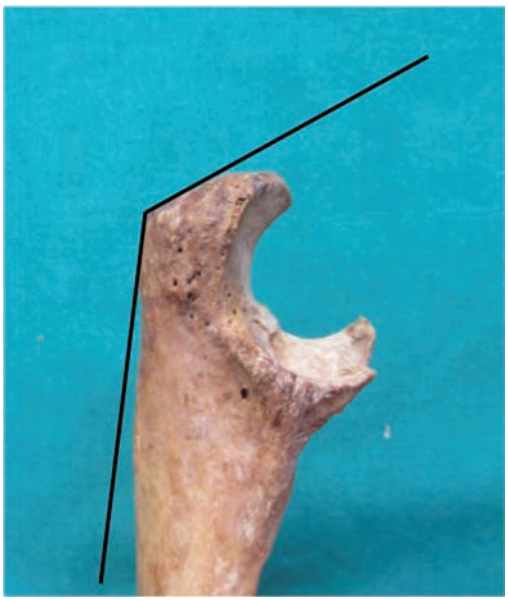

Figure 16.34 Proximal ulna hook angle, lateral view.

Figure 16.36 Proximal ulna varus angulation, posterior view.

scans in order to investigate the morphology of the proximal ulna by measuring three different angles: the hook angle and the angulations of the proximal ulnae on the frontal and sagittal planes (varus and anterior deviation). The hook angle (Fig. 16.34) was calculated between the proximal plane of the ulna, from the tip to the triceps insertion area, and the dorsal plane distal to the triceps insertion. The mean was 95.3° (SD 9.0°) with values ranging from 74.4° to 110.8°. This wide range of values indicates the variety of different shapes of the olecranon process, which can be referred to as flat or upward-tilted and downward-tilted (Fig. 16.35). Moreover, the mean varus angulation of the proximal ulna (Fig. 16.36) in that study was 14.3° (SD 3.6°), the range being 5.8–21.2°. The mean angulation varus point was measured as 75 mm (range 56–86.3 mm) from the posterior olecranon edge, highlighting the different shapes of the proximal ulna on the frontal plane such as a slightly varus deformity and strongly varus-proximal ulna (Fig. 16.37). Lastly, the anterior angulation on the sagittal plane, the so-called PUDA angle (proximal ulna dorsal angulation) (Fig. 16.38), yielded a mean of 6.2°(SD 2.7°) (range 1–11°) with a mean anterior angulation

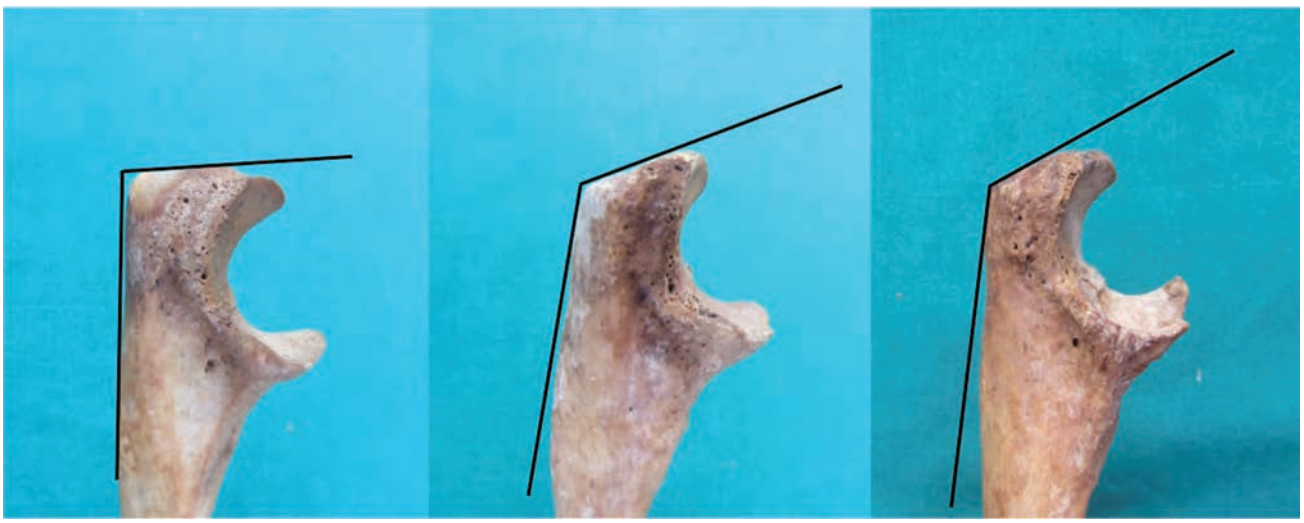

Figure 16.35 Three different olecranon hook angles.

Figure 16.37 Proximal ulna with (a) a slight varus angulation and (b) a strong varus angulation.

Figure 16.38 Proximal ulna dorsal angulation (PUDA angle), lateral view.

point at 44.4 mm (range 31.9–69.3 mm) from the posterior olecranon edge, indicating a straight proximal ulna or a recurvatum proximal ulna (Fig. 16.39).

A number of previous studies have reported marked variations in the varus and PUDA angulations of the proximal ulna. Windisch et al. (2007), who studied 74 cadaveric elbows and focused on the course of the ulna posterior border, detected a mean varus angulation of 17.7° (range 11–28°) placed, on average, 85.4 mm (range 65–110 mm) from the tip of the olecranon. The varus angulation was present in 85% of the ulnae studied, whereas in the remaining specimens the posterior border was either curved radially or was neither well-shaped nor present over the entire length of the ulna. In a previous cadaveric study,

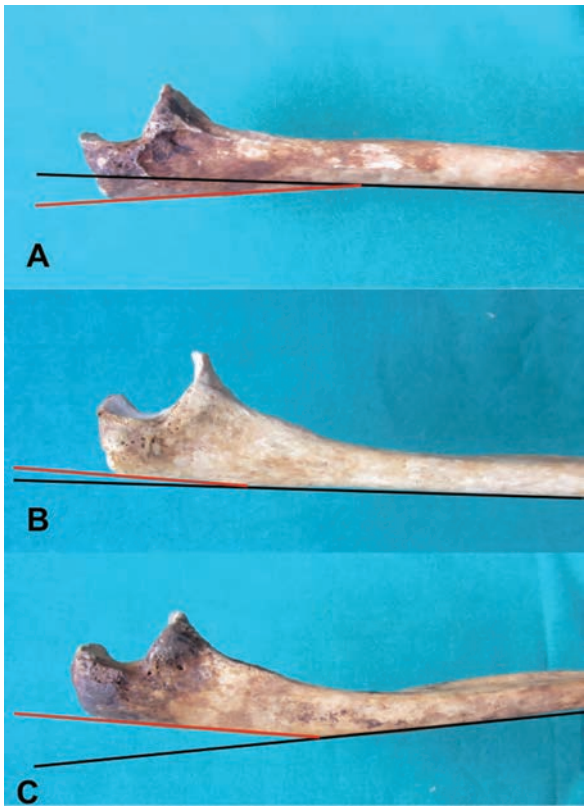

Figure 16.39 (a) Procurvatum proximal ulna; (b) straight proximal ulna; and (c) recurvatum proximal ulna.

Grechenig et al. (2007) had reported similar varus angulations in 83% of the bones and an anterior proximal ulna deviation (4.5°, range 1–14°) in 70% of cases.

The PUDA angle was also confirmed by a radiographic study (Rouleau et al. 2010). It was present in 96% of the lateral radiographs, with a mean value of 5.7° (range 0–14°), placed on average 47 mm (range 34–78 mm) distal to the olecranon tip. As for Grechenig et al. (2007), Rouleau et al. (2010) detected no difference in the PUDA values between the right and left sides. In another study, Rouleau et al. (2012) demonstrated that the PUDA influenced the range of elbow motion (ROM): the increasing width of the PUDA was associated with a decreased maximal elbow extension and global elbow ROM.

When Brownhill et al. (2009) assessed the posterior and lateral offset of the medullary canal in relation to the center of the great sigmoid notch by performing CT scans on 31 cadaveric proximal ulna, they observed that the anatomy of the proximal ulnar varied with a posterior and lateral offset that increased distally to the articulation center (Fig. 16.40).

In a recent study, Giannicola et al. (2015b) measured the proximal ulna bilaterally in 39 skeletally mature subjects (78 elbow) using high-definition MRI scans (1.5 T; 8 channels dedicated array). The purpose of the study was to analyze the degree of coverage provided by the greater sigmoid notch (GSN) to the humeral trochlea, as well as the contribution of the olecranon and coronoid process cartilage tips to this angle and its variations.

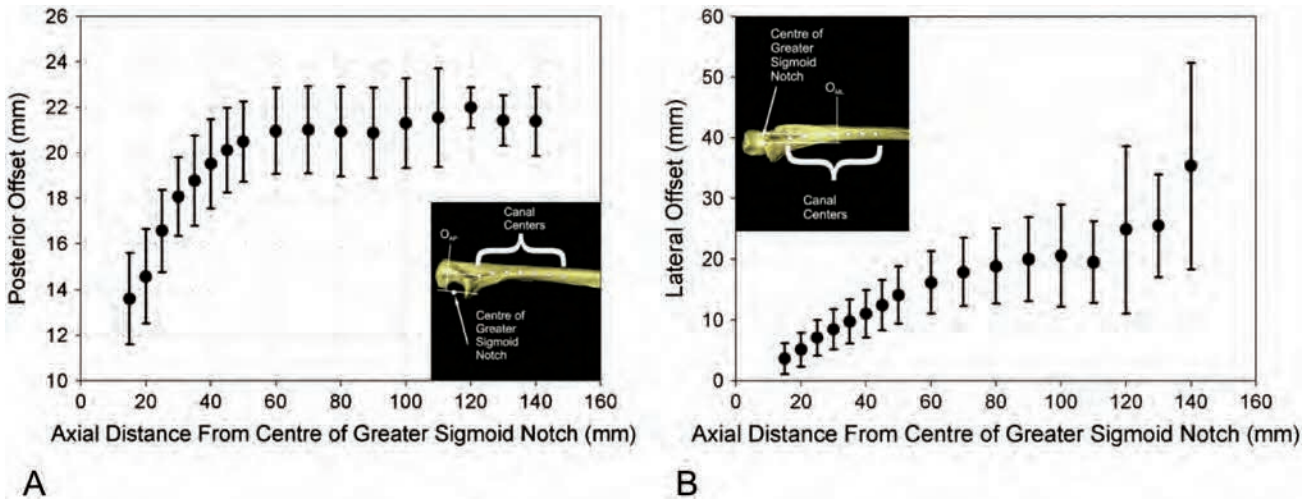

Figure 16.40 (a) Average posterior offset of canal centers versus axial distance from center of greater sigmoid notch. (b) Average lateral offset of canal centers versus axial distance from center of greater sigmoid notch. Note that the scales for the two axes are different.

Source: Brownhill et al. (2009). Reproduced with permission from Elsevier.

All the measurements were taken from a sagittal sequence passing through the coronoid and olecranon tips using a dedicated DICOM viewer. A local coordinate system was established to perform these measurements (Fig. 16.41). Four angles were measured: (1) angle A (olecranon cartilaginous coverage angle), identified by two lines marked from the center of the circle to the olecranon bone–cartilage junction and olecranon cartilage tip; (2) angle B (ulnar bone coverage angle), identified by two lines marked from the center of the circle to the olecranon and the coronoid bone–cartilage junction; (3) angle C (coronoid cartilaginous coverage angle), identified by two lines marked from the center of the circle to the coronoid bone–cartilage junction and coronoid cartilage tip; and (4) greater sigmoid notch coverage angle (GSN-ca), defined as A+B+C. The mean angles A, B, and C were 6° (range 2–12°), 182° (range 153–204°), and 9° (range 2–16°), respectively. The mean GSN-ca was 198° (range 167–222°). There were no significant differences between left and right side or between male and female angle values. No correlations emerged between the two cartilagineous tips and the osseous angle or ulnar dimensions.

On the basis of the variability that emerged, we divided the morphology of the GSN into 2 main types: closed type, with a GSN-ca greater than 180°; and open type, with a GSN-ca less than 180°. We observed open and closed GSN morphologic types in 8% and 92% of cases, respectively. These results define a spectrum of shapes of the contour of the ulnar trochlea notch with different cartilaginous contributions that could be correlated with the predisposition of some individuals to ulnohumeral dislocation during elbow trauma.

These results define a spectrum of shapes of the contour of the ulnar trochlea notch ranging from closed types to open types, with different cartilaginous contributions that could be correlated with the predisposition of some individuals to ulnohumeral dislocation during elbow trauma.

In conclusion, the limited information available in the literature on the anatomical variations of the proximal ulna mostly considers the proximal ulna angle (dorsal hook angle, varus angulation, PUDA angle). Further studies based on standardized morphological measurement methods are therefore warranted to provide an accurate description of the anatomy of the proximal ulna and its possible variants.

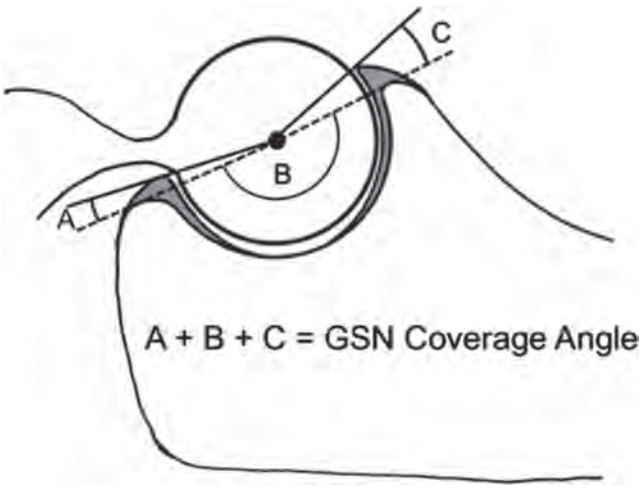

Figure 16.41 The method of measuring the four angles.

Capsule and ligaments

The elbow joint has a synovial membrane-lined joint capsule that contains three articulations: the ulnohumeral joint; the radiohumeral joint; and the proximal radioulnar joint. Medially and laterally, the joint capsule thickens to form the medial or ulnar collateral ligament and the lateral collateral ligament. This section reviews the anatomical variations of the capsule and ligaments of the elbow.

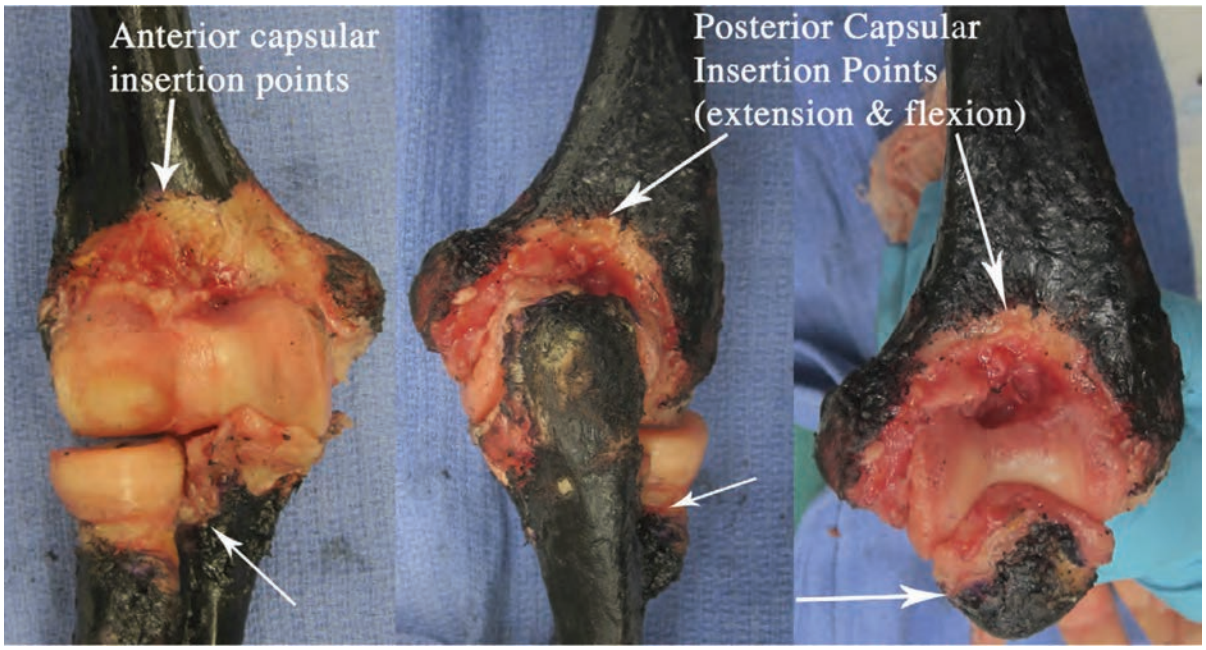

Figure 16.42 Anterior and posterior view of a painted specimen with capsule excised, demonstrating the area covered by the capsule.

Source: Reichel and Morales (2013). Reproduced with permission from Elsevier.

Capsule

The humeral origin of the elbow capsule is proximal to the radial and coronoid fossae anteriorly and to the olecranon fossa posteriorly. Distally, the capsule is attached to the anterior margin of the coronoid and to the anular ligament (AL); posteriorly, it is attached to the articular margin of the sigmoid notch and the proximal aspect of the olecranon (Gray 1918; Morrey and An 1983, 1985) (Fig. 16.42). King et al. (1993) reported transverse and oblique bands in the anterior capsule.

Reichel and Morales (2013) also described three bands in the anterior capsule (Fig. 16.43). The first (the anterolateral band) originates on the anterolateral surface of the distal humerus, near the lateral supracondylar ridge, and continues distally to insert onto the anterior superior AL. The length of this band

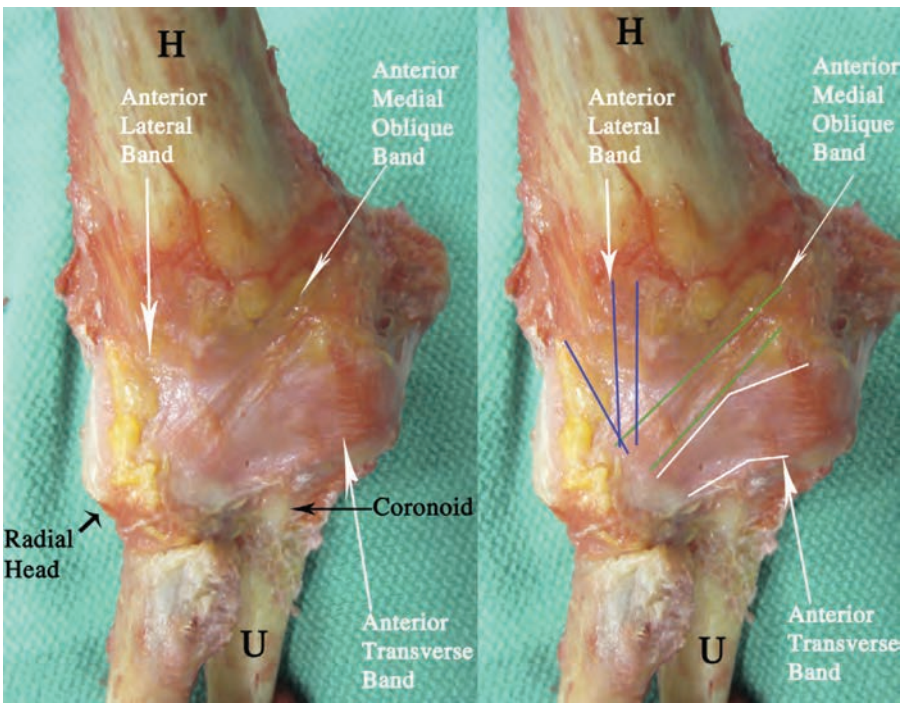

Figure 16.43 Anterior lateral, anterior medial oblique, and anterior transverse bands of the anterior capsule.

Source: Reichel and Morales (2013). Reproduced with permission from Elsevier.

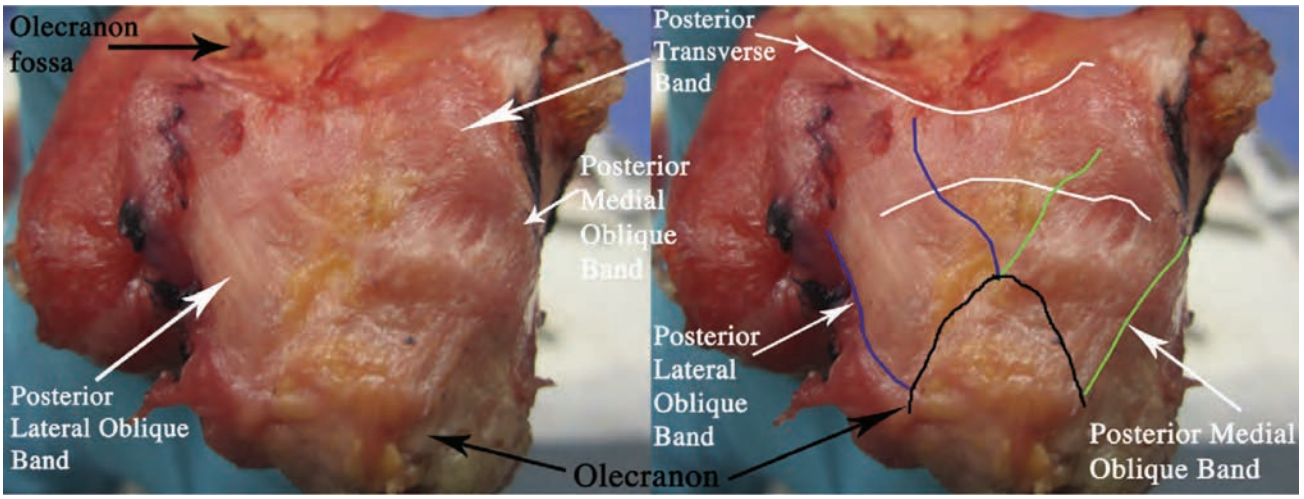

Figure 16.44 Posterior transverse, posterior medial oblique, and posterior lateral oblique bands of the posterior capsule.

Source: Reichel and Morales (2013). Reproduced with permission from Elsevier.

ranges from 15.5 to 24.4 mm (mean 18 mm). The second band (the anteromedial oblique band) originates near the lateral part of the superior medial trochlear ridge and continues laterally and distally to insert onto the central and medial AL. Its length ranges from 15.1 mm to 28.9 mm (mean 20 mm). The last anterior band described by Reichel (the anterior-transverse band) crosses the elbow in a medial to lateral direction from the central and inferior-anterior trochlear ridge to the anteromedial AL and distally to the coronoid tip; the length of this band ranges from 19.7 mm to 38.3 mm (mean 29 mm). Reichel and Morales (2013) observed that all the specimens contained each of these bands although their extent of development varied, the anterolateral band being the least substantial and least developed of the three. In 17% of cases the anterior-transverse band was narrower and thicker, resembling an accessory AL.

Reichel and Morales (2013) also described three distinct posterior bands: the transverse, the medial oblique, and the lateral oblique bands. The transverse band crosses the elbow inferiorly to the olecranon fossa in a medial to lateral direction, originating from the medial trochlear ridge and joining the lateral trochlear ridge. Its length ranges from 17.5 mm to 24.7 mm (mean 21 mm). The other two are opposing bands: the posterior medial oblique originates from the medial posterior trochlear ridge and the posterior lateral oblique originates from the lateral posterior trochlear ridge; both insert onto the posterosuperior ridge of the olecranon tip. The lengths of these two bands fall within the ranges 13.3–21.0 mm (mean 18 mm) and 15.1–20.8 mm (mean 17 mm), respectively. In the posterior capsule the three bands form an inverted triangle (Fig. 16.44).

Medial collateral ligament (ulnar collateral ligament)

The medial collateral ligament (MCL) is most commonly described as comprising three parts (Fig. 16.45): the anterior bundle; the posterior bundle (Bardinet's ligament); and the transverse bundle (Cooper's ligament) (Gray 1918; Williams

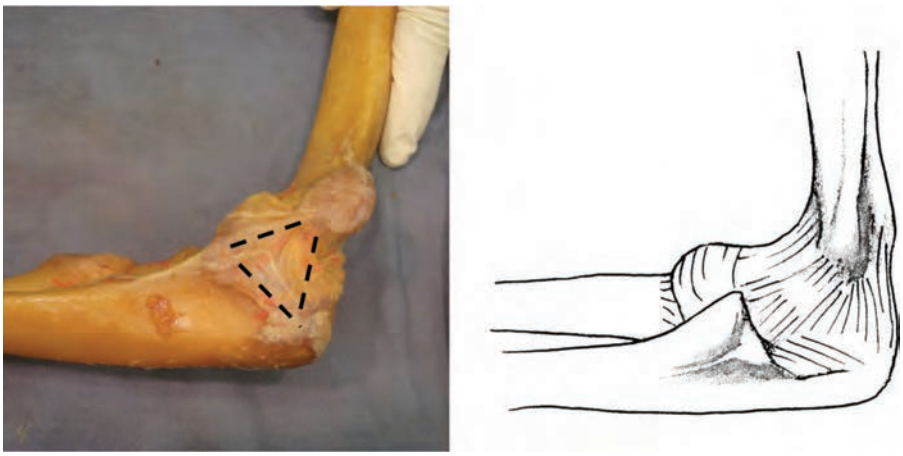

Figure 16.45 Medial collateral ligament (MCL): anterior bundle, posterior bundle and transverse bundle.

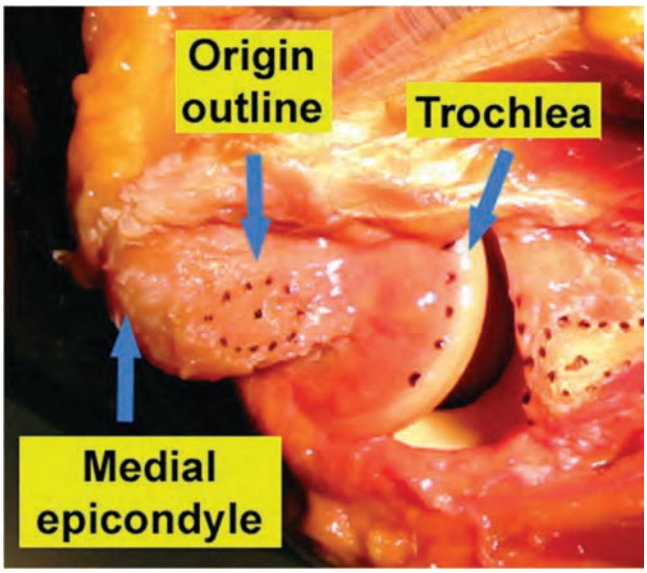

Figure 16.46 Figure shows no attachment of the MCL to the trochlea. The origin has been carefully dissected from its bony attachment. Its outline has been marked with a fine-tipped pen.

Source: Dugas et al. (2007). Reproduced with permission from Elsevier.

and Warwick 1980; Morrey and An 1985). The MCL originates in the central 65% of the anteroinferior surface of the medial epicondyle, just posteriorly to the axis of rotation of the elbow joint (Morrey and An 1985; Ochi et al. 1999).

The anterior bundle (also called anterior oblique ligament or AOL) is the most prominent component and can easily be distinguished from the joint capsule (Morrey and An 1985; Floris 1998); this part originates from the inferior edge of the medial epicondyle and joins the medial aspect of the ulna at the level of the sublime tubercle of the coronoid process. The mean area of attachment of the anterior bundle origin on the medial epicondyle ranges from 25.9 mm^2 to 59.4 mm^2 (mean and SD 45.5±9.3 mm^2) (Dugas et al. 2007). This attachment is round and is located on a flat portion of the anterior and inferior aspect of the medial epicondyle, but is not attached to the medial trochlea (Fig. 16.46) (O'Driscoll et al. 1992; Dugas et al. 2007).

The distances between the center of the origin of the anterior bundle and the center of the medial epicondyle and the humeral cartilage edge fall within the range 10.9–15.3 mm (mean and SD 13.4±1.3 mm) and 15.2–24.2 mm (mean and SD 19.6±2.4 mm), respectively. At the ulnar insertion, the mean area of attachment falls within the range 64.0–199.1 mm^2 (mean and SD 127.8±35.7 mm^2). The insertion is therefore not limited to the prominent portion of the sublime tubercle but extends beyond the sublime tubercle and inserts onto the proximal and medial ulna distally (Dugas et al. 2007). The shape of the insertion is somewhat particular; it is broad proximally at the sublime tubercle and tapered distally (Fig. 16.47). The presence of these distally inserting ligament fibers has been confirmed by histology (Dugas et al. 2007).

The average length of the anterior bundle has been reported in three studies: its mean length is 27.1±4.3 mm as measured by Morrey and An (1985); 21.13±2.79 mm as measured by Regan et al. (1991); and 26.7±3.7 mm as measured by Beckett et al. (2000). The width at its mid-portion is documented in four studies. Morrey and An (1985) reported a mean value of 4.7±1.2 mm, Regan et al. (1991) 7.6 mm, Timmerman and Andrews (1994) 6.0 mm, and Floris et al. (1998) 5.8 mm. Moreover, Dugas et al. (2007) measured the width of the anterior bundle of the MCL at three locations: the proximal, mid-portion and distal insertions. The width is of the range 4.4–9.2 mm (mean and SD 6.8±1.4 mm) proximally, 4.2–9.2 mm (mean and SD 6.8±1.3 mm) at the mid-portion, and 6.2–13.5 mm (9.2±1.6 mm) distally.

The location of the insertion of the anterior bundle of the MCL also varies. Timmerman and Andrews (1994), who studied 10 cadavers, observed that the insertion was 1–2 mm distal to the articular cartilage. In the study by Munshi et al. (2004), 50% of the specimens had an attachment of the anterior bundle that was flush with the articular cartilage, with no separation. In the remaining 50% there was a clear separation between the bundle and the cartilage of the coronoid process. Histological examination of these specimens confirmed that the insertion was 3–4 mm distal to the margin of the joint, although it is unclear whether this was a normal variant or a result of degenerative changes (Munshi et al. 2004). Dugas et al. (2007) reported a mean distance from

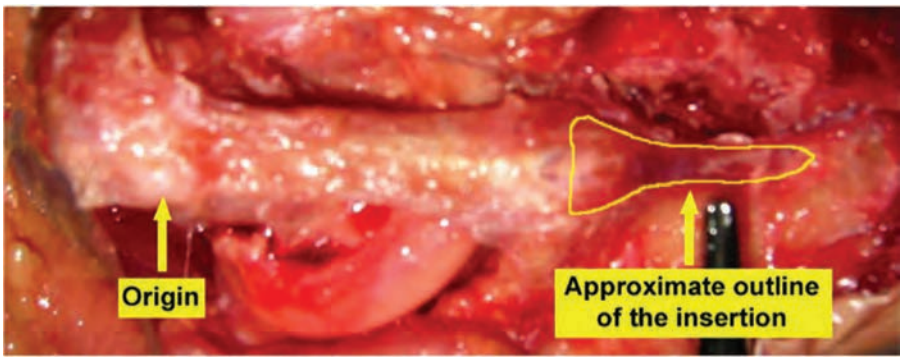

Figure 16.47 The anterior bundle is exposed along its entire length from the origin to the insertion. The approximate insertion is outlined, demonstrating its long shape that is broad proximally and tapered distally.

Source: Dugas et al. (2007). Reproduced with permission from Elsevier.

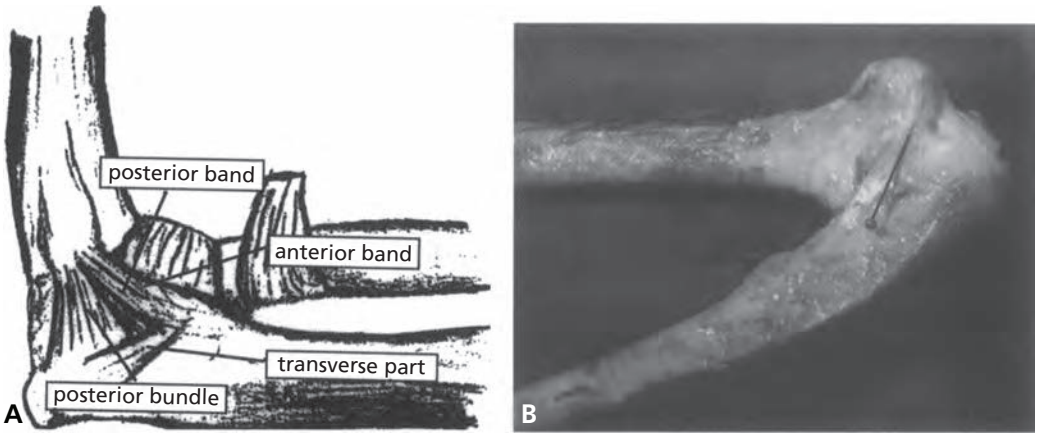

Figure 16.48 Medial collateral ligament complex (on the right, the needle indicates ridge).

Source: Floris et al. (1998). Reproduced with permission from Elsevier.

cartilage to insertion of 2.8±1.4 mm (range 0.3–4.5 mm) in 85% of the specimens analyzed. The mean cross-sectional area, which was assessed only by Regan et al. (1991), measured 12.94±3.07 mm^2.

Upon macroscopic evaluation, a ridge that divided the anterior bundle into two equal parts was identified: the width of the anterior band fell within the range 2.5–4 mm (mean 3 mm), while that of the posterior band was 2–3.5 mm (mean 2.8 mm) (Fig. 16.48) (Floris et al. 1998). In contrast, Munshi et al. (2004) suggested that there is no morphological reason for separating the fibers of the anterior bundle into two distinct layers.

The posterior bundle (also called posterior oblique ligament or POL) is a fan-shaped thickening of the capsule; it originates from the posterior edge of the medial epicondyle and inserts onto the medial olecranon (Morrey and An 1983). The fiber density of this bundle is lower than that of the anterior bundle and the bundle is more distinct upon macroscopic evaluation in joint flexion. Its average length was 16.51±1.52 mm in the study by Regan et al. (1991), 23.2±3.7 mm in the study by Beckett et al. (2000), and 24.2±4.3 mm in the study by Morrey and An (1985). The width in the mid-portion of the ligament fell within the range 5.3±1.1 mm (Morrey and An 1985) to 6 mm (Timmerman and Andrews 1994). The cross-sectional area of the posterior bundle, as measured by Regan et al. (1991), was 8.90±3.36 mm^2.

Lastly, the transverse part (the presence of which varies) is composed of fibers running along the medial joint capsule from the tip of the olecranon to the medial ulna, just distal to the coronoid (Morrey and An 1985; Floris et al. 1998). The mean length of this band is 20.5±3.4 mm (Beckett et al. 2000).

Fuss (1991) observed that it is impossible to identify the origins of the anterior and posterior parts and identified a variant of ulnar insertion of the anterior part, illustrated in a picture (Fig. 16.49) of a specimen in which the anterior band is round and about twice as long as the other bundles, and inserts much further distally along the ulna.

Beckett et al. (2000) performed 39 dissections on embalmed cadavers and described four anatomical variations of the MCL (Fig. 16.50):

- Group I (normal): the classical description with anterior, posterior, and oblique bands was found in 49% of the specimens.
- Group II (strong oblique pattern): the oblique band is expanded into a fan-shaped structure. Its maximum width occupies at least 40% of the length of the anterior band onto which it inserts. This variation was found in 28% of the specimens.
- Group III (extra band pattern): resembled the normal type with an additional band (mean length 39.5±8.5 mm) passing from the posterior capsule to the oblique band of the MCL. This variation was found in 8% of the specimens.
- Group IV (combination pattern). A combination of groups II and III, found in 15% of the specimens.

The so-called classical appearance was found in no more than half of the specimens dissected by Beckett et al. (2000).

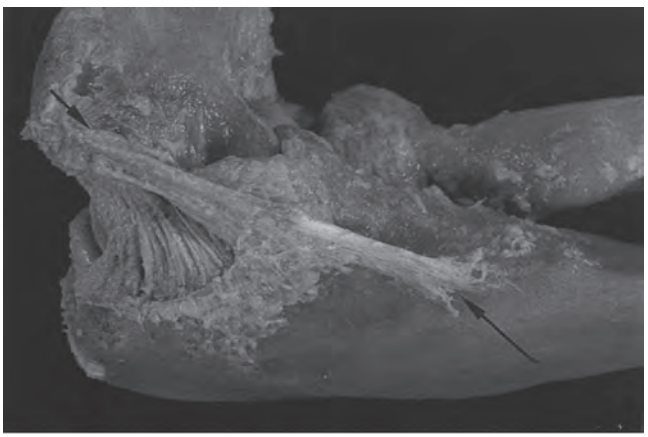

Figure 16.49 Variant of ulnar insertion of the anterior part of the MCL. The anterior band is round and about twice as long as other bundles, and inserts much further distally on the ulna.

Source: Fuss (1991). Reproduced with permission from John Wiley & Sons.

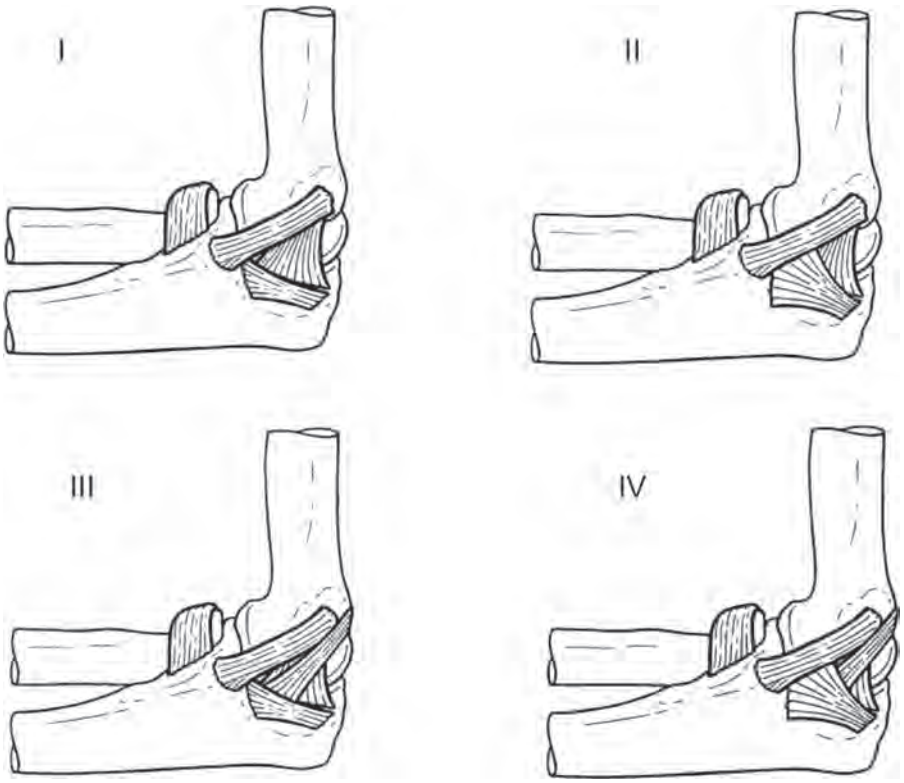

Figure 16.50 Classification of the medial collateral ligament complex: (I) group 1 (classic); (II) group 2 (strong oblique); (III) group 3 (extra band); and (IV) group 4 (combination).

Source: Beckett et al. (2000). Reproduced with permission from John Wiley & Sons.

Lateral collateral ligament

In the most widely accepted description, the lateral collateral ligament (LCL) or lateral collateral ligament complex consists of the lateral ulnar collateral ligament (LUCL), radial collateral ligament (RCL), anular ligament (AL), and accessory lateral collateral ligament (King et al. 1993). The LUCL originates from the inferior surface of the lateral epicondyle and inserts onto the supinator crest of the ulna (Morrey and An 1985). The average length of this band is 45.9±6.3 mm (Beckett et al. 2000). The ulnar part consists of easily identified fibers that are "superficially localized" as described by some authors (O'Driscoll et al. 1991; King et al. 1993), whereas others (Olsen et al. 1996; Imatani et al. 1999) have observed that in the most cases the band passes through the intermediate stratum of the AL and inserts distally onto the proximal part of the supinator crest, blending with fibers from the inferior margin of the AL. Moreover, Regan et al. (1991) and Olsen et al. (1996) occasionally observed various capsular bands between the lateral epicondyle and the olecranon, covering the LCL complex (Fig. 16.51).

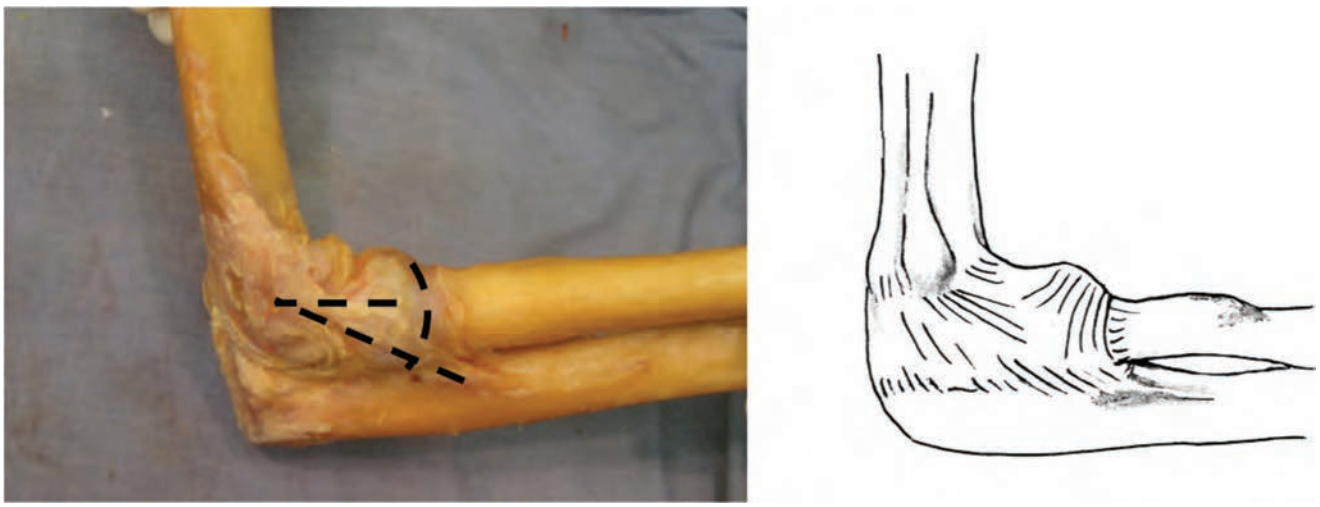

Figure 16.51 The lateral collateral ligament complex: oblique line, lateral ulnar collateral ligament (LUCL); horizontal line, radial collateral ligament (RCL); curved line, anular ligament (AL) and the accessory lateral collateral ligament.

The RCL is a fan-shaped structure that originates from the anteroinferior aspect of the lateral epicondyle and invariably inserts onto and blends with the anular ligament; the mean length of this bundle, as measured by Morrey and An (1983) from the humeral origin to the center of the AL, is 21.2±3.3 mm. Other authors have reported similar values: 19.88±2.95 mm (Regan et al. 1991); 20.5±1.9 mm (Hannouche and Bégué 1999); and 25.7±2.7 mm (Beckett et al. 2000). The mean width of the posterior band measured at its mid-portion ranges from 5.1±1.5 mm (Morrey and An 1985) to 5.2±0.8 mm (Hannouche and Bégué 1999), whereas the mean cross-sectional area as measured by Regan et al. (1991) is 17.01±10.15 mm^2.

The AL is a strong band that encircles the radial head and is confluent with the RCL and LUCL; it is attached to the anterior and posterior margins of the lesser sigmoid notch of the ulna and comprises about four-fifths of the fibro-osseous ring (Morrey and An 1985). Posteriorly, it broadens and is subdivided into several bands with some variations in the extent of its attachment and shape; however, these were not described in detail by the authors (Imatani et al. 1999).

The LCL complex ulnar insertion, which is 2.3±0.4 cm long, begins at the proximal margin of the radial head in 75% of specimens, 2–3 mm distal to the proximal margin in 18% and 2–3 mm proximal to the proximal margin in 7% (Cohen and Hastings 1997). The insertion is located just below the radial notch and progresses along a rough ridge in line with the supinator crest of the ulna. Cohen and Hastings (1997) observed two types of LCL insertions: in 55% of cases the insertion is "bilobed" (Type I), with longitudinal fibers inserting at the level of the radial head; and in the remaining cases (Type II) a second oblique bundle inserts distally onto the ulna (Fig. 16.52). Most of these specimens were characterized by a small but definite gap separating the two bundles. In 45%, the LCL insertion consisted instead of a broad single expansion with a smooth transition between the proximal and distal fibers (Fig. 16.53). The authors did not identify a thin band of ligament extending from the lateral epicondyle to the ulna, which is independent of the AL and is referred to as the LUCL. Moreover, Cohen and Hastings (1997) described two variants of the type II insertion: in the first, a second 3 mm band inserts 4 mm proximally at the level of the distal aspect of the olecranon fossa; and the second is characterized by a narrow and stout band which inserts onto the ulna at the distal margin of the anular ligament.

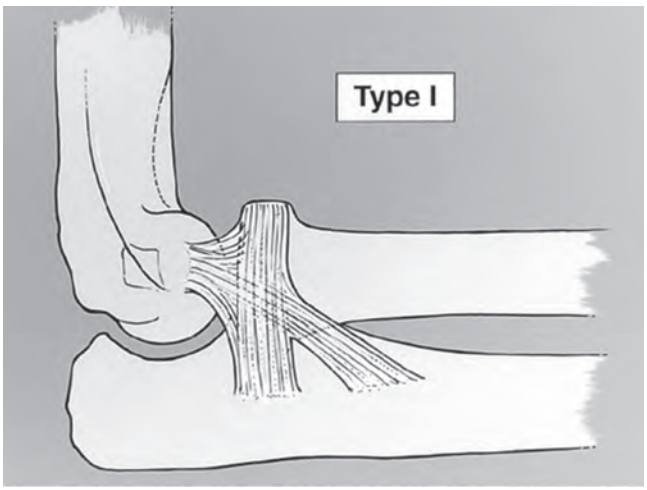

Figure 16.52 Type I LCL insertions: "bilobed", with longitudinal fibers inserting at the level of the radial head. In the other cases a second oblique bundle inserts distally onto the ulna.

Source: Cohen and Hastings (1997). Reproduced with permission from Sapienza University of Rome.

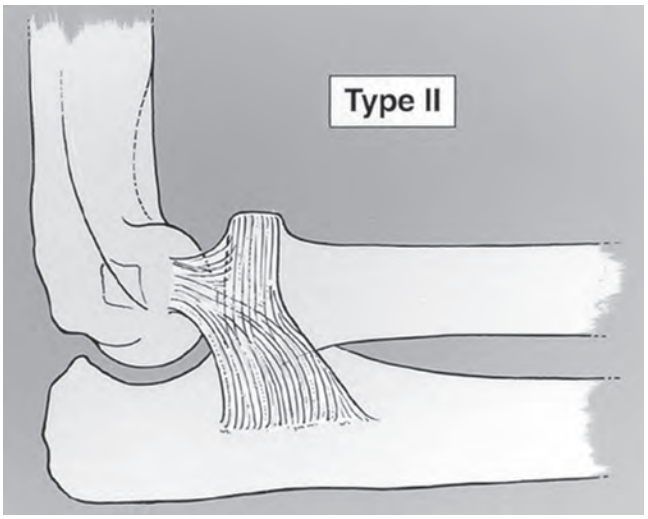

Figure 16.53 Type II LCL insertion: broad single expansion with a smooth transition between the proximal and distal fibers.

Source: Cohen and Hastings (1997). Reproduced with permission from Sapienza University of Rome.

Takigawa et al. (2005) observed a third configuration of the insertion, in which the lateral ligament inserts onto a broad single expansion together with a thin membranous fiber. The authors observed Cohen's Type I configuration in 30% of dissected specimens, Type II in 35% and Type III in 35%. Moreover, they measured the width of the origin, the width of the insertion, and the lengths of the three different LUCLs.

In the study by Bozkurt et al. (2005), the accessory ligament crossed the AL, RCL, and the fibers from the distal thick part of the AL that curved to insert onto the ulna (referred to as the inferior oblique band of the anular ligament). The authors also described other ligamentous structures running proximally in the opposite direction at an oblique angle (referred to as the superior oblique band of the anular ligament) (Fig. 16.54).

Beckett et al. (2000) described four anatomical variations of the LCL (Fig. 16.55):

- Group I: the lateral ulnar collateral ligament is not present. The ligament is fan-shaped, originates from the epicondyle and inserts onto the anular ligament. This variant was found in 23% of the specimens.

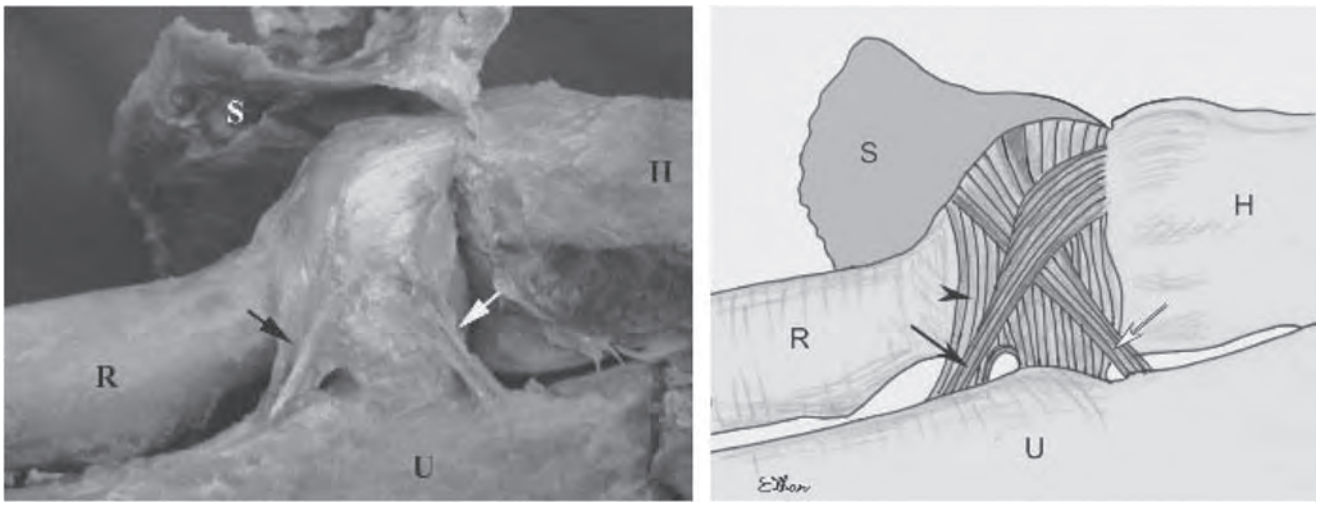

Figure 16.54 Left: Posterolateral view of the left elbow. Black arrow, inferior oblique band of the anular ligament; white arrow, superior oblique band of the anular ligament; R, radius; U, ulna; H, humerus; S, supinator. Right: Schematic drawing of the posterolateral view of the left elbow. The lateral accessory collateral ligament fuses with the distal part of the anular ligament, forming the inferior oblique band. Black arrow, lateral accessory collateral ligament; black arrowhead, distal thick part of the anular ligament; white arrow, superior oblique band of the anular ligament.

Source: Bozkurt et al. (2005). Reproduced with permission from SAGE.

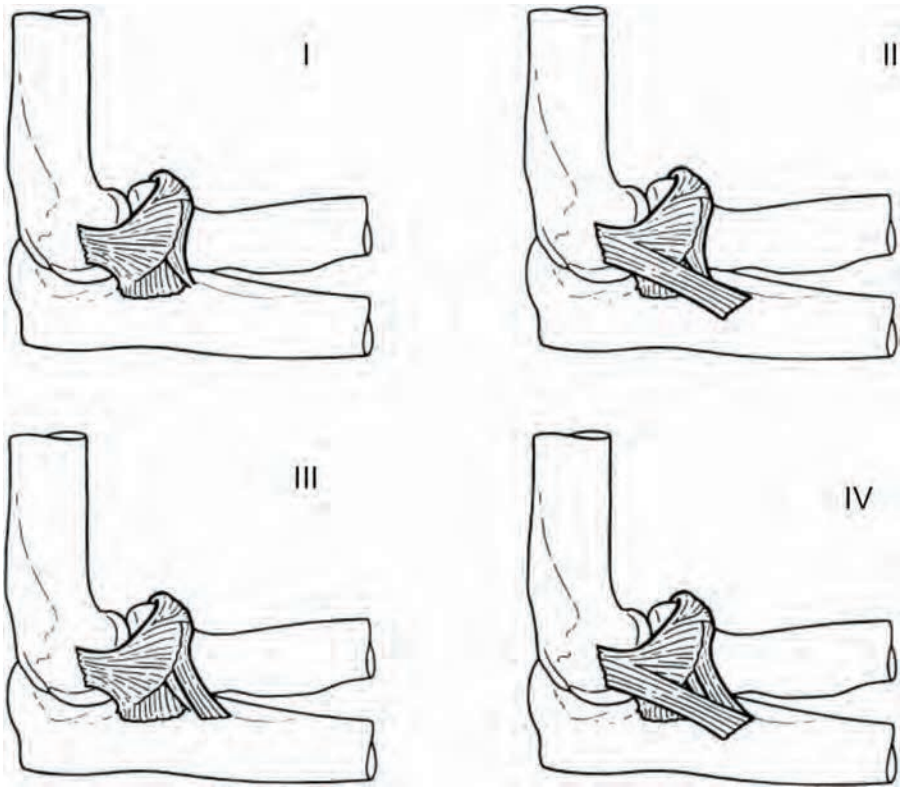

Figure 16.55 Classification of the lateral collateral ligament complex: (I) group 1: LCL + anular ligament; (II) group 2: group 1 + LCL; (III) group 3: group 1 + accessory collateral ligament; and (IV) group 4: group 1 + LUCL + accessory collateral ligament.

Source: Beckett et al. (2000). Reproduced with permission from John Wiley & Sons.

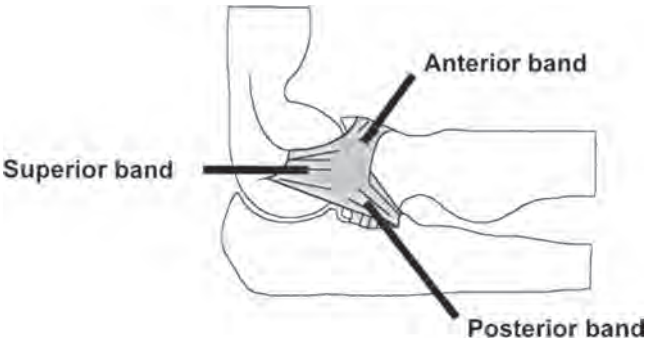

Figure 16.56 Three bands of the Y structure in the LCL complex: superior, anterior, and posterior.

Source: Seki et al. (2002). Reproduced with permission from Elsevier.

- Group II: group I with LUCL, found in 44% of the specimens.
- Group III: group I with the accessory collateral ligament. The average length of the accessory ligament is 43.1±3.3 mm. This group accounted for 25% of the specimens.
- Group IV: a combination of groups II and III. This variant was found in only 7% of the specimens.

The LUCL was identified in almost 50% of the specimens by Morrey and An (1985). This figure contrasts with the incidence reported by O'Driscoll et al. (1991) and Olsen et al. (1996), who found this structure in all their specimens.

According to Olsen et al. (1998), Hannouche and Bégué (1999), Seki et al. (2002), and Takigawa et al. (2005), the LCL is a fan-shaped complex of fibers rather than the discrete ligament bands described by other authors. Seki et al. (2002) suggested that the LCL is a complex of Y-shaped fibers composed of three functional parts: superior, anterior, and posterior (Fig. 16.56). Takigawa et al. (2005) performed a functional subdivision into proximal fibers, which extend from the lateral epicondyle to the anular ligament, and distal fibers, which run from the anular ligament to the supinator crest of the ulna.

References

Ablove RH, Moy OJ, Howard C, Peimer CA, S'Doia S. 2006. Ulnar coronoid process anatomy: possible implications for elbow instability. *Clin Orthop Relat Res* 449: 259–261.

Afshar A. 2011. Os supratrochleare dorsale. *J Hand Surg Eur* 36: 821–822.

Ahlgren SA, Rydholm A. 1975. Patella cubiti. Report of an operated case. *Acta Orthop Scand* 46: 931–933.

Akabori E. 1934. Septal aperture in the humerus in Japanese and in Koreans. *Am J Phys Anthrop* 18: 395–401.

Beckett KS, McConnell P, Lagopoulos M, Newman RJ. 2000. Variations in the normal anatomy of the collateral ligaments of the human elbow joint. *J Anat* 197: 507–511.

Beredjiklian PK, Nalbantoglu U, Potter HG, Hotchkiss RN. 1999. Prosthetic radial head components and proximal radial morphology: A mismatch. *J Shoulder Elbow Surg* 8: 471–475.

Bhanu PS, Sankar KD. 2012. Anatomical note of supratrochlear foramen of humerus in south costal population of Andhra Pradesh. *NMJ* 1: 28–34.

Bozkurt M, Acar HI, Apaydin N, Leblebicioglu G, Elhan A, Tekdemir I, Tonuk E. 2005. The anular ligament: an anatomical study. *Am J Sports Med* 33: 114–118.

Brownhill JR, King GJ, Johnson JA. 2007. Morphologic analysis of the distal humerus with special interest in elbow implant sizing and alignment. *J Shoulder Elbow Surg* 16: S126–S132.

Brownhill JR, Mozzon JB, Ferreira LM, Johnson JA, King GJ. 2009. Morphologic analysis of the proximal ulna with special interest in elbow implant sizing and alignment. *J Shoulder Elbow Surg* 18: 27–32.

Captier G, Canovas F, Mercier N, Thomas E, Bonnel F. 2002. Biometry of the radial head: biomechanical implications in pronation and supination. *Surg Radiol Anat* 24: 295–301.

Caputo AE, Mazzocca AD, Santoro VM. 1998. The nonarticulating portion of the radial head: anatomic and clinical correlations for internal fixation. *J Hand Surg Am* 23: 1082–1090.

Christos P, Marios P, Apostolos S. 2011. Rare cases of humerus septal apertures in Greeks. *Trends Med Res* 6: 178–183.

Cohen MS, Hastings H 2nd. 1997. Rotatory instability of the elbow. The anatomy and role of the lateral stabilizers. *J Bone Joint Surg Am* 79: 225–233.

Cowal LS, Pastor RF. 2008. Dimensional variation in the proximal ulna: evaluation of a metric method for sex assessment. *Am J Phys Anthropol* 135: 469–478.

Doornberg JN, de Jong IM, Lindenhovius AL, Ring D. 2007. The anteromedial facet of the coronoid process of the ulna. *J Shoulder Elbow Surg* 16: 667–670.

Dugas JR, Ostrander RV, Cain EL, Kingsley D, Andrews JR. 2007. Anatomy of the anterior bundle of the ulnar collateral ligament. *J Shoulder Elbow Surg* 16: 657–660.

Floris S, Olsen BS, Dalstra M, Søjbjerg JO, Sneppen O. 1998. The medial collateral ligament of the elbow joint: anatomy and kinematics. *J Shoulder Elbow Surg* 7: 345–351.

Fuss FK. 1991. The ulnar collateral ligament of the human elbow joint. Anatomy, function and biomechanics. *J Anat* 175: 203–212.

Giannicola G, Manauzzi E, Sacchetti FM, Greco A, Bullitta G, Vestri A, Cinotti G. 2012. Anatomical variations of the proximal radius and their effects on osteosynthesis. *J Hand Surg* 37A: 1015–1023.

Giannicola G, Sedati P, Polimanti D, Cinotti G, Bullitta G. 2015a. Contribution of cartilage to size and shape of radial head circumference: magnetic resonance imaging analysis of 78 elbows. *J Shoulder Elbow Surg*, published online 22 September 2015, doi: 10.1016/j.jse.2015.07.003.

Giannicola G, Sedati P, Cinotti G, Bullitta G, Polimanti D. 2015b. The ulnar greater sigmoid notch "coverage angle": bone and cartilage contribution. Magnetic resonance imaging anatomic study on 78 elbows. *J Shoulder Elbow Surg*, published online 1 August 2015, doi: 10.1016/j.jse.2015.06.006.

Glanville EV. 1967. Perforation of the coronoid-olecranon septum. Humero-ulnar relationships in Netherlands and African populations. *Am J Phys Anthrop* 26: 85–92.

Goldfarb CA, Patterson JM, Sutter M, Krauss M, Steffen JA, Galatz L. 2012. Elbow radiographic anatomy: measurement techniques and normative data. *J Shoulder Elbow Surg* 21: 1236–1246.

Gray H. 1918. *Gray's Anatomy*. 20th edition. New York, NY: Lea and Febiger.

Grechenig W, Clement H, Pichler W, Tesch NP, Windisch G. 2007. The influence of lateral and anterior angulation of the proximal ulna on the treatment of a Monteggia fracture: an anatomical cadaver study. *J Bone Joint Surg Br* 89: 836–838.

Gudmundsen TE, Ostensen H. 1987. Accessory ossicles in the elbow. *Acta Orthop Scand* 58: 130–132.

Guitton TG, Van Der Werf HJ, Ring D. 2011. Quantitative measurements of the coronoid in healthy adult patients. *J Hand Surg Am* 36: 232–237.

Hannouche D, Bégué T. 1999. Functional anatomy of the lateral collateral ligament complex of the elbow. *Surg Radiol Anat* 21: 187–191.

Hrdlicka A. 1932. The humerus: septal apertures. *Anthropologie* 10: 31–95.

Imatani J, Ogura T, Morito Y, Hashizume H, Inoue H. 1999. Anatomic and histologic studies of lateral collateral ligament complex of the elbow joint. *J Shoulder Elbow Surg* 8: 625–627.

Itamura JM, Roidis NT, Chong AK, Vaishnav S, Papadakis SA, Zalavras C. 2008. Computed tomography study of radial head morphology. *J Shoulder Elbow Surg*. 17: 347–354.

Kate BR, Dubey PN. 1970. A note on the septal apertures in the humerus of Central Indians. *E Anthropol* 33: 105–110.

King GJ, Morrey BF, An KN. 1993. Stabilizers of the elbow. *J Shoulder Elbow Surg* 2: 165–174.

King GJ, Zarzour ZD, Patterson SD, Jonson JA. 2001. An anthropometric study of the radial head: implications in the design of a prosthesis. *J Arthroplasty* 16: 112–116.

Koslowsky TC, Beyer F, Germund I, Mader K, Jergas M, Koebke J. 2007. Morphometric parameters of the radial neck: an anatomical study. *Surg Radiol Anat* 29: 279–284.

Kuhn S, Burkhart KJ, Schneider J, Muelbert BK, Hartmann F, Mueller LP, Rommens PM. 2012. The anatomy of the proximal radius: implications on fracture implant design. *J Shoulder Elbow Surg* 21: 1247–1254.

Mahaisavariya B, Saekee B, Sitthiseripratip K, Oris P, Tongdee T, Bohez EL, Vander Sloten J. 2004. Morphology of the radial head: a reverse engineering based evaluation using three-dimensional anatomical data of radial bone. *Proc Inst Mech Eng (H)* 218: 79–84.

Mahajan A. 2001. Supratrochlear foramen: Study of humerus in North Indians. *Prof Med J* 18: 128–132.

Mall G, Hubig M, Büttner A, Kuznik J, Penning R, Graw M. 2001. Sex determination and estimation of stature from the long bones of the arm. *Forensic Sci Int*. 117: 23–30.

Matzon JL, Widmer BJ, Draganich LF, Mass DP, Phillips CS. 2006. Anatomy of the coronoid process. *J Hand Surg Am* 31: 1272–1278.

Mays S. 2008. Septal aperture of the humerus in a mediaeval human skeletal population. *Am J Phys Anthropol* 136: 432–440.

McDonald CP, Peters TM, Johnson JA, King GJ. 2011. Stem abutment affects alignment of the humeral component in computer-assisted elbowarthroplasty. *J Shoulder Elbow Surg* 20: 891–898.

Meier LN, Hunt DR. 2006. Incidence of humeral septal aperture and its relation to population and sex. *Am J Phys Anthrop* 42: 129.

Ming-Tzu PA. 1935. Septal apertures in the humerus in the Chinese. *Am J Phys Anthropol* 20: 165–170.

Morrey BF, An KN. 1983. Articular and ligamentous contributions to the stability of the elbow joint. *Am J Sports Med* 11: 315–319.

Morrey BF, An KN. 1985. Functional anatomy of the ligaments of the elbow. *Clin Orthop Relat Res* 201: 84–90.

Munshi M, Pretterklieber ML, Chung CB, Haghighi P, Cho JH, Trudell DJ, Resnick D. 2004. Anterior bundle of ulnar collateral ligament: evaluation of anatomic relationships by using MR imaging, MR arthrography, and gross anatomic and histologic analysis. *Radiology* 231: 797–803.

Nayak SR, Das S, Krishnamurthy A, Prabhu LV, Potu BK. 2009. Supratrochlear foramen of the humerus: An anatomico-radiological study with clinical implications. *Ups J Med Sci* 114: 90–94.

Ndou R, Smith P, Gemell R, Mohatla O. 2013. The supratrochlear foramen of the humerus in a South African dry bone sample. *Clin Anat* 26: 870–874.

Obermann WR, Loose HWC. 1983. The os supratrochleare dorsale: A normal variant that may cause symptoms. *AJR* 141: 123–147.

Ochi N, Ogura T, Hashizume H, Shigeyama Y, Senda M, Inoue H. 1999. Anatomic relation between the medial collateral ligament of the elbow and the humero-ulnar joint axis. *J Shoulder Elbow Surg* 8: 6–10.

O'Driscoll SW, Bell DF, Morrey BF. 1991. Posterolateral rotatory instability of the elbow. *J Bone Joint Surg Am* 73: 440–446.

O'Driscoll SW, Jaloszynski R, Morrey BF, An KN. 1992. Origin of the medial ulnar collateral ligament. *J Hand Surg Am* 17: 164–168.

Olsen BS, Vaesel MT, Søjbjerg JO, Helmig P, Sneppen O. 1996. Lateral collateral ligament of the elbow joint: anatomy and kinematics. *J Shoulder Elbow Surg* 5: 103–112.

Olsen BS, Søjbjerg JO, Nielsen KK, Vaesel MT, Dalstra M, Sneppen O. 1998. Posterolateral elbow joint instability: the basic kinematics. *J Shoulder Elbow Surg* 7(1): 19–29.

Paraskevas GK, Papaziogas B, Tzaveas A, Giaglis G, Kitsoulis P, Natsis K. 2010. The supratrochlear foramen of the humerus and its relation to the medullary canal: A potential surgical application. *Med Sci Monit* 16: BR119–123.

Popovic N, Djekic J, Lemaire R, Gillet P. 2005. A comparative study between proximal radial morphology and the floating radial head prosthesis. *J Shoulder Elbow Surg* 14: 433–440.

Puchwein P, Schildhauer TA, Schöffmann S, Heidari N, Windisch G, Pichler W. 2012. Three-dimensional morphometry of the proximal ulna: a comparison to currently used anatomically preshaped ulna plates. *J Shoulder Elbow Surg* 21: 1018–1023.

Puchwein P, Heidari N, Dorr K, Struger L, Pichler W. 2013. Computer-aided analysis of radial head morphometry. *Orthopedics* 36: e51–57.

Purkait R. 2001. Measurements of ulna a new method for determination of sex. *J Forensic Sci* 46: 924–992.

Rafehi S, Lalone E, Johnson M, King GJ, Athwal GS. 2012. An anatomic study of coronoid cartilage thickness with special reference to fractures. *J Shoulder Elbow Surg* 21: 961–968.

Regan WD, Korinek SL, Morrey BF, An KN. 1991. Biomechanical study of ligaments around the elbow joint. *Clin Orthop Relat Res* 271: 170–179.

Reichel LM, Morales OA. 2013. Gross anatomy of the elbow capsule: a cadaveric study. *J Hand Surg Am* 38: 110–116.

Rouleau DM, Faber KJ, Athwal GS. 2010. The proximal ulna dorsal angulation: a radiographic study. *J Shoulder Elbow Surg*. 19: 26–30.

Rouleau DM, Canet F, Chapleau J, Petit Y, Sandman E, Faber KJ, Athwal GS. 2012. The influence of proximal ulnar morphology on elbow range of motion. *J Shoulder Elbow Surg* 21: 384–388.

Sabo MT, McDonald CP, Ng J, Ferreira LM, Johnson JA, King GJ. 2011. A morphological analysis of the humeral capitellum with an interest in prosthesis design. *J Shoulder Elbow Surg* 20: 880–884.

Santoshkumar DA, GaikwadJyoti R, Laeeque M, Diwan CV. 2011. Determination of sex from ulna by univariate analysis. *Indian J Forens Med Path* 4(3): 119–124.

Seki A, Olsen BS, Jensen SL, Eygendaal D, Søjbjerg JO. 2002. Functional anatomy of the lateral collateral ligament complex of the elbow: configuration of Y and its role. *J Shoulder Elbow Surg* 11: 53–59.

Singhal S, Rao V. 2007. Supratrochlear foramen of the humerus. *Anat Sci Int* 82: 105–107.

Smith GR, Hotchkiss RN. 1996. Radial head and neck fractures: anatomic guidelines for proper placement of internal fixation. *J Shoulder Elbow Surg* 5: 113–117.

Soyer AD, Nowotarski PJ, Kelso TB, Mighell MA. 1998. Optimal position for plate fixation of complex fractures of the proximal radius: a cadaver study. *J Orthop Trauma* 12: 291–293.

Srivastava R, Saini V, Rai RK, Pandey S, Singh TB, Tripathi SK, Pandey AK. 2013. Sexual dimorphism in ulna: An osteometric study from India. *J Forensic Sci* 58: 1251–1256.

Swieszkowski W, Skalski K, Pomianowski S, Kedzior K. 2001. The anatomic features of the radial head and their implication for prosthesis design. *Clin Biomech* 16: 880–887.

Takigawa N, Ryu J, Kish VL, Kinoshita M, Abe M. 2005. Functional anatomy of the lateral collateral ligament complex of the elbow: morphology and strain. *J Hand Surg* 30: 143–147.

Timmerman LA, Andrews JR. 1994. Histology and arthroscopic anatomy of the ulnar collateral ligament of the elbow. *Am J Sports Med* 22: 667–673.

Trotter M. 1934. Septal apertures in the humerus of American Whites and Negroes. *Am J Phys Anthropol* 19: 213–227.

Van Riet RP, Van Glabbeek F, Neale PG, Bortier H, An KN, O'Driscoll SW. 2003. The noncircular shape of the radial head. *J Hand Surg Am* 28: 972–978.

Van Riet RP, Van Glabbeek F, Neale PG, Bimmel R, Bortier H, Morrey BF, O'Driscoll SW, An KN. 2004. Anatomical considerations of the radius. *Clin Anat* 17: 564–569.

Weber MF, Barbosa DM, Belentani C, Ramos PM, Trudell D, Resnick D. 2008. Coronoid process of the ulna: paleopathologic and anatomic study with imaging correlation. *Emphasis on the anteromedial "facet". Skeletal Radiol* 38: 61–67.

Williams P, Warwick R. 1980. *Gray's Anatomy*, 36th edition. Edinburgh: Churchill Livingstone.

Windisch G, Clement H, Grechenig W, Tesch NP, Pichler W. 2007. The anatomy of the proximal ulna. *J Shoulder Elbow Surg* 16: 661–666.

Wood VE, Campbell S. 1994. The supratrochleare dorsale accessory ossicle in the elbow. *J Shoulder Elbow Surg* 3: 395–398.

17 Wrist and hand joints

Benjamin Todd Raines and Jean Oakes
University of Alabama at Birmingham, Birmingham, Alabama, United States

Anatomical variants of the hand and wrist may include osseous, nervous, vascular, and soft tissue structures. The purpose of this chapter is to focus on arthrologic variations. Among the most important considerations for appreciating anatomical variants is avoiding misclassification as pathologic processes.

Anatomical variants within the hand

Skeletal malformations within the hand are quite common and, according to Swanson (1976) and Lister (1993), 31.3% of individuals demonstrate failure of a skeletal hand component to differentiate (Swanson 1976; Lister 1993; Freyschmidt et al. 2003).

Phalanx and metacarpal epiphyses

Although normally narrower than their adjacent metaphyses, phalanx epiphyses of the hand may demonstrate an equal or greater width; this is considered a normal variant. However, note that variations in epiphyseal width may reflect underlying ossification disturbance (Freyschmidt et al. 2003). Similarly, metaphyses may be broader than usual, but this is considered a normal variant (Freyschmidt et al. 2003). Finally, epiphyseal plates of the phalanges usually demonstrate a slightly distal convexity whereas those in the metacarpals show a slight proximal convexity, but these too may vary morphologically (Freyschmidt et al. 2003).

Pseudoepiphyses

Pseudoepiphyses are extra epiphyses, a morphologic variant found most commonly in the distal first metacarpal of up to 65% of normal children and in 20–60% of proximal second metacarpals of normal children. Interestingly, pseudoepiphyses fail to significantly contribute to longitudinal growth of tubular bone. These pseudoepiphyses may be found in otherwise normal children, but may be associated with a systemic disturbance in skeletal growth such as hypothyroidism or Down syndrome (up to 82.4%) (Rochels and Schmidt 1980; Freyschmidt et al. 2003). Pseudoepiphyses are most commonly found in those aged 5–10 years, often close earlier than normal growth plates within the same bone, and do not contribute to longitudinal bone growth (Freyschmidt et al. 2003). Relative frequency of pseudoepiphyses within the hand (Schafer 1952; Freyschmidt et al. 2003): first metacarpal > second metacarpal > fifth metacarpal > fifth middle phalanx > third metacarpal > fourth middle phalanx > first proximal phalanx > fourth metacarpal.

Cone-shaped epiphysis

The cone-shaped epiphysis is a morphologic variant less common within the hands of normal individuals than it is within the foot (Giedion 1968; Freyschmidt et al. 2003). It is hypothesized that the cone shape results from growth arrest within the central portion of the epiphysis, while peripheral components still grow. The condition is most often asymptomatic but may present with symptoms in more significant cases, especially when involving a trophic disturbance (Freyschmidt et al. 2003).

Brachymesophalangia

The most common morphologic variant of the middle phalanx is brachymesophalangia, characterized by an abbreviated and occasionally broadened middle phalanx. It is most common within the fifth finger, and affects roughly 20% of the Japanese population as compared to 0.6–1% of Europeans. Further, aplasia of the middle phalanx has been described in literature to occur in conjunction with a short, hypoplastic distal phalanx and a compensatory long proximal phalanx (Dubost et al. 1960; Freyschmidt et al. 2003). A similar phenomenon may occur with brachymetacarpia, involving an abbreviated metacarpal bone and a compensated proximal phalanx.

Brachyphalangia

Shortening of the phalanges, specifically of the proximal phalanx, is often associated with shortening of other osseous hand structures (Freyschmidt et al. 2003). Brachyphlangia is often seen as a component of various syndromes and, in such cases, is not considered a normal morphologic variant (Freyschmidt et al. 2003).

Bergman's Comprehensive Encyclopedia of Human Anatomic Variation, First Edition. Edited by R. Shane Tubbs, Mohammadali M. Shoja and Marios Loukas.
© 2016 John Wiley & Sons, Inc. Published 2016 by John Wiley & Sons, Inc.

Symphalangia

Absence of the interphalangeal joint is referred to as symphalangia, a hereditary form of dysplasia. Symphalangia results in an end-to-end coalition of the phalanges (Freyschmidt et al. 2003). The ulnar/medial digits are more commonly affected, are often bilateral, and are commonly associated with other skeletal anomalies of the hand. On clinical exam, an absence of skin folds over normal joint locations may be noted; on radiographic imaging, normal joint locations may be marked by a fusiform expansion where the phalanges have coalesced (Freyschmidt et al. 2003). Both the radiographic and clinical aspects are more appreciable in adults; in pediatrics, synchondroses retain a flexible nature on physical exam and may be difficult to differentiate from normal joints on imaging (Freyschmidt et al. 2003). Care is required in distinguishing congenital aplasia from acquired ankyloses, the latter of which is characterized by transverse skin folds overlying the region of ankylosis, and are often either unilateral or asymmetrical (Freyschmidt et al. 2003).

Syndactyly

Fusion of phalanges of separate digits is termed syndactyly, and is most commonly hereditary in nature (Freyschmidt et al. 2003).

Axial deviations

Axial deviations of the phalanges can be congenital in nature as a normal variant or a result of various syndromes, including achondroplasia, trisomies, or dysplasias (Freyschmidt et al. 2003). Regarding congenital, normal variants not concomitant with systemic disease or syndromes, camptodactyly and clinodactyly are the two most common forms (Freyschmidt et al. 2003). Clinodactyly is characterized as ulnar or radial deviation of a distal phalanx because of either a trapezoid-shaped middle phalanx or a delta phalanx (Freyschmidt et al. 2003). Any digit may be affected by clinodactyly, but most often involves radial deviation of the fifth digit (Freyschmidt et al. 2003). One variant of clinodactyly is Kirner deformity, where the distal phalanx of both fifth digits exhibit a dorsal convex bowing, resembling a claw. This deformity may be a sporadic, normal variant, or an inherited autosomal dominant trait (Freyschmidt et al. 2003).

Camptodactyly is characterized by a congenital contracture of individual phalangeal joints (Freyschmidt et al. 2003). Product of a genetic mutation, both sporadic and autosomal dominant forms existing, camptodactyly does not demonstrate any detectable bone changes at onset; however, in chronic cases, the base of the middle phalanx will generate a notch in the neck of the first phalanx (Freyschmidt et al. 2003). Usually affecting the fifth digit and less frequently the fourth, the driving force behind this congenital contracture is an aberrant insertion of the lumbrical muscle or of the superficial digital flexors (Freyschmidt et al. 2003).

Polydactyly

Polydactyly may refer to the presence of either more than five digits on one hand or more than five tubular bones within the metacarpal region, and is often seen in conjunction with an array of other morphologic variants within the hand (Freyschmidt et al. 2003). Osseous structures within supernumerary digits may either reflect normal development and organization, or may be rudimentary elements along a continuum (Freyschmidt et al. 2003).

Polydactyly is classified based on the location of the supernumerary digit or metacarpal bone either as radial, ulnar, or central (second through fourth rays) (Buck-Gramcko and Behrens 1989; Freyschmidt et al. 2003).

Polyphalangia

Similar to polydactyly, polyphalangia is the rare development of one of more duplicate phalanges within a digit (Freyschmidt et al. 2003). For example, Windle (1891) has reported the occurrence of an additional phalanx in the human pollex.

Arachnodactyly

Arachnodactyly is the development of disproportionately long, thin digits, often with premature ossification noted on imaging. On physical examination, when place in the palm of the hand the first digit will extend past the hypothenar eminence/ulnar border of the hand when the first is closed around it (Steinberg sign; Freyschmidt et al. 2003). Arachnodactyly is commonly associated with a number of systemic syndromes so a thorough examination for additional underlying anomalies should be performed (Freyschmidt et al. 2003).

Carpometacarpal variants

The most common etiology for carpometacarpal joint variance is due to four metacarpal base types (Viegas 2001; Phillips 2013). Metacarpal bases shapes have been divided into five types (Phillips 2013):

- Type I: Broad base with articulation with the hamate and one dorsal facet that is in contact with the capitate.
- Type II: Broad base with articulation with the hamate and two facets (dorsal and volar) that articulate with the capitate.
- Type III: Narrow base that solely articulates with the hamate.
- Type IV: Broad base that articulates with the hamate and a single, separate facet that articulates with the capitate.
- Type V: Relatively broad base without any projections or separate articular surface which articulates with the hamate and the capitate.

The thumb

Given the evolutionary significance of the human thumb, morphologic variants are of both anatomic and radiographic significance, as well as of clinical relevance.

A short proximal phalanx in the thumb is associated with a host of systemic syndromes, whereas an abbreviated distal phalanx may be a sign of significant dysplasia (Freyschmidt et al. 2003). The triphalangeal thumb is relatively common within the European population, due to documented incidence of inheritance, and affects roughly 1 in 25,000 (Ferber 1952; Freyschmidt et al. 2003).

Sesamoid bones

There are normally five sesamoid bones within the hand: metacarpophalangeal joint (MCP) of the first, second and fifth digits within the adductor pollicis and flexor pollicis brevis tendons. However, the number and location of sesamoid bones can vary between individuals (Stein et al. 2011).

Osteopoikilosis

Characterized by multiple ossification centers with increased density on imaging, resembling "spotted bone," osteopoikilosis is a generally asymptomatic, autosomal dominant trait with little clinical relevance (Freyschmidt et al. 2003). On occasion, patients may develop cutaneous changes (Freyschmidt and Freyschmidt 1996; Freyschmidt et al. 2003).

Melorheostosis

Often described on radiograph as candle wax dripping down a bone, melorheostosis is characterized by sites of both endosteal and periosteal new bone formation (Freyschmidt et al. 2003). According to Freyschmidt hands are rarely affected by melorheostosis; when it does however occur, it is usually unilateral and isolated to one to two rays (Freyschmidt 2001; Freyschmidt et al. 2003). Additionally, involvement of the rest of the patient's arm usually accompanies hand involvement (Freyschmidt 2001; Freyschmidt et al. 2003).

Anatomical variants of the carpus

Carpal structures on imaging

Radiographic images of carpal bones, especially involving computed tomography, may present with a number of various notches, recesses, and lucencies. These images should be interpreted with caution as both imaging parameters and tissue position play a role and may present cavities on radiograph which fail to truly exist (Freyschmidt et al. 2003). For example, small, round lucencies surrounded by a sclerotic rim or both can often be attributed to nutrient vessels and their canals on cross-section. These canals are known to mimic fractures when viewed tangentially, especially within the scaphoid bone (Freyschmidt et al. 2003).

Bone islands, characterized as small, circumscribed densities within individual carpal bones, may be noted on radiographic examination and are a normal variant. With respect to the wrist, these islands are most commonly found within the scaphoid and triquetrum (Freyschmidt et al. 2003).

Accessory ossicles

Accessory ossicles are secondary ossification centers distinct from the associated underlying bone, and are found in 0.3–1.6% of the normal population (O'Rahilly 1953; Freyschmidt et al. 2003). These extra bones can be congenital, post-traumatic, or degenerative in etiology. Over 20 accessory ossicles involving the wrist have been described in the literature (Timins 1999; Freyschmidt et al. 2003).

When differentiating accessory ossicles from recent traumatic fractures (i.e., avulsion), note that accessory bones will be completely encased in cortical shell and will not demonstrate exposed cancellous bone (Freyschmidt et al. 2003). Freyschmidt proposed that determining exactly what accessory bone is at hand is not the main issue, but rather it is more important to simply determine that an element is an accessory bone. The point is that, no matter what the accessory bone is, it rarely changes clinical decision-making and outcomes, and may simply be referred to as an "unknown bony element" or as an "unnamed accessory bone element" (Freyschmidt et al. 2003).

Carpal boss and os styloideum

A carpal boss is described as a bony protuberance on the dorsum of the wrist, most often lying between the second and third metacarpal bases. A carpal boss may be associated with carpal pain or limitations in wrist mobility. The carpal boss may be derived from degenerative osteophytes or from an os styloideum. The os styloideum is an accessory ossicle of the wrist located between the second and third metacarpal bases and the distal aspects of the capitate and trapezoid. Pain associated with an os styloideum can have multiple etiologies and may be the product of osteoarthritis, concomitant bursitis, an overlying ganglionic cyst, or possibly due to extensor tendon subluxation over the bony protuberance (Conway et al. 1985; Stein et al. 2011). An os styloideum is most appreciable on sagittal images, and should not be mistaken for a fracture (Stein et al. 2011).

Lunate accessories

Both the os hypolunatum and os epilunatum are accessory ossicles of the lunate bone, and careful attention is required to differentiate these variants from fractures. The os hypolunatum is located just proximal to the capitate, positioned between the lunate and scaphoid (Doyle and Bottle 2003; Freyschmidt et al. 2003). The ossiculum of Gruber may be seen just distal to the capitate . The os epilunatum is characterized as a rounded, bony projection from the dorsal horn of the lunate with flattening of the apposing bony margins (Freyschmidt et al. 2003).

Carpal coalitions

Carpal coalitions are osseous, fibrous, or cartilaginous fusions between carpal bones, and may be either congenital or idiopathic in nature. Congenital fusions are a result of incomplete segmentation of a common cartilaginous carpal precursor. Idiopathic coalitions involve adjacent carpal bones in the same row. Females and African Americans have the highest rates of idiopathic coalitions (Timins 1999; Stein et al. 2011). Drews and Gunther (1966) report that 0.11% of Caucasians exhibit carpal coalitions, whereas 1.6% of African Americans and up to 8% of Nigerians are affected (Freyschmidt et al. 2003). Carpal coalitions are usually limited to two bones, and involvement of three or more is a rare anomaly (Freyschmidt et al. 2003). It is important to distinguish congenital coalition from secondary ankylosis due to degenerative or inflammatory processes, often

best achieved via a thorough patient history (Freyschmidt et al. 2003). In some instances, carpal coalitions may not be isolated findings but rather components of syndromes involving concomitant vertebral body fusion or hearing loss (Freyschmidt et al. 2003).

Lunotriquetral coalitions are the most frequent idiopathic carpal coalition, with a prevalence of 0.1% in the general population (Timins 1999; Stein et al. 2011; Phillips 2013). This rate may be 100 times higher in the African American population. Lunotriquetral coalitions are more common among females and are bilateral in 60% of cases (Timins 1999; Stein et al. 2011).

There are a number of lunotriquetral coalition variants, including distal and proximal fusions as well as complete and incomplete fusions (Freyschmidt et al. 2003). Freyschmidt also noted that lunotriquetral coalitions can be associated with Madelung deformity, negating its classification as a normal variant in this context (Freyschmidt et al. 2003). Lunotriquetral coalitions were classified by Minaar as types I–IV (Timins 1999) as follows:

- Type I: proximal fibrous or cartilaginous coalition;
- Type II: incomplete osseous fusion with distal notch;
- Type III: complete osseous fusion; and
- Type IV: complete osseous fusion with other carpal anomalies.

Most lunotriquetral coalitions are asymptomatic and are a result of incidental finding, but type I coalitions may be painful (Stein et al. 2011). Asymptomatic widening of the scapholunate joint may be associated with lunotriquetral coalitions, and is the result of this morphologic variant rather than of ligamentous injury (Metz et al. 1993; Freyschmidt et al. 2003; Stein et al. 2011).

A number of other lunate coalitions have been described, including fusions with the first metacarpal, scaphoid, and trapezoid (Freyschmidt et al. 2003). Delayed ossification of the scaphoid and trapezium after the age of 4–5 years has been identified as a predictor of these coalition patterns (Freyschmidt et al. 2003). One lunate coalition variant, characterized by fusion of the lunate and radius, was described by Becker in 1935 and again by Girod in 1964. This variant also demonstrates an underdeveloped scaphoid (Freyschmidt et al. 2003). Specific radiographic projections of the wrist can create the illusion of lunate coalitions. Elucidation of possible coalition can be achieved through a slight oblique projection in the fourth row on CT imaging (Freyschmidt et al. 2003).

The second-most common carpal coalition is capitohamate fusion, although incidence is significantly less frequent (Timmins 1999; Viegas 2001; Freyschmidt et al. 2003; Stein et al. 2011; Phillips 2013).

Coalitions between the trapezoid and capitate are considered a normal but rare variant (Neiss 1955; Buysch et al. 1971; Freyschmidt et al. 2003). In 1955, Leger described a trapezoid coalition variant displaying fusion with the second metacarpal (Leger 1955; Seibert-Daiker 1975; Freyschmidt et al. 2003).

A number of scaphoid coalitions have been described between neighboring carpals, all as normal variants, including an unusual case described by Krause, Waugh, and Geyer where scapholunate fusion was characterized by a nonunion site at the junction of the middle and distal thirds of the composite bone (Krause 1949; Waugh and Sullivan 1950; Geyer 1962; Freyschmidt et al. 2003).

Pisiform coalitions with either the triquetrum or hamate are rare, but do occur (Freyschmidt et al. 2003).

Bipartite carpals

Bipartite and multipartite carpals are a normal variant within the wrist, but a number of criteria must be met for diagnosis. The order of bipartite carpal frequency is reported as follows: scaphoid > triquetrum > pisiform > trapezium > trapezoid > capitate (Freyschmidt et al. 2003). Note that duplicated carpal bones have been described as part of various enchondral ossification disorders, and are therefore not considered normal variants when under these conditions (Schaaf and Wagner 1962; Freyschmidt et al. 2003).

Controversy exists regarding the congenital nature versus traumatic etiology of bipartite scaphoid bones (Doman and Marcus 1990; Saccomanni 2009). Pfitzner first concluded that bipartite scaphoid was the result of independent ossification nuclei (Pfitzner 1885; Saccomanni 2009). Works by Caffaratti and Bunnell further supported Pfitzner's congenital argument by demonstrating that this rare anomaly could occur bilaterally and provided supplementary factors, such as atraumatic history, equal size and density of both ossicles, absence of degenerative changes in the radial–scaphoid carpal articulation, and even joint-space thereof (Caffaratti 1950; Saccomanni 2009). Among the most convincing evidence for congenital etiology, and therefore considering bipartite scaphoid as a normal morphological variant, is work performed by Doman and Marcus who followed a single case of apparent congenital bipartite scaphoid in a female from childhood through to young adulthood, providing documentation of bipartite retention through serial radiographs (Doman and Marcus 1990; Saccomanni 2009). Saccomanni argued that bipartite scaphoid, at least in some cases, may not be an isolated morphologic variant, but may be attributed to a sporadic form of Holt–Oram-like syndrome (Saccomanni 2009).

A bipartite capitate bone has also been described in literature (Ross 1954; Viehweger 1956; Freyschmidt et al. 2003).

Pfitzner (1885) described a bipartite trapezoid variant, where the two halves were split into dorsal and palmar components (Freyschmidt et al. 2003).

The bipartite capitate has been documented by a number of authors but is generally asymptomatic, not unlike most bipartitions (Ross 1954; Viehweger 1956; Freyschmidt et al. 2003).

Freyschmidt et al. (2003) stated that, to date, no cases of a bipartite hamate have been reported in the literature. A bipartite hamulus has however been described (Greene and Hadied 1981; Freyschmidt et al. 2003).

Lunate morphology

The lunate may vary in both its onset of ossification and its morphologic shape (Phillips 2013). With regards to ossification onset, males have a slightly later window at 1.5–7 years of age compared to 1–6 years of age for females (Phillips 2013). Additionally, double ossification centers as well as a complete absence of the lunate have both been reported in literature (Postacchini and Ippoplito 1975; Poznanski 1984; Phillips 2013).

There are two main "types" or morphologic shapes of the lunate. A type I lunate is characterized by a single facet at the midcarpal joint and is considered the "normal" for classical anatomy. The type II lunate is characterized by an extra medial facet that articulates with the hamate (Viegas et al. 1990; Freyschmidt et al. 2003; Pfirrmann and Zanetti 2005; Stein et al. 2011; Phillips 2013). Types I and II are of equal prevalence, with some studies demonstrating type II lunates in up to 65% of cadaveric specimens (Viegas et al. 1990; Malik et al. 1999; Pfirrmann et al. 2002; Freyschmidt et al. 2003; Yazaki et al. 2008; Stein et al. 2011). Type II lunates can be associated with degenerative changes in the proximal pole of the hamate bone, characterized by cartilaginous erosions and exposed subchondral bone in dissected specimens (Viegas 2001; Stein et al. 2011). As such, the type II lunate can be a possible cause of medial/ulnar wrist pain (Cerezal et al. 2002; Freyschmidt et al. 2003; Stein et al. 2011).

Timins (1999) urges caution in radiographic interpretation, since true lunate morphology cannot always be appreciated. He further advises that lunate morphology is often more clear on coronal MR imaging. In addition, on sagittal MR cuts the volar lunate surface may appear corrugated and irregular. This is a normal variant resulting from numerous insertions and nutrient vessels (Timins 1999).

Bone-specific variations

Hamate

Atypical broadening of the hamate has been described in literature as having two main causes: either duplication of the fifth ray, or broadening and bifurcation of the accessory metacarpal bone (Freyschmidt et al. 2003). This broadening and bifurcation pattern is seen commonly in Ellis–van Crefeld chondroectodermal dysplasia and, as such, is not a normal variant (Freyschmidt et al. 2003). Further, bilateral hyperplasia of the hook of the hamate and the pisiform bones has been described in literature (Viehweger 1957; Freyschmidt et al. 2003).

Scaphoid

Void of any concomitant systemic disease or syndromes, hypoplasia of the scaphoid is a rare variant (Freyschmidt et al. 2003). According to Freyschmidt et al. (2003), there are a number of aplastic scaphoid patterns:

- bilateral scaphoid and lunate aplasia;
- complete left-sided scaphoid aplasia, partial right-sided aplasia with lateral displacement of the lunate bone, and bilateral fusion of the lunate and capitates;
- bilateral scaphoid aplasia combined with abnormal position of the proximal carpal row and atypical articulations; or
- under-development of the scaphoid with ulnar displacement of the lunate, combined with a Wormian bone on the ulnar aspect of both radial epiphyses near the ulnar epiphysis.

Triquetrum

Although most often known for its involvement in carpal coalitions, the triquetrum was noted to be absent in a rare anatomical variant described by Anderson and Bowers (1985) with concomitant scapholunate dissociation and triquetral hypoplasia on the contralateral side (Freyschmidt et al. 2003).

Pisiform

It is common for the pisiform bone to have multiple ossification centers and a late onset of ossification, usually during 8–9 years of age (Freyschmidt et al. 2003). On radiograph, the pisiform may demonstrate a "crumbly" appearance (Freyschmidt et al. 2003).

One interesting morphologic variant of the pisiform involves a bipartite pisiform with an additional bony projection from the distal aspect of the pisiform, terminating at the level of the fourth metacarpal bone (Keats 1979; Freyschmidt et al. 2003).

Pisotriquetral lipping

Pisotriquetral lipping is a normal variant and should be distinguished from degenerative osteophyte formation (Timins 1999).

Anatomical variants of the hand and wrist ligaments and cartilaginous structures

Triangular fibrocartilage complex and intercarpal ligaments

The triangular fibrocartilage complex (TFCC) is composed of six main structures including the triangular fibrocartilage itself, both the volar and dorsal radioulnar ligaments, a meniscus homolog, an ulnar collateral ligament, and the extensor carpi ulnaris tendon sheath (Stein et al. 2011). The purpose of the TFCC is two-fold: it functions to cushion the ulnar head during axial loading as well as to stabilize the ulnar head by anchoring it to the distal radius (Stein et al. 2011). The triangular fibrocartilage is normally thick and biconcave at its central portion, where the lunate articulates distally and the ulna articulates proximally. However, this central, articular region may be thinned or even perforated as a natural variant (Stein et al. 2011). Ulnar variance, the difference in length between the distal radius and ulna, is inversely proportional to the triangular fibrocartilage thickness (Stein et al. 2011). The meniscus homolog component of the TFCC, a fold of connective tissue located between the styloid process, ulnar collateral ligament, and the triquetrum, varies in presence among individuals (Stein et al. 2011). It has been reported that defects within the TFCC and the membranous central portion of the lunotriquetral and scapholunate ligaments

are a common and age-related phenomenon. These defects are rarely seen in those <45 years of age, are present in one-third of those >60, and are most commonly located along the radial aspect of the complex (Viegas and Ballantyne 1987; Zanetti et al. 2000; Pfirrmann and Zanetti 2005; Stein et al. 2011). Although most commonly located along the radial aspect, the literature suggests that ulnar-sided defects are more commonly associated with symptomatic wrists (Pfirrmann and Zanetti 2005).

Imaging signals from ligamentous structures within the hand and wrist are normally hypointense, but moderate-to-bright intensity may be a normal variant, considered a pitfall of imaging, mainly at insertion sites (Stein et al. 2011). As such, the radial and ulnar attachments of the triangular fibrocartilage often demonstrate focal, moderate–high intensity signal for two reportedly different reasons. At the ulnar insertion site, increased signal is the result of separate fiber bundles assimilating (Pfirrmann et al. 2001; Pfirrmann and Zanetti 2005; Stein et al. 2011). At the radial insertion, a curvilinear, intense signal may be due to the presence of hyaline cartilage (Pfirrmann and Zanetti 2005; Stein et al. 2011, fig. 7). Although somewhat beyond the scope of normal anatomic variants, in the presence of myxoid degeneration the TFCC will demonstrate an increased (mild–moderate) signal on imaging (Helms et al. 2009; Stein et al. 2011).

Similar to the increased signal seen at triangular fibrocartilage insertion points, increased signal may be noted at endpoints of all intercarpal ligaments such as the scapholunate or lunotriquetral ligaments (Helms et al. 2009; Stein et al. 2011).

The scapholunate ligament varies in shape based on the imaging projection with the volar aspect being trapezoidal, triangular centrally, and the dorsal component being band-like on coronal images. Further, the scapholunate ligament varies between attaching to the cartilage or cortex of the scaphoid as well as to the lunate in a multitude of combinations (Totterman and Miller 1996; Burns et al. 2011).

Normally characterized by a V-shaped morphology, the lunotriquetral ligament has been described with a number of variant shapes. More specifically, the membranous component of the lunotriquetral ligament is highly variable; although triangular in morphology, it ranges from being broad-based to equilateral, narrow-based, and asymmetric in shape (Smith and Snearly 1994; Yoshioka et al. 2006; Burns et al. 2011) Yoshioka et al. (2006) also describe a linear or "bar-like" morphology of the lunotriquetral ligament as well as an amorphous shape, the latter of which is mostly seen in elderly individuals (Yoshioka et al. 2006; Burns et al. 2011). The dorsal radiolunate ligament may attach to the capitate (Yu et al. 2004).

References

Anderson JW, Bowers WH. 1985. Congenital absence of the triquetrum: a case report. *J Hand Surg* 10A: 620–622.

Buck-Gramcko D, Behrens P. 1989. Klassifikation der polydaktylie fur hand und foot. *Handchir Mikrochir Plast Chir* 21: 195–204.

Burns JE, Tanaka T, Ueno T, Nakamura T, Yoshioka H. 2011. Pitfalls that may mimic injuries of the triangular fibrocartilage and proximal intrinsic wrist ligaments at MR imaging. *Radiographics* 31: 63–78.

Buysch KH, Drewese J, Gunther D. 1971. Synostosen zwischen multangulum minus und capitatum. *Fortsch Rontgenstr* 115: 267–268.

Caffaratti E. 1950. Scafoide bipartito bilaterale del carpo di natura congenita. Quad Rad 13, 159 or Congenital bilateral bipartite carpal scaphoid. *G Batteriol Immunol* 41: 430.

Cerezal L, del Pinal F, Abascal Garcia-Valtuille R, Pereda T, Canga A. 2002. Imaging findings in ulnar-sided wrist impaction syndromes. *Radiographics* 22: 105–121.

Conway WF, Destouet JM, Gillula LA, Bellinghausen HW, Weeks PM. 1985. The carpal boss: an overview of radiographic evaluation. *Radiology* 156: 29–31.

Doman AN, Marcus NW. 1990. Congenital bipartite scaphoid. *J Hand Surg Am* 15A: 869–873.

Doyle JR, Bottle MJ. 2003. *Surgical Anatomy of the Hand and Upper Extremity*. Philadelphia: Lippincott, Williams and Wilkins.

Drews J, Gunther D. 1966. Uber angerborene synostosen im handwurzelberiech. *Radiologe* 6: 64–68.

Dubost E, Picard JM, Ecarlat B, Hernandez C. 1960. Trios forms d'anomalies congenitales des membres. *J Radiol Electrol* 41: 579–583.

Ferber C. 1952. Ein beitrag zur dreigliedrigkeit des daumens. *Z Orthop* 83: 55–64.

Freyschmidt J. 2001. Melorheostosis: a review of 23 cases. *Eur Radiol* 11: 474–479.

Freyschmidt J, Freyschmidt G. 1996. *Haut-, Schleimhaut- und Skeletterkrankungen: SKIBO Disease*. Berlin: Springer.

Freyschmidt J, Brossmann J, Wiens J, Sternberg A. 2003. *Freyschmidt's "Koehler/Zimmer" Borderlands of Normal and Early Pathologic Findings in Skeletal Radiography*, fifth edition. New York: Thieme Verlag.

Geyer E. 1962. Kritische betrachtung zur differentialdiagnose naviculare bipartitum-naviculare-pseudoarthrose. *Mschr Unfallheik* 65: 149–160.

Giedion A. 1968. Zapfenepiphysen. Naturgeschichte und diagnostiche bedeutung einer storung des enchondralen wachstums. In *Ergebnisse der Medizinischen Radiologie* (GlaunerR, RuttimannA, ThurnP, VolgerE, eds). Stuttgart: Thieme.

Greene MH, Hadied AM. 1981. Bipartite hamulus with ulnar tunnel syndrome-case report and literature review. *J Hand Surg* 6: 605–609.

Helms CA, Major NM, Anderson MW et al. (eds) 2009. *Musculoskeletal MRI, second edition*. Philadelphia: Saunders Elsevier.

Keats TE. 1979. *An Atlas of Normal Roentgen Variants that May Simulate Disease, third edition*. Chicago: Year Book.

Krause GP. 1949. Os naviculare bipartitum beider hande. *Fortschr Rontgenstr* 71: 359.

Leger Z. 1955. Beobachtung einer angeborenen synostose zwischen multangulum minus und metakarpale 2. *Z Orthop* 87: 70–76.

Lister G. 1993. *The Hand,* third edition. Edinburgh: Churchill Livingstone.

Malik AM, Schweitzer ME, Culp RW, Osterman LA, Manton G. 1999. MR imaging of the type II lunate bone: frequency, extent, and associated findings. *Am J Roentgenol* 173: 335–338.

Metz VM, Schimmerl SM, Gilula LA, Viegas SF, Saffar P. 1993. Wide scapholunate joint space in lunotriquetral coalition: A normal variant? *Radiology* 188: 557–559.

Neiss A. 1955. Doppelseitige synostose zwischen demo s multangulum minus und demo s capitatum. *Fortschr Geb Rontgenstr* 82: 825.

O'Rahilly RJ. 1953. Survey of carpal and tarsal anomalies. *J Bone Jt Surg* 35A: 626–642.

Pfirrmann CWA, Zanetti M. 2005. Variants, pitfalls and asymptomatic findings in wrist and hand imaging. *European Journal of Radiology* 56: 286–295.

Pfirrmann CW, Theumann NH, Chung CB, Botte MJ, Trudell DJ, Resnick D. 2001. What happens to the triangular fibrocartilage complex during pronation and supination of the forearm? Analysis of its morphology and diagnostic assessment with MR arthrography. *Skeletal Radiol* 30: 677–685.

Pfirrmann CW, Theumann NH, Chung CB, Trudell DJ, Resnick D. 2002. The hamatolunate facet: characterization and association with cartilage lesions – magnetic resonance arthrography and anatomic correlation in cadaveric wrists. *Skeletal Radiol* 31: 451–456.

Pfitzner W. 1885. Beitrage zur kenntniss des menschlichen extremitatenskelts. VIII: Die morphologischen elemente des menschlichen handskeletts. *Zeit Morphol U Anthrop* 2: 77.

Phillips BZ. 2013. Wrist joint anatomy. Available at http://emedicine.medscape.com/article/1899456-overview (accessed 20 October 2015).

Postacchini F, Ippoplito E. 1975. Isolated absence of human carpal bones. *Teratology* 11: 267–271.

Poznanski AK. 1984. *Hand and Radiologic Diagnosis: With Gamuts and Pattern Profile,* second edition. Philadelphia, Pa: W.B. Saunders.

Rochels R, Schmid F. 1980. Morphologische und metrische abweichungen der handknochen beim Down-Syndrome: eine radiologischestudie. *Fortschr Roentgenstr* 133: 30–33.

Ross E. 1954. Os capitatum bipartitum. *Fortschr Rontgenstr* 81: 224–226.

Saccomanni B. 2009. Fracture of the proximal pole of the bipartite carpal scaphoid: a probable holt-oram-like syndrome. *Hand* 4: 140–144.

Schaaf J, Wagner A. 1962. Multiplizitat von handwurzelknochen bei drei geschweistern mit polytoper enchondraler dysostose. *Fortschr Rontgenstr* 97: 497–506.

Schafer H. 1952. Zur rontgenologischen und klinischen bedeutung der pseudoepiphysenbildung am kindlichen handskelett. *Kinderarztl Prax* 20: 77–86.

Seibert-Daiker FM. 1975. Anlage eines os hypolunatum beiderseits bei kongenitaler konkreszenz des scapoideum und trapezium. *Fortschr Rontgenstr* 122: 463–465.

Smith DK, Snearly WN. 1994. Lunotriquetral interosseous ligament of the wrist: MR appearance in asymptomatic volunteers and arthrographically normal wrists. *Radiology* 191: 199–202.

Stein JM, Cook TS, Simonson S, Kim W. 2011. Normal and variant anatomy of the wrist and hand on MR imaging. *Magn Reson Imaging Clin N Am* 19: 595–608.

Swanson AB. 1976. A classification for congenital thumb formations. *J Hand Surg* 1: 8–22.

Timins ME. 1999. Osseous anatomic variants of the wrist: findings on MR imaging. *Am J Roentgenol* 173: 339–344.

Totterman SM, Miller RJ. 1996. Scapholunate ligament: normal MR appearance on three-dimensional gradient-recalled-echo images. *Radiology* 200: 237–241.

Waugh RL, Sullivan RF. 1950. Anomalies of the carpus with particular reference to the bipartite scaphoid (navicular). *J Bone Jt Surg* 32A: 682–686.

Windle BCA. 1891. The occurrence of an additional phalanx in the human pollex. *J Anat Physiol* 26: 99–116.

Viegas SF. 2001. Variations in the skeletal morphologic features of the wrist. *Clin Orthop Relat Res* 383: 21–31.

Viegas SF, Ballantyne G. 1987. Attritional lesions of the wrist joint. *J Hand Surg Am* 12: 1025–1029.

Viegas SF, Wagner K, Patterson R, Peterson P. 1990. Medial (hamate) facet of the lunate. *J Hand Surg An* 15: 564–571.

Viehweger G. 1956. Beitrag zur spaltbildung an den handwurzelknochen. *Fortschr Rontgenstr* 84: 376–377.

Viehweger G. 1957. Doppelseitige hyperplasie des os pisiforme und des hamulus ossis hamate. *Fortschr Rontgenstr* 86: 407.

Yazaki N, Burns ST, Morris RP, Andersen CR, Patterson RM, Viegas SF. 2008. Variations of capitate morphology in the wrist. *J Hand Surg Am* 33: 660–666.

Yoshioka H, Tanaka T, Ueno T, Shindo M, Carrino JA, Lang P, Winalski CS. 2006. High-resolution MR imaging of the proximal zone of the lunotriquetral ligament with a microscopy coil. *Skeletal Radiol* 35: 288–294.

Yu HL, Chase RA, Strauch B. 2004. *Atlas of Hand Anatomy and Clinical Implications*. New York: Mosby.

Zanetti M, Linkous MD, Gilula LA, Hodler J. 2000. Characteristics of triangular fibrocartilage defects in symptomatic and contralateral asymptomatic wrists. *Radiology* 216: 840–845.

Further reading

Boyes JH (ed.) 1970. *Bunnell's Surgery of the Hand*, fifth edition. Philadelphia: J. B. Lippincott.

Kohler A, Zimmer E. 1993. *Borderlands of Normal and Early Pathologic Findings in Skeletal Radiography*, fourth edition. Revised by Schmidt H, Freyschmidt J. New York: Thieme Verlag.

18 Sacroiliac joints

Niladri Kumar Mahato
Ohio University, Athens, Ohio, United States

The sacroiliac joints (SIJ) are unique in several respects. These are the largest axial joints with a substantial surface area. Their basic anatomy will not be discussed in this chapter as detailed descriptions are given in standard anatomical texts. Since the earliest published studies, there has been a major debate about the type of joint the SIJ represents in light of the several diversities related to its synovial and ligamentous components. It can be regarded as partly synovial and partly syndesmotic and not an amphi-arthrodial joint, as we shall subsequently discuss. With an increasing amount of research devoted to exploring the structure of the SIJ, and the advanced and sophisticated techniques being deployed for this purpose, several interesting facts have been revealed about the micro- and macro-anatomy of this joint in recent years. This chapter specifically focuses on the anatomical variations of the SIJ. The SIJ can be seen as quite a "dynamic" structure in the sense that it exhibits a wide range of morphological changes throughout life. This chapter will discuss the different micro- and macro-structural variations associated with the adult SIJ in the context of the size, shape, contour, and joint spaces of the articulating surfaces. We shall also review structural variations of the SIJ in terms of aging, gender, childbearing, and race, and their possible relationship to functional adaptations in an individual. Variations in the innervation patterns of the SIJ and divergences of joint characteristics within a single individual are also considered in this chapter.

The sacroiliac joint (SIJ) can be characterized as atypical in light of the debate following gross anatomical and light microscopic observations of the joint surfaces. Divergent views regarding the type of the SIJ arose from early light microscopic studies that persistently pointed towards structural differences between the sacral and iliac cartilages. The sacral cartilage has consistently been reported as being more fibrous than the iliac cartilage (Brooke 1924; Sashin 1930; Schunke 1938). Studies of the joint articulating interfaces reveal that the iliac surfaces are more fibrous than the sacral surfaces and are covered with fibrocartilage, while the sacral surfaces bear typical articular hyaline cartilage micro- and macrostructures (Puhakka et al. 2004). The composition of the articular cartilages alters throughout life at both the sacral and iliac joint surfaces (Bowen and Cassidy 1981). A number of recent studies have shown that the type, content, and arrangement of collagen at the iliac surfaces are different from those at the sacral surfaces. The structural character of the iliac surface remains predominantly fibrous even in the face of changing micro- and macroscopic surface characteristics in other areas of the SIJ throughout life. Magnetic resonance (MR) imaging and computerized axial tomography (CAT) scans have proved advantageous over conventional X-ray techniques for studying several osseous and non-osseous variations in and around the SIJ (Puhakka et al. 2003; Fortin and Ballard 2009).

Articulation characteristics

Type of joint

The SIJs were first described as true diarthrodial joints by von Luschka in 1864 (Trotter 1937, 1940). Previously, in the mid-eighteenth century Bernhard Albinus and William Hunter had demonstrated that the SIJ is a true joint with a joint cavity and a synovial membrane. Later in 1850, Kolliker found a synovial-like fluid in the cavity (Fick and Bardeleben 1911). In contrast, several anatomical studies revealed that SIJs were rather amphi-arthrodial joints (Braus 1921; Berry 1922). Testut (1889) described these joints as diarthro-amphi-arthrodial. However, most studies have consistently demonstrated that the joint is lined with a synovial membrane and covered by a well-defined fibrous capsule (Sashin 1930). Recently, as sophisticated imaging and microscopic techniques have become available to examine the joint structure, studies investigating the SIJ have revealed that the thickness and texture of the joint surface cartilages change with age and the changes are probably related to posture and load-bearing at these joints transmitted through the spine.

Studies using MR imaging, advanced histological techniques, and immunological cartilage collagen typing have indicated that the SIJ is not a true diarthrodial joint over its entire extent. Puhakka et al. (2004) studied the SIJ micro- and macrostructure using MR imaging along with histological correlations, focusing on different segments of the joint. These areas were designated as proximal, central, and the distal segments in both the sacral and the iliac aspects of the joint. In all observations, the histology of the central portions of the articular cartilages was typically hyaline, with fibrocartilage seen only at the peripheral

Bergman's Comprehensive Encyclopedia of Human Anatomic Variation, First Edition. Edited by R. Shane Tubbs, Mohammadali M. Shoja and Marios Loukas.
© 2016 John Wiley & Sons, Inc. Published 2016 by John Wiley & Sons, Inc.

parts of the articular surface. As Puhakka et al. (2004) wrote, the SIJ could be composed of a superior and dorsal syndesmosis and a ventral C-shaped cartilage-covered articulation, an area that, according to this study, had previously been considered a synovial articulation (Schunke 1938; Warwick and Williams 1973; Resnick 2002). As described in this study, the general histological appearance of the cartilaginous portion of the SIJ samples revealed the anatomical characteristics of a symphysis. In parts of the distal third of the SIJ (confined to the iliac bone), the ventral and dorsal transition zones of the joint resembled some histological traits of a synovial joint. The authors (Puhakka et al. 2003) also indicated that the cartilaginous portion of the SIJ with spondylo-arthropathies demonstrates visible alterations comparable to similar lesions at symphyseal joints (Resnick 1989) and has little in common with those of arthritis in synovial joints (Resnick 2002).

As stated earlier, most of the early studies classifying SIJs were focused on delineating differences between the sacral and iliac cartilages. The iliac cartilage was considered to be more of a fibrocartilage than the hyaline sacral cartilage (Sashin 1930; Schunke 1938; Bowen and Cassidy 1981; Paquin et al. 1983). Using immunostaining, Kampen and Tillman (1998) found different types of collagen fibers associated with the cartilage structure of the SIJ. Puhakka et al. (2004) demonstrated that only the central portions of the cartilaginous joint space represented the diverse types of hyaline cartilage on both the sacral and iliac sides as described and characterized in the earlier publications. The descriptions by Puhakka et al. (2004) of the microscopic appearances of the central parts of the sacral and iliac hyaline cartilage are consistent with previous publications (Lynch 1920; Schunke 1931; Carter and Loewi 1962; Paquin et al. 1983; Kampen and Tillmann 1998). The morphology of the remaining periphery of the cartilage, except for the distal third of the iliac articulation, resembled a structural blending with ligamentous attachment of the SIJ, with microscopic characteristics similar to a symphysis. This study also demonstrated for the first time the presence of Type III collagen in SIJ cartilage such as that seen in peripheral joints. Since both the symphysis pubis and the discovertebral junction contain hyaline cartilage, some investigators argue that classification of the SIJ as a synovial joint should not be based only on the type of cartilage it possesses (Resnick 2002).

Puhakka et al. (2004) suggested that the general histological appearance of the cartilaginous elements indicated that the SIJ was only partly synovial at the distal one-third of the joint, and only on the margins of the iliac joint surfaces. The margins of the articular cartilages in this "synovial" area demonstrated the attachment of a synovial layer, the site of this attachment representing the "transition" zone. Histological data from this study suggest that the SIJ is mostly a symphysis, a fibrous articulation in which bones are attached across the hyaline cartilage with the help of strong fibrous tissue that blend with the hyaline articular cartilage through a fibrocartilaginous transitional zone. Due to the presence of strong interosseous ligaments parts of the SIJ are considered to be syndesmotic, a joint characterized by slightly movable articulation with contiguous bony surfaces opposed by a strong interosseous ligament system. To summarize, the SIJ can exhibit different proportions of synovial, symphyseal, and syndesmosis elements in its anatomy and these can present as normal anatomical variations in the joint structure.

Number of articulating surfaces

Many studies have investigated accessory sacroiliac joints (ASIJ) within the confines of the articulating area of the SIJ. These ASIJ have also been referred to as "axial" or "supernumerary articular facets" in the context of the main joint (Derry 1911; Schunke 1938). From the available data, the prevalence of ASIJs ranges from about 8% to 40% of samples across different studies. Several earlier studies faced difficulties using conventional cadaveric dissection and X-ray techniques to explore the complex SIJ structure as well as the accessory components within the joint mass (Trotter 1940; Puhakka et al. 2004). Some of the earliest comprehensive articles related to ASIJs were authored by Trotter (1937, 1940). As described in detail by Trotter, ASIJs can occur as single or multiple articulating facets on the sacrum, usually at the level of the first or second posterior sacral foramen, and on the ilium, often occupying the medial surface at the level of the posterior superior iliac spine and on the iliac tuberosity, situated just above the auricular surface of the ilium.

ASIJs have often been described as having a superficial component at the level of the posterior second sacral foramen (situated between the posterior superior iliac spine or PSIS and the sacral crest) and a deep component positioned at a level just higher than the first posterior sacral foramen (Hadley 1952). These two segments have also been designated as "axial" and "accessory" joints, respectively (Bakland and Hansen 1984). The axial or superficial joint was found to be more common, caudal in position, and extra-capsular (with reference to the SIJ) in its disposition. The accessory joint was distinguished as a sporadically occurring feature that resembled "true synovial joints" placed at a level higher that the axial/SI joints. Histological investigations by Bakland and Hansen (1984) also revealed the presence of fibrocartilage at the joint surfaces in most samples. The axial joint was designated "syndesmosis" because loose connective tissue was detected histologically in the joint space and because of its articular surface composition. The plane of the ASIJs was reported to range up to 60° relative to the plane of the auricular surface of the sacrum (Hadley 1950, 1952). However, most studies have considered both the superficial and the deep components of accessory joints merely as complex positioning of the ASIJs.

In an important study, Ehara et al. (1988) reported that occurrence of ASIJs was "common" and in most cases the two surfaces of articulation in the ASIJs were congruent. As more sophisticated methods for imaging were applied, the character of the joint surfaces of ASIJs was inspected more closely. Some later investigations focused on distinguishing the "axial" from the "real" ASIJ components (Dijkstra et al. 1989). By

the middle of the twentieth century it was gradually becoming established that the ASIJs: (1) were additional joints lying dorsal to the main SIJ complex; (2) possessed closely approximated, distinct joint spaces with corticated joint margins; and (3) were reported as structures present since birth and having hyaline cartilage-bearing articular surfaces (Peterson 1905; Jazuta 1929) or were being documented as predominantly age-dependent acquired entities containing mainly fibrocartilage articular surfaces (Trotter 1940; Ehara et al. 1988). Investigators have also hypothesized and probed whether weight-bearing patterns and aging could affect the frequency of occurrence of ASIJs and whether ASIJs had any pathological role as a source of localized low back pain (Stewart 1984). Variability in innervations of the SIJ and ASIJ and the motion patterns of these joints have been a focus of intense research in recent years. Investigations have also tried to determine whether the anatomy of the ASIJs could act as a source of low back ache with aging. Prassopoulus et al. (1999) reported that ASIJs were more common in obese people over the age of 60 years, indicating that altered load-bearing stress at the SIJs could lead secondarily to the formation of ASIJs.

Prevalence of ASIJs

Very early osteological studies reported the prevalence of ASIJs in relation to gender, age, and race (Trotter 1937, 1940). Although the numbers of Whites and Blacks in the age-wise samples in Trotter's study were markedly different, she reported occurrences of ASIJs in the two races at 40% and 21%, respectively. Trotter's samples in the two studies included more Black than White individuals between 15 and 45 years of age, whereas the number of Black subjects aged over 55 years was half of the number of White subjects in that group. These studies of Trotter's comprehensive samples of 958 dried pelvic bones reported an increasing incidence of ASIJs with increasing age.

Seligmann (1935) related the incidence of accessory articular facets to age in decades. He also found the incidence of ASIJs to be proportional to age. Some earlier investigators put the incidences of ASIJs as follows: Petersen (1905) reported 16% in a sample of 63 White skeletons; Derry (1911) reported 10.4% in a sample of 192 White skeletons; Jazuta (1929) documented a 27% incidence in 130 White skeletons; and Kaibo (1932) observed a 10% incidence among 50 Japanese skeleton samples.

It is not certain whether an ASIJ is present in the newborn or whether it is an acquired joint. Petersen (1905) and Jazuta (1929) observed hyaline cartilage and joint capsules in some of their specimens, which probably indicated that the ASIJ could be present at birth. Trotter (1937) found fibrocartilage on the articular surface of most of her cadaveric specimens and also observed an increased frequency of ASIJs with age, possibly indicating that the accessory joints are acquired.

Several studies have contributed to our understanding of the prevalence of ASIJs. Ehara et al. (1988) reported a 13% occurrence of ASIJs in CT scan samples obtained from 100 people with no musculoskeletal pathologies, and a 16% incidence in 54 dried osteological samples. Another study (Vleeming et al. 1990a, b) reported an ASIJ incidence of 18% in a sample of 153 individuals. In another detailed study, Prassopoulus et al. (1999) reported the incidence of ASIJs in 102 individuals (19.1%) from scans obtained from 534 patients with no SIJ disease. In the same study, ASIJs were reported to be present unilaterally (10.1%) and bilaterally (9%); in terms of gender, the incidence was 17.7% in male samples and 20% in female scans. This study also reported 24.8% and 12.7% ASIJ cases in the >60 and <60 years age groups, respectively, from the scan samples. Noticeably, 27.4% of the obese samples demonstrated ASIJs whereas 15.7% of normal weight individuals were found to possess these accessory structures. Fortin and Ballard (2009) reported a 3.6% incidence of ASIJ from post-SIJ arthography CT scans of 559 chronic SIJ pain patients. Interestingly, this study also reported the bilateral presence of ASIJs at different levels relative to the sacral auricular surface (Fig. 18.1; Table 18.1). In cases of bilateral ASIJs, the left ASIJs were observed at lower levels than the right. The authors point out that there could be two important reasons why this study detected far fewer ASIJs than previously reported studies involving samples of SIJ chronic pain patients. According to Fortin and Ballard (2009), previous authors could have reported "interlocking articulations" present within the SIJ as ASIJs.

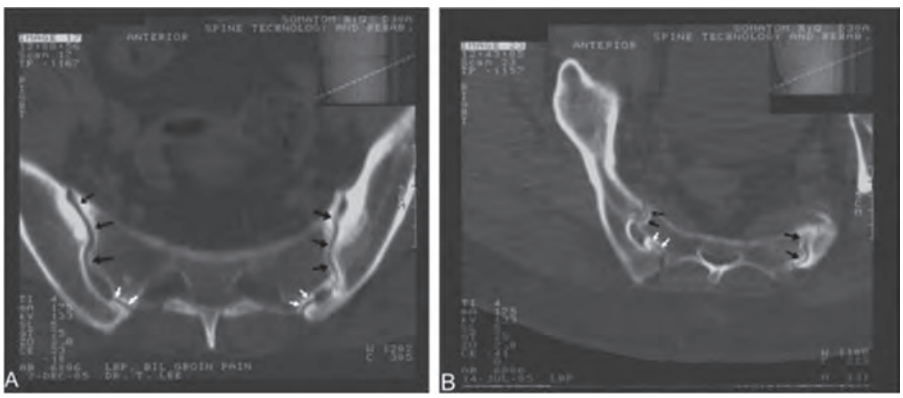

Figure 18.1 Imaging noting accessory sacroiliac joints (arrows).

Source: Fortin and Ballard (2009). Reproduced with permission from John Wiley & Sons.

Table 18.1 Breakdown of 20 patients with ASIJs according to level of the joint, and gender of the patient.

	S1	S1–S2	S2	S2–S3	S3	Unknown
Males with bilateral ASIJs			1		1	
Females with bilateral ASIJs		2	1	2	1	1
Males with unilateral ASIJs	1	1		1		
Females with unilateral ASIJs		1	5	4		

Source: Fortin and Ballard (2009). Reproduced with permission from John Wiley & Sons.

Bowen and Cassidy (1981) and Vleeming et al. (1990a, b) had reported these intricate interdigitating patterns of articulations within the SIJ cavities. Fortin and Ballard also point out that a focal area of degenerating ankylosis within the main SIJ could have been misinterpreted as congenital ASIJs in those populations. Ankylosing degeneration is a common feature after the age of 30 years according to investigations by Resnick et al. (1975) and Vogler et al. (1984). Interestingly, the latter study also suggests that the incidence of ASIJs in symptomatic chronic SIJ pain patients could have been low because ASIJs are congenital in origin rather than acquired due to loading stress at the SIJ. Although the ASIJ is not a rare variant, it might not be very common since normal joint structure or degenerative changes in the SIJ could masquerade as accessory joints.

The occurrence of ASIJs has been reported as 17.5% in studies by Demir et al. (2007a, b) of CT scans from 400 individuals without sacroiliac complaints. These comprehensive studies report the occurrence of ASIJs in relation to samples grouped under gender, age, body mass index (BMI), and childbirth status. There are evident discrepancies in the ASIJ prevalence rates reported from different studies (Walker 1986, 1992), possibly because of different imaging protocols or over- or under-detection of conditions due to overlapping normal joint structure or degenerative changes masquerading as accessory joints.

Anatomy of the ASIJs

The ASIJs have typically been considered false joints situated away from and dorsal to the true synovial portion of the SIJ. The sacral and iliac surfaces are closely approximated with well-defined, corticated joint margins presenting a distinct joint space. The surfaces of the ASIJ facets are mostly flat but can be concave or convex reciprocally. As reported by Trotter (1940), the peripheral outlines of the ASIJs are irregular, ovoid with the long axis of articulation directed along the longitudinal axis of the body. The average dimensions of the long and short axes of the ASIJs were reported as approximately 10 mm and 8 mm, respectively (Trotter 1937). Petersen (1905) reported the existence of spurs of hyaline cartilage in one sample on microscopic examination. Jazuta (1929) was probably the first to report bilateral accessory sacroiliac joints in the pelvis of an adult male. His sample on cadaveric dissection revealed strong ASIJ capsules bilaterally consisting of both joint surfaces covered with hyaline cartilage. Among the earlier studies, Seligmann (1935) documented ASIJs as diarthroses and, from observations on fresh dissecting room material, reported a well-developed capsule, little joint space, and a surface covered with smooth hyaline cartilage detected by microscopy.

Shape of the SIJ

Secondary to the presence of additional joint cavities in the form of ASIJs, common variations of the SIJ are the distinctive patterns of articulation anatomy within the sacroiliac joint cavities. These anatomical forms are described in the following sections.

Iliosacral complex (ILC)

This entity is the commonest anatomical variation, characterized by an iliac projection inserting into a complementary sacral recess within the SIJ articulation. Demir et al. (2007a, b) reported ILCs in 9.5% of a sample of 400 patient scans (7.3% unilateral and 2.2% bilateral). This complementary sacral recess was located at the posterior aspect of the SIJ, extending more or less between the levels of the first and second sacral foramina. The iliosacral complex was more prevalent in patients older than 60 years (17.6%) than the younger age group. BMI was included as a parameter in this study in addition to age, sex, and childbirth: 17% of obese women presented with ILC variations, statistically significantly more than in non-obese women. The ILC variant was more common in men than women in this study but the difference was not statistically significant. Preceding this study, Prassoupoulus et al. (1999) had also reported variations in the anatomy of SIJ articulations in relation to age, gender, obesity, and other parameters. They reported ILCs at both posterosuperior and posteroinferior locations in relation to the main SIJ articulation. There was no statistically significant relationship between ASIJ incidence and obesity in the study by Prassoupoulus et al. (1999).

Bipartite complex

A "bipartite complex" situated at the posterior aspect of the SIJ, extending roughly between the first and the second sacral foramina, is less commonly reported. This complex resembles bipartite iliac plates on CT scans. The variation was more prevalent in males than females, and in individuals aged more than 60 years than in younger people (Prassopoulous et al. 1999). MR imaging of the SIJs also demonstrated an iliac bony channel, bilateral in 3 out of 14 samples (Puhakka et al. 2004). This bony channel was seen as a thick ligamentous structure in one sample, as a localized contrast enhancement in two, and as a cystic lesion in one. The anatomical site of the bipartite complex at the iliac bone, and the anatomical bony channel described by Puhakka et al. (2004), were similarly located. According to the authors, these anatomical variants could simulate joint abnormalities associated with sacroiliitis and also stress fractures at the SIJ (Puhakka et al. 2004).

Semicircular defect

The next variant has been characterized as a semicircular defect in the articular surface. This is more prevalent in the elderly group, in obese patients, and in women (Demir et al. 2007a, b). The semicircular defect variant was described as located at the posterior portion of the SIJ, extending from the level of the first to the second sacral foramen. When this defect is bilateral and appears on the sacral as well as the iliac sides, it anatomically resembles a foramen on CT scans.

Cresenteric defect

The fourth variant is a crescent-shaped iliac bony surface reciprocally accompanied by a bulge in the sacral articular surface. It extends on the posterior aspect of the SIJ and is positioned between the first and second sacral foramina. Demir et al. (2007b) reported this variation only in women and observed it both unilaterally and bilaterally; according to these authors it is more common in the population of >60 years of age.

Ossification centers

The least common anatomical variation reported was identified as ossification centers of the sacral wings located at the anterior portion of the SJ and situated at the level of the first sacral foramen. These centers presented as triangular osseous bodies within the joint space, usually unilaterally (Prassopoulus et al. 1999; Demir et al. 2007a, b).

Width and uniformity of the SIJ space

Trotter (1964) reported the average width of the SIJ. Since then only a few studies have discussed variations in width and uniformity of the SIJ articulation. Data from 400 SIJ scans were analyzed in relation to gender, age, BMI, and childbirth by Demir et al. (2007b) and yielded important observations. This study detailed the joint space characteristics in these groups of samples in relation to the five types of joint anatomy variation discussed above. Vogler et al. (1984) documented detailed SIJ width characteristics under features such as joint uniformity, subchondral sclerosis, erosions, subchondral cysts, osteophyte formation and SIJ symmetry, and bony ankylosis. SIJ ankylosis tends to be more partial than complete; it can be peripheral or central and either bony, fibrous, or chondroid (Walker 1992).

A few investigators have also distinguished between extra-articular (osteophytes) and intra-articular ankylosis. Extra-articular ankylosis has been more frequently reported in in vivo studies (Resnick et al. 1975). These authors believed that true intra-articular ankylosis was exclusive and consistent only with cases of ankylosing spondylitis. Their opinion that intra-articular fusions were distinct from extra-articular osteophytes and that the incidence of ankylosis increased after 50 years of age supported earlier investigations (Brooke 1924). Kapandji (1974) opined that the shape of the articular surfaces of the SIJ was probably related to the posture of the individual and was therefore determined by the prominence of the spinal curvatures. Other important reports have indicated different effects of age and sex on SIJ ankylosis. Focal adhesions between the joint surfaces have been found frequently in adult gross anatomy studies, and light microscopy of the SIJ often demonstrates debris or loose connective tissue in the joint space along with ankylosis (Sashin 1930; Schunke 1938; Resnick et al. 1975; Walker 1986; Bowen and Cassidy 1981; Stewart 1984).

Position of the sacral auricular surface, morphology, and orientation

The position of the sacral auricular surfaces can vary in relation to the body of the sacrum (Mahato 2010, 2011). Alterations in sacral auricular surface positions can be seen in a normal segmented sacrum or can occur because of transitional anomalies at the lumbosacral junctions known as lumbosacral transitional vertebrae (LSTV) variations (Mahato 2013) (Table 18.2). High-assimilation (sacralization) or dissociation (lumbarization) of sacral vertebral segments can lead to anatomical variations in the positioning of the SIJ (Tague 2009) (Fig. 18.2). Variations related to the morphology and orientations of the SIJ have been reported. Weisl (1954) reported numerous variations related to irregularities at the surfaces of both the articular cartilages occurring throughout life. In this detailed report, Weisl (1954) documented the surface dimensions of SIJ articulation and their characteristics from fetal life as they changed through term and then through different decades of life. A cartographic representation of SIJ articular surfaces from different age-grouped cadaveric specimens was created in this study to support a dynamic explanation of age-related changes in the anatomy of the SIJ surfaces. In the same study, Weisl opined that because there were more surface irregularities in older specimens, there was increased interlocking between such irregularities and associated bony ankylosis after 30 years of age.

Although it is generally agreed that SIJ surface irregularities are common anatomical features later in life, ridges and depressions have also been reported in younger subjects (Vleeming et al. 1990a, b). It should be noted that SIJ space asymmetry on one side or bilateral asymmetries are normally observed in

Table 18.2 Detected LSTV samples from studies by the author as Accessory L5-S1 accessory articulation, sacralization and lumbarization. Numbers of osseous samples studied by author (first row) and those obtained from author including published studies (second row; Mahato 2013). Adapted from Mahato (2013) with permission from Elsevier.

Total	LSTV	Uni-/bilateral accessory articulations	Incomplete/ complete L5 sacralization	Incomplete/ complete lumbarization
330	79/330 (24%)	36/79 (46%)	29/79 (36%)	14/79 (18%)
1138	310/1138 (27%)	133/310 (42%)	101/310 (32%)	76/310 (26%)

Figure 18.2 Lateral view of variant sacroiliac joint.

Source: Tague (2009). Reproduced with permission from John Wiley & Sons.

individuals above the age of 30 years, and in some instances could indicate an abnormality (Vogler et al. 1984). Given the frequency of surface alterations reported in the literature, several investigators believe articular cartilage changes to be normal age-related alterations due to accumulated stress (Vleeming et al. 1990a, b). Age- and stress-related SIJ asymmetry, subchondral sclerotic changes, and initiation of cartilage surface irregularities will be discussed (Weisl et al. 1955; Vogler et al. 1984; Walker 1992). Vleeming et al. (1990a) have pointed out that normal intra-articular surface irregularities can be mistaken for osteophytes in a roentgenogram.

Examining fresh cadaveric material, Vleeming et al. (1990a, b) calculated coefficients of friction (COF) of bone-cartilage specimens and concluded that the surface irregularities influence the COF more than the surface texture. This suggests that a greater number of surface irregularities is linked to greater stability. The higher torque on the male SIJ (males SIJs in general and also larger females) was related to the greater number of surface irregularities in men and resulted in more stability as well as greater wear at SIJs with more surface irregularities.

Investigators reporting the complexity and variability of SIJ orientation have pointed to the complex orientation of the joint as an important factor in stability (Solonen 1957; Dijkstra et al. 1989). These studies have stressed the need for imaging of the SIJ at different planes to obtain a complete picture of the joint orientation (Dijkstra et al. 1989; Puhakka et al. 2004; Fortin and Ballard 2009). Several MR imaging studies of SIJ arthritis patients and controls by Bollow et al. (1995, 1998) and Braun et al. (1994, 2000) describe different contrast-enhanced imaging techniques for investigating the joint capsule and synovium of the normal SIJ visualized by oblique coronal sectioning, which could yield better information. Dijkstra et al. (1989) suggested that the SIJ joint surfaces represent a three-dimensional "jigsaw puzzle" that imparts stability. The authors described asymmetries in the size, shape, and direction of the SIJ surfaces, reporting that they can lie on different anatomical planes. They described the SIJ surface orientation as complex and sinusoidal, often with great differences in sacral surface orientation between sides and at different sacral vertebral levels. They emphasized that these variations were normal and had great influence on joint stability and facilitation of load bearing. SIJ motion is limited by the overall inverted wedge shape of the sacral surface as the middle third of the sacral surface is inclined more vertically and the lower third exhibits an outward flare. Surface orientation variability at different levels of the sacrum, together with surface ridges and depressions, has profound implications for SIJ motion and for determining the range of movement achievable by thrusts imparted by manual therapeutic modalities. The physiological implications of complex SIJ articulation have been reviewed comprehensively by Walker (1992).

Auricular cartilage thickness and micro-anatomy

Paquin et al. (1983) demonstrated by electron microscopic, biochemical, and electrophoretic studies that collagen fibers at the sacral surfaces mostly comprise Type I collagen peptides, which are characteristic of hyaline cartilage. According to this electron microscopic (EM) study, the sacral cartilage resembled normal articular cartilage "in all aspects," whereas the iliac cartilage throughout its depth resembled typical articular cartilage only at the superficial zones (Walker 1992). Paquin et al. (1983) opined that the cartilage covering the iliac surfaces was essentially atypical in microstructure. Only a few studies have reported their measurement techniques adequately enough to permit replication. The technique for measuring the gross average thickness of articular cartilage has been generally unclear. Issues such as measurements being taken at maximum width or averaged from several points across the entire surface were not addressed in many earlier studies. Nevertheless, many of the studies cited in this section have documented considerable variability in SIJ cartilage thickness across the entire joint surfaces. The greater thickness (depth) of the sacral than the iliac cartilage was documented even in earlier studies. The sacral surface has been reported as 1.5:1 to 3:1 thicker than its iliac counterpart (Albee 1909; Sashin 1930; Schunke 1938; Carter and Loewi 1962; Paquin et al. 1983). Carter and Loewi (1962) reported that the sacral cartilage itself demonstrated gradual thickening in an anteroposterior direction. Differences in thickness between the sacral and iliac cartilages have been reported even in fetal samples. This observation could indicate that the differences in cartilage thickness are not due to differential life stresses and strains

on the two surfaces. However, the composition and thickness of the articular cartilage either acquired at birth or supposedly changed with life processes could influence the eventual wearing at the SIJ (Bowen and Cassidy 1981; Walker 1986; Ishimine 1989).

SIJ structure and cartilage thickness also differ in species other than humans (Ekman et al. 1986; Gregory et al. 1986). Several of these studies have demonstrated sacral articular cartilage to be thicker and have documented differences in composition between the sacral and iliac auricular cartilages (Paquin et al. 1983; Kampen and Tillman 1998). Sacral cartilage surfaces appear to be smoother than iliac surfaces. Sacral cartilage surfaces contain small, compactly arranged, spindle-shaped cells with their long axes oriented parallel to the free articular surface. The intercellular matrix (ICM) predominantly contains Type I and some Type II collagen fibers that are arranged as thick bundles mostly in the posterior part of the SIJ. The deeper cartilage cells of the sacral surface towards the sacral bone are larger, less compact, round to oval in shape and arranged homogeneously throughout the ICM. The ICM in the deeper planes of the sacral cartilage remains fairly homogeneous with uniform distribution of collagen fibers. The iliac cartilage looks similar to the sacral cartilage in its superficial areas except that it contains predominantly Type II cartilage. Cells in the deeper layers of the iliac cartilage are rounded in shape and often arranged as clusters or columns of chondrocytes within a fibrillar and nonhomogeneous ICM, often with the collagen fibers in a radiating orientation. Typical hyaline cartilage characteristics have been described for regions in the central territories of the SIJ articular cartilages on both sides. These areas surround the true joint recess within the SIJ and allow a complex system of translation and rotation movements at the joint. The cartilage characteristics shift to a predominantly fibrous variety toward the ligamentous attachments at the periphery of the joint. The only exception to this pattern is seen in the dorsal thirds of the iliac surface (Paquin et al. 1998), a common observation at symphyseal joints.

Innervation of the SIJ

Few anatomical texts describe details of SIJ innervation (Fortin et al. 1999; Dreyfuss et al. 1995, 2000, 2004) or variations in the nerve supply to this joint, a fact of potentially great clinical importance in light of the immense load-bearing stresses applied to the SIJ. According to earlier reports the joint is supplied from the sacral plexus, dorsal rami of S1 and S2, from branches of the superior gluteal nerve, or the obturator nerves (Brooke 1924; Schunke 1938). Horwitz (1939) and Solonen (1957) also noted variety in the nerve supply to the joint, from surrounding nerve plexuses such as the lumbosacral plexus and the dorsal and ventral branches from S1 and S2. These nerves are also reported to supply ligaments associated with the joint. Two studies from Japan suggest the involvement of the L4 and L5 ventral rami in the innervation of the SIJ. These studies indicate segmental innervation of the SIJ with the ventral rami of L5, the sacral plexus and S2 supplying the ventrosuperior and ventroinferior regions of the joint respectively, with the dorsal rami of L5 and sacral plexus supplying its dorsosuperior and dorsoinferior parts (Nakagawa 1966; Ikeda 1991). Recent immunocytochemical investigations capable of fine delineation of neural structures in the capsule and ligaments around the joint reveal that previous identifications of structures as neural tissue could have been mistaken (Cohen 2005). These studies indicate that the SIJ is supplied predominantly from the S1–S4 dorsal rami loops to the interosseous, short and long dorsal sacroiliac ligaments, and the capsule, whereas the ventral rami from the sacral plexus supply small parts of the ventral sections of the joint. SIJ innervation has been a subject of much debate. Some experts have claimed the lateral branches of the L4–S3 dorsal rami to be the major sources of innervation to the posterior aspects of the SIJ (Bernard and Cassidy 1991), whereas others indicate L3–S4 as contributing the posterior SIJ nerve supply (Grob et al. 1995; Murata et al. 2000). As indicated in earlier literature, the anterior aspect of the joint is supplied by the obturator and superior gluteal nerves and branches from the lumbosacral trunk (Pitkin and Pheasant 1936).

As stated earlier, some recent literature has also suggested that the anterior part of the joint is supplied by L2–S2 (Bernard and Cassidy 1991), L4–S2 (Solonen 1957) and the L5–S2 ventral rami (Ikeda 1991) or could have no innervation (Fortin et al. 1999). Nerve block procedures have been applied to study the innervation of joints. A similar experimental study on the SIJ has reported that despite blocking the L5 dorsal ramus and S1–S4 lateral branches, the ability to perceive ligamentous probing was retained by 6 out of 10 subjects (Hogan and Abram 1997; Dreyfuss et al. 2000). Neurophysiological studies of cats have indicated that the SIJs could be less pain-sensitive than the lumbar facet joints, but their pain perception thresholds could be higher than those at the anterior portions of the lumbar discs (Yamashita et al. 1990, 1993; Minaki et al. 1996).

SIJ structure and mobility through fetal period and aging

During the embryonic stage at about the second month of life, SIJs appear to be well formed articulations (Bowen and Cassidy 1981). The joint at this stage is surrounded by thin ligaments at the anterior aspect and large thick ligaments in the posterior parts of the articulation. The free surfaces of the sacral and iliac articular cartilages are smooth. The sacral cartilage is clearer, contains large paired chondrocytes characterizing hyaline cartilage, and possesses a clear and homogeneous ICM. The joint allows considerable gliding movements. Schunke (1938) described a fibrous septum inside a narrow newborn joint space that disappears by the first year of life.

The first decade of life sees a proportional enlargement of the SIJ with general somatic growth. Growing flat SIJ articular surfaces allows gliding movements to be performed in all directions. The capsular ligament becomes progressively more fibrous and vascular and subsynovial layers appear in the capsule (Bowen and Cassidy 1981). Since structural alterations in the normal SIJ are distinctly visible during childhood, abnormal variations associated with skeletal impairments at this stage could be diagnostically discernible (Cartel and Imwi 1962).

During the second and the third decades of life, the vascularity of the capsule is reduced and the chondrocyte arrangement and the fibrous characteristics of the ICM typically alter at both articular surfaces. The range of movement at the SIJ is gradually limited with the emergence of articular interdigitations and unevenness, increasing capsular thickening with age. The next two decades are characterized by reduced cellularity and increased fibrous changes in the capsule, fibrillar and erosive alterations in the articular cartilage, and chondrocyte clumping in the deeper planes of the iliac cartilage. During the sixth and seventh decades, collagen fibers in the ICM in both the articular cartilages become more abundant. The sacral chondrocytes are arranged in greater order, as in hyaline cartilage. The iliac cartilage ICM contains more collagen bundles and irregular clumps of chondrocytes occur in the deeper layers. Areas of cartilage calcification, degeneration, and fibrous interdigitations linking across the articular surfaces have been reported. The eighth decade of life is accompanied by extensive marginal para-articular osteophyte formation and fibrous interdigititation, evidence of cartilage degeneration and bony ankylosis resulting in reduced mobility of the SIJ. Formation of ASIJs, intra-articular debris and decrease in cartilage thickness are common accompaniments. Anatomical variations in the distribution and occurrences of all the above-mentioned alterations are not necessarily stratified distinctly with aging and can co-exist, presenting a mixed spectrum of SIJ anatomies at different stages of life.

Age-related differences in ranges of movements at the SIJ have been reported by some studies, though they are insignificant (Egund et al. 1978; Sturesson et al. 1989). More specifically, a decrease in motion with age has been documented by several investigators (Sashin 1930; Schunke 1939; Bowen and Cassidy 1981). SIJ motion has been described variously as gliding in younger subjects, and nodding or rotatory gliding in elderly individuals, the pattern of movement continually changing with increasing age. The effects of age on SIJ mobility and overall SIJ motion detected by observation and manual palpation are among the issues that have yet to be clarified in motion studies (Grieve 1976, 1983; Cyriax 1978; Sherlock 1981; DonTigny 1985; Lee 1989; Woerman 1989; Porterfield and DeRosa 1991).

Complete cavitations or separation of joint surfaces have not been demonstrated before 34 weeks of gestational age (Schunke 1938; Bowen and Cassidy 1981; Walker 1986). Incomplete cavities can be detected by about 12 weeks of fetal life (O'Rahilly and Gardner 1978). Several small cavities have been observed positioned along the entire length of the joint with fibrous septa or bands connecting the surfaces. Coalescence of these small cavities results in the formation of the definitive SIJ cavity. It is not uncommon to find small cavities persisting even in fetuses at term (about 40 weeks of age). No distinct directionality of SIJ cavitation has been reported, although it is documented that cavitation usually commences in the middle of the joint and proceeds outwards (Schunke 1938; Walker 1986; Ishimine 1989). According to Walker (1992), "Whether the fibrous bands disappear, perhaps because of greater motion or simply because of postnatal stress, or whether these bands remain and contribute to the hypo-mobile joints observed by clinicians, cannot be discerned because healthy specimens in the first to third decade of life have not been studied".

Racial and gender differences and pregnancy- and mobility-related variations

Earlier studies investigated incidences of ASIJs and other anatomical variations of the SIJ in distinct racial, gender, and age groups. Trotter (1964) observed that although the sacra in a White group were wider than those in a Black group, the distance between the two iliac bones had essentially no statistically significant bearing on the presence of ASIJs. Morphological and histological studies have demonstrated more joint surface irregularities and apparent pathological changes in male specimens, usually appearing after 30 years of age. Carter and Loewi (1961) and Vleeming et al. (1990a, b) documented gender- and body-weight-specific loading patterns at the SIJs. Their observations indicate that sex differences influence the prime function of the SIJ in women, facilitating vaginal delivery by increasing the pelvic diameter during labor (Lynch 1920; Borell and Fernstrom 1957; Hagen 1974; Joseph 1988; MacLennan 1991). The pubic symphysis increases its mobility as mobility at the SIJ increases during parturition due to the hormonal changes accompanying pregnancy. These studies document symphyseal separation of 2–7 mm to occur. Variable symphyseal width has been observed in non-pregnant women (Vix and Ryu 1971), but Lynch (1920) also observed that "widening of sacro-sciatic spaces was almost a constant phenomenon" and significantly greater during pregnancy. Among other more uncommon variations, the presence of gas in the SIJ, sometimes seen bilaterally, has been identified as an abnormal finding in non-pregnant women (Garagiola et al. 1989). Since the SIJs act as vital linking stations of the pelvic bony ring, mobility at the pelvis has been associated with the range of movement at the SIJ, especially in the context of parturition (Hagen 1974). Increased laxity of the SIJ in pregnant women has been attributed to hormonal shifts and is therefore more frequently associated with women. SIJ dysfunctions are therefore seen more often in women, in addition to the associated aggravation of pain when changing positions and climbing stairs or relapses of SIJ pain episodes during menstruation. Some multiparous women reporting with hypermobile SIJs exhibit various motions such as nodding or rotatory gliding

movements (Meisenbach 1911; Lynch 1920; Hagen 1974; Kogstad and Birnstad 1990). Reported motion ranges at the SIJ obtained from in vivo and in vitro studies (including computer modeling) have been fairly consistent and support data obtained from earlier investigators who used manual pressure on cadaver material to ascertain motion (Pitkin and Pheasant 1936; Clayson et al. 1962).

A synovial recess in the distal third of the joint could explain movements between the opposing bones in this portion of the joint. The observation of localized fibro-cartilaginous fusions dorsally in the middle third could account for the restricted movements here, in agreement with previous reports that translation in the sagittal plane occurs around a horizontal axis located at the center of the ligamentous portion of the joint (Sashin 1930; Cibulka et al. 1988; Sturesson et al. 1989). However, the motion of the sacroiliac joint is probably more complex than simple uni-axial movements (Vogler et al. 1984; Sturesson et al. 1989; Kissling et al. 1990). The fibro-cartilaginous fusion in this portion of the joint is not considered to result from joint degeneration but to be an anatomical construction at a site with minimal motion (Miller et al. 1987). The movement planes within the SIJ have been described using conventional strategies (Weisl 1955; Borell and Fernstrom 1957; Alderink 1991).

On the basis of his radiographic and cartographic studies of changes in articular surface architecture, Weisl (1955) concluded that sacral motion was not just uni-axial in character. He pointed out that motion at the SIJ could not be determined merely by a single factor and suggested that previous reports of axes of rotation (AORs) based on surface morphology could have been "erroneous." He proposed that the surface morphology, degree of congruence between sacra and ilia, and compressibility of the articular cartilage accounted for variations in positioning of the axes and eventually the complex movements occurring at the SIJ. This included the "occasional sliding movement of the sacrum observed in the living" (Weisl 1955; Walker 1992).

More complex ideas about variations related to multiple-axis motion available within the SIJ have evolved out of studies such as that by Wilder et al. (1980). This study takes account of structural variations at the SIJ articular surfaces to calculate the "optimal axes of rotation" and the best-fit AORs for each articulating contour using topography and theoretical modeling. Wilder et al. concluded that a translator motion could occur about a "rough axis" if there was some separation between the SIJ surfaces, and that motion did not occur solely around the axes proposed by earlier studies such as that of Weisl (1955). Importantly, Wilder et al. (1980) suggested that mean separations of 7.25 mm (SD 3.7 mm) in the median plane and 3.4 mm (SD 1.7 mm) in the frontal plane were required for movements at the SIJ.

To summarize, the auricular cartilages of the SIJs change in shape, size, contour, passive motion, and micro-architectural properties with age. Supernumerary articular facets (ASIJs) are common anatomical features associated with SIJs. Cavitation in the SIJ begins during the tenth week of fetal life and is completed during the seventh month of intrauterine life. After the fifth decade, partial extra-articular osteophytes and ankylosis are commonly seen. The sacral and iliac auricular cartilages alter their cellular arrangements and ICM compositions throughout life. Interauricular bands or septa are present during fetal life and in early infancy. Passive movements at the SIJ are greatest at term. Motion is reduced progressively throughout life. Anatomical variability in SIJ innervation has been established. On account of the complex structural diversity associated with this joint, many anatomical variations have been documented as associated with this articulation and could be encountered by future investigators.

References

Albee FH. 1909. A study of the anatomy and clinical importance of the sacroiliac joint. *JAMA* 53: 1273–1275.

Alderink GJ. 1991. The sacroiliac joint: review of anatomy, mechanics and function. *J Orthop Sports Pbys Ther* 13: 71–84.

Bakland OD, Hansen JH. 1984. The "axial sacroiliac joint". *Anat Clin* 6: 29–36.

Bernard TN, Cassidy JD. 1991. The sacroiliac syndrome. Pathophysiology, diagnosis and management. In: *The Adult Spine: Principles and Practice* (Frymoyer JW, ed.). New York: Raven.

Berry RJ. 1922. *Practical Anatomy, Vol. II*. Melbourne and Sidney: Oxford University Publishing.

Bollow M, Braun J, Hamm B, Eggens U, Schilling A, König H, Wolf KJ. 1995. Early sacroiliitis in patients with sponyloarthopathy: evaluation with dynamic gadolinium-enhanced MR imaging. *Radiology* 194: 529–536.

Bollow M, Braun J, Biedermann T, Mutze S, Paris S, Schauer-Petrowskaja C, Minden K, Schmitz SA, Schöntube M, Hamm B. 1998. Use of contrast-enhanced MR imaging to detect sacroiliitis in children. *Skeletal Radiol* 27: 606–616.

Borell U, Fernstrom I. 1957. The movements of the sacro-iliac joints and their importance to changes on pelvic dimensions during parurition. *Acta Obstet Gynecol Scand* 36: 42–57.

Bowen V, Cassidy JD. 1981. Macroscopic and microscopic anatomy of the sacroiliac joint from embryonic life until the eighth decade. *Spine* 6: 620–628.

Braun J, Bollow M, Eggens U, König H, Distler A, Sieper J. 1994. Use of dynamic magnetic resonance imaging with fast imaging in the detection of early and advanced sacroiliitis in spondylarthropathy patients. *Arthritis Rheum* 37: 1039–1045.

Braun J, Khan MA, Sieper J. 2000. Enthesitis and ankylosis in spondylarthropathy: What is the target of the immune response? Ann Rheum Dis 59: 985–994.

Braus H. 1921 Anatomie des Menschen. Em Lehrbuch trudierende und Arzte. Berlin: Springer.

Brooke R. 1924. The sacroiliac joint. *J Anat* 58: 299–305.

Cartel ME, Imwi G. 1962. Anatomical changes in normal sacroiliac joints during childhood and comparison with the changes in Still's disease. *Ann Rheum Dis* 21: 121–143.

Carter ME, Loewi G. 1962. Anatomical changes in normal sacroiliac joints during childhood and comparison with the changes in Still's disease. *Ann Rheum Dis* 21: 121–134.

Cibulka MT, Delitto A, Koldehoff RM. 1988. Changes in innominate tilt after manipulation of the sacroiliac joint in patients with low back pain: An experimental study. *Phys Ther* 68: 1359–1363.

Clayson SJ, Newton IM, Debevec DF, Anger RW, Skowlund HV, Kottke F. 1962. Evaluation of mobility of hip and lumber vertebrae in normal young women. *Arch PhysMed Rehabil* 43: 1–8.

Cohen SP. 2005. Sacroiliac joint pain: A comprehensive review of anatomy, diagnosis, and treatment. *Anesth Analg* 101: 1440–1453.

Cyriax JH. 1978. *Textbook of Orthopedic Medicine. Vol I. Diagnosis of Soft Tissue Lesions*. Seventh edition. London: BalliPre Tindall.

Demir M, Ayfer M, Gümüsburun E, Bayram M, Gürsoy S. 2007a. Anatomical variations with joint space measurements on CT. *Kobe J Med Sci* 53: 209–217.

Demir M, Gümüsburun E, Ayfer M, Bayram M, Gürsoy S. 2007b. Quantative evaluation of anatomical variations of the sacroiliac joint with CT in normal Turkish people. *Minerva Ortopedica e Traumatologica* 58: 361–368.

Derry DE. 1911. Note on accessory articular facets between the sacrum and ilium, and their significance. *J Anat Physiol* 45: 202–211.

Dijkstra PF, Vleeming A, Stoeckart R. 1989. Complex motion tomography of the sacroiliac joint. An anatomical and roentgenological study. *Rofo Fortschr Geb Rontgenstr Neuen BiMgeb Vesahr* 150: 635–642.

DonTigny RL. 1985. Function and pathomechanics of the sacroiliac joint: A review. *Phys Ther* 65: 35–44.

Dreyfuss P, Cole AJ, Pauza K. 1995. Sacroiliac joint injection techniques. *Phys Med Rehabil Clin North Am* 6: 785– 813.

Dreyfuss P, Park K, Bogduk N. 2000. Do L5 dorsal ramus and S1–4 lateral branch blocks protect the sacroiliac joint from an experimental pain stimulus? A randomized, double-blinded controlled trial. Presented at the International Spinal Injection Society 8th Annual Scientific Meeting, San Francisco, CA, September 8–10.

Dreyfuss P, Dreyer SJ, Cole A, Mayo K. 2004. Sacroiliac joint pain. *J Am Acad Orthop Surg* 12: 255– 265.

Egund N, Olsson TH, Schmid H, Selvik G. 1978. Movements in the sacroiliac joints demonstrated with roentgen stereophotogrammetry. *Acta Radiol [Diagn] (Stockh)* 19: 833–846.

Ehara S, El-Koury GY, Bergman RA. 1988. The accessory sacroiliac joint: A common anatomic variant. *AJR* 150: 857–859.

Ekman S, Dalin G, Olsson S-E, Jeffcott LB. 1986. Sacroiliac joint of the horse, 3: Histological appearance. *Anat Hisrol Embryol* 15: 97–107.

Fick R, Bardeleben, KH. 1911. *Handbuch der Anatomie und Mechanik Der Gelenke: Unter Berucksichtigung der Bewegenden Muskeln*. Jena: Fischer.

Fortin JD, Ballard KE. 2009. The frequency of accessory sacroiliac joints. *Clin Anat* 22: 876–877.

Fortin JD, Kissling RO, O'Connor BL, Vilensky JA. 1999. Sacroiliac joint innervation and pain. *Am J Orthop* 28: 68–90.

Garagiola DM, Tarver RD, Gibson L, Rogers RE, Wass JL. 1989. Anatomic changes in the pelvis after uncomplicated vaginal delivery: A CT study of 14 women. *AJR* 153: 1239–1241.

Gregory CR, Cullen JM, Pool R, Vasseur PB. 1986. The canine sacroiliac joint. *Spine* 11: 1044–1048.

Grieve EF. 1983. Mechanical dysfunction of the sacro-iliac joint. *Int Rehabil Med* 5: 46–52.

Grieve GP. 1976. The sacro-iliac joint. *Pbysiotherapy* 62: 383–400.

Grob KR, Neuhuber WL, Kissling RO. 1995. Die innervation des sacroiliacalgelenkes beim mensch. *Z Rheumatol* 54: 117–122.

Hadley LK. 1950. Accessory sacroiliac articulations with arthritic changes. *Radiology* 55: 403–409.

Hadley LK. 1952. Accessory sacroiliac articulations. *J Bone Joint Surg [Am]* 34: 149–155.

Hagen R. 1974. Pelvic girdle relaxation from an orthopaedic point of view. *Acta Orthop Scand* 45: 550–563.

Hogan QH, Abram SE. 1997. Neural blockade for diagnosis and prognosis: A review. *Anesthesiology* 86: 216–241.

Horwitz MT. 1939. The anatomy of (a) the lumbosacral nerve plexus – its relation to variations of vertebral segmentation, and (b) the posterior sacral plexus. *Anat Rec* 74: 91–107.

Ikeda R. 1991. Innervation of the sacroiliac joint. Macroscopial and histological studies. *I Nippon Med Sch* 58: 587–596.

Ishimine T. 1989. Histopathological study of the aging process in the human sacroiliac joint. *Nippon Seikeigeka Gakkai Zusbi* 63: 1074–1084 (in Japanese).

Jazuta K. 1929. Die Nebengelenkflachen an kreuz- und huftbein. *Anat Anz* 68: 137–144.

Joseph J. 1988. The joints of the pelvis and their relation to posture in labour. *Midwives Chron* 101: 63–64.

Kaibo K. 1932. Tiber die akzessorische gelenkfiache des sakroiliakalgelenkes am kreuz- und darmbein. Gyoseki IX: 20–22 (abstract no. 62 in Japanese J Med Sciences I, Anat Vol 2).

Kampen WU, Tillmann B. 1998. Age-related changes in the articular cartilage of human sacroiliac joint. *Anat Embryol (Berl)* 198: 505–513.

Kapandji IA. 1974. *The Physiology of Joints: The Trunk and the Vertebral Column*. Vol 3. London: Churchill Livingston.

Kissling R, Brunner C, Jacob HA. 1990. Mobility of the sacroiliac joint in vitro. *Z Orthop* 128: 282–288 (in German).

Kogstad D, Birnstad N. 1990. Pelvic girdle relaxation: pathogenesis, etiology, definition, epidemiology. *Tidsskr Nos Laegeforen* 110: 2209–2211 (in Norwegian).

Lee D. 1989. *The pelvic girdle*. New York: Churchill Livingstone Inc.

Lynch FW. 1920. The pelvic articulations during pregnancy, labor and puerperium: An X–ray study. *Surg Gynecol Obstet* 30: 575–580.

MacLennan AH. 1991. The role of the hormone relaxin in human reproduction and pelvic girdle relaxation. *Scand J Rheumatol* 20: 7–15.

Mahato NK. 2010. Variable positions of the sacral auricular surface: Classification and importance. *Neurosurg Focus* 28: 12.

Mahato NK. 2011. Relationship of sacral articular surfaces and gender with occurrence of lumbosacral transitional vertebrae. *Spine J* 11: 961–965.

Mahato NK. 2013. Redefining lumbosacral transitional vertebrae (LSTV) classification: Integrating the full spectrum of morphological alterations in a biomechanical continuum. *Med Hypotheses* 81: 76–81.

Meisenbach RO. 1911. Sacroiliac relaxation: With analysis of 84 cases. *Surg Gynecol Obstet* 12: 411–434.

Miller JA, Schultz AB, Andersson GJ. 1987. Load displacement behaviour of sacroiliac joints. *J Orthop Res* 5: 92–101.

Minaki Y, Yamashita T, Ishii S. 1996. An electrophysiological study on the mechanoreceptors in the lumbar spine and adjacent tissues. *Neurol Orthop* 20: 23–35.

Murata Y, Takahashi K, Yamagata M, Takahashi Y, Shimada Y, Moriya H. 2000. Sensory innervation of the sacroiliac joint in rats. *Spine* 16: 2015–2019.

Nakagawa T. 1966. A study on the distribution of nerve filaments over the iliosacral joint and its adjacent region in the Japanese. *I Iap Ortlwp Assoc* 40: 419–430.

O'Rahilly R, Gardner E. 1978. The embryology of moveable joints. In: *The Joints and Synovial Fluid* (Sokoloff L, ed.). New York: Academic Press Inc.

Paquin JD, van der Rest M, Marie PJ, Mort JS, Pidoux I, Poole AR, Roughley PJ. 1983. Biochemical and morphologic studies of cartilage from the adult human sacroiliac joint. *Arthritis Rheum* 26: 887–895.

Petersen O. 1905. Ueber artikulationsflchen an der hinterflchedes os sacrum. *Anat Anz* 26: 521–524.

Pitkin HC, Pheasant HC. 1936. Sacrarthrogenic telalgia I: A study of referred pain. *J Bone Joint Surg* 18: 111–133.

Porterfield JA, DeRosa CP. 1991. Mechanical low back pain: Perspectives in functional anatomy. Philadelphia: WB Saunders Co.

Prassopoulos PK, Faflia CP, Voloudaki AE, Gourtsoyiannis NC. 1999. Sacroiliac joints: Anatomical variants on CT. *J Comput Assist Tomogr* 23: 323–327.

Puhakka KB, Jurik AG, Egund N, Schiottz-Christensen B, Stengaard-Pedersen K, van Overeem Hansen G, Christiansen JV. 2003. Imaging of sacroiliitis in early seronegative spondylarthropathy. Assessment of abnormalities by MR in comparison with radiography and CT. *Acta Radiol* 44: 218–229.

Puhakka KB, Melsen F, Jurik AG, Boel LW, Vesterby A, Egund N. 2004. Magnetic resonance imaging of the normal sacroiliac joint with correlation to histology. *Skeletal Radiol* 33: 15–28.

Resnick D. 1989. Inflammatory disorders of the vertebral column: Seronegative sondyloarthropathies, adult-onset rheumatoid arthritis, and juvenile chronic arthritis. *Clin Imaging* 13: 253–268.

Resnick D. 2002. Rheumatoid arthritis and the seronegative spondyloarthropaties: Radiographic and pathologic concepts. In: *Diagnosis of Bone and Joint Disorders*, fourth edition (Resnick D, ed.). Philadelphia: WB Saunders.

Resnick D, Niwayama G, Goergen TG. 1975. Degenerative disease of the sacroiliac joint. *Invest Radiol* 10: 608–621.

Sashin D. 1930. A critical analysis of the anatomy and the pathologic changes of the sacro-iliac joints. *J Bone Joint Surg* 12: 891–910.

Schunke BB. 1938. The anatomy and development of the sacroiliac joint in man. *Anat Rec* 72: 313–331.

Seligmann SB. 1935. Articulatio sacro-iliaca accessoria. *Anat Anz* 79: 225–241.

Sherlock RA. 1981. A criticism of the article, "Movement of the Sacroiliac Joint." *Clin Orthop* 155: 293–297.

Solonen K. 1957. The sacroiliac joint in the light of anatomical, roentgenological and clinical studies. *Acta Orthop Scand Suppl* 27: 1–115.

Stewart TD. 1984. Pathologic changes in aging sacroiliac joints: A study of dissecting-room skeletons. *Clin Orthop* 183: 188–196.

Sturesson B, Selvik G, Uden A. 1989. Movements of the sacroiliac joints: a roentgen stereophotogrammetric analysis. *Spine* 14: 162–165.

Tague RG. 2009. High assimilation of the sacrum in a sample of American skeletons: Prevalence, pelvic size, and obstetrical and evolutionary implications. *Am J Phys Anthropol* 138: 429–438.

Testut J. 1889. *Traite d'Anatomie Humaine*. Paris: G Doin & Cie.

Trotter M. 1937. Accessory sacroiliac articulations. *Am J Physical Anrthropol* 22: 247–255.

Trotter M. 1940. A common anatomical variation in the sacroiliac region. *J Bone Joint Surg* 2: 293–299.

Trotter M. 1964. Accessory sacroiliac articulations in East African skeletons. *Am J Physical Anrthropol* 22: 137–141.

Vix VA, Ryu CY. 1971. Adult symphysis pubis: normal and abnormal. *Am J Roentgen Radium Ther Nucl Med* 112: 517–527.

Vleeming A, Stoeckart R, Volkers ACW, Snijders CJ. 1990a. Relation between form and function in the sacroiliac joint, part I: Clinical anatomical aspects. *Spine* 13: 130–132.

Vleeming A, Stoeckart R, Volkers ACW, Snijders CJ. 1990b. Relation between form and function in the sacroiliac joint, part II: Clinical anatomical aspects. *Spine* 13: 133–136.

Vogler JB, Brown WH, Helms CA, Genant HK. 1984. The normal sacroiliac joint: A CT study of asymptomatic patients. *Radiology* 115: 433–437.

Walker JM. 1986. Age-related differences in the human sacroiliac joint: Histological study implications for therapy. *J Ortho Sports PhysTher* 7: 325–331.

Walker JM. 1992. The sacroiliac joint: A critical review. *Phys Ther* 72: 903–916.

Warwick R, Williams PL. 1973. Arthrology. In Gray's Anatomy, 35th edition. Philadelphia: WB Saunders.

Weisl H. 1954. The articular surfaces of the sacro-iliac joint and their relation to the movements of the sacrum. Acta Anat (Basel) 22: l–14.

Weisl H. 1955. The movements of the sacroiliac joint. *Acta Anat* 10: 608–621.

Wilder DG, Pope MH, Frymoyer JW. 1980. The functional topography of the sacroiliac joint. *Spine* 5: 575–579.

Woerman AL. 1989. Evaluation and treatment of dysfunction in the lumbar-pelvic-hip complex. In: *Orthopedic Physical Therapy* (Donatelli R, WoodenMJ, eds). New York: Churchill Livingstone Inc.

Yamashita T, Cavanaugh JM, El-Bohy AA, Getchell TV, King AI. 1990. Mechanosensitive afferent units in the lumbar facet joint. *J Bone Joint Surg (Am)* 72: 865–870.

Yamashita T, Minaki Y, Oota I, Yokogushi K, Ishii S. 1993. Mechanosensitive afferent units in the lumbar intervertebral disc and adjacent muscle. *Spine* 18: 2252–2256.

19 Hip joint

Robert Ward
Tufts Medical Center, Boston, Massachusetts, United States

The hip is the proximal joint of the lower extremity formed by the head of the femur and the acetabulum, which stabilizes the body for weight-bearing activity. The femoral neck extends inferolaterally from the femoral head to the femoral shaft and forms the femoral neck angle.

The femoral neck angle is variable with age, stature, and width of pelvis, with an average range of 120–136° (Isaac 1997). Coxa vara is present when the femoral neck angle is less than 120° and coxa valga is noted when this angle is greater than 135°. In the axial plane, the femoral head and neck axis is angled anterior to the transverse axis of the knee, which has been described as the femoral neck anteversion angle, which normally ranges from 15° and 24° (Quesnel 1998). The femoral neck anteversion can be increased (>20°) or decreased (<15°), which is also known as femoral neck retroversion.

The labrum, a fibrocartilaginous ring, attaches to the peripheral rim of the acetabulum and is further stabilized inferiorly by the transverse acetabular ligament as it traverses the acetabular notch. The labrum acts to increase the effective depth of the socket and secures the femoral head in place.

The hip joint capsule attaches directly to the osseous acetabulum, stabilized by the iliofemoral and pubofemoral ligaments anteriorly and the ischiofemoral ligament posteriorly, and the distal joint capsule inserts at the base of the femoral neck. An ischio-trochanteric ligament has been described as a variant hip ligament by Dwight (1873).

Developmental and anatomic variations are often seen in these components of the hip, which can mimic disease or even contribute to the development of pathologic conditions.

Acetabulum

The acetabulum forms a cup with near complete coverage of the femoral head. The labrum, in conjunction with the transverse acetabular ligament at the anteroinferior aspect, forms a complete ring around the acetabulum. The transverse acetabular ligament attaches to the acetabular rim anteriorly and posteriorly and to the ligamentum teres femoris. A normal anterior labral/transverse acetabular ligamentous junction cleft is seen in 32.8% of patients (Dinauer 2004), located more inferior than most labral tears, and is often accompanied by an adjacent periligamentous recess located anteromedial to the ligamentum teres.

The ligamentum teres is a fibrovascular structure that predominantly arises from the transverse acetabular ligament along the inferior acetabulum. The anterior, posterior, and medial bundles comprise the ligamentum teres, which attach to the fovea capitis of the femoral head, providing hip stability in adduction, flexion, and external rotation. The anterior and posterior bundles insert into the periosteum along the ischial and pubic margins of the acetabular notch, respectively (Cerezal 2010). The ligamentum teres may be enlarged (Dwight 1873).

The acetabulum can come in a variety of shapes and sizes. This variation of the acetabulum is known as acetabular dysplasia, which has been seen in up to 20.7% of patients (Dinauer 2004). Klaue et al. (1991) described acetabular dysplasia in two types based on comparison of the acetabulum and femoral head radii. When the radii of the acetabulum and femoral head are similar, the joint is considered congruent; it is dubbed incongruent when they are dissimilar.

Based on the Klaue classification, type I acetabular dysplasia is an incongruent shallow acetabulum that is more vertical than normal, and has a radius of curvature greater than that of the femoral head. In these circumstances, the labrum may shear from the bony acetabular rim in cases of overload. In type II acetabular dysplasia, the acetabulum is congruent but there is deficient coverage of the femoral head since the acetabulum provides less than normal femoral head coverage ("short roof") and has a curvature radius similar to that of the femoral head. Overload forces on the reduced articular coverage, particularly in the upper pole of the femoral head at the superolateral acetabular margin, can lead to increased risk of fatigue fracture and even rim fragment separation.

The orientation of the normal acetabulum opens in the anterolateral direction with lateral anterior and medial posterior acetabular rims, although this can be variable. Acetabular retroversion is seen when the acetabulum is posterolaterally oriented. Acetabular retroversion is seen in 48% of patients, with 18% noted unilateral and 40% bilateral, and is more common

Bergman's Comprehensive Encyclopedia of Human Anatomic Variation, First Edition. Edited by R. Shane Tubbs, Mohammadali M. Shoja and Marios Loukas.
© 2016 John Wiley & Sons, Inc. Published 2016 by John Wiley & Sons, Inc.

in younger patients of age <25 years (Werner et al. 2008). However, Ezoe et al. (2006) only found a 6% prevalence of acetabular retroversion in asymptomatic patients, and the incidence was found to be higher among various hip disorders such as Legg Calves Perthes (42%) and osteoarthritis (20%).

During hip flexion, the anterior acetabular wall and the anterosuperior rim of a retroverted acetabulum lie directly in the femoral neck path and are vulnerable to impingement. This can lead to labral injury, adjacent cartilaginous lesions, and early degenerative changes of the hip (Reynolds et al. 1999; Giori and Trousdale 2003). In contradistinction, acetabular anteverison, when the acetabulum is more anterolaterally directed than normal, can lead to increasing degrees of rotational change, pain, and osteoarthritis (Tonnis and Heinecke 1999).

Embryologic remnants resulting in normal anatomic variants can also be seen within the femoroacetabular joint. Plicae are normal anatomic variants of remnant embryologic capsular or synovial folds seen in joints that form synovial fluid. Plicae may be symptomatic either by mass effect on adjacent structures or by impingement between two structures. Different types of plicae have been described with the flat or villous types mainly confined to the acetabular labrum (labral plicae), the base of the ligament of head of the femur (ligamental plicae) and along the reflecting line of the synovial membrane on the base of the femoral neck (neck plicae) (Fu et al. 1997), with a labral, neck, and ligamental plicae prevalence of 76%, 97%, and 78%, respectively (Bencardino et al. 2011).

The labral plica is felt to be most symptomatic due to its orientation parallel to either the acetabular labrum or the transverse acetabular ligament, and can be entrapped within the hip during movement. The neck plicae, also known as the pectinofoveal fold, can be seen in 95% of patients, can be smooth or irregular, ranges from 1 to 13 mm mediolateral, 1–32 mm anteroposterior, and 7–44 mm in the superoinferior dimensions, and more commonly inserts onto the hip capsule rather than onto the femur (Blankenbaker et al. 2009).

Variations surrounding the acetabulum can also be seen. A supra-acetabular fossa is seen within the superior weight-bearing acetabulum at the 12 o'clock position, and is frequently filled with fibrous tissue (Dubois and Omar 2010). A stellate lesion or crease has been described as a bare area within the acetabular articular surface above the anterosuperior margin of the acetabulum. It is focally discontinuous cartilage seen as a linear indentation in the acetabular roof, and has been found to be more common in young adults but can be seen in elderly patients (Chang and Huang 2013).

Labrum

The labrum is a fibrocartilaginous horseshoe-shaped structure along the anterior, superior, and posterior margins of the acetabular rim. Premature cartilage loss is prevented by the labrum as it seals the margins of the articular hyaline cartilage.

The labrum is normally triangular in cross-section, with the lateral part forming the tip and the broader base attached to the bony acetabulum. The labrum is thinner anteriorly and thicker superiorly and posteriorly (Czerny et al. 1999). Although the labrum is triangular in shape in the majority (66%), it can also be round (11%) and flat (9%), with the triangular shape decreasing with age (Lecouvet et al. 1996).

Labral hypoplasia or absence can be seen in up to 10% of asymptomatic hips (Cotton et al. 1998), and nonvisualization of the labrum increases in incidence with increasing age (Lecouvet et al. 1996). Inversion of the acetabular labrum can occur when a portion of the labrum is interposed within the femoroacetabular joint, and is a recognized cause of secondary osteoarthritis (Harris 1986). In the absence of severe dysplasia, the mechanism by which the labrum inverts is less well documented, and is thought to be congenital, developmental, or acquired (Byrd and Jones 2002). It is also unclear whether the free edge of the labrum inverts or flips inside the joint, becoming entrapped versus intra-articular migration of the labrum over the articular surface.

When abnormal pressure from the femoral head is exerted on the labrum, the labral fibrocartilage can hypertrophy and form surrounding fibrous tissues known as the acetabular labral limbus. The limbus is able to invert and evert, and is a potential block to concentric reduction of the dysplastic hip (Landa et al. 2008). A neolimbus has also been described as a hypertrophied ridge of acetabular articular cartilage that forms in the superolateral aspect of the acetabulum seen in hip dysplasia (Ortolani 1976).

A sublabral sulcus, also known as a sublabral foramen or groove, is a well-defined, smoothly marginated cleft between the labrum and the adjacent articular (hyaline) cartilage, without signs of attempted healing or lateral displacement on probing during intra-operative arthroscopy. A normal sublabral sulcus was found in 22.4% of patients, but was only seen in the posteroinferior labrum (Dinauer et al. 2004).

Saddik et al. (2006) found that in 121 patients with clinically suspected labral tears, 25% were found to have a sublabral sulcus. Of those with a sublabral sulcus, 44% were seen anterosuperiorly, 48% posteroinferiorly, 4% anteroinferiorly, and 4% posterosuperiorly. Studler et al. (2008) found a sublabral sulcus in 18% of patients, with 70% seen at the 8 o'clock and 20% at the 9 o'clock positions, and none of the sulci extended into the substance of the labrum or through the full thickness of the labral base.

As an active stabilizer of the femoroacetabular joint during activity, repetitive impingement and labral tears are frequent causes of hip pain. The majority of labral tears, up to 94.4%, are seen anteriorly or anterosuperiorly, with the remaining seen posterosuperiorly and anteroinferiorly (Dinauer et al. 2004; Saddik et al. 2006; Studler et al. 2008). In addition, 51% of labral tears extend into the labral substance and 49% extend along the entire labral base (Studler et al. 2008). Variants such as a remnant of excess anterior labrum can also lead to an intra-articular

impingement and pain in normal hip morphology patients without a history of hip dysplasia (Beaulé et al. 2009).

The perilabral recess is a potential recess between the joint capsule and the acetabular labrum, and can mimic a labral tear. The recess is larger superiorly where the joint capsule attaches several millimeters above the labrum compared to posteriorly and inferiorly, where the capsule attaches directly to the base of the labrum (Ghebontni et al. 2000).

In addition to anatomic variations of the labrum, different entities adjacent to the labrum also exist. Bone fragments of varying size along the acetabular rim, termed os acetabuli, can be seen in 2–3% of asymptomatic patients, can appear as early as 6 years of age, and may disappear before the age of 20 (Klaue et al. 1991). They are thought to be due to nonunion of secondary ossification centers or ossifications within the acetabular labrum (Hergan et al. 2000).

There are also several accessory ossifications centers of the hip. The os acetabuli anterius (also known as os supertilii, os ad acetabulum, os marginale superius acetabuli, and os coxae quartum) can be found in the anterosuperior margin of the Y-cartilage between the os ilium and pubis, and the os acetabuli posterius can be seen in the posterosuperior or posterior apophyseal cartilage. Some plate-like ossification centers can develop in the center of the acetabular fossa or in the superior and/or inferior rim of the acetabulum (Hergan et al. 2000).

A persistent acetabular fossa ossicle, also known as an os acetabuli centrale, can be bilateral, is located in the center of the Y-cartilage, and can be seen with partial fusion to the acetabulum (Hergan et al. 2000). These acetabular ossicles can mimic disease such as osteochondritis dissecans, post-traumatic intra-articular bone fragments, or osseous loose bodies secondary to degenerative disease (Hergan et al. 2000).

Femur

Morphologic variation and developmental anomalies of the femur and acetabulum can lead to femoral acetabular impingement (FAI), which is a pathologic entity that occurs as a result of abnormal abutment between the femoral neck and the acetabular rim. FAI can lead to early degeneration of the acetabular labrum and articular cartilage, both of which are precursors to osteoarthritis (Ito et al. 2001, 2004; Ganz et al. 2003; Beck et al. 2004a, b; Jager et al. 2004; Tanzer and Noiseux 2004).

Two types of FAI have been described: the first, cam impingement, can be attributed to femoral causes; the second, pincer impingement, is attributable to acetabular causes. Cam impingement occurs when a morphologically abnormal femoral head and/or neck abut the acetabulum during normal and forceful internal rotation (Ito et al. 2001, 2004; Beck et al. 2004a, b; Ganz et al. 2003; Jager et al. 2004). When the anterolateral femoral neck contacts an abnormal acetabular rim, pincer impingement occurs commonly as a result of acetabular retroversion resulting in anterior over-coverage of the femoral head (Reynolds et al. 1999; Ganz et al. 2003).

Although cam impingement is commonly seen in acquired abnormalities of the femur associated with prior surgery, trauma, or slipped capital femoral epiphysis (Klaue et al. 1991; Myers et al. 1999; Leunig et al. 2000; Eijer et al. 2001; Beck et al. 2004a, b; Jager et al. 2004), morphologic variations of the femoral neck and femoral-neck junction are accepted culprits.

As the femoral head and neck internally rotate, the anterior femoral neck has to clear the anterior rim of the acetabulum. This is achieved by normal anterior femoral head-neck offset, where the femoral head is offset anteriorly in relation to the femoral neck. When there is abnormal posterior placement of the femoral head on the femoral neck, the femoral neck is positioned more anteriorly relative to the femoral head and contact and impingement between the anterior femoral neck and anterior acetabular rim occurs during internal rotation. This results in abnormal forces on the acetabular labrum and articular cartilage (Eijer et al. 2001; Ito et al. 2001; Ganz et al. 2003; Beck et al. 2004a, b; Jager et al. 2004; Tanzer and Noiseux 2004).

Other morphologic variations of the femoral head-neck junction, such as the "pistol-grip" deformity and an anterior femoral neck osseous bump, can lead to FAI by the same mechanism of reduced clearance of the abnormal anterolateral femoral head and/or neck by the anterior acetabular rim on internal rotation, resulting in impingement between the anterolateral femoral neck and anterior acetabular rim. The "pistol-grip" deformity of the femoral head-neck junction is described as a flattening of the normal concave surface of the femoral head and femoral head-neck junction, with an osseous bump on the anterolateral femoral neck (Jager et al. 2004; Tanzer and Noiseux 2004).

In contradistinction to cam impingement resulting from anatomic femoral variation, pincer impingement results from acetabular variation. Overcoverage of the femoral head by an abnormally deep acetabulum results in pincer impingement between the anterolateral femoral neck and the anterior acetabular rim. Acetebular retroversion, coxa profunda (a deep acetabular socket), and protrusio acetabuli are entities that increase the relative acetabular depth, and can result in pincer type FAI (Ganz et al. 2003; Siebenrock et al. 2003; Beck et al. 2004a, b; Anderson et al. 2012).

Mechanical abrasion from anterolateral femoral neck impingement by the anterosuperior acetabulum can lead to femoral fibrocystic changes or synovial herniation pits. These are most commonly seen at the anterior junction of the femoral head and neck, with an incidence of up to 33% (Pitt et al. 1982; Leunig et al. 2005).

Muscles

The iliopsoas tendon has been described as a joining of the tendons of the psoas major and iliacus muscles. The psoas major arises from the transverse processes of the lumbar

vertebrae and traverses the pelvic brim inferiorly, eventually inserting on the lesser trochanter of the femur. The iliacus muscle originates from the upper two-thirds of the iliac fossa and the inner portion of the iliac crest. The two sets of muscle fibers converge distally to form a conjoint tendon. A recent cadaveric dissection study (Philippon et al. 2014) indicates that 64% of iliopsoas tendons were bifid, 28% demonstrated a single tendon, and 8% were trifid in configuration. The iliospoas tendon has been implicated as a cause of pain related to internal snapping hip syndrome. Two theories predominate as to the etiology. The snapping had been originally attributed to the partially obstructed motion of the iliopsoas tendon by the iliopectineal eminence. In 2008 however, a dynamic ultrasound-guided study suggested that the snapping mechanism represents the trapping of the iliacus muscle belly between the iliopsoas tendon and the pubic bone during abduction/flexion/external rotation. While returning to the neutral position, the tendon rolls over the iliac muscle, trapping a small portion of the muscle under the tendon until it is abruptly released while returning to its neutral position. A similar type of motion was described for bifid tendons as they rotate over one another during flexion, abduction, and internal rotation (Deslandes et al. 2008).

References

Anderson LA, Kapron AL, Aoki SK, Peters CL. 2012. Coxa profunda: is the deep acetabulum overcovered? *Clin Orthop Relat Res* 470: 3375–3382.

Beck M, Leunig M, Clarke E. 2004a. Femoroacetabular impingement as a factor in the development of nonunion of the femoral neck: a report of three cases. *J Orthop Trauma* 18: 425–430.

Beck M, Leunig M, Parvizi J. 2004b. Anterior femoroacetabular impingement: part II. Midterm results of surgical treatment. *Clin Orthop Relat Res* 418: 67–73.

Bencardino JT, Kassarjian A, Vieira RL, Schwartz R, Meliado JM, Kocher M. 2011. Synovial plicae of the hip: evaluation using MR arthrography in patients with hip pain. *Skel Radiol* 40: 415–421.

Blankenbaker DG, Davis KW, De Smet AA, Keene JS. 2009. MRI Appearance of the Pectinofoveal Fold. *AJR* 192: 93–95.

Byrd JWT, Jones KS. 2002. Osteoarthritis caused by an inverted acetabular labrum: radiographic diagnosis and arthroscopic treatment. *Arthroscopy* 7: 741–747.

Cerezal L, Kassarjian A, Canga A, Dobado MC, Montero JA, Llopis E, Rolon A, Perez-Carro L. 2010. Anatomy, biomechanics, imaging, and management of ligamentum teres injuries. *Radiographics* 30: 1637–1651.

Chang CY, Huang AJ. 2013. MR imaging of normal hip anatomy. *Magn Reson Imaging Clin N Am* 21: 1–19.

Cotten A, Boutry N, Demondion X. 1998. Acetabular labrum: MRI in asymptomatic volunteers. *J Comput Assist Tomogr* 22: 1–7.

Czerny C, Hofmann S, Urban M, Tschauner C, Neuhold A, Pretterklieber M, Recht MP, Kramer J. 1999. MR arthrography of the adult acetabular capsular-labral complex: correlation with surgery and anatomy. *AJR* 173: 345–349.

Deslandes M, Guillin R, Cardinal É, Hobden R, Bureau NJ. 2008. The snapping iliopsoas tendon: new mechanisms using dynamic sonography. *Am J Roentgenol* 190: 576–581.

Dinauer PA, Murphy KP, Carroll JF. 2004. Sublabral sulcus at the posteroinferior acetabulum: a potential pitfall in MR arthrography diagnosis of acetabular labral tears. *AJR* 183: 1745–1753.

Dubois DF, Omar IM. 2010. MR Imaging of the hip: normal anatomic variants and imaging pitfalls. *Magn Reson Imaging Clin N Am* 18: 663–674.

Dwight T. 1873. Abnormal ischio-trochanteric ligament. *J Anat Physiol* 8: 134–136.

Eijer H, Myers SR, Ganz R. 2001. Anterior femoroacetabular impingement after femoral neck fractures. *J Orthop Trauma* 15: 475–481.

Ezoe M, Naito M, Inoue E. 2006. The prevalence of acetabular retroversion among various disorders of the hip. *J Bone Joint Surg* 88: 372–379.

Fu Z, Peng M, Peng Q. 1997. Anatomical study of the synovial plicae of the hip joint. *Clinical Anat* 10: 235–238.

Ganz R, Parvizi J, Beck M. 2003. Femoroacetabular impingement: a cause for osteoarthritis of the hip. *Clin Orthop Relat Res* 417: 112–120.

Ghebontni L, Roger B, El-khoury J, Brasseur JL, Grenier PA. 2000. MR arthrography of the hip: normal intra-articular structures and common disorders. *Eur Radiol* 10: 83–88.

Giori NJ, Trousdale RT. 2003. Acetabular retroversion is associated with osteoarthritis of the hip. *Clin Orthop Rel Res* 417: 263–269.

Harris WH. 1986. Etiology of osteoarthritis of the hip. *Clin Orthop Relat Res* 213: 20–33.

Hergan K, Oser W, Moriggl B. 2000. Acetabular ossicles: normal variant or disease entity? *Eur Radiol* 10: 624–628.

Isaac B, Vettivel S, Prasad R, Jeyseelan L, Chandi G. 1997. Prediction of the femoral neck-shaft angle from the length of the femoral neck. *Clin Anat* 10: 318–323.

Ito K, Minka MA, Leunig M. 2001. Femoroacetabular impingement and the cam-effect. A MRI-based quantitative anatomical study of the femoral headneck offset. *J Bone Joint Surg Br* 83: 171–176.

Ito K, Leunig M, Ganz R. 2004. Histopathologic features of the acetabular labrum in femoroacetabular impingement. *Clin Orthop Relat Res* 429: 262–271.

Jager M, Wild A, Westhoff B. 2004. Femoroacetabular impingement caused by a femoral osseous headneck bump deformity: clinical, radiological, and experimental results. *J Orthop Sci* 9: 256–263.

Klaue K, Durnin CW, Ganz R. 1991. The acetabular rim syndrome: a clinical presentation of dysplasia of the hip. *J Bone Joint Surg Br* 73: 423–429.

Landa J, Benke M, Feldman DS. 2008. The limbus and the neolimbus in developmental dysplasia of the hip. *Clin Orthop Relat Res* 466: 776–781.

Lecouvet FE, Vande Berg BC, Malghem J, Lebon CJ, Moysan P, Jamart J, Maldague BE. 1996. MR imaging of the acetabular labrum: variations in 200 asymptomatic hips. *AJR* 167: 1025–1028.

Leunig M, Beck M, Kalhor M, Kim YJ, Werlen S, Ganz R. 2005. Fibrocystic changes at anterosuperior femoral neck: prevalence in hips with femoroacetabular impingement. *Radiology* 236: 237–246.

Myers SR, Eijer H, Ganz R. 1999. Anterior femoroacetabular impingement after periacetabular osteotomy. *Clin Orthop Relat Res* 363: 93–99.

Ortolani M. 1976. Congenital hip dysplasia in the light of early and very early diagnosis. *Clin Orthop Relat Res* 119: 6–10.

Philippon MJ, Devitt BM, Campbell KJ, Michalski MP, Espinoza C, Wijdicks CA, LaPrade RF. 2014. Anatomic variance of the iliopsoas tendon. *Am J Sports Med* 42(4): 807–811.

Pitt MJ, Graham AR, Shipman JH, Birkby W. 1982. Herniation pit of the femoral neck. *AJR* 138: 1115–1121.

Quesnel T. 1998. Variations of relative anteversion of the femoral neck during walking. *Surg Radiol Anat* 20: 425–429.

Reynolds D, Lucas J, Klaue K. 1999. Retroversion of the acetabulum: A cause of hip pain. *J Bone Joint Surg* 81: 281–288.

Saddik D, Troupis J, Tirman P, O'Donnell J, Howells R. 2006. Prevalence and location of acetabular sublabral sulci at hip arthroscopy with retrospective MRI review. *AJR* 187: 507–511.

Siebenrock KA, Schoeniger R, Ganz R. 2003. Anterior femoro-acetabular impingement due to acetabular retroversion. Treatment with periacetabular osteotomy. *J Bone Joint Surg Am* 85: 278–286.

Studler U, Kalberer F, Leunig M. 2008. MR arthrography of the hip: differentiation between an anterior sublabral recess as a normal variant and a labral tear. *Radiology* 249: 947–954.

Tanzer M, Noiseux N. 2004. Osseous abnormalities and early osteoarthritis: the role of hip impingement. *Clin Orthop Relat Res* 429: 170–177.

Tonnis D, Heinecke A. 1999. Acetabular and femoral anteversion: relationship with osteoarthritis of the hip. *J Bone Joint Surg* 81: 1747–1770.

Werner CM, Copeland CE, Ruckstuhl T, Stromberg J, Seifert B, Turen CH. 2008. Prevalence of acetabular dome retroversion in a mixed race adult trauma patient population. *Acta Orthop Belg* 74: 766–772.

20 Knee joint

Brion Benninger
Western University of Health Sciences, Portland, Oregon, United States

The knee joint is a dynamic specialized weight-bearing synovial modified hinge joint between the two distal femoral condyles and the tibia plateau. The patella, considered the most famous sesamoid bone in the body, articulates with the distal femur sitting anteriorly between the condyles. The arrangement of the femoral condyles, patella, and tibial plateau form three well-recognized compartments: (1) medial femoral condyle and tibial plateau; (2) lateral femoral condyle and tibial plateau; and (3) distal anterior femoral condyle region and patella. In its broadest definition, many consider the entire "knee joint" as a complex of three joints: (1) tibiofemoral; (2) proximal tibiofibular; and (3) patellofemoral. Its function is to allow a desired physiological range of motion and prevent undesirable movement while allowing the body to bear weight during ambulation. While it is often mistakenly considered an unstable joint, in actuality it is an incredibly stable joint because of the impressive architectural integration of musculotendinous and ligamentous structures creating a cocoon-like cinch wrap that provides stability during ambulation with an intact neurovascular system. The knee is a great example that mobility is stability.

Each of the three compartments can become affected by single or multiple pathologies and genetic disorders. Some structures of the knee joint can be absent at birth and some are more highly susceptible to injury depending on the activity chosen and the morphological arrangement. This knee arthrology chapter will include some osteology and musculotendinous structures specific to the knee joint, but advises the reader to review the osteology, muscle, and neurovascular strucures that involve the thigh and leg which are associated with the knee joint complex. Furthermore, dissection, interpretation, and description of knee joint anatomy can be difficult because many of the structures have more than a single attachment point at either end and exist within a multilayered unit, which often is fused or integrated, therefore not complying to homgenous simplicity. Literature on the knee joint is saturated with distilled accounts of anatomy, which is grotesque anatomy rather then detailed observations of an ingenius region of human architecture responsible for locomotion.

Femoral intercondylar notch, condylar orientation, and tibial eminence

Morphological measurements from radiology mediums have enabled researchers to examine detailed osteology regarding the *in situ* knee joint. However, a greater number of specimens need to be examined within ethnic populations, between right and left sides and between sexes, for confident predictable variation patterns. Various investigations have postulated theories based on relatively small numbers. The need to understand specific details of the femoral notch, tibial eminence, and condylar surfaces of both the femur and tibia appears to be critical to manage prevention and provide ideal treatment for the colossal number of knee injuries that afflict populations around the world. The femoral intercondylar notch allows passage of the cruciate ligaments, and much speculation and theories have been proposed regarding the intercondylar notch size in relation to anterior cruciate ligament (ACL) tears, especially in females (Anderson et al. 1987, 2001; Houseworth et al. 1987; Souryal et al. 1988; Souryal and Freeman 1993; LaPrade and Burnett 1994; Koukoubis et al. 1997; Shelborne et al. 1998; Wada et al. 1999; Farrow et al. 2007). However, similar studies confirm that the size of the ACL does not vary in proportion to the size to the intercondylar notch. There has been no evidence to indicate that differences in morphologic notch shape contribute to the sex differences in ACL injuries. When sexes were combined, Wahl et al. (2012) revealed that ACL injured patients had a tibial articular surface that was significantly shorter relative to that of the femur and had a steeper convexity compared with uninjured patients. Interestingly, the distal femoral radius of curvature also differed significantly. A comparison of ACL injured and uninjured male patients demonstrated the tibial and femoral surfaces were more convex and the anteropostero length of the tibial plateau was smaller in the injured group. Risk factors that have been studied for ACL injury between sexes include intercondylar notch and ACL size, length and height of the tibia or thigh, ligamentous laxity, body mass index, and the Q angle (Anderson et al. 1987; Houseworth et al. 1987; Souryal et al. 1988; Shambaugh et al. 1991, Souryal and Freeman 1993,

Bergman's Comprehensive Encyclopedia of Human Anatomic Variation, First Edition. Edited by R. Shane Tubbs, Mohammadali M. Shoja and Marios Loukas.
© 2016 John Wiley & Sons, Inc. Published 2016 by John Wiley & Sons, Inc.

Oöstenberg and Roos 2000; Uhorshak et al. 2003; Chaudhari et al. 2009).

The tibial slope or, more specifically the posterior tibial slope, is being investigated regarding morphological measurements. It is thought the tibial slope could be a contributor to anteroposterior stability of the knee (Hofmann et al. 1991; Dejour and Bonnin 1994; Giffin et al. 2004; Hernigou and Deschamps 2004; Brandon et al. 2006; Hudek et al. 2009). Dejour and Bonnin (1994) reported that the posterior slope had a linear relationship to the degree of anterior tibial translation. Invesigators using cadaveric measurements also reported that there is as much as a 27° difference within the same knee between medial and lateral sides (Grunewald 1916; Genin et al. 1993; Julliard et al. 1993; Jenny et al. 1997). Currently, data suggest the lateral side can differ from the medial and this may have importance in knee replacement design, injury prediction, and prevention. Matsuda et al. (1999) reported posterior tibial slope figures using MRI with an average value of 10.7° (5–15.5°) for the medial plateau and 7.2° (0–14.5°) for the lateral plateau in 27 patients. Hudek et al. (2009) reported the maximal difference was 8.9° and 21% had a mediolateral difference that exceeded 5°. Differences between medial and lateral plateaus have also been reported regarding the meniscal slope (Jenny et al. 1997). Despite controversy, investigators continue to measure the posterior tibial slope and associate it with knee stability (Meister et al. 1997; Giffin et al. 2004; Brandon et al. 2006; Stijak et al. 2008; Todd et al. 2010).

Genu varum, genu valgum, and recurvatum

Lower limb axis (valgus, varus, recurvatum)

The tibiofemoral angle and genu varum and valgum are important for differentiating what will resolve spontaneously from those which require surgery or other forms of treatment for children (Cheema et al. 2003). Children are maximally bowlegged at age 6 months and progress toward an approximate neutral or zero degree knee angle by age 18 months (Heath and Staheli 1993; Green 1994). Increased angles beyond this date often need further evaluation because of the multiple pathologies which cause excessive genu varum and valgum (Cheema et al. 2003). Bowing or genu varum of the lower limb is a normal morphological shape, which commonly occurs in children who are walking under the age of 2 years (Do 2001; Cheema et al. 2003). Prevalence of genu varum is 7.9% and genu valgus 2% from a study conducted on 3000 Iranian children aged 7–11 years. Karimi-Mobarake et al. (2005) reported a difference between gender and rate of angular deformity (genu varum is twice as likely in boys than girls and valgum is three times more likely in girls). Salenius and Vankaa (1975), Cheng et al. (1991), Heath and Staheli (1993), Cahuzac et al. (1995), Arazi et al. (2001), Javid and Hadari (2003), and Omololu et al. (2004) all reported that bilateral angular deformity is more common than unilateral.

Patella

Patella problems are reported to be the most common type of knee complaint in adolescence and young adults (Dejour and Bonnin 1994). Understanding the detailed morphology of the patella will aid in the design of more successful knee replacments, which involve the patella. Wiberg (1941) described a three-category system of the patella:

- Type 1: medial articular facet and lateral articular facet widths are concave and equal;
- Type II: width of medial articular facet is flat or slightly convex and smaller than the width of the lateral articular facet (the most common); and
- Type 3 patella: the width of the medial articular facet being convex and considerably smaller than the width of the lateral articular facet.

Olateju et al. (2013) confirmed this with a study of South Africans from European ancestry.

Patellofemoral malalignment can be caused by bony dysplasias, which include patella alta, baja, tilt, and trochlea dysplasia (Grelsamer and Meadows 1992; Miller et al. 1996; Shabshin et al. 2004). Trochlear dysplasia is associated with >90% of patella dislocations. Trochlear groove depth, inclination, and facet symmetry are postulated to aid in differentiating low- and high-grade dysplasia (Dejour classification system) (Nelitz et al. 2011). The vertical position of the patella was reported to be an important variable associated with patellofemoral malalignment in patients with patella alta (Ward et al. 2007). There are several indices to measure what could be considered as a low- or high-riding patella. Shabshin et al. (2004) used the most popular to date, the Insall and Salvati index (ratio of patellar tendon length to patellar length: TL/PL). They conducted sagittal MRI on 262 knees (females 134, males 128, age range 6–85, mean 44) and concluded that a TL/PL ratio >1.50 or <0.74 defines alta and baja, respectively. Patellar subluxation can be suggestive of a flattened trochlea (Insall and Salvati 1971; Beasley et al. 2004; Shabshin et al. 2004; Ward et al. 2007; Olateju et al. 2013).

Although relatively rare, there have been congenital abnormalities reported regarding absence of the fibula (Thomas and Williams 1987), tibia (Evans and Smith 1926), femur (Gillespie and Torode 1983), and congenital disorders of the knee (Aitken 1959; Amstutz and Wilson 1962). Quantitative measurements of the femoral trochlea have shown to be of limited value for the assessment of trochlear dysplasia; inclination, facet asymmetry, and depth of trochlear groove may help to distinguish between low-grade (Dejour A) and high-grade (Dejour C–D) dysplasia (Dejour et al. 1989; Nelitz et al. 2011).

Capsule

The knee joint capsule is critical to the function of the knee. It creates and maintains a space for the synovial fluid. Often described as a sleeve, it facilitates physiological function by

allowing a safe range of motion. It provides proprioceptive feedback to prevent undesirable range of motion. Lastly, the capsule also acts as an attachment for knee structures and may actually be the origin of some structures (which currently have names lacking histological support or are simply inaccurate).

When a structure in one of the three compartments is damaged, the capsule is highly likely to be injured as well. The capsule can be divided or is often investigated in one of four regions where it is commonly recognized (anterior, posterior, lateral, medial). The quadriceps and patella extensor tendons provide the anterior aspect of the capsule. Nerve fibers from the capsule transmit pain and proprioceptive feedback. The capsule can be excessively lax or taut, leading to pathologies affecting range of motion. The posterior capsule region may be injured in hyperextension trauma; however, injury to the posterior capsule is often associated with meniscal and cruciate ligament regions. The posterior knee capsule is a blind region during arthroscopy, but can be viewed with MRI (Ralphs and Benjamin 1994; De Maeseneer et al. 2003). Morphological measurements addressing variability regarding the extremes of normal has not been reported in formal studies. This would apparently be equivalent to asking an investigator to provide accurate measurements of the abdominal mesentery regarding surface area, angles, thickness, contents, and attachments, then deciding what is uncommon or rare. The capsule can be individually affected by pathology, but its partial or complete absence of congenital conditions is extremely rare on its own.

Bursae and Plicae

Bursae

A bursa is an enclosed sac lined with synovial membrane and containing synovial fluid, and enables structures that are subject to friction to function. Numerous investigators and/or authors have placed a finite number on the bursae of the knee while simultaneously stating that the number can be varied. The detailed morphology of various knee bursae which can be identified with MR and sonography image mediums is being developed. A wave of investigators will undoubtedly document the extent and brevity of the morphology of knee bursae, which will aid understanding of anatomy and diagnosis and treatment of pathology associated with bursae. We will also be able to observe and analyze morphological patterns of knee bursae and better recognize normal and abnormal anatomy of such important structures.

In the knee, bursae can be divided into those that are identified anteriorly, laterally, medially, and posteriorly. Anterior bursae are: (1) prepatella bursae, which lie between the lower patella and skin; (2) deep infrapatella bursae which lie between the tibia and patella tendon; (3) subcutaneous infrapatella bursae which are located between the distal part of the distal aspect of the tibial tuberosity and skin; and (4) suprapatella bursae, found between the femur and quadriceps femoris (a bursa is attached to the articularis genus muscle). Lateral bursae are: (1) gastrocnemius bursae, found between the lateral head of the gastrocnemius and joint capsule; (2) bursae between the lateral (fibular) collateral ligament and tendon of biceps femoris; (3) bursae between lateral (fibular) collateral ligament and the tendon of popliteus; and (4) bursae between the tendon of popliteus and the lateral femoral condyle. Medial bursae are: (1) bursae between the medial head of gastrocnemius and fibrous capsule with a portion extending between the tendon of semimembranosus; (2) bursae between medial (tibial) collateral ligament and the tendons of sartorius, gracilis, and semitendinosus (pes anserine bursae); (3) bursae deep to the medial (tibial) collateral ligament and the capsule femur, medial meniscus, tibia (Brantigan and Voshell 1943), or tendon of semimembranosus; (4) bursae between the tendon of semimembranosus and medial tibial condyle and the medial head of gastrocnemius (semimembranosus bursae); and (5) inconsistant bursae between tendons of semimembranosus and semitendinosus. Posterior bursae are incredibly variable (Gray 1995). The anterior bursae group, pes anserine, and semimembranosus bursae are more commonly involved in clinical conditions.

The prepatellar bursae is described in contemporary anatomy texts as a unicompartmental structure located within the subcutaneous tissue anterior to the patella. The anatomy of the prepatellar bursae has been investigated and reported as being a tricompartmental structure separated by two thin septa oriented in the coronal plane (Dye et al. 2003; Kaufmann et al. 2004; Aguiar et al. 2007). The tricompartments are defined as follows.

- The superficial compartment is designated the prepatellar subcutaneous bursae space, localized between the subcutaneous tissue and an extension of the fascia lata (superficial fascia), and is the structure classically described anatomically.
- The intermediate compartment is the prepatellar subfascial bursae space, situated between the transverse superficial fascia and an intermediate oblique fascia formed by fascial extension of the vastus lateralis and vastus medialis muscles.
- The deep compartment is the prepatellar subaponeurotic bursae space localized between the intermediate oblique fascia and the deep longitudinal fibers of the rectus femoris tendon, which insert directly in the patella (Aguiar et al. 2007).

In a cadaveric study, Dye et al. (2003) identified a trilaminar prepatellar bursa in the coronal plane in 93% of 61 knees. A two-compartment system was identified in 7% of the cases, in which an oblique intermediate fascia was absent. Aguiar et al. (2007) identified trilaminar morphology of the prepatellar bursae in 78% of cases. In 22% of their cases, a bilaminar shape was identified. Histologic analysis of two specimens demonstrated trilaminar morphology separated by two fascia (Aguiar et al. 2007). The oblique intermediate fascia was slightly thicker than the superficial fascia, and the synovial membrane was not visualized. The same histologic finding has been reported by Dye et al. (2003). Although some publications report measurements of the prepatellar bursae, such measurements have

always related to analysis of abnormal bursae which can reach 150–160 mm in the long axis (Donahue et al. 1996; Zambacos et al. 2001).

Synovial plicae

The synovial plicae are normal structures that represent remnants of synovial membranes from the embryologic development of the knee. The prevelance of knee synovial plicae is controversial and dubious at best because plicae are generally documented when they are deemed as the pathological cause and are not routinely documented or measured during arthroscopy or MR imaging. There are three commonly recognized plicae of the knee: (1) suprapatellar plica; (2) infrapatellar plica, also termed the ligamentum mucosum; and (3) mediopatellar plica (Jouanin et al. 1998; Boles and Martin 2001). The mediopatellar plica is thought to be most likely associated with knee symptoms when it is thickened, fibrotic, or bowstrung (Jee et al. 1998). Although many authors neglect to provide the function of plicae, García-Valtuille et al. (2002) reported that some authors have suggested that the synovial plicae may act like eyelids, aiding in lubrication of the joint.

The terms suprapatellar septum, suprapatellar plica, superior plica, septum-like folds, and suprapatellar bursa are used in the literature to report the suprapatellar plica from the border of the suprapatellar bursa to the knee joint cavity. The suprapatellar plica is angled inferiorly from the synovium at the femoral metaphysis to the posterior region of the quadriceps tendon and attaches just above the patella (García-Valtuille et al. 2002). At the superomedial angle of the trochlea, the articular cartilage can be impinged during flexion (Dorfmann et al. 1982). Mechanical factors are thought to determine the morphology of suprapatellar septum perforation, which varies from a fissure to partial or complete loss of the septum (García-Valtuille et al. 2002). Zidorn (1992) classified suprapatellar plicae into four groups on the basis of the following morphologic features:

- type I (septum completum), in which the suprapatellar bursa and knee joint are completely separated by the septum;
- type II (septum perforatum), in which there are one or more openings of varying size in the septum;
- type III (septum residuale), in which there is a remaining fold usually in a medial location; and
- type IV (septum extinctum), in which the septum is completely involuted.

In Zidorn type II plicae, the perforation that allows the joint fluid to circulate between the pouch and the bursa is called a porta. Its location and size are variable. The suprapatellar plica is seen in several forms in adult patients, with a prevalence of 89% at autopsy (Harty and Joyce 1977).

The infrapatellar plica has also been referred to as the ligamentum mucosum, the most commonly noted plica in the knee. It is formed during weeks 8–12 of gestation when the primitive embryologic septum between the medial and lateral compartments of the knee does not completely regress. Its shape, which depends on the degree of regression, has been used as the basis for classifying infrapatellar plica as: (a) having a vertical septum; or as being (b) separate from the anterior cruciate ligament; (c) split or bipartite; or (d) fenestrated (García-Valtuille et al. 2002). At the anterior part of the intercondylar notch, the infrapatellar plica has a tapered femoral attachment and expands as it extends anteriorly and inferiorly through the infrapatellar fat pad where it attaches to the inferior pole of the patella (Kosarek and Helms 1999). Morphologically, it has been noted to be as large as the ACL and can mimick or be mistaken for the ACL in an ACL-deficient knee. It may also be mistaken for focal nodular synovitis, postoperative changes, or a loose body within the infrapatellar fat pad. Familiarity with the infrapatellar plica should eliminate confusion of this anatomic structure with these knee lesions (García-Valtuille et al. 2002).

The mediopatellar plica is also termed the medial plica, plica synovialis patellaris, Iino band, plica alaris, synovial shelf, or patellar meniscus. The mediopatellar plica attaches from the medial wall of the knee joint cavity then angles downward and attaches to the synovium over the infrapatellar fat pad. Occasionally the mediopatellar plica can be attached to the suprapatellar plica and, more commonly, has a separate attachment or exists solely in the absence of the suprapatellar plica. When large, it has been reported to extend over the medial facet of the trochlea or under the medial facet of the patella. Sakakibara (1976) classified mediopatellar plicae into four types on the basis of size. This arthroscopic classification scheme is accepted almost universally because it is simple to use and is assumed to be of clinical significance: type A, which consists of a cord-like elevation in the synovial wall; type B, which has a shelf-like appearance but does not cover the anterior surface of the medial femoral condyle; type C, which is large with a shelf-like appearance and covers the anterior surface of the medial femoral condyle; and type D, in which the plica has a central defect (fenestrated plica).

The lateral patellar plica is the least common and is associated with controversy. It is slender and located 1–2 cm lateral to the patella. It attaches from the lateral wall superior to the popliteus hiatus and angles into the infrapatellar fat pad (Dupont 1997; Kim and Choe 1997). Some believe the lateral patellar plica is uncommon due to lateral subluxation of the patella affording no or minimal space for the lateral plica to develop. Tearse et al. (1998) identified 21 lateral plicae from 3000 arthroscopies where 14 were thought to be pathologically directly relating to the symptoms. A lateral plica could obstruct an arthroscopic approach through the anterolateral portal (García-Valtuille et al. 2002).

There are other synovial structures in the lateral gutter – the lateral alar fold, superolateral fold, and transverse synovial arcuate fold – that should not be confused with a lateral patellar plica. The lateral alar fold is a structure located closer to the patella that represents the equivalent of the medial alar fold. The superolateral fold is a type of suprapatellar plica located on the lateral side of the suprapatellar pouch (Dandy 1990). The transverse synovial arcuate fold is frequently present in the lateral gutter

at the junction between the anteroposterior and vertical aspects of the gutter.

Further studies identifying and measuring plicae using arthroscopy, MR and sonography imaging, and cadaver dissection will better elucidate the many types of plicae of the knee and the morphological variations that exist (Dupont 1997). The majority of investigators agree that broader or larger plicae are associated with knee pathology rather than thin or slender plicae.

Fat pad

The infrapatellar space, also referred to as Hoffa's fat pad, is located between the posterior aspect of the patella tendon and the capsule (Hoffa 1904). It is associated with recesses, which were identified in 15% of a study of 350 knees by Özkur et al. (2005). Regarding the recesses, 65% were linear or ovoid, 9% were pipe-shaped, and 26% were globular in shape. These recesses and their variance can play an important role because they could mimic pathology in a relatively common area of clinical complaint and presentation (Patel et al. 1998). The recesses should not be confused with cysts or synovitis. There are slip-like indentations at the posterior margin of Hoffa's fat pad which are formed by alar folds in all individuals and should not be confused with the recesses above (Fick 1904; Schweitzer et al. 1992; Patel et al. 1998; Vahlensieck et al. 2002; Tschirch et al. 2003).

Menisci

The menisci are fibrocartilaginous structures between the femoral condyles and the tibial plateau, and had their function recognized by King (1936). The medial meniscus is crescent-shaped and occupies 50% of the articular contact within the medial joint space. The lateral meniscus is virtually circular in shape and covers approximately 70% of the articular contact within the lateral joint space. Walker and Erkman (1975) and Fukubayashi and Kurosawa (1980) reported that the menisci covered 59–70% of the joint contact surface area during weight loading. The lateral meniscocapsular ligament is attached to the lateral joint capsule and there are no meniscal attachments at the popliteal hiatus (Kramer and Micheli 2009). Accessory meniscal femoral ligaments are variable, arising in 70–100% of cases at the posterior horn and inserting anterior or posterior to the posterior cruciate ligament (Harner et al. 1995). The Watanabe et al. (1989) classification notes three types of lateral discoid variant. The meniscus is completely vascular at birth with the inner third becoming avascular at 9 months and by 10 years of age the vascularity has progressively moved to the peripheral third of the meniscus, reflecting the adult meniscus (Clark and Ogden 1983; Kocher et al. 2001). The high vascularity of the meniscus in children under 10 years may explain the increased false positive findings on MRI because of the intrameniscal signal changes that mimic meniscal tears (McDermott et al. 1998, 2008; Takeda et al. 1998; Goodwin et al. 2004; Kramer and Micheli 2009).

Young (1889) first described a discoid meniscus, which is a spectrum of meniscal disorders of shape and stability. Discoid lateral menisci are most common in the Japanese population with a prevalence of approximately 15% (Jordan 1996). The United States prevalence is 3–5%. The discoid meniscus is a congenital anomaly found usually in the lateral meniscus (Kaplan 1957a; Clark and Ogden 1983). It has reported incidence of 0.4–16.6%. A meniscus is said to be discoid if there is continuity between the anterior and posterior sides on five or more contiguous 3 mm sagittal MRI sections, which often have a bowtie appearance. The three types of discoid lateral meniscus are complete, incomplete, and the Wrisburg variant. Some investigators include a ring-shaped meniscus as a fourth type. The complete and incomplete types have a firm, normal posterior tibial attachment and are stable. A discoid medial meniscus is much less common, with the incidence reported to be 0.12–0.6% (Chavadaki et al. 2013). Mensical ossicles are reported in 0.15% of patients and are thought to be either developmental or post-traumatic. These small ossific foci are typically found in the posterior horn of the medial meniscus and are associated with meniscal tears (Brantigan and Voshell 1943; Noble 1975; Vahey et al. 1990; Helms 2002; McDermott et al. 2008; Kramer and Micheli 2009; Lee et al. 2010).

The patellomeniscal ligament attaches from the border of the patella distally and attaches to the medial meniscus and coronary ligament. The patella tibial ligament attaches at the medial patella and then travels to attach at the anteromedial aspect of the tibia.

Retinaculum

The patellar retinaculum is a fibrous connective tissue layer, which is formed from structures of the medial and lateral aspects of the knee that condense and/or coalesce to create the retinaculum (Warren and Marshall 1979; Conlan et al. 1993). It is often inaccurately referred to as a ligament. Some of the contributing structures that form the retinaculum come from muscle tendon units and some from fascia of the knee (Starok et al. 1997). Lateral retinaculum is recognized as contributions from the iliotibial band, vastus lateralis fascia, transverse ligament, patellotibial bands, and epicondylopatellar bands. The patellotibial band attaches from the patella at the inferior border of the transverse ligament and attaches to the proximal tibia and lateral meniscus. The epicondylopatella bands extend from the patella at the superior border of the transverse ligament and attach to the lateral epicondyle and intermuscular septum. The lateral or fibular collateral ligament is intimate to the lateral retinaculum, but does not merge with the retinacular complex. Pope et al. (1979) and other investigators report that the lateral retinaculum is an aspect of the lateral or fibular collateral ligament.

The medial retinaculum is recognized as contributions from fascia of sartorius and vastus medialis, superficial component of medial or tibial collateral ligament, and medial patellofemoral ligament (MPFL). The MPFL attaches from the adductor tubercle to the medial patellar margin.

Ligaments

Anterior cruciate ligament (ACL)

The anterior cruciate ligament (ACL) is an intracapsular extrasynovial structure, which attaches into the tibia anterolateral to the anterior tibial spine and twists as it ascends to attach at the posteromedial aspect of the lateral femoral condyle, posterior to the intercondylar notch (Tyler et al. 2010). The ACL is approximately 3.8 cm long and 1.1 cm wide in adults and runs inferomedially, parallel to the intercondylar notch. It is regularly reported to consist of two bundles of fibers: an anteromedial bundle, which is tight in flexion, and a posterolateral bundle, which becomes taut in extension. Many investigators and authors neglect to mention the intermediate bundle reported by Norwood and Cross (1979).

Tena-Arregui et al. (2003) conducted research on fetal knees aged 24–40 weeks, which revealed for the first time the ACL has two distinct bundles in fetal knees. Compared to adult-shaped ACL, the fetal ACL had a more parallel orientation and a broader femoral attachment area compared to adults (Ferretti et al. 2007). Anatomic dissections performed on the fetal knees of fetuses aged 17–23 weeks identified a double-bundle structure as early as the 17th gestational week with a septum separating the two bundles. The bundles were found to be parallel to each other during extension. During flexion, the posterolateral (PL) bundle crossed over the anteromedial (AM) bundle. The literature appears overwhelming regarding limitations of both viewing the ACL in its entirety during arthroscopy when reconstructing a damaged ACL and reproducing the exact morphological shape of the ACL, and replacing its original orientation *in situ* (Noble 1975; Thomas et al. 1985; Houseworth et al. 1987; Noyes et al. 1987; Souryal et al. 1988; Barrack et al. 1989; Amis and Dawkins 1991; Coupens et al. 1992; Souryal and Freeman 1993; LaPrade and Burnett 1994; Meister et al. 1997; Amis and Jakob 1998; Johnson et al. 1998; Shelbourne et al. 1998; Boisgard et al. 1999; Anderson et al. 2001; Rispoli et al. 2001; Buelow et al. 2002; Uhorchak et al. 2003; Crain et al. 2005; Brandon et al. 2006; Colombet et al. 2006; DeFrate et al. 2006; Pfeiffer et al. 2006; Belgin et al. 2007; Luites et al. 2007; Buda et al. 2008; Frikha 2008; Ruiz Santiago et al. 2008; Shen et al. 2008; Siebold and Fu 2008; Stijak et al. 2008; Chaudhari et al. 2009; Quatman and Hewett 2009; Ahn et al. 2010; Bicer et al. 2010; Lee et al. 2010; Todd et al. 2010; Karlsson et al. 2011; Schairer et al. 2011; Scanlan 2012; Wahl et al. 2012).

When the ACL fascicular anatomy is addressed in detail, the literature is unclear. Welsh (1980) and Arnoczky (1983) reported the ACL as being a single broad continuum of fascicles, with different portions taut throughout the range of motion. Odensten and Gillquist (1985) found no evidence of separation into bundles when examining transverse sections histologically. However, Girgis et al. (1975) divided the ACL into two parts: a smaller anteromedial and a larger posterolateral band, which has been accepted as a basis for understanding the function of the ACL (Reiman and Jackson 1987; Arnoczky and Warren 1988). Norwood and Cross (1979) divided the ACL into three functional bundles, mapped their attachments, and described their different actions in resisting rotatory instabilities. The author's own unpublished work on ACL morphology strongly reflects the three categories used by Norwood and Cross (1979). Various ACL lengths have been reported – 39 mm, Kennedy et al. (1974); 38 mm, Girgis et al. (1975); 22 mm, Trent et al. (1976); 31 mm, Norwood and Cross (1979); 31 mm, Odensten and Gillquist (1985) – yielding a mean of 32 mm. The posterior fibers slacken in flexion, leaving the anteromedial fibers to resist anterior tibial glide in the knee at 90° of flexion. Further specific measurements of the anterior, posterior, and intermediate ACL bundle fibers may reveal information useful in prevention and/or treatment of ACL injuries.

Furman et al. (1976) reported that the transection of the anteromedial bundle caused a positive anterior drawer sign and a negative Lachman sign, while the converse was true for the posterolateral bundle. Paley et al. (1986) reported similar findings, except that the anteromedial bundle was also found to affect the Lachman test. This suggests that partial ruptures can affect different bundles, depending on the posture at the time of injury. Furthermore, differential changes between the two clinical tests could allow the diagnosis of partial rupture, and prediction of the affected ACL bundle.

Min et al. (2001) described a case of an ACL coalescing with the lateral part of a discoid medial meniscus. An abnormal attachment of the anterior horn of an otherwise normal medial meniscus into the ACL has also been described, a variant found in 5.5% of knees containing a discoid lateral meniscus (Kim et al. 1995).

The ACL may be deficient in an otherwise normal knee, although congenital absence of the ACL is usually associated with other anomalies of the lower limb including a ring meniscus, complete absence of the menisci, coexisting absence of the PCL, femoral shortening, fibular hemimelia, hypertrophy of the meniscofemoral ligament of Humphrey, hypoplasia of the tibial spines, patella and intercondylar notch, valgus deformity of the knee, and compensatory scoliosis (Ergun et al. 2008). The ACL may be hypoplastic, completely absent, or may be replaced with a fibrous band (Kaelin et al. 1986).

The middle geniculate artery provides a dominant blood supply to the anterior cruciate ligament. The distal aspect of the ACL can frequently receive branches from both the medial and lateral inferior geniculate arteries. Posterior articular branches of the tibial nerve provide innervation to the ACL. The ACL is rich in proprioceptors that identify changes in acceleration, motion,

position, and angular rotation of the knee joint (Barrack et al. 1989; Barrett et al. 1991).

Posterior cruciate ligament (PCL)

The posterior cruciate ligament (PCL) is an intracapsular extrasynovial structure attaching from the posterior tibial intercondylar fossa and posterior horn of the lateral meniscus and ascends to attach at the posterolateral aspect of the medial femoral condyle (Girgis et al. 1975; Harner et al. 1995, 1999; Amis et al. 2006; Kramer et al. 2006; Lopes et al. 2008). It is 32–38 mm long with a cross-sectional area of 11 mm^2 (Harner et al. 1999). The bony insertion sites of the PCL are three times larger than its midsubstance. The average area of the PCL femoral and tibial footprints has been reported by Lopes et al. (2008), Forsythe et al. (2009), and Tajima et al. (2009). Anatomical investigations have divided the PCL into an anterolateral (AL) and posteromedial (PM) bundle based on ligament function in flexion and extension (Girgis et al. 1975; Mejia et al. 2002; Matava et al. 2009).

There is usually no distinct anatomical separation, although each bundle has a different pattern of tension depending on the angle of knee flexion (Edwards et al. 2007). DeFrate et al. (2004), Papannagari et al. (2007), and Voos et al. (2012) report that the PCL may be more accurately described as a continuum of fibers that rotate during the knee flexion and extension cycle. The individual bundle terminology has been utilized in the description of various PCL reconstruction techniques. Takahashi et al. (2006) found the femoral attachment of the AL bundle is 9.6 mm and the PM bundle is 10.6 mm from the articular cartilage using a line drawn parallel to Blumensaat's line. Morgan et al. (1997) reported that the AL bundle originates 13 mm posterior to the medial articular cartilage–intercondylar wall interface and 13 mm inferior to the articular cartilage–intercondylar roof interface. The PM bundle originates 8 mm posterior to the medial articular cartilage–intercondylar wall interface and 20 mm inferior to the articular cartilage–intercondylar roof interface. Forsythe et al. (2009) found a constant "medial intercondylar ridge" in cadaveric specimens that determines the proximal extent of the femoral PCL footprint. A less common bony landmark is the "medial bifurcate ridge" separating the two bundles (Lopes et al. 2008). The two PCL bundles insert as a confluent tendon into a facet on the posterior aspect of the tibia approximately 1.0–1.5 cm distal to the joint line (Edwards et al. 2007; Matava et al. 2009). The posterior horn of the medial meniscus serves as the anterior border of this facet (Voos et al. 2012). The center of the two fiber bundles is located, medial to lateral, 48% of the width of the tibial plateau (Edwards et al. 2007; Matava et al. 2009). Another radiographic study found the common insertion point of the PCL on the tibia is located at 51% of the mediolateral diameter of the tibial plateau with respect to the lateral border and 13–62% inferior to the medial tibial plateau with respect to the sagittal diameter of the tibial plateau (Lorenz et al. 2009).

Moorman et al. (2008) reported in a cadaveric study that the bulk of the PCL inserts in the posterior half of the PCL facet. In the sagittal plane, the center of the PCL lies 7 mm anterior to the posterior cortex of the tibia. At the tibial insertion, the AL bundle is attached to the superolateral portion of posterior intercondylar facet, and the PM bundle is attached to the inferomedial portion of the facet (Harner et al. 1999; Takahashi et al. 2006; Forsythe et al. 2009, Voos et al. 2012). The meniscofemoral ligaments originate from the posterior horn of the lateral meniscus and insert on the medial femoral condyle anteriorly (ligament of Humphrey) and posteriorly (Wrisberg) to the PCL. The PCL and meniscofemoral ligaments combine to make up the PCL complex (Harner et al. 1999). The combined cross-sectional area of the anterior and posterior meniscofemoral ligaments comprises 17.2% of the PCL complex cross-sectional area (Nagasaki et al. 2006). At least one meniscofemoral ligament has been reported in up to 93% of knees. Four investigations have suggested the meniscofemoral ligaments play a role as a secondary stabilizer of the knee against posterior tibial translation (Chhabra et al. 2006).

Tajima et al. (2009) found that the average area of the posteromedial bundle insertion site was larger than that of the anterolateral bundle insertion site. This finding is similar to the observations by Takahashi et al. (2006), who reported the areas of the anterolateral and posteromedial insertion sites to be 46.7±15.6 mm^2 and 115.8±54.6 mm^2, respectively. Interestingly, other investigators have reported the attachment to the tibia from both bundles being relatively equivocal (Harner et al. 1995; Amis et al. 2006; Edwards et al. 2007). Tajima et al. (2009) suggest the differences in their findings could be explained from the fact that they included all peripheral fibers of the posterior cruciate ligament, especially those of the posteromedial bundle which were attached extensively to the distal tibial periosteum, and used a more accurate measurement system (a 3D laser analysis).

The two fiber bundles may be seen as separate structures, resulting in a true "double-barrelled" PCL (Venkatanarasimha et al. 2009). The tibial insertion site has clinical importance and understanding the native morphology is essential (Lizhen et al. 2001; Gill et al. 2003; De Maeseneer et al. 2003; Brandon et al. 2006; Kramer et al. 2006; Chen and Gao 2009; Tajima et al. 2009; Wijdicks et al. 2009; Lee et al. 2010; Todd et al. 2010).

Gill et al. (2003) demonstrated the importance of the tibial placement of the posterior cruciate ligament graft and its relationship to rotational inadequacies, and suggested that the location of the tibial tunnel determines the effective moment arm of the posterior cruciate ligament graft forces relative to the applied loads. Although the two bundles of the PCL appear complex, what is generally agreed upon is that they are located in different planes on the posterior intercondylar fossa and there is a change in slope between the anterolateral and posteromedial insertion sites.

Variants of the PCL are rare. Congenital absence and hypoplasia of the PCL have been reported, as has an abnormally anterior tibial insertion, resulting in an intact but functionally useless ligament (Kaelin et al. 1986). Absence and hypoplasia of

the cruciate ligaments can result in anteroposterior and rotatory instability of the knee. Congenital absence of one or both cruciate ligaments is associated with leg-length discrepancy and, if untreated, is associated with knee stability issues and other pathologies. If treated, it may still lead to subsequent posterior knee subluxation and dislocation, meniscal tears, and retropatellar pain (Kaelin et al. 1986). The failure to diagnose and repair injuries to the posterolateral structures may result in prolonged functional instability of the posterolateral corner of the knee, particularly when associated with a tear of the PCL (Hughston and Jacobson 1985; LaPrade et al. 2002).

Medial or tibial collateral ligament (MCL or TCL)

The medial or tibial collateral ligament is the most frequently injured ligament of the knee. It has been described somewhat consistently as comprising two regions (superficial and deep). Most authors describe the MCL as a relatively wide, flat, superficial portion attaching from the distal medial femur to the proximal anteromedial tibia with no other directly integrating structures. However, the deep component is commonly described attaching to the medial meniscus as well as osseous attachments. Interestingly, those who describe the deep component as a thickening of the capsule still refer to the MCL as a ligament with two components, despite reporting the deep MCL as being an extension of the posterior capsule. Recognized bursae have been described separating the superficial and deep MCL structures, which may strengthen the statement that the deep MCL is inaccurately termed because it is not attached to the superficial MCL structure; at the very least, they should not be considered as a single unit (Brantigan and Voshell 1943; Sims and Jacobson 2004). The superficial medial collateral ligament has one proximal attachment at the femur and two distal attachments at the tibia. Femoral attachment is from a depression posterior to the medial epicondyle and just distal to the adductor tubercle where it descends to attach at the the proximal tibia, anterior to the anterior arm of the semimembranosus tendon, and then extends inferiorly to lie deep to pes anserine musculotendinous unit. It is often separated from the pes anserine via a bursa to finish its distal attachment, anterior to the posteromedial crest of the tibia (Warren et al. 1974; LaPrade et al. 2007a, b).

Warren et al. (1974) described three distinct layers. Layer I is the first fascial plane encountered that circumferentially wraps the knee. Layer II consists of the superficial MCL and layer III is the medial joint capsule. Directly beneath the superficial MCL, the capsule thickens into a vertically oriented band of short fibers representing the deep MCL (Warren et al. 1974; LaPrade et al. 2007a, b). LaPrade et al. (2007ba, b) quantified the attachments of the medial-sided structures and recommended minimizing use of the three-layered anatomy description. The superficial MCL fibers broaden obliquely as they become posterior, thus representing the POL (Robinson et al. 2004; LaPrade et al. 2007a, b). The POL begins midmedially in layer II, blending with the joint capsule, medial meniscus, and semimembranosus tendon sheath before inserting just inferior to the articular surface. This entire area of the knee has been identified as the posteromedial corner or the semimembranosus corner (Robinson et al. 2004; Sims et al. 2004; Griffith et al. 2009a, b).

Variations may appear more common due to the varied terminology more than actual morphological architecture. The superficial MCL is relatively universal in being named the MCL or tibial collateral ligament (TCL). The deep layer has been referred to as the middle third medial capsular ligament (Hughston et al. 1976; Warren and Marshall 1979). Some investigators report that the superficial MCL is a portion of the posterior oblique ligament (POL) (Hughston 1994; Benninger and Delamarter 2012a, b).

As it descends it consists of two separate tibial attachments, separated by the inferior medial genicular artery, vein, and nerve. It has been reported that the proximal tibial aspect of the superficial MCL attaches into the anterior arm of the semimembranosus tendon. The distal tibial superficial MCL attachment helps form the floor of the pes anserine bursa. The deep MCL with its posterior border merges into the central arm of the posterior oblique ligament. It also has distinct meniscofemoral and memiscotibial ligaments associated with it.

Brantigan and Voshell (1943) divided the MCL into an anterior portion (with parallel running fibers) and a posterior portion (with obliquely running fibers). The posterior oblique fibers were continuous with the joint capsule and had direct attachment to the medial meniscus. The MCL complex can be thought of as three linked components: the superficial MCL, the deep MCL, and the posterior oblique ligament (POL), which blends continuously with the former two component (Brantigan and Voshell 1943). Despite the distinct names for the separate components of the MCL, they exist in continuity (Marchant et al. 2011).

During active flexion, both the superficial MCL and the POL are supported by distal expansions of the semimembranosus tendon that attach directly to the ligament (Marchant et al. 2011; Benninger and Delamarter 2012a).

Lateral or fibular collateral ligament (LCL or FCL)

The lateral or fibular collateral ligament (LCL or FCL) is a cord-like structure attached from the lateral femoral epicondyle just proximal to the popliteal groove, which descends to attach anterolaterally at the fibular head (De Lee et al. 1983). The long head of the biceps femoris covers the fibular head attachment and merges with the anterolateral surface of the LCL. The merging of the LCL and biceps femoris tendon (BFT) is often referred to as the conjoint tendon (Lee et al. 2003). The popliteus tendon and the inferior lateral genicular neurovascular structures are deep to the fibular head attachment.

LaPrade and Hamilton (1997) reported that the femoral attachment of the LCL is at a point proximal and posterior to the lateral condyle, and of approximately 7 cm in length. Distally, the main attachment is to the lateral basal aspect of the fibular head as the conjoint tendon, which it forms with the BFT 1 cm proximal to the insertion (Lee et al. 2003; Harish et al.

2006). A bursa is usually present anatomically between the LCL and the BFT, but is not always identified on MRI (LaPrade et al. 2003; Munshi et al. 2003; Harish et al. 2006). On MRI the LCL is easily identified as a low-signal-intensity structure in all standard imaging planes.

LaPrade et al. (2003) found that the average LCL attachment on the femur was just proximal (1.4 mm; range 0.8–2.7 mm) and posterior (3.1 mm; range 2.3–4.4 mm) to the lateral epicondyle. The dominant femoral attachment was a shallow bony depression just posterior to the lateral epicondyle. Some fibers extended proximally and anteriorly over the lateral epicondyle in an expanding manner. LaPrade et al. (2003) reported an average cross-sectional area of the fibular collateral ligament attachment site on the femur of 0.48 cm^2 (0.43–0.52 cm^2). The average distance between the attachments of the fibular collateral ligament and the popliteus tendon on the femur was 18.5 mm (16.8–22.9 mm). As the LCL coursed distally and attached on the lateral aspect of the fibular head, its average attachment was 8.2 mm (6.8–9.7 mm) posterior to the anterior margin of the fibular head and 28.4 mm (25.1–30.6 mm) distal to the tip of the fibular styloid process. The average cross-sectional area of the attachment on the fibular head was 0.43 cm^2 (0.39–0.50 cm^2). The LCL attachment average was 38% (28–46%) of the total width of the fibular head (anterior to posterior) from the anterior edge of the fibular head. The majority of the distal attachment was found in a bony depression that extended to approximately the distal one-third of the lateral aspect of the fibular head. The remaining fibers extended further distally along with the fibularis longus fascia (Sutton 1884; Terry and LaPrade 1994). The average total length of the LCL between attachment sites was 69.6 mm (62.6–73.5 mm).

Ligament of Humphrey/Wrisberg (see meniscofemoral ligaments)

Although Hollinshead (1969) observed the ligament of Wrisberg in 35% of 140 knees, Fabbricciani and Oransky (1992) consistently found it with higher variability in their study. Raheem et al. (2007) reported the posterior meniscofemoral ligament of Wrisberg as less consistenly identified, and demonstrated only in 27% of knees.

Popliteus tendon

The popliteus muscle courses proximally and laterally over the posterolateral knee from its attachment on the posteromedial tibia and becomes the popliteus tendon at the lateral one-third of the popliteal fossa (LaPrade et al. 2003). The popliteofibular ligament is attached to the popliteus complex at the musculotendinous junction. The popliteus tendon lies intraarticular while coursing anterolaterally around the posterior region of the lateral femoral condyle and travels medial to the lateral collateral ligament before attaching on the popliteal sulcus. The average total cross-sectional area of the popliteal sulcus was 3.4 cm^2 (2.9–3.8 cm^2) (LaPrade et al. 2003). The average cross-sectional area of the attachment site of the popliteus tendon was 0.59 cm^2 (0.53–0.62 cm^2) (LaPrade et al. 2003). The popliteus tendon attachment was at the most anterior fifth of the popliteal sulcus, and its attachment was on the proximal half of the sulcus at this position. The popliteus tendon attachment on the femur from the investigation by LaPrade et al. (2003) was always anterior to the LCL femoral attachment. With the knee near extension, the popliteus tendon was anteriorly subluxated from the popliteal sulcus over the lateral aspect of the lateral femoral condyle. It did not completely enter the confines of the popliteal sulcus until the knee was flexed to an average of 112° (105–130°) (LaPrade et al. 2003). The average total length of the popliteus tendon from its femoral attachment to its musculotendinous junction was 54.5 mm (50.5–61.2 mm) (LaPrade et al. 2003). The popliteus musculotendinous unit provides stability to the posterior lateral corner of the knee (Staubli and Birrer 1990; Harner et al. 1998). The tendon pierces the meniscocapsular junction of the posterior third of the lateral meniscus at the popliteal hiatus and inserts into a small sulcus on the lateral aspect of the lateral femoral condyle (Harish et al. 2006). The popliteus tendon and popliteal hiatus were present in all subjects investigated by Raheem et al. (2007). The popliteal hiatus was the bare area of the lateral meniscus where the popliteal tendon crosses the meniscus; there was no capsular attachment (Raheem et al. 2007). It was bound by the two slips of the popliteomeniscal ligament; the upper (superomedial) was attached to the upper border of the lateral meniscus and the lower (inferolateral) to the popliteofibular ligament, the posterior horn of the lateral meniscus, and the coronary ligament.

These bundles of the popliteomeniscal ligaments were present in all subjects, but the superomedial bundle had only two slips in three knees. Most variations occurred in the popliteofibular ligament: it consisted of abundant fibers in 5 knees, an average bundle in 6 knees, and only few slips in 11 knees. The arcuate or popliteal arcuate ligament was found in all knees; one was much stronger and only one had a short lateral collateral ligament. The fabella and the fabellofibular ligament were present in only two knees (Raheem et al. 2007). The popliteus tendon provides support for the arcuate popliteal ligament. The arcuate ligament was present in all specimens (100%) studied by Raheem et al. (2007); one was much stronger and the short lateral collateral ligament was only present in one knee. This is in contrast to the study by Seebacher et al. (1982) where the arcuate ligament alone reinforced the posterolateral part of the capsule in 13% of the knees. The fabella is a sesamoid bone in the lateral head of gastronemius and lies at the point on the posterolateral side of the knee where the multidirectional collagenous tensile stresses meet (Muller 1983).

The fabellofibular ligament

The fabellofibular ligament attaches from the fabella to the styloid process of the fibular head, passing lateral to the popliteofibular ligament (Tyler et al. 2010). The fabellofibular ligament is a variation of the arcuate. The fabellofibular ligament is only present if the fabella is osseous in 8–20% of cases. It is cartilaginous

in 90–92% (Muller 1983). It is separated from the lateral limb of the arcuate ligament by the inferior lateral genicular artery. This ligament has been identified in 24–80% of dissected specimens and in up to 48% of MR studies when imaged in the coronal oblique plane (Seebacher et al. 1982; Yu et al. 1996; Raheem et al. 2007). In the absence of a fabella the ligament may still be present, extending from the lateral femoral condyle to the fibular head. A thin or absent ligament has been associated with the presence of an arcuate ligament, while the arcuate ligament may be absent in the presence of a thick (>5 mm) fabellofibular ligament (Tyler et al. 2010). Minowa et al. (2004) revealed a strong association between an ossified bony fabella and a thick ligament, while in 77.9% of cases a non-ossified fabella was accompanied by a thinned or absent ligament. The fabella and the fabellofibular ligament study revealed a presence in only 10% of the 22 knees dissected, in contrast to the 20% of 35 knees found in the study by Seebacher et al. (1982). The fabella is a sesamoid bone in the lateral head of gastronemius and lies at the point on the posterolateral side of the knee where the multidirectional collagenous tensile stresses meet (Muller 1983).

The popliteomeniscal ligaments

The popliteomeniscal ligaments are described by Kaplan (1961) and LaPrade et al. (2003) as consisting of aponeurotic fibers which arise from the medial side of the tendon and are inserted into the lateral meniscus. They divide into two bundles: superior and inferior (Staubli and Birrer 1990) or the superomedial bundle and the inferolateral bundle (Simonian et al. 1997). The superomedial bundle divides again into an anteroinferior bundle, which is attached to the inferior aspect of the posterior horn of the lateral meniscus, and a posterosuperior bundle, attached to its superior aspect. These fibers form the boundary of the popliteal hiatus. The popliteal hiatus is bounded by the popliteomeniscal ligaments, the popliteofibutar ligament, the posterior horn of the lateral meniscus, and the coronary ligament. In this study, the popliteus tendon and the popliteal hiatus were present in all subjects. The superomedial and inferolateral bundles of the popliteomeniscal ligaments were present in all subjects, but the superomedial bundle only divided into two slips in three knees. Simonian et al. (1997) demonstrated that the popliteomeniscal ligaments function as stabilizers of the lateral meniscus and when torn increase the mobility of the lateral meniscus. Staubli and Birrer (1990) have shown that rupture of these bundles can be diagnosed by a careful functional arthroscopic evaluation of the popliteal hiatus.

The popliteofibular ligament (PFL)

The popliteofibular ligament (PFL) is located in the posterolateral corner of the knee and, with the lateral collateral ligament (LCL), arcuate ligament, fabellofibular ligament, and popliteus tendon, make up the posterolateral structure ligament (PFL) complex (Tyler et al. 2010). The PFL fibers form the inferior portion of the popliteus expansion, attaching at the musculotendinous junction and onto the fibular head, posterior to the LCL. The lateral inferior geniculate artery generally lies deep to the PFL on the surface of the arcuate ligament, but it may also pass through or deep to the arcuate ligament (Ishigooka et al. 2004). The PFL is responsible for the majority of posterolateral rotatory stability within the PLS by preventing posterior translation, external rotation, and varus angulation, and is almost always present in the knee in dissected specimens (Raheem et al. 2007). The PFL may contain a large number of tendon fibers and contain anything from a few slips of tendon fibers to large bundles of fibers (Tyler et al. 2010).

Two types of PFLs have been described: a single-layer PFL (type I) and a two-layer PFL (type II). Type II PFL is further divided into IIa (superficial layer positioned anterior to the deep layer), type IIb (superficial and deep layers lying parallel), and type IIc (the superficial layer positioned posterior to the deep layer). In a study of cadaveric knees a type I PFL was identified in 69.2% of knees and type II in 30.8% (9% IIa, 12.8% IIb, and 9% IIc) (Ishigooka et al. 2004). The PFL may be difficult to evaluate on MRI, but it is typically seen as a band-like structure with a hypo-intense signal and is located between the popliteus tendon and the fibular head (Bolog and Hodler 2007).

The popliteofibular fibers form the inferior portion of the popliteus expansion and are attached at the muscultendinous junction. These fibers are usually very strong and attach to the fibular head behind the LCL (Maynard 2000). LaPrade et al. (2003) and Staubli and Birrer (1990) found that it consisted of anterior and posterior divisions. Varying names have been given to the popliteofibular ligament, which has also been called the short external lateral ligament, the popliteofibular fascicles, and the fibular origin of the popliteus. The popliteofibular ligament was present in all specimens and was oblique to the joint line from anterosuperior to posteroinferior (Fabbricciani and Oransky 1992; Maynard 2000). This study found that most variations occurred in the popliteofibular ligament; it consisted of oblique fibers that were abundant in 5 knees, an average bundle in 6 knees, and only a few slips in 11 knees. Unlike LaPrade et al. (2003), Staubli and Birrer (1990) found that it consisted of anterior and posterior divisions.

The popliteofibular ligament is an integral structure in the posterolateral corner of the knee and plays an important part by preventing posterior translation, varus angulation, and coupled and primary external rotation (Shahane et al. 1999). The coronary ligament is the portion of the capsule that connects the menisci to the tibia. The coronary ligament of the lateral meniscus is longer and more lax than that of the medial meniscus (Last 1950). Rotation of the knee occurs between the menisci and the upper articular surface of the tibia (Last 1950). The coronary ligaments appear to have been neglected in most studies of the posterolateral corner. Excessive rotation may result in injury to the coronary ligament. Injury to the posterior portion of the coronary ligament may result in increased mobility of the lateral meniscus and is associated with posterior knee pain and a gap in the posterior capsule on arthroscopy; if injured, both the popliteomeniscal fibers and the coronary ligament should

be repaired (Covey 2001). In the current study, the coronary or meniscotibial ligament was present in all the knees (100%) but was thicker and appeared stronger in two knees.

The popliteofibular ligament attaches from the musculotendinous junction of the popliteus and formed an average angle of 83° (78–88°) with its medial attachment site (LaPrade et al. 2003). Its average angle to the horizontal plane was 37° (22–40°). The popliteofibular ligament consistently had two divisions (anterior and posterior). Proximomedially, the anterior division of the popliteofibular ligament attached to the popliteus complex at the proximolateral musculotendinous junction. The distolateral attachment of the anterior division was located on the anterior downslope of the medial aspect of the fibular styloid process. In addition, it had fibers extending to the lateral tibia in close proximity to the proximal anterior tibiofibular ligament. The average fibular attachment of the anterior division of the popliteofibular ligament was 2.8 mm (1.2–3.8 mm) distal to the tip of the fibular styloid process on its anteromedial downslope. The average width of the anterior division's attachment on the anteromedial fibular styloid process was 2.6 mm (1.8–3.4 mm). The proximomedial attachment of the posterior division was also located at the lateral aspect of the popliteus musculotendinous junction. The distolateral attachment of the posterior division was at the tip and posteromedial aspect of the fibular styloid process. The average attachment of the posterior division was 1.6 mm (0.6–2.8 mm) distal to the tip of the fibular styloid process on its posteromedial downslope. The average width of the posterior division at its fibular styloid attachment was 5.8 mm (3.6–7.7 mm). In all knees, the posterior division of the popliteofibular ligament was larger than the anterior division (LaPrade et al. 2003).

The oblique meniscomeniscal ligament

The oblique meniscomeniscal ligament attaches from the anterior meniscal horn and passes through the intercondylar notch between the anterior and posterior cruciate ligaments to attach on the contralateral posterior meniscal horn (Tyler et al. 2010). Medial and lateral oblique meniscomeniscal ligaments can be present and are named according to their anterior meniscal origin (i.e., the lateral oblique meniscomeniscal ligament runs from the anterior horn of the lateral meniscus to the posterior horn of the medial meniscus). The oblique meniscomeniscal ligament has no known function in humans, and its presence has no reported pathological consequences. Prevalence of an oblique meniscomeniscal ligament is reported as 2–4% (Dervin and Paterson 1997; Sanders et al. 1999) and it can be misinterpreted as a displaced meniscal flap or bucket handle tear, particularly on sagittal MRI images (Sanders et al. 1999).

The meniscofibular ligament

The meniscofibular ligament is a capsular ligament, attaching from the inferior margin of the posterior third of the lateral meniscus to the fibular head (Bozkurt et al. 2004). Williams et al. (1989) previously reported an incidence of 80% in the population. Recent cadaver studies have found it to be present in 100% (Bozkurt et al. 2004). This ligament may not be identified on MRI if the sagittal slice thickness (usually 3 mm) is greater than the thickness of the ligament (2.6–6.1 mm) (Obaid et al. 2008). It can be mistaken for the inferior popliteomeniscal fascicle, which lies slightly medially and extends from the posterior horn of the lateral meniscus to the capsule (Tyler et al. 2010). Although almost always present, it may only be identified on MRI in a proportion of patients.

The fabellofibular ligament

The fabellofibular ligament attaches from the fabella to the styloid process of the fibular head, passing lateral to the popliteofibular ligament (Tyler et al. 2010). It is separated from the lateral limb of the arcuate ligament by the inferior lateral genicular artery. This ligament has been identified in 24–80% of dissected specimens and in up to 48% of MR studies when imaged in the coronal oblique plane (Seebacher et al. 1982; Yu et al. 1996; Raheem et al. 2007). In the absence of a fabella the ligament may still be present, extending from the lateral femoral condyle to the fibular head. A thin or absent ligament has been associated with the presence of an arcuate ligament, while the arcuate ligament may be absent in the presence of a thick (>5 mm) fabellofibular ligament (Tyler et al. 2010). Minowa et al. (2004) revealed a strong association between an ossified bony fabella and a thick ligament, while in 77.9% of cases a non-ossified fabella was accompanied by a thinned or absent ligament.

The arcuate ligament

The arcuate ligament is a Y-shaped ligament that attaches from the lateral edge of the styloid process of the fibula. It comprises two limbs: a lateral vertical limb, which runs along the lateral aspect of the joint capsule to insert into the lateral femoral condyle, and a medial arcuate limb, which passes posteromedially superficial to the popliteus tendon to insert into the posterior aspect of the capsule where it merges with the fibers of the oblique popliteal ligament (Tyler et al. 2010). Reported incidence of an arcuate ligament falls within the range 48–87% (Yu et al. 1996). In a study correlating MRI, arthrography, and cadaveric specimen dissection, at least one limb was seen in 71% of specimens (Munshi et al. 2003). The lateral limb of the arcuate ligament was seen in 57% of all specimens (present in 50% of specimens with a fabella and in 67% without a fabella). The medial limb of the arcuate ligament was seen in 57% of all specimens (present in 75% of specimens with a fabella and in 33% without a fabella).

Meniscofemoral ligaments

The meniscofemoral ligaments are variants which are present in up to 93% of the population and connect the posterior horn of the lateral meniscus to the lateral aspect of the medial femoral condyle or to the posterior cruciate ligament (PCL) (Gupte et al. 2002; Tyler et al. 2010). The meniscofemoral ligaments are named according to their position relative to the PCL, with the

ligament of Humphrey lying anterior to the PCL and the larger ligament of Wrisberg posterior to the PCL (Amis et al. 2003). The meniscofemoral ligaments attach to the medial femoral condyle in 46% of cases. The anterior (Humphrey) meniscofemoral ligaments attach proximally to the medial femoral condyle between the insertion of the PCL and the edge of the condylar cartilage, and the posterior (Wrisberg) meniscofemoral ligament attach posterior to the PCL on the medial femoral condyle. In 31% of cases the meniscofemoral ligament attaches to the proximal half of the PCL; in 21% of cases, it attaches to the distal half of the PCL (Cho et al. 1999). Distally, the anterior (Humphrey) meniscofemoral ligament attaches to the lateral meniscus more anteriorly than the posterior (Wrisberg) meniscofemoral ligament. The attachments of the meniscofemoral ligaments are separate, consistent with there being two distinct structures rather than two branches of the same structure as was previously thought (Kaplan 1956). The anterior (Humphrey) meniscofemoral ligament is tense in flexion, and the posterior (Wrisberg) meniscofemoral ligament is tense in extension.

A review of the anatomical studies literature (Gupte et al. 2002; Amis et al. 2006) reveals that there was at least one meniscofemoral ligament in 93% of knees examined; an anterior (Humphrey) meniscofemoral ligament was present in 47% of knees, a posterior (Wrisberg) meniscofemoral ligament in 71%, and both an anterior (Humphrey) meniscofemoral ligament and posterior (Wrisberg) meniscofemoral ligament were present in 32% of knees. An anterior (Humphrey) meniscofemoral ligament was present in 21% of cases, and a posterior (Wrisberg) meniscofemoral ligament in 39% of cases. An MRI study by Erbagci et al. (2002) revealed an anterior (Humphrey) meniscofemoral ligaments present in 12% of cases and a posterior (Wrisberg) meniscofemoral ligament present in 42% of cases, which would suggest that meniscofemoral ligaments are not always visualized on MRI.

The incidence of meniscofemoral ligaments decreases with age, raising the possibility that these ligaments might be prone to injury or might undergo age-related degeneration. Very rarely, an anteromedial meniscofemoral ligament is present and can be seen extending from the anterior horn of the medial meniscus to the posterior wall of the intercondylar notch, parallel to the anterior cruciate ligament (ACL) (Soejima et al. 2003). The infrapatallar plica (ligamentum mucosum) may have an appearance similar to that of the anteromedial meniscofemoral ligaments on sagittal oblique images, but tracing its origin from the anterior intercondylar notch through the infrapatellar fat pad to the inferior pole of the patella allows confident differentiation between these two structures. A prominent anterior (Humphrey) meniscofemoral ligament may mimic a double PCL sign (Venkatanarasimha et al. 2009).

Medial patellofemoral ligament (MPFL)

Kaplan (1957b) is credited with describing the medial patellofemoral ligament (MPFL) as the transverse reinforcement between the base of the patella and the tendon of the medial head of the gastrocnemius. Lang and Wachsmuth (1979) termed the MPFL "the retinacular patella transversalia mediale" and Hughston et al. (1984) "the medial patello-epicondylar ligament." During the past decade the majority of authors use the term MPFL. The MPFL generally has a fan-shaped structure and runs from the medial margin of the patella to the medial femoral epicondyle. Although Reider et al. (1981) reported that the MPFL was present in only 6 of 20 (30%) dissected knees, many recent studies have revealed that there was a MPFL in all the dissected knees or in >90% of knees (Nomura et al. 2005). The superficial fibers of the MPFL extended to the posteromedial capsule (Tuxoe et al. 2002; Nomura et al. 2005). The femoral attachment of the MPFL was reported by Smirk and Morris (2003) and Nomura et al. (2005) as being located superoposterior to the medial femoral epicondyle and distal to the adductor tubercle.

Posterior lateral ligament

A supernumerary ligament of the lateral surface of the knee joint has been described. The ligament is known as the ligament of Meckel and Macalister or the peroneosesamoid ligament of Dujarier.

Transverse genicular ligament

The terms transverse genicular ligament (anterior intermeniscal, ligamentum transversum cartilaginis semilunaris, anterior transverse ligament, and jugal ligament) have all been used to describe this structure. Transverse (anterior) intermeniscal ligament attaches the anterior horns of the lateral and medial menisci (Tubbs et al. 2008b). The tendinous attachments of the ligament to the menisci may give the impression of an oblique tear of the anterior horn of the lateral meniscus, particularly on sagittal imaging (Amis et al. 2006). The transverse ligament is of variable thickness and is defined as cord-like when it has a thickness of 3 mm or more at its attachment to the anterior horns of the menisci (Snoeckx et al. 2008). The anterior transverse intermeniscal ligament has been found in 94% of knees at arthroscopy (Sintzoff et al. 1992; Nelson and Laprade 2000).

Posterior oblique ligament

The posterior oblique ligament consists of three attachments from the distal arm of the semimembranosus tendon, referred to as the superficial, central, and capsular ligaments.

A single report exists of an incidental finding at arthroscopy of a three-bundle popliteus tendon, which converged to form a single tendon inserting normally on the tibia (Doral et al. 2006). The quadriceps tendon inserts onto the proximal pole of the patella and is formed by the convergence of four individual muscles. A third head is the most common variation of the gastrocnemius muscle. It has been found in 2.9–5.5% of the population (Iwai et al. 1987) and is composed of muscle or tendon arising from the posteroinferior aspect of the femur to join either the medial or lateral head of gastrocnemius.

The plantaris muscle is a small spindle-shaped muscle originating just proximal to the posterolateral femoral condyle, superior to the origin of the lateral head of gastrocnemius. It descends inferomedially between the gastrocnemius and soleus, passing medial to the Achilles tendon to insert on the posteromedial aspect of the calcaneum. Variations in origin have been described including the inferior linea aspera, the intercondylar notch, the proximal fibula, the oblique line of the tibia, and the fascial covering of the popliteus (Soubhagya et al. 2009).

The termination of the plantaris is also variable, with insertion into the soft tissues between the gastrocnemius and soleus or anterior to the Achilles tendon, the dorsal or medial aspect of the Achilles tendon, and the plantar aponeurosis having been described (Soubhagya et al. 2009). The tendon may be absent (in up to 10% of the population) and, when present, varies in size from a thin fibrous structure to a large muscle belly similar in size to the lateral head of gastrocnemius. With such variety in anatomy and size, the plantaris muscle may be difficult to differentiate from an accessory gastrocnemius. However, the latter can usually be seen joining either the medial or lateral heads of gastrocnemius, while the plantaris can be followed to its more distal termination within the calf.

Several anatomical variations of the biceps femoris muscle and tendon have been reported. The short head may be absent or additional heads may arise from the ischial tuberosity, the linea aspera, or the medial supracondylar ridge of the femur. Recent reports in the literature describe an exclusive insertion of the biceps femoris tendon onto the anterolateral aspect of the proximal tibia, a variant associated with a painful snapping knee (Kristensen et al. 1989; Hernandez et al. 1996; Bagchi and Grelsamer 2003; Tubbs et al. 2008a). Solomon and Stevenson (2008) reported a case of bilateral tibial insertion of the biceps tendon, which was best visualized pre-operatively on axial images. The importance of recognizing this variant relates to accurate preoperative planning for posterolateral corner reconstruction as well as ligament balancing in total knee replacement and revision knee replacements.

The distal semimembranosus tendon divides into five branches at the level of the knee joint (Beltran et al. 2003, Benninger and Delamarter 2012a, b). These branches are: the anterior (tibial) arm, which inserts under the tibial collateral ligament and is best seen on sagittal and coronal images; the direct arm, inserting on the posteromedial tibia and not visualized on imaging; the inferior (popliteal) arm, which inserts above the tibial attachment of the tibial collateral ligament and can be seen on sagittal images; the capsular arm, which is contiguous with the posterior oblique ligament and is seen on axial images; and the oblique popliteal ligament, which blends with the capsule.

Oblique popliteal ligament (OPL)

Despite the fact that nearly 60% of anatomical texts and atlases as well as over 90% of specialty journal articles state that the distal semimembranosus tendon forms the oblique popliteal ligament (Benninger and Delamarter 2012a); none have hypothesized that this structure is itself a tendon (Cave and Porteous 1959; Hollinshead 1961; Hughston and Eilers 1973; Woodburne 1978; Warren and Marshall 1979; Hall-Craggs 1990; Kim et al. 1997; Loredo et al. 1999; Beltran et al. 2003; Sims and Jacobson 2004; Koulouris and Connell 2005; LaPrade et al. 2007a, b; Tank and Gest 2009; Standring 2010; Turman et al. 2010; Benninger and Delamarter 2012b). A macroanalysis using deep dissection of the posterior knee revealed that the distal (medial) attachment of the OPL originated from the semimembranosus muscle-tendon-unit (SMTU) in 100% of the knees (Benninger and Delamarter 2012b). This provided evidence in support of the hypothesis the OPL is indeed a portion of the distal semimembranosus tendon; however, a microanalysis was also necessary to propitiate these findings.

There have been previous studies that have used various staining protocols on the deep tissue of the knee, namely the cruciate ligaments, menisci, and the medial collateral ligament (Amiel et al. 1984). The majority of this research conducted histological studies specifically targeting the morphology of nerve endings in these tissues. The microanalysis of the tendon properties using rabbit anti-PGP9.5/goat anti-rabbit biotinylated immunohistochemistry staining revealed neuronal axons in both the SMTU and the OPL and displayed similar histological patterns in both structures (Amiel et al. 1984; Schultz et al. 1984; Zimny et al. 1985, 1987; Schutte et al. 1987; Wojtys 1990; Katonis et al. 1991; Zimny and Wink 1991). The lateral collateral ligament did not display a positive result for this stain and had a markedly different histology to both the OPL and SMTU. Furthermore, the positive stain for neuronal axons provides grounds that Golgi tendon organs, nervous tissue specific to tendons, may be located in the OPL. These findings support the hypothesis that this structure is a tendon (Benninger and Delamarter 2012b). See also distal semimembranosus muscle variants.

Musculotendinous variations

The popliteus musculotendinous unit is an intra-articular, extrasynovial structure. It is one of the posterolateral structures of the knee, and its actions produce internal rotation of the tibia in the extended knee and external rotation of the femur over the fixed tibia. The popliteus muscle has a triangular attachment on the posteromedial superior tibia, contributing to the floor of the popliteal fossa, and its tendon runs between the knee capsule and synovial membrane to insert into the lateral femoral condyle (Tyler et al. 2010). It also has attachments to the fibular head via the popliteofibular ligament in 98% of knees and an attachment to the posterior aspect of the lateral meniscus in 95% of cases.

A number of variants of the popliteus musculotendinous unit may occur, the most common of these being bifurcation of the popliteus tendon (Tyler et al. 2010). At the proximal femoral

attachment, two separate bundles have been described: a posterior superficial bundle, which is tight in extension, and an anterior deep bundle that is tight in flexion (Bolog and Hodler 2007). Bifurcation of the popliteus may simply represent these bundles continuing as separate structures along the entire course of the tendon. Leal-Blanquet et al. (2008) found a bifurcated popliteus tendon in 0.4% of knees undergoing arthroscopy. The two popliteal fascicles may be equal in size or one may be larger than the other; they usually follow a parallel course, with both fascicles merging distally prior to their tibial insertion (Perez et al. 1999; Leal-Blanquet et al. 2008). In most cases the bifurcation originates proximal to the lateral meniscus, with the origin of bifurcation distal to the meniscus a less frequent finding (Tyler et al. 2010). Popliteal bifurcation appears as two parallel structures of low signal intensity running along the normal course of the popliteus tendon.

One report exists of a three-bundle popliteus tendon, which converged to form a single tendon inserting normally on the tibia (Doral et al. 2006). An accessory popliteus muscle has also been described, originating from the fabella sesamoid bone within the lateral gastrocnemius (Duc et al. 2004). This accessory muscle may be completely separate from the normal popliteus muscle, or it may merge with it distally at its insertion onto the posterior aspect of the proximal tibia (Wagstaffe 1871). These anomalies of the popliteus musculotendinous unit exist as non-pathological normal variants and do not appear to contribute to popliteal entrapment syndrome, despite their proximity to the popliteal vessels (Duc et al. 2004; Doral et al. 2006; Leal-Blanquet et al. 2008). The quadriceps tendon inserts onto the proximal pole of the patella and is formed by the convergence of four individual muscles.

The rectus femoris originates from the anterior inferior iliac spine, while the vastus lateralis, vastus medialis, and vastus intermedius arise from the proximal aspect of the femoral shaft. These muscles produce a layered appearance of the quadriceps tendon, which can be seen on MRI and cadaveric dissection. The normal quadriceps tendon is usually composed of either two or three discrete layers. The number of laminations varies on passing from medial to lateral, with the lateral aspect of the quadriceps tendon usually comprising a single band and two or three discrete layers identified medially. The rectus femoris muscle forms the most superficial layer of the quadriceps tendon, while the vastus intermedius forms the deepest layer. The vastus medialis and vastus lateralis may converge with these muscles, resulting in the formation of a two-layered quadriceps tendon, or may form an additional layer between the rectus femoris and vastus intermedius to produce a three-layered tendon.

An MRI study of the quadriceps tendon of 52 knees revealed that all the normal quadriceps tendons had a laminated appearance with four discrete layers identified in 6% of imaged knees, three layers in 56%, two layers in 30%, and 8% of knees had laminations that were barely perceptible (Zeiss et al. 1992). The overall thickness and width of the quadriceps remains relatively constant, irrespective of the number of layers within it. In cases of partial rupture of the quadriceps tendon, imaging may show discontinuity of one or more layers with at least one layer of the quadriceps tendon remaining intact. The lagest sesamoid bone in the body sits within the quadriceps tendon and allows clinical anatomists to divide the tendon of the quadriceps into a proximal tendon (quadriceps) and a distal tendon (patellar), which is inaccurately referred to as the patella ligament. The latter structure has been reported to be absent from the quadriceps femoris. The overwhelming terminology used clinically is patellar tendon, which originates from the quadriceps muscle unit housing a sesamoid bone of this name.

The gastrocnemius is composed of medial and lateral heads which originate from the distal femur and knee joint capsule. The medial head originates from a concavity in the posterior aspect of the upper part of the medial femoral condyle and adjacent posterior femoral shaft, while the lateral head originates from the side of the lateral femoral condyle and the adjacent distal femoral shaft. A third head is the most common variation of the gastrocnemius muscle. It has been found in 2.9–5.5% of the population and is composed of muscle or tendon arising from the posteroinferior aspect of the femur to join either the medial or lateral head of gastrocnemius (Iwai 1987). Twelve variations have been described (Bergman et al. 1988). While the third head is frequently an asymptomatic normal variant, it may be implicated in popliteal artery or vein entrapment (Koplas et al. 2009). Popliteal entrapment syndrome has a prevalence of 0.165% in young men entering military service, and typically affects athletic young men in whom claudication is caused by anomalous musculature in the popliteal fossa (Bouhoutsos and Daskalakis 1981; Koplas et al. 2009).

A third head arising from the medial head of gastrocnemius is thought to cause popliteal entrapment more frequently than a third head arising from the lateral head. In a study by Koplas et al. (2009), 1039 MRI scans of knees of patients with no history of claudication were analyzed and 2% revealed a third head of gastrocnemius, 95% of which originated just medial to the midline of the distal femur, joining the medial aspect of the lateral head of gastrocnemius. One of the 1039 studies revealed a third head of gastrocnemius that joined the medial head of gastrocnemius. The appearance of the third head varies from fine and thread-like to a large bulky muscle. Several courses of the third head of gastrocnemius causing popliteal entrapment have been described. The third head may originate contralaterally and cross the midline between the artery and vein, thereby causing entrapment. The third head may originate contralaterally and compress the popliteal vessels as it curves around them. The third head may originate from the femoral condyle, passing between the popliteal artery and vein and compressing them between the third head and ipsilateral head of gastrocnemius before inserting into the ipsilateral head of gastrocnemius. The third head of gastrocnemius is a relatively common normal variant, and the majority of cases do not result in popliteal entrapment syndrome.

The biceps femoris long head forms part of the hamstring muscle group and attaches proximally at the inferior aspect of the ischial tuberosity and from the lateral lip of the linea aspera, between the adductor magnus and vastus lateralis. The fibers of the long head form a fusiform belly, which passes obliquely inferolaterally crossing the sciatic nerve. It is joined by fibers from the short head to form an aponeurosis. This distal tendon attaches at the lateral aspect of the fibular head, with a variable slip attaching into the lateral tibial condyle. At its distal attachment, the tendon divides to pass around the lateral collateral ligament. Several anatomical variations of the biceps femoris muscle and tendon have been reported (Tubbs et al. 2008a). The short head may be absent; additional heads may arise from the ischial tuberosity, the linea aspera, or the medial supracondylar ridge of the femur.

Semimembranosus, semitendinosus, and biceps femoris muscles make up the hamstring muscle group. These three muscles originate from the ischial tuberosity as a conjoined tendon and insert distally into the meniscocapsular structures and proximal tibia. The primary action of the hamstrings is flexion of the knee, but the semimembranosus and the biceps femoris also act as joint stabilizers during knee flexion. Two other additional tendinous extensions may occur: an attachment to the posterior horn of the lateral meniscus, which may occur in up to 43% of knees on cadaveric dissection and may be seen as a horizontal structure dorsal to the PCL; and the second additional tendinous extension from the inferior (popliteal) arm to the popliteus muscle aponeurosis, which is not seen on MRI (Kim et al. 1997).

The semimembranosus muscle may be absent or reduced in size. An accessory semimembranosus is a rare variant, which most frequently arises from the sacrotuberous ligament with additional insertions into the adductor magnus or femur. In addition to these variations, it should be noted that the major tendon may contain central fat, which should not be mistaken for a partial tendon rupture.

The sartorius is a strap muscle of the anterior compartment of the thigh, originating from the anterior superior iliac spine and inserting on the upper medial surface of the tibia. It crosses the anterior thigh inferomedially, with its medial edge forming the lateral border of the femoral triangle. The extent of investment by deep fascia is variable although, in the upper thigh, the deep fascia consistently appears to invest the sartorius completely (Burnet et al. 2004). The distal tendon of the sartorius may bifurcate, with an anomalous tendon inserting into the medial femoral condyle, fascia lata, patellar tendon, semitendinosus tendon, medial meniscus, or medial knee joint capsule, in addition to the classically described insertion of the tendon into the tibia (El-Bedawi 1987). The relative lengths of the muscular and tendinous portions are variable and the muscle may be completely absent. The infrapatellar nerve may penetrate or run posterior, anterior, or parallel to the sartorius tendon. Awareness of these anatomical variants is important prior to medial arthrotomy and pes anserinus transplantation (Hunter et al. 1979).

References

Aguiar RO, Viegas FC, Fernandez RY, Trudell D, Haghighi P, Resnick D. 2007. The prepatellar bursa: cadaveric investigation of regional anatomy with MRI after sonographically guided bursography. *Am J Roentgenol* 188: W355–W358.

Ahn JH, Sang HL, Sang HC, Tae KL. 2010. Magnetic resonance imaging evaluation of anterior cruciate ligament reconstruction using quadrupled hamstring tendon autografts comparison of remnant bundle preservation and standard technique. *Am J Sports Med* 38: 1768–1777.

Aitken GT. 1959. Amputation as a treatment for certain lower-extremity congenital abnormalities. *J Bone Joint Surg* 41: 1267–1285.

Amiel D, Frank C, Harwood F. 1984. Tendons and ligaments: a morphological and biochemical comparison. *J Ortho Res* 1: 257–265.

Amis AA, Dawkins GPC. 1991. Functional anatomy of the anterior cruciate ligament: fiber bundle actions related to ligament replacements and injuries. *J Bone Joint Surg Br* 73B: 260–267.

Amis AA, Jakob RP. 1998. Anterior cruciate ligament graft positioning, tensioning and twisting. *Knee Surg Sports Traumatol Arthro* 6: S2–S12.

Amis AA, Bull AM, Gupte CM, Hijazi I, Race A, Robinson JR. 2003. Biomechanics of the PCL and related structures: posterolateral, posteromedial and meniscofemoral ligaments. *Knee Surg Sports Traumatol Arthrosc* 11: 271–281.

Amis AA, Gupte CM, Bull AM, Edwards A. 2006. Anatomy of the posterior cruciate ligament and the meniscofemoral ligaments. *Knee Surg Sports Traumatol Arthrosc* 14: 257–263.

Amstutz HC, Wilson PD Jr. 1962. Dysgenesis of the proximal femur (coxa vara) and its surgical management. *J Bone Joint Surg* 44: 1–24.

Anderson AF, Lipscomb AB, Liudahl KJ, Addlestone RB. 1987. Analysis of the intercondylar notch by computed tomography. *Am J Sports Med* 15(6): 547–552.

Anderson AF, Dome DC, Gautam S, Awh MH, Rennirt GW. 2001. Correlation of anthropometric measurements, strength, anterior cruciate ligament size, and intercondylar notch characteristics to sex differences in anterior cruciate ligament tear rates. *Am J Sports Med* 29: 58–66.

Arazi M, Ögün TC, Memik R. 2001. Normal development of the tibiofemoral angle in children: a clinical study of 590 normal subjects from 3 to 17 years of age. *J Pediatr Ortho* 21: 264–267.

Arnoczky SP. 1983. Anatomy of the anterior cruciate ligament. *Clin Orthop* 172: 19–25.

Arnoczky SP, Warren RF. 1988 *Anatomy of the cruciate ligaments. In: The Cruciat Ligaments* (FeaginJA, ed.). New York: Churchill Livingstone.

Bagchi K, Grelsamer RP. 2003. Partial fibular head resection for bilateral snapping biceps femoris tendon. *Orthopedics* 26: 1147–1149.

Barrack RL, Skinner HB, Buckley SL. 1989. Proprioception in the anterior cruciate deficient knee. *Am J Sports Med* 17: 1–6.

Barrett DS, Cobb AG, Bentley G. 1991. Joint proprioception in normal, osteoarthritic and replaced knees. *J Bone Joint Surg* 73: 53–56.

Beasley LS, Vidal AF. 2004. Traumatic patellar dislocation in children and adolescents: treatment update and literature review. *Curr Opinion Pediatr* 16: 29–36.

Belgin Yildirim F, Soyuncu Y, Oguz N, Turan Aydin A, Sindel M, Ustunel I. 2007. Anterior intermeniscal ligament: An ultrastructural study. *Ann Anat* 189: 510–514.

Beltran J, Matityahu A, Hwang K, et al. 2003. The distal semimembranosus complex: normal MR anatomy, variants, biomechanics and pathology. *Skeletal Radiol* 32: 435–445.

Benninger B, Delamarter T. 2012a. Distal semimembranosus muscle-tendon-unit review: morphology, accurate terminology, and clinical relevance. *Folia Morphol* 72: 1–9.

Benninger B, Delamarter T. 2012b. The "oblique popliteal ligament": a macro- and microanalysis to determine if it is a ligament or a tendon. Anat Res Intern 2012, article ID 151342.

Bergman RA, Afifi AK, Miyauchi R. 1988. *Compendium of Human Anatomical Variations*. Baltimore: Urban and Schwarzenberg.

Bicer EK, Lustig S, Servien E, Selmi TAS, Neyret P. 2010. Current knowledge in the anatomy of the human anterior cruciate ligament. *Knee Surg Sports Traumatol Arthro* 18: 1075–1084.

Boisgard S, Levai JP, Geiger B, Saidane K, Landjerit B. 1999. Study of the variations in length of the anterior cruciate ligament during flexion of the knee: use of a 3D model reconstructed from MRI sections. *Surg Radiol Anat* 21: 313–317.

Boles CA, Martin DF. 2001. Synovial plicae in the knee. *Am J Roentgenol* 177: 221–227.

Bolog N, Hodler J. 2007. MR imaging of the postero-lateral corner of the knee. *Skeletal Radiol* 36: 715–728.

Bouhoutsos J, Daskalakis E. 1981. Muscular abnormalities affecting the popliteal vessels. *Br J Surg* 68: 501–506.

Bozkurt M, Elhan A, Tekdemir I, Tonuk E. 2004. An anatomical study of the meniscofibular ligament. *Knee Surg Sports Traumatol Arthrosc* 12: 429–433.

Brandon ML, Haynes PT, Bonamo JR, Flynn MI, Barrett GR, Sherman MF. 2006. The association between posterior-inferior tibial slope and anterior cruciate ligament insufficiency. *J Arthro Rel Surg* 22: 894–899.

Brantigan OC, Voshell AF. 1943. The tibial collateral ligament: its function, its bursae, and its relation to the medial meniscus. *J Bone Joint Surg* 25: 121–131.

Buda R, Di Caprio F, Giuriati L, Luciani D, Busacca M, Giannini S. 2008. Partial ACL tears augmented with distally inserted hamstring tendons and over-the-top fixation: an MRI evaluation. *Knee* 15: 111–116.

Buelow JU, Siebold R, Ellermann A. 2002. A prospective evaluation of tunnel enlargement in anterior cruciate ligament reconstruction with hamstrings: extracortical versus anatomical fixation. *Knee Surg Sports Traumatol Arthroscopy* 10: 80–85.

Burnet NG, Bennett-Britton T, Hoole AC, Jefferies SJ, Parkin IG. 2004. The anatomy of sartorius muscle and its implications for sarcoma radiotherapy. *Sarcoma* 8: 7–12.

Cahuzac JP, Vardon D, Sales de Gauzy J. 1995. Development of the clinical tibiofemoral angle in normal adolescents. A study of 427 normal subjects from 10 to 16 years of age. *J Bone Joint Surg* 77: 729–732.

Cave AJ, Porteous CJ. 1959. A note on the semimembranosus muscle. *Ann Royal Coll Surg Engl* 24: 251–256.

Chaudhari AM, Zelman EA, Flanigan DC, Kaeding CC, Nagaraja HN. 2009. Anterior cruciate ligament-injured subjects have smaller anterior cruciate ligaments than matched controls a magnetic resonance imaging study. *Am J Sports Med* 37: 1282–1287.

Chavadaki RH, Reddy PK, Reneesh UP, Gurram S. 2013. MRI of the internally deranged knee joint. A prospective study. *J Evol Med Dental Sci* 42: 8186–8206.

Cheema JI, Grissom LE, Harcke HT. 2003. Radiographic characteristics of lower-extremity bowing in children. *Radiographics* 23(4): 871–880.

Chen B, Gao S. 2009. Double-bundle posterior cruciate ligament reconstruction using a non-hardware suspension fixation technique and 8 strands of autogenous hamstring tendons. *J Arthro Rel Surg* 25: 777–782.

Cheng JC, Chan PS, Chiang SC, Hui PW. 1991. Angular and rotational profile of the lower limb in 2630 Chinese children. *J Pediatr Ortho* 11: 154–161.

Chhabra A, Kline AJ, Harner CD. 2006. Single-bundle versus double-bundle posterior cruciate ligament reconstruction: scientific rationale and surgical technique. *Instr Course Lect* 55: 497–507.

Cho JM, Suh JS, Na JB, Cho JH, Kim Y, Yoo WK, Chung IH. 1999. Variations in meniscofemoral ligaments at anatomical study and MR imaging. *Skel Radiol* 28: 189–195.

Clark CR, Ogden JA. 1983. Development of the menisci of the human knee joint: Morphological changes and their potential role in childhood meniscal injury. *J Bone Joint Surg Am* 65: 538–547.

Colombet P, Robinson J, Christel P, Franceschi JP, Djian P, Bellier G, Sbihi A. 2006. Morphology of anterior cruciate ligament attachments for anatomic reconstruction: a cadaveric dissection and radiographic study. *J Arthro Rel Surg* 22: 984–992.

Conlan T, Garth WP, Lemons JE. 1993. Evaluation of the medial soft-tissue restraints of the extensor mechanism of the knee. *J Bone Joint Surg Am* 75A: 682–693.

Coupens SD, Yates CK, Sheldon C, Ward C. 1992. Magnetic resonance imaging evaluation of the patellar tendon after use of its central one-third for anterior cruciate ligament reconstruction. *Am J Sports Med* 20: 332–335.

Covey DC. 2001. Injuries of the posterolateral corner of the knee. *J Bone Joint Surg Am* 83-A(1): 106–118.

Crain EH, Fithian DC, Paxton EW, Luetzow WF. 2005. Variation in anterior cruciate ligament scar pattern: does the scar pattern affect anterior laxity in anterior cruciate ligament-deficient knees? *J Arthro Rel Surg* 21: 19–24.

Dandy DJ. 1990. Anatomy of the medial suprapatellar plica and medial synovial shelf. *J Arthro Rel Surg* 6: 79–85.

De Lee JC, Riley MB, Rockwood CA. 1983. Acute posterolateral rotatory instability of the knee. *Am J Sports Med* 11: 199–207.

De Maeseneer M, Van Roy P, Shahabpour M, Gosselin, R, De Ridder F, Osteaux M. 2003. Normal anatomy and pathology of the posterior capsular area of the knee: findings in cadaveric specimens and in patients. *Am J Roentgenol* 182: 955–962.

DeFrate LE, Gill TJ, Li G. 2004. In vivo function of the posterior cruciate ligament during weightbearing knee flexion. *Am J Sports Med* 32: 1923–1928.

DeFrate LE, Papannagari R, Gill TJ, Moses JM, Pathare NP, Li G. 2006. The 6 degrees of freedom kinematics of the knee after anterior cruciate ligament deficiency an in vivo imaging analysis. *Am J Sports Med* 34: 1240–1246.

Dejour H, Bonnin M. 1994. Tibial translation after anterior cruciate ligament rupture: two radiological tests compared. *J Bone Joint Surg Br* 76: 745–749.

Dejour H, Walch G, Neyret PH, Adeleine, P. 1989. Dysplasia of the femoral trochlea. *Revue de chirurgie orthopedique et reparatrice de l'appareil moteur*, 76: 45–54.

Dervin GF, Paterson RS. 1997. Oblique menisco-meniscal ligament ofthe knee. *Arthroscopy* 13: 363–365.

Do TT. 2001. Clinical and radiographic evaluation of bowlegs. *Curr Opinion Pediatr* 13: 42–46.

Donahue F, Turkel D, Mnaymneh W, GhandurMnaymneh L. 1996. Hemorrhagic prepatellar bursitis. *Skeletal Radiol* 25: 298–301.

Doral MN, Atay AO, Bozkurt M, Ayvaz M, Tetik O, Leblebicioglu G. 2006. Three-bundle popliteus tendon: a non-symptomatic anatomical variation. *Knee* 13: 342–343.

Dorfmann H, Orengo P, Amarenco G. 1982. Pathologie des replis synoviaux du genou: intérêt de l'arthroscopie. *Rev Rhum* 49: 67–73.

Duc SR, Wentz KU, Kach KP, Zollikofer CL. 2004. First report of an accessory popliteal muscle: detection with MRI. *Skeletal Radiol* 33: 429–431.

Dupont JY. 1997. Synovial plicae of the knee: controversies and review. *Clin Sports Med* 16: 87–122.

Dye SE, Campagna-Pinto D, Dye CC, Shifflett S, Eiman T. 2003. Soft tissue anatomy anterior to the human patella. *J Bone Joint Surg* 85: 1012–1017.

Edwards A, Bull AM, Amis AA. 2007. The attachments of the fiber bundles of the posterior cruciate ligaments: an anatomic study. *Arthroscopy* 23: 284–290.

El-Bedawi MG. 1987. An anomalous bifurcation of the sartorius muscle. *Anat Anz* 163: 79–82.

Erbagci H, Yildirim H, Kizilkan N, Gumusburun E. 2002. An MRI study of the meniscofemoral and transverse ligaments of the knee. *Surg Radiol Anat* 24: 120–124.

Ergun S, Karahan M, Akgun U, Kocaoglu B. 2008. A case of congenital anomalies including agenesis of the anterior cruciate ligament. *Acta Orthop Traumatol Turc* 42: 373–376.

Evans EL, Smith NR. 1926. Congenital absence of tibia. *Arch Dis Child* 1: 194–229.

Fabbricciani C, Oransky M. 1992. The popliteus muscle. In: *The Knee and the Cruciate Ligaments: Anatomy, Biomechanics, Clinical Aspects, Reconstruction, Complications, Rehabilitation* (JakobRP, StäubliHU, eds). New York: Springer.

Farrow LD, Chen MR, Cooperman DR, Victoroff BN, Goodfellow DB. 2007. Morphology of the femoral intercondylar notch. *J Bone Joint Surg* 89: 2150–2155.

Ferretti M, Levicoff EA, Macpherson TA, Moreland MS, Cohen M, Fu FH. 2007. The fetal anterior cruciate ligament: an anatomic and histologic study. *Arthroscopy* 23: 278–283.

Fick R. 1904. Anatomie der Gelenke. In: *Handbuch der Anatomie des Menschen* (BardelebenK, ed.). Jena: Gustav Fischer.

Forsythe B, Harner C, Martins CA, Shen W, Lopes OV Jr, Fu FH. 2009. Topography of the femoral attachment of the posterior cruciate ligament: surgical technique. *J Bone Joint Surg Am* 91: 89–100.

Frikha R, Dahmene J, Hamida RB, Chaieb Z, Janhaoui N, Ayeche MLB. 2008. Congenital absence of the anterior cruciate ligament: eight cases in the same family. *Rev Chir Orthop Reparatrice Appar Mot* 91(7): 642–648.

Fukubayashi T, Kurosawa H. 1980. The contact area and pressure distribution pattern of the knee. A study of normal and osteoarthritic knee joints. *Acta Orthop Scand* 51: 871–879.

Furman W, Marshall JL, Girgis FG. 1976. The anterior cruciate ligament. A functional analysis based on postmortem studies. *J Bone Joint Surg Am* 58(2): 179–185.

García-Valtuille R, Abascal F, Cerezal L, García-Valtuille A, Pereda T, Canga A, Cruz A. 2002. Anatomy and MR imaging appearances of synovial plicae of the knee. *Radiographics* 22: 775–784.

Genin P, Weill G, Julliard R. 1993. The tibial slope: proposal for a measurement method. *J Radiol.* 74: 27–33 (in French).

Giffin JR, Vogrin TM, Zantop T, Woo SL, Harner CD. 2004. Effects of increasing tibial slope on the biomechanics of the knee. *Am J Sports Med* 32: 376–382.

Gill TJ, DeFrate LE, Wang C, Carey CT, Zayontz S, Zarins B, Li G. 2003. The biomechanical effect of posterior cruciate ligament reconstruction on knee joint function. Kinematic response to simulated muscle loads. *Am J Sports Med* 31: 530–536.

Gillespie R, Torode IP. 1983. Classification and management of congenital abnormalities of the femur. *J Bone Joint Surg* 65: 557–568.

Girgis FG, Marshall JL, Al Monajem ARS. 1975. The cruciate ligaments of the knee joint: anatomical, functional and experimental analysis. *Clin Orthop* 106: 216–31.

Goodwin DW, Wadghiri YZ, Zhu H, Vinton CJ, Smith ED, Dunn JF. 2004. Macroscopic structure of articular cartilage of the tibial plateau: influence of a characteristic matrix architecture on MRI appearance. *Am J Roentgenol* 182: 311–318.

Gray H. 1995. *Gray's Anatomy*, 38th edition. Editor: Peter LWilliams. London: Churchill Livingston.

Greene WB. 1994. Genu varum and genu valgum in children. *Instruc Course Lect* 43: 151.

Grelsamer RP, Meadows S. 1992. The modified Insall-Salvati ratio for assessment of patellar height. *Clin Orthop* 282: 170–176.

Griffith CJ, LaPrade RF, Johansen S, Armitage BM, Wijdicks CA, Engebretsen L. 2009a. Medial knee injury: Part 1, static function of the individual components of the main medial knee structures. *Am J Sports Med* 37: 1762–1770.

Griffith CJ, Wijdicks CA, LaPrade RF, Armitage BM, Johansen S, Engebretsen L. 2009b. Force measurements on the posterior oblique ligament and superficial medial collateral ligament proximal and distal divisions to applied loads. *Am J Sports Med* 37: 140–148.

Grunewald J. 1916. Die beziehungen zwischen form und funktion der tibia und fibula des menschen und einiger menschenaffen (The relationship between form and function of the human tibia and fibula and selected great apes). *Z Orthop Chir* 35: 675–780.

Gupte CM, Smith A, McDermott ID, Bull AM, Thomas RD, Amis AA. 2002. Meniscofemoral ligaments revisited. *J Bone Joint Surg* 84: 846–851.

Hall-Craggs E. 1990. *Anatomy as a Basis for Clinical Medicine*. Baltimore: Urban and Schwarzenberg.

Harish S, O'Donnell P, Connell D, Saifuddin A. 2006. Imaging of the posterolateral corner of the knee. *Clin Radiol* 61: 457–466.

Harner CD, Xerogeanes JW, Livesay GA, Carlin GJ, Smith BA, Kusayama T, Woo SLY. 1995. The human posterior cruciate ligament complex: an interdisciplinary study ligament morphology and biomechanical evaluation. *Am J Sports Med* 23: 736–745.

Harner CD, Hoher J, Vogrin TM, Carlin GJ, Woo SL. 1998. The effects of a popliteus muscle load on in situ forces in the posterior cruciate ligament and on knee kinematics. A human cadaveric study. *Am J Sports Med* 26: 669–673.

Harner CD, Baek GH, Vogrin TM, Carlin GJ, Kashiwaguchi S, Woo SL. 1999. Quantitative analysis of human cruciate ligament insertions. *Arthroscopy* 15(7): 741–749.

Harty M, Joyce JJ III. 1977. Synovial folds in the knee joint. *Orthop Rev* 7: 91–98.

Heath CH, Staheli LT. 1993. Normal limits of knee angle in white children: genu varum and genu valgum. *J Pediatr Ortho* 13: 259.

Helms CA. 2002. The meniscus: recent advances in MR imaging of the knee. *Am J Roentgenol* 179: 1115–1122.

Hernandez JA, Rius M, Noonan KJ. 1996. Snapping knee from anomalous biceps femoris tendon insertion: a case report. *Iowa Orthop J* 16: 161–163.

Hernigou P, Deschamps G. 2004. Posterior slope of the tibial implant and the outcome of unicompartmental knee arthroplasty. *J Bone Joint Surg Am* 86: 506–511.

Hoffa A. 1904. The influence of the adipose tissue with regard to the pathology of the knee joint. *JAMA* 43(12): 795–796.

Hofmann AA, Bachus KN, Wyatt RW. 1991. Effect of the tibial cut on subsidence following total knee arthroplasty. *Clin Orthop Relat Res* 269: 63–69.

Hollinshead WH. 1961. *Anatomy for Surgeons, Volume 3: The Back and Limbs*. New York: Hoeber-Harper.

Hollinshead WH. 1969. Knee, leg, ankle and foot. In: *Anatomy for Surgeons, Volume 3: The Back and Limbs*, New York: Harper and Rowe Publishers, pp. 763–787.

Houseworth SW, Mauro VJ, Mellon BA, Kieffer DA. 1987. The intercondylar notch in acute tears of the anterior cruciate ligament: a computer graphics study. *Am J Sports Med* 15: 221–224.

Hudek R, Regenfelder F, Koch PP. 2009. Novel measurement technique of the tibial slope on conventional MRI. *Clin Ortho Rel Res* 467: 2066–2072.

Hughston JC. 1994. The importance of the posterior oblique ligament in repairs of acute tears of the medial ligaments in knees with and without an associated rupture of the anterior cruciate ligament. *J Bone Joint Surg Am* 76: 1328–1344.

Hughston JC, Eilers A. 1973. The role of the posterior oblique ligament in repairs of acute medial (collateral) ligament tears of the knee. *J Bone Joint Surg* 55: 923–940.

Hughston JC, Jacobson KE. 1985. Chronic posterolateral instability of the knee. *J Bone Joint Surg* 67: 351–359.

Hughston JC, Andrews JR, Cross MJ, Moschi A. 1976. Classification of ligament instabilities. Part I. the medial compartment and cruciate ligaments. *J Bone Joint Surg Am* 58: 159–172.

Hughston JC, Walsh WM, Puddu G. 1984. *Patellar Subluxation and Dislocation*. Philadelphia: Saunders.

Hunter LY, Louis DS, Ricciardi JR, O'Connor GA. 1979. The saphenous nerve: its course and importance in medial arthrotomy. *Am J Sports Med* 7: 227–230.

Insall J, Salvati E. 1971. Patella position in the normal knee joint. *Radiology* 101: 101–104.

Ishigooka H, Sugihara T, Shimizu K, Aoki H, Hirata K. 2004. Anatomical study of the popliteofibular ligament and surrounding structures. *J Orthop Sci* 9: 51–58.

Iwai SS, Sato S, Yamada T. 1987. Popliteal vein entrapment caused by the third head of the gastrocnemius muscle. *Br J Surg* 74: 1006–1008.

Javid M, Hadavi F. 2003. Normal limit of tibofemoral angle in primary school children in Iran. *Iranian J Ortho Surg* 1: 5.

Jee WH, Choe BY, Kim JM, Song HH, Choi KH. 1998. The plica syndrome: diagnostic value of MRI with arthroscopic correlation. *J Comput Assist Tomogr* 22: 814–818.

Jenny JY, Rapp E, Kehr P. 1997. Proximal tibial meniscal slope: a comparison with the bone slope. *Rev Chir Orthop Reparatrice Appar Mot* 84: 435–438 (in French).

Johnson DL, Urban WP, Caborn DNM, Vanarthos WJ, Carlson CS. 1998. Articular cartilage changes seen with magnetic resonance imaging-detected bone bruises associated with acute anterior cruciate ligament rupture. *Am J Sports Med* 26: 409–414.

Jordan MR. 1996. Lateral meniscal variants: evaluation and treatment. *J Am Acad Ortho Surg* 4: 191–200.

Jouanin T, Dupont JY, Halimi P, Lassau JP. 1982. The synovial folds of the knee joint: anatomical study. *Anatomia Clinica* 4: 47–53.

Julliard R, Genin P, Weil G, Palmkrantz P. 1993. The median functional slope of the tibia: principle, technique of measurement, value, interest. *Rev Chir Orthop Reparatrice Appar Mot* 79: 625–634 (in French).

Kaelin A, Hulin PH, Carlioz H. 1986. Congenital aplasia of the cruciate ligaments. A report of six cases. *J Bone Joint Surg Br* 68: 827–828.

Kaplan EB. 1956. The lateral meniscofemoral ligament of the knee joint. *Bull Hosp Joint Dis* 17: 176–182.

Kaplan EB. 1957a. Discoid lateral meniscus of the knee joint: nature, mechanism, and operative treatment. *J Bone Joint Surg Am* 39: 77–87.

Kaplan EB. 1957b. Factors responsible for the stability of the knee joint. *Bull Hosp Joint Dis* 18: 51–59.

Kaplan EB. 1961. The fabellofibular and short lateral ligaments of the knee joint. *J Bone Joint Surg* 43: 169–179.

Karimi-Mobarake M, Kashefipour A, Yousfnejad Z. 2005. The prevalence of genu varum and genu valgum in primary school children in Iran 2003–2004. *J Med Sci* 5: 52–54.

Karlsson J, Irrgang J. Carola Van Eck F, Samuelsson K, Mejia HA, Fu HF. 2011. Anatomic single- and double-bundle anterior cruciate ligament reconstruction, part 2 clinical application of surgical technique. *Am J Sports Med* 39: 2016–2026.

Katonis P, Assimakopoulos AP, Agapitos MV, Exarchou EI. 1991. Mechanoreceptors in the posterior cruciate ligament: histologic study on cadaver knees. *Acta Ortho Scand* 62: 276–278.

Kaufmann P, Bose P, Prescher A. 2004. New insights into the soft-tissue anatomy anterior to the patella. *Lancet* 363: 586.

Kennedy JC, Weinberg HW, Wilson AS. 1974. The anatomy and function of the anterior cruciate ligament: as determined by clinical and morphological studies. *J Bone Joint Surg Am* 56A: 223–235.

Kim SJ, Choe WS. 1997. Arthroscopic findings of the synovial plicae of the knee. *J Arthro Rel Surg* 13: 33–41.

Kim SJ, Kim DW, Min BH. 1995. Discoid lateral meniscus associated with anomalous insertion of the medial meniscus. *Clin Orthop* 315: 234–237.

Kim YC, Yoo WK, Chung IH, Seo JS, Tanaka S. 1997. Tendinous insertion of semimembranosus muscle into the lateral meniscus. *Surg Radiol Anat* 19: 365–369.

King D. 1936. The function of semilunar cartilages. *J Bone Joint Surg* 18: 1069–1076.

Kocher MS, DiCanzio J, Zurakowski D, Micheli LJ. 2001. Diagnostic performance of clinical examination and selective magnetic resonance imaging in the evaluation of intraarticluar knee disorders in children and adolescents. *Am J Sports Med* 29: 292–296.

Koplas MC, Grooff P, Piraino D, Recht M. 2009. Third head of gastrocnemius: an MR imaging study based on 1039 consecutive knee examination. *Skeletal Radiol* 38: 349–354.

Kosarek F, Helms CA. 1999. The MR appearance of the infrapatellar plica. *Am J Roentgenol* 172: 481–484.

Koukoubis TD, Glisson RR, Bolognesi M, Vail TP. 1997. Dimensions of the intercondylar notch of the knee. *Am J Knee Surg* 10: 83.

Koulouris G, Connell D. 2005. Hamstring muscle complex: an imaging review. *Radiographics* 25: 571–586.

Kramer DE, Micheli LJ. 2009. Meniscal tears and discoid meniscus in children: diagnosis and treatment. *J Am Acad Ortho Surg* 17: 698–707.

Kramer DE, Bahk MS, Cascio BM, Cosgarea AJ. 2006. Posterior knee arthroscopy: anatomy, technique, application. J Bone Joint Surg Am 88 Suppl 4: 110–121.

Kristensen G, Nielsen K, Blyme PJ. 1989. Snapping knee from biceps femoris tendon. A case report. *Acta Orthop Scand* 60: 621.

Lang J, Wachsmuth W. 1979. Praktische Anatomie: Bein und Statik. *Berlin*, Heidleberg New York: Springer.

LaPrade RF, Burnett QM. 1994. Femoral intercondylar notch stenosis and correlation to anterior cruciate ligament injuries a prospective study. *Am J Sports Med* 22: 198–203.

LaPrade RF, Hamilton CD. 1997. The fibular collateral ligamentbiceps femoris bursa. An anatomic study. *Am J Sports Med* 25: 439–443.

LaPrade RF, Muench C, Wentorf F, Lewis JL. 2002. The effect of injury to the posterolateral structures of the knee on force in a posterior cruciate ligament graft: a biochemical study. *Am J Sports Med* 30(2): 233–238.

LaPrade RF, Ly TV, Wentorf FA, Engebretsen L. 2003. The posterolateral attachments of the knee a qualitative and quantitative morphologic analysis of the fibular collateral ligament, popliteus tendon, popliteofibular ligament, and lateral gastrocnemius tendon. *Am J Sports Med* 31: 854–860.

LaPrade RF, Engebretsen AH, Ly TV, Johansen S, Wentorf FA, Engebretsen L. 2007a. The anatomy of the medial part of the knee. *J Bone Joint Surg* 89: 2000–2010.

LaPrade RF, Morgan PM, Wentorf FA, Johansen S, Engebretsen L. 2007b. The anatomy of the posterior aspect of the knee: an anatomic study. *J Bone Joint Surg* 89: 758–764.

Last RJ. 1950. The popliteus muscle and lateral meniscus. *J Bone Joint Surg Br* 32B: 93–99.

Leal-Blanquet J, Gines-Cespedosa A, Monllau JC. 2008. Bifurcated popliteus tendon: a descriptive arthroscopic study. *Int Orthop.* 33: 1633–1635.

Lee J, Papakonstantinou O, Brookenthal KR, Trudell D, Resnick DL. 2003. Arcuate sign of posterolateral knee injuries: anatomic, radiographic, and MR imaging data related to patterns of injury. *Skeletal Radiol* 32: 619–627.

Lee YS, Dong-Il C, Park MJ. 2010. Bilateral PCL hypoplasia resulting in posterior, posterolateral rotatory instability and tears of the lateral meniscus anterior horn. *Orthopedics* 33(12): 924.

Lizhen J, Xi Z, Jilin Z, Hanbing L. 2001. Anatomical observations on the transverse geniculate ligament and the posterior meniscofemoral ligament. *Chinese J Anat* 5: 19.

Lopes OV Jr, Ferretti M, Shen W, Ekdahl M, Smolinski P, Fu FH. 2008. Topography of the femoral attachment of the posterior cruciate ligament. *J Bone Joint Surg Am* 90(2): 249–255.

Loredo R, Hodler J, Pedowitz R, Yeh LR, Trudell D, Resnick D. 1999. Posteromedial corner of the knee: MR imaging with gross anatomic correlation. *Skeletal Radiol* 28: 305–311.

Lorenz S, Elser F, Brucker PU, Obst T, Imhoff AB. 2009. Radiological evaluation of the anterolateral and posteromedial bundle insertion sites of the posterior cruciate ligament. *Knee Surg Sports Traumatol Arthrosc* 17(6): 683–690.

Luites JW, Wymenga AB, Blankevoort L, Kooloos JG. 2007. Description of the attachment geometry of the anteromedial and posterolateral bundles of the ACL from arthroscopic perspective for anatomical tunnel placement. *Knee Surg Sports Traumatol Arthrosc* 15(12): 1422–1431.

Marchant MH, Tibor LM, Sekiya JK, Hardaker WT, Garrett WE, Taylor DC. 2011. Management of medial-sided knee injuries. Part 1: Medial collateral ligament. *Am J Sports Med* 39: 1102–1113.

Matsuda S, Miura H, Nagamine R, Urabe K, Ikenoue T, Okazaki K, Iwamoto Y. 1999. Posterior tibial slope in the normal and varus knee. *Am J Knee Surg* 12(3): 165–168.

Matava MJ, Ellis E, Gruber B. 2009. Surgical treatment of posterior cruciate ligament tears: an evolving technique. *J Am Acad Orthop Surg* 17(7): 435–446.

Maynard MJ. 2000. Posterolateral injuries of the knee. In: *Principles and Practice of Orthopaedic Sports Medicine* (GarrettWE, SpeerKP, KirkendallDT, eds), vol 38. Philadelphia: Lippincott Williams and Wilkins, pp. 675–685.

McDermott ID, Masouros SD, Amis AA. 2008. Biomechanics of the menisci of the knee. *Current Orthopaedics* 22(3): 193–201.

McDermott MJ, Bathgate B, Gillingham BL, Hennrikus WL. 1998. Correlation if MRI and arthoscopic diagnosis of knee pathology in children and adolescents. *J Pediatr Orthop* 18: 675–678.

Meister K, Talley MC, Horodyski MB, Indelicato PA, Hartzel JS, Batts J. 1997. Caudal slope of the tibia and its relationship to noncontact injuries to the ACL. *Am J Knee Surg* 11: 217–219.

Mejia EA, Noyes FR, Grood ES. 2002. Posterior cruciate ligament femoral insertion site characteristics: importance for reconstructive procedures. *Am J Sports Med* 30(5): 643–651.

Miller TT, Staron RB, Feldman F. 1996. Patellar height on sagittal MR imaging of the knee. *AJR* 167: 339–341.

Min BH, Ha HK, Khang SY. 2001. Medial discoid meniscus completely coalesced with the anterior cruciate ligament. *Arthroscopy* 17: E27.

Minowa T, Murakami G, Kura H, Suzuki D, Han SH, Yamashita T. 2004. Does the fabella contribute to the reinforcement of the posterolateral corner of the knee by inducing the development o associated ligaments? *J Orthop Sci.* 9: 59–65.

Moorman CT 3rd, Murphy Zane MS, Bansai S, et al. 2008. Tibial insertion of the posterior cruciate ligament: a sagittal plane analysis using gross, histologic, and radiographic methods. *Arthroscopy* 24(3): 269–275.

Morgan CD, Kalman VR, Grawl DM. 1997. The anatomic origin of the posterior cruciate ligament: where is it? Reference landmarks for PCL reconstruction. *Arthroscopy* 13(3): 325–331.

Muller W. 1983. Posterolateral (popliteus) corner. In: *The Knee: Form, Function and Ligament Reconstruction* (Muller W, ed.). New York: Springer.

Munshi M, Pretterklieber ML, Kwak S, Antonio GE, Trudell DJ, Resnick D. 2003. MR Imaging, MR arthrography and specimen correlation of the posterolateral corner of the knee: an anatomical study. *AJR Am J Roentgenol* 180: 1095–1101.

Nagasaki S, Ohkoshi Y, Yamamoto K, Ebata W, Imabuchi R, Nishiike J. 2006. The incidence and cross-sectional area of the meniscofemoral ligament. *Am J Sports Med* 34(8): 1345–1350.

Nelitz M, Dornacher D, Dreyhaupt J, Reichel H, Lippacher S. 2011. The relation of the distal femoral physis and the medial patellofemoral ligament. *Knee Surg Sports Traumatol Arthro* 19(12): 2067–2071.

Nelson EW, Laprade RF. 2000. The anterior intermeniscal ligament of the knee. An anatomic study. *Am J Sports Med* 28: 74–76.

Noble J. 1975. Congenital absence of the anterior cruciate ligament associated with a ring meniscus. *J Bone Joint Surg* 57: 1165.

Norwood LA, Cross MJ. 1979. Anterior cruciate ligament: functional anatomy of its bundles in rotatory instabilities. *Am J Sports Med* 7: 23–26.

Noyes FR, Mangine RE, Barber S. 1987. Early knee motion after open and arthroscopic anterior cruciate ligament reconstruction. *Am J Sports Med* 15: 149–160.

Obaid H, Gartner L, Haydar AA, Briggs TWR, Saifuddin A. 2008. The meniscofibular ligament: an MRI study. *Eur J Radiol* 73: 159–161.

Odensten M, Gillquist J. 1985. Functional anatomy of the anterior cruciate ligament and a rationale for reconstruction. *J Bone Joint Surg Am* 67A: 257–262.

Olateju OI, Philander I, Bidmos MA. 2013. Morphometric analysis of the patella and of South Africans of European ancestry. *South African J Sci* 109: 1–6.

Omololu B, Tella A, Ogunlade SO, Adeyemo AA, Adebisi A, Alonge TO, Akinpelu AO. 2004. Normal values of knee angle, intercondylar

and intermalleolar distances in Nigerian children. *West Afr J Med* 22: 301–304.

Östenberg A, Roos H. 2000. Injury risk factors in female European football. A prospective study of 123 players during one season. *Scand J Med Sci Sports* 10: 279–285.

Özkur A, Adaletli I, Sirikci A, Kervancioglu R, Bayram M. 2005. Hoffa's recess in the infrapatellar fat pad of the knee on MR imaging. *Surg Radiol Anat* 27: 61–63.

Paley, Holthy R, Jackson RW, Johnston KW. 1986. The functional relation between the two bands of the anterior cruciate ligament and the pivot shift, Lachman and anterior drawer signs. *J Bone Joint Surg* 68: 847–848.

Papannagari R, DeFrate LE, Nha KW, et al. 2007. Function of posterior cruciate ligament bundles during in vivo knee flexion. *Am J Sports Med* 35(9): 1507–1512.

Patel SJ, Kaplan PA, Dussault RG, Kahler DM. 1998. Anatomy and clinical significance of the horizontal cleft in the infrapatellar fat pad of the knee: MR imaging. *AJR* 170: 1551–1555.

Perez CL, Sumillera Garcia M, Sunye Gracia C. 1999. Bifurcate popliteus tendon. *Arthroscopy* 15: 638–639.

Pfeiffer RP, Shea KG, Roberts D, Grandstrand S, Bond L. 2006. Lack of effect of a knee ligament injury prevention program on the incidence of noncontact anterior cruciate ligament injury. *J Bone Joint Surg* 88: 1769–1774.

Pope MH, Johnson RJ, Brown DW, Tighe C. 1979. The role of the musculature in injuries to the medial collateral ligament. *J Bone Joint Surg Am* 61(3): 398–402.

Quatman CE, Hewett ET. 2009. The anterior cruciate ligament injury controversy: is "valgus collapse" a sex-specific mechanism? *Brit J Sports Med* 43: 328–335.

Raheem O, Philpott J, Ryan W, O'Brien M. 2007. Anatomical variations in the anatomy of the posterolateral corner of the knee. *Knee Surg Sports Traumatol Arthrosc* 15: 895–900.

Ralphs JR, Benjamin M. 1994. The joint capsule: structure, composition, ageing and disease. *J Anat* 184: 503.

Reider B, Marshall JL, Koslin B, Ring B, Girgis FG. 1981. The anterior aspect of the knee joint: an anatomical study. *J Bone Joint Surg Am* 63: 351–356.

Reiman PR, Jackson DW. 1987. Anatomy of the anterior cruciate ligament. In: *The Anterior Cruciate Deficent Knee* (JacksonDW, DrezD, eds). St Louis: CV Mosby Co, pp. 17–26.

Rispoli DM, Sanders TG, Miller MD, Morrison WB. 2001. Magnetic resonance imaging at different time periods following hamstring harvest for anterior cruciate ligament reconstruction. *J Arthro Rel Surg* 17: 2–8.

Robinson JR, Sanchez-Ballester J, Bull AMJ, Thomas RWM, Amis AA. 2004. The posteromedial corner revisited: an anatomical description of the passive restraining structures of the medial aspect of the human knee. *J Bone Joint Surg Br* 86: 674–681.

Ruiz Santiago F, Castellano García MDM, Tristán Fernández JM, Tercedor Sánchez J. 2008. Anomalous insertion of anterior cruciate ligament band into the transverse ligament. *Europ J Radiol Extra* 68: 33–35.

Sakakibara J. 1976. Arthroscopic study on Iino's band (plica synovialis mediopatellaris). *J Jpn Orthop Assoc* 50: 513–522.

Salenius P, Vankka E. 1975. The development of the tibiofemoral angle in children. *J Bone Joint Surg* 57: 259.

Sanders TG, Linares RC, Lawhorn KW, Tirman PFJ, Houser C. 1999. Oblique meniscomeniscal ligament: another potential pitfall for a meniscal tear: anatomic description and appearance at MR imaging in three cases. *Radiology* 213: 213–216.

Scanlan SF, Lai J, Donahue JP, Andriacchi TP. 2012. Variations in the three-dimensional location and orientation of the ACL in healthy subjects relative to patients after transtibial ACL reconstruction. *J Ortho Res* 30: 910–918.

Schairer WW, Haughom BD, Morse LJ, Li X, Ma CB. 2011. Magnetic resonance imaging evaluation of knee kinematics after anterior cruciate ligament reconstruction with anteromedial and transtibial femoral tunnel drilling techniques. *J Arthro Rel Surg* 27: 1663–1670.

Schultz R, Miller DC, Kerr CS, Micheli L. 1984. Mechanoreceptors in human cruciate ligaments: a histological study. *J Bone Joint Surg* 66: 1072–1076.

Schutte M, Dabezies EJ, Zimny ML, Happel LT. 1987. Neural anatomy of the human anterior cruciate ligament. *J Bone Joint Surg* 69: 243–247.

Schweitzer ME, Falk A, Berthoty D, Mitchell M, ReSnick D. 1992. Knee effusion: normal distribution of fluid. *AJR* 159: 361–363.

Seebacher JR, Inglis AE, Marshall JL, Warren RF. 1982. The structure of the posterolateral aspect of the knee. *J Bone Joint Surg Am* 64(4): 536–541.

Shabshin N, Schweitzer ME, Morrison WB, Parker L. 2004. MRI criteria for patella alta and baja. *Skel Radiol* 33: 445–450.

Shahane SA, Ibbotson C, Strachan R, Bickerstaff DR. 1999. The popliteofibular ligament. An anatomical study of the posterolateral corner of the knee. *J Bone Joint Surg Br* 81(4): 636–642.

Shambaugh JP, Klein A, Herbert JH. 1991. Structural measures as predictors of injury in basketball players. *Med Sci Sports Exerc* 23: 522–527.

Shelbourne KD, Davis TJ, Klootwyk TE. 1998. The relationship between intercondylar notch width of the femur and the incidence of anterior cruciate ligament tears. A prospective study. *Am J Sports Med* 26: 402–408.

Shen W, Forsythe B, Ingham SM, Honkamp NJ, Fu FH. 2008. Application of the anatomic double-bundle reconstruction concept to revision and augmentation anterior cruciate ligament surgeries. *J Bone Joint Surg* 90: 20–34.

Siebold R, Fu FH. 2008. Assessment and augmentation of symptomatic anteromedial or posterolateral bundle tears of the anterior cruciate ligament. *J Arthro Rel Surg* 24: 1289–1298.

Simonian PT, Sussmann PS, van Trommel M, Wickiewicz TL, Warren RF. 1997. Popliteomeniscal fasciculi and lateral meniscal stability. *Am J Sports Med* 25(6): 849–853.

Sims WF, Jacobson KE. 2004. The posteromedial corner of the knee: medial-sided injury patterns revisited. *Am J Sports Med* 32: 337–345.

Sintzoff SA Jr, Stallenberg B, Gillard I, Gevenois PA, Matos C, Struyven J. 1992. Transverse geniculate ligament of the knee: appearance and frequency on plain radiographs. *Br J Radiol* 65: 766–768.

Smirk C, Morris H. 2003. The anatomy and reconstruction of the medial patellofemoral ligament. *Knee* 10: 221–227.

Snoeckx A, Vanhoenacker FM, Gielen JL, Van Dyck P, Parizel PM. 2008. Magnetic resonance imaging of variants of the knee. *Singapore Med J* 49: 734–744.

Soejima T, Murakami H, Tanaka K, Nagata K. 2003. Anteromedial meniscofemoral ligament. *Arthroscopy* 19: 90–95.

Solomon LB, Stevenson AW. 2008. Tibial insertion of the biceps femoris tendon: anatomical and radiological description of an anatomical variant. *Clin Anat* 21: 802–804.

Soubhagya RN, Krishnamurthy A, Prabhu LV, Madhyastha S. 2009. Additional tendinous origin and entrapment of the plantaris muscle. *Clinics (Sao Paulo)* 64: 67–68.

Souryal TO, Freeman TR. 1993. Intercondylar notch size and anterior cruciate ligament injuries in athletes: A prospective study. *Am J Sports Med* 21: 535–539.

Souryal TO, Moore HA, Evans JP. 1988. Bilaterality in anterior cruciate ligament injuries Associated intercondylar notch stenosis. *Am J Sports Med* 16: 449–454.

Standring S. 2010. *Gray's Anatomy. The Anatomical Basis of Clinical Practice*. Philadelphia: Elsevier.

Starok M, Lenchik L, Trudell D, Resnick D. 1997. Normal patellar retinaculum: MR and sonographic imaging with cadaveric correlation. *Am J Roentgenol* 168: 1493–1499.

Staubli HU, Birrer S. 1990. The popliteus tendon and its fascicles at the popliteal hiatus: gross anatomy and functional arthroscopic evaluation with and without anterior cruciate ligament deficiency. *Arthroscopy* 6: 209–220.

Stijak L, Herzog RF, Schai P. 2008. Is there an influence of the tibial slope of the lateral condyle on the ACL lesion? *Knee Surg Sports Traumatol Arthrosc* 16(2): 112–117.

Sutton JB. 1884. On the nature of certain ligaments. *J Anat Physiol* 40: 34–50.

Tajima G, Nozaki M, Iriuchishima T, Ingham SJ, Shen W, Smolinski P, Fu FH. 2009. Morphology of the tibial insertion of the posterior cruciate ligament. *J Bone Joint Surg* 91: 859–866.

Takahashi M, Matsubara T, Doi M, Suzuki D, Nagano A. 2006. Anatomical study of the femoral and tibial insertions of the anterolateral and posteromedial bundles of human posterior cruciate ligament. *Knee Surg Sports Traumatol Arthrosc* 14: 1055–1059.

Takeda Y, Ikata T, Yoshida S, Takai H, Kashiwaguchi S. 1998. MRI high-signal intensity in the menisci of asymptomatic children. *J Bone Joint Surg Br* 80: 463–467.

Tank PW, Gest TR. 2009. *Atlas of Anatomy*. Philadelphia: Lippincott Williams and Wilkins.

Tearse DS, Clancy WG, Gersoff WK. 1998. The symptomatic lateral synovial plica of the knee. Presented at the 7th Annual Meeting of the Arthroscopy Association of North America, Washington, DC.

Tena-Arregui J, Barrio-Asensio C, Viejo-Tirado F, Puerta-Fonollá J, Murillo-González J. 2003. Arthroscopic study of the knee joint in fetuses. *Arthrosc* 19: 862–868.

Terry GC, LaPrade RF. 1996. The posterolateral aspect of the knee: Anatomy and surgical approach. *Am J Sports Med* 24: 732–739.

Thomas IH, Williams PF. 1987. The Gruca operation for congenital absence of the fibula. *J Bone Joint Surg* 69: 587–592.

Thomas NP, Jackson AM, Aichroth PM. 1985. Congenital absence of the anterior cruciate ligament. A common component of knee dysplasia. *J Bone Joint Surg* 67: 572–575.

Todd MS, Lalliss S, Garcia ES, DeBerardino TM, Cameron, KL. 2010. The relationship between posterior tibial slope and anterior cruciate ligament injuries. *Am J Sports Med* 38: 63–67.

Trent PS, Walker PS, Wolf B. 1976. Ligament length patterns, strength, and rotational axes of the kneejoint. *Clin Orthop* 117: 263–270.

Tschirch FT, Schmid MR, Pfirrmann CW, Romero J, Hodler J, Zanetti M. 2003. Prevalence and size of meniscal cysts, ganglionic cysts, synovial cysts of the popliteal space, fluid-filled bursae, and other fluid collections in asymptomatic knees on MR imaging. *Am J Roentgenol* 180: 1431–1436.

Tubbs RS, Caycedo FJ, Oakes WJ, Salter EG. 2008a. Descriptive anatomy of the insertion of the biceps femoris muscle. *Clin Anat* 19: 517–521.

Tubbs RS, Michelson J, Loukas M, Shoja MM, Ardalan MR, Salter EG, Oakes WJ. 2008b. The transverse genicular ligament: anatomical study and review of the literature. *Surg Radiol Anat* 30: 5–9.

Turman KA, Miller CD, Miller MD. 2010. Semimembranosus tendon viewed through an isolated medial meniscus capsular avulsion: a case report. *Knee Surg Sports Traumatol Arthro* 18: 760–762.

Tuxoe JI, Teir M, Winge S, Nielsen PL. 2002. The medial patellofemoral ligament: a dissection study. *Knee Surg Sports Traumatol Arthro* 10: 138–140.

Tyler P, Datir A, Saifuddin A. 2010. Magnetic resonance imaging of anatomical variations in the knee. Part 1: ligamentous and musculotendinous. *Skel Radiol* 39(12): 1161–1173.

Uhorchak JM, Scoville CR, Williams GN, Arciero RA, Pierre PS, Taylor DC. 2003. Risk factors associated with noncontact injury of the anterior cruciate ligament: A prospective four-year evaluation of 859 west point cadets. *Am J Sports Med* 31: 831–842.

Vahey TN, Bennett HT, Arrington LE, Shelbourne KD, Ng J. 1990. MR imaging of the knee: pseudotear of the lateral meniscus caused by the meniscofemoral ligament. *AJR* 154: 1237–1239.

Vahlensieck M, Linneborn G, Schild H, Schmidt HM. 2002. Hoffa's recess: incidence, morphology and differential diagnosis of the globular-shaped cleft in the infrapatellar fat pad of the knee on MRI and cadaver dissections. *Europ Radiol* 12: 90–93.

Venkatanarasimha N, Kamath A, Mukherjee K, Kamath S. 2009. Potential pitfalls of a double PCL sign. *Skel Radiol* 38: 735–739.

Voos JE, Mauro CS, Wente T, Warren RF, Wickiewicz TL. 2012. Posterior cruciate ligament anatomy, biomechanics, and outcomes. *Am J Sports Med* 40: 222–231.

Wada M, Tatsuo H, Baba H, Asamoto K, Nojyo Y. 1999. Femoral intercondylar notch measurements in osteoarthritic knees. *Rheumatology* 38(6): 554–558.

Wagstaffe WW. 1871. Description of an accessory popliteus muscle in connection with the popliteus. *J Anat Physiol* 6(1): 214–215.

Wahl CJ, Westermann RW, Blaisdell GY, Cizik AM. 2012. An association of lateral knee sagittal anatomic factors with non–contact acl injury: sex or geometry? *J Bone Joint Surg* 94: 217–226.

Walker PS, Erkman MJ. 1975. The role of the menisci in force transmission across the knee. *Clin Orthop Relat Res* 109: 184–192.

Ward SR, Terk MR, Powers CM. 2007. Patella alta: association with patellofemoral alignment and changes in contact area during weight-bearing. *J Bone Joint Surg* 89: 1749–1755.

Warren LF, Marshall JL. 1979. The supporting structures and layers on the medial side of the knee: an anatomical analysis. *J Bone Joint Surg Am* 61A: 56–62.

Warren LF, Marshall JL, Girgis F. 1974. The prime static stabilizer of the medial side of the knee. *J Bone Joint Surg Am* 56: 665–674.

Watanabe AT, Carter BC, Teitelbaum GP, Seeger LL, Bradley Jr WG. 1989. Normal variations in MR imaging of the knee: appearance and frequency. *Am J Roentgenol* 153: 341–344.

Welsh RP. 1980. Kneejoint structure and function. *Clin Orth* 147: 7–14.

Wiberg G. 1941. Roentgenographs and anatomic studies on the femoropatellar joint: with special reference to chondromalacia patellae. *Acta Orthopaedica* 12(1–4): 319–410.

Wijdicks CA, Griffith CJ, LaPrade RF, Spiridonov SI, Johansen S, Armitage BM, Engebretsen L. 2009. Medial knee injury part 2: Load sharing between the posterior oblique ligament and superficial medial collateral ligament. *Am J Sports Med* 37: 1771–1776.

Williams LP, Warwick R, Dyson M, Bannister LH. 1989. *Gray's Anatomy. 37th ed*. Edinburgh: Churchill Livingstone.

Wojtys E. 1990. Innervation of the human knee joint by substance-P fibers. *J Arthro Rel Surg* 6(4): 254–263.
Woodburne RT. 1978. *Essentials of Human Anatomy*. Oxford University Press.
Young RB. 1889. The external semilunar cartilage as a complete disc. *Memoirs Memoranda Anat* 1: 179.
Yu JS, Salonen DC, Hodler J, Haghighi P, Trudell D, Resnick D. 1996. Posterolateral aspect of the knee: improved MR imaging with a coronal oblique technique. *Radiology* 198: 199–204.
Zambacos GJ, Shroff N, Newman PL, Morris RJ. 2001. Massive prepatellar bursa: a case of natural tissue expansion: anatomic and histologic implications. *Plast Reconstr Surg* 108: 267–268.
Zeiss J, Saddemi SR, Ebraheim NA. 1992. MR imaging of the quadriceps tendon: normal layered configuration and its importance in cases of tendon rupture. *AJR* 159: 1031–1034.
Zidorn T. 1992. Classification of the suprapatellar septum considering ontogenetic development. *J Arthro Rel Surg* 8: 459–464.
Zimny M, Wink C. 1991. Neuroreceptors in the tissues of the knee joint. *J Electromyograph Kinesiol* 1: 148–157.
Zimny M, Onge M, Schutte M. 1985. A modified gold chloride method for the demonstration of nerve endings in frozen sections. *Stain Technol* 60: 305–306.
Zimny M, Onge M, Albright D. 1987. The use of agents which improve staining of fresh human fibrocartilage. *Stain Technol* 62: 341–348.

Further reading

Ahmadi B, Shahriaree H, Silver CM. 1979. Severe congenital genu recurvatum. *J Bone Joint Surg A* 61: 622–633.
Arnoczky SP, Warren RF. 1982. Microvasculature of the human meniscus. *Am J Sports Med* 10: 90–95.
Bergamini E, Pillet H, Hausselle J, Thoreux P, Guerard S, Camomilla V, Cappozzo A, Skalli W. 2011. Tibio-femoral joint constraints for bone pose estimation during movement using multi-body optimization. *Gait Posture* 33: 706–711.
Bicos J, Fulkerson JP, Amis A. 2007. Current concepts review the medial patellofemoral ligament. *Am J Sports Med* 35: 484–492.
Blackburn TA, Craig E. 1980. Knee anatomy: a brief review. *Phys Ther* 60: 1556–1560.
Bland-Sutton J. 1897. *Ligaments: Their Nature and Morphology*. Lewis.
Burgkart R, Glaser C, Hyhlik-Dürr A, Englmeier K-H, Reiser M, Eckstein F. 2001. Magnetic resonance imaging-based assessment of cartilage loss in severe osteoarthritis: accuracy, precision, and diagnostic value. *Arthritis Rheumatism* 44: 2072–2077.
Claes S, Vereecke E, Maes M, Victor J, Verdonk, P, Bellemans J. 2013. Anatomy of the anterolateral ligament of the knee. *J Anat* 223: 321–328.
Colombet P, Dejour D, Panisset JC, Siebold R. 2010. Current concept of partial anterior cruciate ligament ruptures. *Revue Chir Orthopédique Traumatol* 96: S329–S338.
Curtis BH, Fisher RL. 1969. Congenital hyperextension with anterior subluxation of the knee surgical treatment and long-term observations. *J Bone Joint Surg* 51: 255–269.
De Sá Pinto AL, De Barros H, Radu PM, Villares SM, Lima FR. 2006. Musculoskeletal findings in obese children. *J Paed Child Health* 42: 341–344.
Devan MR, Pescatello LS, Faghri P, Anderson J. 2004. A prospective study of overuse knee injuries among female athletes with muscle imbalances and structural abnormalities. *J Athl Train* 39: 263.
Donell S. 2006. Patellofemoral dysfunction: Extensor mechanism malalignment. *Current Ortho* 20: 103–111.
Elias DA, White LM. 2004. Imaging of patellofemoral disorders. *Clin Radiol* 59: 543–557.
Fairclough J, Hayashi K, Toumi H, Lyons K, Bydder G, Phillips N, Benjamin M. 2006. The functional anatomy of the iliotibial band during flexion and extension of the knee: implications for understanding iliotibial band syndrome. *J Anat* 208: 309–316.
Ferrone JD. 1976. Congenital deformities about the knee. *Ortho Clin N Am* 7: 323–330.
Gabriel MT, Wong EK, Woo SLY, Furman W, Marshall JL, Girgis FG. 1976. The anterior cruciate ligament: a functional analysis based on postmortem studies. *J Bone Joint Surg Am* 58A: 179–85.
Gardner E, O'Rahilly R. 1968. The early development of the knee joint in staged human embryos. *J Anat* 102: 289.
Gasparutto X, Dumas R, Jacquelin E. 2012. Multi-body optimisation with deformable ligament constraints: influence of ligament geometry. *Comp Meth Biomech Biomed Engineer* 15: 191–193.
Gray DJ, Gardner E. 1950. Prenatal development of the human knee and superior tibiofibular joints. *Am J Anat* 86: 235–287.
Griffith CJ, Wijdicks CA, LaPrade RF. 2013. The lateral collateral ligament and posterolateral corner. In *The Knee Joint: Surgical Techniques and Strategies* (BonninM, AmendolaNA, BellemansJ, MacDonaldSJ, MenetreyJ, eds). Springer.
Heine J. 1926. Über die Arthritis deformans. *Virchows Archiv* 260(3): 521–663.
Jackson DW, Jennings LD, Maywood RM, Berger PE. 1988. Magnetic resonance imaging of the knee. *Am J Sports Med* 16: 29–38.
Johansson E, Aparisi T. 1983. Missing cruciate ligament in congenital short femur. *J Bone Joint Surg Am* 65: 1109–1115.
Juma AH. 2004. Nail-patella syndrome in Saudi Arabia with new features and surgical procedures: the first described study. *Medscape Gen Med* 6(2): 6.
Kalamchi A, Dawe RV. 1985. Congenital deficiency of the tibia. *J Bone Joint Surg* 67: 581–584.
Kale A, Kopuz C, Edýzer M, Aydin ME, Demýr M, Ýnce Y. 2006. Anatomic variations of the shape of the menisci: a neonatal cadaver study. *Knee Surg Sports Traumatol Arthro* 14: 975–981.
Karlen A. 1964. Congenital fibrosis of the vastus intermedius muscle. *J Bone Joint Surg Br* 46: 488–491.
Katz MP, Grogono BJS, Soper KC. 1967. The etiology and treatment of congenital dislocation of the knee. *J Bone Joint Surg* 49: 112–120.
LaPrade RF. 1998. The anatomy of the deep infrapatellar bursa of the knee. *Am J Sports Med* 26: 129–132.
Last RJ. 1952. Specimans from Huntarian collection: synovial cavity of knee joint (speciman 110A); ligaments of knee (specimen S 95A). *J Bone Jt Surg* 33B: 442–445.
Levy BA, Dajani KA, Morgan JA, Shah JP, Dahm DL, Stuart MJ. 2010. Repair versus reconstruction of the fibular collateral ligament and posterolateral corner in the multiligament-injured knee. *Am J Sports Med* 38: 804–809.
Lind M, Jakobsen BW, Lund B, Hansen MS, Abdallah O, Christiansen SE. 2009. Anatomical reconstruction of the medial collateral ligament and posteromedial corner of the knee in patients with chronic medial collateral ligament instability. *Am J Sports Med* 37: 1116–1122.
Machado M, Flores P, Pimenta JCC, Ambrósio J, Silva M, Completo A, Hamid ML. 2010. Development of a planar multibody model of the human knee joint. *Nonlinear Dynamics* 60: 459–478.

Manner HM, Radler C, Ganger R, Grill F. 2006. Dysplasia of the cruciate ligaments: radiographic assessment and classification. *J Bone Joint Surg* 88: 130–137.

Marra MD, Crema MD, Chung M, Roemer FW, Hunter DJ, Zaim S, Guermazi A. 2008. MRI features of cystic lesions around the knee. *Knee* 15: 423–438.

Masouros SD, McDermott ID, Amis AA, Bull AMJ. 2008. Biomechanics of the meniscus–meniscal ligament construct of the knee. *Knee Surg Sports Traumatol Arthro* 16: 1121–1132.

McCarthy CL, McNally EG. 2004. The MRI appearance of cystic lesions around the knee. *Skel Rad* 33(4): 187–209.

McDermott LJ. 1943. Development of the human knee joint. *Arch Surg* 46: 705–719.

Meister BR, Michael SP, Moyer RA, Kelly JD, Schneck CD. 2000. Anatomy and kinematics of the lateral collateral ligament of the knee. *Am J Sports Med* 28: 869–878.

Mérida-Velasco JA, Sánchez-Montesinos I, Espín-Ferra J, Mérida-Velasco JR, Rodríguez-Vázquez, JF, Jiménez-Collado J. 1997. Development of the human knee joint ligaments. *Anat Rec* 248(2): 259–268.

Muehleman C, Bareither D, Huch K, Cole AA, Kuettner KE. 1997. Prevalence of degenerative morphological changes in the joints of the lower extremity. *Osteo Cartil* 5(1): 23–37.

Nomura E, Fujikawa K, Takeda T, Matsumoto H. 1992. Anatomical study of the medial patellofemoral ligament. *Bessatsu Seikeigeka* 22: 2–5 (in Japanese).

Ogata S, Uhthoff HK. 1990. The development of synovial plicae in human knee joints: an embryologic study. *Arthroscopy: J Arthro Rel Surg* 6: 315–321.

Polly DW, Callaghan JJ, Sikes RA, McCabe JM, McMahon K, Savory CJ. 1988. The accuracy of selective magnetic resonance imaging compared with the findings of arthroscopy of the knee. *J Bone Joint Surg Am* 70: 192–198.

Reicher MA, Bassett LW, Gold RH. 1985. High-resolution magnetic resonance imaging of the knee joint: pathologic correlations. *Am J Roentgenol* 145: 903–909.

Rennie WJ, Saifuddin A. 2005. Pes anserine bursitis: incidence in symptomatic knees and clinical presentation. *Skel Radiol* 34: 395–398.

Rudy TW, Livesay GA, Woo SY, Fu FH. 1996. A combined robotic/universal force sensor approach to determine in situ forces of knee ligaments. *J Biomech* 29: 1357–1360.

Saddik D, McNally EG, Richardson M. 2004. MRI of Hoffa's fat pad. *Skel Radiol* 33: 433–444.

Schoenecker PL, Capelli AM, Millar EA, Sheen MR, Haher T, Aiona, MD, Meyer LC. 1989. Congenital longitudinal deficiency of the tibia. *J Bone Joint Surg Am* 71(2): 278–287.

Spinner RJ, Wang H, Angius D, Malik AG, Malghem J, Amrami KK. 2011. A modern perspective on the earliest description of an intraneural ganglion cyst arising from the knee joint. *Clin Anat* 24: 106–112.

Steensen RN, Dopirak RM, McDonald WG. 2004. The anatomy and isometry of the medial patellofemoral ligament implications for reconstruction. *Am J Sports Med* 32: 1509–1513.

Sugita T, Amis AA. 2001. Anatomic and biomechanical study of the lateral collateral and popliteofibular ligaments. *Am J Sports Med* 29: 466–472.

Tan AL, Toumi H, Benjamin M, Grainger AJ, Tanner SF, Emery P, McGonagle D. 2006. Combined high-resolution magnetic resonance imaging and histological examination to explore the role of ligaments and tendons in the phenotypic expression of early hand osteoarthritis. *Ann Rheum Dis* 65: 1267–1272.

Teitge RA, Torga-Spak R. 2004. Medial patellofemoral ligament reconstruction. *Arthrosc* 20(9): 998–1002.

Tolo VT. 1981. Congenital absence of the menisci and cruciate ligaments of the knee. A case report. *J Bone Joint Surg* 63: 1022.

Vasilevska V, Szeimies U, Stäbler A. 2009. Magnetic resonance imaging signs of iliotibial band friction in patients with isolated medial compartment osteoarthritis of the knee. *Skel Radiol* 38: 871–875.

Westphal CJ, Schmitz A, Reeder SB, Thelen DG. 2013. Load-dependent variations in knee kinematics measured with dynamic MRI. *J Biomech* 46: 2045–2052.

Yag M, Debski RE. 2004. Distribution of in situ forces in the anterior cruciate ligament in response to rotatory loads. *J Ortho Res* 22: 85–89.

Yao L, Joonh JK. 1989. Avulsion of the posteromedial tibial plateau by the semimembranosus tendon: diagnosis with MR imaging. *Radiology* 172: 513–514.

Yoshioka H, Stevens K, Genovese M, Dillingham M, Lang P. 2004. Articular cartilage of knee: normal patterns at MR imaging that mimic disease in healthy subjects and patients with osteoarthritis. *Radiology* 231: 31–38.

21 Ankle and foot joints

Takamitsu Arakawa
Kobe Graduate School of Health Sciences, Kobe, Japan

Bones

Ankle (talocrural) joint

A normal variant of articular notching of the anteromedial tibial plafond can be seen. In well-developed notches there was a fold, apparently composed of synovial tissue. The notching increases the surface area for capsular attachment, is variable in size, and could facilitate synovial fluid movement across the joint during ambulation (Ray et al. 1994). A dorsolateral, so-called "squatting facet," is commonly present on the talar neck in individuals who habitually adopt the squatting position. It articulates with the anterior tibial margin in extreme dorsiflexion and may be doubled (Standring 2008).

The anterior border of the trochlear surface of the talus can be straight, slightly concave, convex, or S-shaped (Kelikian 2011). On its lateral surface, the anterior border of the tubercles of the trigonal surface can be replaced by depressions or notches; occasionally, a small accessory articular surface is observed on the anterior segment of the lateral process termed the facies externa accessoria corporis tali. An accessory bone, the os trigonum, may be fused and is then referred to as the trigonal process. An accessory articular surface may be seen in continuity with the posterior calcaneal surface. The lateral surface of the neck of the talus may give insertion to the medial root of the inferior extensor retinaculum. A separation notch can be seen on the inferior surface of the neck of the talus and, if deep enough, near complete or (rarely) complete separation occurs between the middle and anterior calcaneal surfaces. A posterior extension of the articulating surface of the head or an anterior extension of the medial malleloar articulating surface sometimes narrows the medial surface of the neck of the talus. A tubercle can be present anteriorly on the neck of the talus for attachment of the cervical ligament (Kelikian 2011).

Subtalar joint

The calcaneus ranges from 48 to 94 mm in length and 26 to 53 mm in width. One study found that 36.7% of the subjects had three distinct facets on the calcaneus. The anterior facet was missing in 10.2% of subjects; 53.1% demonstrated fusion between the anterior and middle facets. In four cases there was an articulation between the talus and the cuboid bone. At the posterior talocalcaneal articulation, variations were observed in the curvature of the medial side of the joint (Shahabpour et al. 2011). Rarely, all three facets on the upper surface of the calcaneus are fused into one irregular area. A detailed study of patterns of anterior talar articular facets in a series of calcanei revealed four types:

- type I (67%) had one continuous facet on the sustentaculum extending to the distomedial calcaneal corner;
- type II (26%) had two facets, one sustentacular and one distal calcaneal;
- type III (5%) possessed only a single sustentacular facet; and
- type IV (2%) had confluent anterior and posterior facets (Gupta et al. 1977).

A bony crest can be found in the tarsal canal. A large funnel-shaped foramen can be found in the fossa calcaneus. The peroneal tubercle can be flat, prominent, concave, or tunnel-shaped. A well-defined tubercle, the tuberculum ligamneti calcaneofibularis, can be seen in about 50% of individuals behind the midsegment of the facies articularis talaris posterior and posterosuperior to the eminentia retrotrochlearis. A tuberculum ligament talicalcanei can sometimes be present for the attachment of the extension of insertion of the calcaneofibular ligament. A sesamoid bone can be seen in the tendon of peroneous longus and is not the same sesamoid as the more common sesamoid bone found in this same tendon but more distally as it passes over the cuboid tuberosity. On the plantar surface of the cuboid, a gliding facet for the sesamoid bone of the peroneus longus tendon can be seen. A second trochlear facet may be seen. Rarely, if the posterior talar articular surface extends medically over the superior surface of the sustentaculum, then the opening of the tarsal canal is on the medial border of the sustentaculum tali. On the plantar surface of the navicular, an articular facet for the os calcis near its posterior surface can be rarely seen. When the navicular tuberosity is separated from the main navicular mass, it is termed a naviculare secundarium. A true joint between the navicular and cuboid is often seen. A small articular surface is sometimes present on the third cuneiform for the articulation with the fourth metatarsal. The lateral base of the first metatarsal variably articulates with the second metatarsal. Interphalangeal

Bergman's Comprehensive Encyclopedia of Human Anatomic Variation, First Edition. Edited by R. Shane Tubbs, Mohammadali M. Shoja and Marios Loukas.
© 2016 John Wiley & Sons, Inc. Published 2016 by John Wiley & Sons, Inc.

coalition is most often seen between the middle and distal phalanges of the fifth digit (Kelikian 2011). Accessory bones of the subtalar joint are discussed in Chapter 13 on the bones of the lower limb.

Ligaments

Inferior tibiofibular joint

This joint has anterior and posterior tibiofibular ligaments. Clinically, the inferior portions of the anterior tibiofibular ligament (anterior inferior tibiofibular ligament) are the most important.

Anterior inferior tibiofibular ligament

A distal fascicle of this ligament (Bassett's ligament) was found in 83% of specimens and appeared as a single and complete ligament in the remaining 17% (Akseki et al. 2002). A completely separate accessory anteroinferior tibiofibular ligament was present in 22 of the 24 cadaveric specimens. It was parallel and distal to the anterior inferior tibiofibular ligament and had the shape of a parallelogram (Nikolopoulos et al. 2004).

Oh et al. (2006) found the intermalleolar ligament in 81.8% of specimens; it comprised more than two bundles of fibers in all cases. Its medial parts were variable. In 10.4% of specimens, a thin fascicle was observed to connect the margin of the tibia or medial malleolus with the posterior talofibular ligament (Oh et al. 2006). The ligament narrowed laterally and attached with the posterior talofibular ligament to the medial fossa of the lateral malleolus. The intermalleolar ligament appeared as a thick band or as more than two fine parallel bands.

Medial ligament of talocrural joint

This ligament is subdivided into superficial and deep layers. The superficial layer has a trapezoid form in 66.7%, a rectangular form in 19%, and a triangular form in 14.3% (Rodrigo Sepúlveda et al. 2012). In 76.2%, the deep layer was completely covered by the superficial layer; however, in 23.8% this coverage was incomplete (Rodrigo Sepúlveda et al. 2012). The deep anterior tibiotalar ligament can be very small or absent.

Lateral ligaments of the ankle

This complex consists of three ligaments: anterior talofibular, calcaneofibular, and posterior talofibular. In one study, the anterior talofibular ligament was absent in 1 of 20 cases (Raheem and O'Brien 2011). In 1 cadaver out of 42 it was absent bilaterally (Taser et al. 2006). Burks and Morgan (1994) reported that it can have one or two bands. However, other researchers suggested that it can have three bands (Milner and Soames 1997; Uğurlu et al. 2010; Raheem and O'Brien 2011; Boonthathip 2011). According to Milner and Soames (1997), it was single in 38%, doubled in 50%, and tripled in 12%. Uğurlu et al. (2010) found single, doubled, and triple bands in 23%, 59%, and 18% of specimens, respectively.

The calcaneofibular ligament was found to have one band in 72.2%, two bands in 22.2%, and three bands in 5.6% (Kitsoulis et al. 2011). Variation of the calcaneal insertion of this ligament has been found in a typical location in 64.5%, in an anterior location in 25.5%, in a posterior location in 5.5%, and in an inferior location in 4.5% (Laidlaw 1904). The ligament can have a vertical, horizontal, fan-shaped, or oblique configuration.

The posterior talofibular ligament had a tibial slip in four out of five sides (Courvoisier et al. 2008).

An accessory lateral talocrural ligament has been termed the ligament of Bessel–Hagen.

Ligaments of the foot

Jotoku et al. (2006) found that the interosseous talocalcaneal ligament was band-like in 92.5% of examined specimens, and the anterior capsular ligament was present in 95%. The lateral talocalcaneal ligament is seen in about 50% of individuals. When an os trigonum is present, the posterior talocalcaneal ligament arises from it forming the trigoncalcaneal ligament. A lateral band of the dorsolateral calcaneocuboid ligmanet can be seen. Additional bands of the plantar calcaneocuboid ligament can be seen. The short plantar ligament can be split into deep and superficial parts.

The configurations of the dorsolateral calcaneocuboid ligaments vary widely in shape, number, and attachment sites. A constant dorsal ligament and an additional narrower lateral ligament were found in around 50% of cases in one study (Dorn-Lange et al. 2008). The lateral calcaneocuboid ligament is usually stronger than the calcaneocuboid ligament.

Dorsal tarsometatarsal ligaments that connect the base of the medial cuneiform to the base of the second metatarsal are called Lisfranc's ligament. In one study, Lisfranc's ligament had a single bundle in 73% of specimens and two bundles in 27% (Panchbhavi et al. 2013). A transverse band may extend between the ligament connecting the cuboid of the first metatarsal to the dorsal third cuneiform. The second and third interosseous cuneometatarsal ligament are very variable in form.

Bursae

An accessory bursa located behind the calcaneal tendon is known as the supracalcaneal bursa of Poirier. An accessory bursa interposed between the metatarsophalangeal joints has been termed the intermetatarsophalangeal bursa of Gruber.

References

Akseki D, Pinar H, Yaldiz K, Akseki NG, Arman C. 2002. The anterior inferior tibiofibular ligament and talar impingement: a cadaveric study. *Knee Surg Sports Traumatol Arthrosc* 10: 321–326.

Boonthathip M, Chen L, Trudell D, Resnick D. 2011. Lateral ankle ligaments: MR arthrography with anatomic correlation in cadavers. *Clin Imag* 35: 42–48.

Burks RT, Morgan J. 1994. Anatomy of the lateral ankle ligaments. *Am J Sports Med* 22: 72–77.

Courvoisier A, Vialle R, Thévenin-Lemoine C, Mary P, Damsin JP. 2008. The posterior talofibular ligament: an anatomical study with clinical implication in clubfoot surgery. *Surg Radiol Anat* 30: 633–637.

Dorn-Lange NV, Nauck T, Lohrer H, Arentz S, Konerding MA. 2008. Morphology of the dorsal and lateral calcaneocuboid ligaments. *Foot Ankle Int* 29: 942–949.

Gupta SC, Gupta CD, Arora AK. 1977. Pattern of talar articular facets in Indian calcanei. *J Anat* 124: 651–655.

Jotoku T, Kinoshita M, Okuda R, Abe M. 2006. Anatomy of ligamentous structures in the tarsal sinus and canal. *Foot Ankle Int* 27: 533–538.

Kelikian AS. 2011. *Sarrafian's Anatomy of the Foot and Ankle, second edition*. Philadelphia: Wolters Kluwer.

Kitsoulis P, Marini A, Pseftinakou A, Iliou K, Galani V, Paraskevas G. 2011. Morphological study of the calcaneofibular ligament in cadavers. *Folia Morphol (Warsz)* 70: 180–184.

Laidlaw PP. 1904. The varieties of the os calcis. *J Anat Physiol* 38: 133–143.

Milner CE, Soames RW. 1997. Anatomical variations of the anterior talofibular ligament of the ankle joint. *J Anat* 191: 457–458.

Nikolopoulos CE, Tsirikos AI, Sourmelis S, Papachristou G. 2004. The accessory anteroinferior tibiofibular ligament as a cause of talar impingement: a cadaveric study. *Am J Sports Med* 32: 389–395.

Oh CS, Won HS, Hur MS, Chung IH, Kim S, Suh JS, Sung KS. 2006. Anatomic variations and MRI of the intermalleolar ligament. *AJR* 186: 943–947.

Panchbhavi VK, Molina D 4th, Villarreal J, Curry MC, Andersen CR. 2013. Three-dimensional, digital, and gross anatomy of the Lisfranc ligament. *Foot Ankle Int* 34: 876–880.

Raheem OA, O'Brien M. 2011. Anatomical review of the lateral collateral ligaments of the ankle: a cadaveric study. *Anat Sci Int* 86: 189–193.

Ray RG, Gusman DN, Christensen JC. 1994. Anatomical variation of the tibial plafond: the anteromedial tibial notch. *J Foot Ankle Surg* 33: 419–426.

Rodrigo Sepúlveda P, Bruno Capurro S, René Moreno T, Laura Giesen F, Carla Ibarra M, Paula Silva D, Alberto Telias N. 2012. Morphometric study and anatomical variations of the medial ligament of the talocrural joint. *Int J Morphol* 30: 162–169.

Shahabpour M, Devillé A, Van Roy P, Vaes P, De Mey J, De Maeseneer M. 2011. Magnetic resonance imaging of anatomical variants of the subtalar joint. *Surg Radiol Anat* 33: 623–630.

Standring S. 2008. *Gray's Anatomy*. Philadelphia: Elsevier.

Taser F, Shafiq Q, Ebraheim NA. 2006. Anatomy of lateral ankle ligaments and their relationship to bony landmarks. *Surg Radiol Anat* 28: 391–397.

Uğurlu M, Bozkurt M, Demirkale I, Cömert A, Acar HI, Tekdemir I. 2010. Anatomy of the lateral complex of the ankle joint in relation to peroneal tendons, distal fibula and talus: a cadaveric study. *Eklem Hastalik Cerrahisi* 21: 153–158.

Further reading

Dwight T. 1907. *Clinical Atlas. Variations of the Bones of the Hand and Foot*. Philadelphia: JB Lippincott Co.

Klein M. 1994. MR imaging of the ankle: normal and abnormal findings in the medial collateral ligament. *AJR* 162: 377–383.

22 Orbital muscles

Necdet Kocabiyik
Gulhane Military Medical Academy, Ankara, Turkey

Whether extraocular or extrinsic, eye muscles are a series of small muscles that arise from the pre-otic somites in the developing head. These muscles include the superior rectus, inferior rectus, lateral rectus, medial rectus, superior oblique, inferior oblique, and levator palpebrae superiores muscles. The extraocular muscles may sometimes be absent, double or supernumerary bellied, may have muscular bridges or slip/neuromuscular bundles between them, and may also have insertion anomalies or insertion variations (Macalister 1875; Tillaux 1877; Lockwood 1885; Rex 1887; Whitnall 1912; Howe 1923; Posey 1924; MacEwen 1930; Fujita 1938; Banerjee 1950; Bergman et al. 1988; Stager 1996; DeAngelis et al. 1999; DeAngelis and Kraft 2001; Yalçin et al. 2004, 2009; Zinn 2004, 2005; Yalçin and Ozan 2005; Bagheri 2009; Takahashi 2013).

Rectus muscles of the orbit

Lockwood (1885) described the common origin of the superior rectus, the upper half of the medial, and the superior head of the lateral rectus muscles, which is sometimes called "Lockwood's tendon." Lockwood (1885) also demonstrated in detail that the medial and lateral rectus muscles have dual origins. Curnow (1873) described two additional slips of the lateral rectus. One slip arose from the annulus of Zinn and the other, shorter slip attached to the cartilage of the lower eyelid. The abducens nerve innervated both accessory slips.

Tillaux (1877) recognized the differences in distances from these insertions to the limbus. This finding led to the imaginary line connecting the rectus muscle insertions known as the "Tillaux spiral." Refinements in measurement techniques and measurements of large numbers of individuals have changed the absolute numbers Tillaux originally described. Regarding the role of rectus muscle sheaths and pulleys, and the mechanical effect of strabismus procedures, Tillaux (1877) described how cutting the muscle insertion while leaving the fibrous sheath intact would preserve at least part of the rotational effect of a contracting rectus muscle.

The four recti may be poorly developed and may be connected to each other by muscular slips. The inferior rectus may provide a large muscular bundle passing lateral to the optic nerve to join the superior rectus. A fasciculus of the lateral rectus may pass to the inferior rectus. Two additional fasciculi sometimes occur: one passing forward to end on the inferior tarsal plate and another inserting on the lateral wall of the orbit. The lateral rectus may also provide a fascicle that passes across the posterior third of the orbit, beneath the optic nerve, to fuse with the belly of the medial rectus above where this bifid insertion of the medial rectus was observed. The superior rectus may provide a muscular slip that may also arise from the annulus of Zinn, which passes downward and forward across the lateral aspect of the optic nerve to join the inferior rectus. The lateral and medial recti might also be absent (Macalister 1875; MacEwen 1930; Fujita 1938).

Howe (1923) reported how the size and direction of insertions of the recti vary in different individuals; the general direction is however comparatively constant. Zinn (2004) described the origin of three extraocular muscles as a "communal ligament." However, the origin of all rectus muscles is often called the "tendinous ring" or "annulus fibrosus" of Zinn. Zinn (2005) reported that the rectus muscle tendons present insertion into the sclera in a circle, and very close to the cornea.

In addition to the abovementioned extraocular muscle variations, Isomura (1977) asserted that slips corresponding to a retractor bulbi muscle were infrequently present. It was also determined that these slips might be supplied by the abducens and oculomotor nerves. The simplest form of the retractor is the one that may arise from the lateral rectus. The retractor might also be represented by a single muscle bundle between the lateral and superior recti, and a fibrous ring with four muscular slips joined to the deep surface of the four recti (Isomura 1977). In some other reported cases, it was described that the retractor formed a muscular funnel around the optic nerve and inserted onto the back of the eyeball. It was also reported that the retractor might be found divided into four slips that attach to the posterior globe behind and among the four recti (Whitnall 1912). Krasny et al. (2011) reported a child with external ophthalmoplegia and right-sided ptosis. MRI demonstrated the retractor bulbi muscle arising from the annulus of Zinn and inserting onto the posterior aspect of the globe.

Bergman's Comprehensive Encyclopedia of Human Anatomic Variation, First Edition. Edited by R. Shane Tubbs, Mohammadali M. Shoja and Marios Loukas.
© 2016 John Wiley & Sons, Inc. Published 2016 by John Wiley & Sons, Inc.

Valmaggia et al. (1996) reported an elevation deficit in a 6-year-old boy caused by an accessory extraocular muscle. Computed tomography and magnetic resonance imaging had been used to confirm an accessory, fusiform, well-defined, solid structure in the retrobulbar space and a supernumerary intraconal muscle had been detected between the annulus of Zinn and the posterior part of the left globe. This rare anomaly may represent an atavistic retractor bulbi muscle.

von Ludinghausen (1998) found a bilateral variation of the rectus muscles and a unilateral variation of the levator palpebrae muscle in the right and left orbits of a man. The variation was a supernumerary rectus muscle lying in a sagittal orientation between the optic nerve and lateral rectus muscle (in the right orbit) and adjacent to the inferior rectus muscle (in the left orbit). In each orbit, the muscle originated occipitally from the common tendinous ring and frontally joined the terminal part of the inferior rectus near the eyeball. As a further variation in the right orbit, an isolated medial part or belly of the levator palpebrae muscle, which he entitled musculus gracillimus, was also present.

Kakizaki et al. (2006) revealed variable muscles linking the superior and inferior rectus muscles in dissections of the bilateral orbits in a 45-year-old female cadaver who had no known ocular movement disorders. In that case, he observed that the muscles were situated between the optic nerve and the lateral rectus muscle, and they originated from the annulus of Zinn and arose from two heads. He also noticed that one of the heads inserted into the medial inferior side of the superior rectus muscle and the other inserted into the central superior side of the inferior rectus muscle, where each one of the insertion points was located on a distal site of the myoneural junction of each rectus muscle.

Obliquus superior (superior oblique)

Reports concerning obliquus superior variations are rare (Bochdalek 1868; Henle 1873; Le Double 1897; Whitnall 1921; Howe 1923). Henle (1873) found that the superior oblique might be closely accompanied by an offshoot from the levator palpebrae superioris that he called the "obliqui superioris (Albinus)" or "gracillimus orbitis." Some clinicians reported the complete absence of the muscle whereas Le Double (1897) reported accessory slips and Whitnall (1921) reported a doubled muscle. Bochdalek (1868) named an arched slip of muscle fibers passing from the orbital plate of the ethmoid bone across the upper surface of the eyeball to the outer wall of the orbit the "transversus orbitae."

Howe (1923) reported that the insertion of the superior oblique was more variable than that of the recti, not only in position but also in length. He added that the insertion of the inferior oblique was the most irregular of all regarding position, size, and form.

Helveston et al. (1992) reviewed the charts of 82 patients (89 eyes) with superior oblique palsy undergoing surgery on the superior oblique tendon. He concluded that congenital superior oblique palsy was usually associated with a structural abnormality of the superior oblique tendon (87%). He also assumed that acquired superior oblique palsy usually had a normal tendon (92%). In accordance with his findings, he judged that the potential variance in anatomy of the superior oblique tendon should have been considered when undertaking surgery for superior oblique palsy. At the same time, Kim and Hwang (2010) conducted research on congenital superior oblique palsy with superior oblique hypoplasia and classified them as a congenital cranial dysinnervation disorders by the MRI documentation of congenital aplasia of the trochlear nerve. Congenital cranial dysinnervation disorders are developmental abnormalities involving the hypoplasia or aplasia of the cranial nerves with muscle dysinnervation. Kim conducted this research to determine congenital cranial dysinnervation disorders and found out that trochlear nerve was absent on the affected side in 10 patients with confirmed hypoplastic superior oblique muscles.

Obliquus inferior (inferior oblique)

Researchers drew attention to the inferior oblique muscle variations rather than superior oblique muscle variations (Rex 1887; Banerjee 1950; Wilson and Landers 1982; Prakash et al. 1983; Stager 1996; DeAngelis et al. 1999; DeAngelis and Kraft 2001; Yalçin et al. 2004; Yalçin and Ozan 2005; Bagheri et al. 2009). Rex (1887) found an unusual muscle bundle from the inferior oblique (obliquus accessorius inferior) passing from the apex of the orbit to join the inferior rectus, which might be doubled or absent.

Recognizing the variations of the oblique muscles has been important in terms of strabismus operations. For example, Banerjee (1950) observed operative correction of internal strabismus, which had no vertical deviation of the eyes with a girl aged 18 years on exposure of the right lateral rectus. It was found that the right inferior oblique was in a much more anterior position than normal and the two muscles blended just behind the insertion of the lateral rectus; the inferior oblique fibres were medial and inserted via a common tendon into the sclera in the position of a normal lateral rectus. Another example of anomalies caused by oblique muscle variations was observed with a 6-year-old female child who was admitted for strabismus surgery having alternating divergent strabismus. In this example, there was no underaction or overaction of any muscle, including the inferior oblique. While dissecting the lateral rectus muscle, a fleshy mass was noted at the superior border of the lateral rectus muscle. On further dissection, it was realized that the fleshy mass was a part of the inferior oblique muscle, which inserted 5 mm above the upper border of the lateral rectus, and the anterior end of the insertion was 10 mm behind the insertion of the lateral rectus muscle (Prakash et al. 1983).

Distinct from the above examples, Stager (1996) mentioned the neurofibrovascular bundle with adjacent fibrous bands. In

his gross anatomic and microscopic studies, he showed a linear orientation of the neurofibrovascular bundle with adjacent fibrous bands anteriorly joining the inferior oblique and inferior rectus muscles. He concluded that in patients who had undergone anterior transposition surgery, the neurofibrovascular bundle served as the ancillary origin of the inferior oblique.

DeAngelis et al. (1999) assumed that his research showed 17 muscles of 100 inferior oblique muscles that had multiple divisions at the insertion, whereas eight muscles had two bellies 10 or 12 mm from their insertion. Among these eight, four had two distinct (bifid) bellies extending to the insertion, and four had dehiscences in the muscle. Multiple insertions were found in 17% of inferior oblique muscles, and duplication of the inferior oblique muscle at the surgical capture site was found in 8%. He supposed that these duplications might account for some cases of recurrence or persistence of inferior oblique overaction after weakening surgery, due to inadvertent incomplete capture of the muscle during surgery. In another study conducted by DeAngelis and Kraft (2001), an 8% incidence of double-bellied inferior oblique muscles at the surgical capture site (10–12 mm from insertion) in cadaveric specimens was found. They found that in eyes with double-bellied inferior oblique muscles, there was higher incidence of fundus excyclotropia suggesting that the presence of a second belly might alter the physiologic action of the inferior oblique muscle. In this respect, Wilson and Landers (1982) reported a variable right inferior oblique muscle which was found incidentally during an operation on a 59-year-old woman. This variation consisted of parallel muscles (apparently originating from a common origin) inserting separately into the sclera.

Yalçin et al. (2004) observed a muscular bridge between the inferior oblique and inferior rectus muscles in 6.6% of 60 orbits. They observed that the inferior rectus muscle joined to the inferior oblique muscle in 6.6% of orbits dissected. They concluded that the importance of muscular bridges should be appreciated due to the potential of failed inferior oblique or inferior rectus muscle surgery. Yalçin and Ozan (2005) classified the inferior oblique muscle into four groups according to the insertional pattern. In the first group, the muscle was formed of only one belly ("single," five eyes, 8.3%). In the second group, the muscle had a main and a secondary belly ("double," 30 eyes, 50%). In the third group, the muscle had three bellies ("triple," 16 eyes, 26.6%). In the fourth group, the muscle had more than three bellies ("multiple," 9 eyes, 15%). In these four groups of oblique muscles, they found double, triple, and multiple muscle bellies in 91.7% of 60 cadaveric eyes.

The possible association between inferior oblique muscle overaction and inferior oblique muscle mass has been a matter of speculation. Bagheri et al. (2009) conducted case studies to evaluate the anatomical position of the inferior oblique muscle and to determine any association between muscle mass and inferior oblique muscle overaction. In this observational case series, eyes undergoing primary surgery for inferior oblique overaction underwent measurement of inferior oblique muscle borders distance from the limbus and muscle belly circumference, and they found no detectable correlation of inferior oblique overaction with either muscle position or circumference.

Levator palpebrae superioris

Budge (1859) examined the orbits of 85 humans and found the same type of anomalous ocular muscle in five orbitas from three males and one female. He monitored the anomalous ocular muscle, which originated from the belly or the proximal part of the levator palpebrae superioris muscle to attach to the sclera, trochlea, and surrounding tissues. He termed this anatomical structure the "tensor trochleae" muscle (a slip), which was innervated by the superior division of the oculomotor nerve. Bochdalek (1868) assumed that another slip (transversus orbitis) might be found between the medial and lateral walls of the orbita and connecting with the levator in the midline. Macalister (1875) reported that the levator palpebrae superioris might be joined to the superior rectus at its origin. He also added that it might arise from the posterior margin of the frontal part of the roof of the orbit, in front of and above the optic foramen, separate from other muscles. Macalister (1875) described a case of absence of the levator palpebrae superioris but without resultant ptosis. He observed that the levator palpebrae superioris was attached to the upper margin of the tarsal cartilage and into the conjunctiva of the superior palpebral sinus. Moreover, he noted that the levator palpebrae superioris was attached into the ciliary fibers of the orbicularis palpebrarum. Lastly, he found that that levator palpebrae superioris was inserted into all these three anatomical structures.

Isomura (1977) stated that two main branches of the superior division of the oculomotor nerve to the rectus superior muscle united to form a common loop before supplying the levator palpebrae superioris muscle. The loop had a few branches, the thicker of which supplied the levator palpebrae superioris muscle and the smaller of which innervated the variable ocular muscle from the ventral and sometimes dorsal sides.

The reported frequency of these muscles (15 of 20 cases i.e., 75%) is probably high as Isomura (1977) reported the rarity of these muscles (about 3%, 5 in 85 individuals).

Changes during embryogenesis up to 24 months postnatally may result in the levator palpebrae superioris undergoing adaptations (Sevel 1988). A delicate superior transverse fascial expansion is present between the trochlea and the lacrimal gland in the embryo and is represented by the anterior aponeurotic sheath of the superior rectus and levator palpebrae superioris in adults (Ettl et al. 1998). Ettl et al. (1998) observed that the remnants of the fascial sheath system with medial and lateral wall attachments might persist and contribute to the formation of a bipartite levator palpebrae superioris. Sevel (1981) reported that the levator palpebrae superioris develops from multiple foci of mesodermal condensations, which fuse during development. In the light of the information, it can be concluded that

abnormal fusion may contribute to the formation of a bipartite levator palpebrae superioris.

A fasciculus, the retractor glandulae lacrimalis, sometimes passes from levator palpebrae superioris to the lacrimal gland (Bergman et al. 1988). Amonoo-Kuofi and Darwish (1998) identified a supernumerary extraocular muscle located between the superior oblique and levator palpebrae superioris muscles in each orbit of one cadaver. This supernumerary extraocular muscle originated on the inferior surface of the lesser wing of the sphenoid bone and inserted into the skin of the medial one-third of the upper eyelid. This muscle was innervated by a branch from the superior division of the oculomotor nerve. The insertion of the muscle into the upper eyelid produced a crease running obliquely upwards and medially, from the junction of the medial one-third and lateral two-thirds of the lid margin, towards the medial part of the superior orbital fold. The authors suggest the name "levator palpebrae superioris accessorius."

von Ludinghausen et al. (1999) witnessed that the normal fascial connection between levator palpebrae superioris and the lacrimal gland was replaced with muscular slips, which were innervated by the oculomotor nerve. They described these muscles as "bipartite levator palpebrae superioris." The fetal levator palpebrae superioris exhibits a broad aponeurotic insertion on the upper lid and the connective tissue of the lacrimal gland, often with medial and lateral accessory muscular slips or fibrous bands arising from levator palpebrae superioris (Plock et al. 2005).

Loukas and Curry (2006) noticed that the lateral border of otherwise normal right and left levator palpebrae superioris muscles received a broad muscular slip originating from the greater wing of the sphenoid bone to form a retrobulbar arch. Yalçin et al. (2009) studied 60 orbits of 30 embalmed adult human cadavers with which three accessory levator muscle slips of the levator palpebrae superioris muscle were identified. One of these levator muscle slips arose laterally from the origin of the levator palpebrae superioris muscle. It divided into two parts at its anterior end: the main superior and a smaller inferior accessory part. The second had an accessory levator fibromuscular slip, which arose medially from the origin of the levator palpebrae superioris and lost its muscular character after a short course. The third arose from the origin of the levator palpebrae superioris as a thin flat muscle. The authors suppose that the accessory levator muscle slips may be associated with congenital eyelid retraction or blepharoptosis.

References

Amonoo-Kuofi HS, Darwish HH. 1998. Accessory levator muscle of the upper eyelid: Case report and review of the literature. *Clin Anat* 11: 410–416.

Bagheri A, Eshaghi M, Yazdani S. 2009. Relationship of inferior oblique overaction to muscle bulk and position. *J AAPOS* 13: 241–244.

Banerjee BD. 1950. Abnormal insertion of inferior oblique. *Br J Ophthalmol* 34: 756.

Bergman RA, Thompson SA, Afifi AK. 1988. *Compendium of human anatomic variation*. Baltimore: Urban and Schwarzenberg Inc.

Bochdalek VA Jr. 1868. Beitrag zu den anomalen Muskel in der Augenhöle. Braunschweig: von Friedrich Vieweg und Sohn.

Budge J. 1859. Beschreibung eines neuen Muskels und mehrerer Muskel und Knochenvarietäten. *Zeitschrift für Rat Med* 3: 273–278.

Curnow J. 1873. Notes of some irregulatrities in muscles and nerves. *J Anat Physiol* 7: 304–319.

DeAngelis D, Kraft SP. 2001. The double-bellied inferior oblique muscle: Clinical correlates. *J AAPOS* 5: 76–81.

DeAngelis D, Makar I, Kraft SP. 1999. Anatomic variations of the inferior oblique muscle: A potential cause of failed inferior oblique weakening surgery. *Am J Ophthalmol* 128: 485–488.

Ettl A, Koornneef L, Daxer A, Kramer J. 1998. High-resolution magnetic resonance imaging of the orbital connective tissue system. *Ophthal Plast Reconstr Surg* 14: 323–327.

Fujita T. 1938. Eine Muskelanomalie in der orbita. *Okajimas Folia Anat Jap* 16: 301–302.

Helveston EM, Krach D, Plager DA, Ellis FD. 1992. A new classification of superior oblique palsy based on congenital variations in the tendon. *Ophthalm* 99: 1609–1615.

Henle J. 1873. Sinnesapparate. In Handbuch der Systematischen Anatomie des Menschen. Braunschweig: Verlag von Friedrich Vieweg und Sohn.

Howe L. 1923. Variations in the primary insertions of the ocular muscles. *Trans Am Ophthalmol Soc* 21: 124.

Isomura G. 1977. Nerve supply for an anomalous ocular muscle in man. *Anat Anz* 142: 255–265.

Kakizaki H, Zako M, Nakano T, Asamoto K, Miyaishi O, Iwaki M. 2006. An anomalous muscle linking superior and inferior rectus muscles in the orbit. *Anat Sci Int* 81: 197–199.

Kim JH, Hwang JM. 2010. Absence of the trochlear nerve in patients with superior oblique hypoplasia. *Ophthalm* 117: 2208–2213.

Krasny A, Lutz S, Gramsch C, Diepenbruck S, Schlamann M. 2011. Accessory eye muscle in a young boy with external ophthalmoplegia. *Clin Anat* 24: 948–949.

Le Double AF. 1897. *Traité des Variations du Systéme Musculaire de l'Homme et Leur Signification au Point de l'Anthropologie Zoologique, Libraire C*. Paris: Reinwald, Scheicher Freres.

Lockwood C. 1885. The anatomy of the muscles, ligaments, and fasciae of the orbit, including an account of the capsule of Tenon, the check ligaments of the recti, and of the suspensory ligament of the eye. *J Anat Physiol* 20: 2–25.

Loukas M, Curry B. 2006. Bilateral lateral bipartite levator palpebrae superioris muscles. *Clin Anat* 19: 698–699.

Macalister A. 1875. Additional observations on muscular anomalies in human anatomy (third series), with a catalogue of the principal muscular variations hitherto published. *Transactions of the Royal Irish Academy*. Dublin: Ponsonby & Murphy.

MacEwen EM. 1930. Orbital variations. *Anat Rec* 46: 223–232.

Plock J, Contaldo C, von Lüdinghausen M. 2005. Levator palpebrae superioris muscle in human fetuses: anatomical findings and their clinical relevance. *Clin Anat* 18: 473–480.

Posey WC. 1924. Concerning some gross structural anomalies of the muscles of the eye and its adnexia. *Arch Ophthalmol* 53: 344–354.

Prakash P, Nayak BK, Menon V. 1983. Abnormal insertion of inferior oblique. *Indian J Ophthalmol* 31: 21–22.

Rex H. 1887. Über einen abnormen Augenmuskel (Musc. obliquus accessorius inferior). *Anat Anz* 2: 624–630.

Sevel D. 1981. A reappraisal of the origin of the human extra-ocular muscles. *Ophthalmol* 88: 1330–1338.

Sevel D. 1988. Development of the connective tissue of the extraocular muscles and clinical significance. *Graefes Arch Clin Exp Ophthalmol* 226: 246–251.

Stager DR. 1996. The neurofibrovascular bundle of the inferior oblique muscle as its ancillary origin. *Trans Am Ophthalmol Soc* 94: 1073–1094.

Takahashi Y, Kakizaki H, Kohjima K, Nakano T, Asamoto K, Ichinose A, Iwaki M. 2013. Inferior oblique muscle origin: Horizontal location in relation to ala nasi and its gender difference. *Ann Plast Surg* 70: 88–90.

Tillaux P. 1877. Traité d'anatomie topographique avec applications à la chirurgie. Paris: Asselin.

Valmaggia C, Zaunbauer W, Gottlob I. 1996. Elevation deficit caused by accessory extraocular muscle. *Am J Ophthalmol* 121: 444–445.

von Ludinghausen M. 1998. Bilateral supernumerary rectus muscles in the orbit. *Clin Anat* 11: 271–277.

von Ludinghausen M, Miura M, Wuzler N. 1999. Variations and anomalies of the human orbital muscles. *Surg Radiol Anat* 21: 69–76.

Whitnall SE. 1912. An instance of the retractor bulbi muscle in man. *J Anat Physiol* 46: 36–40.

Whitnall SE. 1921. Some abnormal muscles of the orbita. *Anat Rec* 21: 143–152.

Wilson R, Landers J. 1982. Anomalous duplication of the inferior oblique muscle. *Am J Ophthalmol* 93: 521–522.

Yalçin B, Ozan H. 2005. Insertional pattern of the inferior oblique muscle. *Am J Ophthalmol* 139: 504–508.

Yalçin B, Kocabiyik N, Ozan H, Kutoglu T. 2004. Muscular bridge between the inferior oblique and inferior rectus muscles. *Am J Ophthalmol* 137: 121–124.

Yalçin B, Hurmeric V, Loukas M, Tubbs RS, Ozan H. 2009. Accessory levator muscle slips of the levator palpebrae superioris muscle. *Clin Experiment Ophthalmol* 37: 407–411.

Zinn JG. 2004. Anatomical description of the human eye. 1780. *Strabismus 12*: 125, 127–133.

Zinn JG. 2005. Anatomical description of the human eye. *Strabismus* 13: 45–52.

Further reading

Bergman RA, Afifi Ak, Ryosuke Miyauchi. Illustrated encyclopedia of human anatomic variation: Opus I: Muscular system. Available at http://www.anatomyatlases.org/AnatomicVariants/MuscularSystem/Alphabetical/MuscleListing.shtml (accessed 9 October 2015).

23 Middle ear muscles

José Francisco Rodríguez-Vázquez
Complutense University of Madrid, Madrid, Spain

There are two muscles of the tympanic cavity or muscles of the auditory ossicles: the tensor tympani and the stapedius muscles. The tensor tympani muscle, derived from the mesenchyme of the first pharyngeal arch, is innervated by the motor root of the mandibular nerve. The stapedius muscle originates in the second pharyngeal arch by two anlagens (Rodríguez-Vázquez 2005, 2009) and is innervated by the facial nerve. Both muscles occupy bony canals, complicating their study because of the difficult access. The variation of these muscles has an incidence of 4.4% (Wright and Etholm 1973).

Sömmerring (1806) and Le Double (1897) included another two muscles in this region: the external muscle of the malleus or laxator tympani major; and the laxator tympani minor. However, their presence is controversial. Macalister (1875) noted the absence of the laxator tympani major muscle. According to Le Double (1897), both of these muscles are frequently absent. The laxator tympani minor muscle reportedly corresponds to a ligamentous structure connecting the handle and short process of the malleus to the tympanic membrane (Walls 1946). According to Walls (1946), the laxator tympani major muscle is the true laxator muscle and is formed by an inferior tendon attached to the spine of the sphenoid bone, an intermediate fleshy rhomboidal part, and a superior tendon which passes through the petrotympanic fissure to join the anterior process of the malleus. These descriptions actually correspond to the arrangement of the tympanic portions of the sphenomandibular (anterior ligament of the malleus) and discomalleolar ligaments, which join each other in the middle ear and attach in the neck of the malleus above its anterior process (Rodríguez-Vázquez et al. 1992, 1998), but there is no proof of the existence of muscle fibers on them. Romanes (1987) referred to the laxator tympani major muscle when the anterior ligament of the malleus has muscle fibers.

Variations of the tensor tympani muscle

The tensor tympani muscle, a bipennate muscle, has a length of 2 cm. The variations could be classified as: doubled muscle or bifurcated; absent; or having a connection or continuity with the tensor veli palatini muscle

The muscle has been found to be doubled (Macalister 1875; Le Double 1897) or bifurcated into two bellies, that is, medial and lateral (Wright and Etholm 1973). In the latter, the lateral belly had a normal arrangement and the medial belly, with an abnormal arrangement, accompanied the facial nerve in the facial canal up to a level above the oval window, where it joined the stapedius muscle in two out of three observed cases and only on one side.

Kelemen (1943) observed that the tensor tympani muscle was replaced by a fibrous band without striations. No tendon was found to be present.

The tensor tympani muscle was occasionally found to be connected to the tensor veli palatini muscle (Proctor 1967, 1973; Rood and Doyle 1978; Barsoumian et al. 1998; Kierner et al. 2002). However, some authors have denied the existence of such connections (Kolmer 1927; Graves and Edwards 1944). The connection could be tendinous (Proctor 1973; Holborow 1975; Rood and Doyle 1978; Kierner et al. 2002) or muscular (Kessel 1968; Lupin 1969; Kamerer and Rood 1978). We have observed the tensor tympani muscle joining the tensor veli palatini muscle via a tendon in a human fetus, similar to the intermediate tendon of the digastric muscle (Fig. 23.1). This variation is explained by the common origin of both muscles from the internal part of the anlage of the muscles of the first pharyngeal arch. However, others have suggested that this situation could be a secondary fusion of two independent muscles (Rood and Doyle 1978).

Bergman's Comprehensive Encyclopedia of Human Anatomic Variation, First Edition. Edited by R. Shane Tubbs, Mohammadali M. Shoja and Marios Loukas.
© 2016 John Wiley & Sons, Inc. Published 2016 by John Wiley & Sons, Inc.

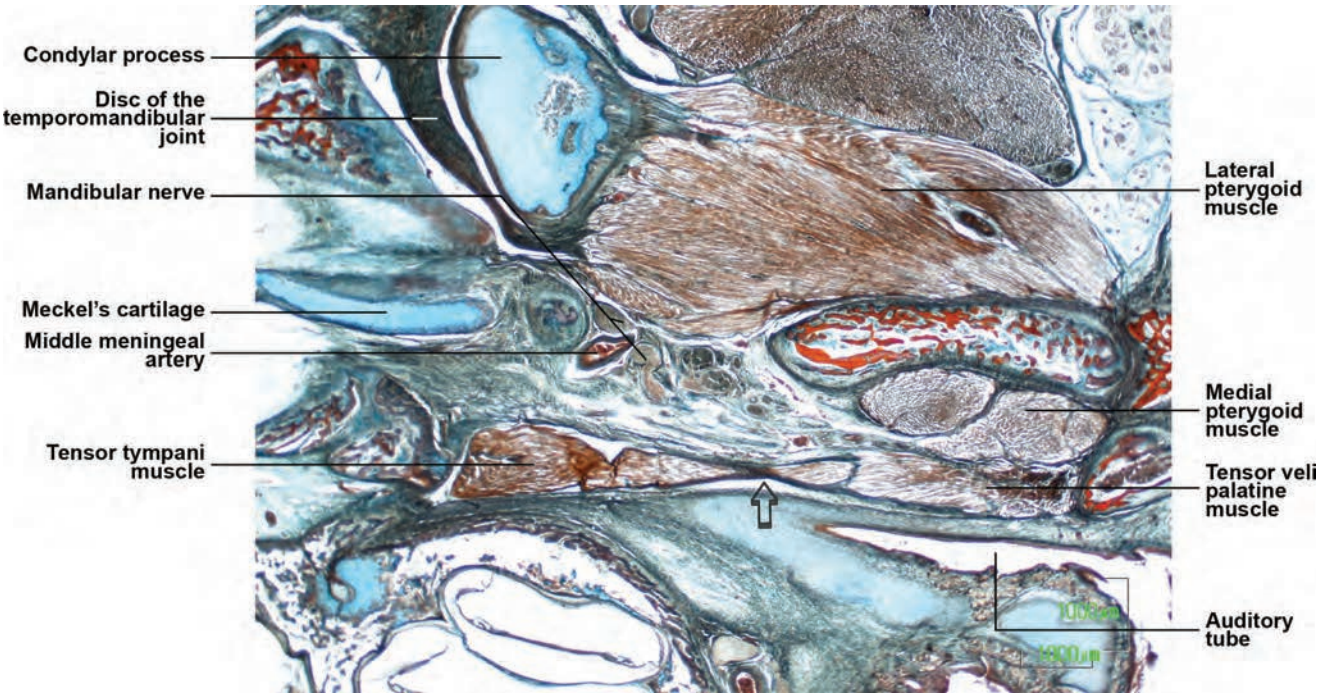

Figure 23.1 Transverse section in a 17-week-old human fetus showing a tendinous connection (arrow) between the tensor tympani and tensor veli palatini muscles.

Variations of the stapedius muscle

The stapedius is the smallest of all the skeletal muscles. The following variations, described in more details in the following paragraphs, have been identified: ectopic muscles; doubled stapedius; presence of the muscular belly and absent tendon; absence or agenesis of the belly, tendon, and the pyramidal eminence; or variations in the tendon.

According to Wright and Etholm (1973), the existence of ectopic muscles is the most common variation of the stapedius. These authors detected variations ranging from a few muscle fibers to well-developed muscle bundles. The ectopic stapedius muscles have been observed along the course of the facial nerve, in the facial canal, and next to the geniculate ganglion near the vertical part of the facial canal.

Le Double (1897), Macalister (1875) and Wright and Etholm (1973) noted doubled stapedius muscles. Wright and Etholm (1973) observed an abnormal muscle above the normal one. The fibers were scarcely developed and the tendon did not penetrate the tympanic cavity.

The absence of the tendon associated with the development of the muscle has been reported (Kelemen 1943; Marquet 1981). While studying a human fetus, Rodríguez-Vázquez et al. (2010) detected unilateral right agenesis of the tendon of the stapedius muscle with the presence of the belly of the muscle in an anomalous arrangement (Fig. 23.2a, c). In this case the pyramidal eminence was not present. This variation was explained by the development of the stapedius in two different anlages: one for the tendon, which derives from the internal segment of the interhyale, and another for the belly, located in the second pharyngeal arch medial to the facial nerve and near the interhyale. Two segments were discerned in the interhyale, forming an angle and delimited by the attachment of the belly of the stapedius muscle. The internal segment formed the tendon. The lateral segment, which normally disappears at the beginning of the fetal period, was attached to the cranial end of Reichert's cartilage (laterohyale) (Rodríguez-Vázquez et al. 2010; Fig. 23.2b). The laterohyale contributes to the formation of the most caudal portion of the vertical part of the facial canal. The regression of the internal segment of the interhyale is the cause for the absence of the tendon. The muscular belly of the stapedius muscle has to develop or be in the right location to form the pyramidal eminence (Rodríguez-Vázquez et al. 2010; Fig. 23.2d).

Complete absence of the stapedius is related to the lack of the tendon and also the lack of the pyramidal eminence (Hough 1958, 1963; Patel 1972; Wright and Etholm 1973). A congenital absence of the tendon, pyramidal eminence, and muscle is one of the most commonly found anomalies in the middle ear. It has an incidence of 1% according to Hough (1963), who reported five cases of total absence of the stapedius muscle in his 500 examinations. This observation could be explained by the regression of the internal segment of the interhyale and the non-formation of the anlage of the belly of the stapedius muscle (Fig. 23.2d). Without the formation of the belly of the stapedius

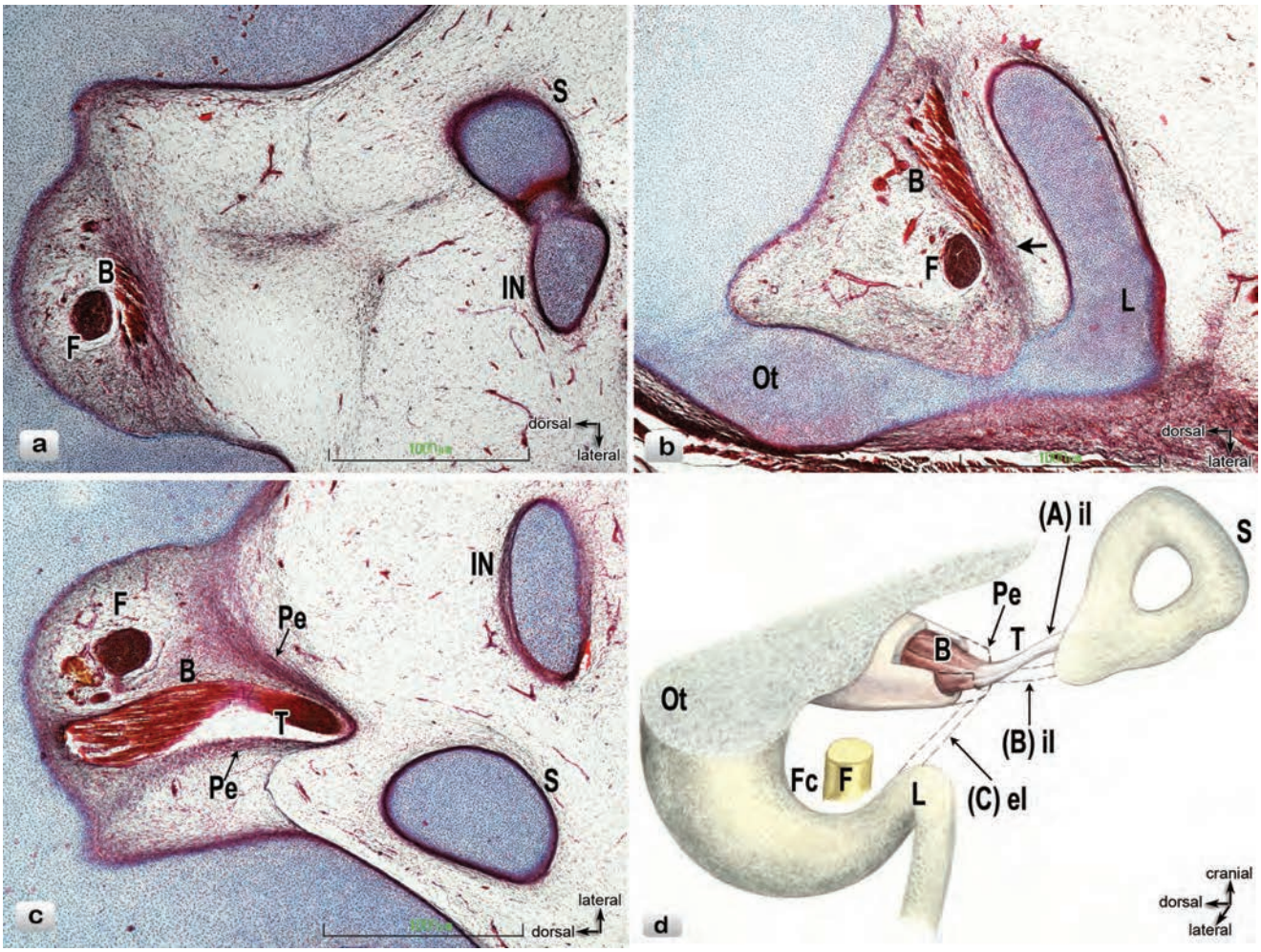

Figure 23.2 Transverse section in a 14-week-old human fetus. (a) Right side. Absence of the tendon of the stapedius muscle and the anlage of the pyramidal eminence, the belly of the stapedius muscle (B) presents an anomalous arrangement. F: facial nerve; IN: incus; S: stapes. (b) Belly of the stapedius muscle (B) with an anomalous arrangement, located in front of the facial nerve (F) and prolonged by a pseudotendon (arrow) attached in the continuity zone of the otic capsule (Ot) and the cranial end of Reichert's cartilage (laterohyale) (L). (c) Left side. The stapedius muscle (belly (B), tendon (T)) and the anlage of the pyramidal eminence (Pe) presented a normal morphology for its stage of development. (d) Variations of the stapedius muscle. A: The variations of the tendon of the stapedius muscle (T) depend on the length and degree of angulation of the internal segment of the interhyale (iI). B: The regression of the internal segment of the interhyale (iI) would give rise to an anomalous arrangement of the belly of the stapedius muscle (B) and the lack of formation of the anlage of the pyramidal eminence (Pe), causing the absence of the tendon of the stapedius muscle as well as the pyramidal eminence. C: The persistence and no regression of the external segment of the interhyale (eI) would join the pseudotendon of the stapedius muscle to the laterohyale (L) to contribute to the formation of the most caudal portion of the vertical part of the facial canal (Fc).

Source: Rodríguez-Vázquez et al. (2010). Reproduced with permission from John Wiley & Sons.

muscle, the mesenchymal tissue would not condense and the pyramidal eminence would therefore not form (Rodríguez-Vázquez et al. 2010).

Hough (1958) and Cremers and Hoogland (1986) reported variations in the length of the tendon of the stapedius muscle that can be explained according to the attachment site of the belly of the stapedius muscle in the interhyale. This feature determines the length of the internal segment of the interhyale and, consequently, the final length of the long or short tendon since this derives from the internal segment of the interhyale (Rodríguez-Vázquez et al. 2010; Fig. 23.2d).

Variations in the arrangement of the tendon have been described (Hough 1963). The stapedius tendon may appear in many positions (Fig. 23.3). It is normally aligned with the posterior crus, but it may be directed far below or above. These variations could be explained by the persistence, to a greater or lesser degree, of the angulation between the tendon and the belly of the stapedius muscle (Rodríguez-Vázquez et al. 2010; Fig. 23.2d).

The calcified tendon has been observed attached to the posterior wall of the tympanic cavity. The head of the stapes is connected to the posterior wall of the tympanic cavity by a bony

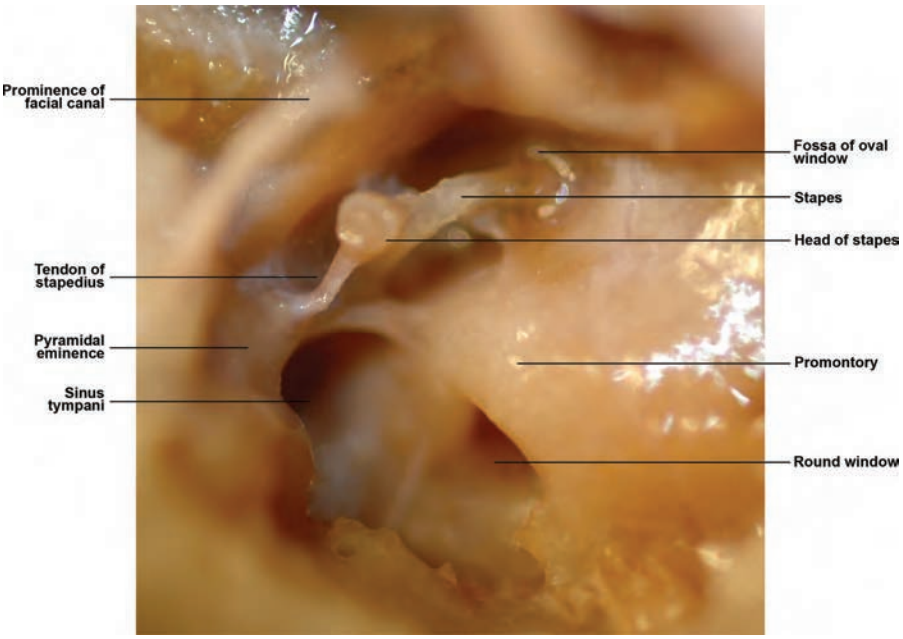

Figure 23.3 Anatomic dissections of the tympanic cavity showing the medial wall. Note a type of angulation of the tendon of the stapedius that emerges from the orifice at the apex of the pyramidal eminence.

bridge (calcification of stapedius tendon) (Podoshin et al. 1972). The persistence and the lack of regression of the external segment of the interhyale, as well as its subsequent ossification, would join the stapedius tendon to the vertical part of the facial canal (Rodríguez-Vázquez et al. 2010).

The tendon could be surrounded by an elongated pyramidal eminence (Schuknecht and Trupiano 1957; Marquet 1981; Cremers and Hoogland 1986) that can reach to the neck of the stapes, and an attachment of the stapes to the pyramidal process with a normal tendon has been reported (Ombredanne 1960; Kinsella and Kerr 1993; Cremers and Hoogland 1986), causing the fixation of the stapes. This variation can be explained by the greater extension of the ossification cone taking place over the mesenchymal condensation, the anlage of the pyramidal eminence, which surrounds the muscle belly and could extend as far as the tendon and even surround it (Rodriguez-Vázquez et al. 2010; Fig. 23.2d).

References

Barsoumian R, Kuehn D P, Moon JB, Canady JW. 1998. An anatomic study of the tensor veli palatini and dilatator tubae muscles in relation to Eustachian tube and velar function. *Cleft Palate Craniofac J* 35: 101–110.

Cremers CWRJ, Hoogland GA. 1986. Congenital stapes ankylosis by elongation of the pyramidal eminence. *Ann Otol Rhinol Laryngol* 95: 167–168.

Graves G, Edwards L. 1944. The Eustachian tube, review of its descriptive, microscopic, topographic and clinical anatomy. *Arch Otolaryngol* 63: 359–397.

Holborow C. 1975. Eustachian tubal function: changes throughout childhood and neuro-muscular control. *J Laryngol Otol* 89: 47–55.

Hough JVD. 1958. Malformations and anatomical variations seen in the middle ear during the operation for mobilization of the stapes. *Laryngoscope* 68: 1337–1379.

Hough JVD. 1963. Congenital malformations of the middle ear. *Arch Otolaryngol* 78: 335–343.

Kamerer D B, Rood SR. 1978. The tensor tympani, stapedius and tensor veli paltini muscles: an electromyographic study. *ORL* 86: 416–421.

Kelemen G. 1943. Malformation involving external, middle and internal ear, with otosclerotic focus. *Arch Otolaryngol* 37: 183–198.

Kessel J. 1968. Vorläufige Mitteilungen ubre einige anatomische Verhältnisse des Mittelohres. *Arch. Ohrenheilkd.* 3: 308–313.

Kierner AC, Mayer R, Kirschhofer KV. 2002. Do the tensor tympani and tensor veli palatini muscles of man form a functional unit? A histochemical investigation of their putative connections. *Hear Res* 165: 48–52.

Kinsella JB, Kerr AG. 1993. Familial stapes superstructure fixation. *J Laryngol Otol* 107: 36–38.

Kolmer W. 1927. Gehörorgan. In: *Handbuch der Mikroskop. Anatomie*. Berlin: Springer Verlag.

Le Double AF. 1897. *Traité des variations de système musculaire de l'homme et de leur signification au point de vue de l'anthropologie zoologique*. Paris: Schleicher Frères.

Lupin AJ. 1969. The relationship of the tensor tympani and tensor palati muscles. *Ann Otol Rhinol Laryngol* 78: 792–796.

Macalister A. 1875. Observations on the muscular anomalies in the human anatomy (Third series), with a catalogue of the principal muscular variations hitherto published. *Trans Roy Irish Acad Sci* 25: 1–130.

Marquet J. 1981. Congenital malformations and middle ear surgery. *J R Soc Med* 74: 119–128.

Ombredanne M. 1960. Chirurgie des surdites congenitales par malformations ossiculares de: 10 nouveaux cas. *Ann Otol Laryngol Chirurg Face* 77: 423–449.

Patel KN. 1972. Ossification of the stapedius tendon. *J Laryngol Otol* 86: 863–865.

Podoshin L, Fradis M, Zisman D. 1972. Congenital anomalies of the stapes. *Arch Otolaryng* 96: 254–255.

Proctor B. 1967. Embryology and anatomy of the Eustachian tube. *Arch Otolaryngol* 86: 503–514.

Proctor B. 1973. Anatomy of the Eustachian tube. *Arch Otolaryngol* 97: 1–8.

Rodríguez-Vázquez JF. 2005 Development of the stapes and associated structures in human embryos. *J Anat* 207: 165–173.

Rodríguez-Vázquez JF. 2009. Development of the stapedius muscle and pyramidal eminence in humans. *J Anat* 215: 292–299.

Rodríguez-Vázquez JF, Mérida-Velasco JR, Jiménez-Collado J. 1992. Development of the human sphenomandibular ligament. *Anat Rec* 233: 453–460.

Rodríguez-Vázquez JF, Mérida-Velasco JR, Mérida-Velasco JA, Jiménez-Collado J. 1998. Anatomical considerations on the discomalleolar ligament. *J Anat* 192: 617–621.

Rodríguez-Vázquez JF, Mérida-Velasco JR, Verdugo-López S. 2010. Development of the stapedius muscle and unilateral agenesia of the tendon of the stapedius muscle in a human fetus. *Anat Rec* 293: 25–31.

Romanes GJ. 1987. *Cunningham Tratado de Anatomía*. Madrid: Interamericana.

Rood SR, Doyle WJ. 1978. Morphology of the tensor veli palatini, tensor tympani and dilatator tubae muscles. *Ann Otol* 87: 202–210.

Schuknecht HF, Trupiano S. 1957.Some interesting middle ear problems. Laryngoscope 67: 395–409.

Sömmerring ST. 1806. Icones Organi Auditus Humani, Table 2, Fig. 10. Francofurti ad Moenum) apud Warrentrapp et Wenner.

Walls EW. 1946. The laxator tympani muscle. *J Anat* 80: 210.

Wright JLW, Etholm B. 1973. Anomalies of the middle-ear muscles. *J Laryngol* 87: 281–288.

24 Facial muscles and muscles of mastication

Koichi Watanabe
Kurume University School of Medicine, Fukuoka, Japan

It is known that some facial muscles are occasionally absent or lack tone and the rates of these occurrences differ among races, ethnic groups, and gender. However, some facial muscles which are not usually observed may occasionally develop; for example, the mandibular marginalis muscle (Hrdlicka 1919; Weaver 1978), the malaris muscle (Burkitt and Lightoller 1927; Weaver 1978; Park et al. 2011), the transverse nuchae muscle (Weaver 1978; Schmidt 1982), and the transverse menti muscle (Weaver 1978) belong to this muscle group.

The fiber types of facial muscles have different functions. Freilinger et al. (1990) classified the facial muscles by their fiber types: type 1, tonic fibers; and type 2, phasic fibers. Type 1 are further classified into three groups as follows: group 1: phasic muscles, containing <20% of type 1 fibers; group 2: intermediate muscles, containing 20–40% of type 1 fibers; and group 3: tonic muscles, containing >40% of type 1 fibers. Group 1 includes procerus, orbicularis occuli, and nasalis muscles. Group 2 includes platysma, zygomaticus major, levator labii superioris, mentalis, orbicularis oris, levator angulioris, and depressor angulioris muscles. Group 3 includes corrugator supercilii, depressor labii inferioris, occipito frontalis, and buccinator muscles.

Facial muscles of the mouth

The positioning or connection of each facial muscle around the mouth has some variations. For example, the appearance of each facial muscle varies widely by gender and race. In particular, a deficiency of the risorius and zygomaticus minor muscles is observed with greater frequency than other facial muscles. A congenital hypoplasia of facial muscles has also been reported, with aplasia or hypoplasia of the depressor anguli oris muscle as an example. This is described in the section on the depressor anguli oris muscle below. As a congenital complex hypoplasia of facial muscles, a case of congenital hypoplasia of risorius, zygomaticus major, zygomaticus minor, and levator labii superioris muscles has been reported (Nada et al. 1998). Fusions with neighboring muscles in the cases of risorius, zygomaticus major, and zygomaticus minor muscles have been reported.

Anatomical variations of each muscle are described in the following sections. However, anatomical variations of the buccinator, depressor labii inferioris, and mentalis muscles have never been reported.

Positioning variations of the facial muscles around the mouth

Shimada and Gasser (1989) reported variations in the positions at the point where facial muscles, such as levator angulioris, zygomaticus major, risorius, buccinators, and depressor anguli oris muscles, converge at the lateral point near the angle of the mouth. They classified the positions into three types as follows: type A: the convergent area is located lateral to the mouth angle; type B: the position is located above the mouth angle; and type C: the position is located below the mouth angle. Among them, type C was the most commonly observed (42.3%) and type B was the next most commonly observed pattern (41.2%). Type A, which was usually described in anatomical textbooks or in an atlas, was the least observed (16.5%). Shimada and Glasser (1989) also reported a difference in distribution among different racial groups. In the Mongoloid population (Japanese), type C was the most frequently observed (45.1%); type B was the most frequently observed in Caucasians (44.2%). Type A had the least incidence in both races.

Pessa et al. (1998) reported seven patterns of muscle distribution composing the nasolabial fold (Fig. 24.1). The most common pattern was type 1, with a combination of levator alae nasi, levator labii superioris, and a single zygomaticus major muscle, observed in 44% of the reported cases.

Orbicularis oris muscle

Lack of continuity of the orbicularis oris muscle is observed in cases of cleft lip (De Mey et al. 1989).

Zygomaticus major muscle

The appearance of the zygomaticus major muscle was reported at almost 100% (Sato 1968; Pessa et al. 1998). However, morphological variations of the zygomaticus major muscle have been reported. The first description of a double zygomaticus major muscle was reported by Santorini in 1775. Subsequently,

Bergman's Comprehensive Encyclopedia of Human Anatomic Variation, First Edition. Edited by R. Shane Tubbs, Mohammadali M. Shoja and Marios Loukas.
© 2016 John Wiley & Sons, Inc. Published 2016 by John Wiley & Sons, Inc.

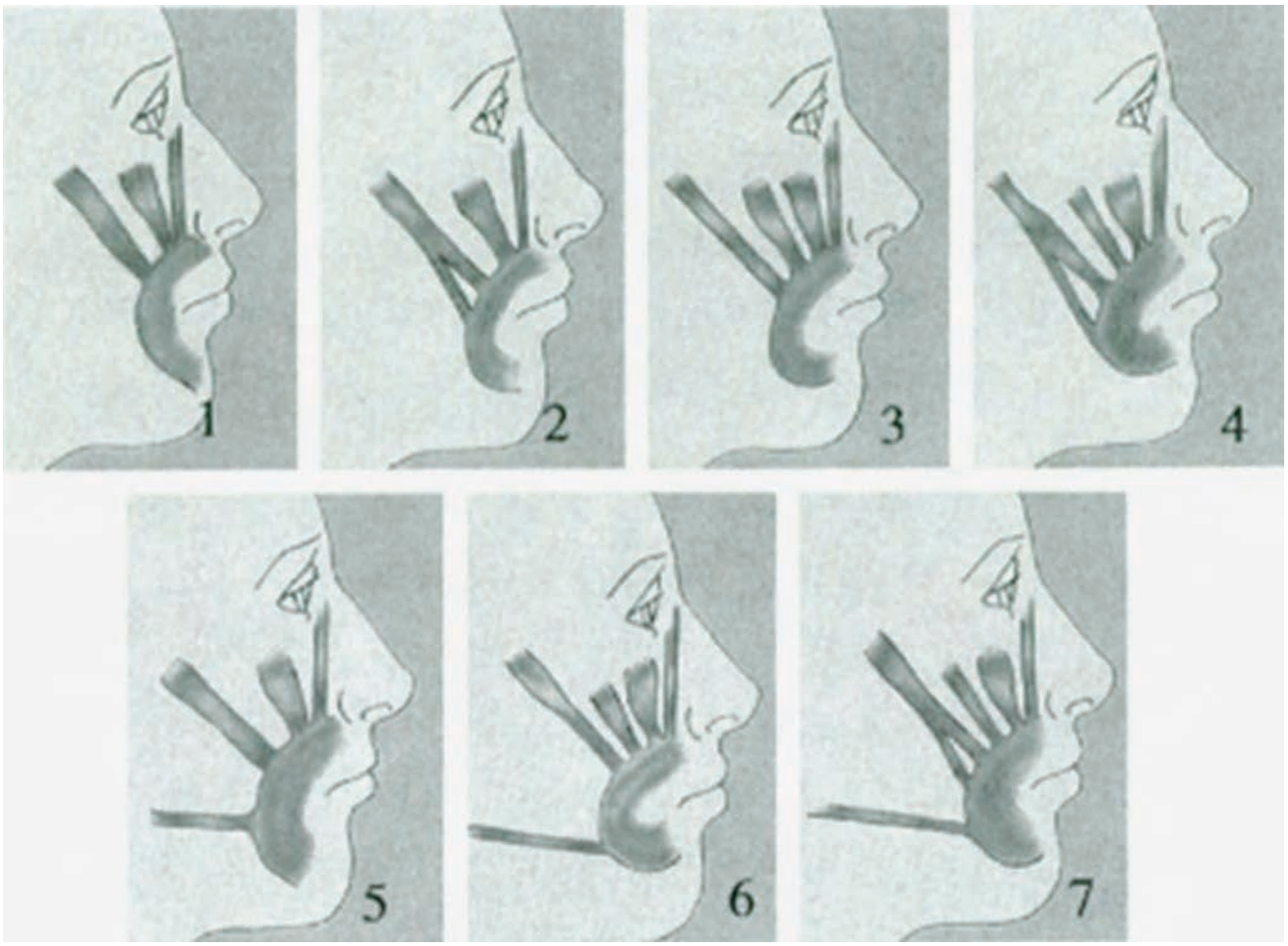

Figure 24.1 Distribution patterns of the mid-facial muscles orbicularis oris, levator labii superioris alaeque nasi, levator labii superioris, zygomaticus minor, zygomaticus major, and risorius as reported by Pessa et al. (1998). Type 1: 44%; type 2: 18%; type 3: 18%; type 4: 14%; type 5: 2%; type 6: 2%; and type 7: 2%. Source: Pessa et al. (1998). Reproduced with permission from Wolters Kluwer Health.

Zufferey (1992) reported cases of a double zygomaticus major muscle in one of ten dissection cases (10%). However, others have reported a higher frequency rate of unusual zygomaticus major muscles. Pessa et al. (1998) reported a double zygomaticus major muscle in 34% of the 50 examined specimens. Hu et al. (2008) reported the appearance rate of bifid zygomaticus major muscles to be 40%. Pessa et al. (1998) reported a gender difference in that this anomaly was dominant in females, but Hu et al. (2008) reported the opposite findings. A difference in thickness between genders has also been reported. McAlister et al. (1998) conducted an ultrasound study, measuring the thickness of the zygomaticus major muscle, and reported that the muscle was significantly thicker in females than in males.

Variations in the zygomaticus major and minor fused muscles, compared with other muscles such as the platysma, levator labii superioris, levator labii superioris alaeque nasi, and risorius muscles, have also been reported (Macalister 1875; Bergman et al. 1995; D'Andrea and Barbaix 2006). A type of muscle fusion around the mouth involving the quadratus labii superioris muscles, which consists of the zygomaticus minor, levator labii superioris, and levator labii superioris alaeque nasi muscles, was also reported (Henle 1871; D'Andrea and Barbaix 2006).

Zygomaticus minor muscle

The zygomaticus minor muscle is often absent. Sato (1968) referred to the previous literature and reported a comparison of the absence rate of the zygomaticus minor muscle among cultures. The absence rate was higher in Europeans (22%), Chinese (15.9%), and the Hottentot (17.7%), and was low in the Japanese. Pessa et al. (1998) reported an extremely high rate of absence of this muscle, with an appearance rate of 36%.

This muscle is sometimes fused with neighboring muscles, such as the zygomaticus major and levator labii superioris muscles. Cases with accessory bands from the risorius or orbicularis occuli muscles, or cases of connecting with the outer fiber of the frontalis, have been reported. Shortening of the muscle, the

entire muscle band arising from the orbicularis occuli, or double or triple at the insertion, have all been reported (Macalister 1875).

Risorius muscle

The risorius muscle often appears to be absent, with a frequency of absence reported as 1–94% (Sato 1968; Pessa et al. 1998). The risorius muscle varies in size and form, and may be separated into double or triple muscles (Macalister 1875).

The risorius muscle may originate from the skin over the upper third of the sternocleidomastoid muscle, from the fascia of the parotid gland, from the fascia over the masseter muscle, from the zygoma, from the external ear, from the platysma, or from the mastoid process (Macalister 1875). Sekine et al. (1988) also reported anomalous cases of the risorius muscle originating from the masseter muscle tendon. In a variation of insertion area, the muscle may also insert into the depressor anguli oris (Macalister 1875).

Fusions with other neighboring muscles, the platysma risorius muscle, the triangularis risorius muscle, and the zygomaticus risorius muscle, have also been reported (Kopsch 1908; D'Andrea and Barbaix 2006).

Depressor anguli oris muscle

The muscle fibers of the anterior border of the bilateral depressor anguli oris sometimes extend under the chin, connect to each other, and form transverse menti muscles. The origin of the muscle may arise separately from the platysma or arise entirely from the bone (Macalister 1875). The fibers of the muscle may continue with the zygomaticus major, lavatory labii superioris, or levator anguli oris muscles (Macalister 1875). Clinically, congenital aplasia or hypoplasia of the depressor anguli oris muscle has been reported. This anomaly is also referred to as "neonatal asymmetric crying facies," and is a recognized asymmetry of the lower lip due to a weakness of the unilateral depressor anguli oris. Its incidence was reported to be 0.31–0.82% (Perlman and Reisner 1973; Papadatos et al. 1974; Alexiou et al. 1976; Singhi et al. 1980; Lahat et al. 2000). Two possibilities for the etiology of this condition have been proposed: muscular aplasia or hypoplasia, or palsy of the marginal mandibular branch of the facial nerve. Based on an electrodiagnostic study, Nelson and Gingrass (1979) reported that hypoplasia of the depressor anguli oris muscle is caused an asymmetrical facial expression, whereas Roedel et al. (1998), using ultrasonography, reported that the muscles developed normally in six out of seven cases. It is generally accepted that aplasia or hypoplasia of the depressor anguli oris is often associated with other anomalies, such as cardiac anomalies. Additionally, anomalies of the urogenital tract, bone, and muscle, neuroblastoma, mediastinal teratoma, trisomy 18, and neuro fibroma type 1 are also associated with this anomaly. However, one report suggested that the frequency of congenital hypoplasia depressor anguli oris associated with other anomalies was not higher than that of the general population (Alexiou et al. 1976).

Depressor labii inferioris muscle

Macalister (1875) reported that the depressor labii inferioris muscle was divided into two or more bundles.

Mentalis muscle

It is said that the size of the mentalis muscle varies in some cases, and the muscle is rarely divided into two bundles.

Levator labii superioris muscle

Macalister (1875) reported the absence of the levator labii superioris muscle, although this is not common. Sato (1968) reported that the levator labii superioris muscle was absent in approximately 4% of males and 2% of females in a study of Japanese subjects. In other variations of this muscle, Macalister (1875) reported that the muscle was divided into a double or triple bicuspid outer head which arises from the zygoma or orbicularis occuli, or that a muscle slip was inserted into the transverse part of the nasalis or levator anguli oris.

Levator labii superioris alaeque nasi muscle

Sato (1968) reported that the levator labii superioris alaeque nasi muscle was absent in 5% of the male and 4% of the female Japanese population.

Macalister (1875) also reported that the levator labii superioris alaeque nasi muscle may have only one head, of internal or nasal origin, and the nasal head of this muscle may be double or separate. However, this muscle usually has one origin: the frontal process of the maxilla. We could not determine which origin he referred to in his report. This muscle may receive the fiber from the frontalis or procerus muscle, and is often inseparable from the levator labii superioris.

Facial muscles around the nose

The procerus, nasalis, and depressor septi muscles belong to the category of muscles around the nose.

Procerus muscle

According to Bergman et al. (1995), the procerus muscle may be absent or more developed on one or both sides. It is also suggested that the attachments vary considerably. It is generally known that the muscle fibers of the procerus decussate with those of the frontalis muscle, and that the procerus muscle rarely separates clearly from the frontalis muscle. The atlas also showed that the bilateral muscles continue over the bridge of the nose (Bergman et al. 1995).

Nasalis muscle

The nasalis muscle consists of two parts: the transverse part and the alar part. The transverse part of the muscle arises from the maxilla, passes upward, medially, and connects to the opposite side of the muscle at the nasal dorsum. The alar part of the nasalis muscle arises from the maxilla and is inserted into the alar

cartilage. The muscle may continue up into the procerus muscle. Detached fibers may form the dilators naris anterior and posterior.

Hur et al. (2010) reported that the transverse part of the nasalis muscle received some muscle fibers from the levator labii superioris alaeque nasi in 90% of the observed specimens. Hur et al. (2010) also reported that the muscle had two patterns of passing: one arising from the maxilla and passing posterior to the levator labii superioris alaeque nasi in 65% of the cases, and the other arising from both the maxilla and the skin of the upper half of the alar facial crease.

Depressor septi nasi muscle

A case of hypertrophy of the depressor septi nasi muscle was reported (Ohtsuka 2005), and hypertrophy of the muscle was confirmed by surgery. Additional reports of anatomical variations concerning this muscle have not been found in the literature.

Facial muscles around the eyes

Two muscles belong to the category of facial muscles around the eyes: the orbicularis oculi and the corrugator supercilii muscle. As inconsistent muscles, the orbitozygomatic muscle and the malaris muscle, which are related to the orbicularis occuli muscle, are included in this chapter.

Orbicularis occuli muscle

A muscle slip inserted into the zygomaticus minor muscle or the entire zygomaticus minor muscle, arising from the orbicularis occuli muscle, has been reported (Macalister 1875). Similarly, a muscle slip inserted into the corrugator supercilii, levator labii superioris, and levator angulioris muscles has also been reported. A slip of platysma muscle, inserted into the orbicularis occuli, has also been reported (Macalister 1875). The transverse glabellae muscle, which extends in the transverse direction across the base of the nose and unites with the bilateral orbicularis oculi muscles, has been described. Absence of the orbital, the rudimentary of the palpebral, and the lacrimal regions and separation of the palpebral and orbital portion of the muscle have also been reported (Macalister 1875; Bergman et al. 1995).

Orbitozygomatic muscle

The orbitozygomatic muscle was recently described as the muscle which originated from the medial canthal tendon at the lower portion of the orbicularis oculi muscle and which inserted into the cheek skin and zygomaticus muscle. Hwang et al. (2002) described this muscle as the orbitozygomatic muscle. However, a description of which muscle slip of the orbicularis occuli inserted into the zygomaticus was not reported in the original article (Macalister 1875). It is reported that this muscle makes the nasojugal fold (Hwang et al. 2002). Park et al. (2012) then confirmed this muscle as the medial muscular band of the orbicularis occuli muscle and classified it into four types as follows: type A: the muscular band attached to the frontalis without being attached to the medial canthal tendon; type B: the band originating from the medial canthal tendon at the lower portion of the orbicularis occuli muscle and inserting into the cheek skin; type C: the band which inserts into the cheek skin and attaches to the frontal belly without being attached to the medial canthal tendon; and type D: the type with no muscular band. The medial muscular band was observed in 65% of the cases and the frequency of each type was reported as follows: type A, 23%; type B, 23%; and type C 19.7% (Fig. 24.2).

Malaris muscle

The malaris muscle is one of the most inconsistent facial muscles, and few reports exist concerning this muscle. This muscle was first described by Henle in 1871 (Zufferey 2013). It was further defined as originating from the superficial temporal fascia,

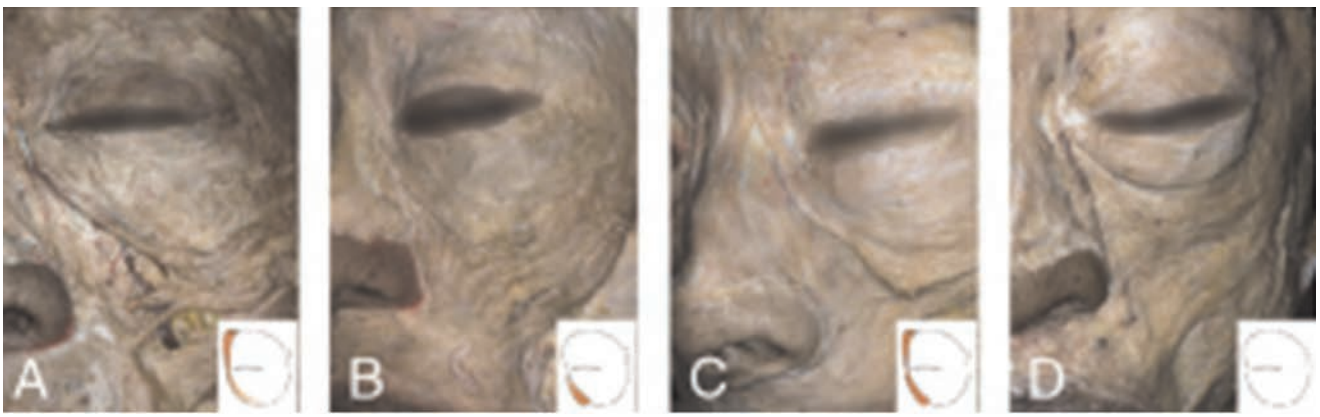

Figure 24.2 Morphological classification of the orbitozygomatic muscle (see text).

Source: Park et al. (2012). Reproduced with permission from Wolters Kluwer Health.

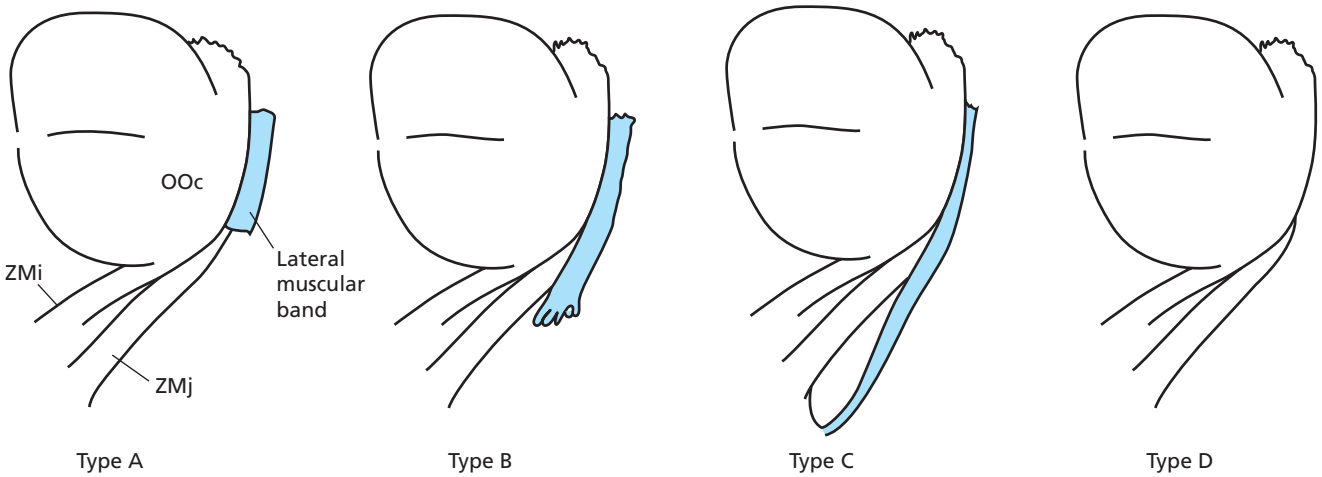

Figure 24.3 Morphological classification of the malaris muscle. Type A: the muscular band terminates at the zygomatic arch; type B: the muscular band terminates at the cheek region; type C: the muscular band terminates at the angle of mouth; type D: there is no muscular band around the orbicularis occuli. OOc: orbicularis occuli muscle: ZMi: zygomaticus minor muscle; ZMj: zygomaticus major muscle.

Source: Park et al. (2011). Reproduced with permission from Wolters Kluwer Health.

running beyond the zygomatic arch and terminating in the fat of the cheek (Park et al. 2011). However, Park et al. (2011) reported a relationship between the orbicularis occuli muscle and the lateral muscular band malaris muscle, and classified them into four types with three types as variations of the malaris muscles and a previously undescribed type (Fig. 24.3). The appearance rate of the muscle was reported as 54.1% in Korean cadavers, and the type in which the muscle terminated at the zygomatic arch was the most prevalent (Park et al. 2011). However, the appearance of this muscle seems to be quite different among racial and ethnic populations. Zufferey (2013) stated that this muscle is rare in the Caucasian population and was found in approximately 10% of the Asian population.

Corrugator supercilii muscle

The corrugator supercilii muscle can be absent, and the appearance of this muscle varies among racial and ethnic populations. Sato (1968) reported that this muscle was found almost entirely in Chinese and European populations, whereas it was sometimes absent in Negro, Malayan people in Southeast Asia, Herero people in Namibia, and Australian populations. Sato (1968) also reported the absence of this muscle in approximately 18% of the Japanese population. The muscle has rarely been observed completely separated from the orbicularis occuli muscle, and constitutes a part of the fibers with the orbicularis occuli or frontalis muscles. The forms are divided into several fasciculi with muscular origins and two or three tendinous slips of bilaminar origins (Macalister 1875). Alfonso et al. (2010) reported two cases of soft tissue masses in glabella which occurred only when crying, and suggested that as the cause of the agenesis of bilateral corrugator supercilii muscles. However, these two cases were diagnosed based upon clinical findings and imaging, but were not confirmed by dissection or surgery. In Bergman's Anatomy Atlas (Bargamn et al. 1995), the absence of an orbital portion of the corrugator muscle was depicted.

Extrinsic muscles of the ear

Three classes of muscle are included in the category of muscles near the ear, including the anterior auricular muscle, the superior auricular muscle, and the posterior auricular muscle.

It is thought that the anterior auricular muscle is the most frequently absent extrinsic auricular muscle (Bergman et al. 1995). This muscle is usually less developed, and sometimes consists of a single muscle bundle or connecting tissue. The other extrinsic auricular muscles, the superior auricular muscle and posterior auricular muscle, are rarely absent (Le Double 1906). A clinical case of agenesis of the posterior and superior auricular muscles was reported (Hoogbergen et al. 1996). This case showed hypermobility of the right ear and agenesis of the posterior and superior auricular muscles, with very thin concha cartilage as confirmed by surgery. Sato (1968) reported that the appearance rate of the posterior auricular muscle in Japanese populations was approximately 90%.

Muscles of the scalp

The occipitofrontalis muscle and temporoparietal muscle belong to the category of muscles near the scalp. As an inconstant muscle, the transverse nuchae muscle is observed in 25–60% of cases.

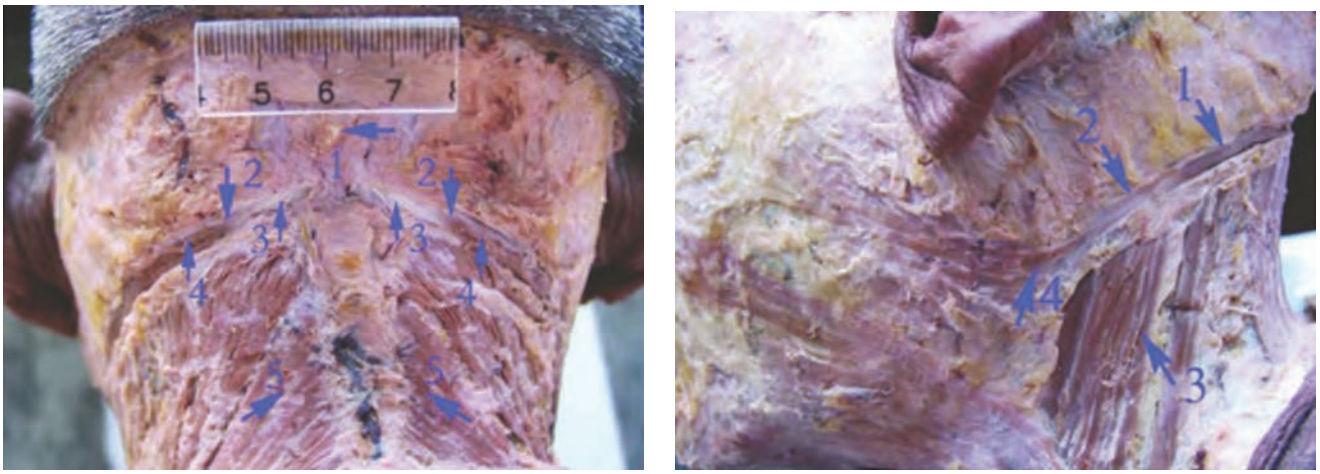

Figure 24.4 A case of transverse nuchae muscle. (a) Origin of the transverse nuchae muscle. 1: external occipital protuberance; 2: transverse nuchae muscle; 3: tendon of transverse nuchae muscle; 4: muscle belly of transverse nuchae muscle; and 5: trapezius. (b) Distribution and insertion of the muscle. 1: muscle belly of the transverse nuchae muscle; 2: the tendon part; 3: the sternocleidomastoid muscle; and 4: tendon transfers into the muscle belly with multiple muscular fasciculi.

Source: Lei et al. (2010). Reproduced with permission from Wolters Kluwer Health.

Occipitofrontalis muscle

The occipitofrontalis muscle has two muscle bellies: the occipital belly and the frontal belly. It is said that both bellies vary in size and extent, or may be absent. The muscle of the two sides may fuse in the midline, and the occipital belly may fuse with the posterior auricular muscle (Clemente 1985). The frontal belly only rarely connects to the occipital belly directly (Kopsch 1908). However, any detailed statistical reports of their variations have not been found in the literature.

Transverse nuchae muscle

Few studies have been reported on the transverse nuchae muscle (Sato 1968; Schmidt 1982; Lei et al. 2010). It is generally recognized that this muscle arises from an external occipital protuberance, runs vertically to anteriorly, and joins to the posterior auricular muscle. However, recent studies showed different findings. Schmidt (1982) reported that the muscle consisted of two bellies, and that the insertion of this muscle was at the fascia of the parotid gland. Lei et al. (2010) reported that the muscle had two sections: one with two muscle bellies as reported by Schmidt (1982), and another with several tendinous structures originating from the membrane of the sternocleidomastoid muscle or the nuchal ligament, and inserted into the superficial fascia of the parotid gland (Fig. 24.4). The presence of this muscle differs greatly from 25% to 60% (Sato 1968; Lei et al. 2010). Sato (1968) reported that the appearance rate varied to some degree among ethnic groups. In his review, the appearance rate in Japanese populations was 32–50%, 40% in Europeans, and 55% in Africans (Sato 1968). The muscle may be a remnant of the platysma muscle.

Platysma muscle

The platysma muscle has various morphological patterns. Both hypoplasia and hyperplasia of the platysma muscle may be observed. An extension to the cranial part of the muscle is rarely observed. Cases in which the platysma muscle extended up to the skin of the lateral cheek crease (Pessa et al. 1998), to the lower eyelid (Bergman et al. 1995), or to the forehead (Macalister 1875) have been reported. Macalister (1875) reviewed the platysma muscle connections to the depressor angulioris, depressor labii inferioris, zygomaticus major, zygomaticus minor, orbicularis occuli, and the auricularis anterior muscle.

At the medial side, both the platysma muscles usually unite at various levels at the midline. Von Lanz and Wachsmuth (1955) classified the patterns of both muscle shapes into eight types. In one report, de Castro (1980) showed interlacing patterns of the bilateral platysma muscle in the midline. He classified the patterns into three types as follows: type 1: interlaces the bilateral muscle fibers just 1–2 cm below the chin; type 2: interdigitates the fibers at the level of the thyroid cartilage, covering the submental region like a single muscle; and type 3: the muscles are separate in the submental region and no interlacing is noted (Fig. 24.5a). Macalister (1875) also mentioned that both sides of the platysma muscle may unite below the level of the thyroid cartilage, and that a transverse slip under the chin may join the muscles. Moreover, Kim et al. (2001) stated that interlacing of both platysma muscles had three types of variations: type A interlacing, with both platysma fibers interlacing each other in the region of the decussation; type B right dominant, where the right platysma fibers cover the left fibers; type C left dominant,

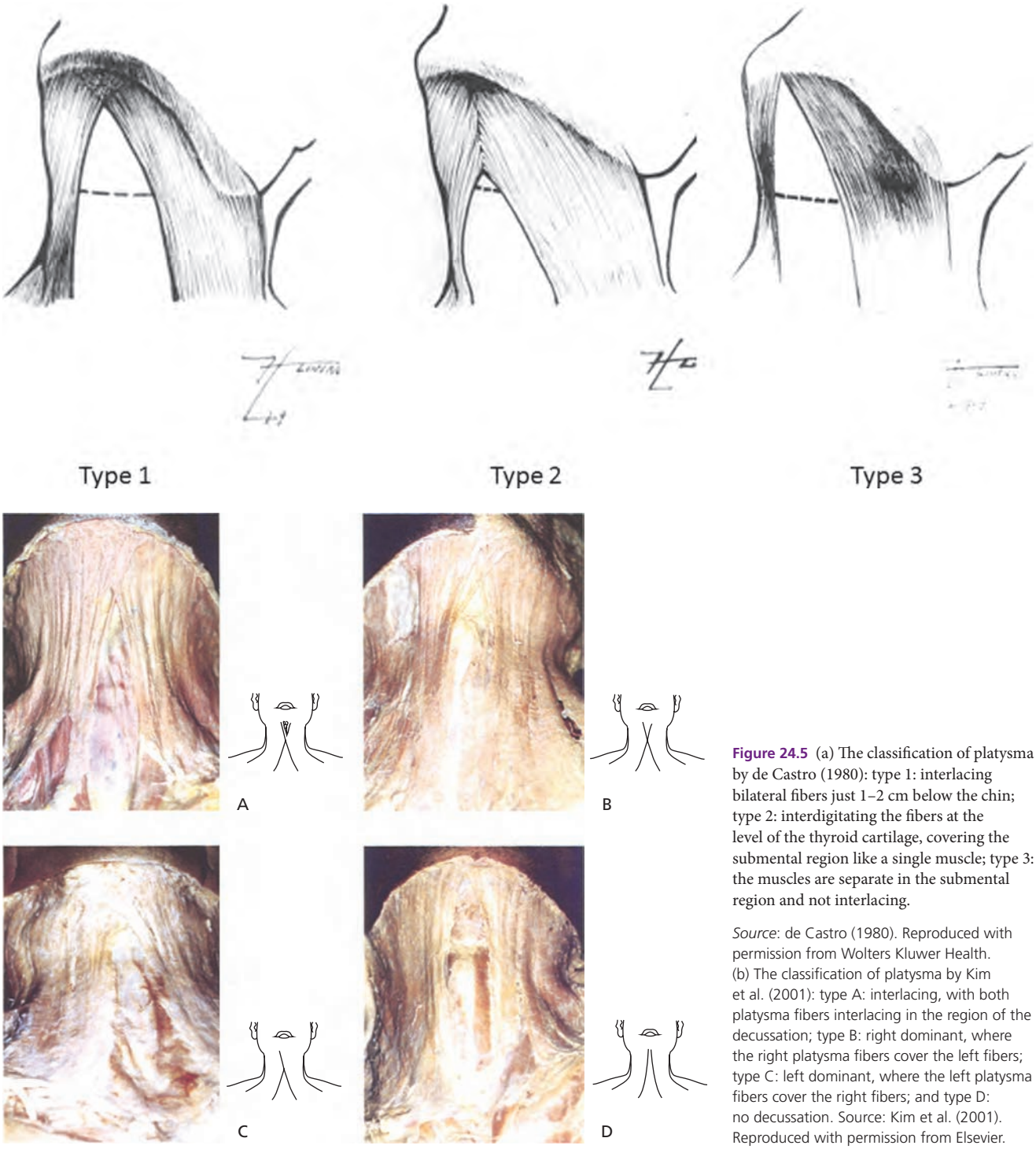

Figure 24.5 (a) The classification of platysma by de Castro (1980): type 1: interlacing bilateral fibers just 1–2 cm below the chin; type 2: interdigitating the fibers at the level of the thyroid cartilage, covering the submental region like a single muscle; type 3: the muscles are separate in the submental region and not interlacing.

Source: de Castro (1980). Reproduced with permission from Wolters Kluwer Health. (b) The classification of platysma by Kim et al. (2001): type A: interlacing, with both platysma fibers interlacing in the region of the decussation; type B: right dominant, where the right platysma fibers cover the left fibers; type C: left dominant, where the left platysma fibers cover the right fibers; and type D: no decussation. Source: Kim et al. (2001). Reproduced with permission from Elsevier.

where the left platysma fibers cover the right fibers; and type D, with no decussation (Fig. 24.5b). In the classification of de Castro (1980), in a comparison among ethnic groups type 1 was the most predominant and type 2 was the next-most prevalent pattern in South Americans and Caucasian populations. However, in Asians (Korean), type 1 and type 2 had the same rate and were the most prevalent patterns (Kim et al. 2001). Differences between genders have also been described, with the platysma muscle being bulky in males and thin in females.

At the lateral side, the muscle fiber may insert into the mastoid process, auricular concha, ear lobe, or occipital bone. Platysma muscles may also unite with the transverse nuchae muscle.

On the caudal side, the platysma muscle may extend down to the deltoid muscle, the upper lobe of the mammary gland, and to the opposite side at the level between the second and the third costal cartilage. Part of the slip may also join the latissimus dorsi (Macalister 1875).

Transverse menti muscle

The transverse menti muscle is inconsistent and runs beneath the chin and connects the bilateral depressor anguli oris muscles (D'Andrea and Barbaix 2006). Weaver (1978) reported that this muscle was found in 9 of 16 cases (56%) of Caucasian cadavers. D'Andrea and Barbaix (2006) reported the frequency of this muscle as 88% in the population. This muscle may be the same as the anomalus menti of Theile.

Muscles of mastication and other inconsistent muscles in the infratemporal fossa

In the masseter, temporalis, and lateral pterygoid muscles, variations of origin and insertion of muscles have been reported. The masseter muscle may fuse with other mastication muscles such as temporalis or buccinators, and is rarely absent. Temporalis minor, which arises anterior to the temporalis muscle and inserts onto the mandibular notch, has rarely been reported.

Pterygoideus proprius, pterygo-spinous, pterygo-fascialis, and spheno-temporalis muscles are inconsistent muscles, which are not involved in the movement of mandibular bone.

Masseter muscle

The masseter muscle consists of a superficial part and a deep part. As variations of this muscle, Macalister (1875) reported two parts of the muscle which were sometimes separated. Furthermore, a bursa was observed between the two parts or between the deep part and the joint capsule, a part of the muscle fibers, which coalesce with the temporalis muscle or the buccinator muscle. Absence of the muscle was reported in the case of phocomelia, a slip of the deep part of the muscle arising from the external lateral ligament of the temporomandibular joint (Macalister 1875).

Temporalis muscle

Temporalis muscles may have more extensive origins than other muscles (Bergman et al. 1995), and the tendon of insertion sometimes extends to the last molar tooth (Macalister 1875). Hypertrophy of the temporalis muscle has been reported. This condition was first reported by Legg in 1880. Usually, temporalis muscle hypertrophy results from psychogenic muscle hyperactivity, can occur on both sides, and is associated with masseter muscle hypertrophy. However, Wilson and Brown (1990) reported unilateral temporalis muscle hypertrophy not associated with masseter muscle hypertrophy. This is an extremely rare condition, and only eight cases have ever been reported (Wilson and Brown 1990; Serrat et al. 1998; Lowry and Helling 2003; Prantle et al. 2005; Ozturk et al. 2007; Wang et al. 2013). The cause of this condition is unclear and is presumed to be idiopathic (Serrat et al. 1998). Wang et al. (2013) summarized the previous reported cases as occurring, on average, at 35 years of age, more commonly in Caucasians, at a slightly higher rate in females, and with no laterality. A so-called temporobuccinator band may be present, which may have the function of pulling the cheek away from the teeth during mastication (Buck 2007).

Temporalis minor muscle

Henle (1871) reported that the temporalis minor muscle arose from the anterior aspect of the temporalis muscle, forming distinct muscle bands to the temporalis muscle, and inserting onto the mandibular notch (Bergman et al. 1995). Additional detailed studies concerning this muscle have not been found in the literature.

Medial pterygoid muscle

The medial pterygoid muscle may extend a fascicle to the masseter muscle and this may give rise to the styloglossus muscle (Bergman et al. 1995).

Lateral pterygoid muscle

Cases of the lateral pterygoid muscle joining to the temporal muscle or digastric muscle have been reported (Macalister 1875). Various studies have been reported concerning the origin and insertion of the muscle. Bertilsson and Ström (1995) surveyed previous reports concerning the lateral pterygoid muscle: 65% of the articles claimed the muscle consisted of two heads, a superior head and an inferior head, while 20% reported only a single head and 10% found three heads (Bertilsson and Ström 1995). According to Fujita et al. (2001), the lateral pterygoid muscle had three heads in 35% of the cases and the remaining 65% had two heads. The second type had a third inner head which originated from the greater wing of the sphenoid, and was separated by the fascia from other heads further than the normal superior and inferior heads.

With regards to the insertion, 60% of the reports stated that the muscle had three insertions, an articular disc, a temporomandibular joint capsule, and a condyle. Thirty percent of the reports found that the majority of the muscle fibers inserted into the condyle and a few fibers inserted into the articular disc. Another 10% of the reports stated that the muscle fibers inserted only into the condyle (Bertilsson and Ström 1995).

Pterygoideus proprius muscle

The pterygoideus proprius muscle was first described by Henle in 1858 as a nearly vertical slip originating from the infratemporal crest of the greater wing of the sphenoid, inserting into the tuber palati or external pterygoid plate (Fig. 24.6; Macalister 1875; Tubbs et al. 2007). In addition, the muscle may send the slip to the pterygo maxillary ligament or to the mandibula (Bergman et al. 1995), and the inferior head of the lateral pterygoid muscle may arise from the slip (Macalister 1875). Akita et al.

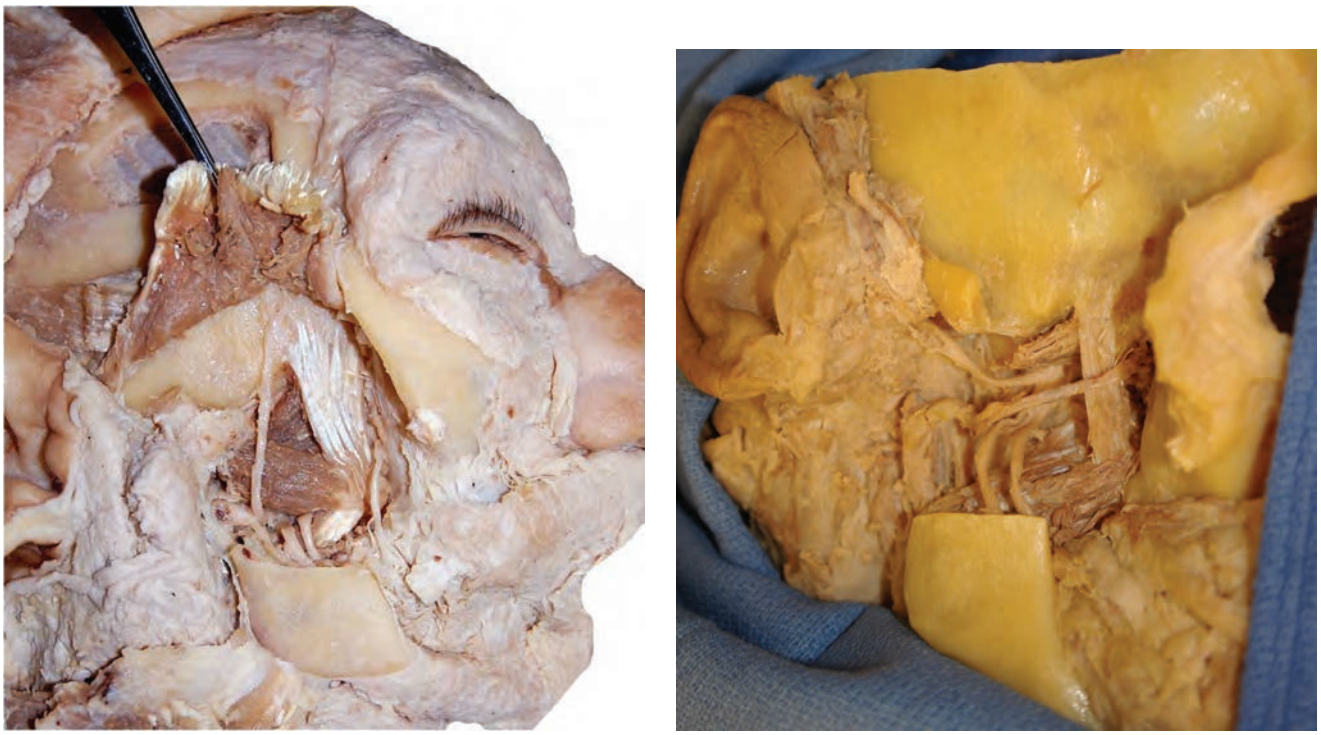

Figure 24.6 Two cases of pterygoideus proprius muscle. Images courtesy of RS Tubbs, Seattle Science Foundation, Seattle, WA.

(2001) reported that the muscle arises from the medial surface of the anteromedial muscle bundle of the temporalis, although they reported that the muscle arose from the infratemporal crest of the greater wing of the sphenoid in one case. The slip consists of a mixture of muscular and tendinous fibers, but sometimes entirely of tendinous fibers. Akita et al. (2001) reported that this muscle was observed in 4.5% of Japanese dissection cases.

Pterygospinous muscle

The pterygospinous muscle is rarely observed with muscle fibers passing along the pterygospinous ligament, or sometimes replacing the ligament (Fig. 24.7). In one case, the course of the pterygospinous muscle arose from the posterior edge of the lateral pterygoid plate between the two pterygoid muscles, and inserted into the spinous process of sphenoid (Macalister 1875; Poland 1890; Nathan 1989). Poland (1890) described this muscle as having 12 different forms.

Pterygofascialis muscle

Poland (1890) described two case studies of the pterygofascialis muscle. According to his description, this muscle arose from the internal lateral ligament of the temporomandibular joint, ran inferiorly, and connected to the posterior margin and outer aspect of the medial pterygoid muscle. Poland (1890) also found a variant of this muscle that also attached to the lateral pterygoid muscle.

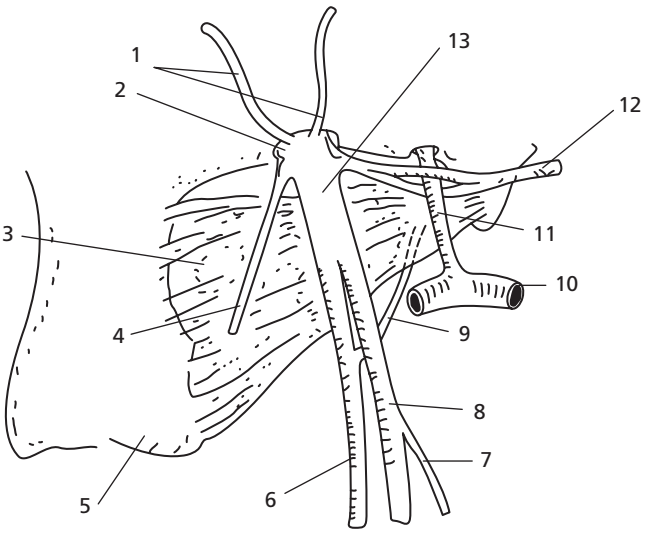

Figure 24.7 Schematic right lateral view showing the attachments and relations of the pterygospinous muscle. 1: temporal nerve; 2: foramen ovale; 3: pterygospinous muscle; 4: buccal nerve; 5: pterygoid process lateral plate; 6: lingual nerve; 7: mylohyoid nerve; 8: inferior alveolar nerve; 9: chorda tympani nerve; 10: maxillary artery; 11: middle meningeal artery; 12: auriculotemporal nerve; 13: mandubular nerve.

Source: Nathan (1989). Reproduced with permission from Elsevier.

Figure 24.8 A case of sphenotemporalis muscle: (a) schematic drawing of (b) cadaveric image. C, condyle of mandible; d, inferior alveolar and lingual nerves; g, great wing of sphenoid bone; l, lateral pterygoid muscle, lower head; m, maxillary artery; p, medial pterygoid muscle; r, ramus of mandible; s, sphenotemporalis muscle; t, squamous temporal bone; u, lateral pterygoid muscle: upper head; za, zygomatic arch anterior; zp, zygomatic arch posterior.

Source: Mack (1984). Reproduced with permission from John Wiley & Sons.

Sphenotemporalis muscle

Mack (1984) described the sphenotemporalis muscle as a newly reported muscle in humans. He reported that this muscle arose from the greater wing of the sphenoid bone, ran in a horizontal plane, and inserted into the anterior aspect of the articular eminence on the surface of the squamous part of the temporal bone (Fig. 24.8).

Other

A muscle extending from the pterygoid fossa to the spine of the sphenoid has been described (Poland 1890). Rarely, the lateral pterygoid is attached to the digastric muscle and a third head may be present and seen attaching to the temporomandibular disc (Lang 1995).

References

Akita K, Shimokawa T, Sato T. 2001. Aberrant muscle between the temporalis and the lateral pterygoid muscles: M. pterygoideus proprius Henle. *Clin Anat* 14: 288–291.

Alexiou D, Manolidis C, Papaevangellou G, Nicolopoulos D, Papadatos C. 1976. Frequency of other malformations in congenital hypoplasia of depressor anguli oris muscle syndrome. *Arch Dis Childhood* 51: 891.

Alfonso I, Miranda LF, Reeves-Garcia J, Checa RM, Guevara C. 2010. Agenesis of the corrugator supercilii: a benign condition. *J Child Neurol* 253: 383–386.

Hrdlicka A. 1919. Morphological anthropometry. *Am J Phys Anthropol* 2: 429.

Bergman RA, Afifi AK, Miyauchi R. 1995. Illustrated Encyclopedia of Human Anatomic Variation. Available at: http://www.anatomyatlases.org/ (accessed 10 October 2015).

Bertilsson O, Ström D. 1995. A literature survey of a hundred years of anatomic and functional lateral pterygoid muscle research. *J Orofac Pain* 9: 17.

Buck WR. 2007. Letter to the Editor. *Clin Anat* 20: 1000.

Burkitt AN, Lightoller GHS. 1927. The facial musculature of the Australian Aboriginal: Part II. *J Anat* 62(1): 33.

Clemente CD. 1985. *Gray's Anatomy, 30th American edition*. Baltimore: Williams and Wilkins.

D'Andrea E, Barbaix E. 2006. Anatomic research on the perioral muscles, functional matrix of the maxillary and mandibular bones. *Surg Radiol Anat* 28(3): 261–266.

de Castro CC. 1980. The anatomy of the platysma muscle. *Plast Reconstr Surg* 66: 680–683.

De Mey A, Van Hoof I, De Roy G, Lejour M. 1989. Anatomy of the orbicularis oris muscle in cleft lip. *Brit J Plast Surg* 42: 710–714.

Freilinger G, Happak W, Burggasser G, Gruber H. 1990. Histochemical mapping and fiber size analysis of mimic muscles. *Plast Reconstr Surg* 86(3): 422–428.

Fujita S, Iizuka T, Dauber W. 2001. Variation of heads of lateral pterygoid muscle and morphology of articular disc of human temporomandibular joint: anatomical and histological analysis. *J Oral Rehabil* 286: 560–571.

Henle J. 1871. Handbuch der Eingeweidelehre des Menschen Vol. 1. Braunschweig: Druck und Verlag von Friedrich Vieweg und Sohn.

Hoogbergen MM, Schuurnian AH, Rijnders W, Kon M. 1996. Auricular hypermobility due to agenesis of the extrinsic muscles. *Plast Reconstr Surg* 98: 869–871.

Hu KS, Jin GC, Youn KH, Kwak HH, Koh KS, Fontaine C, Kim HJ. 2008. An anatomic study of the bifid zygomaticus major muscle. *J Craniofac Surg* 19: 534–536.

Hur MS, Hu KS, Park JT, Youn KH, Kim HJ. 2010. New anatomical insight of the levator labii superioris alaeque nasi and the transverse part of the nasalis. *Surg Radiol Anat* 32: 753–756.

Hwang K, Lee DK, Chung IH, Chung RS, Lee SI. 2002. Identity of "orbitozygomatic muscle". *J Craniofac Surg* 13(2): 202–204.

Kim HJ, Hu KS, Kang MK, Chung IH, Hwang K. 2001. Decussation patterns of the platysma in Koreans. *Brit J Plast Surg* 54: 400–402.

Kopsch F. 1908. *Rauber's Lehrbuch Anatomie des Menshen*. Leiptiz: Gerog Theme.

Lahat E, Heyman E, Barkay A, Goldberg M. 2000. Asymmetric crying facies and associated congenital anomalies: prospective study and review of the literature. *J Child Neurol* 15: 808–810.

Lang J. 1995. *Clinical Anatomy of the Masticatory Apparatus and Peripharyngeal Spaces*. New York: Thieme.

Le Double AF. 1906. *Traité des variations des os de la face de l'homme: et de leur signification au point de vue de l'anthropologie zoologique*. Paris: Vigot Frères.

Lei T, Cui L, Zhang YZ, Shi GJ, Peng P, Wang XH, Gao JH. 2010. Anatomy of the transversus nuchae muscle and its relationship with the superficial musculoaponeurotic system. *Plast Reconstr Surg* 126: 1058–1062.

Lowry TR, Helling E. 2003. Unilateral temporal muscle hypertrophy: a rare clinical entity. *Ear Nose Throat J* 82: 198–199.

Macalister A. 1875. Additional Observations on Muscular Anomalies in Human Anatomy. Third Series With a Catalogue of the Principal Muscular Variations Hitherto Published. *Trans Royal Irish Acad* 25: 1–134.

Mack PJ. 1984. Sphenotemporalis: a new muscle in man. *J Anat* 139: 587.

McAlister RW, Harkness EM, Nicoll JJ. 1998. An ultrasound investigation of the lip levator musculature. *Europ J Orthodont* 20: 713–720.

Nada Y, Sasaki K, Nozaki M, Soejima K. 1998. Congenital partial absence of the facial muscles. *Brit J Plast Surg* 51: 138–141.

Nathan H. 1989. The pterygo-spinous muscle: an aberrant atavic remnant. *Anatomischer Anzeiger* 169: 97.

Nelson DW, Gingrass RP. 1979. Anatomy of the mandibular branches of the facial nerve. *Plast Reconstr Surg* 64: 479–482.

Ohtsuka H. 2005. Hypertrophy of the depressor septi nasi muscle. *Plast Reconstr Surg* 116: 1817.

Ozturk E, Mutlu H, Sonmez G, Sildiroglu HO, Basekim CC, Kizilkaya E. 2007. Unilateral temporalis muscle hypertrophy with contralateral masseteric hypertrophy. *Dentomaxillofac Radiol* 36: 296–297.

Papadatos C, Alexiou D, Nicolopoulos D, Mikropoulos H, Hadzigeorgiou E. 1974. Congenital hypoplasia of depressor anguli oris muscle A genetically determined condition? Arch Dis Child 49: 927–931.

Park JT, Youn KH, Hur MS, Hu KS, Kim HJ, Kim HJ. 2011. Malaris muscle, the lateral muscular band of orbicularis oculi muscle. *J Craniofac Surg* 22: 659–662.

Park JT, Youn KH, Lee JG, et al. 2012. Medial muscular band of the orbicularis oculi muscle. *J Craniofac Surg* 23(1): 195–197.

Perlman M, Reisner SH. 1973. Asymmetric crying facies and congenital anomalies. *Arch Dis Child* 48: 627.

Pessa JE, Zadoo VP, Adrian Jr EK, Yuan CH, Aydelotte J, Garza JR. 1998. Variability of the midfacial muscles: analysis of 50 hemifacial cadaver dissections. *Plast Reconstr Surg* 102: 1888–1893.

Poland J. 1890. Variations of the external pterygoid muscle. *J Anat Physiol* 24(4): 567.

Prantl L, Heine N, Ulrich D, Eisenmann-Klein M. 2005. Recurrence of isolated unilateral temporalis muscle hypertrophy: case report. *Aesth Plast Surg* 29: 574–575.

Roedel R, Christen HJ, Laskawi R. 1998. Aplasia of the depressor anguli oris muscle: A rare cause of congenital lower lip palsy? *Neuropediatrics* 29: 215–219.

Sato S. 1968. Statistical studies on the exceptional muscles of the Kyushu-Japanese. 1. The muscles of the head the facial muscles. *Kurume Med J* 15: 69.

Schmidt HM. 1982. Transversus nuchae muscle: two observations of hitherto unknown deviations of its nerve supply. *Anatomischer Anzeiger* 151: 144.

Sekine J, Hamada N, Toh H, Ohmori T. 1988. An anomalous case of the risorius arising from the masseter tendon. *Okajimas Folia Anat Jap* 65: 29.

Serrat A, Garcia-Cantera JM, Redondo LM. 1998. Isolated unilateral temporalis muscle hypertrophy: A case report. *Intern J Oral Maxillofacial Surg* 27: 92–93.

Shimada K, Gasser RF. 1989. Variations in the facial muscles at the angle of the mouth. *Clin Anat* 2: 129–134.

Singhi S, Sihghi P, Lall KB. 1980. Congenital asymmetrical crying facies. *Clin Pediatr* 19: 673–678.

Tubbs RS, Stetler W, Shoja MM, Loukas M, Salter EG, Oakes WJ. 2007. An unusual muscular variation of the infratemporal fossa. *Folia Morphol* 66: 200.

von Lanz T, Wachsmuth W. 1955. *Praktische Anatomie*. Berlin: Springer-Verlag.

Wang BH, Moon SJ, Wang H, Olivero WC. 2013. Isolated unilateral temporalis muscle hypertrophy: Case report. *J Neurosur Pediatr* 11: 451–453.

Weaver C. 1978. Frequency of occurrence of the transversus menti muscle. *Plast Reconstr Surg* 6: 231–233.

Wilson PS, Brown AMS. 1990. Unilateral temporalis muscle hypertrophy: case report. *Intern J Oral Maxillofac Surg* 19: 287–288.

Zufferey J. 1992. Anatomic variations of the nasolabial fold. *Plast Reconstr Surg* 89: 225–231.

Zufferey JA. 2013. Is the malaris muscle the anti-aging missing link of the midface? *Europ J Plast Surg* 36(6): 345–352.

25 Anterior neck muscles

Hye Yeon Lee[1] and Hee Jun Yang[2]
[1]Yonsei University College of Medicine, Seoul, Korea
[2]Gachon Graduate School of Medicine, Incheon, South Korea

Mylohyoid

Traditionally, the mylohyoid is described as running from the mandible to the hyoid, but it does not always extend to the hyoid bone. Instead, it can fuse with neighboring muscles. Previous studies have described instances of an accessory mylohyoid muscle that inserts along the anterior belly of the digastric on the contralateral side and the left posterior portion of the ipsilateral part of the hyoid, as well as the mylohyoid raphe and the hyoid body. Herniation through the mylohyoid has been reported in around 40% of individuals. Such herniations typically occur near the submandibular or sublingual glands. Division of the mylohyoid by a vein has also been reported. Absence of the mylohyoid is rare. The mylohyoid may not extend to the hyoid bone and may fuse with neighboring muscles. The median raphe may be indistinct. An accessory mylohyoid muscle can be found arising from the left mylohyoid line and inserted into the lower portion of the mylohyoid raphe and hyoid bone. The hypoglossal nerve can innervate the mylohyoid.

Digastric

The mylohyoid and the anterior belly of the digastric remain closely related. They usually exchange some fibers, sometimes resulting in complete fusion between the two muscles or in a digastric originating from the mylohyoid. Both sides of the anterior bellies of the digastric muscle can also be united by conversion of the fascia that typically passes between them into muscular tissue. There is also a close relationship between the stylohyoid and the posterior belly of the digastric, as one or the other occasionally fails to separate from the common mass from which they are derived. Occasionally, the posterior belly fuses completely with the stylohyoid muscle. Fasciculi can also pass from either belly of the two muscles to neighboring structures.

In cases in which the anterior belly is absent, the posterior belly inserts into the angle of the mandible instead of the hyoid. The posterior belly of the digastric can originate from any part of the mastoid groove or even from the outer portion of the superior nuchal line.

Doubling of the anterior belly is a rather common variation. An accessory anterior belly, which may or may not cross the midline, has been reported in 66.7% of individuals; it has often been observed bilaterally or even symmetrically. An accessory anterior belly can arise from the intermediate tendon, the main anterior belly, or the hyoid. Some accessory bellies have their own tendon running from the origin of the main anterior bellies to the hyoid bone with a common fibrous band. An accessory posterior belly may arise from the sternohyoid muscle.

Instances of insertion of additional muscles on an intermediate tendon of the digastric are considered as tri- or quadrigastric muscles. Studies have described a third head arising from the inferomedial aspect of the mandible and inserting on an intermediate tendon of the digastric muscle. Other reports include a trigastric formation involving the splitting of the stylohyoid muscle, through which the external carotid artery passes with its facial and occipital branches. In these cases, the more superficial portion of the stylohyoid accompanies the posterior belly of the digastric and inserts into the intermediate tendon of the digastric muscle. Along the medial border of the anterior belly, an independent muscle between the body of the hyoid and the symphysis of the mandible, termed the mentohyoid, has also been described as the third head of a trigastric muscle. A hyoangularis muscle (Macalister 1871, 1875) has been described traveling from the hyoid to angle of the mandible.

The digastric is frequently divided by a tendinous inscription. In some cases there is no intermediate tendon, the posterior belly inserting onto the styloid process while the anterior belly inserts onto the lateral side of the hyoid body.

Variations of the digastric muscle have been classified into 10 different types according to variations in the anterior and posterior bellies, as well as the intermediate tendon (De-Ary-Pires et al., 2003).

Stylohyoid

The stylohyoid can be absent uni- or bilaterally; it can also be duplicated. Santorini referred to the second muscle as the stylohyoideus nanus. The second slip, the stylohyoideus profundus,

Bergman's Comprehensive Encyclopedia of Human Anatomic Variation, First Edition. Edited by R. Shane Tubbs, Mohammadali M. Shoja and Marios Loukas.
© 2016 John Wiley & Sons, Inc. Published 2016 by John Wiley & Sons, Inc.

varies in its insertion, sometimes accompanying the stylohyoid proper and sometimes inserting into the lesser cornu of the hyoid; in some cases it can even replace the stylohyoid ligament. An accessory muscle arising from the styloid process and inserting onto the lesser horn of the hyoid has been termed the stylochondrohyoideus muscle. A variant of this muscle has been described that enveloped the stylohyoid ligament and inserted into its distal fibers (Lambert et al. 2010).

If the stylohyoid fails to divide near its insertion (which typically permits passage of the intermediate tendon of the digastric), the insertion can comprise a single head passing in front of or behind the digastric tendon.

A bundle of muscle fibers may pass from the tip of the styloid process to the angle of the mandible, forming what some consider the stylomandibularis.

Geniohyoid

Portions of the muscle may be missing. A supernumerary geniohyoid is known as the superior geniohyoid muscle of Ferrein. Mori (1964) found that the muscle is often divided into superficial and deep layers. The muscle can be blended with the geniohyoid of the opposite side. Slips to the genioglossus can occur.

Platysma

With the platysma, a decussation of the two contralateral muscles is usually found across the median line, especially in their upper parts. About 48% of decussations result from interlacing, 34% from covering of the left fibers by the right fibers, and 19% from covering of the right fibers by the left fibers. Additionally, three different degrees of decussation have been noted: the medial fibers interlace with those on the opposite side just below the chin (43–75%); the muscular layer covers the submental region because of fiber interlacing at the level of the thyroid cartilage (15–43%); or the fibers do not interlace (10–14%). Development of the platysma is subject to considerable variation; it sometimes forms a very thin, pale layer largely interspersed among connective tissue and at other times it forms strong, deeply colored bundles with much less intermixing with connective tissue. Its extension upon the face can also vary considerably, sometimes being traceable as high as the zygoma and, dorsally, to behind the ear. On the other hand, the muscle can be considerably reduced in size, especially distally; the lower half can also be completely absent. Also, the facial part of the platysma occupies a larger portion of the face in females than in males. Rarely, a deep transverse layer is found. The platysma is intimately but variably associated with the mentalis.

A rare but notable case of a muscle described as the sphincter colli profundus has been reported. In this case, a muscle sheet arose deep to the platysma from the medial part of the clavicle and inserted into the fascia of the pinna. The platysma was reduced in size and supraclavicularis and mandibulomarginalis muscles were present. Slips arising from the occipital bone and crossing anterior to the sternocleidomastoid muscle have been found merging with the platysma near the midline. This muscle was termed the cleido-occipital platysma muscle by its authors (Kumar et al. 2009) and is probably the same muscle described as the occipital teres muscle, lesser occipital muscle, or corrugator posticus muscle.

Infrahyoid muscles in general

Infrahyoid muscles vary considerably in the extent of their development. Except for the omohyoid, they can be classified as a rectus muscular system; the omohyoid is considered as an obliquus internus muscular system of the trunk muscles of the neck.

A strap-like muscle called the sternohyoideus azygos may be found in the midline of the neck from the posterior surface of the manubrium to the hyoid bone.

Each infrahyoid muscle may be divided longitudinally into two distinct fasciculi, or they may send fasciculi to each other or to the pretracheal layer of the cervical fascia. The infrahyoid muscles can vary in their origins or insertions. Unusual infrahyoid muscles include: the cleidofascialis, which originates from the medial third of the clavicle and inserts into cervical fascia; the cleidohyoideus, which originates behind the origin of the cleidomastoid part of the sternocleidomastoideus and inserts on to the body of the hyoid cartilage; and the m. hyofascialis, which originates from the hyoid and inserts into the omosternoclavicular fascia. The m. cervicocostohumeralis is considered a case of extreme displacement of the omohyoid. This muscle originates from the lesser tubercle of the humerus and inserts along the transverse process of the sixth cervical vertebra and the cartilage of the first rib.

Omohyoid muscle

The omohyoid is the most frequently absent of the infrahyoid muscles. It is more common for one belly than both to be absent. When the inferior belly is absent, the superior belly arises from the clavicle and the resulting muscle is regarded as the cleidohyoideus, which has been observed in 3–6% of cases. The omohyoid and an accessory cleidohyoid can also coexist. When the superior belly is absent, the muscle has been known as the musculus coracocervicalis (of Krause). In contrast to the superior belly the inferior belly may be doubled, with the second belly possibly arising from the coracoid process. A supernumerary bundle of the superior bellies, potentially arising from the sternum, has been found in 3–7% of all cases. A fusion between the sternohyoid muscle and the medial part of the superior belly of a doubled omohyoid muscle has also been reported. A doubled or accessory omohyoid of varying incidence has been noted to arise from the scapular as a flesh belly or a fibrous band and insert on the hyoid bone, the sternohyoid, or the sternothyroid muscle. An accessory omohyoid may or may not comprise an intermediate tendon.

The superior belly sometimes receives slips from the sternum that can insert onto the sternohyoid muscle (1–3%). It may have an accessory slip to the hyoglossus, mylohyoid, or the greater cornu of the hyoid bone. This slip can insert along the mandible or even to the cervical vertebrae. The region between the omohyoid and sternohyoid may be filled with muscle instead of fascia. This primitive sheet of muscle is referred to by various names: the sterno-cleido-omo-hyoid; omosterno-cleido-hyoideus; episterno-cleido-hyoideus superficialis; or the sterno-omo-hyoid. Similar variations of intermediate morphologies between normal and anomalous superior bellies have been reported in 27% of cases in a Japanese population.

An extra fasciculus of the inferior belly can arise from the clavicle (3–10%), the superior transverse scapular ligament (17.2–20%), or the coracoid process or coracoclavicular ligament (c. 7%). The inferior belly can also arise from the scapular spine, acromion, or even the first rib, attaching along the entire length of the clavicle.

The intermediate tendon of the omohyoid may be reduced to a tendinous inscription; in about 10% of cases it is absent. The inferior belly may attach to the supraspinatus muscle (Anderson 1881). The muscle may lie deep to the internal jugular vein (Kasapoglu and Dokuzlar 2007).

Sternohyoid

In some instances the sternohyoid is absent; when present, it can be duplicated or split. It can also comprise a second head from the clavicle, or an accessory slip from the second rib. In addition it can arise from the clavicle and not the sternum, so it may be confused with the cleidohyoid muscle. The sternohyoid can connect with the superior belly of omohyoid muscle. It should be differentiated from a variation of the omohyoid muscle. It can arise from the posterior sternoclavicular ligament, or near the costal cartilage of the first rib. Fibers from both sides of the muscle may decussate or fuse with each other. Part of the muscle has been observed to fuse with the sternothyroid or the anterior belly of the omohyoid. The sternohyoid can give a slip to the mylohyoid, cricoid cartilage, or the hyoid bone. The prelaryngeus obliquus can attach to the sternothyroid. The sternohyoid may fuse at various points or be continuous along most of its length with the contralateral sternohyoid muscle. An occipitohyoid may arise from the occiput and travel superficial to the sternocleidomastoid muscle to attach anteriorly to the hyoid bone.

Sternothyroid

The sternothyroid muscle can comprise a membranous tendon that connects the belly of both sides of the muscle or a muscle strap that fuses both sides of the muscle. The muscle may be duplicated. The medial fibers on both sides of the sternothyroid can form a cruciate pattern. The muscle can exist in two strata or it may be divided longitudinally into bundles; the lateral bundle may terminate at the cervical fascia. The prelaryngeus obliquus can attach to the sternothyroid.

Rennie (1886) described a sternopetrosopharyngeus muscle. This muscle arose from the anterior surface of the manubrium and passed up the right side of the neck, superficial to the sternohyoid, sternothyroid, and omohyoid, and then traveled over the hypoglossal nerve where it passed between the internal and external carotid arteries to run between the digastric and stylohyoid muscles. The muscle then split, with one part ending on the vaginal process of the temporal bone and in contact with the levator veli palati, and two smaller parts ending in the lower border of the superior pharyngeal constrictor muscle. The muscle was supplied by the glossopharyngeal nerve.

Thyrohyoid

The thyrohyoid can insert onto the cricoid cartilage. For this reason, the cricohyoid muscle is often described as a variant of the thyrohyoid. The thyrohyoid is often continuous with the sternothyroid. A keratothyroidhyoid and a basithyrohyoid muscle were described by Shattock (1883). The hypothyroid accessory muscle is a part of the thyrohyoid and is known as the muscle of von Sömmerring.

Levator glandulae thyroidea

A bundle of fibers termed the levator glandulae thyroidea is sometimes found. In standard anatomical texts the levator glandulae thyroidea muscle is described as an accessory muscle, originating from the pharynx or the hyoid bone and inserting into the isthmus or pyramidal lobe of the thyroid gland. A fibrous band is sometimes found attached to the body of the hyoid bone and to the isthmus of the gland or pyramidal lobe. Skandalakis (2004) termed this fibrous band the suspensory ligament of the thyroid gland. According to other authors, when the band is muscular, it is termed the levator glandulae thyroidea (Hollinshead 1969). A report by Kumar et al. (2005) showed an levator glandulae thyroidea with both ligamentous and muscular parts.

Interestingly, several variations of the levator glandulae thyroidea have been reported in the literature regarding the various forms of attachment to the thyroid gland. According to Bergman et al. (1988), the levator glandulae thyroidea is sometimes found passing either from the lower border of the hyoid or from the thyroid cartilage to the lobe, isthmus, or pyramidal lobe of the thyroid gland. Furthermore, a different form of levator glandulae thyroidea includes fibers of the inferior pharyngeal constrictor muscle to the thyroid gland.

Mori (1964) studied the levator glandulae thyroidea. However, there are no reports in the literature correlating the findings of Mori with clinical symptoms or surgical procedures. Although there are no reports establishing the prevalence of the levator glandulae thyroidea in the general population, Lehr (1979) indicated that the prevalence of a levator glandulae thyroidea is 1 in 203 cases (0.49%).

In contrast, Watanabe and Suda (1962) reported a prevalence of levator glandulae thyroidea in 6 out of 7 cadavers (85.7%). A more recent report by Harjeet et al. (2004) indicated that the prevalence of the levator glandulae thyroidea was found to be 19.8%.

In textbooks of anatomy, the levator glandulae thyroidea is described as an occasional unpaired or paired muscle which extends from the hyoid bone to the isthmus of the pyramidal lobe, more frequently on the left side (Hollinshead 1969; Standring et al. 2005). According to Eisler (1900) and Kopsch (1908) the levator glandulae thyroidea could arise from the hyoid bone, thyroid cartilage, or the inferior constrictor muscle. A case has also been reported in which the levator glandulae thyroidea took its origin from the mastoid process (Saadeh et al. 1996).

In his study of 210 levator glandulae thyroidea, Mori (1964) classified the levator glandulae thyroidea into five types according to their origin and insertion: hyopyramidalis; thyreopyramidalis; thyreoglandularis; hyoglandularis; and tracheoglandularis. The most common variation (54.7%) was the thyreoglandularis muscle, originating from the thyroid cartilage and inserting into the sheath of the thyroid gland. The second most common variation (25%) was the hyopyramidalis muscle originating from the hyoid bone and inserting into the tip of the pyramidal lobe. The remaining muscles were the thyreopyramidalis (originating from the thyroid cartilage and inserting onto the tip of the pyramidal lobe), the hyoglandularis (originating from the hyoid bone and inserting onto the sheath of the thyroid gland), and the tracheoglandularis (originating from the upper trachea to insert onto the isthmus of the thyroid gland).

Regionally, a thyreotrachealis muscle has been reported (Sujata et al. 2013). This muscle arose from the anterior surface of the trachea and passed over the thyroid gland to attach to the cricothyroid and inferior constrictor muscles. It was innervated by the ansa cervicalis. According to Eisler (1900) and Keyes (1940), the levator glandulae thyroidea could be innervated either through the ansa cervicalis or through branches of the vagus, most often its external laryngeal branch (McMinn 1994). It is usually assumed that the levator glandulae thyroidea is derived from the infrahyoid musculature but its innervation is not always in accordance with this (Hollinshead 1969). Eisler (1900) classified the levator glandulae thyroidea according to its innervation and based this on proposed embryonic origins. The anterior levator glandulae thyroidea, derived from the cricothyroid muscle, is innervated by the external laryngeal branch of the superior laryngeal nerve. The lateral levator glandulae thyroidea, derived from the thyrohyoid muscles or from the infrahyoid muscle group as a whole, and attached to the hyoid bone, is innervated by the ansa cervicalis. Finally, the posterior levator glandulae thyroidea is innervated similarly to the anterior slips by the superior laryngeal branch of the vagus, and is apparently derived from the inferior constrictor of the pharynx. However, in one case in which the muscle attached to the hyoid bone and was innervated by the superior laryngeal nerve, Eisler (1900) claimed that the muscle was a derivative of the cricothyroid muscle.

Loukas et al. (2008a) reported a levator glandulae thyroidea with three muscular slips and the innervation of the muscle solely from the ansa cervicalis, which does not correspond to the classification scheme of Eisler (1900). Keyes (1940) and Lehr (1979) suggested that the levator glandulae thyroidea is an embryologic derivation of the cricothyroid muscle. According to these authors it is feasible that the thyroid gland, in its passage through the mesoderm, can displace the muscle fibers of origin with the superior laryngeal nerve of the fourth pharyngeal arch (Keyes 1940; Lehr 1979). However, the embryologic mechanism for the development of levator glandulae thyroidea still remains largely unknown.

Sternocleidomastoid

The extent of fusion of the two heads of the sternocleidomastoid varies considerably. The heads are frequently separated into the cleidomastoid and sternomastoid parts; some authors regard this as normal. There may be a supernumerary head from the sternum or clavicle, which can cause significant stenosis of the supraclavicular fossa.

In addition, the muscle frequently separates into other parts that are arranged in two layers: a superficial layer consisting of the superficial sternomastoid, sternooccipital, and cleido-occipital parts, and a deep layer consisting of the deep sternomastoid and cleidomastoid parts. The names indicate the attachments of the various parts. A supernumerary cleido-occipital head, which is more or less separate from the sternocleidomastoid, has been reported at a frequency of 33%. The cleido-occipital muscle may found bilaterally.

Occasionally, the lower portion of the muscle is traversed by a tendinous intersection, a peculiarity of interest in connection with the formation of the muscle by fusion of parts derived from different myotomes.

In many animals, the cleidomastoid portion of the muscle is quite distinct from the sternomastoid portion; this is also frequently found in humans. Other variants of the cleidomastoideus include the cleidoepistrophicus (cleidoaxial muscle of Gruber), which originates from the second cervical vertebra and inserts on the clavicle adjacent to the sternocleidomastoid; the cleidocervicalis, which originates from the carotid tubercle of the fourth cervical vertebra and inserts on the clavicle adjacent to the sternocleidomastoid; and the cleidoatlanticus, which originates from the transverse process of the atlas and inserts on the clavicle about 2 cm away from cleidomastoideus.

The width of the clavicular portion of the muscle is very variable. The origin of the sternocleidomastoideus can spread from the acromial to the sternal end of the clavicle. The sternal head has been observed to extend as far distally as the junction of the

fifth rib. Slips from the muscle can pass to various neighboring structures (e.g., the parotid fascia, thyroid cartilage, angle of the mandible, and the contralateral clavicle); moreover, slips have been found arising from the anterior tubercles of the transverse process of the upper three cervical vertebrae and from the hyoid bone. The entire muscle can be doubled. Rennie (1886) mentioned Macalister's account of an insertion into the tympanic ring.

Cleidocervical or levator claviculae

The cleidocervical or levator claviculae (trachelo-acromial, omocervicalis) muscle travels between the transverse process of the cervical spine and the clavicle in the posterior cervical triangle (Rüdisüli 1995), and is found in 2–3% of individuals. It can originate from the transverse process of the axis (Leon et al. 1995), the transverse process of the sixth cervical vertebra, the anterior tubercle, or the transverse process of the atlas and axis, and attaches to the posterior margin of the clavicle or the middle or lateral third of the posterior surface of the clavicle or the acromion or trapezius. Loukas et al. (2008b) identified this muscle arising from the left transverse processes of C3 and C4.

O'Sullivan et al. described the variation as a muscular slip that originates from the trapezius, traverses anterior to the scalene muscles and inferior belly of the omohyoid and posterior to the spinal accessory nerve before inserting on the posteromedial aspect of the clavicle just lateral to the sternocleidomastoid (O'Sullivan and Kay 1998). The levator claviculae occurs more often unilaterally than bilaterally, with a left-sided predominance (Rubinstein et al. 1999). Capo and Spinner (2007) reported a left-sided levator scapulae, which arose from the anterior tubercle of the C2 transverse process and inserted onto the lateral clavicle. Bilateral reports have also been documented, although they are much less common (Rubinstein et al. 1999). The nerve supply of the levator claviculae has been described as arising from a branch of the fourth cervical nerve and its blood supply as stemming from the ascending cervical artery (Leon et al. 1995).

References

Anderson RJ. 1881. The morphology of the omohyoid muscle. *Dublin J Med Sci* 10: 1–17.

Bergman R, Thompson SA, Afifi AK, Saadek FA. 1988. *Compendium of Human Anatomical Variation*. Baltimore: *Urban Schwarzenberg*.

Capo JA, Spinner RJ. 2007. The levator claviculae muscle. *Clin Anat* 20: 968–969.

Eisler P. 1900. Der M. levator glandulae thyreoidea und verwandte praelaryngeale Muskelbildungen. *Anat Anz* 17: 183–196.

Harjeet A, Sahni D, Jit I, Aggarwal AK. 2004. Shape, measurements and weight of the thyroid gland in northwest Indians. *Surg Radiol Anat* 26: 91–95.

Hollinshead WH. 1969. *Anatomy for Surgeons*, volume 1, second edition. New York: Hoeber Medical Division, Harper & Row.

Kasapoglu F, Dokuzlar U. 2007. An unknown anatomical variation of omohyoid muscle. *Clin Anat* 20: 964–965.

Keyes EL. 1940. Demonstration of the nerve to the levator glandulae thyroidea muscle. *Anat Rec* 77: 293.

Kopsch F. 1908. *Rauber's Lehrbuch der Anatomie des Menschen*. Leipzig: Georg Thieme.

Kumar M, Sundaram S, Fenn A, Nayak SR, Krishnamurthy A. 2009. Cleido-occipital platysma muscle: A rare variant of sternocleidomastoid muscle. *IJAV* 2: 9–10.

Kumar TA, Lekha DS, Kolla S, Rao N, Jothi SS. 2005. Levator glandulae thyroidea: a case report. *J Anat Soc India* 54: 347.

Lambert HW, Atsas S, Dayton TA. 2010. Discovery of a novel variant of the stylochondrohyoideus muscle. *IJAV* 3: 197–199.

Lehr RP. 1979. Musculus levator glandulae thyroidea: An observation. *Anat Anz* 146: 494–496.

Leon X, Maranillo E, Quer M, Sañudo JR. 1995. Case report: Cleidocervical or levator claviculae muscle. A new embryological explanation as to its origin. *J Anat* 187: 503–504.

Loukas M, Merbs W, Tubbs Rs, Curry B, Jordan R. 2008a. Levator glandulae thyroidea muscle with three slips. *Anat Sci Int* 83: 273–276.

Loukas M, Sullivan A, Tubbs RS, Shoja M. 2008b. Levator claviculae. Case report and review of the literature. *Folia Morphol* 67: 307–310.

Macalister A. 1871. The varieties of the styloid muscles. *J Anat Physiol* 5: 28–31.

Macalister A. 1875. Additional observations on muscular anomalies in human anatomy. (third series) with a catalogue of the principal muscular variations hitherto published. *Trans Roy Irish Acad* 25: 1–130.

McMinn RH. 1994. *Last's Anatomy. Head and Neck and Spine*, ninth edition. New York: Churchill Livingstone.

Mori M. 1964. Statistics on the musculature of the Japanese. *Okajimas Folia Anat Jap* 40: 195–300.

O'Sullivan ST, Kay SP. 1998. An unusual variant of the levator claviculae muscle encountered in exploration of the brachial plexus. *J Hand Surg Br* 23: 134–135.

Rennie GE. 1886. On an anomalous muscle in the front of the neck in a human subject: a sterno-petroso-pharyngeus. *J Anat Physiol* 20: 356–358.

Rubenstein D, Escott EJ, Hendbrick LL. 1999. The prevalence and CT appearance of the levator claviculae muscle: A normal variant not to be mistaken for an abnormality. *Am J Neuroradiol* 20: 583–586.

Rüdisüli T. 1995. Demonstration of a musculus levator claviculae. *Surg Radiol Anat* 17(1): 85–87.

Russue IG. 1939. Überzähliges bündel des musculus omohyoidus. *Anat Anz* 88: 420–423.

Saadeh FA, Kawas SH, Haikal FA, Hawi JS. 1996. An unusual levator glandulae thyroidea: A case report and literature review. *J Anat Soc India* 45: 125–128.

Shattock GS. 1883. A "kerato-thyro-hyoid" muscle as a variation in human anatomy. *J Anat Physiol* 17: 124–125.

Skandalakis JE. 2004. *Respiratory System in Skandalakis' Surgical Anatomy*. Athens: Paschalidis Medical Publications.

Standring S, Ellis H, Healy C, Johnson D, Williams A. 2005. *Viscera in Gray's Anatomy*, 39th edition. London: Elsevier Churchill Livingston.

Sujata M, Raju S, Sirisha B, Indira B, Kanchana G, Raghu J. 2013. A thyreotrachealis muscle: a case report. *Eur J Aat* 17: 127–128.

Watanabe S, Suda M. 1962. On the musculus levator glandulae thyroidea of the Ainu. *Saporro Igacu Zasshi* 21: 115–120.

Further reading

Adachi B. 1900. Anatomische untersuchungen an Japanern. *Z Morphol Anthropol* 2: 200–222.

Aktekin M, Kurtoğlu Z, Oztürk AH. 2003. A bilateral and symmetrical variation of the anterior belly of the digastric muscle. *Acta Med Okayama* 57: 205–207.

Anson BJ. 1966. *Morris Human Anatomy*, 12th edition. New York: The Blakiston Division, McGraw-Hill Book Company.

Aziz MA. 1980. Anatomical defects in a case of trisomy 13 with a D/D translocation. *Teratology* 22: 217–227.

Bovero A. 1930. Sur les muscles digastiques de l'os hyoïde. *Arch Ital Biol* 26: 476–485.

Ceccherelli G. 1905. Sur quelques anomalies des muscles peaussiers de la face et de muscle omo-hyoïdien. *Arch Ital Biol* 43: 317–318.

Celik HH, Aldur MM, Ozdemir B, Akşit MD. 2002. Abnormal digastric muscle with unilateral quadrification of the anterior belly. *Clin Anat* 15: 32–34.

Chiba I, Ogawa T, Onodera H, Toshibe T, Saijoh T, Saitoh F, Saitoh M. 1958. Abnormal muscles of sternohyoid and omohyoid. *Iwateidai Kaibou Gyouseki* 3: 87–92.

Civalleri A. 1906. Contribution à l'étude des musculi levatores glandulae thyreoidae et à l'innervation des musculi sternothyreoideus et thyreohyoideus. *Arch Ital Biol* 45: 281–282.

Clemente CD. 1985. *Gray's Anatomy. The Endocrine Gland*. 30th edition. Baltimore: Williams & Wilkins.

Coskun N, Yildirim FB, Ozkan O. 2002. Multiple muscular variations in the neck region: Case study. *Folia Morphol (Warsz)* 61: 317–319.

De-Ary-Pires B, Ary-Pires R, Pires-Neto MA. 2003. The human digastric muscle: patterns and variations with clinical and surgical correlations. *Ann Anat* 185: 471–479.

De Castro CC. 1980. The anatomy of the platysma muscle. *Plast Reconstr Surg* 66: 680–683.

Dratsch S. 1930. Ein fall von variationen des digastric muscle mandibulae. *Anat Anz* 69: 81–82.

Ehrenberg G. 1905. Eine seltene abnormität des platysma. *Anat Anz* 26: 343–347.

Faziogullari Z, Cicekcibasi AE, Unver Dogan N, Yilmaz MT, Buyukmumcu M, Ziylan T. 2010. The levator claviculae muscle and unilateral third head of the sternocleidomastoıd muscle: case report. *Int J Morphol* 28: 929–932.

Feigl GC, Pixner T. 2011. The cleidoatlanticus muscle: A potential pitfall for the practice of ultrasound guided interscalene brachial plexus block. *Surg Radiol Anat* 33: 823–825.

Focacci M. 1903. Contribution à l'étude du muscle inerdiastrique de Bianchi. *Arch Ital Biol* 36: 476.

Gardner E, Gray DJ, O'Rahily R. 1969. *Anatomy, third edition*. Philadelphia: WB Saunders Company.

Gaughran GR. 1963. Mylohyoid boutonniere and sublingual bouton. *J Anat* 97: 565–568.

Gegenbaur C. 1888. *Lehrbuch der Anatomie des Menschen*, third edition. Leipzig: V. Wilhelm Engelmann.

Gruber W. 1847. *Vier Abhandlungen aus dem Gebiete der Medicinisch-Chirurgischen Anatomie*. Berlin: Verlagsort.

Gruber W. 1868. Über die muskeln des unteren schildknorpelrandes (musculi-thyroeoidei marginales inferiores). *Arch Anat Physiol Wissen Med* 1868: 633–634.

Gruber W. 1868. Über den seltenen schildknorpelhorn-giebecken-knorpelmuskel. *Arch Path Anat Physiol Klin Med* 1868: 640–641.

Gruber W. 1868. Über eine neue variante des musculus thyreotrachealis und über den musculus hyo-trachealis. *Arch Path Anat Physiol Klin Med* 1868: 642–645.

Gruber W. 1876. Ein musculus cleido-cervicalis s. tracheloclavicularis imus. *Arch Anat Physiol Wissen Med* 1876: 757–758.

Gruber W. 1876. Ein musculus cleido-epistrophicus bei existenz des musculus cleidomastoideus der norm. *Arch Anat Physiol Wissen Med* 1876: 739–745.

Gruber W. 1876. Über den musculus rectus capitis anticus medius s. minimus. *Arch Anat Physiol Wissen Med* 1876: 746–749.

Gruber W. 1876. Über den musculus rectus capitis anticus medius s. minimus. *Arch Path Anat Physiol Klin Med* 1876: 750–752.

Gruber W. 1876. Vorkommen des musculus cleido-mastoideus als musculus cleido-epistrophicus. *Arch Anat Physiol Wissen Med* 1876: 759–760.

Gruber W. 1876. Ein musculus cleido-atlanticus. *Arch Anat Physiol Wissen Med* 1876: 761.

Gruber W. 1877. Über das neue anheftungsbündel des oesophagus an die glandula thyroidea–musculus thyreo-oesophageus. *Arch Path Anat Physiol Klin Med* 69: 396–398.

Gruber W. 1878. Über einen fall einseitigen vorkommens zweier den musculus omohyoideus substituirender musculi cleidohyoidei. *Arch Path Anat Physiol Klin Med* 73: 342–345.

Gruber W. 1878. Beobachtungen über den mangel des musculus omohyoideus. *Arch Path Anat Physiol Klin Med* 73: 345–346.

Gruber W. 1878. Ein den oberen bauch des omohyoideus (bei Mangel des unteren Bauches des lezteren) repräsenirender Musculus hyofacialis. *Arch Path Anat Physiol Klin Med* 74: 454–456.

Gruber W. 1879. Musculus hyo-fascialis. *Arch Path Anat Physiol Klin Med* 77: 123.

Gruber W. 1880. Musculus digastricus maxillae inferioris mit Urprung sceines vorderen bauches an und hinter der mitte des seitentheiles der masiila im bereiche der strecke zwischen dem ansatze des M. masseter und dem ursprunge des M. depressor anguli oris. *Arch Pat Anat Physiol Klin Med* 81: 449–453.

Gruber W. 1880. Über den musculus trigastricus maxillae inferioris. *Arch Path Anat Physiol Klin Med* 81: 445–449.

Gruber W. 1881. Supernumeräre, der glandula submaxilaris zur stütze dienende schicht des musculus mylohyoideus. *Arch Path Anat Physiol Klin Med* 86: 491–492.

Gruber W. 1885. Auftreten der bäuche des musculus digastricus maxillae inferioris als selbständige muskeln: Musculus mento-hyoideus et M. mastoideo-maxillaris. *Arch Path Anat Physiol Klin Med* 101: 253–255.

Gruber W. 1885. Supernumerärer bauch des musculus sernocleidomastoideus in der richtung des hinteren bauches des digastric muscle maxillae inferioris und abwärts von diesem zum os hyoides. *Arch Path Anat Physiol Klin Med* 102: 538–539.

Hallett CH. 1848. An account of the anomalies of the muscular system met with in the dissecting–room of the University during the years 1846–1847; with general remarks. *Edinburgh Med Surg J* 69: 1–32.

Henle J. 1868. *Handbuch der systematischen anatomie des menschen. 3 Vols*. Braunschweig: Von Friedrich Viewg und Sohn.

Hirako G. 1930. Studies on the constitution of the Ainu race. Part 2. *J Anthrop Soc Nippon* 45: 144.

Huber E. 1918–1919. Überreste des sphincter colli profundus beim Menschen. *Anat Anz* 51: 480–492.

Huber CG. 1930. *Piersol's Human Anatomy*, ninth edition. Philadelphia: LB Lippincott Company.

Hyrtl J. 1887. *Lehrbuch der Anatomie des Menshen*, 19th edition. Wien: Wilhelm Braumüller.

Jackson CM. 1933. *Morris' Human Anatomy*, ninth edition. Philadelphia: P. Blakiston's Son & Co. Inc.

John AB. 1970. The omohyoid muscle and fascia: Morphology and anomalies. *ANZ J Surg* 40: 86–88.

Jordon J. 1963. On the deep stylohyoid muscle in man. *Folia Morphol (Warsz)* 22: 7–10.

Jung A. 1892. Eine noch nicht beschriebene anomalie des musculus omo-hyoideus. *Anat Anz* 7: 582–584.

Kamcevski D, Jenezic O, Seramilac A. 1964. A case of spindle-cell carcinoma of the thyroid gland with peracute clinical course. (Carcinoma fusicellulare glandulae thyroideae.) *Srp Arh Celok Lek* 92: 997–1001.

Kim HJ, Hu KS, Kang MK, Hwang K, Chung IH. 2001. Decussation patterns of the platysma in Koreans. *Br J Plast Surg* 54: 400–402.

Koganei R, Arai SH, Shikinami J. 1902. Statistics on the muscular anomalies. *Tokyo J Med Sci* 17: 127.

Koshy S, Rabi S, Indrasingh I. 2005. Supernumerary cleidocervicalis (levator claviculae) muscle: Case report of its rare incidence with clinical and embryological significance. *Eur J Anat* 9: 103–106.

Koster W. 1869. Verslagen en Mededeelingen der Konink Akademie van Wetenschappen. Afdeeling Letterkunde.

Kudoh H, Kida M. 1991. A case of duplicated omohyoid muscle with an accessory slip of sternothyroid muscle. *Acta Anat Nippon* 66: 323.

Langsam CL. 1941. M. omohyoideus in American Whites and Negroes. *Am J Phys Anthropol* 28: 249–259.

Latarjet A. 1948. *Testut's Traite D'Anatomie Humaine*, ninth edition. Paris: G. Doin & Cie.

Loth E. 1931. *Anthropolgie des Parties Molles*. Paris: Masson et Cie.

Luschka H. 1856. Von ein musculus supraclavicularis beim menschen. *Arch Anat Physiol Wissen Med* 1856: 284.

Malpas P. 1926. Anomalous of the mylohyoid muscle. *J Anat* 61: 64–67.

Mehta V, Arora J, Kumar A, Nayar AK, Ioh HK, Gupta V, Suri RK, Rath G. 2012. Bipartite clavicular attachment of the sternocleidomastoid muscle: A case report. *Anat Cell Biol* 45: 66–69.

Miura M, Kato S, Itonaga I, Usui T. 1995. The double omohyoid muscle in humans: Report of one case and review of the literature. *Okajimas Folia Anat Jap* 72: 81–98.

Mizen KD, Mitchell DA. 2005. Anatomical variability of omohyoid and its relevance in oropharyngeal cancer. *Br J Oral Maxillofac Surg* 43: 285–288.

M'Whinnie AM. 1846. On the varieties in the muscular system of the human body. *London Med Gaz* 11: 185–196.

Nagashima S, Yamaki K, Ohkawa T, Hiramatsu S, Hiranuma S, Yoshikawa H, Miyazaki M. 1989. An extremely rare case of M. cleido-cervicalis and M. cleido-occipitalis. *J Kurume Med Assoc* 52: 680–687.

Nathan H, Luchansky E. 1985. Sublingual gland herniation through the mylohyoid muscle. *Oral Surg Oral Med Oral Pathol* 59: 21–23.

Natsis K, Asouchidou I, Vasileiou M, Papathanasiou E, Noussios G, Paraskevas G. 2009. A rare case of bilateral supernumerary heads of sternocleidomastoid muscle and its clinical impact. *Folia Morphol (Warsz)* 68: 52–54.

Ozgur Z, Govsa F, Ozgur T. 2007a. Bilateral quadrification of the anterior digastric muscles with variations of the median accessory digastric muscles. *J Craniofac Surg* 18: 773–775.

Ozgur Z, Govsa F, Ozgur T. 2007b. The cause of the difference in the submental region: Aberrant muscle bundles of the anterior belly of the digastric muscle. *J Craniofac Surg* 18: 875–881.

Ozgursoy OB, Kucuk B. 2006. Unique variation of digastrics muscle: A confusing landmark for head and neck surgeons. *Acta Otolaryngol* 126: 881–883.

Perrin JB. 1871. A peculiar additional digastric muscle. *J Anat Physiol* 5: 251–256.

Pettersen JC, Koltis GG, White MJ. 1979. An examination of the spectrum of anatomic defects and variations found in eight cases of trisomy 13. *Am J Med Genet* 3: 183–210.

Rai R, Ranade A, Nayak S, Vadgaonkar R, Mangala P, Krishnamurthy A. 2008. A study of anatomical variability of the omohyoid muscle and its clinical relevance. *Clinics* 64: 521–524.

Rani A, Chopra J, Rani A, Verma RK. 2013. Duplicated anterior belly of the digastric muscle. *Singapore Med J* 54: 131–132.

Reid RW. 1886. Anterior belly of the digastric muscle on both sides, arising from the lower border of the horizontal ramus of the inferior maxillary bone. *J Anat Physiol* 21: 78.

Retzius AA. 1837. Bemerkungen über den inneren Bau der Zähne mit besonderer berücksichtigung auf den im zahnknochen vorkommenden röhrenbau. *Arch Anat Physiol Wissen Med* 1837: 486–571.

Reyes G, Contreras C, Ramírez LM, Ballesteros LE. 2007. The digastric muscle's anterior accessory belly: Case report. *Med Oral Patol Oral Cir Bucal* 12: 341–343.

Rodríguez-Vázquez JF, Mérida-Velasco JR, Verdugo-López S, de la Cuadra-Blanco C, Sanz-Casado JV. 2009. Anatomical relationships of the cleidoatlanticus muscle. Interpretation about its origin. *Anat Sci Int* 84: 47–52.

Rosenheimer JL, Loewy J, Lozanoff S. 2000. Levator claviculae muscle discovered during physical examination for cervical lymphadenopathy. *Clin Anat* 13: 298–301.

Ruffini A. 1908. Sul muscolo interdigatrico di Bianchi e sull'aponeurosi soprajoidea od intermediojoidea. Rarissimo caso di mancanza bilaterale del ventre anteriore del m. digastrico della mandibola. *Archiv Ital Anat e di Embriol* 7: 578–601.

Saadeh FA, El-Sabban M, Hawi JS. 2001. Rare variations of the mylohyoid muscle: Case study. *Clin Anat* 14: 285–287.

Sadato S. 1968. Statistical studies on the exceptional muscles of the Kyushu-Japanese. 2. The muscles of the neck. *Kurume M J* 15: 83–95.

Sanchez Y, Sanchez M. 1933. Quelques variations morphologiques des muscles peauciers de la têtê. *L'Assoc Anatomistes Comptes Rendus* 28: 586–592.

Sargon MF, Celik HH. 1994. An abnormal digastric muscle with three bellies. *Surg Radiol Anat* 16: 215–216.

Sargon MF, Onderoğlu S, Sürücü HS, Bayramoğlu A, Demiryürek DD, Oztürk H. 1999. Anatomic study of complex anomalies of the digastric muscle and review of the literature. *Okajimas Folia Anat Jap* 75: 305–313.

Sarikcioglu L, Demir S, Oguz N, Sindel M. 1998. An anomalous digastric muscle with three accessory bellies and one fibrous band. *Surg Radiol Anat* 20: 453–454.

Sarikcioglu L, Donmez BO, Ozkan O. 2001. Cleidooccipital muscle: An anomalous muscle in the neck region. *Folia Morphol (Warsz)* 60: 347–349.

Sasagawa I, Takahashi K, Igarashi A. 1982. A case of the abnormal bundle from the anterior margin of the right and left trapezius and the abnormality in the right omohyoid appeared in a cadaver. *Shigaku* 70: 439–448.

Schaefer EA, Symington J, Bryce TH. 1923. *Quain's Elements of Anatomy*, 11th edition. London: Longmans, Green and Co.

Schwegel. 1858. Die entwickelungsgeschichte der knochen des stammes und der extremitäten, mit rücksicht auf chirurgie, geburtskunde und gerichtliche medicin. Sitzungsberichte der Kaiserlichen Akademie der Wissenschaften zu Wien, pp. 34–51.

Scott-Conner CE, Dawson DL. 2003. *Operative Anatomy*, second edition. Philadelphia: Lippincott Williams & Wilkins.

Sehirli U, Cavdar S. 1996. An accessory mylohyoid muscle. *Surg Radiol Anat* 18: 57–59.

Shah AR, Rosenberg D. 2009. Defining the facial extent of the platysma muscle: A review of 71 consecutive face-lifts. *Arch Facial Plast Surg* 11: 405–408.

Stein M. 1914–1915. Über einen fall von vollkommenem mangel des vorderen digastricusbauches. *Anat Anz* 47: 345–352.

Steinback K. 1923. Über varietäten der unterzungenbein und brustmuskulatur. *Anat Anz* 56: 488–506.

Stracker O. 1908. Die häufigkeit interponierter muskelkörper zwischen den vorderen bäuchen des digastric muscle. *Anat Anz* 33: 227–236.

Su PH, Wang TG, Wang YC. 2012. Ultrasound-guided injection of botulinum toxin in a patient with omohyoid muscle syndrome: A case report. *J Clin Ultrasound* 41: 373–376.

Sukekawa R, Itoh I. 2006. Anatomical study of the human omohyoid m.: regarding intermediate morphologies between normal anomalous morphologies of the superior belly. *Anat Sci Int* 81: 107–114.

Takano T, Takaya M, Iizuka K, Togazawa T, Adachi A. 1955. Statistical study of abnormal muscle of infrahyoid. *lwateidai Kaibou Gyouseki* 2: 113–124.

Tamega OJ, Garcia PJ, Soares JC, Zorzetto NL. 1983. About a case of absence of the superior belly of the omohyoid muscle. *Anat Anz* 154: 39–42.

Taylor J. 1925. An unusual variation of the omo-hyoid muscle. *J Anat* 59: 331–332.

Thiel W. 1954–1955. Eine seltene varietät des venter mastoideus m. biventeris und ihre phylogenetische deutung. *Anat Anz* 101: 16–23.

Tomo S, Toh H, Hirakawa T, Tomo I, Kobayashi S. 1994. Case report: The cleidocervical muscle with speculation as to its origin. *J Anat* 184: 165–169.

Totinai I, Aonuma T. 1944. Abnormal muscles of cleidohyoid and omohyoid. *Iwate Igk Z* 7: 2–8.

Tubbs RS, Salter EG, Oakes WJ. 2004. Unusual origin of omohyoid muscle. *Clin Anat* 17: 578–582.

Turan-Ozdemir S, Oygucu IH, Kafa IM. 2004. Bilateral abnormal anterior bellies of digastric muscles. *Anat Sci Int* 79: 95–97.

Uzun A, Aluclu A, Kavakli A. 2001. Bilateral accessory anterior bellies of the digastric muscle and review of the literature. *Auris Nasus Larynx* 28: 181–183.

Walmsley T. 1918. Observations on the omohyoid muscle. *J Anat* 52: 319–325.

Wang CM. 1950. An anomalous muscle in place of the stylohyoid ligament of a Chinese. *Anat Rec* 107: 375–378.

Weber A. 1918. Signification du muscle stylo-hyoidien profound. *Soc Biol Comptes Rendus Hebdomadaires des Séances et Mémoires* 81: 816–817.

West SH. 1873. A peculiar digastric muscle: a variety of the occipitohyoid. *J Anat Physiol* 8: 150–151.

Wood J. 1867–1868. Variations in human myology observed during the winter session of 1867–68 at King's College, London. *Proc R Soc Lond* 16: 483–525.

Wood J. 1879. On a group of varieties of the muscles of the human, neck, shoulder, and chest with their transitional forms and homologies in the mammalia. *Philos Trans R Soc London* 160: 83–116.

Yamada S. 1934. Über einige variationen der Mm. infrahyoidei und anomalien des clavicularen ansatzes des M. trapezius on den japanischen foeten und neugeborenen. *Acta Anat Nippon* 7: 337–347.

Yamada H, Nishijima T. 1954. A rare case of abnormity in the M. omohyoideus. *Kyushu Shika Z* 11: 187–188.

Yamada H, Kuga H, Ozumi K. 1960. Case report of abnormities in M. omohyoideus and M. sternothyroideus. *Kyushu Shika Z* 14: 390–394.

Yamazaki Y, Shibata M, Ushiki T, Isokawa K, Sato N. 2011. Bilateral, asymmetric anomalies of the anterior bellies of digastric muscles. *J Oral Sci* 53: 523–527.

Yang HJ, Gil YC, Jin JD, Ahn SV, Lee HY. 2012. Topographical anatomy of the suprascapular nerve and vessels at the suprascapular notch. *Clin Anat* 25: 359–365.

Yonekura S. 1954. A study of the muscles of the neck chest, abdomen and back in Japanese fetuses. *Igaku Kenkyu* 24: 1604–1700.

Yoshizuka M, Tanaka I, Sakamoto F, Hirata T, Miyazaki M. 1987. An abnormal case of musculus omohyoideus. *Kurume Igaku Z* 50: 375–378.

26 Pharyngeal muscles

Yujiro Sakamoto
Tokyo Medical and Dental University, Tokyo, Japan

The pharyngeal muscles are composed of three circular muscles (the superior constrictor, the middle constrictor, and the inferior constrictor) and three longitudinal elevator muscles (the stylopharyngeus, the salpingopharyngeus, and the palatopharyngeus) (Thane 1894; Spalteholz 1909; Blount and Lachman 1953; Sinclair 1972; Fleischhauer 1985; Leonhardt 1987; DuBrul 1988; Standring 2005). They are also classified as the muscles of the pharynx and the soft palate (Blount and Lachman 1953; Sinclair 1972; Standring 2005); the palatopharyngeus is also classed among the muscles of the soft palate (Thane 1894; Spalteholz 1909; FIPAT 1998). The constrictors overlap one another and are inserted into the pharyngeal raphe; they have been described as consisting of various parts as the bundles of fibers coming from different areas of the line of the origin can be independent to a considerable degree. At the same time, authors have offered a variety of descriptions of the attachments of the pharyngeal muscles.

Superior constrictor

The superior constrictor arises from the pterygoid hamulus and the adjoining posterior margin of the medial pterygoid plate (the pterygopharyngeal part), the posterior border of the pterygomandibular raphe (the buccopharyngeal part), the posterior end of the mylohyoid line of the mandible (the mylopharyngeal part), and the side of the tongue (the glossopharyngeal part) (Spalteholz 1909; Blount and Lachman 1953; Leonhardt 1987; DuBrul 1988). The upper fibers also arise from the small ligament that bridges the hamular notch (DuBrul 1988), and sometimes from the inferior surface of the petrous part of the temporal bone (Leonhardt 1987) or the bone area anterior to the external opening of the carotid canal (Spalteholz 1909). The lower fibers also arise from the mucous membrane of the mouth (Thane 1894; Leonhardt 1987; DuBrul 1988) and connect to the longitudinal and transverse muscles of the tongue (Leonhardt 1987; DuBrul 1988). The insertion of the most superior fibers reaches the pharyngeal tubercle of the occipital bone (Blount and Lachman 1953; Sinclair 1972). The palatopharyngeal sphincter (Passavant's muscle) is described as lying internal to the superior constrictor (Blount and Lachman 1953; Sinclair 1972; Standring 2005). This muscle arises from the anterior and lateral parts of the upper surface of the palatine aponeurosis and passes lateral to the levator veli palatine. It blends internally with the upper border of the superior constrictor and encircles the pharynx as a sphincter-like muscle. The palatopharyngeal sphincter is also mentioned in connection with the palatopharyngeus. The reported variations of these origins, insertions and other relationships, and their incidences are as follows.

The study by Sakamoto (2009) revealed some variations associated with the superior constrictor from 22 cadavers (44 sides). A longitudinal bundle descended over the dorsal surface of the superior constrictor and spread onto the middle constrictor on the right side twice and on the left four times (13.6%), including two bilateral cases (9.1%). Some fibers arose from the petrous part of the temporal bone, just ventromedial to the carotid canal. The fibers curved either dorsally to join the superior constrictor four times on the right side and four on the left (18.2%), including two symmetrical cases (9.1%), or ventrally to attach to the soft palate with the origin of the superior constrictor on the right side twice and on the left three times (11.4%); these included two symmetrical cases (9.1%). Both ventral and dorsal fibers were found on the right side once and on the left twice (6.8%), including one symmetrical case (4.5%).

The study by Shimada and Gasser (1989) revealed that the pterygomandibular raphe, a prominent, narrow, tendinous band with attachments as described in current textbooks, was not found in 110 adult cadavers. The pterygomandibular raphe was absent with complete continuity of the buccinator and the superior constrictor in 36% of the specimens. Only the upper portion of the raphe could be identified and had a broad, triangular shape in 28%; the two muscles were widely separated by a broad, fascial region in 36%. However, all 50 fetal cadavers exhibited a broad, fascial region that completely separated the two muscles, indicating that changes in the shape of the raphe occur postnatally.

An earlier study by Shimada and Gasser (1988) revealed that the pharyngeal raphe was located between the inferior constrictor in only 47% of 236 adult cadavers and between the superior and middle constrictors in only 40%; it extended from the

Bergman's Comprehensive Encyclopedia of Human Anatomic Variation, First Edition. Edited by R. Shane Tubbs, Mohammadali M. Shoja and Marios Loukas.
© 2016 John Wiley & Sons, Inc. Published 2016 by John Wiley & Sons, Inc.

pharyngeal tubercle through all the constrictor muscles to the esophagus in 13%. The continuous type usually described in anatomy textbooks was found in only 5% of the specimens.

Middle constrictor

The middle constrictor arises from the lesser horn of the hyoid bone (the chondropharyngeal part) and the whole of the upper border of the greater horn (the ceratopharyngeal part) (Spalteholz 1909; Blount and Lachman 1953; Fleischhauer 1985; Leonhardt 1987; DuBrul 1988; Standring 2005; Bergman et al. 2006). The chondropharyngeal part also arises from the lower part of the stylohyoid ligament (Blount and Lachman 1953; Fleischhauer 1985; DuBrul 1988; Standring 2005). The insertion of the most cranial fibers is described as reaching the basilar portion of the occipital bone (Blount and Lachman 1953), and the caudal fibers descend to the lower end of the pharynx (Blount and Lachman 1953; Standring 2005). The middle constrictor also receives fibers from the body of the hyoid bone, the tongue and the posterior part of the mylohyoid line of the mandible (Thane 1894). There is frequently a slip from the lateral thyrohyoid ligament (the syndesmopharyngeus) (Thane 1894), also mentioned in relation to the inferior constrictor. The reported variations and their incidences are as follows.

The study of 22 cadavers, 44 sides by Sakamoto (2009) revealed that, at the origin, the uppermost fibers of the middle constrictor joined the hyoglossus on the right side three times and on the left seven times (22.7%) including three bilateral cases (13.6%), or the stylohyoid on the right side three times and on the left twice (11.4%), including one bilateral case (4.5%).

Inferior constrictor

The inferior constrictor arises from the oblique line of the thyroid lamina (the thyropharyngeal part) and the lateral surface of the cricoid cartilage (the cricopharyngeal part) (Spalteholz 1909; Blount and Lachman 1953; Fleischhauer 1985; Leonhardt 1987; DuBrul 1988; Standring 2005). It is continuous downwards with the circular striated (Blount and Lachman 1953; DuBrul 1988) or longitudinal (Thane 1894) muscles of the esophagus, or the cricopharyngeal part blends with the circular esophageal musculature around the narrowest part of the pharynx (Standring 2005). Some additional fibers arise from the fascia on the lateral aspect of the cricothyroid (Sinclair 1972; Leonhardt 1987) or the tendinous cord that extends between the inferior thyroid tubercle and the cricoid cartilage and loops over the cricothyroid (Spalteholz 1909; Blount and Lachman 1953; Fleischhauer 1985; Standring 2005). The inferior constrictor also arises from the superior thyroid tubercle (Thane 1894; Blount and Lachman 1953), the inferior thyroid horn (Standring 2005), and the cricoid cartilage between the attachment of cricothyroid and the articular facet of the inferior thyroid horn (Standring 2005). The syndesmopharyngeus from the lateral thyrohyoid ligament is frequently observed (Bergman et al. 1988, 2006), as mentioned in relation to the middle constrictor. Some fibers usually continue into the inferior constrictor from the sternothyroid and cricothyroid (Thane 1894; Bergman et al. 1988, 2006), and the inferior constrictor can be more or less united with the fibers from the thyrohyoid (Bergman et al. 1988, 2006). Moreover, an inconstant bundle arises from the first or second tracheal cartilages (Leonhardt 1987). The reported variations of the origins and the other relationships and their incidences are as follows.

A study of 30 cadavers, 60 sides by Sakamoto (2013) revealed that the arcuate tendinous cord linked the origin of the cricoid cartilage with the inferior thyroid tubercle in 36 cases (60.0%) including 14 bilateral (46.7%). The cricothyroid consisted of upper and lower bundles, and the tendinous cord crossed over the upper bundle on the right side eight times and on the left ten times (30.0%), including five symmetrical cases (16.7%), or on both the right side and left sides in nine cases (30.0%), including seven symmetrical cases (23.3%). When the tendinous cord was partly or wholly absent, some fibers of the cricothyroid, especially the lower bundle, connected to the oblique fibers of the inferior constrictor. The study of 22 cadavers, 44 sides by Sakamoto (2009) revealed that at the origin, some of the upper fibers of the inferior constrictor connected directly or tendinously to the sternothyroid on the right side 14 times and on the left 15 (65.9%), including 12 bilateral cases (54.5%), and to the thyrohyroid on the right side six times and on the left seven (29.5%) including three bilateral cases (13.6%).

Stylopharyngeus

The stylopharyngeus arises from the medial side, the base or the posteroinferior surface of the styloid process and spreads out beneath the mucous membrane (Thane 1894; Spalteholz 1909; Blount and Lachman 1953; Sinclair 1972; Fleischhauer 1985; Leonhardt 1987; DuBrul 1988; Standring 2005). It also merges into the constrictors (Blount and Lachman 1953; Standring 2005) or joins the fibers of the palatopharyngeus (Thane 1894; Spalteholz 1909; Blount and Lachman 1953; Sinclair 1972; Leonhardt 1987; Standring 2005). It also attaches to the superior and posterior borders of the thyroid cartilage (Thane 1894; Spalteholz 1909; Blount and Lachman 1953; Sinclair 1972; Leonhardt 1987; Standring 2005), the cricoid cartilage (Spalteholz 1909) and the side of the epiglottis (Spalteholz 1909; Blount and Lachman 1953; Sinclair 1972; Standring 2005). The fibrous capsule of the pharyngeal tonsils can receive slips from the stylopharyngeus (stylotonsillaris), the thyroid cartilage, and the oblique arytenoid muscle (Bergman et al. 2006). The stylopharyngeus is frequently divided into two or three slips (Thane 1894; Bergman et al. 2006). The reported variations and their incidences are as follows.

The study of 22 cadavers, 44 sides by Sakamoto (2009) revealed that the stylopharyngeus was penetrated by the

glossopharyngeal nerve on the right side three times and on the left seven (22.7%), including three bilateral cases (13.6%). The bundle that attached to the intermediate tendon of the posterior belly of the digastrics joined the stylopharyngeus on the left side in one case (2.3%).

Salpingopharyngeus

The salpingopharyngeus arises from the inferior part of the cartilage of the pharyngotympanic (auditory) tube and blends with the palatopharyngeus (Thane 1894; Spalteholz 1909; Sinclair 1972; Fleischhauer 1985; Leonhardt 1987; Bergman et al. 1988; DuBrul 1988; Standring 2005; Bergman et al. 2006) and the remainder of the superior constrictor (Bergman et al. 2006), or is inserted into the wall of the pharynx (Blount and Lachman 1953). The reported variations and their incidences are as follows.

The study of 49 cadavers, 98 sides by Sumida et al. (2012) revealed that the salpingopharyngeus appeared as a muscle bundle 59 times (60.2%), including 21 bilateral cases (42.9%). It originated from the posterior end of the cartilage of the auditory tube and descended to join the palatopharyngeus at a site immediately posterior to the levator veli palatini.

Palatopharyngeus

The palatopharyngeus is composed of two fasciculi separated by the levator veli palatini (Thane 1894; Sinclair 1972; Standring 2005). The thicker anterior (inferior) fascicle arises from the posterior border of the hard palate and the palatine aponeurosis and some fibers interdigitate across the midline. The posterior (superior) fascicle contacts the mucosa of the pharyngeal aspect of the palate and joins the contralateral muscle at the midline. The palatopharyngeus also arises from near the pterygoid hamulus (Spalteholz 1909; Leonhardt 1987; DuBrul 1988) and behind the posterior nasal spine (DuBrul 1988). It is joined by the salpingopharyngeus and is inserted into the posterior border of the thyroid cartilage and the pharyngeal fibrous tissue (Thane 1894; Sinclair 1972; Leonhardt 1987; DuBrul 1988; Standring 2005). The posterior-most fibers attach to the superior thyroid horn and the anterior-most fibers to the pharyngeal raphe (DuBrul 1988). The palatopharyngeus also blends with the other muscles of the pharyngeal wall and decussates with the contralateral muscle (Thane 1894; Sinclair 1972; Leonhardt 1987; Standring 2005). When the palatopharyngeus is referred to as the pharyngopalatinus, the pharynx is described as the origin and the palate as the insertion (Spalteholz 1909; Blount and Lachman 1953). Frequently, a bundle of fibers arises from the basilar part of the occipital bone, or even from the inferior surface of the petrous part of the temporal bone or the spine of the sphenoid bone, and passes downwards to be inserted along with the palatopharyngeus (Bergman et al. 1988, 2006). The study by Whillis (1930) revealed that a constant band of fibers, the palatopharyngeal sphincter, on the same plane as the pharyngopalatinus relative to the pharyngeal constrictors, passes forwards from the superior constrictor muscle and parallel to its upper fibers, lateral to the levator, into the palate, where it is inserted into the palatal aponeurosis. The palatopharyngeal sphincter is also described in relation to the superior constrictor. The reported variations and their incidences are as follows.

The study by Sumida et al. (2012) described the palatopharyngeus as comprising longitudinal and transverse divisions. The transverse division arose from the soft palate and passed dorsally to the pharyngeal raphe. The longitudinal division arose via three fasciculi. The oral fasciculus arose from the palatine aponeurosis 100 times (100.0%) including 50 bilateral (100.0%) and the median line of the soft palate 86 times (86.0%) from 50 cadavers, 100 sides. The posterior fasciculus was located posterior to the levator veli palatini and originated from the median portion of the uvula 40 times (55.6%), including 15 bilateral cases (32.6%) from 46 cadavers, 72 sides. The nasal fasciculus lay on the nasal surface of the levator veli palatini 59 times (76.6%), including 29 bilateral cases (76.3%) from 38 cadavers, 77 sides. The longitudinal division with the salpingopharyngeus and the stylopharyngeus had four insertions, though the epiglottic insertion was mainly formed by the stylopharyngeus. They were inserted into the thyroid cartilage by two bundles 37 times (42.5%), including 14 bilateral cases, or one bundle 50 times (57.5%), including 20 bilateral cases (45.5%), from 44 cadavers, 87 sides. They were inserted into the hypopharynx at the level of the cricopharyngeus with aponeurosis formation 63 times (67.0%), including 25 bilateral cases (53.2%), or without it 11 times (11.7%), including two bilateral cases (4.3%), or did not reach the cricopharyngeus 20 times (21.3%), including six bilateral cases (12.85) from 47 cadavers, 94 sides. They were inserted into the posterior pharyngeal insertion 18 times (18.0%) including one bilateral case (2.0%) from 50 cadavers, 100 sides.

Supernumerary elevator muscles of the pharynx are not uncommon, arising from a neighboring part of the base of the skull and inserted variably into one of the constrictors, or passing between those muscles to the fibrous layer of the pharynx (Thane 1894). Their most frequent origin is from under the surface of the petrous bone in front of the carotid canal, from the vaginal process of the temporal bone (petropharyngeus) or farther back, from the basilar process (occipitopharyngeus), or very rarely from the mastoid process (mastoidopharyngeus) (Thane 1894; Bergman et al. 1988, 2006).

Supernumerary elevator muscles also occur from the spine of the sphenoid bone (sphenopharyngeus) or the pterygoid hamulus (pterygopharyngeus externus) (Thane 1894). Occasionally a small median strip of muscle arises from the pharyngeal tubercle of the occipital bone and descends to the raphe or the posterior wall of the pharynx (azygos-pharyngeus) (Thane 1894; Bergman et al. 1988, 2006). The reported variations and their incidences are as follows.

The study by Shimada et al. (1991) revealed that the petropharyngeal muscle was observed eight times (1.4%) in seven of 614 cadavers, both sides in one case (0.3%) and one side in six cases (1.9%). The studies by Sakamoto (2009) reported that in one head (4.5%) from 22 cadavers, three flat bundles arose from the medial part of the sheath of the styloid process (vaginal process). One of them (right side) merged into the superior constrictor, and the others (both sides) dispersed onto the dorsal surface of the inferior constrictors. Both the bundles from the vaginal process and the petrous part of the temporal bone have been named the petropharyngeus (Thane 1894). However, the name "tympanopharyngeal muscle" (tympanopharyngeus) is better suited to the bundle from the vaginal process.

References

Bergman RA, Thompson SA, Afifi AK, Saadeh FA. 1988. Muscles. In: *Compendium of Human Anatomic Variation: Text, Atlas, and World Literature. Baltimore*, Munich: Urban & Schwarzenberg.

Bergman RA, Afifi AK, Miyauchi R. 2006. Muscles of Head and Neck (Branchiomeric Muscles). In: Illustrated Encyclopedia of Human Anatomic Variation. Available at http://www.anatomyatlases.org/AnatomicVariants/AnatomyHP.shtml (accessed 12 October 2015).

Blount RF, Lachman E. 1953. The digestive system. In: *Morris' Human Anatomy*, 11th edition (Schaeffer JP, ed.) Toronto: The Blakiston Company.

DuBrul EL. 1988. The oropharyngeal system. In: Sicher and DuBrul's Oral Anatomy, 8th edition. St Louis, Tokyo: Ishiyaku EuroAmerica.

FIPAT (Federative International Programme on Anatomical Terminologies). 1998. *Terminologia Anatomica. International Anatomical Terminology*. Second edition. Stuttgart, New York: Georg Thieme Verlag.

Fleischhauer K. 1985. *Der Verdaungsapparat (Apparatus digestorius). In: Bennunghoff Makroskopische und Mikroskopische Anatomie des Menschen*. Band 2, Kreislauf und Eingeweide, 14th/15th editions (Fleischhauer K, Staubesand J, Zenker W eds). München, Wien, Baltimore: Urban & Schwarzenberg.

Leonhardt H. 1987. Verdauungssystem. In: *Rauber/Kopsch Anatomie des Menschen, Band 2, Innere Organe* (LeonhardtH, TillmannB, T öndury G, Zilles K eds). Stuttgart, New York: George Thieme.

Sakamoto Y. 2009. Classifcation of pharyngeal muscles based on innervations from glossopharyngeal and vagus nerves in human. *Surg Radiol Anat* 31: 755–761.

Sakamoto Y. 2013. Interrelationships between the innervations from the laryngeal nerves and the pharyngeal plexus to the inferior pharyngeal constrictor. *Surg Radiol Anat* 35(8): 721–728.

Shimada K, Gasser RF. 1988. Variations of the pharyngeal raphe. *Clin Anat* 1: 285–294.

Shimada K, Gasser RF. 1989. Morphology of the pterygomandibular raphe in human fetuses and adults. *Anat Rec* 224: 117–122.

Shimada K, Yokoi A, Ozawa H, Kitagawa T, Tezuka M. 1991. Observation of the petropharyngeal muscle in Japanese. *Anat Anz* 173: 193–198.

Sinclair DC. 1972. Muscles and Fasciae. In: *Cunningham's Textbook of Anatomy*, 11th edition (Romanes GJ ed.). London: Oxford University Press.

Spalteholz W. 1909. *Gaumen, Schlundkopf. In: Handatlas der Anatomie des Menschen. Band 3, Eingeweide, Gehirn, Nerven, Sinnesorgane. 5 Auflage*. Leipzig: Verlag von S. Hirzel.

Standring S. 2005. *Head and neck. In: Gray's Anatomy*, 39th edition. (Standring S, Ellis H, Healy JC, Johnson D, Williams A eds). Edinburgh, London, New York, Oxford, Philadelphia St Louis, Sydney, Toronto: Elsevier Churchill Livingstone.

Sumida K, Yamashita K, Kitamura S. 2012. Gross anatomical study of the human palatopharyngeaus muscle throughout its entire course from origin to insertion. *Clin Anat* 25: 314–323.

Thane GD. 1894. Myology. In: *Quain's Elements of Anatomy*, 10th edition (Schferäfer EA, Thane GD eds). New York: Longman Green and Co.

Whillis J. 1930. A note on the muscles of the palate and the superior constrictor. *J Anat* 65: 92–95.

27 Soft palate and tongue muscles

Swetal Patel and Marios Loukas
St. George's University, School of Medicine, St. Georges, Grenada

Soft palate

The soft palate is the posterior soft tissue part of the palate. It consists of muscle fibers sheathed in a mucous membrane responsible for closing the airway during the act of swallowing. There are five muscles comprising the soft palate: tensor veli palatini, palatopharyngeus, palatoglossus, levator veli palatini, and the musculus uvulae. In the following sections we discuss the normal anatomy of each of these muscles followed by their perspective anatomical variations.

Tensor veli palatini

The tensor veli palatini (TVP) normally arises from the scaphoid fossa of the pterygoid process, descending down the medial pterygoid plate and then looping around the pterygoid hamulus, inserting into the palatine aponeurosis. It functions to tighten the anterior part of the soft palate and it assists in opening the pharyngotympanic tube. Variations of the tensor veli palatini have been found as follows.

1. Two adjacent origins of the TVP were found: the cranial base origin and the auditory tube cartilage origin. The cranial base origin was always anterior to the auditory tube origin (Abe 2004). Abnormal insertion of the TVP into the cartilage of the Eustachian tube was found to cause a functional obstruction that led to an increase in incidence of otitis media in patients with cleft palate (Matsune et al. 1991).
2. Secondary insertions were found to occur at the maxillary tuber (33.6%) and the submucosal tissue near the palatoglossal arch (37.8%) (Abe 2004). Maxillary insertions were almost always associated with an auditory tube cartilage origin that was wider than the cranial base origin.
3. Macalister (1875) noted the TVP may be split for its whole length. He also noted the TVP receiving a slip from the internal pterygoid muscle, another accessory slip from the outer border of the scaphoid fossa joining the TVP midway, and a slip to the buccinator.

Palatopharyngeus

The palatopharyngeus normally arises from the superior surface of the palatine aponeurosis and the posterior margin of the palatine bone. It then inserts into the upper border of the thyroid cartilage and forms the palatopharyngeal arch behind the palatine tonsil. It functions to elevate the pharynx and larynx and assists in closing the nasopharyngeal isthmus during swallowing. The following are documented variations of the palatopharyngeus.

1. A study performed by Lindman and Ståhl (2002) showed that there were several morphological anomalies regarding the palatopharyngeus. Lindman and Ståhl noted the palatopharyngeus varied in fiber size and amount of connective tissue. Findings pointed towards a pathological process of denervation and degeneration in the patient samples.
2. The palatopharyngeus is composed of the longitudinal and the transverse division. The longitudinal region is known to divide into two fasciculi originating from the palatine aponeurosis and sandwiching the levator veli palatini. Sumida et al. (2012) discovered another fasciculus that originates from the uvula and regarded the salpingopharyngeus as another fasciculus of origin.

The palatoglossus will be discussed in section on the tongue.

Levator veli palatini

The levator veli palatini normally arises from the inferior surface of the petrous temporal bone and the cartilage of the pharyngotympanic tube. It inserts into the superior surface of the palatine aponeurosis. It functions to elevate the posterior part of the soft palate and assists in narrowing the pharynx. Macalister (1875) found the LVP to be split along its length. He described one part arising from the Eustachian tube while the other arose from part of the temporal bone. However, he stated that the muscle could either: be entirely from the Eustachian tube in origin; have a split petrosal part; or have a single origin with two points of insertion. He stated the part arising from the Eustachian tube has been described as another muscle, named the salpingo-staphylinus.

Musculus uvulae

The musculus uvulae arises from the posterior spine of the palatine bone and the dorsal surface of the palatine aponeurosis. It then descends and inserts into the tunica mucosa of the uvula.

Bergman's Comprehensive Encyclopedia of Human Anatomic Variation, First Edition. Edited by R. Shane Tubbs, Mohammadali M. Shoja and Marios Loukas.
© 2016 John Wiley & Sons, Inc. Published 2016 by John Wiley & Sons, Inc.

It assists in closing the nasopharynx by elevating and shortening the uvula. There have been no documented anatomical variations to the musculus uvulae thus far.

In addition to the five main muscles that compose the soft palate there are also four muscles that have been found outside of this normal anatomy. In rare occurrences the soft palate has also been found to consist of the salpingo-pharygeus, peristaphylinus externus, the pterygo-palatinus, and the petro-salpingostaphylinus. The salpingo-pharyngeus is a small muscle found behind the palato-pharyngeus extending from the Eustachian tube to the pharynx, inserting along with the palatopharygeus. The peristaphylinus externus arises from the upper mandibular bone under the first molar tooth and is inserted into the side of the uvula.

Tongue

The tongue consists of eight muscles categorized as either extrinsic or intrinsic. The extrinsic muscles of the tongue serve to change the position of the tongue, while the intrinsic muscles change the shape of the tongue. There are four extrinsic muscles: genioglossus, hyoglossus, styloglossus, and palatoglossus. The four intrinsic muscles of the tongue are: superior longitudinal, inferior longitudinal, verticalis, and transversus. In the following sections we discuss the normal anatomy of each of these lingual muscles followed by their perspective anatomic variations. Other anatomical anomalies regarding the tongue are also discussed in the third and final section.

Genioglossus

The genioglossus arises from the superior genial tubercle on the inner surface of the mandible. It blends with the intrinsic muscles of the tongue from the apex to the root. The following are documented variations of the genioglossus.

1. The genioglossus has been found to send a slip to the epiglottis called the levator epiglottidis.
2. A muscle distinguished as the geniopharyngeus (of Winslow) stretches from the genioglossus to the superior constrictor of the pharynx. Fibers have also been found sent to the stylohyoid ligament.
3. Bergman et al. (1988) defined a fasciculus called the longitudinalis linguae inferior medius. He reported that when parts of the muscle become isolated, this fasciculus can extend from the mental spine to the tip of the tongue.
4. Luschka found a slip of the genio-epiglotticus to be continuous with the styloglossus.

Hyoglossus

The hyoglossus arises from the body and the greater cornu of the hyoid bone and blends into the sides of the tongue between the styloglossus and the inferior longitudinal muscles. It functions to depress the tongue. The following are documented variations of the hyoglossus.

1. Bergman et al. (1998) noted fibers from three muscles, separate from the hyoglossus, that arise from the body, lesser, and greater cornu of the hyoid. The fibers that originate from the body of the hyoid bone and then insert into the dorsum of the tongue are called the basioglossus. In a similar fashion, the fibers originating from the lesser cornu of the hyoid are called the chondroglossus and those from the greater cornu are called the ceratoglossus.
2. Fibers called the triticeoglossus originate from triticeal cartilage and extend to insert into the dorsum of the hyoglossus.
3. The geniohyoid has been found to originate from the fibers of the hyoglossus.

Styloglossus

The styloglossus arises from the styloid process and the stylomandibular ligament. The longitudinal part of the muscle blends dorsally with the inferior longitudinal muscle while the oblique part blends with the hyoglossus. It elevates and retracts the tongue. The following are documented variations of the styloglossus.

1. Macalister (1875) notes that the styloglossus may be doubled or absent on one or both sides. If the styloglossus is absent, it may have been replaced by the myloglossus or the mandibuloglossus.
2. The myloglossus passes from the angle of the jaw to the tongue in proximity to the styloglossus. It is considered an aberrant slip of the styloglossus. In cases where the styloglossus is absent, the myloglossus is found taking its place. It is also found forming a second head for the styloglossus.
3. The muscle is found to arise from the surface of the medial pterygoid, in the form of small bundles of fibers.
4. The styloauricularis and the stylodepressor auriculae are muscle slips originating from the external auditory meatus cartilage and at times ending in the styloglossus.
5. The styloglossus has been found to originate from the stylomaxillary ligament. A second head was found coming from the stylomaxillary ligament and it was suggested that it may send some fibers into the styloglossus.
6. A specimen was described to be a double styloglossus composed of parallel bellies.
7. It is found to send deep fibers to join the genioglossus.
8. In one report the styloglossus sent one slip to its normal insertion and another into the pharynx.
9. The styloglossus has been found absent on one side and on both sides.

Palatoglossus

The palatoglossus arises from the inferior surface of the palatine aponeurosis. It inserts into the lateral aspect and the dorsal surface of the tongue forming the palatoglossal arch. It functions to elevate the back of the tongue and narrows the oropharynx. The following are documented variations of the palatoglossus.

Kuehn (1978) showed lateral radiographs that indicate potential force vectors of palatoglossus in relation to the tongue and

soft palate varied for different specimens. It was found that the region of termination within the tongue was fairly constant across specimens. However, the palatoglossus attachment site in the soft palate varied. In most cases the attachment site was found in the uvula. In some specimens the palatoglossus was found attached to the hard palate. A slip of the tongue musculature attached to the capsule of the palatine tonsil has been termed the amygdaloglossal muscle of Broca.

There has been no documentation of variations within the intrinsic musculature of the tongue.

Other variants of the tongue

Tongue development starts during the fourth week of intrauterine life. It begins in the floor of the primitive cavity with the first, third and fourth pharyngeal arches. Abnormal fusion of the pharyngeal arches can lead to congenital anomalies of the tongue. The literature suggests that tongue malformations are a result of any process that affects the mesenchymal fusion during the latter part of the fourth week of gestation (Surej 2010). Aglossia, macroglossia, bifid tongue, accessory tongue, and long tongue are some of the malformations seen as a result of this process. While isolated cases of these malformations are rare, there have been multiple reported cases of these malformations in association with different clinical syndromes. These various anomalies of the tongue are discussed in the following sections.

Aglossia

Aglossia is the congenital absence of the entire tongue, while microglossia and hypoglossia refer to abnormal smallness of the tongue. The tongue is formed between the fourth and eight week of gestation. When embryogenesis of the lateral lingual swellings and the tuberculum impar fails, aglossia occurs (Salles 2008). Isolated aglossia is rare. This anomaly is commonly associated with limb deformities, cleft palate, situs inversus, and clinical syndromes such as Moebius, Pierre Robin, Hanhart, and hypoglossia-hypodactylia (Stevenson 2006). According to Stevenson (2006) there has been no evidence suggesting that aglossia is hereditary and that no therapy exists for this condition. Boraz used palatal expanders for mandibular expansion, but it failed when their patient lost the ability to talk and swallow. Salles (2008) introduced a multidisciplinary approach to treating aglossia. Their patient received psychological, nutritional, orthodontic, speech, and hearing care.

Absence of the lingual frenulum

During development the tongue is fused to the floor of the mouth. The tongue begins to separate through the process of cellular degeneration. The frenulum becomes absent when this cellular degeneration progresses past its normal limit. This anomaly is found in patients with Ehlers–Danlos syndrome (Gorlin 2001), Rapp–Hodgkin syndrome, and aglossia-adactylia.

Macroglossia

Macroglossia is the enlargement of the tongue. It can be classified as either true macroglossia or relative macroglossia. True and relative macroglossia can then further be classified as either congenital or acquired. True congenital macroglossia includes vascular malformations, muscular enlargement, mucopolysaccharide storage disorders, and congenital tumors. Beckwith–Wiedeman syndrome is an overgrowth syndrome in infants. They usually present with macroglossia along with visceromegaly, diaphragmatic anomalies, omphalocele, and gigantism. Hyalinosis cutis et mucosae is a syndrome where the tongue becomes enlarged and attached to the floor of the mouth. The tongue loses its papillae. Pustular white nodules will also develop on the face. Mannosidosis is a genetic disease that causes mental retardation, skeletal abnormalities, coarse facial features, and macroglossia. Mucopolysaccharidosis is a storage disorder that affects various parts of the body. It is characterized by macrocephaly, hydrocephalus, hepatosplenomegaly, and macroglossia.

True acquired macroglossia includes systemic disorders such as amyloidosis, acquired tumors, and local reactive changes. Lymphoma has been seen to involve the tongue. A case of histiocytic lymphoma was found manifesting as macroglossia (Benjamin 1983).

Systemic amyloidosis macroglossia has been described in several cases of amyloidosis and multiple myeloma. One specific case of a 79-year-old woman who suffered from alpha-lamda-light chain amyloidosis reported macroglossia as the primary finding, which lead to her diagnosis of multiple myeloma (Arweiler 1995). Relative macroglossia occurs when the tongue apears large even though it is normal in size. Relative congenital macroglossia includes trisomy 21 and cretism while relative acquired macroglossia includes edentulousness and myxedema (Vogel 1986).

Bifid tongue

A bifid tongue is when the anterior two-thirds of the tongue is divided longitudinally. Two lateral lingual structures normally grow over the tuberculum impar to form the anterior two-thirds of the tongue. When these two lateral structures fail to fuse, the result is a bifid tongue. Surej (2010) describes a very rare case of a 45-year-old male with an isolated congenital bifid tongue. No other associated congenital orofacial defects were found. The bifid tongue is usually reported in cases of oral-facial-digital syndrome, median mandibular cleft, mandibulofacial dysostosis, cleft palate, and Larsen syndrome (Stevenson 2006). Oral-facial-digital syndrome is characterized by abnormalities that include a lobed tongue, cleft palate, accessory gingival frenulae, hypodontia, and several facial and digital abnormalities.

Smooth, hairy, and geographic tongue

A tongue surface that has lost its papillae, often due to vitamin deficiency rather than variation, is referred to as a smooth tongue. Elongated papillae on the dorsal surface of the tongue

may give the impression of a "hairy" tongue. A map-like surface of the dorsal tongue, where some areas have lost their papillae and are smooth but other areas retain their papillae, has been referred to as a geographic tongue.

Fissured and scrotal tongue, lingua plicata

A fissured tongue (FT) is characterized by having deep fissures in the dorsum of the tongue. The condition is benign and not clinically significant. The fissured tongue can be accentuated when the patient is asked to push the tip of their tongue against the anterior mandibular teeth. A study examining the prevalence of fissured tongue among 2464 Israeli adults of different ethnic origins found the prevalence to be as high as 30.5% (Yarom 2004). However, a study performed in Minnesota of 3611 school children showed the prevalence to be as low as 1.08% (Redman 1970). The varied prevalence of FT among different studies can be attributed to its autosomal dominant mode of inheritance (Kulla-Mikkonen 1988). Kulla-Mikkonen (1987) described two types of fissured tongue: FT with normal appearing filiform papillae and fissured tongue syndrome (FTS). In FTS, the filiform papillae have a smooth surface and are in occurrence with a geographic tongue (Stevenson 2006). A fissured tongue is associated with trisomy 21 and Melkersson–Rosenthal syndrome. It is also seen in immunological and gastrointestinal diseases such as Sjogren and pernicious anemia (Stevenson 2006).

Glossopalatine ankylosis

Glossopalatine ankylosis is characterized by an intraoral band that attaches the anterior portion of the tongue to the hard palate or maxillary alveolar ridge. This causes the tongue tip to have limited mobility and limited extension. The tongue tip is usually cleft. Glossopalatine ankylosis is associated with cleft palate, ankyloglossia superior syndrome, underdeveloped mandible, and hypoplastic upper lip (Gorlin 2001).

Ankyloglossia

Ankyloglossia can be classified as either partial ankyloglossia or total ankyloglossia, both described as having a short and thick frenulum. As mentioned previously, during development the tongue is fused to the floor of the mouth. The tongue begins to separate through the process of cellular degeneration, with the lingual frenulum being the only remaining tissue. As the absence of the lingual frenulum is due to this resorption process progressing too far, ankyloglossia occurs when this resorption process is not completed (Stevenson 2006).

There are varying degrees of ankyloglossia, from a mild form involving only a mucous membrane band to a form where the frenulum and the genioglossus fibers are fibrosed, and finally to total ankyloglossia where the tongue is fused to the floor of the mouth (Horton et al. 1967). In partial ankyloglossia, also known as tongue-tie, a frenulum of variable size exists beginning in the midventral part of the tongue and extending to the tip of the tongue. This frenulum limits the mobility and extension of the tongue. It prevents the tongue from extending past the vermillion border of the lower lip (Stevenson 2006). In total ankyloglossia the tongue is fused to the oral floor. Patients with ankyloglossia to this extent commonly present with associated anomalies of the limb. It has also been reported to be associated with oral-facial-digital syndrome I and a cleft mandible (Gorlin 2001).

Median rhomboid glossitis

Median rhomboid glossitis is characterized by a slightly raised, reddish, rhomboid plaque on the dorsum of the tongue. It lies anterior to the circumvallate papillae and extends to the sulcus terminalis. Its reddish color is due mainly to the absence of filiform papillae. It was believed that this plaque was a result of the persistence of the tuberculum impar (Van der Waal 1979). However, recent investigations have pointed away from a congenital cause. Baughman (1971) suggested the anomaly was due to an inflammatory or degenerative process in adults. Cooke (1975) indicated that this glossitis was due to a candidal species while Van der Waal (1979) postulated that since the area is devoid of papillae it is more susceptible to hosting candidal species. Histological sections show that the epithelium is hyperplastic. The subepithelial area is filled with chronic inflammatory infiltrates (Stevenson 2006).

References

Abe M. 2004. Variations in the tensor veli palatini muscle with special reference to its origin and insertion. *Cleft Palate Craniofac* 41: 474–484.

Arweiler DJ. 1995. Macroglossia as the initial symptom of amyloidosis. *HNO* 43: 318–320.

Baughman RA. 1971. Median Rhomboid Glossitis. A developmental anomaly? *Oral Surg* 31: 56.

Benjamin I. 1983. Histiocytic lymphoma (reticulum-cell sarcoma) of the tongue manifesting as macroglossia. *Hum Pathol* 14: 375–377.

Bergman RA, Thompson SA, Afifi AK. 1988. *Compendium of Human Anatomic Variation: Text, Atlas and World Literature Review*. Baltimore: Urban & Schwarzenberg.

Cooke BE. 1975. Median rhomboid glossitis: candidiasis and not a developmental anomaly. *Br J Dermatol* 93: 399.

Gorlin RJ. 2001. *Syndromes of the Head and Neck*, fourth edition. Oxford: Oxford University Press.

Horton CE, Crawford HH, Adamson JE, Ashbell TS. 1967. Tongue-tie. Presented at the 1967 Annual Meeting of the American Cleft Palate Association, Chicago. Available at: http://digital.library.pitt.edu/c/cleftpalate/pdf/e20986v06n1.03.pdf (accessed 26 October 2015).

Kuehn DP. 1978. Anatomical characteristics of palatoglossus and the anterior faucial pillar. *Cleft Palate J* 15: 349–360.

Kulla-Mikkonen A. 1987. Hematological and immunological features of patients with fissured tongue syndrome. *J Oral Maxillofac Surg* 25: 481.

Kulla-Mikkonen A. 1988. Familial study of fissured tongue. *Scand J Dent Res* 96: 366.

Lindman R, Ståhl P. 2002. Abnormal palatopharyngeal muscle morphology in sleep-disordered breathing. *J Neurol Sci* 15: 195: 11–23.

Macalister A. 1875. Observations on the muscular anomalies in the human anatomy (Third series), with a catalogue of the principal muscular variations hitherto published. *Trans Roy Iri Acad Sci* 25: 1–130.

Matsune S, Sando I, Takahashi H. 1991. Insertion of the tensor veli palatini muscle into the eustachian tube cartilage in cleft palate cases. *Ann Otol Rhinol Laryngol* 100: 439–446.

Redman R. 1970. Prevalence of geographic tongue, fissured tongue, median rhomboid glossitis, and hairy tongue among 3,611 Minnesota schoolchildren. *Oral Surg Oral Med Oral Pathol* 30: 390–395.

Salles F. 2008. Complete and isolated congenital aglossia: case report and treatment of sequelae using rapid prototyping models. *Oral Surg Oral Med Oral Path Oral Rad Endo* 105: 41–47.

Stevenson R. 2006. *Human Malformations and Related Anomalies*. Oxford: Oxford University Press, Inc.

Sumida K, Yamashita K, Kitamura S. 2012. Gross anatomical study of the human palatopharyngeus muscle throughout its entire course from origin to insertion. *Clin Anat* 25: 314–323.

Surej K. 2010. Isolated congenital bifid tongue. *Natl J Maxillofac Surg* 1: 187–189.

Van der Waal I. 1979. Median rhomboid glossitis caused by Candida? *Oral Surg* 47: 31.

Vogel JE. 1986. Macroglossia: a review of the condition and a new classification. *Plast Reconstr Surg* 78: 715.

Yarom N. 2004. Prevalence of fissured tongue, geographic tongue and median rhomboid glossitis among Israeli adults of different ethnic origins. *Oral Path Oral Med* 209: 88–94.

Further reading

Anderson RJ. 1897. A variety of mylopharyngeus and other unusual muscular abnormalities. *J Anat Physiol* 14: 357–359.

Emmanouil-Nikoloussi EN. 1992. Developmental malformations of human tongue and associated syndromes. *Bull du Group Int* 35: 5–12.

Huang M. 1997. Structure of the musculus uvulae: Functional and surgical implications of an anatomic study. *Cleft Palate Craniofac J* 34: 466–474.

28 Prevertebral and craniocervical junction muscles

Yujiro Sakamoto
Tokyo Medical and Dental University, Tokyo, Japan

The scalene muscles comprise the scalenus anterior, the scalenus medius, and the scalenus posterior (Thane 1894; Spalteholz 1910; Grant and Smith 1953; Sinclair 1972; Staubesand 1985; Tillmann 1987). They are also classified as the lateral group of the deep (posterior) cervical muscles (Eisler 1912) or the lateral vertebral muscles (Standring 2005). The scalenus minimus is inconstant; it has been adopted as the fourth scalene muscle (Spalteholz 1910; Eisler 1912; Tillmann 1987) and is treated as one of their variations (Thane 1894; Grant and Smith 1953) or described in relation to the pleura (Wyburn 1972; Johnson 2005). The prevertebral muscles (anterior vertebral muscles) comprise the longus colli, the longus capitis, the rectus capitis anterior, and the rectus capitis lateralis (Thane 1894; Grant and Smith 1953; Sinclair 1972; Staubesand 1985; Tillmann 1987; Standring 2005). They are also classified in the medial group of the deep (posterior) cervical muscles along with the anterior and lateral intertransverse muscles (Eisler 1912). Alternatively, the longus colli and capitis are classified as the anterior vertebral muscles, and the rectus capitis anterior and lateralis as the deep cervical muscles (Spalteholz 1910). The rectus capitis anterior and lateralis are also classified as suboccipital muscles (FIPAT 1998), or the latter is included in the ventral group of the cranial joint muscles (Töndury and Tillmann 1987).

The scalene muscles collectively are considered as the intercostal muscles of the thorax, located in the neck (Bergman et al. 2006). Due to the absence of free ribs, three parts have merged and resemble the abdominal wall; they are not distinctly divided from each other however. The scalene muscles vary in the number of costal and vertebral attachments (Thane 1894; Grant and Smith 1953; Bergman et al. 1988, 2006; Standring 2005), the arrangement of fibers (Thane 1894), the interrelationships caused by the fusion of numerous fasciculi (Bergman et al. 1988, 2006), their degree of separation, and their segmental innervation (Standring 2005). In addition, a poorly defined muscle mass is present in about 30% of cases (Bergman et al. 1988, 2006). The degree of fusion of the various fasciculi likewise varies so much that different authors have subdivided the scalenus mass into different numbers of muscles (Grant and Smith 1953). The problem of definition has been compounded because different authors have described various muscles and their relationships to the scalene mass in different ways (Bergman et al. 1988, 2006).

The most significant and common variations in the prevertebral muscles concern the number of vertebrae to which the tendons of origin and insertion are attached (Bergman et al. 2006). The numbers of vertebrae to which the longus colli and capitis can be attached, and the extent of fusion of the different fasciculi composing them, vary considerably (Grant and Smith 1953), and fusion with the scalenus anterior can occur (Grant and Smith 1953; Bergman et al. 2006). The rectus capitis anterior represents an anterior intertransverse muscle (Sinclair 1972; Bergman et al. 2006) or can be considered its upward continuation (Grant and Smith 1953). The rectus capitis lateralis represents the lateral intertransverse muscle of the space between the transverse process of the atlas and the occipital bone (Grant and Smith 1953; Bergman et al. 2006), the posterior intertransverse muscles (Sinclair 1972; Standring 2005), or the anterior intertransverse muscles (Staubesand 1985; Töndury and Tillmann 1987). The number of attachments and the degree of separation of the several parts of the prevertebral muscles vary (Thane 1894).

Scalenus anterior (anterior scalene)

The scalenus anterior arises from the transverse processes of the third–sixth cervical vertebrae (Thane 1894; Spalteholz 1910; Eisler 1912; Grant and Smith 1953; Sinclair 1972; Staubesand 1985; Tillmann 1987; Bergman et al. 1988, 2006; Standring 2005) and rarely from the second (Tillmann 1987) or seventh (Grant and Smith 1953; Bergman et al. 1988, 2006). It arises from the anterior tubercles of the transverse processes (Thane 1894; Grant and Smith 1953; Sinclair 1972; Staubesand 1985; Tillmann 1987; Standring 2005). It has also been described as arising from the anterior tubercles of the fifth and sixth cervical vertebrae and the posterior tubercles of the third and fourth (Eisler 1912). It is inserted into the scalene tubercle on the inner border or the upper surface of the first rib anterior to the groove for the subclavian

Bergman's Comprehensive Encyclopedia of Human Anatomic Variation, First Edition. Edited by R. Shane Tubbs, Mohammadali M. Shoja and Marios Loukas.
© 2016 John Wiley & Sons, Inc. Published 2016 by John Wiley & Sons, Inc.

artery (Thane 1894; Spalteholz 1910; Eisler 1912; Grant and Smith 1953; Sinclair 1972; Staubesand 1985; Tillmann 1987; Standring 2005), and also in some cases into the second or third rib (Bergman et al. 2006).

The scalenus anterior is rarely absent (Eisler 1912; Tillmann 1987). When it is double, one of the pair is termed the accessory anterior scalene (Bergman et al. 1988, 2006) and the origin is sometimes separated (Tillmann 1987). The scalenus anterior can be penetrated by the fourth–fifth cervical nerves (Eisler 1912) and can be closely associated with the anterior intertransverse muscles or the longus capitis (Bergman et al. 2006); the tendons of its origins can fuse with the former (Eisler 1912) or the latter (Tillmann 1987). A slip from it sometimes passes behind the subclavian artery (Thane 1894; Eisler 1912; Bergman et al. 2006). The scalenus anterior can be split into two parts between which the artery passes through (Eisler 1912; Bergman et al. 2006). In such a case, the muscle can be pierced by the eighth cervical nerve dorsal to the artery, presenting potential entrapment sites for the artery and the nerve (Bergman et al. 2006). The insertion of the scalenus anterior is sometimes close to the scalenus medius and narrows the space between them (Tillmann 1987). Muscle bundles can be exchanged between the scalenus anterior and the scalenus medius (Bergman et al. 2006), and a bundle from the former is joined to the latter (Tillmann 1987) and inserted with it (Eisler 1912). The reported variations of the origins from the transverse processes of the cervical vertebrae, the insertions into the ribs, and the other relationships, are described in the following.

The study of 50 fetal cadavers, 100 sides by Yonekura (1954) revealed that the scalenus anterior arose from the cervical vertebrae as follows: from the second–sixth on the right side once (1.0%); third–fifth on both the right and left sides twice (4.0%); third–sixth, on the right side nine times and on the left eight times (17.0%); fourth–sixth, on the right side 36 times and on the left 37 times (73.0%); fifth–sixth, on the right side once and on the left twice (3.0%); fifth–seventh, on the right and the left sides once each (2.0%). No mention was made of the insertions.

The study of 120 cadavers, 240 sides by Mori (1964) revealed that the scalenus anterior arose from the cervical vertebrae as follows: from the second–fifth on the right and left sides four times each (3.3%); third–fifth, on the right side 53 times and on the left 55 times (45%); and fourth–sixth, on the right side 63 times and on the left 61 (51.6%). By cervical vertebra of origin: the second, eight sides (33.3%); third, 116 sides (48.3%); fourth, 240 sides (100%); fifth, 240 sides (100%), and sixth, 124 sides (51.6%). The scalenus anterior was always inserted into the first rib (100%).

The study of 50 cadavers, 100 sides by Serisawa (1968) revealed that the scalenus anterior arose from the cervical vertebrae as follows: from the second–sixth, on the right side twice (2.0%); third–sixth, on the right side six times and on the left four times (10.0%); third–seventh, on the right side once and on the left twice (3.0%); fourth–sixth, on the right side 25 times and on the left 24 (49.0%); fourth–seventh, on the right side six times and on the left four (10.0%); fifth–sixth, on the right side nine times and on the left ten times (19.0%); and fifth–seventh, on the right side once and on the left six times (7.0%). The scalenus anterior was always inserted into the first rib (100%).

The study of 10 cadavers, 10 left sides by Rusnak-Smith et al. (2001) revealed that the scalenus anterior arose from the cervical vertebrae as follows: from the third–sixth twice (20%); third–seventh twice (20%); fourth–fifth three times (30%); and fourth–sixth three times (30%). The scalenus anterior was always inserted into the first rib (100%).

The study of 26 cadavers, 52 sides by Sakamoto (2012) revealed that the scalenus anterior arose from the cervical vertebrae as follows: from the third–sixth, on the right side 12 times and on the left 11 (44.2%), including 10 symmetrical cases (38.5%); fourth–sixth, on the right side 12 times and on the left 14 times (50.0%), including 10 symmetrical cases (38.5%); and fifth–sixth, on the right side twice and on the left once (5.8%), including one symmetrical case (3.8%). The scalenus anterior was bilaterally inserted into the first rib (100%).

Uemura et al. (2007) revealed that the subclavian arteries passed in front of the scalenus anterior in 16 cases of 15 cadavers, including 2 cases from 2 fetuses. The incidence of this anomaly was reported to be less than 0.7% in adults; among the 14 unilateral cases, the incidence on right side was 18% (2 of 11 cases) and on the left 81.8% (9 of 11 cases); 3 were uncertain.

Scalenus medius (middle scalene)

The scalenus medius arises from the transverse processes of the third–seventh cervical vertebrae and also from the atlas and axis (Thane 1894; Spalteholz 1910; Eisler 1912; Grant and Smith 1953; Sinclair 1972; Staubesand 1985; Tillmann 1987; Bergman et al. 1988, 2006; Standring 2005). It arises from the posterior (Thane 1894; Sinclair 1972; Tillmann 1987; Standring 2005) or anterior (Staubesand 1985) tubercles of the transverse processes, and also from the lateral margin of the groove for spinal nerves (Tillmann 1987) or the lateral edge of the costotransverse lamellae (Grant and Smith 1953; Bergman et al. 1988, 2006). The scalenus medius is inserted into the first rib (Thane 1894; Spalteholz 1910; Sinclair 1972; Tillmann 1987; Standring 2005) or the first–second (Eisler 1912; Grant and Smith 1953; Staubesand 1985), and the insertion rarely extends to the third (Eisler 1912; Tillmann 1987). It is inserted into the upper surface of the first rib dorsal to the groove for the subclavian artery (Spalteholz 1910; Grant and Smith 1953; Sinclair 1972; Staubesand 1985; Tillmann 1987) and between the groove and the tubercle of the rib (Thane 1894; Standring 2005). It is also inserted into the external intercostal membrane of the first intercostal space and the superior margin of the second rib (Tillmann 1987).

Complete absence of the scalenus medius is very rare (Eisler 1912; Tillmann 1987). A bundle from it sometimes connects to the scalenus anterior (Eisler 1912; Tillmann 1987), as mentioned above. The intertransversarius lateralis longus can extend from the posterior tubercles of the third–fifth transverse processes to the tip of the seventh transverse process and divide the muscle fasciculi near their origin into dorsal and ventral parts (Grant and Smith 1953). The scalenus medius is frequently divided into ventral and dorsal portions because the intertransversarius lateralis longus is interposed, whereupon the latter appears to be a component of the scalenus medius (Eisler 1912). The ventral portion arises from the dorsal half of the lateral margin of the transverse processes and its posterior tubercles. It is inserted into the first rib dorsal to the groove for the subclavian artery, the first intercostal space, and the superior margin of the second rib. The dorsal portion arises from the posterior tubercles and is inserted into the tubercle of the first rib and the superior margin of the second. The transversalis cervicis medius arises from the transverse processes of the second and fourth cervical vertebrae and courses between the scalenus medius and scalenus posterior to insert onto the seventh cervical and first thoracic vertebrae (Bergman et al. 1988, 2006). The reported variations of the origins from the transverse processes of the cervical vertebrae, the insertions into the ribs, and the other relationships, are described in the following.

The study of 50 fetal cadavers, 100 sides by Yonekura (1954) revealed that the scalenus medius arose from the cervical vertebrae as follows: from the first–sixth, on the right side three times and on the left twice (5.0%); first–seventh, on the right side 41 times and on the left 42 times (83.0%); second–seventh, on the right and the left sides five times each (10.0%); and third–seventh, on the right and the left sides once each (2.0%). The scalenus medius was inserted into the ribs as follows: into the first, on the right and left sides, 48 cases each (96.0%); and into the second, on the right and the left sides twice each (6.0%).

The study on the origin of the scalenus medius in 60 subjects by Cave (1933) revealed that it arose from the cervical vertebrae as follows: from the first–seventh in 37 cases (61%); second–seventh in nine cases (15%); third–sixth in six cases (10%); and third–seventh in six cases (10%). No exact definition was possible in two cases.

The study of 10 cadavers, 10 left sides by Rusnak-Smith et al. (2001) revealed that the scalenus medius arose from the cervical vertebrae as follows: from the first–seventh five times (50%); second–sixth four times (40%); and second–seventh once (10%). The scalenus medius was always inserted into the first rib (100%).

The study of 26 cadavers, 52 sides by Sakamoto (2012) revealed that the scalenus medius could be divided into dorsal and ventral parts, although they occasionally connected with tendinous or muscular fibers, and reported the origins and insertions of those two parts. The ventral part arose from the cervical vertebrae as follows: from the third–seventh, on the right side six times and on the left four (19.2%), including three symmetrical cases (11.5%); and fourth–seventh, on the right side 20 times and on the left 22 (80.8%), including 19 symmetrical cases (73.1%). The ventral part was inserted into the ribs as follows: into the first, on the right and the left sides 21 cases each (80.8%), including 20 bilateral (76.9%); and first–second, on the right and the left sides five cases each (19.2%), including four symmetrical (15.4%). The dorsal part arose from the cervical vertebrae as follows: from the first–seventh on the right side 20 times and on the left 23 (82.7%), including 20 symmetrical cases (76.9%); second–seventh, on the right side five times and on the left twice (13.5%), including two symmetrical cases (7.7%); and third–seventh, on the right and the left sides once each (3.8%), neither symmetrical (0.0%). The dorsal part was inserted into the first rib (100%).

The study of 51 cadavers, 102 sides by Harry et al. (1997) revealed that in only 14% of necks was there no anatomical variations such as cervical rib, scalenus minimus, abnormal insertion of scalene muscles, or variation in relationship of brachial plexus to scalene muscles. The fifth and sixth cervical nerves together pierced the scalenus anterior on the right side in 10% and on the left in 5% of cases, including 8% bilateral cases, or separately on the right side in 2% and on the left 4%, including 2% bilateral cases. The fifth cervical nerve pierced the scalenus anterior on the right side in 8% and on the left 5%, including 6% bilateral cases. This nerve was located anterior to the scalenus anterior on the right side in 1% and on the left 2% with no bilateral cases. A slip of the scalenus anterior or the scalenus medius inserted on Sibson's fascia on the right side and left in 2% each, neither of them bilateral. The subclavian artery pierced the scalenus anterior in one side.

The study of 93 cadavers 186 sides by Natsis et al. (2006) revealed that the course of the upper trunk of the brachial plexus varied anatomically on the right side 10 times and on the left 14 times (12.9%), including four bilateral cases (4.3%). The fifth cervical nerve ran anteriorly to the scalenus anterior on the right side four times and on the left twice (3.2%), including one bilateral case (1.1%). The fifth and sixth cervical nerves passed anteriorly to the scalenus anterior on the right side once and on the left three times (2.2%), including one bilateral case (1.1%). The fifth and sixth cervical nerves perforated the scalenus anterior on the right side five times and on the left seven (6.5%), including two bilateral case (2.2%). The fifth and sixth cervical nerves passed between the two bellies of the double scalenus anterior on the left side once (0.5%). The fifth cervical nerve passed anteriorly to the scalenus anterior and the sixth nerve on the left side once (0.5%).

The study of 26 cadavers, 52 sides by Sakamoto (2012) revealed that the roots of the brachial plexus passed between the scalenus anterior and the ventral part of the scalenus medius, and there were positional anomalies bilaterally in four cases (15.4%) and unilaterally in six (23.1%). The anomalies were found on the right and left sides seven times each (26.9%),

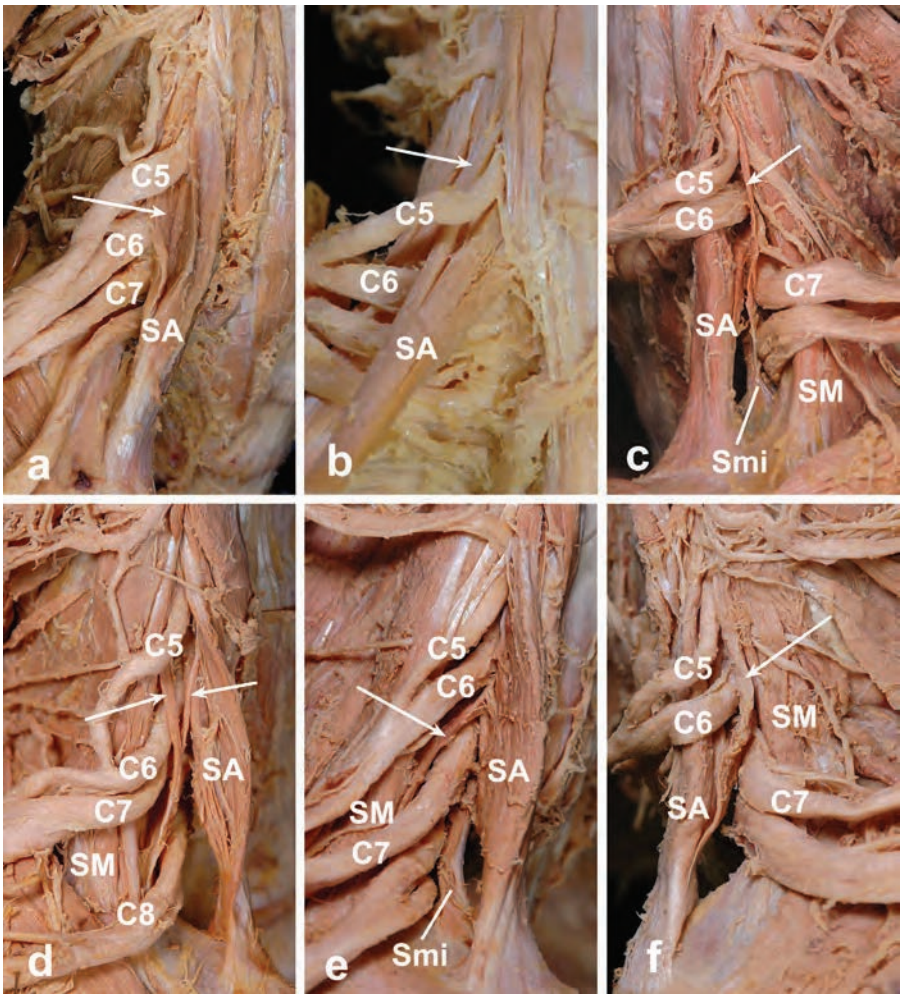

Figure 28.1 The positional anomalies between the scalene muscles and the roots of the brachial plexus. Lateral aspects of the scalenus anterior (SA) and the scalenus medius (SM) on the right (a, b, d, e) and left (c, f) sides. C5–8, ventral ramus of the fifth to eighth cervical nerves; LCa, longus capitis; Smi, scalenus minimus. Arrows indicate the anomalous bundle. One case contains two anomalous bundles (d). Source: Sakamoto (2011). Reproduced with permission from Elsevier.

and one unilateral case contained two anomalies on the right side (1.9%). The scalenus anterior was penetrated by the fifth cervical nerve (Fig. 28.1a) on the right side once and on the left three times (7.6%), including one symmetrical case (3.8%), or passed dorsal to the fifth nerve (Fig. 28.1b) on the right and left sides once each (3.8%) with no symmetrical cases. Some fibers of the scalenus anterior arose from the fourth cervical vertebra and passed dorsal to the fifth and sixth cervical nerves and ventral to the seventh and eighth nerves to join the scalenus minimus (Fig. 28.1c) on the left side once (1.9%) from 52 sides. The ventral part of the scalenus medius was pierced by the sixth and seventh cervical nerves (Fig. 28.1d) on the right side once (1.9%). Some fibers of the scalenus anterior arose from the fourth or fifth cervical vertebra and descended between the sixth and seventh cervical nerves (Fig. 28.1e) on the right side once (1.9%), or the seventh and eighth nerves (Fig. 28.1d) on the right side twice (3.8%) to join the scalenus medius in 52 sides. Some fibers of the scalenus medius arose from the fourth cervical vertebra and descended between the fifth and sixth cervical nerves on the right side twice (3.8%) or the sixth and seventh nerves (Fig. 28.1f) on the left side twice (3.8%) to join the scalenus anterior.

The same study by Sakamoto (2012) revealed the interrelationship between the scalenus medius and the dorsal scapular and long thoracic nerves. The dorsal scapular nerve passed between the ventral and dorsal parts on the right side six times and on the left four times (19.2%), including two symmetrical cases (7.7%); it also pierced the former on the right and the left sides in twelve cases each (46.2%), six of them symmetrical (23.1%), or the latter on the right side three times and on the left twice (9.6%), none of them symmetrical (0.0%). The roots from the fifth and/or sixth cervical nerve to the long thoracic nerve passed between the ventral and dorsal parts on the right side six times and on the left seven times (25.0%), including three symmetrical cases (11.5%), or pierced the ventral part on the right and the left sides 15 times each (57.7%), including nine symmetrical cases (34.6%); the dorsal part was not pierced by these nerve roots.

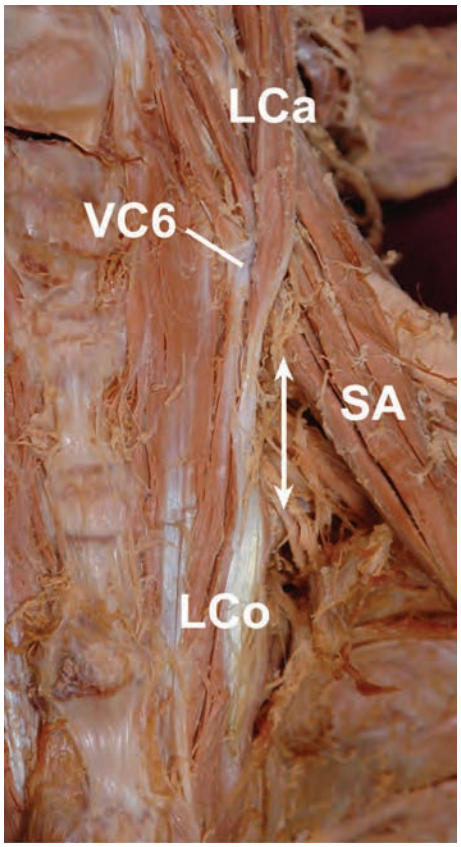

Figure 28.2 Ventral aspect of the anterior vertebral muscles on the left side. The longus capitis (LCa) and the inferior oblique part of the longus colli (LCo) connected with the tendinous fiber (double-headed arrow). SA, scalenus anterior; VC6, transverse process of the sixth cervical vertebra. Source: Sakamoto (2011). Reproduced with permission from Elsevier.

Scalenus posterior (posterior scalene)

The scalenus posterior arises from the posterior tubercles of the transverse processes of the third–seventh (Bergman et al. 1988, 2006), fourth–sixth (Grant and Smith 1953; Sinclair 1972; Staubesand 1985; Standring 2005), fifth–sixth (Eisler 1912), or fifth–seventh (Spalteholz 1910; Tillmann 1987) cervical vertebrae. It is inserted into the outer surface of the second rib (Thane 1894; Spalteholz 1910; Eisler 1912; Grant and Smith 1953; Sinclair 1972; Staubesand 1985; Tillmann 1987; Bergman et al. 1988, 2006; Standring 2005), and sometimes into the first (Eisler 1912; Tillmann 1987), third (Thane 1894; Grant and Smith 1953; Staubesand 1985; Bergman et al. 1988, 2006), or third–fourth (Eisler 1912; Tillmann 1987). Complete absence of the scalenus posterior is not infrequent (Thane 1894; Eisler 1912; Tillmann 1987). It splits into three bundles that are inserted into the first–third ribs (Eisler 1912), or can split into various bundles (Tillmann 1987). It is frequently fused with the scalenus medius (Standring 2005; Bergman et al. 2006) and the first external intercostal muscle (Bergman et al. 1988, 2006). The reported variations of the origins from the transverse processes of cervical vertebrae and the insertions into the ribs are as follows.

The study of 50 fetal cadavers, 100 sides by Yonekura (1954) revealed that the scalenus posterior arose from the cervical vertebrae as follows: from the fourth–fifth, on the right side twice and on the left once (3.0%); fifth–sixth, on the right side once and on the left three times (4.0%); fifth–seventh, on the right side six times and on the left seven (13.0%); sixth–seventh, on the right side 12 times and on the left nine (21.0%); was absent on the right or the left side in six cases each (12.0%); and connected with the scalenus medius on the right side 23 times and on the left 24 (47.0%). The scalenus posterior was inserted into the ribs into the first–second, on the right and the left sides twice each (4.0%); into the second, on the right side 19 times and on the left 17 times (36.0%); and into the third on the left side once (1.0%).

The study of 51 cadavers, 102 sides by Mori (1964) revealed that the scalenus posterior was inserted into the first rib on the right side 9 times and on the left 13 (21.5%); first–second, on the right side 37 times and on the left 34 (69.6%); and first–third, on the right side five times and on the left four (8.8%). No data were reported on its origins.

The study of 10 cadavers, 10 left sides by Rusnak-Smith et al. (2001) revealed that the scalenus posterior arose from the cervical vertebrae as follows: from the fourth–fifth four times (40%); fourth–sixth twice (20%); fifth–sixth twice (20%); and was absent twice (20%). It was inserted into the second rib seven times (70%) and third rib once (10%).

The study of 26 cadavers, 52 sides by Sakamoto (2012) demonstrated the scalenus posterior bilaterally in 19 cases (73.1%), unilaterally in three cases (11.5%), and absent in four (15.4%). The muscle was found on the right side 22 times and on the left 19 (78.8%), and was absent on the right side four times and on the left seven (21.2%). In 22 cadavers, 41 sides it arose from the cervical vertebrae as follows: from the third–fourth on the right side once (2.4%); fourth–fifth on the right side twice (4.9%); fourth–sixth on the right side once and on the left three times (4.9%), including one symmetrical case; fifth on the right side 13 times and on the left 12 times (61.1%), including 10 symmetrical cases; and fifth–sixth on the right side five times and on the left four times (21.9%), including three symmetrical cases. It was inserted into the ribs as follows: into the first, on the right and left sides, one case each (4.9%), which was symmetrical; first–second, on the right side twice and on the left six times (19.5%), including two symmetrical cases; second on the right side 19 times and on the left 10 times (68.3%), including 10 symmetrical cases; and second–third on the right side once and on the left twice (7.3%), including one symmetrical case.

Scalenus minimus

The scalenus minimus (scalenus pleuralis) arises from the anterior border of the transverse process of the seventh cervical vertebra (Thane 1894; Spalteholz 1910; Eisler 1912; Grant and Smith 1953; Wyburn 1972; Tillmann 1987; Bergman et al. 1988, 2006; Johnson 2005), and possibly from the anterior tubercles of the fifth (Eisler 1912; Tillmann 1987) and sixth (Spalteholz 1910; Eisler 1912; Grant and Smith 1953; Tillmann 1987; Bergman et al. 1988, 2006). It is inserted into the inner border of the first rib (Thane 1894; Spalteholz 1910; Eisler 1912; Wyburn 1972; Tillmann 1987; Bergman et al. 1988, 2006; Johnson 2005), dorsal to the scalenus anterior (Eisler 1912) and behind the groove for the subclavian artery (Grant and Smith 1953; Wyburn 1972; Tillmann 1987; Bergman et al. 1988; Johnson 2005), and also sends a process (Sibson's fascia) to the pleural cupola (Grant and Smith 1953). It spreads into the pleural cupola (Eisler 1912; Spalteholz 1910; Johnson 2005) or the fascia supporting it (Thane 1894; Bergman et al. 2006), and joins the cupola through the suprapleural membrane (Bergman et al. 1988). It has been suggested that the suprapleural membrane is the tendon of the scalenus medius (Johnson 2005). The scalenus minimus has also been described as arising from the transverse process of the sixth and seventh cervical vertebrae and the neck of the first rib; the bundle from the latter goes to the pleural cupola (Eisler 1912). The insertion of the scalenus minimus into the first rib can be absent but its insertion into the pleural cupola (the scalenus pleuralis) is constant (Eisler 1912; Tillmann 1987). When the muscle is absent it is replaced by a fibrous band (Grant and Smith 1953; Bergman et al. 1988), Sibson's fascia or the ligamentum costo-pleuro-vertebralis (Eisler 1912; Bergman et al. 2006). Because the insertion into the rib can be absent but the insertion into the pleural cupola cannot, the latter is thought to be the primary insertion for this muscle (Eisler 1912). The scalenus minimus can be double (Eisler 1912). Alongside it, a bundle from the transverse processes of the third and fourth cervical vertebrae has been described as descending ventral to the cervical nerves and dorsal to the origins of the scalenus anterior from fifth and sixth cervical vertebrae, to be inserted into the first rib dorsal to the subclavian artery (Eisler 1912). The scalenus minimus is found in one-third or more of cases (Tillmann 1987): Zuckerkandl found it in 22 out of 60 bodies on both sides, 12 times on the right side only, and nine on the left (Eisler 1912; Grant and Smith 1953). The reported variations of the origins from the transverse processes of cervical vertebrae, the insertions into the rib,s and the other relationships are as follows.

The study of 50 cadavers, 100 sides by Stott (1928) reported the scalenus minimus in 12 cases on both sides (24%), six on the right side only (6%), and nine on the left only (9%).

The study of 50 cadavers, 100 sides by Serisawa (1968) demonstrated the scalenus minimus bilaterally in eight cases (16.0%) and unilaterally in 16 (32.0%), and on the right side 20 times and on the left 12 times (32.0%). The scalenus minimus arose from the sixth–seventh cervical vertebrae on the right side ten times and on the left five (15.0%), including four symmetrical cases, and from the seventh on the right side seven times and on the left four (11.0%) including one symmetrical case. In three bilateral cases it arose from the sixth–seventh on the right side, from the seventh on the left in two cases, and the converse in one. It was always inserted into the first rib and spread into the suprapleural membrane (100%).

The study of 51 cadavers, 102 sides by Harry et al. (1997) demonstrated the scalenus minimus unilaterally on the right side in 24% and on the left in 22%, including 28% bilateral cases. No mention was made of the origins and the insertions.

The study of 26 cadavers, 52 sides by Sakamoto (2012) demonstrated the scalenus minimus (Fig. 28.1c, e) bilaterally in 10 cases (38.4%) and unilaterally in five (19.2%); the muscle was absent in 11 cases. Among the 52 sides it was present on the right side 15 times and on the left 10 times (48.1%). In 15 cadavers, 25 sides it arose from the transverse processes of the cervical vertebrae as follows: from the sixth, on the left side twice (8.0%); sixth–seventh, on the right side six times and on the left three (36.0%), including two symmetrical cases; and seventh, on the right side eight times and on the left six (56.0%), including four symmetrical cases. In four bilateral cases among the 25 sides it arose from the sixth–seventh on the right side and from the sixth on the left in one case; the sixth–seventh on the right side and the seventh on the left in two cases; and the seventh on the right side and the sixth on the left in one. The scalenus minimus was inserted into the first rib (100%) in all 25 sides and lay dorsal to the subclavian artery in all cases and ventral to the cervical nerves as follows: to the seventh, on the right side and the left side one case each (8.0%); eighth, on the right side eight times and on the left seven (60.0%), including six symmetrical cases; and seventh and eighth, on the right side five times and on the left three (32.0%), including two symmetrical cases.

The study by Natsis et al. (2013) revealed that the scalenus minimus arose from the seventh cervical vertebra and was inserted into the first rib unilaterally in three cases (4.1%) from 73 cadavers.

Longus colli

The longus colli is divided into: inferior and superior oblique and vertical (Thane 1894; Tillmann 1987; Standring 2005); or inferolateral, superolateral, and medial (Grant and Smith 1953); or caudal and cranial (Eisler 1912); or lower medial and upper lateral (Spalteholz 1910). The inferior oblique part (inferolateral portion) arises from the fronts or lateral parts of the bodies of the first–second thoracic vertebrae (Thane 1894; Tillmann 1987; Standring 2005) or the first–third (Thane 1894; Grant and Smith 1953; Tillmann 1987; Standring 2005), and is inserted into the transverse processes of the fifth–sixth cervical vertebrae (Thane 1894; Grant and Smith 1953; Tillmann 1987; Standring 2005). The inferior oblique part is inserted into the anterior tubercles of the transverse processes (Thane 1894; Standring 2005). The

vertical part (medial portion) arises from the anterolateral parts or the fronts of the bodies of the first–third thoracic and fifth–seventh cervical (Grant and Smith 1953; Tillmann 1987; Standring 2005) or the first–second or third thoracic and sixth and seventh cervical vertebrae (Thane 1894). It also arises from the transverse processes of the fourth or fifth–seventh cervical vertebrae (Thane 1894). The vertical part is inserted into the anterolateral surfaces or the fronts of the bodies of the second–fourth cervical vertebrae (Thane 1894; Grant and Smith 1953; Tillmann 1987; Standring 2005). The superior oblique part (superolateral portion) arises from the anterior tubercles of the transverse processes of the third–fifth (Thane 1894; Tillmann 1987; Standring 2005) or the third–sixth (Grant and Smith 1953) cervical vertebrae. It also arises from the third thoracic vertebral body (Grant and Smith 1953). The superior oblique part is inserted into the anterolateral surface of the tubercle on the anterior arch of the atlas (Thane 1894; Grant and Smith 1953; Tillmann 1987; Standring 2005).

The caudal part arises from the anterolateral surface of the bodies of the first–third thoracic and the fifth–seventh cervical vertebrae, and is inserted into the transverse processes of the fifth–seventh cervical vertebrae (Eisler 1912). The cranial part arises from the anterior tubercles of the transverse processes of the third–sixth cervical vertebrae and is inserted into the second–fourth cervical vertebral bodies and the tubercle of the anterior arch of the atlas (Eisler 1912). The lower medial part arises from the bodies of the first–third thoracic and the fifth–seventh cervical vertebrae, and is inserted into the second–fifth cervical vertebral bodies and the anterior tubercles of the transverse processes of the fifth–sixth cervical vertebrae (Spalteholz 1910). The upper lateral part arises from the anterior tubercles of the transverse processes of the third–sixth cervical vertebrae and is inserted into the anterior tubercle of the atlas (Spalteholz 1910).

The longus colli can arise from the fourth thoracic vertebral body (Eisler 1912; Tillmann 1987), and rarely from the head of the first–third ribs (Eisler 1912). A slip of the inferior oblique part is sometimes inserted into the head of the first rib (Thane 1894), or its fasciculus can continue into the longus capitis (Thane 1894; Tillmann 1987). The longus colli can fuse with the scalenus anterior (Grant and Smith 1953). The transversalis cervicis anticus is a muscle arising from the front of the transverse processes of some of the fourth–seventh cervical vertebrae, and is inserted into one or more of the first–third (Thane 1894). The reported variations of the attachments to the transverse processes of cervical vertebrae, the bodies of the cervical and thoracic vertebrae, and the other relationships are as follows.

The study of 50 fetal cadavers, 100 sides by Yonekura (1954) revealed the origins and insertions of the three parts of the longus colli. The inferior oblique part arises from the thoracic vertebrae: the first–second on the right and left sides in 31 cases each (62.0%); or the first–third on the right and left sides in 19 cases each (38.0%). The inferior oblique part was inserted into the cervical vertebrae: the fourth–fifth, on the right side once and on the left twice (3.0%); the fourth–sixth, on the right and left sides two cases each (4.0%); the fifth–sixth, on the right side 39 times and on the left 38 times (77.0%); the fifth–seventh, on the right and left sides two cases each (4.0%); and the sixth–seventh, on the right and left sides six cases each (12.0%). The vertical part arises from the cervical and thoracic vertebrae: the fifth–seventh and first–second, on the right side 20 times and on the left 19 (39.0%); the fifth–seventh and first–third, on the right side 10 times and on the left 11 (21.0%); the sixth–seventh and first–second, on the right side 11 times and on the left 12 (23.0%); and the sixth–seventh and first–third, on the right side nine times and on the left eight (17.0%). The vertical part was inserted into the cervical vertebrae: the second–third, on the right and left sides, two cases each (4.0%); the second–fourth, on the right and left sides 20 cases each (40.0%); the third–fourth, on the right and left sides, eight cases each (16.0%); the third–fifth, on the right and left sides, 12 cases each (24.0%); the fourth–fifth, on the right and left sides, seven cases each (14.0%); and the fifth–sixth, on the right and left sides, one case each (2.0%). The superior oblique part arose from the cervical vertebrae: the second–fourth, on the right and left sides, nine cases each (18.0%); the third–fourth, on the right and left sides, 12 cases each (24.0%); the third–fifth, on the right and left sides, 27 cases each (54.0%); and the fourth–fifth, on the right and left sides, two cases each (4.0%). The superior oblique part was inserted into the cervical vertebrae: the first, on the right and left sides, one case each (94.0%); and the first–second, on the right and left sides, three cases each (6.0%).

The study of 26 cadavers, 52 sides by Sakamoto (2012) revealed the origins and insertions of the three parts of the longus colli. The inferior oblique and vertical parts interfused at the origin and arose from the bodies of the upper thoracic and lower cervical vertebrae. Their lowermost origin was the first thoracic vertebra once (1.9%), second 36 times (69.2%), and third 15 times (28.9%). The inferior oblique part was inserted into the fourth–fifth on the right and left sides, one case each (3.8%), not symmetrical (0.0%); fourth–sixth on the right and left sides, two cases each (7.7%) both symmetrical (7.7%); fifth–sixth on the right and left sides, 22 cases each (84.7%), including 21 symmetrical (80.8%); and sixth on the right and left sides, one case each (3.8%), symmetrical (3.8%). In addition to the vertebral bodies, some oblique fibers arising from the anterior tubercles of the cervical transverse processes ascended to join the vertical part. The vertical part arose from the third–sixth on the right and left sides, three cases each (11.5%), including two symmetrical cases (7.7%); fourth–fifth on the right side three times but none on the left (5.8%), no symmetrical cases; fourth–sixth on the right side 11 times and on the left 13 (46.2%), including 10 symmetrical cases (38.5%); fifth on the right side once and none on the left (1.9%), no symmetrical cases; and fifth–sixth on the right and left sides, nine cases each (34.6%), including six symmetrical (23.1%). The vertical part inserted into the bodies of the second–fourth cervical vertebrae. The superior oblique part arose from the second–fourth

on the left side once (1.9%) and not on the right, no symmetrical cases; second, on the right and left sides, two cases each (7.7%), both symmetrical (7.7%); third–fourth on the right side seven times and on the left 10 (32.7%), including five symmetrical cases (19.2%); third–fifth on the right side 14 times and on the left 12 (50.0%), including seven symmetrical cases (26.9%); and third–sixth on the right side three times and on the left once (7.7%), no symmetrical cases. The superior oblique part was always inserted into the anterior tubercle of the first cervical vertebra (100%).

Longus capitis

The longus capitis arises from the anterior tubercles of the transverse processes of the third–sixth cervical vertebrae (Thane 1894; Spalteholz 1910; Eisler 1912; Grant and Smith 1953; Sinclair 1972; Tillmann 1987; Standring 2005). It is inserted into the inferior surface of the basilar part of the occipital bone (Spalteholz 1910; Eisler 1912; Tillmann 1987; Standring 2005) in front of the foramen magnum (Thane 1894), extending anterolaterally from the pharyngeal tubercle (Grant and Smith 1953; Sinclair 1972). It sometimes arises from the axis and rarely the atlas; in contrast, the origin from the sixth can be absent (Tillmann 1987). The longus capitis is often connected with the longus colli (Tillmann 1987) and is occasionally inseparable from it (Bergman et al. 1988, 2006). The longus capitis can fuse with the scalenus anterior (Grant and Smith 1953). In about 4% of cases a muscle, the atlantobasilaris internus or axiobasilaris, extends along the medial border of the longus capitis from the anterior tubercle of the atlas to the base of skull (Grant and Smith 1953; Bergman et al. 1988, 2006). Another muscle, the epistropheobasilaris, is similar but arises from the axis (Bergman et al. 1988, 2006). The atlanticomastoideus or the rectus lateralis accessorius is a cylindrical, ribbon-like, or fusiform muscle extending from the transverse process of the atlas to the mastoid process (Bergman et al. 1988, 2006). The reported variations of the origins from the transverse processes of cervical vertebrae and the other relationships are as follows.

The study of 50 fetal cadavers, 100 sides by Yonekura (1954) revealed that the longus capitis arose from the second–sixth, on the right and left sides, three cases each (6.0%); third–fifth, on the right and left sides, two cases each (4.0%); third–sixth, on the right side 41 times and on the left 40 (81.0%); third–seventh, on the right and left sides, two cases each (4.0%); and fourth–sixth, on the right side twice and on the left three times (5.0%). No mention was made of the insertions.

The study of 26 cadavers (52 sides) by Sakamoto (2012) revealed that the longus capitis arose from the second–sixth on the right side 11 times and on the left nine (38.5%), including seven symmetrical cases (26.9%); and third–sixth, on the right side 15 times and on the left 17 (61.5%), including 13 symmetrical cases (50.0%). The longus capitis was always bilaterally inserted into the occipital bone (100%). The most ventral, superficial fibers of the longus capitis and the inferior oblique part of the longus colli connected with tendinous fibers (Fig. 28.2) on the right side 21 times and on the left 22 (82.7%), including 18 bilateral cases (69.2%).

Rectus capitis anterior

The rectus capitis anterior is a small flat muscle arising from the anterior surface of the lateral mass of the atlas (Spalteholz 1910; Eisler 1912; Grant and Smith 1953; Sinclair 1972; Tillmann 1987; Standring 2005) and the front of the root of its transverse process (Thane 1894; Grant and Smith 1953; Staubesand 1985; Bergman et al. 1988, 2006; Standring 2005). It is inserted into the inferior surface of the basilar part of the occipital bone (Spalteholz 1910; Bergman et al. 1988; Tillmann 1987) immediately anterior to the occipital condyle (Eisler 1912; Grant and Smith 1953; Sinclair 1972; Standring 2005) or the foramen magnum (Staubesand 1985), or between the foramen and the longus capitis (Thane 1894; Bergman et al. 2006). The rectus capitis anterior can be absent or reduced to a few fiber bundles, or it can fail to reach the occipital bone, inserting into the occipitoatlantal ligament (Bergman et al. 1988, 2006). A medial part of the rectus capitis anterior can separate from the primary muscle mass and has been named the rectus capitis minimus (Bergman et al. 1988, 2006).

Rectus capitis lateralis

The rectus capitis lateralis is a short thick muscle arising from the upper surface of the transverse process of the atlas (Thane 1894; Spalteholz 1910; Eisler 1912; Grant and Smith 1953; Sinclair 1972; Staubesand 1985; Töndury and Tillmann 1987; Standring 2005). It is inserted into the inferior surface of the condylar portion of the occipital bone (Bergman et al. 2006) or its jugular process (Thane 1894; Spalteholz 1910; Eisler 1912; Grant and Smith 1953; Sinclair 1972; Staubesand 1985; Töndury and Tillmann 1987; Standring 2005). An accessory bundle, the rectus capitis lateralis longus, arising from the transverse process of the axis and inserting on the occipital bone, has been reported and is known as the muscle of Otto (Bergman et al. 1988, 2006).

References

Bergman RA, Thompson SA, Afifi AK, Saadeh FA. 1988. Muscles. In: *Compendium of Human Anatomic Variation: Text, Atlas, and World Literature. Baltimore*, Munich: Urban & Schwarzenberg.

Bergman RA, Afifi AK, Miyauchi R. 2006. Muscles of head and neck (branchiomeric muscles). In: Illustrated Encyclopedia of Human Anatomic Variation. Available at: http://www.anatomyatlases.org/AnatomicVariants/AnatomyHP.shtml (accessed 13 October 2015).

Cave AJE. 1933. A note on the origin of the m. scalenus medius. *J Anat* 67: 480–483.

Eisler P. 1912. Muskeln des halses, musculi colli. In: *Handbuch der Anatomie des Menscen in acht Bänden; Band 2, Abteilung 2, Teil 1, Bänder, gelenke und Muskeln; Abteilung 2, Teil 1, Die Muskeln des Stammes*. Jena: Gustav Fischer.

FIPAT (Federative International Programme on Anatomical Terminologies). 1998. *Terminologia Anatomica. International Anatomical Terminology. Second edition*. Stuttgart, New York: Georg Thieme Verlag.

Grant JCB, Smith CG. 1953. The musculature. In: *Morris' Human Anatomy*, 11th edition (Schaeffer JP ed.). Toronto: The Blakiston Company.

Harry WG, Bennett JDC, Guha SC. 1997. Scalene muscles and the brachial plexus: anatomical variations and their clinical significance. *Clin Anat* 10: 250–252.

Johnson D. 2005. Thorax. In: *Gray's Anatomy*, 39th edition (Standring S, Ellis H, Healy JC, Johnson D, Williams A eds). Edinburgh, London, New York, Oxford, Philadelphia, St Louis, Sydney, Toronto: Elsevier, Churchill, Livingstone.

Mori M. 1964. Statistics on the musculature of the Japanese. *Okajimas Fol Anat Jap* 40: 196–300.

Natsis K, Totlis T, Tsikaras P, Anastasopoulos N, Skandalakis P, Koebke J. 2006. Variations of the course of the upper trunk of the brachial plexus and their clinical significance for the thoracic outlet syndrome: a study on 93 cadavers. *Am Surg* 72: 188–192.

Natsis K, Totlis T, Diagelos M, Tsakotos G, Vlassis K, Skandalakis P. 2013. Scalenus minimus muscle: overestimated or not? An anatomical study. *Am Surg* 79: 372–374.

Rusnak-Smith S, Moffat M, Rosen E. 2001. Anatomical variations of the scalene triangle: dissection of 10 cadavers. *J Orthop Sports Phys Ther* 31: 70–80.

Sakamoto Y. 2012. Spatial relationships between the morphologies and innervations of the scalene and anterior vertebral muscles. *Annals of Anatomy* 194: 381–388.

Serisawa M. 1968. On the m. scalenus anterior in adult Japanese. *J Nippon Med Sch* 35: 188–202 (in Japanese).

Sinclair DC. 1972. Muscles and fasciae. In: *Cunningham's Textbook of Anatomy*, 11th edition (Romanes GJ ed.) London: Oxford University Press.

Spalteholz W. 1910. Halsmuskeln. In: *Handatlas der Anatomie des Menschen. Band 2, Regionen, Muskeln, fascine, Herz, Blutgefäße. 6 Auflage*. Leipzig: Verlag von S. Hirzel.

Standring S. 2005. Head and neck. In: *Gray's Anatomy*, 39th edition (Standring S, Ellis H, Healy JC, Johnson D, Williams A eds). Edinburgh, London, New York, Oxford, Philadelphia, St Louis, Sydney, Toronto: Elsevier Churchill Livingstone.

Staubesand J. 1985. Muskeln des Thrax. In: *Bennunghoff Makroskopische und Mikroskopische Anatomie des Menschen; Band 1, Cytologie, Histologie, allgemeine Anatomie und Anatomie des Bewegungsapparates*. 1fourth edition (Fleischhauer K, Staubesand J, Zenker W eds). München, Wien, Baltimore: Urban & Schwarzenberg.

Stott CF. 1928. A note on the scalenus minimus muscle. *J Anat* 62: 359–361.

Thane G D. 1894. Myology. In: *Quain's Elements of Anatomy*, 10th edition (Schferäfer EA, Thane GD eds). New York: Longman Green and Co.

Tillmann B. 1987. Hals. In: *Rauber/Kopsch Anatomie des Menschen; Band 1, Bewegungsapparat* (Leonhardt H, Tillmann B, Töndury G, Zilles K eds). Stuttgart, New York: George Thieme.

Töndury G, Tillmann B. 1987. Rumpf. In: *Rauber/Kopsch Anatomie des Menschen; Band 1, Bewegungsapparat* (Leonhardt H, Tillmann B, Töndury G, Zilles K eds). Stuttgart, New York: George Thieme.

Uemura M, Takeuchi A, Suwa F. 2007. Bilateral subclavian arteries passing in front of the scalenus anterior muscle. *Anat Sci Int* 82: 180–185.

Wyburn GM. 1972. The Respiratory System. In: *Cunningham's Textbook of Anatomy*, 11th edition (Romanes GJ, ed.). London: Oxford University Press.

Yonekura S. 1954. A study of the muscles of the neck chest, abdomen and back in Japanese fetuses. *Acta Medica* 24: 1604–1700 (in Japanese).

29 Laryngeal muscles

Eva Maranillo and Jose Sanudo
Complutense University of Madrid, Madrid, Spain

The intrinsic laryngeal muscles have been classically described as arising from two sphincters, external and internal, that surround the cavity of the larynx throughout its embryonic development. The external sphincter gives rise to the cricothyroid muscle, the thyroid cartilage and the inferior constrictor muscles of the pharynx; the internal sphincter is the origin of the rest of the intrinsic muscles and cartilages of the larynx (Fürbringer 1875; Kanthack 1892; Maranillo et al. 2009, 2011).

The two sphincters are interconnected and during their development they dissociate, giving rise to the definitive masses of the individual intrinsic laryngeal muscles. Failure of that process can give rise to a wide range of anatomical variations (Maranillo et al. 2009, 2011).

In order to simplify the many reported variations of the laryngeal muscles, we have tried to categorize them under the main individual muscles whenever possible; fascicles of muscles that do not fit this approach are described in a separate section.

There are five pairs of muscles in addition to the transverse arytenoid. They are all adductors of the vocal folds except for the posterior cricoarytenoid.

Cricothyroid muscle

On the basis of the course of its fibers, this muscle has been considered as comprising of two bellies: oblique and straight. However, some authors have reported three and four bellies (Tourtual 1846; Poirier and Charpy 1903; Mu and Sanders 2008).

The thyroid attachment is normally located on the inner side of the inferior border of the thyroid cartilage. However, the attachment has also been reported on the inner surface of the junction between the lower two-thirds and the upper one-third of the thyroid lamina (Poirier and Charpy 1903).

The cricothyroid muscle can share fibers with neighboring muscles and/or structures: (1) the inferior constrictor of the pharynx; (2) the sternothyroid; (3) the ceratocricoid; (4) the thyrohyoid; (5) the contralateral cricothyroid muscle (Fig. 29.1a); (6) the thyroid gland; (7) the first tracheal rings (*cricotrachealis muscle*); and (8) the remaining intrinsic laryngeal muscles (Gruber 1868c; Macalister 1875; Le Double 1897; Poirier and Charpy 1903).

Superior cricothyroid muscle

This name is reserved for cases of complete independence of the straight belly of the cricothyroid muscle (Fürbringer 1875; Macalister 1875).

Cricotracheal muscle

This very rare muscle arises in the lower border of the cricoid arch below the origin of the cricothyroid muscle, passes behind the isthmus of the thyroid gland, and inserts into the first ring of the trachea. It is considered a supernumerary fascicle of the cricothyroid muscle (Fürbringer 1875; Macalister 1875).

Cricohyoid muscle

This muscle courses from the cricoid arch to the great horn of the hyoid bone or to the posterior aspect of the hyoid body (Fürbringer 1875).

Internal cricoid muscle

This is a small muscle located medially to the cricothyroid and sharing fibers with it. It arises from the outer surface of the cricoid cartilage and the inferior border of a small portion of the thyroid cartilage. It was identified five times by Le Double (1897): one bilateral (one male), and three unilateral (two females and one male), two on the right side and one on the left.

Oblique muscle of the thyroid cartilage prominence

Gruber dissected this for the first time in 1863. It is attached to the lower surface of the thyroid cartilage, near the middle prominence, and to the anterior cricothyroid ligament (Fig. 29.1a–c). This muscle is flattened, fusiform, and sometimes replaced by a fibrous band. Sometimes it is divided into two

Bergman's Comprehensive Encyclopedia of Human Anatomic Variation, First Edition. Edited by R. Shane Tubbs, Mohammadali M. Shoja and Marios Loukas.
© 2016 John Wiley & Sons, Inc. Published 2016 by John Wiley & Sons, Inc.

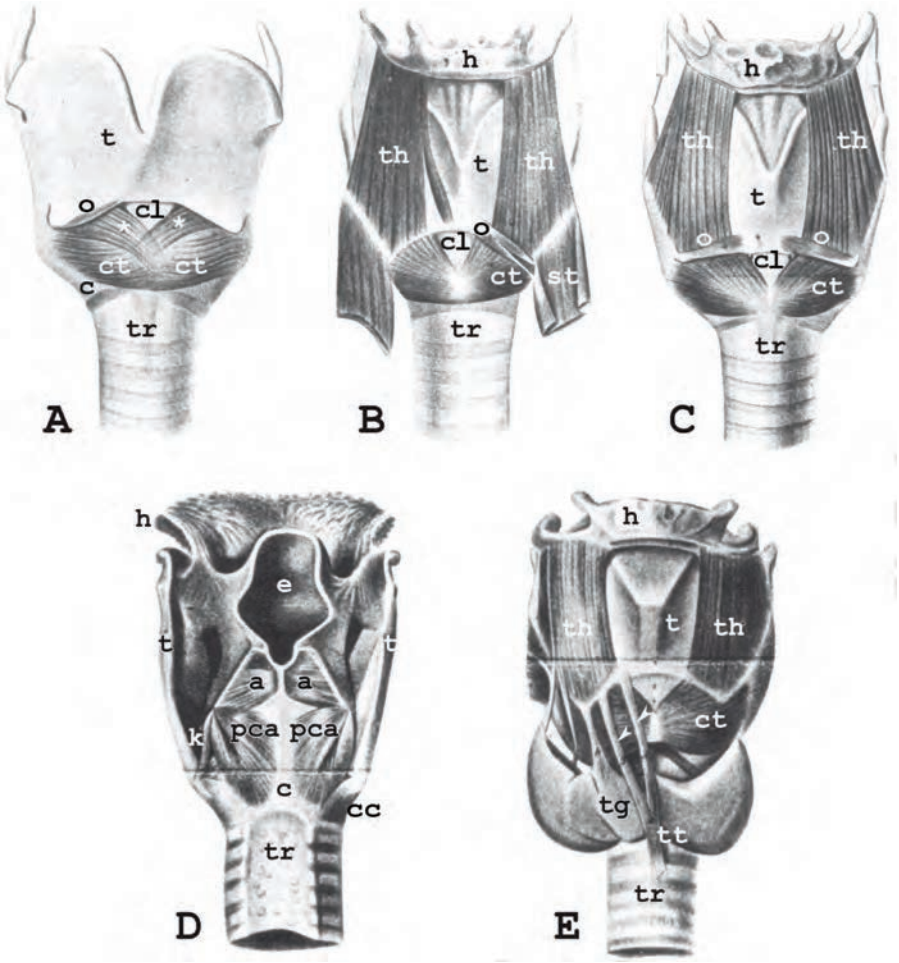

Figure 29.1 Adaptation of Gruber's table XV (1868). (a–c, e) Anterior view of the larynx. (d) Posterior view of the larynx after removing the pharyngeal mucosa. a, arytenoid muscle; c, cricoid cartilage; cl, cricothyroid ligament; ct, cricothyroid muscle; e, epiglottis; h, hyoid bone; o, oblique muscle of the thyroid cartilage prominence; k, ceratoarytenoid muscle; cc, ceratocricoid muscle; pca, posterior cricoarytenoid muscle; st, sternothyroid muscle; t, thyroid cartilage; tg, thyroid gland; th, thyrohyoid muscle; tr, trachea; tt, thyrotracheal muscle; arrowheads, lateral and medial bellies of thyrotracheal muscle; asterisk, fibers from the cricothyroid muscle to the contralateral homonymous muscle.

Source: Gruber 1868a.

bellies by one extra attachment arising from the sternothyroid muscle, *incisurae mediae obliquus bicaudatus* (Fig. 29.1b). It was found six times in 160 subjects (twice on both sides, twice on the right side and twice on the left). It has been considered as the transverse thyroid muscle but less developed (Gruber 1868a; Le Double 1897).

Transverse thyroid muscle

This very rare muscle has been given other names: *thyroideus transversus anomalus*, *thyroideus marginalis inferior*, and *musculus incisurae cartilaginis thyroideae mediae transversus*. It was described first by Gruber in 1845. It passes from one side of the inferior medial thyroid notch to the other, across the upper part of the cricothyroid membrane. It can also be attached along its course in the anterior cricothyroid ligament (Gruber 1868a; Macalister 1875; Poirier and Charpy 1903).

Deep levator muscle of the thyroid gland

This has been reported in 32% of cases. It can be unilateral or more rarely bilateral. It courses from the anteromedial merge of the cricothyroid muscle to the thyroid gland (Fürbringer 1975; Poirier and Charpy 1903).

Thyrotracheal muscle

Gruber described this in 1861. The thyrotracheal muscle arises from the outer surface of the middle part of the thyroid lamina, immediately below the thyrohyoid muscle (Fig. 29.1e). It courses downward, passing over the cricothyroid muscle and over or under the isthmus of the thyroid gland, to be inserted into the anterior surface of the first tracheal ring (Gruber 1868c; Macalister 1875; Poirier and Charpy 1903). It has been reported with two heads, one medial and one lateral, and in some cases with the tracheal attachment prolonged up to the second–fourth tracheal rings (Gruber 1868c; Sujata et al. 2013).

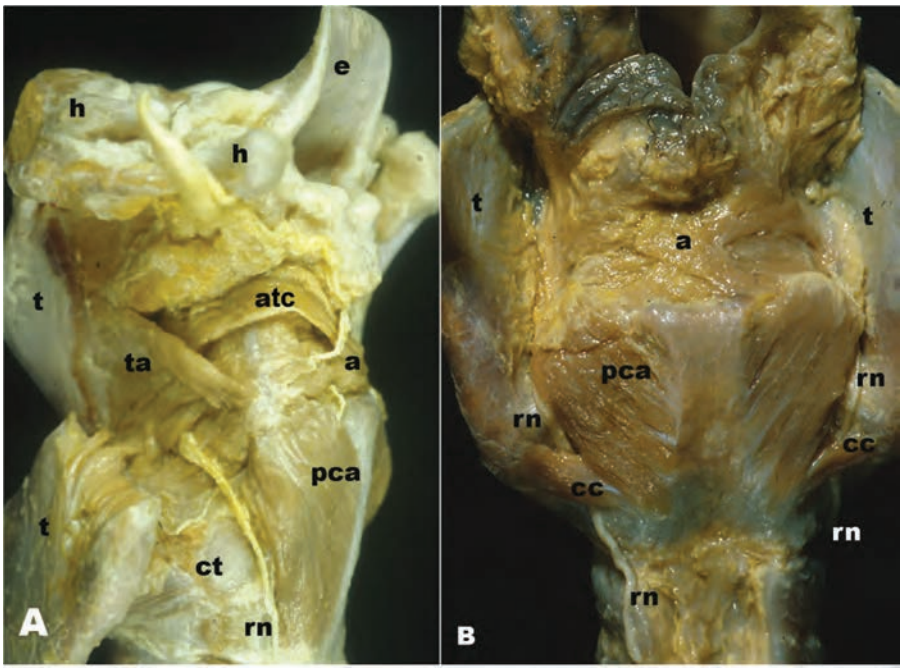

Figure 29.2 (a) Posterolateral view of the left side of the larynx showing over the arythyrocricoid muscle (act) after descending over the thyroid lamina. (b) Dorsal view of the posterior surface of the larynx showing a bilateral ceratocricoid muscle (cc) passing over the recurrent laryngeal nerve (rn). a, arytenoid muscle; ct, cricothyroid joint; e, epiglottis; h, hyoid bone; pca, posterior cricoarytenoid muscle; rn, recurrent laryngeal nerve; t, thyroid cartilage; ta, thyroarytenoid muscle. Adapted from Maranillo et al. (2009) with permission from John Wiley & Sons.

This muscle was found in 21 out 80 larynges (18 times in males and 3 in females) (Gruber 1868c) and 5 times in 8 subjects (Macalister 1875).

Posterior cricoarytenoid muscle

The posterior cricoarytenoid muscle has been reported as comprising two bellies: horizontal or medial and vertical or lateral (Poirier and Charpy 1903; Bryant et al. 1996; Asanau et al. 2011). However, it has recently been considered as comprising three constant bellies or compartments: horizontal, vertical, and oblique (Sanders et al. 1994).

The lateral belly of this muscle can be attached into the inner side of the thyroid cartilage (Poirier and Charpy 1903).

The posterior cricoarytenoid is connected by muscular fascicles with: (1) the cricothyroid joint; (2) the ceratocricoid muscle; (3) the cricopharyngeal muscle; and (4) the remaining intrinsic laryngeal muscles (Macalister 1875; Kanthack 1892; Le Double 1897; Poirier and Charpy 1903).

Ceratoarytenoid muscle

This has also been reported as the posterior thyroarytenoid muscle. Again it was Gruber who first reported it, in 1868. This muscle is situated on the posterior surface of the larynx, between the outer border of the posterior cricoarytenoid muscle and the thyroid cartilage. It courses from the muscular process of the arytenoid cartilage to the posterior border of the lower horn of the thyroid cartilage (Fig. 29.1d). The ceratoarytenoid muscle has been reported in 6% of cases. It has been described as a supernumerary bundle of the posterior cricoarytenoid muscle (Gruber 1868b; Fürbringer 1875; Macalister 1875; Le Double 1897; Poirier and Charpy 1903).

Ceratocricoid muscle

This muscle was described by Tourtual (1846) and is known as the muscle of Merkel. It is a small muscular belly located on the posterior surface of the larynx, lateral to the posterior cricoarytenoid muscle. It is attached between the cricoid lamina and the inferior horn of the thyroid cartilage and also into the capsule of the cricothyroid joint, covering the recurrent laryngeal nerve along its ascending course (Figs 29.1d, 29.2b). It has been reported as a flat or as a fusiform muscle, constituted by one or two fascicles. The reported prevalence of the ceratocricoid muscle ranges from 4.4% to 30% of cases. There are no significant side or sex differences and the muscle is bilateral in 38% of cases. It has been proposed to derive from the cricothyroid or the posterior cricoarytenoid muscle (Luschka 1871; Maranillo et al. 2009).

Cricothyrohyoid muscle

Wells and Thomas described this muscle in 1927 in a Zulu man. It has been named on the basis of its origin and insertion (Fig. 29.3a). It arises from the left superolateral angle of the lamina of the cricoid cartilage under cover of the lateral cricoarytenoid muscle, and passes upward and anteriorly, lying superficial to the thyroarytenoid and thyroepiglottic muscles, to be inserted into a thickened band of fascia that apparently continues above into the lateral part of the middle thyrohyoid ligament (Wells and Thomas 1927).

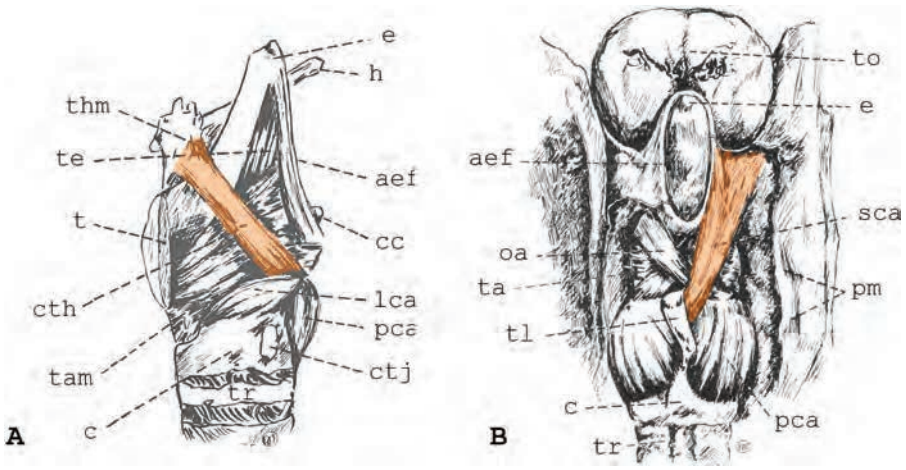

Figure 29.3 Adaptation of figures I and II in Manjome (1959). (a) Left lateral view of the larynx after removal of the thyroid lamina and (b) after removal of the arytenoid muscles (transverse and oblique), the thyroepiglottic, the thyromembranous, the cricothyroid and the cricopharyngeal muscles. a, arytenoid cartilage; aef, arytenoepiglottic fold; aem, major arytenoepiglottic muscle aemi, minor arytenoepiglottic muscle; am, arymembranous muscle; atc, arythyrocricoid fascicle; c, cricoid cartilage; ce, conus elasticus; cm, quadrangular membrane; cph, cricopharyngeal muscle; e, epiglottis; lca, lateral cricoarytenoid muscle; oa, oblique arytenoid muscle; oct; oblique cricothyroid fascicle; pca, posterior cricoarytenoid muscle; rct, right cricothyroid fascicle; sa, syndesmoarytenoid muscle; sta, superior thyroarytenoid muscle; t, thyroid cartilage; ta, transverse arytenoid muscle; tam; thyroarytenod muscle; tc; thyroconoid fascicle; te, major thyroepiglottic; tm, thyromembranous fascicles; temi, variation of the minor thyroepiglottic fascicle. Its origin is lower than normal. v, laryngeal ventricle; vf, vocal fold; vl, vestibular ligament; vm, ventricular muscle.

Source: Manjome (1959).

Lateral cricoarytenoid muscle

The lateral cricoarytenoid muscle can be split into two fascicles: the inferior fascicle attaches on the muscular process of the arytenoid cartilage and the superior fascicle on the outer border of that cartilage (Poirier and Charpy 1903). This muscle can send fibers to the thyroid cartilage, to the quadrangular membrane (cricomembranous muscle), to the epiglottis (cricoepiglottic muscle), and to the remaining intrinsic laryngeal muscles (Fürbringer 1875; Kanthack 1892; Poirier and Charpy 1903).

Internal lateral cricothyroid muscle

This muscle arises from the upper border of the cricoid cartilage or the upper surface of the lateral cricoarytenoid muscle. It courses upwards to join the thyroarytenoid muscle and ends with its fibers in the upper border of the thyroid cartilage (Fig. 29.4f). It appears in 15.6% of cases: 18.4% male, 11.1% female, and 12.5% children (Luschka 1871; Fürbringer 1875; Poirier and Charpy 1903).

Cricomembranous muscle

This muscle arises from the upper border of the lateral cricoarytenoid muscle. It then courses backward and upward, describing a curve of anterosuperior concavity to end in the quadrangular membrane. It is usually covered by the fibers of the thyroarytenoid muscle (Fürbringer 1875; Poirier and Charpy 1903; Manjome 1959).

Cricoepiglotic muscle

This is very rare in humans. It is a small muscle that comes from the upper border of the lateral cricoarytenoid muscle and courses backward and upward, describing a curve of anterior concavity (Fig. 29.5). It ends at the base or at the lateral border of the epiglottis. The thyroarytenoid muscle covers it. This muscle has been reported in 34.4% of cases, more frequently in males (50%) than in females (16.7%) (Fürbringer 1875; Poirier and Charpy 1903).

Syndesmoarytenoid muscle

This arises from the muscular process of the arytenoid and the superior border of the lateral cricoarytenoid muscle to end in the cricothyroid ligament (Fig. 29.4e, 29.6b). It has been reported in 16.6% of cases (Fürbringer 1875; Manjome 1959; Poirier and Charpy 1903).

Superior Cricoarytenoid muscle

This was first described by Wells and Tomas (1927) in a Zulu man. It is named on the basis of its attachments. It arises from the upper part of the cricoid lamina, between the posterior cricoarytenoid muscle and the attachment of the tendon of the esophageal longitudinal muscle, on the right side (Fig. 29.3b). It passes upward and laterally, lying superficial to the arytenoid muscles, to end in the apex of the arytenoid cartilage and in the aryepiglottic fold. This muscle sends fibers to the oblique and transverse arytenoid muscle. It has been considered an aberrant fascicle of the posterior cricoarytenoid muscle (Wells and Thomas 1927).

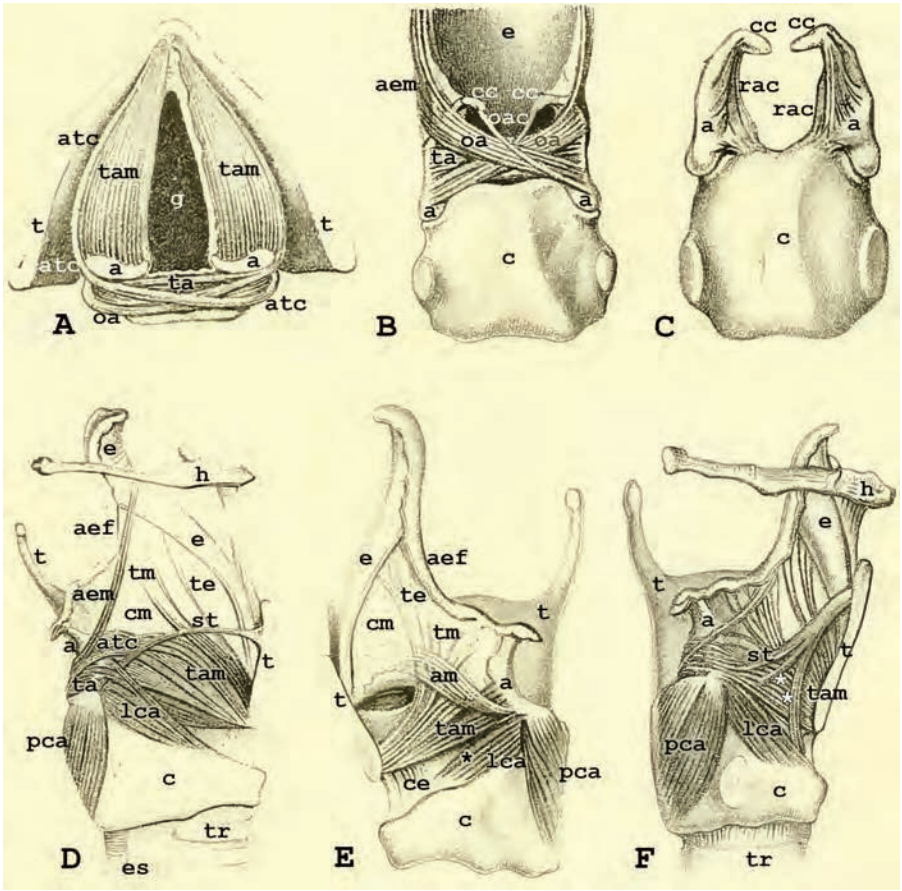

Figure 29.4 Adaptation of Luschka's table VII (1871). (a) Transverse section of the larynx at the level of the glottis. (b) Posterior view of the larynx. The thyroid cartilage and the posterior cricoarytenoid muscles have been removed. (c) Similar to the previous figure but without the epiglottis and the arytenoid muscles (transverse and oblique). (d, f) Right lateral view. (e) Left lateral view. The thyroid lamina on the same side as the view was removed in figures (d–f). a, arytenoid cartilage; aef, arytenoepiglottic fold; aem, major arytenoepiglottic muscle; c, cricoid cartilage; am, arymembranous muscle; atc, arythyrocricoid fascicle; cc, corniculate cartilage; ce, conus elasticus; cm, cuadrangular membrane; e, epiglottis; es, esophagus; g, glottis; h, hyoid bone; lca, lateral cricoarytenoid muscle; oa, oblique arytenoid muscle; oac, oblique arytenocorniculate muscle; pca, posterior cricoarytenoid muscle; rac, straight arytenocorniculate; st, superior thyroarytenoid muscle; t, thyroid cartilage; ta, transverse arytenoid muscle; tam, thyroarytenoid muscle; te, thyroepiglottic muscle; tm, thyromembranous muscle; tr, trachea; black asterisk, syndesmo-arytenoid muscle; white asterisks, internal lateral cricothyroid muscle.

Source: Luschka (1871).

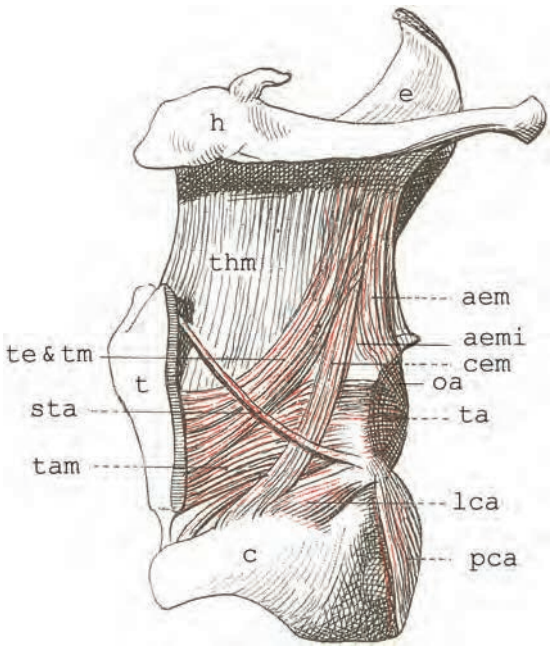

Figure 29.5 Adaptation of figure 233 of Poirier and Charpy (1903). Left lateral view of the larynx after removing the thyroid lamina aem, major arytenoepiglottic muscle; aemi, minor arytenoepiglottic muscle; c, cricoid cartilage; cem, cricoepiglottic muscle; e, epiglottis; h, hyoid bone; lca, lateral cricoarytenoid muscle; oa, oblique arytenoid muscle; pca, posterior cricoarytenoid muscle; sta, superior thyroarytenoid muscle; t, thyroid cartilage; ta, transverse arytenoid muscle; tam, thyroarytenoid muscle; te, thyroepiglottic; tm, thyromembranous muscles; thm, thyrohyoid membrane.

Source: Poirier and Charpy (1903).

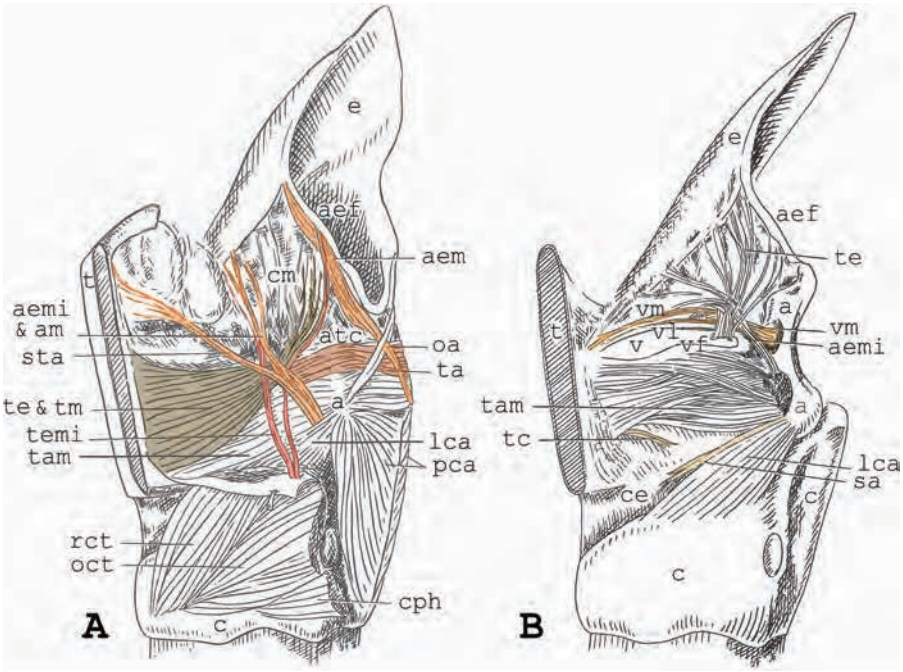

Figure 29.6 Adaptation of figures 1 and 2 of Wells and Thomas (1927). (a) Left lateral view of the larynx. The lamina of the thyroid cartilage has been removed. (b) Posterior view of larynx. The pharyngeal mucosa has been removed. aef, arytenoepiglottic fold; c, cricoid cartilage; cc, corniculate cartilage; cth, cricothyrohyoid muscle; ctj, cricothyroid joint; e, epiglottis; h, hyoid bone; lca, lateral cricoarytenoid muscle; oa, oblique arytenoid muscle; pca, posterior cricoarytenoid muscle; pm, pharyngeal mucosa; sca, superior cricoarytenoid muscle; t, thyroid cartilage; ta, transverse aritenoid muscle; tam, thyroarytenoid muscle; te, thyroepiglottic muscle; thm, thyrohyoid membrane; tl, tendon of longitudinal muscle of esophagus; to, tongue; tr, trachea. Adapted from Well and Thomas (1937) with permission from John Wiley & Sons.

Arytenoid muscle

The arytenoid has two portions: oblique and transverse.

Oblique arytenoid muscle

The volume of this muscle is very variable. One of the two oblique bundles can be absent but the simultaneous absence of both is very rare. Quite often some of their superficial fibers are inserted into the upper border of the lamina of the cricoid cartilage (Poirier and Charpy 1903). The oblique arytenoid muscle can send fibers to the neighboring cartilages and muscles (Kanthack 1892; Le Double 1897; Poirier and Charpy 1903).

Arytenoepiglottic muscle

This is one of the most common supernumerary muscles of the larynx (90.6%) (Fürbringer 1875). It encircles the laryngeal vestibule of the larynx, being an important constrictor muscle. It has been subdivided into two fascicles by Santorini: the major arytenoepiglottic muscle, which continues the oblique fibers in the arytenoepiglottic folds to attach in the lateral border of epiglottis; and the minor arytenoepiglottic muscle, which courses from the upper part of the arytenoid cartilage to the lateral border of epiglottis of the same side in the arytenoepiglottic folds (Figs 29.4d, b, 29.5, 29.6a) (Le Double 1897; Manjome 1959).

Oblique arycorniculate muscle

This muscle was reported for the first time by Luschka (1869) as a fascicle from the oblique arytenoid muscle that ends in the corniculate cartilage (Fig. 29.4b). It was considered a depressor of the corniculate cartilage (Luschka 1871; Fürbringer 1875; Macalister 1875; Le Double 1897).

Straight arycorniculate muscle

This was also reported for the first time by Luschka (1869) as a triangular muscle that originates in the inner border of the base of the arytenoid cartilage and inserts into the corniculate cartilage (Fig. 29.4c). It has been reported in 31% of cases (31.3% male, 22.2% female, 50% children) and is usually bilateral. It is completely covered by the transverse arytenoid muscle, with which it can exchange fibers (Luschka 1871; Fürbringer 1875; Macalister 1875; Le Double 1897; Poirier and Charpy 1903).

Arythyrocricoid muscle

This muscular fascicle connects the oblique and/or transverse arytenoid muscles with the thyroarytenoid and/or the lateral cricoarytenoid muscles, and resembles a sphincter encircling the glottis (Figs 29.2a, 29.4a, d, 29.6a). The arythyrocricoid fascicle has been found in 96.7% of cases (60% bilaterally, 36.7% unilaterally; 20% left side, 16.7% right side) without significant side or

sex differences. The posterior attachment of the muscular slip was observed to be in common with either the transverse arytenoid (34%) or the oblique arytenoid (28%) or with both muscles concurrently (38%). Its fibers terminate by intermingling with those of either the lateral cricoarytenoid muscle (10.6%) or the thyroarytenoid muscle (38.3%) or both (51.1%). These variable attachments mean that there are nine possible variants of this muscular fascicle (Maranillo et al. 2011).

Cricocorniculate muscle

This very rare muscle arises below the upper border of the lamina of the cricoid cartilage, near the midline, and courses vertically or obliquely behind the oblique arytenoid muscle, to end in the corniculate cartilage (Fürbringer 1875; Poirier and Charpy 1903).

Transverse arytenoid muscle

The superficial fibers of this muscle can be more or less oblique, ascending to the corniculate cartilage or descending to the muscular process of the arytenoid cartilage (Poirier and Charpy 1903). The transverse arytenoid muscle can send fibers to the remaining intrinsic laryngeal muscles (Kanthack 1892; Poirier and Charpy 1903).

Arymembranous muscle

The arymembranous muscle courses from the arytenoid cartilage to the quadrangular membrane (Figs 29.4e, 29.6a). It is one of the most common supernumerary muscles with a prevalence of 90.6% (Luschka 1871; Fürbringer 1875; Manjome 1959).

Thyroarytenoid muscle

The extension of its attachment into the inner angle of the thyroid cartilage is variable. Fascicles can be found inserting near the lower part of the posterior border of the thyroid cartilage or in the base of its lower horn. In some cases the fibers of the thyroarytenoid muscle arise from the superior border of the cricoid cartilage or in the cricothyroid ligament (Poirier and Charpy 1903). The thyroarytenoid muscle can be absent. It can send fibers to the epiglottis, to the quadrangular membrane, the cricothyroid ligament, the trachea, and the remaining intrinsic laryngeal muscles (Kanthack 1892; Sömmerring 1791–1796).

Thyroconoid muscle

The fibers of this fascicle arise from the thyroaritenoid muscle and from the inner surface of the thyroid cartilage to end in the conoid ligament (Fig. 29.6b) (Manjome 1959).

Superior thyroarytenoid muscle

This usually arises from the upper third of the inner angle of the thyroid cartilage, and courses backward and downward over the thyroarytenoid muscle to reach the muscular process of the arytenoid cartilage (Figs 29.4d, f, 29.5). It can exchange fibers with the arytenoid muscle (Luschka 1871; Fürbringer 1875; Poirier and Charpy 1903).

Thyrocorniculate muscle

This is a small fascicle that arises from the superficial fibers of thyroarytenoid muscle to insert in the posterior surface of the corniculate cartilage (Poirier and Charpy 1903).

Thyrocuneiform muscle

This is a small supernumerary fascicle that arises from the superficial fibers of the thyroarytenoid muscle to insert in the cuneiform cartilage (Poirier and Charpy 1903).

Thyroepiglottic muscle

This muscle is so common that it can be considered normal. However, some authors have considered it a fascicle of the thyroarytenoid muscle (Tarin 1753). It has been described in two forms: major and minor. The thyroepiglottic major has been reported as a fascicle arising from the inner angle of the thyroid and ending in the lateral border of the epiglottis, joining the oblique arytenoid muscle on the same side (Figs 29.4d, e, 29.5, 29.6a). The thyroepiglottic minor has been reported as similar to the thyroepiglottic major but inserting into the lower portion of the lateral border of the epiglottis, near its root (Fig. 29.6a) (Luschka 1871; Fürbringer 1875; Macalister 1875; Le Double 1897; Poirier and Charpy 1903).

Inferior thyroid muscle

This has also been named the subthyroid muscle. It arises in the lower inner angle of the thyroid cartilage, near the midline, and is attached in the base of the inferior horn of this cartilage. It has been reported with an incidence ranging from 4.6% to 20% (Le Double 1897).

Thyromembranoseous

This muscle has been considered normal by many authors (Figs 29.4d, e, 29.5, 29.6a). It is a specular image of the thyroepliglottic muscle, but attaches in the quadrangular membrane and is covered along its course by the thyroarytenoid muscle (Luschka 1871; Fürbringer 1875; Poirier and Charpy 1903).

Ventricular muscle

This is also known as the superior muscle of the vocal fold. It is a flat muscular fascicle located in the vestibular fold in the inner wall of the laryngeal ventricle (Fig. 29.6b). The vestibular muscle is attached to anterior border of the arytenoid cartilage and the inner angle of thyroid cartilage (Kanthack 1892; Poirier and Charpy 1903; Manjome 1959).

Supernumerary fascicles

Many of the above-mentioned fascicles or muscles have been considered by classical authors as supernumerary muscles. However, a few fascicles are not related to the intrinsic laryngeal

muscles. We now report a small number of these related to different structures associated with the larynx.

Ceratohyoid muscle

As with many other muscles of the larynx, this was first reported by Gruber in 1849. The ceratohyoid is a muscular fascicle that courses from the superior horn of the thyroid cartilage to the great horn of the hyoid bone (Fürbringer 1875; Macalister 1875).

Syndesmothyroid muscle

This muscle, described by Sömmerring (1791–1796), extends between the superior horn of the thyroid cartilage and the posterior thyrohyoid ligament. It has been reported with an incidence of 1% (Macalister 1875; Le Double 1897)

Thyrotriticeal muscle

This muscular fascicle courses from the superior horn of the thyroid to the triticeal cartilage (Macalister 1875).

Genioepiglottic muscle

This is very common and is almost always a continuation of the fibers of the genioglossu,s attaching to the base of epiglottis (Macalister 1875, Le Double 1897).

Glossoepiglottic muscle

This partially or fully replaces the median glossoepiglottic ligament (Le Double 1897).

Hyoepiglottic muscle

This replaces the hyoepiglottic ligament extending from the adhesive part of the upper side of the epiglottis to the posterior border of hyoid bone. It is exceedingly rare in humans, and has been reported only twice in two males (Macalister 1875; Le Double 1897).

Paratoepiglossticus muscle

A paratoepiglossticus muscles has been described by Sood (Sangvichien 2012).

References

Asanau A, Timoshenko AP, Prades JM, Galusca B, Martin C, Féasson L. 2011. Posterior cricoarytenoid bellies: relationship between their function and histology. *J Voice* 25(2): e67–73.

Bryant NJ, Woodson GE, Kaufman K, Rosen C, Hengesteg A, Chen N, Yeung D. 1996. Human posterior cricoarytenoid muscle compartments. Anatomy and mechanics. *Arch Otolaryngol Head Neck Surg* 122(12): 1331–1336.

Fürbringer M. 1875. *Beitrag zur Kenntniss der Kehlkopfmuskulatur*. Jena: Verlag von Hermann Dufft.

Gruber W. 1868a. Über die muskeln des unteren schildknorpelrandes (musculi thyroeoidei marginales inferiores). *Arch Anat Physiol Wissen Med* 12: 635–639.

Gruber W. 1868b. Über den seltenen schildknorpelhorn-gießbeckenknorpelmuskel (musculus keratoarytaenoideus). *Arch Anat Physiol Wissen Med* 12: 640–641.

Gruber W. 1868c. Über eine neue variante des muculus thyreotrachealeis und über den musculus hyo-trachealis. *Arch Anat Physiol Wissen Med* 12: 642–645.

Kanthack AA. 1892. The myology of the larynx. *J Anat Physiol* 26(3): 279–294.

Le Double AF. 1897. *Traité des Variations du Système Musculaire de l'Homme*. Vol I. Paris: Schleicher Frères.

Luschka HV. 1869. Die cartilage interarytenodea des menschlichen stimmorganes. *Arch Anat Physiol* 12: 432–439.

Luschka HV. 1871. *Der Kehlkopf des Menschen*. Tübingen: Verlag der H. Laupp'schen Buchhandlung.

Macalister A. 1875. Additional observations on muscular anomalies in human anatomy. *Trans R Irish Acad Dublin* 25: 28.

Manjome T. 1959. The anatomical studies on the laryngeal muscles of the Japanese. *Nippon Jibiinkoka Gakkai Kaiho* 62(8): 1890–1900.

Maranillo E, Vázquez T, Mirapeix R, León X, Mchanwell S, Quer M, Sañudo JR. 2009. Ceratocricoid muscle: An embryological and anatomical study. *Clin Anat* 22(4): 463–470.

Maranillo E, Rodriguez-Niedenführ M, Hernandez-Morato I, Pascual-Font A, Donat E, McHanwell S, Vázquez T. 2011. The clinical interest of the ary-thyro-cricoid fascicle. *Clin Anat* 24(6): 706–710.

Mu L, Sanders I. 2008. The human cricothyroid muscle: three muscle bellies and their innervation pattern. *J Voice* 23(1): 21–28.

Poirier P, Charpy A. 1903. *Traité d'Anatomie Humaine*. Vol 4. Paris: Masson et Cie.

Sanders I, Wu BL, Mu L, Biller HF. 1994. The innervation of the human posterior cricoarytenoid muscle: evidence for at least two neuromuscular compartments. *Laryngoscope* 104(7): 880–884.

Sangvichien S. 2012. Masterpieces in Congdon anatomy museum. Proceed Anat Assoc Thai Dec: 6–8.

Sömmerring ST. 1791–1796. *Von Bau des menschlichen Körpers*. Am Main: Frankfurt.

Sujata M, Raju S, Sirisha B, Indira B, Kanchana G, Raghu J. 2013 Athyreotrachealis muscle: a case report. *Eur J Anat* 17(2): 127–128.

Tarin M. 1753. *Myographie ou Description des Muscles du Corps Humain*. Paris: Chez Briasson.

Tourtual KT. 1846. Neue Untersuchungen über den Bau des menschlichen Schlund - und Kehlkopfs mit vergleichend–anatomischen Bemerkungen. Leipzig: O. Wigand.

Wells LH, Thomas EA. 1927. A note on two abnormal laryngeal muscles in a Zulu. *J Anat*. 61(3): 340–343.

30 Back muscles

Barclay W. Bakkum[1] and Nathan Miller[2]
[1]Illinois College of Optometry, Chicago, Illinois, United States
[2]National University of Health Sciences, Lombard, Illinois, United States

Trapezius

The trapezius muscle (synonyms: m. cucullaris (Henle), kappenmuskel, mönchskappenmuskel, scarf muscle, cowl muscle) is classically described as having three parts: upper (cleidooccipitalis), middle (horizontal, dorsoscapularis superior), and lower (dorsoscapularis inferior). These may have distinct separations, especially the upper portion from the rest of the muscle and less commonly between the middle and lower portions. The trapezius and sternocleidomastoid muscles develop from the same embryologic anlage; the ventral portion forms the sternocleidomastoid and the dorsal portion makes the trapezius. Fascicles therefore sometimes run from the anterior border of the clavicular portion of this muscle to join the cleido-occipitalis portion of the sternocleidomastoid muscle.

Complete (Allouh et al. 2004) or partial absence (Emsley and Davis 2001; Garbelotti et al. 2001) (either bilaterally or unilaterally) of the trapezius muscle has been observed (Figs 30.1, 30.2). In the case of partial absence, the trapezius muscle may only attach as far superiorly as the axis or as far inferiorly as the spinous process of the third thoracic vertebra.

Figure 30.1 Unilateral absence of trapezius muscle.

Source: D'Alessandro and Bergman (2015). http://www.anatomyatlases.org/.

Other variations in the attachments of the trapezius muscle have been noted. It may send fascicles to the sternum and deltoid muscle. Sometimes the occipital attachment is missing (Standring 2009). The clavicular attachment can vary in its extent, such that it can sometimes reach the mid-clavicle and occasionally blend with the sternocleidomastoid muscle (Figs 30.3, 30.4). When this is the case, the external jugular vein may pass through a defect in this anterior expansion of the trapezius muscle and/or its tendinous attachment to the clavicle. Quite often, the inferior limit of the vertebral attachment of the trapezius muscle is altered. When this is the case, more commonly it extends lower on the right as compared to the left. Asymmetry of the proximal attachment of the trapezius muscle has been reported as 20–25%. One study on 108 Japanese cadavers (216 sides) showed the distribution of spinal attachments described in Table 30.1 (Mori 1964).

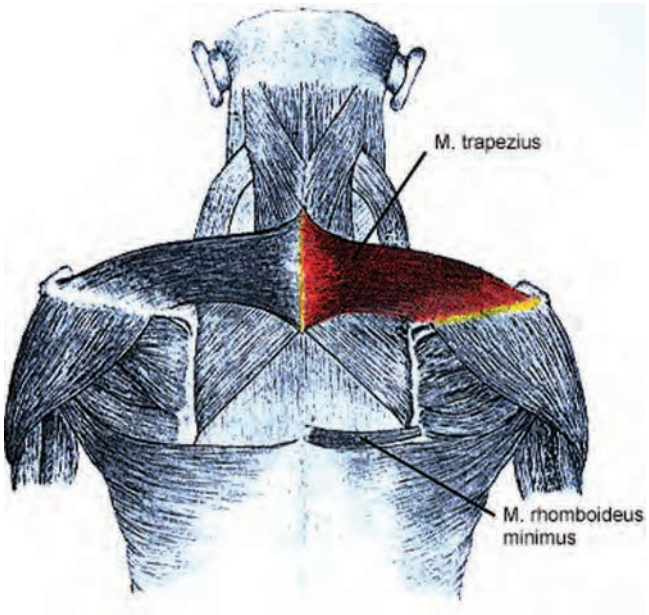

Figure 30.2 Bilateral reduced trapezius muscles along with a rhomboid minimus muscle. Adapted from von Haffner (1903).

Bergman's Comprehensive Encyclopedia of Human Anatomic Variation, First Edition. Edited by R. Shane Tubbs, Mohammadali M. Shoja and Marios Loukas.
© 2016 John Wiley & Sons, Inc. Published 2016 by John Wiley & Sons, Inc.

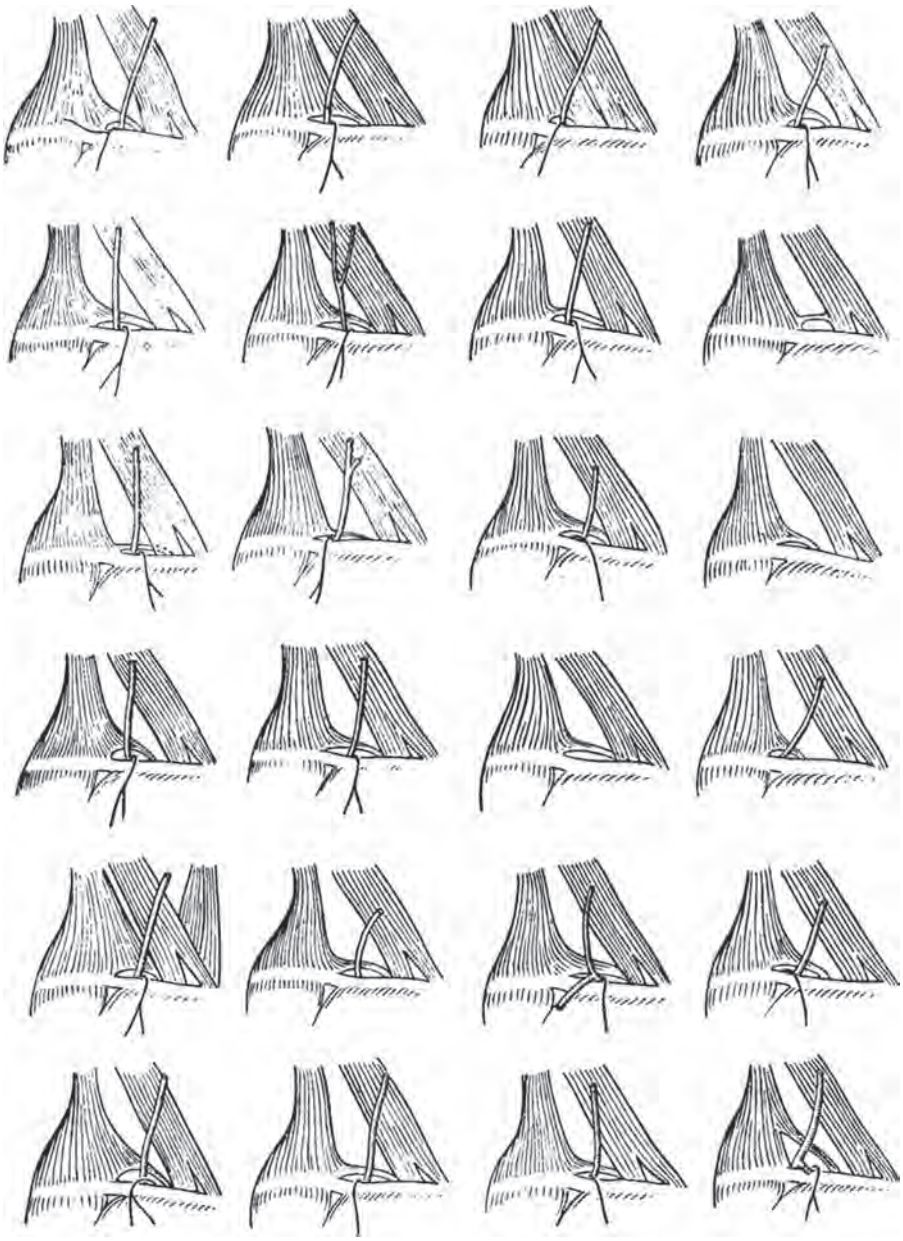

Figure 30.3 Variations of the clavicular attachment of the trapezius muscle.

Source: Mori (1964).

There are many supernumerary clavicular muscles, although their rates of occurrence are small. The supraclavicularis proprius (also known as the tensor laminae superficialis fasciale colli) muscle may be found superficial to and adjacent to the trapezius muscle. It consists of an anterior sheet attaching to the clavicle along with the trapezius muscle and a posterior sheet attaching to the fascia colli superficialis. It has been reported that this muscle may also attach to the fascia in the dorsal scapular region.

Another rare muscle is the sternoclavicularis anticus (also known as the praesternoclavicularis mediale, coracoclavicularis singularis, acromioclavicularis, or preclavicularis lateralis) muscle (Fig. 30.5). When present (in about 3% of the population, according to Gruber 1884), it runs from the manubrium to the anteroinferior aspect of the middle (or even more lateral) portion of the clavicle.

The retroclavicularis proprius (also known as the tensor laminae profundus fasciale colli) muscle is another rare anomalous muscle near the trapezius (Gruber 1884). Another sheet of the panniculus carnosus, known as the dorsofascialis muscle, has been identified superficial to the trapezius muscle (Joshi and Joshi 2001).

The cleido-occipitalis cervicalis muscle is an isolated bundle between the trapezius and sternocleidomastoid muscles that appears to arise as a segregation of the common primordium of those muscles (Rahman and Yamadori 1994; Kwak et al. 2003;

Figs 30.5, 30.6). It runs from the external occipital protuberance and superior nuchal line to the middle of the clavicle. In one case the external jugular vein passed between the tendons of the cleido-occipitalis cervicis and trapezius muscles near the clavicle (Ravindra et al. 2012).

The cleidocervicalis (also known as levator claviculae, omotrachelian, or omocervicalis) muscle is a bundle of fibers lying deep to the cervical portion of the trapezius muscle that may be found in 2% of the population (Koshy et al. 2005; Figs 30.5, 30.7). It attaches proximally to the transverse processes of the upper cervical vertebrae, usually atlas and axis, and attaches distally to the lateral extremity of the clavicle and/or acromion.

Table 30.1 Variations of the spinal attachments of the trapezius. Number of sides: 108.

Lower Limit	Right	Left	Total	%
T8	1	1	2	1
T9	5	2	7	3
T10	22	27	49	22
T11	36	43	79	37
T12	36	29	65	30
L1	7	5	12	6
L2	1	1	2	1

Source: Mori (1964).

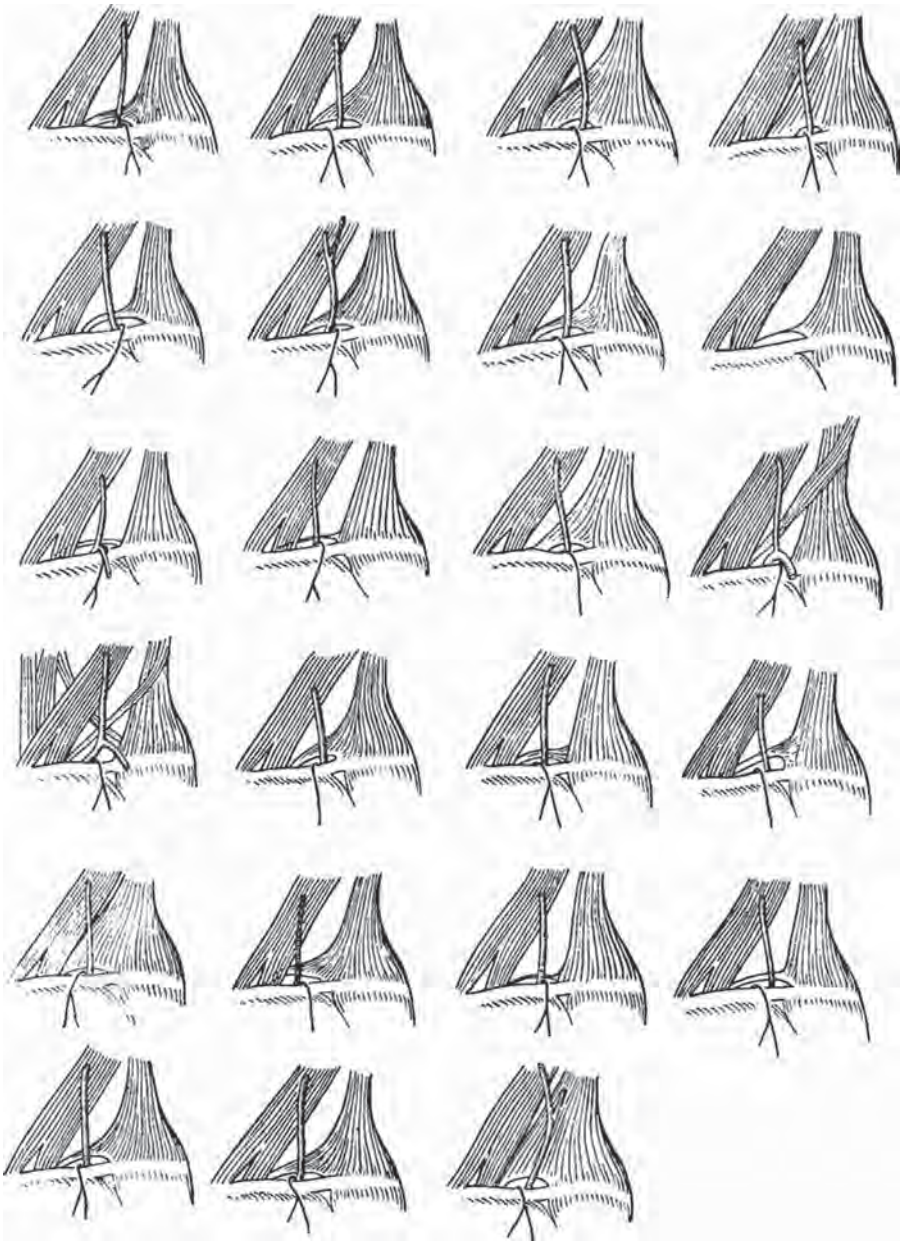

Figure 30.4 More variations of the clavicular attachment of the trapezius muscle.

Source: Mori (1964).

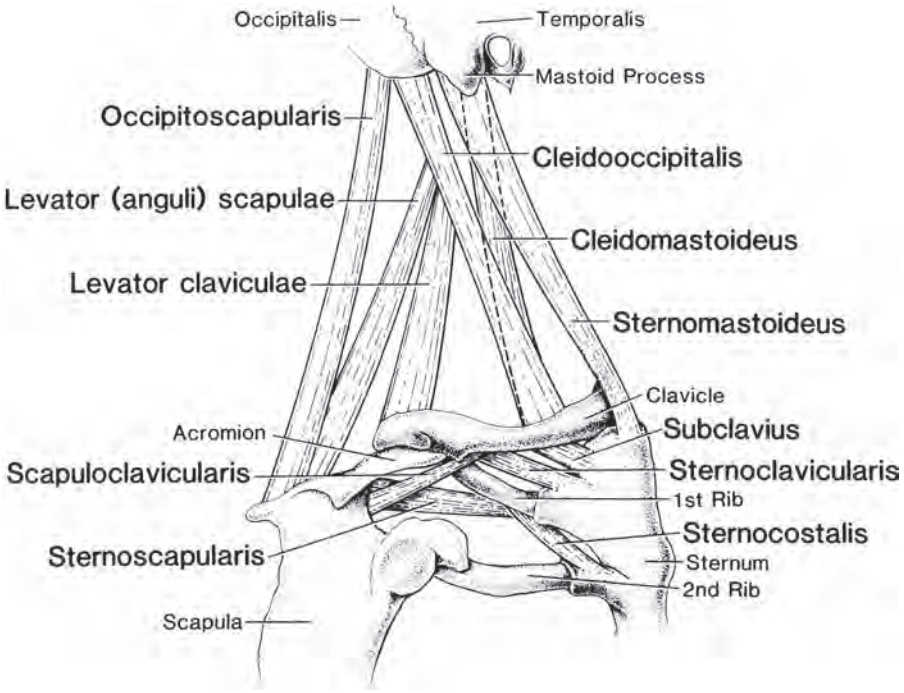

Figure 30.5 Variant muscles of the neck, shoulder, and chest.

Source: Wood (1870).

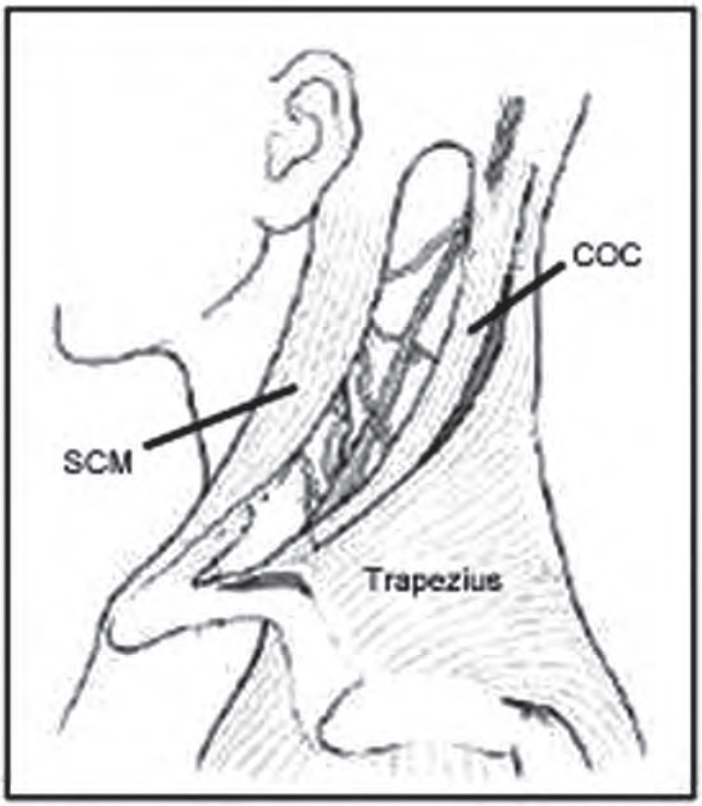

Figure 30.6 Cleido-occipitalis cervicalis muscle. COC, cleido-occipitalis cervicalis muscle; SCM, sternocleidomastoid muscle. Adapted from Kwak et al. (2003).

Figure 30.7 Cleidocervicalis muscle.

Source: D'Alessandro and Bergman (2015). http://www.anatomyatlases.org/.

Table 30.2 Variations in the attachments of the latissimus dorsi. Adapted from Mori (1964).

Vertebral attachment (no sides: 100)				
Upper Limit	**Right**	**Left**	**Total**	**%**
T5	1	1	2	2
T6	9	7	16	16
T7	21	23	44	44
T8	15	15	30	30
T9	4	4	8	8
Costal attachment (no. sides: 60)				
Ribs	**Right**	**Left**	**Total**	**%**
9,10,11,12	13	12	25	42
10,11,12	17	18	35	58
Scapular attachment; percentage of sides				
None	**Right only**	**Left only**	**Both**	
33	8	6	53	

Sometimes there is a small muscle running between the clavicle and the transverse process of the sixth cervical vertebrae known as the trachleoclavicularis (Gruber 1873). Likewise there may be another muscle that connects the scapula and clavicle: the omoclavicularis. It arises from the superior margin of the scapula either deep to or anterior to the origin of the omohyoid muscle and attaches to the posterior surface of the middle of the clavicle by a narrow tendon. In one study it was found in 6 sides of 200 cadavers (Mori 1964).

Latissimus dorsi

The latissimus dorsi muscle (synonyms: breiter Rückenmuskel, grand dorsal) commonly has variations in its attachments. The spinal attachments may go as high as T5 or be so low as to only reach the lumbar levels (Macalister 1875). The costal attachments may reach as superiorly as the eighth rib and may include the ninth intercostal fascia (Wood 1868) or may be restricted to no more than the twelfth rib. Sometimes the attachment to the twelfth rib is lacking (Macalister 1875). The iliac attachment may be reduced to almost a rudiment or expanded to overlap the external abdominal oblique muscle. Often there is a slip of muscle that arises from the inferior angle of the scapula (Standring 2009). Mori (1964) reported the data in Table 30.2 from Japanese cadavers.

Superiorly, a tendinous (or rarely, a muscular) slip may attach to the long head of the triceps brachii muscle. The humeral attachment of the latissimus dorsi muscle may unite with that of the teres major muscle, although these may be separated by a bursa. Scapular fibers of the latissimus dorsi muscle may be continuous with those of the rhomboid major muscle (Bergman et al. 2008), while the costal fibers of the latissimus dorsi muscle may have a separate insertion into the axillary fascia (Langer 1846). An accessory attachment into the anteromedial aspect of the first rib has been described (Miyauchi 1982; Fig. 30.8).

The various portions of the latissimus dorsi muscle may be separated into fascicles. The entire muscle may be absent either unilaterally or bilaterally.

The axillary arch muscle (synonyms: Achselbogen, axillopectoralis, pectorodorsalis, Langer's muscle) is a muscular slip of varying dimensions (7–10 cm in length and 5–15 mm in width; Standring 2009) that may arise from the latissimus dorsi muscle about midway in the posterior axillary fold in 7–8% of the population (Loukas et al. 2009; Figs 30.9–30.13). It crosses the axilla in the axillary fascia anterior to the axillary vessels and brachial plexus to attach to the inferior border of the pectoralis major muscle. It may also have attachments to the short head of the biceps brachii muscle or its fascia, teres major muscle, coracoid process, coracobrachialis muscle (Kalaycioglu et al. 1998) or its fascia, and pectoralis minor muscle (Loukas et al. 2009). Ramsay first described the axillary arch muscle in 1795. In his 1813 article he stated that:

> (t)his body is composed of an oblong muscle, stretched from the pectoral muscle to the latismus (sic) dorsi and teres major, which, in its violent contractions, must prove inconvenient to the axillary arteries, veins, and nerves, which lie within this muscle. It was not known in Edinburgh or London, when I demonstrated it, and is now detected in one of thirty subjects, when dissectors are attentive.

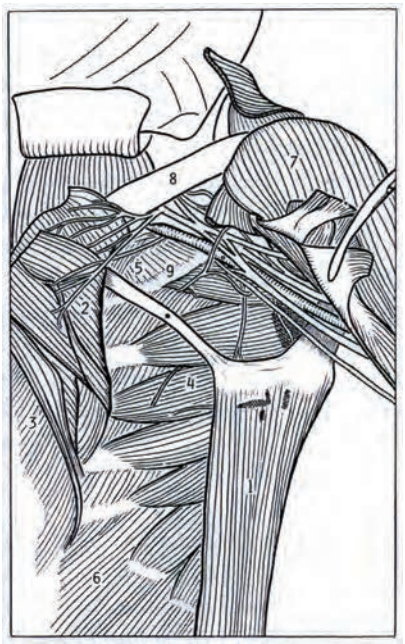

Figure 30.8 Variant attachment of latissimus dorsi muscle to the first rib. *, variant attachment; 1, latissimus dorsi muscle; 2, pectoralis minor muscle; 3, pectoralis major muscle; 4, serratus anterior muscle; 5, external intercostal muscle; 6, external abdominal oblique muscle; 7, deltoid muscle; 8, clavicle; 9, second rib.

Source: Miyauchi (1982).

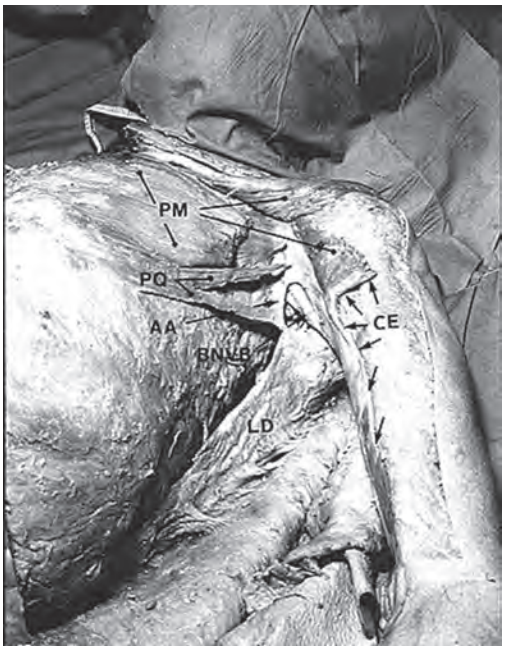

Figure 30.10 Multiple variant muscles of pectoral region. PM, pectoralis major muscle; PQ, pectoralis quartus muscle (double); AA, axillary arch; CE, chondroepitrochlearis muscle; LD, latissiumus dorsi muscle.

Source: Bergman (1991).

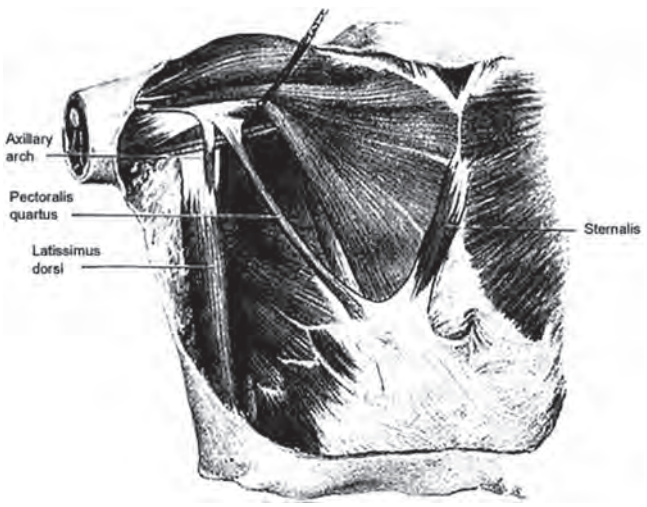

Figure 30.9 Variant muscles of pectoral region. Adapted from Huntington (1905). Reproduced with permission from John Wiley & Sons.

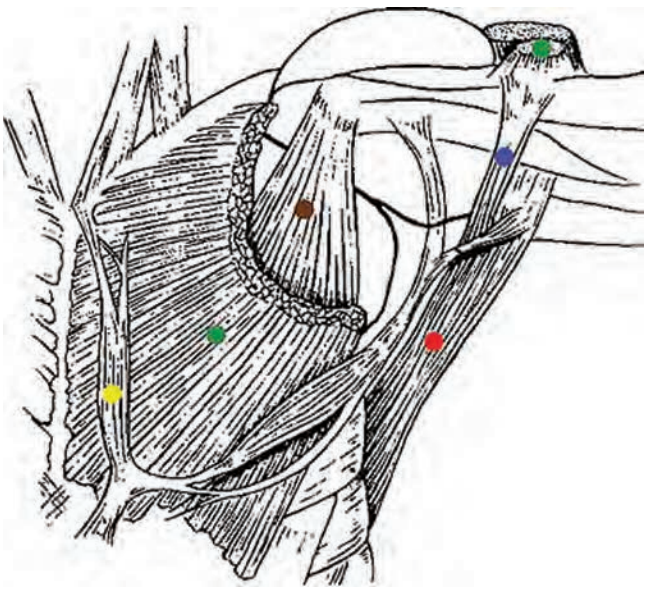

Figure 30.11 Axillary arch (blue dot) extending between pectoralis major (green dots) and latissimus dorsi (red dot) muscles, pectoralis minor muscle (brown dot), and sternalis muscle (yellow dot).

Source: Gehry (1903).

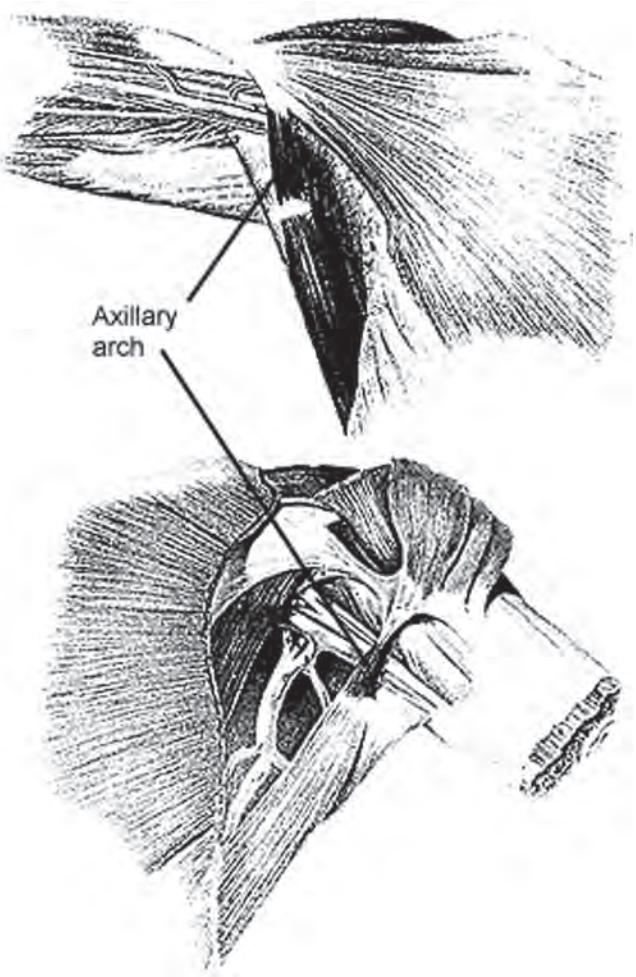

Figure 30.12 Axillary arches. Adapted from Calori (1866).

The axillary arch muscle may be innervated either by the medial pectoral nerve (Loukas et al. 2009) or the thoracodorsal nerve (Kalaycioglu et al. 1998). It receives blood from the lateral pectoral artery (Loukas et al. 2009). This muscle may be palpable on physical exam and can cause neurovascular compression in the region of the axilla. Iamsaard et al. (2012) described a case of a double axillary arch muscle. Axillary arch muscles have also been found to exist with other slips of muscle arising from the fascia over the fifth digitation of the serratus anterior muscle and the interval between the pectoralis major and latissimus dorsi muscles. Lama et al. (2010) described a cadaver that had both axillary arch and chondrohumeralis muscles. An axillary arch muscle has been described that co-existed with a slip of the pectoralis major muscle going to the pectoralis minor muscle.

There are several other variant muscular slips arising from the latissimus dorsi muscle that have been described. In a cadaver with a typical axillary arch muscle, Bhatt et al. (2013) described another slip of muscle that ran from the latissimus dorsi muscle across the posterior aspect of the axilla (behind the neurovascular bundle) to attach to the teres major muscle. An accessory subscapularis-teres-latissimus dorsi muscle has been described (Kameda 1976). The dorsoepitrochlearis (synonym: latissimocondyloideus) muscle may arise from the latissimus dorsi tendon to run through the brachial and antebrachial fascia to attach to the lateral epicondyle of the humerus and olecranon or possibly the long head of the triceps brachii muscle (Haninec et al. 2009; Figs 30.14, 30.15). It may be present in 5% of the population, although this rate of occurrence is disputed (Natsis et al. 2012). An elongation of the costal portion of the latissimus dorsi muscle may attach to the coracoid process. In some cases this slip of muscle may be entirely separate from the latissimus dorsi

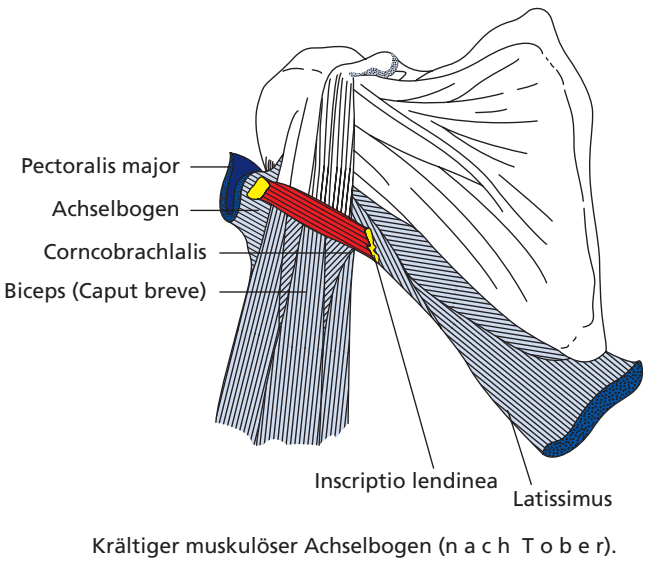

Figure 30.13 Axillary arch (Achselbogen).

Source: Tobler (1902).

Figure 30.14 Dorsoepitrochlearis muscle. Adapted from Perrin (1871). Reproduced with permission from John Wiley & Sons.

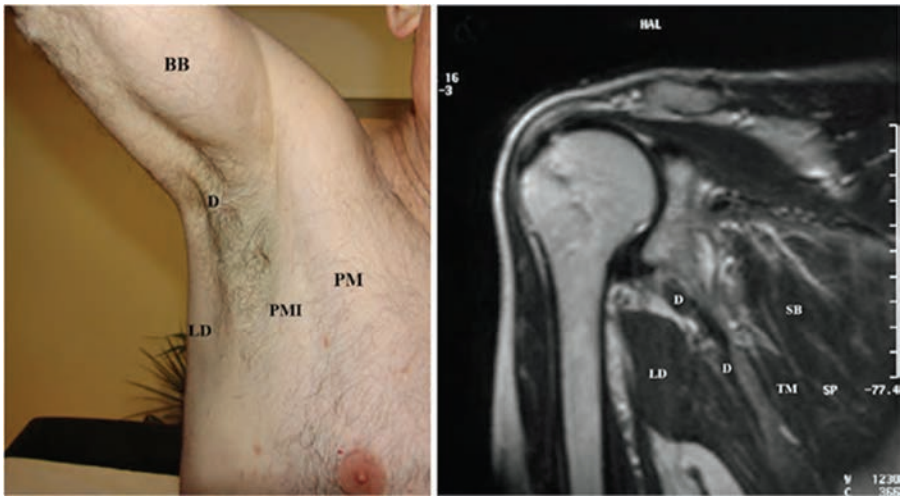

Figure 30.15 (a) Dorsoepitrochlearis muscle in patient with shoulder abducted to 145°. (b) MRI of same patient. D, dorsoepitrochlearis muscle; LD, latissimus dorsi muscle; PM, pectoralis major muscle; PMI, pectoralis minor muscle; BB, biceps brachii muscle; TM, teres major muscle; SB, subscapularis muscle.

Source: Natsis et al. (2012). Reproduced with permission from Springer Science + Business Media and Japanese Orthopaedic Association.

muscle, in which case it is sometimes known as the chondrocoracoid muscle (of Wood). This muscle may attach to the tip of the coracoid process with the pectoralis minor muscle, or the inferior aspect of the coracoid process. Wood (1868) described a case in which the chondrocoracoid muscle not only attached to the inferior aspect of the coracoid process, but also partly into the capsule of the glenohumeral joint with the supraspinatus tendon. This muscle also separated the lateral from the posterior cord of the brachial plexus. Variations of the chondrocoracoid muscle may include one that arose from the fifth, sixth, and seventh ribs that ran to join the muscles, typically attaching to the coracoid process, and another called the levator tendinis latissimus dorsi muscle (of Gruber).

Levator scapulae

The levator scapulae muscle (synonym: m. levator anguli scapulae) has spinal attachments that may arise from either an expanded or contracted number of transverse processes on the cervical or thoracic vertebrae (Loukas et al. 2006; Bergman et al. 2008; Standring 2009). The upper limit of the spinal origin almost always includes the transverse process of C1. The lower limit of the spinal attachment exhibits the most variation. The most frequent attachment at the lower limit of the spinal origin is C4 (66.6%), distantly followed by C3 (26.6%) (Mori 1940, 1964). The lower limit may span from the transverse processes of C2 to C7 (Humphry 1873; Bergman et al. 2008; Lima et al. 2012; Table 30.3).

The superior attachment may not be on any part of the vertebrae. Non-vertebral sites include the temporal bone, either on the squamous part or on the mastoid process, and from the trapezius muscle. Other possible attachments on the vertebrae include the superior articular process of C6, or there may be a second head arising from the spinous processes of the second through fourth thoracic vertebrae (Loukas et al. 2006; Bergman et al. 2008; Lima et al. 2012).

The inferior portion of the levator scapulae muscle sometimes has anomalous slips that can attach to various portions of the scapula (Figs 30.16, 30.17). The inferior attachments of this muscle have also been found in several locations around the back, besides the scapula. It has been found to blend with the muscular attachments of the middle and posterior scalenes (Wood 1867a, b; Humphry 1873; Kamibayashi and Richmond 1998), splenius capitis muscle, serratus posterior superior muscle, scapular spine, scapulothoracic fascia, rhomboid major and minor muscles, and first two ribs (Bergman et al. 2008; Standring 2009). There have been a few cases where the levator scapulae muscle does not have an inferior attachment to the scapula. Such attachments may be between the scapula and the spine, possibly on the second rib, or on both the first and second ribs anterior to the serratus anterior muscle (Bergman et al. 2008; Standring 2009).

The levator scapulae muscle has also been found to split or have aberrant slips. When it splits it is most frequently into two parts, but occasionally into three. Slips of it have been found extending to the splenius capitis, longissimus cervicis, serratus posterior superior, rhomboid major and minor, scalene, and trapezius muscles (Humphry 1873). Humphry also described a rogue slip that passed across the subclavian artery to attach to the subclavius muscle. Macalister (1866) described an example of three muscle slips which arose from

Table 30.3 Variations of vertebral attachment of levator scapulae. Number of sides: 60.

	Right	Left	Total	%
C1–C2	1	1	2	3.3
C1–C3	8	8	16	26.6
C1–C4	20	20	40	66.6
C1–C5	1	1	2	3.3

Source: Mori (1964).

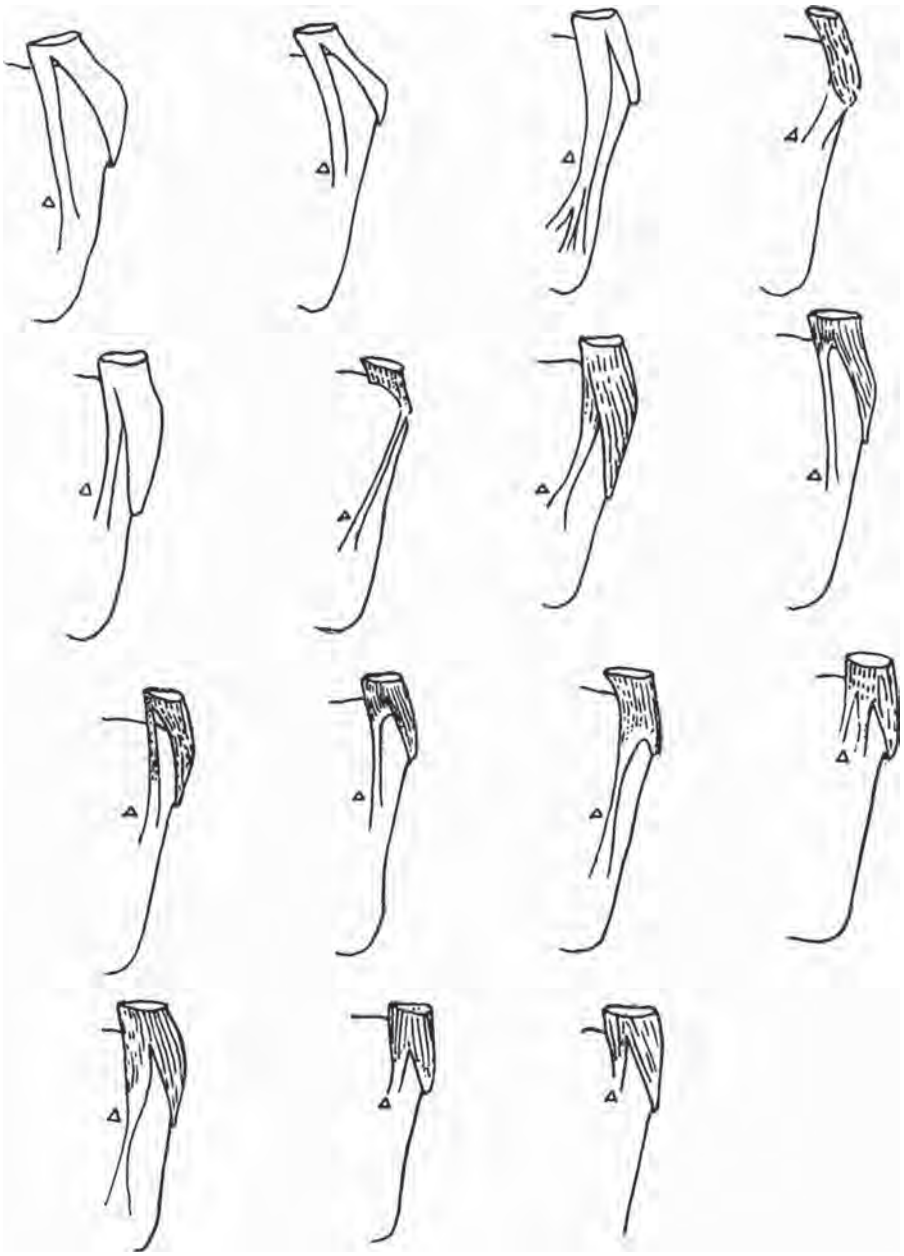

Figure 30.16 Anomalous slips of the inferior portion of the levator scapulae muscle with various scapular attachments.

Source: Mori (1964).

the transverse processes of C3–C5 and remained separate until their attachment to the superior angle of the scapula. One aberrant slip was found extending from the transverse process of C1 to the superior part of the serratus anterior muscle (Bergman et al. 2008).

Wood (1870) noted a case where the levator scapulae muscle had an extended spinal origin on the transverse processes of C1–C6 with three separate insertion sites (Fig. 30.18). In addition to the typical attachment to the superior angle of the scapula, this example also had attachments to the superior border and the root of the spine of the scapula. These two anomalous slips arose from the three lowest digitations of the muscle off the transverse processes of C4–C6. The larger of the two slips attached to the superior border of the scapula, while the smaller slip blended with, and attached superficial to, the rhomboid minor muscle at the root of the scapular spine.

Lima et al. (2012) described a variant of the levator scapulae muscle in which the muscle had its superior attachments on the transverse processes of the upper four cervical vertebrae. As the muscle coursed inferiorly it divided into medial and lateral bands at roughly the midpoint. The medial band attached to the anterior aspect of the rhomboid major muscle. The lateral

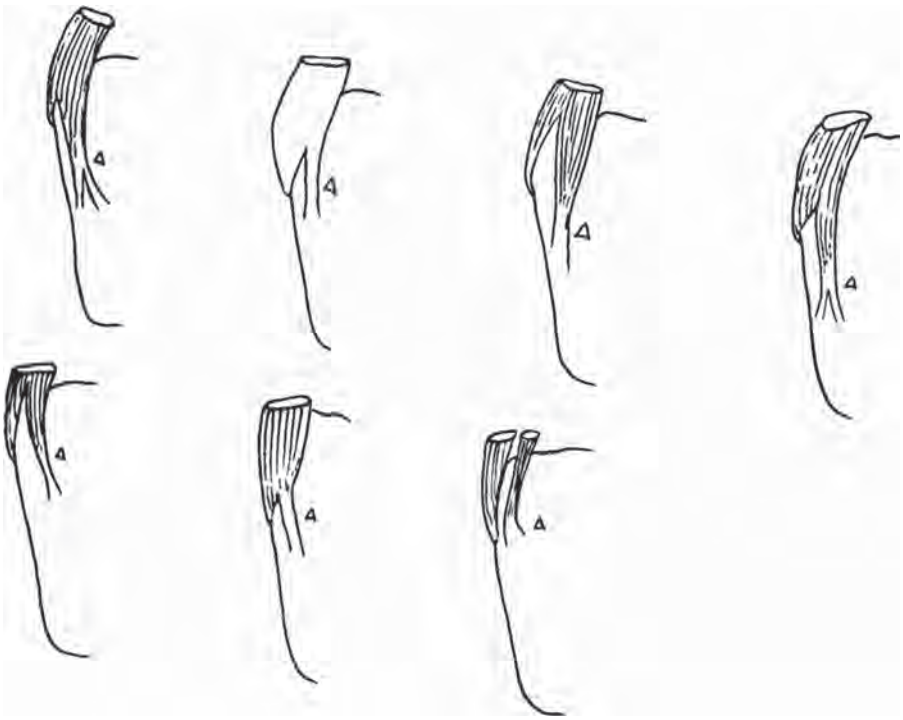

Figure 30.17 More anomalous slips of the inferior portion of the levator scapulae muscle with various scapular attachments.

Source: Mori (1964).

band extended to the superior angle of the scapula and to the aponeurosis of the serratus anterior muscle. Loukas et al. (2006) described a similar variation of the levator scapulae muscle. In this example, the muscle arose from the transverse processes of the C2–C4 vertebrae and divided into medial and lateral bands. The lateral band had a scapular attachment to the superior angle and medial border. The medial band broadened into an aponeurosis and had an inferior attachment on the ligamentum nuchae and on the tendons of the rhomboid major and serratus posterior superior muscles.

Wood (1870) described two slips of the levator scapulae muscle arising from the lower margin of the muscle and the transverse process of C4 (Fig. 30.18). The medial slip, the larger of the two, attached inferiorly via two groups of fibers to the fascia over the serratus posterior superior muscle about the level of the second or third rib and to the posterior surface of the serratus anterior muscle close to its scapular attachment. The lateral slip was smaller and attached to the upper fibers of the serratus anterior muscle.

Several unique slips arising from the anterior surface of the levator scapulae muscle on three separate cadavers have been described by Wood (1870) (Fig. 30.18). In one subject two such slips were found. The longer of the two slips arose from the third digitation off the transverse process of C3 and passed anterior to the fourth digitation of the levator scapulae muscle to attach on the scapula between the attachments of the rhomboid major and serratus anterior muscles. The second slip had a similar spinal attachment as the first, but the inferior attachment was on the serratus posterior superior muscle. In the second subject, the spinal attachment of the aberrant slip was on the anterior surface of the levator scapulae muscle and the transverse process of C3. The inferior attachment was found to be on the posterior surface of the serratus anterior muscle. In the final subject, the aberrant slip arose from the anterior surface of the transverse process of C2 and the levator scapulae muscle with the inferior attachment on the anterior side of the serratus anterior muscle.

Curnow (1873) described an abnormal slip that arose from the posterior tubercle of the transverse process of C3 and extended inferiorly to the first digitation of the serratus anterior muscle. He noted that the levator scapulae muscle on the same specimen had a superior attachment to the transverse processes of the first, second, and fourth cervical vertebrae while skipping the third.

Mori (1964) described the levator scapulae muscle as sometimes having two different abnormal fasciculi; a dorsal fasciculus and a ventral fasciculus (Fig. 30.19). The dorsal fasciculus often had two subtypes. The first subtype arose from the superior attachment on the cervical vertebrae and coursed inferiorly to attach on the serratus posterior superior or the rhomboid major and minor muscles or onto a number of unidentified vertebrae. The second subtype arose abnormally from the mastoid process and ran with the splenius capitis muscle to attach to the superior angle of the scapula. The ventral fasciculus arose from the transverse processes of the upper four cervical vertebrae and attached distally on the

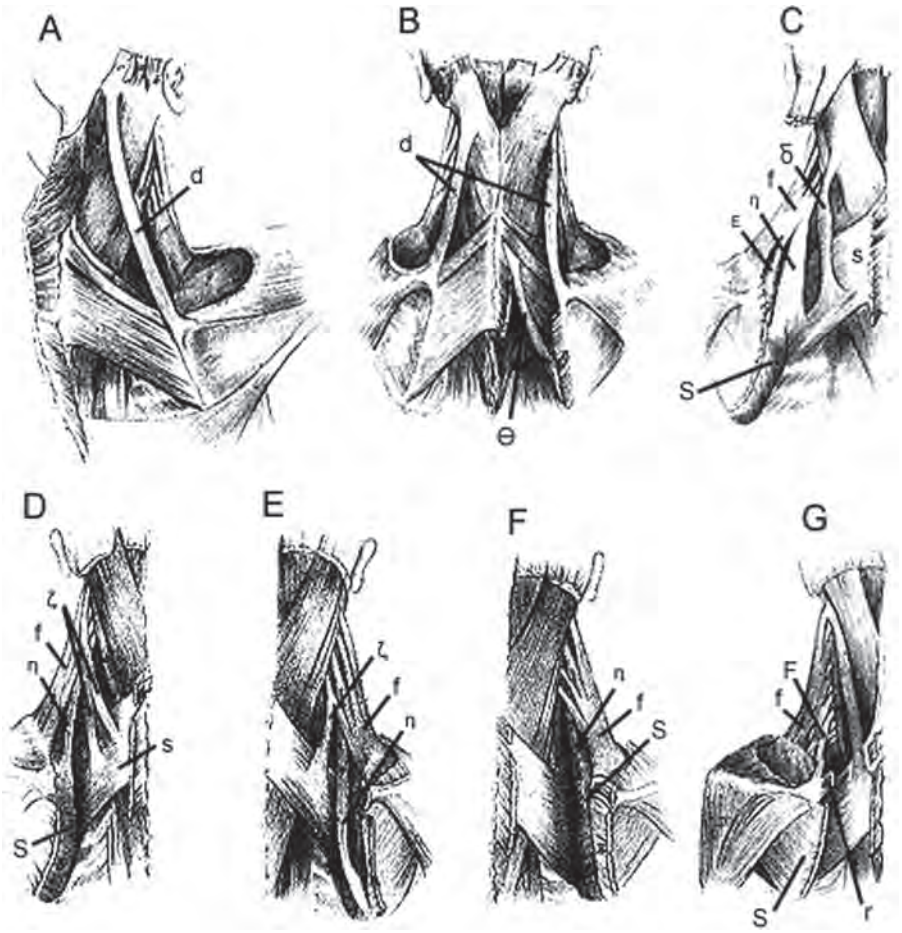

Figure 30.18 Variant muscles of the neck, shoulder, and chest. (a) Back view of the muscle of the human shoulder in a male subject, showing the rhomboid occipitalis variety (d) on the right side. (b) Back view on both sides, showing varieties homologous with occipitoscapular (d,d) and one other anomalous slip (θ) of rhomboid major muscle (R). (c) Back view on left side, showing homologous occipitoscapular muscle (δ) and two slips (ε and η) from levator scapulae muscle (f) to serratus anterior muscle (S) and serratus posterior superior muscle (s). (d) Back view on left side, showing slips (ζ and η) of levator scapulae muscle (f) to serratus posterior superior (s) and serratus anterior (S) muscles. (e) Back view of right side, showing homologous slips (ζ and η) to the same muscles from the front surface of the levator scapulae muscle (f). (f) Back view on right side, showing homologous slip (η) in front of levator scapulae muscle (f) to the serratus anterior muscle (S). (g) Back view on left side, showing slips (F) of levator scapulae muscle (f) to serratus anterior (S) and rhomboid minor (r) muscles. m, subclavius muscle; n, supracostalis muscle; o, omohyoid muscle; P, pectoralis major muscle; p, pectoralis minor muscle; q, supraspinatus muscle; R, rhomboid major muscle; r, rhomboid minor muscle; Rt, rectus thoracicus (continuation of rectus abdominus muscle); S, serratus anterior muscle; s, serratus posterior superior muscle; T, trapezius muscle; t, subscapularis muscle; u, longus capitis muscle; v, rectus capitis anterior muscle; w, rectus capitis lateralis muscle; x, clavicle, its rudimentary representative, or tendinous "inscription"; y, greater tubercle of humerus; 3, acromion or scapular spine; z, metacromion process of scapula; l, transverse process of atlas; θ, an abnormal anomalous muscular slip with the rhomboid major muscle found only in one subject (male). Adapted from Wood (1870).

anterior surface of either the subscapularis or serratus posterior superior muscles.

There have been two cases where the levator scapulae muscle was found to have six distinct parts (Wood 1868) (Fig. 30.18). The first example had six separate and distinct slips arising from the transverse processes of C1–C5. Each of the six slips attached to the superior angle of the scapula. In the second case the spinal origin was again from the transverse processes of the upper five cervical vertebrae but with an additional slip arising from the fascia and belly of the longissimus cervicis muscle. The slips arising from the upper four transverse processes had an inferior attachment to the superior angle of the scapula. The fibers arising from part of the fourth and most of the fifth cervical transverse processes had an unusual inferior attachment along the medial border of the scapula down to the scapular spine where it blended with the serratus anterior muscle. The sixth slip, arising from the longissimus cervicis muscle, blended inferiorly with the rhomboid minor muscle.

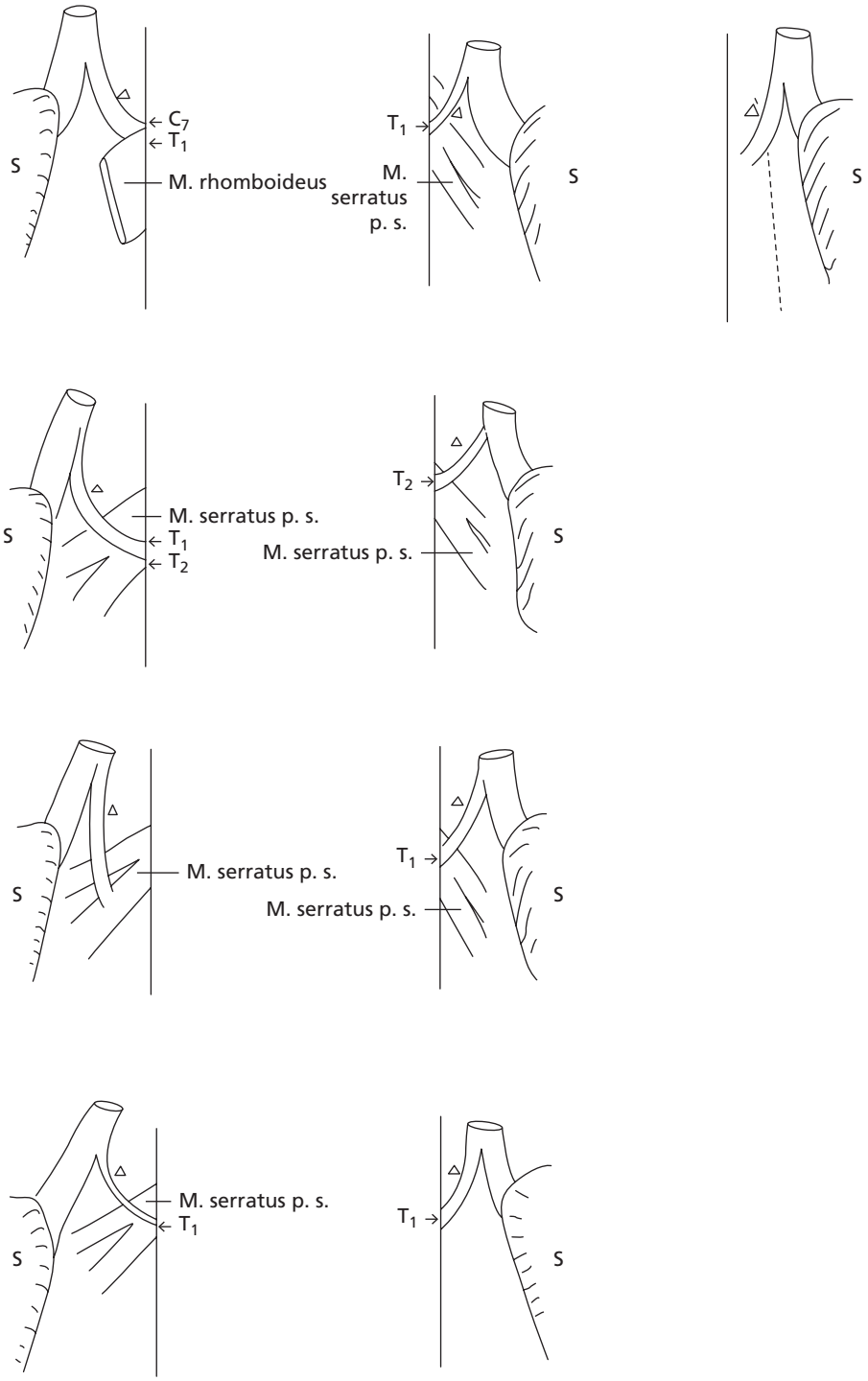

Figure 30.19 Anomalous slips of the inferior portion of the levator scapulae muscle with various non-scapular attachments.

Source: Mori (1964).

Rhomboid major and rhomboid minor

While not having a great number of variations the rhomboid major muscle (synonyms: rhomboideus inferior, grosser Rautenmuskel) and the rhomboid minor muscle (synonyms: rhomboideus superior, kleiner Rautenmuskel) may attach to an increased or decreased number of spinal segments. The upper limits of the spinal attachments extend from the spinous processes of C4–C6 with 60% of the superior-most attachment on C5 (Mori 1964). The lower limits of the spinal attachments vary between the spinous processes of T3 and T6. The spinous processes of T5 (46.6%) and T4 (33.3%) are the most common

Table 30.4 Variations of vertebral attachment of rhomboids. Adapted from Mori (1964).

	Right	Left	Total	%
Upper Limit				
C4	5	5	10	16.7
C5	18	18	36	60
C6	7	7	14	23.3
Lower Limit				
T3	1	1	2	9.3
T4	10	10	20	33.3
T5	14	14	28	46.6
T6	5	5	10	16.6
Scope				
C4–T3	1	1	2	3.3
C4–T4	3	3	6	10
C5–T4	7	7	14	23.3
C5–T5	11	11	22	36.7
C6–T5	3	3	6	10
C6–T6	5	5	10	16.7

sites for these inferior spinal attachments. The distance between superior and inferior attachments to the spinous processes most commonly spans from C5 to T5, a length of eight spinous processes (Table 30.4).

The rhomboid major muscle has been found to have distal attachments ranging from the entire medial border of the scapula to a localized area near the root of the scapular spine (Kamibayashi and Richmond 1998). Three different bands have been described: upper, middle, and lower. The upper and middle bands attach to the medial border of the scapula inferior to the rhomboid minor muscle. The lower band consists of the majority of muscle fibers and attaches strongly to the inferior angle of the scapula. The scapular attachment of the rhomboid major muscle may be in a single arch form, or it may be broken up to form two–three smaller arches. In some cases the upper and middle bands may be absent, which will cause the muscle to lose its characteristic rhombus shape and take on a much more triangular shape (Bergman et al. 2008).

Both the rhomboid major and minor muscles may be divided into separate bundles. There may also be a number of separate slips that will have alternate attachments. Muscular slips have been found running to the latissimus dorsi, teres major, and/or to the infraspinatus muscles (Bergman et al. 2008). One unique muscular slip was described as arising from the superior part of the rhomboid sheet and coursing obliquely across the rhomboid muscles to attach on the inferior angle of the scapula (Bergman et al. 2008). Wood (1870) described a similar slip with the superior attachment on the spinous process of C7 (Fig. 30.18). The slip then passed between the serratus posterior superior and rhomboid major muscles to attach on the inferior angle of the scapula.

The rhomboid major muscle has sometimes been found to split into two planes of fibers. At the spinal attachment the two fiber planes were separate and distinct. Closer to the scapular attachment on the medial border the fibers of the two planes fused into a single group of fibers (Macalister 1866).

A frequent anomaly is the presence of the rhomboid minimus (or minus) muscle. The spinal origin of this muscle is on the spinous processes above the spinal attachments of the latissimus dorsi muscle. The muscle will then run laterally where the fibers will disappear entirely or blend into the fascia of the teres major muscle (Fig. 30.2). Two different studies on Japanese cadavers found the incidence of this muscle to be 11.4% and 16%, respectively (Mori 1964). Other authors have described the rhomboid minumus muscle as extending from the spinous processes of the lower cervical and upper thoracic vertebrae to the scapula and being located just superior to the rhomboid minor muscle (Bergman et al. 2008).

The rhomboid occipitalis muscle (synonyms: rhomboid capitis, rhomboid cervicis, occipitoscapularis) has been reported by several authors (Wood 1867a, b, 1870; Knott 1883; Patten 1935; Rogawski 1990; Bergman et al. 2008; Standring 2009). Wood (1867a, b) was the first to describe the muscle as arising from the occipital bone at the level of the splenius capitis muscle, immediately deep to the cranial attachment of the trapezius muscle on the superior nuchal line (Figs 30.5, 30.18, 30.20). Knott (1883), and later Rogawski (1990), found

Figure 30.20 Rhomboid occipitalis muscle.

Source: D'Alessandro and Bergman (2015). http://www.anatomyatlases.org/.

this muscle with cranial attachments to the medial one-third of the superior nuchal line immediately superior to the occipital attachment of the semispinalis capitis muscle. The rhomboid occipitalis muscle then extended inferiorly, passing between the splenius and trapezius muscles to attach to the medial border of the scapula via short tendinous fibers. This scapular attachment was found blending with, and/or superficial to, the rhomboid major and minor muscles (Wood 1867a, b) or to the medial border of the scapula superior to the rhomboid minor muscle (Knott 1883). The muscle has also been found to have muscular slips extending to the splenius, levator scapulae, serratus posterior superior, and serratus anterior muscles (Wood 1870; Fig. 30.18). Patten (1935) described an example of the rhomboid occipitalis muscle where the distal third of the muscle split into two distinct bands, both of which attached to the fascia over the serratus posterior superior muscle. An accessory slip of the rhomboid occipitalis muscle has been found arising from the transverse process of C1 and/or the fascia over the splenius capitis muscle. This muscular slip then extended inferiorly and laterally to attach either to the superior border of the scapula and/or on the surface of the serratus posterior superior muscle (Bergman et al. 2008). Wood (1870) suggested that the rhomboid occipitalis muscle may frequently be found with another anomalous muscle, the levator claviculae muscle (see section on trapezius).

Serratus anterior

The serratus anterior muscle (synonyms: serratus anticus, serratus magnus (Albinus), serratus anticus major (Henle), grosser Sägemuskel, le grand dentelé) has three parts: upper, middle, and lower. Infrequently, the superior portion is continuous with the levator scapulae muscle. A case of an anomalous attachment of the upper portion of the serratus anterior muscle to the posterior scalene muscle has been reported (Smith et al. 2003). Sometimes the intermediate portion is missing, being replaced by connective tissue. The serratus anterior muscle may fuse with adjacent external intercostal or external abdominal oblique muscles (Standring 2009). Slips from the digitations associated with the sixth and seventh ribs may join the pectoralis minor and/or coracobrachialis muscles and are known as types of axillary arch muscles (see latissimus dorsi muscle section). Complete absence of the serratus anterior muscle has been reported (Chernev and Pessina 2009; Fig. 30.21).

Variations in the attachments of the serratus anterior muscle are common. One historical study found the number of digitations varied between seven and twelve with the inferior most digitation attaching to either the seventh rib (1%), eight rib (40%), ninth rib (38%), tenth rib (10%), or eleventh rib (0.5%). A large study of Japanese cadavers more recently found the lowest rib of attachment being from the sixth to the twelfth ribs, and also that there was a statistically significant gender difference in this attachment site (Morimoto et al. 1992; Table 30.5).

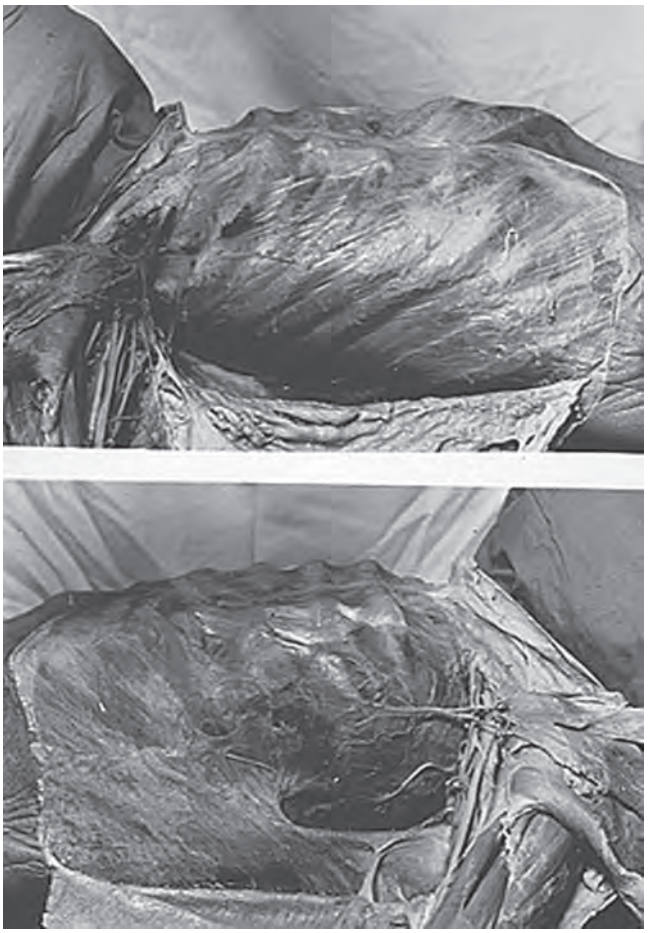

Figure 30.21 Unilateral absence of serratus anterior muscles.

Source: D'Alessandro and Bergman (2015). http://www.anatomyatlases.org/.

Another recent study on 40 cadaver sides only found the lowest attachment ranging between the seventh and tenth ribs (Cuadros et al. 1995). In a small cadaveric study of the uppermost rib attachments (13 sides), Smith et al. (2003) found the superior portion of serratus anterior muscles most frequently

Table 30.5 Variations of rib attachment of serratus anterior. Number of sides: 1618 (1121 males, 497 females).

Lowest rib	Male (%)	Female (%)	Total (%)
6	0	0.2	0.1
7	2.8	5.4	3.6
8	42.5	40.2	41.8
9	39.4	43.3	40.6
10	13.5	10.5	12.5
11	1.7	0.4	1.3
12	0.1	0	0.1

Source: Morimoto et al. (1992). Reproduced with permission from Springer Japan.

attaching both first and second ribs (46%), but also to only first rib (15%), only second rib (31%), and second and third ribs (8%).

The serratus anterior muscle is usually supplied in a segmental fashion by the long thoracic nerve, such that C5 supplies the upper portion of the muscle and C6 and C7 supply the remainder of the muscle (Bertelli and Ghizoni 2005). Nasu et al. (2012) found that the upper portion of the serratus anterior could be innervated by a branch arising from the nerve that supplies the levator scapulae muscle (i.e., the dorsal scapular nerve). This innervation pattern and the observation that the serratus anterior muscle may blend with the levator scapulae muscle (albeit rarely) have led some to suggest that the superior portion of the serratus anterior muscle may be considered as developing from the rhomboid sheet. Besides being mainly supplied by C5, sometimes the upper portion of the serratus anterior muscle has also been found to be supplied by fibers from C4, C6, and/or C7 (Hamada et al. 2008). Nasu et al. (2012) also found that the lower portion of the serratus anterior muscle, as well as being supplied by the long thoracic nerve can also receive input from branches of intercostal nerves. It has also been reported that C8 may supply the lower portion of the serratus anterior muscle. Since the muscles of the upper limb are derived from cervical myotomes, the developing serratus anterior muscle may attach to the trunk before extending into the developing limb bud. This might explain why the long thoracic nerve has a superficial, as opposed to a deep, course along this muscle.

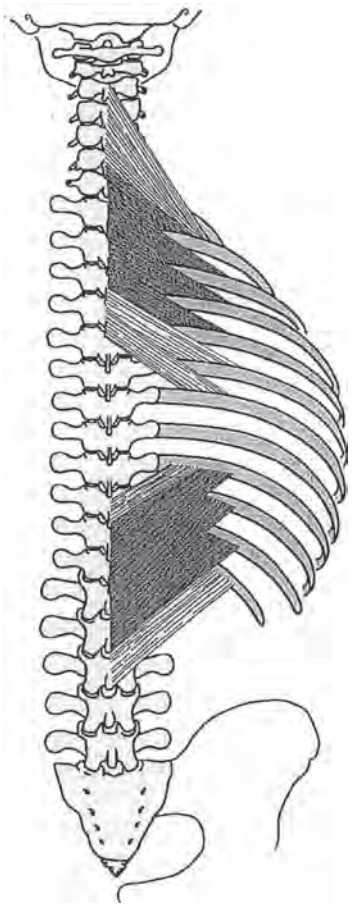

Figure 30.22 Drawing of typical (dark) and variant (light) attachments of the serratus posterior superior (upper fibers) and inferior (lower fibers) muscles.

Source: Vilensky et al. (2001). Reproduced with permission from John Wiley & Sons.

Serratus posterior superior and inferior and supracostalis

The serratus posterior superior and inferior muscles (synonyms: hintere Sägemuskeln, petits dentelés postérieurs) have been reported as completely absent and replaced by fibrous tissue, although very rarely. There are also reports that these muscles may have altered arrangements of their digitations resulting from associated accessory muscles. The posterior serratus muscles may have considerable variation in the number of digitations and the levels of the bony structures to which they attach (Fig. 30.22).

The serratus posterior superior muscle may have between three and six digitations (Standring 2009). Mori (1964) found a range of distributions of attachment sites for the serratus posterior superior muscle (Table 30.6).

The serratus posterior inferior muscle may have as few as two and up to five digitations. Mori (1964) found variations in the attachment sites of this muscle in a Japanese cadaveric population (Table 30.7). It has been reported that the serratus posterior inferior muscle may also arise from the L3 spinous process (Standring 2009).

There are several rare anomalous muscles known as the supracostalis muscles (of Wood) that, along with the serratus posterior muscles, are classified as being remnants of the superficial lamina of the primitive external abdominal oblique muscle. The supracostalis anterior muscle is found on the anterior surface of the thorax in about 5% of the population. It typically runs from the first rib inferiorly to the fourth rib (Figs 30.23, 30.24). Mori (1964) found variations of the attachment sites of this muscle (Table 30.8). Recent evidence suggests that the supracostalis anterior muscle may arise from a single external intercostal muscle that grows to span several intercostal spaces (Nelson et al. 1992).

According to Eisler (Mori 1964) there are three types of supracostalis posterior muscles (Fig. 30.25). Type I, found on the posterior aspect of the chest, has fibers that run parallel to those of the external intercostal muscles. It usually runs from one rib downward to the next lower or second lower rib. Type II is found below and runs parallel to the serratus posterior superior muscle. It has up to three muscular slips and may span several ribs. Type III arises from the eighth to tenth ribs and runs superomedially,

Table 30.6 Variations of attachments of serratus posterior superior. Adapted from Mori (1964).

	Right	Left	Total	%
Spinous process				
Proximal attachment levels (no. sides 99)				
C4–C7	2	2	4	4
C5–C7	5	7	12	12
C4–T1	18	15	33	33
C5–T1	20	21	41	41
C6–T1	2	1	3	3
C4–T2	1	1	2	2
C5–T2	2	2	4	4
Proximal attachment upper limit (no. sides 102)				
C4	24	18	42	41
C5	27	30	57	56
C6	2	1	3	3
Proximal attachment lower limit (no. sides 99)				
C7	7	9	16	16
T1	40	37	77	78
T2	3	3	6	6
Rib				
Distal attachment levels (no. sides 324)				
2nd–4th	44	40	84	26
2nd–5th	72	76	148	46
2nd–6th	10	6	17	5
3rd–4th	4	0	4	1
3rd–5th	34	38	72	22

Table 30.7 Variations of attachments of serratus posterior inferior.

	Right	Left	Total	%
Spinous process: Proximal attachment upper limit (no. sides 100)				
T10	15	16	31	31
T11	31	29	60	60
T12	4	3	7	7
L1	0	1	1	1
L2	0	1	1	1
Rib: Distal attachment upper limit (no. sides 201)				
8th	3	2	5	2
9th	90	90	180	90
10th	6	7	13	7
11th	2	1	3	1
Rib: Distal attachment lower limit (no. sides 206)				
11th	61	30		
12th	145	70		

Source: Mori (1964).

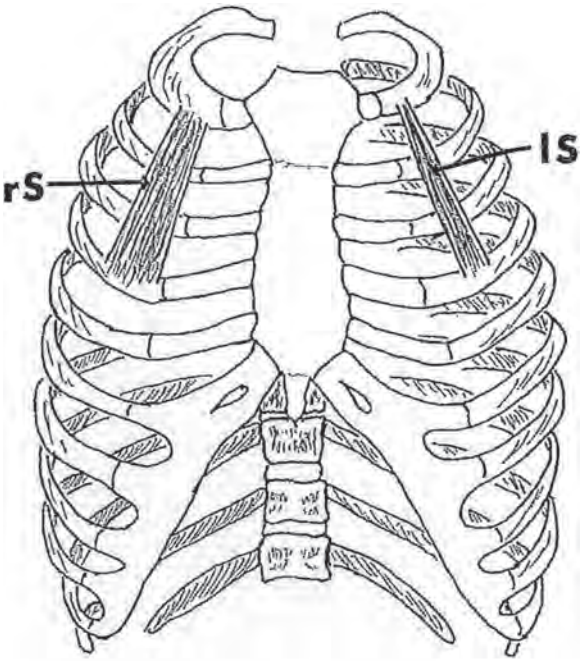

Figure 30.23 Drawing showing position of right (rS) and left (lS) anterior supracostal muscles.

Source: Nelson et al. (1992). Reproduced with permission from John Wiley & Sons.

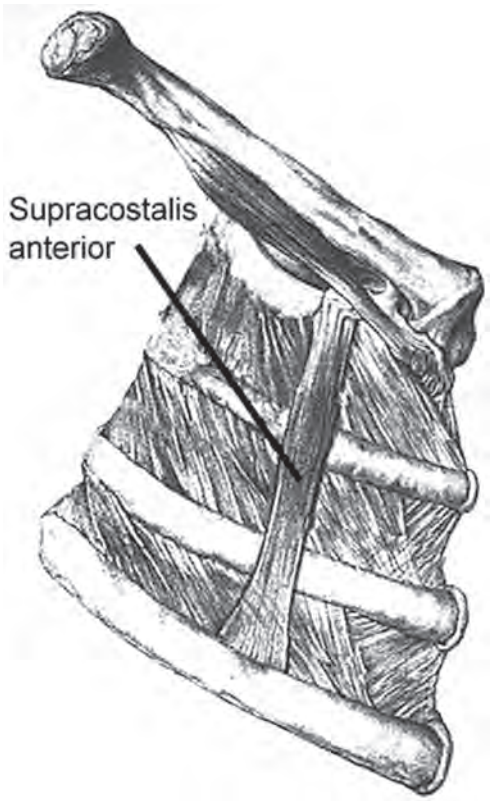

Figure 30.24 Supracostalis anterior muscle. Adapted from Bochdalek Jr (1867).

Table 30.8 Variations of rib attachments of supracostalis anterior. Number of sides: 2400.

	Superior attachment	
Inferior attachment	**1st rib**	**2nd rib**
3rd rib	58 (2.4%)	0
4th rib	47 (1.9%	21 (0.8%)

Source: Mori (1964).

Table 30.9 Variations of rib attachments of supracostalis posterior. Number of sides c. 520.

Type	Sides	%
I	19	3.6
II	17	3.3
III	29	5.6

Source: Mori (1964).

spanning several rib levels. It has a range of degrees of development. If poorly developed, it attaches superiorly to the fascia superficial to the ribs. If it is more robust, it may run to attach superiorly to the fascia of the erector spinae muscle. Mori (1964) found an overall occurrence rate of about 12% for the supracostalis posterior muscle and also reported the rates of occurrence for the three types of this muscle (Table 30.9).

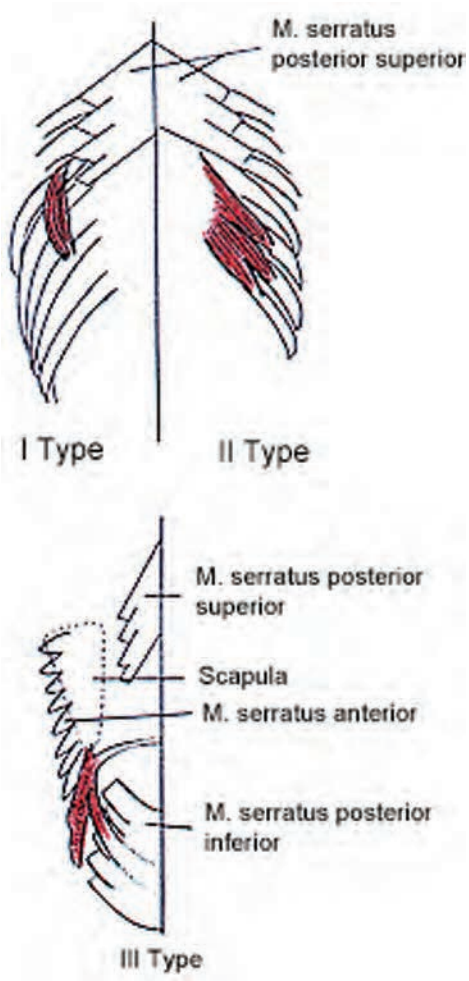

Figure 30.25 Types of supracostalis posterior muscles. Adapted from Mori (1964).

Splenius capitis and cervicis muscles

The spinal attachment of the splenius capitis (synonym: Riemenmuskeln) and splenius cervicis (synonyms: Bauschmuskeln, splenius colli) muscle sheet may be displaced superiorly up to two spinous processes. The spinal attachment to the nuchal ligament may also extend the length of the ligament to the external occipital protuberance (Bergman et al. 2008). Blending of the splenius capitis and cervicis muscles at the attachments on the spinous processes has been noted (Kamibayashi and Richmond 1998). One unique case was reported by Wood (1867a, b) where the spinal attachment of the splenius cervicis muscle was superficial to that of the serratus posterior superior muscle. Although the serratus muscle was located deep to the splenius cervicis muscle, it was superficial to the splenius capitis muscle. It therefore split the two splenius muscles.

The cranial attachment of the splenius capitis muscle is most often on the mastoid process while the splenius cervicis muscle attaches to the transverse processes of the upper cervical vertebrae. Muscular slips from both splenius muscles have been found attaching to the longissimus capitis and/or iliocostalis cervicis muscles. Since the splenius and erector spinae muscle groups are innervated by the lateral branches of the dorsal rami of cervical spinal nerves and these muscle groups sometimes blend, it is supposed that the splenius muscles represent a superficial prolongation of the lateral column of muscles to the head. Both splenius muscles, but especially the splenius cervicis muscle, may send fibers to the levator scapulae muscle (Bergman et al. 2008). A slip of the splenius capitis muscle has been described as running deep to the cleido-occipitalis (see section on trapezius) and rhomboid major muscles to attach to the fascia over the serratus posterior superior muscle (Wood 1870).

The splenius capitis muscle may be separated into superior and inferior parts. The superior part will often overlap the inferior part at their attachments on the spinous processes. The splenius muscle sheet may also be separated into mastoid and occipital divisions. Frequently, there may be asymmetry of the spinal origins of the splenius muscles when compared bilaterally. Absence of the entire splenius muscle sheet has been found at least twice (Bergman et al. 2008; Standring 2009).

Wood (1870) describes a unique muscle found in the cervical region on the left side of a male cadaver. This un-named muscle consisted of superior and inferior slips. The superior slip arose superior to, and directly from, the common attachments of the splenius cervicis and levator scapulae muscles on the atlas. As the superior slip traveled inferiorly it split into two bands at the level of the C7 vertebra. Both bands attached to the fascia covering the serratus posterior superior muscle. The inferior slip arose from the transverse process of C1 and attached inferiorly to the serratus anterior muscle on the anterior surface of the scapula opposite the base of the scapular spine.

The rhombo-atloid muscle (corrected from the rhombo-axoid; Wood 1867a, b) (synonyms: splenius accessories (Krause), adjutor splenii, musculus singularis splenius accessories (Walther), splenius capitis accessories (Bergman et al. 2008), and the splenius colli accessories) is a variable muscle found in the region of the splenius muscles (Fig. 30.26). It usually attaches inferiorly to the spinous process of C7 or T1 deep to and closely associated with the spinal attachment of the rhomboid minor muscle (Macalister 1866; Knott 1883). The spinal attachments of this muscle have also been found attaching to the spinous processes of C6–C7, T1–T2, and T2–T3 (Knott 1883). The rhombo-atloid muscle then extends superiorly, anteriorly, and laterally, superficial to the serratus posterior superior, and splenius cervicis muscles. The superior attachment of the rhombo-atloid muscle is on the transverse process of C1 between the tendons of the splenius cervicis and levator scapulae muscles (Macalister 1866; Wood 1869; Curnow 1873; Knott 1883). If it has a superior attachment on the occipital bone or the mastoid process it is named the splenius capitis accessorius muscle (Bergman et al. 2008). The rhombo-atloid muscle has also been found to have slips combining with fibers from the rhomboid major and the serratus posterior superior muscles (Wood 1867a, b). The incidence of this muscle is reported to be 8% (Knott 1883; Bergman et al. 2008).

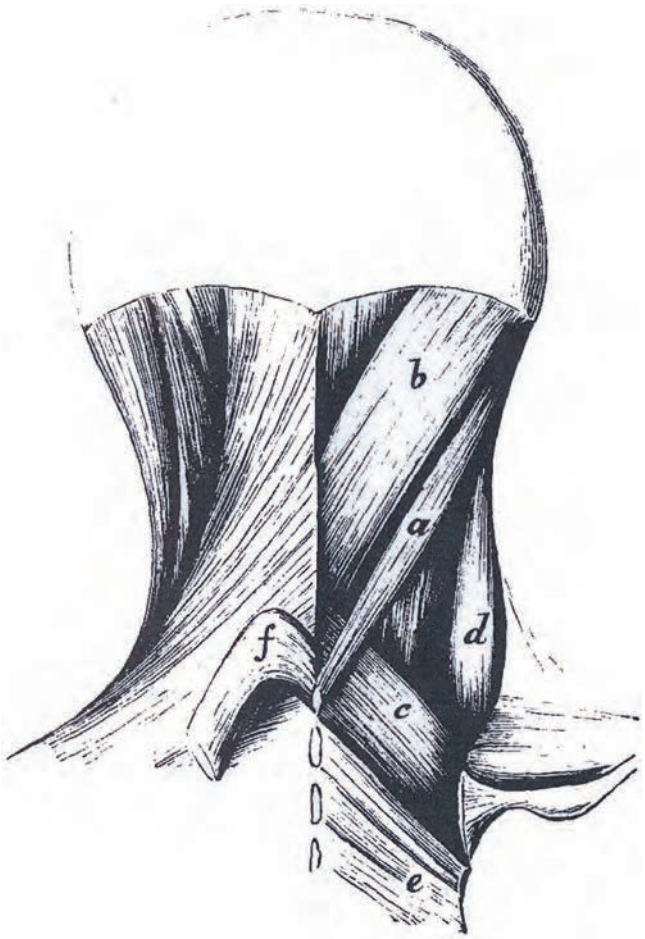

Figure 30.26 Rhombo-atloid muscle (a).

Source: Macalister (1866).

Erector spinae

The erector spinae group of muscles consists of the iliocostalis, longissiumus, and spinalis muscles, all of which have complicated arrangements of superior and inferior attachments (DeFoa et al. 1989; Biedermann et al. 1991; Macintosh and Bogduk 1991; Nomizo et al. 2005; Nomizo and Sakai 2009). The iliocostalis lumborum muscle may vary in the number of lower ribs to which it attaches superiorly (Standring 2009). Likewise, the ilocostalis thoracis and cervicis muscles may show variation in levels of both their superior and inferior attachments.

The longissimus thoracis and cervicis muscles may differ in the specific levels of both their superior and inferior attachments. Sometimes there may be accessory slips of muscle on the deep medial surface of the longissimus thoracis muscle that arise from the lower thoracic vertebrae, mamillary processes, and/or the aponeurosis of the underlying transversospinalis group of muscles. When they form what appears to be a separate muscle that attaches superiorly to the upper two or three thoracic vertebrae, they are known as the transversalis thoracis muscle. Similarly, other extra slips of muscle in the cervical region may arise from the cervical transverse processes and can be known as the transversalis cervicis posterior minor muscle. The longissimus capitis muscle may be divided into two parts, reduced in length, or completely missing. It has also been shown to sometimes arise from the transverse process of atlas or the portion of the longissmus cervicis tendon attaching to atlas.

The spinalis thoracis muscle may vary in the specific levels of its superior and inferior attachment sites. The spinalis cervicis and capitis muscles, while considered typical muscles, are quite variable in their occurrence and appearance. Greiner et al. (2004) classified the conditions of these muscles as absent, blended (with the semispinalis muscle), or distinct (from the semispinalis muscle) (Table 30.10). Miyauchi (1976a) found the

Table 30.10 Variations of the relationship between semispinalis capitis and cervicis.

	M. spinalis cervicis		M. spinalis capitis	
Condition	**Sides**	**%**	**Sides**	**%**
Absent	102	36	196	70
Blended	51	18	80	29
Distinct	131	46	3	1
Totals	284	100	279	100

Source: Greiner et al. (2004). Reproduced with permission from Elsevier.

spinalis cervicis muscle present at a frequency of 82% (49 out of 60 sides) in a Japanese cadaver population. The spinalis capitis (synonym: biventer cervicis) muscle varies in the levels of its inferior attachments, and the spinalis cervicis (synonym: interspinalis cervicalis longus) muscle can vary in the levels of both its superior and inferior attachments. It has been reported that the superior attachment of the spinalis capitis muscle may blend with that of the rectus capitis posterior minor muscle (Martin 1994).

Transversospinalis

The transversospinalis group of muscles consists of the semispinalis, multifidus, and rotatores longus and brevis muscles. The spinal attachments of the semispinalis capitis muscle (synonyms: complexus (Cowper), complexus major (Krause), grand complexus (of Arnold, Cruveilhier)) on the transverse processes of the upper thoracic vertebrae may have an expanded or diminished number of levels (Bergman et al. 2008).

Celik et al. (1997) described a bilateral anomaly of the semispinalis capitis muscle in which there were two muscle bellies. The bellies arose via two tendons from the transverse processes of the three lower cervical and five upper thoracic vertebrae. Both bellies united just before attaching cranially on the inferior nuchal line.

A rare variation of the semispinalis capitis muscle that has been described is that of a second layer, or lamella, deep to the medial part of the main muscle belly (Bergman et al. 2008). This deep layer has spinal attachments from a single or multiple transverse processes of the upper thoracic vertebrae. The superior attachment was found on the occipital bone.

When present, the spinalis capitis muscle commonly blends with the semispinalis capitis muscle (see section on erector spinae). Sometimes the semispinalis capitis muscle consists of two longitudinal portions. When this is the case, the medial portion, which corresponds to the spinalis capitis muscle, may be known as the biventer cervicis muscle and the lateral portion is then known as the complexus muscle (Mayoux-Benhamou et al. 1997; Bergman et al. 2008). Slips from the longissimus thoracis or spinalis thoracis muscles have been found joining the semispinalis capitis muscle (Bergman et al. 2008).

In the thoracolumbar spine, the semispinalis thoracis muscles vary in the number of vertebral segments crossed. Cornwall et al. (2011) described these muscles with the superior attachment on a spinous process and the inferior attachment on a transverse process four or more vertebrae below. The number of vertebral segments crossed varied between four and seven.

The lumbar multifidus muscles may have three–five distinct fascicles, or layers, arising from a single vertebral level. Other sources have indicated that there are no clear divisions of the fascicles and that all the muscles arising from a single spinous process would be removed in a single "sheet" (Hollinshead and Rosse 1997; Cornwall et al. 2011). The deepest fascicles may arise from the root of the spinous process or from the lamina. There is variability as to the inferior attachment of these deep fibers. They have been found extending to the mamillary processes either one or two vertebral segments inferior. The zygapophyseal joints and their capsules, the laminae, and the posterior superior iliac spine have all been found to serve as possible attachment sites of these deep fascicles (Jemmet et al. 2004; Lonnemann et al. 2008).

The more superficial fascicles of the lumbar multifidus muscles have superior attachments on the spinous processes but vary in their inferior attachments. Variations of the inferior attachments include the posterior inferior iliac spine and the iliac crest (Macintosh et al. 1986). In one rare case, a lumbar multifidus muscle was found attaching to the thoracolumbar fascia after coursing through the raphe separating the multifidus lumborum and gluteus maximus muscles (Kay 2000).

While not common, the rotatores longus and brevis muscles may have additional inferior attachments extending to the vertebra immediately above or below the attachment to the transverse process in the thoracic spine (Cornwall et al. 2011). They may also be absent in any region of the spine. Macintosh et al. (1986) and later Cornwall et al. (2011) found the complete absence of the rotatores muscles in the lumbar region deep to the multifidus lumborum muscles.

Suboccipital muscles

There are four muscles in the suboccipital region: rectus capitis posterior major (synonym: rectus capitis posterior superficialis), rectus capitis posterior minor (synonym: rectus capitis posterior profundus), obliquus capitis superior (synonym: obliquus capitis major), and obliquus capitis inferior (synonym: obliquus capitis minimus). It has been reported that doubling or division of the rectus muscles is rather common, but quite rare for the oblique muscles (Tagil et al. 2005; Standring 2009). Splitting of the rectus muscles into three parts has been described, but this appears very rare. There is a case report of

Table 30.11 Variants of the rectus capitis posterior major. Number of cadavers: 104. Data from Mori (1964).

Form	Right side only	Left side only	Both sides
I	7 (3%)	6 (3%)	84 (81%)
II	1 (1%)	2 (2%)	3 (3%)
III	2 (1%)	10 (4%)	3 (3%)

a bilateral doubling of the rectus capitis posterior major muscles with concomitant bilateral absence of the rectus capitis posterior minor muscles (Nayak et al. 2011). Soft tissue connections between the rectus capitis posterior minor muscle and the dura mater have been described (Hack et al. 1995; Rutten et al. 1997). More recently, connections between the dura mater and the rectus capitis posterior major (Scali et al. 2011) and the obliquus capitis inferior (Pontelli et al. 2013) have also been found. These potentially clinically significant myodural bridges between suboccipital muscles and the dura mater may actually be the norm, rather than representing a variation (Kahkeshani and Ward 2012). A soft tissue connection between the rectus capitis posterior minor muscle and the posterior atlanto-occipital membrane has also been described (Zumpano et al. 2006).

Mori (1964) has described three forms of the rectus capitis posterior major muscle in a Japanese cadaver population. Form I is the classic structure of this muscle: inferior attachment on the spinous process of axis and superior attachment on the lateral half of the inferior nuchal line (181 of 208 sides; 87%; Table 30.11). Sometimes there was a gap between these muscles on the right and left sides such that the rectus capitis posterior minor muscle was visible, while in other cadavers there was no gap between these muscles. In Form II of the rectus capitis posterior major muscle, the muscle is divided longitudinally into two bundles (9 of 208 sides; 4.5%). In Form III of this muscle, it receives an accessory slip from an adjacent muscle. The rectus capitis posterior major muscle received a slip from the rectus capitis posterior minor muscle in 17 of 208 sides (8%). In 1 of 208 sides (0.5%) the rectus capitis posterior major muscle received a slip from the obliquus capitis superior muscle. There was therefore a total of 18 of 208 sides (8.5%) of Form III of the rectus capitis posterior major muscle in this population.

Mori (1964) also reported that there were four forms of the rectus capitis posterior minor muscle in a similar Japanese cadaver population. Form I is the classic structure of the muscle: inferior attachment on the posterior tubercle of atlas and superior attachment on the medial aspect of the inferior nuchal line (134 of 214 sides; 62%; Table 30.12). Absence of this muscle was classified as Form II (8 of 214 sides; 3.5%). In Form III of the muscle, it was divided longitudinally into 2 parts (57 of 214 sides; 27%). It was noted that usually the lateral fasciculus was smaller than the medial fasciculus and that the lateral slip sometimes fused with the rectus capitis posterior major muscle. In Form IV of the rectus capitis posterior minor muscle, it received an accessory slip of muscle from either the spinous process of axis or the ligamentum nuchae (15 of 214 sides; 7.5%).

Accessory slips of the spinalis capitis muscle may arise from the suboccipital region, that is, attaching inferiorly to the spinous processes of C2 and sometimes C3, the posterior tubercle of atlas, and/or ligamentum nuchae and attaching superiorly to the occiput. A small muscle has been described running from the spinous process of axis to the mastoid process along the inferolateral border of the obliquus capitis inferior muscle. Recently, another accessory muscle in the suboccipital triangle has been reported that attached inferiorly to the lateral aspect of the spinous process and lamina of axis and ran to attach superiorly to the inferior nuchal line lateral to the attachment site of the rectus capitis posterior major muscle (Loukas and Tubbs 2007). This accessory muscle was perfused by a branch of the vertebral artery and innervated by the suboccipital nerve.

The atlantomastoid muscle is an accessory muscle that arises inferiorly from the transverse process of atlas, runs between the rectus capitis lateralis and obliquus capitis superior muscles, and attaches superiorly to the posterior portion of the mastoid process (Gruber 1867; Figs 30.27, 30.28). In a study of 54 Japanese cadavers, Mori (1964) found an atlantomastoid muscle in 19 of 108 sides (18%), including: bilateral 10 sides (i.e., 5 cadavers; 9%); right side only 5 sides (5%); and left side only 4 (4%). In this same study it was described how the occipital artery ran between the atlantomastoid and obliquus capitis inferior muscles, and sometimes that same artery ran between the longissimus capitis and atlantomastoid muscles. It was also noted that the atlantomastoid muscle was innervated by the same branch of the dorsal ramus of C1 that supplied the obliquus capitis and longissimus capitis muscles, leading the author to speculate that these muscles all have a similar embryologic anlage. In one case in this study a connection between an atlantomastoid muscle and the splenius capitis muscle was found, which the author found more difficult to explain embryologically. He noted that the atlantomastoid muscle has been found in other species: gorilla (Sömmerung); chimpanzee (Gratiolet et Alix); and semnopithecus (Kohbrugge).

Table 30.12 Variants of the rectus capitis posterior minor. Number of cadavers: 107. Data from Mori (1964).

Form	Right side only	Left side only	Both sides
I	16 (7%)	10 (5%)	54 (50%)
II	1 (0.5%)	3 (1%)	2 (2%)
III	11 (5%)	12 (6%)	17 (16%)
IV	0	1 (0.5%)	7 (7%)

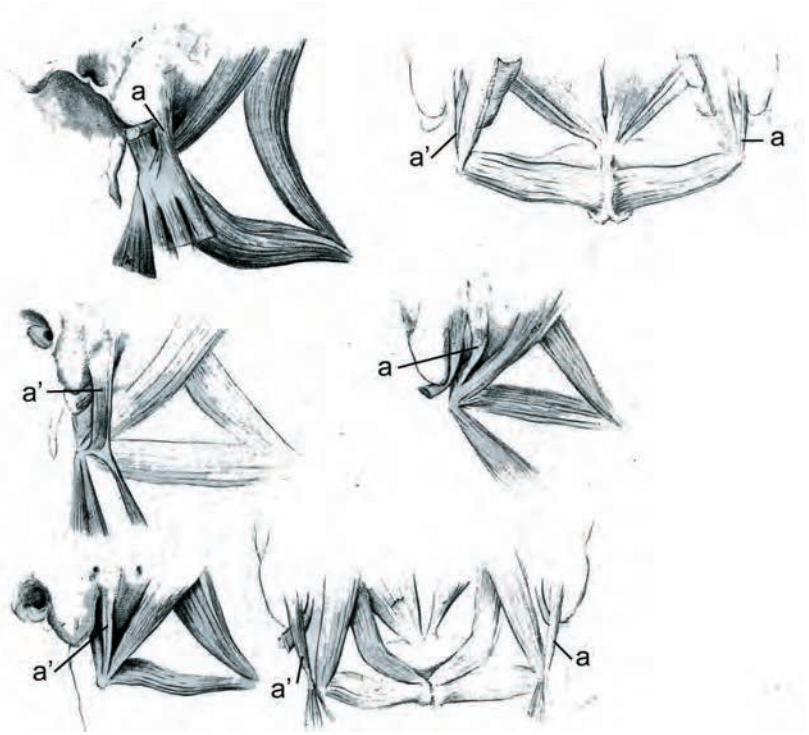

Figure 30.27 Atlantomastoid muscle (a, a′). Adapted from Gruber (1867).

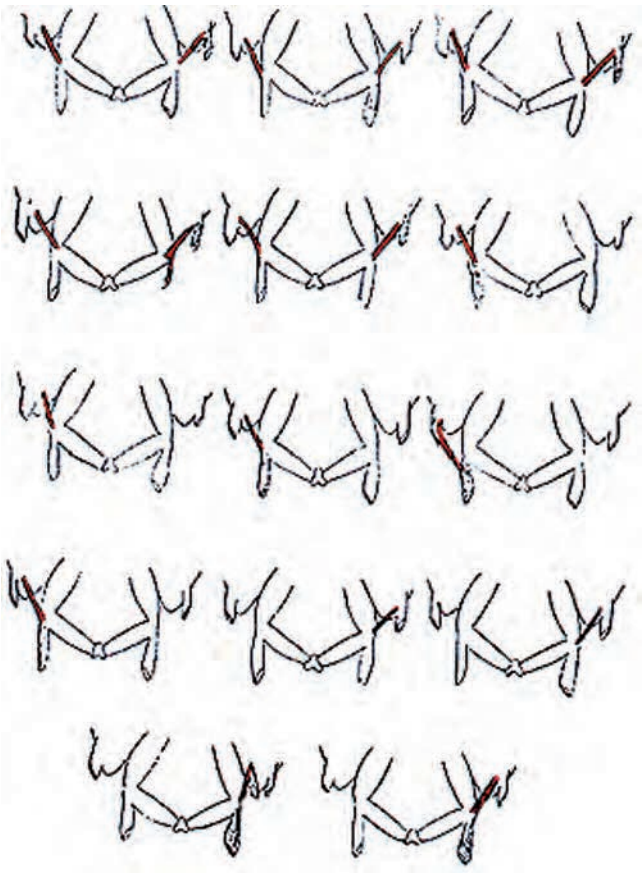

Figure 30.28 Atlantomastoid muscle. Adapted from Mori (1964).

Occipitalis minor (of Santorini)

The occipitalis minor muscle (synonyms: transversus nuchae, occipital transverse, querer Halsmuskel) is a variable muscle found between the occipital protuberances and the auricularis posterior muscle. It may be fused with the auricularis posterior muscle (or even the auricularis superior muscle) and may be located deep or superficial to the cranial fibers of the trapezius muscle. Frequencies of this muscle are apparently quite different in diverse populations (Bergman et al. 1988). It is "always" present in Malays, while it is found in 56% of blacks, 50% of Japanese, and 36% of Europeans. It is absent in Hottentots and Melanesians. Variations in its presentation include a proximal attachment to the external occipital protuberance. Distal attachments may include the parotid fascia. It has even been reported that the occipitalis minor muscle may have an attachment to the angle of the mouth where it can interdigitate with the platysma. This oral attachment may allow it to act as a "risorius" muscle. Turner (1870) described a slender muscle traveling near and parallel to the midline and superficial to the lower fibers of the trapezius muscle. He considered this a remnant of the panniculus carnosus.

Intertransversarii

There are few variations of the different types of intertransversarii muscles. Any of them may be duplicated or missing. Darwish and Ibrahim (2009) described three transversocostal

Figure 30.29 Anterior view of posterior thoracic wall showing three variant intertransverse muscles (1, 2, 3) attaching inferiorly to the necks of the first (a), second (b), and third (c) ribs, respectively.

Source: Darwish and Ibrahim (2009). Reproduced with permission from John Wiley & Sons.

muscles that appear to share a common embryogenesis with the intertransversarii muscles (Fig. 30.29). The first of these, running from the posterior tubercle of the transverse process of the seventh cervical vertebra to the neck of the first rib, seemed to correspond to the posterior intertransverse muscle of the cervicothoracic junction as described by Cave (1937). The other two muscles ran from the lower border of the transverse processes of the first and second thoracic vertebrae to the upper borders of the second and third ribs, respectively. These latter two muscles ran immediately posterior to the corresponding superior costotransverse ligament. Accessory intertransversarii muscles attached to the fourth and sixth cervical vertebrae are known as the transversalis cervicis anticus of Retzius. Similar muscles found between the third and fifth cervical vertebrae are known as Sandifort's muscle or the musculus singularis.

Table 30.13 Frequency of interspinalis at various vertebral levels. Number of sides: 16. Data from Mori (1964).

Level	Frequency
C7–T1	57 (95%)
T1–2	26 (43%)
T2–3	3 (5%)
T10–11	22 (37%)
T11–12	57 (95%)
L4–5	56 (93%)
L5–S1	40 (67%)
S1–2	8 (13%)

Interspinales

There are few variations of the different types of interspinales muscles. Any of them may be duplicated or missing. Miyauchi (1976b) studied the interspinales muscles in a Japanese cadaver population (60 sides). He found interspinales muscles in the cervical (C2/3–C6/7) and in the upper lumbar regions (T12/L1–L3/4) always present, but in the mid-thoracic region (T3/4–T9/10) never present. Variable numbers of these muscles were found at other levels (Table 30.13). In the cervical region, these muscles may span more than two vertebrae (Standring 2009) and may actually be termed the interspinales cervicalis longus muscles, which are synonymous with the spinalis cervicis muscles.

Levatores costarum brevis and longus

In general, the levatores costarum brevis muscles present few variations. There may be missing or duplicated levatores costarum brevis muscles. Variable numbers of levatores costarum longus muscles (more or fewer) is quite common (Steubel 1969). With the presence of lumbar ribs, there may be associated levatores costarum muscles (Bergman et al. 2008).

Quadratus lumborum

The quadratus lumborum muscle (synonyms: m. scalenus lumborum (Meyer, H), ileolumbalis (Meyer, H), rectus abdominis posticus (Luschka)) does not appear to have many variations. The degree of development of its proximal attachments on the vertebrae may differ. Its costal attachment may extend to the eleventh rib. It has been reported that the psoas quartus muscle, a variable structure associated with the iliopsoas muscle, may arise in part from not only the lumbar vertebrae but also the medial aspect of the quadratus lumborum muscle (Tubbs et al. 2006).

References

Allouh M, Mohamed A, Mhanni A. 2004. Complete unilateral absence of trapezius muscle. *McGill J Med* 8: 31–33.

Bergman RA. 1991. Doubled pectoralis quartus, axillary arch, chondroepitrochlearis, and the twist of the tendon of pectoralis major. *Anat Anz* 173: 23–26.

Bergman RA, Thompson SA, Afifi AK, Saadeh FA. 1988. *Compendium of Human Variations*. Baltimore: Urban & Schwarzenberg.

Bergman RA, Afifi AK, Miyauchi R. 2008. Illustrated Encyclopedia of Human Anatomic Variation. Available at: http://www.anatomyatlases.org/AnatomicVariants/AnatomyHP.shtml (accessed 13 October 2015).

Bertelli JA, Ghizoni MF. 2005. Long thoracic nerve: anatomy and functional assessment. *J Bone Joint Surg Am* 87: 993–998.

Bhatt CR, Prajapati B, Patil DS, Patel VD, Singh BGB, Mehta CD. 2013. Variation in the insertion of the latissimus dorsi and its clinical importance. *J Orthop* 10: 25–28.

Biedermann H-J, DeFoa JL, Forrest WJ. 1991. Muscle fibre directions of iliocostalis and multifidus: male-female differences. *J Anat* 179: 163–167.

Bochdalek Jr. 1867. Ein anomaler Musculus supracostalis anterior. *Arch Path Anat Physiol Klin Med* 41: 257–258.

Calori L. 1866. Intorno ad alcune varieté incontrate nelle muscolatura degli arti superiori annatozioni anatomiche. *Mem R Accad Sci Instituto di Bologna S* 26: 137–147, 157–174.

Cave AJE. 1937. The innervation and morphology of the cervical intertransverse muscles. *J Anat* 71: 497–512.

Celik HH, Aktekin M, Sargon M, Cumhur M. 1997. Bilateral anomaly of the semispinalis capitis muscle. *Morphologie* 81: 15.

Chernev I, Pessina MA. 2009. Unilateral complete congenital serratus anterior muscle aplasia: a case report. *PM R* 1: 587–589.

Corner EM. 1901. Proceedings of the Anatomical Society of Great Britain and Ireland, June 1900. A communication of a case of omo-trachelian muscle in a living subject. J Anat Physiol 35: iii.

Cornwall J, Stringer MD, Duxson M. 2011. Functional morphology of the thoracolumbar transversospinalis muscles. *Spine* 36: 1053–1061.

Cuadros CL, Driscoll CL, Rothkopf DM. 1995. The anatomy of the lower serratus anterior muscle: a fresh cadaver study. *Plast Reconstr Surg* 95: 93–97.

Curnow J. 1873. Notes of some irregularities in muscles and nerves. *J Anat Physiol* 7: 304–310.

Darwish HH, Ibrahim AF. 2009. Three muscles in the upper costovertebral region: description and clinical anatomy. *Clin Anat* 22: 352–357.

DeFoa JL, Forrest W, Biedermann H-J. 1989. Muscle fibre direction of longissimus, iliocostalis, and multifidus: landmark-derived reference lines. *J Anat* 163: 243–247.

Emsley JG, Davis, MD. 2001. Partial unilateral absence of the trapezius muscle in a human cadaver. *Clin Anat* 14: 383–386.

Garbelotti SA, Fernando de Sousa Rodrigues C, Sgrott EA, Prates JC. 2001. Unilateral absence of the thoracic part of the trapezius muscle. *Surg Radiol Anat* 23: 131–133.

Gehry K. 1903. Neue beiträge zur geschichte des achselbogens des menschen, eines rudimentes des panniculus der mammalier. *Morphol Jahrb Leipzig* 31: 446–452.

Gruber W. 1867. Ber den Musculus atlantico-mastoideus. *Arch Anat Physiol Wissen Med* 1867: 733–738.

Gruber W. 1873. Sur un muscle cleido-hyoidien et sur un muscle supraclaviculaire singulier chez l'homme. *Bull d l'Acad Imp Sci de St Petersbourg* 18: 154–157.

Gruber W. 1884. Neuer Musculus retro-clavicularis proprius – Tensor laminae produndae fascia colli. *Arch Path Anat Physiol Klin Med* 98: 416–422.

Hack GD, Koritzer RT, Robinson, WL, Hallgren RC, Greenman PE. 1995. Anatomic relation between the rectus capitis posterior minor muscle and the dura mater. *Spine* 20: 2484–2486.

Hamada J, Igarashi E, Akita K, Mochizuki T. 2008. A cadaveric study of the serratus anterior muscle and the long thoracic nerve. *J Shoulder Elbow Surg* 17: 790–794.

Haninec P, Tomáš R, Kaiser R, Ćihák R. 2009. Development and clinical significance of the musculus dorsoepitrochlearis in men. *Clin Anat* 22: 481–488.

Hollinshead W, Rosse C. 1997. *Textbook of Anatomy*, fifth edition. Baltimore: Lippincott Williams and Wilkins.

Humphrey GM. 1873. Lectures on varieties in the muscles of man. *Br Med J* 2: 33–37.

Huntington GS. 1905. The derivation and significance of certain supernumerary muscles of the pectoral region. *J Anat Physiol* 39: 1–54.

Iamsaard S, Uabundit N, Khamanarong K, Sripanidkulchai K, Chaiciwamongkol K, Namking M et al. 2012. Duplicated axillary arch muscle arising from the latissimus dorsi. *Anat Cell Biol* 45: 288–290.

Jemmett RS, Macdonald DA, Agur AMR. 2004. Anatomical relationships between selected segmental muscles of the lumbar spine in the context of multi-planar segmental motion: A preliminary investigation. *Man Ther* 9: 203–210.

Joshi SS, Joshi SD. 2001. Muscle dorso-fascialis – a case report. *J Anat Soc India* 50: 159–160.

Kahkeshani K, Ward PJ. 2012. Connection between the spinal dura mater and the suboccipital musculature: evidence for the myodural bridge and a route for its dissection – a review. *Clin Anat* 25: 415–422.

Kalaycioglu A, Gümüsalan Y, Ozan H. 1998. Anomalous insertional slip of latissimus dorsi muscle: arcus axillaris. *Surg Radiol Anat* 20: 73–75.

Kameda Y. 1976. An anomalous muscle (accessory subscapularis-teres-latissimus dorsi muscle) in the axilla penetrating the brachial plexus. *Acat Anat* 9: 513–533.

Kamibayashi LK, Richmond FJR. 1998. Morphometry of human neck muscles. *Spine* 23: 1314–1323.

Kaye AG. 2000. An extensive literature review of the lumbar multifidus: anatomy. *J Manip Physiol Ther* 8: 102–114.

Knott JF. 1883. Abnormalities in human myology. *Proc Roy Irish Acad* 3: 407–427.

Koshy S, Rabi S, Indrasingh I. 2005. Supernumerary cleidocervicalis (levator claviculae) muscle: case report of its rare incidence with clinical and embryological significance. *Eur J Anat* 9: 103–106.

Kwak H-H, Kim H-J, Youn K-H, Park H-D, Chung I-H. 2003. An anatomic variation of the trapezius muscle in a Korean: the cleidooccipitalis cervicalis. *Yonsei Med J* 44(6): 1098–1100.

Lama P, Potu BK, Bhat KMR. 2010. Chondrohumeralis and axillary arch of Langer: a rare combination of variant muscles with unique insertion. *Romanian J Morphol Embryol* 51: 395–397.

Langer C. 1846. Zur Anatomie des Musculus latissimus dorsi. *Oesterreich Med Wochenschrift* 1846: 454–458, 486–492.

Lima GV, Cabral RH, Andrade DL, Lacerda NSdeO, Araujo VF, Masuko TS. 2012. An unusual anatomical variation of the levator scapulae muscle. *Int J Morphol* 30: 866–869.

Lonnemann ME, Paris SV, Gorniak GC. 2008. A morphological comparison of the human lumbar multifidus by chemical dissection. *J Man Manip Ther* 16: 84–92.

Loukas M, Tubbs RS. 2007. An accessory muscle within the suboccipital triangle. *Clin Anat* 20: 962–963.

Loukas M, Louis Jr RG, Merbs W. 2006. A case of atypical insertion of the levator scapulae muscle. *Folia Morphol* 65: 232–235.

Loukas M, Noordeh N, Tubbs RS, Jordan R. 2009. Variation of the axillary arch muscle with multiple insertions. *Singapore Med J* 50: e88–e90.

Macalister A. 1866. Notes on muscular anomalies in human anatomy. *Proc Roy Irish Acad* 9: 444–469.

Macalister A. 1875. Observations on muscular anomalies in the human anatomy. *(Third series with a catalogue of the principal muscular variations hitherto published.) Trans R Irish Acad Sci* 25: 1–130.

Macintosh JE, Bogduk N. 1991. The attachments of the lumbar erector spinae. *Spine* 16: 783–792.

Macintosh JE, Valencia F, Bogduk N, Munro RR. 1986. The morphology of the human lumbar multifidus. *Clin Biomech* 1: 196–204.

Martin A. 1994. Spinalis capitis, or an accessory paraspinous muscle? *J Anat* 185: 195–198.

Mayoux-Benhamou MA, Revel M, Vallee C. 1997. Selective electromyography of dorsal neck muscles in humans. *Exp Brain Res* 113: 353–360.

Miyauchi R. 1976a. Four cases of rare supernumerary muscles that were found on the anterior chest wall. *Med Bull Fukuoka Univ* 3: 353–365.

Miyauchi R. 1976b. Statistical observations on the musculi interspinales of the Japanese. *Okajimas Folia Anat Jap* 53: 231–244.

Miyauchi R. 1982. A case of the latissimus dorsi muscle with an accessory insertion into the first rib. *Acta Med Nagasaki* 27: 21–29.

Mori M. 1940. Observations on the M. trapezius and the M. pectoralis minor. *Igaku Kenkyu* 14: 85–88 (in Japanese).

Mori M. 1964. Statistics on the musculature of Japanese. *Okajimas Fol Anat Jap* 40: 195–300.

Morimoto I, Hirata K, Yoshida S. 1992. Variability of origin of serratus anterior muscle in Japanese. *Kaibogaku Zasshi J Anat* 67(6): 744–748.

Nasu H, Yamaguchi K, Nimura A, Akita K. 2012. An anatomic study of structure and innervation of the serratus anterior muscle. *Surg Radiol Anat* 34: 921–928.

Natsis K, Totlis, T, Vlasis K, Sofidis G, Lazaridis N, Tsitouridis I. 2012. Dorsoepitrochlearis muscle: an unknown cause of shoulder motion limitation and axilla deformity. *J Orthop Sci* 17: 186–188.

Nayak SR, Swamy R, Krishnamuthry A, Dasgupta H. 2011. Bilateral anomaly of rectus capitis posterior muscles in the suboccipital triangle and its clinical implication. *Clin Ter* 162: 355–356.

Nelson ML, Burkle C, Ricardo R, Shibao S. 1992. Observation of the anterior supracostal muscles. *Anat Rec* 232: 318–321.

Nomizo A, Sakai T. 2009. Segmental level discrepancy of human iliocostalis muscles and their innervation. *Anat Sci Int* 84: 161–169.

Nomizo A, Kudoh H, Sakai T. 2005. Iliocostalis muscles in three mammals (dolphin, goat and human): their identification, structure and innervation. *Anat Sci Int* 80: 212–222.

Patten CJ. 1935. Proceedings of the Anatomical Society of Great Britain and Ireland, November 1933–June 1934. J Anat 69: 147.

Perrin JB. 1871. A rudiment of the dorsal portion of the panniculus carnosus, superficial to the trapezius. *J Anat Physiol* 5: 241.

Rahman HA, Yamadori T. 1994. An anomalous cleido-occipitalis muscle. *Acta Anat* 150: 156–158.

Ravindra SS, Somayaji SN, Nayak SB, Rao MKG. 2012. External jugular vein passing through triangle formed by tendon of cleido-occipitalis cervicalis muscle, trapezius muscle and clavicle – a case report. *Int J Anat Variations* 5: 51–53.

Rogawski KM. 1990. The rhomboideus capitis in man – correctly named rare muscular variation. *Okajimas Folia Anat Jap* 67: 161–164.

Rutten HP, Szpak K, van Mameren H, Ten Holter J, de Jong JC. 1997. Anatomic relation between the rectus capitis posterior minor muscle and the dura mater. *Spine* 22: 924–926.

Scali R, Marsili ES, Pontelli ME. 2011. Anatomical connection between the rectus capitis posterior major muscle and the dura mater. *Spine* 36: E1612–E1614.

Smith R Jr, Nyquist-Battie C, Clark M, Rains J. 2003. Anatomical characteristics of the upper serratus anterior: cadaver dissection. *J Orthop Sports Phys Ther* 33: 449–454.

Standring S. 2009. *Gray's Anatomy*, 40th edition. Edinburgh: Churchill Livingstone.

Steubel R. 1969. Innervation and morphologie der M. levatores costarum. *A Anat Entwickl-Gesch* 128: 211–221.

Tagil SM, Ozçakar L, Bozkurt MC. 2005. Insight into understanding the anatomical and clinical aspects of supernumerary rectus capitis posterior muscles. *Clin Anat* 18: 373–375.

Tobler L. 1902. Der Achselbogen des Menschen, ein Rudiment des Panniculus carnosus der Mammalier. *Morph Jahrbuch* 30(3): 453–507.

Turner W. 1870. A rudiment of the panniculus carnosus superficial to the trapezius. *J Anat Physiol* 5: 116–117.

Vilensky JA, Baltes M, Weikel L, Fortin JD, Fourie LJ, 2001. Serratus posterior muscles: Anatomy, clinical relevance, and function. *Clin Anat* 14(4): 237–241.

von Haffner H. 1903. Eine seltene doppelseitige Anomalie des Trapezius. *Int Monatsschr Anat Physiol* 20: 313–318.

Wood J. 1867a. On human muscular variations in their relation to comparative anatomy. *J Anat Physiol* 1: 44–59.

Wood J. 1867b. Variations in human myology observed during the winter session of 1866–67 at King's College, London. *Proc Roy Soc Lond* 15: 518–546.

Wood J. 1868. Variations in human myology observed during winter session of 1867–68 at King's College, London. *Proc Roy Soc Lond B* 17: 483–525.

Wood J. 1869. On a group of varieties of the muscles of the human neck, shoulder, and chest, with their transitional forms and homologies in the mammalia. *Proc Roy Soc Lond* 18: 1–3, 83–116.

Wood J. 1870. On a group of varieties of the muscles of the human neck, shoulder, and chest, and their transitional forms and homologies in the mammalia. *Phil Trans R Soc (London)* 160: 83–116.

Zumpano MP, Hartwell S, Jagos CS. 2006. Soft tissue connection between rectus capitis posterior minor and the posterior atlantooccipital membrane: a cadaveric study. *Clin Anat* 19: 522–527.

Further reading

Alstead S. 1933. Congenital defect of the pectoral muscles. *Lancet (Lond)* 1: 1179.

Anson BJ. 1966. *Morris' Human Anatomy*, 12th edition. New York: The Blakiston Division, McGraw-Hill Book Company.

Ato T, Gi E. 1959. One case of the M. clavicularis posterior. *Jinruigaku, Jinruiidengaku, Taishitsugaku Ronbumshu* 38: 45 (in Japanese).

Bakirci S, Kafa IM, Uysal M, Sendemir E. 2010. Langer's axillary arch (axillopectoral muscle): a variation of latissimus dorsi muscle. *Int J Anat Variations* 3: 91–92.

Beaton LE, Anson BJ. 1942. Variations in the origin of the m. trapezius. *Anat Rec* 83: 41–46.

Benninghoff A. 1952. *Lehrbuch der Anatomie des Menschen*. Munich: Urban & Schwarzenberg.

Bergman RA, Thompson SA, Saadeh FA. 1988. Anomalous fascicle and high origin of latissimus dorsi compensating for absence of serratus anterior. *Anat Anz* 167: 161–164.

Birmingham A. 1889 Homology and innervation of the achselbogen and pectoralis quartus, and the nature of the lateral cutaneous nerve of the thorax. *J Anat Physiol* 23: 206–223.

Bryce TH. 1899. Note on the varieties of the pectoral sheet of muscle. *J Anat Physiol* 34: 75–78.

Chiaruge G. 1884. Varietá anatomische. 1. Varieta muscolare combinata del grande dorsale e del gran pettorale. *Bollettino/Societa tra e Cultoridelle Science Mediche in Siena* 2: 56–61.

Cramer G, Darby S. 2013. *Clinical Anatomy of the Spine, Spinal Cord, and ANS*, third edition. St Louis: Elsevier Mosby.

David TJ, Winter RM. 1985. Familial absence of pectoralis major, serratus anterior, and latissimus dorsi muscles. *J Med Gen* 22: 390–392.

Dbaly J. 1975. Ein Fall von beiderseitigem Vorkommen des muskelören Achselbogens. *Anat Anz* 137: 75–78.

Delp SL, Suryanarayanan S, Murray WM, Uhlir J, Triolo RJ. 2001. Architecture of the rectus abdominis, quadratus lumborum, and erector spinae. *J Biomech* 34: 371–375.

Deville J. 1848. Anomalie musculaire (grand pectoral et grand dorsal). *Bulletins et Mem de la Société Anatomique de Paris* XXIII: 319–392.

Endres H. 1893. Ueber ein Zwischenmuskelbündel im Gebiete des M. pectoralis major und latissimus dorsi. *Anat Anz* 8: 387–397.

Fitzgerald RR. 1935–36. A case showing the chondro-epitrochlearis muscle. *J Anat* 70: 273–274.

Fritsch G. 1869. Abnorme muskelbundel der achselhöhle. *Arch Anat Physiol Wissen Med* 1869: 367–371.

Gegenbaur C. 1888. *Lehrbuch der Anatomie des Menschen*, third edition. Leipzig: V. Wilhelm Engelmann.

Gérard G, Cordier P. Au sujet d'un cas de fusion des tendons des muscles grand dorsal et grand round. *Soc Biol Comtes Rendus Hebdomadaires des Séances et Mémoires* 83: 927.

Greiner TM, Bedford ME, Walker RA. 2004. Variability in the human M. spinalis capitis and cervicis: frequencies and definitions. *Ann Anat* 186: 185–191.

Griffith TW. 1902. Note on a case of muscular abnormality observed during life. *J Anat Physiol* 36: 387–388.

Gruber W. 1871. Über den Musculus und über die neue Burse mucosa ilio-costocervicalis am Tuberculum der ersten Rippe, und über accidentelle Bursae mucosae am Rücken. *Arch Anat Physiol Wissen Med* 1871: 669–693.

Gruber W. 1880. Ein in der Haut oder Fasciae des Gesichtes und mit seiner Endzacke am Mundwinkel als Musculus risorius endender Musculus occipitalis minor – Santorini. *Arch Path Anat Physiol Klin Med* 80: 83–86.

Guerra AB, Metzinger SE, Xie C, Xie Y, Rigby PL, Naugle T Jr. 2004. Variability of the postauricular muscle complex: analysis of 40 hemicadaver dissections. *Arch Facial Plast Durg* 6: 342–347.

Henle J. 1868. *Handbuch der Systemaischen Anatomie des Menschen, 3 vol*. Braunschweig: von Friedrich Vieweg un Sohn.

Henle J. 1871. *Handbuch der Muskellehre de Menschen, in Handbuch der systematischen Anatomie des Menschen*. Braunschweig: Verlag von Friedrich Vieweg und Sohn.

Hirohashi A, Hayashi K, Akimoto H. 1958. One case of anomaly of the M. trapezius. *Kurume Igakkai Zasshi* 21: 992–996 (in Japanese).

Huber CG, Ed. 1930. *Piersol's Human Anatomy*, ninth edition. Philadelphia: LB Lippincott Company.

Hyrtl J. 1887. *Lehrbuch der Anatomie des Menschen*, 19th edition. Wien: Wilhem Braumüller.

Jackson CM, Ed. 1933. *Morris' Human Anatomy*, ninth edition. New York: Blakiston's Son & Co, Inc.

Kaplan EB. 1945. Langer's muscle of the axilla. *Bull Hosp Joint Dis* 6: 78–70.

Kaneko M, Noriyasu S, Mitsuhashi K. 1978. On a case of musculus supracostalis anterior, Bochdalek Junior, variation (author's transl). *Kaibogaku Zasshi* 53: 157–166 (in Japanese).

Kariya K. 1936. One case of the variation of the M. trapezius approaching the whole absence. *Hokuetsu Igakkai Zasshi* 51: 1139–1142 (in Japanese).

Kasai T, Chiba S. 1977. True nature of the muscular arch of the axilla and its nerve supply. *Kaibogaku Zasshi* 25: 657–669 (in Japanese).

Keith AM 1894. Note of supracostalis anterior. *J Anat Physiol* 27: 333–334.

Khan MM, Darwish HH, Zaher WA. 2008. Axillary arch: a rare variation. *Eur J Anat* 12: 169–173.

Kitano S, Takata N, Sato M. 1957. One case of the variation of the M. rhomboideus minor. *Kurume Igakkai Zasshi* 20: 1045–1048 (in Japanese).

Knapp E. 1966. Über eine seltene Varietät der Nakenmuskulatur (M. splenius accessories). *Anat Anz* 118: 178–180.

Komiya R, Yoshimura H, Honkoku K. 1955. On the anomalies of the insertion of the M. trapezius. *Kurume Igakkai Zasshi* 18: 1042–1044 (in Japanese).

Kopsch F. 1908. *Rauber's Lehrbuch der Anatomie des Menschen*. Leipzig: Georg Thieme.

Kredel L. 1900. Ueber angeborene Halsmuskeldefecte. *Deutche Med Wochenschrift* 56: 398–406.

Kutiyanawala MA, Stotter A, Windle R. 1998. Anatomical variants during axillary dissection. *Brit J Surgery* 85: 393–394.

Laidlaw PP. 1902. A supraclavicularis proprius (Gruber). *J Anat Physiol* 36: 417–418.

Latarjet A. 1948. *Testut's Traite D'Anatomie Humaine*, ninth edition. Paris: G Doin & Cie.

Le Double A. 1891. Du muscle epitrochléo-olécranien et de sa signification au point de vue de l'anthropol. *Bull Soc d'Anthrop Paris* 2: 154–173.

Le Double A. 1893. Les anomalies de muscle grand dorsal. *Bull Soc d'Anthropol Paris* 4: 626–653.

Le Double AF. 1897. *Traité des Variations du Systeme Musculaire de l'Homme et Leur Signification au Point de vue de l'Anthropologie Zoologique*. Paris: Libraire C Reinwald, Scheicher Freres, Paris.

Livini F. 1905. Contribution a la morphologie du M. serratus anterior chez l'homme. *Arch Ital Biol* 44: 115–116.

Livini F. 1905. Contribuzione alla morfolgia des M. rectus abdominis e del M. supra-costalis nell'uomo. *Arch Ital Anat Embriol* 4: 116–117.

Livini F. 1907. Morphologia del M. serratus anterior nell'uomo. *Arch Ital Anat Embriol* 6: 429–441.

LoCascio G. 1915. Contribution a la morphologie de l'arc de Langer. *Arch Ital Biol* 62: 285.
Marciniak T, Serafin K. 1929. On the inervation of axillary arch by the N. intercostobrachialis. *Folia Morphologica (Warsaw)* 1: 23–35.
Miyauchi R. 1982. On the musculus supracostalis anterior. *Okajimas Folia Anat Jap* 59: 45–64.
Miyauchi R. 1986. A case of a rare anomalous muscle of the human anterior thoracic wall. *Okajimas Folia Anat Jap* 63: 331–336.
Miyazima S, Okabe N, Kitagawa Y. 1960. Three cases of the anomalies of the M. Splenius. *Kurume Igakkai Zasshi* 23: 1443–1448 (in Japanese).
Monteiro H. 1926. L'arc axillaire musculaire et ses relations avec le faisceaus pectoreau aberrants. *L'Associ Anatomistes Comptes Rendus* 21: 262–269.
Moore K, Dalley A, Agur A. 2014. *Clinically Oriented Anatomy*, seventh edition. Baltimore: Lippincott Williams & Wilkins.
Mori M, Minoru T. 1949. Studies on the musculature of the back of the fetus, especially comparative studies on it of the twin-fetus, on the M. trapezius. *Kaibogaku Zasshi* 24: 109 (in Japanese).
Mori M, Nazayoshi M. 1938. Two cases of the M. supracostalis anterior. *Kyushi Gakuho* 2: 8–9 (in Japanese).
Mori M, Minoru T. 1950. On the M. latissimus dorsi. *Sotai Taiji no Kaibogakeuteki Kenyu* 11: 1–37 (in Japanese).
Mori M, Minoru T. 1950. On the M. levator scapulae. *Sotai Taiji no Kaibogakeuteki Kenyu* 11: 79–153 (in Japanese).
Mori M, Minoru T. 1950. On the M. rhomboideus. *Sotai Taiji no Kaibogakuteki Kenkyu* 11: 38–78 (in Japanese).
Morrison AB. 1954. The levatores costarum and their nerve supply. *J Anat* 88: 19–24.
Nakajima K, Chiba S, Kobayashi K, Wakatuki E, Kumaki K, Hoshino T. 1999. A rare muscular anomaly in the upper arm: the chondroepitrochlearis muscle with an aberrant type of muscular arch of axilla. *Kaibogaku Zasshi* 74: 209–213 (in Japanese).
Nishi S. 1918. Ein beiträg zur Anatomie des M. ileocostalis (sic): Fasciculi intercostales dorsale beim Mensche. *Arbeite aus Anat Inst Sendai* 1: 1–5.
O'Rahilly R. 1986. *Gardner-Gray-O'Rahilly Anatomy: A Regional Study of Human Structure*, fifth edition. Phildelphia: WB Saunders Company.
Oyama M. 1957. One case of the reduced origin of the M. trapezius. *Tokyo Jikeikai Ikadaigaku Zasshi* 72: 1011–1013 (in Japanese).
Phillips S, Mercer S, Bogduk N. 2008. Anatomy and biomechanics of quadratus lumborum. *Proc Inst Mech Eng H* 222: 151–159.
Phillips WFR. 1913. Innervation of the axillary arch muscle. *Anat Rec* 7: 131–132.
Pichler K. 1916. Ueber den Langer'schen Achselbogen. *Anat Anz* 49: 310–318.
Pichler K. 1916. Achelboden und M. chondro-epitrochlearis bei demselben Trager. *Anat Anz* 49: 383–384.
de Pina L. 1933. Le muscle petit dentelé posterieur et supérieur chex l'homme et les primates. *L'Assoc Anatomistes Comptes Rendus* 28: 523–531.
Pires de Lima JA. 1914. Nova série de observacõs Portuguesas de anomalias musculared. *Arch de Anat e de Anthropol* 1: 231–260.
Pitzorno M. 1911. Contributo alla morphologia dell'arco ascellare musculare di Langer. *Arch Ital Anat Embriol* 10: 129–144.
Pontelli ME, Scali F, Marshall E, Enix D. 2013. The obliquus capitis inferior myodural bridge. *Clin Anat* 26: 450–454.
Princeteau J. 1892. Note pour server a l'historie des anomalies musculaires de creux de l'aisselle. *Soc de Biol, Comptes Rendus Hebdomandaires de Séances et Mémoires*. 44: 202–206.
Pye-Smith I. 1868. Ein aweiter Fall von Musculus supracostalis anterior anomalous. *Arch Path Anat Physiol Klin Med* 43: 142.
Ramsey A. 1812. An account of unusual conformation of some muscles and vessels. *Edinburgh Med Surg J* 8: 281–283.
Rao GRKH, Rao VR. 1956. Dorso-epitrochlearis brachii. *J Anat Soc India* 5: 33–34.
Regnault F. 1902. Les causes des anomalies musculaires. *L'Assoc Anatomistes Comtes Rendus* 4: 19–20.
Rutherford N. 1910. A curious arrangement of the retro-clavicular musculature. *Anat Anz* 37: 148–150.
Sachetello CR. 1977. The axillopectoral muscle (Langer's axillary arch): a cause of axillary vein obstruction. *Surgery* 81: 610–612.
Schaefer EA, Symington J, Bryce TH, Eds. 1923. *Quain's Elements of Anatomy*, 11th edition. London: Longmans, Green, and Co.
Selden BR. 1935. Congenital absence of trapezius and rhomboideus major muscles. *J Bone Joint Surg* 17: 1058–1059.
Serpell JW, Baum M. 1991. Significance of "Langer's axillary arch" in axillary dissection. *Australian New Zealand J Surgery* 61: 310–312.
Sheehan D. 1932. Bilateral absence of trapezius. *J Anat* 67: 180–181.
Shindo H. 1995. Anatomical study of the lumbar multifidus muscle and its innervation in human adults and fetuses. *Nippon Ika Daigaku Zasshi* 62: 439–446 (in Japanese).
Stange P. 1896. Ueber einen Fall von fast vollstandigem Defekt des rechten Musculus cucullaris und des rechten Musculus sternocleidomastoideus. *Deutche Med Wochenschrift* 22: 412–414.
Struthers J. 1854. On some points in the abnormal anatomy of the arm. *British and Foreign Medico-Chirugical Review April* 26: 523–533, July: 224–236.
Takafugi T, Igarashi J, Kanabyashi T, Yokoyama T, Moriya A, Azuma S, Sato Y. 1991. The muscular arch of the axilla and its nerve supply in Japanese adults. *Kaibogaku Zasshi* 66: 511–523 (in Japanese).
Takeshige A, Hirohashi T, Mihashi N, Oribe H, Tsuda H. 1959. On the variation of the M. Splenius. *Kurume Igakkai Zasshi* 22: 33–36 (in Japanese).
Takii T, Mori M. 1952. A study on the tendineal arch of the upper part of the origin of the M. serratus anterior. *Kumamoto Daigaku Igakubu Daiichi Kaibogakujyoshitsu Gyosekishu* 14: D1–D11 (in Japanese).
Testut L. 1884. *Les Anomalies Musculaires Chez l'Homme Expliques par l'Anatomic Comparée*. Paris: Masson.
Tochiuchi I, Tsukahara K. 1944. On the anomaly of the M. levator scapulae. *Iwate Ikakusenmongakko Zasshi* 7: 36–92 (in Japanese).
Tsuda M. 1939. Supernumerous muscle-bundle of the M. infrahyoidei and M. trapezius. *Iwate Igakusenmongakko Zasshi* 3: 186–189 (in Japanese).
Tubbs RS, Oakes WJ, Salter EG. 2006. The psoas quartus muscle. *Clin Anat* 19: 678–680.
Turner W. 1867. On the musculus sternalis. *J Anat Physiol* 1: 246–253.
Vastarini-Cresi G. 1906. Nouvelle variété de musculus supraclavicularis chez l'homme et sa signification probable. *Arch Ital Biol* 46: 290–291.
Vilde J. 1924–1925. Ueber eine bisher unbekannte Ursprungsmöglichkeit des Musculus serratus posterior inferior. *Anat Anz* 59: 464–467.
von Saar FG. 1903. Zur vergleichenden Anatomie der Brustmuskeln und des Deltamuskels. *Arch f Anat u Enwickelungsgeschichte* 1903: 153–202.
Voto SJ, Weiner DS. 1987. The chondroepitrochlearis muscle. *J Ped Orthopedics* 7: 213–214.

Weil M. 1869. Faisceau supplémentaire du grand pectoral s'unissant dan l'aisselle par une expansion aponévrotiqueé un autre faisceau longeant le grand dorsal. *Lyon Méd* 1: 558–559.

Weissberg H. 1932. Ueber einen Fall von muskulosem Achselbogen. *Anat Anz* 74: 105–117.

Wood J. 1865. Additional varieties in human myology. *Proc Roy Soc London B* 14: 378–392.

Wood J. 1866. Variations in human myology observed during the winter session of 1865–66 at King's College, London. *Proc Roy Soc Lond* 15: 229–244.

Yamada F. 1933. One case of the variation of the M. levator scapulae. *Aichi Igakki Zasshi* 40: 1351–1354.

Yamada F. 1934. Ein Fall von variation des M. levator scapulae beim Menschen. *Nagoya J Med Sci* 8: 19–23.

Yamada F. 1934. Some variations of the infrahyoid muscles and insertion of the trapezius into the clavicle. *Kaibogaku Zasshi* 7: 337–347 (in Japanese).

31 Scapulohumeral muscles

Clare Lamb
University of Dundee, Dundee, United Kingdom

The scapulohumeral muscles are the rotator cuff (subscapularis, infraspinatus, supraspinatus and teres minor), teres major and deltoid. Variations have been recorded for all of the scapulohumeral muscles. Supraspinatus is the least variable of the rotator cuff muscles and subscapularis is the most variable. There is still debate concerning the exact origin of some of the variants with identical structures being described by several authors but given different names and attributed to variation of different muscles. Several of the variants detailed below are muscular slips passing between the scapulohumeral muscles, making determination of the exact nature of the variation more difficult.

Subscapularis

Subscapularis has the largest number of reported variations of all of the rotator cuff muscles. The most reported variation of subscapularis is duplication, with a prevalence of 5% of individuals showing this variation (Gruber 1859). The duplicated muscle has been named as subscapularis minor or secundus (Gruber 1859) or as an accessory subscapularis (Le Double 1897). An example of this accessory muscle is given by Testut (1894) who describes a muscle slip originating from the tendon of subscapularis and inserting directly into the surgical neck of the humerus. Subscapularis may also separate into several small slips and the muscle can form two distinct parts with a larger, thicker lower segment divided from the smaller, upper segment by a deep fissure (Macalister 1867). Accessory muscle slips may be separated from the main muscle by the axillary and subscapular nerves (Breisch 1986).

Accessory muscle tissue may pass from the lateral border of the scapula (Aasar 1947; Yoshinaga et al. 2008), the superolateral aspect of subscapularis (Breisch 1986), and the lateral border of subscapularis (Downie et al. 2010). The accessory muscle may insert into the joint capsule (Yoshinaga et al. 2008; Downie et al. 2010), or to the humerus at or below the lesser tubercle (Aasar 1947; Breisch 1986). Namking et al. (2013) report a rare finding of an accessory muscle that originated from the joint capsule and lesser tubercle close to the attachment of subscapularis and inserted into latissimus dorsi. There is debate whether all of the accessory tissue ascribed to subscapularis actually originates from subscapularis or are instead remnants of latissimus dorsi (Kameda 1976; Yoshinaga et al. 2008).

Rarer variants include a muscular slip arising from the tendon of subscapularis to pass into the axillary fascia or the skin of the base of the axilla (Le Double 1897). A small muscular slip (subscapulo-capsular) has been described that inserted into the joint capsule or inferior border of the neck of the humerus (Macalister 1867). Kameda (1976) reports the presence of an accessory 'subscapularis-teres-latissimus' muscle in 3.8% of individuals. This muscle could take three distinct forms, either arising from the surface of subscapularis, from latissimus dorsi, or from both. The accessory muscle then fused with the insertion of subscapularis.

There may be a muscular slip connecting subscapularis to pectoralis major (Macalister 1875) or a tendon from subscapularis to the short head of biceps or long head of triceps (Le Double 1897). Henle (1858) reported a slip of muscle passing from an abnormal tubercle on the humerus to attach to the fascia of the internal brachial ligament to terminate on the joint capsule, blending its fibers with subscapularis as it did so. Henle (1858) classed this as a variation of subscapularis, but Wood (1867) suggests that equivalent muscles he observed during dissection were a form of accessory coracobrachialis (coracocapsularis) muscles. Slips have also been observed passing from the coracoid process and attaching to the fascia of subscapularis or interdigitating with the muscle fibers, which have been classed as either a variant of subscapularis (Henle 1858), of coracobrachialis (Aasar 1947), or of deltoid (Macalister 1875). Cervicohumeralis muscle (costohumeralis from C6, C7 vertebrae and the first rib to the humerus, noted by Gruber 1860) has been reported to blend with the insertion of subscapularis at the lesser tubercle of the humerus (Ransom 1885; Weber and Collin 1905).

MRI analysis of the insertion of the tendon of subscapularis has shown considerable variation between individuals, with only 20% of the subscapularis muscles studied inserting into the lesser tubercle (normal or type 1). Cash et al. (2009) identified three types of insertion, with the majority of individuals

Bergman's Comprehensive Encyclopedia of Human Anatomic Variation, First Edition. Edited by R. Shane Tubbs, Mohammadali M. Shoja and Marios Loukas.
© 2016 John Wiley & Sons, Inc. Published 2016 by John Wiley & Sons, Inc.

showing insertion into the bicipital groove (type 2) and insertion across the greater tuberosity (type 3). Boon et al. (2004) found that in all of the 43 shoulders in their study there was a band of tissue passing between subscapularis and supraspinatus. The tissue did not appear to insert into the greater tubercle but instead interdigitated with supraspinatus, lending support to the idea of a rotator cuff extension around the joint as suggested by Jost et al. (2000).

Infraspinatus

Few variations have been described and usually relate infraspinatus to supraspinatus or teres minor muscles. Infraspinatus muscle fibers may blend with those of teres minor forming a single muscle (Macalister 1875; Aasar 1947), or the insertion of infraspinatus may blend with the insertion of supraspinatus (Minagawa et al. 1998; Curtis et al. 2006). Infraspinatus and teres minor have been reported to share a common fascial envelope (Chafik et al. 2013). The presence of accessory slips passing to deltoid from infraspinatus (Macalister 1875) and from deltoid to infraspinatus (Thiele 1843) have also been reported. Infraspinatus may separate into two parts, with the upper part described as infraspinatus minor (muscle of Knott) (Aasar 1947), or into two overlapping laminae (Macalister 1875). Infraspinatus has been described as having two heads with the oblique head being more active during movement than the transverse head (Hughes et al. 2012). In rare cases, infraspinatus may be absent (Bing 1902). An accessory muscle between the deltoid and infraspinatus has been termed the scapulohumeralis digastricus of Gruber.

Supraspinatus

Rare reports of variation only, Macalister (1875) calls supraspinatus "singularly invariable." The muscle bulk of suprapinatus may form two sections, with separate slips passing from the most anteromedial area of the supraspinous fossa (Volk and Vangness 2001). A posterolateral extension of supraspinatus has been described that passed over the bicipital groove to blend with the tendon of subscapularis (Clark and Harryman 1992; Boon et al. 2004). Interdigitation with the insertion of infraspinatus has also been found (Minagawa et al. 1998; Curtis et al. 2006). The tendon of pectoralis minor may pass over the superior surface of the coracoid process to blend with supraspinatus (Macalister 1867; Le Double 1897; Musso et al. 2004; Moineau et al. 2008; Uzel et al. 2008). Supraspinatus may receive a slip from pectoralis major (Macalister 1875; Le Double 1897). The insertion of supraspinatus is also reported to vary with insertion to both greater and lesser tubercles (Kolts 1992), and insertion into the middle facet of the greater tubercle described (Minagawa et al. 1998). In rare cases, supraspinatus can be absent (Bing 1902).

Teres minor

Few variants of teres minor have been reported. Teres minor may divide into two, with a separate upper part described as the "teres minimus" (Gruber 1875). Accessory slips have been reported to cover the lower parts of the greater tubercle and insert into the upper part of the surgical neck of the humerus (Gruber 1875, Jain et al. 2012). Teres minor has been found fused to infraspinatus (Macalister 1875; Mori 1964), or deriving an extra origin from the infraspinous fascia (Aasar 1947). Slips may also pass to deltoid (Aasar 1947). The fascia surrounding teres minor has been reported to show two distinct and equally common variants, with an inflexible fascial sheet enveloping teres minor alone or a common fascial compartment for teres minor and infraspinatus (Chafik et al. 2013). Teres minor may also be absent (Petit 1733; Mori 1964).

Teres major

The most commonly reported variation is accessory tissue associated with latissimus dorsi. Teres major may be fused to latissimus dorsi at the inferior angle of the scapula (Macalister 1875), or fuse with the tendon of latissimus dorsi (Gérard and Cordier 1920; Aasar 1947; Mori 1964; Iamsaard et al. 2012). If the whole of teres major fuses to the tendon of latissimus dorsi then the terminal tendon of teres major may be absent (Iamsaard et al. 2012). The terminal ends of teres major and latissimus dorsi have been observed to fuse, attach to the long head of triceps, and insert into the scapula between the coracoid process and the insertion of subscapularis (Meek 1915). Muscular slips have been reported passing between teres major and the long head of triceps (Macalister 1875; Le Double 1897; Quandros et al. 2013), and between teres major and fascia of the shoulder capsule and the brachial fascia (Blandin 1838; Macalister 1875). Fibres of teres major have been observed fusing with the lower fibers of rhomboid major (Macalister 1875; Le Double 1897).

Tissue slips have been reported passing from latissimus dorsi (Bhatt et al. 2013) and biceps brachii to teres major (Aggarwal et al. 2009). A muscular slip from latissimus dorsi and teres major that inserted into the tendon of coracobrachialis has also been described (Macalister 1875). Mori (1964) reported one case where an anomalous muscle slip originated from the infraglenoid tubercle of the scapula and inserted into the tendon of teres major. In rare cases teres major may be absent (Macalister 1867).

Deltoid

Deltoid shows variation in all the parts of the muscle, with clavicular (Otto 1830), middle (Gruber 1872), and acromial (Macalister 1875) parts reported absent or reduced in size. In rare cases deltoid may also show fasciculation into separate sections from 6–7 in number (Macalister 1875) to 18–20 (Jenty 1757).

The separation of acromial, clavicular, and spinal parts of deltoid may be complete or partial (Mori 1964). The clavicular fibers of pectoralis major have been observed to fuse with the clavicular fibers of deltoid (Perrin 1871; Macalister 1875). The most posterior fibers of deltoid have been reported to be separated from the rest of the muscle by a distinct fascial sheath (Chudzinski 1885; Kayikçioglu et al. 1993; Kamburoğlu et al. 2008).

Deltoid fibers may form a "basio-deltoideus" from the infraspinatus fascia or axillary border of the scapula, or a "costo-deltoideus" (of Calori) joining the upper part of deltoid to the clavicle or acromion process (Macalister 1875; Aasar 1947). Gruber (1865) describes an "acromioclavicularis" that arose from the acromion of the scapula and inserted into the clavicular head of deltoid. Deltoid fibers may blend with trapezius, infraspinatus, latissimus dorsi, and teres major (Macalister 1875; Aasar 1947). Additional muscular slips (infraspinatohumeralis) may arise from the vertebral or axillary borders of the scapula and expand into the fascia of the arm (Calori 1867). The tendon of deltoid has also been observed to be in continuity with the lateral intermuscular septum, lateral aspect of brachialis, and the deep brachial fascia (Rispoli et al. 2009). Macalister (1875) describes one case of deltoid inserting into the long head of biceps brachii to create a single muscular ribbon from the acromion of the scapula to the radius. Fibers of deltoid attached to the fascia of the supraspinatus have been termed the fasciculus infraspinatus deltoideus of Gruber.

Supernumerary heads of biceps brachii may take origin from the deltoid (Kosugi et al. 1992; Schoenleber and Spinner 2006) and the tendon of deltoid (Vijayabhaskar et al. 2008). In rare cases, deltoid may be absent (Bing 1902).

References

Aasar YH. 1947. *Anatomical Anomalies*. Cairo: Fouad I University Press.

Aggarwal A, Kaur H, Sahni D, Aggarwal A. 2009. Four-headed biceps brachii muscle with variant course of musculocutaneous nerve: anatomical and clinical insight. *Int J Anat Var* 2: 127–130.

Bhatt CR, Prajapati B, Patil DS, Patel VD, Singh BG, Mehta CD. 2013. Variation in the insertion of latissimus dorsi and its clinical importance. *J Orthop* 10: 25–28.

Bing R. 1902. Veberangeborene muskeldefecte. *Virchows Archiv* 170: 175–228.

Blandin FP. 1838. *Nouveaux Eléments d'Anatomié Descriptive*. Vol 1: 461. Paris: J.B. Bailliere.

Boon JM, de Beer MA, Botha D, Maritz NGJ, Fouche AA. 2004. The anatomy of the subscapularis tendon insertion as applied to rotator cuff repair. *J Shoulder Elbow Surg* 3: 65–69.

Breisch EA. 1986. A rare human variation: the relationship of the axillary and inferior subscapular nerves to an accessory subscapularis muscle. *Anat Record* 216: 440–442.

Calori L. 1867. Di alcone varietà muscolari dell'avambraccio. Memorie dell'Acc. *delle Scienze dell'Inst di Bologna* 7: 359–381.

Cash CJC, MacDonald KJ, Dixon AK, Bearcroft PWP, Constant CR. 2009. Variation in MRI appearance of the insertion of the tendon of subscapularis. *Clin Anat* 22: 489–494.

Chafik D, Galatz LM, Keener JD, Kim HM, Yamaguchi K. 2013. Teres minor muscle and related anatomy. *J Shoulder Elbow Surg* 22: 108–114.

Chudzinski TH. 1885. Une anomalie du muscle deltoide. *Bulletins de la Société d'anthropologie de Paris* 8: 10–11.

Clark JM, Harryman DT. 1992. Tendons, ligaments, and capsule of the rotator cuff. Gross and microscopic anatomy. *J Bone Joint Surg* 74: 713–725.

Curtis AS, Burbank KM, Tierney JJ, Scheller AD, Curran R. 2006. The insertional footprint of the rotator cuff: an anatomic study. *Arthroscopy* 22: 603–609.

Downie SA, Lee MM, Pace A, Park ME, Shapiro D, Stone JA, Baker EW, Haramati N, Olson TR. 2010. Two cadaver-cases of accessory subscapularis muscles with multiple brachial plexus anomalies and axillary artery variations. Abstracts from the Joint Meeting of the American Association of Clinical Anatomists and the International Society for Plastination. *Clin Anat* 23: 1013–1014.

Gérard G, Cordier P. 1920. Au sujet d'un case de fusions des tendons des muscles grand dorsal et grand rond. *Soc Biol Comptes Rendus Hebdomadiares des Séances et Memoires* 83: 927.

Gruber W. 1859. Die Musculi subscapulares (major et minor) und die neuen supernumerären schulter-muskeln des menschen. Mémoires prés. *l'Académie Impériale des Sciences de St Pétersbourg pars Divers Savants* 8: 219–58.

Gruber W. 1860. Die supernumeraeran Brustmuskeln des Menschen. Mémoires prés. *l'Académie Impériale des Sciences de St Pétersbourg* 2:10.

Gruber W. 1865. Neue supernumeräre schüsselbeinmuskeln. *Archiv Anat Phys Wissen Med* 2: 703–718.

Gruber W. 1872. Mangel der mittlern portion des musculus deltoideus. *Archiv Anat Physiol Klin Med* 54: 186–187.

Gruber W. 1875. Ein Musculus teres minimus scapulae. *Archiv Anat Physiol Wissen Med* 2: 593–598.

Henle J. 1858. *Handbuch der Muskellehre des Menschen, in Handbuch der systematischen anatomie des Menschen*. Braunschweig: Verlag von Friedrich Vieweg und Sohn.

Hughes PC, Green RA, Taylor NF. 2012. Differentiation of the two heads of infraspinatus during functional testing. Abstracts presented at the Australian and New Zealand Association of Clinical Anatomists. *Clin Anat* 25: 530–543.

Iamsaard S, Thunyaharn N, Chaisiwamongkol K, Boonruangsri P, Uabundit N, Hipkaeo W. 2012. Variant insertion of the teres major muscle. *Anat Cell Biol* 45: 211–213.

Jain M, Shukla L, Kaur D. 2012. Extended insertion of teres minor muscle: a rare case report. *Eur J Anat* 16: 224–225.

Jenty CN. 1757. A Course of Anatomico-Physiological Lectures on the Human Structure and Animal Oeconomy vol 3: 232. Printed for James Rivington and James Fletcher at the Oxford Theatre in Paternoster Row.

Jost B, Koch PP, Gerber C. 2000. Anatomy and functional aspects of the rotator cuff interval. *J Shoulder Elbow Surg* 9: 336–340.

Kamburoğlu HO, Boran OF, Sargon MF, Keçik A. 2008. An unusual variation of deltoid muscle. *Int J Shoulder Surg* 2: 62–63.

Kameda Y. 1976. An anomalous muscle (accessory subscapularis-teres-latissimus muscle) in the axilla penetrating the brachial plexus in man. *Acta Anat (Basel)* 96: 513–533.

Kayikçioglu A, Celik HH, Yilmaz E. 1993. An anatomic variation of the deltoid muscle (case report). *Bull Assoc Anat (Nancy)* 77: 15–16.

Kolts I. 1992. A note of the anatomy of the supraspinatus muscle. *Archiv Orthop Trauma Surg* 111: 247–249.

Kosugi K, Shibata S, Yamashita H. 1992. Supernumerary head of biceps brachii and branching pattern of the musculocutaneous nerve in Japanese. *Surg Radiol Anat* 14: 175–185.

Le Double AF. 1897. *Traité des Variations du Systéme Musclaire de l'homme et de le Signification au Point de Vue de l'Anthropologie Zoologique*. Second edition. Libraire C. Reinwald, Schleicher Freres: Paris.

Macalister A. 1867. Notes on an instance of irregularity in the muscles around the shoulder joint. *J Anat Physiol* 1: 316–319.

Macalister A. 1875. Observations on the muscular anomalies in the human anatomy. Third Series with a catalogue of principal muscular variations hitherto published. *Trans Royal Irish Acad Sci*: 1–130.

Meek MO. 1915. Some rare muscular anomalies. *J Anat Physiol* 49: 376–377.

Minagawa, H, Itoi E, Konno N, Kido T, Sano A, Urayama M, Sato K. 1998. Humeral attachment of the supraspinatus and infraspinatus tendons: an anatomic study. *Arthroscopy* 14: 302–306.

Moineau G, Cikes A, Trojani C, Boileau P. 2008. Ectopic insertion of the pectoralis minor: implication in the arthroscopic treatment of shoulder stiffness. *Knee Surg Sports Traum Arthro* 16: 869–871.

Mori M. 1964. Statistics on the musculature of the Japanese. *Okajimas Folio Anat Japonica* 40: 195–300.

Musso F, Azerrdo R A, Tose D, Marchiori JGT. 2004. Pectoralis minor muscle. An unusual insertion. *Braz J Morph Sci* 21: 139–140.

Namking M, Mo-thong W, Chaijaroonkhanarak W, Khamanarong K, Woraputtaporn W. 2013. A rare variation of the posterior cord brachial plexus branching coexisting with the intercalated ectopic muscle. *Anat Sci Int* 88: 115–117.

Otto AW. 1830. *Lehrbuch der pathologisches Anatomie des Menschen und der Thiere*. First edition. Berlin: A Rücher.

Perrin JB. 1871. Notes on some variations of the pectoralis major, with its associate muscles. *J Anat Physiol* 5: 233–240.

Petit M. 1733. Remarques sur en enfant nouveau-ne. *Memoires de Mathematique et de Physique: Tires des registres de l'Académie Royale des Sciences*, pp. 1–22.

Quandros LS, Babu A, Bhat N, Ankolekar VH, D'Souza AS. 2013. Variant musculo-tendinous slip between teres major and triceps brachii. *Online J Health Allied Sci* 12(3).

Ransom WB. 1885. Notes on some variations of the shoulder muscles. *J Anat Physiol* 19: 508–509.

Rispoli DM, Athwal GS, Sperling JW, Cofield RH. 2009. The anatomy of the deltoid insertion. *J Elbow Shoulder Surg* 18: 386–390.

Schoenleber SJ, Spinner RJ. 2006. An unusual variant of the biceps brachii. *Clin Anat* 19: 702–703.

Testut L. 1894. *Traité d'Anatomie Humaine*. Paris: Masson.

Thiele F. 1843. Myologie et angeologie. In *Encyclopédie Anatomique*, 10 volumes (Jourdan AJL, ed.). Paris: Prix-de-change.

Uzel AP, Bertino R, Cix P, Boileau P. 2008. Bilateral variation of the pectoralis minor muscle discovered during practical dissection. *Surg Radiol Anat* 30: 679–682.

Vijayabhaskar P, Baral P, Vaishya R, Shrestha RN. 2008. Supernumerary head of biceps brachii: a rare occurrence in the Nepalese population. *Kathmandu Uni Med J* 6: 225–227.

Volk AG, Vangness CT Jr. 2001. An anatomic study of the supraspinatus muscle and tendon. *Clin Orthop Rel Res* 384: 280–285.

Weber A, Collin R. 1905. Un muscle huméro-transversaire observé chez l'homme. *Bibliog Anat* 14: 190–192.

Wood J. 1867. On human muscular variations and their relation to comparative anatomy. *J Anat Physiol* 6: 44–59.

Yoshinaga K, Kawai K, Tanii I, Imaizumi K, Kodama K. 2008. Nerve fiber analysis on the so-called accessory subscapularis muscle and its morphological significance. *Anat Sci Int* 83: 55–59.

32 Arm muscles

Keiichi Akita and Akimoto Nimura
Tokyo Medical and Dental University, Tokyo, Japan

Coracobrachialis

This muscle generally originates from the coracoid process with the short head of the biceps brachii. Superficial and deep coracobrachialis muscles are observed in primates, and the musculocutaneous nerve runs through them. The coracobrachialis in humans is therefore considered as a compound muscle comprising two muscles (Koizumi 1989). Various authors have reported that the musculocutaneous nerve does not always traverse it (4%, Koizumi 1934; 6%, Ishimi 1950; 3.5–6.5%, Becker 1963; 4%, Koizumi 1989). In some cases, the superficial part of the muscle is completely separated from the deep part by this nerve (10%, Koizumi 1934; 16%, Ishimi 1950).

The superficial and deep layers of the coracobrachialis can be separated as follows (Mori 1964): (1) the muscle is completely separated into superficial and deep layers in 16%; (2) it is incompletely separated into layers in 8%; and (3) it shows no signs of separation in 76%.

The proximal region of the deep part of the muscle occasionally inserts into the surgical neck of the humerus or the capsule of the shoulder joint, in which case it is recognized as an accessory head (the coracobrachialis superior or brevis). The coracocapsularis (Wood 1864) originates from the coracoid process and inserts into the shoulder capsule. The distal portion is sometimes extended to form the coracobrachialis inferior or longus (Wood 1864). This portion is sometimes attached to the medial intermuscular septum and/or even to the medial epicondyle (El-Naggar and Al-Saggaf 2004; Potu et al. 2008). The muscle is sometimes connected to the brachialis muscle or the medial head of the triceps brachii. It is sometimes fused with the brachialis, and a muscle bundle can adjoin the medial head of the triceps brachii (Gupta et al. 2012). An accessory muscle, the coracobrachialis accessorius, originates from the posterior margin of the coracoid process and inserts into the tendinous part of latissimus dorsi (the coracobrachialis minor or secundus (Gruber), the cracobrachialis brevis s. rotator humeri (Wood 1864), le court coracobrachialis (Cruveilhier)). In some cases the coracobrachialis is absent (Nishi 1952). The deep layer of the coracobrachialis can originate from the insertion of the pectoralis major (Mori 1964).

The coracobrachialis is generally innervated by the musculocutaneous nerve. It is subdivided into three parts according to the innervating branches (Koizumi 1989): (1) the part innervated by branches arising from the main trunk of the musculocutaneous nerve; (2) the part innervated by branches arising from the lateral cord of the brachial plexus running ventral to the main trunk; and (3) the part innervated by branches arising from the lateral cord of the brachial plexus running dorsal to the main trunk.

Biceps brachii

This muscle is usually composed of the long head and short head. The long head originates from the supraglenoid tubercle of the scapula and the short head from the tip of the coracoid process of the scapula. The biceps brachii muscle is very variable. There is sometimes a humeral head in addition to the normal two heads. The most common slip arises from the ventral surface of the humerus around the insertion of the coracobrachialis. Additional heads can also originate from the tendon of the pectoralis major muscle and the capsule of the shoulder joint. A biceps with more than two heads reportedly occurs in about 8% of Chinese, 10% of white Europeans, 12% of black Africans, and 18% of Japanese (Kudo and Bando 1956), or in about 14% of Chinese 18% of white Europeans, 13% of black Africans, and 18% of Japanese (Nishi 1952). Occasionally there are three additional accessory slips, which can appear singly or in combination so that the muscle can appear to have three, four, or five heads. A third head is reported with various frequencies: 14.2% (Koganei et al. 1903); 20.6% (Adachi 1909/1910); 26% (Koizumi 1934); 20% (Ishimi 1950); 13.1% (Kosugi et al. 1985); and 23.0% (Higashi and Sone 1988). A fourth head is found in around 1–4% (Adachi 1909/1910; Tamura 1971; Higashi and Sone 1988), and fifth and sixth heads are rare (Higashi and Sone 1988). When additional heads are fully developed they arise close together from the neck of the humerus, below the lesser tubercle and the tendon of the pectoralis major. A third head of the biceps brachii is found in 20% (Mori 1964).

Bergman's Comprehensive Encyclopedia of Human Anatomic Variation, First Edition. Edited by R. Shane Tubbs, Mohammadali M. Shoja and Marios Loukas.
© 2016 John Wiley & Sons, Inc. Published 2016 by John Wiley & Sons, Inc.

The origins of the additional heads are reported (if present) as: (1) the distal portion of the deltoid tuberosity in 8%; (2) the area near the insertion point of the coracobrachialis in 6%; and (3) the tendon of the pectoralis major in 4% (Mori 1964). The tendon of the long head of the biceps brachii is sometimes separated, and these origins are separately attached to the supraglenoid tubercle and the posterosuperior capsulolabral tissue (Hyman and Warren 2001; Enad 2004). In addition, many reports have described variations (Curnow 1873; Macalister 1875; Meyer 1914; Miura 1956; Ohki et al. 1958; Takeshige et al. 1960; Kosugi et al. 1992; Asvat et al. 1993; Nakatni et al. 1998; Santo Neto et al. 1998; Dirim et al. 2008; Poudel and Bhattarai 2009).

The long head is sometimes less developed or absent. In these specimens, the tendon can arise from the bicipital groove, the greater tubercle, the lesser tubercle, the capsule of the joint, or the tendon of the pectoralis major. An accessory slip may arise from the deltoid muscle. The short head can also be less developed or absent.

The muscle generally inserts onto the tuberosity of the radius and the fascia of forearm. At its distal end, various muscular or tendinous slips have been reported. The slips connect with the lower end of the humerus, ulna, radius, antebrachial fascia, or neighboring muscles. Such supernumerary slips can be divided from the brachialis, the brachioradialis, or the humeral head of the pronator teres. An additional slip can also arise from the medial border of the biceps muscle. Absence of the biceps brachii has been reported (Nishi 1952).

The musculocutaneous nerve is sometimes absent or fused with the median nerve; in such individuals the coracobrachialis and the biceps brachii are innervated by branches of the median nerve (Koizumi 1989), and supernumerary heads of the biceps brachii can occur (Ferner 1938; Serizawa et al. 1978; Watanabe et al. 1985; Higashi and Sone 1988).

Brachialis

This muscle generally originates from the ventral surface of the distal half of the humerus. It is frequently subdivided into two or more parts and is sometimes absent (Wood 1866; Macalister 1875). It tends to be subdivided into lateral and medial parts or into superficial and deep parts. It can also be joined with the fibers of adjacent muscles. A third and/or fourth head of the biceps brachii may fuse with the brachialis (Machida 1961). The medial part of the origin of the brachialis can fuse with the insertion of the coracobrachialis, and its lateral part can partly fuse with the brachioradialis or the extensor carpi radialis (Machida 1961; Wood 1864, 1867, 1868; Vadgaonkar et al. 2010). The brachiofascialis (Wood 1864) is a slip from the biceps brachii running to insert into the deep fascia over the pronator teres muscle (Reid and Taylor 1879). Anterior interosseous nerve syndrome can be caused by a fibrous band arising from the deep fasciae of the brachialis and the pronator teres (Hill et al. 1985).

The muscle generally inserts into the coronoid process and the tuberosity of the ulna. When the muscle is divided, the distal insertions can be variable. The insertion parts can also be attached to the radius, a tendinous band between the radius and the coronoid process, or the fascia of the forearm. The insertion part also joins the forearm muscles originating from the medial epicondyle. A deep muscular part of the brachialis can attach to the capsule of the elbow joint and is called the capsularis subbrachialis or the artecularis cubiti anterior (Nishi 1966).

The brachialis muscle is generally innervated by the musculocutaneous nerve. However, in more than 50% of specimens, it is also innervated by the radial nerve and sometimes by the median nerve (Ouchi and Kasai 1953; Kasai and Hirai 1959; Machida 1961; Ip and Chang 1968). According to Machida (1961) it is innervated by (1) only the muculocutaneous nerve (6%); (2) the musculocutaneous nerve and the radial nerve (54%); (3) the musculocutaneous nerve, the radial nerve, and the median nerve (32%); and (4) the musculocutaneous nerve and the median nerve (8%). In all cases where there is innervation by both the musculocutaneous and the radial nerves, nervous branches are connected to each other within the muscle.

Macalister (1875) reported the following variations of the biceps brachii:

1. The muscle can be entirely absent.
2. The short head can be absent.
3. The long head was found to be deficient by Otto, Lauth, Henle, Hyrtl, and Macalister.
4. The lacertus fibrosis was found to be absent (Macalister).
5. The radial insertion was found to be absent von Haller (1768).
6. Variation (5), with an insertion into the elbow capsule and the coronoid process, was found by Gruber in a case of a congenitally absent radius.
7. The two heads are separate for the entire length of the muscle (Macalister); a similar case was reported by Stephanus and Riverius (1545); in another case the muscle was split for three-quarters of its course.
8. The long head was found doubled by Moser.
9. The long head can arise from the capsular ligament.
10. The long head can arise from the bicipital groove.
11. A doubled coracoid head was described by Wood (1864) and by Macalister.
12. This variable portion can join the main body of the muscle, or it may unite with the normal coracoid head before that portion of the biceps joins the long head.
13. An extension of the coracoid part of the coracoacromial ligament was found six times by Macalister.
14. Macalister reported a slip to the short head from the insertion tendon of pectoralis minor.
15. The most common of all variations of this muscle is the occurrence of a third head, and the most common third head arises from the interval between the coracobrachialis and brachialis.

16. Macalister found a third head arising directly from the brachialis, which crossed the brachial artery.
17. A separate slip from coracobrachialis continuous with the short head was described by Wood and Macalister.
18. A humeral head starting from the insertion of coracobrachialis was reported by Macalister.
19. A third head arises between the insertion of the deltoid and the origin of supinator longus (brachioradialis).
20. This has been found as a separate muscle, distinct for its whole length as far as its insertion from the biceps, and described with the brachioradialis by Gruber (1866), Theile, Hyrtl, and Wagner; Wood and Pietsch described it as imperfectly separate.
21. A head as in (19) above but continuous with the deltoid was found by Macalister.
22. In another similar case, Macalister found the usual long head absent.
23. The same variation can join the supinator longus (brachioradialis) instead of the deltoid.
24. A variant of an internal third head (15) was described by Hyrtl where the accessory part arose from the medial intermuscular septum.
25. An instance of the origin of the long tendon of the biceps from the tendon of pectoralis major was described by Koster.
26. A third head from the greater tuberosity was described by Meckel.
27. The long head can attach to the greater tuberosity of the humerus.
28. von Haller (1768) described a third head arising from the outer margin of the bicipital groove by a tendon.
29. Macalister found an accessory third head arising from the upper border of the pronator teres and inserted with the biceps.
30. A series of four heads was found by Macalister; in this case, a typical third humeral origin head coexisted with a head from the greater tuberosity similar to (26).
31. Wood (1864) found a four-headed muscle in which the lateral and humeral origins coexisted; see (15) and (19).
32. Another quadricipital arrangement was seen by Macalister, where the short head was doubled, and the medial humeral head (15) coexisted with the greater tuberosity head (26) but without the long tendon.
33. Henle found a quinqueceps (five-headed) variant with the normal heads and the third humeral head coexisting with one from the deltoid, and a fifth from the middle of the bicipital groove as high as the tendon of the pectoralis major.
34. In another four-headed biceps found by Macalister, the two normal heads and the medial humeral coexisted with an origin from the outer (lateral) lip of the bicipital groove.
35. Among the unusual insertions, Macalister noted a slip from the lateral head inserted separately into the radius.
36. A normal-arising biceps was seen by Wood (1864) to have three insertions: a normal outer portion, giving off a radial tendon and a superficial semilunar fascia; a middle smallest portion inserted into the fascia, over the supinator and the bursa of the radial tuberosity; and the inner division, which ended in a strong trifurcating tendon, sent a slip to the coronoid origin of the pronator teres (one into the coronoid insertion of the brachialis and one into the coronoid attachment of the flexor digitorum superficialis).
37. Kelly found a small tendon detached from the lower end of the biceps, giving origin to part of the flexor carpi radialis.
38. A slip from biceps to the internal intermuscular septum was described by Quain.
39. Kelly reported a tendinous slip arising from the long head of an otherwise normal biceps. Becoming fleshy, the slip was inserted at the lowest part of the antecubital fossa by three tendons: one into the fascia over the brachioradialis; a second into the semilunar fascia; and the third dipped into the bottom of the fossa between the pronator teres and the supinator muscle.
40. In a somewhat similar case to (39), the muscle was inserted by two slips: one into the bursa over the tubercle of the radius under the normal tendon, and the other into the coronoid process.
41. Another and larger accessory biceps muscle was described by Pietsch, which arose from three heads: one from the lateral side of the humerus; one from its medial side; and one from the short head of the biceps itself. These three were inserted by a separate tendon into the radius at its tubercle behind the ordinary biceps tendon.
42. Macalister reported a slip from the biceps to brachialis, running downward and a little inward.
43. Theile described a tricipital muscle in which there were two coracoid heads and a slip from the capsular ligament with no long head.
44. Macalister found one biceps, which inserted by four slips (as well as the normal insertion) into the internal (medial) brachial ligament, the capsule of the elbow joint, the coronoid process, and the pronator teres.
45. A slip arising from the biceps and crossing the brachial artery is sometimes traceable down as far as the fascia over the pronator teres, and was described by Struthers as a "brachio-fascialis."
46. Macalister saw a simple fascicle of the biceps inserting into the origin of the pronator teres three times. Gruber found in a case of deficient radius a biceps possessing a weak coracoid head, two humeral origins, and two insertions (one radial and one ulnar).

Triceps brachii

The triceps brachii muscle generally arises by three heads. The tendinous long head originates from the infraglenoid tubercle of the scapula and the glenoid labrum. All three heads are inserted together by a broad tendon into the posterior part of

the proximal surface of the olecranon of the ulna. The fleshy lateral and medial heads originate from the dorsal surface of the humerus. There are sometimes abnormal muscle bundles, which originate from the tendon of the latissimus dorsi and insert into the brachial fasciae, the olecranon of the ulna, or the lateral epicondyle of the humerus. These supernumerary muscle bundles are recognized as the dorsoepitrochlearis, the latissimocondyloideus, or the accessorium tricipitis (Tountas and Bergman 1993). They are common among anthropoids. There is usually a tendinous connection between the long head and the tendon of the latissimus dorsi (Koizumi 1934; Ishimi 1950). The proximal end of the lateral head is usually located more proximal to that of the medial head. However, the proximal end of the medial head can exceptionally be extended proximal to that of the lateral head (2%, Koizumi 1934). The fibers of the long head can sometimes extend to the capsule of the shoulder joint, or distally to the lateral border of the scapula, and are longer than usual. The long head can originate from only the capsule of the shoulder joint (Ishimi 1950). It can be divided into two parts (Ishimi 1950). There is sometimes an anomalous muscular fascicle between the lateral and long heads of the triceps (Prabhu et al. 2012). The medial head sometimes extends over the ulnar groove. The deep layer of the triceps brachii can be attached to the capsule of the elbow joint, in which event it is recognized as the articularis cubiti or the subanconeus muscle (Tubbs et al. 2006).

The epitrochleoanconeus (the epitrochleo-olecranonis, the epitrochleocubital, the artecularis cubiti posterior (Nishi 1966), or the anconeus sextus) originates from the medial epicondyle and inserts to the olecranon of the ulna. This abnormal muscle bundle is observed in 5% of cases (Mori 1964). It can often be recognized as a part of the triceps brachii. However, it extends over the groove for the ulnar nerve, which usually innervates it. It should therefore be recognized as a variant muscle bundle of the flexor carpi ulnaris (Inoue 1934). The triceps brachii and epitrochleoanconeus can be fused with the anconeus.

The triceps brachii is generally innervated by the radial nerve. Sometimes, its medial head is also innervated by branches of the ulnar nerve (21%, Fuchino 1960).

Macalister (1875) described the following variations of the triceps brachii. A fourth head arises from the medial part of the humerus by a long, slender tendon and by an aponeurotic expansion from the capsule of the shoulder; this head blends with the medial head. The long head is frequently split, one part attached to the capsule and the other to the spine or axillary border of the scapula; or the first slip splits the capsular ligament. A slip from the tendon of the latissimus dorsi has been seen several times. This slip is the remains of the tricipiti accessorius or the dorsiepitrochlearis.

Macalister also reported a tendon of union for the lower border of the latissimus dorsi to the long head; a fleshy slip of connection from the costal fibers of latissimus dorsi into the same part of the triceps; the triceps occasionally attaching to the anconeus; a slip from the long head up to the coracoid process; a slip from the subscapularis; a small slip connected to the capsule of the shoulder has been seen, continuing up to the upper portion of the glenoid cavity; a doubled fourth head, one from the coracoid process and one from the capsule of the shoulder; fusion of the lateral head with the origin of the extensor carpi ulnaris (there can be a second lateral head); a slip from the long head, the anconeus quintus, which is present in 5% of bodies, joining the latissimus dorsi; an accessory or fourth head arising from the medial aspect of the humerus above or near the deep head and inserting at the axillary border of the scapula, the tendon of the latissimus dorsi, from the coracoid process, or even the capsule of the shoulder joint; occasionally the medial head of the triceps extending distally to form an arch across the ulnar groove; and finally, the tendon of insertion of the triceps brachii can contain a sesamoid bone, the patella cubiti (sesamum cubiti or "elbow disk").

The epitrochleo-olecranonis (epitrochleoanconeus, epitrochleocubital, or anconeus sextus (Gruber)), a muscle distinct from the triceps, extends from the medial epicondyle of the humerus and arches across the groove for the ulnar nerve to insert on the olecranon process. It occurs in no more than about 25% of bodies and takes the place of the fibrous arch normally passing between the epicondylar and ulnar heads of the flexor carpi ulnaris. Mori found this muscle in 5% of 96 arms. The triceps brachii and epitrochleo-olecranonis can be fused with the anconeus.

Anconeus

The anconeus generally originates from the posterior surface of the lateral epicondyle of the humerus. If present, it is usually blended with the triceps brachii and there is seldom a clear border between the anconeus and the medial head. It is also fused in various degrees with the extensor carpi ulnaris or the epitrochleoanconeus (see the section on triceps brachii).

The anconeus is generally innervated by the radial nerve branch to the medial head of the triceps brachii, and therefore can be considered as a division of the triceps brachii.

References

Adachi B. 1909/1910. Beiträge zur Anatomie der Japaner. Die Statistik der Muskelvarietäten. *Zeieschrift für Morphologie und Anthropologie* 12: 261–312.

Asvat E, Candler P, Sarmiento E. 1993. High incidence of the third head of biceps brachii in South African populations. *J Anat* 182: 101–104.

Becker AE. 1963. Variation of the M. coracobrachialis. *Acta Morphol Neerl Scand* 5: 217–220.

Curnow J. 1873. Notes of some irregularities in muscles and nerves. *J Anat Physiol* 7: 304–309.

Dirim B, Brouha SS, Pretterklieber ML, Wolff KS, Frank A, Pathria MN, Chung CB. 2008. Terminal bifurcation of the biceps brachii muscle and tendon: anatomic considerations and clinical implications. *AJR Am J Roentgenol* 191: W248–255.

El-Naggar MM, Al-Saggaf S. 2004. Variant of the coracobrachialis muscle with a tunnel for the median nerve and brachial artery. *Clin Anat* 17: 139–143.

Enad JG. 2004. Bifurcate origin of the long head of the biceps tendon. *Arthroscopy* 20: 1081–1083.

Ferner H. 1938. Der Nervus musculocutaneous, seine Verlaufsvarietäen am Oberarm und deren Beziehung zur Entwicklung eines Capt tertium musculi bicipitis. *Z Anat Entwickl–Gesch* 108: 567–586.

Fuchino K. 1960. Studies on muscles of the upper arm and forearm of the Japanese. Studies on the nerve distribution of the muscles of the upper arm. *Med J Kagoshima Univ* 12: 7–31.

Gruber W. 1866. Über den Musculus epitrochleo-anconeus des Menschen und der Säugethiere. *Mem. de l'Acadèmie Impèriale des Sciences de St Petersbourg* 10: 1–26.

Gupta G, Singh K, Chhabra S, Srivastava SK, Gupta V. 2012. Accessory coracobrachialis: a case report with its morphological and clinical significance. *Surg Radiol Anat* 34: 655–659.

Higashi N, Sone C. 1988. A study on the accessory head of the biceps brachii in man. *Acta Anat Nippon* 63: 78–88.

Hill NA, Howard FM, Huffer BR. 1985. The incomplete anterior interosseous nerve syndrome. *J Hand Surg A* 10: 4–16.

Hyman JL, Warren RF. 2001. Extra-articular origin of biceps brachii. *Arthroscopy* 17: E29: 1–2.

Inoue R. 1934. Relationship among muscles, blood vessels and nerves of forearm in Japanese. *Acta Anat Nippon* 7: 1155–1207.

Ip MC, Chang KSF. 1968. A study on the radial supply of the human brachialis muscle. *Anat Rec* 162: 363–370.

Ishimi S. 1950. Studies on the musculacture of the upper extremities of the Japanese fetus. Report on the muscles of the brachium. *Igaku Kenkyu* 20: 766–778.

Kasai T, Hirai S. 1959. The nerve distribution of the brachial muscle – composition of the diploneural muscle. *Acta Anat Nippon* 34: Appendix 12.

Koganei Y, Arai, S, Shikinami S. 1903. Statics of anomaly muscles. *Tokyo J Med Sci* 17: 127–131.

Koizumi K. 1934. Studies on the sholder and brachial muscle. *JNMS* 5: 1063–1083.

Koizumi M. 1989. A morphological study on the coracobrachialis muscle. *Acta Anat Nippon* 64: 18–35.

Kosugi K, Kounoda M, Kageyama I, Fukushima O, Hayakawa T. 1985. Anatomical study of the supernumerary head on the biceps brachii muscle. *Jikeikai Med J* 100: 641–650.

Kosugi K, Shibata S, Yamashita H. 1992. Supernumerary head of biceps brachii and branching pattern of the musculocutaneous nerve. *Surg Rad Anat* 14(2): 175–185 (in Japanese).

Kudo K, Bando K. 1956. Varietäten-Statistik des M. biceps brachii beim nordchinesischen Weibe. *Okajimas Folia Anat Jap* 28: 299–301.

Macalister A. 1875. Observations on muscular anomalies in the human anatomy. (Third series with a catalogue of the principal muscular variations hitherto published.) *Trans R Irish Acad Sci* 25: 1–130.

Machida N. 1961. Studoj pri la double nervoprovizitaj muskoloj će homa supra membro: La braka muskolo. *J NUMA* 20: 7–16.

Meyer AW. 1914. Spolia Anatomica. *J Anat Physiol* 48: 107–160.

Miura Y. 1956. Anatomical studies on the variations of the M. biceps brachii. *Tokyo Jikeikai Ikadaigaku Kaibogaku Kyoshitsu Gyosekishu* 14: 5–20 (in Japanese).

Mori M. 1964. Statistics on the musculature of Japanese. *Okajimas Fol Anat Jap* 40: 195–300.

Nakatani T, Tanaka S, Mizukami S. 1998. Bilateral four-headed biceps brachii muscles: The median nerve and brachial artery passing through a tunnel formed by a muscle slip from the accessory head. *Clin Anat* 11(3): 209–212.

Nishi S. 1952. Miologio de la Japano. Statistika raporto pri muskolanomalioj ĉe jaoanoj. II. Muskoloj de malsupra membro. *Gumma J Med Sci* 2: 1–13.

Nishi S. 1966. Kelkaj Muskolvarioj Ĉirka Ŭ La Kubutartiko. *Acta Anat Nippon* 41: 246.

Ohki T, Abe Y, Sekisawa G. 1958. On the supernumeral heads of the M. biceps brachii. *Iwate Ikadaigaku Kaibogakukyoshitsu Gyosekishu* 5: 93–97 (in Japanese).

Ouchi H, Kasai T. 1953. Distribution of inner nerves in brachialis. *Acta Anat Nippon* 28: Appendix 7.

Potu BK, Rao MS, Nayak SR, Vollala VR, Mandava AK, Thomas H. 2008. Variant insertion of coracobrachialis muscle in a South Karnataka cadaver. Cases Journal I: 291.

Poudel PP, Bhattarai C. 2009. Study on the supernumerary heads of biceps brachii muscle in Nepalese. *Nepal Med Coll J* 11: 96–98.

Prabhu LV, Asif M, Murlimanju BV, Anup Rao K, Shivaprakash S. 2012. Anomalous fascicle of triceps brachii muscle and its clinical importance in relation to radial nerve entrapment. *Clin Ter* 163: 123–124.

Reid RW, Taylor S. 1879. Anatomical variations. Reports St Thomas's Hospital 9: 46–47.

Santo Neto H, Camilli JA, Andrade JC, Meciano Filho J, Marques MJ. 1998. On the incidence of the biceps brachii third head in Brazilian white and blacks. *Anat Anz* 180(1): 69–71.

Serizawa M, Hagura N, Eto M. 1978. On the third head to the biceps brachii muscle and its relation to the lateral cutaneous nerve of the forearm. *Dokkyo J Med* 5: 303–312.

Stephanus C, Riverius S. 1545. *De dissection partium corporis humani*. Paris: Apud Simoneum Colinzeum.

Takeshige A, Miyazima S, Minakawa T, Hayashida T, Nakamura K. 1960. Variation of the M. biceps brachii. *Kurume Igakkai Zasshi* 23: 865–868 (in Japanese).

Tamura H. 1971. A case of the brachial biceps with the two accessory heads bilaterally. *Acta Anat Nippon* 46: 12–16.

Tountas CP, Bergman RA. 1993. *Anatomic Variation of the Upper Extremity*. New York: Churchill Livingstone.

Tubbs RS, Oakes WJ, Salter EG. 2006. The subanconeus muscle. *Folia Morphol (Warsz)* 65 (1): 22–5.

Vadgaonkar R, Rai R, Nayak SR, D'Costa S, Saralaya V, Dhanya. 2010. An anatomical and clinical insight on brachialis with emphasis on portal's muscle. *Romanian J Morph Embryol* 51: 551–553.

Von Haller A. 1748. *Operum Anatomici Argumenti Minorum*. Lausanne: Francisci Grasset & Socier.

Watanabe M, Tkatsuji K, Sakamoto N, Morita Y, Ito H. 1985. Two cases of fusion of the musculocutaneous and median nerves. *Acta Anat Nippon* 60: 1–7.

Wood J. 1864. On some varieties in human myology. *Proc Roy Soc Lond B* 13: 299–303.

Wood J. 1866. Variations in human myology observed during the winter session of 1865–1866 at King's College, London. *Proc Royal Soc London* 15: 229–244.

Wood J. 1867. On human muscular variations and their relation to comparative anatomy. *J Anat Physiol* 1: 44–59.

Wood J. 1868. Variations in human myology observed during the winter session of 1867–68 at King's College, London. *Proc Roy Soc Lond B* 17: 483–525.

33 Forearm muscles

Keiichi Akita and Akimoto Nimura
Tokyo Medical and Dental University, Tokyo, Japan

Pronator teres

An extension of the origin of this muscle in a proximal direction, to a supracondylar process or to a ligament that connects it to the medial epicondyle, has been reported. In such cases the course of the brachial artery is usually changed; accompanied by the median nerve, it passes behind the process, deep to the accessory portion of the muscle, and reaches the antecubital space. When the bifurcation of the brachial artery is high, it is usually the ulnar artery that passes deep to the process or ligament (of Struthers). Even in the absence of a supracondylar process, an accessory bundle or head can arise from the median intermuscular septum, humerus, fascia of the arm, or adjacent muscle. The coronoid head is absent in 3% or rudimentary in 6% (Inoue 1934). The two heads of the muscle can be completely separated, and the coronoid and the humeral heads can also be divided (Macalister 1875b). Many muscular variations have been reported (Barrett 1935; Giannelli 1899; Ishimi 1951; Macalister 1875a, b).

Possible positional relationships between the median nerve and the pronator teres are: (1) the median nerve passes between the humeral and ulnar heads of the muscle in 95% in cases; (2) the nerve passes between the muscle and the flexor digitorum profundus in 0.25% of cases; and (3) the nerve passes through the humeral head in 0.25% of cases (Mori 1964). Variations among the blood vessels, nerves, and the muscle have been reported (Bianchi 1906; Inoue 1934).

The radial insertion is sometimes more extensive than usual (Ishimi 1951). In addition, the insertion of the pronator teres can send a slip into the radial origin of the flexor digitorum superficialis (Macalister 1875a, b). Fasciculi can also extend to the long flexor of the thumb.

Macalister reported the following variations for this muscle:

1. It can be split into separate coronoid and condyloid muscles for its entire length (Albinus).
2. The coronoid head can be absent.
3. The two heads can be separated for their entire length but insert in common.
4. There is doubled coronoid head, the second lying posterior to the artery (Macalister 1868). Kelly found a similar muscle but both heads were posterior to the median nerve.
5. The coronoid head was twice found attached to brachialis anticus (brachialis).
6. The coronoid head can attach to the palmaris longus (instead of the pronator).
7. A single slip from the coronoid process can give origin to two slips, one of which goes into the pronator and the other to the flexor carpi radialis.
8. An accessory medioulnar origin was found by Brugnone.
9. The condyloid origin has been found with a sesamoid bone in it, with an accessory origin from the semilunar fascia of the biceps, or with an accessory slip from brachialis anticus (brachialis).
10. Macalister (1866) once found a triple origin: one head from the biceps tendon, between its usual tendon and its semilunar fascia; one from the humerus from about three and a half inches above the condyle to about an inch and a half above it; and one (a short narrow tendon) from the tip of the medial condyle.
11. A high origin, like the second head of the previous variation, was reported by Struthers, and was nearly separate throughout its length from the rest of the muscle.
12. A case of the humeral head not detached was described by Nuhn.
13. A more complex case of high origin is described by Hyrtl, in which there was one origin from the intermuscular ligament, one from the medial condyle, and one from the humerus at the intersection of coracobrachialis, lying over the brachialis-anticus.
14. A high humeral origin has been found to coexist with a supracondyloid process of the humerus by Gruber, Struthers, Schwegl, and Voss of Christiania (Oslo); in the latter case an additional humeral head lay above the supracondylar process.
15. Macalister found the insertion of the pronator teres sending a slip into the radial origin of the flexor sublimis (flexor digitorum superficialis).

Bergman's Comprehensive Encyclopedia of Human Anatomic Variation, First Edition. Edited by R. Shane Tubbs, Mohammadali M. Shoja and Marios Loukas.
© 2016 John Wiley & Sons, Inc. Published 2016 by John Wiley & Sons, Inc.

Flexor carpi radialis

At its origin, the flexor carpi radialis can receive an additional slip from the tendon of insertion of the biceps brachii or its tendinous extension, the brachialis, the coronoid process of the ulna, or the anterior oblique line on the radius (accessory muscle of Calori) (Carleton 1934).

Its insertion is subject to frequent variations, the most common being partial or total attachment to the trapezium. In an embryonic study, all cases were partly inserted into the trapezium (Ishimi 1951). It can also be partly inserted into the flexor retinaculum or navicular bone, and sometimes a supplementary slip to the third metacarpal is extended to the fourth.

A small muscle originating from the radius usually inserts on the fibrous sheath of the tendon of the flexor carpi radialis. This muscle terminates distally to the base of the second or third metacarpal bone (Gruber 1872a, b; Wood 1867a). The terminal tendon is inserted into the second metacarpal in 90% of cases, sends a slip to the third metacarpal in 7.5%, and was absent in 2.5% (Mori 1964). The small muscle, which originates proximal to the proximal end of the insertion of the pronator teres, is called the flexor carpi radialis profundus. The muscle that originates distal to the end is called the flexor carpi radialis brevis. The flexor carpi radialis is sometimes doubled and sometimes absent. Muscular variations have also been reported (Macalister 1868, 1875c; Ito et al. 1981; Yoshida et al. 1983; Saadeh et al. 1990; Spinner 1970).

Macalister reported the following variations for this muscle.

1. With a triple origin, one head came from a slip of the biceps tendon and one from the deep surface of the semilunar fascia (this head was separated from the second or usual head by the median nerve), and the third head was from the ulna, below the coronoid process, and was likewise separated from the foregoing by the median nerve.
2. The radial head of this muscle was joined to the radial origin of the flexor sublimis.
3. A coronoid head was observed in which the pronator teres had no such slip.
4. Macalister found a coronoid head in common in one instance; in both these cases the coronoid was separated from the condyloid origin by the median nerve, and in the former case by the brachial artery. In another example of (3) which Macalister observed in 1868, the nerve alone separated the parts.
5. A case of second head from a special slip of the biceps tendon (Kelly).
6. The muscle was inserted in whole or in part into the trapezium as described by Albinus, Fleishmann, Loschge, Hyrtl, Wood, Theile, Henle, and Macalister; into the anular ligament and scaphoid as described by Fleishmann; into the bases of the third and fourth metacarpals; and into the scapho-trapezium bone in a case in which only a thumb and two fingers were present, described by Friedlowsky (1869).

Palmaris longus

This is probably the most variable muscle in the body. It is absent in about 20% of bodies (white), 4% (black), and 4% of Japanese (Adachi 1909–10). The palmaris longus is absent more often in the female and on the left side in both sexes. There have been many reports of its rates of absence (Inoue 1934; Takeda et al. 1955; Hojo 1976; Suzuki 1955, 1957).

It can be digastric or fleshy throughout its entire length. It can have a proximal tendon as well as a distal one; it can be fleshy distally and tendinous proximally (palmaris longus inversus), or it can be reduced to a mere tendinous band. Occasionally, there are two palmaris longus muscles, one having the normal form and the other having one of the forms referred to previously. Alternatively, the second can arise from the medial intermuscular septum, the biceps or brachialis, the fascia of the forearm proximally or one of the neighboring muscles, the coronoid process or the radius. It can be doubled at its proximal end, the additional slip arising from one of the sites just indicated.

The insertion is equally variable. It can be attached to the fascia of the forearm, the tendon of the flexor carpi ulnaris, the flexor retinaculum, the pisiform bone, the scaphoid bone, the short abductor of the thumb, the fascia and muscles of the hypothenar eminence, one of the flexor tendons, or near the metacarpophalangeal joint. A doubled distal insertion is known as the palmaris longus bicaudatus of Gruber. If the palmaris longus is absent, the palmar aponeurosis should not be absent. In these cases, the palmar aponeurosis is connected with the flexor retinaculum and the tendons of the flexor digitorum superficialis and the flexor carpi radialis (Eguchi and Shima 1959; Takeuchi and Noda 1961).

There have been numerous variations of the palmaris longus reported (Gruber 1868, 1872c, d; Krueg 1872; Macalister 1875b; Schaeffer 1909; Morrison 1916; Thompson et al. 1921; Nakano 1922; Nikolajew 1932–33; Reimann et al. 1944; Pales 1946; Madsen 1947; George 1953; Bigot 1954; Stewart 1954; Moriya 1956; Gaillard 1958; Ikeda et al. 1958; Suzuki et al. 1958; Nakano and Matsumoto 1959; Ashby 1964; Mori 1964; Feret et al. 1965; Jeffery 1971; Roberts 1972; Still and Kleinert 1973; Carr et al. 1977; Brones 1978; Stark et al. 1979; Carroll and Montero 1980; Dorin and Mann 1984; Saadeh and Bergman 1986; Cassell and Bergman 1990; Celik et al. 1996; Ari et al. 1997; Claassen et al. 2013).

The palmaris profundus arises from the lateral edge to the middle of the anterior surface of the radius in its middle third, external to flexor digitorum superficialis and deep to pronator teres. Its tendon passes beneath the flexor retinaculum and broadens in the palm to insert into the deep side of the palmar aponeurosis. The abnormal muscle can cause compressive neuropathy of the anterior interosseous nerve and the median nerve in the distal forearm and wrist. It has been described in many reports (Dyreby and Engber 1982; Fatah 1984; Floyd et al. 1990; King and O'Rahilly 1950; Lahey and Aulicino 1986; Meyer and Pflaum 1987; Sahinoglu et al. 1994; Schlafly and Lister 1987; Takisawa et al. 1979; Yoshida et al. 1984).

Flexor carpi ulnaris

Because its two heads are completely independent and are usually supplied by the ulnar nerve, it has been suggested that this muscle is formed of two fused elements. An additional slip of origin from the medial side of the coronoid process is often present. Partial insertion into the flexor retinaculum has been recorded and its attachment to the fifth metacarpal can extend to the fourth or even to the third metacarpal by the radial expansion of a pisimetacarpal band of fibers. Extension of these fibers to the capsule of the fifth metacarpophalangeal joint has been observed (see the section on pronator quadratus). The occurrence of a slip connecting the tendon with the abductor of the little finger has also been reported.

Variations of this muscle have been described (Jansen 1850; Wood 1866; Calori 1868; Curnow 1873; Macalister 1875c; Gruber 1881b; Hirasawa et al. 1979).

The epitrochleoanconeus is a small anomalous muscle closely associated with the flexor carpi ulnaris (see also the section on triceps brachii in Chapter 32). It arises from the posterior surface of the medial epicondyle of the humerus and is inserted into the olecranon process. It is superficial to the ulnar nerve from which it receives its innervation, and takes the place of the fibrous arch of deep fascia usually found in the same location. The muscle appears to be normally present in other mammals, but only in about 25% (Galton 1875) or 3% (Inoue 1934) in humans.

Variations of flexor carpi ulnaris reported by Macalister include having an origin from the triceps; with a slip to the fourth metacarpal bone; or having a slip to the anular ligament, without or with a coexisting palmaris longus. The latter form was seen by Harrison and Macalister and the former was seen by Winslow and also by Macalister. In a case described by Koster, the flexor carpi ulnaris was inserted into the interosseus membrane. Friedlowsky described a muscle that sent a slip into the anular ligament, and the palmaris longus was suppressed.

Flexor digitorum superficialis

The flexor digitorum superficialis is formed from two heads: humeroulnar and radial. This muscle has a very complicated structure and is generally composed of two planes: superficial and deep. The superficial plane is divided into two parts, which end in tendons for the middle and ring fingers. The deep plane is also divided into two parts, which terminate at the index and little fingers.

Some reported variations in this muscle seem to represent remnants of connections between the two planes of muscle. These types of variations have been considered retrogressive. The slips very frequently connect the superficialis with the flexor pollicis longus or flexor digitorum profundus, as muscular slips occasionally pass between the superficial and deep flexors of the fingers. Sometimes a slip derived but separated from the superficialis, or one arising directly from the coronoid process, ends on a tendon that joins one of the tendons of the deep flexor (accessorius profundus digitorum of Gantzer). Tendinous slips frequently connect the tendons of the two muscles. There are detailed reports of the connections between the superficial and deep planes (Ohtani 1979; Yamada 1986). On the other hand, the occasional separation of individual muscle bellies has been considered a progressive variation.

The extensive origin of the muscle from the radius is a human feature. The radial head is very variable. Complete absence has been recorded: it is absent in 7.5% and poorly developed in 12.5% (Mori 1964). One or more of the muscle's distal divisions, for example the radial head of the index finger, can be deficient or absent. The belly to the middle finger can be absent or reinforced by a slip from the radial tuberosity. The most common example of this is the absence of the belly for the little finger. Normally, this is the smallest division of the muscle; it arises from the side of the intermediate tendon. In the absence of the fourth belly of the muscle, its place can be taken by a muscle arising from the medial collateral ligament of the ulna, the deep flexor, the transverse carpal ligament and palmar aponeurosis or the ligament alone, or the fourth lumbrical. A slip has been seen passing from the superficial aspect of the muscle to the palmaris longus, or replacing it if absent, and ending in the fascia of the forearm or palmar aponeurosis. A slip (radiopalmaris) can arise directly from the radius beneath the sublimis and attach to the palmar aponeurosis or the common sheath of the flexor tendons.

The origin of the tendons from the flexor digitorum superficialis is somewhat variable: a slip from the deep part of the muscle sometimes forms the chief part of the ring finger division, or there can be a slip from the deep part to the middle finger tendon. The radial head sometimes supplies the tendon to the fourth digit. The tendon for the third digit arises only from the extreme radial side of the radial head and is reinforced by a tendon arising from the epicondyle. An accessory slip is sometimes present, passing from the tuberosity of the ulna to the index and middle finger portions. Another slip can arise from the muscle and attach to the tendon of the brachioradialis. Very rarely, the whole muscle is digastric. Cases have been reported in which the medial and deep tendons are replaced by a sheet of muscle (representing a second superficial flexor) and in which the tendon has failed to divide within the flexor sheath. An anomalous muscle (palmar flexor digitorum superficialis accessorius) can arise from the palmar fascia and the distal border of the transverse carpal ligament and end in a tendon that joins the flexor tendon of the index finger at the level of the metacarpophalangeal joint.

Many variations of this muscle have also been reported (Wood 1866, 1867b; Macalister 1868, 1875c; Carrel 1872; Curnow 1873; Badolle 1874; Gruber 1887b; Kater 1902; Graper 1917/18; Nakano 1923; Mainland 1927; Inoue 1934; Ishimi 1950; Chowdhary 1951; Iwami 1951; Ouchi and Kasai 1953; Takeshige et al. 1959; Tountas and Halikman 1976; Cassell and Bergman 1990; Swamy et al. 2013).

The muscle is innervated by the median nerve. However, according to detailed observations of the innervating patterns, it can be derived from two different origins: the proximal belly of the index finger is derived from the forearm muscle anlage, but the others are derived from the hand muscle anlage (Yamada 1986). Macalister (1875c) reported the following variations in the flexor digitorum sublimis (superficialis):

1. Absence of the tendon for the little finger by Wood and Macalister.
2. Suppression of the radial origin (Wood).
3. A deep slip to the anular ligament, coexisting with the palmaris longus.
4. A doubled coronoid origin: the upper slip fleshy, the lower tendinous.
5. Otto saw a slip from the insertion of the pronator teres to the radial origin.
6. From the outside of the coronoid origin a slip arose which, becoming tendinous, became the sole origin of the first lumbrical (Wood). Wood also described a case in which the lumbrical had a second usual origin, and a third instance in which a muscular slip joined this tendon to the indicial tendon of the profundus.
7. A muscular band sometimes connects the origins of the flexor sublimis and flexor pollicis longus (Wood and Macalister).
8. Turner noticed the variation in the length of the radial origin of this muscle; it ranges from half an inch to four inches.
9. In a case in which this muscle sent no tendon to the little finger, Kelly found its representative to arise from the front of the synovial sheath of the fourth perforating tendon.
10. Macalister found the index perforated flexor as a separate muscle arising from the coronoid process (also noted by Wood).
11. Macalister and Wood both found cases in which the separate muscle was digastric.
12. A similar digastric muscle, supplying both the index and middle fingers, has been described.
13. The entire muscle was found to be digastric by Dursy.
14. A separate coronoid tendon joining the radial origin was seen by Wood.
15. Wood also found a separate fusiform muscle for the little finger arising from the medial condyle of the humerus.
16. Macalister found the tendons for the index and little finger arising from a separate digastric muscle, with a condyloid and coronoid origin.
17. Wood found all the tendons connected to separate bellies: the first being digastric and condyloid, the second radial and coronoid, the third and fourth condyloid.
18. Macalister (1868) described a case in which the radial head and part of the condyloid went to the middle finger; a tendon from the muscle a few inches below the condyle (becoming fleshy) supplied the ring finger, and the remainder supplied the index and little fingers.
19. A slip from this muscle to the palmar fascia coexisting with a feeble palmaris longus was found by Rosenmüller, Wood, and Macalister.
20. Wood saw a doubled tendon for the middle digit.
21. In the absence of the little finger tendon, Wood found the perforated flexor for this finger supplied by the fourth lumbrical.
22. Macalister found the little finger slip of the flexor sublimis (superficialis) coalescing with, and not split by, the corresponding tendon of the flexor profundus.
23. Cross slips joining the muscle bundles for separate digits were found by Turner.
24. The same author reported a slip from the flexor sublimis to the medial side of the palmaris longus, crossing under that muscle, and joining the tendon of the supinator longus (the brachioradialis at the lower end of the forearm.)

Flexor digitorum profundus

The flexor digitorum profundus generally originates from the upper three-quarters of the anterior and medial surfaces of the body of the ulna and the interosseous membrane of the forearm. This muscle often originates from the proximal radius (33%: Inoue 1934; 16%: Ishimi 1951). The number of its bellies can be increased. The various ways in which the superficial and deep flexors can be united have already been noted under the m. flexor digitorum superficialis, with which the flexor digitorum profundus is fused in 11% of cases (Mori 1964). A muscular slip originating from the cronoid and running as a long tendon on one or another (usually index or middle) of the tendons of the muscle has been reported in 40% of cases (Mori 1964). The flexor digitorum profundus receives a muscular slip from the epicondyle of the humerus in 0.5% and from the flexor pollicis longus in 12.5% (Mori 1964). In addition, there is often a connection with the flexor pollicis longus, generally in the form of a slip passing to the index finger tendon of the deep flexor. The separation of the index finger tendon from the others is a distinctively human characteristic, correlated with the specialization of the index finger. The degree of freedom of the muscle varies. It can be quite independent, forming a flexor indicis profundus (Ishimi 1951; Takeuchi and Noda 1962; Winkelman 1983). There is sometimes no tendon to the middle finger.

Many reports have described the variations of this muscle (Wood 1867b, 1868; Gruber 1875b, 1886a; Macalister 1875; Dylersky 1967). The variations of the connecting muscles are well known as Gantzer's muscle (Gantzer 1813a; see m. flexor pollicis longus). Macalister reported the following variations in the flexor digitorum profundus:

1. Cleft, the flexor indicis profundus being separate (Wood).
2. An origin from the radius along the entire border of the flexor pollicis (Kelly).
3. A coronoid fasciculus of origin with the coronoid head of the sublimis (Wood).

4. In one subject a separate muscle arose from the coronoid process and received fibers from the medial part of the front of the radius. It passed beneath the anular ligament and divided into two: one to join the tendon of the flexor pollicis longus and the other the tendon of the index perforans (Wood).
5. Some of the fibers to the index finger arose from the radius (Wood).
6. Macalister saw a detached muscular slip of the profundus becoming tendinous and joining that of the sublimis or the index, in the palm, as described by Wood.
7. Wood saw the fourth lumbrical arising from a special tendon of this muscle.
8. Sömmerring found a similar slip which expanded on the synovial sheath of the tendons, giving origin to the first lumbrical.
9. A distinct pyriform muscle, arising from the coronoid process, constitutes the accessorius ad flexorem profundus of Gantzer. This can form a common coronoid origin for the flexor sublimis and profundus, or a special one for the latter. It sometimes joins the perforating tendon of the index finger (6 times in 72 subjects; Wood), the perforating tendon of the middle (8 out of 72; Wood), that of the ring finger alone (Turner), those of the ring and little (1 out of 36; Wood), that of the little finger alone (Turner), those of the index or ring fingers, or those of the index and little. Macalister saw all nine of these varieties.
10. Macalister described a pear-shaped muscle arising from the medial condyle under the flexor sublimis, which ended in a long tendon and united with the little finger slip of the flexor profundus, opposite the metacarpophalangeal articulations.
11. Methods of union between this muscle and the flexor pollicis longus are common. Macalister saw a tendon joining the indicial part of profundus with the pollicis, or another muscular slip.
12. Macalister reported a slip from the ulnar side of the flexor profundus running to join the little finger tendon of the flexor digitorum sublimis (superficialis).
13. The tendon was sometimes divided into five slips, two of which united to form the tendon for the ring finger.
14. A special head arose from the medial condyle (Theile).
15. An origin from the radius was seen by Theile, Hallett, Henle, and by Macalister.
16. In one subject the palmaris longus arose from the flexor digitorum profundus (described by Fleischmann).

Flexor pollicis longus

The flexor pollicis longus is unique to humans. In other primates there is only one common deep flexor that provides a tendon to the thumb (Homma and Sakai 1992). In some cases, this condition is exactly reproduced in humans; in others, the muscle is fused with the index tendon of the flexor digitorum profundus (as in the gorilla and chimpanzee). The belly of this muscle can be partially fused with that of the flexor digitorum profundus (Ishimi 1951). This muscle is sometimes absent (Wagstaffe 1872; Hall 1903; Usami 1987).

Fleshy slips are sometimes present uniting the belly of the flexor pollicis longus with the flexor digitorum superficialis or profundus. These muscular slips are well known as Gantzer's muscles (Gantzer 1813a, b). The frequencies of this aberrant muscle differ among races (Wood 1867a; Le Double 1897; Adachi 1909–10; Inoue 1934; Mori 1964). These, as well as humeral and coronoid heads, are indications of the original connection between the divisions of the deep flexor sheet of muscles. The accessory coronoid head is subject to some variation, occasionally being divided distally into two or three slips passing to the flexor pollicis longus, flexor digitorum profundus, flexor digitorum superficialis, or pronator teres. Gantzer's muscle originates from various sites (Mori 1964): the medial epicondyle of the humerus in 24%; the coronoid process of the ulna in 68%; and both the medial epicondyle and the coronoid process in 8%. The aberrant muscle recognized as the accessory head of the flexor pollicis longus has been reported in 55–71% of cases; however, it has also been recognized as the accessory head of the flexor digitorum profundus (Adachi 1909–10; Morimoto et al. 1993). Detailed investigations of the innervations indicate that Gantzer's muscle is closely related to the proximal belly of the index finger muscle of the flexor digitorum superficialis and the flexor digitorum profundus (Homma 1981; Yamada 1986; Kida 1988). Variations of this muscle including Gantzer's muscle have also been reported (Gruber 1872e; Macalister 1875c; Dykes and Anson 1944; Wilkinson 1953; Mangini 1960; Linburg and Comstock 1979; Malhotra et al. 1982). According to Macalister, the following variations of the flexor pollicis longus have been observed.

1. It has been seen with an accessorius ad pollicem (Gantzer), present in 40 out of 102 subjects (Wood). This can be distinct from the coronoid head of the sublimis (superficialis) or with it; and it occasionally receives a slip from the condyloid fibers of the sublimis. Macalister found Gantzer's muscle to be present in two out of every five subjects.
2. Both Macalister and Wood found the flexor pollicis longus (fpl) providing a tendon to the first lumbrical.
3. A common slip from the coronoid process was found to provide the coronoid head of the pronator teres and a fleshy belly to the flexor pollicis, deep to which a slip for the flexor sublimis arose.
4. Another common coronoid slip was found to trifurcate and terminate in the three-flexor pollicis, profundus, and sublimis.
5. A slip from the medial condyle can form an accessory head.
6. A coronoid head was found arising from the place where the second head of the pronator teres usually arises. The pronator head was absent. The slip was joined by a fasciculus from the flexor sublimis (superficialis), which passed beneath the ulnar artery and ended in the flexor pollicis.

7. A head can arise from brachialis.
8. A head can arise from the middle of the superficial layer of the pronator teres.
9. Sömmerring saw the flexor pollicis longus doubled.
10. A common condyloid head provided a slip to flexor pollicis and to the indicial slip of the flexor profundus.
11. A slip from the coronoid process was found to end in two parts: one to the pronator teres, the second forming a belly 3 inches (9.5 cm) long which ran to the flexor pollicis. In this case a separate slip went to the profundus.
12. The fpl has been seen to provide a tendon to the index finger which did not join with the indicial tendon of the flexor profundus; running separately in the sheath, it was inserted onto the ungual (distal) phalanx.
13. Cases of slips, sent from this muscle to the flexor profundus, have been described by Loschge, Wood, and Macalister.
14. An accessory muscle arose partly from the proundus and partly from the sublimis (superficialis), became tendinous just proximal to the anular ligament, and divided into two: one to flexor pollicis, and one to the flexor profundus of the index finger.
15. The absence of the fpl was described by Gegenbaur.
16. In a case of a double thumb, Gruber found it sent a slip to both digits.

Pronator Quadratus

In very rare instances, even when the radius is normal, the absence of a pronator quadratus has been noted. It is occasionally laminated into two or more layers consisting of fasciculi running in different directions: two layers in 13% of cases, three in 1%, and four in 1% (Inoue 1934). It can continue down on the carpus or metacarpus, in some cases as a radiocarpal fasciculus and in others as an ulnocarpal fasciculus. Aberrant fibers arising from its distal edge can insert into the thenar muscle mass and act as an accessory adductor of the thumb. The pronator quadratus can also extend in a proximal direction on the radius and be joined to the pronator teres or flexor carpi radialis brevis.

The pronator quadratus muscle can be also distinguished between the superficial head and the deep head (Johnson 1976; Koebke 1984; Stuart 1996). The superficial head runs transversely from the ulna to the radius, whereas the deep head runs obliquely from the proximal ulnar origin to the distal radial insertion (Johnson 1976; Koebke 1984; Gordon 2004). Double or more muscle fascicles were found in the superficial or deep heads in 80% of speciments (Sakamoto 2014).

The radiocarpeus (radiocapien (Fano), court radial anterieur (Le Double), flexor carpi radialis brevis vel profundus (Wood), flexor carpi radialis brevis) is a small penniform muscle, present in about 16% of individuals (all sources), which arises from the radius (usually from its volar border and surface) proximal to the pronator quadratus. It can extend proximally to the ulna or medial epicondyle and have additional attachment sites. It is inserted by a tendon on one or more carpal bones or one or more metacarpals, or both. The radiocubitocarpien (radialis internus brevis biceps) arises from two heads, from the radius and ulna, and terminates distally on the carpus (Calori 1870). It originates from the anterior surface of the radius and the proximal border of the flexor retinaculum, and inserts on the deep surface of the palmar aponeurosis.

A small muscle called the ulnocarpeus brevis (the flexor carpi ulnaris or cubitocarpeus) is rare. It originates from the ulna on its medial or volar surface and is inserted to the pisiform bone, the hamulus, the proximal end of the fifth metacarpal bone, the capsule of the carpal articulations, or the abductor digiti minimi (the abductor manus or the abductor digiti quinti). This muscle is found in 1.9% of cases (Mori 1964).

M. tensor capsulae radiocubitalis (inferioris) is a small muscular slip that arises from the volar aspect of the distal radius, crosses superficial to pronator quadratus in a distal direction, and inserts into the radioulnar capsule. The uncipisiformis extends from the pisiform to the tip of the hamulus of the os hamatum (see the abductor digiti minimi).

Variations of this muscle have been described in many reports (Wood 1867a; Macalister 1871, 1875b; Gruber 1872b, f, g, 1881a, 1885a, b, 1886b; Carleton 1934–35; Jeffery 1971; Claassen et al. 2013).

Brachioradialis

This muscle generally originates from the upper two-thirds of the humerus, between the brachialis and triceps. The brachioradialis is often united with the brachialis at its origin (2–3%, Inoue 1934). Its origin can also extend proximally as far as the insertion of the deltoid, with which it is sometimes connected. It can also be joined to the extensor carpi radialis longus and abductor pollicis longus. It can be divided, with the second belly attached distally to the radius (in the neighborhood of the tuberosity) or even to the ulna. The tendon can be split into two or three slips, occasionally allowing the radial nerve to pass through and becoming a potential entrapment site for the radial nerve (Spinner and Spinner 1996). A tendinous slip can also extend to the fascia of the forearm (Calori 1868).

The muscle is generally inserted into the lateral side of the base of the styloid process of the radius. The insertion can ascend on the lateral face of the radius or be extended distally to the navicular, trapezium, or base of the third metacarpal bone. Alternatively, the brachioradialis can be joined to the supinator.

An accessory brachioradialis arises adjacent to brachioradialis, inserts on the radial tuberosity, and acts as a true supinator (the supinator longus accessorius: Lauth 1830; the brachioradialis brevis minor: Gruber 1887a). It can also insert into the supinator or the tendon of pronator teres, or onto the ulna. It can be doubled or absent.

Variations have been described in many reports (Calori 1866, 1867; Gruber 1867; Macalister 1875c; Nishida 1941; Ishimi 1951; Baur 1971; Yogesh et al. 2011).

Extensor carpi radialis longus and brevis

The extensor carpi radialis longus originates in line with the brachioradialis from the distal third of the lateral supracondylar ridge of the humerus, from the lateral intermuscular septum, and from the common tendon of the extensor muscles of the forearm. The extensor carpi radialis brevis originates from the lateral epicondyle of the humerus and from the common tendon of the extensor muscles of the forearm. The origin of the extensor carpi radialis longus is primarily composed of a muscular portion and only thin, short tendons. To the contrary, that of the extensor carpi radialis brevis is composed of a thick tendinous portion without any muscular portion (Nimura 2014). These muscles are often fused to each other, with many varieties in the partial to complete fusion patterns (Ishimi 1951). In lower mammals, the two extensores carpi radiales are usually represented by one muscle. Human cases have been reported in which the muscles were fused however, the common belly having two or three tendons inserted into the metacarpal bones.

A trigastric radialis longus has been reported inserting partially on the base of the first metacarpal and partially on the base of the second. There is often incomplete fusion, effected by cross slips from one muscle to the other. The longus and brevis are noted for exchange of fleshy and tendinous slips. These connecting fasciculi can be replaced by distinct muscles connected with one or both of the radial extensors.

The extensor carpi radialis intermedius is a rare muscle that arises independently from the epicondyle of the humerus between the two usual muscles and is inserted into the second and third metacarpals. More frequently, the accessory muscle is represented by a slip from one or both of the radial extensors and is inserted, in the same way, onto the second or third metacarpal or both of these bones.

The extensor carpi radialis accessorius is an additional muscle sometimes seen arising from the humerus, with or below the long radial extensor, and inserting most frequently onto the metacarpal bone of the thumb (Kosugi et al. 1985). The musculus extensor atque abductor pollicis accessory (of Mingazzini) arises from the lateral epicondyle and inserts onto the proximal phalanx of the thumb.

The muscle of the radial extensors can be divided. However, it is more commonly one of the tendons that splits into two or sometimes three prior to insertion. The tendons can be attached to the second and third metacarpal bones. Occasionally, a slip also passes to the fourth metacarpal or to the trapezium. The extensor carpi radialis longus can be joined to the abductor pollicis longus or to some of the interosseous muscles.

Variations of these muscles have been described in many reports (Wood 1864, 1865, 1866, 1867a, b, 1868; Calori 1868; Curnow 1873; Macalister 1875c; Gruber 1877, 1885c; Shepherd 1880a; Inoue 1934; Baumann 1947; Matsushima and Ikuta 1959; Kaneff 1969; Kosugi et al. 1987a, b; Wood 1988; Yoshida 1994; Mitsuyasu et al. 2004; Nayak et al. 2007).

Supinator

The supinator consists of two layers of fibers with the deep branch of the radial nerve running between them. The two layers originate in common from the lateral epicondyle of the humerus, the radial collateral ligament of the elbow joint, the anular ligament of the proximal radioulnar joint, the supinator crest on the ulna, and a tendinous aponeurosis covering the surface of the muscle. The supinator is generally not clearly divided into layers, but sometimes the division is clearer than usual. The superficial layer is inserted into the lateral edge of the radial tuberosity and the oblique line of the radius, and the deep layer onto the back part of the medial surface of the radius. An accessory fasciculus originating from the lateral epicondyle can be inserted into the tendon of insertion of the biceps, the bursa under the tendon, and the tuberosity of the radius. Variations of the muscle have been described in several reports (Halbertsma 1862; Clason 1869; Macalister 1875b; Carrington et al. 1883; Ishimi 1951).

The proximal part of the superficial layer of the muscle can be tendinous, forming a fibrous arch that can cause paralysis of the posterior interosseous nerve (Spinner 1968).

Macalister (1875b) reported the following variations in the supinator: it muscle can be doubled (Sandifort); there is sometimes a cleft where the posterior interosseus nerve perforates it; a slip can insert on the tubercle of the radius; a similar slip was found joining the pronator teres (Clason); a second or supinator brevis accessorius (Halbertsma) was found; and a slip from the lower border of the brachialis was inserted onto the tubercle of the radius. Dursey described a slip from this muscle inserted into the biceps tendon and a slip into the bursa tubercularis of the radius.

Extensor digitorum communis

The extensor digitorum mainly originates from the lateral epicondyle of the humerus, generally divides distally into four tendons, and is inserted into the index to fifth fingers. Variations of this muscle include the occasional deficiency of one or more of the tendons of insertion or an increase in numbers, supplying the five fingers. If one of the tendons is absent, the tendon to the fifth digit is variable: (1) it is absent; (2) it is divided from that to the fourth digit; and (3) it runs parallel with that to the fourth digit (Ebisawa 1960a, b; Yamamoto and Sato 1960). Any digit can receive two tendons. A hand with tendons doubled to the second, third, and fifth fingers has been reported (Wood 1868). Statistical data concerning variations of the terminal tendons of the extensor digitorum have been published (Mori 1964). The fleshy part of the muscle can comprise two to four bellies, one for each tendon of insertion. Tendinous slips can leave the muscle and join those of the extensor indicis or extensor pollicis longus.

Three types of intertendinous connections can be seen between the extensor digitorum communis: transverse, transfer,

and aberrant and membranous. Transverse and transfer connections are observed from the index to little fingers. Membranous connections between the index and middle finger are frequent (Ebisawa 1960a, b; Yamamoto and Sato 1960). Sometimes there are no such connections (junctura tendinea). There can be an intertendinous connection between the extensor digitorum communis and the extensor pollicis longus (Takeuchi et al. 1978; Steichen and Petersen 1984).

Variations of this muscle have been reported (Gantzer 1813a; Calori 1867; Bankart et al. 1869; Gruber 1875a, 1878, 1879, 1881b, 1882b, c, d, 1885d, 1887c, 1888; Macalister 1875c; de Vilhena 1933; Straus 1941; Straus and Temkin 1943; Sunderland 1945; Baumann 1947; Scheldrup 1951; Ebisawa 1954; Jones and Suffolk 1959; Schenk 1964; Egawa and Hashimoto 1966; Spinner and Olshansky 1973; Culver 1980; Chiu 1981; Kosugi et al. 1984; Steichen and Peterson 1984; Ishizuki et al. 1986; von Schroeder et al. 1990; Tanaka et al. 2007; Mitsuyasu et al. 2004; Nayak et al. 2007; Bettencourt Piers et al. 2013).

Mori provides statistical data on the condition of the terminal tendon of the extensor digitorum: the tendon for the third digit is doubled in 2.5% of cases; the fourth digit 5.0%; and the fifth digit 12.5%. The tendons of the second and fourth digits are doubled in 2.5% of cases; the fourth and fifth digits in 2.5%; the third, fourth, and fifth digits in 15%; and the third and fifth digits in 2.5% of Mori's cases.

The junctura tendinae can be absent between the index and middle fingers in 10% of cases; between the ring and little fingers in 2.5%; and between the middle and ring fingers in 10%. The terminal tendon for the little finger is absent in 4% of subjects.

Macalister's observations of the extensor communis digitorum complement those of Mori as follows.

1. The little finger tendon can be absent.
2. The tendon for each finger can be doubled.
3. There can be partial doubling of the ring finger tendon.
4. Exclusive doubling of the index tendon can be observed.
5. The tendon for the middle finger only can be doubled.
6. The tendon for the middle finger can be trebled.
7. The middle and ring can be doubled, the contiguous portions being joined by a vinculum.
8. The index tendon can be doubled, and the ulnar (side) tendon can be joined to the middle finger tendon.
9. All tendons can be united by vincula (Wood described the occurrence of this, one of the index tendons being the only one free).
10. Albinus reported a separate belly for each tendon (the same was reported by Brugnone, Meckel, and Wood).
11. A special (accessory) belly for the index finger tendon was reported by Henle, Wood and Macalister.
12. The little finger tendon can be doubled.
13. The ring and little finger tendons are both doubled.
14. The index and little finger tendons are both doubled.
15. In one case, Wood reported two tendons to the index and little fingers and four to the ring finger.
16. This muscle sent a slip in the groove with the extensor secundi internodii pollicis (extensor pollicis longus), which it joined at the base of the first phalanx of the thumb (Macalister and Wood).
17. Wood saw a similar slip going to the indicator (first finger).
18. The extensor digitorum communis (edc) could send one, two, or three slips to substitute for the extensor digiti minimi when this muscle was absent.
19. The tendon for the second finger, which normally arises from extensor carpi radialis brevis, can be deficient.
20. It can have two bellies, one supplying the second and third and one to the fourth and fifth.
21. The third and fourth bellies can be split into two parts, each with a tendon inserted into their respective fingers.
22. Sömmerring saw it send a slip that joined extensor digiti minimi.
23. Rüdinger had a case in which there was a remarkable subdivision of the extensor muscles: eleven extensor tendons for the fingers between this muscle, the extensores medii et tertii digiti, and the indicator. (See also the section on extensor indicis.)

Extensor digiti minimi (proprius) (manus)

The extensor digiti minimi chiefly originates from the common extensor tendon. A thin fibrous slip from the lateral epicondyle of the humerus, continuous with the common tendon, is occasionally present. More rarely, there is a supplementary origin from the dorsal surface of the ulna. The belly of the muscle is sometimes doubled. The insertion with a single tendon occurs in only 15–18%. The tendon of this muscle is usually divided (74%) and gives a slip to the fourth digit in 10.3% (Yoshida 1985). An ulnar slip of this tendon has been observed to end on the base of the fifth metacarpal. The muscle can be absent (Yoshida 1985). Fusion with the tendon of the extensor digitorum is frequent, and in these cases the tendon comes from the common extensor.

The extensor digiti minimi accessorius is observed in 4%, when the extensor digiti minimi divides into two slips (Mori 1964). The ulnar part extends onto the back of the fifth metacarpal to the base of the first phalanx of the little finger and is the extensor digiti minimi; the radial slip extends to the dorsal carpal ligament and inserts into it, and this becomes the extensor digiti minimi accessorius.

Variations have been also described (Calori 1867; Flower and Murie 1867; Wood 1868; Macalister 1875c; Gruber 1885d, e, f; Baumann 1947; Mori 1964; Bettencourt Piers et al. 2013). Macalister reported the following variations. The muscle can be absent and substituted by: a slip of the extensor communis; a slip by the extensor carpi ulnaris; or with no substitute. The muscle can have two tendons, both inserted into the little finger (a very common arrangement). Wood and Macalister found both muscle and tendon doubled. It can have a double

tendon, the lateral going to the ring finger and the other to the little finger (cases of this type were seen by Vesalius, Meckel, M'Whinnie, Hallett, Theile, and Wood). Wood found this variation 13 times in 106 cases, one in every eight individuals. Macalister found it in more than one in 14 Irish subjects. It was also found with a treble tendon, two going to the little finger and one to the ring finger. Finally, the muscle can receive an accessory slip from the common extensor (Sömmerring).

Extensor carpi ulnaris

The extensor carpi ulnaris generally originates from the lateral epicondyle of the humerus, from the dorsal border of the ulna, and from the deep fascia of the forearm. The muscle is generally inserted onto the prominent tubercle at the ulnar side of the base of the fifth metacarpal bone. The extensor carpi ulnaris, being the ulnar marginal element of the primitive extensor sheet, corresponds to the two peroneal muscles in the leg. Several variations have been reported: (1) the muscle is occasionally doubled throughout; (2) there can be a partial attachment of its tendon to the base of the third or fourth metacarpal bone; (3) an additional tendon can replace an absent extensor digiti quinti; and (4) an independent muscle, the ulnaris digiti minimi or ulnaris digiti quinti, has been observed arising from the lower part of the dorsal surface of the ulna and inserting into the base of the proximal phalanx of the little finger.

An anomalous slip between the extensor carpi ulnaris tendon and the extensor aponeurosis of the fifth finger has been observed (Barfred and Adamsen 1986).

There have been several reports of variations of this muscle (Wood 1868; Macalister 1875c; Gruber 1885g; Inoue 1934; Baumann 1947; Ishimi 1951; Gloobe and Liberty 1973; Roman-Liu et al. 2004).

Macalister reported the following variations: an extensor carpi ulnaris has been found receiving a slip from the triceps; it can send a tendon to replace that of a suppressed extensor minimi digiti; it can give origin, from its tendon, to an abductor minimi digiti; it can send a slip to be inserted into the septum in the posterior anular ligament, between its usual insertion and the extensor minimi digiti; and it can send a slip (the ulnaris quinti) to the tendinous aponeurosis on the back of the little finger (Henle, Meckel, and Wood). Wood stated it had a frequency of 12%.

Abductor pollicis longus

The abductor pollicis longus generally originates from the lateral part of the posterior surface of the body of the ulna, the interosseous membrane and the middle third of the posterior surface of the body of the radius. The muscle is generally inserted into the radial side of the base of the first metacarpal. The most common variations in the muscles of the thumb occur in the long abductor and consist of an extensive cleavage of its tendon, or even of the whole muscle, into separate parts. On the other hand, it can be reduced to a small slip arising only from the radius. The slips into which its tendon is divided can be attached to the flexor retinaculum, scaphoid, trapezium, abductor pollicis brevis, opponens pollicis, or first phalanx or the tendon can be inserted onto the base of the first metacarpal bone.

In a few cases (6%), the abductor pollicis longus has only a single tendon which is inserted upon the radial side of the first metacarpal bone. In the remaining cases (94%), the muscle has an accessory tendon to be inserted into the abductor pollicis brevis, onto the trapezium, and into the carpalmetacarpal joint (Kimura 1958). The accessory tendon can be inserted onto the opponens pollicis (Lacy et al. 1951).

A rare muscle, the abductor pollicis tertius, originates from the dorsal aspect of the radius with the abductor pollicis longus and is inserted, after fusion with the abductor pollicis brevis, onto the fist metacarpal.

Variations of this muscle have been described in many reports (Jansen 1850; Calori 1867; Wood 1867a; Macalister 1875c; Petit 1880; Shepherd 1880b; Debierre 1888; Pires de Lima 1914; Baumann 1947; Schuldt 1947–48; Stein 1951; Coleman et al. 1953; Baba 1954; Chopra et al. 1954–55; Giles 1960; Martinez and Omer 1985; Jackson et al. 1986; Patel and Desai 1988; Rayan and Mustafa 1989; Oudenaarde 1991; Imaeda and Cooney 1992; Abu-Hijleh 1993; Nayak et al. 2007; Paul and Das 2007).

Macalister (1875c) reported the following variations of the extensor ossis metacarpi pollicis (abductor pollicis longus). It has a double tendon very often, both inserted together, or one is inserted onto the trapezium connected to the tendon of the short abductor pollicis (brevis). This is not uncommon and occurs in about 1 in every 12 subjects. A triple tendon (either: two into the metacarpal and one into the trapezium; one into the metacarpal, one into the trapezium, and one into the opponens pollicis; or two into the metacarpal and one into the opponens pollicis) has been observed. Cloquet (1836) found it sending a slip into the origin of abductor pollicis brevis (Wood found this 7 times in 36 subjects). A doubled muscle, one-half of which went exclusively to the abductor pollicis, and a triple tendon, which sent a slip to abductor pollicis were both observed. An example with four tendons, three to the metacarpal bone and one to the abductor indicis was noted by Macalister. The muscle has been found fused with the extensor primi internodii (extensor pollicis brevis).

A doubled muscle with normal insertion was observed, as well as one in which the inner (medial) segment was normal while the outer (lateral) had four tendons (three of which went into the first metacarpal bone and one gave origin to part of the opponens pollicis).

Macalister found the muscle fused with the extensor primi (extensor pollicis brevis) and giving off two tendons. Carver found it with three slips from a single tendon, one to the distal phalanx of the thumb, one to the second phalanx, and one to the scaphoid bone. Fleischmann described it as digastric, but the case seemed to be rather one of the examples of the extensor carpi radialis accessorius; a digastric example was also described

by Sömmerring. Macalister found it doubled: one muscle with four tendons, one to the trapezium, one to the lateral part of the abductor brevis pollicis, one to the opponens, and the fourth to the metacarpal. The second went entirely to the metacarpal bone, which coexisted with a slip from the extensor secundi (extensor pollicis longus) to the first phalanx. Macalister also found a slip inserted into the anular ligament.

Extensor pollicis brevis

The extensor pollicis brevis generally originates from the posterior surface of the body of the radius and from the interosseous membrane. The muscle is generally inserted into the base of the first phalanx of the thumb. It is a muscle peculiar to humans and is sometimes absent (Wood 1867a, 1868; Macalister 1875c), being fused with the abductor longus (Inoue 1934; Ishimi 1951; Kosugi et al. 1985; Yoshida and Fukuyama 1979; Homma and Sakai 1992). On the other hand, its tendon is often united with that of the long extensor and is inserted with it, or it continues as an independent slip to the base of the distal phalanx. In a study of 118 forearms, the extensor pollicis brevis inserted onto the proximal phalanx in 72%, both phalanges in 21.2%, and the terminal phalanx in only 6.8%. It has been reported absent in 6.3% of cases. In another study, the muscle was absent in 5 of 120 limbs. It can terminate in two tendons, one of which attaches to the base of the first metacarpal.

There have been several descriptions of variations of this muscle (Wood 1864; Henle 1871; Dubreuil-Chambardel 1919; McGregor 1926; Baumann 1947; Stein 1951; Chopra et al. 1954–56; Giles 1960; Kaplan 1981; Dawson and Barton 1986; Jackson et al. 1986; Yoshida 1990; Tountas and Bergman 1993; Bahm et al. 1995; Lutz et al. 1997).

Macalister (1875c) reported the following variations for extensor pollicis brevis. It has been found absent by Wood (1867a, 1868) once in 36 specimens and three times in 36 specimens; this was also reported by Moser and found by Macalister. Theile and Henle have seen it fused with abductor pollicis longus, as have Wood and Macalister. Its tendon can pass distally to the ungual distal phalanx. The tendon has been described as split, and Macalister has found the entire muscle cleft with each part normally attached. Wood found it replaced by a tendon from the styloid process of the radius to its normal site of insertion. A slip to the tendon of the extensor secundi (extensor pollicis longus) at the base of the ungual phalanx was observed, as was the tendon going entirely to the ungual phalanx, or a slip going to the metacarpal bone at its head. It was also found receiving a slip from the abductor, which passed it onto the second phalanx.

Extensor pollicis longus

The extensor pollicis longus generally originates from the dorsolateral surface of the ulna and from the interosseous membrane, and is generally inserted into the base of the last phalanx of the thumb. It could be one of the least variable muscles of the forearm (Kosugi et al. 1989). Doubling of the extensor longus is not infrequent, and the ulnar portion of the muscle sometimes passes beneath the dorsal anular ligament with the common extensor (Kosugi et al. 1985). The extensor pollicis longus is reported to be absent in about 1.5% of individuals. A slip from the tendon of the long extensor to the extensor indicis is occasionally seen. A rarer variation is an additional extensor between the extensor indicis and extensor pollicis longus, with a double tendon and insertion into both digits. This additional extensor can replace the extensor pollicis longus or extensor indicis. In lower primates, the extensor longus and indicis are fused and inserted into other digits, and terminate as the extensor digitorum profundus. These primitive and remnant muscles contribute to occurrences of several variations (Yoshida 1990, 1995).

Variations of this muscle have been described in many reports (Calori 1867; Wood 1868; Macalister 1875c; Reid and Taylor 1879; Shepherd 1880b; Gruber 1881b, 1882b, 1885c, h; Breglia 1886; Debierre 1888; Dubreuil-Chambardel 1919; Kawai 1935; Straus and Temkin 1943; Baumann 1947; Krishnamurti 1962; Kaplan and Nathan 1969; Salama and Weissman 1975; Yoshida 1978; Yoshida and Fukuyama 1979; Yoshida et al. 1984; Lutz et al. 1997; Nayak et al. 2007; Paul and Das 2007).

Macalister (1875c) reported the following variations. It can receive a slip of extensor digitorum communis which runs in the same way in the radius (Wood). Macalister found the muscle doubled with both tendons inserting as usual. It was also found giving a slip to the base of the first phalanx in a case where the extensor pollicis longus was absent. A slip from the extensor pollicis longus to the first phalanx was seen to coexist with a slip from the extensor pollicis brevis to the second phalanx.

Extensor indicis

The muscle generally originates from the posterior surface of the body of the ulna and from the interosseous membrane, and is usually inserted into the extensor aponeurosis of the second digit. Its origin can shift from the ulna to the radius, carpus, or interosseous membrane. It can have two heads or be doubled completely. Its tendon is occasionally double; rarely, one of the slips passes to the thumb or ring finger; more commonly it passes to the middle finger. This last slip, forming an extensor digiti III, occurred as a separate muscle (2–5%) arising from the ulna, or from the posterior ligament of the wrist joint below the indicator. An extensor digiti IV is a rarer variation. These slips of the deep or short extensor appear to be reversions to a primitive arrangement in which the muscle provides tendons to the whole series of digits. The tendons can also be poorly developed. The muscle of the index finger is rarely absent.

The extensor digiti medii originates from the ulna beneath the extensor indicis, with which it is fused in 10% of bodies. It sends a tendon to the extensor aponeurosis of the middle finger or sends slips to the middle finger and index finger.

The extensor digitorum brevis or extensor digitorum brevis manus resembles the muscle of the same name on the dorsum of the foot. It can have from one to four fasciculi. The most common fasciculus provides a tendon to the extensor of the index finger. This arrangement is nearly as frequent for the middle finger. The fasciculi usually arise from the bones of the ulnar half of the carpus (lunate, triquetrum, hamate, and capitate) and from the dorsal ligaments joining the bones. The tendons are inserted either into the corresponding extensor tendons or onto the metacarpals (Gama 1976, 1983). The muscle is found in 1.6–3.2% of bodies (Kosugi et al. 1984; Yoshida et al. 1984).

There are reports of an extensor indicis et medii communis, which originates from the distal third of the ulna with two tendons inserting into the index and long fingers (von Schroeder and Botte 1991, 1995; Yalcin et al. 2006).

This muscle is very variable because in humans the proper extensor muscles to the third and fourth fingers are absent, in contrast to other mammals. There have been many reports about these variations (Jansen 1850; Calori 1867; Flower and Murie 1867; Wood 1868; Henle 1871; Curnow 1873; Jacob 1873; Macalister 1875c; Shepherd 1880b; Gruber 1881b, 1882a, b; Breglia 1886; Poiriér 1887; Sebileau 1887; Spourgitis 1895; Barkley-Smith 1896; Le Double 1897; Riche 1897; Smith 1897; Chudzinski 1898; Bühler 1902; Tenchini 1903; Manno 1907; de Vilhena 1933; Shiraki 1934; Cauldwell et al. 1943; Straus and Temkin 1943; Tsubaki and Onuki 1953; Moriya 1956; Jones 1959; Kuwahata and Sakamoto 1959; Bhadkamkar and Mysorekar 1960; Dunn and Evarts 1963; Bingold 1964; Peeling 1966; Souter 1966; Glasgow 1967; Lunda and Cihak 1967; Ritter and Inglis 1969; Ross and Troy 1969; Asi et al. 1971; Binns 1972; Hart 1972; Kuczynski 1972; Watanabe et al. 1972; Riodan and Stokes 1973; Spinner and Olshansky 1973; Still and Kleinert 1973; Reef and Brestin 1975; Nomura et al. 1976; Pitt 1976; Zientarski 1976; Maguire 1977; Varian and Pennington 1977; Yoshida 1978, 1990; Fukuzawa and Mitani 1979; Lucas 1979; Stith and Browne 1979; Culver 1980; Chiu 1981; Murakami and Todani 1982; Gahhos and Ariyan 1983; Bromley 1986; Gebuhr and Klareskov 1987; Ogura et al. 1987; Shaw and Manders 1988; Kuschner et al. 1989).

Macalister (1875c) reported the following variations of the extensor indicis. Macalister found it absent (as did Cheselden and Moser), with a doubled tendon (Wood and Macalister), with a doubled muscle and tendon, with a slip from the extensor digitorum communis (Wood), and with origins from the radius, carpus, and interosseous ligament and none from the ulna (Wood). Macalister found a doubled tendon coexisting with an accessory slip from the common extensor, but also inserted by fascia into the back of the hand or into the posterior anular ligament (Moser). A digastric indicator, whose second belly was on the back of the hand, was observed by Rosenmüller. It can be partly unified with the extensor medii digiti or be inseparable from it; Meckel found it with tendons to the second, third, and fourth fingers. Gantzer once saw it doubled, and one of these muscles arose from the radius.

References

Abu-Hijleh MF. 1993. Extensor pollicis tertius: an additional extensor muscle to the thumb. *Plast Reconstructive Surg* 92: 340–343.

Adachi B. 1909–10. Beiträge zur Anatomie der Japaner. XII. Die Statistik der Muskelvarietäten. *Zeitschr Morphol Anthropol* 12: 261–312.

Ari I, Sendemir E, Kurt MA, Ikiz I. 1997. A rare case of a multiple variation of the muscles in the upper and lower extremities. *Acta Anat Nippon* 72: 521–524.

Ashby BS. 1964. Hypertrophy of the palmaris longus muscle: Report of a case. *J Bone Joint Surg B* 46: 230–232.

Asi O, Yamashita H, Tagawa N, Hanamura H. 1971. One case of extensor digitorum brevis manus. *Cent Jpn J Orthop Traumat* 14: 625–628 (in Japanese).

Baba MA. 1954. The accessory tendon of the abductor pollicis longus muscle. *Anat Rec* 119: 541–574.

Badolle M. 1874. Anomalie du Fléchisseur sublime. *Lyon Med* 15: 500.

Bahm J, Szabo Z, Foucher G. 1995. The anatomy of de Quervains's disease. A study of operative findings. *Internat Orthop* 19: 209–211.

Bankart J, Pye-Smith PH, Phillips JJ. 1869. Note of abnormalities observed in the dissection room during sessions of 1866–7, 1867–68. *Guy's Hospital Report* 14: 436–455.

Barfred T, Adamsen S. 1986. Duplication of the extensor carpi ulnaris tendon. *J Hand Surg* (A) 11: 423–425.

Barkley-Smith E. 1896–97. Some points in the anatomy of the dorsum of the hand with special reference to the morphology of the extensor brevis digitorum manus. *J Anat Physiol* 31: 45–48.

Barrett JH. 1935–36. An additional (third and separate) head of the pronator teres muscle. *J Anat* 70: 577–578.

Baumann JA. 1947. Valeur, variation, et équivalences des muscles extenseurs, interosseux, adducteurs, et abducteurs de la main et du pied chez l'homme. *Acta Anat* 4: 10–16.

Baur R. 1971. Innervation des M. brachioradialis aus dem N. musculocutaneous als seltene Varietät. *Anat Anz* 128: 108–110.

Bettencourt Piers MA, Casal D, Mascarenhas de lemos L, Godinho CE, Pais D, Goyri-O'Neill J. 2013. An unusual variety of the extensor digiti muscles: report with notes on repetition strain injuries. *Acta Med Port* 26: 278–283.

Bhadkamkar AR, Mysorekar VR. 1960. Bilateral extensor digitorum brevis muscle in the hand. *J Anat Soc India* 9: 104–105.

Bianchi A. 1906. Faisceau accessorie du m. pronator teres du nerf médian et de l'artère humérale àla région du coude. *Arch Ital Biol* 45: 283–284.

Bigot A. 1954. Note sur la frequence du muscle petit palmaire chez le Tamoul de Pondicéry. *Bull Mem Soc Anthropol de Paris* 5: 81–84.

Bingold AC. 1964. An extensor indicis brevis. *Brit J Surg* 51: 236–237.

Binns JH. 1972. Two cases of extensor digitorum brevis manus. *Hand* 4: 263–264.

Breglia A. 1886. Di una rara anomalia del plesso brachiale. *Rivista Internazionale di Medicina e Chururgia* 4: 337–344.

Bromley GS. 1986. Rare coincidence of bilateral extensor digitorum brevis manus and bilateral capitates-hamate synostosis. *J Hand Surg (A)* 11: 37–40.

Brones MF. 1978. Anatomical variations of the palmaris longus, causing carpal tunnel syndrome. Case reports. *Plast Reconstruct Surg* 62: 798–800.

Bühler A. 1902. Beziehungen regressiver und progressiver Vorgägne tiefen Fingerstecker und den Musculi interossei dorsales der menschlichen Hand. *Morphol Jahrb* 29: 563–581.

Calori L. 1866. Intorno ad alcune varieta incontrate nella muscolatura degli arti superiori annotazioni anatomische. *Mem Accad Sci d Istituto di Bologna S2* VI: 157–174.

Calori L. 1867. Di alcune varieta muscolari dell'avambraccio e dell'eminenza ipothenar. *Mem Accad Scienze Istituto di Bologna S2* 7: 383–393.

Calori L. 1868. Delle anomalie più importanti di ossa, vasi, nervi, e muscoli occorse nell'ultimo biennio fascendo anatomia del corpo umano. *Mem R Accad Sci Istituto di Bologna S2*. 8: 417–482.

Calori L. 1870. Degli usi del muscolo pronatore quadrato e di un muscolo sopranumerario cubito-radio-carpeo nell'uomo. *Mem R Accad Sci Instituto di Bologna S2* 10: 647–657.

Carleton A. 1934–35. Flexor carpi radialis brevis vel profundus. *J Anat* 69: 292–293.

Carr ND, O'Callaghan JD, Vaughn R. 1977. An unusual flexor of the fifth finger. *Acta Anat* 98: 376–379.

Carrel M. 1872. Anatomy anormale. 1. Biceps humeral trifide. *Lyon Med* 10: 43–44.

Carrington RE, Horrocks P, White WH. 1883. Abnormalities observed in the dissecting room of Guy's hospital during the sessions 1880–81 and 1881–82. Guy's Hosp Reports 46: 57–81 (volume 26 of the third series).

Carroll MP, Montero C. 1980. Rare anomalous muscle cause of carpal tunnel syndrome. *Orthop Rev* 9: 83–85.

Cassell MD, Bergman RA. 1990. An unusual palmaris longus muscle substituting for the ring finger slip of flexor digitorum superficialis serving the ring finger. *Anat Anz* 171(3): 201–204.

Cauldwell EW, Anson BJ, Wright RR. 1943. The extensor indicis proprius muscle. A study of 263 consecutive specimens. *Q Bull Northwestern Univ Med School* 17: 267–279.

Celik HH, Sargon MF, Yilmaz E, Kayikcioglu A. 1996. Bitendinous palmaris longus muscle. *Bull Assoc Anat (Nancy)* 80(250): 15–16.

Chiu DTW. 1981. Supernumerary extensor tendon to the thumb: A report on a rare anatomic variation. *Plastic and Reconstructive Surg* 68(6): 937–939.

Chopra RP, Singh S, Makhni SS. 1954–55. The insertion of the abductor pollicis longus and extensor pollicis brevis. *J Anat Soc India* 7: 105–109.

Chowdhary DS. 1951. A rare anomaly of m. flexor digitorum sublimis. *J Anat* 85: 100–101.

Chudzinski T. 1898. Observations sur les variations musculaire dans les races humaines. *Mem Soc L'Anthropol Paris* 2(2): 227.

Claassen H, Schmitt O, Schulze M, Wree A. 2013. Variation in the hypothenar muscles and its impact on ulnar tunnel syndrome. *Surg Radiol Anat* 35: 893–899.

Clason E. 1869. Om muskelanomalier. *Upsala Lakareforening Forhandlingar* IV: 244–248.

Cloquet H. 1836. *Traite D'Anatomie Descriptive*. Paris: Crochard.

Coleman SS, Macafee DK, Anson BJ. 1953. The insertion of the abductor pollicis longus muscle. An anatomical study of 175 specimens. *Q Bull Northwestern Univ Med Sch* 27: 117–122.

Culver J. 1980. Extensor pollicis and indicis communis tendon: a rare anatomic variation revisited. *J Hand Surg* 5: 548–549.

Curnow J. 1873. Notes of some irregularities in muscles and nerves. *J Anat Physiol* 7: 304–309.

Dawson S, Barton N. 1986. Anatomical variations of the extensor pollicis brevis. *J Hand Surg (B)* 11: 378–381.

de Vilhena. 1933. Le muscle surnuméaire extenseur commun du pouce et de l'index. *L'Assoc Anatomistes Comptes Rendus* 28: 685–702.

Debierre C. 1888. Anomalie des muscles radiaux externes et du long abducteur du pouce de l'homme. *Soc Biol, Comptes Rendus Hebdomadaires des Séances et Mémoires* 40: 547–550.

Dorin D, Mann RJ. 1984. Carpal tunnel syndrome associated with abnormal palmaris longus muscle. *South Med J* 77: 1210–1211.

Dubreuil-Chambardel L. 1919. Des muscles flechisseurs et extenseurs sur un pouce a trois phalanges. *Bull Mem Soc Anthropol Paris* 10: 45–47.

Dunn AW, Evarts CM. 1963. The extensor digitorum brevis manus muscle. *Clin Ortho* 28: 210–212.

Dykes J, Anson BJ. 1944. The accessory tendon of the flexor pollicis longus muscle. *Anat Rec* 90: 83–87.

Dylersky I. 1967. Contribution to the ontogenesis of the flexor digitorum superficialis and the flexor digitorum profundus in man. *Folia Morphol Praha* 15: 330–335.

Dyreby JR, Engber WD. 1982. Palmaris profundus: Rare anomalous muscle. *J Hand Surg* 7: 513–517.

Ebisawa K. 1954. The tendons of the extensors of the fingers. *Kaibogaku Zasshi* 29: 164 (in Japanese).

Ebisawa K. 1960a. The form of the tendons of the extensors on the dorsum of the hand. *Nihon Ikadaigaku Zasshi* 19: 831–846 (in Japanese).

Ebisawa K. 1960b. Studoj pri la ekstensoraj tendenoj de mano, precipe pri la tendena anastomozo ĉe homo. *J NUMA* 19: 831.

Egawa T, Hashimoto K. 1966. An anomalous extensor Indicis muscle: A case report. *Bull NY Hosp Joint Dis* 27: 116–119.

Eguchi T, Shima S. 1959. On the palmaris longus and the aponeurosis palmaris. *Nihon Ikadaigaku Zasshi* 18: 2681–2691 (in Japanese).

Fatah MF. 1984. Palmaris profundus of Frohse and Fränkel in association with carpal tunnel syndrome. *J Hand Surg B* 9: 142–144.

Feret J, Jagiello W, Wisniewski A. 1965. Morphologic variation of the long palmar muscle (M. palmaris longus) in man. *Folia Morphol (Warsaw)* 24: 64–69.

Flower WH, Murie J. 1867. Account of the dissection of a Bush woman. *J Anat Physiol* 1: 202–208.

Floyd T, Burger RS, Sciaroni CA. 1990. Bilateral palmaris profundus causing bilateral carpal tunnel syndrome. *J Hand Surg A* 15: 364–366.

Friedlowsky A. 1869. Ergebnisse der anatomischen untersuchung von zwie extremitdtem mit angeborener dreizahl der finger. *Weiner Akad Sitzungsberichte Math Natur* 59: 527–548.

Fukuzawa G, Mitani S. 1979. An anomalous extensor digitorum brevis manus. A case report. *Clin Orthop Surg* 14: 1228–1233 (in Japanese).

Gahhos FN, Ariyan S. 1983. Extensor indicis brevis manus: a rare anatomical variation. *Ann Plast Surg* 10: 326–328.

Gaillard J. 1958. Fréquence du muscle petit palmaire (M. Palmaris longus) chez les Melano-Indiens. *L'Assoc Anatomistes, Comptes Rendus* 45: 371–377.

Galton JC. 1875. On the epitrochleo-anconeus or anconeus sextus (Gruber). *J Anat Physiol* 9: 169–175.

Gama C. 1976. Musculus extensor digitorum brevis manus. *Int J Surg* 61: 31–40.

Gama C. 1983. Extensor digitorum brevis manus: a report of 38 cases, and a review of the literature. *J Hand Surg* 8: 575–582.

Gantzer CFL. 1813a. De Musculorem Varietat. Thesis, J. F. Starkii, Berolini.

Gantzer CFL. 1813b. *Dissertatio Anatomica Musculorum Varietatis Sistens*. Berlin: Joannis Fridrici.

Gebuhr P, Klareskov B. 1987. Extensor digitorum brevis manus. *Acta Orthop Scand* 58: 85–86.

George R. 1953. Co-incidence of palmaris longus and plantaris muscles. *Anat Rec* 116: 521–523.

Giannelli L. 1899. Sur une anomalie peu commune du muscle rond pronateur. *Arch Ital Biol* 31: 186.

Giles KW. 1960. Anatomical variations affecting the surgery of De Quervain's disease. *J Bone Joint Surg* 42B: 352–355.

Glasgow EF. 1967. Bilateral extensor digitorum brevis manus. *Med J Australia* 54: 24–25.

Gloobe H, Liberty S. 1973. Bilateral agenesis of extensor carpi ulnaris. *Hand* 5: 175–176.

Gordon KD, Pardo RD, Johnson JA, King GT, Miller TA. 2004. Electromyographic activity and strength during maximum isometric pronation and supination efforts in healthy adults. J Orthop Res 22: 208–213.

Graper L. 1917/18. Eine sehr Varietät des M. flexor digitorum sublimis. *Anat Anz* 50: 80–84.

Gruber W. 1867. Uber die varietaten des musculus brachioradialis. *Bull Acad Imp Sci St Petersbourg* 12: 527–528.

Gruber W. 1868. Über die Varietäten des Musculus palmaris longus. *Mém l'Acad Imp Sci St Petersbourg S7*, 11: 1–26.

Gruber W. 1872a. Un muscle radial interne long bicaude chez l'homme, remplacant par une portion surnuméraire le palmaire grele, qui manqué. *Bull L'Acad Imp Sci St Petersbourg* 17: 318–319.

Gruber W. 1872b. Sur les varietes du muscle radial interne court. *Bull L'Acad Imp Sci St Petersbourg* 17: 379–380.

Gruber W. 1872c. Sur quelques varieties du muscle palmaire grele. *Bull l'Acad Imp Sci St Petersbourg* 17: 291–294.

Gruber W. 1872d. Un muscle radial interne long bicaude chez l'homme, remplacant par une portion surnumeraire le palmaire grele, qui manque. *Bull l'Acad Imp Sci St Petersbourg* 17: 318–319.

Gruber W. 1872e. Zergleiderung eines linken Armes mit Duplicitat des Daumens. *Bull Acad Imp Sci St Petersbourg* 17: 24–31.

Gruber W. 1872f. Ein spanner der unteren Radiocubitalkapsel: tensor capsulae radiocubitalis inferioris. *Arch Path Anat Physiol Klin Med* 54: 186–187.

Gruber W. 1872g. Nachträge zu den Varietäten des Musculus radialis internus brevis. *Bull l'Acad Imp Sci St Petersbourg* 17: 380–388.

Gruber W. 1875a. Über den Musculus extensor digitorum communis manus anomalous mit 5 Sehnen zu allen Fingern, und über den Musculus extensor digitorum longus pedis anomalous mit 5 Sehnen zu allen Zehen. *Arch Anat Physiol Wissen Med* 1875: 204–210.

Gruber W. 1875b. Ein Fall des Vorkommens des Musculus flexor pollicis longus beim Menschen: als Tensor bursae mucosae tendinum mm. flexorum, oder als Kopf des M. flexor digitorum profundus manus. *Arch Anat Physiol Wissen Med* 1875: 211–214.

Gruber W. 1877. Über den Muskulus radialis externus accessorius. *Arch Anat Physiol Wissen Med* 1877: 388–389.

Gruber W. 1878. Musculus extensor digitorum communis manus anomalous mit 5 Sehnen zu allen Fingern. *Arch Path Anat Physiol Klin Med* 72: 500–501.

Gruber W. 1879. Nachtrag zum Vorkommen des Musculus extensor digitorum communis manus mit 5 Sehnen zu allen Fingern. *Arch Path Anat Physiol Klin Med* 77: 129–130.

Gruber W. 1881a. Ein musculus ulnaris brevis beim Menschen. *Arch Path Anat Physiol Klin Med* 86: 15–19.

Gruber W. 1881b. Über den dem constanten Musculus extensor pollicis et indicis gewisser Säugetiere homologen supernumerären Muskel beim Menschen. *Arch Path Anat Physiol Klin Med* 86: 471–491.

Gruber W. 1882a. Über den zum Extensor pollicis et indicis singularis gewordenen extensor pollicis longus beim Menschen. *Arch Path Anat Physiol Klin Med* 90: 103–108.

Gruber W. 1882b. Uber einen zum Extensor indicis et pollicis singularis gewordenen Extensor indicis proprius beim Menschen. Dasypeus Bildung. *Arch Path Anat Physiol Klin Med* 95: 180–183.

Gruber W. 1882c. Über einen anomalen, den constanten Musculus extensor digitorum communis manus zu allen 5 Fingern bei den Säugetieren Genera Myogale und Fiber Homologen Muskel beim Menschen. *Arch Path Anat Physiol Klin Med* 90: 88–97.

Gruber W. 1882d. Über anomale, dem constanten Musculus extensor digitorum communis manus zum 2–4. Fingern bei Asplax und Dasypus, und dem constanten Musculus extensor digitorum communis manus zum 1–4. Fingern bei Echidna homologe Muskeln beim Menschen. *Arch Path Anat Physiol Klin Med* 90: 97–103.

Gruber W. 1885a. Der musculus ulno-carpeus externus (eine neue Variante des Musculus ulnaris externus brevis) und sein Homologen, der musculus peroneo-cuboideus. *Arch Path Anat Physiol Klin Med* 99: 475–478.

Gruber W. 1885b. Ein musculus tensor ligamenti carpi dorsalis. *Arch Path Anat Physiol Klin Med* 101: 259–260.

Gruber W. 1885c. Über die im Bereiche des Lig. carpi dorsale schon congenital und in der Norm vorkommende Communication der Sehnenscheide fur den Extensor pollicis longus mit der fur die Radialis externi (nach 500 Untersuchungen), und uber einen Fall von Hygroma proliferum dieser mit einander communicirender Sehenenscheiden. *Arch Path Anat Physiol Klin Med* 101: 245–253.

Gruber W. 1885d. Düplicität des Musculus extensor digiti quinti et quarti proprius manus. *Arch Path Anat Physiol Klin Med* 101: 260–262.

Gruber W. 1885e. Zweibäuchiger Extensor digiti V proprius manus mit Insertion eines seiner Bäuche an die Basis des Metacarpal V, und die ihm homologe Variante des Peroneus III. *Arch Path Anat Physiol Klin Med* 99: 480–483.

Gruber W. 1885f. Absoluter Mangel des Extensor digiti quinti proprius manus bei mangel seiner Vagina im ligamentum carpi dorsale: ganz ausnahmsweise und nur beim Menschen (2 Fall) bei Vorkommen des muskels dennoch Mangel der Vagina constant bei den Prosimiae. *Arch Path Anat Physiol Klin Med* 99: 484–488.

Gruber W. 1885g. Mangel des Musculus ulnaris externus bis auf einen Sehnenstreifen. *Arch Path Anat Physiol Klin Med* 99: 478–480.

Gruber W. 1885h. Beobachtung eines Schnenrisses des Musculus extensor pollicis longus in 3 Hillen. *Archiv f Pathologische Anatomic u Physiologic u f klinische Medicin* 102(l): 1–2.

Gruber W. 1886a. Musculus flexor digitorum profundus mit Mangel einer Sehne zum Mittlefinger. *Arch Path Anat Physiol Klin Med* 103: 472–474.

Gruber W. 1886b. Ein Tensor capsulae radio-carpalis dorsalis. *Arch Path Anat Physiol Klin Med* 103: 474–475.

Gruber W. 1887a. Auftreten des Musculus radialis externus accessorius als Musculus supinator longus II. s. accessorius. *Arch Path Anat Physiol Klin Med* 107: 478–480.

Gruber W. 1887b. Auftreten des Zeigefingerbauches des flexor digitorum sublimis al Venter bifissus digastricus biceps. *Arch Path Anat Physiol Klin Med* 110: 559–561.

Gruber W. 1887c. Seltener Extensor proprius digiti quinti manus bei dem Menschen und bei den Menschen und bei Säugethieren. *Arch Pathol Anat Physiol Klin Med* 107: 478–480.

Gruber W. 1888. Vagina propria im ligamentum carpi dorsale fur den Bäuch des Extensor digitorum communis manus zum Zeigefingern

beim Menschen – und dieselbe analoge Vagina fur den Bäuch desselben Muskels fur die 2. Zehe des Vorderfusses bei Phascolarctos cinereus. *Arch Path Anat Physiol Klin Med* 114: 369–371.

Halbertsma HJ. 1862. Ontleedkundige Aanteekeningen. Verslagen en Medadeelingen der Koninklijke Akademie van Wetenschappen, *Afdeeling Natuurkunde* 13: 330–347.

Hall HS. 1903. Complete absence of the superficial flexors of the thumb and concurrent anomalies. *J Anat Physiol* 37: 287–289.

Hart JAL. 1972. Extensor digitorum brevis manus. *Hand* 4: 265–267.

Henle J. 1871. *Handbuch der Muskellehre des Menschen. In Handbuch der Systematischen Anatomie des Menschen*. Braunschweig: Verlag von Friedrich Vieweg und Sohn.

Hirasawa Y, Sawamura H, Sakakida K. 1979. Entrapment neuropathy due to bilateral epitrochleoanconeus muscles. A case report. *J Hand Surg* 4: 181–184.

Hojo T. 1976. A case of the duplicate palmalis longus muscle. *Acta Anat Nippon* 51: 422–425.

Homma T. 1981. Innervation of the accessory head of the flexor pollicis longus et digitorum profundus (Gantzer's muscle). *Acta Anat Nippon* 56: 287–288.

Homma T, Sakai T. 1992. Hand muscles concerning thumb movement in the primates – significance of the human hand. *Primate Research* 8: 25–31.

Johnson RK, Shrewsbury MM. 1976. The pronator quadratus in motions and in stabilization of the radius and ulna at the distal radioulnar joint. J Hand Surg 1: 205–209.

Ikeda A, Nagaoka A, Kimura M. 1958. On the variation of the abductor digiti minimi and the palmaris longus. *Hiroshima Daigaku Igakubu Kaibogaku Daiichi Koza Gyosekishu* 2: 96–100 (in Japanese).

Imaeda T, Cooney WP. 1992. Functional anatomy and biomechanics of the thumb. *Hand Clinics* 8: 9–15.

Inoue R. 1934. Relationship among muscles, blood vessels and nerves of forearm in Japanese. *Acta Anat Nippon* 7: 1155–1207.

Ishimi S. 1950. Studies on the musculacture of the upper extremities of the Japanese fetus. Report on the muscles of the brachium. *Igaku Kenkyu* 20: 766–778.

Ishimi S. 1951. Studies on the musculacture of the upper extremities of the Japanese fetus. II. Report on the muscles of the forearm and hand. *Igaku Kenkyu* 21: 1073–1085.

Ishizuki M, Furyua K, Kumakura T. 1986. Extensor digitorum brevis manus associated with attrition rupture of a common extensor tendon. *J Hand Surg* (A) 11(4): 582–584.

Ito R, Ajiri T, Nakanishi H, Matsumoto Y, Kaneuchi Y, Inokuchi S. 1981. A case of the Flexor carpi radialis profundus. *Showa Univ J Med* 41: 345–346.

Iwami S. 1951. Two cases of anomalous flexor digitorum superficialis. *Igaku Kenyu* 21: 36–37 (in Japanese).

Jackson WT, Viegas SF, Coon TM, Stimpson KD, Frogameni AD, Simpson JM. 1986. Anatomical variations in the first extensor compartment of the wrist. *J Bone Joint Surg* 68A: 923–926.

Jacob M. 1873. Extenseur propre de l'index envoyant un faiseau au médius. *Lyon Med* 13: 36.

Jansen JH. 1850. Waarnemingen van anomale spieren. *Nederlandsch Lancet* 1850: 431–437.

Jeffery AK. 1971. Compression of the deep palmar branch of the ulnar nerve by an anomalous muscle: Case report and review. *J Bone Joint Surg B* 53: 718–723.

Jones BV. 1959. An anomalous extensor indicis muscle. *J Bone Joint Surg* (B) 41: 763–765.

Jones BV, Suffolk I. 1959. An anomalous extensor indicis muscle. *J Bone Joint Surg* (B) 41: 763–765.

Kaneff A. 1969. Sehr seltene Kombination von Muskelvärietäten der radialen und dorsalen Muskelgruppen eines menschlichen Vorderarmes. *Anat Anz* 125: 535–538.

Kaplan EB. 1981. *Anatomical variations of the forearm and hand. In The Hand*, Vol. 1 (TubianaR, ed.) Philadelphia: WB Saunders Company.

Kaplan EB, Nathan P. 1969 Accessory extensor pollicis longus. *Bull NY Hosp Joint Dis* 30: 202–207.

Kater NW. 1902. Two cases of supernumerary radio-palmar muscle-muscle surnumeraire radio-palmaire of Testut. *J Anat Physiol* 36: 76.

Kawai M. 1935. Accessory tendon from the terminal tendon of the M. extensor pollicis longus. *Kaibogaku Zasshi* 8: 261–275 (in Japanese).

Kida M. 1988. The morphology of Gantzer's muscle, with special reference to the morphogenesis of the flexor digitorum superficialis. *Acta Anat Nippon* 63: 539–546.

Kimura K. 1958. Variations of the tendons of insertion of the abductor pollicis longus muscle in Japanese. *Acta Anat Nippon* 33: 523–527.

King TS, O'Rahilly R. 1950. M. palmaris accessorius and duplication of m. palmaris longus. *Acta Anat* 10: 327–331.

Koebke VJ, Werner J, Piening H. 1984. The quadrate pronator muscle: a morphological and functional analysis. Anat Anz 157: 311–318.

Kosugi K, Fujishima A, Koda M, Tokudome M. 1984. Anatomical study on the variation of the extensor muscles of the forearm. 2. M. extensor digitorum manus brevis. *Tokyo Jikekai Med J* 99: 877–883 (in Japanese).

Kosugi K, Kounoda M, Kageyama I, Tokudome M. 1985. Anatomical study of the variations of the extensor muscles of the forearm. 4 M. extensor pollicis brevis. *Jikeikai Med J* 100: 63–70.

Kosugi K, Shibata S, Yamashita H. 1987a. Anatomical study on the variation of extensor muscles of human forearm. 6. M.extensor carpi radialis longus. *Jikeikai Med J* 34: 51–60.

Kosugi K, Shibata S, Yamashita H. 1987b. Anatomical study on the variation of extensor muscles of forearm. 7. M.extensor carpi radialis brevis. *Jikeikai Med J* 34: 61–69.

Kosugi K, Shibata S, Yamashita H. 1989. Anatomical study of the variation of the extensor muscles of the human forearm. 1. The relationship between differentiation and variation. *Jikeikai Med J* 36: 93–111.

Krishnamurti A. 1962. Anomalous insertion of extensor pollicis longus. *J Anat Soc India* 11: 90–91.

Krueg G. 1872. Ein accessorischer palmaris longus mit doppelter Endsehne. *Wiener med Wochenschrift* 49: 1229.

Kuczynski K. 1972. Development of the hand and some anatomical anomalies. *Hand* 4: 1–9.

Kuschner SH, Gellman H, Budinger A. 1989. Extensor digitorum brevis manus. An unusual cause of exercise-induced wrist pain. *J Sports Med* 17: 440–441.

Kuwahata T, Sakamoto F. 1959. One case of variation of the M. extensor indicis. *Kagoshima Daigaku Igaku Zasshi* 11: 1440–1442 (in Japanese).

Lacy T III, Goldstein LA, Tobin CE. 1951. Anatomical and clinical study of the variations in the insertions of the abductor pollicis longus tendon, associated with stenosing tendovaginitis. *J Bone Joint Surg* 33A: 347–350.

Lahey MD, Aulicino PL. 1986. Anomalous muscles associated with compression neuropathies. *Orthopaedic Review* 15(4): 199/19–28/208.

Lauth EA. 1830. Varietes dans la distribution des muscles de l'homme. *Mem de la Soc d'Histoire Naturelle de* Strasbourg T1: 1830.

Le Double AF. 1897. *Traité des variations du Systeme Musculaire de l'Homme et leur Signification au Point de Vue de l'Anthropologie Zoologique*. Vol 2. Paris: Schleicher Freres.

Linburg RM, Comstock BE. 1979. Anomalous tendon slips from the flexor pollicis longus to the flexor digitorum profundus. *J Hand Surg* 4: 79–83.

Lucas GL. 1979. An intratendinous cyst in the extensor digitorum brevis manus tendon. *J Hand Surg* 4: 176–177.

Lunda O, Cihak R. 1967. Clinical significance of muscle extensor digitorum manus brevis and similar variations. *Rozhl Chir Praha* 46: 652–658.

Lutz BS, Ingianni G, Durmus C. 1997. A rare insertion variant of the extensor pollicis brevis tendon. A case report. *Handchir Mikrochir Plast Chir.* 29: 79–82 (in German).

Macalister A. 1868. On the nature of the coronoid portion of pronator radii teres. *J Anat Physiol* 2: 8–12.

Macalister A. 1871. The varieties of the pronator quadratus. *J Anat Physiol* 5: 32–34.

Macalister A. 1875a. On the nature of the coronoid portion of pronator radii teres. *J Anat Physiol* 2: 8–12.

Macalister A. 1875b. Observations on muscular anomalies in the human anatomy. Third series with a catalogue of the principal muscular variations hitherto published. *Trans Roy Irish Acad Sci* 25: 1–130.

Macalister A. 1875c. Additional observations on muscular anomalies in human anatomy. Third series with a catalogue of the principal muscular variations hitherto published. *Trans Roy Irish Acad Sci.* 25: 131–134.

Madsen E. 1947. Musculus palmaris longus inversus. *Nordisk Medicin* 37: 855–856.

Maguire WB. 1977. Les muscles anormaux de la main. *Commun GEM Ann Chir* 31: 371.

Mainland D. 1927. An uncommon abnormality of the flexor digitorum sublimis muscle. *J Anat* 62: 86–89.

Malhotra VK, Singh NP, Tewari SP. 1982. The accessory head of the flexor pollicis muscle and its nerve supply. *Anat Anz* 151: 503–505.

Mangini U. 1960. Flexor pollicis longus muscle. *J Bone Joint Surg* (A) 42(3): 467–470.

Manno A. 1907. Un cas de M. extensor digitorum brevis de la main. *Arch Ital Biol* 47: 482.

Martinez R, Omer GE. 1985. Bilateral subluxation of the base of thumb secondary to an unusual abductor pollicis longus insertion: a case report. *J Hand Surg* 10A: 396–399.

Matsushima R, Ikuta T. 1959. An anomalous case of extensor carpi radialis brevis and longus. *Studies Depart Anatomy, Hiroshima Univ School Med* 4: 17–19 (in Japanese).

McGregor AL. 1926. A contribution to the morphology of the thumb. *J Anat* 60: 266–269.

Meyer FN, Pflaum BC. 1987. Median nerve compression at the wrist caused by a reversed palmaris longus muscle. *J Hand Surg A* 12: 369–371.

Mitsuyasu H, Yoshida R, Shah M, Patterson RM, Viegas SF. 2004. Unusual variant of the extensor carpi radialis brevis muscle: a case report. *Clin Anat* 17: 61–63.

Mori M. 1964. Statistics on the musculature of the Japanese. *Okajimas Fol Anat Jap* 40: 195–300.

Morimoto I, Hirata K, Yoshida S. 1993. Variability of origin of serratus anterior muscle in Japanese. *Acta Anat Nippon* 67: 744–748.

Moriya M. 1956. The variation of the M. palmaris longus and the extensor indicis. *Tokyo Jikeikai Ikadaigaku Zasshi* 71: 2035–2041 (in Japanese).

Morrison JT. 1916. A palmaris longus muscle with a reversed belly forming an accessory flexor muscle of the little finger. *J Anat Physiol* 50: 324–326.

Murakami Y, Todani K. 1982. The extensor indicis brevis muscle with an unusual ganglion. *Clin Orthop Rel Res* 162: 207–209.

Nakano T. 1922. Beiträge zur Anatomie der Chinesen. Die Statistik der Muskelvarietäten. *Okajimas Folia Anat Jap* 1: 274–282.

Nakano T. 1923. Beiträge zur Anatomie der Chinesen. Die Statistik der Muskelvarietäten. *Okajimas Folia Anat Jap* 1: 273–282.

Nakano Y, Matsumoto T. 1959. On the variation of the muscle of the forearm (anomaly of the M. palmaris longus). Kaibogaku Zasshi 34: Supplement 69 (in Japanese).

Nayak SR, Madhan Kumar SJ, Krishnamurthy A, Prabhu LV, Ranade AV, Rai R, Ramanathan L. 2007. An additional radial wrist extensor and its clinical significance. *Ann Anat* 189: 283–286.

Nikolajew PW. 1932–33. Zur Frage über die funktionale Bedeutsamkeit der Mm. palmaris longi beim Menschen. *Anat Anz* 75: 145–160.

Nimura A. 2014. Joint capsule attachment to the extensor carpi radialis brevis origin: an anatomical study with possible implications regarding the etiology of lateral epicondylitis. J Hand Surg Am. 39: 219–225.

Nishida K. 1941. Ueber den Bau des M. brachioradialis und seiner Anstazsehne. *Arbeite aus der med Fakultät Okayama* 6: 492–498.

Nomura S, Torisu T, Kitajima T. 1976. A case of the extensor digitorum brevis manus. *Seikei-Geka* 27: 148–149 (in Japanese).

Ogura T, Inoue H, Tanabe G. 1987. Anatomic and clinical studies of the extensor digitorum brevis manus. *J Hand Surg* (A) 12: 100–107.

Ohtani O. 1979. Structure of the flexor digitorum superficialis. *Okajimas Folia Anat Jap* 56: 276–288.

Ouchi H, Kasai T. 1953. Distribution of inner nerves in brachialis. Acta Anat Nippon 28: Appendix 7.

Oudenaarde EV. 1991. Structure and function of the abductor pollicis longus muscle. *J Anat* 174: 221–227.

Pales L. 1946. Les variations de fréquence du muscle petit palmaire (m. palmaris longus) dons les races humaines esai de mise au point de la questions. *Bull Mem Soc Anthropol de Paris* 7: 157–184.

Patel MR, Desai SS. 1988. Anomalous muscles of the first dorsal compartment of the wrist. *J Hand Surg* 13A: 829–831.

Paul S, Das S. 2007. Variant abductor pollicis longus muscle: a case report. Acta Medica (Hradec Kralove) 50: 213–215.

Peeling WB. 1966. Short extensor muscles of the hand. *Brit J Surg* 53: 359–360.

Petit A. 1880. Anomalie musculaire: Un digastric muscle de l'avantbras droit. *Bulletins et Mem de la Société Anatomique de Paris* LV(1): 114–115.

Pires de Lima JA. 1914. Nova série de observações Portugesas de anomalias musculares. *Arch de Anat e de Anthropol* 1(3): 231–260.

Pitt T. 1976. An unusual hand "tumour" extensor digitorum brevis. *Brit J Plast Surg* 29: 368–369.

Poiriér P. 1887. Muscle court extenseur des doights (pédieux de la main). *Bullétins et Mémoires de la société Anatomique de Paris* 1887 (12): 880–881.

Rayan GM, Mustafa E. 1989. Anomalous abductor pollicis longus insertion in the thenar muscles. *J Hand Surg* (A) 14: 550–552.

Reef T, Brestin SG. 1975. The extensor digitorum brevis manus and its clinical significance. *J Bone Joint Surg* (A) 57: 704–706.

Reid RW, Taylor S. 1879. Anatomical variations. *Reports St Thomas' Hospital* 9: 48.

Reimann AF, Daseler EH, Anson BJ, Beaton LE. 1944. The palmaris longus muscle and tendon. A study of 1600 extremities. *Anat Rec* 89: 495–505.

Riche P. 1897. Le nerf cubital et les muscles de l'éminence thénar. *Bull Mem Soc Anat Paris* 5: 251–252.

Riodan DC, Stokes HM. 1973. Synovitis of the extensors of the fingers associated with extensor digitorum brevis manus muscle. *Clin Orthop Rel Res* 95: 278–280.

Ritter MA, Inglis AE. 1969. The extensor indicis proprius syndrome. *J Bone Joint Surg* (A) 51: 1645–1648.

Roberts PH. 1972. An anomalous accessory palmaris longus muscle. *Hand* 4: 40–41.

Roman-Liu D, Tokarski T, Wójcik K. 2004. Quantitative assessment of upper limb muscle fatigue depending on the conditions of repetitive task load. *J Electromyogr Kinesiol.* 14: 671–682.

Ross AJ, Troy CA. 1969. The clinical significance of the extensor digitorum brevis manus. *J Bone Joint Surg B* 51: 473–478.

Saadeh FA, Bergman RA. 1986. Doubled palmaris longus muscle (with accessorius ad flexorem digiti minimi). *Anat Anz* 161: 393–395.

Saadeh FA, Kawas SH, Bergman RA. 1990. A doubled flexor carpi radialis muscle. *Gegenbaurs Morphol Jahrbuch (Leipzig)* 136: 201–204.

Sahinoglu K, Cassell MD, Miyauchi R, Bergman RA. 1994. Musculus comitans nervi mediani (Palmaris profundus). *Ann Anat* 176: 229–232.

Salama R, Weissman SL. 1975. Congenital bilateral anomalous band between flexor and extensor pollicis longus tendons. *Hand* 7: 25–26.

Sakamoto K, Nasu H, Nimura A. Hamada J, Akita K. 2015. An anatomic study of the structure and innervation of the pronator quadratus muscle. Anat Sci Int 90: 82–88.

Schaeffer JP. 1909. On the variations of the palmaris longus muscle. *Anat Rec* 3: 275–278.

Scheldrup EW. 1951. Tendon sheath patterns in the hand: an anatomical study based on 367 hand dissections. *Surg Gynecol Obstet* 93: 16–22.

Schenk RR. 1964. Variations of the extensor tendons of the fingers. Surgical significance. *J Bone Joint Surg* (A) 46: 103–110.

Schlafly B, Lister G. 1987. Median nerve compression secondary to bifid reversed palmaris longus. *J Hand Surg A* 12: 371–373.

Schuldt HH. 1947–48. Ein zweibäuchiger Musculus abductor tertius des rechten *Daumens Anat Anz* 96: 418.

Sebileau P. 1887. Sur le muscle pédieux de la man. *Bullétins et Mémories de la Société Anatomique de Paris* 1887(12): 852–853.

Shaw JA, Manders EK. 1988. Extensor digitorum brevis manus muscle: a clinical reminder. *Orthop Review* 17: 867–869.

Shepherd FJ. 1880a. Notes of abnormalities observed in the dissecting-room of McGill University from October 1875 to May 1879. *Ann Report Montreal General Hospital* 1: 71–93.

Shepherd FJ. 1880b. Anatomical variations: An account of a few of the more interesting abnormalities that have occurred in the dissecting-rooms during the last seven years; with remarks on their morphological significance, and their bearing on the practice of surgery. *St Bartholomews Hospital Reports* 16: 69–105.

Shiraki Y. 1934. On the rare variations of the muscles, peroneus quartus and M. extensor digiti brevis. *Aichi Igakkai Zasshi* 41: 511–514 (in Japanese).

Smith EB. 1897. Some points in the anatomy of the dorsum of the hand, with special reference to the morphology of the extensor brevis digitorum manus. *J Anat Physiol* 31: 45–58.

Souter WA. 1966. The extensor digitorum brevis manus. *Brit J Surg* 53: 821–823.

Spinner M. 1968. The arcade of Frohse and its relationship to posterior interosseous nerve paralysis. *J Bone Joint Surg B* 50: 809–881.

Spinner M. 1970. The anterior interosseous nerve syndrome with special attention to its variations. *J Bone Joint Surg* (A) 52: 84–94.

Spinner M, Olshansky K. 1973. The extensor indicis proprius syndrome: A clinical test. *Plast Reconstr Surg* 51: 134–138.

Spinner RJ, Spinner M. 1996. Superficial radial nerve compression at the elbow due to an accessory brachioradialis muscle: A case report. *J Hand Surg (Am)* 21(3): 369–372.

Spourgitis J. 1895. Sur un rameau musculaire très rare fourni par le nerf cubital. *Bull Soc Anatomique Paris* 9: 410–411.

Stark HH, Otter TA, Boyes JH, Richard TA. 1979. "Atavistic contrahentes digitorum" and associated muscle abnormalities of the hand: A cause of symptoms. *J Bone Joint Surg* A 61: 286–289.

Steichen JB, Peterson DP. 1984. Junctura tendinum between extensor digitorum communis and extensor pollicis longus. *J Hand Surg* (A) 9: 674–676.

Stein AH. 1951. Variations of the tendons of insertion of the abductor pollicis longus and extensor pollicis brevis. *Anat Rec* 110: 49–55.

Stewart SF. 1954. Reverse palmaris longus. *J Bone Joint Surg B* 36: 689–690.

Still JM Jr, Kleinert HE. 1973. Anomalous muscles of nerve entrapment in the wrist and hand. *J Plast Reconstr Surg* 52: 394–400.

Stith JS, Browne PA. 1979. Extensor digitorum brevis manus: a case report and review. *Hand* 11: 217–223.

Straus WL Jr. 1941. Phyologeny of the human forearm extensors. *Hum Biol* 13: 203–238.

Straus WL Jr, Temkin O. 1943. Vesalius and the problem of variability. *Bull Hist Med* 14: 609–633.

Sunderland S. 1945. The actions of the extensor digitorum communis, interosseous and lumbrical muscles. *Am J Anat* 77: 189–209.

Suzuki M. 1955. Studies on the M. palmaris longus. Its statistics and heredity. Nihon Jinruigakkai Nihon Minzokugakkai Kyokai Rengotaikai. 9 1955. *Jinruigaku Zasshi* 63: 155–157 (in Japanese).

Suzuki M. 1957. On the palmaris longus of the Sado population. *Jinruigaku Shuho* 18: 159–162 (in Japanese).

Suzuki M, Morimoto I, Shimasaki H. 1958. On the doubled M. palmaris longus and its accessory muscle-bundle. Medical Journal of Shinshu University. 3: 157–163 (in Japanese).

Swamy R, Rao M, Kumar N, Sirasanagandla S, Nelluri V. 2013. Unusual branching pattern of axillary artery associated with the high origin of ulnar artery. *Ann Med Health Sci Res* 3: 265–267.

Takeda R, Takeishi M, Ezaki T. 1955. The platysma in the Kyushu Japanese population. *J of Krume Med Asc* 18: 379–384.

Takeshige Y, Kitano Y, Kono T, Kurematsu K, Oka S. 1959. Ueber die veiderseitige anomalie des musculus digiti secondi et quinti des M.flexor digitorum supereicialis. *J Krume Med Ass* 22: 22–32.

Takeuchi R, Noda Y. 1961. Pri la malesto de M. palmaris longus kaj lastato de manplata aponeŭrozo. *J NUMA* 20: 953–959.

Takeuchi R, Noda Y. 1962. La varioj de Mm. flexor digitorum superficialis kaj profundus, viditaj ĉe unu kaj sama individuo. *J NUMA* 21: 295–301.

Takeuchi S, Kato S, Komiya Y, Hayami H. 1978. Two cases of the surplus slip of the extensor digitorum tendon to the thumb. *Acta Anat Nippon* 53: 377–378.

Takisawa A, Fujimaki N, Jinguji Y. 1979. A rare case of M. palmaris profundus. *Acta Anat Nippon* 54: 136–139.

Tanaka T, Moran SL, Zhao C, Zobitz ME, An K-N, Amadio PC. 2007. Anatomic variation of the 5th extensor tendon compartment and extensor digiti minimi tendon. *Clin Anat* 20: 677–682.

Tenchini L. 1903. Sur un noveau muscle surnuméraire de la région postérieure de l'avant-bras humain (M. extensor digiti indicis et medii) associé a un faisceau manieux. *Arch Ital Biol* 39: 481.

Thompson JW, McBatts J, Danforth CH. 1921. Hereditary and racial variations in the musculus palmaris longus. *Am J Phys Anthropol* 4: 205–218.

Tountas CP, Halikman LA. 1976. An anomalous flexor digitorum sublimis muscle. A case report. *Clin Orthop Rel Res* 121: 230–233.

Tountas CP, Bergman RA. 1993. *Extensor pollicis brevis. In Anatomic Variations of the Upper Extremity*. New York: Churchill Livingstone.

Tsubaki H, Onuki H. 1953. Some variations of the muscles (M. omohyoideus, M. extensor indicis and some unknown muscle in leg). *Acta Anat Nippon 28: Supple Kanto 6* (in Japanese).

Usami F. 1987. Bilateral congenital absence of the flexor pollicis longus with craniofacial abnormalities. *J Hand Surg* (Am) 12: 603–604.

Varian JPW, Pennington DG. 1977. Extensor digitorum brevis manus used to restore function to a ruptured extensor pollicis longus. *Brit J Plast Surg* 30: 313–315.

von Schroeder HP, Botte MJ. 1991. The extensor medii proprius and anomalous extensor tendons to the long finger. *J Hand Surg* 16: 1141–1145.

von Schroeder HP, Botte MJ. 1995. Anatomy of the extensor tendons of the fingers: Variations and multiplicity. *J Hand Surg* 20: 27–34.

von Schroeder HP, Botte MJ, Gellman H. 1990. Anatomy of the junctturae tendinum of the hand. *J Hand Surg* 15A: 595–602.

Wagstaffe WW. 1872. Partial deficiency of the tendon of the long flexor of the thumb. *J Anat Physiol* 6: 212–214.

Watanabe H, Abe M, Kunishima I. 1972. A case of the extensor digitorum brevis manus. *Seikei-Geka* 23: 1060–1061 (in Japanese).

Wilkinson JL. 1953. The insertions of the flexores pollicis longus et digitorum profundus. *J Anat* 87: 75–88.

Winkelman NZ. 1983. An accessory flexor digitorum profundus indicis. *J Hand Surg* 8: 70–71.

Wood J. 1864. On some varieties in human myology. *Proc Roy Soc Lond B* 13: 299–303.

Wood J. 1865. Additional varieties in human myology. *Proc Roy Soc Lond B* 14: 378–392.

Wood J. 1866. Variations in human myology observed during the winter session of 1865–66 at King's College, London. *Proc Roy Soc Lond B* 15: 229–244.

Wood J. 1867a. On human muscular variations and their relation to comparative anatomy. *J Anat Physiol* 1: 44–59.

Wood J. 1867b. Variations in human myology observed during the winter session of 1866–67 at King's College, London. *Proc Roy Soc Lond B* 15: 518–546.

Wood J. 1868. Variations in human myology observed during the winter session of 1867–68 at King's College, London. *Proc Roy Soc Lond B* 16: 483–525.

Wood VE. 1988. The extensor carpi radialis intermedius tendon. *J Hand Surg* (A) 13: 242–245.

Yalcin B, Kutoglu T, Ozan H, Gurbuz H. 2006. The extensor indicis et medii commuins. *Clin Anat* 19: 112–114.

Yamada T. 1986. Re-evaluation of the Flexor digitorum superficialis. *Acta Anat Nippon* 61: 283–298.

Yamamoto T, Sato Y. 1960. Studoj pri la ekstensoraj tendenoj de mano, precipe pri la tendena anastomozo ĉe homo. (La 2a raporto.) *J NUMA* 19: 3930.

Yogesh A, Marathe R, Pandit S. 2011. Musculocutaneous nerve substituting for the distal part of radial nerve: A case report and its embryological basis. *J Neurosci Rural Pract* 2: 74–76.

Yoshida Y. 1978. Studies on the Extensor Indicis Muscle in Man. *Acta Anat Nippon* 53: 1–15.

Yoshida Y. 1985. A study on the extensor digiti minimi muscle in man. *Acta Anat Nippon* 60: 185–196.

Yoshida, Y. 1990. Anatomical study on the extensor digitorum profundus muscle in the Japanese. *Okajimas Folia Anat Jap* 66: 339–354.

Yoshida Y. 1994. Anatomical studies on the extensor carpi radialis longus and brevis muscles in Japanese. *Okajimas Folia Anat Jap* 71: 127–136.

Yoshida Y. 1995. Anatomical studies on the extensor pollicis et indicis accesorius muscle and the extensor indicis radialis muscle in Japanese. *Okajimas Folia Anat Jap* 71: 35–364.

Yoshida Y, Fukuyama U. 1979. Phylogeny of forearm extensor musles in tetrapods. *J Kanazawa Med Univ* 4: 122–130.

Yoshida Y, Yasutaka S, Seki T. 1983. Studies on the flexor carpi radialis profundus and palmaris profundus muscles in man. *Acta Anat Nippon* 58: 58–67.

Yoshida Y, Yasutaka S, Seki T. 1984. Studies on the extensor digitorum brevis manus muscle in man. *Acta Anat Nippon* 59: 313–321.

Zientarski B. 1976. A rare variation of the extensor indicis muscle. *Folia Morphol,* Warsaw 35: 401–493.

34 Hand intrinsic muscles

Mirtha A. Gonzalez[1] and David T. Netscher[2]
[1, 2]Baylor College of Medicine, Houston, Texas, United States
[2]Weill Medical College, Cornell University, New York, New York, United States

The hand is a complicated and unique structure in the human body. It performs many functions from delicate, precise actions to heavy labor. The hand is made up of a large number of muscles that help to perform various functions. Marius Fahrer stated "extrinsic muscles are said to be strong, pluriarticular, little differentiated motors, supplying mainly the force required for common power movements, without real precision. The short intrinsic muscles are said to be essentially the motors of fine movements." The intrinsic muscles of the hand include the muscles of the palm, the thumb, the little finger, the lumbrical muscles, and the interosseous muscles. They are crucial to motor control of the hand and have been observed to have multiple variations.

Sir William Osler stated that "variability is the law of life," and in this chapter the variations of the intrinsic muscles of the hand are explored in detail. The normal anatomy of the intrinsic muscles of the hand is briefly presented to allow for comparison. However, the chapter is focused on the observed variations of the intrinsic muscles of the hand. To facilitate the presentation of the various observed findings their descriptions will be subdivided into: origin; insertion; course and structure; numerical; and neurovascular variations. In the concluding section, the implications of these variations are discussed to determine why this variability may prove to be clinically important. A multitude of variations have been observed and, while the clinical ramifications they present may lead to confusion, they are nonetheless relatively uncommon. Because of the high frequency of these variations, vigilance is necessary even when performing common procedures (e.g., nerve decompression or tendon repair) in order to recognize abnormal anatomy and avoid injury.

Thenar muscles

There are four thenar muscles: the abductor pollicis brevis; flexor pollicis brevis; opponens pollicis; and the adductor pollicis (listed in order from superficial to deep). The bellies of these muscles form a thick, fleshy area directly proximal to the thumb, and together their synergistic actions help in opposition of the thumb. The thenar muscles are innervated by the median and ulnar nerves. The motor branch of the median nerve innervates the abductor pollicis brevis, the opponens pollicis, and the superficial head of the flexor pollicis brevis. The deep head of the flexor pollicis brevis and the adductor pollicis are innervated by the ulnar nerve (Kaplan 1965).

Abductor pollicis brevis

Normal

Origin: Palmar surface of the flexor retinaculum and the trapezium (Fig. 34.1a).

Insertion: Fibers converge into a flat tendon with two layers (superficial and deep). The superficial layer joins the aponeurosis of the extensor pollicis longus along the lateral band. The deep layer inserts on the radial side of the base of the proximal phalanx of the thumb.

Variations

Origin: May arise from the scaphoid bone and from a slip off of the abductor pollicis longus (Doyle and Botte 2003).

Insertion: No specific variations have been described.

Course and structure: Accessory slips:

1. The muscle may receive slips from the scaphoid or styloid process of the radius.
2. An accessory slip may join the muscle with the abductor pollicis longus.
3. The muscle may have attachments to other neighboring structures including palmaris longus, extensor carpi radialis longus, accessory extensor carpi radialis, opponens pollicis, flexor pollicis brevis, the adductor pollicis, scaphoid, extensor pollicis longus or extensor pollicis brevis, although these attachments are rare (Fig. 34.1b).
4. A cutaneous slip is frequently present, attached to the skin over the proximal part of the thenar eminence and inserted distally on the radial side of the proximal phalanx of the thumb (Bergman et al. 2006; Fig. 34.1c).

Bergman's Comprehensive Encyclopedia of Human Anatomic Variation, First Edition. Edited by R. Shane Tubbs, Mohammadali M. Shoja and Marios Loukas.
© 2016 John Wiley & Sons, Inc. Published 2016 by John Wiley & Sons, Inc.

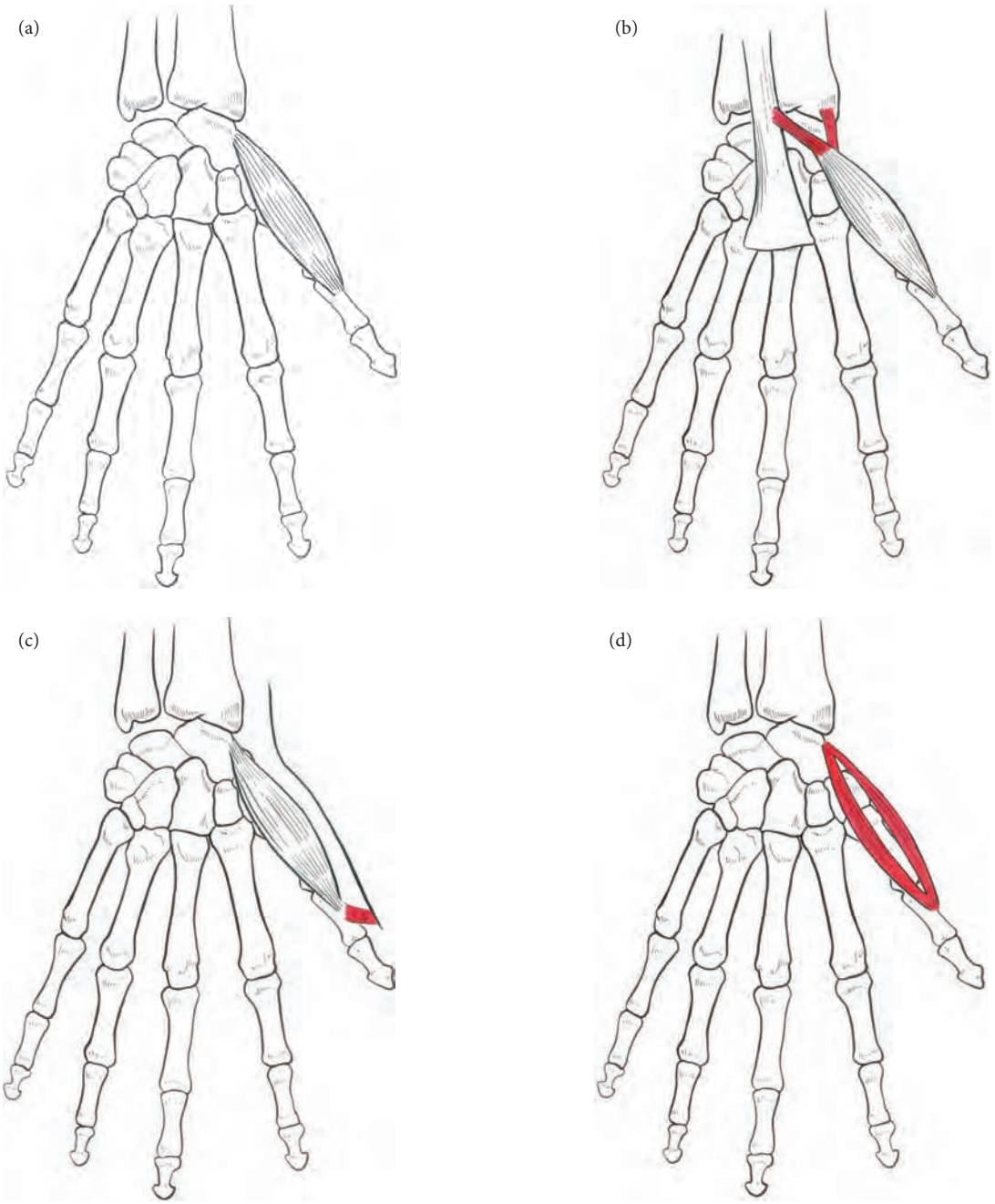

Figure 34.1 Abductor pollicis brevis: (a) normal; (b) tendon slip from palmaris longus or from radial styloid, scaphoid, and other tendons; (c) accessory slip to skin; and (d) muscle divided into two separate heads.

Numerical:

1. May be absent (Doyle and Botte 2003).
2. May be doubled (Tountas and Bergman 1993). The abductor pollicis brevis can be divided completely into two (two separate heads). This is in distinction from the two layers present at its point of insertion (Doyle and Botte 2003; Fig. 34.1d).
3. A third head may arise from the opponens pollicis (Wood 1868; Tountas and Bergman 1993).

Neurovascular: The median nerve may join with a branch of the radial nerve to provide innervation to the muscle (Kaplan 1965).

Flexor pollicis brevis

Normal

Origin: Has two heads (Fig. 34.2), superficial and deep, divided by the tendon of flexor pollicis longus. The superficial head arises from the trapezium, the flexor retinaculum, and the tendon sheath of the flexor carpi radialis. The deep head arises

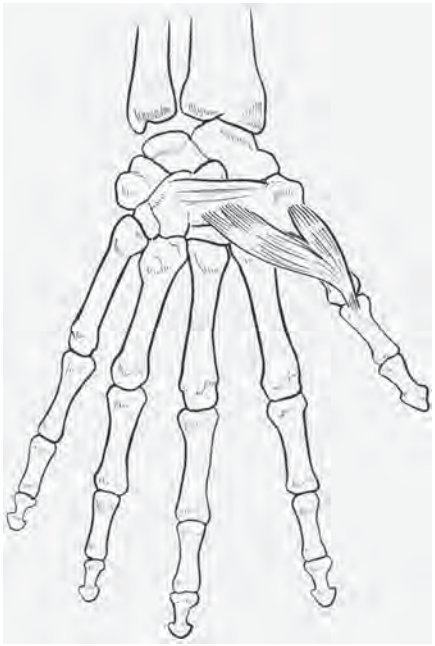

Figure 34.2 Flexor pollicis brevis: normal. Variations of the flexor pollicis brevis exist only in the lack of definition (mergence) with adjacent thenar muscles and potential separation into more muscles bellies.

from the trapezoid, capitate, and the palmar ligaments of the distal carpal row.

Insertion: Superficial head: inserts on the radial side of the volar aspect of the proximal phalanx of thumb. Deep head: passes deep to the tendon of the flexor pollicis longus, joins the superficial head on the sesamoid bone and base of the proximal phalanx of the thumb.

Variations

Origin: No specific variations have been described.

Insertion: No specific variations have been described.

Course and structure:

1. The superficial head has been reported incorporated into the opponens pollicis (Doyle and Botte 2003).
2. The superficial head may be fused with abductor pollicis brevis (Tountas and Bergman 1993).
3. The muscle may be inseparably joined to adductor pollicis.
4. A superficial slip may connect the two heads of the muscles (Wood 1868).

Numerical:

1. May be absent (Bergman et al. 1984).
2. Either (superficial/deep heads) or both heads may be doubled or absent (Kaplan 1965; Tountas and Bergman 1993).
3. An additional head has been found arising from the ulnar side of the base of the thumb metacarpal and the adjacent carpal ligaments. It inserts onto the ulnar side of the base of the proximal phalanx (Doyle and Botte 2003).

Neurovascular: An interesting pattern of innervation has been reported for this muscle. The muscle is located at the terminal aspect of both the motor branch of the ulnar nerve and the recurrent motor branch of the median nerve. The location of the muscle contributes to its dual innervation, as it forms in a "watershed" area of innervation supplied by the two nerves.

1. The superficial head may be innervated by the median, ulnar, or both nerves. In a study of 30 patients, 13 muscles were innervated by the median nerve, 10 by the ulnar nerve, and 7 by both nerves (Tountas and Bergman 1993).
2. The deep head is innervated primarily by the ulnar (16 of 24 cases), by the median (3 of 24 cases), or by both nerves (5 of 24 cases) (Tountas and Bergman 1993).

Opponens pollicis

Normal

Origin: Palmar surface of the flexor retinaculum and the trapezium (Fig. 34.3a).

Insertion: Radial aspect of the palmar surface of the shaft of the thumb metacarpal.

Variations

Origin: No specific variations have been described.

Insertion: No specific variations have been described.

Course and structure: It may fuse with the flexor pollicis brevis (Doyle and Botte 2003).

Numerical: (1) May be absent (rare) (Doyle and Botte 2003) or (2) may be doubled (Doyle and Botte 2003) (Fig. 34.3b).

Neurovascular: The muscle has been reported to have dual innervation, with the deep branch of the ulnar nerve contributing to its innervation (Doyle and Botte 2003).

Adductor pollicis

Normal

Origin: Two heads, oblique and transverse (Fig. 34.4). The oblique head arises from the capitate, bases of the ring and long finger metacarpals, intercarpal ligaments, and sheath of the flexor carpi radialis. The transverse head arises from the distal two thirds of the palmar surface of the long finger metacarpal (Doyle and Botte 2003).

Insertion: Oblique and transverse heads converge via the ulnar sesamoid of the thumb metacarpalphalangeal joint to insert on the ulnar side of the base of the proximal phalanx of the thumb (Doyle and Botte 2003).

Variations

Origin: The transverse head has been found to originate from the long and ring finger metacarpal bones (Bergman et al. 2006).

Insertion: (1) May insert distally onto the proximal phalanx and the dorsal thumb expansion; or (2) a slip may cross deep to the tendon of the flexor pollicus longus via the radial sesamoid to insert on the radial side of the base of the proximal phalanx of the thumb.

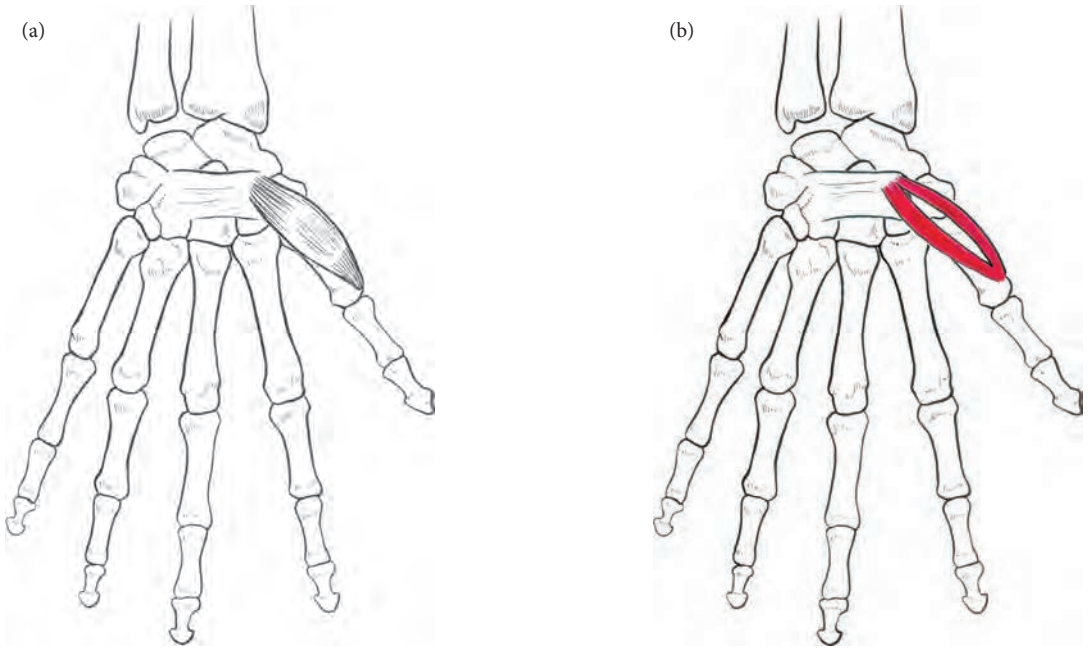

Figure 34.3 Opponens pollicis: (a) normal; and (b) muscle divided into two separate heads.

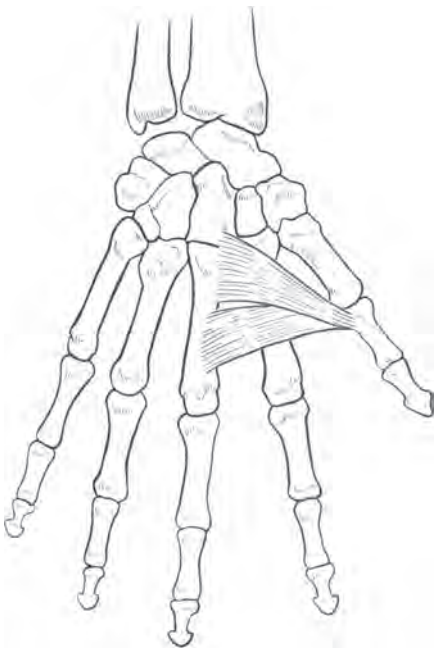

Figure 34.4 Adductor pollicis: normal.

Course and structure:

1. The two heads (oblique and transverse) can be coalesced to varying degrees (Doyle and Botte 2003).
2. Fasciculi can form a transversus manus muscle (Tountas and Bergman 1993). It is closely related to the adductor pollicis. It arises from the volar plate of the metacarpalphalangeal joint of the long finger and connects to the base of the thumb proximal phalanx or in its vicinity (Tountas and Bergman 1993; Doyle and Botte 2003).

Numerical:

1. The muscle can be split into additional bellies (Tountas and Bergman 1993).
2. An accessory head may be present that arises dorsal and radial to the oblique head from the base of the index metacarpal and inserts into the ulnar aspect of the thumb dorsal aponeurosis (Doyle and Botte 2003).

Neurovascular: May be innervated by the median nerve (Kaplan 1965).

Hypothenar muscles

The hypothenar eminence contains the muscles on the opposite side of the palm from the thenar muscles. They are the abductor digiti minimi, flexor digiti minimi, and the opponens digiti minimi. These muscles control the actions of the little finger, and receive their innervation from the ulnar nerve.

Abductor digiti minimi

Normal

Origin: Has two muscle bellies, originating from the pisiform, terminal tendon of the flexor carpi ulnaris, and the pisohamate ligament (Kaplan 1965; Doyle and Botte 2003; Fig. 34.5).

Insertion: Two tendons: one to the ulnar side of the base of the proximal phalanx of the small finger and the other continues to the ulnar border of the dorsal aponeurosis of the

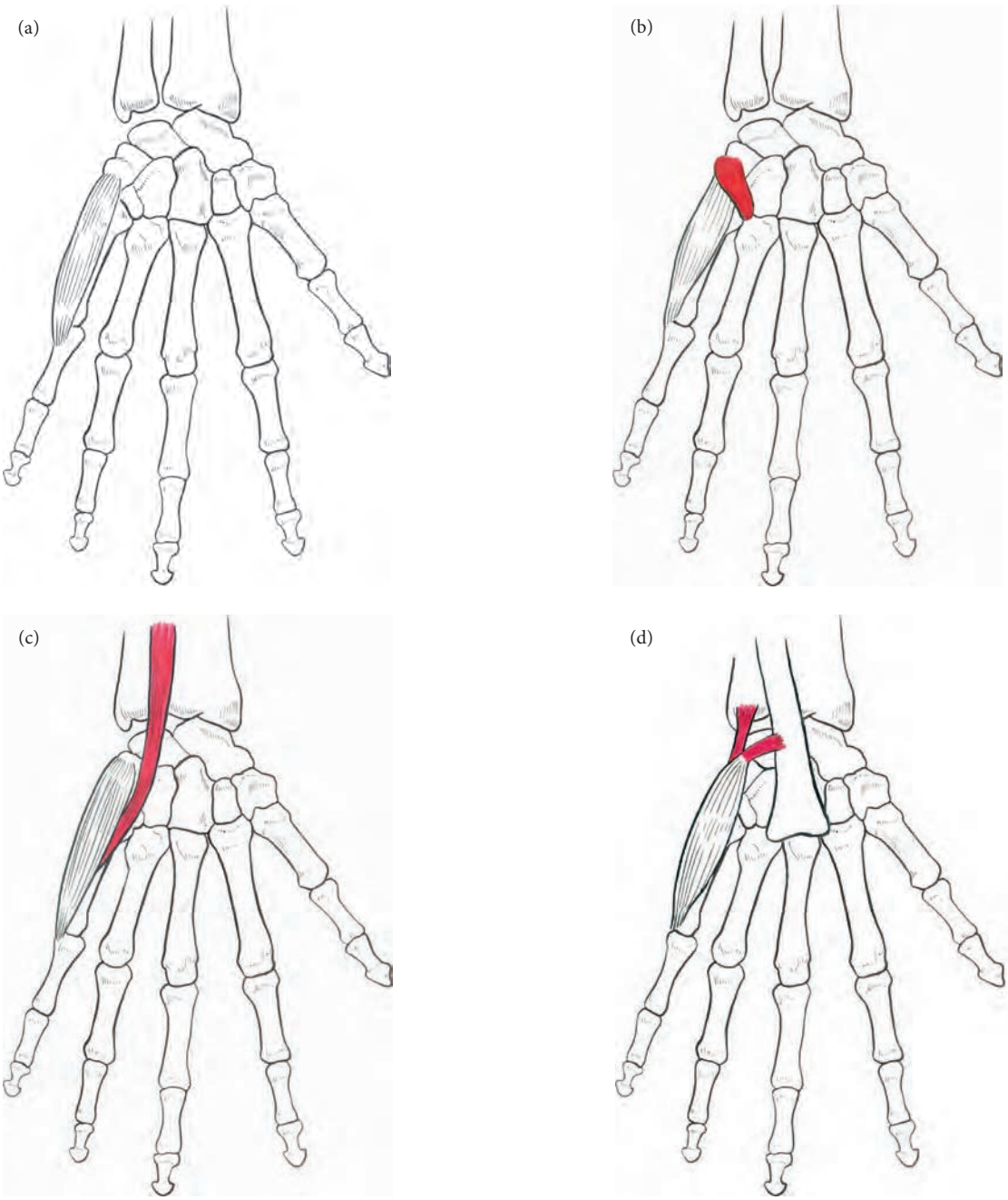

Figure 34.5 Abductor digiti minimi: (a) normal; (b) slip to pisiuncinatus; (c) accessory abductor digiti minimi (may have numerous sources of origin); and (d) slip to palmaris longus or to multiple other locations.

extensor digiti minimi through the lateral band. Of note, the abductor digiti minimi functions as the dorsal interosseous of the small finger by abducting the digit. The dorsal interossei and the abductor digiti minimi are also similar in that both have dual insertions to proximal phalanx and the lateral band.

Variations

The abductor digiti minimi is considered the most variable of all the hypothenar muscles (Soldado-Carrera et al. 2000).

Origin:

1. May have a single origin; has been described as arising only from the pisiform (Macalister 1875).
2. The muscle may have three origins, different from its usual sites of origin. It may arise from the pisiform, extensor retinaculum, and the tendon of the extensor carpi ulnaris (Wood 1866; Macalister 1875).
3. May extend over the entire pisiform bone (Kaplan 1965).
4. May originate high on the fascia of the forearm and therefore course through the Guyon canal (Wood 1868).

Insertion: A part of the muscle may insert only onto the metacarpal of the small finger (Doyle and Botte 2003).

Course and structure:

1. It may be united with the flexor digiti minimi (Kaplan 1965; Tountas and Bergman 1993).
2. It may receive a separate slip from multiple locations (Tountas and Bergman 1993): (a) pisimetacarpeus: slip from the pisiform bone to the metacarpal bone; (b) pisiuncinatus (pisohamatus): a small muscle occurring in 2–5% of hands which extends from the pisiform bone to the hook of the hamate bone (Fig. 34.5b); or (c) pisiulnaris: may extend from the pisiform bone to the flexor retinaculum.

Numerical:

1. May be absent (Tountas and Bergman 1993).
2. May only have a single belly (Kaplan 1965).
3. May be doubled (Tountas and Bergman 1993).
4. The most common accessory muscle belly associated with the hypothenar muscles is the accessory abductor digiti minimi (Soldado-Carrera et al. 2000; Fig. 34.5c).
   a. An accessory head of the abductor digiti minimi is a common variation occurring in as many as 24% of all wrists. Frequent sites of origin include the palmar carpal ligament, tendon of the palmaris longus, tendon of the flexor carpi ulnaris, ulna, and radius. The accessory muscle usually inserts into the abductor digiti minimi, ulnar, and volar to the pisiform bone, near the origin of the abductor digiti minimi muscle (Macalister 1875; Tountas and Bergman 1993; Timins 1999; Fig. 34.5d).
   b. The accessory muscle may originate from the antebrachial fascia of the forearm; in these cases it may traverse the Guyon canal.
   c. A muscle was found with a second head arising from the flexor retinaculum. It was separate from the rest of the muscle as far as the insertion (Wood 1866).

Neurovascular: No specific variations have been described.

Flexor digiti minimi

Normal

Origin: Hook of the hamate and flexor retinaculum (Fig. 34.6).

Insertion: Ulnar side of the base of the proximal phalanx of the small finger.

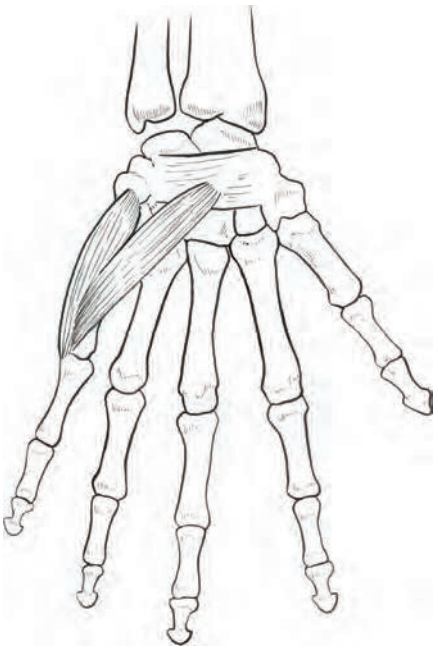

Figure 34.6 Flexor digiti minimi: normal.

Variations

Origin: May arise from the volar aspect of the transverse fibers of the distal antebrachial fascia (Wingerter et al. 2003).

Insertion: May insert on the ulnar side of the base of the proximal phalanx of the small finger and the head of the small finger metacarpal. The opponens digiti minimi muscle was absent in the cadaver with this variation (Saadeh and Bergman 1988).

Course and structure:

1. The flexor digiti minimi may be very small; in these instances the abductor digiti minimi is usually larger than normal (Doyle and Botte 2003).
2. As with the flexor pollicis brevis, the flexor digiti minimi also frequently merges and fuses with adjacent muscles (Bergman et al. 1984; Tountas and Bergman 1993).
3. May be replaced by the abductor or opponens digiti minimi muscles (Bergman et al. 1984; Tountas and Bergman 1993).
4. Accessory slips:
   a. A tendinous slip may arise from the flexor digiti minimi that attaches to the extensor aponeurosis or to the head of the small finger metacarpal (Tountas and Bergman 1993).
   b. A slip may arise from the flexor digiti minimi that courses to the metacarpal shaft between the opponens digiti minimi and the palmar interosseous (Kaplan 1965).
   c. May receive an accessory slip that arises from the hook of the hamate. In a patient with this variant, the anomalous slip coursed through the deep branch of the ulnar nerve causing its compression (Spinner et al. 1996).
   d. May receive a slip that arises from the flexor carpi radialis muscle (De Smet 2002).
5. The muscle may be replaced by a tendinous band that arises from flexor carpi ulnaris and inserts onto the base of the small finger proximal phalanx and the hook of the hamate (Doyle and Botte 2003).

Numerical: (1) May be absent (Doyle and Botte 2003; Wingerter et al. 2003); or (2) may be duplicated (Wingerter et al. 2003).

Neurovascular: No specific variations have been described.

Opponens digiti minimi

Normal

Origin: Hook of the hamate and flexor retinaculum (Fig. 34.7).

Insertion: Ulnar side and palmar surface of the metacarpal of the small finger.

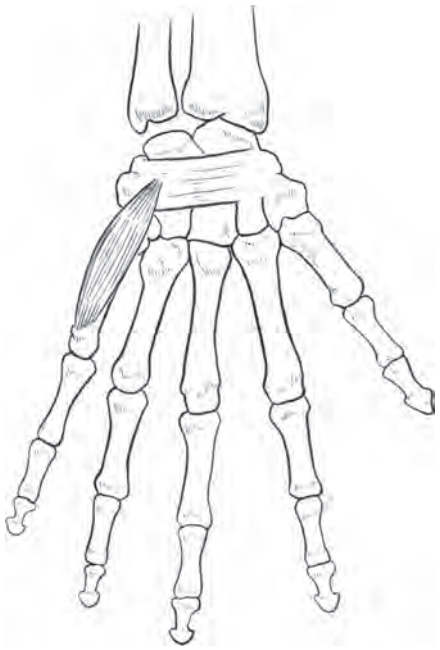

Figure 34.7 Opponens digiti minimi: normal.

Variations

Rarely described, except for the following.

Course and structure:

1. May be fused with neighboring muscles including the abductor digiti minimi or the flexor digiti minimi (Tountas and Bergman 1993; Doyle and Botte 2003).
2. May receive accessory slips (Tountas and Bergman 1993).
3. May be divided into two layers by the deep branches of the ulnar artery and nerve (Doyle and Botte 2003).

Lumbricals

The lumbricals consist of four muscles (Fig. 34.8a) and show frequent variations (20% of individuals; Tountas and Bergman 1993). The median nerve innervates the first and second lumbricals. The deep branch of the ulnar nerve innervates the third and fourth lumbricals.

First lumbrical

Normal

Origin: Radial side and palmar surface of the flexor digitorum profundus tendon of the index finger.

Insertion: Lateral band on the radial side of the extensor digitorum of the index finger.

Variations

Origin:

1. Has been found arising from the tendon of the flexor pollicis longus (Tountas and Bergman 1993).
2. May have a bipennate origin (Bergman et al. 2006): (a) may arise from the flexor digitorum superficialis of the index finger and the flexor pollicis longus; or (b) a case was described in which the origin of one of the muscles was normal and the origin of the second was a fine tendon that arose near the origin of flexor digitorum superficialis in the forearm.

Insertion:

1. May insert on the proximal phalanx of the index finger (Doyle and Botte 2003; Bergman et al. 2006).
2. May have a bifurcarted insertion. The tendon of the first lumbrical is attached both to proximal phalanx and to the lateral band on the radial side of the index finger (Bergman et al. 2006).

Course and structure: accessory slips:

1. An accessory fascicle may arise from the muscular belly of the flexor digitorum superficialis or the flexor digitorum profundus and join the first lumbrical, forming an independent lumbrical for the index finger (Kaplan 1965; Tountas and Bergman 1993; Bergman et al. 2006; Fig. 34.8b).
2. An accessory slip may arise from the tendon of flexor pollicis longus (Fig. 34.8c), the thumb metacarpal, opponens pollicis, or the palmar carpal ligament (Tountas and Bergman 1993; Bergman et al. 2006).
3. A slip may arise connecting the first lumbrical to the first palmar interosseous causing the muscle to look bipinneform (Wood 1866; Bergman et al. 2006).

Numerical: May be absent (Macalister 1875) or may be doubled. One lumbrical inserted to its usual site. The extra lumbrical split into two parts at its insertion. One part was found to insert on the tendon of the flexor digitorum superficialis (near where the muscle splits to insert on the index finger) and the other part joined the lumbrical near its normal insertion on the lateral band (Wood 1866, 1868).

Neurovascular: No specific variations have been described.

Second lumbrical

Normal

Origin: Radial side and palmar surface of the flexor digitorum profundus tendon of the long finger.

Insertion: Lateral band on the radial side of the extensor digitorum of the long finger.

Variations

Origin: May have a bipennate origin, arising from the flexor digitorum profundus tendons on the ulnar side of the index finger and the radial side of the long finger (Wood 1866; Tountas and Bergman 1993).

Insertion: May have a bifurcated insertion:

1. May insert on the radial side of the extensor digitorum of the long finger and the ulnar side of the extensor digitorum of the index finger (Wood 1866).
2. The tendon of the second lumbrical may attach to both to the proximal phalanx and to the lateral band on the radial side of the extensor digitorum of the long finger (Bergman et al. 2006).

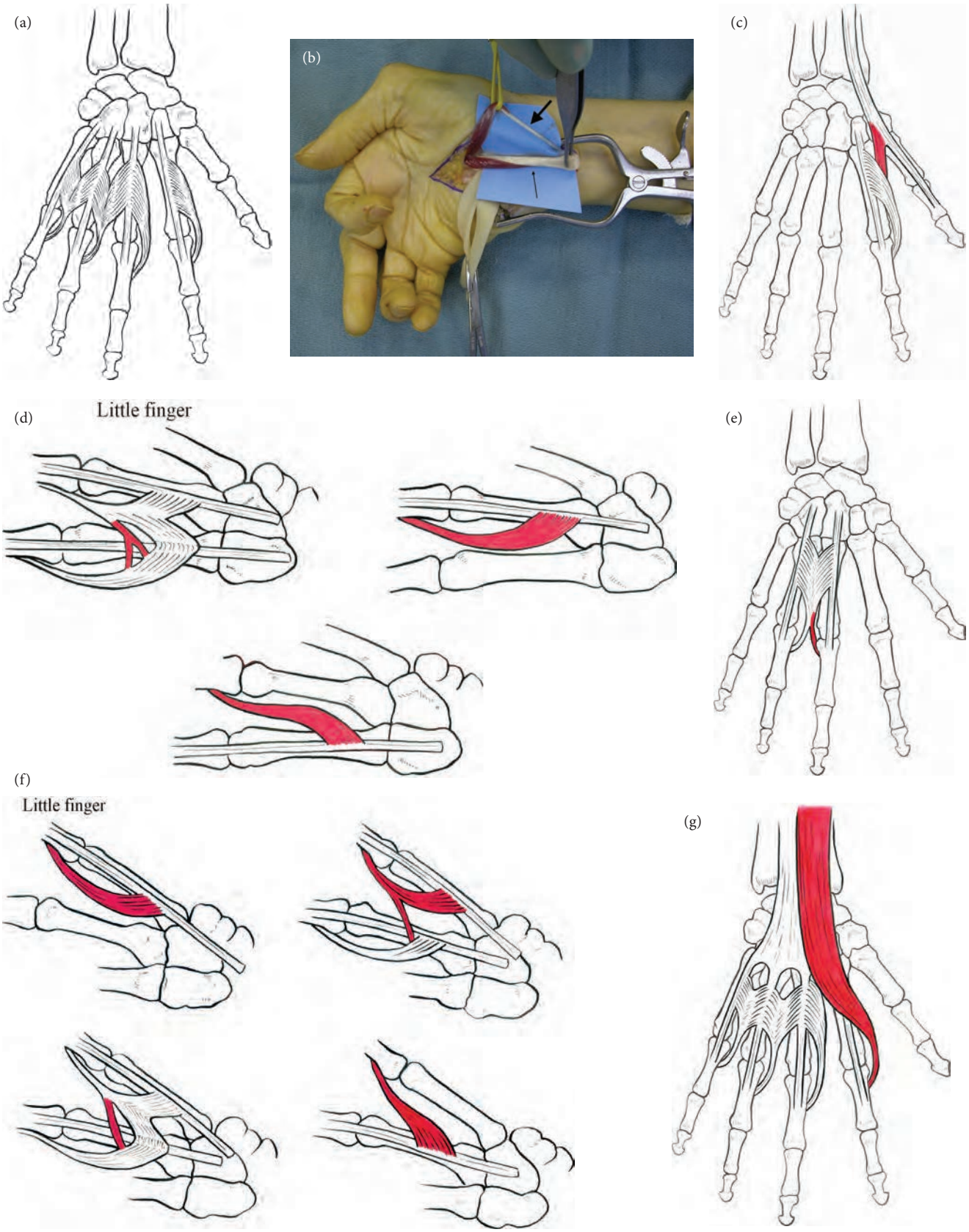

Figure 34.8 Lumbricals: (a) normal; (b) clinical photograph showing an accessory lumbrical to the index finger originating from flexor digitorum profundus (fine arrow: flexor digitorum profundus with normal first lumbrical; bold arrow: accessory lumbrical); (c) slip from the flexor pollicus longus to index finger lumbrical; (d) different origins of third lumbrical; (e) third lumbrical with double insertion; (f) different origins of fourth lumbrical; and (g) lumbrical originating more proximally in the forearm from either flexor digitorum superficialis or flexor digitorum profundus.

Course and structure: No specific variations have been described.

Numerical: (1) May be absent (Kaplan 1965; Bergman et al. 2006); or (2) may be doubled (Tountas and Bergman 1993).

Neurovascular: No specific variations have been described.

Third lumbrical

Normal

Origin: Bipenniform: arising from the flexor digitorum profundus tendons on the ulnar side of the long finger and the radial side of the ring finger.

Insertion: Lateral band on the radial side of the extensor digitorum of the ring finger.

Variations

Origin:

1. May arise from one tendon only (Fig. 34.8d; Tountas and Bergman 1993; Eladoumikdachi et al. 2002b): (a) may originate from the radial side of the ring finger flexor digitorum profundus tendon; or (b) may originate from ulnar side of the long finger flexor digitorum profundus tendon.
2. The origin may be more proximal, arising from the flexor retinaculum, or from a separate tendon that originates from either the superficial or deep flexor digitorum (Tountas and Bergman 1993).

Insertion:

1. The entire third lumbrical has been seen going to the ulnar side of the long finger. This was found in a subject with an absent fourth lumbrical (Wood 1868; Kaplan 1965).
2. May have a bifurcated insertion; may insert on the ulnar side of the extensor digitorum of the long finger and the radial side of the extensor digitorum of the ring finger (Wood 1868; Tountas and Bergman 1993; Doyle and Botte 2003; Fig. 34.8e).
3. May insert onto the proximal phalanx (Doyle and Botte 2003).

Course and structure: accessory slips: may receive fibers from the second or fourth lumbricals (Eladoumikdachi et al. 2002b).

Numerical: (1) May be absent (Kaplan 1965); or (2) may be doubled (Tountas and Bergman 1993).

Neurovascular: May receive variable innervation from the median and ulnar nerve (Doyle and Botte 2003).

Fourth lumbrical

Normal

Origin: Bipenniform: arising from the flexor digitorum profundus tendons on the ulnar side of the ring finger and radial side of the small finger.

Insertion: Lateral band on the radial side of the extensor digitorum of the small finger.

Variations

Origin:

1. May arise from one tendon only (Fig. 34.8f); may originate from the ulnar side of the tendon of flexor digitorum profundus of the ring finger (Zancolli and Cozzi 1992; Tountas and Bergman 1993; Bergman et al. 2006).
2. The origin may be more proximal, arising from the flexor retinaculum, or from a separate tendon that originates from either the superficial or deep flexor digitorum (Tountas and Bergman 1993).

Insertion:

1. May insert on the lateral band on the ulnar side of the extensor digitorum of the ring finger (Wood 1866; Doyle and Botte 2003).
2. May insert onto the capsule of the metacarpal joint, the tendon of the flexor digitorum superficialis, or the extensor expansion of the ring finger (Tountas and Bergman 1993; Doyle and Botte 2003; Bergman et al. 2006).
3. May have a bifurcated insertion; may insert into the ulnar side of the ring finger and the radial side of the small finger through the lateral bands (Wood 1868; Bergman et al. 2006).

Course and structure:

1. May pass through the Guyon canal.
2. Has been found to be replaced by a bundle of fibers from the third interosseous muscle (Bergman et al. 2006).
3. The fourth lumbrical may substitute for the small finger flexor digitorum superficialis, which itself is noted to be absent relatively frequently (Tountas and Bergman 1993; Bergman et al. 2006).

Numerical: May be absent (Kaplan 1965; Bergman et al. 2006) or may be doubled (Tountas and Bergman 1993).

Accessory slips: May receive fibers from the third lumbrical (Eladoumikdachi et al. 2002b).

Neurovascular: No specific variations have been described.

Unclassified variations

All the lumbricals may be absent (Macalister 1875). Wood reported that he found 19 variations in the lumbricals of 102 individuals (5.3%). The lumbricals may be decreased in number from four to two–three, or completely absent (occurs rarely) (Bergman et al. 2006). The lumbricals may originate more proximally in the carpal tunnel or the forearm from either the deep or superficial flexor digitorum (Tountas and Bergman 1993; Fig. 34.8g). Five lumbricals have been reported (Bergman et al. 2006): in one case, the long finger had two lumbricals, the ring finger had two lumbricals, and the little finger had none; in another case, the long finger had two lumbricals and the rest of the lumbricals were normal. Macalister found 12.5% of subjects to have this variation (Macalister 1875). The origins and insertions of the lumbricals were noted to increase in variability from the radial to ulnar side. The first lumbrical was noted to have the least variability of origin, while the third and fourth lumbricals showed the highest variability of origin (Zancolli and Cozzi 1992; Eladoumikdachi et al. 2002b).

The lumbricals are a complex set of muscles, the description of which can be convoluted and difficult to understand. This next section will provide an overview of the lumbricals

to allow for a more straightforward presentation of a complex subject.

Origin

Variations in origin are common, especially for the third and fourth lumbrical:

- First and second lumbricals: unipennate, arise from the flexor digitorum profundus (FDP) tendon of the ring and long fingers, respectively.
- Third and fourth lumbricals: bipennate, arise from the FDP tendon of the long/ring fingers and the small/ring fingers, respectively.

Insertions

The classic description is that all insert exclusively into the radial lateral band of the corresponding finger. They most frequently insert on the radial side of the corresponding digit, but occasionally they may have an ulnar-sided insertion. Zancolli and Cozzi (1992) have described how different distal insertions exist. Possible distal insertions of the lumbricals include bone (proximal phalanx), volar plate "assemblage nucleus," and extensor apparatus (consisting of the lateral band, the oblique fibers, and/or the transverse fibers). In a study by Netscher, all lumbricals except one were found attached to the lateral band. Of those attached to the lateral band, 25% attached exclusively, 44% inserted onto either the oblique or transverse fibers of the extensor mechanism, or both. Netscher also noted that the lumbricals could have attachments to bone, volar plate, or both (Eladoumikdachi et al. 2002b).

Dorsal interossei

There are four dorsal interossei (Fig. 34.9). Most dorsal interossei are bipennate in origin and split into superficial and deep muscle bellies distally at their insertions. The superficial head is bipennate and the deep head has been found to be fusiform and often multipennate. The deep branch of the ulnar nerve innervates all the dorsal interossei.

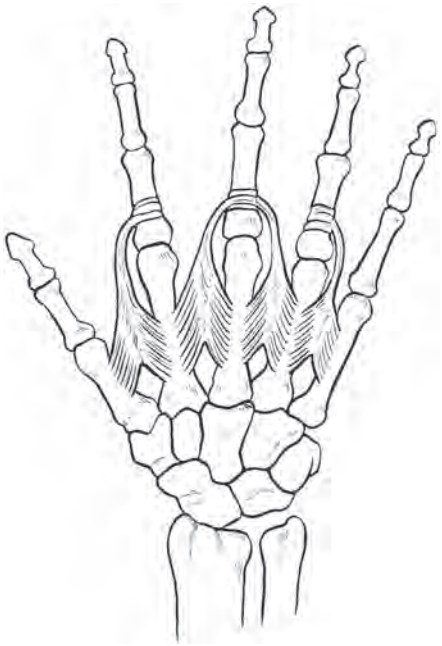

Figure 34.9 Dorsal interossei: normal.

First dorsal interosseous

Normal

Origin: Two heads, arise from the ulnar side of the thumb metacarpal and the radial side of the index finger metacarpal.

Insertion: Divides into superficial and deep muscles bellies, which insert onto the radial side of the base of the index finger proximal phalanx and the lateral band of the index finger, respectively.

Variations

These are rarely described, except for the following.

Insertion: Eyler and Markee described how most of the muscle consisted of the superficial belly. They reported in their cases that 100% of the muscle fibers insert onto the base of the proximal phalanx of the index finger (Eyler and Markee 1954; Doyle and Botte 2003).

Course and structure: The presence of the deep head of the muscle is variable (Eyler and Markee 1954; Doyle and Botte 2003):

1. The deep muscle belly may fuse with the superficial muscle belly to insert onto the base of the index finger proximal phalanx.
2. The deep muscle belly may be a distinct muscle with insertion into the lateral band of the index finger.

Numerical: May be doubled (Wood 1868).

Neurovascular: May be innervated by the radial or musculocutaneous nerve (Doyle and Botte 2003); or may be innervated by the median nerve, noted in 3% of limbs (Tountas and Bergman 1993). This may be associated with a Martin–Gruber anastomosis (median to ulnar nerve crossover in the forearm) or with the Riche–Cannieu anastomosis (median to ulnar nerve crossover in the palm).

Second dorsal interosseous

Normal

Origin: Two heads, arising from the ulnar side of the index finger metacarpal and the radial side of the long finger metacarpal.

Insertion: Divides into superficial and deep muscle bellies, which insert onto the radial side of the base of the long finger proximal phalanx and the lateral band of the long finger, respectively.

Variations

These are rarely described, except for the following.

Insertion: Inserts more frequently onto the proximal phalanx of the long finger (Tountas and Bergman 1993). Eyler and Markee reported in their cases that 60% of the muscle fibers insert onto the base of the long finger proximal phalanx. The remaining 40% of fibers insert into the lateral band of the long finger (Eyler and Markee 1954; Doyle and Botte 2003).

Numerical: May have three heads (Tountas and Bergman 1993).

Third dorsal interosseous

Normal

Origin: Two heads, arising from the ulnar side of the long finger metacarpal and the radial side of the ring finger metacarpal.

Insertion: Divides into superficial and deep muscle bellies, which insert onto the ulnar side of the base of the long finger proximal phalanx and the lateral band of the long finger, respectively.

Variations

These are rarely described, except for the following.

Insertion:

1. Eyler and Markee reported in their cases that 94% of the muscle fibers insert into the lateral band of the long finger. The remaining 6% of fibers insert onto the base of the long finger proximal phalanx.
2. Of all the dorsal interossei, it is the least likely to have a bony insertion (Eyler and Markee 1954; Doyle and Botte 2003).

Numerical: Smith described the third dorsal interosseous as having only one muscle belly. The distal insertion was to the lateral band of the long finger (Smith 1999; Eladoumikdachi et al. 2002a).

Fourth dorsal interosseous

Normal

Origin: Two heads, arising from the ulnar side of the ring finger metacarpal and the radial side of the small finger metacarpal.

Insertion: Divides into superficial and deep bellies, which insert onto the ulnar side of the base of the ring finger proximal phalanx and the lateral band of the ring finger, respectively.

Variations

These are rarely described, except for the following.

Insertion: Eyler and Markee reported in their cases that 40% of the muscle fibers insert onto the base of the long finger proximal phalanx. The remaining 60% of fibers insert into the lateral band (Eyler and Markee 1954; Doyle and Botte 2003).

Numerical: May be completely absent in the interspaces (Doyle and Botte 2003); or may have additional or reduced muscle bellies (Kaplan 1965, Doyle and Botte 2003). Netscher described that the dorsal interossei (75% of cases) may have two heads and may therefore have both distal attachments to the lateral band and the proximal phalanx (Eladoumikdachi et al. 2002b).

Neurovascular:

1. May be innervated partially by the posterior interosseous branch of the radial nerve (Kaplan 1965; Doyle and Botte 2003).
2. May be innervated by intercommunication between the musculocutaneous and median nerves (Doyle and Botte 2003).
3. The superficial and deep muscle bellies can be separately innervated by small nerve branches (Doyle and Botte 2003).

Palmar interossei

There are three palmar interossei (Fig. 34.10). They occupy the palmar aspect of the intermetacarpal spaces, which is shared with the dorsal interossei. They receive their innervation from the deep branch of the ulnar nerve. The palmar interossei have only one head.

First palmar interosseous

Normal

Origin: Ulnar side of index finger metacarpal.

Insertion: Lateral band on the ulnar side of the index finger.

Variations

These are rarely described, except for the following.

Insertion: May insert onto the index finger proximal phalanx, although this is not common.

Coarse and structure: accessory slips: May receive a few additional fibers coming from the adjacent long finger metacarpal (Eladoumikdachi et al. 2002a).

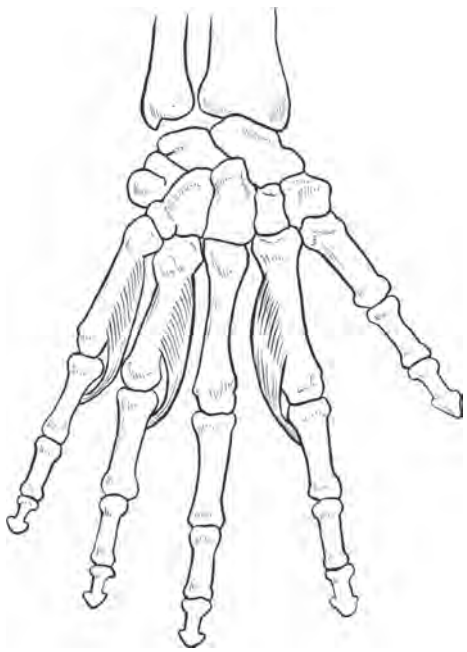

Figure 34.10 Palmar interossei: normal.

Second palmar interosseous

Normal

Origin: Radial side of the ring finger metacarpal.

Insertion: Lateral band on the radial side of the ring finger.

Variations

These are rarely described, except for the following.

Insertion: May insert onto the ring finger proximal phalanx, although this is not common.

Coarse and structure: accessory slips: may receive a few additional fibers coming from the adjacent third metacarpal bone (Eladoumikdachi et al. 2002a).

Third palmar interosseous

Normal

Origin: Radial side of the small finger metacarpal.

Insertion: Lateral band on the radial side of the small finger.

Variations

These are rarely described, except for the following.

Insertion: Insertions vary, largely insert on the lateral band. Eyler and Markee reported that 90% of the muscle fibers insert on the lateral band. The remaining 10% of fibers insert onto the base of the small finger proximal phalanx (Eyler and Markee 1954; Doyle and Botte 2003).

Unclassified variations

Origin: May have a bipennate origin (Kaplan 1965).

Numerical:

1. One or all palmar interossei may be missing (Kaplan 1965).
2. May be doubled (Doyle and Botte 2003).
3. A small muscular belly connected with the flexor pollicis brevis muscle has been considered to be an additional palmar interosseous muscle (Kaplan 1965).
4. Four palmar interossei have been described (Doyle and Botte 2003). The fourth palmar interossei is the muscle or fibers that pass from the base of the thumb metacarpal to the base of the thumb proximal phalanx. These fibers have been considered as part of the adductor pollicis muscle.
5. The palmar interossei can have one or more muscle bellies. Classically, the palmar interossei have one muscle belly, with its distal insertion on the lateral band. Smith noted that the palmar interossei do not have superficial and deep bellies, therefore none can be inserted into the proximal phalanx (Doyle and Botte 2003). He stated that the palmar interossei have only one muscle belly that inserts distally on the lateral band (Eladoumikdachi et al. 2002a). Netscher found that the palmar interossei may have more than one muscle belly, each with a different insertion. Netscher noted that classically the palmar interossei insert distally onto the lateral band only, although they can also insert onto bone and volar plate (Eladoumikdachi et al. 2002a). Netscher reported that the palmar interossei (36% of cases) may have two heads and may therefore have distal attachments to both the lateral band and the proximal phalanx. Three heads, each with a different destination, have been described (Eladoumikdachi et al. 2002b).

Neurovascular: The more radially located interossei are occasionally supplied by branches of the median nerve (Eyler and Markee 1954).

Overview

The interossei have also been frequently described as having a large number of variations, especially with respect to distal insertions. The classic description of the dorsal interossei is that they all (except for the third) have superficial and deep heads. The superficial head is bipennate, originating from adjacent surfaces of the metacarpals and the deep head originates from the radial side of the corresponding metacarpals.

The palmar interossei have a unipennate origin from the radial side of the corresponding metacarpals, except for the first palmar interosseous. In the dorsal interossei with two heads, the deep head inserts on the lateral band and the superficial head spirals around and inserts on the base of the proximal phalanx. All the palmar interossei and the third dorsal interosseous are said to insert distally only onto the lateral band.

However, in reality, one cannot be as rigid in the descriptions of the distal insertions as previously mentioned. The two distal insertions may come from functionally separate fleshy parts, superficial and deep heads, or they may merge into one muscle.

Furthermore, where there are distinct superficial and deep heads, some have referred to the deep heads as palmar interossei (based on their capacity to either abduct or adduct the digit rather than on their unipennate origin from the metacarpal and their dorsal insertions to the lateral band; Fig. 34.11). Additionally, the distal insertions may have more destinations than previously described, traveling not only to the bony proximal phalanx and to the lateral band of the extensor expansion, but also to the volar plate ("assemblage nucleus" of Zancolli). Traditionally, the first dorsal interosseous inserts primarily onto bone and the palmar interossei insert into the lateral band. The remaining dorsal interossei have varying combinations of bone and expansion attachments. Although the latter may be an oversimplification, it explains the finding that when the muscle attaches to both proximal phalanx and extensor expansion it does so with two anatomically and functionally separate tendons. This dual insertion explains how a single muscle is simultaneously able to perform multiple seemingly opposing functions, namely metacarpal joint flexion and interphalangeal joint extension, as well as abduction and adduction of the fingers.

Palmaris brevis

The palmaris brevis is a small muscle layer located between the hypothenar fascia and the skin. It helps deepen the hypothenar eminence, thereby increasing the security of the

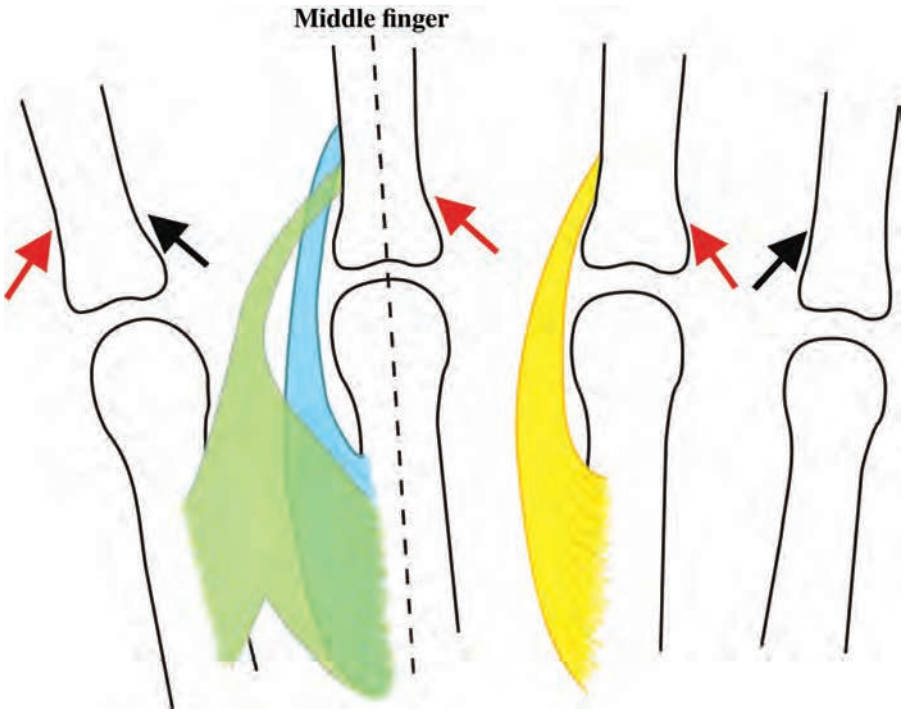

Figure 34.11 Dorsal and palmar interossei. Green represents the bipennate superficial head of the dorsal interosseous muscle; blue represents its unipennate deep head. In contrast, the yellow palmar interosseous is a unipennate muscle. With the Middle finger as a reference axis, the dorsal interossei abduct from this axis (red arrows) and the palmar interossei (black arrows) adduct.

palmar grip by steadying the skin. It is innervated by the ulnar nerve.

Normal

Origin: Ulnar border of the palmar fascia and flexor retinaculum (Fig. 34.12a; Doyle and Botte 2003).

Insertion: Dermis of the ulnar border of the hand (Doyle and Botte 2003).

Variations

These are rarely described, except for the following.

Origin: May originate radially from slips off the scaphoid and trapezium (Fig. 34.12b).

Insertion: May insert onto the pisiform bone (Tountas and Bergman 1993; Fig. 34.12c).

Course and structure: May be joined to flexor digiti minimi brevis (Tountas and Bergman 1993); or may be found deeper than its usual location and not directly attached to the dermis (Das and Paul 2000).

Numerical: may be absent (about 2% of individuals; Tountas and Bergman 1993); or may be doubled (Bergman et al. 2006; Fig. 34.12d). When doubled, the supranumary muscle is called the palmaris brevis profundus; it arises transversely from the flexor retinaculum and the palmar aponeurosis (Tountas and Bergman 1993).

Extensor digitorum brevis manus

This muscle is an anatomic variant of the finger extensor musculature; found on the dorsum of the hand, it occurs in 2–3% of the population and has a slight male predominance. The muscle has a single belly and is innervated by the posterior interosseous nerve (Ranade et al. 2008).

Most common

Origin: The carpal bones (scaphoid or lunate) or the metacarpals.

Insertion: Ulnar side of the extensor digitorum of the index finger, sometimes replacing the extensor indicis proprius.

Variations

Origin: May arise from the dorsal carpal ligaments, the wrist joint capsule, distal radius, or the ulna (Paraskevas et al. 2002); or may arise from the wrist capsule deep to the extensor retinaculum (Paraskevas et al. 2002).

Insertion: May insert onto the extensor digitorum of the long (second-most common), ring, or small fingers (Paraskevas et al. 2002; Ranade et al. 2008); or may have multiple insertions into more than one finger (index and long finger; third-most common finding; Ranade et al. 2008).

Numerical: May be doubled, the size of each belly is variable (Paraskevas et al. 2002). It may have one–four fascicles (Doyle and Botte 2003). The fascicle that provides the tendon to the extensor of the index finger is the most common.

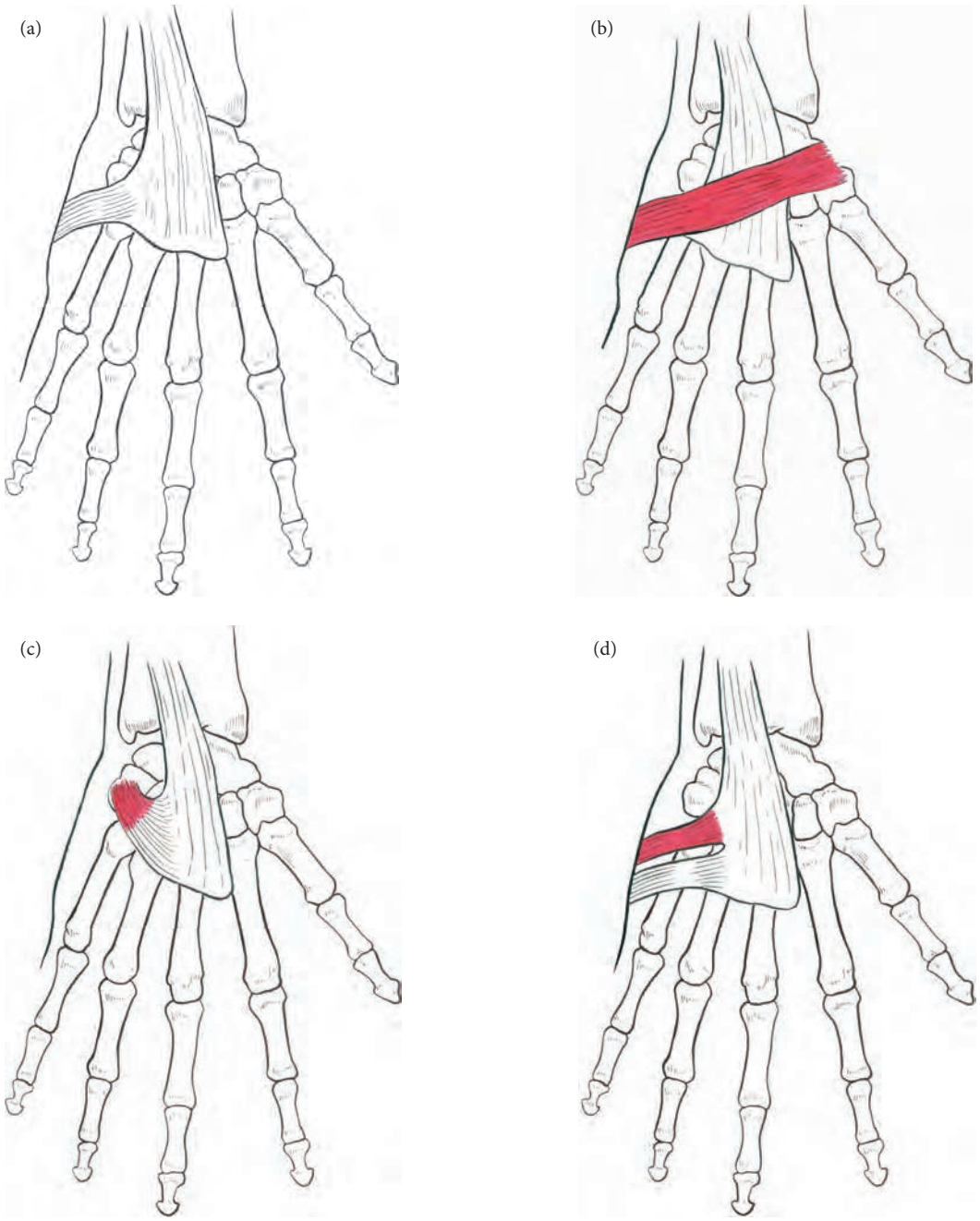

Figure 34.12 Palmaris brevis: (a) normal; (b) slip originating from scaphoid and trapezium; (c) insertion onto pisiform bone; and (d) doubled muscle.

Clinical implications

Nerve entrapment

Thenar muscle

Abductor pollicis brevis: Duplication of the muscle may cause compression neuropathy of the recurrent motor branch of the median nerve (Tountas and Bergman 1993).

Unspecified thenar muscle: An accessory slip attached from the palmaris longus to the thenar muscles has been noted to cause compression of the median nerve, resulting in sensory neuropathy and pain at the wrist (Fig. 34.13a, b).

Hypothenar muscles

Abductor digiti minimi: To traverse into the hand, n abductor digiti minimi with a proximal origin in the antebrachial fascia must pass through Guyon canal, causing compression. The anatomic relationships of accessory bellies could be involved in entrapment neuropathies of the ulnar and median nerves, particularly when the muscle is hypertrophied (Timins 1999; Soldado-Carrera et al. 2000; Fig. 34.14;a, b). The accessory abductor digiti minimi may compress the deep palmar branch of the ulnar nerve (Tountas and Bergman 1993).

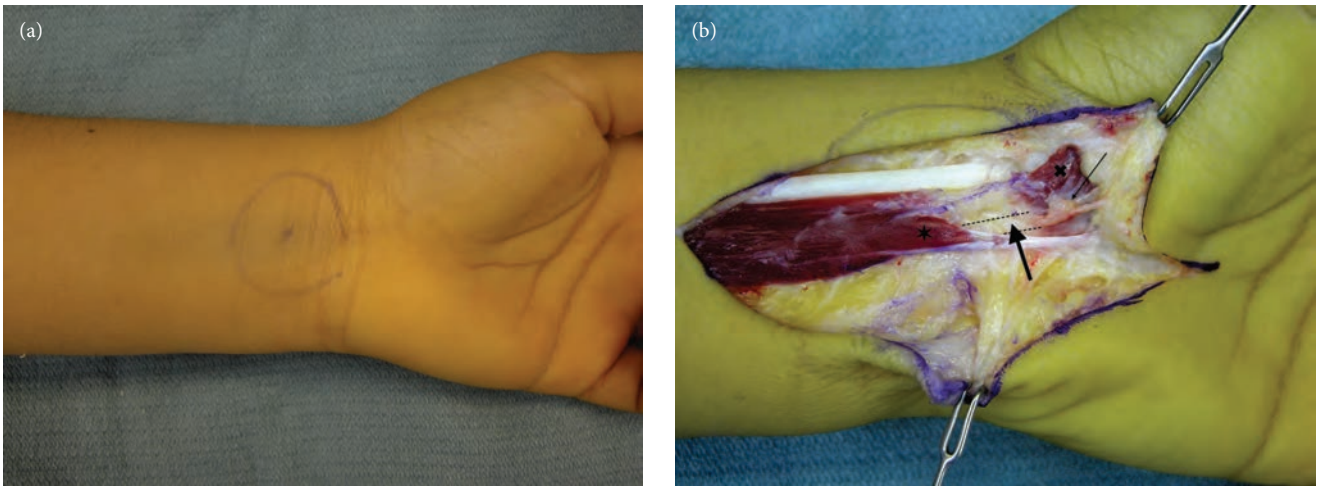

Figure 34.13 Accessory slip from palmaris longus to thenar muscle: (a) site of prominent Tinel sign and exquisite tenderness radiating up into the fingers, thumb, and palm; and (b) intraoperative photograph showing compression on median nerve (bold arrow) and its palmar cutaneous branch (fine arrow) by an abnormally long palmaris longus muscle belly (*) and proximal origin of the thenar muscles (X) from palmaris longus in the forearm fascia.

An accessory abductor digiti minimi is the muscle variant most commonly found in Guyon canal (Dodds et al. 1990; Fig. 34.15). The accessory muscle may pass through the Guyon canal. Compression of the ulnar nerve in the Guyon canal occurs when the muscle hypertrophies in the canal or with traumatic compression between the muscle and the pisohamate ligament. Compression can cause both motor and sensory neuropathy at the wrist (Tountas and Bergman 1993).

Flexor digiti minimi: Ulnar nerve compression can result from an enlarged or duplicated muscle (Wingerter et al. 2003). An anomalous tendinous extension of the muscle has been found to split the deep branch of the ulnar nerve resulting in compression of a branch of the nerve (Spinner et al. 1996). An accessory flexor digiti minimi has been reported to pass through Guyon canal causing compression (Madhavi and Holla 2003).

Opponens digiti minimi: An accessory opponens digiti minimi has been reported to pass through Guyon canal and take origin in the forearm fascia causing compression (Madhavi and Holla 2003) (Fig. 34.16a, b).

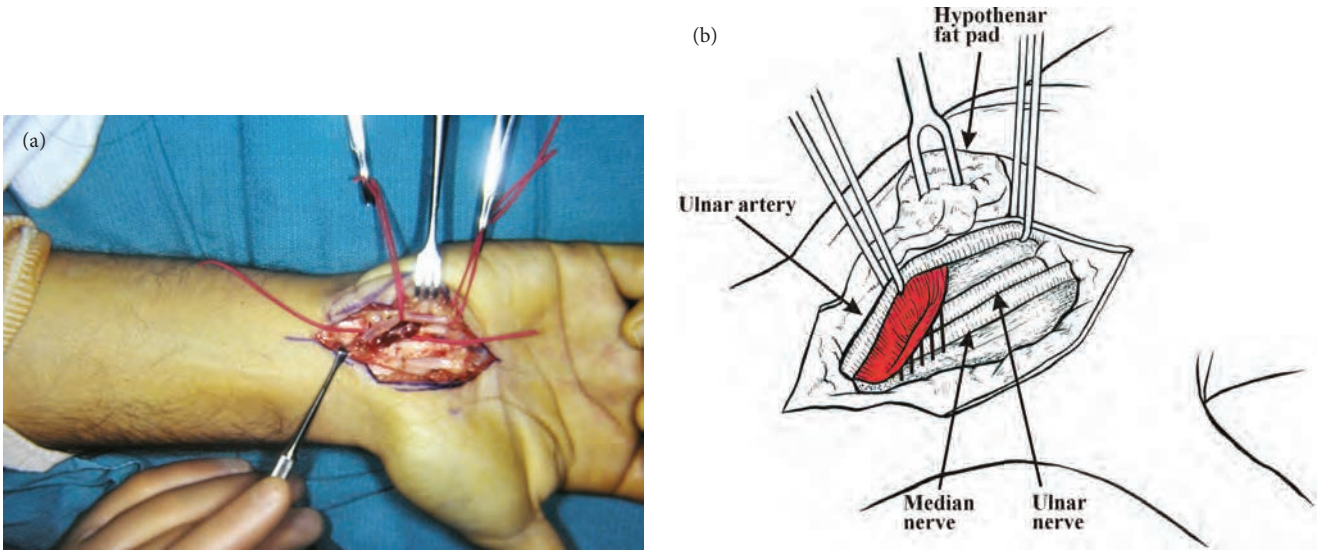

Figure 34.14 Abnormal origin of abductor digiti minimi: (a) muscle has been detached radially from the transverse carpal ligament; and (b) line diagram of (a) demonstrating the reflected abductor digiti minimi (hatch marks) from its radial attachment. The abnormal muscle passed deep to the ulnar artery, but superficial to the ulnar nerve and caused ulnar and median nerve compression with electrodiagnositc verification of conduction delay in Guyon canal and the carpal tunnel.

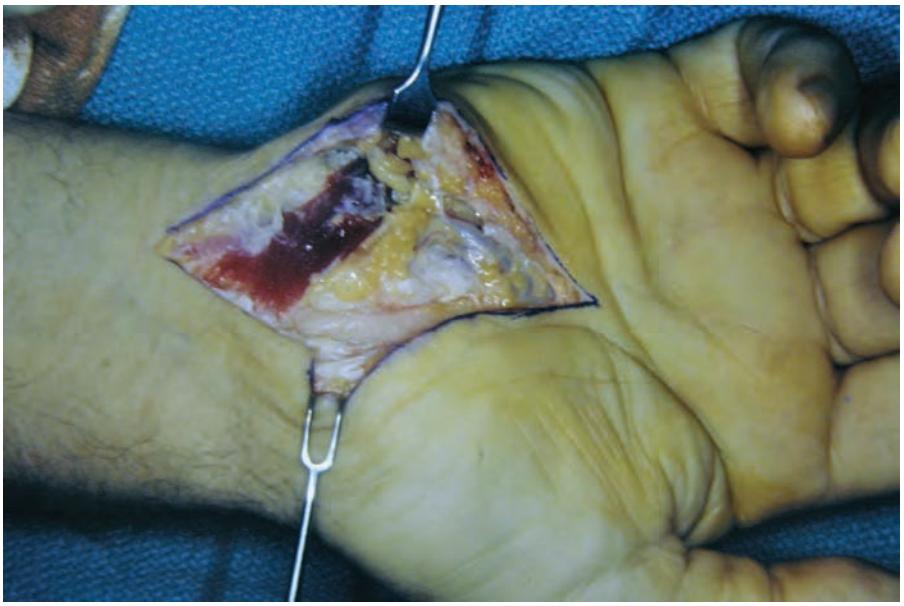

Figure 34.15 Accessory abductor digiti minimi taking origin in the forearm, traversing through the Guyon canal causing ulnar nerve compression.

Lumbricals

An anomalous first lumbrical originating from the flexor digitorum superficialis may cause carpal tunnel syndrome by compressing and irritating the median nerve as it crosses the nerve or by passing through a bifurcated median nerve (Tountas and Bergman 1993). An anomalous lumbrical muscle originating high on the profundus tendon of the long finger travels proximal to the transverse carpal ligament, causing carpal tunnel syndrome as it crosses the median nerve. In as many as 22% of individuals, the lumbrical muscles originate within the carpal tunnel and may cause median nerve compression (Fig. 34.17)

In a study by Timins, it was found that the four lumbricals originated distal to the carpal tunnel with the fingers in extension. Flexion of the fingers can pull the proximal aspect of the lumbrical muscles within the carpal tunnel, despite an otherwise normal location of the muscles with the fingers extended. Correct diagnosis of a proximal lumbrical origin therefore requires that the wrist be assessed with the fingers extended (Timins 1999). This finding was also confirmed by Delgado, who found that a more proximal lumbrical insertion may cause the lumbricals to move into the carpal tunnel upon flexion, causing nerve compression (Delgado Serrano et al. 2005).

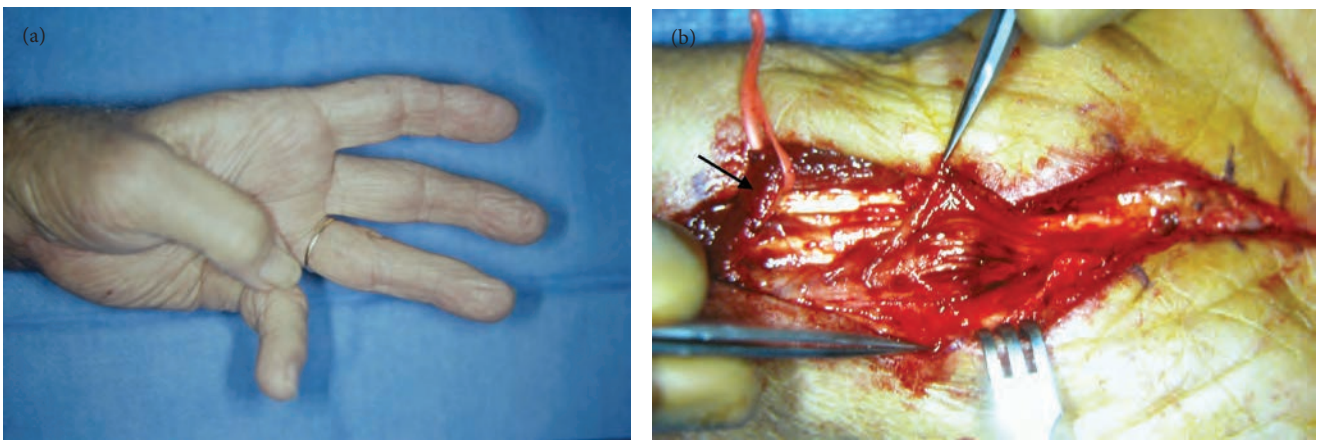

Figure 34.16 Abnormal opponens digiti minimi. (a) Clinical photograph of patient with severe carpal tunnel symptoms. He was unable to effectively oppose the little finger; he had no ulnar nerve symptoms. (b) Intraoperative photograph. An abnormal opponens digiti minimi (retracted and demonstrated by the arrow) originated from the forearm fascia, crossing over the median nerve in the distal forearm where there was tight compression, demonstrated by pseudoneuroma formation. Although the muscle traversed the Guyon canal, there was no electrodiagnostic evidence of ulnar entrapment neuropathy.

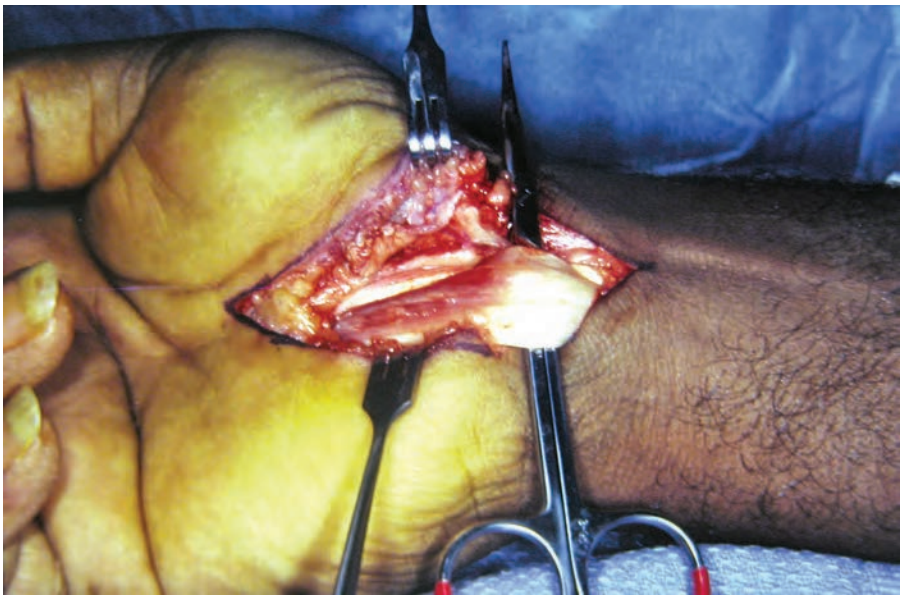

Figure 34.17 Lumbrical with a more proximal origin causing compression of the median nerve in the carpal tunnel. This finding may be more common in people who perform manual labor and have lumbrical hypertrophy.

Anomalous lumbricals passing through the carpal canal have been reported to produce carpal tunnel syndrome by organizing hematoma on the muscle via a closed disruption (Tountas and Bergman 1993). Anomalous lumbricals passing through the Guyon canal can cause compression neuropathy on the ulnar nerve.

Palmaris brevis

When doubled, the accessory muscle (the palmaris brevis profundus) may be located in the Guyon canal between the superficial and deep branches of the ulnar nerve and found to be attached to the pisiform, thereby producing ulnar nerve compression (Tountas and Bergman 1993; Fig. 34.18). An abnormally thickened muscle can cause ulnar nerve compression (Mackinnon and Dellon 1998).

Innervation

Interossei

The variation in innervation of the dorsal interossei can allow for continued function of the interosseous muscles in the presence of ulnar nerve laceration or severe neuropathy (Doyle and Botte 2003).

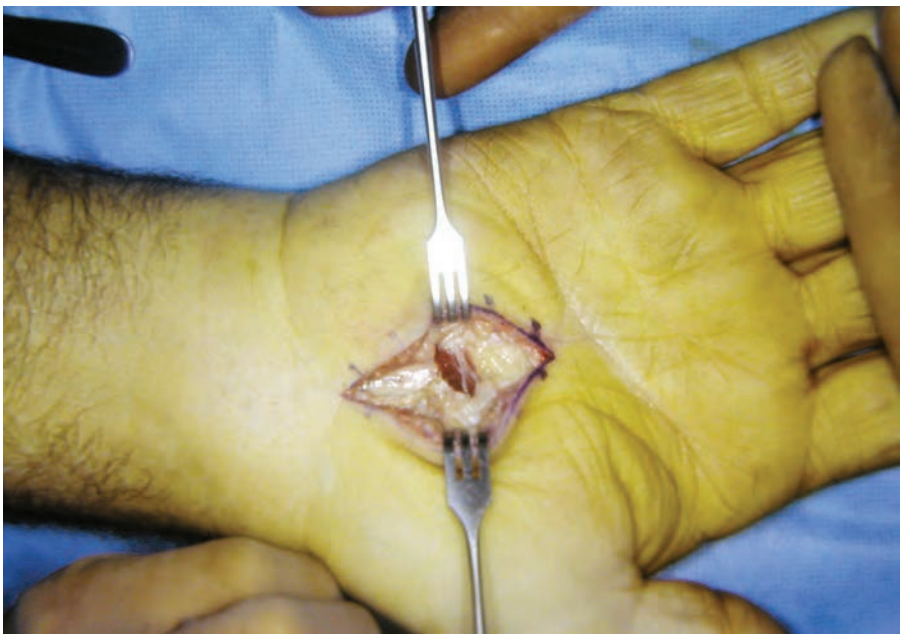

Figure 34.18 Palmar subcutaneous muscle causing median nerve compression. While the muscle was not dissected out in full, it could have represented an accessory palmaris brevis or the muscle extending out to the scaphoid bone.

Figure 34.19 Abnormal lumbrical. (a) An infant with multiple trigger fingers was found to have a lumbrical muscle traversing into the flexor tendon sheath (arrow). (b) Upon further exploration, the lumbrical muscle inserted onto the flexor digitorum superficialis tendon within the sheath. The mechanical problem was resolved by excision of the tendon and attached lumbrical muscle.

Biomechanical effects

Thenar muscles

The muscles that form the thenar eminence (abductor pollicis brevis muscle, opponens pollicis, and flexor pollicis brevis) play an important role in hand functions, especially for fine motor functions of the thumb. Absence of the FPB and APB can cause problems with thumb opposition and pinching (Koca et al. 2012). These muscles may be variably absent in the hypoplastic thumb, which result in functional deficits.

Lumbricals

Lumbricals abnormally attached to or within the flexor tendon sheath can cause trigger finger (Fig. 34.19a, b).

Interossei

When performing index pollicization for an absent thumb, it is vital to detach all distal insertions (both superficial and deep heads from the base of the proximal phalanx and the lateral band) of the first dorsal interosseous and reattach them as a group into the extensor apparatus of the index finger to allow for full force of the muscle (Zancolli and Cozzi 1992). The size, insertions, and amount of muscle fibers (at each point of insertion) of the superficial and deep muscle bellies of the dorsal interossei affect the function of interphalangeal joint extension and proximal phalanx abduction (Doyle and Botte 2003).

Patients with an absent thumb demonstrate increased abnormalities on the radial aspect of the hand and have a gradual transition from normal to abnormal anatomy (ulnar to radial). Reconstruction in these patients may be complicated by the absence of the index finger dorsal interosseous.

Other muscles

Palmaris brevis: An anomalous attachment can reduce gripping function of the palm due to lack of deepening of the hollow of the palm (Das and Paul 2000).

Extensor digitorum brevis manus: May function to assist in extension of other fingers.

Functional substitution

Extensor digitorum brevis manus

May replace the extensor indicis proprius and may therefore be the only muscle responsible for independent extension of the index finger (Ranade et al. 2008). If present, this muscle should not be excised inadvertently when exploring an unexplained dorsal wrist mass. Prior to any resection, testing for index finger extension should be performed (Fig. 34.20).

Vascular effects

Hypothenar muscles

Abductor digiti minimi: Accessory muscle bellies may cause ulnar artery thrombosis or fibrosis (Soldado-Carrera et al. 2000). The abductor digiti minimi with an additional head, as it passes distally, may cover the ulnar artery, causing its compression (Tountas and Bergman 1993).

Mass appearance

Thenar muscles

Abductor pollicis brevis: Duplication of the muscle may simulate a soft tissue tumor of the hand (Tountas and Bergman 1993).

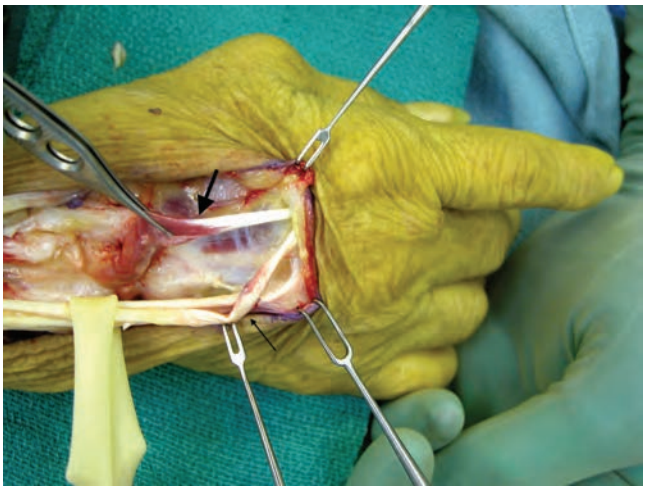

Figure 34.20 Extensor digitorum brevis manus (EDBM) replacing extensor indicis proprius. Forceps retraction on EDBM produces index finger extension (bold arrow). Extensor digitorum communis (fine arrow) to index finger is lightly retracted to permit visualization.

Hypothenar muscles

Abductor digiti minimi: An anomalous fascicle or duplication of the muscle may simulate a soft tissue tumor in the lower third of the forearm (Soldado-Carrera et al. 2000).

Flexor digiti minimi: Duplication of the muscle may simulate soft tissue tumors of the hand (Tountas and Bergman 1993).

Opponens digiti minimi: Duplication of the muscle may simulate soft tissue tumors of the hand (Tountas and Bergman 1993).

Lumbricals

A variant lumbrical was noted to produce a radial palmar swelling (Tountas and Bergman 1993).

Other muscles

Palmaris brevis: Duplication of the muscle may simulate a soft tissue tumor of the hand (Tountas and Bergman 1993).

Extensor digitorum brevis manus:

1. May simulate a soft tissue tumor. When the hand is actively extended at the wrist and fingers, the muscle (EDBM) will bulge on the dorsum. This characteristic bulging of the muscle when the wrist is in extension can be used to distinguish it from other masses of the wrist. Most other masses become less distinct when the wrist is in extension and appear more prominent when the wrist is in flexion, as is the case with a dorsal wrist ganglion.
2. Its resemblance of a soft tissue mass, and may mimic neoplastic, inflammatory, and infectious masses arising on the dorsum of the wrist (Ranade et al. 2008).
3. Mimics exostosis or a synovial cyst (Jacobina et al. 2007).

Camptodactyly

Lumbricals

Anomalous insertion of the fourth lumbrical has been associated with camptodactyly. Frequent variability in the origin and insertion of the ulnar lumbricals may correlate with the common finding of little and ring finger camptodactyly (Eladoumikdachi et al. 2002b).

Interosseous

The fourth palmar interosseous may insert onto the ring finger, rather than to the radial side of the small finger, in patients with camptodactyly (Tountas and Bergman 1993).

References

Bergman RA, Thompson SA, Afifi AK. 1984. *Catalog of Human Variation*. Baltimore: Urban & Schwarzenberg.

Bergman RA, Afifi AK, Miyauchi R. 2006. Illustrated encyclopedia of human anatomic variation, opus I: Muscular system. Available at http://www.anatomyatlases.org (accessed 15 October 2015).

Das S, Paul S. 2000. An anomalous palmaris brevis muscle and its clinical implications. *The Internet Journal of Surgery* 9(2), 9 pp.

Delgado Serrano PJ, Abad Morenilla JM, Dudley Porras AF, García Olea Á. 2005. Síndrome del túnel carpiano asociado a variaciones anatómicas de músculos del antebrazo y mano. *Patología del Aparato Locomotor* 3: 81–86.

De Smet L. 2002. Median and ulnar nerve compression at the wrist caused by anomalous muscles. *Acta Orthop Belg* 68: 431–438.

Dodds GA, Hale D, Jackson WT. 1990. Incidence of an anatomic variance in Guyon's canal. *J Hand Surg (Am)* 15: 352–355.

Doyle JR, Botte MJ. 2003. *Surgical Anatomy of the Hand and Upper Extremity*. Philadelphia: Lippincott Williams & Wilkins.

Eladoumikdachi F, Valkov PL, Thomas J, Netscher DT. 2002a. Anatomy of the intrinsic hand muscles. Revisited: Part I. Interossei. *Plast Reconstr Surg* 110: 1211–1224.

Eladoumikdachi F, Valkov PL, Thomas J, Netscher DT. 2002b. Anatomy of the intrinsic hand muscles revisited: Part II. Lumbricals. *Plast Reconstr Surg* 110: 1225–1231.

Eyler DL, Markee JE. 1954. The anatomy and function of the intrinsic musculature of the fingers. *J Bone Joint Surg Am* 36: 1–9.

Jacobina C, Bastos P, Siqueira S, Issa M, Baumfeld D, Orlandi C, Barroso T Duarte P, Villela R, Nelson, A, Toledo J, Teixeira M, Finch F. 2007. Extensor digitorum brevis manus: A rare muscle on the dorsum of the hand. *Braz J Morphol Sci* 24: 208–210.

Kaplan EB. 1965. *Functional and Surgical Anatomy of the Hand*. Second edition. Philadelphia: JB Lippincott.

Koca K, Ekinci S, Ege T, Ozyurek S, Kurklu M, Battal B, Basbozkurt M. 2012. Bilateral congenital absence of flexor pollicis brevis and abductor pollicis brevis muscles with bilateral thenar atrophy: A case report. *Clin Med Insights Arthritis Mudsculoskeletal Disord* 5: 59–62.

Macalister A. 1875. Additional observations on muscular anomalies in human anatomy (third series), *with a catalogue of muscular variations hitherto published*. 25: 1–134.

Mackinnon SE, Dellon AL (eds). 1998. *Ulnar nerve entrapment at the wrist. Surgery of the Peripheral Nerve*. New York: Thieme Medical Publishers.

Madhavi C, Holla SJ. 2003. Anomalous flexor digiti minimi brevis in Guyon's canal. *Clin Anat* 16: 340–343.

Paraskevas G, Papaziogas B, Spanidou S, Papadopoulos A. 2002. Unusual variation of the extensor digitorum brevis manus: A case report. *Eur J Orthop Surg Traumatol* 12: 158–160.

Ranade AV, Rai R, Prabhu LV, Rajanigandha. 2008. Incidence of extensor digitorum brevis manus muscle. *Hand* 3: 320–323.

Saadeh FA, Bergman RA. 1988. An unusual accessory flexor (opponens) digiti minimi muscle. *Anat Anz* 165: 327–329.

Smith RJ. 1999. Intrinsic contracture. In: *Green's Operative Hand Surgery*, fourth edition (DP Green, RN Hotchkiss, CW Pederson, eds). New York: Churchill Livingston.

Soldado-Carrera F, Vilar-Coromina N, Rodríguez-Baeza A. 2000. An accessory belly of the abductor digiti minimi muscle: A case report and embryologic aspects. *Surg Radiol Anat* 22: 51–54.

Spinner RJ, Lins RE, Spinner M. 1996. Compression of the medial half of the deep branch of the ulnar nerve by an anomalous origin of the flexor digiti minimi. *J Bone Joint Surg Am* 78: 427–430.

Timins ME. 1999. Muscular anatomic variants of the wrist and hand: Findings on MR imaging. *AJR Am J Roentgenol* 172: 1397–1401.

Tountas CP, Bergman RA. 1993. Anatomic Variations of the Upper Extremity. New York: Churchill Livingstone.

Wingerter S, Gupta S, Le S, Shamasunder S, Bernstein S, Rabitaille W, Kukuyeva Y, Downie S. 2003. Unusual origin of the flexor digiti minimi brevis muscle. *Clin Anat* 16: 531–533.

Wood J. 1866. Variations in human myology observed during the winter session of 1865–66 at King's College, London. *Proc Roy Soc Lond B* 15: 229–244.

Wood J. 1868. Variations in human myology observed during the winter session of 1867–68 at King's College, London. *Proc Roy Soc Lond B* 17: 483–525.

Zancolli EA, Cozzi EP. 1992. *Atlas of surgical anatomy of the hand*. New York: Churchill Livingstone.

35 Thoracic wall muscles

Michael Snosek and Marios Loukas
St. George's University, School of Medicine, St. Georges, Grenada

Many of the supernumerary muscles of the anterior thoracic wall region may be traced back to the abnormal development of the pectoral muscle mass. The pectoral muscle mass develops from the hypaxial part of the associated somites. It is this primitive muscle mass that gives rise to the pectoralis major and minor. A disturbance in the normal development and differentiation of this muscular sheet anywhere along its developmental continuum may result in partial or complete absence of a muscle or give rise to aberrant or supernumerary musculature. Pectoral muscle variations are said to be more frequent than any other skeletal muscles (Clark 1915). These muscular variants may be divided into a group superficial to the plane of the pectoralis major muscle and a group deep to the plane of this muscle.

The wide range of nomenclature used to describe these muscular variations is the cause of much confusion. For example, a segmented portion of the pectoralis major muscle that inserts onto the humerus and originates from the ribs might be called costohumeralis; if it originates from the costal cartilages it might be called chondrohumeralis; likewise, if it takes it origin from the lateral aspect of the sternum it will aptly be called sternohumeralis. It should be readily apparent that all three muscles represent the same supernumerary muscular variant with varied origin of their medial-most fibers. Likewise, the lateral attachment points can vary widely, giving rise to a multitude of new muscle names such as sternocoracoideus, sternoepicondylaris, or sternofascialis. This concept was clearly demonstrated by Huntington (1901) in his description of a series of retroclavicular muscle, where one parent muscle (sternochondroscapularis) gives rise to four new muscular variations based simply on varied attachments (Fig. 35.1).

Pectoralis major

The pectoralis major muscle develops from the ventral sheet of the pectoral mass and grows onto the thorax. The muscle may be divided into a clavicular head, which takes its origin from the anterior aspect of the proximal clavicle, a sternoclavicular head from the anterior surface of the ipsilateral half of the sternum and second–sixth costal cartilages, and an abdominal head from the aponeurosis of the external oblique muscle. The clavicular and sternocostal fibers are separated by a varying gap, which is more prominent with hypoplasia of one of the heads. The origins of the sternocostal heads may include the first and seventh costal cartilages and the sternal end of the sixth rib, and their attachments on the sternum may interdigitate with the contralateral muscle. The abdominal head varies in its extent of attachment to the thorax and external oblique muscle, and is sometimes absent completely. The muscle inserts into the lateral lip of the intertubercular groove through a flat bilaminar tendon. Fibers from the clavicle, manubrium, and upper five costal cartilages form the anterior lamina and course laterally to insert into the lateral lip of the intertubercular groove. The posterior lamina is formed by fibers from the sixth and sometimes seventh costal cartilages, sixth rib, and external oblique aponeurosis. The fibers contributing to the posterior lamina ascend superiorly and wrap around the lowermost fibers of the superior lamina to insert higher on the intertubercular groove. This wrapping of the lowermost fibers around the upper fibers results in a twisting orientation of the pectoralis major tendon and gives its inferior margin; this forms the anterior axillary fold, which has a rounded appearance (Landry 1958; Flaherty et al. 1999; Standring 2008).

Morphological variations of the pectoralis major are very common. Aside from the completely distinct and hence named anatomical variants of the pectoral muscle mass, incompletely separated segments, partial or complete absence, or accessory segments have also been reported in the past. The most common variation of the pectoralis major muscle is the absence of the sternocostal head with associated hypertrophy of the clavicular head and absence of the pectoralis minor muscle. Absence of the clavicular head alone is rare (Clark 1915; Mosconi and Kamath 2003), although it may occur concomitantly with the occurrence of supernumerary muscles such as the sternoclavicularis or infraclavicularis (Bryce 1899). Complete absence of the pectoralis major associated with accompanying skeletal and vascular deficits is consistent with Poland's syndrome (see section on Poland's syndrome). Complete absence of pectoralis major excluding Poland's syndrome is extremely rare (0.01%; Bergman 2014). Barge (1927) reported a case of complete

Bergman's Comprehensive Encyclopedia of Human Anatomic Variation, First Edition. Edited by R. Shane Tubbs, Mohammadali M. Shoja and Marios Loukas.
© 2016 John Wiley & Sons, Inc. Published 2016 by John Wiley & Sons, Inc.

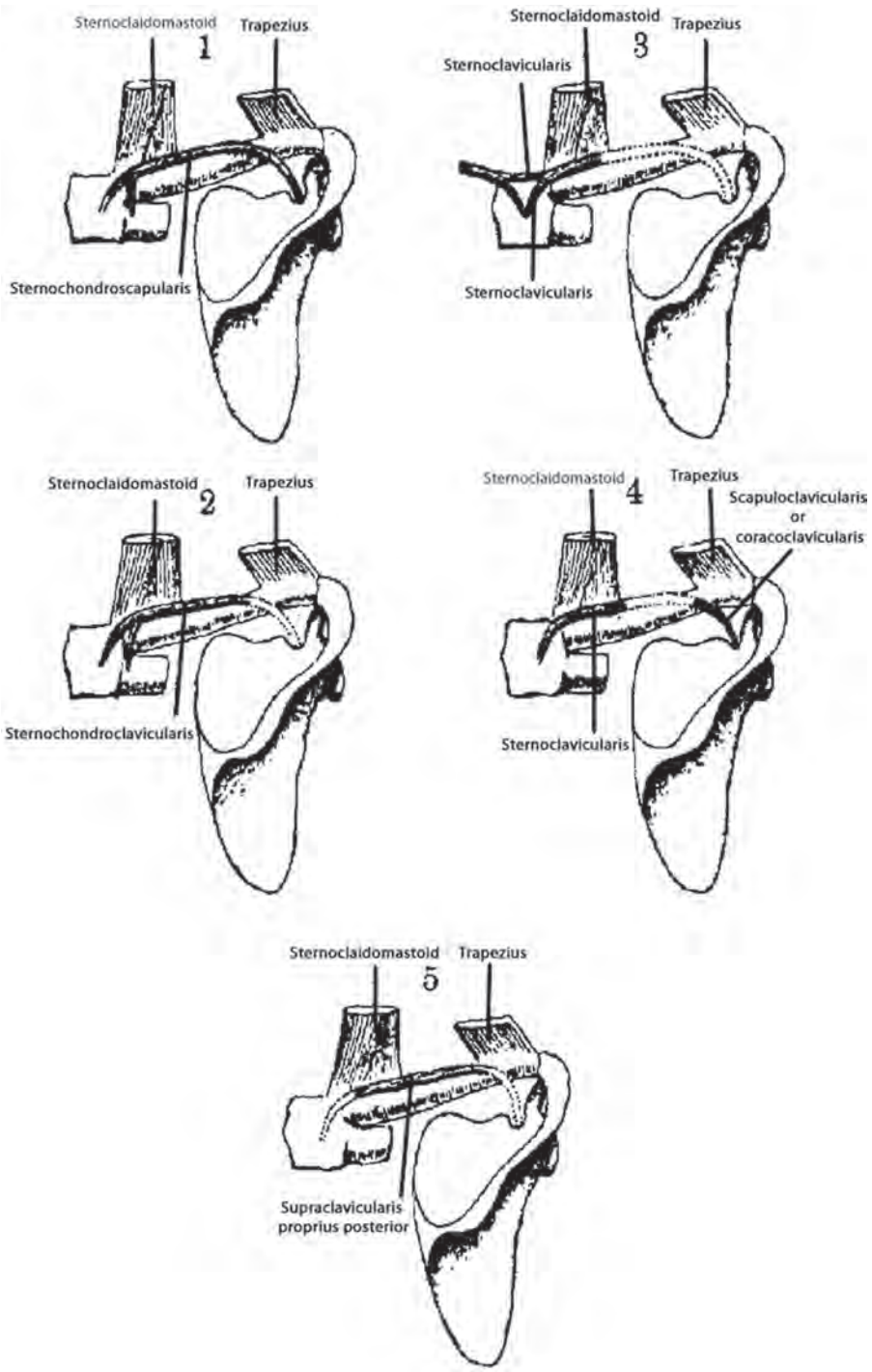

Figure 35.1 Series of retroclavicular supernumerary muscles possible based on various attachments points: 1, sternochondroscapularis; 2, sternochondroclavicularis; 3, sternoclavicularis; 4, formation of sternoclavicularis and scapuloclavicularis as a result of loss of the central portion of a larger sternochondroscapularis muscle seen in (1); 5, formation of supraclavicularis proprius posterior by loss of distal attachments to scapula and sternum.

Source: Huntington (1901). Reproduced with permission from John Wiley & Sons.

deficit of pectoralis major and minor muscles on the left side, which were replaced by a tough fascial membrane. Masconi and Kamath (2003) reported a case of complete absence of pectoralis major on the right side, along with partial deficit on the left side, and bilateral absence of the lateral pectoral nerves. Complete absence of pectoralis major alongside serratus anterior muscle absence has also been reported (Fig. 35.2; Dayal et al. 2014). Such cases of muscle absence frequently present with fibrous, tendinous, or fatty tissue remnants. Partial or complete deficits in the pectoralis major muscle frequently present with little to no functional deficits due to compensatory action of surrounding muscles, although decreased peak torque and average power in horizontal adduction of the ipsilateral arm have been reported (Lee and Chun 1991).

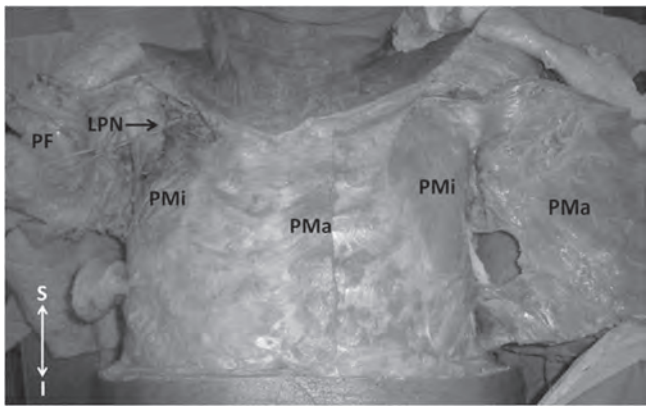

Figure 35.2 Absence of the pectoralis major on the right side. The pectoralis major has been cut and reflected laterally on the left side. LPN, lateral pectoral nerve; PF, pad of fat; PMa, pectoralis major; PMi, pectoralis minor; S, superior; I, inferior. Source: Dayal et al. (2013). Reproduced with permission from Springer Japan.

Loukas et al. (2006) reported an accessory head of the pectoralis major muscle originating from the serratus anterior muscle (Fig. 35.3). An accessory head of the pectoralis major muscle has also been reported to attach proximally from the shoulder joint capsule and, after running for a short distance with the tendon of the long head of the biceps brachii muscle, it attached to and blended with the superior fibers of the pectoralis major tendon as it inserted in its usual fashion to the intertubercular groove (Hammad and Mohamed 2006). A double pectoralis major muscle has been reported where the sternocostal head was composed of two strata – superficial and deep – one on top of the other (Macalister 1867; Sarikcioglu et al. 2004).

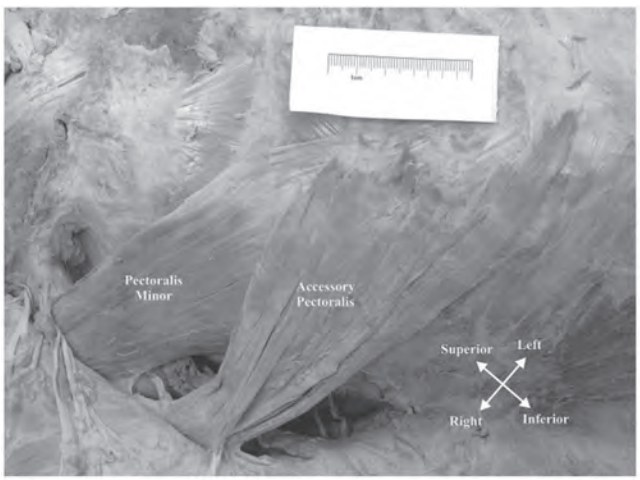

Figure 35.3 Fibers of the right-sided AcPM arising from fibers of the serratus anterior muscle. Note the relatively large width of the muscle belly as compared to the pectoralis minor muscle.

Source: Loukas et al. (2006).

Unusual attachment points of the pectoralis major muscle have been documented. The distal tendon has been reported to insert onto the brachial fascia, the greater or lesser tubercles of the humerus, coracoid process, the shoulder joint capsule without actually penetrating it, pectoralis minor or biceps brachii muscle, and the medial epicondyle of the humerus (Testut 1884; Hollinshead 1956; Sarikcioglu et al. 2004; Tubbs et al. 2008; Bergman 2014). The clavicular head can extend laterally to insert onto the deltoid muscle (Vollala et al. 2009; Bergman 2014). An interesting case was presented by Yazar et al. (1998) where two fibrous bands from the posterior aspect of the pectoralis major near its lateral border, crossed the axilla and attached to the brachial fascia of the posterior arm. These fibrous bands were reported to be in intimate contact with the median nerve and the brachial vein, with possible implications for compression syndromes and surgical operations of the axilla.

Pectoralis minor

The pectoralis minor muscle is said to attach to the coracoid process superiorly and ribs three–five inferiorly. Some variations to these attachment points have been noted. Cases of the pectoralis minor attaching to the humeral tuberosities, clavicle, the costocoracoid membrane, coracoacromial ligament, coracohumeral ligament, superior glenoid margin, supraspinatus tendon, or the shoulder joint capsule, instead of or in conjunction with its usual attachment to the coracoid process, have been reported (Wood 1866; Taylor 1898; Grant 1940; Bergman et al. 1988; Homsi et al. 2003; Tubbs et al. 2005; Uzel et al. 2008). Tubbs et al. (2005) reported a unilateral case of the pectoralis minor muscle attaching to the shoulder joint capsule directly in the absence of the coracohumeral ligament. Such presentation fits with Grant's suggestion that the coracohumeral ligament is a detached portion of a much longer pectoralis minor tendon as it attaches onto the humerus, resembling the arrangement found in other animals where the pectoralis minor has no attachment to the coracoid process (Grant 1940). Uzel et al. (2008) reported a bilateral case of the pectoralis minor with varied insertions (Figs 35.4, 35.5). The left muscle inserted onto the shoulder joint capsule similarly to that reported by Tubbs et al. (2005), while the right muscle inserted on the coracohumeral ligament and the supraspinatus tendon. Insertion of the tendon into the clavicle is extremely rare. Wood (1866) noted a case where a slip from the first rib attached to the clavicle, and one from the second rib attached to the costocoracoid membrane. Taylor (1898) noted a slip coming from the second rib to the clavicle in his specimen, which had a well-marked deficiency in the sternocostal portion of the pectoralis major at the level of the second rib. Note that Taylor's case also exhibited a well-developed sternalis muscle on the same side as the aberrant slip of the pectoralis minor, which is also frequently associated with pectoralis major deficits; this made the source of the deficit unclear (see section

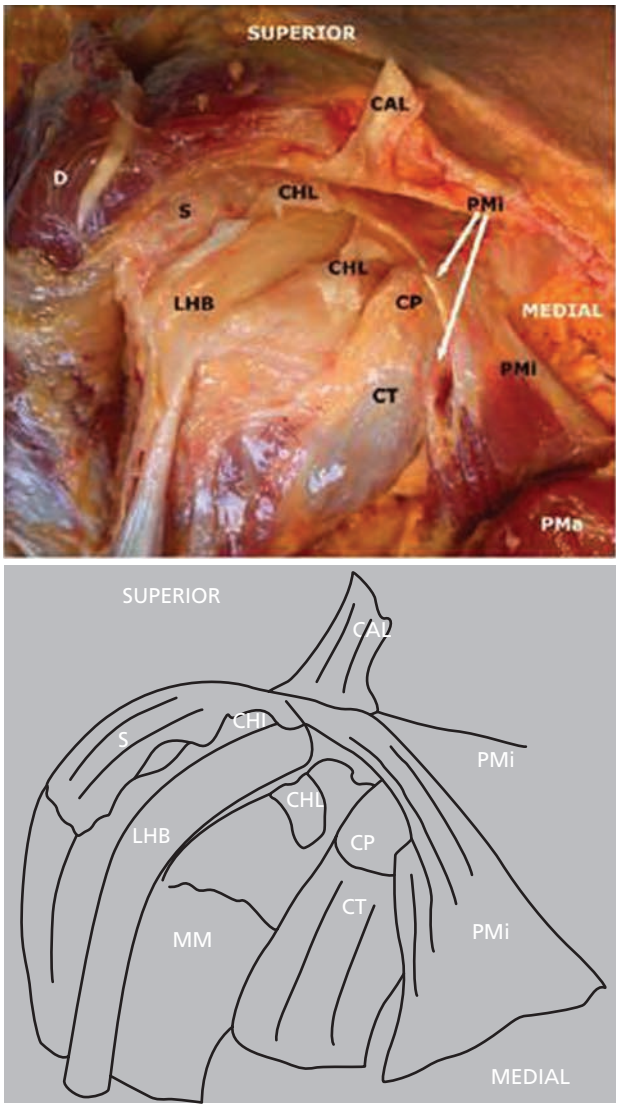

Figure 35.4 The right shoulder presents type 2 of the proximal insertion of pectoralis minor of the three types variation described by Le Double. CAL, coracoacromial ligament; CHL, coracohumeral ligament; S, supraspinatus; D, deltoid; LHB, long head of the biceps; CP, coracoid process; PMi, pectoralis minor; PMa, pectoralis major; CT, conjoined tendon; HH, humeral head; C, capsule.

Source: Uzel et al. (2008). Reproduced with permission from Springer Science and Business Media.

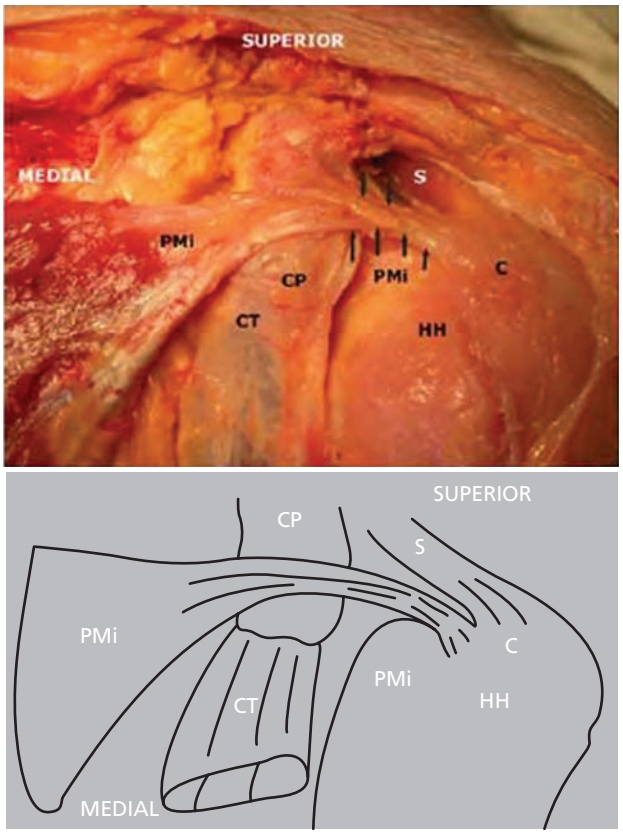

Figure 35.5 The left shoulder presents type 1 of the proximal insertion of pectoralis minor of the three types of variation described by Le Double. Abbreviations as for Figure 35.4.

Source: Uzel et al. (2008). Reproduced with permission from Springer Science and Business Media.

on Sternalis). A bundle joining the pectoralis minor to the latissims dorsi muscle has been termed Chassaignac's muscle.

The costal attachments can also vary, extending as far superiorly as the first intercostal aponeurosis and as far down as the sixth rib. According to Wood (1866), such upward extension of the pectoralis minor muscle is critical to the formation of the sternoclavicularis (see section on Sternocalvicularis). Turan-Ozdemir and Cankur (2004) noted an unusual case on right side of a male cadaver where the muscle attached inferiorly to the fifth rib alone, with usual superior attachment to the coracoid process.

Anomalous insertions of the pectoralis minor are often thought to be clinically insignificant, but Low and Tan (2010) reported a symptomatic case in 20-year-old male patient who presented with shoulder pain and snapping sensation with shoulder shrugging. A thickened ectopic pectoralis minor tendon was found with MRI to course over the coracoid process and insert on the supraspinatus muscle. The clicking sensation was attributed to the tendon snapping over the coracoid process during shoulder shrugging. A similar case of an ectopic tendon inserting onto the supraspinatus muscle presented with pain, stiffness, and diminished range in external rotation, necessitating complete tenotomy (Moineau et al. 2008). Pectoralis minor has also been linked to neurovascular obstruction due to its close proximity to the axillary vessels and brachial plexus. Wright (1945) coined the term "pectoralis minor syndrome," referring to the neurovascular deficits noted during hyperabduction of the arm as a result of compression by the pectoralis minor (Sanders and Rao 2007). The tendon of the

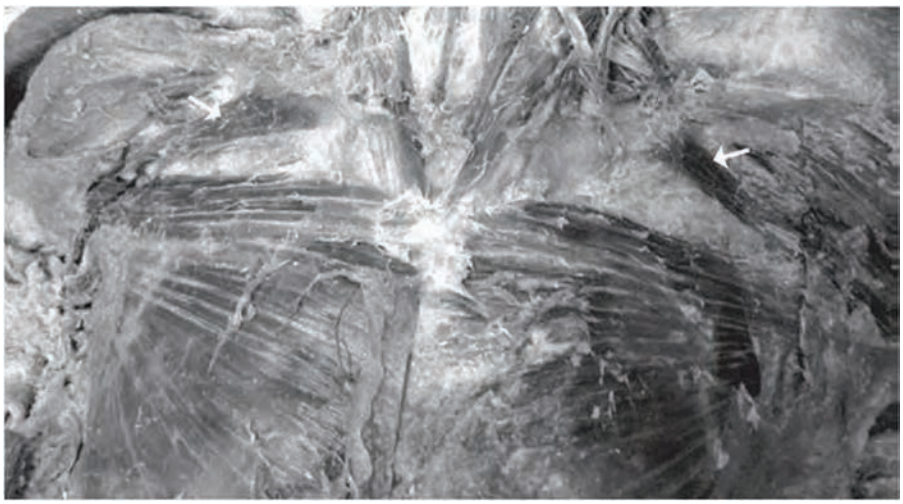

Figure 35.6 Bilateral hypoplasia of the clavicular heads of the pectoralis major muscle. On the right side, the inferior-medial half of the clavicular head is absent, while on the left side, the inferior-medial three-quarters of the clavicular head is aplastic. The residual clavicular heads on both sides are shown (arrows) as well as the wide gaps between the clavicular and sternocostal heads.

Source: Paraskevas and Raikos (2010).

pectoralis minor has also been used for acromioclavicular joint reconstruction, by inverting superiorly a transected tendon up to the clavicle (Moinfar and Murthi 2007). Although to date no study has explored the use of an ectopic pectoralis minor tendon as a source for alternate autographs, it seems feasible due to its insignificant physiological function. The pectoralis minor is commonly used as a surgical landmark, so any perturbation to its normal presentation may cause confusion and complications during surgical procedures.

Absence of the pectoralis minor alone is rare (Clark 1915; Mysnyk and Johnson 1991), but occurs frequently with pectoralis major deficits and as part of Poland's syndrome (see section on Pectoralis major).

Poland's syndrome

Poland's syndrome is a rare congenital anomaly characterized by a hypoplasia of the chest wall and associated thoracic wall musculatures, neurovascular abnormalities, and hypoplasia of the musculature of the ipsilateral upper limb. Defects in the upper limb can include webbing of the fingers (syndactyly), symbrachydactyly, and ectrodactyly (Standring 2008). The syndrome is named after Alfred Poland, a British surgeon who first described this deformity in 1841. Poland syndrome usually presents unilaterally, although bilateral occurrence has been reported (Poland 1841; Karnak et al. 1998; Moir and Johnson 2008; Baban et al. 2009). It has a right-sided propensity and affects males more frequently than females. The incidence is reported to be one in 7000–100,000 persons (Fokin and Robicsek 2002).

The most common muscular anomalies of the thorax associated with Poland's syndrome are the absence of the sternocostal head of the pectoralis major muscle, or complete absence of the pectoralis major. Absence of the pectoralis minor is less frequent, but has been noted along with complete pectoralis major absence (Stylianos et al. 2012). Deficiencies in the clavicular head of the pectoralis major muscle are also extremely rare (Fig. 35.6; Paraskevas and Raikos 2010). The underlying cause of the syndrome is unclear, but may include disruption of the arterial blood supply to the subclavian vessels in early embryonic life or disruption in development of the lateral plate mesoderm (Bavinck and Weaver 1986; Standring 2008).

Pectoralis minimus

The pectoralis minimus (sternocostocoracoidian, sternochondrocoracoideus, chondrocoracoideus ventralis, or sternochondrocoracoideus ventralis) is a variant muscle of the thorax. It attaches medially to the first (Turgut et al. 2000; Soni et al. 2008; Ebenezer and Rathinam 2013) or second rib (Turgut et al. 2000; Rai et al. 2008) and runs laterally to insert on the coracoid process (Huntington 1904; Rai et al. 2008; Soni et al. 2008; Ebenezer and Rathinam 2013; Fig. 35.7). Turgut et al. (2000) reported an interesting case of bilateral pectoralis minimus muscles with varied insertions. On the right side the muscle took origin from the first costal cartilage and inserted onto the shoulder joint capsule. On the left side the muscle originated from the second costal cartilage and inserted via two tendinous slips that divided on the coracoid process. The thicker slip inserted onto the shoulder joint capsule, while the thinner part inserted on the lateral third of the clavicle and fascia of subclavius muscle. The deltoid branch of the thoracoacromial artery and the venae commitantes passed between the two tendinous slips at their bifurcation.

Innervation is by way of the lateral pectoral nerve (Soni et al. 2008). Some authors have noted that branches of the thoracoacromial vessels passed both superficial and deep to the variant muscle and are at risk of impingement or compression (Turgut et al. 2000; Rai et al. 2008; Fig. 35.8). The possibility of impingement of these vessels exists during hyperabduction of the shoulder, leading to pain with movements and possible mechanical alterations to muscular dynamics of the joint.

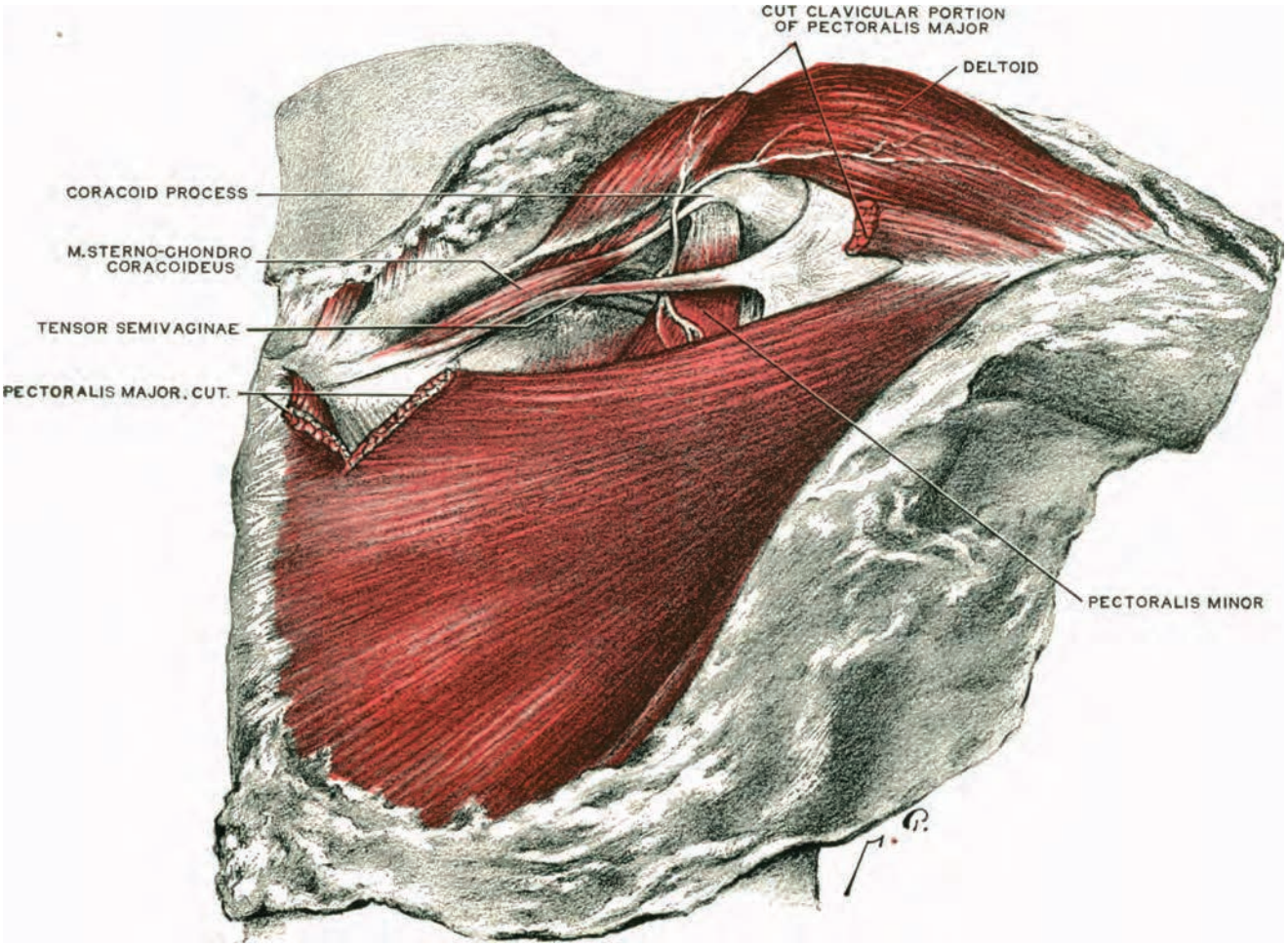

Figure 35.7 Columbia University Museum. Adult human subject. Left pectoral region with tensor semivaginae (sternohumeralis) and sternochondrocoracoideus ventralis (pectoralis minimus).

Source: Huntington (1904).

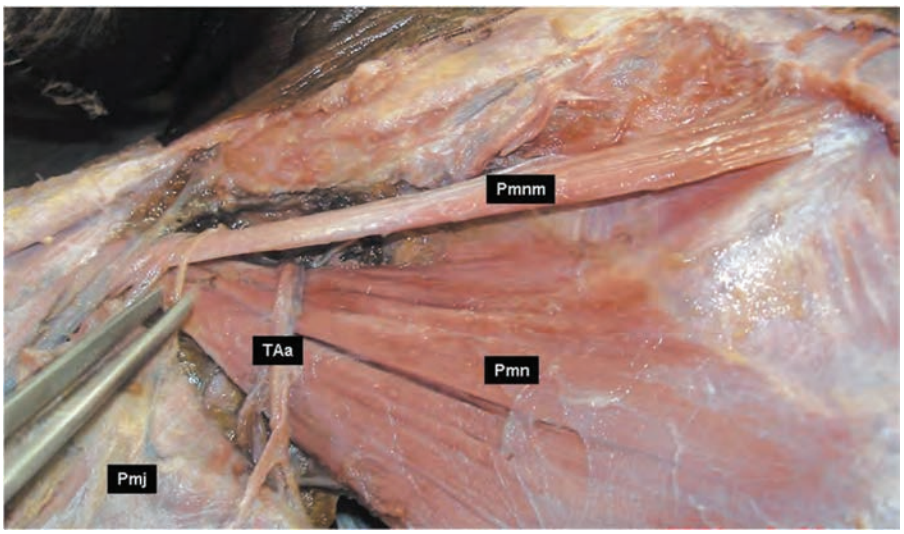

Figure 35.8 Dissection of right pectoral region showing *Pectoralis minimus* muscle. Pmj, *Pectoralis major* muscle; Pmn, *Pectoralis minor* muscle; Pmnm, *Pectoralis minimus* muscle; TAa, pectoral branch of thoracoacromial artery.

Source: Rai et al. (2008).

Pectoralis intermedius

Pectoralis tertius (xiphihumeralis)

The pectoralis tertius is derived from the entopectoral muscle sheet; it is usually absent in mammals but is quite distinct in the rat where it takes its origin from the xiphoid process and inserts onto the coracoid process (xiphihumeralis; Diogo and Wood 2012). In humans it is reported to take origin from the lower ribs and inserts onto the humerus or coracoid process, bearing a striking resemblance to the pectoralis quartus. Unlike the pectoralis quartus, which is innervated by the medial pectoral nerve, the tertius was reported by del Sol and Vasquez (2009) to be supplied by the lateral pectoral nerve instead. These same authors also state that the pectoralis intermedius and pectoralis quartus as described by other authors are in fact none other than the pectoralis tertius described by them (del Sol and Vasquez 2009; Fig. 35.9), making classification difficult.

Pectoralis quartus

The pectoralis quartus muscle is believed to be a segmented portion of the pectoralis major muscle (Birmingham 1889). It often presents as a slender muscle belly running along with or just under the inferolateral margin of pectoralis major, to which it may be loosely connected (Birmingham 1889; Huntington 1904; Fig. 35.10). It takes its origin from the lower ribs, the lateral border of the pectoralis major muscle, or the rectus sheath, and inserts into the bicipital groove or fascia of the upper arm (Wood 1866; Birmingham 1889; Bonastre et al. 2002; Hardy and Fabrizio 2009). Arican et al. (2006) reported a case where the muscle inserted as an aponeurosis to the intertubercular groove and tendon of the short head of the biceps brachii muscle. Bonastre et al. (2002) reported an interesting case of pectoralis quartus occurring alongside an axillary arch, in which case the pectoralis quartus muscle inserted into the inferior medial aspect of the axillary arch instead of the usual bicipital groove insertion (Fig. 35.11). A similar case was reported by Bergman (1991), where a double pectoralis quartus inserted into an axillary arch. Hardy and Fabrizio (2009) noted a case of a pectoralis quartus muscle occurring along another accessory thoracic muscle on the left side of a 60-year-old male cadaver. The pectoralis quartus arose from the fifth costal cartilage overlying the origin of the pectoralis minor muscle and coursed superiorly to insert into the fascia of the coracobrachialis muscle, while the accessory muscle arose from the aponeurosis of the external abdominal oblique muscle and inserted into the fascia of the coracobrachialis muscle deep to the pectoralis quartus insertion. The accessory muscle also exhibited a 180° rotation of its distal tendon, resulting in its deep surface facing anterior at insertion. Both muscles were innervated by the medial pectoral nerve. A variation of the pectoralis quartus named the chondrofascialis has been suggested to be an intermediate form between pectoralis quartus and chondroepitrochlearis, due to its insertion into the fascia of the arm but without connection to the pectoralis major as in the pectoralis quartus or the humerus as in the chondroepitrochlearis (Barcia and Genoves 2009; Fig. 35.12).

The presence of this muscle has been linked to complications during axillary lymphadenectomy by limiting the surgical field (Petrasek et al. 1997; Natsis et al. 2010; Totlis et al. 2012). The pectoralis quartus muscle has been found to be innervated by the medial pectoral nerve (Birmingham 1889; Sawada et al. 1991; Hardy and Fabrizio 2009), and has a prevalence of 2.8% (Natsis et al. 2010) although according to Bonastre et al. (2002) much higher rates (11–16%) have been reported in the past.

Figure 35.9 Dissected right pectoral region showing pectoralis tertius muscle. 1, Pectoral tertius muscle; 2, pectoral minor muscle; 3, pectoral major muscle; 4, serratus anterior muscle; 4, axillary fossa; 5, tendon of the latissimus dorsi muscle.

Source: del Sol and Vasquez (2009).

Chondroepitrochlearis

The chondroepitrochlearis (costoepitrochlearis, thoracoepicondylaris, chondrofascialis, chondrohumeralis, chondrobrachialis, or costohumeralis) is a muscular slip arising from the lower ribs, the inferolateral aspect of pectoralis major, or the aponeurosis of the external oblique muscle (Knott 1880; Voto and Weiner 1987; Lama et al. 2010; Table 35.1), which after crossing the axilla inserts on the medial intermuscular septum or the medial epicondyle of the humerus (Knott 1880; Voto and Weiner 1987; Jaijesh 2005; Lama et al. 2010). The distal attachment is frequently via a long slender tendon, but the muscle may remain fleshy to its insertion (Bryce 1899; Flaherty et al. 1999). This variant has a high predilection to occur together with an axillary arch muscle (of Langer) (Chiba et al. 1983; Lin 1988; Bergman 1991; Spinner et al. 1991; Lama et al. 2010), although it has been reported to occur alone (Voto and Weiner 1987; Flaherty et al. 1999; Sarikcioglu et al. 2004; Jaijesh 2005; Samuel and Vollala

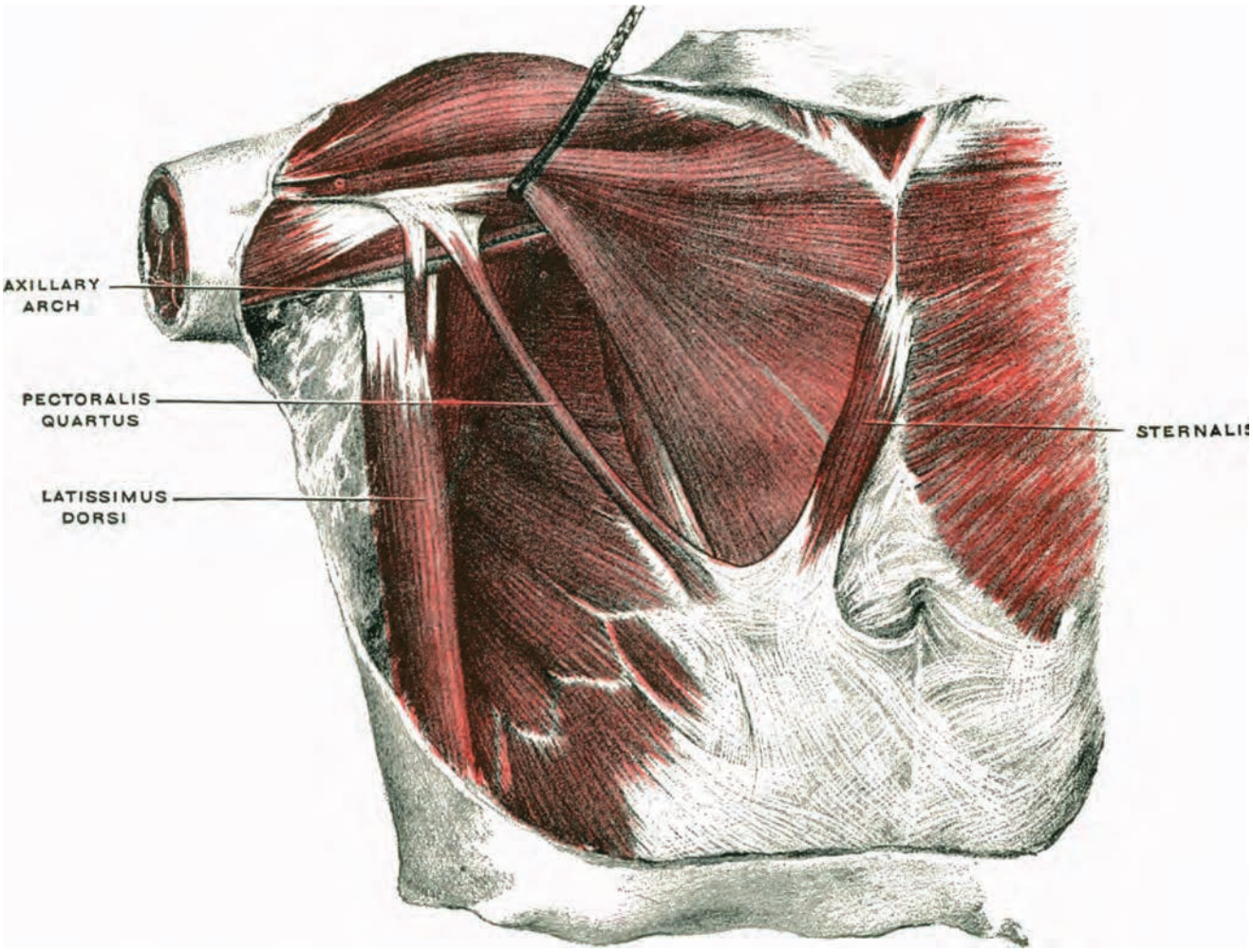

Figure 35.10 Columbia University, Study Collection. Adult human subject. Pectoral region with sternalis, pectoralis quartus, and axillary arch.

Source: Huntington (1904).

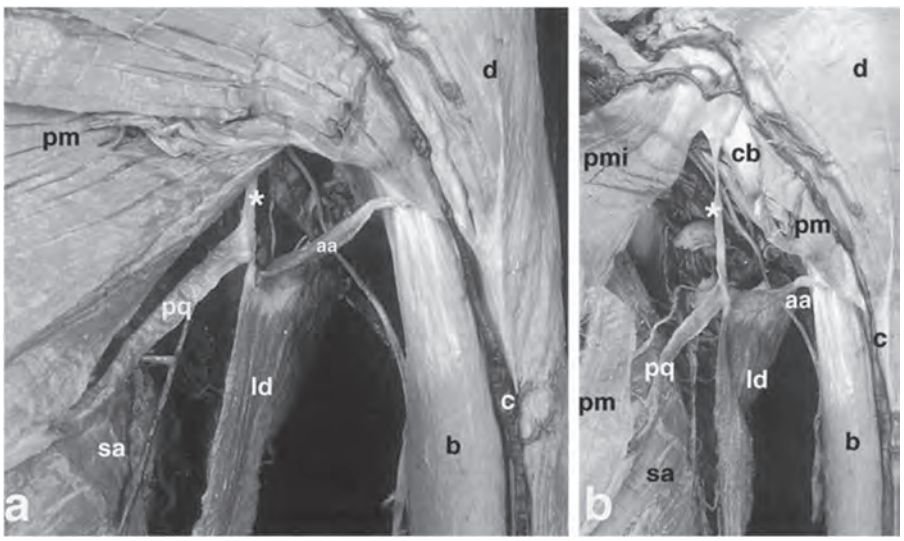

Figure 35.11 (a) Anterior view of the axillary region showing the pectoralis quartus (pq) and the axillary arch (aa) with its additional fibrous band (*). (b) Anterior view of the axillary region after reflecting pectoralis major (pm) to show the insertion of the additional fibrous band (*) of the axillary arch muscle into the coracoid process between pectoralis minor (pmi) and coracobrachialis (cb). b, biceps brachii muscle; c, cephalic vein; d, deltoid muscle; ld, latissimus dorsi muscle; sa, serratus anterior muscle.

Source: Bonastre et al. (2002). Reproduced with permission from John Wiley & Sons.

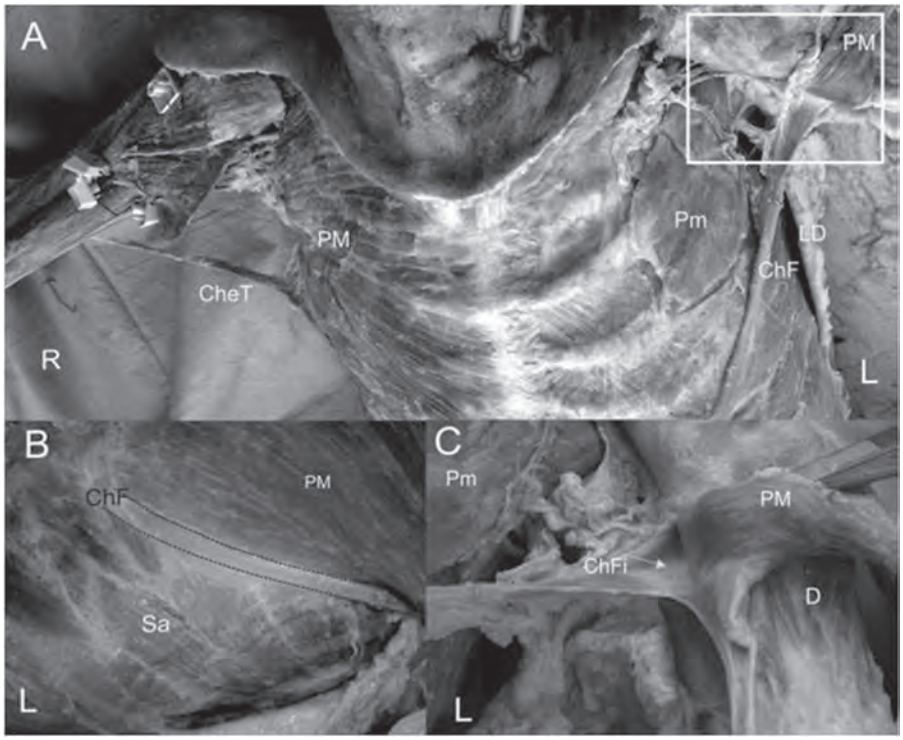

Figure 35.12 (a) Frontal view showing chondroepitrochlearis (CheT), sectioned pectoralis major (PM) in the right side (R) and the chondrofascialis (ChF), pectoralis minor (Pm), latissimus dorsi (LD), and the PM reflected in the left side (L). (b) Shows the close relation between PM and ChF (plotted line), serratus anterior (Sa). (c) Detailed photograph obtained from the white square on (a), where (D) is the deltoid muscle, and the arrow shows the fascial insertion (ChFi) of ChF underneath the reflected PM.

Source: Barcia and Genoves (2009). Reproduced with permission from John Wiley & Sons.

2008). Unilateral presentation is most common although bilateral presentation has been documented (Lin 1988; Flaherty et al. 1999). Recent reports suggest prevalence rates of around 0.5–0.84% (Flaherty et al. 1999; Natsis et al. 2012); Le Double (1897) suggested rates as high as 12–20%, although such rates have not been confirmed. Presence of the chondroepitrochlearis has been associated with certain chromosomal abnormalities including trisomy-13 and -18 (Bersu and Ramirez-Castro 1977; Aziz 1980).

It is frequently confused with the pectoralis quartus muscle due to their similar proximal attachments and course through the axilla, but may be differentiated based on its inferior attachments on the medial aspect of the humerus versus the superior attachments of the pectoralis quartus. Landry (1958) regarded this muscle as the inferior aspect of the pectoralis major muscle which has not undergone its normal anatomical rotation as it inserts into the proximal humerus. Accordingly, he concluded that the chondroepitrochlearis muscle must occur concurrently with a non-rotated distal tendon of the pectoralis major muscle. This association has been confirmed by some authors (Lin 1988; Bergman 1991; Spinner et al. 1991; Flaherty et al. 1999; Samuel and Vollala 2008), although others report no such association (Chiba et al. 1983; Voto and Weiner 1987; Jaijesh 2005; Lama et al. 2010). The chondroepitrochlearis has also been considered a separated pars abdominalis of the pectoralis major muscle (Tobler 1902; Chiba et al. 1983). Lama et al. (2010) reported a rare case of the chondroepitrochlearis occurring along with the axillary arch (Fig. 35.13). The two variants jointed together after taking origin from the pectoralis major and latissimus dorsi muscles, respectively, and, after crossing superficially over the neurovascular bundle of the axilla, the common tendon inserted into the brachial fascia and the lateral lip of the intertubercular groove. Chiba et al. (1983) also observed this variant along with the axillary arch; in this case the chondroepitrochlearis arose via two slips from the lower costal cartilages. The upper slip crossed the axilla and connected to an aponeurotic sheet, where it abruptly turned down as a long slender tendon to insert into the medial intermuscular septum and medial epicondyle of the humerus. The other slip inserted onto the axillary arch which itself was connected to the aponeurotic sheet. Bryce (1899) reported a case with multiple supernumerary muscles on the right hemithorax of a female cadaver including the chondroepitrochlearis, sternalis, and sternoclavicularis, and a deficit in the sternal portion of pectoralis major muscle.

Any aberrant muscle crossing the axilla including the chondroepitochlearis is of great importance clinically. The chondroepitrochlearis has been reported to cause nerve impingement (Spinner et al. 1991) or shoulder contractures (Lin 1988), complicate procedures such as an axillary lymphadenectomy (Natsis et al. 2010, 2012), or cause functional impairment by limiting full abduction of the shoulder joint, necessitating surgical release (Voto and Weiner 1987; Di Gennaro et al. 1998).

The arterial supply is via the lateral thoracic artery (Sarikcioglu et al. 2004; Samuel and Vollala 2008; Barcia and Genoves 2009)

Table 35.1 Reported cases of chondroepitrochlearis muscle with attachment points and innervation.

Study	No. muscles observed (width × length cm)	Medial attachment	Lateral attachment	Innervation
Calori 1867	1	Pectoralis major	Intermuscular septum	
Knott 1880	1	Sixth costal cartilage	Medial epicondyle	
Bryce 1899	1	Sixth costal cartilage	Intermuscular septum	
Aziz 1980	2	Fourth–sixth ribs	Medial epicondyle	
Chiba et al. 1983	1	Lower costal cartilages	Intermuscular septum, medial epicondyle Axillary arch	Ansa pectoralis
Voto and Weiner 1987	1	Third–tenth costal cartilage	Medial epicondyle	
Spinner et al. 1991	1 (3.5 × 31)	Sixth–seventh ribs	Brachial fascia Medial epicondyle	Medial pectoral n. Branch of median n.
Flaherty et al. 1999	2 (1.7 × 35)	Fifth costal cartilage	Intermuscular septum Medial epicondyle	Medial pectoral n.
Sarikcioglu et al. 2004	1	Fifth–sixth costal cartilage	Medial epicondyle	Medial pectoral n.
Jaijesh 2005	1	Sixth costal cartilage	Medial epicondyle	Medial pectoral n.
Loukas et al. 2005	1 (1.0 × 12)	Pectoralis major	Medial epicondyle Intermuscular septum	Medial pectoral n.
Samuel and Vollala 2008	1 (0.5 × 15)	Pectoralis major	Medial epicondyle Intermuscular septum	Medial pectoral n.
Barcia and Genoves 2009	1	Costal cartilage	Medial epicondyle	Medial pectoral n.
Lama et al. 2010	1 (1.5 × 18)	Pectoralis major at rib five	Lateral lip intertubercular groove Brachial fascia	
Natsis et al. 2012	1	Costal cartilages	Medial epicondyle	
Redler et al. 2012	1 (1.5 × 11)	Pectoralis major ?	Intermuscular septum Brachial fascia Coracobrachialis muscle	

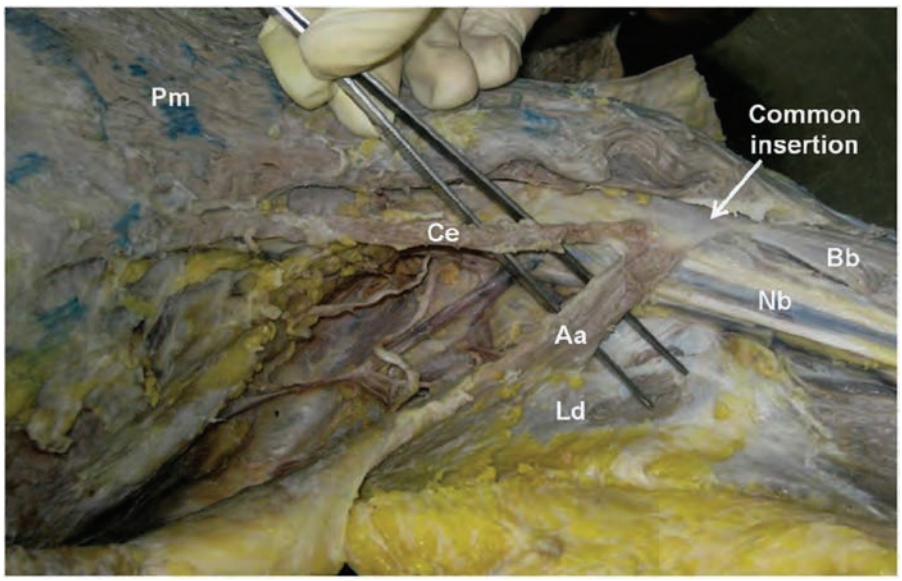

Figure 35.13 A muscular slip from the inferior border of the pectoralis major muscle (Pm), known as the chondroepitrochlearis (Ce), was separated from the main course of the pectoralis major muscle and crossed the neurovascular bundle of the axilla (Nb) before its insertion. In the same axilla, another variant muscular slip from the anteroinferior border of the lattissimus dorsi muscle (Ld), known as the axillary arch (Aa), arises and also runs superficial to the neurovascular bundle of the axilla. These two rare variant muscle slips, after crossing the Nb, were joined to form a single aponeurotic sheath and inserted into the fascia covering the biceps brachii muscle (Bb) and also onto the lateral lip of the intertubercular sulcus of the humerus.

Source: Lama et al. (2010). Reproduced with permission from the Romanian Society of Morphology.

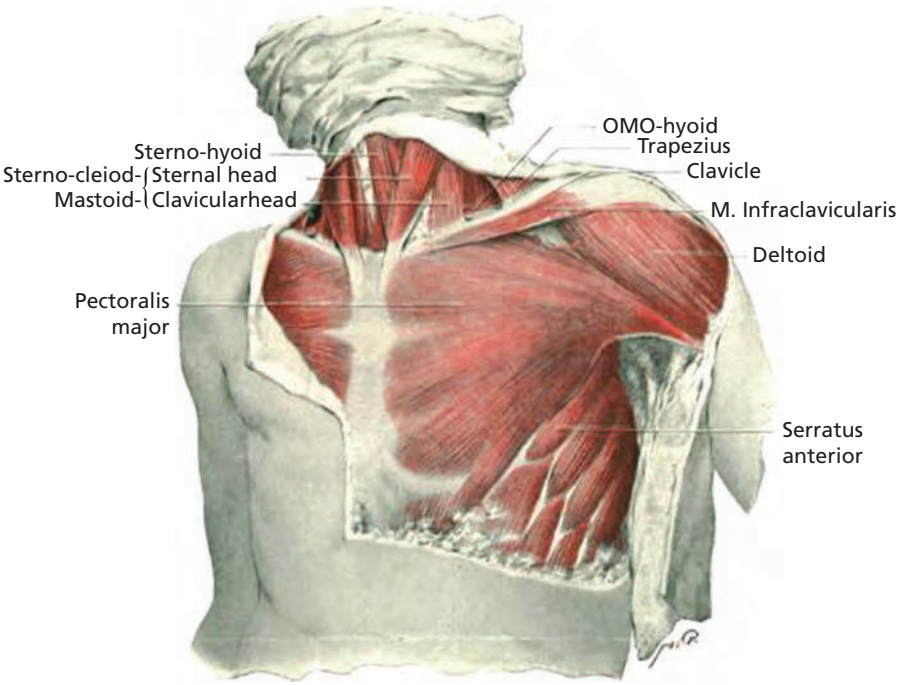

Figure 35.14 Adult human subject. Left pectoral region with infra-clavicularis.

Source: Huntington (1904).

or from a branch of the thoracoacromial trunk (Loukas et al. 2005). Innervation is furnished by the medial pectoral nerve (Spinner at al. 1991; Flaherty et al. 1999; Jaijesh 2005; Loukas et al. 2005; Samuel and Vollala 2008; Barcia and Genoves 2009), or a branch of the ansa pectoralis (Chiba et al. 1983). Dual innervation from the medial pectoral nerve and a branch from the Y-junction of the medial and lateral roots of the median nerve have also been reported (Spinner et al. 1991).

Costocoracoideus (chondrocoracoideus)

A muscular variant arising via slips from ribs six–eight or the rectus sheath and inserting with the short head of the biceps brachii muscle to the coracoid process (Bergman 2014). Diogo et al. (2009) note that the costocoracoideus and sternocoracoideus muscles are present in other taxa, but suggest that in humans these are represented by the costocoracoid ligament and the subclavius muscle, respectively.

Infraclavicularis

The infraclavicularis muscle is a rare muscular variant of pectoral muscle mass origin. As the name implies, it lies inferior to and runs more or less parallel to the clavicle. The muscle originates from the ventral surface of the medial part of the clavicle or the anterior sternoclavicular ligament and fans out laterally to insert into the distal clavicle and deltopectoral fascia (Ingalls 1913). A well-developed infraclavicularis muscle may often be associated with an underlying large deltopectoral triangle, which this muscle often bridges (Huntington 1904; Fig. 35.14). Innervation is supplied by the lateral pectoral nerves and the muscle is believed to be an aberrant or displaced part of the clavicular head of the pectoralis major muscle (see section on Sternalis m.).

Interclavicularis anticus digastricus

See section on Sternoclavicularis.

Supraclavicularis proprius (tensor fascia colli)

This muscle takes its origin from the cervical fascia overlying the clavicular head of the sternocleidomastoid and sternoclavicular joint, and inserts to the distal end of the clavicle (Knott 1880; Ottone and Medan 2009; Fig. 35.15) or the fascial sheath of the trapezius muscle at the level of the acromion process (Laidlaw 1902). Knott (1880) described a sheath about the muscle from the deep cervical fascia which held the muscle in place. In his report, Laidlaw (1902) agreed with Gruber's proposed action of this muscle as tensing the superficial layer of the cervical fascia for which he aptly termed it "tensor fascia colli." Ottone and Medan (2009) report the frequency of occurrence to be 0.64% after finding 1 case in 156 body halves. The muscle is innervated by a small twig from the supraclavicular nerve (Laidlaw 1902).

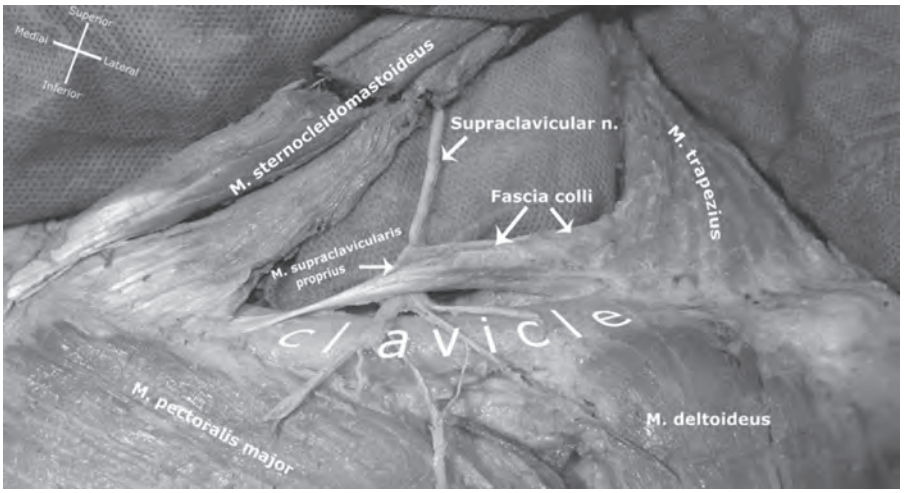

Figure 35.15 The supraclavicularis proprius muscle over the lower portion of the left supraclavicular fossa.

Source: Ottone and Medan (2009).

Sternoclavicularis

The sternoclavicularis muscle (sternoclavicularis anticus, sternoclavicularis anterior, supraclavicularis, or preclavicularis medialis) takes its origin from the manubrium, the anterior sternoclavicular ligament, or the first or second costal cartilage, and passes laterally beneath the clavicular head of the pectoralis major muscle to insert onto the ventral surface of the distal end of the clavicle. It is separated from the subclavius muscle by the costocorocoid membrane (Wood 1866; Bryce 1899; Huntington 1904; Fig. 35.16). Presence of the sternoclavicularis muscle is frequently associated with deficits in the clavicular or upper part of the sternal head of the pectoralis major (Dwight 1887; Bryce 1899; Sakuma et al. 2007). Wood (1866) believed the sternoclavicularis to be closely allied to the upward extension of the pectoralis minor muscle, from which it differentiates. When present bilaterally, a tendinous band can unite the medial ends of the muscles, forming a digastric muscle (*interclavicularis anticus digastricus*) (Dwight 1887; Bryce 1899; Sakuma et al. 2007). Innervation is afforded by the lateral pectoral nerve (Bryce 1899; Huntington 1904; Sakuma et al. 2007). Laidlaw (1902) described a case of supraclavicularis muscle which he believed did not differ from the sternoclavicularis muscle described by others but for its origin which lacked the sternal attachment; he considered the two to be variations of the same muscle. His case took origin from the cervical fascia overlying the distal end of the sternocleidomastoid muscle and the sternoclavicular joint, and after running superior to the clavicle it inserted into the fascia about the acromium process. A supraclavicular branch of the fourth cervical nerve passed between this muscle and the clavicle, giving off a small branch for innervation in the process. However, his innervation pattern and suggested derivative from a displaced fascicle of the platysma or sternocleidomastoid are in stark contrast to the recent descriptions offered for sternoclavicularis, which align it with the pectoral muscle group.

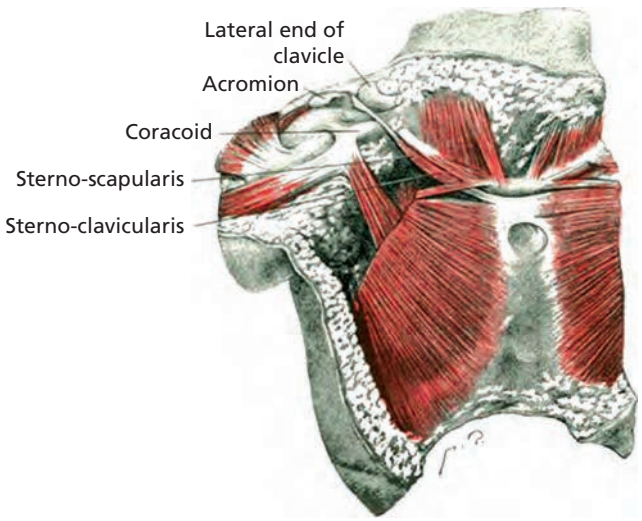

Figure 35.16 Columbia University, Study Collection. Adult human subject. Pectoral region with sternalis, pectoralis quartus and axillary arch.

Source: Huntington (1904).

Costoclavicularis

The costoclavicularis is described as originating from the second rib and, after coursing superiolaterally below the inferior margin of the subclavius muscle, it inserts into the inferior surface of the middle of the clavicle. Mori (1964) found 3 cases in 367 cadavers for a prevalence rate of less than 1%.

Sternoscapularis (sternoacromialis)

The sternoscapularis originates from the sternum and ascends laterally to pass between the clavicle and the corocoid process, and insert onto the medial border of the acromion (Huntington 1904; Fig. 35.16). The insertion on the acromion is just dorsal to the acromioclavicular joint. The innervation

is said to come from the lateral pectoral nerves. Absence of the subclavius muscle has been reported with sternoscapularis (Huntington 1904).

Supracostalis anterior

The supracostalis anterior muscle presents deep to the pectoral muscles, spanning across two or more intercostal spaces on the anterior chest wall. Its attachments may include ribs one or two, scalene muscle, or the deep fascia of the neck (Bergman 2014). Mori (1964) found 126 cases of this muscle in 2400 body halves (5.2%). Their attachments included the first (83%) or second (17%) rib superiorly and third (46%) or fourth (54%) rib inferiorly. The majority of the cases spanned two intercostal spaces (63%) with the remaining spanning three (37%). Tachibana and Miyauchi (1989) found the muscle in 14 out of 316 body halves (4.4%), all with innervation by the external muscular branch of the first intercostal nerve. In three of these cases the external muscular branch included the lateral cutanous branch. Keith (1894) stated that the supracostalis anterior is a rudiment of the external abdominal oblique muscle based on his observations of monkeys, and suggested it be named the obliques externus thoracis. More recent reports suggest it is derived from the intercostal muscles. Nelson et al. (1992) reported a bilateral case where the muscles took origin from the first rib and inserted into the fourth rib. They were able to determine the innervation to one of the muscle as a collateral branch of the second intercostal nerve, and suggested the muscle might be derived from the external intercostal muscles. Tachibana and Miyauchi (1989) believed the muscle was derived from the first external intercostal muscle based on their innervation pattern.

A similar muscle, the supracostalis posterior, may be found on the dorsal aspect of the thorax (Mori 1964).

Sternohumeralis

The sternohumeralis (or sternochondrohumeralis or tensor semivaginae articulationis humeroscapularis) lies in the interval between pectoralis major and pectoralis minor. It arises from the first, first and second, second and third, or third and fourth rib cartilages and from the border of the sternum, to be inserted by an aponeurosis into the capsule of the shoulder joint, the wall of the subacromial bursa (Bergman 2014), or the fascia deep to the deltoid muscle (Huntington 1904; Fig. 35.7). This muscular variant is believed to be a displaced segment of the pectoralis major, and its presence is frequently associated with deficiencies in the latter, relative to the size of the variant structure. This may present as a more or less pronounced gap between the sternal and clavicular heads of the pectoralis major muscle. These deficiencies are seemingly due to diversion of some of the deeper fibers normally entering the pectoralis major to form the variant muscle (Huntington 1904). Innervation is furnished by branches from the lateral pectoral nerve (Huntington 1904).

Transpleuralis subclavius

Allen (1950) reported two flat muscular bands passing through the oblique fissure of a right lung, extending from the sixth rib to the central tendon of the diaphragm posterior to the caval opening.

Transversus thoracis (sternocostalis, triangularis sternae)

Mori (1964) and Jelev et al. (2011) have done extensive analysis on the morphological variations of the transversus thoracis muscle. Jelev et al. (2011) found the muscle to range from 1 to 7 slips on each side of the thorax, with over 80% of the bodies having 4–5 slips (Figs 35.17, 35.18). The muscle radiates out from the sternum to as far as the first rib superiorly and seventh rib inferiorly, with most frequent attachments superiorly to the second (39–45%) and third rib (38–50%) and inferiorly to the fifth (1–16%) and sixth rib (76–92%) (Mori 1964; Satoh 1971; Jelev et al. 2011).

Subclavius

Mori (1964) reports two types of variations of the subclavius muscle in his investigation of 72 hemithoraces. In type I variation (12/72 sides, 16.8%) the lateral end is divided into two

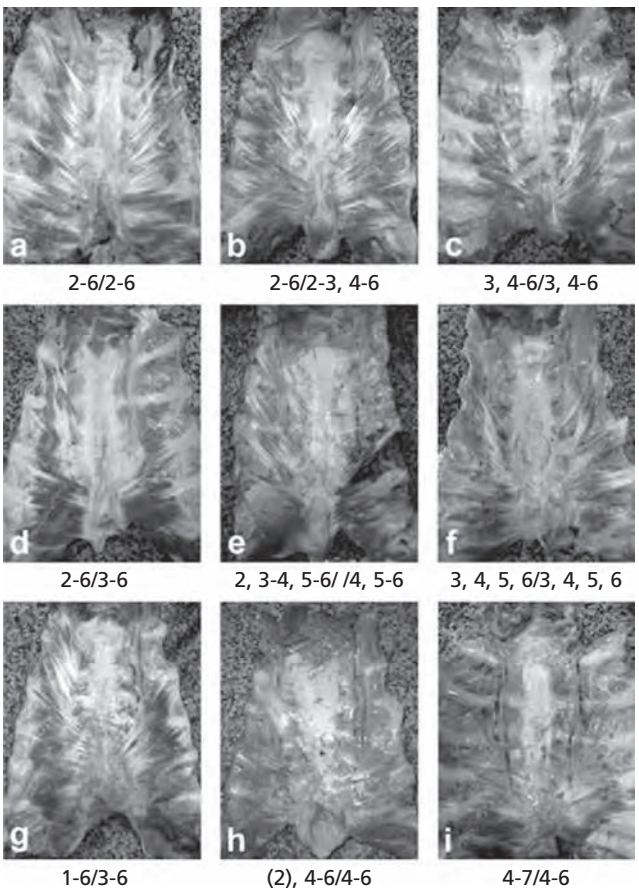

Figure 35.17 Photographs of various forms of the transversus thoracis muscle indicating highest and lowest level of rib insertion on each side.

Source: Jelev et al. (2011). Distributed under the terms of the Creative Commons CC-BY-2.0 licence.

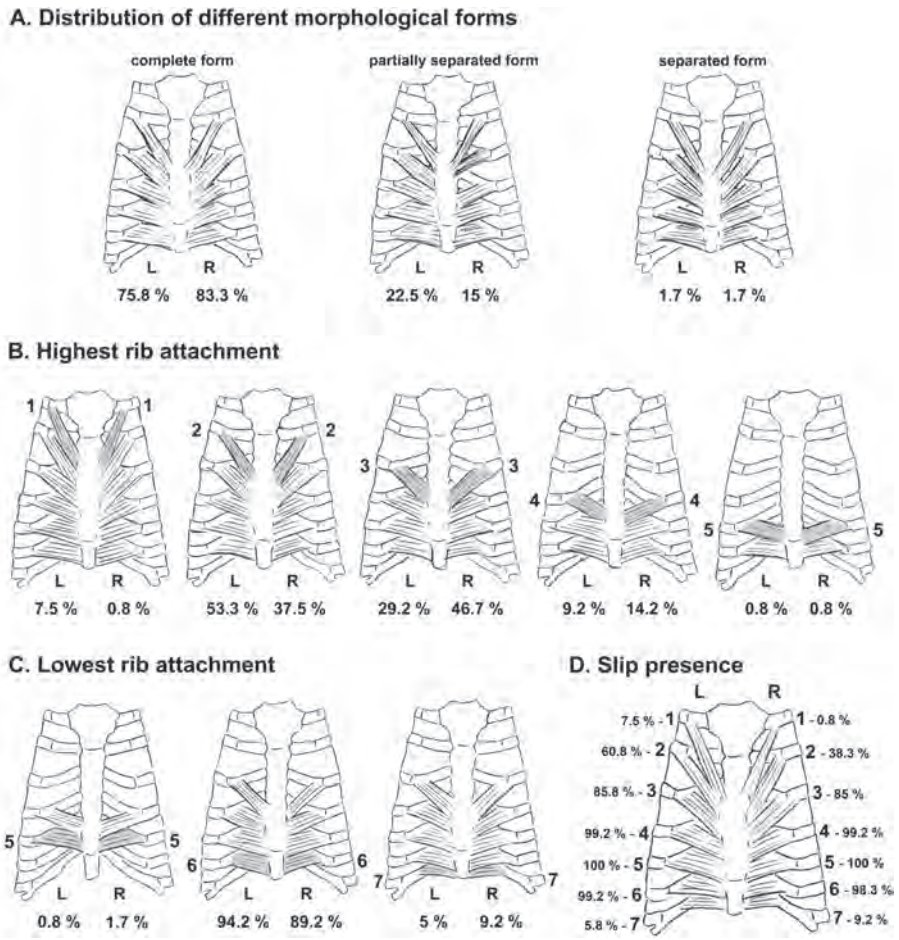

Figure 35.18 Schemes showing numerical distribution of different characteristics of the transversus thoracis muscle.

Source: Jelev et al. (2011). Distributed under the terms of the Creative Commons CC-BY-2.0 licence.

portions, where one inserts onto the inferior aspect of the clavicle and the other into the root of the coracoid process. In type II variation (6/72 sides, 8.3%) the lateral end inserts into the middle third of the inferior aspect of the clavicle then continues on to the superior margin of the scapula or the root of the coracoid process as in type I. Complete absence of the subclavius muscle has been reported, in which case it was be replaced by a strong fibrous band (Crerar 1892). A bursa is occasionally seen between the tendon of subclavius and the first rib.

Subclavius posticus (scapulocostalis minor)

The subclavius posticus originates from the first costal cartilage and courses posterolaterally along the dorsal surface of the clavicle to insert onto the superior margin of the scapula opposite the omohyoid muscle. Prevalence ranges between 1 and 7% (Mori 1964).

Levator costae primae

The levator costae primae is a slender muscle, originating from the superior border of the scapula and the suprascapular ligament, coursing anteriorly to insert via a rounded tendon onto the sternal end of the first rib. It is innervated by the suprascapular nerve. A bilateral case has been reported by Macdonald Brown (1880).

Diaphragm

The dome-shaped diaphragm is composed of a central tendon and peripheral muscular portion. The muscular portion of the diaphragm attaches to the sternum, lower six costal cartilages, and lumbar vertebrae. Over the posterior abdominal wall the diaphragm arches over the psoas major and quadratus lumborum muscles, creating fascia thickenings called the medial and lateral arcuate ligament, respectively. Centrally, two vertically oriented bands of muscle called the right and left crus attach the lumbar portion of the diaphragm to the lumbar vertebrae and contribute to the formation of the hiatus for the esophagus and arch over the abdominal aorta. The thickened portions of the crura, which arch over the abdominal aorta, are called the median arcuate ligament. The right crus which takes its origin

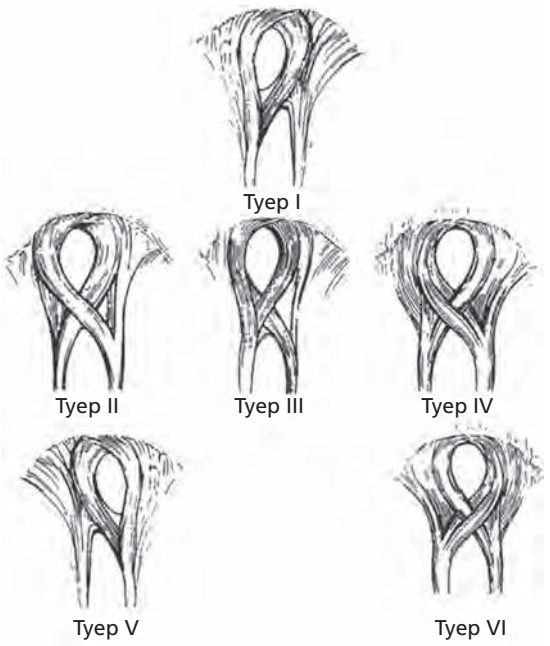

Figure 35.19 Diagrammatic representation of the different types of diaphragmatic crura observed in this study. Adapted from Loukas et al. (2008).

from the upper three lumbar verterbral bodies and intervening intervertebral disks (IVD) is typically larger than the left crus, which originates from the first and second lumbar vertebrae and intervening disk. Botros et al. (1990) found that in 98% of the cases they examined the right crus was divided into a medial, middle, and lateral bundle, while 90% of the left crus had only a medial and lateral bundle. The two crura may not communicate with each other.

Variations in size, thickness, and attachments are common. The average thickness of the muscular portion is 5 mm (Shirkhoda 2011). Variations in the crura have also been reported. Loukas et al. (2008) examined 200 human diaphragms and identified six morphological patterns of crural contributions to the formation of the esophageal hiatus (Fig. 35.19), while Botros et al. (1990) examined 50 diaphragms and identified five patterns. In Type I identified by Loukas et al. (2008), the hiatus was formed by the muscular contributions arising solely from the right crus, and was found in 45% of the cases compared to only 10% by Botros et al. (1990). Type II (20%) exhibited equal muscular contributions from both crura and was found in 10% in the latter study. In type III (15%), the right and left muscular contributions arose from the right crus with an additional small contribution from the left crus and was found in 62% of cases by Botros et al. (1990). In type IV (10%), the right and left muscular contributions arose from the right crus with two additional (anterior and posterior) bands coming from the left crus. This pattern was not identified in the later study. Type V (5%) demonstrated contributions coming solely from the left crus, and was present in 2% of Botros' cases. In type VI (5%), the right and left muscular contributions originated from the left crus with two additional bands, one from the right crus and one from the left crus. This pattern was also not found by Botros et al. (1990); however, they described an additional pattern where neither crus contributed directly to the hiatus except posteriorly and the hiatus was bounded by a V-shaped band from the median arcuate ligament. This pattern was observed in 16% of the cases and none by Loukas et al. The high prevalence of type I esophageal hiatus identified by Loukas et al. (2008) has been confirmed by others (Shehata 1966). Sirasanagandla et al. (2014) reported a case of duplicated right crus, where the medial right crus originated from the anterolateral surface of the upper three lumbar vertebrae and associated (IVD), while the lateral right crus took origin from the IVD between the third and fourth lumbar vertebrae.

Defects of the diaphragm can be congenital, age related, or associated with other pathological conditions. Congenital defects can range from small areas of thinning of the muscular diaphragm with no loss of continuity to large defects leading to herniation of abdominal organs into the thorax. Hernias in the posterolateral part of the diaphragm (Bochdalek hernias) are much more common than in the anterior part (Morgagni hernias), with left presentation being twice as common as the right (Hollinshead 1956; Gale 1985). A supernumerary muscle bundle that can obturate Bochdalek's trigone (hiatus of Tuffier and Lejars; Costolumbar hiatus of Henle) is known as the small muscle of Theile and Müller. The prevalence of diaphragmatic defects increases with age, particularly after age 60. Caskey et al. (1989) reported that 56% of patients between 60 and 80 years have acquired such defects. These defects are often asymptomatic and discovered accidentally on diagnostic imaging. A positive association has been reported between diaphragmatic defects and emphysema (Caskey et al. 1989). Cases of accessory diaphragm have also been reported, where an incomplete musculotendinous membrane resembling a diaphragm partitions the hemithorax (usually right; da Silva et al. 2012). Portions of the lower lobe of the right lung often grow into the space between the two layers of the diaphragm. This accessory diaphragm may present in various stages of development, ranging from small muscular bands running through the fissures of the lung and attaching to the central tendon to full duplication of the hemidiaphragm (Hollinshead 1956). Wille et al. (1975) reported that in 20 out of 21 cases (his own 6 cases and 15 others from the literature) of accessory diaphragm the condition was on the right side and affected males more frequently than females. Left-sided accessory diaphragms have been reported by others (Kenanoglu and Tuncbilek 1978). An accessory diaphragm is believed to form due to faulty migration of the septum transversum, which traps part of the developing lung bud, and may be associated with other vascular and pulmonary anomalies (Kenanoglu and Tuncbilek 1978; da Silva et al. 2012). Symptomatic cases have been treated by resecting the accessory diaphragm and lobectomy (Ausin et al. 2010).

Roos bands/muscles

A fibromuscular band/muscle can be found anterior to the T1 nerve root. This results in a tunnel for the nerve to travel through before combining with the C8 nerve root. Spears et al. (2011) identified such structures in 41% of cadavers. These muscles arise in the neck and insert onto the first rib.

Sternalis

During the four centuries since it was first reported by Barthelemy Cabrol (Cabrolius) in 1604, numerous reports of the sternalis muscle (musculus sternalis, episternalis, parasternalis, presternalis, rectus sternalis, rectus sterni, rectus thoracis, rectus thoracicus superficialis, superficial rectus abdominis, sternalis brutorum, japonicas, or thoracicus; Fig. 35.15) have been published, highlighting its wide range of presentations (Turner 1867; Cunningham 1888; Barlow 1935; Bradley et al. 1996; O'Neill and Folan-Curran 1998; Jelev et al. 2001; Raikos et al. 2011b; Ge et al. 2014). Despite its well-documented existence, the infrequent presentation of the sternalis muscle has led to its continued obscurity and absence from mainstream anatomical, surgical, and radiological texts. Much disagreement remains about this muscle's embryological origin, function, and innervation. Even the task of giving it a universally accepted anatomical name has historically proven challenging, with at least a dozen different variants used in the past to describe it. The nomenclature used in the literature for the sternalis muscle has changed throughout history and continues to evolve today as new variants are found, making historical comparisons difficult. Substantial technological progress in medical imaging and surgical procedures during the last century has once again brought the sternalis muscle into relevance. Although the surgical and radiological anatomy of the anterior thoracic musculature has been well described, recent scientific reports concerning its mimicking of focal densities in the medial breast on mammography, leading to suspicion of a neoplasm, are re-emphasizing the importance of this structure in everyday clinical practice.

A clinician's familiarity with this muscular variant and its inclusion in differential diagnosis may avoid unnecessary invasive procedures and undue stress to patients. The sternalis muscle has major implications in breast and thoracic surgery. When undetected prior to surgery it can interfere with procedures, leading to longer operative times. When detected pre-operatively, it can be used as a muscular flap in reconstructive surgery and improve aesthetic results in breast augmentation by providing extra cover for the prosthesis.

Historical background

Barthelemy Cabrol, a sixth century French surgeon (Eycleshymer et al. 1917), was the first to note a longitudinal band-like muscle located deep to the skin and fat and superficial to the sternum (Turner 1867; Fig. 35.20). Over a century later, in 1726, Du Puy was one of the first to describe its detailed morphology

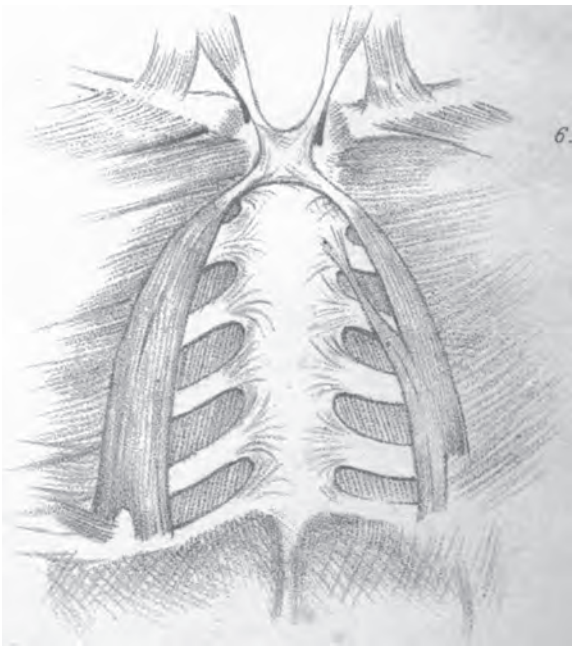

Figure 35.20 Original drawing of bilateral sternalis muscle.

Source: Turner (1867).

(Turner 1867). Following his publication, other authors including Weitbrecht, Albinus, De la Faye, Wilde, and Boerhave began to publish their findings on this rare variant (as reported by Turner 1867). Sandifort is reported to have been the first to use the name *thoracicus* on the basis of Boerhave's observations and drawings of specimens with the sternalis muscle present (Turner 1867). The report by Albinus in 1734 is also noteworthy as he first proposed that the sternalis muscle was somehow connected to the rectus abdominis muscle (Turner 1867). Many prominent anatomists of the late seventeenth and eighteenth centuries supported this view and began referring to the muscle as the *rectus sternalis* or *sternalis brutorum* (as reported by Turner 1867). Not everyone at that time shared this view, believing instead that the sternalis was a downward extension or continuation of the sternocleidomastoid muscle since they appeared closely associated at the clavicle and upper part of the sternum (Turner 1867). Turner (1867) believed the sternalis muscle was associated with the panniculus carnosus on the basis of his comparative anatomical studies of animals. He noted that some animals had a well-developed panniculus carnosus over the ventral thoracic wall, closely resembling that of the platysma muscle in humans, which is also believed to be derived from the panniculus carnosus. Even Charles Darwin, the father of evolutionary biology, weighed in on the issue, supporting Turner's view in his book *The Descent of Man* by stating that the sternalis was "closely allied to the panniculus" (Darwin 1871).

According to Wallace (1886), the nerve supply to the sternalis muscle had not been thoroughly investigated and reported until

1884 when Cunningham traced the nerve branches from the sternalis back to the medial pectoral nerve (formerly referred to as internal anterior thoracic nerve). However, Cunningham himself gave credit to Hallett (1848) as the first to comment on the nerve supply to the sternalis, although Hallett had attributed the innervation to the third, fourth, and fifth intercostal nerves (Cunningham 1888). Cunningham's work on tracing the innervation of the sternalis muscle back to the medial pectoral nerve supported the view that the sternalis muscle belonged to the pectoral group of muscles. This view was first proposed by Bardeleben in 1876 and was popularized by Abraham's 1883 study of 11 anencephalic fetuses of which six had sternalis muscles (Abraham 1883; Cunningham 1884, 1888). From his study, Abraham suggested a connection between fetal deformities and the frequency of this muscular variation (55% in his study). He also noted that aberrations in the pectoralis major muscles were common when well-developed sternalis muscles were present, suggestive of their close or identical primitive muscular layer origin (Abraham 1883). Shepherd (1885) substantiated those findings with his own dissections of anencephalic fetuses with sternalis muscles, all of which were supplied by the medial pectoral nerve (Wallace 1886).

The debate over the innervation and homology of the sternalis muscle which began in the nineteenth century continues to the present day. During this time, alternative names have been used for the sternalis muscle to more accurately represent its location, origin and insertion, and morphology including: musculus sternalis, episternalis, parasternalis, presternalis, rectus sternalis, rectus sterni, rectus thoracis, rectus thoracicus superficialis, superficial rectus abdominis, sternalis brutorum, japonicas, and thoracicus (Hallett 1848; Turner 1867; Humphry 1873, Raikos et al. 2011b; Jelev et al. 2001).

Prevalence

Cadaveric investigations reveal that the sternalis muscle has an overall prevalence of around 7.8% in the general population (Snosek et al. 2014; Table 35.2); however, there is great variation both within and between different geographic populations. For example, some of the highest rates have been reported in the Asian population (11.5%), compared to 8.4% in populations of African descent and 4.4% in those of European descent. Interestingly, the reported prevalence within the Asian population ranges from 1% in Taiwanese to 23.5% in Northern Chinese (Jelev et al. 2001). The discrepancies in reported prevalence rates and in geographic variability in particular could be explained by the muscle's inherent physical variability and by the small sample size commonly associated with full body dissections. This physical variability could lead to small, slender, poorly defined, and frequently fibrous sternalis-like structures often being missed during dissection, leading to inaccurate reporting of its prevalence.

There is no evident correlation between the presence of the sternalis muscle and the general muscularity of the individual, since the muscle has been reported in both very muscular and fairly feeble individuals (Turner 1867). Females have a slightly higher rate of occurrence than males (8.6% and 7.5%, respectively; Table 35.2), although others report no gender difference (Cunningham 1888; Yap 1921; Barlow 1935). Barlow also pointed out that although most authors report the genders of the specimens with sternalis muscle present, most fail to report the ratio of males to females in the sample population from which the sternalis-positive specimens were obtained (Barlow 1935). Without this ratio, any statistical analysis from such sample populations is of little significance for determining differences in the occurrence of the sternalis muscle between the genders.

Table 35.2 Cadaveric prevalence rates of sternalis muscle for males and females. Male, female, and combined prevalence rates from cadaveric investigations based on review of the literature. Only studies with adult cadaveric population where the male to female ratio was noted are included in this data.

	No. male bodies			No. female bodies			
Study	Examined	Sternalis found	%	Examined	Sternalis found	%	Overall % (M + F)
Adachi 1909	137	16	11.7	46	11	23.9	14.8
Locchi 1930	217	23	10.6	86	7	8.1	9.9
Barlow 1935	422	23	5.5	113	10	8.8	6.2
Mori 1964	350	36	10.3	25	3	12.0	10.4
Bergman et al. 1988	562	36	6.4	438	38	8.7	7.4
Jeng and Su 1998	151	2	1.3	56	0	0	1.0
Londhe et al. 2010	9	0	0	1	1	100	10.0
Raikos et al. 2011b	29	1	3.4	16	0	0	2.2
Chaijaroonkhanarak et al. 2013	70	9	12.9	47	1	2.1	8.5

Source: Snosek et al. (2014). Reproduced with permission from John Wiley & Sons.

Clinical reports of this muscular variant based on various imaging modalities and surgical procedures indicate a lower prevalence (0.6%) than is inferred from cadaveric studies. Various factors could contribute to this underreporting of prevalence, including improper positioning of the patient, inadequate resolution of the images obtained, and a general lack of knowledge and awareness of this muscular variant among radiologists and surgeons. Even if the sternalis muscle is found and documented, such cases could often go unreported due to its benign nature.

The lowest rates have been reported from mammography studies (0–0.02%); however, this only includes studies of women as no data are available for males (Table 35.3). In one such study, the authors found no cases of the sternalis muscle from a review of medical records of 1580 women who had undergone mammographic imaging, compared to three confirmed cases out of 75 cadavers (4.0%) examined (Saeed et al. 2002). Demirpolat et al. (2010) reviewed 10 years worth of records from the mammography unit and reported only 10 cases among 52,930 female patients (0.018%). Bradley et al. (1996) evaluated 32,000 women who had received craniocaudal projection mammography screening and reported only four cases of the sternalis muscle (0.0001%). These cases presented as an unusual or irregular structure in the medial aspect of the breast and caused some diagnostic concern, warranting further investigation. However, studies using multidetector computed tomography (MDCT) have reported prevalence rates (6.4%) in line with those seen in dissection rooms (Table 35.3). Young Lee et al. (2006) retrospectively reviewed MDCT chest scans performed on 1387 Korean patients (790 males, 597 females), and found the sternalis muscle was present in 86 cases (6.2%) of which 42 were males (5.3%) and 44 were females (7.4%). In a similar study of 948 Japanese patients' MDCT chest scans (511 males, 437 females), the sternalis muscle was present in 100 patients (10.5%) of which 43 were male (8.4 %) and 57 were female (13%) (Shiotani et al. 2012). The unusually high prevalence rate could be attributed to the entire sample population being of Japanese origin which has previously been reported to have prevalence rates ranging from 4.1 to 15.6% (Jelev et al. 2001). Most recently, Ge et al. (2014) reviewed MDCT chest scans of 3091 males and 2909 females in a sample of 6000 Chinese patients. They confirmed the sternalis muscle in 187 males and 160 females (6.0% and 5.5%, respectively), for a combined prevalence rate of 5.8%. These MDCT studies have reported prevalence rates that are much higher than those from other clinical modalities, suggesting that MDCT is a highly sensitive identifier of this muscular variant, bringing cadaveric and clinical prevalence rates more in line with one another.

Results from surgeons during operations seem to support the previous notion that the sternalis muscle is clinically underreported. In one retrospective study of 1152 operative case records dating from 1990 to 2000 from women undergoing modified radical mastectomies, only eight cases (0.7%) of sternalis muscle were confirmed (Harish and Gopinath 2003). The authors state that the low prevalence rate could have been attributable to the surgeons' lack of awareness of the sternalis muscle, resulting in failure to identify it during surgery, or the inherent variability in its development, where smaller less-developed muscles with relatively thin and scant fibers could have been unintentionally removed with the breast tissue during the procedure (Harish and Gopinath 2003). Another study reported similarly low rates from breast augmentation surgery (Khan 2008; Table 35.3). The general lack of awareness by clinicians of this muscular variant was documented by Bailey and Tzarnas

Table 35.3 Clinical prevalence rates of sternalis muscle for males and females. Adult male, female, and combined prevalence rates from clinical investigations based on review of the literature.

		No. males			No. females			
Study	**Modality used**	**Examined**	**Sternalis found**	**%**	**Examined**	**Sternalis found**	**%**	**Overall prevalence (%)**
Bradley et al. 1996	Mammography				32,000	4	0.01	0.01
Saeed et al. 2002	Mammography				1,580	0	0	0.0
Demirpolat et al. 2010	Mammography				52,930	10	0.02	0.02
X-ray total					86,510	14	0.02	0.02
Harish and Gopinath 2003	Breast surgery				1,152	8	0.7	0.7
Khan 2008	Breast surgery				1,150	3	0.3	0.3
Surgery total					2,302	11	0.48	0.48
Young Lee et al. 2006	CT (MDCT)	790	42	5.3	597	44	7.4	6.2
Shiotani et al. 2012	CT (MDCT)	511	43	8.4	437	57	13.0	10.5
Ge et al. 2014	CT (MDCT)	3,091	187	6.0	2,909	160	5.5	5.8
CT Total		4,392	272	6.2	3,943	261	6.6	6.4

Source: Snosek et al. (2014). Reproduced with permission from John Wiley & Sons.

(1999), who surveyed physicians, residents, and medical students and found near-uniform unfamiliarity on the topic. Other surgical reports of the sternalis come from single case reports (Nuthakki et al. 2007; Marques et al. 2009; Salval et al. 2012; Nguyen and Ogawa 2012), so few data on its true prevalence rate are available. Furthermore, nearly all mammographic and breast augmentation data come from female patients and little, if any, prevalence data are available for males, making comparisons and statistical analysis difficult.

Morphology

Numerous descriptions and classifications of the sternalis exist in the literature today, demonstrating the highly variable nature of this muscular variant. Presumably because of its rare occurrence, most authors' descriptions and analyses are based on relatively few cases, often a single case report. This has led to a wide range of descriptions and terminologies which, although accurate as they are reported from first-hand experience, fail to demonstrate any common attributes and characteristics of the sternalis muscle in general. Often, these reports even seem to contradict one another. Occasional structures are more likely to present variations in arrangement, and only by observing multiple variations side by side can one generalize about morphology and draw conclusions about their homology.

Physical characteristics

The sternalis muscle presents as a parasternal mass deep to the superficial fascia of the anterior thoracic wall and superficial to the pectoral fascia overlying the pectoralis major muscle (Fig. 35.21). It has been reported to be cord-like, flat band (Turner 1867; Shah 1968), or irregular and flame-like in shape (Bradley et al. 1996). A unilateral sternalis muscle is more common (67%) than bilateral (33%), with preferential occurrence on the right side (64% right, 36% left; Snosek et al. 2014; Tables 35.4, 35.5). The variable presentation of the sternalis is most evident in its attachments and physical dimensions. Its reported origin or superior attachment includes a combination of the sternum, the inferior border of the clavicle, the sternocleidomastoid fascia, pectoralis major, and the upper ribs and their costal cartilages; the insertion or inferior attachment includes structures such as the lower ribs and their costal cartilages, pectoralis major, rectus abdominis sheath, and the external abdominal oblique aponeurosis (Snosek et al. 2014; Table 35.6). Although the superior and inferior attachments are predominantly considered as the origins and insertions, respectively, some early authors regarded the inferior attachment as the origin instead (Turner 1867; Wallace 1886). The superior tendon is often slender and more rounded than the inferior tendon, which is frequently broad and flat as it inserts into the rectus abdominis sheath and external abdominal oblique aponeurosis (Turner 1867). The size of the muscle belly is also highly variable, ranging from a few scattered fibers to large muscle bellies visible on external examination (Jelev et al. 2001). Large sternalis muscles are often associated with deficits in the medial aspect of the

Table 35.4 Thoracic presentation. Frequency of unilateral and bilateral sternalis muscle presentation based on review of the literature. F, some or all data was obtained from fetal dissections. Cited by *Cunningham (1888); **Barlow (1935).

	No. bodies with	
Study	**Unilateral**	**Bilateral**
Hallet 1848**	1	0
Gruber 1860**	2	3
Turner 1867	12	9
Humphry 1873	1	0
Curnow 1874	2	1
Malbranc 1878*	2	0
Abraham 1883 (F)	2	3
Cunningham 1884	1	0
Shepherd 1885 (F)	3	3
Wallace 1886	1	0
Lamont 1887	3	2
Dwight 1887	4	2
Dwight 1887 (F)	0	1
Cunningham 1888	12	4
Cunningham 1888 (F)	0	1
Shepherd 1889 (F)	1	1
Le Double 1890	11	15
Hepburn 1896	1	0
Christian 1898**	0	2
Flint 1902	0	2
Huntington 1904	1	0
Adachi 1909	16	11
Ingalls 1913	0	1
Yap 1921	2	3
Yap 1921 (F)	0	6
de Pina 1928**	5	4
Locchi 1930	25	5
Patten 1934a,b	2	0
Barlow 1935	28	5
Harper 1936 (F)	2	1
Mori 1964	25	14
Shen et al. 1992	0	1
O'Neill and Folan-Curran 1998	0	1
Jeng and Su 1998	0	2
Jelev et al. 2001	2	1
Saeed et al. 2002	1	2

(continued)

Table 35.4 *(continued)*

Study	No. bodies with	
	Unilateral	Bilateral
Arraez-Aybar et al. 2003	1	0
Kumar et al. 2003	0	1
Gupta and Harjeet 2004	0	1
Motabagani et al. 2004	0	2
Ibrahim et al. 2005	0	1
Schulman and Chun 2005	2	0
Young Lee et al. 2006	63	23
Das et al. 2006	1	0
Goktan et al. 2006	0	1
Nuthaki et al. 2007	1	0
Khan 2008	2	0
Natsis et al. 2008	0	1
Sarikcioglu et al. 2008	0	1
Bhat et al. 2009	1	0
Georgiev et al. 2009	1	1
Jetti et al. 2009	1	0
Rahman et al. 2009	1	0
Demirpolat et al. 2010	10	0
Mehta et al. 2010	1	0
Londhe et al. 2010	1	0
Vaithianathan et al. 2011	0	1
Raikos et al. 2011a	0	1
Raikos et al. 2011b	1	0
Pinhal-Enfield et al. 2011	1	0
Salval et al. 2012	0	1
Shiotani et al. 2012	75	25
Nguyen and Ogawa 2012	1	0
Hung et al. 2012	0	1
Hung et al. 2012 (F)	1	0
Silveira et al. 2012	2	0
Simhadri et al. 2012	1	0
Anjamrooz 2013	1	0
Chaijaroonkhanarak et al. 2013	9	1
Kobayashi et al. 2013	2	0
Ge et al. 2014	229	118
TOTALS	577 (67%)	286 (33%)

Source: Snosek et al. (2014). Reproduced with permission from John Wiley & Sons.

Table 35.5 Unilateral presentation. Frequency of right- and left-sided presentation of the sternalis muscle based on review of the literature. F, some or all data was obtained from fetal dissections. Cited by *Barlow (1935).

Source	Right	Left	Crossed
Gruber 1860*	1	1	
Turner 1867	5	2	5
Humphry 1873	1	0	
Curnow 1874	2	0	
Abraham 1883 (F)	2	0	
Shepherd 1885 (F)	0	3	
Wallace 1886	1	0	
Dwight 1887	3	1	
Shepherd 1889 (F)	0	1	
Le Double 1890*	6	5	
Hepburn 1896	0	1	
Huntington 1904	1	0	
Adachi 1909	10	6	
Yap 1921	1	1	
de Pina 1928*	1	4	
Locchi 1930*	17	8	
Patten 1934a,b	2	0	
Barlow 1935	17	11	
Harper 1936 (F)	2	0	
Mori 1964	17	8	
Saeed et al. 2002	1	0	
Arraez-Aybar et al. 2003	0	1	
Shulman and Chun 2005	0	2	
Young Lee et al. 2006	35	28	
Das et al. 2006	0	1	
Nuthakki et al. 2007	1	0	
Khan 2008	2	0	
Bhat et al. 2009	0	1	
Georgiev et al. 2009	0	1	
Jetti et al. 2009	1	0	
Rahman et al. 2009	1	0	
Demirpolat et al. 2010	10	0	
Mehta et al. 2010	1	0	
Londhe et al. 2010	1	0	
Raikos et al. 2011b	0	1	
Pinhal-Enfield et al. 2011	1	0	
Shiotani et al. 2012	45	28	2
Nguyen and Ogawa 2012	0	1	
Hung et al. 2012 (F)	1	0	
Silveira et al. 2012	0	2	
Simhadri et al. 2012	1	0	
Anjamrooz 2013	1	0	
Chaijaroonkhanarak et al. 2013	9	0	
Kobayashi et al. 2013	2	0	
Ge et al. 2014	148	81	
TOTALS	350 (64%)	199 (36%)	7

Source: Snosek et al. (2014). Reproduced with permission from John Wiley & Sons.

Table 35.6 Attachment points for sternalis muscle. The following data report all attachment points observed by each author in their study and not necessarily on each and every specimen, due to authors reporting attachments for the whole set of observed specimens. SCM apon., sternocleidomastoid muscle and aponeurosis; Manub., nanubrium sterni; Manub-stern. junction, manubriosternal junction; Pec. major, pectoralis major muscle; apon., aponeurosis; F, some or all data were obtained from fetal dissections.

		Superior attachments						Inferior attachments						
Study	No. sternalis muscles observed	SCM apon. /fascia	Manub.	Manub– stern. junction	Sternum body	Pec. major /fascia	Upper ribs /cartilage	Lower ribs	Lower costal cartilage	External oblique apon.	Rectus abdominis sheath	Pec. major /fascia	Serratus anterior	Sternum body
Hallett 1848	2	X	X		X	X			3–6th		X			
Turner 1867	30	X	X		X	X		6th	5–7th	X				X
Humphry 1873	1	X	X						3–5th					
Curnow 1874	4	X							5th		X			
Abraham 1883 (F)	8		X		X	X	X		X	X		X		
Shepherd 1885	9	X	X		X				3–4th	X				X
Wallace 1886	1	X				X			3–6th					X
Dwight 1887 (F)	10	X	X			X	2–3rd	3–7th			X	X		X
Shepherd 1889 (F)	3	X	X		X			5–7th		X		X		
Hepburn 1896	1	X	X						5th	X				
Flint 1902	4	X				X			6th		X			X
Huntington 1904	1		X		X					X				
Ingalls 1913	2	X			X				6th			X		X
Yap 1921 (F)	20	X	X		X		X		X	X	X	X		
Patten 1934a,b	2	X			X	X					X	X		
Barlow 1935	38	X			X	X	X		X		X	X		X
Harper 1936 (F)	4		X		X	X	2–3rd	5th	4–5th	X				
O'Neill and Folan-Curran 1998	2	X	X						6–7th	X		X		
Jeng and Su 1998	4		X						6th					
Jelev et al. 2001	4	X	X						X			X		
Arraez-Aybar et al. 2003	1				X	X						X		

(continued)

Table 35.6 *(continued)*

Study	No. sternalis muscles observed	Superior attachments						Inferior attachments						
		SCM apon. /fascia	Manub.	Manub– stern. junction	Sternum body	Pec. major /fascia	Upper ribs /cartilage	Lower ribs	Lower costal cartilage	External oblique apon.	Rectus abdominis sheath	Pec. major /fascia	Serratus anterior	Sternum body
Kumar et al. 2003	2		X						2–6th	X				
Gupta and Harjeet 2004	2			X					6–7th		X			
Motabagani et al. 2004	4	X	X	X					5–7th	X				
Ibrahim et al. 2005	2	X				X				X				
Nuthakki et al. 2007	1			X								X		
Natsis et al. 2008	2				X	X	2–3rd				X			
Sarikcioglu et al. 2008	3	X			X	X			6–7th	X				
Bhat et al. 2009	1	X				X				X		X	X	
Georgiev et al. 2009	3			X	X				3–4th			X		
Jetti et al. 2009	1	X								X	X			
Rahman et al. 2009	1						2nd		7th					
Londhe et al. 2010	1		X							X				
Raikos et al. 2011a	2	X				X			10–12th	X				
Raikos et al. 2011b	1	X							X					
Vaithianathan et al. 2011	2		X		X			7–8th	7–8th	X				
Pinhal-Enfield et al. 2011	1		X						6th		X			
Hung et al. 2012 (F)	1		X						5th					
Hung et al. 2012	2		X									X		
Nguyen and Ogawa 2012	1	X						X		X	X			
Simhadri et al. 2012	1					X					X			
Anjamrooz 2013	1	X						X	X		X			
TOTALS	184													

Source: Snosek et al. (2014). Reproduced with permission from John Wiley & Sons.

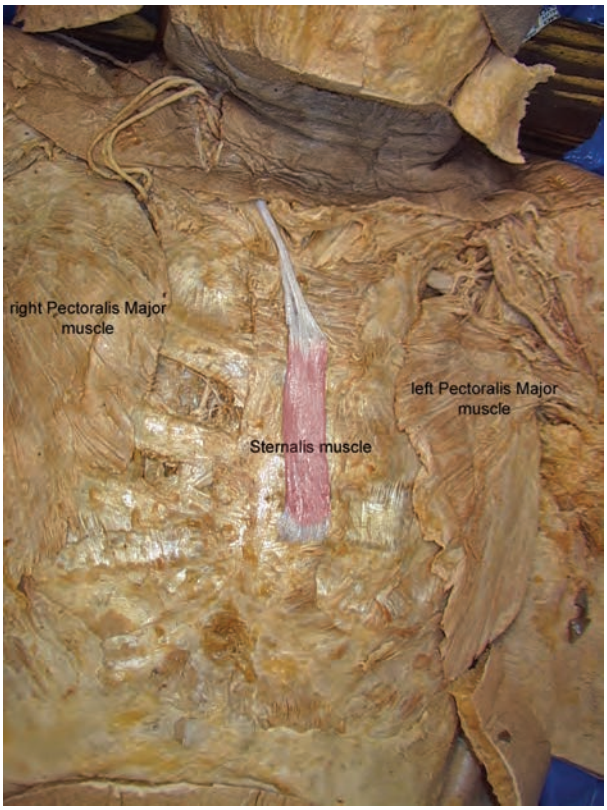

Figure 35.21 A rare occurrence of a unilateral sternalis muscle crossing the midline, observed during routine cadaveric dissection.

Source: Loukas et al. (2004).

ipsilateral pectoralis major muscle, where the medial margins fail to reach the sternum and often begin lateral to the sternalis muscle near to or on the costochondral joints. The resulting defect exposes the medial aspect of the costal cartilages and affords direct contact with the overlying sternalis muscle (Turner 1867; Cunningham 1884; Huntington 1904; O'Neill and Folan-Curran 1998). Its maximum reported length ranges from a relatively short muscle of only 2.4 cm to very long specimens of 26.0 cm, the maximum width 0.48–7.0 cm, and the maximum depth 0.01–0.6 cm. The physical dimensions as reported in the literature are summarized in Table 35.7 (Snosek et al. 2014).

Nerve supply

The nerve supply to the muscle has been reported to come from the pectoral (medial or lateral) (51.9%; Fig. 35.22) or intercostal nerves (43.1%; Fig. 35.23), with rare instances of both nerves contributing to the innervation (5%) (Snosek et al. 2014; Table 35.8). Dual innervation is not only rare but has also not been observed and documented since 1964, and could be more apparent than real as discussed below.

On the basis of years of cadaveric observations, Kida et al. (2000), among others (Wallace 1886; Lamont 1887; Cunningham 1888; Patten 1934a, b; Harper 1936; Kida and

Table 35.7 Adult morphological presentations based on review of literature. Reported maximum adult morphological dimensions of the sternalis muscle. Morphological data from studies based on fetuses are not included.

Study	Max length (cm)	Max width (cm)	Max depth (cm)
Hallett 1848	c. 15	c. 5	c. 1.25
Turner 1867		0.5–3.8	
Wallace 1886	16.50	2.5	
Dwight 1887		1.27–6.35	
Hepburn 1896		1.5	
Flint 1902		1.0–4.0	0.01–0.02
Huntington 1904	11.50	2.75	
Ingalls 1913		1.0–2.0	
Yap 1921	4.0–10.0	1.5–2.5	
Patten 1934a,b	6.0–11.0	1.5–2.0	
O'Neill and Folan-Curran 1998	23.0–26.0	2.5–4.6	
Jeng and Su 1998	13.0–15.2		
Jelev et al. 2001	12.0–14.4	1.5–2.6	
Saeed et al. 2002	8.0–13.0	1.0–2.5	
Arraez-Aybar et al. 2003	13.00	7.0	0.5
Kumar et al. 2003	11.0–13.5	2.5–5.5	
Motabagani et al. 2004	8.0–12.0	1.5–2.5	
Ibrahim et al. 2005	19.00	3	
Shulman and Chun 2005	12.0–15.0	6.0–9.0	
Kabay et al. 2005	8.00	2.0	
Young Lee et al. 2006	2.0–13.0	0.48–3.99	0.12–0.57
Nuthakki et al. 2007	2.40	1.7	0.6
Khan 2008		3.5	
Bhat et al. 2009	12.30		
Jetti et al 2009	10.00	1.5	
Rahman et al. 2009	9.00	1.9	
Mehta et al. 2010	16.50	4.3	
Vaithianathan et al. 2011	6.0–10.5	0.8–2.0	
Raikos et al. 2011b	13.50	1.9	
Pinhal-Enfield et al. 2011	15.00	2.5	
Salval et al. 2012	12.00	2.0	0.5
Shiotani et al. 2012	(mean) 7.79	(mean) 1.94	(mean) 0.28
Nguyen and Ogawa 2012	5.0–6.0		
Silveira et al. 2012	11.8–18.0	0.8–1.8	
Simhadri et al. 2012	12.50	2.5	
Anjamrooz 2013	15.00	2.4	
Ge et al. 2014	1.35–22.0	0.2–7.11	0.1–1.24

Source: Snosek et al. (2014). Reproduced with permission from John Wiley & Sons.

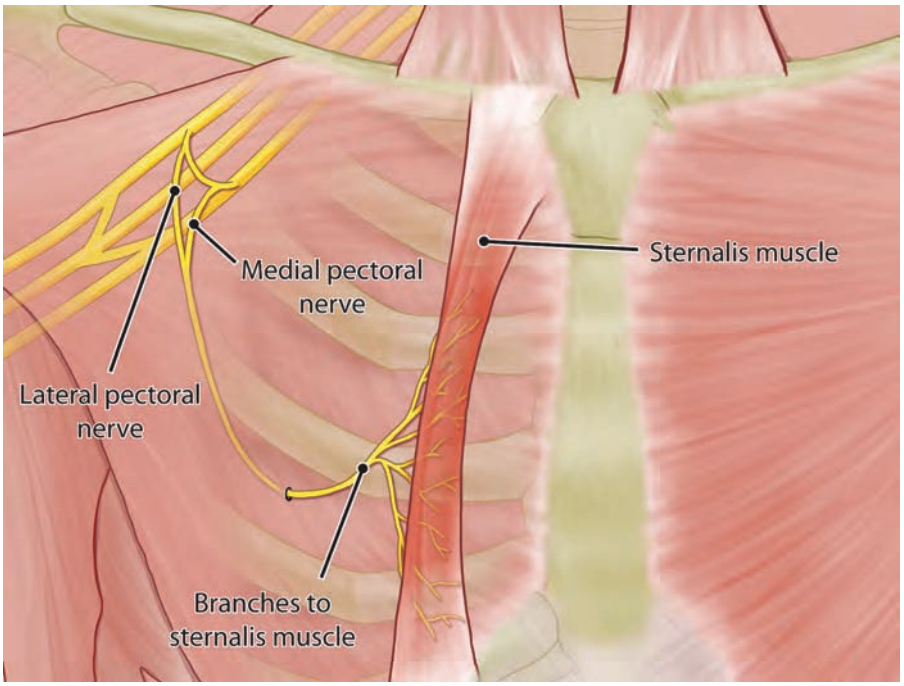

Figure 35.22 Sternalis muscle with innervation from medial and/or lateral pectoral nerves.

Source: Snosek et al. (2014). Reproduced with permission from John Wiley & Sons.

Kudoh 1991; Kumar et al. 2003), believe that the innervation is derived from the pectoral nerves. They state that the sternalis muscle is innervated by very fine twigs of the pectoral nerves approaching the muscle at its lateral border and lying immediately beneath the pectoral fascia. The authors noted that unless a very careful and specific dissection for such branches is carried out, the mere task of delineating the lateral border of the sternalis muscle is likely to damage these fine twigs and make them difficult to distinguish from the surrounding connective tissue (Kida et al. 2000). Proponents of intercostal nerve innervation base their argument on numerous surgical and cadaveric observations of intercostal nerve branches supplying the sternalis (O'Neill and Folan-Curran 1998; Jeng and Su 1998; Schulman and Chen 2005; Georgiev et al. 2009). There is a lack of agreement among the proponents of intercostal nerve innervation as to the specific branches of the intercostal nerves that supply the sternalis muscle. Some report the anterior cutaneous branches innervating the sternalis (Jeng and Su 1998; Jelev et al. 2001;

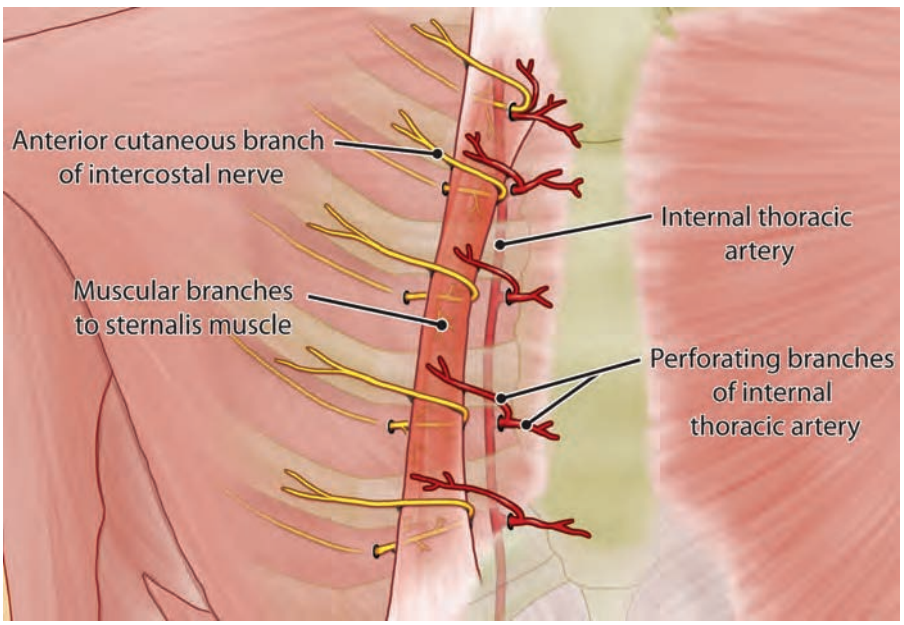

Figure 35.23 Sternalis muscle with innervation from intercostal nerves and arterial blood supply from perforating branches of interal thoracic artery.

Source: Snosek et al. (2014). Reproduced with permission from John Wiley & Sons.

Table 35.8 Innervation of the sternalis muscle based on review of the literature. Reported frequency of innervation to sternalis muscles. n, nerve; F, some or all data were obtained from fetal dissections. Cited by *Cunningham (1888); **Barlow (1935); ***O'Neill and Folan-Curran (1998).

Study	Total sternalis observed	No. muscles with innervation from			
		Pectoral n.	Intercostal n.	Dual innervation	Not noted
Hallet 1848	1		1		
Bardeleben 1876***	2		2		
Malbranc 1878*	2	1	1		
Krause 1880**	1		1		
Cunningham 1884	1	1			
Shepherd 1885	9	6		1	2
Wallace 1886	1	1			
Lamont 1887	7	5		1	1
Dwight 1887	8	2	3		3
Bardeleben 1888**	10		10		
Cunningham 1888	10	15			5
Cunningham 1888 (F)	2	2			
Shepherd 1889 (F)	3	2		1	
Le Double 1890**	4	1	3		
Fick 1891**	5		4	1	
Hepburn 1896	1		1		
Christian 1898**	4	1	2	1	
Eisler 1901**	17	17			
Flint 1902	4		2		2
Huntington 1904	1				1
Ingalls 1913	2				2
Yap 1921	8	5	1		2
Yap 1921 (F)	12	4	1		7
Locchi 1930**	35	20			15
Patten 1934a,b	2	2			
Slobodin 1934–35***	6	3	3		
Barlow 1935	38	3	13	1	21
Harper 1936 (F)	4	3			1
Fukuyama 1940***	32	15	17		
Misra 1954***	6		6		
Rao and Rao 1954	4		4		
Kacker 1960***	6		6		
Mori 1964	27	12	5	10	
Blees 1968***	1		1		
Kida and Kudoh 1991	2	2			
Shen et al. 1992	2		2		
O'Neill and Folan-Curran 1998	2		2		
Jeng and Su 1998	4		4		
Kida et al. 2000	40	40			

(continued)

Table 35.8 *(continued)*

Study	Total sternalis observed	No. muscles with innervation from			
		Pectoral n.	Intercostal n.	Dual innervation	Not noted
Jelev et al. 2001	4		2		2
Saeed et al. 2002	5		5		
Arraez-Aybar et al. 2003	1		1		
Kumar et al. 2003	2	2			
Gupta and Harjeet 2004	2		2		
Motabagani et al. 2004	4		4		
Ibrahim et al. 2005	2		2		
Natsis et al. 2008	2		2		
Sarikcioglu et al. 2008	3		2		1
Jetti et al. 2009	1		1		
Georgiev et al. 2009	3		3		
Mehta et al. 2010	1		1		
Londhe et al. 2010	1		1		
Vaithianathan et al. 2011	2		2		
Simhadri et al. 2012	1		1		
Hung et al. 2012 (F)	1	1			
Hung et al. 2012	2		2		
Anjamrooz 2013	1		1		
Chaijaroonkhanarak et al. 2013	11		11		
TOTALS	375	166 (51.9%)	138 (43.1%)	16 (5%)	65

Source: Snosek et al. (2014). Reproduced with permission from John Wiley & Sons.

Georgiev et al. 2009), while others claim the muscular branches are separate from the anterior cutaneous nerves supplying the skin over the anterior thoracic wall (O'Neill and Folan-Curran 1998). It is also probable that some sternalis muscles appear on first inspection to be innervated by the intercostal nerves and are documented as such. However, upon closer dissection, these nerves could simply be the anterior cutaneous nerves that perforate through the muscle to provide cutaneous innervation to the skin, with no contribution to the sternalis muscle itself.

Others have documented the path of the intercostal nerves with little or no association with the sternalis muscle, other than close proximity. Ingalls (1913) reported that in his specimen the intercostal nerves perforated the pectoralis major muscle and ran medially towards the sternum deep to the sternalis muscle to emerge at its medial border, where they changed course sharply to run laterally and superficially over the sternalis muscle to reach their cutaneous terminations. However, he noted that one of the nerves took a more direct route and pierced the upper tendon of the sternalis muscle to reach the skin. No muscular branches from the intercostal nerves to the sternalis were observed and innervation was attributed to the pectoral nerves alone (Ingalls 1913).

Occasionally authors have reported that the sternalis muscles receive dual innervation from both pectoral and intercostal nerves. This occurrence is rare (5%; Snosek et al. 2014; Table 35.8) and, aside from a few reports (each of a single case) from the nineteenth and early twentieth centuries, only Mori (1964) has reported multiple cases of such innervation. Some authors such as Eisler (1901) were skeptical about the reported dual innervation or even the purely intercostal innervation of the sternalis muscle. Eisler emphasized that upon closer inspection these cases received pectoral nerve innervation, with intercostal nerves merely perforating the sternalis muscle as described previously (Huntington 1904). Conflicting reports on the nerves and their specific branches innervating the sternalis muscle highlight the need for further investigation in this area.

Blood supply

The blood supply is primarily derived from the perforating branches of the internal thoracic artery (Flint 1902; Jeng and Su 1998; Jelev et al. 2001; Motabagani et al. 2004; Schulman and Chen 2005; Georgiev et al. 2009; Nguyen and Ogawa 2012; Snosek et al. 2014; Fig. 35.23), with additional supply from intermuscular connections from the pectoral branch of the thoracoacromial artery (Schulman and Chen 2005).

Classification

Jelev et al. (2001) outlined four basic morphological characteristics that must be satisfied for a muscle to be accepted as the sternalis: (1) location between the superficial fascia of the anterior thoracic region and the pectoral fascia; (2) origin from the sternum or infraclavicular region; (3) insertion onto the lower ribs, costal cartilages, aponeurosis of the external abdominal oblique muscle or the sheath of rectus abdominis; and (4) innervation by the anterior thoracic (pectoral) and/or intercostal nerves. It is important to note that other variants of the anterior thoracic wall have been described in the literature and heralded as new and never previously seen variants; however, upon closer inspection and application of the four characteristics mentioned above, they bear a striking resemblance to the sternalis muscle. Some of these potentially misclassified sternalis muscles include the oblique pectoralis anterior (Huber et al. 2012) and the rectus thoracis bifurcalis (Mehta et al. 2010). The oblique pectoralis anterior muscle was noted to lie anterior to pectoralis major, extending from the sternum to the inferior ribs and the rectus sheath; aside from the innervation, which was not noted in the study, its description is consistent with the characteristics of the sternalis muscle. However, the authors state that it is a "unique case of an anomalous slip of pectoralis major" that "had not previously been described in the literature" (Huber et al. 2012).

In the case of the rectus thoracis bifurcalis, the authors state that their case lacks any attachment to the sternum (which fails to satisfy its classification as a sternalis muscle) yet go on to state that the "superior attachment was to the manubrium sterni in the vicinity of the jugular notch" (Mehta et al. 2010) which is part of the sternum (Standring 2008). The authors admit that its location in the subcutaneous plane, intercostal nerve innervation, and inferior attachments to the external abdominal oblique aponeurosis are consistent with the sternalis muscle. Another supernumerary muscle of the anterior thoracic wall bearing many similarities to (and correctly classified by the authors as) a variant of the sternalis muscle was aptly termed the "sternomastalis muscle" due to its insertion into the breast tissue and the nipple-areola complex (Kale et al. 2006). These and other variants of the anterior thoracic wall fitting the description of the sternalis muscle are crucial in a review of this normal variant to complete the picture of its varied morphology and to help anatomists and clinicians correctly identify such anomalous structures. Incorrect classification and superfluous creation of new variations with the inevitable new terminology leads to confusion and frustration for all.

To help classify the sternalis muscle into identifiable types, a system was proposed in 2001 based on the morphology of the muscle bellies. Eight types were identified, four unilateral and four bilateral variations (Jelev et al. 2001). This classification has rarely been adopted in the literature however, most likely because of its restrictive nature as many presentations of the sternalis fail to fit into a single category. Raikos et al. (2011b) published a modified classification based on Jelev's work, which included a new sub-type for the double-bellied midline-crossing specimen they found, but this classification has not been used much in the literature either. Ge et al. (2014) offered their own modified system, which classified each hemi-thorax separately. The total categories were expanded to three: I, simple sternalis (single head and single belly); II, double-headed/multi-headed sternalis; and III, double-bellied/multi-bellied sternalis, each with three subtypes for a total of nine subtypes. This system included subtypes that classified midline-originating bellies, which was absent from previous classifications.

Snosek et al. (2014) proposed a new classification based on each hemi-thorax separately similar to that of Ge et al. (2014). This proposed system is based on three categories to which every sternalis muscle can be categorized. These categories include simple type, mixed type, and other. The simple types include six variations of the sternalis muscle: single, double, bicipital diverging, bicipital converging, single midline crossing, and double midline crossing (Fig. 35.24). The mixed type category includes any and all variations (only the six most common variations are shown) that present with more than one of the simple type variations on a specific hemi-thorax, including: double sternalis with single midline cross; bicipital diverging with single midline cross; bicipital diverging with double cross; double with single bicipital converging; and double with single bicipital converging and single bicipital diverging (Fig. 35.25). Each variation in this category must explicitly state the simple types that are involved. The "other" category is meant to allow classification of sternalis muscles that fail to conform to any other subdivisions previously mentioned, and includes variations such as: criss-crossed, midsagital, and right–left bicipital converging sternalis (Fig. 35.26). No categories are exhaustive and additions can be made as new variations are documented. For example, the simple type category may be expanded to include triple and quadruple sternalis muscles when such rare cases are found. The classification presented here is illustrated for right hemi-thorax only, but all the variations may be adapted to left hemi-thorax as well (Snosek et al. 2014).

Homology

One of the most debated aspects of the sternalis muscle has always been its embryological origin and ipso facto its innervation, as once it is established in the fetus it does not change (Khan 2008). By finding agreement on the most common source of innervation, as variations and anomalous neural branches will inevitably be found, we can therefore speculate on its origin. Different hypotheses have been proposed as to the homology of

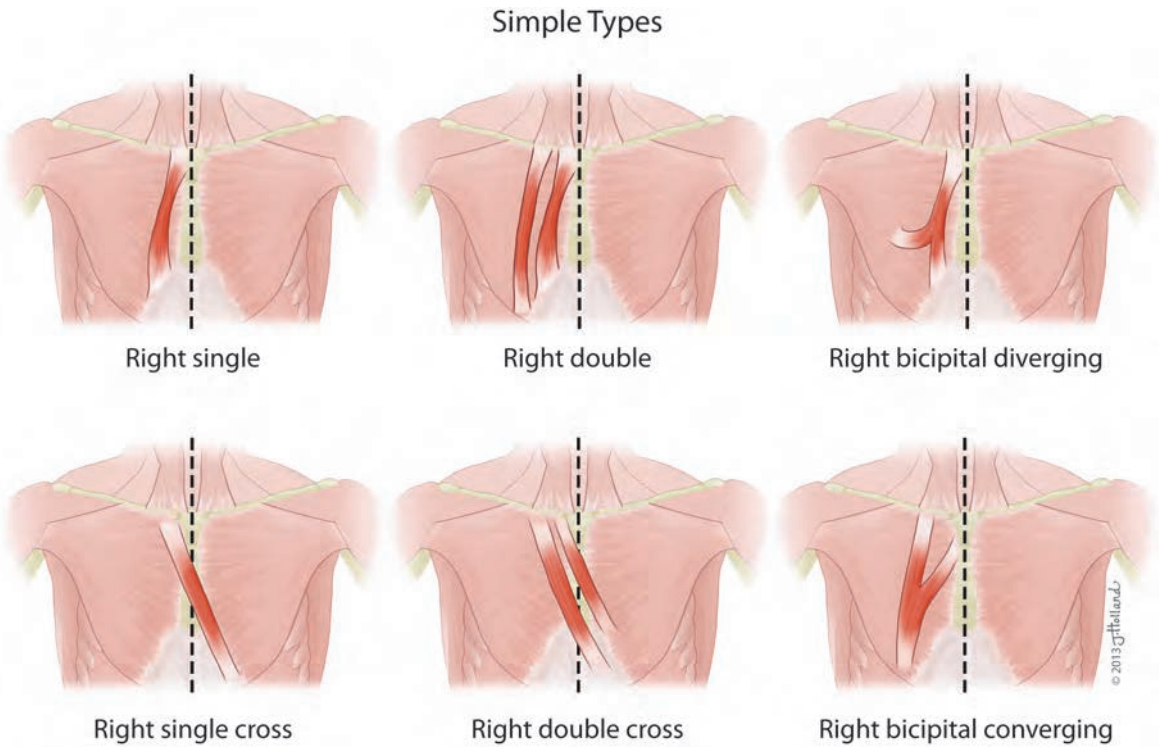

Figure 35.24 A sample of the most common "simple" types of right sternalis muscle.

Source: Snosek et al. (2014). Reproduced with permission from John Wiley & Sons.

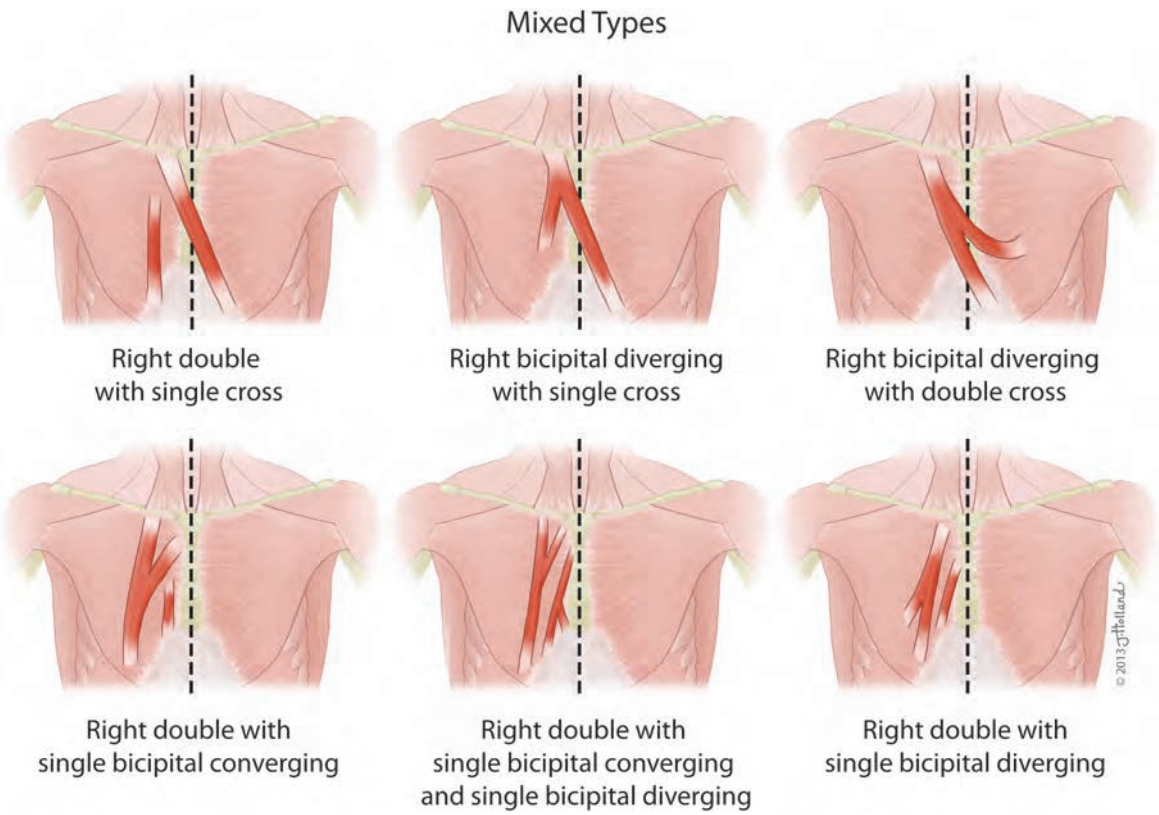

Figure 35.25 A sample of the most common "mixed" types of right sternalis muscle.

Source: Snosek et al. (2014). Reproduced with permission from John Wiley & Sons.

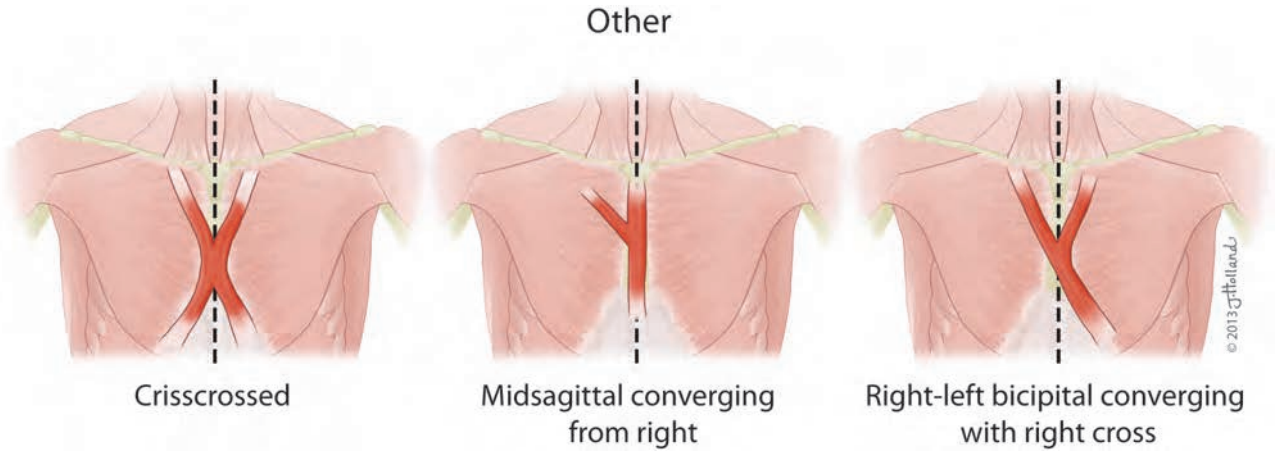

Figure 35.26 A sample of the most common "other" types of right sternalis muscle.

Source: Snosek et al. (2014). Reproduced with permission from John Wiley & Sons.

this muscle, with their respective proponents presenting empirical evidence. The four most commonly proposed hypotheses suggest it is derived from adjacent musculature: the panniculus carnosus; the sternocleidomastoid; the pectoralis major; or the rectus abdominis. The latter two have received the most support thanks to the pectoral nerve (pectoralis major derived) or intercostal nerve (rectus abdominis derived) innervation observed on cadaveric inspection (O'Neill and Folan-Curran 1998; Kida et al. 2000).

The sternalis muscle was once believed to be derived from the panniculus carnosus, which is a thin sheet of skeletal muscle located immediately beneath the superficial fascia and acting to move the overlying skin. It is considered vestigial in humans but is very prominent in other mammals, for example in herd animals which use it to thwart pesky insects on their skin. The platysma muscle is seen as one of the few remnants in humans of this prominent muscular sheet, and it was proposed that the sternalis muscle was a further extension or another remnant of this sheet (Turner 1867; Parsons 1893; Barlow 1935); however, this view is no longer supported.

The hypothesis that the sternalis was a downward extension of the sternocleidomastoid muscle was based on observations of the close association or continuity of their tendons at the clavicle and upper part of the sternum (Turner 1867; Humphry 1873; Flint 1902). Turner agreed that the two muscles shared similar attachment points on the basis of his own observations but believed it was merely incidental rather than proof of true homology (Turner 1867), an idea reiterated by others (Huntington 1904).

Proponents of the rectus abdominis origin of the sternalis suggest that it is an upward extension of that muscle. Earlier reports did not support these findings. In his work spanning years of detailed note-taking on 21 cases of sternalis muscle, Turner did not find a single case in which its fibers were continuous with those of rectus abdominis, although their attachment points were in close proximity. The inferior attachment of the sternalis was frequently associated with the external abdominal oblique aponeurosis, which lies in a plane superficial to the rectus abdominis. Furthermore, Turner argued that the sternalis muscle did not exhibit the transverse tendinous intersections characteristic of the rectus abdominis (Turner 1867), although such tendinous intersections were reported by at least two separate anatomists in the nineteenth century (Hallet 1848). Supporters of the rectus-derived sternalis hypothesis point to evidence from the dissection room, where the sternalis was noted to be innervated by branches of the intercostal nerves in common with the rectus abdominis nerve supply (Hallet 1848; Dwight 1887; Bardeleben 1888; Barlow 1935; O'Neill and Folan-Curran 1998; Jevel et al. 2001). However, while it is frequently perforated by branches of the intercostal nerves (of various segmental levels, depending on the position of the muscle) on their way to becoming the anterior cutaneous nerves, few cases of actual nerve endings being disseminated within the substance of the sternalis muscle have been reported (O'Neill and Folan-Curran 1998). It seems that the innervation is often inappropriately attributed to the intercostal nerves merely because they exist in close proximity to or actually traverse through the muscle itself on the way to their cutaneous distributions. This was further supported by Kida et al. (2000), who emphasized the delicate nature of the innervation of the sternalis muscle by pectoral nerve branches and their propensity to damage during routine dissections of the pectoral musculature (as described in the previous section), leading to its true nerve supply often being overlooked (Cunningham 1888).

There is also strong support for the hypothesis that the sternalis is derived from the pectoralis major muscle. Interestingly,

this hypothesis did not garner much support until the late nineteenth century, when Cunningham (1884) traced the small twigs innervating the sternalis muscle back to the pectoral nerves. He gives credit to PS Abraham, a curator of the Museum of the Royal College of Surgeons in Dublin, who first suggested the hypothesis in 1883 on the basis of his study of 11 anencephalic fetuses of which six had sternalis muscles that "attained development rarely seen in adults" (Cunningham 1884). In four of these six cases the sternalis muscle was found to lie in the same plane as, and was intimately attached to, the sternal fibers of the pectoralis major, which incidentally was deficient in its most medial aspect and attachment to the sternum and costal cartilages (Abraham 1883). It is unclear whether the prominent development of the sternalis muscle hindered the complete development of the pectoralis major or if its development was a compensatory response to a primary deficiency in the latter. His research not only demonstrated a correlation between anencephaly in fetuses and the presence of the sternalis muscle, but also supported the view that "the muscle in question is an aberrant portion of the great pectoral muscle" (Cunningham 1884). According to Cunningham himself, this hypothesis had previously been ignored because it was difficult to imagine that the pectoralis major was related to a muscle with such contrasting fiber direction and axial attachments. However, he held the notion that this muscular variant was merely a displaced and rotated segment of the pectoral muscle mass; it is therefore not surprising that many sternalis muscle occurrences, especially the more developed cases, are coupled with atypical development of or deficiencies in the medial aspect of the pectoralis major muscle (Turner 1867; Cunningham 1884; Huntington 1904). The larger the displaced segment of the pectoral muscle mass, the larger the deficit that would result and correspondingly the larger the sternalis muscle.

The literature contains many examples of the sternalis muscle with aberrant or accessory muscular slips continuous with the pectoralis major muscle (Turner 1867; Shepherd 1885; O'Neill and Folan-Curran 1998; Jelev et al. 2001). These muscular connections could be examples of incomplete or partial rotation of the segments of the pectoralis muscle, and could range from only a few muscular fibers to large fascicles resulting in obvious deficits in the pectoralis major muscle. As these displaced segments migrate from their normal course they are free to make connections with adjacent structures, resulting in the apparent continuity with the sternal head of the sternocleidomastoid superiorly or the rectus abdominis inferiorly. These connections then lend themselves to logical interpretation of homology as described above, but are likely to be secondarily acquired and morphologically unimportant (Huntington 1904).

It must be noted that the sternalis muscle is a variation prone to a range of morphological presentations and must not be confined by a single description. Likewise, as new and previously undocumented presentations of this variant are observed, one must be careful not to invent new variations but merely add a subtype or class to the existing classification of sternalis variants. In fact, the sternalis muscle can be viewed as a type of a much larger group of variations caused by a disturbance of the normal processes of pectoral muscle development, which include similar variations such as the pectoralis minimus, pectoralis tertius, infraclavicularis, and chondroepitrochlearis (Huntington 1901, 1904; Ingalls 1913; Bergman et al. 1988).

References

Abraham PS. 1883. Note on the occurrence of the musculus sternalis in human anencephalous fetuses. *Trans Acad Med Ireland* 1: 301–304.

Adachi B. 1909. Beitrage zur anatomie der Japaner. *Z Morphol Anthropol* 12: 261–312.

Allen L. 1950. Transpleural muscles. *J Thoracic Surg* 19: 290–291.

Anjamrooz SH. 2013. Biceps sternalis: A Y-shaped muscle on the anterior chest wall. *J Cardiothorac Surg* 8: 38–41.

Arican RY, Coskun N, Sarikcioglu L, Sindel M, Oguz N. 2006. Coexistence of the pectoralis quartus and pectoralis intermedius muscles. *Morphologie* 290: 157–159.

Arraez-Aybar LA, Sobrado-Perez J, Merida-Velasco JR. 2003. Left musculus sternalis. *Clin Anat* 16: 350–354.

Ausin P, Caro AG, Sanchez M, Gea J. 2010. Accessory diaphragm dividing the thoracic cavity between native lung and pulmonary sequestration. *Eur J Cardiothorac Surg* 37: 236.

Aziz MA. 1980. Anatomical defects in a case of trisomy 13 with a D/D translocation. *Teratology* 22: 217–237

Baban A, Torre M, Bianca S, Buluggiu A, Rossello MI, Calevo MG, Valle M, Ravazzolo R, Jasonni V, Lerone M. 2009. Poland syndrome with bilateral features: case description with the review of the literature. *Am J Med Genet A* 149A: 1597–1602.

Bailey PM, Tzarnas CD. 1999. The sternalis muscle: A normal finding encountered during breast surgery. *Plast Reconstr Surg* 103: 1189–1190.

Barcia JM, Genoves JM. 2009. Chondrofascialis versus pectoralis quartus. *Clin Anat* 22: 871–872.

Bardeleben K. 1876. Der Musculus sternalis. *Z Anat Entwicklungsgesch* 1: 424–458.

Bardeleben K. 1888. Die morphologische Bedeutung des Musculus "sternalis." *Anat Anz* 3: 324–333.

Barge JAJ. 1927. Ein Fall von vollstandigem Defekt der beiden Brustmuskeln. *Anat Anz* 64: 102–119.

Barlow RN. 1935. The sternalis muscle in American whites and negroes. *Anat Rec* 61: 413–426.

Bavinck JN, Weaver DD. 1986. Subclavian artery supply disruption sequence: hypothesis of a vascular etiology for Poland, Klippel-Feil and Moebius anomalies. *Am J Med Genet* 23: 903–918.

Bergman RA. 1991. Doubled pectoralis quartus, axillary arch, chondroepitrochlearis, and the twist of the tendon of pectoralis major. *Anat Anz* 173: 23–26.

Bergman RA. 2014. Anatomy atlases: illustrated encyclopedia of human anatomic variation. http://www.anatomyatlases.org/ (accessed 16 October 2015).

Bergman RA, Thompson SA, Afifi AK, Saageh FA. 1988. *Compendium of human anatomic variations*. Baltimore, Munich: Urban and Schwarzenberg.

Bersu ET, Ramkez-Castro JL. 1977. Anatomical analysis of the developmental effects of aneuploidy in man. The 18-trisomy syndrome: I. Anomalies of the head and neck. *Am J Med Genet* 1: 173–193.

Bhat KM, Potu BK, Gowda S. 2009. Sternalis muscle revisited in South Indian male cadaver: a case report. *Cases J* 2: 6318–6320.

Birmingham AJ. 1889. Homology and innervation of the achselbogen and pectoralis quartus, and the nature of the lateral cutaneous nerve of the thorax. *Anat Physiol* 23: 206–223.

Blees G. 1968. A peculiar type of sternalis muscle. *Acta Morphol Neerl Scand* 7: 69–72.

Bonastre V, Rodriguez-Niedenfuhr M, Choi D, Sanudo JR. 2002. Coexistence of a pectoralis quartus muscle and an unusual axillary arch: case report and review. *Clin Anat* 15: 366–370.

Botros KG, Bondok AA, Gabr OM, el-Eishi HI, State FA. 1990. Anatomical variations in the formation of the human esophageal hiatus. *Anat Anz* 71: 193–199.

Bradley FM, Hoover HC Jr, Hulka CA, Whitman GJ, McCarthy KA, Hall DA, Moore R, Kopans DB. 1996. The sternalis muscle: An unusual normal finding seen on mammography. *Am J Roentgenol* 166: 33–36.

Bryce TH. 1899. Note on a group of varieties of the pectoral sheet of muscle. *J Anat Physiol.* 34(1): 75–78.

Calori L. 1867. Varieta dei muscoli del trunco e descrizione di una pettorina di fanciullo singolare per varie anomalie. *Accad Sci Istituto di Bologna S* 27: 383–393.

Caskey CI, Zerhouni EA, Fishman EK, Rahmouni AD. 1989. Aging of the diaphragm: a CT study. *Radiology* 171: 385–9.

Chaijaroonkhanarak W, Amarttayakong P, Pannangrong W, Umka J, Namking M, Chaisiwamongkol K, Kondo H, Prachaney P. 2013. Incidence of the sternalis muscle in Northeastern Thais. *Srinagarind Med J* 28: 62–65.

Chiba S, Suzuki T, Kasai T. 1983. A rare anomaly of the pectoralis major: the chondroepitrochlearis. *Okajimas Folia Anat Jap* 60: 175–186.

Christian HA. 1898. Two subjects in which the sternalis muscle existed. *Johns Hopkins Hosp Bull* 9: 235.

Clark E. 1915. Congenital variation of the pectoral muscles, with report of a case. *J Anat Physiol* 49: 155–164.

Crerar JW. 1892. Note on the absence of the subclavius muscle. *J Anat Physiol* 26(4): 554.

Cunningham DJ. 1884. The musculus sternalis. *J Anat Physiol* 18: 208–210.

Cunningham DJ. 1888. The musculus sternalis. *J Anat Physiol* 22: 391–407.

Curnow J. 1874. Notes of some irregularities in muscles and nerves. *J Anat Physiol* 7: 304–310.

da Silva TK, Marchiori E, da Rosa Silva G, Lago LN, Bello RM. 2012. Accessory diaphragm associated with single pulmonary vein in an asymptomatic patient: 64-multidetector CT findings. *Lung* 190: 353–354.

Darwin C. 1871. *The Descent of Man, and Selection in Relation to Sex*. New York: D. Appleton and Company.

Das S, Paul S, Mandal AK. 2006. Anomalous musculoskeletal morphology of anterior chest wall: A case report. *Arch Med Sci* 4: 289–291.

Dayal S, Bhat R, Shankar N. 2014. Complete unilateral right-sided absence of the pectoralis major and serratus anterior muscles in an adult male cadaver of South Indian origin. *Anat Sci Int* 89(1): 53–56.

de Pina L. 1928. Le muscle presternal chez les Portugais. *Ann Anat Path* 5: 1028.

del Sol M, Vasquez B. 2009. Anatomical and clinical considerations of the pectoralis tertius muscle in man. *Int J Morphol* 27: 715–718.

Demirpolat G, Oktay A, Bilgen I, Isayev H. 2010. Mammographic features of the sternalis muscle. *Diagn Interv Radiol* 16: 276–278.

Di Gennaro GL, Soncini G, Andrisano A, Valdiserri L. 1998. The chondroepitrochlearis muscle: case report. *Chir Organ Mov* 83: 419–423.

Diogo R, Wood BA. 2012. Comparative Anatomy and Phylogeny of Primate Muscles and Human Evolution. Science Publishers.

Diogo R, Abdala V, Aziz MA, Lonergan N, Wood BA. 2009. From fish to modern humans – comparative anatomy, homologies and evolution of the pectoral and forelimb musculature. *J Anat* 214: 694–716.

Dwight T. 1887. Muscular abnormalities. *J Anat Physiol* 22(1): 96–102.

Ebenezer DA, Rathinam BAD. 2013. Rare multiple variations in brachial plexus and related structures in the left upper limb of a Dravidian male cadaver. *Anat Cell Biol* 46: 163–166.

Eisler P. 1901. Der Musculus sternalis. *Z Morph Anthropol, Bd. 3*, 8: 21.

Eycleshymer AC, Shoemaker DM, Moodie RL. 1917. *Anatomical Names, Especially the Basle Nomina Anatomica*. New York: William Wood and Company.

Flaherty G, O'Neill MN, Folan-Curran J. 1999. Case report: bilateral occurrence of a chondroepitrochlearis muscle. *J Anat* 194(2): 313–315.

Fick R. 1891. Drei falle von Musculus sternalis. *Anat Anz* 6: 601–606.

Flint JM. 1902. On the use of clay models to record variations found in the dissecting room, with a note of two cases of m. sternalis and its influence on the growth of m. pectoralis major. *J Med Res* 8: 496–501.

Fokin AA, Robicsek F. 2002. Poland's syndrome revisited. *Ann Thorac Surg* 74: 2218–2225.

Fukuyama U. 1940. Der Musculus sternalis bei den Nordchinesen. *Okajimas Folia Anat Jap* 19: 69–92.

Gale ME. 1985. Bochdalek hernia: prevalence and CT characteristics. *Radiology* 156: 449–452.

Ge Z, Tong Y, Zhu S, Fang X, Zhuo L, Gong X. 2014. Prevalence and variance of the sternalis muscle: a study in the Chinese population using multi-detector CT. *Surg Radiol Anat* 36(3): 219–224.

Georgiev GP, Jelev L, Ovtscharoff VA. 2009. On the clinical significance of the sternalis muscle. *Folia Med* 51: 53–56.

Goktan C, Orguc S, Serter S, Ovali GY. 2006. Musculus sternalis: A normal but rare mammographic finding and magnetic resonance imaging demonstration. *Breast J* 12: 488–489.

Grant JCB. 1940. *A Method of Anatomy, second edition*. Baltimore: Williams and Wilkins.

Gruber W. 1860. Die supernumiraren brustmuskeln des menschen. *Mem Acad Imp St Petersburg* 3: 12.

Gupta M, Harjeet. 2004. Bilateral sternales in relation to body of sternum. *Nepal Med Coll J* 6: 62–63.

Hallett CH. 1848. Muscular system of the human body. *Edinburgh Med Surg J* 69: 1–31.

Hammad RB, Mohamed A. 2006. Unilateral four-headed pectoralis muscle major. *McGill J Med* 9: 28–30.

Hardy MA, Fabrizio PA. 2009. An accessory muscle of thoracic wall. *IJAV* 2: 93–95.

Harish K, Gopinath KS. 2003. Sternalis muscle: Importance in surgery of the breast. *Surg Radiol Anat* 25: 311–314.

Harper WF. 1936. The sternalis muscle in the anencephalous foetus. *J Anat* 70: 317–320.

Hepburn D. 1896. Abnormalities of muscles, nerves, heart, vessels, and ligaments. *J Anat Physiol* 30: 570–583.

Hollinshead H. 1956. *Anatomy for Surgeons, Vol 2: The Thorax, Abdomen and Pelvis*. New York: Hoeber-Harper.

Homsi C, Rodrigues MB, Silva JJ, Stump X, Morvan G. 2003. Anomalous insertion of the pectoralis minor muscle: ultrasound findings. *J Radiologie* 84: 1007–1011.

Huber KM, Boyd TG, Quillo AR, Wilhelmi BJ. 2012. Implications of anomalous pectoralis muscle in reconstructive breast surgery: The oblique pectoralis anterior. Eplasty 12:e44.

Hung LY, Lucaciu OC, Wong JJ. 2012. Back to the debate: sternalis muscle. *Int J Morphol* 30: 330–336.

Huntington GS. 1901. The morphological significance of certain periclavicular supernumerary muscles. *Annals NY Acad Sci1* 4: 53–66.

Huntington GS. 1904. The derivation and significance of certain supernumerary muscles of the pectoral region. *J Anat Physiol* 39: 1–68.

Ibrahim AF, Makarem SA, Darwish HH. 2005. Bilateral sternalis muscles. *Neurosci* 10: 171–173.

Ingalls NW. 1913. Musculi sternales and infraclavicularis. *Anat Rec* 7: 203–206.

Jaijesh P. 2005. Unilateral appearance of a chondro-epitrochlearis muscle – a case report. *Indian J Plast Surg* 38(2): 164–166.

Jelev L, Georgiev G, Surchev L. 2001. The sternalis muscle in the Bulgarian population: classification of sternales. *J Anat* 199: 359–363.

Jelev L, Hristov S, Ovtscharoff W. 2011. Variety of transversus thoracis muscle in relation to the internal thoracic artery: an autopsy study of 120 subjects. *J Cardiovasc Surg* 27: 6–11

Jeng H, Su SJ. 1998. The sternalis muscle: An uncommon anatomical variant among Taiwanese. *J Anat* 193: 287–288.

Jetti R, Pamidi N, Vollala VR, Vasavi R, Nerella VM. 2009. Right sternalis muscle. *Intern J Anat Variations* 2: 41–42.

Kabay B, Akdogan I, Ozdemir B, Adiguzel E. 2005. The left sternalis muscle variation detected during mastectomy. *Folia Morphol* 64: 338–340.

Kacker GN. 1960. Sternalis muscle in U.P. Indian subjects. *J Anat Soc Ind* 9: 101–103.

Kale SS, Herrmann G, Kalimuthu R. 2006. Sternomastalis: a variant of the sternalis. *Ann Plast Surg* 56(3): 340–341.

Karnak I, Tanyel FC, Tunçbilek E, Unsal M, Büyükpamukçu N. 1998. Bilateral Poland anomaly. *Am J Med Genet* 75(5): 505–507.

Kenanoglu A, Tuncbilek E. 1978. Accessory diaphragm in the left side. *Pediat Radiol* 7: 172–174.

Keith A. 1894. Note on the supracostalis anterior. *J Anat Physiol* 28: 333–334.

Khan UD. 2008. Use of the rectus sternalis in augmentation mammoplasty: Case report and literature search. *Aesthetic Plast Surg* 32: 21–24.

Kida MY, Kudoh H. 1991. Innervation of the sternalis muscle accompanied by congenital partial absence of the pectoralis major muscle. *Okajimas Folia Anat Jap* 67: 449–455.

Kida MY, Izumi A, Tanaka S. 2000. Sternalis muscle: Topic for debate. *Clin Anat* 13: 138–140.

Knott JF. 1880. Muscular anomalies. *J Anat Physiol* 15(1): 139–140.

Kobayashi S, Tomizawa Y, Manaka Y. 2013. Incidental finding of the sternalis muscle on chest multidetector-row computed tomography (MDCT): The diagnostic value of additional post processed MDCT images for an uncommon muscular variant. *Intern Med* 52: 1137–1139.

Kumar H, Rath G, Sharma M, Kohli M, Rani B. 2003. Bilateral sternalis with unusual left-sided presentation: A clinical perspective. *Yonsei Med J* 44: 719–722.

Laidlaw PP. 1902. A supraclavicularis proprius (Gruber). *J Anat Physiol* 36: 417–418.

Lama P, Potu BK, Bhat KM. 2010. Chondrohumeralis and axillary arch of Langer: a rare combination of variant muscles with unique insertion. *Rom J Morphol Embryol* 51: 395–397.

Lamont JC. 1887. Notes on the nervous supply of the musculus sternalis. *J Anat Physiol* 21: 514–515.

Landry SO. 1958. The phylogenetic significance of the chondroepitrochlearis muscle and its accompanying pectoral abnormalities. *J Anat* 92: 57–61.

Le Double AF. 1897. *Traite de Variations due Systeme Musculaire de l'Homme*. Paris: Schleider Freres.

Le Double A. 1890. Sur trente-trois muscles presternaux. *Bull Soc Anthropol Paris* 1: 533.

Lee YH, Chun SI. 1991. Congenital absence of pectoralis major: a case report and isokinetic analysis of shoulder motion. *Yonsei Med J* 32: 87–90.

Lin C. 1988. Contracture of the chondroepitrochlearis and the axillary arch muscles. *J Bone Joint Surg Am* 70A: 1404–1406.

Locchi R. 1930. Recherches d'anatomie ethnique sur le 'musculus sternalis'. *C R Assoc Anat* 25: 212.

Londhe SR, Jadhav AS, Koti MN. 2010. Unilateral rectus stermalis muscle a case presentation. *Anat Karnataka* 4: 51–53.

Loukas M, Louis RG Jr, Kwiatkowska M. 2005. Chondroepitrochlearis muscle, a case report and a suggested revision of the current nomenclature. *Surg Radiol Anat* 27: 354–356.

Loukas M, South G, Louis Jr RG, Fogg QA, Davis T. 2006. A case of an anomalous pectoralis major muscle. *Folia Morphol* 65: 100–103.

Loukas M, Wartmann Ch T, Tubbs RS, Apaydin N, Louis Jr RS, Gupta AA, Jordan R. 2008. Morphologic variation of the diaphragmatic crura: a correlation with pathologic processes of the esophageal hiatus? *Folia Morphol* 67: 273–279.

Low SC, Tan SC. 2010. Ectopic insertion of the pectoralis minor muscle with tendinosis as a cause of shoulder pain and clicking. *Clin Radiol* 65: 254–256.

Macalister A. 1867. Notes on an instance of irregularity in the muscles around the shoulder joint. *J Anat Physiol* 1(2): 316–319.

Macdonald Brown J. 1880. Variations in myology. *J Anat Physiol* 14(4): 512–513.

Malbranc M. 1876. In sachen des sternal muskels. Z Anat Entwicklungsgesch, Bd. ii. p. 310.

Marques EF, Souza JA, Graziano L, Bitencourt AGV, Senaga C, Fontes CEM. 2009. Sternalis muscle simulating a breast nodule. *Rev Bras Ginecol Obstet* 31: 492–495.

Mehta V, Arora J, Yadav Y, Suri RK, Rath G. 2010. Rectus thoracis bifurcalis: A new variant in the anterior chest musculature. *Romanian J Morph Embrio* 51: 799–801.

Misra BD. 1954. The sternalis muscle. *J Anat Soc Ind* 3: 47–48.

Moineau G, Cikes A, Trojani C, Boileau P. 2008. Ectopic insertion of the pectoralis minor: implication in the arthroscopic treatment of shoulder stiffness. *Knee Surg Sports Traumatol Arthrosc* 16: 869–71.

Moinfar AR, Murthi AM. 2007. Anatomy of the pectoralis minor tendon and its use in acromioclavicular joint reconstruction. *J Shoulder Elbow Sug* 16: 339–46.

Moir CR, Johnson CH. 2008. Poland's syndrome. *Semin Pediatr Surg* 17: 161–166.

Mori M. 1964. Statistics on the musculature of the Japanese. *Okajimas Fol Anat Jap* 40: 195–300.

Mosconi T, Kamath S. 2003. Bilateral asymmetric deficiency of the pectoralis major muscle. *Clin Anat* 16: 346–349.

Motabagani MA, Sonalla A, Abdel-Meguid E, Bakheit MA. 2004. Morphological study of the uncommon rectus sterni muscle in German cadavers. *East Afr Med J* 81: 130–133.

Mysnyk MC, Johnson DE. 1991. Congenital absence of the pectoralis muscles in two collegiate wrestling champions. *Clin Orthop* 265: 183–186.

Natsis K, Vlasis K, Totlis T, Paraskevas G, Tsikaras P. 2008. An unusual bilateral sternalis muscle. *Chirurgia* 103: 231–232.

Natsis K, Vlasis K, Totlis T, Paraskevas G, Noussios G, Skandalakis P, Koebke J. 2010. Abnormal muscles that may affect axillary lymphadenectomy: surgical anatomy. *Breast Cancer Res Treat* 120: 77–82.

Natsis K, Totlis T, Sofidis G. 2012. Chondroepitrochlearis: an abnormal muscle that may affect axillary lymphadenectomy. *ANZ J Surg* 82: 286–287.

Nelson ML, Burkle C, Ricardo R, Shibao S. 1992. Observation of the anterior supracostal muscles. *Anat Rec* 232: 318–321.

Nuthakki S, Gross M, Fessell D. 2007. Sonography and helical computed tomography of the sternalis muscle. *J Ultrasound Med* 26: 247–250.

Nguyen DT, Ogawa R. 2012. The sternalis muscle-incidental finding of a rare chest wall muscle variant during keloid excision-chest wall reconstruction. Eplasty 12:e36.

O'Neill MN, Folan-Curran J. 1998. Case report: bilateral sternalis muscles with a bilateral pectoralis major anomaly. *J Anat* 193: 289–292.

Ottone NE, Medan C. 2009. A rare muscle anomaly: the supraclavicularis proprius muscle. *Folia Morphol* 68: 55–57.

Paraskevas GK, Raikos A. 2010. Bilateral pectoral musculature malformations with concomitant vascular anomaly. *Folia Morphol (Warsz)* 69: 187–191.

Parsons FG. 1893. On the morphology of the musculus sternalis. *J Anat Physiol* 27: 505–507.

Patten CJ. 1934a. Right sternalis muscle with expanded fenestrated tendon. *J Anat* 68: 424–425.

Patten CJ. 1934b. Right sternalis muscle, narrow and spindle-shaped. *J Anat* 68: 426.

Petrasek AJ, Semple JL, McCready DR. 1997. The surgical and oncologic significance of the axillary arch during axillary lymphadenectomy. *Can J Surg* 40: 44–47.

Pinhal-Enfield G, Varricchio P, DeFouw D, Vasan NS. 2011. Sternalis muscle: importance of its awareness in chest imaging and clinical significance. *Int J Anat Variat* 4: 106–108.

Poland A. 1841. Deficiency of the pectoral muscles. *Guys Hosp Rep* 6: 191–193.

Rahman NA, Das S, Maatoq Sulaiman I, Hlaing KP, Haji Suhaimi F, Latiff AA, Othman F. 2009. The sternalis muscle in cadavers: Anatomical facts and clinical significance. *Clin Ter* 160: 129–131.

Rai R, Ranade AV, Prabhu LV, Prakash, Rajanigandha V, Nayak SR. 2008. Unilateral pectoralis minimus muscle. A case report. *Int J Morphol* 26: 27–29.

Raikos A, Paraskevas GK, Tzika M, Faustmann P, Triaridis S, Kordali P, Kitsoulis P, Brand-Saberi B. 2011a. Sternalis muscle: An underestimated anterior chest wall anatomical variant. *J Cardiothorac Surg* 6: 73–76.

Raikos A, Paraskevas GK, Yusuf F, Kordali P, Ioannidis O, Brand-Saberi B. 2011b. Sternalis muscle: A new crossed subtype, classification, and surgical applications. *Ann Plast Surg* 67: 646–648.

Redler LH, Kim HM, Tang P, Ahmad CS. 2012. An anomalous accessory pectoralis major muscle: a case report. *Am J Sports Med* 40: 2149–2153.

Rao VS, Rao GRKH. 1954. The sternalis muscle. *J Anat Soc Ind* 3: 49–51.

Saeed M, Murshid KR, Rufai AA, Elsayed SE, Sadiq MS. 2002. Sternalis. An anatomic variant of chest wall musculature. *Saudi Med J* 23: 1214–1221.

Sakuma E, Omi K, Takeda N, Hasegawa H, Mori K, Mabuchi Y, Soji T. 2007. Bilaterally existing sternoclavicularis anticus muscles. *Anat Sci Int* 82: 237–241.

Salval A, Scevola A, Baruffaldi Preis FW. 2012. Sternalis muscle: An uncommon finding during aesthetic breast surgery. *Aesthet Surg J* 32: 903–905.

Samuel VP, Vollala VR. 2008. Unusual pectoralis major muscle: The chondroepitrochlearis. *Anat Sci Int* 83: 277–279.

Sanders RJ, Rao NM. 2007. Pectoralis minor obstruction of the axillary vein: report of six patients. *J Vasc Surg* 45: 1206–1211.

Sarikcioglu L, Yildirim FB, Chiba S. 2004. Unilateral occurrence of a chondroepitrochlearis muscle. *Clin Anat* 17: 272–275.

Sarikcioglu L, Demirel BM, Oguz N, Ucar Y. 2008. Three sternalis muscles associated with abnormal attachments of the pectoralis major muscle. *Anat* 2: 67–71.

Satoh J. 1971. The M. transversus thoracis in man and monkey. *Okajimas Folia Anat Jap* 48(2): 103–137.

Sawada M, Ishibashi Y, Suzuki T, Chiba S. 1991. Case reports on the pectoralis quartus and the pectoralis intermedius muscles. *Kaibogaku Zasshi* 66: 99–105.

Schulman MR, Chun JK. 2005. The conjoined sternalis-pectoralis muscle flap in immediate tissue expander reconstruction after mastectomy. *Ann Plast Surg* 55: 672–675.

Shah AC. 1968. The sternalis muscle. *Indian J Med Sci* 22(1): 46–47.

Shehata R. 1966. The crura of the diaphragm and their nerve supply. *Acta Anat (Basel)* 63: 49–54.

Shen CL, Chien CH, Lee SH. 1992. A Taiwanese with a pair of sternalis muscles. *Kaibogaku Zasshi* 67: 652–654.

Shepherd FJ. 1885. The musculus sternalis and its occurrence in (human) anencephalous monsters. *J Anat Physiol* 19: 310–319.

Shepherd FJ. 1889. Musculus sternalis and its nerve-supply. *J Anat Physiol* 23: 303–307.

Shiotani M, Higuchi T, Yoshimura N, Kiguchi T, Takahashi N, Maeda H, Aoyama H. 2012. The sternalis muscle: Radiologic findings on MDCT. *Jap J Radiol* 30: 729–734.

Shirkhoda A. 2011. *Variants and Pitfalls in Body Imaging: Thoracic, Abdominal and Women's Imaging, second edition*. Baltimore: Lippincott Williams & Wilkins.

Silveira D, Sousa LM, Siqueira SL, Oliveira BVM, Silva AT, Costa JP, Araujo DC, Costa GAR, Araujo BA. 2012. Sternalis muscle: An anatomic variation of the anterior chest wall. *J Morphol Sci* 29: 76–78.

Simhadri D, Suseelamma D, Praveen Kumar M. 2012. Uncommon variation in musculature of the chest wall. *Anat Physiol* 2: 113–115.

Sirasanagandla SR, Nayak SB, Bhat KM, Surendran S, Regunathan D, Kumar N, Shetty SD, Patil J. 2014. Duplicated right crus of the diaphragm: a cadaveric case report. *J Can Chiropr Assoc* 58: 39–44.

Slobodin SG. 1934–35. Zur frage über den Musculus sternalis. *Anat Anz* 79: 207–211.

Snosek M, Tubbs S, Loukas M. 2014. Sternalis muscle, what every anatomist and clinician should know. *Clin Anat* 27: 866–890.

Soni S, Rath G, Suri R, Kumar H. 2008. Anomalous pectoral musculature. *Anat Sci Int* 83: 310–313.

Spears J, Kim DC, Saba SC, Mitra A, Schneck C, Mitra A. 2011. Anatomical relationship of Roos' type 3 band and the T1 nerve root. *Plast Reconstr Surg* 128(6): 1257–1262.

Spinner RJ, Carmichael SW, Spinner M. 1991. Infraclavicular ulnar nerve entrapment due to a chondroepitrochlearis muscle. *J Hand Surg* 7: 315–317.

Standring S. (ed.) 2008. *Gray's Anatomy*, 40th edition. Edinburgh: Elsevier.

Stylianos K, Constantinos P, Alexandros T, Aliki F, Nikolaos A, Demetriou M, Petros P. 2012. Muscle abnormalities of the chest in Poland's syndrome: variations and proposal for a classification. *Surg Radiol Anat* 34: 57–63.

Tachibana G1, Miyauchi R. 1989. Nerve supply to and the true nature of anterior supracostal muscle: three cases of the anterior supracostal muscle innervated by the external muscular branch of the first intercostal nerve having lateral cutaneous branch. *Anat Anz* 169(4): 235–245.

Taylor AE. 1898. Case of clavicular insertion of the pectoralis minor. *J Anat Physiol* 32(2): 218.

Testut L. 1884. *Les Anomalies Musculaires chez l'Homme*. Paris: Masson.

Tobler L. 1902. Der aschelbogen des menschen, ein rudiment des panniculus carnosus der mammalier. *Morph J* 30: 453–507.

Totlis T, Iosifidou R, Pavlidou F, Sofidis G, Natsis K, Bousoulegas A. 2012. Complicated axillary lymphadenectomy due to a pectoralis quartus muscle. *Chirurgia (Bucur)* 107: 397–398.

Tubbs RS, Oakes WJ, Salter EG. 2005. Unusual attachment of the pectoralis minor muscle. *Clin Anat* 18: 302–304.

Tubbs RS, Shoja MM, Shokouhi G, Loukas M, Oakes WJ. 2008. Insertion of the pectoralis major into the shoulder joint capsule. *Anat Sci Int* 83: 291–293.

Turan-Ozdemir S, Cankur NS. 2004. Unusual variation of the inferior attachment of the pectoralis minor muscle. *Clin Anat* 17: 416–417.

Turgut HB, Anil A, Peker T, Barut C. 2000. Insertion abnormality of bilateral pectoralis minimus. *Surg Radiol Anat* 22: 55–57.

Turner W. 1867. On the musculus sternalis. *J Anat Physiol* 1: 246–253.

Uzel AP, Bertino R, Caix P, Boileau P. 2008. Bilateral variation of the pectoralis minor muscle discovered during practical dissection. *Surg Radiol Anat* 30: 679–682.

Vaithianathan G, Aruna S, Rajila RH, Balaji T. 2011. Sternalis "mystery" muscle and its clinical implications. *Ital J Anat Embryol* 116: 139–143.

Vollala VR, Nagabhooshana S, Bhat SM, Potu BK, Rodrigues V, Pamidi N. 2009. Multiple arterial, neural and muscular variations in upper limb of a single cadaver. *Rom J Morphol Embryol* 50: 129–35.

Voto SJ, Weiner DS. 1987. The chondroepitrochlearis muscle. *J Pediatr Orthop* 7: 213–214.

Wallace D. 1886. Nerve supply of musculus sternalis. *J Anat Physiol* 21: 153–154.

Wille L, Holthusen W, Willich E. 1975. Accessory diaphragm. Report of 6 cases and review of the literature. *Pediatr Radiol* 4: 14–20.

Wood J. 1866. Variations in human myology observed during the Winter Session of 1865–6 at King's College, London. Proc Royal Soc 15: 229–244.

Wright IS. 1945. The neurovascular syndrome produced by hyperabduction of the arms: the immediate changes produced in 150 normal controls, and the effects on same persons of prolonged hyperabduction of the arms, as in sleeping, and in certain occupations. *Am Heart J* 29: 1–19.

Yap SE. 1921. Musculus sternalis in Filipinos. *Anat Rec* 21: 353–371.

Yazar F, Kirici Y, Ozan H. 1998. Accessory insertions of pectoralis major muscle to the brachial fascia: a case report. *Kaibogaku Zasshi* 73: 637–9.

Young Lee B, Young Byun J, Hee Kim H, Sook Kim H, Mee Cho S, Hoon Lee K, Sup Song K, Soo Kim B, Mun Lee J. 2006. The sternalis muscles: Incidence and imaging findings on MDCT. *J Thorac Imaging* 21: 179–183.

36 Abdominal wall muscles

Tsuyoshi Saga and Nagahiro Takahashi
Kurume University School of Medicine, Fukuoka, Japan

Anterior abdominal muscles

The rectus abdominis and pyramidalis muscles belong to the anterior abdominal muscles. Variations in the morphology of rectus abdominis have been reported; these include higher-than-normal locations of its insertions, differing numbers of tendinous intersections within the muscle, variations in the rectus sheath formed by the aponeuroses of the three lateral abdominal muscles, and inconsistencies in the shape and height of the arcuate line.

Pyramidalis muscle defects have been reported with some frequency. The size of this muscle is also highly variable; it can insert into the linea alba as high as the umbilicus, or can be only 1.5 cm in height.

An inconstant muscle, the rectus abdominis lateralis – which lies between the internal and external abdominal oblique muscles – arises from the middle and lower portions of the tenth rib and inserts into the iliac crest.

Rectus abdominis muscle

The rectus abdominis muscle usually inserts into the cartilages of the fifth, sixth, and seventh ribs (Clemente 1985); however, variations in its insertions have been described. There have been reports of the rectus abdominis inserting into the third and fourth rib, into the sternum, and into the fourth rib alone (Macalister 1875). Kopsch and Rauber (1919) described the rectus abdominis muscle inserting as high as the fourth, third, and second ribs, and even into the clavicle. Insertion of some of the inner muscle fibers into the linea alba has also been reported (Macalister 1875). The muscle can be doubled or send slips to the deep inguinal ring.

There are typically three tendinous intersections within the rectus abdominis muscle (Clemente 1985); however, this can vary from two to five in some cases. According to Sato (1968), the most frequent number of tendinous intersections differs between studies; while the majority of authors report three as the most frequently observed number of tendinous intersections (Loth 1912; Kita 1931; Sato 1968), some report four (Loth 1912; Nakamura 1935; Mori 1964). Sato (1968) did not observe differences in the number of tendinous intersections in rectus abdominis between sides (right/left) or genders in 684 cases.

The composition of the rectus sheath superior to the arcuate line is generally as follows: the aponeurosis of the internal abdominal oblique muscle divides into two layers, the superficial layer fuses with the aponeurosis of the external oblique muscle and forms the anterior rectus sheath, while the deep layer fuses with the aponeurosis of the transversus abdominis muscle and forms the posterior rectus sheath. The anterior and posterior sheaths then enclose the rectus abdominis muscle and connect at the midline to form the linea alba. However, anatomic variations in the rectus sheath have been reported. Monkhouse and Khalique (1986) studied 40 cases and reported two patterns (Fig. 36.1) in addition to the generally recognized configuration of the rectus sheath described above (Type 1). In one variation, the aponeurosis of the internal abdominal oblique does not split; instead, it fuses in its entirety with the aponeurosis of the external abdominal oblique muscle to form the anterior rectus sheath, whereas the posterior rectus sheath consists only of the aponeurosis of the transversus abdominis muscle (Type 2). In another variation, the aponeurosis of the transversus abdominis muscle splits into two layers, the more superficial of which fuses with the aponeuroses of the external and internal abdominal obliques to form the anterior rectus sheath, while only the posterior layer of the aponeurosis of the transversus abdominis forms the posterior rectus sheath (Type 3). Monkhouse and Khalique (1986) reported that the Type 1 configuration occurred in 60% of cases (24/40), Type 2 in 27.5% (11/40), and Type 3 in 12.5% (5/40). However, this result differs markedly from the findings of McVay and Anson (1940), who reported that the anatomic configuration corresponding to Type 3 in Monkhouse's classification system was the most commonly seen pattern, occurring with a frequency of 77% (43 of 56 cases). The anatomic arrangement corresponding to Type 1 in Monkhouse's classification was only seen in 3.6% of cases (2 of 56). The remaining 11 cases differed from the Type 2 in Monkhouse and Khalique's classification system, with both the internal abdominal oblique and transversus abdominis aponeuroses contributing fibers to both the posterior and anterior rectus sheaths (McVay and Anson 1940).

Bergman's Comprehensive Encyclopedia of Human Anatomic Variation, First Edition. Edited by R. Shane Tubbs, Mohammadali M. Shoja and Marios Loukas.
© 2016 John Wiley & Sons, Inc. Published 2016 by John Wiley & Sons, Inc.

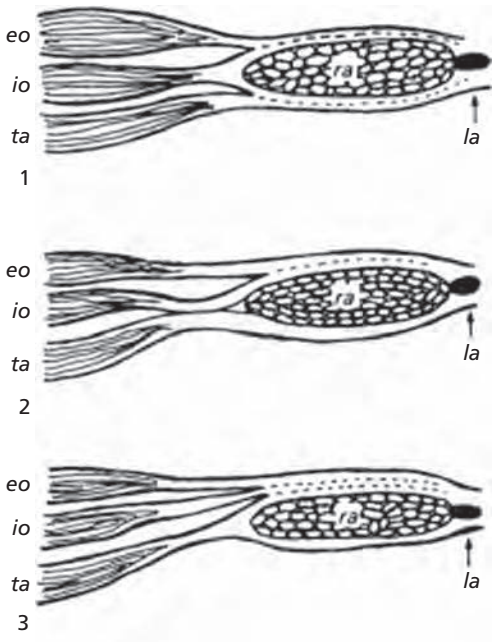

Figure 36.1 Anatomic variations in the rectus sheath above the arcuate line as reported by Monkhouse and Khalique (1986): types 1, 2, and 3.

Source: Monkhouse and Khalique (1986). Reproduced with permission from John Wiley & Sons.

Although it is usually located approximately equidistant between the pubic crest and umbilicus, the position of the arcuate line can be highly variable. It has been reported to be located as high as the umbilicus, and to have the configuration of a small foramen (McVay and Anson 1940). The arcuate line is typically higher laterally than medially, although cases in which it is higher medially, or approximately the same height both laterally and medially, have also been reported. McVay and Anson (1940) reported that the maximum height of the lateral side of the arcuate line was 130 mm, the minimum height was 40 mm, and its average height was 80 mm above the pubic crest. Monkhouse and Khalique (1986) found that the distance from the pubic crest to the arcuate line ranged from 30 to 126 mm on the medial side and from 46 to 130 mm on the lateral side, with mean distances of 63 mm and 87 mm, respectively. The distance from the umbilicus was 16–95 mm on the medial side and 30–112 mm on the lateral side, and the mean distances were 48 mm and 65 mm, respectively.

Rectus abdominis lateralis

Macalister (1875) credits Kelch with first describing the rectus abdominis lateralis. When this muscle is present, it arises from the middle and lower portions of the tenth rib, lies between the internal and external abdominal oblique muscles, and inserts into the iliac crest. There have been very few studies of this muscle. The only study examining the frequency with which this inconstantly present muscle occurs in a population is that by Sato (1968), who found that the rectus abdominis lateralis was present in 50 (approximately 9%) of 536 Japanese cadavers. The distribution was similar between genders, with 9.88% (32/324) of males and 8.49% (18/212) of females having a rectus abdominis lateralis muscle. The appearance rate between the right and left sides was not reported (Sato 1968). Additional muscle bundles in association with the external and internal abdominal oblique muscles are also mentioned in the section on the external abdominal oblique muscle.

Pyramidalis muscle

The pyramidalis muscle is a small, triangular-shaped muscle located in the lower abdomen between the layers of the anterior rectus sheath. Usually, this muscle arises from the anterior aspect of the pubis and anterior pubic ligament, runs superiormedially, and inserts into the linea alba approximately halfway between the umbilicus and the pubic symphysis. However, this muscle is absent in approximately 10% of cases. Anson et al. (1938) examined 165 subjects and reported that 10.8% of them lacked a pyramidalis muscle (Fig. 36.2). He also reported the rates of pyramidalis deficiency seen in previous studies, which ranged from 0% (Chudzinski 1898; Nakano 1923) to 27.2% (Aneel cited by Vallois 1926). Totaling the results of investigations before Anson's results in a 13.1% pyramidalis deficiency rate, 414 of 3154 sides lacked a pyramidalis muscle (Anson et al. 1938). In contrast, Dickson (1999) reported an extremely high rate of pyramidalis deficiency; the muscle was present in only 18/60 (30%) of the cases studied. He suggested that this might be due to his study population, which consisted of females of northern European origin. However, since his findings were based on observation of the muscle during gynecological surgery rather than dissection, the possibility exists that he failed to detect the muscle in some cases when it was actually present. Sinha and Kumar (1985) examined the rate of both bilateral and unilateral absence in 31 Indian male cadavers and found that 5.88% lacked the pyramidalis muscle bilaterally and 2.94% lacked it unilaterally. The bilateral absence rate was approximately twice as high as the unilateral rate. Supernumerary muscles have also been reported. A case with two pyramidalis muscles on one side and one on the other side (Winslow 1732; Cruveilher 1837), a case with two muscles on one side and none on the other side (Chudzinski 1898), a case with double muscles on both sides (Hallett 1848; Le Double 1897), and a case with more than two muscles on one side (Horner 1840) have all been reported (Anson et al. 1938).

Anson et al. (1938) found that the average size of the pyramidalis muscle was 6.82 cm in length and 1.98 cm in width, and the observed muscle lengths in the range 1.5–12 cm. These findings were similar to those of earlier studies, in which the average length and width ranged from 6.2 to 7.17 cm and 1.60 cm to 2.35 cm, respectively. In a relatively recent report, Sinha and Kumar (1985) found a similar mean length of 6.18 cm and width of 1.61 cm. Cases of the superior portion of the tendon

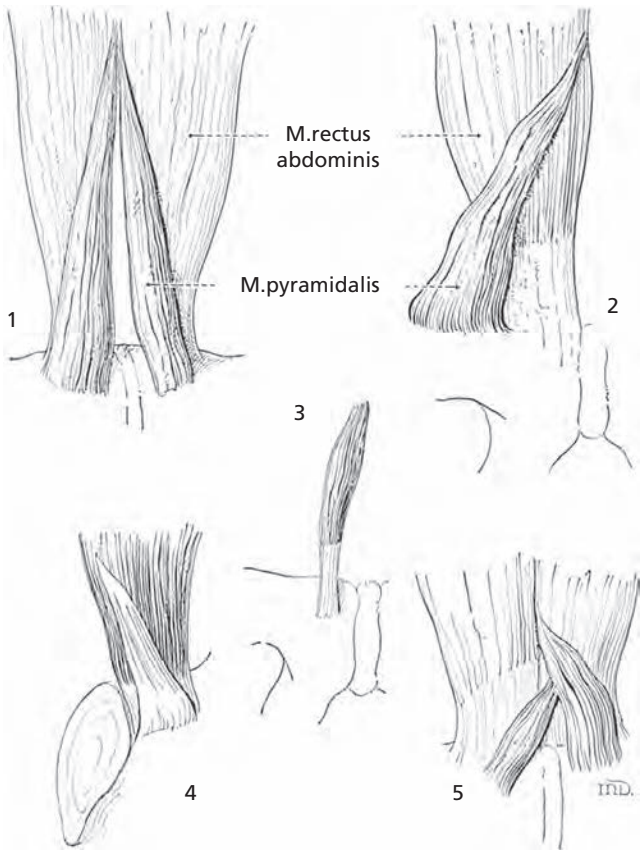

Figure 36.2 Morphological variations of the pyramidalis muscle (Anson et al. 1938). 1, long muscles of normal form; 2, the base of the muscle has been reflected laterally from the symphysis; 3, a quadrilateral rather than pyramidal muscle shape, with the inferior one third aponeurotic; 4, a triangular-shaped muscle in the normal position but almost entirely aponeurotic in structure; and 5, a muscle that arose lateral to the symphysis, crossed the midline, and inserted between the rectus abdominis and pyramidalis on the opposite side of the linea alba.

Source: Anson et al. (1938). Reproduced with permission from John Wiley & Sons.

or muscle reaching as high as the umbilicus, and of the inferior portion of the muscle occupying the entire pubic crest, have been described in Macalister's review (Macalister 1875). Moreover, Anson et al. (1938) also investigated bilateral (right/left) differences in pyramidalis muscle length and found that the muscles were approximately the same length in 40%, the right muscle was longer in 30%, and the left muscle was longer in 30% of his examinations. However, this was in contrast to the findings of Hallett (1848), who reported that the right muscle was almost always longer than the left (Anson et al. 1938).

The pyramidalis muscle is generally innervated by the subcostal nerve (the twelfth thoracic nerve; Clemente 1985); however, Tokita (2006) reported variations in its innervation. In his examination of 67 sides (50 bodies) he found nine different patterns of pyramidalis muscle innervation, which involved spinal nerves Th12–L2.

Lateral abdominal muscles

There are three lateral abdominal muscles: the external abdominal oblique muscle, the internal abdominal oblique muscle, and the transversus abdominis muscle. In addition, the cremaster muscles arise from the internal abdominal oblique.

The external abdominal oblique muscle forms the outer layer of the lateral abdominal wall, and its inferior aponeurosis forms the inguinal ligament. The internal abdominal oblique muscle forms the middle layer of the abdominal wall. The deepest muscular layer of the abdominal wall consists of the transversus abdominis muscle, and deep to this are the transversalis fascia and peritoneum.

The three large muscles of the lateral abdominal wall have many anatomic variations in their lateral portions, mainly in their attachments to the ribs (in other words, the origin of the external abdominal oblique and insertion of the internal abdominal oblique muscle are highly variable). However, their medial portions which form the rectus sheath (in other words, the insertion of the external abdominal oblique muscle and origin of the internal abdominal oblique muscle), are highly consistent. Additional muscle bundles have occasionally been observed in the external and internal abdominal oblique muscles. The entire absence of these muscles has only been reported in cases of congenital deficiency (Guthrie 1896).

External abdominal oblique muscle

The external abdominal oblique muscle generally originates from the ribs and its aponeurosis forms the inguinal ligament and anterior layer of the sheath of rectus abdominis. The number of ribs from which it originates is highly variable. Generally, the external abdominal oblique muscle arises from seven to nine ribs, with the fourth rib being the most superior and the twelfth rib being the most inferior. However, there are many reports of variations in its highest and/or lowest rib of origin.

Macalister (1875) reviewed many anatomic variations of the external abdominal oblique muscle. He described twelve different forms of this muscle, including: variations in the superior extent and the numbers of ribs comprising its origin; a partial absence of the origin from some ribs; a double origin from the same rib; and additional muscle deep to the external abdominal oblique muscle or between the external and internal abdominal oblique muscles.

Mori (1964) reported that in 166 Japanese adults (332 cases, right and left side) the most superior portion of the origin of the external abdominal oblique muscle was the fourth rib in 0.6%, fifth rib in 83.1%, and sixth rib is 16.3% of cases. A similar result was reported by Miyauchi et al. (1983). However, in the fetus, two different researchers reported that the most superior portion of the origin was only the fifth (77.0%) or sixth ribs (23.0%); Yonekura (1954) found 77.0% and 23.0% and Kikuchi (1986) found 87.5% and 12.5% of fetal external abdominal oblique muscles had their most superior point of origination from the fifth and sixth ribs, respectively. The most inferior site of origin

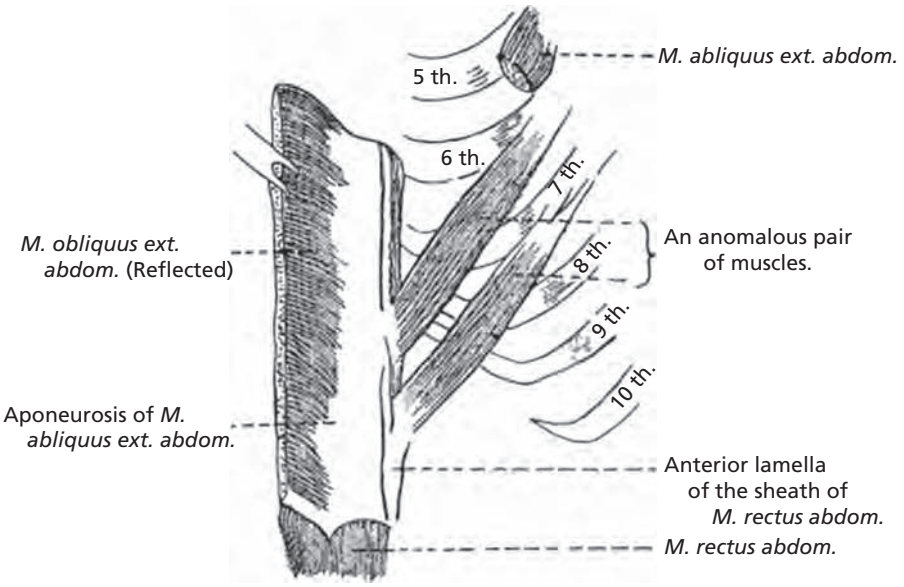

Figure 36.3 The variation of M. obliquus externus abdominis. Two additional muscle bundles originated from the left sixth and seventh ribs and inserted to the anterior lamella of the sheath of rectus abdominis in a male cadaver.

Source: Sugiura (1935). Reproduced with permission from Nagoya Journal of Medical Science.

of the external abdominal oblique muscle is the twelfth rib in adults, but in the fetus the origin ends at the eleventh rib and fibers do not originate from the twelfth rib in 34.0% of cases (Yonekura 1954). The superior portions of the origin of the external abdominal oblique interdigitate with portions of the serratus anterior muscle that arise from the same region. Moreover, the inferior portions of its origin cross the latissimus dorsi muscle to form Gerdy's Line. The level at which the serratus anterior and external abdominal oblique muscles cross was reported by Murata et al. (1971); they found that these muscles crossed at the fifth rib in 85.0%, sixth rib in 100%, seventh rib in 100%, eighth rib in 98.8%, ninth rib in 71.6%, tenth rib in 14.8%, and eleventh rib in 0.3% of cases.

Occasionally, additional muscle bundles arise from the ribs in association with the external and internal abdominal oblique muscles (Fig. 36.3). These additional muscle bundles have been given various names, including "Federkieldicker Muskel" (Weitbrecht 1735, quoted by Sugiura 1935), "M. rectus lateralis abdominis" (Kelch 1813), "M. obliquus externus secundus s. accessorius" (Gruber 1875), "M. obliquus externus profundus s. minor" (Knott 1880) or "M. obliquus externus abdominis minor s. secundus" (Knott 1883). Old reports by Macalister (1875) and Knott (1880, 1883) briefly mention several types of musculus obliquus abdominis externus profundus. Macalister (1875) describes a case in which this muscle was doubled on the left side, with the deeper muscle passing from the three most inferior ribs (except the twelfth) to the crest of the ilium, precisely parallel to the normal muscle and separated from it by a layer of fascia. Knott (1883) reported that this muscle arose from the ninth and tenth ribs at the costochondral junction and inserted between the middle and lateral thirds of the inguinal ligament. Nakayama and Okuda (1952) presented detailed figures of the obliquus abdominis externus profundus, and described two cases of this muscle occurring in Japanese adults. In one case of a 36-year-old male, the muscle originated from the eleventh rib and ran between the external and internal abdominal obliques (width 1 cm and length 13 cm) before inserting into the ventral side of the iliac crest near the anterior superior iliac spine. In another case of an 84-year-old female, the muscle had two heads that both originated from the fascia of the internal abdominal oblique muscle just below the eleventh rib; these fused to form one muscle (width 0.5 cm and length 9.5 cm) and then attached to the inner surface of the aponeurosis of the external abdominal oblique muscle near the iliac crest. A similar anatomic arrangement on both sides of the abdomen has been reported in one Japanese adult cadaver (Fig. 36.4; Shimazaki 1959).

The frequency of the occurrence of obliquus abdominis externus profundus has been reviewed by Miyauchi et al. (1986). They describe inconsistencies in the literature in the frequencies with which this muscle reportedly occurs. Loth (1912, 1879) found the obliquus abdominis externus profundus in 3.8% of Blacks and 7% of Caucasians, and Nakayama and Okuda (1952), Kudo and Otobe (1952), and Yonekura (1954) found it in 1.9%, 3%, and 2% of their study populations, respectively. In contrast, Kodama (1986) reported that this muscle occurred in about 36.5% of the cases studied. Based on his findings, Kodama (1986) suggested that this additional muscle should be classified into one of three categories based on its innervation.

There are two other inconstantly present muscles associated with the external abdominal oblique: the interfoveolar muscle, which consists of muscle fibers within the interfoveolar ligament and has been observed in 46% of Chinese people (Kudo and Otobe 1952); and the saphenous muscle, which attaches at both ends to the inguinal ligament and loops around the saphenous

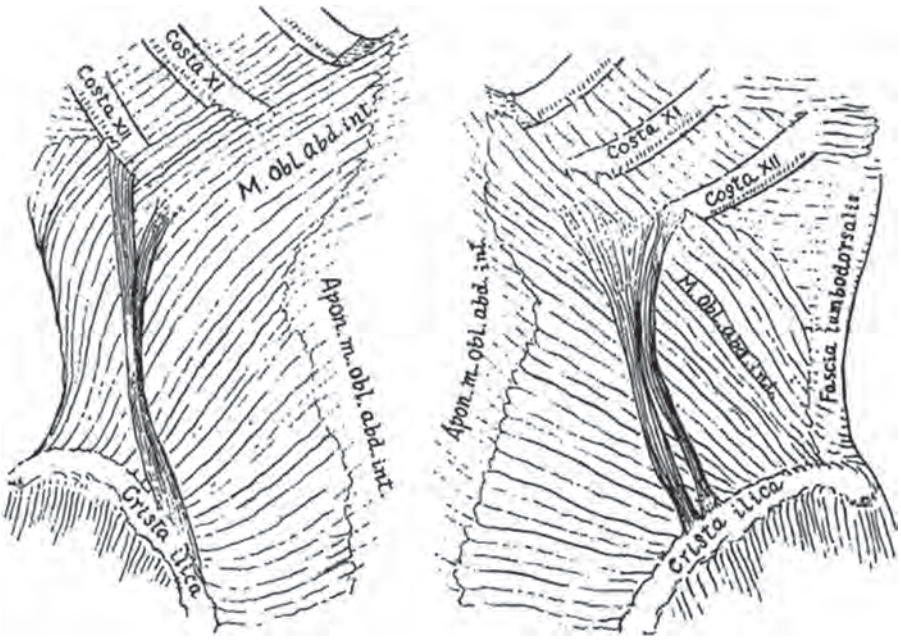

Figure 36.4 The two additional bundles as the obliquus abdominis externus profundus in a cadaver of a 70-year-old male. Additional muscle was found in both sides of abdomen. Source: Shimazaki (1959).

vein (Fig. 36.5; Tyrie 1894). A very small muscle slip from the pubic bone to the trasversalis fascia and crossing anterior to the interfoveloar ligament/muscle at a near right angle was termed the pubotrasversalis muscle by Luschka (1879).

Internal abdominal oblique muscle

The internal abdominal oblique muscle lies deep to the external abdominal oblique muscle. It originates from the thoracolumbar fascia, the anterior two-thirds of the iliac crest and the lateral two-thirds of the inguinal ligament. The superior bundle of this muscle inserts on the inferior border of the most inferior three or four (two–five in Macalister 1875) ribs, and becomes continuous with the internal intercostals. The middle bundle of this muscle runs towards the midline and its aponeurosis forms part of the sheath of rectus abdominis. The inferior portion of this muscle runs diagonally towards the inferior linea alba and the most inferior bundle of this muscle forms the cremaster.

Macalister (1875) reviewed several anomalous configurations of the internal abdominal oblique muscle. He described six anatomical variations, which included variations in the number of costal attachments, fusion of the internal abdominal oblique and transversus abdominis muscles, and the presence of tendinous inscriptions in the internal abdominal oblique near its costal insertions.

Macalister (1875) reported that the costal attachments of the internal abdominal oblique varied from two to five, with three being the most common (occurring in about 78% of people) and 4 being present in about 17% of people. Based on studies in a Polish population, Loth (1912) reported that the most superior costal insertion of this muscle was the eighth rib in 1.5%, the

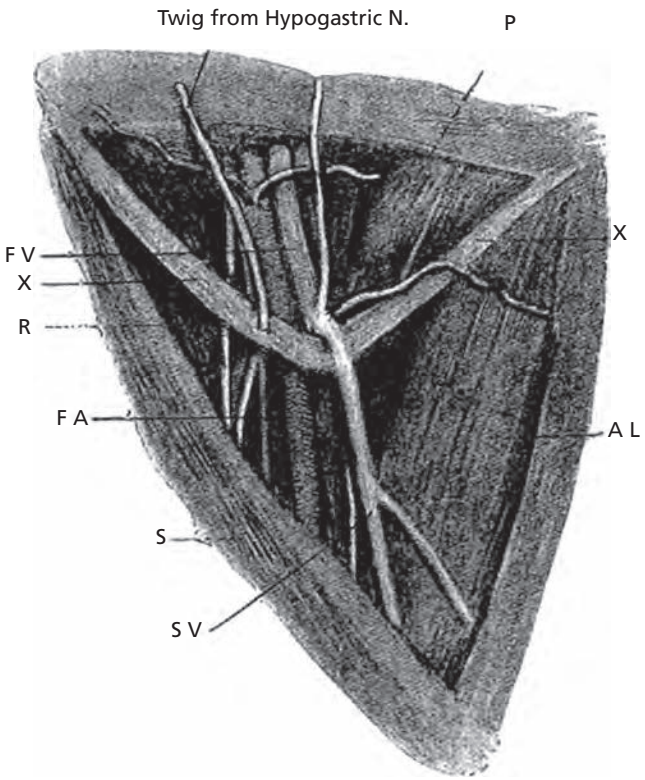

Figure 36.5 The saphenous muscle in a 65-year-old male. This muscle attaches loops around the saphenous vein (indicated by X–X). AL, adductor longus; FA: femoral artery; FV: femoral vein; P: pectineus; R: rectus femoris; S: sartorius; SV; saphenous vein; X: saphenous muscle.

Source: Tyrie (1894). Reproduced with permission from John Wiley & Sons.

ninth in 1.0%, the tenth in 66.5%, and the eleventh rib in 31% of cases. In 200 Japanese adults, Mori (1964) found that the most superior costal insertion on the right side was the tenth rib in 56% and the eleventh rib in 34% of cases and, on the left side, was the tenth rib in 64% and the eleventh rib in 36% of cases. After studying 100 fetuses, Yonekura (1954) reported that the most superior costal insertion was the eighth, ninth, tenth, and eleventh rib in 2.0%, 40.0%, 55.0%, and 3.0% of cases, respectively. Kikuchi (1986) reported that the tenth rib was the most superior point of insertion in all 40 fetuses.

Knott (1883) described two cases in which the internal abdominal oblique muscle and the transversus abdominis were fused. He described the internal abdominal oblique as so closely connected to the transversus abdominis that he could not satisfactorily separate their adjacent surfaces.

Knott (1883) also described tendinous inscriptions opposite the apex of the tenth or eleventh rib in several cases. In another two instances, isolated cartilaginous slips opposite the tenth costal cartilage were observed by Knott (1883), and he commented that similar observations had been reported by Henle (1871) and Macalister (1875). Macalister (1875) mentioned that where this muscle is continuous with the tenth intercostal muscle, the line of the tenth rib is often extended medially by a tendinous inscription which has been observed to contain a slender cartilaginous slip perfectly separate from the cartilage of the rib. In addition, Macalister (1875) also reported partial deficiencies in the anterior and superior parts of this muscle.

Cremaster muscle

Macalister (1875) described the cremaster muscles arising in whole or in part from the fascia transversalis (in Gruber), or from the transversalis muscle with a special spino-pubal slip, or doubled, or in separate fasciculi. Knott (1883) reported that the only variation of this muscle which he has noted is an origin almost wholly continuous with the lower fibers of the transversus abdominis. In the female, a few muscular fibers descending the round ligament of the uterus are analogous to the lateral part of the cremaster in males. According to Kawamitsu et al. (2004), surgeons currently tend to regard the cremaster as a muscular cylinder that envelopes the spermatic cord; however, anatomists have historically regarded it as a slender muscular fasciculus consisting of muscular arches or loops, that lies not around the cord but only in front of it.

Transversus abdominis

The transversus abdominis is the deepest muscular layer of the lateral abdominal wall. It lies immediately beneath the internal abdominal oblique muscle and generally originates from the inner surfaces of the cartilages of the six or seven most inferior ribs, from the lumbodorsal fascia, from the anterior two-thirds of the inner lip of the iliac crest, and from the lateral one-third of the inguinal ligament. The insertion of this muscle is mainly the sheath of rectus abdominis.

Macalister (1875) reviewed several anomalous configurations of the transversus abdominis, including the entire or partial absence of this muscle, fusion with the internal abdominal oblique, and variation in the number of costal origins. In one rare case, the transversus abdominis was absent without any other anatomic anomalies. He reported that the transversus abdominis usually has five costal origins, but may also arise from the six or seven lowest ribs in some cases. As mentioned above, the origin of this muscle was described by Knott in 1883. He showed that in 29/36 cases there were six costal origins, 4/36 cases had four costal origins, and 3/36 cases had five costal origins. In 40 Japanese fetuses, the transversus abdominis arose from the seven lowest ribs in 36 and from the six lowest ribs in four (Kikuchi 1986). In another variation, described by both Macalister (1875) and Knott (1883), the spermatic cord traveled through the lower part of the transversus abdominis and the muscle fibers normally associated with the inguinal ligament were absent.

Chandler and Schadewald (1944) made detailed observations of the inguino-hypogastric region of 220 body-halves, and found that the transversus abdominis muscle seldom arose from the whole of the inguinal ligament and its fibers ran parallel or oblique to the ligament. Moreover, they described the inferior edge of the muscle as forming an arch that forms part of the roof of the inguinal canal.

Gruber (1873a, b) reported a tensor laminae posterioris vaginae musculi rectus that was composed of muscle slips arising inferiorly from the trasversalis fascia and traveling cephalad to fan out and interdigitate at right angles with the transversus abdominis. This muscle has also been termed the puboperitonealis.

In a relatively recent report, Urquhart et al. (2005) reported five anatomic variations of the transverse abdominal muscle in separate specimens. These included complete and partial detachment of the muscle from the iliac crest and an abrupt change in fascicle orientation, absence of fascicles below the iliac crest, passage of the iliohypogastric and ilioinguinal nerves through the septa, and fusion of the lower fascicles with the internal abdominal oblique muscle.

An accessory muscle arising from the pecten pubis and inserted into the fascia of the transversus abdominis is known as the pubotransverse muscle of Luschka.

Posterior abdominal muscles

The posterior abdominal muscles are quadratus lumborum, psoas major, psoas minor, and iliacus. Few anatomical variations of quadratus lumborum have been reported. Psoas major and iliacus share the compound iliopsoas tendon, which inserts into the lesser trochanter of the femur. Separation or fusion of these muscles, and the presence of aberrant muscular slips, have been reported as anatomical variations. Psoas minor is an inconsistent muscle, and is often absent.

Quadratus lumborum

There are few known anatomical variations of quadratus lumborum. This muscle usually arises from the iliolumbar ligament and iliac crest and inserts into the inferior border of the twelfth rib and the transverse processes of the first through fourth lumbar vertebrae via small tendons of insertion, which can vary in number and thickness (Macalister 1875). The insertions of quadratus lumborum have been found to consist of the bodies of both the tenth and eleventh thoracic vertebrae, the body of the eleventh thoracic vertebra only, or the eleventh rib (Macalister 1875). Two components of the muscle have been described: fibers extending from the ribs and separate fibers from the transverse processes.

Iliopsoas muscle

Iliopsoas consists of two muscles: iliacus and psoas major. These two muscles join together and end in a tendon that inserts into the lesser trochanter of the femur. Recently, anatomical variations of the iliopsoas tendon have been reported by some authors as the cause of "snapping hip." Tatu et al. (2001) described the iliopsoas tendon as consisting of three elements: a main tendon, an accessory tendon, and the proper tendon of iliacus. The main tendon consists primarily of the tendon of psoas major. The accessory tendon consists of fibers from the iliacus muscle, except for the most medial and inferior fibers arising from iliacus which merge with the main tendon. The most lateral fibers of the iliacus muscle attach to the lesser trochanter independently of the tendon. Tatu et al. (2001) described two cases of completely split or bifid psoas major tendons out of 24 cases studied. Phillippon et al. (2014) examined 53 cadavers and found three types of iliopsoas tendons: single-, double-, and triple-banded. The proportions of these types in the study population were 28.3%, 64.2%, and 7.5%, respectively. Polster et al. (2008) used MRI to examine patients with a snapping hip and reported that there was a longitudinal cleft in the iliopsoas tendon in these patients. The author also performed a cadaver dissection study and found that, in one of three cases, the crossing fibers ended at the level of the femoral head-neck junction instead of joining to the psoas major tendon. Other authors have also described anatomical variations of the iliopsoas tendon. Shu and Safran (2011) reported a bifid iliopsoas tendon, similar to that described by Polster et al. (2008).

Iliacus

The iliacus muscle is one of the muscles that comprises iliopsoas. Anatomical variations of iliacus are rare; however, some variations, such as agenesis, aberrant muscular slips, and muscular fusion, have been reported. Aleksandrova et al. (2013) reviewed the previous reports and classified the variations into ten types (A to J) based on criteria that included partial muscular agenesis, the presence of aberrant muscle slips, the relationship between iliacus and psoas major, and the relationship between aberrant slips and the femoral nerve (Fig. 36.6).

Type A is partial agenesis of the iliacus. The course of the femoral nerve is basically normal in this classification. To our knowledge only one case of this type has been reported, described by Aleksandrova et al. (2013) themselves. The case was a 58-year-old male with some muscle slips absent in the most anterior and middle portions of iliacus.

Type B is complete separation of iliacus and psoas major, with the femoral nerve following a normal course. This type of anomaly has been described in the older literature. Macalister described the psoas major as perfectly separated from the iliacus.

In contrast to type B, type C is complete fusion of the iliacus and psoas major. Fabrizio (2011) reported one case in which the iliacus and psoas major were fused at the level of the superior one-third of the ilium. The femoral nerve ran along the superior margin of the blended muscles at their uppermost connection.

Type D is aberrant slips of higher origin with the femoral nerve running on the surface of the slip. Aleksandrova et al. (2013) reported one case of this type, in which partial agenesis of the iliacus muscle was combined with aberrant slips arising from beyond the iliac crest. The psoas quartus muscle, an extremely rare muscle that has only been reported twice in the literature (Clarkson and Rainy 1889; Tubbs et al. 2006), may belong to this classification. Tubbs and Salter (2006) described a case with a psoas quartus muscle that arose from the transverse process of the L3 vertebra and the anteromedial aspect of the quadratus lumborum, and united with the psoas major and iliacus muscles at the level of the inguinal ligament (Fig. 36.7). In the case described by Clarkson and Rainy (1889), muscle slips arose from both the anterior surface of the quadratus lumborum and the transverse process of the fifth lumbar vertebra. The psoas tertius was also present in this case (Clarkson and Rainy 1889). This muscle arose from the inner surface of the twelfth rib and the transverse process of the first through fourth lumbar vertebrae, ran deep to the quadratus lumborum and iliacus muscles, and ended in tendinous fibers that fused with the tendon of the psoas major and psoas quadratus near the level of the inguinal ligament.

Type E is called the iliacus minor muscle (Winslow) or iliocapusularis (Harrison) muscle. The femoral nerve runs normally in this classification. According to Macalister (1875) this muscle is a small detached portion of the iliacus, arising from the anterior inferior spine of the ilium and inserting into the anterior inter-trochanteric line. Das and Singh (1950) described the difference between the iliacus minor, which inserts entirely into the inter-trochanteric line, and the ilio-capsularis, which inserts entirely into the ilio-femoral ligament. In some recent studies of hip surgery, the authors claimed that ilio-capsularis was a constant muscle observed in all cases (Ward et al. 2000; Babst et al. 2011). Babst et al. (2011) suggested that the ilio-capsularis muscle was particularly important in dysplastic hips, where contractions of this muscle would help to stabilize the femoral head in a deficient acetabulum. This muscle may therefore be hypertrophied in dysplastic hips and atrophied in stable and well-constrained hips.

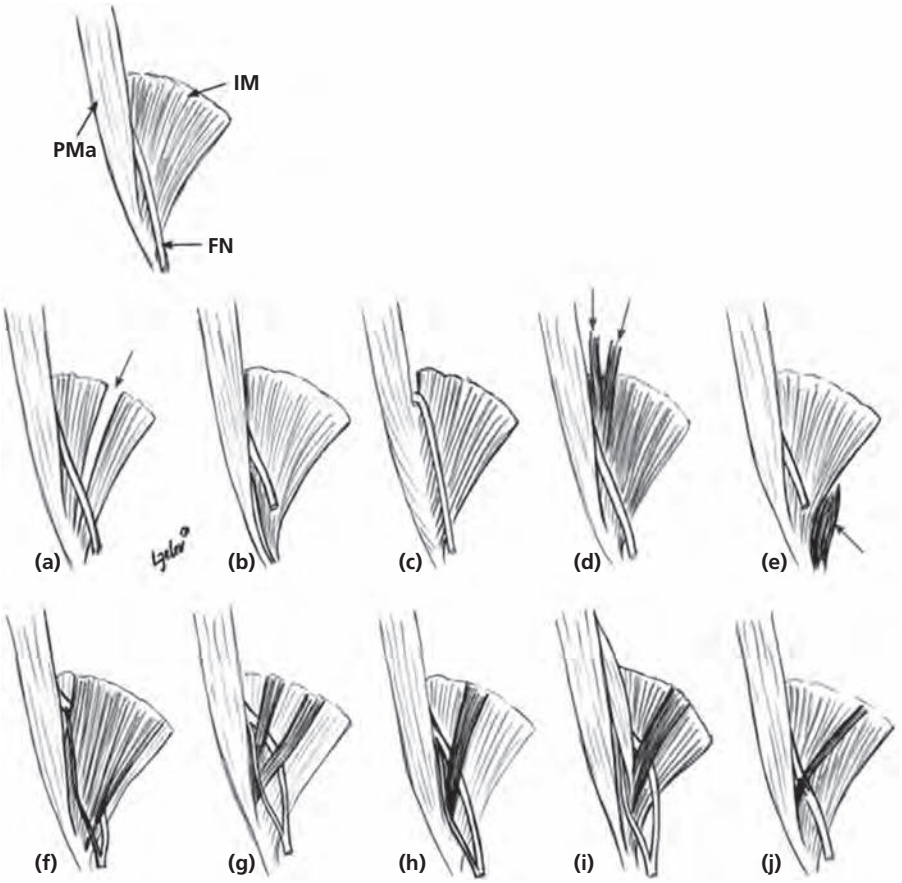

Figure 36.6 The variations of iliacus: (a) partial agenesis; (b) complete separation of iliacus and psoas major; (c) complete fusion of iliacus and psoas major; (d) aberrant slips of higher origin; (e) presence of iliacus minor (iliocapsularis); (f) splitting of the iliacus into deep and superficial layers; (g) presence of two large aberrant slips; (h) presence of a single large aberrant slip; (i) presence of an accessory iliacus joining the accessory psoas major; and (j) presence of a small muscular slip piercing the femoral nerve. IM: iliacus muscle; PMa: psoas major; FN: femoral nerve.

Source: Aleksandrova et al. (2013). Reproduced with permission from the International Journal of Anatomical Variations.

Type F is the condition in which the iliacus muscle is split into deep and superficial layers. The femoral nerve splits into two, with one branch running between the two layers of the iliacus muscle. This classification has only been described in the older literature, and there have not been any reports with detailed figures or pictures.

Type G is when the iliacus has two large, aberrant, superficial slips. The femoral nerve is split in two and aberrant muscle slips run between the two nerve branches. Rao et al. (2008) reported one case of bilateral iliacus variations. On the left side there were two aberrant slips on the surface of the iliacus muscle, the iliacus minimus on the medial side and the accessory iliacus muscle on the lateral side. The femoral nerve was split into two and its branches ran on the medial and lateral side of the two muscles. The larger portion of the nerve ran on the lateral side (between the muscles slips and iliacus) and the smaller portion of the nerve ran superficial to the muscle slips on the medial side.

Type H is a single large aberrant slip of the iliacus muscle with the main trunk of the femoral nerve running between the aberrant muscle slip and iliacus. D'Costa et al. (2008) reported the muscle slip originating from the middle third of the inner lip of the iliac crest and inserting with the iliopsoas complex at the lesser trochanter. The L4 root of the femoral nerve ran between the muscle slip and iliacus, whereas the L2 and L3 roots ran superficial to the aberrant muscle slip. Rao et al. (2008) reported bilaterally abnormal iliacus muscles. On the right side, the iliacus muscle had one additional slip and the femoral nerve split into two parts in order to enclose the aberrant muscle slip and then fused again to form a single trunk.

Type I has two aberrant muscular slips and the femoral nerve is split into two portions that run both superficial and deep to these muscle slips, enclosing them. Jelev et al. (2005) reported one case of this type. The medial side of the aberrant slip was located lateral to the normal psoas major muscle, originated from the left costal process of the L3 vertebra and from the intertransverse ligament between L3 and L4, and inserted with a short tendon to the common iliopsoas tendon. This muscle has been described as the "accessory psoas major muscle" (Le Double 1897; Rickenbacker et al. 1985; Jelev et al. 2005). The lateral side of the aberrant slip arose from the middle third of the iliac crest and inserted into the tendon of the above-mentioned aberrant slip ("accessory psoas major muscle"). The author named this muscular slip the "accessory iliacus muscle" (Jelev et al. 2005). Jelev et al. (2005) described the "accessory iliopsoas muscle" as a combination of the aberrant accessory psoas major and accessory iliacus muscles.

Figure 36.7 A case of psoas quartus muscle.

Source: Tubbs et al. (2006). Reproduced with permission from John Wiley & Sons.

Figure 36.8 A case of iliacus minimus muscle.

Source: Tubbs and Salter (2006). Reproduced with permission from John Wiley & Sons.

Type J has a small muscular slip piercing the femoral nerve. Spratt et al. (1996) first reported this type of anomaly, and named it "iliacus minimus." Spratt et al.'s case (1996) had an aberrant muscular slip originating from the iliolumbar ligament, piercing the femoral nerve, and splitting into two tendons that went to the lesser trochanter of the femur and the medial thigh. This muscle is presumed to have variations in its insertion. It may insert into the lesser trochanter of the femur or end by joining the iliopsoas muscle. The former insertion was reported by both Spratt et al. (1996) and Aristotle et al. (2013). In 2006, Tubbs and Salter reported a similar case of an aberrant muscle slip that arose from the iliolumbar ligament, traveled on the iliacus, and pierced the femoral nerve. However, it ended by fusing with the iliopsoas muscle at the level of inguinal ligament, and did not reach the lesser trochanter (Fig. 36.8). Aleksandrova et al. (2013) also reported a similar case, in which the muscle slip ended by joining the iliopsoas tendon.

An aberrant slip of the iliacus has been described as arising from the dorsal ilium, immediately below and external to the anterior inferior iliac spine, and from the hip joint capsule to travel behind the rectus femoris and blend with the ilacus muscle.

Psoas major

Both complete separation and complete fusion of the iliacus and psoas major have been reported. Macalister described psoas major as perfectly separated from iliacus. Fabrizio (2011) reported one case in which iliacus and psoas major were blended together at the level of the superior one-third of the ilium. Psoas major may be divided longitudinally into fascicles (Bergman et al. 1988). Jelev et al. (2005) reported one case in which psoas major was split longitudinally into three parts: a superior part arising from the body of the L1 vertebra and the intervertebral disc between L1 and L2; a middle part arising from the

L2/L3 intervertebral disc; and an inferior part arising from the lower borders of the L3 to S3 vertebrae. Macalister (1875) also described anomalous cases in which psoas major originated from the fifth lumbar vertebra. Bergman et al. (1988) described an "aberrant psoas major fascicle" arising from the L4 body, L5 transverse process and descending posterior to the psoas major muscle to be inserted just posterior to the psoas minor insertion onto the pubic bone.

Psoas minor

Psoas minor is an inconsistent muscle that is often absent. The frequency of appearance of this muscle differs between races. Ghandhi et al. (2013) reviewed previous reports and found that this muscle had a prevalence of 33.4–52% in the studied populations. Comparison among races is difficult because the reported prevalences are highly variable, even between researchers studying the same race. For example, Mori (1964) reviewed reports of the prevalence of psoas minor in Japanese populations and found that the prevalence ranged from 35% to 55%. However, Hanson et al. (1999) compared the prevalence of psoas minor between young black and white men and found that psoas minor was absent in 91% of black subjects but in only 13% of white subjects. Seib (1934) studied 500 cadavers (1000 sides) and found the psoas minor present in 38.6%. This author also found that the muscle was absent more frequently in females, regardless of side or race. Psoas minor is consistently absent in those with Trisomy-18 (Agichani et al. 2013).

This muscle may be replaced by tendon (Macalister 1875; Bergman et al. 1988) or may have a remarkably long tendon (Ghandhi et al. 2013). Guerra et al. (2012) reported that the tendon comprised 57% of the total length of the muscle. The average proportion of the total length comprising the tendon was 60% in females and 54% in males (Guerra et al. 2012). Agichani et al. (2013) found that the average length of the muscle belly of psoas minor was 7.85 cm (right, 7.56 cm; left, 8.14 cm) and the length of the tendon was 13.13 cm (right, 13.56 cm; left, 12.7 cm). This result also shows that a large proportion of the total length of the muscle consists of tendon.

Some variations in the origin and insertion of psoas minor have been reported. The origin of the muscle may consist of two heads, which may split partially or completely prior to insertion (Ghandhi et al. 2013). Part of the split muscle may lie deep to the other part (Macalister 1875; Bergman et al. 1988). The psoas minor has been reported to originate as a ramification of the fibers of the psoas major (Macalister 1875). Although this muscle is generally described as inserting into the iliopectineal eminence, some variations in its insertion have been reported: the pectineal line of the femur (Bankart et al. 1869; Guerra et al. 2012); the arched line; the iliac fascia; and the pectineal ligament. The insertion may be, in many cases, present at more than one of these points (Muttarak and Peh 2000; Guerra et al. 2012; Ghandhi et al. 2013).

Ghandhi et al. (2003) describes insertion of psoas minor into the iliac fascia, inguinal ligament, and the neck of the femur or lesser trochanter in unison with psoas major in the cases with two heads at its origin. In a case with a bifurcation in its tendinous insertion, the additional aberrant band inserted into the synchondrosis between the fifth lumbar vertebra and the sacrum (Kraychete et al. 2007; Ghandhi et al. 2013). As an additional variation of psoas minor, Joshi et al. (2010) reported psoas accessories that arose from the deep surface of the tendon of psoas minor and continued on the superficial surface of the psoas major until its insertion. This variation was observed in 25% of the cases. Ghandhi et al. (2013) found psoas accessories in 15% of cases.

References

Agichani S, Sontakke Y, Joshi SS, Joshi SD. 2013. Morphology of psoas minor muscle-reviewed. *J Evolution Med Dent Sci* 2: 5867–5869.

Aleksandrova JN, Malinova L, Jelev L. 2013. Variations of the iliacus muscle: report of two cases and review of the literature. *IJAV* 6: 149–152.

Anson BJ, Beaton LE, McVay CB. 1938. The pyramidalis muscle. *Anat Rec* 72: 405–411.

Aristotle S, Sundarapandian S, Felicia C. 2013. Accessory iliacus muscle with splitting of the femoral nerve: a case report. *OA Case Reports* 2(6): 56.

Babst D, Steppacher SD, Ganz R, Siebenrock KA, Tannast M. 2011. The iliocapsularis muscle: an important stabilizer in the dysplastic hip. *Clin Ortho Rel Res* 469: 1728–1734.

Bankart J, Pye-Smith PH, Phillips JJ. 1869. Notes of abnormalities observed in the dissecting room during the winter sessions of 1866–7 and 1867–8. *Guy's Hosp Rep* 14: 436–455.

Bergman RA, Thompson SA, Afifi AK, Saadeh FA. 1988. *Compendium of Human Variation*. Baltimore: Urban Schwarzenberg.

Bergman RA, Afifi AK, Jew JJ, Reimann PC. 2012. Anatomy Atlases. Illustrates encyclopedia of Human Anatomic variation: Opus I: Muscular system: Extensor carpi ulnaris. Available at: http:/anatomyatlases.org (accessed 20 October 2015).

Chandler SB, Schadewald M. 1944. Studies on the inguinal region. I. The conjoined aponeurosis versus the conjoined tendon. *Anat Rec* 89: 339–343.

Chudzinski T. 1898. *Observations sur les variations musculaires dans les races humaines. Mem Soc d'Anthrop Paris*. Paris: Compte.

Clarkson RD, Rainy H. 1889. Unusual arrangement of the psoas muscle. *J Anat Physiol* 23: 504.

Clemente CD. (ed.) 1985. *Gray's Anatomy*. Philadelphia: Williams Wilkins/Waverly Incorporated.

Cruveilhier, J. 1837. *Anatomie Descriptive. Vols 1–3*. Paris: Bechet.

Das N, Singh B. 1950. Iliacus minor; a report. *Ind Med Gaz* 85(11): 492.

D'Costa S, Ramanathan LA, Madhyastha S, Nayak SR, Prabhu LV, Rai R. 2008. An accessory iliacus muscle: a case report. *Rom J Morphol Embryol* 49: 407–409.

Dickson MJ. 1999. The pyramidalis muscle. *J Obst Gynecol* 19(3): 300.

Fabrizio PA. 2011. Anatomic variation of the iliacus and psoas major muscles. *IJAV* 4: 28–30.

Gandhi S, Gupta N, Thakur A, Anshu A, Mehta V, Suri RK, Rath G. 2013. Anatomical and clinical insight of variation morphologies of psoas minor muscle: A case report. *Int J Cur Res Rev* 5: 106–110.

Gruber W. 1873a. Sur quelques muscles surnumeraires de l'abdomen chez l'homme. *Bull l'Acad Imp Sci St Petersbourg* 18: 142–147.

Gruber W. 1873b. Un cas de muscle oblique interne de l'abdomen, prive completement de sa portion inguinal. *Bull l'Acad Imp Sci St Petersbourg* 18: 157–158.

Gruber W. 1875. Zwei neue fälle eines rudimentären Musculus obliquus externus abdominis II. *Arch Path Anat Physiol Klin Med* 65: 16–21.

Guerra DR, Reis FP, Bastos ADA, Brito CJ, Silva RJDS, Aragão JA. 2012. Estudio Anatómico del Músculo Psoas Menor en Fetos Humanos. *Inter J Morphol* 30: 136–139.

Guthrie L. 1896. Case of congenital deficiency of the abdominal muscles, with dilation and hypertrophy of the bladder and uterus. *Trans Path Soc London* 47: 139–145.

Hallett CH. 1848. An account of the anomalies of the muscular system met with in the dissecting-room of the University during the years 1846–1847; with general remarks. *Edinburgh Med Surg J* 69: 1–32.

Hanson P, Magnusson SP, Sorensen H, Simonsen EB. 1999. Anatomical differences in the psoas muscles in young black and white men. *J Anat* 194: 303–307.

Henle J. 1871. *Handbuch der Muskellehre des Menschen, in Handbuch der systematischen Anatomy des Menschen*. Braunschweig: Verlag von Friedrich Vieweg und Sohn.

Horner WE. 1840. *A treatise on special and general anatomy (Vol. 2)*. Philadelphia: Lea Blanchard.

Jelev L, Shivarov V, Surchev L. 2005. Bilateral variations of the psoas major and the iliacus muscles and presence of an undescribed variant muscle-accessory iliopsoas muscle. *Ann Anat* 187: 281–286.

Joshi SD, Joshi SS, Dandekar UK, Daini SR. 2010. Morphology of psoas minor and psoas accessorius. *J Anat Soc India* 59: 31–34.

Kawamitsu T, Miyaki T, Hayashi S, Terayama H, Itoh M. 2005. The cremaster and the inguinal anatomy. *Jap Res Soc Clin Anat* 5: 54–55.

Kelch WG. 1813. *Beiträge zur Pathologischen Anatomie*. Berlin: Salfeild.

Kikuchi Y. 1986. Morphological studies on the muscles of the abdomen in Japanese fetuses. *J Nippon Med School* 53: 280–290 (in Japanese).

Kita G. 1931. The rectus abdominis of the Japanese. *Acta Anat Nippon* 3: 1491.

Knott JF. 1880. Muscular anomalies. *J Anat Physiol* 15: 139–140.

Knott JF. 1883. Muscular anomalies, including those of the diaphragm, and subbiaphragmatic regions of the human body. *Proc Sci Royal Irish Acad* 2: 727–641.

Kodama K. 1986. Morphological significance of the supracostal muscles, and the superficial intercostal nerve: A new definition. *Acta Anat Nippon* 61: 107–129 (in Japanese).

Kopsch F, Rauber A. 1919. Lehrbuch und atlas der anatomie des menschen. Leipzig: Georg Thieme.

Kraychete DC, Rocha APC, Castro P. 2007. Psoas muscle abscess after epidural analgesia: case report. *Revista Brasileira Anestesiologia* 57: 195–198.

Kudo K, Otobe I. 1952. Statistics on the anatomy of Northern Chinese. The lateral abdominal muscles and others. *Hirosaki Igaku* 3:103–108.

Le Double AF. 1897. *Traite des variations du systeme musculaire de l'homme et de leur signification au point de vue de l'anthropologie, zoologique (Vol. 2)*. Paris: Schleicher Frères.

Loth E. 1912. *Beiträge zur Anthropologie der Negerweichteile (Muskelsystem)*. Stuttgart: Strecker Schröder.

Loth E. 1931. *Anthropologie des Parties Molles*. Paris: Masson Cies.

Luschka H. 1879. Der musc. pubo-transversalis des menschen. *Arch Anat Physiol Wissen Med* 12: 227–231.

Macalister A. 1875. Additional Observations on Muscular Anomalies in Human Anatomy. (Third Series) With a Catalogue of the Principal Muscular Variations Hitherto Published. *Trans Royal Irish Acad* 25: 1–134.

McVay CB, Anson BJ. 1940. Composition of the rectus sheath. *Anat Rec* 77: 213–225.

Miyauchi R, Kurihara K, Tachibana G. 1986. On the human obliquus abdominis externus profundus. *Acta Med Nagasaki* 31: 59–75.

Monkhouse WS, Khalique A. 1986. Variations in the composition of the human rectus sheath: a study of the anterior abdominal wall. *J Anat* 145: 61.

Mori M. 1964. Statistics on the musculature of the Japanese. *Okajimas Folia Anat Jap* 40: 195–300.

Murata K, Abe K, Honma T. 1971. M. serratus anterior of Japanese. 2. The area of its origin and its interdigitation with the M. obliquus externus abdominis. *Anat Sci Inter* 46: 193–196.

Muttarak M, Peh WC. 2000. CT of unusual iliopsoas compartment lesions. *Radiographics* 20: S53–S66.

Nakamura S. 1935. Ueber den M. rectus abdominis und den M. pyramidalis der Japaner (aus Kyushu). *J Kumamoto Med Assoc* 11: 1251.

Nakano T. 1923. Beitrage zur Anatomie der Chinesen. Die Statistik der Muskelvarietaten. *Folia Anat Jap* 1: 273–282.

Nakayama T, Okuda S. 1952. On the M. obliquus abdominis externus profundus. *Kaibogaku Zasshi* 27: 89–94 (in Japanese).

Philippon MJ, Devitt BM, Campbell KJ, Michalski MP, Espinoza C, Wijdicks CA, Laprade RF. 2014. Anatomic variance of the iliopsoas tendon. *Am J Sports Med* 42: 807–811.

Polster JM, Elgabaly M, Lee H, Klika A, Drake R, Barsoum W. 2008. MRI and gross anatomy of the iliopsoas tendon complex. *Skel Radiol* 37: 55–58.

Rao TR, Vanishree KP, Rao S. 2008. Bilateral variation of iliacus muscle and splitting of femoral nerve. *Neuroanatomy* 7, 72–75.

Rickenbacker J, Landholt AM, Theiler K. 1985. *Applied Anatomy of the Back*. Heidelberg: Springer.

Sato S. 1968. Statistical studies on the anomalous muscles of the Kyushu Japanese. 3. The muscles of the back, breast and abdomen. *Kurume Med J* 15: 209.

Seib GA. 1934. Incidence of the m. psoas minor in man. *Am J Phys Anthropol* 19: 229–246.

Shimazaki H. 1959. A case of M. obliquus abdominis externus profundus. *Shinshu Igakukai Zasshi* 8: 1436–1438.

Shu B, Safran MR. 2011. Case report: bifid iliopsoas tendon causing refractory internal snapping hip. *Clin Ortho Rel Res* 469: 289–293.

Sinha DN, Kumar V. 1985. Study of human pyramidalis muscle in Indian subjects. *Anthro Anz* 43(2): 173–177.

Spratt JD, Logan BM, Abrahams PH. 1996. Variant slips of psoas and iliacus muscles, with splitting of the femoral nerve. *Clin Anat* 9: 401–404.

Sugiura R. 1935. On a superfluous pair of muscles accompanying the M. obliquus externus abdominis sinister. *Nagoya J Med Sci* 8: 139–143.

Tatu L, Parratte B, Vuillier F, Diop M, Monnier G. 2001. Descriptive anatomy of the femoral portion of the iliopsoas muscle. Anatomical basis of anterior snapping of the hip. *Surg Radiol Anat* 23: 371–374.

Tokita K. 2006. Anatomical significance of the nerve to the pyramidalis muscle: A morphological study. *Anat Sci Int* 81: 210–224.

Tubbs RS, Salter EG. 2006. The iliacus minimus muscle. *Clin Anat* 19: 720–721.

Tubbs RS, Oakes WJ, Salter EG. 2006. The psoas quartus muscle. *Clin Anat* 19: 678–680.

Tyrie CCB. 1894. Musculus saphenous. *J Anat Physiol* 28: 288–290.

Urquhart DM, Barker PJ, Hodges PW, Story IH, Briggs CA. 2005. Regional morphology of the transversus abdominis and obliquus internus and externus abdominis muscles. *Clin Biomech* 20: 233–241.

Vallois HV. 1926. Valeur et signification du muscle pyramidal de l'abdomen. *Arch Anat Histol Embryol* 5: 497–525.

Ward WT, Fleisch ID, Ganz R. 2000. Anatomy of the iliocapsularis muscle: relevance to surgery of the hip. *Clin Ortho Rel Res* 374: 278–285.

Winslow JB. 1732. *Exposition anatomique de la structure du corps humain T. 1 and 2*. Paris: Chez Guillaume Desprez et Jean Desessartz.

Yonekura S. 1954. A study of the muscles of the neck, chest, abdomen and back in Japanese fetuses. *Igaku Kenkyu (Acta Medica)* 24: 1604–1700 (in Japanese).

Further reading

Anson BJ (ed.) 1966. *Morris' Human Anatomy*, 12th edition. New York: The Blakiston Division, McGraw-Hill Book Company.

Budge J. 1859. Beschreibung eines neuen Muskels und mehrerer Miskel- und Knochenvarietäten. *Z für Rat Med* 3: 273–278.

Gruber W. 1880. Ein mit seiner inguinalen Portion durch die ganze Regio inguinalis sich herab erstreckender Musculus transversus abdominis. *Arch Path Anat Physiol Klin Med* 80: 88–91.

Gruber W. 1887. Ein rudimentärer Musculus obliquus abdominis externus accessorius. *Arch Path Anat Physiol Klin Med* 110: 561.

Henle J. 1873. Sinnesapparte, in Handbuch der systematischen Anatomie des Menschen. Braunschweig: Verlag von Friedrich Vieweg und Sohn.

Latarjet A. 1948. *Testut's Traité D'Anatomie Humaine*, ninth edition. Paris: G. Doin Cie.

Nussbaum N. 1894. Vergleichend anatomische beiträge zur kenntnis der augenmuskeln. *Anat Anz* 8: 208–210.

Schaefer EA, Symington J, Bryce TH (eds). 1923. *Quain's Elements of Anatomy*, 11th edition. London: Longmans, Green and Co.

Warwick R, Williams PL (eds). 1973. *Gray's Anatomy*, 35th ed. New York: Longman.

37 Pelvic diaphragm and external anal sphincter

Howe Liu and Yasser Salem
University of North Texas Health Science Center, Fort Worth, Texas, United States

The pelvic diaphragm is a funnel-shaped structure formed by the levator ani and (ischio) coccygeus muscles, with a diaphragmatic fascia covering both muscles superiorly and inferiorly. The diaphragmatic fascia is part of the parietal pelvic fascia. Its margins follow the line of attachments of the levator ani and coccygeus. Its lateral margin becomes a thickened white band known as the tendinous arch, which extends from the lower pubic symphysis to the ischial spine and separates the obturator internus fascia from the diaphragmatic fascia.

The pelvic diaphragm is bounded by the pubic bone anteriorly, coccygeus posteriorly, and the tendinous arches on either side of pelvic wall. The diaphragm is pierced by the rectum and the urethra in both females and males and by the vagina in females. The external anal sphincter is a ring-shaped muscle that surrounds the anus to control anal closure.

Variations of the pelvic diaphragm and external anal sphincter are very rare, but minor variations have been reported through cadaver studies and clinical examination using magnetic resonance imaging (MRI).

Levator ani muscle

Normal anatomy

The levator ani is a thin flat muscle that originates on the lower part of the pubic symphysis, superior fascia of the urogenital diaphragm, obturator fascia, back of the pubic bone, and ischium. It inserts on the pelvic visceral organs, tendinous arch, coccygeus, and sacrum (Moore et al. 2010; Standring 2008). It can be regarded as comprising three divisions which, in an anteromedial to posterolateral direction, are: pubococcygeus (puboviscerallis); puborectalis; and iliococcygeus (Corton 2005; Shobeiri et al. 2009). There is consensus about the origin and insertion of the iliococcygeus, but slight differences among authors about the other two divisions (Kearney et al. 2004; Corton 2005).

The puboccygeus muscle is the main part of the levator ani. Some of its fibers in the most posterior portion extend to the coccyx and sacrum (Standring 2008), but in view of its vaginal, perineal, and anal attachments it can more accurately be called the puboviscerallis and further subdivided into three parts: pubovasginalis; puboperinealis; and puboanalis (Kearney et al. 2004; Corton 2005). Some researchers have suggested that the term "pubococcygeus" be abandoned and replaced with "puboviscerallis" (Kearney et al. 2004; Corton 2005). The puboviscerallis originates from the inner surface of the pubic bone and travels posteriorly and horizontally. It inserts onto the lateral wall of the vagina or lateral side of the prostate (pubovaginalis muscle in females or levator prostate in males), the perineal body (puboperinealis muscle), and the intersphincteric groove between the external and internal anal sphincters (puboanalis muscle) (Kearney et al. 2004; Corton 2005). In this chapter, we prefer to use "puboviscerallis." During pelvic contraction, the puboviscerallis can elevate the urethra, pull the perineum anteriorly (via the puboperinealis) and elevate the anus to narrow the urogenital hiatus with the rest of the levator ani muscle (via the puboanalis). However, puboviscerallis elevation of the urethra can also contribute to urinary continence (via the pubovaginalis).

The puborectalis muscle originates from the left and right pubic bones, traveling posteriorly and inferiorly to the anorectal junction to form a U-shaped muscular puborectal sling (Courtney 1950; Lawson 1974). The puborectalis can be considered as part of the anal sphincter complex (Corton 2005). Its primary action is to maintain fecal continence by pulling the anorectal junction anteriorly (resting contraction) and contributing to the formation of the anorectal angle (Moore et al. 2010). During defecation, voluntary relaxation of the puborectalis will therefore reduce the anterior bending of the anorectal junction and allow for easy passage of feces through the junction.

The most posterior portion of the levator ani muscle is the iliococcygeus, originating from the posterior portion of the tendinous arch (arcus tendineus) and inner surface of the ischial spine. This portion inserts onto the coccyx and the fibrous anococcygeal raphe (body or ligament) or iliococcygeal raphe (Kearney et al. 2004; Corton 2005). The function of the iliococcygeus is to support the pelvic organs during relaxation of the levator ani muscle.

The levator ani receives its blood supply primarily from the middle rectal artery (DiDio et al. 1986; Nano et al. 2000), followed by the internal pudendal artery (DiDio et al. 1986) and

Bergman's Comprehensive Encyclopedia of Human Anatomic Variation, First Edition. Edited by R. Shane Tubbs, Mohammadali M. Shoja and Marios Loukas.
© 2016 John Wiley & Sons, Inc. Published 2016 by John Wiley & Sons, Inc.

inferior gluteal artery (DiDio et al. 1986; Zhang et al. 2005). It is innervated mainly from the second–fourth sacral spinal nerve roots through the levator ani nerve (arising directly from the pudendal nerve or S3 and/or S4 nerve roots), the perineal nerve (a branch from the pudendal nerve in the pudendal canal), and the inferior rectal nerve (a branch from the pudendal nerve or directly from the S3–S4 spinal roots) (Sato 1980; Moore 2010; Grigorescu et al. 2008). The levator ani and perineal nerves supply the superior levator ani muscle surface (Grigorescu et al. 2008; Wallner et al. 2008; Zhang et al. 2005), while the inferior rectal nerve innervates the inferior levator ani muscle surface and the external anal sphincter (Grigorescu et al. 2008). Both the pubovisceralis and puborectalis are innervated primarily by branches of the pudendal nerve (76.5%), while the iliococcygeus is innervated directly by the S3 and/or S4 spinal roots (64.7%). However, direct innervation to the levator ani muscle from the pudendal nerve is controversial. Barber et al. (2002) found that in 12 dissected female cadavers the levator ani was not directly innervated by the pudendal nerve, but rather by a nerve originating from the sacral nerve roots (S3–S5) and traveling along the superior surface of the pelvic floor.

Attachment of the levator ani muscle

Among the three portions of the levator ani muscle, the pubococcygeus (pubovisceralis) and puborectalis exhibit variations while the iliococcygeus does not. By studying the insertion of the puboanalis (part of the pubovisceralis or pubococcygeus) in 46 cadavers, Arakawa et al. (2004) found that the muscle inserts on the conjoined longitudinal muscles (the intersphincteric groove between the external and internal anal sphincters) through a tight connection with its associated smooth muscles (37/46) or through a definite complex with little or no tissue connection (9/46). Recently, Tansatit et al. (2013) re-examined the origin of the puborectalis with 10 hemipelvis specimens and found that the muscle inserts on either the obturator internus fascia (4/10) or the superior pubic ramus (6/10).

Using MRI, Tunn et al. (2003) studied the levator ani muscle attachment in 20 healthy female subjects and found no attachment to the pubic bone in four of them. Hoyte et al. (2004) found using a dynamic MRI that genetic defects in the levator ani muscle are most likely to occur in the iliococcygeus, possibly weakening the area and making it less stable and consequently contributing to perineal herniation.

Variants of the levator ani muscle are not common. Shepherd (1889) reported a 30-year-old female with no trace of the levator ani, its place being taken by pelvic fascia. Niikura et al. (2010) reported a variant muscle from the sacrum to the coccyx called the sacrococcygeus ventralis; it appeared medial to the coccygeus muscle by the 12th week of fetal life. By the 18–20th week this muscle has increased in size, fused with the dorsal end of the levator ani muscle and become part of it. The sarcococcygeus ventralis is not usually present in adults (Niikura et al. 2010). It has been referred to as the curvator coccyges. However, Nair et al. (2011) reported a bilateral appearance of this muscle in a 65-year-old cadaver. It originated at the ventral lateral surface of the sacrum at the S3 level, inserted on the ventral surface of the coccyx, and was innervated by a branch from the sacral plexus (Nair et al. 2011).

Blood supply and innervation of the levator ani muscle

Variations of the vascular supply to the levator ani are seldom reported. A branch from the ipsilateral obturator artery or inferior vesicle artery, called the accessory pudendal artery (APA), was found to provide blood supply to the muscle (Secin et al. 2005; Allan et al. 2012). There are two types of APA, apical and lateral, distinguished by their arterial supply to the prostate. The apical APA can send branches to supply the levator ani and even the external anal sphincter (Secin et al. 2005). Regarding innervation of the levator ani muscle, a variant rectal nerve was identified by Shafik et al. (1995) and Zhang et al. (2009) as the "accessory rectal nerve" only in male cadavers. This variant nerve is a branch off the pudendal nerve when it crosses the back of the sacrospinous ligament and innervates the visceral side of the levator ani muscle (Zhang et al. 2009). However, the concurrent appearance of an accessory pudendal artery and the accessory rectal nerve to the levator ani has not been reported.

Coccygeus (also known as ischiococcygeus)

The coccygeus is located between the levator ani anteriorly and the sacrospinous ligament posteriorly. It presents as a triangular musculotendinous sheet with its apex attached to the sacrospinous ligament and the tip of the ischial spine, and its base attached to the lateral board of the coccyx and the fifth sacral vertebra. The action of this muscle is to assist the levator ani in supporting the pelvic organs. Its innervation is via the coccygeal nerve off the levator ani nerve, which is a branch off the pudendal nerve.

The coccygeus is a degenerate muscle in humans. It can vary among individuals from fully to poorly developed or almost completely tendinous rather than muscular, blending with the sacrospinous ligament. Because the coccygeus muscle is so close to the sacrospinous ligament, the latter was considered by Piloni et al. (1997) to be a degenerate portion of the coccygeus or an aponeurosis of the muscle, since the muscle and ligament are coextensive and approximate geographically. A rectococcygeus muscle of Treitz can arise from the anterior surface of the coccyx and mingle with the muscle coats of the rectum.

External anal sphincter

The external anal sphincter (EAS) is a circular muscle with fibers from the anococcygeal ligament posteriorly that extend forward to encircle the anus and insert onto the perineal body anteriorly. Histologically, it can be divided into subcutaneous,

superficial, and deep portions, but in gross view these three portions cannot be differentiated (Mahadevan 2011). The distal edge of the EAS is longer than that of the internal anal sphincter, so the intersphincter groove is generated between these two edges (Mahadevan 2011). Fibers from the medial portions of the levator ani muscle (puboanalis and puborectalis) travel posteriorly to blend with the periphery of the EAS, becoming the anococcygeal ligament (Ayoub 1979). The deep portion of the EAS blends with the puborectalis sling behind the recto-anal junction. The blended area is palpable during digital examination of the rectum (Mahadevan 2011). The action of the EAS is to maintain basic muscle tone in order to sustain closure of the anus. The blood supply to the EAS is mainly from the inferior rectal artery. Its innervation is primarily from the inferior anal nerve (inferior rectal nerve) (Moore 2006; Mahadevan 2011), and occasionally from the perineal nerve (off the fourth sacral spinal root or the pudendal nerve) or the anococcygeal nerve (off the S4 spinal root) (Sato 1980). In general, anatomical variations of the EAS in terms of origin, insertion, blood, and nerve supply are uncommon. However, the EAS can have fibers that cross and branch in several directions and extend posteriorly with fibers of the superficial portion above (Gorsch 1968). Anterior muscular extensions of the EAS can occur, especially in males. Uncrossed posterior extensions of the subcutaneous EAS can also connect with the coccyx.

References

Allan R, García NA, Montenegro JM, Álvarez-Alberó JN. 2012. Prevalence of accessory pudendal artery. *Clin Anat* 25: 983–985.

Arakawa T, Murakami G, Nakajima F, Matsubara A, Ohtsuka A, Goto T, Teramoto T. 2004. Morphologies of the interfaces between the levator ani muscle and pelvic viscera, with special reference to muscle insertion into the anorectum in elderly Japanese. *Anat Sci Int* 79: 72–81.

Ayoub FS. 1979. Anatomy of the external anal sphincter in man. *Acta Anat* 105: 25–36.

Barber DM, Bremer RE, Thor KB, Dolber PC, Kuehl TJ, Coates KW. 2002. Innervation of the female levator ani muscles. *Am J Obst Gynecol* 187: 64–71.

Corton MM. 2005. Anatomy of the pelvis: How the pelvis is built for support. *Clin Obst Gynecol* 3: 611–626.

Courtney H. 1950. Anatomy of the pelvic diaphragm and anorectal musculature as related to sphincter preservation in anorectal surgery. *Am J Surg* 79: 155–173.

DiDio JAL, Diaz-Franco C, Schemainda R, Bezerra AJ. 1986. Morphology of the middle rectal arteries. A study of 30 cadaveric dissections. *Surg Radiol Anat* 8: 229–236.

Gorsch RV. 1968. The sigmoid, rectum, and anal canal. In *Clinical Symposia Anthology* (Walton JH, Netter FH eds). New Jersey: CIBA.

Grigorescu BA, Lazarou G, Olson TR, Downie SA, Powers K, Greston WM, Mikhail MS. 2008. Innervation of the levator ani muscles: description of the nerve branches to the pubococcygeus, iliococcygeus, and puborectalis muscles. *Int Urogynecol J Pelvic Floor Dysfunc* 19: 107–116.

Hoyte L, Jakab M, Warfield SK, Shott S, Flesh G, Fielding JR. 2004. Levator ani thickness variations in symptomatic and asymptomatic women using magnetic resonance-based 3-dimensional color mapping. *Am J Obst Gynecol* 191: 856–861.

Kearney R, Sawhney R, DeLancey JO. 2004. Levator ani muscle anatomy evaluated by origin-insertion pairs. *Obst Gynecol* 104: 168–173.

Lawson J. 1974. Pelvic anatomy. I. Pelvic floor muscles. *Ann R Coll Surg England* 54: 244–252.

Mahadevan V. 2011. The anatomy of the rectum and anal canal. *Surgery* 29: 5–10.

Moore KL. 2010. *Essential Clinical Anatomy*, fourth edition. Philadelphia, PA: Lippincott Williams & Wilkins.

Nair V, Nair RV, Mookambika RV, Mohandas Rao KG, Krishnaraja Somayaji S. 2011. Persistent sacrococcygeus ventralis muscle in an adult human pelvic wall: a variation for surgeons to note. *J Chinese Med Ass* 74: 567–569.

Nano M, Dal Corso HM, Lanfranco G, Ferronato M, Hornung JP. 2000. Contribution to the surgical anatomy of the ligaments of the rectum. *Dis Colon Rectum* 43: 1592–1597.

Niikura H, Zin ZW, Cho BH, Murakami G, Yaegashi N, Lee JK, Li CA. 2010. Human fetal anatomy of the coccygeal attachments of the levator ani muscle. *Clin Anat* 23: 566–574.

Piloni V, Bassotti G, Fioravanti P, Amadio L, Montesi A. 1997. Dynamic imaging of the normal pelvic floor. *Int J Colorectal Dis* 12: 246–253.

Sato K. 1980. A morphological analysis of the nerve supply of the sphincter ani externus, levator ani and coccygeus. *Kaibogaku Zasshi* 55: 187–223.

Secin PF, Karanikolas N, Touijer AK, Salamanca JI, Vickers AJ, Guillonneau B. 2005. Anatomy of accessory pudendal arteries in laparoscopic radical prostatectomy. *J Urol* 174: 523–526.

Shafik A, el-Sherif M, Youssef A, Olfat ES. 1995. Surgical anatomy of the pudendal nerve and its clinical implications. *Clin Anat* 8:110-115.

Shepherd FJ. 1889. Some vascular anomalies observed during the session 1888–89. *J Anat Physiol* 24: 69–71.

Shobeiri SA. 2009. Appearance of the levator ani muscle subdivisions in endovaginal three-dimensional ultrasonography. *Obst Gynecol* 114: 66–72.

Standring S. 2008. *Gray's Anatomy: The Anatomical Basis of Clinical Practice, Expert Consult.* London, UK: Churchill Livingstone.

Tansatit T, Apinuntrum P, Phetudom T, Phanchart P. 2013. New insights into the pelvic organ support framework. *Eur J Obst Gynecol Repro Biol* 166: 221–225.

Tunn R, Delancey JO, Howard D, Ashton-Miller JA, Quint LE. 2003. Anatomic variations in the levator ani muscle, endopelvic fascia, and urethra in nulliparous evaluated by magnetic resonance imaging. *Am J Obst Gynecol* 188: 116–121.

Wallner C, van Wissen J, Maas CP, Dabhoiwala NF, DeRuiter MC, Lamers WH. 2008. The contribution of the levator ani nerve and the pudendal nerve to the innervation of the levator ani muscles: a study in human fetuses. *Eur Urol* 54: 1136–1142.

Zhang J, Lu LG, Wu YJ. 2005. Anatomic observation of inferior gluteal artery. *Chinese J Cosmet Surg (Zhonghua Zheng Xing Wai Ke Za Zhi)* 21: 44–46.

38 Perineal muscles

R. Shane Tubbs[1] and Koichi Watanabe[2]
[1]Seattle Science Foundation, Seattle, Washington, USA
St George's University, School of Medicine , St Georges, Grenada
University of Dundee, Dundee, UK
[2]Kurume University School of Medicine, Fukuoka, Japan

The corpora cavernosum or ischial tuberosity may receive fibers derived from the external anal sphincter.

Superficial transverse perineus

This muscle may be absent or poorly developed. It often receives fibers from the puborectalis or external anal sphincter (Fig. 38.1). Specifically, the superficial portion of the external anal sphincter muscle usually merges with the bulbocavernosus muscle, but some fibers may extend laterally as far as the ischiopubic rami and the ischial tuberosities in conjunction with or independent of the thin superficial transverse perineal muscles (Gorsch 1968). There are often strong connections between it and the bulbocavernosus. Sometimes, fibers that pass around the anal canal on the left side cross over to insert anteriorly or laterally on the right side and vice versa. This muscle is frequently poorly developed. Sometimes it consists of several separate fasciculi, and it may be inserted wholly or in large part into the bulbocavernosus or external anal sphincter. The muscle has been reported to be duplicated bilaterally.

Deep transverse perineus

This muscle is variably present and is seen more often in females. A second muscle sometimes exists in front of this muscle, and is termed the transversus perinei alter.

Bulbospongiosus

The posterior part of the muscle is often distinct from the anterior part. The posterior part may be absent, which is more often seen in females. These posterior fibers have been termed the compressor bulbi. The deeper fibers of the muscle may be quite separate from the superficial fibers and be regarded as a separate muscle termed the compressor hemisphericum bulbi, which surrounds the bulb. Fibers from the ischila tuberosities may join the bulbocavernosus to form the so-called ischiobulbosi. There are frequently connections between the bulbocavernosus and the superficial transverse perineus. A muscular slip is occasionally found arising from the fascia at the lower border of gluteus maximus or upper fascia lata, and inserts under the origin of bulbocavernosus in the albuginea of the penile urethra in males. This variation is not found in females.

A fasciculus from the external anal sphincter may extend and join the bulocavernosus muscle or extend toward the base of the scrotum to be termed the retractor scroti (Piersol 1916). Specifically, these fibers are extensions from the superficial portion of the external anal sphincter. The muscle of Jarjavay is an accessory muscle bundle that reinforces the bulbocavernosus.

Ischiopubicus

This muscle arises at the sides of the deep perineal interspace and arises from the inferior rami of the ischium and pubis. It passes anteriorly to attach to the arcuate ligament of the pubis. It may be absent or wanting.

Ischiocavernosus

This muscle is obviously larger in the male. Some of the more anterior fiber bundles may extend to the dorsal surface of the penis and form a pubocavernosus (or levator penis) muscle. Fibers from the superficial part of the external anal sphincter can travel superolaterally, superficial to the superficial transverse perineal muscle, to attach to the medial surface of the ischiocavernosus muscle, and more than one fascicle may be present.

A compressor venae dorsalis has been described, composed of a few fascicles that arise from the sheath of the corpus cavernosum urethrae and from the median raphe, and unite with those of the opposite side by a tendon that passes over the dorsal vein.

Bergman's Comprehensive Encyclopedia of Human Anatomic Variation, First Edition. Edited by R. Shane Tubbs, Mohammadali M. Shoja and Marios Loukas.
© 2016 John Wiley & Sons, Inc. Published 2016 by John Wiley & Sons, Inc.

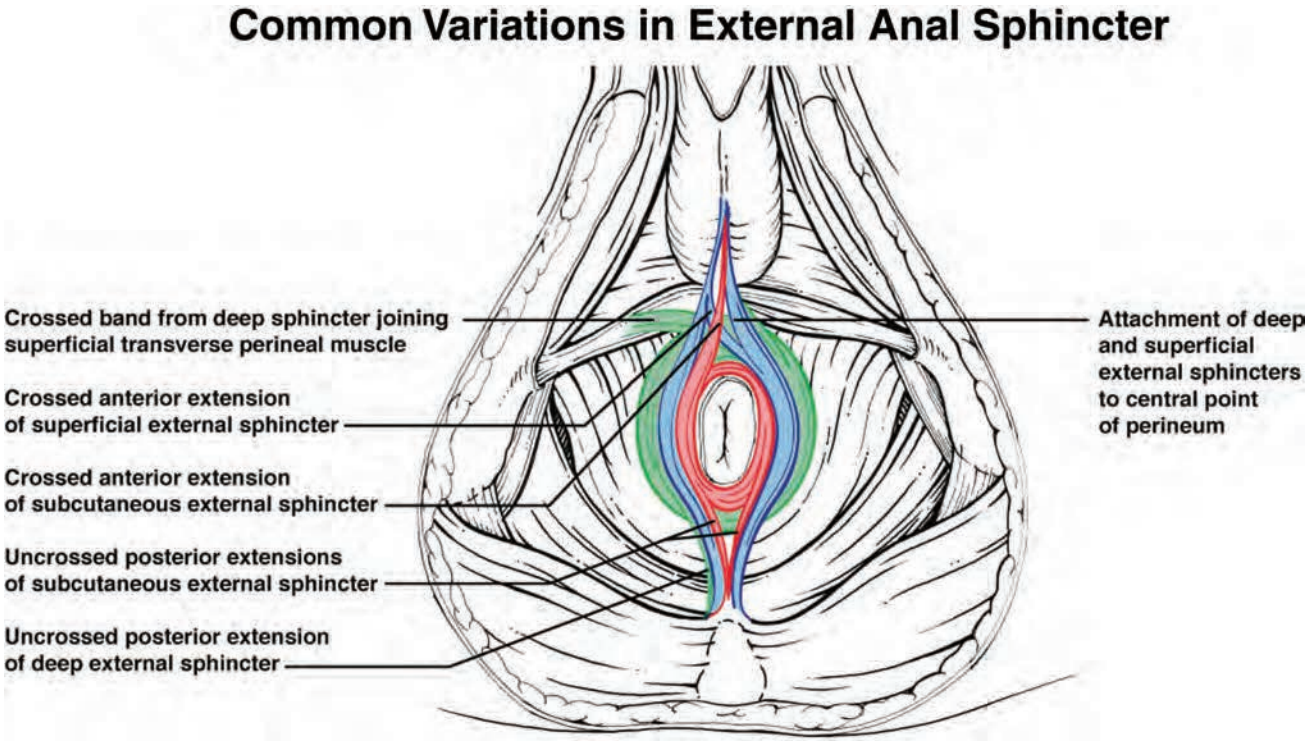

Figure 38.1 Various muscular variations of the perineal region.

Source: Gorsch (1968).

References

Gorsch RV. 1968. The sigmoid, rectum, and anal canal. In *Clinical Symposia Anthology* (Walton JH, Netter FH eds). Summit, New Jersey: CIBA.

Piersol GA. 1916. *Human Anatomy*. Philadelphia: J.B. Lippincott & Co.

Further reading

Gruber W. 1876. Über einen anomalen Musculus transverse perinei superficialis. *Arch Path Anat Physiol Klin Med* 67: 353–358.

Gruber W. 1876. Neuer Fall eines ausserhalb des Regio perinealis entsprungenen Musculus transversus perinei superficialis. *Arch Path Anat Physiol Klin Med* 68: 287–290.

Houston, W. 1831. Two newly discovered muscles for compressing the dorsal vein of the penis of man and other animals. *Am J Med Sci* 8: 477–478.

Macalister A. 1875. Observations on muscular anomalies in the human anatomy. Third series with a catalogue of the principal muscular variations hitherto published. *Trans Roy Irish Acad Sci* 25: 1–130.

39 Gluteal muscles and lateral rotators of the hip

Helen Nicholson, Stephanie Woodley and Natasha Flack
University of Otago, Dunedin, New Zealand

Gluteus maximus

Attachments

In addition to the commonly recognized areas of attachment, the muscle belly of gluteus maximus may also originate from a variety of other sites. These include the superficial lamina of the posterior layer of the thoracolumbar fascia (Frick et al. 1991; Vleeming et al. 1995), the fascia covering multifidus and that which is medial to the long posterior sacroiliac ligament (Stern 1972), the posterior surfaces of the posterior sacroiliac ligaments (Gray 1858; Knox 1831), and the aponeuroses of erector spinae (Macalister 1871; Knott 1883; Woodburne and Burkel 1988), iliocostalis lumborum (*sacro-lumbalis*) (Testut 1884) or latissimus dorsi (Knox 1831). An additional attachment has also been reported from the ischial tuberosity (Macalister 1871; Testut 1884).

While gluteus maximus normally arises from the posterior surface of the sacrum and the lateral aspect of the coccyx, its attachment may not encompass the whole of the lower sacrum (Le Double 1897) and/or coccyx (Macalister 1871; Knott 1883; Le Double 1897).

The gluteal aponeurosis is usually recognized as a site of attachment for gluteus maximus (Stern 1972; Ramirez et al. 1984; Nork et al. 2005). However, the extent of the aponeurotic attachment is variable (Stern 1972; Ramirez et al. 1984) and can be extensive in some individuals (Stern 1972).

Distally gluteus maximus attaches to the iliotibial tract and the gluteal tuberosity. There are two main variations of the distal attachment, one via an ascending tendon and the other directly into bone. The ascending tendon receives muscle fibers from the deep, superior half of the muscle, and the majority of the inferior half of the muscle. It may attach along the lateral lip of the linea aspera (Frick et al. 1991), extending between 14% and 32% down the length of the femur (Stern 1972) or into the lateral intermuscular septum of the thigh (Ramirez et al. 1984). There is also a direct insertion of the deep muscular fibers of the superior half of the muscle belly into the bone (Stern 1972; Ramirez et al. 1984) which can extend as far as 33% down the length of the femur (Stern 1972). Superiorly, the femoral insertion of gluteus maximus may insert as high as the upper part of the greater trochanter (Macalister 1871).

Similar to the insertion into the femur, the distal insertion of gluteus maximus into the iliotibial tract can be either muscular (Winslow 1763) or tendinous (Frick et al. 1991) in nature. The superficial fibers of the superior half of the muscle and a small number of superficial fibers from the inferior half of the muscle insert directly into the fascia lata (Stern 1972) or iliotibial tract (Ramirez et al. 1984). The ascending tendon (when present) secondarily joins with the iliotibial tract (Ramirez et al. 1984).

Morphology

The thickness of the muscle varies throughout, with the medial part (range 17.1–18.1 mm) being thicker than the lateral (range 14.5–15.7 mm) or inferior (range 14.5–14.7 mm) regions (n=20 from 10 cadavers, 7 male; Hwang et al. 2009). Quantitative data on muscle morphology are presented in Table 39.1.

A duplicated and/or divided gluteus maximus has been reported by Macalister (1867). Furthermore, the muscle belly of gluteus maximus may consist of two parts (Macalister 1866, 1871; Le Double 1897) that are separated by a cellular lamina (Macalister 1866). More recently a case of a separate fibrous sacroiliac (cranial or superior) part and a muscular coccygeo-femoral (caudal or inferior) part have been described (Kirici and Ozan 1999) with the coccygeo-femoral portion of the muscle having distal tendinous attachments to the origin of the short head of the biceps femoris muscle. Gluteus maximus is formed by the fusion of several fetal muscle components and it has been suggested that this appearance is a result of inadequate fusion between these elements during the prenatal period (Kirici and Ozan 1999). Interestingly, when examined using magnetic resonance imaging (MRI) up to five parts of the muscle have been identified: two superficial and three deep (cranial, intermediate, and caudal) portions (Jaegers et al. 1992).

Accessory muscles

The muscle fibers attaching to the posterior sacrum and coccyx may be separated from the rest of the muscle and referred to as the homologue of the agitator caudae of quadrupeds

Bergman's Comprehensive Encyclopedia of Human Anatomic Variation, First Edition. Edited by R. Shane Tubbs, Mohammadali M. Shoja and Marios Loukas.
© 2016 John Wiley & Sons, Inc. Published 2016 by John Wiley & Sons, Inc.

Table 39.1 Morphometric data for gluteus maximus reported by dissection and imaging. Standard deviation in parentheses.

Reference	No. specimens and sex	Mean muscle volume (cm^3)	Mean muscle length (mm)	Mean muscle PCSA (cm^2)	Other
Lippert (1962)	50 (M: 31; F: 19)			M: 313.8 (90.6) F: 215.1 (84.0)	
Brand et al. (1986)	2 (M: 1; F: 1)			M: 59.8 F: 32.3	
Friederich and Brand (1990)	2 (M: 1; F: 1)[a]	M: 864.0 F: 327.0	M: 168.3 F: 158.3	M: 59.8 F: 32.3	
Jaegers et al. (1992)	6 lower limbs of participants (MRI; M: 4; F: 2)	839.1 (201.1)			
Duda et al. (1996)	4 (M: 2; F: 2)	643.8 (230.6)			Mean femoral attachment area: 1110.5 (428.2) mm^2
Nork et al. (2005)	9		271.0 (13)		Mean muscle width: 162.0 (18.0) mm
Grimaldi et al. (2009b)	24 lower limbs of participants (MRI) M: 12; F: 12	Upper GMax L: 352.0 (106.0); R: 359.0 (125.0) Lower GMax L: 453.0 (130.0); R: 495.0 (158.0)			
Ward et al. (2009)	18		26.9 (6.4)	33.4 (8.8)	Mean muscle mass: 547.2 (162.2) g
Preininger et al. (2012)	186 lower limbs of participants (CT) M: 96; F: 90	M: 565.0 (140.0); F: 445.0 (92.4)			

CT, computed tomography; F, female; L, left limb; M, male; MRI, magnetic resonance imaging; R, right limb; SD, standard deviation.

[a]Same cadavers as examined by Brand et al. (1986)

(Macalister 1866, 1871; Testut and Latarjet 1928). These fibers may be synonymous with the "coccygeofemoral" muscle observed by Testut (1884). The muscle is located along the lower border of gluteus maximus and is either completely separate or partially fused with gluteus maximus. It attaches proximally to the lateral coccyx and S5 vertebra and distally to the femur below gluteus maximus. Deep muscular fibers originating from the posterior sacroiliac ligaments that were distinctly separated (via connective tissue) from the rest of the superficial part of the muscle were recorded in 5 of 40 cases (Knott 1883).

A gluteoperinealis muscle may also exist (Gruber 1878b; Knott 1883) attaching from the aponeurosis overlying gluteus maximus and inserting into the urethral bulb and bulbocavernous muscle of the perineum. Sripanidkulchai et al. (2012) reported this muscle attaching to the perineal body.

Gluteus medius

Attachments

Minor variations are reported in the location of the bony proximal and distal insertion sites of gluteus medius (for review, see Flack et al. 2012; Fig. 39.1). Variations are described regarding the proximal attachment to the iliac crest. The muscle may attach to the anterior three-quarters of the crest (Duparc et al. 1997), more posteriorly between 55 mm and 68 mm from the anterior superior iliac spine (mean 61±4 mm; Zhang et al. 2008) or along the entire length of the crest (Gottschalk et al. 1989; Little and Lyons 1983; Nork et al. 2005).

The gluteus medius muscle attaches distally to the greater trochanter by two tendinous components. The most commonly denoted femoral insertion site is the lateral surface of the greater trochanter, with a second site of attachment to the superior (Srivastava and Joshi 1969; Duparc et al. 1997; Standring 2008) or posterior aspect (Flack et al. 2014) of the trochanter, or more specifically the posterosuperior trochanteric facet (Woodburne and Burkel 1988; Pfirrmann et al. 2001; Robertson et al. 2008). The tendinous footprint is larger for the lateral (438.0±57.5 mm^2) compared to the posterosuperior (196.5±48.4 mm^2) attachment (Robertson et al. 2008).

Where the two parts of the distal tendon have not been identified, the distal tendinous insertion has been variably reported as attaching to the anterosuperior (Gottschalk et al. 1989; Connell 2003), posteromedial (Molini et al. 2011), or superior (Little and Lyons 1983) aspect of the greater trochanter, or its apex (Pérez et al. 2004). The mean area of the tendinous footprint onto the greater trochanter has been reported to vary between 535.0±98.6 mm^2 and

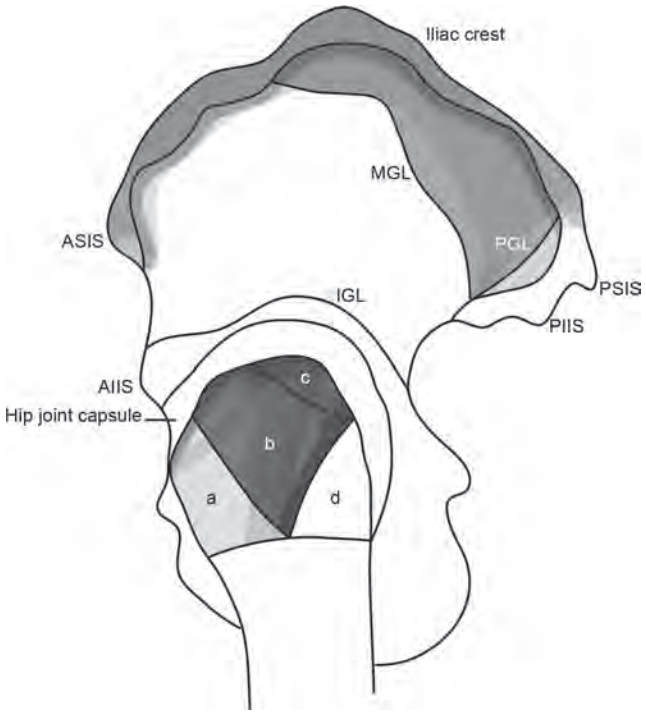

Figure 39.1 Minor variations in the location of the bony proximal and distal insertion sites of gluteus medius. Shaded areas denote sites of bony insertion as described in anatomical textbooks and scientific articles. Areas common to more than one publication are indicated by darker regions. AIIS, anterior inferior iliac spine; ASIS, anterior superior iliac spine; IGL, inferior gluteal line; MGL, middle gluteal line; PGL, posterior gluteal line; PIIS, posterior inferior iliac spine; PSIS, posterior superior iliac spine; a, anterior facet; b, lateral facet; c, posterosuperior facet; d, posterior facet of the greater trochanter.

Source: Flack et al. (2012). Reproduced with permission from John Wiley & Sons.

1071±309.71 mm^2 (Duda et al. 1996; McConnell et al. 2003; Woyski et al. 2013) and, as demonstrated by McConnell et al. (2003), can be highly variable within a population (n=34, mean 935, range 658–1294 mm^2).

The mean width of the distal attachment of gluteus medius to the lateral aspect of the greater trochanter (along the oblique line) may be significantly longer in males (males 34.6±1.8 mm; females 27.1±3.1 mm; Flack et al. 2014). Similarly, a smaller cross-sectional area of the tendinous femoral attachment has been reported in women (Woyski et al. 2013) although in their study of six specimens Duda et al. (1996) were unable to identify any sex-related differences.

Morphology

Gluteus medius may comprise two (Henle 1858; Srivastava and Joshi 1969; Duparc et al. 1997), three (Winslow 1763; Knox 1831; Gottschalk et al. 1989; Jaegers et al. 1992; Al-Hayani et al. 2009), or up to four (Flack et al. 2014) anatomical compartments (Fig. 39.2). Variations in muscle morphology are summarized in Table 39.2.

Musculotendinous length may be significantly longer in males than females (Flack et al. 2014). It is unclear whether there are sex-related differences in total muscle volume as Preininger et al. (2012) report increased volumes in men (males 333±69 cm^3, females 250±41 cm) while Flack et al. (2014) were unable to detect a significant difference.

Fusion

Anteriorly, the borders of gluteus medius and gluteus minimus may fuse with one another (Knox 1831; Gray 1858; Frick et al. 1991; Duparc et al. 1997). Such a fusion has been termed the suspensory ligament of the greater trochanter (of Gunther). Some muscle fibers of gluteus medius may insert distally onto the tendon of gluteus minimus (Akita et al. 1993; Flack et al. 2014; Fig. 39.3). This has been reported to occur in 7.5% of specimens (Duparc et al. 1997) and is sometimes referred to as a separate, independent muscle bundle of gluteus medius (Akita et al. 1993). Complete fusion of gluteus medius with gluteus minimus is rare (Macalister 1866; Testut 1884). Finally, fusion may occur between the anterior muscular border of gluteus medius and the proximal part of the deep surface of tensor fascia lata (Gray 1858; Clark and Haynor 1987; Akita et al. 1992).

Posteriorly, the muscle bellies of gluteus medius and piriformis are sometimes adjoined (Henle 1858; Macalister 1871; Chiba 1992; Akita et al. 1994). Alternatively, fibers from the gluteus medius muscle may insert into the tendon of piriformis (Winslow 1763; Windisch et al. 2007; Flack et al. 2014), the tendons blend at their insertion onto the greater trochanter (Henle 1858; Macalister 1866), or a combination of these variations occurs simultaneously (Flack et al. 2014; Fig. 39.4).

Distally, the gluteus medius tendon may be anatomically continuous with that of gluteus minimus (Winslow 1763; Steel 1980; Pfirrmann et al. 2001) with some authors reporting that this occurs in 100% of cases (Nazarian et al. 1987; Flack et al. 2014). The gluteus medius tendon may also be continuous with the proximal tendon of vastus lateralis in 13.5–100% of hips (Nazarian et al. 1987; Heimkes et al. 1992) or with both vastus lateralis and gluteus minimus over the lateral aspect of the greater trochanter in 34.6% of cases (Heimkes et al. 1992).

There may also be between one and three independent muscle layers present on the deep surface of gluteus medius, each with their own distinct distal attachment into the lateral surface of the aponeurosis of gluteus minimus (Akita et al. 1993).

Accessory muscles

A gluteus medius accessorius muscle has been reported (Jazuta 1931). This triangular-shaped muscle arises from the outer surface of the iliac crest below the origins of tensor fascia lata and gluteus medius. It lies between gluteus medius and minimus but does not fuse with either muscle.

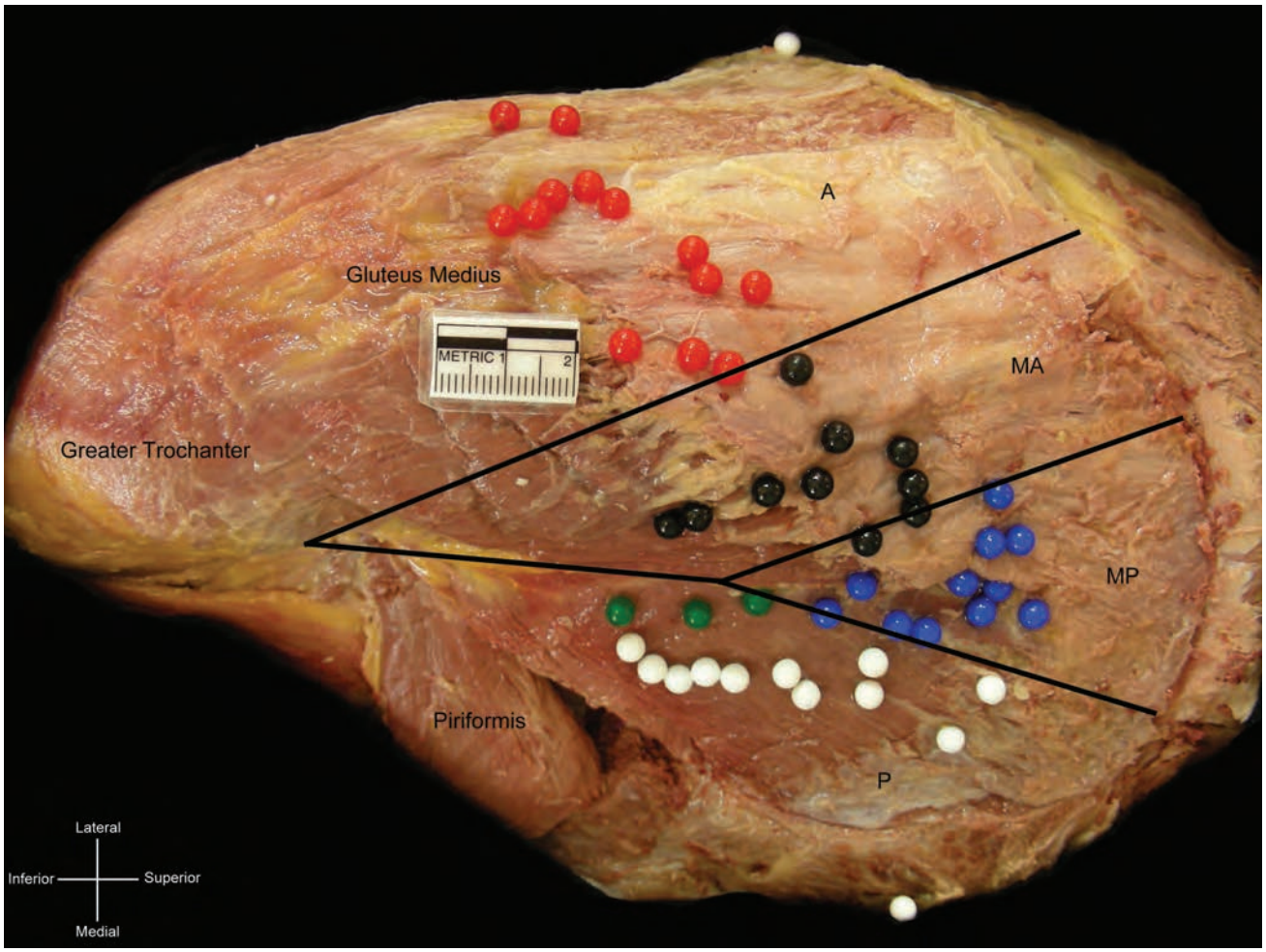

Figure 39.2 Architectural features of gluteus medius. The attachment sites, fascicle direction, fascicle length, and nerve supply (pins, each representing a single nerve entry point) divide the muscle into four anatomical compartments. A, anterior compartment; MA, mid-anterior compartment; MP, mid-posterior compartment; P, posterior compartment.

Source: Flack et al. (2014). Reproduced with permission from John Wiley & Sons.

Its distal tendon consists of two parts; the superficial portion fuses with the tendon of gluteus medius and the deep part inserts independently onto the greater trochanter. The muscle is reported to be 10 cm long and 1 cm thick (Jazuta 1931). Henle (1858) made similar observations that allude to a muscle being that of gluteus medius accessorius. In his account, a number of deep muscle fibers belonging to gluteus medius insert onto a distinct, short, and narrow tendon which attaches to the gluteus medius tendon as well as the upper edge of the greater trochanter.

The anterior fibers of gluteus medius may also be separate from the rest of the muscle, forming a distinct scansorial muscle (Macalister 1866) and inserting onto the upper part of the greater trochanter (Macalister 1871). A similar description by Duparc et al. (1997) reports an anterior muscle bundle attaching from the anterior superior iliac spine and the anterior edge of the greater trochanter in 3 of 40 specimens.

Gluteus minimus

Attachments

There are few detailed accounts of the proximal attachments of gluteus minimus and no significant variations recorded (Beck et al. 2000). However, variations are apparent in the distal attachments of this muscle (for review see Flack et al. 2012; Fig. 39.5). In addition to the most commonly denoted attachment to the anterior surface of the greater trochanter, gluteus minimus has also been reported to attach to the anterosuperior angle (Woodburne and Burkel 1988; Gottschalk et al. 1989), anterolateral ridge (Beck et al. 2000; Walters et al. 2000; Al-Hayani 2009), lateral surface with gluteus medius (Basarir et al. 2008), and the superior aspect of the greater trochanter with gluteus medius (Little and Lyons 1983). The distal insertional footprint varies between an irregular L-shape and a triangular area (Beck et al. 2000), and the mean attachment width of the distal tendon onto the greater trochanter is 21.5±3.0 mm (Flack et al. 2014).

Table 39.2 Morphometric data for gluteus medius reported by dissection and imaging. Standard deviation in parentheses.

Reference	No. specimens and sex	Mean muscle volume (cm^3)	Mean muscle length (mm)	Mean muscle PCSA (cm^2)	Other
Lippert (1962)	50 (M: 31; F: 19)			M: 17.9 (6.9); F: 12.8 (3.6)	
Jensen and Metcalf (1975)	2	Specimen 1: L: 298.4 (0.8); R: 258.6 (2.1) Specimen 2: L: 434.9 (4.3); R: 364.0 (8.2)			
Brand et al. (1986)	2 (M: 1; F: 1)			M: 62.4; F: 33.2	
Delp et al. (1990)	3		125.0[a]		
Friederich and Brand (1990)	2 (M: 1; F: 1)[b]	M: 411.0; F: 159.0	M: 130.0; F: 113.3	M: 62.4; F: 33.2	
Jaegers et al. (1992)	6 lower limbs of participants (MRI) M: 4; F: 2	398.9 (60.5)			
Heimkes et al. (1993)	6			27.8	
Duda et al. (1996)	4 (M: 2; F: 2)	242.5 (110.9)			
Duparc et al. (1997)	12		135.0 (17.0)		
McConnell et al. (2003)	34				Mean tendon length 55.9 mm; mean tendon width 16.8 mm
Inan et al. (2005)	11 lower limbs of participants (MRI) M: 0; F: 11	130.4 (24.0)			
Nork et al. (2005)	9		179.0 (18.0)		Mean muscle width 136.0 (19.0) mm (range 110.0–180.0)
Ward et al. (2008)	16		199.9 (28.6)	33.8 (14.4)	Mean muscle mass 273.5 (76.9) g
Grimaldi et al. (2009a)	24 lower limbs of participants (MRI) M: 12; F: 12	L: 317.0 (75.0); R: 305.0 (88.0)			
Preininger et al. (2011)	204 lower limbs of participants (MRI) M: 104; F: 100	289.0 (72.0; range 142.0–466.0)			
Liu et al. (2012)	19 lower limbs of participants (CT) M: 7; F: 12		145.5 (9.6)	17.4 (5.1) – 23.6 (6.4)	Cross-sectional area was measured at 3 levels in the muscle
Preininger et al. (2012)	186 lower limbs of participants M: 90; F: 96	M[c]: 333.0 (68.6; range 139.0–473.0) F: 250.0 (40.9; range 150.0–332.0)			
Flack et al. (2014)	12 (M: 6; F: 6)	138.6 (57.8)	131.4 (17.4)	27.6 (11.6)	Mean muscle width 142.1 (9.7) mm

CT, computed tomography; F, female; L, left side; M, male; MRI, magnetic resonance imaging; R, right side; SD, standard deviation.

[a]Musculotendon length; [b]same cadavers as used by Brand et al. (1986); [c]significantly larger in males than females ($P < 0.001$)

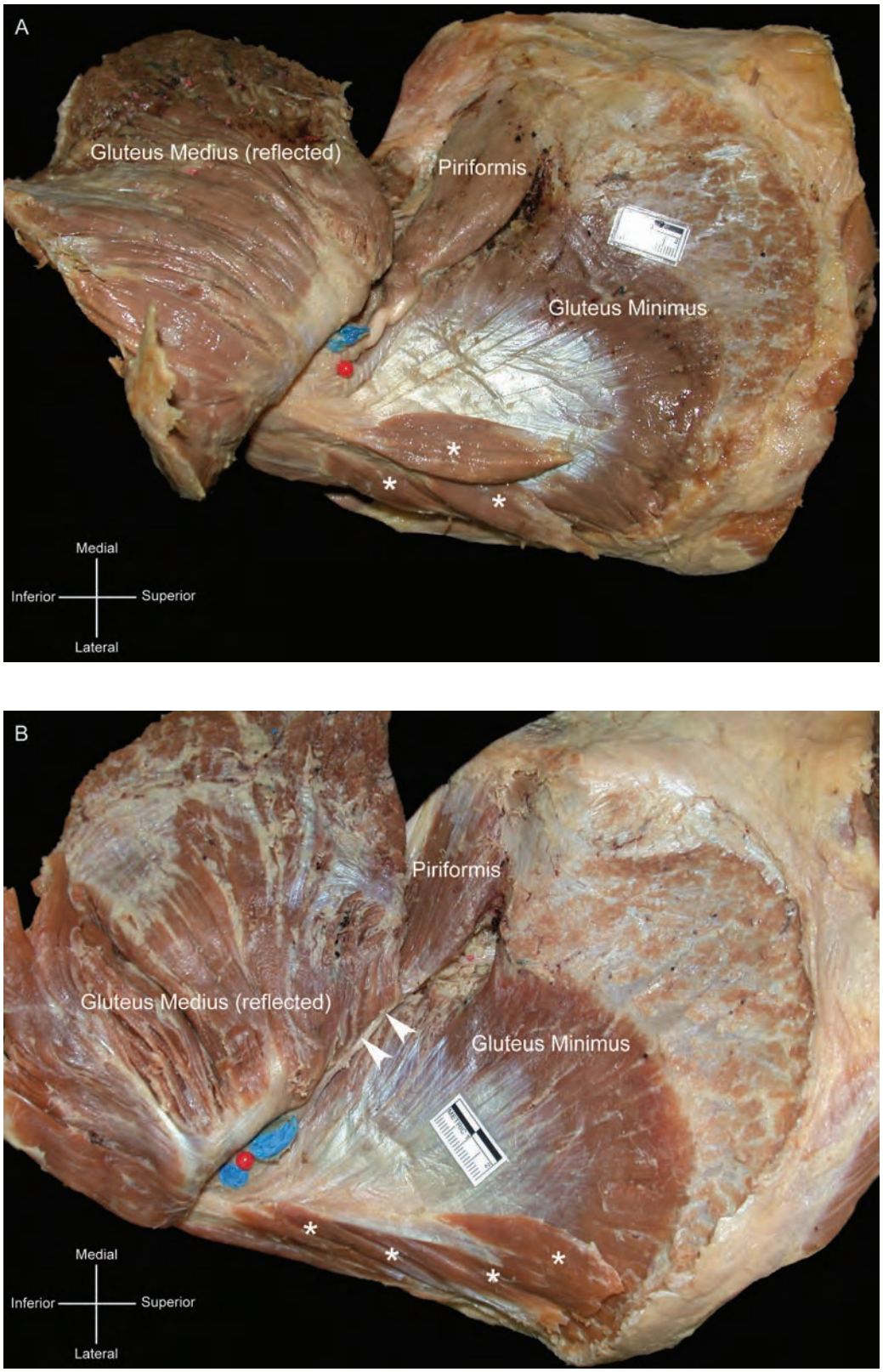

Figure 39.3 (a, b) Distal insertion of gluteus medius muscle fibres (asterisks) onto the tendon of gluteus minimus. Figure B also shows fusion of gluteus medius muscle fibers with the distal tendon of piriformis (arrowheads). Blue latex has been injected into the subgluteus medius bursa(e).

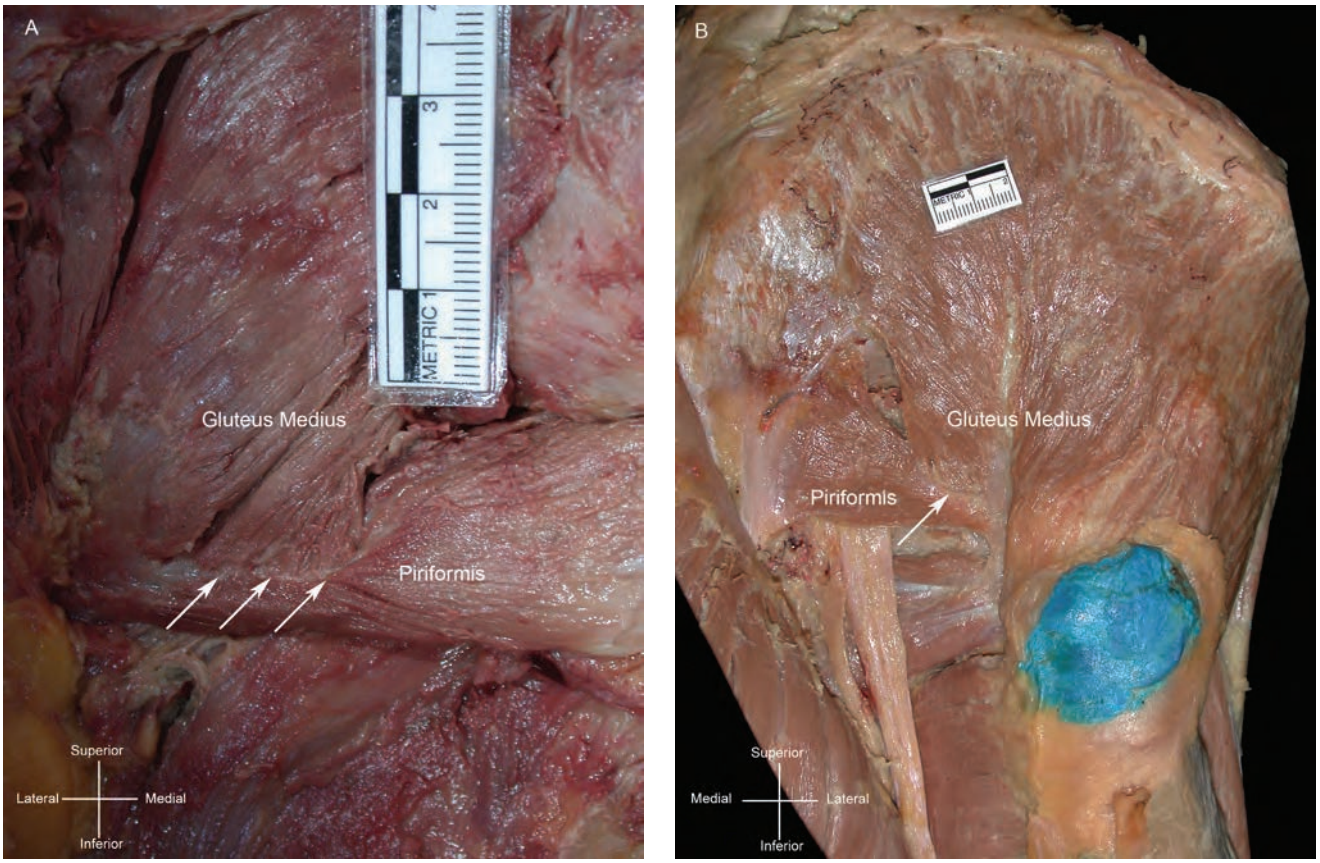

Figure 39.4 Posterior fusion of gluteus medius muscle fibres (a) with those of piriformis and (b) into the tendon of insertion of piriformis. Blue latex has been injected into the deep subgluteus maximus bursa.

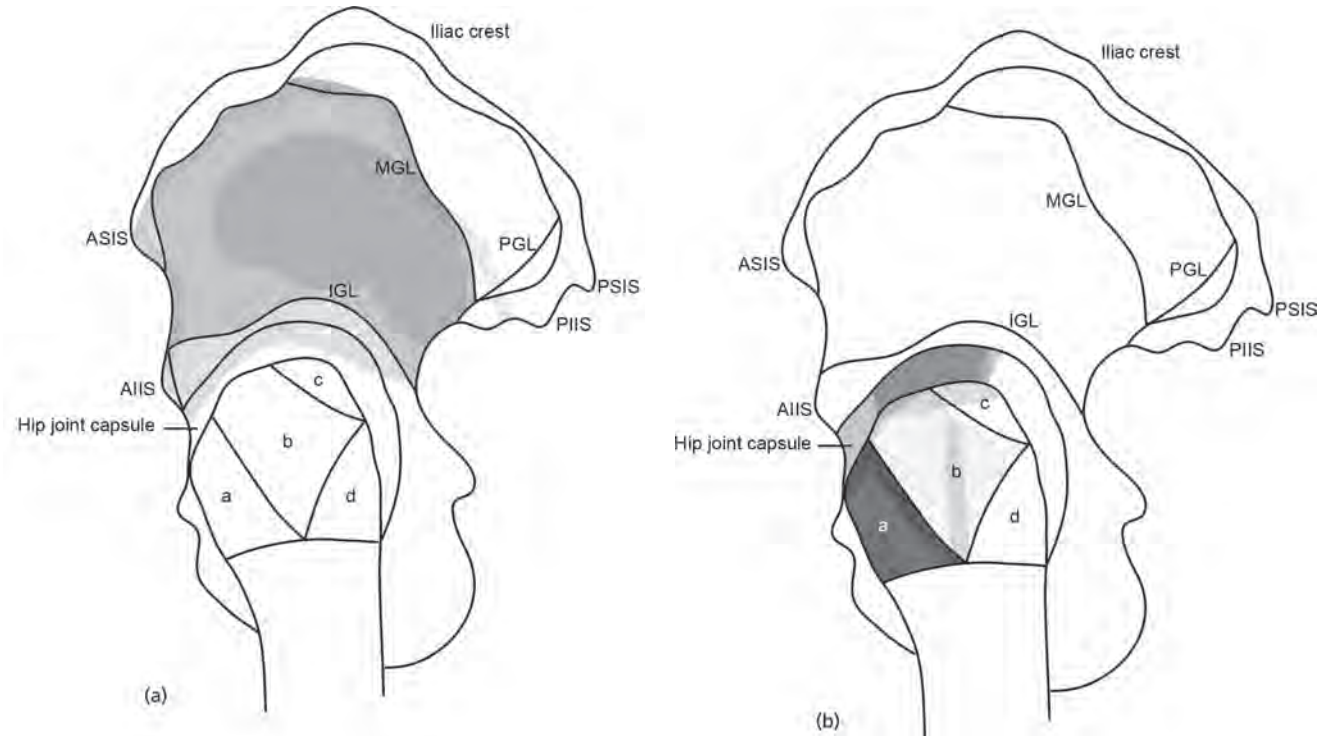

Figure 39.5 Minor variations in the location of the bony (a) proximal and (b) distal insertion sites of gluteus minimus. Shading and abbreviations as for Figure 39.1.

Source: Flack et al. (2012). Reproduced with permission from John Wiley & Sons.

Association with the hip joint capsule

Gluteus minimus may attach to either the anterior (Harty 1982; Dall 1986; Pfirrmann et al. 2001; Robertson et al. 2008; Flack et al. 2014), and/or superior (Steel 1980; Dall 1986; Walters et al. 2000; Pfirrmann et al. 2001; Flack et al. 2014) aspect of the hip joint capsule. This attachment can be muscular (Macalister 1875; Walters et al. 2000; Pfirrmann et al. 2001; Weber and Ganz 2002; Rabi and Vettivel 2003; Flack et al. 2014) and/or tendinous in nature (Nazarian et al. 1987; Beck et al. 2000; Rabi and Vettivel 2003; Connell 2003; Woodley et al. 2008; Flack et al. 2014). The site of attachment may be intermingled with capsular fibers originating from vastus lateralis (Duparc et al. 1997). The size of the tendinous capsular insertion is irregular and varies between the range of 10-15 mm mediolaterally and 20–25 mm craniocaudally (Beck et al. 2000). The muscular insertion into the capsule is likewise variable with up to 19 (mean = 5) fascicles inserting at this location (Flack et al. 2014).

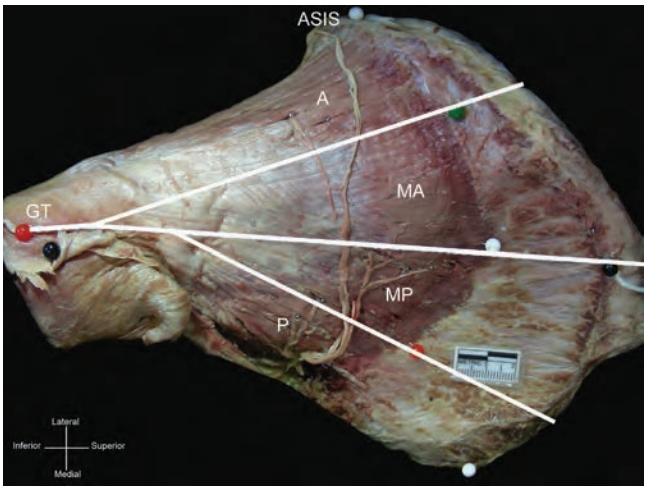

Figure 39.6 Photograph showing the compartments of gluteus minimus.

A, anterior compartment; ASIS, anterior superior iliac spine; GT, greater trochanter; MA, mid-anterior compartment; MP, mid-posterior compartment; P, posterior compartment.

Source: Flack et al. (2014). Reproduced with permission from John Wiley & Sons.

Morphology

There is debate as to whether gluteus minimus comprises different parts. Jaegers et al. (1992) were unable to distinguish any muscle divisions using MRI, which contrasts to the descriptions of two parts (anterior and posterior; Macalister 1871; Standring 2008), or up to four parts based on architectural parameters and secondary innervation patterns (Flack et al. 2014; Fig. 39.6). Quantitative data showing variation in muscle morphology can be found in Table 39.3.

Fusion

Anteriorly, the muscle belly of gluteus minimus is often fused with gluteus medius (Gray 1858; Gardner et al. 1975; Frick et al. 1991; Duparc et al. 1997) but complete fusion of gluteus medius and minimus is rare (Macalister 1866). The posterior component of gluteus minimus may be joined to gemellus superior (Macalister 1871) or piriformis (Macalister 1871; Knott 1883; Frazer 1904; Gardner et al. 1975), with some authors stating fusion is specifically with the tendon of piriformis (Gray 1858; Flack et al. 2014).

Distally, the gluteus minimus tendon may blend with that of gluteus medius (Winslow 1763; Nazarian et al. 1987; Pfirrmann et al. 2001; Flack et al. 2014) or be connected to vastus lateralis over the greater trochanter (Macalister 1871). In the latter situation there may also be contributions from the distal tendon of gluteus medius in up to 35% of cases (Heimkes et al. 1992). At its origin from the iliac fossa, the fibers of tensor fascia lata may blend with the fibers of gluteus minimus (Kaplan 1958).

Table 39.3 Morphometric data for gluteus minimus reported by dissection and imaging. Standard deviation in parentheses.

Reference	No. specimens and sex	Mean muscle volume (cm^3)	Mean muscle length (mm)	Mean muscle PCSA (cm^2)	Other
Brand et al. (1986)	2 (M: 1; F: 1)			M: 26.9; F: 24.2	
Jaegers et al. (1992)	6 lower limbs of participants (MRI) M: 4; F: 2	102.5 (30.1)			
Duda et al. (1996)	Mean muscle volume 4 (M: 2; F: 2) Mean femoral attachment area 6 (M: 4; F: 2)	55 (20.82)			Mean femoral attachment area 504.8 (121.3) mm^2
Friederich and Brand (1990)	2[a] (M: 1; F: 1)	M: 138.0; F: 72.0	M: 86.7; F: 81.7	M: 26.9; F: 24.2	
Grimaldi et al. (2009a)	24 lower limbs of participants (MRI) M: 12; F: 12	L: 86 (21) R: 79 (21)			
Flack et al. (2014)	12 (M: 6; F: 6)	36.7 (17.6)	117.9 (12.7)	14.1 (11.1)	Muscle width 66.1 (10.6) mm

F, female; L, left side; M, male; MRI, magnetic resonance imaging; R, right side; SD, standard deviation.

[a]Same cadavers as examined by Brand et al. (1986)

Table 39.4 Details of variations of accessory muscles associated with gluteus minimus.

Reference	Proximal insertion	Distal insertion	Frequency	Other notes
Macalister (1866)	AIIS	Hip joint capsule; anterior intertrochanteric line above the LT	Not specified	Gluteus quartus
Macalister (1867)	Not specified	Anteroinferior portion of the root of the GT	N=1	A distinct scansorius muscle; posterior and parallel to TFL; separated from the anterior border of GMin
Knott (1883)	A deep inner lamina of GMin; Differentiated anterior segment of GMin, up to the ASIS	Tendon of GMin; GT with tendon of GMin; Partly into the GT with tendon of GMin and partly to the side of vastus lateralis	N=3; N=1; N=1	Gluteus accessories; separated from GMin by a thin layer of adipose tissue Gluteus quartus/scansorius; differentiated anterior segment of GMin
Testut (1884)	ASIS	Anterior GT, hip joint capsule and almost to the LT, or the "subiliac tendon"	"Frequent" (not specified)	Gluteus quartus/scansorius/ accessory; found anterior to gluteus minimus
Gruber (1887)	AIIS	Hip joint capsule; anterior intertrochanteric line above the lesser trochanter	Not specified	Gluteus quartus
Beck et al. (2000)	Lateral edge of the iliac crest (between ASIS iliac tubercle) and fascia covering GMin	Tendon of GMin; Covered by GMin fascia	12.5%; 31.25%	Accessory muscle; Present along the anterior edge of GMin

AIIS, anterior inferior iliac spine; ASIS, anterior superior iliac spine; GMin, gluteus minimus; GT, greater trochanter; LT, lesser trochanter; TFL, tensor fascia lata.

Accessory muscles

A number of accessory muscles associated with gluteus minimus have been identified within the literature and are sometimes referred to as gluteus quartus or scansorius. The attachment sites and frequency (when provided) of each muscle variant are provided in Table 39.4.

Piriformis

Piriformis has been a source of interest for more than a century, particularly in relation to so-called "piriformis (muscle) syndrome." Characterized by low back and/or buttock pain and sciatica (Sayson et al. 1994; Benzon et al. 2003), the pathogenesis of this syndrome is uncertain (Chen 1994; Papadopoulos and Khan 2004; Jawish et al. 2010) and diagnosis is often one of exclusion (Indrekvan and Sudmann 2002; Benzon et al. 2003; Papadopoulos and Khan 2004; Cassidy et al. 2012). It has been proposed that anatomical variants of piriformis may contribute to the cause of symptoms, due to compression or entrapment of the sciatic nerve or its divisions within the piriformis muscle (Pecina 1979; Benzon et al. 2003). The variation in the relationship between piriformis and the sciatic nerve is described first before providing details of attachments and morphology.

Relationship between piriformis and the sciatic nerve

The classification devised by Beaton and Anson (1937) is commonly used to describe variation in the relationship between piriformis and the sciatic nerve (Table 39.5; Fig. 39.7), although anatomical anomalies between these two structures were recognized prior to this time (e.g., Paterson 1893; Testut 1884; Le Double 1897; Parsons and Keith 1897; Bardeen 1901; Trotter 1932; Fukumoto 1935). Although emphasis is placed on the common fibular and tibial nerves, they are usually accompanied by all, or elements of, the inferior gluteal nerve and posterior cutaneous nerve of thigh (Chiba 1992; Akita et al. 1994; Chiba et al. 1994;

Table 39.5 Classification of the relationship between piriformis and the sciatic nerve.

Classification	Beaton and Anson (1937)	Contemporary description
Type A	Undivided nerve below undivided muscle	Normal passage of sciatic nerve, passing anterior to piriformis and exiting the pelvis inferior to the muscle via the infrapiriformis fossa
Type B	Divisions of nerve between and below undivided muscle	Common fibular nerve traverses through piriformis and the tibial nerve passes inferior to the muscle
Type C	Divisions above and below undivided muscle	Common fibular nerve exits superior to piriformis and the tibial nerve passes inferior to the muscle
Type D	Undivided nerve between heads	Sciatic nerve passes through piriformis
Type E	Divisions between and above heads	Common fibular nerve exits superior to piriformis and the tibial nerve passes through the muscle
Type F	Undivided nerve above undivided muscle	Sciatic nerve passes superior to piriformis

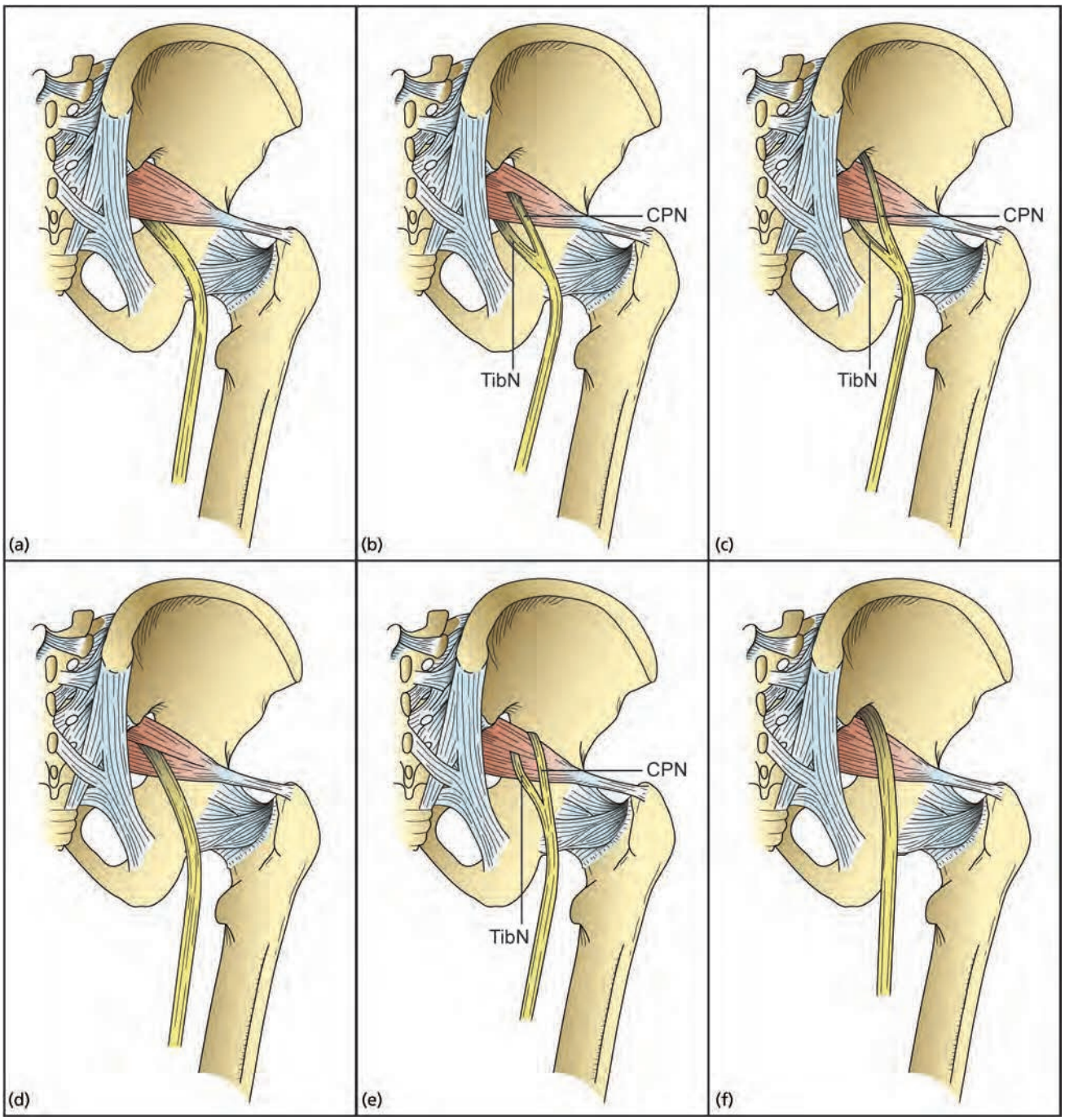

Figure 39.7 Line drawings of piriformis variations. Adapted from Beaton and Anson (1937), with permission from John Wiley & Sons.

CPN, common peroneal nerve; TibN, tibial nerve.

Gabrielli et al. 1997; Uluutku and Kurtoglu 1999). With respect to the type A subcategory, the sciatic nerve may be "undivided" in nature (Beaton and Anson 1937); however, the common fibular and tibial divisions can also separate prior to emerging beneath piriformis (Misra 1954; Nizankowski et al. 1972; Chiba 1992; Okraszewska et al. 2002; Jawish et al. 2010; Ogeng'o et al. 2011; Patel et al. 2011).

Variations of piriformis relative to the sciatic nerve

Numerous case reports document variations in the passage of the sciatic nerve relative to piriformis. Most are dissection-based and note type B variation (Arifoglu et al. 1997; Kirici et al. 1999; Kirici and Ozan 1999; Demiryurek et al. 2002; Paval and Nayak 2006; Jawish et al. 2010; Sharma et al. 2010; Khan and Khan 2011; Battaglia et al. 2012; Hamid and Rekha 2012;

Retamal et al. 2012; Pais et al. 2013 (case series)), with a few surgical reports describing types C (Kobbe 2008; Battaglia et al. 2012) and D (Chen 1994; Kosukegawa et al. 2006; Kobbe 2008), respectively.

The prevalence of variation and the normal passage of the sciatic nerve, reported in 43 studies that each included 10 or more specimens/patients, is summarized in Table 39.6. Of the 6466 total cases, variation is ascribed to 16.5% (1067) in keeping with the findings of Smoll and Ebroll (2010). Of the variations, type B accounts for the largest proportion (77.5%), followed by type C (8.2%) and type D (3.2%). Types E and F are rare, being reported in only 0.5% (Nizankowski et al. 1972; Lee and Tsai 1974) and 0.7% (Lee and Tsai 1974; Ndiaye et al. 2004; Natsis et al. 2014) of specimens, respectively. The infrequency of types E and F may be a reflection of the fact that Beaton and Anson (1937) originally deemed these two categories to be hypothetical in nature.

The rate of type B variation appears to be consistently higher in Chinese (32.9%; P'an 1941) and Japanese (33.5–34.6%; Fukumoto 1935; P'an 1941; Chiba 1992; Chiba et al. 1994) populations (Table 39.6). Trotter (1932) noted slightly more overall variation in European Americans (54.7%) compared to African Americans (45.3%).

As reported in 17 studies (with a total of 3424 specimens), the distribution of variants with respect to laterality was documented in 611/3424 (17.8%) specimens. Variations occurred bilaterally in approximately 45% of these cases (Table 39.7), compared to about 40% in those presenting with a normal course of the nerve. Slightly more cases of variation have been documented in the right (314) compared to left (297) limbs (Table 39.7). Of the nine studies (total of 1911 specimens) that include details on sex distribution, males account for 60% (206) of the reported variation (344) compared to females (40%, 138; Table 39.8). This is slightly different to the spread of normal cases (55% male, 45% female). Further interpretation of these data is not possible as only two of the studies (Parsons and Keith 1897; Nizankowski et al. 1972) state the sex of all of the included specimens.

Other neurovascular-related variants

There is a single report of the sciatic nerve lying posterior to piriformis in a woman with suspected piriformis syndrome (Sayson et al. 1994). The superior gluteal nerve may perforate piriformis in 8–10% of cases (Chiba 1992; Akita et al. 1994) or pass inferior to the muscle in 10% (Uluutku and Kurtoglu 1999).

Some examples of differences in type B sciatic nerve variation have been documented. In addition to the common fibular nerve, part of the tibial nerve can pass through piriformis, with the remaining tibial component passing inferior to the muscle (two specimens; Chiba 1992). The inferior gluteal vein may also perforate the tibial nerve as it emerges below piriformis (one specimen; Natsis et al. 2014) or the tibial nerve may exit inferior to the gemellus superior muscle rather than piriformis (Mas et al. 2003; Guvencer et al. 2009). Other unusual findings are the common fibular nerve passing either between piriformis and obturator internus or coursing through obturator internus, with the tibial nerve emerging below gemellus inferior (Sabnis 2012).

With respect to type C variation, a rare finding is noted whereby the common fibular nerve forms a neural loop with the respective parts passing superior and inferior to piriformis before joining together to descend with the tibial nerve, which emerges beneath piriformis (Spinner et al. 2001; Retamal et al. 2012).

Attachments

Piriformis arises as three digitations (Standring 2008) from the projections of bone lying between the four ventral sacral foramina (Drake et al. 2010). Attachment to only two sacral vertebrae may occur, observed in two individuals who had rheumatoid arthritis (Knott 1883) or in persons with a short and narrow sacrum (Le Double 1897). An additional slip to S1 or to the coccyx is possible (Le Double 1897). Instead of the usual digitations, there has been one report of insertion via a single, long slip medial to the ventral sacral foramina. In this report, the grey sympathetic rami and branches of the lateral sacral artery pierced the muscle (Smoll and Ebrall 2010).

Muscle morphology

Division into two or more muscle bellies

In the type B variant Beaton and Anson (1937) state that the common fibular nerve passes between the "undivided muscle," yet the diagrams in this paper suggest division of piriformis into superior and inferior parts. Two studies (Pecina 1979; Delabie et al. 2013) report the presence of both types of muscle morphology (undivided and divided). Although the prevalence of each presentation is inconclusive, division into two parts is most likely an anomaly.

Some authors comment that piriformis is split into two distinct heads by the common fibular nerve (Beaton and Anson 1938; Lee and Tsai 1974; Kirici and Ozan 1999; Kirici et al. 1999; Demiryurek et al. 2002; Benzon et al. 2003; Kosukegawa et al. 2006; Paval and Nayak 2006; Jawish et al. 2010; Khan and Khan 2011; Rastogi et al. 2011; Natsis et al. 2014). This characteristic is also alluded to in photographs (Gabrielli et al. 1994, 1997; Pokorny et al. 1998; Ugrenovic et al. 2005; Vincente et al. 2007; Pecina et al. 2008; Ogeng'o et al. 2011) and line drawings (Chiba 1992; Fig. 39.8)

When two muscle bellies are present, the superior belly is usually larger accompanied by a smaller inferior belly (Chiba 1992; Chen 1994; Kirici et al. 1999; Demiryurek et al. 2002; Vincente et al. 2007; Khan and Khan 2011; Martin et al. 2011; Cassidy et al. 2012). The superior belly may be partially superposed to the inferior belly (Vincente et al. 2007) and occasionally the two parts may be positioned superficial and deep as reported in 5 of 12 specimens (Natsis et al. 2014). Each muscle belly may have a distinct tendon blending to a common insertion, a variation described in a total of 41 of 57 cases (Pecina 1979; Chen 1994; Vincente et al. 2007; Pecina et al. 2008; Cassidy et al. 2012; Natsis et al. 2014; Fig. 39.8). It has been suggested that compression of neural tissue between the tendinous components or edge

Table 39.6 Relationship between piriformis and the sciatic nerve reported by dissection and surgical examination.

Reference	Country of origin of population	No. specimens and sex (if known)	Type A	Type B	Type C	Type D	Total variation, number (% of specimens)
Paterson (1893)	Scotland	23	20 (87)[a]	3 (13)			3 (13)
Parsons and Keith (1897)	England	138[b] (M: 76; F: 36)	118 (85.5)	17 (12.3)	–	3 (2.2)	20 (14.5)
Bardeen (1901)	America	246 (M: 172; F: 74)	220 (89.4)[a]	25 (10.2)	1 (0.4)	–	26 (10.6)
Trotter (1932)	America	464	400 (86.2)				64 (13.8)[c]
Fukumoto (1935)	Japan	306	200 (65.4)[d]	106 (34.6)			106 (34.6)
Beaton and Anson (1938)	America	240	216 (90)	17 (7.1)	5 (2.1)	2 (0.8)	24 (10)
P'an (1941)	China	140	92 (65.7)	46 (32.9)	–	2 (1.4)	48 (34.3)
Misra (1954)	India	300	262 (87.4)[d]	18 (6)	12 (4)	8 (2.6)	38 (12.6)
Kubota et al. (1960)	Japan	38	33 (86.8)[a]	–	5 (13.2)		5 (13.2)
Nizankowski et al. (1972)	Poland	200 (M: 110; F: 90)	181 (90.5)	8 (4)	3 (1.5)	5 (2.5)	19(9.5)
Lee and Tsai (1974)	Taiwan	168 (M: 146; F: 22)	118 (70.2)	33 (19.6)	7 (4.2)	3 (1.8)	50 (29.8)
Pecina (1979)	Croatia	130	102 (78.5)	27 (20.7)	1 (3.3)		28 (21.5)
Chiba (1992)	Japan	511	328 (64.2)	173 (33.8)	10 (2)	–	183 (35.8)
Chiba et al. (1994)	Japan	442	285 (64.5)	148 (33.5)	9 (2)		157 (35.5)
Gabrielli et al. (1994)	Brazil	60 (M and F)	52 (86.7)	6 (10)	2 (3.3)	–	8 (13.3)
Georgiadis et al. (1996)	America	42	40 (95.2)	2 (4.8)			2 (4.8)
Gabrielli et al. (1997)	Brazil	80 (M: 58; F: 22)	69 (86.3)	9 (11.2)	2 (2.5)	–	11 (13.7)
Pokorny et al. (1998)	Czech Republic	51	41 (80.4)	7 (13.7)	2 (3.9)	1 (2.0)	10 (24.4)
Benson and Schutzer (1999)	America	15 (surgical) (M: 5; F: 10)	14 (93.3)	1 (6.7)			1 (6.7)
Uluutku and Kurtoglu (1999)	Turkey	50 fetal (M: 14; F: 36)	37 (74)	8 (16)	5 (10)		13 (26)
Fishman et al. (2002)	America	76	65 (85.5)[a]				11 (14.5)[c]
Indrekvam & Sudmann (2002)	Norway	19 (surgical) (M: 5; F: 14)	15 (78.9)				4 (21.1)[c]
Okraszewska et al. (2002)	Poland	36 (M: 19; F: 17)	29 (80.6)	2 (5.6)	2 (5.6)	3 (8.2)	7 (19.4)
Benzon et al. (2003)	America	66	65 (98.5)	1 (1.5)			1 (1.5)
Ndiaye et al. (2004)	Senegal	20	19 (95)	–	–	–	1 (5)
Agur and Dalley (2005)[d]	–	640[e]	557 (87)	78 (12.2)	3 (0.5)	–	81 (12.7)
Ugrenovic et al. (2005)	Serbia and Montenegro	200 fetal (M: 114; F: 86)	192 (96)	5 (2.5)	3 (1.5)		8 (4)
Pokorny et al. (2006)	Czech Republic	91	72 (79.1)	13 (14.3)	4 (4.4)	2 (2.2)	19 (20.9)
Chukwuanukwu et al. (2007)	Nigeria	52	50 (96.2)	2 (3.8)			2 (3.8)
Vincente et al. (2007)	Brazil	40 (M: 32; F: 14)	34 (85)	6 (15)			6 (15)
Jia et al. (2008)	China	104 (M: 66; F: 38)	76 (73)				28 (27)[c]
Pecina et al. (2008)	Croatia	10 (surgical) (M: 3; F: 7)	7 (70)[a]	3 (30)			3 (30)

(continued)

Table 39.6 *(continued)*

Reference	Country of origin of population	No. specimens and sex (if known)	Type A	Type B	Type C	Type D	Total variation, number (% of specimens)
Guvencer et al. (2009)	Turkey	50 (M: 25)	38 (76)[f]	7 (16)	4 (8)	–	11 (24)
Inayat et al. (2010)	Pakistan	60 (M: 60)	53 (88.3)[d]	4(6.7)	3 (5)		7 (11.7)
Brooks et al. (2011)	Brazil ("mixed ethnic origins")	40 (M: 16; F: 4)	36 (90)	0	0	4 (10)	4 (10)
Muthu Kumar et al. (2011)	India	50	50 (100)	–	–	–	0
Ogeng'o et al. (2011)	Kenya	164	147 (89.6)	13 (7.9)	4 (2.4)		17 (10.4)
Patel et al. (2011)	India	86	81 (94.2)	5 (5.8)			5 (5.8)
Rastogi et al. (2011)	India	80	78 (97.5)	2 (2.5)			2 (2.5)
Sabnis (2012)	India	140	139 (99.3)[a]		1 (0.7)		1 (0.7)
Delabie et al. (2013)	France	104	94 (90.6)	10 (9.6)			10 (9.6)
Natsis et al. (2014)	Greece	294	275 (93.5)	12 (4.1)	1 (0.3)	1 (0.3)	15 (5.1)[g]
Sulak et al. (2014)	Turkey	400 fetal (M: 206; F: 194)	392 (98)	5 (3.5)	3 (1.5)		8 (2)
Totals		6466	5392	827	87	34	1055[h]

F, female; M, male

[a]Calculated from reported data; [b]sex of 26 specimens unknown; [c]total variation provided, no information on classification subtypes; [d]absolute numbers calculated from reported percentages; [e]data missing for approximately two specimens; [f]data missing from one specimen; [g]an additional four variations were observed that do not fit classification of Beaton and Anson (1937); [h]12 additional cases of variation have been reported in this literature as types E (*n*=5) and F (*n*=7).

Table 39.7 Relationship between piriformis and the sciatic nerve, unilateral and bilateral variation. L, left; R, right; B, bilateral.

Reference	No. specimens	No. type A (L, R, B)	No. type B (L, R, B)	No. type C (L, R, B)	No. type D (L, R, B)	Total variation (L, R, B, number (% of specimens))
Parsons and Keith (1897)	138	58, 60, –	9, 8, –	–	2, 1, –	11, 9, –, 20 (14.5)
Trotter 1932	464	–	–	–	–	30, 34, 21, 64 (13.8)
Beaton and Anson (1938)	240	–	–	–	–	13, 11, 8, 24 (10)
P'an (1941)	140	45, 47, 36	24, 22, 13	–	1, 1, –	25, 23, 13, 48 (34.4)
Nizankowski et al. (1972)	200	88, 93, –	5, 3, –	0, 3, –	4, 1, –	11, 8, –, 19 (9.5)[a]
Pecina (1979)	130	–	14, 13, 9	–[b]		14, 13, –, 28[b] (21.5)
Chiba (1992)	511[c]	170, 157, 126	78, 93, 37	6, 4, 2	–	84, 100, 39, 183 (35.8)
Chiba et al. (1994)	442	148, 137, 113	68, 80, 35	5, 4, 2	–	73, 84, 37, 157 (35.5)
Gabrielli et al. (1994)	60	28, 24, 24	1, 5, 1	1, 1, 1	–	2, 6, 2, 8 (13.3)
Pokorny et al. (1998)	51	21, 20, –	4, 3, –	2, 0, –	1, 0, –	7, 3, –, 10 (24.4)
Uluutku and Kurtoglu (1999)	50 fetal	18, 19, –	4, 4, –	3, 2, –		7, 6, –, 13 (26)
Vincente et al. (2007)	40	17, 17, 17	3, 3, 3	–	–	3, 3, 3, 6 (15)
Patel et al. (2011)	86	–	3, 2, 1	–	–	3, 2, 1, 5 (5.8)
Sabnis (2012)	140	–	–	0, 1, –	–	0, 1, –, 1 (0.7)
Natsis et al. (2014)	294	–	7, 5, 3	0, 1, –	1, 0, –	8, 7[d], 3, 14 (4.8)
Sulak et al. (2014)	400 fetal	196, 196, –	3, 2, –	1, 2, –	–	4, 4, –, 8 (2)
Totals	3424	1560 (789, 771, 316)	466 (223, 243, 102)	41 (20, 21, 7)	12(9, 3, 0)	611 (297, 314, 138)

Variations are classified according to Beaton and Anson (1937); all studies are dissection-based a3 cases of variation were classified as Type E (2L, 1R); bL/R data not available for 1 specimen; cdata missing from 3 male specimens, right side; dOne case of Type F variation, right side included

Table 39.8 Relationship between piriformis and the sciatic nerve, male (M) and female (F) variations.

References	No. specimens	No. type A (M, F)	No. type B (M, F)	No. type C (M, F)	No. type D (M, F)	Total variation (M, F, number (% of all specimens))
Parsons and Keith (1897)	138[a]	69, 28	6, 7	–	1, 1	7, 8, 20 (14.5)[a]
Trotter (1932)	464					53, 11, 64 (13.8)
Kubota et al. (1960)	38			4, 1		4, 1, 5 (13.2)
Nizankowski et al. (1972)	200	99, 82	4, 4	2, 1	2, 3	10, 9, 19 (9.5)[b]
Pecina (1979)	130	–	21, 6	0, 1		21, 7, 28 (21.5)
Chiba (1992)	511	179, 149	94, 79	4, 6		98, 85, 183 (35.8)
Uluutku and Kurtoglu (1999)	50 fetal	8, 29	5, 3	1, 4		6, 7, 13 (26)
Patel et al. (2011)	86		2, 3			2, 3, 5 (5.8)
Natsis et al. (2014)	294		4, 5	0, 1	0, 1	5[c], 7, 12 (4.1)[d]
Totals	1911	643 (355, 288)	243 (136, 107)	25 (11, 14)	8 (3, 5)	344 (206, 138)

[a]Sex of 26 specimens unknown, 5 of which were included in types B–D variation; [b]three cases of variation were classified as type E (2 male, 1 female); [c]one case of type F variation, male included; [d]type B variation, 3 of 12 cases were bilateral but sex is unknown

Variations are classified according to Beaton and Anson (1937); all studies are dissection-based

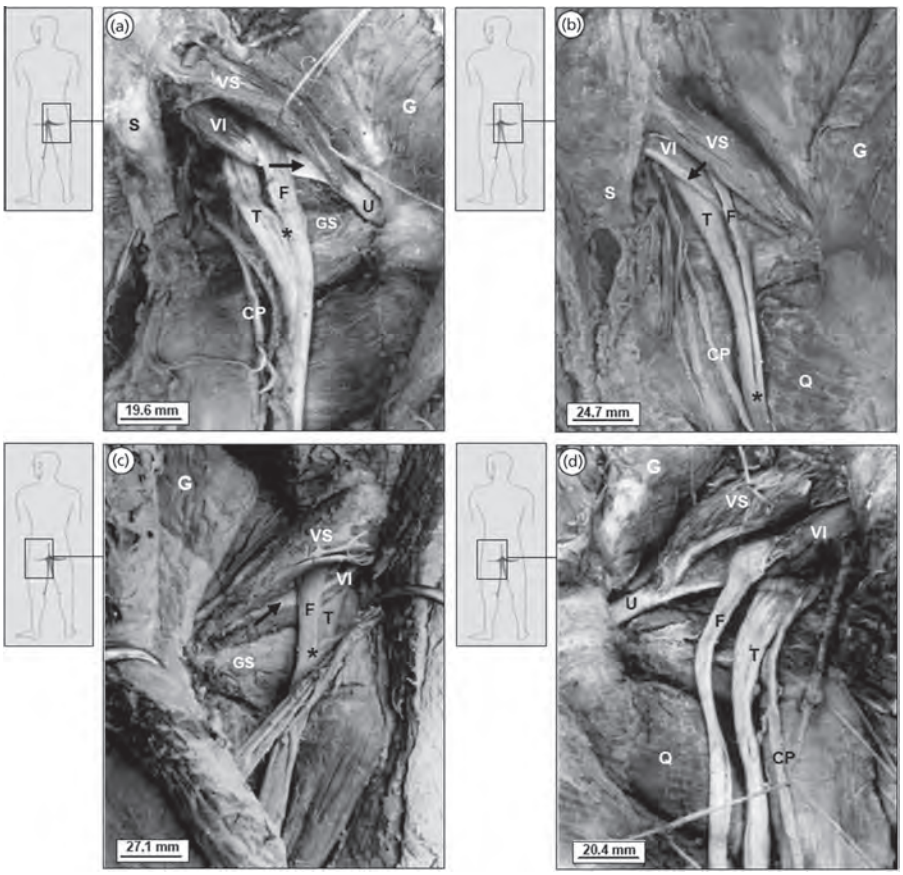

Figure 39.8 Variants of the piriformis with splitting of the sciatic nerve in the gluteal region. (a) Note the gluteus medius (G), sacrum (S), upper head of the piriformis (VS), lower head of the piriformis (VI), tibial nerve (T), common fibular nerve (F), superior gemellus (GS), fusion of the nerves (*), and posterior femoral cutaneous nerve (CP). (b) Note the more distal fusion of the nerves (*) and the tendinous lower head of the piriformis (arrow). The quadratus femoris (Q) is also seen. (c) The lower head of the piriformis is again tendinous (arrow) and note the more proximal nerve fusion (*). (d) The nerves are separated throughout. Adapted from Vincente et al. (2007).

of the muscle can cause symptoms, particularly during internal rotation of the hip (Pecina et al. 2008; Natsis et al. 2014).

Infrequently, the presence of two distinct piriformis muscle bellies may be accompanied by duplication of surrounding muscles such as the gemellus superior (Arifoglu et al. 1997), both gemelli and quadratus femoris (Tanyeli et al. 2006), or gluteus maximus (Kirici and Ozan 1999).

As a consequence of the different branching patterns of divisions of the sciatic nerve, piriformis can be divided into three muscle bellies by components of the common fibular and tibial nerves. This has been reported in 5 of 511 (Chiba 1992) and 1 of 294 (Natsis et al. 2014) specimens, respectively.

Association with surrounding muscles

Piriformis can fuse with the posterior fibers of gluteus minimus (Macalister 1866; Knott 1883; Frazer 1904; Gardner et al. 1975) or its distal tendon (Gray 1858; Flack et al. 2014). Occasionally an association is evident between the piriformis and gluteus medius muscles (Le Double 1897; Chiba 1992; Akita et al. 1994; Machado et al. 2003) with fusion noted along the lower border of piriformis almost to its insertion (Frazer 1904). Alternatively, the piriformis tendon can join with the muscle fibers of gluteus medius (Winslow 1763; Windisch et al. 2007; Flack et al. 2014). Rarely, both muscle bellies (Henle 1858; Macalister 1866; Chiba 1992; Akita et al. 1994) or tendons may fuse at their insertion onto the greater trochanter (Henle 1858; Macalister 1866; Flack et al. 2014).

An association with the gemellus superior may also exist (Knott 1883) and has been reported in up to 29.5% of cases (Machado et al. 2003; Windisch et al. 2007). When two piriformis muscle bellies are present, it is the tendon of the lower belly that blends with the gemellus superior, an anomaly seen in 5 of 511 specimens (Chiba 1992). Both the piriformis and gemellus superior tendons may also blend with that of obturator internus prior to insertion at the greater trochanter (Windisch et al. 2007). A conjoint piriformis-obturator internus tendon measuring 0.5–2.0 cm has been consistently reported in one study (Solomon et al. 2010) but observed in only 10% (3/29) of specimens in another (Pine et al. 2011).

Variations in the number of muscles

The piriformis muscle has been reported as missing in 2 of 6 specimens (Duda et al. 1996). However, this observation has been questioned and could be attributed to the existence of a very small muscle (Duda et al. 1996) or due to fusion with surrounding muscles (Testut 1884).

Two types of accessory muscle, not associated with variations in the sciatic nerve, have been described: an additional muscle superior to piriformis and an anomalous digastric muscle. The additional muscle superior to piriformis varies from a small accessory slip arising from the sacrotuberous ligament (Ravindranath et al. 2008) to a more substantial muscle (Fig. 39.9) originating from the border and inner surface (Prasad et al. 2005) or posterosuperior aspect (Tubbs and Salter 2006) of the greater sciatic foramen, or the posterior rim of the iliac bone inferior to the posterior iliac spine (Natsis et al. 2014). Running almost parallel to piriformis, the accessory muscle inserts into the greater trochanter independently (Prasad et al. 2005) or via the main piriformis tendon (Ravindranath et al. 2008), or into the posterior capsule of the hip joint together with piriformis (Tubbs and Salter 2006). In the latter case the quadratus femoris muscle was absent, and in all instances the sciatic nerve emerged inferior to piriformis (Fig. 39.9).

Figure 39.9 Right gluteal region in a cadaver. Note the piriformis (P) and sciatic nerve (S). A variant gluteal muscle (arrow) is seen just lateral to the piriformis muscle. Note the superior gluteal nerve exiting deep to the variant muscle and crossing superficial to the forceps.

Source: Tubbs and Salter (2006). Reproduced with permission from John Wiley & Sons.

Several digastric muscle variants have been described in association with piriformis and biceps femoris. The proximal muscle belly can arise from the lower fibers of piriformis (Moore 1922) or as a small accessory muscle below piriformis (Stevenson 1922; Seelaus 1927). Exiting through the greater sciatic foramen, a tendon forms and passes inferiorly through the posterior thigh. A second, small distal muscle belly is formed, being a derivative of the biceps femoris (Moore 1922; Fig. 39.10, Table 39.9).

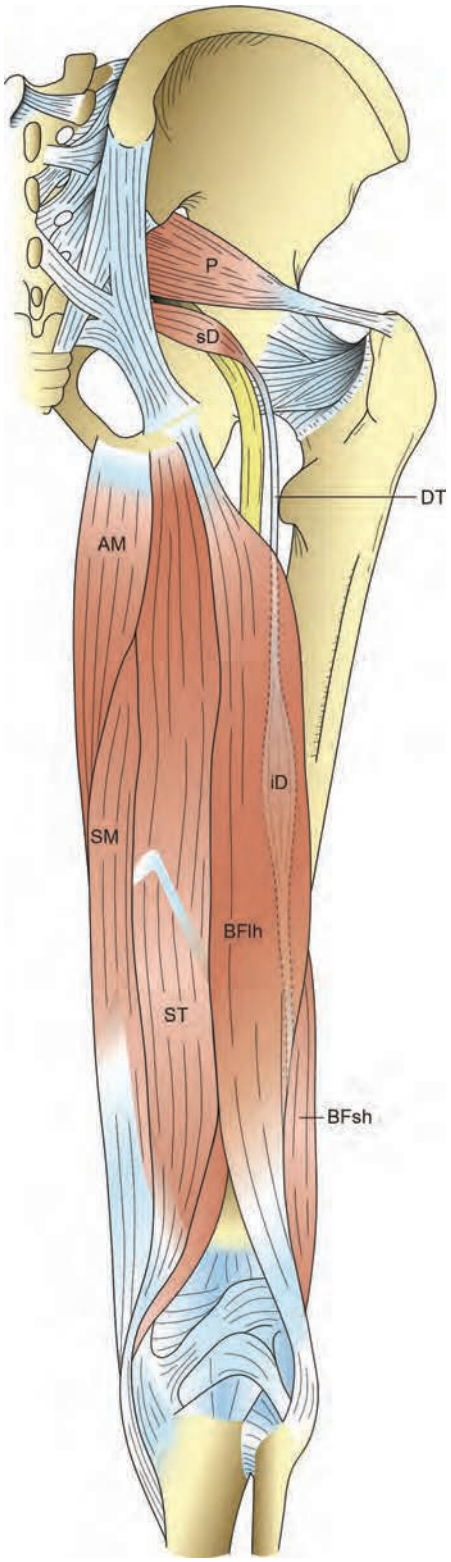

Figure 39.10 Line drawing showing an example of a digastric muscle variant in association with piriformis and biceps femoris long head, posterior view.

AM, adductor magnus; BFlh, long head of biceps femoris; BFsh, short head of biceps femoris; DT, long inter-belly tendon of digastric muscle; iD, inferior belly of digastric muscle; P, piriformis; sD, superior belly of digastric muscle; SM, semimembranosus; ST, semitendinosus.

Obturator internus

Variations of obturator internus are rare.

Attachments

Slight variations in the pelvic attachment of obturator internus have been described. Accessory slips arising from the sacrotuberous ligament or the inner surface of the ischium above the ischial spine (Knott 1883) may occur as well as the usual origin from the obturator membrane and its bony margins (Standring 2008). The muscle normally leaves the pelvis through the lesser sciatic foramen; however, a single report describes it passing behind the midpoint of the sacrotuberous ligament (Kirici et al. 1999). On leaving the pelvis, obturator internus immediately forms a tendon that inserts into the anterosuperior medial aspect of the greater trochanter. In some situations, tendinous bands form within the muscle and occasionally fibers from obturator internus join the gemellus inferior muscle belly (Aung et al. 2001; Fig. 39.11).

Variations concerning fusion of the tendon of obturator internus with the gemelli and other tendons and its attachment to the greater trochanter are described in the following sections.

Morphology

The volume of the obturator internus muscle varies over the range 5–20 mL (Duda et al. 1996) and the thickness of its muscle belly over 4.5–7 mm (Ersoy et al. 2004). Based on magnetic resonance imaging of living women, Morris et al. (2012) have shown that the volume of obturator internus decreases with age.

There are no records of obturator internus being absent, although the muscle may be divided into two parts (Gruber 1878a).

Gemelli

Gemellus superior

The gemellus superior is the smaller of the two gemelli. It normally arises from the ischial spine but may sometimes come from the upper border of the greater sciatic notch (Aasar 1947).

The gemellus superior may be missing unilaterally or bilaterally (Terry 1942; Bajka et al. 2004) and is more commonly absent than the gemellus inferior muscle (Duda et al. 1996). Wood (1867) reports the muscle as being absent either unilaterally or bilaterally in 5.7% of a British population, Testut and Latarjet (1928) report that the gemellus superior is absent in 8% of American Caucasians and 6% of American Africans, while Terry (1942) reports a higher rate of 8.6% in American Caucasians and 14.5% in American Africans. In all cases, absence was reported as being more common in men than women. Absence of the muscle has not been recorded in Chinese or Japanese populations.

Double gemelli superior may also occur (Arifoglu et al. 1997; Kirici et al. 1999; Tanyeli et al. 2006) and are often associated

Table 39.9 Attachments and innervation of digastric muscle variant associated with piriformis and biceps femoris. Adapted from Akita et al. (1992), with permission from John Wiley & Sons.

				Innervation	
Reference	**Side**	**Origin**	**Insertion**	**Superior belly**	**Inferior belly**
Moore (1922)	R	Lower anterior fibers of piriformis	Junction of BFlh and BFsh	Small branch of sciatic nerve	Twigs from nerve to BFsh
Stevenson (1922)	R	Anterior aspect of S3 and S4 vertebrae and dorsolateral surface of sacrospinous ligament	Angle between BFlh and BFsh	Small branch of anterior division of S2	Twig from tibial nerve
Seelaus (1927)	R	Anterior surface of S4 and margin of S4 foramen	Lateral surface of BFlh	Not determined	Small branch from tibial side of sciatic nerve
Niizima (1937)	L	Spina ossis ischia and inner surface of ilium	BFsh	Fine nerve from S2	Branch from common peroneal nerve
Suda and Takahashi (1957)	L	Pelvic surface of sacrum	Medial surface of BFsh	Branch from anterior primary rami of S2	Branch from common peroneal nerve

BFlh, biceps femoris long head; BFsh, biceps femoris short head; L, left; R, right

with duplication of piriformis and/or gemellus inferior. When gemellus superior is duplicated, both muscles may arise from the ischial spine (Arifoglu et al. 1997) or the upper of the pair of muscles may arise from the body of the ischium (Tanyeli et al. 2006).

The gemellus superior can fuse with piriformis (Knott 1883; Chiba 1992; Machado et al. 2003; Windisch et al. 2007) or gluteus minimus (Testut and Latarjet 1928). In the case of fusion with piriformis, this may occur as frequently as 29% (Machado et al. 2003; Windisch et al. 2007).

Gemellus inferior

The gemellus inferior arises from the upper part of the ischial tuberosity at the margin of the lesser sciatic notch and is rarely

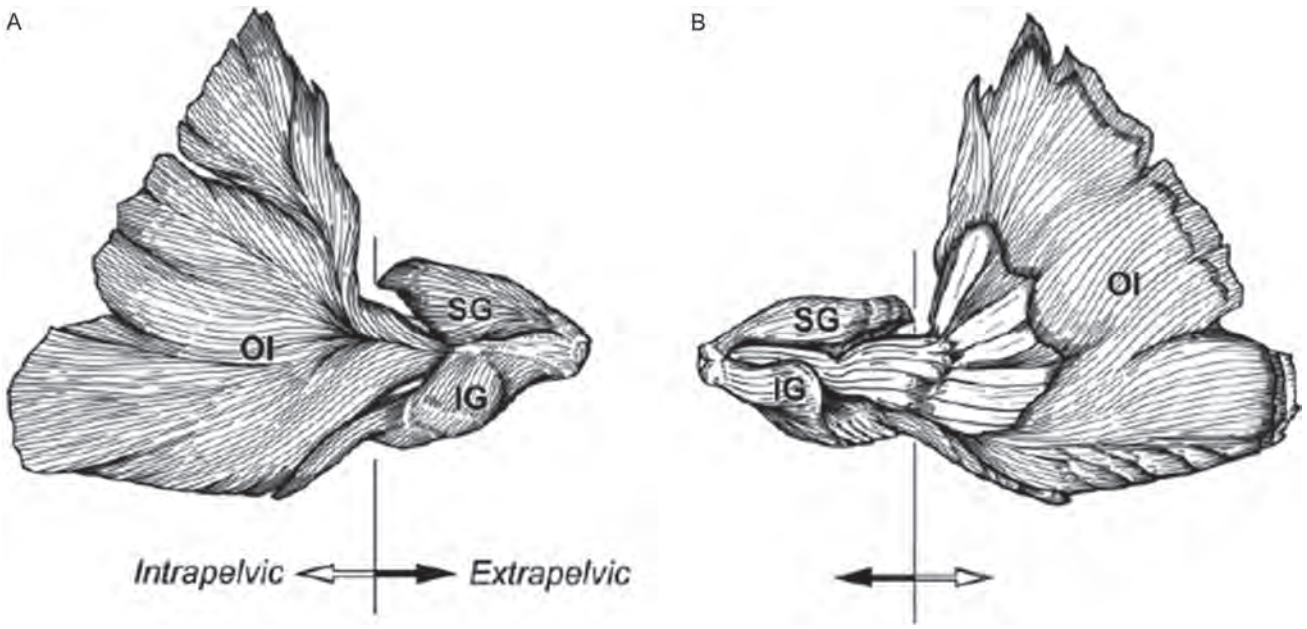

Figure 39.11 Schematic drawings of the obturator internus muscle (OI) and its variable fusion with the superior (SG) and inferior gemellus (IG) muscles. (a) Fusion of the gemelli muscles across the tendon of the obturator internus (OI), and (b) the tendon of OI separating the SG and IG muscles.

Source: Aung et al. (2001). Reproduced with permission from John Wiley & Sons.

absent (Charpey and Nicolas 1912). Duplication of gemellus inferior may occur (Tanyeli et al. 2006), and in this situation the upper part may arise from the ischial spine and the lower from the ischial tuberosity. It has been suggested that duplication of the gemelli may contribute to "piriformis syndrome" by compressing the sciatic nerve (Arifoglu et al. 1997).

The inferior gemellus may also fuse with quadratus femoris (Testut and Latarjet 1928).

Attachment of obturator internus and the gemelli to the femur

The tendons of the gemelli typically fuse with that of obturator internus to form a conjoined tendon. The three tendons are usually described as coming together in the same plane. A study by Shinohara (1995) however reports that this only occurs in 36% of cases. In 64% of cases the gemellus superior and/or inferior muscles cover the superficial surface of the obturator internus tendon (Fig. 39.12). In the extreme situation the gemelli run over the obturator tendon as an aponeurotic sheet, creating a "gemellus pocket" between the tendon and aponeurosis (Shinohara 1995). The depth of the pocket varies, but may be as much as 20 mm (Fig. 39.13).

The femoral attachments of the gemelli may be separate from that of obturator internus or can be continuous, with muscle fibers from each gemellus intertwined with those from obturator internus. The fibers of the two gemelli may also fuse on the posterior surface of obturator internus (Aung et al. 2001; Fig. 39.11).

Variation in the exact attachment of the conjoined tendon to the greater trochanter also occurs (Ito et al. 2012) and this knowledge is important when considering less invasive posterior approaches for total hip arthroplasty. The footprint of the tendon may be either elliptical or scaphoid in shape, with its anterior attachment site located 9–23 mm from the anteroinferior surface of the greater trochanter (Ito et al. 2012).

Fusion of the obturator internus with other tendons is common. In a study of 20 hips, the tendon of obturator internus was observed to fuse with the piriformis tendon in all of the specimens (Solomon et al. 2010). However, in other studies the incidence of fusion is reported to fall within the range 10–30% (Windisch et al. 2007; Pine et al. 2011). In some instances the tendon of obturator internus may fuse with the tendons of both piriformis and gluteus medius (Windisch et al. 2007) before inserting onto the greater trochanter.

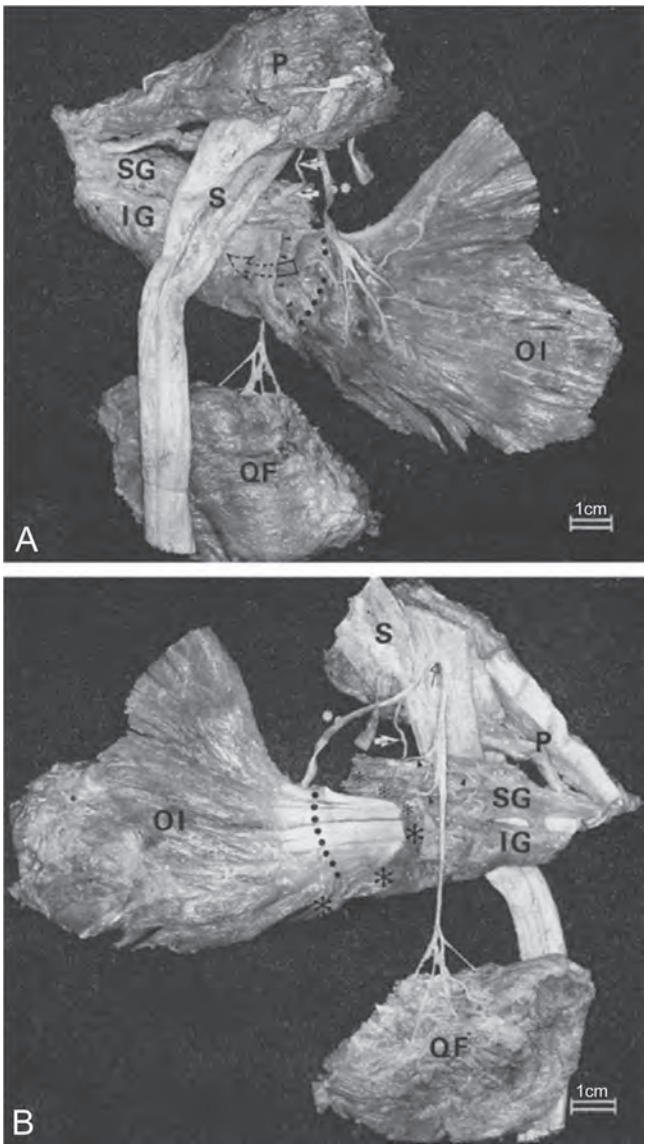

Figure 39.12 Cadaveric views of the obturator internus (OI) and superior and inferior gemellus muscles. (a) OI traveling anterior to the tendons of the gemelli muscles, and (b) a muscular fusion of the gemelli muscles posterior to the OI muscle.

P, piriformis muscle; S, sciatic nerve; SG, gemellus superior; QF, quadratus femoris.

Source: Shinohara (1995). Reproduced with permission from John Wiley & Sons.

Quadratus femoris

Variation in the attachment of quadratus femoris is rare. The quadratus femoris muscle can range in volume from 20 to 40 mL, being larger in males (Duda et al. 1996). The area of attachment to the intertrochanteric crest of the femur also varies over the range 123–733 mm^2 (Duda et al. 1996). Furthermore, when the adductor minimus muscle is absent, the femoral attachment of quadratus femoris extends more caudally along the intertrochanteric crest (Tubbs et al. 2011).

Bilateral or unilateral absence of quadratus femoris has been reported (Fig. 39.14) (Bellamy 1874; Stibbe 1929; Tubbs & Salter 2006; Liu et al. 2011) with a frequency of approximately 1% (Testut and Latarjet 1928). When quadratus femoris is absent there may be an increase in the volume of gemellus inferior (Bellamy 1874; Testut and Latarjet 1928). However, quadratus

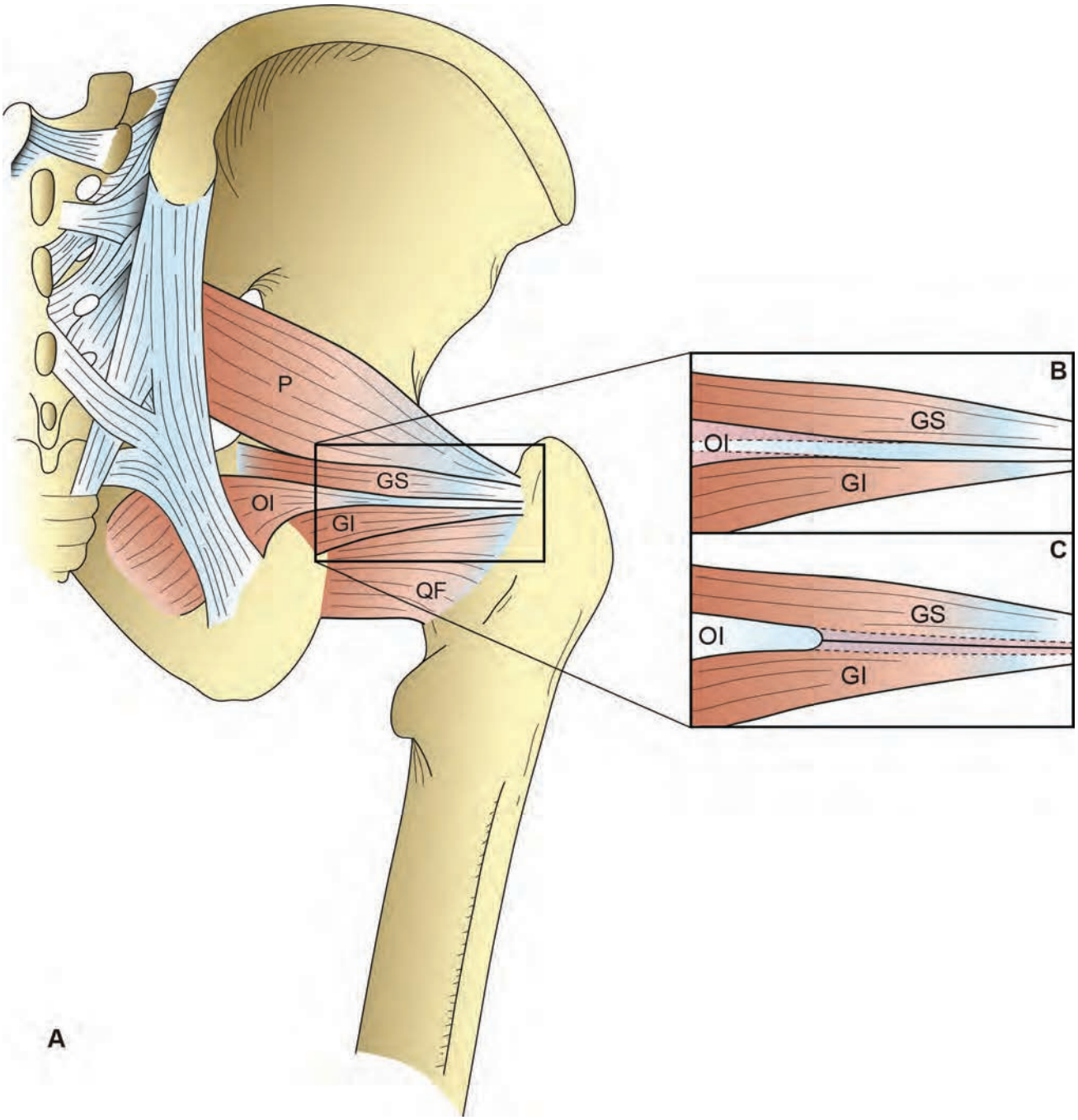

Figure 39.13 Drawing of variations in arrangements of obturator internus (OI) and gemelli, posterior view.

GI, gemellus inferior; GS, gemellus superior; P, piriformis; QF, quadratus femoris.

A) The textbook arrangement of gemellus superior (GS) and gemellus inferior (GI) joining the upper and lower borders, respectively, of the obturator internus (OI) tendon. B) The gemelli partially cover the OI tendon anteriorly. C) The gemelli completely cover the OI tendon anteriorly, forming a pocket.

femoris may be absent without any compensatory change in gemellus size (Arora and Gupta 2012).

Unilateral duplication of quadratus femoris has also been observed (Tanyeli et al. 2006). In this case report, both muscles were observed to arise from the ischial tuberosity and attach to the intertrochanteric crest (Fig. 39.15). Macalister (1866) reported that the muscle could be divided into two or occasionally three separate parts, but it is unclear whether this represents a division or duplication.

Quadratus femoris has also been reported to fuse with either the gemellus inferior or adductor magnus (Charpy and Nicolas 1912).

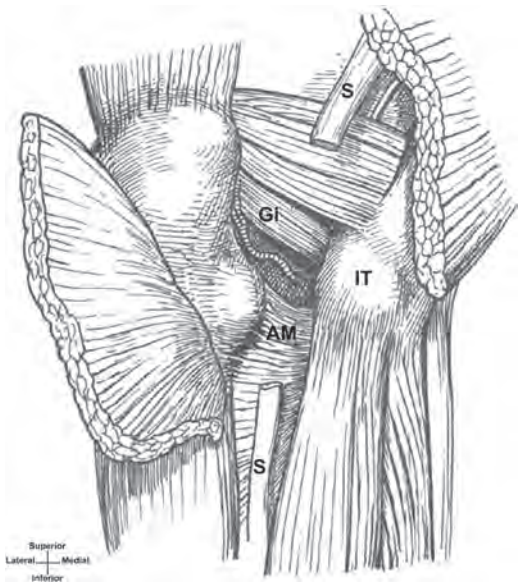

Figure 39.14 Absence of the quadratus femoris muscle. Note the sciatic nerve (cut, S), inferior gemellus (GI), ischial tuberosity (IT), and adductor magnus (AM).

Source: Stibbe (1929). Reproduced with permission from John Wiley & Sons.

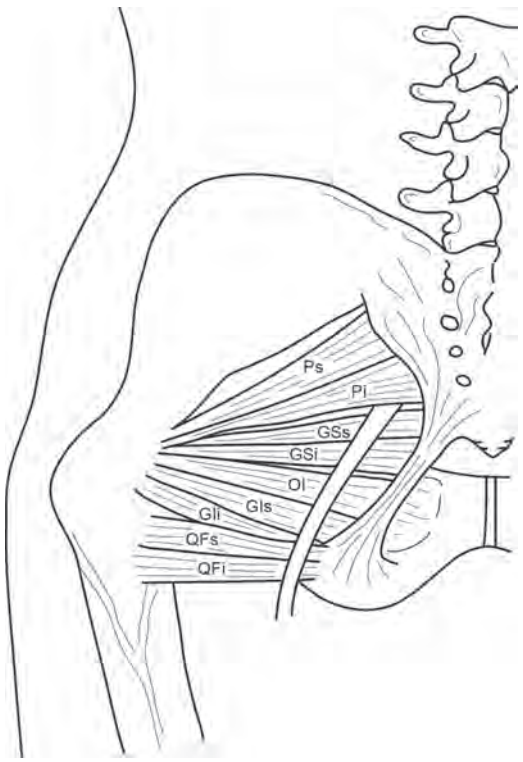

Figure 39.15 Multiple duplications of the left short lateral rotators of the hip joint: piriformis (Ps and Pi), superior gemellus (GSs and GSi), obturator internus (OI), inferior gemellus (GIs and GIi) and quadratus femoris (QFs and QFi). Line drawing of multiple duplications of the left muscles.

Source: Adapted from Tanyeli et al. (2006).

References

Aasar YH. 1947. *Anatomical Anomalies*. Cairo: Fouad I University Press.

Agur AM, Dalley AF. 2005. *Grant's Atlas of Anatomy*. Philadelphia: Lippincott Wiliams & Wilkins.

Akita K, Sakamoto H, Sato T. 1992. Innervation of an aberrant digastric muscle in the posterior thigh: Stratified relationships between branches of the inferior gluteal nerve. *J Anat* 181: 503–506.

Akita K, Sakamoto H, Sato T. 1993. Innervation of the anteromedial muscle bundles of the gluteus medius. *J Anat* 182: 433–438.

Akita K, Sakamoto H, Sato T. 1994. Arrangement and innervation of the glutei medius and minimus and the piriformis: A morphological analysis. *Anat Rec* 238: 125–130.

Al-Hayani A. 2009. The functional anatomy of hip abductors. *Folia Morphol (Warsz)* 68: 8–103.

Arifoglu Y, Sürüc HS, Sargon MF, Tanyeli E, Yazar F. 1997. Double superior gemellus together with double piriformis and high division of the sciatic nerve. *Surg Radiol Anat* 19: 407–408.

Arora K, Gupta S. 2012. A case report on absence of the quadratus femoris muscle. *GCSMC J Med Sci* 1: 71–72

Aung HH, Sakamoto HH, Akita K, Sato T. 2001. Anatomical study of the obturator internus, gemelli and quadratus femoris muscles with special reference to their innervation. *Anat Rec* 263: 41–52.

Bajka M, Manestar M, Hug J, Szekely G, Haller U, Groscurth P. 2004. Detailed anatomy of the abdomen and pelvis of the visible human female. *Clin Anat* 17: 252–260.

Bardeen CR. 1901. A statistical study of the variations in the formation and position of the lumbo-sacral plexus in man. *Anat Anz* 19: 209–239.

Basarir K, Ozsoy MH, Erdemli B, Bayramoglu A, Tuccar E, Dincel VE. 2008. The safe distance for the superior gluteal nerve in direct lateral approach to the hip and its relation with the femoral length: A cadaver study. *Arch Orthop Trauma Surg* 128: 645–650.

Battaglia PJ, Scali F, Enix DE. 2012. Co-presentation of unilateral femoral and bilateral sciatic nerve variants in one cadaver: A case report with clinical implications. *Chiropr Man Therap* 20: 34.

Beaton LE, Anson BJ. 1937. The relation of the sciatic nerve and of its subdivisions to the piriformis muscle. *Anat Rec* 70: 1–5.

Beaton LE, Anson BJ. 1938. The sciatic nerve and the piriformis muscle: their inter-relation possible cause of coccygodynia. *J Bone Joint Surg Am* 20: 686–688.

Beck M, Sledge JB, Gautier E, Dora CF, Ganz R. 2000. The anatomy and function of the gluteus minimus muscle. *J Bone Joint Surg Br* 82: 358–363.

Bellamy E. 1874. Note on the absence of the quadratus femoris muscle and on a spine possessing a sixth lumbar vertebra, the first rib being rudimentary. *J Anat Physiol* 9: 185–186.

Benson ER, Schutzer SF. 1999. Posttraumatic piriformis syndrome: diagnosis and results of operative treatment. *J Bone Joint Surg Am* 81: 941–949.

Benzon HT, Katz JA, Benzon HA, Iqbal MS. 2003. Piriformis syndrome: Anatomic considerations, a new injection technique, and a review of the literature. *Anesthesiology* 98: 1442–1448.

Brand RA, Pedersen DR, Friederich JA. 1986. The sensitivity of muscle force prediction to changes in physiologic cross-sectional area. *J Biomech* 19: 589–596.

Brooks JBB, Silva CAC, Soares SA, Kai MR, Cabral RH, Fragoso YD. 2011. Anatomical variations of the sciatic nerve in a group of Brazilian cadavers. *Revista Dor Sao Paulo* 12: 332–336.

Cassidy L, Walters A, Bubb K, Shoja MM, Tubbs RS, Loukas M. 2012. Piriformis syndrome: Implications of anatomical variations, diagnostic techniques, and treatment options. *Surg Radiol Anat* 34: 479–486.

Charpy A, Nicolas A. 1912. *Traite d'Anatomie Humaine*. Paris: Masson et Cie.

Chen WS. 1994. Bipartite piriformis muscle: An unusual cause of sciatic nerve entrapment. *Pain* 58: 269–272.

Chiba S. 1992. Multiple positional relationships of nerves arising from the sacral plexus to the piriformis muscle in humans. *Kaibogaku Zasshi* 67: 691–724.

Chiba S, Ishibashi Y, Kasai T. 1994. Perforation of dorsal branches of the sacral nerve plexus through the piriformis muscle and its relation to changes of segmental arrangements of the vertebral column and others. *Kaibogaku Zasshi* 69: 281–305.

Chukwuanukwu TOG, Ukoha UU, Chukqujekwu IE, Asomugha AL, Oranusi CK, Anyabolu AE, Nzeako HC, Nwajagu GI, Ashaolu JO. 2007. Bilateral high division of the sciatic nerve: Incidence and clinical implications in Nigeria. *Trop J Med Res* 11: 12–13.

Clark JM, Haynor DR. 1987. Anatomy of the abductor muscles of the hip as studied by computed tomography. *J Bone Joint Surg Am* 69: 1021–1031.

Connell DA, Bass C, Sykes CJ, Young D, Edwards E. 2003. Sonographic evaluation of gluteus medius and minimus tendinopathy. *Eur Radiol* 13: 1339–1347.

Dall, D. 1986. Exposure of the hip by anterior osteotomy of the greater trochanter. A modified anterolateral approach. *J Bone Joint Surg Br* 68: 382–386.

Delabie A, Peltier J, Havet E, Page C, Foulon P, Le Gars D. 2013. Relationships between piriformis muscle and sciatic nerve: Radioanatomical study with 104 buttocks. *Morphologie* 97: 12–18.

Delp SL, Bleck EE, Zajaz FE, Bollini G. 1990. Biomechanical analysis of the chiari pelvic osteotomy: Preserving hip abductor strength. *Clin Orthop* 254: 189–198.

Demiryurek D, Bayramoglu A, Erbil M, Aldur MM, Sargon MF. 2002. Bilateral divided piriformis muscle together with the high division of the sciatic nerve. *Gazi Medical Journal* 13: 41–44.

Drake R, Vogl AW, Mitchell AWM. 2012. *Gray's Basic Anatomy*. Edinburgh: Churchill Livingstone.

Duda GN, Brand D, Freitag S, Lierse W, Schneider E. 1996. Variability of femoral muscle attachments. *J Biomech* 29: 1185–1190.

Duparc F, Thomine JM, Dujardin F, Durand C, Lukaziewicz M, Muller JM, Freger P. 1997. Anatomic basis of the transgluteal approach to the hip-joint by anterior hemimyotomy of the gluteus medius. *Surg Radiol Anat* 19: 61–67.

Ersoy M, Sagsoz N, Bozkurt MC, Apaydin N, Elhan A, Tekdemir I. 2004. Important anatomical structures used in paravaginal defect repair: Cadaveric study. *Eur J Obstet Gynecol Reprod Biol* 112: 206–213.

Fishman LM, Dombi GW, Michaelsen C, Ringel S, Rozbruch J, Rosner B, Weber C. 2002. Piriformis syndrome: Diagnosis, treatment, and outcome: A 10-year study. *Arch Phys Med Rehabil* 83: 295–301.

Flack NAMS, Nicholson HD, Woodley SJ. 2012. A review of the anatomy of the hip abductor muscles, gluteus medius, gluteus minimus, and tensor fascia lata. *Clin Anat* 25: 697–708.

Flack NAMS, Nicholson HD, Woodley SJ. 2014. The anatomy of the hip abductor muscles. *Clin Anat* 27(2): 241–253.

Frazer E. 1904. The insertion of the pyriformis and obturator internus, and formation of the posterior circular capsular fibers and upper retinaculum of Weitbrecht. *J Anat Physiol* 38: 170–185.

Frick H, Leonhardt H, Starck D. 1991. *Human Anatomy 1 General Anatomy, Special Anatomy: Limbs, Trunk Wall, Head and Neck. (D Meyer, trans)*. New York: Thieme Medical Publishers, Inc.

Friederich JA, Brand RA. 1990. Muscle fiber architecture in the human lower limb. *J Biomech* 23: 91–95.

Fukumoto N. 1935. Uber den m. piriformis und n. ischiadicus von Japanern. *Fukuoka Igaky Zasshi* 28: 39.

Gabrielli C, Ambrosio JD, Prates JC, Olave E. 1994. Relacoes topograficas entre o nervo isquiatico e o musculo piriforme. *Rev Bras Ciênc Morfol* 11: 8–12.

Gabrielli C, Olave E, Mandiola E, Rodrigues CF. 1997. Trayecto del nervio gluteo inferior asociado a la division alta del nervio isquiatico. *Revista Chilena de Anatomía* 15: 79–83.

Gardner E, Gray DJ, O'Rahilly R. 1975. *Anatomy. A Regional Study of Human Structure*, fourth edition. Philadelphia: W.B. Saunders Company.

Georgiadis GM, Olexa TA, Ebraheim NA. 1996. Entry sites for antegrade femoral nailing. *Clin Orthop Relat Res* 330: 281–287.

Gottschalk F, Kourosh S, Leveau B. 1989. The functional anatomy of tensor fasciae latae and gluteus medius and minimus. *J Anat* 166: 179–189.

Gray H. 1858. *Anatomy Descriptive and Surgical*. London: John W. Parker and Son.

Grimaldi A, Richardson C, Stanton W, Durbridge G, Donnelly W, Hides J. 2009a. The association between degenerative hip joint pathology and size of the gluteus medius, gluteus minimus and piriformis muscles. *Man Ther* 14: 605–610.

Grimaldi A, Richardson C, Durbridge G, Donnelly W, Darnell R, Hides J. 2009b. The association between degenerative hip joint pathology and size of the gluteus maximus and tensor fascia lata muscles. *Man Ther* 14: 611–617.

Gruber W. 1878a. Ein Musculus obturator internus biceps. *Virchows Archiv fur Pathologische Anatomie und Physiologie und fur Klinische Medizin* 73: 348–350.

Gruber W. 1878b. Ueber den Gesäss-Mittelfleischmuskel (Musculus gluteo-perinealis). *Archiv für pathologische Anatomie und Physiologie und für Klinische Medicin* 74: 456–460.

Gruber W. 1887. Ueber einen Musculus glutaeus quartus bei dem Menschen (1. u. 2. Fall) und einen homologen Muskel bei Säugethieren. *Archiv für pathologische Anatomie und Physiologie und für Klinische Medicin* 107: 480–484.

Guvencer M, Iyem C, Akyer P, Tetik S, Naderi S. 2009. Variations in the high division of the sciatic nerve and relationship between the sciatic nerve and the piriformis. *Turk Neurosurg* 19: 139–144.

Hamid S, Rekha RS. 2012. An anatomical variation of unilateral higher division of sciatic nerve with bifid piriformis and its clinical implications. *Indian J Res Rep Med Sci* 2: 23–25.

Harty M. 1982. Symposium on surface replacement arthroplasty of the hip. Anatomic considerations. *Orthop Clin North Am* 13: 667–679.

Heimkes B, Posel P, Bolkart M. 1992. The transgluteal approaches to the hip. *Arch Orthop Trauma Surg* 111: 220–223.

Heimkes B, Posel P, Plitz W, Jansson V. 1993. Forces acting on the juvenile hip joint in the one-legged stance. *J Pediatr Orthop* 13: 431–436.

Henle J. 1858. *Handbuch der Systematichen Anatomie des Menschen*. Brunswick: Druck und Verlag von Friedrich Vieweg und Sohn.

Hwang K, Nam YS, Han SH, Hwang SW. 2009. The intramuscular course of the inferior gluteal nerve in the gluteus maximus muscle and augmentation gluteoplasty. *Ann Plast* 63: 361–365.

Inan M, Alkan A, Harma A, Ertem, K. 2005. Evaluation of the gluteus medius muscle after a pelvic support osteotomy to treat congenital dislocation of the hip. *J Bone Joint Surg Am* 87: 2246–2252.

Inayat Q, Ilahi M, Chishti AT, Humma Z. 2010. Topographical variations of the sciatic nerve in Pakistani population. *Medical Forum Monthly* 21: 10–13.

Indrekvam K, Sudmann E. 2002. Piriformis muscle syndrome in 19 patients treated by tenotomy: A 1 to 16 year follow-up study. *Int Orthop* 26: 101–103.

Ito Y, Matsushita I, Watanabe H, Kimura T. 2012. Anatomic mapping of short external rotators shows the limit of their preservation during total hip arthroplasty. *Clin Orthop* 470: 1690–1695.

Jaegers SMHJ, Dantuma R, de Jongh HJ. 1992. Three-dimensional reconstruction of the hip muscles on the basis of magnetic resonance images. *Surg Radiol Anat* 14: 241–249.

Jawish RM, Assoum HA, Khamis CF. 2010. Anatomical, clinical and electrical observations in piriformis syndrome. *J Orthop Surg Res* 5: 3–9.

Jazuta KM. 1931. Glutaeus medius accessories. *Anat Anz* 72: 10–11.

Jensen RH, Metcalf WK. 1975. A systematic approach to the quantitative description of musculo-skeletal geometry. *J Anat* 119: 209–221.

Jia M, Xia Q, Sun J, Zhou Q, Wang W. 2008. Anatomical study of sciatic nerve and common peroneal nerve compression. *Neural Regeneration Research* 3: 621–624.

Kaplan EB. 1958. The iliotibial tract: Clinical and morphological significance. *J Bone Joint Surg Am* 40: 817–832.

Khan Y, Khan T. 2011. A rare case of bilateral high division of sciatic nerve (of different types) with unilateral divided piriformis and unusual high origin of genicular branch of common fibular nerve. *Int J Anat Var* 4: 63–66.

Kirici Y, Ozan H. 1999. Double gluteus maximus muscle with associated variations in the gluteal region. *Surg Radiol Anat* 21: 397–400.

Kirici Y, Yazar F, Ozan H. 1999. The neurovascular and muscular anomalies of the gluteal region: an atypical pudendal nerve. *Surg Radiol Anat* 21: 393–396.

Knott JF. 1883. Muscular anomalies, including those of the diaphragm, and subdiaphragmatic regions of the human body. *P Roy Irish Acad* 3: 627–641.

Knox R. 1831. *A system of human anatomy: on the basis of the "Traite d'anatomie descriptive" of M. H. Cloquet*. Second edition. Edinburgh: Maclachlan and Stewart.

Kobbe P, Zelle BA, Gruen GS. 2008. Case report: Recurrent piriformis syndrome after surgical release. *Clin Orthop* 466: 1745–1748.

Kosukegawa I, Yoshimoto M, Isogai S, Nonaka S, Yamashita T. 2006. Piriformis syndrome resulting from a rare anatomic variation. *Spine* 31: 664–666.

Kubota K, Noguchi I, Nakano T. 1960. Rare types of relation between the sciatic nerve and the piriformis muscle. *Okajimas Folia Anat Jap* 36: 329–343.

Le Double AF. 1897. *Traité des variations du système musculaire de l'home et de leur signification au point de vue de l'anthropologie zoologique, volume two*. Paris: Schleicher Frères.

Lee CS, Tsai TL. 1974. The relation of the sciatic nerve to the piriformis muscle. *J Formos Med Assoc* 73: 75–80.

Lippert H. 1962. Wachstum und rückbildung menschlicher skelemuskeln. *Zeitschrift für Anatomie und Entwicklungsgeschichte Bd* 123: 9–31.

Little JW 3rd, Lyons JR. 1983. The gluteus medius-tensor fascia latae flap. *Plast Reconstr Surg* 71: 366–370.

Liu H, Fletcher J, Garrison MK, Holmes C. 2011. Bilateral absence of quadratus femoris and semimembranosus. *International Journal of Anatomical Variations* 4: 40–42.

Liu R, Wen X, Tong Z, Wang K, Wang C. 2012. Changes of gluteus medius muscle in the adult patients with unilateral developmental dysplasia of the hip. *BMC Musculoskelet Disord* 13: 101–107.

Macalister A. 1866. Notes on muscular anomalies in human anatomy. *P Roy Irish Acad* 9: 444–469.

Macalister A. 1867. Further notes on muscular anomalies in human anatomy, and their bearing upon homotypical myology. *P Roy Irish Acad* 10: 121–164.

Macalister A. 1871. Additional observation on muscular anomalies in human anatomy (third series), with a catalogue of the principal muscular variations hitherto published. *Transactions of the Royal Irish Academy* 25: 1–134.

Macalister A. 1875 Observations on the muscular anomalies in the human anatomy. Third series with a catalogue of the principal muscular variations hitherto published. *Trans Roy Irish Acad Sci* 25: 1–130.

Machado FA, Babinski MA, Brasil FB, Favorito LA, Abidu-Figueiredo M, Costa MG. 2003. Variaciones anatomicas entre el nervio isquiatico y el musculo piriforme durante el periodo fetal humano. *Int J Morphol* 21: 29–35.

Martin HD, Shears SA, Johnson JC, Smathers AM, Palmer IJ. 2011. The endoscopic treatment of sciatic nerve entrapment/deep gluteal syndrome. *Arthroscopy* 27: 172–181.

Mas N, Ozeksi P, Ozdemir B, Kapakin S, Sargon MF, Celik HH, Yener N. 2003. A case of bilateral high division of the sciatic nerves, together with a unilateral unusual course of the tibial nerve. *Neuroanatomy* 2: 13–15.

McConnell T, Tornetta P 3rd, Benson E, Manuel J. 2003. Gluteus medius tendon injury during reaming for gamma nail insertion. *Clin Orthop* 407: 199–202.

Misra BD. 1954. The relation of the sciatic nerve to the piriformis in Indian cadavers. *J Anat Soc India* 3: 28–33.

Molini L, Precerutti M, Gervasio A, Draghi F, Bianchi S. 2011. Hip: Anatomy and US techniques. *J Ultrasound* 14: 99–108.

Moore AT. 1922. An anomalous connection of the piriformis and biceps femoris muscles *Anat Rec* 23: 306–309.

Morris VC, Murray MP, Dlancey JOL, Ashton-Miller JA. 2012. A comparison of the effect of age on levator ani and obturator internus muscle cross-sectional areas and volumes in nulliparous women. *Neurourol Urodyn* 31: 481–486.

Muthu Kumar T, Srimathi, Rani A, Latha S. 2011. A cadaveric study of sciatic nerve and it's level of bifurcation. *J Clin Diag Res* 5: 1502–1504.

Natsis K, Totlis T, Konstantindis GA, Paraskevas G, Piagkou M, Koebke J. 2014. Anatomical variations between the sciatic nerve and the piriformis muscle: A contribution to surgical anatomy in piriformis syndrome. *Surg Radiol Anat* 36(3): 273–280.

Nazarian S, Tisserand P, Brunet C, Müller ME. 1987. Anatomic basis of the transgluteal approach to the hip. *Surg Radiol Anat* 9: 27–35.

Ndiaye A, Sakho Y, Fall F, Dia A, Sow ML. 2004. Sciatic nerve in gluteal portion: application of sciatic nerve post injection lesion. *Morphologie* 88: 135–138.

Niizima M. 1937. Ein fall von iiberzahligem kopf des m. biceps femoris beim menschen. *Okaj Fol Anat Jap* 16: 187–192.

Nizankowski C, Slociak J, Szybejko J. 1972. Variations in the anatomy of the sciatic nerve in man. *Folia Morphol (Warsz)* 31: 507–513.

Nork SE, Schär M, Pfander G, Beck M, Djonov V, Ganz R, Leunig M. 2005. Anatomic considerations for the choice of

surgical approach for hip resurfacing arthroplasty. *Orthop Clin North Am* 36: 163–170.
Ogeng'o JA, El-Busaidy H, Mwika PM, Khanbhai MM, Munguti J. 2011. Variant anatomy of sciatic nerve in a black Kenyan population. *Folia Morphol (Warsz)* 70: 175–179.
Okraszewska E, Migdalski L, Jedrzejewski KS, Bolanowski W. 2002. Sciatic nerve variations in some studies on the Polish population and its statistical significance. *Folia Morphol (Warsz)* 61: 277–282.
Pais D, Casal D, Bettencourt Pires MA, Furtado A, Bilhim T, Angelica-Almeida M, Goyri-O'Neill J. 2013. Sciatic nerve high division: Two different anatomical variants. *Acta Med Port* 26: 208–211.
P'an MT. 1941. The relation of the sciatic nerve to the piriformis muscle in the Chinese. *Am J Phys Anthropol* 28: 375–380.
Papadopoulos EC, Khan SN. 2004. Piriformis syndrome and low back pain: A new classification and review of the literature. *Orthop Clin North Am* 35: 65–71.
Parsons FG, Keith A. 1897. Sixth annual report of the Committee of Collective Investigation of the Anatomical Society of Great Britain and Ireland 1895–96. *J Anat Physiol* 31: 31–44.
Patel S, Shah M, Vora R, Zalawadia, A, Rathod SP. 2011. A variation in the high division of the sciatic nerve and its relation with piriformis muscle. *Natl J Med Res* 1: 27–30.
Paterson AM. 1893. The origin and distribution of the nerves to the lower limb. *J Anat Physiol* 28: 84–95.
Paval J, Nayak S. 2006. A case of bilateral high division of sciatic nerve with a variant inferior gluteal nerve. *Neuroanatomy* 5: 33–34.
Pecina HI, I. Boric Smoljanovic T, Duvancic D, Pecina M. 2008. Surgical evaluation of magnetic resonance imaging findings in piriformis muscle syndrome. *Skeletal Radiol* 37: 1019–1023.
Pecina M. 1979. Contribution to the etiological explanation of the piriformis syndrome. *Acta Anat* 105: 181–187.
Pérez M M, Llusá M, Ortiz JC, Lorente M, Lopez I, Lazaro A, Pérez A, Götzens V. 2004. Superior gluteal nerve: Safe area in hip surgery. *Surg Radiol Anat* 26: 225–229.
Pfirrmann CWA, Chung CB, Theumann, NH, Trudell DJ, Resnick D. 2001. Greater trochanter of the hip: Attachment of the abductor mechanism and a complex of three bursae: MR imaging and MR bursography in cadavers and MR imaging in asymptomatic volunteers. *Radiology* 221: 469–477.
Pine J, Binns M, Wright P, Soames, R. 2011. Piriformis and obturator internus morphology: A cadaveric study. *Clin Anat* 24: 70–76.
Pokorny D, Sosna A, Veigl P, Jahoda D. 1998. Anatomic variability of the relation of pelvitrochanteric muscles and sciatic nerve. *Acta Chir Orthop Traumatol Cech* 65: 336–339.
Pokorny D, Jahoda D, Veigl D, Pinskerova V, Sosna A. 2006. Topographic variations of the relationship of the sciatic nerve and the piriformis muscle and its relevance to palsy after total hip arthroplasty. *Surg Radiol Anat* 28: 88–91.
Prasad AM, Nayak BS, Deepthinath R, Vallala VR, Bhat S. 2005. Clinically important variations in the lower limb: A case report. *Eur J Anat* 9: 167–169.
Preininger B, Schmorl K, von Roth P, Winkler T, Schlattmann P, Matziolis G, Perka C, Tohtz S. 2011. A formula to predict patients' gluteus medius muscle volume from hip joint geometry. *Man Ther* 16: 447–451.
Preininger B, Schmorl K, von Roth P, Winkler T, Matziolis G, Perka C, Tohtz S. 2012. The sex specificity of hip-joint muscles offers an explanation for better results in men after total hip arthroplasty. *Int Orthop* 36: 1143–1148.
Rabi S, Vettivel S. 2003. Gluteus minimus muscle: Insertion to hip joint capsule in south indian fetuses. *Eur J Anat* 7: 135–137.
Ramirez OM, Hurwitz DJ, Futrell JW. 1984. The expansive gluteus maximus flap. *Plast Reconstr Surg* 74: 575–768.
Rastogi R, Budhiraja V, Asthana AK. 2011. Common peroneal component of sciatic nerve piercing piriformis muscle: Piriformis syndrome versus sciatica. *Medico-Legal Update: An International Journal* 11: 104–105.
Ravindranath Y, Manjunath KY, Ravindranath R. 2008. Accessory origin of the piriformis muscle. *Singapore Med J* 49: 217–218.
Retamal P, Galaz C, Cabezas J, Cruzat C, Olave E. 2012. Variaciones del nervio isquiatico en relacion al musculo piriforme. *Int J Morphol* 30: 1252–1255.
Robertson WJ, Gardner MJ, Barker JU, Boraiah S, Lorich DG, Kelly BT. 2008. Anatomy and dimensions of the gluteus medius tendon insertion. *Arthroscopy* 24: 130–136.
Sabnis AS. 2012. Anatomical variations of sciatic nerve bifurcation in human cadavers. *J of Clin Res Lett* 3: 46–48.
Sayson SC, Ducey JP, Maybrey JB, Wesley RL, Vermillion D. 1994. Sciatic entrapment neuropathy associated with an anomalous piriformis muscle. *Pain* 59: 149–152.
Seelaus HK. 1927. On certain muscle anomalies of the lower extremity. *Anat Rec* 35: 185–191.
Sharma T, Singla RK, Lalit M. 2010. Bilateral eventration of sciatic nerve. *JNMA J Nepal Med Assoc* 50: 309–312.
Shinohara H. 1995. Gemelli and obturator internus muscles: different heads of one muscle? *Anat Rec* 243: 145–150.
Smoll N, Ebrall P. 2010. The piriformis muscle and its relationship to the autonomics of the pelvis: A single bilateral case. *Chiropr J Aust* 40: 86–87.
Solomon LB, Lee YC, Callary SA, Beck M, Howie DW. 2010. Anatomy of piriformis, obturator internus and obturator externus: implications for the posterior surgical approach to the hip. *J Bone Joint Surg Br* 92: 1317–1324.
Spinner RJ, Thomas NM, Kline DG. 2001. Failure of surgical decompression for a presumed case of piriformis syndrome. Case report. *J Neurosurg* 94: 652–654.
Sripanidkulchai K, Pannagrong W, Amarttayakong P, Tumsan Y, Chaichun A. 2012. Glutoperineus muscle: A rare cases in the gluteal region. Proceed Anat Assoc Thai Dec 6–8.
Srivastava HC, Joshi AD. 1969. Insertions of piriformis, obturator internus and gluteus medius muscles on the femur. *J Anat Soc India* 18: 91–93.
Standring S. 2008. *Gray's Anatomy: The Anatomical Basis of Clinical Practice*, 40th edition. Edinburgh: Churchill Livingstone.
Steel HH. 1980. Gluteus medius and minimus insertion advancement for correction of internal rotation gait in spastic cerebral palsy. *J Bone Joint Surg Am* 62: 919–927.
Stern JTJr. 1972. Anatomical and functional specializations of the human gluteus maximus. *Am J Phys Anthropol* 36: 315–340.
Stevenson PH. 1922. On an anomalous digastric muscle in the thigh of a Chinese. *Anat Rec* 23: 281–290.
Stibbe E P. 1929. Complete absence of the quadratus femoris. *J Anat* 64: 97.
Suda M, Takahashi K. 1957. A rare case of an anomalous digastric muscle in the thigh. *Sapporo Med J* 14: 134–137.
Sulak O, Sakalli B, Ozguner G, Kastamoni Y. 2014. Anatomical relation between sciatic nerve and piriformis muscle and its bifurcation level during fetal period in human. *Surg Radiol Anat* 36(3): 265–272.

Tanyeli E, Pestemalci T, Uzel M, Yildirim M. 2006. The double deep gluteal muscles. *Saudi Med J* 27: 385–386.

Terry RJ. 1942. Absence of superior gemellus muscle in American whites and Negroes. *Am J Phys Anthropol* 29: 47–56.

Testut JL. 1884. *Les anomalies musculaires chez l'homme expliquées par l'anatomie compare leur importance en anthropologie*. Paris: G. Masson.

Testut L, Latarjet A. 1928. *Traité d'Anatomie Humaine*, eighth edition. Paris: G. Doin & Cie.

Trotter M. 1932. The relation of the sciatic nerve to the piriformis muscle in American whites and Negroes. *Anat Rec* 52: 321–323.

Tubbs RS, Salter EG. 2006. A variant gluteal muscle. *Clin Anat* 19: 729.

Tubbs RS, Griessenauer C, Marshall T, Dennison CP, Shoja MM, Loukas M, Apaydin N, Cohen-Gadol AA. 2011. The adductor minimus muscle revised. *Surg Radiol Anat* 33: 429–432.

Ugrenović S, Jovanović I, Krstić V, Stojanović V, Vasović L, Antić S, Pavlović S. 2005. The level of the sciatic nerve division and its relations to the piriform muscle. *Vojnosanit Pregl* 62: 45–49.

Uluutku MH, Kurtoglu Z. 1999. Variations of nerves located in deep gluteal region. *Okajimas Folia Anat Jap* 76: 273–276.

Vincente EJD, Viotto MJS, Barbosa CAA, Vincente PC. 2007. Study on anatomical relationships and variations between the sciatic nerve and piriformis muscle. *Revista Brasileira de Fisioterapia* 11: 197–202.

Vleeming A, Pool-Goudzwaard AL, Stoeckart R, van Wingerden JP, Snijders CJ. 1995. The posterior layer of the thoracolumbar fascia. Its function in load transfer from spine to legs. *Spine* 20: 753–758.

Walters J, Solomons M, Davies J. 2000. Gluteus minimus: Observations on its insertion. *J Anat* 198: 239–242.

Ward SR, Eng CM, Smallwood LH, Lieber RL. 2009. Are current measurements of lower extremity muscle architecture accurate? *Clin Orthop* 467: 1074–1082.

Weber M, Ganz R. 2002. The anterior approach to hip and pelvis. Modified Smith–Petersen approach and its possibilities for extension. *Orthopedics and Traumatology* 10: 245–257.

Windisch G, Braun EM, Anderhuber F. 2007. Piriformis muscle: Clinical anatomy and consideration of the piriformis syndrome. *Surg Radiol Anat* 29: 37–45.

Winslow JB. 1763. *An Anatomical Exposition of the Structure of the Human Body (G Douglas, trans)*, fifth edition. London: Alexander Donaldson and John Reid.

Wood J. 1867. Variation in human myology observed during the winter session of 1867–1868 at King's College, London. Proc Roy Soc Lond B 16: 483–525.

Woodburne RT, Burkel WE. 1988. *Essentials of Human Anatomy*, eighth edition. New York: Oxford University Press.

Woodley SJ, Mercer SR, Nicholson HD. 2008. Morphology of the bursae associated with the greater trochanter of the femur. *J Bone Joint Surg Am* 90: 284–294.

Woyski D, Olinger A, Wright B. 2013. Smaller insertion area and inefficient mechanics of the gluteus medius in females. *Surg Radiol Anat* 35(8): 713–719.

Zhang X, Shen H, Qin X, Wang Q. 2008. Anterolateral muscle sparing approach total hip arthroplasty: An anatomic and clinical study. *Chung Hua I Hsueh Tsa Chih* 121: 1358–1363.

40 Thigh muscles

Maira du Plessis and Marios Loukas
St. George's University, School of Medicine, St. Georges, Grenada

Anterior compartment

Tensor fascia lata

The tensor fascia lata attaches by muscular and tendinous components from the external aspect of the iliac crest and anterior superior iliac spine to the fascia lata around the area of the head of the fibula (Lizars 1827). Its proximal attachment may extend as far as the fascia of gluteus medius and the length may vary considerably (Standring 2009), or it may be absent. This muscle is occasionally found doubled longitudinally, partially or completely. Accessory slips have been reported proceeding from the iliac crest, inguinal ligament, or aponeurosis of the abdominal wall. Union with gluteus maximus has been observed.

Scansorius

The scansorius is a muscle found mainly in non-human primates and runs from the anterior superior iliac spine, the lateral lip of the iliac crest, and the fascia lata that covers the muscle, passing in the same plane as gluteus medius, and inserts into the oblique line on the lateral surface of the greater trochanter (Ochiltree 1912).

Musculus saphenous

Tyrie (1894) reported the presence of a muscle (of Tyrie) attaching to the inguinal ligament (Poupart's ligament) laterally and to the medial border of sartorius about an inch long. The muscle was found bilaterally in a 65-year-old male and looped under the arch made by the saphenofemoral junction. It passed superficial to pectineus, adductor longus, and brevis, as well as the femoral artery. A tendinous attachment to the medial aspect of the inguinal ligament was seen as its termination. The attachment points of the muscle were tendinous with fleshy muscular belly in between (Tyrie 1894). Unlike the remaining muscles of the anterior compartment, it was innervated by the iliohypogastric nerve. Figure 40.1 illustrates the muscle and its nerve supply as well as the relationship to the great saphenous vein which lead to its naming.

Sartorius

Sartorius may be absent, partially absent (Fig. 40.2), or duplicated in its entire length; it may also be bifurcated proximally or distally. An extra proximal head may attach to the pectineal line, iliopectineal eminence (Brock 1879), femoral sheath, a notch below the anterior superior iliac spine, inguinal ligament, or even the pubic symphysis (Bergman et al. 1988). These heads may join the sartorius anywhere; even the most distal third of the muscle and can be substantial in thickness (Brock 1879). Additional tendons may attach distally to the anteromedial aspect of the patella, medial condyle of the femur (Fig. 40.3), capsule of the knee joint, fascia of the leg or medial meniscus (Kedzia et al. 2011). The partial bifurcation of the distal half of the muscle varies in size and can be anything from 50% of the muscle or less (Figs 40.4–40.6; Garbelotti et al. 1999; Kedzia et al. 2011). Caution should be applied in identifying additional heads as the deeper muscles of the superior aspect of the anterior thigh are prone to layering. Shape differences have also been described as being either conical or rectangular (Kedzia et al. 2011). A doubled sartorius where the muscle may be completely divided longitudinally into two parts is rare (Bergman et al. 1988). This accessory portion inserts into the fascia lata, the femur above the medial condyle, the ligament of the patella, the tendon of semitendinosus, or the tendon of the main belly, and may arise from the same points as the additional heads of bifid muscles (Bergman et al. 1988).

Separate or accessory heads of origin occasionally arise from the notch below the anterior superior spine, the iliopectineal line, the pubic bone close to the symphysis, or the inguinal ligament.

The tendon of insertion has been found to end in the fascia lata, capsule of the knee joint, and fascia of the leg. When the muscle is divided the second tendon may insert into one of the areas just mentioned above. Mori describes the distal part of the muscle as having five forms as follows.

1. The boundary of the muscular part and the terminal tendon is clear, and the terminal tendon is moderate in size in 62%.

Bergman's Comprehensive Encyclopedia of Human Anatomic Variation, First Edition. Edited by R. Shane Tubbs, Mohammadali M. Shoja and Marios Loukas.
© 2016 John Wiley & Sons, Inc. Published 2016 by John Wiley & Sons, Inc.

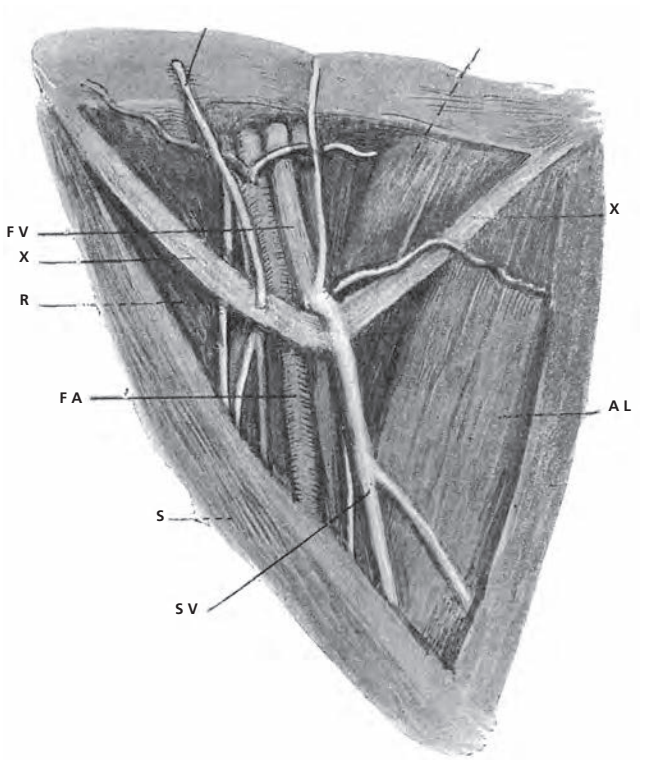

Figure 40.1 The musculus saphenous (X) in its relationship to the femoral (FV) and saphenous (SV) veins. It blends with the sartorius (S) laterally and the adductor longus (AL) medially. The pectineus (P) and iliopsoas (R) lies deep to it.

Source: Tyrie (1894). Reproduced with permission from John Wiley & Sons.

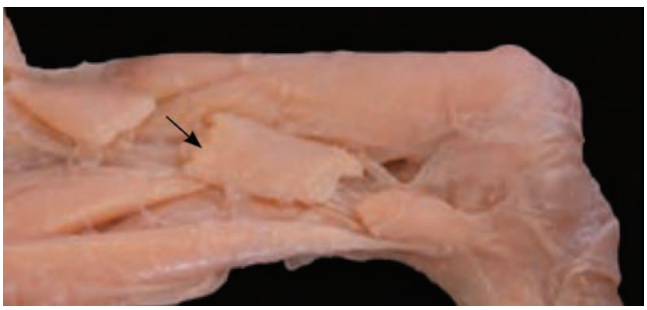

Figure 40.2 Discontinuous sartorius muscle (arrow).

Source: Kedzia et al. (2011). Reproduced with permission from Wroclaw Medical University, Poland.

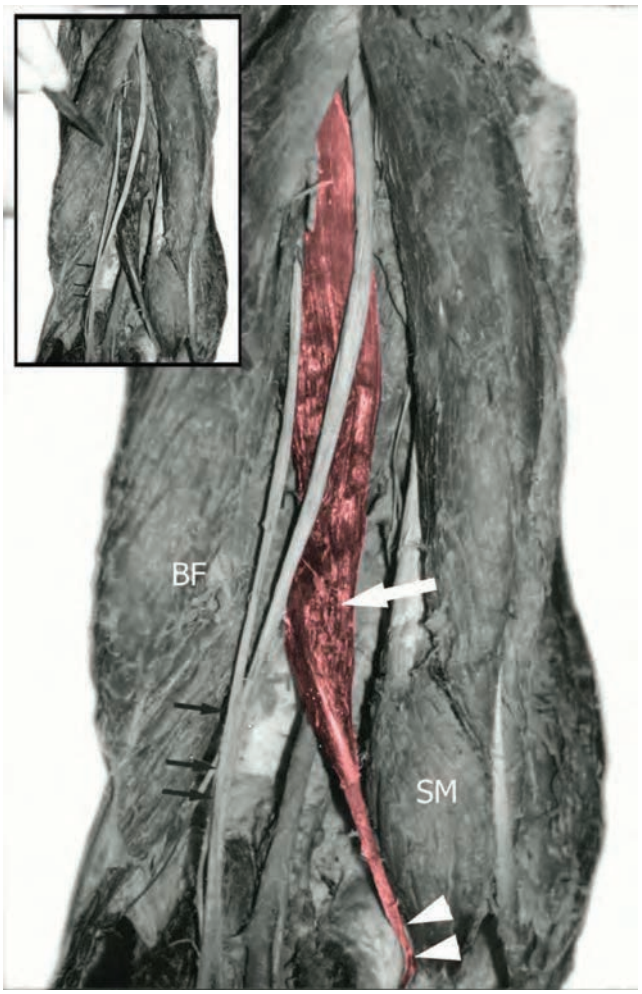

Figure 40.3 The belly of the supernumerary semitendinosus muscle (arrow) lies deep to the retracted biceps femoris muscle (BF). The divided sciatic nerve is superficial to the muscle (black arrows). The adjacent semimembranosus (SM) is apparent at its insertion (arrowheads).

Source: Paraskevas et al. (2010). Reproduced with permission from John Wiley & Sons.

2. The boundary of the muscular part and the terminal tendon is not clear (not well defined), but the length of the terminal tendon is moderate in 26%.
3. The terminal tendon is very short, and the muscle fibers appear to be inserted directly into the tibia in 12%.
4. The distal portion of the muscle is longitudinally divided into two parts, and the tendon of the secondary slip is attached to the anterior wall of the adductor canal in 15/320 thighs or 4.7%.

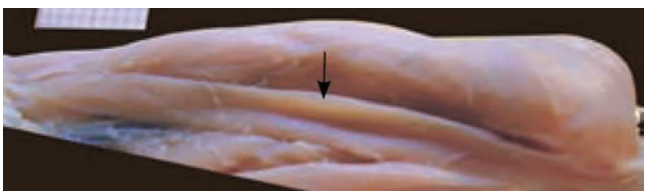

Figure 40.4 Initial process of muscle bifurcation in the sartorius muscle (arrow).

Source: Kedzia et al. (2011). Reproduced with permission from Wroclaw Medical University, Poland.

5. The distal half of the sartorius has no muscle fibers, but is a collagenous, fibrous band. The fibrous band is attached to the fascia over the vastus medialis in 2/320 or 0.6%.
6. Macalister reports the variations in the sartorius muscle as follows:
   1. absent (Meckel);
   2. doubled (by Otto, by Rosenmüller, by Gantzer and by Sömmerring);
   3. doubled, the lower of the two representatives being inserted into the femur (Meckel) or into the tendon of the normal one (Huber);
   4. splitting of the lower border into two parts (Horner);
   5. much broader than usual (Horner);
   6. crossing the thigh more transversely than usual (Quain);
   7. ending in the fascia lata;
   8. with two heads: one from the anterior superior iliac spine, and another, perfectly separate, below it, from the incisura semilunaris;
   9. with a central tendinous intersection (Kelch and by Hyrtl);
   10. with its tendon inserted into the medial side of the capsule of the knee, and not extending any further; or
   11. with some of its medial fibers arising from the splitting of the iliac portion of the fascia lata, which forms its sheath, as it forms the outer wall of the triangle of scarpa.

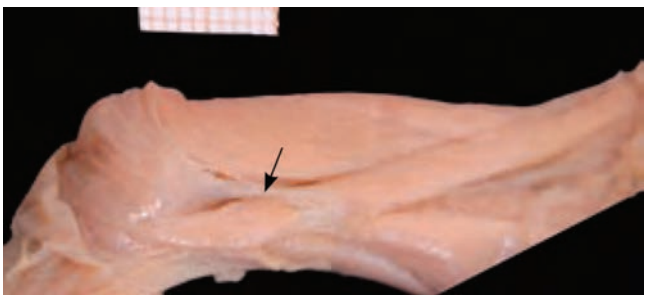

Figure 40.5 Sartorius muscle with extra tendon present (arrow).

Source: Kedzia et al. (2011). Reproduced with permission from Wroclaw Medical University, Poland.

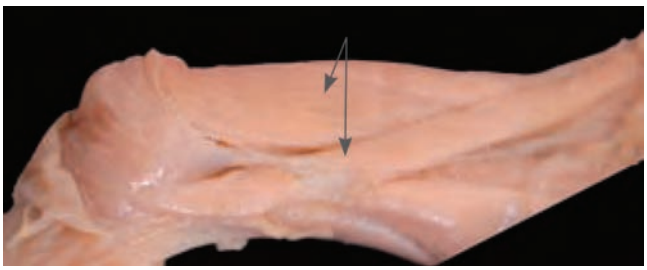

Figure 40.6 Muscle fragment from sartorius indicating partial duplication.

Source: Kedzia et al. (2011). Reproduced with permission from Wroclaw Medical University, Poland.

Pectineus

The pectineus muscle may be separated into two layers superficial (lateral/ventral) and deep (medial/dorsal) (Ochiltree 1912; Standring 2009). The two parts of the muscle receive separate nerve supplies and have different actions (Bergman et al. 1988). It may be partially or completely attached to the capsule of the hip joint proximally or originate from adductor brevis (Ochiltree 1912; Standring 2009). Accessory fascicles from pectineus may fuse to obturator externus, iliacus, adductor longus, the capsule of the hip, or lesser trochanter (Bergman et al. 1988). If lamellated, the superficial part is supplied by the femoral nerve and the deep part by a branch of the obturator nerve. The muscle may be partially (superficial) or entirely supplied by the accessory obturator nerve (Patterson 1891).

Quadriceps femoris

Rectus femoris

An additional head was reported running from the iliofemoral ligament deeply and superficially attached to the tendon of the gluteus minimus muscle as it attached into the femur (Tubbs et al. 2006). This tendon may attach to the anterior aspect of the greater trochanter in an inferolateral direction. This "femoral head" (Figs 40.7, 40.8) can have some variation in its size and shape and may even be bilaminar in some cases (Tubbs et al. 2006). Accessory rectus femoris muscle has been reported and attaches proximally to the edge of the acetabulum and distally into the ventral aspect of the vastus lateralis (Tubbs et al. 2004). Slips of muscle may arise from the inguinal ligament and terminate the proximal part of the vastus medialis muscle (Tubbs et al. 2004). Absence of the acetabular attachment (reflected head), doubled origin from the anterior inferior iliac spine, and origin from the anterior superior iliac spine have also been reported. The muscle may be bilaminar and have continuity between the reflected and straight heads. The muscle belly may be very short and fuse to vastus medialis (Fig. 40.9), become buried beneath a fused tendon formed by vastus lateralis and medialis, or even be absent (Stringer et al. 2012).

Vasti muscles

In some, vastus medialis is larger distally while vastus lateralis is larger proximally (Willan et al. 2002). Some authors report extensive variation among the vasti, in particular to their relationship and position to each other. It appears that these muscles exhibit great variation in the size, shape, and fascicle arrangement that may not be easily observed gross morphologically (Willan et al. 2002). The vastus lateralis and intermedius are fused proximally for 25–35% of their length (Finni et al. 2008).

Vastus lateralis

Some fibers may arise from the tendon of gluteus maximus and the lateral intermuscular septum between vastus lateralis and the short head of biceps femoris. The mass of muscle forming the vastus lateralis longus is attached to a strong aponeurosis

Figure 40.7 Left anterior thigh showing femoral head of the rectus femoris muscle anterior to the forceps (the forceps are distal to the scissors). The normal rectus femoris muscle belly is seen just medial to the scissors that are embedded in the vastus intermedius muscle. Medial to the rectus femoris muscle note the sartorius muscle (long arrow) and great saphenous vein (short arrow).

Source: Tubbs et al. (2004). Reproduced with permission from John Wiley & Sons.

on the deep surface of the distal part (Standring 2009). Vastus lateralis obliquus has its distal fibers interdigitated with the lateral retinaculum and the iliotibial tract and then joins longus (Fig. 40.10) to attach to the superolateral border of the patella (Beviloqua-Grossi et al. 2006). It narrows into a flat tendon which attaches to the base and lateral border of the patella, where it blends into the rest of the muscles forming the quadriceps tendon (Standring 2009; Becker et al. 2010). It sends an expansion to the capsule of the knee joint which descends to the lateral condyle of the tibia and blends with the iliotibial tract (Dwight 1887; Patil et al. 2007; Becker et al. 2009). Descriptions of the size and extent of the proximal attachment vary. Reports on variations of these attachment sites range between attachment only to the gluteal tuberosity and additionally to the posterolateral aspect of the femur. Variations of the distal attachment sites include mainly the base and lateral border of the patella; some suggestions have been made that it could be both sites or either of the two. Attachment to the lateral epicondyle of the tibia has also been observed (Becker et al. 2009). Vastus lateralis may be doubled with a neurovascular bundle separating the two parts (Dwight 1887). In this case one head attaches to the outer surface of the greater trochanter, the line to the linea aspera, and from the lateral surface of the femur approx midshaft (Dwight 1887). The other head attaches to the upper part of the anterior intertrochanteric line, anterior greater trochanter and anterior border of the femur, or from the hip joint capsule anterior surface just below the anterior superior iliac spine (Dwight 1887). It appears to have a degree of asymmetry, being larger on the right than on the left (Willan et al. 2002). Some variation has been found in the degree of fusion to vastus intermedius (Willan et al. 1990, 2002; Finni et al. 2008; Becker et al. 2009; Standring 2009), the vast majority of reports showing a clear fascial plane between them (Becker et al. 2009; Waligora et al. 2009). Additional bellies of vastus lateralis have been reported when the two are fused. Suggestions that the vastus lateralis have four components instead of two and that the longus and obliquus should be considered as separate muscles have also been made (Becker et al. 2010). In both these instances, the divisions appear to be functional and there is insufficient evidence to support either of these suggestions. In one reported case, the vastus lateralis had a bone embedded and was tightly attached to the muscle fibers of the belly (Pires de Lima 1913).

Vastus intermedius

It may be fused to vastus medialis proximal to the lower part of the intertrochanteric line, and have been reported as fused to vastus lateralis to varying degrees (Willan et al. 1990, 2002; Finni et al. 2008; Becker et al. 2009; Standring 2009). It may descend as far as half an inch to an inch above the knee or, more commonly, it does not extend below a point three to four inches above the knee. This muscle is usually inseparable from the vastus medialis, so much so that some have regarded them as one. Vastus intermedius and articularis genus are frequently united or, when no articularis genus is present, deep fibers are (rarely) attached to the synovial membrane of the knee.

Vastus medialis

Regardless of the difference in fiber orientation and proposed action, there is not enough evidence to support the theory that the vastus medialis longus and obliquus (Fig. 40.11) are separate muscles (Peeler et al. 2005; Waligora et al. 2009). It has however been suggested that the two parts, if present, serve different actions (Hubbard et al. 1997), with longus performing extension and obliquus serving more of a stabilizer role. A clear separation has only been shown in 22% of individuals studied (Hubbard et al. 1997; Peeler et al. 2005).

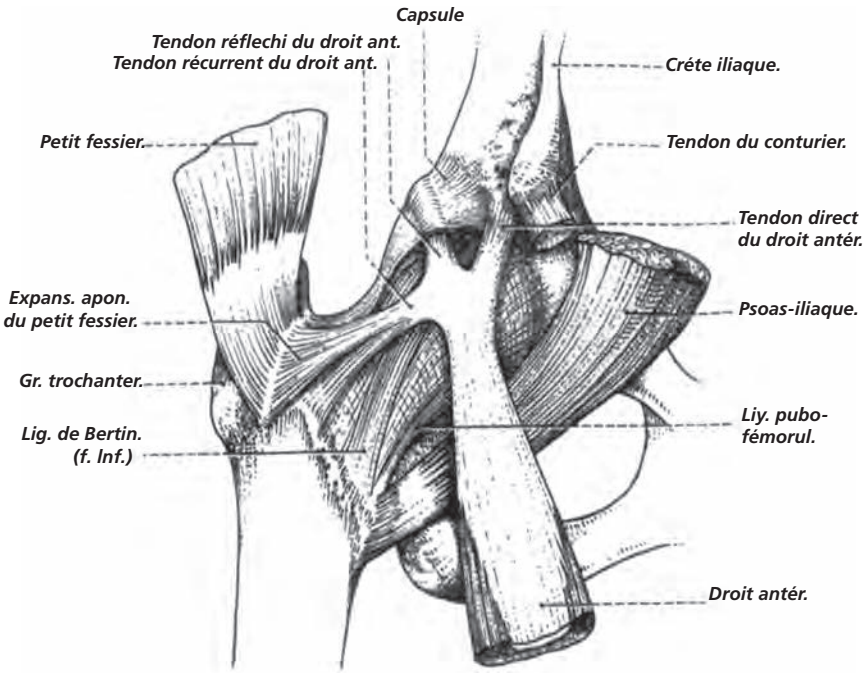

Figure 40.8 Drawing of the femoral head ("tendon recurrent du droit arjt") of the rectus femoris as shown by Paturet (1951).

Source: Tubbs et al. (2006).

Descriptions of distal attachment of the quadriceps as a whole are highly variable (Waligora et al. 2009). The tendon may form three laminae, corresponding to a similar division in the muscles. The superficial tendon may insert into the anterior portion of the base and superior third of the anterior surface of the patella (Standring 2009). Alternatively, it attaches in part to the base of the patella and continue further to attach to the tibial tuberosity (Waligora et al. 2009). It may also fuse to the tendon of the vastus intermedius and form a unilaminar suprapatellar tendon that may or may not receive fibers from either the vasti medialis or lateralis (Waligora et al. 2009). All three tendons may join to form a single attachment that continues over the patella (Standring 2009). The vasti are sometimes bilaminar (Bergman et al. 1988). In the case of the vastis lateralis, this is an accentuation of a normal feature. The vasti may be continuous with the rectus femoris, and all three parts may be united into a common fleshy mass (Bergman et al. 1988). The entire quadriceps femoris has been reported to be absent.

Macalister reported the variations of the quadriceps as follows:

1. an origin from the anterior superior spine of the ilium joining the straight head;
2. a split curved head, part being outside, and a part between the layers of the hip-joint capsule;
3. a double origin from the inferior spine;
4. a continuity of the acetabular and spinous heads; or with no acetabular origin;
5. a bursa between the lateral tendon and the brim of the acetabulum (Isenflamm);
6. a double long head (Diemerbröck), which Macalister also found; and
7. a large fasciculus of its tendon, passing across the front of the patella, was separated from the bone by the deepest part of the prepatellar bursa.

The relation of this muscle to the rest of the extensor is variable; sometimes at its insertion it is inseparable from the vastus intermedius. At other times Macalister saw the two vasti uniting over the tendon of this muscle, forming a canal in which the rectus tendon ran to its insertion. Alternatively, the vastus lateralis may be inserted into the outer border of its tendon, while the vastus medialis and vastus intermedius lie beneath.

Articularis genus

The articularis genus is found to be liable to atrophy, absence, splitting, or fusion with vastus intermedius. The muscle may be inserted at either side of the knee, or into the upper part of the synovial membrane; its lateral slips, when split, are usually equal.

Medial compartment

Gracilis

Some fibers from the lower part of the tendon continue into the deep fascia of the leg, and it often sends a muscular slip that blends with the medial head of gastrochnemius tendon (Standring 2009). Occasionally, the gracilis supplies fibers to the fascia lata and to the fascia of the leg. A biceps gracilis has been

Figure 40.9 Right and left thigh dissections in a 92-year-old female showing a unilateral short rectus femoris muscle belly on the left side.

Source: Stringer et al. (2012). Reproduced with permission from International Journal of Anatomical Variations.

reported with normal upper head and a lower head arising from the ramus of the ischium (Bergman et al. 1988).

Adductor longus

Adductor longus may occasionally be doubled or fused to adductor magnus (Bergman et al. 1988; Standring 2009). The muscle may even extend as far as the knee, fusing to the tendon of adductor magnus and making their attachments inseparable (Bergman et al. 1988).

Adductor brevis

Adductor brevis may be divided into two or three separate parts, or may be integrated into adductor magnus (Bergman et al. 1988; Standring 2009). This division may be complete or

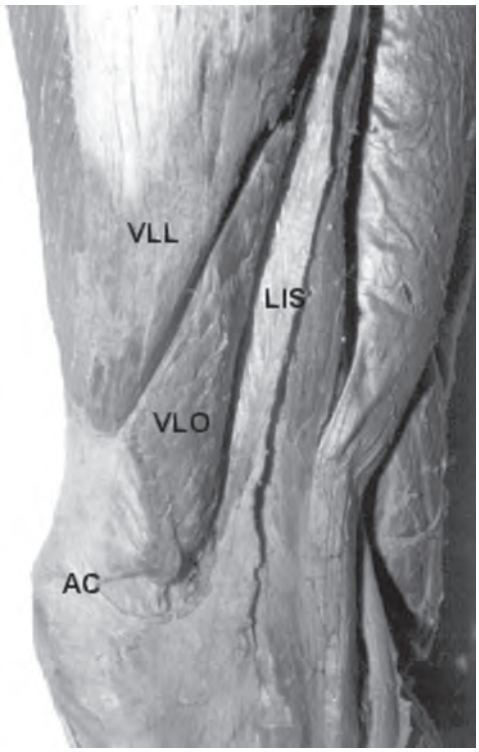

Figure 40.10 Lateral view of the right thigh showing the origin of the obliquus portion of the vastus lateralis muscle (vastus lateralis obliquus, VLO) in the lateral intermuscular septum (LIS) and its insertion in the superiolateral border of the patella (P). VLL, vastus lateralis longus.

Source: Beviloqua-Grossi et al. (2006). Reproduced under the terms of the Creative Commons CC-BY-2.0 licence from Springer Science and Business Media.

partial and have varying degrees; if split the proximal attachment stays usual, but distally the attachment to the linea may be more toward the midline than in a non-split muscle (Ochiltree 1912). Adductor brevis may also provide a slip to adductor magnus and obturator externus (Bergman et al. 1988).

Adductor magnus

The fibers from the pubic or ischiopubic ramus are short and horizontally oriented, attaching to the gluteal tuberosity medially to gluteus maximus distally. This part of the muscle is located in a plane anterior to the rest and is sometimes referred to as the adductor minimus (quartus). These fibers may insert into a line leading from the greater trochanter to the linea aspera, and have been advocated as a separate muscle (Ochiltree 1912). The ischiocondylar part of the muscle is vertical and varies in its degree of separation from the rest. At its upper border the adductor magnus may fuse with quadratus femoris (Bergman et al. 1988; Standring 2009) or with either or both the long or short adductor. Irregular slips from both adductor magnus and biceps femoris may insert into the tendon of adductor magnus and onto the adductor tubercle (Bergman et al. 1988). A particular variant slip was reported by Tubbs and Zehren (2006) attaching from the medial lip of the linea aspera adjacent to the biceps short head. The slip was 15 cm long and 1 cm thick; of particular note is that it compressed the popliteal vein causing an aneurysm (Tubbs and Zehren 2006). Similar slips have been reported by both Gray (1945) and Hildebrand (1978) but was not associated with venous compression.

Obturator externus

The external obturator muscle shows little variation. Sometimes part of the muscle is isolated above the point of exit of the obturator nerve. The muscle may be divided into three parts, a subdivision that has been described by some authors as the normal arrangement, and may also be connected to adductor brevis (Bergman et al. 1988).

Posterior compartment

The posterior compartment contains the three hamstring muscles: biceps femoris, semimembranosus, and semitendinosus (Anson and McVay 1971). It is by far the most variable of the thigh compartments and all the muscles cross both the hip and knee joints. The distal tendons of all the hamstring muscles display a large amount of variation in the morphology of the tendinous bands. Bands arising from the tendons of each muscle vary greatly in number, origin, and attachment, and may arise as high as 10 cm above the insertion point (Yasin et al. 2010).

Biceps femoris

The main part of the narrow tendon distally splits to surround the lateral collateral ligament and attaches to the head of the fibula (Anson and McVay 1971; Standring 2009; Paraskevas et al. 2010) and sometimes onto the tibia. The rest of the tendon splits into three flat bands attaching to and around the collateral ligament and lateral tibial condyle (Standring 2009). There is some support for the suggestion that the two parts of the biceps represent separate muscles, which fused in humans. In rare cases, the parts do remain separate either partially or entirely and the short head may be completely absent. The normal attachment of the muscle to the crural fascia represents an extension to the leg that is found in some mammals. The crural extension may be seen as muscular slips (tensor fascia suralis) attached to either fascia, gastrochnemius, or the achilles tendon. Accessory slips have been noted which arise from various sources including the sacrum, coccyx, sacrotuberous ligament, ischial tuberosity, linea aspera, medial supracondylar line, gluteus maximus, gluteal ridge of the femur, adductor magnus, or vastus lateralis. In 41% of limbs studied, the long head took origin from the sacrotuberous ligament and may attach to the lateral intermuscular septum posteriorly (Bergman et al. 1988).

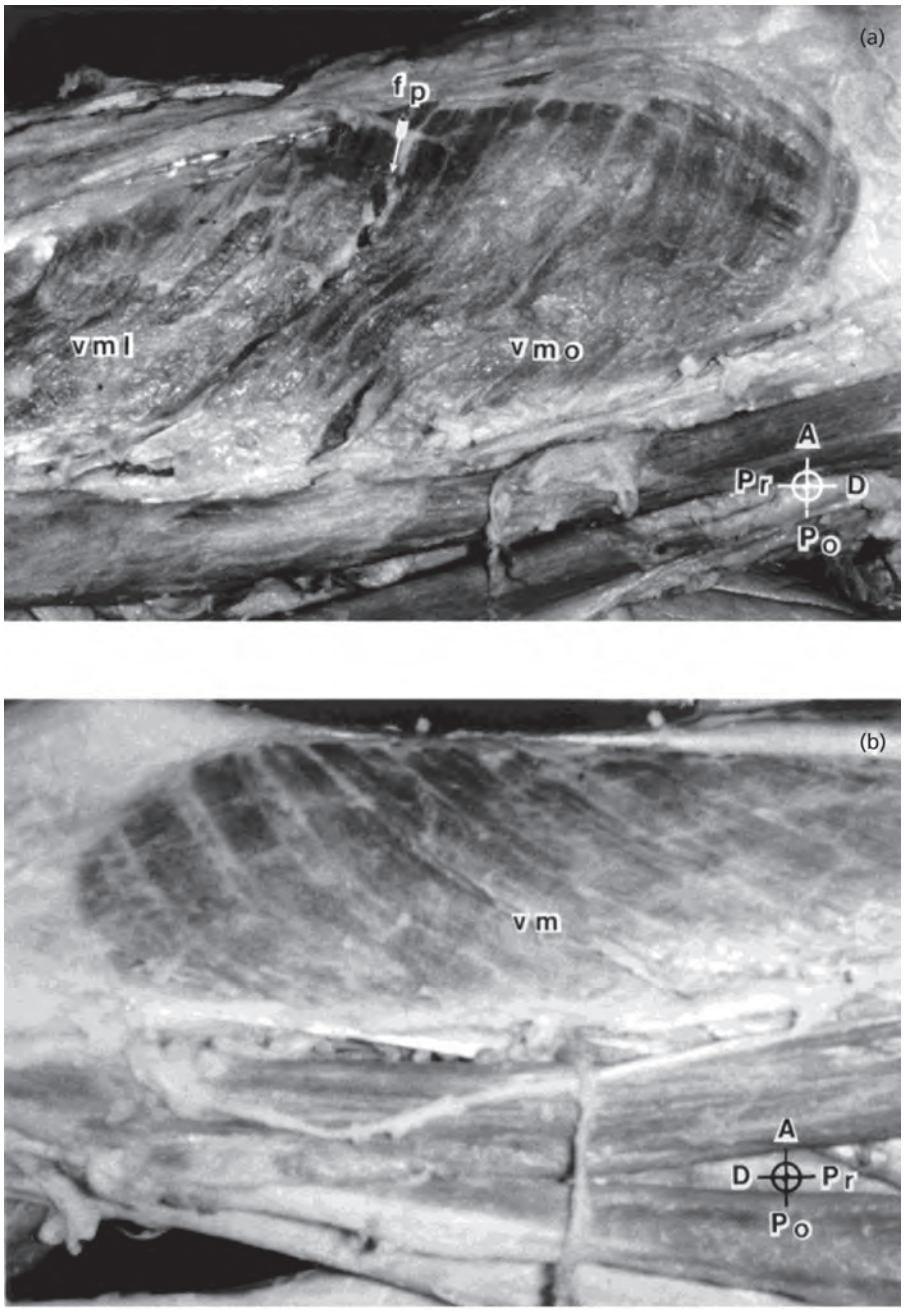

Figure 40.11 (a) VM muscle dissection showing areolar fascial plane as defined by Lieb and Perry (1968). A, anterior; D, distal; fp, fascial plane; Po, posterior; Pr, proximal; vml, vastus medialis longus; vmo, vastus medialis oblique. (b) VM muscle dissection showing no fascial plane. vm, vastus medialis.

Source: Hubbard et al. (1997). Reproduced with permission from John Wiley & Sons.

Semitendinosus

A tendinous intersection can usually be found near the midpoint of the muscle which may receive a muscular slip from the biceps long head; it may also be partly fused with the semimembranosus. Complete separation of the semitendinosus from the biceps has been reported and accessory slips have been observed arising from the coccyx, sacrotuberous ligament, or ischial tuberosity (Fig. 40.12; Fraser et al. 2013) joining the belly of the muscle. The semitendinosus took origin from the sacrotuberous ligament without biceps in 39% of limbs studied, but may also form a joint tendon with biceps (Bergman et al. 1988). A rare variation is one in which a slip arises from the

Figure 40.12 Right posterior thigh depicting the semitendinosus muscle (asterisk) and variant origin (arrow) in situ. (L: lateral; I: inferior; M: medial; S: superior).

Source: Fraser et al. (2013) Reproduced with permission from International Journal of Anatomical Variations.

linea aspera below the semitendinosus and ends on the medial condyle and back of the knee joint (Bergman et al. 1988; Paraskevas et al. 2010). The tendon may also receive reinforcements via slips of muscle from the quadratus femoris muscle; in this report it was not attached to the ischial tuberosity but was separated from it by a bursa. Tensor fascia suralis (ischioneuroticus) is a slip that leaves the belly of the semitendinosus (or any of the other hamstrings) and ends in a tendon that joins the fascia of the leg (Bergman et al. 1988). Supernumerary semitendinosus has been observed originating from lateral ridge of the linea aspera between the tendinous attachments of the short head of biceps and adductor magnus muscle (Gray 1945). Distally it is covered by the long head of biceps femoris, and runs obliquely from lateral to medial to insert into the medial tibial condyle. Additional cord-like tendinous heads of semitendinosus was also found and arose from the ischial tuberosity close to 8 mm from the main attachment. This fused with the belly and continued together to its usual distal attachment (Standring 2009).

Semimembranosus

The muscle varies in size and may be doubled, absent, or occasionally split along its length. Up to four bellies have been reported inserting into the adductor magnus, planum popliteum, and tibia. It may also arise proximally from the sacrotuberous ligament or coccyx and send slips to the femur or adductor magnus, the tendon of which it may join or even split along its entire length (Standring 2009). The second belly may have the form of a small fleshy slip with proximal and distal tendons, or it may arise from the sacrotuberous ligament. The distal tendon may be inserted in various ways. One method is by attachment of a slip to the main tendon, with a larger slip going to the oblique popliteal ligament and a delicate reflected slip inserted onto the medial supracondylar ridge. It may also be partly fused to the semitendinosus (Bergman et al. 1988).

It has been reported that the semitendinosus, semimembranousus, and long head of biceps may originate via a common tendon (Fig. 40.13), attached superiorly to the sacrotuberous ligament, and can be continuous with the intermuscular septum. This may pass cranially to split and envelope the piriformis muscle. Gray reported a supernumerary hamstring muscle observed as originating from the linea aspera bilaterally (Figs 40.14, 40.15), between the origin of the short head of biceps and the insertion of the adductor magnus as well as from a septum between it and these muscles. The bony attachment of this muscle extended along the femur for a distance (17 cm) and the muscle passed medially and inferiorly behind the popliteal vessels, and in front of the long flexors of the leg. It then inserted into the dorsal aspect of the capsule of the knee joint medial to gastrocnemius and into deep fascia covering the medial head of origin of this muscle (Gray 1945).

Two muscles that cross the popliteal fossa from lateral to medial – one arising from the short and the other from the long head of the biceps femoris – have also been observed. Others have reported a muscle arising as fleshy bundles from the adductor magnus and from the linea aspera between attachments of the adductor magnus and short head of the biceps muscle, which inserted into the medial condyle of the femur and into the dorsal part of the capsule of the knee joint. It was proposed to be a supernumerary semitendinosus muscle and could be regarded as a femoral head (Gray 1945).

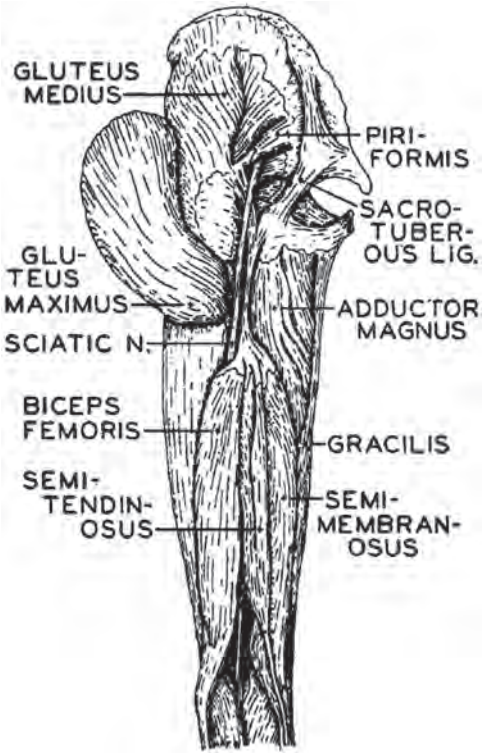

Figure 40.13 A sketch of the dorsal aspect of the left thigh. The gluteus maximus muscle has been reflected to show the common tendon of origin for the hamstring muscles.

Source: Gray (1945). Reproduced with permission from John Wiley & Sons.

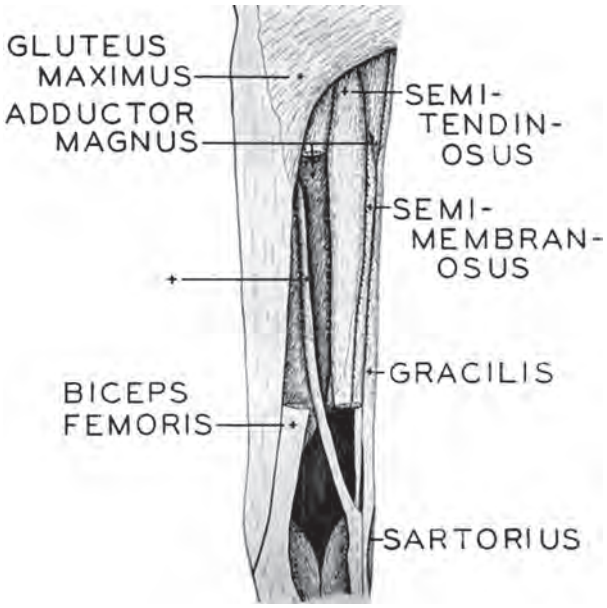

Figure 40.14 A sketch of the dorsal aspect of the left thigh. The distal portions of the semimembranosus and semitendinosus and the intermediate part of the long head of the biceps femoris have been removed to show the anomalous muscle ('+') arising from the deep surface and attaching to the sartorius tendon.

Source: Gray (1945). Reproduced with permission from John Wiley & Sons.

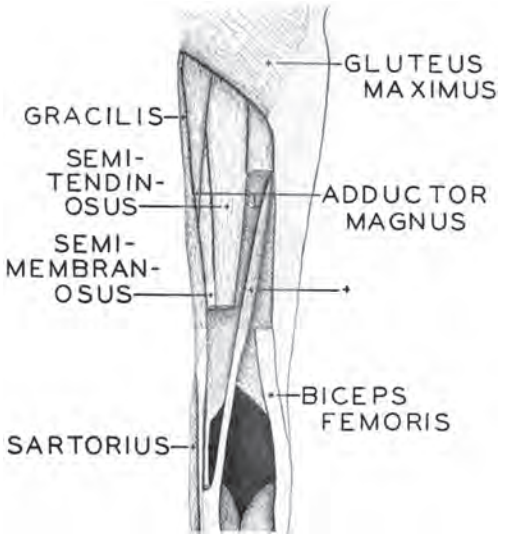

Figure 40.15 Sketch of the dorsal aspect of the right thigh. The intermediate part of the long head of the biceps feinoris and the distal parts of the semitendinosus wild semimembranosus muscles have been removed. Anomalous muscle at '+'.

Source: Gray (1945). Reproduced with permission from John Wiley & Sons.

References

Anson BJ, McVay CB. 1971. *Surgical Anatomy. Vol 2, 5th edition*. Philidelphia PA: WB Saunders Company.

Becker I, Woodley SJ, Baxter GD. 2009. Gross morphology of the vastus lateralis muscle: an anatomical review. *Clin Anat* 22: 436–450.

Becker I, Baxter GD, Woodley SJ. 2010. The vastus lateralis muscle: An anatomcal investigation. *Clin Anat* 23: 575–585.

Bergman RA, Thomson SA, Afifi AK, Saadeh FA. 1988. Compendium of Human Variation. Text, Atlas and World Literature. Munich, Germany: Urban and Baltimore: Schwarzenberg.

Beviloqua-Grossi D, Monteiro-Pedro V, de Vasconcelos RA, Arakaki JC, Berzin F. 2006. The effect of hip abduction on the EMG activity of vastus medialis obliquus, vastus lateralis longus and vastus lateralis obliquus. *J NeuroEng Rehab* 3: 13.

Brock GS. 1879. A two-headed sartorius. *J Anat Physiol* 13: 578.

Dwight T. 1887. Muscular abnormalities (Notes on muscular abnormalities). *J Anat Physiol* 22: 96–102.

Finni T, Havu M, Sinha S, Usenius J-P, Cheng S. 2008. Mechanical behavior of the quadripecs femoris muscle tendon unit during low-load contractions. *J Appl Physiol* 104: 1320–1328.

Fraser PR, Wood AR, Rosales AA. 2013. Anatomical variation of the semitendinosus muscle origin. *Int J Anat Var* 6: 225–227.

Garbelotti JS, Rodrigues CFS, Nobeschi L, Seiji F, Olave E. 1999. Anatomical variation of the sartorius muscle (Spanish). *Rev Chil Anat* 17: 95–97.

Gray DJ. 1945. Some anomalous hamstring muscles. *Anat Rec* 91: 33–38.

Hildebrand R. 1978. Discovery of a variant in the region of the adductor magnus and the short head of the biceps femoris. *Anat Anz* 144: 48–50.

Hubbard JK, Sampson HW, Elledge JR. 1997. Prevalence of vastus medialis oblique muscle in human cadavers. *Anat Rec* 249: 135–142.

Kedzia A, Walek E, Podlesry K, Dudek K. 2011. Muscular sartorius metrology in the fetal period. *Adv Clin Exp Med* 20: 567–574.
Lizars J. 1827. *A System of Anatomical Plates of the Human Body, Accompanied with Descriptions, and Physiological & Surgical Observations*. Edinburgh: WH Lizars.
Ochiltree AB. 1912. Some muscular anomalies in the lower limb. *J Anat Physiol* 47: 31–34.
Paraskevas GK, Raikos A, Loannids O. 2010. Supernummerary semitendinosus muscle: a rare case presentation and its clinical significance. *Clin Anat* 23: 909–910.
Patil S, Grigaris P, Shaw-Dunn J, Reece AT. 2007. Innervation of vastus lateralis muscle. *Cin Anat* 20: 556–559.
Patterson AM. 1891. The pectineus muscle and its nerve-supply. *J Anat Physiol* 26: 43–47.
Paturet G. 1951. *Traite d'Anatomie Humaine*. Vol. 2. Paris: Masson et Cie.
Peeler J, Cooper J, Porter MM, Thliveris JA, Anderson JE. 2005. Structural parameters of the vastus medialis mucle. *Clin Anat* 18: 281–289.
Pires de Lima JA. 1913. On a bone found in the muscle vastus externus of the thigh. *J Anat Physiol* 47: 414–424.
Standring S. (ed.) 2009. *Gray's Anatomy: The Anatomical Basis of Clinical Practice*. 40th edition. China: Churchill Livingstone Elsevier.
Stringer MD, Kano M, Fausett C, Samallia L. 2012. Unilateral short rectus femoris muscle belly. *Int J Anat Var* 5: 56–58.
Tubbs RS, Zehren S. 2006. Popliteal vein aneurysm due to an anomalous slip of the adductor magnus. *Clin Anat* 19: 722–723.
Tubbs RS, Salter G, Oaks WJ. 2004. Femoral head of the rectus femoris muscle. *Clin Anat* 17: 276–278.
Tubbs RS, Stelter Jr. W, Savage AJ, Shoja MM, Shakeri AB, Loukas M, Salter EG, Oaks WJ. 2006. Does a third head of rectus femoris muscle exist? *Folia Morphol* 65: 377–380.
Tyrie CCB. 1894. Musculus Saphenus. *J Anat Physiol* 28: 288–290.
Waligora AC, Johanson NA, Hirsch BE. 2009. Clinical anatomy of the quadriceps femoris and extensor apparatus of the knee. *Clin Orthop Relat Res* 467: 3297–3306.
Willan PLT, Ransome JA, Mahon M. 2002. Variability in the human quadriceps muscles: Quantitative study and review of clinical literature. *Clin Anat* 15: 116–128.
Willian PLT, Mahon M, Golland JA. 1990. Morphological variations of the human vastus lateralis muscle. *J Anat* 168: 235–239.
Yasin MN, Charalambous CP, Mills SP, Phaltankar PM. 2010. Accessory bands of hamstring muscle tendons. *Clin Anat* 23: 862–865.

Further reading

Hayashi A, Maruyama Y. 2001. Lateral intermuscular septum, of the thigh and short head of the biceps femoris muscle: An anatomic investigation with new clinical applications. *Plast Recontr Surg* 108: 1646–1654.
Hepburn D. 1893. Complete separation of the two heads of biceps flexor cruris muscle. *J Anat Physiol* 27: 282–284.
Macchi V, Vigato E, Porzionato A, Tiengo C, Stecco C, Parenti A, Morra A, Bassetto F, Mazzoleni F, de Caro R. 2008. The gracillis muscle and its use in clinical reconstruction: An anatomical, embryological, and radiological study. *Clin Anat* 21: 696–704.
Magallal A, Wang C, Shipkov C, Hocuoq C, Recchihuito J, Brown S, Rohrich RJ, Michel S. 2011. Redeining the vascular anatomy and clinical applications of the sartorius muscle and myocutaneous flap. *Plast Reconstr Surg* 127: 1946–1956.
Smith J, Sayeed YA, Finnoff JT, Levy BA, Martonoli C. 2011. The bifurcating distal biceps femoris tendon: potential pitfall in musculoskeletal sonography. *J Ultrasound Med* 30: 1156–1166.
Smith TO, Nichols R, Harle D, Donell ST. 2009. Do the vastus medialis obliquus and vastus medialis longus really exist? A systematic review. *Clin Anat* 22: 183–199.
Tubbs RS, Caycado FJ, Oaks WJ, Salter EG. 2006. Descriptive anatomy of the insertion of the biceps femoris muscle. *Clin Anat* 19: 517–521.
Vegas MR, Martin-Hevas C. 2013. The superolateral thigh flap: Cadaver and computed tomographic Angiographic studies with clinical series. *Plast Reconstr Surg* 131: 310–322.
Woodley SJ, Mercer SR. 2005. Hamstring muscles: architecture and innervation. *Cells Tissues Organs* 179: 125–141.

41 Leg muscles

H. Wayne Lambert
West Virginia University School of Medicine, Morgantown, West Virginia, United States

Anterior compartment

Tibialis anterior

The origin of the tibialis anterior muscle may extend proximally to the lateral femoral condyle (Le Double 1897; Jackson,1914; Bejjani and Jahss 1985); however, the muscular variants of the tibialis anterior are primarily related to its tendinous insertions which exhibit bifurcations, extensions of attachment, and loss of attachment (Wood 1863; Macalister 1875; Giani 1909; Hallisy 1930; Musial 1963a; Mori 1964; Luchansky and Paz 1986; Arthornthurasook and Gaew-Im 1990; Brenner 2002; Kelikian 2011). Bifurcation usually involves only the tendon, but may reach the distal muscle fibers in rare instances (Macalister 1875; Testut 1884; Bardeen 1906; Hallisy 1930; Bergman et al. 1988; Kelikian 2011). The distal attachments usually insert inferomedially into the base of the first metatarsal and medial part of the medial (first) cuneiform, but variants can extend to reach the navicular, talus, or calcaneus proximally, or the head of the first metatarsal (Fig. 41.1) or the base of the proximal phalanx of the big toe distally, as well as inserting into the inferior extensor retinaculum, plantar and dorsal aponeurosis of the foot, or capsule of the ankle joint (Wood 1863, 1865, 1866b; Macalister 1875; Knott 1883; Testut 1884; Hallisy 1930; Mori 1964; Luchansky and Paz 1986; Bergman et al. 1988; Kelikian 2011). The lack of the distal attachment to the base of the first metatarsal has also been reported (Giani 1909; Hallisy 1930; Brenner 2002).

Notable variants of the tibialis anterior

- Tensor of the dorsal fascia of the foot (musculus tensor fasciae dorsalis pedis muscle of Wood): This variant muscle arises from the lower third of the fibula and inserts into the inferior extensor retinaculum and dorsal fascia of the foot (Wood 1863; Bahnsen 1868; Knott 1883; Le Double 1897; Bejjani and Jahss 1985).
- Anterior tibiofascialis muscle (musculus tibiofascialis anticus of Macalister): This variant muscle is similar to the previously mentioned tensor of the dorsal fascia of the foot; however, the anterior tibiofascialis muscle arises from the lower third of the tibia. The tibiofascialis anterior muscle lies superficial to the tibialis anterior, arises from the lower third of the tibia and inserts on the deep surface of the inferior extensor retinaculum or dorsal fascia of the foot (Macalister 1875; Bergman et al. 1988; Kelikian 2011). A recent study depicted the tibiofascialis anticus as a tendinous slip from the tibialis anterior muscle, traveling superficial to the inferior extensor retinaculum and inserting into the dorsal fascia of the foot (Jain et al. 2013).
- Anterior tibiotalus muscle (musculus tibioastragalus anticus of Gruber): The anterior tibiotalus muscle lies deep to the tibialis anterior, originates from the lateral lower third of the tibia and interosseous membrane, and pierces the capsule of the ankle joint to insert into the anterosuperior aspect of the neck of the talus (astragalus). This muscle may have additional attachments into the navicular and talonavicular joint or the medial malleolus (Gruber 1871; Seelaus 1927; Kelikian 2011).

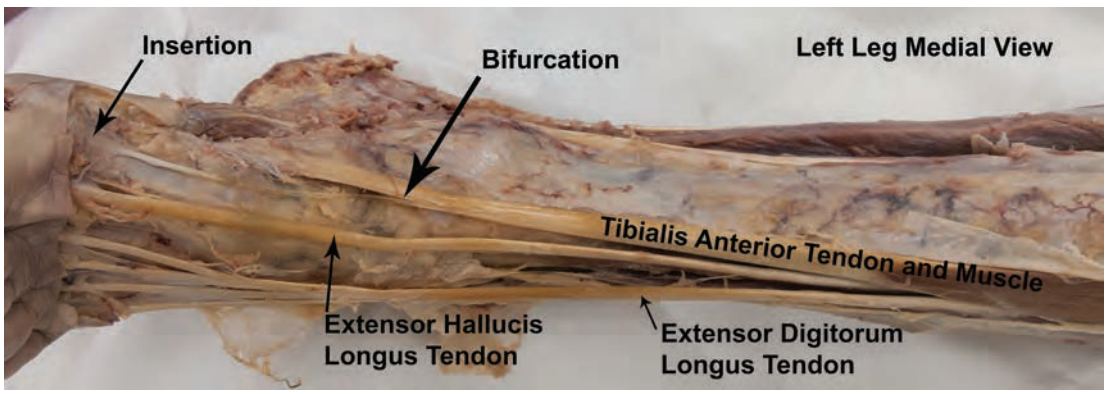

Figure 41.1 A bifurcation of the tibialis anterior tendon is shown extending distally to insert into the head of the first metatarsal within the left leg. This variant tendinous insertion was reported by Wood in 1863.

Bergman's Comprehensive Encyclopedia of Human Anatomic Variation, First Edition. Edited by R. Shane Tubbs, Mohammadali M. Shoja and Marios Loukas.
© 2016 John Wiley & Sons, Inc. Published 2016 by John Wiley & Sons, Inc.

Extensor hallucis longus

The muscular belly of the extensor hallucis longus is unipennate; however, this muscle occasionally splits into two or three separate muscular bellies and associated tendons (the so-called extensor tricaudatus of Gruber; Gruber 1876; Hallisy 1930; Mori 1964; Al-saggaf 2003; Bergman et al. 1988; Kelikian 2011). Most reported variants of the extensor hallucis longus possess the standard insertion into the dorsum of the base of the distal phalanx of the big toe, but also exhibit one or more accessory tendinous slips that insert into neighboring bones or muscles/tendons (Wood 1866b; Macalister 1875; Gruber 1875a, 1876; Knott 1883; Hallisy 1930; Baumann 1947; Mori 1964; Bergman et al. 1988; Al-saggaf 2003; Kelikian 2011). The most common insertion includes one to two additional slip(s) inserting into base of the proximal hallucal phalanx, either distal to, medial to, or directly into the extensor hallucis brevis tendon (Macalister 1866, 1875; Wood 1866b; Knott 1883; Hallisy 1930; Al-saggaf 2003; Kelikian 2011). Other reported insertions of these tendons include the dorsal aspect of the distal segment of the first metatarsal, the capsule of the first metatarsophalangeal joint, or joining the extensor digitorum longus tendon to terminate into its normal insertion point, the base of the proximal phalanx of the big toe, or the extensor expansion of the second toe (Wood 1866a; Gruber 1875a; Bardeen 1906; Hallisy 1930; Mori 1964; Tate and Pachnik 1976; Boyd et al. 2006; Kelikian 2011).

Notable variants of the extensor hallucis longus

- Musculus extensor primi internodii hallucis of Wood (extensor hallucis capsularis): This variant muscle is seen when an accessory tendinous slip, usually arising from the extensor hallucis longus muscle and rarely from the tibialis anterior or even the extensor digitorum longus muscles, inserts into the proximal phalanx of the big toe (Wood 1863, 1865, 1866a, b; Macalister 1866, 1875; Knott 1883; Hallisy 1930). It is rarely found as a separate muscle distinct from the extensor hallucis longus muscle, but this rare variant is shown in Figure 41.2 (Wood 1863, 1866b; Macalister 1866, 1875; Hallisy 1930). Prevalence of the musculus extensor primi internodii hallucis varies from 29.3% (85 of 290 feet; Hallisy 1930), to 54.0% (27 of 54 feet; Gruber 1875a); 80.6% (58 of 72 feet; Wood 1866b), with approximately 90% of these variants originating from the extensor hallucis longus and the remainder primarily from the tibialis anterior (Wood 1866b; Gruber 1875a; Hallisy 1930; Kelikian 2011). Recently, a similar muscle has been described as the extensor hallucis capsularis due to inserting into the capsule of the metatarsophalangeal joint, with a prevalence of 80–88% (Tate and Pachnik 1976; Lundeen et al. 1983; Bibbo et al. 2004; Boyd et al. 2006; Kelikian 2011). Like the musculus extensor primi internodii hallucis of Wood, the extensor hallucis capsularis arises from the extensor hallucis longus in approximately 90% of cases (Tate and Pachnik 1976; Lundeen et al. 1983; Bibbo et al. 2004; Boyd et al. 2006; Kelikian 2011). However, Boyd et al. (2006) reported the extensor hallucis capsularis only inserts into the base of the proximal phalanx in 1% of cases (Boyd et al. 2006; Kelikian 2011).
- Musculus extensor primi metatarsal of Gruber: This exceedingly rare variant muscle is seen when an accessory tendinous slip, usually arising from the extensor hallucis longus muscle and rarely from the tibialis anterior or even the extensor digitorum longus muscles, inserts into the dorsal aspect of the distal segment of the first metatarsal (Gruber 1875a; Bardeen 1906; Hallisy 1930). Like the musculus extensor primi internodii hallucis, this tendinous slip usually arises from the extensor hallucis longus. Hallisy (1930) reported this variant in 2 of 290 feet, an incidence of 0.69, and it has been documented by other researchers (Gruber 1875a; Knott 1883; Hallisy 1930; Lundeen et al. 1983).

Extensor digitorum longus

The muscular variants of the extensor digitorum longus are primarily related to its tendinous insertions, which may exhibit bifurcations or additional tendinous slips or may even be absent within a toe (Wood 1866b; Macalister 1875; Gruber 1875b, c; Testut 1884; Le Double 1897; Baumann 1947; Shigematsu et al. 1956; Bhadkamkar and Mysorekar 1961; Bergman et al. 1988; Kelikian 2011). Bifid tendons usually insert within the same toe, but one of these tendons may enter adjacent toes, including the

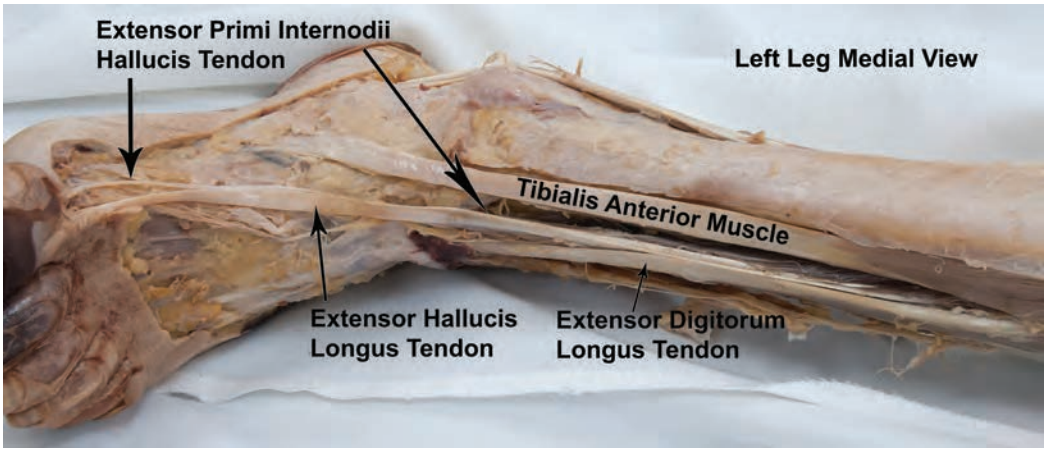

Figure 41.2 The extensor primi internodii hallucis muscle of Wood is shown arising as a separate muscle in a left leg. Its muscle belly is shown arising between the tibialis anterior and extensor digitorum longus muscles with proximal attachments to their investing fascia and the interosseous membrane. Its tendon courses parallel to the extensor hallucis longus tendon to insert into the proximal phalanx of the big toe.

big toe, often contributing to the extensor hallucis longus or brevis tendons (Bergman et al. 1988; Kelikian 2011). The additional tendinous slips have been found to insert within their corresponding metatarsal bones, the extensor digitorum brevis tendons, and the extensor expansion (dorsal aponeurosis), or into the fibularis (peroneus) tertius, to insert and reinforce the fifth metatarsal (Wood 1866b; Macalister 1875; Bergman et al. 1988; Stevens et al. 1993; Kelikian 2011). Conversely, several cadaveric studies have reported a lack of insertion of the extensor digitorum longus muscle into one toe, either the third, fourth, or fifth (little) toes, replaced by the extensor digitorum brevis or an unusually large fibularis tertius, respectively (Macalister 1875; Stevenson 1921; Takeuchi et al. 1960; Chaney et al. 1996; Sakuma et al. 2004; Plochocki and Bodeen 2010).

Fibularis (peroneus) tertius

The fibularis tertius is specific to humans, but it varies in size from being as large as the extensor digitorum longus to being absent (Wood 1866a, b; Macalister 1875; Le Double 1897; Reimann 1981; Bejjani and Jahss 1985; Bergman et al. 1988; Kramer et al. 1989; Stevens et al. 1993; Chaney et al. 1996; Joshi et al. 2006; Witvrouw et al. 2006; Rourke et al. 2007; Kelikian 2011). According to previous studies (listed in Table 41.1), the fibularis tertius muscle is present in approximately 91.3% of the cadaveric specimens (Wood 1866a, b; Macalister 1875; Le Double 1897; Reimann 1981; Bejjani and Jahss 1985; Kramer et al. 1989; Stevens et al. 1993; Chaney et al. 1996; Joshi et al. 2006; Rourke et al. 2007), though recent surface palpation studies have suggested a lower incidence (49.1–81.5%), depending on the population studied (Witvrouw et al. 2006; Ramirez et al. 2010; Ashaolu et al. 2013).

This muscle usually inserts into the base of the fifth metatarsal (Fig. 41.3), but it often sends an additional tendinous slip to insert onto the superior surface of the shaft of the fifth metatarsal (Fig. 41.3), base or shaft of the fourth metatarsal, the investing fascia over the fourth interosseous space, fifth proximal phalanx, the extensor expansion (dorsal aponeurosis) of the fifth toe, or converges with the extensor digitorum longus tendon to insert into the fifth toe (Stevenson 1921; Kramer et al. 1989; Joshi et al. 2006; Witvrouw et al. 2006; Rourke et al. 2007; Kelikian 2011; Jana and Roy 2011). Other variants include the fibularis quartus inserting solely on the base of the fourth metatarsal (Le Double 1897; Bejjani and Jahss 1985; Kelikian 2011). Doubling of the fibularis tertius tendon has been documented previously in approximately 1–2% of specimens, and this rare variant is shown in Figure 41.4b (Macalister 1875; Werneck 1957; Stevens et al. 1993; Rourke et al. 2007; Lambert and Atsas 2010;

Table 41.1 Historical prevalence of fibularis (peroneus) tertius muscle in previous cadaveric studies.

Study	Method	No. limbs	FQ	Prevalence (%)
Kramer et al. 1989	Cadaveric	169	157	92.9
Reimann 1981	Cadaveric	200	180	90.0
Bejjani and Jahss 1985*	Cadaveric	759	694	91.4
Stevens et al. 1993	Cadaveric	40	38	95.0
Chaney et al. 1996	Cadaveric	282	257	91.1
Joshi et al. 2006	Cadaveric	220	197	89.5
Rourke et al. 2007	Cadaveric	82	77	93.9
Total		1752	1600	91.3

*Bejjani and Jahss (1985) summarized the combined results of Wood (1866a, b), Macalister (1875), and Le Double (1897) in their translation of Le Double's (1897) research.

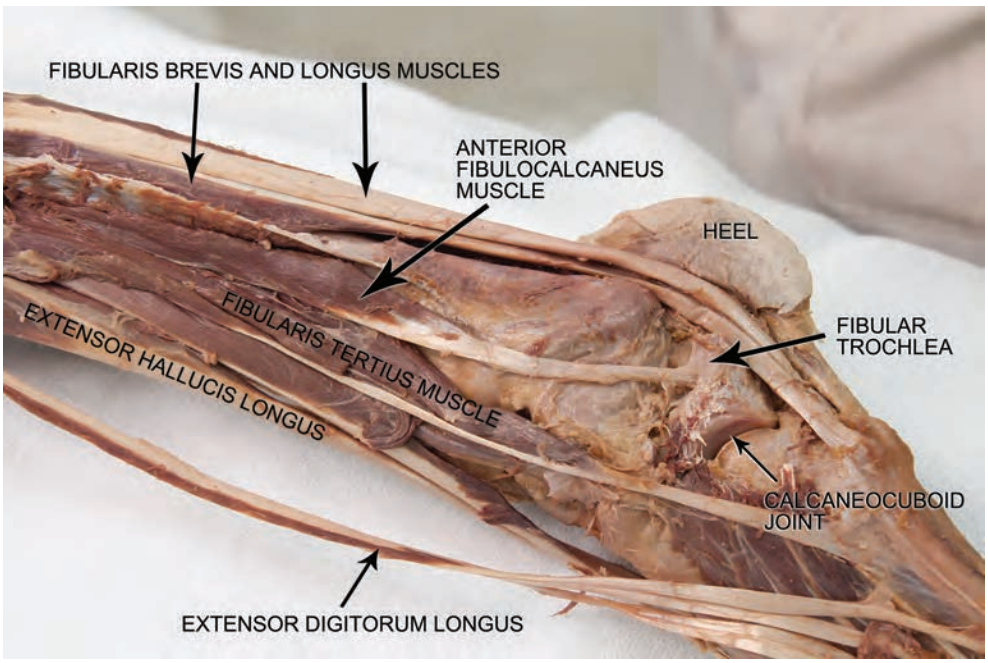

Figure 41.3 The fibularis tertius muscle is shown inserting into its normal insertion point, the base of the fifth metatarsal proximally, as well as sending a distally expanding tendinous slip to insert onto the superior surface of the shaft of the fifth metatarsal. The anterior fibulocalcaneus muscle is also shown arising from the lower half of the fibula and the investing fascia of the fibularis tertius, coursing anterior to the lateral malleolus, and inserting into the fibula (peroneal) trochlea of the calcaneus.

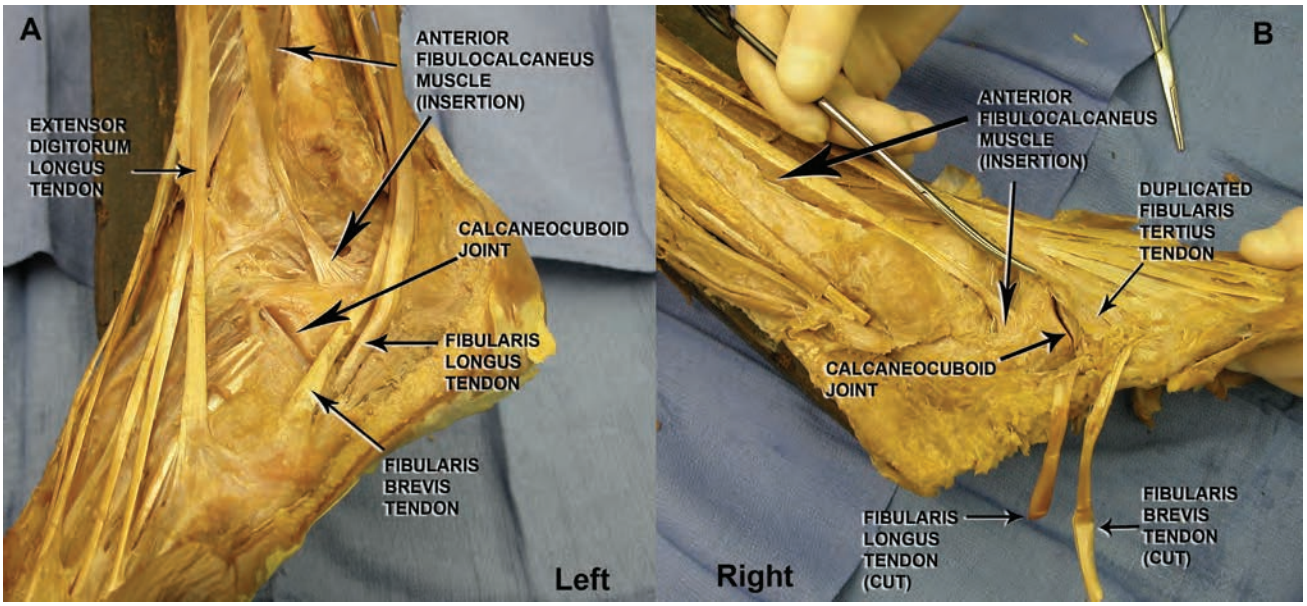

Figure 41.4 (a) The anterior fibulocalcaneus muscle is shown coursing anterior to the lateral malleolus and inserting into the fibula (peroneal) trochlea of the calcaneus in the left leg. (b) The insertion of anterior fibulocalcaneus muscle is also shown in the right leg. A duplicated fibularis tertius tendon is also present, indicated by the scissors.

Source: Lambert and Atsas (2010). Reproduced with permission from John Wiley & sons.

Jana and Roy 2011). Duplication of the entire muscle is exceedingly rare, but has been seen bilaterally (Le Double 1897; Bejjani and Jahss 1985). At its origin, the fibularis tertius is usually associated with the extensor digitorum longus muscle, but it may arise as completely separate muscle (Macalister 1875; Le Double 1897; Shigematsu et al. 1956; Bhadkamkar and Mysorekar 1961; Sokołowska-Pituchowa et al. 1974; Reimann 1981; Bejjani and Jahss 1985; Joshi et al. 2006).

Notable variants of the fibularis tertius

Peroneus (fibularis) quinti digiti: In the rare case of the extensor digitorum longus muscle lacking a tendon to the fifth toe it may be replaced by the peroneus quinti digiti, which is a variant muscle arising from a common muscle belly with the peroneus tertius to insert into the extensor expansion of the fifth toe. Le Double cites an 1887 talk by Boyer and Dubois when discussing this muscular variant (Le Double 1897; Bejjani and Jahss 1985).

Anterior fibulocalcaneus

This anterior compartment muscle arises from the fibula, anterior intermuscular septum, and investing fascia of the fibularis tertius, passes anterior to the lateral malleolus, and inserts into or near the fibular (peroneal) trochlea of the calcaneus, as shown in Figures 41.3 and 41.4. The length of this muscle varies as it can arise as far proximally as the head of the fibula or originate from the lower half of the fibula (Lambert and Atsas 2010; Lambert et al. 2011a). It is innervated by the deep fibular nerve (Lambert et al. 2011a).

Lateral compartment

Fibularis (peroneus) longus

The fibularis longus may have superficial and deep bellies (Mehta et al. 2011). The fibular collateral ligament may represent a primitive femoral attachment of the fibularis longus muscle due to fasciculi which have been documented to arise from the lateral femoral condyle in rare cases (Bergman et al. 1988). Variations in the investing fascia of the proximal attachments (origins) of the fibularis longus muscle has gained recent attention due to the potential of compression of the common fibular nerve at the neck of the fibula (Dellon et al. 2002). Moreover, the fibularis longus may be fused to the fibularis brevis near its origin in the upper half of the lateral surface of the fibula (Jayakumari et al. 2006). The distal attachments usually insert into the lateral tubercle of the base of the first metatarsal and plantar aspect of the medial cuneiform, but variants can send additional tendinous slips into the head or neck of the first metatarsal, the bases of the second through fifth metatarsals, or the intermediate cuneiform (Macalister 1875; Gruber 1884, 1887a, b, c; Cunningham and Brooks 1889; Picou 1894a, b; Bardeen 1906; Lamont 1908; Bhargava et al. 1961; Musial 1963b; Alken and Arnold 1970; Bergman et al. 1988; Raheja et al. 2005; Jayakumari et al. 2006; Patil et al. 2007; Cromeens and Reeves 2011; Kelikian 2011; Verma et al. 2011; Verma and Arora 2012). Furthermore, the fibularis longus tendon may serve as the origin of flexor digiti minimi brevis, third plantar interosseous, second or third dorsal interosseous, or the medial head of the

first dorsal interosseous muscles (Wood 1865; Lamont 1908; Harbeson 1938; Bergman et al. 1988; Verma et al. 2011). Within the fibularis longus tendon, a sesamoid bone is often found in close approximation to the cuboid tubercle (Picou 1894b; Le Double 1897; Cromeens and Reeves 2011; Kelikian 2011). At the location of this cuboidal sesamoid, an anteriorly projecting fibrous expansion called the anterior frenular ligament may connect the fibularis longus tendon to the base of the fifth metatarsal and the origin of the flexor digiti minimi brevis muscle in approximately 63.0–83.3% of specimens (Picou 1894b; Le Double 1897; Patil et al. 2007; Cromeens and Reeves 2011; Kelikian 2011). The posterior frenular ligament may also be located at the cuboidal sesamoid to connect the fibularis longus tendon posteriorly to the cuboid bone in 10–13.3% of specimens (Picou 1894b; Le Double 1897; Patil et al. 2007; Cromeens and Reeves 2011; Kelikian 2011). In approximately 22–36% of feet, the tibialis posterior sends a tendinous slip to attach to the fibularis longus tendon at its insertion on the base of the first metatarsal (Picou 1894b; Musial 1963a; Lohrmann et al. 1997; Bloome et al. 2003; Raheja et al. 2005; Kelikian 2011).

Fibularis (peroneus) brevis

The fibularis brevis may have superficial and deep bellies (Mehta et al. 2011).The tendon of the peroneus brevis usually inserts into the base of the fifth metatarsal near its tuberosity, but variants may deviate to insert on the dorsum of the fifth metatarsal, into the fourth dorsal interosseous muscle, or attach to the flexor digiti minimi brevis (Wood 1866b; Gruber 1887b; Javadekar 1961; Musial 1963b; Bergman et al. 1988). Its tendon may also bifurcate, with one part joining the fibularis tertius tendon or even giving origin to the abductor digiti minimi muscle (Wood 1866a, b; Macalister 1875; Bergman et al. 1988). The fibularis brevis tendon often sends a tendinous slip to the base of the fifth proximal phalanx or the extensor expansion (dorsal aponeurosis) of the little toe, and this fibularis quartus variant, fibularis (peroneus) digiti minimi, is discussed in the next section (Wood 1865, 1866a, b; Macalister 1875; Le Double 1897; Bhargava et al. 1961; Reimann 1981; Bareither et al. 1984; Bejjani and Jahss 1985; Raheja et al. 2005; Jadhav et al. 2013).

Fibularis (peroneus) quartus

The fibularis quartus (peroneocalcaneus externum muscle of Otto) is a variant muscle within the lateral leg compartment that arises from the lower third of the fibula, fibularis longus muscle, and/or fibularis brevis muscle, and travels posterior to the lateral malleolus. Its distal insertion has shown great variability, most often inserting onto the lateral surface of the calcaneus on the retrotrochlear eminence (Kelikian 2011; Clarkson et al. 2013). The fibularis quartus was first described by Otto in 1816 (Kelikian 2011) and has since been called the "peroneus sextus, peroneus calcaneus externus, peroneocuboidian, peroneus accessorius, peroneus medius" (Le Double 1897; Bejjani and Jahss 1985) as well as the "peroneus muscle of the tarsus" (Hecker 1923). Anatomists, surgeons, and radiologists have discovered slight variations in the distal insertion of the fibularis quartus, which has resulted in both increased and ambiguous nomenclature (Macalister 1866; Wood 1866b; Sobel et al. 1990; Saupe et al. 2007; Clarkson et al. 2013). Reported points of insertion include (from proximal to distal): retrotrochlear eminence of the calcaneus; the fibular (peroneal) trochlea of the calcaneus; tendons of fibularis longus and brevis muscles; cuboid; and fifth metatarsal (Sobel et al. 1990; Cheung et al. 1997; Zammit and Singh 2003; Gumusalan and Ozbag 2007; Clarkson et al. 2013). With so many variations within the insertion of the fibularis quartus muscle, two studies attempted to resolve the nomenclature issues by suggesting that the fibularis quartus muscle inserts onto the lateral aspect of the calcaneus, often named the peroneocalcaneus externum muscle, and the variants of the muscle have other distal attachments (Sobel et al. 1990; Buschmann 1991; Cheung and Rosenberg 2001; Zammit and Singh 2003; Wang et al. 2005; Sookur et al. 2008).

The confusion in the fibularis quartus nomenclature has led to great disparities in its reported prevalence (Trono et al. 1999; Clarkson et al. 2013). As Table 41.2 summarizes, the fibularis quartus muscle has been reported to be present in 11.5% of legs in cadaveric, MRI, and ultrasound studies (Wood 1865, 1866b; Pozzi 1872; Gruber 1879; Hecker 1923; Sobel et al. 1990;

Table 41.2 Historical prevalence of fibularis quartus (FQ) muscle in previous cadaveric, magnetic resonance imaging, and ultrasound studies. Adapted from Clarkson et al. (2013) with permission from Elsevier.

Study	Method	No. limbs	FQ	Prevalence (%)
Wood 1865	Cadaveric	32	5	15.6
Wood 1866b	Cadaveric	70	2	2.9
Pozzi 1872	Cadaveric	28	4	14.3
Gruber 1879	Cadaveric	982	118	12.0
Hecker 1923	Cadaveric	63	10	15.9
Sobel et al. 1990	Cadaveric	124	27	21.8
Chaney et al. 1996	Cadaveric	269	8	3.0
Cheung et al. 1997	MRI	136	14	10.3
Rosenberg et al. 1997	MRI	31	2	6.5
Chepuri et al. 2001	Ultrasound/MRI	32	7	21.9
Borne et al. 2002	MRI	63	7	11.1
Zammit and Singh 2003	Cadaveric/MRI	182	12	6.6
Saupe et al. 2007	MRI	65	11	16.9
Tubbs et al. 2008	Cadaveric	89	1	1.1
Prakash et al. 2011	Cadaveric	70	3	4.3
Athavale et al. 2012	Cadaveric	92	20	21.7
Nascimento et al. 2012	MRI	211	16	7.6
Clarkson et al. 2013	Cadaveric	277	58	20.9
Total		2816	325	11.5

Chaney et al. 1996; Cheung et al. 1997; Rosenberg et al. 1997; Chepuri et al. 2001; Borne et al. 2002; Zammit and Singh 2003; Saupe et al. 2007; Tubbs et al. 2008; Prakash et al. 2011; Athavale et al. 2012; Nascimento et al. 2012; Clarkson et al. 2013), although recent studies report a higher incidence (20.9–21.9%; Sobel et al. 1990; Chepuri et al. 2001; Athavale et al. 2012; Clarkson et al. 2013). Believed to be an evolutionary acquisition for bipedal gait, the fibularis quartus muscle is unique to humans, assisting with eversion of the lateral border of the foot, pronation of the foot against the walking surface, and lateral stabilization of the ankle (Hecker 1923; Wachter and Beekman 1983; Athavale et al. 2012). Although often identified in asymptomatic individuals, the presence of the fibularis quartus muscle has been shown to cause lateral ankle pain, ankle instability, fibular tenosynovitis, subluxation of the fibular (peroneal) tendons, and longitudinal splitting of the fibularis brevis tendon, especially following inversion ankle sprains (Regan and Hughston 1977; Trono et al. 1999; Sammarco and Brainard 1991; Donley and Leyes 2001; Martinelli and Bernobi 2002; Zammit and Singh 2003; Lotito et al. 2011; Clarkson et al. 2013).

Notable variants of the fibularis quartus

- Fibulocuboideus (peroneocuboideus) of Chudzinski: The fibulocuboideus variant was originally described by Theophile H. Chudzinski in 1875 (Chudzinski 1875). It is named by its distal attachment into the cuboid bone, which has been reported to insert into its lateral surface (Donley and Leyes 2001), its tuberosity (Gray 1918; Nascimento et al. 2012), or its distal lip of the peroneal sulcus (Clarkson et al. 2013), as seen in Figure 41.5. The fibulocuboideus muscle is exceedingly rare; in fact, in studies where it has been identified, its estimated prevalence is 0.57%, or 5 fibulocuboideus muscles identified in 877 leg dissections (Sobel et al. 1990; Cheung et al. 1997; Donley and Leyes 2001; Zammit and Singh 2003; Saupe et al. 2007; Athavale et al. 2012; Clarkson et al. 2013). A novel variant, the fibulocalcaneocuboideus (peroneocalcaneocuboideus) muscle, has also been identified, which sends an additional fascial slip into the retrotrochlear eminence of the calcaneus (Clarkson et al. 2013).
- Peroneus accessorius (peroneoperoneolongus) of Hecker: The peroneus accessorius muscle arises from the fibularis brevis or fibularis longus muscle and inserts back into either the fibularis longus or brevis tendon. This fibularis quartus variant was originally described as the peroneoperoneolongus muscle by Hecker (1923) due to its insertion into the fibularis longus tendon. (Hecker 1923; White et al. 1974; Regan and Hughston 1977; Sobel et al. 1990; Jayakumari et al. 2006; Saupe et al. 2007; Sookur et al. 2008; Carroll 2008; Clarkson et al. 2013).
- Peroneus (fibularis) digiti minimi (quinti) of Huxley: The peroneus digiti minimi has been described as a small slip derived from the tendon of the peroneus brevis that arises proximal or distal to the lateral malleolus or a completely separate muscle arising from the lower fourth of the fibula (Wood 1866b; Macalister 1875; Raheja et al. 2005). This fibularis quartus variant earns its name by inserting into the extensor (dorsal) aponeurosis of the little toe, the base and head of the dorsal surface of the fifth metatarsal, or the base of the fifth proximal phalanx (Wood 1866b; Macalister 1875; Testut 1921; Hecker 1923; Bareither et al. 1984; Sobel et al. 1990; Jadhav et al. 2013). Reported incidence of the peroneus digiti minimi varies from 15.5% to 79.5%, and this tendinous slip can be seen extending off the fibularis brevis tendon in Figure 41.3 (Wood 1866b; Bhargava et al. 1961; Reimann 1981; Bareither et al. 1984; Bejjani and Jahss 1985; Jadhav et al. 2013).
- Peroneotalocalcaneus muscle of Tubbs: The peroneotalocalcaneus muscle is another fibularis quartus variant in which the distal insertion bifurcated to insert into the superior surface of the talus as well as the retrotrochlear eminence of the calcaneus (Tubbs et al. 2008).

Posterior compartment: superficial muscles

Gastrocnemius

The medial and lateral heads of the gastrocnemius may consist of two layers throughout their entire length: conversely, both muscular heads may be replaced by fibrous bands (Macalister

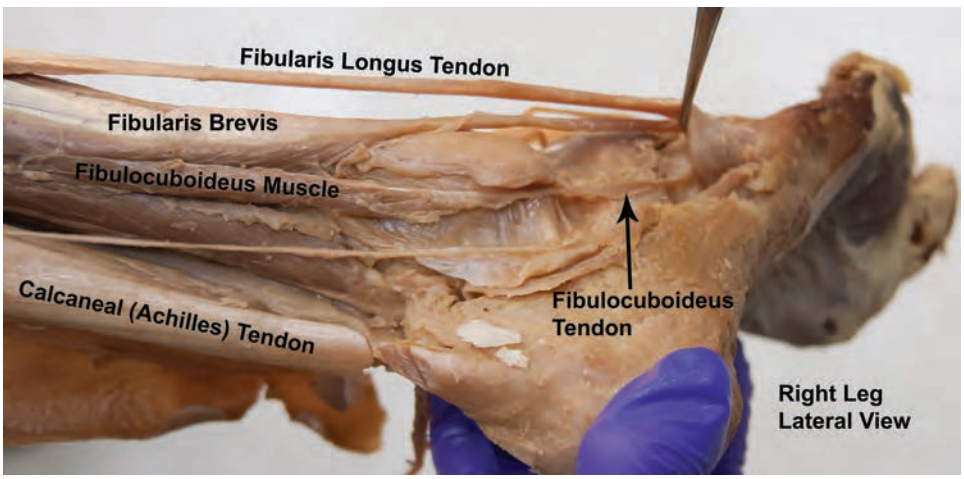

Figure 41.5 An exceedingly rare fibulocuboideus variant of the fibularis quartus muscle is shown arising from the muscle belly of the fibularis brevis, the lower third of the fibula, and the posterior intermuscular septum in the right leg. It courses posterior to the lateral malleolus, and its tendon inserts onto the cuboid bone at the distal lip of the fibular (peroneal) sulcus, which contains the fibularis longus tendon.

1875; Le Double 1897; Bejjani and Jahss 1985). The lateral head of the gastrocnemius can be absent or poorly developed, sometimes represented by a tendinous band (Shepherd 1880; Le Double 1897; Bejjani and Jahss 1985; Bergman et al. 1988). The tendons of each head of the gastrocnemius may stay separated until merging in the distal leg, close to their insertion into the calcaneal (Achilles) tendon (Le Double 1897; Bejjani and Jahss 1985; Bergman et al. 1988). In addition, the gastrocnemius and the soleus muscles may not fuse until just proximal to their insertion into the calcaneal tuberosity, and have even been seen inserting into the calcaneus separately (Bankart et al. 1869; Pye-Smith et al. 1871; Testut 1884; Le Double 1897; Bejjani and Jahss 1985). Finally, a sesamoid bone may exist in the lateral head of the gastrocnemius in approximately 9.4–17% of specimens, but is rarely found within the medial head (Macalister 1875; Pfitzner 1892; Le Double 1897; Bejjani and Jahss 1985).

Notable variants of the gastrocnemius

- Gastrocnemius tertius (caput tertium) of Kelch: A third head of the gastrocnemius, gastrocnemius tertius or caput tertium, may arise from the popliteal surface of the femur, namely the linea aspera, lateral epicondyle, knee joint capsule, or midfibula, or even from the long head of biceps femoris muscle, semitendinosus muscle, or the crural fascia (Kelch 1813; Macalister 1875; Walsham 1880; Le Double 1897; Frey 1919; Parsons 1920; Kato and Tofukuji 1954; Bejjani and Jahss 1985; Bergman et al. 1988, 1995; Somayaji et al. 1998; Gupta and Bhagwat 2006; Dave et al. 2012). The gastrocnemius tertius may originate from more than one location or divide near its termination to insert into both heads of gastrocnemius. The gastrocnemius tertius may cross the popliteal neurovascular structures and has been shown to cause clinical problems, such as intermittent claudication, arterial stasis and aneurysm (popliteal vascular entrapment syndrome), venous stasis, and impaired nerve function (Hamming 1959; Liu et al. 2005; Paval et al. 2005; Yildirim et al. 2011; Sirasanagandla et al. 2013; Simsek et al. 2014). The prevalence of the gastrocnemius tertius muscle has been reported to occur in 1.9–5.5% of specimens, based on cadaveric and MRI studies (Kelch 1813; Frey 1919; Parsons 1920; Kato and Tofukuji 1954; Mori 1964; Bergman et al. 1988, 1995; Koplas et al. 2009; Yildirim et al. 2011; Dave et al. 2012).

Soleus

The soleus normally arises from the posterior aspect of the head and superior part of the fibula (fibular head), and the soleal line and medial border of the tibia (tibial head). The soleus may be completely absent, as observed by Danseux in 1884, and the tibial head may be absent in 14% of specimens (Testut 1884; Le Double 1897; Mori 1964; Bejjani and Jahss 1985; Bergman et al. 1988). Duplication of both the tibial and fibular heads of the muscle has been reported, with the accessory head usually arising deep (anterior) to the soleus muscle (Macalister 1875; Le Double 1897; Bejjani and Jahss 1985; Bergman et al. 1988; Sawant et al. 2013).

Notable variants of the soleus

- Accessory soleus muscle of Cruveilhier (musculus accessories): The accessory soleus muscle was first described by Cruveilhier in 1843, and was previously called the musculus accessorius (Cruveilhier 1843; Bankart et al. 1869; Pye-Smith et al. 1871; Davies-Colley et al. 1873; Hatzantonis et al. 2011). The accessory soleus usually arises from the soleal line of the tibia, but also can originate from the deep (anterior) surface of the soleus muscle or the proximal third of the fibula (Le Double 1897; Bejjani and Jahss 1985; Bergman et al. 1988; Lorentzon and Wirell 1987; Buschmann et al. 1991; Brodie et al. 1997; Kendi et al. 2004; Sookur et al. 2008; Hatzantonis et al. 2011). This muscle descends anterior or anteromedial to the calcaneal (Achilles) tendon, and usually inserts one of three types of distal attachments, according to Hatzantonis et al. (2011): Type A displays a separate tendinous or fleshy insertion into the calcaneus, medial to the calcaneal tendon; Type B displays a distal tendinous attachment to the calcaneal tendon; and Type C represents a distal tendinous or fleshy attachment to the medial surface of the calcaneus, as depicted in Figure 41.6 (Le Double 1897; Bejjani and Jahss 1985; Lorentzon and Wirell 1987; Yu and Resnick 1994; Brodie et al. 1997; Sookur et al. 2008; Hatzantonis et al. 2011). This variant muscle has a documented prevalence of 0.7–5.5% according to cadaveric studies (Brodie et al. 1997; Sookur et al. 2008; Hatzantonis et al. 2011). Clinically, it is often detected as a soft-tissue, mass-occupying lesion in the posteromedial aspect of the ankle commonly detected in athletes in the second or third decade of life. These individuals present with pain due to localized compartment syndrome or inadequate blood supply from the posterior tibial artery (Buschmann et al. 1991; Brodie et al. 1997; Sookur et al. 2008; Hatzantonis et al. 2011). The accessory soleus muscle travels superficial to the flexor retinaculum, distinguishing it from the tibiocalcaneus internus muscle which passes deep to the flexor retinaculum (Hecker 1924; Sookur et al. 2008; Kelikian 2011).
- Tibiocalcaneus internus muscle of Testut: The tibiocalcaneus internus muscle is exceedingly rare and has only been reported by a few researchers (Testut 1892; Hecker 1924; Sammarco and Conti 1994). This muscle is very similar to the Type C accessory soleus muscle in that it originates from the soleus line and medial crest of the tibia, lies deep (anterior) to the soleus muscle, and inserts on the medial surface of the calcaneus about 2 cm anterior to the calcaneal (Achilles) tendon (Hecker 1924; Kelikian 2011). The passage of the tibiocalcaneus internus muscle deep to the flexor retinaculum, or within the tarsal tunnel, which is what distinguishes this muscle from the accessory soleus muscle (Hecker 1924; Sookur et al. 2008; Kelikian 2011). The location of the tibiocalcaneus internus within the tarsal tunnel is superficial (posterior) to the neurovascular bundle, which is similar to the course of the flexor digitorum accessorius longus or FDAL muscle (Sookur et al. 2008). It is therefore important to investigate the distal attachment to distinguish between the tibiocalcaneus internus, which inserts into the

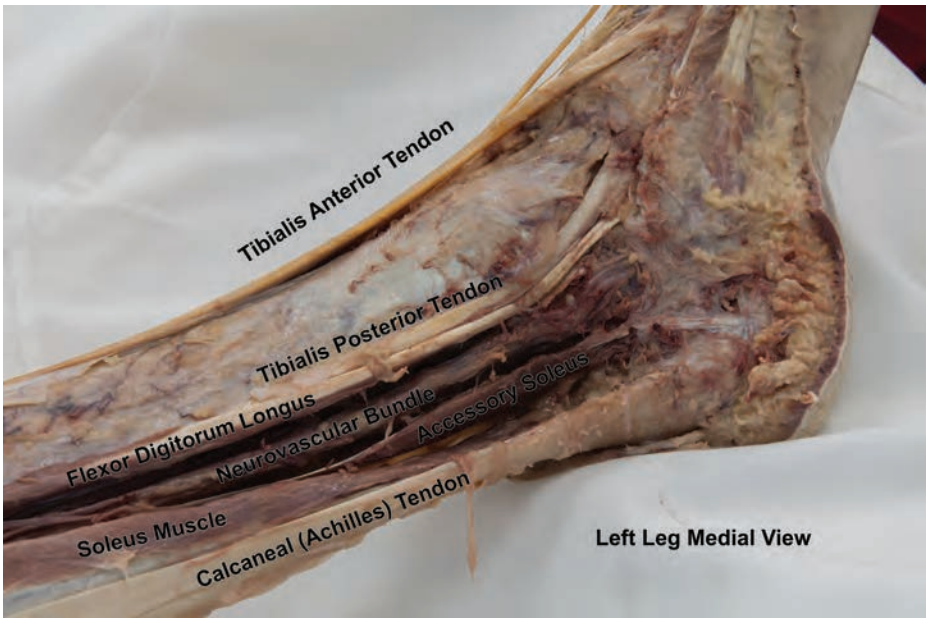

Figure 41.6 A type C accessory soleus muscle is shown in a left leg descending anteromedial to the calcaneal tendon. Its tendon bifurcates to insert onto the medial surface of the calcaneus.

medial aspect of the calcaneus, and the FDAL muscle, which inserts into the quadratus plantae and/or flexor digitorum longus muscles (Sammarco and Conti 1994; Sookur et al. 2008; Kelikian 2011).

- Peroneotibialis muscle of Gruber: Gruber (1878) described the pereoneotibialis muscle as a tensor of the tendinous arch of the soleus, originating from the medial side of the fibula and inserting into the superior aspect of the soleal line of the tibia or the tendinous arch of the soleus muscle, as shown in Figure 41.7 (Gruber 1878; Bergman et al. 1988). Gruber (1878) identified the peroneotibialis muscle in 128 of 860 (14.9%) legs; it usually occurs bilaterally but, when unilateral, is more frequently found in the right limb (Gruber 1878; Bergman et al. 1988).

Plantaris

The plantaris muscle can vary in appearance from a thin fibrous band to a robust muscle belly equal in size to the lateral head of the gastrocnemius at its origin (Cruveilhier 1843; Le Double 1897; Daseler and Anson 1943; Bejjani and Jahss 1985). The plantaris usually originates from the oblique popliteal ligament and lateral aspect of the lateral condyle of the femur slightly above the origin of the lateral head of the gastrocnemius; however, it has been shown to arise from the lateral supracondylar line or even inferior lateral bifurcation of the linea aspera of the femur, the intercondylar fossa of the femur, the investing fascia of the popliteus, the lateral head of the gastrocnemius, the superior aspect of the fibula between the flexor hallucis longus and fibularis longus muscles, the soleal line of the tibial beneath the

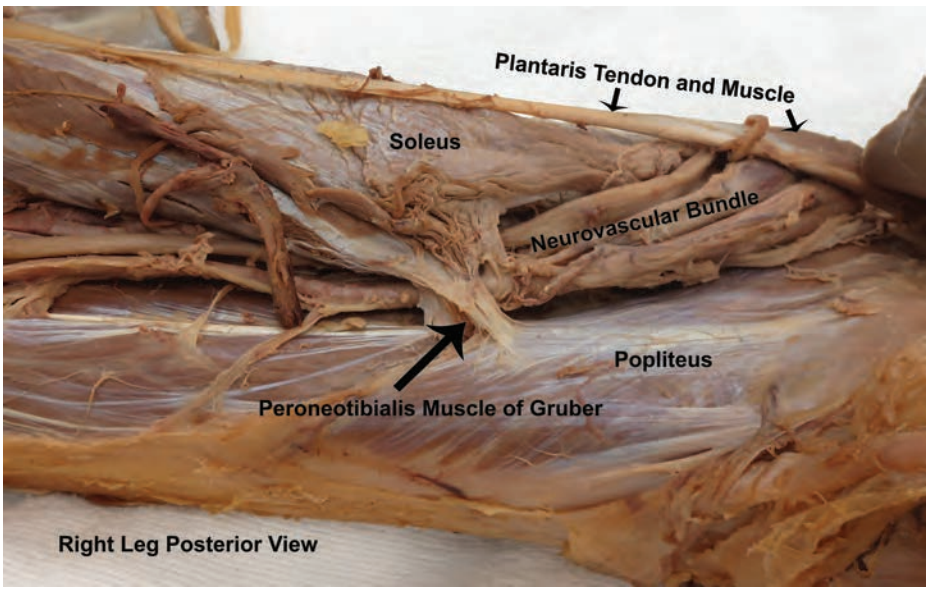

Figure 41.7 The pereoneotibialis muscle of Gruber is shown originating from the medial side of the fibula and a tendinous slip from the popliteus muscle and inserting into the superior aspect of the tendinous arch of the soleus muscle (Gruber 1878; Bergman et al. 1988). Note how this variant muscle and the medial aspect of the soleus arches posterior to the neurovascular bundle, creating a location for potential entrapment of the posterior tibial artery and tibial nerve. Photo by H. Wayne Lambert, Ph.D., West Virginia University.

soleus, and the crural fascia (Macalister 1875; Le Double 1897; Daseler and Anson 1943; Bejjani and Jahss 1985; Rana et al. 2006; Upasna and Kumar 2011). The plantaris muscle may interdigitate with the lateral head of the gastrocnemius in 19.6% of legs or send a strong fibrous extension to the patella in 10.9% of legs, which may contribute to patellofemoral pain syndrome (Wood 1866b; Freeman et al. 2008). The distal attachment of the plantaris varies rarely as it usually inserts into the posterosuperior aspect of the calcaneus via the calcaneal (Achilles) tendon; however, it has been shown to insert into neighboring structures along its normal course deep to the gastrocnemius and superficial to the medial aspect of the soleus muscle, including the investing fascia of the gastrocnemius and soleus, the flexor retinaculum, the dorsomedial border of the calcaneal tendon near or at its insertion, or even distally into the fascia overlying the calcaneus or the plantar aponeurosis (Le Double 1897; Daseler and Anson 1943; Bejjani and Jahss 1985; Sawant et al. 2012).

According to Cruvelhier (1843), the plantaris muscle is often missing and is sometimes doubled (Cruveilhier 1843; Le Double 1897; Daseler and Anson 1943; Bejjani and Jahss 1985). A historical review of cadaveric studies (Table 41.3) reveals that the plantaris is present in 92.6% of legs or, conversely, absent in 7.4% of legs (Gruber 1879; Schwalbe and Pfitzner 1894; Le Double 1897; Danforth 1924; Daseler and Anson 1943; Moss 1988; Saxena and Bareither 2000; Freeman et al. 2008; Venter et al. 2011).

Notable variants of the plantaris

- Accessory plantaris muscle (bicipital plantaris of Hall): When the plantaris muscle has two muscular slips originating from its previously mentioned variable sites of origin, this additional muscle belly transforms this normally fusiform muscle into a biceps, which was first reported by Hall in 1808 (Cruveilhier 1843; Le Double 1897; Bejjani and Jahss 1985). According to Herzog (2011), the accessory plantaris muscle has a prevalence of 6.3% in 1000 consecutive MRI exams of the knee; however, the paucity of cadaveric studies identifying this muscle suggests a much lower incidence (Cruveilhier 1843; Rana et al. 2006; Herzog 2011; Upasna and Kumar 2011; Sawant et al. 2012). In fact, in a cadaveric study of 750, Daseler and Anson (1943) did not report the identification of an accessory plantaris muscle.
- Tensor fasciae plantaris of Wood (tibiotarsalis muscle): Tensor fasciae plantaris arises from the soleal line of the tibia deep (anterior) to the soleus muscle and inserts into the fascia overlying the calcaneus (Bergman et al. 1988). Anderson (1880) described a similar muscle, which he called the tibiotarsalis muscle, which arises from the soleal line of the posterior aspect of the tibia and inserts in the plantar fascia. Due to its insertion, he considered this muscle to be a variant of the tensor fasciae plantaris muscle (Anderson 1880).

Table 41.3 Historical prevalence of the plantaris muscle in previous cadaveric dissection studies.

Study	Method	No. limbs	Plantaris	Prevalence (%)
Gruber 1879	Cadaveric	1400	1295	92.5
Schwalbe and Pfitzner 1894	Cadaveric	520	488	93.8
Le Double 1897	Cadaveric	420	397	94.5
Danforth 1924	Cadaveric	1084	992	91.5
Daseler and Anson 1943	Cadaveric	750	700	93.3
Moss 1988	Cadaveric	300	285	95.0
Saxena and Bareither 2000	Cadaveric	40	39	97.5
Freeman et al. 2008	Cadaveric	46	40	87.0
Venter et al. 2011	Cadaveric	302	267	88.4
Total		4862	4503	92.6

Posterior compartment: deep muscles

Popliteus

The popliteus muscle usually originates from the lateral surface of the lateral condyle of the femur and the posterior arch of the lateral meniscus of the knee, but it also regularly attaches to the apex and head of the fibula through the popliteofibular ligament (Macalister 1875; Higgins 1895; Last 1950; Hadziselmovic and Gluhbegovic 1969; Lovejoy and Harden 1971; Fetto et al. 1977; Feipel et al. 2003; Paraskevas et al. 2006; Chuncharunee et al. 2012). The proximal attachments of the popliteus muscle regularly exhibit fibrous connections to the posterior knee joint capsule, the arcuate popliteal ligament, and the oblique popliteal ligament (Last 1950; Fetto et al. 1977; Feipel et al. 2003). Proximal attachments to the posterior cruciate and posterior meniscofemoral ligaments are less common (Feipel et al. 2003). The popliteus muscle inserts into the posterior (popliteal) surface of the tibia, immediately superior to the soleus line. The absence of the popliteus muscle has been reported only twice (Ringhoffer 1860; Le Double 1897; Bejjani and Jahss 1985), and the popliteus muscle may be doubled, which was first reported by Fabrice d'Aquapendente in 1687 (Fabrice 1687; Macalister 1875; Le Double 1897; Bejjani and Jahss 1985; Bergman et al. 1988).

Notable variants of the popliteus

Accessory popliteus muscle of Fabrice (popliteus biceps): An accessory popliteus muscle is rare, and possesses two muscular slips or (even less often) two distinct muscular heads (Calori 1866; Wood 1866b; Wagstaffe 1872; Macalister 1875; Bergman et al. 1988; Duc et al. 2004). This duplicated muscle has been called the small or proximal popliteus or even popliteus minor (Calori 1866; Wood 1866b), popliteus biceps (Gruber 1875d), popliteus geminus (Fabrice 1687), and accessory popliteal muscle (Wagstaffe 1872; Le Double 1897; Bejjani and Jahss 1985; Duc et al. 2004). Accessory slips may originate both proximally

and distally to the popliteus muscle from the posterosuperior part of the lateral femoral condyle medial to the origin of the plantaris muscle, the lateral head of the gastrocnemius near its sesamoid bone, posterior knee joint capsule, or the posterior cruciate ligament of the knee (Le Double 1897; Bejjani and Jahss 1985; Bergman et al. 1988). It may insert into the medial border of the tibia along with the medial fibers of the popliteus near the soleal line (Le Double 1897; Bejjani and Jahss 1985; Bergman et al. 1988). Gruber identified the accessory popliteus in 11 of 695 legs for a prevalence of 1.6% (Gruber 1875d; Bartoníček 2005). Moreover, rare bifurcation of the popliteal tendon in the vicinity of the lateral meniscus has been documented in 6 of 1549 (0.4%) knee arthroscopies (Burman 1968; Perez Carro and Sumillera Garcia 1999; Leal-Blanquet et al. 2009).

Tibialis posterior

Variations of the tibialis posterior muscle are rare; however, this muscle may be absent as reported by Budge or duplicated (Macalister 1875; Le Double 1897; Bejjani and Jahss 1985; Bergman et al. 1988). The muscular variants of the tibialis posterior are primarily related to its tendinous insertions, which usually divide into three components: anterior, middle, and posterior (Musial 1963a; Lewis 1964; Martin 1964; Bloome et al. 2003; Kelikian 2011). The anterior component is the largest and has a broad insertion into the navicular tuberosity, inferior surface of the medial (first) cuneiform, and the intervening inferior joint capsule (Lewis 1964; Martin 1964; Kelikian 2011). The insertion into the medial cuneiform may be absent (Bergman et al. 1988). The anterior component may send a tendinous slip to the abductor hallucis muscle (Bloome et al. 2003; Kelikian 2011). Within the anterior component of the tibialis posterior tendon, a fibrocartilaginous or bony sesamoid bone, which absorbs pressure and assists in the gliding mechanism of this tendon, was identified in 23% of 348 adult feet (Bloome et al. 2003; Semple et al. 2009). The middle component is very deep (superior) and diverts to insert into the middle (second) and medial (third) cuneiform bones as well as the cuboid bone laterally. In addition, the middle component sends a tarsometatarsal extension anteriorly, located deep (superior) to the fibularis longus tendon, to insert into the bases of the second, third, fourth, and (less often) the fifth metatarsal bones in 64% of feet according to Bloome et al. (2003). This metatarsal extension of the middle component of the tibialis posterior tendon attaches to the flexor digitorum brevis muscle at its origin in 82% of feet; in approximately 22–36% of feet, it sends an additional tendinous slip to the attach to the fibularis longus tendon at its insertion into the base of the first metatarsal (Picou 1894b; Le Double 1897; Musial 1963a; Lewis 1964; Martin 1964; Bejjani and Jahss 1985; Lohrmann et al. 1997; Bloome et al. 2003; Raheja et al. 2005; Kelikian 2011). The attachment of the medial component to the flexor digitorum brevis may be a cause of hallux valgus (Gunal et al. 1994). The middle component has also been shown to insert into the plantar calcaneonavicular (spring) ligament in 36% of feet (Bloome et al. 2003; Kelikian 2011). The posterior component of the posterior tibialis tendon is recurrent, originating proximal to the insertion into the navicular tuberosity and running posterolateral to insert into the anterior border of the sustentaculum tali of the calcaneus (Lewis 1964; Martin 1964; Bloome et al. 2003; Kelikian 2011).

Notable variants of the tibialis posterior

Accessory tibialis posterior (tibialis secundus of Bahnsen): An accessory tibialis posterior muscle has been reported only three times, found initially by Bahnsen and later by Le Double in two separate legs (Bahnsen 1868; Macalister 1875; Le Double 1897; Bejjani and Jahss 1985; Bergman et al. 1988). Bahnsen called this muscle the tibialis secundus and reported that it arose from the posterior aspect of the tibia distal to the normal tibialis posterior muscle and the soleal line, and inserted into flexor retinaculum (Bahnsen 1868; Le Double 1897; Bejjani and Jahss 1985; Bergman et al. 1988). In January of 1885, Le Double found an accessory tibialis posterior arising from the posterior aspect and medial edge of the right tibia, 6 cm distal to the soleal line of the tibia (Le Double 1897; Bejjani and Jahss 1985). Its distal tendon exhibited characteristics of the normal middle component of the tibialis posterior tendon as it trifurcated to insert into the fibularis longus tendon, base of the second metatarsal, and cuboid (Le Double 1897; Bejjani and Jahss 1985). Within this same right leg, the main tibialis posterior tendon inserted into the navicular tuberosity, representing the normal anterior component of this tendinous insertion (Le Double 1897; Bejjani and Jahss 1985). In February of 1879, Le Double found a similar accessory tibialis posterior in the right leg; however, this variant muscle bifurcated to insert in the base of the second metatarsal and distal tendon of the tibialis posterior muscle at the location of its sesamoid bone (Le Double 1897; Bejjani and Jahss 1985).

Flexor digitorum longus

Accessory muscular bundles have been seen joining the flexor digitorum longus proximal to the ankle after arising from the tibialis posterior muscle, the crura fascia, or the tibia itself (Gies 1868; Le Double 1897; Bejjani and Jahss 1985). However, most of the muscular variants of the flexor digitorum longus are primarily related to its tendinous insertions, which may exhibit additional tendinous slips or may even be absent within a toe (Turner 1865; Flower and Murie 1867; Gies 1868; Testut 1884; White 1884; Gruber 1887d, e; Le Double 1897; Focacci 1903; Barlow 1949; Martin 1964; Bejjani and Jahss 1985; Bergman et al. 1988; Kelikian 2011). The flexor digitorum longus usually divides to insert into the bases of the distal phalanges of the lateral four digits, but occasionally the tendon to the second toe is absent, replaced by a tendon from the flexor hallucis longus muscle (Wood 1866b; Macalister 1875; Le Double 1897; Bejjani and Jahss 1985; Bergman et al. 1988). Moreover, the flexor digitorum longus may send a tendinous slip to the big toe, which is rare (Macalister 1875; Le Double 1897; Bejjani and Jahss 1985). However, most of the variants of the flexor digitorum longus concern the tendinous connections that intermingle between

the flexor digitorum longus and flexor hallucis longus tendons, which will is discussed in the following section (Turner 1865; Schultze 1867; Le Double 1897; Martin 1964; Bejjani and Jahss 1985; Bergman et al. 1988; LaRue and Anctil 2006; Kelikian 2011).

Flexor hallucis longus

The connection extending from the flexor hallucis longus (FHL) to insert into the flexor digitorum longus tendons is constant but highly variable in its insertion (Turner 1865; Schultze 1867; Le Double 1897; Martin 1964; Bejjani and Jahss 1985; Bergman et al. 1988; LaRue and Anctil 2006; Kelikian 2011). Through two separate studies with a total of 150 leg dissections, Turner (1865) and Schultze (1867) found the flexor hallucis longus sent a tendinous slip to the flexor digitorum longus in all 150 legs, although Martin (1964) did see the absence of these tendinous connections in two specimens (Turner 1865; Schultze 1867; Macalister 1875; Le Double 1897; Martin 1964; Bejjani and Jahss 1985; Bergman et al. 1988; Kelikian 2011). More specifically, the tendinous slips of the FHL inserted into the flexor digitorum longus tendon after its segmentation into digital slips at the following locations: (1) the tendon for the second toe in 43/150 (28.7%) legs; (2) tendons to the second and third toes in 78/150 (52.0%) legs; (3) tendons to the second through fourth toes in 28/150 (18.7%) legs; and (4) tendons to the second through fifth toes in 1/150 (0.7%) legs (Turner 1865; Schultze 1867; Macalister 1875; Le Double 1897; Bejjani and Jahss 1985; Bergman et al. 1988; Kelikian 2011).

Flower and Murie (1867) also identified the latter insertion pattern in which the tendons of both the flexor digitorum longus and the FHL insert into the lateral four toes (Flower and Murie 1867; Macalister 1875; Le Double 1897; Bejjani and Jahss 1985; Bergman et al. 1988; Kelikian 2011). Interestingly, the flexor digitorum longus can also send tendinous slips to insert into the flexor hallucis longus tendon, although less frequently according to Turner (1865) who reported this tendinous connection in 6/50 (12.0%) legs, Wood (1866a) in 6/29 (20.5%) legs, and Schultze (1867) in 29/100 (29.0%) legs (Turner 1865; Wood 1866a; Schultze 1867; Macalister 1875; Le Double 1897; Bejjani and Jahss 1985; Bergman et al. 1988; LaRue and Anctil 2006; Kelikian 2011).

Flexor digitorum accessorius longus muscle

The flexor digitorum accessorius longus (FDAL) has a variable proximal attachment to the tibia, fibula, tibia and fibula, the posterior intermuscular septum, or any of the musculature in the deep posterior compartment of the leg (Macalister 1875; Testut 1884; Le Double 1897; Bejjani and Jahss 1985; Porter 1996; Jaijesh et al. 2006; Sookur et al. 2008). After coursing posterior to the medial malleolus and underneath the flexor retinaculum (within the tarsal tunnel), the FDAL ends in the sole of the foot inserting into the flexor digitorum longus and/or quadratus plantae muscles, as shown in Figure 41.8 (Bergman et al. 1988; Mellado et al. 1997; Cheung and Rosenberg 2001; Jaijesh et al. 2006; Sookur et al. 2008). The incidence of the FDAL muscle has been reported as 6% of asymptomatic individuals during MRI studies (Cheung et al. 1999) and 2–8% of lower limbs in cadaveric studies (Wood 1866b; Driver 1914; Lewis 1962; Nathan et al. 1975; Peterson et al. 1995; Cheung and Rosenberg 2001; Sookur et al. 2008). The FDAL muscle has been mistakenly portrayed as being synonymous with the fibulocalcaneus internus muscle due to both muscles coursing within the tarsal tunnel deep to the flexor retinaculum (Schaeffer 1953; Bergman et al. 1988; Cheung and Rosenberg 2001; Lambert et al. 2011b), despite the original 1884 work by French physician Leo Testut describing the differences between the fibulocalcaneus internus and FDAL muscles (Testut 1884; Mellado et al. 1997). The course of these anomalous muscles helps distinguish between

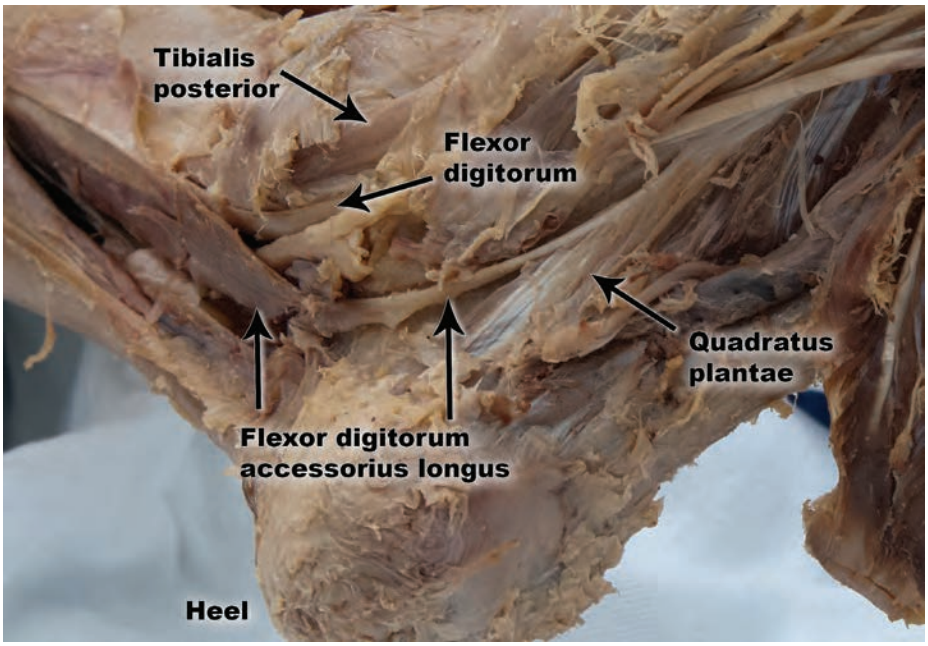

Figure 41.8 The flexor digitorum accessorius longus (FDAL) muscle is shown coursing posterior to the medial malleolus and inserting into the second layers of muscles within the sole of the left foot. More specifically, the FDAL tendon is forming the medial border of the quadratus plantae proximally and inserting distally into the flexor digitorum longus tendon. Within the tarsal tunnel, the FDAL muscle lies deep to the flexor retinaculum and superficial to the posterior tibial artery and the tibial nerve, and it has been seen to act as a space-occupying lesion within this fibro-osseous tunnel.

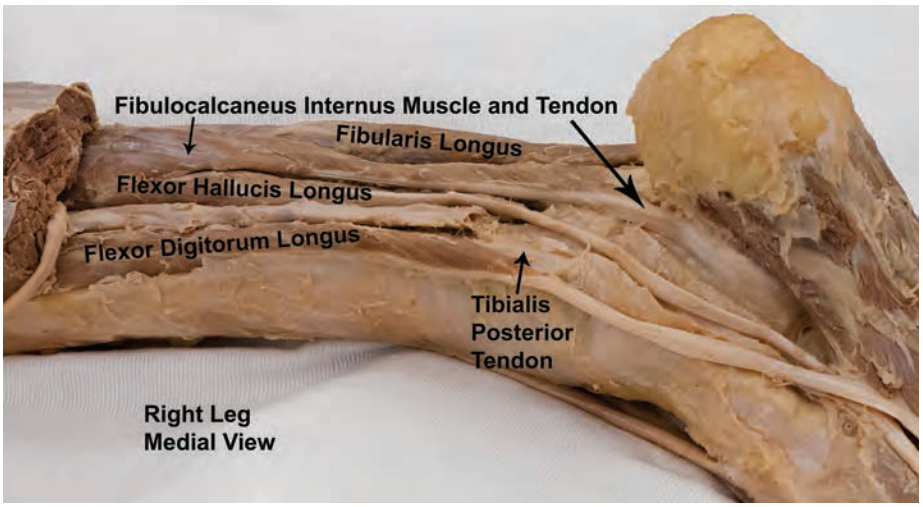

Figure 41.9 The fibulocalcaneus (peroneocalcaneus) internus muscle is shown in its normal position, located lateral to the flexor hallucis longus muscle within the right leg. However, this large example of the fibulocalcaneus internus muscle is shown arising more proximal than previously reported, originating from the medial and posterior aspect of the upper third of the fibula and the investing fascia of the flexor hallucis longus muscle. This variant muscle assumes its normal course, traveling posterior to the medial malleolus, lying deep to the flexor retinaculum within the tarsal tunnel, and inserting into the inferior aspect of the medial calcaneus just distal to the coronoid fossa, a small depression between the anterior tuberosity and the anterior apex of the sustentaculum tali.

the fibulocalcaneus internus and the FDAL; the fibulocalcaneus internus runs lateral to the FHL, as shown in Figure 41.9, while the FDAL lies medial and posterior to the flexor hallucis longus muscle when traversing the tarsal tunnel (Macalister 1875; Testut 1884; Perkins 1914; Bejjani and Jahss 1985; Cheung and Rosenberg 2001; Lambert et al. 2011b). Finally, the fibulocalcaneus internus muscle is separated from the posterior tibial artery and tibial nerve by the FHL; however, the FDAL is intimately related to the neurovascular bundle lying immediately superficial to it, as depicted in 41.8 (Peterson et al. 1995; Mellado et al. 1997; Gumusalan and Kalaycioglu 2000; Cheung and Rosenberg 2001; Sookur et al. 2008; Lambert et al. 2011b). Knowledge of the defining characteristics of these variant muscles, including the origin, course, position within the tarsal tunnel, and insertion, is therefore necessary to distinguish between the fibulocalcaneus internus and FDAL muscles (Lambert et al. 2011b).

Fibulocalcaneus (peroneocalcaneus) internus muscle of Macalister

The fibulocalcaneus (peroneocalcaneus) internus muscle arises from the medial aspect of the lower third of the fibula, just distal to the origin of the flexor hallucis longus muscle, and inserts generally into the inferior aspect of the medial calcaneus (Curnow 1873; Macalister 1875; Testut 1884; Hartmann 1888; Thane 1891; Le Double 1897; Perkins 1914; Bejjani and Jahss 1985; Lambert et al. 2011b). More specifically, this distal attachment varies from the sustentaculum tali of the calcaneus (Macalister 1875; Best et al. 2005; Seipel et al. 2005; Kelikian 2011), a small tubercle on the medical surface of the calcaneus distal to the sustentaculum tali (Curnow 1873; Thane 1891; Perkins 1914; Mellado et al. 1997; Cheung and Rosenberg 2001; Carroll 2008; Sookur et al. 2008; Amini 2011), or distal to the coronoid fossa, a small depression between the anterior tuberosity and the anterior apex of the sustentaculum tali, as shown in Figure 41.9 (Lambert et al. 2011b).

During its course, this variant muscle parallels and remains lateral to the FHL, travels posterior to the medial malleolus, and lies within the tarsal tunnel, or deep to the flexor retinaculum (Curnow 1873; Macalister 1875; Testut 1884; Hartmann 1888; Thane 1891; Le Double 1897; Perkins 1914; Bejjani and Jahss 1985; Kelikian 2011; Lambert et al. 2011b). Despite its associated eponymous description, the fibulocalcaneus internus muscle of Macalister was originally discovered by German anatomist Johann Friedrich Meckel in 1815 (Meckel 1815; Sarrafian 1993; Lambert and Atsas 2010; Kelikian 2011; Lambert et al. 2011b). Concerning its function, the fibulocalcaneus internus muscle assists in plantar flexion of the foot at the ankle joint and may aid in supination, or inversion of the foot (Perkins 1914; Lambert et al. 2011b). Clinically, this muscle has been associated with posterior ankle pain and impingement (Best et al. 2005; Seipel et al. 2005) and may be involved with tarsal tunnel syndrome (Mellado et al. 1997; Seipel et al. 2005; Duran-Stanton and Bui-Mansfield 2010; Lambert et al. 2011b). This muscle is exceedingly rare, with only one unilateral muscle detected in 100 asymptomatic volunteers during an MRI study (Mellado et al. 1997). Some radiologists have called it "the least common of all accessory muscles of the ankle" (Cheung and Rosenberg 2001).

References

Alken R, Arnold G. 1970. Ein doppelseitiger, akzessorischer muskel der peroneusgruppe. *Z Orthop* 108: 38–42.

Al-saggaf S. 2003. Variations in the insertion of the extensor hallucis longus muscle. *Folia Morphol* 62(2): 1–9.

Amini B. 2011. Peroneocalcaneus Internus Muscle. Roentgen Ray Reader. Available at: http://roentgenrayreader.blogspot.com/2011/02/peroneocalcaneus-internus-muscle.html (accessed 22 October 2015).

Anderson RJ. 1880. Vorkommen eines musculus tibio-tarsalis sive tensor fasciae plantaris. *Arch Pathol Anat Physiol Klin Med* 81: 574–575.

Arthornthurasook A, Gaew-Im K. 1990. Anterior tibial tendon insertion: an anatomical study. *J Med Assoc Thai* 73: 692–696.

Ashaolu JO, Olorunyomi OI, Opabunmi OA, Ukwenya VO, Thomas MA. 2013. Surface anatomy and prevalence of fibularis tertius muscle in a south-western Nigerian population. *Forens Med Anat Res* 1(2): 25–29.

Athavale SA, Gupta V, Kotgirwar S, Singh V. 2012. The peroneus quartus muscle: clinical correlation with evolutionary importance. *Anat Sci Int* 87: 106–110.

Bahnsen G. 1868. *Zeitschrift fur Rationelle Medicin, Dritte Reihe*. Leipzig and Heidelberg: Verlag.

Bankart J, Pye-Smith PH, Phillips JJ. 1869. Notes of abnormalities observed in the dissecting room during the winter sessions of 1866–7 and 1867–8. *Guys Hospital Reports* 14: 436–455.

Bardeen CR. 1906. Development and variation of the nerves and the musculature of the inferior extremity and of the neighboring regions of the trunk in man. *Am J Anat* 6(1): 259–390.

Bareither DJ, Schuberth JM, Evoy PJ, Thomas GJ. 1984. Peroneus digiti minimi. *Anat Anz.* 155: 11–15.

Barlow TE. 1949. An unusual anomaly of m. flexor digitorum longus. *J Anat* 83: 224–226.

Bartoníček J. 2005. Rare bilateral variation of the popliteus muscle. Anatomical case report and review of the literature. *Surg Radiol Anat* 27: 347–350.

Baumann JA. 1947. Valeur, variation, et equivalences des muscles extenseurs, interosseux, adducteurs et abducteurs de la main et du pied chez l'homme. *Acta Anat* 4: 10–16.

Bejjani FJ, Jahss MH. 1985. Le Double's study of muscle variations of the human body part I: muscle variations of the leg. *Foot Ankle* 6(3): 111–134.

Bergman RA, Thompson SA, Afifi AK, Saadeh FA. 1988. *Compendium of Human Anatomic Variation*. Baltimore, Munich: Urban & Schwarzenberg.

Bergman RA, Walker CW, El-Khoury GY. 1995. The third head of gastrocnemius in CT images. *Ann Anat* 177: 291–294.

Best A, Giza E, Linklater J, Sullivan M. 2005. Posterior impingement of the ankle caused by anomalous muscles: A report of four cases. *J Bone Joint Surg Am* 87(9): 2075–2079.

Bhadkamkar AR, Mysorekar VR. 1961. Anomalous peroneus tertius and extensor digitorum longus muscles. *J Anat Soc India* 10: 37–38.

Bhargava KN, Sanyal KP, Bhargava SN. 1961. Lateral musculature of the leg as seen in hundred Indian cadavers. *Ind J Med Sci* 15: 181–185.

Bibbo C, Arangio G, Patel DV. 2004. The accessory extensor tendon of the first metatarsophalangeal joint. *Foot Ankle Int* 25(6): 387–390.

Bloome DM, Marymont JV, Varner KE. 2003. Variations on the insertion of the posterior tibialis tendon: A cadaveric study. *Foot Ankle Int* 10: 780–783.

Borne J, Fantino O, Besse JL, Clouet P, Tran Minh V. 2002. Aspect IRM des variantes anatomiques des muscles, tendons et ligaments de la cheville. *J Radiol* 83(1): 27–38.

Boyd N, Brock H, Meier A, Miller R, Mlady G, Firoozbakhsh K. 2006. Extensor hallucis capsularis: frequency and identification on MRI. *Foot Ankle Int* 27(3): 181–184.

Brenner E. 2002. Insertion of the tendon of the tibialis anterior muscle in feet with and without hallux valgus. *Clin Anat* 15: 217–233.

Brodie JT, Dormans JP, Gregg JR, Davidson RS. 1997. Accessory soleus muscle: A report of 4 cases and review of literature. *Clin Orthop Relat Res* 337: 180–186.

Burman M. 1968. The high-bellied popliteus muscle. An anomaly of the popliteus muscle. *J Bone Joint Surg Am* 50: 761–762.

Buschmann WR. 1991. Congenital variations of the peroneus quartus muscle: An anatomical study by Sobel et al. *Foot Ankle* 11(5): 342.

Buschmann WR, Cheung Y, Jahss MH. 1991. Magnetic resonance imaging of anomalous leg muscles: Accessory soleus, peroneus quartus, and the flexor digitorum longus accessorius. *Foot Ankle* 12(2): 109–116.

Calori L. 1866. Di alcune nuovi muscoli sopranumerarii degli arti. *Mem R Accad Sci Istituto di Bologna* 6: 137–147.

Carroll JF. 2008. Accessory muscles of the ankle. Radsource MRI Web Clinic. Available at: http://www.radsource.us/clinic/0811 (accessed 22 October 2015).

Chaney DM, Lee, MS, Khan MA, Krueger WA, Mandracchia VJ, Yoho RM. 1996. Study of ten anatomical variants of the foot and ankle. *J Am Podiatr Med Assoc* 86(11): 532–537.

Chepuri NB, Jacobson JA, Fessell DP, Hayes CW. 2001. Sonographic appearance of the peroneus quartus muscle: correlation with MR imaging appearance in seven patients. *Radiology* 218: 415–419.

Cheung Y, Rosenberg ZS. 2001. MR imaging of the accessory muscles around the ankle. *Magn Reson Imaging Clin N Am* 9: 465–473.

Cheung Y, Rosenberg ZS, Ramsinghani R, Beltran J, Jahss MH. 1997. Peroneus quartus muscle: MR imaging features. *Radiology* 202: 745–750.

Cheung Y, Rosenberg ZS, Colon E, Jahss M. 1999. MR imaging of the flexor digitorum accessorius longus. *Skeletal Radiol* 28(3): 130–137.

Chudzinski TH. 1875. Contributions a panatomie du negre. *Rev de Soc d'Anthrop De Paris* 2: 398–414.

Chuncharunee A, Chanthong P, Lucksanasombool P. 2012. The patterns of proximal attachments of the popliteus muscle: Form and function. *Med Hypotheses* 78: 221–224.

Clarkson MJ, Fox JN, Atsas S, Daney BT, Dodson SC, Lambert HW. 2013. The clinical implications of novel variants of the fibularis (peroneus) quartus muscle inserting onto the cuboid bone: peroneocuboideus and peroneocalcaneocuboideus. *J Foot Ankle Surg* 52(1): 118–121.

Cromeens B, Reeves R. 2011. Anomalous peroneus (fibularis) longus muscle: An atypical insertion and incomplete distal tendon. *Clin Anat* 24(8): 997–999.

Cruveilheir J. 1843. *Traité d'Anatomie Descriptive, second edition*. Paris: Béchet Jeune.

Cunningham DJ, Brooks J. 1889. The peroneus quinti digiti. *Proc R Irish Acad*, Ser 3.1: 78–81.

Curnow J. 1873. Notes of some irregularities in muscles and nerves. *J Anat Physiol* 7: 307.

Danforth CH. 1924. The heredity of unilateral variations in man. *Genetics* 9: 199–210.

Daseler EH, Anson BJ. 1943. The plantaris muscle: An anatomical study of 750 specimens. *J Bone Joint Surg Am* 25(4): 822–827.

Dave MR, Yagain VK, Anadkat S. 2012. Unilateral third/accessory head of the gastrocnemius muscle: A case report. *Int J Morphol* 30(3): 1061–1064.

Davies-Colley N, Taylor F, Dalton BN. 1873. Notes of abnormalities observed in the dissecting room from October 1870 to June 1872. *Guys Hospital Reports* 16: 389–399.

Dellon AL, Ebmer J, Swier P. 2002. Anatomical variations related to decompression of the common peroneal nerve at the fibular head. *Ann Plastic Surg* 48(1): 30–34.

Donley BG, Leyes M. 2001. Peroneus quartus muscle: a rare cause of chronic lateral ankle pain. *Am J Sports Med* 29: 373–375.

Driver J. 1914. The morphology of the long accessorius muscle. *Anat Rec* 8: 341.

Duc SR, Wentz KU, Käch KP, Zollikofer CL. 2004. First report of an accessory popliteal muscle: Detection with MRI. *Skeletal Radiol* 33(7): 429–431.

Duran-Stanton AM, Bui-Mansfield LT. 2010. Magnetic resonance diagnosis of tarsal tunnel syndrome due to flexor digitorum accessorius longus and peroneocalcaneus internus muscles. *J Comput Assist Tomogr* 34: 270–272.

Fabrice d'Aquapendente. 1687. *De Motu Locali Animalium. Opera Anatomica et Physioloca*. Lipsiae: Dailly.

Feipel V, Simonnet ML, Rooze M. 2003. The proximal attachments of the popliteus muscle: A quantitative study and clinical significance. *Surg Radiol Anat* 25: 58–63.

Fetto JF, Marshall JL, Ghelman B. 1977. An anomalous attachment of the popliteus tendon to the lateral meniscus. *J Bone Joint Surg Am* 59: 548–549.

Flower WH, Murie J. 1867. Account of the dissection of a Bush woman. *J Anat Physiol* 1: 202–208.

Focacci M. 1903. Etude morphologique sur les fléchisseurs longus du pied. *Arch Ital Biol* 39: 486–487.

Freeman AJ, Jacobson NA, Fogg QA. 2008. Anatomical variations of the plantaris muscle and a potential role in patellofemoral pain syndrome. *Clin Anat* 21(2): 178–181.

Frey H. 1919. Musculus gastrocnemius tertius. *Gegenbaurs Morphol Jahrbuch* 50: 517–530.

Giani R. 1909. Der m. tibialis anticus und die pathogenese des statisch-mechanischen plattfuossees. *Z Orthop Chir* 23: 564–586.

Gies T. 1868. Der flexor digitorum pedis communis longus und seine varietäten. *Arch Anat Physiol Wissen Med* 1868: 231–239.

Gray H. 1918. Anatomy of the Human Body, 20th edition (WH Lewis, ed.). Philadelphia: Lea & Febiger.

Gruber W. 1871. *Uber einen musc. Tibio-astragalus anticus des menschen*. Arch Anat Physiol Wissen Med 1871: 663–693.

Gruber W. 1875a. Uber die varietäten des musculus extensor hallucis longus. *Arch Anat Physiol Wissen Med* 1875: 565–589.

Gruber W. 1875b. Uber den musculus extensor digitorum communis manus anomalus mit 5 sehnen zu allen fingern, und über den musculus extensor digitorum longis pedis anomalus mit 5 sehnen zu allen zehen. *Arch Anat Physiol Wissen Med* 1875: 204–210.

Gruber W. 1875c. Ein musculus extensor digiti II pedis longus. *Arch Path Anat Physiol Klin Med* 65: 23–25.

Gruber W. 1875d. Über den musculus popliteus biceps. *Arch Anat Physiol Wissen Med* 1875: 599–605.

Gruber W. 1876. Ein neuer fall von musculus extensor hallucis longus tricaudatus. *Arch Anat Physiol Wissen Med* 1876: 750–752.

Gruber W. 1878. Nachträge über den musculus peroneotibialis. *Arch Anat Physiol Wissen Med* 1878: 481–485.

Gruber W. 1879. *Beobachtungen aus der Menschlichen und Vergleichenden Anatomie*. Berlin, A. Hirschwald.

Gruber W. 1884. Ein neuer musculus peroneo-calcaneus externus anterior. *Arch Path Anat Physiol Klin Med* 95: 177–179.

Gruber W. 1887a. Musculus peroneus longus and brevis zu einem muskel verschmolzen. *Arch Path Anat Physiol Klin Med* 107: 485–487.

Gruber W. 1887b. Ein musculus peroneus brevis mit insertion an den calcaneus, bei abgabe einer mit einem fleischbauche versehenen fussrückensehne zur 5. *Arch Path Anat Physiol Klin Med* 107: 485–487.

Gruber W. 1887c. Dreibäuchiger musculus peroneus longus. *Arch Path Anat Physiol Klin Med* 109: 5.

Gruber W. 1887d. Ein musculus flexor brevis digiti II pedis. *Arch Path Anat Physiol Klin Med* 109: 6–8.

Gruber W. 1887e. Ein musculus flexor brevis digiti IV pedis. *Arch Path Anat Physiol Klin Med* 109: 8.

Gumusalan Y, Kalaycioglu A. 2000. Bilateral accessory flexor digitorum longus muscle in man. *Ann Anat* 182: 573–576.

Gumusalan Y, Ozbag D. 2007. A variation of fibularis quartus muscle: musculus fibulocalcaneus externum. *Clin Anat* 20: 998–999.

Gunal I, Sahinoglu K, Bergman RA. 1994. Anomalous tibialis posterior muscle as an etiologic factor of hallux valgus. *Clin Anat* 7(1): 21–25.

Gupta RK, Bhagwat SS. 2006. An anomalous muscle in the region of the popliteal fossa: A case report. *J Anat Soc India* 55(2): 65–68.

Hadziselmovic V, Gluhbegovic N. 1969. Vergleichende anatomische untersuchungen des musculus popliteus. *Anat Anz* 125: 388–399.

Hallisy JE. 1930. The muscular variations in the human foot: A quantitative study. *Am J Anat* 45(3): 411–442.

Hamming JJ. 1959. Intermittent claudication at an early age, due to an anomalous course of the popliteal artery. *Angiol* 10: 369–371.

Harbeson AE. 1938. Further studies on the origin of the first dorsal interosseous muscle of the foot from the tendon of the peroneus longus. *J Anat* 72: 463–464.

Hartmann H. 1888. Anomalie du flechisseur proper du gros orteil. *Bull Soc Anat Paris* 10: 223–225.

Hatzantonis C, Agur AMR, Naraghi A, Gautier S, McKee N. 2011. Dissecting the accessory soleus muscle: A literature review, cadaveric study, and imaging study. *Clin Anat* 24(7): 903–910.

Hecker P. 1923. Study on the peroneus of the tarsus. *Anat Rec* 26: 79–82.

Hecker P. 1924. Etude sur le pèronier du tarse: variations des pèroniers latèraux. *Arch Anat Histol Embryol.* 3: 327–359.

Herzog RJ. 2011. Accessory plantaris muscle: Anatomy and prevalence. *HSSJ* 7(1): 52–56.

Higgins H. 1895. The popliteus muscle. *J Anat Physiol* 29: 569–573.

Jackson CM. 1914. *Morris's Human Anatomy, fifth edition*. Philadelphia: P. Blakiston's Son & Co.

Jadhav SD, Gosavi SN, Zambare BR. 2013. Study of Peroneus digiti minimi quinti in Indian population: A cadaveric study. *Rev Arg de Anat Clin* 5(2): 67–72.

Jaijesh P, Shenoy M, Anuradha L, Chithralekha KK. 2006. Flexor accessorius longus: A rare variation of the deep extrinsic digital flexors of the leg and its phylogenetic significance. *Indian J Plast Surg* 39: 169–171.

Jain A, Sikka A, Goyal N. 2013. Tibiofascialis anticus – a rare variation. *Indian J Med Case Rep* 2(2): 8–10.

Jana R, Roy TS. 2011. Variant insertion of the fibularis tertius muscle is an evidence of the progressive evolutionary adaptation for the bipedal gait. *Clin Prac* 1(4): e81.

Javadekar BS. 1961. Peroneus digiti minimi. *J Anat Soc India* 10: 44.

Jayakumari S, Suri RK, Rath G, Arora J. 2006. Accessory tendon and tripartite insertion pattern of fibularis longus muscle. A case report. *Int J Morphol* 24: 633–636.

Joshi SD, Joshi SS, Athavale SA. 2006. Morphology of peroneus tertius muscle. *Clin Anat* 19(7): 611–614.

Kato M, Tofukuji S. 1954. A case of the gastrocnemius tertius. *Jikeikai Ikadaigaku Kaibogakukyoshitsu Gyosekishu* 11: 1–5.

Kelch WG. 1813. *Beiträge zur pathologischen Anatomie. Abweichung des Biceps Femoris*. Berlin: C. Salfeld.

Kelikian AS. (ed.) 2011. *Sarrafian's Anatomy of the Foot and Ankle, third edition*. Philadelphia: Lippincott, Williams & Wilkins.

Kendi TK, Erakar A, Oktay O, Yildiz HY, Saglik Y. 2004. Accessory soleus muscle. *J Am Podiatr Med Assoc* 94: 587–589.

Knott JF. 1883. Muscular anomalies, including those of the diaphragm and subdiaphragmatic regions of the human body. *Proc Roy Irish Acad* 3: 627–641.

Koplas MC, Grooff R, Piraino D, Recht M. 2009. Third head of the gastrocnemius: An MR imaging study based on 1039 consecutive knee examinations. *Skeletal Radiol* 38(4): 349–354.

Kramer E, Linschka M, Genber H. 1989. Gross anatomy and evolutionary significance of the human peronius III. *Anat Embryol* 155: 291–302.

Lambert HW, Atsas S. 2010. An anterior fibulocalcaneus muscle: An anomalous muscle discovered in the anterior compartment of the leg. *Clin Anat* 23(8): 911–914.

Lambert HW, Atsas S, Dodson SC, Daney BT, Billings HJ, Campbell FR. 2011a. The anterior fibulocalcaneus muscle: Confirmation of its presence in the anterior leg compartment. *Clin Anat* 24(8): 1029.

Lambert HW, Atsas S, Fox JN. 2011b. The fibulocalcaneus (peroneocalcaneus) internus muscle of Macalister: Clinical and surgical implications. *Clin Anat* 24(8): 1000–1004.

Lamont JC. 1908. Note on a tendon found in association with the insertion of the peroneus longus, and the origin of the first dorsal interosseus muscles. *J Anat Physiol* 42: 236.

LaRue BG, Anctil EP. 2006. Distal anatomical relationship of the flexor hallucis longus and the flexor digitorum longus tendons. *Foot Ankle Int* 7: 528–532.

Last RJ. 1950. The popliteus muscle and the lateral meniscus. *J Bone Joint Surg Br* 32-B: 93–99.

Leal-Blanquet J, Ginés-Cespedosa A, Monllau JC. 2009. Bifurcated popliteus tendon: A descriptive arthroscopic study. *Int Orthop* 33(6): 1633–1635.

Le Double AF. 1897. *Traité des Variations du Système Musculaire de l'homme et de Leur Signification an Point de l'anthropologie Zoologique, vol. 2*. Paris: Schleicher Frères.

Lewis OJ. 1962. The comparative morphology of m. flexor accessorius and the associated long flexor tendons. *J Anat* 96: 321.

Lewis OJ. 1964. The tibialis posterior tendon in the primate foot. *J Anat* 98(2): 209–218.

Liu PT, Moyer AC, Huettl EA, Fowl RJ, Stone WM. 2005. Popliteal vascular entrapment syndrome caused by a rare anomalous slip of the lateral head of the gastrocnemius muscle. *Skeletal Radiol* 34: 359–363.

Lohrmann S, Flöel H, Christ B. 1997. Insertion of musculus tibialis posterior into musculus peroneus (fibularis) longus. *Ann Anat* 197: 161–163.

Lorentzon R, Wirell S. 1987. Anatomic variations of the accessory soleus muscle. *Acta Radiol* 28: 627–629.

Lotito G, Pruvost J, Collado H, Coudreuse JM, Bensoussan L, Curvale G, Viton JM, Delarque A. 2011. Peroneus quartus and functional ankle instability. *Ann Phys Rehabil Med* 54: 282–292.

Lovejoy JF, Harden TP. 1971. Popliteus muscle in man. *Anat Rec* 169(4): 727–730.

Luchansky E, Paz Z. 1986. Variations in the insertion of tibialis anterior muscle. *Anat Anz* 162: 129–136.

Lundeen RO, Latva D, Yant J. 1983. The secondary tendinous slip of the extensor hallucis longus (extensor ossis metatarsal hallucis). *J Foot Surg* 22: 142–144.

Macalister A. 1866. On muscular anomalies in human anatomy, and their bearing upon homotypical myology. *Proc R Irish Acad* 10: 121–164.

Macalister A. 1875. Observations on muscular anomalies in the human anatomy. *Trans R Irish Acad* 25: 1–130.

Martin BF. 1964. Observations on the muscles and tendons of the medial aspect of the sole of the foot. *J Anat* 98: 437–453.

Martinelli B, Bernobi S. 2002. Peroneus quartus muscle and ankle pain. *Foot Ankle Surg* 8: 223–225.

Meckel JF. 1815. *Handbuch der Menschlichen Anatomie*. Halle und Berlin: Buchhandlung des Hallischen Waisenhauses.

Mehta V, Suri RK, Arora J, Dave V, Rath G. 2011. Supernumerary peronei in the leg musculature-utility for reconstruction. *Chang Gung Med J* 34: 62–65.

Mellado JM, Rosenberg ZS, Beltran J, Colon E. 1997. The peroneocalcaneus internus muscle: MR imaging features. *Am J Roentgenol* 169: 585–588.

Mori M. 1964. Statistics on the musculature of the Japanese. *Okajimas Fol Anat Jap* 40: 195–300.

Moss ALH. 1988. Is there an association between an absence of palmaris longus tendon and an absence of plantaris tendon? *Eur J Plast Surg* 11: 32–34.

Musial WW. 1963a. Variations of the terminal insertions of the anterior and posterior tibial muscles in man. *Folia Morphol* 22: 237–247.

Musial WW. 1963b. Variations of the terminal insertions of the peroneus longus and brevis muscles in man. *Folia Morphol* 22: 294–302.

Nascimento SRR, Costa RW, Ruiz CR, Wafae N. 2012. Analysis on the incidence of the fibularis quartus muscle using magnetic resonance imaging. *Anat Res Int* 2012: 485149.

Nathan H, Gloobe H, Yosipovitch Z. 1975. Flexor digitorum accessorius longus. *Clin Ortho Relat R* 113: 158–161.

Paraskevas G, Papaziogas B, Kitsoulis P, Spanidou S. 2006. A study on the morphology of the popliteus muscle and arcuate popliteal ligament. *Folia Morphol* 65(4): 381–384.

Parsons FG. 1920. Note on an abnormal muscle in the popliteal space. *J Anat* 54: 307–314.

Patil V, Frisch NC, Ebraheim NA. 2007. Anatomical variations in the insertion of the peroneus (fibularis) longus tendon. *Foot Ankle Int* 28: 1179–1182.

Paval J, Vollala VR, Bairy KL. 2005. Sciatic nerve entrapment in the popliteal fossa: A case report. *Neuroanat* 4: 41–42.

Perez Carro L, Sumillera Garcia M. 1999. Bifurcated popliteus tendon. *Arthroscopy* 15: 638–639.

Perkins JD. 1914. An anomalous muscle of the leg: peronaeocalcaneus internus. *Anat Rec* 8: 21–25.

Peterson DA, Stinson W, Lairmore JR. 1995. The long accessory flexor muscle: an anatomical study. *Foot Ankle Int* 16(10): 637–640.

Pfitzner W. 1892. *Dieses ambeine de menschilchen korpers, morphologishe arbeiten*. Jena: Specieller Theil.

Picou R. 1894a. Insertions inférieures du péronier lateral. *Bull Soc Anat Paris* 8(7): 254–259.

Picou R. 1894b. Quelques condérations sur les insertions du muscle long péronier lateral à la plante du pied. *Rev Orthop Bull Soc Anat Paris* 8(7): 254–259.

Plochocki JH, Bodeen M. 2010. Unusual supernumerary muscle in the anterior compartment of the leg. *Clin Anat* 23(1): 104–105.

Porter RW. 1996. An anomalous muscle in children with congenital talipes. *Clin Anat* 9: 25–27.

Pozzi S. 1872. Sur une variété fréquente du muscle court péronier lateral chez l'homme (anomalie réversive). *Bull Soc d'Anthrop Paris* 2(7): 155–161.

Prakash R, Narayanswamy C, Singh DK, Rajini T, Vankatiah J, Singh G. 2011. Anatomical variation of peroneal muscles: A cadaveric study in an Indian population and a review of the literature. *JAPMA* 101(6): 505–508.

Pye-Smith PH, Howse HG, Davies-Colley JNC. 1871. Notes of abnormalities observed in the dissecting room during the winter sessions of 1868–69 and 1869–70. *Guy's Hospital Reports* 16: 147–165.

Raheja S, Choudhry R, Singh P, Tuli A, Kumar H. 2005. Morphological description of combined variation of distal attachments of fibularis in a foot. *Surg Radiol Anat* 27: 158–160.

Ramirez D, Gajardo C, Caballero P, Zavando D, Cantín M, Galdames IS. 2010. Clinical evaluation of fibularis tertius muscle prevalence. *Int J Morphol* 28(3): 759–764.

Rana KK, Das S, Verma R. 2006. Double plantaris muscle: A cadaveric study with clinical importance. *Int J Morphol* 24(3): 495–498.

Regan TP, Hughston JC. 1977. Chronic ankle "sprain" secondary to anomalous peroneal tendon: a case report. Clin Orthop Relat Res 123: 52–54.

Reimann R. 1981. Der variable streckappar at der kleinan zehe. *Geganbaurs Mophol Jahrb* 127: 188–209.

Ringhoffer VD. 1860. Beschreibung einer menschlichen missgeburt. *Arch Path Anat Physiol Klin Med* 19: 28–43.

Rosenberg ZS, Beltran J, Cheung YY, Colon E, Herraiz F. 1997. MR features of longitudinal tears of the peroneus brevis tendon. *Am J Roentgenol* 168: 141–147.

Rourke K, Dafydd H, Parkin IG. 2007. Fibularis tertius: Revisiting the anatomy. *Clin Anat* 20(8): 946–949.

Sakuma E, Kato H, Honda N, Mabuchi Y, Soji T. 2004. A rare anomaly of the extensor digitorum longus. *Anat Sci Int* 79(4): 235–238.

Sammarco GJ, Brainard JB. 1991. A symptomatic anomalous peroneus brevis in a high-jumper: a case report. *J Bone Joint Surg Am* 73: 131–133.

Sammarco GJ, Conti SF. 1994. Tarsal tunnel syndrome caused by an anomalous muscle. *J Bone Joint Surg Am* 76(9): 1308–1314.

Sarrafian SK. (ed.) 1993. *Anatomy of the Foot and Ankle: Descriptive, Topographic, Functional, second edition*. Philadelphia: JB Lippincott Co.

Saupe N, Mengiardi B, Pfirrmann CW, Vienne P, Seifert B, Zanetti M. 2007. Anatomic variants associated with peroneal tendon disorders: MR imaging findings in volunteers with asymptomatic ankles. *Radiology* 242: 509–517.

Sawant SP, Shaikh ST, More RM. 2012. A rare variation of the plantaris muscle. *Int J Biol Med Res* 3(4): 2437–2440.

Sawant SP, Shaikh ST, Lele SD, Rizvi R, Menon SR, Uma R. 2013. Study of the variant soleus muscle. *Int J Cur Res Rev* 5(1): 86–89.

Saxena A, Bareither D. 2000. Magnetic resonance and cadaveric findings of the incidence of the plantaris tendon. *Foot Ankle Int* 21(7): 570–572.

Schaeffer JP. (ed.) 1953. *Morris' Human Anatomy, 11th edition*. New York: The Blakiston Company.

Schultze FE. 1867. Die sehnenverbindung in der planta des menschen und der säugethiere. *Z Wissen Zool* 17: 1–22.

Schwalbe G, Pfitzner W. 1894. *Varietäten, Statistik und Anthropologie Arbeiten*. Strausbourg: Deutsche Med Wchnschr.

Seelaus HK. 1927. On certain muscle anomalies of the lower extremity. *Anat Rec* 35: 187–191.

Seipel R, Linklater J, Pitsis G, Sullivan M. 2005. The fibulocalcaneus internus muscle: an unusual cause of posterior ankle impingement. *Foot Ankle Int* 26: 890–893.

Semple R, Murley GS, Woodburn J, Turner DE. 2009. Tibialis posterior in health and disease: A review of structures and function with specific reference to electromyographic studies. *J Foot Ankle Res* 2: 24.

Shepherd FJ. 1880. Notes of abnormalities observed in the dissecting room of McGill University, from October 1875 to May 1879. Annual Report, *Montreal General Hospital* 1: 71–93.

Shigematsu M, Tsubakihara M, Maruyama S. 1956. On the m. extensor digitorum longus. *Kurume Igakkai Zasshi* 19: 1297–1302.

Simsek E, Bugra O, Teber MA, Katircioglu SF. 2014. What should be the first treatment of popliteal artery entrapment syndrome? *Ann Thorac Cardiovasc Surg* 20(2): 169–172.

Sirasanagandla SR, Potu BK, Nayak BS, Bhat KMR. 2013. Popliteal vessels entrapment by a variant accessory belly of medial head of gastrocnemius. *Anatom Physiol* 3(1): 116–117.

Sobel M, Levy ME, Bohne WH. 1990. Congenital variations of the peroneus quartus muscle: an anatomic study. *Foot Ankle* 11: 81–89.

Sokołowska-Pituchowa J, Miśkiewicz CZ, Skawina A, Makoś K, Gorczyca J. 1979. The third peroneal muscle in human fetuses. *Folia Morphol* 38: 489–498.

Somayaji SN, Vincent R, Bairy KL. 1998. An anomalous muscle in the region of the popliteal fossa: Case report. *J Anat* 192: 307–308.

Sookur PA, Naraghi AM, Bleakney RR, Jalan R, Chan O, White LM. 2008. Accessory muscles: Anatomy, symptoms, and radiographic evaluation. *Radiographics* 28: 481–499.

Stevens K, Platt A, Ellis H. 1993. A cadaveric study of the peroneus tertius muscle. *Clin Anat* 6(2): 106–110.

Stevenson PH. 1921. On an unusual anomaly of the peroneus tertius in a Chinese. *Anat Rec* 22(1): 81–83.

Takeuchi R, Kawashima T, Kagano T, Kaku S. 1960. Kelkaj muskolanomalioj ce malsupra membro de japanoj. *J Nihon Univ Med Assoc* 19: 2340–2350.

Tate R, Pachnik RL. 1976. The accessory tendon of extensor hallucis longus: Its occurrence and function. *J Am Podiatr Med Assoc* 66(12): 899–907.

Testut L. 1884. *Les Anomalies Muscularis Chez l'Hommes Expliquées par l'Anatomie Comparée: Leur Importance en Anthropologie*. Paris: Masson.

Testut L. 1892. *Les Anomalies Musculaires Considérées du Point de Vue de la Ligature des Artéres*. Paris: Doin.

Testut L. 1921. *Traitd d' Anatomie Humaine, seventh edition*. Paris: Doin.

Thane GD. 1891. Proceedings of the Anatomical Society of Great Britain and Ireland. *J Anat Physiol XXV* (N.S. Vol. V): xiii–xv.

Trono M, Tueche S, Quintart C, Libotte M, Baillon JM. 1999. Peroneus quartus muscle: a case report and review of the literature. *Foot Ankle Int* 20: 659–662.

Tubbs RS, May WR, Shoja MM, Loukas M, Salter EG, Oakes WJ. 2008. Peroneotalocalcaneus muscle. *Anat Sci Int* 83: 280–282.

Turner W. 1865. On variability in human structure, with illustrations, from the flexor muscles of the fingers and toes. *Trans R Soc Edinburgh* 24(1): 175–189.

Upasna A, Kumar A. 2011. Bicipital origin of plantaris muscle: *A case report. IJAV* 4: 177–179.

Venter G, van Schoor A, Bosman MC. 2011. Clinical applications of the plantaris muscle in reconstructive surgery. *Clin Anat* 24(7): 924.

Verma P, Arora AK. 2012. An anatomic variant insertion of peroneus longus in a cadaver: A case report. *IJAV* 5: 18–19.

Verma P, Arora AK, Sharma RK, Bhatia BS, Agnihotri G. 2011. A variation at the insertion of peroneus longus: A case report. *Case Study Case Rep* 1: 99–103.

Wachter S, Beekman S. 1983. Peroneus quartus: a case report. *J Am Podiatr Med Assoc* 73: 523–524.

Wagstaffe WW. 1872. Description of an accessory muscle in connection with the popliteus. *J Anat Physiol* 6: 214–215.

Walsham WJ. 1880. Anatomical variation: An account of a few of the more interesting abnormalities that have occurred in the dissecting rooms during the last seven years; with remarks on their morphological significance, and their bearing on the practice of surgery. *St Bartholomew's Hospital Reports* 16: 69–105.

Wang XT, Rosenberg ZS, Mechlin MB, Schweitzer ME. 2005. Normal variants and diseases of the peroneal tendons and superior peroneal retinaculum: MR imaging features. *RadioGraphics* 25: 587–602.

Werneck HJL. 1957. Contribuciccao paro o estudo de alguns aspectos morfologicos de M fibularis tertius. *An Fac Med Univ Minas Gerais* 17: 417–520.

White AA 3rd, Johnson D, Griswold DM. 1974. Chronic ankle pain associated with the peroneus accessorius. *Clin Orthop Relat Res* 103: 53–55.

White S. 1884. Note respecting the course of the flexor longus digitorum pedis. *J Anat Physiol* 18: 118–119.

Witvrouw E, Borre KV, Willems TM, Huysmans J, Broos E, De Clerq D. 2006. The significance of peroneus tertius muscle in ankle injuries: A prospective study. *Am J Sports Med* 34(7): 1159–1163.

Wood J. 1863. On some varieties in human myology. *Proc Roy Soc Lond* 13: 299–303.

Wood J. 1865. Additional varieties in human myology. *Proc Roy Soc Lond* 14: 378–392.

Wood J. 1866a. Variations in human myology observed during the winter session of 1865–1866 at King's College, London. *Proc R Soc Lond* 15: 229–244.

Wood J. 1866b. Variations in human myology observed during the winter session of 1867–1868 at King's College, London. *Proc R Soc Lond* 15: 518–546.

Yildirim FB, Sarikcioglu L, Nakajima K. 2011. The co-existence of the gastrocnemius tertius and accessory soleus muscle. *J Korean Med Sci* 26(10): 1378–1381.

Yu JS, Resnick D. 1994. MR imaging of the accessory soleus muscle appearance in six patients and a review of the literature. *Skeletal Radiol* 23: 525–528.

Zammit J, Singh D. 2003. The peroneus quartus muscle: anatomy and clinical relevance. *J Bone Joint Surg* 85: 1134–1137.

42 Intrinsic muscles of the foot

Rene M. Kafka, Ian L. Aveytua, Regina C. Fiacco, Garen M. Ream, Anthony C. DiLandro, and Anthony D'Antoni
New York College of Podiatric Medicine, New York, New York, United States

Muscles of the dorsal aspect of foot

Extensor digitorum brevis muscle

The extensor digitorum brevis muscle is frequently variable with respect to its number of muscular heads (e.g., presence of accessory heads) and tendons. The muscle can also receive slips from the flexor digitorum longus muscle (Hallisy 1930) and dorsal interossei (Macalister 1875).

The muscular head arrangement of the extensor digitorum brevis varies from two to five heads (Bergman et al. 1984, 1988; Kelikian 2011; Sirasangandla et al. 2013). A head with a single tendon to the first toe is sometimes referred to as the extensor hallucis brevis and its fibers may be entirely separate from or fused with the fibers of the extensor digitorum brevis muscle (Macalister 1875). When there are only two heads present, these heads have been found to insert in one of the following arrangements: first and fourth toes (Fig. 42.1); second and third toes (Fig. 42.2); or first and fifth toes (Fig. 42.3) (Sirasangandla et al. 2013).

When the muscle comprises three heads, the heads are typically present in one of two arrangements: associated with the first, second, and third digits (Fig. 42.4); or associated with the second, third, and fourth digits (Fig. 42.5) (Sirasangandla et al. 2013). Other arrangements have been described however, especially in the presence of accessory muscular or tendinous components (Kelikian 2011).

Sirasangandla et al. (2013) described the extensor digitorum brevis muscle in 44 formalin-fixed feet. Forty of these feet (90.9%) had four muscle bellies (Fig. 42.6), 36 (81.8%) had single tendons associated with the first and second, third and fourth digits. Four (9.09%) had only three muscle heads that each terminated in a single tendon to the three most medial toes. Chaney et al. (1996) reported similar findings: 63.9% (186/291) of specimens had four heads with tendons inserting on the four most medial toes (Fig. 42.6), and 17.2% (50/291) of specimens had three heads with tendons inserting onto the second, third, and fourth toes. In the same study, Chaney et al. (1996) described a variable muscle belly and tendon to the fifth toe that was present in 18% (51/284) of specimens (Fig. 42.7).

Figure 42.1 Extensor digitorum brevis muscle with two heads: one attached to the first proximal phalanx and the other attached to the fourth proximal phalanx.

This variable component inserted on the lateral side of the flexor digitorum longus tendon. Chaney et al. (1996) quotes Le Double's (1897) discussion regarding cases of the extensor digitorum brevis supplying the fifth toe. However, Chaney et al. (1996) mentioned that Le Double (1897) was unable to find this variation in his study of 74 specimens.

Bergman's Comprehensive Encyclopedia of Human Anatomic Variation, First Edition. Edited by R. Shane Tubbs, Mohammadali M. Shoja and Marios Loukas.
© 2016 John Wiley & Sons, Inc. Published 2016 by John Wiley & Sons, Inc.

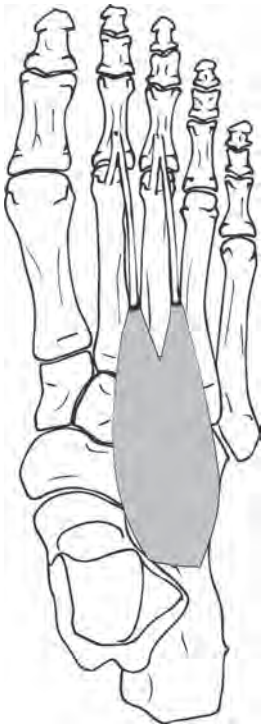

Figure 42.2 Extensor digitorum brevis muscle with two heads: one attached to the second proximal phalanx and the other attached to the third proximal phalanx.

Figure 42.4 Extensor digitorum brevis muscle with three heads: one attached to the first proximal phalanx and the other two attached to the second and third proximal phalanges.

Figure 42.3 Extensor digitorum brevis muscle with two heads: one attached to the first proximal phalanx and the other attached to the fifth proximal phalanx.

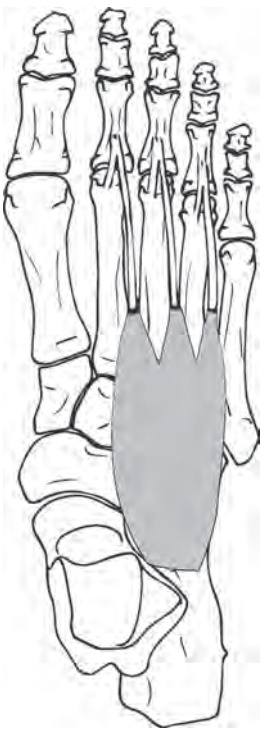

Figure 42.5 Extensor digitorum brevis muscle with three heads: one attached to the second proximal phalanx and the other two attached to the third and fourth proximal phalanges.

Figure 42.6 Extensor digitorum brevis muscle with four heads attaching to the proximal phalanges of digits one through four.

Figure 42.7 Extensor digitorum brevis muscle with five heads attaching to all five proximal phalanges.

The extensor digitorum brevis muscle may also have variations in the number of tendons from muscle heads. While the typical arrangement is a one-to-one relationship, many authors have reported two-to-one and three-to-one relationships of tendons to muscle bellies. For example, Chaney et al. (1996) reported that 11 of 291 limbs (3.8%) had bifid tendons inserting on variable individual digits. In their sample, Sirasangandla et al. (2013) reported that four feet (9.09%) had brevis muscle heads with multiple tendons and three (6.81%) demonstrated four muscle heads with five tendons. The second toe received both tendons in two cases. The third toe received both tendons in one case. Additionally, one foot had four muscle bellies with six tendons. In this instance, the second muscle belly diverged into three tendons inserting into three points: the proximal phalanx of the second toe, the fascia over the shaft of the third metatarsal, and the lateral side of the extensor digitorum longus tendon to the second toe.

Accessory fascicles that arise between normal tendons may also be present in the extensor digitorum brevis muscle. These muscles may replace an absent head or tendon in a muscle with fewer than the typical four heads. They may also have a fifth belly, usually to the fifth digit (Kelikian 2011). These additional muscles can originate from the talus and navicular bones or from the lateral cuneiform bone (Bergman et al. 1984, 1988). They occur most frequently between the first and second toes. In this arrangement, the slip typically inserts on the medial aspect of the head of the proximal phalanx of the toe (Kelikian 2011). Chaney et al. (1996) reported that 15% (44/291) of their specimens had more than four brevis tendons. The most common accessory tendon was to the second digit, followed by the third and the fourth digits.

Muscles of the plantar aspect of foot

First plantar layer

Abductor hallucis muscle

The abductor hallucis muscle has variations in bony attachments, soft-tissue insertions and origins, and the presence of an accessory abductor hallucis muscle. A recent study by Aga-

Figure 42.8 Abductor hallucis muscle with a single insertion onto the first proximal phalanx.

wany and Meguid (2010) found four categories of insertions in 15 cadaveric feet, three of which were purely bony:

1. a single tendinous insertion at the proximal phalanx of the first toe (46.7%, 7/15; Fig. 42.8);
2. a slip to the medial sesamoid bone and one to the base of the proximal phalanx (33.3%, 5/15; Fig. 42.9);
3. a single insertion onto the medial sesamoid bone (6.7%, 1/15; Fig. 42.10); and
4. a superficial tendinous slip attached to the base of the proximal phalanx and a deep, fleshy slip attached to the metatarsophalangeal joint capsule of the first toe (13.3%, 2/15; Fig. 42.11).

Brenner (1999) found similar variations of abductor hallucis muscle insertions in his cadaveric study of 109 formalin-fixed feet and defined three types:

1. single point of insertion on the medial aspect of the proximal phalanx of the first toe (38.5%, 42/109);
2. insertions on the medial sesamoid ligament and the medial sesamoid bone (59.6%, 65/109); and
3. insertion on the medial sesamoid bone (1.8%, 2/109).

Additionally, authors of several textbooks have reported an occasional variation with an additional slip attached to the base of the proximal phalanx of the second toe, as well as a similar variant with slips attached to the proximal phalanges of both the second and third toes (Bergman et al. 1984, 1988)

Soft-tissue anomalies include the description by Macalister (1875) of a single muscular slip inserting onto the flexor hallucis longus tendon, as well as a slip passing to the skin of the "ball of the great toe." Additionally, in a surgical intervention study by Asirvatham and Stevens (1997) for severe, recalcitrant pediatric metatarsus adductus, five cases of anomalous insertion of the tibialis anterior into the abductor hallucis tendon were found out of 29 feet (17%).

In their case report, Bhansali and Bhansali (1997) reported a male with juvenile rheumatoid arthritis that had an accessory abductor hallucis muscle excised to relieve entrapment of the tibial nerve. This accessory muscle originated from under the surface of the fascia covering the tibial nerve, passed deep to the nerve through the tarsal tunnel and merged with the abductor hallucis muscle.

Figure 42.9 Abductor hallucis muscle with a slip to the medial sesamoid bone and one to the base of the proximal phalanx.

Figure 42.10 Abductor hallucis muscle with a single insertion onto the medial sesamoid bone.

Flexor digitorum brevis muscle

The flexor digitorum brevis muscle has been reported to have variations in 63% of limbs (Bergman et al. 2006). These variations occurred most frequently in the slips to the fourth and fifth digits and were relatively uncommon in the more medial slips (Barnes 2003).

The most commonly described variation was the absence of the muscle belly and tendon to the fifth toe (Fig. 42.12). Authors have reported the frequency of this absence ranging from 2% to 100% (Aasar 1947; Lobo et al. 2008). Kelikian (2011) and Bergman et al. (1984, 1988) defined the belly and tendon to the fifth digit as being absent in 21.5% and 21% of cases, respectively. Yalçin and Ozan (2005) found a similar frequency of 18% (6/33). Nathan and Gloobe (1974) observed a comparable rate of absence in their study of 100 feet, where 23 specimens had no fibers to the fifth toe. Aasar (1947) and Le Double (1897) reported lower frequencies of 2% and 10%, respectively.

Several authors described a greater frequency of this particular variation. Kura et al. (1997) conducted a study of 11 fresh-frozen feet and found that 4 feet (36%) did not have this lateral-most muscular component. Chaney et al. (1996) found 63% (181/284) of specimens without this slip to the fifth toe. Moreover, a Nepalese study of 30 cadavers demonstrated this absence of the intrinsic flexor muscle bilaterally in all specimens (Lobo et al. 2008).

Less frequently observed, the muscle bellies and tendons were absent to both the fourth and fifth digits (Fig. 42.13). Nathan and Gloobe (1974) described this variation in 3% (3/100) of feet, corroborated by Kelikian (2011).

The fourth and fifth muscle bellies and tendons have also been described to be present, but notably smaller and thinner. Nathan and Gloobe (1974) reported that 23% (23/100) of specimens had small, thin slips to the fifth toe alone and 3% (3/100) had similarly slender slips to both the fourth and fifth toes. The former variation was observed in 6 of 33 feet (18%) in a study by Yalçin and Ozan (2005). This lateral-most intrinsic tendon may also be so small that it inserts into the plantar fascia before reaching the bony tissue of the toe (Macalister 1875).

The single, cadaveric case study by Claassen and Wree (2003) had both types of the aforementioned variation: the right foot had no flexor digitorum brevis to the fifth toe, and the left foot

Figure 42.11 Abductor hallucis muscle with a superficial tendinous slip attached to the base of the proximal phalanx and a deep, fleshy slip attached to the first metatarsophalangeal joint capsule.

Figure 42.12 Flexor digitorum brevis muscle with only three heads. The head and tendon to the fifth digit is absent.

possessed a notably smaller and thinner belly and tendon to the fifth toe.

Extrinsic muscles and other soft tissues of the foot may contribute slips to the lateral portions of the flexor digitorum brevis. These same tissues may contribute directly to the fourth and fifth toes when intrinsic flexor digitorum slips are absent. The flexor digitorum longus, quadratus plantae, the intermuscular septum or combinations of these soft tissues are the most common sources. Nathan and Gloobe (1974) reported that the flexor digitorum contributes to the brevis's fifth tendon 20% of the time (20/100) and to the fourth and fifth toes in 3% of cases (3/100). Moreover, the same study demonstrated a sole origin of the flexor digitorum brevis to the fourth and/or fifth toe from the flexor digitorum longus in 5% of specimens; in one case, the lateral brevis muscle component arose from the intermuscular septum. Additionally, an independent flexor digitorum brevis muscle to the fifth digit may arise from the tibialis posterior muscle (Aasar 1947; Bergman et al. 1984, 1988; Barnes 2003; Asomugha et al. 2005).

Yalçin and Ozan (2005) described an additional variation of origin in one cadaver. The flexor digitorum brevis originated from deep and superficial heads, where the deep head diverged to form the muscle bellies and tendons for intermediate phalanges of digits two and five. The superficial head remained as a single belly but with two tendons, which inserted onto the third and fourth middle phalanges.

Lastly, the insertions of the flexor digitorum brevis muscle have also been described as having unique variations. The tendons may not split at the base of the proximal phalanges, but rather run parallel to the flexor digitorum longus muscle until they reach their insertions on the middle phalanges of the lesser digits (Chaney et al. 1996; Kelikian 2011). Kelikian (2011) reported that this insertional variation occurred 5% of the time. Yalçin and Ozan (2005) reported a single case where the tendon split into two slips, but one inserted on the proximal phalanx of the fifth toe and the other fused with the flexor digitorum longus to insert on the distal phalanx.

Abductor digiti minimi muscle

Variations of the abductor digiti minimi are additional muscular components that arise from or are in close proximity to the abductor muscle.

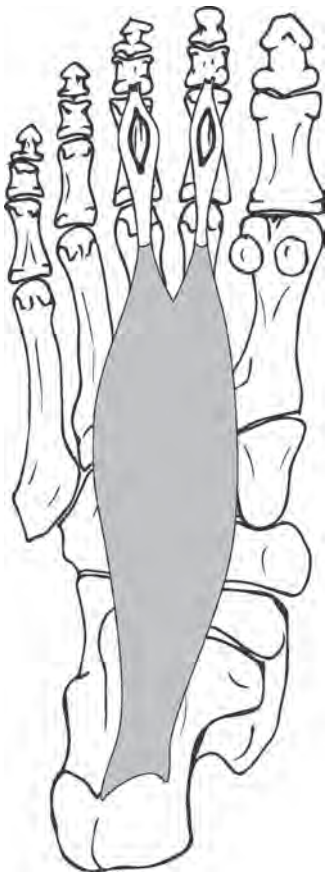

Figure 42.13 Flexor digitorum brevis muscle with only two heads. The heads and tendons to the fourth and fifth digits are absent.

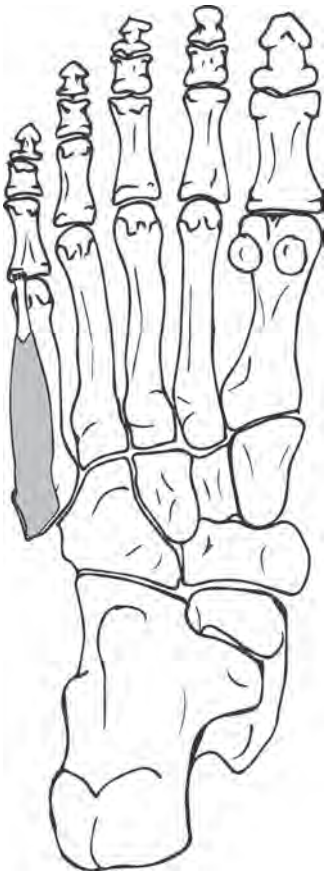

Figure 42.14 Unnamed muscle belly deep to the abductor digiti minimi muscle. This accessory muscle originated on the styloid process of the fifth metatarsal and inserted on the fifth proximal phalanx.

An unnamed muscle belly that originated from the styloid process of the fifth metatarsal, deep to and separate from the fibers the abductor digiti minimi muscle, has been reported (Fig. 42.14; Bergman et al. 1984, 1988; Kelikian 2011). This accessory muscle followed the same course as the abductor and inserted as a conjoined tendon on the proximal phalanx of the fifth toe (Fig. 42.14; Kelikian 2011). It may also insert on the metatarsal bone (Bergman et al. 1984, 1988).

The abductor osis metatarsi digit minimi (also called the abductor os metatarsi digiti minimi) is a variable slip of muscle off the abductor digiti minimi. It is a fusiform-shaped muscle that inserts onto the styloid process of the fifth metatarsal bone (Fig. 42.15; Bergman et al. 1984, 1988; Kelikian 2011). Sometimes its insertion extends to the middle or anterior part of the fifth metatarsal bone. Bergman (1984, 1988) stated that this distal insertion occurred 40% of the time when the accessory muscle was present. According to Le Double (1897), the abductor osis metatarsi digit minimi was found in 43% of the time in 65 feet and 45% of the time in 40 feet.

The abductor accessories digiti minimi muscle shares a similar course and insertion to the abductor ossi metatarsi digiti minimi, but originates separately from the abductor digiti minimi off the posterolateral tuberosity of the calcaneus. In its course, it may also share fibers with the flexor digiti minimi brevis. (Macalister 1875).

Chaney et al. (1996) considered both separate and conjoined origins of the abductor digiti minimi to be the abductor os metatarsi digiti minimi. With this combined definition, this muscle was observed in 45.5% (125/275) of cadaveric feet.

Second plantar layer

Quadratus plantae muscle

Hur et al. (2011) dissected 50 formalin-fixed cadavers to study the morphology of the quadratus plantae muscle. The quadratus plantae was found in 49 of 50 (98%) of cadavers. They found three types of origins: two heads in 40 of 50 cadavers (80%); a single medial head in 5 of 50 cadavers (10%); and a single lateral head in 4 of 50 cadavers (8%). These authors found that the muscle inserted into both the tendons of flexor digitorum longus and flexor hallucis longus muscles in 48 of 50 (96%) cadavers and into the tendon of flexor digitorum longus alone in 2 of 50 (4%) cadavers (Hur et al. 2011). When

Figure 42.15 Abductor osis metatarsi digit minimi muscle (also called the abductor os metatarsi digiti minimi muscle) is a fusiform-shaped muscle that inserts onto the styloid process of the fifth metatarsal.

the tendon of the quadratus plantae muscle inserted onto both the flexor digitorum longus and flexor hallucis longus muscles, superficial fibers of the muscle were connected to the flexor digitorum longus; however, the majority of the muscle fibers were attached to the lateral side of the flexor hallucis longus (Hur et al. 2011).

Claassen and Wree (2003) dissected a 75-year-old male cadaver with multiple variations in each foot. A single muscle variant in the right foot arose from the quadratus plantae muscle just anterior to the muscle's origin on the calcaneus. This variant muscle inserted onto the distal phalanx of the fifth toe. In the left foot, this muscle variation replaced a missing tendon slip for the flexor digitorum longus muscle. In the right foot the variant replaced a missing superficial and a missing deep intrinsic flexor tendon.

Lewis (1962) dissected a series of 18 cadaveric feet and found that the quadratus plantae muscle contributed to tendons two and three of the flexor digitorum longus muscle in 4 of 18 (22%) cadavers, and tendons two, three, and four of the flexor digitorum longus muscle in 14 of 18 (78%) cadavers.

Athavale et al. (2012), Hur et al. (2011) and Lewis (1962) have all described a muscle variant called the flexor digitorum accessories longus muscle. Athavale et al. (2012) found this variant muscle in 2 of 47 (4%) cadavers, one in the right and one in the left foot. The muscle originated in the inferior area of the posterior compartment of the leg from fascia that covered the flexor hallucis longus muscle. The muscle belly traversed the tarsal tunnel and eventually combined with the tendon of the flexor digitorum longus muscle. Hur et al. (2011) reported that this variant muscle combined with the medial head of the quadratus plantae muscle creating the tendon of insertion. Lewis (1962) reported that the quadratus plantae muscle inserted directly onto the flexor digitorum accessorius muscle in 3 of 18 (17%) cadavers. This variant muscle may be a significant cause of tarsal tunnel syndrome if it compresses the tibial nerve in the tarsal tunnel (Bowers et al. 2009). A reinforcing muscle bundle of the quadratus plantae has been termed the peroneocalcaneus muscle of Macalister.

Lumbrical muscles

The first lumbrical muscle of the foot can originate from the tendon of the tibialis posterior muscle as well as the tendon of the flexor hallucis longus muscle (Macalister 1866). The other lumbricals can originate from the tendon of the flexor hallucis brevis muscle in lieu of the tendon of the flexor digitorum longus muscle (Macalister 1866). The third and fourth lumbricals can also have two separate muscle bellies rather than one (Bergman et al. 1988).

In their study of 25 formalin-fixed feet, Oukouchi et al. (1992) found that in some instances the lumbrical tendons were directly fused with or interspersed into the medial terminal tendons of the extensor digitorum longus muscle, and inserted into the dorsal-proximal portion of the middle and distal phalanges. Furthermore, an "accessory" insertion of the lumbrical muscles was also noted by Oukouchi et al. (1992) to insert into the base of the proximal phalanx. The first lumbrical sent this accessory slip in 3 of 25 cadavers (0.12%), the second lumbrical was found in 2 of 25 (0.08%), the third lumbrical was found in 3 of 25 (0.12%), and the fourth lumbrical was found in 4 of 25 cadavers (0.16%) (Oukouchi et al. 1992). Macalister stated that the insertion of the fourth lumbrical can terminate by sending two tendons to two different locations (Bergman et al. 1988). These locations were specifically identified in the third and fourth lumbricals as inserting into the bases of the proximal phalanx on the medial and lateral side of the muscle (Oukouchi et al. 1992). The third lumbrical therefore inserted into the base of the proximal phalanx on the second and third toe, while the fourth lumbrical inserted into the base of the proximal phalanx of the third and fourth toe. This variation was found in 1 of 25 (0.04%) feet for both the third and fourth lumbricals (Oukouchi et al. 1992).

Occasionally, one or more lumbricals may be absent. In their longitudinal study, Chaney et al. (1996) examined cadaveric, formalin-fixed feet and found an absence of one or more lumbricals in 45.5% (117/257) of specimens. They found that three lumbricals were present 27.2% (69/257) of the time, two lumbricals were present 12.1% (31/257) of the time, one lumbrical was present 3.5% (9/257) of the time, and none were present 3.1% (8/257) of the time (Chaney et al. 1996). In a study performed on 11 fresh-frozen feet, Kura et al. (1997) found that the second and fourth lumbricals were absent in 9% (1/11) of specimens. Similarly, Schmidt et al. (1963) studied 100 formalin-fixed feet comprising 400 lumbricals. They found that the fourth lumbrical was most commonly absent 3% (12/400) of the time, followed by the third lumbrical 2.5% (10/100), then the second lumbrical 2.25% (9/100), and lastly the first lumbrical was absent 0.25% (1/400) of the time. In total, an absence of one or more lumbricals occurred in 8% (32/400) of feet (Schmidt et al. 1963).

Third plantar layer

Flexor hallucis brevis muscle

Le Double (1897) noted that the lateral head of the flexor hallucis brevis muscle could become somewhat fixed or indistinguishable from the oblique head of the adductor hallucis muscle. The medial head can have a tendinous slip that inserts into the first cuneiform (Le Double 1897).

The distal insertion for the tendon of the medial head of the flexor hallucis brevis muscle may unite with the tendon of the abductor hallucis muscle (Le Double 1897). A slip can arise from the tendon of the lateral head and attach into the second toe's proximal phalanx (Fig. 42.16; Le Double 1897). The flexor digitorum longus tendon can send an extension into the flexor hallucis brevis tendon (Le Double 1897).

Adductor hallucis muscle

The adductor hallucis muscle can have extensive variations in both its oblique and transverse heads. Authors have reported

Figure 42.16 Flexor hallucis brevis muscle with medial and lateral heads. The tendon of the lateral head has a small slip that is attached to the second proximal phalanx.

a greater range of variations in the transverse head compared to the oblique. Complete absence of the entire muscle has also been observed (Cralley and Schuberth 1979; Kura et al. 1997; Standring 2009).

In some variants the oblique head has been found to be inseparable from the lateral head of the flexor hallucis brevis muscle at its insertion (Le Double 1897). A fascicle has also been observed from the lateral border of the oblique adductor to the lateral aspect of the proximal phalanx of the second toe at the base (Macalister 1875; Le Double 1897).

Arakawa et al. (2003) classified the oblique head of the adductor hallucis muscle into four types: A, B, C and D. Type A, 47% (43/91), was further subdivided into subtypes 1, 2, and 3. In subtype 1, the origin arises from the fibrous sheath of the tendon of the fibularis (peroneus) longus muscle (Macalister 1875; Arakawa et al. 2003), long plantar ligament, bases of the second, third, and fourth metatarsal bones, and lateral cuneiform bone. In subtype 2, there is no origin on the long plantar ligament and in subtype 3, the muscle does not attach to the cuneiform bone. Type B, 33% (30/91), originates more laterally from the base of the fifth metatarsal bone by an aponeurotic slip in addition to the common origin sites as those found in type A. Type C, 9% (8/91) arises laterally from the base of the fifth metatarsal bone and medially from the divided tendon of the tibialis posterior muscle, medial intermuscular septum, and plantar tarsometatarsal ligaments. Extended between the medial cuneiform bone and the base of the second metatarsal bone or the divided tendon of the fibularis longus, type C inserts onto the first dorsal interosseous muscle in addition to the common origin sites. Type D, 11% (10/91), has many origins. The oblique head originates from the divided tendon of the tibialis posterior muscle, the medial intermuscular septum, the plantar tarsometatarsal ligament between the medial cuneiform bone and the base of the second metatarsal bone, or divided tendon of peroneus longus. Type D then inserts to the first dorsal interosseous muscle, in addition to the common origin sites (Arakawa et al. 2003).

There exist many more variations of the transverse head of the adductor hallucis muscle due to the bipedal nature of human locomotion. Some variations include: origin only from the fifth–fourth or fourth–third plantar plate and corresponding deep transverse metatarsal ligaments (Le Double 1897; Cralley and Schuberth 1979); origin only from the joint of the fifth toe; and an absent transverse component replaced by an extremely thin contractile band. A proximal extension reaching the anterior border of the oblique adductor, as well as an additional muscle located in the first interosseous space, has been observed. This additional muscle is small and triangular, measuring about 1 cm and originating from the distal third of the plantar border or the second metatarsal. It is located between the first dorsal interosseous and oblique adductor, courses anteromedially, and inserts on the tendon of the transverse adductor (Le Double 1897). This head usually has a fleshy origin from the intermuscular septa of the third and fourth muscle layers and from the fibular syndesmosis of Henkel, a portion of the plantar aponeurosis, which extends to the plantar ligament of the fourth toe (Le Double 1897; Cralley and Schuberth 1979) which was also noted in a case report (Mehta et al. 2011). Nowhere does this muscle originate from bony attachments (Cralley and Schuberth 1979).

Arakawa et al. (2003) suggested that the transverse head be classified into types A, B, and C based on its origins. In type A, 40% (36/91), narrow type, the muscle originates from the capsules of the third and fourth metatarsophalangeal joints and the deep transverse metatarsal ligaments. In type B, 30% (27/91), lateral type, the origin is the same as type A with an added attachment to the fifth metatarsolphalangeal joint and the deep transverse metatarsal ligament. In type C, 30% (27/91), wide type, the transverse head originates from the aponeurosis between the third plantar interosseous muscle and the fourth dorsal interosseous muscle. Type C can also originate from the deep band of the plantar aponeurosis as well as the capsules of the third, fourth, and occasionally fifth metacarphophalangeal joints (Arakawa et al. 2003).

In general the insertion of the transverse head varies from 4 to 16 mm in width and fans out directly to the epimysium

and to the tendon fibers of the oblique head in 12% (11/91) of specimens (Cralley and Schuberth 1979). Arakawa et al. (2003) described the insertion of the transverse head to be into the lateral sesamoid bone of the great toe, the capsule of the joint, and lateral surface of the first proximal phalanx. When present, this insertion into the first proximal phalanx is referred to as opponens hallucis muscle when off either the oblique head (Barnes 2003) or transverse head (Standring 2009). In contrast, occasionally 12% (11/91) found the insertion into the tendon of the oblique head of adductor hallucis or the conjoined tendon of oblique head of flexor hallucis brevis. This insertion is often more "cord-like" (Cralley and Schuberth 1979).

Flexor digiti minimi brevis muscle

The most frequently reported variation of the flexor digiti minimi brevis muscle concerns deep fibers from the muscle belly that course anterolaterally to insert on the lateral border of the fifth metatarsal shaft and sometimes on the head (Macalister 1875; Bergman et al. 1984, 1988; Barnes 2003). Bergman et al. (1984, 1988) note that this variation occurs in a "great majority of cases." These variable muscle fibers may be found as separate and independent from the belly of the flexor digiti minimi brevis muscle.

Macalister (1875) referred to these variable muscles fibers, whether separate or arising from the flexor digiti minimi brevis muscle, as the opponens minimi digiti muscle. Additional textbooks acknowledge the occasional existence of the opponens minimi digiti (Hollinshead 1982; Barnes 2003; Kelikian 2011). Kelikian (2011) called these muscle fibers the opponens digiti quiniti, but described how this muscle is not consistently considered a unique muscle from the flexor digiti minimi brevis. *Nomina Anatomica* did not include this muscle (Kelikian 2011). However, it is listed as an "inconstant" variant in the recent *Terminologia Anatomica*.

Macalister (1875) described additional variations of the flexor digiti minimi. This third-layer muscle may share fibers with a first-layer muscle, the abductor digiti minimi, or any of its various slips: the abductor ossis metatarsi minimi digiti and abductor accessorious digiti minimi. The flexor digiti minimi may also originate solely from fibularis longus tendon sheath (Macalister 1875).

A recent, cadaveric case study identified a variation of the flexor digiti minimi brevis with two muscle bellies (medial and lateral orientations; Mehta et al. 2011).

Fourth plantar layer

Interosseous muscles

Manter (1945) examined 149 feet and grouped the extensive variations of pedal interosseous muscles into five categories. The first category included variations in the usual bipennate shape of the dorsal interossei. He found that the usually bipennant dorsal interossei occasionally had a unipennate shape that originated from a single metatarsal bone. The first and second interossei kept their relationship to the second metatarsal bone, but lost their origins from the first and third metatarsal bones. The first interosseous muscle had this variation in 17 cases (11.4%) and the second in 11 cases (7.4%). The third and fourth dorsal interossei shifted their origin laterally to the fourth and fifth metatarsal bones in 3.4% (5/149) and 22.8% (34/149) of specimens, respectively. Rarely, the fourth dorsal interosseus muscle originated from the lateral side of the fourth metatarsal bone (2/149, 1.3%).

The second category included variations of the dorsal extensions of the plantar interossei. In 15.5% (23/149) of specimens, the second dorsal interosseous muscle was partially or wholly absent from third metatarsal bone and was replaced by a dorsal extension of first plantar interosseous muscle. In one case, the third plantar interosseous extended dorsally on the fifth metatarsal bone when the fourth dorsal interosseous muscle shifted medially to the fourth metatarsal bone (Manter 1945).

Accessory origins comprise the third category. The most frequent variation is a plantar slip extending from the third dorsal interosseous muscle to the first plantar interosseous muscle (17/149, 11.4%). The second dorsal interosseous may extend plantarly, covering the first plantar interosseous without creating an attachment to it. Additionally, the dorsal interosseous can receive tendinous slips from the extensor digitorum brevis, fibularis brevis and fibularis tertius muscles. Kalin and Hirsch (1987) corroborated the findings of Manter (1945) with detailed descriptions of soft tissue origins for ten feet. However, the findings of Kalin and Hirsch (1987) were that all dorsal and plantar interossei demonstrated variations in origins from neighboring soft tissues, including a "ligamentous meshwork" and adjacent muscles. Neighboring muscles that gave rise to interosseous muscles were primarily adjacent interossei muscles, with a few notable exceptions:

- the first and second dorsal interossei received slips from the tendon of the fibularis longus muscle;
- in the case of the first dorsal interosseous muscle, two specimens had fibers that arose from the flexor hallucis brevis muscle; and
- the second plantar interosseous muscle took partial origin from the oblique head of the adductor hallucis muscle (Kalin and Hirsch 1987).

Additionally, Manter (1945) observed instances of fusing and doubling of muscle bellies. Fusions may occur between the muscle bellies of the plantar interosseous and the third dorsal interosseous, as well as the first plantar interosseous and the second dorsal interosseous muscles. Muscle doubling was only observed in the second dorsal interosseous muscle (Manter 1945).

The fourth category includes bifid tendon insertions, where the tendon slips and inserts into both the medial and lateral metatarsal bones. This variation was found in all dorsal and plantar interossei, but was most frequently seen with the second dorsal interosseous muscle that inserted on both the second and third toes (5/149, 3.4%; Manter 1949). Hallisy (1930) studied the muscles of the foot and found a bifid tendon insertion of the first dorsal and third plantar interossei muscles.

Oukouchi et al. (1992) and Kelikian (2011) described tendinous insertions onto the extensor expansions as well as the bases of the proximal phalanges. However, Manter (1945) did not find any such insertions in his sample of 149 feet.

References

Aasar YH. 1947. *Anatomical Anomalies*. Cairo: Fouad University Press.

Agawany AE, Meguid EA. 2010. Mode of insertion of the abductor hallucis muscle in human feet and its arterial supply. *Folia Morphol* 69: 54–61.

Arakawa T, Tokita K, Miki A, Terashima T. 2003. Anatomical study of human adductor hallucis muscle with respect to its origin and insertion. *Ann Anat* 185: 585–592.

Asirvatham R, Stevens PM. 1997. Idiopathic forefoot-adduction deformity: medial capsulotomy and abductor hallucis lengthening for resistant and severe deformities. *J Pediatr Orthop* 17: 496–500.

Asomugha AL, Chukwuanukwu TO, Nwajagu GI, Ukoha U. 2005. An accessory flexor of the fifth toe. *Niger J Clin Pract* 8: 130–132.

Athavale SA, Geetha GN, Swathi. 2012. Morphology of flexor digitorum accessorius muscle. *Surg Radiol Anat* 34: 367–372.

Barnes DJ. 2003. *Anatomy of the Lower Extremity*. New Delhi: CBLS.

Bergman RA, Thompson SA, Afifi AK. 1984. *Catalog of Human Variation*. Baltimore and Munich: Urban & Schwarzenberg.

Bergman RA, Thompson SA, Afifi AK. 1988. *Compendium of Human Anatomic Variation*. Baltimore and Munich: Urban & Schwarzenberg.

Bergman RA, Afifi AK, Miyauchi R. 2006. Illustrated Encyclopedia of Human Anatomic Variation, Muscular System, Opus. Available at: http://www.anatomyatlases.org/AnatomicVariants/AnatomyHP.shtml (Accessed 22 October 2015).

Bhansali RM, Bhansali RR. 1997. Accessory abductor hallucis causing entrapment of the posterior tibial nerve. *J Bone Joint Surg* 69: 479–480.

Bowers CA, Mendicino RW, Catanzariti AR, Kernick ET. 2009. The flexor digitorum accessories longus: a cadaveric study. *J Foot Ankle Surg* 48: 111–115.

Brenner E. 1999. Insertion of the abductor hallucis muscle in feet with and without hallux valgus. *Anat Rec* 254: 429–434.

Chaney DM, Lee MS, Khan MA, Krueger WA, Mandrachia VJ, Yoho RM. 1996. Study of ten anatomy variants of the foot and ankle. *J Am Podiatr Med Assoc* 86: 532–537.

Claassen H, Wree A. 2003. Isolated flexor muscles of the little toe in the feet of an individual with atrophied or lacking 4th head of the m. extensor digitorum brevis and lacking the 4th tendon of the m. extensor digitorum longus. *Ann Anat* 185: 81–84.

Cralley JC, Schuberth JM. 1979. The transverse head of adductor hallucis. *Ann Anat* 146: 400–409.

Hallisy JE. 1930. The muscular variation in the human foot: a quantitative study. *Am J Anat* 45: 411–442.

Hollinshead WH. 1982. Anatomy for Surgeons, Volume 3: The Back and Limbs. Philadelphia: Harper & Row.

Hur MS, Kim JH, Woo JS, Choic BY, Kim HJ, Lee KS. 2011. An anatomic study of the quadratus plantae in relation to tendinous slips of the flexor hallucis longus for gait analysis. *Clin Anat* 24: 768–773.

Kalin PJ, Hirsch BE. 1987. The origins and functions of the interosseous muscles of the foot. *J Anat* 152: 83–91.

Kelikian AS. 2011. *Sarrafian's Anatomy of the Foot and Ankle: Descriptive, Topographic, Functional. Third edition*. Philadelphia: Lippincott Williams & Wilkins.

Kura H, Luo ZP, Kitaoka HB, An KN. 1997. Quantitative analysis of the intrinsic muscles of the foot. *Anat Rec* 249: 141–151.

Le Double AF. 1897. *Traité des Variations du Système Musculaire de l'Homme et de leur Signification au Point de vue de l'Anthropologie Zoologique, Vol II*. Paris: Schleicher Freres.

Lewis OJ. 1962. The comparative morphology of m. flexor accessorius and associated long flexor tendons. *J Anat* 96: 321–333.

Lobo SW, Menezes RG, Mamata S, Baral P, Hunnargi SA, Kanchan T, Bodhe AV, Bhat NB. 2008. Phylogenetic variation in flexor digitorum brevis: a Nepalese cadaveric study. *Nepal Med Coll J* 10: 230–232.

Macalister A. 1866. On muscular anomalies in human anatomy, and their bearing on homotypical myology. *Proc R Ir Acad* (1836–1869)10: 126–164.

Macalister A. 1875. Additional observations on muscular anomalies in human anatomy (third series): With a catalogue of the principal muscular variations hitherto published. Part 1 of Transactions of the Royal Irish Academy, pp. 126–130.

Manter JT. 1945. Variations of the interosseous muscles of the human foot. *Anat Rec* 93: 117–124.

Mehta V, Gupta A, Arora J, Nayyar A, Suri RK, Rath G. 2011. An atypical composition of adductor hallucis co-existent with an accessory plantar muscle and duplication of flexor digiti minimi pedis. *Clin Ter* 162: 361–363.

Nathan H, Gloobe H. 1974. Flexor digitorum brevis: anatomical variations. *Ann Anat* 135: 295–301.

Oukouchi H, Murakami T, Kikuta A. 1992. Insertions of the lumbrical and interosseous muscles in the human foot. *Okajimas Folia Anat Jap* 69: 77–83.

Schmidt R, Reissig D, Heinrichs HJ. 1963. Die m. lumbricales am fuss des menschen. *Ann Anat* 113: 450–453.

Sirasangandla SR, Swamy RS, Nayak SB, Somayaji NS, Rao MKG, Bhat KMR. 2013. Analysis of the morphometry and variations in the extensor digitorum brevis muscle: an anatomic guide for muscle flap and tendon transfer surgical dissection. *Anat Cell Biol* 46: 198–202.

Standring S. 2009. *Gray's Anatomy, 40th edition*. Edinburgh: Churchill Livingstone.

Yalçin B, Ozan H. 2005. Some variations of the musculus flexor digitorum brevis. *Anat Sci Int* 80: 189–192.

43 Internal carotid artery and the anterior cerebral circulation

Paul M. Foreman, Christoph J. Griessenauer, John P. Deveikis, and Mark R. Harrigan
University of Alabama at Birmingham, Birmingham, Alabama, United States

Internal carotid artery

The internal carotid artery (ICA) originates at the bifurcation of the common carotid artery (CCA) into the ICA and external carotid artery (ECA). The CCAs most commonly derive from the aortic arch on the left and the innominate artery on the right. The CCAs ascend in the neck with the internal jugular vein and vagus nerve within the carotid sheath. While the bifurcation of the CCA can be located anywhere between T2 and C1, it is typically located at the level of C3 or C4, corresponding to the upper border of the thyroid cartilage (Morris 1997; Osborn 1999) The CCAs usually give rise to only the ICA and ECA; occasionally the superior thyroid, ascending pharyngeal, or occipital arteries arise directly from the CCA (Osborn 1999).

Various authors classify the segments of the ICA using numbering systems. In this chapter we utilize the system reported by Bouthillier et al. (1996): cervical segment (C1); petrous segment (C2); lacerum segment (C3); cavernous segment (C4); clinoidal segment (C5); ophthalmic segment (C6); and communicating segment (C7).

Cervical segment (C1)

The cervical carotid begins at the carotid bifurcation, ascends in the neck, and ends at the skull base. The ICA receives approximately 80% of the flow from the CCA with only 20% funneled into the external carotid artery. The ICA travels up the carotid sheath along with encircling sympathetic fibers, the internal jugular vein and the vagus nerve. The C1 segment can be divided into the carotid bulb, a focal dilation of the ICA at the origin, and the ascending cervical segment. The diameter of the ascending cervical segment remains relatively constant throughout its course. The cervical segment may be coiled or looping in 15% of cases (Osborn 1999). The cervical segment of the ICA usually contains no branches.

Variations are rare and include positional abnormalities, agenesis/hypoplasia, anomalous branches, fenestration/duplication, and carotid-vertebrobasilar anastomosis. Positional anomalies usually involve the level of the CCA bifurcation, which can be anywhere from T2 up to C1 (Osborn 1999). The ICA may rarely arise directly from the aortic arch, giving rise to all of the branches normally supplied by the ECA before continuing as the ICA (Morimoto et al. 1990). Agenesis and hypoplasia of the ICA can assume different forms depending on the degree of the maldevelopment and whether it is bilateral or unilateral. Congenital absence of the ICA may be associated with other congenital anomalies, such as anencephaly or basal telangiectasia (Pascual-Castroviejo et al. 1995), which are frequently associated with intracranial aneurysms (Lee et al. 2003). Agenesis of the ICA occurs rarely in just 0.01% of cases (Chen et al. 1998) and is associated with an absent carotid canal on imaging (Quint et al. 1989). Agenesis more frequently involves the left ICA (Tasar et al. 2004). Bilateral involvement occurs in <10% of ICA agenesis cases (Tasar et al. 2004) and in 25% of cases is associated with intracranial aneurysms (Cali et al. 1993). Congenital carotid artery hypoplasia is much less common than acquired diffuse narrowing and has an incidence of 0.079% (Tasar et al. 2004). Congenital hypoplasia can be distinguished from acquired stenosis by the presence of a small petrous carotid canal (Quint et al. 1989). Hypoplastic ICAs may end as an ophthalmic artery (Makowicz et al. 2013). Anomalous branches of the ICA include the ascending pharyngeal artery, superior thyroid artery, occipital artery, posterior meningeal artery, persistent stapedial artery, and the vidian artery (Teal et al. 1973). Duplication and fenestration of the cervical ICA has been reported (Glasscock et al. 1993; Chess et al. 1995) and involves segmental division of the vessel to form two separate lumens with endothelial walls (Makowicz et al. 2013).

Petrous segment (C2)

The petrous segment begins the carotid canal in the skull base and continues to the posterior edge of the foramen lacerum. The vertical subsegment transitions into the horizontal subsegment by taking a 90° bend known as the genu. Sympathetic fibers (internal carotid nerve) follow the ICA as it enters the skull base. The internal carotid artery plexus of Rektorzik is a venous plexus that surrounds the petrous ICA (San Millan

Bergman's Comprehensive Encyclopedia of Human Anatomic Variation, First Edition. Edited by R. Shane Tubbs, Mohammadali M. Shoja and Marios Loukas.
© 2016 John Wiley & Sons, Inc. Published 2016 by John Wiley & Sons, Inc.

Ruiz et al. 2002). Petrous ICA branches are found in a minority of cadaveric dissections, and in 23% of angiographic studies (Quisling and Rhoton 1979).

The Vidian artery represents a small branch that arises from the horizontal petrous ICA in 30% of cases and travels anteriorly within the Vidian (pterygoid) canal along the floor of the sphenoid sinus with the nerve of the same name to the pterygopalatine fossa, where it anastomoses with branches of the internal maxillary artery (IMA). The periosteal branch is found in 8% of specimens arising at the entrance of the ICA into the carotid canal (Paullus et al. 1977). While the carticotympanic artery is a commonly described branch of the petrous ICA, its existence has been disputed (Paullus et al. 1977). It is reported to arise from the petrous ICA and anastomose with the ascending pharyngeal artery via the inferior tympanic artery (Quisling and Rhoton 1979).

Variants of the petrous segment include an aberrant ICA, the persistent stapedial artery, and carotid-vertebrobasilar anastomoses. An aberrant ICA is more posterior and lateral than usual, passing through the middle ear cavity. This variant is found more often in woman, most frequently involves the right side (Caldemeyer et al. 1998), and is bilateral in 15% of cases (Windfuhr 2004). The aberrant ICA is thought to arise from the ascending pharyngeal artery supplying collateral flow to a segmentally atretic internal carotid (Lasjaunias and Santoyo-Vazquez 1984). This vessel is formed as a result of the fusion of the inferior tympanic branch of the ascending pharyngeal artery with the caroticotympanic artery (Roll et al. 2003; Sauvaget et al. 2006). This anomaly is usually asymptomatic but can occasionally produce tinnitus or auditory conduction abnormalities (Makowicz et al. 2013). Knowledge of the possibility of an aberrant ICA is critical when planning tympanic membrane incision or middle ear surgery, in order to avoid ICA injury (Makowicz et al. 2013). The persistent stapedial artery appears as a branch of the vertical segment of the petrous ICA that travels through the middle ear and gives rise to the middle meningeal artery (Pahor and Hussain 1992). It is observed in 0.48% of temporal bone sections in post-mortem examinations (Roll et al. 2003). It is associated with an abnormal course of the ICA, potentially due to traction forces or secondary fusion (Silbergleit et al. 2000; Sauvaget et al. 2006). Imaging findings can include absence of a foramen spinosum and a soft tissue lesion in the proximal part of the tympanic segment of the facial nerve (Makowicz et al. 2013). Most persistent stapedial arteries are asymptomatic, although they may produce tinnitus and dizziness (Makowicz et al. 2013).

Lacerum segment (C3)

The C3 segment is a short portion of the ICA that crosses over the foramen lacerum, connecting the petrous to the cavernous segment of the ICA. The foramen lacerum is a 1-cm-long fibrocartilaginous floor over which the ICA passes (Paullus et al. 1977). The lacerum segment is separated from the cavernous segment by the petrolingual ligament, which is a small fold of periosteum that extends from the lingula of the sphenoid bone to the petrous apex (Tauber et al. 1999), continuous with the periosteum of the carotid canal (Bouthillier et al. 1996). The trigeminal ganglion is just above it, so the C3 segment is sometimes termed the trigeminal segment (Ziyal et al. 1998). This segment is usually without subsegments, branches, or variants.

Cavernous segment (C4)

The cavernous segment forms an S-shaped siphon and travels from the superior margin of the petrolingual ligament, through the cavernous sinus where it is surrounded by areolar tissue, fat, postganglionic sympathetic fibers, and the interconnecting venous chambers, to the proximal dural ring. The artery is positioned against the lateral surface of the body of the sphenoid bone in the carotid suclus (Resnick et al. 1997). A thin layer of bone separates the artery from the sinus in almost 90% of cases, and this layer of bone is absent in almost 10% with the carotid bulging into the sinus (Resnick et al. 1997).

Subsegments of the cavernous ICA include the posterior vertical, posterior bend, horizontal, anterior bend, and anterior vertical parts (Rhoton 2002b). The branches of the cavernous ICA are variable, but often include the posterior trunk, the lateral trunk, and the medial branch group (Inoue et al. 1990). The posterior trunk (also known as the meningohypophyseal artery) arises distal to the foramen lacerum from the posterior bend of the cavernous ICA (Rhoton 2002b). The combination of tentorial artery, the inferior hypophyseal artery, and dorsal meningeal artery arise from the meningohypophyseal trunk in about 70% of cases (Rhoton 2002b). The tentorial artery is always present in dissections (Tran-Dinh 1987). It gives rise to the marginal tentorial artery (of Bernasconi and Cassinari 1957) which travels posteriorly along the medial edge of the tentorium (Rhoton 2002a), and the basal tentorial artery which travels laterally along the border between the tentorium and the petrous ridge and anastomoses with the middle meningeal artery and the dural arteries of the posterior fossa (Morris 1997). The inferior hypophyseal artery extends superiorly and medially to supply the posterior lobe of the pituitary gland (Bernasconi and Cassinari 1957). It anastomoses with the superior hypophyseal artery, the medial branch group, and the contralateral inferior hypophyseal artery. A total of 75% of dissections have the dorsal meningeal artery arising from the meningohypophyseal trunk, going through Dorello's canal and giving off lateral and dorsal clival branches (Tsitsopoulos et al. 1996). The recurrent artery of foramen lacerum is a variable branch of the posterior trunk that may connect to the carotid branch of the ascending pharyngeal artery (Lasjaunias 1987).

The lateral trunk is also known as the inferolateral trunk, artery of the inferior cavernous sinus, or lateral main stem. It arises from the lateral aspect of the horizontal cavernous segment superior to the abducens nerve in about 66% of dissections (Inoue et al. 1990) and typically gives off four branches: (1) anteromedial branch which potentially anastomoses with the recurrent meningeal branch of the ophthalmic artery; (2) anterolateral

branch which anastomoses with the artery of the foramen rotundum; (3) posterior branch which anastomoses with the cavernous branches of the middle and accessory meningeal arteries; and (4) superior branch, which joins the ophthalmic artery (Lasjaunias 1987). The medial branch group is known as the capsular arteries of McConnell. It arises from the most superior portion of the cavernous segment in about 28% of dissections, and supplies the pituitary gland (Inoue et al. 1990). Other cavernous ICA branches include the ophthalmic artery in about 8% of cases (Parkinson 1964), the recurrent artery of the foramen lacerum, and the artery of the Gasserian ganglion.

Variants of the cavernous ICA include kissing intrasellar ICAs, intercavernous ICA anastomoses, aberrant branches, and persistent carotid-vertebrobasilar anastomoses. Kissing intrasellar ICAs occur when the cavernous ICA approach within 4 mm of each other within the sella in some 10% of cases (Hayreh 2006), sometimes associated with acromegaly (Renn and Rhoton 1975). When a large collateral vessel connects the cavernous carotid arteries, hypoplasia or agenesis of the ICA can be associated (Sacher et al. 1986; Quint et al. 1989; Midkiff et al. 1995; Chen et al. 1998). Aberrant origin of the cerebellar arteries from the cavernous segment has been reported, and is hypothesized to result from an abnormal regression of fetal carotid-vertebrobasilar anastomoses (Shoja et al. 2012).

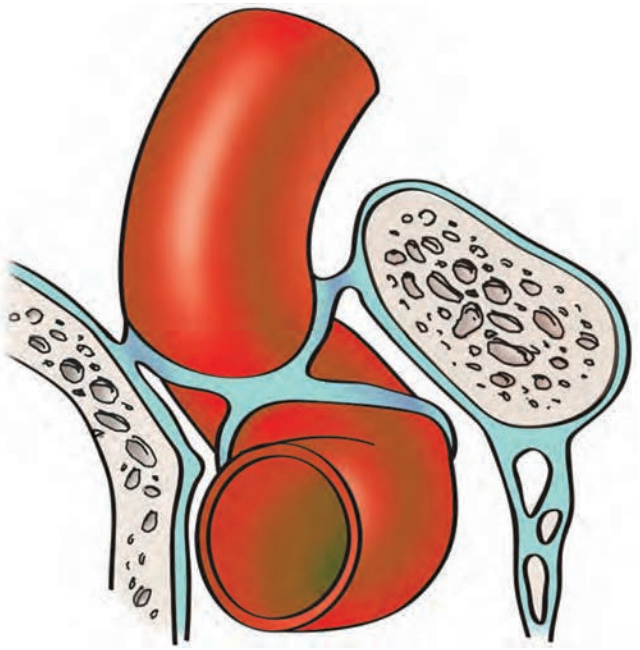

Figure 43.1 Clinoidal segment of ICA. The clinoidal segment is defined by the proximal and distal dural rings. The space between the dural rings is wide on the lateral aspect of the ICA and small on the medial aspect, where the dural rings come closest together. The medial part of the distal dural ring is incomplete; this region is known as the "carotid cave."

Clinoidal segment (C5)

The clinoidal segment is a small wedge-shaped portion of the ICA between two dural rings (Fig. 43.1). The clinoidal ICA is inferior and medial to the anterior clinoid process, and is surrounded by a dural ring containing the clinoid veous plexus and venous tributaries of the cavernous sinus (Tran-Dinh 1987). The clinoidal segment of the ICA contains no subsegments or reported variants, but the ophthalmic artery may rarely arise from the clinoidal segment (Osborn 1999).

Ophthalmic segment (C6)

The ophthalmic segment becomes intradural at the distal dural ring and extends superior and posterior to the spenoid sinus, inferior and lateral to the optic nerve, extending to the origin of the posterior communicating artery. The optic strut is a bony process that extends from the base of the anterior clinoid to the body of the sphenoid bone. The optic strut separates the cavernous from the ophthalmic segments (Kobayashi et al. 1989). The ophthalmic segment contains no subsegments. Branches include the ophthalmic artery, the superior hypophyseal artery, and perforating branches.

The ophthalmic artery arises from the anterior surface of the ICA at the level of the anterior clinoid process. The artery originates at or above the distal dural ring in ≥90% of cases, or from the cavernous segment in about 8% of cases (Parkinson 1964). The artery enters the optic canal inferior and lateral to the optic nerve. The artery continues in the orbit inferior and lateral to the optic nerve in 83% of cases, and then continues medially toward the globe. In 17% of cases, the ophthalmic artery remains medial and inferior to the optic nerve (Parkinson 1964). The ophthalmic artery has been reported to be duplicated by Uchino et al. (2013).

Ophthalmic artery branches are highly variable, and frequently anastomose with the branches of the external carotid artery. Ophthalmic artery branches include the ocular, orbital, and extraorbital groups. The ocular group consists of the central retinal artery and the ciliary arteries. The central retinal artery arises from the ophthalmic artery as a single trunk or in common with a posterior ciliary artery, then penetrates the optic nerve sheath to supply the retina (Gonzalez et al. 2003). The central retinal artery is a true end-artery, with no appreciable collateral circulation. Occlusion of the central retinal artery can be expected to cause loss of vision. The ciliary arteries are divided into posterior and anterior ciliary arteries. The orbital group includes the lacrimal artery and muscular branches. The lacrimal artery arises from the ophthalmic artery adjacent to the optic nerve and passes along the lateral rectus muscle to supply the lacrimal gland and conjunctiva. It can anastomose with branches of the superficial temporal and internal maxillary artery (Tsutsumi and Rhoton 2006). The lacrimal artery gives rise to a recurrent meningeal artery, which extends back through the superior orbital fissure, and anastomoses with the middle meningeal artery (Gray 1901). Zygomaticofacial branches connect to deep temporal and transverse facial branches in the external carotid territory (Gray 1901). The muscular branches

supply the extraocular muscles and periosteum of the orbit. The extraorbital branches include the ethmoidal arteries, palpebral artery, and the terminal ophthalmic artery. The ethmoidal arteries supply the upper nasal mucosa and anastomose with branches of the sphenopalatine branches of the internal maxillary artery. They also contribute through the cribriform plate to supply dura of the anterior fossa, including the anterior falx artery, which supplies the falx via the foramen caecum. The posterior ethmoidal artery can anastamose with the sphenopalatine branch of the internal maxillary artery. The palpebral artery divides into medial, inferior medial, and superior medial palpebral branches (Parkinson 1964) which can anastomose with the branches of the superficial temporal and internal maxillary artery. The terminal ophthalmic artery divides into the supratrochlear branch, which connects to branches of the superficial temporal artery, and the dorsal nasal branch, which connects to branches of the facial artery. The anterior ethmoidal artery is absent on one side in 14% and both sides in 2% of cases and can arise from a common stem with the posterior ethmoidal. When the anterior ethmoidal is absent, it is usually replaced by a branch of the posterior ethmoidal artery. The posterior ethmoidal can be small or absent and, in such cases, can be replaced with a branch of the anterior ethmoidal, contralateral posterior ethmoidal, or branches of the sphenopalatine artery (Lang 1989). Both ethmoidal arteries can also arise from the middle meningeal artery. The middle meningeal may be replaced by a branch of the ophthalmic artery, the so-called sphenoidal artery.

One or two superior hypophyseal arteries arise from the ophthalmic segment of the ICA, usually near the ophthalmic artery origin (Lang and Kageyama 1990). A single large superior hypophyseal artery divides into multiple smaller branches in 42% of cases, or two or three hypophyseal arteries in the remaining cases (Lang and Kageyama 1990). The arteries then anastomose with branches of the contralateral superior hypophyseal artery and posterior communicating arteries at the pituitary stalk, supplying stalk and anterior pituitary (Lang and Kageyama 1990). The posterior pituitary is supplied by inferior hypophyseal branch of the meningohypophyseal artery (Gibo et al. 1981b).

Several perforating branches arising from the ophthalmic segment of the ICA not included with the superior hypophyseal arteries arise from the posterior or medial surface of the ICA and supply the optic tract, chiasm, and nerve, and the floor of the third ventricle (Gibo et al. 1981b).

Most anatomic variants of the ophthalmic segment of the ICA consist of anomalous origins of the ophthalmic artery. The most common variant is a middle meningeal artery origin of the ophthalmic, seen in nearly 16% of cases in a dissection series (Hayreh 1963). Conversely, an ophthalmic origin of the middle meningeal artery is seen in about 0.5% of the angiograms (Gabriele and Bell 1967). Other reported anomalous origins of the ophthalmic include the cavernous ICA, the MCA, ACA, PCA, and the basilar artery (Parkinson 1964). A fenestrated segment can occur in the ophthalmic segment of the ICA (Krisht et al. 1994).

Communicating segment (C7)

The communicating segment begins just proximal to the origin of the posterior communicating artery and ends with the bifurcation of the ICA into the ACA and the MCA. The C7 segment of the ICA contains no subsegments. Branches include the posterior communicating artery and the anterior choroidal artery. The posterior communicating artery arises from the posterior surface aspect of the ICA distal to the ophthalmic artery and proximal to the ICA bifurcation (Gibo et al. 1981b). Posteromedially it connects to the PCA between the P1 and P2 segments. The number of perforating arteries numbering from 4 to 14 (average of 7.8) arise from the posterior communicating artery (Gibo et al. 1981b). These perforators supply the floor of the third ventricle, the posterior perforated substance, optic tract, pituitary stalk, and optic chiasm (Alvarez et al. 1990), as well as the thalamus, hypothalamus, and internal capsule. These anterior thalamoperforators can be differentiated from the posterior thalamoperforators that arise from the P1 segment of the posterior cerebral. The largest and the most constant perforator is the premamillary artery (Pedroza et al. 1987).

The anterior choroidal artery (Fig. 43.2) arises from the posterolateral ICA, distal to the posterior communicating artery

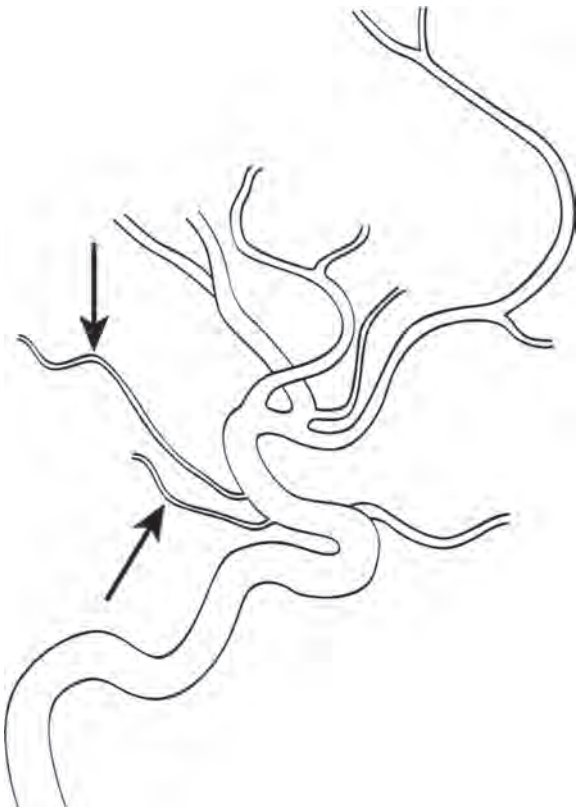

Figure 43.2 Anterior choroidal artery. On a lateral angiogram, the anterior choroidal artery (upper arrow) has a characteristic undulating appearance as it passes around the cerebral peduncle. The posterior communicating artery (lower arrow) travels inferior to the anterior choroidal artery.

and proximal to the ICA bifurcation (Gibo et al. 1981b). The vessel is duplicated in 4% of cases (Tripathi et al. 2003). The anterior choroidal artery has a cisternal segment and an intraventricular segment. The cisternal segment travels posteriorly, first medially, then laterally around the cerebral peduncle. It then angles upward as it passes through the choroidal fissure to enter the temporal horn of the lateral ventricle. This cisternal segment gives rise to an average of eight perforating branches (Tripathi et al. 2003), which supply brain structures that are most vulnerable to ischemic injury with anterior choroidal artery occlusion. The intraventricular segment travels with the choroid plexus in the lateral ventricle, anastomosing with branches of the lateral posterior choroidal artery from the posterior cerebral artery. The artery then travels up and around the thalamus, and in some cases it reaches as far as the foramen of Monro and connects to branches of the medial posterior choroidal artery, also from the posterior cerebral artery. Arterial branches from the intraventricular segment irrigate the optic tract, lateral geniculate body, and thalamus (Rhoton et al. 1979a).

The anterior choroidal artery supplies the optic tract, cerebral peduncle, lateral geniculate body, uncus, and temporal lobe (Gibo et al. 1981b). The brain structures supplied by these branches include the optic radiation, globus pallidus, midbrain, thalamus, and posterior limb of the internal capsule. Occlusion of the anterior choroidal artery can affect the the posterior limb of the internal capsule, the retrolenticular portion of the internal capsule, the internal portion of the globus pallidus, and the lateral thalamus (Morandi et al. 1996). The severity of neurologic change after occlusion of the vessel may vary depending on possible anastomoses with the posterior choroidal arteries from the PCA (and, less commonly, the ACA or MCA).

Variations of the posterior communicating artery include a persistent fetal origin, infundibulum, hypoplasia/absence, and fenestration. Fetal origin is filling of the PCA primarily via the ICA with a prominent P-comm artery that has the same diameter as the P2 segment of the PCA, with hypoplastic ipsilateral P1 segment (Fig. 43.3). This is present in 18–22% of cases (Pedroza et al. 1987). An infundibulum is a conical or funnel-shaped dilatation at the origin of an artery, and is found most commonly at the junction of the posterior communication artery and ICA (Fig. 43.4). At this location, an infundibulum is defined as a symmetric bulge at the origin of the P-comm, with a diameter of 3 mm or less (Taveras and Wood 1976; Takahashi et al. 1990). Some have also found infundibula at the P-comm-PCA junction, the P2 segment, in the anterior communicating artery complex, the ophthalmic artery origin, and at the origin of the anterior choroidal artery. Infundibula are found in 7–15% of angiograms (Saltzman 1959; Waga and Morikawa 1979; Ohyama et al. 1994) and 25% of cases have bilateral infundibula. Benign infundibula should be round or conical in shape, ≤3 mm in the maximum diameter, without aneurysmal neck, and with a posterior communicating artery arising from its apex (Takahashi et al. 1990).

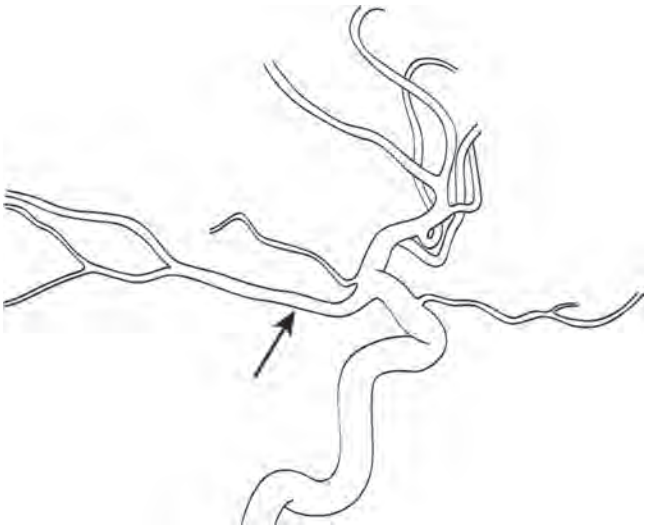

Figure 43.3 Fetal configuration of the posterior communicating artery. A "fetal" variant of the posterior communicating artery is defined as the diameter of the posterior communicating artery equaling the diameter of the P2 segment to which it connects.

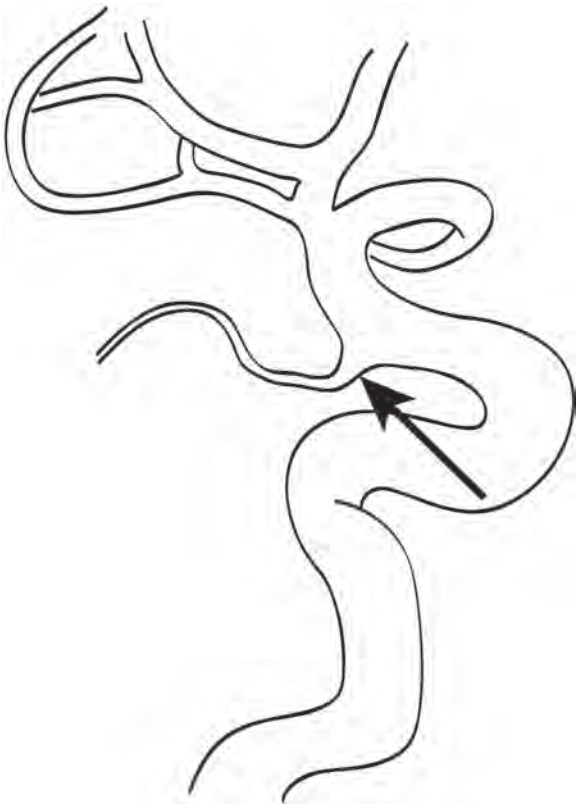

Figure 43.4 Posterior communicating artery infundibulum (arrow).

Hypoplasia of the P-comm artery is seen in 34% of the dissections (Pedroza et al. 1987) but complete absence of the P-comm artery is found in only 0.6% of the dissections (Saeki and Rhoton 1977). Fenestration of the P-comm artery is sometimes seen (Alpers et al. 1959).

Variants of the anterior choroidal artery include ectopic origin, absence, and hyperplasia. Ectopic origin occurs in 4% of the dissections (Rhoton et al. 1979a). The anterior choroidal artery may originate from the MCA or PCA, or rarely from the ICA proximal to the posterior communicating artery (Cooper 1954). The anterior choroidal artery is absent in 3% of angiograms (Moyer and Flamm 1992). A hyperplastic anterior choroidal artery supplies part of the PCA territory in 2.3% of angiograms (Moyer and Flamm 1992).

Circle of Willis

The circle of Willis consists of interconnecting vessels encircling the pituitary infundibulum providing important collateral circulation from right to left and between anterior and posterior circulations. In reality it is a nonagon rather than a circle. Despite a circle of Willis being present in some 90% of individuals, a well-developed and symmetric circle is found in less than half of cases (Wolpert 1997). In 60%, at least one component of the circle is relatively hypoplastic and diminished in its capacity to provide collateral flow (Osborn 1999). An incomplete circle of Willis results in asymmetric blood flow and can be a factor in the development of intracranial aneurysms and in ischemic stroke (Krabbe-Hartkamp et al. 1998). Fenestrations may occur in all cerebral vessels, but are most common in the Circle of Willis (Makowicz et al. 2013). Fenestrations can be associated with aneurysms (Kowada et al. 1972; de Gast et al. 2008), and patients with aneurysms are more likely to have asymmetry or an anomaly of the circle (Hendrikse et al. 2005). The presence of a nonfunctional anterior collateral pathway in the circle of Willis in patients with ICA occlusive disease is strongly associated with ischemic stroke (Alpers and Berry 1963). The primary variations in the vessels of the circle of Willis include absence, hypoplasticity, duplication, triplication, and persistence of the embryonic pattern. A hypoplastic P-comm artery and a fetal origin of the PCA are the most common variants, occurring in 16.7% and 10.6%, respectively (Kapoor et al. 2008).

Anterior cerebral artery

Several classification systems for the ACA have been described. The conventional and most common system includes three segments: A1, from ICA to anterior communicating artery; A2, from anterior communicating artery to the anterior extent of the genu of the corpus callosum; and A3, distal branches.

A1 segment and anterior communicating artery complex

The A1 segment (i.e., the precommunicating segment; Osborn 1999) travels superomedially from the ICA bifurcation to its junction with the anterior communicating artery (AC) within or just inferior to the interhemispheric fissure. It is usually superior to the optic chiasm or optic nerves and inferior to the anterior perforated substance. The AC complex is highly variable and usually takes one of four patterns.

Branches of the A1 include the perforators, AC artery branches, and the recurrent artery of Heubner. A1 perforating branches include 2–15 superior branches comprising the medial lenticulostriate arteries that travel into the anterior perforated substance and supply the anterior hypothalamus, septum pellucidum, anterior commissure, fornix, and the anterior striatum (Hoksbergen et al. 2003), and inferior branches supply the optic chiasm and optic nerves.

Perforating branches of the AC include subcallosal, hypothalamic, and chiasmatic branches (Rhoton et al. 1979b). A single subcallosal branch is usually the largest branch of the AC, supplying the septum pellucidum, columns of the fornix, corpus callosum, and lamina terminalis (Serizawa et al. 1997). The hypothalamic branches are smaller and multiple. A chiasmatic branch is present in 20% of cases (Rhoton et al. 1979b).

The recurrent artery of Heubner, most often an A2 branch, may arise from the A1 segment in up to 17% of cases and from the ACA–AC junction in 35% of cases (Dunker and Harris 1976; Gomes et al. 1986). See A2 Segment, Branches below for further discussion of the artery of Heubner.

Variants

Some degree of asymmetry is present in the majority of cases. The left and right A1 segments are asymmetric in size in up to 80% of cases (Morris 1997). Right A1 segments tend to be longer, more tortuous, deviated, and more narrow than left A1 segments (Zurada et al. 2010). Approximately 10% of the A1 segments are hypoplastic (defined as having a diameter of ≤1.5 mm; Hoksbergen et al. 2003). Complete absence of one A1 segment is seen in 1–2% of cases (Osborn 1999). A persistent olfactory artery is a rare anomaly in which a persistent primitive olfactory artery travels from the ICA, along the olfactory tract, to supply the distal ACA territory (Marinkovic et al. 1986). This variant represents an abnormal course of the proximal ICA with the proximal segment running anteriorly along the olfactory tract before taking an upward turn to return to the usual location of the ACA (Uchino et al. 2003). This variant may be associated with aneurysm formation in the region of the "hairpin turn" (Moffat 1967). In rare cases an infraoptic A1 may be present in which the A1 segment travels inferior to or through the optic nerve (Bollar et al. 1988; Maurer et al. 1991; Nozaki et al. 1998). This variant is also associated with aneurysms. Fenestration of the A1 segment is rare, occurring in 0–4% of anatomical studies, and is also associated with aneurysms (Minakawa et al. 1985; Suzuki et al. 1992; Given and Morris 2002). An accessory

ACA represents an atypical branch of the ICA that courses under the optic nerve and ACA to give rise to the orbitofrontal and frontopolar arteries (Choudhari 2002). Anomalous origins of the A1 from the cavernous ICA (Ladzinski et al. 1997), from the ICA at or proximal to the ophthalmic artery (Singer et al. 1997), and from the contralateral ICA (Spinnato et al. 1999) have been reported.

Some 227 AC complex variations have been described (Burbank and Morris 2005). An AC in which a single vessel forms a link between two non-anomalous ACAs is present in only about 40% of cases (Busse 1927; Dunker and Harris 1976; Rhoton et al. 1979b; Burbank and Morris 2005). Anomalous AC anatomy is present in the remaining 60% of cases. These patterns included the plexiform (i.e., multiple complex vascular channels, 33%), dimpled (i.e., incomplete fenestration, 33%), fenestration (21%), duplication (18%), string (18%), fusion (12%), median artery of the corpus callosum (6%), and azygos ACA (3%) (Rhoton et al. 1979b). The AC artery is absent in about 5% of cases (Perlmutter and Rhoton 1976).

A2 segment

The A2 segment extends in a vertical direction from the AC toward the most anterior position, the genu of the corpus callosum. The left and right A2 segments usually travel together in the interhemispheric fissure, although the right A2 is more often (72% of cases) anterior to the left A2 in the sagittal plane (Marinkovic et al. 1990).

Branches

Branches include perforators, the recurrent artery of Heubner, the orbitofrontal artery, and the frontopolar artery. Perforating branches of the A2 segment are located along the first 5 mm of the segment, and penetrate the brain at the gyrus rectus and olfactory sulcus (Dunker and Harris 1976).

The recurrent artery of Heubner, which is a large lenticulostriate artery, arises from the A2 segment in most (57–78%) cases (Dunker and Harris 1976; Hoksbergen et al. 2003). It doubles back and runs in the opposite direction to the A1 segment to enter the lateral anterior perforated substance lateral to the ICA bifurcation (Gomes et al. 1986). This artery irrigates the head of the caudate nucleus, anterior limb of the internal capsule, and the anterior third of the putamen (Perlmutter and Rhoton 1978). Although it is often not large enough to be seen on angiography, it is regularly identified during surgery of the AC complex and inadvertent occlusion of the vessel can occur by pinching the vessel during retraction of the frontal lobe. Isolated infarction of the territory of this vessel can be clinically silent, or produce a hemiparesis that is most prominent in the face and upper extremity (Morris 1997).

The orbitofrontal artery is the first cortical branch of the A2 segment, and may appear as two or three vessels rather than single branch (Marinkovic et al. 1990). The artery runs close to the midline in an anterior direction to the gyrus rectus, olfactory bulb, and medial aspect of the inferior frontal lobe.

The frontopolar artery may also appear as a group of vessels and usually arises from the distal A2 segment, below the corpus callosum. It travels anteriorly and superiorly towards the frontal pole.

Variants

Variants include bihemispheric ACA, azygos ACA, duplicated A2, and the superior anterior communicating artery. In the bihemispheric ACA, one A2 segment is hypoplastic and the other A2 vessel irrigates both the hemispheres. This is present in up to 7% of cases (Marinkovic et al. 1990).

An azygos ACA is defined as a single unpaired A2 segment that arises from the junction of the A1s (Fig. 43.5). It is present in ≤1% of the general population (Ostrowski et al. 1960). Baptista classified three types: (1) an unpaired, single ACA; (2) "bihemispheric" ACA giving branches to both hemispheres; and (3) an additional vessel from the AC accompanied by two hypoplastic A2 arteries (LeMay and Gooding 1966). As many as 41% of patients with an azygos ACA have a terminal aneurysm (Baptista 1963; Huber et al. 1980) and this anomaly is also associated with holoprosencephaly, agenesis of the corpus callosum, hydranencaphaly, and septo-optic dyplasia (Cinnamon et al. 1992; Makowicz et al. 2013). In addition, the azygos ACA is associated with bilateral frontal ischemic stroke (Huh et al. 2007).

A duplicated A2 occurs when more than one A2 segment is present, and has been reported in up to 13% of cases (Osborn 1999). In some cases, this may represent persistence of the primitive median artery of the corpus callosum (Osborn 1999) which is found in 6% of cases (Rhoton et al. 1979b).

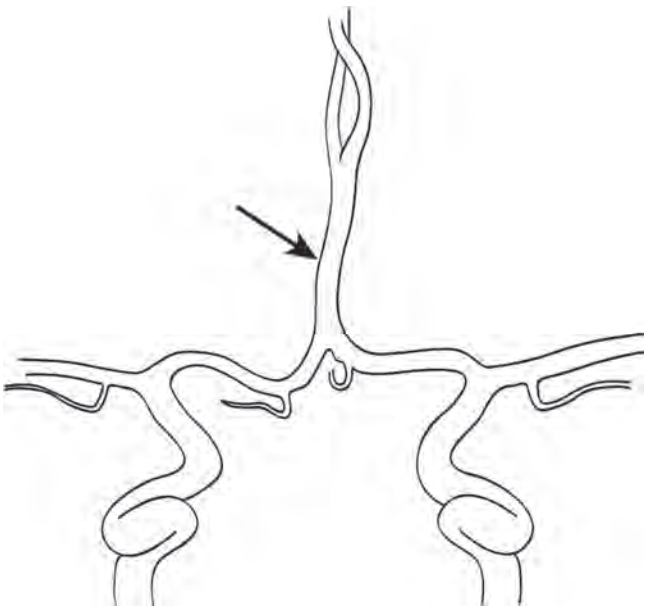

Figure 43.5 Azygos anterior cerebral artery. An azygos anterior cerebral artery is defined as both A1 segments joining to form single A2 segment.

The superior anterior communicating artery is an anomalous communicating vessel between the ACAs near the corpus callosum, and has been associated with aneurysms (Osaka and Matsumoto 1978).

A3 segments

The A3 segments include all the ACA branches distal to the origin of the pericallosal and callosomarginal arteries. The distal ACA branches have extensive anastomoses with distal branches of the MCA and PCA. These connecting arteries, in the furthest reaches of the intracranial arterial circulation, are the watershed zones. The corresponding territories of the brain are the most vulnerable to ischemia during hemodynamic failure.

The distal ACA branches may be further subdivided into A4 and A5 segments (Fischer 1938; Marinkovic et al. 1990); the A3 segment in this system is defined as the part of the ACA that extends around the genu of the corpus callosum, and the A4 and A5 segments comprise the part of the ACA that travels posteriorly over the corpus callosum. The A4 and A5 segments are separated by the coronal suture (Marinkovic et al. 1990).

Branches

The A3 segments consist of five primary branches. The pericallosal artery is the main trunk of the ACA as it passes posteriorly over the corpus callosum. It gives off multiple small branches ("short callosal arteries"; Marinkovic et al. 1990) that extend laterally along the corpus callosum and anastomose with the splenial artery (the "posterior pericallosal branch"), a branch of the PCA. Infrequently, a "long callosal artery" is present, which is a branch of, and runs parallel to, the pericallosal artery (Marinkovic et al. 1990).

The callosomarginal artery is the second-largest distal branch of the ACA, after the pericallosal artery. It travels superiorly over the cingulate gyrus to run in a posterior direction within the cingulate sulcus. It is absent in 18% of hemispheres (Marinkovic et al. 1990).

The internal frontal branches are a group identified according to which part of the superior frontal gyrus they supply. They may arise from the pericallosal or the callosomarginal artery and include: the anterior internal frontal arteries, the middle internal frontal arteries, and the posterior internal frontal arteries.

The paracentral artery arises from the pericallosal or callosomarginal artery midway between the genu and splenium of the corpus callosum, to supply the paracentral lobule.

The parietal arteries are the final and most distal branches of the ACA. They supply the medial aspect of the hemisphere above the corpus callosum and most of the precuneus (Yasargil and Carter 1974). They connect with the parieto-occipital branch of the PCA and can be divided into the superior parietal artery and inferior parietal artery.

Variants

Variants include branches to the contralateral hemisphere and are found in 64% of brains (Marinkovic et al. 1990). While the anatomy of the distal ACA branches is highly variable, true developmental anomalies in this region are uncommon (Osborn 1999).

Middle cerebral artery

Most classification schemes divide the MCA into four segments. The authors of this chapter favor the following system: M1, from ICA to the 90° vertical turn within the sylvian fissure; M2, from the MCA's 90° vertical turn to the circular sulcus of the insula; M3, from the circular sulcus to the superficial aspect of the sylvian fissure; and M4, as the cortical branches.

M1 segment

The M1 segment (also known as the horizontal or sphenoidal segment; Gloger et al. 1994a) arises from the ICA and travels in a lateral direction, parallel to the sphenoid wing, and terminates by dividing into the M2 segments. The diameter of the M1 segment at its origin is usually twice the diameter of the A1 segment (Osborn 1999). The MCA bifurcates in 71% of cases, trifurcates in 20% of cases, and divides into four branches in 9% of cases (Gibo et al. 1981a).

Branches

Branches include the lateral lenticulostriate arteries and the anterior temporal artery. Approximately 80% of the lenticulostriates that arise from the MCA arise from the M1 segment. These branches average 10 in number (Gibo et al. 1981a; Umansky et al. 1985), and most arise from the superior aspect of the M1 segment. They enter the anterior perforated substance to supply the anterior commissure, internal capsule, caudate nucleus, putamen, globus pallidus, and substantia innominata.

The anterior temporal artery typically arises near the midpoint of the M1 segment. Less commonly, it arises from the inferior division (an M2 segment) or as part of an M1 trifurcation. It travels in an anterior and inferior direction over the temporal tip and does not usually enter the sylvian fissure itself (Osborn 1999). It supplies the anterior temporal lobe.

Variants

Variants include MCA duplication, an accessory MCA, aplasia, early branching, and fenestration. MCA duplication is an anomaly that consists of a large MCA branch arising from the ICA proximal to the ICA bifurcation, and has a frequency of 0.2–2.9% (Grand 1980). This vessel travels parallel and inferior to the main M1 segment and primarily supplies the anterior temporal lobe (Grand 1980; Komiyama et al. 1998). This variant is associated with aneurysms (Umansky et al. 1988; Uchino et al. 2004). Power (1850) reported a case where the left and right MCA arose from the left ICA and the left and right ACA arose from the right ICA.

An accessory MCA arises from the ACA and runs parallel to the M1 segment, and has a prevalence of 0.3–4.0% (Grand

1980; Takahashi et al. 1994). There is a classification scheme for accessory MCAs (Jain 1964): type 1 arises from the ICA (i.e., MCA duplication); type 2 from the A1 segment; and type 3 from the A2 segment. The accessory MCA primarily supplies the orbitofrontal area (Gloger et al. 1994b) and is also associated with aneurysms (Abanou et al. 1984; Umansky et al. 1988). This anomaly should be not be confused with a large recurrent artery of Heubner (Morioka et al. 1997).

Aplasia of the MCA is rare and is associated with aneurysms (Takahashi et al. 1989). Early branching of the MCA occurs when the MCA bifurcates close to its origin from the ICA (Parmar et al. 2005). Fenestration of the M1 segment has been reported but is uncommon (Komiyama et al. 1998).

M2 segment

The M2 segments (also known as insular segments) travel from the main division point of the M1 segment, over the insula within the sylvian fissure, and terminate at the circular sulcus of the insula. The MCA divisions are equal in diameter and size in 18% of the hemispheres; the superior division is larger in 28% of the hemispheres and the inferior division is larger in 32% of the hemispheres (Gloger et al. 1994a).

Branches

The cortical area supplied by the superior division extends from the orbitofrontal area to the posterior parietal area. The cortical area supplied by the inferior division extends from the temporal pole to the angular area. The M2 segments number from six to eight arteries at the point of transition into the M3 segments.

Variants

The M2 segment of the MCA contains no variants.

M3 segment

The M3 segments (also known as opercular segments) begin at the circular sulcus of the insula and end at the surface of the sylvian fissure. These vessels travel over the surface of the frontal and temporal opercula to reach the external surface of the sylvian fissure.

Branches

The M3 branches, together with the M2 vessels, give rise to the stem arteries, which in turn give off the cortical branches. There are usually eight stem arteries per hemisphere, and each one typically gives rise to one to five cortical branches (Gloger et al. 1994a).

Variants

The M3 segment of the MCA contains no variants.

M4 segment

The M4 segment (also known as cortical branches) begins at the surface of the sylvian fissure and extends over the surface of the cerebral hemisphere.

Branches

The smallest cortical branches arise from the anterior sylvian fissure and the largest emerge from the posterior sylvian fissure (Gloger et al. 1994a). The cortical branches can be grouped according to the region of the cortex that they supply; any given region may have a single artery or several arteries supplying it. The following 12-subdivision system is in common usage (Gloger et al. 1994a; Han et al. 1994; Osborn 1999). Although each branch is discussed as a single artery, any given cortical artery may actually exist as several branches (up to five) from a single stem artery.

The orbitofrontal artery may arise from the M1 or M2 segment, and may share a common origin with the prefrontal artery. It travels within the anterior horizontal ramus of the sylvian fissure to supply the orbital surface of the frontal lobe.

The prefrontal artery may share a common origin with the orbitofrontal artery. It supplies the opercular part of the inferior frontal gyrus and most of the middle frontal gyrus, in addition to supplying part of the inferior frontal gyrus and the inferior part of the precentral gyrus.

The central artery (aka Rolandic artery) travels within the central sulcus. It may share a common origin with the anterior parietal artery and is the largest MCA branch to the frontal lobe (Gloger et al. 1994a). It supplies the superior part of the precentral gyrus and the inferior half of the postcentral gyrus.

The anterior parietal artery may arise with the central artery or the posterior parietal artery and travels in the postcentral sulcus. It supplies the superior part of the postcentral gyrus, the upper part of the central sulcus, the anterior part of the inferior parietal lobule, and the anteroinferior part of the superior parietal lobule.

The posterior parietal artery represents the most posterior ascending branch of the MCA. It may share a common trunk with the anterior parietal artery or the angular artery and supplies the posterior part of the superior and inferior parietal lobules, including the supramarginal gyrus.

The angular artery is the terminal and largest branch of the MCA. It emerges from the posterior end of the sylvian fissure to travel over the superior temporal gyrus, and terminates over the superior half of the occipital lobe supplying the posterior part of the superior temporal gyrus, parts of the supramarginal and angular gyri, and superior parts of the lateral occipital lobe.

The temporo-occipital artery may share an origin with the angular artery. It supplies the posterior half of the superior temporal gyrus, the posterior extent of the middle and inferior gyri, and the inferior parts of the lateral occipital lobe.

The posterior temporal artery leaves the posterior sylvian fissure and crosses over the superior and middle temporal gyri. It supplies the middle and posterior parts of the superior temporal gyrus, the posterior third of the middle temporal gyrus, and the posterior extent of the inferior temporal gyrus. The middle temporal artery emerges from the middle of the sylvian fissure and supplies the middle parts of the temporal gyri. The anterior temporal artery passes inferiorly and posteriorly over the temporal

lobe and terminates in the middle temporal sulcus, supplying the anterior parts of the superior, middle, and inferior temporal gyri. The temporopolar artery supplies the anterior pole of the temporal lobe.

Variants

The M4 segment of the MCA contains no variants.

References

Abanou A, Lasjaunias P, Manelfe C, Lopez-Ibor L. 1984. The accessory middle cerebral artery (AMCA). Diagnostic and therapeutic consequences. *Anat Clin* 6: 305–309.

Alpers BJ, Berry RG. 1963. Circle of Willis in cerebral vascular disorders. The anatomical structure. *Arch Neurol* 8: 398–402.

Alpers BJ, Berry RG, Paddison RM. 1959. Anatomical studies of the circle of Willis in normal brain. *AMA Arch Neurol Psychiatry* 81: 409–418.

Alvarez H, Rodesch G, Garcia-Monaco R, Lasjaunias P. 1990. Embolisation of the ophthalmic artery branches distal to its visual supply. *Surg Radiol Anat* 12: 293–297.

Baptista AG. 1963. Studies on the arteries of the brain. II. the anterior cerebral artery: some anatomic features and their clinical implications. *Neurology* 13: 825–835.

Bernasconi V, Cassinari V. 1957. Angiographical characteristics of meningiomas of tentorium. *Radiol Med (Torino)* 43: 1015–1026.

Bollar A, Martinez R, Gelabert M, Garcia A. 1988. Anomalous origin of the anterior cerebral artery associated with aneurysm–embryological considerations. *Neuroradiology* 30: 86.

Bouthillier A, van Loveren HR, Keller JT. 1996. Segments of the internal carotid artery: a new classification. *Neurosurgery* 38: 425–432.

Burbank NS, Morris PP. 2005. Unique anomalous origin of the left anterior cerebral artery. *AJNR Am J Neuroradiol* 26: 2533–2535.

Busse O. 1927. Aneurysmen und bildungsfehler der a. communicans anterior. *Virchows Arch Pathol Anat* 229: 178–189.

Caldemeyer KS, Carrico JB, Mathews VP. 1998. The radiology and embryology of anomalous arteries of the head and neck. *AJR Am J Roentgenol* 170: 197–203.

Cali RL, Berg R, Rama K. 1993. Bilateral internal carotid artery agenesis: a case study and review of the literature. *Surgery* 113: 227–233.

Chen CJ, Chen ST, Hsieh FY, Wang LJ, Wong YC. 1998. Hypoplasia of the internal carotid artery with intercavernous anastomosis. *Neuroradiology* 40: 252–254.

Chess MA, Barsotti JB, Chang JK, Ketonen LM, Westesson PL. 1995. Duplication of the extracranial internal carotid artery. *AJNR Am J Neuroradiol* 16: 1545–1547.

Choudhari KA. 2002. Fenestrated anterior cerebral artery. *Br J Neurosurg* 16: 525–529.

Cinnamon J, Zito J, Chalif DJ, Gorey MT, Black KS, Scuderi DM, Hyman RA. 1992. Aneurysm of the azygos pericallosal artery: diagnosis by MR imaging and MR angiography. *AJNR Am J Neuroradiol* 13: 280–282.

Cooper IS. 1954. Surgical occlusion of the anterior choroidal artery in Parkinsonism. *Surg Gynecol Obstet* 92: 207–219.

de Gast AN, van Rooij WJ, Sluzewski M. 2008. Fenestrations of the anterior communicating artery: incidence on 3D angiography and relationship to aneurysms. *AJNR Am J Neuroradiol* 29: 296–298.

Dunker RO, Harris AB. 1976. Surgical anatomy of the proximal anterior cerebral artery. *J Neurosurg* 44: 359–367.

Fischer E. 1938. Die lageabweichungen der vorderen hirnarterie im gefässbild. *Zentralbl Neurochir* 3: 300–313.

Gabriele OF, Bell D. 1967. Ophthalmic origin of the middle meningeal artery. *Radiology* 89: 841–844.

Gibo H, Carver CC, Rhoton AL, Jr, Lenkey C, Mitchell RJ. 1981a. Microsurgical anatomy of the middle cerebral artery. *J Neurosurg* 54: 151–169.

Gibo H, Lenkey C, Rhoton AL, Jr. 1981b. Microsurgical anatomy of the supraclinoid portion of the internal carotid artery. *J Neurosurg* 55: 560–574.

Given CA, 2nd, Morris PP. 2002. Recognition and importance of an infraoptic anterior cerebral artery: case report. *AJNR Am J Neuroradiol* 23: 452–454.

Glasscock ME, 3rd, Seshul M, Seshul MB, Sr. 1993. Bilateral aberrant internal carotid artery case presentation. *Arch Otolaryngol Head Neck Surg* 119: 335–339.

Gloger S, Gloger A, Vogt H, Kretschmann HJ. 1994a. Computer-assisted 3D reconstruction of the terminal branches of the cerebral arteries. I. Anterior cerebral artery. *Neuroradiology* 36: 173–180.

Gloger S, Gloger A, Vogt H, Kretschmann HJ. 1994b. Computer-assisted 3D reconstruction of the terminal branches of the cerebral arteries. II. Middle cerebral artery. *Neuroradiology* 36: 181–187.

Gomes FB, Dujovny M, Umansky F, Berman SK, Diaz FG, Ausman JI, Mirchandani HG, Ray WJ. 1986. Microanatomy of the anterior cerebral artery. *Surg Neurol* 26: 129–141.

Gonzalez LF, Walker MT, Zabramski JM, Partovi S, Wallace RC, Spetzler RF. 2003. Distinction between paraclinoid and cavernous sinus aneurysms with computed tomographic angiography. *Neurosurgery* 52: 1131–1139.

Grand W. 1980. Microsurgical anatomy of the proximal middle cerebral artery and the internal carotid artery bifurcation. *Neurosurgery* 7: 215–218.

Gray H. 1901. *Gray's Anatomy*. Philadelphia: Running Press.

Han DH, Gwak HS, Chung CK. 1994. Aneurysm at the origin of accessory middle cerebral artery associated with middle cerebral artery aplasia: case report. *Surg Neurol* 42: 388–391.

Hayreh SS. 1963. Arteries of the orbit in the human being. *Br J Surg* 50: 938–953.

Hayreh SS. 2006. Orbital vascular anatomy. *Eye* 20: 1130–1144.

Hendrikse J, van Raamt AF, van der Graaf Y, Mali WPTM, van der Grond J. 2005. Distribution of cerebral blood flow in the circle of Willis. *Radiology* 235: 184–189.

Hoksbergen AW, Legemate DA, Csiba L, Csati G, Siro P, Fulesdi B. 2003. Absent collateral function of the circle of Willis as risk factor for ischemic stroke. *Cerebrovasc Dis* 16: 191–198.

Huber P, Braun J, Hirschmann D, Agyeman JF. 1980. Incidence of berry aneurysms of the unpaired pericallosal artery: angiographic study. *Neuroradiology* 19: 143–147.

Huh JS, Park SK, Shin JJ, Kim TH. 2007. Saccular aneurysm of the azygos anterior cerebral artery: three case reports. *J Korean Neurosurg Soc* 42: 342–345.

Inoue T, Rhoton AL, Jr, Theele D, Barry ME. 1990. Surgical approaches to the cavernous sinus: a microsurgical study. *Neurosurgery* 26: 903–932.

Jain KK. 1964. Some observations on the anatomy of the middle cerebral artery. *Can J Surg* 7: 134–139.

Kapoor K, Singh B, Dewan LI. 2008. Variations in the configuration of the circle of Willis. *Anat Sci Int* 83: 96–106.

Kobayashi S, Kyoshima K, Gibo H, Hegde SA, Takemae T, Sugita K. 1989. Carotid cave aneurysms of the internal carotid artery. *J Neurosurg* 70: 216–221.

Komiyama M, Nakajima H, Nishikawa M, Yasui T. 1998. Middle cerebral artery variations: duplicated and accessory arteries. *AJNR Am J Neuroradiol* 19: 45–49.

Kowada M, Yamaguchi K, Takahashi H. 1972. Fenestration of the vertebral artery with a review of 23 cases in Japan. *Radiology* 103: 343–346.

Krabbe-Hartkamp MJ, van der Grond J, de Leeuw FE, de Groot JC, Algra A, Hillen B, Breteler MM, Mali WP. 1998. Circle of Willis: morphologic variation on three-dimensional time-of-flight MR angiograms. *Radiology* 207: 103–111.

Krisht AF, Barrow DL, Barnett DW, Bonner GD, Shengalaia G. 1994. The microsurgical anatomy of the superior hypophyseal artery. *Neurosurgery* 35: 899–903.

Ladzinski P, Maliszewski M, Majchrzak H. 1997. The accessory anterior cerebral artery: case report and anatomic analysis of vascular anomaly. *Surg Neurol* 48: 171–174.

Lang J. 1989. *Clinical Anatomy of the Nose, Nasal Cavity and Paranasal Sinuses*. New York: Thieme.

Lang J, Kageyama I. 1990. The ophthalmic artery and its branches, measurements and clinical importance. *Surg Radiol Anat* 12: 83–90.

Lasjaunias P. 1987. *Functional Anatomy of Craniofacial Arteries*. New York: Springer–Verlag.

Lasjaunias P, Santoyo-Vazquez A. 1984. Segmental agenesis of the internal carotid artery: angiographic aspects with embryological discussion. *Anat Clin* 6: 133–141.

Lee JH, Oh CW, Lee SH, Han DH. 2003. Aplasia of the internal carotid artery. *Acta Neurochir (Wien)* 145: 117–125.

LeMay M, Gooding CA. 1966. The clinical significance of the azygos anterior cerebral artery (ACA). *Am J Roentgenol Radium Ther Nucl Med* 98: 602–610.

Makowicz G, Poniatowska R, Lusawa M. 2013. Variants of cerebral arteries – anterior circulation. *Pol J Radiol* 78: 42–47.

Marinkovic S, Milisavljevic M, Kovacevic M. 1986. Anatomical bases for surgical approach to the initial segment of the anterior cerebral artery. Microanatomy of Heubner's artery and perforating branches of the anterior cerebral artery. *Surg Radiol Anat* 8: 7–18.

Marinkovic S, Milisavljevic M, Marinkovic Z. 1990. Branches of the anterior communicating artery. Microsurgical anatomy. *Acta Neurochir (Wien)* 106: 78–85.

Maurer J, Maurer E, Perneczky A. 1991. Surgically verified variations in the A1 segment of the anterior cerebral artery. Report of two cases. *J Neurosurg* 75: 950–953.

Midkiff RB, Boykin MW, McFarland DR, Bauman JA. 1995. Agenesis of the internal carotid artery with intercavernous anastomosis. *AJNR* 16: 1356–1359.

Minakawa T, Kawamata M, Hayano M, Kawakami K. 1985. Aneurysms associated with fenestrated anterior cerebral arteries. Report of four cases and review of the literature. *Surg Neurol* 24: 284–288.

Moffat DB. 1967. A case of peristence of the primitive olfactory artery. *Anat Anz* 121: 477–479.

Morandi X, Brassier G, Darnault P, Mercier P, Scarabin JM, Duval JM. 1996. Microsurgical anatomy of the anterior choroidal artery. *Surg Radiol Anat* 18: 275–280.

Morimoto T, Nitta K, Kazekawa K, Hashizume K. 1990. The anomaly of a non-bifurcating cervical carotid artery. Case report. *J Neurosurg* 72: 130–132.

Morioka M, Fujioka S, Itoyama Y, Ushio Y. 1997. Ruptured distal accessory anterior cerebral artery aneurysm: case report. *Neurosurgery* 40: 399–401.

Morris P. 1997. *Practical Neuroangiography*. Baltimore: Williams & Wilkins.

Moyer DJ, Flamm ES. 1992. Anomalous arrangement of the origins of the anterior choroidal and posterior communicating arteries. Case report. *J Neurosurg* 76: 1017–1018.

Nozaki K, Taki W, Kawakami O, Hashimoto N. 1998. Cerebral aneurysm associated with persistent primitive olfactory artery aneurysm. *Acta Neurochir (Wien)* 140: 397–401.

Ohyama T, Ohara S, Momma F. 1994. Fatal subarachnoid hemorrhage due to ruptured infundibular widening of the posterior communicating artery: case report. *Neurol Med Chir (Tokyo)* 34: 172–175.

Osaka K, Matsumoto S. 1978. Holoprosencephaly in neurosurgical practice. *J Neurosurg* 48: 787–803.

Osborn AG. 1999. *Diagnostic Cerebral Angiography, second edition*. Phliadelphia: Lippincott Williams & Wilkins.

Ostrowski AZ, Webster JE, Gurdjian ES. 1960. The proximal anterior cerebral artery: an anatomic study. *Arch Neurol* 3: 661–664.

Pahor AL, Hussain SS. 1992. Persistent stapedial artery. *J Laryngol Otol* 106: 254–257.

Parkinson D. 1964. Collateral circulation of cavernous carotid artery: anatomy. *Can J Surg* 7: 251–268.

Parmar H, Sitoh YY, Hui F. 2005. Normal variants of the intracranial circulation demonstrated by MR angiography at 3T. *Eur J Radiol* 56: 220–228.

Pascual-Castroviejo I, Viano J, Pascual-Pascual SI, Martinez V. 1995. Facial haemangioma, agenesis of the internal carotid artery and dysplasia of cerebral cortex: case report. *Neuroradiology* 37: 692–695.

Paullus WS, Pait TG, Rhoton AI, Jr. 1977. Microsurgical exposure of the petrous portion of the carotid artery. *J Neurosurg* 47: 713–726.

Pedroza A, Dujovny M, Artero JC, Umansky F, Berman SK, Diaz FG, Ausman JI, Mirchandani HG. 1987. Microanatomy of the posterior communicating artery. *Neurosurgery* 20: 228–235.

Perlmutter D, Rhoton AL, Jr. 1976. Microsurgical anatomy of the anterior cerebral-anterior communicating-recurrent artery complex. *J Neurosurg* 45: 259–272.

Perlmutter D, Rhoton AL, Jr. 1978. Microsurgical anatomy of the distal anterior cerebral artery. *J Neurosurg* 49: 204–228.

Power JH. 1850. Surgical Anatomy of the Arteries, and Descriptive Anatomy of the Heart by the late Valentine Flood, M.D. Dublin: Fannin and Co.

Quint DJ, Boulos RS, Spera TD. 1989. Congenital absence of the cervical and petrous internal carotid artery with intercavernous anastomosis. *AJNR Am J Neuroradiol* 10: 435–439.

Quisling RG, Rhoton AL, Jr. 1979. Intrapetrous carotid artery branches: radioanatomic analysis. *Radiology* 131: 133–136.

Renn WH, Rhoton AL, Jr. 1975. Microsurgical anatomy of the sellar region. *J Neurosurg* 43: 288–298.

Resnick DK, Subach BR, Marion DW. 1997. The significance of carotid canal involvement in basilar cranial fracture. *Neurosurgery* 40: 1177–1181.

Rhoton AL, Jr. 2002a. The cavernous sinus, the cavernous venous plexus, and the carotid collar. *Neurosurgery* 51: S375–410.

Rhoton AL, Jr. 2002b. The sellar region. *Neurosurgery* 51: S335–374.

Rhoton AL, Jr, Fujii K, Fradd B. 1979a. Microsurgical anatomy of the anterior choroidal artery. *Surg Neurol* 12: 171–187.

Rhoton AL Jr, Saeki N, Perlmutter D, Zeal A. 1979b. Microsurgical anatomy of common aneurysm sites. *Clin Neurosurg* 26: 248–306.

Roll JD, Urban MA, Larson TC, 3rd, Gailloud P, Jacob P, Harnsberger HR. 2003. Bilateral aberrant internal carotid arteries with bilateral persistent stapedial arteries and bilateral duplicated internal carotid arteries. *AJNR Am J Neuroradiol* 24: 762–765.

Sacher M, Som PM, Shugar JM, Leeds NE. 1986. Kissing intrasellar carotid arteries in acromegaly: CT demonstration. *J Comput Assist Tomogr* 10: 1033–1035.

Saeki N, Rhoton AL, Jr. 1977. Microsurgical anatomy of the upper basilar artery and the posterior circle of Willis. *J Neurosurg* 46: 563–578.

Saltzman GF. 1959. Infundibular widening of the posterior communicating artery studied by carotid angiography. *Acta Radiol* 51: 415–421.

San Millan Ruiz D, Gailloud P, Rufenacht DA, Delavelle J, Henry F, Fasel JH. 2002. The craniocervical venous system in relation to cerebral venous drainage. AJNR. *American journal of neuroradiology* 23: 1500–1508.

Sauvaget E, Paris J, Kici S, Kania R, Guichard JP, Chapot R, Thomassin JM, Herman P, Tran Ba Huy P. 2006. Aberrant internal carotid artery in the temporal bone: imaging findings and management. *Arch Otolaryngol Head Neck Surg* 132: 86–91.

Serizawa T, Saeki N, Yamaura A. 1997. Microsurgical anatomy and clinical significance of the anterior communicating artery and its perforating branches. *Neurosurgery* 40: 1211–1218.

Shoja MM, Loukas M, Tubbs RS, D'Antoni A, DiLandro A, Cure JK. 2012. An aberrant cerebellar artery originating from the internal carotid artery. *Surg Radiol Anat* 34: 285–288.

Silbergleit R, Quint DJ, Mehta BA, Patel SC, Metes JJ, Noujaim SE. 2000. The persistent stapedial artery. *AJNR Am J Neuroradiol* 21: 572–577.

Singer RJ, Abe T, Taylor WH, Marks MP, Norbash AM. 1997. Intracavernous anterior cerebral artery origin with associated arteriovenous malformations: a developmental analysis: case report. *Neurosurgery* 40: 829–831.

Spinnato S, Pasqualin A, Chioffi F, Da Pian R. 1999. Infraoptic course of the anterior cerebral artery associated with an anterior communicating artery aneurysm: anatomic case report and embryological considerations. *Neurosurgery* 44: 1315–1319.

Suzuki M, Onuma T, Sakurai Y, Mizoi K, Ogawa A, Yoshimoto T. 1992. Aneurysms arising from the proximal (A1) segment of the anterior cerebral artery. A study of 38 cases. *J Neurosurg* 76: 455–458.

Takahashi S, Hoshino F, Uemura K, Takahashi A, Sakamoto K. 1989. Accessory middle cerebral artery: is it a variant form of the recurrent artery of Heubner? *AJNR Am J Neuroradiol* 10: 563–568.

Takahashi S, Suga T, Kawata Y, Sakamoto K. 1990. Anterior choroidal artery: angiographic analysis of variations and anomalies. *AJNR Am J Neuroradiol* 11: 719–729.

Takahashi T, Suzuki S, Ohkuma H, Iwabuchi T. 1994. Aneurysm at a duplication of the middle cerebral artery. *AJNR Am J Neuroradiol* 15: 1166–1168.

Tasar M, Yetiser S, Tasar A, Ugurel S, Gonul E, Saglam M. 2004. Congenital absence or hypoplasia of the carotid artery: Radioclinical issues. *Am J Otolaryng* 25: 339–349.

Tauber M, van Loveren HR, Jallo G, Romano A, Keller JT. 1999. The enigmatic foramen lacerum. *Neurosurgery* 44: 386–391.

Taveras JM, Wood EH. 1976. *Diagnostic Neuroradiology, second edition*. Baltimore: Williams & Wilkins.

Teal JS, Rumbaugh CL, Segall HD, Bergeron RT. 1973. Anomalous branches of the internal cartoid artery. *Radiology* 106: 567–573.

Tran-Dinh H. 1987. Cavernous branches of the internal carotid artery: anatomy and nomenclature. *Neurosurgery* 20: 205–210.

Tripathi M, Goel V, Padma MV, Jain S, Maheshwari MC, Gaikwad S, Gupta V, Chandra PS, Mehta VS. 2003. Fenestration of the posterior communicating artery. *Neurol India* 51: 75–76.

Tsitsopoulos PD, Tsonidis CA, Petsas GP, Hadjiioannou PN, Njau SN, Anagnostopoulos IV. 1996. Microsurgical study of the Dorello's canal. *Skull Base Surg* 6: 181–185.

Tsutsumi S, Rhoton AL, Jr. 2006. Microsurgical anatomy of the central retinal artery. *Neurosurgery* 59: 870–879.

Uchino A, Sawada A, Takase Y, Kudo S. 2003. MR angiography of anomalous branches of the internal carotid artery. AJR. *American journal of roentgenology* 181: 1409–1414.

Uchino M, Kitajima S, Sakata Y, Honda M, Shibata I. 2004. Ruptured aneurysm at a duplicated middle cerebral artery with accessory middle cerebral artery. Acta Neurochir (Wien) 146: 1373–1375.

Uchino A, Saito N, Kurita H, Ishihara S. 2013. Double ophthalmic arteries arising from the internal carotid artery. *Surg Radiol Anat* 35: 173–5.

Umansky F, Gomes FB, Dujovny M, Diaz FG, Ausman JI, Mirchandani HG, Berman SK. 1985. The perforating branches of the middle cerebral artery. A microanatomical study. *J Neurosurg* 62: 261–268.

Umansky F, Dujovny M, Ausman JI, Diaz FG, Mirchandani HG. 1988. Anomalies and variations of the middle cerebral artery: a microanatomical study. *Neurosurgery* 22: 1023–1027.

Waga S, Morikawa A. 1979. Aneurysm developing on the infundibular widening of the posterior communicating artery. *Surg Neurol* 11: 125–127.

Windfuhr JP. 2004. Aberrant internal carotid artery in the middle ear. *Ann Otol Rhinol Laryngol Suppl* 192: 1–16.

Wolpert SM. 1997. The circle of Willis. *AJNR Am J Neuroradiol* 18: 1033–1034.

Yasargil MG, Carter LP. 1974. Saccular aneurysms of the distal anterior cerebral artery. *J Neurosurg* 40: 218–223.

Ziyal IM, Salas E, Wright DC, Sekhar LN. 1998. The petrolingual ligament: the anatomy and surgical exposure of the posterolateral landmark of the cavernous sinus. *Acta Neurochir (Wien)* 140: 201–205.

Zurada A, St Gielecki J, Tubbs RS, Loukas M, Zurada-Zielinska A, Maksymowicz W, Nowak D, Cohen-Gadol AA. 2010. Three-dimensional morphometry of the A1 segment of the anterior cerebral artery with neurosurgical relevance. *Neurosurgery* 67: 1768–1782.

44 Vertebrobasilar arteries

R. Shane Tubbs[1-3] and Marios Loukas[3]
[1]Seattle Science Foundation, Seattle, Washington, USA
[2]University of Dundee, Dundee, UK
[3]St George's University, School of Medicine, St Georges, Grenada

Vertebral and basilar arteries

With complete absence of both internal carotid arteries, the vertebrobasilar system supplies the anterior and middle cerebral arteries (Fig. 44.1). In about 4% of individuals, the pars atlantica segment of the vertebral artery gives rise to the posterior inferior cerebellar artery. At the level of the posterior arch of the atlas, the vertebral artery is 6–20 mm lateral to the midline. Tsai et al. (1975) has stated that, occasionally, the occipital artery carries the main inflow to the basilar artery.

The basilar artery may be absent (Fig. 44.2) or internally septated (Fig. 44.3; Tubbs et al. 2008). Very rarely, the two vertebral

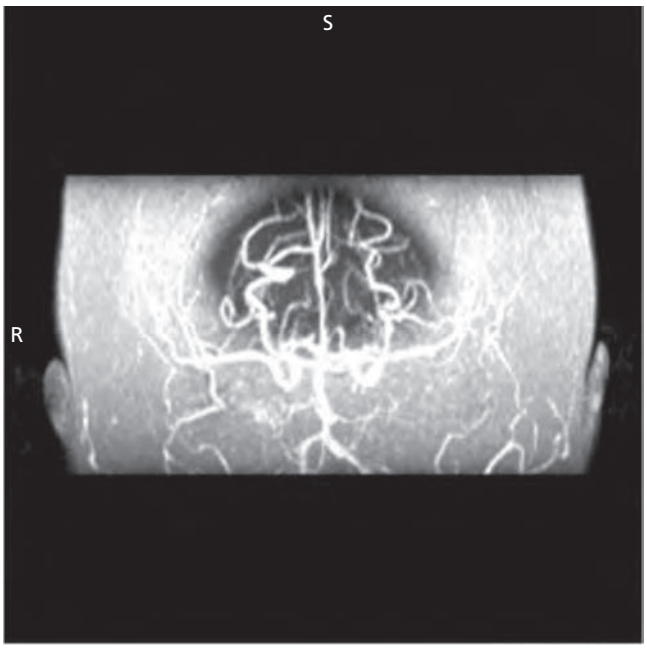

Figure 44.1 Coronal MRA of the circle of Willis illustrating absence of the left and right internal carotid arteries with the anterior circulation filled entirely from the vertebrobasilar system.

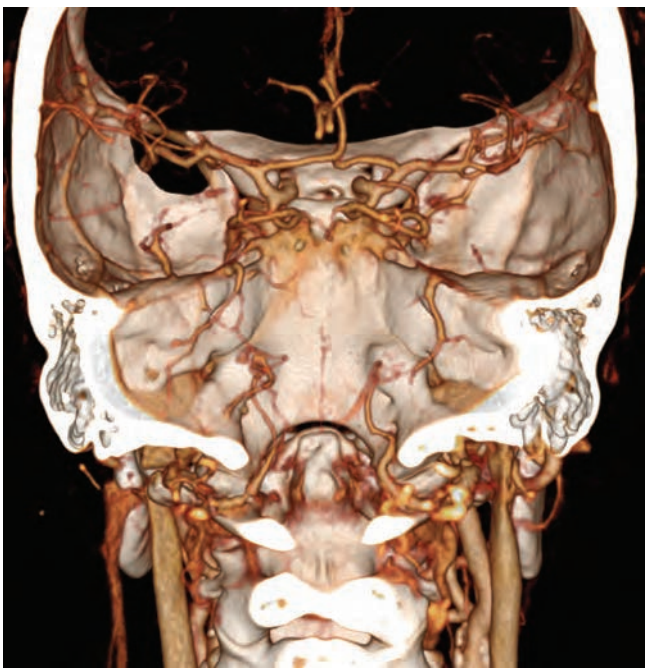

Figure 44.2 Absence of the basilar artery on CTA.

Figure 44.3 Septation (running over pin) of the basilar artery just beyond the union of the left and right vertebral arteries.

Bergman's Comprehensive Encyclopedia of Human Anatomic Variation, First Edition. Edited by R. Shane Tubbs, Mohammadali M. Shoja and Marios Loukas.
© 2016 John Wiley & Sons, Inc. Published 2016 by John Wiley & Sons, Inc.

arteries fail to unite to form the basilar artery; the basilar may therefore appear to be doubled. The two longitudinal trunks may be united by anastomoses between them. Fenestration of the basilar artery is found in 1.33% of dissection and 0.12% of angiograms. The vertebral artery may exist as several vessels that eventually unite, or it may form an arterial ring traversed by the hypoglossal nerve.

One of the anterior spinal branches (usually the left) is occasionally absent, in which case it is replaced by branches from the contralateral vertebral artery. Occasionally, a spinal branch arises to supply the cervical enlargement of the spinal cord.

The basilar artery may exist as two longitudinal trunks that may be united by anastomoses. Occasionally, the basilar splits into two vessels that reunite. When the two vessels fuse, the resulting single vessel may have a median sagittal partition. In some subjects, the basilar passes through a foramen in the dorsum sellae. An aberrant branch (persistent fetal trigeminal artery) may arise that pierces the dorsum sellae and joins the internal carotid. In one case of a rudimentary vertebral artery that stopped short of the skull, the basilar arose as a branch of the internal carotid in the neck and entered the cranial cavity through the hypoglossal canal. The basilar may give rise to the middle meningeal artery (Shah and Hurst 2007). The vertebral artery on the contralateral side ended as a posterior inferior cerebellar artery.

The posterior spinal arteries may be missing. The posterolateral spinal artery arises from the posterior inferior cerebellar in 73% of individuals or from the vertebral artery in 20% (Stopford 1916).

Superior cerebellar artery

The superior cerebellar artery (SCA) is duplicated in 14% of hemispheres; in these cases, the duplicate vessels correspond to the rostral and caudal trunks. Although rare, absence of the SCA has been reported. The SCA can give rise proximally to a perforating artery that travels to the interpeduncular fossa.

Anterior inferior cerebellar artery

The origin of the vessel is single in 72% of cases, a duplicate in 26%, and triplicate in 2% (Harrigan and Deveikis 2013). Origin of the AICA from the ICA has been reported. Sunderland (1948) reported that the anterior inferior cebellar artery ran basal to the abducens nerve on the right side in 84% and on the left side in 73%. Stopford (1916) found this arrangement on the right side in 86% and on the left side in 81%. In three cases, Sunderland found that the anterior inferior cerebellar artery ran through the abducent nerve on the left side. In 16 of 260 of Sunderland's (1948) cases, the abducens nerve was deeply indented by the artery in the basal part of its course without adverse effect.

Posterior inferior cerebellar

The posterior inferior cerebellar artery (PICA) is the largest branch of the vertebral artery and leaves before the junction of the vertebral arteries to form the basilar artery. This artery may arise from the basilar or may be absent unilaterally. Extradural origin of the PICA is found in 5–20% of cases. Origins of the PICA from the ICA, the posterior meningeal artery, a hypoglossal artery, and a proatlantal artery have been reported. The PICA is duplicated in some 2.5–6% of cases (Harrigan and Deveikis 2013). The PICA is hypoplastic in 5–16% of hemispheres (Harrigan and Deveikis 2013). The PICA is sometimes absent. An AICA–PICA trunk is a normal variant. In 0.2% of cases, the vertebral artery terminates in PICA. The posterior inferior cerebellar artery may provide the posterior spinal artery (Harrigan and Deveikis 2013).

The posterior inferior cerebellar artery may arise from the internal carotid artery, and the embryonic explanation postulated is the persistence of a primitive communicating vessel (presegmental artery) between the anterior and posterior circulation. The posterior inferior cerebellar artery may arise from the posterior meningeal artery.

The most frequent origin of the posterior inferior cerebellar artery is from the intracranial segment of the vertebral artery. This origin of the posterior inferior cerebellar artery is not considered rare. This artery arises from the upper third of the basilar artery in 2% of cases, from the middle third in 46%, and from the lower third in 52% of cases (Harrigan and Deveikis 2013). Brunner also found the vessel to be duplicated in 11.1%.

Posterior cerebral artery

Occasionally, the proximal part of one of the posterior cerebral arteries is greatly reduced in size. The blood reaches the terminal region of the vessel from the internal carotid via the posterior communicating artery.

The posterior cerebral may course below, rather than over, the oculomotor nerve. It may be absent and replaced by an accessory contralateral vessel. The posterior cerebral may provide the anterior cerebral artery. The posterior cerebral artery may arise on one side, from the internal carotid, by an enlargement of the posterior communicating branch

Side-to-side asymmetry of the P1 segments is common, being present on about half of angiograms. When a fetal P-comm artery is present, the ipsilateral P1 is typically hypoplastic (Harrigan and Deveikis 2013).

In some persistent carotid-vertebrobasilar anastomoses, the PCA may be supplied by branches from the carotid system. Duplication, fenestration, and a bilateral shared origin of the PCA and SCA may be seen involving the P1 segment of the posterior cerebral artery. Absence of the P1 is rare.

There may be a prominent perforating branch (artery of Percheron) that supplies portions of both the ipsilateral and contralateral thalamus and potentially mid-brain, as well. Large perforating arteries can arise from a hypoplastic P1 segment. The P2 segment can give rise to a quadrigeminal artery, which may give off a branch to the superior cerebellum.

In rare cases, the parieto-occipital, posterior temporal, or calcarine arteries may arise directly from the ICA. Similarly,

anomalous anterior choroidal artery supply to temporal, parietal, and occipital cortical regions normally supplied by branches of the PCA can occur. In the ambient cistern, the P2 segment can give rise to an anterior temporal branch that supplies the uncus. This latter branch may give rise to a posterior lateral choroidal artery to the temporal horn.

The calcarine artery is duplicated in 10% of cases, and arises from the parieto-occipital artery in 10% of cases (Harrigan and Deveikis 2013). It can arise from the posterior cerebral artery and can travel deep in the calcarine sulcus or superficial over the medial edge of the calcarine cortex. The calcarine and parieto-occipital arteries can give rise to posterior temporal branches that extend out laterally and inferiorly.

The splenial artery (posterior pericallosal artery) arises from the parieto-occipital artery in 62% of cases, but may arise from the calcarine (12%), medial posterior choroidal (8%), posterior temporal (6%), P2 or P3 segments (4% each), or the lateral posterior choroidal artery (4%) (Harrigan and Deveikis 2013). The parieto-occipital artery arises from the P3 segment in about half of the population (Harrigan and Deveikis 2013). This vessel can arise from the calcarine, posterior lateral choroidal, or splenial arteries. The lateral posterior choroidal artery arises from the P3 segment in 11% of cases (Harrigan and Deveikis 2013). The posterior medial choroidal artery can arise from the distal P1 segment and can be duplicated. The posterior communicating artery may be absent, or the branch representing it may fail to join the posterior cerebral artery.

Posterior communicating artery

This artery may be absent on one or both sides or replaced by a branch from the middle cerebral artery. The posterior communicating artery is sometimes joined with the middle cerebral artery instead of the trunk of the internal carotid. The posterior cerebral artery frequently arises by an enlarged posterior communicating artery from the internal carotid artery, and is connected only by a slender vessel with the basilar (on the right side in 5.5%, on the left side only in 4.5%, and on both sides in 2% of cases studied; Harrigan and Deveikis 2013).

The middle cerebral artery can be derived from the posterior communicating artery. The posterior communicating artery is sometimes absent, or the branch representing it fails to join the posterior cerebral. The anterior choroidal artery is occasionally derived from the middle cerebral or posterior communicating.

Lang found accessory hypophyseal arteries arising from the posterior communicating artery, which ran to the tuber cinereurn and contributed to the supply of the infundibulum. There were also anastomoses with the superior hypophyseal artery.

Labyrinthine artery

The labyrinthine artery, which enters the internal acoustic meatus, can arise from multiple sources including the anterior inferior cerebellar artery, the basilar artery, the vertebral artery, or the posterior inferior cerebellar artery. Additionally, the vessel may be duplicated with each branch arising from a different source.

References

Harrigan M, Deveikis JP. 2013. *Cerebrovascular Disease and Neurointerventional Technique, second edition*. New York: Humana Press.

Shah QA, Hurst RW. 2007. Anomalous origin of the middle meningeal artery from the basilar artery: a case report. *J Neuroimaging* 17(3): 261–263.

Sunderland S. 1948. Anatomy of Base of Brain. Montefiore Medical Library. *Neurovascular Rel Anam Base Brain* 1948: 243–257.

Tsai FY, Mahon J, Woodruff V. 1975. Congenital absence of bilateral vertebral arteries with occipital-basilar anastomosis. *Am J Roentgenol* 124: 281–286.

Tubbs RS, Shaffer WA, Loukas M, Shoja MM, Harrigan MR, Oakes WJ. 2008. Intraluminal septation of the basilar artery: incidence and potential clinical significance. *Folia Morphol* 67: 193–195.

Further reading

Anderson RJ. 1879. A new abnormality in connection with the vertebral artery. *J Anat Physiol* 14: 248–249.

Atkinson WJ. 1949. The anterior inferior cerebellar artery. Its variations, pontine distribution, and significance in the surgery of cerebellopontine angle tumors. *J Neurol Neurosurg Psychiatry* 12: 137–151.

Bell RH, Swigart LL, Anson BJ. 1950. The relation of the vertebral artery to the cervical vertebrae. Based on a study of 200 specimens. *Q Bull NW Uni Med School* 24: 184–185.

Bergman RA, Thompson SA, Afifi AK, Saadeh FA. 1988. *Compendium of Human Anatomic Variation: Catalog, Atlas and World Literature*. Baltimore and Munich: Urban & Schwarzenberg.

Berry R, Anderson J. 1910. A case of nonunion of the vertebrals with consequent abnormal origin of the basilaris. *Anat Anz* 35: 54–65.

Distelmaier P, Wappenschmidt J. 1976. An atypical termination of the vertebral artery and of the inferior posterior cerebellar artery. *Forschritte Röntgenstrahlen* 124(3): 253–256.

Gillilan LA. 1958. The arterial blood supply of the human spinal cord. *J Comp Neurol* 110: 75–103.

Giuffrè R, Sherkat S. 2000. Maldevelopmental pathology of the vertebral artery in infancy and childhood. *Child's Nerv Sys* 16: 627–632.

Hassler O. 1966. Blood supply to the human spinal cord. A microangiographic study. *Arch Neurol* 15: 302–307.

Kielbasinski G. 1976. Arteries of the inferior part of the vermis cerebelli in man. *Folia Morphol, Warsaw* 35: 149–157.

Kielbasinski G. 1977. Course and area supplied by the anterior inferior cerebellar arteries in man. *Folia Morphol, Warsaw* 36: 181–190.

Nizankowski C, Noczynski L, Suder E. 1982. Variability of the origin of ramifications of the subclavian artery in humans (studies on the Polish population). *Folia Morphol* 41: 281–294.

Ogawa T, Fujita H, Inugami A, Shishido F, Higano K. 1991. Anomalous origin of the posterior inferior cerebellar artery from the posterior meningeal artery. *Am J Neuroradiology (AJNR)* 12: 186.

Okahara M, Kiyosue H, Mori H, Tanoue S, Sainou M, Nagatomi H. 2002. Anatomic variations of the cerebral arteries and their embryology: a pictoral review. *Eur Radiol* 12(10): 2548–2561.

Paterson AM. 1884. Notes on abnormalities, with special reference to the vertebral arteries. *J Anat Physiol* 18: 295–303.

Rath G, Prakash R. 1984. Double vertebral artery in an Indian cadaver. *Clin Anat* 6: 117–119.

Schaefer EA, Symington J, Bryce TH (eds) 1915. Quain's Anatomy, 11th edition. London: Longmans, Green and Co.

Siqueira M, Piske R, Ono M, Marino R Jr. 1993. Cerebellar arteries originating from the internal carotid artery. *AJNR* 14: 1229–1235.

Stopford JSB. 1916. The arteries of the pons and medulla oblongata. *J Anat Physiol* 50: 133–164.

Takahashi M, Wiison G, Hanafee W. 1968. The anterior inferior cerebellar artery: its radiologic anatomy and significance in the diagnosis of extra-axial tumors of the posterior fossa. *Radiology* 90: 281–287.

Tanohata K, Maehara T, Noda M, Sugiyama S, Okazaki A. 1987. Anomalous origin of the posterior meningeal artery from the lateral medullary segment of the posterior inferior cerebellar artery. *Neuroradiology* 29: 89–92.

Waddington MM. 1974. *Atlas of Cerebral Angiography with Anatomic Correlation*. Boston: Little, Brown and Co.

Wolf BS, Newman CM, Khilnani MT. 1962. The posterior inferior cerebellar artery on vertebral angiography. *Am J Roentgenol* 87: 322–337.

45 Persistent fetal intracranial arteries

Soner Albay
Suleyman Demirel University Faculty of Medicine, Isparta, Turkey

Ventrally, the first to third arches and corresponding roots of the aortic arch give rise to arteries that become the external and internal carotids (Carlson 2013). In the fourth week of embryo development the major arterial supply to the brain comprises the longitudinal neural arteries, which run ventrally along the brain from the midbrain through the caudal end of the hindbrain (Carlson 2013). The vertebral arteries form through connections of the lateral branches of the dorsal intersegmental arteries. There are connections between these two major arterial groups. Occasionally, arteries that usually disappear during or after embryological development persist into adulthood (Bergman et al. 2013). The exact causes of persistence of these primitive vessels are not completely clear.

Primitive carotid-vertebrobasilar anastomoses – the trigeminal, otic, hypoglossal, and proatlantal intersegmental arteries – are recognized as presegmental vessels during the embryonic period. Presegmental arteries connect the primitive internal carotid arteries with the bilateral longitudinal neural arterial plexus in the hindbrain area. This plexus is supplied cranially by the primitive trigeminal artery and caudally by the primitive proatlantal intersegmental artery. Laterally, each longitudinal neural arterial plexus receives the primitive otic artery and primitive hypoglossal artery (Vasovic et al. 2010). Usually, bilateral longitudinal neural arterial plexuses unite and form the basilar artery in the 7–12 mm crown-rump-length embryo (Padget 1948). Ordinarily, the otic artery disappears at the fourth week of embryogenesis, followed soon after by disappearance of the hypoglossal and trigeminal arteries. The proatlantal intersegmental artery maintains the posterior circulation until the vertebral arteries are fully developed, between seven and eight weeks (Okahara et al. 2002). When these anastomoses fail to regress, they become congenital persistent anastomoses.

Trigeminal artery

The first sign of the trigeminal artery appears in the 20-somite (3 mm) embryo. The trigeminal artery persists for the longest embryonic period, usually being obliterated by the 11.5–14 mm stage (Padget 1948). Failure of this regression is thought by some authors to follow occlusion of the proximal portion of the internal carotid artery in the fetus, which inevitably results in persistence of the trigeminal artery so that an adequate blood supply to the forebrain is maintained via retrograde transport of blood from the basilar to the carotid artery (Figs 45.1–45.3; Azab et al. 2012).

Neither sex is significantly prone to persistent carotid-basilar anastomoses, which can occur on either side, in patients of any age, and can be multiple. Persistence of the trigeminal artery is the most common case and accounts for approximately 80–85% of persistent anastomoses (Vasovic et al. 2012). The trigeminal artery is the largest of the fetal carotid-basilar anastomotic arteries with an incidence of approximately 0.2%, and persists for the

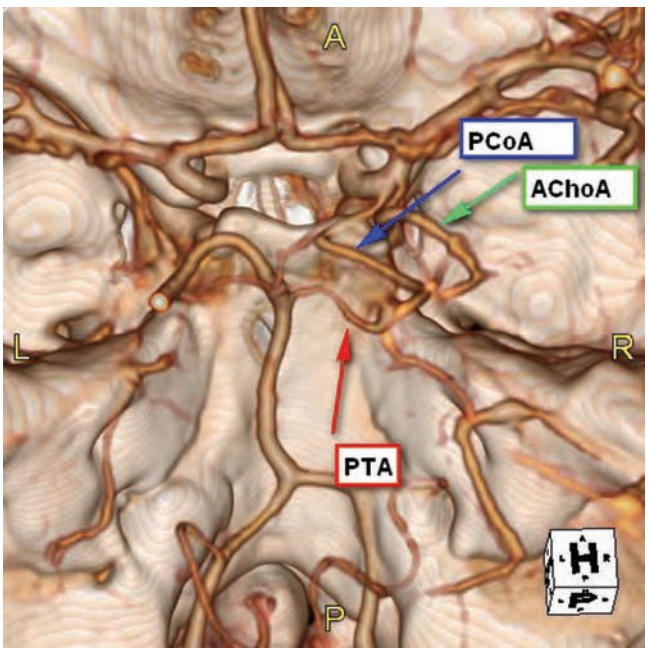

Figure 45.1 CTA image noting a persistent trigeminal artery (PTA). Also note the posterior communicating (PCoA) and anterior choroidal arteries (AChoA).

Bergman's Comprehensive Encyclopedia of Human Anatomic Variation, First Edition. Edited by R. Shane Tubbs, Mohammadali M. Shoja and Marios Loukas.
© 2016 John Wiley & Sons, Inc. Published 2016 by John Wiley & Sons, Inc.

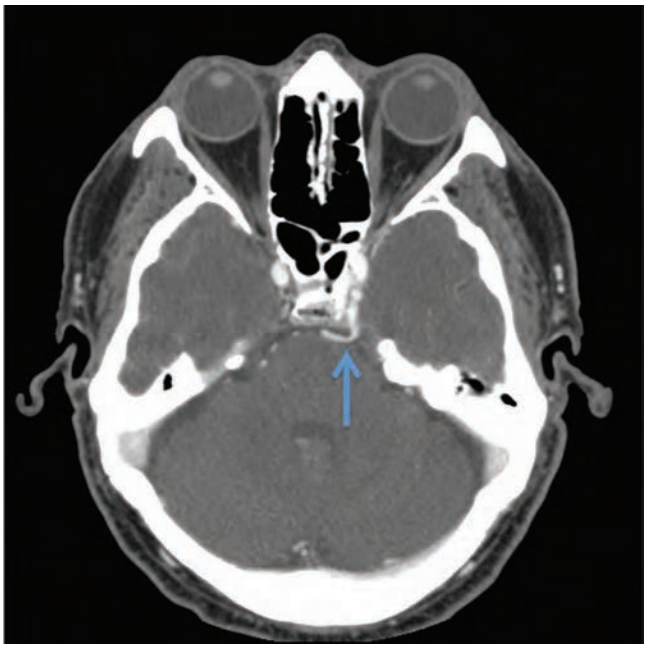

Figure 45.2 CT noting a persistent trigeminal artery (arrow).

Figure 45.3 Cadaveric skull base (brain removed) noting a persistent trigeminal artery (arrow). For reference, note the left oculomotor nerve crossing the left side of this artery.

longest embryonic period (Takese et al. 2004). The incidence of persistent trigeminal arteries estimated on cerebral angiograms is 0.1–1.0% (Azab et al. 2012). The artery usually involutes after the posterior communicating artery develops. Descriptions of the persistent trigeminal artery date back to 1844 in the original work and drawings by Quain. It was demonstrated angiographically for the first time by Sutton about one century later (Azab et al. 2012).

The persistent trigeminal artery usually originates from the cavernous portion of the internal carotid and can reach the posterior cranial fossa in two ways: (1) in about 50% of cases it penetrates the sella turcica, runs in its own groove, and perforates the dura mater near the clivus; or (2) in the other half it runs extradurally after leaving the cavernous sinus, between the sensory trigeminal root and lateral side of the sella. It communicates with the basilar artery between the origin of the superior cerebellar and anterior inferior cerebellar arteries (Vasovic et al. 2012).

Variants have also been described; persistent trigeminal artery variants are arteries that originate directly from the precavernous portion of the internal carotid but terminate as cerebellar arteries rather than anastomosing with the basilar artery (Ali et al. 2008). The incidences reported in the recent study of O'uchi and O'uchi (2010), including 103 cases of persistent trigeminal artery and so-called primitive trigeminal artery variants, were as follows: 0.29% persistent trigeminal artery, 0.34% primitive trigeminal artery variants, and 0.03% unclassified type of persistent trigeminal artery. However, a case reported by Samra and colleagues was the only instance of persistent trigeminal arteries in a series of 1500 angiograms (0.06%), while De Bondt and colleagues found them in 2.2% of cases (Vasovic et al. 2012). They were on the left side in six cases of a series of seven; in another series they were on the right side in five cases and on the left in three. The persistent trigeminal artery originated from the right internal carotid artery in 15 cases and from the left internal carotid in 15 (Vasovic et al. 2012). A recent study demonstrated that the laterality of origin of all persistent trigeminal arteries comprised 16 right- and 32 left-sided cases. A bilateral persistent trigeminal artery case was also described (O'uchi and O'ouchi 2010).

A persistent trigeminal artery can originate from the left or right internal carotid. The most common sites of origin are the posterior bend or lateral wall of the intracavernous carotid artery (Parkinson and Shields 1974; Azab et al. 2012). In one autopsy case, the persistent trigeminal artery originated from the posterior bend of the cavernous internal carotid artery to run posteriorly in the posterolateral space of the cavernous sinus (Ohshiro et al. 1993). Salas et al. (1998) reported the vessel to originate from the posterolateral aspect of the ascending cavernous segment of the internal carotid artery just medial to the sixth nerve, to make an acute inferolateral angle and follow a course below the sixth nerve immediately at the point of leaving the internal carotid to exit the cavernous sinus by piercing the reticular layer of the sinus wall, forming a posterior loop around

the sphenopetrous (Gruber's) ligament, then running in the medial wall of the trigeminal (Meckel's) cave (Salas et al. 1998). However, some reports describe an origin from the medial wall of the cavernous internal carotid artery. Suttner et al. (2000) found a persistent trigeminal artery arising from the superomedial portion of the distal horizontal segment of the intracavernous carotid, coursing medially and immediately posteroinferiorly, to continue between the posterior bend of the carotid artery laterally and the pituitary gland medially. It was described as passing the junction of the posterior clinoid process and the pituitary gland to exit the posterior wall of the cavernous sinus (Suttner et al. 2000).

In relation to the dorsum sellae, approximately 50–59% of all cases of persistent trigeminal artery penetrate the sella turcica, course along their own groove, perforate the dura near the clivus, and then join the basilar artery. Thinning of the sellar floor and abnormalities of the dorsum sellae are frequent findings. In the remaining 41–50% of cases the persistent trigeminal artery runs lateral to the sella turcica (Ohshiro et al. 1993). Ohshiro et al. classified persistent trigeminal arteries into two types: a medial type in which the artery runs through the dorsum sellae and perforates the dura mater near the clivus; and a lateral type in which it runs between the sensory root of the trigeminal nerve and the lateral side of the sella to penetrate the dura mater medial to Meckel's cave (Ohshiro et al. 1993). Inoue and colleagues reported that both the trigeminal and abducens nerves ran lateral to the persistent trigeminal artery in one specimen. Tulsi and Locket reported one case in which the trigeminal artery followed a medial course, crossing below the level of the pituitary fossa and piercing the dura of the dorsum sellae; in two other cases in their study, the artery followed a course lateral to the abducens nerve and pierced the dura of the posterior fossa just medial to the sensory root of the trigeminal nerve (Azab et al. 2012).

Salas et al. (1998) classified the persistent trigeminal artery by its relationship to the abducens nerve, distinguishing a lateral (petrosal) from a medial (sphenoidal) variation. When the artery courses lateral to the sixth cranial nerve it arises from the posterolateral aspect of the cavernous carotid and crosses underneath that nerve, which it can displace superiorly. This petrosal variant of the persistent trigeminal artery pierces the dura just medial to the sensory root of the trigeminal nerve. When the artery courses medial to the abducens nerve, it arises from the posteromedial aspect of the cavernous carotid artery and pierces the dura of the dorsum sellae (sphenoid variation) (Salas et al. 1998).

Clinically, the lateral variant can be associated with brainstem ischemia, ophthalmoplegia, and trigeminal neuralgia. The medial variant can be associated with posterior fossa symptoms secondary to a steal phenomenon (Azab et al. 2012).

Branches from a persistent trigeminal artery have been described in adult anatomical specimens (Azab et al. 2012). Khodadad demonstrated pontine branches from the trunk of the artery in brains of 4–6- and 8-month fetuses. He suggested that persistent trigeminal arteries could become functionally and clinically significant if they persisted (Khodadad 1976). Ohshiro et al. reported a case in which two branches from the cisternal portion of the persistent trigeminal artery were present. One branch sent a feeding artery to the left trigeminal nerve root and a perforating artery to the pons (Ohshiro et al. 1993). The other perforated directly into the pons. Salas et al. described four pontine perforating branches originating from the intradural segment of the artery (Salas et al. 1998). It is highly probable that these branches are functioning vessels in the brainstem even in adult cases since occlusion of the persistent trigeminal artery leads to ischemic lesions in the brainstem (Ohshiro et al. 1993; Kwon et al. 2010). Perforating arteries originating from the persistent trigeminal artery could be important supplies to the hindbrain (Azab et al. 2012).

Arakawa et al. (2007) reported one case in which the anterior inferior cerebellar artery arose from the internal carotid artery passing medial to the abducens nerve. This artery gave off a small branch communicating to the basilar artery, passed lateral to the trigeminal nerve root, and continued backward to the dorsal surface of the cerebellum; the anterior inferior cerebellar artery was therefore considered a branch of the persistent trigeminal artery (Arakawa et al. 2007). In the other case reported by these authors, the persistent trigeminal artery gave off medial and lateral branches to the basilar artery. These branches supplied the basal pons and the lateral surface of the trigeminal nerve root (Arakawa et al. 2007).

In a review of various anatomical descriptions, the origins of the persistent trigeminal artery and the meningohypophyseal trunk were found to be common or separate, and the artery could give rise to vessels normally arising from that trunk (Salas et al. 1998). In the case reported by Ohshiro et al. (1993) the meningohypophyseal trunk and the artery of the inferior cavernous sinus branched off at the origin of the persistent trigeminal artery. The authors suggested that the persistent trigeminal artery, the meningohypophyseal trunk, and the artery of the inferior cavernous sinus could be closely linked in the embryo (Ohshiro et al. 1993). Suttner et al. (2000) described a case in which the persistent trigeminal artery gave off two branches: the inferior hypophyseal artery medially, and the dorsal meningeal artery to the clivus inferolaterally. The tentorial artery arose directly from the intracavernous carotid artery at its posterior bend (Suttner et al. 2000). Dwight Parkinson pointed out that the meningohypophyseal trunk could be a remnant of an earlier carotid basilar connection above the sixth nerve, distinct from the true persistent trigeminal artery below the sixth nerve (Azab et al. 2012). Parkinson and Shields (1974) analyzed the differences between the persistent trigeminal artery and meningohypophyseal trunk and stressed their separate origins, emphasizing that the trunk has three main branches while the artery has none.

Other anomalies include a duplicated superior cerebellar artery and hypoplastic anterior inferior cerebellar artery (Parkinson and Shields 1974), bilateral absence of the posterior inferior cerebellar

artery, and a fenestrated oculomotor nerve around the posterior cerebral artery (Ohshiro et al. 1993). A persistent trigeminal artery has been reported in the context of neurofibromatosis type 1, Klippel–Feil syndrome (Paksoy et al. 2004), and Moyamoya disease (Azab et al. 2012). The incidence of this artery is much higher among children with posterior fossa malformations, hemangiomas, arterial anomalies, coarctation of the aorta, and other cardiac defects and eye abnormalities (PHACE syndrome) (12–16%) than reported from other large cerebral angiographic series (0.1–0.2%; Pascual-Castroviejo et al. 2011).

A headache is the usual initial symptom, evidencing a persistent trigeminal artery. There are also other presentations, such as acute subarachnoid hemorrhage, consciousness disturbance, sixth cranial nerve palsy, different visual field defects, diplopia, hemiparesis, and symptoms suggestive of vertebrobasilar insufficiency. Cerebrovascular anomalies of the persistent trigeminal artery include an infraoptic course of the A1 segment of the anterior cerebral artery (Turkoglu et al. 2011), absence of the common carotid artery (Rossitti and Raininko 2001), absence of internal carotid artery (Hattori et al. 1998), an occluded internal carotid artery, hypoplastic basilar and vertebral arteries, bilateral occlusion of the vertebral artery, and a primitive otic artery (Azab et al. 2012). Davis et al. (1956) first reported an aneurysm of the persistent trigeminal artery. Others have reported that approximately 13.8–27.8% of patients with persistent trigeminal artery also have intracranial aneurysms (Chen et al. 2010), 2% arising from the persistent primitive trigeminal artery itself (Vasovic et al. 2012).

A more recent analysis of 103 persistent trigeminal artery patients detected among 16,415 magnetic resonance angiographies reported an incidence of 3.9% cerebral aneurysms in those patients (O'uchi and O'uchi 2010). Cerebral aneurysms associated with the persistent trigeminal artery have been reported in relation to the bifurcations formed by this artery and either the internal carotid (Li et al. 2004; Onizuka et al. 2006; Memis et al. 2007) or the basilar artery (Azab et al. 2012). Aneurysms in the persistent trigeminal artery were at its origin and distal to it, at its mid-portion, or at its junction with the basilar artery bifurcation. If an aneurysm located at the junction with the internal carotid artery ruptures, or if there is spontaneous or traumatic rupture of the persistent trigeminal artery near its anomalous origin, a carotid–cavernous fistula results (Vasovic et al. 2012). This fistula (Cook et al. 2000; Oka et al. 2000) and a persistent trigeminal artery cavernous sinus fistula (Tokunaga et al. 2004) can develop either spontaneously or after a traumatic event and are best treated by endovascular occlusion (Azab et al. 2012).

Stapedial artery

A persistent stapedial artery is a rare congenital vascular anomaly of the middle ear (Guinto et al. 1972). The incidence of this anomaly was 0.02–0.05% in a surgical series (Steffen 1968) and slightly higher (0.48%) in a temporal bone study.

The vascular structures named ventral pharyngeal arteries, a pair of symmetrical arterial sprouts extending craniolaterally from the aortic sac at the midline to the mandibular nerve root, supply the first and second branchial arches and are important in the formation of the stapedial and external carotid arteries (Lefournier et al. 1999). The stapedial artery is transiently present in fetal life and connects the branches of the future external and internal carotid arteries. It arises at 4–5 weeks of fetal life from the hyoid artery, which is a derivative of the second branchial arch, near its origin from the proximal internal carotid artery. It extends cranially and passes through the mesenchymal primordium of the stapes and forms the obturator foramen of the stapes. The distal remnant of the stapedial artery beyond the stapes is the superior tympanic artery, a branch of the middle meningeal artery (Lefournier et al. 1999). During the tenth week of gestation (40 mm embryo), the stapedial artery trunk disappears and the obturator foramen of the stapes remains empty (Hitier et al. 2013).

If the stapedial artery persists in postnatal life, the middle meningeal artery typically arises from it. The foramen spinosum remains hypoplastic or aplastic, which is an indirect sign of a persistent stapedial artery; however, the foramen spinosum is absent in up to 3% of skull base CT studies (Ginsberg et al. 1994). It can be a normal variation, particularly when the middle meningeal artery arises from the ophthalmic artery. The persistent stapedial artery arises from the petrous part of the internal carotid artery, enters the anteromedial hypotympanum, and is contained in the Jacobson canal. After leaving the osseous canal it crosses the cochlear promontory and passes through the obturator foramen of the stapes. It then enters the fallopian canal through a dehiscence just behind the cochleariform process and travels anteriorly in the anterior facial canal. This leads to prominence of the tympanic part of the facial nerve, another indirect sign of a persistent stapedial artery. The persistent stapedial artery finally exits just before the geniculate ganglion, entering the extradural space of the middle cranial fossa (Jain et al. 2004).

The stapedial artery gives rise to two branches after it enters the cranial cavity. The upper, supraorbital, branch becomes the middle meningeal artery and also transiently anastomoses with the ophthalmic artery. The lower, maxillomandibular, division has two branches, mandibular and infraorbital, which persist in adult life as the inferior alveolar and infraorbital arteries, respectively. This lower division leaves the cranial cavity via the foramen spinosum. Normally, anastomoses develop between the ventral pharyngeal arteries and the lower division branches of the stapedial artery, which involutes during the tenth week of fetal life with reversal of flow at the foramen spinosum level (Silbergleit et al. 2000).

Stapedial arteries can persist as four types of anatomical variations. The hyoido-stapedial artery is the typical and most-described form: failure of anastomosis between the mandibular artery and the ventral branch of the stapedial artery leads to the persistence of the stapedial artery trunk (hyoid artery) and

agenesis of the spinosum foramen. In adulthood, the hyoido-stapedial artery goes along the promontory in a bony canal or a mucous fold. It follows through the obturator foramen of the stapes and enters the tympanic portion of the facial canal just behind the cochleariform process. It follows the facial canal and usually enlarges it to emerge 2 mm posterior to the geniculate ganglion and become the middle meningeal artery (Hitier et al. 2013).

The pharyngo-stapedial artery results from regression of the hyoid artery with a persistent stapedial artery. This stapedial artery is supplied by the inferior tympanic, which comes from the pharyngeal artery (Hitier et al. 2013).

The stapedial artery with aberrant carotid artery arises when a persistent stapedial artery is associated with agenesis of the cervical part of the internal carotid artery and carotid foramen. The intracranial carotid is therefore supplied by the inferior tympanic artery. This artery enters the skull through the tympanic canal, passes through the middle ear, and joins the horizontal intrapetrous part of the carotid artery through the intermediary of the hyoid artery. This situation is called a persistent stapedial artery with aberrant internal carotid artery (Celebi et al. 2012).

The pharyngo-hyo-stapedial artery arises when the stapedial artery persists with supply from the inferior tympanic and hyoid arteries, the latter arising from a normal internal carotid artery. In the only case described by Lefournier et al. (1999), the ascendant pharyngeal artery (which provides the inferior tympanic artery) had an abnormal origin from the internal carotid artery.

A branch of the stylomastoid artery going through the arch of the stapes in adults has been described by several authors, referred to as the "stapedial artery." According to Bossy, the stapedial artery as a branch of the stylomastoid artery is unrelated to the embryological stapedial artery, which gives the shape of the stapedial arch (Hitier et al. 2013).

Jain et al. (2004) indicated that identification of the persistent stapedial artery, along with the labyrinthitis ossificans, was important for two reasons. First, the presence of the artery correlated with the patient's conductive hearing loss, probably attributable to stapes ankylosis because of pulsations of the persistent stapedial artery; the management plan was therefore changed. Second, the treating surgeon was alerted if the patient underwent stapedectomy to correct stapes ankylosis or was considered for a cochlear implant because of labyrinthitis ossificans. A persistent stapedial artery has been known to prevent successful cochlear implantation and to cause unexpected hemorrhaging during middle ear interventions if not detected at pre-procedure imaging. It usually manifests as a pulsatile mass in the middle ear cavity, an incidental finding during middle ear surgery, or pulsatile tinnitus. It can also manifest as conductive hearing loss due to associated stapes ankylosis. However, it can in rare instances erode the otic capsule and result in sensorineural hearing loss (Jain et al. 2004). A persistent stapedial artery can be associated with an aberrant internal carotid artery or other middle ear anomalies, especially of the stapes and facial nerve. Rarely, it has been detected in patients with trisomy 13, second branchial arch anomalies, Paget disease, otosclerosis, or thalidomide deformities (Boscia et al. 1990). Differential diagnosis of the persistent stapedial artery includes a glomus tympanicum tumor, an aberrant carotid artery, or a high rising jugular bulb if there is a vascular mass in the middle ear or a facial nerve schwannoma if there is facial nerve enlargement (Silbergleit et al. 2000).

The stapedial artery in humans is initially dedicated to the vascularized meninx and disappears as the middle meningeal artery becomes a branch of the maxillary artery. It persists when the maxillary artery fails to supply meningeal vascularization. It is usually but not always associated with an absence of the spinosum foramen. A persistent stapedial artery can be coagulated if necessary, as it is usually of small diameter. Nevertheless, if other malformations are detected, an arteriography is useful before any surgical decision (Hitier et al.2013).

Hypoglossal artery

The hypoglossal artery is a rarely described member of the carotid-basilar family anastomoses (Vasovic et al. 2008). It belongs to the group of segmental arteries, which establish dorsoventral anastomoses during early fetal life (Vlychou et al. 2003). Although these segmental arteries are normally obliterated after the 40th day, sporadically one remains patent resulting in a carotid-basilar anastomosis during adult life (Vlychou et al. 2003).

Batujeff presented the first anatomical description of this vestigial vessel (Vasovic et al. 2008). Murayama and colleagues reported the first case of bilateral persistent primitive hypoglossal arteries (Murayama et al. 1985).

Lie suggested the term "hypoglossal artery" for the vessel, which follows the hypoglossal nerve on its pathway through its bony canal (Fig. 45.4). The author also described the diagnosis criteria of the variation (Memis and Guney 2001). The artery is situated dorsolaterally in the hypoglossal canal in relation to the rootlets of the hypoglossal nerve, or it pierces these rootlets when it is located in the subarachnoid space (Vasovic et al. 2008).

The origin of the persistent primitive hypoglossal artery is different from that of the cervical portion of the internal carotid artery. The hypoglossal artery can arise from internal carotid at the level of atlas (Kodama et al. 1976). It usually originates from the cervical portion of the internal carotid between the C1 and C2 vertebrae (Andoh et al. 2001), from the C2 (Ahn et al. 2005) or C3 vertebra level, or between C3 and C5 (Nishida et al. 2000). There have also been reports about the persistent primitive hypoglossal artery as a terminal or dorsal branch of the internal carotid (Vasovic et al. 2008), external carotid (Nakamura et al. 2000), or right common carotid artery (Stern et al. 1978).

Up to 1999 there are about 160 cases reported in the literature (Luh et al. 1999). This is a rare embryological anastomosis

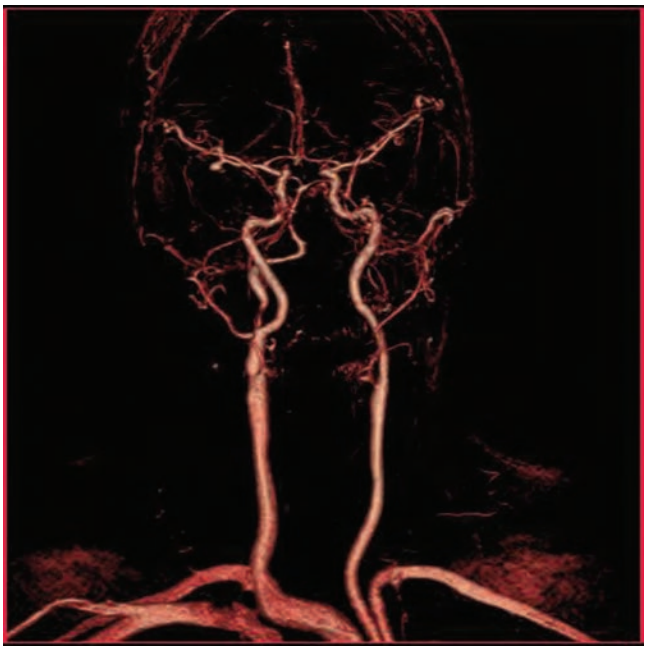

Figure 45.4 Angiography noting a right-sided hypoglossal artery joining the basilar artery.

between the internal carotid and basilar arteries, and the reported angiographic frequency ranges from 0.027% to 0.1% (Vasovic et al. 2008). There is no significant sex difference in occurrence (Vasovic et al. 2008).

Reports of a persistent otic artery as a branch of the persistent primitive hypoglossal artery are rare (Jukic-Basic et al. 2001).

In 26.9% of cases with persistent primitive hypoglossal artery there is an associated intracranial aneurysm (Kanematsu et al. 2004) but, according to Baltsavias et al. (2007), only 16 patients with an aneurysm on the persistent primitive hypoglossal artery itself have been reported in the literature.

Primitive ophthalmic arteries

The embryogenesis of the ophthalmic artery is highly complex. Vascularization of the optic cup is derived from two branches of the primitive internal carotid artery called the primitive ventral and dorsal ophthalmic arteries (Sade et al. 2004). The ventral ophthalmic artery arises from the future anterior cerebral artery and the dorsal from the carotid siphon (Ogawa et al. 1990). Later, these arteries anastomose near the optic nerve. The ventral ophthalmic artery makes an additional anastomosis with the supracavernous portion of the internal carotid. Meanwhile, both these primitive arteries partially regress, the ventral ophthalmic artery at its proximal portion and the dorsal at the level of the superior orbital fissure (Sade et al. 2004). This final configuration gives rise to the primitive ophthalmic artery (Vignaud et al. 1974; Willinsky et al. 1987).

When the embryo reaches 18 mm, the stapedial artery, which arises from the primitive hyoidal branch of the petrous internal carotid artery, gives rise to the maxillofacial and supraorbital branches (Dilenge and Ascherl 1980). At the 20 mm stage the supraorbital branch anastomoses with the primitive ophthalmic artery. By 40 mm, the anastomosis is complete and the primitive ophthalmic artery starts to assimilate the supraorbital branch. This branch not only supplies the intraorbital extraocular contents but also participates in forming the middle meningeal artery.

The dorsal ophthalmic artery usually regresses and the ventral forms the normal ophthalmic artery (Padget 1948). If the dorsal persists it usually arises from the inferolateral trunk, a tiny branch of the cavernous segment of the internal carotid (Willinsky et al. 1987). In a study of 826 patients, the incidence of a dorsal ophthalmic artery was 0.42%, six right-sided and one left-. Three of these seven variants were male. Only one case among the 826 had bilateral dorsal ophthalmic arteries (Uchino et al. 2013). The ventral ophthalmic artery persists more commonly than the dorsal. Only this study explains the incidence of the dorsal ophthalmic artery, and suggests right-side predominance but no gender predominance.

Proatlantal intersegmental artery

There are numerous variations in the nomenclature used to designate the proatlantal intersegmental artery: suboccipital, suboccipital intersegmental, first segmental, first cervical segment, first cervical intersegmental, primitive cervical segmental, and primitive proatlantal intersegmental artery. Some authors have used Latin terms: "arteria intersegmentalis proatlantica," "arteria proatlantoidea," and "arteria intersegmentalis proatlantis". Olry and Haines (2004) proposed the name "supraatlantal artery." Padget, discussing the nomenclature of the embryonic intersegmental vessels, specifically gave the name "proatlantal intersegmental artery" to the first (the most cranial of eight) cervical intersegmental artery (suboccipital intersegmental vessel) (Padget 1954). The second pair is called the "first cervical intersegmental artery," so there are seven pairs of cervical intersegmental arteries. Okahara et al. (2002) proposed that the type I proatlantal artery is the true persistent proatlantal intersegmental artery, while type II is a persistent primitive first cervical intersegmental artery. These persistent arteries – the proatlantal intersegmental and first cervical intersegmental (Fig. 45.5) – were named by Lasjaunias and colleagues as "proatlantal artery type I" and "proatlantal artery type II," respectively. This terminology is still used (Arráez-Aybar et al. 2011).

The proatlantal artery is a vestige of the embryonic precursors of the craniocervical junction arteries present in the human embryo at approximately 24 days and usually disappearing between the 35th and 40th days of gestation (Padget 1948). Rarely, these anastomoses persist into adult life, but it is important to recognize them because of their possible clinical or

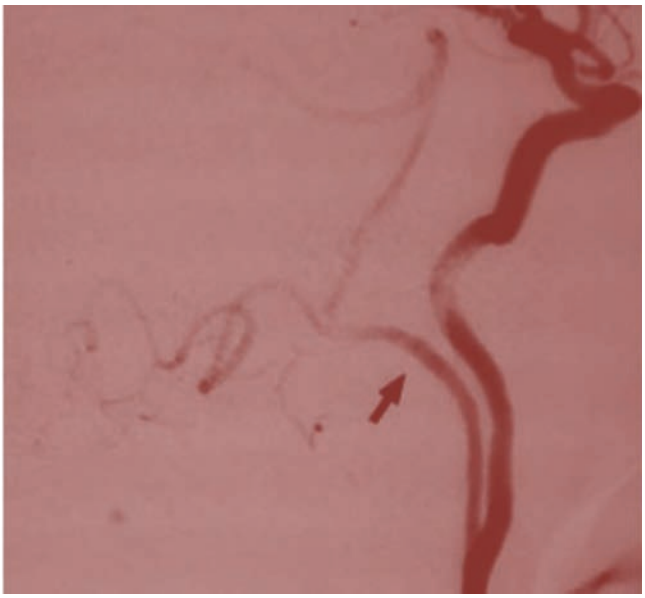

Figure 45.5 Angiography noting a persistent proatlantal artery (arrow).

Figure 45.6 Angiography example of a persistent otic artery.

presurgical implications (Guerri-Guttenberg et al. 2009). Persistence of the proatlantal artery into adult life could be explained embryologically by a primary error in the development of the vertebral artery (Arráez-Aybar et al. 2011).

The proximal vertebral arteries are hypoplastic in 46% of those with a persistent proatlantal artery (Kolbinger et al. 1993). Purkayastha et al. (2005) suggested that bilateral proatlantal intersegmental arteries are extremely rare: only five cases have been reported in the literature, including theirs.

Otic artery

The least common persistent intracranial artery is the otic artery. The most frequently used name for this artery is the "primitive persistent otic artery," but it is also called the "acoustic artery" (Vasovic et al. 2010). It is normally the first to regress during further development of the embryo (Vasovic et al. 2008). The diagnostic criterion for the artery is that it must arise from the petrous portion of the internal carotid, pass through the internal auditory meatus (Fig. 45.6), and anastomose with the internal carotid and vertebrobasilar branches, usually the basilar artery. Only eight cases had been reported in the literature up to 1995. Until 1999, only one case was diagnosed by angiography (Oktay et al. 2003). There was another in 2003; an otic artery associated with multiple intracranial aneurisms was demonstrated angiographically (Patel et al. 2003). In the literature there is only one case of an otic artery joining the posterior inferior cerebellar artery (Luh et al. 1999; Albay et al. 2012).

The caroticotympanic artery is said to be a morphological remnant of the hyoid artery (Vasovic et al. 2010). This branch arises from the petrous portion of the internal carotid artery and enters the tympanic cavity through a foramen in the wall of the vertical portion of the carotid canal; angiographically, it cannot be seen due to the density of the petrous portion of the temporal bone (Tubbs et al. 2007). The incidence of the otic artery has not been reported in the literature because it is very rare and this area is difficult to image. In a study of 7382 carotid artery angiograms, the otic artery was observed in only one (Tubbs et al. 2011).

Persistent primitive olfactory artery

A persistent primitive olfactory artery, which is highly associated with cerebral aneurysms, is very rare (Nozaki et al. 1998; Vasovic et al. 2013). It represents a continuation of the cranial branch of the primitive internal carotid artery (Vasovic et al. 2013). It arises from the terminal portion of the internal carotid and courses anteromedially along the ipsilateral olfactory tract and makes a hair-pin curve posterior to the olfactory bulb (Padget 1948), becoming the distal anterior cerebral artery (variant 1) or the ethmoidal artery (variant 2). It is suggested that a relatively frequent location of an aneurysm on the hair-pin bend of the persistent primitive olfactory emphasizes the importance of hemodynamic stress in this vessel (Nozaki et al. 1998; Yamamoto et al. 2009; Vasovic et al. 2013).

Usually, the primitive olfactory artery regresses and remains as the recurrent artery of Heubner during early gestation (Padget 1948), but when it persists there is no ipsilateral recurrent artery of Heubner (Uchino et al. 2011).

The incidence of the artery was not reported before the study of Uchino et al. (2011). This retrospective study, performed on 3626 magnetic resonance angiographic images, gave the incidence of the persistent artery as 0.14% (Uchino et al. 2011). The same study indicated that there was no significant laterality and gender difference, and only in one case were the arteries seen bilaterally (Uchino et al. 2011).

The persistent primitive olfactory artery is usually asymptomatic, but two patients who had suffered from anosmia have been reported (Nozaki et al. 1998). According to Vasovic et al. (2013), 67 cases had been reported in the literature up to that time. The variation is more frequent in males and on the left side (Vasovic et al. 2013). Only five bilateral cases have been reported (Vasovic et al. 2013). The incidences of the persistent primitive olfactory artery are given as 0.64% in the Serbian and 0.14% in the Japanese populations (Uchino et al. 2011), and 0.29% in the Korean population (Vasovic et al. 2013).

References

Ahn JH, Choe WJ, Park HI, Lee CH. 2005. Persistent hypoglossal artery. *J Korean Neurosurg Soc* 38: 312–315.

Albay S, Kastamoni Y, Koyuncu E. 2012. Embriyonal kalinti arterler. *SDU Tip Fak Derg* 19(2): 62–67.

Ali S, Radaideh MM, Shaibani A, Russell EJ, Walker MT. 2008. Persistent trigeminal artery terminating in the posterior inferior cerebellar artery: Case report. *Neurosurgery* 62: 746–748.

Andoh K, Tanohata K, Moriya N, Hagiwara H, Lee J, Sato M, Yoshida T, Nagashima T. 2001. The posterior inferior cerebellar artery arising from the extracranial segment of the internal carotid artery via the hypoglossal canal without an interposed segment of the basilar artery. *Clin Imaging* 25: 86–89.

Arakawa T, Koizumi M, Terashima T, Honma S, Kawai K, Kodama K, Miki A. 2007. Two anatomical autopsy cases of direct communication between a persistent primitive trigeminal artery and an anterior inferior cerebellar artery. *Ann Anat* 189: 489–498.

Arráez-Aybar LA, Navia-Álvarez P, Méndez-Cendón JC. 2011. A case of a type II proatlantal artery with arteriovenous malformation. *Surg Radiol Anat* 33: 85–89.

Azab W, Delashaw J, Mohammed M. 2012. Persistent primitive trigeminal artery: a review. *Turk Neurosurg* 22(4): 399–406.

Baltsavias GM, Chourmouzi D, Tasianas N, Drevelengas A, Damianovski D, Jovkovski S. 2007. Ruptured aneurysm of a persistent primitive hypoglossal artery treated by endovascular approach: case report and literature review. *Surg Neurol* 68: 338–343.

Bergman RA, Afifi AK, Miyauchi R. 2013. Persistent Embryologic Arteries. Available at: http://www.anatomyatlases.org/AnatomicVariants/Cardiovascular/Text/Arteries/PersistentEmbryologic.shtml (accessed 23 October 2015).

Boscia R, Knox RD, Adkins WY. 1990. Holgate RC. Persistent stapedial artery supplying a glomus tympanicum tumor. *Arch Otolaryngol Head Neck Surg* 116: 852–854.

Carlson BM. 2013. *Human Embryology and Developmental Biology, fifth edition*. Philadelphia: Elsevier Saunders.

Celebi I, Oz A, Yildirim H, Bankeroglu H, Basak M. 2012. A case of an aberrant internal carotid artery with a persistent stapedial artery: association of hypoplasia of the A1 segment of the anterior cerebral artery. *Surg Radiol Anat* 34: 665–670.

Chen YC, Li MH, Chen SW, Hu DJ, Qiao RH. 2010. Incidental findings of persistent primitive trigeminal artery on 3-dimensional time-of-flight magnetic resonance angiography at 3.0 T: An analysis of 25 cases. *J Neuroimaging* 21(2): 152–158.

Cook BE Jr, Leavitt JA, Dolan JW, Nichols DA. 2000. Carotid cavernous fistula associated with persistent primitive trigeminal artery. *J Neuroophthalmol* 20: 264–265.

Davis RA, Wetzel N, Davis L. 1956. An analysis of the results of intracranial vascular lesions by carotid artery ligation. *Ann Surg* 143: 641–648.

Dilenge D, Ascherl GF Jr. 1980. Variations of the ophthalmic and middle meningeal arteries: relation to the embryonic stapedial artery. *AJNR Am J Neuroradiol* 1: 45–53.

Ginsberg LA, Pruett SW, Chen MY, Elster AD. 1994. Skull base foramina of the middle cranial fossa: reassessment of normal variation with high resolution CT. *AJNR Am J Neuroradiol* 15: 283–291.

Guerri-Guttenberg RA. 2009. Fetal carotid-vertebrobasilar anastomoses: persistent hypoglossal artery associated with further variations of the circle of Willis. *Surg Radiol Anat* 31: 311–315.

Guinto FC, Garrabrant EC, Radcliffe WB. 1972. Radiology of the persistent stapedial artery. *Radiology* 105: 365–369.

Hattori T, Kobayashi H, Inoue S, Sakai N. 1998. Persistent primitive trigeminal artery associated with absence of internal carotid artery. *Surg Neurol* 50: 352–355.

Hitier M, Zhang M, Labrousse M, Barbier C, Patron V, Moreau S. 2013. Persistent stapedial arteries in human: from phylogeny to surgical consequences. *Surg Radiol Anat* 35(10): 883–891.

Jain R, Gandhi D, Gujar S, Mukherji SK. 2004. Case 67: Persistent stapedial artery. *Radiology* 230(2): 413–416.

Jukic-Basic N, Jelic M, Basic V, Jukic T, Vinter I. 2001. Persistent hypoglossal artery. *J Anat* 198: 315–316.

Kanematsu M, Satoh K, Nakajima N, Hamazaki F, Nagahiro S. 2004. Ruptured aneurysm arising from a basilar artery fenestration and associated with a persistent primitive hypoglossal artery. Case report and review of the literature. *J Neurosurg* 101: 532–535.

Khodadad G. 1976. Persistent trigeminal artery in the fetus. *Radiology* 121: 653–656.

Kodama N, Ohara H, Suzuki J. 1976. Persistent hypoglossal artery associated with aneurysms. Report of two cases. *J Neurosurg* 45: 449–451.

Kolbinger R, Heindel W, Pawlik G, Erasmi-Korber H. 1993. Right proatlantal artery type 1, right internal carotid occlusion, and left internal carotid stenosis: case report and review of literature. *J Neurosci* 117: 232–239.

Kwon JY, Lee EJ, Kim JS. 2010. Brainstem infarction secondary to persistent trigeminal artery occlusion: Successful treatment with intravenous rt-PA. *Eur Neurol* 64 (5): 311.

Lefournier V, Vasdev A, Bessou P, Boubagra K. 1999. A persistent pharyngohyostapedial artery: embryologic implications. *AJNR Am J Neuroradiol* 20(2): 271–274.

Li MH, Li WB, Pan YP, Fang C, Wang W. 2004. Persistent primitive trigeminal artery associated with aneurysm: Report of two cases and review of the literature. *Acta Radiol* 45: 664–668.

Luh GY, Dean BL, Tomsick TA, Wallace RC. 1999. The persistent fetal carotid-vertebrobasilar anastomoses. *AJR Am J Roentgenol* 172(5): 1427–1432.

Memis A, Guney B. 2001. Persistan hipoglossal arterin MR anjiyografi ile görüntülenmesi. *Tanısal ve Girişimsel Radyoloji* 7(2): 248–251.

Memis A, Demirpolat G, Biceroglu S. 2007. Persistent trigeminal artery aneurysm: Treatment with coil embolization. *J Vasc Interv Radiol* 18: 459–461.

Murayama Y, Fujimoto N, Matsumoto K. 1985. Bilateral persistent primitive hypoglossal arteries associated with a large ruptured aneurysm on one side. *Surg Neurol* 24: 498–502.

Nakamura M, Kobayashi S, Yoshida T, Kamagata M, Sasaki T. 2000. Persistent external carotid-vertebrobasilar anastomosis via the hypoglossal canal. *Neuroradiology* 42: 821–823.

Nishida C, Ashikaga R, Araki Y, Nakamatsu K, Ono Y, Fujii K, Nishimura Y. 2000. Persistent hypoglossal artery associated with arteriovenous malformation: case report. *Eur Radiol* 33: 59–62.

Nozaki K, Taki W, Kawakami O, Hashimoto N. 1998. Cerebral aneurysm associated with persistent primitive olfactory artery aneurysm. *Acta Neurochir (Wien)* 140(4): 397–401.

O'uchi E, O'uchi T. 2010. Persistent primitive trigeminal arteries (PTA) and its variant (PTAV): Analysis of 103 cases detected in 16,415 cases of MRA over 3 years. *Neuroradiology* 52: 1111–1119.

Ogawa T, Miyauchi T, Kato T, Tamakawa Y. 1990. Internal carotid origin of double ophthalmic arteries. *Neuroradiology* 32: 508–510.

Ohshiro S, Inoue T, Hamada Y, Matsuno H. 1993. Branches of the persistent trigeminal artery: An autopsy case. *Neurosurgery* 32: 144–148.

Oka Y, Sadamoto K, Tagawa M, Kumon Y, Sakaki S, Fujita M. 2000. Transvenous embolization of carotid-cavernous sinus fistula associated with a primitive trigeminal artery case report. *Neurol Med Chir (Tokyo)* 40: 61–64.

Okahara M, Kiyosue H, Mori H, Tanoue S, Sainou M, Nagatomi H. 2002. Anatomic variations of the cerebral arteries and their embryology: a pictorial review. *Eur Radiol* 12: 2548–2561.

Oktay O, Kitis O, Oran I, Memis A. 2003. Persistan fetal carotid-vertebrobaziler anastomozlar. *Tanisal ve Girisimsel Radyoloji* 9: 382–387.

Olry R, Haines DE. 2004. Nomenclature of persistent carotid vertebrobasilar anastomoses. *J Hist Neurosci* 13: 190–192.

Onizuka M, Kazekawa K, Tsutsumi M, Kodama T, Aikawa H, Ikou M, Tomokiyo M, Matsubara S, Nii K, Tanaka A. 2006. Hyperform remodeling balloon for the balloon occlusion test of persistent primitive trigeminal artery aneurysm: case report. *Neurol Med Chir (Tokyo)* 46: 541–543.

Padget DH. 1948. The development of the cranial arteries in the human embryo. *Contr Embryol Carneg Inst* 32: 205–262.

Padget DH. 1954. Designation of the embryonic intersegmental arteries in reference of the vertebral and subclavian stem. *Anat Rec* 119: 349–356.

Paksoy Y, Seker M, Kalkan E. 2004. Klippel–Feil syndrome associated with persistent trigeminal artery. Spine (Phila Pa 1976) 29(9): 193–196.

Parkinson D, Shields CB. 1974. Persistent trigeminal artery. Its relationship to the normal branches of the cavernous carotid. *J Neurosurg* 40: 244–248.

Pascual-Castroviejo I, Alvarez-Linera J, Coya J, Viano J, Pascual-Pascual SI, Velazquez-Fragua R, Lopez-Gutierrez JC. 2011. Pascual-Castroviejo type II syndrome (P–CIIS). Importance of the presence of persistent embryonic arteries. *Childs Nerv Syst* 27(4): 617–625.

Patel AB, Gandhi CD, Bederson JB. 2003. Angiographic documentation of a persistent otic artery. *AJNR Am J Neuroradiol* 24(1): 124–126.

Purkayastha S, Jayadevan ER, Gupta AK, Bodhey NK. 2005. Cerebral arteriovenous malformation embolized through persistent primitive hypoglossal artery. A case report. *Interv Neuroradiol* 11: 241–246.

Rossitti S, Raininko R. 2001. Absence of the common carotid artery in a patient with a persistent trigeminal artery variant. *Clin Radiol* 56: 79–81.

Sade B, Tampieri D, Mohr G. 2004. Ophthalmic artery originating from basilar artery: a rare variant. *Am J Neuroradiol* 25: 1730–1731.

Salas E, Ziyal IM, Sekhar LN, Wright DC. 1998. Persistent trigeminal artery: An anatomic study. *Neurosurgery* 43: 557–562.

Silbergleit R, Quint DJ, Mehta BA, Patel SC, Metes JJ, Noujaim SE. 2000. The persistent stapedial artery. *Am J Neuroradiol* 21: 572–577.

Steffen TN. 1968. Vascular anomalies of the middle ear. *Laryngoscope* 78: 171–197.

Stern J, Correll JW, Bryan N. 1978. Persistent hypoglossal artery and persistent trigeminal artery presenting with posterior fossa transient ischaemia attacks. Report of 2 cases. *J Neurosurg* 49: 614–619.

Suttner N, Mura J, Tedeschi H, Ferreira M, Wen H, de Oliveira E, Rhoton AL Jr. 2000. Persistent trigeminal artery: A unique anatomic specimen: analysis and therapeutic implications. *Neurosurgery* 47: 428–434.

Takase T, Tanabe H, Kondo A, Nonoguchi N, Tane K. 2004. Surgically treated aneurysm of the trunk of the persistent primitive trigeminal artery: case report. *Neurol Med Chir (Tokyo)* 44: 420–423.

Tokunaga K, Sugiu K, Kameda M, Sakai K, Terasaka K, Higashi T, Date I. 2004. Persistent primitive trigeminal artery-cavernous sinus fistula with intracerebral hemorrhage: Endovascular treatment using detachable coils in a transarterial doublecatheter technique. Case report and review of the literature. *J Neurosurg* 101: 697–699.

Tubbs RS, Hansasuta A, Loukas M, Louis RG Jr, Shoja MM, Salter EG, Oakes WJ. 2007. Branches of the petrous and cavernous segments of the internal carotid artery. *Clin Anat* 20: 596–601.

Tubbs RS, Verma K, Riech S, Mortazavi MM, Shoja MM, Loukas M, Curé JK, Zurada A, Cohen-Gadol AA. 2011. Persistent fetal intracranial arteries: a comprehensive review of anatomical and clinical significance. *J Neurosurg* 114(4): 1127–1134.

Turkoglu E, Arat A, Patel N, Kertmen H, Baskaya MK. 2011. Anterior communicating artery aneurysm associated with an infraoptic course of anterior cerebral artery and rare variant of the persistent trigeminal artery: A case report and literature review. *Clin Neurol Neurosurg* 113 (4): 335–340.

Uchino A, Saito N, Kozawa E, Mizukoshi W, Inoue K. 2011. Persistent primitive olfactory artery: MR angiographic diagnosis. *Surg Radiol Anat* 33(3): 197–201.

Uchino A, Saito N, Takahashi M, Kozawa E, Mizukoshi W, Nakajima R, Okano N. 2013. Persistent dorsal ophthalmic artery and ophthalmic artery arising from the middle meningeal artery diagnosed by MR angiography at 3 T. *Surg Radiol Anat* 35(9): 775–782

Vasovic L, Milenkovic Z, Jovanovic I, Cukuranovic R, Jovanovic P, Stefanovic I. 2008. Hypoglossal artery: a review of normal and pathological features. *Neurosurg Rev* 31(4): 385–396.

Vasovic L, Arsic S, Vlajkovic S, Jovanovic I, Jovanovic P, Ugrenovic S, Andjelkovic Z. 2010. Otic artery: a review of normal and pathological features. *Med Sci Monit* 16(5): 101–109.

Vasovic L, Jovanovic I, Ugrenovic S, Vlajkovic S, Jovanovic P, Stojanovic V. 2012. Trigeminal artery: a review of normal and pathological features. *Childs Nerv Syst* 28(1): 33–46.

Vasovic L, Trandafilovic M, Vlajkovic S, Jovanovic I, Ugrenovic S. 2013. Persistent primitive olfactory artery in Serbian population. *Biomed Res Int* 2013: 903460.

Vignaud J, Hasso AN, Lasjaunias P, Clay C. 1974. Orbital vascular anatomy and embryology. *Radiology* 111: 617–626.

Vlychou M, Georganas M, Spanomichos G, Kanavaros P, Artinopoulos C, Zavras GM. 2003. Angiographic findings and clinical implications of persistent primitive hypoglossal artery. *BMC Med Imaging* 3(1): 2.

Willinsky R, Lasjaunias P, Berenstein A. 1987. Intravcavernous branches of the internal carotid artery (ICA): comprehensive review of their variations. *Surg Radiol Anat* 9: 201–215.

Yamamoto T, Suzuki K, Yamazaki T, Tsuruta W, Tsurubuchi T, Matsumura A. 2009. Persistent primitive olfactory artery aneurysm. *Neurol Med Chir (Tokyo)* 49(7): 303–305.

Further reading

Lee MR, Chuang YM, Chen WJ, Lin CP. 2009. Meticulous blood pressure control is mandatory for symptomatic primitive trigeminal artery. *Am J Emerg Med* 27(5): 634.

McKenzie JD, Dean BL, Flom RA. 1996. Trigeminal-cavernous fistula: Saltzman anatomy revisited. *Am J Neuroradiol* 17: 280–282.

Nishio A, Nishijima Y, Komiyama M, Hara M. 2001. Primitive trigeminal artery variant aneurysm treated with Guglielmi detachable coils: Case report. *Neurol Med Chir (Tokyo)* 41: 446–449.

Raphaeli G, Bandeira A, Mine B, Brisbois D, Lubicz B. 2009. A rare variant of persistent trigeminal artery: Cavernous carotidcerebellar artery anastomosis: a case report and a systematic review. *Cerebellum* 8: 445–447.

46 Common carotid and cervical part of the internal carotid arteries

R. Shane Tubbs[1-3] and Marios Loukas[3]
[1]Seattle Science Foundation, Seattle, Washington, USA
[2]University of Dundee, Dundee, UK
[3]St George's University, School of Medicine, St Georges, Grenada

Common carotid artery

The right common carotid artery may be absent. The artery may obliquely cross the lower part of the trachea above the level of the sternum. This occurs on the right side when the right brachiocephalic artery is situated to the left of the midline, when the right common carotid artery arises as the second branch of the aortic arch, or when the right and left common carotid arteries arise as common stem from the aorta. It occurs on the left side when the left common carotid artery arises from the brachiocephalic artery.

The left common carotid artery varies more than the right, arising either from the brachiocephalic artery or from a common stem with the right common carotid artery. In those cases where the right subclavian artery is a separate branch of the aorta, the two carotid arteries most frequently arise by a common trunk.

The right common carotid artery, when arising from the aorta, sometimes runs behind the trachea or the esophagus to the right side of the neck. The origin of the right common carotid artery may be above or below the usual point, depending on whether the brachiocephalic artery bifurcates higher or lower than usual. A low bifurcation of the brachiocephalic artery is somewhat more common. The common carotid artery sometimes follows a very tortuous course, forming one or more distinct loops in the neck.

The common carotid arteries may bifurcate higher or lower than usual; a high bifurcation is more common. The bifurcation can occur as high as the hyoid bone (3/400, Poynter 1922) or even the styloid process, or as low as the cricoid cartilage (18/400, Poynter 1922) or within 3.7 cm of its origin. The artery may not bifurcate but provide branches usually derived from the external carotid artery as it ascends in the neck. A common carotid artery may be absent, the external and internal carotid arteries arising directly from the arch of the aorta or from the termination of the brachiocephalic artery.

As a very rare occurrence, the carotid artery can ascend in the neck without dividing into the two usual branches, either the external or internal carotid arteries being absent. Power (1850) described some cases where, instead of bifurcating, the common carotid trifurcates into the internal and external carotid arteries and superior thyroid artery.

The common carotid artery may provide one or more of the branches usually derived from the external carotid. Examples are: superior thyroid, thyroidea ima, and cases in which a vertebral or inferior thyroid artery is a branch of the common carotid artery.

The vagus nerve may run in front of the common carotid artery instead of behind it. The common carotid arteries may give rise to an esophageal artery.

Cervical internal carotid artery

Looping of the internal carotid artery may occur in up to 30% of individuals. Rarely, the internal carotid artery can form a loop around a transverse process of a cervical vertebra. Tortuosity and coiling of the internal carotid artery may be seen infancy. Tortuosity of this vessel is usually unilateral and more often found on the left side. The vessel may be elongated. The carotid sinus may be found associated with only the internal carotid artery (Lang 1993). The internal carotid artery may be duplicated (Killien et al. 1980).

The internal carotid artery rarely provides branches in the neck. However, the ascending pharyngeal, occipital, transverse facial, and lingual arteries, as well as a laryngeal and a meningeal artery, have all been reported to arise from the internal carotid artery prior to its entry into the carotid canal. The internal carotid artery gave rise to the hypoglossal artery. There have also been reports of the internal carotid artery giving rise to the basilar artery (Morris and Moffat 1956).

The internal carotid artery is occasionally absent uni- or bilaterally. When absent, branches of the maxillary artery may

Bergman's Comprehensive Encyclopedia of Human Anatomic Variation, First Edition. Edited by R. Shane Tubbs, Mohammadali M. Shoja and Marios Loukas.
© 2016 John Wiley & Sons, Inc. Published 2016 by John Wiley & Sons, Inc.

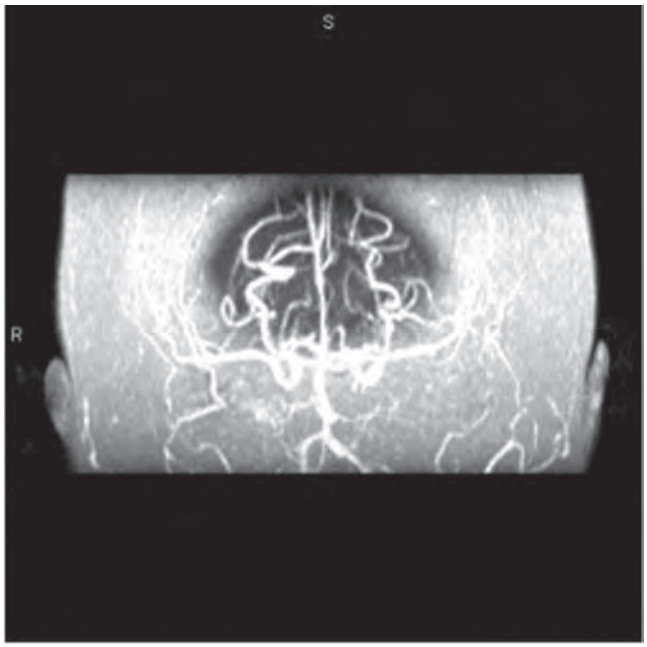

Figure 46.1 Bilateral absence of the internal carotid arteries. Note that the anterior circulation is provided exclusively from the vertebrobasilar system.

replace the internal carotid artery. The carotid canal(s) may be absent (Fig. 46.1).

In a dissection study of 200 half-necks (or sides), the internal carotid artery ran dorsolateral to the external carotid artery in 38%, dorsal to the external carotid artery in 38.5%, and dorsomedial to the external carotid artery in 23.5% of cases.

References

Killien FC, Wyler AR, Cromwell LD. 1980. Duplication of the internal carotid artery. *Neuroradiology* 19: 101–102.

Lang J. 1993. *Clinical Anatomy of the Cervical Spine*. New York: Thieme.

Morris ED, Moffat DB. 1956. Abnormal origin of the basilar artery from the cervical part of the internal carotid artery and its embryological significance. *Anat Rec* 125: 701–711.

Power JH. 1850. *Surgical Anatomy of the Arteries and Descriptive Anatomy of the Heart by the Late Valentine Flood, MD*. Dublin: Fannin and Co.

Poynter CWM. 1922. Congenital anomalies of the arteries and veins of the human body with bibliography. *The University Studies of the University of Nebraska, Lincoln* 22: 1–106.

Further reading

Adachi B. 1928. *Das Arteriensystem der Japaner*. Kyoto: Kenkyusha Press.

Bergman RA, Thompson SA, Afifi AK, Saadeh FA. 1988. *Compendium of Human Anatomic Variation: Catalog, Atlas and World Literature*. Baltimore and Munich: Urban & Schwarzenberg.

Chess MA, Barsotti JB, Chang JK, Ketonen LM, Westesson PL. 1995. Duplication of the extracranial internal carotid. *Am J Neuroradiol AJNR* 16: 1545–1547.

Flemming EE. 1895. Absence of left internal carotid. *J Anat Physiol* 29: 22–24.

Lasjaunias P, Santoyo-Vasquez A. 1984. Segmental agenesis of the internal carotid artery: angiographic aspects with embryological discussion. *Anat Clin* 6: 133–141.

Lie TA. 1968. Congenital anomalies of the carotid arteries. *Exerpta Medica* 30: 84–93.

Orr AE. 1907. A rare anomaly of the carotid arteries (internal and external). *J Anat Physiol* 41: 51.

Priman J, Christie DH. 1959. A case of abnormal internal carotid artery and associated vascular anomalies. *Anat Rec* 134: 87–95.

Roope AP. 1913. Anomalous internal carotid artery. *J Indiana State Med Assoc* 6: 162.

Rosen IW, Mills DF, Nadel HI, Maiserman DD. 1975. Angiographic demonstration of congenital absence of both internal carotid arteries. Case report. *J Neurosurg* 42: 478–482.

Thompson JA. 1898. An anomalous position of the internal carotid artery. *Milwaukee Med J* 6: 12.

Turnbull I. 1962. Agenesis of the internal carotid artery. *Neurology (Minneapolis)* 12: 588–590.

47 External carotid artery

Selcuk Tunali
TOBB University of Economics and Technology, Ankara, Turkey
University of Hawaii, Honolulu, Hawaii, United States

The external carotid artery (ECA) can be absent unilaterally or bilaterally. When it is unilaterally absent, its branches usually arise from the upward continuation of the common trunk or from the contralateral vessel (Bergman et al. 1996).

The ECA arises from the bifurcation of the common carotid artery (CCA), usually at the level of the third and fourth cervical vertebrae. However, this bifurcation is sometimes higher or lower than usual. Lippert and Pabst (1985) reviewed the level of bifurcation of the CCA as follows: C4, 35%; C3–C4 disc, 30%; C3, 12%; C4–C5 disc, 12%; C5, 5%; C2–C3 disc, 4%; C5–C6 dis, 1%; and C2 <1% (Fig. 47.1)

Zümre et al. (2005) studied 40 fetuses and reported the bifurcation level of the CCA as 55% at the C3 level, 35% at C4, and 10% at C5 on the right side, and 60% at the C3 level and 40% at C4 on the left.

Gomez and Arnuk (2013) reported a case where the CCA had an intrathoracic bifurcation at the T3 level. Gailloud et al. (2000) reported a 72-year-old male with bilateral intrathoracic carotid bifurcation. The right CCA was extremely short, dividing after approximately 1.5 cm into the right internal and external carotid arteries. The right carotid bifurcation was therefore in a thoracic location at a level corresponding to T4. The left carotid bifurcation was also intrathoracic, at a vertebral level corresponding to T2. Horowitz et al. (2003) reported a case of a left ECA that arose directly from the aortic arch, along with a type II proatlantal-vertebral artery anastomosis.

Gluncic et al. (2001) reported a high origin of the ECA. In their case the right CCA bifurcated at the level between the second and the third cervical vertebrae. Ueda et al. (1984) reported the bifurcation of a CCA as the upper margin of the C2 vertebra. Adachi (1928) depicted the ECA as traveling between the digastric and stylohyoid muscles.

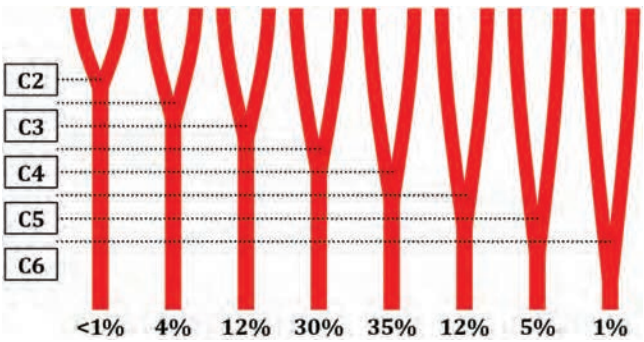

Figure 47.1 Illustration showing the bifurcation of the common carotid artery.

Redrawn after Lippert and Pabst (1985).

Superior thyroid artery

The superior thyroid artery (STA) is almost always considered to be present. It has been reported to arise from the common carotid in 18% of cases, the point of division of the common carotid in 36%, and the external carotid in 36%. It can also arise from the subclavian or the common carotid (41/292 or 14% of cases, Quain; 9%, Livini; 7% Poynter), or share a common origin with the facial or with the lingual and facial (Bergman et al. 1988). The STA can arise from a common trunk with the lingual artery as the thyrolingual trunk, or with the lingual and facial arteries as the thyrolinguofacial trunk. According to Lippert and Pabst (1985), the prevalence of a thyrolingual trunk from the ECA is 2% and from the CCA is <0.1%; the prevalence of a thyrolinguofacial trunk from the ECA is <1%. The origin of the thyrolingual trunk from the ECA has been reported with incidences ranging from 0.7% to 3% (Budhiraja and Rastogi 2010). Ongeti and Ogeng'o (2012) studied the origin of the STA in 46 cadavers of black Kenyans; in 13.1% it originated from the CCA. There was asymmetric origin of the artery in three (6.5%) cadavers. It originated from the ECA on the left and the CCA on the right in two cadavers. Interestingly, Natsis et al. (2011) reported that the STA originated from the ECA in 39% of a Greek population and from the CCA at the level of the carotid bifurcation in the other 61%.

Bergman's Comprehensive Encyclopedia of Human Anatomic Variation, First Edition. Edited by R. Shane Tubbs, Mohammadali M. Shoja and Marios Loukas.
© 2016 John Wiley & Sons, Inc. Published 2016 by John Wiley & Sons, Inc.

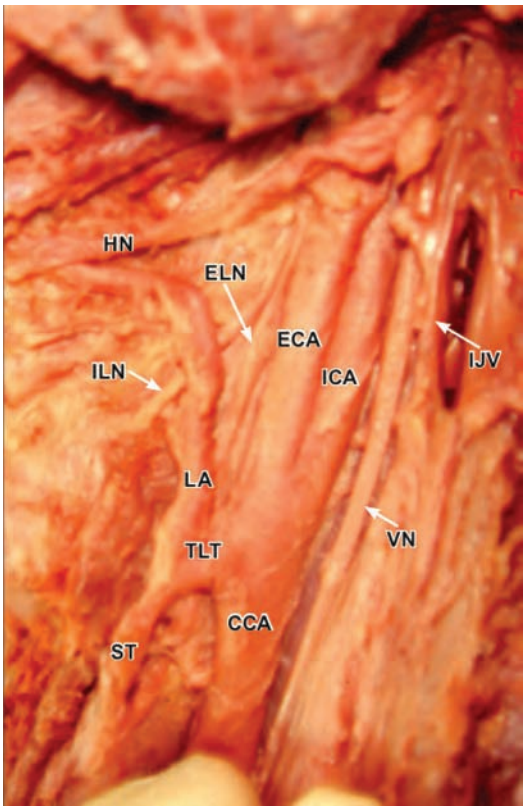

Figure 47.2 Photograph of specimen showing variant thyrolingual trunk arising from left common carotid artery. TLT: thyrolingual trunk; LA: lingual artery; ST: superior thyroid artery; CCA: common carotid artery; ECA: external carotid artery; ICA: internal carotid artery; VN: vagus nerve; IJV: internal jugular vein; HN: hypoglossal nerve; ELN: external laryngeal nerve; ILN: internal laryngeal nerve.

Source: Budhiraja and Rastogi (2010). Reproduced with permission from International Journal of Anatomical Variations.

Figure 47.3 Common trunk for superior thyroid, lingual and facial arteries. 1: common carotid artery; 2: internal carotid artery; 3: external carotid artery; 4: common trunk; 5: superior thyroid artery; 6: lingual artery; 7: facial artery; 8: submandibular gland.

Source: Satishkumar et al. (2013). Reproduced with permission from International Journal of Anatomical Variations.

Mehta et al. (2010) reported an absent STA on the right side and a left STA originating from the left CCA. Budhiraja and Rastogi (2010) reported a thyrolingual trunk arising from the left CCA in a male cadaver aged about 60 years (Fig. 47.2). Satishkumar et al. (2013) reported a thyrolinguofacial trunk on the left side of a female cadaver (Fig. 47.3). Geraci et al. (2009) reported an unusual origin of the STA and ascending pharyngeal artery from a common trunk arising from the CCA, which is very rare. In a case described by Aggarwal et al. (2006), the STA and the occipital artery had a common origin and the ascending pharyngeal artery originated from the occipital artery. The STA can be doubled and can supply the sternocleidomastoid muscle (Lang 1993).

The superior laryngeal artery (SLA) usually arises from the STA (88%). Alternatively, it can arise from the ECA (10%), the lingual artery (1%), or the thyrolingual/thyrolinguofacial trunk (1%). During its course the SLA enters the larynx either through the thyrohyoid membrane (75%), through a foramen on the thyroid cartilage (20%), or between the thyroid and cricoid cartilages (5%) (Lippert and Pabst 1985). In the study by Rusu et al. (2007), the SLA originated from the superior thyroid artery in 68% and directly from the ECA in 32%. In the same study, an aberrant SLA entered the larynx through a foramen on the thyroid cartilage (foramen thyroideum) in 5%.

Nayak and Soumya (2008) reported a case where there were two SLAs on the left side. One of them took its origin from the STA and the other directly from the ECA. Both arteries pierced the thyrohyoid membrane along with the internal laryngeal nerve (Fig. 47.4).

Facial artery

The facial artery is frequently rudimentary and it is rarely absent (Ezure et al. 2011). It can terminate as a submental artery, that is, not reaching the face, or as a labial or alar nasi (lateral nasal) artery and not as the angular artery. In its absence it can be replaced by either the nasal branch of the ophthalmic artery at the medial side of the orbit, the transverse facial, or the maxillary artery. The buccal, posterior alveolar, or infraorbital artery can also be larger than usual, compensating for a deficiency of the facial artery.

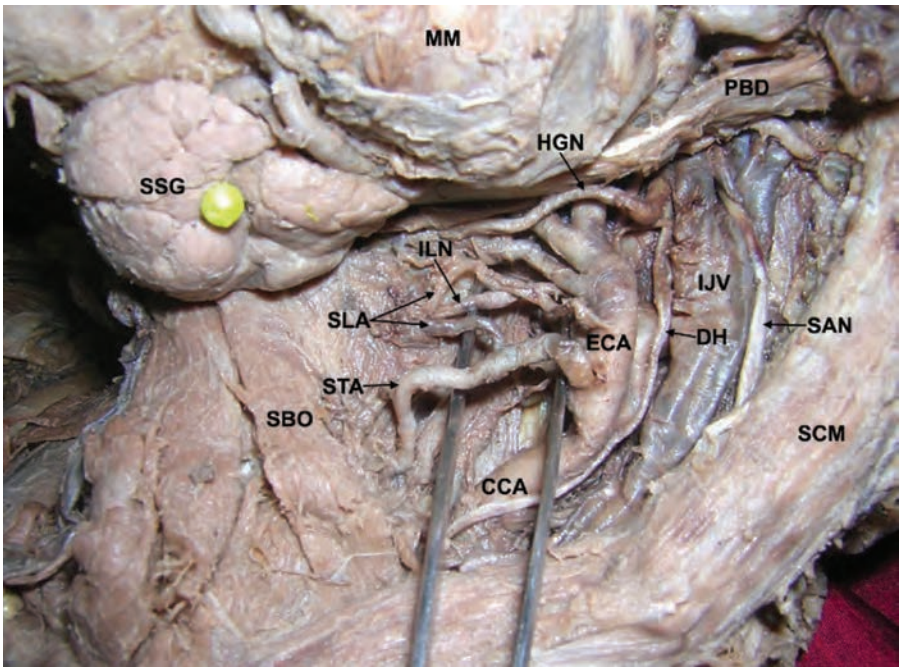

Figure 47.4 The left carotid triangle showing the variations of the superior laryngeal arteries and the spinal accessory nerve. The veins accompanying the branches of external carotid artery have been removed for better exposure. MM: masseter muscle; SSG: submandibular salivary gland; PBD: posterior belly of digastrics; SCM: sternocleidomastoid muscle; SBO: superior belly of omohyoid; CCA: common carotid artery; ECA: external carotid artery; STA: superior thyroid artery; SLA: superior laryngeal arteries; IJV: internal jugular vein; SAN: spinal accessory nerve; ILN: internal laryngeal nerve; HGN: hypoglossal nerve; DH: descendens hypoglossi.

Source: Nayak and Soumya (2008). Reproduced with permission from International Journal of Anatomical Variations.

The facial artery can pierce the masseter muscle (Lang 1993). When it is larger than usual, the facial artery can replace the frontal branches of the ophthalmic or nasal artery; on the other hand, the submental branch of the facial sometimes arises from the lingual artery. The ascending palatine branch of the facial artery can arise from the ECA. Unusual branches of the facial include the ascending pharyngeal, superior laryngeal, tonsillar, sternocleidomastoid, maxillary, or sublingual arteries. The facial artery sometimes replaces the lingual artery and supplies the sublingual gland. The facial artery's inferior and superior labial branches are sometimes poorly developed or absent, in which case they are replaced by the contralateral vessel, which is usually enlarged.

The facial artery can arise by a common trunk with the lingual artery. Occasionally, it arises above its usual position, then descends beneath the angle of the jaw to assume its ordinary course. The arch formed above the submandibular gland can extend some distance beneath the ramus of the jaw, lying between the lateral pterygoid and styloglossus muscles. The angular artery is frequently small and is variable in its distribution. It is usually the terminal branch of the facial artery.

Midy et al. (1986) described three types of the proximal facial artery. The first type arose at the level of the angle of the mandible, ran around the submandibular gland to the mandible, and then entered the face. The second type arises from the ECA rather distally, deep to the posterior belly of the digastric artery, continues along the inner circumference of the mandible, and finally travels through the submandibular gland. The latter type is the most common and travels in a groove along the lateral border of the submandibular gland and medial to the mandible.

Lingual artery

This artery often arises from the common carotid along with the facial and less frequently with the superior thyroid. The lingual and facial (Faller 1946; 10–20%), lingual and superior thyroid, or all three arteries can arise from a common trunk. Alternatively, a common trunk can supply the lingual, superior thyroid, and maxillary arteries (14%, Haller; 20%, Quain; 25%, Livini; 20%, Dall'Acqua; 15%, Poynter) or with the ascending pharyngeal (0.5%, Livini) (Bergman et al. 1996).

The lingual sometimes branches from the facial. It can also give rise to both the facial and the maxillary as well as to the submental, ascending palatine, superior laryngeal, or accessory superior thyroid arteries.

Its hyoid branch is sometimes absent; when present, this branch varies inversely in size with the hyoid branch of the superior thyroid artery. The lingual is occasionally replaced, totally or partially, by a branch of the maxillary or the submental branch of the facial. The lingual artery sometimes pierces the origin of the hyoglossus rather than passing beneath the posterior border of the muscle, or it can travel external to the muscle. The sublingual branch can arise from the facial and then pierce the mylohyoid muscle. The lingual artery occasionally provides the following unusual branches: the superior laryngeal, the submental, and the ascending palatine arteries.

Superficial temporal artery

The superficial temporal artery occasionally gives rise to the maxillary above the zygomatic arch, or to a tympanic artery (Power 1850).

If it is small, it is replaced by the posterior auricular. When larger, it can give rise to branches normally provided by the facial such as the lateral nasal and superior and inferior labial. Its transverse facial branch is sometimes doubled. Its anterior temporal branch is occasionally larger than the posterior branch and can take the place of a defective facial artery. The posterior branch may be absent, in which case the occipital or posterior auricular artery takes over its distribution. The transverse facial artery can arise directly from the ECA.

Sometimes the orbital branch of the superficial temporal artery is larger than usual and extends to the eyelids. Cruveilhier saw it communicate with the supraorbital artery and supply a large part of the forehead.

Maxillary artery

The origin of this artery is usually constant, but very rarely it is a branch of the facial artery. After it crosses behind the neck of the mandible, it has been seen to pierce the medial pterygoid muscle in its upward course.

Quain reported a case where the maxillary artery provided two vessels that entered the cranial cavity (one branch through the foramen rotundum and the second through the foramen ovale) to compensate for the absence of the internal carotid. The maxillary artery can be doubled.

The relationship of the maxillary artery to the lateral pterygoid muscle is important for surgery. The maxillary artery is medial to the lateral pterygoid muscle in about 30–45% of cases and lateral to the lateral pterygoid in about 55–70%. The maxillary artery can pierce the lower head of the lateral pterygoid. The number of branches arising from the maxillary artery is frequently reduced because two or more take origin from a common trunk.

The anterior deep temporal branch of the maxillary sometimes exists as a temporobuccal trunk, which divides into the anterior deep temporal (behind the nerve of the same name) and buccal arteries. The anterior deep temporal can substitute for the lacrimal artery; the middle deep temporal branch of the maxillary can exist (less than 20%) as a temporomasseteric trunk, which gives rise to the middle deep temporal and a branch to the masseter muscle (Fig. 47.5).

Lang (1995) listed the following variations of the maxillary artery:

1. The maxillary artery may divide into three trunks which give off the inferior alveolar, masseteric and buccal, and posterior superior alveolar arteries.
2. The maxillary artery may be absent and replaced by a large ascending palatine artery.
3. The facial artery may arise from the maxillary artery.
4. The maxillary artery may arise from the facial artery.
5. The maxillary artery may ascend within the parotid gland before traveling to the pterygopalatine fossa.
6. The maxillary artery can pierce the temporalis muscle.

Middle meningeal artery (MMA)

The MMA may be absent. In 99% of individuals, the MMA enters the cranial cavity via the foramen spinosum. When this foramen is hypoplastic or absent, especially when the MMA has an alternative origin, the artery enters the foramen ovale along with the mandibular division of the trigeminal nerve. Also, rarely, it can enter through the petrosphenoid fissure or through the superior orbital fissure (Bergman et al. 1988; Bruner and Sherkat 2008). If the foramen spinosum is absent the artery enters the foramen ovale, which is typically the foramen for the mandibular division of the trigeminal nerve. In about 50% of cases the MMA gives rise to an accessory meningeal artery, which also enters the skull via the foramen ovale, or the emissary sphenoidal foramen (20% of cases). It may also supply a palatine branch. The artery may or may not supply the trigeminal (semilunar) ganglion, which usually gets its blood supply from the internal carotid or, less often, the accessory meningeal artery. The anterior division of the MMA occasionally gives rise to a medial branch (0.8% of cases). This branch enters the skull through the superior orbital fissure or a small foramen in the greater wing of the sphenoid to anastomose with the ophthalmic artery.

The entire ophthalmic system of arteries occasionally arises from the middle meningeal artery. On the other hand, if absent, the MMA may be replaced by branches from the lacrimal or ophthalmic arteries. The MMA may give rise to the lacrimal artery. The communicating branch of the MMA may join the lacrimal artery and replace the entire ophthalmic artery in about 2% of individuals. In about 1% of cases the entire lacrimal artery arises from the frontal branch of the middle meningeal artery, Not infrequently, a branch from the anastomotic region of the ophthalmic artery runs backward through the superior orbital fissure and takes part in the blood supply of nerves, bone, and dura in the cavernous sinus. The foramen spinosum may be hypoplastic or absent in a case of an aberrant MMA.

One of the best described origins (0.5%) is the ophthalmic artery (ophthalmic MMA) (Bruner and Sherkat 2008). In such cases, the MMA passes through the lateral end of the superior orbital fissure or a foramen in the greater wing of the sphenoid (Manjunath 2001). The earliest observations of this origin can be traced back to the nineteenth century by Curnow (1873) and Zuckerkandl (1876). Another very rare origin from the persistent stapedial artery (stapedial MMA) was reported as early as 1836 by Hyrtl (House and Patterson 1964).

The stapedial artery may also persist. This vessel has also been associated with an aberrant internal carotid artery. The persistent stapedial artery courses through the tympanic cavity, between the crura of the stapes, and enters the facial canal distal to the geniculate ganglion. It enters the middle cranial fossa by

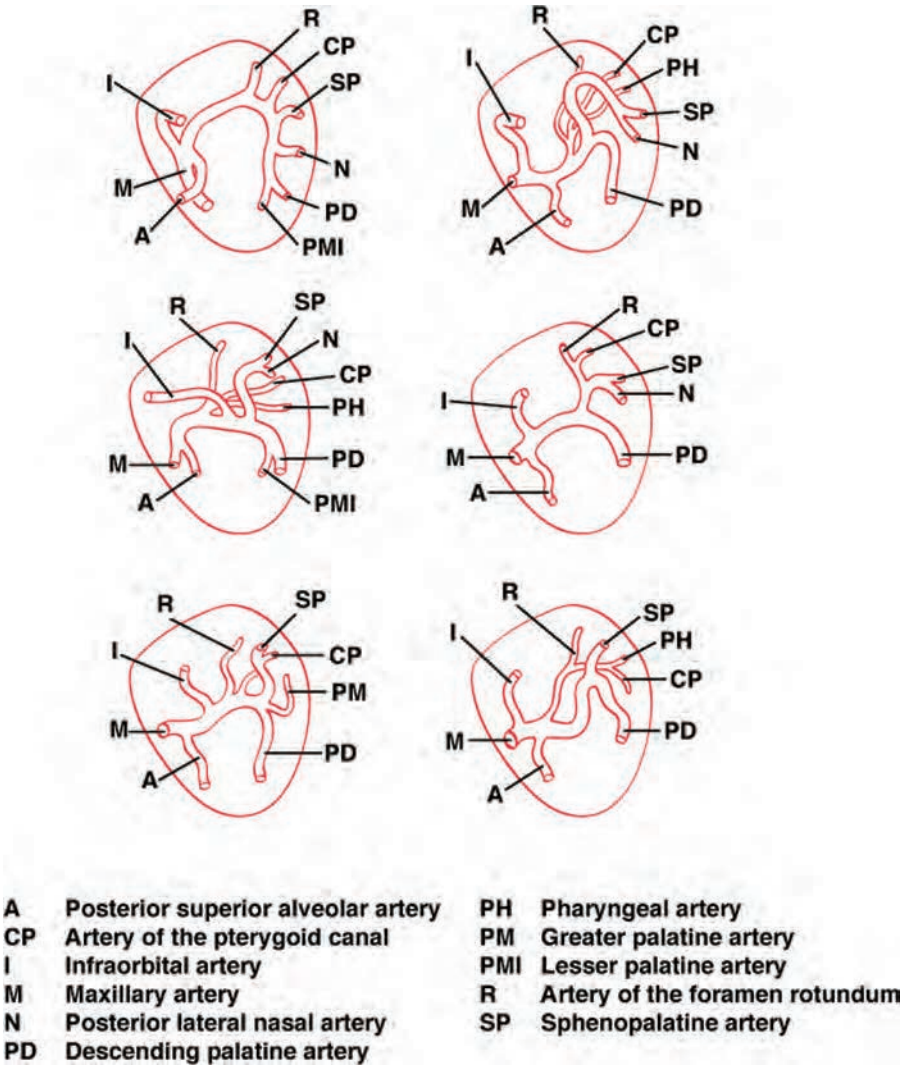

Figure 47.5 Variations of the branches of the maxillary artery in the right pterygopalatine fossa.

Source: adapted after Mandiola et al. (1979).

the facial hiatus, which is the opening for the greater petrosal nerve, and becomes the MMA. In both of these cases, the variants of origin of the middle meningeal artery, the foramen spinosum will be tiny, or absent. Ginsberg et al. (1994) found the foramen spinosum absent in 3.2%, and asymmetry of size was observed in 20 (16%) of their patients.

In most individuals, the MMA arises from the maxillary artery branch of the external carotid artery. Other origins, including branches of the internal carotid artery, are rare. An origin from the petrous segment, prepetrous and suprasellar segment, or the cavernous segment of the internal carotid artery has also been reported (Manjunath 2001; Omeis et al. 2005). On extremely rare occasions, the MMA originates from the basilar artery or the superior cerebellar artery. This could be related to insufficient supply provided by the maxillary artery (Ohata et al. 2006; Shah and Hurst 2007; Kumar and Mishra 2012). It has also been reported to originate from the ascending pharyngeal artery (Manjunath 2001).

Generally, the MMA gives rise to three branches: anterior (bregmatic), middle (obelic), and posterior (lambdoidal). However, the middle branch does not consistently arise from the MMA, and many variations have been described regarding its origin. The most famous classification of these variations is the Adachi classification. According to this, the middle branch can arise from the anterior branch (Adachi type I), posterior branch (Adachi type II), or both (Adachi type III). Giuffrida-Ruggeri proposed a slightly different classification: type I, type IIa, and type IV are similar to Adachi type I, II, and III, respectively; type IIb is associated with low division of the MMA into its terminal branches; and type III is similar to type I but with low division of the MMA (Giuffrida-Ruggeri 1912; Bergman et al. 1988).

Because the origin of the middle branch is variable, many anatomists only consider two branches of the MMA: anterior and posterior (Bruner and Sherkat 2008; Alkhazali 2009; Adeeb et al. 2012). The length of the MMA from its origin

to its terminal division ranges between 0.21 and 4.1 cm, so it might divide before entering the cranial cavity and be associated with a double foramen spinosum (Bergman et al. 1988; Alkhazali 2009). Its diameter ranges between 0.2 and 0.39 cm (Alkhazali 2009).

In 50% of cases the MMA gives rise to an accessory meningeal artery, which also enters the skull via the foramen ovale or the emissary sphenoidal foramen. On other occasions it gives rise to a palantine, ophthalmic (2%), or lacrimal branch (1%). The latter can also arise from the anterior branch of the MMA (Bergman et al. 1988).

The length of the anterior branch ranges between 2.52 and 3.58 cm and its diameter between 0.21 and 0.45 cm (Alkhazali 2009). A bony groove, or less commonly a bony canal for the anterior branch, might be seen unilaterally or bilaterally (Chandler and Derezinski 1935; Alkhazali 2009). The length of the canalized portion (when present) ranges between 0.1 and 2.05 cm and its diameter between 0.35 and 1.92 cm (Alkhazali 2009). The entrance to the bony canal can be located up to 20 mm inferior (mostly), superior, anterior, or inferior to the pterion (Chandler and Derezinski 1935).

The anterior branch can also give rise to a medial branch (0.8%) that enters the superior orbital fissure or small foramen in the greater wing of the sphenoid to anastomose with the ophthalmic artery (Bergman et al. 1988; Alkhazali 2009).

Rarely, the anterior branch is absent and is replaced by the ophthalmic meningeal artery, which supplies part of the dura (Alkhazali 2009). On other occasions the anterior branch arises from the ophthalmic division instead of the MMA (Manjunath 2001). Double anterior branches have also been reported; in these cases the lateral anterior branch has the same course as the anterior branch. The medial anterior branch courses along the mandibular and maxillary nerves on the lateral aspects of the foramen ovale and foramen rotundum, and either supplies the dura along the side of the sella turcica or bends laterally to anastomose with branches from the anterior meningeal artery (Chandler and Derezinski 1935).

During its course, the anterior branch can also bifurcate into two ascending branches above the level of the lesser wing of the sphenoid. One or both of these branches may be contained in a bony canal or course on a groove (Chandler and Derezinski 1935).

In some cases, the ascending anterior branch emerges from one canal to enter another after a short interval, during which it lies superficial to the bony plate of the cranium (Chandler and Derezinski 1935).

The length of the posterior branch ranges between 3.2 and 4.9 cm, and its diameter between 0.1 and 0.36 cm (Alkhazali 2009).

Kanavel and Davis (1922) classified the variations of the posterior branch into six types: type I, the posterior branch is given off midway between the foramen spinosum and the pterion; type II, it is given off at a higher level, near the region of the pterion; type III, it is given off at a lower level, very soon after the MMA emerges from the foramen spinosum; type IV, two posterior branches arise separately; type V, two posterior branches arise by bifurcation of a single stem; and type VI, no posterior branch is identified (Kanavel and Davis 1922; Chandler and Derezinski 1935). A bony canal containing the posterior branch can also be found (Chandler and Derezinski 1935).

Rarely, the MMA is absent and is replaced by a branch from the lacrimal or the ophthalmic artery (Alkhazali 2009). The anterior tympanic artery can arise from the middle meningeal artery.

Accessory meningeal artery (AMA)

The artery distributes branches to the medial pterygoid muscle, superior head of the lateral pterygoid, tensor veli palatini, parts of the sphenoid bone, middle cranial fossa, root of the mandibular division of the trigeminal nerve, and the otic ganglion.

It has been suggested that the name AMA, which was used to reflect the complementary function of this artery, is a misnomer as the artery makes a very limited contribution to blood supply (10%). For this reason, and in view of its anatomical course, the authors suggest changing its name to pterygomeningeal artery (Vitek 1989).

The AMA is present in 96% of individuals and arises equally frequently from either the maxillary (MA) or the MMA. If the MA passes behind the lateral pterygoid muscle, the AMA arises from the MA; when the MA passes in front of the lateral pterygoid muscle, the AMA arises from the MMA (Bergman et al. 1988). Rarely, the AMA arises from the superior cerebellar artery (Komiyama et al. 1998). The AMA can also be duplicated (Bergman et al. 1988).

The MMA and AMA have been reported to supply the trigeminal (semilunar) ganglion in some individuals (Bergman et al. 1988). The AMA can also supply the posterior nasal cavity (Duncan and Dos Santos 2003).

In a very rare case, the MMA gave rise to the posterior superior alveolar artery extracranially, which then gave rise to an unusually large pterygoid branch (Kresimir Lukic et al. 2001).

Artery of the pterygoid canal

The artery of the pterygoid canal can arise from the internal carotid artery, and not the maxillary, in up to 30% of cases.

Ascending pharyngeal artery

The ascending pharyngeal artery (APA) can originate from the ECA or the common carotid artery (approximately 65–80%), from the occipital artery (20–14%), or from the common carotid artery (9–7%). Lippert and Pabst (1985) reviewed its origin and, from reports in the literature, concluded that the APA arises from the ECA in 70%, occipital artery in 20%, internal carotid

artery in 8%, and facial artery in 2%. Power (1850) found it arising from the superior thyroid artery. It is occasionally doubled or tripled and can give rise to the ascending palatine or superior laryngeal arteries (Bergman et al. 1996). When arising from the external carotid artery, Lang (1995) found that the APA (with a diameter of 0.9–2.3 mm) arose from its anteromedial, medial, and posteromedial surfaces in 15.9, 41.4, and 22.7% of individuals, respectively.

Cavalcanti et al. (2009) studied the course and branching pattern of the APA in 20 cadavers. In 80% of the specimens it originated from the ECA; it originated from the internal carotid artery, CCA bifurcation, occipital artery, and a trunk common to the lingual and facial arteries in 5% each. Although the number of specimens was limited, the results were consistent with previous studies on larger series.

The APA is a small but important artery that supplies multiple cranial nerves and anastomotic channels to the anterior and posterior cerebral circulations. Anastomoses to the internal carotid artery are either direct via the lateral clival branch of the jugular artery or the recurrent artery of the foramen lacerum, or indirect via the superior pharyngeal branch to the inferolateral trunk, the clival branches to the meningohypophyseal trunk, or the inferior tympanic branch to the caroticotympanic branch. Anastomoses to the vertebral artery are through the hypoglossal branch and the musculospinal branch. Anastomoses to the occipital artery can be either indirect through the odontoid arch system or direct through a common trunk. Lastly, the APA can be connected to the maxillary artery at the level of the descending palatine artery through the middle pharyngeal branch or the pterygovaginal artery to the accessory meningeal artery (Hacein-Bey et al. 2002).

The APA has potential anastomoses to all neighboring major arteries. A 60-year-old woman underwent angiography and embolization for a glomus tympanicum tumor. At the end of the embolization the patient had posterior circulatory stroke. The check angiogram revealed nearly total devascularization of the tumor; there was also filling of the left vertebral artery through an anastomotic channel. MRI confirmed the infarct in the posterior circulation. The anastomoses to the vertebral artery in this case were through the musculospinal artery (Sawlani et al. 2009). At its termination near the anterior arch of the atlas, the APA gave off transverse branches that anastomosed with the anterior ascending arteries to the odontoid process (Haffajee 1997).

Wei et al. (2004) reported a case of complete occlusion of the internal carotid artery associated with an aberrant ipsilateral APA originating from the proximal internal carotid artery, which mimicked a stenotic internal carotid artery on sonography.

Uchino and Suzuki (2011) reported an extremely rare case, diagnosed using magnetic resonance angiography, where the posterior inferior cerebellar artery was supplied by the jugular branch of the APA which passes through the medial side of the jugular foramen pars vascularis.

The APA is sometimes connected to the internal jugular vein via an arteriovenous fistula. Tomsick and Tomsick (2008) reported a 32-year-old female with a rare direct arteriovenous fistula from the APA to the internal jugular vein. Chaloupka et al. (1992) and Fox and Allcock (1978) reported similar cases; Takahashi et al. (1974) reported an arteriovenous fistula between the APA and the sigmoid sinus.

Occipital and posterior auricular arteries

The occipital artery can be a branch of the internal carotid, thyrocervical trunk, inferior thyroid, vertebral, or the ascending cervical branch of the inferior thyroid artery (Power 1850). The posterior auricular artery (12%), ascending pharyngeal artery, stylomastoid and posterior meningeal branches can arise from the occipital artery (Bergman et al. 1996). The occipital artery can travel superficial to the sternocleidomastoid muscle.

Lippert and Pabst (1985) reviewed the origins of occipital and posterior auricular arteries: in 85% of cases the two arteries originated separately from the ECA; in 14% they both formed an occipitoauricular trunk; in 1% a superficial occipital artery ran superficial to the sternocleidomastoid; and in <0.1% the occipital artery originated from the internal carotid. Power (1850) reported a transverse facial artery arising from the posterior auricular artery.

Iwai et al. (2012a) investigated the origin of the occipital artery using three-dimensional computed tomographic angiography on 265 patients with cancer of the head and neck. The occipital artery originated from the internal carotid artery in approximately 0.2%.

Uchino et al. (2011) retrospectively reviewed MRA images of 2866 patients that included the carotid bifurcation. They observed six cases (seven arteries) of variant origin of the occipital artery, which represented an incidence of 0.21%. The occipital artery arose from the internal carotid artery in four patients (five arteries), from the carotid bifurcation in one, and from the vertebral artery in one. Five of the seven variant arteries occurred on the right side.

Iwai et al. (2012b) reported an 87-year-old male who presented with advanced tongue cancer, exhibiting a variant origin of the occipital artery from the internal carotid artery 8.8 mm distal from the carotid bifurcation.

The occipital artery can form anastomoses with neighboring arteries. Alexander et al. (2014) reported a case of occipital artery anastomosis to the vertebral artery causing pulsatile tinnitus. The occipital artery can also form arteriovenous fistulas. Chae et al. (2001) reported a case of a fistula between the posterior auricular artery and the internal jugular vein, which caused pulsatile tinnitus in the right orbital region two months after an accident.

The external carotid artery can give rise to the vertebral artery.

References

Adachi B. 1928. *Das Arteriensystem der Japaner*. Kyoto: Kenkyusha Press.

Adeeb N, Mortazavi MM, Tubbs RS, Cohen-Gadol AA. 2012. The cranial dura mater: a review of its history, embryology, and anatomy. *Childs Nerv Syst* 28: 827–837.

Aggarwal NR, Krishnamoorthy T, Devasia B, Menon G, Chandrasekhar K. 2006. Variant origin of superior thyroid artery, occipital artery and ascending pharyngeal artery from a common trunk from the cervical segment of internal carotid artery. *Surg Radiol Anat* 28: 650–653.

Alexander MD, English J, Hetts SW. 2014. Occipital artery anastomosis to vertebral artery causing pulsatile tinnitus. *J Neurointerv Surg* 6(2): e15.

Alkhazali TJ. 2009. Anatomical variation in the course, branches, and metrical measurement of the grooves, of the middle meningeal artery inside the skull. *Tikrit Med J* 15: 38–41.

Bergman RA, Thompson SA, Afifi AK, Saadeh FA. 1988. *Compendium of Human Anatomic Variation: Catalog, Atlas and World Literature*. Baltimore and Munich: Urban & Schwarzenberg.

Bergman RA, Afifi AK, Miyauchi R. 1996. Illustrated Encyclopedia of Human Anatomic Variation: Opus II: Cardiovascular System: Arteries: Head, Neck, and Thorax. Available at http://www.anatomyatlases.org/AnatomicVariants/Cardiovascular/Text/Arteries (accessed 23 October 2015).

Bruner E, Sherkat S. 2008. The middle meningeal artery: from clinics to fossils. *Childs Nerv Syst* 24: 1289–1298.

Budhiraja V, Rastogi R. 2010. Variant origin of thyrolingual trunk from left common carotid artery. *Int J Anat Var (IJAV)* 3: 44–45.

Cavalcanti DD, Reis CV, Hanel R, Safavi-Abbasi S, Deshmukh P, Spetzler RF, Preul MC. 2009. The ascending pharyngeal artery and its relevance for neurosurgical and endovascular procedures. *Neurosurgery* 65: 114–120.

Chae SW, Kang HJ, Lee HM, Hwang SJ. 2001. Tinnitus caused by traumatic posterior auricular artery-internal jugular vein fistula. *J Laryngol Otol* 115: 313–315.

Chaloupka JC, Kibble MB, Hoffman JC. 1992. Ascending pharyngeal artery-internal jugular vein fistula complicating radical neck dissection. *Neuroradiology* 34: 524–525.

Chandler SB, Derezinski CF. 1935. The variations of the middle meningeal artery in the middle cranial fossa. *Anat Rec* 62: 309–319.

Curnow J. 1873. Two instances of irregular ophthalmic and middle meningeal arteries. *J Anat Physiol* 8: 155–156.

Duncan IC, Dos Santos C. 2003. Accessory meningeal arterial supply to the posterior nasal cavity: another reason for failed endovascular treatment of epistaxis. *Cardiovasc Intervent Radiol* 26: 488–491.

Ezure H, Mori R, Ito J, Otsuka N. 2011. Case of completely absent facial artery. *IJAV* 4: 72–74.

Faller A. 1946. Variation in site and form of branching of the carotid artery. *Schweiz Med Wochenschrift* 76: 1156–1158.

Fox AJ, Allcock JM. 1978. Successful embolization of a fistula between the ascending pharyngeal artery and internal jugular vein. *Neuroradiology* 15: 149–152.

Gailloud P, Murphy KJ, Rigamonti D. 2000. Bilateral thoracic bifurcation of the common carotid artery associated with Klippel–Feil anomaly. *AJNR Am J Neuroradiol* 21: 941–944.

Geraci C, Mulè G, Mogavero M, Geraci G, Foraci AC, Cerasola G. 2009. Aberrant origin of the superior thyroid artery and ascending pharyngeal artery from a common trunk arising from the common carotid artery in a hypertensive patient with dizziness. *Minerva Cardioangiol* 57: 684–686.

Ginsberg LE, Pruett SW, Chen MYM, Elster AD. 1994. Skull-base foramina of the middle cranial fossa: Reassessment of normal variation with high-resolution CT. *AJNR* 15: 283–291.

Giuffrida-Ruggeri V. 1912. Über die endocranischen furchen der arteria meningea media beim menschen. *Zeitschrift Morphol Anthropol* 15: 401–412.

Gluncic V, Petanjek Z, Marusic A, Gluncic I. 2001. High bifurcation of common carotid artery, anomalous origin of ascending pharyngeal artery and anomalous branching pattern of external carotid artery. *Surg Radiol Anat* 23: 123–125.

Gomez CK, Arnuk OJ. 2013. Intrathoracic bifurcation of the right common carotid artery. *BMJ Case Rep pii*: bcr2012007554. doi: 10.1136/bcr-2012-007554.

Hacein-Bey L, Daniels DL, Ulmer JL, Mark LP, Smith MM, Strottmann JM, Brown D, Meyer GA, Wackym PA. 2002. The ascending pharyngeal artery: branches, anastomoses, and clinical significance. *AJNR* 23: 1246–1256.

Haffajee MR. 1997. A contribution by the ascending pharyngeal artery to the arterial supply of the odontoid process of the axis vertebra. *Clin Anat* 10: 14–18.

Horowitz M, Bansal S, Dastur K. 2003. Aortic arch origin of the left external carotid artery and type II proatlantal fetal anastomosis. *AJNR* 24: 323–325.

House HP, Patterson ME. 1964. Persistent stapedial artery: report of two cases. *Trans Am Acad Ophthalmol Otolaryngol* 68: 644–646.

Iwai T, Izumi T, Inoue T, Maegawa J, Fuwa N, Mitsudo K, Tohnai I. 2012b. Occipital artery arising from the anterior aspect of the internal carotid artery identified by three-dimensional computed tomography angiography. *Iran J Radiol* 9: 103–105.

Iwai T, Izumi T, Inoue T, Maegawa J, Mitsudo K, Tohnai I. 2012a. Incidence of the occipital artery arising from the internal carotid artery identified by three-dimensional computed tomographic angiography. *Br J Oral Maxillofac Surg* 50: 373–375.

Kanavel AB, Davis LE. 1922. Surgical anatomy of the trigeminal nerve. *Surg Gynecol Obstet* 34: 357–366.

Komiyama M, Kitano S, Sakamoto H, Shiomi M. 1998. An additional variant of the persistent primitive trigeminal artery: accessory meningeal artery–antero-superior cerebellar artery anastomosis associated with moyamoya disease. *Acta Neurochir (Wien)* 140: 1037–1042.

Kresimir Lukic I, Gluncic V, Marusic A. 2001. Extracranial branches of the middle meningeal artery. *Clin Anat* 14: 292–294.

Kumar S, Mishra NK. 2012. Middle meningeal artery arising from the basilar artery: report of a case and its probable embryological mechanism. *J Neurointerv Surg* 4: 43–44.

Lang J. 1993. *Clinical Anatomy of the Cervical Spine*. New York: Thieme.

Lang J. 1995. *Clinical Anatomy of the Masticatory Apparatus and Peripharyngeal Spaces*. New York: Theime.

Lippert H, Pabst R. 1985. *Arterial variations in man. Classification and frequency*. Munich: J. F. Bergmann Verlag.

Mandiola E, Delgado A, Chatain I. 1979. Contribucion al studio de la fossa pterigopalatina/I contenido vascular y tecnica de abordaje por la via transantral. *Rev Otorhinolaryngol* 39: 39–46.

Manjunath KY. 2001. Anomalous origin of the middle meningeal artery: a review. *J Anat Soc India* 50: 179–183.

Mehta V, Suri RK, Arora J, Rath G, Das S. 2010. Anomalous superior thyroid artery. *Kathmandu Univ Med J* 8: 429–431.

Midy DB, Mauruc P, Vergnes PC. 1986. A contribution to the study of the facial artery, its branches and anastomoses; application to the anatomic vascular bases of facial flaps. *Surg Radiol Anat* 8: 99–107.

Natsis K, Raikos A, Foundos I, Noussios G, Lazaridis N, Njau SN. 2011. Superior thyroid artery origin in Caucasian Greeks: A new classification proposal and review of the literature. *Clin Anat* 24: 699–705.

Nayak SB, Soumya KV. 2008. Neurovascular variations in the carotid triangle. *Int J Anat Var (IJAV)* 1: 17–18.

Ohata K, Nishio A, Takami T, Goto T. 2006. Sudden appearance of transdural anastomosis from middle meningeal artery to superior cerebellar artery during preoperative embolization of meningioma. *Neurol India* 54: 328.

Omeis I, Crupain M, Tenner M, Murali R. 2005. Anomalous origin of the middle meningeal artery from the petrous segment of the internal carotid artery associated with multiple cerebrovascular abnormalities. *Internet J Radiol* 4: 2.

Ongeti KW, Ogeng'o JA. 2012. Variant origin of the superior thyroid artery in a Kenyan population. *Clin Anat* 25: 198–202.

Power JH. 1850. *Surgical Anatomy of the Arteries and Descriptive Anatomy of the Heart by the Late Valentine Flood, MD*. Dublin: Fannin and Co.

Rusu MC, Nimigean V, Banu MA, Cergan R, Niculescu V. 2007. The morphology and topography of the superior laryngeal artery. *Surg Radiol Anat* 29: 653–660.

Satishkumar PS, Archana BS, Deepak JS. 2013. Variant formation of external jugular vein and branching pattern of external carotid artery. *Int J Anat Var* 6: 140–142.

Sawlani V, Browing S, Sawhney IM, Redfern R. 2009. Posterior circulation stroke following embolization of glomus tympanicum: relevance of anatomy and anastomoses of ascending pharyngeal artery. A case report. *Interv Neuroradiol* 15: 229–236.

Shah QA, Hurst RW. 2007. Anomalous origin of the middle meningeal artery from the basilar artery: a case report. *J Neuroimaging* 17: 261–263.

Takahashi M, Gito Y, Kowada M. 1974. Arteriovenous fistula between the ascending pharyngeal artery and the sigmoid sinus. Report of a case with spontaneous regression. *Neuroradiology* 7: 245–248.

Tomsick SD, Tomsick TA. 2008. Direct ascending pharyngeal artery to jugular vein arteriovenous fistula. A case report. *Interv Neuroradiol* 14: 191–194.

Uchino A, Suzuki C. 2011. Posterior inferior cerebellar artery supplied by the jugular branch of the ascending pharyngeal artery diagnosed by MR angiography: report of two cases. *Cerebellum* 10: 204–207.

Uchino A, Saito N, Mizukoshi W, Okada Y. 2011. Anomalous origin of the occipital artery diagnosed by magnetic resonance angiography. *Neuroradiology* 53: 853–857.

Ueda S, Kohyama Y, Takase K. 1984. Peripheral hypoglossal nerve palsy caused by lateral position of the external carotid artery and an abnormally high position of bifurcation of the external and internal carotid arteries: a case report. *Stroke* 15: 736–739.

Vitek JJ. 1989. Accessory meningeal artery: an anatomic misnomer. *AJNR Am J Neuroradiol* 10: 569–573.

Wei CJ, Chang FC, Chiou SY, Teng MM, Hu HH, Chung CP, Chou YH, Chang CY. 2004. Aberrant ascending pharyngeal artery mimicking a partially occluded internal carotid artery. *J Neuroimaging* 14: 67–70.

Zuckerlandl E. 1876. *Zür Anatomie der orbitalarterien. Medicinische Jahrbücher der K.K*. Gesellschaft der Ärzte zu Wien 343–350.

Zümre O, Salbacak A, Ciçekcibaşi AE, Tuncer I, Seker M. 2005. Investigation of the bifurcation level of the common carotid artery and variations of the branches of the external carotid artery in human fetuses. *Ann Anat* 187: 361–369.

Further reading

Anson BJ (ed.) 1966. *Morris's Human Anatomy, 12th edition*. New York: Blakiston Division, McGraw-Hill Book Co.

Bien G. 1907. Eine seltene Varietät der Arteria maxillaris interna. *Anat Anz* 30: 421–426.

Dall'Acqua U. 1901. L'artere temporale superficielle de l'homme. *Arch Ital Biol* 36: 347–348.

Dall'Acqua U, Meneghetti A. 1905. Ricerche di anatomia comparata sulle arteria della faccia. *Arch Ital Anat Embriol* 4: 161–182, 306–365.

Dall'Acqua U, Meneghetti A. 1906. Recherches d'anatomie comparée sur les artères de la face. *Arch Ital Biol* 46: 302–304.

Dall'Acqua U, Meneghetti A. 1907. Recherches d'anatomie comparée sur les artères de la face. *Arch Ital Biol* 47: 484–486.

Demarquay, T. 1845. *Anomalies Artèrielles*. Bull Mém Soc Anatomique Paris 1845: 41.

Grönroos H. 1902. Eine seltene anorddung der arteria maxillaris externa bei einem erwachsenen. *Anat Anz* 20: 9–16.

Grote G. 1901. Die varietäten der arteria temporalis superficialis. *Z Morph Anthrop* 3: 1–20.

Henle J. 1868. *Handbuch der Systematischen Anatomie des Menschen*. Braunschweig: Von Friedrich Vieweg und Sohn.

Howe L. 1880. Unusual position of the arteria anguli nasi. *Buffalo Med and Surg J* 20: 495–498.

Huber GC. (ed.) 1930. *Piersol's Human Anatomy, ninth edition*. Philadelphia: L.B. Lippincott Co.

Joessel S. 1878. Neue anomalien der carotis externa und der maxillaris interna. *Arch Anat Physiol Wissen Med* 1878: 433–437.

Kadyi H. 1881. Abnormer verlauf der art. lingualis. *Medizinische Jahrbücher* 1881: 44–45.

Kalantroff J. 1887. Anomaly of internal maxillary artery. *Russkaia Meditsina, St Petersbourg* 12: 225–227 (in Russian).

Kren O. 1931–32. Über eine seltene anomalie der arteria lingualis nebst einer kurzen zusammenfassung ihrer häufigsten topographischen varietaten. *Anat Anz* 73: 107–110.

Lasker GW, Opdyke DL, Miller H. 1951. The position of the internal maxillary artery and its questionable relation to the cephalic index. *Anat Rec* 109: 119–126.

Latarjet A. 1948. *Testut's Traite d'Anatomie Humaine, ninth edition*. Paris: G. Doin & Cie.

Lauber H. 1901. Über einige varietäten im verlaufe der arteria maxillaris interna. *Anat Anz* 19: 444–448.

Long JJ. 1890. The relation of the internal maxillary artery to the external pterygoid muscle. Collective investigation in the anatomical department of Trinity college, Dublin. *Trans Roy Acad Med Ireland* 8: 520–521.

Lurje AS. 1947. On the topographical anatomy of the internal maxillary artery. *Acta Anat* 2: 219–231.

Mériel F. 1903. Anomalies de l'artère linguale au point de vue opératoire. *Bull Mém Soc Anatomique de Paris* 5: 573–575.

Monjardino A. 1906. Anomalia da arteria maxillar interna. *J Sociedade das Sciencias Medicas de Lisboa* 70: 181–182.

Morestin H. 1894. Anomalie de l'artère linguale. *Bull Mém Soc Anatomique Paris* 8: 680–681.

Navarro JAC, Filho JLT, Zorzetto NL. 1982. Anatomy of the maxillary artery in (and) to the pterygomaxillopalatine fossa. *Anat Anz* 152: 413–433.

Nizankowski C. 1972. Seltenes Fall eines gemeinsamen stammes der schilddrüzenzungengesichtsschlagader beim menschen. *Anat Anz* 132: 530–534.

Polonskaja R. 1935. Zur fraga der morphologie der art. maxillaris externa bei vertretern der weissen und der gelben rasse. *Anat Anz* 80: 331–339.

Poynter CWM. 1922. Congenital anomalies of the arteries and veins of the human body with bibliography. *The University Studies of the University of Nebraska, Lincoln* 22: 1–106.

Robineau M. 1897. Anomalies de la glande parotide, de l'artère maxillaire interne et du nerf facial. *Bull Mém Soc Anatomique Paris* 1897: 384–385.

Rouvière H, Vallois H. 1908. Note sur le mode de termiaison de l'artère sublinguale chez l'homme (Terminaison de la branche maxillaire de la sublinguale). *Biblio Anat* 18: 106–109.

Schaefer EA, Symington J, Bryce TH, Eds. 1915. *Quain's Anatomy, 11th edition*. Londond: Longmans, Green, and Co.

Shepherd FJ. 1889. *Abnormal lingual artery*. Medical News, Philadelphia 1889: 305.

Skopakoff C. 1968. Über die variabilat im verlauf der a. maxillaris. *Anat Anz* 123: 534–546.

Tokarski S. 1931. Les variations de l'artere maxillare interne chez l'homme expliquées par les variations chez les primates. *Assoc Anatomistes Comptes Rendus* 26: 507–510.

von Textor J 1857. Ungewöhnlicher ursprung der inneren kieferschlagader. *Verhandlungen der Physikalisch-Medicinische Gesellschaft in Wurtzburg* 7: 230–233.

48 Vertebral artery

Bernard George[1] and Michaël Bruneau[2]
[1]Hôpital Lariboisière, Paris, France
[2]Hôpital Erasme, Brussels, Belgium

Anatomical variations in the origin, size, course, and branching of the vertebral artery (VA; Fig. 48.1) are common. Such variations need to be known and recognized by any clinician dealing with pathologies related to this vessel. The VA is the first branch of the subclavian artery (SCA) originating from its posterior aspect. It is divided into four segments:

1. V1 or ostial segment from the vessel's origin to its entrance into the C6 transverse foramen, accompanied by one or two vertebral veins traveling anterior to it.
2. V2 or transverse foramen segment from C6 to the C2 transverse foramen, accompanied by the vertebral venous plexus and the vertebral nerve.
3. V3 or suboccipital segment from C2 to the foramen magnum (FM) dura.
4. V4 or intradural segment from the FM to the junction with the opposite VA to form the basilar trunk (BT).

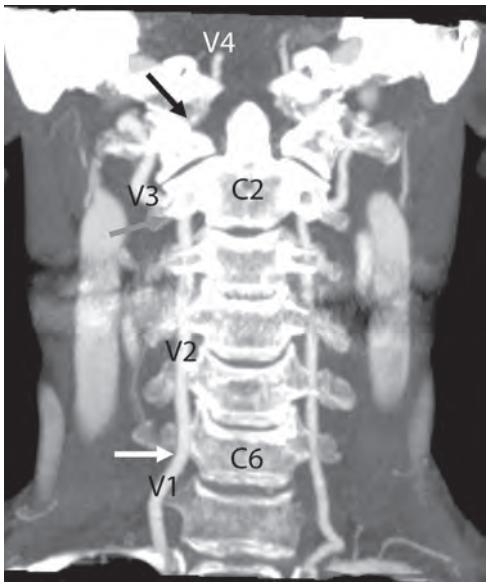

Figure 48.1 Normal anatomy of the vertebral artery. Arrows indicate the limits of the different segments.

Origin

SCA and branches

The VA can be the second branch of division of the SCA after the inferior thyroid artery and before the cervical artery (Satti et al. 2007). It can arise from the inferior thyroid artery, the thyrocervical trunk (Matula et al. 1997), or the costocervical trunk. The VA may also give rise to the inferior thyroid artery.

Aortic arch

The left VA originates from the aortic arch in 5–8% of individuals (Osborn 1999; Lasjaunias and Ter Brugge 2001a; Goray et al. 2005). The most frequent site is between the common carotid artery (CCA) and the SCA. It can also arise distal to the SCA. It is less common for the right VA to originate from the aorta (Lemke et al. 1999; Akdeniz et al. 2007; Satti et al. 2007). The VA can arise from the ascending aorta or between the right SCA and CCA (in the absence of the brachiocephalic trunk) or between the left CCA and left SCA (Wasserman et al. 1992) or even distal to the left SCA (Stoesslein et al. 1982). In the latter two cases it runs behind the esophagus to enter the right C6 transverse foramen (Schwarzacher and Krammer 1989). A bilateral aortic origin of the VA has been reported in four cases (Schwarzacher and Krammer 1989; Al-Okaili and Schwartz 2007). The VA may give rise to the superior intercostal artery (Walsham 1882).

Other origins

The VA has also been reported to originate from the CCA, the internal carotid artery (ICA), or the external carotid artery (ECA) (Flynn 1968; Huber and Peipgras 1976; Yanik et al. 2004; Goray et al. 2005; Ugurlucan et al. 2006).

Double origin

In this case the VA has two branches of origin. They are usually unilateral, but one case of bilateral double origin from the SCA has been reported (Ionete and Omojola 2006). Both

Bergman's Comprehensive Encyclopedia of Human Anatomic Variation, First Edition. Edited by R. Shane Tubbs, Mohammadali M. Shoja and Marios Loukas.
© 2016 John Wiley & Sons, Inc. Published 2016 by John Wiley & Sons, Inc.

branches of origin can arise from the SCA or one each from the SCA and another vessel, aortic arch, or brachiocephalic trunk (Komiyama et al. 1999; Shhadeh et al. 2007; Thomas et al. 2008). The two branches can enter the same foramen or different transverse foramina; usually the medial one enters at the higher level. The branches fuse at C5–C6 in 42.3% of cases, C4–C5 in 30.8%, C3–C4 in 15.4% and C6–C7 in 11.5% (Komiyama et al. 1999). This anomaly is equally frequent on both the right and left sides.

Transverse segment

Abnormal level of entrance into the transverse canal

Figure 48.2 depicts an abnormal level of entrance into the transverse canal. Instead of the C6 transverse foramen, the VA enters another foramen in 7% of cases: C5 (5%); C4 (1%); C7 (0.8%); and C3 (0.2%) (Bruneau et al. 2006a, 2011). Other authors have indicated higher frequencies up to 13% (Daseler and Anson 1959; Brink 1984; Anson 1995; Matula et al. 1997; Lasjaunias and Ter Brugge 2001a). In this anomaly, the VA runs in front of the transverse processes and behind the longus colli (cervicis) muscle before entering the upper foramen. The anomaly has two clinical implications. One is the need for caution in exposing the transverse process surgically since the VA is not protected inside the foramen, so cutting the longus colli muscle confidently along the transverse process entails a risk of injury to the vessel. The other is the association with a fibrous band (generally part of the longus colli muscle) compressing the VA intermittently at the level of its entrance during head extension. This anomaly is readily detected by CT and MRI (Fig. 48.2).

Loops

There are two types of loops: medial and lateral (Bruneau et al. 2006c). Medial loops occur either at the level of the intervertebral discs, sometimes being responsible for nerve root irritation (Figs 48.3, 48.4), or at the level of the vertebral bodies (Fig. 48.5). In both cases the VA can be injured during anterior approaches to the cervical spine (e.g., discectomy, foraminotomy, corpectomy). The incidence of medial loops is about 1%. Lateral loops (Fig. 48.6) are generally due to compression by osteophytic spurs, potentially leading to stenosis or even occlusion (Fig. 48.7; Bruneau et al. 2011).

Bone anomalies

The anterior branch of the transverse process can be very thin or even absent (5%; Kawashima et al. 2003).

A high-riding VA is sometimes observed at the base of the C2 vertebral body where the VA bends laterally to join the C2 transverse foramen. It results in a narrowing of the isthmus of the axis (Neo et al. 2003; Bruneau et al. 2011); screwing through the isthmus is very dangerous in such cases (Fig. 48.8).

Suboccipital segment

Variations at this level are more frequent and can include not only VA but also posteroinferior cerebellar artery (PICA) anomalies.

Duplications and fenestrations

Duplication (Fig. 48.9a) is the division of the VA into two parts, one following the usual course and the other one piercing the dura to run intradurally (Lasjaunias 1983; Lasjaunias and Ter Brugge 2001b; Sim et al. 2001; Bruneau et al. 2011). In fact, the intradural part corresponds to the persistence of one of the embryological intersegmental arteries, which becomes the radicular artery. The global incidence of duplications is 0.7% (Suzuki 1978; Rieger and Huber 1983; Eisenberg et al. 1986; Hashimoto et al. 1987; Takasato et al. 1992). They are almost invariably observed at the C1–C2 level. Either both parts (intradural and extraspinal) or only the intradural part can persist, the latter giving the "intradural course of the VA."

Fenestrations (Fig. 48.9b) are sometimes confused with duplications; these correspond to the VA dividing after a short distance into two channels running into the transverse foramen. This is a rare anomaly with only five cases in the literature (Lasjaunias 1983; Sim et al. 2001; Bruneau et al. 2011), mostly observed above C3.

Bone anomalies

Anomalies of the VA are more frequent in patients having osseous anomalies of the cranio-cervical junction (CCJ) (Fig. 48.10; Yamazaki et al. 2005). The groove of the VA in the posterior arch of atlas can be partially (posterior or lateral bridges) or totally converted to a tunnel (Fig. 48.11) by calcification or ossification of the posterior atlanto-occipital membrane (1–3%) (Hasan et al. 2001; Gupta 2008). This anomaly obviously leads to difficulties in the surgical exposure of the VA at this level.

Intradural segment

Fenestrations

Figure 48.12 depicts how fenestrations can occur in association with aneurysms and dissection (Bernard et al. 2007).

Rete vertebralis

This is an exceptional anomaly presenting as a network through the lateral and anterior spinal arteries. It can be associated with the lack of ICA (Hyogo et al. 1996; Mahadevan et al. 2004).

Termination

The VA can end at the PICA (Fig. 48.13), the occipital artery or a spinal artery (Cagnie et al. 2005a, b; Bruneau et al. 2006a). This is only observed on both sides in exceptional cases (Burger et al. 2007).

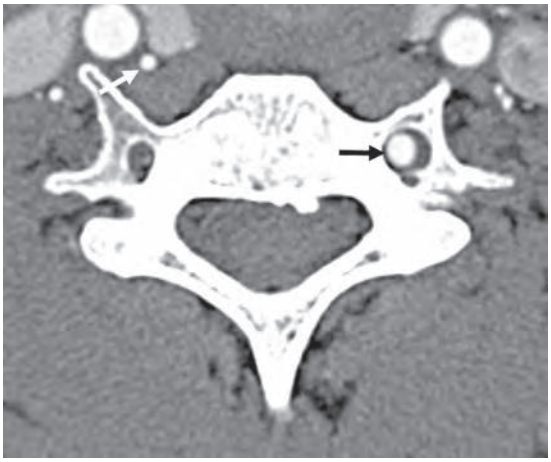

(a)

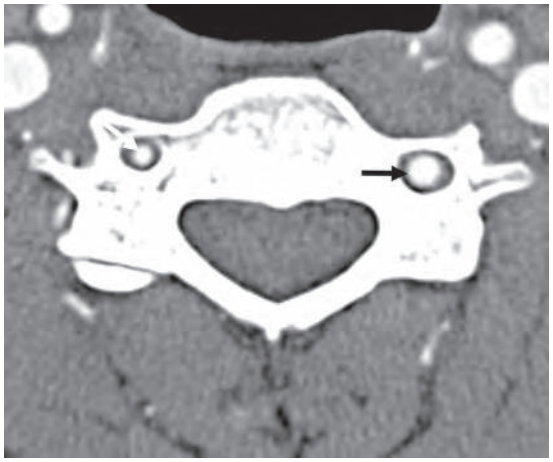

(b)

(c)

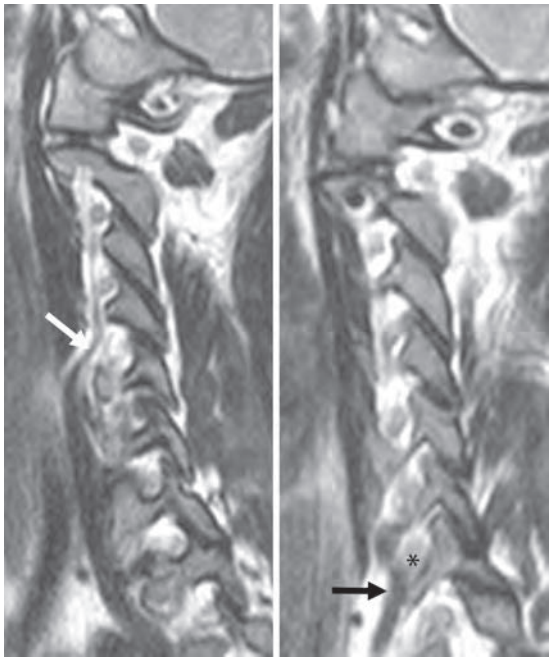

(d)

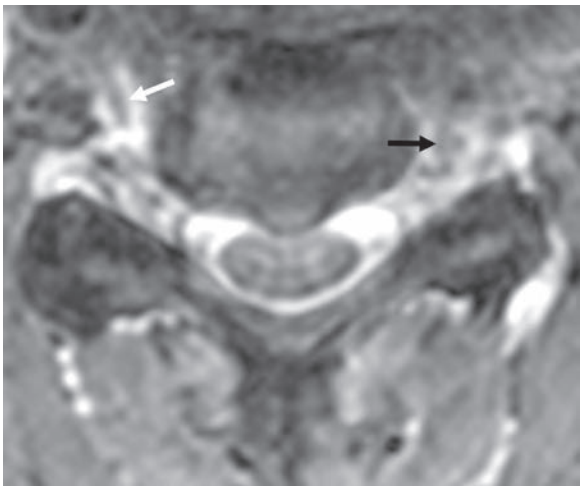

(e)

Figure 48.2 Abnormal level of entrance into the transverse canal viewed on CTA (a–c) and MRI (d–e). (a) Axial image at the C6 level: the right vertebral artery (white arrow) is located in front of the transverse process while the other (black arrow) fills the transverse foramen. Notice also the caliber difference, the left vertebral artery being dominant. A small transverse foramen, as observed on the right side in contrast to the left, is suspected of being an abnormal level of entrance. (b) Axial image at the C4 level: the right vertebral artery has entered the transverse foramen. (c) CTA sagittal reconstructions of the right (white arrow) and left (black arrow) vertebral arteries. CTA sagittal reconstructions displayed the levels of entrance clearly. (d) MRI sagittal views allow the trajectories of both vertebral arteries to be analyzed; this requires more attentive analysis than CTA however because a single image provides a limited view of the artery. We can observe that the right vertebral artery (white arrow) has a curved trajectory just before entering the C4 transverse foramen. The left vertebral artery (black arrow) is visible on a shorter segment where the artery becomes closer to the C7 nerve root (asterix), indicating entrance at the C6 transverse foramen. (e) MRI axial view, T2-weighted image. It is difficult to be convinced of the exact position of the arteries on a single image, especially since the signal intensity of the artery can vary. The position is only located precisely by analyzing all consecutive images for defining trajectory of the vertebral artery. Both arteries are indicated by arrows.

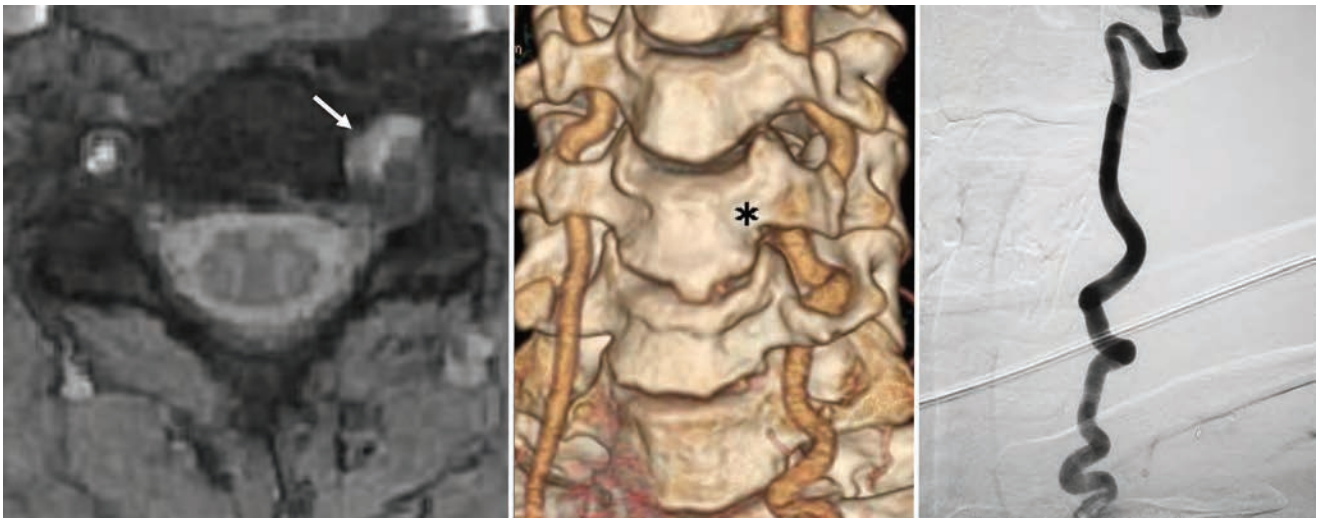

Figure 48.3 Medial foraminal loop of a dominant vertebral artery on the left side at the C5–C6 level. The loop is observed on axial T2-weighted MRI. Anatomical relationships with the bony structures are best viewed on 3D CT scan reconstructions. Angiography also displays the loop and confirms the absence of origin of the anterior spinal artery at this level, which would have been a contraindication for vertebral artery transposition. Notice also the abnormal level of entrance of the right vertebral artery at the C5 level, clearly visible on the 3D CT scan reconstruction.

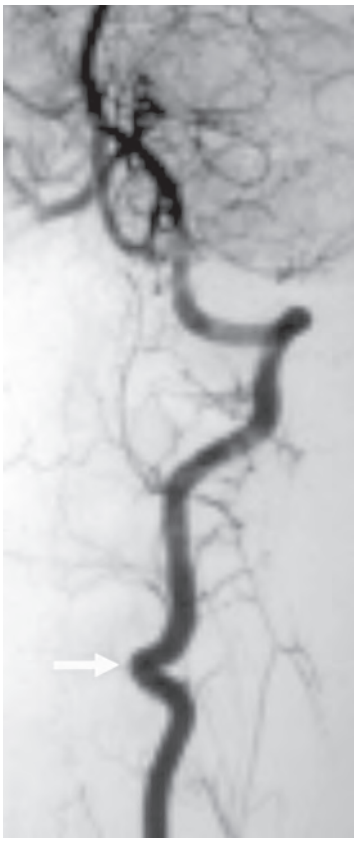

Figure 48.4 Another medial foraminal loop of the vertebral artery viewed by angiography at the C4–C5 level. This loop was responsible for a radiculopathy.

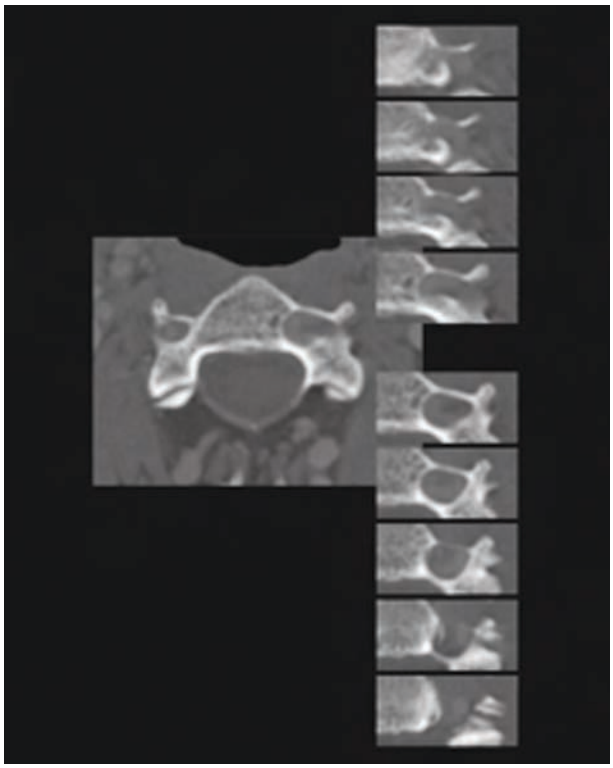

Figure 48.5 The vertebral artery forms a loop inside the vertebral body, as observed on sequential views. Reprinted with permission of Springer from Bruneau M, De Witte O, Regli L, George B. 2011. Anatomical variations. In Pathology and surgery around the vertebral artery. George B, Bruneau M, Spetzler RF (eds), chapter 7, pp 53–74. Springer (Paris).

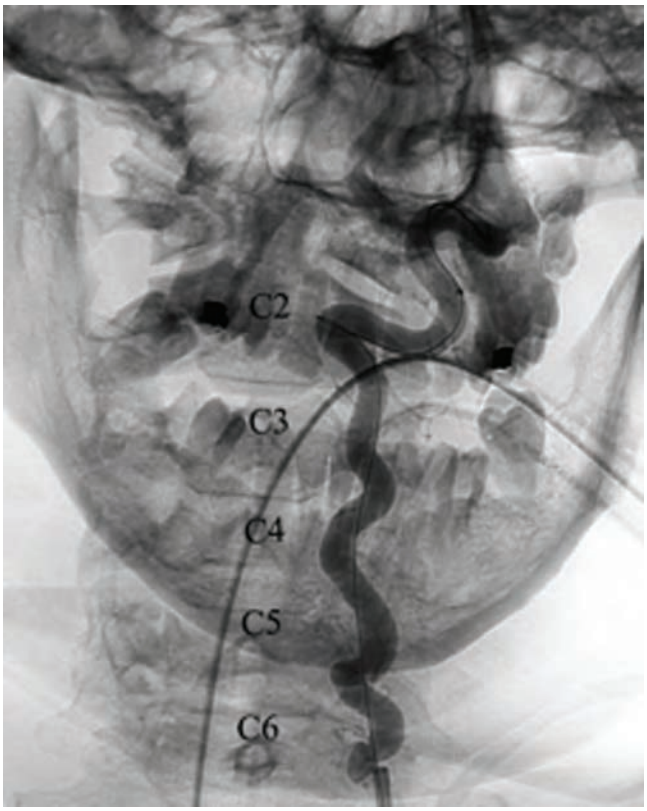

Figure 48.6 Lateral loops are visible at each subaxial level due to osteophytes. Reprinted with permission of Springer from Bruneau M, De Witte O, Regli L, George B. 2011. Anatomical variations. In Pathology and surgery around the vertebral artery. George B, Bruneau M, Spetzler RF (eds), chapter 7, pp 53–74. Springer (Paris).

Size, hypolasia, atresia

On average, the diameter of the left VA is slightly greater than the right (5 mm and 4.1 mm, respectively; Krayenbühl 1982; Peltier et al. 2003). In 20–40% of cases (George 2001; Peltier et al. 2003; Bruneau et al. 2006b) one VA is clearly smaller than the contralateral VA; the former is called a minor VA and the latter a dominant VA. A small VA is called either hypoplastic or atretic. A hypoplastic VA has a diameter of less than 2–3.5 mm (Touboul et al. 1986; Matula et al. 1997; Jeng and Yip 2004; Park et al. 2007) but always joins the opposite VA to form the BT (Fig. 48.14). In contrast, an atretic VA does not end at the BT but at the PICA, the occipital artery or a spinal artery (Cagnie et al. 2005a, b; Bruneau et al. 2006a). Very often it is associated with persistent congenital caroticovertebral anastomoses (Lasjaunias and Ter Brugge 2001b; Burger et al. 2007; Hachem et al. 2008).

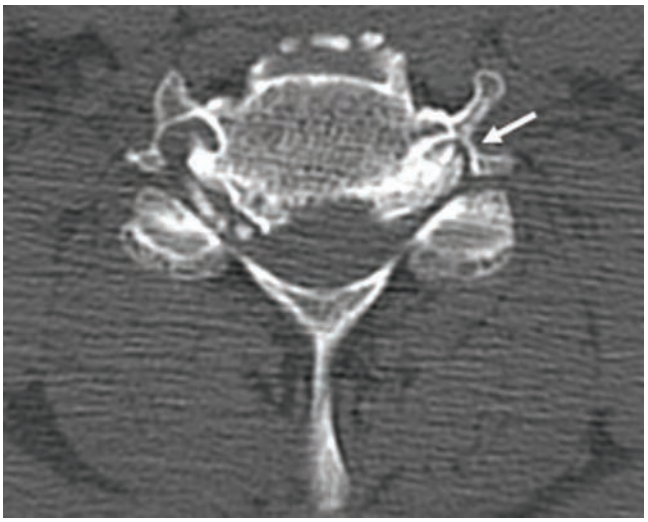

(a)

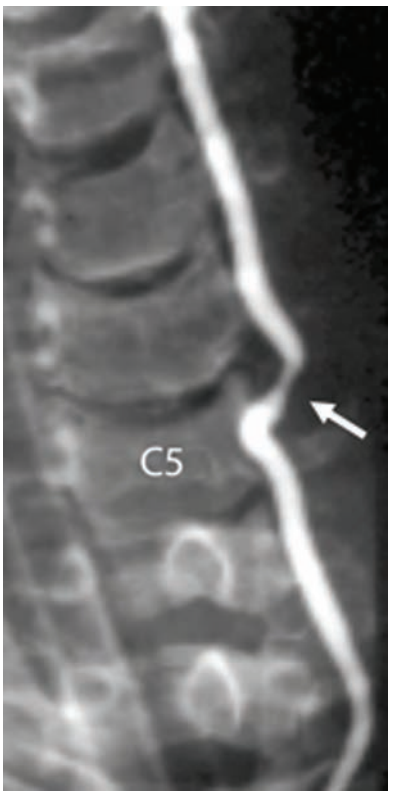

(b)

Figure 48.7 The vertebral artery can be occluded by osteophytic formations extending inside the transverse foramen (a, arrow) and compressed by fibrous bands (b). Figure 7a reprinted with permission of Springer from Bruneau M, De Witte O, Regli L, George B. 2011. Anatomical variations. In Pathology and surgery around the vertebral artery. George B, Bruneau M, Spetzler RF (eds), chapter 7, pp 53–74. Springer (Paris).

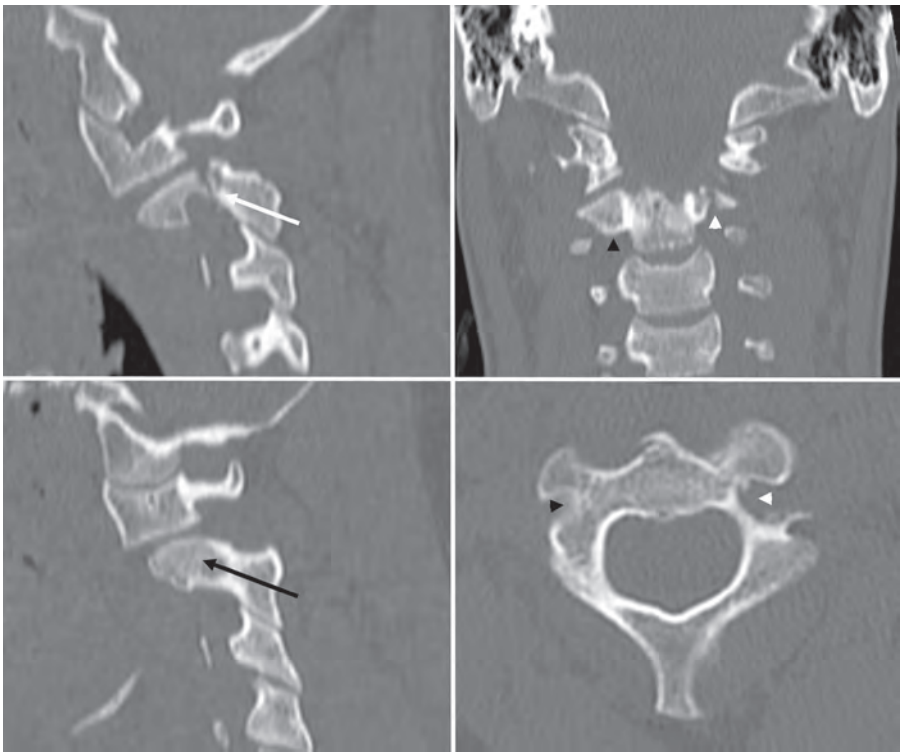

Figure 48.8 High-riding vertebral artery on the left side. Arrows indicate screw trajectories on sagittal reconstruction. On the left side (white arrow), a high-riding vertebral artery narrows the pedicle and prevents screw insertion. In contrast, on the right side, the pedicle is larger and a screw (black arrow) can be inserted. The location of the vertebral artery at the bottom of the C2 vertebral body is observed on coronal and axial views. The impression of the left vertebral artery (white arrowhead) is clearly wider than the right (black arrowhead).

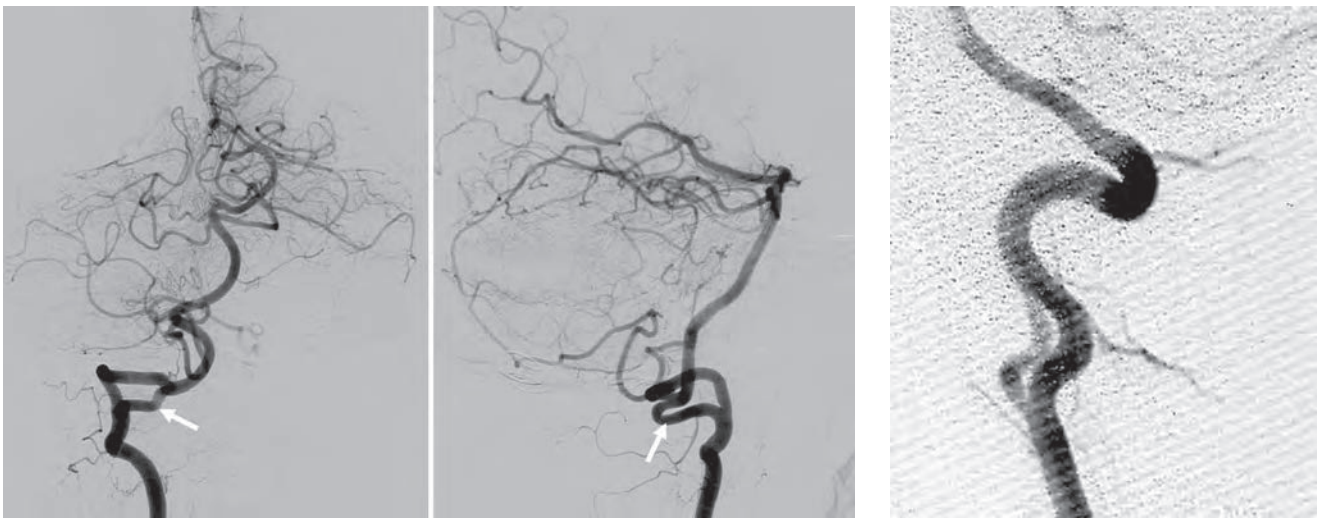

(a) (b)

Figure 48.9 Vertebral artery V3 segment (a) duplication and (b) fenestration.

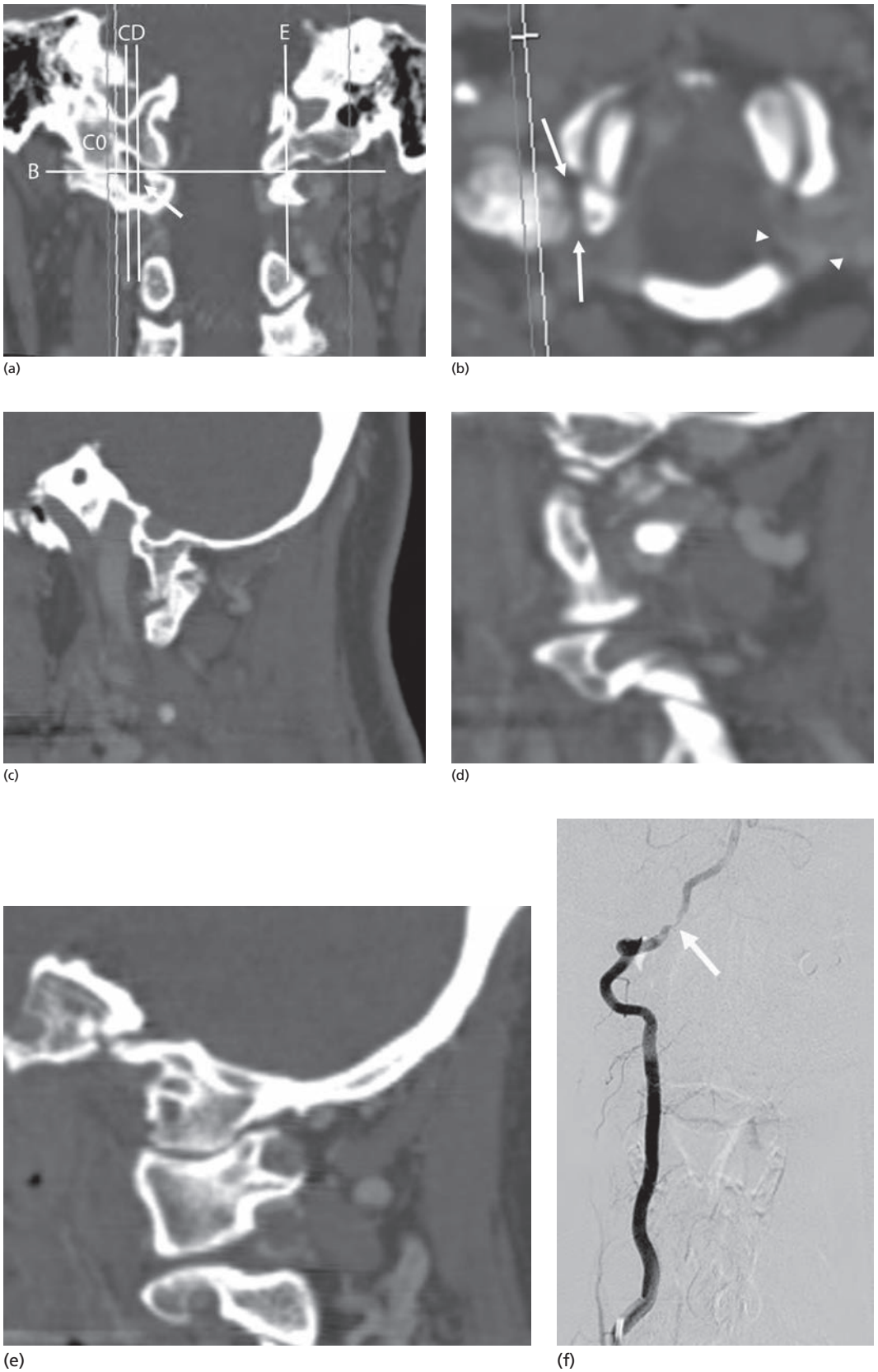

Figure 48.10 Abnormal trajectory of the right vertebral artery in the presence of a congenital anomaly of the craniocervical junction. (a) Lines B–E represent the level of section of the following images. (b) The right vertebral artery passes between the arrows, lateral to the right occipital condyle. The left vertebral artery has a normal trajectory between the arrowheads, running transversely above the C1 posterior arch. (c–e) Sagittal reconstructions on the (c, d) abnormal and (e) normal sides. (f) On angiography, an arterial stenosis is observed (arrow) where the artery passes through the bone.

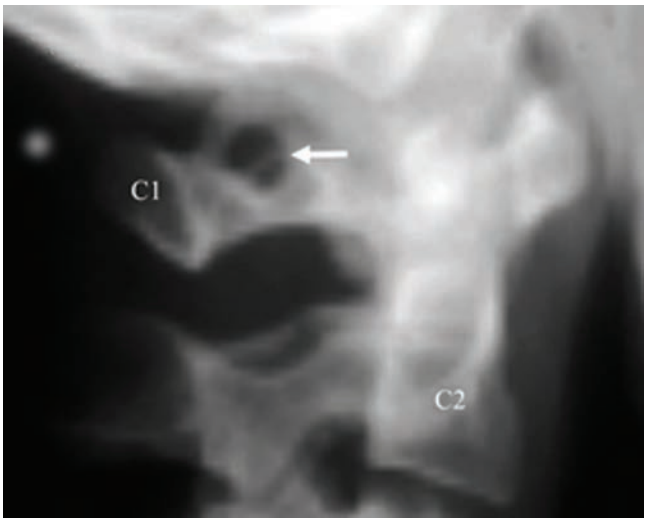

Figure 48.11 Ossification of the atlanto-occipital membrane turning the groove of the vertebral artery into a tunnel (arrow). Reprinted with permission of Springer from Bruneau M, De Witte O, Regli L, George B. 2011. Anatomical variations. In Pathology and surgery around the vertebral artery. George B, Bruneau M, Spetzler RF (eds), chapter 7, pp 53–74. Springer (Paris).

Figure 48.12 Fenestration at the origin of the basilar artery.

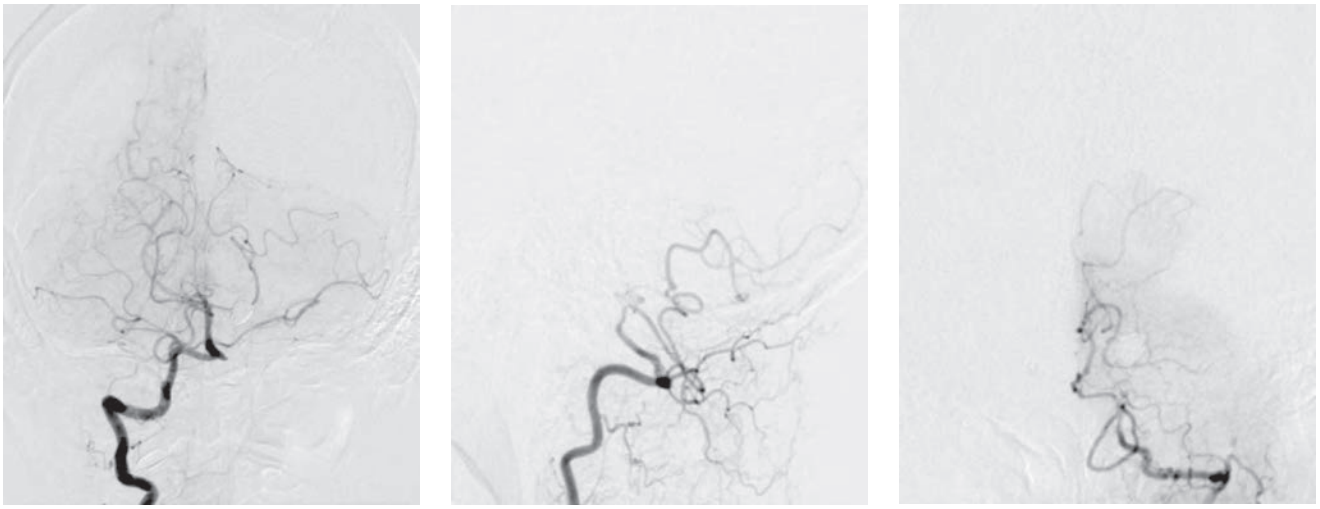

Figure 48.13 If the vertebral artery ends at the PICA, the contralateral vertebral artery supplies the cerebellar hemisphere on the abnormal side and forms the basilar trunk on its own.

Figure 48.14 The left vertebral artery (small arrows) is hypoplasic compared to the right (wide arrow) and participates in the formation of the basilar trunk.

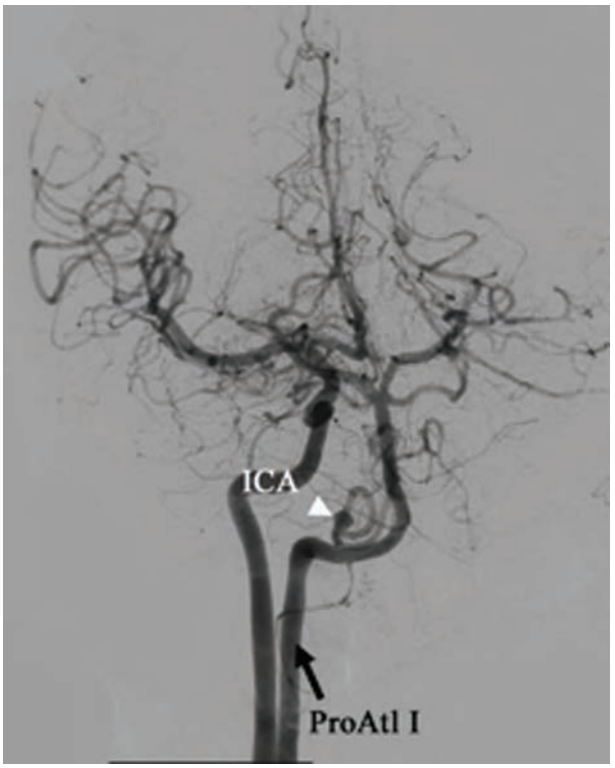

(a)

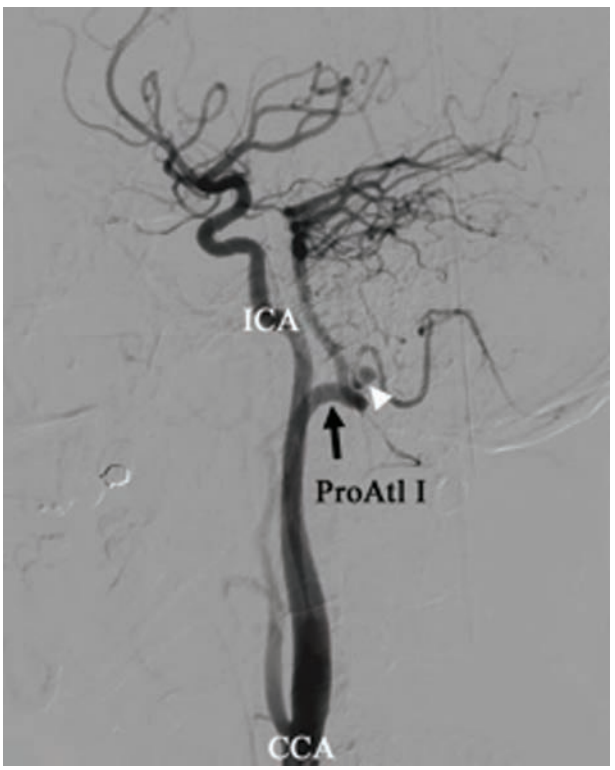

(b)

Figure 48.15 Proatlantal artery type I. Arrowhead indicates an aneurysm at the PICA origin. Reprinted with permission of Springer from Bruneau M, De Witte O, Regli L, George B. 2011. Anatomical variations. In Pathology and surgery around the vertebral artery. George B, Bruneau M, Spetzler RF (eds), chapter 7, pp 53–74. Springer (Paris).

Anastomoses

Persistent congenital anastomoses between the carotid and the vertebrobasilar systems are usually associated with proximal and distal abnormalities such as agenesis, hypoplasia, moya moya syndrome, and congenital aneurysms (Gilmartin 1963; Springer et al. 1974; Kodama et al. 1976; Kwak et al. 1983; Garza-Mercado et al. 1990; Yamamoto et al. 1991; Fantini et al. 1994; Hatayama et al. 1999; Nishida et al. 2000; Katayama et al. 2001; Wagner 2001). At the cervical level they are related to abnormal development and fusion of the embryological intersegmental arteries. They are exceptional except for the proatlantal artery (Pasco 2004). The more cranial the anastomosis, the more frequent it is. They are usually named according to the corresponding cranial nerve except the first one, which is the posterior communicating artery. The next three anastomoses are called, from cranial to caudal, the trigeminal artery (following the Vth nerve), the otic artery (following the VIIth and VIIIth nerves) and the hypoglossal artery (following the XIIth nerve); in fact they connect the ICA to the BT and not to the VA. These anastomoses are usually unilateral but can be bilateral (Tanaka et al. 1983; Lui et al. 1987; Al-Memar and Thrush 1998; Lode 2000; Woodcock et al. 2001).

Proatlantal artery

Two types of proatlantal artery (PA) have been described (Lasjaunias and Ter Brugge 2001b): PA type I (Fig. 48.15) and PA type II. They correspond to the persistence of the first and

second intersegmental arteries and are therefore located at the level of the second or third vertebral body (Purkayastha et al. 2005). PA type I connects the ICA to the VA before its penetration into the posterior fossa at the foramen magnum level. PA type II originates from the ECA and joins the horizontal or vertical part of the V3 VA segment (Pasco et al. 2004). Bilateral proatlantal arteries are extremely rare (Kurose et al. 1990; Woodcock et al. 2001; Gumus et al. 2004; Purkayastha et al. 2005).

Branches

Along the cervical part of the VA, one muscular (lateral) and one radicular or segmental interspace (medial) artery arises from the VA at each level. Variations in size and distribution between these branches are frequent but with a balance; if one branch is small or absent at a particular level, there is compensation via connections with the cranial and/or caudal branches (Fig. 48.16). If the VA is proximally occluded the muscular branches can bypass the occluded segment and re-inject the VA distally. This is usually clearly visible in the distal part of the VA through muscular branches of the ECA and the cervical arteries.

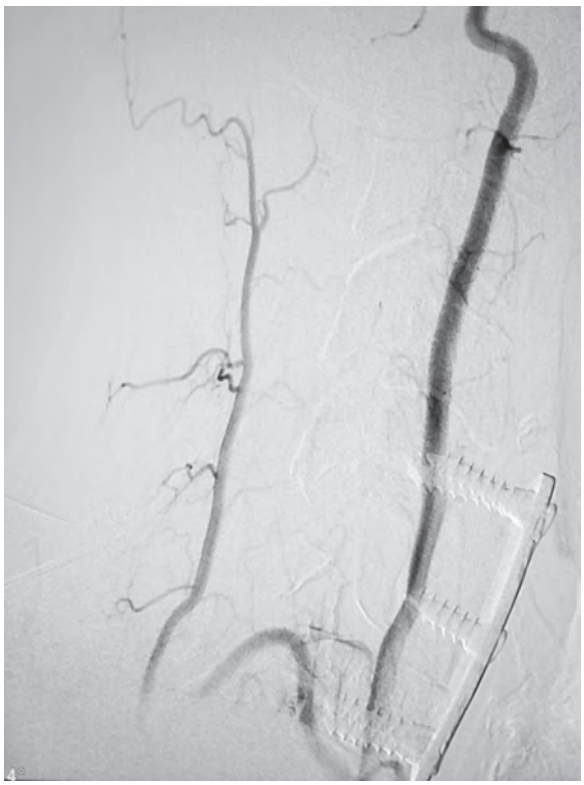

Figure 48.16 Right atretic vertebral artery ending at a muscular branch. Dominant left vertebral artery.

Anterior radiculomedullary and meningeal arteries

Two radicular arteries can be particularly important. One is the anterior radiculomedullary artery, the principal and often the only supply to most of the spinal cord (Fig. 48.17a). It can arise from any VA whatever its size and at any level below C3. Obviously, its surgical obliteration leads to complete tetraplegia. This medullary branch can also arise from another branch of the SCA. The other branch is the third segmental interspace artery, also called the anterior meningeal artery (Fig. 48.17b). It runs inside the dura lateromedially up to the FM. It is the main supply to the FM dura and therefore to FM meningiomas.

Posterior meningeal artery

The posterior meningeal artery branches from the VA either extradurally or intradurally at the foramen magnum level (Campero and Rhoton 2011).

Anterior spinal artery

This artery originates from the VA on each side just before they join to form the BT. In some cases it is a tiny vessel on one side, just connecting the opposite side to the VA.

Posteroinferior cerebellar artery (PICA)

There are many variations of the PICA (Fig. 48.18). It can be absent or its territory supplied by the anteroinferior cerebellar artery (AICA) or the superior cerebellar artery (SCA) (Fujii et al. 1980; Lister et al. 1982; Cullen et al. 2005). A common origin of both PICAs from a dominant VA has been reported (Cullen et al. 2005) with two variations: one is a common trunk supplying both cerebellar hemispheres and the other gives a bilateral vermian supply only. The PICA can arise from the hypoglossal, proatlantal, or posterior meningeal arteries (Manabe et al. 1991; Ogawa et al. 1991; Ahuja et al. 1992) or even from the internal carotid artery (Bruneau et al. 2011) or from one channel of a fenestrated VA (Bruneau et al. 2011). The most common anomaly in the origin of the PICA is an extracranial origin, which is observed in 5–20% of cases (Lasjaunias et al. 1985; Salas et al. 1998; Fine et al. 1999). This rarely occurs bilaterally.

The PICA can arise from any part of the V3 VA segment. If it originates between C1 and C2 it follows the course of the C2 radicular artery and penetrates the dura at that level. If it originates from the VA above C1 it runs along the VA and the C1 nerve root and penetrates the FM dura with these elements. The PICA can also originate on either side (extra- or intradural) of the FM dura, proximal to its regular origin. It can have a double origin (1.45–2%; Osborn 1999; Lesley et al. 2007) or one origin can be extracranial and the other intracranial (Kwon et al. 2007). It can be fenestrated (Theodosopoulos and Lawton 2000). It can give origin to the posterior meningeal artery (Tanohata et al. 1987).

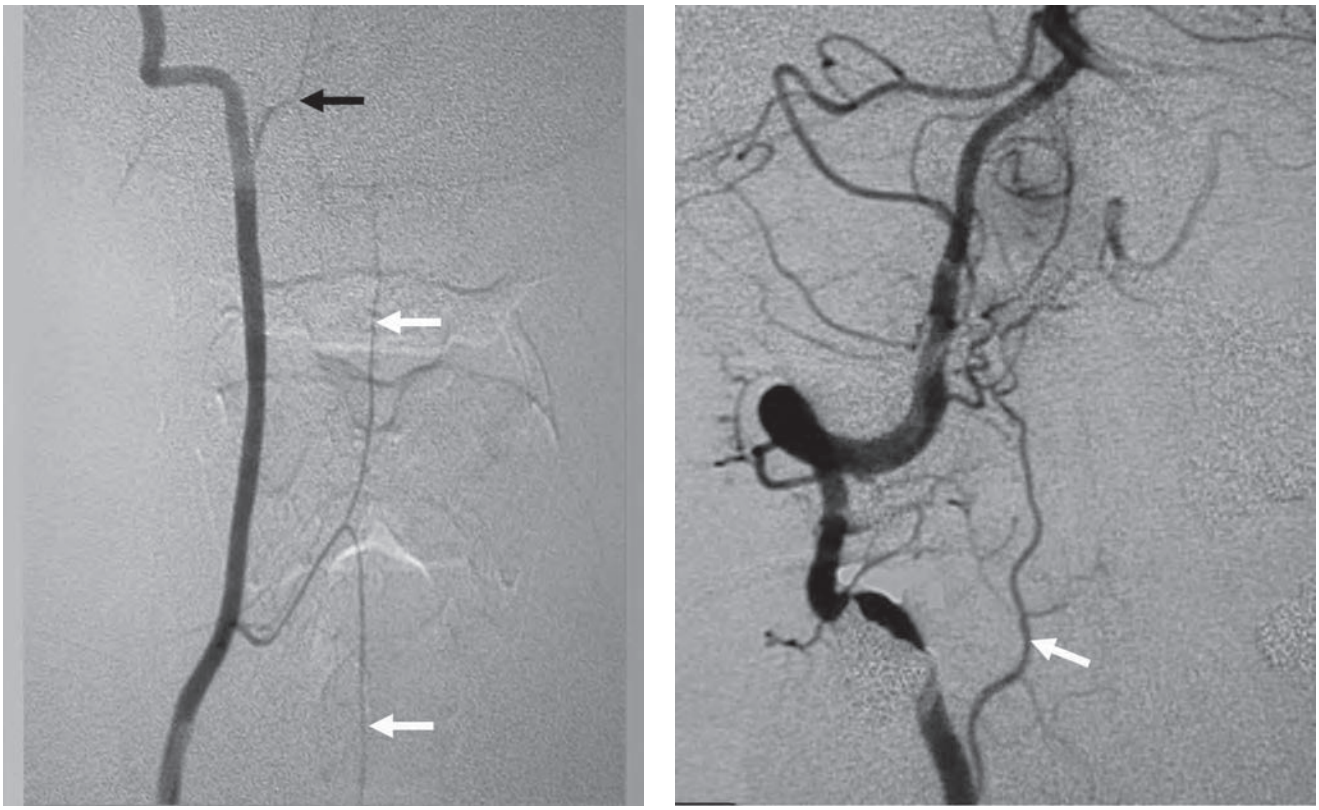

(a) (b)

Figure 48.17 (a) The vertebral artery gives off the anterior spinal artery (white arrows) at the C4–C5 level and the anterior meningeal artery (black arrow) at the C2–C3 level. (b) The anterior meningeal artery (white arrow) is wider in this case of foramen magnum meningioma.

Source: Bruneau and George (2011a, b). Reproduced with permission from Springer Verlag France.

Figure 48.18 On the left side, a common PICA-AICA trunk is visible. On the right side, vermian and hemispheric PICA branches are distinct.

References

Ahuja A, Graves VB, Crosby DL, Strother CM. 1992. Anomalous origin of the posterior inferior cerebellar artery from the internal carotid artery. *AJNR* 13(6): 1625–1626.

Akdeniz B, Yilmaz E, Pekel N, Ergul BU. 2007. Anomalous origin of the right vertebral artery from the ascending aorta in the presence of an aberrant right subclavian artery. *Int J Cardiovasc Imaging* 23(1): 39–42.

Al-Memar A, Thrush D. 1998. Unilateral hypoglossal nerve palsy due to aneurysm of the stump of persistent hypoglossal artery. *J Neurol Neurosurg Psych* 64(3): 405.

Al-Okaili R, Schwartz ED. 2007. Bilateral aortic origins of the vertebral arteries with right vertebral artery arising distal to left subclavian artery: case report. *Surg Neurol* 67(2): 174–176.

Anson JA. 1995. Surgery for vertebrobasilar insufficiency. In *Neurovascular Surgery* (eds LP Carter, MG Hamilton). New York: McGraw-Hill.

Bernard TJ, Mull BR, Handler MH, Harned RK, Filley CM, Kumpe DA, Tseng BS. 2007. An 18-year-old man with fenestrated vertebral arteries, recurrent stroke and successful angiographic coiling. *J Neurol Sci* 260(1–2): 279–282.

Brink B. 1984. Approach to the second segment of the vertebral arteries. In *Vertebrobasilar Arterial Occlusive Disease: Medical and Surgical Management* (ed. BR Berguer). pp 257–264. New York: Raven Press.

Bruneau M, George B. 2011a. Chapter 13. In *Pathology and Surgery around the Vertebral Artery* (eds George B, Bruneau M, Spetzler RF), pp 143–164. Paris: Springer.

Bruneau M, George B. 2011a. Surgical approaches to the V3 segment of the vertebral artery. Chapter 25. In *Pathology and Surgery around the Vertebral Artery* (eds George B, Bruneau M, Spetzler RF), pp 329–360. Paris: Springer.

Bruneau M, Cornelius JF, George B. 2006a. Anterolateral approach to the V3 segment of the vertebral artery. *Neurosurgery* 58(1 Suppl): ONS29–35.

Bruneau M, Cornelius JF, George B. 2006b. Anterolateral approach to the V1 segment of the vertebral artery. *Neurosurgery* 58(4 Suppl 2): ONS215–219.

Bruneau M, Cornelius JF, Marneffe V, Triffaux M, George B. 2006c. Anatomical variations of the V2 segment of the vertebral artery. *Neurosurgery* 59(1 Suppl 1): ONS20–24.

Bruneau M, De Witte O, Regli L, George B. 2011. Anatomical variations. In *Pathology and Surgery around the Vertebral Artery* (eds BM George, RF Spetzler). pp. 53–74 Paris: Springer.

Burger IM, Siclari F, Gregg L, Gailloud P. 2007. Bilateral segmental agenesis of the vertebrobasilar junction: developmental and angiographic anatomy. *AJNR* 28(10): 2017–22.

Cagnie B, Barbaix E, Vinck E, D'Herde K, Cambier D. 2005a. A vertebral artery without atlantic and intradural sections: a case report and a review of the literature. *Ann Anat* 187(3): 271–275.

Cagnie B, Barbaix E, Vinck E, D'Herde K, Cambier D. 2005b. Extrinsic risk factors for compromised blood flow in the vertebral artery: anatomical observations of the transverse foramina from C3 to C7. *Surg Radiol Anat* 27(4): 312–316.

Campero A, Rhoton AL. 2011. Anatomy of the vertebral artery. In *Pathology and Surgery around the Vertebral Artery* (eds BM George, RF Spetzler). pp. 29–40 Paris: Springer.

Cullen SP, Ozanne A, Alvarez H, Lasjaunias P. 2005. The bihemispheric posterior inferior cerebellar artery. *Neuroradiology* 47(11): 809–812.

Daseler EH, Anson BJ. 1959. Surgical anatomy of the subclavian artery and its branches. *Surg Gynecol Obstet* 108(2): 149–174.

Eisenberg RA, Vines FS, Taylor SB. 1986. Bifid origin of the left vertebral artery. *Radiology* 159(2): 429–430.

Fantini GA, Reilly LM, Stoney RJ. 1994. Persistent hypoglossal artery: diagnostic and therapeutic considerations concerning carotid thromboendarterectomy. *J Vasc Surg* 20(6): 995–999.

Fine AD, Cardoso A, Rhoton AL, Jr. 1999. Microsurgical anatomy of the extracranial–extradural origin of the posterior inferior cerebellar artery. *J Neurosurg* 91(4): 645–652.

Flynn RE. 1968. External carotid origin of the dominant vertebral artery. Case report. *J Neurosurg* 29(3): 300–301.

Fujii K, Lenkey C, Rhoton AL, Jr. 1980. Microsurgical anatomy of the choroidal arteries. Fourth ventricle and cerebellopontine angles. *J Neurosurg* 52(4): 504–524.

Garza-Mercado R, Cavazos E, Urrutia G. 1990. Persistent hypoglossal artery in combination with multifocal arteriovenous malformations of the brain: case report. *Neurosurgery* 26(5): 871–876.

George B, Cornelius J. 2001. Vertebral artery: Surgical anatomy. In *Operative Techniques in Neurosurgery* (ed RF Spetzler). pp. 168–181 Philadelphia: W.B. Saunders.

Gilmartin D. 1963. Hypoglossal artery associated with internal carotid stenosis. *Br J Radiol* 36: 849–851.

Goray VB, Joshi AR, Garg A, Merchant S, Yadav B, Maheshwari P. 2005. Aortic arch variation: a unique case with anomalous origin of both vertebral arteries as additional branches of the aortic arch distal to left subclavian artery. *AJNR* 26(1): 93–95.

Gumus T, Onal B, Ilgit ET. 2004. Bilateral persistence of type 1 proatlantal arteries: report of a case and review of the literature. *AJNR* 25(9): 1622–1624.

Gupta T. 2008. Quantitative anatomy of vertebral artery groove on the posterior arch of atlas in relation to spinal surgical procedures. *Surg Radiol Anat* 30: 239–42.

Hachem K, Abi Khalil S, Slaba S, Jebara V, Ghossain M. 2008. Non invasive imaging of bilateral vertebral arteries agenesis. *J Mal Vasc* 33(1): 26–29.

Hasan M, Shukla S, Siddiqui MS, Singh D. 2001. Posterolateral tunnels and ponticuli in human atlas vertebrae. *J Anat* 199(3): 339–343.

Hashimoto H, Ohnishi H, Yuasa T, Kawaguchi S. 1987. Duplicate origin of the vertebral artery: report of two cases. *Neuroradiology* 29(3): 301–303.

Hatayama T, Yamane K, Shima T, Okada Y, Nishida M. 1999. Persistent primitive hypoglossal artery associated with cerebral aneurysm and cervical internal carotid artery stenosis: case report. *Neurol Med Chir (Tokyo)* 39(5): 372–375.

Huber G, Piepgras U. 1976. Origin of the left vertebral artery from the left external carotid artery (author's transl). *Rofo* 125(1): 63–66.

Hyogo T, Nakagawara J, Nakamura J, Suematsu K. 1996. Multiple segmental agenesis of the cerebral arteries: case report. *Neuroradiology* 38(5): 433–436.

Ionete C, Omojola MF. 2006. MR angiographic demonstration of bilateral duplication of the extracranial vertebral artery: unusual course and review of the literature. *AJNR* 27(6): 1304–1306.

Jeng JS, Yip PK. 2004. Evaluation of vertebral artery hypoplasia and asymmetry by color–coded duplex ultrasonography. *Ultrasound Med Biol* 30(5): 605–659.

Katayama W, Enomoto T, Yanaka K, Nose T. 2001. Moyamoya disease associated with persistent primitive hypoglossal artery: report of a case. *Pediatr Neurosurg* 35(5): 262–265.

Kawashima M, Tanriover N, Rhoton AL, Jr., Matsushima T. 2003. The transverse process, intertransverse space, and vertebral artery in anterior approaches to the lower cervical spine. *J Neurosurg* 98(2 Suppl): 188–194.

Kodama N, Ohara H, Suzuki J. 1976. Persistent hypoglossal artery associated with aneurysms. Report of two cases. *J Neurosurg* 45(4): 449–451.

Komiyama M, Nakajima H, Yamanaka K, Iwai Y. 1999. Dual origin of the vertebral artery: case report. *Neurol Med Chir (Tokyo)* 39(13): 932–937.

Krayenbühl H. 1982. *Cerebral Angiography*. Stuttgart, New York: Georg Thieme Verlag.

Kurose K, Kishi H, Nishijima Y. 1990. Type 2 proatlantal artery associated with a ruptured aneurysm: case report. *Neurol Med Chir (Tokyo)* 30(3): 191–193.

Kwak R, Emori T, Yamamoto N, Kadoya S. 1983. Moyamoya disease associated with persistent primitive trigeminal artery: Report of two cases. *No To Shinkei* 35(3): 237–242.

Kwon BJ, Jung C, Im SH, Lee DH, Han MH. 2007. Double origin of the posteroinferior cerebellar artery: angiographic anatomy and endovascular treatment of concurrent vertebrobasilar dissection. *Neurosurgery* 61(5 Suppl 2): 242–248.

Lasjaunias P. 1983. *Craniofacial and Upper Cervical Arteries: Collateral Circulations and Angiographic Protocols*. Baltimore, London: Williams and Wilkins.

Lasjaunias P, Ter Brugge KG. (eds) 2001a. *Surgical Neuroangiography*. Berlin: Springer-Verlag.

Lasjaunias P, Ter Brugge KG. 2001b. The pharyngo-occipital system. In *Surgical Neuroangiography* (eds Lasjaunias P, Ter Brugge KG) pp. 165–224. Berlin: Springer-Verlag.

Lasjaunias P, Vallee B, Person H, Ter Brugge K, Chiu M. 1985. The lateral spinal artery of the upper cervical spinal cord. Anatomy, normal variations, and angiographic aspects. *J Neurosurg* 63(2): 235–241.

Lemke AJ, Benndorf G, Liebig T, Felix R. 1999. Anomalous origin of the right vertebral artery: review of the literature and case report of right vertebral artery origin distal to the left subclavian artery. *AJNR Am J Neuroradiol* 20(7): 1318–1321.

Lesley WS, Rajab MH, Case RS. 2007. Double origin of the posterior inferior cerebellar artery: association with intracranial aneurysm on catheter angiography. *Am J Roentgenol* 189(4): 893–897.

Lister JR, Rhoton AL Jr, Matsushima T, Peace DA. 1982. Microsurgical anatomy of the posterior inferior cerebellar artery. *Neurosurgery* 10(2): 170–199.

Lode I. 2000. Persistence of both proatlantal arteries with occlusion of the internal carotid arteries. A case report. *Acta Radiol* 41(5): 410–411.

Lui CC, Liu YH, Wai YY, Tsai CC. 1987. Persistence of both proatlantal arteries with absence of vertebral arteries. *Neuroradiology* 29(3): 304–305.

Mahadevan J, Batista L, Alvarez H, Bravo-Castro E, Lasjaunias P. 2004. Bilateral segmental regression of the carotid and vertebral arteries with rete compensation in a Western patient. *Neuroradiology* 46(6): 444–449.

Manabe H, Oda N, Ishii M, Ishii A. 1991. The posterior inferior cerebellar artery originating from the internal carotid artery, associated with multiple aneurysms. *Neuroradiology* 33(6): 513–515.

Matula C, Trattnig S, Tschabitscher M, Day JD, Koos WT. 1997. The course of the prevertebral segment of the vertebral artery: anatomy and clinical significance. *Surg Neurol* 48(2): 125–131.

Neo M, Matsushita M, Iwashita Y, Yasuda T, Sakamoto T, Nakamura T. 2003. Atlantoaxial transarticular screw fixation for a high-riding vertebral artery. *Spine* 28(7): 666–670.

Nishida C, Ashikaga R, Araki Y, Nakamatsu K, Ono Y, Fujii K, Nishimura Y. 2000. Persistent hypoglossal artery associated with arteriovenous malformation: a case report. *Eur J Radiol* 33(1): 59–62.

Ogawa T, Fujita H, Inugami A, Shishido F, Higano S, Uemura K. 1991. Anomalous origin of the posterior inferior cerebellar artery from the posterior meningeal artery. *AJNR* 12(1): 186.

Osborn AG. (ed.) 1999. The vertebrobasilar system. In *Diagnostic Cerebral Angiography* pp. 173–194. Philadelphia: L.W. Wilkins.

Park JH, Kim JM, Roh JK. 2007. Hypoplastic vertebral artery: frequency and associations with ischaemic stroke territory. *J Neurol Neurosurg Psychiatry* 78(9): 954–958.

Pasco A, Papon X, Bracard S, Tanguy JY, Ter Minassian A, Mercier P. 2004. Persistent carotid-vertebrobasilar anastomoses: how and why differentiating them? *J Neuroradiol* 31(5): 391–396.

Peltier J, Toussaint P, Deramond H, Gondry C, Bruniau A, Gontier MF, Le Gars D. 2003. The dural crossing of the vertebral artery. *Surg Radiol Anat* 25(3–4): 305–310.

Purkayastha S, Gupta AK, Varma R, Kapilamoorthy TR. 2005. Proatlantal intersegmental arteries of external carotid artery origin associated with Galen's vein malformation. *Am J Neuroradiol* 26(9): 2378–2383.

Rieger P, Huber G. 1983. Fenestration and duplicate origin of the left vertebral artery in angiography. Report of three cases. *Neuroradiology* 25(1): 45–50.

Salas E, Ziyal IM, Bank WO, Santi MR, Sekhar LN. 1998. Extradural origin of the posteroinferior cerebellar artery: an anatomic study with histological and radiographic correlation. *Neurosurgery* 42(6): 1326–1331.

Satti SR, Cerniglia CA, Koenigsberg RA. 2007. Cervical vertebral artery variations: an anatomic study. *AJNR* 28(5): 976–980.

Schwarzacher SW, Krammer EB. 1989. Complex anomalies of the human aortic arch system: unique case with both vertebral arteries as additional branches of the aortic arch. *Anat Rec* 225(3): 246–250.

Shhadeh A, Sair HI, Kanamalla US. 2007. Bifid direct aortic arch origin of left vertebral artery: a unique vascular variant. *J Vasc Interv Radiol* 18(8): 1051–1053.

Sim E, Vaccaro AR, Berzlanovich A, Thaler H, Ullrich CG. 2001. Fenestration of the extracranial vertebral artery: review of the literature. *Spine* 26(6): E139–142.

Springer TD, Fishbone G, Shapiro R. 1974. Persistent hypoglossal artery associated with superior cerebellar artery aneurysm. Case report. *J Neurosurg* 40(3): 297–299.

Stoesslein F, Porstmann W, Schueler F, Schoepke W. 1982. Aberrant vertebral artery originating from the descending aorta: a new congenital steal syndrome in coarctation. *Eur J Radiol* 2(2): 157–159.

Suzuki S, Kuwabara Y, Hatano R, Iwai T. 1978. Duplicate origin of left vertebral artery. *Neuroradiology* 15(1): 27–29.

Takasato Y, Hayashi H, Kobayashi T, Hashimoto Y. 1992. Duplicated origin of right vertebral artery with rudimentary and accessory left vertebral arteries. *Neuroradiology* 34(4): 287–289.

Tanaka Y, Hara H, Momose G, Kobayashi S, Kobayashi S, Sugita K. 1983. Proatlantal intersegmental artery and trigeminal artery associated with an aneurysm. Case report. *J Neurosurg* 59(3): 520–523.

Tanohata K, Maehara T, Noda M, Katoh H, Sugiyama S, Okazaki A. 1987. Anomalous origin of the posterior meningeal artery from the lateral medullary segment of the posterior inferior cerebellar artery. *Neuroradiology* 29(1): 89–92.

Theodosopoulos PV, Lawton MT. 2000. Fenestration of the posteroinferior cerebellar artery: case report. *Neurosurgery* 47(2): 463–465.

Thomas AJ, Germanwala AV, Vora N, Prevedello DM, Jovin T, Kassam A, Horowitz M. 2008. Dual origin extracranial vertebral artery: case report and embryology. *J Neuroimaging* 18(2): 173–176.

Touboul PJ, Bousser MG, LaPlane D, Castaigne P. 1986. Duplex scanning of normal vertebral arteries. *Stroke* 17(5): 921–923.

Ugurlucan M, Sayin OA, Surmen B, Alpagut U, Dayioglu E, Onursal E. 2006. Common carotid trunk and right vertebral artery originating from the right common carotid artery in a patient with carotid stenosis. *J Card Surg* 21(4): 423–424.

Wagner AL. 2001. Isolated stenosis of a persistent hypoglossal artery visualized at 3D CT angiography. *AJNR* 22(8): 1613–1614.

Walsham WJ. 1882. Abnormal origin and distribution of the upper seven right intercostal arteries with remarks. *J Anat Physiol* 16: 441–445.

Wasserman BA, Mikulis DJ, Manzione JV. 1992. Origin of the right vertebral artery from the left side of the aortic arch proximal to the origin of the left subclavian artery. *AJNR* 13(1): 355–358.

Woodcock RJ, Cloft HJ, Dion JE. 2001. Bilateral type 1 proatlantal arteries with absence of vertebral arteries. *AJNR* 22(2): 418–420.

Yamamoto S, Sunada I, Matsuoka Y, Hakuba A, Nishimura S. 1991. Persistent primitive hypoglossal artery aneurysms: report of two cases. *Neurol Med Chir (Tokyo)* 31(4): 199–202.

Yamazaki M, Koda M, Aramomi MA, Hashimoto M, Masaki Y, Okawa A. 2005. Anomalous vertebral artery at the extraosseous and intraosseous regions of the craniovertebral junction: analysis by three-dimensional computed tomography angiography. *Spine* 30(21): 2452–2457.

Yanik B, Conkbayir I, Keyik B, Hekimoglu B. 2004. A rare anomalous origin of right vertebral artery: findings on Doppler sonography. *J Clin Ultrasound* 32(4): 211–214.

49 Thoracic aorta

Veysel Akgun[1], Salih Hamcan[2], Yalcin Bozkurt[3], and Bilal Battal[1]
[1]Gulhane Military Medical Academy, Ankara, Turkey
[2]Agri Military Hospital, Agri, Turkey
[3]Golcuk Military Hospital, Kocaeli, Turkey

The variations of the thoracic aorta represent a group of entities that can be either isolated or associated with other cardiovascular anomalies. These anomalies can be clinically silent or lead to severe morbidity or even mortality; it is therefore important to know their clinical significance. In this chapter, we review the variations of the thoracic aorta and its branches and briefly discuss the variations of the ostia of the coronary arteries.

Embryology

Knowledge of the basic embryology of the thoracic aorta is essential for understanding its potential anatomical variations. In this section, we briefly review the basic embryological concepts.

A pair of angioblastic cords canalize and form endothelial tubes in the third week of embryonic life; they quickly fuse and form a single cardiac tube. This cardiac tube develops segments of dilatations and constrictions, named the truncus arteriosus, bulbus cordis, primitive ventricle, primitive atrium, and sinus venosus, respectively, from the cephalad to the caudad direction (Fig. 49.1).

The spiral septum, also named the aorticopulmonary septum, separates the truncus arteriosus into aorta and pulmonary trunk in a cephalad-to-caudad direction. The truncus arteriosus is continuous with the aortic sac cranially, which gives rise to six paired aortic arches. Some of these arches regress and disappear but several portions normally persist.

The first, second and fifth aortic arches regress almost totally. The third pair of aortic arches form the common carotid arteries and part of the internal carotids. The left fourth aortic arch forms the left aortic arch. The aortic sac contributes to the proximal part of the aortic arch while the left dorsal aorta contributes to the distal part. The right fourth aortic arch forms the proximal subclavian artery; the distal subclavian artery originates from the dorsal aorta and the right seventh intersegmental artery. The left subclavian artery is formed by the left seventh intersegmental. The left and right pulmonary arteries are derivatives of the sixth aortic arches on both sides. The left sixth aortic arch also forms the ductus arteriosus. The embryological double aortic arch has an aortic arch and a potential ductus arteriosus on each side (Fig. 49.2).

As the embryological right arch regresses, the normal configuration of a left aortic arch with a left descending aorta and

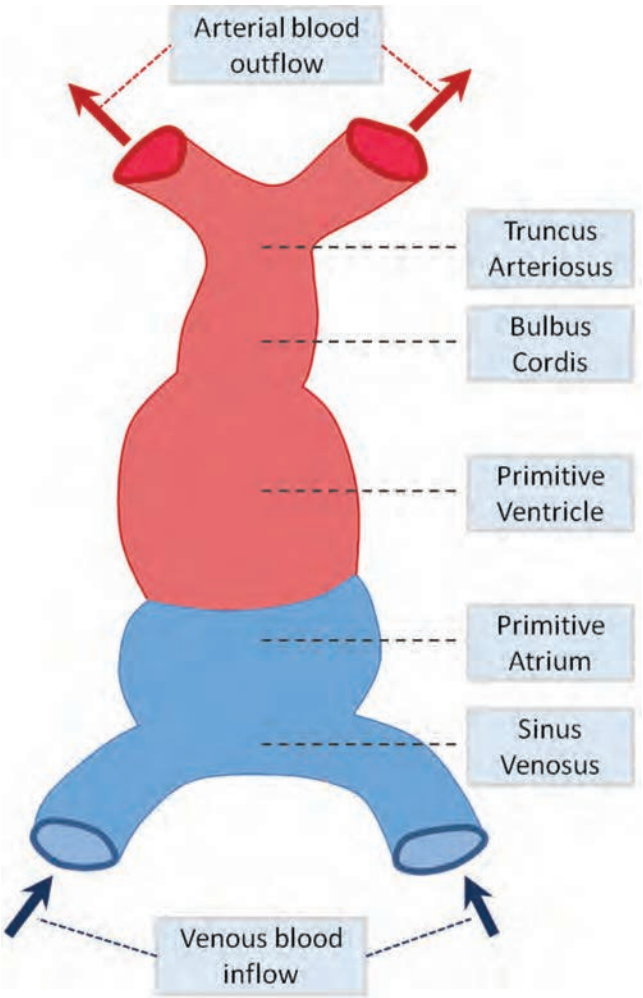

Figure 49.1 Schematic illustration of endocardial heart tube.

Bergman's Comprehensive Encyclopedia of Human Anatomic Variation, First Edition. Edited by R. Shane Tubbs, Mohammadali M. Shoja and Marios Loukas.
© 2016 John Wiley & Sons, Inc. Published 2016 by John Wiley & Sons, Inc.

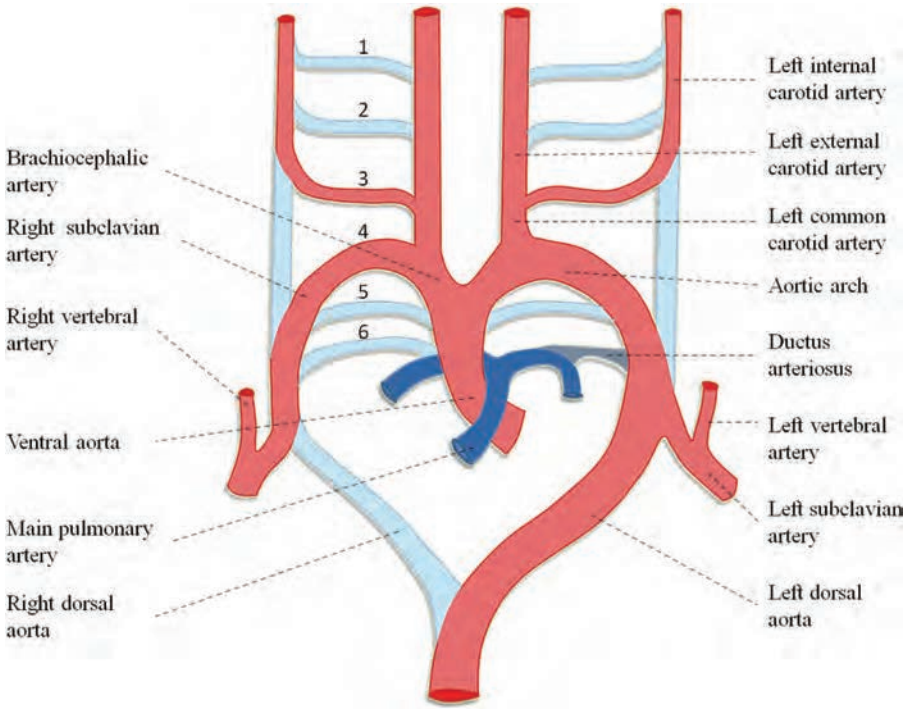

Figure 49.2 Schematic illustration of the embryological development of the arcus aorta and its branches.

a left ligamentum arteriosum forms. The right subclavian artery fuses superiorly with the right common carotid and inferiorly with the brachiocephalic artery. The two dorsal aortae fuse in the abdomen and the fusion progresses toward the thorax. The right thoracic dorsal aorta gradually regresses, leaving only the left dorsal as the descending thoracic aorta (Arey 1984; Moore and Persaud 1993; Soler 1998; Stojanovska et al. 2012).

Aortic valve

The normal aortic valve has three equal-sized cusps. Abnormal valve morphology can be manifest as a unicuspid, bicuspid, or quadricuspid aortic valve. Of these three variations the bicuspid aortic valve is the most common, seen in 2% of the general population (Roberts 1970).

Cusps of the bicuspid aortic valve can be unequal in size. The most frequently encountered variant comprises three developmental cusps with underdevelopment and/or fusion of a commissure between two of them. A bicuspid aortic valve with two cusps, sinuses, and commissures is less commonly seen (Fig. 49.3; Sievers and Schmidtke 2007).

The unicuspid aortic valve is much less common, with an estimated incidence of 0.02%. It can be seen as a unicuspid commissural or a unicuspid unicommissural valve. A unicuspid commissural valve has three undeveloped commissures and a centrally located orifice, whereas a unicuspid unicommissural valve has one true unfused commissure and two rudimentary commissures (Roberts and Ko 2005). Both unicuspid and bicuspid aortic valves are more commonly seen in men than women (Roberts and Ko 2005).

The quadricuspid aortic valve is an uncommon morphological abnormality. Its frequency on necropsy is estimated at only 1 in 8000 (Simonds 1923).

Coronary arteries

Coronary artery anomalies can be classified according to different perspectives as major or minor, as critical, severe, relevant, or benign, or anatomically as anomalies of origin, intrinsic anatomy, or termination. In this section we review the variations of the coronary arteries according to the location of their ostia. To discuss other variations of the coronary arteries is beyond the scope of this chapter.

Originating from the opposite sinus/coronary artery or non-coronary sinus

In this anomaly, the coronary artery arises from the opposite aortic sinus or coronary artery directly, or rarely from a non-coronary sinus. The coronary artery follows one of four courses before it perfuses its usual myocardial territory. Three of these courses are transseptal, prepulmonic, and retroaortic, are accepted as benign or clinically insignificant, and are also referred to as non-malignant anomalies (Fig. 49.4). The last course is interarterial; it is considered clinically significant and is also referred to as a malignant anomaly. It is potentially lethal and can lead to sudden cardiac death in young adults (Figs 49.5, 49.6).

A

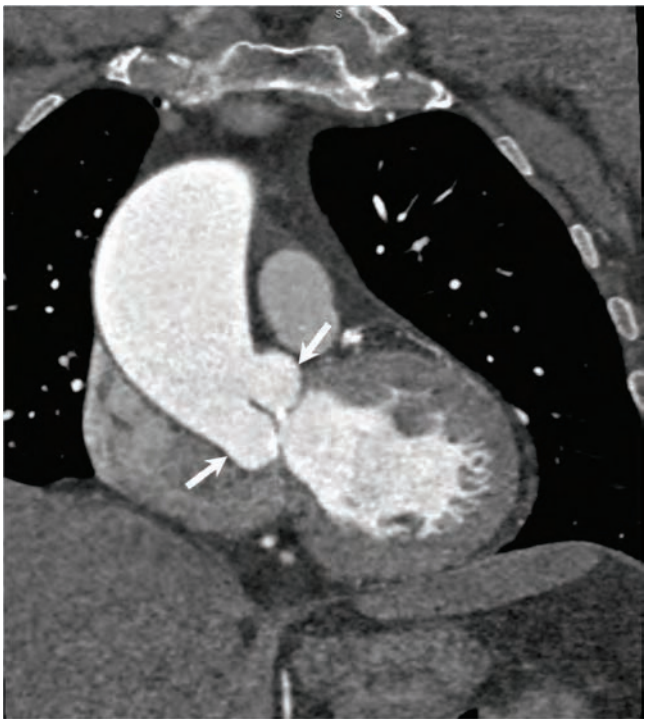

B

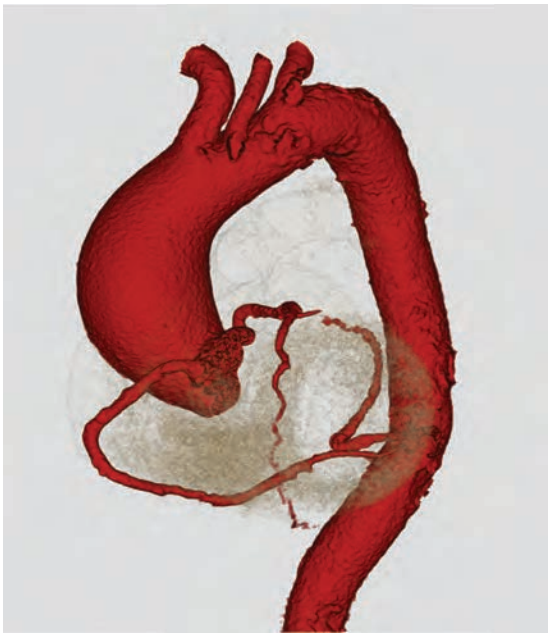

C

Figure 49.3 (a) Oblique axial, (b) coronal, and (c) volume-rendered (VR) computed tomography angiography (CTA) images reveal a bicuspid aortic valve and enlargement of the ascending aorta.

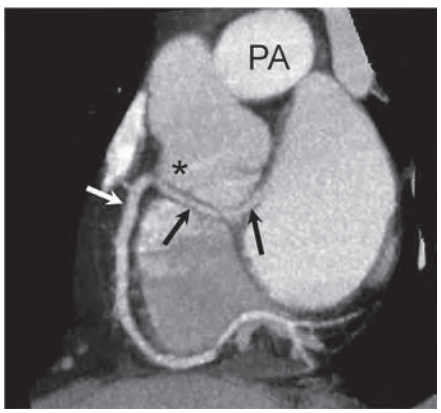

A

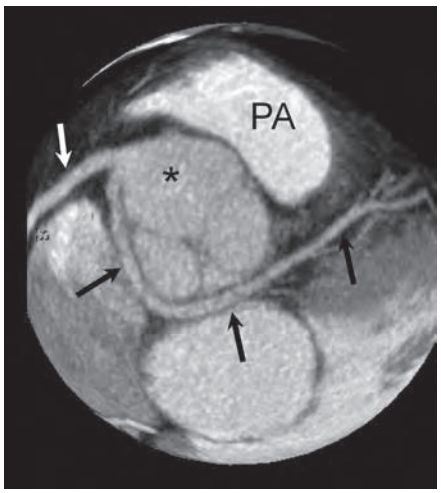

B

Figure 49.4 Aberrant origin of left main coronary artery (LMCA). (a) Oblique axial and (b) three-dimensional (3D) maximum-intensity-projection (MIP) CTA images reveal aberrant origin of the LMCA (black arrows) from right sinus valsalva (*) and its retroaortic course. White arrow: right coronary artery (RCA); PA: main pulmonary artery.

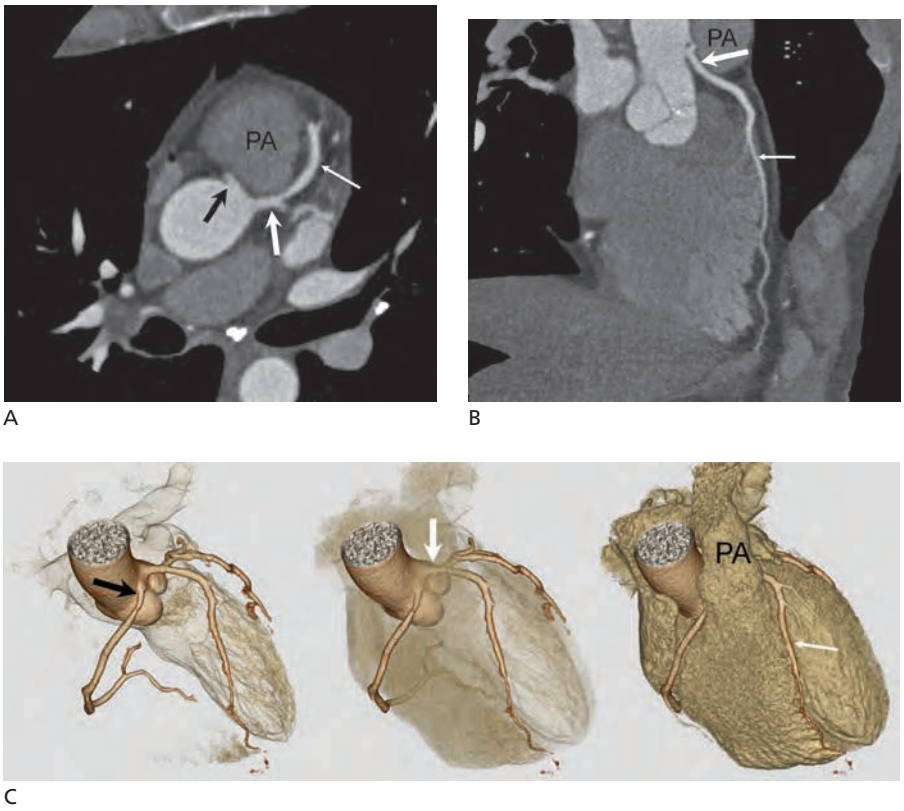

Figure 49.5 High origin of coronary arteries and malign RCA origin anomaly. (a) Oblique axial, (b) oblique coronal, and (c) VR CTA images reveal high take-off of both RCA (black arrow) and LMCA (thick white arrow) above the coronary sinus, and the RCA arising from the left coronary sinus and having an interarterial course between the aorta and main pulmonary artery (PA). Thin white arrow: left anterior descending artery (LAD).

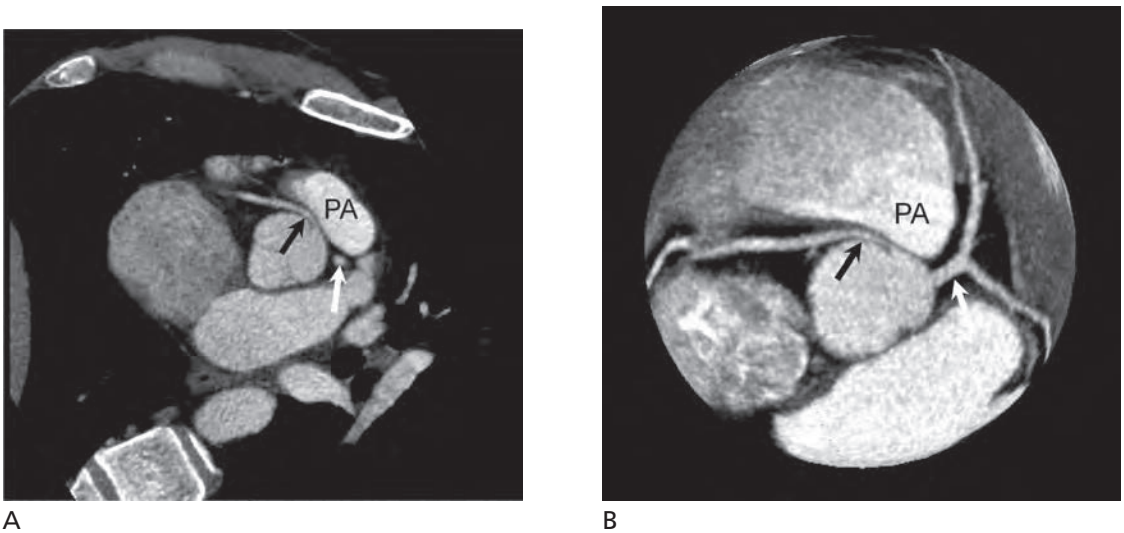

Figure 49.6 Malignant origin of RCA. (a) Oblique axial and (b) 3D MIP CTA images demonstrate aberrant origin of RCA (black arrow) from left sinus valsalva and its interarterial course between the aorta and main pulmonary artery (PA). White arrow: LMCA.

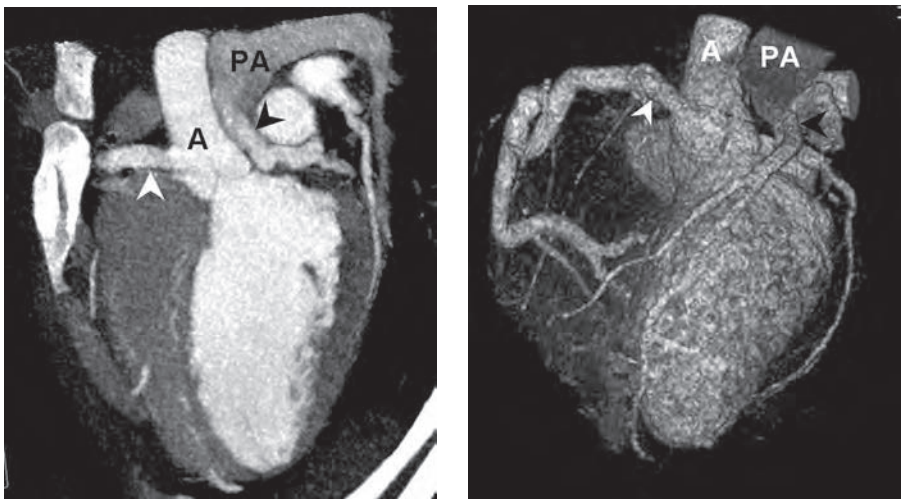

A B

Figure 49.7 (a) Oblique coronal MIP and (b) VR CTA images reveal abnormal LMCA (black arrowhead) originating from the pulmonary artery (PA). There is minor enhancement in the lumen of the PA, indicating retrograde blood flow toward the PA. A: aorta; white arrowheads: RCA.

Source: Akgun et al. (2010). Reproduced with permission from Eurasian Journal of Medicine.

The left main coronary artery (LMCA) originates from the right coronary sinus separately, or as a common trunk with the right coronary artery (RCA). In most cases it has an interarterial course. The RCA can arise from the left coronary sinus and follow an interarterial course. It can also arise directly from a single coronary artery originating from the left sinus of valsalva and follow either an interarterial or a retroaortic course. An anomalous origin of a coronary artery from the non-coronary sinus is rare and can accompany other cardiac anomalies such as transposition of the great arteries or the tetralogy of Fallot (Hoffman et al. 2006; Kim et al. 2006; O'Brien et al. 2007; Pannu et al. 2003; Hlavacek et al. 2010).

Originating from the pulmonary artery

Any of the coronary branches can arise from the pulmonary trunk. The most common type is the left coronary artery arising from the pulmonary artery (anomalous left coronary artery from the pulmonary artery, or ALCAPA) while the right coronary artery arises from the right aortic sinus as usual. This anomaly is also named the Blend White Garland syndrome. The reported incidence of ALCAPA is 1 in 300,000 live births (Fig. 49.7; Akgun et al. 2010). The RCA can also arise from the pulmonary artery (anomalous right coronary artery from the pulmonary artery, or ARCAPA). In either anomaly there is a dilated coronary artery arising from the pulmonary artery and multiple collateral vessels with left-to-right shunt from the coronary to the pulmonary artery. It is treated by implanting the anomalous coronary artery onto the aorta (Fernandes et al. 1992a, b; Dodge-Khatami et al. 2002).

Coronary ostial location

The RCA and LMCA ostia are usually located in the middle of the aortic sinuses. Rarely, they are located in the anterior or posterior thirds or upper portions of the corresponding sinuses. A low coronary artery origin refers to an ostium located at the lower end of the aortic sinus. A high coronary artery origin refers to an ostium located approximately 10 mm or more above the sinotubular junction and is seen in 6% of adults (Fig. 49.5). Finally, a commissural ostium is an ostium located within 5 mm of the aortic valve apposition at the aortic annulus (Vlodaver et al. 1972; Fernandes et al. 1992a, b; Dodge-Khatami et al. 2002).

Coronary ostial number

Although there are usually individual coronary ostia, there are several ostial variations for the RCA and LMCA. In one of the most common of these variations, instead of there being one LMCA ostium, the left anterior descending (LAD) and left circumflex (LCX) arteries have separate ostia arising from the left sinus of valsalva (Fig. 49.8). There can also be two ostia off the right sinus of valsalva, one for the RCA and the second for the conus branch directly arising from aorta (Pannu et al. 2003; Kim et al. 2006).

Single coronary artery

A single coronary artery ostium occurs with an incidence of 0.06% and can arise from any aortic sinus. The single artery course can vary, with the proximal RCA or LMCA dividing into branches following the distributions of the RCA, LMCA, LAD, and LCX to their respective myocardial territories (Desmet et al. 1992; Ishii et al. 2010).

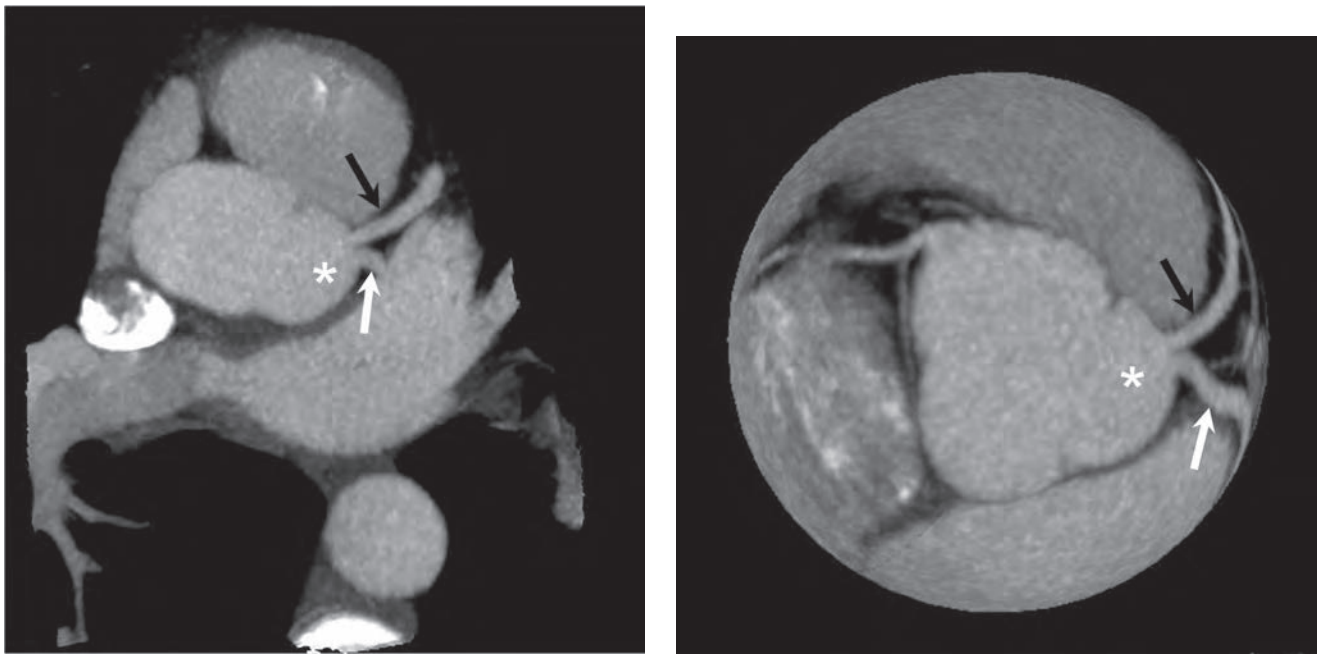

Figure 49.8 Separately originating LAD and left circumflex artery (LCX). (a) Oblique axial and (b) 3D MIP CTA images reveal separate origins of LAD (black arrow) and LCX (white arrow) from the left sinus of valsalva (*).

Hypoplasia of the ascending aorta

An interruption in the partitioning of the truncus arteriosus during the embryological period can result in this anomaly (Figs 49.9, 49.10). Hypoplasia of the ascending aorta is an uncommon congenital malformation that is almost always a part of hypoplastic left heart syndrome, which comprises a wide spectrum of cardiac malformations such as hypoplasia or atresia of the aortic and mitral valves and/or hypoplasia of the left ventricle. This variation is usually associated with a patent ductus arteriosus and juxtaductal coarctation (Bardo et al. 2001).

Aortic arch anomalies are the most common congenital anomalies of the thoracic aorta. In this section we review variations of the aortic arch on the basis of its embryological development.

Aortic arch branching variations

Left aortic arch: normal branching pattern

The normal left aortic arch develops with the interruption of the hypothetical arch distal to the right subclavian artery. It is characterized by a rightward ascending aorta turning toward the left and posterior, crossing over the left main bronchus and to the left of the trachea. The descending aorta courses adjacent to the spine on the left side (Weinberg 2006).

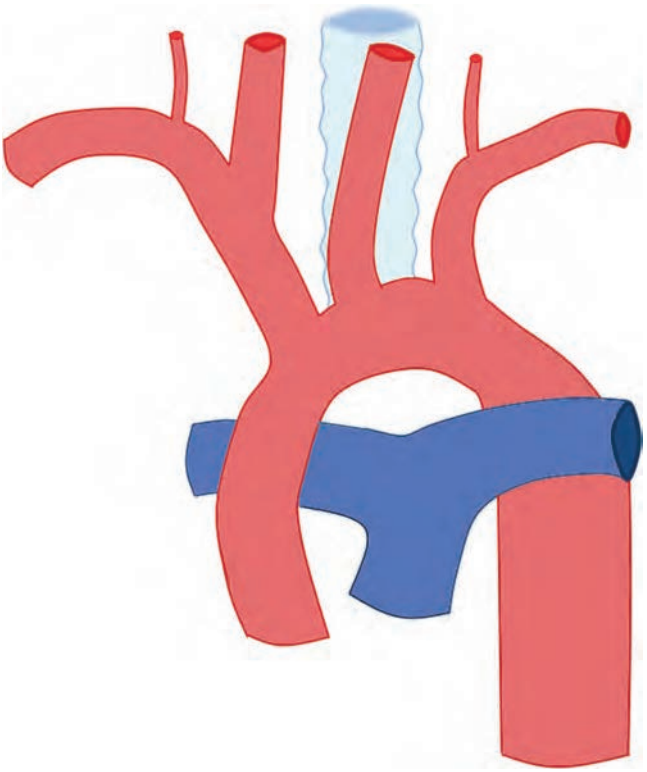

Figure 49.9 Hypoplasic ascending aorta and arcus aorta.

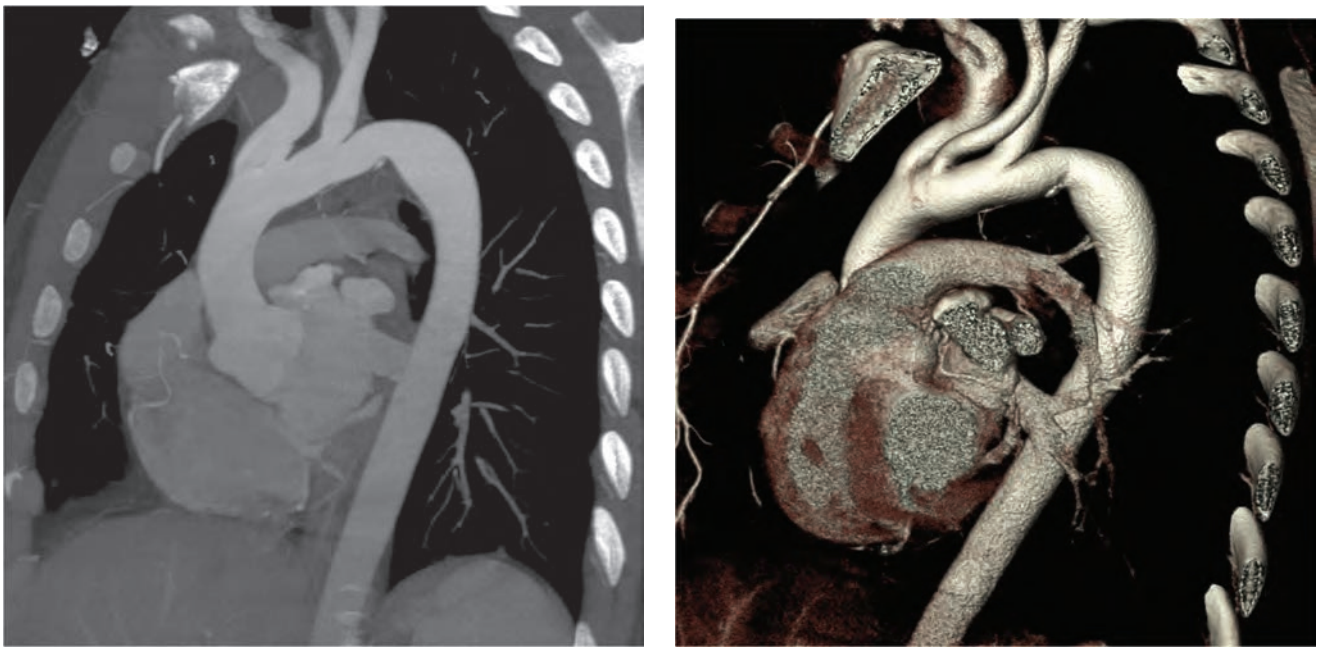

A B

Figure 49.10 (a) Oblique sagittal MIP and (b) VR CTA images reveal hypoplasic ascending aorta and arcus aorta.

Bovine arch

A bovine arch is the most common variant of the aortic arch. In the most frequent form of this variation, the brachiocephalic artery shares a common origin with the left common carotid artery. Its name comes from the similarity to the branching pattern of the aortic arch in bovines; some authors have stressed that the term should not be used however, as the pattern seen in man is not similar to what is found in ruminant animals (Layton et al. 2006). There are two main forms of bovine arch in humans. In the first, the brachiocephalic artery and the left common carotid artery have a common origin and only two great vessels originate from the aortic arch. In the second form, the left common carotid artery originates from the brachiocephalic artery directly and more distally. This variation is extremely rare in humans, however (Figs 49.11, 49.12; Lippert and Pabst 1985; Osborn 1999; Habel and Budras 2003; Shaw et al. 2003; Deutsch 2005).

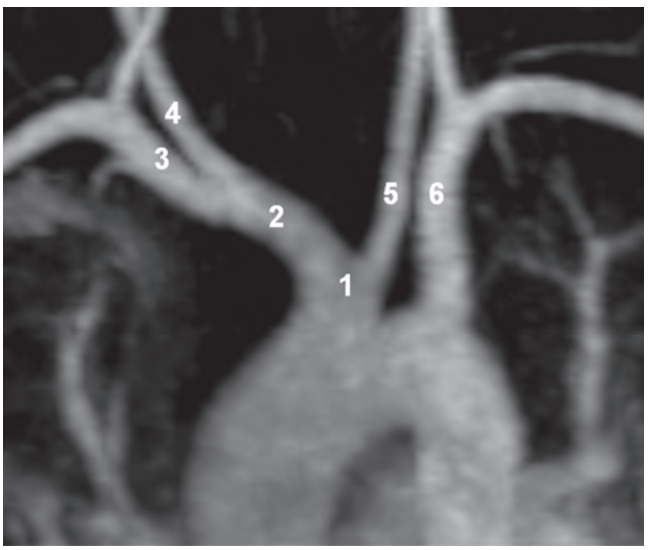

Figure 49.11 Bovine arch. 3D magnetic resonance angiography image demonstrates aortic arch with two branches. 1: common trunk; 2: brachiocephalic truncus (BT); 3: right subclavian artery (RSC); 4: right common carotid artery (RCC); 5: left common carotid artery (LCC): 6: left subclavian artery (LSC).

Variant right subclavian artery

This is one of the most common variants of the aortic arch and is seen in 0.5–2% of the population (Ramaswamy et al. 2008). Embryologically, a left aortic arch with aberrant right subclavian artery results from interruption of the right arch between the right common carotid and right subclavian arteries. The aberrant right subclavian artery is the last main branch of the aortic arch (Fig. 49.12). In most cases it courses behind the esophagus (Fig. 49.13). However, it can also be located in front of the trachea or between the trachea and esophagus (Loukas et al. 2006). The origin of the aberrant vessel can exhibit a focal enlargement known as the diverticulum of Kommerell (Fig. 49.14). This diverticulum is a residue of the right dorsal aortic artery root and can lead to an aneurysm (Asherson 1979).

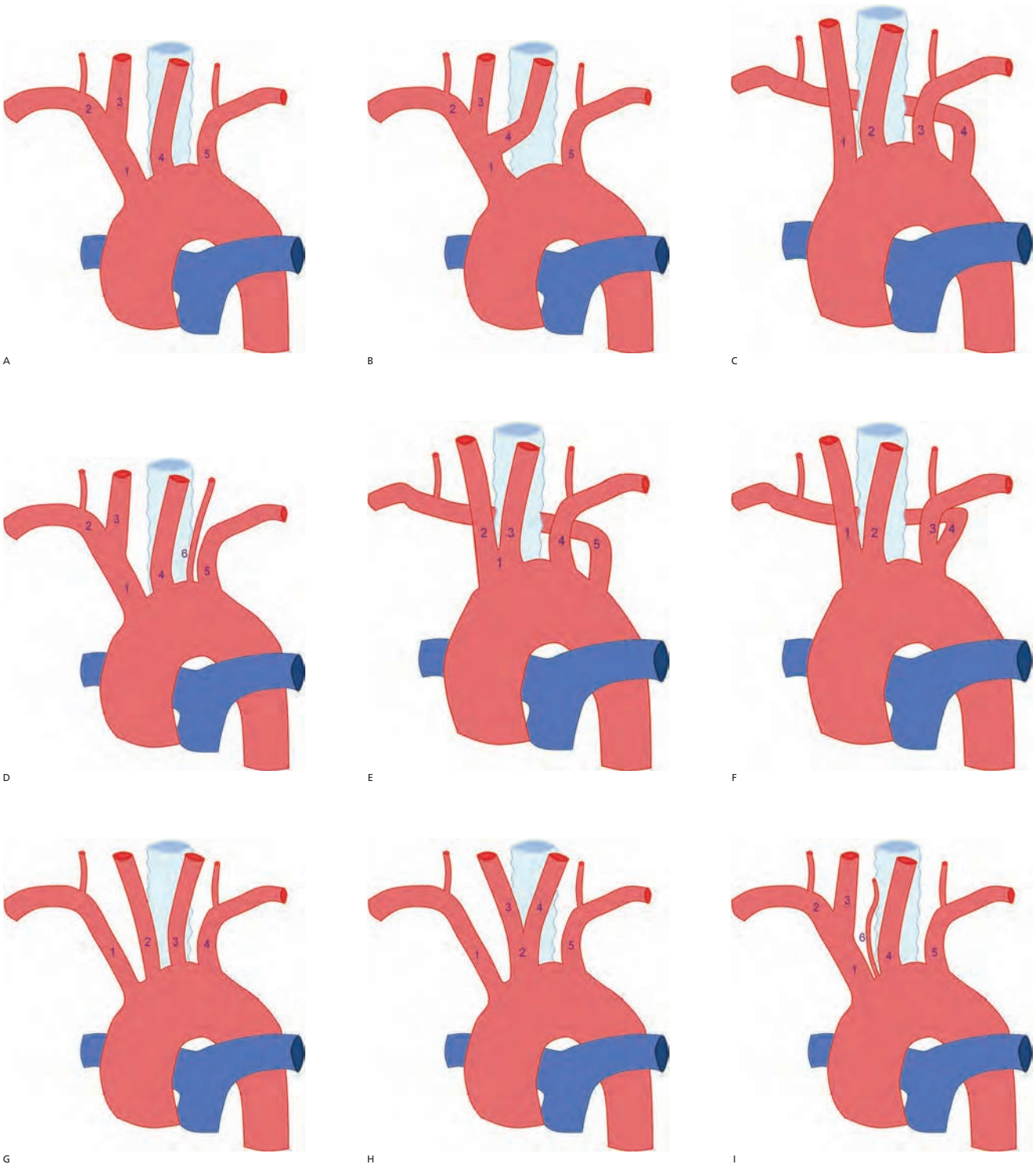

Figure 49.12 The branching patterns of the aortic arch. (a) Normal aortic arch with three branches (1: BT; 2: RSC; 3: RCC; 4: LCC: 5: LSC). (b) Aortic arch with two branches. The first branch (1: common trunk) is constituted by 2 (RSC), 3 (RCC), 4 (LCC) and the second branch is LSC. (c) Aberrant RSC artery (4), aortic arch with four branches (1: RCC; 2: LCC; 3: LSC). (d) Aortic arch with four branches. Left vertebral artery (6) arises directly from the aortic arch (1: BT; 2: RSC; 3: RCC; 4: LCC; 5: LSC). (e) Aortic arch with three branches including common origin for common carotids (1) and aberrant RSC (5) (2: RCC; 3: LCC; 4: LSC). (f) Aortic arch with two branches (avian form) including common origin of common carotids (1: RCC; 2: LCC) and subclavian arteries (3: LSC; 4: aberrant-origin RSC). (g) Aortic arch with four branches. Absence of BT. (1: RSC; 2: RCC; 3: LCC; 4: LSC). (h) Aortic arch with three branches. Common trunk (2) of common carotid arteries. (1: RSC; 3: RCC; 4: LCC; 5: LSC). (i) Aortic arch with four branches. Thyroidea ima artery (6) arises directly from the aortic arch. (1: BT; 2: RSC; 3: RCC; 4: LCC; 5: LSC.)

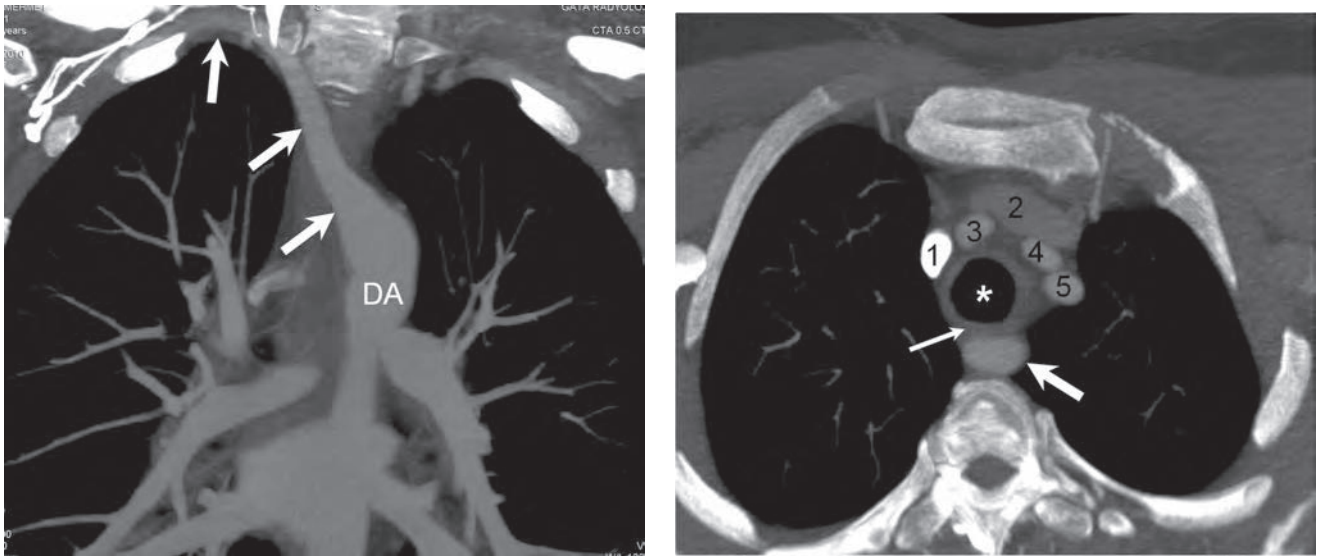

A B

Figure 49.13 Aberrant RSC artery. (a) Coronal and (b) axial MIP CTA images reveal aberrant origin of RSC artery (thick arrows) from the distal aortic arch. The aberrant RSC artery courses behind the esophagus (thin arrow). DA: descending aorta; 1: right brachiocephalic vein; 2: left Brachiocephalic vein; 3: RCC; 4: LCC; 5: LSC.

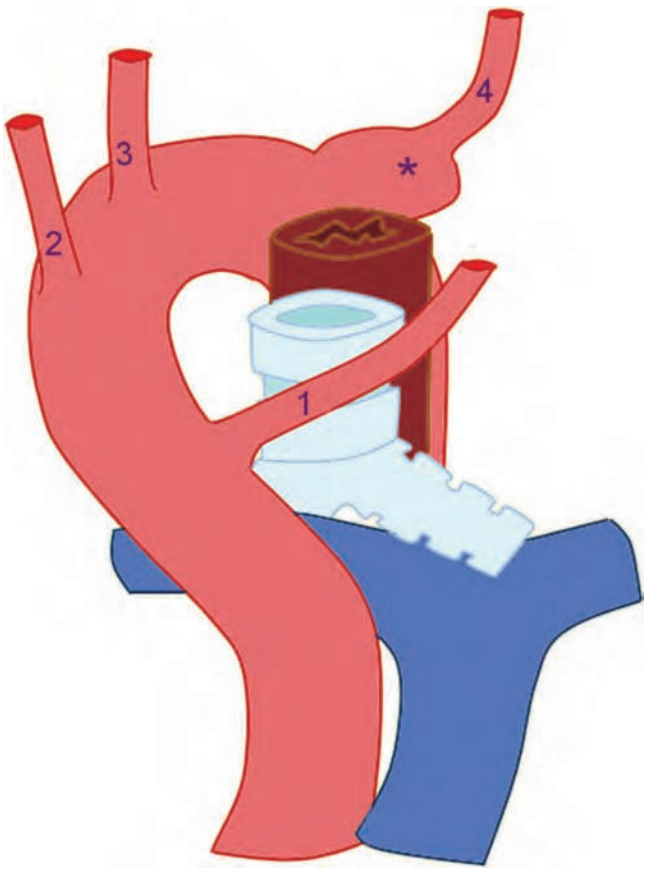

Figure 49.14 Kommerell's diverticulum. Type 1 right aortic arch with aberrant LSC artery originating from a Kommerell's diverticulum (*). 1: LCC; 2: RCC; 3: RSC; 4: aberrant LCC.

Although it is usually asymptomatic it can occasionally lead to dysphagia, also known as dysphagia lusoria (Maldonado et al. 2010; Hellinger et al. 2011; Murillo et al. 2012; Stojanovska et al. 2012).

Miscellaneous rare aortic arch branching variations

Other rare aortic arch branching variations include the following (Ergun et al. 2013; Fig. 49.12).

1. An aortic arch with two branches: the first is the common trunk that divides into the right subclavian, right common carotid, and left common carotid arteries and the second is the left subclavian artery.
2. The left vertebral artery arises directly from an arch that has four branches.
3. Common origin for common carotid arteries, arch with three branches: right subclavian artery, common trunk for right and left common carotid arteries, and left subclavian artery.
4. Common origin for common carotid arteries and aberrant right subclavian artery, arch with three branches: bicarotid trunk, left and right subclavian arteries as the last branch of the arcus aorta.
5. Common origin of common carotid arteries and subclavian arteries, arch with two branches — avian form – common stem for right and left common carotid arteries, common stem for right and left subclavian arteries.
6. Absence of brachiocephalic trunk, arch with four branches.
7. An additional branch from the arcus aorta (thyroidea ima artery), arch with four branches.
8. Doubled brachiocephalic arteries.
9. Brachiocephalic artery arising from the descending aorta (Power 1850).

10. All branches of the aortic arch arising from its left side and the right carotid and right subclavian arteries crossing the midline (Power 1850).

Double aortic arch

A double aortic arch is the most common cause of a vascular ring and can be associated with congenital heart disease. Persistence of the fourth aortic arches on both sides leads to the left and right aortic arches encircling the trachea and esophagus by forming a vascular ring. These arches fuse posteriorly, usually on the left side, after each has given rise to a subclavian and common carotid artery. The right-sided limb in a double aortic arch is usually larger and located higher than the left. The left limb can be atretic and take the form of a fibrous cord that completes the vascular ring. In either case there can be symptoms such as stridor and/or dysphagia due to tracheal and/or esophageal compression. A double aortic arch can be right arch dominant (the most common form), left arch dominant, or isodominant (Figs 49.15–49.17; Schlesinger 2005; Kafka et al. 2006).

Isolation of the subclavian artery

This anomaly occurs when the subclavian artery and aortic arch are separated from each other. Imaging of the vascular structure reveals loss of continuity between the subclavian artery and the aortic arch. The isolated subclavian artery is filled with collaterals derived from the ductus arteriosus or from the vertebral artery; this is also called the subclavian steal phenomenon (Stojanovska et al. 2012).

Right aortic arch

A right aortic arch is explained by the aortic arch crossing over the right main bronchus and is relatively common. It occurs in approximately 0.04–0.1% of the population (Hastreiter et al. 1966). Regression of the left instead of the right dorsal aorta leads to a right aortic arch which can be associated with congenital cardiac anomalies, esophageal atresia, and tracheaesophageal fistula (Canty et al. 1997; Allen et al. 2006).

There are additional subtypes based on the site of the ductus arteriosus. The ductus arteriosus can be located on the right

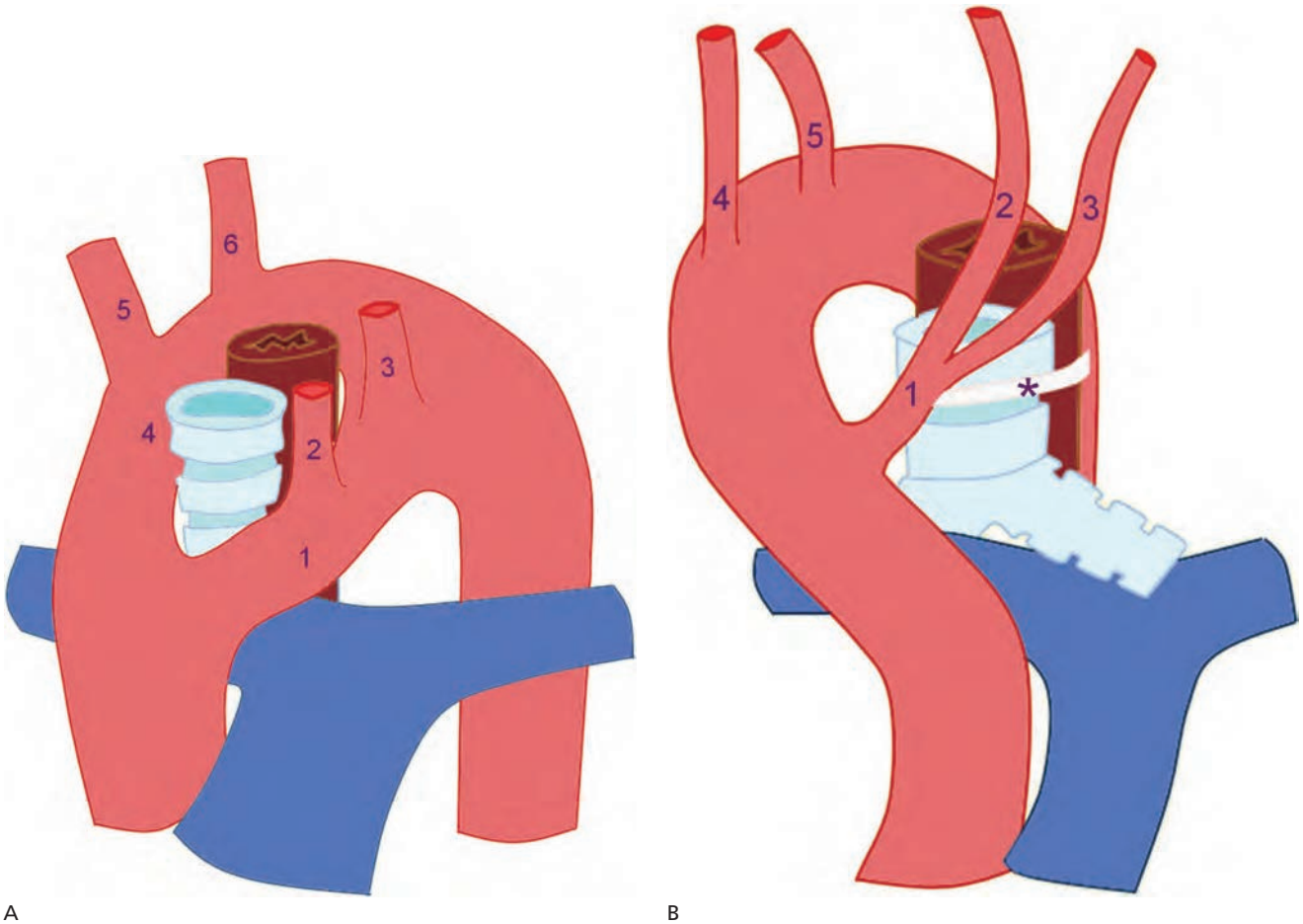

A B

Figure 49.15 Double aortic arch. (a) Right arch dominant type. 1: left limb; 2: LCC; 3: LSC; 4: right limb; 5: RCC; 6: RSC. (b) Left limb (*) atretic type. 1: BT; 2: LCC; 3: LSC; 4: RCC; 5: RSC.

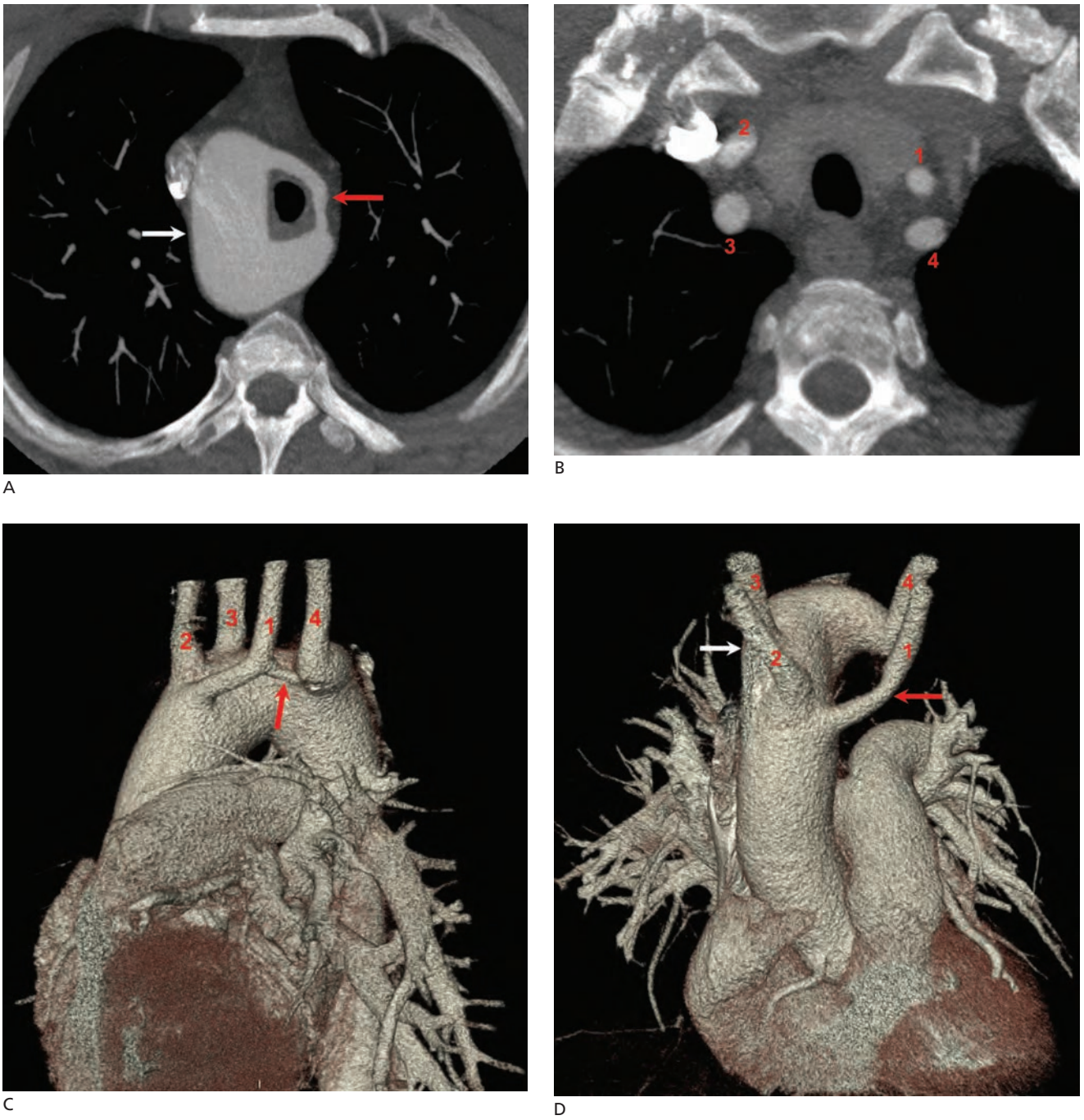

Figure 49.16 (a, b) Axial and (c, d) VR CTA images demonstrate left limb hypoplasic double aortic arch. 1: LCC; 2: RCC; 3: RSC; 4: LSC arteries; white arrow: right limb; red arrow: hipoplasic left limb.

or left or can be bilateral. The circumflex retresophageal aorta is the name given to a right aortic arch that crosses the midline behind the esophagus before descending, resulting in the descending and ascending aorta lying on different sides of the spine (Stojanovska et al. 2012). In the right aortic arch there is no aortic knob in the ordinary left location and the descending aorta opacity is along the right paraspinal space.

Right aortic arch with mirror image branching (type I)

A right aortic arch with mirror image branching is the second-most common type of arch anomaly (Weinberg 2006) and is often associated with other congenital heart anomalies (Knight and Edwards 1974; Backer and Mavroudis 2000). In the hypothetical double arch model defined by Edwards (1948) this anomaly results from interruption and regression of the dorsal

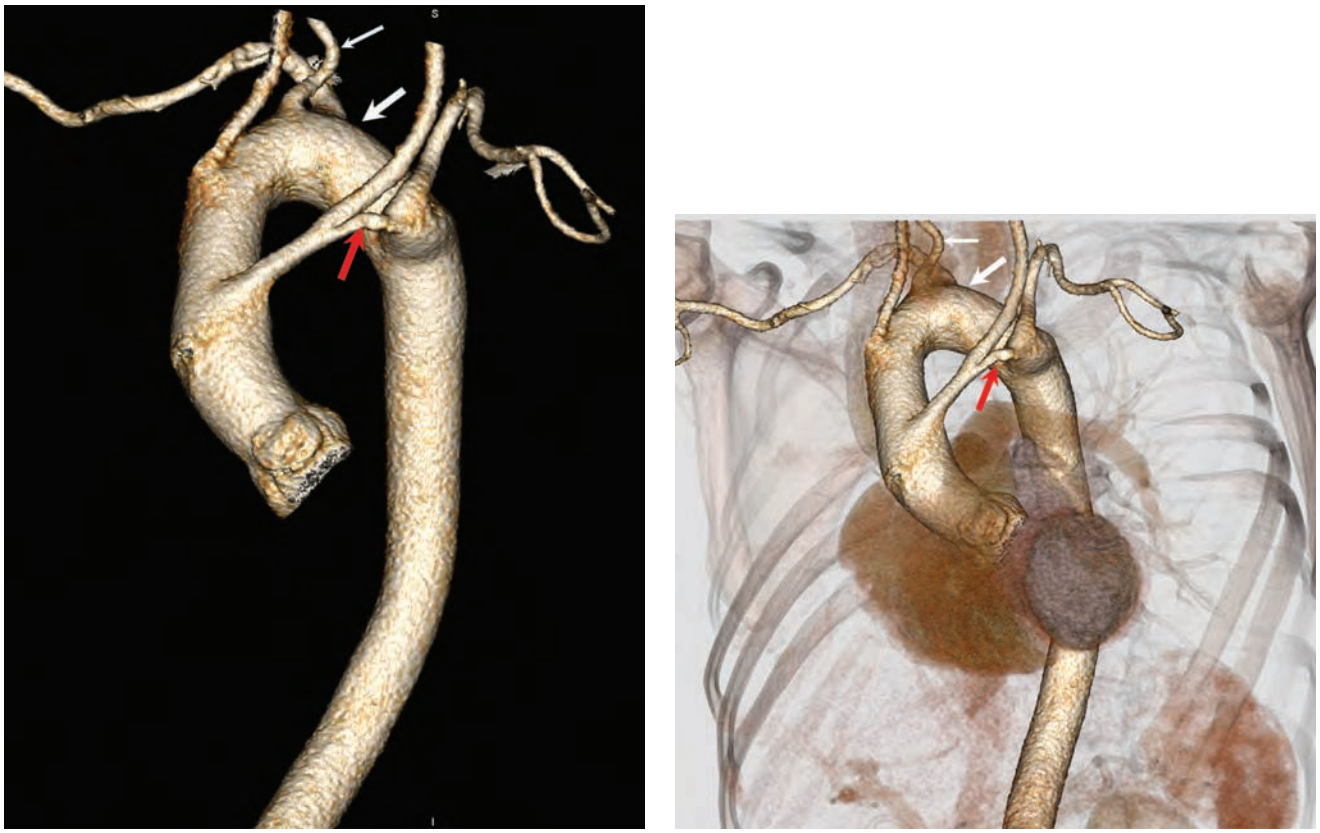

A B

Figure 49.17 (a, b) VR CTA images reveal left limb hypoplasic double aortic arch. Thin white arrows: right vertebral artery originating from right limb of the double aortic arch; thick white arrow: cervical extending right limb; red arrow: hypoplasic left limb.

segment of the left arch between the left ductus arteriosus and the descending aorta, leading to mirror image branching of the aortic arch. In this branching pattern the left brachiocephalic artery is the first branch, followed by the right common carotid and the subclavian arteries (Figs 49.18, 49.19). Some types of this anomaly differ according to the location of the ductus arteriosus. A true mirror image includes a right ductus crossing between the aortic arch or proximal descending aorta and the right pulmonary artery (Weinberg 2006). However, there is usually a left ductus arteriosus that does not form a complete vascular ring. The left-sided ductus arteriosus usually originates from the brachiocephalic artery instead of the descending aorta (Ramos-Duran et al. 2012).

Right aortic arch with an aberrant left subclavian artery (type II)

A right aortic arch with aberrant left subclavian artery results from interruption of the left arch between the left common carotid and left subclavian artery. The anomalous left subclavian artery usually courses retroesophageally and originates either as the last branch of the right aortic arch or from the Kommerell diverticulum, which is a remnant of the dorsal left aortic arch and leads to esophageal compression (Figs 49.14, 49.20). Infrequently, a right aortic arch can be accompanied by an aberrant left subclavian artery without a Kommerell diverticulum (Van Son 2002). In this anomaly the order of branching from proximal to distal is: left common carotid, right common carotid, right subclavian, and left subclavian artery (Figs 49.18, 49.20).

A right aortic arch with an aberrant brachiocephalic artery is very rare. This anomaly is similar to a right aortic arch with aberrant left subclavian artery and retroesophageal diverticulum (Garti and Aygen 1979). The order of branching is: right carotid, right subclavian, and finally a retroesophageal brachiocephalic artery.

Right aortic arch with isolation of the left subclavian artery (type III)

The right aortic arch with isolation of the left subclavian artery is the least common type of anomaly associated with the right aortic arch (Edwards 1948). It results from interruption of the aortic arch at two levels, proximal and distal to the left subclavian artery (Van Dyke and White 1994). The isolated left subclavian artery can be continuous either with the left vertebral

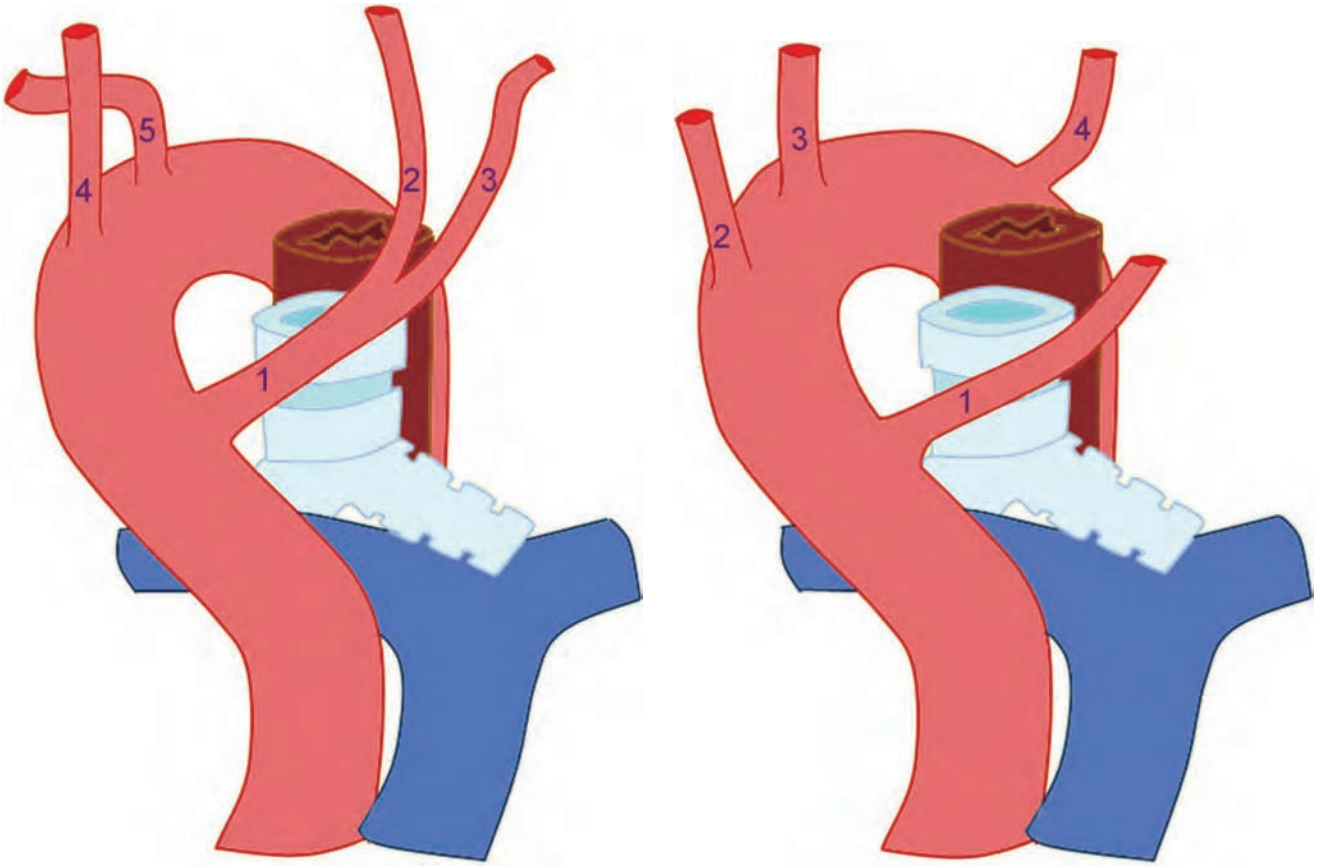

A B

Figure 49.18 Right aortic arch. (a) Type 1 right aortic arch with mirror image branching. 1: BT; 2: LCC; 3: LSC; 4: RCC; 5: RSC. (b) Type 2 right aortic arch. 1: LCC; 2: RCC; 3: RSC; 4: aberrant LSC.

artery or with the pulmonary artery via the ductus arteriosus. It can be filled with collaterals such as the external carotid, vertebral, thyrocervical trunk, and axillary arteries. Patients with isolated left subclavian artery can present with symptoms of left upper extremity ischemia (Stojanovska et al. 2012).

Aortic coarctation

In aortic coarctation there is a congenital constriction of the aortic lumen at the junction between the aortic arch and the descending aorta. This anomaly is usually classified as preductal (infantile type) or postductal (adult type) (Fig. 49.21).

In the preductal form, in addition to the focal constriction a long segment of the aortic arch can exhibit hypoplasia proximal to the ductus arteriosus, which often remains patent (Fig. 49.22). This type usually presents with congestive heart failure in infancy. A ventricular septal defect can also coexist and lead to pulmonary arterial hypertension.

In the postductal form, the obstruction occurs distal to the ductus arteriosus due to a shelf-like indentation in the posterolateral aortic wall. A bicuspid aortic valve is seen in 85% of cases and can be complicated by aortic stenosis, regurgitation, or both (Fig. 49.23).

In coarctation, the formation of collateral pathways usually via intercostal arteries is mostly seen because of a high-pressure gradient across the area of constriction. Dilated intercostal arteries can lead to inferior notching of the third to sixth ribs, a classic radiographic finding. These collateral pathways include (Fig. 49.23):

1. internal thoracic arteries originating from the subclavian arteries and connecting with the descending thoracic aorta;
2. thoracoacromial and descending scapular arteries arising from the subclavian arteries and connecting with the descending thoracic aorta; and
3. vertebral arteries arising from the subclavian arteries and connecting with the descending thoracic aorta.

Aortic coarctations with or without aortic arch hypoplasia are usually associated with intracardiac anomalies such as mitral stenosis, left ventricular hypoplasia or endocardial fibroelastosis, or subaortic or aortic stenosis, also known as Shone's syndrome (Shone et al. 1963).

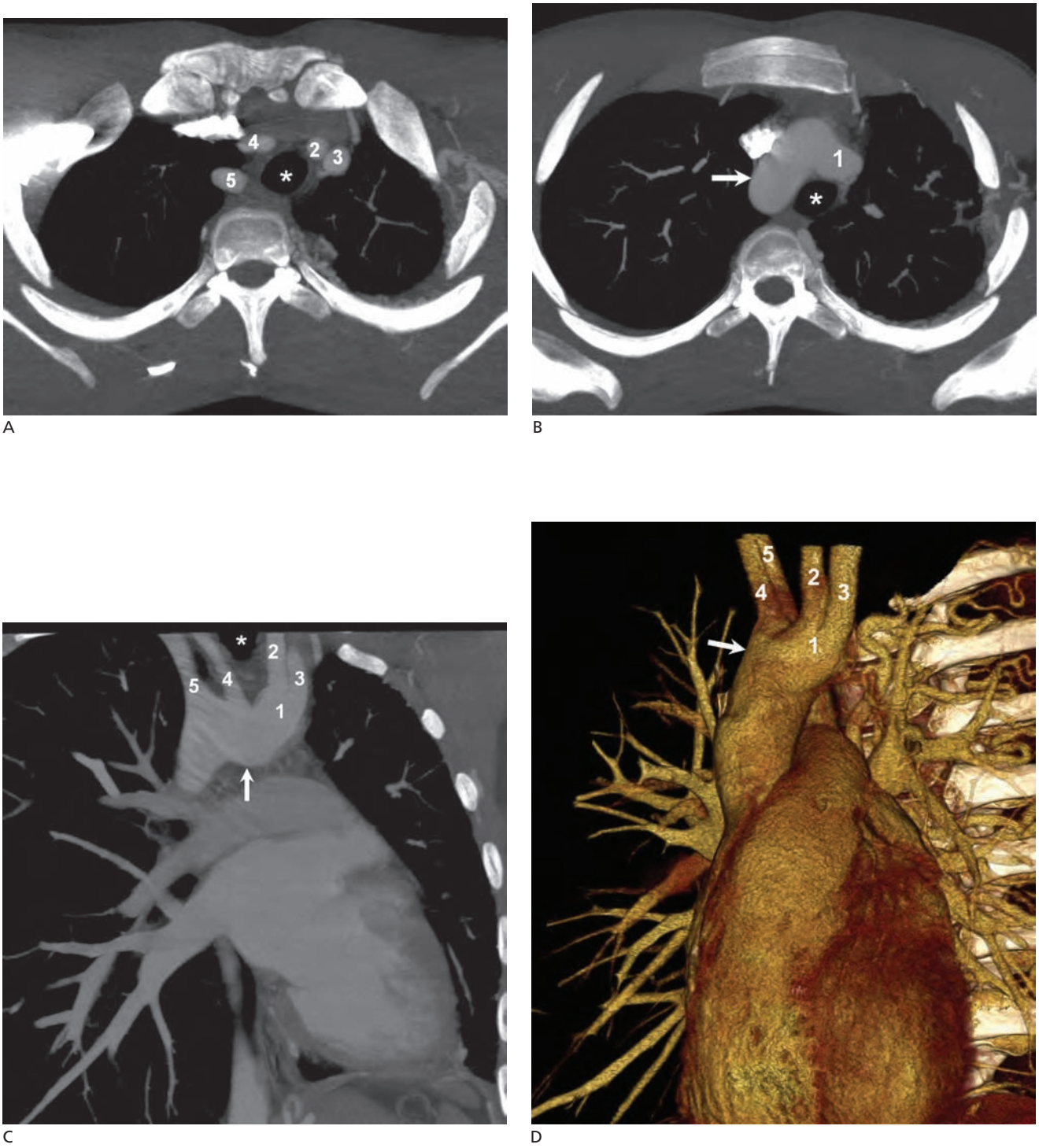

Figure 49.19 Type 1 right aortic arch with left pulmonary artery agenesis. (a, b) Axial and (c) oblique coronal MIP, and (d) VR CTA images demonstrate mirror image branching pattern of the right aortic arch (white arrow). 1: BT; 2: LCC; 3: LSC; 4: RCC; 5: RSC; *: trachea.

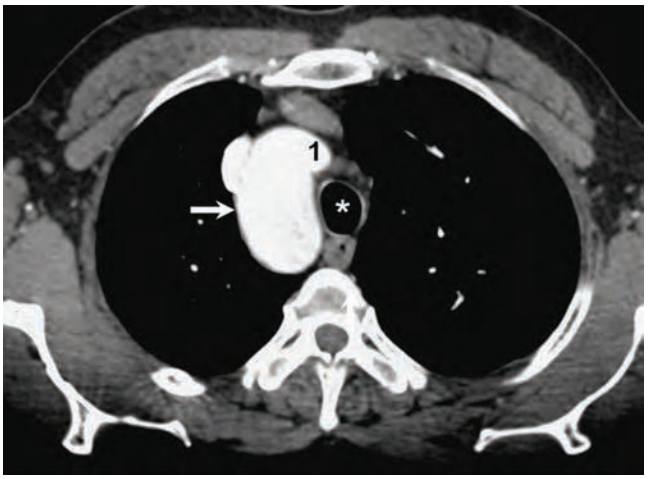

A

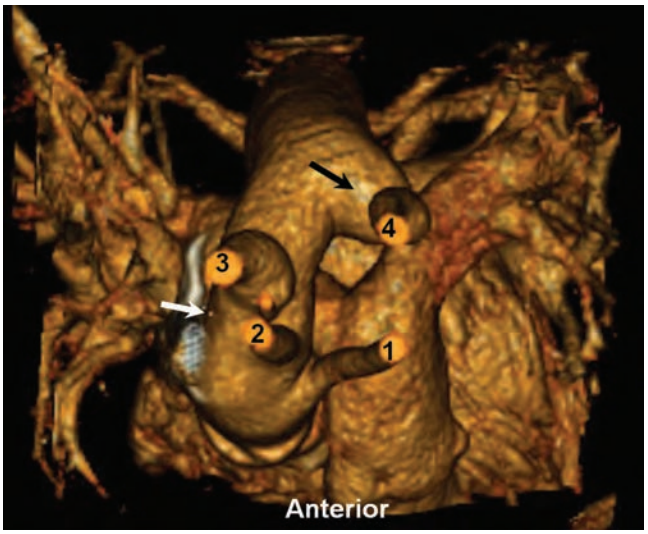

B

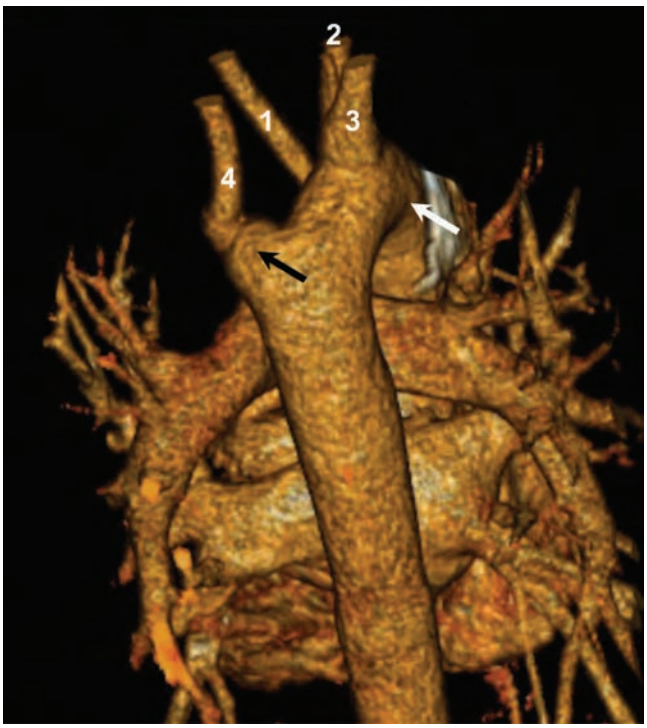

C

Figure 49.20 Type 2 right aortic arch. (a) Axial, (b) superior view, and (c) posterior view VR CTA images reveal right aortic arch (white arrow) with aberrant LSC artery and Kommerell's diverticulum (black arrow). 1: LCC; 2: RCC; 3: RSC; 4: aberrant LSC; *: trachea.

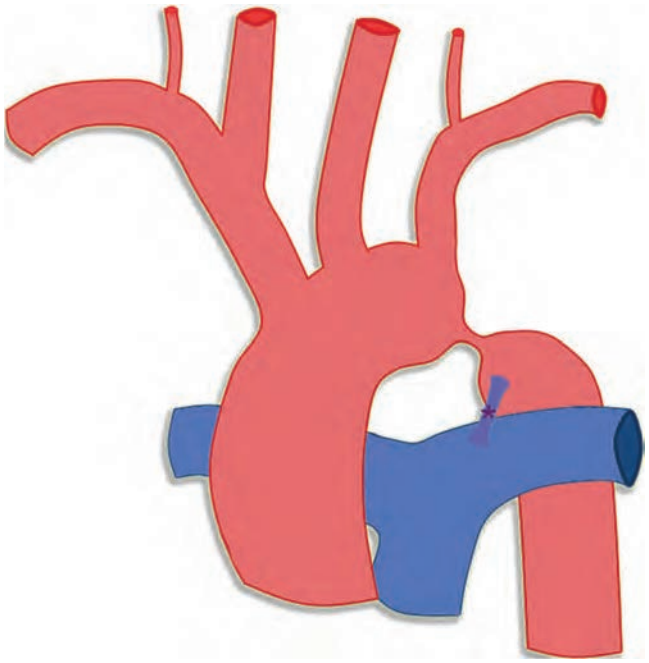

A

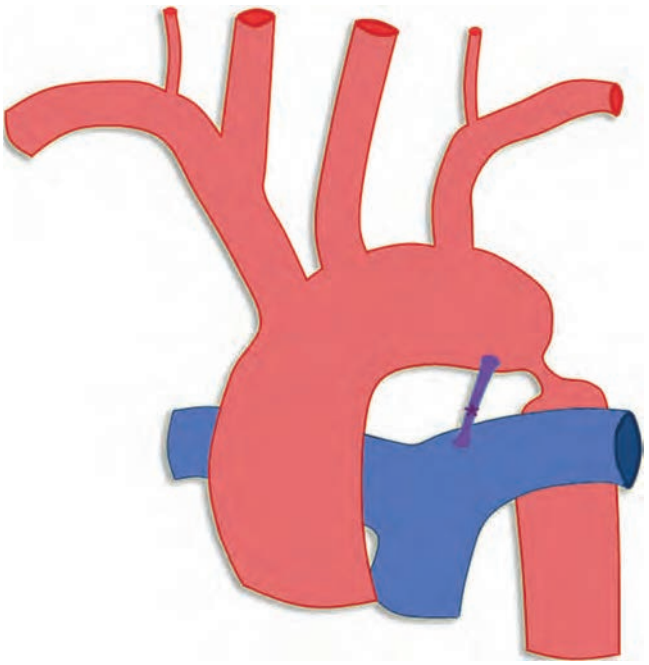

B

Figure 49.21 Aortic coarctation: (a) preductal and (b) postductal type. *: ductus (ligamentum) arteriosus.

A

B

C

Figure 49.22 (a) Oblique sagittal MIP, (b) VR, and (c) CTA images reveal preductal aortic coarctation (white arrows) with patent ductus arteriosus (black arrow). (*)=LSC

Figure 49.23 Aortic coarctation. (a) Oblique sagittal MIP and (b) VR CTA images reveal an aortic coarctation at the proximal descending aorta. There are multiple collateral pathways including the internal thoracic artery, thoracoacromial artery and intercostal arteries. (c) Axial CT image demonstrates coexistence of the bicuspid aortic valve.

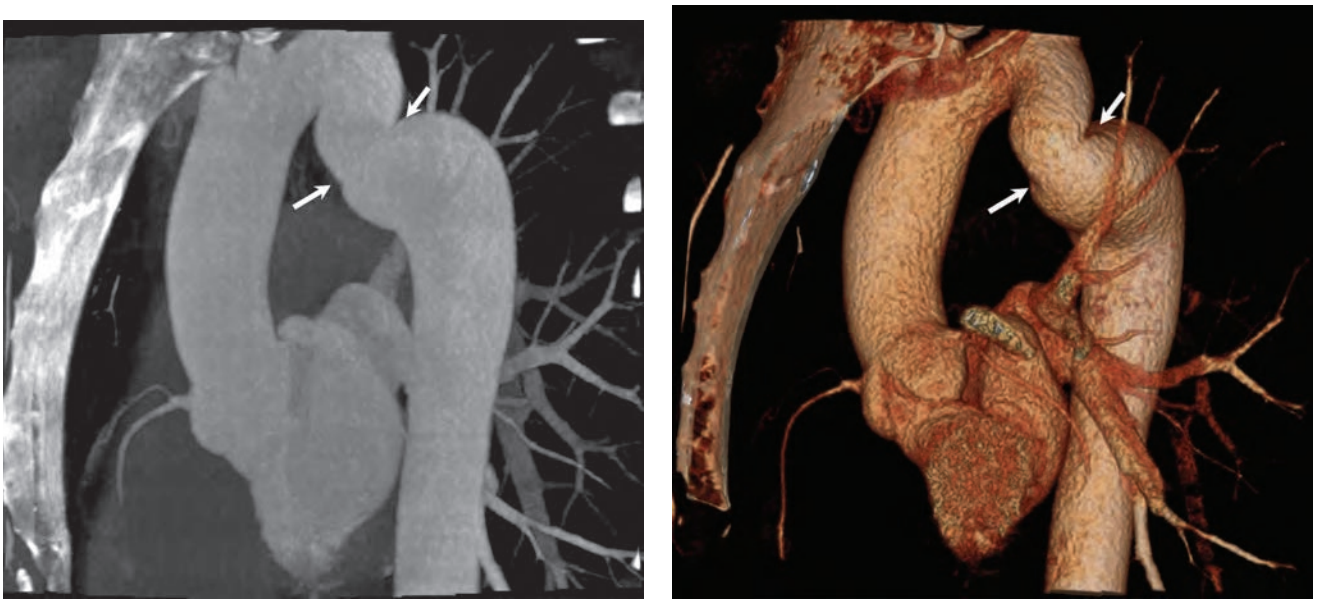

A B

Figure 49.24 Aortic pseudocoarctation. (a) Oblique sagittal MIP and (b) VR CTA images reveal aortic pseudocoarctation (arrows) and the elongation of the aorta.

Aortic pseudocoarctation

Aortic pseudocoarctation is an uncommon congenital anomaly characterized by kinking of a tortuous aortic arch at the level of the ligamentum arteriosus (Fig. 49.24). It occurs when the third and seventh aortic dorsal segments fail to fuse. Due to absence of a significant pressure gradient there is no systemic collateral, in contrast to coarctation of the aorta (Gay et al. 1969).

Interruption of the aortic arch

In an interrupted aortic arch there is complete discontinuity of the aortic lumen between the ascending and descending aorta. Interrupted aortic arches are rare and account for less than 1.5% of congenital heart anomalies. They are classified into three types, reflecting the level of interruption (Fig. 49.25; Monro 1994): type A, distal to the left subclavian artery (Fig. 49.26); type B, between the left common carotid and left subclavian artery; and type C, between the brachiocephalic trunk and left common carotid artery.

A patent ductus arteriosus invariably coexists and provides distal aortic flow. There can be a concurrent ventricular septal defect. An aberrant right subclavian artery (retroesophageal), originating from the descending aorta, also often coexists. A right-sided descending aorta with interrupted arch is almost always associated with Di George syndrome. Power (1850)

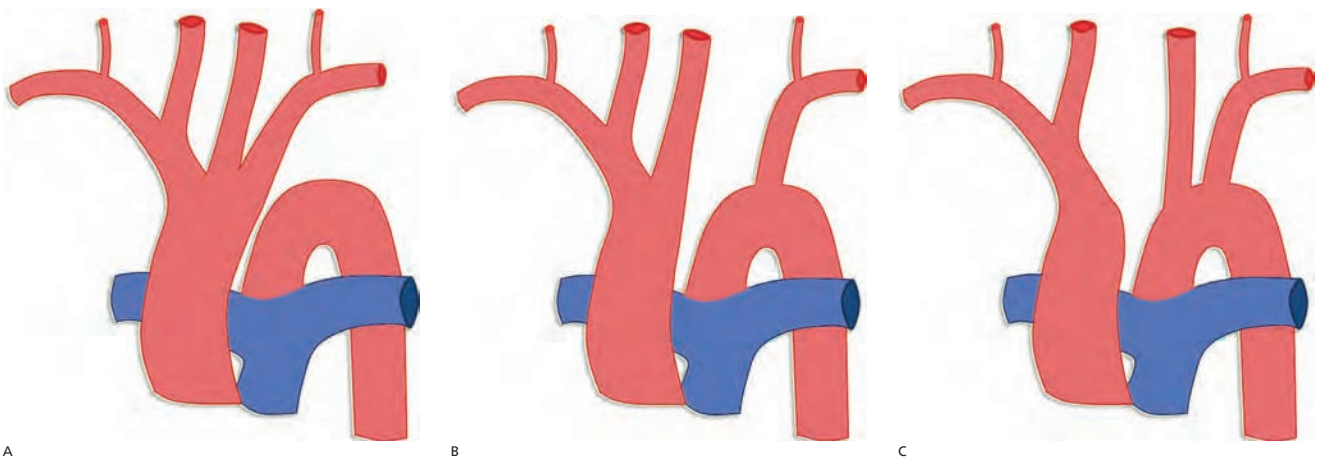

A B C

Figure 49.25 Aortic interruption: (a) type A, (b) type B, and (c) type C.

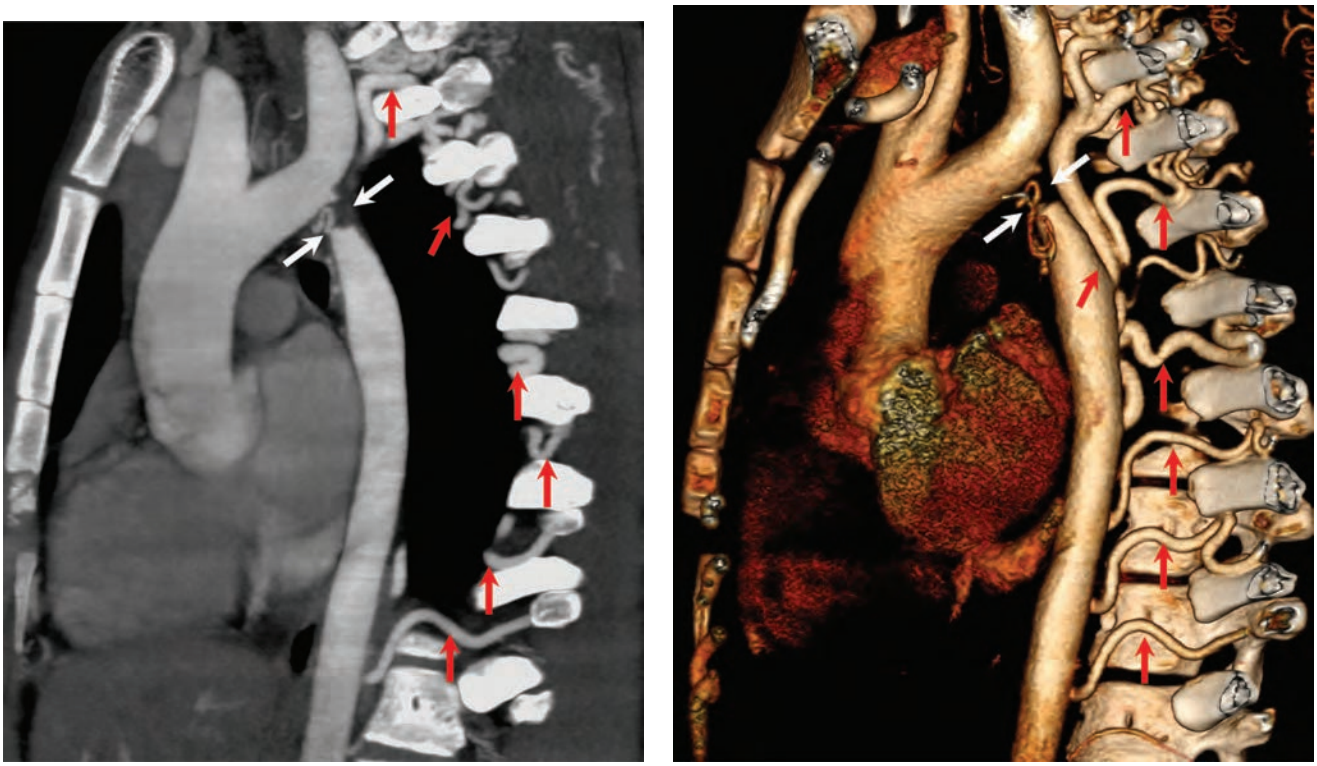

Figure 49.26 Type A aortic interruption. (a) Oblique sagittal and (b) volume-rendered (VR) CTA images reveal aortic interruption (white arrows) after the origin of the LSC artery. There are multiple enlarged collateral vascular structures (red arrows) between the branches of the LSC artery and descending aorta.

reported an ascending aorta that supplied the head and neck and a descending aorta that was a continuation of the pulmonary artery.

Cervical aortic arch

A cervical aortic arch is characterized by an elongated aortic arch that runs upward above the sternum, usually seen on the right side (Fig. 49.17). This abnormality can be attributed to abnormal regression of the fourth dominant arch with persistence of the first, second, or third arch, or by the lack of normal caudal migration of the fourth arch. It is commonly associated with a retroesophageal descending aorta contralateral to the arch, and an aberrant subclavian artery originating from the descending aorta. It can form a vascular ring if the ligamentum arteriosum is present on the side opposite the arch. Although it is usually asymptomatic, it occasionally causes dysphagia and respiratory symptoms. This anomaly can also be a part of syndromes such as Di George or Turner syndromes (Predey et al. 1989; Soler et al. 1998).

Aortic spindle

In the segment of the aorta between the left subclavian artery and the ductus arteriosus the fetal aorta is considerably narrowed and is named the aortic isthmus. Beyond the attachment of the ductus arteriosus the aorta presents a fusiform dilation known as the aortic spindle, an indentation or angle at the point of junction of the two parts in the concavity of the arch (Fig. 49.27). This condition can persist into adulthood (Fisher et al. 1997).

Ductus diverticulum

The aortic isthmus can appear in different ways. One is the ductus diverticulum, which consists of a focal dilatation along the anteroinferior surface of the isthmic region of the aortic arch (Gotway and Dawn 2003). Although a ductus diverticulum is usually believed to be a remnant of the closed ductus arteriosus, it has been suggested that it could actually be a remnant of the right dorsal aortic root (Grollman 1989). Sometimes a prominent ductus diverticulum looks like a traumatic pseudoaneurysm, but smooth margins with softly sloping symmetric shoulders and a slight convexity help to distinguish the two entities (Figs 49.28, 49.29).

Besides the well-known classic diverticulum another type of this entity is an atypical ductus diverticulum, which has a shorter and steeper slope superiorly and a more classically gentle slope inferiorly. Like the classic diverticulum it also has

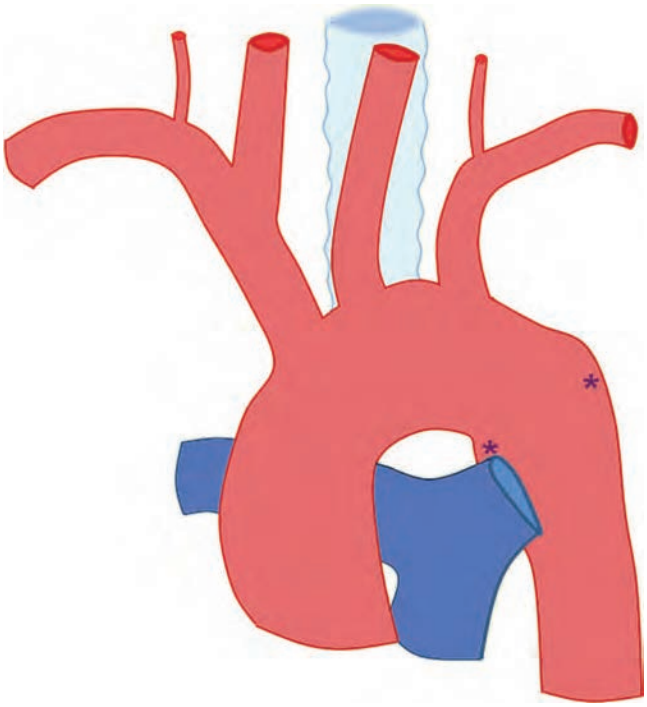

Figure 49.27 Aortic spindle. A circumferential bulge (*) in the proximal descending aorta.

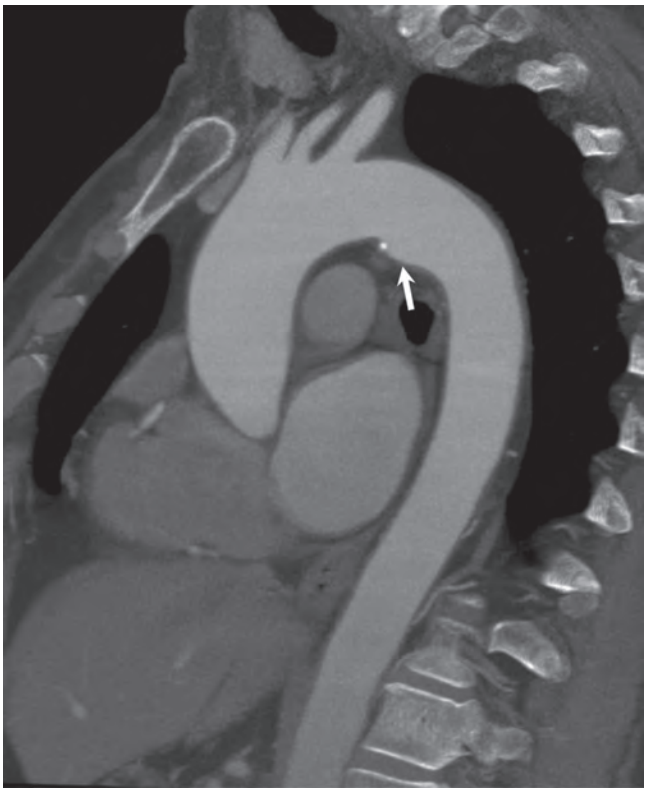

Figure 49.29 Ductus diverticulum. Oblique sagittal maximum-intensity-projection (MIP) computed tomography angiography (CTA) image demonstrates diverticular outpouching (arrow) at the anteromedial aspect of the aorta.

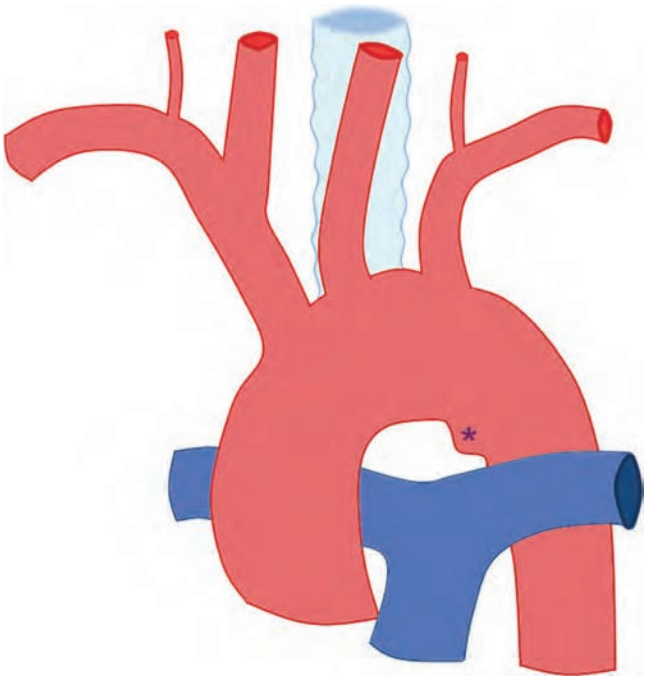

Figure 49.28 Ductus diverticulum. A developmental outpouching (*) at the anteromedial aspect of the aorta at the site of the previous ductus arteriosus.

smooth, uninterrupted margins that distinguish it from a pseudoaneurysm (Parmley et al. 1958; Hunink and Bos 1995).

Patent ductus arteriosus

The ductus arteriosus is derived from the left sixth aortic arch. It connects the main or left pulmonary artery to the descending aorta. In the fetal circulation, it carries deoxygenated blood from the right ventricle to the descending aorta and finally to the placenta (from the pulmonary to the systemic circulation). In normal circumstances it closes functionally 48 hours after birth and anatomically several weeks later. Its closure is mediated by the release of vasoactive substances such as acetylcholine and bradykinin and by variations in pH, oxygen tension, and prostaglandin levels. Interruption of this process leads to the anomaly called patent ductus arteriosus (Figs 49.30, 49.31). A patent ductus arteriosus carries a portion of the oxygenated blood from the aorta to the pulmonary circulation.

A patent ductus arteriosus can be associated with other anomalies such as transposition of the great vessels. In these cases it is sometimes the only pathway by which oxygenated blood mixes with deoxygenated blood, and is essential for the survival of the patient (Goo et al. 2003; Leschka et al. 2007).

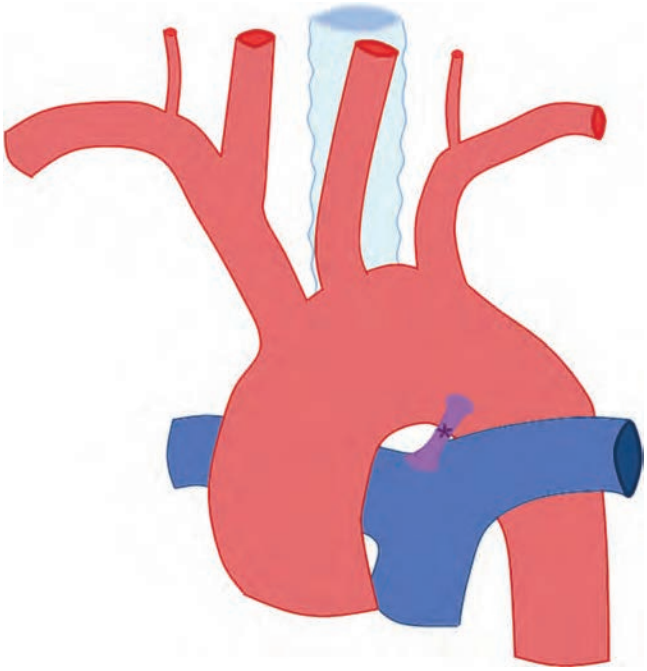

Figure 49.30 Patent ductus arteriosus (*) connects the distal main pulmonary artery to the descending aorta.

A

B

Figure 49.31 Patent ductus arteriosus and ductus diverticulum. (a) Oblique sagittal and (b) volume-rendered (VR) CTA images reveal patent ductus arteriosus (white arrow that connects the main pulmonary artery to the proximal descending aorta). A diverticular outpouching (black arrow) is also prominent at the site of the origin of the PDA.

Double descending aorta

In embryological development, the dorsal vessels initially form a paired symmetric system as the right and left primitive aortae, which then fuse to form a single descending aorta. In this anomaly there are two basic types of variation. The first type consists of complete separation of the two dorsal aortae. The second is a double-lumen descending aorta with a dividing septum coursing from a point distal to the ductal ligament to the aortic bifurcation.

In the first type, the bilateral intercostal arteries and the visceral branches arise from only one descending aorta, and only blind-ended rudimentary openings for the intercostal and visceral arteries can be present in the opposite aorta. Walsham (1882) described a long posterior vertical branch of the thoracic aorta that gave rise to almost all the posterior intercostal arteries on the right side.

In the second type the paired arterial branches originate from the corresponding ipsilateral trunks, whereas the unpaired arteries originate from only one aorta (Formanek et al. 1991; Karadeli and Ulu 2009).

Vertebral arteries

The vertebral artery develops from longitudinal arterial channels communicating with the cervical intersegmental arteries. All intersegmental arteries regress except for the seventh, which forms the proximal part of the subclavian artery and the origin of the vertebral artery (Newton and Mani 1974; Moore

and Persaud 1993). A left vertebral artery of aortic origin can result from persistence of the dorsal division of the left sixth intersegmental as the first part of the vertebral artery (Shoja 2006).

The vertebral artery usually originates from the posterior superior part of the ipsilateral subclavian artery, although it can originate from the aortic arch, the common, internal, or external carotid arteries, or subclavian artery branches such as the thyrocervical trunk. The left vertebral artery originates from the aortic arch in 3.1–8.3% of the population (Singla et al. 2010). When the left vertebral artery originates directly from the arch, it usually enters the transverse foramen of the fourth or fifth cervical vertebra instead of the sixth (Schwarzacher and Krammer 1989).

The aortic origin of the right vertebral artery is a rare anatomical variant. The right vertebral artery can originate: (1) from the first part of the subclavian; (2) directly from the aortic arch; (3) from the right common carotid; or (4) from the brachiocephalic trunk (Singla et al. 2010).

Thyroidea ima artery

The course of the thyroidea ima artery in the superior mediastinum and lower neck is hazardous for median surgical approaches to these areas. The artery has a variable origin and a highly variable rate of occurrence. It occurs in 4–10% of the population.

The thyroidea ima artery can arise from any of the following sources: aortic arch, brachiocephalic trunk, common carotid, internal thoracic, pericardiacophrenic, subclavian, thyrocervical trunk, inferior thyroid, or transverse scapular artery. In most cases it emerges from the brachiocephalic trunk, and less often from the right common carotid artery, aortic arch, internal thoracic artery, or left common carotid artery. It usually arises from the right side (Ziolkowski et al. 1994).

Bronchial arteries

The origin and course of the bronchial arteries vary greatly (Battal et al. 2010, 2011; Morita et al. 2010; Akgun et al. 2014). Knowledge of the variations of bronchial arterial anatomy is crucial in thoracoscopic surgery and interventions in pulmonary hemorrhage cases (Mori 2001; Remy-Jardin et al. 2004; Battal et al. 2011).

In early embryonic life, six symmetric pairs of pharyngeal arch arteries develop in conjunction with the branchial pouches supplying blood to the brachiocephalic structures. Regression and growth of the different pharyngeal arch components lead to the normal mature configuration.

Morita et al. (2010) devised a bronchial artery classification system based on the parent artery (Fig. 49.32):

- Type I: bronchial arteries originate directly from the thoracic aorta.
- Type II: bronchial arteries include both the common trunk of the right intercostal and right bronchial arteries (i.e., right IBT) and the common trunk of the right intercostal and left bronchial arteries (i.e., right intercostal–left bronchial trunk, or left IBT) originating from the thoracic aorta.
- Type III: bronchial arteries originate from the thoracic aorta with a common trunk of both bronchial arteries (CTB).
- Type IV: bronchial arteries originate from the subclavian artery.

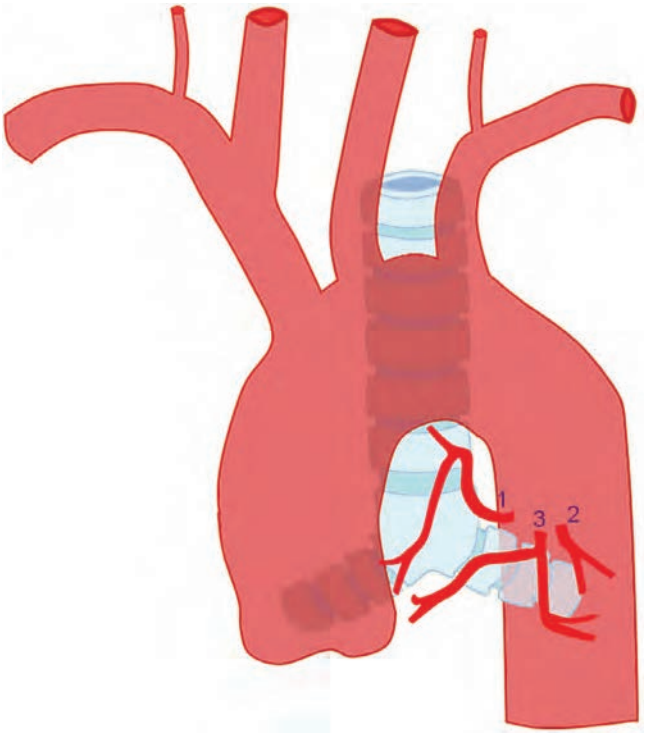

Figure 49.32 Bronchial artery origin types. 1: intercostal bronchial trunk (IBT), the common trunk of the right intercostal and right bronchial arteries; 2: bronchial artery originating from the thoracic aorta independently; 3: common trunk of right and left bronchial arteries (CTB).

There are also other classification systems based on the location of the ostia of the bronchial arteries on the circumferential wall of the thoracic aorta. Cauldwell et al. (1948) classified the classical bronchial artery branching patterns into four groups (Fig. 49.33):

1. two on the left and one on the right presenting as an IBT (40.6% of cases);
2. one on the left and one IBT on the right (21%);
3. two on the left and two on the right (one IBT and one bronchial artery) (20%); and
4. one on the left and two on the right (one IBT and one bronchial artery) (9.7%).

Most of the orthotopic bronchial arteries arise from the descending thoracic aorta, between the level of the upper endplate of vertebra T5 and the lower endplate of T6. Bronchial arteries that originate outside of these levels are defined

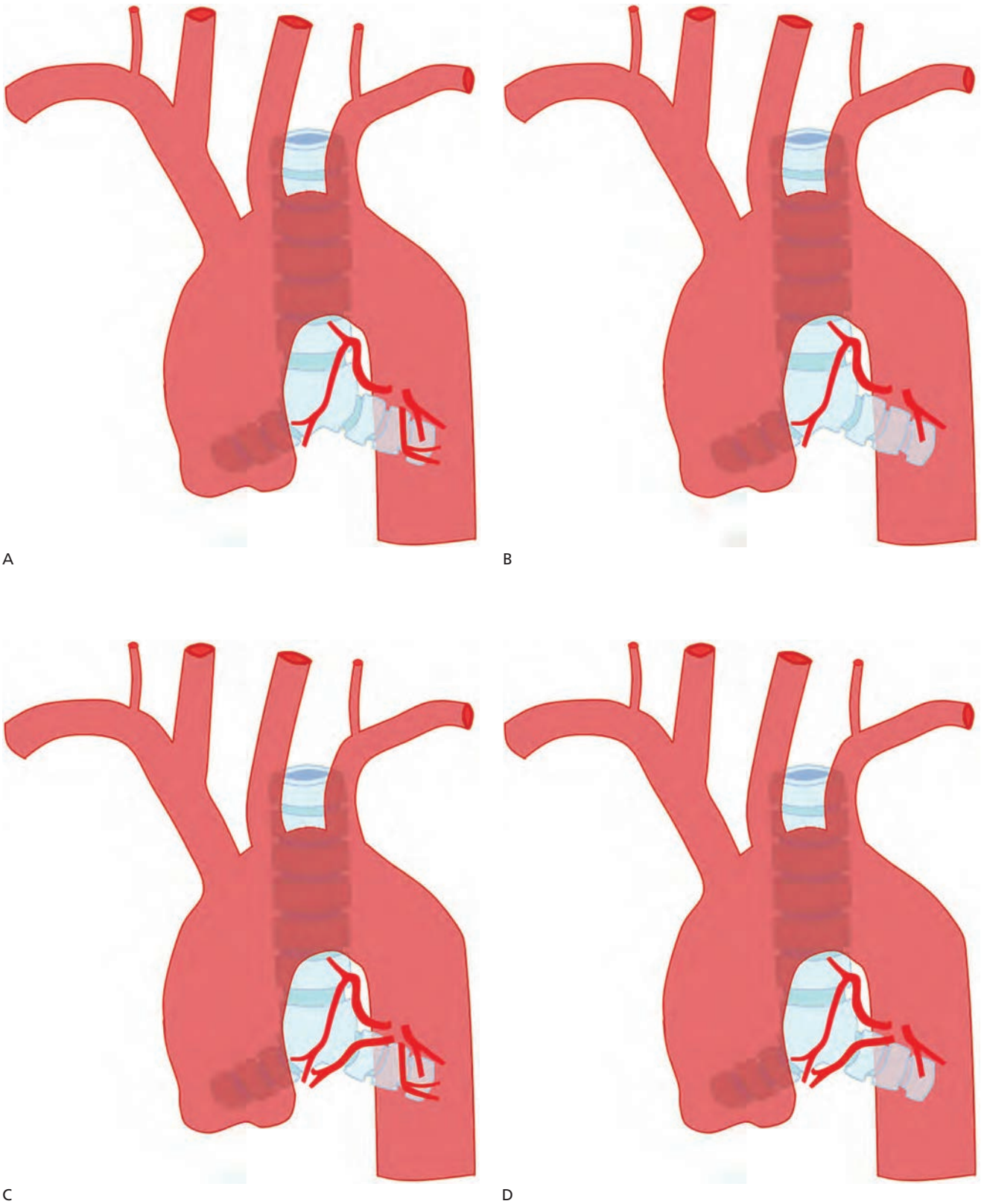

Figure 49.33 Cauldwell's classification of bronchial artery branching patterns. (a) Type 1 branching pattern; two on the left and one on the right that presents as an IBT. (b) Type 2 branching pattern; one on the left and one IBT on the right. (c) Type 3 branching pattern; two on the left and two on the right (one IBT and one bronchial artery). (d) Type 4 branching pattern; one on the left and two on the right (one IBT and one bronchial arteries).

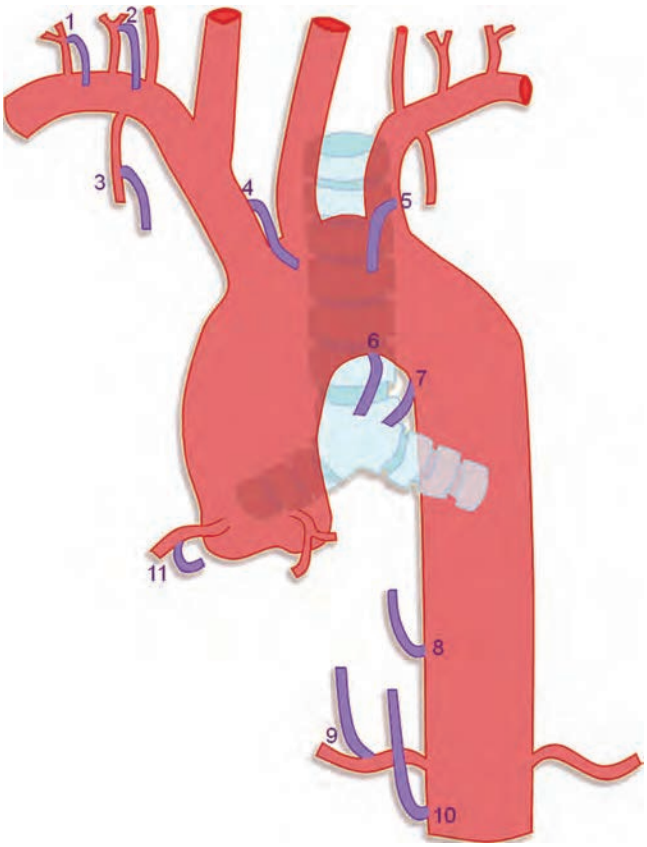

Figure 49.34 Ectopic bronchial arteries. They can originate from the costocervical trunk (1), thyrocervical trunk (2), internal mammary artery (3), brachiocephalic artery (4), subclavian artery (5), aortic arch (6), descending aorta above T3–T4 intervertebral disk level (7), descending aorta below T5–T6 intervertebral disk level (8), inferior phrenic artery (9), abdominal aorta (10), or coronary artery (11).

as ectopic. Ectopic locations of bronchial arteries include the aortic arch, internal thoracic artery, thyrocervical trunk, subclavian artery, costocervical trunk, brachiocephalic artery, coronary artery, pericardiacophrenic artery, inferior phrenic artery, and abdominal aorta (Figs 49.34–49.38). There are significantly more bronchial arteries in men than women (Battal et al. 2010, 2011; Loukas et al. 2011; Osiro et al. 2012; Akgun et al. 2013).

Spinal arteries

The arterial supply to the spinal cord derives from intradural vessels at each spinal level during the embryological period. These vessels have dorsal and ventral roots. The ventral radicular branches join in the midline and form the anterior spinal artery, which is by far the most important spinal artery since it supplies most of the spinal cord.

The anterior spinal artery and two posterolateral spinal arteries arise from the vertebral and deep cervical arteries in the cervical region. More inferiorly, they originate from the posterior intercostal or lumbar arteries. Circumflex vessels (arteria vaso corona) connect the anterior and posterior arterial systems in lateral margins of the cord.

During development, a few radicular arteries become dominant and provide most of the flow to the spinal cord through the anterior spinal artery. Five to eight of these vessels typically persist in adults. The largest and most frequently identified of the anterior vessels is the great artery of Adamkiewicz. Its level of origin is variable. It is usually on the left side, between T8 and L1–2. It provides much of the blood flow to the lower thoracic cord and the lumbar enlargement.

In general, larger numbers of smaller vessels serve as the posterior spinal arteries. The cervical and upper thoracic spinal cord is richly vascularized by a plexus arising from branches of the ascending cervical and vertebral arteries (Doppman et al. 1969; Goshgarian 2003).

Esophageal arteries

The arterial vasculature of the gastrointestinal tract is divided into two components, intramural and extramural. The intramural vascular distribution is generally well developed with plexuses in the different layers of the bowel wall. The extramural arterial supply for the esophagus is derived from the thoracic aorta or its major branches.

The extramural arterial supply to the human esophagus is divided into three major segments – the cervical, thoracic, and abdominal esophagus – with numerous anastomoses.

The cervical esophagus is supplied by the inferior thyroid artery, which is usually a branch of the thyrocervical trunk. An additional, individually variable supply is provided by small branches of other arteries such as the subclavian, common carotid, vertebral, superior thyroid, and costocervical trunk.

The thoracic esophagus receives blood from branches of the aorta, the bronchial arteries, and the right intercostal arteries. At the level of the bifurcation of the trachea, the main supply comes from branches of the bronchial arteries that descend on the ventral side of the esophagus. Approximately 50% of all cases have accessory esophageal branches originating directly from the aorta, the internal mammary, the common carotid, and the upper intercostal arteries. Below the bifurcation of the trachea the blood supply originates from two esophageal branches that arise directly from the right ventral side of the aorta. Both branches run to the dorsal side of the esophagus and give right and left branches. These also divide into ascending and descending branches that anastomose between themselves and with the descending branches of the lower thyroid and ascending branches of the left gastric and left lower phrenic arteries.

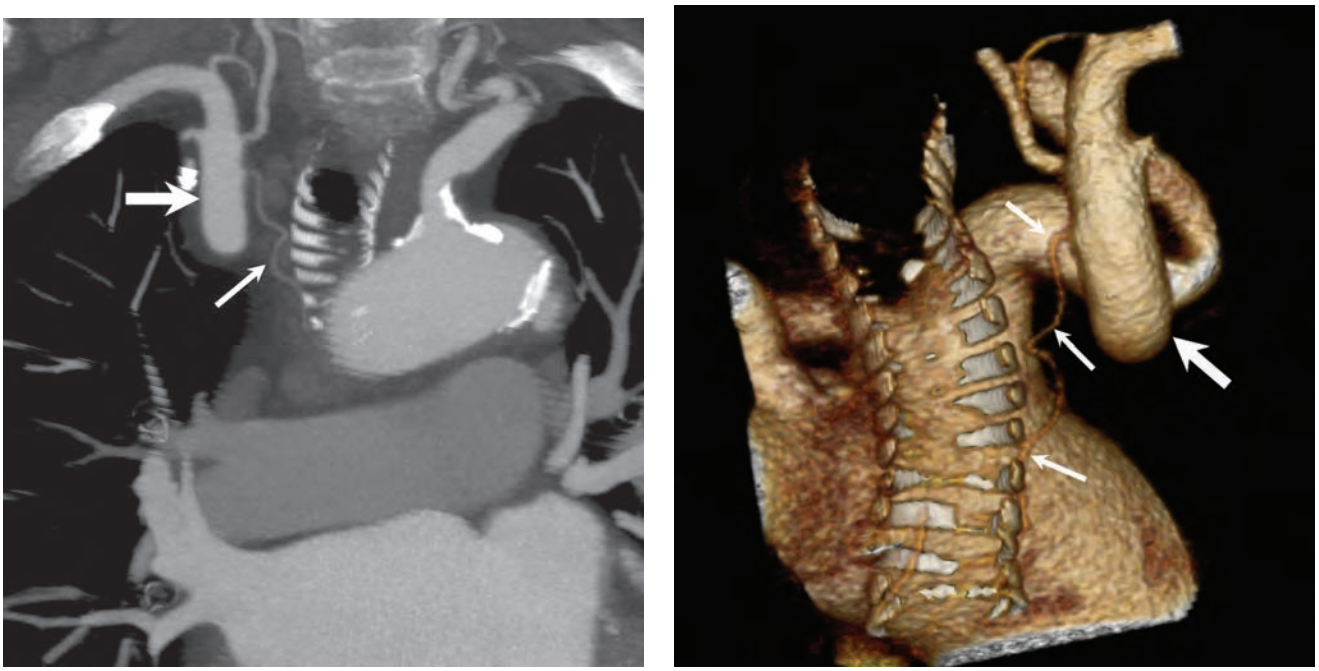

A B

Figure 49.35 (a) Coronal MIP and (b) posterior view VR CTA images reveal aberrant right bronchial artery (thin arrows) originating from the RSC artery (thick arrow).

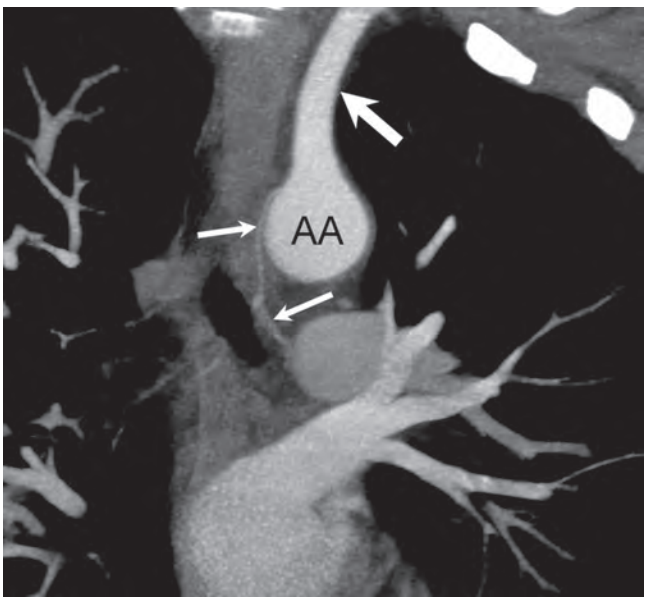

Figure 49.36 Coronal MIP CTA image reveals aberrant bronchial artery (thin arrows) originating from the superior surface of the aortic arch (AA). Thick arrow: RSC artery.

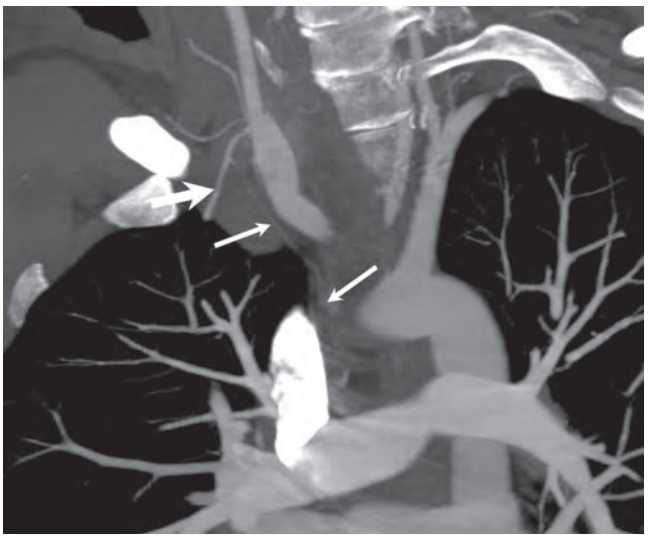

Figure 49.37 Coronal MIP CTA image reveals aberrant bronchial artery (thin arrows) originating from the right internal mammary artery (thick arrow).

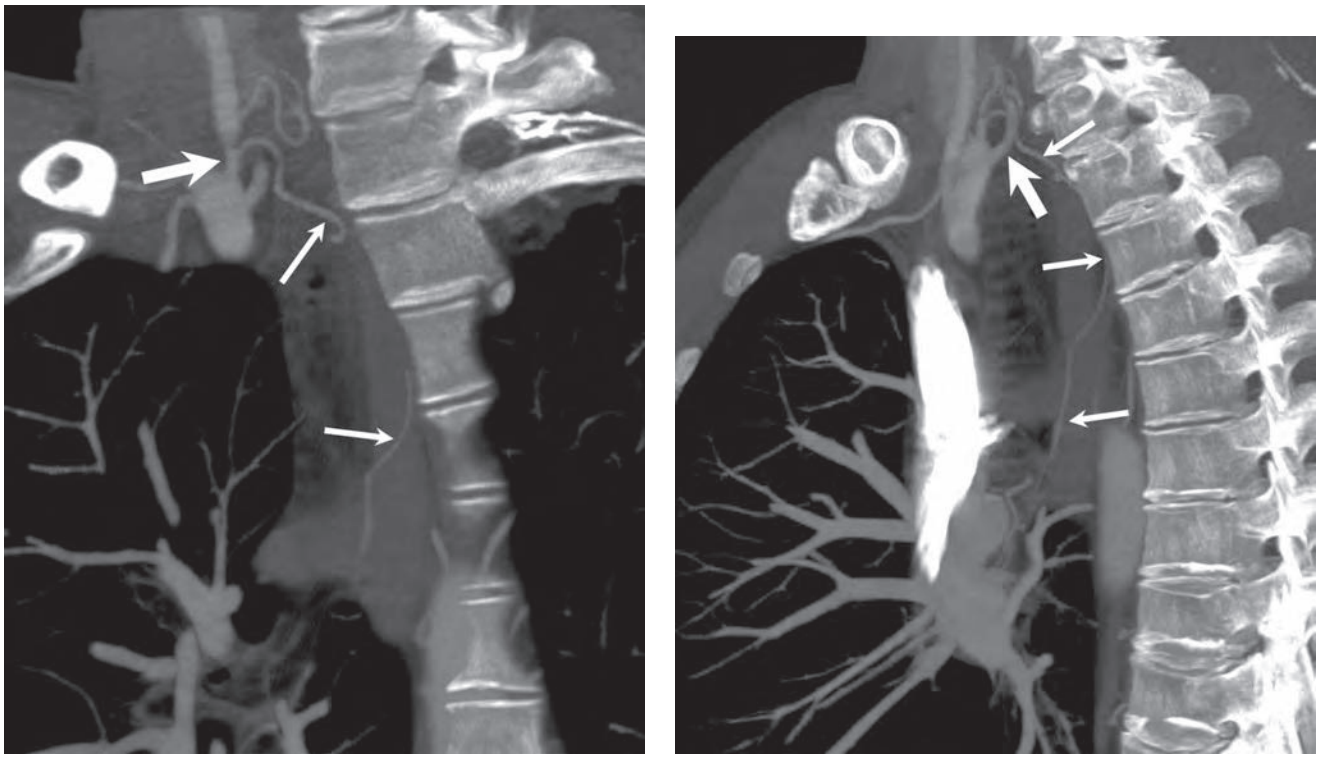

A B

Figure 49.38 (a) Oblique coronal and (b) sagittal MIP CTA images reveal aberrant bronchial artery (thin arrows) originating from the right thyrocervical trunk (thick arrow).

Esophageal branches of the left gastric and left inferior phrenic arteries supply the abdominal esophagus. They run alongside the right anterolateral and dorsal aspect of the esophagus and anastomose with the lower two esophageal branches from the thoracic aorta (Shapiro and Robillard 1950).

Superior phrenic arteries

The superior phrenic arteries are generally two small arteries distributed to the posterior part of the upper surface of the diaphragm. They can originate directly from the thoracic aorta or as a branch of either the proximal or distal segment of the tenth intercostal artery. In the first type, originating directly from the thoracic aorta, the superior phrenic artery usually terminates after a short course within the medial and posterosuperior surfaces of the diaphragm (Loukas et al. 2007).

Systemic arteries in pulmonary sequestration

Pulmonary sequestration entails nonfunctioning lung parenchyma that does not communicate with the tracheobronchial tree and receives blood from a systemic artery. The anomaly is further classified into intralobar and extralobar types.

Although they are sometimes congenital, most intralobar sequestrations are acquired secondary to chronic inflammation and bronchial obstruction due to recurrent pneumonias. This form is the most common and accounts for up to 75% of cases. It is rarely associated with other anomalies.

In contrast to intralobar sequestration, extralobar sequestration is always congenital, has a separate pleural investment, and is often associated with other anomalies (Lacey et al. 1999).

The arterial supply in both types of pulmonary sequestration is most commonly received from the descending aorta (Fig. 49.39). This type of vascularization is much more common in the intralobar type. More than one artery can supply the sequestration, or the artery can be split into branches before entering the parenchyma. Other origins of the aberrant arterial supply (in descending order) are the abdominal aorta, intercostal arteries, pulmonary artery, subclavian artery, internal mammary artery, pericardiophrenic artery, celiac artery, splenic artery, left gastric artery, ascending aorta, and suprarenal artery (Savic 1979).

As mentioned above, knowledge of the basic embryology of the thoracic vasculature is essential for understanding its variations. In this chapter we have primarily discussed the variations of the thoracic aorta and the origins of its clinically important branches. Besides the arteries discussed in the text there are also numerous fine branches of the thoracic aorta such as intercostal, subcostal, and pericardial which exhibit a range of variations. These variations are almost never clinically significant however, so are not detailed in the text.

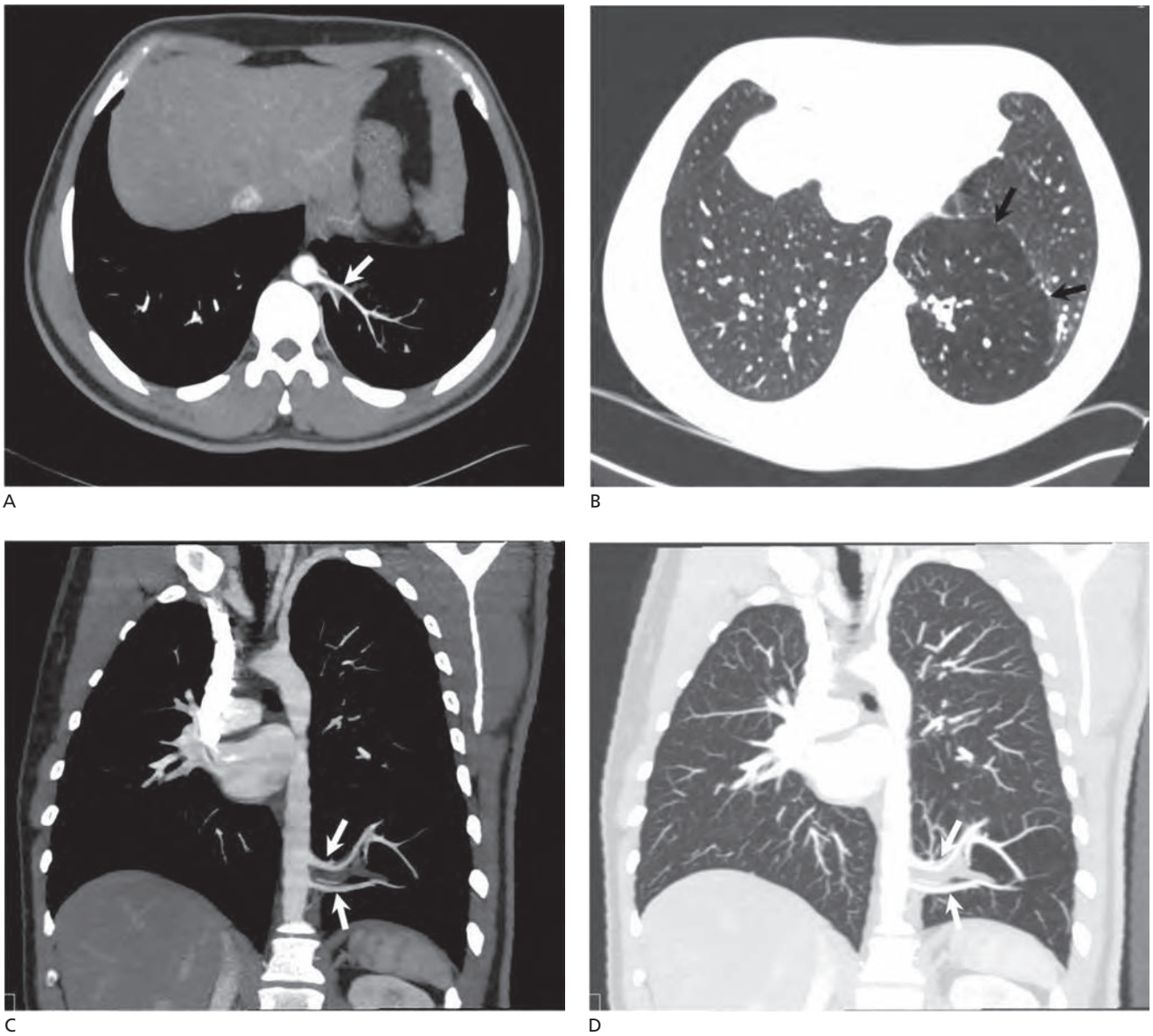

Figure 49.39 Axial (a) mediastinal window, (b) parenchymal window, and coronal (c) mediastinal window, (d) parenchymal window CTA images demonstrate left lower zone lung sequestration (black arrows), which has two systemic arterial supplies (white arrows) originating from the distal descending aorta.

References

Akgun V, Battal B, Karaman B, Ors F, Saglam M, Tasar M. 2010. A case of anomalous left coronary artery arising from the pulmonary artery in adulthood: multidetector computed tomography coronary angiography findings. *EAJM* 42: 100–102.

Akgun V, Battal B, Sari S. 2014. Bronchial arteries: normal anatomy, variation and radiologic evaluation. *Surg Radiol Anat* 36(1): 103–104.

Allen SR, Ignacio R, Falcone RA, Alonso MH, Brown RL, Garcia VF, Inge TH, Ryckman FC, Warner BW, Azizkhan RG, Tiao GM. 2006. The effect of a right-sided aortic arch on outcome in children with esophageal atresia and tracheesophageal fistula. *J Pediatr Surg* 41: 479–483.

Arey JB. 1984. Embryology of the heart and great vessels. In: *Cardiovascular Pathology in Infants and Children* (ed. Arey JB). Philadelphia: W B Saunders, p. 9–54.

Asherson N. 1979. David Bayford. His syndrome and sign of dysphagia lusoria. *Ann R Coll Surg Engl* 61: 63–67.

Backer CL, Mavroudis C. 2000. Congenital Heart Surgery Nomenclature and Database Project: vascular rings, tracheal stenosis, pectus excavatum. *Ann Thorac Surg* 69: S308–S318.

Bardo DME, Frankel DG, Applegate KE, Murphy DF, Saneto DO. 2001. Hypoplastic left heart syndrome. *RadioGraphics* 21: 705–717.

Battal B, Saglam M, Ors F, Akgun V, Dakak M. 2010. Aberrant right bronchial artery originating from right coronary artery: MDCT angiography findings. *Br J Radiol* 83: e101–104.

Battal B, Akgun V, Karaman B, Bozlar U, Tasar M. 2011. Normal anatomical features and variations of bronchial arteries: an analysis with 64-detector-row computed tomographic angiography. *J Comput Assist Tomogr* 35: 253–259.

Canty TG Jr, Boyle EM Jr, Linden B, Healey PJ, Tapper D, Hall DG, Sawin RS, Foker JE. 1997. Aortic arch anomalies associated with long gap esophageal atresia and tracheesophageal fistula. *J Pediatr Surg* 32: 1587–1591.

Cauldwell EW, Siekert RG, Lininger RE, Anson BJ. 1948. The bronchial arteries: an anatomic study of 150 human cadavers. *Surg Gynecol Obstet* 86: 395–412.

Desmet W, Vanhaecke J, Vrolix M, Van de Werf F, Piessens J, Willems J, de Geest H. 1992. Isolated single coronary artery: a review of 50,000 consecutive coronary angiographies. *Eur Heart J* 13: 1637–1640.

Deutsch L. 2005. Anatomy and angiographic diagnosis of extracranial and intracranial vascular disease. In: *Vascular Surgery* (ed. Rutherford RB). Philadelphia: Elsevier Saunders.

Dodge-Khatami A, Mavroudis C, Backer CL. 2002. Anomalous origin of the left coronary artery from the pulmonary artery: collective review of surgical therapy. *Ann Thorac Surg* 74: 946–955.

Doppman JL, Di Chiro G, Ommaya AK. 1969. *Selective arteriography of the spinal cord*. St Louis, Mo: Warren H. Green.

Edwards JE. 1948. Anomalies of the derivatives of the aortic arch system. *Med Clin N Am* 32: 925–49.

Ergun E, Simşek B, Koşar PN, Yılmaz BK, Turgut AT. 2013. Anatomical variations in branching pattern of arcus aorta: 64-slice CTA appearance. *Surg Radiol Anat* 35: 503–509.

Fernandes ED, Kadivar H, Hallman GL, Reul GJ, Ott DA, Cooley DA. 1992a. Congenital malformations of the coronary arteries: the Texas Heart Institute experience. *Ann Thorac Surg* 54: 732–740.

Fernandes J, Rutkowski M, Sanger JJ. 1992b. Anomalous origin of the left coronary artery. Use of thallium perfusion scans in the evaluation of successful revascularization. *Clin Nucl Med* 17: 177–179.

Fisher RG, Sanchez-Torres M, Whigham CJ, Thomas JW. 1997. "Lumps" and "bumps" that mimic acute aortic and brachiocephalic vessel injury. *Radiographics* 17: 825–834.

Formanek AG, Weisner KM, Lantz PE. 1991. Anomaly of the descending aorta: a case of persistent double dorsal aorta. *AJR Am J Roentgenol* 156: 1033–1035.

Garti IJ, Aygen MM. 1979. Right aortic arch with aberrant left innominate artery. *Pediatr Radiol* 8: 48–50.

Gay WA Jr, Young WG Jr, Durham NC. 1969. Pseudocoarctation of the aorta: a reappraisal. *J Thorac Cardiovasc Surg* 58: 739–745.

Goo HW, Park I-S, Ko JK, Kim YH, Seo DM, Yun TJ, Park JJ, Yoon CH. 2003. CT of congenital heart disease: normal anatomy and typical pathologic conditions. *RadioGraphics* 23: S147–S165.

Goshgarian HG. 2003. Blood supply of the spinal cord. In: *Spinal Cord Medicine: Principles and Practice* (eds Lin VW, Cardenas DD, Cutter NC, et al.). New York: Demos Medical Publishing.

Gotway MB, Dawn SK. 2003. Thoracic aorta imaging with multislice CT. *Radiol Clin North Am* 41: 521–543.

Grollman JH. 1989. The aortic diverticulum: a remnant of the partially involuted dorsal aortic root. *Cardiovasc Intervent Radiol* 12: 14–17.

Habel RE, Budras KD. 2003. Thoracic cavity. In: *Bovine Anatomy: An Illustrated Text*. Hanover, Germany: Schlütersche GmbH & Co.

Hastreiter AR, Serratto M, Arevalo F, Miller RA. 1966. Long-term hemodynamic studies in postoperative patients with transposition of the great vessels. Results of the venous switching operation. *Circulation* 33(4 Suppl): 34–51.

Hellinger JC, Daubert M, Lee EY, Epelman M. 2011. Congenital thoracic vascular anomalies: evaluation with state-of-the-art MR imaging and MDCT. *Radiol Clin North Am* 49: 969–996.

Hlavacek A, Loukas M, Spicer D, Anderson RH. 2010. Anomalous origin and course of the coronary arteries. *Cardiol Young* 20: 20–25.

Hoffman U, Pena AF, Cury RC, Abbara S, Ferencik M, Moselewski F, Siebert U, Brady TJ, Nagurney JT. 2006. Cardiac CT in emergency department patients with acute chest pain. *RadioGraphics* 26: 963–980.

Hunink MGM, Bos JJ. 1995. Triage of patients to angiography for detection of aortic rupture afterblunt chest trauma: cost-effectiveness analysis of using CT. *AJR* 165: 27–36.

Ishii Y, Suzuki T, Kobayashi T, Arakawa H. 2010. Single coronary artery with right ventricular fistula: case report and literature review. *Congenit Heart Dis* 5: 56–59.

Kafka H, Uebing A, Mohiaddin R. 2006. Adult presentation with vascular ring due to double aortic arch. *Congenit Heart Dis* 1: 346–350.

Karadeli E, Ulu E. 2009. CT of double descending thoracic aorta in an adult female. *Diagn Interv Radiol* 15: 179–181.

Kim SY, Seo FB, Do K-H, Heo JN, Lee JS, Song JW, Choe YH, Kim TH, Yong HS, Choi SI, Song KS, Lim TH. 2006. Coronary artery anomalies: classification and ECG-gated multi-detector row CT findings with angiographic correlation. *RadioGraphics* 26: 317–334.

Knight L, Edwards JE. 1974. Right aortic arch: types and associated cardiac anomalies. *Circulation* 50: 1047–1051.

Lacey DE, Shaw NJ, Pilling DW, Walkinshaw S. 1999. Outcome of congenital lung abnormalities detected antenatally. *Acta Paediatr* 88: 454–458.

Layton KF, Kallmes DF, Cloft HJ, Lindell EP, Cox VS. 2006. Bovine aortic arch variant in humans: clarification of a common misnomer. *AJNR* 27: 1541–1542.

Leschka S, Oechslin E, Husmann L, Desbiolles L, Marincek B, Genoni M, Prêtre R, Jenni R, Wildermuth S, Alkadhi H. 2007. Evaluation of congenital heart disease in children and adults with 64 section CT. *RadioGraphics*. 27: 829–846.

Lippert H, Pabst R. 1985. Aortic arch. In: *Arterial Variations in Man: Classification and Frequency*. Munich, Germany: JF Bergmann-Verlag.

Loukas M, Louis RG Jr, Gaspard J, Fudalej M,Tubbs RS, Merbs W. 2006. A retrotracheal right subclavian artery in association with a vertebral artery and thyroidea ima. *Folia Morphol (Warsz)* 65: 236–241.

Loukas M, Louis RG Jr, Wartmann CT, Tubbs RS, Esmaeili E, Bagenholm AC, Merbs W, Curry B, Jordan R. 2007. Superior phrenic artery: an anatomic study. *Surg Radiol Anat* 29: 97–102.

Loukas M, Hanna M, Chen J, Tubbs RS, Anderson RH. 2011. Extracardiac coronary arterial anastomoses. *Clin Anat* 24: 137–142.

Maldonado JA, Henry T, Gutiérrez FR. 2010. Congenital thoracic vascular anomalies. *Radiol Clin North Am* 48: 85–115.

Monro JL. 1994. Interruption of aortic arch. In: *Surgery for Congenital Heart Defects*, second edition (eds Stark J, de Leval M). Philadelphia: WB Saunders.

Moore KL, Persaud TV. 1993. *The Developing Human*. Philadelphia: WB Saunders.

Mori K. 2001. The mediastinal courses of the bronchial arteries: helical CT evaluation. *Nippon Igaku Hoshasen Gakkai Zasshi* 61: 156–162.

Morita Y, Takase K, Ichikawa H, Yamada T, Sato A, Higano S, Takahashi S. 2010. Bronchial artery anatomy: preoperative 3D simulation with multidetector CT. *Radiology* 255: 934–943.

Murillo H, Lane MJ, Punn R, Fleischmann D, Restrepo CS. 2012. Imaging of the aorta: embryology and anatomy. *Semin Ultrasound CT MR* 33: 169–190.

Newton TH, Mani RL. 1974. The vertebral artery. In: *Radiology of Skull and Brain* (eds Newton TH, Potts DG). St Louis, Mo: Mosby.

O'Brien JPO, Srichai MB, Hecht EM, Kim DC, Jacobs JE. 2007. Anatomy of the heart at multidetector CT: what the radiologist needs to know. *RadioGraphics* 27: 1569–1582.

Osborn AG. 1999. *The aortic arch and great vessels. In: Diagnostic Cerebral Angiography*, second edition. Philadelphia: Lippincott Williams & Wilkins.

Osiro S, Wear C, Hudson R, Ma XX, Zurada A, Michalak M, Loukas M. 2012. A friend to the airways: a review of the emerging clinical importance of the bronchial arterial circulation. *Surg Radiol Anat* 34: 791–798.

Pannu HK, Flohr TG, Corl FM, Fishman EK. 2003. Current concepts in multi-detector row CT evaluation of the coronary arteries: principles, techniques, and anatomy. *RadioGraphics* 23: S1111–1125.

Parmley LF, Mattingly TW, Manion WC, Janke EJ. 1958. Nonpenetrating traumatic injury of the aorta. *Circulation* 17: 1086–1092.

Power JH. 1850. *Surgical Anatomy of the Arteries and Descriptive Anatomy of the Heart by the Late Valentine Flood*, M.D. Dublin: Fannin and Co.

Predey TA, McDonald V, Demos TC, Moncada R. 1989. CT of congenital anomalies of the aortic arch. *Semin Roentgenol* 24: 96–113.

Ramaswamy P, Lytrivi ID, Thanjan MT, Nguyen T, Srivastava S, Sharma S, Ko HH, Parness IA, Lai WW. 2008. Frequency of aberrant subclavian artery, arch laterality, and associated intracardiac anomalies detected by echocardiography. *Am J Cardiol* 101: 677–682.

Ramos-Duran L, Nance JW Jr, Schoepf UJ, Henzler T, Apfaltrer P, Hlavacek AM. 2012. Developmental aortic arch anomalies in infants and children assessed with CT angiography. *AJR Am J Roentgenol* 198: W466–474.

Remy-Jardin M, Bouaziz N, Dumont P, Brillet PY, Bruzzi J, Remy J. 2004. Bronchial and nonbronchial systemic arteries at multi-detector row CT angiography: comparison with conventional angiography. *Radiology* 233: 741–749.

Roberts WC. 1970. The congenitally bicuspid aortic valve: a study of 85 autopsy cases. *Am J Cardiol* 26: 72–83.

Roberts WC, Ko JM. 2005. Frequency by decades of unicuspid, bicuspid, and tricuspid aortic valves in adults having isolated aortic valve replacement for aortic stenosis, with or without associated aortic regurgitation. *Circulation* 111: 920–925.

Savic B, Birtel FJ, Tholen W, Funke HD, Knoche R. 1979. Lung sequestration: report of seven cases and review of 540 published cases. *Thorax* 34: 96–101.

Schlesinger AE, Krishnamurthy R, Sena LM, Guillerman RP, Chung T, DiBardino DJ, Fraser CD Jr. 2005. Incomplete double aortic arch with atresia of the distal left arch: distinctive imaging appearance. *AJR Am J Roentgenol* 184: 1634–1639.

Schwarzacher SW, Krammer EB. 1989. Complex anomalies of the human aortic arch system: unique case with both vertebral arteries as additional branches of the aortic arch. *Anat Rec* 225: 246–250.

Shapiro AL, Robillard GL. 1950. The esophageal arteries: their configurational anatomy and variations in relation to surgery. *Ann Surg* 131: 171–175.

Shaw JA, Gravereaux EC, Eisenhauer AC. 2003. Carotid stenting in the bovine arch. *Catheter Cardiovasc Interv* 60: 566–569.

Shoja MM, Tubbs RS, Khaki AA, Shokouhi G, Farahani RM, Moein A. 2006. A rare variation of the vertebral artery. *Folia Morphologica* 65: 167–170.

Shone JD, Sellers RD, Anderson RC, Adams P Jr, Lillehei CW, Edwards JE. 1963. The developmental complex of "parachute mitral valve," supravalvular ring of left atrium, subaortic stenosis, and coarctation of aorta. *Am J Cardiol* 11: 714–725.

Sievers HH, Schmidtke C. 2007. A classification system for the bicuspid aortic valve from 304 surgical specimens. *J Thorac Cardiovasc Surg* 133: 1226–1233.

Simonds JP. 1923. Congenital malformations of the aortic and pulmonary valves. *Am J Med Sci* 166: 584–595.

Singla RK, Sharma T, Sachdeva K. 2010. Variant origin of left vertebral artery. *International Journal of Anatomical Variations* 3: 97–99.

Soler R, Rodriguez E, Requejo I, Fernández R, Raposo I. 1998. Magnetic resonance imaging of congenital abnormalities of the thoracic aorta. *Eur Radiol* 8: 540–546.

Stojanovska J, Cascade PN, Chong S, Quint LE, Sundaram B. 2012. Embryology and imaging review of aortic arch anomalies. *J Thorac Imaging* 27: 73–84.

Van Dyke CW, White RD. 1994. Congenital abnormalities of the thoracic aorta presenting in the adult. *J Thorac Imaging* 9: 230–244.

Van Son JA, Konstantinov IE. Burckhard F. 2002. Kommerell and Kommerell's diverticulum. *Tex Heart Inst J* 29: 109–112.

Vlodaver Z, Neufeld HN, Edwards JE. 1972. Pathology of coronary disease. *Semin Roentgenol* 7: 376–394.

Walsham WJ. 1882. Abnormal origin and distribution of the upper seven right intercostal arteries with remarks. *J Anat Physiol* 16: 441–445.

Weinberg PM. 2006. Aortic arch anomalies. *J Cardiovasc Magn Reson* 8: 633–643.

Ziolkowski M, Bieganska-Dembowska D, Kurlej W. 1994. Variations in the number and in origin of the thyroid arteries. *Folia Morphol (Warsz)* 53: 105–110.

50 Coronary arteries

Horia Muresian
Cardiovascular Surgery, San Donato Milan, Italy
University Hospital of Bucharest, Bucharest, Romania

Coronary artery anomalies and variations (CAAs) constitute an important topic, especially in view of the continual deployment of newer and more accurate diagnostic and imaging techniques paralleled by the development of surgical and percutaneous procedures. Beyond mere anatomical description, the associated pathophysiological mechanisms, clinical significance and prognosis demand a thorough understanding of the CAAs. Numerous classifications have emerged from recent developments to provide the tools needed to inform complex clinical judgments and therapeutic decisions. However, there is no clear distinction between "major" and "minor" CAAs. New mechanisms along with their resultant hemodynamic effects are continually being identified, resulting in detailed descriptions that allow for more efficient treatments. Consequently, the list of CAAs remains open; the percentages pertaining to their incidence and prevalence are re-evaluated and revisited, and there is a need for pertinent dialogue among the specialists involved – even marginally – in diagnosing and treating these cardiac conditions.

The following pages, presenting the anomalies and variations of the coronary arteries and veins, are founded on the concept of clinical anatomy. Their aim is to endow the reader with the principles required to achieve a comprehensive approach to any modified coronary pattern, assisting the physician to solve the dilemma between "doing too much" and "not doing enough." Not least, the reader will become better oriented and will find this a useful guide among the multitude of articles and cases often presented with too many classifications, nomenclatures, and interpretations.

The most appropriate and practical scheme includes the description of the normal coronary arterial disposition based on qualitative and quantitative criteria and the definition of a coronary abnormality after the normal features have been excluded, in order to generate a classification scheme (Angelini 2007). The features of the normal coronary arterial anatomy in humans are listed in Table 50.1.

Although there are essentially two coronary arteries – left and right – the former divides into the anterior interventricular branch (left anterior descending or LAD) and the circumflex branch (Cx). The resultant three coronary stems (Fig. 50.1) are designated "the three elementary coronary trunks" (Table 50.2) and all CAAs are eventually described on this basis (Angelini 2002). The definition of a coronary artery or trunk should not take its origin and proximal course into account, but focus on the intermediate and distal segments and target tissues of distribution.

Another important detail refers to the nomenclature of the aortic (and pulmonary) sinuses (Table 50.3). A positional nomenclature of the facing sinuses of the aorta relative to the heart complicates the classification and is unnecessary (Shaher and Puddu 1966; Gittenberger-de Groot et al. 1983). The numerical nomenclature (Fig. 50.1) also allows the coronary arterial disposition in congenitally malformed hearts to be described properly.

For a better understanding of coronary arterial variations, it is important to highlight the existence of preferential coronary pathways, that is, the most possible paths the coronaries can follow (Muresian 2009). These correspond to areas occupied by the *anlage* of the future coronary arteries and where a major coronary trunk or significant anastomotic channel is most likely to be found (McAlpine 1975; Loukas et al. 2009a, b). As well as the coronary sulcus crossed at right angles by the anterior and posterior interventricular sulci, the following routes are also described: the periaortic route with a preaortic and a retroaortic component (Fig. 50.2a), the preinfundibular (precardiac) route (Fig. 50.2b), the intraseptal (supracristal) route (Fig. 50.2c), and the atrial routes with the L-loop (retrocardiac) and M-loop (Kawashima and Sasaki 2003; Fig. 50.2d).

A useful classification based on a hierarchical scheme, and with the purpose of establishing a unified reporting system, was offered by Dodge-Khatami and associates (Dodge-Khatami et al. 2000; Table 50.4). An in-depth classification, including newer concepts as well as recently reported variations, is further developed in this chapter (Angelini 2007; Table 50.5).

Bergman's Comprehensive Encyclopedia of Human Anatomic Variation, First Edition. Edited by R. Shane Tubbs, Mohammadali M. Shoja and Marios Loukas.
© 2016 John Wiley & Sons, Inc. Published 2016 by John Wiley & Sons, Inc.

Table 50.1 Normal features of the coronary artery anatomy in humans. Adapted from Angelini et al. (2007) with permission from LWW.

Feature	Range	Notes
Number of ostia	2–4	Accepted normal separate ostia are the separate origin of the LAD and Cx, of the conus artery or, rarely, the first septal branch*
Location of ostia	Right and left aortic sinuses (sinus 1 and 2) in the upper midsection (or not less than 5 mm from commissure)	(See also Table 50.3) The numeric definition of the aortic sinuses and the spatial orientation *in situ* (anatomically appropriate orientation)
Shape of ostium	Circular, oval; may appear double-barreled in cases with very short common trunk of the LCA, or when the RCA and the conus artery share a common ostium	The presence of a diaphragm or a slit-like ostium are considered abnormal
Size of ostium	Must be measured against the proximal emerging coronary trunk	See also the section on COSA (congenital ostial stenosis or atresia)
Proximal orientation	45–90° (off the aortic wall); see also Figure 50.5.	The most acute angle must be sought and determined in imaging techniques. See also section on 'Acute take-off of the circumflex branch (ATO-Cx)'
Proximal common trunk	Only the left coronary artery (Cx + LAD). All other variations are named "mixed trunks"	The common origin of the RCA and the conus artery not included in this classification
Proximal tract	Direct, from ostium to destination	Meandering coronary arteries must be considered as a separate condition. See text, 'Multiple concomitant coronary arterial anomalies'
Mid-course	Subepicardial	But not all myocardial bridges compress or deform the coronary arteries; see text, sections 'Muscular bridging' and 'Subendocardial coronary course'
Branches	Adequate for the dependent myocardium	Variations may however appear with different coronary typology/ dominance or in cases with split RCA or twin Cx
Essential territories	RCA: RV free wall; LAD: anteroseptal; OM: LV free wall	The distal territory remains the most constant while the origin and are highly variable midcourse
Termination	Capillary bed	Directly visible subepicardial and intramyocardial anastomoses between the main coronary trunks are considered normal

LAD: left anterior descending artery (anterior interventricular branch); Cx: circumflex branch; RCA: right coronary artery; LCA: left coronary artery (common trunk); OM: obtuse marginal branch; LV: left ventricle; RV: right ventricle
*Separate origin of the first septal branch from sinus #2 (the left aortic sinus) is considered normal, while other locations such as sinus #1 (right aortic sinus) are considered abnormal (see text, 'Anomalies of intrinsic coronary arterial anatomy')

Table 50.2 The three elementary coronary trunks. Adapted from Muresian (2009) with permission from Texas Heart Institute, Houston.

Coronary artery	Minimally required features	Notes
Anterior interventricular branch (LAD)	Situated at the level of anterior interventricular sulcus; subepicardial location (but not infrequently intramyocardial); follows the septum providing septal branches; accompanied by a conspicuous venous branch (the great cardiac vein).	These represent the essential features of the anterior interventricular branch, no matter what origin it might have (e.g., not always from the aortic sinus 2, as in TGA). Its proximal course can also be very different (preinfundibular, interarterial between the aorta and pulmonary trunk or intraseptal). The anterior interventricular artery can be split or doubled or it may give off few diagonal branches. It may also show an important and longer recurrent tract at level of the posterior interventricular sulcus. Even in complex cardiac malformations, such as in criss-cross hearts with a "horizontal" interventricular septum, the LAD always follows the septum.
Circumflex branch (Cx)	Situated at the level of the left coronary sulcus; subepicardial location; provides at least one marginal branch.	In some instances, the circumflex branch might have a more "atrial" or a more "ventricular" course (i.e., lying not exactly at the level of the coronary sulcus). The surgeon should be aware of these anatomical variations, especially in complex congenital cardiac diseases when such anatomical variations might limit or impede certain surgical maneuvers.
Right coronary artery (RCA)	Situated at the level of the right coronary sulcus; subepicardial location; provides at least the right ("acute") marginal branch.	Variations in caliber and length of the RCA should be interpreted taking into account the conus artery (which may have a separate origin or be of considerable dimensions; cf. "the third coronary"). The conus artery may also originate at the level of the aortic sinus #1 (e.g., TGA) The RCA might practically end (or become insignificant) after giving off the right (acute) marginal branch. The origin and course of the sinus node artery are very important for the surgeon (e.g., the atrial switch procedures Mustard or Senning).

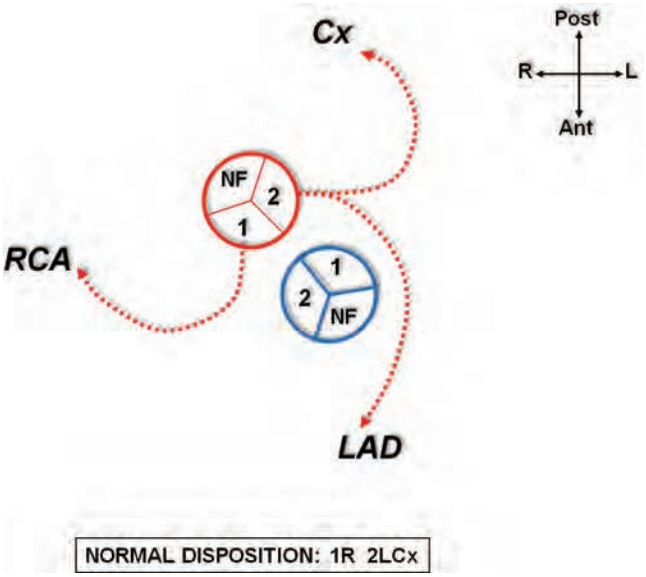

Figure 50.1 The 3 elementary coronary trunks. Cx: circumflex branch (of the left coronary artery); LAD: left anterior descending/anterior interventricular branch; RCA: right coronary artery; 1, 2, and NF: sinus #1, #2 or non-facing of both the aortic root (red) or pulmonary trunk (blue).

Table 50.3 Systematic classification of the sinuses of the arterial roots.

Arterial root	Numeric nomenclature	Nomina anatomica	Actual disposition in the adult heart
Aortic root	#1	Right	Anterior
	#2	Left	Left posterior
	Non-facing/sinus 3	Posterior/ non-coronary	Right posterior
Pulmonary root	#1	Left	Posterior
	#2	Right	Right anterior
	Non-facing/sinus 3	Anterior	Left anterior

Source: Muresian (2009).

Table 50.4 Main categories of coronary artery anomalies.

Coronary anomaly	Abbreviation
Anomalous pulmonary origin of the coronaries	APOC
Anomalous aortic origin of the coronaries	AAOC
Congenital atresia of the left main coronary artery	CALM
Coronary arteriovenous fistula	CAVF
Coronary artery bridging	CB (MB)
Coronary artery aneurysms	CAn
Coronary stenosis	

Note that the correct denomination is "anomalous or abnormal aortic or pulmonary connection" and not origin, as the coronary arteries do not appear as outgrowths from the aorta or pulmonary trunk

Source: Dodge-Khatami et al. (2000). Reproduced with permission from Elsevier.

Table 50.5 Classification of coronary artery anomalies in human hearts. see text for a detailed presentation and description of each major category from A through E

A	Anomalies of origination and course
B	Anomalies of intrinsic coronary arterial anatomy
C	Anomalies of coronary termination
D	Anomalous anastomotic vessels
E	Multiple (combined) coronary arterial anomalies
F	Coronary anomalies in congenital heart disease

Anomalies of origin and course

Absent left main trunk

An absent left main trunk (a split origin of the left coronary artery is depicted in Fig. 50.3) is considered a benign variation necessitating selective catheterization of the LAD and Cx during coronarography. Failure to view one of the major trunks can be wrongly interpreted as absence or occlusion that trunk. Cases in which either the LAD or the Cx has an ectopic origin constitute the so-called "secondary absence of the left main trunk".

Left coronary artery common trunk variations

Variations of the common trunk of the left coronary artery include differences in length, major branches, or angle of division. The length of the common trunk can range from a few millimeters up to 25 mm. The angle of origin from the aorta is clinically relevant. The angle of division into the LAD and Cx is also relevant for surgery and percutaneous interventions. The pattern of division is also important: the common trunk can trifurcate, giving rise to an intermediate branch (ramus intermedius or RI), or alternatively divide into four branches: LAD; first diagonal (D1); RI; and Cx. Its emerging branches can be almost equal or totally different in caliber (Fig. 50.4).

Anomalous location of coronary ostium

An anomalous location of coronary ostium within or near the proper aortic sinus can be of the type: high, low, or commissural (Fig. 50.5). Although it is not an anomaly *per se*, an unusual location of the ostium and proximal tract of the main trunk (of the left or right coronary artery) can predispose to scissoring mechanisms during the cardiac cycle or to earlier atherosclerotic or fibrotic changes, and obviously makes catheterization and percutaneous techniques more difficult. It is very important to identify a high origin of the ostium before performing an aortotomy. Lower ostia can be inadvertently occluded during aortic valve replacement, especially with very diseased valves. This possibility should also be taken into account when a transcatheter aortic valve implantation (TAVI) procedure is considered. A commissural or near-commissural location of the ostium (generally less than 5 mm away from the commissure) can make

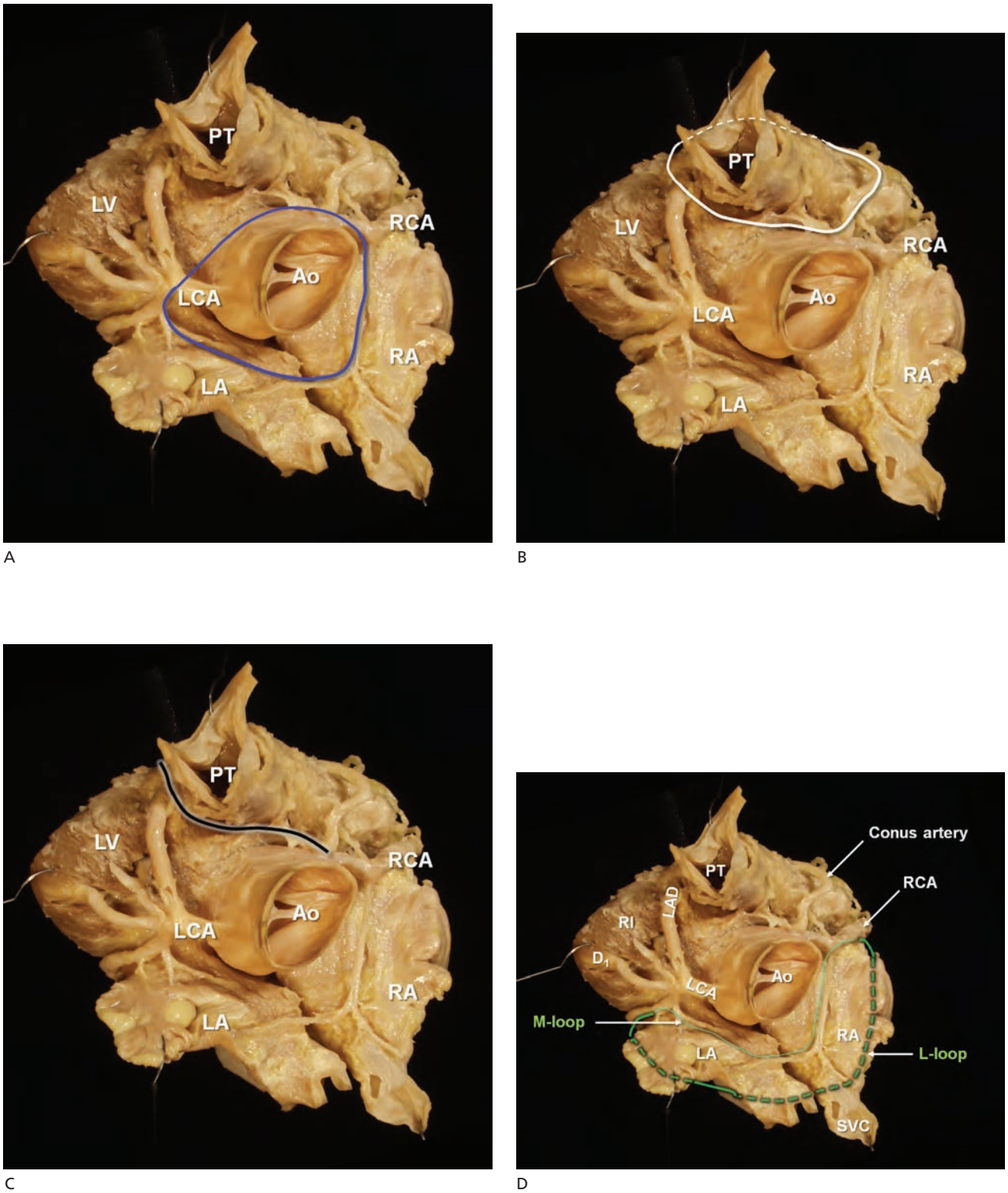

Figure 50.2 The coronary preferential pathways: (a) the periaortic route; (b) the periinfundibular route; (c) the intraseptal route; and (d) the atrial L-loop (retrocardiac) and M-loop. The M-loop follows the atrial arteries including the sinuatrial node artery (which in this specimen is doubled, with one branch originating from the Cx and the other from the RCA). Ao: aortic root; D_1: first diagonal branch; LA: left atrium; LAD: left anterior descending branch; LCA: left coronary artery (left main trunk); LV: left ventricle; PT: pulmonary trunk; RA: right atrium; RCA: right coronary artery; SVC: superior vena cava; RI: ramus intermedius.

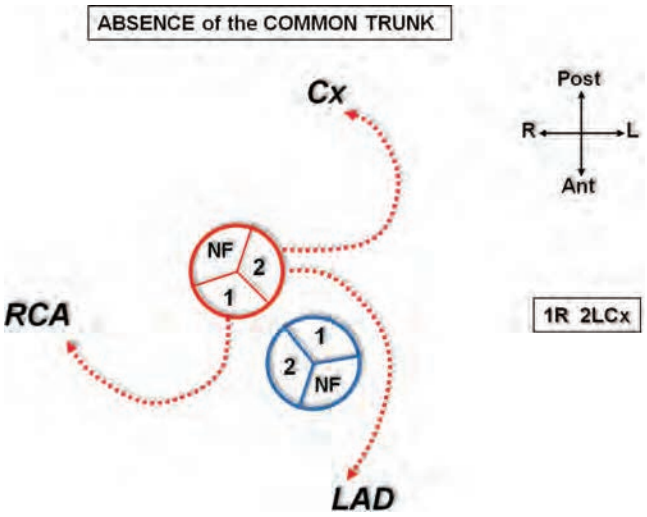

Figure 50.3 Absence of the common trunk of the LCA/split LCA. Abbreviations as for Figure 50.1.

coronary re-implantation difficult in both pediatric and adult heart surgery. The orientation of the right and left coronary ostia can vary in the horizontal as well as the vertical plane (Angelini et al. 1999); consequently, the disposition of the proximal tract of the RCA or LCA and the angles of division of their proximal branches can vary markedly.

Anomalous location of coronary arterial ostium

An anomalous location of coronary arterial ostium outside the normal facing ("coronary") aortic sinuses can be of the type described in the following sections.

LCA from NF sinus

The LCA ostium is located closer to the commissure between the non-facing sinus and sinus #2 (Fig. 50.6). The proximal tract of the LCA is tangential to the aortic root and prone to lateral compression, or this segment can be intussuscepted and hypoplastic, potentiating thrombosis at this level (Ishikawa et al. 1990).

RCA from NF sinus

The RCA courses around the aortic root to reach the coronary sulcus (Vlodaver et al. 1975). Cases in which the left or right coronary artery originates from the NF sinus are very rare in hearts with normal ventriculo-arterial concordance (Fig. 50.7).

Origin of both coronary arteries from the ascending aorta

The RCA (more frequently) and the LCA (or the LAD and Cx separately) can originate from the ascending aorta (Fig. 50.8), up to the level of the brachiocephalic trunk. The usual location is on the left anterior aspect of the ascending aorta. In contrast to the "high" origin from or near the proper aortic sinus, a coronary artery originating from the ascending aorta has a proximal tract either tangential to the aorta or intramural, intussuscepted.

Origin of LCA from the ascending aorta

Ascending aortography is needed to identify the apparently missing coronary trunk. Cannulation of the LCA or angioplasty can be difficult in such cases (Fig. 50.9; Rosenthal et al. 2012).

Origin of RCA from the ascending aorta

The RCA originates distally to aortic sinus #2 (left sinus) and courses around the aortic root, eventually reaching its normal anatomical position in the right coronary sulcus (Fig. 50.10; Jin et al. 2012).

Origin of RCA from the ascending aorta and LCA from the NF sinus

The RCA originates distally to sinus #2 (left aortic sinus) and travels between the aortic root and the pulmonary trunk. The LCA originates from the NF sinus and follows a tangential course around the aortic root (Fig. 50.11; Lee et al. 2009).

Origin of LCA from the brachiocephalic trunk

The LCA travels the left anterior aspect of the ascending aorta, eventually gaining its usual anatomical position and bifurcating normally (Santucci et al. 2001; Duran et al. 2008).

Origin of coronary arteries from the aortic arch, right carotid artery, subclavian artery, internal thoracic artery, bronchial artery, descending thoracic aorta

Such anomalies are usually present in cases with associated complex congenital heart defects and anomalies. As stated by Angelini et al. (1999), the disposition of the ectopic proximal coronary trunk in such cases reproduces patterns seen in other species, which result from the atypical hemodynamic factors in congenitally malformed hearts.

Origin of the coronary arteries from the right ventricle

In the same way as noted above, this condition has never been observed in otherwise normal hearts. It is characteristic of cases with pulmonary atresia and an intact ventricular septum, with multiple right ventricular sinusoids draining into the coronary vessels during systole.

Origin of LCA from the left ventricular outflow tract (LVOT)

In a recently reported case the LCA originated from the left ventricular outflow tract (LVOT), with an occlusive membrane over the ostium (Pirelli et al. 2008). This can be interpreted as a late-development case of congenital atresia of the left main trunk (CALM).

Origin of RCA from the LVOT

Few cases have been reported with the RCA originating just below the aortic valve. The flow is retrograde from the left

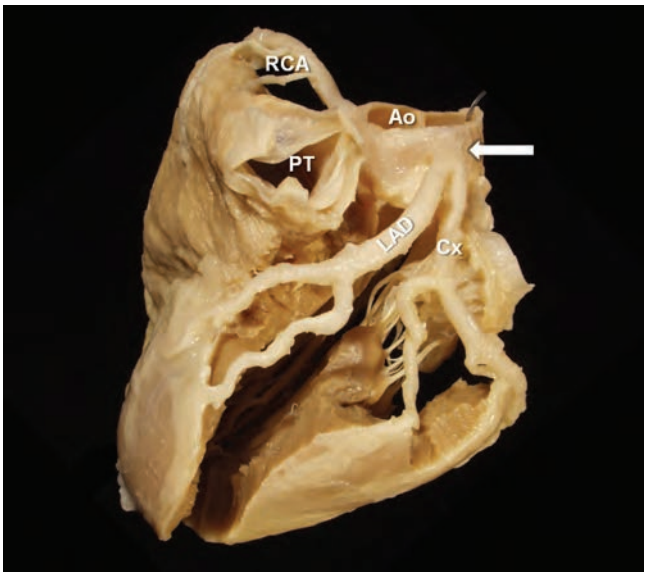

A

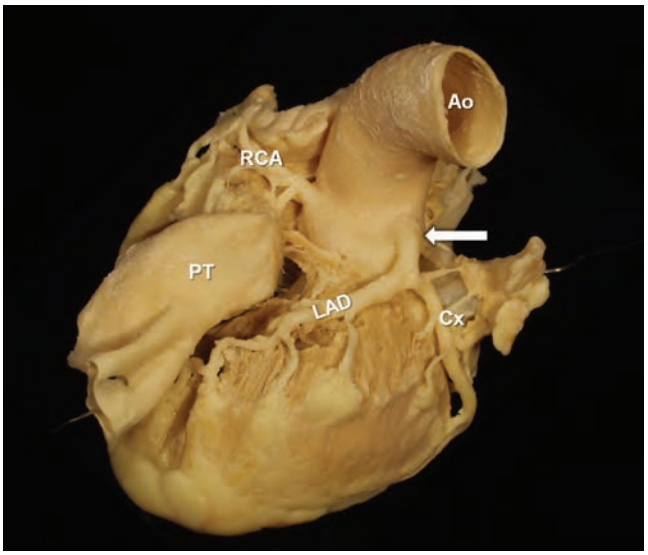

B

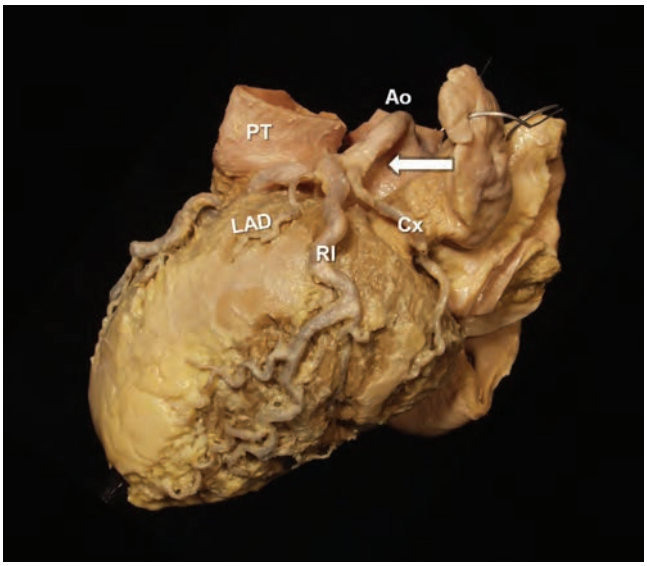

C

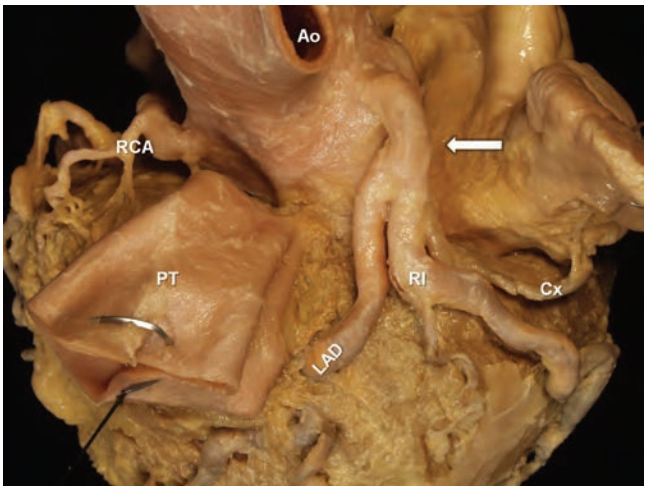

D

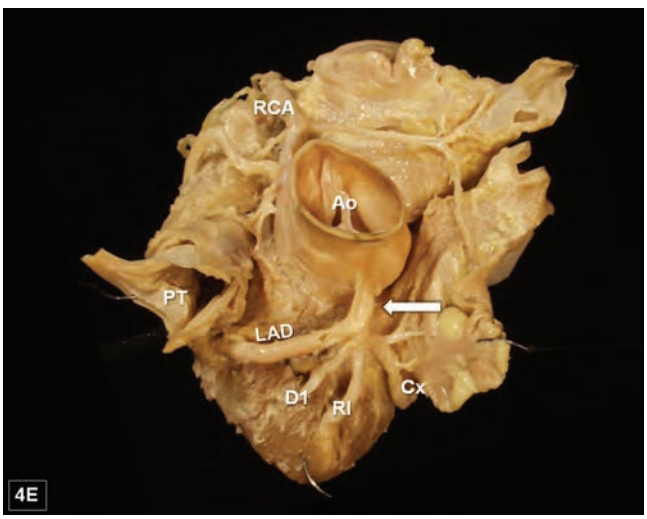

E

Figure 50.4 Variations of the common trunk (white arrow): (a) short trunk bifurcating at acute angle; (b) long trunk with LAD and Cx at almost 90°; (c) trifurcation of a long trunk with a conspicuous ramus intermedius (RI) and a slender Cx; there is also a myocardial bridge over the proximal LAD. A wide angle is noted between the LAD and RI; (d) trifurcation of the common trunk (note the higher origin of the LCA and the atypical trifurcation with a large RI coursing as an obtuse marginal; the Cx appears slender, terminating as a left atrial branch); and (e) quadrifurcation of the common trunk with four branches of equal caliber: LAD, D1, RI and Cx. Abbreviations as for Figures 50.1 and 50.2.

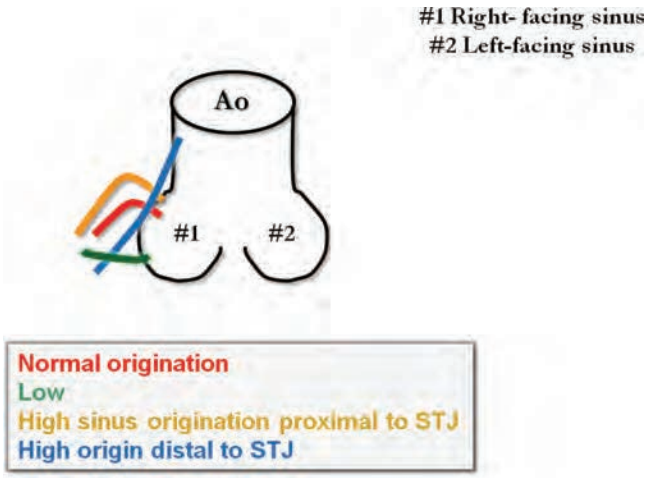

A

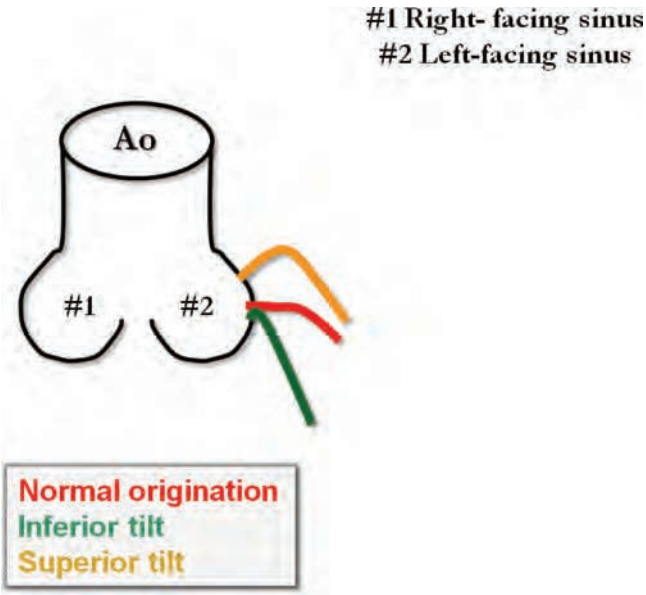

B

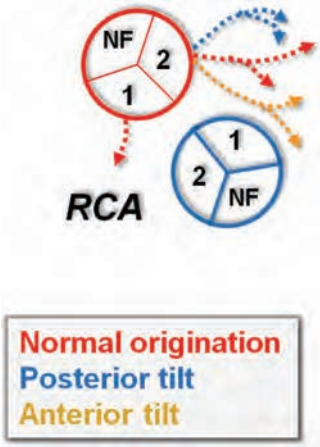

C

Figure 50.5 Anomalous location of RCA ostium within or near the proper aortic sinus. (a) Variations of RCA origin (red: normal origination of RCA; green: low origin; orange: high sinus origin proximal to sinutubular junction (STJ) but with angled proximal tract of the RCA; blue: high origin distal to the sinutubular junction with tangential/intramural tract of proximal RCA). (b) Variations of LCA origin in vertical plane (red: normal origination of LCA; green: inferior tilt; orange: superior tilt). (c) Variations of LCA origin in horizontal plane (red: normal origination; orange: anterior tilt; blue: posterior tilt).

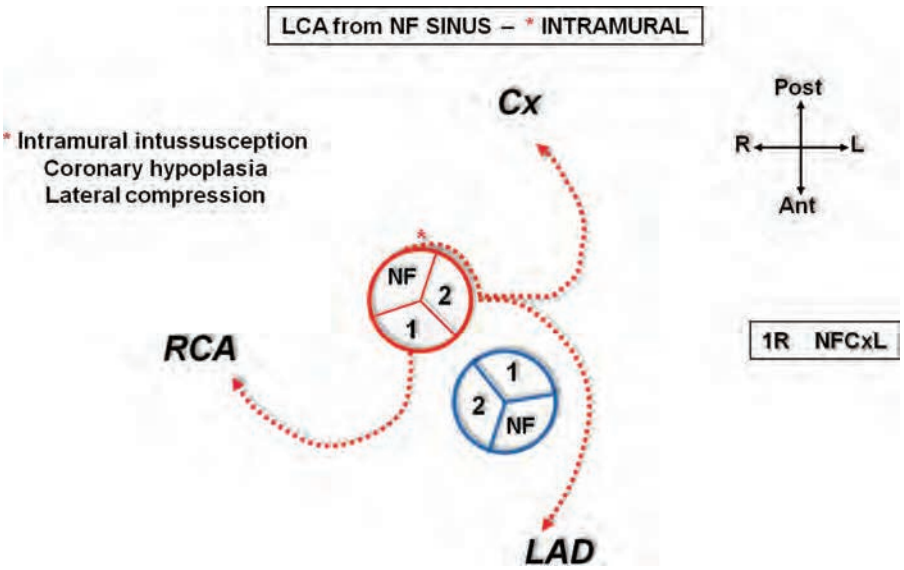

Figure 50.6 Origination of LCA from the aortic NF sinus. The proximal tract is hypoplastic, intussuscepted, intramural, and prone to lateral compression. The middle and sital tracts of the LAD and Cx are normal.

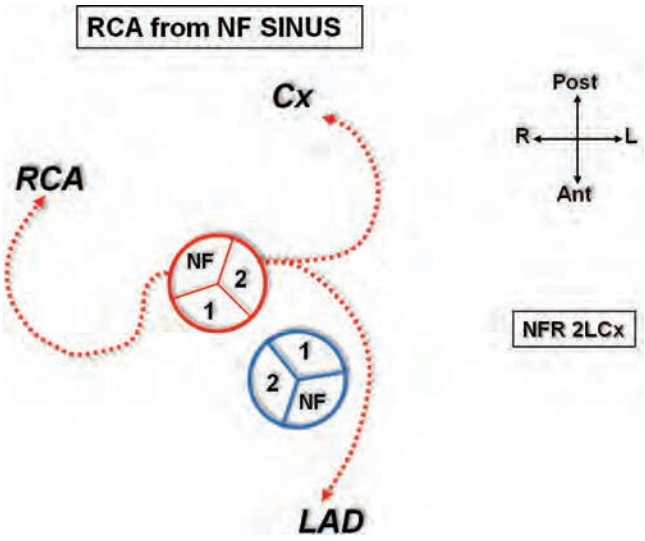

Figure 50.7 Origination of RCA from the aortic NF sinus. The RCA courses around the aortic root, eventually reaching its normal anatomic position in the right coronary sulcus.

system (mainly from the LAD) into the RCA and into the LVOT (Lauer et al. 2001; Ippisch and Kimball 2010). This condition should be differentiated from aorta-to-left ventricular tunnel or sinusoidal-coronary collaterals.

Origin of the coronary arteries from the pulmonary trunk or its branches

The common name is "abnormal pulmonary origin of the coronaries" or APOC (see Table 50.4). The following conditions can occur:

- **ALCAPA**: abnormal left coronary artery from pulmonary artery (actually from the pulmonary trunk). The LCA can originate from the NF sinus of the pulmonary trunk (Fig. 50.12; Sodian et al. 2008) or from pulmonary sinus #1 (posterior-facing sinus), the latter being more frequently reported (Fig. 50.13; Vesterlund et al. 1985). The blood flow is retrograde through the LAD, Cx, and LCA. An abnormal origin from the pulmonary trunk or artery can cause myocardial ischemia (or infarction), mitral insufficiency, congestive heart failure, and death in early infancy. The main pathophysiological mechanism is impoverishment of the left ventricular myocardial blood flow due to retrograde flow toward the pulmonary trunk through intercoronary anastomoses; surgical creation of a two-artery coronary system is therefore mandatory. ALCAPA can serve as a paradigm: during the neonatal period, high pulmonary vascular resistance and resultant pulmonary artery pressure ensure antegrade flow from the pulmonary trunk (PT) toward the anomalous coronary artery; as this pressure decreases, the flow eventually reverses with resultant left-to-right shunting (into the PT). In the face of this coronary steal, myocardial perfusion becomes dependent on the RCA via the intercoronary collaterals. The rapidity of this sequence classically divides the clinical picture into two types: infantile and adult. Few or no collaterals characterize the infantile type: myocardial ischemia ensues rapidly, the patients presenting all the signs of myocardial ischemic dysfunction. These infants present with poor feeding, probably due to angina, tachypnea, tachycardia, and over heart failure, although such clinical findings are difficult to distinguish from those caused by cardiomyopathy or endocardial fibroelastosis. There are often electrocardiographic signs of anterolateral infarction along with signs of left ventricular hypertrophy and a marked increase in myocardial enzymes. Cardiomegaly and interstitial pulmonary edema are evident on the chest X-ray. A prompt surgical decision is needed,

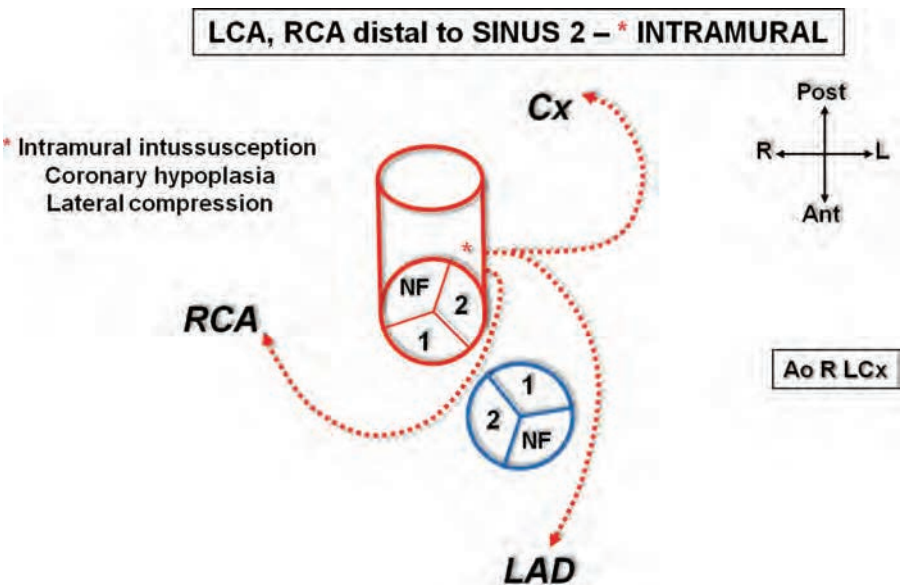

Figure 50.8 Origination of both coronary arteries from the ascending aorta. Both coronary arteries arise from the ascending aorta "above" the left sinus (sinus #2). The proximal tracts can be intussuscepted.

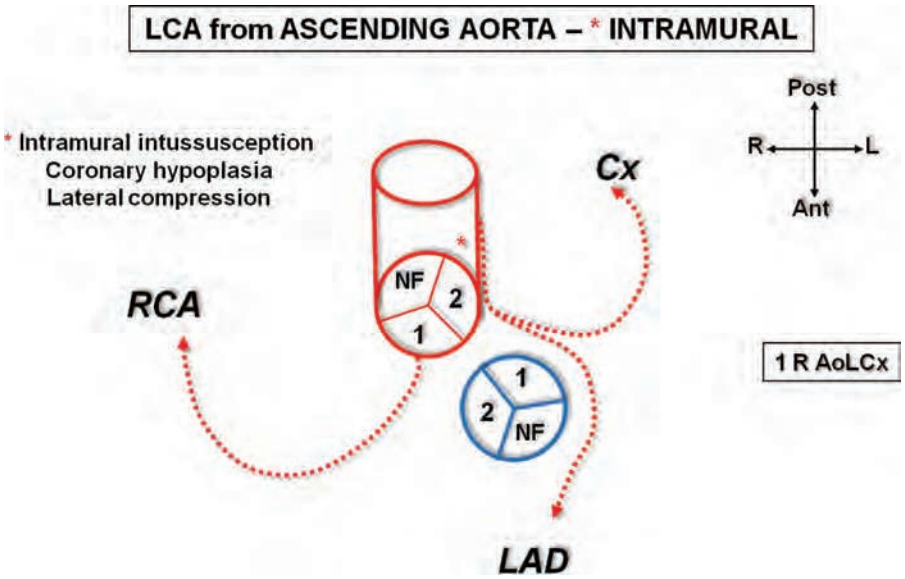

Figure 50.9 LCA arising from the ascending aorta. The proximal tract is intramural/intussuscepted. The bifurcation takes place at the base of the aortic root. Branches are normal.

otherwise premature deterioration and death supervene. The adult type accounts for roughly 10–15% of patients; well-developed and large collaterals aid survival. Clinical presentation with fatigue, dyspnea, palpitations, and effort angina can develop beyond the age of 20 years, but in some cases the patients remain asymptomatic with a nonspecific cardiac murmur (apical pansystolic) as a consequence of mitral regurgitation (this sometimes dominates the clinical picture). The ECG is abnormal, revealing signs of an old anterolateral infarction, and there can be cardiomegaly. The ejection fraction can remain within normal limits but anterolateral hypokinesia is evident. Surgery should aim to eliminate the abnormal origin of the coronary and ideally restore a two-vessel system: re-implantation into the aorta, coronary artery transfer, tunnel operation, subclavian-to-left coronary artery anastomosis, or coronary artery bypass grafting. Nowadays, ligation of the proximal left coronary artery is accepted only as an interim measure.

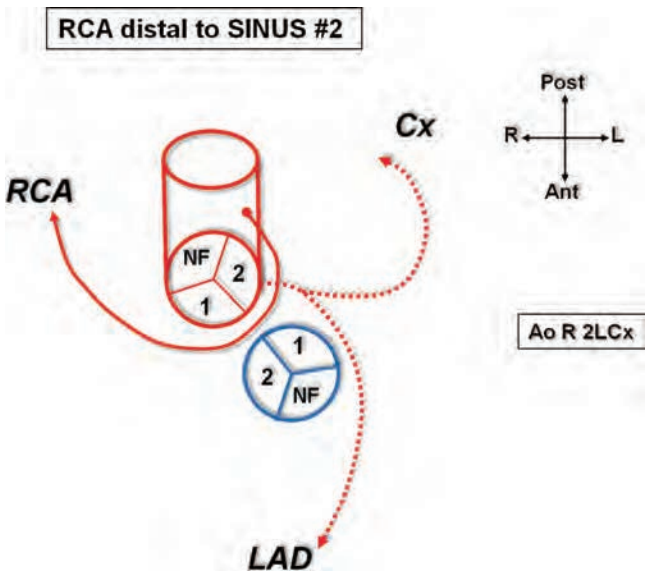

Figure 50.10 RCA with high aortic origin. The RCA originates from the ascending aorta "above" the left sinus (sinus #2). The RCA and LCA do not cross (as they might appear in the figure).

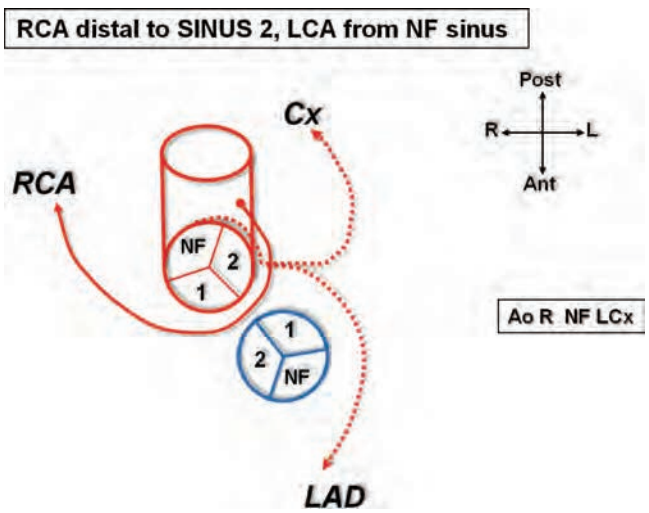

Figure 50.11 RCA with high aortic origin and LCA with posterior origin from the aortic NF sinus. This particular disposition appears more severe as both coronary main trunks are prone to intussusception or lateral compression.

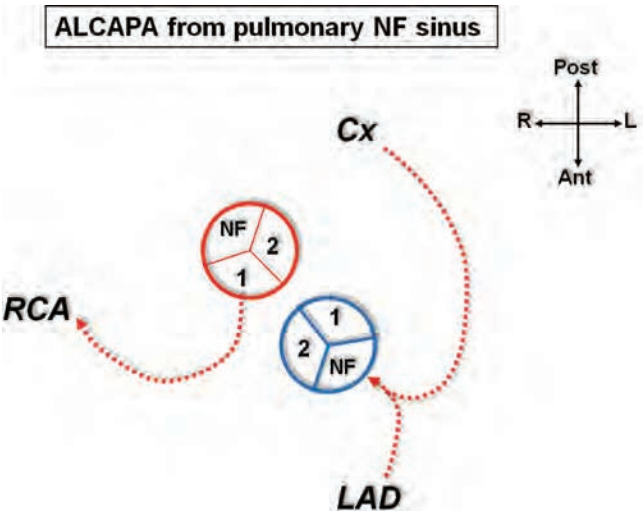

Figure 50.12 ALCAPA (from pulmonary NF sinus). The RCA has a normal origin and course. The LCA arises from the pulmonary NF sinus (pulmonary left anterior sinus). Blood flow is retrograde through the LAD and Cx.

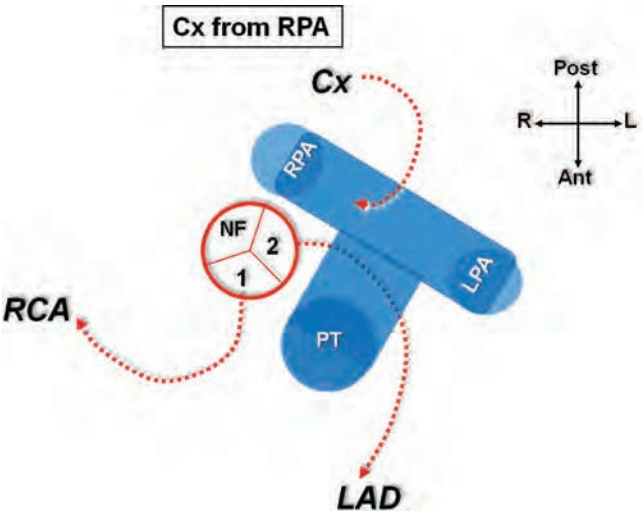

Figure 50.14 Origin of the Cx branch from the right pulmonary artery. The LAD and the RCA depict normal origins and courses. The Cx descends from its origin from the right pulmonary artery toward the aortic root and gets its normal anatomic position in the left coronary sulcus. Blood flow in retrograde through the Cx. RPA: right pulmonary artery; LPA: left pulmonary artery; PT: pulmonary trunk.

The hemodynamic consequences are protean and a straightforward classification presents challenges. Such consequences (among others) depend on: the pulmonary versus the systemic pressure; the presence and extent of atherosclerotic coronary disease; the type of collaterals between the RCA and LCA (epicardial versus intramyocardial, the former favoring fistulous flow, the latter being more beneficial for myocardial nutrition); the remodeling of the left ventricle; the possible obstruction of the anomalous ectopic ostium; and the coronary typology and dominance within the individual patient.

- **ACxPA**: abnormal origin of the circumflex branch from the pulmonary artery (Fig. 50.14). The Cx usually originates in one of the pulmonary arteries (Korosoglu et al. 2008).
- **ALADPA**: abnormal origin of the LAD from the pulmonary artery (trunk). The LAD originates from pulmonary sinus #1 (posterior-facing sinus; Fig. 50.15). The isolated origin of the Cx or LAD from the pulmonary trunk (or main branches) entails a less severe condition than ALCAPA (Vesterlund et al. 1985).

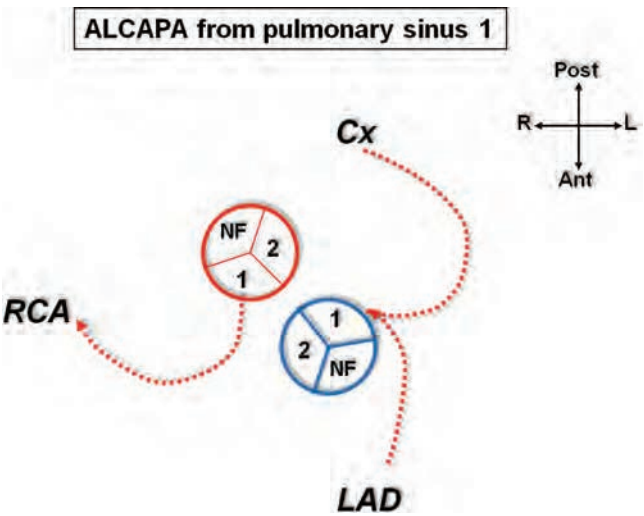

Figure 50.13 ALCAPA (from pulmonary sinus #1). The LCA originates from the pulmonary sinus #1 (posterior sinus) and depicts a tangential proximal tract. Blood flow in retrograde through the LAD and Cx.

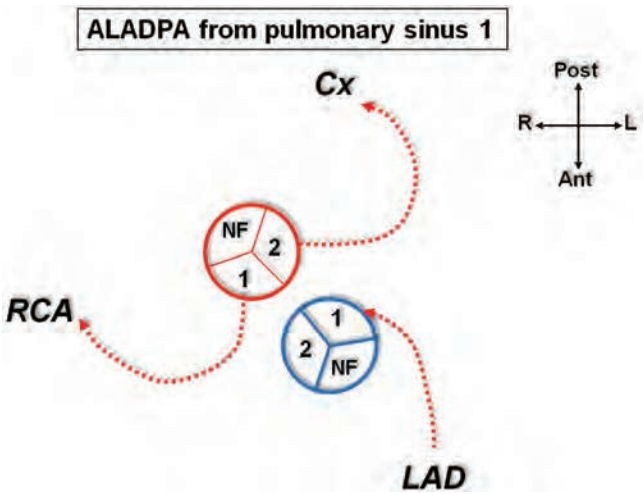

Figure 50.15 ALADPA (abnormal origin of the LAD form the pulmonary trunk). The LAD originates from the pulmonary sinus #1. Blood flow is retrograde through the LAD but, taking into account the numerous and conspicuous anastomoses especially at septal level and around the apex, this condition may not be always well tolerated.

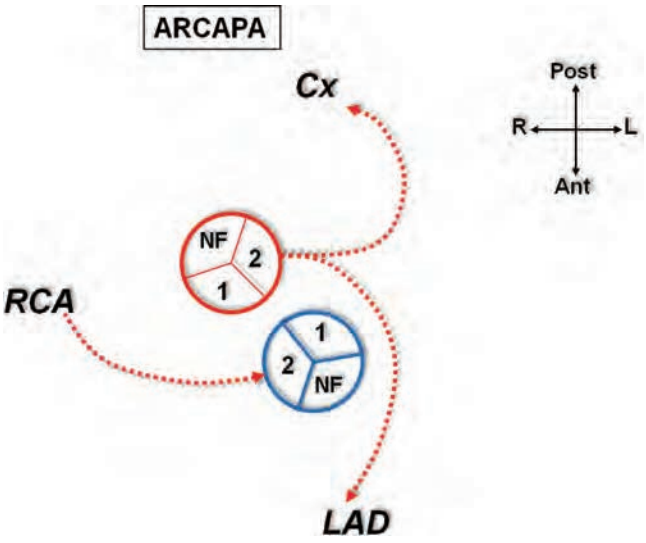

Figure 50.16 ARCAPA (origin of the RCA from the pulmonary sinus #2 (right anterior)). As with ALADCAPA, conspicuous anastomoses develop at septal level.

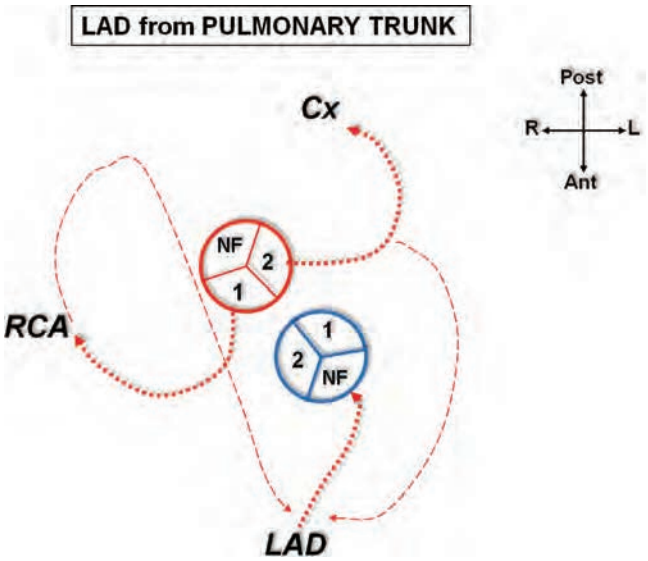

Figure 50.18 LAD with origin in pulmonary non-facing sinus. This condition is less severe than ALCAPA. The numerous collateral branches ensure a proper filling of the LAD.

- **ARCAPA**: abnormal origin of the RCA from the pulmonary artery (Fig. 50.16; Winner et al. 2011). Conspicuous anastomoses develop between the LAD and RCA, especially at the septal level.
- **AOCAP**: abnormal origin of (both) coronary arteries from the pulmonary trunk (Fig. 50.17; Ochos-Ramirez et al. 2005). This condition is considered extremely rare but fatal, with survival times ranging from 9 hours to 1 year of age. The medical literature reveals only three cases that survived after corrective surgery (Urcelay et al. 1994). Earlier attempts at surgical correction were unsuccessful (Keeton et al. 1983).

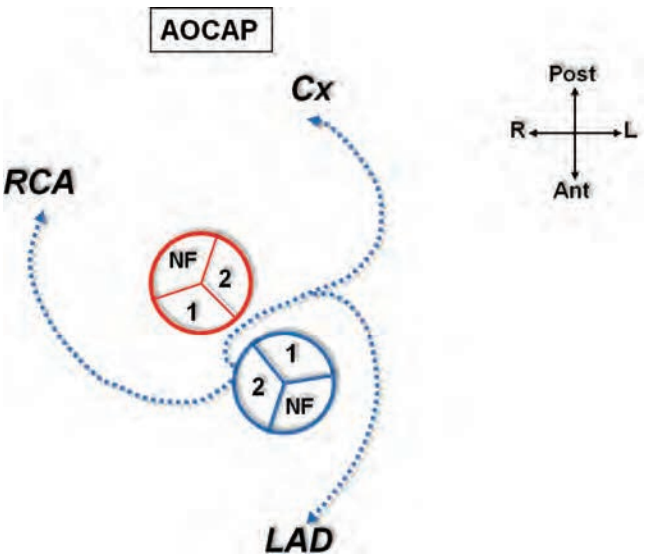

Figure 50.17 AOCAP (abnormal origin of both coronary arteries from the pulmonary trunk (sinus #2)). Note the interarterial course of the LCA prior to its bifurcation.

Abnormal origin of coronary artery outside facing sinuses

An abnormal original of coronary artery outside the facing sinuses could include: pulmonary NF sinus; pulmonary trunk; or pulmonary artery. The most frequently encountered variant is the origin of the LAD from the pulmonary NF sinus (Fig. 50.18). Flow is retrograde in the LAD, with collateral circulation developing from the RCA and Cx (Probst et al. 1976). For ALCAPA from the NF sinus, see above (Fig. 50.12).

Abnormal origin from improper (opposite) aortic sinus

Abnormal origin from improper (opposite) aortic sinus, with possible mixed trunks or single coronary artery is known as ACAOS (abnormal coronary artery from the opposite sinus). In these cases the definition of each main coronary trunk is based on the middle tract and its territory of distribution (since the origin and proximal tract are obviously either displaced or mixed). The paths traveled by each trunk toward the corresponding target tissues follow the previously presented "preferential coronary pathways" (Fig. 50.2).

RCA from sinus #2 (left aortic sinus)

An RCA with an interarterial course and intramural initial segment is prone to angulation and lateral compression (Fig. 50.19) with consequent myocardial ischemia (Ho and Strickman 2002; De Luca et al. 2004; Andreou et al. 2009; Chen et al. 2010); in some cases the aortic ostium is slit-like. Besides the

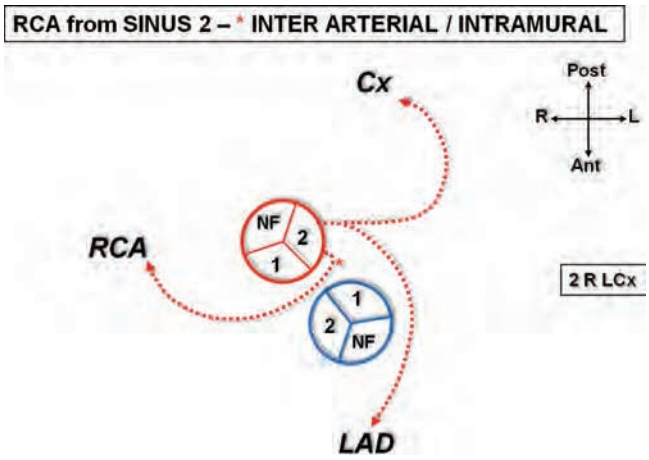

Figure 50.19 Origination of RCA from opposite aortic sinus (sinus #2). The interarterial/intramural course and slit-like ostium can precipitate myocardial ischemia.

interarterial route, other routes for the aberrant RCA have been described: retrocardiac (posterior coronary sulcus); retroaortic; posterior interventricular sulcus (the wraparound coronary); and intraseptal (see 'Mixed trunks and single coronary artery' below).

LCA from sinus #1

The LCA can travel between the arterial trunks (Fig. 50.20a); the route can be intraseptal (Fig. 50.20b) or preinfundibular (Fig. 50.20c). In the former case the artery follows an intramural tract with intussusceptions and lateral compression (Angelini 2009; Slim et al. 2009). The intussuscepted proximal tract of the intramural/interarterial LCA (Fig. 50.21) is especially prone to lateral compression and usually indicates a hypoplastic segment (Angelini et al. 2008b). Alternative routes for the aberrant LCA include interventricular sulcus or retroarotic (see 'Mixed trunks and single coronary artery' below).

LAD from sinus #1

The most usual route is preinfundibular (Fig. 50.22). Alternatively, an accessory LAD with anomalous origin (Fig. 50.23) is sometimes spared by the atherosclerotic process (Canga et al. 2010). Other routes described are: intraseptal; interarterial (intramural); interventricular sulcus.

Cx from sinus #1

Another abnormality is the Cx originating from sinus #1, usually with a retroaortic course (Fig. 50.24; Braat 2007; Uznanska-Loch 2012). A similar situation is encountered when the Cx originates from the RCA (mixed trunk; Fig. 50.25; Plastiral et al. 2008). In another variation, the Cx originates from sinus #1 and takes a retroaortic course and an accessory LAD takes an interarterial course (Fig. 50.26; Groothuis et al. 2011).

Mixed trunks and single coronary artery

A single coronary artery is defined as only one ostium present, and the coronary artery originating from it vascularizes the entire heart. This anomaly can present either with no intrinsic abnormalities of the artery or with associated intrinsic modifications such as aneurysm or anomalous communication with a cardiac chamber. The incidence is about 0.024%. The single coronary artery can present under various forms:

- Type I, "true single coronary": one artery supplies the entire heart.
- Type II: the single artery divides into RCA and LCA (actually there are two coronary arteries with a common aortic origin).
- Type III: comprises other atypical patterns.

However, a proper classification should consider the sinus of origin of the single ostium and the pathways followed by each coronary trunk. The pathological significance of this anomaly emanates from lesions or disease processes affecting its proximal course, which can induce dramatic events. In addition, the single coronary artery can appear isolated (Shirani and Roberts 1993) or be part of the larger picture of complex malformations of the heart (tetralogy of Fallot, DORV, persistent truncus arteriosus, pulmonary atresia with intact septum, TGA, etc.).

In single coronary type I from sinus #1, the artery begins as an RCA, giving off the known branches of the RCA including the posterior/inferior interventricular branch (the PDA). The artery proceeds to give off the posterior left ventricular branches, the obtuse marginal, and eventually the LAD and diagonal branches (Fig. 50.27). The blood flow is antegrade through all branches.

In single coronary type II from sinus #2, the common trunk divides to give off the LAD and a mixed trunk that continues as a Cx, which gives off the obtuse marginal and proceeds in the posterior portion of the coronary sulcus where it generates the posterior/inferior interventricular branch. The most distal segment is an RCA proper but with retrograde flow (Fig. 50.28). A variant of single coronary artery type II from sinus #2 is illustrated in Figure 50.29: the common trunk generates a preinfundibular RCA and an LCA that appears normal. A pattern similar to type II single coronary artery is encountered in ACAOS with an LCA from sinus #1 and an intramural interarterial tract (Fig. 50.21). Another variant of type II single coronary is from sinus #1 with the LCA following an interarterial course (Fig. 50.30). The single coronary artery type II from the NF sinus bifurcates into a retroaortic LCA and an RCA that circumvents the posterior and right aspects of the aortic root (Fig. 50.31).

Other forms of single coronary artery have been described, some of which can be considered as variations of ACAOS with mixed trunks. For example: all three elementary coronary trunks with origin in sinus #1 but with separate ostia, retroaortic Cx, and preinfundibular LAD and first septal branch originating in the RCA (Fig. 50.32; Al-Mohaissen et al. 2010). Practically the same disposition but with a common ostium at the level of sinus #1 can be considered another form of single coronary artery (Fig. 50.33; Mihl et al. 2010). A variation of the former is with an intraseptal LAD (Fig. 50.34; Pascual et al. 1999). A further

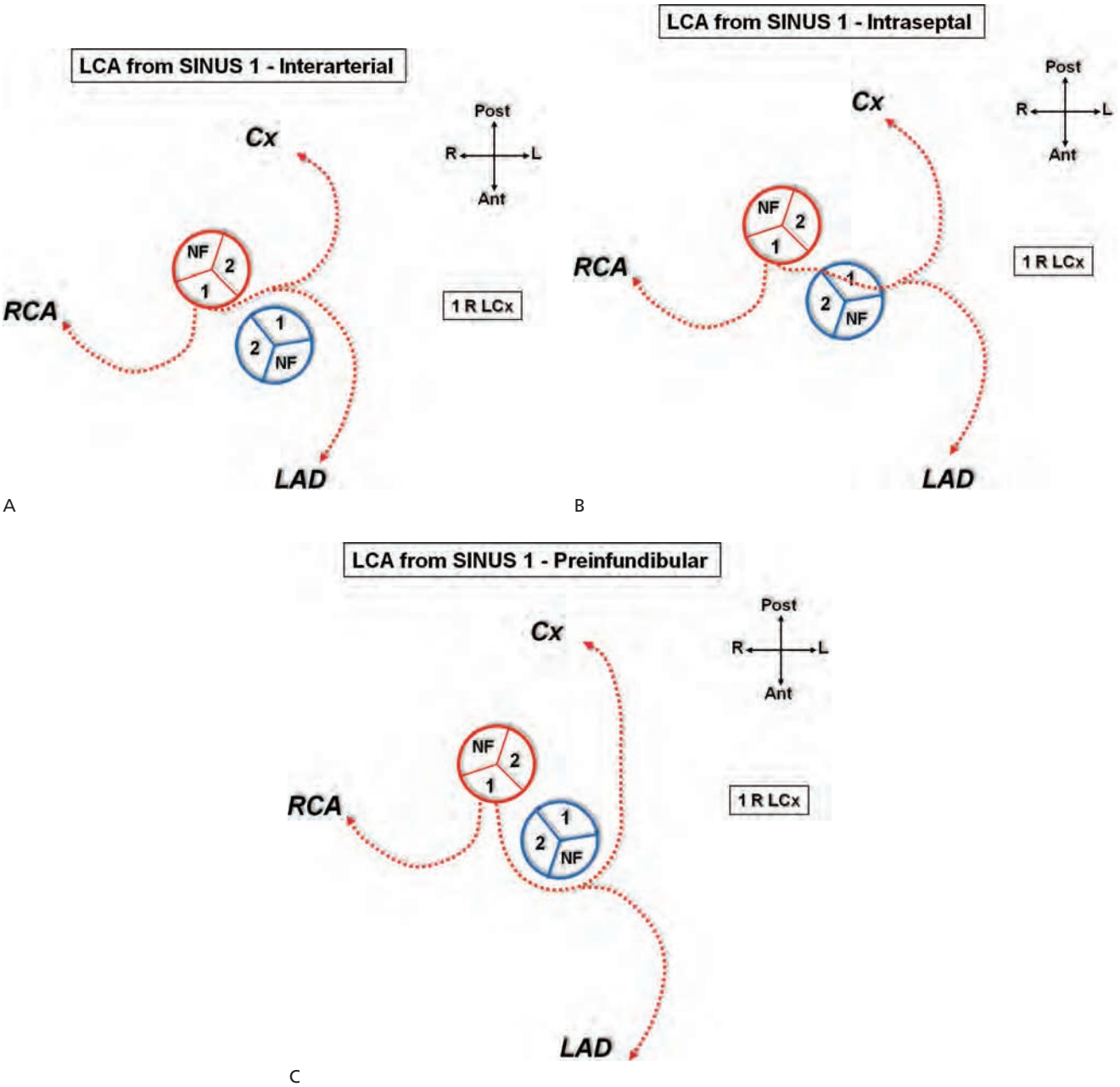

Figure 50.20 Origination of LCA from opposite aortic sinus (sinus #1). The paths followed by the LCA with aberrant origin can be: (a) interarterial; (b) intraseptal; or (c) preinfundibular. In (a) and (b), the angle of take-off is acute, sometimes associating an intramural tract. Although benign, the preinfundibular course should be recognized before or during surgery.

variation is with an intraseptal LCA (Fig. 50.35; Liesting et al. 2012). In one recently described case of a patient with a quadricuspid aortic valve (Fig. 50.36), a common trunk generated the RCA and Cx (with retroaortic Cx) and a juxtaposed ostium of the LAD (with interarterial course), all from sinus #1 (Wang et al. 2012). The "absent Cx" case (Fig. 50.37) looks similar to a mixed trunk of RCA and Cx, where the branches of the Cx are given off by the continuation of the RCA in the left coronary sulcus (Yameen et al. 2011). It is also very similar to a single coronary artery except for the separate origin of the LAD. Consequently, the distinction between single coronary artery and mixed trunks is not straightforward in ACAOS cases.

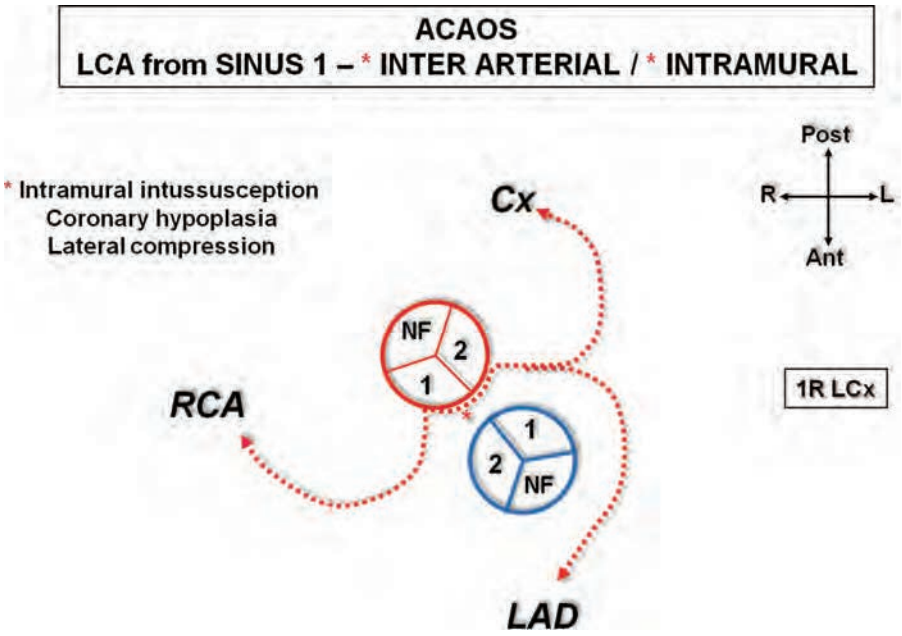

Figure 50.21 LCA from sinus #1 with intramural course. The LCA apparently detaches from the aortic wall at the level of the proper sinus (i.e., sinus #2). However, this is only apparent as it actually originates from sinus #1 and has a long intramural tract all around the anterior third of the aortic root. The intramural segment is usually hypoplastic, intussuscepted and prone to lateral compression, stretching. and elongation.

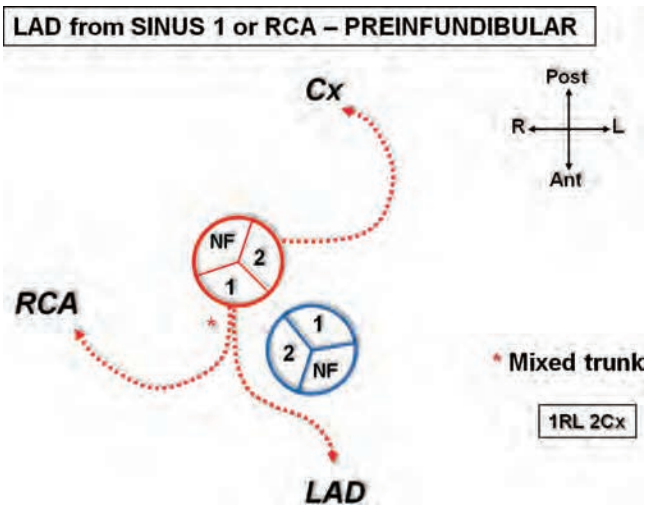

Figure 50.22 LAD with origin in sinus #1 and preinfundibular course. The same precautions apply as in the case with preinfundibular course of the LCA.

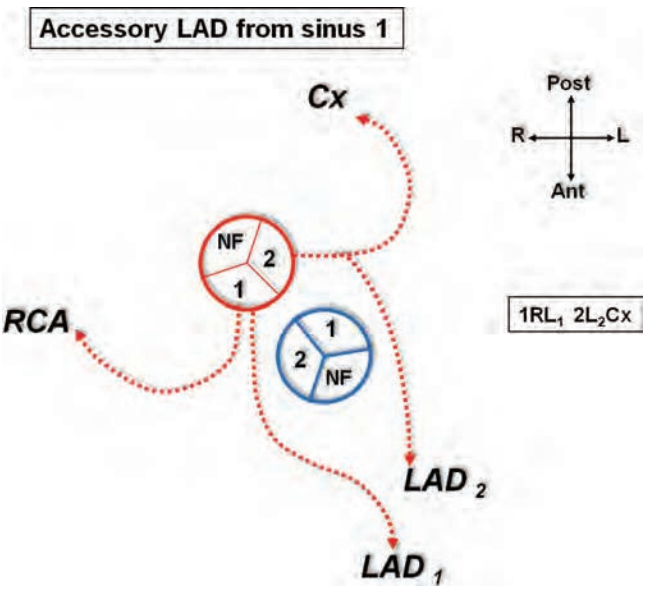

Figure 50.23 Accessory LAD from sinus #1 and preinfundibular course. In cases with accessory or split LADs, the longer LAD usually gives off less branches. Most of the septal arteries and diagonal branches originate from the short LAD. The case presented is clinically significant as the accessory LAD was free of atherosclerosis, resembling more an arterialized collateral vessel.

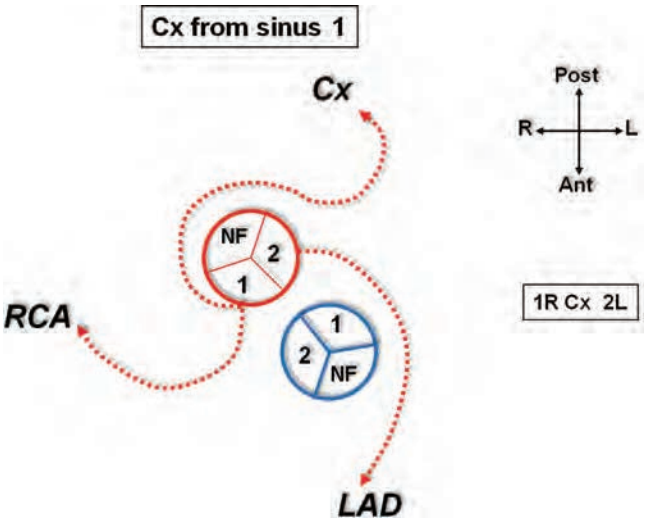

Figure 50.24 The Cx originates from sinus #1 and the Cx has a retroaortic course. Except for the shape and disposition of the ostium, this anomaly is benign. The course of the Cx around the aortic root is usually not prone to compression or scissoring mechanisms, requiring only precautions during surgery.

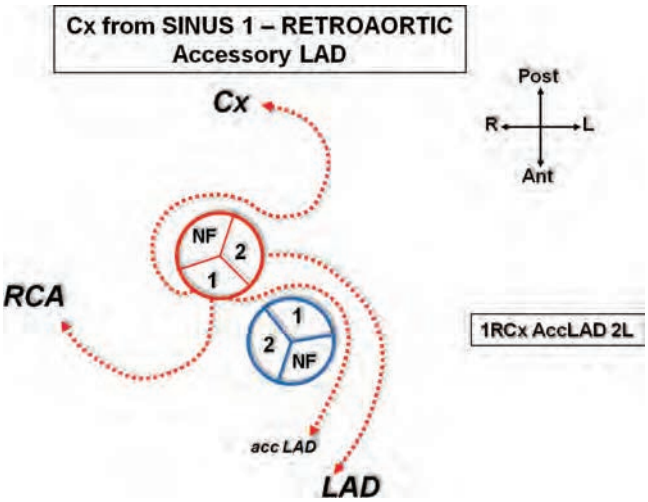

Figure 50.26 Cx with origin in opposite aortic sinus accompanied by an accessory LAD from the same sinus #1. It is important to distinguish the territories of vascularization of each trunk, as some of the main septal arteries may arise from the accessory LAD. Moreover, the disposition, dimension, and characteristics of each aotic ostium are of clinical relevance.

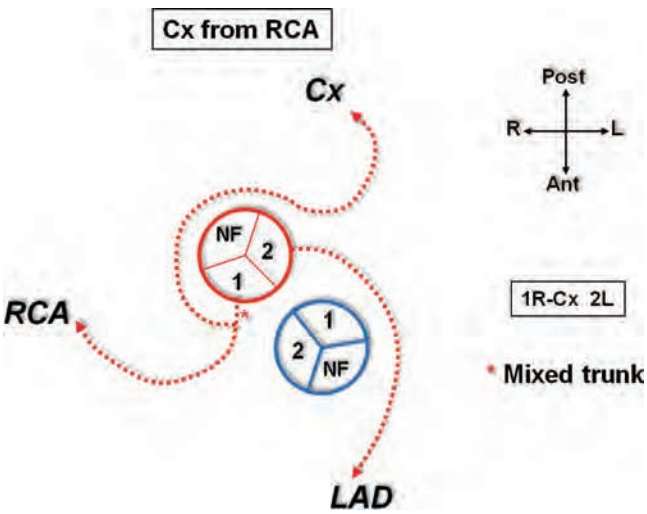

Figure 50.25 Cx with origin in the proximal RCA. This is an example of a mixed trunk giving off a normal RCA and an aberrant Cx. As in Figure 50.24, the disposition of the Cx is benign. Atherosclerotic lesions affecting the ostium or the proximal tract of the common trunk are clinically significant.

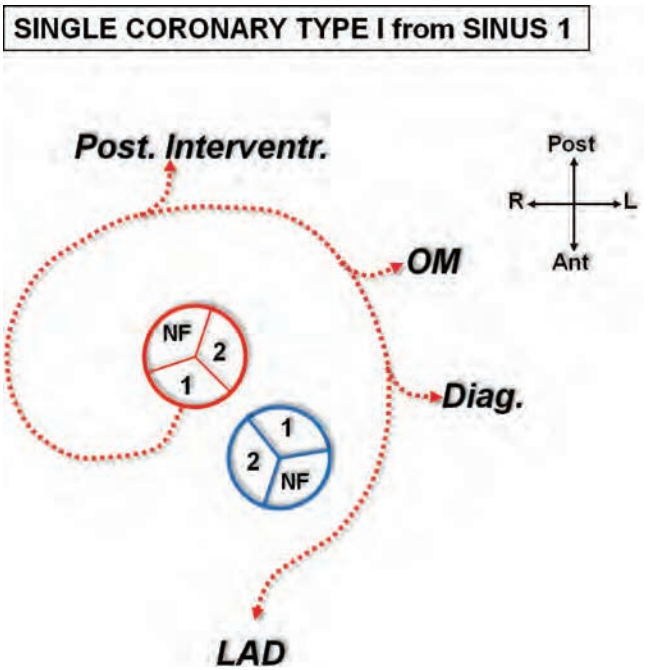

Figure 50.27 Single coronary type I. This is actually the genuine "single coronary" where a coronary trunk winds around the heart, giving off all the major branches, with a blood flow antegrade through all the main trunks and their divisions. Diag: diagonal branches; OM: obtuse marginal branch of the left ventricle; Post. interventr.: "posterior" (actually inferior) interventricular branch.

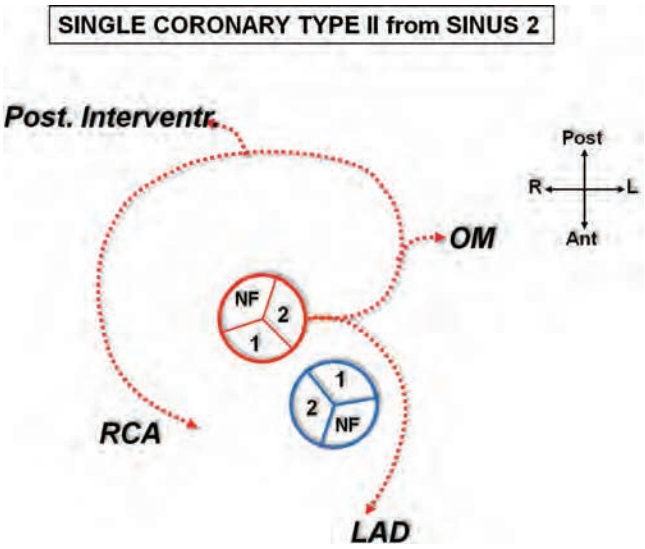

Figure 50.28 Single coronary type II. This actually represents a common origin of all the major trunks from sinus #2; the Cx and RCA constitute a mixed trunk. The blood flows in retrograde through the main trunk of the RCA. It is evident that a clear distinction between the single coronary pattern and the various forms of mixed trunks is not straightforward.

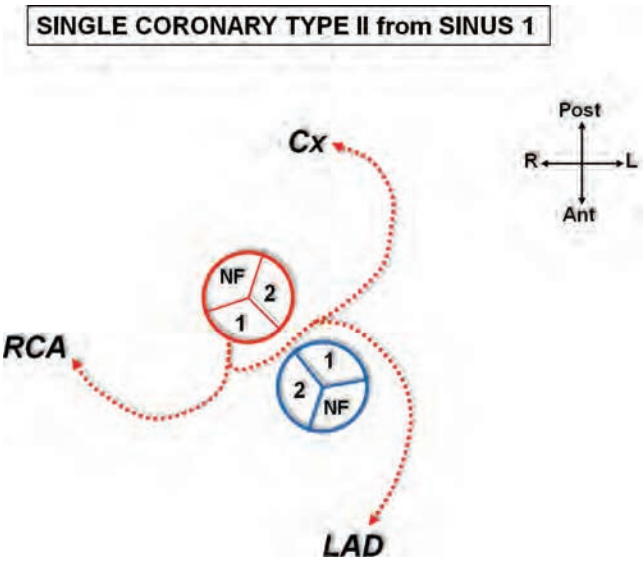

Figure 50.30 Single coronary type II from sinus #1. This disposition is similar to that reported with abnormal origin of left coronary artery from the opposite (aortic) sinus. Compare to Figure 50.21.

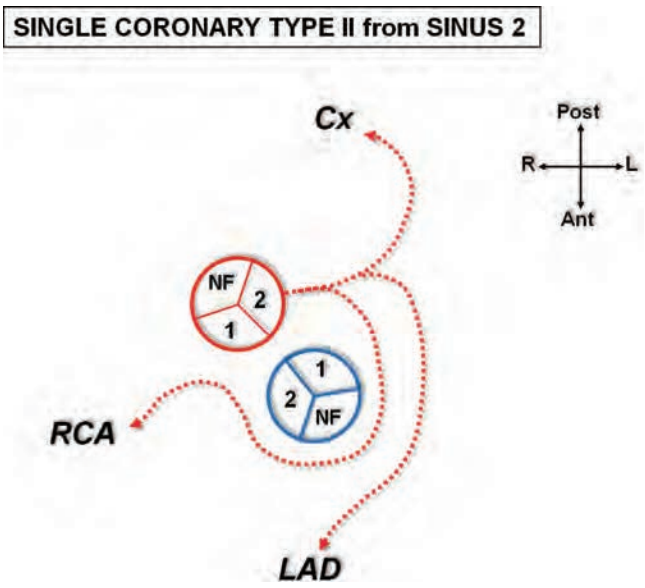

Figure 50.29 Single coronary type II from sinus #2. The same observations as in Figure 50.28: a common trunk gives origin to all three main coronary trunks with the RCA depicting a preinfundibular course. Blood flows in antegrade through all vessels.

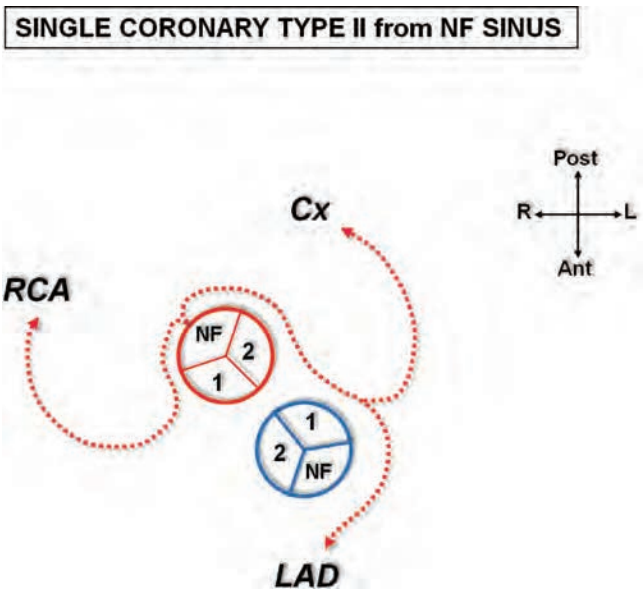

Figure 50.31 Single coronary from aortic NF sinus.

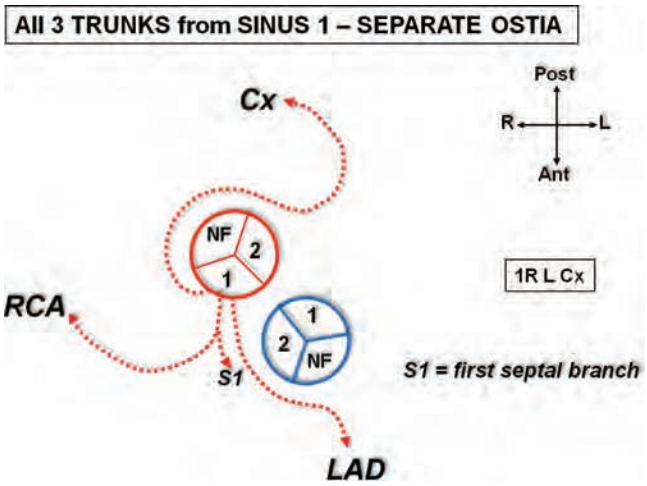

Figure 50.32 Separate origins of all trunks from sinus #1. This disposition is similar to single coronary type II from sinus #1. The first septal artery arises from the RCA. The LAD crosses anterior to the infundibulum while the Cx has a retroaortic course.

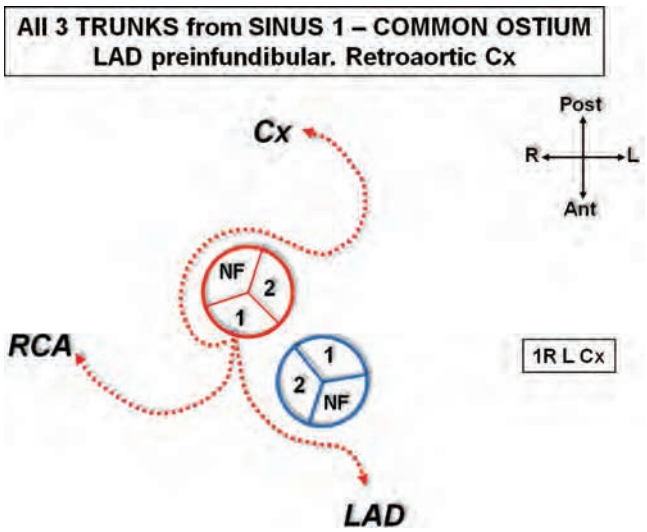

Figure 50.33 All trunks with common ostium in sinus #1 (variation). This is a pattern similar to that presented in Figure 50.32 and, except for the location of the ostia, the disposition of the main trunks is similar. The clinical relevance may however be different in the case of stenosis of the common ostium.

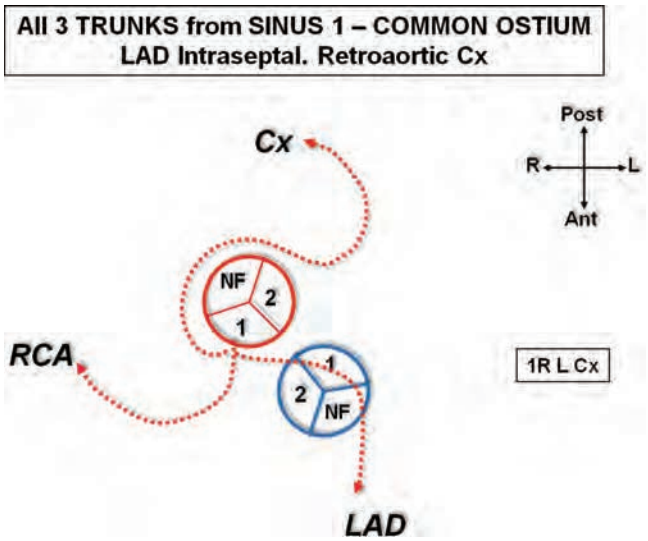

Figure 50.34 All trunks with origin at the level of sinus #1 (variation). There is an added abnormal intraseptal course of the LAD.

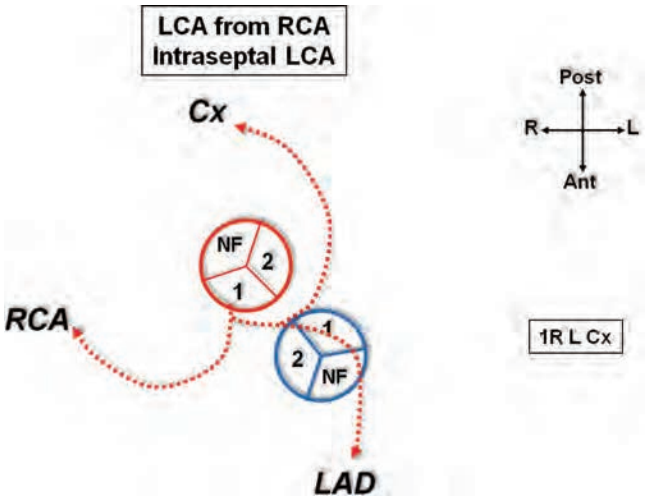

Figure 50.35 LCA from RCA and intraseptal LAD. A mixed trunk gives origin to a normal RCA and an aberrant LCA: the Cx runs between the arterial trunks while the LAD has an intraseptal proximal tract.

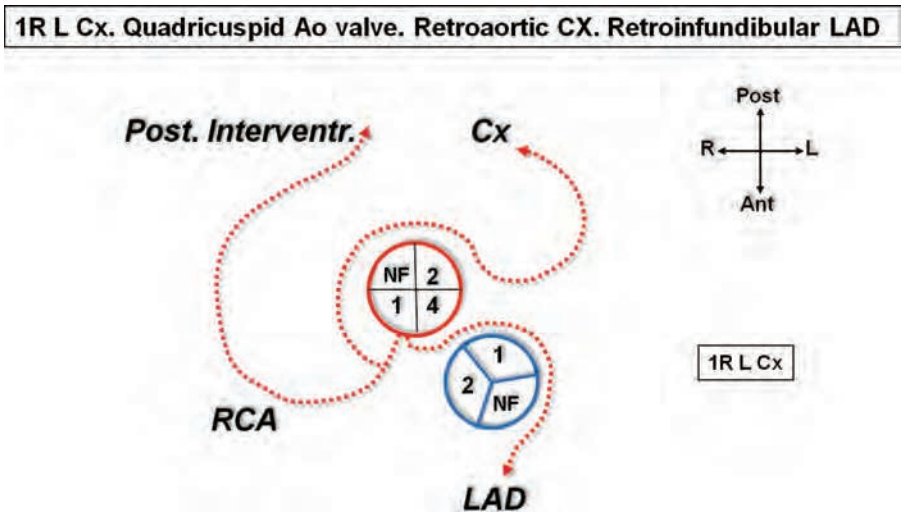

Figure 50.36 Complex variation with quadricuspid aortic valve. A mixed trunk gives origin to a normal RCA and a retroarotic Cx; the LAD has aberrant origin and interarterial course.

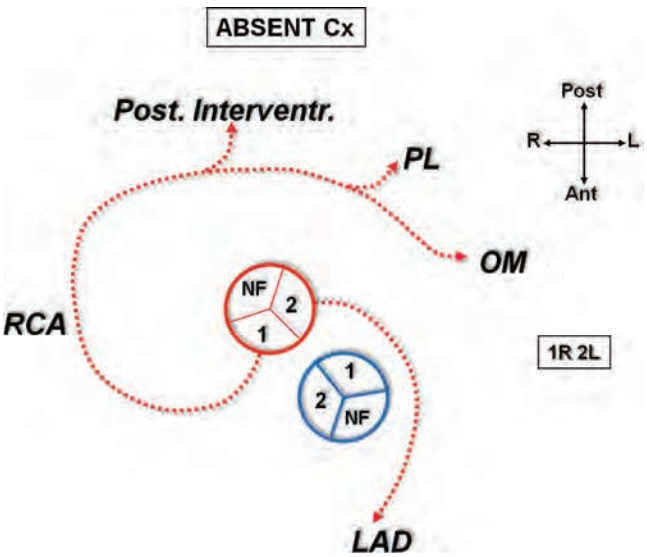

Figure 50.37 Absent Cx. This disposition resembles the single coronary type I except for the separate origin of the LAD. A common trunk begins as an RCA traveling the right and then the left coronary sulcus; the distal part gives origin to the posterolateral branches and the obtuse marginal branch of the left ventricle. As in the case of single coronary type I, the blood flow through the arterial trunk traveling the left coronary sulcus is retrograde (if this trunk is seen as a Cx branch).

Acute take-off of the circumflex branch (ATO-Cx)

An acute take-off of the circumflex branch (ATO-Cx; Angelini et al. 2008a) represents a newly identified coronary pattern that could hinder percutaneous interventions. Angiographically, the angle between the main trunk of the LCA and the Cx is ≤45° in two orthogonal, caudal projections (Fig. 50.38). However, no adverse effects have been reported to result from this variant.

Anomalies of intrinsic coronary arterial anatomy

There are numerous intrinsic congenital anomalies of the coronary arteries that can affect any portion of their tract from ostium to termination. Some of these are difficult to distinguish from acquired conditions, and a more detailed analysis is sometimes required; see the following sections.

Congenital coronary ostial stenosis or atresia (COSA)

Congenital coronary ostial stenosis or atresia (COAS; Angelini 2012) is a group of anomalies which indicates a congenital defect causing ostial or proximal coronary obstruction, more frequently affecting the LCA (L-COSA). Clearly, the condition must be distinguished from acquired forms such as those associated with atherosclerosis, syphilis, Kawasaki, or Takayasu disease. The collateral vessels connecting the main coronary trunks are one or two full-diameter arteries, while numerous anastomotic vessels develop in acquired cases (smaller than the recipient vessels with which they eventually connect). There

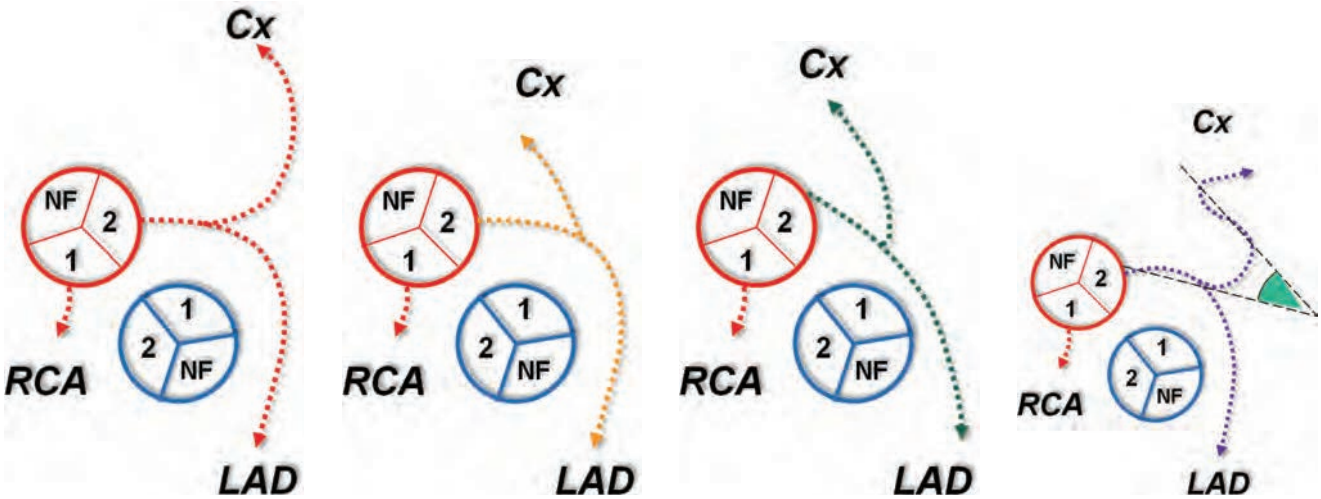

Figure 50.38 Acute take-off of the Cx. (a) Normal bifurcation of the LCA and the normal origination of the Cx; (b) normal-appearing acute take-off; (c) posterior origination of the Cx and acute take-off; and (d) sinuous S-shaped take-off of the Cx and the angle as measured angiographically.

can be an ostial dimple or no vestigial sign. The ostial rudiment can appear normally located or ectopic. In the latter situation, the proximal segment of the coronary artery can adopt any of the forms described under ACAOS (see section "Anomalous location of coronary arterial ostium"). The absence of signs of ischemia (clinical or stress-induced) favors a diagnosis of COSA; no revascularization is generally indicated. However, superimposed atherosclerotic modifications or fibrotic changes can induce ischemia later in life (Shen et al. 2012). Ultrasound and CT scans provide additional information about the atretic ostium and proximal segment of the abnormal coronary artery.

Coronary ostial dimple

This is defined as a depression in the aortic wall opposite a sinus with only one coronary ostium or at the level of the NF sinus, leading to no coronary artery. Its significance needs careful interpretation, as it is well known that the proximal tracts of the coronary arteries do not appear as outgrowths from the aorta; instead, the primitive coronary system connects to the aorta secondarily (Bogers et al. 1989). In COSA (see previous section), the dimple is connected to an atretic proximal coronary segment. The coronary ostial dimple must be distinguished from incipient aortic dissection.

Coronary ectasia and aneurysm (CAn)

The terms ectasia and CAn generally refer to enlargement of the coronary artery; morphologically, a greater than 50% increase in diameter is measured. Peak blood flow velocity is reduced. Coronary flow reserve is probably decreased due to repetitive distal embolization from mural thrombi (and not caused by stenotic segments between ectatic portions). Complications can develop progressively and become manifest, even in old age (Lee et al. 2012a). Secondary ectasia develops in cases with fistulous communications (and in older ALCAPA patients with coronary-cameral fistulas); in such cases the flow velocity is increased. It is not always easy to differentiate between congenital and acquired forms of CAn. Minor forms of ectasia appear to be related to myocardial hypertrophy (aortic stenosis, hypertension, and athlete's heart). Pediatric CAn cases pose difficult problems regarding long-term management and surgical/interventional indications.

Absent coronary artery

True congenital absence of a coronary artery/trunk should lead to hypoplasia of the dependent myocardial territory, but the term frequently denotes *apparently* missing coronary arteries or branches. The most frequent reasons for an apparently missing coronary artery are coronary artery ectopia and coronary occlusion with lack of demonstrable collateral retrograde filling. With the advent of CT scanning (MDCT and CT coronary angiogram), such cases are becoming increasingly rare.

Absent Cx

Two types have been described. The first refers to a "superdominant RCA:" the RCA gives off the posterior/inferior interventricular branch (PDA) and branches to the posterior aspect of the left ventricle and ends by giving off obtuse marginal branch(es). Such conditions must be differentiated from occlusion of the Cx: in congenital absence of the Cx, the branches are supplied by the RCA (Yameen et al. 2011; Guo and Xu 2012; Hongsakul and Suwannanon 2012). Reported cases also have intraoperative confirmation (Ali et al. 2009). The other type involves true absence of the Cx, usually accompanied by signs of myocardial ischemia in infants.

Congenital absence of the left main (CALM)

Such cases are rare; CALM is one of the least-frequently observed variations with very few cases presented in the literature (Amaral et al. 2000; Gebauer et al. 2008), although they usually require surgical correction. Clinical diagnosis is usually delayed because of the nonspecific and broad-spectrum symptoms, which range from asymptomatic to life-threatening (Blackman et al. 1981). Syncope, tachyarrhythmia, failure to thrive, or a sudden cardiac arrest can present during infancy or childhood in some patients (Singh et al. 2005; Sohn et al. 2010). Although CALM is frequently described as atresia of the LCA, the trunk of the LCA and, importantly, the distal LCA branches are indeed present while the left main ostium is atretic. Congenital atresia of the LCA needs to be differentiated from single coronary artery, in which a single common trunk located at any aortic sinus supplies the entire heart: in CALM, the three main coronary trunks (RCA, LAD, and Cx) are normally developed (none is absent; Pirelli et al. 2008).

Absent RCA

No ostium of the RCA is present. The territory of the RCA is supplied by a continuation of the Cx over the right coronary sulcus (Leitch and Caves 1975). The disposition resembles the single coronary artery type (Alderson 1972) except there is no proximal trunk of the RCA (compare with Fig. 50.28).

Absent LAD

The following situations can be found. There is a large first septal branch (S1) with origin in the proximal LAD or sinus #2. The remaining LAD is small and short or even absent (Fig. 50.39a). In another variant, two smaller LADs run the anterior interventricular sulcus (Fig. 50.39b). Another condition entails a large proximal LAD giving off the D1 and S1. The D1 gives off anterolateral branches to the left ventricle. Distal to the S1, the LAD appears slender and terminates early (Fig. 50.39c). In the last condition, the RCA provides anterior septal branches via an intraseptal route, preinfundibular route (Fig. 50.39d), or a wrap-around-the-apex inferior/posterior interventricular branch (Fig. 50.39e). Apparent absence of the LAD must be distinguished from an occluded LAD.

Absent PDA

The inferior/posterior interventricular branch (erroneously called the "posterior descending branch;" for practical clinical reasons the abbreviation PDA will be used in this chapter) travels the posterior interventricular sulcus for variable distances. The disposition is usually longitudinal, toward the apex of the heart. The PDA is usually a single trunk originating from the distal RCA or Cx. It can be doubled, with one branch from the RCA and another from the Cx. Other conditions included under the term "absent RCA" are as follows: split RCA, where one branch follows the distal RCA at the crux and travels the proximal interventricular sulcus terminating close to the crux cordis; or the distal branch of the PDA originates earlier from the RCA and obliquely travels the inferior aspect of the RV, toward the apex (Fig. 50.40). There is therefore no clearly formed PDA, although there are branches to the PDA territory of vascularization, albeit with different origins. In other cases, the PDA is almost absent and is replaced by a long LAD that passes around the apex of the heart, reaching the *crux cordis* (Fig. 50.41).

Coronary hypoplasia

The definition should include the angiographic appearance of a coronary branch or trunk with a smaller diameter with respect to the apparent area of dependent myocardium, and the demonstration of a locally reduced coronary reserve or presence of ischemia (Roberts and Glick 1992; Zugibe et al. 1993; Sim et al. 2009). Morphological data must be interpreted with caution, taking into account the coronary typology and dominance and always comparing the diameter of the hypoplastic vessel with the other main coronary trunks. The clinical condition is called hypoplastic coronary artery disease (HCAD). It is very uncommon, but leads to myocardial infarction or sudden death.

Muscular bridging (MB)/intramural coronary artery

The presence of two main coronary trunks is a recently evolved acquisition among animals (e.g., not all avian species have two coronary arteries). With respect to the course of the coronary arteries, mammalian hearts can be classified as follows:

- Type A: rat, guinea pig, hamster: intramyocardial course. In these species there is a characteristic septal branch with origin at the proximal right or left coronary artery.
- Type B: human, sheep, dog, cat: predominantly epicardial and frequently intramural course.
- Type C: horse, cow, pig: entirely epicardial arteries (Muresian 2009).

It is still difficult to establish a direct correlation of the species mentioned above with cardiac pathology and disease.

A distinction must be made between myocardial bridging and the intraseptal course of a coronary branch (most frequently the anterior interventricular branch). In the former case, an epicardial coronary branch runs beneath a muscular slip varying in length, resembling a normal tract albeit with a possible slight angulation. In the latter case the artery, besides being located deep within the septum, also follows an anomalous course.

A more detailed analysis reveals that different types of myocardial bridges can be encountered, depending on:

- the location of the bridge: over the LAD (the most frequent, especially in its midportion), over the Cx (Fig. 50.42), over one of their branches, over the RCA, right marginal branch, variant Cx or third coronary artery;
- the number of bridges: single or multiple (over the same coronary branch or over different coronaries) (Fig. 50.43);
- the width of the bridge: narrow (usually slender and weak although sometimes highly compressive) or wide;
- the origin, disposition and course of the muscular fibers: superficial bridges (crossing the artery either perpendicularly

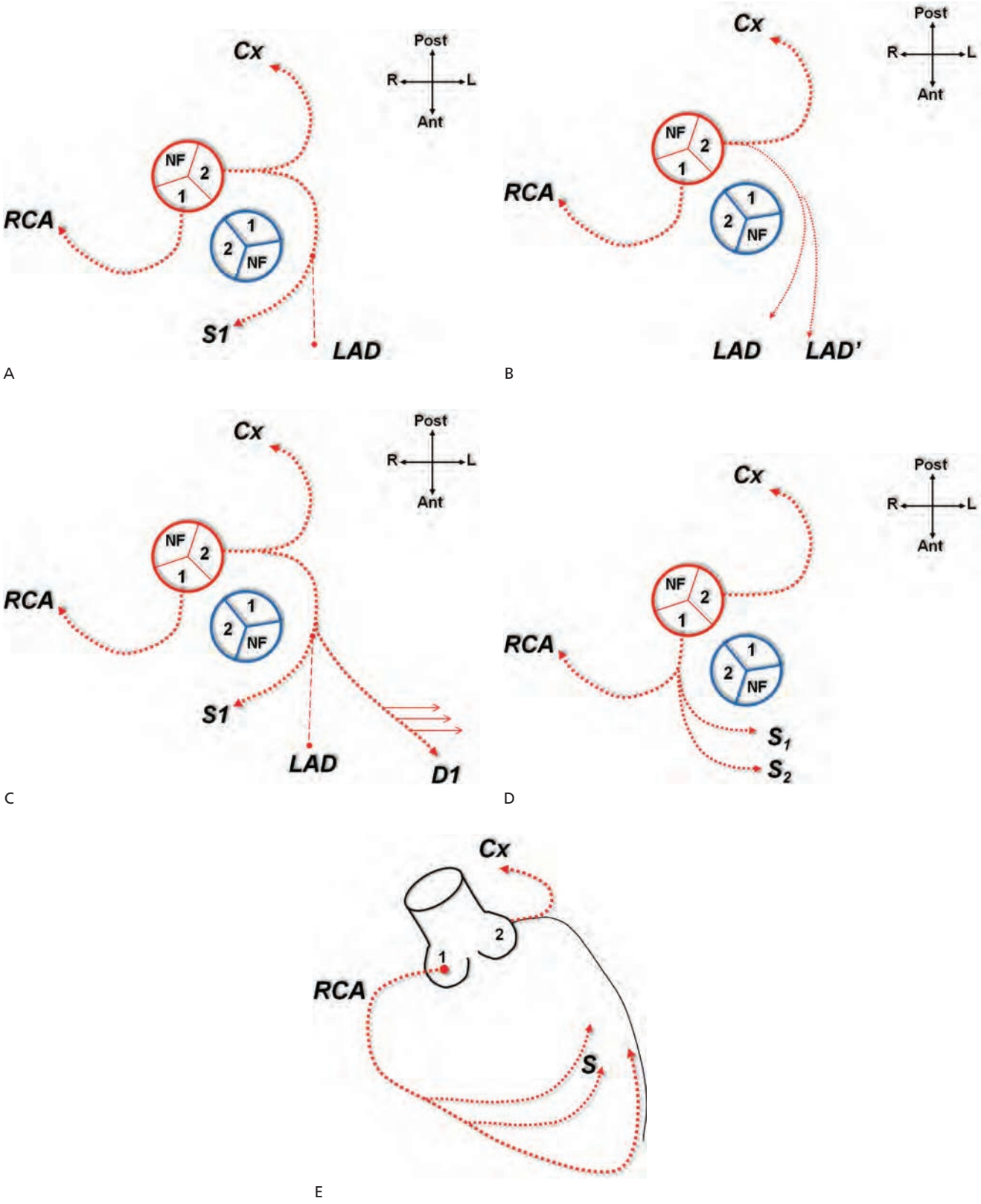

Figure 50.39 Absent LAD. (a) The LAD can be recognized only in the very proximal part terminating as the first septal branch (S1). The remainder portion cannot be recognized. This particular case may also be interpreted as absent LAD associated with a distinct origin of a large proximal septal branch. (b) Two smaller branches run the anterior interventricular sulcus, none of which appear as a true LAD. (c) The proximal LAD originates in a normal fashion. The LAD gives off a large septal branch and another artery running the left ventricle and giving off diagonal branches. The main trunk of the LAD terminates early. (d) The RCA gives off the first septal branches. These branches course either anterior to the infundibulum or through the septum. (e) The branches of the LAD are substituted by arteries from the RCa traveling the septum or around the septum

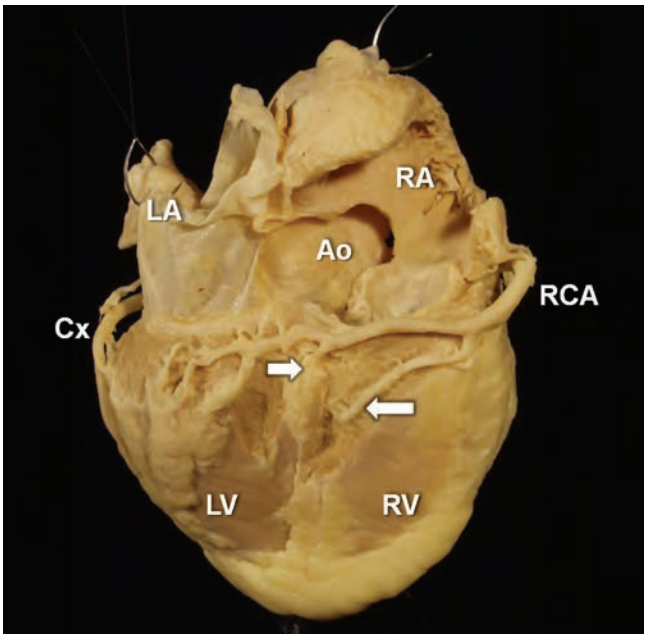

Figure 50.40 Absent PDA. The RCA travels the right coronary sulcus and proceeds to the left, almost reaching the obtuse margin of the left ventricle. There is no distinct PDA. Instead, two branches with an oblique disposition (white arrows) vascularize the territory of the PDA.

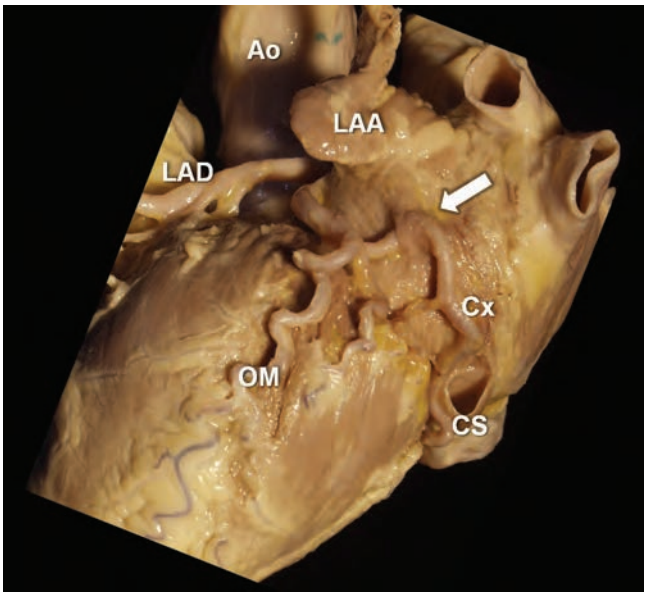

Figure 50.42 Myocardial bridge over the Cx (white arrow). The Cx runs in a more superior location, being partially covered by a muscular bridge constituted by left atrial myocardium. Ao: aortic root; Cx: circumflex branch; CS: coronary sinus. LAA: left atrial appendage; LAD: left anterior descending; OM: obtuse marginal.

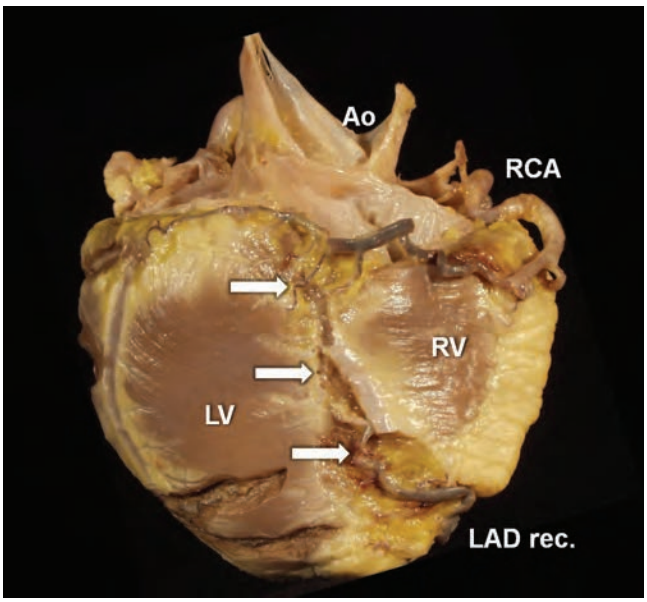

Figure 50.41 Absent RCA and long LAD. The LAD has a long recurrent course reaching the crux cordis (white arrows). All septal branches are given off by the LAD.

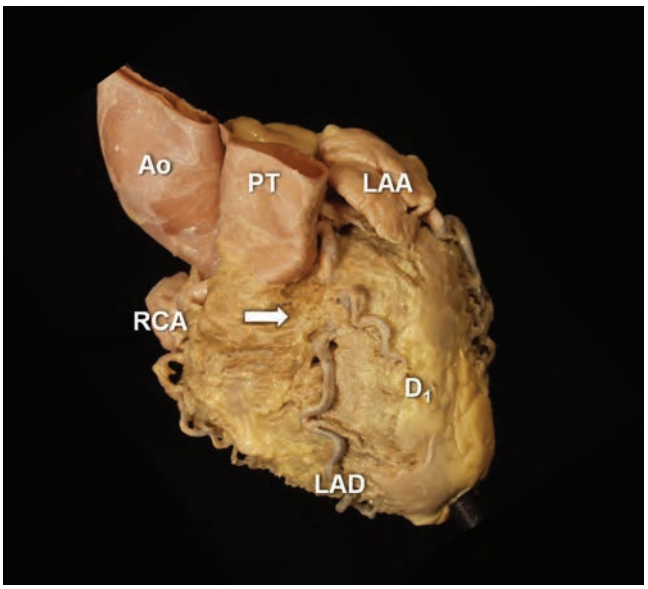

Figure 50.43 Myocardial bridge over the LAD and origin of first diagonal (D_1).

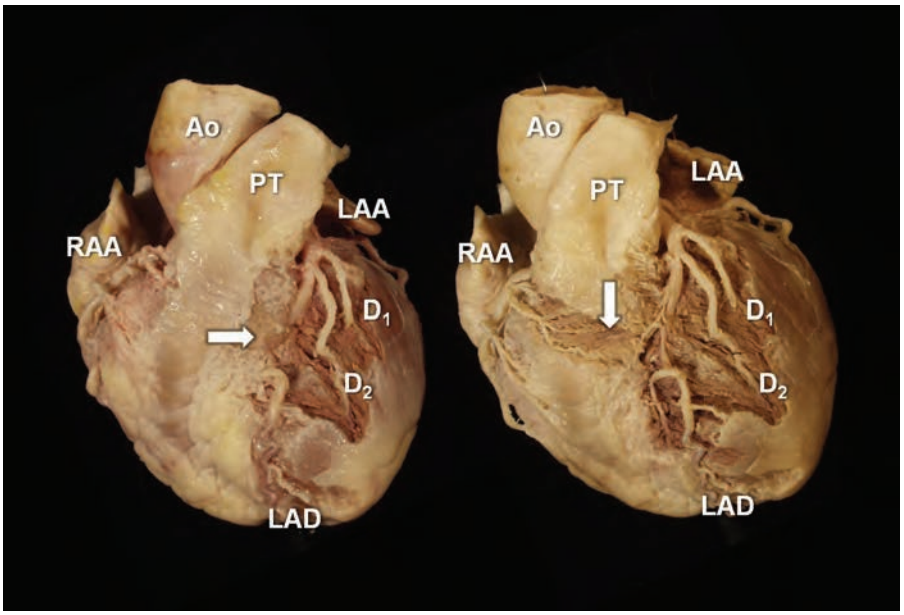

Figure 50.44 Anatomical aspect of the bridged artery. The middle tract of the LAD is covered by a conspicuous myocardial bridge (white arrow, left panel). Under the bridge the artery appears hypoplastic (right panel). Conspicuous anastomoses connecting the RCA and LAD are easily visible (white arrow, right panel). The LAD distal to the bridge appears normal.

or at acute angles and apparently not constricting the underlying artery); deeper and more conspicuous and compressive bridges (muscle bundles arising at the level of the right ventricular infundibulum or apical trabeculae, crossing the LAD transversally, obliquely or helically, and terminating in the interventricular septum);

- the type of myocardium constituting the bridge: atrial or ventricular;
- the clinical picture in the given patient: MB in persons with no apparent cardiovascular disease versus MB in patients with cardiovascular pathologies such as hypertrophic cardiomyopathy (compression of both the LAD and septal branches) or coronary atherosclerosis (e.g., MB over the LAD can precipitate ischemia in a patient with atherosclerotic coronary arteries);
- the aspect of the artery beneath the MB: rectilinear profile or looping of the artery ("the U-sign"); normal diameter or hypoplastic coronary arterial segment (Fig. 50.44).

From the above it is evident that many variations and associations are possible, making the various statistics difficult to compare. From a practical point of view it is obvious that an MB represents only one preliminary element in a more complex and individualized clinical-diagnostic framework.

The claimed consequences of myocardial bridging are heterogeneous. At the benign end of the spectrum are MBs as variants of the normal condition and compatible with excellent long-term survival. On the other hand, MB has been linked to myocardial ischemia, infarction, exercise-induced tachycardia, conduction disturbances, and sudden death. The relationship between atherosclerosis and myocardial bridges is also still controversial: while some authors indicate that atherosclerosis is uncommon within a MB, others report the opposite. Taking into account the multitude of anatomical forms, one cannot accept only "the protective effect" of the intramural portion of a given coronary artery; atherosclerosis can probably develop as easily (or even more easily) when some forms of myocardial bridging are present. Experimentally created myocardial bridges confirm the ischemic distress induced by compression of the coronary artery.

Subendocardial coronary course (SEC)

Although some authorities describe this condition as intermediate in the spectrum of coronary malpositions, ranging from subendocardial location to intramyocardial and eventually to coronary-cameral fistula (Angelini et al. 1999), the following details should be underlined: the coronary segment in cases of SEC is morphologically normal (not hypoplastic, or looping, or with altered parietal structure); a SEC apparently does not predispose the arterial segment to any particular pathological alteration; and, not least, this seems to be a benign condition that requires no preventive treatment or special follow-up. Until the advent of the newer imaging modalities such as MDCT and cardiac MRI, the SEC was mostly an intraoperative finding, as subendocardial locations could not be properly diagnosed or predicted by angiography alone (Scheffel et al. 2007; Zalamea et al. 2009; Andrade et al. 2010; Cristopher and Duraikannu 2011).

The RCA can follow an "intra-atrial" course while the LAD can reach the subendocardial aspect of the RV.

A SEC can complicate or hinder surgical or percutaneous procedures, such as: pacemaker implantations; invasive electrophysiology testing (Rosamond et al. 2007); cannulation for cardiopulmonary bypass; surgical procedures on the tricuspid

valve; or the dissection and preparation of the LAD with a view to coronary bypass grafting, especially on the beating heart when the RV can be inadvertently open (Tovar et al. 1997).

Coronary crossing

Very few angiographic reports describe crossing coronary arteries; this condition affects secondary epicardial branches but none of the three elementary coronary trunks (Yilmaz and Demir 2005).

Anomalous origin of posterior interventricular branch

Anomalous origin of posterior interventricular branch from the anterior interventricular branch or from a septal branch (PDA from LAD or from S). In cases of "absent PDA" (see section "Absent PDA" above) the LAD courses over the apex and continues as a PDA (blood flow is retrograde in the PDA) for various distances. However, acquired and congenital forms must be clearly distinguished. The diameters of the LAD and PDA must be taken into account: an occluded PDA will be filled in retrograde fashion by an LAD that tapers towards the apex of the heart; in contrast, in a congenital form, the LAD over the cardiac apex will retain its caliber.

The anterior two-thirds or even three-quarters of the interventricular septum are vascularized by the anterior septal branches (branching from the LAD) while the remaining posterior inferior aspect is vascularized by the posterior septal branches originating from the PDA. Hence, the septal arteries are not transit vessels. On rare occasions, a large septal artery travels the septum and reappears in subepicardial position as a distal PDA (Fig. 50.45).

Split RCA (double RCA)

The denomination "double RCA" is considered incorrect by some authors as the RCA is actually split, forming two separate portions of the PDA (Fig. 50.46). The first (proximal or anterior division of the RCA) gives off branches to the anterior RV wall (Sawaya et al. 2008), courses obliquely over the posterior inferior aspect of the RV and terminates as the distal PDA (the latter vascularizes the distal posterior septum and can provide branches to the posterior LV wall). The second (distal or posterior) branch of the bifurcation follows the regular path of the RCA in the coronary sulcus and terminates as the uppermost portion of the PDA. There can be even more branches coursing obliquely over the posterior RV and substituting for the PDA and its terminal branches (Fig. 50.47). Other cases have been reported, in which two actually separate RCAs arise from a common ostium in sinus #1 (right sinus). The distal pattern includes two parallel PDAs (Selcoki et al. 2010). It is important to recognize the territory of vascularization of each major branch of the division of the RCA, both for a correct diagnosis and for properly oriented surgical or percutaneous therapy.

Other conditions relating to the split RCA illustrate various coronary artery typologies. A proximal PDA from the RCA and a distal PDA from the LAD represents a coronary arterial typology: a short PDA and a long LAD with a recurrent course around the cardiac apex. In fact, the Nomina Anatomica designates this portion "the posterior apical artery" and it should not be included among CAAs. Another condition involves two parallel PDAs, one originating in the RCA and the other in the Cx. This also represents a coronary arterial typology pattern, the so-called codominance, and should not be considered a CAA.

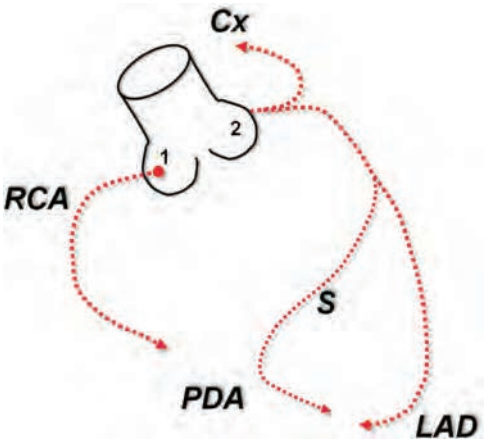

Figure 50.45 Anomalous origination of the PDA. The proximal portion of the PDA originates in the RCA in the usual manner. The distal PDA takes origin from a large septal artery that crosses the septum and emerges at the level of the distal inferior interventricular sulcus. 1: aortic sinus #1 (right-facing aortic sinus); 2: aortic sinus #2 (left-facing aortic sinus); S: septal artery.

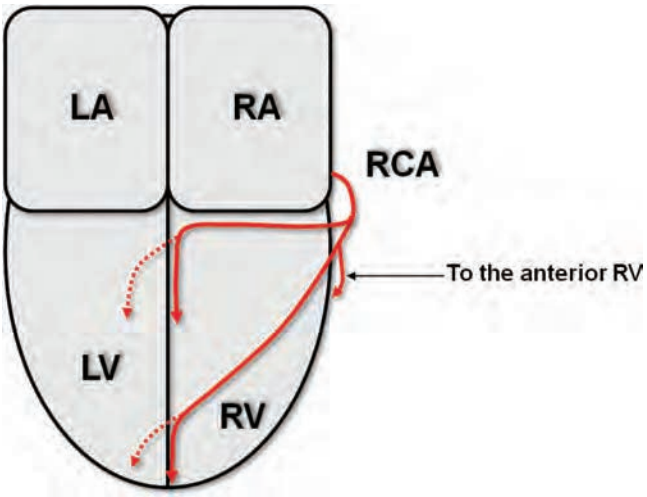

Figure 50.46 Split RCA. The proximal branch of the RCA gives off branches to the right ventricle and, after an oblique tract over the inferior RV wall, terminates as a distal PDA. The remainder division of the RCA occupies the proximal interventricular sulcus running longitudinal the proximal sulcus; it may also give additional branches to the posterior left ventricle.

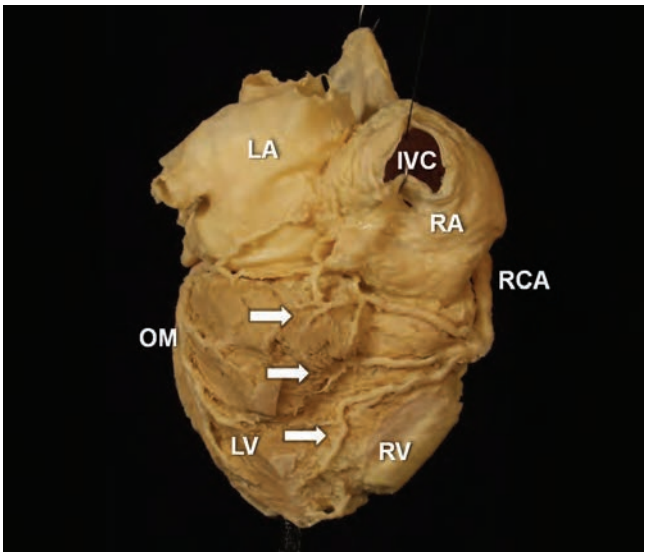

Figure 50.47 Split RCA (variation). There is no distinct PDA. The RCA divides into three branches with an almost horizontal disposition (white arrows).

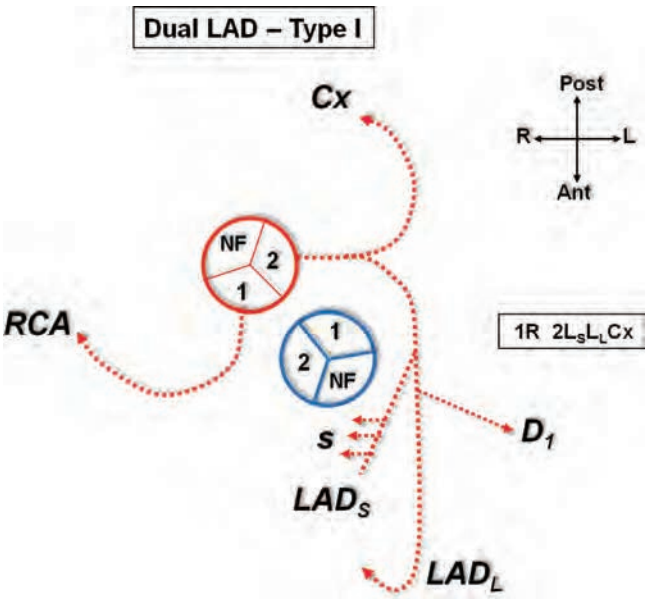

Figure 50.48 Split (dual) LAD type I. There are two LADs: a short and a long LAD. The short LAD (LAD_S) gives off the septal branches and travels the right aspect of the AIVS. The long LAD (LAD_L) gives off the diagonal branches and travels the remainder AIVS (on the left of the LAD_S), sometimes winding around the apex. The distal septal branches are given off by the long LAD.

Split LAD and other conditions affecting the LAD

The classical split LAD comprises cases of the LAD giving off a large septal artery or the presence of two parallel LADs. However, numerous other cases have been described. The presence of an accessory LAD from sinus #1 taking a preinfundibular route has already been described (Fig. 50.23).

Numerous other cases are included in the category "dual LAD" and comprise six types to date (Figs 50.48–50.54). The original classification by Spindola-Franco et al. (1983) was recently updated with new categories (Maroney and Klein 2012; Moreno-Martinez et al. 2012). In types I–III, the LAD originates in the LCA and divides into two branches, the short and the long LAD, the former giving off most of the septal and diagonal branches. In types IV–VI the long LAD originates in the RCA (or sinus #1) and the short in the LCA (or sinus #2) (Table 50.6). The path followed by the long LAD is preinfundibular, intramyocardial (intraseptal), or interarterial (between the aortic and pulmonary roots). Such aberrant courses can predispose the artery to the same complications as described above, generated by similar mechanisms: compression, scissoring, shearing, etc. Interventionalists must be aware of all the possible variations both for a correct diagnosis (avoiding confusion between the lack of visualization of the additional LAD and an occluded segment of a normal LAD) and for possible pitfalls resulting from the anomalous course of the LAD (Lee et al. 2012c).

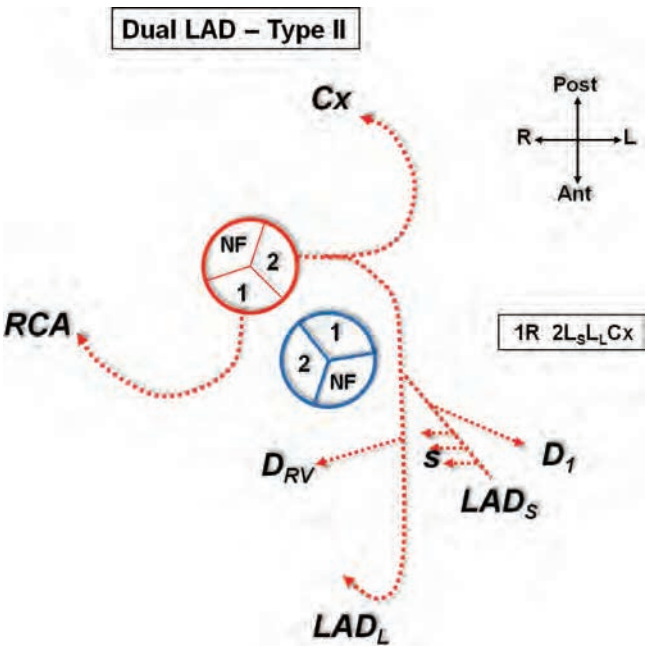

Figure 50.49 Split (dual) LAD type II. The disposition is reversed as compared to Figure 50.48: the short LAD is on the left side of the AIVS and gives off the septal and diagonal branches. The long LAD travels the remainder AIVS (on the right of the short LAD), giving off only some distal septal branches and diagonal branches of the right ventricle (D_{RV}).

Twin Cx

Twin Cx (or doubled circumflex branch of the left coronary artery) is defined as two circumflex branches, which may or may not have closely related origins, eventually traveling to the

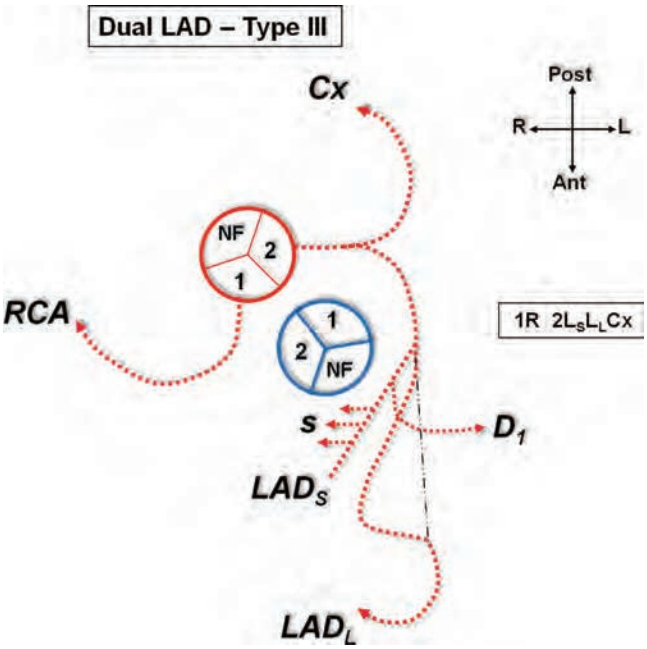

Figure 50.50 Split (dual) LAD type III. The short LAD is similar to type I (Fig. 50.48). The long LAD passes deep into the septum as a septal branch, only to emerge distally at apical level and eventually wind around the apex.

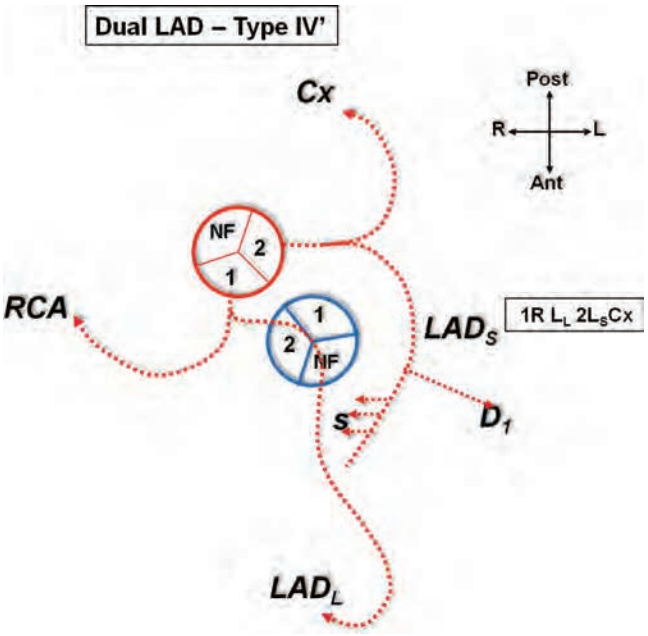

Figure 50.52 Split (dual) LAD type IV (variation). The general disposition is as presented in Figure 50.51. The long LAD has an intraseptal (supracristal) course.

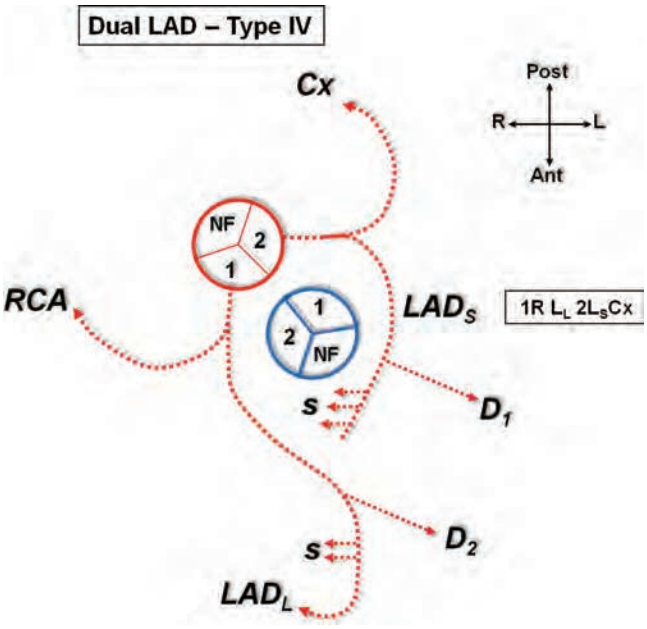

Figure 50.51 Split (dual) LAD type IV. The short LAD originates in a normal manner from the LCA. It gives off septal and diagonal branches. The long LAD originates from the RCA, runs a preinfundibular course and reaches the middle-distal AIVS. Some of the distal septal and diagonal branches may originate from the distal long LAD.

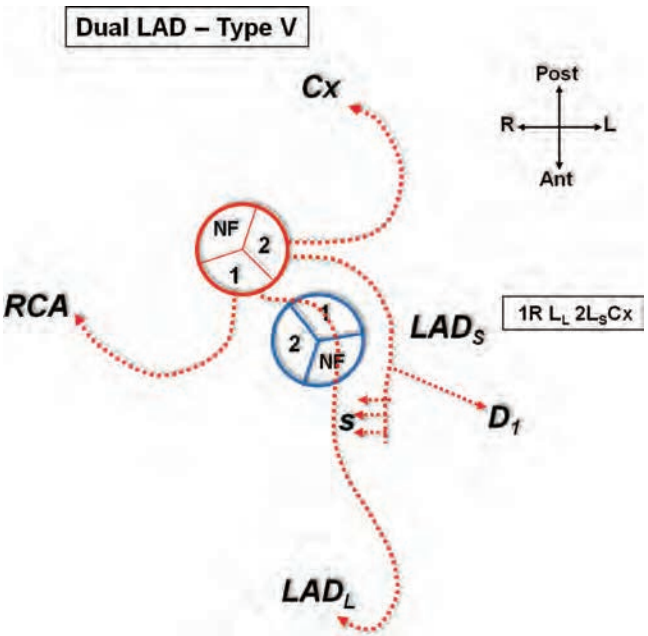

Figure 50.53 Split (dual) LAD type V. The origin of the long LAD is in sinus #1. The LAD has an intraseptal course reaching the middle-distal AIVS. The septal and diagonal branches are given off by the short LAD, which has a separate origin in sinus #2.

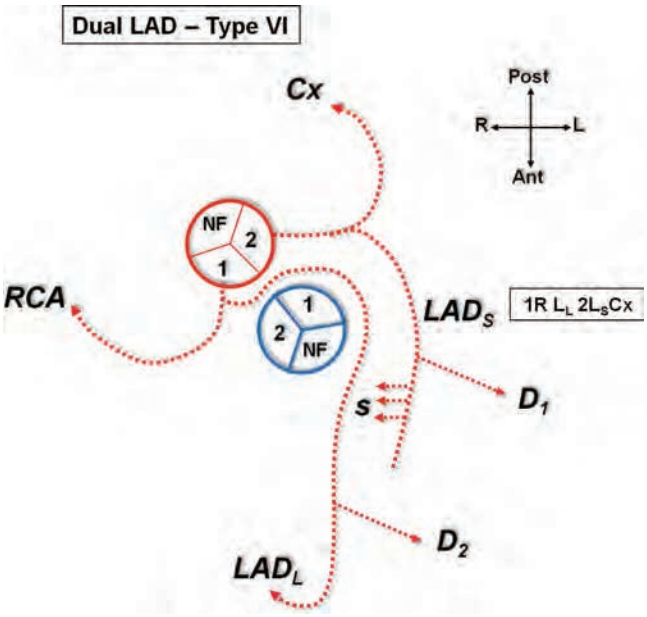

Figure 50.54 Split (dual) LAD type VI. The LCA divides in two branches: Cx and a short LAD. The latter gives off proximal diagonal and septal branches. The long LAD originates in the proximal RCA, courses between the arterial roots and travels the AIVS toward the apex, where it may give off distal septal and diagonal branches.

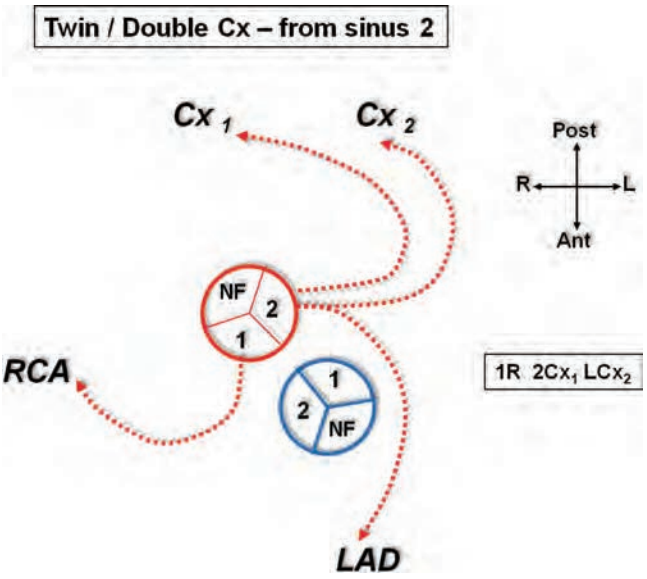

Figure 50.55 Twin Cx. There is an additional Cx branch (Cx_1) with origin in sinus #2. It travels superior to the normal Cx.

left coronary sulcus. The Cx branches can originate separately from sinus #2 (left sinus) (Tekbas et al. 2011; Fig. 50.55) or the additional Cx can originate from the RCA (van der Velden et al. 2008) (Fig. 50.56). The supernumerary Cx is placed in a more "atrial" position (i.e., superior to the normal Cx). This anomaly is considered benign; however, in clinical practice one must be alert to the possibility of an additional Cx, especially in cases in which the posteriolateral left ventricular myocardium remains apparently avascular during left coronary opacification (despite normal wall motion in that area).

Woven coronary arteries

This is an extremely rare anomaly characterized by the twisting courses of multiple thin channels along the vessel, in any coronary artery, with a TIMI=III (a normal thrombolysis in myocardial infarction) blood flow (Sane and Vidaillet 1988; Berman et al. 1990; Kaya et al. 2006; Soylu et al. 2012). This anomaly is difficult to recognize because of its rarity. It is usually mistaken for coronary thrombosis or dissection. It can actually result from coronary dissection; however, reported cases differ regarding the presence or absence of myocardial ischemia in the territory of the woven vessel. The angiographic appearance is quite characteristic, as indicated by the name. This condition appears not to be amenable to any revascularization procedure due to the diffuse involvement of the vessel.

Table 50.6 Types of dual LADs: classification.

	Origin			Branches supplied	
Type	s/LAD	L/LAD	Course of L/LAD	s/LAD	L/LAD
I	Proximal LAD		Epicardial course on the LV side of the AIVS re-enters the distal AIVS	S	D
II			Epicardial course on the RV side of the AIVS re-enters the distal AIVS	S + D	D_{RV}
III			Intramyocardial course; terminates as S branch or re-enters the distal AIVS	D ± S	S
IV	LCA	RCA	Preinfundibular or intraseptal, re-enters the distal AIVS	D + S (distal)	D + S (proximal)
V	Sinus #2	Sinus #1	Intraseptal re-enters the distal AIVS	D + S (distal)	D + S (proximal)
VI	LCA	RCA	Epicardial interarterial enters the middle/distal AIVS	D + S (distal)	D + S (proximal)

s/LAD: short LAD; L/LAD: long LAD; p/LAD: proximal LAD; S: septal branches; D: diagonal branches; D_{RV}: right ventricular diagonal branches; sinus #1: right-facing aortic sinus; sinus #2: left-facing aortic sinus; AIVS: anterior interventricular sulcus

Source: Lee et al. (2012). Reproduced under the terms of the Open Access Licence CC-BY-2.0.

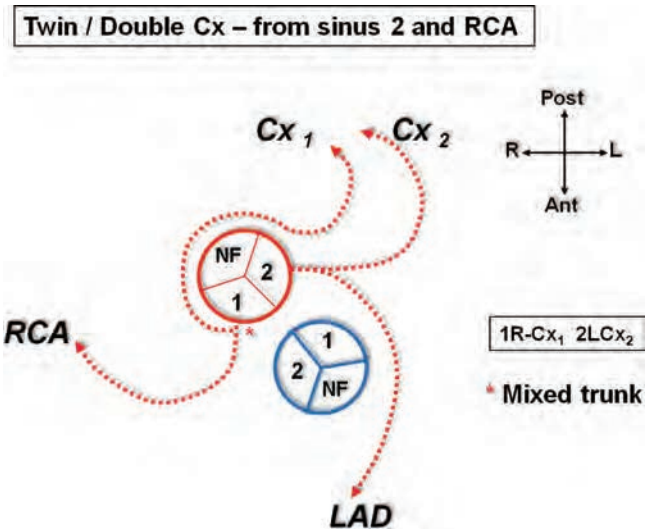

Figure 50.56 Twin Cx; the additional Cx originates from the RCA. The additional Cx labeled Cx_1 takes off from the proximal portion of the RCA and winds around the aortic root. In correspondence with the aortic sinus #2 (left sinus), it comes to occupy the left coronary sulcus, superior to the normal Cx (Cx_2).

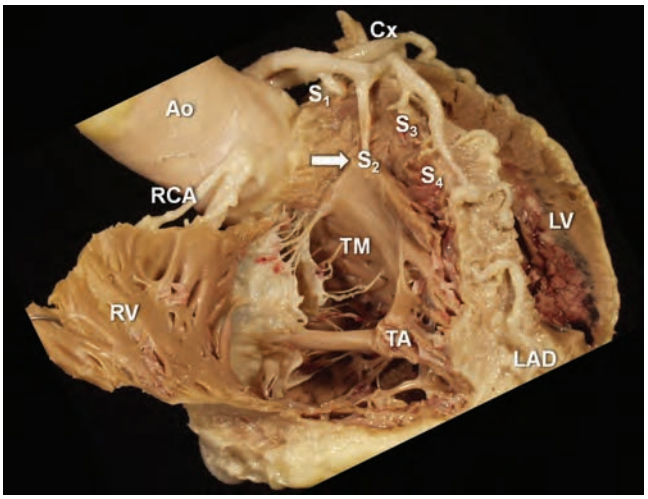

Figure 50.57 The main septal branch. Anatomical specimen in which the pulmonary infundibulum was removed (as for the Ross operation). The right ventricle is wide open. The first septal branches (S_1 through S_4) were dissected. This figure demonstrates the fact that the main septal branch is not always the first: indeed, the second septal artery (S_2) appears larger and longer while the first (S_1) has a very proximal origin and vascularizes the right aspect of the superior septum. S_2 vascularizes most of the septum, the medial papillary muscle group of the tricuspid valve (TM), and proceeds toward the base of the anterior papillary muscle of the tricuspid valve (TA). Abbreviations as for previous figures.

Ectopic origination of the first septal branch

This situation resembles the normal coronary arterial disposition in some species (Fernandez et al. 2008; Clauss et al. 2006; Durán et al. 1991, 2005, 2007), in which the first septal artery is a large vessel vascularizing most of the septum and can have a separate origin from one of the aortic facing sinuses (sinus #1 or #2) or from the most proximal tract of either the RCA or the LCA. In human hearts the disposition of the anterior septal branches (from the LAD) can vary: these arteries do not follow the expected decreasing pattern (e.g., S1 larger than S2, larger than S3, and so on). Instead, there are one or two (rarely three) major septal arteries with important territories of vascularization: the main part of the septum; the tricuspid medial group of papillary muscles; the atrioventricular node and adjacent area (comprising portions of the muscular part of the aortic root); the base of the tricuspid anterior papillary muscle; and through a separate branch a portion of the RV aspect of the upper interventricular septum. Interventionalists have called this septal vessel "the first septal unit," and it is variously and selectively approached in the treatment of septal hypertrophy (alcoholization) or preserved during surgical procedures such as Ross or Konno. However, as stated above, the main septal branch (MSB) is not always the first septal (Hosseinpour et al. 2001; Muresian 2001, 2006, 2009; Fig. 50.57). Consequently, the ectopic origination of the S1 must always be distinguished from the caliber of the S1, which might or might not be the MSB in the given patient. The S1 can originate from the left coronary system (sinus #2, LCA, Cx, or RI) or from the right (RCA, sinus #1). In cases with ectopic origin, it is more important to follow the course of the artery, the anatomical relationships, and the major branches of division. Septal arteries originating from the aortic sinuses usually indicate a low ostium, a surgically relevant detail. In surgical procedures for left ventricular restoration, revascularization of the MSB (and as many septal branches as possible) represents a principal condition: an ectopic origin of the MSB can therefore exclude this vessel from revascularization.

Anomalies of coronary termination

Inadequate arteriolar/capillary ramifications

Lack of adequate branching or capillary termination of one or more coronary trunks is rarely documented *in vivo* but can be one cause of the syndrome. Absence of septal branches from the proximal portion of the LAD was recently reported (De-Giorgio et al. 2013) as a cause of sudden death. Corroboration by various imaging modalities can draw the attention of the physician toward such an anomaly with a potentially grim prognosis; otherwise, it is difficult to diagnose.

Coronary arteriovenous fistulae (CAVF)

Under this category are included the abnormal communications/terminations of one or more coronary main trunks or branches with (or into) a cardiac chamber or any segment of the systemic or pulmonary circulation. To elucidate the normally occurring connections in the coronary vascular system, a schematic representation is presented in Figure 50.58. The CAVF can arise from the RCA, LCA, Cx, diagonal, obtuse marginal

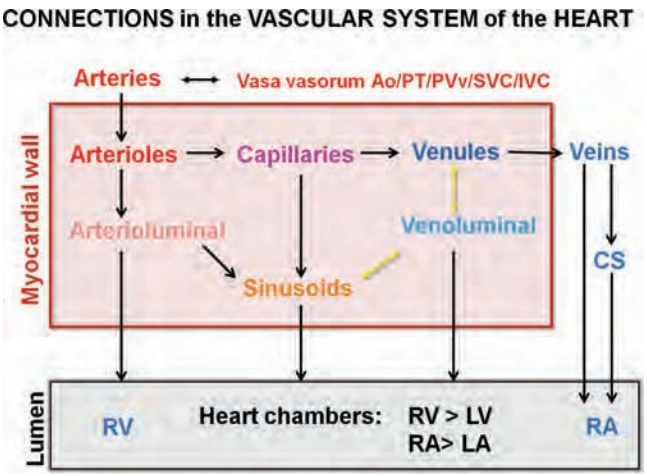

Figure 50.58 Connections in the vascular system of the heart. This scheme provides the essential features of the various types of vessels that can be found in the walls of the cardiac chambers, as well as the connections between them. Most of the veins drain through the epicardial veins, eventually reaching the RA directly or through the CS. Numerous channels called Thebesian vessels ensure the direct venous drainage with the various heart chambers, more in the atria (in the RA more than in the LA) than in the ventricles (in the RV more than in the LV). The sinusoids and arterioluminal vessels open more frequently into the RV cavity. In some conduits, blood flow is bidirectional (yellow arrows).

branch, infundibular artery, or single coronary artery, putting one or more of these arteries in communication with the right or left heart chambers (communication with the LV being the least common), the cardiac veins, pulmonary trunk or branch, coronary sinus, caval veins, or persistent left superior vena cava. A good review of the sites of termination of solitary CAVFs is presented by Said (2010) and Said et al. (2011). The CAVFs can be single or multiple, congenital or acquired, and are sometimes associated with congenital cardiac malformations such as the tetralogy of Fallot, atrial septal defects, ventricular septal defects, patent ductus, or pulmonary atresia with intact ventricular septum. In this latter case the CAVFs create additional shunting of blood from the RV into the sinusoids, coronary artery, coronary veins, coronary sinus, right atrium, and again the RV (circular shunt; Freedom and Harrington 1974).

The hemodynamic consequences depend on multiple factors including: the location of the CAVF (proximal or distal); the number of fistulae (single versus multiple); the anatomical modifications acquired over time (dilated coronary artery, fibrosed vein, development of pulmonary hypertension, etc.); and various hemodynamic parameters such as exercise-inducing intramyocardial arteriolar dilatation and increased systemic venous impedance and hypertensive status versus hypotension (the latter adversely influencing the balance between nutrient and fistulous flow).

Diagnostic imaging should reveal numerous particulars but not least the following: nutrient flow to the myocardium (the existence of adequate coronary arterial branching); hypoplastic coronaries; aneurysmal dilatation of the proximal coronary arteries; and the consequences for the cardiac chambers (dilatation, remodeling, local contractility, valvar insufficiency). Consequently, there is no algorithm for the proper diagnosis and follow-up of CAVFs and a properly oriented clinical judgment is mandatory.

One of the complications of myocardial infarction is coronaro-cameral communication (not a congenital CAVF), in which a ruptured coronary artery, or more frequently a vein, communicates with a heart chamber. The smaller anatomical but not functional connections should be called "coronaro-cameral micro-communications" (Angelini et al. 1999).

The coronary artery proximal to the CAVF dilates progressively with eventual development of an aneurysm; other important modifications include mural thrombi ± branch embolization and occlusion; intimal ulceration; and accelerated atherosclerotic changes. It is now generally agreed that surgical or percutaneous correction should be performed between the ages of 5 and 15 years (although some authors report spontaneous closures).

Several CAVFs can develop after cardiac surgery in the context of pericarditis, pleuropericarditis, and atelectasis during the postoperative period.

Some particular cases of CAVF have been reported: dual fistulas of the ascending aorta and coronary artery to the pulmonary trunk (Kim et al. 2011), persistence of the Thebesian veins (Jung et al. 2012), a giant coronary sinus aneurysm secondary to a right coronary arteriovenous fistula leading to a pseudomitral stenosis (Gaudino et al. 2011), a bilateral CAVF to the pulmonary trunk (Kwoon et al. 2010), "the snake heart" (Wallia et al. 2010), multiple CAVFs emptying into the LV through the entire LV wall (Lee et al. 2012b), a Cx-to-LV fistula (Teno et al. 1993), a LV and coronary sinus (McGarry et al. 1981), a local pulmonary malformation caused by a bilateral coronary artery and bronchial artery fistulae to the left pulmonary artery (Cijan et al. 2000), a fistula with aneurysmal termination in the pulmonary trunk (Darwazah et al. 2005), a CAVF associated with sinus node dysfunction (Endoh et al. 1990), and a fistula with the SVC (Galbraith et al. 1981) or rare multiple fistulae (Takechi et al. 2012).

Anomalous anastomotic vessels

As revealed by numerous studies, but especially by the superb work of Baroldi and Scomazzoni (1967), there are multiple anastomoses between the coronary arteries at both epicardial and intramyocardial level. However, not all are functionally adapted or angiographically visible. Ischemic heart disease leads to a progressive recruitment of collaterals by arteriogenesis (i.e., arterializations of previously existing inter-coronary communications). The so-called congenital "anomalous collaterals" are anastomotic communications with diameters >1 mm

connecting adjacent and non-obstructed coronary arteries. The pathophysiological mechanism leading to the development of these vessels is generally obscure, although a previous transient coronary occlusion cannot be ruled out. These vessels appear in principle to have a protective role. Angiographically visible larger-than-expected communications can result from the progression of coronary disease in a major trunk, leading to enlargement of previously developed (but less functional) anastomoses.

However, abnormal origination of a coronary artery (e.g., the PDA continuing the LAD over the apex) must be distinguished from conspicuous enlargement of collaterals between a patent and a diseased coronary arterial trunk (e.g., occlusion of the RCA at the aortic ostium with retrograde filling from enlarged anastomoses with the LAD and septal branches).

Multiple concomitant coronary arterial anomalies (and atypical anomalies)

Coronary arterial anomalies in the various types of congenital cardiac malformations are not discussed in this section.

More recent reports include combinations of anomalies in the same patient, obviously more difficult to fit into a proper classification. It is clinically interesting that there can be more than one coronary anomaly and that some of them can be clinically silent. Some examples are summarized below.

- Bilateral origin of a split LAD combined with atypical branching of the Cx (Schanzenbacher and Strotmann 2002), in which the long LAD originates in the proximal RCA, courses intraseptally, and enters the anterior interventricular sulcus (AIVS). The short LAD originates as the common trunk of the LCA, reaches the AIVS, but makes a 180° turn after giving off a large septal branch. The ascending loop continues as a Cx (Fig. 50.59).
- Giant single coronary artery terminating in a fistula (Adamo and Adamo 2006).
- Ectopic RCA with anomalous Cx (Ramsdale et al. 2005). The RCA originates from the ascending aorta above the right sinus (sinus #1) in a common trunk with the Cx; the RCA proceeds tangentially to reach the right coronary sulcus while the Cx follows a retroaortic course. The LAD has a high origin from sinus #2 near the sinutubular junction.
- Anomalous right-sided left main coronary artery and dual LAD type IV (Cruz et al. 2010).
- Cx from RCA plus myocardial bridge over the LAD (Selcoki et al. 2009).
- Cx originating from sinus #1 with retroarotic course + LAD from sinus #1 with preinfundibular course + hypertrophic cardiomyopathy (Bush et al. 2005).
- Cx from sinus #1 with retroarotic course + LAD from sinus #1 with preinfundibular course (La Vecchia et al. 2002).
- Preinfundibular anomalous branch from the LAD ending in a blind aneurysmal pouch in the pulmonary trunk (Moosa et al. 1988).

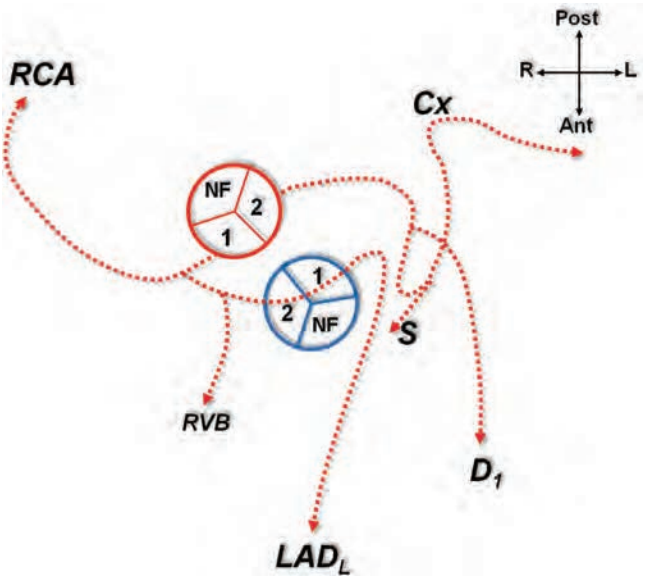

Figure 50.59 Multiple or rare anomalies. The figure illustrates the presence of a split LAD associated with an atypical Cx. The Long LAD (LAD_L) takes off from the RCA at acute angle, has an intraseptal course and emerges in the AIVS; it also gives off a branch for the right ventricle (RVB). The vessels originating from the aortic sinus #2 enter the proximal AIVS and gives off a diagonal branch (D_1); it then makes a wide loop from the convexity of which arises the first septa branch (S). This winding vessel can therefore be called a short LAD. After emitting the septal branch, the artery turns back to occupy the left coronary sulcus as a normal Cx; however, it terminates early as a left ventricular (obtuse marginal) branch. As in other cases depicting rare or "atypical" anomalies, it is difficult to define clearly the individual arterial branches; not only is the proximal tract of the arterial trunk altered, but also the middle and even distal segments.

- Meandering coronary arteries/coronary tortuosity (Zegers et al. 2007). Excessive tortuosity of the coronary arteries can lead to diminished pressure and flow distal to the redundant segment and potentially precipitate ischemia. On the other hand, long-term cyclic flexion of the coronary arteries can predispose to accelerated progression of atherosclerosis.

Coronary anomalies in congenital heart disease

This topic is not part of the subject of the present chapter.

Coronary typology and dominance

This is a highly debated subject among various categories of specialists who see the distribution of the coronary trunks in different ways. The anatomist is more inclined to contemplate the epicardial distribution, unless performing a deeper dissection or using the corrosion-cast technique. The surgeon identifies only the epicardial trunks. The angiographist sees different

patterns of coronary arterial distribution but without the necessary landmarks (e.g., the exact position of the interventricular sulcus, the location of the papillary muscles, the wall thickness, the exact landmarks of the septum) or visualizing both coronary arteries at the same time. The territories corresponding to the three major coronary trunks can be readily visualized with scintigraphy or MRI, but the actual disposition of each main trunk is not readily available. Consequently, most classifications regarding coronary dominance are based on the epicardial distributions of some of the major branches, especially of the PDA (the posterior/interior interventricular branch). This is an oversimplification and has little clinical value. The corrosion-cast technique (Baroldi and Scomazzoni 1967) and the techniques of advanced, submacroscopic dissection (Muresian 2009) targeting the dependent myocardial territory of each major coronary trunk lead to a more realistic image. Not least, the findings have many more clinical implications.

For any classification it is primarily important to consider the three elementary coronary trunks and their reciprocal relationships, comprising diameter, length, global territory of distribution, and the particular regions of the heart vascularized by these branches (e.g., the papillary muscles of the mitral valve, the interventricular septum, the conduction tissue). A direct consequence is that the frequently used reporting scheme of "one-, two- or three-vessel disease" has little significance (if any); it is important to know which of the three elementary coronary trunks is the major one (by following the above-mentioned criteria) and to what degree it is affected. For example, a "one-vessel disease" of a large LAD that has a long recurrent tract up to the *crux cordis* in a patient with a short and slender RCA and Cx would be equivalent to a severe form of "three-vessel disease" in an individual with LAD, RCA, and Cx of nearly the same length and caliber.

The classification offered by Baroldi and Scomazzoni will be followed:

- Type I: right preponderance. The RCA supplies the RV and posterior septum and may distribute to the posterior LV wall. The following subtypes are described.
  - Type Iα: the RCA terminates with the PDA without giving branches to the LV. A recurrent tract of the LAD can contribute to the vascularization of the distal posterior septum (Fig. 50.60).
  - Type Iβ: the RCA terminates between the interventricular sulcus and the obtuse margin of the LV, supplying about one-half of the posterior LV (Fig. 50.61).
  - Type Iγ. The RCA terminates at the left margin of the heart and the posterior LV is almost entirely vascularized by the RCA (Fig. 50.62).
- Type II: left preponderance. The LCA supplies the entire septum and LV and may extend to the posterior wall of the RV (Fig. 50.63).
- Type III: balanced. Both the LCA and RCA contribute to the vascularization of the posterior septum. There are two PDAs originating from the RCA and Cx respectively (Fig. 50.64).

As stated above, possible variations must be taken into account. There are classical type Iγ cases, with a long RCA traveling toward the left margin of the heart, in which the LAD has a long recurrent tract reaching almost to the *crux cordis*. Moreover, the RCA has a long course but gives off slender branches near the coronary sulcus. The Cx is not visible on the posterior

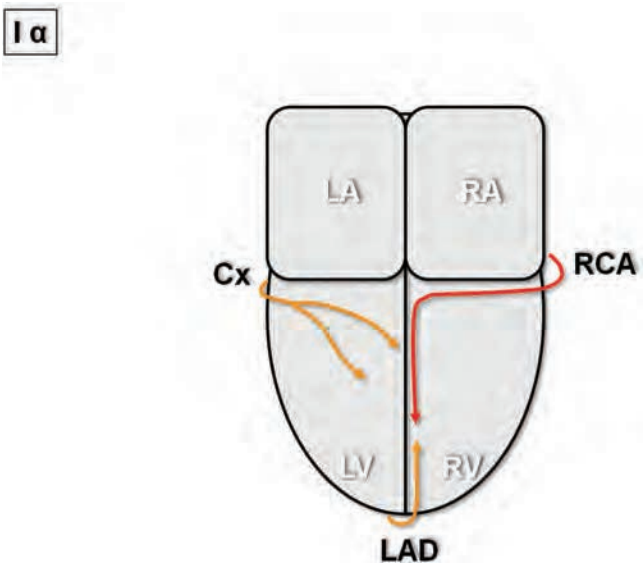

Figure 50.60 Coronary arterial typology and dominance. Posterior inferior aspect of the heart. The RCA and its branches are depicted in red. The left coronary system with the Cx and LAD (and branches) are depicted in orange. Coronary arterial typology and dominance: type Iα. Right coronary dominance. The RCA ends at the level of the inferior interventricular sulcus by giving off the PDA.

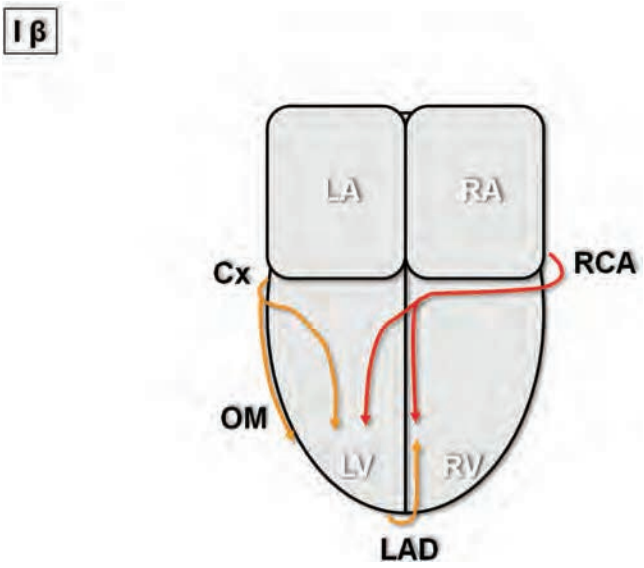

Figure 50.61 Coronary arterial typology and dominance: type Iβ. The RCA vascularizes a portion of the posterior inferior LV wall and most of the posterior septum.

aspect of the LV, but conspicuous marginal branches wind around the obtuse margin and supply most of the posterior LV (Fig. 50.65). This is an example of an apparent "extreme right preponderance." The entire septum and the LV (including the posterior papillary muscle of the mitral valve) are vascularized by branches of the LCA (Cx and LAD).

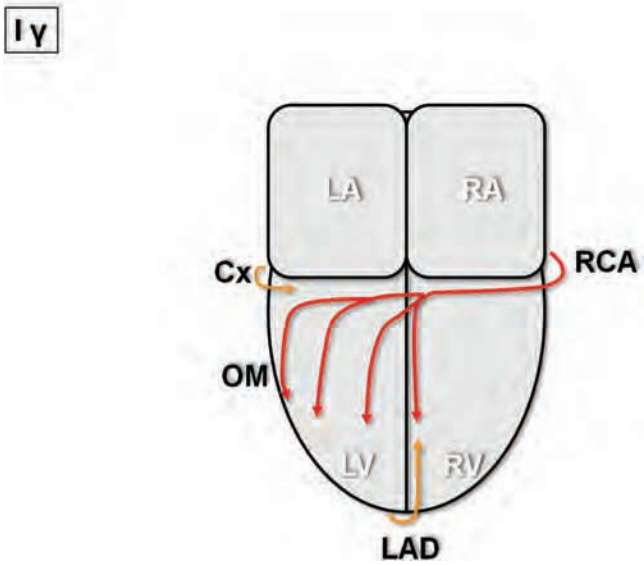

Figure 50.62 Coronary arterial typology and dominance: type Iγ. The RCA appears superdominant, as it vascularizes most of the posterior inferior LV wall.

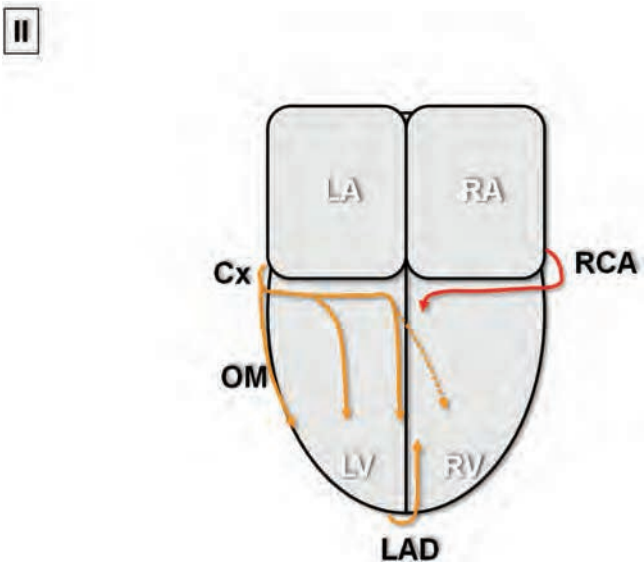

Figure 50.63 Coronary arterial typology and dominance: type II. Left coronary dominance. The Cx travels the left coronary sulcus and gives off the OM, LV posterior inferior branches of the LV, the PDA and sometimes branches to the RV. The RCA is short and slender. The LV and the entire septum are vascularized by the LCA.

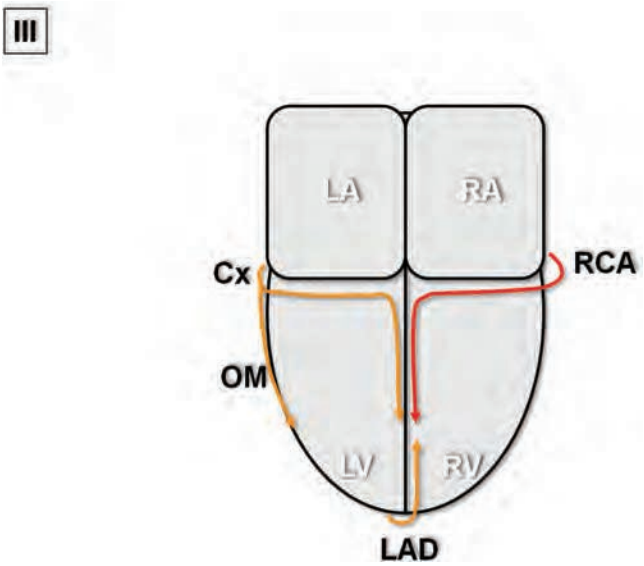

Figure 50.64 Coronary arterial typology and dominance: type III. Balanced type: both the RCA and Cx give off a PDA. The posterior septum is vascularized by branches from the left and right system. However, corrosion cast studies revealed that the participation of the RCA to the vascularization of the septum is limited to the right ventricular side of the septum in the posterior third or quarter.

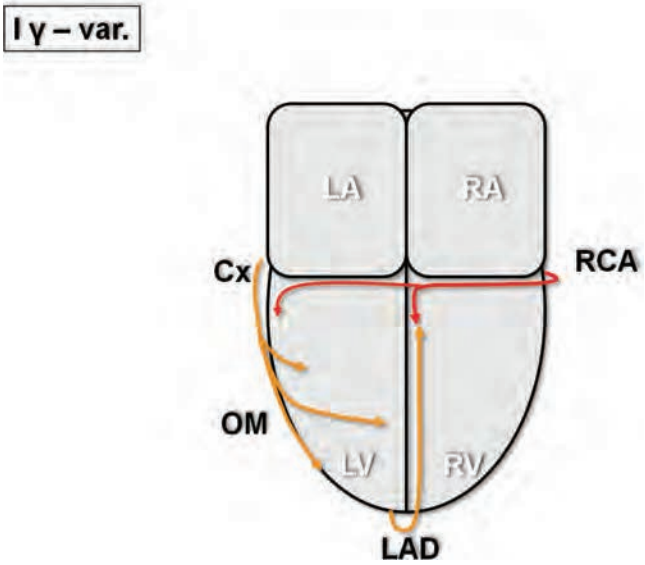

Figure 50.65 Coronary arterial typology and dominance: variation of type Iγ. The RCA travels the right and the left coronary sulcus, reaching the obtuse margin of the heart (as in type Iγ in Fig. 50.62). In this particular case the LAD depicts a long recurrent course, reaching the crux cordis. Consequently, the entire septum is vascularized by the LAD. Moreover, although not reaching the posterior aspect of the heart, the Cx gives off a conspicuous OM and posterior LV branches (with an oblique disposition over the LV). The territory of vascularization of the RCA is limited to the area in the neighborhood of the coronary sulcus. The LV, including the posterior papillary muscle group of the mitral valve and the septum, are vascularized by the left coronary system. Consequently, this represents only an apparent right coronary dominance.

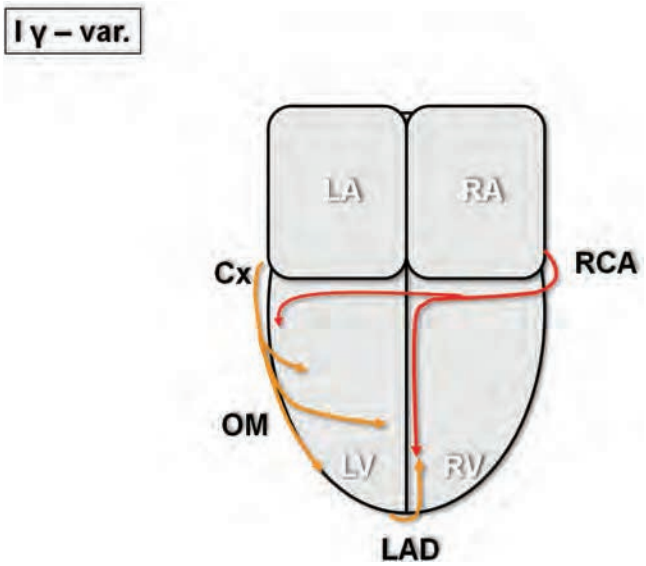

Figure 50.66 Coronary arterial typology and dominance: variation of type Iγ. There is the same disposition of the Cx branch; the RCA again reaches the obtuse margin of the LV. In this particular case, the LAD is shorter and terminates at the level of the apex. The PDA with RCA origin vascularizes most of the posterior part of the septum. However, even in this case the major portions of the posterior LV wall (including the posterior papillary muscle group of the mitral valve) are vascularized by the left coronary system.

The same condition as above but with a short LAD, terminating at the apex and with a similar disposition of the Cx and its branches, is also presented (Fig. 50.66). In this case most of the posterior LV is vascularized by the LCA, but the posterior septum and part of the posterior papillary muscle of the mitral valve are vascularized by the RCA.

The classification algorithm focuses mainly on the posterior distribution of the coronary branches, but it is also important not to overlook the distribution to the remaining cardiac areas. Diagonal and marginal branches can each have large and important territories of vascularization (including the anterolateral papillary muscle of the mitral valve). The right ventricular branches can also have larger territories (e.g., a large conus artery or a "third coronary"). The atrial branches and the artery for the sinus node, the artery supplying the atrioventricular node, etc. all represent all significant elements that should complete the picture of the coronary typology. This remains a subject for future investigations (in both clinical and experimental settings).

The conus artery (the right accessory artery; the adipose artery of Vieussens; "the third coronary artery") is an arterial branch belonging to the right coronary system and is present in 23–51% of cases (Baroldi and Scomazzoni 1967). It can originate from the proximal tract of the RCA or from aortic sinus #1 (right), either sharing a common ostium with the RCA or arising from a separate one (Fig. 50.67). This vessel supplies the anterior wall of the right ventricle, usually terminating at the level of the AIVS and thus offering a collateral route between the left and right coronary systems. Variations in the distribution pattern and territory of the conus artery are frequent (Edwards et al. 1981). Some authors have called this artery "the third coronary artery," although it should be considered only as the first anterior branch of the RCA, sometimes with an independent origin. The term "third coronary artery" should be reserved for rarer cases in which a more conspicuous artery with separate origin in sinus #1 (Uyan et al. 2003; Koteshwara et al. 2012) vascularizes most of the anterior RV wall and gives off one or more arteries of the conus (Fig. 50.68). Consequently, the various statistics are difficult to compare; some authorities include only the latter case under the term "third coronary artery," while others use it to denote all cases with a distinct conus artery (irrespective of its epicardial length and diameter).

When comparing the diameters of the RCA and LCA at the origin, and when evaluating coronary dominance, awareness of the possible existence of a conus or "third coronary" artery is important.

Extracardiac circulation

There are two types of coronary collaterals arteries: the endomural-forming anastomoses between the epicardial arteries; and the extracardiac. The extracardiac coronary arterial anastomoses have received little attention however, despite being known to exist in the setting of multiple diseases and having been demonstrated in normal individuals regardless of their age (Loukas et al. 2011). These extracardiac anastomoses usually take origin either from the bronchial arteries, or from the internal thoracic arteries, the latter arrangement described by von Haller as long ago as 1803. These anastomoses can also develop from other arteries adjacent to the heart (Loukas et al. 2011). The typical anastomoses include: bronchial arteries and the atrial branches of the coronary arteries; right internal thoracic artery and the right coronary artery; left internal thoracic artery; and the anterior interventricular artery.

In view of the increased reporting of coronary anomalies (in type as well as number), very few percentages regarding the frequency of particular CAAs have been offered in this chapter. The aim of this presentation is to help the physician be aware of each known coronary anomaly or variation, irrespective of its frequency. Needless to say, with the advent of new diagnostic techniques besides angiography, the statistics regarding CAAs are continually changing.

The text and the illustrations were conceived to offer a basic understanding of the anatomical dispositions of altered coronary patterns and to endow the reader with a comprehensive guide pertaining to pathophysiological mechanisms, the alleged or established consequences, and the clinical significance of the CAAs. Not least, some principles of therapy have been added.

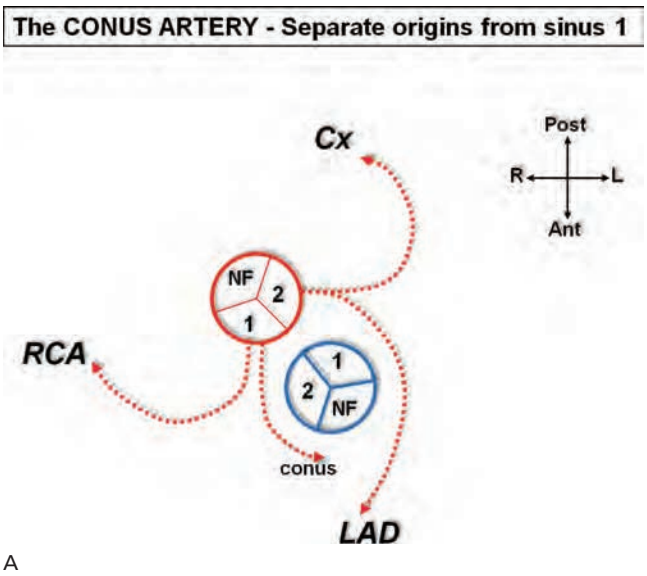

A

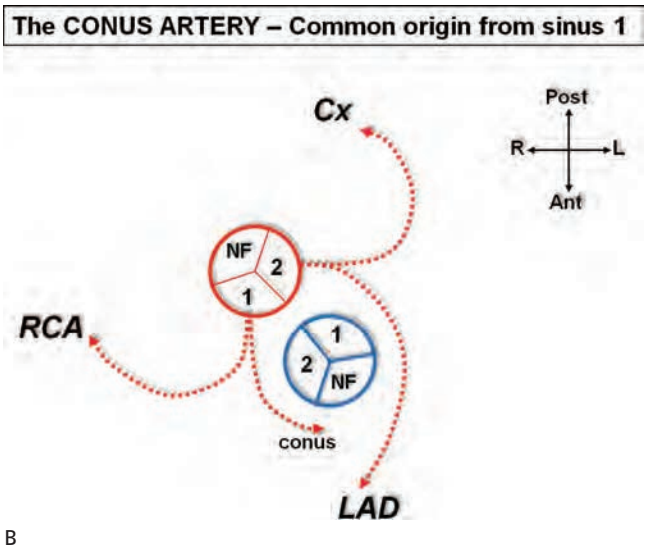

B

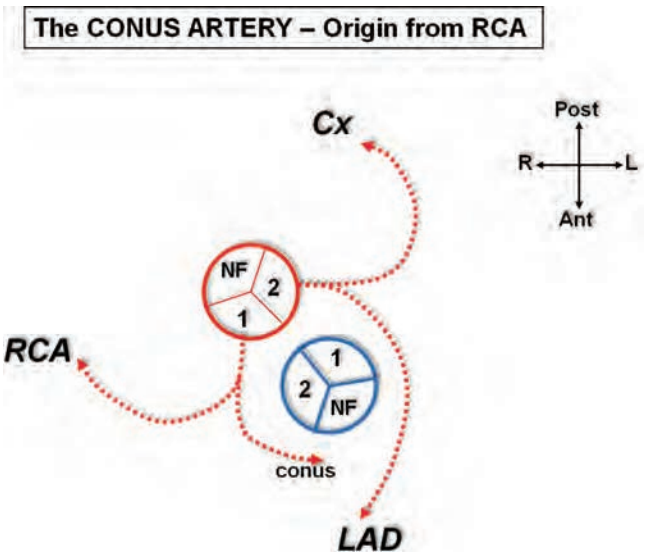

C

Figure 50.67 Variations of origination of the conus artery: (a) the conus artery has separate origin in the right aortic sinus (sinus #1); (b) the conus artery and the RCA share a common ostium in sinus #1; and (c) the conus artery arises from the proximal portion of the RCA.

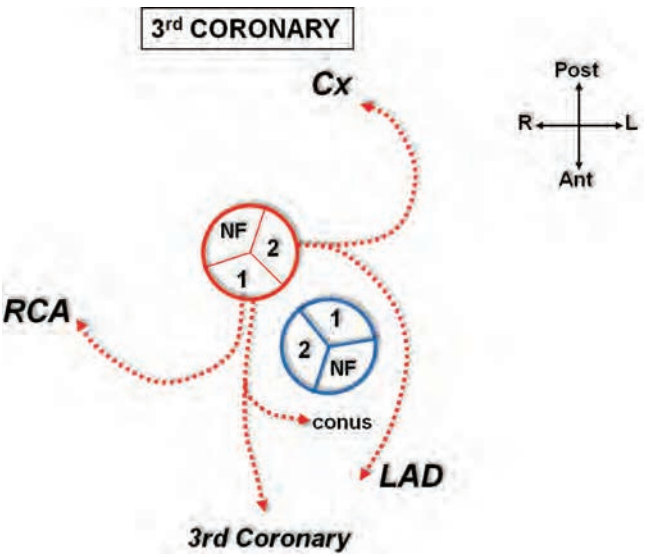

Figure 50.68 The third coronary artery. A more conspicuous artery with origin in sinus #1 gives off the conus artery and proceeds over the surface of the RV, vascularizing a great area of its anterior wall. The term "third coronary artery" should be applied only in such cases.

List of abbreviations

ACAOS: abnormal coronary artery (origin) from the opposite (aortic) sinus
ACxPA: abnormal circumflex from the pulmonary artery
ACV: anterior cardiac vein(s)
AIV: anterior interventricular vein
AIVS: anterior interventricular sulcus
AL: anterolateral papillary muscle of the mitral valve
ALADPA: abnormal LAD from the pulmonary artery
ALCAPA: abnormal left coronary artery from the pulmonary artery
AML: anterior mitral leaflet
Ao: aortic root
AOCAP: abnormal origin of both coronaries from the pulmonary trunk
APOC: abnormal pulmonary origin of the coronaries
ARCAPA: abnormal right coronary artery from the pulmonary artery
ATO-Cx: acute take-off of the circumflex branch
AVN: atrioventricular node
CAA: coronary artery anomalies and variations
CALM: congenital atresia/absence of the left main
CAn: coronary aneurysm and ectasia
CAVF: coronary arteriovenous fistula
COSA: congenital coronary ostial stenosis or atresia
CS: coronary sinus
CVS: coronary (cardiac) venous system
Cx: circumflex branch of the left coronary artery
$D_{1,2}$ etc.: diagonal branches of the LAD
D_{RV}: diagonal branch of the right ventricle
FO: fossa ovalis
GCV: great cardiac vein
IIV: inferior interventricular vein (middle cardiac vein)
IVC: inferior vena cava
LA: left atriu
LAA: left atrial appendage
LAD: left anterior descending artery (the correct term is anterior interventricular branch)
LAD_L: long LAD (in cases with dual LAD)
LAD_S: short LAD (in cases with dual LAD)
LCA: left coronary artery ("left main trunk")
L-COSA: congenital coronary ostial stenosis or atresia of the left coronary artery
LMV: left marginal vein (vein of the obtuse margin of the left ventricle)
LPA: left pulmonary artery
LPV: left posterior vein (posterior vein of the left ventricle)
LV: left ventricle
MB: myocardial bridging/muscular bridging
M-CVS: major cardiac venous system
m-CVS: minor cardiac venous system
OV: oblique vein of the left atrium (Marshall)
PDA: posterior descending artery (the correct term is inferior interventricular artery)
PL: posterior (posteromedial) papillary muscle of the mitral valve
PT: pulmonary trunk
R-COSA: congenital coronary ostial stenosis or atresia of the right coronary artery
RI: ramus intermedius (intermediate branch of the left coronary artery)
RMV: right marginal vein (vein of the acute margin of the right ventricle)
RPA: right pulmonary artery
RV: right ventricle
RVOT: right ventricular outflow tract
S: septal branch (generic term)
$S_{1,2}$ etc.: septal branches (of the LAD)
SAN: sinuatrial node
SCV: small cardiac vein
SEC: subendocardial coronary course
Sinus #1: right-facing sinus (of the aortic or pulmonary root)
Sinus #2: left-facing sinus (of the aortic or pulmonary root)
SVC: superior vena cava
TA: anterior papillary muscle of the tricuspid valve
TM: medial papillary muscle group of the tricuspid valve
Tr: tricuspid valve

References

Adamo L, Adamo M. 2006. Giant single coronary artery with terminal fistulous aneurysm: a rare entity. *Heart* 92: 1419.

Alderson JD. 1972. Single coronary artery and dissecting aneurysm of ascending aorta following resection of coarctation of aorta. *Thorax* 27: 90–92.

Ali FS, Khan SA, Tai JM, Fatmi SH, Dhakam SH. 2009. Congenital absence of left circumflex artery with a dominant right coronary artery. BMJ case Rep 2009: bcr08.2008.0772 doi: 10.1136/bcr.08.2008.0772.

Al-Mohaissen M, Heilbron B, Leipsic J, Ignaszewski A. 2010. Anomalous origin of the entire coronary system by three separate ostia within the right coronary sinus – a rarely observed coronary anomaly. *Can J Cardiol* 26: e206–e208.

Amaral F, Tanamati C, Granzotti JA, Haddad JL, LeiteJ R, Barbero-Marcial M. 2000. Congenital atresia of the ostium of the left coronary artery. Diagnostic difficulty and successful surgical revascularization in two patients. *Arquivos Brasileiros de Cardiologia* 74: 339–342.

Andrade JG, Heilbron BG, Leipsic JA. 2010. Intracavitary right coronary artery. *Can J Cardiol* 26: 211–212.

Andreou AY, Ioannides MA, Avraamides PC, Georgiou GM. 2009. Aberrant right coronary artery origin from aortic sinus with interarterial course manifesting acute myocardial infarction. *Exp Clin Cardiol* 14: 50–52.

Angelini P. 2002. Coronary artery anomalies – current clinical issues. *Tex Heart Inst J* 29: 271–278.

Angelini P. 2007. Coronary artery anomalies: an entity in search of an identity. *Circulation* 115: 1296–1305.

Angelini P. 2009. Anomalous origin of the left coronary artery from the opposite sinus lf Valsalva. Typical and atypical features. *Tex heart Instit J* 36: 313–315.

Angelini P. 2012. Congenital coronary artery ostial disease. A spectrum of anatomic variants with different pathophysiologies and prognoses. *Tex Heart Instit J* 39: 5509.

Angelini P, Villason S, Chan AV, Diez JG. 1999. Normal and anomalous coronary arteries in humans. In: *Coronary Artery Anomalies. A Comprehensive Approach* (eds AngeliniP, FairchildVD). Philadelphia: Lippincott Williams and Wilkins.

Angelini P, Trujillo A, Sawaya F, Lee V-V. 2008a. "Acute Takeoff" of the circumflex artery. A newly recognized coronary anatomic variant with potential clinical consequences. *Tex Heart Instit J* 35: 28–31.

Angelini P, Walmsley RP, Liberos A, Ott DA. 2008b. Symptomatic anomalous origination of the left coronary artery from the opposite sinus of Valsalva. Clinical presentations, diagnosis, surgical repair. *Tex Heart Instit J* 33: 171–179.

Baroldi G, Scomazzoni G. 1967. The normal coronary arterial anastomotic circulation, and: Coronary typology. In: *Coronary Circulation in the Normal and the Pathologic Heart*. Office of the Surgeon General. Department of the Army. Washington DC. p. 47–58 and p. 35–46.

Berman AD, Kim D, Baim DS. 1990. Woven right coronary artery: Case report and therapeutic implications. *Cathet Cardiovasc Diagn* 21: 258–259.

Blackman MS, Schneider B, Sondheimer HM. 1981. Absent left main coronary artery in association with pulmonary atresia. *Br Heart J* 46: 449–451.

Bogers AJ, Gittenberger-de Groot AC, Poelmann RE, Peault BM, Huysmans HA. 1989. Development of the origin of the coronary arteries, a matter of ingrowth or outgrowth? *Anat Embryol (Berl)* 180: 437–441.

Braat HJM. 2007. A coronary anomaly. *Netherlands Heart J* 15: 267–268.

Bush HS, Nolan J, Shen MHY. 2005. Use of CT angiography for evaluation of 3 coronary ostia originating from the right sinus of Valsalva in a patient with hypertrophic obstructive cardiomyopathy. *Tex heart Instit J* 32: 246–247.

Canga Y, Guvenc TS, Ilhan E, Satilmis S, Altay S, Karatas MB, Durmus G, Hasdemir H. 2010. Providing insights into atherosclerosis: a case of multivessel coronary artery disease with an anomalous straightforward vessel spared from atherosclerosis. *Int J angiol* 19: e91–e93.

Chen KJ, Teefy P, Kiaii B, Vezina WC, Chu MWA. 2010. Roboti coronary artery bypass for aberrant right coronary artery stenosis. *Can J Cardiol* 26: e326–e327.

Cijan A, Zorc-Pleskovic R, Zorc M, Klokocovnik T. 2000. Local pulmonary malformation caused by bilateral coronary artery and bronchial artery fistulae to the left pulmonary artery in a patient with coronary artery disease. *Tex Heart Instit J* 27: 390–394.

Clauss SB, Walker DL, Kirby ML, Schimel D, Lo CW. 2006. Patterning of coronary arteries in wildtype and connexin43 knockout mice. *Dev Dyn* 235: 2786–2794.

Cristopher J, Duraikannu C. 2011. Case report: intra-atrial course of right coronary artery: evaluation by dual-source CT. *Indian J Radiol* 21: 57–59.

Cruz C, Mclean D, Janik M, Raggi P, Zafari AM. 2010. A rare coincidence of two coronary anomalies in an adult. Cardiology Research and Practice Volume 2010 Article ID 376067, doi: 10.4061/2010/376067.

Darwazah AK, Hussein IH, Hawari MH. 2005. Congential circumflex coronary arteriovenous fistula with aneurysmal termination in the pulmonary artery. *Tex heart Instit J* 32: 56–59.

De Luca L, Bovenzi F, De Luca I. 2004. Congenital coronary artery anomaly simulating an acute aortic dissection. *Heart* 90: e11.

De-Giorgio F, Grassi VM, Vetrugno G, Arena V. 2013. Sudden death in a young female with an under-recognised coronary anomaly. *Diagnostic Pathology* 8(41), doi: 10.1186/1746-1596-8-41.

Dodge-Khatami A, Mavroudis C, Backer CL. 2000. Congenital heart surgery nomenclature and database project: anomalies of the coronary arteries. *Ann Thorac Surg* 69: S270–S297.

Durán AC, Sans-Coma V, Cardo M, Arqué JM. 1991. The blood supply to the interventricular septum of the heart in Soricoidea (Mammalia). *Zool Anz* 227: 279–285.

Durán AC, Fernández-Gallego T, Fernández B, Fernández MC, Arqué JM, Sans-Coma V. 2005. Solitary coronary ostium in the aorta of Syrian hamsters. A morphological study of 130 cases. *Cardiovasc Pathol* 14: 303–311.

Durán AC, Arqué JM, Fernández B, Fernández MC, Fernández-Gallego T, Sans-Coma V. 2007. Separate origin of the main components of the left coronary artery in Syrian hamsters (Mesocricetus auratus). *J Vet Med A Physiol Pathol Clin Med* 54: 297–301.

Duran NE, Duran I, Aykan AC. 2008. Congential anomalous origin of the left main coronary artery from the innominate artery in a 73-year-old woman. *Can J Cardiol* 24: e108.

Edwards BS, Edwards WD, Edwards JE. 1981. Aortic origin of conus artery. Evidence of postnatal coronary development. *Br Heart J* 45: 555–558.

Endoh R, Maruyama T, Akahana K, Kolke S, Sasaki Y, Furuta S, Homma T. 1990. Coronary artery fistula with left or right ventricular communication and sinus-node dysfunction. *Tex heart Instit J* 17: 51–55.

Fernandez B, Duran AC, Fernandez C, Fernandez-Gallego T, Icardo JM, Sans-Coma V. 2008. The coronary arteries of the C57BL/6 mouse strains: implications for comparison with mutant models. *J Anat* 212: 12–18.

Freedom RM, Harrington DP. 1974. Contributions of intramyocardial sinusoids in pulmonary atresia and intact ventricular septum to a right-sided circular shunt. *Br Heart J* 36: 1061–1065.

Galbraith AJ, Werner D, Cutforth RH. 1981. Fistula between left coronary artery and superior vena cava. *Br Heart J* 46: 99–100.

Gaudino M, Anselmi A, Lombardo A, Marano R, Possati G. 2011. Giant coronary sinus aneurysm secondary to right coronary arteriovenous fistula leading to pseudo-mitral stenosis. *Arch Med Sci* 3: 533–535.

Gebauer R, Cerny S, Vojtovic P, Tax P. 2008. Congenital atresia of the left coronary artery: myocardial revascularization in two children. *Interact Cardiovasc Thorac Surg* 7: 1174–1175.

Gittenberger-de Groot AC, Sauer U, Oppenheimer-Dekker A, Quagebeur J. 1983. Coronary arterial anatomy in transposition of the great arteries: a morphological study. *Pediatr Cardiol* 4: 15–24.

Groothuis JGJ, Appelman YE, Meijerink MR, van Rossum AC. 2011. Coronary anomaly diagnosed by computed tomography coronary angiography in a patient with atypical chest pain. *Neth Heart J* 19: 93–94.

Guo J, Xu M. 2012. Congenital absence of the left circumflex artery associated with inferior myocardial infarction. *Intern Med* 51: 71–74.

Ho JS, Strickman NE. 2002. Anomalous origin of the right coronary artery from the left coronary sinus. Case report and literature review. *Tex Heart Instit J* 27: 37–39.

Hongsakul K, Suwannanon R. 2012. Congenital absence of the left circumflex artery detected by computed tomography coronary angiography: a case report. Case Reports in Vascular Medicine. Hindaqi Publishing Corporation Volume 2012, Article ID 204657, doi: 10.1155/2012/204657.

Hosseinpour AR, Anderson RH, Ho YS. 2001. The anatomy of the septal perforating arteries in normal and congenitally malformed hearts. *J Thorac Cardiovasc Surg* 121: 1046–1052.

Ippisch HM, Kimball TR. 2010. Anomalous origin of the right coronary artery from the left ventricle. *J Am Soc Echocardiogr* 23: 222.e1.

Ishikawa T, Otsuka T, Suzuki T. 1990. Anomalous origin of the left main coronary artery from the noncoronary sinus of Valsalva. *Pediatr Cardiol* 11: 173.

Jin S-A, Seong S-W, Kim SS, Lee YD, Choi UL, Choi S-W, Jeong J-O. 2012. Successful percutaneous coronary intervention in an anomalous origin of the right coronary artery from the ascending aorta above the left sinus of Valsalva. *Korean Circ J* 42: 497–500.

Jung Y, Kim H-J, Yoon C-H. 2012. Severe form of persistent Thebesian veins presenting as ischemic heart disease. *Korean Circ J* 42: 714–717.

Kawashima T, Sasaki H. 2003. The morphological significance of the human sinuatrial nodal branch. *Heart Vessels* 18: 213–219.

Kaya D, Kilit C, Onrat E. 2006. An uncommon congenital anomaly of coronary arteries misdiagnosed as intracoronary thrombus: Woven coronary artery disease. *Anadolu Kardiyol Derg* 6: 383–384.

Keeton BR, Keenan JM, Monro JL. 1983. Anomalous origin of both coronary arteries from the pulmonary trunk. *Br Heart J* 49: 397–399.

Kim M-J, Kwon H-Y, Hwang C-S, Kang J-H, Kim H-J, Kim S-M, Lee G-H, Kim T-I, Cho K-I. 2011. Dual fistulas of ascending aorta and coronary artery to pulmonary artery. *Korea Circ J* 41: 213–216.

Korosoglu G, Ringwald G, Giannitsis E, Katus HA. 2008. Anomalous origin of the left circumflex coronary artery from the pulmonary artery. A very rare congenital anomaly in an adult patient diagnosed by cardiovascular magnetic resonance. *J Cardiovasc Mag Res* 10: 4, doi: 10.1186/1532-429X-10-4.

Koteshwara P, Smiti S, Binu TR, Padmakumar RP. 2012. A rare coronary artery anomaly: duplication of right coronary artery with separate ostium on 64-row multidetector computed tomography. *Singapore Med J* 53: e125

Kwoon SH, OH JH, Hwang S-J, Kim SJ, Kim MG, Kim KS. 2010. Bilateral coronary artery fistulae to main pulmonary artery. *Tex heart Instit J* 37: 127–128.

La Vecchia L, Favero L, Fontanelli A. 2002. Anomalous origin of left anterior descending and circumflex artery from two separate ostia in the right aortic sinus. *Heart* 88: 322.

Lauer B, Thiele H, Schuler G. 2001. A new coronary anomaly: origin of the right coronary artery below the aotic valve. *Heart* 85: 486.

Lee AS, Huang CL, Shyu MY. 2012a. Ventricular fibrillation during coronary angiography in a patient with left dominant coronary artery ectasia. *Exp Clin Cardiol* 17: 79–80.

Lee D-Y, Park S-H, Bae MH, Lee JH, Yang DH, Park H-S, Cho Y, Chae S-C, Jun J-E. 2012b. Multiple fistula emptying into the left ventricle through the entire left ventricular wall. *J Cardiovasc Ultrasound* 20: 108–111.

Lee JJ, Kim D-H, Byun S-S, Choi W-G, Lee C-W, Yi S-M, Kwan J, Park K-S, Lee W-H. 2009. A case of acute myocardial infarction with the anomalous origin of the right coronary artery from the ascending aorta above the left sinus of Valsalva and left coronary artery from the posterior sinus of Valsalva. *Yonsei Med J* l50: 164–168.

Lee Y, Lim Y-H, Shin J, Kim K-S. 2012c. A case report of type VI dual left anterior descending coronary artery anomaly presenting with non-ST segment elevation myocardial infarction. *BMC Cardiovascular Disorders* 12: 101. Available at: http://www.biomedcentral.com/1471-2261/12/101 (accessed 27 October 2015).

Leitch AG, Caves PK. 1975. A case of Marfan's syndrome with absent right coronary artery complicated by aortic dissection and right ventricular infarction. *Thorax* 30: 352–354.

Liesting C, Brugts JJ, Kofflard MJM, Dirkali A. 2012. Acute coronary syndrome in patient with a single coronary artery arising from the right sinus of Valsalva. *World J Cardiol* 4: 264–266.

Loukas M, Bilinsky S, Bilinsky E, Matusz P, Anderson RH. 2009a. The clinical anatomy of the coronary circulation. *Clin Anat* 22: 146–160.

Loukas M, Groat C, Khangura R, Owens DG. Anderson RH. 2009b. The normal and abnormal anatomy of the coronary arteries. *Clin Anat* 22: 114–128.

Loukas M, Hanna M, Chen J, Tubbs RS, Anderson RH. 2011. Extracardiac coronary arterial anastomosis. *Clin Anat* 24: 137–142.

Maroney J, Klein LW. 2012. Report of a new anomaly of the left anterior descending artery: Type VI dual LAD. *Cathet Cardiovasc Interv* 80: 626–629.

McAlpine WA. 1975. *Heart and Coronary Arteries*. Berlin, Heidlberg, New York: Springer-Verlag.

McGarry KMJ, Stark J, Macartney FJ. 1981. Congenital fistula between left ventricle and coronary sinus. *Br Heart J* 45: 101.

Mihl C, Alzand BSN, Winkens MH. 2010. A rare coronary anomaly: one ostium fits all. *Cardiol Res Pract* 2010 pii: 476760.

Moosa YA, Peniston RL, Lewis JF, Lowery RC, Curry CL. 1988. Anomalous coronary artery originating from the left anterior descending artery and ending in a blind aneurysm. *J Natl Med Assoc* 80: 1139–1142.

Moreno-Martinez FL, Aladro-Miranda IF, Ibargolin-Hernandez RS, Vega-Fleites LF, Nodarse-Valdivia JR, Lara-Perez NR, Aguero-Sanchez A, Gonzalez-Chinea R. 2012. Angioplastia de circunfleja en paciente con doble arteria desecendente anterior tipo IV. Propuesta para actualizar la classificacion de Spindola-Franco. *Arch Cardiol Mex* 82: 297–302.

Muresian H. 2001. The vascularization of the pulmonary infundibulum (Abstract). Verhandlungen der Anatomischen Gesellschaft Muenster 2001. *Ann Anat* 183: S125–126.

Muresian H. 2006. The Ross procedure: new insights into the surgical anatomy. *Ann Thorac Surg* 81: 495–501.

Muresian H. 2009. *The Clinical Anatomy of the Coronary Arteries. An Anatomical Study on 100 Human Heart Specimens*. Bucharest: Editura Enciclopedica.

Ochos-Ramirez E, Valdez-Garza HE, Reyes-Gonzalez R, Matteos-Corral D, Sanchez-Sigel D, Gonzalez-Lopez V. 2005. Double anomalous coronary origin from the pulmonary artery. Successful surgical correction in an infant. *Tex Heart Instit J* 32: 348–350.

Pascual DA, Soria F, Valdes M. 1999. Unusual congenital coronary anomaly and myocaridal ischemia. *Heart* 82: e7.

Pirelli L, Yu P-J, Srichai MB, Khvilivitzky K, Angelini P, Grau JB. 2008. Ectopic origin of left coronary ostium from left ventricle, with occlusive membrane. A previously unreported anomaly with an embryologic interpretation. *Tex Heart Instit J* 35: 162–165.

Plastiral SC, Kampessi O, Gotzmanidou M, Kastanis P. 2008. Anomalous origin of the left circumflex artery from the right coronary artery: a case report. *Cases Journal I*: 336 doi: 10.1186/1757-1626-1-336.

Probst P, Pachinger O, Koller H, Niderberger M, Kaindl F. 1976. Origin of anterior descending branch of left coronary artery from pulmonary trunk. *Br Heart J* 38: 523–325.

Ramsdale DR, Lowe R, Hamilton M. 2005. Ectopic right coronary artery with anomalous left circumflex artery. *Heart* 2005, doi: 10.1136/hrt.2005.075796.

Roberts WC, Glick BN. 1992. Congenital hypoplasia of both right and left circumflex coronary arteries. *Am J Cardiol* 170: 121–123.

Rosamond T, Wetzel LH, Lakkireddy D, Ferrell R, Tadros P. 2007. Intracameral right coronary artery: detection by 64 slice coronary computed tomographic angiography and implications for radiofrequency ablation of atrial dysarhythmias. *Pacing Clin Electrophysiol* 30: 1571–1574.

Rosenthal RL, Carrothers IA, Schussler JM. 2012. Benign or malignant anomaly? Very high takeoff of the left main coronary artery above the left coronary sinus. *Tex Heart Instit J* 39: 538–541.

Said SAM. 2010. Congenital solitary fistulas characterized by their drainage sites. *World J Cardiol* 26: 6–12.

Said SAM, Nijhuis RLG, op den Akker JW, Kimman GP, Van Houwelingen KG, Gerrits D, Huisman AB, Slart RHJA, Nicastia DM, Koomen EM, Tans AC, Al-Windy NYY, Sonker U, Slagbloom T, Pronk AC. 2011. Diagnostic and therapeutic approach of congenital solitary coronary artery fistulas in adults; Dutch case series and review of literature. *Neth Heart J* 19: 183–191.

Sane DC, Vidaillet JH. 1988. "Woven" right coronary artery: A previous undescribed congenital anomaly. *Am J Cardiol* 61: 1158.

Santucci PA, Bredikis AJ, Kavinsky CJ, Klein LW. 2001. Congenital origin of the left main coronary artery from the innominate artery in a 37-year-old man with syncope and right ventricular dysplasia. *Catheter Cardiovasc Interv* 52: 378–381.

Sawaya FJ, Sawaya JI, Angelini P. 2008. Split right coronary artery. Its definition and its territory. *Tex Heart Instit J* 35: 477–480.

Schanzenbacher P, Strotmann J. 2002. Bilateral origin of a split left anterior descending coronary artery combined with atypical branching of the left circumflex artery. *Heart* 88: 70.

Scheffel H, Vetter W, Alkadhi H. 2007. Intra-atrial course of the right coronary artery: a previously missed anomaly. *Eur Heart J* 28: 1919.

Selcoki Y, Er O, Eryonucu B. 2009. Coexistence of myocardial infarction with normal coronary arteries and a left circumflex artery anomaly originating from the right coronary artery with a bridge in the left anterior descending artery. *Clinics* 64: 707–710.

Selcoki Y, Yilmaz OC, Er O, Eryonucu B. 2010. Double right coronary artery: a report of two cases. *Clinics* 65: 449–451.

Shaher RM, Puddu GC. 1966. Coronary arterial anatomy in complete transposition of the great vessels. *Am J Cardiol* 17: 355–361.

Shen TC, Chou HH, Tsai KT. 2012. Ectopic and atretic ostium of left main coronary artery from interleaflet triangle between left and noncoronary cusps. *Tex Heart Instit J* 39: 60–62.

Shirani J, Roberts WC. 1993. Solitary coronary ostium in the aorta in the absence of other major congenital cardiovascular anomalies. *J Am Coll Cardiol* 21: 137.

Sim DS, Jeong MH, Choi S et al. 2009. Myocardial infarction in a young man due to a hypoplastic coronary artery. *Korean Circ J* 39: 163–167.

Singh C, Singh H, Kumar A, Banerji AK, Aggarwal N, Bharadwaj P. 2005. Congenital atresia of left main coronary artery. *Indian Heart J* 57: 255–257.

Slim A, Thurlow J, Blevins J, Martinho S, Markelz B. 2009. Discovery of a symptomatic left anomalous coronary artery from the opposite sinus and postoperative considerations. Hindawi Pulbishing Corporation. Case Reports in Medicina Vol 2009, Article ID 509063, doi: 10.1155/2009/509064.

Sodian R, Rassoulian D, Beiras-Fernandez A, Loeff M, Schmitz C, Reichart B, Daebritz S.2008. ALCAPA with the ectopic oriffice at the non-facing sinus. Successful anatomic repair by creation of an autologous extrapulmonary tunnel. *Tex Heart Instit J* 35: 32–35.

Sohn SY, Jang GY, Choi BM. 2010. Congenital atresia of the left main coronary artery in an infant. *Univ-Sci B (Biomed & Biotechnol)* 11: 539–541.

Soylu K, Meric M, Zengin H, Yuksel S, Kaya MG. 2012. Woven right coronary artery. *J Card Surg* 27: 345–346.

Spindola-Franco H, Grose R, Solomon N. 1983. Dual left anterior descending coronary artery: angiographic description of important anatomic variants and surgical implications. *Am Heart J* 105: 445–455.

Takechi M, Yan J, Hitomi J. 2012. Rare coronary anastomoses between the aorta, pulmonary trunk, left coronary artery and subclavian artery. *Clin Anat* 25: 969–972.

Tekbas EO, Cakici M, Yuce M Alici H, Davutoglu V. 2011. Twin circumflex arteries with left sinus of Valsalva origin: a case report *Int J Angiol* 20: 101–102.

Teno LAC, Santos JLA, Bestetti RB, Zanardi AMCT, Ceccon C, Castilho OT. 1993. Congenital circumflex coronary artery fistula with drainage into the left ventricle. *Tex Heart Instit J* 20: 304–306.

Tovar E, Borsari A, Landa D, Weinstein P, Gazzamiga A. 1997. Ventriculotomy repair during revascularization of intracavitary anterior descending coronary arteries. *Ann Thor Surg* 64: 1194–1196.

Urcelay GE, Iannettoni MD, Ludomirsky A, Mosca RS, Cheatham JP, Danford DA, Bove EL. 1994. Origin of both coronary arteries from the pulmonary artery. *Circulation* 90: 2379–2384.

Uyan C, Akdemir R, Uyan AP, Erbilen E. 2003. Aberrant origin of the right ventricular coronary artery: A case report. *Exp Clin Cardiol* 8: 108–109.

Uznanska-Loch B, Plewka M, Peruga JZ, Krzeminska-Pakula M, Kasprzak JD. 2012. Non-invasive detection of concomitant coronary artery anomaly and atherosclerotic coronary disease, using transthoracic Doppler echocardiography. *Arch Med Sci* 1: 162–165.

van der Velden LBJ, Bar FWHM, Meursing BTJ, Oude Ophius TJM. 2008. A rare combination of coronary anomalies. A rare combination of coronary anomalies. *Neth Heart J* 16: 387–389.

Vesterlund T, Thomsen PEB, Hansen OK. 1985. Anomalous origin of the left coronary artery from the pulmonary artery in an adult. *Br Heart J* 54: 110–112.

Vlodaver Z, Neufeld HN, Edwards JE. (eds) 1975. Patterns of origin of coronary arteries. In: *Coronary Arterial Variations in the Normal Heart and in Congenital Heart Disease*. New York: Academic Press Inc.

Wallia I, Arora HS, Barkar EA, Delgado EA III, Frazier OH. 2010. Snake heart. A case of atavism in a human being. *Tex Heart Instit J* 37: 687–690.

Wang N, Zhang C, Zhang A, Chen B, Du F. 2012. Quadricuspid aortic valve with anomalous coronary artery. Comprehensive evaluation with multidetector computed tomography. *THIJ* 39(2): 303–305.

Winner MW, Raman SV, Sun BC, Crestanello JA. 2011. Preoperative assessment of anomalous right coronary artery arising from the main pulmonary artery. Case Reports in Medicine 2011: article 642126, doi: 10.1155/2011/642126.

Yameen M, Monali W, Jaydeepa S, Tanuj G, Arjun K. 2011. Superdominant right coronary artery with absent left circumflex artery. Biomedical Imaging and Intervention Journal 7: doi: 10.2349/biij.7.1.e2.

Yilmaz H, Demir I. 2005. Crossing epicardial coronary arteries. *Heart* 91: 1523.

Zalamea RM, Entrikin DW, Wannenburg T, Carr JJ. 2009. Anomalous intracavitary right coronary artery shown by cardiac CT: a potential hazard to be aware of before various interventions. *J Cardiovasc Comput Tomogr* 3: 57–61.

Zegers ES, Meursing BTJ, Zegers EB, Oude Ophuis AJM. 2007. Coronary tortuosity: a long and winding road. *Neth Heart J* 15: 191–195.

Zugibe FT, Zugibe FT Jr, Costello JT, Breithaupt MK. 1993. Hypoplastic coronary artery disease within the spectrum of sudden unexpected death in young and middle age adults. *Am J Forensic Med Pathol* 14: 276–283.

51 Pulmonary arteries

M. Cumhur Sivrikoz
Eskişehir Osmangazi University Medical Faculty, Eskişehir, Turkey

Main pulmonary artery

The pulmonary tract starts at the conus arteriosus of the right ventricle. Over a distance of nearly 5 cm, it moves upwards on the left side of the ascending aorta and separates into the right and left pulmonary artery branches beneath the aortic arch and in front of the left main bronchus. These separate branches proceed towards the hilum of the right and left lungs on the horizontal plane surrounded by the pericardial sac.

Right pulmonary artery

The right pulmonary artery is longer than the left and a significant portion of it lies inside the pericardial sac. In the transverse plane, it advances behind the ascending aorta and the superior vena cava, in front of the trachea, reaching the right lung hilus. The phrenic nerve lies on the lateral border of the superior vena cava and proceeds downwards; the right pulmonary artery enters the lung hilus at the point where the nerve passes through its anterior portion. When the right pulmonary artery enters the lung hilus, the right main bronchus lies posterior to it, the superior pulmonary vein anterior to it, and the azygos vein superior to it.

Left pulmonary artery

After originating at the bifurcation, the left pulmonary artery follows a transverse path in front of the left main bronchus. It is shorter than the right pulmonary artery, but the portion that lies outside the pericardial sac is longer. Anterior to the left pulmonary artery there is the superior pulmonary vein; the vagus nerve lies superior to this. The left pulmonary artery and the aortic arch are connected to each other through the ligamentum arteriosum. During fetal life there is a shunt between the pulmonary artery and the aortic arch through the ductus arteriosus contained within this ligament. After birth the shunt normally closes. However, it sometimes remains patent, leading to a clinical condition known as "patent ductus arteriosus." If it stays patent for a long period, pulmonary hypertension might develop; in such cases the shunt needs to be closed either by non-invasive means or by surgical intervention. Bech et al. (2010) reported a child with CHARGE (coloboma, congenital heart defects, choanal atresia, retardation, genital and ear anomalies) syndrome who was found to have the left subclavian artery arise from the left pulmonary artery.

As the pulmonary artery approaches the left hilus, it crosses from the anterior side of the descending aorta. When it enters the hilus, the superior pulmonary vein is at its anterior and the left main bronchus at its posterior side.

Lobar branch of pulmonary artery

The first pneumonectomy was performed by Nissen in 1931, followed by Graham in 1933. During the following years, Archibald in 1933 and Rienhoff in 1936 performed pneumonectomies by mediastinal dissection. In 1940, Blades and Kent performed the first lobectomy operation.

Resective lung surgery has been performed for more than 80 years. During this time, the diagnostic and therapeutic alternatives have diversified due to increasing numbers of invasive and non-invasive approaches. The anatomical variations of the pulmonary arterial system are of the utmost importance for the performance of diagnostic and therapeutic procedures. In this section we elaborate on the intralobar anatomies of the right and left pulmonary arteries together with their possible variations.

Right pulmonary artery

Upper lobe

The first branch of the right pulmonary artery after its entry to the hilus is called the anterior trunk, superior trunk, or upper division. The anterior trunk is the major branch for the upper lobe and is found in all patients. Together with the upper lobe bronchus it proceeds toward the lungs and, starting from the anterior of the bronchus, it passes to its lateral side and reaches the lung. During its progress toward the lungs it usually separates into two branches 1 cm from its origin. Milloy et al. (1963) reported that the anterior trunk usually originates from a single root; it originates from two different roots in 3.6% of patients. Very rarely, it can be in the form of three different branches. In 10% of patients the anterior trunk is the only branch of the pulmonary artery that goes to the upper lobe. It gives branches

Bergman's Comprehensive Encyclopedia of Human Anatomic Variation, First Edition. Edited by R. Shane Tubbs, Mohammadali M. Shoja and Marios Loukas.
© 2016 John Wiley & Sons, Inc. Published 2016 by John Wiley & Sons, Inc.

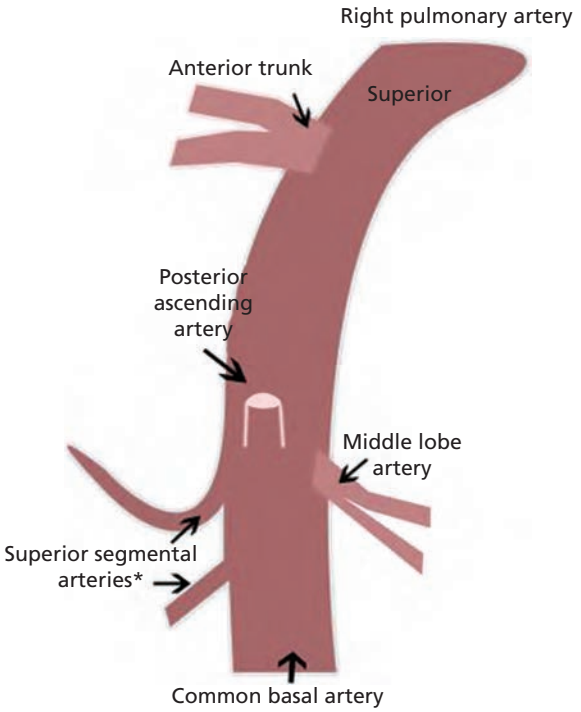

Figure 51.1 Right pulmonary artery: two separate superior segmental arteries* to the right lower lobe, but there was no posterior ascending artery to the right upper lobe.

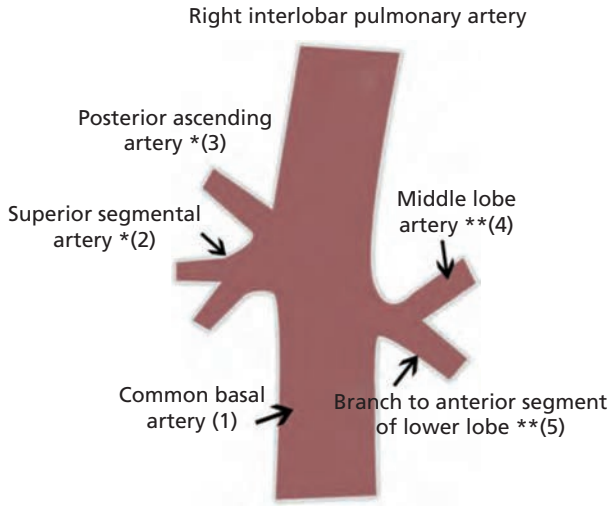

Figure 51.2 Right interlobar pulmonary artery: the posterior ascending artery of the upper lobe and the superior segmental artery of the right lower lobe originated from a common root*. The middle lobe artery and anterior segment artery of the lower lobe originated from the same stem**. 1, common basal artery; 2, superior segmental artery*; 3, posterior ascending artery*; 4, middle lobe artery**; 5, branch to anterior segment of lower lobe**.

to apical, posterior, and sometimes to anterior segments (Fig. 51.1).

After the pulmonary artery gives off its first branch, it proceeds downward on the lateral side of the intermediary bronchus that lies between the upper lobe bronchus and middle and lower lobe bronchi. This portion of the pulmonary artery is called the interlobar pulmonary artery and extends to the posterolateral aspect of the oblique fissure. At this point it divides into upper lobe, middle lobe, and lower lobe branches. The branch that goes to the upper lobe at the level of the interlobar portion is the second branch supplying the upper lobe, referred to as the ascending artery or posterior ascending artery. It originates from the posterolateral aspect of the pulmonary artery on the opposite side from the middle lobe artery. It then extends on the anterior side of the intersection of the intermediary bronchus and the upper lobe bronchus. This branch feeds the posterior segment and is of smaller caliber than the anterior trunk. According to Rice (2008), this branch is seen in 90% of patients. It occurs as a single branch in 60% of patients, a double branch in 20%, and three branches in 1%.

The posterior ascending artery usually starts from a higher level than the middle lobe artery, but in 40% of patients it starts at the same level and in 12% at a lower level.

According to Rice (2002) and Boyden and Hartman (1946), the posterior ascending artery originates from a common root with the lower lobe superior segment artery in 12% and 6–14% of patients, respectively. Cory and Valentine (1959) demonstrated that the posterior ascending artery of the upper lobe and the superior segmental artery of the right lower lobe originate from the same root in only 1.53% of cases. In our series of cases in 2011, we found this type of variation in 1.81% (Figs 51.2, 51.3).

Boyden and Hamre (1951) also reported that in 2–6% of patients the posterior ascending artery originates from a common root with the middle lobe artery.

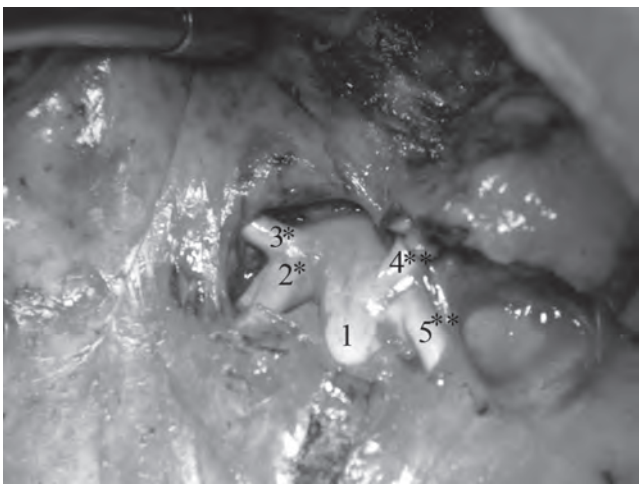

Figure 51.3 Right interlobar pulmonary artery: 1, common basal artery; 2, superior segmental artery*; 3, posterior ascending artery*; 4, middle lobe artery**; 5, branch to anterior segment of lower lobe**.

Rice (2008) reported that in 25% of patients there is an "anterior ascending artery" which feeds the anterior segment of the upper lobe. The anterior ascending artery originates from the lateral aspect of the pulmonary artery and is found at the same level as the middle lobe artery. In 99% of cases it is single, and in 1% it arises from a common root with the middle lobe artery.

Middle lobe

The middle lobe artery is the branch of the pulmonary artery supplying the middle lobe. Its starting point generally corresponds to the junction of the major and minor fissures. It originates from the anteromedial aspect of the interlobar portion of the pulmonary artery and from opposite the posterior ascending artery and lower lobe superior segment artery. The starting point of the artery is located superior to the lower lobe superior segment artery. Wragg et al. (1968) reported that the middle lobe artery was single in 46.5% of patients. In 51% it occurs as two separate branches and in 2.5% it has three branches. In our 2011 cases, the middle lobe artery and the anterior segmental artery of the lower lobe originated from the same common root in the same patient (Figs 51.2, 51.3).

A novel variation was seen in 2.85% of our right upper lobectomy patients. After originating from the interlobar portion of the artery, the medial segment of the middle lobe artery turned posterior to the back of the middle lobe bronchus (Figs 51.4, 51.5).

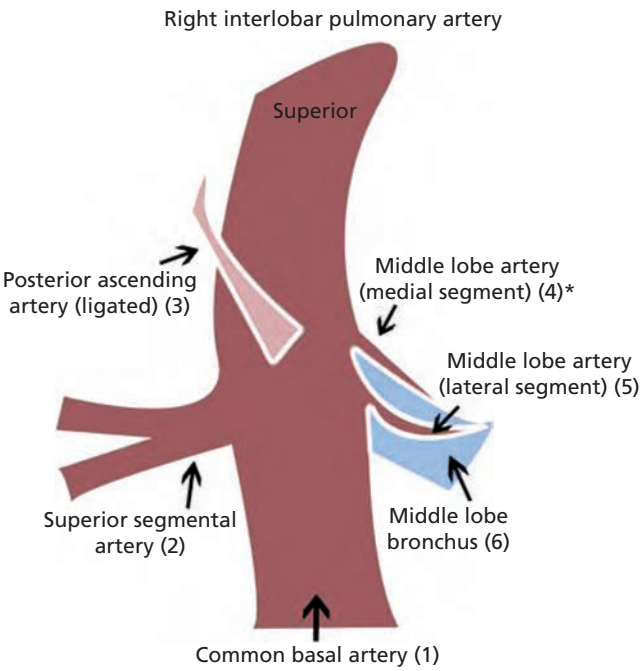

Figure 51.4 Right interlobar pulmonary artery: after originating from the interlobar portion of the artery, the medial segment of the middle lobe artery* turned posterior to the back of the middle lobe bronchus. 1, Common basal artery; 2, superior segmental artery; 3, posterior ascending artery (ligated); 4, middle lobe artery (medial segment)*; 5, middle lobe artery (lateral segment); 6, middle lobe bronchus.

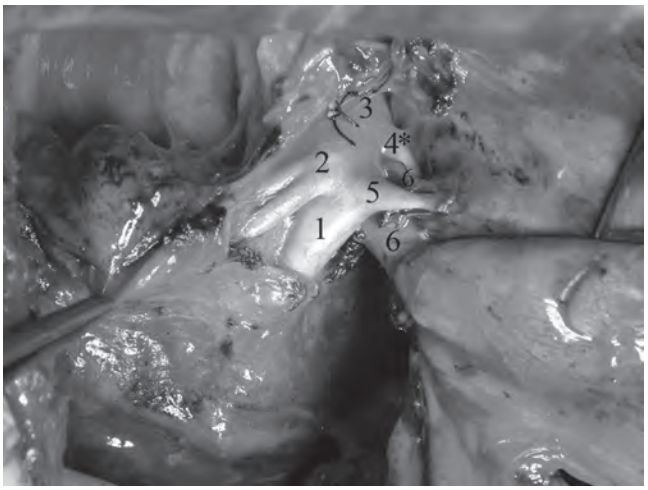

Figure 51.5 Right interlobar pulmonary artery: 1, common basal artery; 2, superior segmental artery; 3, posterior ascending artery (ligated); 4, middle lobe artery (medial segment)*; 5, middle lobe artery (lateral segment); 6, middle lobe bronchus.

Lower lobe

The first branch that the pulmonary artery extends to the lower lobe is the superior segment artery. It starts from the posterolateral aspect of the interlobar pulmonary artery and from the side opposite the middle lobe artery. In the medical literature, the starting point is at the level of the middle lobe artery or lower. In our cases in 2011, the superior segmental artery of the right lower lobe originated proximal to the middle lobe artery in 12.5% of right lower lobectomies (Fig. 51.6).

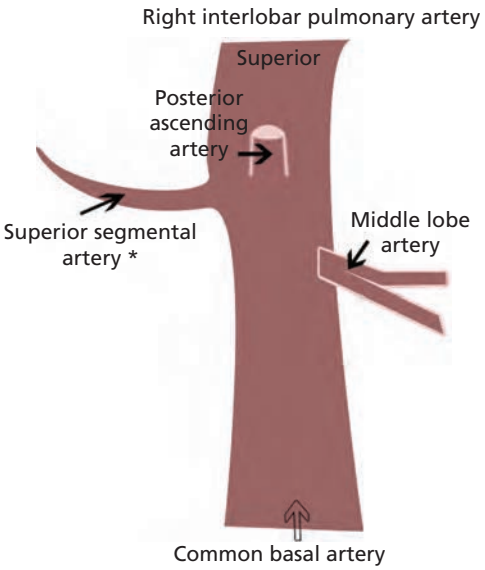

Figure 51.6 Right interlobar pulmonary artery: the superior segmental artery* of the right lower lobe originated from superior to the middle lobe artery.

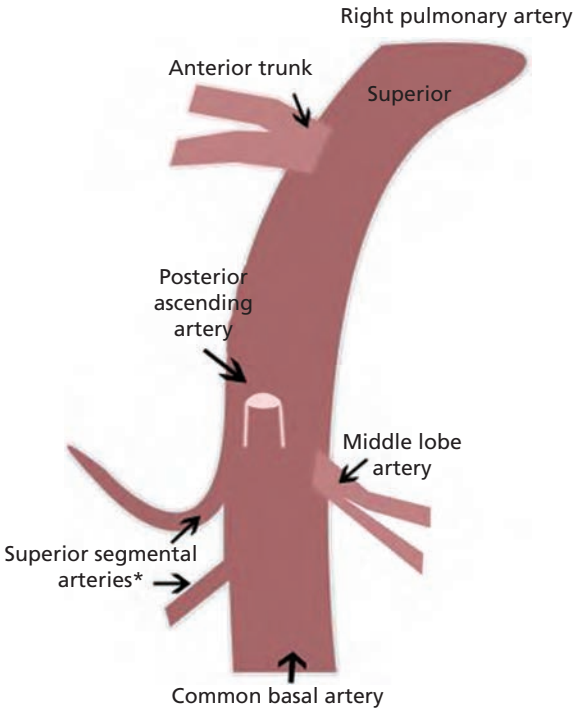

Figure 51.7 Right pulmonary artery: two separate superior segmental arteries* to the right lower lobe.

Wragg et al. (1968) reported that this artery had a single root in 78% of patients and bifurcated. In 21% there were two branches and in 1% patients there were three. Cory and Valentine (1959) explained that there were two separate superior segmental arteries in 6.97%. In our 2011 series, the incidence of two separate superior segmental arteries to the right lower lobe was 12.5% (Fig. 51.7).

According to Rice (2008), it can originate from basal segment arteries in 12–14% of patients, and in 6% it originates from the pulmonary ascending artery of the upper lobe. In one of our 2011 patients there were also two separate superior segmental arteries to the right lower lobe and there was no posterior ascending branch to the right upper lobe. Both variations were observed in the same patient (Fig. 51.1). A retrobronchial artery (of Hovelacque) has been described that is an accessory branch of the right pulmonary artery and supplies the dorsal segment of the right upper lobe. The artery has also been called the dorsal fissural artery of Cordier and Cabral and the ascending artery of the superior lobe of Appleton.

Basal segment arteries extend to the lower lobe on the posterolateral aspect of the bronchus in the form of a common basal trunk. The common basal trunk first divides into lower lobe anterior and medial segments, then feeds the posterior and lateral segments.

Left pulmonary artery

Upper lobe

After the left pulmonary artery enters the lung hilus, it gives off branches to the upper lobe after the superior, posterior, and interlobar portions. The most commonly seen pattern is three–four branches. According to Milloy et al. (1968) the left upper lobe is fed by one–seven different branches. Kent and Blades (1942a, b) reported this figure as four–seven. Boyden and Hartman (1946) stated that the upper lobe is fed by four–eight different roots. In the medical literature, three branches are seen in 46% of patients and four branches in 36%. In our 2011 cases, three branches were seen in 56.25%, four branches in 37.5%, and five segmental branches in 6.25%, entering the left upper lobe separately. Maciejewski and Kutnik (1990) demonstrated that five segmental branches penetrate the upper lobe in 19%. Cory and Valentine (1959) found this type of variation in 0.93% of cases (Fig. 51.8).

The anterior branches of the left upper lobe divide into two groups. These are the anterior trunk and posterior arterial branches. The anterior trunk is short and thick, and usually originates as separate branches from the pulmonary artery. According to Rice (2008), the anterior trunk has two branches in 70% of patients. In 1% of cases the only arterial source to the upper lobe is the anterior trunk. The first segments feed the anterior segment while it also feeds the lingula in 25% of cases.

After the pulmonary artery gives off its anterior trunk branches, it passes through the posterolateral aspect of the upper lobe bronchus and progresses downward, neighboring the bronchus. It crosses the intermediary bronchus in the interlobar region and proceeds anteriorly. In the interlobar portion of the pulmonary artery, the posterior arterial branches that

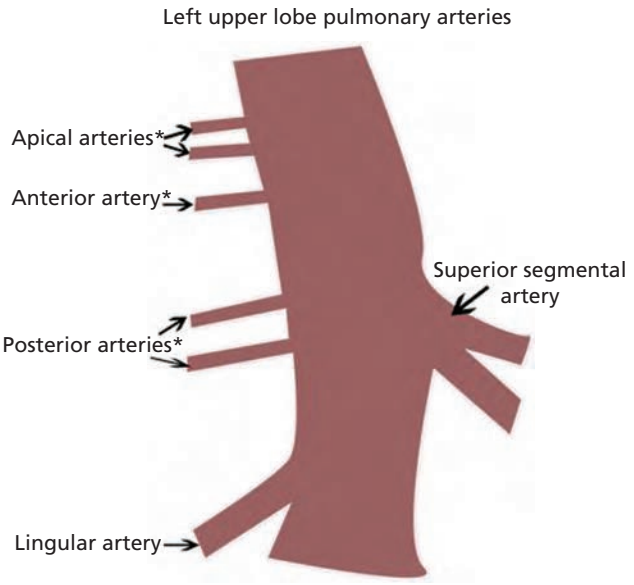

Figure 51.8 Left upper lobe pulmonary arteries: five upper lobe segmental arteries* which enter the upper lobe separately.

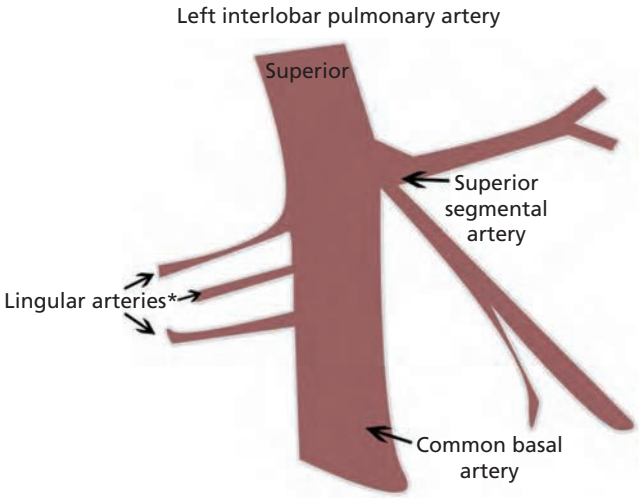

Figure 51.9 Left interlobar pulmonary artery: three lingular branches* which enter the lingula separately.

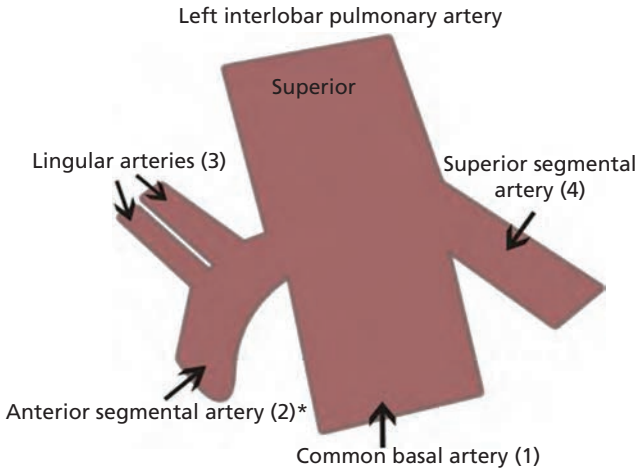

Figure 51.10 Left interlobar pulmonary artery: two lingular arteries and one anterior segment artery of the left lower lobe originated from the same root from the interlobar pulmonary artery at the same level as the superior segment artery of the left lower lobe. 1, common basal artery; 2, anterior segmental artery*; 3, lingular artery; 4, superior segmental artery.

constitute the second group appear. According to Rice (2008), these branches appear one by one in 65% of cases. In 35% there is a common root. The posterior arterial branches comprise one branch in 5% of cases, two branches in 46%, three branches in 36%, four branches in 12% and five branches in 1%.

Lastly, the lingular artery originates from the interlobar portion of the pulmonary artery. The lingular artery branch can originate as a single root or as multiple roots from the lower portion of the upper lobe superior segment artery. In our cases in 2011, there were three lingular branches in 6.25% that entered the lingula separately. Maciejewski and Kutnik (1990) encountered this variation in 1 of 100 cadavers. Cory and Valentine (1959) demonstrated that three lingular arteries entered the lingular segment in 1 of 107 (0.93%) upper lobectomy patients (Fig. 51.9).

In addition, we saw that two lingular arteries and one anterior segment artery of the left lower lobe originated from the same root from the interlobar pulmonary artery at the same level as the superior segment artery of the left lower lobe (Fig. 51.10).

Lower lobe

The first branch the pulmonary artery gives off to the left lower lobe is the superior segment artery. In the interlobar portion of the pulmonary artery it originates from the posterolateral aspect and usually from the proximal part of the lingular branches. In 35% of cases it originates at the same level as the lingular artery or at a more distal level. Wragg et al. (1968) reported that the superior segment artery is in the form of a single branch in 72% of cases. This single branch divides into a bifurcation or a trifurcation after passing through a short segment. The superior segment artery can also be seen as two separate branches in 26% of cases and three separate branches in 2%. In our cases in 2011, two separate branches were seen in 7.14%. Cory and Valentine (1959) demonstrated that 15% of lower lobes present this type of variation (Fig. 51.11).

The lower lobe superior segment artery generally originates directly from the pulmonary artery. However, Rice (2008) reported that in 12% of cases it originates from the basal segment arteries and in 3% from the posterior arterial branches of the upper lobe.

The basal segment arteries extend to the lower lobe in the form of a common basal trunk formed after the lingula and superior segment arteries. The common basal trunk gives branches to the anteromedial, posterior, and lateral segments of the lower lobe.

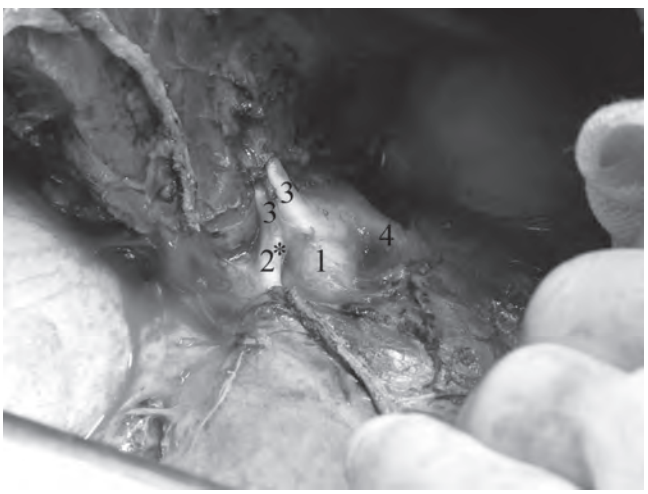

Figure 51.11 Left interlobar pulmonary artery: 1, common basal artery; 2, anterior segmental artery*; 3, lingular artery; 4, superior segmental artery.

References

Bech AP, Akker J, Matthijsse PR. 2010. Isolation of the left subclavian artery from the pulmonary artery in a patient with CHARGE association. *Congenit Anom* 50: 200–202.

Boyden EA, Hartman JF. 1946. An analysis of variations in the bronchopulmonary segments of the left upper lobes of fifty lungs. *J Anat* 79: 321.

Boyden EA, Hamre CJ. 1951. An analysis of variations in the bronchovascular patterns of the middle lobe in fifty dissected and twenty injected lungs. *J Thorac Cardiovasc Surg* 21: 172.

Cory RAS, Valentine EJ. 1959. Varying patterns of the lobar branches of the pulmonary artery. *Thorax* 14: 267–280.

Kent EM, Blades B. 1942a. The anatomic approach to pulmonary resection. *Ann Surg* 116: 782–794.

Kent EM, Blades B. 1942b. The surgical anatomy of the pulmonary lobes. *J Thoracic Surg* 12: 18.

Maciejewski R, Kutnik B. 1990. Branches of the left pulmonary artery vascularizing the left upper pulmonary lobe. *Acta Anat* 138: 224–229.

Milloy FJ, Wragg LE, Anson BJ. 1963. The pulmonary artery supply to the right upper lobe of the lung based upon a study of 300 laboratory and surgical specimens. *Surg Gynecol Obstet* 116: 34.

Milloy FJ, Wragg LE, Anson BJ. 1968. The pulmonary artery supply to the upper lobe of the left lung. *Surg Gynecol Obstet* 126: 811–824.

Rice TW. 2002. Anatomy of the lung. In: *Thoracic Surgery* (eds Pearson FG, Cooper JD, Deslauriers J, Ginsberg RJ, Hiebert C, Patterson GA, Urschel HC). Philadelphia: Churchill Livingstone, pp. 427–441.

Rice TW. 2008. Anatomy of the lung. In: *Pearson's Thoracic and Esophageal Surgery* (eds Patterson GA, Cooper JD, Deslauriers J, Lerut AT, Luketich JD, Rice TW, Pearson FG). Philadelphia: Churchill Livingstone, pp. 401–414.

Wragg LE, Milloy FJ, Anson BJ. 1968. Surgical aspects of the pulmonary artery supply to the middle lobe and lower lobe of the lungs. *Surg Gynecol Obstet* 127: 531–537.

Further reading

Boyden EA. 1956. The trachea and lungs. In: *Anatomy for Surgeons* (ed. Hollinshead WH). New York: Harper and Brother, pp. 40–97.

Fukuhara K, Akashi A, Shigeru N, Tomita E. 2008. Preoperative assessment of the pulmonary artery by three-dimensional computed tomography before video-assisted thoracic surgery lobectomy. *Eur J Cardiothorac Surg* 34: 875–877.

Le Roux BT. 1962. Anatomical abnormalities of the right upper bronchus. *J Thorac Cardiovasc Surg* 44: 225–227.

Shields TW. 2005. Surgical anatomy of the lungs. In: *General Thoracic Surgery* (eds Shields TW, LoCicero J, Ponn RB, Rusch VW). Philadelphia: Lippincott Williams & Wilkins, pp. 59–73.

Sivrikoz MC, Tulay CM. 2011. Variations of lobar branches of pulmonary arteries in thoracic surgery patients. *Surg Radiol Anat* 33: 509–514.

52 Subclavian artery

Selcuk Tunali
TOBB University of Economics and Technology, Ankara, Turkey
University of Hawaii, Honolulu, Hawaii, United States

This chapter covers the variations of the origin of the subclavian artery and related variations of its branches except for the vertebral artery; vertebral artery variations are discussed in Chapter 48 (Vertebral artery).

Variations of the subclavian artery (SA) should also be considered along with variations of the aortic arch. In most cases (70%) the left SA emerges from the aortic arch, whereas the right SA is a branch of the brachiocephalic trunk. In some cases both carotid arteries form a trunk (bicarotid trunk) and the right and left SAs can emerge individually from the aortic arch (<0.1%); or the right SA is a branch of the bicarotid trunk (<0.1%) or originates from it (<0.1%). In some cases a left brachiocephalic trunk is observed where the left SA emerges from it (<0.1%). In very rare cases, there is no brachiocephalic trunk and the aortic arch gives rise to four branches: right SA; right common carotid; left common carotid; and left SA (<0.1%) (Lippert and Pabst 1985).

In a large series of 1000 patients with normal left-sided aortic arches who underwent computed tomographic angiography, 20.8% of the aortic arches had variations. The prevalence of an aberrant right SA was 0.6%, coexistence of aberrant right SA and bicarotid trunk was 0.7%, and the thyroidea ima artery arose from the aortic arch in 0.1%. The frequency of variations of aortic arch branching was similar in males and females (20% and 22.1%). The incidence of aberrant right SA was higher among females than males, whereas other variations were equal or similar in frequency in both genders (Karacan et al. 2013).

When there is a right aortic arch the left SA demonstrates two principal variations: (1) when the left SA arises as the first major vessel of the right aortic arch, it crosses the anterior aspect of the trachea to reach the left side; and (2) when the left SA arises as the last branch of the aortic arch, it crosses the posterior aspect of the esophagus to reach the left side. The left SA does not arise directly from the aortic arch but from a diverticulum, a remnant of the fourth left branchial arch (Bergman et al. 1996).

Mligiliche and Isaac (2009) reported a case where the aortic arch had three branches: bicarotid trunk; left SA; and right SA (in order of appearance). The right SA was the last branch of the aortic arch, taking origin more posteriorly, about 3 cm from the origin of the left subclavian artery. It attained the right upper limb by crossing obliquely behind the esophagus as it reached the thoracic inlet (Figs 52.1, 52.2).

The right SA followed a retrotracheal course in 0.2–2% of the population. Loukas et al. (2006) reported a retrotracheal right SA that originated distally along the left aortic arch and coursed between the trachea and the esophagus. The aortic arch also gave rise to a common trunk, which subsequently bifurcated to

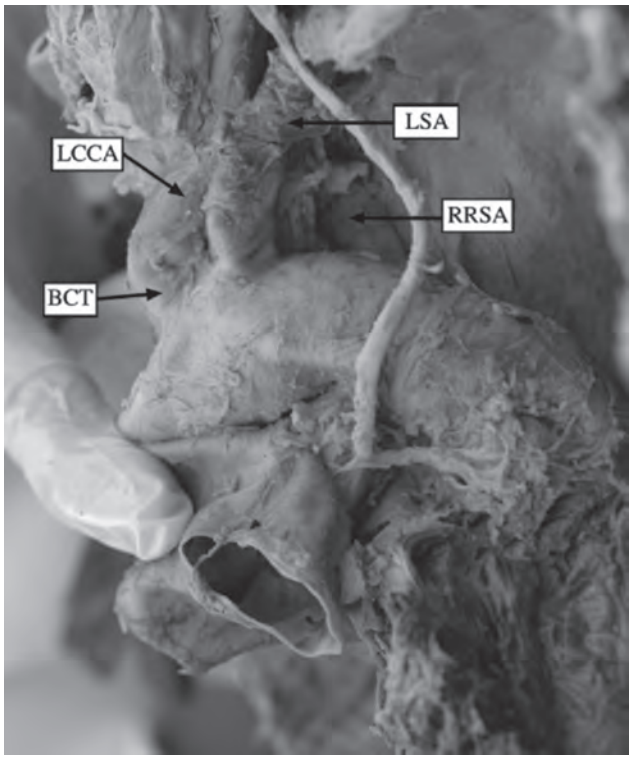

Figure 52.1 Left lateral view of the aortic arch variant. The left common carotid artery (LCCA) passes cranially along the left side of the trachea. The left subclavian artery (LSA) originates from the convexity of the aortic arch and follows a normal course. The anomalous right subclavian artery (RRSA) arises from the posterior wall of the aortic arch.

Source: Mligiliche and Isaac (2009). Reproduced with permission from International Journal of Anatomical Variations.

Bergman's Comprehensive Encyclopedia of Human Anatomic Variation, First Edition. Edited by R. Shane Tubbs, Mohammadali M. Shoja and Marios Loukas.
© 2016 John Wiley & Sons, Inc. Published 2016 by John Wiley & Sons, Inc.

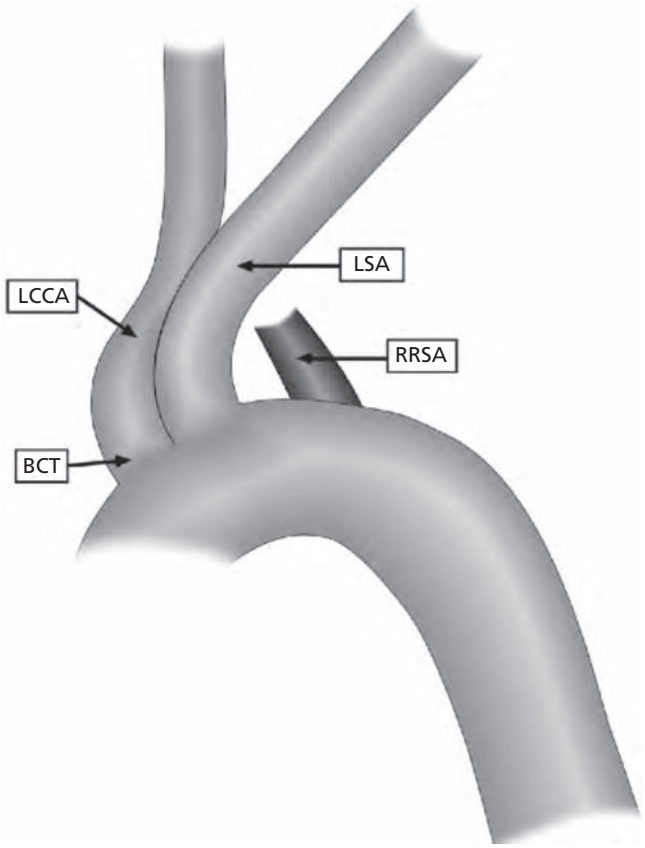

Figure 52.2 A line drawing of Figure 52.1. The left common carotid artery (LCCA), the left subclavian artery (LSA), and the anomalous right subclavian artery (RRSA).

Source: Mligiliche and Isaac (2009). Reproduced with permission from International Journal of Anatomical Variations.

Figure 52.3 Three-dimensional VR CT angiogram in oblique coronal plane shows four supraaortic branches originating separately from right-sided aortic arch. LCCA: left common carotid artery; RCCA: right common carotid artery; RSA: right subclavian artery; ALSA: aberrant left subclavian artery. Left vertebral artery had two separate origins, one segment originating from the left common carotid artery (arrow head) and the other segment from aberrant left subclavian artery (thick arrow); both segments united at C6 vertebral level to continue as the left vertebral artery (thin arrow). The right vertebral artery (RVA) was originating from the right subclavian artery.

Source: Oguz et al. (2010). Reproduced with permission from International Journal of Anatomical Variations.

yield to a right vertebral artery and a left thyroidea ima, replacing the left inferior thyroid artery.

Oguz et al. (2010) reported a right-sided aortic arch with aberrant left SA in a 7-year-old boy. The patient was admitted to hospital with gastroesophageal reflux with no dysphagia and manifested no symptoms of these vascular variations. Interestingly, the left vertebral artery had double origins, one from the left common carotid and the other from the left SA (Fig. 52.3).

A remnant of the left fourth aortic arch that forms the origin of the aberrant left SA is sometimes dilated as an aortic diverticulum called Kommerell's diverticulum. In the literature, an atherosclerotic aneurysm and the rupture of Kommerell's diverticulum have been reported in adults (Fig. 52.4).

Isolation of the left SA or an unusual origin from the pulmonary artery has been documented in several cases, especially in association with a right-sided aortic arch. Similar variants involving the right SA are less frequent. Mosieri et al. (2004) reported an unusual origin of the right SA from the pulmonary artery in association with D-transposition of the great arteries. Such cases can be counted on the fingers of one hand.

Variations in the origin of the SAs are mostly encountered in cases with right-sided aortic arches and transposition of the great arteries. These patients usually present with vascular symptoms, so it is questionable whether such origins should be considered variations or anomalies.

In cases in which the right SA is the last branch of the aortic arch, it can either pass between the trachea and the esophagus or follow a pretracheal course to reach the right side. Sometimes, when the SA passes between the trachea and esophagus, it compresses both the artery and the esophagus, giving rise to a "disease" named "dysphagia lusoria" (Bergman et al. 1996). Arteria lusoria, the term used for an aberrant right SA from a left aortic arch, is the most common aortic arch anomaly/variation, occurring in 0.5–2.5% of individuals. In these cases four vessels arise sequentially from the aortic arch: the right common carotid artery; the left common carotid artery; the left SA; and the aberrant right SA, which crosses upwards and to the right in the posterior mediastinum. It results from disruption of the complex remodeling of the paired branchial arches, typically of the right dorsal aorta distal to the sixth cervical intersegmental artery.

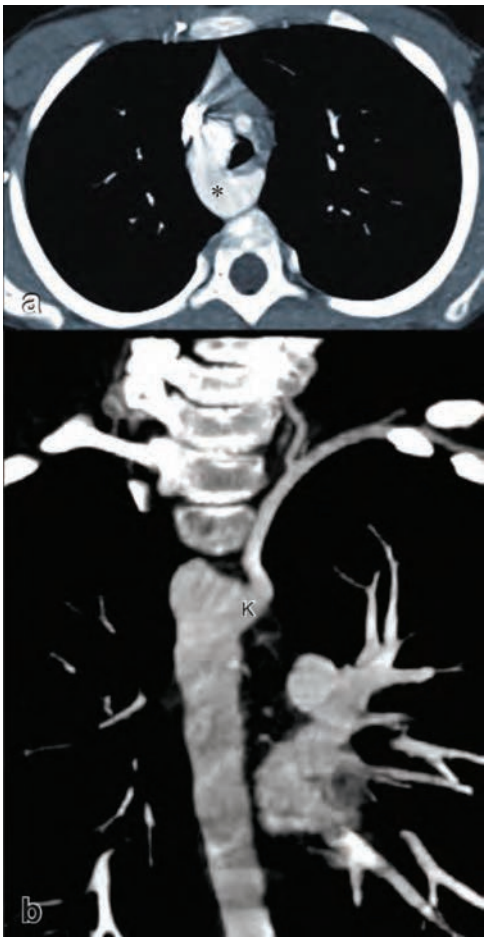

Figure 52.4 (a) Axial CT image shows right aortic arch (asterisk). (b) Coronal MIP image shows ALSA arising from a diverticulum of Kommerell (K).

Source: Oguz et al. (2010). Reproduced with permission from International Journal of Anatomical Variations.

It is usually asymptomatic. When symptomatic, it produces dysphagia lusoria or dyspnea and chronic coughing. Treatment for symptomatic relief of dysphagia lusoria and for prevention of complications due to aneurysmal dilatation is indicated (Myers et al. 2010).

Trunk formation of the subclavian artery

In about 85% of cases, four branches of the SA – inferior thyroid, transverse cervical, and two internal thoracic arteries – form a common trunk; the vertebral artery and costocervical trunk are separate. In 30% of cases (the usual textbook definition) the thyrocervical trunk is formed by the inferior thyroid, suprascapular, and transverse cervical arteries. A trunk formed by only the inferior thyroid and suprascapular arteries is equally common (30%). A trunk formed by the internal thoracic, inferior thyroid, and suprascapular arteries is seen in 8%. Two trunks can sometimes be formed: the inferior thyroid with suprascapular artery and transverse cervical with internal thoracic (1%); the inferior thyroid with transverse cervical artery and suprascapular with internal thoracic artery (4%); the inferior thyroid with internal thoracic artery; and suprascapular with transverse cervical artery (1%) (Lippert and Pabst 1985).

Internal thoracic artery

The internal thoracic artery (ITA) is always reported as present. Murray et al. (2012) evaluated 120 female patients with preoperative imaging using either CTA or color duplex ultrasound. In all patients the ITA was present, and in two it was duplicated (1% of overall cases). The ITA always arose from the subclavian artery.

Indeed, the ITA usually arises as a direct branch of the subclavian artery. However, it can also originate from the thyrocervical trunk (10%) or from a common trunk with the inferior thyroid and suprascapular arteries (8%), the suprascapular artery (4%), the transverse cervical artery (1%), the inferior thyroid artery (1%), or the suprascapular and transverse cervical arteries (1%) (Lippert and Pabst 1985). The suprascapular artery can arise from the ITA. Power (1850) found the ITA arising from both the aorta and brachiocephalic artery.

Henriquez-Pino et al. (1997) studied the ITAs of 100 cadavers. The ITA was present in all cases, originating directly from the subclavian artery or from a common trunk with other arteries. Its average length was 20.4 cm and the most frequent level of termination was at the sixth intercostal space; it existed as a bifurcation in 93% and as a trifurcation in 7%. The pericardiacophrenic artery originated from the ITA in 89%. The lateral costal branch was present in 15%.

In a study of 32 human fetuses (18 female, 14 male) from the 21st to the 24th week of intrauterine life, the right ITA arose from the ascending (68.7%), arcuate (21.9%), or descending (3.2%) parts of the subclavian artery. In other cases (6.2%) it was a branch of the thyrocervical trunk. The left ITA was a branch of the ascending (78.1%) or the arcuate (21.9%) parts of the subclavian artery (Wiśniewski et al. 2004).

Pietrasik et al. (1999) studied the branching pattern of 56 ITAs (28 right, 28 left) in cadavers. They reported eight types of ITA branches forming two main groups: proper (solitary) branches and common trunks. The proper branches have been divided into sternal, perforating, intercostal, and mediastinal. Collectively they account for 83.53% of left ITA and 81.66% of right ITA branches. The difference in numbers of branches between the left and right ITAs was statistically significant: the left ITA gave off more sternal and intercostal branches than the right. The authors also observed that mediastinal branches arising directly from the ITA account for 1.58% of branches. They found four types of common trunk: sternal/perforating; sternal/intercostal; perforating/intercostals; and sternal/perforating/

intercostal, together accounting for 18.34% of the right ITA branches and 16.47% of the left.

The internal thoracic can give rise to a lateral internal thoracic artery as it enters the thorax. The lateral internal thoracic runs about midway between the spine and the sternum or somewhat forward, spans up to six intercostal spaces, and anastomoses with the intercostal arteries in those spaces. A lateral internal thoracic artery can arise from the costocervical trunk, thyrocervical trunk, or ascending cervical. The possible existence of this vessel must be remembered when paracentesis is performed (Bergman et al. 1996). Yoshida et al. (1997) reported an unusual case of a patient in whom postoperative angiography following coronary artery bypass grafting revealed a lateral origin of the right ITA and a usual origin of the left ITA, both of which were patent and did not follow a tortuous course.

A thymic branch usually arises from the ITA. The blood supply to the thymus is normally from the inferior thyroid, internal thoracic, pericardiacophrenic, or anterior intercostal arteries. Cahill (1998) reported a thymic artery that branched from the anterior aspect of the right common carotid approximately 1 cm above the bifurcation of the brachiocephalic artery. It traveled inferiorly through a plexus of inferior thyroid veins for 6 cm in front of the brachiocephalic artery and crossed the anterior surface of the trachea, where it divided into two branches that supplied the right and left lobes of the thymus. Between the sixth and seventh weeks of gestation the thymus descends in close relation successively to the internal carotid, the common carotid, and the brachiocephalic trunk. It is therefore not surprising that the thymic blood supply occasionally comes from the common carotids.

The ITA usually terminates by bifurcating into the musculophrenic and superior epigastric arteries. However, in a study of 62 cadavers, a third branch arose from the medial border of the ITA at the level of the sixth costal cartilage. As it descended it inclined medially towards the angle between the xiphoid process and the seventh costal cartilage, giving off two or three fine branches to the lower sternum. It then passed deep to this angle and could be observed on the anterior surface of the xiphoid process, terminating in fine branches distributed to the inferior aspect of the xiphoid cartilage. It is proposed that this branch at the "trifurcation" of the ITA be termed the xiphoid branch. It was noted in 61.3% of cases: an incidence of 30.7% on the right, 21% on the left, and 9.7% bilateral (Lachman and Satyapal 1999).

Inferior thyroid artery

The blood supply to the thyroid gland is of great clinical relevance. According to Lippert and Pabst (1985) the inferior thyroid artery (InTA) is absent in 3% of cases. When it is absent, the superior thyroid artery or thyroidea ima artery supplies its area.

Different studies have reported absence rates of 1–6% for the InTA. In a case in which the left InTA was absent, the branches of the right InTA crossed the isthmus to supply the ventral and dorsal surfaces of the left lobe of the thyroid gland (Sherman and Colborn 2003). Moriggl and Sturm (1996) reported the absence of both InTAs and of the left superior thyroid artery in an 89-year-old female cadaver; the right superior thyroid artery came from the right common carotid. A large lowest thyroid artery originated from the left internal thoracic artery at the level of the first intercostal space to supply most of the thyroid gland. The InTA can supply the trapezius muscle and is known as the artery of Cruveilhier.

The InTA originates from the subclavian artery medial to the anterior scalene muscle in 95% of cases, from the thyrocervical trunk in 85%, directly from the subclavian artery in 8%, via a common stem with the vertebral artery in 1%, and via a common stem with the internal thoracic artery in 1%. It can also originate from the subclavian artery, but dorsal or lateral to the anterior scalene muscle in 1%; in this event, <1% of cases are via a common trunk with the suprascapular artery or the costocervical trunk and 0.1% are directly from the subclavian artery. The InTA also emerges from the common carotid artery in 1% of cases; on the right side it can originate from the bifurcation of the brachiocephalic trunk (Lippert and Pabst 1985).

In other studies, the InTA was reported to arise from the thyrocervical trunk in 90.5%, the subclavian artery in 7.5%, and very rarely from the common carotid, aortic arch, brachiocephalic, internal thoracic, pericardiacophrenic, or vertebral, or as a common stem with the contralateral InTA (Bergman et al. 1996).

Mariolis-Sapsakos et al. (2014) reported a unique case of a 56-year-old patient undergoing total thyroidectomy and level VI lymph node dissection for papillary thyroid carcinoma, with aberrant origin of both inferior thyroid arteries from the common carotids.

Accessory InTAs have also been reported. Cigali et al. (2008) reported an accessory InTA originating from the left suprascapular artery; both superior and inferior thyroid arteries were present. Sedy (2008) reported an accessory InTA. On the right side, he found a doubled inferior thyroid artery, both arising separately from the thyrocervical trunk. The lower artery was in a typical location whereas the upper was recognized as accessory. On the left side, only a single inferior thyroid artery was present (Fig. 52.5).

Banneheka et al. (2010) reported an interesting case of a middle thymothyroid artery arising from the anterior aspect of the right common carotid in a 71-year-old Japanese male cadaver. It soon divided into a thyroidea ima artery, a branch supplying the sternoclavicular joints, and a thymic branch. Twigs from these three main branches also supplied the sternohyoid and sternothyroid muscles, right inferior parathyroid gland and some deep cervical lymph nodes.

The thyroidea ima artery, regardless of its origin, is reported to occur in 4–10% people. However, there are reports of a much lower incidence (0.4%). The thyroidea ima artery can arise from the aortic arch, the brachiocephalic trunk, the common carotid, the internal thoracic, the pericardiacophrenic, the subclavian,

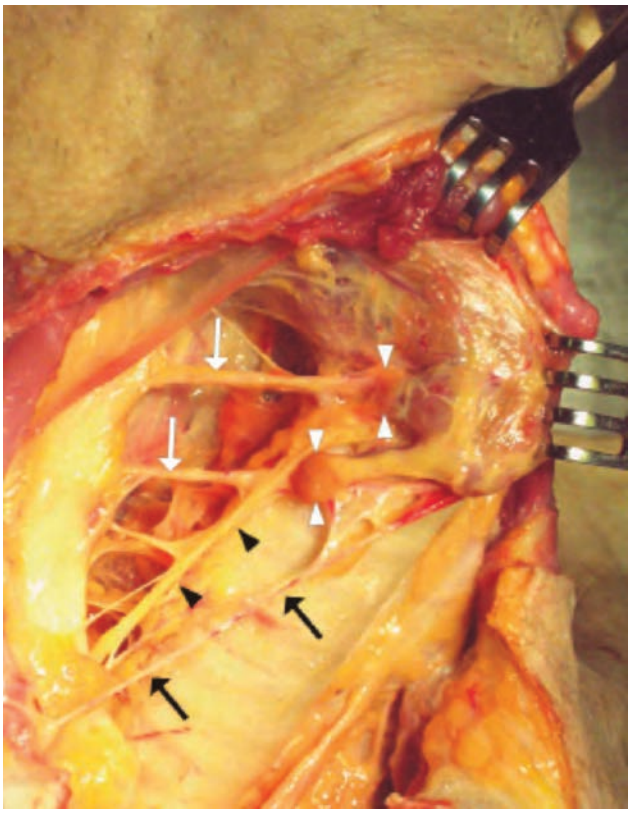

Figure 52.5 Dissection of the neck showing accessory inferior thyroid artery, right side view, thyroid gland shifted medially. White arrows: doubled right inferior thyroid arteries (the superior one is the accessory inferior thyroid artery); white arrowheads: parathyroid glands; black arrowheads: recurrent laryngeal nerve; black arrows: inferior thyroid vein.

Source: Sedy (2008). Reproduced with permission from International Journal of Anatomical Variations.

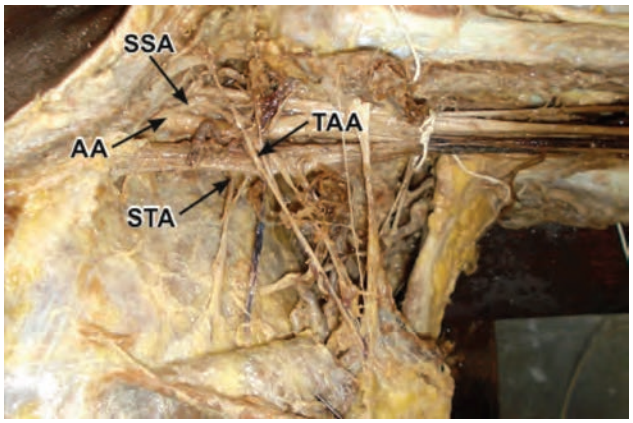

Figure 52.6 Suprascapular artery arising directly from the first part of axillary artery. SSA: suprascapular artery; AA: axillary artery; TAA: thoracoacromial artery; STA: superior thoracic artery.

Source: Adibatti and Prassana (2010). Reproduced with permission from International Journal of Anatomical Variations.

the thyrocervical trunk, the inferior thyroid or the transverse scapular artery. It usually, but not always, arises from the right side (Natsis et al. 2009).

The ascending cervical artery usually arises from the InTA but its origin can vary. Oztürk et al. (1998) reported a variant ascending cervical artery branching from the superficial cervical artery, nearly 1 cm lateral to its origin from the thyrocervical trunk. Tubbs et al. (2004) reported an ascending cervical artery continuing as the occipital artery. The ascending cervical was enlarged from its origin and supplied segmental branches through the intervertebral foramina. At the upper cervical spine the ascending cervical artery continued as the occipital artery, providing the branches normally seen stemming from this artery.

Suprascapular artery

The suprascapular artery usually arises from the thyrocervical trunk. In about 2% of cases it emerges directly from the subclavian artery. It forms common trunks with the internal thoracic and inferior thyroid arteries in 8%; with the internal thoracic artery alone in 4%; and with the internal thoracic and transverse cervical artery in 1% of cases (Lippert and Pabst 1985; Bergman et al. 1996). It can also arise from the axillary artery, accessory inferior thyroid artery, subscapular artery, costocervical trunk, or the thoracoacromial artery. The suprascapular artery can arise from the dorsal scapular artery. The suprascapular artery can also be duplicated bilaterally or even absent (Atsas et al. 2011).

Adibatti and Prasanna (2010) reported a variant suprascapular artery emerging from the first part of the axillary artery on the left side of a male cadaver. Similar observations were made in 1.6% of cases studied (Fig. 52.6).

Atsas et al. (2011) reported a variant suprascapular artery occurring unilaterally on the left side. In this case, the artery arose from the proximal end of the internal thoracic artery which, in turn, originated from the first part of the subclavian. The thyrocervical trunk was present and contained its other normal branches: inferior thyroid, transverse cervical, and ascending cervical arteries (Fig. 52.7).

A bilateral variant origin of the suprascapular artery from the first part of the axillary artery was reported in a nearly 65-year-old male cadaver. The suprascapular artery on both sides ascended for about 1 cm above the medial third of the clavicle and then passed obliquely behind the clavicle. It then passed between the trunks of the brachial plexus to reach the suprascapular notch, where it was accompanied by the suprascapular nerve. The artery and nerve passed together beneath the transverse scapular ligament (Shukla et al. 2012; Figs 52.8, 52.9).

Chen and Adds (2011) reported an accessory suprascapular artery on the left side of a 94-year-old formalin-embalmed Caucasian female. In this case, the suprascapular artery (proper) was

Figure 52.7 The cadaveric dissection shows the variant origin of the suprascapular artery (SSA) arising off the internal thoracic artery (ITA). The thyrocervical trunk (TCT) is present and contains its remaining branches: inferior thyroid, transverse cervical, and ascending cervical arteries. VA: vertebral artery; SSN: suprascapular nerve; STSL: superior transverse scapular ligament.

Source: Atsas et al. (2011). Reproduced with permission from International Journal of Anatomical Variations.

identified as emerging from a thyrothoracic trunk (a thyrocervical trunk, which also gives off the internal thoracic artery) and passing over the brachial plexus and superior transverse scapular ligament before supplying the supraspinatus. During deeper dissection, an artery was found to arise from the third part of the subclavian artery, passing deep to the inferior trunk of the brachial plexus and superior transverse scapular ligament

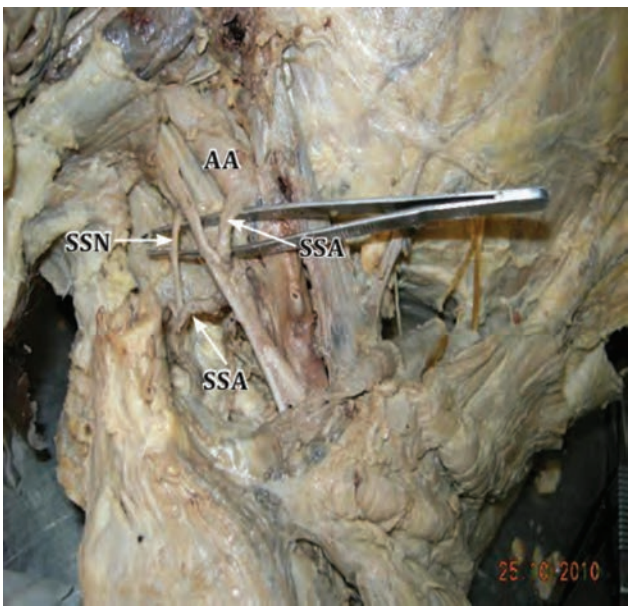

Figure 52.8 Photograph showing the right suprascapular artery arising from the first part of the axillary artery. SSA: suprascapular artery; AA: axillary artery; SSN: suprascapular nerve.

Source: Shukla et al. (2012). Reproduced with permission from International Journal of Anatomical Variations.

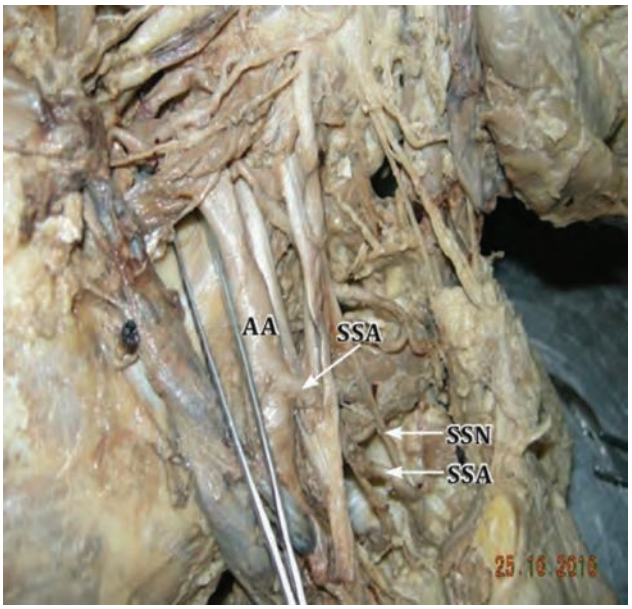

Figure 52.9 Photograph showing the left suprascapular artery arising from the first part of the axillary artery. SSA: suprascapular artery; AA: axillary artery; SSN: suprascapular nerve.

Source: Shukla et al. (2012). Reproduced with permission from International Journal of Anatomical Variations.

before forming a direct anastomosis with the suprascapular artery beneath the supraspinatus. They termed it the "accessory suprascapular artery". It accompanied the suprascapular nerve under the superior transverse scapular ligament. A cervicodorsal trunk gave origin to the superficial cervical and dorsal scapular arteries, and was found in 30% of cases. A cervicoscapular trunk gave rise to the superficial cervical and suprascapular arteries in 22% of cases, and a dorsoscapular trunk provided origins for the dorsal scapular and suprascapular arteries in 4% of cases. Weiglein et al. (2005) used novel terminology to report the arteries of the posterior cervical triangle. In their study, a cervico-dorso-scapular trunk gave origin to the superficial cervical artery, the dorsal scapular artery, and the suprascapular artery, and was found in 24% of cases.

Transverse cervical artery

The transverse cervical artery arises from the subclavian artery in about 61% of cases and from the thyrocervical trunk in about 38% (Bergman et al. 1996). It can form common trunks with other branches of the subclavian artery. In this case there are usually two trunks: the inferior thyroid with the transverse cervical artery and the suprascapular with the internal thoracic (4%); the inferior thyroid with the suprascapular artery and the transverse cervical with the internal thoracic (1%); or the inferior thyroid with the internal thoracic and the suprascapular

with the transverse cervical (1%) (Lippert and Pabst 1985). Lang (1993) described a common trunk with the costocervical trunk in 0.26% of specimens.

When transverse cervical artery is absent (6%) it is compensated by branches from the dorsal scapular or superficial cervical artery, costocervical trunk, or the distal or third part of the subclavian or even the axillary artery. The dorsal scapular artery, which usually arises from the second part of the subclavian artery as an individual branch (70%), can also emerge from the transverse cervical artery (30%) (Bergman et al. 1996).

Costocervical trunk

This trunk commonly arises from the third part of the subclavian artery; however, it can also arise from other parts of the subclavian. The usual branches are the supreme intercostal and the deep cervical arteries. It is absent in 8–10% of cases so its main branches can arise independently, most frequently from the second part of the subclavian artery (Bergman et al. 1996).

The supreme intercostal artery can also arise from the thyrocervical trunk or the deep cervical, inferior thyroid, second intercostal, or axillary arteries. The left supreme intercostal artery has been reported as a branch of the aortic arch in cases with four arch branches. In one case it arose from a lateral internal thoracic artery (Bergman et al. 1996).

Lang (1993) included the following variations of the costocervical trunk:

1. an origin from the second part of the subclavian artery in 42% (usually on the right side);
2. accessory deep cervical arteries in 23%, usually on the left and sometimes duplicated or even triplicated;
3. an origin of the costocervical or deep cervical artery from the transverse cervical artery;
4. absence of the costocervical trunk in 5% of cases;
5. an approximately 1%, the deep cervical artery arises from the subclavian artery and the highest intercostal artery from the internal thoracic artery;
6. an origin from the third segment of the subclavian artery in 1%;
7. in 0.8% of specimens, the costocervical trunk arose from the vertebral artery and in 0.32%, it arose from the suprascapular artery; and
8. in 0.16% it arose from the inferior thyroid artery.

Other

An artery of Casali can be present, which supplies the apex of the lung (Casali 1912). Direct branches can also leave the subclavian artery to supply the stellate ganglion (Tubbs et al. 2002). Other direct branches may be present, supplying the scalene muscles and known as the scalene artery of Stahel.

References

Adibatti M, Prasanna LC. 2010. Variation in the origin of suprascapular artery. *Int J Anat Var (IJAV)* 3: 178–179.

Atsas S, Fox JN, Lambert HW. 2011. The rare origin of the suprascapular artery arising off the internal thoracic artery in the presence of the thyrocervical trunk: clinical and surgical implications. *Int J Anat Var (IJAV)* 4: 182–184.

Banneheka S, Chiba S, Fukazawa M, Tokita K, Arakawa T, Suzuki R, Miyawaki M, Kumaki K. 2010. Middle thymothyroid artery arising from the common carotid artery: case report of a rare variation. *Anat Sci Int* 85: 241–244.

Bergman RA, Afifi AK, Miyauchi R. 1996. Illustrated Encyclopedia of Human Anatomic Variation: Opus II: Cardiovascular System: Arteries: Head, Neck, and Thorax. Subclavian Arteries. Available at: http://www.anatomyatlases.org/AnatomicVariants/Cardiovascular/Text/Arteries/Subclavian.shtml (accessed 16 November 2015).

Cahill DR. 1998. Anomalous thymic branch of the right common carotid artery. *Clin Anat* 11: 346–348.

Casali R. 1912. Osservazioni sui rami collaterali della succlavia. *Bibl Anat* 22: 2–41.

Chen D, Adds P. 2011. Accessory suprascapular artery. *Clin Anat* 24: 498–500.

Cigali BS, Ulucam E, Bozer C. 2008. Accessory inferior thyroid artery and internal thoracic artery originating from the thyrocervical trunk. *Anat Sci Int* 83: 283–285.

Henriquez-Pino JA, Gomes WJ, Prates JC, Buffolo E. 1997. Surgical anatomy of the internal thoracic artery. *Ann Thorac Surg* 64: 1041–1045.

Karacan A, Türkvatan A, Karacan K. 2013. Anatomical variations of aortic arch branching: evaluation with computed tomographic angiography. *Cardiol Young* 22: 1–9.

Lachman N, Satyapal KS. 1999. Origin and incidence of xiphoid branch of the internal thoracic artery. *Surg Radiol Anat* 21: 351–354.

Lang J. 1993. *Clinical Anatomy of the Cervical Spine*. New York: Thieme.

Lippert H, Pabst R. 1985. *Arterial Variations in Man. Classification and Frequency*. Munich: J. F. Bergmann-Verlag.

Loukas M, Louis RG Jr, Gaspard J, Fudalej M, Tubbs RS, Merbs W. 2006. A retrotracheal right subclavian artery in association with a vertebral artery and thyroidea ima. *Folia Morphol (Warsz)* 65: 236–241.

Mariolis-Sapsakos T, Kalles V, Papapanagiotou I, Bonatsos V, Orfanos N, Kaklamanos IG, Manolis E. 2014. Bilateral aberrant origin of the inferior thyroid artery from the common carotid artery. *Surg Radiol Anat* 36(3): 295–297.

Mligiliche NL, Isaac ND. 2009. A three branches aortic arch variant with a bi-carotid trunk and a retro-esophageal right subclavian artery. *Int J Anat Var (IJAV)* 2: 11–14.

Moriggl B, Sturm W. 1996. Absence of three regular thyroid arteries replaced by an unusual lowest thyroid artery (A. thyroidea ima): a case report. *Surg Radiol Anat* 18: 147–150.

Mosieri J, Chintala K, Delius RE, Walters HL 3rd, Hakimi M. 2004. Abnormal origin of the right subclavian artery from the right pulmonary artery in a patient with D-transposition of the great vessels and left juxtaposition of the right atrial appendage: an unusual anatomical variant. *J Card Surg* 19: 41–44.

Murray AC, Rozen WM, Alonso-Burgos A, Ashton MW, Garcia-Tutor E, Whitaker IS. 2012. The anatomy and variations of the internal thoracic (internal mammary) artery and implications in autologous

breast reconstruction: clinical anatomical study and literature review. *Surg Radiol Anat* 34: 159–165.

Myers PO, Fasel JH, Kalangos A, Gailloud P. 2010. Arteria lusoria: developmental anatomy, clinical, radiological and surgical aspects. *Ann Cardiol Angeiol (Paris)* 59: 147–154.

Natsis KI, Tsitouridis IA, Didagelos MV, Fillipidis AA, Vlasis KG, Tsikaras PD. 2009. Anatomical variations in the branches of the human aortic arch in 633 angiographies: clinical significance and literature review. *Surg Radiol Anat* 31: 319–323.

Oguz B, Yigit AE, Oguz KK, Haliloglu M. 2010. MDCT angiography of right-sided aortic arch with aberrant left subclavian artery and duplicated left vertebral artery. *Int J Anat Var (IJAV)* 3: 15–18.

Oztürk AH, Bayramoğlu A, Celik HH, Yener N. 1998. An anomalous ascending cervical artery. *Okajimas Folia Anat Jap* 75: 259–261.

Pietrasik K, Bakon L, Zdunek P, Wojda-Gradowska U, Dobosz P, Kolesnik A. 1999. Clinical anatomy of internal thoracic artery branches. *Clin Anat* 12: 307–314.

Power JH. 1850. *Surgical Anatomy of the Arteries and Descriptive Anatomy of the Heart by the Late Valentine Flood, MD*. Dublin: Fannin and Co.

Sedy J. 2008. An incidental finding of the accessory inferior thyroid artery. *Int J Anat Var (IJAV)* 1: 10–11.

Sherman JH, Colborn GL. 2003. Absence of the left inferior thyroid artery: clinical implications. *Clin Anat* 16: 534–547.

Shukla L, Gaur N, Soni G. 2012. Bilateral variation in the origin of suprascapular artery. *Int J Anat Var (IJAV)* 5: 14–15.

Tubbs RS, Salter G, Wellons JC 3rd, Oakes WJ. 2002. Blood supply of the human cervical sympathetic chain and ganglia. *Eur J Morphol* 40: 283–288.

Tubbs RS, Salter G, Oakes WJ. 2004. Continuation of the ascending cervical artery as the occipital artery in man. *Anat Sci Int* 79: 43–45.

Weiglein AH, Moriggl B, Schalk C, Künzel KH, Müller U. 2005. Arteries in the posterior cervical triangle in man. *Clin Anat* 18: 553–557.

Wiśniewski M, Krakowiak-Sarnowska E, Szpinda M, Sarnowski J. 2004. The internal thoracic artery in human foetuses. *Folia Morphol (Warsz)* 63: 19–23.

Yoshida K, Ohshima H, Murakami F, Tomida Y, Matsuura A, Hibi M, Kawamura M, Notoya A. 1997. Lateral origin of the right internal thoracic artery: report of a case. *Surg Today* 27: 664–665.

53 Upper limb arteries

Anthony Olinger
Kansas City University of Medicine and Biosciences, Kansas City, Missouri, USA

Variations in the branching and origins of the arteries of upper limb are numerous and therefore the subject of many anatomical studies (Rodríguez-Niedenführ et al. 2001a, b, 2003). Anatomic variation of the major arteries of the upper limb have been reported in 11–24.4% of cases (Uglietta and Kadir 1989). The variety with which these studies present this information is not always consistently based on the criteria that define the anomaly and the often differing terminology, and therefore leads to conflicting reports of incidence and description. Some investigators have chosen to report on whole branching patterns of the vasculature, while others have decided to focus on the incidence of specific vessels and their anomalous origins or courses. Furthermore, some studies are strictly case reports describing a single anomaly while others have focused entirely on the incidence of variant branching. Many studies concentrate of the clinical implications of the anatomical variation while other focus primarily on the development that led to the anomaly in the first place (Singer 1933; Rodríguez-Niedenführ et al. 2001a, b, 2003).

The goal of this chapter is to sort through all of these reports and describe the anatomical variations of the arterial supply to the upper limb using the Terminologia Anatomical as a foundation for terminology and generally agreed-upon notions of anatomical morphological concepts, in order to eliminate the confusion that has been present in the literature since these anomalies were first discovered. The chapter begins with the axillary artery and works distally to the arteries of the hand, attempting to dispense the information in a consistent pattern covering reports of incidence, single case reports of anomalies, and then clinical implications.

Axillary artery

The axillary artery is the continuation of the subclavian artery distal to the first rib. The axillary artery begins at the first rib and then becomes the brachial artery distal to the teres major muscle. The axillary artery is classically divided into three parts by the pectoralis minor muscle: part one of the vessel is proximal to the pectoralis minor; part two is deep to the pectoralis minor; and part three is distal to the pectoralis minor muscle, but proximal to the teres major muscle. The axillary artery classically has six branches: the superior (supreme) thoracic artery, which originates from the first part of the axillary artery; the lateral thoracic artery and thoracoacromial truck, which originate from the second part of the axillary artery; and the subscapular artery and anterior and posterior humeral circumflex arteries, which all originate from the third part of the axillary artery.

Variation in the axillary artery is common (Zagorsky 1809; Calori 1877; Walsham 1880; Winslow 1883a; Heuston 1885; Guerra 1887; Potherat 1888; Hitzrot 1901; Ferrari 1902–03; Bovero 1907; Poynter 1922; P'an 1940; Cayotte and Quereux 1953; Bhargava 1956; Jakubowicz and Bruska 1980; Bergman et al. 1988) and typically described in one of two ways: as either a branching pattern for the whole vessel or as the frequency by which specific branches originate from specific locations off of the artery. Both will be described. Some studies report a very high percentage when describing variability of the axillary artery (90% of the time; Lippert and Pabst 1985) while others report somewhat lower numbers (3.7% of the time; Saeed et al. 2002).

Lippert and Pabst (1985) have mapped out the branching of variant branches of the axillary artery and assigned rough estimates of the frequency of those variations based on original reports (Adachi 1928; deGaris and Swartley 1928; Trotter et al. 1930; Charles et al. 1931; Coulouma 1934; Miller 1939; Huelke 1959; Lanz and Wachsmuth 1959; Skopakoff 1959b; Smith-Agreda 1959; Keen 1961; Anson 1963; Mojab et al. 1976; Wachtler 1978). The following three paragraphs discuss those findings.

The classic description above actually only appears in about 10% of cases (Fig. 53.1). The most common variations observed in cadavers involve the branches of the axillary artery originating from common trunks (Fig. 53.2). Approximately 20% of the time the posterior humeral circumflex artery originates from the subscapular artery (Fig. 53.2a) and about 20% of the time both the anterior and posterior humeral circumflex artery originate as a common trunk (Fig. 53.2b). The lateral thoracic artery forms a common trunk with the thoracoacromial artery about 10% of the time (Fig. 53.2c); the lateral thoracic artery also originates as a common trunk with the subscapular artery about 10% of the time (Fig. 53.2d). Approximately 2% of the

Bergman's Comprehensive Encyclopedia of Human Anatomic Variation, First Edition. Edited by R. Shane Tubbs, Mohammadali M. Shoja and Marios Loukas.
© 2016 John Wiley & Sons, Inc. Published 2016 by John Wiley & Sons, Inc.

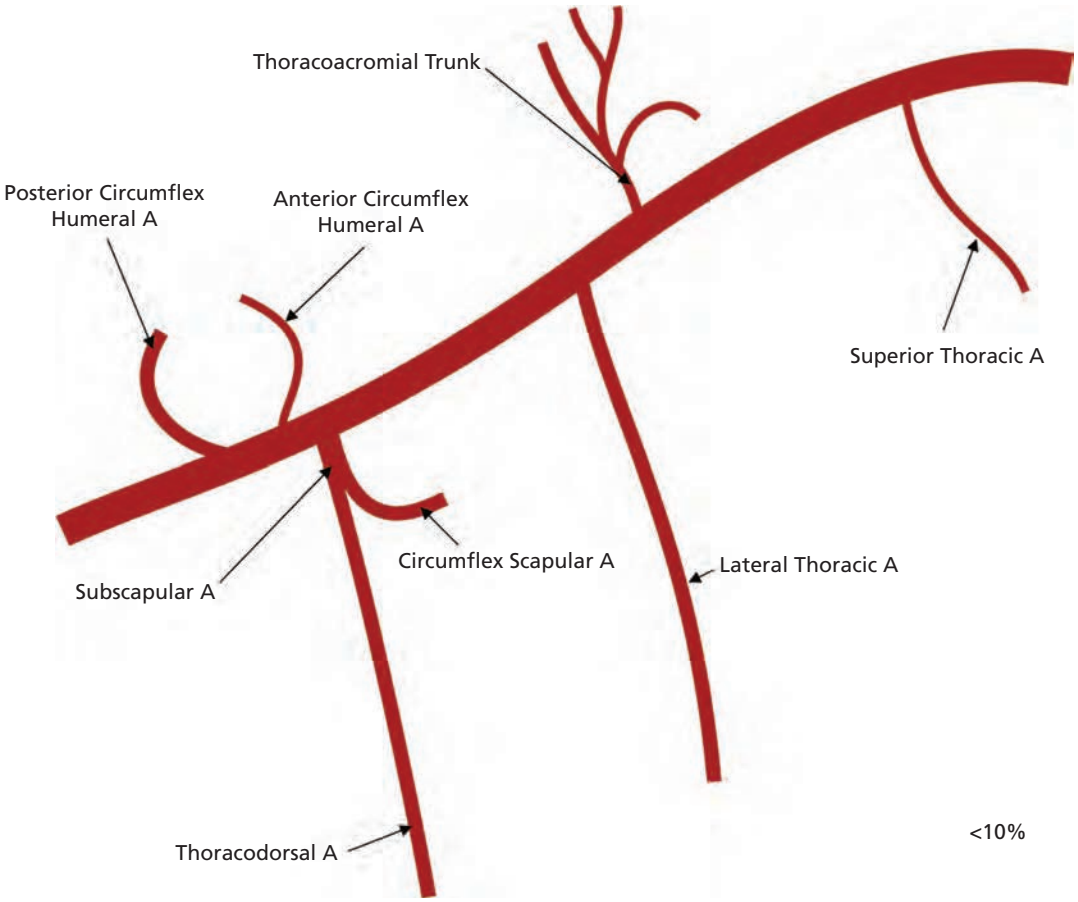

Figure 53.1 Classic branching pattern of the axillary artery.

time the lateral thoracic, thoracoacromial, anterior and posterior humeral circumflex and subscapular will originate as a common trunk (Fig. 53.2e). Occasionally, when the anterior and posterior humeral circumflex arteries originate as a common trunk, the lateral thoracic artery will also originate with the thoracoacromial trunk (Fig. 53.2f).

The next major pattern of axillary artery variations involve the high or proximal origin of arteries that should branch more distally down the upper limb. These occur approximately 22% of the time. Approximately 13% of the time the deep brachial artery will originate from the axillary artery, where it typically arises from the brachial artery proper (Fig. 53.3a). In approximately 5% of cases the deep brachial artery will arise from the posterior humeral circumflex artery (Fig. 53.3b). Finally, in roughly 4% of cases the axillary artery will produce a superficial brachial artery while still in the axilla (Fig. 53.3c).

The remaining variation patterns of the axillary artery include the deep brachial artery arising from the posterior humeral circumflex artery, which arises from the brachial artery rather than the axillary artery (Fig. 53.4a). This variation pattern occurs approximately 7% of the time. In roughly 6% of cases, the lateral thoracic artery will be doubled and both branches will arise from the second part of the axillary artery (Fig. 53.4b). It is estimated that in 4% of cases the thoracodorsal artery and circumflex scapular artery, which typically arise from the axillary artery as a common trunk called the subscapular artery, will arise from the third part of the axillary artery as separate branches (Fig. 53.4c). In approximately 3% of cases the thoracodorsal artery will arise as a small branch from the lateral thoracic artery, either with or without the presence of an even smaller branch from the subscapular artery (Fig. 53.4d). In roughly 1% of cases the superior thoracic artery will produce a long descending branch that travels with the lateral thoracic artery (Fig. 53.4e). Finally in less than 1% of cases the suprascapular artery, which is typically a branch of the thyrocervical trunk of the subclavian artery, will arise from the second part of the axillary artery near the thoracoacromial trunk (Fig. 53.4f).

The other method for examining the variability of the branching of the axillary artery, rather than looking at the entire branching pattern of the artery, is to observe the frequency by which specific branches arise specifically from the axillary artery.

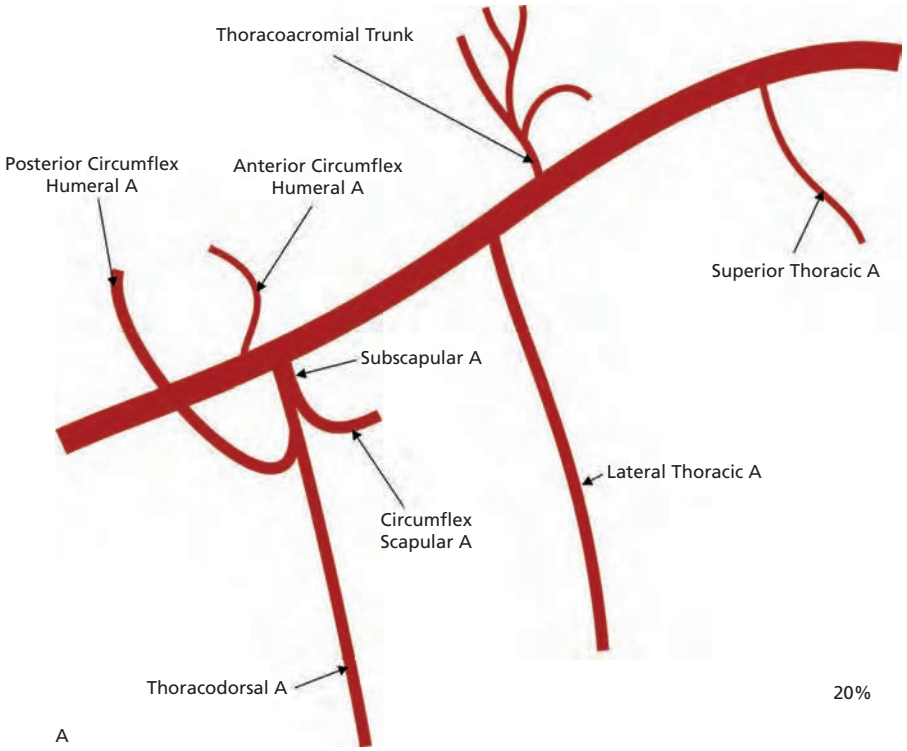

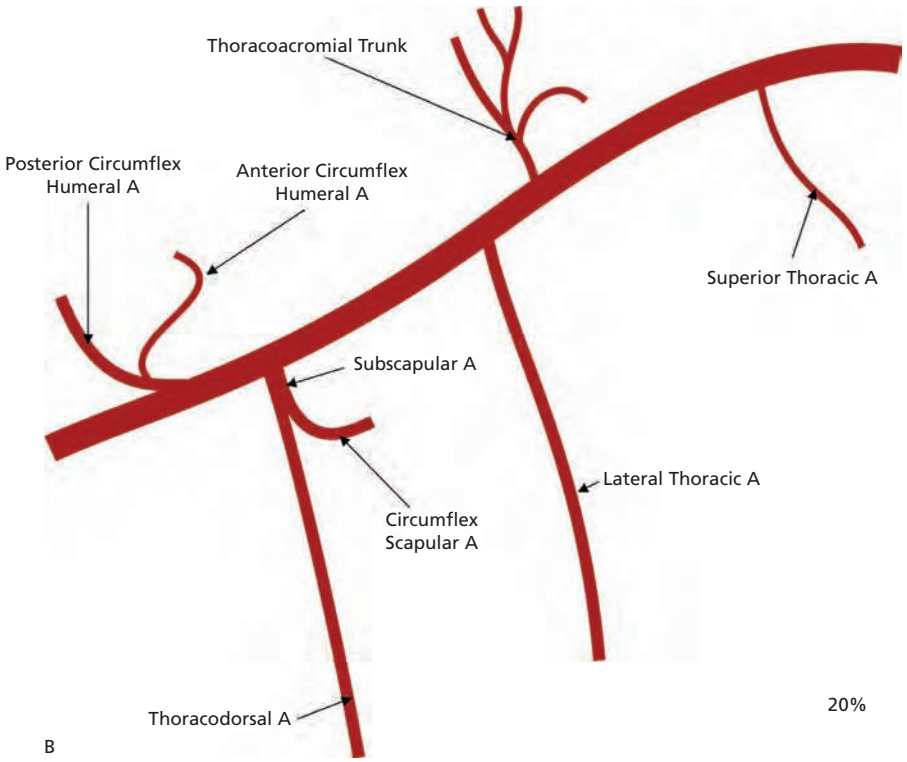

Figure 53.2 Anomalous branching patterns of the axillary artery involving a common trunk: (a) posterior humeral circumflex artery originating from the subscapular artery (20%); (b) anterior and posterior humeral circumflex arteries originating as a common trunk (20%)

(continued)

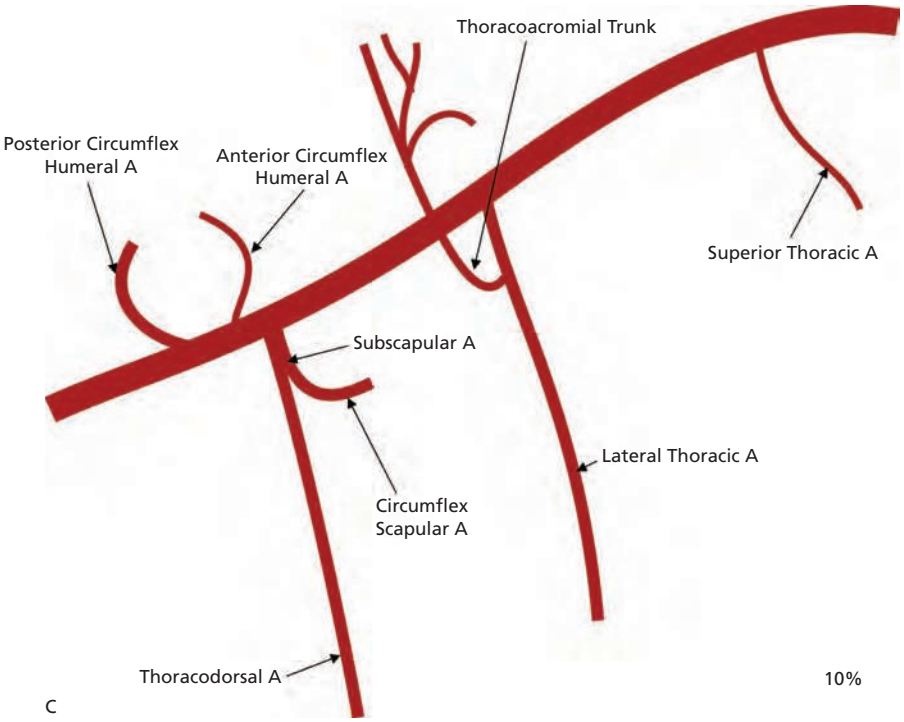

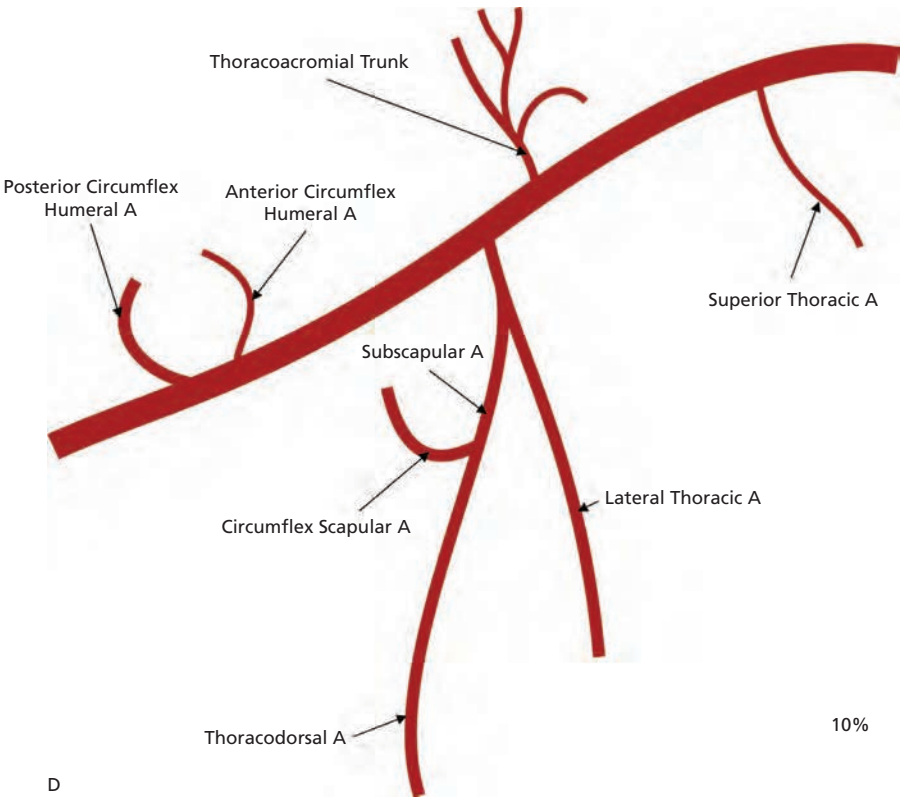

Figure 53.2 *(continued)* (c) lateral thoracic artery originating as a common trunk with the thoracoacromial artery (10%); (d) lateral thoracic artery originating from the subscapular artery (10%)

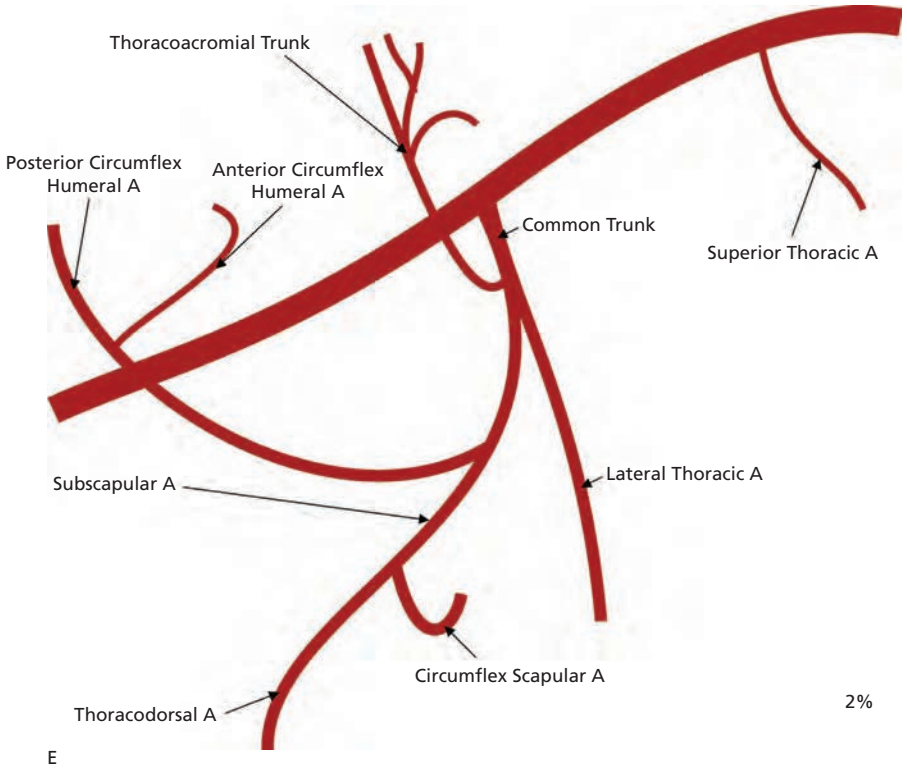

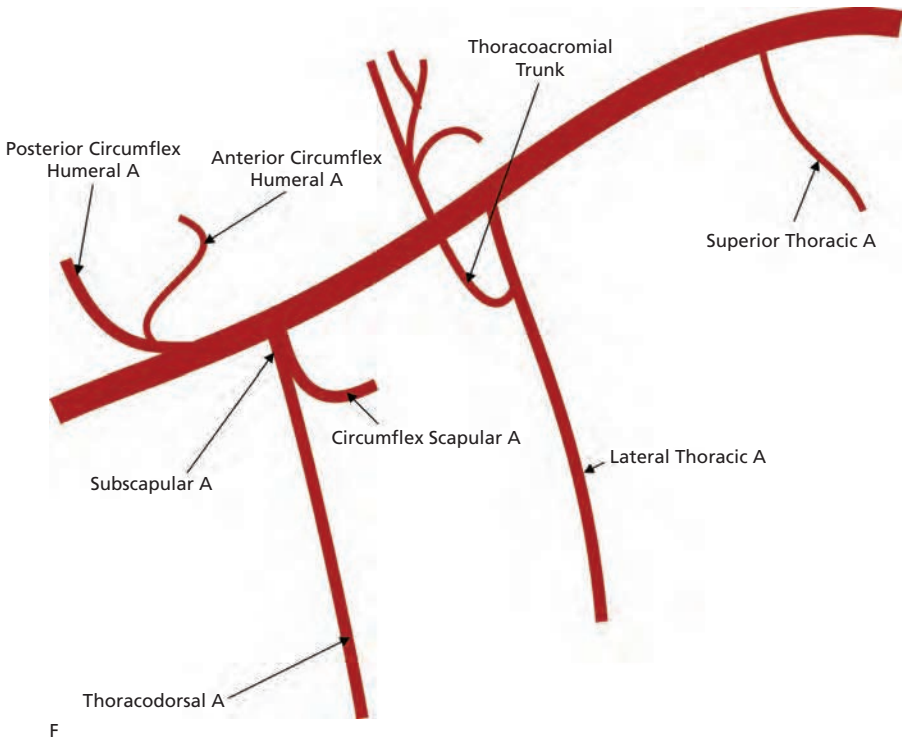

Figure 53.2 *(continued)* (e) lateral thoracic, thoracoacromial, anterior and posterior humeral circumflex and subscapular arteries originate as a common trunk (2%); and (f) combination of anterior and posterior humeral circumflex arteries originating as a common trunk and lateral thoracic artery originating as a common trunk with the thoracoacromial artery.

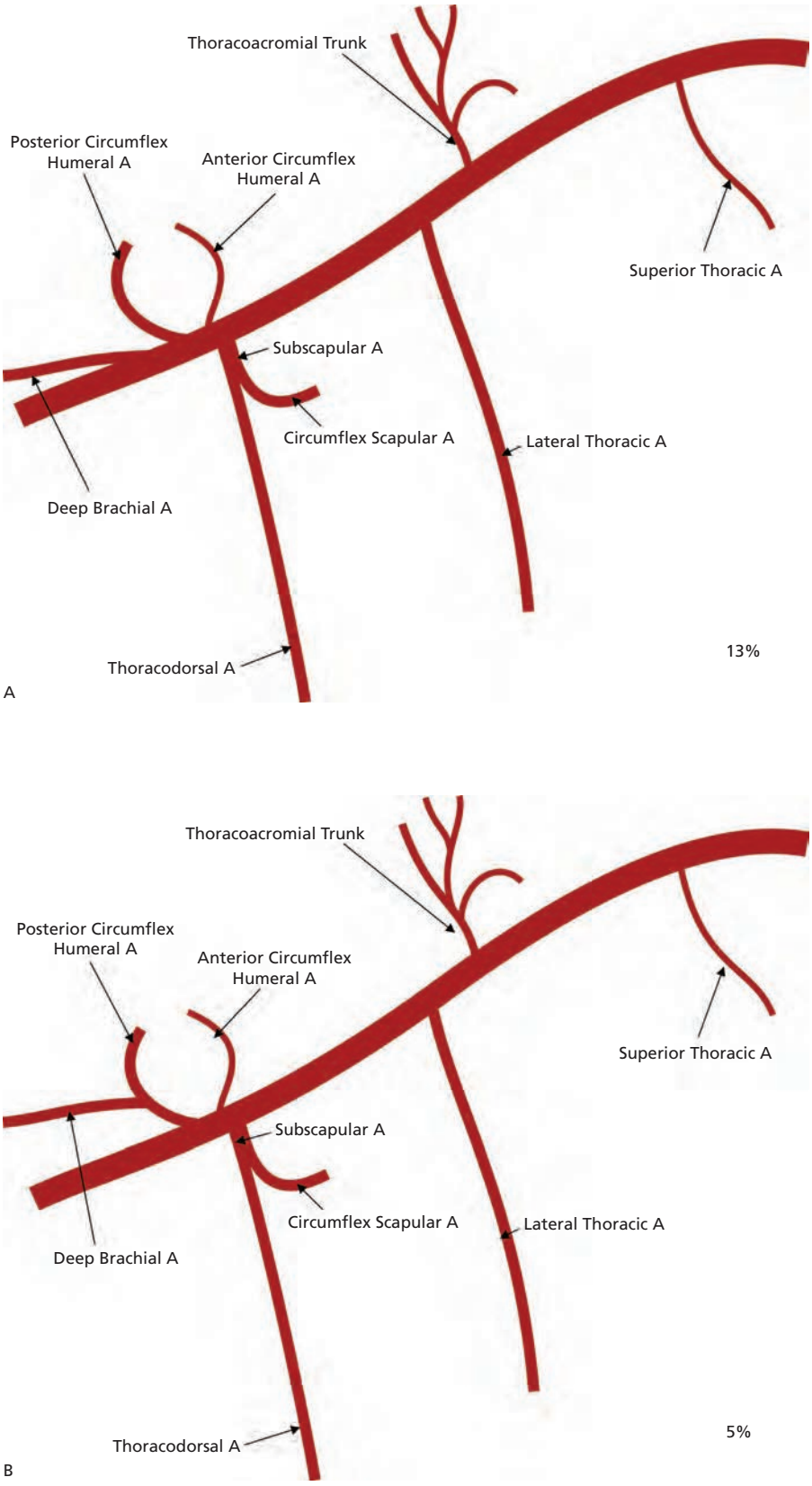

Figure 53.3 Anomalous branching of the axillary artery involving proximal branching that classically takes place more distally. Deep brachial artery originates (a) from the axillary artery rather than the brachial artery (13%); and (b) from the posterior humeral circumflex artery (5%).

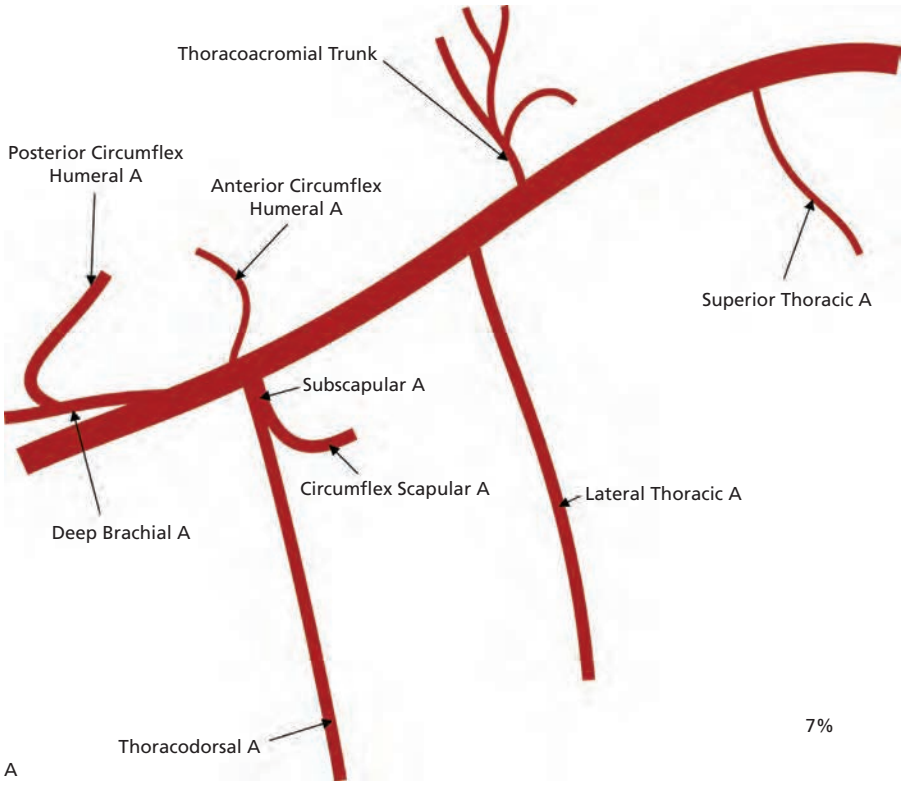

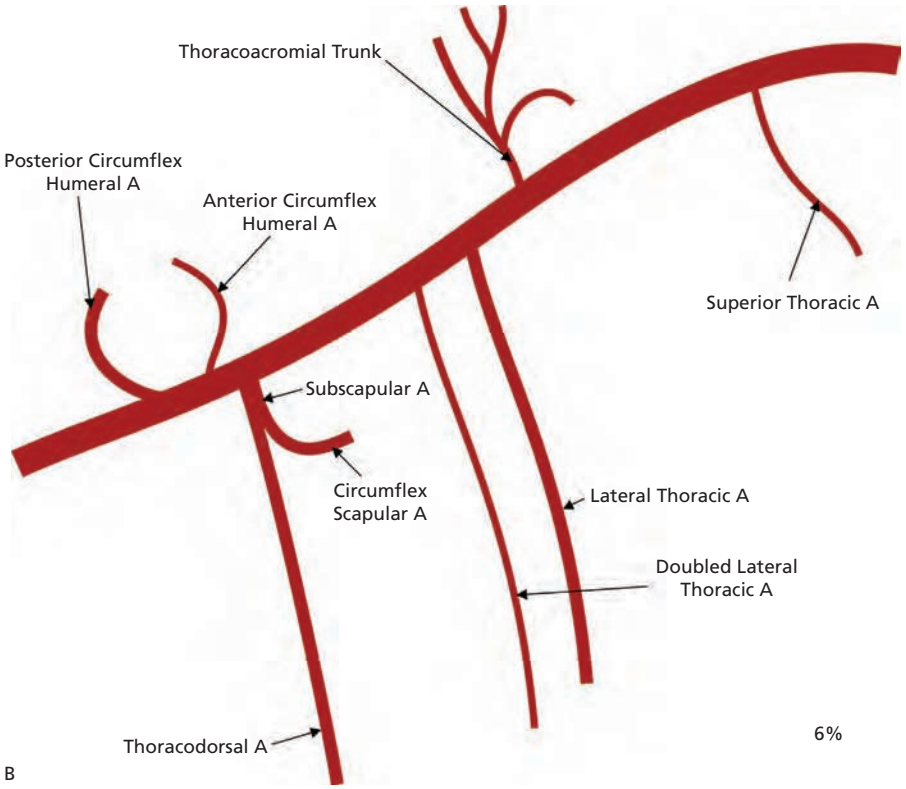

Figure 53.4 *(continued)* Remaining anomalous branching of the axillary artery: (a) deep brachial artery originating from the posterior humeral circumflex artery (7%); (b) double lateral thoracic artery (6%)

(continued)

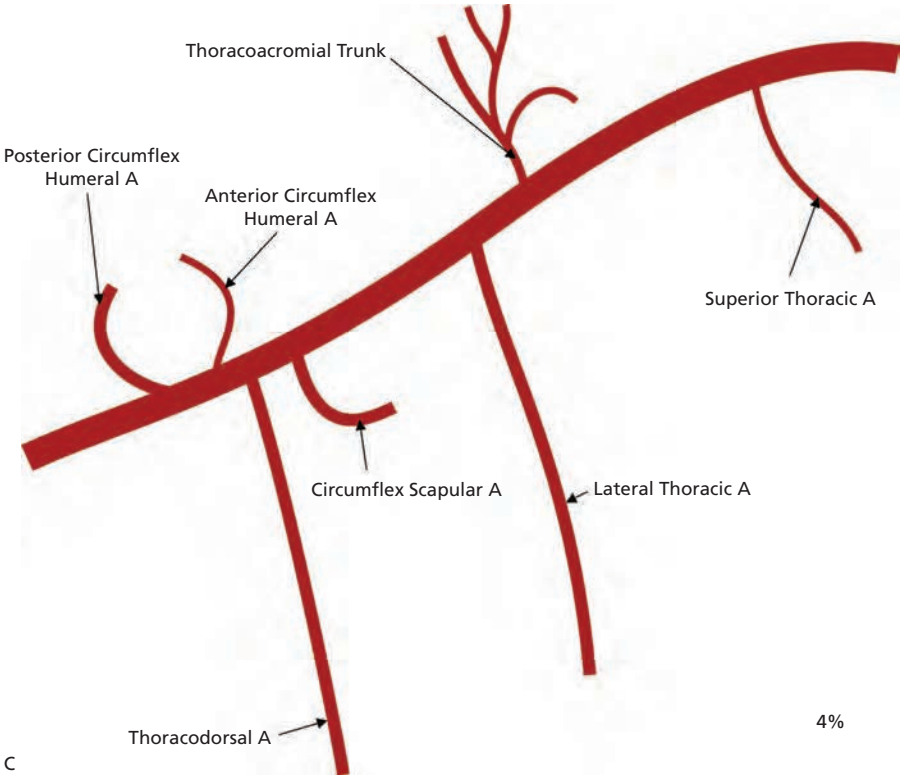

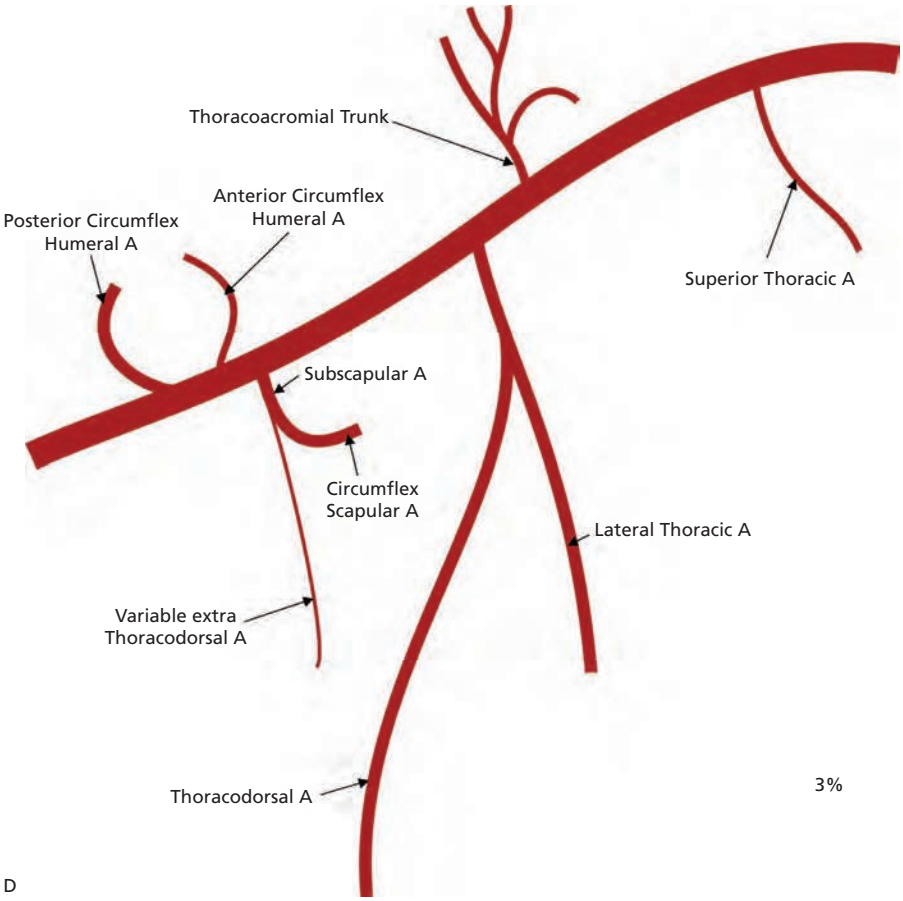

Figure 53.4 *(continued)* (c) thoracodorsal artery and circumflex scapular artery originating separately with no subscapular artery (4%); (d) thoracodorsal artery originating from the lateral thoracic artery with variable additional thoracodorsal artery from the subscapular artery (3%)

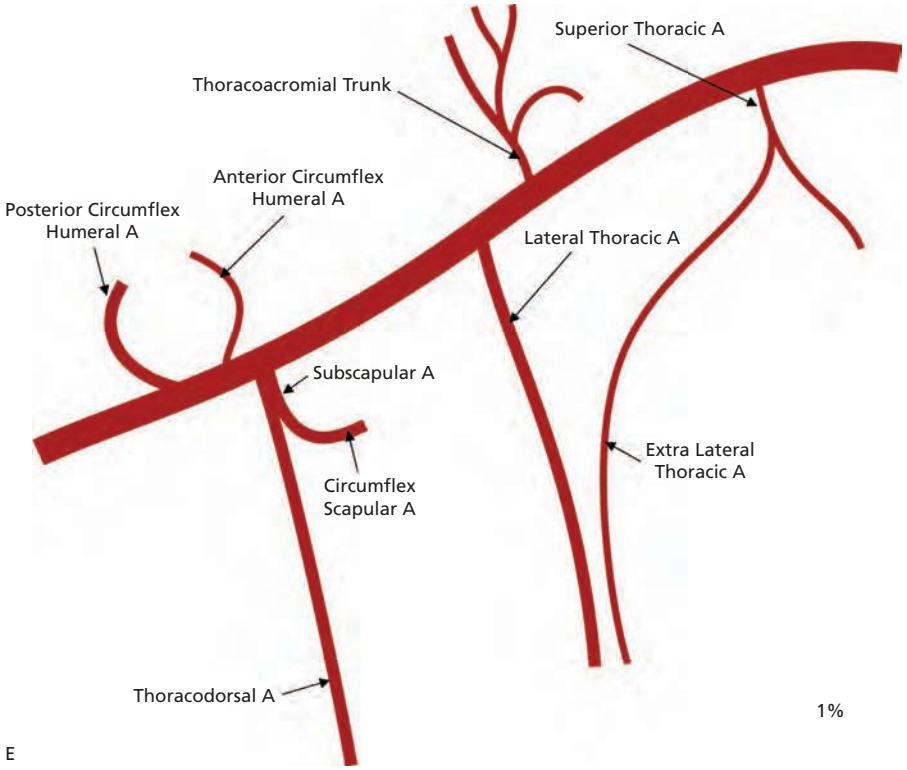

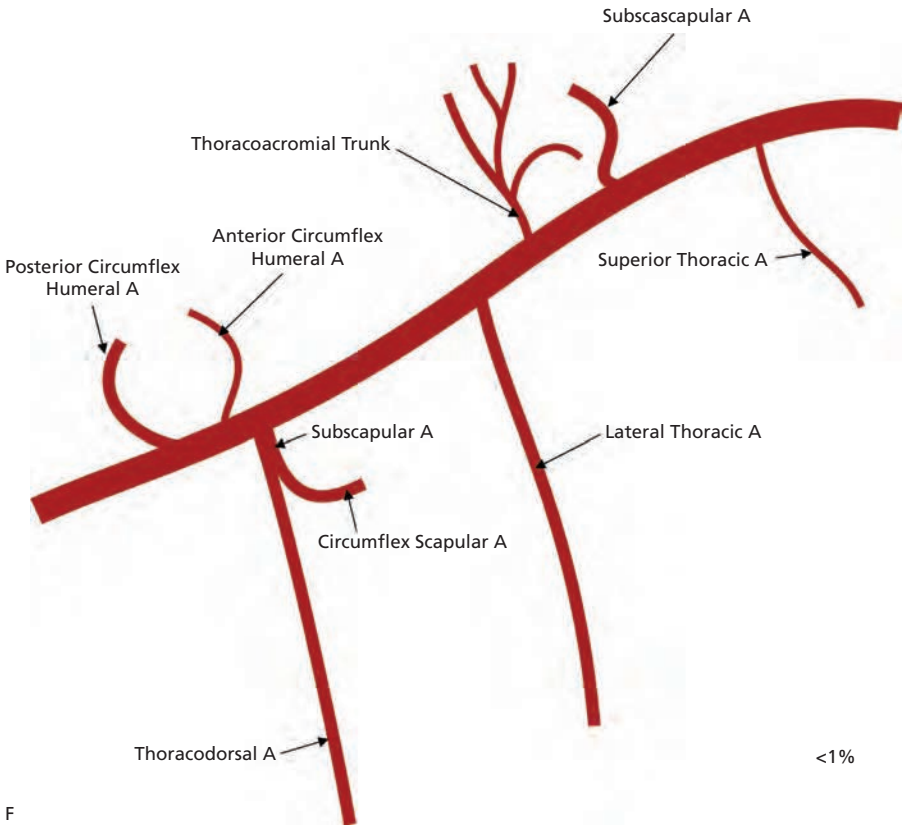

Figure 53.4 *(continued)* (e) additional branch from the superior thoracic artery (1%); and (f) suprascapular artery from the axillary artery (<1%).

There is typically not much variation of the superior thoracic artery beyond absence of the vessel completely, which can occur as much as 63.7% of the time (Baral et al. 2012). As mentioned above, approximately 1% of the time the superior thoracic artery will produce a branch that travels with the lateral thoracic artery (Lippert and Pabst 1985).

Given that the thoracoacromial trunk typically has multiple branches to structures such as the acromion, clavicle, deltoid, and pectoral muscles, it seems logical that there would be variation in the branching patter of those vessels. The most common variation involves the pectoral branches originating directly off of the axillary artery. The lateral thoracic and superior thoracic artery may also arise from the thoracoacromial trunk (Baral et al. 2012).

The majority of variation involving the branches of the axillary artery involves the distal half of the vessel. The lateral thoracic artery originates from the axillary artery as it is classically described from the second half of the artery 78.3% of the time (Olinger and Benninger 2010). The lateral thoracic artery arises from the subscapular artery 4.2% of the time (Olinger and Benninger 2010). The remainder of the time the lateral thoracic artery produces additional branches including the thoracodorsal artery, circumflex scapular artery, subscapular artery, and posterior circumflex humeral artery. Baral et al. (2009) also report observing a large common trunk from the second part of the axillary artery that gave rise to the lateral thoracic, thoracodorsal, subscapular, and anterior and posterior circumflex humeral arteries. Lengele and Dhem (1989) also report observing this phenomenon whereby the axillary artery is anterior to the median nerve roots and a large common trunk produces the majority of the branches of the distal two-thirds of the axillary artery. The lateral thoracic artery was described by Erdogmus and Govsa (2005) as having seven distinct branching patterns in its supply to the upper portion of the serratus anterior muscle.

The subscapular artery also originates from the axillary artery as it is classically described from the third part of the axillary artery 78.3% of the time (Olinger and Benninger 2010). The subscapular artery arises from the lateral thoracic artery 5.4% of the time (Olinger and Benninger 2010). The subscapular artery is absent 2.4% of the time with the thoracodorsal and circumflex scapular arteries arising individually from the lateral thoracic artery (Olinger and Benninger 2010). The remainder of the time the subscapular artery is responsible for producing the posterior circumflex humeral artery (12%; Olinger and Benninger 2010). Jesus et al. (2008) have described the subscapular artery as being present 96.7% of the time and absent 3.3% of the time. Jesus et al. (2008) also described the subscapular artery as having collateral branches (one branch: 31.1%; two branches: 29.3%) that supply the subscapularis muscle. The subscapular artery has been observed originating from the third part of the axillary artery (as is classically described) 81% of the time, from the second part of the axillary artery 13% of the time, and from the first part of the axillary artery 3% of the time (Rowsell et al. 1984). Rowsell et al. (1984) have reported that the circumflex scapular artery arises from the subscapular artery 100% of the time, the thoracodorsal artery arises from the subscapular artery 97% of the time, the muscular branches to the subscapularis arise from the subscapular artery 74% of the time, the cutaneous branches arise from the subscapular artery 28% of the time, the posterior circumflex humeral artery arises from the subscapular artery 28% of the time, the anterior circumflex humeral artery arises from the axillary artery 4% of the time, and branches to the teres major muscle arise from the subscapular artery 4% of the time. Al-Fayez et al. (2010) report observing a large common trunk that arose from the axillary artery and traveled deep to the median nerve roots, while the rest of the axillary artery traveled anterior to the median nerve roots. The large common trunk gave rise to the anterior and posterior circumflex humeral, subscapular, and deep brachial arteries, which then went on to produce its two terminal branches. Maral et al. (1993) describe a specific variation of the branching of the thoracodorsal artery and the clinical implications of variation.

There is little variation of the anterior circumflex humeral artery, but the posterior circumflex humeral artery originates from several different locations. The posterior circumflex humeral artery originates from the third part of the axillary artery (as it is classically described) 77.1% of the time (Olinger and Benninger 2010). The posterior circumflex humeral artery arises from the subscapular artery 12% of the time, the deep brachial artery 8.4% of the time, and from the lateral thoracic artery 1.2% of the time (Olinger and Benninger 2010). The posterior circumflex humeral artery was also observed arising from the subscapular artery by Durgun et al. (2002). The posterior circumflex scapular artery also varies in its distribution. Classically the posterior circumflex humeral artery travels through the quadrangular space of the posterior shoulder and, when the posterior circumflex humeral artery arises from the axillary artery, subscapular artery, and lateral thoracic artery, it travels through the quadrangular space. However, when the posterior circumflex humeral artery arises from the deep brachial artery it travels through the triangular interval 85.7% of the time (Olinger and Benninger 2010).

The termination of the axillary artery was found to be anomalous in 14.3% of cases (Pandey and Shukla 2004). The axillary artery divided into medial and lateral branches at its termination in 6.2% of cases. The axillary artery divided into superficial and deep branches in 3.15 of cases. The axillary artery branched into medial, lateral, and intermediate branches in 2.5% of cases, and the axillary artery tapered significantly in 2.81% of cases.

The remaining studies that describe variability of the axillary artery are case reports of single specimen descriptions of variations.

The axillary artery may give rise to the radial artery, which was accompanied by variations of the vasculature of the hand (Gonzalez-Compta 1991).

The axillary artery has been observed as a double axillary artery bilaterally. This variation included an axillary artery that was very close to the classic description and an axillary artery

that did not follow the classic branching pattern of the axillary artery (Jurjus et al. 1999).

An accessory thoracodorsal artery has been observed arising from the axillary artery just distal from the lateral thoracic artery, with a classical thoracodorsal artery arising from the subscapular artery (Saadeh 1984).

Ozan et al. (1994), Natsis et al. (2006), and Panagouli et al. (2009) describe rare cases whereby a branch called the superficial ulnar artery arises from the axillary artery at the level of the median nerve rots, which then travels distally down the arm into the forearm to supply structures of the forearm.

The axillary artery has also been observed branching into superficial and brachial arteries proximal to the teres major, where the vessel would have become the brachial artery (Cavdar et al. 2000). Similar findings were observed by VijayaBhaskar et al. (2006).

Lee and Kim (2008) observed the anomalous branching of the subscapular artery bilaterally in one case whereby a very large subscapular artery arose from the second part of the axillary artery and produced the lateral thoracic artery and posterior circumflex humeral artery, in addition to the thoracodorsal and circumflex scapular artery.

The special relationship between the axillary artery and the brachial plexus can also be quite anomalous depending on the course and distribution of the axillary artery (Aizawa et al. 1995, 1996).

Brachial artery

The brachial artery is the continuation of the axillary artery distal to the teres major muscle. The brachial artery produces the deep brachial artery, superior and inferior ulnar collateral arteries, and some muscular and skeletal branches to the surrounding musculature and humerus. The deep brachial artery and superior ulnar collateral artery branch from the brachial artery superiorly, while the inferior ulnar collateral artery branches more distally down the arm.

Variation of the brachial artery is very common and has been reported in numerous publications (Sandifort 1777; Meckel 1816; Struthers 1848; Maestre 1864; Henle 1868; Charles 1873, 1875; Krause 1876; Cappi 1879; Bonora and Casati 1880; Dean 1880; Shepherd 1883; Winslow 1883b; Ruge 1884; Esquerdo 1887; Schwalbe 1889, 1895; Rossi 1890; Cocchi 1891; Janosík 1891; Bayer 1893; Souligoux 1893; Carson 1895; Zuckerkandl 1895; Bertacchini 1896; Jaschtschiniski 1897; Brême 1899; Müller 1903; Göppert 1904; Georgievski 1905; Gérard 1905; Gérard and Breucq 1905; Herrington 1905; Hofer and Hofer 1910; Schaefer et al. 1915; Forster 1917–18; Dubreuil-Chambardel 1926; Barta and Petrovits 1927; Dieulaufe and Cahuzac 1931; Polonskaja 1932; Brunati 1937; Siegbauer 1940; Bianchi 1943; Maruyama 1944; Latarjet 1948; Rauber and Kopsch 1948; Weathersby 1956a; Jurjus et al. 1986; Bassett et al. 1994; Yucel 1999).

According to Poynter (1922) there are major variations involving the brachial artery in 25% of cases, which typically have an explanation based on embryology. Poynter (1922) described two main classes of arterial arm variation. One involved the brachial artery traveling anterior to the median nerve; the other main variation involves the doubling of the brachial artery into a superficial and deep brachial artery. Power (1850) described a brachial artery that divided into two branches in the arm to reunite as a single trunk, which then divided normally into ulnar and radial branches.The brachial artery traveling anterior to the median nerve can either occur at the median nerve roots in the axillary where it is called superficial brachial artery superior, despite the fact that when this typically happens it is actually the axillary artery in this position more so than the brachial artery (Olinger et al. 2012). In the other version of superficial brachial artery, the artery travels posterior to the median nerve roots but then travels anterior to the median nerve more distally in the arm.

When the brachial artery is doubled in the arm or possesses a high bifurcation of the vessel, according to Poynter (1922) the superficial and deep brachial artery can reunite distally, superficial brachial artery can become the radial artery with or without anastomoses, superficial brachial artery can become the ulnar artery, median artery or both, and finally the superficial brachial artery can become both the radial artery and superficial antebrachial artery. Jurjus et al. (1986) observed a double brachial artery that produced a deep brachial artery with no collateral branches. One of the branches of the double brachial artery continued as a radial artery, the other as a common interosseous artery.

When the brachial artery is positioned anterior to the median nerve it is described as superficial brachial artery. This variation typically occurs 9% of the time and is accompanied by little variation distally along the course of the vessel. The superficial brachial artery still produces the ulnar and radial arteries in the cubital fossa. Typically the deep brachial artery will originate from some large common trunk that produces the subscapular artery and also both humeral circumflex arteries.

Lippert and Pabst (1985) have reported the frequencies of classically described brachial artery versus superficial brachial artery and the relationship to the median nerve based on various reports (Adachi 1928; Schwyzer and de Garis 1935; McCormack et al. 1953; Lanz and Wachsmuth 1959; Skopakoff 1959a, b; Smith-Agreda 1959; Wankoff 1961; Anson 1963; Seldinger 1964; Kadanoff and Balkansky 1966; Handa et al. 1967; Loetzke and Kleinau 1968; Pabst and Lippert 1968; Maraspin 1971). Those findings are as follows.

Classic arrangement of the brachial artery and median nerve occur 75% of the time (Fig. 53.5a), with 3% of cases being a classically positioned brachial with a lack of typical median nerve (Fig. 53.5b). In 5% of cases the brachial artery is posterior to the median nerve roots, but then crosses anterior to the median nerve in the arm (Fig. 53.6a). In 2% of cases the brachial artery is anterior to the median nerve roots in the axilla and remains anterior

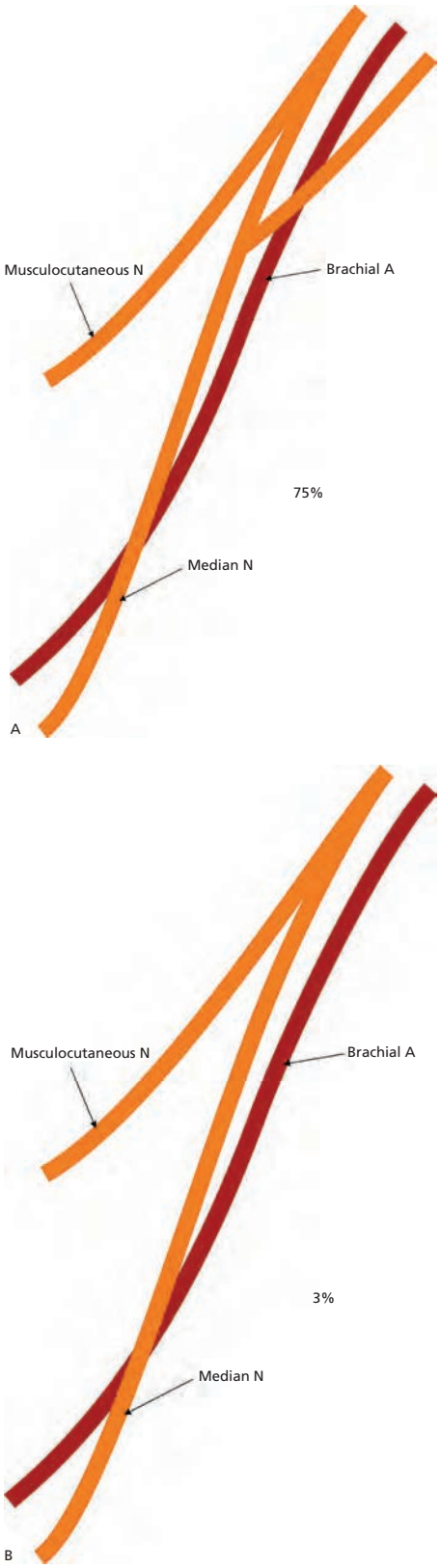

Figure 53.5 Relationship between brachial artery and median nerve: (a) classic arrangement between the brachial artery and median nerve (75%); (b) brachial artery posterior to an atypical median nerve (3%).

to the median nerve throughout the arm (Fig. 53.6b). In 1% of cases the brachial artery is posterior to the median nerve roots in the axilla but then travels anterior to a communicating branch between the musculocutanous nerve in the arm (Fig. 53.6c). The median nerve does not form correctly in the axilla 1% of the time, and the superficial brachial artery travels anterior to the median nerve more distally in the arm (Fig. 53.6d).

In 13% of cases the brachial artery possesses two main arterial stems, a brachial artery and superficial brachial artery. In 8% of cases the brachial artery will split in the arm and send one branch anterior to the median nerve and one posterior to the median nerve (Fig. 53.7a). In 4% of cases the brachial artery and superficial brachial artery will split the median nerve roots in the axilla sending one branch anterior and one branch posterior (Fig. 53.7b). Less than 1% of the time the brachial artery will split in the arm and send one branch anterior and one posterior to a communicating branch between the musculocutaneous nerve and median nerve (Fig. 53.7c). Less than 1% of the time the brachial artery will split in the arm and send both branches anterior to the median nerve in the arm (Fig. 53.7d).

Sometimes the brachial artery is doubled in the arm and will exist as a superficial and deep branch or as a medial and lateral branch. Doubling of the brachial artery is sometimes simply an early bifurcation of the brachial artery into the radial and ulnar arteries, while other times one of the branches (superficial, deep, medial, or lateral) will go on to branch into the radial and ulnar arteries. Celik et al. (1996) report an early bifurcation of the brachial artery into radial and ulnar arteries near the median nerve roots. Other times, when the brachial artery is doubled into superficial and deep branches, the superficial brachial artery will persist as what is called the median artery or interosseous artery.

The superficial brachial artery will often continue as the radial artery; more than half the time than it continues as the ulnar artery. Several studies do however report cases whereby the superficial brachial artery continues as the ulnar artery or superficial ulnar artery (Pabst and Lippert 1968; Aharinejad et al. 1997; Nakatani et al. 1998). A study by Yang et al. (2008) reports the different classifications of superficial brachial artery and the frequencies of each variation. Yang et al. (2008) examined 304 upper limbs and observed superficial brachial artery in 12.2% of subjects. Each of the three types observed by Yang et al. (2008) showed a superficial brachial artery anterior to the median nerve roots and an actual brachial artery deep to the median nerve roots. Type I of the Yang et al. (2008) study described the superficial brachial artery anterior to the median nerve roots, with the majority of the branches of the distal part of the axillary artery originating from the deep branch of the doubled brachial artery in 8.9% of subjects. Type II of the Yang et al. (2008) study was similar to Type I, except the subscapular and its branches came from the axillary artery rather than the deep branch of the doubled brachial artery and occurred 2.3% of the time. Finally, Type III of the Yang et al. (2008) study had the doubled brachial artery splitting distal to the convergence of

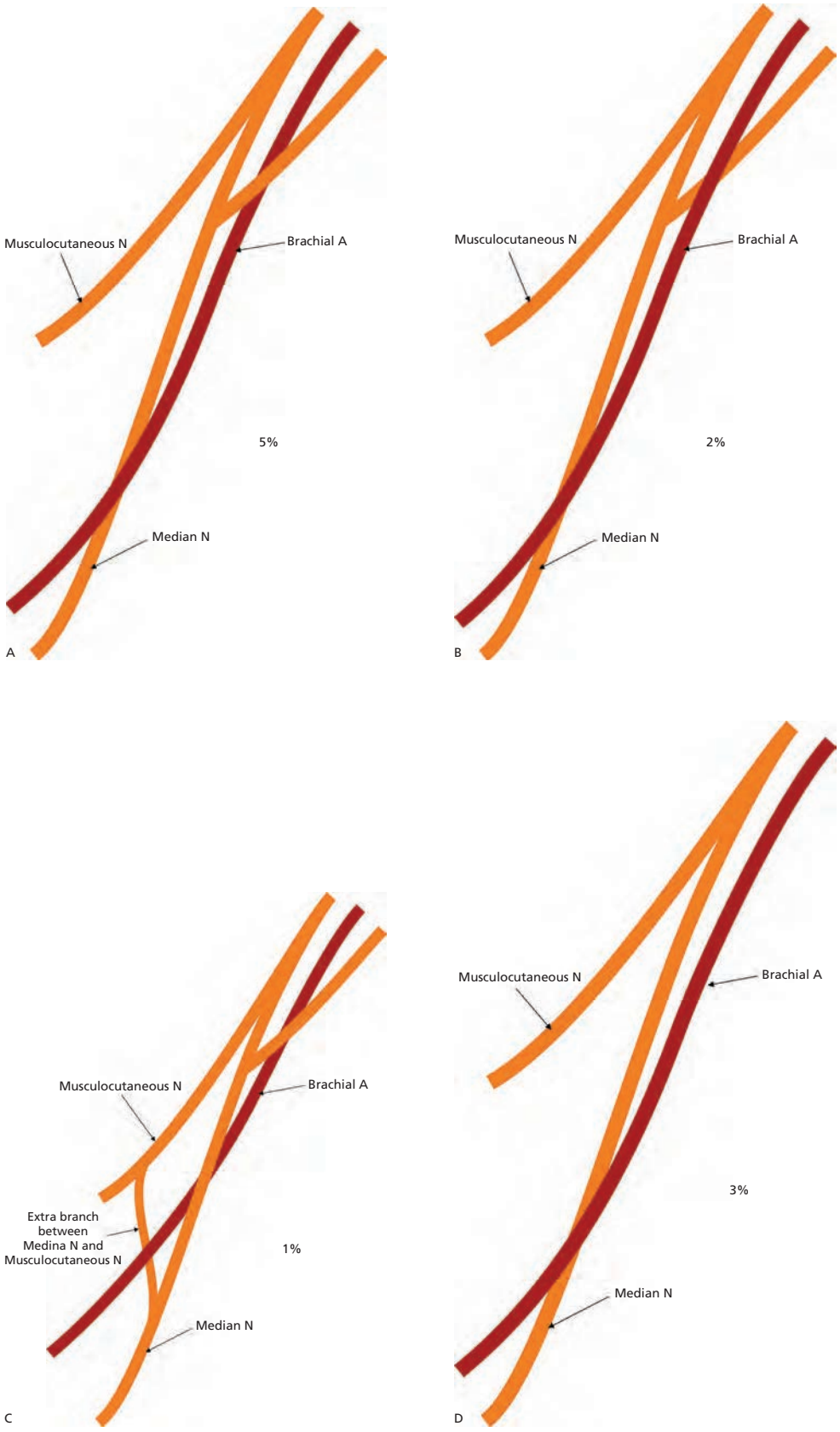

Figure 53.6 Relationship between brachial artery and median nerve: (a) brachial artery posterior to the median nerve crosses anterior to the median nerve in the brachium (5%); (b) brachial artery anterior to the median nerve throughout the brachium (2%); (c) brachial artery posterior to the median nerve but anterior to an additional branch between the musculocutaneous nerve and median nerve (1%); and (d) brachial artery travels anterior to the irregularly formed median nerve (1%)

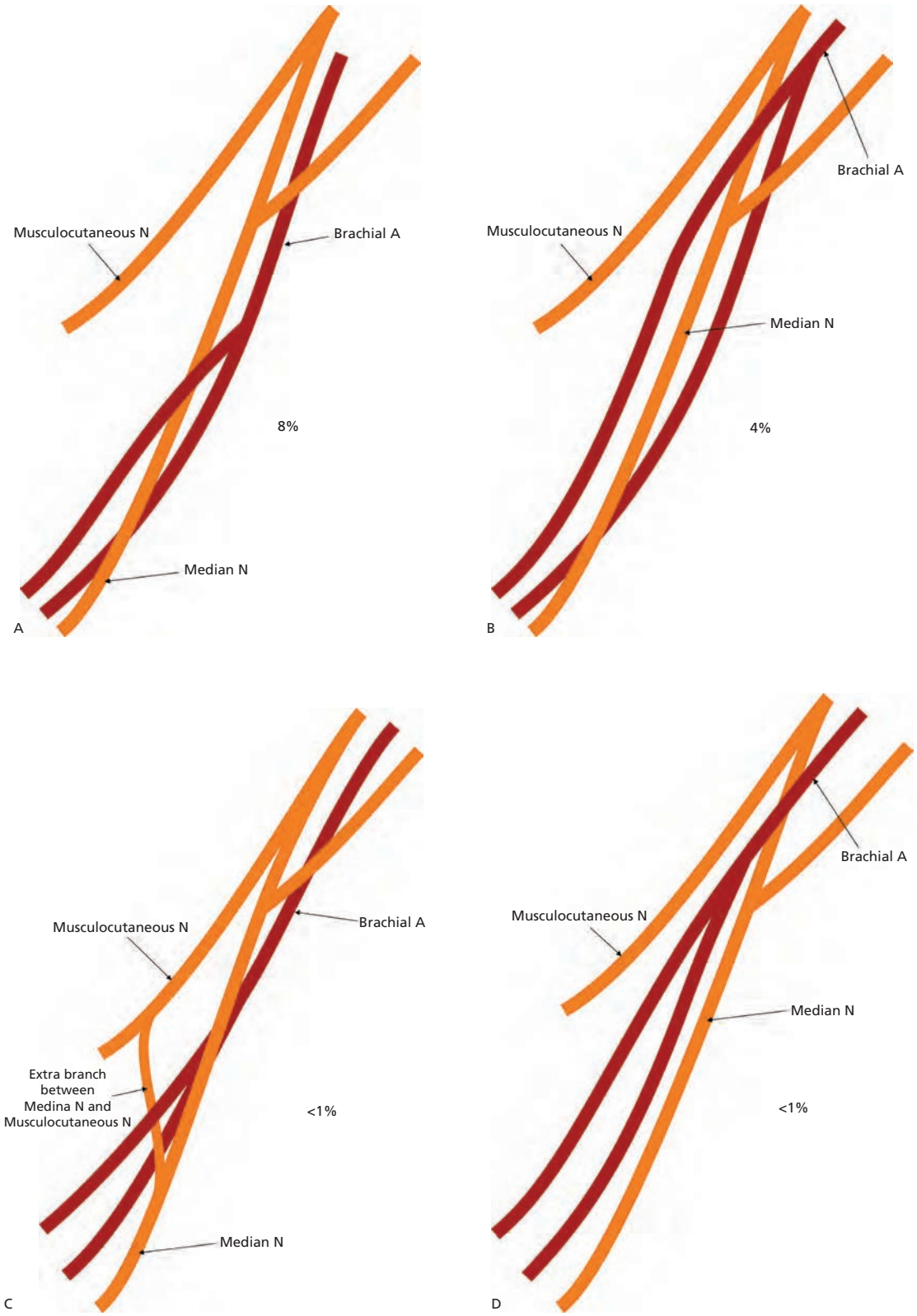

Figure 53.7 Two arterial stems of the brachial artery deep and superficial branches (13%) and the relationship to the median nerve: (a) superficial branch superficial to the median nerve and deep branch deep to the median nerve (8%); (b) superficial branch superficial to the roots of the median nerve (4%); (c) superficial branch superficial to an additional branch between the musculocutaneous nerve and median nerve (<1%); and (d) both superficial and deep branches superficial to the median nerve (<1%).

the median nerve roots, but with one branch clearly superficial to the other and the deep branch producing the majority of the branches of the distal axillary artery 1.0% of the time.

The superficial brachial artery has been observed taking rare courses through the arm including around the ulnar nerve and then back to travel with the median nerve (Yoshinaga et al. 2003). Goswami et al. (2013) describe a superficial and deep brachial artery whereby the superficial brachial artery was located more medially and branched into the radial and ulnar arteries in the cubital fossa. The deep brachial artery was more lateral and traveled deep to the pronator teres and terminated as the common interosseous artery. Aughsteen et al. (2011) report a case of a doubled brachial artery with a medial and lateral branch; the larger medial branch gave rise to the superficial ulnar artery and radial artery. The radial artery gave rise to the common interosseous artery and traveled deep to the pronator teres muscle (Baral et al. 2012). The smaller lateral branch traveled into the cubital fossa and produced all of the branches of a classically described brachial artery. Yucel (1999) reports a case of a unilateral brachial artery that split into radial and ulnar arteries 5 cm distal to its origin. The radial artery started on the medial side of the arm then crossed the ulnar artery to get to the lateral forearm. The inferior ulnar collateral artery arose from the ulnar artery rather than the brachial artery.

The brachial artery has also been observed trifurcating into three branches in the arm and forearm, often accompanied by variability of the courses of the vessels. Loetzke and Kleinau (1968) describe a simultaneous appearance of the superficial brachial artery, radial artery and superficial dorsal artery of the forearm. Malcic-Gürbüz et al. (2002) describe a trifurcation of the brachial artery into the radial, ulnar, and superior ulnar collateral artery in the arm. Vollala et al. (2008a) describe a trifurcation of the brachial artery whereby the radial artery traveled deep to the pronator teres.

Ciervo et al. (2001) describe a very rare variation whereby the brachial artery was completely absent and replaced by an unnamed tortuous branch that coursed between the coracobrachialis and the triceps brachii muscle, before rejoining a seemingly classic brachial artery that bifurcated into the radial and ulnar arteries proximal to the cuibital fossa. Neither the deep brachial artery nor the ulnar collateral artery were present in this subject.

The deep brachial artery classically originates from the brachial artery and then divides into the radial collateral and middle collateral artery of the elbow anastomosis deep to the lateral and long head of the triceps brachii muscle. The deep brachial artery was classified by Charles et al. (1931) into seven types. The deep brachial artery can originate from the brachial artery as a single branch, double branch, or triple branch (Type I, Type Ia, and Type Ib, respectively; Fig. 53.8a–c). The deep brachial artery can originate from the brachial artery as a common trunk with the superior ulnar collateral artery (Type II; Fig. 53.8d). The deep brachial artery can originate at the teres major muscle between axillary and brachial arteries (Type III; Fig. 53.8e). The deep brachial artery can originate from the axillary artery (Type IV; Fig. 53.8f). Nayak et al. (2008) also report observing the variation whereby the deep brachial artery originates from the axillary artery. The deep brachial artery can originate as a common trunk with the posterior circumflex humeral artery (Type V; Fig. 53.8g). The deep brachial artery can originate as a branch of the subscapular artery from the axillary artery (Type VI; Fig. 53.8h). Finally, the deep brachial artery can be entirely absent (Type VII; Fig. 53.8i). Olinger and Benninger (2010) disrobe the deep brachial artery and posterior circumflex humeral artery originating from the axillary artery as a common trunk, Charles et al. (1931) Type V, occurring 8.4% of the time. Celik et al. (2004) have observed and reported on Charles et al. (1931) Type Ia and Type II variations of the brachial artery, and go on to report that Type Ia variation is observed 0.7% of the time and Type II occurring 22.3% of the time.

According to Basset et al. (1994) the brachial artery can be compressed by the bicipital aponeurosis to the extent that it can cause pain and obliterate the radial pulse.

The principle blood supply to the hand in the developing embryo is a branch of the brachial artery called the median artery (Fig. 53.9). The median artery is reported to persist in as many as 8% of the population (Dubreuil-Chambardel 1922; Duval and Loescher 1959; Misra 1955), while other studies suggest that frequency to be much smaller (Baral et al. 2012). The median artery should become the anterior interosseous artery, leaving the radial and ulnar arteries as the principle blood supply to the hand. The median artery and anterior interosseous artery have been observed supplying the superficial palmar arterial arch. The median artery has been observed supplying the digits directly in the absence of palmar arch. The median artery is also capable of traveling through the carpal tunnel, where it has been shown to be involved with complications secondary to thrombosis (Maxwell et al. 1973; Levy and Pauker 1978; Barfred et al. 1985). The median artery may also travel very superficially through the forearm, making it much more susceptible to injury (Rossi 1890).

According to Lippert and Pabst (1985; based on the original research of Adachi 1928; Anson 1963; Pabst and Lippert 1968), the median artery originates from the ulnar artery distal to the origin of the common interosseous artery 3% of the time (Fig. 53.10a) and proximal to the common interosseous artery 2% of the time (Fig. 53.10b). The median artery originates from the common interosseous artery 2% of the time (Fig. 53.10c) and from the anterior interosseous artery 1% of the time (Fig. 53.10d). Less than 1% of the time, the median artery originates from the radial artery (Fig. 53.10e) or from some kind of anastomosis between the radial and brachial arteries (Fig. 53.10f). Poornima and Dakshayani (2011) report observing a persistent median artery accompanied by a variety of muscular anomalies.

According to Rossi (1890) a small branch may arise from the brachial artery near the origin of the deep brachial artery, travel distally through the arm and join with the radial artery; this is referred to as the vas aberrans.

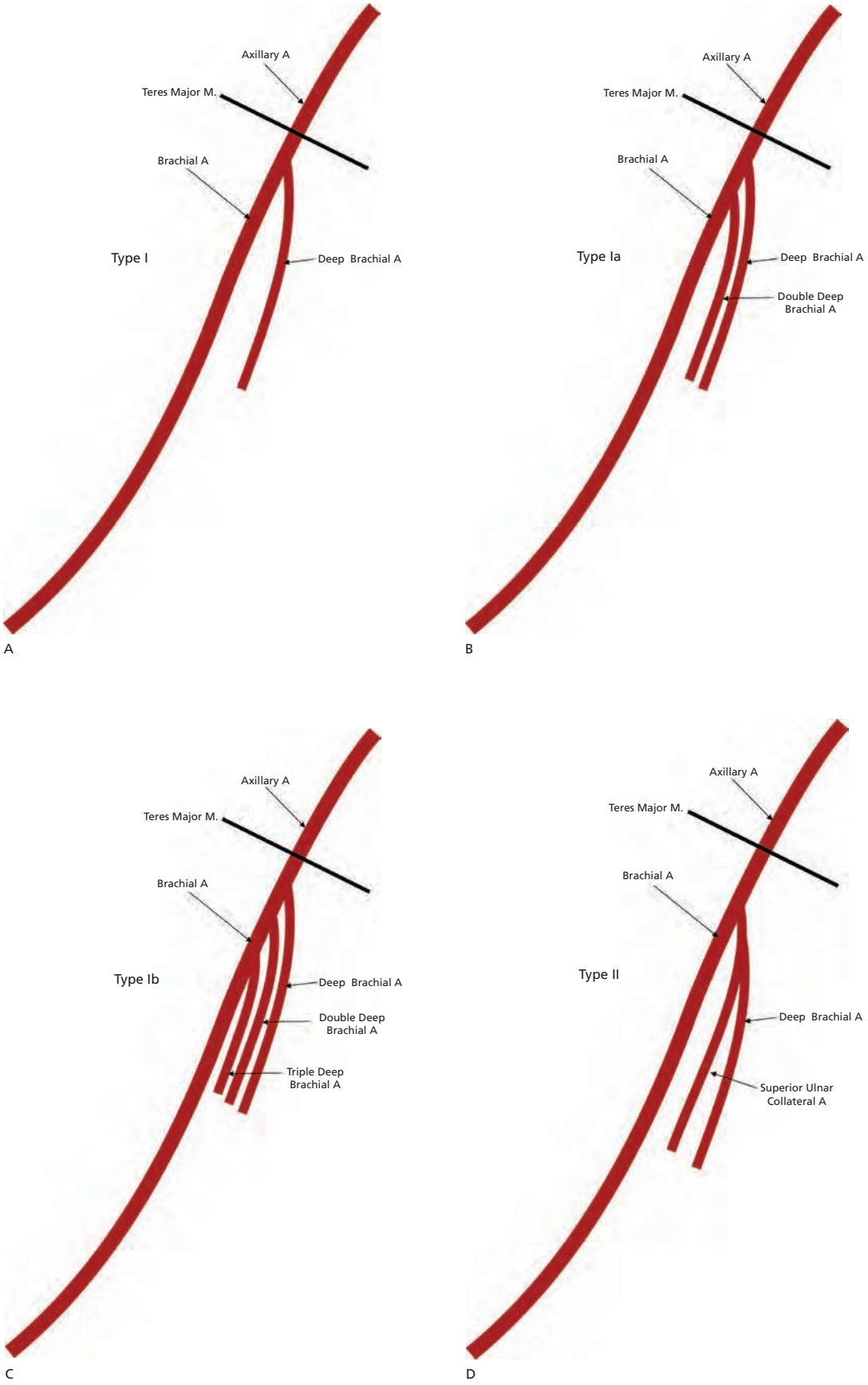

Figure 53.8 Typing of the deep brachial artery: (a) type Ia deep brachial artery, single artery; (b) type Ib deep brachial artery, doubled artery; (c) type Ic deep brachial artery, tripled artery; (d) type II deep brachial artery as a common trunk with the superior ulnar collateral artery.

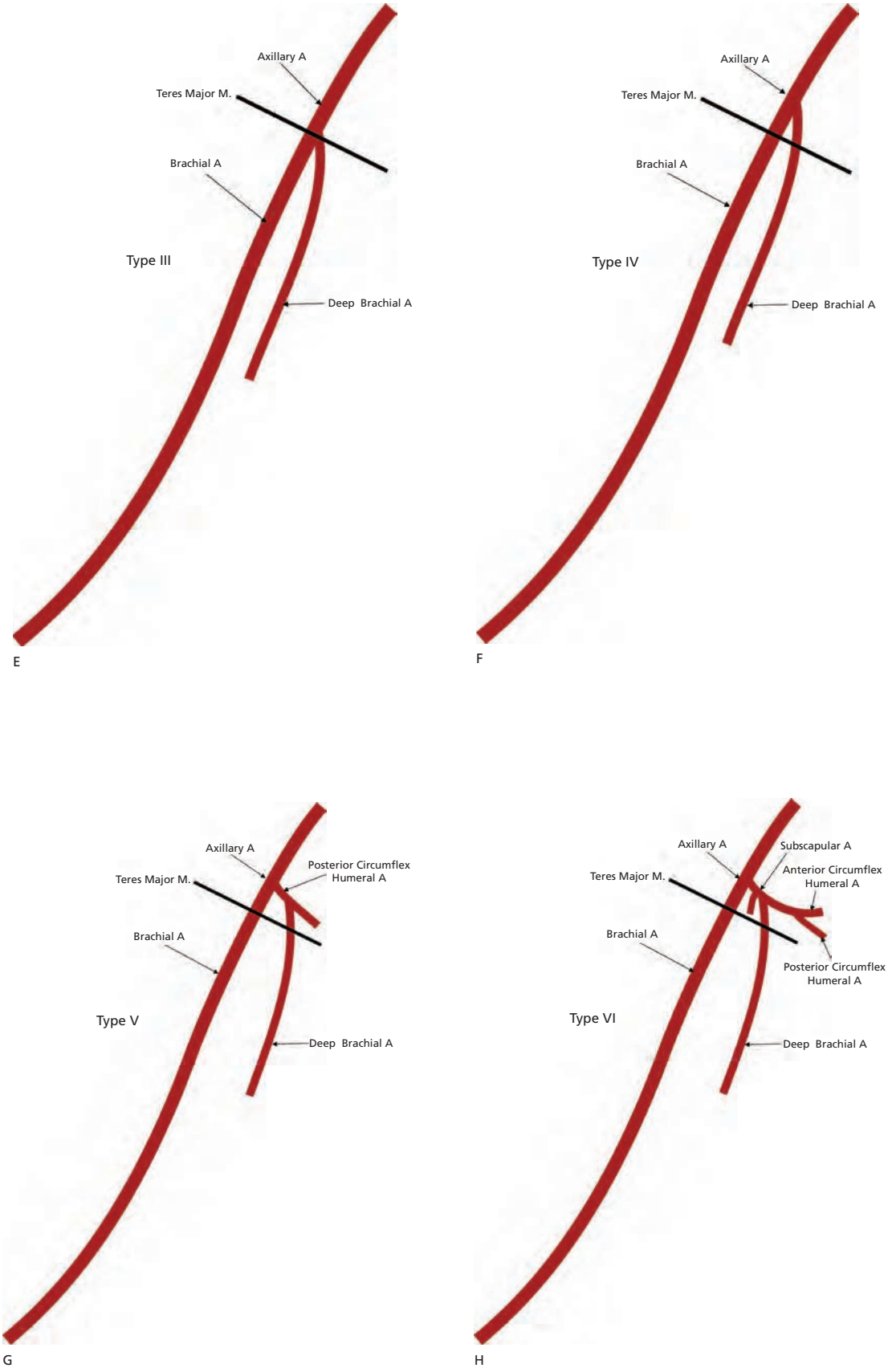

Figure 53.8 *(continued)* (e) type III deep brachial artery originating at the teres major m.; (f) type IV deep brachial artery originates from the axillary artery; (g) type V deep brachial artery originates from the posterior humeral circumflex artery; (h) type VI deep brachial artery originates from the subscapular artery.

(continued)

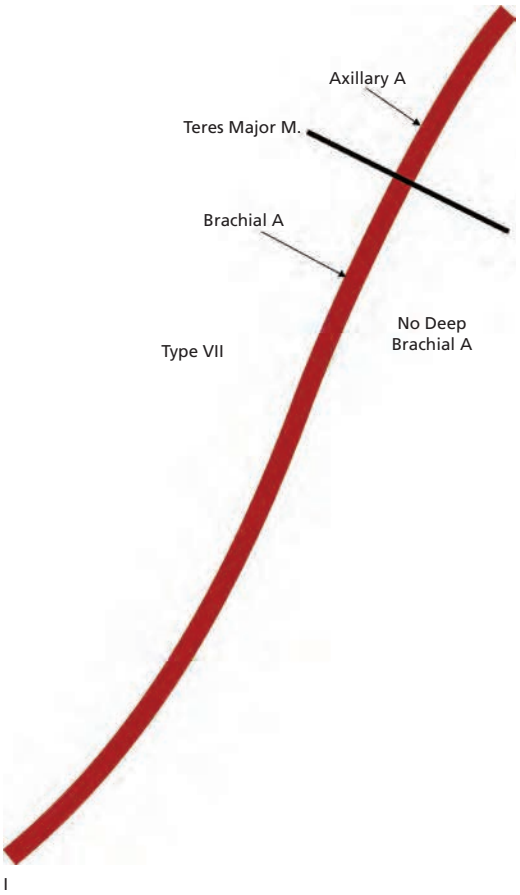

Figure 53.8 *(continued)* (i) type VII, no deep brachial artery.

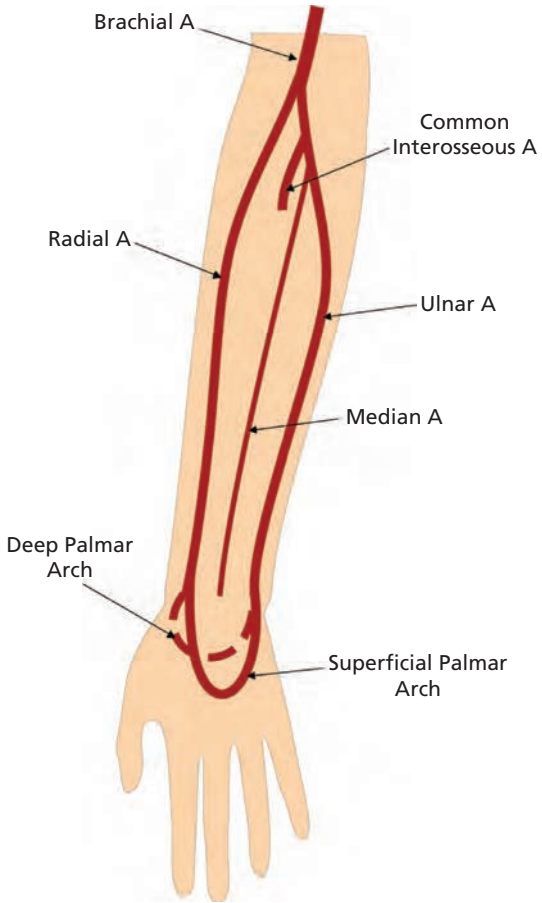

Figure 53.9 Illustration of the median artery in the development of the upper limb.

Radial artery

The radial artery is classically the smaller of the two terminal branches of the brachial artery. It typically arises in the cubital fossa with the ulnar artery. The radial artery produces the radial recurrent artery, which feeds into the elbow anastomosis, then courses though the forearm supplying the musculature of the forearm. The radial artery produces a palmar carpal branch, and a palmar branch then travels through the floor of the anatomical snuffbox and travels posteriorly around the first metacarpal. While it is posterior to the first metacarpal the radial artery produces the dorsalis pollicis artery, first dorsal metacarpal artery, and princeps pollicis artery before entering the hand. The radial artery is the primary blood supply to the deep palmar arterial arch.

Variation of the radial artery is common and has been reported in numerous publications (Yelloly 1801; Gruber 1864, 1870a–c; Chuquet 1876; Schneck 1879; Kadyi 1881; Park 1883; Winslow 1883c; Thomson 1884; Charles 1894; Salvi 1898; Bartels 1900; Sussloff 1903; Dibailoff 1904; Pitzorno 1907; Brick 1909; Sankott 1919–20a, b; Guerrier and Paleirac 1951; Coleman and Anson 1961; Mozersky et al. 1973; Gajisin et al. 1983; Earley 1986), and the majority of variation is based on the development of the vessel (Senior 1926).

According to Lippert and Pabst (1985; based on the original work of Adachi 1928; McCormack et al. 1953; Lanz and Wachsmuth 1959; Smith-Agreda 1959; Turner 1959; Anson 1963; Weathersby 1956a; Kadanoff and Balkansky 1966; Loetzke and Kleinau 1968; Pabst and Lippert 1968), the classic branching pattern of the radial and ulnar arteries occurs 84% of the time (Fig. 53.11). The radial, ulnar, and common interosseous artery all arise directly from the brachial artery 70% of the time (Fig. 53.12a). Approximately 6% of the time, the radial and ulnar arise together from the superficial brachial artery (Fig. 53.12b). The radial artery may arise from the superficial brachial artery 5% of the time, with the ulnar and common interosseous arteries arising from the brachial artery (Fig. 53.12c); when this happens (approximately 3% of the time), there is an extensive anastomosis between the radial and the brachial artery proper (Fig. 53.12d). The radial artery may be doubled in the forearm with a deep version, traveling the classic course of the radial artery, and a superficial radial artery traveling superficially toward the

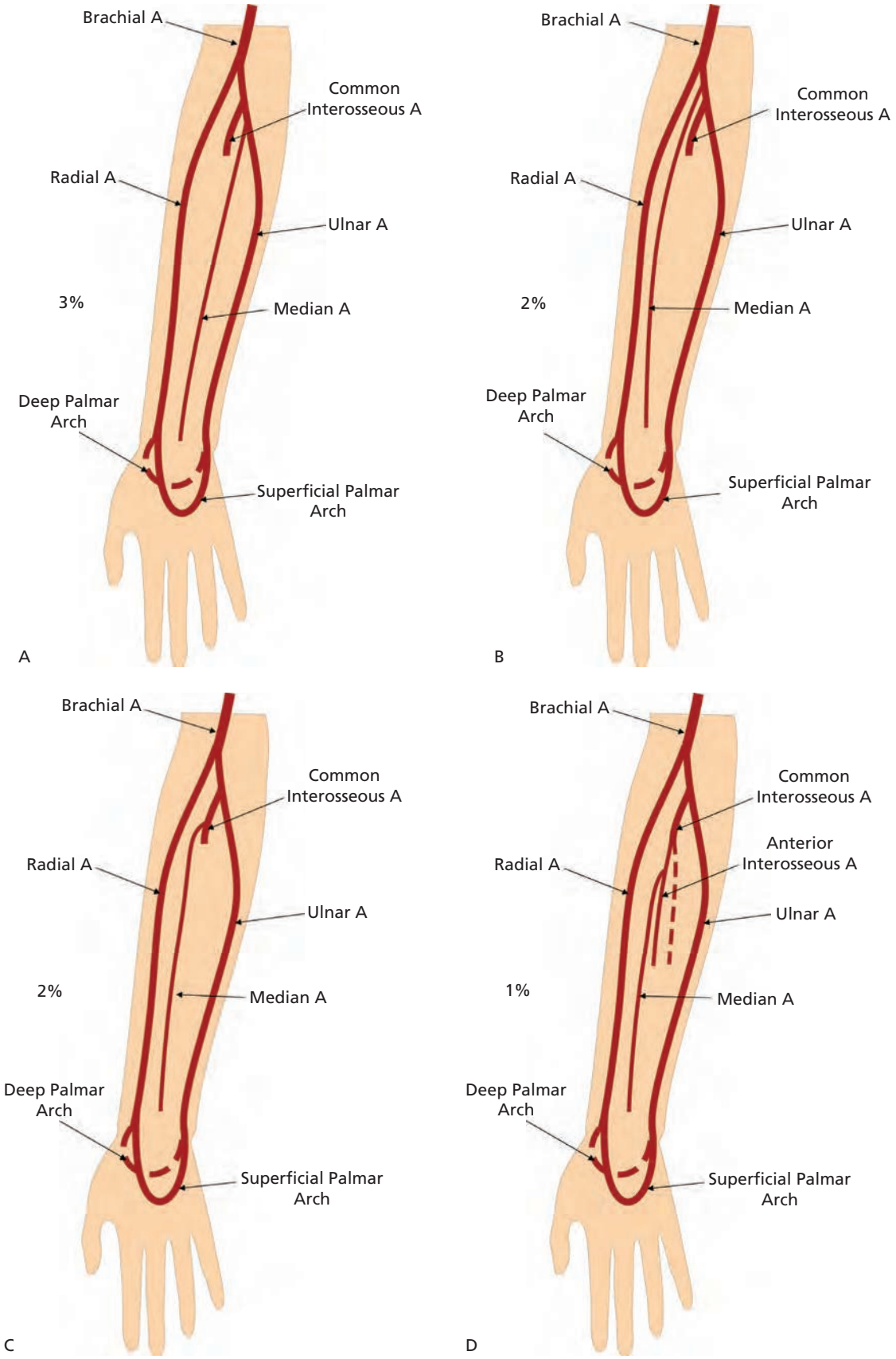

Figure 53.10 Persistence of the median artery: (a) median artery originates from the ulnar artery distal to the common interosseous artery (3%); (b) median artery originates from the ulnar artery proximal to the common interosseous artery (2%); (c) median artery originates from the common interosseous artery (2%); (d) median artery originates from the anterior interosseous artery (1%).

(continued)

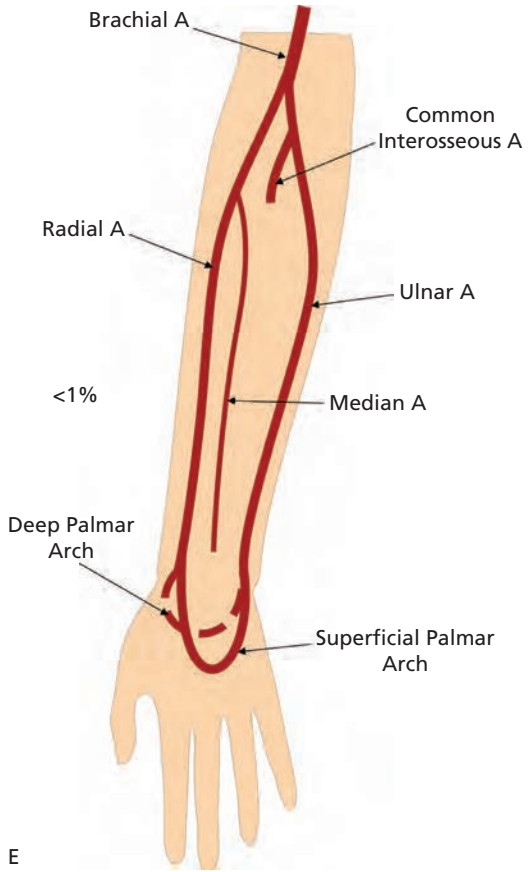

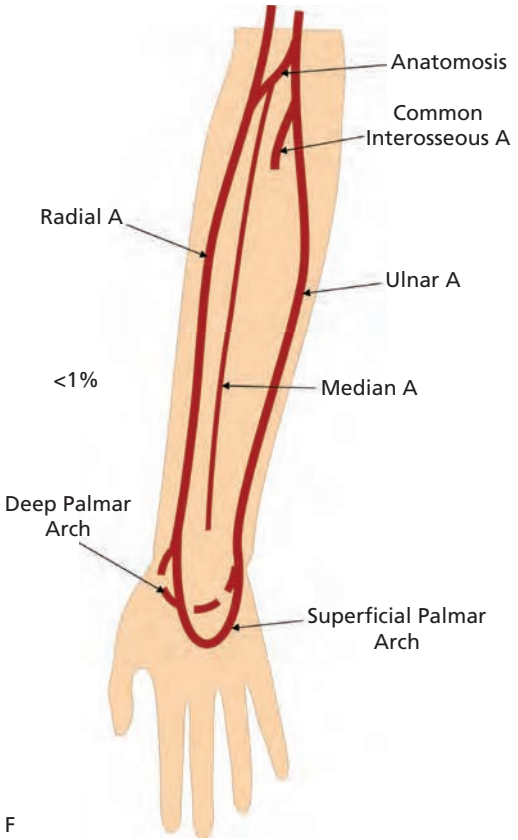

Figure 53.10 *(continued)* (e) median artery originates from the radial artery (<1%); and (f) median artery originates from an anomalous anastomosis between the radial and ulnar arteries (<1%).

hand, which occurs 1% of the time. In this case of superficial radial artery, the palmar branch may carry out the typical role of the radial artery (Sachs 1987).

A high origin of the radial artery is the most common variation of the radial artery with an overall incidence of 14.3% when examined on cadavers, and 9.8% when examined on radiology (Pelin et al. 2006). Celik et al. (2001) examined arteriograms and have reported the incidence of high origin of the radial artery from the brachial artery at 8.6% and high origin of the radial artery from the axillary artery at 1.2%. High origin of the radial artery typically refers to the radial artery arising from the axillary artery and can occur unilaterally (Yagain et al. 2012) and bilaterally (Icten et al. 1996; Gonzalez-Compta 1991). Both cases by Icten et al. (1996) and Gonzalez-Compta (1991) also described a variety of vascular anomalies in the hand. Muresian et al. (2008) report a case of high origin of the radial artery from the brachial artery, whereby the radial artery was occluded at the level of the elbow and collateral circulation filled the part of the radial artery distal to the occlusion. The radial artery may also arise from the deep brachial artery (Mehta et al. 2008). Loukas and Curry (2006) found a radial artery that arose from the thoracodorsal artery.

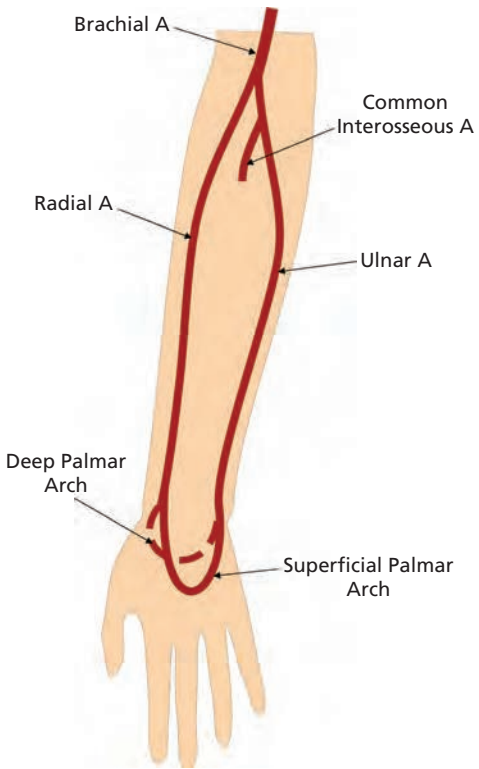

Figure 53.11 Classic branching pattern of the radial and ulnar arteries.

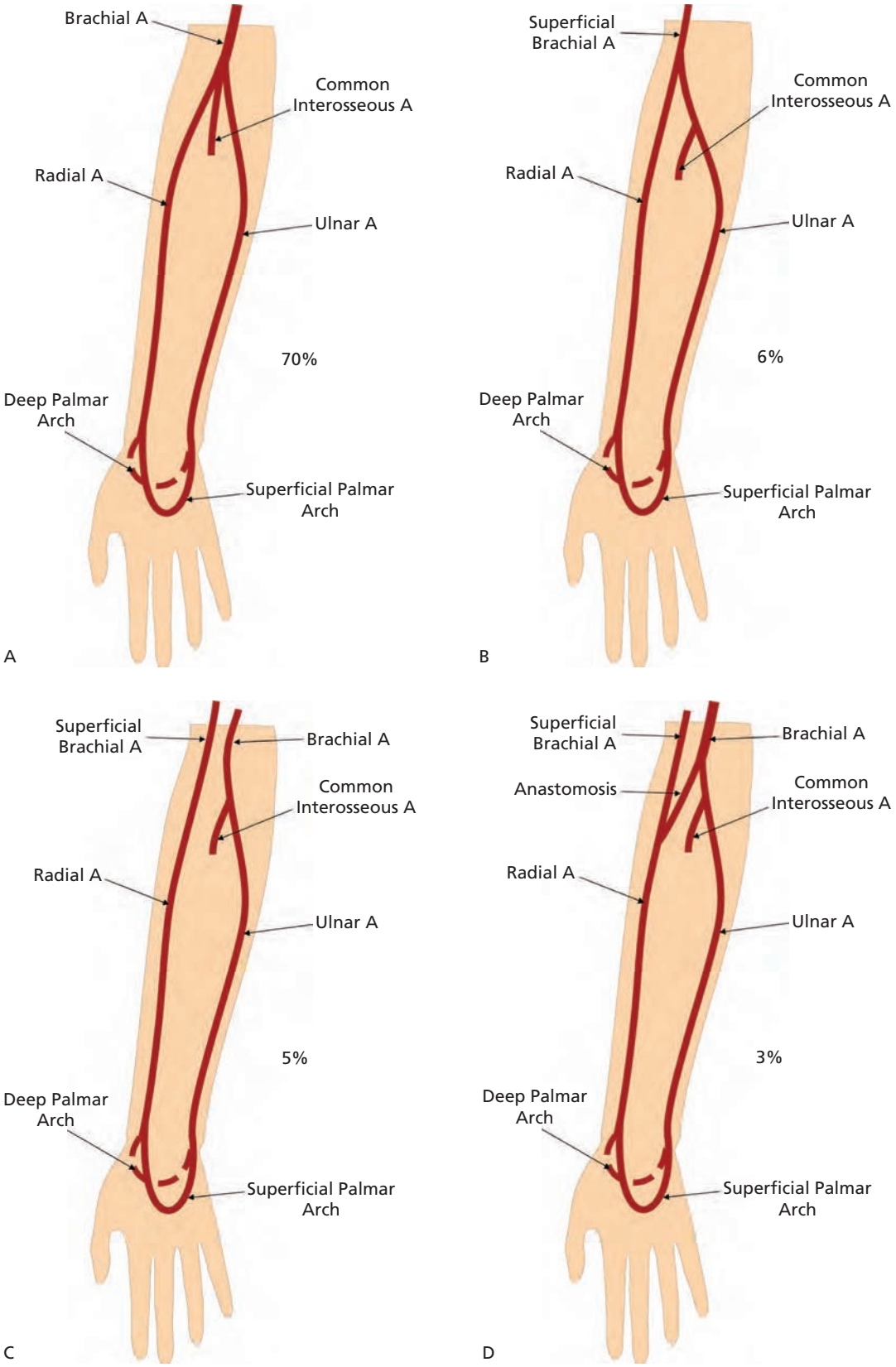

Figure 53.12 Variable branching of the radial and ulnar arteries. (a) Ulnar, radial and common interosseous arteries all arise directly from the brachial artery (70%); (b) radial and ulnar arteries arise from the superficial brachial artery (6%); (c) radial artery arises from the superficial brachial artery with ulnar and common interosseous arteries arising from the brachial artery (5%); and (d) when the radial artery arises from the superficial brachial artery with ulnar and common interosseous arteries arising from the brachial artery, there is an anastomosis between the radial and brachial arteries (3%).

The radial recurrent artery has been reported to be absent, in which case it is typically replaced by a branch from the superior ulnar collateral artery (Cilley 1881). Durgun et al. (2002) report observing an arciform anastomosis between the radial and ulnar arteries, with a radial recurrent artery arising from the anastomosis.

The radial artery has been described as following a variant course through the forearm, whereby the radial artery originated from the medial side of the brachial artery 12 cm superior to the cubital fossa, then passed over the median nerve twice while deep to the brachioradialis muscle (Pelin et al. 2006).

Poteat (1986) reports a case that involves compete absence of the radial artery unilaterally, which left the anterior interosseous artery to supply the forearm and hand. There was also no visible deep palmar arterial arch in this subject.

In addition to variation involving the branching pattern, course, and distribution of the radial artery, the branches of the radial artery are also capable of anomalous position and supply (Radzikowski and Szulczyk 1972). The superficial palmar branch of the radial artery has been observed traveling superficial to and in contact with the flexor retinaculum to join with the ulnar artery (Tagil et al. 2012). The common interosseous artery, which typically arises from the ulnar artery has been observed arising from the radial artery (SatheeshNaik and Lokanadham 2013).

According to Lippert and Pabst (1985; based on the original work of Adachi 1928; Dimtza 1956; Lanz and Wachsmuth 1959; Coleman and Anson 1961; Anson 1963; Varro et al. 1978; Doscher et al. 1983), the radial artery travels between the first and second metacarpal bones to enter the palm 96% of the time (Fig. 53.13a). In 2% of cases the radial artery will split and send a branch between the first and second metacarpal and a branch between the second and third metacarpals, which both end up in the palm (Fig. 53.13b). In 1% of cases the radial artery can travel between the second and third metacarpals to enter the palm (Fig. 53.13c). Finally, in the case of a superficial radial artery, the superficial radial artery travels between the first and second metacarpals while the deep branch travels between the second and third metacarpals; this occurs 1% of the time (Fig. 53.13d).

Variation involving the radial artery has been shown to be clinically significant, especially with respect to transradial approach to coronary procedures (Dogan et al. 2005; Valsecchi et al. 2006; Cavolli et al. 2007; Nie et al. 2009; Norgaz et al. 2012).

Lo et al. (1986) report an incidence of 16% of Down's syndrome patients possessing an anomalous radial arterial pattern. Eight of the 77 subjects possessed an enlarged anterior interosseous artery, seven of which possessed no actual radial artery. Three of the patients possessed a small radial artery and dominant ulnar artery. One of the patients possessed a radial artery that ended in the musculature of the forearm with no contribution to the hand.

Charles (1903) reported a case of a superficial radial artery, superficial to all of the forearm musculature.

Ulnar artery

The ulnar artery is classically the larger of the two terminal branches of the brachial artery. The ulnar artery typically arises in the cubital fossa with the radial artery. The ulnar artery produces an anterior and posterior ulnar recurrent artery, as well as the common interosseous artery which gives rise to the anterior and posterior interosseous artery, as well as the interosseous recurrent artery. The ulnar artery produces muscular branches as it travels distally through the forearm, then gives rise to a palmar and dorsal carpal branch. The ulnar artery produces a small deep palmar branch that anastomoses with the deep palmar arterial arch, then enters the hand deep to the palmar aponeurosis and forms the superficial palmar arterial arch.

Variations in the course, branching, and distribution of the ulnar artery are common and are therefore the topic of numerous publications (Ramsay 1813; Guyon 1861; Gruber 1867, 1871; Winslow 1883d; Stocquart 1887; Souligoux 1895; Poynter 1922; Bianchi 1943; Maruyama 1944; Blunt 1959; Anson 1966). The ulnar artery can be duplicated or absent.

According to Lippert and Pabst (1985; based on the original work of Adachi 1928; McCormack et al. 1953; Weathersby 1956b; Lanz and Wachsmuth 1959; Smith-Agreda 1959; Turner 1959; Anson 1963; Kadanoff and Balkansky 1966; Loetzke and Kleinau 1968; Pabst and Lippert 1968), the classic branching pattern of the radial and ulnar arteries occurs 84% of the time (Fig. 53.9). In 70% of cases the ulnar, radial and common interosseous artery all branch directly from the brachial artery (Fig. 53.10a). In 3% of cases the ulnar, radial, and common interosseous artery all branch from the brachial artery with extensive anastomosis in the cubital fossa (Fig. 53.10d). According to Lippert and Pabst (1985) 8% of the time a superficial ulnar artery is observed both joining with the ulnar artery and replacing the ulnar artery.

Superficial ulnar artery is a very common anatomical variation with a prevalence of 0.7–9.4% (Sieg et al. 2006). Some cadaveric studies have reported observing a superficial ulnar artery in 4.2% of cases (Dartnell et al. 2007). The superficial ulnar artery has been observed originating from both the brachial artery (Aharinejad et al. 1997; Nakatani et al. 1998) and axillary artery (Ozan et al. 1994). The superficial ulnar artery has also been observed originating from the axillary artery bilaterally (Jacquemin et al. 2001). Yazar et al. (1999) observed a bilateral superficial ulnar artery whereby the left originated from the axillary artery crossed over the median nerve and joined into the radial artery in the hand forming the superficial palmar arterial arch. The right superficial ulnar artery originated from the brachial artery and had an anomalous communication with the superficial palmar arterial arch. Both sides were also accompanied by inverted palmaris longus muscles (Yazar et al. 1999). The superficial nature of the superficial ulnar artery makes it susceptible to accidental intra-arterial injections (Hazlett 1949). Vollala et al. (2009) report observing a superficial ulnar artery in a single cadaver who also had a persistent median artery and

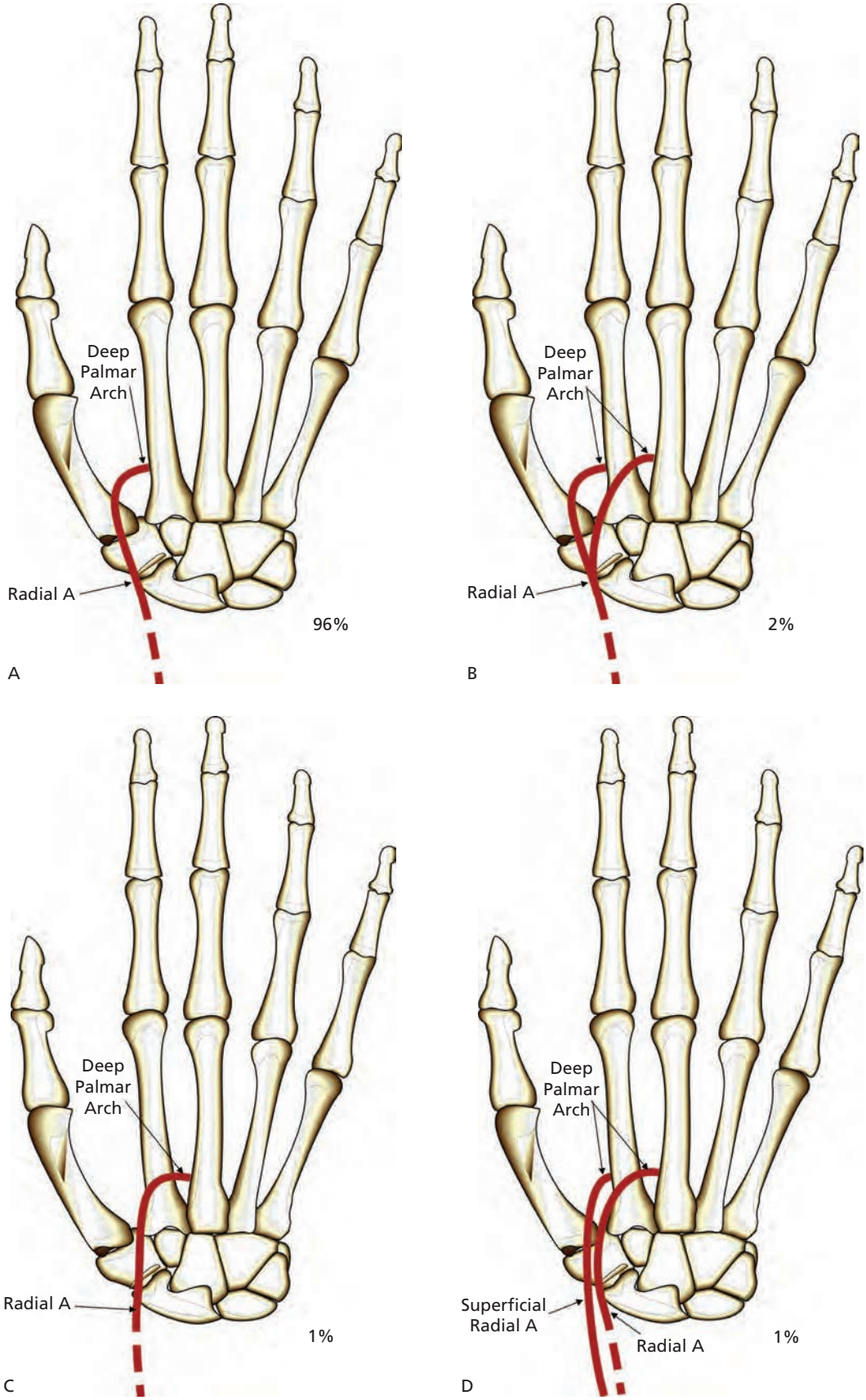

Figure 53.13 Relationship of the radial artery to the metacarpal bones: (a) radial artery travels between the first and second metacarpal bones to enter the palmar hand (96%); (b) radial artery sends two branches to the deep palmar arch, one between the first and second metacarpals and one between the second and third metacarpals (2%); (c) radial artery travels between second and third metacarpal bones to form the deep palmar arch (1%); and (d) the superficial radial artery travels between the first and second metacarpals while the radial artery travels between the second and third metacarpal bones.

a variant superficial palmar arch, as well as a number of other muscular and neural variations.

The branches of the ulnar artery, including the common interosseous and ulnar recurrent arteries, have also been shown to be capable of variation (Radzikowski and Szulczyk 1972). Variations include anterior and posterior interosseous arteries arising separately from the ulnar, common interosseous arising from the axillary artery, common interosseous arising from the high radial artery, and interosseous recurrent originating from the common interosseous rather than the posterior interosseous artery (Henle 1868; Salvi 1898; Schaefer et al. 1915; Latarjet 1948; Anson 1966; Bergman et al. 1988).

Arteries of the hand

The arterial supply to the hand exists as the superficial and deep palmar arterial arches as well as a network of arteries on the dorsum of the hand that arise from the dorsal carpal arch. The superficial palmar arterial arch is classically primarily supplied by the ulnar artery, with some anastomoses to the deep palmar arterial arch and the radial artery. The superficial palmar arterial arch produces palmar metacarpal arteries which meet with the palmar metacarpal arteries from the deep palmar arterial arch and form common palmar digital arteries, which then branch into proper palmar digital arteries. In addition, the superficial palmar arterial arch produces a palmar digital artery that supplies the lateral aspect of the fifth digit. The deep palmar arterial arch is classically primarily supplied by the radial artery with some anastomoses to the superficial palmar arterial arch and the ulnar artery. The deep palmar arterial arch produces palmar metacarpal arteries which meet with the palmar metacarpal arteries from the superficial palmar arterial arch and form common palmar digital arteries, which then branch into proper palmar digital arteries. The deep palmar arterial arch also produces perforating branches that travel between the metacarpal bones and form an anastomosis with the dorsal metacarpal arteries. The dorsal carpal arch is classically produced by dorsal carpal branches from the radial and ulnar arteries, as well as the anterior and posterior interosseous arteries. The dorsal carpal arch produces dorsal metacarpal arteries which communicate with the perforating branches from the deep palmar arterial arch, and then go on to produce dorsal digital arteries.

Variation of the supply, branching, and distribution of the arteries of the hand are common and are therefore the subject of numerous publications (Henle 1868; Winslow 1883d; Schwalbe 1895; Jaschtschinski 1897; Tandler 1897; Schaefer et al. 1915; Barbosa Sueiro 1916, 1917; Poynter 1922; Maruyama 1944; Latarjet 1948; McCormack et al. 1953; Weathersby 1955; Mestdagh 1980; Bergman et al. 1988; Ebner and Hammer 1988).

According to Lippert and Pabst (1985; based on the original work of Adachi 1928; Dimtza 1956; Lanz and Wachsmuth 1959; Edwards 1960; Coleman and Anson 1961; Anson 1963; Pabst and Lippert 1968; Little et al. 1973; Mozersky et al. 1973; Kamienski and Barnes 1976; Varro et al. 1978; Libersa et al. 1982; Doscher et al. 1983), the superficial palmar arterial arch exists as a complete or closed arch 42% of the time and as an incomplete or open arch 58% of the time. This finding differs dramatically from the findings of Ikeda et al. (1988) who, based on their analysis of 220 cadaver hands, report that complete superficial palmar arches occur 96.4% of the time with only 3.6% of superficial palmar arches incomplete. Furthermore, Al-Turk and Metcalf (1984) report that the superficial palmar arch is complete 84% of the time and incomplete 16% of the time. The classic description that is seen in text books only occurs 35% of the time (Fig. 53.14a). In 4% of cases the median artery communicates with the ulnar artery, forming a complete superficial palmar arch (Fig. 53.14b). In 2% of cases a deep branch from either the dorsum of the hand or from the deep palmar arch communicates with the ulnar artery to form a complete superficial palmar arch (Fig. 53.14c). In 1% of cases the radial, ulnar, and median arteries all contribute to the superficial palmar arch (Fig. 53.14d).

In the instance of an incomplete superficial arch, 37% of the time the radialis indicis artery and three palmar metacarpal arteries arise from the ulnar artery (Fig. 53.15a). This finding was also observed by Vollala et al. (2009) whereby the superficial palmar arch was supplied exclusively by the ulnar artery with no contribution from the radial artery at all. Baral et al. (2012) also reported observing this variation 31.3% of the time. In 13% of cases the radialis indicis artery arises from the radial artery and the three palmar metacarpal arteries arise from the ulnar artery (Fig. 53.15b). In 4% of cases the median artery produces the radialis indicis artery and first palmar metacarpal artery and the medial two palmar metacarpal arteries arise from the ulnar artery, with no contribution from the radial artery (Fig. 53.15c). In 3% of cases, the radialis indicis artery and first palmar metacarpal artery arise from the radial artery and the medial two palmar metacarpal arteries arise from the ulnar artery (Fig. 53.15d). In 1% of cases, the radialis incicis artery arises from the radial artery, the first palmar metacarpal artery arises from the median artery, and the medial two palmar metacarpal arteries arise from the ulnar artery (Fig. 53.15e).

According to Lippert and Pabst (1985; based on the original work of Adachi 1928; Dimtza 1956; Lanz and Wachsmuth 1959; Coleman and Anson 1961; Anson 1963; Little et al. 1973; Mozersky et al. 1973; Kamienski and Barnes 1976; Varro et al. 1978; Libersa et al. 1982; Doscher et al. 1983) there are four primary variations of the deep palmar arterial arch. In 79% of cases the ulnar artery has only one deep branch which meets up with the deep arch, which then produces the princeps pollicis, and three palmar metacarpal arteries all arise from the deep palmar arterial arch, as is classically described in text books (Fig. 53.16a). In 13% of cases the ulnar artery produces two deep palmar branches, which both supply the deep palmar arch (Fig. 53.16b). In 5% of cases the anterior interosseous, radial, and ulnar arteries all contribute to the deep palmar arterial arch (Fig. 53.16c). In only 3% of cases the deep palmar arch is incomplete or open, and the radial artery and deep palmar branch

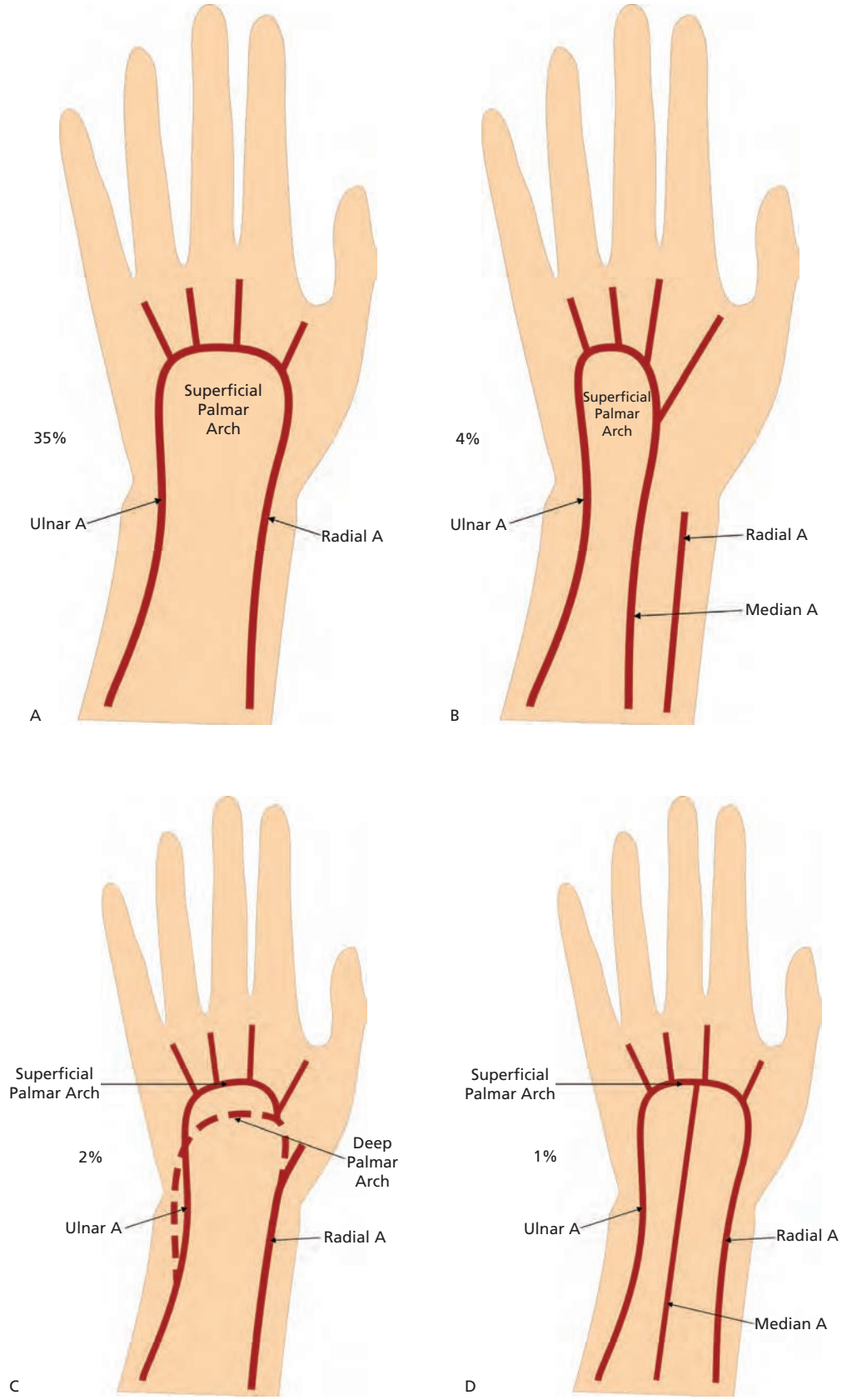

Figure 53.14 Variations of the superficial palmar arterial arch when the arch is complete: (a) classic arrangement of the complete (closed) superficial palmar arch (35%); (b) ulnar artery and median artery form the superficial palmar arch (4%); (c) deep branch from the from the dorsum of the hand, or deep palmar arch communicates with the ulnar artery to form the superficial palmar arch (2%); and (d) ulnar, radial, and median arteries all contribute to the superficial palmar arch (1%).

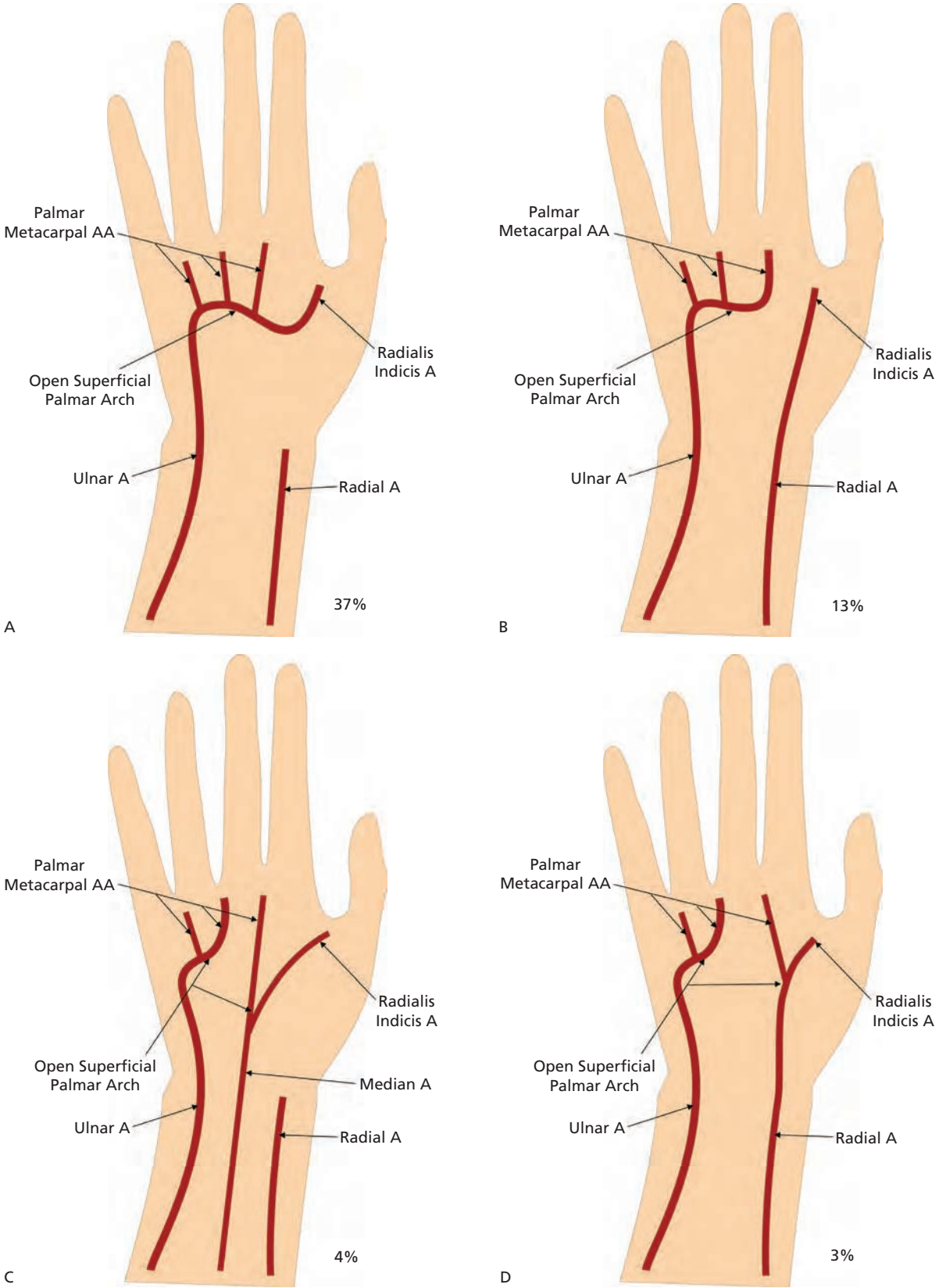

Figure 53.15 Variations of the superficial palmar arch when the arch is incomplete: (a) incomplete superficial palmar arch (37%); (b) radialis indicis artery arises from the radial artery with the remaining branches arising from the incomplete superficial palmar arch (13%); (c) median artery produces the radialis indicis artery and the first palmar metacarpal artery with the remaining branches coming from the incomplete superficial palmar arch (4%); (d) ulnar artery produces second and third palmar metacarpal arteries while the radial artery produces the radialis indicis and first palmar metacarpal artery (3%)

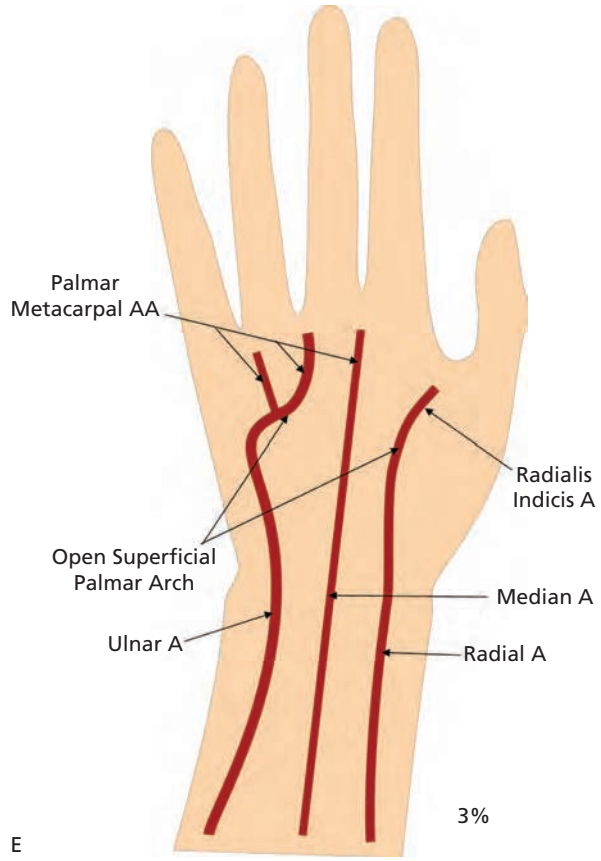

Figure 53.15 *(continued)* (e) ulnar artery produces second and third palmar metacarpal arteries, the median artery produces the first palmar metacarpal artery, and the radial artery produces the radialis indicis (3%).

from the ulnar split produce the palmar metacarpal arteries (Fig. 53.16d). According to Ikeda et al. (1988), based on their analysis of 220 cadaver hands, the deep palmar arch was complete in 76.9% of cases. Baral et al. (2012) report that it is very infrequent (0.9%) for the radial artery to be the only contribution to the deep palmar arch.

According to Lippert and Pabst (1985; based on the original work of Adachi 1928; Lanz and Wachsmuth 1959; Edwards 1960; Anson 1963; Libersa et al. 1982; Al-Turk and Metcalf 1984) the classic description of the deep and superficial palmar arterial arches both producing palmar metacarpal arteries, which converge in the palm to form the common palmar digital arteries, only occurs 30% of the time. In 10% of cases the palmar metacarpal arteries can form an anastomosis directly with the proper palmar digital arteries. In 60% of cases, the palmar metacarpal arteries from the deep palmar arterial arch from no functional anastomosis at all with either the common or proper palmar digital arteries, and therefore do not supply the digits at all. Several different varieties of variation of this anatomy exist, for example in 77% of cases the radialis indicis and all three palmar metacarpal arteries arise from the superficial palmar arch with no contribution from the deep arch (Fig. 53.17a). In 11% of cases the radialis indicis arises from the deep palmar arch and the three palmar metacarpal arteries arise from the superficial palmar arch (Fig. 53.17b). In 10% of cases the princeps pollicis artery arises from the deep palmar arch, while the radialis indicis and all three palmar metacarpal arteries arise from the superficial palmar arch with no contribution from the deep arch (Fig. 53.17c). In 2% of cases the radialis indicis and first palmar metacarpal arteries arise from the deep palmar arterial arch, and the remaining two palmar metacarpal arteries arise from the superficial palmar arch (Fig. 53.17d).

According to Lippert and Pabst (1985; based on the original work of Adachi 1928; Dimtza 1956; Lanz and Wachsmuth 1959; Coleman and Anson 1961; Anson 1963; Varro et al. 1978; Doscher et al. 1983) the arterial supply to the dorsum of the hand is less relevant than the palmar side; however, several variations have been observed. In 50% of cases the dorsal carpal branch from the radial artery meets up with the anterior interosseous artery to form the dorsal carpal arch (Fig. 53.18a). In 30% of cases the anterior interosseous and a dorsal carpal branch from the radial and ulnar arteries, and contribute to the dorsal carpal arch (Fig. 53.18b). In 8% of cases the entire dorsal carpal arch is supplied by the dorsal carpal branch from the radial artery (Fig. 53.18c). The classic description, whereby the dorsal carpal arch is formed by a dorsal carpal branch from the radial and ulnar arteries, only occurs 5% of the time (Fig. 53.18d). In 3% of cases the dorsal carpal arch is formed by the anterior interosseous artery and a dorsal carpal branch from the ulnar artery, with no contribution from the radial artery (Fig. 53.18e). Finally, in 4% of cases the dorsal carpal arch and dorsal metacarpal arteries are all absent (Fig. 53.18f). Despite the variability of blood supply to the dorsum of the hand, Gajisin et al. (1983) report that the anatomical complex on the dorsum of the hand responsible for extension of the digits is adequate.

Ideka et al. (1998) report that the princeps pollicis artery, or first metacarpal artery, is absent 2.4% of the time. Earley (1986) suggests that to use the terms princeps pollicis and radialis indicis arteries are misnomers, while Al-Turk and Metcalf (1984) describe them as prevalent but variable in their origin and frequency. Vollala et al. (2008b) report observing a small arterial circle at the base of the thumb in addition to fully developed superficial palmar arch.

Al-Turk and Metcalf (1984) describe seeing different branching patterns in one hand versus the other 52% of the time, while the patterns were identical between right and left hands 48% of the time.

Jyoti et al. (2008) report having observed a case of a double superficial palmar arch as well as a double deep palmar arch of similar caliber formed by the branching on the deep branches of both the radial and ulnar arteries.

Spinner et al. (1996) report observing a case whereby a common palmar digital artery penetrated a proper palmar digital nerve, resulting in neurovascular symptoms.

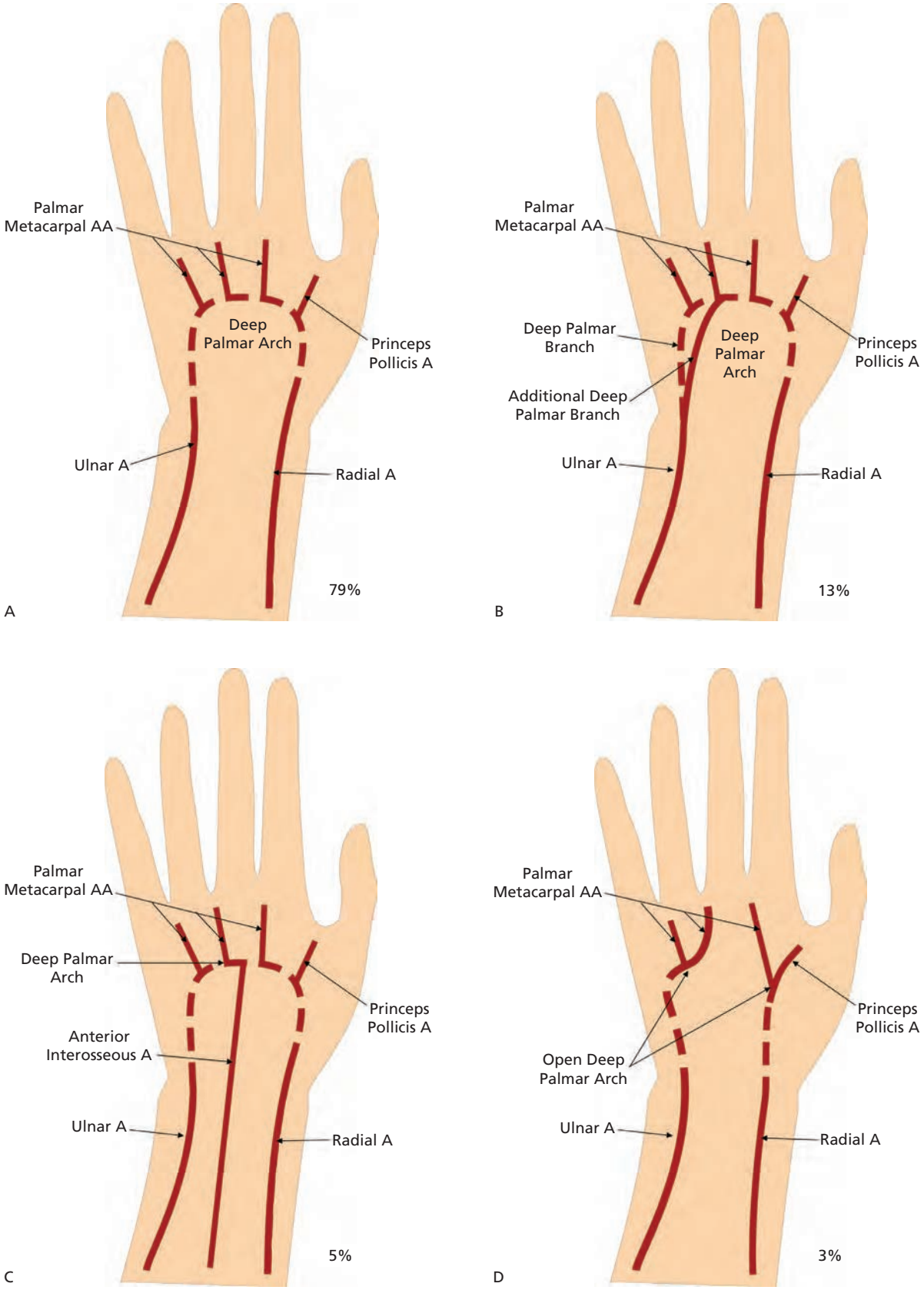

Figure 53.16 Variations of the deep palmar arterial arch: (a) the ulnar artery has only one deep branch that contributes to the deep palmar arch (79%); (b) the ulnar artery produces two deep branches that contribute to the deep palmar arch (13%); (c) the deep palmar arch is formed by the ulnar, radial, and anterior interosseous arteries (5%); and (d) in the case of an incomplete deep palmar arch the ulnar artery produces the second and third palmar metacarpal arteries and the radial artery produces the princeps pollicis and first palmar metacarpal arteries (3%).

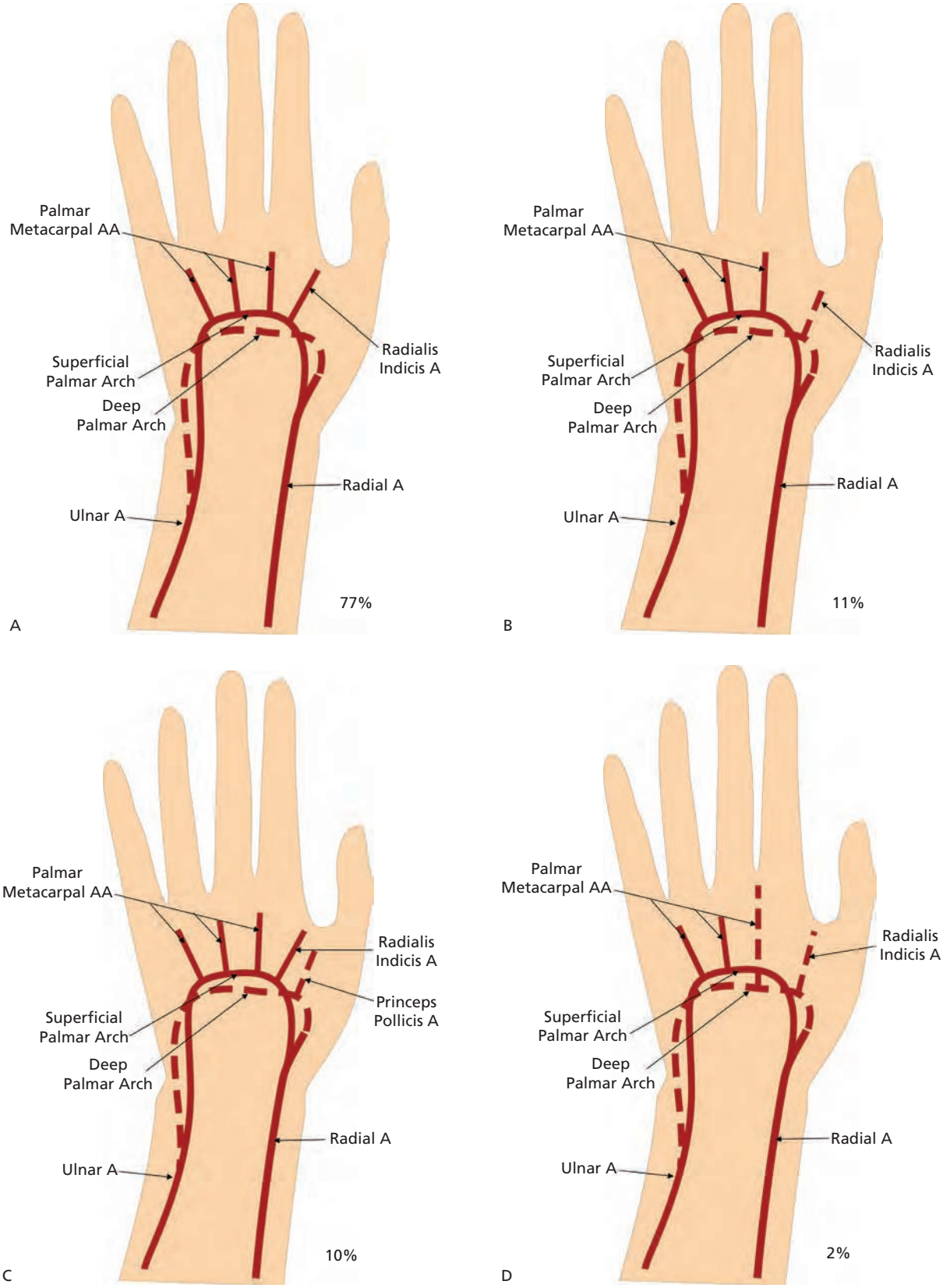

Figure 53.17 Variations between the superficial and deep palmar arterial arches: (a) the radialis indicis artery and all three palmar metacarpal arteries arise from the superficial palmar arch with no contribution from the deep palmar arch (77%); (b) the palmar metacarpal arteries arise from the superficial palmar arch with the radialis indicis arising from the radial artery (13%); (c) the radialis indicis artery and all three palmar metacarpal arteries arise from the superficial palmar arch and the priceps pollicis artery arises from the deep palmar arch (10%); and (d) the radialis indicis artery and first palmar metacarpal artery arise from the deep palmar arch while the second and third palmar metacarpal arteries arise from the superficial palmar arch (2%).

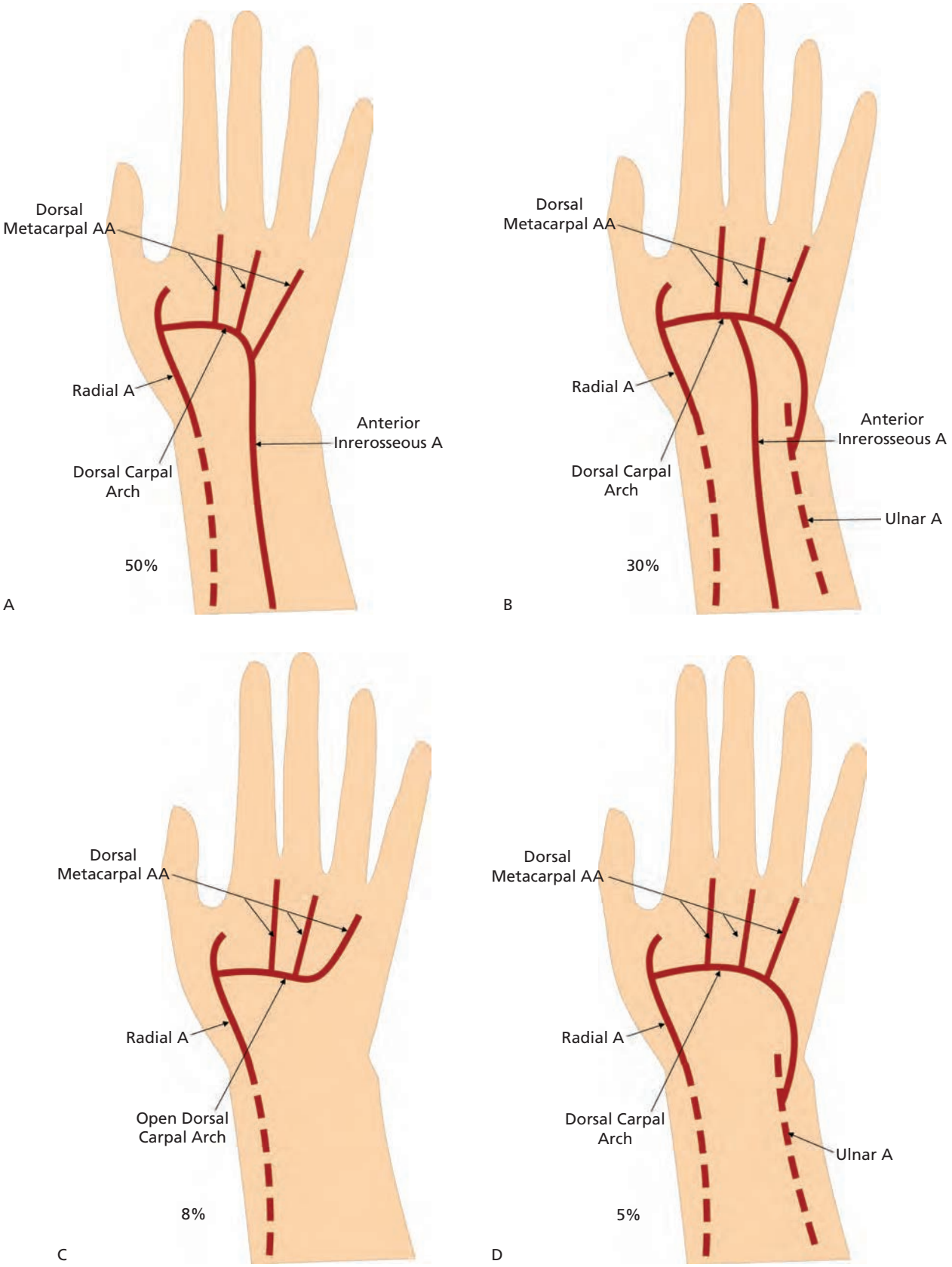

Figure 53.18 Variations of the dorsal carpal arch: (a) dorsal carpal branch of the radial artery meets up with the anterior interosseous artery to form the dorsal carpal arch (50%); (b) radial and ulnar arteries each produce a dorsal carpal branch which meets up with the anterior interosseous artery to form the dorsal carpal arch (30%); (c) dorsal carpal arch is incomplete and only formed by the dorsal carpal branch from the radial artery (8%); (d) the classic description whereby the dorsal carpal arch is formed by a dorsal carpal branch from the radial and ulnar arteries (5%)

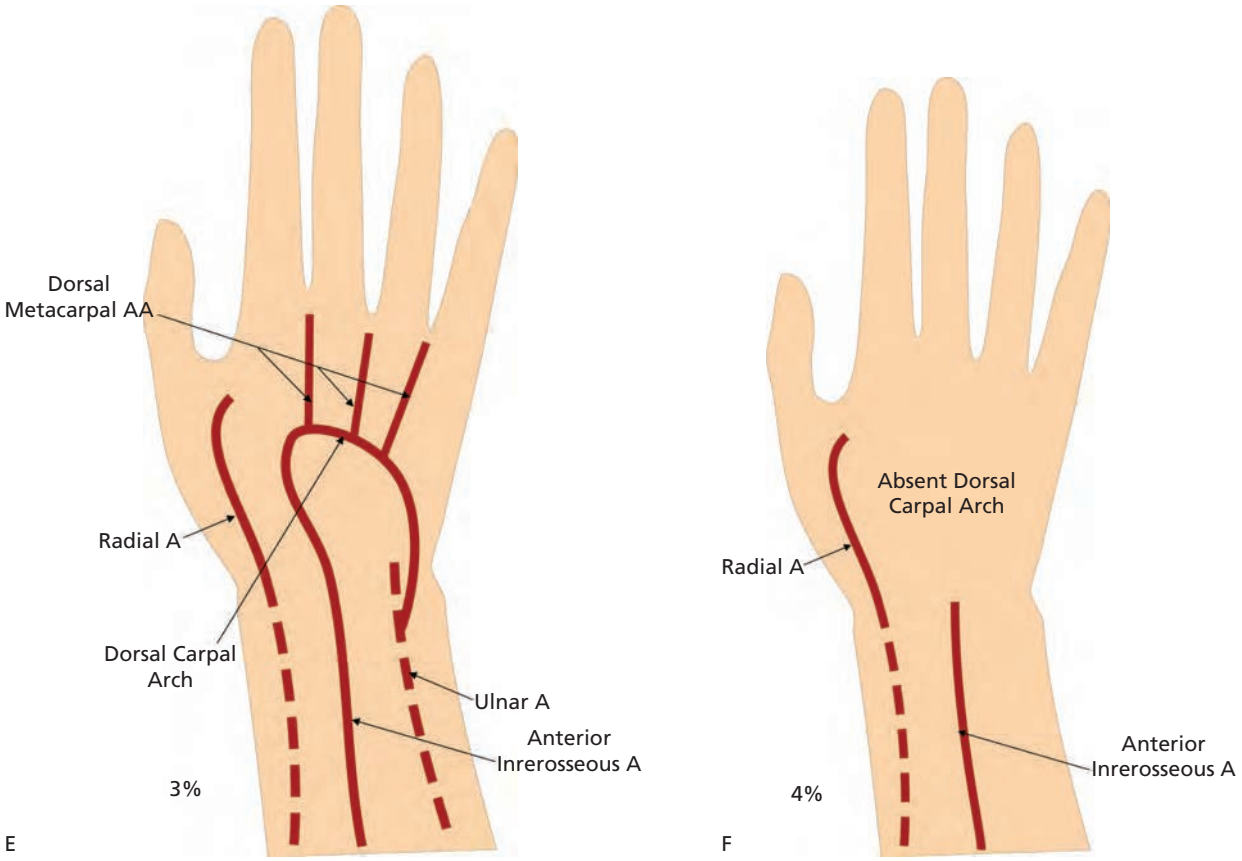

Figure 53.18 *(continued)* (e) the dorsal carpal arch is formed by the anterior interosseous artery and a dorsal carpal branch from the ulnar artery (3%); and (f) complete absence of the dorsal carpal arch (4%).

References

Adachi B. 1928. *Das Arteriensystem der Japaner*. Vol I. Kyoto: Maruzen.

Aharinejad S, Nourani F, Hollensteiner H. 1997. Rare case of high origin of the ulnar artery from the brachial artery. *Clin Anat* 10: 253–258.

Aizawa Y, Ohtsuka K, Kumaki K. 1995. Examination on the courses of the arteries in the axillary region I. The course of the subscapular artery system, especially the relationships between the arteries and the posterior cord of the brachial plexus. *Kaibogaku Zasshi* 70: 554–568.

Aizawa Y, Ohtsuka K, Kumaki K. 1996. Examination on the courses of the arteries in the axillary region II. The course of the axillary artery in the case of Adachi's C–type brachial plexus. *Kaibogaku Zasshi* 71: 92–105.

Al-Fayez M, Kaimkhani Z, Zafar M, Darwish H, Aldahmash A, Al-Ahaideb A. 2010. Multiple arterial variations in the right upper limb of a Caucasian male cadaver. *Int J Morphol* 28: 659–665.

Al-Turk M, Metcalf WK. 1984. A study of the superficial palmar arteries using the Doppler ultrasonic flowmeter. *J Anat* 139: 27–32.

Anson BJ. 1963. *An Atlas of Human Anatomy*, second edition. Philadelphia: Saunders.

Anson BJ. 1966. *Morris' Human Anatomy*, 12th edition. New York: The Blakiston Division, McGraw-Hill Book Company.

Aughsteen A, Hawamdeh H, Al-Khayat M. 2011. Bilateral variations in the branching pattern of the brachial artery. *Int J Anat Var* 4: 187–170.

Baral P, Vijayabhaskar P, Roy S, Kumar S, Ghimire S, Shrestha U. 2009. Multiple arterial variations in upper limb. *Kathmandu Univ Med J* 7: 293–297.

Baral P, Satheesha K, Vijayabhaskar P, Shetty H, Baral R, Shrestha R, Banstola D, Lobo S. 2012. A study of variations of the arterial system of the upper limbs in Nepalese cadavers. *Int J AJ Inst Med* 2012: Sci 3–9.

Barbosa Sueiro MB. 1916. Arcadas arteriais palmares. *Arquivo Anat Anthropol* 2: 389–414.

Barbosa Sueiro MB. 1917. Arcadas arteriais palmares. *Arquivo de Anat Anthropol* 3: 97–124.

Barfred T, Hojlund A P, Bertheussen K. 1985. Median artery in carpal tunnel syndrome. *J Hand Surg (Am)* 10: 864–867.

Barta E, Petrovits L. 1927. Das ligamentum supracondyloideum. *Anat Anz* 63: 177–184.

Bartels P. 1900. Über eine Ösebildung der Arteria recurrens radialis für den Nervus radialis profundus, kombiniert mit anderen Abnormitäten. *Anat Hefte* 15: 203–212.

Bassett FH, Spinner RJ, Schroeter TA. 1994. Brachial artery compression by the lacertus fibrosus. *Clin Ortho* 307: 110–116.

Bayer L. 1893. Beitrag zur vergleichenden Anatomie der Oberarmarterien. *Morph Jahrbuch* 19: 1–41.

Bergman RA, Thompson SA, Afifi AK, Saadeh FA. 1988. *Compendium of Human Anatomic Variation: Catalog, Atlas and World Literature*. Baltimore and Munich: Urban & Schwarzenberg.

Bertacchini P. 1896. Un cas d'anomalie artérelle du bras et d'apophyse susépitrochléenne de l'humérus associés. *Arch Ital Biol* 26: 159.

Bhargava I. 1956. Anomalous branching of axillary artery. *J Anat Soc India* 5: 78–80.

Bianchi L. 1943. Considerazioni sopra un caso di arteria brachio-ulnare superficiale. *Anat Anz* 94: 73–88.

Blunt MJ. 1959. The vascular anatomy of the median nerve in the forearm and hand. *J Anat* 93: 15–22.

Bonora C, Casati L. 1880. Anomalia dell'Arteria omerale ed aneurisma della piegatura del braccio. *Raccoglitore Medico* 13: 175–188.

Bovero, A. 1907. Morphologie des arteres de la glande mammaire. *Arch Ital Biol* 48: 486–487.

Brême G. 1899. Casuistischer Beitrag zur Kenntniss der Anomalien der Armarterien. *Zeitschr für Morphol Anthropol* 1: 483–494.

Brick AI. 1909. On conradial arteries. *Khururgiia* 25: 576–593 (in Russian).

Brunati J. 1937. Sur les bifurcations hautes de l'artère humerale. *Ann Anat Path* 14: 873–882.

Calori L. 1877. Sul variato rapporto vascolare delle due radici del nervo mediano e sulle condizioni atte a produrlo. *Mem Accad Sci Instituto di Bologna* 8: 443–456.

Cappi E. 1879. Di un'anomalia della arterie omerali. *Annali Universali di Medicina e Chirurgia* 47: 267–268.

Carson ER. 1895. Rare anomaly of the brachial artery. *Med Rec* 48: 911

Cavdar S, Zeybek A, Bayramicli M. 2000. Rare variation of the axillary artery. *Clin Anat* 13: 66–68.

Cavolli R, Eryilmaz S, Kaya B, Ozyurda U. 2007. Report of the anatomic variation of the brachial artery in a patient undergoing transradial cardiac catheterization. *J Vasc Nurs* 25: 19–20.

Cayotte J, Quereux P. 1953. Ramescence anormale des artères axillaire et fémorale. *Assoc Anatomistes Comptes Rendus* 40: 968–972.

Celik HH, Sargon MF, Konan A, Kural E. 1996. High brachial artery bifurcation: a report of two cases. *Bull Assoc Anat* 80: 13–14.

Celik HH, Gormus G, Aldur MM, Ozcelik M. 2001. Origin of the radial and ulnar arteries: variations in 81 arteriograms. *Morphologie* 85: 25–27.

Celik HH, Aldur MM, Tunali S, Ozdemir MB, Aktekin M. 2004. Multiple variations of the deep artery of arm: double deep artery of arm and deep artery of arm with the superior ulnar collateral artery. A case report. *Morphologie* 88: 188–90.

Charles CM, Penn L, Holden HF, Miller RA, Alvis EB. 1931. The origin of the deep brachial artery in American white and American negro males. *Anat Rec* 50: 299–302.

Charles G. 1903. Note on an abnormality of the radial artery. *Indian Med J* 38: 259–260.

Charles JJ. 1873. Notes on some cases of abnormal arrangement of arteries of the upper extremity. *J Anat Physiol* 7: 300–301.

Charles JJ. 1875. Abnormalities in the arteries of the upper extremity. *J Anat Physiol* 9: 180–181.

Charles JJ. 1894. A case of absence of the radial artery. *J Anat Physiol* 28: 449–450.

Chuquet 1876. Anomalie des artères de l'avant-bras. *Bull Méms Soc Anatomique Paris* 1876: 726.

Ciervo A, Kahan M, Pangilinan AJ, Dardik H. 2001. Absence of the brachial artery: a report of rare human variation and review of upper extremity arterial anomalies. *J Vasc Surg* 33: 191–194.

Cilley JL. 1881. A few anomalies observed in the Medical College of Ohio dissecting-rooms. *Cinn Lancet Clin* 8: 349.

Cocchi A. 1891. Contribuzione allo studio dell'anastomosi tra radiale e cubitale alla piegatura dell cubito nella divisione prematura dell'arteria brachiale. *Atti dell Accademia dei Fisiocritici in Siena* 3: 247–261.

Coleman SS, Anson BJ. 1961. Arterial patterns in the hand based upon a study of 650 specimens. *Surg Gyn Obst* 113: 409–424.

Coulouma B. 1934. Resultat de cent quatre observations su la disposition des branches de l'axillaire. *Bull Assoc Anat* 29: 193–199.

Dartnell J, Sekaran P, Ellis H. 2007. The superficial ulnar artery: incidence and calibre in 95 cadaveric specimens. *Clin Anat* 20: 929–932.

Dean MH. 1880. Arterial anomalies. *Med Rec* 17: 384.

DeGaris CF, Swartley WB. 1928. The axillary artery in white and negro stocks. *Am J Anat* 41: 353–397.

Dibailoff SI. 1904. Anomaly of the radial artery. *Prakticheskii Vrach* 1904: 682 (in Russian).

Dieulaufe R, Cahuzac M. 1931. Un cas d'anomalies artèrielles due membre superieur. *Ann Anat Path Paris* 8: 661–662.

Dimtza A. 1956. Die Arteriographie der hand. *Radiol Clin* 25: 205–220

Dogan OF, Karcaaltincaba M, Duman U, Akata D, Besim A, Boke E. 2005. Assessment of the radial artery and hand circulation by computed tomography angiography: a pilot study. *Heart Surg Forum* 8: E28–33.

Doscher W, Viswanathan B, Stein T, Margolis IB. 1983. Hemodynamic assessment of the circulation in 200 normal hands. *Ann Surg* 198: 776–779.

Dubreuil-Chambardel L. 1922. Variations de l'artére médiane, en rapport avec les variations des grosses artéres du membre supèrieur. *Bull Mém Soc Anthrop Paris* 3: 9–11.

Dubreuil-Chambardel L. 1926. *Variations des Artères du Membre Superieur*. Paris: Masson et Cie.

Durgun B, Yucel AH, Kizilkanat ED, Dere F. 2002. Multiple arterial variation of the human upper limb. *Surg Radiol Anat* 24: 125–128.

Duval JM, Loescher JP. 1959. L'artére du nerf médian et ses variations. *Assoc Anatomistes Comptes Rendus* 46: 231–236.

Earley MJ. 1986. The arterial supply of the thumb, first web and index finger and its surgical application. *J Hand Surg Br* 11: 163–174.

Ebner I, Hammer H. 1988. Aspekte der arteriellen Gefässbeziehungen im Hohlhandbereich (Arterial connections in the palma manus). *Acta Anat* 131: 297–304.

Edwards EA. 1960. Organization of the small arteries of the hand and digits. *Am J Surg* 99: 837–846.

Erdogmus S, Govsa F. 2005. Distal variations of the neurovascular pedicle of the serratus anterior muscle as a flap. *Surg Radiol Anat* 27: 100–107.

Esquerdo A. 1887. De algunas anomalías arteriales. *Arch Cirugía* 1: 86–89.

Ferrari G. 1902–03. Anomalie di rapporti e distribuzione dell' arteria ascellare. *Atti della Accademia delle scienze mediche e naturali in Ferrara* 77: 259–262.

Forster A. 1917–18. Über zwei Fälle einer seltenen Arterienvarietät an der Ansatzsehne des Biceps brachii. *Anat Anz* 50: 193–194.

Gajisin S, Zbrodowski A, Grodecki J. 1983. Vascularization of the extensor apparatus of the fingers. *J Anat* 137: 315–322.

Georgievski IV. 1905. Kazuistik vysokogo proischozdenija i podkoznago polozenija tyl'noj v–tvi lucevoj arteri. *Chirurgija* 18: 319–317.

Gérard G. 1905. Anomalies artérielles. Considérations sur les anomalies de l' artère du nerf médian. A propos de trois cas nouveaux. *Biblio Anat* 14: 156–163.

Gérard G, Breucq E. 1905. Sur un cas de bifurcation précoce de l'artère humérale. *Biblio Anat* 14: 164–170.

Gonzales-Compta X. 1991. Origin of the radial artery from the axillary and associated hand vascular anomalies. *J Hand Surg* 16: 293–296.

Göppert E. 1904. Die Beurteilung der Arterienvarietaten der oberen Gliedmasse bei den Säugetieren und beim Menschen auf entwicklungsgeschichtlicher und vergleichend-anatomischer Grundlage. *Erg Anat Entw'gesch* 14: 170–233.

Goswami P, Tigga A, Bharihoke V. 2013. Variant course and branching of right brachial artery: a case study. *Int J Res Med Sci* 1: 62–65.

Gruber W. 1864. Zur Anatomie der Arteria radialis. *Arch Anat Physiol Wissen Med* 1864: 434–455.

Gruber W. 1867. Über die Arteria mediana antibrachii superficialis, Arteria ulnaris antibrachii superficialis und Duplicität der arteria ulnaris. *Arch Anat Physiol Wissen Med* 67: 668–687.

Gruber W. 1870a. Dreiwurzelige arteria radialis. *Arch Anat Physiol Wissen Med* 70: 180–188.

Gruber W. 1870b. Rudimentare arteria radialis. *Arch Anat Physiol Wissen Med* 70: 189–196.

Gruber W. 1870c. Subcutaner verlauf des ramus dorsalis der arteria radialis am underarm- und handwurzelrücken. *Arch Anat Physiol Wissen Med* 70: 484–489.

Gruber W. 1871. Duplicität der arteria ulnaris – neuer fall. *Arch Anat Phys Wissen Med* 71: 286–296.

Guerra P. 1887. Anomalie rinvenute in cadaveri di delinquenti e di normale. *Ateneo Medico Parmense* 1: 278–292.

Guerrier Y, Paleirac R. 1951. Le tronc artèriel antibrachial. *Assoc Anatomistes Comptes Rendus* 38: 566–575.

Guyon F. 1861. Note sur une disposition anatomique propre a la face antérieure de la région du poignet et non encore décrite. *Bull Mém Soc Anat Paris* 6: 184–186.

Handa J, Kikuchi H, Handa H. 1967. Persistierende karotido-basilare Anastomose: Die A. primitive hypoglossica. *Fortschr Rontgenstr* 107: 421–422.

Hazlett JW. 1949. The superficial ulnar artery with reference to accidental intra-arterial injection. *CMAJ* 61: 289–293.

Henle J. 1868. *Handbuch der Systematischen Anatomie des Menschen*. Braunschweig: Von Friedrich Vieweg und Sohn.

Herrington M. 1905. High bifurcation of the brachial artery with reunion at the elbows. *Johns Hop Hosp Bull* 16: 65–66.

Heuston FT. 1885. Notes on some anatomical anomalies. *Trans Roy Acad Med Ireland* 3: 453–456.

Hitzrot JM. 1901. A composite study of the axillary artery in man. *Johns Hop Hosp Bull* 12: 136–145.

Hofer K, Hofer G. 1910. Über den verlauf der arteria brachialis mit dem nervus medianus zwischen den beiden köpfen des musculus pronator teres. *Anat Anz* 36: 510–514.

Huelke DF. 1959. Variation in the origins of the branches of the axillary artery. *Anat Rec* 35: 33–41.

Icten N, Sullu Y, Tuncer I. 1996. Variant high-origin radial artery: a bilateral case. *Surg Radiol Anat* 18: 63–66.

Ikeda A. Ugawa A, Kazihara Y, Hamada N. 1988. Arterial patterns in the hand based on three-dimensional analysis of 220 cadaver hands. *J Hand Surg* 13: 501–509.

Jacquemin G, Lemaire V, Medot M, Fissette J. 2001. Bilateral case of superficial ulnar artery originating from the axillary artery. *Surg Radiol Anat* 23: 139–143.

Jakubowicz M, Bruska M. 1980. A case of variations in arterial vascularization of the upper limb. *Folia Morphol* 39: 55–59.

Janosík J. 1891. Cérvy krevni a nervy horni koncetiny u cloveka a nekterych zvirat. (Sur les vaisseaux sanguins et les nerfs des membres supérieurs l'homme et chez quelques autres animaux). *Sbornik Lekarsky* 4: 244–255.

Jaschtschiniski SN. 1897. Morphologie und topographie des arcus volaris sublimis und profundus des menschen. *Anat Hefte* 7: 161–188.

Jesus RC, Lopes MCH, Demarchi GTS, Ruiz CR, Wafae N, Wafae GC. 2008. The subscapular artery and thoracodorsal branch: an anatomical study. *Folia Morphol* 67: 58–62.

Jurjus A, Sfeir R, Bezirdjian R. 1986. Unusual variation of the arterial pattern of the human upper limb. *Anat Rec* 215: 82–83.

Jurjus AR, Correa-De-Aruaujo R, Bohn RC. 1999. Bilateral double axillary artery: Embryological basis and clinical implications. *Clin Anat* 12: 135–140.

Jyoti A, Kumar SR, Vandana M, Gayatri R, Vijay K. 2008. Unilateral duplication of palmar arterial arches: a case report. *Ital J Anat Embryol* 113: 257–263.

Kadanoff D, Balkansky G. 1966. Zwei Fälle mit seltenen varietäten der arterien der oberen extremität. *Anat Anz* 118: 289–296.

Kadyi H. 1881. Eine rudimentäre arteria radialis. *Medizinische Jahrbücher* 1881: 43–44.

Kamienski RW, Barnes RW. 1976. Critique of the Allen test for continuity of the palmar arch assessed by Doppler ultrasound. *Surg Gynecol Obstet* 142: 861–864.

Keen JA. 1961. A Study of the arterial variations in the limbs, with a special reference to the symmetry of vascular patterns. *Am J Anat* 108: 245–261.

Krause E. 1876. *Varietäten des aortensystems. In Handbuch der Systematischen Anatomie des Menschen* (ed. HenleJ). Braunschweig: Von Friedrich Vieweg und Sohn.

Lanz T, Wachsmuth W. 1959. *Praktische Anatomie*. Berlin, Göttingen, Heidelberg: Springer.

Latarjet A. 1948. *Testut's Traite d'Anatomie Humaine*, ninth edition. Paris: G. Doin & Cie.

Lee JH, Kim DK. 2008. Bilateral variations in the origin and branches of the subscapular artery. *Clin Anat* 21: 783–785.

Lengele B, Dhem A. 1989. Unusual variations of the vasculonervous elements of the human axilla. Report of three cases. *Arch Anat Histol Embryol* 72: 57–67.

Levy M, Pauker M. 1978. Carpal tunnel syndrome due to thromosed persisting median artery, a case report. *Hand* 10: 65–68.

Libersa CL, Francke JP, Mauppin JM, Bailleul JP, Gamglin P. 1982. The arterial supply to the palm of the hand (arteriae palme manus). *Anat Clin* 4: 33–45.

Lippert H, Pabst R. 1985. *Arterial Variations in Man: Classification and Frequency*. Munich: Bergmann Verlag.

Little JM, Zylstra PL, West J, May J. 1973. Circulatory patterns in the normal hand. *Brit J Surg* 60: 652–655.

Lo RNS, Leung MP, Lau KC, Yeung CY. 1986. Abnormal radial artery in Down's syndrome. *Arch Dis Child* 61: 885–890.

Loetzke HH, Kleinau W. 1968. Gleichzeitiges Vorkommen der Aa. brachialis superficialis, radialis und antebrachialis dors. superfic. sowie deren Aufzweigungen. *Anat Anz* 122: 137–141.

Loukas M, Curry B. 2006. A case of an atypical radial artery. *Clin Anat* 19: 706–707.

Maestre A. 1864. Notable anomalía de la arteria humeral. *La España Médica* 9: 330–331.

Malcic-Gürbüz J, Gürünlüoğlu R, Ozdoğmuş O, Yalin A. 2002. Unique case of trifurcation of the brachial artery: its clinical significance. *Clin Anat* 15: 224–227.

Maral T, Celik H, Hayaran M, Kecik A. 1993. An anatomical variation of the thoracodorsal artery with comments on flaps based on the axillary artery. *Eur J Plast Surg* 16: 231–233.

Maraspin LE. 1971. A report of an anomalous bifurcation of the right axillary artery in man. *Vasc Surg* 5: 133–136.

Maruyama K. 1944. Seltene Varietät der Arterien der oberen Extremität bei einem Japaner (A. brachialis superficialis lateralis inferior, A. antebrachialis superficialis mediano–ulnaris, Arcus volaris superficialis vom Typus mediano-ulnaris). *Okajima's Folia Anat* 22: 551–567.

Maxwell JA, Kepes JJ, Ketchem LD. 1973. Acute carpal tunnel syndrome secondary to thrombosis of a persistent median artery. *J Neurosurg* 38: 774–777.

McCormack LJ, Cauldwell EW, Anson BJ. 1953. Brachial and antebrachial arterial patterns: A study of 750 extremities. *Surg Gynecol Obst* 96: 43–54.

Meckel JF. 1816. Ueber den regelwidrigen Verlauf der Armpulsadern Dtsch Arch Physiol 2: 117–131.

Mehta V, Arora J, Suri R, Rath G. 2008. Unilateral anomalous arterial pattern of human upper limb. Anatomical description and clinical implications. *Sul Qab Univ Med J* 8: 227–230.

Mestdagh H. 1980. Anatomie des Arcus volaris profundus beim Menschen. *Anat Anz* 147: 180–187.

Miller RA. 1939. Observations upon arrangement of the axillary artery and brachial plexus. *Am J Anat* 64: 143–163.

Misra BD. 1955. The arteria mediana. *J Anat Soc* 4: 48.

Mojab K, Ghosh BC, Moss GS. 1976. Bilateral subclavian and axillary artery anomaly. *Am Surg* 42: 585–588.

Mozersky DJ, Buckley CJ, Hagood CO, Capps WF, Dannemiller FJ. 1973. Ultrasonic evaluation of the palmar circulation. A useful adjunct to radial artery cannulation. *Am J Surg* 126: 810–812.

Müller E. 1903. Beiträge zur morphologie des gefässsystems. 1. Die armarterien des menschen. *Anat Hefte* 22: 379–574.

Muresian H, Dorobat B, Filipoiu F. 2008. Acute upper limb ischemia in patient with aberrant radial artery. *EJVES* 16: 23–24.

Nakatani T, Tanaka S, Mizukami S. 1998. Superficial ulnar artery originating from the brachial artery and its clinical importance. *Surg Radiol Anat* 20: 383–385.

Natsis K, Papadopoulou AL, Paraskevas G, Totlis T, Tsikaras P. 2006. High origin of a superficial ulnar artery arising from the axillary artery: anatomy, embryology, clinical significance and a review of the literature. *Folia Morphol (Warsz)* 65: 400–405.

Nayak SR, Krishnamurthy A, Kumar M, Prabhu LV, Saralaya V, Thomas MM. 2008. Four-headed biceps and triceps brachii muscles, with neurovascular variation. *Anat Sci Int* 83: 107–111.

Nie B, Zhou YJ, Li GZ, Shi DM, Wang JL. 2009. Clinical study of arterial anatomic variations for transradial coronary procedure in Chinese population. *Chin Med J* 122: 2097–2102.

Norgaz T, Gorgulu S, Dagdelen S. 2012. Arterial anatomic variations and its influence on transradial coronary procedural outcome. *J Interv Cardiol* 25: 418–424.

Olinger A, Benninger B. 2010. Branching patterns of the lateral thoracic, subscapular, and posterior circumflex humeral arteries and their relationship to the posterior cord of the brachial plexus. *Clin Anat* 23: 407–412.

Olinger A, Borman W, Benninger B. 2012. 2. A possible relationship between reliability of thoracic outlet syndrome diagnostic testing and the position of the axillary artery. *Surg Radiol Anat* 34: 499–507.

Ozan H, Simsek C, Onderoglu S, Kirici Y, Basar R. 1994. High division of the axillary artery: a rare case of superficial ulnar artery. *Acta Anat* 151: 68–70.

P'an, MT. 1940. The origin of the branches of the axillary artery in the Chinese. *Am J Phys Anthropol* 27: 269–279.

Pabst R, Lippert H. 1968. Beiderseitiges Vorkommen von A. brachialis superficialis, A. ulnaris superficialis und A. mediana. *Anat Anz* 123: 223–226.

Panagouli E, Tsaraklis A, Gazouli I, Anagnostopoulou S, Venieratos D. 2009. A rare variation of the axillary artery combined contralaterally with an unusual high origin of a superficial ulnar artery: description, review of the literature and embryological analysis. *Ital J Anat Embryol* 114: 145–156.

Pandey SK, Shukla VK. 2004. Anatomical variation in origin and course of the thoracoacromial trunk and its branches. *Nepal Med Coll J* 6: 88–91.

Park R. 1883. A record of the principal anatomical anomalies noticed during the dissection of one hundred subjects. *Ann Anat Surg* 8: 269.

Pelin C, Zagyapan R, Mas N, Karabay G. 2006. An unusual course of the radial artery. *Folia Morphol* 65: 410–413.

Pitzorno M. 1907. Di una varietà dell'arteria radiale. *Studi Sassaresi* 5: 23–30.

Polonskaja R. 1932. Zur frage der arterienanastomosen im gebiete der ellenbogenbeuge des menschen. *Anat Anz* 74: 303–317.

Poornima G, Dakshayani K. 2011. Multiple "retrogressive" variations in upper limb. *Int J Anat Var* 4: 109–111.

Poteat WL. 1986. Report of a rare human variation: absence of the radial artery. *Anat Rec* 214: 89–95.

Potherat E. 1888. Anomalie de l'axillaire. *Bull Mém Soc Anat Paris* 1888: 296–298.

Power JH. 1850. *Surgical Anatomy of the Arteries, and Descriptive Anatomy of the Heart by the late Valentine Flood*, M.D. Dublin: Fannin and Co.

Poynter CWM. 1922. Congenital anomalies of arteries and veins of the human body with bibliography. *Univ Studies Univ Nebraska* 22: 1–106.

Radzikowski A, Szulczyk P. 1972. The radial recurrent and ulnar recurrent arteries. *Folia Morphol* 31: 109–116.

Ramsay A. 1813. Account of unusual conformation of some muscles and vessels. *Edinb Med Surg J* 8: 281–283.

Rauber A, Kopsch F. 1948. *Rauber–Kopsch Lehrbuch und Atlas der Anatomie des Menschen*. Leipzig: Theime.

Rodríguez-Niedenführ M, Burton GJ, Deu J, Sañudo JR. 2001a. Development of the arterial pattern in the upper limb of staged human embryos: normal development and anatomic variations. *J Anat* 199: 407–417.

Rodríguez-Niedenführ M, Vazquez T, Nearn L, Ferreira B, Parkin IG, Sañudo JR. 2001b. Variations of the arterial pattern in the upper limb revisited: a morphologic and statistical study, with a review of the literature. *J Anat* 199: 547–566.

Rodríguez-Niedenführ M, Vazquez T, Parkin IG, Sañudo JR. 2003. Arterial patterns of the human upper limb: update of anatomical variations and embryological development. *Eur J Anat* 1: 21–28.

Rossi U. 1890. Anomalie Arteriose: Lo Sperimentale. *Giornale Italiano di Scienze Mediche* 65: 3–14.

Rowsell AR, Davies DM, Eisenberg N, Taylor GI. 1984. The anatomy of the subscapular-thoracodorsal arterial system: Study of 100 cadaver dissections. *Br J Plast Surg* 37: 574–576.

Ruge G. 1884. Beiträge zur Gefässlehre des Menschen. *Gegenbaurs Morphologisches Jahrbuch* 9: 329–388.

Saadeh FA. 1984. Accessory thoracodorsal artery. *Anat Anz* 157: 319–321.

Sachs M. 1987. The arteria radialis superficialis. An unusual variatioin of the arterial radialis of man and its phylogenetic significance. *Acta Anat* 128: 110–123 (in German).

Saeed M, Rufai A, Elayed S, Sadiq M. 2002. Variations in the subclavian-axillary arterial system. *Saudi Med J* 23: 206–212.

Salvi G. 1898. Arteriae dorsales carpi. Atti della Societia Toscana di Scienze Naturali, Residente in Pisa. *Mem* 17: 167–185.

Sandifort Ed. 1777. Brachiales arteriae binae ex subclavia enatae p. 127. Observationes Anatomico-Pathologicae, Apud P.v.d. Eykk et D. Vygh, Leiden.

Sankott AM. 1919–20a. Über eine neue varietät der art radialis. *Anat Anz* 52: 502–511.

Sankott AM. 1919–20b. Zweiter beitrag zur kasuistik der varietäten der art. radialis. *Anat Anz* 53: 397–398.

SatheeshNaik K, Lokanadham S. 2013. Unusual origin of unilateral arterial trunk from radial artery – case report. *Int J Cur Res Rev* 5: 82–84.

Schaefer EA, Symington J, Bryce TH. 1915. *Quain's Anatomy*, 11th edition. London: Longmans, Green and Co.

Schneck J. 1879. Hereditary variation in the radial arteries. *Chicago Med J Exam* 39: 475–476.

Schwalbe E. 1889. Beitrag zur kenntniss der arterienvarietäten des menschlichen arms. *Morphologichen Arbeiten* 8: 1–47.

Schwalbe E. 1895. Zur vergleichenden anatomie der unterarmarterien, speciell des arcus volaris sublimis. *Morphologisches Jahrbuch* 23: 412–451.

Schwyzer AG, de Garis CF. 1935. Three diverse patterns of the arteria brachialis superficialis in man. *Anat Rec* 63: 405–416.

Seldinger SI. 1964. Arteries of the extremities. In: *Handbuch Medizinischer Radiologie* (eds Diethelm L, Olsson O, Strnad F, Vieten H, Zuppinger A). Vol. 10, part 3. Berlin: Springer, p. 400–472.

Senior HAD. 1926. A note on development of the radial artery. *Anat Rec* 55: 403–409.

Shepherd FJ. 1883. On some anatomical variations with remarks on their morphology. *Ann Anat Surg* 8: 175.

Sieg P, Jacobsen HVC, Hakin SG, Hermes D. 2006. Superficial ulnar artery: Curse or blessing in harvesting fasciocutaneous forearm flaps. *Head Neck* 28: 447–452.

Siegbauer F. 1940. Lehrbuch der Normalen Anatomie des Menschen. Wien, Berlin: Urban & Schwarzenberg.

Singer E. 1933. Embryology pattern persisting in the arteries of the arm. *Anat Rec* 55: 403–409.

Skopakoff C. 1959a. Über die Variabilität der Ab- und Verzweigung der A. brachialis superficialis. *Anat Anz* 106: 356–368.

Skopakoff C. 1959b. Uber die variabilität der abzweigung der hauptäste der Aa. axillaris et brachialis. *Anat Anz* 107: 294–304.

Smith-Agreda V. 1959. Posililidades genotipicas en ciretas ramos de ditribucion de las arterias del miembro superior. *Ann Anat (Granada)* 8: 53–74.

Souligoux C. 1893. Anomalie de l'artère humérale. *Bull Mém Soc Anat Paris* 7: 278.

Souligoux C. 1895. Anomalie de l'artère cubitale. *Bull Mém Soc Anat Paris* 1895: 657.

Spinner RJ, Varela CD, Urbaniak JR. 1996. Digital nerve penetration by a digital artery in a patient with neurovascular symptoms: A case report. *J Hand Surg (Am)* 21: 1101–1103.

Stocquart A. 1887. Les anomalies de l'artère cubitale. *Arch Méd Chirurgie Pratiques* 2: 85–86.

Struthers J. 1848. On a peculiarity of the humerus and humeral artery. *Month J Med Sci* 8: 264–267.

Sussloff KI. 1903. On subcutaneous position of the radial artery in the lower one half of the forearm. *Russkii Vrach* 2: 1420–1422 (in Russian).

Tagil SM, Bozkurt MC, Kuvat SV, Cicekcibasi AE. 2012. A variant course of the superficial palmar branch of the radial artery. *Surg Radiol Anat* 34: 871–873.

Tandler J. 1897. Zur anatomie der arterien der hand. *Anat Hefte* 7: 263–282.

Thomson A. 1884. Note on two instances of abnormality in the course and distribution of the radial artery. *J Anat Physiol* 18: 265–269.

Trotter M, Henderson JL, Gass H, Brua RS, Welsman S, Agress H, Curtis GH, Westbrook ER. 1930. The origin of the branches of the axillary artery in whites and American negroes. *Anat Rec* 46: 133.

Turner RS. 1959. The angle of origin of the ulnar artery. *Anat Rec* 134: 761–768.

Uglietta JP, Kadir S. 1989. Arteriographic study of variant arterial anatomy of the upper extremities. *Cardiovasc Intervent Radiol* 12: 145–148.

Valsecchi O, Vassileva A, Musumeci G, Rossini R, Tespili M, Guagliumi G, Mihalcsik L, Gavazzi A, Ferrazzi P. 2006. Failure of transradial approach during coronary interventions: anatomic considerations. *Catheter Cardiovasc Interv* 67: 870–878.

Varro J, Laszlo H, Varga G. 1978. Anatomy of the hand arteries based on angiographic studies. *Magyar Traumat Orthop* 21: 127–134.

VijayaBhaskar P, Ritesh R, Shankar PR. 2006. Anomalous branching of the axillary artery: a case report. *Kathmandu Univ Med J* 4: 517–519.

Vollala VR, Nagabhooshana S, Bhat SM. 2008a. Trifurcation of the brachial artery with variant course of radial artery: rare observation. *Anat Sci Int* 83: 307–309.

Vollala VR, Nagabhooshana S, Bhat SM, Rodrigues V, Rao M, Pamidi N, Surendran S. 2008b. Rare anatomical variant: arterial circle in the palm and at the base of the thumb. *Rom J Morphol Embryol* 49: 585–587.

Vollala VR, Nagabhooshana S, Rao M, Potu BK, Pamidi N, Bolla SR. 2009. Unorthodox superficial palmar arch observed in a South Indian cadaver: a case report. *Cases J* 2: 6362.

Wachtler F. 1978. Eine seltene varietat im gefab-nevenbundel der axilla. *Anat Anz* 143: 450–455.

Walsham WJ. 1880. A large branch from the brachial artery distributed as the ulnar in the palm; the ulnar in the forearm derived from the brachial as usual. *St Bartholomews Hosp Rep* 16: 91–92.

Wankoff W. 1961. Die frage der typenbestimmung der a. brachialis superficialis im lichte einer neuen varietat, die beim menschlichen fotus beobachtet wurde. *Anat Anz* 110: 265–269.

Weathersby HT. 1955. The artery of the index finger. *Anat Rec* 122: 57–64.

Weathersby HT. 1956a. Anomalies of brachial and antebrachial arteries of surgical significance. *South Med J* 49: 46–49.

Weathersby HT. 1956b. Unusual variation of the ulnar artery. *Anat Rec* 124: 245–248.

Winslow R. 1883a. A study of the malformations, variations, and anomalies of the circulatory apparatus in man. *Ann Anat Surg* 7: 18–19.
Winslow R. 1883b. A study of the malformations, variations, and anomalies of the circulatory apparatus in man. *Ann Anat Surg* 7: 19–21.
Winslow R. 1883c. A study of the malformations, variations, and anomalies of the circulatory apparatus in man. *Ann Anat Surg* 7: 21–22.
Winslow R. 1883d. A study of the malformations, variations, and anomalies of the circulatory apparatus in man. *Ann Anat Surg* 7: 91–92.
Yagain VK, Dave MR, Anadkat S. 2012. Unilateral high origin of radial artery from axillary artery. *Folia Morphol* 71: 121–124.
Yang HJ, Gil YC, Jung WS, Lee HY. 2008. Variations of the superficial brachial artery in Korean cadavers. *J Korean Med Sci* 23: 884–887.
Yazar F, Kirici Y, Ozan H, Aldur MM. 1999. An unusual variation of superficial ulnar artery. *Surg Radiol Anat* 21: 155–157.
Yelloly J. 1801. A peculiarity in the course of the radial artery. *Med Phys J* 5: 82–83.
Yoshinaga K, Tanii I, Kodama K. 2003. Superficial brachial artery crossing over the ulnar and median nerves from posterior to anterior: embryological significance. *Anat Sci Int* 78: 177–180.
Yucel HH. 1999. Unilateral variation of the arterial pattern of the upper extremity with a muscle variation of the hand. *Acta Med Okayama* 53: 61–65.
Zagorsky P. 1809. Observationum anatomicarum quadrigae de singulari arterium aberratione. *Mem de l'Acad Imperiale Sci St Petersbourg* 1: 386.
Zuckerkandl E. 1895. Zur anatomie und entwicklungsgeschicte der arterien des vorderarmes. *Anat Hefte* 4: 1–98.

54 Abdominal aorta

Daisy Sahni[1], Anjali Aggarwal[1], Tulika Gupta[1], Harjeet Kaur[1], Richa Gupta[1], Kunal Chawla[1], Narbada Saini[1], Shallu Garg[1], Anjali Singla[1], Arpan Deep[2], Harsimran Jit Singh[1], Devendra Shekhawat[1] and Megha Rapotra[1]

[1]Postgraduate Institute of Medical Education & Research, Chandigarh, India

[2]Children's of Alabama, Birmingham, Alabama, USA

Abdominal aorta

Origin and length

The uppermost limit of the abdominal aorta is level with the lower border of the T12 vertebra (Feller and Woodburne 1961). The present authors found two cases with a difference among 50 bodies dissected. The abdominal aorta started at the disk between T11 and T12 in one case, while in the second the origin was at the disk between T12 and L1. The mean aortic length has been reported as 13.2±1.39 cm (9.5–16.6 cm) (Heidsieck 1928; George 1935). Pennington and Soames (2005) reported it to be 16.1±1.5 cm with a range of 12.7–18.2 cm and stated that the celiac artery, superior mesenteric artery (SMA), and both renal arteries all arise from the proximal half of the abdominal aorta within 45 mm of each other, with the origin of the renal arteries being most consistent. The present authors found the mean aortic length to be 15.6±2.29 cm (11.5–24.4 cm). The length of the abdominal aorta is approximately one-third of the total descending aorta (Yahel and Arsenburg 1998).

Aortic course

The aorta lies in the midline as it enters the abdomen, but it usually deviates very slightly to the left in its descent (Hollinshed 1956). In a study of 100 specimens by Fellar and Woodburne (1961) the aorta followed a straight course in 59, deviated to the left in 24, and deviated to the right in the remaining 17.

Tortuosity

Wadhwa and Soni (2012) reported that the abdominal aorta follows a tortuous course with deviation to the right opposite the first and second lumbar vertebrae, and deviation to the left opposite the third and fourth. Marked tortuosity was found in five patients among the 20 aortograms studied by Gerlock and Gonchorenko (1979). In our series of 50 cases left tortuosity was observed in 16% and right tortuosity in 6%, while 2% exhibited anterior tortuosity (Fig. 54.1). In one case the abdominal aorta had an S-shaped curvature. The first convexity was toward the right and the inferior mesenteric artery emerged from its midpoint; the renal arteries arose from the midpoint of the second convexity, which was toward the left side (Fig. 54.2).

Diameter

The aortic diameter gradually decreases between the diaphragm and its bifurcation: it is wider just below the superior mesenteric artery origin then narrows caudally (Dixon et al. 1984; Pearce et al. 1993; Lederle et al. 1997; Fleischmann et al. 2001). The aortic diameter was 19.4±3.8 mm (11.4–31.9 mm) at the origin, 18.9±3.1 mm (13.0–24.9 mm) at the midpoint, and 20.7±3.9 mm (13.1–28.3 mm) at the termination. In their study of 15 cadavers, Pennington and Soames (2005) found that the external aortic diameter decreased from 24.9±4.8 mm at the level of the celiac trunk to 24.4±4.2 mm at the level of the superior mesenteric artery (SMA) and 21.5±5.5 mm at the level of the IMA. In their angiographic study, Kahraman et al. (2006) reported the internal aortic diameter of the suprarenal segment (1 cm above the renal artery) to be 19.0±2.5 mm, of the infrarenal segment (1 cm below the renal artery) to be 15.7±2.8 mm, and of the distal infrarenal segment (1 cm above the aortic bifurcation) to be 14.2±2.4 mm. Shah et al. (1978) reported the diameter of the distal aorta to be 1.8 cm. In their study of 389 CT scans, Pearce et al. (1993) concluded that at all levels and in each decade the aortic diameter is significantly greater in men than women (p<0.0001). The aortic diameter increases with age at all levels.

Aortic bifurcation

The most common point of the aortic bifurcation is opposite the lower part of L4 (Quain 1844; Ssoson-Jaroschewitsch 1926; Adachi 1928; Heidiseck 1928; George 1935), although the termination has been reported to vary from the upper third of L2 to the upper third of S1 (Power 1850; Poirer and Charpy 1902; von Bardeleben 1906; Gray 1932; Feller and Woodburne 1961; Lerona and Tewfink 1975; Bergman et al. 1988; Pearce 1993;

Bergman's Comprehensive Encyclopedia of Human Anatomic Variation, First Edition. Edited by R. Shane Tubbs, Mohammadali M. Shoja and Marios Loukas.
© 2016 John Wiley & Sons, Inc. Published 2016 by John Wiley & Sons, Inc.

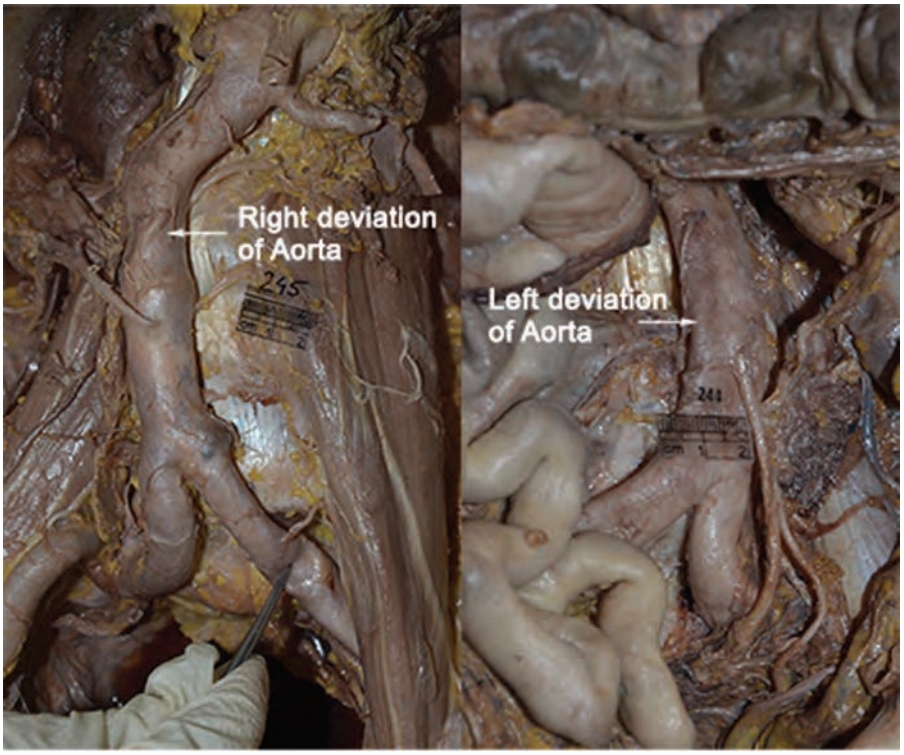

Figure 54.1 Two cases illustrating lateral tortuosity in the course of the abdominal aorta. In first case a right deviation is against the third–fifth lumbar vertebrae, while in the second case a left deviation is present from the second–fourth lumbar vertebrae.

Kornreich et al. 1997; Pennigton and Soames 2005). Prakash et al. (2011) reported the aortic bifurcation at L4 in 54%, L5 in 26%, and L3 in 20% of 50 cases studied. The present authors in their study of 50 cadavers found the aortic bifurcation at the disk between L4 and L5 in 77.5%, L4 in 15%, L5 in 5%, and L3 in 2.5%. A higher division is less common, although the aorta has been reported to divide as high as the second lumbar vertebra.

According to Quain (1844), in 10 out of every 13 subjects examined the bifurcation of the aorta was found within 1.2 cm above or below the level of the highest part of the iliac crest. In our study the bifurcation occurred below the highest point of the iliac crest in all but one case.

Termination of the aorta into external and internal iliac branches on both sides with bilateral absence of the common iliac arteries has been reported by some authors (Mansfield and Howard 1964; Shetty et al. 2013).

A distal shift of the aortic bifurcation from the upper third of the L4 vertebra at birth to the middle third of L4 in subjects below 25 years of age and the lower third of the fourth lumbar vertebra in those above 25 years was noted by Ssoson-Jaroschewitsch (1926).

Usual branches

The branches of the abdominal aorta can be classed as follows:

- Ventral branches (these are unpaired): celiac trunk; superior mesenteric artery; anferior mesenteric artery.
- Lateral branches (these are paired): inferior phrenic; middle suprarenal; renal; and gonadal.
- Dorsal branches: lumbar arteries; and median sacral artery.
- Terminal branches: common iliac arteries.

Unusual branches

Ucerler and Ikiz (2006) reported a case in which branches of the celiac trunk arose from the aorta via two different trunks: the upper gastrophrenic trunk and the lower hepatosplenic trunk. A bronchial artery can arise from the celiac trunk (Bergman et al. 1988).

Shivarama et al. (2012) reported a case of a 66-year-old male with multiple variations in the branches of the abdominal aorta. The celiac trunk gave rise to inferior phrenic arteries bilaterally while the left gastric was a direct branch of the abdominal aorta, which also gave off the accessory left renal artery. The right testicular artery arose as an anterior branch of the abdominal aorta. Direct branches of the abdominal aorta sometimes include an accessory inferior phrenic artery, splenic, hepatic, accessory hepatic, supreme pancreatic, accessory superior mesenteric, inferior suprarenals, accessory gonadal, accessory and fifth lumbar, internal iliac, external iliac, umbilical, and/or accessory median sacral (Bergman et al. 1988). In a study of 50 cadavers, the present authors found unilateral quadruple middle suprarenal arteries in one case, a unilateral accessory inferior suprarenal in one, a left gastric artery in one, an accessory renal artery unilaterally in 15 and bilaterally in two, two accessory unilateral renal arteries in a single case and a unilateral accessory testicular artery in five.

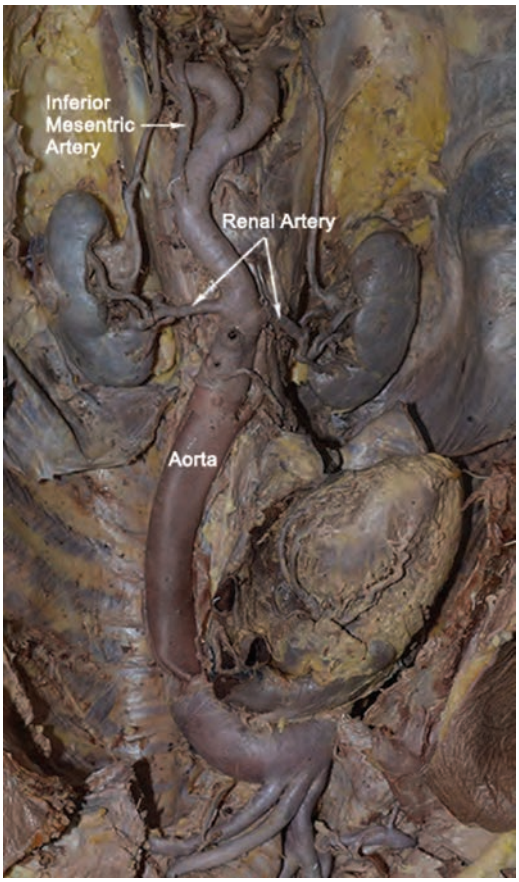

Figure 54.2 An abdominal aorta with an S-shaped curvature. The first convexity is toward the right side and the inferior mesenteric artery emerged from its midpoint, while the second convexity is toward the left side and the renal arteries emerged from its midpoint.

Celiac trunk

The celiac trunk (CT), the first unpaired branch of the abdominal aorta, originates from the anterior wall of the aorta just below the aortic hiatus of the diaphragm at the level of the intervertebral disk between T12 and L1 (Williams et al. 1995).

The emergence of the CT from the abdominal aorta has been reported to lie at the level of the intervertebral disk between the T12 and L1 vertebrae in 73.3–100% of cases (Pennington and Soamer 2005, 100%; Wadhwa and Soni 2010, 73.3%; Yang et al. 2011, 93.5%). Kao et al. (1992) reported a high level origin of the CT at the level of T12 in 48% of celiac angiograms and Yang et al. (2011) at the level of the T11–12 intervertebral space in 6.55% of their cases. A low level of origin of the CT is extremely rare. Nayak et al. (2013) reported a case where the CT arose opposite the L2 vertebrae. The present authors observed the CT to lie at the level of the T12 vertebra in 62.5% of 50 cases and between the T12 and L1 vertebrae in 30%. It lay at the level of L1 and the disk between L1 and L2 in 2.5% and 5% of cases, respectively.

The distance between the CT and the aortic hiatus ranges between 11.5 and 12.5 mm (Cavdar et al. 1997; Uysal et al. 2010). The present authors observed that the CT originated 25.3±1.17 mm (1.93–54.63 mm) below the aortic hiatus. Most commonly (54.0%) it lay below the hiatus at a distance ranging from 20.1 to 30 mm. In only one case was the distance less than 5 mm, that is, 1.93 mm. It lay between the crura of the diaphragm at a mean distance of 15.4±8.67 mm (0.9–34.02 mm) from the right crus and 10.4±10.86 mm (1.29–7.09 mm) from the left.

The length of the CT from its origin to the point where the trunk gives off its main branches ranges from 5 to 40 mm, 8 to 40 mm, and 10 to 15 mm according to Rio-Branco (1912), Michels (1951b) and Latarjet and Ruiz-Liard (1989), respectively. Orts Llorca (1944) found it to be up to 12 mm. Malnar et al. (2010) reported the length of the CT to be 1.9±0.08 cm when it trifurcated and 2.0±0.08 cm when it bifurcated.

The diameter of the celiac trunk ranges from 4 to 10 mm, 3 to 12 mm and 10 to 12 mm according to Rio-Branco (1912), Michels (1951b) and Pignataro (1969), respectively. The mean diameter of the CT was reported to be 7 mm, 6 mm and 6.2 mm by Fumagalli and Cavallotti (1983), Latarjet and Ruiz-Liard (1989) and Gosai et al. (2013), respectively.

The present authors observed that in the classical type of CT, that is, three branches radiating from one point, its length from the origin to the point where the trunk gave off its three main branches was 13.21±3.74 mm with a range of 8.54 to 19.8 mm, and its mean diameter at its origin was 5.74±1.14 mm with a minimum of 4.74 mm and maximum of 7.87 mm. In non-classical CTs, that is, when the left gastric artery (LGA) arises at its first branch and then the CT continues for a while before dividing into the common hepatic (CHA) and splenic (SA) arteries, the length of the CT from its origin to the point of bifurcation into CHA and SA was 19.72±5.66 mm (8.81–28.89 mm). The length from its origin to the point where it gave off the first branch, the LGA, was 10.57±5.66 mm (2.53–22.89 mm), and from the LGA to the terminal point of bifurcation of the CHA and SA was 9.16±3.77 mm with a range of 4.43–15.63 mm.

The distance between the origin of the celiac trunk and the superior mesenteric artery on the aorta varies considerably from 1 to 22 mm according to Michels (1952) and from 1 to 18 mm according to Saeed and Rufai (2001) and Petrella et al. (2007). The present authors observed it to vary from 2.14 to 30.1 mm (13.34±4.89 mm).

The first description of normal and aberrant anatomies of the celiac trunk (CT or truncus celiacus) was given by Haller in 1756 and anatomical variations of the CT were classified for the first time by Adachi in 1928. He noted six types of division of the CT and superior mesenteric artery (SMA). Since then, many reports have demonstrated a plethora of other variations. The CT can divide into 2, 3, 4, 5, or even 6 branches.

Branching pattern of the CT

Variations in the branching pattern of the CT can be categorized into the following types depending upon the number of arteries arising from it (Gielecki et al. 2005) (Fig. 54.3).

1. Bifurcation of the CT: division into two branches, with variable origin of one of the normal three branches. This pattern

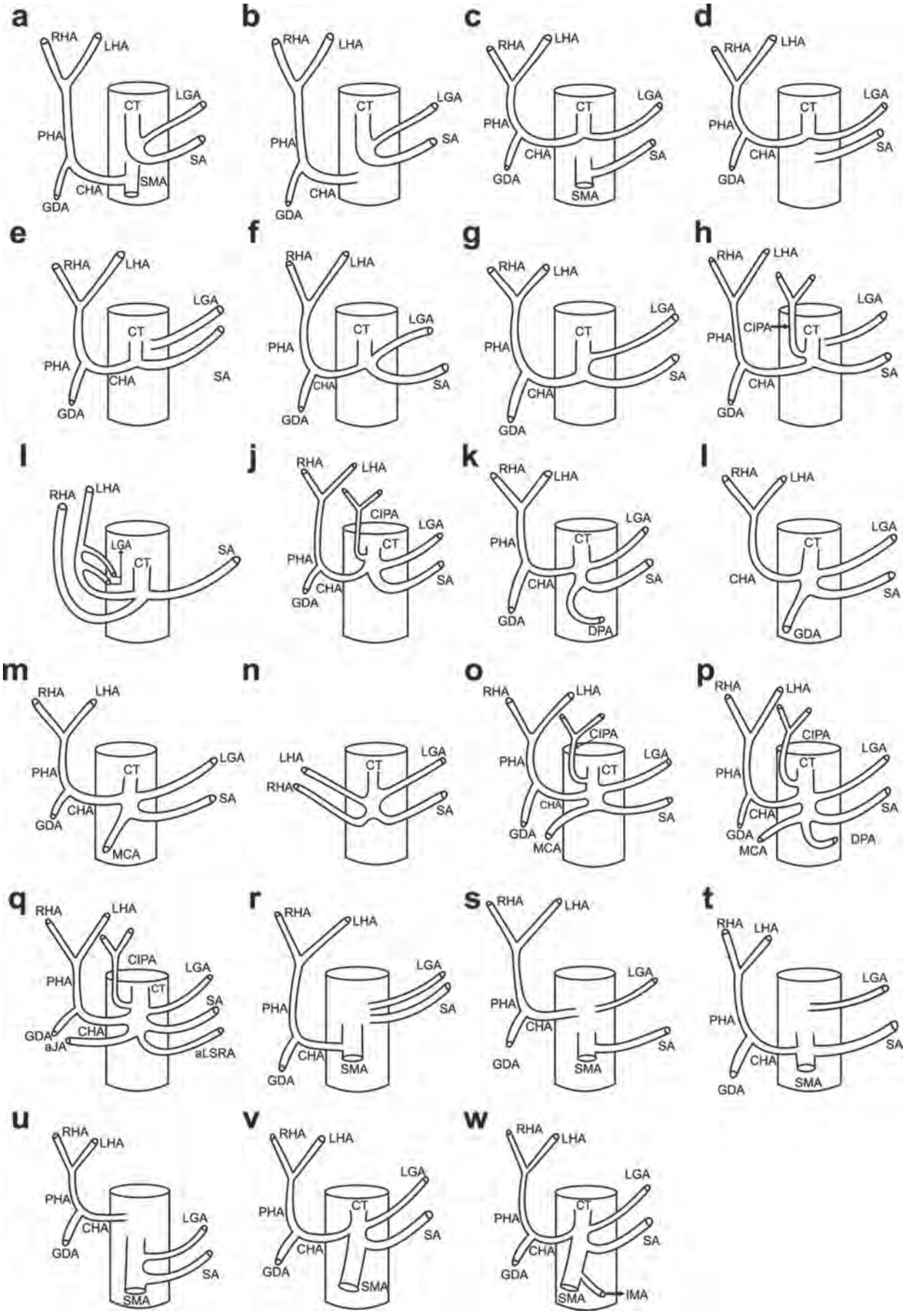
a
RHA
LHA
CT
LGA
PHA
SA
SMA
CHA
GDA
b
RHA
LHA
CT
LGA
PHA
SA
CHA
GDA
c
RHA
LHA
CT
LGA
PHA
CHA
SA
GDA
SMA
d
RHA
LHA
CT
LGA
PHA
CHA
SA
GDA
e
RHA
LHA
LGA
CT
PHA
CHA
SA
GDA
f
RHA
LHA
CT
LGA
PHA
CHA
SA
GDA
g
RHA
LHA
LGA
CT
PHA
SA
CHA
GDA
h
RHA
LHA
LGA
CIPA
PHA
CT
SA
CHA
GDA
i
RHA
LHA
LGA
CT
SA
j
RHA
LHA
CIPA
LGA
CT
PHA
SA
CHA
GDA
k
RHA
LHA
LGA
CT
PHA
CHA
SA
GDA
DPA
l
RHA
LHA
CT
LGA
CHA
SA
GDA
m
RHA
LHA
PHA
CT
LGA
SA
GDA
CHA
MCA
n
LHA
CT
LGA
RHA
SA
o
RHA
LHA
CIPA
PHA
CT
LGA
CHA
SA
GDA
MCA
p
RHA
LHA
CIPA
LGA
PHA
CT
CHA
SA
GDA
DPA
MCA
q
RHA
LHA
CIPA
PHA
LGA
CT
SA
GDA
CHA
aJA
aLSRA
r
RHA
LHA
LGA
PHA
SA
CHA
SMA
GDA
s
RHA
LHA
LGA
PHA
CHA
SA
GDA
SMA
t
RHA
LHA
LGA
PHA
SA
CHA
GDA
SMA
u
RHA
LHA
PHA
CHA
LGA
GDA
SA
SMA
v
RHA
LHA
LGA
PHA
CT
SA
CHA
GDA
SMA
w
RHA
LHA
LGA
PHA
CT
SA
CHA
GDA
SMA
IMA

has been reported in 4–12% of specimens in cadaveric studies and 7.5–9% in angiographic studies. The variable branch usually arises either from the SMA or directly from the aorta. In the present study conducted on 50 cadavers, it was observed in 4% of cases (Fig. 54.3a–e).

a. Bifurcation of the CT into the left gastric artery (LGA) and splenic artery (SA) with variable origin of the common hepatic artery (CHA) has been reported in 2–8% of cases. The CHA arises from the SMA in 2–6% of cadaveric and 2.6–4% of angiographic studies, or from the aorta in 0.02–2% of cases (Vandamme and Bonte 1985; Nelson et al. 1988; Petrella et al. 2007; Winston et al. 2007; Silveira et al. 2009; Chitra 2010; Song et al. 2010; Ugurel et al. 2010) (Fig. 54.3a, b).
b. Bifurcation of the CT into the LGA and CHA with a variable origin of the SA is a less common variant with a range of 0.18–2%. The SA arises either from the SMA (0.16–1%) or more commonly from the aorta (0.02–2%) (Song et al. 2010; Ugurel et al. 2010; Prakash et al. 2012) (Fig. 54.3c, d).
c. Bifurcation of the CT into the CHA and SA with a variable origin of the LGA, which then usually arises directly from the aorta. This is a more common CT bifurcation, observed in 2–8% of cases in previous reports (Vandamme and Bonte 1985; Winston et al. 2007; Petrella et al. 2007; Silveira et al. 2009; Chitra 2010; Song et al. 2010; Ugurel et al. 2010; Prakash et al. 2012) (Fig. 54.3e). The present authors observed a case where the CT bifurcated into the CHA and SA and the LGA originated directly from the aorta (Fig. 54.4). In one angiographic study, the LGA was seen to arise from the SMA in 0.02% of cases (Song et al. 2010).

2. Trifurcation of the CT: This is the most common type of division, seen in 44–95% of cases. The CT divides into the LGA, CHA, and SA. The three branches radiate from a single point (termed classical) in 11–30%; more frequently (in 70–90% of cases), a non-classical type of trifurcation is seen in which the LGA arises from the CT as its first branch and then the CT continues for a while before dividing into the CHA and SA (Vandamme and Bonte 1985; Nelson et al. 1988; Petrella et al. 2007; Winston et al. 2007; Silveira et al. 2009; Chitra 2010; Malnar et al. 2010; Song et al. 2010; Ugurel et al. 2010; D'Souza et al. 2012; Prakash et al. 2012) (Figs 54.3f, g, 54.5). Trifurcation of the CT into the CHA, SA, and common inferior phrenic artery (CIPA) was observed in a study in 2% of cases; the LGA in these cases arose directly from the aorta (Chitra 2010) (Fig. 54.3h). The present authors observed a case where the CT trifurcated into the right hepatic artery (RHA) and left hepatic artery (LHA), and the SA and LGA arose from the LHA (Figs 54.3i, 54.6).
3. Quadrificaton of the CT: The celiac trunk branches into four arteries, three of which are normal branches (i.e., LGA, CHA, and SA) and the fourth is anomalous. The anomalous branch can be one of the two inferior phrenics (right and left inferior phrenic arteries) or a trunk common to them (Fig. 54.3j). These are the most common additional arteries arising from the CT, seen in 20–48% of reported cases (Vandamme and Bonte 1985; Nelson et al. 1988; Nayak et al. 2008; Chitra 2010; Salve and Ratanprabha 2011; Ashalata 2011). The additional branch can also be the dorsal pancreatic artery in 2–12% (Vandamme and Bonte 1985; Nelson et al. 1988; Chitra 2010), the gastroduodenal artery in 2–6% (Petrella et al. 2007; Chitra 2010), the middle colic artery in 1.2–4.8% (Vandamme and Bonte 1985; Nelson et al. 1988; Silveira et al. 2009; Petrella et al. 2007; Chitra 2010), the accessory hepatic artery in 1.12% (Petrella et al. 2007), the RHA in 4% or the LHA in <1% (Winston et al. 2007) (Fig. 54.3k–m). The present authors found a case in which there was quadrification of the CT into the LGA, SA, RHA, and LHA (Figs 54.3n, 54.7).
4. Pentafurcation of the CT: In 2–5% of cases, in addition to the normal three branches, two more arteries – a common trunk of the inferior phrenic artery (CIPA) and a middle colic artery – were also seen to originate from the CT, resulting in pentafurcation (Chitra 2010; D'Souza et al. 2010) (Fig. 54.3o).

Figure 54.3 Schematic representation of variant branching pattern of the celiac trunk. Bifurcation of the CT into (a) the LGA and SA with the CHA arising from the SMA; (b) the LGA and SA with the CHA arising directly from the aorta; (c) the LGA and CHA with the SA arising from the SMA; (d) the LGA and CHA with the SA arising from the aorta; and (e) the CHA and SA with the LGA arising from the aorta. Trifurcation of the CT (f) from a point into the LGA, CHA and SA; (g) with the LGA arising as its first branch, then continuing for some distance before bifurcating into the CHA and SA; (h) into the CIPA, CHA and SA with the LGA arising directly from the aorta; and (i) into the RHA, LHA and SA with the LGA arising from the LHA. Quadrification of the CT into (j) the LGA, SA, CHA and CIPA; (k) the LGA, SA, CHA and DPA; (l) the LGA, CHA, SA and GDA; (m) the LGA, CHA, SA and MCA; and (n) the LGA, SA, RHA and LHA. (o) Pentafurcation of the CT into the LGA, CHA, SA, CIPA and MCA. Hexafurcation of the CT into (p) the LGA, CHA, SA, CIPA, MCA and DPA; and (q) the LGA, CHA, SA, CIPA, aLSRA and aJA. (r) The CT is absent and (r) the LGA and SA arise directly from the aorta and the CHA from the SMA; (s) the LGA and CHA arise from the aorta and the SA from the SMA; (t) the LGA arises from the aorta and the CHA and SA arise from the SMA; and (u) the CHA arises from the aorta and the LGA and SA arise from the SMA. (v) The CT and SMA form a common trunk. (w) The CT, SMA, and IMA form a common trunk of origin. CT: celiac trunk; CHA: common hepatic artery; SA: splenic artery; LGA: left gastric artery; SMA: superior mesenteric artery; LHA: left hepatic artery; RHA: right hepatic artery; GDA: gastroduodenal artery; CIPA: common inferior phrenic artery; DPA: dorsal pancreatic artery; MCA: middle colic artery; aLSRA: accessory left suprarenal artery; aJA: accessory jejunal artery; SDA: supraduodenal artery; IMA: inferior mesenteric artery.

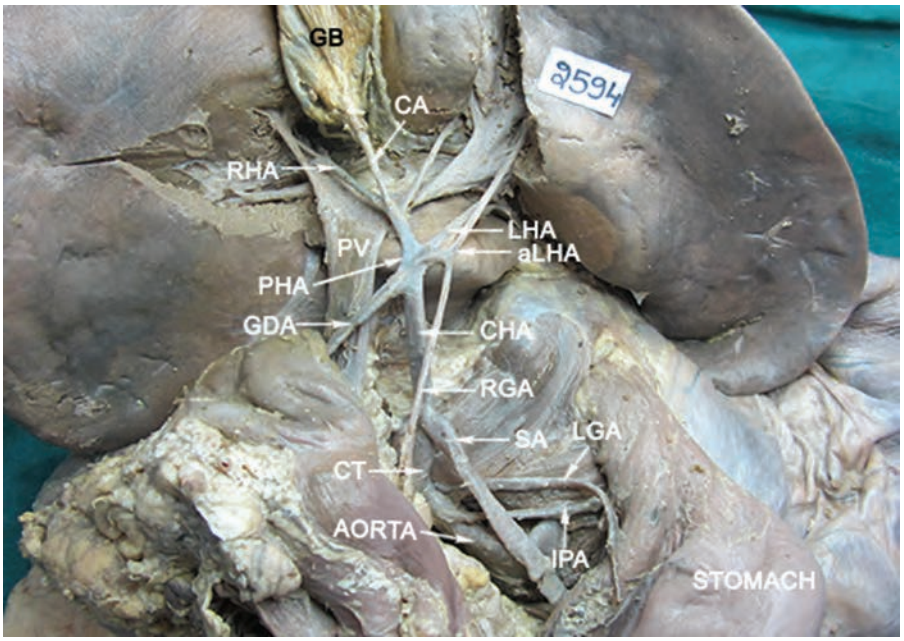

Figure 54.4 Dissection on the visceral surface of the liver illustrating the bifurcation of the CT into the CHA and SA. The LGA arises directly from the abdominal aorta at the level of origin of the IPA. The CHA gives off the GDA and continues as the PHA, which bifurcates into the RHA and LHA. An accessory LHA arises from the PHA stem and gives off the RGA. The CA arises from the RHA. Abbreviations as for Figure 54.3 and CA: cystic artery; IPA: inferior phrenic artery; RGA: right gastric artery; GB: gall bladder; CD: cystic duct; CBD: common bile duct; CHD: common hepatic duct; PV: portal vein.

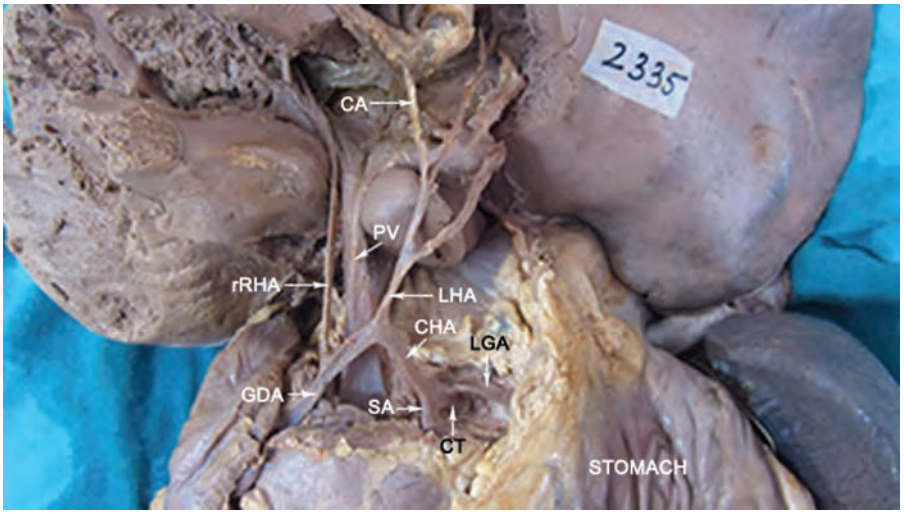

Figure 54.5 Dissection on the visceral surface of the liver illustrating the normal branching pattern of the CT. The CT first gives off the LGA, then continues for some distance before bifurcating into the CHA and SA. The CHA bifurcates into the LHA and GDA. The RHA is replaced from the GDA and the CA arises from the LHA. Abbreviations as for Figures 54.3 and 54.4.

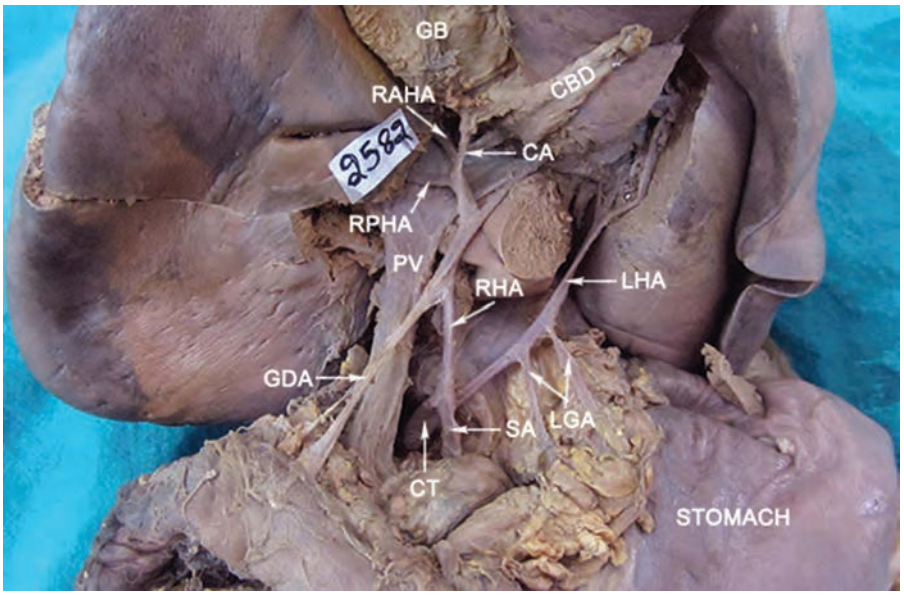

Figure 54.6 Dissection on the visceral surface of the liver illustrating trifurcation of the CT into the RHA, LHA, and SA. Two left gastric arteries arise from the LHA and the GDA arises from the RHA. The CA arises from the RHA. Abbreviations as for Figures 54.3 and 54.4.

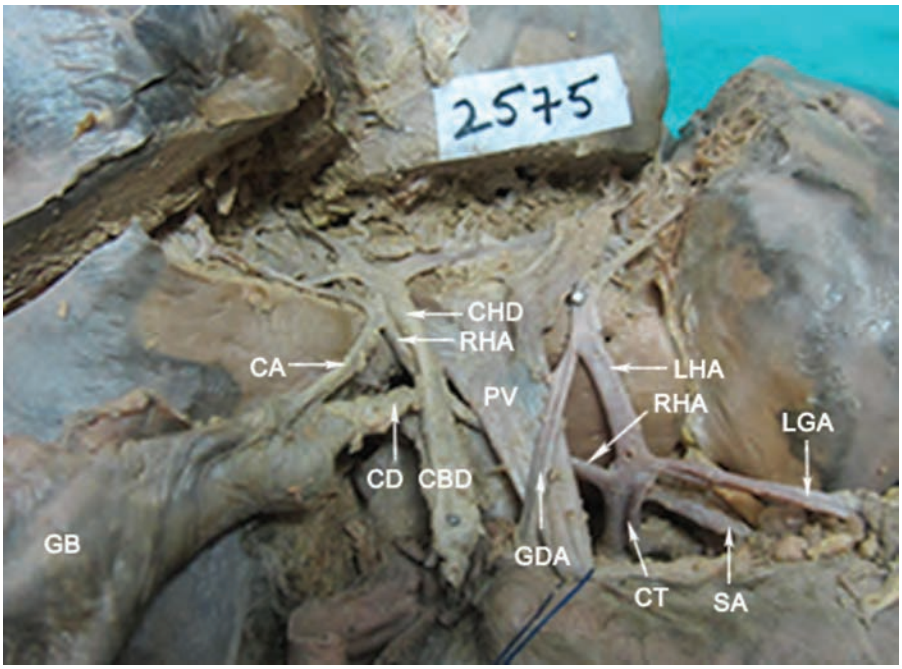

Figure 54.7 Dissection on the visceral surface of the liver illustrating quadrification of the CT into the LGA, LHA, RHA, and SA. The RHA crosses posterior to the PV to reach the hilum of the liver. The GDA arises from the LHA and the CA from the RHA. Abbreviations as for Figures 54.3 and 54.4.

5. Hexafurcation of the CT: In one study (Chitra 2010), in 2% of cases the dorsal pancreatic artery – in addition to the above-mentioned branches in pentafurcation – arose from the CT, resulting in hexafurcation (Fig. 54.3p). Hexafurcation of the CT into its normal three branches plus three additional arteries (accessory left suprarenal, inferior phrenic, and accessory jejuna) was found in one case (Paraskevas and Raikos 2011) (Fig. 54.3q).
6. Agenesis of the CT: The celiac trunk is absent in 0.1–4% of cases (Vandamme and Bonte 1985; Petrella et al. 2007; Song et al. 2010; Ugurel et al. 2010; Prakash et al. 2012). Branches that normally arise from it then usually arise separately from the aorta. Other origins of the arteries of the CT have been seen in such situations. In one case the LGA and SA arose from the aorta and the CHA from the SMA (Vandamme and Bonte 1985) (Fig. 54.3r). In another case, the LGA and CHA arose from the aorta and the SA from the SMA (Song et al. 2010) (Fig. 54.3s). In a few cases of agenesis of the CT, two of the arteries of the CT arose from the SMA and the third from the aorta (LGA, SA from SMA, and CHA from the aorta; CHA, SA from the SMA, and the LGA from the aorta) (Song et al. 2010; Samarawickrama 2010; Varma et al. 2010) (Fig. 54.3t, u).
7. Others:
   a. Celicomesenteric trunk: In 1–2% of cases, the CT and SMA have a common origin from the abdominal aorta (Nelson et al. 1988; Winston et al. 2007; Malnar et al. 2010; Song et al. 2010) (Fig. 54.3v). The celicomesenteric trunk, in addition to its normal branches, gave off the CIPA and left gastroepiploic arteries in one case (Ciçekcibaşi et al. 2005).
   b. Celico-bimesenteric trunk: the celiac, superior mesenteric, and inferior mesenteric arteries can be joined together by one continuous longitudinal anastomosis (Nonent et al. 2001) (Fig. 54.3w).
   c. Hepatogastrophrenic and hepatosplenomesenteric trunk: a case has been observed where the CT gave off the IPA, LGA, and a stem to the CHA, and the SMA gave off the SA and another stem to the CHA. The CHA was therefore formed by the union of two stems, one from the CT and other from the SMA (Hemanth et al. 2011).
   d. A branch of the CT can pass through the esophageal hiatus of the diaphragm to supply the lower medial quarter of the right lung (Bergman et al. 1988).

Left gastric artery

The left gastric artery (LGA) arises from the celiac trunk (CT) in about 90% of cases. Most commonly, it arises as the first branch of the celiac trunk in 60–100% (Rio-Branco 1912; Eaton 1917). In about 25% of cases, the LGA takes origin from the distal end of the CT along with the hepatic and splenic arteries, forming the tripod of Haller (Nelson et al. 1988; Malnar et al. 2010; Song et al. 2010; Ugurel et al. 2010; D'Souza et al. 2012; Prakash et al. 2012).

The LGA arises directly from the abdominal aorta in 0.5–15% of cases (Eaton 1917, 4.5%; Lipshutz, 1917, 15%; Kiss 1926, 0.5%; Michels 1955, 2.5%; Naidich et al. 1978, 1.8%; Lippert and Pabst 1985, 3%; Vandamme and Bonte 1990, 6%). The present authors observed it in one out of 50 cases studied (Fig. 54.4).

Pamidi et al. (2008) reported a case in which the LGA arose from the abdominal aorta and gave origin to two rare branches, the left gastroepiploic artery and left inferior phrenic artery. After forming a common trunk with one (Cavdar et al. 1997) or both of the inferior phrenics (Matusz et al. 2013), the LGA can arise directly from the abdominal aorta.

Other less frequently reported sources of origin of the LGA include the splenic artery (Michels 1955, 6%), hepatic artery (Tsagareishvili 1959, two out of 250 cases), left inferior phrenic artery (Testut and Laterjet 1958) or superior mesenteric artery (Naidich et al. 1978, 0.2%). Michels (1955) reported the LGA to arise from the CT in 96% of cases and directly from the aorta in 2.5%. He reported three odd derivations of the LGA: origins from the splenic, the left hepatic, and the replaced right hepatic artery.

Two left gastric arteries of almost equal caliber arising from the celiac trunk were reported in two out of 500 cases by Naidich et al. (1978). The present authors observed a case in which there were two left gastric arteries arising from the left hepatic artery (Fig. 54.6).

Salve and Ratanprabha (2011) reported a case where a common trunk arose from the celiac artery and trifurcated into two gastric arteries and an accessory hepatic artery.

The average distance of the origin of the LGA from the origin of the CT was reported to be 12.3 mm by Petrella et al. (2007). The present authors observed it to be 10.57±5.66 mm (range 2.53–22.89 mm). The diameter of the LGA has been reported to be 2.4–4.2 mm in the literature (Vandamme and Bonte 1985; Yildirim et al. 1998; Silveria et al. 2009; Malnar et al. 2010; Ashalata 2011). The present authors observed a mean diameter of 3.43±0.70 mm with the range 1.98–5.42 mm.

Course and branching

The mode of branching and the distribution of the left gastric artery follow a fairly uniform pattern. The LGA courses forward, upward and to the left behind the upper part of the lesser omentum. When it approaches the cardiac end of the stomach it abruptly turns caudally, that is, reverses its direction and passes between the two layers of the lesser omentum. The LGA gives off either a single large vessel or 1–3 small ascending esophageal branches that supply the cardio-esophageal end of the stomach before dividing into its two terminal branches (Michels 1955).

The LGA usually terminates by dividing into two main branches, anterior and posterior (Adachi 1928; Michels 1955; El-Eishi et al. 1973; Naidich et al. 1978; Okada et al. 2010). The anterior branch gives off two or three branches and is distributed to the anterior surface of the stomach. During its course along the lesser curvature, the posterior branch gives off branches to the posterior surface and, in most cases, anastomoses with the right gastric artery (Adachi 1928; Michels 1955; E1-Eishi et al. 1973; Eckmann and Krahn 1984). In some instances, where there is no anastomosis between the left and right gastric, the secondary division of the two vessels enters the muscular coat of the stomach and anastomosis is effected in the submucous layer. Nelson et al. (1988) reported the LGA to arise from the CT in all the 50 cases he studied, but he found an ascending esophageal branch and anterior and posterior gastric branches in 72%.

Accessory left gastric artery

The accessory left gastric artery is a variant gastric artery present in addition to a normal LGA. It supplies the cardia and fundus of the stomach and usually arises from the left hepatic artery. The incidence of this anatomical variant has been reported to be 3–20% (Michels 1955, 3%; Nakamura et al. 1980, 14.2%; Ishigami et al. 2006, 21.2%). The present authors observed one such case out of 50 studied where, in addition to the normal LGA from the CT, there was an additional LGA arising from the LHA (Fig. 54.8).

Michels (1951b) reported the accessory left gastric artery to arise from the splenic artery in 6% of cases, the left hepatic artery in 3%, the iliac artery in 2% and the hepatic artery in one case.

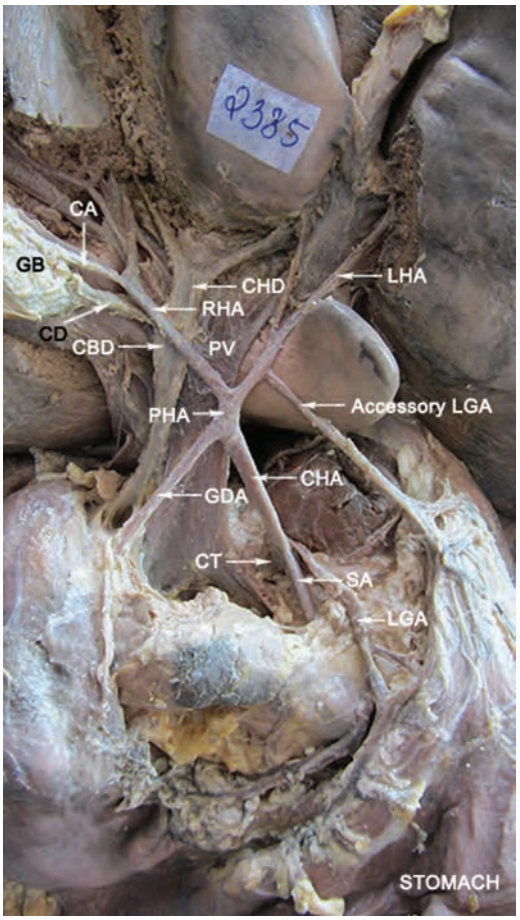

Figure 54.8 Dissection on the visceral surface of the liver illustrating the normal branching pattern of the CT into the LGA, CHA, and SA. An accessory LGA arises from the LHA and the CA arises from the RHA. Abbreviations as for Figures 54.3 and 54.4. PHA: proper hepatic artery; aLGA: accessory left gastric artery

The incidence of an esophageal branch arising from this accessory left gastric artery was reported to be 71–92% (Nakamura et al. 1980; Ishigami et al. 2006).

Inconstant branches

Inconstant branches arising from the LGA include: common hepatic artery; accessory/replaced LHA; right hepatic artery; inferior phrenic artery as well as the following:

- A common hepatic artery arising from the LGA is the least common variation. Since it was first described by Adachi in 1928, who reported it in one out of 252 cases, fewer than 10 cases have been published in the literature. Michels (1955) reported it in one out of 200 cases and Song et al. (2010) observed it in 0.16% of cases.
- An aberrant left hepatic artery (replaced/accessory) arising from the LGA has been reported in 3.8–20% of cases (Adachi 1928; Michels 1966; Suzuki et al. 1971; Rygaard et al. 1986; Nelson et al. 1988; Hiatt et al. 1994; Gruttadauria et al. 2001; Covey et al. 2002; López-Andújar et al. 2007; Chen et al. 2009). Because the LHA frequently originates from the LGA, the early anatomists followed the nomenclature of Haller and designated the left gastric the "gastrohepatic artery" (Michels 1951b).
- An accessory right hepatic artery arising from the LGA is extremely rare and was observed in one out of 600 cases by Covey et al. (2002). One such case was also reported by Panagouli and Venieratos (2011).
- The LGA gives rise to one or both the inferior phrenic arteries in 1.4–4% of cases (Michels 1955; Piao et al. 1998; Loukas et al. 2005b; Basile et al. 2008).

Common hepatic artery

The hepatic artery (HA) and its variations have been extensively described in the literature, beginning with Haller's description in 1756. Michels (1966) proposed an internationally recognized classification of 10 types of HA variations, which has served as a benchmark for further studies of this artery. Subsequently, other hepatic arterial variants have been reported, not included in the Michels classification.

Normally, the common hepatic artery (CHA) arises from the celiac trunk (CT) and divides into the gastroduodenal artery (GDA) and the proper hepatic artery (PHA). The PHA then bifurcates into the right (RHA) and left (LHA) hepatic arteries at the hilum of the liver. This is found in 52–80% of individuals (Michels 1966; Macdonald et al. 2005; Chen et al. 2009; Kishi et al. 2010) (Fig. 54.8). Often, the hepatic artery exhibits incomplete branching and one or other of its usual branches arises from a source other than the CHA from the CT. Such a vessel is said to be aberrant. Aberrant hepatic arteries are of two types: replaced and accessory. A replaced hepatic artery is a substitute for the normal hepatic artery, which is lacking; an accessory hepatic artery appears in addition to that normally present. Aberrant hepatic arteries are found in approximately 45% of individuals (Michels 1966; Suzuki et al. 1971; Hiatt et al. 1994; Gruttadauria et al. 2001; Covey et al. 2002; Macdonald et al. 2005; Abdullah et al. 2006; Chen et al. 2009; Kishi et al. 2010).

Origin

Various origins of the CHA have been reported in about 4% of individuals. These include a replaced CHA (rCHA) arising from the superior mesenteric artery (SMA) and running behind the portal vein (PV) in 0.86–3% of cases (Michels type IX, 4.5%). This is the most common site of variant origin of the CHA. The present authors observed one such case out of 100 studied. A replaced CHA arising directly from the aorta has been reported in 0.2–2% and from the left gastric artery (LGA) in 0.16–1% of individuals (Michels type X, 0.5%). When it arises from the LGA, the rCHA passes though the ligamentum venosum to reach the liver (Suzuki et al. 1971; Hiatt et al. 1994; Winter et al. 1995; Gruttadauria et al. 2001; Covey et al. 2002; Abdullah et al. 2006; López-Andújar et al. 2007; Song et al. 2010; Ugurel et al. 2010; Ozsoy et al. 2011) (Fig. 54.9a). A CHA arising from an anastomosis connecting the CT to the SMA was also reported by Makisalo et al. (1993) (Fig. 54.9b).

Another uncommon variant is an absent CHA, in which one or both of the hepatic arteries originate from either the CT or the aorta. This type of variation has been referred to as a double hepatic artery in the literature and has been reported in about 1–5% of cases. The GDA in these cases usually originates from either of the hepatic arteries (Makisalo et al. 1993; Abdullah et al. 2006; Ozsoy et al. 2011). The present authors observed two such cases in which the CHA was absent and both the hepatic arteries originated directly from the CT (Fig. 54.9c). In one the GDA originated from the LHA, while in the other it arose from the RHA and the LGA from the LHA (Figs 54.6, 54.7). Rygaard et al. (1986) reported two cases in which the CHA was absent and the LHA arose from the LGA: the RHA arose from the aorta in one case and from the CT in the other (Fig. 54.9d, e).

Course

Variations in the course of the CHA from a normal origin have also been observed. The CHA has a retroportal course, that is, behind the portal vein (PV), in 0.15% of individuals (Song et al. 2010). The present authors also observed one such case. A CHA passing though the pancreatic parenchyma (transpancreatic course) has also been reported (Song et al. 2010).

Branching pattern

Variant branching patterns of the CHA have been reported in 0.5–8% of individuals. These include trifurcation of the CHA into the GDA, RHA, and LHA in 2.8% of individuals (Covey et al. 2002). The present authors observed it in 8% of livers (Fig. 54.10). Quadrification of the CHA into the GDA, RHA, LHA, and middle hepatic artery (MHA) was observed in 0.5% of individuals (Covey et al. 2002). In another study, the CHA terminated at the porta into seven branches: five were hepatic arteries, one was a superior pancreaticoduodenal artery, and the

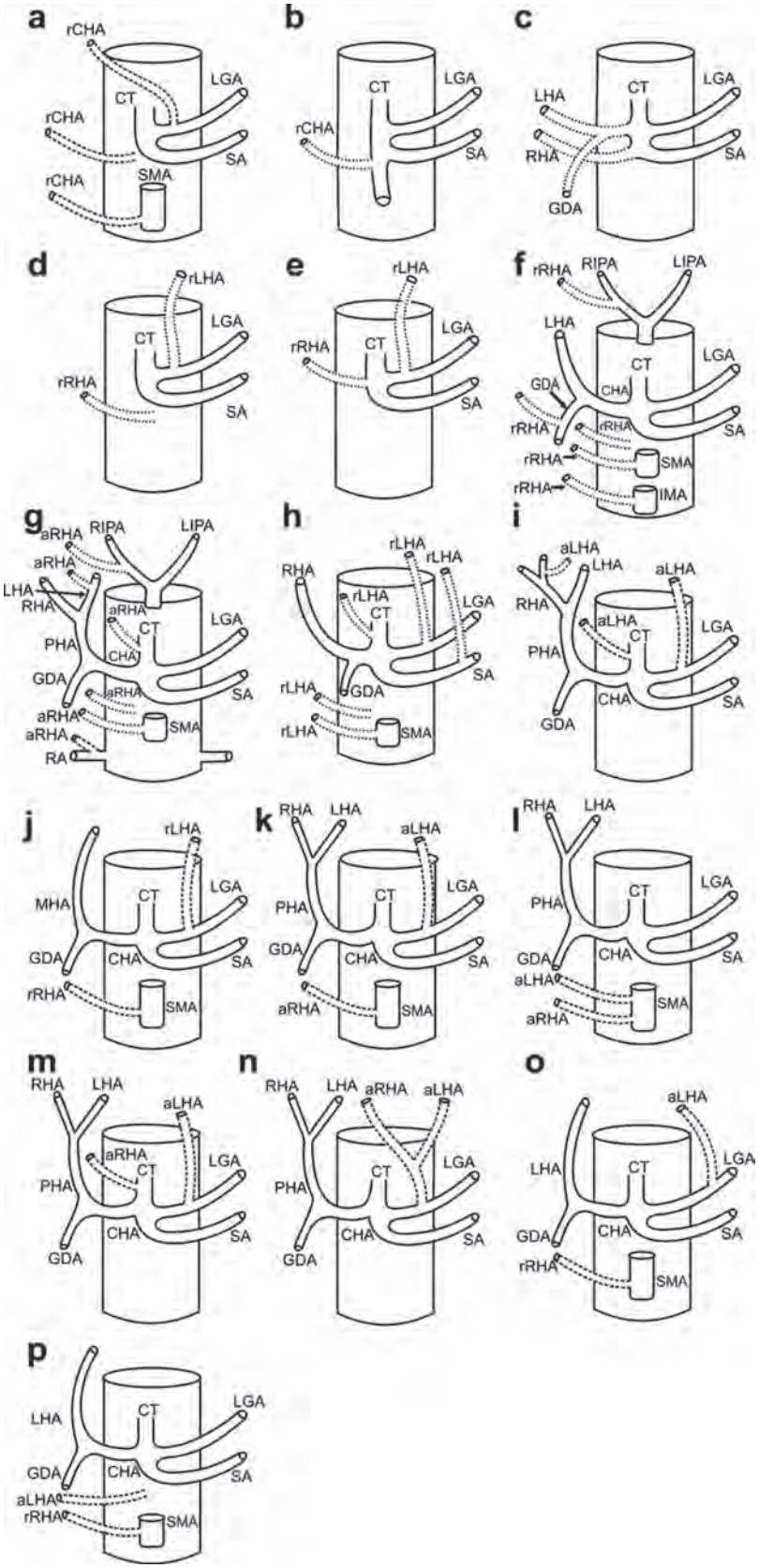

Figure 54.9 Schematic representation summarizing variant patterns of origin of hepatic arteries. (a) Various sources of origin of replaced CHA. (b) The CHA arises from an anastomosis connecting the CT and SMA. The CHA is absent, and (c) the RHA and LHA arise directly from the CT with the GDA arising from the LHA; (d) the LHA is replaced from the LGA and the RHA from the aorta; and (e) the LHA is replaced from the LGA and the RHA from the CT. f. Various sources of origin of (f) replaced RHA; (g) accessory RHA; (h) replaced LHA; and (i) accessory LHA. (j) The CHA arises from the CT, gives off the GDA, and continues as the MHA. The LHA is replaced from the LGA and the RHA is replaced from the SMA. (k) The CHA arises from the CT, gives off the GDA, and continues as the PHA. The PHA at the hilum of the liver bifurcates into the RHA and LHA. An accessory LHA arises from the LGA and an accessory RHA from the SMA. (l) The CHA arises from the CT, gives off the GDA, and continues as the PHA. The PHA at the hilum of the liver bifurcates into the RHA and LHA. An accessory LHA and RHA are present and both arise from the SMA. (m) The CHA arises from the CT, gives off the GDA, and continues as the HA. The PHA at the hilum of the liver bifurcates into the RHA and LHA. An accessory LHA arises from the LGA and an accessory RHA from the CT. (n) The CHA arises from the CT, gives off the GDA, and continues as the PHA. The PHA at the hilum of the liver bifurcates into the RHA and LHA. An accessory RHA arises from the LGA and an accessory LHA from this accessory RHA. (o) The CHA arises from the CT, gives off the GDA, and continues as the LHA. The RHA is replaced from the SMA and an accessory LHA arises from the LGA. (p) The CHA arises from the CT, gives off the GDA, and continues as the LHA. The RHA is replaced from the SMA and an accessory LHA arises from the aorta. Abbreviations as for Figures 54.3 and 54.4, and rCHA: replaced common hepatic artery; SMA: superior mesenteric artery; rLHA: replaced left hepatic artery; aLHA: accessory left hepatic artery; rRHA: replaced right hepatic artery; aRHA: accessory right hepatic artery; MHA: middle hepatic artery; CIPA: common inferior phrenic artery; DPA: dorsal pancreatic artery; MCA: middle colic artery; RA: renal artery; IMA: inferior mesenteric artery.

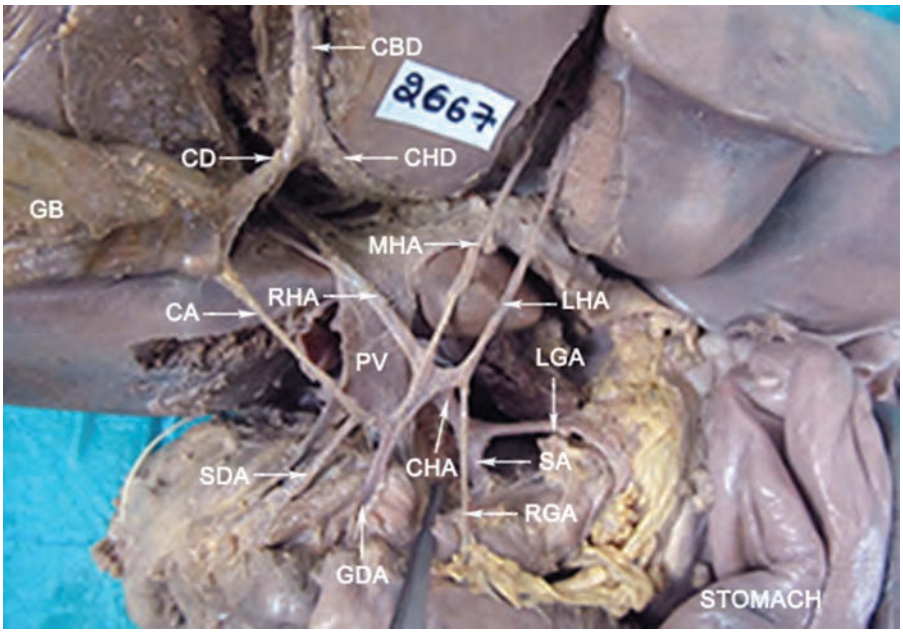

Figure 54.10 Dissection on the visceral surface of the liver illustrating trifurcation of the CT into the LGA, CHA and SA. The CHA trifurcates into the RHA, LHA, and GDA. The RGA arises from the LHA and the CA from the SDA. Abbreviations as for Figures 54.3 and 54.4.

other was a right gastroepiploic artery (Rajendran et al. 2011). Early origins of the right or left hepatic arteries have also been reported. In these cases, the RHA or LHA originates from the CHA before giving off the GDA (Gurgacz et al. 2011).

Right hepatic artery

An aberrant right hepatic artery has been reported in 8.4–18% of individuals. It usually arises from the SMA and runs posterior to the main portal vein in the portocaval space and ascends posterolateral to the common bile duct. This is the most common hepatic arterial variant, occurring with a frequency of 7–18% (Michels 1966; Suzuki et al. 1971; Hiatt et al. 1994; Gruttadauria et al. 2001; Covey et al. 2002; Macdonald et al. 2005; Abdullah et al. 2006; Chen et al. 2009; Kishi et al. 2010). Other sources of origin of the aberrant RHA have also been reported in the literature.

A replaced RHA (rRHA) arising from the SMA has been reported in 6.9–17% of individuals (Michels type III, 11%) (Michels 1966; Suzuki et al. 1971; Rygaard et al. 1986; Makisalo et al. 1993; Hiatt et al. 1994; Gruttadauria et al. 2001; López-Andújar et al. 2007; Chen et al. 2009; Kishi et al. 2010; Ugurel et al. 2010; Ozsoy et al. 2011). The present authors observed it in 5% of cases. Various other sources of origin of the rRHA have also been reported, including single cases where the rRHA originated from the inferior mesenteric artery (IMA) (Abdullah et al. 2006), right inferior phrenic artery (Covey et al. 2002), celiac trunk (Kishi et al. 2010), dorsal pancreatic artery (Kishi et al. 2010), and middle colic artery (Ugurel et al. 2010). An rRHA arising from the GDA has been reported in 1–6% (Jones and Hardy 2001; Kishi et al. 2010) and directly from the aorta in 0.71–1% of individuals (Gruttadauria et al. 2001; Lee et al. 2003; Ugurel et al. 2010) (Fig. 54.9f). The present authors observed one case out of 100 where the rRHA arose from the GDA (Fig. 54.5).

An accessory RHA (aRHA), like the rRHA, frequently arises from the SMA and has been reported in 0.6–7% of individuals (Michels type VI, 7%) (Michels 1966; Suzuki et al. 1971; Rygaard et al. 1986; Makisalo et al. 1993; Hiatt et al. 1994; Gruttadauria et al. 2001; López-Andújar et al. 2007; Chen et al. 2009; Kishi et al. 2010; Ugurel et al. 2010; Ozsoy et al. 2011). Other reported sources of origin include single cases with the aRHA arising from the right phrenic artery (Covey et al. 2002), dorsal pancreatic artery (Kishi et al. 2010), LGA (Gruttadauria et al. 2001; Covey et al. 2002; Panagouli and Venieratos 2011), CT (Gruttadauria et al. 2001; Covey et al. 2002) and renal artery (Gruttadauria et al. 2001). An aRHA arising from the GDA has been reported in 1–4% of cases (Rygaard et al. 1986; Gruttadauria et al. 2001; Covey et al. 2002; Lee et al. 2003) and directly from the aorta in 1–3% of cases (Lee et al. 2003; Ozsoy et al. 2011). An aRHA arising from the LHA and crossing posterior to the PV bifurcation to reach the right lobe of the liver has also been observed in 5–26% of livers (Daseler et al. 1947; Rela et al. 1998) (Fig. 54.9g).

Left hepatic artery

Aberrant left hepatic arteries have been reported in 4–18% of individuals (Michels 1966; Suzuki et al. 1971; Rygaard et al. 1986; Makisalo et al. 1993; Hiatt et al. 1994; Gruttadauria et al. 2001; López-Andújar et al. 2007; Chen et al. 2009; Kishi et al. 2010; Ugurel et al. 2010; Ozsoy et al. 2011). The aberrant LHA usually originates from the LGA and passes through the lesser sac to enter the umbilical fissure of the liver via the fissure for

the ligamentum venosum. This is the second most common hepatic arterial variant, occurring in 3.8–11% of individuals.

A replaced LHA (rLHA) arising from the LGA has been reported in 3.8–11% of individuals (Michels type II, 10%) (Michels 1966; Suzuki et al. 1971; Rygaard et al. 1986; Covey et al. 2002; López-Andújar et al. 2007; Kishi et al. 2010; Ozsoy et al. 2011). The present authors observed it in 4% of cases. Other sources of origin of the rLHA include the CT in 0.5–1% (Jones and Hardy 2001; Kishi et al. 2010), GDA in 1%, SMA in 0.5%, splenic artery in 2% (Jones and Hardy 2001), and directly from the aorta in 0.5–0.13% of individuals (Jones and Hardy 2001; Gruttadauria et al. 2001) (Fig. 54.9h).

An accessory LHA (aLHA) arising from the LGA has been reported in 3.9–10.7% of individuals (Michels type V, 8%) (Michels 1966; Suzuki et al. 1971; López-Andújar et al. 2007; Kishi et al. 2010; Ozsoy et al. 2011). The present authors observed it in 10% of cases. Makisalo et al. (1993) reported a case in which the aLHA arose from the CT, and another in which it arose from the LGA and wound around the esophagus to reach the liver at the umbilical fissure. An aLHA arising from anterior division of the RHA has been reported by Covey et al. (2002) and Wu et al. (2004) (Fig. 54.9i).

Right and left hepatic arteries

Right and left hepatic arteries with aberrant origins have also been reported to coexist. Both can be replaced or accessory in origin, or one can be replaced and the other accessory. These include the following.

1. Both the RHA and LHA are replaced: the rRHA and rLHA usually arise from the SMA and LGA, respectively (Michels type IV, 1%), in 0.5–4.5% of individuals (Michel 1966; Suzuki et al. 1971; Rygaard et al. 1986; Covey et al. 2002; López-Andújar et al. 2007; Kishi et al. 2010; Ozsoy et al. 2011). In these cases, the CHA usually gives off the GDA and continues as the middle hepatic artery (MHA) (Fig. 54.9j). A case has been reported where the CHA continued as the MHA and the rRHA originated from the root of the CT and ran posterior to the PV and common bile duct (CBD) to reach the liver, and the rLHA arose from the LGA (Hlaing and Othman 2012).
2. Both RHA and LHA are accessory: the aRHA and aLHA arising from the SMA and LGA, respectively (Michels type VII, 1%), in 0.5–1% of cases (Michels 1966; Rygaard et al. 1986; Gruttadauria et al. 2001; López-Andújar et al. 2007; Kishi et al. 2010; Ozsoy et al. 2011) (Fig. 54.9k). Gruttadauria et al. (2001) observed a case in which both the aRHA and aLHA arose from the SMA and another in which the aRHA arose from the CT and the aLHA from the LGA (Fig. 54.9l, m). Covey et al. (2002) reported a case where the aRHA originated from the LGA and the aLHA arose from this aRHA (Fig. 54.9n).
3. Replaced RHA or LHA are associated with an accessory LHA or RHA: the replaced RHA arising from the SMA and the accessory LHA from the LGA or vice versa (Michels type VIII, 1%), in 0.3–3% of individuals (Fig. 54.9o). A replaced or accessory RHA arising from the SMA along with an accessory or replaced LHA originating from the aorta was reported 0.29% of cases by Gruttadauria et al. (2001) (Fig. 54.9p).

Combined variations

Yamaki et al. (1995) reported a case in which the CT was absent and the LGA, SA, and CHA arose directly from the aorta. An accessory LHA was also present and arose from the LGA.

Karakaya et al. (2009) observed a case in which both the CT and CHA were absent. The rRHA arose from the SMA and the rLHA from the LGA, which itself originated from the aorta.

A rCHA arising from the SMA along with an aLHA originating from the LGA has also been reported in 1–3% of cases (Lee et al. 2003; López-Andújar et al. 2007).

Cystic artery

The cystic artery (CA) normally arises as a single stem from the right hepatic artery (RHA), right and posterior to the hepatic duct within Calot's triangle. It typically divides into two branches, one of which passes onto the free and the other onto the attached surface of the gall bladder. Variations are frequent and are based on the origin, position, and number of cystic arteries. These are found in 25–50% of cases (Callot 1891; Ramirez 1953; Moore 1958; Cimmino et al. 1992).

Multiple cystic arteries

Double cystic arteries were reported in the earlier literature in 11–20% of cases (Brewer 1900; Belou 1915; Lipshutz 1917; Flint 1923; Daseler et al. 1947; Futara et al. 2001; Mlakar 2003). Michels (1951b) found a higher percentage of double cystic arteries in 25% of the 200 cases he studied. Both the cystic arteries can arise from the hepatic artery, one from the hepatic artery and other from an abnormal source, or both can arise from an anomalous source. According to Michels (1951b), double cystic arteries typically represent separate origins for the superficial and deep branches of this artery. As a rule, the deep cystic artery arises from the RHA while the superficial cystic artery can arise from various other sources.

Lippert and Pabst (1985) reported double cystic arteries in 20% of cases. Both cystic arteries originated from the RHA in 13% of these. One of the two cystic arteries arose from the RHA and the other from various other sources including the left hepatic artery (LHA) in 2%, gastroduodenal artery (GDA) in 3%, and common hepatic artery (CHA) in 1% of cases. Both the cystic arteries arose from the LHA in <1% and one from the LHA and the other from the GDA in <1%.

Tripling of the cystic artery is apparently quite rare (0.28%). One case each was reported by Brewer (1900), Daseler et al. (1947) and Michels (1951b), while four were observed by Browne (1940).

The present authors observed double cystic arteries in 6% of their cases. One arose from the RHA and the other from the GDA in 4%, and the LHA in 1%. In one case, the two cystic

arteries originated from the right anterior and right posterior hepatic arteries respectively.

Variations in origin of the CA

The most common source of origin of the CA is the RHA, with a range of 70–80% (Daseler et al. 1947; Chen et al. 2000; Sugita et al. 2008; Bakheit 2009) (Figs 54.4, 54.6–54.8).

Michels (1951b) reported a single cystic artery in 75% of cases; in 70% it was a branch of the right hepatic artery or aberrant right hepatic artery. It arise from another source in only 5% of cases: the LHA, middle hepatic artery (MHA), CHA, GDA, or retroduodenal artery.

Other reported sources of origin of the CA include the CHA with a frequency of 0.6–3% (Daseler et al. 1947; Michels 1951b; Chen et al. 2000), LHA in 2–6.3% (Michels 1951b; Daseler et al. 1947; Anson 1963; Chen et al. 2000; Bakheit 2009), GDA in 1.4–4% (Daseler et al. 1947; Michels 1951b; Anson 1963; Harris and Pellegrini 1994; Chen et al. 2000; Bakheit 2009) and the proper hepatic artery in 2.2–4% of cases (Harris and Pellegrini 1994; Chen et al. 2000). A more frequent origin of the CA from the CHA was observed by Anson in 1963 (26.9%) and Bakheit in 2009 (17%). The present authors observed the CA originating from the RHA in 87%, the GDA in 5%, and the LHA in 2% of cases (Figs 54.4, 54.10).

Rarely, the cystic artery originates from the superior mesenteric artery (Anson 1963, 0.3%; Chen et al. 2000, 1.4%; Molmenti et al. 2003), superior pancreaticoduodenal artery (Anson 1963, 0.3%; Harris and Pellegrini 1994, 0.2%; Chen et al. 2000, 1.4%), right gastric artery (Anson 1963, 0.1%), or directly from the celiac artery (Anson 1963, 0.3%; Chen et al. 2000, 1.4%).

Relationship of the CA to Calot's triangle

Cystic arteries have been classified into seven subtypes on the basis of their relationship to the Calot triangle according to a modified Suzuki classification. Types 1, 2, and 3 of this modified Suzuki classification were associated with one, two, and three or more cystic arteries, respectively. Each type was further subdivided as follows:

- Type 1a: One CA courses through the Calot triangle. This is the most commonly observed relationship, reported in 35–80% (Ata 1991; Hugh et al. 1992; Scott-Conner and Hall 1992; Balija et al. 1999; Suzuki et al. 2000; Sugita et al. 2008).
- Type 1b: One CA courses outside the Calot triangle, which has been reported in 3–22% of cases (Ata 1991; Hugh et al. 1992; Scott-Conner and Hall 1992; Balija et al. 1999; Suzuki et al. 2000; Sugita et al. 2008).
- Type 2a: Two cystic arteries coursing through the Calot triangle have been reported in 4–12% of cases (Ata 1991; Hugh et al. 1992; Scott-Conner and Hall 1992; Balija et al. 1999; Suzuki et al. 2000; Sugita et al. 2008).
- Type 2b: One CA coursing through the Calot triangle and the other outside it has been reported in 6–18% of cases (Ata 1991; Hugh et al. 1992; Scott-Conner and Hall 1992; Balija et al. 1999; Suzuki et al. 2000; Sugita et al. 2008).
- Type 2c: Both cystic arteries course entirely outside the Calot triangle.
- Type 3a: All cystic arteries course through the Calot triangle.
- Type 3b: All but one cystic artery course through the Calot triangle. Ding et al. (2007) observed one such case out of 600.
- Type 3c: Two or more cystic arteries course outside the Calot triangle.

Chen et al. (2000) found that 86.1% of cystic arteries in his study coursed through the Calot triangle, including all those originating from the right hepatic artery. Only 54% of the cystic arteries that originated from the left, bifurcation, proper, and common hepatic arteries ran through the triangle. None of the cystic arteries that originated from the gastroduodenal, celiac, superior mesentery, or superior pancreaticoduodenal arteries passed through it.

Relationship of the CA to bile ducts

When the cystic artery arises from the RHA it passes posterior to the common hepatic duct (CHD) in 70–80% of cases and anterior to it in 20–30% (Chen et al. 2000; Larobina and Nottle 2005). Chen et al. (2000) reported that among cystic arteries originating from locations other than the right hepatic artery, 29.4% ran posterior to the CHD and 11.8% ran anterior to it.

Right gastric artery

The right gastric artery (RGA) is usually described as arising from the hepatic artery after the gastroduodenal artery (GDA) has been given off. It can also arise from the hepatic artery before the origin of the GDA.

According to Michels (1955), variations in the origin of the RGA are due to the various modes in which the hepatic artery gives off its main branches. Most commonly, the RGA arises from the hepatic trunk shortly after the latter has given off the GDA and before it divides into its main right and left branches. When the origin of the RGA is delayed, it arises from the proximal portion of the left hepatic; when advanced, it arises from the proximal portion of the GDA or from the hepatic trunk before the latter is given off. In the series of 200 specimens examined by Michels (1955), the main sources of origin of the RGA were the common hepatic artery (40%) and left hepatic artery (40.5%). Other sources of origin were the right hepatic artery (5.5%), middle hepatic artery (5%), and gastroduodenal artery (8%). In one case the RGA arose as a branch of the retroduodenal artery.

The right gastric artery most commonly arises from the proper hepatic artery (PHA) in 40–65% of cases (Browne 1940, 42.2%; Lippert and Pabst 1985, 50%; Nelson et al. 1988, 92%; Wang and Yang 2009, 63.5%). Other frequently reported sources of origin of the RGA include the left hepatic artery (LHA) in 15–26% (Lippert and Pabst 1985, 15%; Nelson et al. 1988, 26%; Wang and Yang 2009, 19.2%) and the gastroduodenal artery in 45–22% (Lipshutz 1917, 22%; Nelson et al. 1988, 16%; Wang and Yang 2009, 4.5%). Less frequently, the RGA arises from the right hepatic artery (RHA) in 5–6% (Lippert and Pabst 1985, 5%;

Nelson et al. 1988, 6%) or the middle hepatic artery in 1.3–6% (Nelson et al. 1988, 6%; Wang and Yang 2009, 1.3%).

The present authors observed that the RGA originated more commonly from the LHA (57%) than the PHA (28%) (Figs 54.4, 54.10). Other sources of origin were the GDA in 9% and RHA in 4% of cases.

Two right gastric arteries were reported by Browne (1940) in 1.43% of cases. Wang and Yang (2009) found one such case out of 156; both arteries originated from the PHA. Reeves (1920) found the RGA absent in only one out of 62 cases. The RGA normally courses down toward the lesser curvature of the stomach and continues from right to left along the lesser curvature between the layers of the lesser omentem. In most instances it terminates by anatomizing with the posterior branch of the LGA.

Gastroduodenal artery

The gastroduodenal artery (GDA) is a fairly constant trunk and is almost always a branch of the common hepatic artery (92–95%) (Lipshutz 1917; Michels 1951b). Haller in 1745 first described the GDA accurately and presented a usable nomenclature for the pancreatic arcades. Meckel et al. (1832) described the principal variant anatomies of the GDA.

After studying 200 cadaveric dissections, Michels (1955) correlated atypical origins of the GDA with variations in the mode of branching of the celiac trunk (CT); he reported that the GDA originated from a normal celiac common hepatic artery (CHA) before its bifurcation into the right (RHA) and left (LHA) hepatic arteries in 75% of cases. In about half of these cases it arose at a trifurcation of the CHA into the RHA, LHA, and GDA. It arose from the RHA after the origin of the LHA in 3.5% and from the LHA after the origin of the RHA in 1%. In 11% of cases it originated from the celiac LHA when the RHA was replaced from the superior mesenteric artery (SMA), and in 7% from the celiac RHA when the LHA was replaced from the left gastric artery (LGA). In 1% the GDA arose from the celiac middle hepatic artery when both the RHA and LHA were replaced from other sources. In 2.5% of the cases examined by Michels, the GDA originated from other sources including the CT (1.5%) and SMA (1%). When it arises from the SMA it loops around the common bile duct (CBD) to reach the anterior surface of the pancreas.

Daseler et al. (1947) reported that the GDA arose from a normal CHA in 75.4% of cases, an aberrant CHA in 3.8%, an accessory LHA in 0.4%, and separately from the celiac trunk in 0.2%. The GDA was absent in 2.8% of their cases.

A variant origin of the GDA directly from the celiac trunk was also reported by Lipshutz (1917) (3.61%) and by Petrella et al. (2007) (6.74%), from the SMA by Huu et al. (1976), and from an aberrant hepatic artery arising from the SMA by Eaton (1917). Prudhomme et al. (1997) reported a variant origin of the GDA from the LHA in one of 35 cases studied. The present authors observed a variant origin of the GDA from the RHA in 6% of cases and one case each in which the GDA arose from the LHA and the splenic artery (SA) (Figs 54.6, 54.7, 54.11).

Browne (1940) found the GDA to be absent in 2.88% of cases and observed that the region usually supplied by it was perfused by the left gastroepiploic, inferior pancreaticoduodenal, SMA, and collaterals from the hepatic artery itself. Del Campo (1931) reported a case in which the inferior pancreaticoduodenal artery replaced an absent GDA.

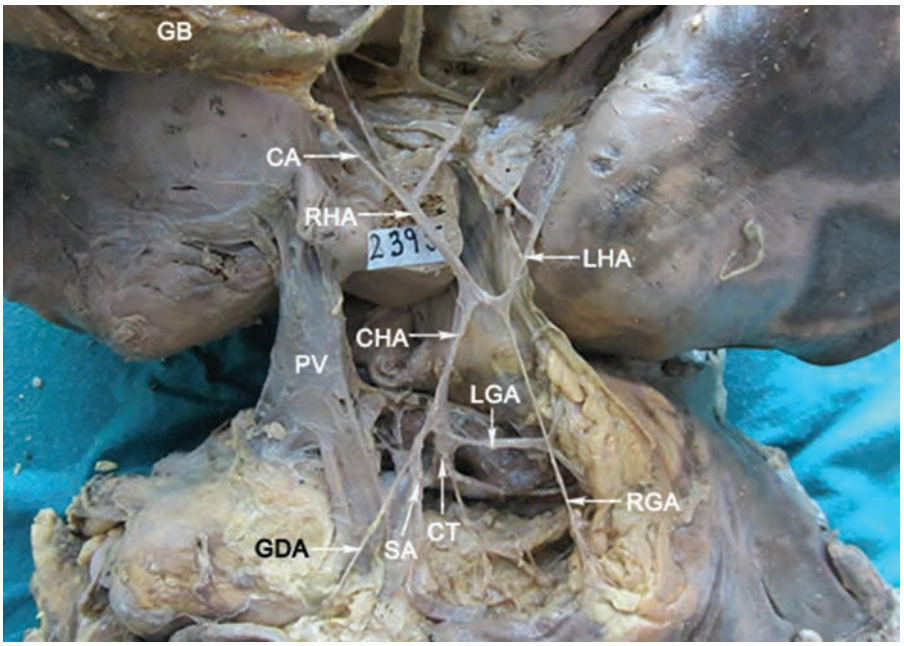

Figure 54.11 Dissection on the visceral surface of the liver illustrating the normal branching pattern of the CT into the LGA, CHA, and SA. The GDA arises from the SA. Abbreviations as for Figures 54.3 and 54.4.

Li and Ren (2011) reported a case in which the GDA and SA originated as a common trunk (the gastroduodenal-splenic trunk) from the anterior surface of the abdominal aorta.

Course of the GDA

After its origin, the GDA descends behind the first part of the duodenum to the lower border of the pylorus where it divides into the right gastroepiploic and anterior superior pancreaticoduodenal arteries. The GDA typically lies to the left of the CBD but can course down in front of the duct. Browne (1940) reported it to lie anterior to the CBD in 27.6% of cases.

Relationship between the GDA and bile duct

The relationship of the GDA to the bile duct was classified into four anatomical types by Prudhomme et al. (1997):

- Type 1: The GDA originates to the left of the bile duct and progressively separates from it throughout its course (Prudhomme et al. 1997, 63%; Chen et al. 2007, 42%).
- Type 2: The two structures come close together without crossing (Prudhomme et al. 1997 20%; Chen et al. 2007 19%).
- Type 3: The course of the GDA is oblique below and to the right. It crosses in front of the bile duct at the posterior surface of the first part of the duodenum (Proudhomme et al. 1997, 14%; Chen et al. 2007, 27%).
- Type 4: The GDA originates near the convergence of the hepatic ducts, crosses the bile duct below the first part of the duodenum and then runs along its right border (Proudhomme et al. 1997, 12%; Chen et al. 2007, 3%).

Branches of the GDA

- Major branches: posterior superior pancreaticoduodenal, right gastroepiploic, and anterior superior pancreaticoduodenal
- Small branches: retroduodenal and supraduodenal
- Inconstant branches: cystic artery, middle colic artery, and replaced/accessory right hepatic artery.

Supraduodenal artery (SDA)

Wilkie (1911) first described the supraduodenal artery (SDA) stemming from the gastroduodenal artery as the source of supply to roughly the upper two-thirds of the anterior and upper one-third of the posterior wall of the first part of the duodenum (Fig. 54.10). The artery is not always present. It was reported to be present in 70% of cases by Shapiro and Robillard (1946), 30% by Thompson (1933), and 20% by Browne (1940) and coursed anterior to or to the left of the common bile duct in the hepatoduodenal ligament.

There is diversity in the origin of the supraduodenal artery. Its usual source is the gastroduodenal artery. Shapiro and Robillard (1946) observed this in 60% of cases and Bianchi and Albanese (1989) in 26.6%. Michels (1962) observed that it arose as a direct branch of the posterior superior pancreaticoduodenal artery (50%) or the GDA (25%) in 75% of cases.

It also frequently originates from the common hepatic or one of its branches in 12–53.3% of cases (Shapiro and Robillard 1946, 25%; Michels 1962, 12%; Bianchi and Albanese 1989, 53.3%). Less frequent sources of origin include the right gastric artery (Shapiro and Robillard 1946, 12%; Michels 1962, 19%; Bianchi and Albanese 1989, 6.6%), cystic artery (Shapiro and Robillard 1946, 3%; Bianchi and Albanese 1989, 10%), hepatogastroduodenal anastomosis (Shapiro and Robillard 1946, 3%) and pericholedochal plexus (Bianchi and Albanese 1989, 6.6%).

Shapiro and Robillard (1946) reported that, in cases where the SDA was of negligible size or missing, there were multiple retroduodenal branches of the GDA; Bianchi and Albanese (1989) observed that in cases where the SDA was absent it was substituted by the right gastric artery (RGA).

Bianchi and Albanese (1989) reported the SDA to be a single artery in 83.3%, double in 6.6%, and triple in 3.3% of cases.

Evrard (1932), Reeves (1920), and Wilkie (1911) considered the SDA as a terminal branch and as having no anastomoses with neighboring arteries. However, Williams (1928) found extra- and intra-parietal anastomoses in 46.6% of cases, more frequently with the RGA than the posterior superior pancreaticoduodenal artery (PSPDA). Bianchi and Albanese (1989) observed anastomoses of the SDA with the RGA in 46.6%, the PSPDA in 23%, the pericholedochal plexus in 20%, and the GDA in 6.6%.

Retroduodenal arteries (RDA)

These are small branches, either single or multiple, arising from the retroduodenal portion of the GDA or PSPDA.

According to Wilkie (1911), who first described it, the RDA usually arises from the retroduodenal portion of the GDA and supplies the posterior surface of the first part of the duodenum and sometimes also the second. Voisin and Devambez (1949) reported this origin of the RDA in only 27% of cases, and wrote that it can arise from many other sources.

Posterior superior pancreaticoduodenal artery (PSPDA)

This was first described by Haller in 1745 as the right superior pancreaticoduodenal artery. The artery was designated the retroduodenal artery by Edwards (1941) and Michels (1951b). Its occurrence is almost constant with a frequency of 96–100% (Petren 1929; Edwards 1941; Pierson 1943; Woodburne and Olsen 1951; Michels 1952; Thomford et al. 1986). It almost invariably arises from the retroduodenal portion of the GDA (Edwards 1941; Falconer and Griffiths 1950; Woodburne and Olsen 1951; Peri et al. 1969; Okahara et al. 2010). The caliber of the artery usually ranges from 1 to 3 mm (Rio-Branco 1912; Kosinski 1928; Michels 1952; Peri et al. 1969) but can be larger (Donatini 1990).

Variant origins of the PSPDA

1. As the posterior branch of the superior pancreaticoduodenal artery (SPDA) (Pitzorno 1920; Kosinski 1928; Evrard 1932; Calas et al. 1955; Vandamme et al. 1967; Bertelli et al. 1995).

This has been reported in 5.33–9.1% of cases (Kosinski 1928; Calas et al. 1955; Vandamme et al. 1967).

2. From the hepatic artery (Kosinski 1928; Woodburne and Olsen 1951; Vandamme et al. 1967). This was first reported by Haller (1745). It encompasses several different possibilities including:
   a. from the common hepatic artery: the incidence of this origin has been reported between 0.67% (Calas et al. 1955) and 7.5% of cases (Evrard 1932);
   b. from the proper hepatic artery: Calas et al. (1955) found it in 8%;
   c. from the right hepatic artery: this pattern of origin has been reported in 2–4% of cases (Michels 1952; Bertocchi and Bianco 1955; Vandamme et al. 1967; Bertelli et al. 1996a);
   d. from the left hepatic artery: this arrangement had only been reported by Haller (1756) until Bertelli et al. (1996a) detected it in two of their cases;
   e. from a replaced common hepatic artery arising from the superior mesenteric artery (Michels 1962): according to Vandamme et al. (1967), this origin occurs in 3% of cases; or
   f. from an accessory or a replaced right hepatic artery arising from the superior mesenteric artery; this has been reported in about 3–4% of cases (Edwards 1941; Falconer and Griffiths 1950; Woodburne and Olsen 1951; Michels 1952; Vandamme et al. 1967; Bertelli et al. 1995).
3. From the superior mesenteric artery in 3–5% of cases (Vandamme et al. 1967; Nebesar et al. 1969; Bertelli et al. 1996a).
4. From the dorsal pancreatic artery: this is a rare occurrence, reported in 1–2% (Woodburne and Olsen 1951; Michels 1962; Vandamme et al. 1967).
5. From the splenic artery: this was observed by Thomford et al. (1986) and Petren (1929) in 3.45% and 7.14% of cases, respectively.

The following sources of origin of the PSPDA are considered extraordinary since each has only been reported only: from a cystic artery arising from the gastroduodenal artery (Kosinski 1928); from the right gastroepiploic artery (Calas et al. 1955); from the celiac trunk (Barbin and Guntz 1971); from an anastomotic trunk between the splenic artery and an accessory hepatic artery stemming from the superior mesenteric artery (Schlyvitch 1937); through two roots coming from the splenic artery and from the gastroduodenal artery (Petren 1929); and as a branch of the trifurcation of the gastroduodenal artery, together with the anterior superior pancreaticoduodenal artery and the right gastroepiploic artery (Quinlan 1983).

The PSPDA has been reported as double in 10.7–20% of cases (Petren 1929; Moretti 1965), triple in 5% (Michels 1962; Moretti 1965), and even quadruple (Michels 1962).

Course of the PSPDA

After it originates from the GDA the PSPDA descends anterior to the retroduodenal CBD in 75% of cases and curves around it, crossing it dorsally to its intrapancreatic portion, then descends toward the left forming on arterial hook around the duct (Pierson 1943). This spiral and descending course of the PSPDA around the common bile duct was called the "vascular arch of Gregoire" by Peri et al. (1969). While crossing posterior to the CBD, the PSPDA is rarely situated close to it, being separated from it by a layer of pancreatic parenchyma between 3 and 12 mm thick (Farisse et al. 1966).

The relationship between the origin of the PSPDA and the CBD is variable. Rio-Branco (1912) found the artery arising to the left or in front of the CBD in 80% of cases and to its right in only 20%. The comparable figures of Petren (1929) were 86% and 14% respectively. Falconer and Griffiths (1950) found the artery to be invariably in front of the CBD.

Instead of crossing anterior to the suprapancreatic portion of the CBD, the PSPDA sometimes crosses it posteriorly. According to Woodburne and Olsen (1951) and Vandamme et al. (1967), this variation always occurs when the PSPDA detaches from an accessory right hepatic artery coming from the superior mesenteric artery or from the dorsal pancreatic artery, since in these cases the artery is already situated behind the pancreas from its beginning.

There is no anastomosis between the PSPDA and the posterior inferior pancreaticoduodenal artery in 5–20% of cases (Edwards 1941; Calas et al. 1955). In these cases, the PSPDA branches into numerous minute arteries (Haller 1756; Falconer and Griffiths 1950; Woodburne and Olsen 1951).

Anterior superior pancreaticoduodenal artery (ASPDA)

The origin and relations of the ASPDA are amazingly constant. It has been reported to be one of the terminal branches of the GDA and occurs in almost 100% in various series (Woodburne and Olsen 1951; Thomford et al. 1986; Okahara et al. 2010). The ASPDA was reported to be missing in 1–2.5% of cases (Evrard 1932; Couinaud and Huguet 1966). Shapiro and Robillard (1946) reported that the ASPDA was present in all except one case, in which it was replaced by large branches from the inferior pancreaticoduodenal artery. A double ASPDA was reported by Petren (1929) in 7.1% of cases and in as many as 35% by Moretti (1965). Nebesar et al. (1969) found that the ASPDA could even be triple or quadruple.

Variant origins of the ASPDA

Other sources of origin of the ASPDA that are to be considered extremely unusual include the following.

1. Petren (1929) found it in all of his 28 cases; it arose from the GDA except in one case where it originated from the SMA.
2. Pitzorno (1920) reported a common trunk of origin of the ASPDA and transverse pancreatic artery from the GDA.
3. From a replaced RHA arising from the SMA (Nebesar et al. 1969).
4. From the celiac trunk (Issajew 1932).
5. From an anastomotic trunk running behind the pancreas, connecting the SA and SMA, and another connecting the hepatic artery and SMA (Pitzorno 1920).

6. From the GDA as a branch of trifurcation together with the PSPDA and gastroepiploic artery (Quinlan 1983).
7. From the proper hepatic artery (Kosinski 1928).
8. From the splenic artery (Thomford et al. 1986).

Course of the ASPDA

The ASPDA runs along the anterior groove formed by the duodenum and the lateral border of the head of the pancreas (Michels 1962; Nebesar et al. 1969) or along the anterior surface of the gland (Woodburne and Olsen 1951; Basmajian 1906). In the latter case, it runs weaving downward, parallel with the inner edge of the duodenum, a distance of 1–2.5 cm from it (according to Petren 1929; Pierson 1943).

The ASPDA can form a groove in the substance of the gland (Evrard 1932; Belli et al. 1958) and can sometimes become intrapancreatic with a very thin layer of parenchyma covering it (Pierson 1943). The artery reaches the lower flexure of the duodenum and turns backward. At this point, it can:

1. pierce the gland (Pierson 1943; Michels 1962; Vandamme et al. 1967);
2. surround the lower edge of the pancreas (Piquand 1910; Petren 1929; Schlyvitch 1937; Falconer and Griffiths 1950); or
3. surround the lateral edge of the pancreas (Pitzorno 1920; Schlyvitch 1937; Paturet 1958; Vandamme et al. 1967; Quinlan 1983).

The ASPD artery never remains on the anterior surface of the pancreas, according to Schlyvitch (1937). In contrast, according to Petren (1929), Evrard (1932), and Pierson (1943), in 24–39% of cases it runs anterior to the pancreas throughout its course. In 61% of cases the ASPDA goes along the posterior surface of the uncinate process and anastomoses with the anterior inferior pancreaticoduodenal artery (AIPDA). This anastomosis is lacking in 14% of cases (Shapiro and Robillard 1946; Boijsen 1983).

Collateral branches arising from the ASPDA include the transverse pancreatic artery in 8–10% of cases (Falconer and Griffiths 1950; Woodburne and Olsen 1951), retroduodenal artery (Voisin and Devambez 1949; Bertelli et al. 1995), cystic artery (Kosinski 1928), accessory cystic artery (Flint 1923), choledochal branches (Barbin and Guntz 1971) and anterior duodeno-pyloric branch (Villemin 1921).

Right gastroepiploic artery (RGEA)

Anatomical variations of the RGEA are very rare. It usually arises as a larger terminal branch of the GDA. According to Michels (1955) it occasionally arises from the SMA either as a separate branch (1.5%) or together with the middle colic and inferior pancreaticoduodenal arteries (1%).

In the series reported by Daseler et al. (1947), the GDA was absent in 2.8% of cases and, in such cases, the RGEA arose from the SMA. Sakamoto et al. (1999) reported a case where the RGEA originated from the SMA.

The RGEA courses from right to left between the two layers of the greater omentum to approach the greater curvature of the stomach. Its site of termination on the greater curvature of the stomach is variable (Paturet 1958), the most frequent site being the middle part of the curvature (Poirier and Charpy 1901; Testut and Latarjet 1949; Michels 1955; Paturet 1958; Mercier and Vanneuville 1968; Rouviere 1970).

Yamato et al. (1979) classified the gastroepiploic arcade formed between the RGEA and left gastroepiploic artery into four types:

- Type 1: a continuous well-developed arcade (34.5%);
- Type 2: the RGEA and LGEA terminate close to one another with slender plexiform anastomoses between them (15%);
- Type 3: the two arteries terminate at a distance from each other and no extra or intramural anastomoses are seen (44.5%); and
- Type 4: there are indirect anastomoses via an epiploic artery.

Levasseur and Couinaud (1968) identified a prominent continuous arcade in 37% of cases, a continuous arcade but of small diameter in 27%, and absence of an arcade in 36%. According to Michels (1955), these anastomoses are lacking in 10% of cases.

Inconstant branches of the GDA

- Cystic artery: a cystic artery (CA) arising from the GDA has been reported in 0.5–4% of cases (Flint 1923; Michels 1952; Sarkar and Roy 2000). The present authors observed this at a higher frequency (8.5%) (Fig. 54.10).
- Middle colic artery: rarely, the GDA gives origin to the middle colic artery (Hollinshed 1971; Gupta et al. 2013).
- Aberrant RHA: the GDA gives rise, rarely, to an aberrant right hepatic artery. The present authors have observed one such case (Fig. 54.5).

Splenic artery

The splenic artery (SA) is the largest branch of the celiac trunk (CT). It typically originates from the CT via the hepatosplenogastric trunk. This most prevalent mode of origin has been reported in 44–95% of cases (Michels 1942; Vandamme and Bonte 1985; Matoba et al. 2003; Pandey et al. 2004; Petrella et al. 2007; Ugurel et al. 2010; Song et al. 2010; Prakash et al. 2012).

Variations of origin

There are known deviations from the classical pattern of origin of the SA from the CT. In the absence of a hepatic artery origin, the SA usually arises along with the LGA in the gastrosplenic trunk. This variant has been noted in 2–8% individuals (Vandamme and Bonte 1985; Petrella et al. 2007; Winston et al. 2007; Silveira et al. 2009; Song et al. 2010; Ugurel et al. 2010). Another form of origin from the CT is in conjunction with the hepatic artery as the hepatosplenic trunk. The reported incidence of this variant is 2–8% (Michels 1942; Vandamme and Bonte 1985; Petrella et al. 2007; Winston et al. 2007; Silveira et al. 2009; Song et al. 2010; Ugurel et al. 2010). Michels (1942) found a hepatosplenogastropancreatic trunk in which a dorsal pancreatic artery was an addition to the typical hepatosplenogastric trunk in 8% of cases.

Although infrequent, origins from sources other than the CT occur. The SA can arise directly from the SMA, and the SMA can arise as a combined splenomesenteric trunk from the aorta. This origin has been recorded in 0.18–2% of cases by different groups (Rossi and Cova 1904; Michels 1942; Bertocchi and Bianco 1955; Pandey et al. 2004) (Fig. 54.3c).

The SA, HA, and SMA can issue together from the aorta as the hepatosplenomesenteric trunk. This has been found in 0.68–1.7% of individuals (Ugurel et al. 2010; Samarawickrama 2010; Song et al. 2010; Varma et al. 2010; Salve and Ratanprabha 2011) (Fig. 54.3t). A direct origin from the aorta has been noted in 0.36–8.1% of cases (Lipshutz 1917; Michels 1942; Vandamme and Bonte 1985; Pandey et al. 2004; Petrella et al. 2007; Song et al. 2010; Prakash et al. 2012) (Fig. 54.3d, r). Gangadhara et al. (2013) found a rare case of origin from the gastrosplenicophrenic trunk from the aorta.

Studying 83 cases, Lipshutz (1917) observed two instances of unusual origin of the SA from the LGA. Occasionally the SA arises from the middle colic, right hepatic, left hepatic, common hepatic, or accessory right hepatic arteries (Michels 1942).

Occasional instances of a double SA have been reported. Michels (1955) found a double SA in two cases among 500 bodies investigated, both arising from the CT; the upper SA was much smaller. Redmond et al. (1989) also found the double SA in one case out of 127 dissected. The second SA arose directly from the aorta. In both studies the accessory SA was observed supplying the upper pole of the spleen.

Course

Michels (1942) stated that, as a rule, the SA arises from the CT to the right of the midline and therefore crosses the aorta to course to the left to reach the spleen. Michels (1942) divided the course of the SA from its origin to the spleen into four segments: suprapancreatic, pancreatic, prepancreatic, and prehilar.

- Suprapancreatic segment: This short segment (1–3 cm) is the descending portion of the artery from the origin to the pancreas and usually lies above the latter. This segment can follow an ascending or horizontal and at times retropancreatic course.
- Pancreatic segment: The SA courses retroperitoneally to the left along the upper border of the neck and body of the pancreas behind the omental bursa. The relationship of this segment to the pancreas is predominantly suprapancreatic (57–90%). It can follow a retropancreatic (2.8–36%), prepancreatic (2–18.4%), or intrapancreatic (0–4.6%) course (Michels 1942; Franz 1896; Lippert and Pabst 1985; Vandamme and Bonte 1985; Redmond et al. 1989; Ozan and Ondergolu 1997; Pandey et al. 2004). In the intrapancreatic type, the SA courses through the gland throughout its variable extent.
- Prepancreatic segment: This segment is represented by the part of artery toward the tail of the pancreas, where the SA leaves the upper border of the organ and runs on its anterior surface.
- Postpancreatic (prehilar) segment: This is the portion of the SA situated between the tail of the pancreas and the hilum of the spleen.

Tortuosity

The SA generally exhibits a tortuous course. Totuosity can occur in the form of continuous irregular serpentine curves; one or more spirals; one or more (1–6) loops or half-circle twists; or superimposed coils. When the artery has multiple loops, some can be placed in the horizontal and others in the vertical plane. Loops or spirals often lie in the groove on the upper dorsal surface of the pancreas, completely or partly covered by the gland. Tortuosity is most marked in the pancreatic and prepancreatic segments (Michels 1945; Sylvester et al. 1995). Michels (1945) found the SA slightly curved in 45%, looped or coiled in 40%, and straight in 15% of cases. However, Sahni et al. (2003) found the SA tortuous in only 10% of adults; according to them, the characteristic tortuosity of the SA appears to develop with age. Tortuosity could account for its variable relationship with the pancreas.

The length of the SA varies from 8 to 32 cm (average 13 cm) and the caliber from 5 to 11 mm. This artery is considered the widest of all branches of the CT. However, in a series of 200 cadavers studied by Sahni et al. (2003), the diameter of the hepatic artery surpassed that of the SA in 10%.

Branches

The constant branches are the pancreatic, superior and inferior splenic terminals, short gastric, and left gastroepiploic. Inconstant branches are the superior and inferior polar, accessory left gastric, and posterior gastric arteries. The SA can also give off branches derived from other sources such as the middle colic, left gastric, and left hepatic arteries.

Pancreatic branches (3–7) arise from the SA during its course along the upper border of the pancreas. Three branches, namely the dorsal pancreatic, greater pancreatic, and caudal pancreatic arteries, have extensive distributions.

Dorsal pancreatic artery

The credit for describing the dorsal pancreatic artery (DPA) for the first time goes to Haller (1745), who referred to it as arteria pancreatica suprema. This artery was called different names in the literature before acquiring its final name, the dorsal pancreatic artery, in the Nomina Anatomica (International Anatomic Nomenclature Committee 1989). The DPA has been visualized in 64–100% of individuals in various dissection and angiographic studies (Vergoz 1921; Kirk 1931; Woodburne and Olsen 1951; Amaifi and Cefaly 1958; Bouchet and Martin 1961; Milon et al. 1979; Toni et al. 1985; Thomford et al. 1986). Although usually single, instances of numerical variations are not uncommon. Double DPAs have been observed in 3.38–26.9% of cases (Bouchet and Martin 1961; Vandamme et al. 1967; Toni et al. 1985). Triple and quadruple DPAs, although not as frequent as double DPAs, have also been reported. Vandamme et al. (1967)

found a triple DPA in 5% of cases. Toni et al. (1988b) visualized four DPAs in 3% of 72 patients undergoing selective celiac angiography.

The caliber of the artery varies between 1 mm and 1 cm with a mean value of 1–3 mm (Kosinski 1928; Pierson 1943; Michels 1962).

Origin

The dorsal pancreatic artery most commonly arises from the SA, but remarkable variations in the incidence of this origin have been reported (70% by Vergoz 1921; 52% by Bertocchi and Bianco 1955; 100% by Amaifi and Cefaly 1958; 28.8% by Bouchet and Martin 1961; 78% by Delagrange and Barbin 1966; 76.9% by Thomford et al. 1986; 13.5% by Toni et al. 1988b; 100% by Sahni et al. 2003). The site of origin from the SA usually lies within its proximal third (42–44%), but in 7.8–23.2% of cases an origin from the distal part of the SA has been recorded (Kupie et al. 1967; Toni et al. 1985) (Figs 54.3k, p; 54.12a).

The DPA has frequently been found to originate from other sources. An origin from the celiac trunk (CT) has been seen in 3–33% cases. It most commonly issues from the CT where it divides into the splenic and common hepatic arteries (Vergoz 1921; Falconer and Griffiths 1950; Michels 1951a; Bouchet and Martin 1961; Delagrange and Barbin 1966) (Fig. 54.12b).

The common hepatic artery (CHA) has been seen giving off the DPA in 0–25% of individuals (Pierson 1943; Kupie et al. 1967; Vandamme et al. 1967) (Fig. 54.12c).

An origin from the SMA has been noted in 1.8–25% of cases, usually close to the origin of the latter from the aorta (Pitzorno 1920; Del Campo 1931; Falconer and Griffiths 1950; Woodburne and Olsen 1951; Bertocchi and Bianco 1955; Bouchet and Martin 1961; Delagrange and Barbin 1966; Vandamme et al. 1967; Thomford et al. 1986) (Fig. 54.12d).

Less frequently, the DPA arises from: an accessory right hepatic artery arising from the SMA in 0.6–7% of cases (Pitzorno 1920; Michels 1951a; Bouchet and Martin 1961; Delagrange and Barbin 1966; Milon et al. 1979); as a common trunk with the inferior pancreaticodeuodenal artery in 6–8% (Kosinski 1928; Melliére 1968), and the gastroduodenal artery in 0.6–3.8% (Vergoz 1921; Kosinski 1928; Falconer and Griffiths 1950; Michels 1951a; Vandamme et al. 1967; Thomford 1986) (Fig. 54.12e–g). Occasionally, the artery arises from unusual sources such as the right gastroepiploic, aorta, right gastric, left gastric, left inferior phrenic, posterior superior pancreaticoduodenal, or middle colic artery (Haller 1745; Michels 1945, 1951a; Falconer and Griffiths 1950; Delagrange and Barbin 1966; Toni et al. 1988b) (Fig. 54.12h–n).

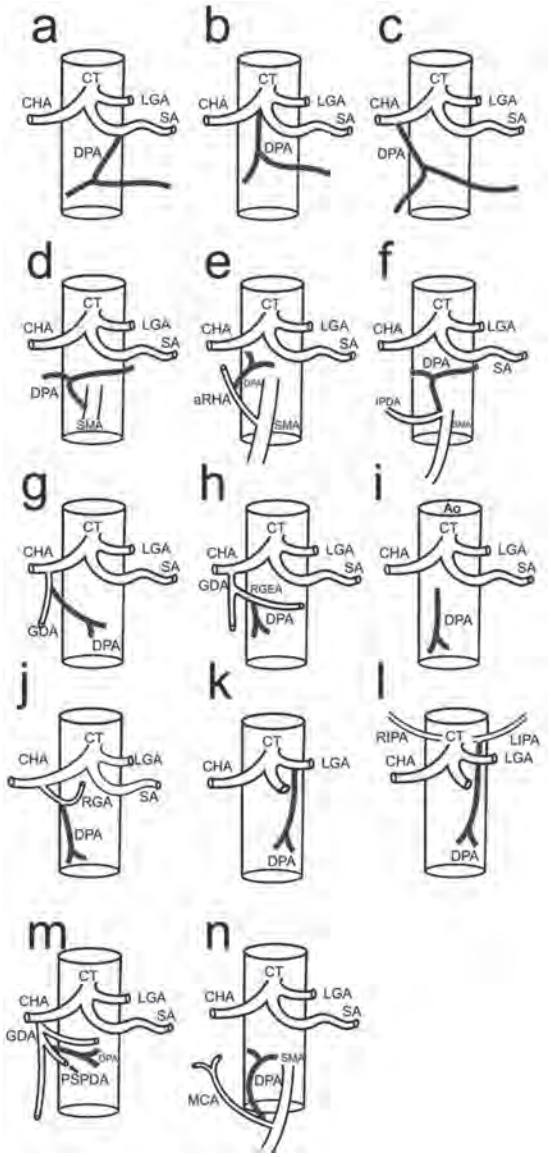

Figure 54.12 Schematic representation of variant patterns of origin of the dorsal pancreatic artery, from the (a) SA; (b) CT; (c) CHA; (d) SMA; and (e) aRHA. Common trunk of origin (f) with the IPDA. Origin from the (g) GDA; and (h) RGEA. Origin (i) independently from the Ao; (j) from the RGA; (k) from the LGA; (l) from the LIPA; (m) from the PSPDA; and (n) from the MCA. Abbreviations as for Figures 54.3 and 54.4, and aRHA: accessory right hepatic artery; IPDA: inferior pancreaticoduodenal artery; RGEA: right gastro-epiploic artery; AO: aorta; LIPA: left inferior phrenic artery; RIPA: right inferior phrenic artery; PSPDA: posterior superior pancreaticoduodenal artery.

Course

The site of origin decides the course of the artery. A DPA of high origin from the celiac, hepatic or SA descends behind the neck (Kosinski 1928; Pierson 1943; Falconer and Griffiths 1950) or, rarely, the body of pancreas (Woodburne and Olsen 1951). While descending, the artery bends more toward the left if it arises from the CHA or right when it originates from the SA. It lies on the left of the portal vain (PV) and crosses posterior to the splenic vein. An artery of low origin from the SMA exhibits an ascending course. The length of the arterial trunk usually ranges from 1–3 cm. When the origin is from the

SMA, the length of the trunk depends upon the level of origin of the SMA from the aorta (varies from a few millimeters to several centimeters).

Branches

On reaching the lower edge of the pancreas at the junction of the neck and body near the angle between the splenic and superior mesenteric veins, the DPA divides in the form of an inverted "T" into two terminal branches. The level of the division usually lies against the L1 vertebra but can vary from the inferior edge of T12 to the middle third of L2. The right terminal branch usually runs behind the superior mesenteric vein. Less frequently, it divides into two sub-branches, one running behind and the other in front of the vein, or both run anterior to the vein (Pitzorno 1920; Del Campo 1931; Bouchet and Martin 1961). The right branches can run onto the anterior aspect of the head of the pancreas where it can form an anastomotic arch with the anterior superior pancreaticoduodenal or right gastroepiploic artery (Bertelli et al. 1995). In one case, Makomaska-Szaroszyk and Fiedor (1989) noticed the DPA giving a branch that anastomosed with the right branch of the MCA.

The left terminal branch of the DPA actually represents the transverse pancreatic artery (TPA), which runs along the inferior edge of the body toward the tail of the pancreas (Del Campo 1931; Michels 1951a; Woodburne and Olsen 1951; Bouchet and Martin 1961; Vandamme et al. 1967; Milon et al. 1979).

The DPA has been found to give off collateral branches to the uncinate process in 60% of individuals (Michels 1945; Woodburne and Olsen 1951; Vandamme et al. 1967). Other collateral branches related to the pancreas are suprapancreatic branches, which run along the superior edge of the pancreas and sometimes anastomose with the superior pancreatic branch of the gastroduodenal artery (Vandamme et al. 1967; Melliére 1968; Vandamme and Bonte 1986; Bertelli et al. 1997).

The DPA sometimes gives off collateral branches to the colon: the middle colic artery in 4–10% of cases (Michels 1945; Woodburne and Olsen 1951; Vandamme 1967); left colic artery in 4% (Michels 1945; Melliére 1968; Inoue et al. 1986); right colic artery (Michels 1945); and left colic branches in 0.3% (Milon et al. 1979).

Pancreaticoduodenal arteries such as the posterior inferior pancreaticoduodenal (in 2.5–8.57% of cases), anterior inferior pancreaticoduodenal (in about 0.7–2.5%), and posterior superior pancreaticoduodenal (in about 1–2%) have been seen arising from the DPA (Woodburne and Olsen 1951; Calas et al. 1955; Michels 1962; Vandamme et al. 1967; Bertelli et al. 1997).

Among the rare branches reported in the literature are the accessory right hepatic artery, epiploic branches, gastric branches, and jejunal arteries (Michels 1945; Bouchet and Martin 1961; Vandamme et al. 1967; Melliére 1968; Gordon et al. 1978). The DPA occasionally sends anastomotic branches to the SMA, posterior pancreaticoduodenal arch, anterior pancreaticoduodenal arch, middle colic artery, supraduodenal artery, inferior pancreaticoduodenal artery, and inferior mesenteric artery (Pitzorno 1920; Pierson 1943; Michels 1951a; Bouchet and Martin 1961; Delagrange and Barbin 1966; Melliére 1968; Inoue et al. 1986).

Toni et al. (1985) observed the DPA anastomosing with the greater pancreatic artery in 20% of cases and the caudal pancreatic artery in 7%, directly or mediated by the transverse pancreatic artery.

Greater pancreatic artery

The incidence of the greater pancreatic artery (pancreatica magna artery) ranges between 64 and 98% (Woodburne and Olsen 1951; Bolognese et al. 1979; Toni et al. 1985; Vandamme and Bonte 1986). Its width averages 2 mm (Vandamme and Bonte 1986).

The greater pancreatic artery (GPA) usually issues from the middle third of the SA and enters the substance of the pancreas at the junction of the middle and distal third of the gland. Less frequently, the artery has been reported to originate from the proximal or distal third of the SA (Toni et al. 1985) or left gastroepiploic artery (LGEA) (Vandamme and Bonte 1986). Occasionally, it has been seen arising from the SMA or hepatic artery (Thomford et al. 1986).

The greater pancreatic artery has been found double in 33–54% individuals (Toni et al. 1985; Vandamme and Bonte 1986) and even triple in 3% (Toni et al. 1985). Immediately after its origin, it enters the substance of the pancreas, passes behind the pancreatic duct, and subdivides into multiple branches, some of which course to the right to anastamose with branches of the transverse pancreatic artery (TPA) (90%) while others course to the left to anastamose with the caudal pancreatic (CPA). Multiple anastamoses can occur.

Caudal pancreatic arteries

Caudal pancreatic arteries (arteria caudae pancreatis) have been reported in 66–95% of cases (Woodburne and Olsen 1951; Delagrange and Barbin 1966; Bolognese et al. 1979; Ebner and Anderhuber 1985). The number of caudal pancreatic arteries (CPA) varies between one and four. One CPA has been recorded in 32–36% of cases, two in 46%, three in 8–20%, and four in 2% (Toni et al. 1985; Vandamme and Bonte 1986).

These branches can arise from the distal end of the splenic trunk or from its terminal branches or the left gastroepiploic artery. Vandamme et al. (1967) found it arising from the common trunk formed by the left gastroepiploic artery and the inferior splenic branch (50%), SA (21%), left gastroepiploic artery (20%), and inferior or superior splenic branches (9%). Multiple CPAs can have different origins. Michels (1955) identified double caudal pancreatic branches, one arising from the splenic artery and the other from one of its terminal branches. As it courses within the tail of the pancreas it anastomoses usually with the transverse pancreatic artery and less frequently with the greater pancreatic or dorsal pancreatic (Toni et al. 1985).

An accessory spleen located in the pancreaticolineal ligament sometimes receives its blood supply from the CPA. When the

tail of the pancreas contacts the spleen, this artery is reported to be short (Michels 1955). Ebner and Anderhuber (1985) found no visible anastomosis with the arteries of the pancreatic body in 33% of cases. In such cases, CPAs carry the only blood supplies to the tail of the pancreas.

Posterior gastric artery

The posterior gastric artery (PGA) was first described by Walther in 1740 and was named as the posterior gastric by Haller in 1745. There is extreme variability regarding its prevalence. The PGA has been detected in 4–99% of individuals (Piquand 1910; Rossi and Cova 1904; Laude et al. 1972; Suzuki et al. 1978; Didio et al. 1980; Pitynski et al. 1996; Sahni et al. 2003; Loukas et al. 2007).

Many authors claim the splenic artery (SA) as the exclusive origin of the PGA (Lippert and Pabst 1985; Trubel et al. 1988; Sahni et al. 2003). Loukas et al. (2007) found an alternative origin from the left gastric artery (in 41.8% of 120 cadavers). In fact, the left gastric artery was the most common source, followed by the SA (25.5%) and celiac trunk (10.2%). The PGA can arise from the superior polar branch of the SA (Okabayashi et al. 2006).

Loukas et al. (2007) found double PGAs in 22.4% cadavers issuing from the LGA and SA. Okabayashi et al. (2006) found cases of double PGA, both arising from the SA.

The PGA usually arises from the SA at variable levels. The most common site of origin from the SA is the middle of its pancreatic portion (47.8%) followed by the distal third (34.2%) and proximal third (18.4%). The origin from the SA usually lies within 3.1–9.2 cm of the origin of the latter from the celiac trunk (CT). However, Berens et al. (1991) found the origin of the artery origin to lie within 3 cm of the beginning of the SA. The PGA usually arises from the upper border of the SA (84.2%). It can issue from the anterior (7.9%) or even posterior (7.9%) aspects of the SA (Suzuki et al. 1978).

The PGA can be tortuous. Loukas et al. (2007) found them tortuous in 75% of specimens.

The average diameter of the artery varies between 1 and 3 mm (Weisz and Bianco 1957). Rossi and Cova (1904) found the caliber larger than that of the short gastric arteries, at times even matching that of the LGA.

The PGA courses retroperitoneally, superiorly and to the left, to reach the diaphragm where it enters the gastrophrenic ligament to approach the cardiac portion of the stomach (Suzuki et al. 1978). Many authors differ regarding its area of distribution. According to Suzuki et al. (1978) and Loukas et al. (2007), it supplies the fundus and superior portion of the posterior wall of the gastric body near the cardiac region, whereas Pitynski et al. (1996) found the PGA supplying part of the posterior wall of the stomach along with the posterior wall of the abdominal portion of the esophagus. The PGA has also been referred to as the accessory left gastric artery or ascending posterior esophagogastric artery. In addition to the esophagus and stomach, it can supply a superior polar artery to the spleen. Sahni et al. (2003) found a superior polar branch in 1.5% of cases (Fig. 54.13). Its terminal branches anastomose with branches of the left gastric, left gastroepiploic, and short gastric arteries (Sahni et al. 2003).

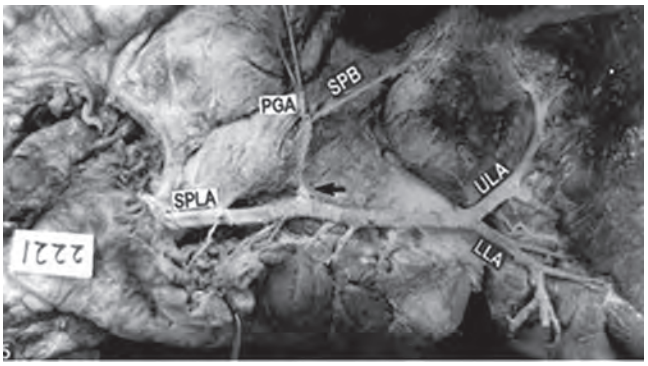

Figure 54.13 Illustration of the posterior gastric artery and superior polar branch having a common trunk of origin from the splenic artery. SPLA: splenic artery; PGA: posterior gastric artery; SPB: superior polar branch; ULA: upper lobar artery; LLA: lower lobar artery.

Source: Sahni et al. (2003). Reproduced with permission from John Wiley & Sons.

Short gastric arteries

The short gastric arteries (arteriae gastricae breves, fundic branches) are multiple vessels numbering 1–25 (Gregorczyk et al. 2008) but more commonly 4–6. These vessels can arise from the splenic trunk, the superior polar artery or its branches, the superior terminal, inferior terminal or their penultimate and ultimate branches, the inferior polar arteries, or the left gastroepilploic and its branches (Michels 1955; Sahni et al. 2003). Michels (1955) claimed the superior or inferior terminal branches of the SA as the commonest source. Helm (1915) found them arising more commonly from either the left gastroepiploic artery before it reaches the stomach or from the proper splenic branches of the SA. Gregorczyk et al. (2008) demonstrated origins from a variety of sources, namely the left inferior phrenic (IPA), accessory left hepatic, left gastric, left middle suprarenal, and posterior gastric arteries.

The short gastric vessels are usually very slender. Helm (1915) found their caliber to be 0.5 mm or less.

These vessels pass from left to right from between the layers of the phrenicolineal to the gastrolienal ligament; on reaching the cardiac end of the stomach, they irrigate the anterior and posterior surfaces of the stomach (the posterior more profusely) and anastomose with branches of the left gastric, left gastroepiploic, and IPA, or accessory left gastric if present. These arteries can anastomose with cardioesophageal branches of the accessory left gastric or aberrant left hepatic stemming from the left gastric, if present.

Left gastroepiploic artery

The left gastroepiploic artery (LGEA) is considered the most varied of splenic branches. Sahni et al. (2003) found this artery

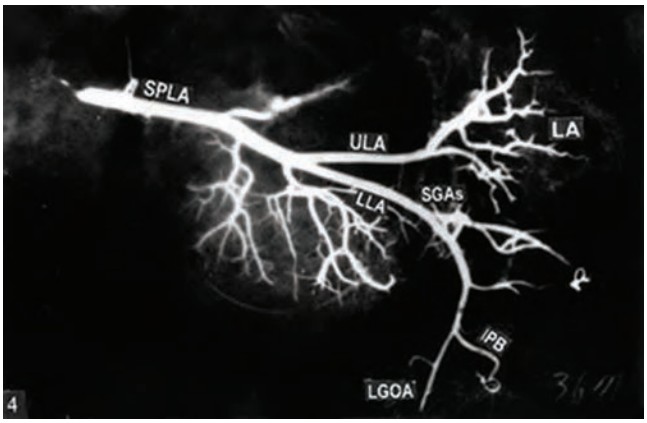

Figure 54.14 Iillustration of the left gastro-omental (epiploic) and inferior polar arteries arising from the inferior lobar (terminal) branch of the splenic artery. Abbreviations as for Figure 51.13 and SGAs: short gastric arteries; LA: lobular arteries; IPB: inferior polar branch; LGOA: left gastro-omental artery.

Source: Sahni et al. (2003). Reproduced with permission from John Wiley & Sons.

in 81% of cases. In a series 100 spleens, Michels (1942) found it arising most commonly from gastroepiploic SA (72%) 1–4 cm proximal to its terminal division. In the remaining cases the artery issued from the gastroepiploic inferior splenic terminal, superior splenic terminal, and the middle portion of the SA. Sahni et al. (2003) found the LGEA arising from the SA or one of its splenic terminal branches (Fig. 54.14).

There is sometimes an unusual origin from the interior of the spleen. However, Vandamme and Bonte (1988) and Ndoye et al. (2008) reported the inferior splenic polar branch as the commonest site of origin (66-68.35%). Ndoye et al. (2008) even found it arising from the common splenogastroepiploic trunk in 11.4% of cases.

Although it is usually single, there can be two or three LGEAs. When multiple LGEAs are present, the main artery usually comes from the SA or its branches and other accessory LGEAs commonly stem from the polar arteries.

The artery can run close to the greater curvature of the stomach or as far as 2 cm from it. It commonly ends by anastomosing with the RGEA; however, in 10% of individuals, no anasatomosis could be found. The artery can be tortuous, looped, and rarely coiled (Michels 1955).

Branches of LGEA

Gastric branches of the LGEA comprise 2–4 fundic branches and multiple short gastric branches for the anterior and posterior surfaces of the stomach.

While descending along the greater curvature it irrigates the greater omentum through many short and long descending epiploic branches. Some epiploic branches can communicate with like branches of the right gastroepiploic and left colic arteries.

It also furnishes pancreatic rami to the tail of the pancreas. In few instances it supplies an accessory spleen located in the pancreaticolienal or splenicocolic ligament (Michels 1955).

Superior polar artery

Michels (1942) found a superior polar artery (SPoA) to the superior extremity of the spleen in 65% of specimens. The artery can arise from the first, second, third, or fourth segment of the SA. Most commonly it arises from the main splenic trunk proximal to its primary division (75%) and, less frequently, from the superior terminal branch or its subbranches (20%). Occasionally, the inferior terminal splenic branch gives off this artery. Sahni et al. (2003) found it arising from the SA in 51% of cases and from the posterior gastric artery in 1.5%. Michels (1955) found it originating separately from the CT in 2/500 dissections and interpreted such cases as double SAs. Occasionally one or more SPoAs arise from the short gastric artery, left gastric artery, or its posterior esophageal branches.

The length of the artery falls within the range 2–12 cm, width 1–5 mm, and the number of branches 2–13. Frequently this artery is very long (10–13 cm), thin, and thread-like. Like the parent splenic trunk, the SPoA also exhibits characteristic tortuosity. Occasionally it sends many branches to the diaphgramatic surface of the spleen. It can give origin to the short gastric branches and, rarely, to the left inferior phrenic artery and pancreatic branches.

Inferior polar branch

Michels (1942) found inferior polar arteries (IPoA) to the inferior extremity of the spleen in 82% of spleens investigated. Sahni et al. (2003) found this artery in 79.4% of female and 88.5% of male cadavers. Inferior polar arteries can arise directly from the left gastroepiploic artery, superior terminal, inferior terminal, or their sub-branches, the left gastroepiploic artery being the commonest source. The number varies from one to five. All branches can arise from a single source or sometimes from multiple sources. IPoAs are usually narrower than SPoAs. Sometimes an IPoA is voluminous and enters the spleen through its own hilum. At times the caliber of these vessels matches that of the left gastroepiploic artery or even surpasses it; in such instances, it becomes difficult to decide whether the IPoA arises from the left gastroepiploic artery or vice versa. Michels (1942) encountered cases in which the caliber of the IpoA was twice that of the left gastroepiploic artery. Like the SpoA, the IPoA is not free from tortuosity which can take the form of undulation, looping, or (rarely) coiling. Branching occurs as the artery reaches the surface of the spleen, usually in a dichotomous manner. Michels (1942) observed crawling branches to the renal or colic surface of the spleen. It usually anastomoses with the inferior terminal or its branches, with the LGEA or other polar arteries. Anastomosis can even occur within the substance of the spleen.

Splenic terminal branches

According to Michels (1942), the SA usually (80%) divides into the superior and inferior terminal splenic branches as it approaches the spleen in the phrenicolineal ligament. Sometimes a third terminal is also present (20%). These are long end divisions of the SA, with ultimate and penultimate branches. The distance of the terminal dividing point from the spleen is relatively constant (2–6 cm). When the SA divides terminally near the spleen (1–2 cm from the hilum) it is called a magistral splenic artery; this occurs in about 30% of individuals. When the division of the SA occurs further (2–12 cm) from the hilum in the prepancreatic segment, as in about 70% of individuals, it is called a distributing type.

Usually these arteries enter the spleen through its gastric surface but can enter through the renal surface (60%). These terminal arteries vary in length over the range 1–12 cm.

The superior terminal is usually larger than the inferior. There can be a very thin transverse anastomosis between the superior and inferior terminals, between the inferior terminal and the inferior polar, or between the superior terminal and superior polar arteries. Penultimate or ultimate branches sink into the spleen at different points. Subdivision of the main terminal can be absent, simple or complicated.

Sometimes the splenic trunk does not form superior and inferior terminal branches but becomes divided into many branches differing in caliber and length. The left gastroepiploic artery and inferior polar artery frequently take origin from the inferior terminal arteries.

Superior mesenteric artery

The superior mesenteric artery (SMA), the second unpaired branch, classically arises from the anterior aspect of the abdominal aorta. The vessel supplies part of the duodenum and a portion of the head and, frequently, an extensive area of the body of pancreas, the entire small intestine, and the large intestine up to the right two-thirds of the transverse colon.

Origin

Patterns of origin of the SMA are far more varied than described in standard textbooks of anatomy or surgery. The vessel may be absent or doubled (Powers 1850). The origin of the artery is commonly located at the level opposite the lower third of the first lumbar vertebra. However, the level can range from the lower border of the twelfth thoracic vertebra to the disk between the second and third lumbar vertebrae (Adachi 1928; George 1935; Cauldwell and Anson 1943). Prakash et al. (2011) reported an atypical level of origin in 24% of cases. During routine multidetector computed tomographic angiography of a patient, Matusz et al. (2013) noticed an exceptional origin of the celiac trunk (CT) and SMA from the thoracic part of the aorta, approximately 21 mm and 9 mm above the aortic hiatus, respectively.

The different levels of origin of the SMA could account for the wide variations in the interval between the aortic hiatus and SMA (range 20.6–59.3 mm; average 33.5 mm) (Prakash et al. 2011).

Usually the SMA arises as a single vessel from the ventral aspect of the aorta inferior to the origin of the CT. The celiacmesenteric interval on the external surface of the aorta varies over the range 1–31 mm. According to most researchers, the average distance lies between 13 mm and 16 mm (George 1935; Cauldwell and Anson 1943; Anson and McVay 1971; Songür et al. 2010). However, in most of the cases (60%) examined by Michels (1955), this distance ranged between 1 mm and 6 mm. Likewise, in two large case series studies by Brunet et al. (1993) and Katz-Summercorn and Bridger (2013), much lower average distances of 3.88 mm and 3.4 mm, respectively, were noted. Even a zero distance between the two vessels was recorded in 57.6% of 99 cadavers investigated by Katz-Summercorn and Bridger (2013). In the same series they found a case in which the CT and SMA arose adjacent to each other in the same horizontal plane. In the current series of 50 cadavers, the average distance measured was 10 mm.

The artery arises at a distance ranging from 75 to 138 mm (average 109.8 mm) cranial to the aortic bifurcation (Yahel and Arensburg 1998).

Songür et al. (2010) recorded the average external diameter of the artery as 7.7 mm (range 5–11 mm). However, Pennington and Soames (2005) reported higher values (9.1 mm) and in the same case series the average internal diameter recorded was 7.3 mm (range 5.8–10.0 mm). The vessel geometry can also vary. The average projection angles of the artery are 77° (range 30–110°) with the horizontal plane, 3° (range 5–90°) with the sagittal plane, and 80° (range 30–120°) with the coronal plane (Pennington and Soames 2005).

Variations in origin

Although the SMA usually arises as an independent branch from the aorta, different modes of origin are not uncommon. The following variations have been found.

1. Celiacomesenteric trunk (CMT): at times the SMA fuses with the CT at its origin to form a celiacomesenteric trunk (CMT). The incidence of this anomaly has been reported as 1–2% (Higashi and Sone 1987; Kaneko 1990; Cavdar et al. 1997; Nelson et al. 1988; Çiçekcibaşi et al. 2005; Winston et al. 2007; Varma et al. 2009; Malnar et al. 2010; Song et al. 2010). In contrast to these studies, Tsukamoto (1929) found an exceptionally high percentage of this variation (11%) (Fig. 54.3v).
2. The SMA can arise jointly with one or any two components of the CT: it shares a common trunk of origin with the splenic artery (SA) to form a splenomesenteric trunk in 0.16–1% of cases (Song et al. 2010; Ugurel et al. 2010; Prakash et al. 2012) (Fig. 54.3c). It fuses with both splenic and hepatic arteries to form a hepatosplenomesenteric trunk in 0.68–1.7% of subjects (Chen et al. 2009; Song et al. 2010; Ugurel et al. 2010;

Varma et al. 2010) (Fig. 54.3t). A common stem of origin shared by the left gastric artery, SA, and SMA is another anomalous type.

3. Celiaco-bimesenteric trunk: Nonent et al. (2001) found an extremely unusual variation in which the SMA took origin jointly with the CT and inferior mesenteric artery (IMA) from the aorta at the level of the second lumbar vertebra, and named this variation the celiaco-bimesenteric trunk (Fig. 54.3w).
4. Another variation in the mode of origin, although rare (incidence less than 0.1%), is an SMA stemming jointly with the IMA as a common trunk from the aorta (Adachi 1930; Gwyn and Skilton 1966; Lippert and Pabst 1985; Kitamura et al. 1987; Yamasaki et al. 1990; Nonent et al. 2001; Osawa et al. 2004; Yi et al. 2008). The common trunk usually arises from the abdominal aorta at the level from which the normal SMA would arise. Maleux et al. (2010) reported a case in which the common trunk of the SMA and IMA arose at the level of the fifth lumbar vertebra. In such cases the IMA almost always emerges as the first branch of the SMA within 1.0–4.0 cm from its origin. However, in the case reported by Gwyn and Skilton (1966), the IMA arose as a second colic branch from the SMA. Osawa et al. (2004) found a rare case in which the IMA and common hepatic artery stemmed from the SMA, forming a common hepatomesenteric trunk.

Delannoy (1923) reported two SMAs arising from the aorta. One divided into jejunal and ileal branches and the other supplied the ascending and the transverse colon. He considered them a duplicated SMA. Pillet et al. (1993) named the arteries which supply the ascending and transverse colon the middle mesenteric artery. Milnerowicz et al. (2012) also reported a similar case. Power (1850) stated that the SMA can arise from the internal iliac artery.

Complete absence of the SMA is extremely rare. Wu et al. (2013) discovered this variation in one patient during multidetector computed tomography. This was associated with compensatory dilated IMA.

Course

After its origin from the aorta, the SMA runs behind the body of the pancreas, proceeding downward anterior to the uncinate process and horizontal part of the duodenum. The superior mesenteric vessels emerge from beneath the pancreas in the neck region and enter the root of the mesentery. Sometimes the uncinate process is absent or completely encircles the superior mesenteric vessels, disturbing its relationship with the vessels (Sugiura et al. 1987). The retropancreatic portion of the SMA can give off small rami to the head of the pancreas.

The contour of the SMA can vary. The first part of the artery for an inch or more can be indented in a spiral form (Michels 1955).

Branches

The constant branches of the SMA are the inferior pancreaticoduodenal artery (IPDA); middle colic artery (MCA); right colic artery (RCA); ileocolic artery (ICoA); and intestinal (jejunal and ileal) arteries. The classical picture in which all these branches arise separately from the SMA was found in only 22% of cadavers by Nelson et al. (1988), in 28.7% by Sonneland et al. (1958), and in one-third of 200 cadavers investigated by Michels et al. (1965).

Inferior pancreaticoduodenal artery

Origin

The inferior pancreaticoduodenal artery (IPDA) commonly arises directly as the first right branch of the SMA (Fig. 54.15a). When the accessory right hepatic arises from the SMA, the IPDA is usually the second right branch of the latter. Opinions differ regarding the side of origin of the IPDA from the SMA. The vessel usually arises from the right or posterior surface of the SMA, although occasionally from its left side (Michels 1955). Takamuro et al. (1998) emphasized that, irrespective of the side of origin, the point at which the IPDA splits into anterior and posterior divisions is consistently located to the right side of the SMA. Another common source of the IPDA is the first jejunal branch of the SMA (Fig. 54.15b). The incidence of origin from the SMA or first jejunal artery recorded in certain large series ranges from 60 to 70% (Pierson 1943; Shapiro and Robillard 1946; Woodburne and Olsen 1951; Michels 1955). The IPDA and first jelunal artery can emerge as a common trunk from the SMA. Bertelli et al. (1997) named it the pancreaticoduodenojejunal trunk (PDJ). This type of origin has been found in 17.4–30.43% cases (Kosinski 1928; Petren 1929; Meyer 1953; Delagrange and Barbin 1966; Martin and Couppié 1963; Thomford et al. 1986; Donatini 1990).

Less frequently, the IPDA arises from the accessory right hepatic artery (aRHA), dorsal pancreatic artery (DPA), or a common stem with the second or third jejunal artery and middle colic artery (MCA) (Kosinski 1928; Shapiro and Robillard 1946; Woodburne and Olsen 1951; Vandamme et al. 1967; Bertelli et al. 1996a) (Fig. 54.15c–g).

Numerical variations of IPDA are rare. Michels (1955) observed instances of a double IPDA. The present authors found two IPDAs in one cadaver, both emanating separately from the SMA (Fig. 54.16).

In relation to the pancreas the IPDA stem usually arises at the level of the lower edge of its neck but occasionally there is a high retropancreatic origin. Ziegler (1942) found a high origin in 50% of 24 bodies, and its branches characteristically distributed downward in a fan-shaped manner over the anterior surface of the pancreas. Shapiro and Robillard (1946) observed such a fan-shaped distribution in 14% of cases.

Branches

Irrespective of the source of origin, the IPDA stem ascends posterior to the superior mesenteric vessels to reach the posterior surface of the head of the pancreas and, at a variable distance, bifurcates into the anterior inferior pancreaticoduodenal (AIPDA) and posterior inferior pancreaticoduodenal arteries

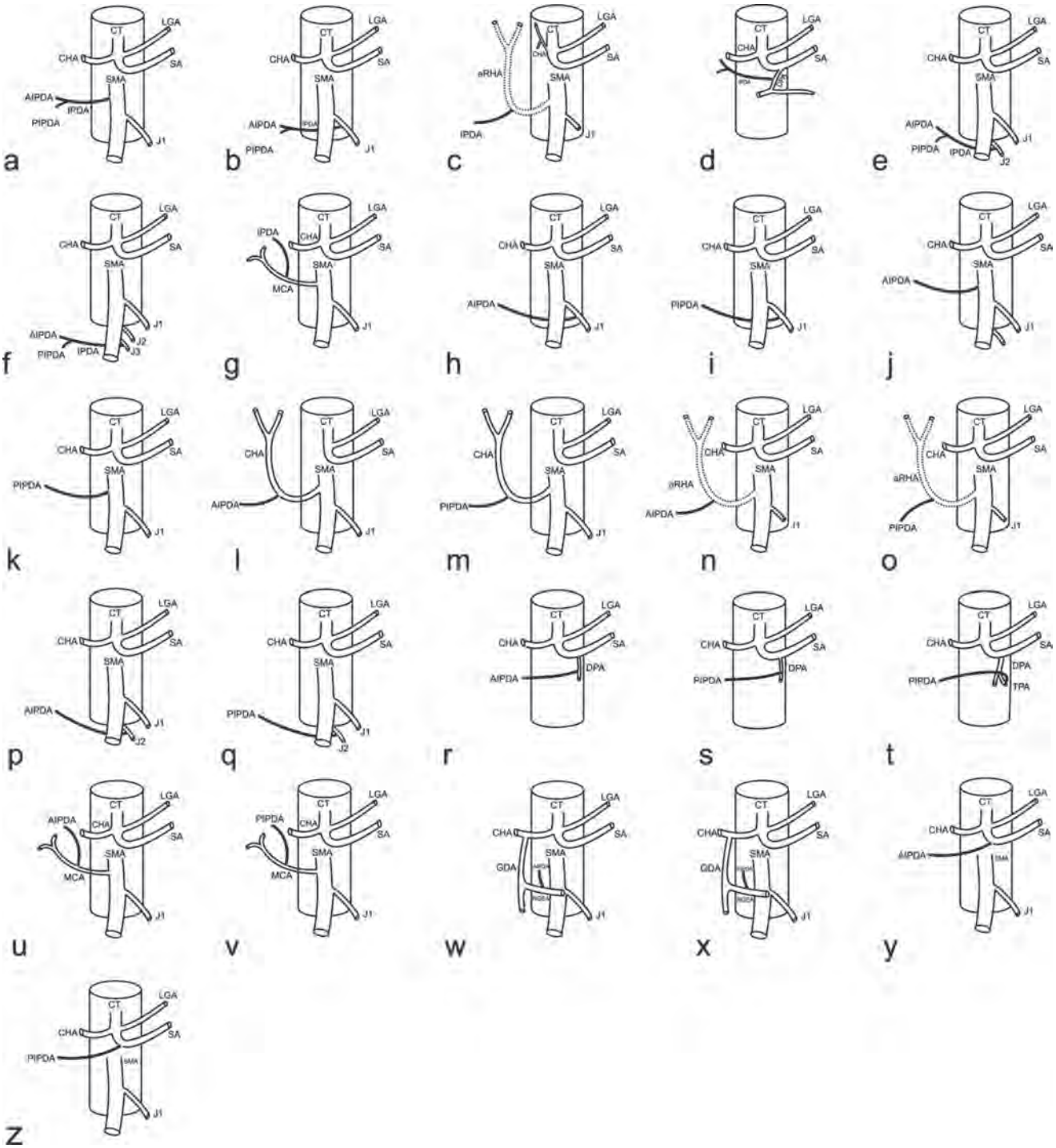

Figure 54.15 Schematic representation of variant patterns of origin of the inferior pancreaticoduodenal arteries: (a) IPDA from SMA; (b) IPDA from J1; (c) IPDA from aRHA; (d) IPDA from DPA; (e) IPDA from J2; (f) IPDA from J3; (g) IPDA from MCA; (h) AIPDA from J1; (i) PIPDA from J1; (j) AIPDA from SMA; (k) PIPDA from SMA; (l) AIPDA from aberrant CHA; (m) PIPDA from aberrant CHA; (n) AIPDA from aRHA; (o) PIPDA from aRHA; (p) AIPDA from J2; (q) PIPDA from J2; (r) AIPDA from DPA; (s) PIPDA from DPA; (t) PIPDA from TPA; (u) AIPDA from MCA; (v) PIPDA from MCA; (w) AIPDA from RGEA; (x) PIPDA from RGEA; (y) AIPDA from SA; (z) PIPDA from SA. Abbreviations as for previous figures and IPDA: inferior pancreaticoduodenal artery; AIPDA: anterior inferior pancreaticoduodenal artery; PIPDA: posterior inferior pancreatico duodenal artery: J1: first jejunal artery; J2: second jejunal artery; J3: third jejunal artery; RGEA: right gastro-epiploic artery. Adapted from Woodburne and Olsen (1951).

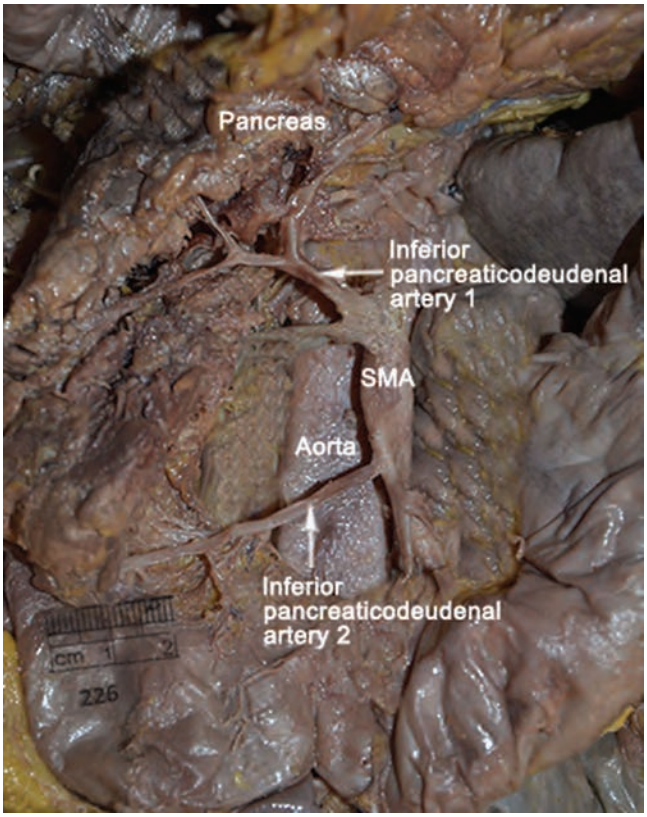

Figure 54.16 Cadaveric dissection revealing two inferior pancreaticoduodenal arteries arising separately from the SMA.

(PIPDA). Other uncommon branches are the jejunal arteries and right gastroepiploic artery. Rarely, it anastamoses with the first jejunal artery.

The constancy of the AIPDA has often been noted; however, Calas et al. (1955) and Thomford et al. (1986) could not detect it in 2% and 6.7% of cases, respectively. The PIPDA occurs in 90–100% of cases (Pierson 1943; Shapiro and Robillard 1946; Woodburne and Olsen 1951; Calas et al. 1955; Thomford et al. 1986).

Variations in origins of the anterior and posterior inferior pancreaticoduodenal arteries

Both divisions of the IPDA, instead of stemming from it, can arise independently from the same or different sources. Alternate sources of the AIPDA and PIPDA include the following.

1. First jejunal artery: the AIPDA or PIPDA have been seen shooting from the first jejunal artery in 5.4–40% and 3.6–30% of cases, respectively (Kosinski 1928; Woodburne and Olsen 1951; Meyer 1953; Calas et al. 1955; Thomford et al. 1986). Bertelli et al. (1997) named this pattern an incomplete pancreaticoduodenojejunal trunk because it lacks either the PIPDA or AIPDA (Fig. 54.15h, i).
2. The superior mesenteric artery (SMA): the frequency of origin of the AIPDA from the SMA has been reported as 1.8–50%. Estimates of its incidence differ among the techniques employed (dissections v. angiographies). Dissection studies report lower percentages ranging from 1.8 to 16%. The incidence of origin of the PIPDA from the SMA ranges from 8 to 56.6%. The incidence observed in dissection or corrosion cast studies ranges between 8 and 25% (Kosinski 1928; Falconer and Griffiths 1950; Woodburne and Olsen 1951; Martin and Couppié 1963; Vandamme et al. 1967; Thomford et al. 1986; Nebesar et al. 1969) (Fig. 54.15j, k).
3. The common hepatic artery (CHA): Vandamme et al. (1967) found the AIPDA and PIPDA arising from the CHA (shooting aberrantly from the SMA) in 2.48% and 1.86% of cases, respectively (Fig. 54.15l, m).
4. Accessory RHA (aRHA): several anatomists reported an origin from the aRHA coming from the SMA. The frequency reported for the AIPDA is 0.7–3.1% and for the PIPDA is 1.8–8% (Kosinski 1928; Woodburne and Olsen 1951; Calas et al. 1955; Vandamme et al. 1967; Martin and Couppié 1963) (Fig. 54.15n, o).
5. Second jejunal artery: the AIPDA arises more commonly from the second jejunal artery (2–6.6%) than its posterior counterpart (Kosinski 1928; Meyer 1953; Calas et al. 1955) (Fig. 54.15p, q).
6. Dorsal pancreatic artery (DPA): the AIPDA originates from the DPA in 0.7–2.5% of cases and the PIPDA in 2.5–8.57% (Kosinski 1928; Woodburne and Olsen 1951; Meyer 1953; Calas et al. 1955; Martin and Couppié 1963; Vandamme et al. 1967) (Fig. 54.15r, s). The PIPDA has been seen originating as a common trunk with transverse pancreatic artery in 1.42% of cases (Martin and Couppié 1963; Meyer 1953) (Fig. 54.15t).
7. Occasionally the AIPDA and PIPDA arise from unusual sources such as the middle colic, right gastroepiploic or splenic artery (Fig. 54.15u–z). Even the third jejunal artery and celiac trunk sometimes give origin to the AIPDA (Kosinski 1928; Woodburne and Olsen 1951; Calas et al. 1955).

The caliber of the AIPDA falls within the range 1–2.5 mm (Kosinski 1928) and its length 1–5 cm (Moretti 1965). The caliber of the PIPDA ranges between 1 and 2.3 mm (Kosinski 1928). The course of the PIPDA is usually very short but, when it takes origin from the pancreaticoduodenojejunal trunk or jejunal arteries, it is longer.

The AIPDA is variably related to the head of the pancreas. It is retropancreatic in 61–74% (Petren 1929; Yi et al. 2010), subpancreatic running along the inferior edge of the gland in 25% (Meyer 1953), and prepancreatic in 23-39% of cases (Petren 1929; Meyer 1953; Yi et al. 2010). It rarely passes through the substance of the pancreas and exhibits an intrapancreatic course (Meyer 1953). It can even lie inferior to the uncinate process (Belli et al. 1958). The posterior vessel retains its posterior position and can be embedded in the pancreatic substance. The AIPDA usually courses parallel to the PIPDA but almost always 20–30 mm inferior to it (Murakami et al. 1999).

The AIPDA and PIPDA can give off a transverse pancreatic artery, a branch to the uncinate process, a small branch to the duodenojejunal flexure called the angular duodenal artery, anastomotic branches to the hepatic, SA or first jejunal arteries, right gastroepiploic artery, dorsal pancreatic artery, and CT (Schlyvitch 1937; Pierson 1943; Michels 1951a; Meyer 1952, 1953; Quinlan 1983).

Pancreatic arcades

The AIPDA and PIPDA anastomose typically with the anterior and posterior superior pancreaticoduodenal arteries, respectively, to form the anterior and posterior panrceaticoduodenal arcades in relation to the head of pancreas. The arcades are usually considered complete. The anterior anastomosis is absent in 5–50% and the posterior anastomosis in 5–20% of subjects examined in different studies (Edwards 1941; Shapiro and Robillard 1946; Falconer and Griffiths 1950; Donatini 1990). Anterior arcades up to four in number have been found. Lippert and Pabst (1985) reported two arcades as the commonest variant (79%), three arcades in 16%, and four in 5% of individuals. Posterior arcades are more commonly single, but are double in 10% of individuals (Lippert and Pabst 1985).

Arcades vary not only in number but also in origin. Anterior arcades invariably have a superior origin from the anterior superior pancreaticoduodenal artery. This is more variable for the posterior arcades, which can arise from the gastroduodenal, common hepatic, proper hepatic artery, or right hepatic arteries. Inferior origins of the anterior and posterior arcades are usually formed by divisions of the IPDA.

Posterior arcades typically lie further from the pancreaticoduodenal groove than anterior ones (Hollinshead 1971). Their positions can vary. The pancreatic and duodenal branches arise from them, the latter sometimes embedded in the pancreas. Takamuro et al. (1998) observed that in individuals with a common trunk of the IPDA and jejunal artery, the jejunal artery supplies a portion of the fourth part of the duodenum. When the jejunal artery originates directly from the SMA, the IPDA supplies the entire length of the fourth part of the duodenum. When the AIPDA and PIPDA arise independently from the SMA, the jejunal artery supplies the anterior aspect and the PIPDA the posterior aspect of the duodenum.

Middle colic artery

The middle colic artery (MCA) varies greatly in number, origin, and course. It usually arises as a single vessel from the front or concave right side of the SMA below the origin of the inferior pancreaticoduodenal artery (IPDA) inferior to the uncinate process of the pancreas. The level of origin from the SMA can be higher than usual, in which case the MCA descends with the SMA between the duodenum and pancreas or sometimes even passes through the pancreas (Hollinshead 1971).

The present authors found the MCA arising from the SMA at an average distance of 4.7 cm (range 1.9–7.9 cm), distal to the origin of the latter from the aorta. The distance from the lower border of the pancreas ranged from 0.69 cm to 5.4 cm (average 3.0 cm).

Absence of the MCA has been recorded in 0–5% of cases (Steward and Rankin 1933; Mayo 1955; Sonneland et al. 1958; Michels 1955; Garcia-Ruiz et al. 1996). Branches of the SMA or IMA often replace the MCA. In 5% of specimens with no MCA, Steward and Rankin (1933) found it was replaced by a large branch from the left colic artery (LCA). In our series of 50 cadavers, the artery was absent in 6% of cases (Fig. 54.17a).

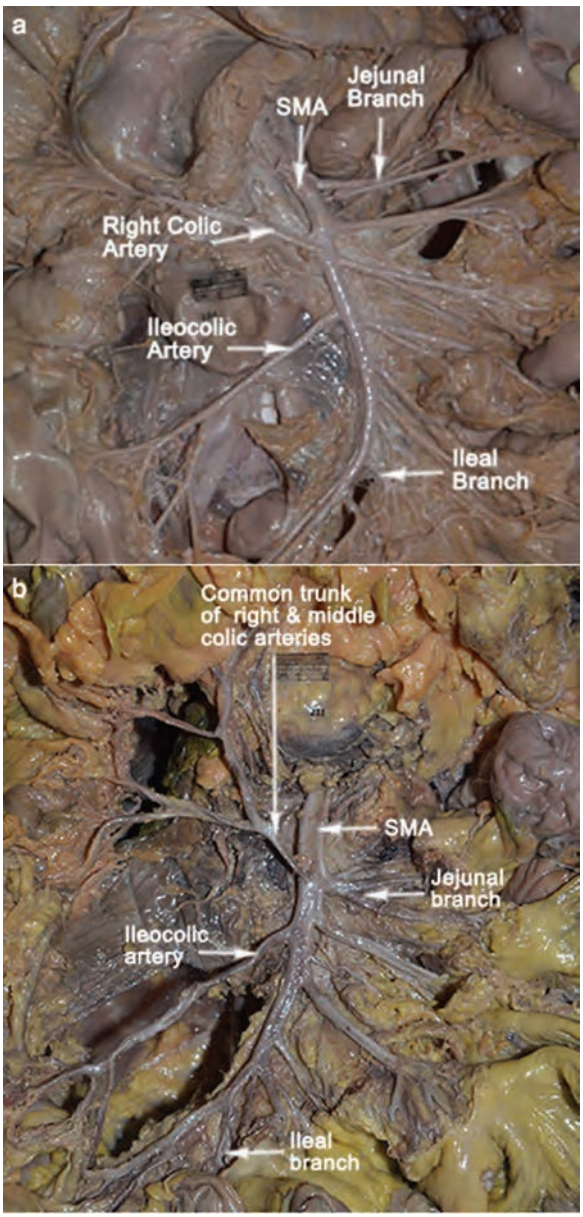

Figure 54.17 Cadaveric dissection revealing (a) absence of the middle colic artery; and (b) common trunk of origin of the right colic and middle colic arteries from the SMA.

Origin

The MCA originates from the SMA in 78–99% of cases studied by various research groups (Steward and Rankin 1933; Basmajian 1955; Sonneland et al. 1958; Michels 1965; Nelson et al. 1988; Garcia-Ruiz et al. 1996). When the MCA is single, it can arise either independently from the SMA or in company with its other colic branches. The most prevalent pattern (58–94.6%) is direct independent origin from the SMA (Sonneland et al. 1958; Nelson et al. 1988; Garcia-Ruiz et al. 1996).

Sonneland et al. (1958) gave a detailed account of the modes of origin of the MCA. In their large series of 600 cadavers, the classical single MCA arising directly from the SMA was present in 59.7% of cases. The other patterns in decreasing order of frequency were the MCA sharing common stem with: the right colic artery (26.7%); the ICoA and right colic arteries (1.0%); and the right colic (RCA) and left colic arteries (0.2%). Among 50 cadavers investigated, Nelson et al. (1988) found the MCA arising along with the RCA in 6% and with the ICoA in 4.6% of cases.

The authors in the current series found a single MCA originating from the SMA as an independent artery in 92% of cases, along with the RCA in 2% and with the ICoA in 2% (Fig. 54.17b).

The MCA can arise aberrantly from various sources. Instead of the SMA it can stem directly from the aorta (Yoshida et al. 1993). This deserves special mention. The term "middle mesenteric artery" is reserved for the vessel originating directly from the aorta between the SMA and IMA. Lawdahl and Keller (1987) used the term "third mesenteric artery" for such a vessel. The MCA also arises from the celiac trunk (CT) or one of its branches in 1.2–4.8% of cases (Vandamme and Bonte 1985; Nelson et al. 1988; Amonoo-Kuofi 1995; Yildirim et al. 2004; Petrella et al. 2007). This origin was first described by Tandler (1904). Michels (1955) found it arising from the CT on several occasions, in two of which the superior pancreaticoduodenal and right gastroepiploic arteries arose from the SMA via a common trunk.

Other atypical occasional sources are the splenic artery (SA) (Yamada et al. 1963; Murokami et al. 1998), replaced right hepatic artery (Michels 1955), common hepatic artery (Wadhwa and Barua 2008), inferior mesenteric artery (Benton and Cotter 1963), inferior pancreaticoduodenal artery (Hollinshead 1971), dorsal pancreatic artery (Pierson 1943; Michels 1951a; Woodburne and Olsen 1951; Bouchet and Martin 1961; Vandamme et al. 1967), gastroduodenal artery (Gupta et al. 2013), and left colic artery. Occasionally an enlarged DPA is prolonged as the MCA into the transverse mesocolon (Michels 1955).

Accessory middle colic artery

An accessory MCA is a rather frequent additional arterial supply to the transverse colon. The reported incidence varies from 3.6 to 18% (Steward and Rankin 1933; Sonneland et al. 1958; Nelson 1988; Garcia-Ruiz et al. 1996; Chitra 2010). Steward and Rankin (1933) found the additional artery arising above the main MCA in 3.6% of cases. Nelson et al. (1988) found two MCAs but of different origin in 18% of cases. Sonneland et al. (1958) described various modes of origin of double MCA in different combinations with other branches of the SMA. They found both arteries issuing from the SMA in 3.7% of cases; one issuing from SMA and other from a common stem with the RCA (1.5%); both issuing from a common trunk with the ICoA (1.3%); one issuing from the SMA and the other from a common trunk with the ICoA and RCA (0.3%); and both issuing from a common trunk with the LCA (0.2%).

The authors in the current series found double MCAs, both stemming from the SMA, in 2% of cases (Fig. 54.18).

Occasionally even three MCA are seen. Sonneland et al. (1958) found a triple MCA in 1.6% of their specimens.

Course

Usually the MCA courses downward and forward between two layers of the transverse mesocolon at a variable distance from the gut wall, and bifurcates into right and left branches. An MCA of more proximal origin from the SMA or from aberrant sources

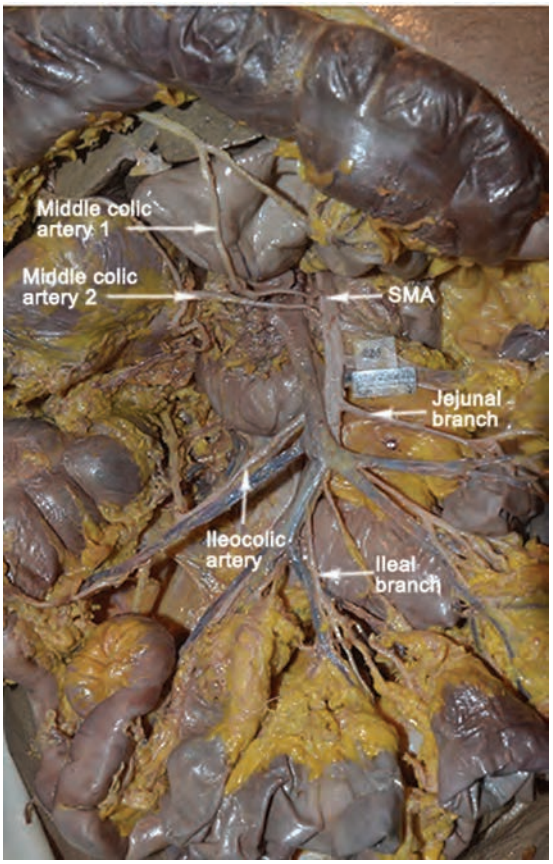

Figure 54.18 Cadaveric dissection indicating absence of the right colic artery and presence of two middle colic arteries arising separately from the SMA.

can pass through the head of the pancreas or between the head and the duodenum. The right and left branches anastomose with the ascending branch of the RCA and right branch of the LCA, respectively, to form an arterial arcade from which vasa recta are given off to the transverse colon except for its splenic flexure. Trifurcation and even tetrafurcation of the MCA can be present (Steward and Rankin 1933). Steward and Rankin (1933) observed variable positions of the anastomosis between the MCA and LCA. There are occasional failures of this anastomosis (Merkel 1918; Lochhart-Mummery 1923; Robillard and Shapiro 1947).

In the mesocolon the artery, whenever single, runs to the right of the midline as a rule (Anson and McVay 1971) so that the left branch crosses the midline. However, when associated with a superiorly placed RCA, the MCA quite frequently passes toward the middle of the transverse colon. Occasionally the entire artery is directed toward the splenic flexure and encroaches upon the territory of the left colic branch of the IMA. In 37% of cases, Steward and Rankin (1933) encountered a large branch of the MCA or accessory MCA that ran toward the splenic flexure and reinforced the marginal artery to supply the left side of the transverse colon and splenic flexure. Sometimes an accessory MCA takes a parallel course with a marginal branch of the LCA, forming the arch of Riolan (artery of Riolan).

Steward and Rankin (1933) stated that the longer the MCA trunk and its branches, the greater the distance between the point of bifurcation and the wall of colon. Whenever two MCAs are present, this distance is relatively shorter (range 7–17.7 cm, average 11.7 cm).

Collateral branches of the middle colic artery

In his extensive work, Michels (1955) found many cases in which the MCA, and an accessory MCA of celiac axis or SMA origin, gave rise to the dorsal pancreatic or transverse pancreatic branches. The MCA can also give collateral branches to irrigate the submesocolic portion of the pancreas and its uncinate process (Delagrange and Barbin 1966).

Right colic artery

The right colic artery (RCA) typically arises from the right concave surface of the SMA, usually as an independent branch or a common trunk with other intestinal arteries. It is considered to be one of the most inconstant colic arteries and reports of frequency vary (10.7–98% of cases). In 18% of the cases studied by Steward and Rankin (1933) there was no artery corresponding in its course to the RCA. Michels (1955) failed to identify it in 2% and Sonneland et al. (1958) in 12.6% of cases. In 50 bodies studied by us, the vessel was absent in 6% (Fig. 54.18).

Origin

Out of 600 bodies studied, Sonneland et al. (1958) found the typical single vessel in 78% and Nelson et al. (1988) in 82%. When the RCA was single, Steward and Rankin (1933) found it originated directly from the SMA in 40% of cases. The authors in the current study found an independent origin directly from the SMA in 82%. The artery can arise along with other colic arteries. Sonneland et al. (1958) described a variety of patterns of origin. In their case series, the artery stemmed as a common trunk with: the iliocolic artery (ICoA) in 26.3%; the MCA in 23.8%; both the MCA and ICoA in 0.9%; and the left colic artery (LCA) in 0.2%. Steward and Rankin (1933) and Michels (1955) identified the origin of the vessel from the MCA in 30% and 52% of cases, respectively, and from the ICoA in 12% and 8%, respectively. The current authors found the RCA originated as a common trunk with the ICoA in 10% and with the MCA in 2% of cases (Figs 54.17b, 54.19).

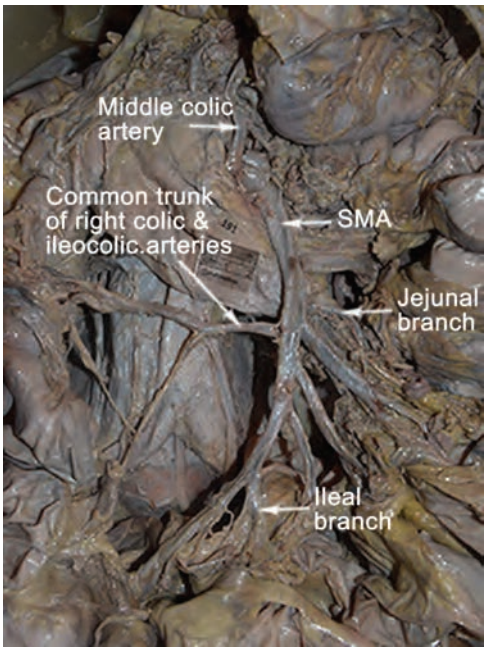

Figure 54.19 Cadaveric dissection revealing a common trunk of origin of the right colic and ileocolic arteries from the SMA.

Accessory right colic arteries

Like the MCA, the RCA can be multiple. Sonneland et al. (1958) found two vessels in 8.7% and three in 0.7% of cases. In a case series of 50 cadavers, Nelson et al. (1988) found two RCAs of different origin in 16%.

Sonneland et al. (1958) observed great variability in the origins of multiple RCAs. In cases with double RCA, one shared a stem with the MCA and the other with the ICoA (5.7%); one originated from the SMA and the other arose along with the ICoA (1.5%); both RCAs arose with the MCA and ICoA (1.0%); or both RCAs arose with the ICoA (0.5%). In all three cases of Sonneland et al. (1958) with triple RCAs, the vessel shared a common trunk of origin with the ICoA. In the present series double RCAs were found in 4% of cases, one arising from the MCA and the other from the ICoA.

Sonneland et al. (1958) stated that in cases of double RCA, the distance of origin of the more proximal vessel from the SMA origin varies between 1.5 and 9 cm (average 6.2 cm). In cases with multiple RCAs, the distance of the artery from the SMA to the colon wall is shorter than for a single vessel. In the current series, the length of the RCA from origin to bifurcation averaged 6.01 cm (range 2.54–8.17 cm).

The RCA courses more or less transversely towards the ascending colon behind the parietal peritoneum or within the ascending mesocolon, if it exists. Close to the medial margin of the ascending colon the vessel divides into ascending and descending branches; the former anastomoses with the right branch of the MCA while the latter anastomoses with the ascending colic branch of the ICoA. From the arterial arcade so formed, vasa recta arise and supply the upper two-thirds of the ascending colon. The ileocolic artery sometimes fails to anastomose with the RCA, resulting in discontinuity of the marginal artery. Steward and Rankin (1933) observed failure of anastomosis between the ICoA and RCA in 5% of 40 cadavers investigated.

Iliocolic artery

The iliocolic artery (ICoA) arises from the right concave side of the SMA about halfway down its length. The artery can arise directly from the SMA or share a common stem of origin with colic branches of the latter. In 600 cadavers dissected by Sonneland et al. (1958) the artery issued independently from the SMA in 63.2% of cases, and in 36% branched off as a common stem with the RCA or MCA or both. Solanke (1970) found it invariably the lowest branch of the SMA.

The ICoA passes to the right retroperitoneally and, at variable distances from the colon, it divides into ascending and descending branches. The ascending branch anastomoses with the RCA and the descending branch divides into the ileal, ascending colic, appendicular, and cecal arteries. The termination varies. The ICoA can divide directly into the ascending colic, common cecal, and ileal branches, or the anterior cecal, posterior cecal, appendicular, and ileal branches. In a case series of 100 cadavers studied by Solanke (1970), the ICoA soon after its origin divided into medial and lateral branches of equal caliber in 16% of cases.

Branches of the iliocolic artery: 1. Ascending colic artery

The ascending colic artery is usually the first branch given off by the ICoA, although one of the cecal branches can be the first. This branch ascends parallel to the ascending colon and typically anastomoses with the descending branch of the RCA. It forms the origin of the marginal artery. This part of the anastomosis is the most variable. Steward and Rankin (1933) observed failure of anastomosis in 5% of their specimens and Michels et al. (1963) in 10% of cases. The ascending colic artery can form an arterial arcade with other branches of the ICoA. From this anastomotic loop other branches of the ICoA can arise.

Branches of the iliocolic artery: 2. Cecal arteries

Cecal arteries, anterior and posterior to the corresponding surfaces of the cecum, issue in variable ways from the ICoA or its branches. The anterior cecal and posterior cecal arteries, ACA and PCA, respectively, can arise from a common cecal trunk or separately from the same or different sources.

Ures et al. (1979) found both cecal arteries arising from the common cecal trunk, issuing from the ileal artery in 61.2% and from the RCA in 15% of cases. Michels et al. (1963) found a common cecal artery arising from the arterial arcade between the ileal and colic branches of the ICoA in most cases (76%). A common cecal trunk from the iliocolic artery or its ascending or descending divisions or colic branch has been observed (Veeresh et al. 2012).

Two cecal arteries can arise separately from the same or different sources. Both can arise directly from the iliocolic artery. Ures et al. (1979) found both cecal arteries arising from the ileal artery in 13.8%, the PCA from the RCA and the ACA from the ileal artery in 8.7%, and the ACA from the RCA and the PCA from the ICoA in 1.2% of cases. An arterial arcade between the ileal and colic branches of the ICoA occasionally give off cecal arteries. The posterior cecal artery passes posterior to the iliocecal junction to the posterior surface of the cecum. Infrequently, there are two or three additional cecal arteries.

The anterior cecal artery runs on the anterior surface at or a little above the upper border of the iliocecal junction and raises a fold of the peritoneum, the superior iliocecal fold. The appendicular artery can arise from the cecal arteries.

Branches of the iliocolic artery: 3. Appendicular artery

Variability in the origin of the appendicular artery is known. Many research workers claim this artery arises solely from the ICoA, either directly or through one of its sub-branches (Koster and Weintrobb 1928; Bruce et al. 1964; Robinson 1965; Pitynski et al. 1992). Shah and Shah (1946) found that among the 70% of their cases with a single appendicular artery, the artery arose as a direct branch from the ICoA in 31.7%. Solanke (1970) claimed the ICoA as the most common source (50%). In all cases with a double ICoA (13%), the appendicular artery stemmed from the medial ICoA. In cases with a single appendicular artery, Shah and Shah (1946) found an origin from the anterior cecal artery (ACA) in 20%, whereas Solanke (1970) found this origin in only 1% of cases. The incidence of origin from the posterior cecal artery (PCA) was given as 8.3% by Solanke (1970). A branch from the PCA supplies the appendix either totally or partially but almost always supplies the part close to its base. An origin from the ileal branch has been recorded in 32–35% of cases (Solanke 1970). Other relatively less frequently reported sources are the ascending colic branch of the ICoA (3%) and the arterial loop between the ascending colic and ileal branches (1%). Michels (1955) found one unusual case in which the appendicular artery arose from the dorsal pancreatic artery of celiac origin.

Branches of the iliocolic artery: 4. Accessory appendicular arteries

The appendicular artery is usually singular but there are various observations regarding the number. Kelly and Hurdon (1905) first drew attention to an accessory appendicular artery. Koster and Weintrob (1928) and Bruce et al. (1964) emphasized the presence of a single appendicular artery. In most studies the incidence of double appendicular arteries ranges between 7.5% and 44% (Shah and Shah 1946; Michels 1955; Ajmani and Ajmani 1983). However, the highest ever reported incidence of accessory appendicular arteries was 80 of 100 Nigerian cadavers by Solanke (1970). Kelly and Hurdon (1905) demonstrated that in 66% of appendices studied, the main appendicular artery supplied the distal three-quarters and the accessory supplied the proximal quarter of the appendix.

In his detailed study of the appendicular artery, Solanke (1970) found accessory vessels varying in number from one to nine. Mostly, the ICoA is the source of the accessory arteries. Other sources could be the cecal branches, ileal branch, ascending colic branch, or an arterial loop.

Course of the appendicular artery

In Solanke's (1970) series, among appendices that received more than one arterial supply the main appendicular artery supplied the whole length of the organ in 8.7% of specimens, the distal three-quarters in 53.7%, distal half in 26.3%, and distal quarter in 9%. In 66% of the appendices examined by Kelly and Hurdon (1905), the main appendicular artery supplied the distal three-quarters and the accessory artery supplied the proximal quarter. The terminal part of the main artery supplying the tip is usually an end artery. The main appendicular artery forms arterial loops variably with other branches of the iliocolic artery.

In addition to the main appendicular artery, the base of the appendix can be supplied by a small branch of the anterior or posterior cecal artery. Arterial anastomoses could serve as an alternate route for circulation. The artery gives off a recurrent branch that anastomoses with the posterior cecal artery.

From its origin, the artery usually descends dorsal to the terminal part of the ileum. It passes ventral to the ileum to reach the appendix in less than 1% of individuals (Lippert and Pabst 1985). In cases in which the artery is duplicated, one artery can run dorsal and the other ventral to the ileum. The artery runs an arcuate course in the mesoappendix. Usually it terminates at the tip of the appendix. Solanke (1970) found it turned around the tip and continued along the free border of the organ for 2 cm in 1% of cases. The main artery, while running in the free border of the mesoappnedix, gives off branches ranging in number from to 1 to 10. Anastomotic connections are usually found among the appendicular branches.

Branches of the iliocolic artery: 5. Ileal artery

The ileal branch ascends to the left toward the terminal ileum and unites with the last intestinal branch of the SMA, forming a double or triple arc from which several vasa recta are given off to the last part of the ileum. It also anatomoses with other branches of the iliocolic artery via secondary loops. There is sometimes a gap between the blood supply of the ileum from the cecal and ileal branches of the ileocolic artery. Michels et al. (1963) regarded this blood supply as precarious if the gap was 3–5 cm long. Such a gap was present in 16% of specimens.

Jejunal and ileal branches

Intestinal branches of the SMA vary in number from 10 to 24 (Dwight 1903; Michels 1962). The first jejunal branch is typically small while the succeeding 4–6 are usually large and arise close to each other to irrigate the upper half of the jejunoileum. The remaining branches are small. The distribution of origin of arteries from the SMA varies greatly. In the authors' current series of 50 cadavers, the number ranged from 5 to 17 (average 11.6). In most cases (84%) the arteries arose from the middle third of the SMA, resulting in a maximum concentration in the middle portion. In 12% the upper third of the SMA issued most of the branches and in 2% the lower third had the maximum concentration. In the remaining 2%, small branches emanated along the whole length of the SMA. The length varied from 3 to 10 cm (average 5.6 cm).

The first jejunal artery usually anastomoses with the IPDA or gives origin to the inferior pancreaticoduodenal artery (IPDA). Within the mesentery, these branches divide into ascending and descending branches and anastamose with branches of the immediate next artery to form a series of arterial arcades. The last ileal branch anastomoses with an ileal branch of the ICoA. Primary arcades give rise to straight arteries, which bifurcate and anatomose to form secondary arcades.

The arcades are usually primary and secondary in the upper part of the jejunum, but increase in number from three to five in the middle third of the jejunoileum with an average of four (Michels 1955). In 8% of the authors' series, the maximum numbers of arcades were in the upper third of the SMA. Sometimes there are no arcades between the first and second or second and third jejunal arteries, or the jejunal arcades are so narrow that very little circulation is possible between two adjacent arteries.

The vasa recta divide as they approach the small intestine to send branches alternately to each side of it. According to many researchers this is not a prevailing pattern in man (Dwight 1903; Michels 1955). Michaels (1955) divided the vasa recta into short and long arteries, depending upon whether they entered at the mesenteric border or ran anteriorly or posteriorly before entering the intestinal wall. Short branches usually (in 93% of cases) arise from long branches, although many of the latter do not give short branches. In 10% of cases, Michels (1955) found that the long branches bifurcated and gave rise to both anterior and posterior branches. The vasa recta are traditionally considered as end arteries. Rarely, consecutive vessels anastomose with each other (7 out of 479; Michels et al. 1963). Adjacent vessels can be connected by tiny longitudinal channels on the gut surface, their

chief anastomosis being intramural. Michels et al. (1963) found visible anastomoses occasionally around the antimesenteric border. This border was relatively avascular in most bodies, but the anastomoses were well developed in some.

Collateral branches of the jejunal artery, the first jejunal artery, and even the SMA and posterior pancreaticoduodenal arcade send twigs to the fourth part of the duodenum (Shapiro and Robillard 1946).

The main trunk of the IPDA or its anterior and posterior divisions have been found to arise from the second or third jejunal arteries (Kosinski 1928; Woodburne and Olsen 1951; Meyer 1953; Calas et al. 1955; Martin and Couppié 1963; Vandamme et al. 1967) (Fig. 54.15b, e, f, h, i, p, q).

Aberrant branches of the SMA

Occasionally the SMA gives accessory branches or branches normally derived from other sources to the liver, stomach, spleen, pancreas, gall bladder, suprarenal glands, and hindgut-derived parts of the colon. The most frequent aberrant branches are dorsal pancreatic, transverse pancreatic, and aberrant right hepatic (replaced or accessory).

A dorsal pancreatic artery (DPA) originating from the SMA has been observed in 1.8–25% of cases by various researchers (Pitzorno 1920; Del Campo 1931; Falconer and Griffiths 1950; Woodburne and Olsen 1951; Bertocchi and Bianco 1955; Bouchet and Martin 1961; Delagrange and Barbin 1966; Vandamme and van der Schuren 1976; Thomford et al. 1986).

The transverse pancreatic artery can become displaced from the DPA and take origin from the SMA (Michels 1955).

A replaced RHA frequently arises from the SMA; the recorded incidence varies over the range 6.9–17% (Michels 1955; Suzuki et al. 1971; Rygaard et al. 1986; Kemeny et al. 1986; Makisalo et al. 1993; Hiatt et al. 1994; Gruttadauria et al. 2001; Chen et al. 2009; Kishi et al. 2010; Ugurel et al. 2010).

An accessory RHA originating from the SMA is also a frequent variation and has been reported in 0.6–7% of individuals (Michels 1955; Suzuki et al. 1971; Rygaard et al. 1986; Rong and Sindelar 1987; Makisalo et al. 1993; Hiatt et al. 1994; Gruttadauria et al. 2001; López-Andújar et al. 2007; Chen et al. 2009; Kishi et al. 2010; Ugurel et al. 2010, Ozsoy et al. 2011).

The common hepatic artery arises in 0.9–5% of individuals (Michels 1966; Hiatt et al. 1994; Gruttadauria et al. 2001; Koops et al. 2004; Abdullah et al. 2006; López-Andújar et al. 2007).

The gastroduodenal artery (GDA) is another artery arising anomalously from the SMA. Michels (1955) reported two such instances. In a series of 400 dissected bodies, Huu et al. (1976) observed the origin of the GDA from the SMA in four cases. In 10 cases with double GDAs, one normal artery stemmed from the CT and other from the SMA. In cases with double GDAs, the vessel of mesenteric origin was dominant. The right gastroepiploic artery can arise from the SMA instead of the GDA (Michels 1955; Sakamoto et al. 1999).

The splenic artery (SA) can arise from the SMA (Rossi and Cova 1904; Michels 1942; Bertocchhi and Bianco 1955; Pandey et al. 2004). Jain and Motwani (2013) reported a rare case of accessory SA and LCA arising jointly from a common stem from the SMA.

Other less frequently reported aberrant arteries are the proper hepatic (Covey et al. 2002); right anterior hepatic (Nagino et al. 1993); replaced left hepatic (Chaib et al. 2010); cystic (Daseler et al. 1947; Katada et al. 2008); left gastric (Ray et al. 1998); right renal (Dalçik et al. 2000; Bamac et al. 2011; Lacout et al. 2012); and middle suprarenal (Gagnon 1964; Honma and Kudo 2012).

Koizumi and Horiguchi (1990) found an accessory colic artery arising from the SMA more proximal than the first jejunal artery in 49.2% of 65 subjects. This artery anastomosed with the marginal artery at the splenic flexure and was named the "superior left colic artery."

Cases of accessory LCA arising from the SMA and replacing the left colic branch of the IMA have been reported (Sierocinski 1975; Vandamme and van der Schuren 1976; Roberts et al. 1984). In the authors' current series an accessory LCA emanated from the SMA in 8%.

Occasionally the LCA and superior rectal arteries arise from the SMA, wholly or partially replacing the IMA (Sierocinski 1975; Vandamme and van der Schuren 1976).

Vandamme and van der Schuren (1976) described an accessory transverse colic artery arising from the left border of the proximal segment of the SMA for the left half of the transverse mesocolon, which joined the marginal artery proximal to the splenic flexure.

Superior mesenteric-celiac trunk anastomosis

Anastomosis between the CT and SMA or their branches can occur. This anastomosis, the Arc of Buhler, was described for the first time by Buhler (1904). Such CT-SMA communications are not very unusual. McNulty et al. (2001) reported three variants of such anastomosis among 300 visceral angiograms: (1) anastomosis between the GDA and branches of the IPDA; (2) dorsal pancreatic artery (DPA) anastomoses with the anterior and posterior pancreaticoduodenal arcades via a right transverse branch of the DPA (Kirk's arcade); and (3) direct anastomosis between the CT and SMA. Grabbe and Bucheler (1980) detected 14 cases of CT-SMA arterial links in 350 visceral angiograms (4.0%). Later, Saad et al. (2005) found it in 3.3% of cases.

Superior mesenteric–inferior mesenteric anastomosis

As for connections with the CT, SMA-IMA links have been described, although in low frequencies of 0–18% (Steward and Rankin 1933; Michels et al. 1963; Bertelli et al. 1996b; Garcia-Ruiz et al. 1996). Bertelli et al. (1996b) identified three categories of intermesenteric connections: (1) direct type: communication between the SMA and IMA; (2) indirect type: connection between the MCA and LCA (the most common variant); and (3) connection of one of the two mesenteric arteries with the main branch of the other.

Inferior mesenteric artery

The IMA arises as the last ventral unpaired branch of the abdominal aorta. It is a short artery that supplies a very long territory from the splenic angle of the colon to the mid rectum. Because it acts like too short a string for too long a bowel, its branches have a fan-like course (Skandalakis et al. 2004). It arises at the level of the L3 vertebra and courses toward the left side. Its first branch is the left colic artery which divides into superior and inferior divisions followed by two or three sigmoidal arteries, while the trunk continues downward as the superior rectal artery (Fig. 54.20). Variations in the mesenteric arteries are rare according to Bellini (1894), but many other authors have found that the standard picture of the IMA is only seen in 15–16% (Michels et al. 1965; Nelson et al. 1988) to 30–40% of cases (Goligher 1949; Basmajian 1955).

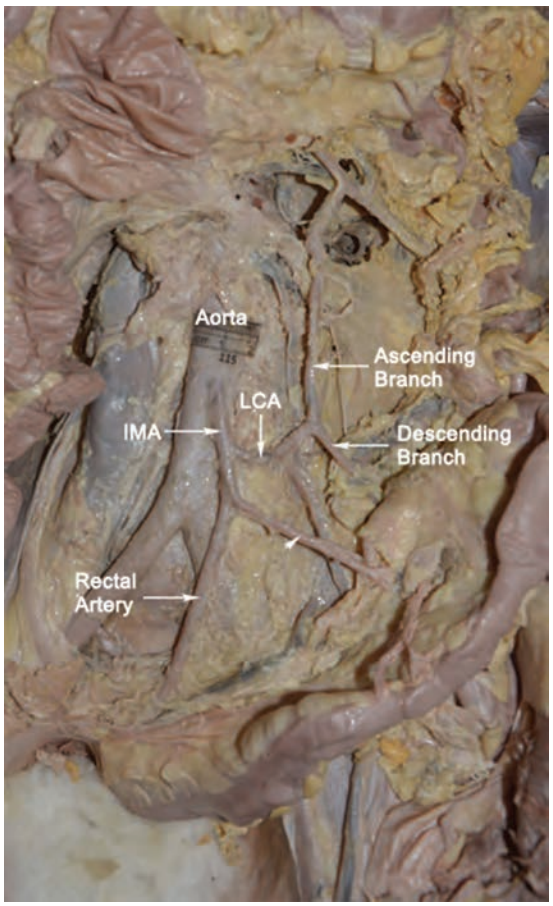

Figure 54.20 Typical branching pattern of the inferior mesenteric artery (IMA) is seen with the left colic artery (LCA) as first branch, which divides into ascending and descending branches supplying part of the transverse colon, splenic flexure, and descending colon. The second branch is the common sigmoid trunk dividing (arrow head) into two sigmoidal branches. The IMA continues downward as the superior rectal artery.

Origin

Benton and Cotter (1963) first reported duplication of the IMA; both vessels had separate origins from the aortic trunk. A second case was reported by Bergman et al. (1988), with two IMA trunks originating from the aorta 2.6 cm apart.

Absence of the IMA, though extremely rare, has been reported (Fleischman in 1815 as cited by Henle 1871; Jacques 1895; Merkel 1918; Cunningham 1921; Morris 1923; Adachi 1928; Mori et al. 1960). A common trunk of the IMA with other vessels can be interpreted as absence of the IMA. Common celico-bimesenteric or celicomesenteric trunks (CMT) were found by Cavdar et al. (1997) and Nonent et al. (2001). A common hepatomesenteric trunk (CHMT) was reported by Osawa et al. (2004). The CHMT divided into the common hepatic artery, SMA, and IMA while the splenic artery branched from the abdominal aorta and the left gastric arose from the splenic. There are reports of the IMA arising from the superior mesenteric artery (SMA) (Kitamura et al. 1987; Yamasaki et al. 1990; Shuang-Qin et al. 2008; Yoo et al. 2011). According to Lippert and Pabst (1985) the frequency of this variation is less than 0.1%. A common origin of the IMA and a single main renal artery has been reported (Garti et al. 1986). The IMA and accessory renal artery can arise as a common trunk from the aorta (Bergman et al. 1988). An anomalous origin of the IMA from the common iliac artery was described first in the literature by Petsche (1736), and later by Sher et al. (1999) and Nassar et al. (2012). Power (1850) reported a left common iliac artery that arose from the IMA.

The IMA is a ventral branch arising from the middle of the ventral aspect of the aorta. Zebrowski et al. (1971) found two cases with the IMA arising from the left side and one case from the right side of the aorta out of 115 cases studied.

The predominant level of origin of the IMA is the third lumbar vertebra (Michels et al. 1965). However, the point of origin of the IMA is more variable than the points of origin of the celiac trunk and the SMA (Yahel and Arensberg 1998). Cauldwell and Anson (1943) stated that the unpaired branches of the abdominal aorta usually vary no more than one-half to two-thirds of the height of a vertebra from the standard positions. George (1935) found there was rarely a deviation of more than one vertebral level in these origins. He observed the vertebral level of the origin of the IMA in 107 cadaveric dissections. These ranged from the lower third of the L2 vertebra to the lower third of the L4 vertebra, with the mean opposite the middle of L3. In a study of 115 inferior mesenteric arteries, Zebrowski et al. (1971) found the origin at the level of L3 in 67% of cases, the disk between L3 and L4 in 20%, L4 in 8%, the disk between L2 and L3 in 4%, and the disk between L4 and L5 in 1%. Adachi (1928) (n=53) and Taniguchi (1931) (n=100) also reported this level to be at the middle of L3 in their respective series on Japanese subjects, while Heidsieck (1928) (n=98) found the level of origin at the lower third of L3 in German subjects. Poirier and Charpy (1902) and also Testut (1931) gave the location as opposite the disk below the L3 vertebra, and von Bardeleben (1906) gave it as opposite the disk

above, but none of these claims were supported by a later series of cases (George 1935). The present authors found the vertebral level of origin of the IMA at L3 in 52% of cases while in 30% ($n = 15$) it was at L4. In the remaining cases, the level of origin was located at the disk between L3 and L4, L2, the disk between L1 and L2, and L1, in 10%, 4%, 2%, and 2% of cases, respectively. The vertebral level of origin shifts distally with advancing age; there is a distal shift of one-quarter of the height of vertebra in subjects aged 60 years or more (George 1935).

The distance between the SMA and IMA origins is 5–7 cm, the same as the width of two vertebrae and two disks (George 1935; Michels et al. 1965; Yahel and Arensberg 1998; Songür et al. 2010; present authors). In a single case the present authors found this distance to be 2.6 cm.

The distance between the midpoint of the T12 vertebra and the IMA origin ranges from 9 to 14 cm (Pennington and Soames 2005). The distance between the origin of the IMA and the aortic bifurcation (IMA-AB) is between 3 and 7 cm (Quain 1844; Poirier and Charpy 1902; Piersol 1916; Heidsicek 1928; Tetsut 1931; Gray 1932; George 1935; Cauldwell and Anson 1943; Griffiths 1956; Michels et al. 1965; Anson and McVay 1971; Hollinshead 1971; Yahel and Arsenburg 1998; Williams et al. 2000; Songür et al. 2010). It has been observed that an IMA-AB distance of 5 cm or more often coincides with a low division of the aorta (Quain 1844).

The diameter of the IMA at origin is 3–8 mm with a mean of 5 mm (Michels et al. 1965; Songür et al. 2010; present authors). The average length of the IMA before the origin of its first branch varies between 2 and 7 cm (Griffiths 1956; Michels et al. 1965; Zebrowski et al. 1971; Sher et al. 1999; Michiya et al. 2006).

Left colic artery (LCA)

The standard pattern of the LCA arising directly from the IMA is seen in about 30–60% of cases (Goligher 1949; Nelson et al. 1988; Niculescu et al. 2005). The left colic artery can arise from a branch of the middle colic artery supplying the proximal descending colon, to an origin from a common trunk with the sigmoid artery supplying the distal descending colon (Nelson et al. 1988). The most common origin of the LCA in 53–56% of cases is via a common trunk with the sigmoid artery (Michels et al. 1965; Griffiths 1956; Nelson et al. 1988).

Absence of the LCA has been cited by some authors with frequencies ranging from 0.7% to 12% (Griffiths 1956; Sonneland et al. 1958; Cheng et al. 2006). Nelson et al. (1988) found the LCA absent in one of 50 cases. In this case the splenic flexure and descending colon were supplied by multiple small retroperitoneal arteries emanating from the renal fascia, the pancreas and diffuse retroperitoneal connective tissue, collectively called Turner's plexus. As per Vandamme et al. (1982), the LCA was absent in 12% of preparations and its function was taken over by the colosigmoid artery. This anastomoses with the right colic artery or accessory right colic artery, arising from the SMA or, exceptionally, from the area of the celiac trunk.

The left accessory colic artery (two or more left colic arteries) is rare. Its incidence varies: 2% (present authors); 4% (Nelson et al. 1988); 5% (Vandamme et al. 1982); 7.5% (Amonoo-Kuofi et al. 1995); and a very high 25% (Calas et al. 1955) or even 49.2% (Koizumi and Horiguchi 1990). The behavior of the LCA could be influenced by the presence of an accessory left colic artery or branch from the middle colic artery group. If an accessory left colic vessel is present the normal LCA can be absent (12%), atrophic, or displaced, and the sigmoid artery and paracolic arcades are usually reinforced by this accessory vessel (Vandamme et al. 1982). The present authors observed a normal LCA and sigmoidal vessels in all cases, despite the presence of an accessory LCA. Both the accessory and normal LCAs supplied the splenic flexure and descending colon (Fig. 54.21).

A left accessory aberrant (anomalous origin) colic artery (Fig. 54.22) arising from the SMA was reported by Sonneland et al. (1958) in 0.4%, Vandamme et al. (1982) in 0.6%, Lippert and Pabst (1985) in 1%, Nelson et al. (1988) in 4%, and in 8% by the present authors. In all such cases the contribution of the SMA

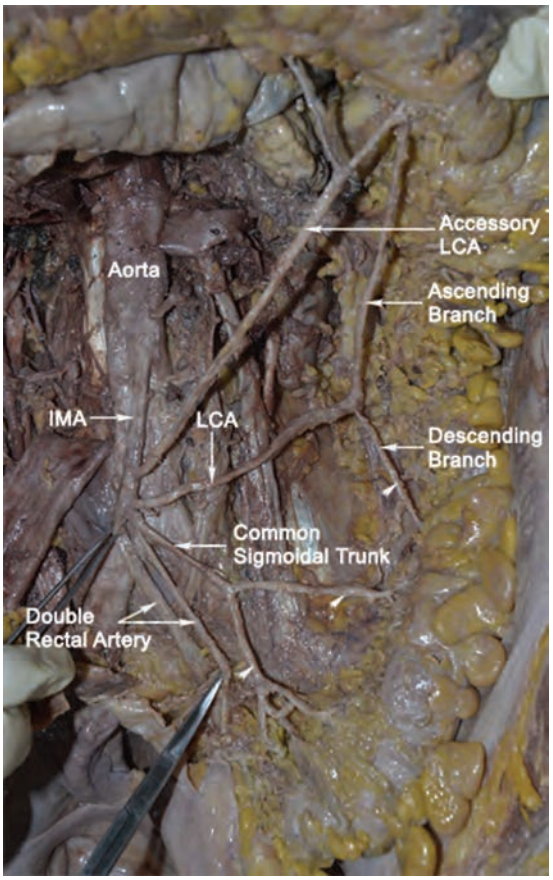

Figure 54.21 Three sigmoidal branches are given (arrow heads). The first sigmoidal artery is a branch of the left colic artery (LCA). The two lower branches are from the common sigmoidal trunk from the IMA. This trunk also gives the accessory rectal artery. The first branch of the inferior mesenteric artery (IMA) is the accessory LCA.

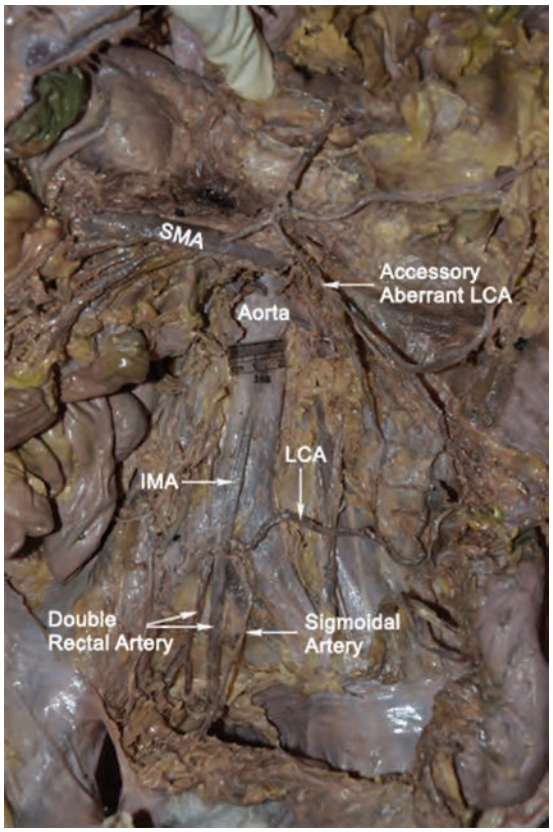

Figure 54.22 A single sigmoidal artery is given off by the left colic artery (LCA). The LCA supplies only the lowest part of the descending colon, while the upper part is supplied by the aberrant accessory LCA arising from the superior mesenteric artery.

to the formation of the marginal artery is dominant, as the left accessory colic artery supplies the flexure and proximal part of the descending colon.

The branches of the left colic artery are the ascending and descending branches, also called the superior left colic and inferior left colic arteries (Rusu et al. 2008) (Fig. 54.20). The ascending branch of the LCA can extend up to the splenic flexure in some cases; in others it passes above the flexure and supplements the vascular supply to the left transverse colon. Michels et al. (1965) found that the ascending branch reached the splenic flexure in 86% and the mid region of the descending colon in only 14%. The third branch of the LCA, the left middle colic artery, is found in 38% of cases (Michels et al. 1965). Niculescu et al. (2005) found the left middle colic artery in 50% of the 100 cases studied, either as a direct origin from the IMA in 12% or through a common trunk (88%) with the left superior colic artery (84%) or the left inferior colic artery (4%).

Sigmoid arteries usually arise from the lateral aspect and spread fan-like toward the sigmoid colon, usually up to 15 cm in length (Toupet 1951). The number of branches to the sigmoid varies considerably from one to seven, with most having two or three (Greenberg 1950; Basmajian 1955; Michels et al. 1965; Nelson et al. 1988).

Classical types of sigmoid arteries are found in only one-third of cases (Toupet 1951). The sigmoidal arteries can arise from left colic artery or its branch, the IMA trunk, or from the left middle colic artery when present. The reported incidence of origin of the sigmoid artery from the LCA varies from 22.5% to 55% (Drummond 1914; Goligher 1949; Greenberg 1950; Griffiths 1956). Niculescu et al. (2005) found a trunk of the sigmoid arteries in all 100 cases arising from the IMA as a direct branch (96%), or through a common trunk with the middle left colic artery and dividing immediately into two (26%), three (68%), or rarely four, five or six branches (6%).

Zebrowski et al. (1971) reported the following variations:

- The IMA divided into the LCA and common rectal sigmoid trunk. Two sigmoid arteries originated from the common rectal-sigmoid trunk independently, dividing dichotomously into secondary branches running to the sigmoid colon.
- The IMA divided into two large arterial trunks: rectal-sigmoid and colosigmoid, each of which gave off one large sigmoid artery; these arteries divided further on the walls of the sigmoid colon, usually five or six, producing typical arcades.
- The common colosigmoid trunk gave off two sigmoid arteries and the rectal-sigmoid trunk gave one sigmoid artery.

The present authors found the following patterns in the origin of the sigmoid vessels:

1. two sigmoid arteries arising as a common sigmoid trunk from the IMA or separately (60%) (Fig. 54.20);
2. two sigmoid arteries arising as a common sigmoid trunk through trifurcation of the IMA into the LCA, superior rectal, and common trunk of the sigmoid artery (32%) (Fig. 54.23);
3. three sigmoid arteries, two as a common trunk from the IMA and one from the descending branch of the LCA (2%) (Fig. 54.21);
4. four sigmoid arteries arising independently from the LCA (2%) (Fig. 54.24); or
5. one sigmoid artery arising from the (a) IMA (Fig. 54.19) or (b) LCA (4%) (Fig. 54.22).

The sigmoidea ima artery has been described as a distinct branch of the IMA by some authors (Cunningham 1921; Rankin et al. 1935). It arises about 1–3 cm above the main bifurcation of the IMA into the superior rectal arteries. Any branches above are regarded as sigmoidal arteries. Greenberg (1950) found it to be a constant branch that arose either from the IMA or the superior rectal artery. It was absent in only 8% of cases.

Superior rectal artery

The superior rectal artery is a continuation of the trunk of the IMA beyond the left common iliac vessels (Figs 54.20–54.24). It is considered the most important end branch of the IMA. It divides into two main branches in 80% of cases and is the main arterial blood supply to the rectum (arterial variations in Lippert and Pabst 1985). The superior rectal artery usually divides

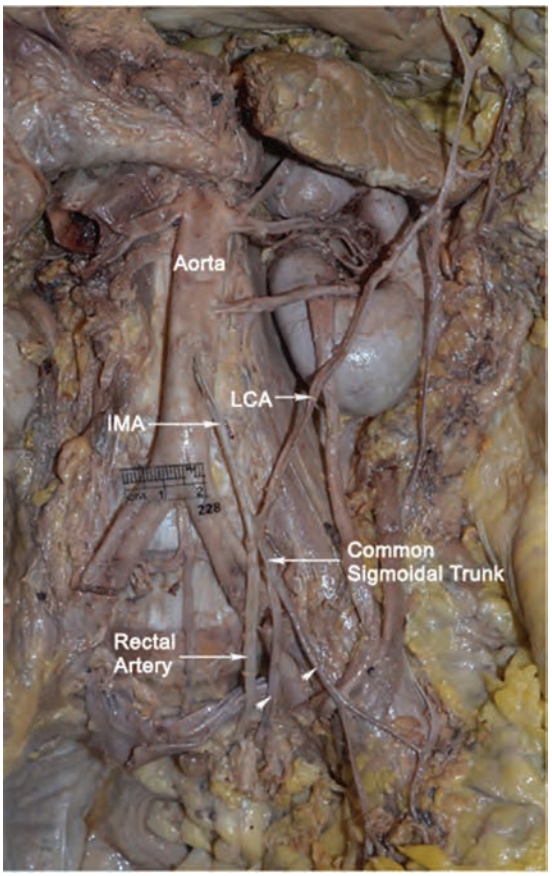

Figure 54.23 The inferior mesenteric artery (IMA) trifurcates into the left colic artery (LCA) and the common sigmoidal trunk, dividing into two sigmoid arteries (arrow heads) and the rectal branches.

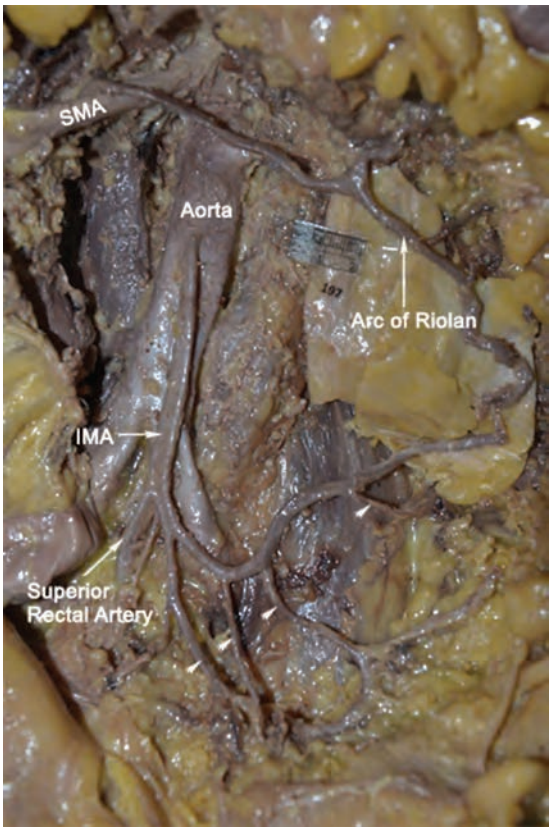

Figure 54.24 Four sigmoidal arteries (arrow heads) are seen arising sequentially from the left colic artery (LCA) as it courses upward to join the accessory middle colic artery; a branch from the superior mesenteric artery forms the "Arc of Riolan."

opposite S2 or S3, just below the peritoneal reflection (Michels et al. 1965). Pope and Judd (1929) found the point of bifurcation 18 cm from the origin of the IMA. The two branches are seldom equal in size; the right branch is usually larger and frequently gives a large branch to the posterior surface of the rectum (Quenu 1893). According to Vandamme et al. (1982) the IMA ends by dividing into two superior rectal arteries in 86% of cases; sometimes (10%) it trifurcates however, and the third branch is usually a posterior rectal artery. In 4% of cases the division was difficult to interpret.

Sudeck's Point

In 1907, on the basis of injections and radiological studies, Sudeck observed that if the inferior mesenteric artery is ligated just above the origin of the last sigmoidal, few of the rectal vessels become filled as there is no marginal communication between the last sigmoidal artery and the superior rectal arteries. This ligature position, "Sudeck's critical point," has been substantiated by many workers (Hartmann 1909; Rubeshch 1910; Drummond 1913; Forgue and Milhaud 1923; Sunderland 1942; Balice 1949; Toupet 1951; etc.) Anastomosis between the last sigmoidal and superior rectal arteries was found to be poor or absent by Archibald (1908), Steward and Rankin (1933), Greenberg (1950), Basmajian (1955) and McGowan (1955).

The validity of Sudek's point was disregarded by Bacon and Smith (1948), Dixon (1948), Ault et al. (1952), Pope and Judd (1926), Pope and Buie (1929) and Goligher (1949). According to Vandamme et al. (1982), there is always a critical point from the gross anatomical point of view, but with modern surgical techniques it has lost its importance. Griffiths (1956) opines that Sudeck's point is devoid of anatomical or surgical significance. Most contemporary surgeons regard Sudeck's point as irrelevant.

Blood supply to the splenic flexure

The splenic flexure is typically supplied by the LCA, which divides into two branches near it; one branch goes to the flexure while the other goes to the right side to anastomose with the left branch of the middle colic artery. According to Griffiths (1956) a truly critical point exists at the splenic

flexure where the marginal artery is very small from the functional point of view. Meyers (1976) broadens the definition of Griffiths's point as the site of (a) communication of the LCA with the marginal artery; and (b) anastomotic bridging between the branches of the LCA. The marginal artery supplying the descending colon is dependent upon the collateral circulation at this critical point on the splenic flexure. In an arteriographic study, Meyers (1976) detected the anastomosis at Griffiths's point in 48%; it was poor in 9% and absent in 43%. Anastomosis between the two branches of the LCA is good in 61%, tenuous in 32%, and absent in 7% (Michels et al. 1965). These authors found that the ascending branch reaches the splenic flexure in 86% of cases. Kahn and Abrams (1964) found from 136 aortograms and selected inferior mesenteric arteriograms that the IMA supplies the splenic flexure in 44% of cases; in a further 10%, its supply extends proximal to the flexure. The SMA, either through the large branches of the middle colic artery or by the accessory middle colic artery, was found to supply the splenic flexure in 37% of cases by Steward and Rankin (1933); in the other 63% of their cases, the ascending branch of the LCA passed above the flexure and supplemented the marginal artery. In 27% the ascending branch failed to reach the flexure.

An aberrant supply to the splenic flexure is frequent because of the intimate relationship of the celiac trunk and its branches with the flexure. The aberrant vessels reported are the celiacocolic trunk, splenocolic trunk, hepatocolic trunk, pancreatocolic branch, gastrocolic artery, and omentocolic artery (Michels et al. 1965).

Communications with superior mesenteric artery

Marginal artery

Griffiths (1956) defined the marginal artery (Fig. 54.25) as an artery that runs alongside the mesenteric border of the colon and from which the vasa recta arise. It is supplied with blood by branches of the inferior and superior mesenteric arteries and therefore forms an important anastomosis between them, as described by von Haller (originally 1786, reprinted 1966) and later by Drummond (1914), whose name it carries. Griffiths (1956) found the marginal artery in 100% of his specimens and called it "the functional vessel of the colon." Steward and Rankin (1933) also reported that the marginal artery is quite constant and fails only in a few cases (5%). In the arteriographic study by Toupet (1951), the marginal artery was absent in the sigmoid flexure in two-thirds of cases.

The distance of the marginal artery from the wall of the colon is inconstant; it varies among specimens and in different parts of the same specimen from a fraction of 1 cm to 8 cm. As a rule the marginal artery is situated furthest from the colon wall at the points of bifurcation of the large artery. It was situated nearer the colonic wall in the left half of the transverse colon and the descending colon (Griffiths 1956). Roberts et al. (1984) described the precolic position of the marginal artery, with the artery situated anterior to the descending colon.

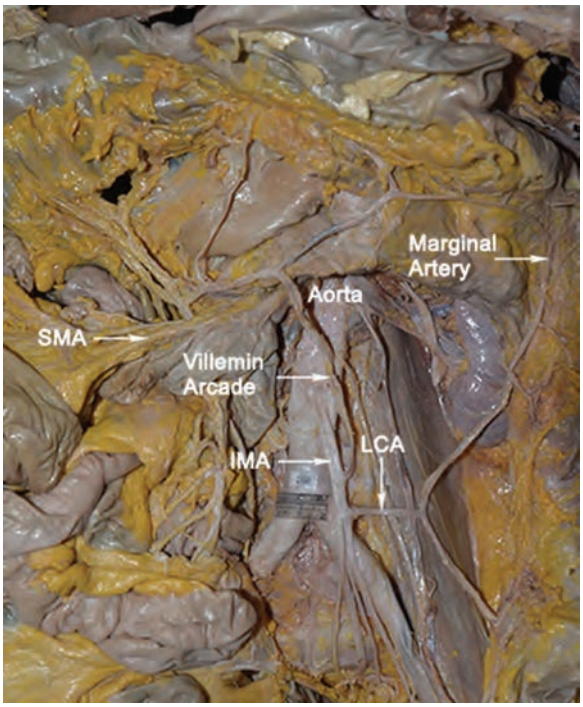

Figure 54.25 The Villemin arcade, formed by a branch given off as the IMA crosses the inferior mesenteric vein (not seen in the picture) and ascends to join the superior mesenteric artery. The marginal artery is seen on the left side.

Arc of Riolan

Communication between the superior and inferior mesenteric arteries was first mentioned by Galen and later drawn by Vesulius, but credit for the description goes to Jean Riolan, after whom this communication is called the "arc of Riolan" (Fig. 54.24; Gourley and Gering 2005). The Riolan arcade is between the right transverse branch of the right colic artery and the ascending branch of the left colic artery; the middle colic artery, when present, forms the right pillar of the Riolan arcade (Douard et al. 2006). Steward and Rankin (1933) found a direct communication between the middle colic and left colic arteries in 60% of cadavers, communication with the left colic artery via an accessory middle colic artery in 10%, and via a prominent left branch of the middle colic artery in the remainder. Two different interpretations of Riolan's arch can be found in the literature: one as a synonym for the marginal artery, and the other as a rare distinct anatomical entity connecting the SMA with the IMA (Lange et al. 2007).

The Villemin arcade

The Villemin arcade (Fig. 54.25) is found in 12–18% of cases (Villemin and Huard 1924; Vandamme and Bonte 1990). The IMA can give a branch at the point where it crosses the inferior mesenteric vein; this branch runs along the upper part of the vein to connect with the superior mesenteric artery.

Aberrant branches of the IMA

The IMA can give rise to the middle colic artery, accessory middle colic artery, accessory right hepatic artery, accessory renal artery, or a common artery for both umbilical arteries (Bergman et al. 1988).

Inferior phrenic artery

Inferior phrenic arteries (IPA) are the first paired branches of the abdominal aorta that supply many organs including the diaphragm, suprarenal glands, esophagus, stomach, liver, inferior vena cava, and retroperitoneum.

Origin

Variations in the origin of the IPA are very common. The right and left IPAs can arise separately from the same or different sources or by a common stem.

The right inferior phrenic artery (RIPA) arises from the abdominal aorta in 28–55% of cases and the incidence of aortic origin recorded for left inferior phrenic artery (LIPA) is 21–53% (Adachi 1928; Pick and Anson 1940; Grieg et al. 1951; Piao et al. 1998; Loukas et al. 2005a). An origin of the RIPA and LIPA through a common trunk from the aorta has been reported in 14–31% of cases (Adachi 1928; Pick and Anson 1940; Piao et al. 1998; Loukas et al. 2005a; Kimura et al. 2007) (Fig. 54.26a–d). Although IPAs are considered the first paired branches of the abdominal aorta, this is not always the case. Kimura et al. (2007) investigated the exact site of origin from the aorta and found that the supra celiac region (32%) was the most common site, followed in order of frequency by the interval between the CT and SMA (17%) and between the SMA and right renal artery (8%). Pick and Anson (1940) and Grieg et al. (1951) found the aortic origin slightly more frequent on the right than the left side. In contrast, Loukas et al. (2005a) found the LIPA arising more frequently from the aorta than the RIPA.

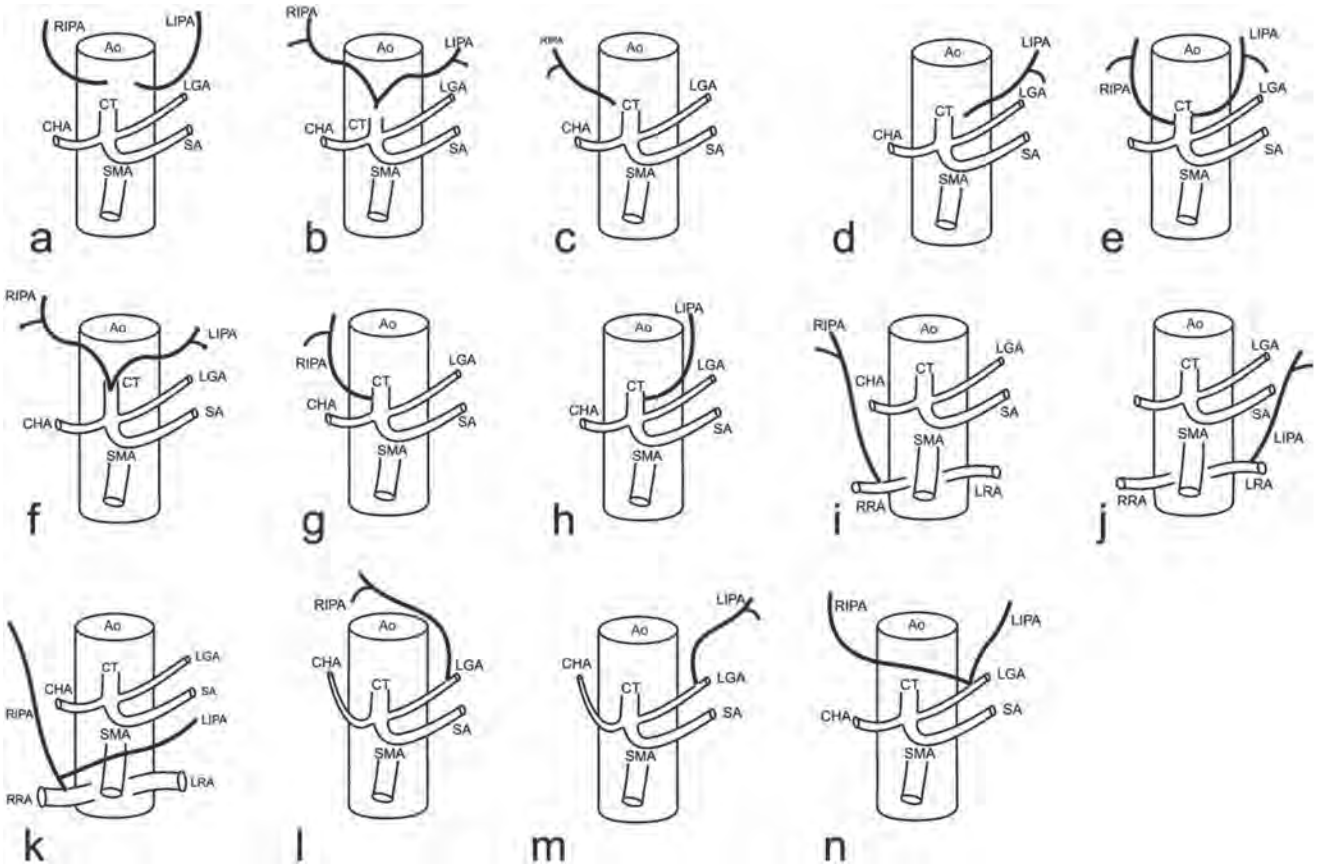

Figure 54.26 Schematic diagram illustrating variant patterns of origin of inferior phrenic arteries: (a) the RIPA and LIPA taking origin independently from the Ao; (b) the RIPA and LIPA taking origin as a common trunk from the Ao; (c) unilateral origin of the IPA (RIPA) from the Ao; (d) unilateral origin of the IPA (LIPA) from the Ao; (e) the RIPA and LIPA taking origin separately from the CT; (f) the RIPA and LIPA taking origin as a common trunk from the CT; (g) unilateral origin of the PA (RIPA) from the CT; (h) unilateral origin of the IPA (LIPA) from the CT; (i) the RIPA taking origin from the RRA; (j) the LIPA taking origin from the LRA; (k) the RIPA and LIPA taking origin as a common trunk from the RRA; (l) the RIPA taking origin from the LGA; (m) the LIPA taking origin from the LGA; and (n) the RIPA and LIPA taking origin as a common trunk from the LGA. Adapted from Loukas et al. (2005a).

An origin of the RIPA from the CT has been recorded in 27–41.4% of cases and the LIPA in 21.2–52.2% (Adachi 1928; Pick and Anson 1940; Grieg et al. 1951; Piao et al. 1998; Loukas et al. 2005a). The RIPA and LIPA can arise independently from the CT (20–37%) or through a common trunk (8–13%). Direct origin from the CT is more common on the left than on the right side (Adachi 1928; Pick and Anson 1940; Grieg et al. 1951; Piao et al. 1998; Loukas et al. 2005a; Kimura et al. 2007). Loukas et al. (2005a) claimed that the celiac axis origin of the IPA is more frequent than the direct origin from the aorta (Fig. 54.26e–h).

Less frequently, the IPA has been found to arise from the renal artery. A RIPA emanating from the right renal artery has been recorded in 8.5–17% of subjects (Adachi 1928; Pick and Anson 1940; Piao et al. 1998; Loukas et al. 2005a; Kimura et al. 2007). A renal origin of the left artery is much less common than the right. A LIPA originating from the left renal artery has been seen in up to 5% of cases (Pick and Anson 1940; Loukas et al. 2005a). The right superior polar renal arteries sometimes issue an IPA, particularly the right one. Pick and Anson (1940) found such an origin in 2% of 200 specimens dissected. Topaz et al. (2010) found both the RIPA and LIPA arising through a common stem from the right renal artery in three cases (Fig. 54.26i–k).

The left gastric artery (LGA) is another source of the IPA encountered by many researchers. An origin of the RIPA from the LGA has been observed in 2–3% and of the LIPA in 0.65–2% of subjects (Pick and Anson 1940; Piao et al. 1988; Loukas et al. 2005a; Kimura et al. 2007; Tanaka et al. 2008). A RIPA and LIPA arising from a common trunk stemming from the LGA was observed in 1.35% of 74 cadavers by Adachi (1928) (Fig. 54.26l–n).

Tanaka et al. (2008) found a LIPA coming from an accessory LGA arising from the left hepatic artery in 0.1% of 761 patients undergoing transcatheter arterial chemoembolization for hepatocellular carcinoma.

Piao et al. (1998) found a RIPA and LIPA arising from a common stem from the middle suprarenal artery in one case.

Less frequent sources of origin are the dorsal pancreatic artery (Kimura et al. 2007); superior mesenteric artery (Khan 1967; Loukas et al. 2005a; Gwon et al. 2007), LHA (Song et al. 2006; Tanaka et al. 2008), hepatic artery proper (Adachi 1928; Loukas et al. 2005a; Song et al. 2006; Tanaka et al. 2008), aberrant suprarenal arteries (Bakheit and Motabagani 2004), intercostal arteries, splenic artery (Basile et al. 2008), spermatic arteries (Pick and Anson 1940), contralateral IPA (Hieda et al. 2009; Ozbulbul et al. 2011), first lumbar artery (Power 1850), celiacomesentericophrenic trunk (Nayak 2006a) and gastrosplenicophrenic trunk (Nayak 2006b).

Numerical variations and vertebral level of origin

Multiple inferior phrenic arteries are not unusual. Piao et al. (1998) found two cases with double IPAs on the left side. In one case, one LIPA arose from the middle suprarenal artery and the other from the aorta. In another case, right, left, and accessory left had a common origin from the LGA. The levels of origin of these arteries vary from the middle of the twelfth thoracic to the second lumbar vertebra (Pick and Anson 1940).

Dimensions

The RIPA is usually wider than the LIPA. According to data derived from angiographic measurements by Khan (1967) the average internal diameter of the proximal part of the RIPA is 2.2 mm (range 1.4–3.2 mm) and of the LIPA 2 mm (range 1.4–2.8 mm). The length of the trunk of the IPA varies considerably depending upon the origin. According to Loukas et al. (2005a), an IPA of aortic, RA, and LGA origin is longer on the right than the left side, whereas an LIPA of hepatic artery origin is longer than its right counterpart.

Course and branches

Irrespective of origin, each IPA crosses the crus of the diaphragm obliquely to reach the dorsal part of the central tendon, where it branches into ascending and descending branches. The ascending branch has been named by many authors as the anterior or medial branch, likewise the descending branch as posterior or lateral (Pick and Anson 1940; Clemente 1985; Williams 1999; Gwon et al. 2007).

The ascending branches on two sides supply the under surface of the diaphragm and anastomose with the artery on the opposite side, variably communicating with the internal mammary, intercostal, musculophrenic, and pericardiophrenic arteries. As the ascending branch of the RIPA passes behind the inferior vena cava, it shoots off inferior vena caval and diaphragmatic hiatal branches and usually contacts the bare area of the liver and potentially communicates with the intrahepatic arteries. All liver segments have the potential for such communication, but it commonly occurs with the caudate lobe and posterior segment. The frequency of communication with other lobes is relatively less. The ascending branches of the LIPA pass behind the esophagus and irrigate its hiatal portion.

Descending branches of the RIPA and LIPA irrigate the diaphragm and can communicate with the intercostal and musculophrenic arteries. The ascending branch of the LIPA passes deep to the esophagus. Loukas et al. (2005a) found that the abdominal part of the esophagus is supplied variably from the LIPA in 11% of subjects either from the trunk or descending branch. In 12% of cases, the LIPA gave twigs to the superior pole of the spleen. The esophageal branch can arise from an accessory LIPA (Piao et al. 1988) instead of the normal LIPA.

The LIPA has the potential to communicate with the intrahepatic arteries, particularly of the lateral segment. In addition to the above-mentioned branches, the IPA also gives off the superior suprarenal artery. Occasionally it gives off an an accessory renal artery.

Superior suprarenal artery

The main trunk or posterior branch of the IPA commonly gives off the superior suprarenal artery (SSRA). The incidence of

origin from the IPA ranges from 79% to 92% (Toni et al. 1988a; Manso and Didio 2000; Loukas et al. 2005a). An origin of the SSRA from the IPA is relatively more common on the right than on the left side. In a study of 100 aortography cases by Toni et al. (1988a), the RIPA gave off the right SSRA in 92% and the LIPA gave off the left SSRA in 79%. These arteries arise more commonly from the posterior branch than the main trunk of the IPA (Manso and DiDio 2000). The present authors found the SSRA arising consistently from the IPA in all cases.

These arteries can also arise from other sources. The right SSRA has been found to arise aberrantly from the CT in 5–6.7% of cases and the aorta in 3–3.3%. Incidences of origin of the left SSRA from the CT and aorta have been quoted as 2–6.7% and 10–16%, respectively (Toni et al. 1988a; Manso and DiDio 2000).

In an aortography study, Toni et al. (1988a) discovered an unusual origin of the left SSRA from the intercostal artery in 3% of cases. Occasionally the SSRA arises from the testicular artery (Onderoglu et al. 1993).

If multiple and arising from the IPA, SSRAs usually arise as a series of laterally directed short vessels near the medial border of the gland. One can be larger than the other(s) or all can be comparable in size. Each IPA gives off 5–10 SSRAs, which tend to subdivide before piercing the gland. Irrespective of source, the total number of SSRAs usually ranges from three to eight (Manso and DiDio 2000). The present authors found the number varied from 1 to 11 on the right side and 1 to 7 on the left. Anson and McVay (1936) found 50 or even more branches entering the gland (Hollinshead 1971).

SSRAs supply 30–50% of the total gland (Gagnon 1957, 1966; Diard et al. 1972). We found these arteries entering the superior pole of the gland in 22% of cases on the right side and 14% on the left, and the superomedial border of the gland in 78% of cases on the right side and 86% on the left.

The average diameters of the right and left SSRAs are 1.07±0.11 mm and 1.09±0.11 mm, respectively (Toni et al. 1988a).

Middle suprarenal arteries

The middle suprarenal arteries (MSRA) are paired branches that classically arise from the anterolateral surface of the aorta above the origin of the renal arteries (Hollinshead 1971; Standring et al. 2008). These arteries are the most variable among the three suprarenal arteries (Harrison et al. 1990). The incidence of this artery varies extremely. Gagnon (1964) found the MSRA in 78% of cases and Manso and DiDio (2000) in 96%. Piatre et al. (1941) noticed the absence of vessels in a remarkably high number of cases (50% on the right side and 33.3% on the left). In our study, the arteries were found in 84%. When the artery is absent, it is usually replaced by the superior or inferior suprarenal arteries (Bergman et al. 1988).

The MSRAs have been reported to arise from variety of sources; most commonly they arise directly from the aorta. The incidence of aortic origin varies between 50 and 95% (Gagnon 1964; Toni et al. 1988a; Manso and DiDio 2000) and the artery arises at various levels. Gagnon (1964) observed an origin above the renal artery in 50%, at the level of the renal artery in 20%, and below the level of the renal artery in 12%.

The MSRA can arise indirectly from other aortic branches in the vicinity of the suprarenal gland. An origin from the IPA is not infrequent. Manso and DiDio (2000) found this origin bilaterally in 26.7% of cases. Loukas et al. (2005a) found than an origin from the inferior phrenic artery origin was more common on the right side (35%) than the left (18%).

Other less frequent sources are the celiac trunk (2.5–7%), superior mesenteric artery (3%), inferior suprarenal artery (6.7%), and renal artery (3.3%) (Gagnon 1964; Toni et al. 1988a; Manso and DiDio 2000). The artery can even arise from the superior suprarenal artery. Manso and DiDio (2000) found this origin in 3.3% of cases on the right and 10% on the left side. Exceedingly rare cases of origin of the left MSRA from the lumbar artery have also been found (Gagnon 1964). Reddy et al. (2011) reported a case in which the right MSRA and right testicular artery originated as a common trunk from the abdominal aorta.

We found cases of aberrant origin of the right MSRA from the IPA (46%), renal artery (10%), and testicular artery (4%), and of the left MSRA from the IPA (52%), aorta, renal artery (2%), and testicular artery (6%). The classical origin from the aorta (24%) was less common than the aberrant origin (Figs 54.27, 54.28).

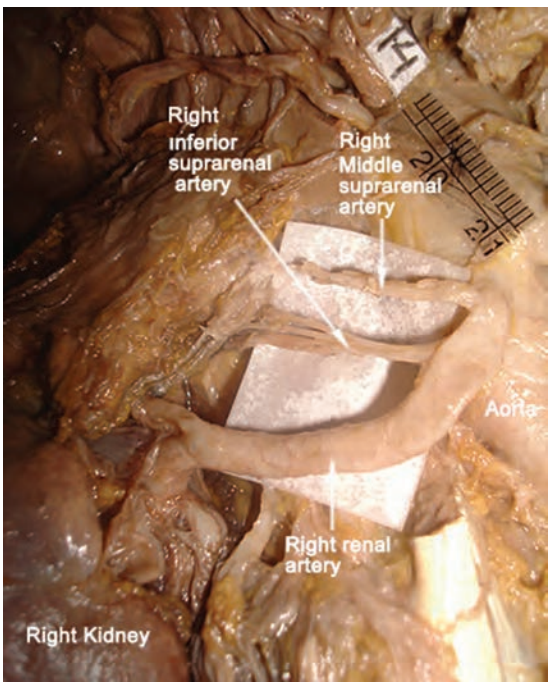

Figure 54.27 Cadaveric dissection revealing the right middle and inferior suprarenal arteries arising from the right renal artery.

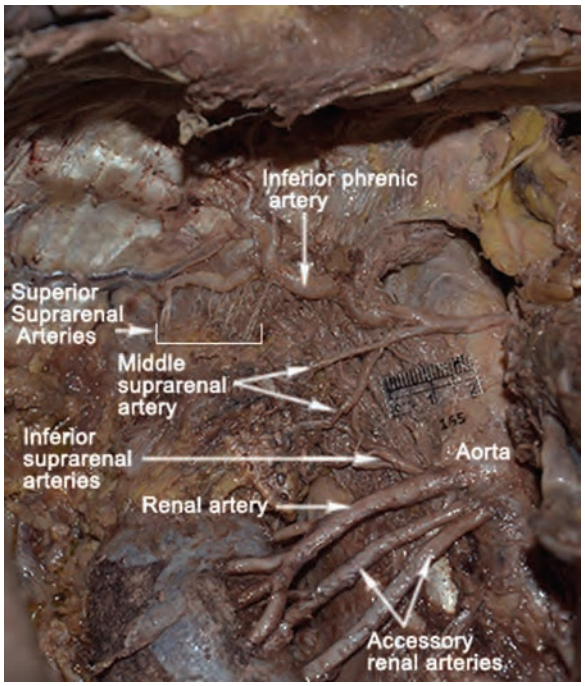

Figure 54.28 Cadaveric dissection revealing the middle suprarenal artery arising aberrantly from the inferior phrenic artery. Two right accessory renal arteries are also present.

The right and left MSRA are usually single, although a multiplicity of the arteries can occur (Gagnon 1964; Manso and DiDio 2000). Gagnon (1964) found four arteries on the right side in one case and on the left side in three cases.

The average diameters of the right and left MSRAs are 1.50±0.13 mm and 1.48±0.13 mm, respectively (Toni et al. 1988a).

The arteries can enter the suprarenal gland as a single stem or divide into multiple branches before entering its medial and inferior aspects. The MSRA supplies the middle portion of the suprarenal gland (Diard et al. 1972). Bergman et al. (1988) reported a case in which the anteromedial part of the organ was infused by both the middle and inferior suprarenal arteries.

Renal artery

Classically, the paired renal arteries (RA) originate from the lateral wall of the aorta just below the origin of the superior mesenteric artery (SMA) at the level of the intervertebral disk between L1 and L2 (Anson 1966; Williams et al. 1989; Kadir 1991). The level of origin of the RA can vary from T12 to L4 (Kadir 1991; Ozkan et al. 2006; Alghizzi 2011). The authors in the current study observed a maximum incidence of origin of the RA at the level of L1 (right side 86%; left side 80%). Different levels were found in the remaining cases (T12, right side in 2%; L1–L2, right side in 2% and left side in 4%; L2, right side in 10% and left in 10%; L3, left side in 6%).

Although the right kidney lies caudad to the left, the ostium of the right RA usually lies cephalad to that of the left (49.1–65% of cases; Garcier et al. 2001; Saldarriaga et al. 2008). In the current study, the authors observed such variation in 24% of cases. Both RAs have a symmetrical level of the ostium in 10–50% of cases (Keen 1981; Beregi et al. 1999; Saldarriaga et al. 2008). However, our study revealed quite a low incidence of this variation (6%). In one study, the RA originated in an unusual way, both sides sharing a common stem of origin from the aorta (Glodny et al. 2009).

Occasionally, RAs have been found to arise aberrantly from the common iliac artery (Halloul et al. 2001), celiac axis (Garti and Meiraz 1980; Nachiappan et al. 2011), splenic artery (Kruyt, 1992), SMA (Dalçik et al. 2000), or inferior mesenteric artery (Armstrong et al. 1979). In a case report by Çilingiroglu et al. (2013), the origin of the RA from the aorta was displaced to the level of the aortoiliac bifurcation in close proximity to the median sacral artery.

Dimensions

The diameter of the RA varies from 3 to 9 mm (Anson 1966; Aytac et al. 2003; Chiaganama et al. 2013). The authors in the current study found a similar mean value of the RA diameter (8 mm). The calibers of accessory renal arteries (3–5.5 mm) are narrower than that of the main renal vessel (Aytac et al. 2003; Banerjee et al. 2007; Saldarriaga et al. 2008). The findings of the current study are consistent with the foregoing.

The length of the RA varies from 3 to 5 cm, with the right RA longer than the left in most cases (Anson 1966; Saldarriaga et al. 2008). The authors in the current study corroborated this (right RA length 5.8 cm and left RA length 5.3 cm). Similarly, the length of the right accessory RA (5.6 cm) was greater than that of the left (4.5 cm). These dimensions observed in our study are consistent with the findings of Miclaus and Matusz (2012).

Variations in number

Multiple RAs can occur. The incidence of accessory RAs has been reported as 25–30% (Williams et al. 1989; Ozkan et al. 2006; Kummuru et al. 2012). The number of additional RAs can vary from one to three and they can be present either unilaterally or bilaterally. Accessory RAs have been found more frequently on the left side (Satyapal et al. 2001; Saldarriaga et al. 2008). The authors in the current study also reported a higher incidence of accessory RAs on the left side (28%) than the right (18%). Bilateral multiple renal vessels have been seen in 2–10% of subjects (Satyapal et al. 2001; Dhar and Lal 2005; Gawish et al. 2007).

In addition to double RAs, instances of triple and quadruple RAs have also been quoted in the literature. Triple RAs have been found in 0.6–1.1% of subjects (Merklin and Michels 1958; Satyapal et al. 2001; Bordei and Antohe 2002; Khamanarong et al. 2004; Şener et al. 2005). Miclaus and Matusz (2012)

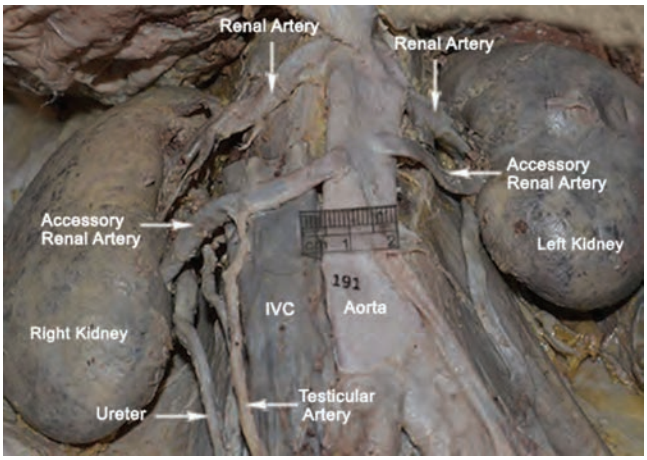

Figure 54.29 Cadaveric dissection revealing bilateral accessory renal arteries originating from the aorta caudal to the main renal artery. The right accessory renal artery lies anterior to the IVC and gives origin to the right testicular artery. IVC: inferior vena cava.

described a rare case with bilateral quadruple RAs. In the current study, the authors observed triple RAs in 2% of cases (Figs 54.28–54.30).

Accessory RAs can arise from the aorta as high as the diaphragm to as low as the internal iliac artery (Bergman et al. 1988). Accessory RAs arise above the usual trunk more frequently than below. However, in a study by Mamatha and D'Souza (2011), a right accessory RA was seen arising below the main RA. Similarly, Şener et al. (2005) reported a case of bilateral triple RA in which the second accessory RA arose below the main RA. Giavroglou and Kokkinakis (2005) reported a case of origin of a left accessory RA from the opposite RA. Loukas et al. (2005b) observed a common origin of the accessory RA and

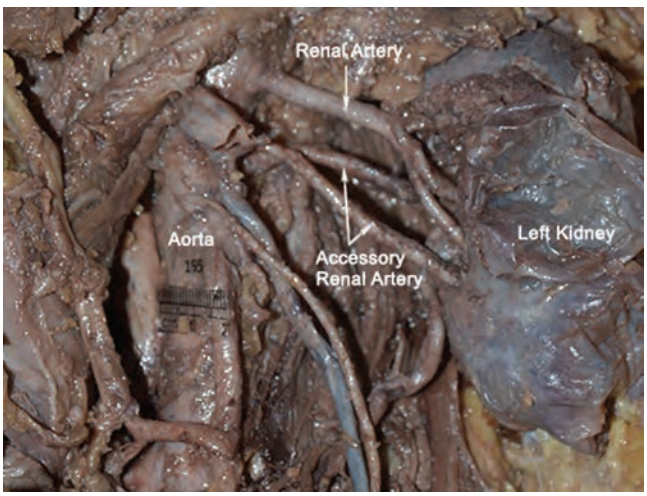

Figure 54.30 Cadaveric dissection revealing two left accessory renal arteries originating from the aorta, caudal to the main renal artery.

IMA. Even the IPA can sometimes give origin to an accessory RA (Bergman et al. 1988).

Course

The renal vasculature was discovered by Hunter (1794), but a detailed account became available only with the corrosion cast studies in the 1950s. Classically, a single RA arising from the abdominal aorta supplies the kidney on the same side. Near the hilum of the kidney each RA divides into four branches – two anterior (superior and inferior) and two posterior (superior and inferior) – which supply different renal segments (Gerard 1921). However, many variations have been reported in the literature in addition to the above-mentioned typical branching pattern. Instead of four branches, the RA has been found giving rise to three branches (anterior, superior, and posterior; Poirier and Charpy 1901; Testut and Latarjet 1958; Williams et al. 1989) or even two branches (anterior and posterior; Schmerber 1895; Paturet 1958; Terminologia Anatomica 1998).

The branching of the RA can vary from a prehilar to a hilar pattern. Prehilar segmental branching was reported in 11.66–17% of cases (Harrison et al. 1978; Budhiraja et al. 2011). Shoja et al. (2008) described many different types of prehilar branching pattern such as fork, duplicate, triplicate, and ladder. Hilar branching has been reported in around 10% of cases (Paturet 1958; Calas et al. 1963; Guntz 1967; Daescu et al. 2012). However, in most cases (53.3–82%) a single hilar artery with no extrarenal branching pattern is present (Sampaio and Passos 1992; Tong-Un and Sripaoraya 2004).

Variations have also been observed in the entry points of accessory renal vessels. Bordei et al. (2004) reported that in cases with a double RA there can be a primary aortic hilar renal branch and the accessory RA can originate anywhere from the hilar point to either of the poles. Similarly, a triple RA can enter the kidney as two aortic hilar and a third superior or inferior renal polar branch. Quadruple renals can comprise two hilar and two polar, three hilar and one polar, or one hilar and three polar arteries (Bergman et al. 1988).

Polar arteries are specific to the superior and inferior poles of the kidneys. The incidence of inferior polar RAs is approximately twice that of superior polar RAs (Albarran 1909; Weinstein et al. 1940; Kummuru et al. 2012). The superior polar artery can originate either from the aorta (7%) or the RA (12%). It supplies the apical segment exclusively and can also give rise to inferior suprarenal branches. We observed a superior polar artery arising from either the aorta or the RA in 6% of cases. Sometimes this artery even provides branches to the suprarenal gland before entering the superior pole of the kidney (Bergman et al. 1988). In the current study, the right inferior phrenic and inferior suprarenal arteries were found to arise from the superior polar artery. Similarly, the inferior polar artery can originate from the aorta (95.5%) or RA (1.4%) (Neri et al. 2009). In the current study, the authors noted an inferior polar artery in 10% of cases (Figs 54.31, 54.32).

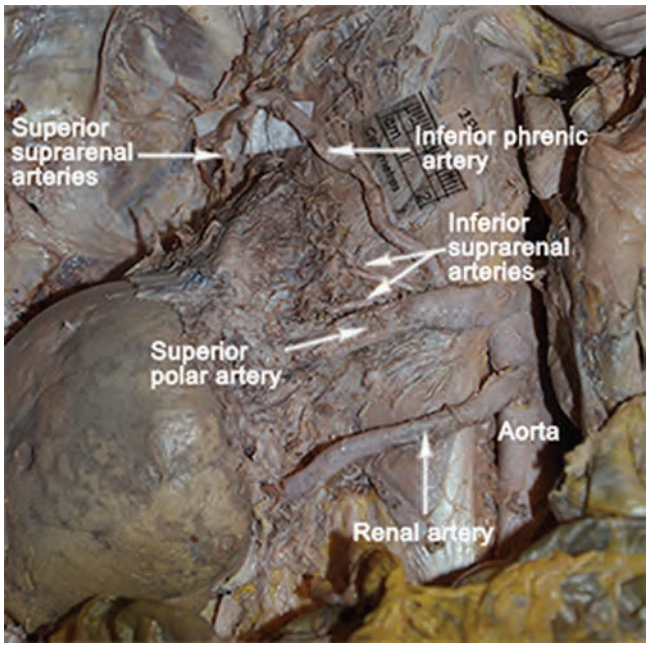

Figure 54.31 Cadaveric dissection revealing the right inferior phrenic and right inferior suprarenal arteries arising from the right superior polar renal artery.

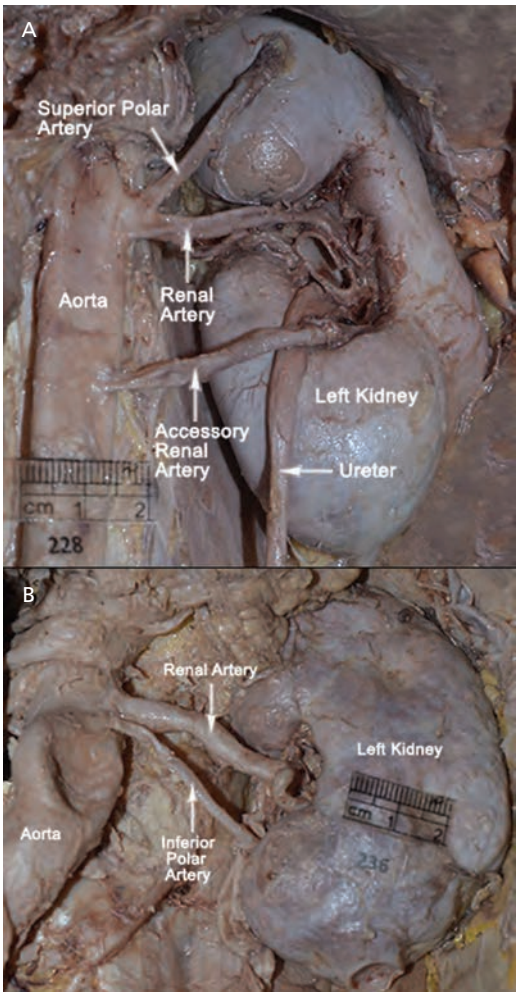

Figure 54.32 Cadaveric dissections revealing (a) the left kidney with one superior renal polar artery and one accessory renal artery in addition to the main renal artery; and (b) the left inferior polar renal artery.

Relationship of renal vessels to renal vein, pelvis, and ureter

The RA typically courses behind the inferior vena cava (IVC). However, in some studies the right RA lay anterior to the IVC and criss-crossed the right renal vein in more than one-third of cases (Testut and Latarjet 1958). In case of multiple RAs, the more caudal vessels often take a precaval course (Bergman et al. 1988). Exceptionally, in one case with one accessory RA in the current study, the authors observed the IVC lying anterior to the main RA and posterior to the accessory RA (Fig. 54.29).

If there are two main RAs, one frequently becomes retropelvic (Albarran 1909; Bergman et al. 1988; Singh et al. 1998). The main RA can divide into pre- and retropelvic trunks and, during its course, the retropelvic artery can give off branches similar to those arising from the prepelvic artery (Glodny et al. 2009).

Branches

Inferior suprarenal arteries

The inferior suprarenal arteries (ISRA) typically arise from the upper border of the renal artery (RA), rarely from the posterior face, and very rarely from the anterior face (Hollinshead 1971; Bordei et al. 2003). These vessels irrigate 30–50% of the total gland, particularly the inferior portion (Diard et al. 1972). The incidence of its origin from the RA varies from 60 to 95.5% (Toni et al. 1988a; Manso and DiDio 2000; Bordei et al. 2003). This branch can arise from any part of the RA. In their study of 120 cases, Bordei et al. (2003) gave a detailed account of its origin from different parts of the RA. The artery arose from the main trunk prior to the terminal division in 48.33% of cases; as one of the terminal branches in 4.17%; from the anterior division in 8.33%; and from the posterior division in 1.67% (Bordei et al. 2003).

Even the renal polar arteries can give off ISRAs. Manso and DiDio (2000) observed the origin of the left ISRA from the left superior and inferior polar arteries in 3.3% and 3.3% of cases, respectively. Toni et al. (1988a) observed its origin from the right polar arteries in 2%.

The ISRA can arise from aberrant sources. The most common aberrant source has been reported as the aorta with an incidence varying from 3.5 to 31.7% (Toni et al. 1988a; Manso and DiDio 2000; Bordei et al. 2003). Bordei et al. (2003) found an arterial trunk arising from the aorta, which divided into the middle suprarenal, inferior suprarenal, and RA, in a 7-month-old fetus. The ISRA can also arise from the testicular artery. In two separate studies by Manso and DiDio (2000) and Bordei et al. (2003)

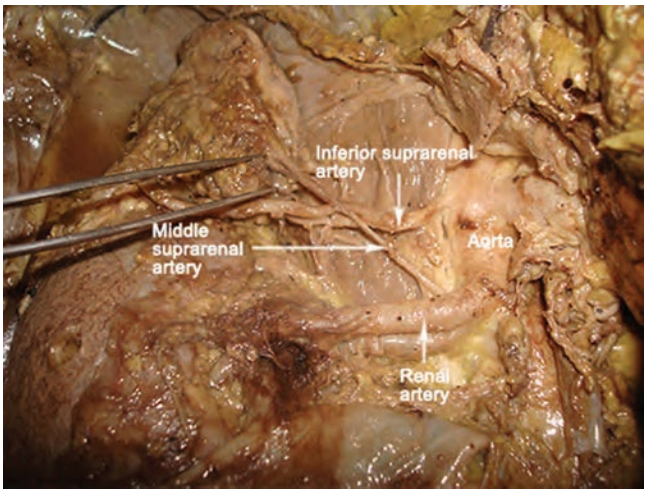

Figure 54.33 Dissection revealing the right inferior suprarenal artery arising from the aorta and the right middle suprarenal artery arising from the renal artery. The two arteries cross each other before entering the substance of the gland.

the left ISRA was found to arise from the artery in 6.6% and 3.33% cases, respectively (Hagopian 1953). Panyanetinad (2011) noted a common trunk of the testicular artery and ISRA arising from the right RA. Bordei et al. (2003) found an ISRA arising from the celiac trunk either separately or in common with the middle suprarenal artery in 4.17% of cases.

ISRAs can be one or multiple. Bordei et al. (2003) found single, double, and triple ISRAs in 75.83%, 17.5%, and 6.67% of cases, respectively. Manso and DiDio (2000) saw single, double, and triple ISRAs in 6.6%, 51.6%, and 10% of cases, respectively. They also recorded four arteries in 1.6%.

In our study, the ISRA was present in 82% of cases on the right side and 68% on the left. The number of ISRAs ranged from one to seven on the right and one to four on the left. On the right side, they issued from the RA in 76%, the testicular artery in 2%, the aorta in 2%, and the renal polar artery in 2%. On the left side they arose from the RA in 64% and the aorta in 4% (Figs 54.28, 54.31, 54.33).

The ISRA has been found to give rise to a superior polar renal branch in 15.83% of cases (Bordei et al. 2003).

The average diameters of the right and left ISRAs reported by Toni et al. (1988a) are 0.91±0.07 mm and 0.89±0.05 mm, respectively. The diameters found in the authors' current series were on the higher side (right, 1.60±1.24 mm; left, 1.23±1.0 mm).

Aberrant branches from the RA

The RA can give rise to branches normally derived from other sources such as the inferior phrenic artery (Piao et al. 1988; Loukas et al. 2005a; Kalthur et al. 2011), hepatic artery (Michael et al. 1991), middle suprarenal artery (Kalthur et al. 2011), gonadal artery (Lippert and Pabst 1985; Singh et al. 1998; Asala et al. 2001; Ciçekcibaşi et al. 2002; Salve and Ratanprabha 2011), pancreatic artery, some colic branches, and one or more lumbar arteries.

Gonadal arteries

The gonadal arteries are two long slender vessels arising from the anterolateral aspect of the abdominal aorta, a little inferior to the origin of the renal arteries at the level of the second lumbar vertebra. Variations in the origins of the testicular and ovarian arteries are common and have been reported by several authors (Adachi 1928; Hollinshead 1971; Bergman et al. 1988; Onderoglu et al. 1993; Brohi et al. 2001; Ciçekcibaşi et al. 2002; Bhaskar et al. 2006; Petru et al. 2007). The common variations are in the level, source of origin, number, and unusual course of the artery. The present authors have found the right testicular artery in 76.31% and left testicular artery in 78.94% of cases arising from the abdominal aorta. Anatomical variations in the testicular arteries were noticed in 4.7–14.7% of specimens (Asala et al. 2001; Pai et al. 2008; Salve and Ratanprabha 2011).

Variations in origin

There are reports of high origins of the gonadal arteries (Onderoglu et al. 1993; Ozan et al. 1995; Loukas and Stewart 2004; Xue et al. 2005; Paraskevas et al. 2011). The present authors have found a right upper testicular artery originating from the aorta, 1.53 mm above the level of origin of the renal artery, in 2.63% cases (Fig. 54.34). Shinohara et al. (1990) also reported a case where the testicular artery originated 1 cm superior to the origin of the IPA. In another study, the testicular artery arose from the aorta cephalad to the renal vein in 9.87% of cases (Notkovich 1956). There was a rare case of bilateral high origin of testicular arteries from the abdominal aorta, cephalad to the origin of the renal arteries (Li et al. 2012). Among three cases, Pai et al. (2008) found the testicular artery to originate as high as the origin of the renal artery and to arch over the ipsilateral renal

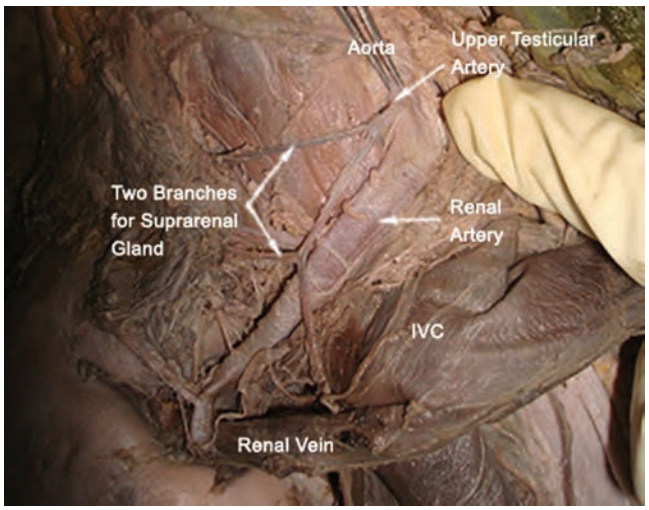

Figure 54.34 Cadaveric dissection revealing the origin of the right upper testicular artery from the aorta above the origin of the renal artery. The artery passes in front of the renal artery and also gives two branches to the right suprarenal gland.

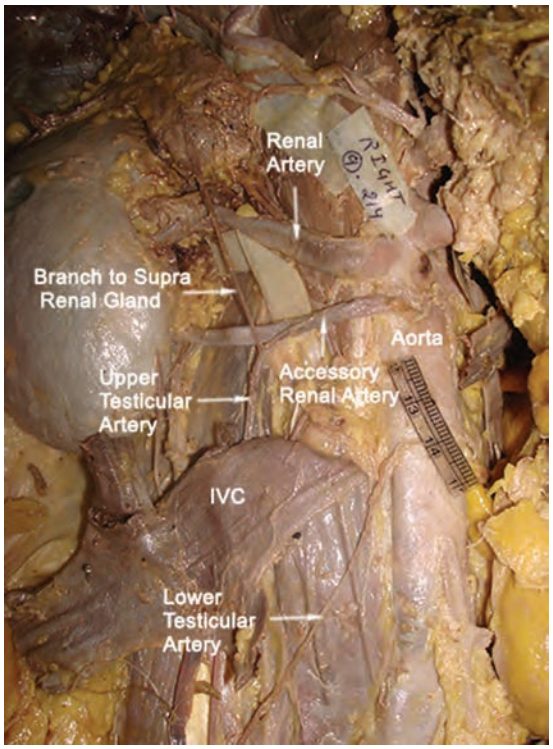

Figure 54.35 Picture illustrating double right testicular arteries. The upper testicular artery takes origin from the accessory renal artery, and gives a branch to the suprarenal gland, and the lower testicular artery arises from the aorta.

vein. In one case, the ovarian arteries were found to originate from the abdominal aorta at a level inferior to the corpus of the L1 vertebra bilaterally (Sulak et al. 2005). Occasionally, gonadal arteries arise from two or three roots, which subsequently merge into one (Bergman et al. 1988).

A case has been reported in which the right testicular and middle suprarenal arteries originated from a common trunk with a retrocaval course (Reddy et al. 2011). In the 2.63% of cases with doubled right testicular arteries, the present authors found the upper right testicular artery arising from the accessory renal artery and giving a branch to the right suprarenal gland (Fig. 54.35). Filipovic et al. (2012) observed two left testicular arteries, medial and lateral; the lateral debranched from the common trunk together with the left inferior suprarenal artery. Adachi (1928) also reported that the testicular and the suprarenal arteries arose from a common trunk with a frequency of 1 in 26 suprarenal glands. The origin of the inferior phrenic and suprarenal arteries from a high-origin testicular artery has also been described (Shinohara et al. 1990; Onderoglu et al. 1993; Brohi et al. 2001). In another report, a common trunk of the right testicular and right inferior suprarenal arteries took origin from the right RA (Panyanetinad 2011).

The gonadal arteries have been reported to arise from the renal or middle suprarenal arteries, one of the lumbar arteries, the common or internal iliac artery, or the superior epigastric artery (Notkovich 1956; Bergman et al. 1988; Deepthinath et al. 2006; Sylvia et al. 2009). Shoja et al. (2007) observed gonadal arteries arising from the main or accessory renal artery in 5–6% of cases. Gonadal arteries of renal origin were reported in 3.33% cases on the right side and 1.66% on the left, and of middle suprarenal origin in 3.3% of cases on the left side (Wadhwa and Soni 2010). The prevalence of gonadal arteries of renal origin has been variably reported within the range 3–16% (Pick and Anson 1940; Cauldwell and Anson 1943; Anson and Kurth 1955; Notkovich 1956). Petru et al. (2007) reported 16 cases of gonadal arteries originating from the renal artery; in 75% of them this variation was unilateral while in 25% it was bilateral. Although there are reports of unilateral aberrant origins of testicular arteries from the RAs (Notkovich 1956; Bergman et al. 1992; Ravery et al. 1993; Deepthinath et al. 2006), a bilateral aberrant origin from additional renal arteries is rare (Çiçekcibaşi et al. 2002). In various studies, the right testicular artery was found to arise from the right renal artery in 6% of cases (Lippert and Pabst 1985) and from the right accessory renal artery in 10% (Singh et al. 2011). Bakheit (2012) reported a case where both the ovarian arteries originated bilaterally from the accessory renal arteries. Sylvia et al. (2009) reported a case where the right testicular artery arose from the right renal artery and the left testicular artery from the left lower renal artery. In another study, Panagouli et al. (2012) found the testicular artery taking origin from the lower polar renal artery bilaterally in 1.3% of cases. Otulakowski and Woźniak (1975) found an aberrant testicular artery that originated from the main renal artery and passed posterior to the IVC. The present authors have found right and left testicular arteries taking origin from the renal arteries in 2.63% and 5.26% of cases, respectively. We also found accessory renal arteries giving origin to the right and left testicular arteries in 2.63%. There is a report of the right testicular artery arising from the right common iliac artery approximately at the L5–S1 level (Mamatha et al. 2011). Another study reported the origin of the ovarian artery from the proximal internal iliac artery (Richard and Bruce 2012) and an aberrant ovarian artery was also found arising from the right common iliac artery (Kim et al. 2013).

Testicular arteries can arise from a common stem; they can be double, triple, or quadruple throughout or in a particular part of their course (Bergman et al. 1988; Loukas and Stewart 2004; Rusu 2006). Bergman et al. (1988) observed double gonadal arteries in 17% of cases and claimed that the medial one is usually of aortic origin and the lateral can be either from the aorta or the renal artery. Cauldwell et al. (1943) reported double testicular arteries in 10.3% of cases. The present authors have found double testicular arteries in 15.7% of cases on the right side and 10.52% on the left. They also reported that on the right side, both upper and lower testicular arteries took origin from the aorta in 10.52% of cases (Fig. 54.36); in 2.63%, the lower right testicular arteries arose from the aorta, the upper right from the renal arteries in 2.63% (Fig. 54.37), and from accessory

renal arteries in 2.63% (Fig. 54.35). On the left side, in 2.63% of cases both the left testicular arteries took origin from aorta (Fig. 54.38) and in 7.89% the upper testicular arteries took origin from the renal arteries and the lower testicular arteries from the aorta (Fig. 54.39). Filipovic et al. (2012) also observed two

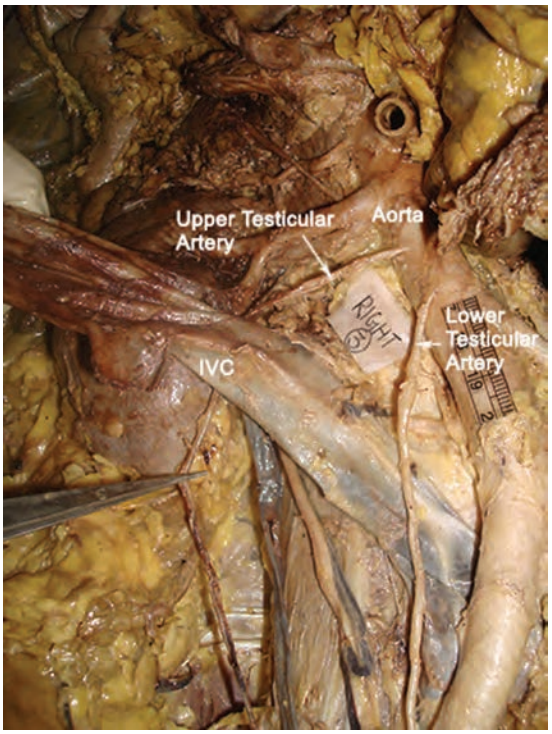

Figure 54.36 Cadaveric dissection revealing the origin of the upper and lower right testicular arteries from the aorta. The upper testicular artery passes behind the IVC and the lower testicular artery passes in front of it.

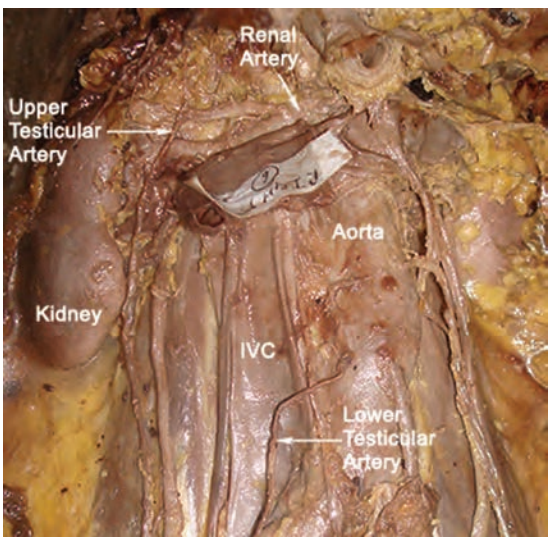

Figure 54.37 Cadaveric dissection revealing double right testicular arteries; the right upper testicular artery takes origin from the right renal artery and the right lower testicular artery arises from the aorta.

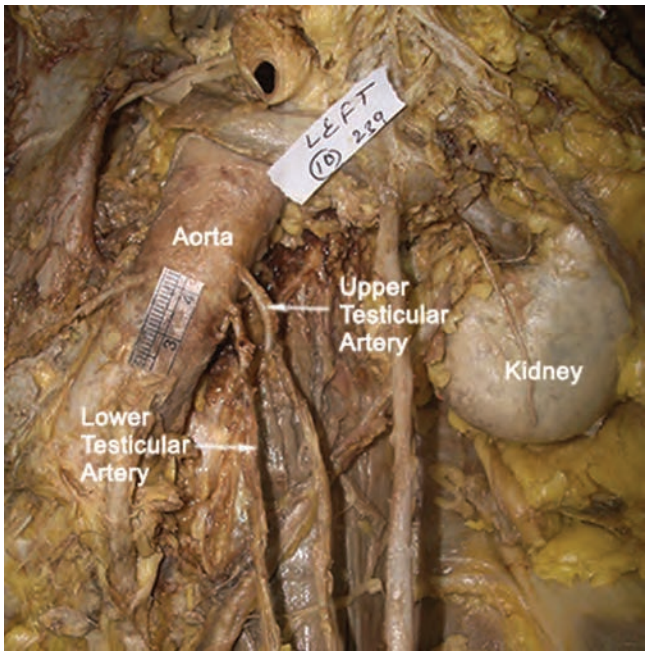

Figure 54.38 Cadaveric dissection revealing double left testicular arteries; both arise from the aorta.

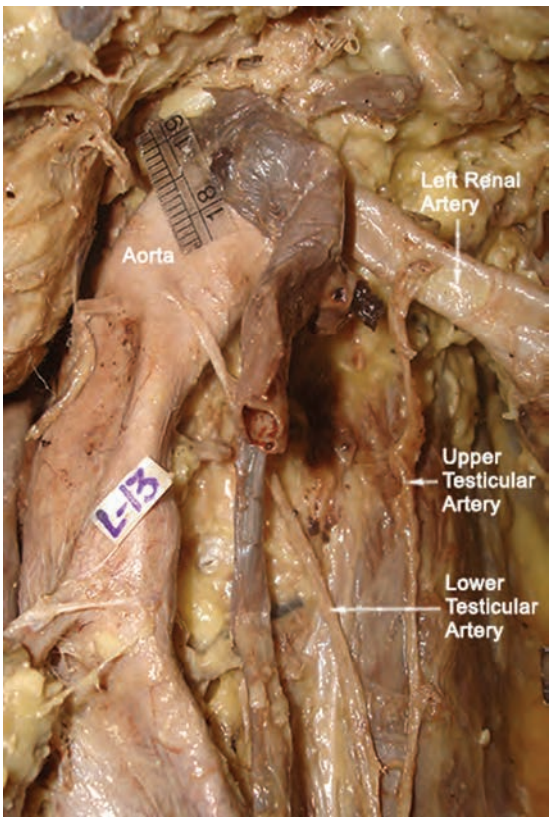

Figure 54.39 Cadaveric dissection revealing the origin of the left upper testicular artery from the left renal artery and the left lower testicular artery from the aorta.

left testicular arteries, medial and lateral, of which the medial originated from an accessory renal artery while the lateral arose from the common trunk together with the left inferior suprarenal artery. Deepthinath et al. (2006) reported a double left testicular artery, one originating from an accessory renal artery and the other from the main renal artery. The gonadal artery can also give rise to a branch to the kidney. Power (1850) stated that the spermatic artery can arise from the capsular, external, or internal iliacs or epigastric arteries.

Course and variations

The right testicular and ovarian arteries run behind the IVC (Bergman et al. 1988; Sulak et al. 2005). Wadhwa and Soni (2010) also found the right testicular artery passing behind the IVC in 10% of cases. The present authors also found the right testicular artery running behind the IVC in 13.15% of cases (Fig. 54.40).

Arching of the gonadal artery above the renal vein has been described by older and more recent authors (Notkovich 1956; Nathan et al. 1976; Grine and Kramer 1981; Naito et al. 2006; Rusu 2006). The gonadal arteries were arched in 1.6% of cases (Gupta et al. 2011). A testicular artery was seen to arise at the lower level and arch around the renal vein to descend in 6% (Notkovitch 1956) and 22% (Kamina 1974) of cases. This type of variation was previously reported by Pick and Anson (1940) and Anson and Kurth (1955). The left testicular artery arching over the left renal vein was reported in 6.7% of cases by Naito et al. (2006) and 3.8% by Bandopadhyay and Saha (2009).

In a rare case, the left testicular artery took its origin just behind the upper part of the left renal vein and then passed between its two divisions and came out of the hilum (Satheesha 2007). Another study reported a similar case of a right testicular artery passing through the bifid renal vein (Mirapeix et al. 1996). The present authors have found two left testicular arteries, with the upper one passing through the two divisions of the left renal vein (Fig. 54.41).

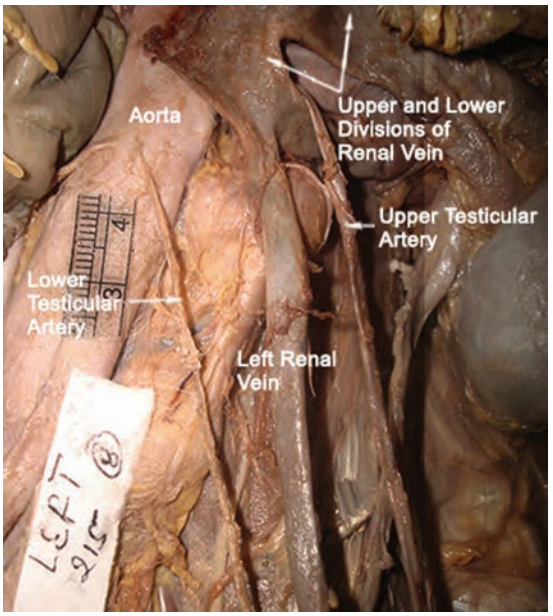

Figure 54.41 Cadaveric dissection revealing double left testicular arteries arising from the aorta. The upper testicular artery passes through the two divisions of the left renal vein.

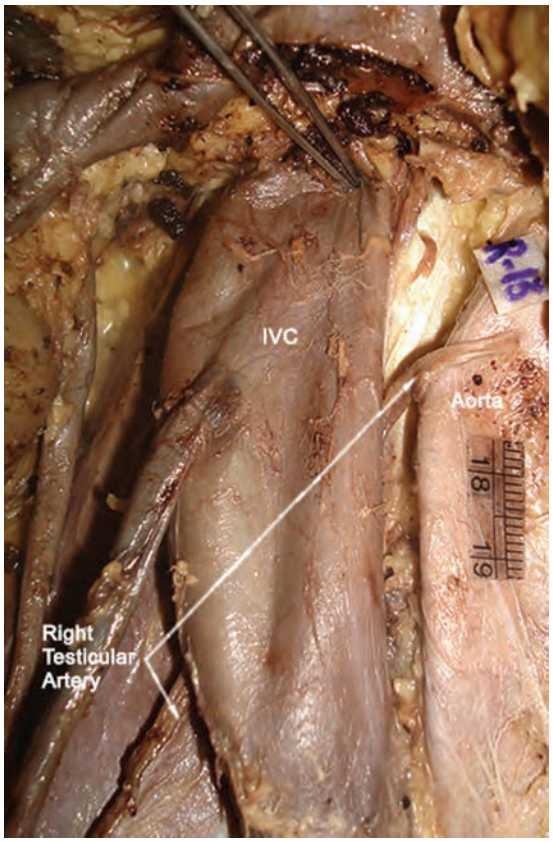

Figure 54.40 Cadaveric dissection revealing the right testicular artery coursing behind the inferior vena cava.

Lumbar arteries

Number and origin

Lumbar arteries are somatic segmental branches of the abdominal aorta and correspond to the intercostal branches of the thoracic aorta (Young 1905). There are four pairs of lumbar arteries arising from the posterolateral aspect of the aorta opposite the lumbar vertebrae (Arslan et al. 2011; present authors). The first pair arises between the celiac trunk and the superior mesenteric artery, the second below the renal artery, the third between the gonadal artery and the inferior mesenteric artery (IMA), and the fourth just below the IMA (Anson 1966). The present authors found four pairs of lumbar arteries arising at the L1,

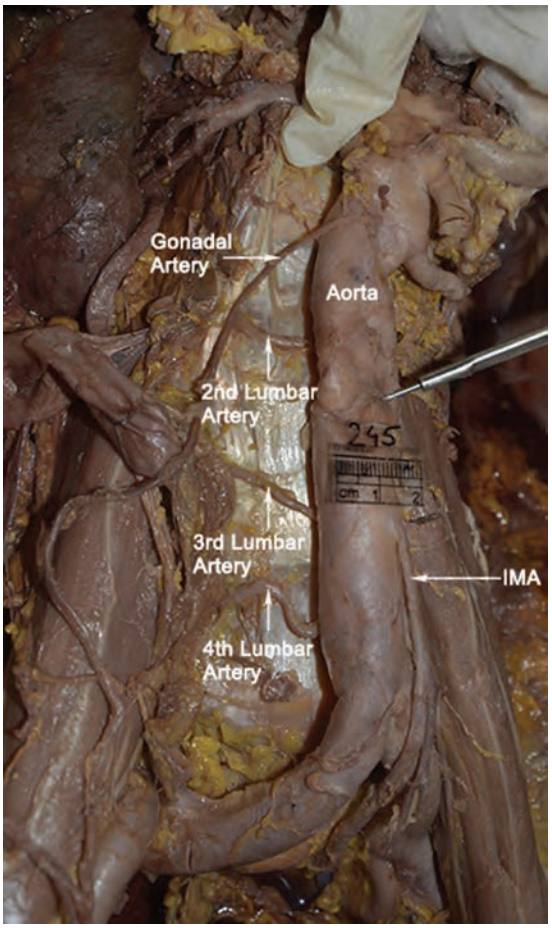

Figure 54.42 The right second, third, and fourth lumbar arteries can be seen arising from the aorta. The fourth lumbar artery is tortuous.

L2, L3, and L4 vertebral levels in 84% of cases, whereas in the remaining 16% the first, second, third, and fourth pairs arose at L1, L2–L3 disk, L3–L4 disk, and L4–L5 disk, respectively.

The number of lumbar arteries ranges from one to five pairs (Anson 1966; Hollinshead 1971; Ratcliffe 1980, 1982; Bergman et al. 1988; Seker et al. 2005; Standring et al. 2008). Three pairs of lumbar arteries were reported in 60% (*n*=102) and 11.5% (*n*=95) of cases by Baniel et al. (1995) and Songür et al. (2010), respectively. The present authors found tortuous fourth right lumbar arteries in 4% of cases (*n*=50) (Fig. 54.42). The incidence of a fifth pair of lumbar arteries varies from 52% (*n*=100) to 100% (*n*=16) (Ratcliffe 1982; Caglar et al. 2004). The fifth pair of lumbar arteries (arteria lumbalis ima) exhibits variable origins if present. It can arise from the aorta (2 cm above the bifurcation), medial, iliolumbar artery, fourth lumbar artery, or common iliac artery (Anson 1966; Caglar et al. 2004).

Pattern of origin

One or more pairs of lumbar arteries can arise as a common stem from the back of the aorta (Young 1905; Bergman et al. 1988; Arslan et al. 2011). In a study on 120 fetuses, variations in the location and formation of lumbar arteries were seen in 14 cases. In 75% of these the fourth pair of lumbar arteries arose as a common trunk from the aorta, while the rest of the lumbar arteries originated separately from the aorta. A common stem for each pair of lumbar arteries was found in 25% of cases, with the fourth trunk trifurcating into two lumbar arteries and a median sacral artery. In another 10% of cases, common stems for fourth and fifth lumbar pairs were found with trifurcation of the lower common stem into two lumbars and a median sacral artery (Seker et al. 2005). Ratcliffe (1982) reported a common stem for the fourth pair of lumbar arteries in 15% of cases. In 13.3% of these the third pair of lumbar arteries also arose from a single, posterior midline trunk. The present authors found a common trunk arising from the aorta and further trifurcating into fourth right lumbar, left lumbar, and median sacral arteries in three cases (Fig. 54.43). In one such case, the third lumbar artery also originated as a common trunk from the aorta.

Young (1905) reported a single case of a right lower lumbar artery arising from the aorta and on the left side; a common trunk arose near the commencement of the left common iliac artery, dividing into median sacral and left lowest lumbar arteries. Ratcliffe (1982) found a high bifurcation of the aorta with the fourth lumbar artery arising from the median sacral artery in 2% of cases (*n*=100). The present authors found a case of high bifurcation of the aorta, with the fourth pair of lumbar arteries

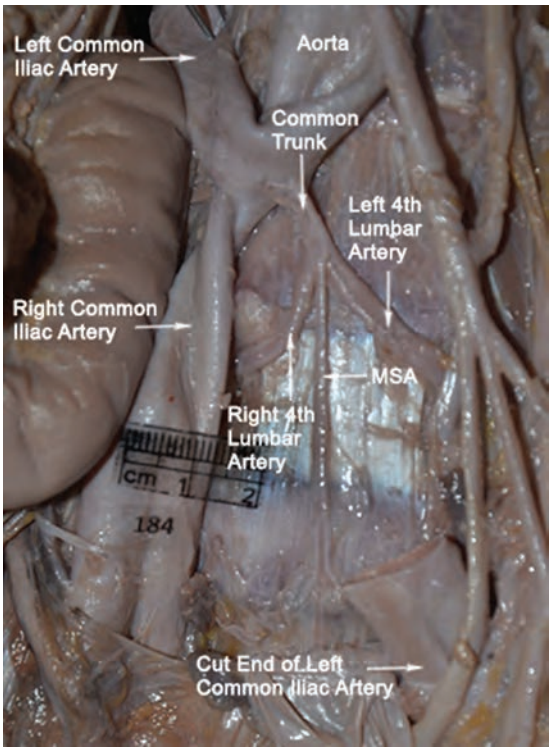

Figure 54.43 A common trunk trifurcating into the median sacral artery (MSA) and the right and left fourth lumbar arteries.

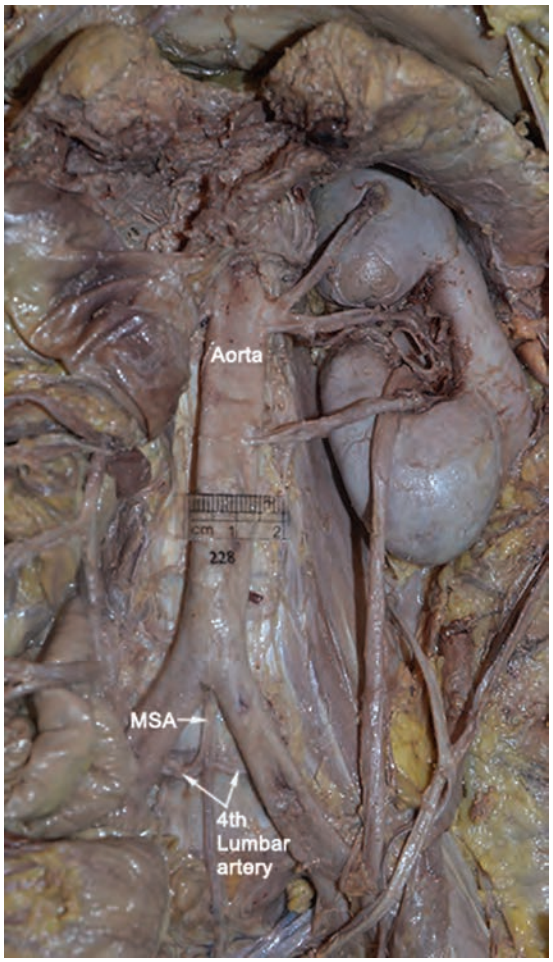

Figure 54.44 High bifurcation of the aorta with the median sacral artery giving rise to the fourth pair of lumbar arteries. This origin is 1.5 cm below the bifurcation of the aorta.

arising from the median sacral artery about 1.5 cm below the bifurcation of the aorta (Fig. 54.44). The first lumbar artery can be joined at its origin with the lowest intercostal artery (Bergman et al. 1988).

Dimensions of the lumbar arteries

The right lumbar arteries are longer than the left because of the leftward location of the aorta with respect to the midline. The diameter of the lumbar arteries is approximately 2 mm (Anson 1966) but it increases from L1–L4 with the average diameters of the first, second, third, and fourth pairs to be 2.4 mm, 2.2 mm, 2.6 mm, and 3.2 mm respectively (Arslan et al. 2011). The present authors found larger average lumbar artery diameters (first 3.37±0.7 mm; second 3.51±0.73 mm; third 3.57±0.82 mm; fourth 4.08±3.83 mm) than other workers. Ratcliffe (1980) states that the fifth pair of lumbar arteries is much smaller than the others, and is reinforced by lumbar branches from the iliolumbar artery and communicating vessels from the fourth lumbar arteries. In contrast, Caglar et al. (2004) observed the diameter of the fifth pair of lumbar arteries to be the largest (2.9 mm).

Distance of lumbar arteries from the tendinous arch

The distance of origin of the lumbar arteries from the tendinous arch (fibrous band arching of the psoas muscle over a lumbar artery) increased gradually from the L1 to L4 segments. For the right and left sides, these distances were 31.8 mm and 22.5 mm at L1 and 40.9 mm and 31.8 mm at L4 (Arslan et al. 2011).

Distance of lumbar arteries from bifurcation of the aorta

The present authors observed that the average distances of the origins of the fourth right and left lumbar arteries from the bifurcation of the aorta were 12.51±7.32 mm and 12.28±7.21 mm. The corresponding measurements for the first pair were 74.22±18.53 mm and 74.35±18.74 mm.

Course and structures supplied

Each lumbar artery runs posterolaterally around the body of the lumbar vertebra deep to the sympathetic trunk and the psoas major muscle, and through intervals between the lumbar transverse processes to reach the abdominal wall. The first two pairs also pass through or behind the crura of the diaphragm. Each lumbar artery gives off vertebral branches to the bodies of the vertebrae and adjoining ligaments, muscular branches to the psoas major, quadratus lumborum, and oblique muscles of the abdomen, a dorsal branch to the lumbar portion of the erector spinae, and a spinal branch to supply the contents of the vertebral canal. It also gives off small renal branches passing in front of the kidney and supplying its capsule.

Anomalous branches

The first lumbar artery can give off the inferior phrenic and middle suprarenal arteries. In some cases the gonadal artery arises from the lumbar arteries (Bergman et al. 1988).

Median sacral artery

The median sacral artery (MSA) arises from the dorsal aspect of the aorta a little above its bifurcation and is described as one of the terminal branches of the aorta (Hollinshed 1971; Standring et al. 2008). The MSA (a sacral mediana) was formerly called the middle sacral artery by Anson (1966). In lower mammals this artery is large and supplies the tail, so it is called the anterior caudal artery (Kudo et al. 1984). According to Quain (1844), the MSA represents the caudal prolongation of the aorta of mammals; the lateral branches of the MSA correspond to the intercostal and the lumbar arteries.

Agenesis of the MSA was reported in 2.1% of cases in a study conducted on 95 abdominal aortas (Songür et al. 2010). Duplication of the MSA has also been reported in the literature

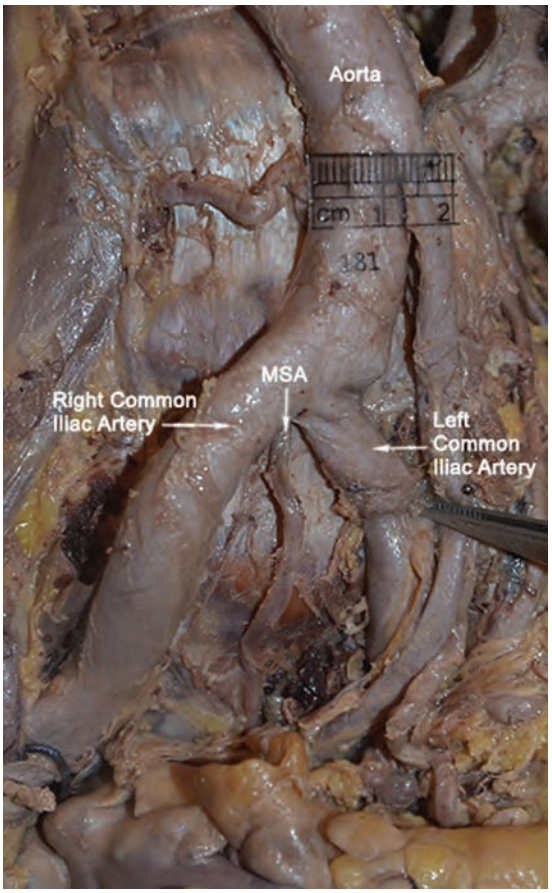

Figure 54.45 The median sacral artery (MSA) arising from the right common iliac artery.

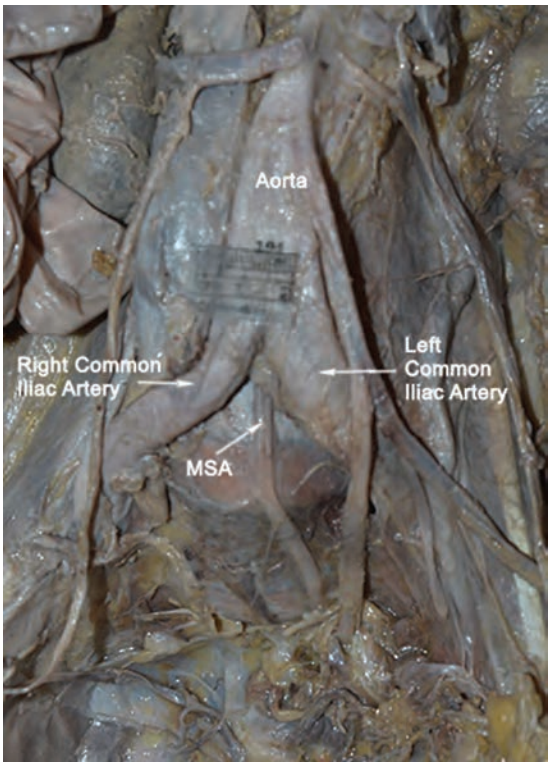

Figure 54.46 The median sacral artery (MSA) arising from the left common iliac artery.

(Hollinshed 1971). The origin of the MSA is variable. It is not always directly connected with the aorta but can arise from one of its branches such as the third, fourth, or fifth lumbar arteries or their common stems, or one of the common iliac arteries, more frequently the left (Young 1896). In our series of 50 cases the MSA was a direct branch of the aorta in most (90%), whereas in three (6%) the MSA arose from a common trunk for the fourth lumbar arteries, which trifurcated into the right and left lumbar arteries and the MSA (Fig. 54.43). In the remaining cases (4%) it took origin from the right (2%) and left (2%) common iliac arteries (CIA) (Figs 54.45, 54.46).

The site of origin is also inconstant. Different levels of origin have been reported such as above the bifurcation of the aorta (Anson 1966), at the aortic bifurcation usually at the L3–L4 disk space, or at the upper portion of L4 (Kudo et al. 1984). The origin is usually 1 cm above the bifurcation of the aorta (Anson 1966), but in a few cases out of 400 studied the exact point was as high as 2.5 cm above the bifurcation (Young 1896). The mean distance of the MSA origin from the bifurcation of the aorta was 0.8±0.38 cm (range 0.12–1.5 cm) as found by the authors, whereas in two cases (4%) the MSA arose from the bifurcation of the aorta (Fig. 54.47). The average distance between the origins of the MSA and the IMA was 3.2±0.78 cm (range 5.5–1.7 cm).

The MSA is a relatively small vessel (2.3–2.8 mm in diameter), as observed in a study conducted of 10 cadavers (Guvencer et al. 2009). Wieslander et al. (2006) found the average width of MSA to be 2 mm (1–4 mm) in a study of 52 unembalmed female cadavers. We found the average diameter of the MSA to be 3.65±0.97 mm (range 2.5–8.9 mm).

The median sacral artery descends in the midline, anterior to the fourth and fifth lumbar vertebrae, sacrum, and coccyx, and ends in the coccygeal body (Standring et al. 2008). In a study conducted on 52 female cadavers, the MSA was found to be left of the midline at the sacral promontory (MSP) in most (61.2%), right of the MSP in 30.6%, and crossing the midline in 8.2% (Wieslander et al. 2006). In a study of ten fresh female cadavers, Flynn et al. (2005) reported that in most cases (70%) the MSA was in close proximity to the midline, and to the left and right of the midline in 20% and 10%, respectively.

At the level of the fifth lumbar vertebra, the MSA is crossed by the left common iliac vein. Anterior to this vertebra the MSA anastomoses with a lumbar branch of the iliolumbar artery; anterior to the sacrum it anastomoses with the lateral sacral arteries and sends branches into the anterior sacral foramina (Standring et al. 2008).

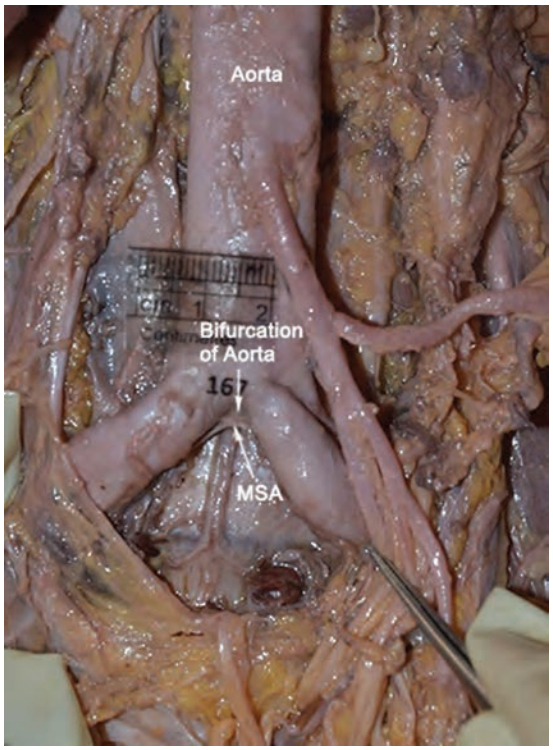

Figure 54.47 The lower end of the aorta (ventral aspect) revealing the origin of the median sacral artery (MSA) at the bifurcation of the aorta.

Branches of the MSA

1. Right and left lateral sacral arteries: these are usually small twigs, serially arranged, passing laterally, and anastomosing with the lateral sacral branches of the internal iliac artery. They give off small spinal branches that pass into the anterior sacral foramina and supply the sacral canal and dorsum of the sacrum (Anson 1966).
2. Rectal branches: these are small twigs that can pass ventrally into the fusion fascia and extraperitoneal connective tissue surrounding the rectum. They can anastomose with other rectal arteries (Anson 1966).
3. Small mesial branches: these pass into the fold of the mesorectum and ramify upon the posterior surface of the intestine; others on each side spread over the sacrum and anastomose with the lateral sacral arteries, occasionally sending small offshoots into the anterior sacral foramina (Young 1896).
4. Small lumbar artery (arteria lumbalis ima): at the level of the fifth lumbar vertebra the MSA gives off a small lumbar artery, small branches of which reach the anorectum via the anococcygeal ligament (Standring et al. 2008).
5. Terminal branches of the MSA form a network of small arteries exhibiting little aneurysmal dilatation in front of the tip of the coccyx, called the coccygeal gland (Luschka's gland). From there, small branches pass through the mesorectum to supply the posterior surface of the rectum (Warwick and Williams 1973).
6. Aberrant branches: the MSA can also furnish an accessory renal or accessory middle rectal artery, or a renal artery if there is a pelvic kidney (Bergman et al. 1988). The authors found that in 2% of cases the MSA gave origin to the fourth pair of lumbar arteries (Fig. 54.44). The lowest (fifth) lumbar arteries (aa. lumbales ima) can also arise from the MSA; when not a branch of the aorta, this artery courses laterally dorsal to the common iliac arteries and veins on the fifth lumbar vertebra. If they are long they supply the psoas and iliacus muscles and can anastomose with the deep circumflex iliac, iliolumbar, and fourth lumbar segmental arteries. A dorsal branch can pass between the last lumbar vertebra and sacrum to supply the erector spinae and gluteus muscles (Anson 1966). In exceptional cases, the MSA can give rise to the sciatic artery.

Common iliac artery

The common iliac arteries (iliaca communis) traditionally arise opposite the left side of the body of the fourth lumbar vertebra as terminal branches from the bifurcation of the abdominal aorta. The level of bifurcation can be as low as the disk between the fourth and fifth lumbar vertebrae. The two branches diverge at average angles of 60° and 68° in males and females, respectively, and terminate opposite the lumbosacral articulation by bifurcating into the external and internal iliac arteries (Anson 1966).

The common iliac arteries are occasionally absent bilaterally. In such cases, the external and internal iliac arteries arise directly from the abdominal aorta at the level of the intervertebral disk between the fourth and fifth lumbar vertebrae (Mansfield and Howard 1964; Bergman et al. 1988; Shetty et al. 2013). Unilateral absence of the right (RCIA) or left common iliac artery (LCIA) has also been reported (Dumanian et al. 1965; Llauger et al. 1995; Dabydeen et al. 2008).

The common iliac arteries (CIA) can vary in length. They can be as short as 1.2 cm or as long as 11 cm; the usual length is between 3.7 and 7.5 cm (Bergman et al. 1988). In the authors' study of 50 cadavers, the average lengths of the RCIA and LCIA were 8.7 cm (range 4.5–16.9 cm) and 8.6 cm (range 4–16.9 cm), respectively. These differences in length could depend upon the aorta bifurcating above or below the usual point or upon the common iliac arteries dividing higher or lower than usual. A low bifurcation of the aorta is more common than a high one, as is also the case with the common iliacs (Bergman et al. 1988). The RCIA is usually longer than the left because the bifurcation of the aorta lies to the left of the midline (Anson 1966).

The average diameters of the RCIA and LCIA are documented as 9.6 mm (range 7–14 mm) and 9.5 mm (range 6–16 mm) respectively (Anson 1966). However, the diameters of these arteries in the present series are higher, that is, 15.2 mm (range 11.4–18.5 mm) and 15.5 mm (range 11.5–22.3 mm) on the right and left side, respectively.

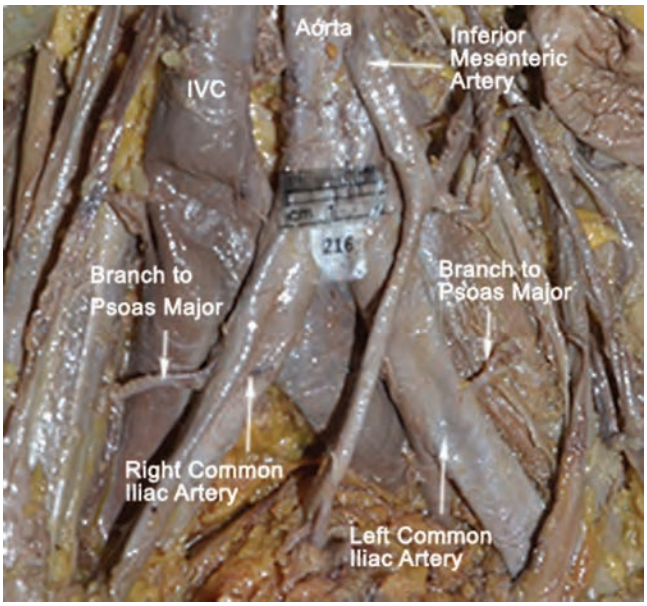

Figure 54.48 Cadaveric dissection revealing the right and left common iliac arteries furnishing branches to the corresponding psoas major muscle. IVC: inferior vena cava.

Branches of the common iliac artery

Each CIA terminates as internal and external iliac arteries, a few small branches distributing to the peritoneum and extraperitoneal connective tissue and lymphatic nodes. As the ureter crosses the CIA, it receives an important branch that anastomoses with other ureteral arteries supplying that structure (Hollinshed 1971; Standring et al. 2008). This artery can also furnish branches to the psoas major and adjacent nerve tissue (Standring et al. 2008). The present authors found the artery to the psoas major stemming from the CIA bilaterally in 2% of cases (Fig. 54.48).

The CIA has been found to provide the iliolumbar artery in 3.7–4.8% of cases (Chen et al. 1999; Kiray et al. 2010). Occasionally a lateral or median sacral, a lumbar, or an accessory or replaced renal artery, if there is a low-lying kidney or a gonadal artery, can arise from the common iliac artery (Bergman et al. 1988; Standring et al. 2008). In our series, the common iliac artery furnished the median sacral artery in 4% of cases, one case each from the right and left common iliacs (Figs 54.45, 54.46). Halloul et al. (2001) reported an anomalous contralateral origin of the right main renal artery from the LCIA. A rare case of origin of an aberrant ovarian artery from the RCIA has also been reported (Kim et al. 2013).

References

Abdullah SS, Mabrut JY, Garbit V, De La Roche E, Olagne E, Rode A, Morin A, Berthezene Y, Baulieux J, Ducerf C. 2006. Anatomical variations of the hepatic artery: study of 932 cases in liver transplantation. *Surg Radiol Anat* 28: 468–473.

Adachi B. 1928. *Anatomie der Japaner I, Das Arteriensystem der Japaner*. Band II. Kyoto: Verlag der Kaiserlich-Japanischen Universitat zu Kyoto.

Adachi B. 1930. Das Fehlen der A. mesenterica inferior bei einem Japaner. *Anat Anz* 69: 431–433.

Ajmani ML, Ajmani K. 1983.The position, length and arterial supply of vermiform appendix. *Anat Anz (Jena)* 153: 369–374.

Albarran J. 1909. *Medicine Operatiore des Voies Urinouris 4*. Paris: Masson & Cie.

Alghizzi HJK. 2011. The variation of renal artery anatomy in the Iraqi population: An angiographic study of 358 middle Euphrates Iraqi patients attending the catheterization laboratory in Hilla province. *Karbala J. Med* 4(1,2): 933–938.

Amaifi M, Cefaly F. 1958. Studio anatomochirurgico del pancreas. *Rass Ital Chir Med* 7: 805–813.

Amonoo-Kuofi HS, el-Badawi MG, el-Naggar ME. 1995. Anomalous origins of colic arteries. *Clin Anat* 8: 288–293.

Anson BJ. 1963. *An Atlas of Human Anatomy*, second edition. Philadelphia: W.B. Saunders.

Anson BJ. 1966. *Morris' human anatomy. In: The Cardiovascular System: A Complete Systematic Treatise*, 12th edition. New York: The Blakiston Division, McGraw-Hill Book Co.

Anson BJ, McVay CB. 1936. The topographical positions and the mutual relations of the visceral branches of the abdominal aorta. *Anat Rec* 67: 7–15.

Anson BJ, Kurth LE. 1955. Common variations in the renal blood supply. *Surg Gyn Obst* 100: 157–62.

Anson BJ, McVay CB. 1971. *Surgical Anatomy, vol 1*, fifth edition. Philadelphia: W.B. Saunders.

Archibald, E. 1908. Operative treatment of cancer of rectum. *JAMA* 50: 573.

Armstrong BG, Hunt TH, Price CW, Resnick MI. 1979. Common origin of inferior mesenteric and accessory renal artery. *Urology* 14: 298–299.

Arslan M, Comert A, Acar HI, Ozdemir M, Ehlan A, Tekdemir I, Tubbs RS, Ugur HS. 2011. Surgical view of the lumbar arteries and their branches: An anatomical study. Operative Neurosurgery 68: ons16–ons22.

Asala S, Chaudhary SC, Masumbuko-Kahamba N, Bidmos M. 2001. Anatomical variations in the human testicular blood vessels. *Ann Anat* 183: 545–549.

Ashalata K. 2011. Variations of the branches of the celiac trunk: a case report. *Asian J Med Sci* 2: 148–150.

Ata AH. 1991. Cystic artery identification during laparoscopic cholecystectomy. *J Laparoendosc Surg* 1: 313–318.

Ault GW, AF Castro, RS Smith. 1952. Clinical study of ligation of the inferior mesenteric artery in left colon resections. *Surg Gynecol Obstet* 94: 223–228.

Aytac SK, Yigit H, Sancak T, Ozcan H. 2003. Correlation Between the diameter of the main renal artery and the presence of an accessory renal artery: sonographic and angiographic evaluation. *J Ultrasound Med* 22: 433–439.

Bacon HE, Smith CH. 1948. The arterial supply of the distal colon pertinent of abdominoperineal proctosigmoidectomy, with preservation of the sphincter mechanism. *Ann Surg* 127: 28–38.

Bakheit MA. 2009. Prevalence of variations of the cystic artery in the Sudanese. *East Mediterr Health J* 15: 1308–1312.

Bakheit MA. 2012. Bilateral origin of ovarian arteries from accessory renal arteries. *Saudi Med J* 33: 1122–1124.

Bakheit MA, Motabagani MA. 2004. Anomalies of the renal, phrenic, suprarenal arteries. *Saudi Med J* 25: 376–378.

Balice G. 1949. L'anatomia chirurgica del l'arteria mesenterica inferior ed il punto del sudeck. *Gior Ital Chir* 5: 1.

Balija M, Huis M, Nikolic V, Stulhofer M. 1999. Laparoscopic visualization of the cystic artery anatomy. *World J Surg* 23: 703–707.

Bamac B, Colak T, Ozbek A,Gundogmus UN. 2011. A report of unusual origin of right renal artery. *Int J Anat Variat* 4: 95–97.

Bandopadhyay M, Saha A. 2009. Three rare variations in the course of the gonadal artery. *Int J Morphol* 27: 655–658.

Banerjee S, Cho M, Gupta S, Brilakis ES. 2007. Aberrant take off a right accessory renal artery, identified during an aorto iliac intervention. *Vasc Dis Management* 4: 4–5.

Baniel J, Foster RS, Donohue JP. 1995. Surgical anatomy of the lumbar vessels. *J Urol* 153: 1422–1425.

Barbin JY, Guntz M. 1971. La circulation arterielle visceral, Essai de systematization. *CR Assoc Anat* 153: 819–945.

Bardeleben von K. 1906. *Lehrbuch der Systematischen Anatomie des Menschen*. Berlin: Urban 7 Schwarzenberg.

Basile A, Tsetis D, Montineri A, Puleo S, Massa Saluzzo C, Runza G, Copplino F, Ettorre GC, Patti MT. 2008. MDCT anatomic assessment of right inferior phrenic artery origin related to potential supply to hepatocelleular carcinoma and its embolization. *Cardiovasc Intervent Radiol* 31: 349–358.

Basmajian JV. 1955. The main arteries of the large intestine. *Surg Gynecol Obstet* 101: 585–591.

Basmajian JV. 1971. Mesenteric vessels duodenum and pancreas. In: *Grant's Method of Anatomy* (ed. Basmajian JV). Baltimore: Williams and Wilkins.

Belli L, De Marzo V, Tiberio G, Morisi M. 1958. Contributo allo studio della circolazione arteriosa intrapancreatica. *Biol Lat* 11: 375–394.

Bellini A. 1894. Observations et notes sur le trajet des arteres. *Bull Soc Anat De Paris* 8: 696.

Belou P. 1915. *Anattomia de los Conductos Biliarees y de la Arteria Cistca*. Buenos Aires: Imp. Oceana.

Benton RS, Cotter WB. 1963. A hitherto undocumented variation of the inferior mesenteric artery in man. *Anat Rec* 145: 171–173.

Beregi JP, Mauroy B, Willoteaux S, Mounier-Vehier C, Remy-Jardin, M. 1999. Anatomic variation in the origin of the main RA: spiral CTA evaluation. *Eur Radiol* 9: 1330–1334.

Berens AS, Aluisio FV, Colborn GL, Gray SW, Skandalakis JE. 1991. The incidence and significance of the posterior gastric artery in human anatomy. *J Med Assoc Ga* 80: 425–428.

Bergman RA, Thompson SA, Afifi AK, Saadeh FA. 1988. Compendium of Human Anatomic Variation: Text, Atlas, and World Literature. In: *Cardiovascular System*. Baltimore, Munich: Urban and Schwarzenber.

Bergman RA, Cassell MD, Sahinoglu K, Heidger PM Jr. 1992. Human doubled renal and testicular arteries. *Ann Anat* 174: 313–315.

Bertelli E, Di Gregorio F, Bertelli L, Mosca S. 1995. The arterial blood supply of the pancreas: a review. I. The superior pancreaticoduodenal and the anterior superior pancreaticoduodenal arteries. An anatomical and radiological study. *Surg Radiol Anat* 17: 97–106.

Bertelli E, Di Gregorio F, Bertelli L, Civeli L, Mosca S. 1996a. The arterial blood supply of the pancreas: a review. II. The posterior superior pancreaticoduodenal artery. An anatomical and radiological study. *Surg Radiol Anat* 18: 1–9.

Bertelli L, Lorenzini L, Bertelli E. 1996b. The arterial vascularization of the large intestine: anatomical and radiological study. *Surg Radiol Anat* 18: 51–59.

Bertelli E, Bertelli L, Di Gregorio F, Orazioli D, Bastianini A. 1997. The arterial blood supply of the pancreas: a review. IV. The anterior inferior and posterior pancreaticoduodenal and minor sources of blood supply for the head of pancreas. An anatomical review and a radiological study. *Surg Radiol Anat* 19: 203–212.

Bertocchi A, Bianco V. 1955. La circolazione arteriosa delle vie biliari extraepatiche, del duodeno, pancreas e della milza. *Giorn Accad Med Torino* 118: 141–148.

Bhaskar PV, Bhasin V, Kumar S. 2006. Abnormal branch of the testicular artery. *Clin Anat* 19: 569–570.

Bianchi HF, Albanese EF. 1989. The supraduodenal artery. *Surg Radio Anat* 11: 37–40.

Boijsen E. 1983. Pancreatic angiography In: *Angiography* (ed. Abrams HL). Boston: Little, Brown.

Bolognese A, Di Giorgio A, Stipa V. 1979. Arterial vascularization of the pancreas; anatomical findings by means of vascular injection of plastic material. *Surg Ital* 9: 346–351.

Bordei P, Antohe DS. 2002. Anatomical study of triple renal arteries. *Morphologie* 86: 37–41.

Bordei P, Antohe DS, Sapte E, Iliescu D. 2003. Morphological aspects of the inferior suprarenal artery. *Surg Radiol Anat* 25: 247–251.

Bordei P, Sapte E, Iliescu D. 2004. Double renal arteries originating from the aorta. *Surg Radiol Anat* 26: 474–479.

Bouchet Y, Martin R. 1961. Considérations sur l'artère pancreatica magna ou pancréatique dorsale. *C R Ass Anat* 111: 174–180.

Brewer GE. 1900. *Some observations upon the surgical anatomy of the gallbladder and ducts*. Baltimore: Johns Hopkins Press.

Brohi RA, Sargon ME, Yener N. 2001. High origin and unusual suprarenal branch of a testicular artery. *Surg Radiol Anat* 23: 207–208.

Browne EZ. 1940. Variations in origin and course of the hepatic artery and its branches. *Surgery* 8: 424.

Bruce J, Walmsley R, Ross JA. 1964. *Manual of Surgical Anatomy*. Edinburgh, London: Brace and Livingstone.

Brunet C, Moutardier V, Di Marino V. 1993. La region dite du "bouton coelio-mésentérique", étude anatomo-chirurgicale. *J Chir (Paris)* 2: 10–13.

Budhiraja V, Rastogi R, Asthana AK. 2011. Variant origin of superior polar artery and unsual hilar branching pattern of renal artery with clinical correlation. *Folia Morphol (Warsz)* 70: 24–28.

Buhler A. 1904. Uber eine Anastomose zwischen den Stammen der Art. Celiaca und der Art. Mesenterica superior. *Gegenbaurs Morph Jb* 32: 185–188.

Caglar S, Dolgun H, Ugur HS, Torun F, Attar A, Uz A, Tekdemir I, Ehlan A. 2004. Extraforaminal lumbar arterial anatomy. *Surg Neurol* 61: 29–33.

Calas F, Martin R, Bouchet Y, Polliack D. 1955. Les arteres de la tete du pancreas. *CR Assoc Anat* 89: 362–367.

Calas F, Martin R, Convert A. 1963. Contribution a l'étude de la vascularisation du rein. *CR Assoc Anat (Nancy)*, 117.

Callot JF. 1891. De la Cholecystectomie. Med. Frc de Paris, Dissertation.

Cauldwell EW, Anson BJ. 1943. The visceral branches of the abdominal aorta: topographical relationships. *Am J Anat* 73: 27–57.

Cavdar S, Sehirii U, Pekin B. 1997. Celiaco mesenteric trunk. *Clin Anat* 10: 231–234.

Chaib E, de Souza Y, Maruyama MY, Marinucci L, Aranha MR, Isabela A de Siqueira, Chen L, de Campos Carvalho M, Albuquerque L. 2010. Left hepatic artery arising from the superior mesenteric artery: a case study of a rare anatomic variation. *The Open Anatomy Journal* 2: 76–78.

Chen H, Yano R, Emura S, Shoumura S. 2009. Anatomic variation of the celiac trunk with special reference to hepatic artery patterns. *Ann Anat* 191: 399–407.

Chen JY, Shyu JF, Uen YH, Hsiao WC, Su CH, Shyr YM, Wu CW, Lui WY, Liu JC, Chen TH. 2007. Surgical anatomy of the gastroduodenal artery in Chinese adults and its clinical applications. *Hepatogastroenterology* 54: 1458–1461.

Chen RS, Liu YX, Liu CB, Hu YS, Xu DC, Zhong SZ, Li ZH. 1999. Anatomic basis of iliac crest flap pedicled on the iliolumbar artery. *Surg Radiol Anat* 21: 103–107.

Chen TH, Shyu JF, Chen CH, Ma KH, Wu CW, Lui WY, Liu JC. 2000. Variations of the cystic artery in Chinese Adults. *Surg Laparos, Endosc and Percutan Tech* 10(3): 154–157.

Cheng BC, Chang S, Huang J, Mao ZF, Wang ZW, Lu SQ, Wang TS, Wu XJ, Hu H, Xia J, Kang GJ, Xiao YG, Lin HQ. 2006. Surgical anatomy of the colic vessels in Chinese and its influence on the operation of esophageal replacement with colon. *Zonghua Yi Xue Za Zhi* 86: 1453–1456.

Chiaganama NO, Ekpo EU, Egbe NO, Nzotta CC, Okwara KK. 2013. Aging and the average diameter of the renal artery using computed tomography angiography (CTA). *SA Radiogr* 51: 23–25.

Chitra R. 2010. Clinically relevant variations of the celiac trunk. *Singapore Med J* 51: 216–219.

Ciçekcibaşi AE, Salbacak A, Seker M, Ziylan T, Buyukmumcu M, Uysal II. 2002. The origin of gonadal arteries in human fetuses: anatomical variations. *Ann Anat* 184: 275–279.

Ciçekcibaşi AE, Uysal II, Seker M, Tuncer I, Buyumumcu M, Salbacak A. 2005. A rare variation of the celiac trunk. *Ann Anat* 187: 387–391.

Çilingiroğlu M, Marmagkiolis K, Wholey M. 2013. Successful recanalization of a left common iliac artery chronic total occlusion adjacent to an ectopic renal artery at the aortoiliac bifurcation. *Arch Turk Soc Cardiol* 41: 347–350.

Cimmino, PT, Boccheti T, Izzo L. 1992. Anatomo-surgical considerations in laparoscopic cholecystectomy. *G Chir* 13: 149.

Clemente CD. 1985. *Anatomy of the Human Body*, 30th edition. Baltimore: Williams and Wilkins.

Couinaud C, Huguet. 1966. La greffe du duodeno-pancreas chez l'homme. Ire partie: Etudeanatomicque. *J Chir* 92: 293–312.

Covey AM, Brody LA, Maluccio MA, Getrajdman GI, Brown KT. 2002. Variant hepatic arterial anatomy revisited: Digital subtraction angiography performed in 600 patients. *Radiology* 224: 542–547.

Cunningham DJ. 1921. *Textbook of Anatomy*, fifth edition. New York: William Wood and Company.

D'Souza AS, Vijyalakshmi, Hemalatha, Pugazhandhi, Mamatha H. 2012. Anatomical variations in the branches of the celiac trunk. *JCDR* 6(3): 333–335.

Dabydeen D, Shabashov A, Shaffer K. 2008. Congenital absence of the right common iliac artery. *Radiol Case Reports* 3: 47.

Daescu E, Zahoi DE, Motoc A, Alexa A, Baderca F, Enache A. 2012. Morphological variability of the renal artery branching pattern: a brief review and an anatomical study. *Rom J Morphol Embryol* 53: 287–291.

Dalçik C, Çolak T, Özbek A, Dalçik H. 2000. Unusual origin of the right renal artery: A case report. *Surg Radiol Anat* 22: 117–118.

Daseler EH, Anson BJ, Hambley WC, Reimann AF. 1947. The cystic artery and constituents of the hepatic pedicle. A study of 500 specimens. *Surg Gyencol Obstet* 85: 47–63.

Deepthinath R, Satheesha Nayak B, Mehta RB, Bhat S, Rodrigues V, Samuel VP, Venkataramana V, Prasad AM. 2006. Multiple variations in the paired arteries of the abdominal aorta. *Clin Anat* 19: 566–568.

Del Campo JC. 1931. Cireulacion del duodeno. *Anales Facultad Med Montevideo* 16: 1–27.

Delagrange AB, Barbin JY. 1966. Contributiona l'étude de la vascularisation artèriélle du pancéas. *C R Ass Anat* 135: 297–306.

Delannoy E. 1923. Artere mesenterique superieure double. *Bull Mem Soc Anat Paris* 93: 346.

Dhar P, Lal K. 2005. Main and accessory renal artery – a morphological study. *Internet J Biol Anthropol* 110: 101–110.

Diard F, Levot J, Tavernier J. 1972. L'arteriographic surrenalienne. *Bordeaux Medical* 12: 1435–1448.

Didio LJ, Christforidis AJ, Chandnani PC. 1980. Posterior gastric artery and its significance as seen on angiograms. *Am J Surg* 139: 333–337.

Ding YM, Wang B, Wang WX, Wang P, Yan JS. 2007. New classification of the anatomic variations of cystic artery during laparoscopic cholecystectomy. *World J Gastroenterol* 13: 5629–5634.

Dixon AK, Lawrence JP, Mitchell JRA. 1984. Age-related changes in the abdominal aorta shown by CT. *Clin Radiol* 35: 33–37.

Dixon CF. 1948. Anterior resection for malignant lesions of the upper part of the rectum and lower part of the sigmoid. *Ann Surg* 128: 425–442.

Donatini B. 1990. A systematic study of the vascularization of the pancreas. *Surg Radiol Anat* 12: 173–180.

Douard R, Chevallier JM, Delmas V, Cugnenc PH. 2006. Clinical interest of digestive arterial trunk anastomoses. *Surg Radiol Anat* 28: 219–227.

Drummond H. 1913. The arterial supply of the rectum and pelvic colon. *Brit J Surg* 1: 677–685.

Drummond H. 1914. Some points relating to the surgical anatomy of the arterial supply of large intestine. *Proc R Soc M London* 7: 185–193.

Dumanian AV, Frahm CJ, Benchik FA, Wooden TF. 1965. Intermittent claudication secondary to congenital absence of iliac arteries. *Arch Surg* 91: 604–606.

Dwight T. 1903. The branches of superior mesenteric artery to jejunum and ileum. *Anat Anz* 23: 184.

Eaton PB. 1917. The celiac axis. *Anat Rec* 13: 369.

Ebner I, Anderhuber F. 1985. Arterielle Gefässversorgung der Cauda pancreatis unter besonderer Berücksichtigung der cauda-corporealen Gefässbeziehungen. *Acta Anat* 121: 115–123.

Eckmann I, Krahn V. 1984. Untersuchuhung zur Haufigkeit verschiedener Ursprungsstellen der arteria gastric dextra. *Anat Anz* 155: 65–70.

Edwards LF. 1941. The retroduodenal artery. *Anat Rec* 81: 351–355.

El-Eishi HI, Ayoub SF, Adb-El-Khalek M. 1973. The arterial supply of the human stomach. *Acta Anat* 86: 565–580.

Evrard HL. 1932. Les arteres du duodenum et du pancreas. Paris, these 640.

Falconer CWA, Griffiths E. 1950. The anatomy of the blood-vessels in the region of the pancreas. *Br J Surg* 37: 334–344.

Farisse J, Cannoni M, Gau M, Miliani P, Niel J, Richelme H. 1966. Sur les arteres de la papille duodenale. *CR Ass Anat* 134: 384–395.

Feller I, Woodburne RT. 1961. Surgical anatomy of the abdominal aorta. *Ann Surg* 154: 239–252.

Filipovic B, Stijak L, Filipovic B. 2012. An unusual origin of the double left testicular artery in a male cadaver: a case report. *J Med Case Rep* 6: 267.

Fleischmann D, Hastie TJ, Danneger FC, Paik DS, Tillich M, Zarins CK, Rubin GD. 2001. Quantitative deyermination of age-related geometric changes in the normal abdominal aorta. *J Vasc Surg* 33: 97–105.

Flint ER. 1923. Abnormalities of the right hepatic, cystic, and gastroduodenal arteries, and of the bile-ducts. *Br J Surg* 10: 509–519.

Flynn MK, Romero AA, Amundsen CL, Weidner AC. 2005. Vascular anatomy of the presacral space: A fresh tissue cadaver dissection. *Am J Obst Gynecol* 192: 1501– 1505.

Forgue E, Milhaud 1923. La circulation du segment sigmoido-rectal. La valeur reelle du point de sudeck. Contribution a la technique de l'extirpation abdomino-perineale du rectum. *Rev Chir* 61: 61.

Franz K. 1896. Ueber die Configuration der Arterien in der Umgebung des Pankreas. *Anat Anz* 12: 470–472.

Fumagalli Z, Cavallotti C. 1983. *Anatomía Umana Nórmale*. Padova: PiccinNuova Libraría.

Futara G, Ali A, Kinfu Y. 2001. Variations of the hepatic and cystic arteries among Ethiopians. *Ethiop Med J* 39: 133–142.

Gagnon R. 1957. The arterial supply of the human adrenal gland. *Rev Can Biol* 16: 421–433.

Gagnon R. 1964. Middle suprarenal arteries in man: a statistical study of two hundred human adrenal glands. *Rev Can Biol* 23: 461–467.

Gagnon R. 1966. Les arteres surrenales inferieures chez l'homme. *Rev Can Biol* 25: 135–144.

Gangadhara, Manivannan K, Rao NS, Rao HRK. 2013. Hepatomesentric trunk and gastro-splenico-phrenic trunk: a rare anatomic variation. *J Evol Med Dent Sci* 2: 5799–5804.

Garcia-Ruiz A, Milsom JW, Ludwig KA, Marchesa P. 1996. Right colonic arterial anatomy. Implications for laparoscopic surgery. *Dis Colon Rectum* 39: 906–911.

Garcier JM, De Fraissinette B, Filaire M, Gayard P, Therre T, Ravel A. 2001. Origin and initial course of the renal artery: a radiological study. *Surg Radiol Anat* 23: 51–55.

Garti I, Meiraz D. 1980. Ectopic origin of main renal artery. *Urology* 15: 627–629.

Garti I, Nissenkorn I, Lerner M. 1986. Common origin of inferior mesenteric and main renal artery. *Eur Urol* 12: 215–216.

Gawish AE, Donia F, Samhan M, Halim MA, Al-Mousawi M. 2007. Outcome of renal allografts with multiple arteries. *Transplant Proc* 39: 1116–1117.

George R. 1935. Topography of the unpaired visceral branches of the abdominal aorta. *J Anat* 69: 196–205.

Gerard G. 1921. *Manuel d'Anatomie Humaine*, second edition. Paris: Masson e Cie Éditeurs.

Gerlock AJ Jr, Goncharenko V. 1979. Hazards of straight catheter aortography in the tortuous abdominal aorta. *Rev Interam Radiol* 4: 131–134.

Giavroglou C, Kokkinakis H. 2005. Main arterial supply of a kidney from the opposite renal artery: an unusual case. *Acta Radiol* 46: 567–568.

Gielecki J, Zurada A, Sonpal N, Jablonska B. 2005. The clinical relevance of celiac trunk variations. *Folia Morphol* 64: 123–129.

Glodny B, Tröbinger MG, Hofmann KJ, Rehder P, Trieb T, Petersen A. 2009. Right accessory renal artery arising from a left additional common renal artery stem. *Cardio Vasc Interv Rad* 32: 804–806.

Goligher JC. 1949. The blood supply to the sigmoid colon and rectum with reference to the technique of rectal resection with restoration of continuity. *Brit J Surg* 37: 157–162.

Gordon DH, Martin EC, Kim YH, Kutcher R. 1978. Accessory blood supply to the liver from the dorsal pancreatic artery: an unusual anatomic variant. *Cardiovasc Radiol* 1: 199–201.

Gosai P, Kanani S, Patel J, Shah R, Nirvan A. 2013. A study of morphology of celiac trunk in 100 cadavers. *Int J Med Sci Public Health* 2: 915–918.

Gourley EJ, Gering SA. 2005. The meandering mesenteric artery: A historic review and surgical implications. *Dis Colon Rectum* 48: 996–1000.

Grabbe VE, Bucheler E. 1980. Die Buhlersche Anastomose. *Fortschr Rontgenstr* 132: 541–546.

Gray H. 1932. *Anatomy, Descriptive and Applied*, 25th edition. London: John William Parker.

Greenberg MW. 1950. Blood supply of the recto sigmoid and rectum. *Ann Surg* 131: 100–107.

Gregorczyk M, Dąbkowska A, Tarka S, Ciszek B. 2008. The anatomy of the fundic branches of the stomach: preliminary results. *Folia Morphol* 67: 120–125.

Grieg HW, Anson BJ, Coleman SS. 1951. The inferior phrenic artery. Types of origin in 850 body-halves and diaphragmatic relationship. *Q Bull Northwestern Univ Med School* 25: 345–350.

Griffiths JD. 1956. Surgical anatomy of the blood supply of the distal colon. *Ann R Coll Med* 19: 241–246.

Grine FE, Kramer B. 1981. Arched gonadal arteries in the South African Negro. *J Anat* 132: 387–390.

Gruttadauria S, Floglieni CS, Doria C, Luca A, Lauro A, Marino IR. 2001. The hepatic artery in liver transplantation and surgery: vascular anomalies in 701 cases. *Clin Transpl* 15: 359–363.

Guntz M. 1967. Radio-anatomie del'artère rénale. Déduction chirurgicales. *CR Assoc Anat* 148: 623– 631.

Gupta A, Singal R, Singh D. 2011. Variations of gonadal artery: embryological basis and clinical significance. *Int J Biol Med Res* 2: 1006–1010.

Gupta I, Ray A, Basu P. 2013.Variant origin of the middle colic artery from the gastroduodenal artery. *Int J Anat Variation* 6: 13–17.

Gurgacz AM, Horbaczewska A, Klimek-Piotrowska W, Walocha. 2011. Variations in hepatic vascularisation: lack of a proper hepatic artery. Two case reports. *Folia Morphol* 70: 130–134.

Guvencer M, Dalbayrak S, Tayefi H, Tetik S, Yilmaz M, Erginoglu U, Baksan O, Guran S, Nader S. 2009. Surgical anatomy of the presacral area. *Surg Radiol Anat* 31: 251–257.

Gwon DI, Gi-Young K, Yoon H, Sung K, Lee JM, Ryu SJ, Seo MH, Shim J, Lee GJ, Kim HK. 2007. Inferior phrenic artery: anatomy, variations, pathologic conditions, and interventional management. *Radiographics* 27: 687–705.

Gwyn DG, Skilton JS. 1966. A rare variation of the inferior mesenteric artery in man. *Anat Rec* 156: 235–238.

Hagopian AC. 1953. An abnormal inferior suprarenal artery. *Yale J Biol Med* 26: 78–79.

Haller Von A. 1745. Arteriae Celiacae. In: *Iconum Anatomicarum* (ed. Haller Von A). Gottingae: Vandenhoeck.

Haller Von A. 1756. Addenda. In: *Iconum Anatomicarum* (ed. Haller Von A). Gottingae: Vandenhoeck.

Halloul Z, Meyer F, Buerger T. 2001. Ectopic vascularization of the right kidney by a contralateral origin of the main renal artery from the left common iliac artery: report of a case. *Surg Today* 31: 371–373.

Harris HW, Pellegrini CA. 1994. Surgical Disease of the Biliary Tract and Pancreas–Multidiskiplinary Management Year Book. Braasch and Tompkins, St Louis, Mosby.

Harrison CB, Kaplan JJ, Scherz HC, Packer MG, Jones J. 1990. Microvascular auto transplantation of the intra-abdominal testis. *J Urol* 144: 506–507.

Harrison LH, Flye MW, Seigle HF. 1978. Incidence of anatomical variants in renal vasculature in the presence of normal renal function. *Ann Surg* 188: 83–89.

Hartmann H. 1909. Some considerations upon high amputation of the rectum. *Ann Surg* 50: 1091–1094.
Heidsicek E. 1928. Zur skeletopie der grossen äste der bauchaorta. *Anat Anz* 66: 6–24.
Helm HM. 1915. The gastric vasa brevia. *Anat Rec* 9: 637.
Hemanth K, Garg S, Yadav TD, Sahni D. 2011. Hepato-gastro-phrenic trunk and hepato-spleno-mesenteric trunk: A rare anatomic variation. *Trop Gastroenterol* 32: 56–59.
Henle FGJ. 1871. *Handbuch der systematischen anatomie des Menschen*. Gefasslehre, Braunschweig: F. Vieweg and Sohn.
Hiatt JR, Gabbay J, Busittil RW. 1994. Anatomy of the hepatic arteries in 1000 cases. *Ann Surg* 220: 50–52.
Hieda M, Toyota N, Kakizawa H, Ishikawa M, Horiguchi J, Ito K. 2009. The anterior branch of the left inferior phrenic artery arising from the right inferior phrenic artery: an angiographic and CT study. *Cardiovasc Intervent Radiol* 32: 250–254.
Higashi N, Sone C. 1987. A case of celiac-mesenteric trunk. *Kaibogaku Zasshi* 62: 550–556.
Hlaing KPP, Othman F. 2012. Complex pattern of a variant hepatic artery. *Singapore Med J* 53: 186–187.
Hollinshead WH. 1956. Vessels and nerves associated with the posterior abdominal wall. In: *Anatomy for Surgeons: Volume 2, The Thorax, Abdomen and Pelvis*. New York: Paul. B. Hoeber Inc. pp 589–595.
Hollinshead WH. 1971. *Anatomy for Surgeons*. Vols 1–3, second edition. New York, Harper and Row Publishers.
Honma S, Kudo M. 2012. The middle suprarenal artery arising from the superior mesenteric artery. *Surg Radiol Anat* 34: 93–95.
Hugh TB, Kelly MD, Li B. 1992. Laparoscopic anatomy of the cystic artery. *Am J Surg* 163: 593–595.
Hunter J. 1794. A treatise on the blood, inflammation, and gun-shot wounds. Republished in 2007. *Clin Orthop Relat Res* 458: 27–34.
Huu N, Tam NT, Minh NK. 1976. Gastro-duodenal artery arising from the superior mesenteric artery. *Bull Assoc Anat (Nancy)* 60: 779–786.
Inoue K, Yamani T, Odajima G. 1986. A rare case of anastomosis between the dorsal pancreatic and the inferior mesenteric arteries. *Okajimas Folia Anat Jap* 63: 45–46.
International Anatomic Nomenclature Committee. 1989. *Nomina Anatomica*. New York: Churchill Livingstone.
Ishigami K, Yoshimitsu K, Irie H, Tajima T, Asayama Y, Hirakawa M, Honda H. 2006. Accessory left gastric artery from left hepatic artery shown on MDCT and conventional angiography: correlation with CT hepatic arteriography. *AJR* 187: 1002–1009.
Issajew PO. 1932. Ein fall von anomalie der celiaca und mesenterica sup. *Anat Ber* 23: 70.
Jacques P. 1895. Quelques anomalies arterielles. *Bull Soc Anat De Paris* 9: 252.
Jain P, Motwani R. 2013. Morphological variations of superior mesenteric artery: a cadaveric study. *Int J Anat Res* 1: 83–87.
Jones RM, Hardy KJ. 2001. The hepatic artery: a reminder of surgical anatomy. *J R Coll Surg Edinb* 46: 168–170.
Kadir S. 1991. *Atlas of Normal and Variant Angiographic Anatomy*. Philadelphia: W.B. Saunders Company.
Kahn P, Abrams HL. 1964. Inferior mesenteric arterial patterns: angiographic study. *Radiology* 82: 429–441.
Kahraman H, Ozaydin M, Varol E, Aslan SM, Dogan A, Altinbas A, et al. 2006. The diameters of the aorta and its major branches in patients with isolated coronary artery ectasia. *Tex Heart J Inst J* 33: 463–468.
Kalthur SG, Sarda R, Bankar M. 2011. Multiple vascular variations of abdominal vessels in a male cadaver: embryological perspective and clinical importance. *J. Morphol Sci* 28: 152–156.
Kamina P. 1974. *Anatomie Gynécologique et Obstétricale*, second edition. Paris: Maloine SA Éditeur.
Kaneko O. 1990. The arterial distribution to the abdominal digestive organs in human fetuses. *J Nippon Med Sch* 57: 448–464.
Kao GD, Whittington R, Coia L. 1992. Anatomy of the celiac axis and superior mesenteric artery and its significance in radiation therapy. *J Radiol Oncol Boil Phys* 25: 131–134.
Karakaya AF, Kantarci M, Yalcin A, Demir B, Yuce I. 2009. A rare variation of hepatic arteries (Michels Type IV): MDCT angiographic findings. *EAHN* 41: 63–65.
Katada Y, Kishino M, Ishihara K, Takeguchi T, Shibuya H. 2008. Anomalous arterial supply to the gallbladder from the superior mesenteric artery: angiography and computed tomography findings in two cases. *Acta Radiol* 49: 987–990.
Katz-Summercorn A, Bridger J. 2013. A cadaveric study of the anatomical variation of the origins of the celiac trunk and the superior mesenteric artery. A role in median arcuate ligament syndrome. *Clin Anat* 26: 971–974.
Keen EN. 1981. Origin of renal artery from the aorta. *Acta Anat (Basel)* 110: 285–286.
Kelly HA, Hurdon E. 1905. *The Vermiform Appendix and its Diseases*. Philadelphia: WB Saunders.
Kemeny MM, Hogan JM, Goldberg DA. 1986. Continuous hepatic artery infusion with an implantable pump: problems with hepatic arterial anomalies. *Surgery* 99: 501–504.
Khamanarong K, Prachaney P, Utraravichien A, Tongun T, Sripaoraya K. 2004. Anatomy of renal arterial supply. *Clin Anat* 17: 334–336.
Khan PC. 1967. Selective angiography of the inferior phrenic arteries. *Radiology* 88: 1–8.
Kim WK, Yang SB, Goo DE, Kim YJ, Chang YW, Lee JM. 2013. Aberrant ovarian artery arising from the common iliac artery: case report. *Korean J Radiol* 14: 91–93.
Kimura S, Okazaki M, Higashihara H, Nozaki Y, Haruno M, Urakawa H, Koura S, Shinagawa Y, Nonokuma M. 2007. Analysis of the origin of the right inferior phrenic artery in 178 patients with hepatocellular carcinoma treated by chemoembolization via the right inferior phrenic artery. *Acta Radiol* 48: 728–733.
Kiray A, Akcali O, Tayefi H, Kosay C, Ergur I. 2010. Anatomical variations of iliolumbar artery and its relation with surgical landmarks. *Acta Orthop Traumatol Turc* 44: 464–468.
Kirk E. 1931. Untersuchungen üiber die grobere und feinere topographische Verteilung der Arterien, Venen und Ausführungsgänge in der menschlichen Bauchspeicheldrüse. *Z Ges Anat* 94: 822–875.
Kishi Y, Imamura H, Sugawara Y, Sano K, Kaneko J, Kokudo N, Makuuchi M. 2010. Evaluation of donor vasculobiliary anatomic variations in liver graft procurements. *Surgery* 147: 309–339.
Kiss F. 1926. Uber einige varietaten der arteria hepatica und Arteria cystic. *Z Anat Entw Gesch* 81: 601–619.
Kitamura S, Nishiguchi T, Sakai A, Kumamoto K. 1987. Rare case of the inferior mesenteric artery arising from the superior mesenteric artery. *Anat Rec* 217: 99–102.
Koizumi M, Horiguchi M. 1990. Accessory arteries supplying the human transverse colon. *Acta Ansat (Basel)* 137: 246–251.
Koops A, Wojciechowski B, Broering DC, Adam G, Krupski-Burdien G. 2004. Anatomic variations of the hepatic arteries in 604 selective

celiac and superior mesenteric angiographies. *Surg Radiol Anat* 26: 239–244.

Kornreich L, Hadar H, Sulkes J, Gornish M, Ackerman J, Gadoth N. 1997. Effect of normal ageing on the sites of aortic bifurcation and inferior vena cava confluence: a CT study. *Surg Radiol Anat* 20: 63–68.

Kosinski C. 1928. Quelquesobservations sur je, rameaux du tronc caeliaque et des arteres mesenteriques chez l'homme. *CR Assoc Anat* 23: 241–260.

Koster H, Weintrob M. 1928. The blood supply of appendix. *Arch Surg* 17: 577–586.

Kruyt RH. 1992. Vascularization of left kidney by single vessel originating from splenic artery. *Urology* 39: 487–489.

Kudo S, Chuang VP, Walace S, Bechtel W, Mir S. 1984. Middle sacral arteriogaphy diagnostic and therapeutic implications. *Radiology* 151: 65–67.

Kummuru H, Sree Lekha D, Jothi SS, Rajeswararao N, Sujatha N. 2012. Presence of renal artery variations and its surgical correlations. *Int J Med Clin Res* 3: 176–179.

Kupie EA, Marshall WH, Abrams HL. 1967. Splenic arterial patterns: angiographic analysis and review. *Invest Radio* l2: 70–98.

Lacout A, Thariat J, Marcy P. 2012. Main right renal artery originating from the superior mesenteric artery. *Clin Anat* 25: 977–978.

Lange JF, Komen N, Akkerman G, Nout E, Horstmanshoff H, Schlesinger F, Bonjer J, Kleinrensink GJ. 2007. Riolan's arch: confusing misnomer, and obsolete. A literature survey of the connection (s) between the superior and inferior mesenteric arteries. *Am J Surg* 193: 742–748.

Larobina M, Nottle PD. 2005. Extrahepatic biliary anatomy at laparoscopic cholecystectomy: Is aberrant anatomy important? *ANZ J Surg* 75: 392–395.

Latarjet M, Ruiz-Liard A. 1989. *Anatomia Humana*, second edition. Sao Paulo: Medicina Panamericana Editora do Brasil Ltda.

Laude M, Libersa C, Rozan R. 1972. Radio-anatomie du tronc de l'artere splenique chez l'homme. A propos de 100 cas. *Bull Anat* 154: 1050–1055.

Lawdahl RB, Keller FS. 1987. The middle mesenteric artery. *Radiology* 165: 371–372.

Lederle FA, Johnson GR, Wilson SE, Gordon IL, Chute EP, Littooy FN, Krupski WC, Bandyk D, Barone GW, Graham LM, Hye RJ, Reinke DB. 1997. Relationship of age, gender, race and body size to infrarenal aortic diameter. *J Vasc Surg* 26: 595–601.

Lee SS, Kim TK, Byun JH, Kim PN, Kim AY, Lee SG, Lee MG. 2003. Hepatic arteries in potential donors for living related liver transplantation: Evaluation with multi-detector row CT Angiography. *Radiology* 227: 391–399.

Lerona PT, Tewfink HH. 1975. Bifurcation level of the aorta: landmark for pelvic irradiation. *Radiology* 115: 735.

Levasseur JC, Couinaud C. 1968. Etude de la distribution des arteres gastriques. Incidences chirurgicales. *J Chir* 95: 57–78.

Li J, Ren ZF. 2011. Gastroduodenal-splenic trunk: an anatomical vascular variant. *Rom J Morphol Embryol* 52: 1385–1387.

Li J, Ren ZF, Sun T. 2012. Bilateral high origins of testicular arteries: a rare variant. *Rom J Morphol Embryol* 53: 427–429.

Lippert H, Pabst R. 1985. *Arterial variations in man: classification and frequency*. Munchen: Bergmann Verlag.

Lipshutz B. 1917. A composite study of the celiac axis artery. *Ann Surg* 65: 159–169.

Llauger J, Sabate JM, Guardia E, Escudero J. 1995. Congenital absence of the right common iliac artery: CT and angiographic demonstration. *Eur J Radiol* 21: 128–130.

Lochhart-Mummery P. 1923. *Diseases of rectum and colon and their surgical treatment*. London: Bailliere, Tindall and Cox.

López-Andújar R, Moya A, Montalvá E, Berenguer M, De Juan M, San Juan F, Pareja E, Vila JJ, Orbis F, Prieto M, Mir J. 2007. Lessons learned from anatomic variants of the hepatic artery in 1081 transplanted livers. *Liver Transpl* 13: 1401–1404.

Loukas M, Stewart D. 2004. A case of an accessory testicular artery. *Folia Morphol* 63: 355–357.

Loukas M, Hullett J, Wagner T. 2005a. Clinical anatomy of the inferior phrenic artery. *Clin Anat* 18: 357–365.

Loukas M, Aparicio S, Beck A, Calderon R. Kennedy M. 2005b. Rare case of right accessory renal artery originating as a common trunk with the inferior mesenteric artery: a case report. *Clin Anat* 18: 530–535.

Loukas M, Wartmann CT, Louis RG, Tubbs RS, Ona M, Curry B, Jordan R, Colborn GL. 2007. The clinical anatomy of the posterior gastric artery revisited. *Surg Radiol Anat* 29: 361–366.

Macdonald DB, Haider MA, Khalili K, Kim TK, O'Malley M, Greig PD, Grant DR, Lockwood G, Cattral MS. 2005. Relationship between vascular and biliary anatomy in living liver donors. *Am J Roentgenol* 185: 247–252.

Makisalo H, Chaib E, Krokos N, Calne SR. 1993. Hepatic arterial variations and liver-related diseases of 100 consecutive donors. *Transpl Int* 6: 325–329.

Makomaska-Szaroszyk E, Fiedor P. 1989. A rare case of anastomosis between the dorsal pancreatic artery and the middle colic artery. *Folia Morphol (Warsz)* 48: 147–149.

Maleux G, Vaninbroukx J, Demedts I, Heye S. 2010. Common trunk of superior and inferior mesenteric artery at the level of the fifth lumbar vertebra. *J Vasc Interv Radiol* 21: 296–298.

Malnar D, Klasan GS, Mileti D Snjeàna Bajek S,Vrani TS, Arbanas J, Bobinac D, Bobinac M. 2010. Properties of the celiac trunk – anatomical study. *Coll Antropol* 34: 917–921.

Mamatha S, D'Souza AS. 2011. Bilateral accessory renal artery with a rare origin of the testicular artery: An embryological basis. *J Clin Diag Res* 5: 1267–1269.

Mamatha Y, Prakash BS, Padmalatha K. 2011. Rare variant origin of right testicular artery – A case report. *Asian J Med Sci* 2: 65–67.

Mansfield AO, Howard JM. 1964. Absence of both common iliac arteries. A case report. *Anat Rec* 150: 363–364.

Manso JC, DiDio LJA. 2000. Anatomical variations of the human suprarenal arteries. *Ann Anat* 182: 483–488.

Martin R, Couppié G. 1963. Étude des variations des branches du tronc artériel pancréatico-duodéno-jéjunal. *Arch Anat Pathol* 11: A29–A32.

Matoba M, Tonami H, Kuginuki M, Yokota H, Takashima Yamamoto I. 2003. Comparison of high-resolution contrast-enhanced 3D MRA with digital subtraction angiography in the evaluation of hepatic arterial anatomy. *Clin Radiol* 58: 463–468.

Matusz P, Iacob N, Miclaus GD, Pureca A, Ples H, Loukas M, Tubbs SR. 2013. An unusual origin of the celiac trunk and the superior mesenteric artery in the thorax. *Clin Anat* 26: 975–979.

Matusz P, Loukas M, Iacob M, Ples H. 2013. Common stem origin of left gastric, right and left inferior phrenic arteries, in association with a hepatosplenomesenteric trunk, independently arising from the abdominal aorta: Case report using MDCT angiography. *Clin Anat* 26: 980–983.

Mayo CW. 1955. Blood supply of the colon: surgical considerations. *Surg Clin North Am* 35: 1117–1121.

McGowan JR. 1955. Collateral circulation in the sigmoid colon. *Arch Surg* 71: 531–537.

McNulty JG, Hickey N, Khosa F, O'Brien P, Callaghan JP. 2001. Surgical and radiological significance of variants of Buhler's anastomotic artery: a report of three cases. *Surg Radiol Anat* 23: 277–280.

Meckel JF, Jourdan AJL, Doane A. 1832. *Manual of General, Descriptive, and Pathological Anatomy (Volume 1)*. Philadelphia: Carey and Lea.

Melliére D. 1968. Variations des artères hépatiques et du carrefour pancréatique. *J Chir* 95: 5–42.

Mercier R, Vanneuville G. 1968. *Anatomie radiologique de l'aorte abdominale et des ses brances terminales et collaterales*. Paris: Expansion Scientifique.

Merkel FD. 1918. *Anatomie des Menschen*. Wiesbaden: JF Bergmann.

Merklin RJ, Michels NA. 1958. The variant renal and suprarenal blood supply with data on the inferior phrenic, urethral and gonadal arteries. *J Int Coll Surg* 29: 41–76.

Meyer, P. 1952. Contribution à l'étude de la première artère jéjunale. *Assoc Anat Comptes Rendus* 39: 250–257.

Meyer P. 1953. Etude du tronc artériel pancréatico-duodéno-jéjunal.*CR Ass Ant* 40: 99–119.

Meyers MA. 1976. Griffiths' Point: critical anastomosis at the splenic flexure significance in ischemia of the colon. *Am J Roentgenol* 126: 77–94.

Michael AB, Mark BC, Peter W. 1991. An aberrant right hepatic artery from the right renal artery: Anatomical vignette. *Cardio Vasc Intervent Radiol* 14: 349–351.

Michels NA. 1942. The variational anatomy of the spleen and splenic artery. *Am J Anat* 70: 21–72.

Michels NA. 1945. Variations in blood supply of liver, gallbladder, stomach, duodenum and pancreas. *J Intenat Coll Surg* 8: 502–504.

Michels NA. 1951a. Blood supply of pancreas. *Anat Rec* 109: 326.

Michels NA. 1951b. The hepatic, cystic and retroduodenal arteries and their relations to the biliary ducts. *Ann Surg* 133: 503–524.

Michels NA. 1952. Blood supply of the stomach. *Anat Rec* 112: 361.

Michels NA. 1955. *Blood Supply and Anatomy of the Upper Abdominal Organs with a Descriptive Atlas*. Philadelphia, Montreal: JB Lippincott Company.

Michels NA. 1962. The anatomic variation of the arterial pancreatic, bladder, bile duct, liver, pancreas and parts of small and large intestine. *J Int Surg* 18: 13–40.

Michels NA. 1966. Newer anatomy of the liver and its variant blood supply and collateral circulation. *Am J Surg* 112: 337–347.

Michels NA, Siddharth P, Kornblith PL, Parke WW. 1963. The variant blood supply to the small and large intestines: its importance in regional resections. A new anatomic study based on four hundred dissections with a complete review of the literature. *J Int Coll Surg* 39: 127–170.

Michels NA, Siddharth P, Kornblith PL, Parke WW. 1965. The variant blood supply to the descending colon, rectosigmoid and rectum based on 400 dissections. Its importance in regional resections: A review of medical literature. *Dis Col Rect* 8: 251–278.

Michiya K, Satoshi M, Takehiro O, Kana M, Ken O, Tsutomu N, Yasuhiro O, Keijiro A. 2006. Preoperative assessment of vascular anatomy of inferior mesenteric artery by volume-rendered 3D-CT for laparoscopic lymph node dissection with left colic artery preservation in lower sigmoid and rectal cancer. *World J Gastroenterol* 12: 1442–1446.

Miclaus GD, Matusz P. 2012. Bilateral quadruple renal artery. *Clin Anat* 25: 973–979.

Milnerowicz S, Milnerowicz A, Taboła R. 2012. A middle mesenteric artery. *Surg Radiol Anat* 34: 973–975.

Milon D, Milon J, Le Guerrier A, Lanchou G. 1979. Contribution à l'étude de l'artére pancrtéatique dorsale. *CR Ass Anat* 63: 561.

Mirapeix R, Sanudo JR, Ferreira B, Domenechmateu JM. 1996. A retrocaval right testicular artery passing through a hiatus in a bifid right renal vein. *J Anat* 189: 689–690.

Mlakar B, Gadzijev EM, Ravnik D, Hribernik M. 2003. Anatomical variations of the cystic artery. *Eur J Morphol* 41: 31–34.

Molmenti EP, Pinto PA, Klenin J, Klein AS. 2003. Normal and variant arterial supply of the liver and gallbladder. *Pediat Transpl* 7: 80–82.

Moore F. 1958. Variations in the origin and course of the right hepatic and cystic arteries. *Med J* 33: 319.

Moretti S. 1965. Le arterie della testa del pancreas. *Ann Radiol Diagn* 38: 569–594.

Mori Y, Ito I, Hatashita S, Yoshikawa K. 1960. An anomalous case of the mesenteric arteries. absence of a mesenterica inferior. *J Osaka Med Coll* 20: 77–79.

Morris H. 1923. *Human Anatomy*, seventh edition. Philadelphia: P. Blakiston Son and Co.

Murakami G, Hirata K, Takamuro T, Mukaiya M, Hata F, Kitagawa S. 1999.Vascular anatomy of the pancreticoduodenal region: a review. *L Hepatobiliary Pancreat Surg* 1: 55–68.

Murokami T, Mabuchi M, Giuvarasteanu I, Kikuta A, Ohtsuka A. 1998. Coexistence of rare arteries in the human celiac-mesenteric system. *Acta Med Okayama* 52: 239–244.

Nachiappan S, Franks S, Thomas P. 2011. Single ectopic main right renal artery originating from the celiac axis. *JCSR* 12: 10.

Nagino M, Hayakawa N, Kitagawa S, Dohke M, Nimura Y. 1993. Right anterior hepatic artery arising from the superior mesenteric artery. *Hepatogastroenterology* 40: 407–409.

Naidich JB, Naidich TP, Sprayregen S, Hyman RA, Pudlowski RM, Stein HL. 1978. The origin of the left gastric artery. *Radiology* 126: 623–626.

Naito M, Terayama H, Nakamura Y. 2006. Left testicular artery arching over the ipsilateral renal vein. *Asian J Androl* 8: 107–10.

Nakamura H, Uchida H, Kuroda C, Yoshioka H, Tokunaga K, Kitatani T, Sato T, Ohi H, Hori S. 1980. Accessory left gastric artery arising from left hepatic artery: Angiographic study. *AJR* 134: 529–532.

Nassar L, Atweh LA, Jurjus A, Kutoubi AA. 2012. Unusual arterial pattern of the gastrointestinal tract: inferior mesenteric artery arising from the lliac artery and corkscrew external lilac. *Vas Endovasc Surg* 46: 418–421.

Nathan H, Tobias PV, Wellsted MD. 1976. An unusual case of right and left testicular arteries arching over the left renal vein. *Brit J Urol* 48: 135–138.

Nayak BS. 2006a. Common celiac-mesenterico-phrenic trunk and renal vascular variations. *Saudi Med J* 27: 1884–1896.

Nayak BS. 2006b. Hepatomesenteric trunk and gastro-splenico-pyretic trunk. *Int J Anat variat* 1: 2–3.

Nayak SR, Prabhu LV, Krishnamurthy A, Ganesh Kumar C, Ramanathan LA, Acharya A, Sinha AP. 2008. Additional branches of celiac trunk and its clinical significance. *Rom J Morphol Embryol* 49(2): 247–249.

Nayak SB, Patil J, Thangarajan R, Prabhu GS. 2013. Long celiac trunk and its low origin and unusual branched: a case report. *OA Case Reports* 2: 77.

Ndoye JM, Savadogo J, Ndiaye A, Mane L, Diop M, Ndiaye A, Dia A, Sow ML. 2008. The left gastroepiploic artery: A splenic origin but a variable birthplace. *Morphologie* 92: 11–15.

Nebesar RA, Kornblith PL, Pollard JJ, Michels NA. 1969. *Celiac and Superior Mesenteric: A Correlation of Angiograms and Dissections*. Boston: Little, Brown.

Nelson TM, Pollak R, Jonasson O, Abcarian H. 1988. Anatomic variants of the celiac, superior mesenteric and inferior mesenteric arteries and their clinical relevance. *Clin Anat* 1: 75–91.

Neri E, Cosottini M, Caramella D. 2009. *MR Angiography of the Body. Technique and Clinical Applications*. Berlin, Heidelberg: Springer-Verlag.

Niculescu MC, Niculescu V, Ciobanu IC, Daescu E, Jianu A, Sisu AM, Petrescu CI, Motoc A. 2005. Correlations between the colic branches of the mesenteric arteries and the vascular territories of the colon. *Romanian Journal of Morphology and Embryology* 46: 193–197.

Nonent M, Larroche P, Forlodou P, Senecail B. 2001. Celiac bimesenteric trunk: Anatomic and radiologic description: case report. *Radiology* 220: 489–491.

Notkovich H. 1956. Variations of the testicular and ovarian arteries in relation to the renal pedicle. *Surg Gynecol Obstet* 103: 487–495.

Okabayashi T, Kobayashi M, Nishimori I, Yuri K, Miki T, Takeuchi Y, Onishi S, Hanazaki K, Araki K. 2006. Autopsy study of anatomical features of the posterior gastric artery for surgical contribution. *World J Gastroenterol* 12: 5357–5359.

Okada Y, Nishi N, Matsuo Y, Watadani T, Kimura F. 2010. The common hepatic artery arising from the left gastric artery. *Surg Radiol Anat* 32: 703–705.

Okahara M, Mor H, Kiyosue H, Yamada Y, Sagar Y, Matsumoto S. 2010. Arterial supply to the pancreas; variations and cross-sectional anatomy. *Abdom Imaging* 35: 134–142.

Onderoglu S, Yuksel M, Arik Z. 1993. Unusual branching and course of the testicular artery. *Ann Anat* 175: 541–544.

Orts Llorca F. 1944. *Anatomia Humana*. Barcelona: La Semana Grafica.

Osawa T, Feng XY, Sasaki N, Nagato S, Matsumoto Y, Onodera M, Nara E, Fujimura A, Nozaka Y. 2004. Rare case of the inferior mesenteric artery and the common hepatic artery arising from the superior mesenteric artery. *Clin Anat* 17: 518–521.

Otulakowski B, Woźniak W. 1975. A case of origin of the testicular artery from the renal artery, and course of the testicular artery behind the inferior vena cava. *Folia Morphol (Warsz)* 34: 349–351.

Ozan H, Onderoglu S. 1997. Intrapancreatic course of the splenic artery with combined pancreatic anomalies. *Surg Radiol Anat* 19: 409–411.

Ozan H, Gümüşalan Y, Onderoglu S, Simşek C. 1995. High origin of gonadal arteries associated with other variations. *Ann Anat* 177: 156–160.

Ozbulbul NI, Yurdakul M, Tola M. 2011. Does the right inferior phrenic artery have a supplying role in liver cirrhosis without hepatocellular carcinoma? A 64-slice CT study. *Diagn Interv Radiol* 17: 239–242.

Ozkan UL, Ouzkurt F, Tercan O, Kzlkl Ç, Troppmann C, Koç Z, Koca N. 2006. Renal artery origins and variations: angiographic evaluation of 855 consecutive patients. *Diagn Interv Radiol* 12: 183–186.

Ozsoy, Zeytunlu M, Kilic M, Alper M, Sozbilen M. 2011.The results of vascular and biliary variations in Turks liver donors: comparison with others. ISR Surg, article ID 367083, doi: 10.5402/2011/367083.

Pai MM, Vadgaonkar R, Rai R, Nayak SR, Jiji PJ, Ranade A, Prabhu LV, Madhyastha S. 2008. A cadaveric study of the testicular artery in the South Indian population. *Singapore Med J* 49: 551–555.

Pamidi N, Varma S, Vollala VR. 2008. Anomalous branching pattern of Celiac trunk. *IJAV* 1: 8–9.

Panagouli E, Venieratos D. 2011. Right accessory hepatic artery arising from the left gastric artery: a case report. *Rom J Morphol Embryol* 52(3): 1143–1145.

Panagouli E, Lolis E, Venieratos Otula D. 2012. Bilateral origin of the testicular arteries from the lower polar accessory renal arteries. *Int J Morphol* 30: 1316–1320.

Pandey SK, Bhattacharya S, Mishra RN, Shukla VK. 2004. Anatomical variations of the splenic artery and its clinical implications. *Clin Anat* 17: 497–502.

Panyanetinad O. 2011. Rare combined variations of renal, testicular and suprarenal arteries. *IJAV* 4: 17–19.

Paraskevas GK, Raikos A. 2011. Multiple aberrant celiac trunk ramifications. *Singapore Med J* 52(7): e147–e149.

Paraskevas GK, Ioannidis O, Raikos A, Papaziogas B, Natsis K, Spyridakis I, Kitsoulis P. 2011. High origin of a testicular artery: a case report and review of the literature. *J Med Case Reports* 5: 75.

Paturet G. 1958. *Traite d'Anatomie Humaine*. Paris: Masson et Cie Editeurs.

Pearce WH, Slaughter MS, Le Maire S, Salyapongse N, Feinglass J, McCharthy WJ, Yao JST. 1993. Aortic diameter as a function of age, gender and body surface area. *Surgery* 114: 691–697.

Pennington N, Soames RW. 2005. The anterior visceral branches of the abdominal aorta and their relationship to the renal arteries. *Surg Radiol Anat* 27: 395–403.

Peri G, Veralli E, Trivellini G. 1969. La vascolarizzazione del pancreas. *Arch It Chir* 95: 287–300.

Petrella S, de Sousa Rodriquz CF, Sgrott EA, Fernandes GJM, Marques SR, Prates JC. 2007. Anatomy and variations of the celiac trunk. *Int J Morphol* 25: 249–257.

Petren T. 1929. Die arterien und venen des duodenums und des pankreaskopfes beim menschen. *Z Ges Anat* 90: 234–277.

Petru B, Elena S, Dan I, Constantin D. 2007. The morphology and the surgical importance of the gonadal arteries originating from the renal artery. *Surg Radiol Anat* 29: 367–371.

Petsche JZ. 1736. Sylloge anatomica. In Disputations Physico-Medico-Anatomico-Chirurgicae Selectee (ed. Vgl. A. von Haller). Tomus IV, Neapel 1756, s. 6: 762–786.

Piao DX, Ohtsuka A, Murakami T. 1998. Typology of abdominal arteries, with special references to inferior phrenic arteries and their oesophageal branches. *Acta Med Okayama* 52: 189–196.

Piatre F, Giraud D, Dupret S. 1941. *Practica Anatomoquirurgica Ilustrada. Fasc III, Los Organos Retroperitoneales (Spanish transl)*. Barcelona: Salvat Edit.

Pick JW, Anson BJ. 1940. The inferior phrenic artery. Origin and suprarenal branches. *Anat Rec* 81: 413–27.

Piersol GA. 1916. *Human Anatomy*, seventh edition. Philadelphia, London: Lippincott Co.

Pierson JM. 1943. The arterial blood supply of the pancreas. *Surg Gynec Obster* 77: 426–432.

Pignataro E. 1969. L'angiografia selettiva del tronco celiaco e dell'arteria mesenterica superiore. *Min Med* 60: 2369–2398.

Pillet J, Reigner B, Lhoste P, Pillet JC, Mercier P, Cronier P. 1993. Arterial vascularization of the colon. The middle mesenteric artery. *Bull Assoc Anat (Nancy)* 77: 27–30.

Piquand G. 1910. Recherches sur l'anatomie du tronc coeliaque et de ses branches. *Bibliogr Anat* 19: 159–201.

Pitynski K, Skawina A, Gorczyca J, Kitlinski M, Kitlinski Z. 1992. Arterial vascularization of the vermiform appendix in human fetus. *Folia Morphol (Warsz)* 51: 159–164.

Pitynski K, Skawina A, Lipczynski W, Polakiewicz J, Walocha J. 1996. The posterior gastric and superior polar arteries in human fetuses. *Folia Morphol* 55: 43–49.

Pitzorno M. 1920. Morfologia delle arterie del pancreas. *Arch Ital Anat Embriol* 18: 1–48.

Poirier P, Charpy A. 1901. *Traite d'Anatomie Humaine, tome IV*. Paris: Masson.

Poirier P, Charpy A. 1902. *Traite d'Anatomie Humaine*. second ed, vol. II, part 2. Paris: Masson.

Pope CE, Buie LA. 1929. A description of the arterial blood supply of the pelvic colon. *Trans Am Proct Soc* 30: 78.

Pope CE, Judd ES. 1929. The arterial blood supply of the sigmoid, rectosigmoid and rectum. *Surg Clin North Am* 9: 957.

Power JH. 1850. *Surgical Anatomy of the Arteries, and Descriptive Anatomy of the Heart by the late Valentine Flood*, M.D. Dublin: Fannin and Co.

Prakash V, Mokhasi, Rajini T, Shashirekha M. 2011. The abdominal aorta and its branches: anatomical variations and clinical implications. *Folia Morphol* 70: 282–286.

Prakash V, Rajini T, Mokhasi V, Geethanjali BS, Sivacharan PV, Shashirekha M. 2012. Coeliac trunk and its branches: anatomical variations and clinical implications. *Singapore Med J* 53: 329–331.

Prudhomme M, Canovas F, Godlewski G, Bonnel F. 1997. The relationships of the bile duct and the retroduodenal arteries and their importance in the surgical treatment of hemorrhagic duodenal ulcer. *Surg Radio Anat* 19: 227–230.

Quain R. 1844. *Anatomy of the arteries of the human body*. London: Taylor and Walton.

Quenu E. 1893. Des arteres du rectum et de l'anus chez 1'homme et chez la femme. *Bull Soc Anat Paris* 7: 703.

Quinlan R. 1983. Anatomy, embryology, and physiology of the pancreas. In: *Surgery of the Alimentary Tract* (eds Shackelford RT, Zuidema GD). Philadelphia, London, Toronto: WB Saunders.

Rajendran SS, Anbumani SK, Subramaniam A, Balaji MST, Rajendran HSR. 2011. Variable branching pattern of the common hepatic artery and the celiac artery. *JCDR* 5: 1433–1436.

Ramirez FR. 1953. A new anatomic guide for safe ligation of the cystic artery. *Surg Gynecol Obst* 100: 633.

Rankin FW, Bargen JA, Buie LA. 1935. *Colon, Rectum and Anus*. Philadelphia: WB Saunders.

Ratcliffe JF. 1980. The arterial anatomy of the adult human lumbar vertebral body: a microarteriographic study. *J Anat* 131: 57–79.

Ratcliffe JF. 1982. The anatomy of the fourth and fifth lumbar arteries in humans: an arteriographic study in one hundred live subjects. *J Anat* 135: 753–761.

Ravery V, Cussenot O, Desgrandchamps F. 1993. Variations in arterial blood supply and the risk of hemorrhage during percutaneous treatment of lesions of the pelviureteral junction obstruction: Report of a case of testicular artery arising from an inferior polar renal artery. *Surg Radiol Anat* 15: 355–359.

Ray CE Jr, Gupta AK, Shenoy SS. 1998. Left gastric artery arising from the superior mesenteric artery: case reports. *Angiology* 49: 1017–1022.

Reddy S, Bhat SM, Mathew JG, Shetty PC, Gorantla VR, Jetti R, Vollala VR. 2011. A common trunk of origin of the right testicular and middle suprarenal arteries with a retrocaval course. *Indian J Surg* 73: 314–315.

Redmond HP, Redmond JM, Rooney BP, Duignan JP, Bouchier-Hayes DJ. 1989. Surgical anatomy of the human spleen. *Br J Surg* 76: 198–201.

Reeves TB. 1920. A study of the arteries supplying the stomach and duodenum and their relation to ulcer. *Surg Gynecol Obstet* 30: 375–385.

Rela M, McCall JL, Heaton ND. 1998. Accessory right hepatic artery arising from the left: implications for liver transplantation. *Transpl* 66: 792–794.

Richard AR, Bruce M. 2012. Aberrant right ovarian artery from proximal internal iliac artery in uterine artery embolization patient. *O J Rad* 2: 117–119.

Rio-Branco P. 1912. *Essai sur l'anatomie et al medicine operatoire du tronc celiaque et de ses branches, de l'artere hepatique en particulier*. Paris: Stenienhiel.

Roberts WH, Engen PC, Mitchell DA. 1984. When the marginal artery is not marginal. *Anat Anz* 155: 269–272.

Robillard GL, Shapiro AL. 1947. Variational anatomy of middle colic artery; its significance in gastric and middle colonic surgery. *J Internat Coll Surg* 10: 157–169.

Robinson JO. 1965. *Surgery*, first edition. London: Longman, Green.

Rong GH, Sindelar WF. 1987. Aberrant peripancreatic arterial anatomy: considerations in performing pancreatectomy for malignantneplasms. *Am Surg* 53: 726–729.

Rossi G, Cova E. 1904. Studio morfologico delle arterie dellostomacho. *Archo Ital Anat Embriol* 3: 576–579.

Rouviere H. 1970. *Anatomie Humaine*. Paris: Masson.

Rubesch R. 1910. Uber der vermeidugn der darmgangrun bie rectumoperationen. *Beitr Klin Chir* 67: 480.

Rusu MC. 2006. Human bilateral doubled renal and testicular arteries with a left testicular arterial arch around the left renal vein. *Rom J Morphol Embryol* 47: 197–200.

Rusu MC, Vlad M, Voinea LM, Curca GC, Sisu AM. 2008. Detailed anatomy of a left accessory aberrant colic artery. *Surg Radiol Anat* 30: 595–599.

Rygaard H, Forrest M, Mygind T, Baden H. 1986. Anatomic variants of the hepatic arteries. *Acta Radiol Diagn* 27: 425–427.

Saad WE, Davies MG, Sahler L, Lee D, Patel N, Kitanosono T, Sasson T, Waldman D. 2005. Arc of Buhler: incidence in asymptomatic individuals. *Vas Endovascular Surg* 39: 347–349.

Saeed M, Rufai AA. 2001. Duplication of hepatic artery. *Saudi J Gastroenterol* 7: 103–108.

Sahni D, Jit I, Gupta NM, Gupta M, Harjeet. 2003. Branches of the splenic artery and splenic arterial segments. *Clin Anat* 16: 371–377.

Sakamoto H, Akita K, Sato T. 1999. An anomalous right gastroepiploic artery arising from the superior mesenteric artery. *Surg Radiol Anat* 21: 283–286.

Saldarriaga B, Pinto SA, Ballesteros LE. 2008. Morphological expression of the renal artery: A direct anatomical study in a Colombian halfcaste population. *Int J Morphol* 26: 31–38.

Salve VM, Ratanprabha C. 2011. Multiple variations of branches of abdominal aorta. *Kathmandu Univ Med J* 33: 72–76.

Samarawickrama MB. 2010. Hepatosplenomesenteric trunk; a rare variation of the celiac trunk. *Galle Medical J* 15: 39–41.

Sampaio FJ, Passos MA. 1992. Renal artery: anatomic study for surgical and radiologicalpractice. *Surg Radiol Anat* 14: 113–117.

Sarkar AK, Roy TS. 2000. Anatomy of the cystic artery arising from the gastrodudenal artery and its choledochal branches: A case report. *J Anat* 197: 503–506.

Satheesha NB. 2007. Abnormal course of left testicular artery in relation to an abnormal left renal vein: A case report. *Kathmandu Uni Med J* 5(17): 108–109.

Satyapal KS, Haffejee AA, Singh B, Ramsroop L, Robbs JV, Kalideen JM. 2001. Surg Radiol Anat 23: 33–38.

Schlyvitch B. 1937. Untersuchungen uber den anastomotischen kanal zwischen der arteria celiaca and mesenterica superior und damit in zusammenhang stehende Fragen. *Z Anat Entwicklungsgesch* 107: 709–737.

Schmerber F. 1895. Recherches anatomiques sur l'artère renale. Thesis, Lyon.

Scott-Conner CE, Hall TJ. 1992. Variant arterial anatomy in laparoscopic cholecystectomy. *Am J Surg* 163: 590–592.

Seker M, Ciçekcibaşi AE, Salbacak A, Buyukmumcu M. 2005. A morphometric study and variations on the lumbar arteries of human fetuses. *Annals of Anatomy* 187: 135–140.

Şener E, Uzun AH, Özışık K, Çetin L, Emir M. 2005. Bilateral triple renal arteries. *Ankara Üniversitesi Tıp Fakültesi Mecmuası* 58: 18–19.

Shah MA, Shah M. 1946. The arterial supply of the veriform appendix. *Anat Rec* 95: 457–460.

Shah PM, Scarton HA, Tsapogas. 1978. Geometric anatomy of the aortic common iliac bifurcation. *J Anat* 126: 461–468.

Shapiro AL, Robillard GL. 1946. Morphology and variation of the duodenal vasculature. *Arch Surg* 52: 571–602.

Sher S, Mukerjee A, Skillman JJ, Ducksoo K. 1999. Anomalous origin of the inferior artery from common iliac artery. *Vas Endovas Surg* 33: 109–112.

Shetty S, Kantha L, Sheshgiri C. 2013. Bilateral absence of common iliac artery– a cadaveric observation. *Int J Anat Var* 6: 7–8.

Shinohara H, Nakatani T, Fukuo Y, Morisawa S, Matsuda T. 1990. Case with a high-positioned origin of the testicular artery. *Anat Rec* 226: 264–266.

Shivarama CH, Shivarama B, Shetty R.K, Avadhani R. 2012. Multiple variations of branches of abdominal aorta: a case study. *NUJHS* 2: 48–50.

Shoja MM, Tubbs RS, Shakeri AB, Oakes WJ. 2007. Origins of the gonadal artery: embryologic implications. *Clin Anat* 20: 428–432.

Shoja MM, Tubbs RS, Shakeri A, Loukas M, Ardalan MR, Khosroshahi HT, Oakes WJ. 2008. Perihilar branching patterns and morphologies of the RA: a review and anatomical study. *Surg Radiol Anat* 30: 375–382.

Shuang-Qin, Li JY, Terayama H, Naito M, Iimura A, Itoh M. 2008. A rare case of inferior mesenteric artery arising from the superior mesenteric artery, with a review of the review of the literature. *Surg Radio Anat* 30: 159–165.

Sierocinski W. 1975. Arteries supplying the left colic flexure in man. *Folia Morphologica* 34: 117–124.

Silveira LA, Silveira FB, Fazan VP. 2009. Arterial diameter of the celiac trunk and its branches. Anatomical study. *Acta Cir Bras* 24: 43–47.

Singh G, Ng YK, Bay BH. 1998. Bilateral accessory renal artery associated with some anomalies of the ovarian arteries: a case study. *Clin Anat* 11: 417–420.

Singh R, Jaiswal A, Shamal SN, Singh SP. 2011. Variation in the origin of the testicular arteries and drainage of the right testicular vein. *Int J Morphol* 29: 614–616.

Skandalakis LJ, Skandalakis PN, Mirilas PS. 2004. *Surgical Anatomy: The Embryonic and Anatomic Basis of Modern Surgery*. Vol. 2. Thessaloniki: PMP.

Solanke TF. 1970. The position, length and content of the vermiform appendix in Nigerians. *Br J Surg* 57: 100–102.

Song SY, Chung JW, Lim HG, Park JH. 2006. Nonhepatic arteries originating from the hepatic arteries: angiographic analysis in 250 patients. *J Vasc Interv Radiol* 17: 461–469.

Song SY, Chung JW, Yin YH, Jae HJ, Kim HC, Jeon UB, Cho BH, So YH, Park JH. 2010. Celiac axis and common hepatic artery variations in 5002 patients: systematic analysis with spiral CT and DSA. *Radiology* 255: 278–288.

Songür A, Toktas M, Alkoc O, Acar T, Uzun I, Bas O, Ozen AO. 2010. Abdominal aorta and its branches: morphometry variations in autopsy cases. *Eur J Gen Med* 7: 321–325.

Sonneland J, Anson BJ, Beaton. 1958. Surgical anatomy of the arterial supply of the colon from the superior mesenteric artery based upon a study of 600 specimens. *Surg Gynecol Obstet* 106: 385–398.

Ssoson-Jaroschewitsch AJ. 1926. Zur chirurgischen anatomie der aortabifurkation. *Z Anat Ent* 79: 44–57.

Standring S, Borley NR, Collins P, Crossman AR, Gatzoulis MA, Healy JC et al. 2008. Posterior abdominal wall and retroperitoneum. In: *Gray's Anatomy. The Anatomical Basis of Clinical Practice*, 40th edition. NewYork: Churchill Livingstone.

Steward JA, Rankin FW. 1933. Blood supply of the large intestine its surgical considerations. *Arch Surg* 26: 843–891.

Sugita R, Yamazaki T, Fujita N, Naitoh T, Kobari M, Takahashi S. 2008. Cystic artery and cystic duct assessment with 64-detector row CT before laparoscopic cholecystectomy. *Radiology* 248: 124–131.

Sugiura Y, Shima S, Yonekawa H, Yoshizumi Y, Ohtsuka H, Ogata T. 1987. The hypertrophic uncinate process of the pancreas wrapping the superior mesenteric vein and artery: a case report. *Jap J Surg* 17: 182–185.

Sulak O, Albay S, Tagil SM, Malas MA. 2005. Ovarian arteries with bilateral unusual courses. *Saudi Med J* 26: 1456–1458.

Sunderland S. 1942. Blood supply of the distal colon. *Aus New Zeal J Surg* 11: 253–263.

Suzuki K, Prates JC, DiDio LJ. 1978. Incidence and surgical importance of the posterior gastric artery. *Ann Surg* 187: 134–136.

Suzuki M, Akaishi S, Rikiyama T, Naitoh T, Rahman MM, Matsuno S. 2000. Laparoscopic cholecystectomy, Calot's triangle, and variations in cystic arterial supply. *Surg Endosc* 14: 141–144.

Suzuki T, Nakayasu A, Kawabe K, Takeda H, Honjo I. 1971. Surgical significance of anatomic variations of the hepatic artery. *Am J Surg* 122: 505–512.

Sylvester PA, Stewart R, Ellis H. 1995.Tortuosity of the human splenic artery. *Clin Anat* 8: 214–218.

Sylvia S, Kakarlapudi SV, Vollala VR, Potu BK, Jetti R, Bolla SR, Rao M, Pamidi N. 2009. Bilateral variant testicular arteries with double renal arteries. *Cases J* 2: 114.

Takamuro T, Murakami G, Hirata K. 1998. Arterial supply of the first, second, third and fourth portion of duodenum: An anatomical study with special reference to the minimal invasive pancreaticoduodenectomy. *Jap J Gastroenterol Surg* 31: 825–835.

Tanaka R, Ibukuro K, Akita K. 2008. The left inferior phrenic artery arising from left hepatic artery or left gastric artery: radiological and anatomical correction in clinical cases and cadaver dissection. *Abdom Imag* 33: 328–333.

Tandler J. 1904. Uber die varietäten der Celiac und deren Entwicklung. *Anat Hefte* 25: 473–500.

Taniguchi T. 1931. Beitrag zur Topographie der grossen aste der bauchaorta. *Fol Anat Jap* 9: 201–214.

Terminologia Anatomica. 1998. *Federative Committee on Anatomical Terminology*. Stuttgart, New York: Thieme.

Testut L. 1931. *Traite d'Anatomie Humaine*, eighth edition. Paris: Hoeber–Harper.

Testut L, Laterjet A. 1949. *Traite d'Anatomie Humaine*. Paris: Doin.

Testut L, Latarjet A. 1958. *Tratado de Anatomia Humana*, ninth edition. Barcelona: Salvat.

Thomford NR, Chandnani PC, Taba AM, Chablani VN, Busnardo AC. 1986. Anatomic characteristics of the pancreatic arteries: radiologic observations and their clinical significance. *Am J Surg* 151: 690–693.

Thompson J. 1933. Arteries in hepatic pedicle. *Univ Calfornia Publ Anat* 1: 55.

Tong-Un T, Sripaoraya K. 2004. Anatomy of renal arterial supply. *Clin Anat* 17: 334–336.

Toni R, Favero L, Bolzani R, Roversi R, Vezzadini P. 1985. Further observations on the anatomic variation in the arteries of the human pancreas. *IRCS Med Sci* 13: 605–606.

Toni R, Mosca S, Favero L, Ricci S, Roversi R, Toni G, Vezzadini P. 1988a. Clinical anatomy of the suprarenal arteries: a quantitative approach by aortography. *Surg Radiol Anat* 10: 297–302.

Toni R, Favero L, Mosca S, Ricci S, Roversi R, Vezzadini P. 1988b. Quantitative clinical anatomy of the pancreatic arteries studied by selective celiac angiography. *Surg Radiol Anat* 10: 53–60.

Topaz O, Topaz A, Polkampally P R, Damiano T, King CA. 2010. Origin of a common trunk for the inferior pyretic arteries from the right renal artery: A new anatomic vascular variant with clinical implications. *Cardiovasc Revasc Med* 11: 57–62.

Toupet A. 1951. Quelque considerations sur la vascularization des colons et leurs abaissements dans la chirurgie du colon gauche et du rectum. *Rev Chir* 70: 70.

Trubel W, Rokitansky A, Turkof E, Firbas W. 1988. Correlations between posterior gastric artery and superior polar artery in human anatomy. *Anat Anz* 167: 219–223.

Tsagareishvili A. 1959. Variants of the origin of the left gastric artery and their practical significance in stomach resection. *Vestin Khir Grekova* 83: 104–107.

Tsukamoto N. 1929. The branches of the abdominal visceral arteries in Japanese. *Kaibogaku Zasshi Asshi* 2: 780–829.

Ucerler H, Ikiz AA. 2006. Multiplicity of the variations in ventral branches of abdominal aorta. *Ital J Anat Embryol* 111: 15–22.

Ugurel MS, Battal B, Bozlar U, Nural MS, Tasar M, Ors F, Saglam M, Karademir I. 2010. Anatomical variations of hepatic arterial system, celiac trunk and renal arteries: an analysis with multidetector CT angiography. *Brit J Radiol* 83: 661–667.

Ures J, Stacchini A, Prates JC, Gatto IM, Ures S. 1979. Angiographic anatomy of the cecal artery. *Arq Gastroenterol* 16: 8–11.

Uysal II, Ciçekcibaşi AE, Yilmaz MT, Seker M, Sanli O. 2010. Multiple variations of the abdominal aorta in single cadaver. *Singapore Med J* 51: e94–97.

Vandamme JP, van der Schuren G. 1976. Re-evaluation of the colic irrigation from the superior mesenteric artery. *Acta Anat* 95: 578–588.

Vandamme JP, Bonte J. 1985. The branches of the celiac trunk. *Acta Anat (Basel)* 122(2): 110–114.

Vandamme JP, Bonte J. 1986. Systematization of the arteries in the splenic hilus. *Acta Anat* 125: 217–224.

Vandamme JP, Bonte J. 1988. The blood supply of the stomach. *Acta Anat* 131: 89–96.

Vandamme JP, Bonte J. 1990. *Vascular anatomy in abdominal surgery*. Stuttgart: Georg Thieme.

Vandamme JP, Van der Schueren G, Bonte J. 1967. Vascularisation du pancreas: proposition de nomenclature P.N.A. et angioarchitecture des ilots. *CR Ass Anat* 137: 1184–1189.

Vandamme JP, Bone J, Schueren G. 1982. Re-evaluation of the colic irrigation from the inferior mesenteric artery. *Acta Anat (Basel)* 112: 18–30.

Varma KS, Pamidi N, Vollala VR. 2009. Common celiacomesenteric trunk: a rare anatomic variation. *J Vasc Bras* 8: 271–273.

Varma KS, Pamidi N, Vollala VR, Bolla SR. 2010. Hepato-splenomesenteric trunk: a case report. *Rom J Morphol Embryo* l51: 401–402.

Veeresh H, Halasagi SS, Pai SR, Mavishettar GF. 2012. A study of arterial supply of cecum in humans. *J Evolu Dent Med Sci* 1: 812.

Vergoz M. 1921. Artère principale. *Bull Mém Soc Anat Paris* 18: 97–99.

Villemin F. 1921. Sur la circulation arterielle du duodenum. *CR Assoc Anat* 16: 223–228.

Villemin F, Huard P. 1924. Ka constitution de l'arc de Treitz. *CR Ass Anat Strasbourg* 263–267.

Voisin MM, Devambez L. 1949. Contribution l' etude de la vascularisation arterielle du bulbe duodenal. *CR Assoc Anat* 36: 691–696.

Von Bardeleben K. 1906. *Lehrbuch der Systematischen Anatomie des Menschen*. Berlin: Urban & Schwarzenberg.

Von Haller A. 1966. The large intestine. In: First Lines of Physiology. A Reprint of the 1786 Edition (ed. Cullen WW). New York, London: Johnson Reprint Corporation, Sources of Science 32.

Wadhwa S, Barua MP. 2008. Anomalous middle colic artery originating from common hepatic artery: a case report. *Clin Anat* 21: 798–799.

Wadhwa A, Soni S. 2010. A study of gonadal arteries in 30 adult human cadavers. *Clin Med Insights Repro Health* 4: 1–5.

Wadhwa A, Soni S. 2012. An accessory renal artery from a tortuous abdominal aorta: A case report. *J Clin Diagn Res* 6: 1292–1293.

Wang X, Yang R. 2009. Angiographic findings of extrahepatic branches originating from hepatic artery and its clinical significance. *Chin J Cancer Res* 21: 61–67.

Warwick R, Williams PL. 1973. *Gray's Anatomy*, 35th edition. Philadelphia: Saunders.

Weinstein BB, Countess EH, Derbes VJ. 1940. *Urol Cutan Rev* 44: 137–139.

Weisz R, Bianco V. 1957. Richerche anatomiche e considerazioni chirurgiche sull'arteria splenica. *Boll Soc Piemont Chir* 27: 805.

Wieslander CK, Rahn DD, McIntire DD, Marinis SI, Wai CY, Schaffer JI, Corton MM. 2006. Vascular anatomy of the presacral space in unembalmed female cadavers. *Am J Obst Gynecol* 195: 1736–1741.

Wilkie DP. 1911. The blood supply of the duodenum with special reference to the supraduodenal artery. *Surg Gynecol Obstet* 13: 399–405.

Williams PL. 1999. *Gray's Anatomy*, 38th edition. London: Churchill Livingston.

Williams PL, Warwick R, Dyson M, Bannister LH (eds). 1989. *Gray's Anatomy*, 37th edition. Edinburgh, London, and New York: Churchill Livingstone.

Williams PL, Bannister LH, Beny MM, Collins P, Dyson M, Dussek JE, Fergusen MWJ. 1995. *Gray's Anatomy*. London: Churchill Livingstone.

Williams PL, Dyson M, Dussak JE, Bannister LH, Berry MM, Collins P, Ferguson MWJ. 2000. *Gray's Anatomy*, 38th edition. Edinburgh, London: ELBS with Churchill Livingstone.

Williams TB. 1928. Vascular studies of the pylorus. *Anat Rec* 38: 273–285.

Winston CB, Lee NA, Jarnagin WR, Teitcher J, DeMatteo RP, Fong Y, Blumgart LH. 2007. CT angiography for delineation of celiac and superior mesenteric artery variants in patients undergoing hepatobiliary and pancreatic surgery. *Am Roentgenol* 108: W13–W19.

Winter TC, Nghiem HV, Freeny PC, Hommeyer SC, Mack LA. 1995. Hepatic arterial anatomy: Demonstration of normal supply and

vascular variants with three- dimensional CT angiography. *Radiographics* 15: 771–780.

Woodburne RT, Olsen LL. 1951. The arteries of the pancreas. *Anat Rec* 111: 255–270.

Wu WH, Wan YL, Lee L, Yang YM, Huang YT, Cehn CL, Fan SF. 2004. First two cases of living related liver transplantation with complicated anatomy of blood vessels in Beijing. *World J Gastroenterol* 10: 2854–2858.

Wu Y, Peng W, Wu H, Chen G, Zhu J, Xing C. 2013. Absence of the superior mesenteric artery in an adult and a new classification method for superior-inferior mesenteric arterial variations. *Surg Radiol Anat* 36(5): 511–515.

Xue HG, Yang CY, Ishida S, Ishizaka K, Ishihara A, Ishida A, Tanuma K. 2005. Duplicate testicular veins accompanied by anomalies of the testicular arteries. *Ann Anat* 187: 393–398.

Yahel J, Arensburg B. 1998. The topographic relationships of the unpaired visceral branches of the aorta. *Clin Anat* 11: 304–309.

Yamada M, Nojiri I, Kosugi M. 1963. Two anomalies: 1) middle colic artery from the splenic artery, 2) anomalous hepatic duct combined with arterial anomalies. *Acta Anat Nippon* 38(IV): 7 (in Japanese).

Yamaki K, Tanaka N, Matsushima T, Miyaxaki K, Yoshizuka M. 1995. A rare case of absence of the celiac trunk: the left gastric, the splenic, the common hepatic and the superior mesenteric arteries arising independently from the abdominal aorta. *Ann Anat* 177: 97–100.

Yamasaki M, Nakao T, Ishizawa A, Ogawa R. 1990. A rare case of the inferiormesenteric artery and some colic arteries in man. *Anat Anz* 171: 343–349.

Yamato T, Hamanaka Y, Hirata S, Sakai K. 1979. Oesophagoplasty with an autogenous tubed gastric flap. *Am J Surg* 137: 597–602.

Yang IY, Oraee S, Viejo C, Stern H. 2011. Computed tomography celiac trunk topography relating to celiac plexus block. *Reg Anesth Pain Med* 36: 21–25.

Yi N, Yi S-Q, Wang H-X, Ogawa Y, Ohta T, Ozaki N, Itoh M. 2010. Anterior inferior pancreaticoduodenal artery running between the dorsal and ventral pancreas: morphological and embryological viewpoint. *Open Anat J* 2: 79–85.

Yi SQ, Li J, Terayama H, Naito M, Iimura A, Itoh M. 2008. A rare case of inferior mesenteric artery arising from the superior mesenteric artery, with a review of the review of the literature. *Surg Radiol Anat* 30: 159–165.

Yildirim M, Ozan H, Kutoglu T. 1998. Left gastric artery originating directly from the aorta. *Surg Radiol Anat* 20: 303–305.

Yildirim M, Celik HH, Yildiz Z, Tatar I, Aldur MM. 2004. The middle colic artery originating from the celiac trunk. *Folia Morphol (Warsz)* 63: 363–365.

Yoo SJ, Ku MJ, Cho SS, Yoon SP. 2011. A case of inferior mesenteric artery arising from the superior mesenteric artery in a Korean woman. *J Korean Med Sci* 26: 1382–1385.

Yoshida T, Suzuki S, Sato T. 1993. Middle mesenteric artery; an anomalous origin of a middle colic artery. *Surg Radiol Anat* 15: 361–363.

Young AH. 1896. Abnormalities of the middle sacral artery and their morphological significance. *J Anat Physiol* XXXX: 169–175.

Young AH. 1905. Observations on the lumbar arteries. *J Anat Physiol* 39: 295–300.

Zebrowski W, Augustyniak E, Zajac S. 1971. Variation of origin and branches of the inferior mesenteric artery and its anastomoses. *Folia Morphol* 30: 510–517.

Ziegler HR. 1942. Excision of the head of the pancreas for carcinoma with studies of its blood supply. *Surg Gynecol Obstet* 74: 137–145.

55 Renal arteries

Priti L. Mishall
Albert Einstein College of Medicine, Bronx, New York, USA

Renal arterial variations are extensive and occur because the embryonic development of the kidneys is complex. Embryological development is the basis for variability in the position and source of the blood supply, the branching pattern of the blood vessels, the location of entry of the blood vessels into the kidneys, and the relationships of the renal arteries throughout their course with adjacent structures. Anatomical variation in the renal arterial system has significant clinical implications in, for example, endoscopic surgery, radiodiagnostic procedures including renal angiography, and renal vascular interventions such as those required during transplantation surgery (Satyapal et al. 2001). Knowledge of the variations in renal vessels is also essential for exploring renal trauma, vascular reconstruction procedures, repair of abdominal aortic aneurysms, and treating systemic diseases such as renal artery stenosis and renal hypertension (Kaplan et al. 1999; Garcier et al. 2001; Satyapal et al. 2001; Tao et al. 2013).

Historical background

Variations of the renal vessels have intrigued investigators for centuries. In 1552, Eustachius was the first to write about multiple renal arteries (Graves 1969; Çiçekcibaşi et al. 2005). Bartholin (1655–1738), who described the Bartholin glands in females, was the first to report anatomical variations in the origin of the renal arteries (Beregi et al. 1999; Çiçekcibaşi et al. 2005).

Subsequently, innumerable articles have been published focusing on the arrangement of the renal vasculature relative to both normal and congenitally malformed kidneys. The most detailed and striking work was the literature review of 10,967 kidneys by Merklin and Michels (1958). There have been other notable contributions, specifically covering multiple renal arteries (Gray 1906; Eisendrath and Strauss 1910; Pick and Anson 1940; Edsman 1957; Sykes 1963; Olsson and Wholey 1964; Bergman et al. 1988; Satyapal et al. 2001; Vilhova et al. 2001; Beyer and Daily 2004; Bordei et al. 2004; Tao et al. 2013). Extensive studies of the segmental distribution and branching pattern of renal arteries are to be found in Graves (1954), Shoja et al. (2008) and Bordei et al. (2012). Diagnostic angiographic studies have been performed to elucidate the branching pattern of the renal arteries (Boijsen 1959; Odman and Ranniger 1968), and there has been detailed work on the blood supply to the kidney via the hilar and polar arteries (Sampaio and Passos 1992; Khamanarong et al. 2004). Investigations of the corresponding vertebral level and circumferential origin of the renal arteries from the abdominal aorta were reviewed by Aubert and Koumare (1975) and Ozan et al. (1997).

Normal anatomy of the renal arteries

Typically, the renal arteries originate from the aorta at the level of the second lumbar vertebra. In addition to supplying the renal parenchyma, the renal artery also perfuses the renal pelvis, the fatty capsule, the upper part of the ureter, and the adrenal gland (Boijsen 1959; El-Galley and Keane 2000). The right renal artery is longer than the left and takes a long inferior path passing posterior to the inferior vena cava (IVC) and right renal vein to reach the hilum. The left renal artery traverses posterior to the renal vein and runs slightly superiorly to reach the more superiorly situated kidney. According to Merklin and Michels (1958), the average lengths of the right and left renal arteries are in the range 0.5–8 cm and 0.5–6 cm, respectively.

Single-origin renal artery from abdominal aorta

Origin: vertebral level

The origin of the renal arteries from the aorta varies relative to vertebral level. Since these structures are bilateral there are variations in the origins of both the right and left renal arteries: they can arise at higher, lower, or equal vertebral levels. These differences have been reported in many adult studies and a single fetal study. A wide range of variations has been reported with individual case reports documenting the level of origin of a renal artery as high as the thoracic vertebrae.

Bergman's Comprehensive Encyclopedia of Human Anatomic Variation, First Edition. Edited by R. Shane Tubbs, Mohammadali M. Shoja and Marios Loukas.
© 2016 John Wiley & Sons, Inc. Published 2016 by John Wiley & Sons, Inc.

The close relationship between the renal arteries and other branches arising from the abdominal aorta, especially the superior mesenteric artery, makes it necessary to distinguish the renal from the mesenteric arteries to avoid inadvertent injury (Beregi et al. 1999).

Knowing the corresponding vertebral level of origin of the renal arteries helps to identify these vessels on CT images and MRI angiographies. Interventional radiologists need to be aware of the variations of origin to ensure accurate interpretation of the selective renal angiograms that are widely performed to evaluate conditions of the renal arteries such thrombosis, stenosis, aneurysms, and renal hypertension (Aubert and Koumare 1975; Beregi et al. 1999).

The pioneering work of Aubert and Koumare (1975) using aortography negative films demonstrated that the origin of the renal arteries varies between the upper border of lumbar vertebra 1 (L1) and the lower border of L2 in 95.8% (604 out of 630) of specimens. In a spiral CT angiography study of 200 renal arteries, Beregi et al. (1999) found that the right (88%) and the left (87%) renal artery originated between the lower one-third of the L1 vertebra and the lower border of L2 respectively.

Studies of the origins of right versus left renal arteries with respect to vertebral levels have revealed the following. In an angiographic study of 855 patients, Özkan et al. (2006) revealed that the right and left renal arteries originated between the upper margin of L1 and the lower margin of L2 in 98% and 97% of the patients, respectively. In the same study they found that 23% of right and 22% of left renal arteries originated at the intervertebral disk between L1 and L2 (Özkan et al. 2006). Aubert and Koumare (1975) found that 14.49% (91/628) of right and 13.37% (87/632) of left renal arteries arose at the same level, that is, at the disk between L1 and L2. Renal angiographic studies by Edsman (1957) demonstrated that the right and left renal arteries originate at the disk between L1 and L2 in 31.5% (86/273) and 34.4% (86/250) respectively. The above findings establish that the vast majority of right and left renal arteries arise between the L1 and L2 vertebrae and generally at the level of the disk between them.

In a dissection study on 180 fetal renal arteries, Çiçekcibaşi et al. (2005) found that the right and the left renal arteries originated between the upper margin of L1 and the upper one-third of L2 in 96% and 97.9%, respectively.

Incidental individual findings on aortography have reported origins of the renal artery from the thoracic aorta at the body of T11 (Doppman 1967; Tegtmeyer 1969). In another case report, Fernet et al. (1987) found a renal artery origin at the disk between T11 and T12.

Aubert and Koumare (1975) summarized the work of previous authors, stating that the renal arteries originate from the abdominal aorta below the superior mesenteric artery at the level of L1. Angiographic studies by Edsman (1957) and Kincaid (1966) concluded that the renal artery arises from the aorta usually at the level of the lower third of L1 with a variation of one vertebral body cephalad or caudad.

Origin: Renal ostium on the abdominal aorta

The position of the renal ostium or opening into the renal artery on the inner aspect of the abdominal aorta is variable. As a consequence, the origins of the right and left renal arteries do not always correspond. Also, the proximity of one or both renal ostia (2 mm) to the origin of the superior mesenteric artery (SMA) can confuse interventional radiologists during selective renal catheterization (Odman and Ranniger 1968).

When endovascular procedures such as balloon angioplasty and stent implantation are performed to treat renal artery stenosis, it is extremely important for the clinician to have accurate information about the origin of the renal artery from the abdominal aorta in order to place the stent perpendicular to the relevant ostium (Beregi et al. 1999). Many studies of adults and a single fetal study document variability in the origins of the right and left renal arteries from the inner aspect of the abdominal aorta.

Circumferential location of the renal ostium on the wall of the abdominal aorta

Most authors have used the terms anterior or ventral, lateral, anterolateral, and posterolateral to describe the circumferential position of the ostia of the renal arteries. In dissections of 30 abdominal aorta specimens, Ozan et al. (1997) found that the renal ostia were on the lateral wall in 48.3% (29 out of 60) and the anterolateral wall in 31.6% (19 out of 60); the remaining 16.67% (10 out of 60) were located on the anterolateral-lateral border and one each on the posterolateral and posterolateral posterior borders of the abdominal aorta. In another study, Odman and Ranniger (1968) performed postmortem aortic dissections on 110 cadavers and documented that 36.36% (40 out of 110) of the right renal ostia and 10.91% (12 out of 110) of the left renal ostia were located on the ventral aspect of the abdominal aorta. The ostium of the right renal artery in 27.27% (30 out of 110) of cases, and the ostium of the left renal artery in 52.72% (58 out of 110), was located on the lateral aspect of the abdominal aorta. The authors also observed that the right renal ostia arose more frequently from the ventral midline of the abdominal aorta than the left. During translumbar aortography the catheter is introduced from the left of the spine and is directed anteriorly to the right. The likliehood of causing accidental injury to the ventrally originating right renal artery than the left is therefore greater (Odman and Ranniger 1968).

In a dissection study of 180 fetal renal arteries, Çiçekcibaşi et al. (2005) revealed that the right renal artery originated from the lateral and anterolateral walls of the abdominal aorta in 73.0% and 26.9% of cases, respectively, while the left renal artery originated from the lateral and anterolateral wall in 90.3% and 9.6%, respectively. These findings are similar to those from studies conducted on adults, suggesting that there are no significant changes in circumferential position of the renal arterial ostia during postpartum development.

Vertical relationship of the origins of the right and left renal arteries

In a study by Merklin and Michels (1958) on 185 autopsy kidneys, the renal arteries originated at the same level in 30% of specimens, the right artery was higher than the left in 47%, and the left was higher than the right in 23%. In another study on 60 organ blocks of the abdominal aorta with renal arteries and kidneys, Kosiński (1994) found that in 72% cases the right renal artery originated superior to the left and in 56% it was closer to the median plane of the body, which passed through the center of the aortic lumen and wall or very close to it. Ozan et al. (1997) performed cadaveric dissections on 30 abdominal aortae and found that the right renal ostium was located superior to the left in 53.3% of specimens, while in 10% the right and left renal ostia were located at the same level.

In a dissection study on 180 fetal renal arteries, Çiçekcibaşi et al. (2005) found that the origin of the right renal artery from the inner aspect of the abdominal aorta was superior to the left renal artery in 53.8%, at the same level in 34.6%, and inferior in 11.5%.

When describing an arterial phase of renal angiography, Kincaid (1966) mentioned the relationship of the renal artery origin to the vertebrae and found that the renal arteries arose from the lateral aspect of the abdominal aorta at a level between the mid-portion of L1 and the upper third of L2. The author further concluded that the right renal artery arises higher on the aorta than the left.

Although in most people the right kidney sits in a lower position in the retroperitoneum than the left, data indicate that the right renal artery has a higher point of origin from the aorta than the left (Pick and Anson 1940; Ross et al. 1961; Lippert and Pabst 1985; El-Galley and Keane 2000). Interestingly, variations in the locations of renal ostia on the aortic wall result from developmental variability in the origin of the mesonephric arteries (Felix 1912; Bremer 1915; Bauer 1968; Ozan et al. 1997).

Morphometry of the renal artery

The morphometric parameters of the renal artery are especially important for renal transplantation surgery, because variations affect the surgical outcome. Variability in the length and diameter of the renal vessels has significant clinical implications.

Length of renal artery

In a study by Ross et al. (1961) on 34 cadavers, the average lengths of the right and left renal arteries were 39 mm and 33 mm respectively; the longest right and left renal arteries were 81 mm and 58 mm, respectively, and the shortest were 8 mm and 9 mm, respectively. Hazırolan et al. (2011) noted that the average length of the renal artery was usually 4–6 cm.

Diameter of renal artery

Merklin and Michels (1958) reported that the caliber of the right and left renal artery is usually the same, the average diameter being 5.5 mm with a range of 4–7 mm. In an angiographic study on 28 right and 29 left renal arteries in males, Edsman (1957) found that the lumens on both sides had the same diameter, averaging 7.9 mm, while in females the average lumen diameter from 21 right and 17 left renal arteries was 6.4 mm. The renal artery is therefore wider in males than in females. Weld et al. (2005) found that the diameter of the renal artery ranged from 4 to 12 mm with an average of 7.9 mm. As reported by Hazırolan et al. (2011), the average diameter of the renal artery was 5–6 mm.

The left kidney is the preferred side for retrieval of the donor kidney during renal transplantation because the left renal vein is typically longer and less fragile (Urban et al. 2001; Shakeri et al. 2007; Sezer and Hoscoskun 2012). The minimum length of the renal artery suitable for transplantation was found by Ross et al. (1961) to be 20 mm and that for the renal vein was 30 mm. The length of the renal artery is therefore crucial during transplantation as a long right renal artery can cause kinking at the anastomotic site (Sezer and Hoscoskun 2012).

Course of renal artery

Sound knowledge of the topographic relationship of the renal artery to the renal vein and the pelvis of the ureter is of the utmost importance to surgeons before they perform renal transplantation operations if they are to avoid injuries due to misidentification of the structures. It is equally important for radiologists to understand the close association of structures around the renal artery in order to draw relevant clinical conclusions from such diagnostic and therapeutic procedures as renal angiography and balloon angioplasty.

The renal artery originates from the abdominal aorta and travels through the hilum of the kidney. Before entering the hilum it divides into segmental branches. At the hilum these branches are in close relationship with the expanded part of the ureter, the pelvis. Throughout its course, the renal artery is accompanied by the returning renal vein.

Studies by many investigators on the course of the renal artery broadly identify the variations described in the following sections.

Straight or tortuous course of the renal artery from its origin at the abdominal aorta to the hilum of the kidney

Hegedus (1972) performed three-dimensional angiography on 120 renal arteries and found that the course of the artery from the aorta to the hilum was either straight (38.8%) or tortuous (61.2%). The author also observed that in 32 bilateral examinations, 50% (16/32) of renal arteries were tortuous and symmetrical.

Relationship of the renal artery to the renal vein

Anson and Daseler (1961) studied 125 specimens of kidneys with aorta, renal artery, and renal vein and found that the renal artery lay dorsal to the renal vein in 47.6% of the sides. The authors also observed the relationship of the cranial or caudal origin of the renal artery relative to the renal vein and found

that in 42% of specimens the renal artery originated cranial and dorsal to the renal vein; further, along its path it turned ventral to the renal vein at the hilum of the kidney. In 2.4% of the specimens it originated caudal and dorsal to the renal vein and, along its path, moved ventral to enter the hilum.

Relationship of the renal artery and its branches to the pelvis of the ureter

During kidney development the renal pelvis rotates from a primitively anterior orientation to a mature medial position. Failure of the kidney to rotate medially causes the inferior branch of the renal artery to obstruct the pelviureteral junction (Ravery et al. 1993). Rao et al. (2006) reported that 15–52% of upper urinary tract obstructions occur as a consequence of arteries anterior or posterior to the ureteropelvic junction. Bergman et al. (1988) reported that in 2 out of 124 kidney dissections, the main renal artery was retropelvic and followed a fan-like distribution.

Branching pattern of renal artery

Before it enters the hilum of the kidney, the renal artery typically branches into five segmental arteries. Graves (1954) described the segments of the kidney. He performed detailed and extensive studies on the branching pattern of the segmental arteries, outlined the extent of their distribution, and proposed a classification for the variations in their branching pattern.

In the following section we give a brief description of the segments of the kidney, the distribution of the segmental arteries, and their clinical significance. The term *peri-hilar* branching is broadly used to describe the branching of the renal artery before the artery enters the hilum of the kidney. Notable studies of the peri-hilar branching pattern were performed by Graves (1954) through his groundbreaking work on the segmental arteries. Weld et al. (2005) introduced the term 'presegmental artery' to describe the main renal artery that divides into two or more segmental arteries before entering the hilum. In their study on branching of the renal artery, Fine and Keen (1966) considered only three primary segmental arteries (upper, lower, and posterior) instead of the five proposed by Graves. Shoja et al. (2008) studied a single main and multiple renal arteries and classified their peri-hilar branching into eight cardinal patterns on the basis of their morphology. This is followed by a discussion of the variations in the perihilar branching patterns, as seen in the above studies, and of the relationship of the segmental arteries to the pelvis of the ureter.

Segments of the kidney and clinical significance of the segmental arteries

Kidneys have a segmental distribution of their blood supply similar to those of the lungs, liver, and spleen. According to Graves (1956) the kidney typically has five vascular segments: (1) apical/superior, the upper pole in both the anterior and posterior planes; (2) upper, the central area; (3) middle, the area between the upper and the lower pole; (4) lower/inferior, forming the lower pole in both the anterior and posterior planes; and (5) posterior, the area between the apical and the lower pole in the posterior plane (Graves 1956).

Graves (1954) found that the main renal artery, which arises from the abdominal aorta, splits into anterior and posterior divisions prior to reaching the hilum. The anterior division further branches into four segmental branches that supply the apical/superior, upper, middle, and inferior segments of the kidney, while the posterior division supplies the posterior segment of the kidney.

Each of these segmental arteries enters the hilum and branches into a lobar artery that supplies the pyramids of the kidney. Each lobar artery divides to form two to three interlobar arteries. The interlobar artery passes between the renal pyramids and arches over the base of the pyramid to form the arcuate artery. Each arcuate artery gives off interlobular arteries, which branch to become the glomerular capillaries that form the filtration unit of the kidney. Variations in the distribution of those intrarenal branches of the renal arteries are beyond the scope of this chapter.

In contrast, the intrarenal veins have no segmental distribution and there is free anastomosis between them within the substance of the kidney (Graves 1954; Kincaid 1966).

Each segmental artery is an end artery (Brödel 1901; Graves 1954; El-Galley and Keane 2000; Shakeri et al. 2007). This implies lack of collateral circulation between adjacent renal segments. Blockage of a segmental renal artery will therefore result in loss of the blood supply to that particular segment of the kidney. The kidneys receive 20% of the cardiac output (Kadir 1991). Understanding the risks associated with injury to the vascular supply of the kidney will help the surgeon to plan cautiously for renal transplantation surgeries and laparoscopic procedures. An accidental ligature of the segmental artery can result in ischemic necrosis and loss of function of the corrsponding renal segment. In contrast, careful and deliberate clamping of the segmental artery during a surgical procedure provides a bloodless plane and minimizes the risk of injury to the rest of the kidney. Identification of the following two safe avascular planes on the kidney has therefore assisted in minimizing the blood loss during surgery: first, an area situated approximately one-third of the distance between the posterior and anterior surfaces; and second, an area between the posterior segment and polar segments to gain access to the upper or lower pole of the kidney (El-Galley and Keane 2000; Urban et al. 2001).

Variations in peri-hilar branching patterns

There are variations in the branching patterns of the peri-hilar arteries; mapping the peri-hilar branching pattern is therefore crucial in donor renal transplanation (Hazırolan et al. 2011).

Branching of the apical segmental artery

Graves (1954) studied 30 postmortem specimens by injecting polyester resin into the renal vessels; the kidneys with the

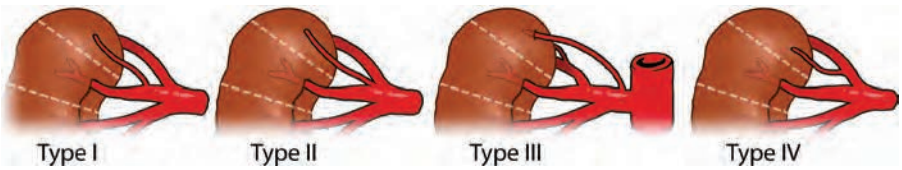

Figure 55.1 Variations in the origin of apical segmental artery in right kidney. Type I: arises from the upper segmental artery; Type II: arises from the junction between the anterior and posterior division of the main stem renal artery; Type III: arises at the junction of the main renal artery with the aorta, enters the apical segment outside the hilum; Type IV: arises from the posterior division (Adapted from Graves (1954) with permission from John Wiley & Sons).

surrounding tissue were then removed *en bloc*. The branching of the apical segmental artery is the most variable and was classified by Graves (1954) into the following four types (Fig. 55.1):

- Type I: in 43.3% of specimens it arises from the upper segmental artery;
- Type II: in 23.3% it arises from the junction between the anterior and posterior division of the main stem renal artery;
- Type III: in 23.3% it arises at the junction of the main renal artery with the aorta, entering the apical segment outside the hilum; and
- Type IV: in 10.0% it arises from the posterior division.

In an exhaustive study of the origin of the apical segmental artery in 185 kidneys, Merklin and Michels (1958) identified 43.3% Type 1, 23.3% Types 2 and 3 and 10% Type 4.

Origin of the upper, middle and lower segmental arteries

Graves (1954) also observed variations in the branching of the upper, middle, and lower segmental arteries and divided them into three groups (Fig. 55.2):

- Group I: in 53.3% of specimens the lower segmental artery arises first; the upper and middle have a common origin;
- Group II: in 30.3% the upper segmental artery arises first; the middle and lower have a common origin; and
- Group III: in 16.6% the upper, middle, and lower segmental arteries all arise from a common point.

In their study of 185 kidneys, Merklin and Michels (1958) observed similar frequencies of variations in the origins of the upper, middle, and lower segemental arteries: 53.5% in group I and 16.6% in each of groups II and III. In a study on 73 formalin-fixed cadaveric kidneys, Weld et al. (2005) found that the prevalences of three, four, or five segemental arteries were 21.9%, 34.2%, and 31.5%, respectively. The vast majority (83.6%) of kidneys possessed upper, middle, and inferior/lower segemental arteries, while apical and posterior segemental arteries were seen in 64.4% and 75.3% of specimens.

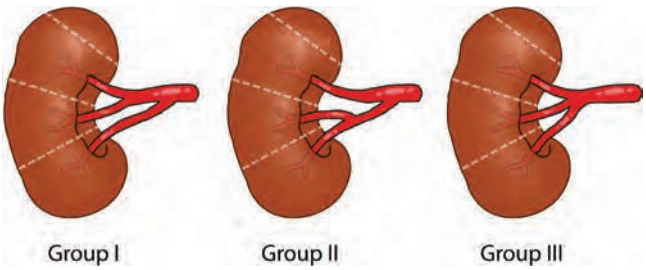

Figure 55.2 Variations in the origin of the upper, middle and lower segmental arteries in right kidney. Group I: lower segmental artery arises first, the upper and middle have a common origin; Group II: upper segmental artery arises first, the middle and lower have a common origin; Group III: upper, middle and lower segmental arteries all arise from a common point (Adapted from Graves (1954) with permission from John Wiley & Sons).

Branching of the presegmental arteries

In a study on 73 formalin-fixed cadaveric kidneys, Weld et al. (2005) found that the prevalances of presegmental arteries were zero, one, and two in 49.3%, 31.5%, and 19.2% of specimens, respectively.

Surgical resection of tumors on the poles of the kidney can be succesfully performed by selective ligation of the segmental artery with minimal injury to the rest of the organ. In kidneys with a presegmental artery, clamping of the presegmental branch will result in a non-selective larger area of obstruction to the blood flow than segmental clamping. Occlusion of a presegmental artery can therefore be beneficial only in surgeries that require removal of larger renal tumors, where there is significant overlap between two or more renal segments.

Primary branches of the renal arteries

Fine and Keen (1966) studied 107 renal arteries by resin casts and introduced the concept of primary and secondary branches of the renal artery as an alternative to the anterior and posterior division terminology proposed by Graves (1954). According to Fine and Keen (1966), the renal artery divides into three primary branches (Fig. 55.3) – upper, lower, and posterior – while the intermediate and middle branches were recognized as secondary branches and the apical/suprahilar branch originated from either the primary or the secondary branches. On the basis of the origin of the first primary branch, the authors established four patterns: P1 (53%), where the posterior artery was the first branch of the renal artery; L1 (38%), where the lower artery was the first branch of the renal artery; U1 (5%), where the first branch was a separate aortic branch or a branch from the renal artery; and triple pattern (4%), where the renal artery divided into three branches.

Morphological variations in peri-hilar branching arteries

Fine and Keen (1966) described the variations in morphology of the posterior division of the renal artery, while Shoja et al. (2008) categorized the morphological variations in the branching of

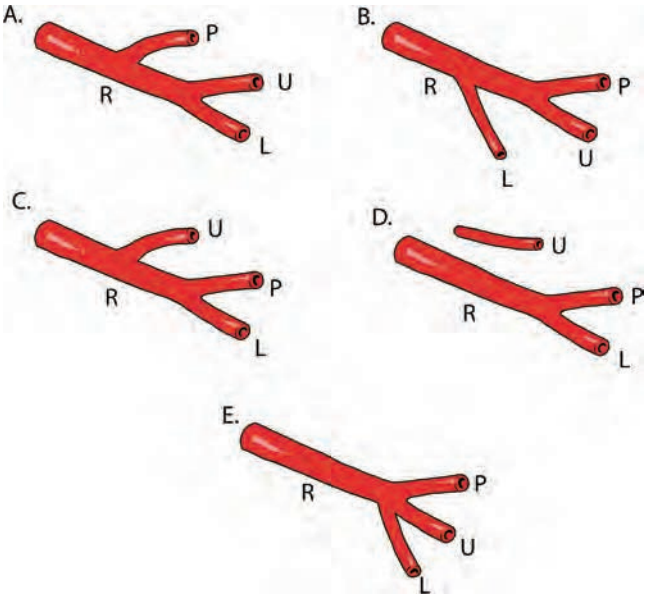

Figure 55.3 Primary Branching patterns of renal arteries. A: posterior artery (P) was the first branch of renal artery, B: lower artery (L) was the first branch of the renal artery, C: first branch (U) arises from the renal artery, D: first branch (U) arises as a separate aortic branch and E: triple pattern (U, L, P) (Adapted from Fine and Keen (1966) with permission from John Wiley & Sons).

the main renal artery by classifying them into two main types, ladder and fork.

In their study of 107 renal arterial casts, Fine and Keen (1966) recognized magistral, bifurcating, and cruciate as three common patterns of the posterior division of the renal arteries (Fig. 55.4). The authors found that in the magistral type (50%), the posterior artery curves and gives two branches; the bifurcating type (30%) entails two arteries that traverse superiorly and inferiorly; and the cruciate type (10%) demonstrates upper and lower vessels arising from a common point.

Shoja et al. (2008) performed renal arteriograms on 81 kidneys to visualize the morphology of the branching pattern of the main renal artery and classified it into two types, ladder and fork. The ladder type, in which the arteries branch in sequence, was seen in 7.4% of cases, while in the fork type (92.6%) the branches arise from a common point, bifurcating in 80.2% or trifucating in 12.4%.

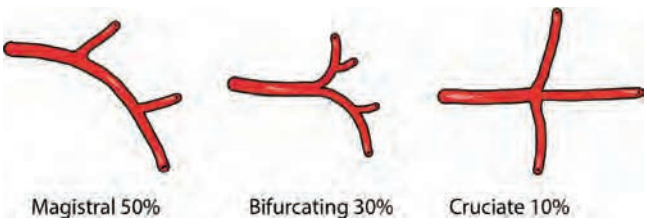

Figure 55.4 Three common posterior artery patterns. A. Magistral (50%), Bifurcating (30%) and Cruciate (10%) (Adapted from Fine and Keen (1966) with permission from John Wiley & Sons).

The authors used the terms primary, secondary, and tertiary branches to indicate the first division of the renal artery and their subsequent divisions. They expanded the scope of the peri-hilar branching pattern by including both the primary and secondary branchings in their observations, whereas Fine and Keen (1966) in the earlier study excluded the secondary branching pattern. Shoja et al. (2008) demonstrated eight cardinal perihilar branching patterns that were characteristic of 83% of the observed morphological patterns. They also observed that patterns I, V, and VI were seen more commonly with a single main renal artery.

Relationship of the segmental arteries to the pelvis of the ureter

In an angiographic study of 120 renal arteries, Hegedus (1972) found that the renal artery divides into primary and secondary branches, the former passing ventral to the renal pelvis in 19.2% (23 patients) and dorsal in 33.3% (40 patients). Secondary branches passed dorsal to the renal pelvis in 15% (18 patients) while in 10% (12 patients) the relationship of the branches was indeterminate because the contrast medium failed to enter the pelvis. The branching of the renal artery in relation to the pelviureteric junction is important in pyelotomy. Ravery et al. (1993) reported that accidental injury to the renal vessels resulted in hemorrhage in 2–3%.

Multiple origin or termination of the renal arteries

The classically described single renal artery, arising from the abdominal aorta and supplying the kidney, is seen in 70–75% of the population. The overall incidence of kidneys with more than one renal artery was found to be 30% (Shakeri et al. 2007; Hazırolan et al. 2011) with a wide spectrum of distribution over the range 9–76% (Macalister 1883; Anson et al. 1947; Sykes 1963; Satyapal et al. 2003; Khamanarong et al. 2004; Özkan et al. 2006).

On the basis of the number, the renal arteries can be:

- Double: 7% (Eisendrath and Strauss 1910), 17.2% (Geyer and Poutasse 1962), 18.7% (Vilhova et al. 2001), 17% (Khamanarong et al. 2004), or 20% (Bordei et al. 2004);
- Triple: 0.5% (Eisendrath and Strauss 1910), 2.5% (Pick and Anson 1940), 2.1% (Geyer and Poutasse 1962), 1% (Khamanarong et al. 2004), or 3% (Vilhova et al. 2001);
- Quadruple: 1% (Pick and Anson 1940).

Multiple-origin renal arteries can be unilateral or bilateral:

- Bilateral double renal arteries: 9.5% (Pick and Anson 1940), 11% (Bordei et al. 2004);
- Bilateral triple renal arteries: 0.5% (Pick and Anson 1940);
- Bilateral five renal arteries: single case report (Kinnunen 1985).

We now focus on variations of multiple arteries, taking account of their origins (the aorta or its branches) and terminations (hilum or poles) as described in the literature, the inconsistencies in nomenclature, the differing statistical data about prevalence, the developmental basis of the variations, and their clinical significance.

Source of origin

Renal arteries with multiple origins can arise from the abdominal aorta or any of its branches. More than one additional renal artery can arise directly from the abdominal aorta besides the main renal artery. Renal arteries can also originate from the "aortic branches." These are broadly referred to as multiple, additional, supernumerary, aberrant, supplementary, anomalous, extra, or plural renal arteries.

Additional renal artery

The literature reveals many different terminologies used to describe multiple origins of renal arteries. Table 55.1

Table 55.1 Additional renal arteries: literature review.

Nomenclature	Author	Type of study	Sample size	Prevalence (%)
Multiple renal arteries	Macalister 1883	Literature review	–	–
Multiple renal arteries, accessory renal arteries	Young and Thompson 1904	Cadaveric	Case reports	–
Multiple renal arteries, accessory renal arteries	Gray 1906	Cadaveric	Case report	–
Accessory renal arteries	Eisendrath and Strauss 1910	Cadaveric	200	14
Double/multiple renal arteries, accessory renal arteries	Bremer 1915	Literature review	–	–
Anomalous renal arteries, accessory renal arteries	Gillaspie et al. 1916	Cadaveric	23	43
Accessory renal arteries	Hellström 1927	Clinical cases	50	22
Supernumerary renal arteries	Pick and Anson 1940	Cadaveric	430	32.25
Accessory renal arteries	Edsman 1954	Renal arteriography	388	16.24
Aberrant renal arteries, accessory renal arteries	Graves 1956	Plastic cast, renal angiography	60	–
Anomalous renal arteries, accessory renal arteries, multiple renal arteries	Hollinshed 1956	Literature review	–	–
Supplementary renal arteries, Multiple renal arteries	Boijsen 1959	Clinical renal angiography	638	23.8
Accessory renal arteries, multiple renal vessels	Anson and Daseler 1961	Cadaveric	100	25
Double renal arteries, triple renal arteries	Ross et al. 1961	Cadaveric	68	26.5
Multiple renal arteries	Geyer and Poutasse 1962	Trans lumbar aortograms	400	23.6
Accessory renal arteries	Sykes 1963	Cadaveric, arterial cast	71	8.4
Multiple renal arteries, supplementary renal arteries	Bauer and Robbins 1967	Angiography and cast	143	32
Multiple renal arteries, accessory renal arteries	Jeffery 1972	Patient arteriography	Case report	–
Two or more arteries, multiple renal arteries	Aubert and Koumare 1975	Aortographic negatives	715	12.1
Multiple renal arteries	Fox and Yalin 1979	Renal transplants	184	14.7
Accessory renal arteries	Tisnado 1979	Renal arteriography	Case report	–
Supernumerary renal arteries	Bergman et al. 1988	Literature review	–	–
Multiple renal arteries	Coen and Raftery 1992	Donor population	403	31
Accessory renal arteries	Baniel et al. 1995	Surgical	102	24
Plural renal arteries	Vilhova et al. 2001	Post vital angiography; aortography with selective angiography	66; 35	28.1; 25.7
Additional renal arteries (ARA)	Satyapal et al. 2001	Clinical, Cadaveric	440	27.7
Plural renal arteries, double renal arteries	Vilhova 2002	Aortography with selective angiography	35	33
Double renal arteries, supplementary renal arteries	Bordei et al. 2004	Cadaveric	272	20
Multiple renal arteries, additional renal arteries, extra renal artery	Özkan et al. 2006	Non-selective renal angiography	855	Multiple arteries, 24
Accessory renal arteries	Tao et al. 2013	Dual-energy computed tomography (DECT) angiography	756	11.4

summarizes the various names/terms used by investigators for this purpose.

It is clear that a plethora of terms have been used to describe the multiple origins of the renal arteries from the abdominal aorta. The current review suggests the term "additional renal artery (ARA)" for renal arteries with multiple origins, as defined by Satyapal et al. (2001). An ARA is an artery other than the main renal artery that arises from the aorta and terminates in the hilum of the kidney. Double and triple renal arteries are therefore denoted "first additional renal artery" and "second additional renal artery", respectively.

On the other hand, renal arteries arising from aortic branches are named "aberrant," "accessory," or "anomalous renal arteries." The current review recommends the unifying term "accessory renal arteries" suggested by Satyapal et al. (2001) for all renal arteries arising from aortic branches.

Additional renal arteries have larger diameters than accessory renal arteries, which can arise from the suprarenal or gonadal vessels (Hollinshed 1956). ARAs are more common on the left than the right (Bergman et al. 1988; Satyapal et al. 2001; Vilhova 2002; Shakeri et al. 2007). In a study on 440 cadavers, Satyapal et al. (2001) found a greater prevalence of ARAs in men (33.1%) than women (20.2%). However, Aubert and Koumare (1975) and Tao et al. (2013) reported no significant sex difference in the prevalence of additional renal arteries. In 74 *en-block* cadaveric dissections, Satyapal et al. (2001) reported the prevalences of ARAs in African, White, Indian, and "colored" populations as 36.5%, 35.3%, 18%, and 18.5% respectively.

Table 55.1 indicates differences in the reporting of ARA prevalences that can be attributed to differences in the study approaches – cadaveric, renal cast, CT, selective angiographies, abdominal aortography, clinical cases – employed by the investigators (Lippert and Pabst 1985).

Accessory renal artery

Accessory renal arteries arise from branches of the aorta including branches from the thoracic aorta and the inferior phrenic, celiac, superior mesenteric, inferior mesenteric, common iliac, and external or internal iliac arteries. The literature review revealed a number of incidental cadaveric and angiographic reports of accessory renal arteries.

Nathan (1963) reported an accessory renal artery arising from the right common iliac artery. In an angiographic study, Gulsun et al. (2000) reported an interesting finding of pelvic kidneys supplied by three arteries arising from bilateral common iliac and ipsilateral internal iliac arteries. Gillaspie et al. (1916) described an accessory renal artery arising from the celiac plexus to supply the upper pole. Loukas et al. (2005) reported a case of accessory renal arteries originating from the common trunk of the inferior mesenteric artery along with an additional renal artery. Gesase (2007) reported a case of accessory renal artery arising from the inferior mesenteric artery in a normal kidney, while Olsson and Wholey (1964) and Tisnado (1979) reported accessory renal arteries originating from the inferior mesenteric artery with congenitally abnormal kidneys. Gulsun et al. (2000) mentioned the study of Dretler et al. who found, in 33 ectopic kidneys, 12 cases of double accessory arteries (one artery from the bifurcation, one from the ipsilateral or contralateral common iliac artery), 17 cases of single artery (arising distal to the aorta), and 3 with triple blood supplies (arising from the bifurcation and the common and internal iliac arteries). Doppman (1967), Tegtmeyer (1969), and Hazırolan et al. (2011) reported accessory renal arteries arising from the thoracic abdominal aorta. Giavroglou and Kokkinakis (2005) reported an interesting case of an accessory renal artery arising from opposite renal artery and supplying the lower pole.

Role of embryology in multiple renal arteries

Knowledge of the embryonic development of the kidney forms the basis for understanding the cause of ARAs. The kidneys are derived from the embryonic urogenital ridge in the intermediate mesoderm (Kinnunen 1985). The urogenital ridge is supplied by a network of capillaries called "rete arteriosum urogenitale" (Felix 1912; Bremer 1915; Derrick 1960) which arise from the abdominal aorta, later named the segmental lateral splanchnic arteries (Shakeri et al. 2007). With the initial development of the metanephric kidney in the sacral region and its subsequent ascent to its final destination in the lumbar region, the caudal branches of the lateral splanchnic vessels degenerate in favor of more proximal vessels that are relatively close to the position of the kidney (Bremer 1915; Cocheteux et al. 2001). Failure of regression of the lateral splanchnic vessels can give rise to ARAs anywhere between the eleventh thoracic and fifth lumbar vertebral levels (Anson et al. 1936; Graves 1956; Kinnunen 1985). The lower/inferior pole of the kidney is the more frequently affected pole with ARAs, which represent persistent lower splanchnic arteries that arise directly from the aorta and have larger diameters than the superior polar arteries (Atasever et al. 1992 ; Kocabiyik et al. 2004). Chemical factors including degree of oxygenation, nutrients, availability of transcription factors, and hemodynamic selection, along with the genetic disposition of the individual, have been identified as critical regulators in the development of the renal vasculature (Shakeri et al. 2007).

ARAs and accessory renal arteries are "essential" vessels of the kidney. Even though they are called additional/accessory arteries they are not to be considered optional, since blockage in any accessory artery compromises the kidney functionally in the same way as blockage of the main renal artery (Graves 1954). The presence of ARAs increases the challenge and complexity of diagnostic and surgical procedures. The advantages and disadvantages of ARAs in transplantation surgeries are much debated. ARAs are end arteries lacking a collateral circulation. Failure of the donor ARA to undergo re-anastomosis successfully with the recipient arteries can therefore lead to loss of vascular supply in the corresponding segment of the kidney. As a consequence, the transplanted kidney can suffer ischemic injury (Khamanarong et al. 2004). Various reports indicate that kidneys with renal arterial variations are prone to higher failure

rates than those with a single renal artery (Bayazit et al. 1992; Çiçekcibaşi et al. 2005; Tao et al. 2013). There are higher incidences of renal artery stenosis and vascular thrombosis in ARAs (Çiçekcibaşi et al. 2005).

In order to prevent strictures forming after an anastomosis is performed during renal transplantation surgery, the main renal artery needs to be at least 1 cm long (Sampaio and Passos 1992; Çiçekcibaşi et al. 2005). Geyer and Poutasse (1962) and Davis (1963) concluded that ARAs are more commonly associated with hypertension. Although in recent years kidneys with more than two separate renal arteries have been successfully used for transplantation, post-operative complications with poorer prognosis have been reported (Spanos et al. 1973; Fox and Yalin 1979; Bozkurt 2013). Ectopic kidneys with abnormal morphology, location and malrotation also tend to have more ARAs. They commonly present with clinical symptoms of urinary tract infection, renal calculi, renovascular hypertension, ureteropelvic obstruction, and vesicoureteral reflex (Gulsun et al. 2000).

Hilar and polar arteries

The term hilar or polar artery indicates the mode by which the renal artery terminates in the kidney. Polar arteries can have aortic or renal origin. The following five categories can be distinguished: aortic hilar; Aortic upper polar; renal upper polar; aortic lower polar; and renal lower polar. Table 55.2 provides a systematic review of the hilar and polar arteries as described by various investigators.

Ravery et al. (1993) found that about 22% of the two polar arteries arise from the abdominal aorta and that the prevalence of lower polar arteries in the general population is about 9%. Other sources for the origins of polar arteries are the suprarenal, inferior phrenic, and gonadal vessels (Khamanarong et al. 2004; Gesase 2007). Like the segmental artery, the polar artery provides a blood supply to the corresponding upper and lower poles of the kidney. In his study of 71 renal arterial casts, Sykes (1963) found that in 86.3% of specimens the renal artery entered the kidney by penetrating the cortex of the inferior pole. Blockage of these polar arteries can lead to segmental ischemia. In their study of 185 kidney dissections, Merklin and Michels (1958) found that the main renal artery gave rise to the upper and lower polar arteries in 12.0% and 1.4% of specimens, respectively. The superior polar artery more commonly has a renal origin (Kadir 1991; Budhiraja et al. 2010). Tao et al. (2013) in a study on 756 kidneys by dual-energy computed tomography angiography found that 14.6% of renal arteries directly entered the upper pole, lower pole, or hilum of the kidney. In a study on 200 kidneys, Eisendrath and Strauss (1910) found upper polar arteries and lower polar arteries in 3.5% and 2.5% of the specimens, respectively.

Course of hilar and polar arteries

Bordei et al. (2004) performed a study on 272 kidneys to access the course of double hilar arteries in 51 specimens. The course of the double hilar artery was either parallel (17.6%), obliquely descending (11.6%), or obliquely ascending (9.8%) (total 39%), while in the remaining 61% of specimens it was divergent (19.5%), straight/sinuous (9.8%), or convergent (21.6%).

Persisting embryonic lateral segmental arteries that arise from the aorta and supply the kidney constitute the polar arteries. Inferior polar arteries are more prevalent than superior polar arteries. An inferior polar artery running anterior to the pelvis of the ureter can compress the ureter and cause hydronephrosis (Pick and Anson 1940). The constriction causes distention of the renal pelvis and secondary renal infection (Skandalakis 1972). Whether the smooth muscle of the uretero-pelvic junction is weak, the inferior polar artery is responsible for the obstruction, or abnormal fascia-like bands associated with the polar vessels obstruct the ureteropel-

Table 55.2 Hilar and polar arteries: literature review

			Prevalence (%)				
Authors	**No. kidneys**	**Type of study**	**Aortic hilar**	**Aortic upper polar**	**Renal upper polar**	**Aortic lower polar**	**Renal lower polar**
Eisendrath 1920	218	Cadaveric	54.6	5.9	22.2	13.1	2.1
Lloyd 1935	144	Cadaveric	59.7	10.4	18.0	7. 0	0.7
Merklin and Michels 1958	185	Cadaveric	64.3 (1); 15 (2)	1.1	1.8	6.5	10.3
Sampaio and Passos 1992	266	Cadaveric	53.3 (1), 7.9 (2); 1.9 (3)	6.8	–	5.3	–
Vilhova 2002	35	Selective renal angiography	83	17	–	–	–
Khamanarong et al. 2004	534	Cadaveric	82.0 (1), 17.0 (2), 1.0 (3)	7.0	–	3.0	–
Çiçekcibaşi et al. 2005	180 fetal renal arteries	Dissection	75.0 (1), 11.1 (2)	3.3	–	10.5	–

vic juncture, is controversial (Hollinshed 1956). Polar arteries can be accidentally injured during surgical procedures. Earlier, polar arteries were considered additional arteries and were clamped or ligated to treat hydronephrosis; this resulted in segmental ischemia and necrosis of the ureter. Segmental ischemia and ureteral necrosis often occur because lower polar arteries are lost during renal transplantation. Using the microsurgical method, Wolters et al. (2001) anastomosed the polar artery to the inferior epigastric artery and succeeded in preserving the blood supply to the ureter. The superior polar artery supplies the capsule of the kidney and the perinephric fat. Sometimes it arises from the suprarenal artery; inferior phrenic arteries entering the kidney at the upper pole can be small and multiple (Hollinshed 1956; Anson and Daseler 1961). Furthermore, during the renal transplantation procedure, polar vessels can increase the failure rate because of urinary leakage and thrombosis of the renal vessels (Bayazit et al. 1992). Surgeons should be careful in dissecting the fat in the polar region to avoid accidental injury to the artery (Atasever et al. 1992). Accessory renal arteries can arise from the internal spermatic or ovarian arteries; they can be small and single and enter the lower pole of the kidney (Anson and Daseler 1961). Rao et al. (2006) reported a case of prehilar branching of the renal arteries with an unusual relationship to the renal pelvis: bilateral obliquely running superior polar arteries penetrating the poles directly. A similar case of vertical trajectory of two superior polar arteries causing upper pole infarction has also been reported (Beyer and Daily 2004).

References

Anson BJ, Daseler EH. 1961. Common variations in renal anatomy, affecting blood supply, form, and topography. *Sur Gyn Obstet* 112: 439–449.

Anson BJ, Richardson GA, Minear WL. 1936. Variations in the number and arrangements of the renal blood vessels, a study of the blood supply of four hundred kidneys. *J Urol* 36: 211–219.

Anson BJ, Cauldwell EW, Pick JW. 1947. The blood supply of the kidney, suprarenal gland, and associated structures. *Sur Gyn Obstet* 84: 313–320.

Atasever A, Celik HH, Durgun B, Yilmaz E. 1992. Unrotated left kidney associated with an accessory renal artery. *J Anat* 181: 507–508.

Aubert J, Koumare K. 1975. Variations of origin of the renal artery: a review covering 403 aortographies. *Eur Urol* 1: 182–188.

Baniel J, Foster RS, Donohue JP. 1995. Surgical anatomy of the lumbar vessels: implications for retroperitoneal surgery. *J Urol* 153: 1422–1425.

Bauer FW. 1968. The aortic origin of renal arteries in man and other mammals. *Arch Path* 86: 230–233.

Bauer FW, Robbins SL. 1967. A postmortem study comparing renal angiograms and renal artery casts in 58 patients. *Arch Path* 83: 307–314.

Bayazit M, Göl MK, Zorlutuna Y, Tasdemir O, Bayazit K. 1992. Bilateral triple renal arteries in a patient with iliac artery occlusion : a case report. *Surg Radiol Anat* 14: 81–83.

Beregi JP, Mauroy B, Willoteaux S, Mounier-Vehier C, Rémy-Jardin M, Francke JP. 1999. Anatomic variation in the origin of the main renal arteries: spiral CTA evaluation. *Eur Radiol* 9: 1330–1334.

Bergman RA, Thompson SA, Afifi AK, Saadeh FA. 1988. *Compendium of Human Anatomic Variation: Text, Atlas and World Literature*. Baltimore, Munich: Urban & Schwarzenberg.

Beyer RW, Daily PO. 2004. Renal artery dissection associated with Gz acceleration. *Aviat Space Environ Med* 75: 284–287.

Boijsen E. 1959. Angiographic studies of the anatomy of single and multiple renal arteries. *Acta Radiol Supplement* 183: 1–135.

Bordei P, Şapte E, Iliescu D. 2004. Double renal arteries originating from the aorta. *Surg Radiol Anat* 26: 474–479.

Bordei P, Sapte E, Iliescu D, Brânzaniuc K, Baz R, Dina C. 2012. Morphological assessments on the arteries of the superior renal segment. *Surg Radiol Anat* 34: 137–144.

Bozkurt B. 2013. Favorable outcome of renal grafts with multiple arteries: a series of 198 patients. *Transplantation proceedings* 45: 901–903.

Bremer JL. 1915. The origin of the renal artery in mammals and its anomalies. *Am J Anat* 18: 179–200.

Brödel M. 1901. The intrinsic blood vessels of the kidney and their significance in nephrectomy. *Bull Johns Hopkins Hosp* 12: 10–13.

Budhiraja V, Rastogi R, Asthana AK. 2010. Renal artery variations: embryological basis and surgical correlation. *Rom J Morphol Embryol* 51: 533–536.

Çiçekcibaşi AE, Ziylan T, Salbacak A, Şeker M, Büyükmumcu M, Tuncer I. 2005. An investigation of the origin, location and variations of the renal arteries in human fetuses and their clinical relevance. *Ann Anat* 187: 421–427.

Cocheteux B, Mounier-Vehier C, Gaxotte V, McFadden EP, Francke JP, Beregi JP. 2001. Rare variations in renal anatomy and blood supply: CT appearances and embryological background. A pictorial essay. *Eur Radiol* 11: 779–786.

Coen LD, Raftery AT. 1992. Anatomical variations of the renal arteries and renal transplantation. *Clin Anat* 5: 425–432.

Davis GD, Kincaid W, Hunt JC. 1963. Roentgenologic evaluation of multiple renal arteries. *Am J Roentgenol Radium Ther Nucl Med* 90: 583–592.

Derrick JR. 1960. The association of aberrant renal arteries and systemic hypertension. *Surgery* 48: 907–912.

Doppman J. 1967. An ectopic renal artery. *Br J Radiol* 40: 312–313.

Edsman G. 1954. Accessory vessels of the kidney and their diagnosis in hydronephrosis. *Acta Radiol* 42: 26–32.

Edsman G. 1957. Angionephrography and suprarenal angiography; a roentgenologic study of the normal kidney, expansive renal and suprarenal lesions and renal aneurysms. Acta Radiol Supplementum: 1–141.

Eisendrath DN. 1920. The relation of variations in the renal vessels to pyelotomy and nephrectomy. *Ann Surg* 71: 726–743.

Eisendrath DN, Strauss DC. 1910. The surgical importance of accessory renal arteries. *J Am Med Assoc* 55: 1375–1377.

El-Galley RES, Keane TE. 2000. Embryology, anatomy, and surgical applications of the kidney and ureter. *Surg Clin North Am* 80: 381–401.

Felix W. 1912. *Manual of Human Embryology: Development of Urinogenital Organs*. Philadelphia: J.P. Lippincott.

Fernet M, Goldlust D, Salama J, Chevrel J. 1987. A case of ectopic right renal artery: a radiologic-anatomic variant. *Surg Radiol Anat* 9: 319–320.

Fine H, Keen EN. 1966. The arteries of the human kidney. *J Anat* 100: 881–894.

Fox M, Yalin R. 1979. Renal transplantation with multiple arteries. *Br J Urol* 51: 333–336.

Garcier JM, Fraissinette B, Filaire M, Gayard P, Therre T, Ravel A, Boyer L. 2001. Origin and initial course of the renal arteries a radiological study. *Surg Radiol Anat* 23: 51–55.

Gesase AP. 2007. Rare origin of supernumerary renal vessels supplying the lower pole of the left kidney. *Ann Anat* 189: 53–58.

Geyer JR, Poutasse EF. 1962. Incidence of multiple renal arteries on aortography: Report of a series of 400 patients, 381 of whom had arterial hypertension. *JAMA* 182: 120–125.

Giavroglou C, Kokkinakis H. 2005. Main arterial supply of a kidney from the opposite renal artery: an unusual case. *Acta Radiol* 46: 567–568.

Gillaspie C, Miller LI, Baskin M. 1916. Anomalous renal vessels and their surgical significance. *Anat Rec* 11: 77–86.

Graves FT. 1954. The anatomy of the intrarenal arteries and its application to segmental resection of the kidney. *Br J Surg* 42: 132–139.

Graves FT. 1956. The aberrant renal artery. *J Anat* 90: 553–558.

Graves FT. 1969. The arterial anatomy of the congenitally abnormal kidney. *Br J Surg* 56: 533–541.

Gray GM. 1906. Multiple renal arteries. *Anat Anz 29*: 29: 266–270.

Gulsun M, Balkanci F, Cekirge S, Deger A. 2000. Pelvic kidney with an unusual blood supply: angiographic findings. *Surg Radiol Anat* 22: 59–61.

Hazırolan T, Oz M, Karaosmanoğlu AD, Oğuz BS, Canyiğit M. 2011. CT angiography of the renal arteries and veins: normal anatomy and variants. *Diagn Interv Radiol* 17: 67–73.

Hegedus V. 1972. Arterial anatomy of the kidney. A three-dimensional angiographic investigation. *Acta Radiol* 12: 604–618.

Hellström J. 1927. Relation of abnormally running renal vessels to hydronephrosis and an investigation of the arterial condition of 50 kidneys. *Acta Chir Scand* 61: 289–293.

Hollinshed WH. 1956. Anatomy *for Surgeons: The Thorax, Abdomen and Pelvis*. New York: A Hoeber-Harper Book.

Jeffery RF. 1972. Unusual origins of renal arteries. *Radiology* 102: 309–310.

Kadir S. 1991. *Atlas of Normal and Variant Angiographic Anatomy*. Philadelphia: WB Saunders Co.

Kaplan DB, Kwon CC, Marin ML, Hollier LH. 1999. Endovascular repair of abdominal aortic aneurysms in patients with congenital renal vascular anomalies. *J Vasc Surg* 30: 407–415.

Khamanarong K, Prachaney P, Utraravichien A, Tong-Un T, Sripaoraya K. 2004. Anatomy of renal arterial supply. *Clin Anat* 17: 334–336.

Kincaid OW. 1966. Normal Renal Angiogram: Renal Angiography. Chicago: Year Book Medical Publishers.

Kinnunen J. 1985. Ten renal arteries. *Eur J Radiol* 5: 300–301.

Kocabiyik N, Yalcin B, Yazar F, Ozan H. 2004. A persistent mesonephric artery: A rudimentary accessory renal artery (An embryonic remnant). *Gazi Medical Journal* 15: 75–78.

Kosiński H. 1994. Variability of places of origin of the human renal arteries. *Folia Morphol (Warsz)* 53: 111–116.

Lippert H, Pabst R. 1985. *Arterial Variations in Man: Classification and Frequency*. Munchen: J. F. Bergmann, Verlag.

Lloyd LW. 1935. The renal artery in Whites and American Negroes. *Am J Phys Anthropol* 20: 153–163.

Loukas M, Aparicio S, Beck A, Calderon R, Kennedy M. 2005. Rare case of right accessory renal artery originating as a common trunk with the inferior mesenteric artery: a case report. *Clin Anat* 18: 530–535.

Macalister A. 1883. Multiple renal arteries. *J Anat Physiol* 17: 250–252.

Merklin RJ, Michels NA. 1958. The variant renal and suprarenal blood supply with data on the inferior phrenic, ureteral and gonadal arteries: a statistical analysis based on 185 dissections and review of the literature. *J Int Coll Surg* 29: 41–76.

Nathan H. 1963. Aberrant renal artery producing developmental anomaly of kidney associated with unusual course of gonadal (ovarian) vessels. *J Urol* 89: 570–572.

Odman P, Ranniger K. 1968. The location of the renal arteries. *Am J Roentgenol* 104: 283–288.

Olsson O, Wholey M. 1964. Vascular abnormalities in gross anomalies of kidneys. *Acta Radiol Diagn (Stockh)* 2: 420–432.

Ozan H, Alemdaroglu A, Sinav A, Gumusalan Y. 1997. Location of the ostia of the renal arteries in the aorta. Surg Radiol Anat (English ed.) 19: 245–247.

Özkan U, Oğuzkurt L, Tercan F, Kızılkılıç O, Koc Z, Koca N. 2006. Renal artery origins and variations: angiographic evaluation of 855 consecutive patients. Diagn Interv Radiol 183–186.

Pick JW, Anson BJ. 1940. The renal vascular pedicle. An anatomical study of 430 body-halves. *J Urol* 44: 411–434.

Rao M, Bhat SM, Venkataramana V, Deepthinath R, Bolla SR. 2006. Bilateral prehilar multiple branching of renal arteries: a case report and literature review. *Kathmandu Univ Med J* 4: 345–348.

Ravery V, Cussenot O, Desgrandchamps F, Teillac P, Martin-Bouyer Y, Lassau JP, Le Duc A. 1993. Variations in arterial blood supply and the risk of hemorrhage during percutaneous treatment of lesions of the pelviureteral junction obstruction: report of a case of testicular artery arising from an inferior polar renal artery. *Surg Radiol Anat* 15: 355–359.

Ross JA, Samuel E, Millar DR. 1961. Variations in the renal vascular pedicle. *Br J Urol* 33: 478.

Sampaio FJ, Passos M. 1992. Renal arteries: anatomic study for surgical and radiological practice. *Surg Radiol Anat* 14: 113–117.

Satyapal KS, Haffejee AA, Singh B, Ramsaroop L, Robbs JV, Kalideen JM. 2001. Additional renal arteries incidence and morphometry. *Surg Radiol Anat* 23: 33–38.

Satyapal KS, Kalideen JM, Singh B, Haffejee AA, Robbs JV. 2003. Why we use the donor left kidney in live related transplantation. *S Afr J Surg* 41: 24–26.

Sezer TO, Hoscoskun C. 2012. Vascular Surgery. In: Vascular Complications After Renal Transplantation (ed. DDY). Online: InTech.

Shakeri AB, Tubbs RS, Shoja MM, Pezeshk P, Farahani RM, Khaki AA, Ezzati F, Seyednejad F. 2007. Bipolar supernumerary renal artery. *Surg Radiol Anat* 29: 89–92.

Shoja MM, Tubbs SR, Shakeri A, Loukas M, Ardalan MR, Khosroshahi HT, Oakes WJ. 2008. Peri-hilar branching patterns and morphologies of the renal artery: a review and anatomical study. *Surg Radiol Anat* 30: 375–382.

Skandalakis J. 1972. *Embryology for Surgeons: The Embryological Basis for the Treatment of Congenital Defects*. Philadelphia, London, Toronto: WB Saunders company.

Spanos PK, Simmons RL, Kjellstrand CM, Buselmeier TJ, Najarian JS. 1973. Kidney transplantation from living related donors with multiple vessels. A problem revisited. *Am J Surg* 125: 554–558.

Sykes D. 1963. The arterial supply of the human kidney with special reference to accessory renal arteries. *Br J Surg* 50: 368–374.

Tao XF, Zhu JQ, Wu YW, Tang GY, Shi YZ, Zhang L, Lin Y, Wang ZQ. 2013. Dual-energy computed tomography angiography for evaluating the renal vascular variants. *Chin Med J (Engl)* 126: 650–654.

Tegtmeyer CJ. 1969. Thoracic origin of a single renal artery. *JAMA* 209: 1223.

Tisnado J. 1979. Renal artery originating from the inferior mesenteric artery. *Br J Radiol* 52: 752–754.

Urban BA, Ratner LE, Fishman EK. 2001. Three-dimensional volume-rendered CT angiography of the renal arteries and veins: normal anatomy, variants, and clinical applications. *RadioGraphics* 21: 373–386.

Vilhova I. 2002. The frequency of different plural renal arteries rare variants. Annales Universitatis Mariae Curie–Skłodowska. *Sectio D, Medicina* 57: 68–73.

Vilhova I, Kryvko YY, Maciejewski R. 2001. The radioanatomical research of plural renal arteries. *Folia Morphol (Warsz)* 60: 337–341.

Weld KJ, Bhayani SB, Belani J, Ames CD, Hruby G, Landman J. 2005. Extrarenal vascular anatomy of kidney: Assessment of variations and their relevance to partial nephrectomy. *Urology* 66: 985–989.

Wolters HH, Schult M, Chariat M, Senninger N, Dietl KH, Heidenreich S. 2001. The anastomosis between renal polar arteries and arteria epigastrica inferior in kidney transplantation: an option to decrease the risk of ureter necrosis? *Transplant Internat* 14: 442–444.

Young AH, Thompson P. 1904. Abnormalities of the renal arteries, with remarks on their development and morphology. *J Anat Physiol* 38: 1–15.

56 Internal iliac arteries

Richard Tunstall
The University of Warwick, Coventry, United Kingdom

The point of origin and branching pattern of the internal iliac artery shows considerable variation. Surgeons and interventionalists need to be aware of both variant vessels and vessel origins in order to reduce the incidence of iatrogenic damage and avoid ischemic damage during arterial ligation/embolism. Many current anatomical texts report that the internal iliac divides into anterior and posterior divisions with visceral and parietal branches arising from them (Standring 2008; Drake et al. 2009; Moore et al. 2014). In reality, however, the branching pattern of the internal iliac varies considerably and the traditional notion of anterior and posterior divisions is not often observed. Multiple evidence-based systems categorizing the internal iliac branching pattern have been suggested and are presented here (Adachi 1928; Ashley and Anson 1941; Yamaki et al. 1998).

A wealth of information relating to the internal iliac arterial system began emerging in the late nineteenth century, and continues to be produced. In 1988 Bergmann reviewed the work of multiple authors and reported considerable variance (Quain 1844; Henle 1868; Hyrtl 1887; Gegenbaur 1888; Gérard 1901; Paterson 1909; Chalier 1912; Schaefer et al. 1915; Lipshutz 1918; Senior 1925; Huber 1930; Jackson 1933; Ashley and Anson 1941; Curtis et al. 1942; Latarjet 1948; Dufour et al. 1951; Braithwaite 1952a; Gouazé et al. 1956; Anson 1966; Roberts and Krishinger 1967; Gardner et al. 1969; Nitschke and Preuss 1971; Pac et al. 1977). Briefly, Bergmann et al. (1988) reported that the length of the internal iliac varied over the range 12–90 mm and was related to both the length of the common iliac arteries and the level of internal iliac artery bifurcation into anterior and posterior divisions. The bifurcation of the internal iliac artery occurred anywhere between the pelvic brim and the upper border of the sacrosciatic foramen and in some cases no separate anterior and posterior division appeared, leaving the normal branches to arise directly from a main trunk. It was also noted that branches could exchange origins, highlighting the extent of variability. A range of unusual branches were reported arising from the internal iliac artery including the superior mesenteric, vesicoprostatic (also supplied the testes), prostatic (also supplied the rectum) or inferior epigastric artery, a common trunk for the superior vesical and profunda penis arteries, or an independent penile artery supplying the profunda penis arteries.

Recent advances in medical imaging combined with further cadaveric studies from around the world have added to the already substantial knowledge base in this area. This chapter reviews the currently available literature base and reports the variability in origin, course, and branching pattern of the internal iliac artery and its branches. The results of both large and small studies will be presented alongside case reports that highlight key variants of interest. Variability in the location, level, and type of aortic and common iliac bifurcation will also be considered, since both impact on internal iliac artery morphology. At relevant points, similar datasets have been combined and tabulated and meta-analysis performed in order to simplify comparisons. The embryological development of the iliac arterial system has also been reviewed to help explain variant morphology or the presence of aberrant vessels.

Aorto-iliac arterial system

Aortic bifurcation

The reported level of the aortic bifurcation into common iliac arteries in cadaveric studies ranges from L3-L5 with the L4 vertebral body being the most common site in 67.4% of 1231 specimen. In 90% of cases the bifurcation is located between the L4 to L5 vertebral levels (Table 56.1).

Table 56.1 Level of aortic birfurcation relative to the lumbar vertebral bodies as measured in cadaveric specimens.

Author	Cadaveric origin	Total (*n*)	Frequency (%)				
			L3	L3–L4 disc	L4	L4-L5 disc	L5
Dwight (1894–95)	America	500	2.8	3.5	76	5	11.5
Quain (1899)	Europe	400	3	6	62	14	11
Lipshutz (1918)	America	181	4	9	59	20	8
Shafiroff et al. (1959)	America	150	3	4	63	20	10
Total		1231	3.1	5.2	67.4	12.0	10.6

Source: Bergman et al. (1988).

Bergman's Comprehensive Encyclopedia of Human Anatomic Variation, First Edition. Edited by R. Shane Tubbs, Mohammadali M. Shoja and Marios Loukas.
© 2016 John Wiley & Sons, Inc. Published 2016 by John Wiley & Sons, Inc.

Table 56.2 Common iliac artery length (mm) as measured in embalmed cadaveric specimens. Bleich et al. (2007) used fresh cadaveric specimens.

Author	Cadaveric origin	Total (*n*)	Length (mm); range or mean±SD	Frequency (%)
Quain (1899)	Europe	400	25–101	100
Lipshutz (1918)	America	181	25–40	15.2
			40–50	36.0
			50–60	27.2
			60–70	5.8
			70–80	10
			80–90	5.2
Shafiroff et al. (1959)	America	150	40–70	81
Terek et al. (2004)	Turkish	22 (right)	60.9±11.5	–
		22 (left)	66.2±12.5	–
Bleich et al. (2007)	America	37 (right)	25–91 (55.2 mean)	–
		37 (left)	30–94 (57.0 mean)	–

Source: Bergman et al. (1988).

Common iliac artery

Cadaveric studies have demonstrated the length of the common iliac artery lies within the range 25–101 mm (Table 56.2). Quain (1844) reported the length of most internal iliac arteries as 25–40 mm, which broadly agrees with the results of Lipshutz (1918). More recent studies show mean vessel length ranges of 55.2–66.2 mm, with the left common iliac artery being slighty longer than the right. Lipshutz (1918) reported the left common iliac often bifurcated at a lower level than the right and that common iliac vessels over 6 cm in length tended to be tortuous.

Common iliac bifurcation and level of internal iliac artery origin

Cadaveric studies have shown the level of internal iliac artery origin sits at the L5–S1 intervertebral disc in 76.6% of 441 cadavers studied (Table 56.3). In a study of 40 adult Indian cadaveric pelves, Shivakumar et al. (2010) reported the level of origin ranged from the L4–L5 disc to the middle of S2 vertebrae, which represents the maximum range of variance reported in the literature.

Table 56.3 Bifurcation point of common iliac artery relative to the lumbar-sacral vertebrae, as measured in formalin-fixed cadaveric specimens.

			Frequency (%)		
				L5–S1	
Author	Cadaveric origin	Total (*n*)	L5	Disc	S1
Lipshutz (1918)	American	181	14.5	85.5	0
Shafiroff et al. (1959)	American	150	18	82	0
Naveen et al. (2011)	Indian	60	1.7	40	58.3
Mamatha et al. (2012)	Indian	50	2	72	24
Total	441		12.5	76.6	10.7

Source: Bergman et al. (1988).

Alternative reference points have been used to define the level of internal iliac artery origin. In a study of 50 formalin-fixed cadaveric pelvic halves in India, Mamatha et al. (2012) reported that the internal iliac artery originated above the level of the greater sciatic notch in 98% of specimens and below it in 2%. The distance of the internal iliac artery origin from the greater sciatic notch was either 2 cm (in 28%), 2.5 cm (in 36%), 3 cm (in 18%), or 3.5 cm (in 16%) above (superior to) the notch, or 1 cm (in 2%) below the notch. In a cadaveric study of 34 limbs from 17 cadavers, Jusoh et al. (2010) reported the distance of the common iliac artery bifurcation point from the sacral ala fell within the range 43–53 mm. Fatu et al. (2006) studied 100 internal iliac arteries in 50 Romanian cadavers (30 male: 20 female) and reported the internal iliac artery origin to be 29–36 mm from the mid-sagittal plane, with the average distance being slightly greater in females (32.8 mm) compared to males (31.9 mm).

Length and location of the internal iliac artery

The length of the internal iliac artery, as determined by the distance from its point of origin to the emergence of its first branch/division, is highly variable. The distance to the emergence of the first branch and the level at which the internal iliac artery further divides is relevant to interventionalists avoiding iatrogenic damage following internal iliac artery ligation for hemostasis.

Cadaveric studies have reported the length of the internal iliac artery to fall within the range 0–90 mm (Table 56.4). Quain (1844) reported that the majority of internal iliac arteries measured 25–40 mm in length, whereas Fatu et al. (2006) reported an average length of 49±3 mm and a diameter of 4–11 mm ($n = 100$; 60 male: 40 female). Lipshutz (1918) noted that if the aorta divided lower it did not follow that the internal iliac was shorter; indeed, in such cases the internal iliac artery also tended to divide lower. Shafiroff et al. (1959) reported that the internal iliac artery on the right was frequently longer than that on the left, and that its length

Table 56.4 Length of the internal iliac artery as determined by the distance from the common iliac bifurcation to the appearance of the first branch/division. Measured in formalin-fixed cadaveric specimens.

Author	Cadaveric origin	Total (*n*)	Length range±SD (mm)	Frequency (%)
Quain (1844)	Europe	338	13–75	–
Lipshutz (1918)	America	181	15–25	13.5
			25–35	28
			35–45	37.6
			45–55	11.2
			55–67	9.5
Adachi (1928)	Japan	121	44.3±1.3	–
Shafiroff et al. (1959)	America	150	10–30	21
			30–50	60
			50–70	13
Terek et al. (2004)[a]	Turkish	22 right	40.2±8.3	–
		22 left	38.4±7.2	–
Fatu et al. (2006)	Romania	100	49±3 (range 20–90)	–
Bleich et al. (2007)[b]	America	54 right	27.0±10.1 (range 0–49)	–
		54 left	26.8±10.7 (range 0–52)	
Shivakumar et al. (2010)	India	40	20–62	–
Naveen et al. (2011)	India	60	37±4.6 (range 13–54)	–

Source: Bergman et al. (1988).

[a]Terek et al. (2004) reported on fresh cadaveric specimens; [b]Bleich et al. (2007) reported on 37 fresh cadavers and 17 embalmed.

was inversely proportional to that of the common iliac artery. Jusoh et al. (2010) reported that the distance from the common iliac bifurcation to the origin of the anterior division of internal iliac artery lay within the range 1–6 cm and to the posterior division 0–6 cm, based upon a study of 34 limbs from 17 cadavers. Bleich et al. (2007) studied 54 female cadavers (37 unembalmed: 17 embalmed; mean age 79.6±12.7 years) and noted a significant difference in internal iliac artery length in embalmed versus fresh specimens (Table 56.5). The authors state that the exact cause of this, either shortening during embalming or the stretching of fresh tissues, was not elucidated; they go on to suggest a safe distance for internal iliac artery ligation is 50 mm from the iliac bifurcation. This allows sufficient distance for the safe emergence of the first posterior division branches which, in 63% of subjects, was a common trunk for the iliolumbar, superior gluteal, and lateral sacral arteries. The 50 mm measurement takes into account the distance to the appearance of the first posterior branch, the cranio-cadual width of the first branch (mean 4.6 mm, range 2-9 mm on the left; mean 5.3 mm, range 2–12 mm on the right), plus two standard deviations.

In a similar study Terek et al. (2004) studied the left and right sides of 22 fresh Turkish female cadavers and recorded the distance of the posterior division of the internal iliac artery from the sacral promontory and the pelvic midline (Table 56.6). No significant age-related differences were noted. The only

Table 56.5 Comparison of the length (mm) of the left and right internal iliac arteries in 17 embalmed and 37 unembalmed specimens. Adapted from Bleich et al. (2007) with permission from Elsevier.

Side	Cadaver type	Total (*n*)	Length (mm)		
			Mean±SD	Median	Range
Left	Fresh	37	29.0±9.6	29.5	7–52
	Embalmed	17	21.8±11.6[a]	24	0–38
	Total	54	26.8±10.7	27	0–52
Right	Fresh	37	29.0±10.4	29.5	0–49
	Embalmed	17	22.6±8.1[b]	24.5	0.31
	Total	54	27.0±10.1	27.5	0–49

[a]$p<0.001$; [b]$p<0.002$ for comparison of lengths in embalmed vs unembalmed

Table 56.6 Distance of the posterior division of the internal iliac artery (mm) from the sacral promontory and the pelvic midline. Adapted from Terek et al. (2004) with permission from John Wiley & Sons.

Measured distance	Length right side (mm)	Length left side (mm)
From sacral promontory to the posterior division of the internal iliac artery	42.0±7.9*	47.6±7
From the pelvic midline to the posterior division of internal iliac artery	35.3±6.3	38.1±4.9
Aortic bifurcation to internal iliac artery	60.9±11.5	66.2±12.5
Length of internal iliac artery to the appearance of posterior division	40.2±8.3	38.4±7.2

*$p<0.018$ when comparing left–right measurements; Mann-Whitney U Test

significant left–right difference was the distance from the sacral promontory to the posterior division of internal iliac artery was significantly shorter on the right side compared to the left (p=0.018, Mann–Whitney U-test). The authors suggest that the point of origin of the posterior division of the internal iliac can be identified intra-operatively as approximately 4–4.5 cm from either the sacral promontory or the common iliac bifurcation, or 3.5 cm from the pelvic midline.

Variability of the aortico-iliac tree

The structure of the aortico-iliac arterial tree is variable. Examples include the unilateral absence of an internal iliac artery (Mehl et al. 1969; Harb 2006), absence of the common iliac artery (Paterson 1909; Adachi 1928; Llauger et al. 1995; Greebe 1977; Kara et al. 2008) or absence of a common iliac artery with the lower limb blood supply arising from the ipsilateral renal artery (Greebe 1977). Some variants are thought to be related to the embryological development of the regional vascular system (see "Embryology") such as a persistent sciatic artery (see section "Persistent sciatic artery"). Such variants may prove non-problematic and only be discovered incidentally, whereas others are symptomatic and cause regional ischemia, nerve entrapment, or claudication.

The true incidence of variance in this region has not been determined; a series of case reports will therefore be used to demonstrate a range of possible variants. Both Adachi (1928) and Greebe (1977) reported a single observation of the absence of the common iliac artery, and therefore a quadrification of the aorta into the internal and external iliac arteries (Fig. 56.1).

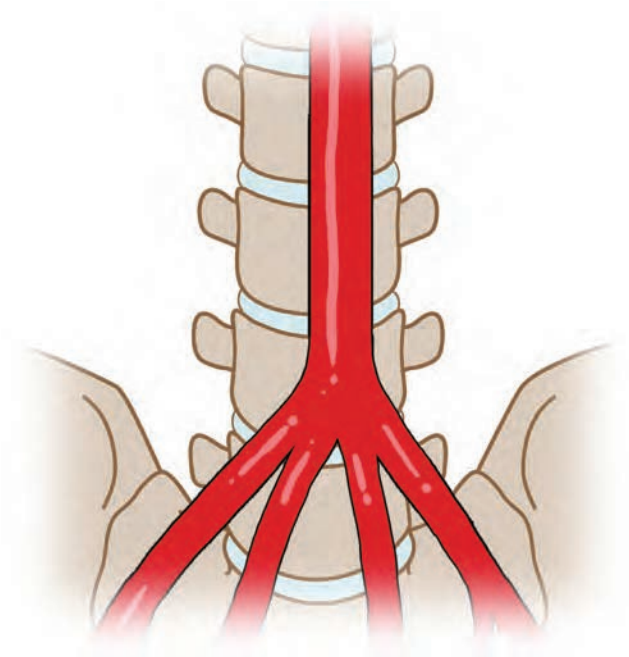

Figure 56.1 Case report of an abdominal aortic quadrification into right and left external and internal iliac arteries. Adapted from Adachi (1928).

Figure 56.2 Variant origin of the right internal and external iliac arteries with absence of the right common iliac artery. The right external iliac artery (REIA) branches from the aorta at the level of the last lumbar artery and caudally the aorta bifurcates into the right internal iliac (RIIA) and left common iliac (LCIA) arteries. LIIA: left internal iliac artery; LEIA: left external iliac artery; MSA: median sacral artery.

Source: Kara et al. (2008). Reproduced with permission from Springer Science and Business Media.

Kara et al. (2008) reported the absence of the right common iliac artery in a 53-year-old male, instead the right external iliac artery arose from the aorta at the level of the last lumbar artery and caudally the aorta bifurcated into the right internal iliac and left common iliac arteries (Fig. 56.2). In addition, the median sacral artery was noted to be a branch of both the right internal iliac and left common iliac arteries.

Paterson (1909) reported the case of a 60-year-old male cadaver in which there was no recognizable left common, external, or internal iliac artery branching from the aorta (Fig. 56.3). Both the femoral artery and distal part of the internal iliac artery were visible and fed by tributary vessels from the aorta. All of the normal branches of the internal iliac artery, except the iliolumbar, were reported present.

The location of the aortic bifurcation can also vary. Harb et al. (2006) reported the case of a 46-year-old male who had an aortic bifurcation located posterior to the inferior vena cava, together with a bilateral congenital absence of internal iliac arteries and prominent lumbar arteries which were thought to be compensating for the absent internal iliac arteries (Fig. 56.4).

Several case reports document the absence of an internal or external iliac artery. Koyama et al. (2003) reported the left

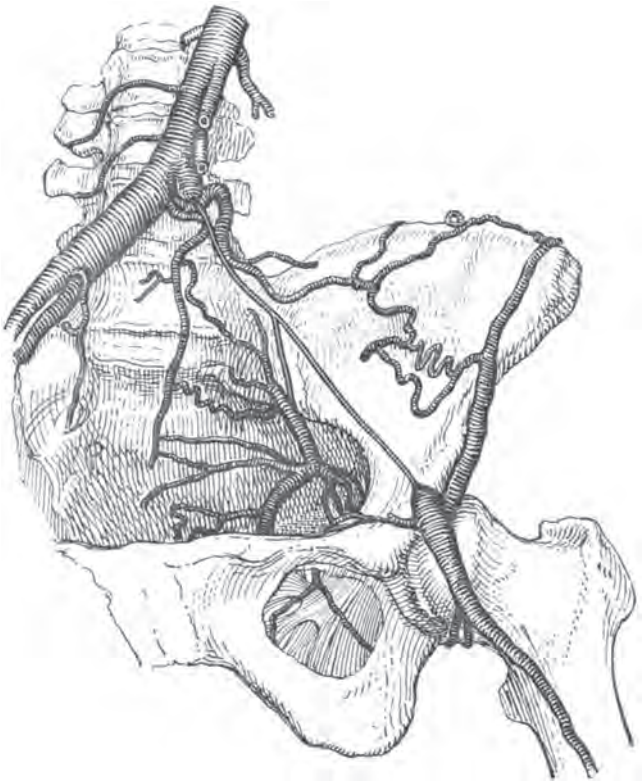

Figure 56.3 Case report of a left-sided absence of the common, internal, and external iliac arteries in a 60-year-old male English cadaver.

Source: Paterson (1909).

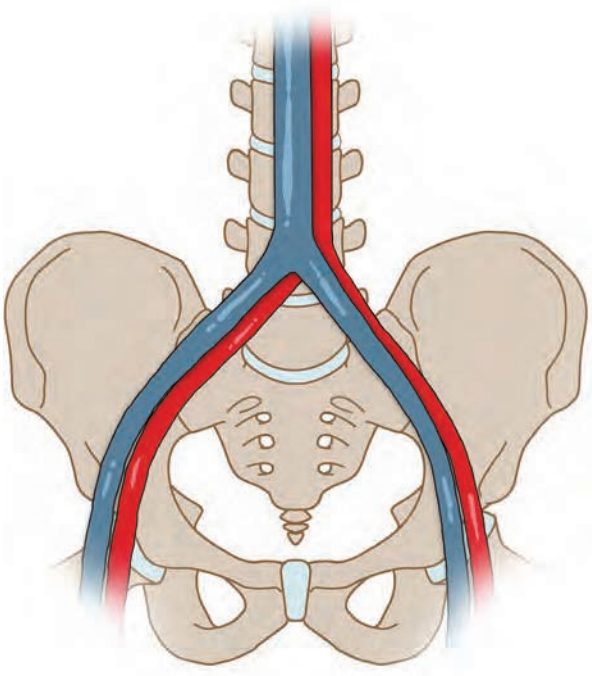

Figure 56.4 Bilateral congenital absence of the internal iliac arteries, with an aortic bifurcation located posterior to the inferior vena cava. Adapted from Harb et al. (2006).

Figure 56.5 Arteriogram demonstrating an absence of the left common iliac artery, and a left femoral arterial system fed by a continuation of the left internal iliac artery.

Source: Koyama et al. (2003). Reproduced with permission from Elsevier.

external iliac artery to be absent in a 51-year-old male patient and, instead, the left common iliac led directly into a left internal iliac artery which subsequently fed into the left femoral artery (Fig. 56.5). Okamoto et al. (2005) reported the case of a 92-year-old Japanese female cadaver in which the left external iliac artery was a continuation of the left internal iliac artery (Fig. 56.6). The authors reported that the left common iliac artery did not bifurcate and instead passed into the pelvic cavity, looped posterior to the S1 spinal nerve, gave rise to the branches

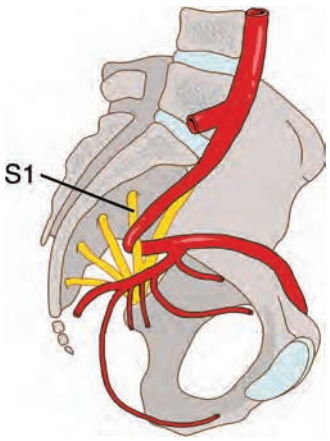

Figure 56.6 Case report of a 92-year-old female Japanese cadaver in whom the left external iliac artery was absent; instead, the left internal iliac artery provided its normal branches, passed under the left S1 nerve root, and then continued out of the pelvic cavity as the left external iliac artery which then formed the left femoral artery. Adapted from Okamoto et al. (2005).

normally associated with the internal iliac artery, and then continued out of the pelvic cavity as the left external iliac artery, which subsequently became the left femoral artery. Similar variations have been reported by other authors. Tamisier et al. (1990) reported the case of a 47-year-old male patient in which the femoral artery was a continuation of a pelvic artery that followed the same course as the internal iliac artery. Link et al. (2009) reported the case of a cadaver in which the left-sided external iliac artery was absent; instead, a single dominant vessel supplied the pelvic organs via an intra-pelvic course, and then continued over the pelvic brim as the left external iliac and into the anterior thigh as the left femoral artery (Fig. 56.7). Vessels on the right side were normal in course and origin.

Collateral arterial vessels have been shown able to compensate for the absence of internal iliac vessels. Kawashima et al. (2006) reported the case of a 91-year-old Japanese female cadaver with a hypoplastic right external iliac artery and enlarged right obturator and iliolumbar arteries, thought to be compensating for the reduced right external iliac arterial supply to the lower limb. It was noted that the obturator artery joined the right femoral at the level of the inguinal ligament, and the iliolumbar artery arose from the internal iliac artery via a common stem with the lateral sacral and connected to the right femoral artery via the deep circumflex iliac artery.

Complex vascular malformations may form during embryology, some of which are compatible with life and normal limb development. Goldny et al. (2009) presented the case of a persistent right-sided single aberrant abdominal umbilical artery, or patent impar umbilical artery, branching from the abdominal aorta at vertebral level L2 in an 18-year-old female. The right impar umbilical artery ran in place of the right iliac arterial system and a communicating vessel connected it to the left femoral artery across the anterior pelvis (Fig. 56.8).

Figure 56.7 Patient arteriogram showing an absence of the left external iliac artery and a dilated left internal iliac artery that is continuous distally with the left femoral artery.

Source: Link et al. (2009). Reproduced with permission from Elsevier.

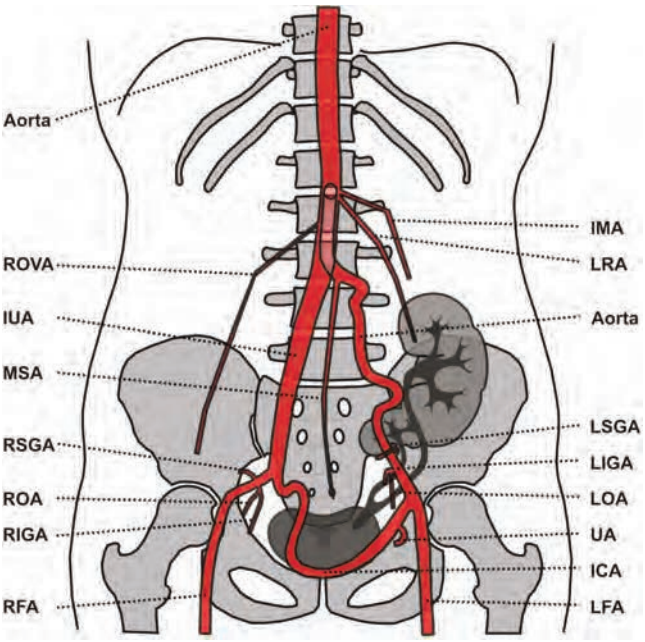

Figure 56.8 Persistent right-sided single aberrant abdominal umbilical artery, or patent impar umbilical artery, branching from the abdominal aorta at L2 in an 18-year-old female. ICA: inferior communicating artery; IMA: inferior mesenteric artery; IUA: impar umbilical artery; LFA: left femoral artery; LOA: left obturator artery; LIGA: left inferior gluteal artery; LRA: left renal artery; LSGA: left superior gluteal artery; MSA: median sacral artery; RFA: right femoral artery; RIGA: right inferior gluteal artery; ROA: right obturator artery; ROVA: right ovarian artery; RSGA: right superior gluteal artery; UA: umbilical artery.

Source: Goldny et al. (2009). Reproduced under the terms of the Creative Commons CC-BY-2.0 licence.

Embryology

The development of the lower limb vascular system has been studied in detail (Senior 1919–20, 1925; Arey 1963) and is discussed by Mandell et al. (1985) and Lippert and Pabst (1985). Briefly, during early embryonic development the common iliac arteries develop from the fifth dorsal branches/lumbar arteries of the aorta. The aorta caudal to the fifth branch regresses to form the median sacral artery. The umbilical arteries initially develop from the paired fourth ventral branches of the aorta, although their origin changes during development. Specifically, a longitudinal anastomotic connection develops joining the umbilical artery to the fifth dorsal branch of the aorta in the region of the developing internal iliac artery, and the original aortic origin of the umbilical artery eventually disappears. The latter change of origin is relevant when considering different

systems for classifying the branching pattern of the internal iliac artery based upon its branches.

The external iliac artery buds from the common iliac artery and the distal portion of the common iliac artery continues as the internal iliac artery. The developing regional vasculature initially forms a rich capillary plexus, from which the normal adult arterial pattern is formed via enlargement and persistence of the most appropriate vascular channels and regression of less important channels (Fitzgerald 1978). It is likely that variants in the arterial patterns of the pelvis and lower limb are most likely due to the selection of unusual/different vascular channels from primary capillaries (Arey 1963; Fitzgerald 1978). Variation in embryological vessel regression and persistence can lead to other unusual variants. Honma et al. (2013) reported the rare case of an 88-year-old Japanese male cadaver in which an arterial connection was present on the left side between the superior and inferior gluteal arteries (Fig. 56.9). The authors suggest that such an anastomotic ring is an embryonic remnant from the capillary plexus from which the pelvic arterial system develops. Such an anastomotic loop could be responsible for failed attempts at internal iliac artery embolization.

The lower limb bud receives arterial blood from the dorsal inter-segmental arterial system via a capillary plexus. A single dorsal axial/sciatic/ischiadic artery is formed following joining, selection, and enlargement of the most appropriate channels. The sciatic artery is the main arterial supply to the early stage lower limb. It passes distally along the dorsal pelvis and lower limb. The femoral arterial system develops later as a branch of the external iliac artery and eventually takes over from the sciatic artery. In the adult the proximal part of the sciatic artery forms the inferior gluteal artery, the middle section forms parts of the perforating arteries of the profunda femoris system, and the distal part contributes to the popliteal, peroneal, and anterior tibial arteries.

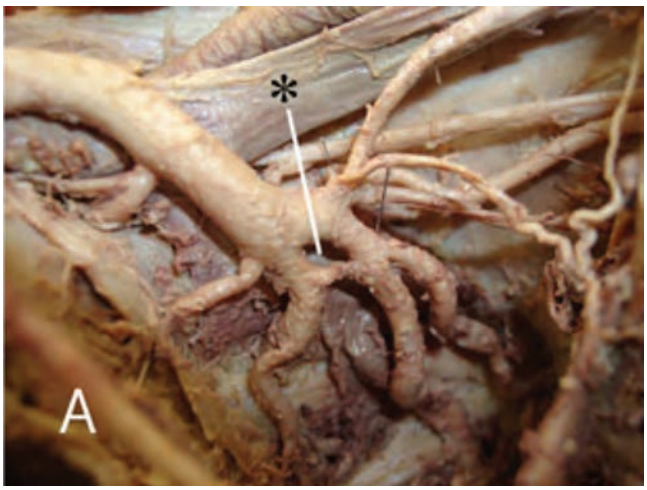

Figure 56.9 Case report of an arterial connection between the left superior and inferior gluteal branches of the internal iliac artery forming an anastomotic ring (*). IGA: inferior gluteal artery; SGA: superior gluteal artery; IIA: internal iliac artery.

Source: Honma et al. (2013). Reproduced with permission from Springer Science and Business Media.

Persistent sciatic artery

The sciatic artery provides the initial blood supply to the developing lower limb. This normally regresses by the end of the third month of embryonic development and the femoral system takes over. A lack of regression leads to persistent sciatic artery that is often accompanied by an underdeveloped femoral arterial system. The proximal part of the regressed sciatic artery normally forms the inferior gluteal artery. A persistent sciatic artery therefore represents a direct continuation of the internal iliac artery into the lower limb, and is often large in diameter (Job 1933; Mandell et al. 1985; Marincola et al. 2012). A persistent sciatic artery often gives rise to the superior gluteal and internal pudendal arteries, and then passes into the gluteal region through the infrapiriform part of the greater sciatic foramen where it can accompany either the sciatic nerve (within or outside of its sheath) or the posterior cutaneous nerve of the thigh.

A persistent sciatic artery may be asymptomatic or may be associated with acute or chronic limb ischemia, buttock mass, limb claudication, aneurysm formation, rupture and sudden death, nerve compression, hemi-hypertrophy of the limb, embolus, or thrombosis (Williams et al. 1983; Mandell et al. 1985; Marincola et al. 2012). The extent to which a persistent sciatic artery perfuses the limb varies from a small contributor/collateral vessel to the main blood supply if accompanied by anomalies in the femoral arterial system (Williams et al. 1983; Savov and Wassilev 2000) (Figs 56.10). Marincola et al. (2012) presented the case report of a 64-year-old male with signs of ischemia in the right foot. CT angiography revealed bilateral persistent sciatic arteries, which originated as a continuation of an enlarged internal iliac artery (Fig. 56.11). The right-sided vessel was the predominant vascular supply to the right lower limb and the right femoral artery and its branches ended in the muscles of the thigh. A similar smaller persistent sciatic vessel was noted in the left lower limb.

The presence of a sciatic artery is also relevant to procedures where internal iliac artery ligation or embolization is used to control bleeding, since full ligation in the presence of a dominant persistent sciatic vessel could cause significant limb ischemia. In such cases embolization of individual branches of the internal iliac artery is necessary (Hiki et al. 2007). Early cases of persistent sciatic artery were reported in European, Japanese, and African American cadavers (Green 1832; Bryan 1914; Senior 1925; Adachi et al. 1928; Job 1933). A literature review by Williams et al. (1983) revealed that a total of 52 cases of the condition have been reported (Table 56.7). The authors reported that complete persistence was the most common pattern (79%), and it was often accompanied by hypoplasia of the femoral artery (61%). In 1984 the estimated incidence of discovering a persistent sciatic artery on angiogram was 0.025–0.6% (Donovan and Sharp 1984).

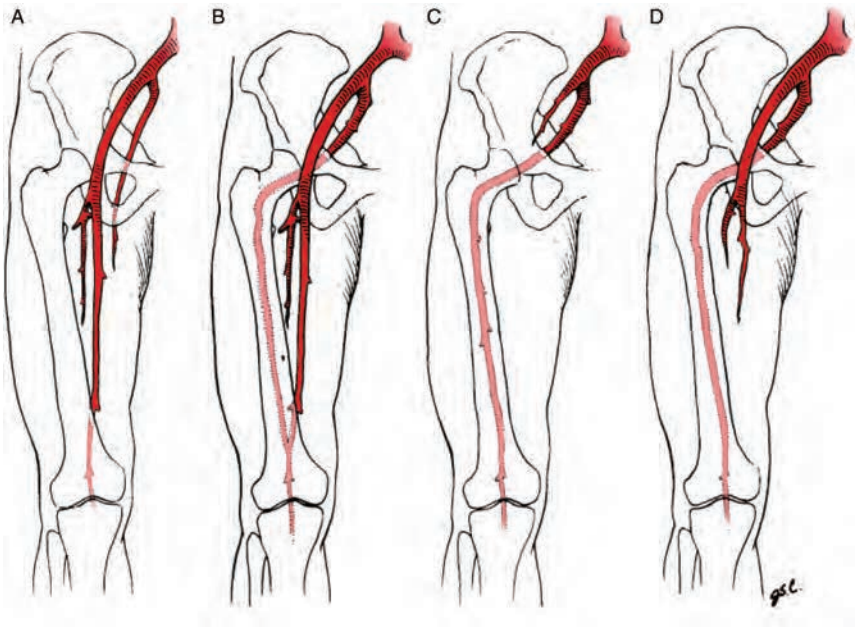

Figure 56.10 Variation in the size and distribution of the persistent sciatic artery and femoral arteries. (a) Incomplete sciatic artery with normal femoral artery; (b) large sciatic and femoral arteries joining to form the popliteal artery; (c) hypoplastic femoral artery with a large complete sciatic artery; and (d) partial femoral artery with large complete sciatic artery. Adapted from Williams et al. (1983) with permission from Elsevier.

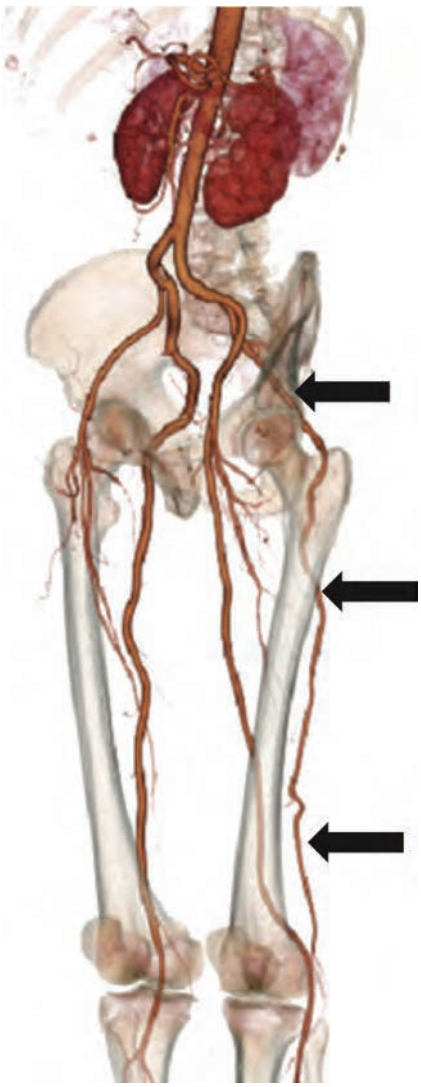

Figure 56.11 Volume-rendered 3D reconstruction of a CT-angiographic study of a 64-year-old male with bilateral persistent sciatic artery. A large right-sided persistent sciatic artery (*) continues from the right internal iliac and provides the main blood supply to the right lower limb. Note the right femoral artery is small and ends at mid-thigh level. The left persistent sciatic artery (black arrows) is smaller and ends by joining with the left popliteal artery of the femoral system posterior to the knee.

Source: Marincola et al. (2012). Reproduced under the Open Access licence.

Table 56.7 Relative incidence of persistent sciatic artery up until 1983 (*n*=52). Complete: persistence of all of the sciatic artery; incomplete: persistence of only the proximal part of the sciatic artery, therefore forming a collateral to the limb; hypoplastic: present but not normal size or pursuing its normal course. Adapted from Williams et al. (1983) with permission from Elsevier.

Artery	Morphology	Total (*n*)	Frequency (%)
Sciatic	Complete	41	79
	Incomplete	4	8
	Unknown	7	13
Femoral	Normal	5	10
	Hypoplastic	32	61
	Absent femoral and iliac systems	3	6
	Unknown	12	23

Persistent sciatic artery is most often unilateral although bilateral persistence (Fig. 56.11) occurs with an estimated incidence of 12–32% of all cases of persistence (reviewed by Savov and Wassilev 2000; based on work by McLellan and Morettin 1982; Freeman et al. 1986; Madson et al. 1995; Balachandra et al. 1998). In 2000 Savov and Wassilev reported a further case of bilateral persistence in a 65-year-old cadaver in which the sciatic arteries arose from an extremely large anterior trunk of the internal iliac artery.

Collateral connections of the internal iliac arteries and its branches

The internal iliac artery and its branches can receive collateral connections from regional parietal arteries and the branches of the internal iliac artery can connect to partner vessels across the midline. The main collateral arteries to the internal iliac system have been shown to be between branches of the internal iliac itself or regional non-internal iliac system artereis such as the middle sacral, circumflex femoral, deep circumflex iliac, inferior epigastric, and fifth lumbar arteries (Shafiroff et al. 1959; Chait et al. 1968; Hassen-Khodja et al. 1987) (Table 56.8). Chait et al. (1968) reported that in some cases anastomoses became functional/observable immediately after vessel occlusion, and in others it was noted that blood flow remained visible distal to a ligated internal iliac artery.

Collateral vessels are thought to be responsible for continued bleeding following vessel embolization/ligation (Binder and Mitchell 1960) and, in the long term, collateral vessels have been shown to re-establish blood supply to pelvic structures following intraoperative internal iliac artery ligation to control hemorrhage. For example, Nakai et al. (2011) reported the case of an 80-year-old male who, following internal iliac artery embolization, suffered buttock claudication. Over time the claudication subsided and was associated with a dilation of the superior gluteal artery. The authors postulated that this was through development of collateral connections via arteries

Table 56.8 The collateral blood supplies to the main branches of the internal iliac artery. Data from (1) Shafiroff et al. (1959) and (2) Chait et al. (1968). Shafiroff et al. (1959) studied the collateral arteries in 150 cadaveric specimens via intra-arterial injection of red lead suspension with one or both internal iliac arteries occluded. Chait et al. (1968) studied the pelvic arteries and collaterals in 19 patients (aged 9–49 years) via angiography following internal or common iliac artery ligation or occlusion.

Main branch of internal iliac artery	Collateral Arterial Vessel	Author
Iliolumbar	Gluteal; lumbar; deep circumflex iliac; lateral circumflex femoral; spinal	1
	Last lumbar; deep circumflex iliac	2
Lateral sacral	Spinal; median sacral; inferior gluteal; superior gluteal	1
	Lateral sacral (contralateral); median sacral	2
Superior gluteal	Lateral sacral; deep circumflex iliac; lateral circumflex femoral; inferior gluteal	1
	Lateral circumflex femoral; deep circumflex iliac; last lumbar;	2
Internal pudendal	External pudendal; inferior gluteal	1
Obturator	Medial circumflex femoral; inferior epigastric; iliolumbar; inferior gluteal	1
	Medial circumflex femoral	2
Inferior gluteal	Medial and lateral circumflex femoral; first perforating (thigh)	1
	Medial circumflex femoral	2
Umbilical	Vesical; ureteric	1
Uterine	Ovarian	1
Middle rectal	Superior rectal; inferior rectal	1
	Superior rectal	2

such as the circumflex femoral. Clark et al. (1985) presented a study of 19 female patients who underwent bilateral internal iliac artery ligation to control obstetric hemorrhage. Bleeding was only fully controlled in 42% and continued in the remaining 58%, suggesting the presence of collateral vessels from a source other than the internal iliac system. Both the advantages and disadvantages of regional collateral arteries were demonstrated by Gür et al. (2013) who reported the case of a 53-year-old male with right lower limb claudication and impotence secondary to an occluded right external iliac artery. Angiography revealed the right internal iliac artery was dilated and supplying the right lower limb via a dilated obturator and circumflex femoral arteries, with the consequent negative effect of diverting blood from the penis.

Hassen-Khodja et al. (1987) studied the angiograms of 200 atherosclerotic patients and found multiple routes for collateral circulation with the internal iliac system. Five collateral arteries were reported to have major anastomotic roles: the iliolumbar, superior gluteal, inferior gluteal, internal pudendal, and obturator arteries. Other collateral branches were reclassified as

the central system of anastomotic collaterals that anastomosed with arteries passing to the viscera. These included the umbilical and middle rectal arteries, arteries supplying the genitourinary organs (e.g., bladder/uterus/vagina) and parietal collateral arteries (e.g., superior and inferior lateral sacral arteries) which anastomose with each other at the midline. The authors presented six main collateral routes of circulation that had either afferent or efferent circulatory potential as follows.

1. The iliolumbar artery anastomosed with the circuit formed by the lumbar arteries and the 11th or 12th posterior intercostal arteries (afferent system). It also anastomosed with the deep circumflex iliac artery branching from the external iliac artery (efferent system).
2. The superior gluteal artery (afferent system) anastomosed with the lumbar arteries via a deep branch and also anastomosed with the deep femoral artery via a superficial branch (efferent system).
3. The inferior gluteal artery (efferent system) anastomosed with the first perforating branch deep femoral artery via a descending collateral branch.
4. The internal pudendal artery anastomosed with the inferior rectal artery, which itself anastomosed with the deep femoral artery (efferent system) and numerous perineal collateral vessels were noted (both efferent and afferent).
5. The obturator artery anastomosed with the femoral artery via the external pudendal arteries and its anastomosis with the inferior epigastric artery (efferent systems). It forms part of the central system via its pubic branch (both afferent and efferent).
6. The central anastomotic system corresponded to the numerous anastomoses between visceral and parietal arteries, although many are not very effective. The anastomosis of the middle rectal with the inferior mesenteric artery could represent a major afferent system.

Branching pattern of the internal iliac artery

The main parietal and visceral branches arising from the internal iliac artery are relatively consistent and can be identified by following them to their destination/region of supply. However, the pattern of internal iliac artery branching is highly variable and multiple classification systems/methods have been devised. Jastschinski (1891a) was the first to categorize the branching pattern of the internal iliac artery based upon a study of 396 Polish cadavers. Arterial branches were organized into three main categories:

1. vessels of large calibre (e.g., superior gluteal, inferior gluteal, and internal pudendal arteries);
2. vessels of medium calibre (e.g., obturator artery); and
3. vessels of small calibre (e.g., iliolumbar and lateral sacral arteries).

Jastschinski (1891a) noted that only large-calibre vessels (Category 1) were sufficiently regular in origin to enable their pattern of origin to be grouped into types, of which four were identified and ordered numerically based upon their frequency of observation (Table 56.9). In general, the gluteal and pudendal arteries are normally present. However, it should be noted that variability may also occur in the large calibre vessels as highlighted by Reddy et al. (2007) who reported the case of a male Indian cadaver with no right inferior gluteal artery.

In 1918 Lipshutz studied 181 dissections of pelvic halves from 93 cadavers (72 male white: 11 female white; 7 male black: 3 female black) and presented an alternative five group classification system based upon the origin of the inferior gluteal, superior gluteal, internal pudendal, and obturator arteries (Fig. 56.12). The ordering of the five types was based upon their frequency of observation (Table 56.10). Similar results were presented by Shafiroff et al. (1959) in their study of 150 cadaveric specimens. Lipshutz (1918) also reported that there was a tendency for types I and II to be more common on the right side with types III, IV, and V being more common on the left. The five branching patterns were described as follows.

- Type I (40%): The superior gluteal artery was the largest branch and arose as the dorsal or posterior trunk of the internal iliac artery. The internal pudendal and inferior gluteal arteries arose as a common trunk caudal to superior gluteal. Jastschinski (1891a) found this type present in 38% (20% right side, 18% left side) of subjects studied. The obturator, vesical, middle hemorrhoidal, and uterine arteries arose as separate branches from the caudal continuation of the internal iliac

Table 56.9 The branching pattern of the internal iliac artery based upon a study of 396 Polish cadavers. S: superior gluteal artery; I: inferior gluteal artery; P: internal pudendal artery; U: umbilical artery. Adapted from Jastschinski (1891a).

Type	I	II	III	IV
	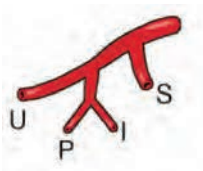	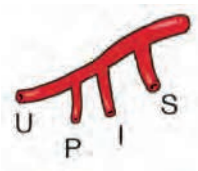		
Frequency (%)	38	28	24	9

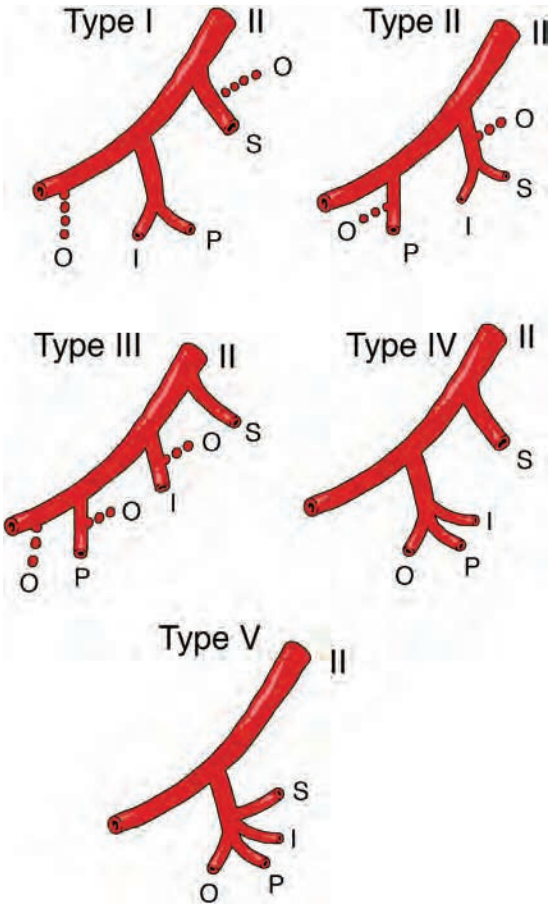

Figure 56.12 Five types of internal iliac artery branching based upon a study of 181 cadaveric pelvic halves from 93 cadavers. II: internal iliac artery; I: inferior gluteal artery; S: superior gluteal artery; P: internal pudendal artery; O: obturator artery.

Source: Lipshutz (1918). Reproduced with permission from Wolters Kluwer Health.

artery. In 45% of this group the obturator artery arose in a common trunk with the inferior epigastric artery from the external iliac, and arose 16 times as a separate branch from the superior gluteal artery. In one subject the obturator artery was as a branch of the femoral artery.

Table 56.10 Frequency of Type I–V branching patterns of the internal iliac artery. Data from Lipshutz (1918) and Shafiroff et al. (1959).

	Frequency (%) Lipshutz 1918 (*n*=181)			Frequency (%) Shafiroff et al. 1959 (*n*=150)
Type	Right side	Left side	Total	Total
I	24	16	40	36
II	14	10	24	20
III	7	10	17	18
IV	3	8	11	14
V	2	5	7	12

- Type II (24%): The superior and inferior gluteal arteries arose from the internal iliac artery as a common trunk. The internal pudendal, obturator, and uterine arteries arose as separate branches from the caudal continuation of the internal iliac artery. In 40% of this group the obturator artery arose as a separate branch from the common trunk of the superior and inferior gluteal arteries. It also arose via a common trunk with the inferior epigastric artery from the external iliac artery (*n*=3). In all cases the common trunk for the superior and inferior gluteal arteries exited the pelvis via the greater sciatic foramen superior to piriformis. In two subjects the internal pudendal artery was a separate branch of the common trunk for the superior and inferior gluteal arteries after the trunk had exited the pelvis.
- Type III (17%): The superior gluteal, inferior gluteal and internal pudendal arteries were separate branches of the internal iliac artery. The origin of the obturator artery was variable, occurring as a branch of the internal iliac artery (*n*=17), inferior gluteal artery (*n*=4), internal pudendal artery (*n*=5), a common trunk with the inferior epigastric artery (*n*=4); and the middle rectal artery (*n*=2).
- Type IV (11%): The obturator, internal pudendal, and inferior gluteal arteries arose from the internal iliac artery as a common trunk and the superior gluteal artery arose as a separate branch dorsal to the common trunk. The superior gluteal artery was usually larger than the trunk for the inferior gluteal, obturator, and internal pudendal arteries.
- Type V (7%): The superior gluteal, inferior gluteal, obturator, and internal pudendal arteries arose as a common trunk from the internal iliac artery.

In 1925 Dubreuil-Chambardel conducted a study of 440 cadaveric specimens and reported ten different branching patterns of the internal iliac artery based upon the gluteal, internal pudendal and sacral arteries (Fig. 56.13) and ten different branching patterns based upon the visceral branches of the anterior division (Fig. 56.14).

In 1928 Adachi published the results of a study based upon 121 Japanese cadaveric specimens. Adachi classified the branching of the internal iliac using four of its main branches; the umbilical, superior gluteal, inferior gluteal, and internal pudendal arteries (Fig. 56.15). This classification system has since proved the standard for many years. Based upon the embryological origins of vessels, Adachi suggested the umbilical artery was a continuation of the main stem of the internal iliac artery, and the superior gluteal, inferior gluteal, and internal pudendal arteries branched from it. The main differences in the Adachi system compared to that of Jastschinski (1891a) were that the Jastschinski Types II and III swapped positions due to the relative predominance of Jastschinski Type III over Type II in the Adachi study. Adachi also added subgroups to existing groups and a new fifth group. Each main branching pattern was described as follows.

- Type 1: The superior gluteal artery arose separately from the internal iliac artery, and the inferior gluteal and the internal

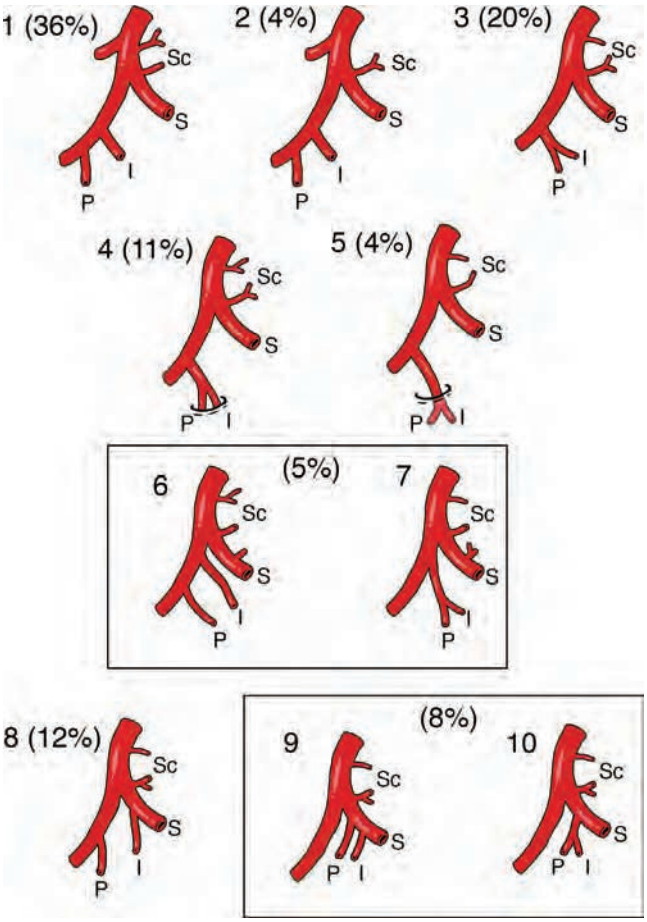

Figure 56.13 Ten types of variation in the branching pattern of the internal iliac artery based upon four main branches. Based on 440 observations, relative frequency (%) of each type is shown. S: superior gluteal artery; I: inferior gluteal artery; p: internal pudendal artery; Sc: lateral sacral arteries. Adapted from Dubreuil-Chambardel (1925).

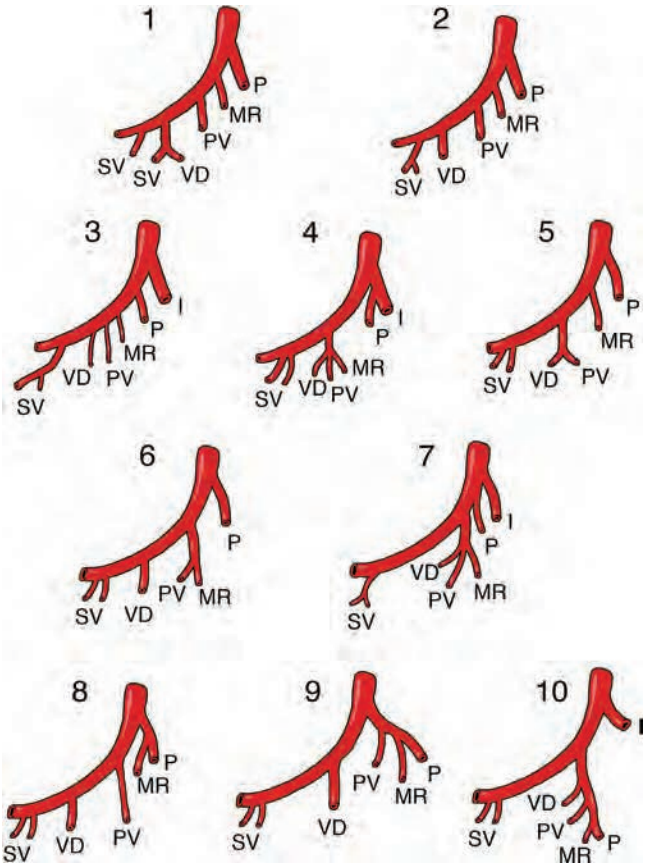

Figure 56.14 Ten types of variation in the origin of the visceral branches of the internal iliac artery. Based on 440 observations. P: internal pudendal artery; MR: middle rectal artery; PV: prostatovesical artery; VD: vesicodeferential artery; SV: superior vesical artery; I: inferior gluteal artery. Adapted from Dubreuil-Chambardel (1925).

pudendal artery arose from a common trunk. Type 1a refers to bifurcation of the common trunk within the pelvis. Type 1b refers to bifurcation of the common trunk below the pelvic floor.

- Type 2: The internal pudendal artery arose separately from the internal iliac artery and the superior and inferior gluteal arteries arose via a common trunk. In type 2a the superior and inferior gluteal arteries arose from a common trunk within the pelvis. In type 2b the gluteal arteries arose outside of the pelvis.
- Type 3: The superior gluteal, inferior gluteal, and internal pudendal arteries arose separately from the internal iliac artery.
- Type 4: The superior gluteal, inferior gluteal, and internal pudendal arteries arose via a common trunk. In type 4a the trunk first gives origin to the superior gluteal artery before bifurcating into the other two branches. In Type 4b the internal pudendal artery is the first vessel branching from the common trunk, which then divides into superior and inferior gluteal arteries.
- Type 5: The internal pudendal and the superior gluteal arteries arose from a common trunk, and the inferior gluteal arose separately from the internal iliac.

A meta-analysis of 22 studies (representing 5331 specimens) of internal iliac artery branching patterns categorized according to the Adachi (1928) system showed type 1 to be the majority branching pattern (54.4%), after which the order of frequency was type 3 > type 2 > type 4 > other > type 5 (Table 56.11), demonstrating that Jastschinski (1891) was correct in the ordering of branching types. Recent studies on Indian cadavers (Shivakumar et al. 2010; Naveen et al. 2011; Ramakrishnan et al. 2012; Vishnumukkala et al. 2013) suggest that the Indian population may have a higher percentage of type 1 variants (74.8%) as compared to the Western/Japanese population (53.9%).

Internal iliac artery branching based upon the full Adachi classification

In 1967 Roberts and Krishinger reviewed a series of publications classifying the branching patterns of the internal iliac artery according to the full Adachi (1928) system, including subgroups.

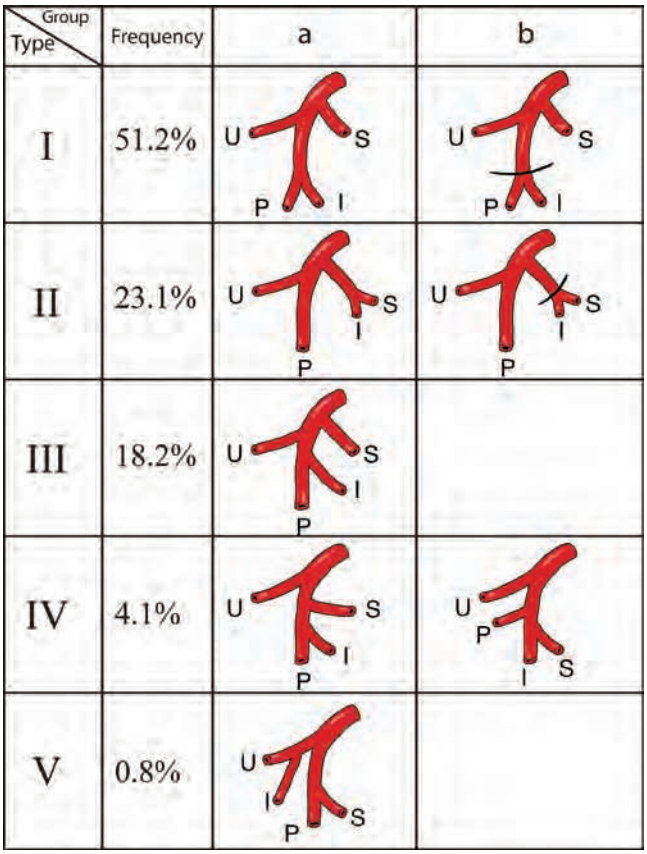

Figure 56.15 The Adachi 1928 classification of the internal iliac artery branching into five types, with subgroups, based upon 121 cases (2.5% of observed cases were classified as "other" and excluded from classification). Groups Ib and IIb were defined by a common trunk branching below the pelvic floor. I: inferior gluteal artery; S: superior gluteal artery; P: internal pudendal artery; U: umbilical artery. Adapted from Adachi (1928).

In cases where the original authors had used a different classification/grouping system it was standardized to the Adachi system. The addition of more recent data yields 788 observations from 7 studies (Table 56.12). Type 1a branching is the most common (50.9%), followed by type III and then type IIa.

Sex differences

Braithwaite (1952a) studied 169 cadaveric pelvic halves from white British subjects, classified internal iliac branching pattern according to the Adachi (1928) system, and compared males and females (Table 56.13). The addition of more recent data for comparison yielded a total of 264 specimens (76 female: 188 male) from three studies. There was a greater incidence of type IIa branching in females versus males and type Ia branching in males versus females. In general, type III branching predominated over type II. Braithwaite (1952a) also reported that the superior gluteal, inferior gluteal, and internal pudendal arteries were relatively constant in their origins, yet the obturator artery was more variable.

Alternative systems of classification

Alternative systems for classifying internal iliac artery branching patterns have been suggested. Ashley and Anson (1941) developed a classification system that included the obturator artery; however, the wide variability in obturator artery origin yielded a complex system with 9 types and 49 subtypes (Fig. 56.16) rendering the system difficult to use. Odano (1962) classified internal iliac artery branching using the visceral branches. The common stem of the umbilical and vesiculo-deferential arteries formed the superior pelvic trunk and a common trunk from the inferior pelvic trunk gave rise to vessels such as the prostatic, inferior vesicular, and middle rectal.

Following a review of the literature, Lippert and Pabst (1985) reported variations in internal iliac branching (Lipshutz 1918; Adachi 1928; Ashley and Anson 1941; Anson 1963; Fischer 1959; Roberts and Krishinger 1967; Nitschke and Preuss 1971; Narverud and Mhyre 1974; Pac et al. 1977; Becken 1984) and presented a four-group classification system with subgroups (Fig. 56.17). The umbilical artery was reported to be the main branch of the internal iliac artery, with all other branches being side branches. The most common branching pattern (Type 2a, 35%) corresponds to an Adachi Type I pattern.

In 1998 Yamaki et al. published the results of a study investigating 645 cadaveric pelvic halves from Japanese cadavers. The authors attempted to classify the internal iliac artery branching pattern according to Adachi's 1928 scheme, but found that not all specimens matched the original scheme. The authors therefore created a revised classification system consisting of the original five types but with multiple subgroups, of which there were 19 (Fig. 56.18). No significant differences between male and female specimens or between left and right sides were reported. In the original Adachi publication of 1928 the umbilical artery was classified as a continuation of the main stem of the internal iliac artery. Yamaki et al. (1998) suggested a new classification system based upon the exclusion of the umbilical artery and the use of only the internal pudendal and superior and inferior gluteal arteries. This was justified by the fact the umbilical artery originates as a ventral branch of the dorsal aorta and connects to the internal iliac artery through a capillary network, whereas the common iliac artery originates as a dorsal branch of the dorsal aorta. The exclusion of the umbilical artery simplified the categorization of branching patterns and gave rise to four main groups, into which the original and modified Adachi systems could be fitted (Fig. 56.19). Within this system, the umbilical artery can arise from the internal iliac artery or any subsequent branch. The four groups were described as follows.

- Group A: The internal iliac artery divides into two branches, the superior gluteal artery and a common trunk for the inferior gluteal and internal pudendal arteries. This group includes Type I-Groups 1–4, Type III-Groups 1 and 2, and Type IV-Groups 1 and 2 of the modified Adachi classification.

Table 56.11 Frequency of observation of the five main internal iliac branching patterns classified according to the Adachi 1928 system.

			Frequency (%); type of internal iliac artery branching (Adachi 1928)					
Author	**Cadaver origin**	**Total (*n*)**	**I**	**II**	**III**	**IV**	**V**	**Other**
Jastschinski (1891a)[c]	Poland	396	38	24	28	9	–	–
Lipshutz (1918)[c]	America	181	51	24	17	7	–	–
Adachi (1928)[a]	Japan	121	51.2	23.1	18.2	4.1	0.8	2.5
Tsukamoto (1929)[a]	Japan	287	56.5	8.4	22.0	12.9	–	–
Miyaji (1935)[a]	Japan	179	70.4	11.7	9.5	8.4	–	–
Arai (1936)[a]	Japan	500	52.4	19.4	24.0	4.2	–	–
Hoshiai (1938)[a]	Japan (fetal)	379	55.1	16.1	26.1	2.6	–	–
Ashley & Anson (1941)[c]	America	260	58.1	17.3	9.6	7.7	–	7.3
Suzuki (1951)[a]	Japan	490	53.2	18.8	24.1	3.7	0.2	–
Braithwaite (1952a)	Europe	169	58.5	15.3	22.5	3.6	–	–
Yasukawa (1954)[a]	Japan	544	53.7	18.4	23.9	4.0	–	–
Shafiroff et al. (1959)	America	150	50	20	18	12	–	–
Fischer (1959)	Europe	50	50	26	16	8	0	0
Roberts & Krishinger (1967)	America	167	51	26.8	14.4	7.2	0	0
Morita et al. (1974)[a]	Japan (fetal)	267	49.1	22.5	21.7	6.7	0	0
Iwasaki et al. (1987)[a]	Japan	251	54.2	19.5	24.3	2	0	0
Yamaki et al. (1998)	Japan	645	58	13.6	22.8	5.4	0.2	0
Fatu et al. (2006)	Europe	100	60	20	10	1	8	0
Shivakumar et al. (2010)	Indian	40	89	11	0	0	0	0
Naveen et al. (2011)	Indian	60	83.5	6.6	9.9	0	0	0
Ramakrishnan et al. (2012)	Indian	50	60	8	30	2	0	0
Vishnumukkala et al. (2013)	Indian	45	66.7	2.2	24.4	4.4	2.2	0
Total		5331	54.4	17.8	21.4	5.57	0.23	0.58[b]

[a]Japanese language data reviewed and presented by Yamaki et al. (1998); [b]Includes observations that were unclassified by the author; [c]Data converted to Adachi types.

Table 56.12 Frequency of observation of the types of internal iliac branching pattern classified according to the full Adachi (1928) system, including subgroups. Data from 1941–67 adapted from Roberts & Krishinger (1967).

			Frequency (%); type of internal iliac artery branching (Adachi 1928)								
Author	**Cadaver origin**	**Total (*n*)**	**Ia**	**Ib**	**IIa**	**IIb**	**III**	**IVa**	**IVb**	**V**	**Other**
Ashley & Anson (1941)	America	247	49.7	0	17.3	0	11.9	7.3	7.7	0	0
Braithwaite (1952a)	Europe	169	48.5	10	11.8	3.5	22.5	2.4	1.2	0	0
Fischer (1959)	Europe	50	46	4	12	14	16	2	6	0	0
Roberts & Krishinger (1967)	America	167	45	6	25	1.8	14.4	5.4	1.8	0	0
Naveen et al. (2011)	India	60	76.9	6.6	6.6	0	9.9	0	0	0	0
Ramakrishnan et al. (2012)	India	50	52	8	8	0	30	2	0	0	0
Vishnumukkala et al. (2013)	India	45	57.8	8.8	2.2	0	24.4	4.4	0	2.2	0
Total		788	50.9	5.2	15.1	2.0	16.7	4.5	3.4	0.1	0.0

Table 56.13 Frequency of observation of the types of internal iliac branching pattern in male versus female cadavers categorized using the full Adachi (1928) system.

			Frequency (%); type of internal iliac artery branching (Adachi 1928)								
Author	**Sex**	**Total (*n*)**	**Ia**	**Ib**	**IIa**	**IIb**	**III**	**IVa**	**IVb**	**V**	**Other**
Braithwaite (1952a)	Female	61	40.9	8.2	18.0	6.5	21.3	3.2	1.6	0	0
	Male	108	52.7	11.1	8.3	1.8	23.1	1.8	0.9	0	0
Ramakrishnan et al. (2012)	Female	10	40	10	20	0	30	0	0	0	0
	Male	40	55.0	7.5	5.0	0	30.0	2.5	0	0	0
Vishnumukkala et al. (2013)	Female	5	60	20	0	0	20	0	0	0	0
	Male	40	57.5	7.5	2.5	0	25	0	0	2.5	0
Total	Female	76	42.0	9.2	17.1	5.2	22.4	2.6	1.3	0.0	0.0
	Male	188	54.2	9.6	6.4	1.0	25.0	1.6	0.5	0.5	0.0

- Group B: The internal iliac artery divides into two branches, the internal pudendal artery, and a common trunk for the superior gluteal and inferior gluteal arteries. This group includes Type II-Groups 1–4 and Type IV-Groups 3 and 4 of the modified Adachi classification.
- Group C: The internal iliac artery simultaneously divides into three major branches. This group includes Type III-Groups 3 and 4 and Type IV-Groups 5 and 6 of the modified Adachi classification.
- Group D: The internal iliac artery divides into the inferior gluteal artery and a common trunk for the superior gluteal and internal pudendal arteries. This group includes Type V of the modified Adachi classification.

No significant differences were noted between sides or sexes (Fig. 56.19). A recent study by Bilhim et al. (2011) on 42 pelvic sides from 21 male patients using medical imaging confirmed the results of Yamaki et al. (1998).

Case reports of internal iliac artery variant branching and locations

Shetty et al. (2011) reported the case of a 60-year-old male Indian cadaver in which the posterior division of the internal iliac artery terminated as the superior and inferior gluteal arteries with the ventral ramus of first sacral nerve descending between them. In addition, the obturator artery arose close to the bifurcation of the posterior division and subsequently passed deep to the internal iliac vein along the lateral pelvic wall, was crossed by the ureter and ductus deferens on its medial side, and then coursed downward and forward, deep to the internal pudendal artery.

Badagabettu et al. (2013) reported the case of a 65-year-old male Indian cadaver in which the right internal iliac artery divided into three main trunks that gave origin to the iliolumbar and lateral sacral arteries (trunk 1), the inferior gluteal and internal pudendal arteries (trunk 2), and the superior vesical and obturator arteries (trunk 3). In the same specimen the superior gluteal and middle rectal arteries arose directly from the main part of the internal iliac artery. The superior gluteal artery entered the gluteal region through the greater sciatic foramen by passing above the lumbosacral trunk, instead of passing between the lumbosacral trunk and the S1 ventral ramus. The superior vesical artery supplied the territory of the inferior vesical artery, since the inferior vesical artery was absent.

Branches of the internal iliac arterial system

The internal pudendal, umbilical, and superior and inferior gluteal arteries show sufficient regularity of origin to allow classification into groups. The points of origin of the remaining branches of the internal iliac artery are highly variable. Naguib et al. (2008) performed magnetic resonance angiographic studies of 49 females (mean age 47.0±4.7 years; range 38–57 years) prior to uterine artery embolization. In total, 98 internal iliac vessel systems were studied and the number of each type of vessel detected and their point of origin recorded (Table 56.14). The main point of origin for each vessel was either from the main stem of the internal iliac artery or its anterior or posterior division. Similarly, Shafiroff et al. (1959) studied 150 cadaveric specimens, classified internal iliac artery branching according to the Lipshutz (1918) system, and reported the point of origin of all branches of the iliac system (Table 56.15; Fig. 56.20).

Bleich et al. (2007) studied 54 American female cadavers (37 unembalmed; 17 embalmed; mean age 79.6±12.7 years) and recorded the first branch of the posterior division. In the majority of cadavers (61.5% left side, 63.0% right side) the first branch was a common trunk for the iliolumbar, lateral sacral, and superior gluteal arteries (Table 56.16). In the remaining specimens, posterior division branches arose independently from the internal iliac with the iliolumbar forming the first branch in 28.3%,

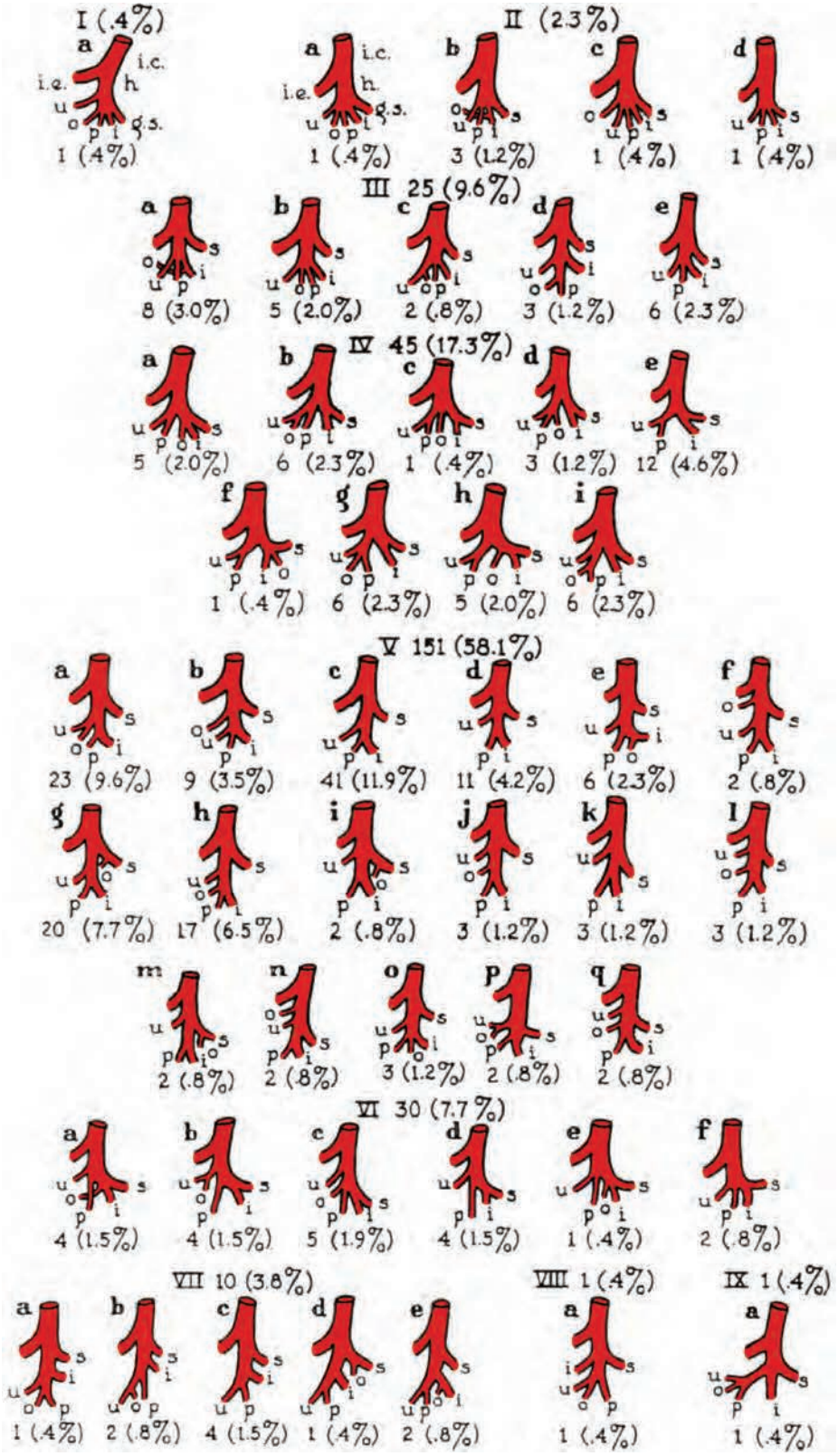

Figure 56.16 Classification of the branching pattern of the internal iliac artery into nine types, with 49 subtypes in total, following a study of 130 specimens (260 sides; 100 white American: 30 Black American). Frequency data (%) is shown. Classification is based upon 5 main branches; S: superior gluteal artery; I: inferior gluteal artery; P: internal pudendal artery; U: umbilical artery; O: obturator artery. Adapted from Ashley and Anson (1941), with permission from John Wiley & Sons.

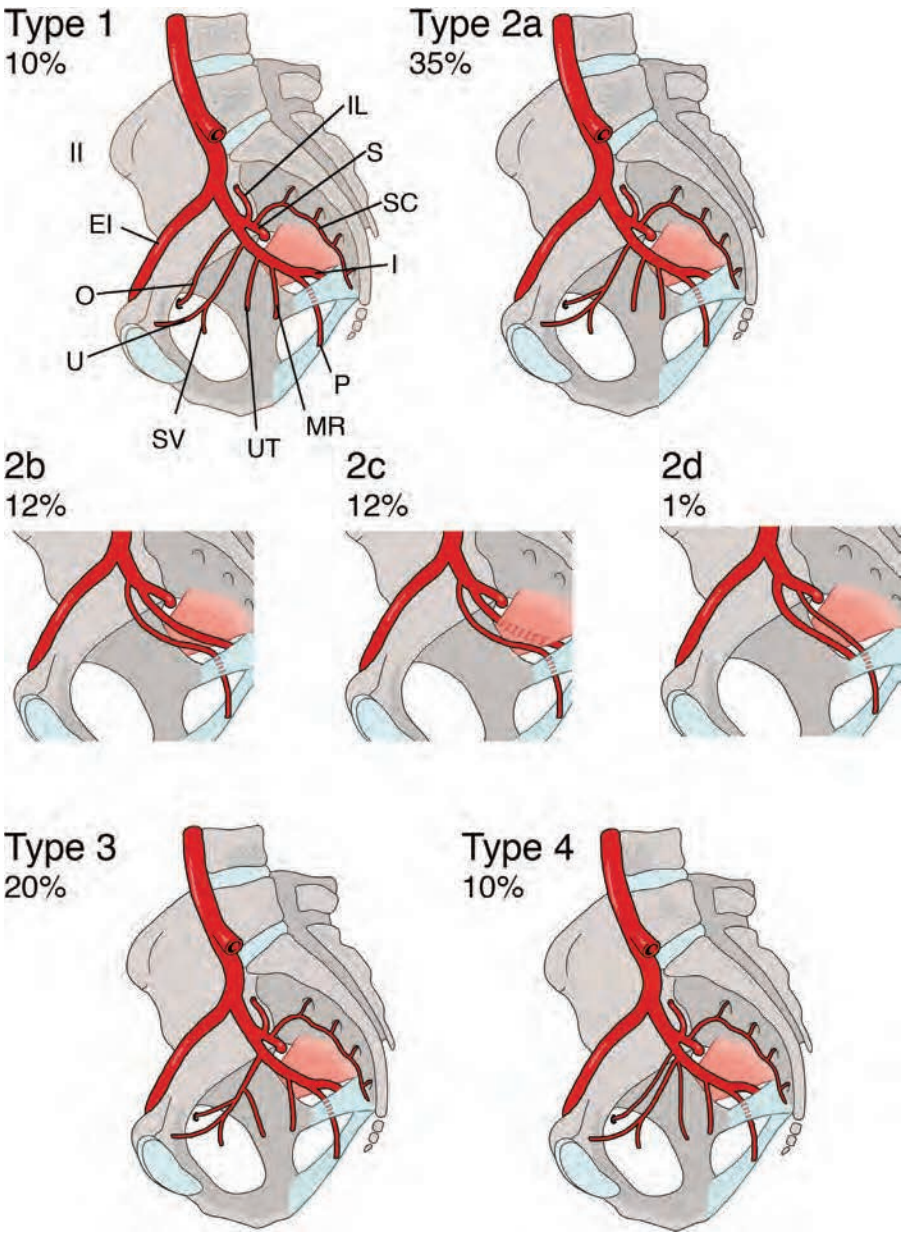

Figure 56.17 Four main types of internal iliac branching based upon a review of the literature. Type 1: all arteries branch from a single main stem (internal iliac artery); Type 2a–d the internal iliac artery divides into two main divisions (anterior and posterior) from which the branches arise; Type 2a: anterior division ends as the inferior gluteal and internal pudendal arteries (posterior division ends as the superior gluteal artery); Type 2b: anterior division ends as the internal pudendal artery; posterior division ends as the superior and inferior gluteal arteries, which leave through the supra- and infrapiriform foramen, respectively; Type 2c: same branching as 2b except the posterior division ends as a common trunk that divides into superior and inferior gluteal arteries after passing through the suprapiriform foramen; Type 2d: the anterior division ends as the inferior gluteal artery; posterior division ends as the superior gluteal and internal pudendal arteries; Type 3: internal iliac artery divides into three stems which give off all other branches; Type 4: internal iliac artery divides into four or more stems which branch to give the other arteries. Adapted from Lippert and Pabst (1985).

the lateral sacral in 5.7%, and the superior gluteal artery in 3.8% of specimens.

Hypogastric trunk

The term hypogastric trunk was historically used to describe a trunk arising from the internal iliac artery that gave rise to vessels including the vaginal, middle rectal, and superior and inferior vesical arteries. Parsons and Keith (1897) studied 56 specimens and reported the hypogastric trunk to be present in 76.7%. A total of 66% of observed hypogastric trunks branched from the anterior division. In 23.3% no trunk was present, and in the remaining 10.7% of cases it came from the internal iliac artery before its division into two. The term hypogastric trunk is now rarely used.

Obturator artery

The origin point of the obturator artery is highly variable and has been studied in detail due to its clinical significance in pelvic and abdominal wall surgery. Indeed, Lipshutz (1918) commented that "Probably no artery in the human body of proportionate size has so voluminous a literature as the obturator artery," a fact which most likely still holds true. The embryological origin of the obturator artery from the capillary plexus of the pelvis helps explain the wide variability of its origin (Senior 1919–20, 1925; Sanudo et al. 1993). The obturator artery is known to supply the adductor, psoas, and obturator muscles and parts of the hip joint, but it can also supply the bladder, rectum, and erectile tissues of the perineum as shown

Type	Total Frequency	Group 1	Group 2	Group 3	Group 4	Group 5	Group 6
I	58.0%	46.8%	2.8%	8.2%	0.2%		
II	13.7%	5.6%	5.6%	1.7%	0.8%		
III	22.9%	9.5%	8.7%	3.0%	1.7%		
IV	5.4%	3.1%	0.3%	0.9%	0.5%	0.6%	0%
V	0.2%	0.2%					

Figure 56.18 Branching pattern of the internal iliac artery based upon a modified version of the Adachi (1928) system in which multiple subgroups have been added to the original five types. Based upon a study of 645 cadaveric pelvic halves from Japanese cadavers. Frequency data (%) is provided. Adapted from Yamaki et al. (1998).

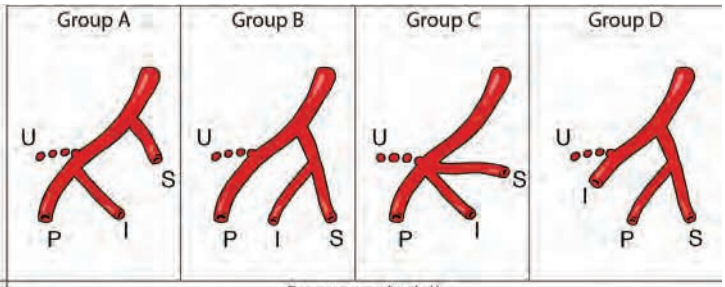

	n	Frequency (% (n))			
Right Side	327	79.2 (259)	15.3(50)	5.5 (18)	0
Left Side	318	79.9 (254)	14.8 (47)	5.0 (16)	0.3 (1)
Male	426	80.1 (341)	13.4 (57)	6.6 (28)	0
Female	219	78.5 (172)	18.3 (40)	2.7 (6)	0.5 (1)
Total	645	79.5 (513)	15.0 (97)	5.3 (34)	0.2 (1)
Bilhim et al. 2010	42	61.9 (26)	31 (13)	7.1 (3)	0 (0)

Figure 56.19 Branching pattern of the internal iliac artery based upon the exclusion of the umbilical artery and the use of only the internal pudendal artery (P), superior gluteal artery (S), and inferior gluteal (I) artery. In this classification system the umbilical artery (U) can arise from any branch or part of the internal iliac system. Based upon a study of 645 cadaveric pelvic halves from Japanese cadavers. Data are presented as frequency (*n* %). Adapted from Yamaki et al. (1998) with additional data from Bilhim et al. (2010).

by Pick et al. (1942) in a study of 320 cadavers and Park et al. (2009). Other unusual branches of the obturator artery can include the iliolumbar, superior and inferior vesical, uterine, vaginal, dorsal penile, ureteric, perineal, circumflex femoral, external pudendal, and inferior epigastric arteries (Quain 1844; Henle 1868; Hyrtl 1887; Gegenbaur 1888; Pfitzner 1889; Delitzin 1896; Robinson 1902; Schaefer et al. 1915; Lipshutz 1918; Cordier and Pardoen 1921; Poynter 1922; Huber 1930; Chandler and Kreuscher 1932; Jackson 1933; Dschau 1936–37; Curtis et al. 1942; Pick et al. 1942; Latarjet 1948; Howe et al. 1950; Batteur 1951; Crock 1965; Anson 1966; Gardner et al. 1969; Pac et al. 1977) (Fig. 56.21). Furthermore, the ligamentun teres femoris artery arises from the obturator in about 54% of subjects and the acetabular branch of the obturator artery may be absent.

Morphology

There is little published data on the morphology of the obturator artery. In a study of 60 pelvic halves from 30 cadavers, Maneesha et al. (2012) reported that the length of the obturator artery originating from the anterior division of the internal iliac artery fell within the range 40–88 mm, from the posterior division 70–115 mm, and from external iliac/inferior epigastric arteries 30–40 mm.

Origin from the internal and external iliac arterial systems

The obturator artery can arise from most parts and branches of the internal iliac arterial system, the inferior epigastric artery, the external iliac artery and, although rare, has also been reported to arise from the femoral artery (Lipshutz 1918;

Table 56.14 Variability in the origin of the main branches of the internal iliac artery as detected in 49 female patients (98 pelvic halves) using magnetic resonance angiography based upon data from Naguib et al. (2008). Figures represent the number of each artery/point of origin detected on scans, and percentages are relative to the total number of each type of main vessel detected. IIA: internal iliac artery.

Artery (total number detected)	Artery of origin	No. samples (*n*) (% of detected vessels)
Uterine artery (95)	Anterior division of IIA	86 (90%)
	Main stem of IIA	2 (2%)
	Internal iliac bifurcation point	1 (1%)
	Posterior division of IIA	1 (1%)
	Anterior division via common stem with obturator artery	4 (4%)
	Anterior division via common stem with internal pudendal	1 (1%)
Superior gluteal artery (98)	Posterior division of the IIA	98 (100%)
Inferior gluteal artery (98)	Anterior division of IIA	83 (85%)
	Posterior division of IIA	15 (15%)
Lateral sacral arteries (86)	Posterior division of IIA	78 (91%)
	Main stem of the IIA	6 (7%)
	Anterior division of IIA	1 (1%)
	Inferior gluteal artery (from posterior division)	1 (1%)
Iliolumbar arteries (84)	Main stem of the IIA	42 (50%)
	Posterior division of IIA	37 (44%)
	Point of IIA bifurcation	5 (6%)
Superior vesical artery (21)	Anterior division of IIA	21 (100%)
Middle rectal artery (11)	Anterior division of IIA	11 (100%)
Internal pudendal arteries (96)	Anterior division of IIA	91 (95%)
	Indirect origin from the anterior division	3 (3%)
	Main stem of IIA	1 (1%)
	Posterior division of IIA	1 (1%)
Obturator arteries (81)	Anterior division of IIA	53 (65%)
	Inferior epigastric artery	21 (26%)
	Posterior division of IIA	3 (4%)
	Anterior division via common segment with the uterine artery	4 (5%)

Dubreuil-Chambardel 1925; Pick et al. 1942; Lanz and Wachsmuth 1959). Based upon an analysis of 5781 cases from 22 studies, the most common origin point for the obturator artery is from the internal iliac arterial system (70.3%, range 57.7–81.0%) with 28.7% (range 19.0–43.3%) originating from the external iliac arterial system (Table 56.17). Further sub-categorization shows the most common origin to be from the anterior division of the internal iliac artery (31.5%, range 20.3–70%) based upon 1109 specimens from 7 studies (Table 56.18). An analysis of 7816 specimens from 30 studies showed the second most common origin to be the inferior epigastric artery branching from the external iliac artery (23%, range 2.6–43.3) (Table 56.19).

In 2011 Sanudo et al. suggested a six-point classification system (Type A–F) for single-rooted obturator arteries based upon the frequency of observation of different origin points following a study of 116 cadavers (232 sides). A meta-analysis of 11 studies reviewed by Sanudo et al. (2011), together with the author's own dataset, revealed that the most common origin point for the obturator artery was from the anterior division of the internal iliac (Type A, 37.6% of cases, *n*=618/1642, range 20.9–60.2%) with the next most common being from the inferior epigastric artery (Type B, 22.9% of cases, *n*=741/3240, range 12.6–32.3%).

Dubreuil-Chambardel (1925) presented six different origin points for the obturator artery from the external iliac or femoral arterial systems, with the most common origin being from a short common trunk with the inferior epigastric artery (24.8% of 440 specimens) (Fig. 56.22). Rare points of origin included the medical circumflex femoral artery in 0.45% of cases and the profunda femoris artery. In all cases, the obturator artery passed over the pelvic brim into the pelvic cavity to exit via the

Table 56.15 Variation in the origin of the main branches of the internal iliac artery as observed in a study of 150 cadaveric specimens. The ischiopudendal trunk refers to a common trunk giving rise to the obturator, inferior gluteal, and internal pudendal arteries. IIA: internal iliac artery. Adapted from Shafiroff et al. (1959) with permission from Elsevier.

	Artery of origin	
Artery	**>10% incidence**	**<10% incidence**
Middle rectal (seen in 84% of specimens)	Internal pudendal; inferior gluteal; anterior division of IIA	Obturator; deferential
Inferior vesical (seen in 78% of specimens)	Anterior division of IIA; umbilical; prostatic; vaginal	Vesicodeferential; internal pudendal
Obturator	Common trunk with inferior epigastric or superior and inferior gluteal; internal pudendal	Common trunk with superior and inferior gluteal and internal pudendal
Superior gluteal	Posterior division of IIA; common trunk with inferior gluteal	Common trunk with inferior gluteal, obturator and internal pudendal
Inferior gluteal	Ischiopudendal trunk; anterior division of IIA; common trunk with superior gluteal	Common trunk with superior gluteal, obturator and internal pudendal
Internal pudendal	Ischiopudendal trunk; anterior division of IIA	Middle rectal; uterine; common trunk with gluteal artery
Uterine*	Anterior division of IIA; internal pudendal; inferior vesical	Obturator; middle rectal
Deferential*	Anterior division of IIA; internal pudendal; prostatic	Middle rectal (in this case the deferential artery replaced the testicular artery)
Prostatic*	Anterior division of IIA; middle rectal; inferior gluteal; inferior vesical	Obturator; umbilical; ischiopudendal trunk
Vaginal*	Uterine; anterior division of IIA; ischiopudendal trunk; inferior gluteal	Obturator; internal pudendal

*homologous arteries

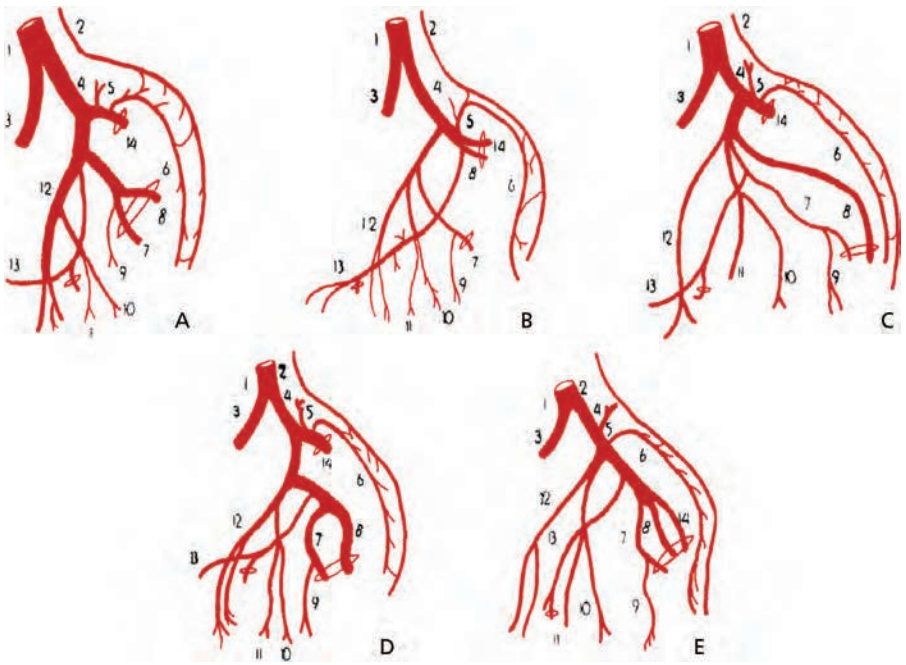

Figure 56.20 Variations in the branching pattern of the internal iliac artery as determined from a study of 150 cadaveric specimens. The five main branching patterns of the internal iliac artery, as first classified by Lipshutz 1918, are shown with additional branches added. 1: common iliac artery; 2: middle sacral artery; 3: external iliac artery; 4: internal iliac artery; 5: iliolumbar artery; 6: lateral sacral artery; 7: internal pudendal artery; 8: inferior gluteal artery; 9: middle rectal artery; 10: inferior vesical artery; 11: uterine or deferential artery; 12: umbilical artery; 13: obturator artery; 14: superior gluteal artery. Adapted from Shafiroff et al. (1959).

Table 56.16 The first branch of the posterior division of the internal iliac artery and its frequency of occurrence on both left and right sides. From a study of 54 female US cadavers; 37 unembalmed: 17 embalmed; mean age 79.6±12.7 years. Adapted from Bleich et al. (2007) with permission from Elsevier.

Branch of posterior division of internal iliac artery	Left % (*n*)	Right % (*n*)
Common trunk for iliolumbar, lateral sacral and superior gluteal	61.5 (32)	63.0 (34)
Iliolumbar	26.9 (14)	29.6 (16)
Lateral sacral	5.8 (3)	5.6 (3)
Superior gluteal	5.8 (3)	1.8 (1)

obturator foramen. Other rare variants have also been observed, for example Pai et al. (2012) reported the case of an Indian cadaver in which the obturator and inferior vesical artery arose via a common trunk from the external iliac artery.

There is a low incidence of the obturator artery arising directly from the external iliac artery with studies reporting frequencies of 1.1% (Braithwaite 1952a) to 3.5% (Biswas et al. 2010). Other authors have reported similar frequencies: 1.3% (Jakubowicz and Czarniawska-Grzesinska 1996); 1.7% (Lipshutz 1918); 1.8% (Sanudo et al. 2011); and 2.4% (Reid 1836, citing Cloquet). A meta-analysis of data by Saundo et al. (2011) found the mean frequency to be 1.7% with a range of 0.6–5.1%. Case reports also exemplify this variant. Nayak and Kv (2009) reported the right obturator artery to originate from the right external iliac artery in a 60-year-old male Indian cadaver and Sarikcioglu and Sindel (2002) reported the same in a 55-year-old male cadaver. El-Sawaf (2010) reported the obturator artery to originate from the external iliac artery on the right and from the inferior epigastric artery on the left in a female Egyptian cadaver. The obturator artery has also been seen to originate from the external iliac artery and then give origin to the inferior epigastric artery (Nagabhooshana et al. 2008).

Sex differences

An analysis of multiple studies has shown that the origin of the obturator artery from the external iliac system is more common in females (33.2%) compared to males (28.0%) (Table 56.20). Biswas et al. (2010) studied 56 formalin-fixed East Indian cadaveric pelvic halves (18 female: 38 male) and reported a relatively higher frequency of obturator artery origin from the superior gluteal artery in females compared to males (22.2%: 13.2%, respectively). Similar results were reported by Braithwaite (1952a) (16.4%: 6.4%; female: male) following a study of 169 cadaveric pelvic halves (61 female: 108 male) and by Ramakrishnan et al. (2012) (30%: 10%; female: male) following a study of 50 Indian pelvic halves (10 female: 40 male).

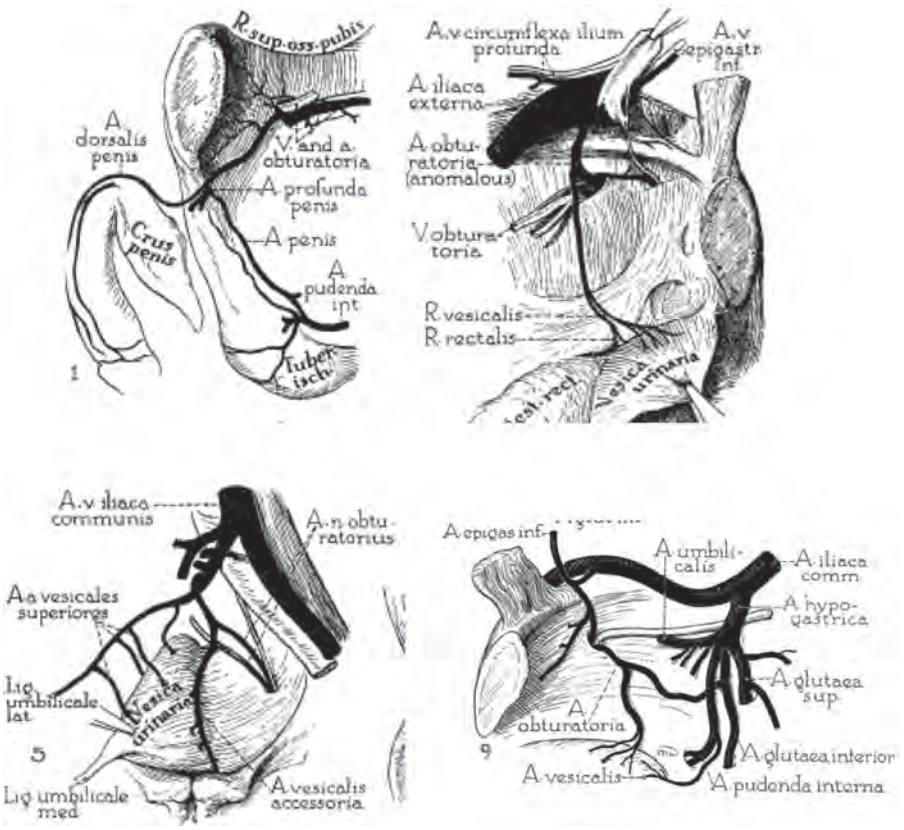

Figure 56.21 Variations in the origin of the obturator artery origin and its branching pattern as observed in a study of 640 pelvic halves from 320 cadavers. Adapted from Pick et al. (1942) with permission from John Wiley & Sons.

Table 56.17 Frequency of the obturator artery originating from the internal and external iliac systems. Adapted from Dubreuil-Chambardel (1925).

			Internal iliac system		External iliac system	
Author and country of study	**Year**	**Total (n)**	**Cases (*n*)**	**%**	**Cases (*n*)**	**%**
Cloquet (France)	1817	500	348	69.6	152	30.4
Hesselbach (Germany)	1819	64	37	57.7	27	43.3
Breschet (France)	1819	63	51	81.0	12	19.0
Quain (England)	1844	361	246	68.6	115	31.4
Schlöbig (Germany)	1844	112	78	69.6	34	21.0
Hoffmann (Switzerland)	1878	400	270	67.5	130	32.5
Wyeth and Wardwell (England)	1878	52	34	66.0	18	34.0
Hartmann (Germany)	1881	180	146	81.0	34	19.0
Krusche (Estonia)	1885	80	63	78.8	17	20.0
Pfitzner (France)	1889	226	141	62.4	85	37.0
Jastschinski (Poland)	1891	1034	723	70.0	311	30.0
Dwight (America)	1895	500	371	74.2	129	25.8
Levi (Italy)	1902[a]	110	82	74.8	28	25.2
Dubreuil-Chambardel (France)	1925	440	310	70.5	130	29.5
Original total (%)		4122	2900	70.4	1222	29.6
Lipshutz (America)	1918	181	141	77.9[a]	40	22.1
Pick et al. (America)	1942	640	447	69.9	188	29.4
Braithwaite (England)	1952[b]	169	123	72.7	35	20.6
Roberts & Krishinger (America)	1967	79	58	73.5	21	26.5
Namking et al. (Thailand)	2007	204	158	77.5	46	22.5
Pai et al. (India)	2009	98	77	80.2	21	21.4
Biswas et al. (India)	2010	56	41	73.1	15	26.8
Sanudo et al. (Japan)	2011	232	115	69.2	69	30.8
Updated total (%)		5781	4060	70.3	1657	28.7

[a]Incomplete dataset presented by Lipshutz (1918), therefore number provided calculated from the raw dataset provided by the author; [b]Braithwaite (1952a) noted that in 6.5% of specimens the obturator artery originated from both the internal and external iliac arteries; these data are not included in the table.

Biswas et al. (2010) reported a higher percentage of obturator vessels originating from the anterior division of the internal iliac in males compared to females (50%: 33.3%), whereas Pai et al. (2009) following a study of 98 Indian cadaveric specimens (62 male: 36 female) reported the opposite (69.4%: 54.8%; female: male) (Table 56.21). Sanudo et al. (2011) reported no significant difference in obturator artery origin between genders (127 female: 105 male) or left and right sides, based upon a study of 116 cadavers (232 sides). Similarly, Braithwaite (1952a) reported no further sex differences; likewise, none were reported by Namking et al. (2007) following a study of 204 Thai pelvic halves (111 from 56 males; 93 from 43 females).

Single and multiple rooted obturator arteries

In most cases (96.6%: Sanudo et al. 2011) the obturator artery arises as a single root; however, less commonly it can arise as a double root (0.7%: Dubreuil-Chambardel 1925; 1%: Quain 1844; Dwight 1894–95; Pick et al. 1942; Lippert and Pabst 1985; 3%: Sanudo et al. 2011; 6.1%: Lipshutz 1918; Kawai et al. 2008; 6.5%: Braithwaite 1952a) or even triple root from both the internal and external iliac systems (seen in 0.4%: Sanudo et al. 2011). Nasu and Chiba (2009) reported the case of a triple-rooted left obturator artery arising from the left superior and inferior gluteal arteries and the inferior epigastric artery.

Double-rooted vessels can arise from both the internal and external iliac arteries. Namking et al. (2007) reported such an origin in 5.4% of 204 Thai cadaveric specimens and Pai et al. (2009) reported the same in 2% of 98 Indian cadaveric specimens (62 male: 36 female). In an analysis of the literature Sanudo et al. (2011) reported that the frequency of double-rooted obturator arteries fell within the range 1–2% (Jaschtschinski 1891b; Dubreuil-Chambardel 1925; Levi 1902a, b; Adachi 1928; Pick et al. 1942; Lippert and Pabst 1985; Pai et al. 2009) and that all double-rooted obturator arteries consistently possessed a small anastomotic vessel joining the two roots. The authors go on to suggest that such small roots

Table 56.18 Frequency (%) of the obturator artery originating from different parts of the internal and external iliac arterial systems. The hypogastric trunk is a historical term that refers to a trunk giving rise to the superior and inferior vesical arteries, vaginal and middle rectal arteries. –, data are not available or were not categorized in this manner.

	Parsons and Keith (1897)	Pick et al. (1942)	Braithwaite (1952a)	Roberts and Krishinger (1967)	Biswas et al. (2010)	Ramakrishnan and Elezy (2012)	Maneesha et al. (2012)	Total
Artery of origin	***n*=55**	***n*=640**	***n*=169**	***n*=79**	***n*=56**	***n*=50**	***n*=60**	***n*=1109**
Internal iliac system								
Internal Iliac trunk	9.1	23.3	0	3.8	0	0	3.3	14.3
Anterior division	36.4	20.3	41.4	53.2	44.6	40	70	31.5
Posterior division	14.5	3.3	0	16.5	12.5	0	10	5.0
Superior gluteal	0	11.1	10	0	16.0	14	0	9.4
Inferior gluteal	0	8.8	4.7	0	0	0	0	5.8
Internal pudendal	0	2.8	3.8	0	0	18	0	3.0
Iliolumbar	0	0.3	3.0	0	0	10	0	1.1
Hypogastric trunk	16.4	–	–	–	–	–	–	–
External iliac system								
External iliac	0	2.0	1.1	1.2	3.5	0	3.3	1.8
Inferior epigastric (from external iliac)	18.1	26.7	19.5	25.3	23.3	0	6.7	22.6
Inferior epigastric (from femoral)	0	0.6	0	0	0	0	0	0.3
External and internal iliac	0	0	6.5	0	0	0	0	1.0

Table 56.19 Frequency of the obturator artery originating from the inferior epigastric artery. Data in the left side of the table adapted from Poynter (1922). Data in the right part are additional.

Author	Total (n)	Frequency (%)	Author	Total (n)	Frequency (%)
Cloquet (1817)	500	30.4	Parsons & Keith (1897)	55	18.1
Breschet (1819)	63	19	Lipshutz (1918)	181	19.3
Hesselbach (1819)	64	43.3	Dubreuil-Chambardel (1925)	440	29.5
Quain (1844)	361	31.4	Adachi (1928)	692	12.6
Schlöbig (1844)	112	21	Pick et al. (1942)	640	27.3
Isaacs (1855)	706	18.3	Braithwaite (1952a)	169	19.5
Wyeth and Wardwell (1877)	52	34	Roberts & Krishinger (1967)	79	25.3
Hoffmann (1878)	400	32.5	Gilroy et al. (1997)	105	15.2
Hartmann (1881)	180	19	Pai et al. (2009)	98	14.3
Krusche (1885)	80	20	Darmanis et al. (2007)	80	36
Pfitzner (1889)	226	37.6	Jakubowicz & Czarniawska-Grzesinska (1996)	76	2.6
Jastschinski (1891b)	404	24	Mamatha et al. (2012)	50	12
Dwight (1894–95	500	25	Kawai et al. (2008)	706	10.5
Levi (1902a)	109	21.1	Biswas et al. (2010)	56	23.2
Poynter (1922)	400	26.2	Sanudo et al. (2011)	232	28
			Overall Total	7816	23.0

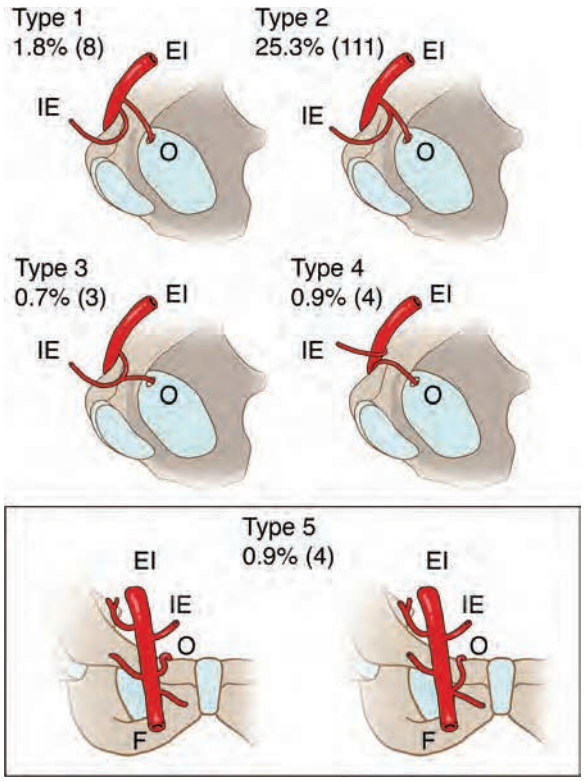

Figure 56.22 Variation in the origin of the obturator artery from the external iliac and femoral arteries. Figures show % frequency (*n*). Based on a study of 440 cases. The obturator artery arose from the external iliac system in 130 of 440 cases (29.5%). EI: external iliac artery; O: obturator artery; IE: inferior epigastric artery; F: femoral artery. Type 1: branches directly from the external iliac artery. Type 2: Arises via a common trunk with the inferior epigastric artery: (a) trunk is a few millimeters in length (24.8%, *n*=109) and (b) trunk is 4–5 cm in length (0.5%, *n*=2). Type 3: obturator artery branches from the inferior epigastric artery. Type 4: obturator artery branches from the femoral artery under the inguinal ligament. Type 5: (a) branches from the femoral artery in the femoral triangle; (b) branches from the profunda femoris artery; and (c) branches from the medial circumflex femoral artery (observed in 2 cases of 440). Adapted from Dubreuil-Chambardel (1925).

Table 56.20 Frequency of the obturator artery originating from the external iliac arterial system by sex. The total number of specimens (*n*) studied in each category is shown. Adapted from Dubreuil-Chambardel (1925).

	Male	Female
Author	**% (total *n*)**	**% (total *n*)**
Cloquet (1817)	24.4 (250)	31.4 (250)
Quain (1844)	29.8 (181)	33.9 (180)
Schlöbig (1844)	28.4 (74)	34.2 (38)
Krusche (1885)	25.9 (63)	37.5 (16)
Pfitzner (1889)	38.3 (163)	35.6 (39)
Jastschinski (1891b)	26.3 (572)	34.6 (462)
Braithwaite (1952a)	28.7 (108)	24.6 (61)
Biswas et al. (2010)	23.7 (38)	33.4 (18)
Total	28.0 (1449)	33.2 (1064)

of the obturator artery can easily be missed in macroscopic studies, resulting in an artificially lower reported incidence of multiple-rooted vessels.

There is some lack of clarity as to how to distinguish between a true double-rooted obturator artery and the presence of iliopubic vessels that anastomose with the obturator artery during dissection. Kawai et al. (2008) determined the fate/destination of the pubic branches of the inferior epigastric artery in 706 pelvic halves and showed pubic vessels to be present in 79.3% (*n*=560/706) of cases, with a number of different possible arrangements. For example, in 10.5% of cases (*n*=59/560) the pubic vessels formed the only obturator artery and in 21.6% of cases (*n*=121/560) the pubic vessels anastomosed with the obturator artery originating from the internal iliac artery.

Table 56.21 Comparison of the frequency of the obturator artery originating from the internal and external iliac arterial systems between males and females. Based upon a study of 62 male and 36 female specimens. Adapted from Pai et al. (2009).

			Frequency % (*n*)		
Artery			**Male % (*n*)**	**Female % (*n*)**	**Total % (*n*)**
Internal iliac	Anterior division		54.8 (34)	69.4 (25)	60.2 (59)
	Posterior division	Separate branch	8.1 (5)	5.6 (2)	7.1 (7)
		With superior gluteal	11.3 (7)	8.3 (3)	10.2 (10)
		With iliolumbar	1.6 (1)	0 (0)	1.0 (1)
External iliac		Separate branch	6.5 (4)	2.8 (1)	5.1 (5)
		With inferior epigastric	14.5 (9)	13.9 (5)	14.3 (14)
Internal and external iliac			3.2 (2)	0 (0)	2.0 (2)

Table 56.22 Frequency of the obturator artery originating from the external iliac artery in either a bilateral or unilateral pattern. Adapted from Dubreuil-Chambardel (1925).

		Frequency of obturator artery arising from the external iliac artery system % (*n*)		
			Unilaterally	
Author	Total (*n*)	Bilaterally	Right	Left
Cloquet (1817)	250	24.8 (62)	11.2 (28)*	
Hesselbach (1819)	32	–	37.5 (12)	46.9 (15)
Quain (1844)	159	15.7 (25)	11.3 (18)	12.6 (20)
Pfitzner (1889)	105	–	33.3 (35)	34.3 (36)
Dubreuil-Chambardel (1925)	130	31.5 (41)	20.8 (27)	16.9 (22)
Total uni-/bilateral origin	539	23.7 (128)	–	–
Total unilateral origin by side (R/L)	426	–	21.6 (92)	21.8 (93)

*Figure represents the total number of unilateral observations on both left and right sides; no breakdown was provided so excluded from totals.

Differences in left vs right-sided origin

The origin point of the obturator artery can vary between the left and right sides of the same specimen. The occurrence of a symmetrical pattern of obturator artery origin has been reported in 9% (Dubreuil-Chambardel 1925), 15.4% (Ashley and Anson 1941), 15.7% (Quain 1844), 20.3% (Pick et al. 1942), 28.5% (Biswas et al. 2010), and 57.4% (Sanudo et al. 2011) of cadaveric specimens studied. Pai et al. (2009) studied 98 (62 male: 36 female) embalmed Indian pelvic halves and found a bilateral pattern of origin from the internal iliac artery in 45%: 50% (male: female) of specimens and a bilateral pattern of origin from the external iliac/inferior epigastric in 17%: 20% (male: female). Reid 1836 (citing Cloquet's 1817 study of 250 specimens) reported the obturator artery arose bilaterally from the internal iliac arterial system in 64% of cases, bilaterally from the inferior epigastric system in 24.8% of cases, from the internal iliac on one side and the inferior epigastric on the other in 11.2% of cases, and bilaterally from the external iliac in 2.4% of cases. In a review of the literature, Dubreuil-Chambardel (1925) (Table 56.22) reported that bilateral origin from the external iliac system occurred in 23.7% of 539 specimens and unilateral origin from the external iliac system occurred equally on the left (21.8%) and right sides (21.6%) of 426 specimens. All observed cases of double or triple rooted obturator artery have been reported to be unilateral (Saundo et al. 2011).

Origin from the branches of the internal iliac artery

The obturator artery can take origin from multiple parts of the internal iliac system. Dubreuil-Chambardel (1925) reported 16 different points of origin of the obturator artery from the internal iliac arterial system from a study of 440 specimens (Fig. 56.23). The point of origin was shown to vary widely, from the proximal to distal ends of the internal iliac system, with vessels arising as either individual arteries or as common trunks with other main arteries. The most common level of origin was reported to be between the internal pudendal and inferior gluteal arteries in 60% of specimens.

An analysis of 7 studies totalling 1109 observations has shown the obturator artery most commonly originates from the anterior division of the internal iliac artery (31.5%, range 20.3–70%), followed by the inferior epigastric artery (22.6%, range 0–26.7%), and then the main trunk of the internal iliac artery (14.3%, range 0–23.3%). Similarly, Biswas et al. (2010) also reported the anterior division of the internal iliac artery as the most common point of obturator artery origin.

Origin from common arterial trunks

The obturator artery can arise as a common trunk with other vessels of the internal and external iliac systems (Figs 56.22, 56.23). Dubreuil-Chambardel (1925) reported the most frequent common trunk from the external iliac system was with the inferior epigastric artery, totalling 25.3% of 440 observations. Conversely, Jakubowicz and Czarniawska-Grzesinska (1996) studied 76 specimens and found the inferior epigastric and obturator arteries arose as a common trunk in only 4% of cases. Maneesha et al. (2012) studied 60 pelvic halves and reported the obturator artery to arise from a common trunk with combinations of the middle rectal, vaginal, inferior gluteal, and internal pudendal arteries (Table 56.23). Rusu et al. (2010) studied 30 pelvic halves and 50 angiograms, and reported one case (1.25%) of the obturator artery arising from a common trunk with the descending lumbar artery, the latter normally being a branch of the iliolumbar artery. Other reported examples include the obturator artery arising as a:

- common trunk with inferior gluteal and internal pudendal in 11% of cases (Lipshutz 1918);
- common trunk with inferior and superior gluteal and internal pudendal arteries in 7.2% of cases (Lipshutz 1918);

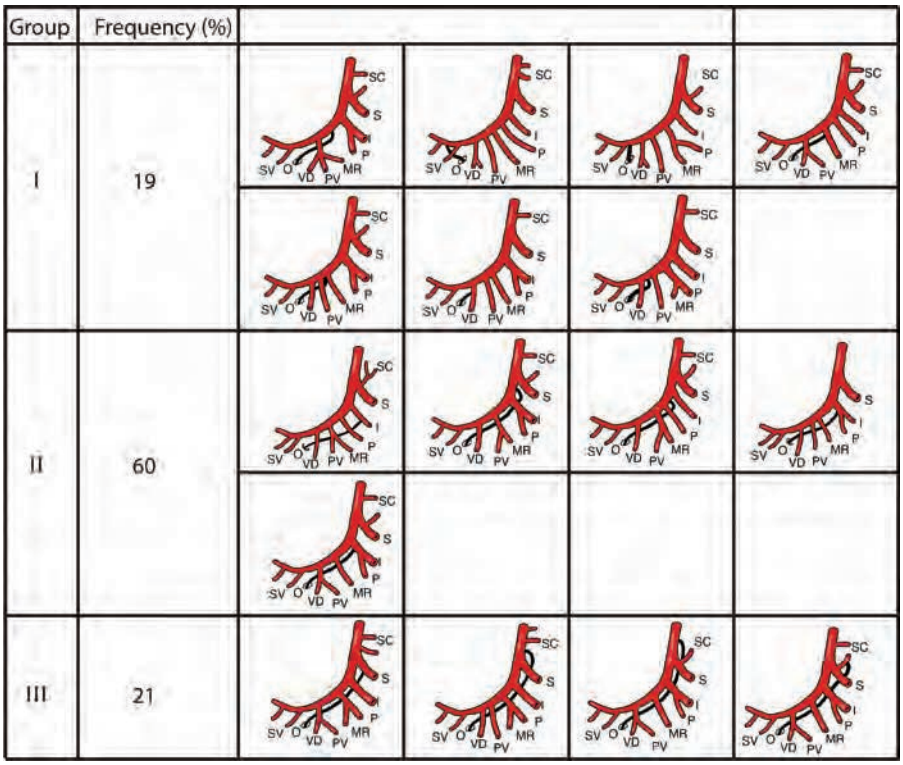

Figure 56.23 Variation in the origin of the obturator artery (black line) from the internal iliac arterial system. Three groups were determined according to the level of origin of the obturator artery relative to other vessels: Group 1: level with or below the internal pudendal artery; Group 2: level with the internal pudendal and inferior gluteal arteries; Group 3: level with or above the superior gluteal artery. The table shows the frequency of the three main groupings for the point of origin of the obturator artery. IL: iliolumbar artery; S: superior gluteal artery; I: inferior gluteal artery; P: internal pudendal artery; MR: middle rectal artery; PV: prostatovesical artery; VD: vesicodeferential artery; SV: superior vesical artery; O: obturator artery; Sc: lateral sacral artery. In all cases the obturator artery exited the pelvis via the obturator foramen. Adapted from Dubreuil-Chambardel (1925).

- branch from a common trunk for the inferior and superior gluteal arteries in 9.9% of cases (Lipshutz 1918);
- common trunk with the inferior gluteal and internal pudendal arteries in 10% (Ramakrishnan et al. 2012) and 18% of cases (Maneesha et al. 2012);
- branch of the middle rectal artery originating from the anterior division of the internal iliac artery in 3.6% of cases (Parsons and Keith 1897);
- branch of the middle rectal artery originating from the internal iliac artery in 1.8% (Parsons and Keith 1897); or
- common trunk with the inferior vesical artery in 8% of cases (Maneesha et al. 2012).

The origin of the obturator artery from the posterior division of the internal iliac artery appears less common (5%, range 0–16.5%, 1109 observations) although this low figure may be due to the way in which the posterior division is classified, if at all. Mamatha et al. (2012) reported the obturator artery to originate from the posterior division in 14% of a study of 50 Indian cadaveric pelves and Jusoh et al. (2010) reported a frequency of 6% following a study of 34 limbs from 17 cadavers. Conversely, a study of 316 formalin-fixed Indian cadavers showed only a single incidence (0.3%) of the obturator artery (left-sided) arising from the posterior division of the internal iliac, 8 mm distal to the internal iliac bifurcation (Kumar and Rath 2007).

Table 56.23 Frequency of the obturator artery originating from a common trunk of the anterior division of the internal iliac artery in a study of 60 Indian pelvic halves (30 cadavers).

Arteries sharing common trunk with the obturator	Frequency (%)
Vaginal and internal pudendal	3.3
Inferior gluteal	1.7
Inferior gluteal and internal pudendal	1.7
Internal pudendal and middle rectal	1.7
Superior vesical	1.7

Source: Maneesha et al. (2012) distributed under the terms of the Creative Commons Attribution License.

The obturator artery can originate from the external iliac artery via a common trunk with the inferior epigastric and medial circumflex femoral arteries. Sanudo et al. (1993) noted that in addition to the two observations of this arrangement in their study, there were six previously reported cases, all of which arose from the femoral artery within the femoral triangle region (Thompson 1882–83; Quain 1844; Duclaux 1902; Adachi 1928; Dschau 1936–37). Three different branching patterns were reported.

1. In three cases all three arteries arose from a common trunk from the femoral artery (Thompson 1882–83; Adachi 1928; Sanudo et al. 1993).
2. In four cases the inferior epigastric and obturator arteries arose as a common trunk from the medial circumflex femoral artery (Quain 1844; Duclaux 1902; Adachi 1928; Sanudo et al. 1993).
3. In one case the inferior epigastric and obturator arteries arose separately from the medial circumflex femoral artery (Dschau 1936–37).

Saundo et al. (1993) observed this arrangement in the right lower limb of a 64-year-old male cadaver and the left lower limb of a 73-year-old female cadaver. The authors reported that in the female the trunk divided directly into three arterial branches and in the male the trunk first divided into a single descending branch, the medial circumflex femoral artery, and an ascending branch that further divided into the obturator and inferior epigastric arteries. In both cases, the obturator artery followed a medial course to the obturator foramen by passing over the external iliac vein and behind the lacunar ligament. It supplied an anastomotic pubic branch to the inferior epigastric artery and a small-diameter additional obturator artery was seen originating from the iliolumbar artery and anastomosing with the obturator artery as it entered the obturator foramen. The authors provided an embryological explanation for variability in the origin of the obturator artery (Senior 1919–20, 1925; Arey 1963; Fitzgerald 1978).

In 1997 Bilic and Sahin studied 100 cadavers of new-born age and reported a single case (1%) in which the obturator artery arose from the medial side of the external iliac artery, approximately 1 cm proximal to the inguinal ligament via a common arterial trunk with the inferior epigastric arteries, profunda femoris artery, and medial circumflex femoral arteries. The common trunk divided into ascending and descending branches; the ascending branch gave rise to the obturator and inferior epigastric arteries, and the descending branch gave rise to the profunda femoris artery from which arose the medial circumflex femoral artery. The obturator artery passed medially over the external iliac vein and then inferomedially over the lateral wall of the pelvic cavity toward the obturator foramen.

Iliopubic anastomoses and corona mortis

There is no clear definition of, nor distinction between, an iliopubic anastomosis, a corona mortis, or a double-rooted obturator artery originating from the internal and external iliac arterial systems that unites prior to the obturator foramen. Most variants of this type will therefore be discussed within this section.

Iliopubic anastomoses and aberrant origins of the obturator artery are relevant to pelvic and orthopedic surgeons and to those operating on the abdominal wall/inguinal canal and on femoral hernia, especially in the region of the retroinguinal/Bogros space. Collectively, arteries and veins that pass over the iliopubic ramus (pelvic brim/iliopectineal line) and lacunar ligament to access the obturator foramen are often referred to as the corona-mortis or "crown of death," since inadvertent laceration results in profuse bleeding (Tornetta et al. 1996; Berberoglu et al. 2001). Corona mortis vessels have been reported to pass across the retropubic region and be oriented vertically behind the superior pubic ramus (Tornetta et al. 1996). The importance of such anastomoses is demonstrated by clinical cases. For example, Garrido-Gómez et al. (2012) reported a fall in a 70-year-old female resulted in fracture of the iliopubic ramus and bleeding from the distal portion of a branch of the left obturator artery. Similarly, Larsson et al. (2010) reported the case of a 53-year-old female patient who suffered serious hemorrhage following damage to the retropubic corona mortis during a routine tension-free vaginal tape procedure to treat stress incontinence.

The anastomoses between the pubic branches of the inferior epigastric and obturator arteries are variable in origin and route. Dubreuil-Chambardel (1925) presented six different variants for the anastomoses between the external iliac arterial system and the obturator artery (Fig. 56.24). Similar anastomostic patterns were shown by Namking et al. (2007) and Kawai et al. (2008). Berberoglu et al. (2001) studied the corona mortis in 14 cadaveric specimens and 36 pelvic halves from 28 patients via laparoscopy. In 62% of cases, the obturator artery branched prior to the obturator foramen and the branches anastomosed with vessels from the inferior epigastric artery in the retropubic region. The majority of the branches were <1 mm diameter. Smith et al. (2009) reported corona mortis, defined as an obturator artery originating from the external iliac system, in 29% of 100 pelvic halves (from 50 patients) studied using CT imaging. A study of black South Africans by Missankov et al. (1996) showed 44% of retropubic anastomoses were an obturator artery arising from the inferior epigastric artery and 25% were an obturator artery arising from the external iliac artery. Missankov et al. (1996) also reported that black South African subjects appeared to exhibit a higher incidence of

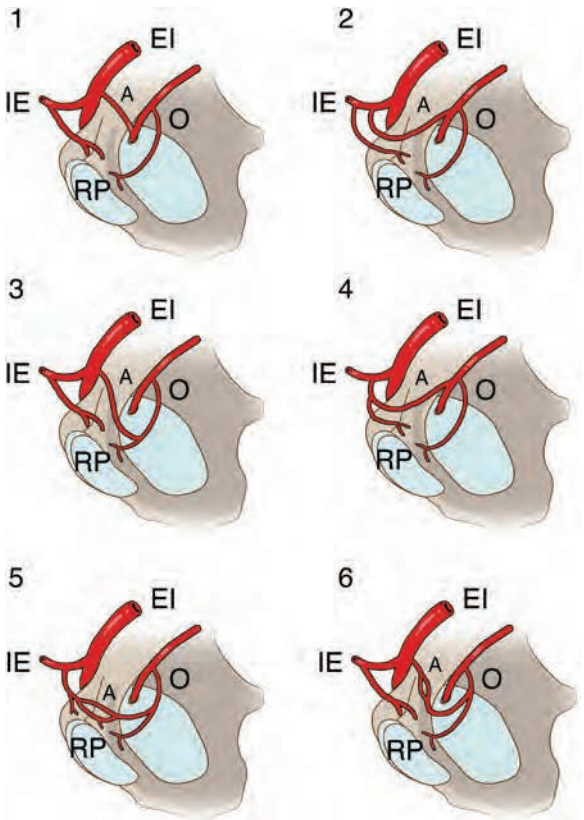

Figure 56.24 Six variations in the anastomoses between the external iliac artery and the obturator artery originating from internal iliac artery. A: anastomotic arteries; EI: external iliac artery; IE: inferior epigastric artery; RP: pubic/retropubic arterial branches; O: obturator artery. Adapted from Dubreuil-Chambardel (1925).

variations of the pubic anastomoses compared to North American, European and Japanese populations. A study of 66 pelvic halves from 33 Thai cadavers showed corona mortis, which was defined as aberrant obturator arteries/branches connecting the inferior epigastric and obturator arteries across the pelvic brim, to be present in 13.6% of cases (Pungpapong and Thum-umnauysuk 2005) and a study of 80 cadaveric pelvic halves by Darmanis et al. (2007) showed 36% had an arterial communication between the obturator artery and the external iliac/inferior epigastric system. Similarly, frequencies of retropubic arterial anastomoses have been reported by Teague et al. (1996) (43% of 78 pelvic halves) Hong et al. (2004) (34% of 50 pelvic halves), and Tornetta et al. (1996) (34% of 50 pelvic halves).

In a large study of 353 Japanese cadavers (706 pelvic halves), Kawai et al. (2008) were specific in determining the difference between an obturator vessel arising from the inferior epigastric and the presence of pubic vessels/anastomoses between the obturator and inferior epigastric artery (Table 56.24). A total of 560 (79.3%) specimens showed pubic branches, of which 74.6% (527) were branches of the inferior epigastric artery crossing over the pelvic brim. Of these cases, the most common pattern (58.4%) was for no anastomoses to be present between the pubic branches of the inferior epigastric and the obturator artery. Anastomoses were reported between the pubic branches of the inferior epigastric artery and the obturator artery in 21.6% of specimens. In 3.0% of specimens two obturator arteries were seen arising independently from both the internal iliac and inferior epigastric arteries with no anastomosis present, and in 10.5% of specimens the obturator artery arose solely from the inferior epigastric artery. Kawai et al. (2008) suggest the intimate relationship and connections between the obturator and inferior epigastric arteries is due to the close developmental relationship between their pubic branches. The authors also emphasize that the difficulty in identifying very small arterial roots could mean multiple-rooted obturator arteries probably occur more frequently than reported. In support of this, Biswas et al. (2010) studied 56 formalin-fixed East Indian cadaveric pelvic halves and concluded that the reason no multiple-rooted obturator arteries were observed was most likely due to the difficulty in identifying vessels of small calibre.

Location and course of the obturator artery

Lipshutz (1918) reported the variability of the relationship of the obturator artery to the femoral ring as follows.

1. An obturator artery arising from the external iliac artery bears little or no relation to the femoral region.
2. An obturator artery arising from the femoral artery usually courses between the femoral vein and the lacunar ligament, dorsal and caudal to the femoral ring. In about half of the cases in the literature, the obturator artery courses along the outer half or two-thirds of the femoral ring where it can be injured. To avoid injury, the iliopubic ligament should be incised as near as possible to the lacunar ligament.
3. An obturator artery arising from a common trunk with the inferior epigastric artery varies in its relationship to the femoral ring. Specifically, (a) if it arises from the central portion of the artery, between the external iliac artery and the inguinal ligament, or from the summit of the common trunk of the inferior epigastric and obturator arteries, it pursues an arched course and is usually related to the lateral border of the femoral ring; and (b) if it arises at or above the inguinal ligament it lies at the medial border or middle of the femoral ring. It is usually related to the lateral side of a femoral hernia.

According to Jastschinski (1891b) the obturator artery courses transversely across a femoral hernia in 22% of cases, and in two cases passed transversely across the femoral ring. In female subjects the obturator artery passes more frequently along the lateral border of the femoral ring compared to the medial.

Ovarian artery

The ovarian artery normally originates as a lateral branch of the abdominal aorta (Standring 2008; Moore et al. 2014); however, a series of patient case reports based upon arteriographic studies have demonstrated the ovarian artery originating from the proximal part of the right internal iliac artery in a 45-year-old Caucasian female patient (Reed and McLucas 2012), from the right common iliac artery in a 46-year-old Vietnamese patient (Kim 2013), and from the right external iliac artery in a 35-year-old Korean patient. In all patients the aberrant ovarian artery also provided a significant supply to the uterus.

Middle rectal artery

The middle rectal artery is variable in presence, origin, and size (Lipshutz 1918; Roberts and Krishinger 1967; DiDio et al. 1986; Sato and Sato 1991; Bilhim et al. 2013). The literature has reported a variable frequency of presence ranging from 12% to 94% of cases studied (Drummond 1914; Chiarugu 1936; Widmer 1955; Boxall et al. 1963; Roberts and Krishinger 1967; Ayoub 1978; DiDio et al. 1986; Sato and Sato 1991; Jones et al. 1999; Lin et al. 2010; Bilhim et al. 2013). The middle rectal artery can arise from the internal iliac, inferior vesical, internal pudendal, sciatic, or inferior gluteal arteries or other branches of the internal iliac system as single or multiple vessels (Parsons and Keith 1897; DiDio et al. 1986; Bilhim et al. 2013). In a study of 440 specimens, Dubreuil-Chambardel (1925) reported that when present the middle rectal artery was singular in 74%, duplicate in 21%, and three or four arteries in 5% of specimens. Ashley and Anson (1941) reported that multiple middle rectal arteries often arose from several branches of the internal iliac artery in the same body-half, although no frequency figures were reported. Sato and Sato (1991) reported a single case (1.2%) of duplicate middle rectal arteries in a study of 81 pelvic halves and Lipshutz (1918) reported 15% of 181 pelvic halves showed a double middle rectal artery.

The most common origin for the middle rectal artery is from the internal pudendal artery followed by the inferior gluteal artery (Table 56.25) and, where present, often arises (70%, n=56/80) in common with the prostatic artery via a prostatorectal trunk (Bilhim et al. 2013). Lipshutz (1918) reported the middle rectal artery was seen in 72% of 181 pelvic halves with 54% of those

Table 56.24 Destination/fate of the pubic branches of the inferior epigastric artery as observed in a study of 706 cadaveric pelvic halves from 353 cadavers. Frequency figures are calculated as a proportion of the total number of specimens in which pubic branches were identified (*n*=560). Adapted from Kawai et al. (2008) with permission from Elsevier.

Artery of origin of inferior epigastric artery	Total (*n*)	Fate of the pubic branch of the inferior epigastric artery		Observed (*n*)	Frequency (*n*/560 %)
External iliac artery	701	(a) Anastomosis with obturator artery from internal iliac	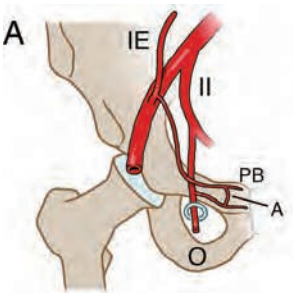	121	21.6
		(b) No anastomosis with obturator artery	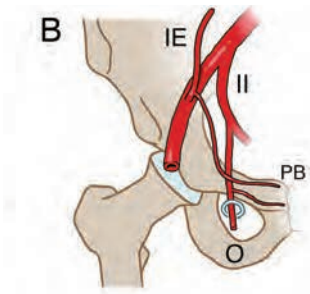	327	58.4
		(c) Forms second obturator artery; no anastomosis with obturator artery from internal iliac artery	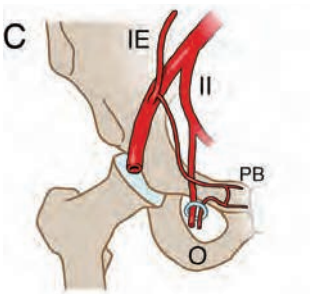	17	3.0
		(d) Becomes obturator artery	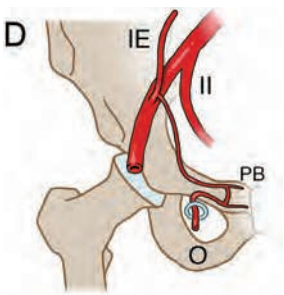	59	10.5
		(e) No pubic branches from inferior epigastric artery	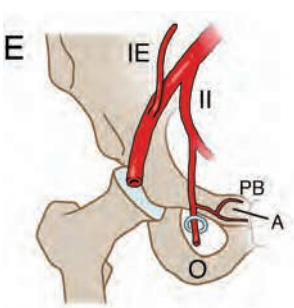	33	5.9

Artery of origin of inferior epigastric artery	Total (*n*)	Fate of the pubic branch of the inferior epigastric artery		Observed (*n*)	Frequency (*n*/560 %)
		No pubic branches identified from either the inferior epigastric or obturator arteries		144	–
Obturator artery	3	(f) Forms the proximal part of the inferior epigastric artery	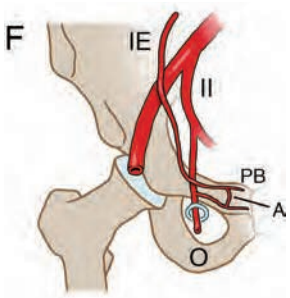	3	0.5
Not clear	2	No pubic branches identified		2	–

Table 56.25 Frequency of the middle rectal artery originating from the parts and branches of the internal iliac arterial system in a series of cadaveric studies. *n*: the total number of middle rectal arteries observed in a given study. The total number of specimens/patients studied were DiDio et al. (1986) 30; Sato & Sato (1991) 81; Lin et al. (2010) 32; Bilhim et al. (2013) 167.

Artery of origin	Frequency % (*n*=28) DiDio et al. (1986)	Frequency % (*n*=18) Sato & Sato (1991)	Frequency % (*n*=18) Lin et al. (2010)	Frequency % (*n*=80) Bilhim et al. (2013)
Internal iliac	17.9	15.8	11.1	–
Internal pudendal	40.0	63.2	66.7	60.0
Inferior gluteal	26.7	21.1	22.2	21.3
Superior gluteal	3.3	–	–	–
Inferior vesical	3.3	–	–	–
Middle sacral	3.3	–	–	–
Common trunk with gluteal and pudendal	–	–	–	16.2
Obturator	–	–	–	2.5

observed originating from the internal pudendal, 22.7% from inferior gluteal, 5.5% from internal pudendal, 2.8% from obturator, 2.8% from anterior division of internal iliac, 2.2% inferior gluteal, and 1.7% from vesicodeferential artery. Parsons and Keith (1897) reported on the origin of 45 middle rectal arteries and noted the most common origin to be from the anterior division of the internal iliac artery followed by the hypogastric trunk (Table 56.26). Roberts and Krishinger (1967) reported 65.5% of 79 cadaveric pelvic halves studied possessed a middle rectal artery and, where present, it originated from the internal pudendal artery in 63% of cases, with the vaginal artery in 1 case, and from either the internal pudendal, ischiopudendal trunk, or the inferior gluteal artery in 89% of cases. Ashley and Anson (1941) reported that the middle rectal artery originated from the internal pudendal artery in 40.9% of 66 sides studied, from the inferior gluteal artery in 22.7% of sides and, less frequently, from the obturator, umbilical, internal iliac, and vesical arteries. In a study of 30 cadavers, DiDio et al. (1986) showed the origin of the middle rectal artery was identical in 72.7% of cases where the artery was seen bilaterally.

Table 56.26 Frequency of the middle rectal artery originating from the internal iliac system based upon 45 observations. The hypogastric trunk historically described a trunk arising from the internal iliac artery that gave rise to vessels including the vaginal, middle rectal, superior vesical, and inferior vesical arteries. Adapted from Parsons and Keith (1897) with permission from John Wiley & Sons.

Artery of origin	Frequency (%)
Anterior division of the internal iliac artery	33.3
Hypogastric trunk of the internal iliac artery	22.2
Common origin with the internal pudendal	13.3
Obturator artery	8.9
Common origin with the inferior gluteal artery	4.4
Common origin with the inferior vesical artery	4.4
Common origin with the uterine artery	4.4
Common origin with the superior vesical artery	2.2

Several studies show the middle rectal artery may give origin to the vaginal, seminal vesical, prostatic, and inferior lateral sacral arteries (Quain 1844; Henle 1868; Hyrtl 1887; Engelman 1898; Dall'Acqua and Meneghetti 1907; Schaefer et al. 1915; Lipshutz 1918; Huber 1930; Jackson 1933; Latarjet 1948; Clegg 1955; Boxall et al. 1963; Anson 1966; Gardner et al. 1969; Pac et al. 1977; Sato and Sato 1991) and Lipshutz (1918) reported the case of a middle rectal artery supplying the posterior vaginal wall. in a study of 81 cadaveric specimens, Sato and Sato (1991) reported that 52.6% of the middle rectal arteries observed gave branches to the inferior bladder and the vagina or prostate, whereas the remaining 47.4% supplied the rectum alone.

The presence of the middle rectal artery may be sex-dependent. Jones et al. (1999) reported unilateral middle rectal arteries to be present in only 53% of female specimens compared to 80% of male specimens following a study of 28 cadaveric specimens. Sato and Sato (1991) also reported a slightly higher incidence of middle rectal artery in males (37.9%) compared to females (28.6%). Conversely, no significant sex differences were reported in studies by Widmer (1955) or DiDio et al. (1986).

The middle rectal artery may be present unilaterally or bilaterally, although a unilateral pattern appears more common. Sato and Sato (1991) studied 81 pelvic halves from 43 cadavers and identified the middle rectal artery in 34.9% of subjects. Of these subjects the arteries were unilateral in 80% (n=12) and bilateral in 20% (n=3). Similarly Bilhim et al. (2013) reported the middle rectal artery to be present in 35.9% of 167 male patients undergoing arteriography and was unilateral in 66.6% and bilateral in 33.3% of cases. Lin et al. (2010) observed the middle rectal artery in 43.8% of 32 whole pelves; 18 vessels were identified, of which 71.4% were unilateral and 28.6% were bilateral. The opposite was reported by DiDio et al. (1986) who showed the middle rectal artery to be present in 56.7% of 30 cadavers (15 male: 15 female), which was bilateral in 64.7% and unilateral in 35.3% of cases (4 right-sided: 2 left-sided).

Route and morphology

Starting from its origin the middle rectal artery passes vertically downward before turning through 90° to travel transversely to the rectum, although the exact route of travel can vary depending upon its point of origin (Boxall et al. 1963). Bilhim et al. (2013) reported the middle rectal arteries were visible as paraprostatic ridges in the male or posterior to the superior portion of the vagina in the female. Jones et al. (1999) identified middle rectal arteries in 60.7% of 28 cadavers (17 female: 10 male) and, of those identified, 70.6% approached the rectum from a lateral direction, 17.6% from anterolateral, and 11.8% from posterolateral. The same authors also reported the middle rectal arteries to sit a median of 2 cm (range 0–7 cm) above the pelvic floor, and that 82.4% crossed the mesorectal plane independent of any connective tissues whereas 17.6% were part of a connective-tissue-associated neurovascular bundle.

Once adjacent to the rectum, the middle rectal artery anastomoses with the superior rectal and inferior mesenteric artery in 87.5% of cases (Bilhim et al. 2013). The external diameter of the middle rectal artery at its origin has been reported as a mean of 1.27±0.15 mm (range 1.0–1.5 mm) (Lin et al. 2010) and 1.7 mm (range 1–3 mm) (DiDio et al. 1986) and a median of 1 mm (range 0.5–2.0 mm) (Jones et al. 1999). Interestingly, Lin et al. (2010) noted that the middle rectal artery narrowed as it approached the visceral pelvic fascia, after which it was almost invisible. The authors suggest this latter finding might explain the apparent absence of the vessel in certain subjects. The middle rectal artery varies in length with reports of a mean of 80.4 mm (Sato and Sato 1991) and 69.5 mm (range 28–112 mm) (DiDio et al. 1986).

Inferior epigastric artery

The inferior epigastric artery and its cutaneous perforator arteries can be harvested with overlying tissues and skin for graft surgery; a knowledge of potential variance in its origin is therefore important. It normally arises from the external iliac arterial system (Standring 2008; Moore et al. 2014), but has been reported to arise solely from the internal iliac system in common with the obturator artery (Fig. 56.25). Multiple authors (Redfern 1850; Adachi 1928; Ishizeki et al. 1982; Kawai et al. 2008) have reported the inferior epigastric artery arising as a common trunk with the obturator from the anterior division of the internal iliac. In a large study

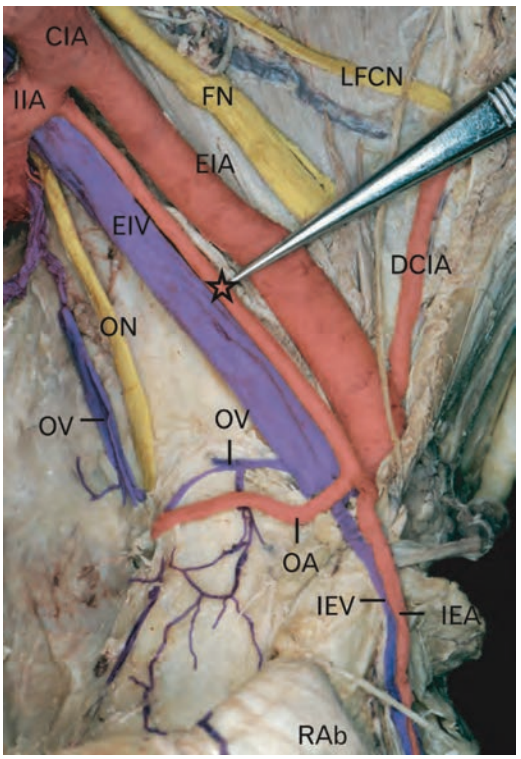

Figure 56.25 Case report of an 84-year-old female Korean cadaver with a left-sided inferior epigastric artery originating from a common trunk with the obturator artery. EIV: external iliac vein; IEV: inferior epigastric vein; OV: obturator vein; CIA: common iliac artery; IIA: internal iliac artery; EIA: external iliac artery; IEA: inferior epigastric artery; DCIA: deep circumflex iliac artery; OA: obturator artery; *: common trunk for inferior epigastric and obturator arteries; RAb: Rectus abdominis muscle; ON: obturator nerve; LFCN: lateral femoral cutaneous nerve; FN: femoral nerve.

Source: Won et al. (2012).

Table 56.27 The four different types of origin (branching patterns) of the uterine artery (Type I–IV) from the internal iliac arterial system and their frequency of origin based upon study of 53 African female cadavers (aged 3–65 years). The origin of the uterine artery was categorized using a modified version of the system used by Gomez-Jorge et al. (2003). Adapted from Obimbo et al. (2010) with permission from Elsevier.

Type	Frequency (%)	Description
I	18.9	First branch of the anterior division of the internal iliac
II	70.8	Second or third branch of the anterior division of the internal iliac
III	10.4	From a trifurcation with other arteries (including inferior gluteal, inferior vesical, superior vesical, middle rectal)
IV	0	First branch of internal iliac trunk

of 353 Japanese cadavers (706 pelvic halves), Kawai et al. (2008) showed that the inferior epigastric artery arose from the internal iliac system in 0.4% (3/706) of cases, representing two bodies (Table 56.27). In both cases the inferior epigastric arteries were 2 mm in diameter, arose from the obturator arteries around the midpoint of its route across the lateral pelvic wall, then ascended medial to the deep inguinal ring onto the deep surface of rectus abdominis. Won et al. (2012) reported the case of an 84-year-old female Korean cadaver in which the left obturator and inferior epigastric arteries arose directly from the internal iliac artery 3 mm below its origin from the common iliac artery. Power (1850) reported other origins of the inferior epigastric artery including the femoral and deep femoral arteries. The deep iliac circumflex arteries can be doubled, or arise from the inferior epigastric or femoral arteries (Power 1850).

Uterine artery

The uterine artery normally branches from the internal iliac artery either alone or in combination with other vessels such as the internal pudendal, vaginal, middle rectal, superior vesical, or inferior vesical artery. It may be doubled or composed of multiple parts and can give rise to the superior vesical, inferior vesical, urethral, and vaginal arteries (Quain 1844; Henle 1868; Hyrtl 1887; Gegenbaur 1888; Lipshutz 1918; Schaefer and Symington 1915; Huber 1930; Jackson 1933; Corfier et al. 1939; Curtis et al. 1942; Latarjet 1948; Borell and Fernström 1953, 1954; Anson 1966; Gardner et al. 1969; Gladykowska-Rzeczycka and Mieszkowska 1977; Pac et al. 1977; Pelage et al. 1999). Lipshutz (1918) reported a further case in which the uterine artery arose via a common trunk with the obturator artery.

Gomez-Jorge (2003) described the course of the uterine artery following a study of 257 patient arteriograms (514 uterine arteries). Briefly, a descending segment passes downward and laterally, a transverse segment advances medially and a marginal or ascending segment runs along the side of the uterus. Similarly, Pelage et al. (2005) described the uterine artery as having a characteristic U-shape, with a descending segment that parallels the lateral pelvic wall, a transverse segment that crosses the distal ureter at the level of the cervix, and an ascending segment that courses along the uterine margin at the medial edge of the broad ligament. Following a study of 53 African cadavers, Obimbo et al. (2010) reported that the uterine artery ascended as a single branch in 76.4%, bifurcated in 17.1% and trifurcated in 6.7% of cases. Bifurcation and trifurcation of the uterine artery are linked to spontaneous abortion and small gestational size. Obimbo et al. (2010) also reported that the uterine artery branched consistently from the medial aspect of the internal iliac artery and passed anterior to the ureter in 96.2% and posterior to it in 3.8% of cases, all of which were observed in the left hemi-pelvis.

The uterine artery commonly gives off ascending (marginal) and descending (cervicovaginal) branches as it approaches the lateral cervix. Dubreuil-Chambardel (1925) documented five different branching patterns of the uterine artery (Fig. 56.26),

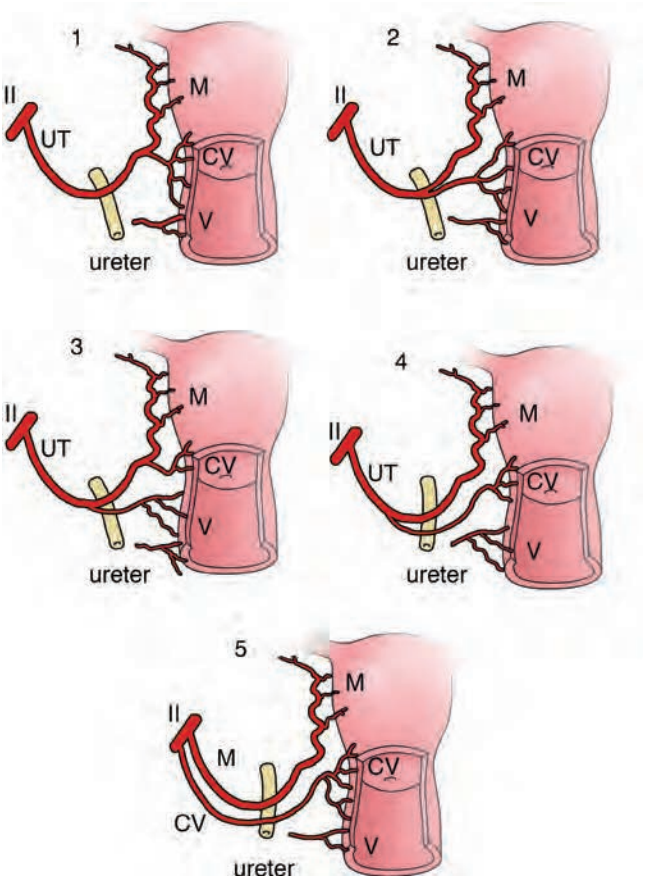

Figure 56.26 Five variations in the course and branching of the uterine artery. Type I: uterine artery dominant and gives origin to marginal and cervico/vaginal branches after crossing the ureter. A small vaginal artery is present. Type II: similar to Type 1 except the uterine artery divides at the ureter. Type III: uterine artery dominant and gives origin to the marginal artery and separate cervical and vaginal branches. A small vaginal artery is also present. Type IV: uterine artery branches into the marginal and cervical/vaginal arteries before the ureter. Vaginal artery supplies more than half of the vaginal wall. Type V: internal iliac artery gives origin to the marginal and cervical/vaginal branches. Cervicovaginal artery supplies most of the vaginal wall. A small vaginal artery is present. M: marginal artery; CV: cervicovaginal artery; V: vaginal artery. Adapted from Dubreuil-Chambardel (1925).

and reported that the cervicovaginal branch arose directly from the uterine artery in 91% of cases while in 9% it arose directly from the internal iliac artery. In a study of 375 patient angiograms, Pelage et al. (1999) observed the cervicovaginal artery arising from the uterine artery in 201 (53%, 112 left, 89 right) of 375 arteries; intramural branches were identified in all cases.

Lippert and Pabst (1985) reviewed the literature relating to the blood supply of the female genital tract (Adachi 1928; Borell and Fernström 1954; Fernström 1955; Karlsson and Jonsson 1980; Koritke et al. 1967; Becken 1984) and summarized that 90% of observed cases possessed the normal pattern of arterial supply as outlined in standard texts, and that the blood supply:

- to the uterine fundus was from the uterine artery in 90% and the ovarian artery in 10% of cases;
- to the uterine tube was from the tubal branch of the uterine artery in 60%, the tubal branch of the ovarian artery in 30%, and both the uterine and ovarian arteries in 10% of cases; and
- to the ovary was from the ovarian artery alone in 40%, the ovarian and uterine arteries in 56%, and the uterine artery alone in 4% of cases.

The origin point of the uterine artery is variable. Parsons and Keith (1897) reported on 18 observations of the uterine artery; in 50% of cases it arose from the hypogastric trunk, in 16.9% of cases it was a separate branch of the anterior division of the internal iliac artery, in 11% of cases it arose with the inferior vesical artery from the hypogastric trunk, and in 5.5% of cases it arose in common with the middle rectal artery. In two cases the uterine arteries were duplicated on a single side; in the first case one artery arose from the hypogastric trunk and the other from the anterior division of the internal iliac artery, and in the second case one artery arose with the inferior vesical artery and the other with the middle rectal artery. In a study of 48 cadaveric specimens, Roberts and Krishinger (1967) noted that the most common origin for the uterine artery was the anterior division of the internal iliac artery (56%) followed by the umbilical artery (40%), with 2% coming from either a common trunk with internal pudendal artery or a common trunk with the vaginal and inferior vesical arteries.

Several different classification systems for the origin of the uterine artery have been presented. Gomez-Jorge et al. (2003) identified 514 uterine arteries in 257 patients via angiography; 196 uterine arteries (38%) were visible, and their origins were classified into four types. The most common origin was as the first branch of the inferior gluteal artery (45%, Type 1) followed by a trifurcation from a common trunk with the superior and inferior gluteal arteries (43%, Type 3). Similarly, Holub et al. (2005) studied 100 right uterine arteries in 100 female Czech patients during laparoscopic retroperitoneal dissection and 81% were classified into four types of origin (19% could not be classified; Fig. 56.27). The most common origin was from the umbilical artery alone (45.6%). Obimbo et al. (2010) studied 53 African female cadavers and categorized uterine artery origin according to a modified version of the Gomez-Jorge (2003) system (Table 56.27), reporting that the most common origin was as the second or third branch of the internal iliac anterior division (Type 2, 70%).

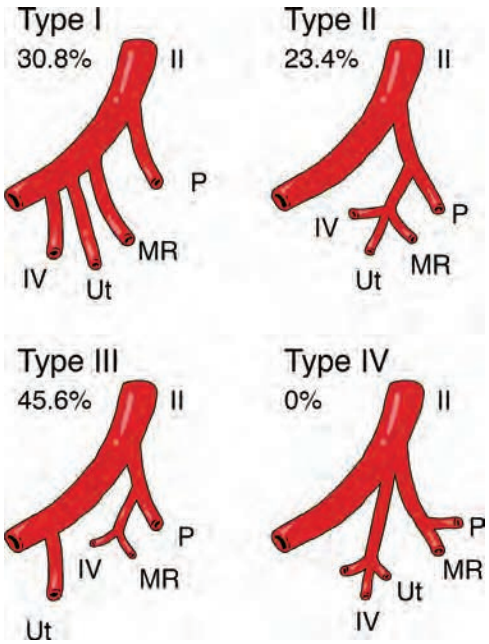

Figure 56.27 Frequency of origin of the uterine artery from four different types of branching pattern of the internal iliac arterial system based on a laparoscopic study of 100 right uterine arteries in 100 female patients in the Czech republic; 81% were classified into 4 types. Type I: visceral branches (uterine, inferior vesical, and medial rectal arteries) arise from the umbilical artery. Type II: uterine and inferior vesical arteries arise from the internal pudendal artery. Type III: uterine artery arises from the umbilical artery. Inferior vesical artery and middle rectal artery arise from the internal pudendal artery. Type IV: uterine and inferior vesical arteries arise from the obturator artery and the middle rectal artery is a branch of the internal pudendal artery. II: internal iliac artery; P: internal pudendal artery; Ut: uterine artery; MR: middle rectal artery; IV: inferior vesical artery. Adapted from Holub et al. (2005) with permission from John Wiley & Sons.

In rare instances the uterine artery may be absent and replaced by alternative vessels. In an angiographic study of 43 patients, 1 patient (2.3%) was reported to have an absence of the right uterine (Baba et al. 2012). Saraiya et al. (2002) described a case in which the left uterine artery was absent and replaced by an enlarged artery of the round ligament that took origin from the inferior epigastric artery arising from the external iliac.

Anastomoses

Rich anastomoses have been demonstrated between the uterine, vaginal, ovarian, and cervical arteries. For example, CT examination of the uterine vasculature in five Chinese cadaveric uteruses following intra-arterial injection of colored plastic showed anastomoses between the ovarian branch of the uterine artery and the uterine branch of the ovarian artery in all specimens (Ouyang et al. 2012; Fig. 56.28). The uterine artery can also anastomose with its contralateral partner or the ovarian artery. Such

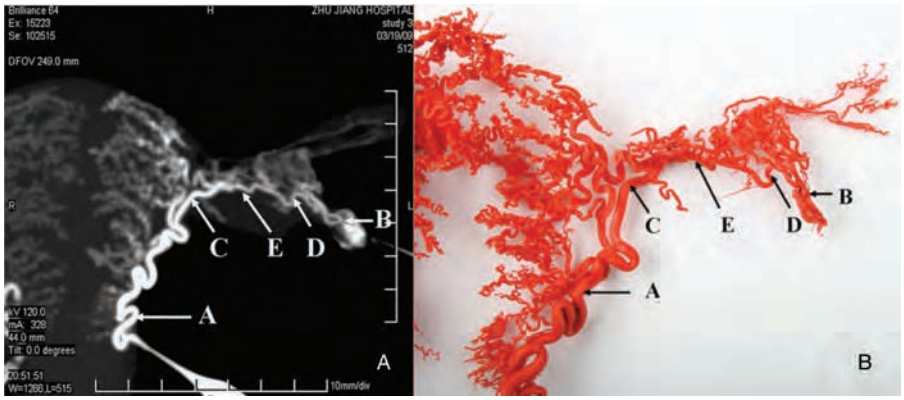

Figure 56.28 Anastomoses between the ovarian branch of the uterine artery and the uterine branch of the ovarian artery in a cadaveric uterus demonstrated on (a) CT scan and (b) corrosion cast following intra-arterial injection of contrast medium. A: left uterine artery; B: left ovarian artery; C: ovarian branch of uterine artery; D: ovarian branch of ovarian artery; E: ovarian artery-to-uterine artery anastomoses.

Source: Ouyang et al. (2012). Reproduced with permission from Springer Science and Business Media.

anastomoses often result in the failure of uterine artery embolization procedures (Pelage et al. 2005). Anastomoses between contralateral uterine arteries around the uterine cervix and fundus have been demonstrated in excised uteri via intra-arterial plastic injection (Lindenbaum et al. 1978; Ouyang et al. 2012). Similarly, a study of the blood supply to the lower uterus and vagina in 39 female cadaveric pelves, following intra-arterial injection of colored latex, demonstrated anastomoses between the vaginal, cervical, and uterine arteries along the lateral border of the vagina and uterus (Palacios Jaraquemada et al. 2007). Rare or unexpected anatomoses may also exist, for example Nair et al. (2012) reported the case of a 48-year-old female patient in whom the right uterine artery was connected to the right obturator artery.

Dubreuil-Chambardel (1925) documented five types of anastomosis between the ovarian and uterine arteries (Fig. 56.29). Mocquot and Rouvillois (1938) reported four types of arterial blood supply to the ovary, all of which had anastomosis with the uterine artery: types 1 and 2, where the uterine and ovarian arteries provided relatively equal supply occurred commonly and with equal frequency; and types 3 and 4, where either the ovarian or uterine artery predominated, were rarer (Fig. 56.30).

Functional anastomoses have been demonstrated between the uterine and ovarian arteries (Lindenbaum et al. 1978; Karlsson and Jonsson 1980; Matson et al. 2000). Karlsson and Jonsson (1980) demonstrated anatomoses in 46.9% of 32 patients undergoing angiography and Matson et al. (2000) showed uterine artery embolism resulted in retrograde flow through the ovarian artery. The latter authors suggested such anastomoses may cause continued fibroid bleeding following uterine artery embolism, or may result in retrograde passage of an embolic material to the ovary, aorta, or renal artery. An angiographic study of 43 patients demonstrated uterine-ovarian artery anastomoses in 58% (21.7% right, 37.5% left) of the 23 patients with uterine fibroids, and 47.4% (21% right, 26.3% left) of the 20 patients with hemorrhage (Baba et al. 2012). Similarly, an angiographic

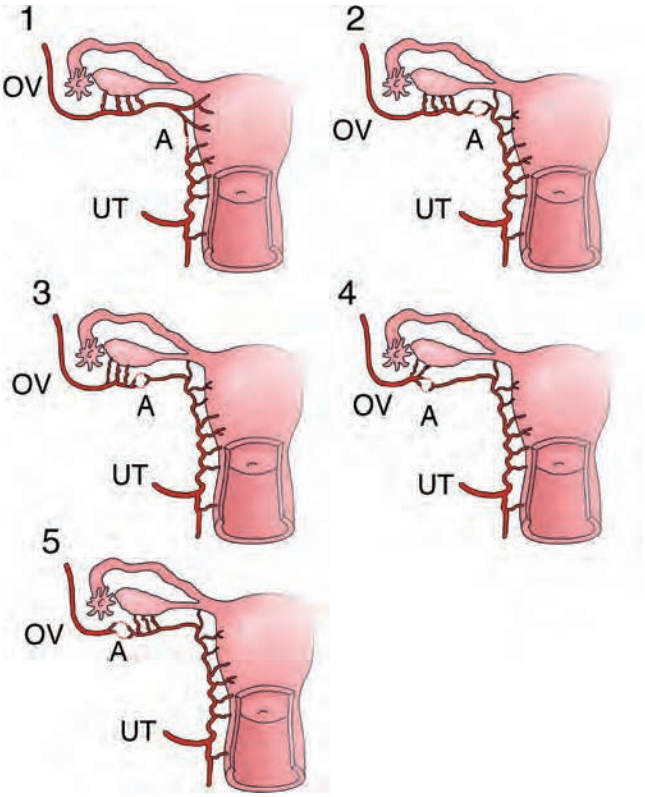

Figure 56.29 Five variations in the position of the anastomoses between uterine and ovarian arteries. In some cases the ovarian and/or uterine arteries exceed their usual area of supply. In all variants except Type I the uterine artery is the main supply to the uterine tube. Type I: anastomoses sit along the body of the uterus. A dominant ovarian artery supplies the uterine tube and extends onto the body of the uterus. Type II: anastomoses sit between the ovary and uterus and are not related to either organ. Type III: anastomoses occur at the distal pole of the ovary. Type IV: anastomoses occur at the midpoint of the ovary. Type V: anastomoses occur at the tubular pole of the ovary. A dominant uterine artery supplies the uterine tube and the ovary. UT: uterine artery; OV: ovarian artery; A: anastomotic vessels. Adapted from Dubreuil-Chambardel (1925).

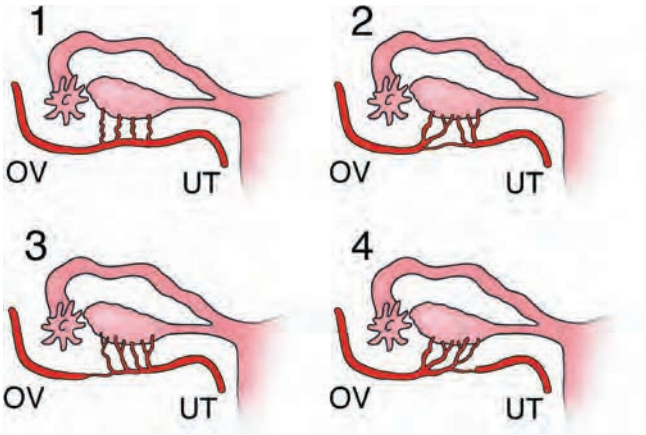

Figure 56.30 The four types of anastomosis between the ovarian and uterine arteries and the variation in arterial supply to the ovary. Type 1: the anastomosis between the ovarian and uterine arteries gives rise to arterial vessels that equally supply the ovary. Type 2: the ovarian and uterine arteries each directly supply the ovary and also anastomose with each other. Type 3: the primary source (sole source) of blood to the ovary is the uterine artery which has a small anastomotic branch with the ovarian artery. Type 4: the ovarian artery is the sole source of the blood supply to the ovary and it gives off a small anastomotic branch, which joins the uterine artery or the tubal branch of the uterine artery. UT: uterine artery; OV: ovarian artery.

Source: Mocquot and Rouvillois (1938).

study of 76 female patients demonstrated anastomoses between ipsilateral ovarian and uterine arteries were present in 46% of patients, which occurred via intramural or tubal artery anastomoses (Razavi et al. 2002). Gomez-Jorge at al. (2003) studied 514 uterine arteries in 257 patients via angiography, and found that anastomoses between the tubal and ovarian arteries were observed in 11% only after embolization, in 5% both before and after embolization, and in 14% only prior to embolization; anastomoses were not seen in 70% of patients.

Pelage et al. (1999) studied 375 angiograms of uterine arteries from 197 patients and found the uterine artery was 2–5 mm in width and identified three types of anastomoses:

- Type 1: transversal anastomoses between right and left uterine arteries (10%);
- Type 2: anastomoses between the uterine and ovarian arteries (11%) (6 left, 9 right, 7 both sides); and
- Type 3: a round ligament artery branching from the proximal inferior epigastric artery was an anastomotic supplier to a previously embolized uterine artery in one patient (0.5%).

Palacios Jaraquemada et al. (2007) studied the arterial supply to 39 female reproductive tracts via injection of colored latex and noted three main arterial pedicles (upper, middle, and lower) provided the arterial supply and their origins were from the internal iliac (100%), uterine (67%), and internal pudendal artery (71%), respectively (Table 56.28). In 38.5% of pelves there was a direct anastomosis between the uterine arteries across the midline anterior to the cervico-isthmal junction of the uterus and the uterine artery was reported to be duplicated in one case.

Table 56.28 The origin point of the three main arterial pedicles supplying the female reproductive tract as determined by a study of 39 female reproductive tracts via injection of colored latex.

Pedicle/supply	Origin	Origin and frequency (%)
Upper	Uterine artery	100% internal iliac artery
Middle	Cervical artery	67% uterine artery 23% vaginal artery (from uterine) 10% inferior vesical artery
Lower	Upper vaginal artery Middle vaginal artery Lower vaginal artery	18% uterine artery 11% internal iliac artery 71% internal pudendal artery (75% as ascending branches; 25% as descending branches)

Source: Palacios Jaraquemada et al. (2007). Reproduced with permission from John Wiley & Sons.

Vaginal artery

The vaginal artery normally originates from the uterine artery as one or multiple branches. It can also originate from the internal iliac, middle rectal, superior vesical, inferior vesical, inferior gluteal, or obturator artery, the ischiopudendal trunk, or via a common trunk with the uterine artery (Quain 1844; Henle 1868; Hyrtl 1887; Schaefer and Symington 1915; Lipshutz 1918; Huber 1930; Jackson 1933; Corfier et al. 1939; Curtis et al. 1942; Latarjet 1948; Anson 1966; Gardner et al. 1969; Gladykowska-Rzeczycka and Mieszkowska 1977; Pac et al. 1977). Lipshutz (1918) reported 40% of vaginal arteries to be duplicate, with the proximal artery arising from the anterior division of the internal iliac, uterine, or internal pudendal artery and the more distal branch arising from the internal pudendal, obturator, or inferior gluteal artery, the ischiopudendal trunk, or as a common trunk with the middle rectal artery.

In a study of cadaveric specimens, Roberts and Krishinger (1967) reported the vaginal artery was more variable than the uterine in its site of origin and that it was usually smaller in size than the uterine. The vaginal artery arose most commonly as a branch of the internal pudendal artery, followed by the uterine artery and then the ischiopudendal trunk. In one specimen, it arose in common with a sizeable middle rectal artery. Both the uterine and the vaginal arteries may be represented by more than one branch. A study of 375 angiograms from 197 patients showed the vaginal artery arose from the anterior division of the internal iliac artery just below the uterine artery in 50% of cases (50 left, 32 right, 52 both sides; Pelage et al. 1999). In 9% of the patients studied, the vaginal artery arose from a common trunk formed with the uterine artery.

The vaginal artery supplies a variable territory. Dubreuil-Chambardel (1925) showed the vaginal artery to supply an area ranging from the distal vagina to the majority of the vagina. Palacios Jaraquemada et al. (2007) studied the arterial supply of 39 female reproductive tracts. It was shown that the vaginal arteries formed the lower pedicle supply to the vagina, and their origin varied with the most common being from the internal

pudendal artery (71%; Table 56.28). The authors also reported that all observed vaginal arteries sat dorsal to the ureter.

Prostatic/prostatovesical artery

The prostatic artery can originate from various different branches of the internal iliac arterial system including the obturator, inferior vesical, superior vesical, internal pudendal, umbilical, or even the dorsal artery of the penis (Clegg 1955; Roberts and Krishinger 1967). The prostatic artery normally travels inferiorly, medially, and anteriorly (Lipshutz 1918). Lipshutz (1918) reported 10% of prostatic arteries to arise from middle rectal artery, 5% from the inferior gluteal artery, 15% from the obturator artery, 10% from the ischiopudendal trunk, and 30% from the anterior division of the internal iliac artery. It can also branch from the umbilical artery or arise as a common trunk with the inferior vesical artery. Roberts and Krishinger (1967) studied 79 specimens and noted the origin of the prostatic artery on 17 sides. In 13 of the 17 sides the arteries were duplicate, making 30 observations in total. The most common origin was from the ischiopudendal trunk (37.7%) followed by the obturator artery (23.3%) (Table 56.29).

Clegg (1955) studied the origin of the prostatovesical artery and, of the 17 arteries identified, reported that 52.9% originated from the common trunk for the inferior gluteal and internal pudendal arteries, 11.8% from the origin of the umbilical artery, 11.8% from the umbilical artery, 11.8% from a common trunk with vesicodeferential artery, 5.9% from the internal pudendal artery, and 5.9% from the obturator artery (Fig. 56.31). The course of the artery was reported to be relatively constant; it passed inferiorly, anteriorly, and medially toward the prostate on the anteroinferior surface of the bladder where it divided into the prostatic and inferior vesical branches.

Table 56.29 Frequency of the prostatic artery originating from the branches of the internal iliac arterial system. 30 vessels were identified in a total of 9 specimens (17 sides; duplicate vessels were identified in 13 sides). Adapted from Roberts & Krishinger (1967).

Artery of origin	Frequency (%)
Ischiopudendal trunk	37.7
Obturator	23.3
Inferior vesical	13.3
Superior vesical	13.3
Internal pudendal	10.0
Dorsal artery of penis	3.3

Vesicodeferential artery

The vesicodeferential artery provides the main supply to the seminal vesicles. Clegg (1955) reported that 58.8% of 17 vesicodeferential arteries identified in a study originated from the origin of the umbilical artery, 11.8% from the superior vesical artery, 11.8% from the first centimeter of the umbilical artery, 5.9% from the umbilical artery distal to the superior vesical, 5.9% from the anterior division of the internal iliac artery before the umbilical artery, and 5.9% from the gluteopudendal trunk. Dubreuil-Chambardel (1925) reported the vesicodeferential artery arose with the internal iliac system in 94% of cases; of these, it often branched from the internal pudendal artery or was in a common trunk with the superior vesical artery. In a review of the literature, Bergmann et al. (1988) reported that the vesicodeferential artery was seen in 72.7% of specimens (n=70) and that it arose from the umbilical artery in 94% of cases. The superior vesical artery was also reported to branch from it.

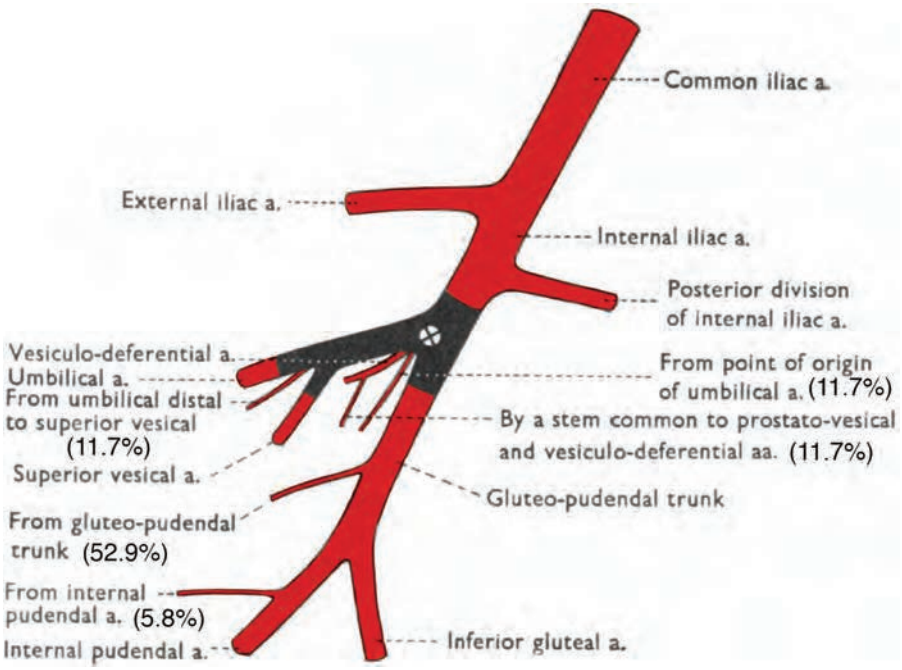

Figure 56.31 Frequency of the prostatovesical artery originating from different parts of the internal iliac arterial system based on a cadaveric study. Figures represent the frequency of origin of the prostatovesical artery from different vessels, based on a total of 17 observed arteries. The shaded area represents the region from which the vesicodeferential artery arises, with 'X' marking the most frequent location. Adapted from Clegg (1955) with permission from John Wiley & Sons.

Vesical arteries

Superior vesical

The number of superior vesical arteries has been shown to vary from one to five (Levi 1902a; Dubreuil-Chambardel 1925) with the most common number being two (Table 56.30). Ashley and Anson (1941) studied 66 cadaveric pelvic halves, and reported that the superior vesical arteries were commonly two to three in number and all were derived from the umbilical artery. Robinson (1902) reported the origin of the superior vesical artery to be mainly from the umbilical artery, although a case in which superior vesical artery originated from the obturator artery was also reported. In a review of the literature, Bergman et al. (1988) reported the superior vesical arteries to commonly arise from the umbilical artery, although they could also arise from the uterine, vesicodeferential, and the obturator arteries.

Pelage et al. (1999) studied 375 uterine arteries in 197 patients using angiography. In 92% of cases the vesical artery arose from the anterior division of the internal iliac artery, usually above the uterine artery. Parsons and Keith (1897) reported on 58 observations of the superior vesical artery. In 44 cases (75.9%) it arose from the hypogastric trunk; in two of these cases the artery was duplicated, in nine cases (15.5%) it arose from the anterior division of the internal iliac artery and in one of these it was duplicated, in four cases (7%) it arose from the internal iliac artery, and in one case it arose from the hypogastric trunk in common with the middle rectal artery.

Rare variants in origin have also been reported. Following a study of 353 Japanese cadavers (706 pelvic halves), Kawai et al. (2008) reported a rare variant in which the inferior epigastric arose from a common trunk, with the obturator artery and either the superior vesical artery or both the superior and inferior vesical arteries arising from the same arterial trunk. Lipshutz (1918) reported the superior vesical artery to arise as a common trunk with the uterine. Similarly, Pelage et al. (1999) studied 375 uterine arteries in 197 patients and reported three cases (1%) in which the vesical artery arose as a common trunk with the uterine artery; it subsequently coursed downward and medially to reach the lateral part of the bladder where it gave off three terminal branches.

Powers (1850) reported umbilical arteries that united as a single trunk and unilateral absence of this vessel.

Table 56.30 Frequency of observation of singular or multiple superior vesical arteries. Adapted from Dubreuil-Chambardel (1925).

Number of superior vesical arteries	Frequency (%)	
	Levi (1902a)	Dubreuil-Chambardel (1925)
1	10	9
2	70	74
3	12	9
4	8	6
5	0	2

Middle and inferior vesical

The middle vesical arteries are variable in presence and origin and the inferior vesical arteries are mainly variable in origin. In a review of the literature (Quain 1844; Henle 1868; Hyrtl 1887; Schaefer and Symington 1915; Lipshutz 1918; Huber 1930; Jackson 1933; Curtis et al. 1942; Latarjet 1948; Braithwaite 1951, 1952b; Clegg 1955; Gouazé et al. 1957; Anson 1966; Gardner et al. 1969; Shehata 1976; Gladykowska-Rzeczycka and Mieszkowska 1977; Pac et al. 1977), Bergmann et al. (1988) reported the following.

- The middle vesical artery arose from the umbilical artery in 75% of 132 cases.
- The middle vesical was bilateral in 50% and unilateral in 50% of a study of 66 specimens and, when unilateral, it occurred with almost equal frequency from the right (18 of 33 cases) and left (15 of 33 cases) sides.
- The inferior vesical may arise in common with the middle rectal artery, from a common trunk with the internal pudendal and superior gluteal, or as a branch from the internal pudendal. It is usually a single branch.
- Anastomoses between the inferior vesical and uterine arteries were found in 60–70% of subjects reported.
- Large anastomoses have been noted between the superior and inferior vesical arteries in many specimens.

The inferior vesical artery is variable in its point of origin. Palacios Jaraquemada et al. (2007) studied the arterial supply to 39 female urogenital tracts via injection of colored latex and noted that the inferior vesical artery originated from the lower vaginal pedicle/vaginal artery in 90% of cases and branched directly from the internal iliac artery in 10% (Table 56.28). Ashley and Anson (1941) studied 66 cadaveric pelvic halves and reported that in most cases the inferior and middle vesicle arteries were derived from, in order of frequency, the pudendal, inferior gluteal, hypogastric, or middle rectal arteries. Parsons and Keith (1897) reported on 58 observations of the inferior vesical artery; in 68.9% of cases it arose independently from the hypogastric trunk, in 22.4% from the anterior division of the internal iliac artery, in 3.5% from the internal iliac artery, in 3.5% with the middle rectal artery; and in 1.7% with the superior vesical artery. In the cases where the inferior vesical artery arose from the middle rectal artery, duplicate inferior vesical arteries were present, one of which came directly from the hypogastric trunk. In a study of 181 specimens, Lipshutz (1918) reported the inferior vesical artery arose in 34 subjects as a separate branch from the prostatic artery and arose three times as a branch of the vaginal, eight times as a branch of the umbilical artery distal to the uterine artery, nine times as a branch of the vesicodeferential artery, and five times as a branch of the internal pudendal artery. It was also reported to give rise to the dorsalis penile or accessory profunda penis arteries. The accessory pudendal arteries can also arise from the inferior vesical artery (Benoit et al. 1999).

Jusoh et al. (2010) reported that the inferior vesical artery originated from an obturator artery arising from the posterior division of the internal iliac artery in 6% of 34 observations

from 17 cadavers. Similarly, Pai et al. (2012) reported the case of a middle-aged Indian cadaver in which the inferior vesical artery originated from a common stem with the obturator artery, and the common stem arose from the external iliac artery. The inferior vesical artery has also been reported to be absent (Badagabettu et al. 2013) and its territory instead supplied by the superior vesical artery.

Internal pudendal artery

Variability in the origin of the internal pudendal artery from the internal iliac system has been discussed in detail (see "Branching pattern of the internal iliac artery") in relation to the branching pattern of the internal iliac artery. Further to this, Lipshutz (1918) reported the internal pudendal artery arose in 40% of cases from a common stem with the inferior gluteal, in 24% as a separate branch of the anterior division of the internal iliac artery, in 17% as a common trunk with the inferior gluteal and obturator arteries, and in 7% as a common trunk with the superior gluteal, inferior gluteal, and obturator arteries. Lipshutz (1918) also noted the internal pudendal artery to branch from the middle rectal artery in four subjects and to branch from the uterine artery in two subjects. Kawanishi et al. (2007) studied the angiograms of 282 internal pudendal arteries from 145 patients (eight were not visible) and classified them into five types; the most common origin (53% of observations) was from the anterior division of the internal iliac artery between the iliopectineal line and greater sciatic notch (Type 1; Fig. 56.32). It was suggested that the presence of a bilateral variation from the predominant Type 1 arrangement might result in earlier onset of erectile dysfunction by up to 10 years compared to matched subjects.

Accessory pudendal artery

The accessory pudendal artery normally assists the internal pudendal artery in its function, although in 6% of 145 patients studied angiographically it was found to be the main blood supply to the penis (Kawanishi et al. 2007). Anastomoses between the accessory pudendal and pudendal arteries/cavernous arteries of the penis have been demonstrated in approximately 70% of cases where accessory vessels are present (Droupy et al. 1997; Benoit et al. 1999).

The accessory pudendal artery is variable in presence and can be unilateral or bilateral. Following a review of the literature, Allan et al. (2012) suggest that the detection rate of the accessory pudendal artery varied depending upon the method of detection used. Angiographic detection ranged from 7% of 195 patients (Rosen et al. 1990) to 29.8% of 121 patients (Park et al. 2009), whereas laparoscopic detection ranged from 25% of 285 patients (Secin et al. 2005) to 30% of 325 patients (Secin et al. 2007). Accessory pudendal arteries have been identified in as little as 4% of 2399 men undergoing a radical retropubic prostatectomy (Rogers et al. 2004) to as many as 85% of subjects in a study of 20 cadavers (Droupy et al. 1997; Benoit et al. 1999). Early cadaveric studies showed the frequency of presence varied from 21.7% (Adachi 1928) to 30% (Levi 1902a) to 41% (Dubreuil-Chambardel 1925). A range of other results relating to the presence of the accessory pudendal artery have been reported:

- 25% of 285 patients during laparoscopy; 92 accessory pudendal arteries were identified (Secin et al. 2005);
- 25.7% of 70 patients during laparoscopic radical prostatectomy; 23 accessory pudendal arteries were identified, 8 on the left, 5 on the right, and 5 with accessory arteries on both sides (Matin 2006);
- 27% of 15 cadaveric specimens; 6 accessory arteries were identified; 2 pelves had unilateral arteries and 2 had bilateral arteries (Allan et al. 2012);
- 29.2% of 24 male patients via angiography (Bruhlmann et al. 1982); and
- 70% in a study of 10 cadavers (Breza et al. 1989).

The accessory pudendal artery can originate from the internal iliac artery or one of its branches (Secin et al. 2007). An angiographic study of 24 male patients revealed 29.2% had accessory pudendal arteries arising from either the obturator, superior vesical, or umbilical artery (Bruhlmann et al. 1982). The most commonly reported origin is either the obturator or inferior vesical artery. Allan et al. (2012) studied 15 cadaveric specimens and found six arteries in four patients; four (66%) originated from the obturator artery and two (33%) from the inferior vesical artery. Droupy et al. (1997) and Benoit et al. (1999) reported accessory pudendal arteries (33 arteries in total from 20 cadavers) to be present in 85% of specimens studied; of these, 45.5% originated from the inferior vesical artery, 36.4% from the obturator artery, and 18.2% from the external pudendal artery. Whang et al. (2012) studied 127 Korean patients using CT angiography followed by laparoscopic surgery and found 12.6% had accessory pudendal arteries, of which 56.2% originated from the obturator artery and 43.8% from the inferior vesical artery. Park et al. (2009) studied 121 patients using CT angiography and identified 44 accessory pudendal arteries in 36 patients (29.8%) (Table 56.31). Of those with accessory pudendal arteries, single arteries were seen in 80.6% of patients and multiple arteries were seen in 19.4%. The most common origin was the intrapelvic part of the obturator artery (77%), followed by the internal iliac artery or one of its branches such as the inferior vesical artery (23%). Accessory pudendal arteries were seen on the right side in 52% of patients and on the left side in 48% of patients.

Several authors have further categorized accessory pudendal arteries as being either apical or lateral according to their relationship to the prostate. Secin et al. (2005) identified 92 accessory pudendal in 25% of 285 patients; of these, 10% of patients had lateral accessory pudendal arteries that coursed along the lateral aspect of the prostate (40% of observed arteries), 13% of patients had an apical accessory pudendal artery that emerged through the levator ani fibers near the apical region of the prostate (52% of observed arteries); and 1.7% of patients had both apical and lateral arteries (7% of observed arteries).

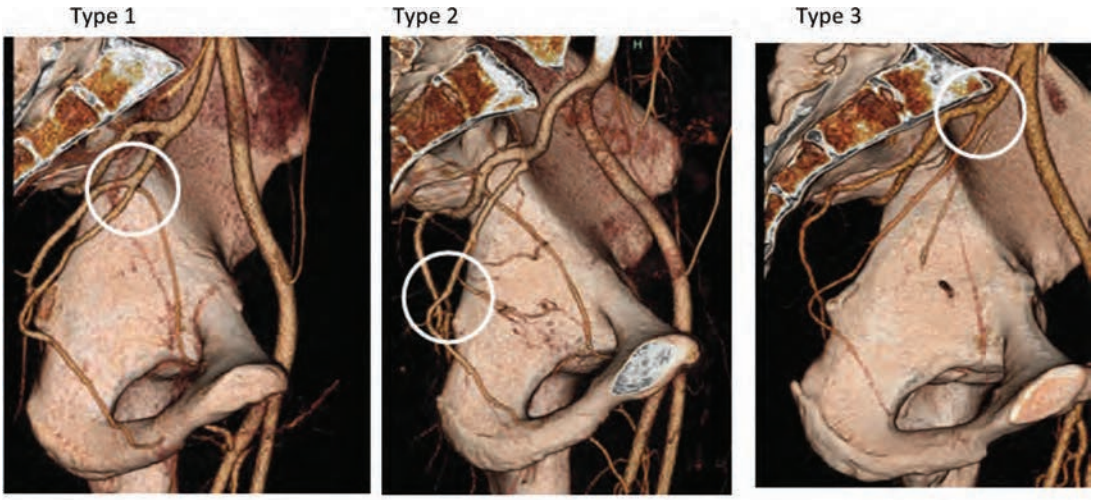

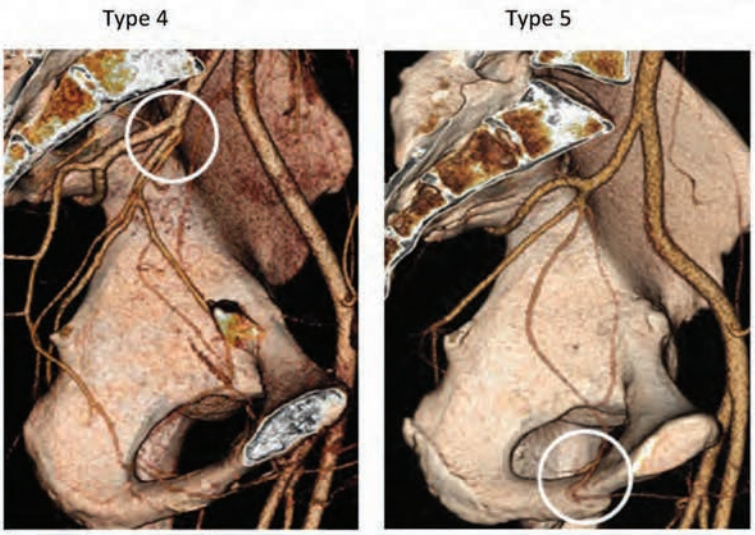

Type	Frequency (%)	Point of origin
1	53	From the anterior trunk of internal iliac artery between the iliopectineal line and greater sciatic notch
2	13	From the anterior trunk of internal iliac artery at the level of the greater sciatic notch or distal
3	11	From the internal iliac artery proximal to the iliopectineal line level
4	14	Together with the superior and inferior gluteal arteries, within 1 cm of each other
5	6	Penile blood supply dependent on arteries other than the internal pudendal artery e.g. the obturator artery

Figure 56.32 The origin point of the internal pudendal artery classified into five types. Based upon the CT angiographic study of 282 internal pudendal arteries from 145 patients.

Source: Kawanishi et al. (2007). Reproduced with permission from John Wiley & Sons.

Table 56.31 Number of lateral and apical accessory pudendal arteries observed in a study of 121 patients. 44 accessory pudendal arteries were observed in 36 patients. Lateral accessory pudendal arteries coursed along the lateral aspect of the prostate in intimate contact with prostate. Apical accessory pudendal arteries emerged near the anterolateral region of the prostatic apex close to the pubic bone. Adapted from Park et al. (2009).

Type of accessory pudendal artery	Single accessory pudendal arteries	Multiple accessory pudendal arteries			Total *n* (%)
		Bilateral same	Bilateral different	Three different	
Apical	24	6	1	2	33 (75)
Lateral	5	4	1	1	11 (25)
Patient number	29	5	1	1	36

Park et al. (2009) also classified 44 accessory pudendal arteries in the same way, but reported 75% of those observed to be apical and only 25% to be lateral.

Lateral sacral arteries

The lateral sacral arteries vary in diameter, number, and distribution (Lipshutz 1918). Bergman et al. (1988) reviewed the literature (Quain 1844; Henle 1868; Hyrtl 1887; Gegenbaur 1888; Chalier 1912; Schaefer and Symington 1915; Lipshutz 1918; Huber 1930; Jackson 1933; Curtis et al. 1942; Latarjet 1948; Anson 1966; Gardner et al. 1969; Pac et al. 1977) and reported the lateral sacral arteries to commonly branch from the posterior division of the internal iliac and to arise individually or via common trunks. In some cases the superior branches of the lateral sacral arteries were absent and replaced by branches from the common iliac, internal iliac, iliolumbar, or sciatic arteries. When the inferior branches were absent they were replaced by branches from the middle rectal, superior gluteal, and inferior gluteal arteries. The lateral sacral artery may give rise to the inferior vesical and middle rectal arteries. Extensive anastomoses are frequently seen between the sacral arteries on the anterior sacrum (Gillilan 1958). The variance of the lateral sacral arteries may be due to their irregular development (Poynter 1922).

Dubreuil-Chambardel (1925) reported five types of origin and branching pattern for the lateral sacral arteries passing to the S1–S4 sacral foramen (Fig. 56.33). Most commonly (59% of cases) there are two arteries, one passing to S1 and the second branching to S1–S3. The author also reported the following in relation to the origin of the lateral sacral arteries.

- The first lateral sacral artery took origin from the internal iliac artery in 43% of cases (alone in 40% and in a common trunk with the iliolumbar artery in 3%) and from the superior gluteal artery in 55% of cases (alone in 48% or in a common trunk with the iliolumbar artery in 7%).
- The second lateral sacral artery took origin from the superior gluteal artery in 63% of cases, the inferior gluteal artery in 31%, and the internal iliac artery in 4%.
- The third and fourth lateral sacral arteries normally took origin from inferior gluteal artery and, very rarely, the superior gluteal artery.

Levi (1902a) studied 87 subjects and reported 34.5% had a single lateral sacral artery, 55.2% had two lateral sacral arteries, and 10.3% had three lateral sacral arteries. Lipshutz (1918) reported the lateral sacral arteries arose as a single common trunk in 51% of subjects, with 88% of these arising from the superior gluteal artery and 12% from the internal iliac artery. A total of 10% of cases had three lateral sacral arteries and the

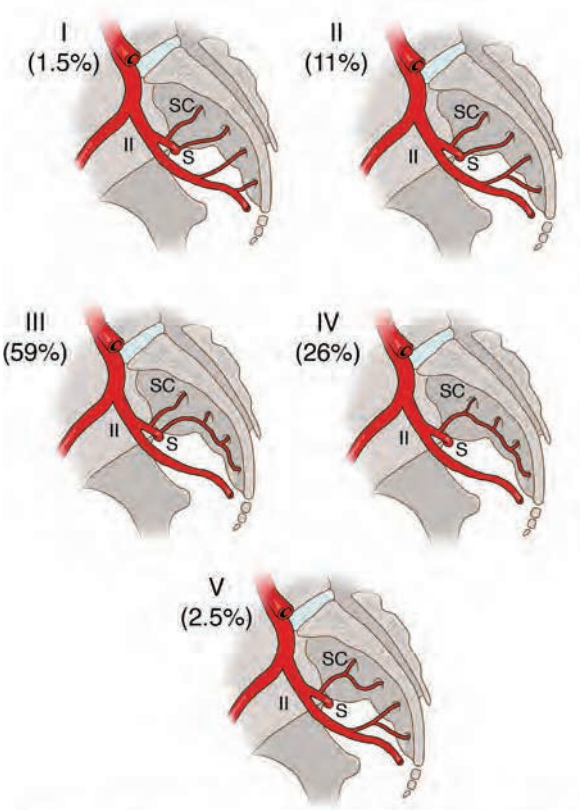

Type	Arrangement
I	Four lateral sacral arteries; S1, S2, S3, S4
II	Three lateral sacral arteries; S1, S2 (S3, S4)
III	Two lateral sacral arteries; S1, (S2, S3, S4)
IV	One lateral sacral artery; (S1, S2, S3, S4)
V	Two lateral sacral arteries; (S1, S2) (S3, S4)

Figure 56.33 Five types of origin of the four lateral sacral arteries (S1, S2, S3, and S4) and the relative frequency (%) of occurrence of each pattern. S: superior gluteal; I: inferior gluteal; SC: lateral sacral arteries in the S1–S4 positions. Adapted from Dubreuil-Chambardel (1925).

additional vessels often entered the second sacral foramen. It was also noted that the lateral sacral artery arose caudal to the iliolumbar artery, apart from in six cases when it arose as a common trunk with the iliolumbar artery. Similarly, Parsons and Keith (1897) reported a common origin for the lateral sacral and iliolumbar arteries in 17% of 53 cases. Gillilan (1958) noted a single case of the lateral sacral arteries arising from the obturator artery. Parke et al. (1994) studied 40 pelvic halves from 20 cadavers and noted that in 77.5% the segmental arteries passing to S1 arose as an independent branch from the posterior division of the internal iliac artery.

Parsons and Keith (1897) made 53 observations of the lateral sacral artery and reported that in 50.9% of cases two arteries were seen on a single side arising via a common trunk, in 47.2% there were two separate arteries on one side, while in one case three arteries were present. A total of 92.6% of the common arterial trunks arose from the posterior division of the internal iliac artery and 7.4% arose from the main internal iliac artery. Of the 25 cases in which there were two separate arteries, both branched from the posterior division of the internal iliac artery in 68% of cases, both branched from the internal iliac artery in 4% of cases, and they originated from different parts of the internal iliac system in 28% of cases (the upper artery usually coming from the main internal iliac artery and the lower artery from the posterior division of the internal iliac artery).

Iliolumbar artery

The iliolumbar artery forms an important supply to the iliac bone, psoas major, quadratus lumborum, muscles of the iliac fossa, the vertebral canal, and spinal cord (Harrington 2001). Knowledge of its position, course, and point of origin is relevant to those conducting interventional intra-arterial procedures or spinal surgeons, since iatrogenic injury can result in serious adverse consequences (reviewed in Rusu et al. 2010). In a literature review (Quain 1844; Henle 1868; Hyrtl 1887; Gegenbaur 1888; Robinson 1902; Chalier 1912; Schaefer and Symington 1915; Lipshutz 1918; Huber 1930; Jackson 1933; Curtis et al. 1942; Latarjet 1948; Anson 1966; Gardner et al. 1969; Pac et al. 1977), Bergman et al. (1988) noted that the iliolumbar artery is variable in size and is usually the first branch of the posterior division of the internal iliac artery. It has also been reported to arise from the superior gluteal, lumbar, median sacral, and lateral sacral arteries. The superior lateral sacral artery can branch from the iliolumbar artery and, in some cases, it can be partially replaced by one of the lumbar arteries or be absent. Feneis and Dauber (2000) noted the iliolumbar artery can give origin to the descending lumbar branch to psoas and quadratus lumborum, the iliac branch to both iliacus and the iliac fossa, and the spinal branch to the vertebral canal structures. The iliolumbar artery can be doubled (Power 1850).

The origin of the iliolumbar artery is variable, although most originate directly from the main trunk of the internal iliac artery (96.3%, Chen et al. 1999; 61%, Heye 2006; 28.3%, Bleich et al. 2007; 50%, Naguib et al. 2008). Yiming et al. (2002) studied 10 cadavers and found the iliolumbar artery arose from the internal iliac artery in all specimens. Chen et al. (1999) reported the iliolumbar artery to arise from internal iliac artery in 96.3% of cases and from the common iliac artery in 3.7% of cases. Kiray et al. (2010) studied 42 formalin-fixed specimens and reported that the iliolumbar artery arose from the internal iliac artery in 71.4% of cases, the posterior trunk of internal iliac artery in 19%, the common iliac artery in 4.8%, and from two different points from internal iliac artery in 4.8%. The authors also noted that the iliolumbar artery passed anterior to the lumbosacral trunk in 52.4% of cases, cleaved it in 35.7%, and passed posterior to it in 11.9%. Furthermore, 4.8% of iliolumbar arteries passed anterior to the obturator nerve and 95.2% passed posterior to it. The exception to these findings were presented by Mamatha et al. (2012) who studied 50 cadaveric pelves, and found the iliolumbar artery branched from the main trunk of the internal iliac artery in 6% of cases.

Lipshutz (1918) reported the iliolumbar artery to be a branch of the internal iliac artery in 52% of cases and of the superior gluteal in 38% of cases. Less-frequent origins included the anterior division of the internal iliac artery in three cases, the common iliac artery in four cases, the external iliac in two cases, a common trunk with the lateral sacral artery from the internal iliac artery in six cases, and absent in five cases. The author also reported that the distance between the iliolumbar and superior gluteal arteries fell within the range 1–3 cm.

Parsons and Keith (1897) made 57 observations of the iliolumbar artery; in 61.4% of cases it branched from the internal iliac artery (in one of these cases the artery was duplicate) and in 29.8% it arose with the lateral sacral artery directly from the posterior division of the internal iliac artery. In an additional two cases the artery was duplicate; in the first case one artery arose from the posterior division of the internal iliac artery and the other from the inferior gluteal artery, in the second case one artery arose from the internal iliac artery and the other from the posterior division of the internal iliac artery. In one case the iliolumbar artery was a branch of the obturator artery, itself a branch of the internal iliac artery.

Following a study of 30 pelvic halves and 50 angiograms, Rusu et al. (2010) categorized the level of iliolumbar artery origin into five levels (A–E). The most common level was found to be the main trunk of the internal iliac artery (Level C, 52.2%) followed by the posterior trunk of the internal iliac artery (Level E, 32.5%) (Fig. 56.34), which was in general agreement with the work of previous authors. Rusu et al. (2010) also noted that arteries with a higher level of origin took a more horizontal course to the iliac fossa, and those with lower origins took an oblique course. A descending lumbar branch, supplying psoas major and quadratus lumborum, was seen branching separately from the internal iliac artery or its posterior division in 48.8% of cases, between levels A–D. The authors suggest the descending lumbar branch might easily be confused for the iliolumbar artery on an arteriogram.

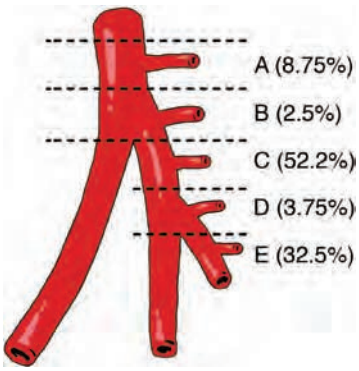

Figure 56.34 The five levels of iliolumbar artery origin from the common and internal iliac arterial systems and the relative frequency of each, based upon a study of 30 cadaveric pelves and 50 patient angiograms. Level A: from the common iliac artery; Level B: from the common iliac artery bifurcation (classified as a trifurcated common iliac artery; Level C: from the internal iliac artery; Level D: from the internal iliac artery bifurcation (classified as a trifurcated internal iliac artery); Level E: from the posterior trunk of the internal iliac artery. Adapted from Rusu et al. (2010) with permission from John Wiley & Sons.

Two studies have reported the morphology of the iliolumbar artery. Rusu et al. (2010) reported the diameter of the iliolumbar artery fall within the range 1.2–2.3 mm and, following a study of 42 cadaveric specimens, Kiray et al. (2010) reported the following:

- mean diameter at origin of 3.7±0.7 mm;
- mean distance between origin of the iliolumbar artery and its bifurcation into iliac and lumbar branches of 13.2±5.5 mm;
- distance between the origin of the iliolumbar artery and the lower edge of lumbar fifth vertebra of 43.2±12.6 mm; and
- distance between origin of the iliolumbar artery and the bifurcation point of the common iliac artery of 28.7±12.6 mm; Harrington (2001) reported this distance as 20 mm.

References

Adachi B. 1928. *Das Arteriensystem der Japaner*. Kyoto: Maruzen Co.

Allan R, Garcia NA, Montenegro JM, Alvarez-Albero JNM. 2012. Prevalence of accessory pudendal artery. *Clin Anat* 25: 983–985.

Anson BJ. 1963. An Atlas of Human Anatomy, second edition. Philadelphia: Saunders Publishing.

Anson BJ. 1966. Morris' Human Anatomy, 12th edition. New York: The Blakiston Division, McGraw-Hill Book Company.

Arai S. 1936. The distribution pattern of the hypogastric artery in Japanese. Acta Anat Nippon 9: 81 (in Japanese).

Arey LB. 1963. The development of peripheral blood vessels. In *The Peripheral Blood Vessels* (eds OrbisonJL, SmithDE). Baltimore: Williams and Wilkins.

Ashley FL, Anson BJ. 1941. The hypogastric artery in American whites and negroes. *Am J Physical Anthropol* 28: 381–395.

Ayoub SF. 1978. Arterial supply to the human rectum. *Acta Anat (Basel)* 100: 317–327.

Baba Y, Hayasho S, Ikeda S, Nakajo M, Yoshinaga M. 2012. Visualization of utero-ovarian anastomoses: Comparison between patients with and without uterine fibroid. *J Biomedical Science and Engineering* 5: 767–770.

Badagabettu SN, Kumar N, Shetty SD, Sirasanagandla SR. 2013. Variant branching pattern of the right internal iliac vessels in a male: A case report. *Arch Clin Exp Surg* 3(3): 197–200.

Balachandra S, Singh A, Al-Ani O, Baqi N. 1998. Acute limb ischemia after transplantation in a patient with persistent sciatic artery. *Transplantation* 66: 651–652.

Batteur M. 1951. Un cas exceptionel de variation de l'artère obturatrice. *Assoc Anatomistes Comptes Rendus* 38: 116.

Becken LW. 1984. In: Praktische Anatomie (eds LanzT, WachsmuthW). Vol II Part 8a. Berlin: Springer.

Benoit G, Droupy S, Quillard J, Paradis V, Giuliano F. 1999. Supra and infralevator neurovascular pathways to the penile corpora cavernosa. *J Anat* 195: 605–615.

Berberoglu M, Uz A, Ozmen MM, Bozkurt C, Erkuran C, Taner S, Tekin A, Tekdemir I. 2001. Corona mortis: An anatomic study in seven cadavers and an endoscopic study in 28 patients. *Surg Endosc* 15: 72–75.

Bergman RA, Thompson SA, Afifi AK, Saadeh FA. 1988. *Compendium of Human Anatomic Variation: Catalogue, Atlas and World Literature*. Baltimore and Munich: Urban and Schwarzenberg.

Bilhim T, Casal D, Furtado A, Pais D, O'Neill JEG, Pisco JM. 2011. Branching patterns of the male internal iliac artery: imaging findings. *Surg Radiol Anat* 33(2): 151–159.

Bilhim T, Pereira JA, Tinto HR, Fernandes L, Duarte M, O'Neill J, Pisco JM. 2013. Middle rectal artery: myth or reality? Retrospective study with CT angiography and digital subtraction angiography. *Surg Radiol Anat* 35: 517–522.

Bilic S, Sahin B. 1997. Rare arterial variation: a common trunk from the external iliac artery for the obturator, inferior epigastric and profunda femoris arteries. *Surg Radiol Anat* 19: 45–47.

Binder SS, Mitchell GA. 1960. The control of intractable pelvic haemorrhage by ligation of the hypogastric artery. *Southern Med J* 53: 837–843.

Biswas S, Bandopadhyah M, Adhikari A, Kundu P, Roy R. 2010. Variation of the origin of the obturator artery in Eastern Indian population. *J Anat Soc India* 59: 168–172.

Bleich AT, Rahn DD, Wieslander CK, Wa CY, Roshanravan SM, Corton MM. 2007. Posterior division of the internal iliac artery: Anatomic variations and clinical applications. *Am J Obs Gyn* 197: 658.e1–658.e5.

Borell U, Fernström I. 1953. Uterine artery adnexal branches. Arteriography study in human subjects. *Acta Radiol* 40: 561–582.

Borell U, Fernström J. 1954. The ovarian artery: An arteriographic study in human subjects. *Acta Radiol Diagn Stockholm* 42: 253–265.

Boxall TA, Smart PJG, Griffiths JD. 1963. The blood-supply of the distal segment of the rectum in anterior resection. *Br J Surg* 50: 399–404.

Braithwaite JL. 1951. The arterial supply of the urinary bladder. *J Anat* 85: 431.

Braithwaite JL. 1952a. Variations in origin of the parietal branches of the internal iliac artery. *J Anat* 86: 423–430.

Braithwaite JL. 1952b. The arterial supply of the male urinary bladder. *Br J Urol* 24: 61–71.

Breschet G. 1819. Considerations et observations anatomiques et pathologiques sur la hernie femorale, ou merocele. (Memoire Sur la Hernie Crurale), second thesis, pp. 41–205. Paris: Libraire pour la Partie de Medicine.

Breza J, Aboseif SR, Orvis BR, Lue TF, Tanagho EA. 1989. Detailed anatomy of penile neurovascular structures: Surgical significance. *J Urol* 141: 437–443.

Bruhlmann W, Pouliadis G, Zollikofer C. *Hauri D.* 1982. Arteriography of the penis in secondary impotence. *Urol Radiol* 4: 243–249.

Bryan RC. 1914. Aneurysm of the sciatic artery. *Ann Surg* 60: 463–475.

Chait A, Moltz A, Nelson JH. 1968. The collateral arterial circulation in the pelvis. *American Journal of Roentgenology* 102: 392–400.

Chalier A. 1912. Anomalies des arteres renales et du bassinet. *J Urol Paris* 1: 103–104.

Chen RS, Liu YX, Liu CB, Hu YS, Xu DC, Zhong SZ, Li ZH. 1999. Anatomic basis of iliac crest flap pedicled on the iliolumbar artery. *Surg Radiol Anat* 21: 103–107.

Chiarugi G. 1936. *Istituzioni di Anatomia dell'Uomo*, IV edition. Milano: Soc Ed Libraria.

Clark SL, Phelan JP, Yeh S-Y, Bruce SR, Paul RH. 1985. Hypogastric artery ligation for obstetric hemorrhage. *Obstet Gynaecol* 66(3): 353–356.

Clegg EJ. 1955. The arterial supply of the human prostate and seminal vesicles. *J Anat* 89(2): 209–216.

Cloquet H. 1817. *Recherches anatomiques sur les Hernies de l'Abdomen*. Paris: Libraire Mequignon-Marvis.

Cordier G, Pardoen L. 1921. Deux variétés d'origine de l'artère obturatrice. *Soc Biol Comptes Rendus Hebdomadaires Seances Mem* 84: 896–897.

Corfier P, Devos L, Delcroix A. 1939. L'anastomose arterielle uteroovarienne. Assoc Anatomistes Comptes Rendus 48–79.

Crock HV. 1965. A revision of the anatomy of the arteries supplying the upper end of the human femur. *J Anat* 99: 77–88.

Curtis AH, Anson BJ, Ashley FL, Jones T. 1942. The blood vessels of the female pelvis in relation to gynecological surgery. *Surg Gynecol Obstet* 75: 421–423.

Dall'acqua U, Meneghetti A. 1907. Recherches d'anatomie comparee sur les arteres de la face. *Arch Ital Biol* 47: 484–486.

Darmanis S, Mansoor ALA, Bircher M. 2007. Corona mortis: an anatomical study with clinical implications in approaches to the pelvis and acetabulum. *Clin Anat* 20: 433–439.

Delitzin S. 1896. Über eine complicierte anomalie im gebiete der arteria obturatoria und epigastrica inferior. *Arch Anat Physiol Wissen Med* 413–422.

DiDio LJA, Diaz-Franco C, Schemainda R, Bezerra AJC. 1986. Morphology of the middle rectal arteries: A study of 30 cadaveric dissections. *Surg Radiol* 8: 229–236.

Donovan DL, Sharp WV. 1984. Persistent sciatic artery: Two case reports with emphasis on embryologic development. *Surgery* 95: 363–366.

Drake RL, Vogl W, Mitchell AWM. 2009. Gray's Anatomy for Students, second edition. Philadelphia: Elsevier.

Droupy S, Benoit G, Giuliano F, Jardin A 1997. Penile arteries in humans. *Surg Radiol Anat* 19: 161–167.

Drummond H. 1914. The arterial supply of the rectum and pelvic colon. *Br J Surg* 1: 677–685.

Dschau F. 1936–37. Eine bisher unbekannte Varietät der arteria obturatoria und pudenda accessoria mit einer Varietät der arteria circumflexa femoris medialis. *Anat Anz* 83: 25–29.

Dubreuil-Chambardel L. 1925. *Traité des Variations du System Artériel Variations des Artères du Pelvis et du Membre Inferieur*. Paris: Masson et Cie.

Duclaux, H. 1902. Anomalies de l'épigastrique et de l'obturatrice. *Bull Mém Soc Anat Paris* 4: 58–59.

Dufour R, Rigaud A, Gouaze A. 1951. Variations du mode de division du tronc de l'artère hypogastric en fonction due sexe. *Assoc Anatomistes Comptes Rendus* 38: 449–456.

Dwight T. 1894–95. Statistics of variations with remarks on the use of this method in anthropology. *Anat Anz* 10: 209–215.

El-Sawaf ME. 2010. Unrecorded origin of external pudendal artery with variant obturator vessels. *Int J Anat Var* 3: 141–143.

Engelman G. 1898. Ein fall von mangel einer coronararterie. *Anat Anz* 14: 348–350.

Fatu C, Puisoru M, Fatu IC. 2006. Morphometry of the internal iliac artery in different ethnic groups. *Ann Anat* 188: 541–546

Feneis H, Dauber W. 2000. *Pocket Atlas of Human Anatomy. Based on the International Nomenclature, fourth edition*. Stuttgart: Thieme.

Fernström I. 1955. Arteriography of the uterine artery. *Acta Radiol Diagn Stockholm* 122: 1–128.

Fischer W. 1959. Anatomisch-rontgenologische untersuchungen uber die verteilung und anastomosen bildung der visceralen und parietalen weiblichen beckenarterien. *Z Geburtsh Gynak* 154: 321–340.

Fitzgerald MJT. 1978. Human Embryology. New York: Harper International.

Freeman MP, Tisnado J, Cho SR. 1986. Persistent sciatic artery. Report of three cases and literature review. *Br Radiol* 59: 217–223.

Gardner E., Gray DJ, O'Rahilly R. 1969. Anatomy, third edition. Philadelphia: Saunders Co.

Garrido-Gómez J, Pena-Rodríguez C Martín-Noguerol T, Hernández-Cortes P. 2012. Corona mortis artery avulsion due to a stable pubic ramus fracture. *Orthpedics* 35(1): e80–e82.

Gegenbaur C. 1888. Lehrbuch der Anatomie des Menschen, third edition. Leipzig: V. Wilhelm Engelmann.

Gérard G. 1901. Variabilité des rapports vasculaires du bassinet. *Assoc Anatomistes Comptes Rendus* 3: 147–154.

Gillilan LA. 1958. The arterial blood supply of the human spinal cord. *J Comp Neurol* 110(1): 75–103.

Gilroy AM, Hermey DC, DiBenedetto LM, Marks SC, Page DW, Lei QF. 1997. Variability of the obturator vessels. *Clin Anat* 10: 328–332.

Gladykowska-Rzeczycka J, Mieszkowska M. 1977. Vascular variation in the genitor-urinary system. *Folia Morphol Warsaw* 36: 113–116.

Goldny B, Henninger B, Hofmann K, Trieb T, Petersen J, Rehder P. 2009. CT appearance of a patent impar umbilical artery in an adult woman and related anomalies: a case report and review of the literature. *Cases Journal* 2(65): 1–6.

Gomez-Jorge J, Keyoung A, Levy EB, Spies JB. 2003. Uterine artery anatomy relevant to uterine leiomyomata embolization. *Cardiovasc Intervent Radiol* 26: 522–527.

Gouazé A, Sentenae M, Odano R. 1956. Contribution a l'étude de l'irrigation artérielle de la prostate. *Assoc Anatomistes Comptes Rendus* 43: 374–381.

Gouazé A, Odano R, Chantepie G. 1957. Contribution a l'étude de la vascularsation artérielle de la vessie. *Assoc Anatomistes Comptes Rendus* 44: 331–340.

Greebe J. 1977. Congenital anomalies of the iliofemoral artery. *J Cardiovasc Surg* 18: 317–23.

Green PH. 1832. On a new variety of the femoral artery. *Lancet* 1: 730–1.

Gür S, Oguzkurt L, Kaya B, Tekbas G, Ozkan U. 2013. Impotence due to external iliac steal syndrome: treatment with percutaneous transluminal angioplasty and stent placement. *Korean J Radiol* 14(1): 81–85.

Harb Z, Williams S, Rutter P. 2006. Bilateral congenital absence of internal iliac arteries, prominent lumbar arteries, and a ruptured mycotic aneurysm of the abdominal aorta. *Ann R Coll Surg Engl* 88(4): W3–W5.

Harrington JF. 2001. Far lateral disc excision at L5–S1 complicated by iliolumbar artery incursion: Case report. *Neurosurgery* 48: 1377–1380.

Hartmann R. 1881. *Lehrbuch. d. Anat. des Menschen*. Strassburg: Pb. R Schulz & Co.

Hassen-Khodjal R, Batt M, Michetti C, Le Bas P. 1987. Radiologic anatomy of the anastomotic systems of the internal iliac artery. *Surg Radiol Anat* 9: 135–140.

Henle J. 1868. Handbuch der Systematischen Anatomie des Menschen, Bd I–III. Braunschweig: Von Friedreich Vieweg und Sohn.

Hesselbach AC. 1819. *Die Dicherste Art des Bruchschnittes in der Leiste*. Wurzburg: Pb. Bamberg.

Hiki T, Okado Y, Wake K, Fujiwara A, Kaji Y. 2007. Embolization for a bleeding pelvic fracture in a patient with persistent sciatic artery. *Emergency Radiology* 12: 55–57.

Hoffmann CE. 1878. *Lehrbuch. d. Anat. d. Menschen*. Erlangen: Pb. E. Besold.

Holub Z, Lukac J, Kliment L, Urbanek S. 2005. Variability of the origin of the uterine artery: laparoscopic surgical observation. *J Obstet Gynaecol Res* 31(2): 158–163.

Hong HX, Pan ZJ, Chen X, Huang ZJ. 2004. An anatomical study of corona mortis and its clinical significance. *Chin J Traumatol* 7: 165–169.

Honma S, Aimi Y, Kudo M. 2013. Ring formation of the internal iliac artery. *Surg Radiol Anat* 35: 169–171.

Hoshiai H. 1938. Anatomical study on the pelvic arteries in Japanese fetus. Acta Mat Nippon 11: 61–72 (in Japanese).

Howe WW, Lacey T, Schwartz RP. 1950. A study of the gross anatomy of the arteries supplying the proximal portion of the femur and the acetabulum. *J Bone Joint Surg* 32A: 856–866.

Huber GC. 1930. *Piersol's Human Anatomy, ninth edition*. Philadelphia: Lippincott Co.

Hyrtl J. 1887. *Lehrbuch der Anatomic des Menschen*, 19th edition. Wien: Wilhelm Braumtiller.

Isaacs CE. 1855. On the anomalies of the arteries. *Am J Med Sci* 30: 400–401.

Ishizeki K, Sakakura Y, Iida S, Tachibana T, Nawa T. 1982. A rare case of the inferior epigastric artery originated from the obturator artery (author's translation). *Kaibogaku Zasshi* 57: 47–50.

Iwasaki Y, Shoumura S, Ishizaki N, Emura S, Yamahira T, Ito M, Isono H. 1987. The anatomical study on the branches of the internal iliac artery: Comparison of the findings with Adachi's classification. *Kaibogaku Zasshi* 2(6): 640–645 (in Japanese).

Jackson CM. 1933. *Morris' Human Anatomy, ninth edition*. Philadelphia: Blakiston's Son and Co.

Jakubowicz M, Czarniawska-Crzesinska M. 1996. Variability in origin and topography of the inferior epigastric and obturator arteries. *Folia Morphol Warsz* 55(2): 121–126.

Jastschinski S. 1891a. Die typischen verzweigungformen der arteria hypogastrica. *Month Int J Anat Physiol* 8: 111–126.

Jastschinski S. 1891b. Die abweichungen der arteria obturatoria nebst erklärung ihres entstehens. *Int Monats Anat Physiol* 8: 367–386.

Job T. 1933. Persistence of a left ischiatic artery. *Anat Rec* 58(1): 101–105.

Jones OM, Smeulders N, Wiseman O, Miller R. 1999. Lateral ligaments of the rectum: an anatomical study. *Brit J Surg* 86: 487–489.

Jusoh AR, Rahman NA, Latiff AA, Othman F, Das S, Ghafar NA, Suhaimi FH, Hussan F, Sulaiman IM. 2010. The anomalous origin and branches of the obturator artery with its clinical implications. *Rom J Morphol Embryol* 51(1): 163–166.

Kara E, Yildiz A, Ozturk NC, Ozturk H. 2008. An extremely rare bifurcation pattern of the caudal abdominal aorta: case report demonstrated by angiography. *Surg Radiol Anat* 30: 689–691.

Karlsson S, Jonsson K. 1980 Angiography of the ovarian artery in adnexal lesions. *Acta Radiol Diagn Stockholm* 21: 739–746.

Kawai K, Honma S, Koizumi M, Kodama K. 2008. Inferior epigastric artery arising from the obturator artery as a terminal branch of the internal iliac artery and consideration of its rare occurrence. *Ann Anat* 190: 541–548.

Kawanishi Y, Muguruma H, Sugiyama H, Kagawa J, Tanimoto S, Yamanaka M, Kojima K, Numata A, Kishimoto T, Nakanishi R, Kanayama H. 2007. Variations of the internal pudendal artery as a congenital contributing factor to age at onset of erectile dysfunction in Japanese. *Brit J Urol Int* 101(5): 581–587.

Kawashima T, Sato K, Sasaki H. 2006. A human case of hypoplastic external iliac artery and its collateral pathways. *Folia Morphol* 65(2): 157–160.

Kim WK, Yang SB, Goo DE, Kim YJ, Chang Y-W, Lee JML. 2013. Aberrant ovarian artery arising from the common iliac artery: case report. *Korean J Radiol* 14(1): 91–93.

Kiray A, Ackali O, Tayefi H, Kosay C, Ergur I. 2010. Anatomical variations of iliolumbar artery and its relation with surgical landmarks. *Acta Orthop Traumatol Turc* 44(6): 464–468.

Koritke JG, Gillet JY, Pietri J. 1967. Les arteres de la tropme utreine chez la femme. *Arch Anat Histol Embryol Norm Exp* 50: 47–70.

Koyama T, Kawada T, Kitanaka Y, Katagiri K, Ohno M, Ikeshita M, Yamate N. 2003. Congenital anomaly of the external iliac artery: A case report. *J Vasc Surg* 37(3): 683–685.

Krushche T. 1885. Anatomische Untersuchungen uber der Art. Obturatoria. Dorpat.

Kumar D, Rath G. 2007. Anomalous origin of obturator artery from the internal iliac artery. *Int J Morphol* 25(3): 639–641.

Lanz T, Wachsmuth W. 1959. *Praktische Anatomie, Vol 1 Part 3*, second edition. Berlin: Springer.

Larsson P-G, Teleman P, Persson J. 2010. A serious bleeding complication with injury of the corona mortis with the TVT–Secur procedure. *Int Urogynecol J* 21: 1175–1177.

Latarjet A. 1948. *Testut's Traite D'Anatomie Humaine, ninth edition*. Paris: G. Doin and Cie.

Levi G. 1902a. Observations sur les variations de arteries iliaques. *Arch Ital Biol* 37: 489.

Levi G. 1902b. Morfologia delle arterie iliache. *Arch Ital Anat Embriol* 1: 120–173, 295–346, 523–605.

Lin M, Chen W, Huang L, Ni J, Yin L. 2010. The anatomy of lateral ligament of the rectum and its role in total mesorectal excision. *World J Surg* 34: 594–598.

Lindenbaum E, Brandes JM, Itskovitz J. 1978. Ipsi- and contralateral anastomosis of the uterine arteries. *Acta Anatomica* 102: 157–161.

Link DP, Garza AS, Monsky WL. 2009. Congenital single, pelvic iliac artery: a case report. *J Vasc Interv Radiol* 20(9): 1231–1234.

Lippert H, Pabst R. 1985. Arterial Variations in Man: Classification and Frequency. München: JF Bergman.

Lipshutz B. 1918. A composite study of the hypogastric artery and its branches. *Ann Surg* 67(5): 584–608.

Llauger J, Sabate JM, Guardia E, Escudero J. 1995. Congenital absence of the right common iliac artery: CT and angiographic demonstration. *Eur J Radiol* 21: 128–130.

Madson DI, Wilkerson DK, Ciocca RG, Graham AM. 1995. Persistent sciatic artery in association with varicosities and limb length discrepancy: An unrecognized entity? *Am Surg* 61: 387–392.

Mamatha H, Hemalatha B, Vinodini P. Souza ASD, Suhani S. 2012. Anatomical study on the variations in the branching pattern of internal iliac artery. Indian J Surg. Online publication, doi: 10.1007/s12262-012-0785-0.

Mandell VS, Jaques PF, Delany DJ, Oberheu V. 1985. Persistent sciatic artery: clinical, embryologic, and angiographic features. *Am J Roent* 144: 245–249.

Maneesha S, Tripta S, Richpal S, Kaur AA. 2012. Variations of obturator artery in man. *Anat Physiol* 2(3): 1–4.

Marincola BC, Napoli A, Anzidei M, Marotta E, Boni F, Cartocci G, Bertaccini L, Noce V, Pacile MA, Catalano C. 2012. Persistence of the sciatic artery: a case report of a combined (complete and incomplete) type causing leg ischemia. Case Rep Vasc Med 2012: article ID 196798, doi: 10.1155/2012/196798.

Matin SF. 2006. Recognition and preservation of accessory pudendal arteries during laparoscopic radical prostatectomy. *Urology* 67: 1012–1015.

Matson M, Nicholson A, Bello A-M. 2000. Anastomoses of the ovarian and uterine arteries: a potential pitfall and cause of failure of uterine embolization. *Cardiovasc Intervent Radiol* 23: 393–396.

McLellan GL, Morettin LB. 1982. Persistent sciatic artery: clinical, surgical, and angiographic aspects. *Arch Surg* 117: 817–822.

Mehl R. 1969. Retro-iliac artery ureter. *J Urol* 102: 27.

Missankov AA, Asvat R, Maoba KI. 1996. Variations of the pubic vascular anastomoses in Black South Africans. *Acta Anatomica* 155: 212–214.

Miyaji K. 1935. Uber die A. hypogastrica. *Arbeit Mat Institut Kanazawa* 20: 85–93 (in Japanese).

Mocquot P, Rouvillois C. 1938. La vascularisation artérielle de l'ovaire étudiée en vue de la chirurgie conservatrice. *J Chir* 51: 161–176 (original article in French).

Moore KL, Dalley AF, Agur AMR. 2014. *Clinically Oriented Anatomy, seventh edition*. Philadelphia: Lippincott Williams and Wilkins.

Morita S, Kato S, Sugawara E. 1974. Corrosions-anatomical studies on the arterial system of the Japanese fetus. VIII. The common iliac arteries and the branches of the internal iliac artery. *Acta Mat Nippon* 49: 79 (in Japanese).

Nagabhooshana S, Vollala VR, Rodrigues V, Bhat S, Pamidi N, Lobo SW. 2008. Anatomical variation of obturator vessels and its practical risk: a case report from an anatomic study. *J Vasc Bras* 7(3): 275–277.

Naguib NN, Nour-Eldin A, Hammerstingl RM, Lehnert T, Floeter J, Zangos S, Vogl TJ. 2008. Three-dimensional reconstructed contrast-enhanced MR angiography for internal iliac artery branch visualization before uterine artery embolization. *J Vasc Interv Radiol* 19: 1569–1575.

Nair SB, Sidhu HS, Watkinson AF. 2012. Variant obturator artery complicating uterine artery embolization. *Clin Radiol* 67: 290–291.

Nakai M, Nakata K, Sato M, Ikoma A, Minamiguchi H, Kawai N, Sonomura T, Hatada A, Nishimura Y, Okamura Y. 2011. Sequential dilatation of the superior gluteal artery following coil embolization of the internal iliac artery and endovascular abdominal aneurysm repair: a case report. *Ann Vasc Dis* 4(2): 134–138.

Namking M, Woraputtaporn W, Buranarugsa M, Kerdkoonchorn M. 2007. Variation in origin of the obturator artery and corona mortis. *Siriraj Med J* 59: 12–15.

Narverud G, Myhre HO. 1974. Congenital hypoplasia of the lower limb arteries. A report of two cases. *Scandanavian J Thoracic Cardiovasc Surg* 8: 70–72.

Nasu H, Chiba S. 2009. Rare case of femoral artery ramification and origin of the obturator artery. *Anat Sci Int* 84: 323–326.

Naveen NS, Murlimanju BV, Kumar V, Jayanthi KS, Rao K, Pulakunta T. 2011. Morphological analysis of the human internal iliac artery in south Indian population. *Online J Health Allied Sci* 10(1): 1–4.

Nayak S, Kv S. 2009. Variant obturator vessels. *Int J Anat Var* 2: 111–112.

Nitschke T, Preuss F. 1971. Die Hauptaste der A. Iliaca int. bei Mensch und Haussaugetieren in vergleichend-anatomisch haufigster Rei henfolge. *Anat Anz* 128: 439–453.

Obimbo MM, Ogeng'o JA, Saidi H. 2010. Variant anatomy of the uterine artery in a Kenyan population. *Int J Gynaecol Obstet* 111(1): 49–52.

Odano, R. 1962. Essai de systematisation des branches viscerales pelviennes de l'artere hype gastrique chez l'homme. *J Med Bordeaux* 139: 722–726.

Okamoto K, Wakebe T, Saiki K, Nagashima S. 2005. Consideration of the potential courses of the common iliac artery. *Anat Sci Int* 80: 116–119.

Ouyang Z, Liu P, Yu Y, Chen C, Song X, Liang B, Zhong G, Liu C, Li Z. 2012. Role of ovarian artery-to uterine artery anastomoses in uterine artery embolization: initial anatomic and radiologic studies. *Surg Radiol Anat* 34: 737–741.

Pac L, Hamplova M, Pelcova O. 1977. An atypical case of arising of some parietal branches of the arteria iliaca interna in man. *Anat Anz* 141: 450–454.

Pai MM, Krishnamurthy A, Prabhu LV, Pai MV, Kumar SA, Hadimani GA. 2009. Variability in the origin of the obturator artery. *Clinics* 64(9): 897–901.

Pai NV, Ambiye MV, Khambatta S. 2012. Variation in the origin of inferior vesical artery from a variant obturator artery. *Int J Anat Var* 5: 8–10.

Palacios Jaraquemada JM, Monaco RG, Barbosa NE, Ferle L, Iriarte H, Conesa A. 2007. Lower uterine blood supply: extrauterine anastomotic system and its application in surgical devascularization techniques. *Acta Obstet Gynecol* 86: 228–234.

Park BJ, Sung DJ, Kim MJ, Kim YH, Chung KB, Kang SH, Cheon J. 2009. The incidence and anatomy of accessory pudendal arteries as depicted on multidetector-row CT angiography: clinical implications of preoperative evaluation for laparoscopic and robot-assisted radical prostatectomy. *Korean J Radiol* 10: 587–595.

Parke WW, Whalen JL, Van Demark RE, Kambin P. 1994. The infraaortic arteries of the spine: their variability and clinical significance. *Spine* 19(1): 1–5.

Parsons FG, Keith A. 1897. Sixth Annual Report of the Committee of Collective Investigation of the Anatomical Society of Great Britain and Ireland 1895–96. The mode of origin of the branches of the internal iliac artery. *J Anat Phys* 31: 31–44.

Paterson AM. 1909. Obliteration of the left common, external, and internal iliac arteries. *J Anat Phys* 44(1): 56–57.

Pelage J-P, Le Dref O, Soyer P, Jacob D, Kardache M, Dahan H, Lassau J-P. 1999. Arterial anatomy of the female genital tract: variations and relevance to transcatheter embolization of the uterus. *Am J Roentgen* 172: 989–994.

Pelage J-P, Cazejust J, Pluot E, Le Dref O, Laurent A, Spies JB, Chagnon S, Lacombe P. 2005. Uterine fibroid vascularization and clinical relevance to uterine fibroid embolization. *Radiographics* 25: s99–s117.

Pfitzner W. 1889. Über die ursprungsverhältnisse der arteria obturatoria. *Anat Anz* 4: 504–514.

Pick JW, Anson BJ, Ashley FL. 1942. The origin of the obturator artery. A study of 640 body halves. *Am J Anat* 70(2): 317–343.

Power JH. 1850. *Surgical Anatomy of the Arteries, and Descriptive Anatomy of the Heart by the late Valentine Flood, M.D.* Dublin: Fannin and Co.

Poynter RCWM. 1922. Congenital anomalies of the arteries and veins of the human body with bibliography. *The University Studies of the University of Nebraska Lincoln* 22: 1–106.

Pungpapong S, Thum-umnauysuk S. 2005. Incidence of corona mortis; preperitoneal anatomy for laparscopic hernia repair. *J Med Assoc Thai* 88(4): s51–s52.

Quain R. 1844. *The Anatomy of the Arteries of the Human Body and Its Application to Pathology and Operative Surgery*. London: Taylor and Walton.

Quain R. 1899. The Anatomy of the Arteries of the Human Body. Report of Committee of Collective Investigation of the Anatomical Society, London, 1891–1892. J Anat Physiol 27.

Ramakrishnan PK, Elezy MA. 2012. Variations in the branching pattern of internal iliac artery. *Anatomica Karnataka* 6(1): 16–22.

Razavi MK, Wolanske KA, Hwang GL, Sze DY, Kee ST, Dake MD. 2002. Angiographic classification of ovarian artery-to-uterine artery anastomoses: initial observations in uterine fibroid embolization. *Radiol* 224: 707–712.

Reddy S, Ramana VV, Rao M. 2007. Absence of inferior gluteal artery: A rare observation. *Int J Morphol* 25(1): 95–98.

Redfern P. 1850. Origin of the epigastric and obturator arteries by a common trunk from the internal iliac; with an inquiry into the amount of danger occasioned by various positions of arteries in the ordinary operations for femoral and inguinal herniae. *Monthly J Med, Edin* 9: 203–222.

Reed RA, McLucas B. 2012. Aberrant right ovarian artery from proximal internal iliac artery in uterine artery embolization patient. *Open Journal of Radiology* 2: 117–119.

Reid J. 1836. On the varieties of the obturator artery, and the relation of these to the femoral ring. *Edin Med Surg J* 45: 65–70.

Roberts WH, Krishingner GL. 1967. Comparative study of human internal iliac artery based on Adachi classification. *Anat Rec* 158(2): 191–196.

Robinson B. 1902. Note on the distribution of the branches of the internal iliac artery and the zones of exsanguination resulting from its deligation. *Ann Surg* 35(2): 189–206.

Rogers CG, Trock BP, Walsh PC. 2004. Preservation of accessory pudendal arteries during radical retropubic prostatectomy: surgical technique and results. *Urology* 641: 148–151.

Rosen MP, Greenfield AJ, Walker TG, Grant P, Guben JK, Dubrow J, Bettmann MA, Goldstein I. 1990. Arteriogenic impotence: findings in 195 impotent men examined with selective internal pudendal angiography. Young Investigator's Award. *Radiology* 174(3 Pt 2): 1043–1048.

Rusu MC, Cergan R, Dermengiu D, Curca GC, Folescu R, Motoc AGM, Jianu AM. 2010. The iliolumbar artery-anatomic considerations and details on the common iliac artery trifurcation. *Clinical Anatomy* 23: 9–100.

Sanudo JR, Roig M, Rodriguez A, Ferreira B, Domenech JM. 1993. Rare origin of the obturator, inferior epigastric and medial circumflex femoral arteries from a common trunk. *J Anat* 183: 161–163.

Sanudo JR, Mirapeix R, Rodriguez-Niedenfuhr, Maranillo E, Parkin IG, Vazquez T. 2011. Obturator artery revisited. *Int Urogynecol J* 22: 1313–1318.

Saraiya PV, Chang TC, Pelage J-P, Spies JB. 2002. Uterine artery replacement by the round ligament artery: an anatomic variant discovered during uterine artery embolization for leiomyomata. *J Vasc Intervent Radiol* 13(9 pt1): 939–941.

Sarikcioglu L, Sindel M. 2002. Multiple vessel variations in the retropubic region. *Folia Morphol* 61(1): 43–45.

Sato K, Sato T. 1991. The vascular and neuronal composition of the lateral ligament of the rectum and the rectosacral fascia. *Surg Radiol Anat* 13: 17–22.

Savov JD, Wassilev WA. 2000. Bilateral persistent complete sciatic artery. *Clin Anat* 13: 456–460.

Schaefer EA, Symington J, Bryce TH. 1915. *Quain's Anatomy, 11th edition*. London: Longmans, Green and Co.

Schlöbig SFJ. 1844. Observations quadem de varia arteria obturatoriae origine atque decursu. Leipzig.

Secin FP, Karanikolas N, Touijer K, Salamanca JIM, Vickers AJ, Guilloneau B. 2005. Anatomy of accessory pudendal arteries. *J Urol* 174(2): 523–526.

Secin FP, Touijer K, Mulhall J, Guillonneau. 2007. Anatomy and preservation of accessory pudendal arteries in laparoscopic radical prostatectomy. *Eur Urol* 51: 1229–1235.

Senior HD. 1919–20. The development of the human femoral artery, a correction. *Anat Res* 17: 271–279.

Senior HD. 1925. An interpretation of the recorded arterial anomalies of the human pelvis and thigh. *Am J Anat* 36: 1–46.

Shafiroff BGP, Grillo EB, Baron H. 1959. Bilateral ligation of the hypogastric arteries. *American Journal of Surgery* 98: 34–40.

Shehata, R. 1976. The arterial supply of the urinary bladder. *Acta Anat* 96: 128–134.

Shetty AS, Jetti R, Shivaram B, Madhyastha S. 2011. Variant branching pattern of the posterior division of internal iliac artery: a case report. *Galle Medical Journal* 16(2): 37–38.

Shivakumar AH, Sathyamurthy B, Raju GM, Vijayanath V. 2010. Internal iliac artery and its variations. *Anatomica Karnatka* 41: 15–20.

Smith JC, Gregorius JC, Breazeale BH, Watkins GE. 2009. The corona mortis, a frequent vascular variant susceptible to blunt pelvic trauma: identification at routine multidetector CT. *J Vasc Interv Radiol* 20(4): 455–460.

Standring S. 2008. *Gray's Anatomy: The Anatomical Basis of Clinical Practice*, 40th edition. London: Churchill Livingstone.

Suzuki H. 1951. The mode of branching of the internal iliac artery in Japanese. *Jikeikai Ikadaigaku Kaibougaku Kyoshitsu Gyosekishu* 5: 1–49 (in Japanese).

Tamisier D, Melki JP, Cormier JM. 1990. Congenital anomalies of the external iliac artery: Case report and review of the literature. *Ann Vasc Surg* 4: 510–514.

Teague DC, Graney DO, Routt ML. 1996. Retropubic vascular hazards of the ilioinguinal exposure: A cadaveric and clinical study. *J Orthop Trauma* 10: 156–159.

Terek MC, Saylam C, Orhan M, Yilmaz A, Oztekin K. 2004. Surgical anatomy of the posterior division of the internal iliac artery: The important point for internal iliac artery ligation to control pelvic haemorrhage. *Austr NZ J Obstet Gynaecol* 44: 374–375.

Thompson A. 1882–83. Origin of the internal circumflex from the deep epigastric artery. *J Anat* 17: 379–383.

Tornetta P, Hochwald N, Levine R. 1996. Corona mortis. Incidence and location. *Clin Orthop Relat Res* 329: 97–101.

Tsukamoto N. 1929. Studies on the arterial system in pelvic cavity of Japanese. *Acta Mat Nippon* 2: 830–852 (in Japanese).

Vishnumukkala TR, Yalakurthy S, Bharath CHNV, Raj SSJD, Puttagunta B, Kannan M. (2013) The parietal branching pattern of the internal iliac artery. *Int J Biol Med Res* 4(1): 2792–2797.

Whang SY, Sung DJ, Lee SA, Park BJ, Kim MJ, Cho SB, Kim YH, Cheon J. 2012. Preoperative detection and localization of accessory pudendal artery with contrast enhanced MR angiography. *Radiol* 262(3): 903–911.

Widmer O. 1955. Die rectalarterien des menschen. *Anat Entwicklungsg* 118: 398–416.

Williams LR, Flanigan DP, O'Connor RJA, Schuler JJ. 1983. Persistent sciatic artery: clinical aspects and operative management. *Am J Surg* 145(5): 687–693.

Won H-S, Won H-J, Oh C-S, Han S-H, Chung I-H, Kim D-H. 2012. The inferior epigastric artery arising from the internal iliac artery via a common trunk with the obturator artery. *Anat Cell Biol* 45(4): 285–287.

Wyeth JA, Wardwell WL. 1877. Notes upon the surgical anatomy of the obturator artery. The difference of its relations in the male and female, with a consideration of its importance in the operation for relief of femoral hernia. *Med Rec* 12: 630–631.

Yamaki KI, Saga T, Doi Y, Aida K, Yoshizuka M. 1998. A statistical study of the branching of the human internal iliac artery. *Kurume Med J* 45: 333–340.

Yasukawa S. 1954. An anatomical study on the hypogastric artery in Japanese. *Jikeikai Ikadaigaku Kaibougaku Kyoshitsu Gyosekishu* 12: 1–43 (in Japanese).

Yiming A, Baqué P, Rahili A, Mayer J, Braccini AL, Fontaine A, Leplatois A, Clave A, Bourgeon A, de Peretti F. 2002. Anatomical study of the blood supply of the coxal bone: radiological and clinical application. *Surg Radiol Anat* 24: 81–86.

57 Lower limb arteries

Akshal Patel
Penn State, Hershey, Pennsylvania, United States

The major arterial variants of the lower extremities exist due to differential embryologic destinies of the primordial vessels. In that sense there is no strict "abnormal" pattern, rather, the observed differences between individuals should be anticipated even in healthy states. It is important to understand and identify the alternate vascular pathways, and the subject is of interest to a myriad of surgical and endovascular specialists. Vascular surgeons require knowledge of which vessels are truly at risk and which can be used for bypass. Plastic surgeons commandeer large areas of skin and the associated vascular tree for grafting and reconstructive procedures. Endovascular specialists use the major limb vessels as access sites for a number of diagnostic and interventional procedures. Occasionally, redirection of flow from the "standard" or "classical" model can contribute to the formation of aneurysms, fistulae, and complications related to ischemia.

This chapter will first outline the embryology of major arterial conduits into the lower extremity. Following this, it will move sequentially down the leg, highlighting the arterial variants of the thigh, knee/popliteal fossa and foot–ankle complex.

Embryonic development of the lower extremity vascular enlage

The limb bud typically appears at the end of the fourth week of prenatal life. Blood supply originates from intersegmental arteries arising from the aorta and form a fine capillary network throughout the mesenchyme. The primordial vascular pattern consists of a primary axial artery and its branches, which drain into a peripheral marginal sinus. Blood in the marginal sinus drains into peripheral veins. A concerted and programmed balance between angiogenesis, vasculogenesis and apoptosis dictates the angioarchitecture of the lower extremity. The arteries of the lower limb derive from the fifth lumbar artery. Specifically, the sciatic or axial artery is the chief artery of the lower limbs at the first stages (6–9 mm crown–rump length) of the development and arises from the dorsal root of the umbilical artery. During development, the primary axial artery is proximally and gradually replaced by the femoral artery, a branch of the external iliac artery. The sciatic artery regresses to become the inferior gluteal artery. At early stages an anastomotic network is formed between the femoral artery and the sciatic artery; the deep femoral artery is one of the branches of this network. The distal sciatic becomes the popliteal artery and peroneal branch. The anterior tibial artery branches from the popliteal, while uniting with the popliteal transforms the distal femoral artery into the posterior tibial artery.

Persistent sciatic artery

This is a rare variant that represents a lack of regression or involution of the sciatic artery (axial artery) in favor of development of the femoral artery. The incidence of this variant ranges from 0.025% to 0.04% and less than 100 cases have so far been reported in the literature. There are various phenotypes of this variant and relate to the varying degrees to which the femoral artery supply is supplanted by the sciatic artery. George Paraskevas et al. (2004) give the following classification for the various types of the persistent axis artery: type I, a complete axial artery and a normal femoral artery; type II, a complete axial artery and an incomplete femoral artery; type IIa, a superficial femoral artery which does not, however, reach the popliteal artery; type IIb, no superficial femoral artery; type III, an incomplete axial artery; only the upper half of the artery can be found with a normal femoral network.; type IV, an incomplete axial artery in which only the lower half can be found, with the coexistence of a normal femoral network; and type V, a sciatic artery branching from the medial sacral artery, with an existing superficial femoral artery. Power (1850) reported that Green mentioned a case of the sciatic artery giving rise to the popliteal artery.

Femoral artery

This vessel represents the major inflow tract into the lower extremity, barring instances of the sciatic artery variant noted above. The femoral artery may arise from the inferior gluteal or internal iliac, leave the pelvis, and traverse the back of the thigh with the sciatic nerve to the popliteal space. Under these circumstances, the external iliac ends in the deep femoral or lateral circumflex, or some other branch of the femoral.

The femoral vein may remain on the medial side of the artery throughout its course in the thigh. The femoral artery may give

Bergman's Comprehensive Encyclopedia of Human Anatomic Variation, First Edition. Edited by R. Shane Tubbs, Mohammadali M. Shoja and Marios Loukas.
© 2016 John Wiley & Sons, Inc. Published 2016 by John Wiley & Sons, Inc.

rise to the inferior epigastric, deep circumflex iliac, lateral femoral circumflex, medial femoral circumflex, iliolumbar, accessory femoral circumflex (medial and lateral), descending branch of the lateral femoral circumflex, and fourth or lowest perforating artery (great femoral nutrient or arteria femoris magna). Thomson (1882) reported a case of a common trunk from the femoral artery they gave rise to the medial femoral circumflex and inferior epigastric arteries. Musgrove (1882) has reported a femoral artery that split into equal parts to reunite distally. The splitting occurred distal to the origin of the deep femoral artery and the reunion occurred 13 cm distally. This author mentioned that Quain (1844) found this variant in one of 1200 bodies. The femoral artery can be doubled and can then unite and form the popliteal artery (Power 1850). Power (1850) states that Sandifort reported a case where the femoral split into two just below the inguinal ligament. The continuations of these vessels were the fibular and posterior tibial arteries. Power also cites Portal as having reported a similar case with a high duplication, where the distal vessels gave rise to two popliteal arteries.

Proximal branches

Superficial inferior epigastric artery (SIEA)

The origin of this vessel is approximately 2–5 cm below the inguinal ligament and is most often seen within 1 cm of the midpoint. Rather than a singular takeoff, it often shares a common branch with the superficial circumflex iliac artery (discussed in the following section), but there are reports of this vessel arising from either the pudendal artery or profunda femoris artery as another pattern. The diameter of this vessel falls within the range 1.1–2.5 mm and the average pedicle length is 3–8 cm. In a classic cadaveric study, this vessel was absent in 35% of subjects. In 48% of cases the SIEA was noted to share a common trunk with the superficial circumflex artery, in contrast to being an independent trunk from the femoral artery which was seen in only 17% of cases (Taylor and Daniel 1975). When it was seen as a singular branch the mean diameter was 1.1 mm, but when seen as a combined trunk with another vessel the mean diameter was 1.4 mm.

Recent studies are conflicting as to the prevalence of this artery. One small anatomic study demonstrated the SIEA in >90% of dissections. Eighteen out of twenty cadavers possessed a SIEA that arose as a common trunk from either the superficial circumflex artery (14/20), the deep circumflex artery (4/20), or the superficial external pudendal artery (7/20). A more recent study in 278 patients reported a lack of discernible vessel in 42%, corroborating the findings of earlier reports (Taylor and Daniel 1975; Hester et al. 1984; Stevenson et al. 1984; Reardon et al. 2004; Fathi et al. 2008; Sinna et al. 2010)

Superficial circumflex iliac artery (SCIA)

As opposed to the SIEA, this vessel is relatively constant and is seen arising from the femoral artery in 83.3% of cases. The diameter of this vessel falls within the range 1.2–3 mm. A new classification system delineates three SCIA variants based on cadaveric analysis of 216 iliac regions: type 1 or archetype, where a true vessel originates below the inguinal ligament and may have one or more branches; type 2 vessels are branches from the deep circumflex artery, which is a branch itself from the internal iliac artery; and type 3 is the designation used for complete absence of this artery (seen in 17% of dissections; Penteado 1983; Thein et al. 1997; Sinna et al. 2010; Ghassemi et al. 2013).

Superfical external pudendal artery (SEPA)

Two studies suggest that this vessel originates from the femoral artery in 98–100% of cases; rarely (0–2%) will it be found as a branch of the profunda femoris (Dias et al. 1987; Patil et al. 1987; La Falce et al. 2006). Another anatomic study found that the SEPA has a common origin/trunk with the superficial epigastric artery in 15% of cases. It invariably arises from the medial aspect of the femoral artery, pierces the thigh fascia and travels superiomedially toward the pubis, and then on to the umbilicus. It ramifies into 3–4 branches. One study reports that duplication occurs with a frequency of 46%, and this produces superior and inferior divisions. It also reports a large variation in the distance between the inguinal ligament (IL) and the origin of this vessel (0.8–8.5 cm). In specimens with a duplication pattern, the distance between the arteries fell within the range 0–4.3 cm (La Falce et al. 2006).

Deep branches

Profunda femoris (deep femoral artery)

The profunda femoris artery may rarely be absent (Young 1879). Young (1879) found that in the absence of this vessel, all of its normal branches arose from the femoral artery. It arises from the lateral aspect of the femoral artery in 23–86% of cases, from the posterolateral aspect in 30%, and the posterior aspect in 46% (Fig. 57.1). Boltri et al. (1979) reported two cases where the DFA origin was on the medial side. The mean distance of its origin from the midpoint of the IL lies within the range 3.2–5.3 cm (Prakash et al. 2010). Power (1850) reported that the profunda can be duplicated and that it can arise from the external iliac within the pelvis.

Medial circumflex femoral artery (MCFA)

This vessel arises from the profunda femoris in 58–81% of specimens (Fig. 57.1; Adachi et al. 1928; Suder and Nizankowski 1985; Emura et al. 1989; Colborn et al. 1995; Massoud and Fletcher 1997; Gautier et al. 2000; Tanyeli et al. 2006; Ciftcioğlu et al. 2009) and, less commonly, from the femoral artery in 18–26% of specimens. There is one case of a common trunk or trifurcation pattern involving the femoral artery, the profunda and the MCFA (Uzel et al. 2008). Kopuz refers to a case where the MCFA shares a common trunk with the SIEA (Ciftcioğlu

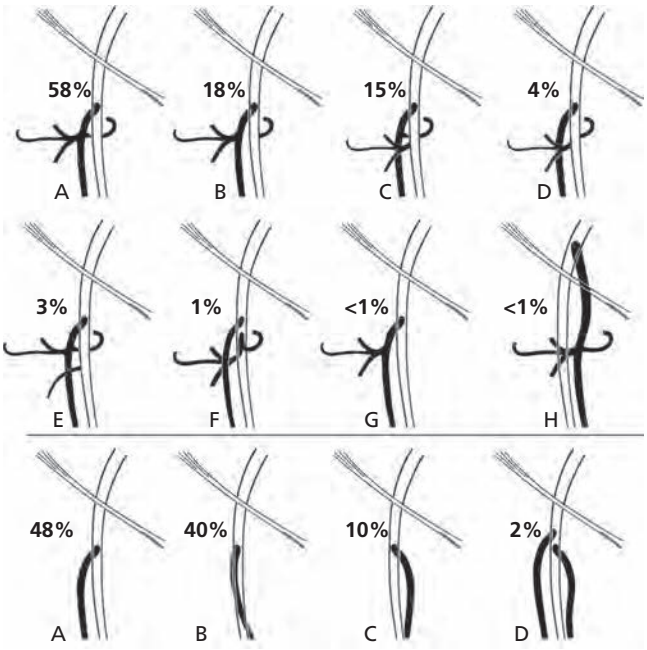

Figure 57.1 Rows 1 and 2 illustrate the major variations of the profunda femoris and its branches: (a) the circumflex and profunda femoris arteries all arise from a common trunk; (b) the femoral artery gives rise to the medial femoral circumflex artery; (c) the femoral artery gives rise to the lateral femoral circumflex artery; (d) the femoral artery gives rise to both circumflex arteries; (e) similar to (a) or (b) but a large branch of the lateral circumflex artery arises from the femoral artery; (f) both circumflex arteries arise from a common trunk separate from the profunda femoris artery; (g) absence of the medial circumflex artery with this territory supplied by a branch of the obturator artery; (h) the external iliac artery gives rise to the profunda femoris artery and, sometimes, together with the inferior epigastric artery. Row 3 illustrates the major variations of the course of the profunda femoris artery: (a) lateral or dorsolateral position of the profunda femoris artery in relation to the femoral artery; (b) a dorsal position of the profunda femoris artery to the femoral artery; (c) the main part of the profunda femoris artery is dorsomedial or medial to the femoral artery; and (d) branches of the profunda femoris are located medial and lateral to the femoral artery. Adapted from Lippert and Pabst (1985).

et al. 2009). The medial femoral circumflex may be absent, in which case the distal supply is from the obturator artery.

Lateral circumflex femoral artery (LCFA)

This vessel arises from the profunda femoris in 67–81% of specimens and from the femoral in 2.8–23.9% (Fig. 57.2; Adachi et al. 1928; Massoud and Fletcher 1997; Uzel et al. 2008). Uzel et al. (2008) describe variants where the LCFA arises as a common trunk with the profunda femoris.

Knee vascular variants

The knee is furnished by numerous vessels which arise from the popliteal artery. We will then discuss anterior knee supply and posterior knee supply separately.

1. Branching of the popliteal artery at the lower border of the popliteal muscle (95%).

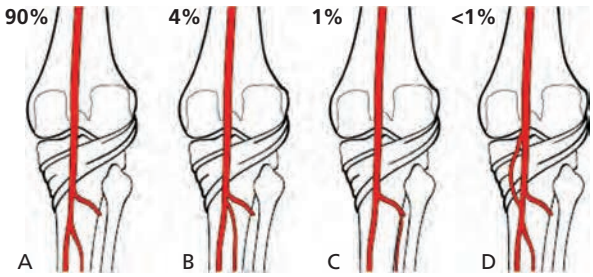

a. the "normal" situation as described in textbooks
b. "trifurcation" or very short stems of the anterior, posterior tibial and peroneal arteries
c. trunk to the anterior tibial and peroneal arteries
d. "island" formation of a branch

2. Branching of the popliteal artery proximal to the upper margin of the popliteal muscle (5%).

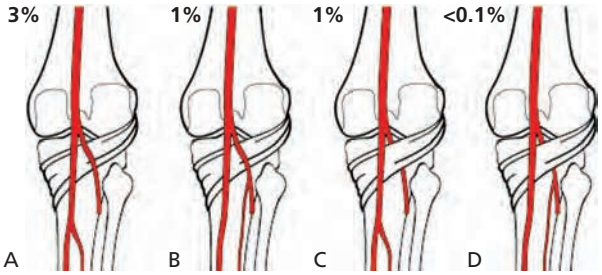

a. otherwise as normal
b. combined with a trunk formation (Tr. peroneotibialis anterior)
c. the anterior tibial artery runs ventrally to the popliteal muscle
d. trunk formation; interosseaou and anterior tibial artery

Figure 57.2 Major branching patterns of the popliteal artery and its branches. Adapted from Lippert and Pabst (1985).

Anterior knee joint

Anatomical variations of this region are controversial and not well studied. The arterial network consists of the inosculation of seven major vessels: the superior lateral genicular artery (SLGA); the superior medial genicular artery (SMGA); the middle genicular artery (MGA); the inferior lateral genicular artery (ILGA); the inferior medial genicular artery (IMGA); the descending genicular artery (DGA); and the anterior tibial recurrent artery (ATRA). The vascularization pattern can be considered in light of the patellar rete, the lateral tibial condylar, intercondylar and medial femoral condylar nutrient supply.

Patellar rete

If the patella can be considered a clock face, then the irrigation arises from sources at the 1, 3, 5, 7, and 11 o'clock positions: at 1 o'clock, the DGA; at 3 the SMGA; at 5 the IMGA; at 7 the ATRA; and at 11 the SLGA. The number of vessels converging on this region may vary between 5 and 6 (Scapinelli 1968; Shim and Leung 1986; Brick and Scott 1989). The convergence points are on a "circular" artery on the ventral patella, which acts as

the circumpatellar anastomosis of the rete. The SLGA and the SMGA migrate toward each other along the superior margin of the patella, anterior to the attachment of the quadriceps tendon, and anastomose with branches of the DGA. Before reaching the inferior border of the patellar ligament, the inferior genicular arteries divide into three branches: the ascending parapatellar artery, the oblique prepatellar artery, and the transverse infrapatellar artery. The ascending division unites with branches of the superior genicular arteries on the lateral surface of the patella. The oblique division converges centripetally towards the anterior surface of the patella, completing the ring of the "circular" artery. The transverse division anastomoses behind the ligamentum patellae, sending patellar interosseous ramifications (Kirschner et al. 1997).

Intercondylar space

This space derives the majority of its irrigation from three sources; in order of importance these are the MGA, the accessory MGA, and distal branches of the inferior genicular arteries. The MGA, known classically as the azygos artery of Hyrtl (1881), is the dominant supplier. It typically arises perpendicular to the popliteal artery on its anterior or anterolateral aspect. In 33–40% of cases from cadaveric studies, the MGA shares a common trunk with the LSGA (Scapinelli 1997). Duplications of this vessel have been reported as well as a very rare case of a triplication pattern. When duplicated, the lesser or inferior vessel is known as the accessory MGA and its origin is seen 1.5–2 cm distal to the main MGA (Arnoczky 1985; Simank et al. 1995).

Medial femoral condyle

The two principal suppliers to this region are the DGA and the SMGA, although these vessels are rarely co-dominant. The DGA is the main supplier and splits off the superficial femoral artery proximal to the adductor hiatus. It has three major branches: the muscular branch, the osteoarticular branch, and the saphenous branch. Yamamoto et al. (2010) found the DGA to be present in 89% of their specimens and the SMGA to be present in 100%. The frequency of the osteoarticular branch was 89%, whereas the frequency of the saphenous branch was 79%. As a neurovascular bundle, the DGA and saphenous nerve travel together within the adductor canal, deep to the Sartorius muscle. It branches from the superficial femoral artery 10.5–17.5 cm above the condyle. In contrast, the SMGA branches from the popliteal artery 3.5–6.5 cm above the knee joint (Kirschner et al. 1998; Yamamoto et al. 2010). After leaving the popliteal artery, the SMGA crosses from behind the adductor magnus tendon to connect with the osteoarticular branch of the DGA.

Lateral tibial condyle

Two vessels ramify on the tibial condyle: the ILGA and the ATRA (Dubreuil-Chambardel 1925; Scapinelli 1968; Shim and Leung 1986). The distal branches of these arteries anastomose both in front and behind the lateral intercondylar tubercle. The ILGA invariably originates from the popliteal artery and travels horizontally around the condyle under the lateral collateral ligament. It lies 6–10 mm below the joint interline when behind this ligament, but then rises to above the joint once beyond it. Rarely crossing the midline on its way to the retropatellar fat pad, the vessel sends 4–6 ascending and descending collaterals (Hannouche et al. 2006). The ATRA arises invariably from the anterior tibial artery 6–8 cm below the joint interline and ascends in an oblique fashion toward the condyle (Sanders and Alston 1986). It divides asymmetrically to provide a large medial vessel which fans over the tibial tuberosity and a diminutive lateral branch that supplies the fibular head (Menck et al. 1992).

Posterior knee joint/popliteal fossa variants

The popliteal artery is a continuation of the aforementioned axial or sciatic artery. The adult form of the popliteal artery is a fusion of the developing femoral vessel plexus and the regressing axial vessel plexus. The distal popliteal-axial configuration initially sits deep to the developing popliteus muscle but disappears at about the 20–22 mm embryo stage. The definitive configuration, which is now the distal popliteal artery proper, forms superficial to the popliteus muscle, after the medial head of the gastrocnemius muscle has migrated medially over the popliteal fossa. The distal popliteal artery represents the union of the immature anterior and posterior tibial vessels. To summarize, the distal segments of the axial or sciatic artery persist as the popliteal artery and the peroneal artery. The anterior tibial artery develops from the popliteal vessels and the posterior tibial artery develops similarly but as an anastamosis with distal primitive/primordial femoral artery.

Variations of the popliteal artery are seen in 6.4–18.2% of cases, combining data gathered since 1940 and encompassing anatomic/cadaveric reports as well as angiographic studies of this region (Fig. 57.2) (Kropman et al. 2011). Kim et al. (1989) formulated a classification system, a modification of the criteria documented by Lippert and Pabst, which neatly summarizes the major variant patterns. They proposed three major categories (I, II, III) and three subtypes (A, B, C) within each category.

- In category I, A type (literature incidence: 81.8–93.6%) represents the classic or usual pattern where the popliteal artery divides at the level of the inferior border of the popliteus muscle to give the anterior tibial artery (AT), which runs laterally towards the fibula and later terminates in the lower calf as the dorsalis pedis artery (DP). The remainder of the vessel continues on as the tibioperoneal trunk and terminates at the origin of the peroneal artery (PR). The latter travels down the interosseous membrane, to end above the ankle. The posterior tibial (PT) artery courses down the posterior calf and terminates at the level of the calcaneus, splitting into the medial and lateral tarsal arteries (see below). Type B (0–6%) represents a functional trifurcation of the AT, PR, and PT offshoot in close (0.5–1 cm) proximity to each other. Type C (0.1–5%) represents the situation where the posterior tibial artery is the first branch point and the resultant anterior tibioperoneal trunk bifurcates into the AT and PR.

- In category II, the altitudinal variation here represents a high division of the popliteal artery by which we mean it occurs proximal to the interior border of the popliteus muscle. Type A (1.2–5%) here is when the AT arises at or above the patella, and its trajectory heads either in front or behind the popliteus muscle. Type B variant (0.4–5.9%) represents a PT arising at or above the patella, and is similar to the type I-C in that an anterior tibioperoneal trunk is present. Type C variant (0–0.2%) represents a high peroneal artery and is extremely rare.
- Category III includes the special instance where the proximal portions of the AR or the PT are congenitally hypoplastic/filiform or aplastic. Due to the paucity of supply from these vessels the distal runoff is altered, namely the peroneal artery will replace the distal irrigation of the anterior tibial/dorsalis pedis and posterior tibial arteries. Type A (0–5.1%) is where the PT is hypoplastic, type B (0–5%) is where the AT/DP is hypoplastic, and type C (0–0.8%) is where both the PT and AT are hypoplastic (Morris et al. 1960; Keen 1961; Bardsley and Staple 1970; Pirker 1970; Mauro et al. 1988; Kim et al. 1989; Prayer et al. 1990; Day and Orme 2006; Kil and Jung 2009; Ozgur et al. 2009).

Senior described this variant as the peronea magna, which is believed to be an engorged peroneal artery in the setting of missing anterior and posterior tibial arteries (Jung et al. 2008). To briefly summarize, the three most common variations encountered in the literature are a high origin of the anterior tibial, a high origin of the trifurcation, and a hypoplastic or aplastic posterior tibial artery. A large angiographic analysis by Kil and Jung (2009) is the first report evaluating differences between right and left limbs simultaneously. Notably, there appears to be no right–left predominance of variants. However, it was documented that if branching pattern was "non-classical" on extremity then there is a 28% chance that the opposite side also contains a variant. In these cases, 76% of the variants were of the same category and subtype (Kil and Jung 2009).

Foot and ankle vascular variants

The arterial variations in this region of the lower extremity are numerous due to the rich distal collateral anastomoses. For the sake of completeness, we tour the embryology of this region briefly before examining the variants.

At the 14 mm embryologic stage, the axial artery can be divided into three arbitrary segments. The first, most proximal segment is the sciatic artery proper which lies proximal to the ramus communicans superius, an artery that connects the developing femoral artery and the regressing axial artery. Note that the femoral artery occupies the ventral compartment of the thigh and the axial artery, soon to be considered the sciatic segment, occupies the dorsal compartment. At this stage a small artery budding off the femoral artery anteriorly can be noted, known as the ramus saphenous. This vessel represents the future supreme genicular artery. The next segment of the axial artery is named the poplitea profunda, because it lies deep or anterior to the popliteus muscle, and ends as it gives of a branch known as the ramus perforans cruris. This ramus passes the proximal end of the tibiofibular interspace. The most distal segment, beyond the ramus perforans cruris, becomes the interosseous artery, a vessel that is anatomically inserted between the interosseous membrane anteriorly and the tibialis posterior muscle posteriorly. Two branches bud off the primitive popliteal to lie superficial or posterior to the flexor hallucis longus muscle: the superficial posterior tibial artery and the superficial posterior peroneal artery. The former ends in the plantar compartment of the foot although the latter ends in the ankle, giving off medial and lateral branches.

At the 17.8 mm embryologic stage, the ramus perforans cruris has given off an ascending branch called the recurrent tibial artery lying anterior to the tibial plateau and a descending branch called the anterior tibial artery lying anterior to the interosseous membrane. The anterior tibial artery ends in the dorsal foot plexus of vessels. Four major arteries to the foot are now delineated. Two were described above, namely the superficial posterior artery and the superficial posterior peroneal artery. The interosseous artery and the anterior tibial artery complete the vascular runoff. The interosseous artery divides into two branches. The dorsal ramus is called the perforans tarsi, which passes through the talo-calcaneal mass and is joined distally by the anterior tibial artery, forming the rudimentary dorsal arterial plexus. The plantar ramus becomes the lateral plantar artery and anastomoses with the terminal superficial posterior peroneal artery to form the deep plantar arch. The terminal branch of the superficial posterior tibial artery becomes the medial plantar artery.

At the 18 mm embryologic stage, the sciatic artery continues to involute and the femoral artery enlarges. We also see the formation of the ramus communicans inferior, which connects the proximal superficial posterior peroneal artery with the distal interosseous artery. This vessel sits between the tibialis posterior muscle ventrally and the flexor hallucis longus dorsally. Also noted at this stage is the development of the superficial popliteal vessel (see previous section on popliteal variants).

At the 22 mm embryologic stage, the sciatic artery has all but disappeared and the femoral artery has assumed the role of major blood supply to the lower extremity. The superficial popliteal artery is more formed and has a communicating branch, the ramus communicans medius, to the anterior tibial artery. Both the interosseous artery and the superficial posterior peroneal artery have regressed. The former disappears along with the ramus perforans tarsi. The latter loses its distal medial branch whereas the lateral branch unites with the ramus communicans inferius, which is the future peroneal artery. In the adult, the peroneal artery sends a perforating branch forward to join the anterior tibial artery. The lateral plantar artery is now only a branch of the superficial posterior tibial artery.

Anatomic variations of the foot and ankle vessels have been studied extensively and the complexity is immense. Three main

vessels feed this region: the anterior tibial artery (ATA), the posterior tibial artery (PTA), and the peroneal artery. Any combination of these vessels can be thin (filiform), atrophic, or absent. If either the ATA or the PTA or both are diminished then the peroneal artery and its major arborizations (the anterior and posterior peroneal arteries) hypertrophy to serve the distal foot (Dubreuil-Chambardel 1925). The frequency of a thinned or absent ATA is reported to fall within the range 2.4–7.1% (Dubreuil-Chambardel 1925; Adachi et al. 1928). The frequency of a thinned or absent PTA is reported to fall within the range 0.98–1.42% (Dubreuil-Chambardel 1925; Adachi et al. 1928). The peroneal artery has never been reported as being absent, rather very thin or with missing branches and runoff vessels (Edwards 1960). The frequency of finding a thin peroneal artery is reported as 2.8–3.8% (Dubreuil-Chambardel 1925). The following discussion is divided into variant anatomy based on the foot's dorsal supply and the foot's plantar supply.

Dorsal variants

The dorsal arterial system is highly variable and rarely appears as the textbook classic or "expected" pattern (Huber 1941). A number of authors have attempted to classify or capture the variants based on cadaveric, radiographic, or surgical findings.

Dorsalis pedis artery (DPA)

This artery can be thin (3%, Adachi et al. 1928) or absent (12%, Huber 1941). In terms of its origin, it is most commonly seen as a continuation of the ATA (Fig. 57.3). In approximately 5% however, the ATA can be atrophic and the DPA will arise from the perforating branch of the peroneal artery or possess shared supply from both the perforating branch and the ATA (0.5%, Huber 1941). Dubreuil-Chambardel (1925) describes a very rare case where the PTA is the origin vessel of the DPA, which passes around the medial malleolus to reach the dorsal surface of the foot. Although the first dorsal metatarsal artery continues to be supplied by the DPA, the second, third, and fourth dorsal metatarsal arteries are now supplied by the perforating branch of the peroneal artery.

The DPA course is also variable; medial deviation is described to occur in 3.5% of specimens (Huber 1941) and lateral deviation in 0.4–5.5% of specimens (Dubreuil-Chambardel 1925; Adachi et al. 1928). If the rete of the dorsalis pedis persists beyond the embryonic stage, then what Adachi coined the "grundform" pattern emerges. The transverse (mesiolateral) components of this pattern are formed by the proximal lateral tarsal artery, the distal lateral tarsal artery, and the arcuate artery. These are connected by longitudinal or sagittal anastomotic branches and the DPA, which typically continue as the dorsal metatarsal arteries.

Lateral tarsal arteries (LTAs)

The proximal and distal lateral tarsal arteries are co-dominant in only 10% of cases, and the proximal artery tends to be the larger-caliber vessel most of the time (84% vs 6%; Adachi et al. 1928). The origin of the proximal LTA is variable. In Huber's study of 200 feet, the most common site of origin was at the level of the junction of the talar head and neck (58%), followed by the ankle joint (19.5%), and then below the talonavicular joint (19%). The artery was absent in 1.5% and filiform in 1.5%. Rarely, it was seen as a continuation of the perforating branch of the peroneal artery (Huber 1941).

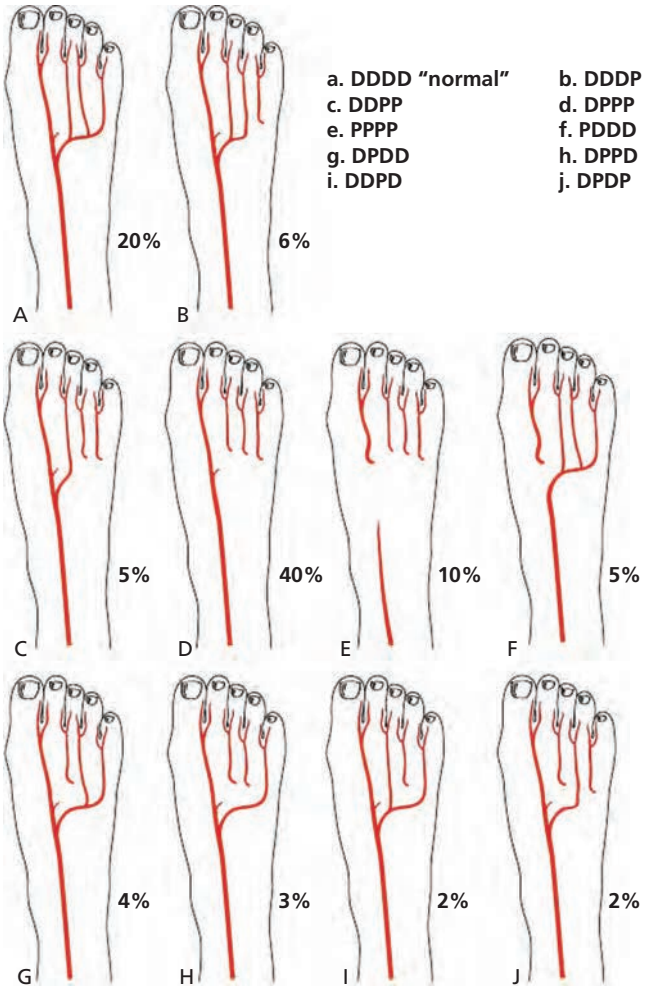

Figure 57.3 Dorsal foot: (a–k) represent the more common anatomic variations; a more dorsal (D) or plantar (P) origin of the arteries on the dorsal side of the foot are shown. Adapted from Lippert and Pabst (1985).

The arcuate artery

The DPA and the arcuate artery are intimately related and the variant pattern of these vessels is dependent on each other. Huber proposed a classification system for arcuate artery variations based on the level of origin of the vessel and the number of dorsal metatarsal artery runoffs.

- Group A (35%) comprised those specimens with the arcuate artery arising at the level of the first metatarsal joint. The most frequent subtype in this group was when the arcuate artery supplied the second, third, and fourth dorsal metatarsal arteries (16.5%).

- Group B (19%) comprised those specimens with the arcuate artery arising at the level of the cuneonavicular joint. The subtype distribution was similar to that of group A, with the arcuate artery supplying all three dorsal metatarsals in most cases (9%).
- Group C was indicative of no arcuate artery being present (34%).
- Group D was indicative of no DPA being seen (12% as noted above).

As can be gleaned from Huber's work, the disposition of the second–fourth dorsal metatarsal is dependent on the arcuate artery and more proximally by the presence of an adequate DPA. Note that these vessels have a double origin and therefore a dual supply, dorsal and plantar. Interestingly, in Huber's series the dorsal rete is the major contributor whereas in Adachi's series the plantar proximal or posterior perforating artery is the major contributor. This highlights the impact of race or ethnicity on the vascular variants (Adachi et al. 1928).

First dorsal metatarsal artery (FDMA)

While studying appropriate harvest locations for free-flaps, May et al. (1977) outlined two basic patterns for the origin of the FDMA. Type 1, seen in 78%, describes the FDMA arising from the DPA at the base of metatarsals 1 and 2. Type 2, seen in 22%, describes the FDMA arising deeply from the descending portion of the DPA or from the plantar vessels. Both variants travel dorsal or superficial to the transverse metatarsal ligament and, after giving off small branches to the surrounding skin, muscle, and joint tissues, dive over this ligament and subsequently form the distal communicating artery (DCA). This vessel represents the key anastomosis with the plantar circulation. In 38% of cases the DCA directly connected to the first plantar metatarsal artery (FPMA), in 26% the DCA connected with the plantar digital artery of the first toe, and in 28% the DCA connected with the plantar digital artery of the second toe.

FDMA variants have been stratified in relation to the muscular anatomy, source of supply (dorsal or plantar), and course. We will examine each in turn, starting with two studies that examine variants relative to the first dorsal interosseous muscle.

Seeking sites of tissue transfer from the foot, Gilbert (1976) reported variations of the FDMA based on the path of this vessel through or adjacent to the first dorsal interosseous muscle proximally and its relation to the deep transverse metatarsal ligament distally. This classification has five major types: Ia, Ib, IIa, IIb, and III. Types Ia and Ib were the most common variant encountered in Gilbert's series (together making up 66%) and in these cases both metatarsal arteries arise independently. Types IIa and IIb cumulatively represented 22% of cases, but here the metatarsal arteries arise from a common trunk located under the first dorsal interosseous muscle. In type III, seen only in 12% of feet, the FDMA is slender and irrigation is chiefly from a well-developed plantar metatarsal artery. Type Ia represents the situation in which the FDMA travels superficial to the main belly of the first dorsal interosseous muscle, whereas in type Ib the FDMA pierces the main portion of this muscle. In both types IIa and IIb, the FDMA lies dorsal to the muscle. Differentiating type IIa from type IIb is the presence of an atrophic superficial branch in the former. The slender FDMA of type III passes through the first dorsal interosseous muscle.

In a slighter smaller cadaveric study of 40 feet, Murakami (1971), Hinenoya et al. (1987), and Horie et al. (1988) reported a different classification system for the FDMA variants. Eight types are described, anatomically defined by the location of the FDMA relative to the first dorsal interosseous muscle and branching of the FDMA relative to the insertion of the adductor hallucis muscle. With types Ia, Ib, Ic, Id, and V, there is a common trunk for the first dorsal and first plantar metatarsal arteries. In types II, III, and IV the two metatarsal arteries arise independently. For types Ia, Ib, Ic, and Id the common trunk lies deep to the medial head of the first dorsal interosseous muscle. In type V the common trunk passes above the muscle. When there is a distinct origin for the FDMA branch it sits above the muscle in type II, below the muscle in type III, and pierces the muscle in type IV. The relative frequencies of these types in this series are: Ia 5%, Ib 5%, Ic 12.5%, Id 25%, II 25%, III 17.5%, IV 7.5%, and V 2.5%.

The FDMA can be considered from the viewpoint of local blood supply, whether it is principally irrigated from the dorsal system or the plantar system. In classical studies the dorsal system is reported to be the major source in 76.5–80% of specimens and the plantar system the minor source in 8.5–19.1% of specimens; they are rarely co-dominant, in just 0.3% of specimens (Adachi et al. 1928). Leung and Wong (1983) described seven distinct arterial patterns as observed in a clinical series during toe-transfer operations. The patterns were organized on the basis of arterial supply from the dorsalis pedis artery and the deep plantar arch. The most common variation (28.6% of cases, type I) demonstrated is a FDMA, fed by the horizontal portion of the dorsalis pedis artery, which lies superficial to the first dorsal interosseous muscle and the deep transverse metatarsal ligament (TML). It ends in two branches, one for the first/big toe and one for the second toe. The second most common pattern (25.7% of cases, type II) demonstrated is that of an FDMA which ramifies through the first dorsal interosseous muscle. In the type III (seen in 14%) variant, the FDMA arises deep from the vertical portion of the dorsalis pedis artery but soon passes above the deep TML. Type IV (5%) is a combination of type I and III, where there is a small superficial FDMA branch and a deep FDMA branch from the horizontal and vertical segments of the dorsalis pedis artery respectively. Type V (8%) is similar to type III; however, the FDMA passes below the deep TML rather than above it. Types VI (1%) and VII (4%) represent atretic variants, either an absence of the FDMA or an absence of the dorsalis pedis artery altogether, respectively.

Tibial plantar hallucal artery

This vessel has variable origin. Adachi has documented this vessel arising from the first dorsal metatarsal artery, the first

plantar metatarsal artery, the tibial superficial plantar artery, and several combinations of these. In 40% of feet the origin was from the first plantar metatarsal artery; in 35% it was from the fibular branch of the first plantar metatarsal artery; in 13% it was from the tibial branch of the first plantar metatarsal artery; in 5% it was seen from both those branches; in 2% it was seen either from the tibial superficial plantar artery alone or in combination with the first dorsal metatarsal artery; and in 5% it was seen from the first dorsal metatarsal and the tibial branch of the first plantar metatarsal arteries (Adachi et al. 1928).

Dorsomedial/dorsotibial hallucal artery

This vessel possesses either a plantar or dorsal origin. Ethnic/racial/genetic differences explain the large range published, being of plantar origin 4.3–98.7% of the time and dorsal origin in 0.9–95.7% of cases (Dubreuil-Chambardel 1925; Adachi et al. 1928). The oldest study describes how the distal portion of this artery is fed by the first dorsal metatarsal artery (Poirer and Charpy 1902).

Dorsal metatarsal arteries II, III, and IV

These vessels have a double origin, which is to be expected toward the distal segments of the arterial tree. For the second artery, plantar source is observed in 33.5–56.5% and a dorsal source in 36–55%. For the third artery, plantar source is observed in 23–59.9% and a dorsal source in 35.6–59%. For the fourth artery, plantar source is observed in 37.5–63.4% and dorsal source in 33.9–40.5%. Dual origin is seen in 2.6–7.3% of cases in one study (Adachi et al. 1928) and 0.5–10.5% cases in another (Huber 1941).

Perforating artery of the sinus tarsi

This vessel is always present, although it has a highly variable origin (Mulfinger and Trueta 1970). It can arise from the dorsalis pedis artery (39.2–52%), the lateral tarsal artery (21.7–32%), the anterior lateral malleolar artery (9–11.7%), or has a double supply from the perforating branch of the peroneal artery proximally and the lateral tarsal artery distally (15.8%) (Dubreuil-Chambardel 1925; Adachi et al. 1928).

Medial tarsal arteries

These vessels are not only highly variable in size and origin, but they also vary widely in number present. Huber (1941) reported the presence of two equal branches in 42% of feet. This system anastomoses with the medial plantar artery system on the medial side of the foot.

Anterior medial and lateral malleolar arteries

Documented variations of these vessels are relative to their origin above, below or at the ankle joint articular interline. The origin of the anterior medial malleolar artery is above the interline in 20–37%, below the interline in 3–52%, and at the interline in 44–60% of feet. The origin of the anterior lateral malleolar artery is above the interline in 3–40%, below the interline in 52–60%, and at the interline in 31–65% of feet (Dubreuil-Chambardel 1925; Adachi et al. 1928). Adachi writes that the lateral artery is larger caliber than the medial artery in 69% of cases and of equal size in 24%.

Perforating or anterior branch of the peroneal artery

There is a variable irrigation pattern for this vessel. It becomes the dorsalis pedis in 3% of feet or continues as the lateral tarsal artery in 0.5% of feet (Huber 1941). Rarely, it may also terminate in conjunction with the anterior tibial artery to form the dorsalis pedis artery.

Plantar variants/plantar arterial network

Posterior tibial artery

Variations of this vessel at the level of the ankle are dependent on its bifurcation into medial and plantar arteries. The level of this bifurcation relative to the sustentacular tali is seen proximal to the posterior border of this ligament in 29–30% feet, distal in 4–9%, and directly under the ligament is most commonly seen in 61–67% (Adachi et al. 1928). An alternative description of this bifurcation takes into account the posterior tibial nerve neurovascular bundle. In the majority of cases (86.5%), the posterior tibial artery bifurcates distal to the division of the posterior tibial nerve. The division of the neurovascular bundle is congruent in 11.5% of cases and, very rarely, the artery will divide proximal to the nerve (Adachi et al. 1928).

Medial plantar artery

This vessel splits into a superficial branch and deep branch, which are the sources of the variants. The superficial branch divides again into a medial marginal plantar artery to the big toe, the superficial tibial plantar artery, and the common plantar digital artery. The latter may have a very separate and isolated origin to medial plantar artery (Adachi et al. 1928). The former typically continues on as the plantar hallucal artery (Poirer and Charpy 1902). Distally, the superficial arc is typically filiform or frail and is present in 5–30% of feet (Dubreuil-Chambardel 1925; Adachi et al. 1928). The deep or profunda branch divides again into two branches, tibial and lateral. Adachi notes that the profunda branch is seen to arise as a solitary artery in 63% of cases, shares a common trunk with the superficial tibial plantar artery in 28%, or is part of a trifurcation system consisting of the superficial tibial plantar artery, the common trunk to the plantar digital arteries, and the profunda trunk in 9%.

Lateral plantar artery

The most important contribution of this vessel is the formation of the deep plantar arch (Fig. 57.4). The deep transverse component of the lateral plantar artery unites with the deep plantar branch of the dorsalis pedis artery in variable locations to fashion the deep arch. Adachi documented seven types of arch based on the junction point, which is typically narrowed, between the lateral plantar supply and the dorsalis pedis supply.

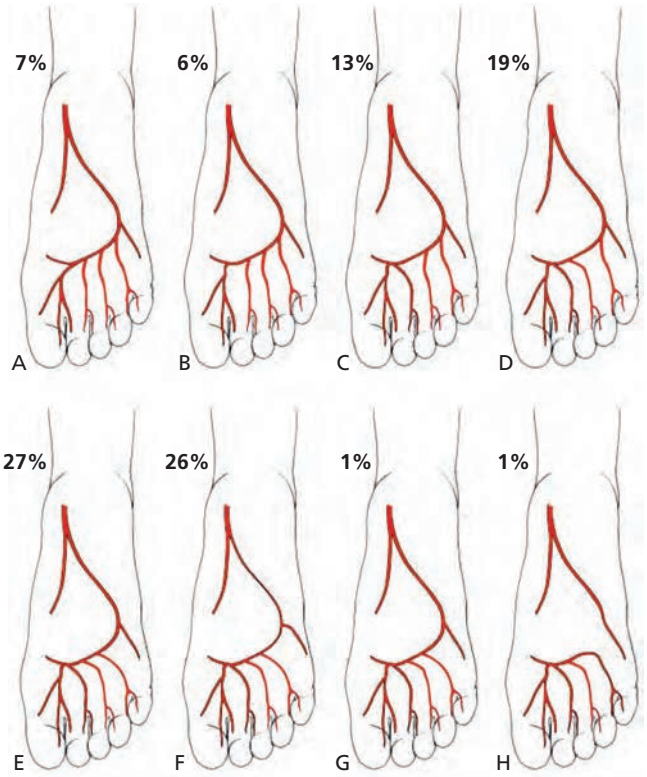

Figure 57.4 Plantar arch: (a) all plantar metatarsal and common digital arteries arise from the lateral plantar artery; (b) the first plantar metatarsal artery arises from the deep plantar branch; (c) the first and second plantar arteries arise from the deep plantar arch; (d) the first through third plantar metatarsal arteries arise from the deep plantar arch; (e) all plantar metatarsal arteries arise from the deep plantar branch; (f) the deep branch also reaches the lateral aspect of the foot; (g) an equally strong plantar arch is found in all areas; and (h) the plantar arch is not closed. Adapted from Lippert and Pabst (1985).

Type A arches are formed entirely by the dorsalis pedis, which supplies the plantar metatarsal arteries 1–4 as well as the fibular plantar marginal artery (25.3%). The type B arch possesses a junction point so that the dorsalis pedis supplies the metatarsal arteries but the lateral plantar artery supplies the fibular plantar marginal artery (32.3%). Moving more medially, type C arches have a junction point between the plantar metatarsal arteries 3 and 4 (14.6%). Type D arches have a junction point between the plantar metatarsal arteries 2 and 3 (14.6%). Type E arches have a junction point between the plantar metatarsal arteries 1 and 2 (6.1%). The type F arch is entirely irrigated by the lateral plantar artery (7%). Several other authors highlight the inconsistency of the junction point. In a study of 203 feet, Dubreuil-Chambardel (1925) noted a pure lateral plantar formation in 4% and a pure dorsalis pedis formation in 40.2%. In 66 feet, Manno (1905) noted a pure dorsalis pedis formation in 48.4% but no pure plantar supply. In a study involving 130 feet, Adachi et al. (1928) noted a type A rate of 25.3% and a type F rate of 7%. In a study of 361 feet, Vann (1943) reported a pure lateral plantar formation in 15.2% and a pure dorsalis pedis formation in 80.8%.

Plantar metatarsal arteries

These vessels may be missing or atretic. Adachi et al. (1928) reported the frequencies of absence of plantar metatarsals as: I: 2.3%; II: 2.3%; III: 0%; IV: 6.1%. From an examination of 40 feet, Murakami (1971) summarized the variant anatomy and developed the concept of superficial and deep plantar metatarsal and intermetatarsal arteries. The most commonly seen arteries are the superficial plantar metatarsal arteries: II, 85%; III, 82.5%; IV, 62.5%; and V, 80%. Deep plantar metatarsal arteries are encountered with the following frequencies: II, 22.5%; III, 30%; IV, 57.5%; and V, 37.5%. Superficial intermetatarsal arteries are encountered with the following frequencies: II, 32.5%; III, 25%; III, 22.5%. Deep intermetatarsal arteries are encountered with the following frequencies: II, 32.5%; III, 57.5%; and IV 67.5%. The lateral marginal plantar artery is often considered as part of this group of intermetatarsal vessels, but may originate from the lateral plantar artery. It is noted to be present in 22.5% of specimens (Pyka and Coventry 1961).

References

Adachi B, Hasebe K, Daigaku K, Igakubu. 1928. *Das Arteriensystem der Japaner*. Kyoto: Kaiserlich-Japanische Universität zu Kyoto.

Arnoczky SP. 1985. Blood supply to the anterior cruciate ligament and supporting structures. *Orthop Clin North Am* 16: 15–28.

Bardsley JL, Staple TW. 1970. Variations in branching of the popliteal artery. *Radiology* 94: 581–587.

Boltri F, Ardissone F, Barile C. 1979. Apropos of 2 unusual variations of origin and course of the deep femoral artery. *Minerva Chir* 34: 705–708.

Brick GW, Scott RD. 1989. Blood supply to the patella. Significance in total knee arthroplasty. *J Arthroplasty* 4: 75–79.

Ciftcioğlu E, Kale A, Kopuz C, Edizer M, Aydin E, Demir MT. 2009. Medial circumflex femoral artery with different origin and course: A case report and review of the literature. *Folia Morphol (Warsz)* 68: 188–191.

Colborn GL, Mattar SG, Taylor B, Skandalakis JE, Lumsden AB. 1995. The surgical anatomy of the deep femoral artery. *Am Surg* 61: 336–346.

Day CP, Orme R. 2006. Popliteal artery branching patterns: an angiographic study. *Clin Radiol* 61: 696–699.

Dias AD, Thatte RL, Patil UA, Dhami LD, Prasad S. 1987. The uses of the SEPA flap in the repair of defects in the hands and fingers. *Br J Plast Surg* 40: 348–359.

Dubreuil-Chambardel L. 1925. *Les Variations du Corps Humain*. Paris: E. Flammarion.

Edwards EA. 1960. Anatomy of the small arteries of the foot and toes. *Acta Anat (Basel)* 41: 81–96.

Emura S, Shoumura S, Ishizaki N, Yamahira T, Ito M, Chen HY, Isono H. 1989. The anatomical study on the branches of the femoral artery (II). Comparison with the findings of Adachi's classification. *Kaibogaku Zasshi* 64: 196–205.

Fathi M, Hatamipour E, Fathi HR, Abbasi A. 2008. The anatomy of superficial inferior epigastric artery flap. *Acta Cir Bras* 23: 429–434.

Gautier E, Ganz K, Krugel N, Gill T, Ganz R. 2000. Anatomy of the medial femoral circumflex artery and its surgical implications. *J Bone Joint Surg Br* 82: 679–683.

Ghassemi A, Furkert R, Prescher A, Riediger D, Knobe M, O'Dey D, Gerressen M. 2013. Variants of the supplying vessels of the vascularized iliac bone graft and their relationship to important surgical landmarks. *Clin Anat* 26: 509–521.

Gilbert A. 1976. Composite tissue transfers from the foot: Anatomic basis and surgical technique. In: Symposium on Microsurgery (eds DanillerAI, StrauchB). St Louis: CV Mosby.

Hannouche D, Duparc F, Beaufils P. 2006. The arterial vascularization of the lateral tibial condyle: Anatomy and surgical applications. *Surg Radiol Anat* 28: 38–45.

Hester TR Jr, Nahai F, Beegle PE, Bostwick J 3rd. 1984. Blood supply of the abdomen revisited, with emphasis on the superficial inferior epigastric artery. *Plast Reconstr Surg* 74: 657–670.

Hinenoya H, Kikuta A, Murakami T. 1987. Pedal arteries of monkeys, with special reference to the plantar metatarsal arteries. *Acta Med Okayama* 41: 267–274.

Horie M, Murakami T, Kikuta A. 1988. Deep plantar arteries of some mammals, with special reference to the plantar metatarsal arteries. *Acta Med Okayama* 42: 97–103.

Huber JF. 1941. The arterial network supplying the dorsum of the foot. *Anat Rec* 80: 373.

Hyrtl J. 1881. Lehrbuch der Anatomie des Menschen. Wien: Wilhelm Braumüller.

Jung W, Oh CS, Won HS, Chung IH. 2008. Unilateral arteria peronea magna associated with bilateral replaced dorsalis pedis arteries. *Surg Radiol Anat* 30: 449–452.

Keen JA. 1961. A study of the arterial variations in the limbs, with special reference to symmetry of vascular patterns. *Am J Anat* 108: 245–261.

Kil SW, Jung GS. 2009. Anatomical variations of the popliteal artery and its tibial branches: Analysis in 1242 extremities. *Cardiovasc Intervent Radiol* 32: 233–240.

Kim D, Orron DE, Skillman JJ. 1989. Surgical significance of popliteal arterial variants. A unified angiographic classification. *Ann Surg* 210: 776–781.

Kirschner MH, Menck J, Nerlich A, Walser R, Buhren V, Hofmann GO. 1997. The arterial blood supply of the human patella. Its clinical importance for the operating technique in vascularized knee joint transplantations. *Surg Radiol Anat* 19: 345–351.

Kirschner MH, Menck J, Hennerbichler A, Gaber O, Hofmann GO. 1998. Importance of arterial blood supply to the femur and tibia for transplantation of vascularized femoral diaphyses and knee joints. *World J Surg* 22: 845–851.

Kropman RH, Kiela G, Moll FL, de Vries JP. 2011. Variations in anatomy of the popliteal artery and its side branches. *Vasc Endovascular Surg* 45: 536–540.

La Falce OL, Ambrosio JD, Souza RR. 2006. The anatomy of the superficial external pudendal artery: A quantitative study. *Clinics (Sao Paulo)* 61: 441–444.

Leung PC, Wong WL. 1983. The vessels of the first metatarsal web space. An operative and radiographic study. *J Bone Joint Surg Am* 65: 235–238.

Lippert H, Pabst R. 1985. Arterial Variations in Man: Classification and Frequency. München: JF Bergman.

Manno A. 1905. Arteriae plantares pedis mammalium. *Int Monatsschr Anat Physiol* 22: 293–359.

Massoud TF, Fletcher EW. 1997. Anatomical variants of the profunda femoris artery: An angiographic study. *Surg Radiol Anat* 19: 99–103.

Mauro MA, Jaques PF, Moore M. 1988. The popliteal artery and its branches: Embryologic basis of normal and variant anatomy. *AJR Am J Roentgenol* 150: 435–437.

May JW Jr, Chait LA, Cohen BE, O'Brien BM. 1977. Free neurovascular flap from the first web of the foot in hand reconstruction. *J Hand Surg [Am]* 2: 387–393.

Menck J, Bertram C, Lierse W. 1992. Sectorial angioarchitecture of the human tibia. *Acta Anat (Basel)* 143: 67–73.

Morris GC Jr, Beall AC, Berry WB, Feste J, De Bakey ME. 1960. Anatomical studies of the distal popliteal artery and its branches. *Surg Forum* 10: 498–502.

Mulfinger GL, Trueta J. 1970. The blood supply of the talus. *J Bone Joint Surg Br* 52: 160–167.

Murakami T. 1971. On the position and course of the deep plantar arteries, with special reference to the so-called plantar metatarsal arteries. *Okajimas Folia Anat Jap* 48: 295–322.

Musgrove J. 1892. Bifurcation of the femoral artery with subsequent union. *J Anat Physiol* 26: 239–244.

Ozgur Z, Ucerler H, Aktan Ikiz ZA. 2009. Branching patterns of the popliteal artery and its clinical importance. *Surg Radiol Anat* 31: 357–362.

Paraskevas G, Papaziogas B, Gigis J, Mylonas A, Gigis P. 2004. The persistence of the sciatic artery. *Folia Morphol (Warsz)* 63: 515–518.

Patil UA, Dias AD, Thatte RL. 1987. The anatomical basis of the SEPA flap. *Br J Plast Surg* 40: 342–347.

Penteado CV. 1983. Venous drainage of the groin flap. *Plast Reconstr Surg* 71: 678–684.

Pirker E. 1970. Radiographic anatomy of the arterial variations in the lower extremity and their frequency. *Fortschr Geb Rontgenstr Nuklearmed* 112: 731–745.

Poirer P, Charpy A. 1902. Traite d'Anatomie Humaine. Paris: Masson.

Power JH. 1850. *Surgical Anatomy of the Arteries, and Descriptive Anatomy of the Heart by the late Valentine Flood, M.D*. Dublin: Fannin and Co.

Prakash, Kumari J, Kumar Bhardwaj A, Jose BA, Kumar Yadav S, Singh G. 2010. Variations in the origins of the profunda femoris, medial and lateral femoral circumflex arteries: A cadaver study in the Indian population. *Rom J Morphol Embryol* 51: 167–170.

Prayer L, Karnel F, Schurawitzki H. 1990. Angiographic demonstration of the branching of the popliteal artery in the arteries of the lower extremity: variations and frequency distribution. *Rontgenpraxis* 43: 100–103.

Pyka RA, Coventry MB. 1961. Avascular necrosis of the skin after operations on the foot. *J Bone Joint Surg Am* 43: 955–960.

Quain R. 1844. Anatomy of the arteries of the human body. London: Ramsay.

Reardon CM, O'Ceallaigh S, O'Sullivan ST. 2004. An anatomical study of the superficial inferior epigastric vessels in humans. *Br J Plast Surg* 57: 515–519.

Sanders RJ, Alston GK. 1986. Variations and anomalies of the popliteal and tibial arteries. *Am J Surg* 152: 531–534.

Scapinelli R. 1968. Studies on the vasculature of the human knee joint. *Acta Anat (Basel)* 70: 305–331.

Scapinelli R. 1997. Vascular anatomy of the human cruciate ligaments and surrounding structures. *Clin Anat* 10: 151–162.

Shim SS, Leung G. 1986. Blood supply of the knee joint. A microangiographic study in children and adults. Clin Orthop 119–125.

Simank HG, Graf J, Schneider U, Fromm B, Niethard FU. 1995. Demonstration of the blood supply of human cruciate ligaments using the plastination method. *Z Orthop Ihre Grenzgeb* 133: 39–42.

Sinna R, Hajji H, Qassemyar Q, Perignon D, Benhaim T, Havet E. 2010. Anatomical background of the perforator flap based on the deep branch of the superficial circumflex iliac artery (SCIP Flap): A cadaveric study. *Eplasty* 10: 11.

Stevenson TR, Hester TR, Duus EC, Dingman RO. 1984. The superficial inferior epigastric artery flap for coverage of hand and forearm defects. *Ann Plast Surg* 12: 333–339.

Suder E, Nizankowski C. 1985. Variations in the origin of the deep femoral arteries in human fetuses. *Folia Morphol (Warsz)* 44: 262–269.

Tanyeli E, Uzel M, Yildirim M, Celik HH. 2006. An anatomical study of the origins of the medial circumflex femoral artery in the Turkish population. *Folia Morphol (Warsz)* 65: 209–212.

Taylor GI, Daniel RK. 1975. The anatomy of several free flap donor sites. *Plast Reconstr Surg* 56: 243–253.

Thein T, Kreidler J, Stocker E, Herrmann M. 1997. Morphology and blood supply of the iliac crest applied to jaw reconstruction. *Surg Radiol Anat* 19: 217–225.

Thomson A. 1882. Origin of internal circumflex from the deep epigastric. *J Anat Physiol* 17: 379.

Uzel M, Tanyeli E, Yildirim M. 2008. An anatomical study of the origins of the lateral circumflex femoral artery in the Turkish population. *Folia Morphol (Warsz)* 67: 226–230.

Vann MH. 1943. A note on the formation of the plantar arterial arch of the human foot. *Anat Rec* 85: 269.

Yamamoto H, Jones DBJr, Moran SL, Bishop AT, Shin AY. 2010. The arterial anatomy of the medial femoral condyle and its clinical implications. *J Hand Surg Eur Vol* 35: 569–574.

Young AH.1879. Abnormal arrangement of the branches of the femoral artery. Note on the absence of the profunda femoris. *J Anat Physiol* 13: 154–156.

58 Arteries of the spinal cord

Marius C. Bosman and Albert van Schoor
University of Pretoria, Pretoria, South Africa

Because of the clinical importance, the arterial blood supply to the spinal cord has been exhaustively examined and discussed via cadaver-based, angiographic, and advanced imaging studies (Romanes 1965; Lazorthes et al. 1971; Dommisse 1973; Rodriguez-Baeza et al. 1989; Gövsa et al. 1996; Koshino et al. 1999; Biglioli et al. 2000; Lo et al. 2002; Kudo et al. 2003; Yoshioka et al. 2003; Kawaharada et al. 2004; Nijenhuis et al. 2007; Backes et al. 2008; Melissano & Chiesa 2009; Melissano et al. 2009; Soubeyrand et al. 2011; Gao et al. 2013).

The scientific literature and anatomical writings all come to the same basic conclusions regarding the blood supply to the spinal cord. The spinal cord is completely dependent upon three segmented longitudinal arterial trunks – one anterior longitudinal and two posterior longitudinal arterial trunks – that extend from the medulla oblongata to the conus medullaris and is linked by a sacral anastomosis (Lazorthes et al. 1971; Dommisse et al. 1973; Boll et al. 2006). These are the single anterior and two posterior spinal arteries, respectively.

The anterior spinal artery is formed by the fusion of the two branches from the vertebral arteries and is situated over the ventral median fissure of the spinal cord (Fig. 58.1). It has been shown to be structurally continuous with multiple large anterior radicular arteries that join and support it along its course (these are also known as the anterior radiculomedullary arteries) (Morishita et al. 2003). Several studies have shown an uninterrupted course of the anterior spinal artery along the entire ventral length of the spinal cord, up to the cauda equina (Romanes 1965; Dommisse 1973; Carmichael & Gloviczki 1999; Biglioli et al. 2000; Kudo et al. 2003; Morishita et al. 2003). However, there is significant narrowing at intervals throughout its course, making the blood supply to the spinal cord segmental and dependent on the support from anterior radiculomedullary arteries taking blood from segmental spinal arteries to the anterior spinal artery (Romanes 1965; Lazorthes et al. 1971; Turnbull 1972; Dommisse 1973; Biglioli et al. 2000; Morishita et al. 2003; Gao et al. 2013).

The posterior spinal arteries are situated on the posterolateral aspect of the spinal cord, at the base of the dorsal nerve roots. They have been shown to either originate from the posterior inferior cerebellar arteries or directly from the vertebral arteries, prior to the latter uniting to form the basilar artery (Stopford 1916).

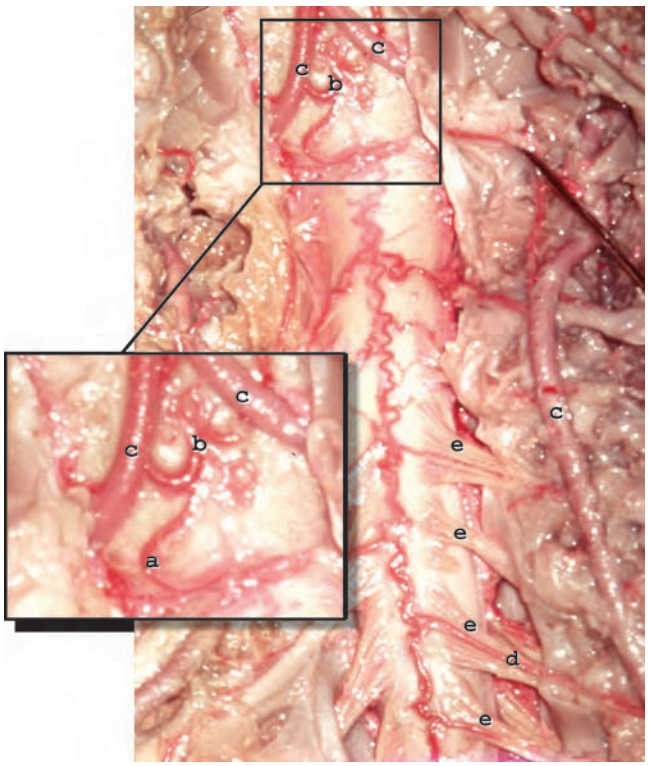

Figure 58.1 Anterior spinal artery (a) found on ventral surface of spinal cord and formed, in this case, from a transverse intervertebral anastomosis with a single root (b). This variation occurs in 0.75% cases and forms between the two vertebral arteries (c). A large anterior radiculomedullary artery (d) can be seen coursing on the ventral roots (e) to join the anterior spinal artery.

Source: Dommisse (1973). Reproduced with permission from Department of Anatomy, University of Pretoria.

Each of the three longitudinal trunks gives rise to transverse pial branches which may form arterial anastomoses between the spinal arteries and from which perforating branches enter and

Bergman's Comprehensive Encyclopedia of Human Anatomic Variation, First Edition. Edited by R. Shane Tubbs, Mohammadali M. Shoja and Marios Loukas.
© 2016 John Wiley & Sons, Inc. Published 2016 by John Wiley & Sons, Inc.

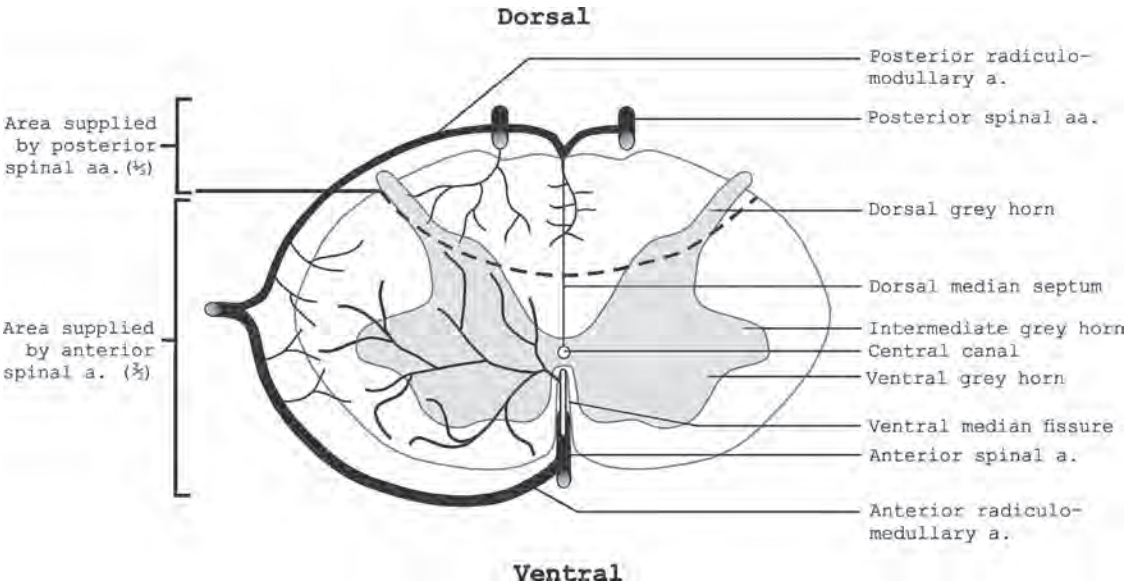

Figure 58.2 Segmental arterial supply of the spinal cord illustrating the areas of supply of the anterior and posterior spinal arteries.

Source: Bosman (2008). Reproduced with permission from Department of Anatomy, University of Pretoria.

supply the spinal cord. Additionally, the anterior spinal artery gives off branches that enter the ventral median fissure to supply the central regions of the spinal cord (Romanes 1965). The anterior radicular/radiculomedullary arteries also give off branches that supply the peripheral spinal cord. Another longitudinal trunk is associated with the most rostral extent of the posterolateral arterial axis of the spinal cord: the lateral spinal arteries found anterior to the dorsal nerve roots (Lasjaunias et al. 1985; Siclari et al. 2007; Morigaki et al. 2012).

On a cross-section through the spinal cord, the anterior spinal artery supplies two-thirds of the spinal cord while the posterior spinal arteries are only responsible for one-third and supply the dorsal white columns and dorsal gray horn. The ventral median fissure allows the branches of the anterior spinal artery to reach much deeper levels of the cord and is responsible for the lateral and ventral white columns, as well as the majority of the gray matter (Fig. 58.2) (Bosman 2008).

The arterial supply of the spinal cord can therefore be divided into a ventral and dorsal component. The ventral component includes the anterior spinal artery, anterior radicular/radiculomedullary arteries, anterior perforating vessels of the ventral median fissure, and the perforating pial vessels. Similarly, the dorsal component of supply consists of the two posterolaterally situated posterior spinal arteries, posterior radicular/radiculomedullary arteries, and perforating pial vessels. Anastomoses between the anterior and posterior components are minimal. Some links in the cervical and lumbar regions have been reported; however, an absence of arterial communications in the thoracic region has been previously described (Suh & Alexander 1939; Turnbull et al. 1966; Lazorthes et al. 1971; Turnbull 1971; Dommisse 1973). A pronounced communication does exist at the distal end of the cord where arterial circles cross the lateral surface of the conus medullaris, forming a "cruciate anastomosis" between the anterior and posterior arterial trunks (Fig. 58.3) (Dommisse 1973).

Throughout their course down the spinal cord, the spinal arteries are serially reinforced by large anterior and/or posterior radicular arteries that branch from segmental spinal branches, originating from vertebral, deep cervical, intercostal, lumbar, iliolumbar, and lateral sacral arteries. These segmental spinal arteries enter the vertebral canal through the intervertebral foramina and travel along the ventral and dorsal roots as the anterior and posterior radicular arteries. Some of these radicular arteries continue and join the anterior and/or posterior spinal arteries, providing a further source of blood supply to the spinal cord; these are known as radiculomedullary arteries. During fetal development, the anterior and posterior radicular branches of the segmental spinal arteries connect with, and support, the longitudinal channels at right angles. Due to the differential growth between the spinal cord and the vertebral column, the relationship between segmental and longitudinal blood vessels changes. The vertebral column extends more rapidly in a caudal direction when compared to the spinal cord, displacing the origin of the arteries in that direction. While this differential growth is taking place, the size of radicular arteries diminish to where most radicular arteries only provide blood supply to the nerve root itself. The number of large radicular arteries decreases to the point that, in the adult, only about 6–8 radicular arteries make functional connections with the anterior spinal artery and 10–23 supply the posterior spinal arteries (Carmichael & Gloviczki 1999). The 31 pairs of segmental spinal

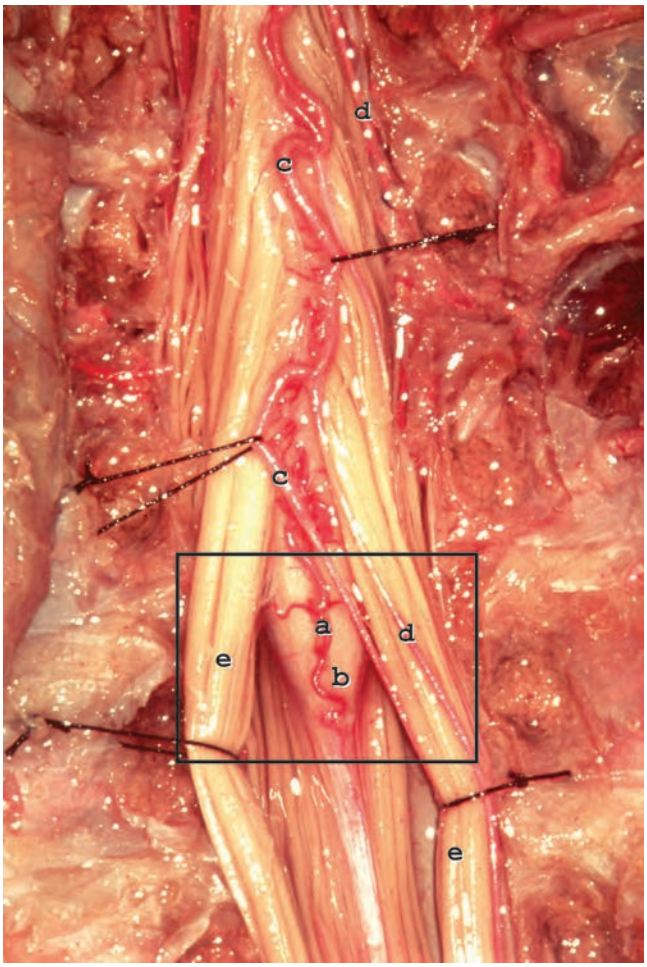

Figure 58.3 The "cruciate anastomosis" (a) around the conus medullaris (b), connecting the anterior spinal artery (c) with the two posterior spinal arteries (not shown here). Also visible is large radiculomedullary arteries (d) and the sacral nerve roots (e).

Source: Dommisse (1973). Reproduced with permission from Department of Anatomy, University of Pretoria.

arteries which enter the vertebral canal through the intervertebral foramina can therefore be classified into three types:

1. proper radicular branches (anterior and posterior radicular arteries), which end within the roots or on the dura mater before reaching the spinal cord;
2. pia mater radicular branches, which do not penetrate beyond the arterial systems surrounding the spinal cord; and
3. radiculomedullary arteries, which are the only arteries that truly vascularize the spinal cord by joining and supporting the three longitudinal vascular channels as well as providing blood supply to the ventral and dorsal roots.

Examination of these radiculomedullary arteries has shown that their distribution is more or less fixed with three clearly distinguishable spinal cord segments: the superior or cervicothoracic segment, the intermediate or midthoracic segment, and the inferior or thoracolumbar segment (Lazorthes et al. 1971).

Arterial supply to the cervicothoracic segment

The cervical and upper two thoracic segments of the spinal cord receive a rich blood supply from branches of the subclavian and superior intercostal arteries. Of these, the most important are the vertebral arteries which branch from the subclavian arteries. The superior cervical segments is supplied by the anterior spinal artery originating and descending from the intracranial vertebral artery, which rarely descends past the C4 segment (Lazorthes et al. 1971). The anterior spinal artery is commonly formed rostrally from the junction of the two spinal branches, each originating from one vertebral artery. This usually occurs intracranially or near the midline on the anterior aspect of the medulla oblongata, at the level of the olive (Tveten 1976; Rodriguez-Baeza et al. 1989; Gövsa et al. 1996). In 66.25% of cases the two spinal branches joined at the junction between the medulla oblongata and spinal cord, while in 12.5% of cases it extended up to levels C2 and C3 of the cervical spinal cord before joining. In two cases (2.5%), the two spinal arteries did not fuse and remained duplicated (Gövsa et al. 1996). The anterior spinal artery has also previously been reported as being duplicated in the cervical segment of the spinal cord (Brugieries et al. 1990). Considering that the anterior spinal artery begins as segmented pairs of arteries and, because it is derived from a pair of longitudinal channels, it is not surprising that at least a portion of the artery is frequently doubled (Carmichael & Gloviczki 1999).

Occasionally, one of the paired vertebral branches is much smaller or even absent, and at other times two or more very slender spinal vessels may branch from one of the vertebral arteries to unite with a large branch coming from the other side (Stopford 1916; Lasjaunias et al. 1985). In a study of 80 human cadaver brains, the anterior spinal artery pattern was classified into three types:

- Type I (75% of cases) is characterized by the presence of a left and right spinal branch originating from the vertebral arteries. These were further subdivided into Type Ia (or "balanced") where the two spinal branches were basically of equal diameter (43.5% of cases), Type Ib (or "right dominant") where the diameter of the right spinal branch were significantly larger than the left (17.5% of cases), and Type Ic (or "left dominant") where the opposite is true (15% of cases) (Fig. 58.4a–c) (Gövsa et al. 1996). Another study reported that the right dominant pattern was more frequent (32.2% of cases) as opposed to a "balanced" type (22.6%) or left-dominant pattern (22.6%) (Rodriguez-Baeza et al. 1989), while Lanz and Wachmuth (1979) stated that the frequency for left or right dominance was equal (10%). Other studies reported the presence of Gövsa and co-workers' Type I classification in 85% (Stopford 1916), 54.6% (Miyadi-Tosihiko 1931), and 77.4% of cases (Rodriguez-Baeza et al. 1989).
- Type II is characterized by the presence of only one spinal branch, which either originates from the right vertebral artery (8.8% of cases) or the left vertebral artery (0.25% of

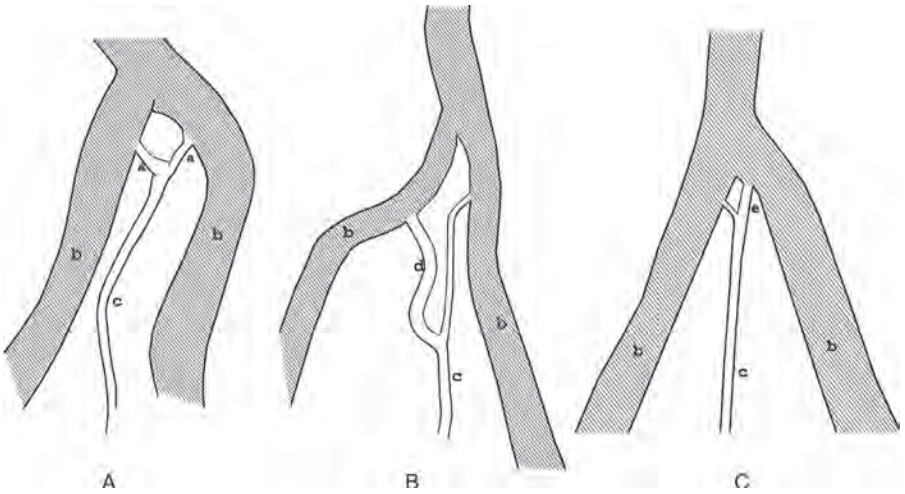

Figure 58.4 (a) Balanced type (43.5%): both anterior spinal branches (a) are of equal caliber. Vertebral arteries (b); anterior spinal artery (c). (b) Right-dominated type (17.5%): the right anterior spinal branch's (d) caliber is wider than the left. (c) Left-dominated type (15%): left anterior spinal branch (e) is the widest. Adapted from Gövsa et al. (1996).

cases) (Fig. 58.5a, b). A unilateral origin of the anterior spinal artery was also previously reported in 9.7% of cases (Rodriguez-Baeza et al. 1989). A single instance was observed where the two spinal branches formed a duplicate anterior spinal artery without any visible connections in the cervical area (Fig. 58.6) (Gövsa et al. 1996).

- Type III is characterized by the origin of the anterior spinal artery from a transverse intervertebral anastomosis with a single (0.75% of cases) (Fig. 58.7) or double root (0.6% of cases) (see Fig. 58.1) (Gövsa et al. 1996). This type was much more common in another study on 31 human cadavers, where it was reportedly seen in 12.9% of cases (Rodriguez-Baeza et al. 1989).

Stopford (1916) found the anterior spinal artery to originate solely from the right vertebral artery, without the contribution from a left spinal branch in 3% of cases. The inverse was seen in 9% of cases. The anterior spinal artery arose from a single spinal branch that originated at the angle formed by the junction of the two vertebral arteries in 3% of cases. The pattern of origin that coincided with the Type Ia or "balanced" classification (as discussed by Gövsa et al. 1996) was found in only 11% of the cases. In the rest of the sample, a right-sided dominance (Type Ib) existed in 43% and a left-sided dominance (Type Ic) was the most common, with 46% of cases. In two instances, the left spinal branch had a double origin, while only one such case was

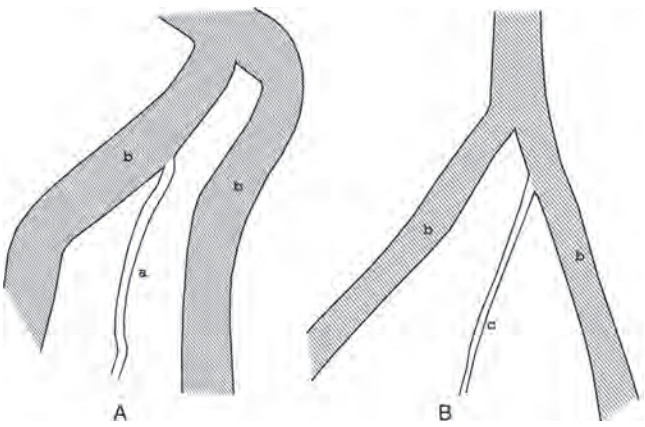

Figure 58.5 (a) A single anterior spinal artery (a) originating from the right vertebral artery (b). (B) A single anterior spinal artery (c) originating from the left side. Adapted from Gövsa et al. (1996).

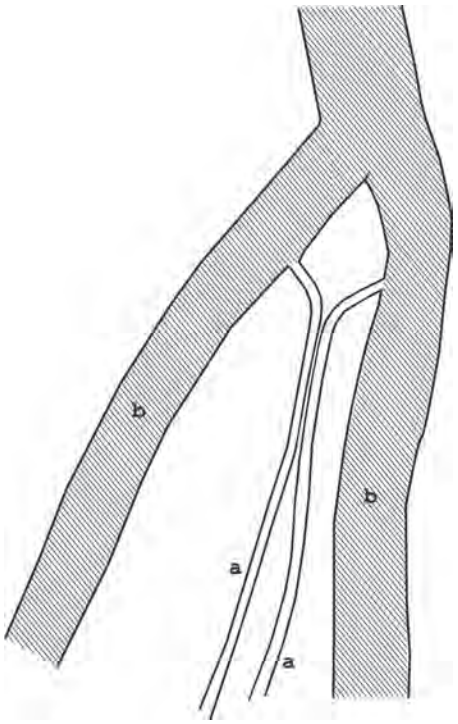

Figure 58.6 Duplicate anterior spinal arteries (a) originating from the vertebral arteries (b). Adapted from Gövsa et al. (1996).

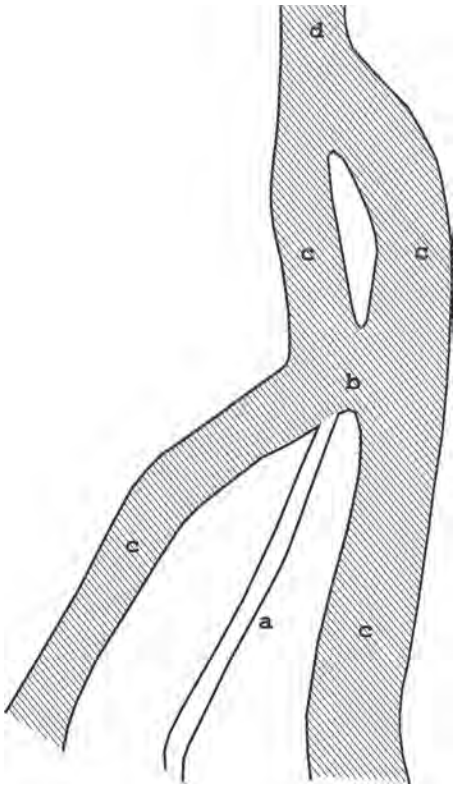

Figure 58.7 A single anterior spinal artery (a) branching from an intervertebral anastomosis (b). Also visible are the vertebral arteries (c) and basilar artery (d). Adapted from Gövsa et al. (1996).

found on the right side. The origin of the right spinal branch was from the extreme upper part of the vertebral artery (i.e., in the region of the cephalic extremity of the olivary eminence) in 51% of cases. In 29% the origin was in the mid-olivary region and in 20% it was at the level of the caudal extremity of, or slightly below, the olive. The frequency of origin of the left spinal branch from the three abovementioned levels on the vertebral artery was 59%, 28%, and 13% respectively. Failure of the left and right spinal branches to join results in two anterior spinal arteries on the ventral surface of the spinal cord, and this was seen in 6% of cases. The two trunks will frequently have communications between them. This was found to be most often at the normal level of junction between the two spinal branches. Some variation in the arterial pattern of the cervical anterior spinal artery has been described, and is best described by Figure 58.8.

Bulbar branches of the anterior spinal artery

There are three sets of the bulbar branches that were described by Stopford (1916). These are:

1. A set of branches arising from the right and left spinal branches before fusing. These form a fine network on the upper part of the pyramids where their terminal filaments end. A few filaments penetrate the upper part of the ventral median fissure.
2. Branches that originate directly from the anterior spinal artery (or arteries in the case of duplication) and pass directly into the ventral median fissure.
3. Branches that also originate from the anterior spinal artery (or arteries) but pass laterally on the pyramids, similar to the pontine branches of the basilar artery.

After repeated division, these branches penetrate the pyramids or the ventrolateral sulcus. When the branch of origin of one side is absent, its bulbar supply is invariably taken over by the ipsilateral vertebral artery (Stopford 1916).

The middle cervicothoracic segment is supported by radiculomedullary arteries from the vertebral artery (running within the transverse foramina of the cervical vertebrae), while the lower cervicothoracic segment is supplied by a branch of the costocervical trunk (Lazorthes et al. 1971). A very small amount of blood entering the spinal arteries at the cervical level actually reaches the lower thoracic or lumbar segments of the spinal cord. The arterial supply of the spinal cord from the midthoracic segments caudally relies heavily on support from radiculomedullary arteries (Turnbull 1972).

In a study by Dommisse (1973), the number of anterior radiculomedullary arteries supplementing the anterior spinal artery was counted on 35 dissected cadavers. It was found that they were concentrated between C4 and C7, and the average number of arteries in the sample were 3.4 with a right-sided preponderance of 5: 4 and an average diameter of 0.31 mm. In studies as far back as the late nineteenth century, Adamkiewicz (1881) and Kadyi (1889) examined the presence of anterior radiculomedullary arteries in the cervical segment of the spinal cord. They reported that there are usually three (at C4, C5, and C8) and two (between C4 and C7, but most commonly at C5 and C6), respectively. Neither of the latter two authors specified whether these anterior radiculomedullary arteries were predominantly found on the left or right sides of the body. Table 58.1 is a summary of the number and position of anterior radiculomedullary arteries reported in the literature.

The posterior longitudinal arterial trunks remain duplicated as the pair of posterior spinal arteries. These can be found throughout embryological development, along the origins of the dorsal nerve roots. The presence of a median dorsal artery is mentioned (Carmichael & Gloviczki 1999), but no record of this variation was been found.

The posterior spinal arteries originate from the posterior inferior cerebellar arteries in 73% of cases. In 20% it originates from the right vertebral artery before the latter unites with the left vertebral artery to form the basilar artery. In 18% of cases it originates from the left vertebral artery only. The right posterior spinal artery had a double origin, from both the posterior inferior cerebellar artery and the vertebral artery in 9% of cases, while it had a similar double origin in 7% of cases on the left (Stopford 1916). It was seen in dissections of 35 spinal cords that the posterior spinal arteries were continuous in their course from its origin at the medulla oblongata to the conus medullaris. They lie in relation to the posterior nerve roots, frequently

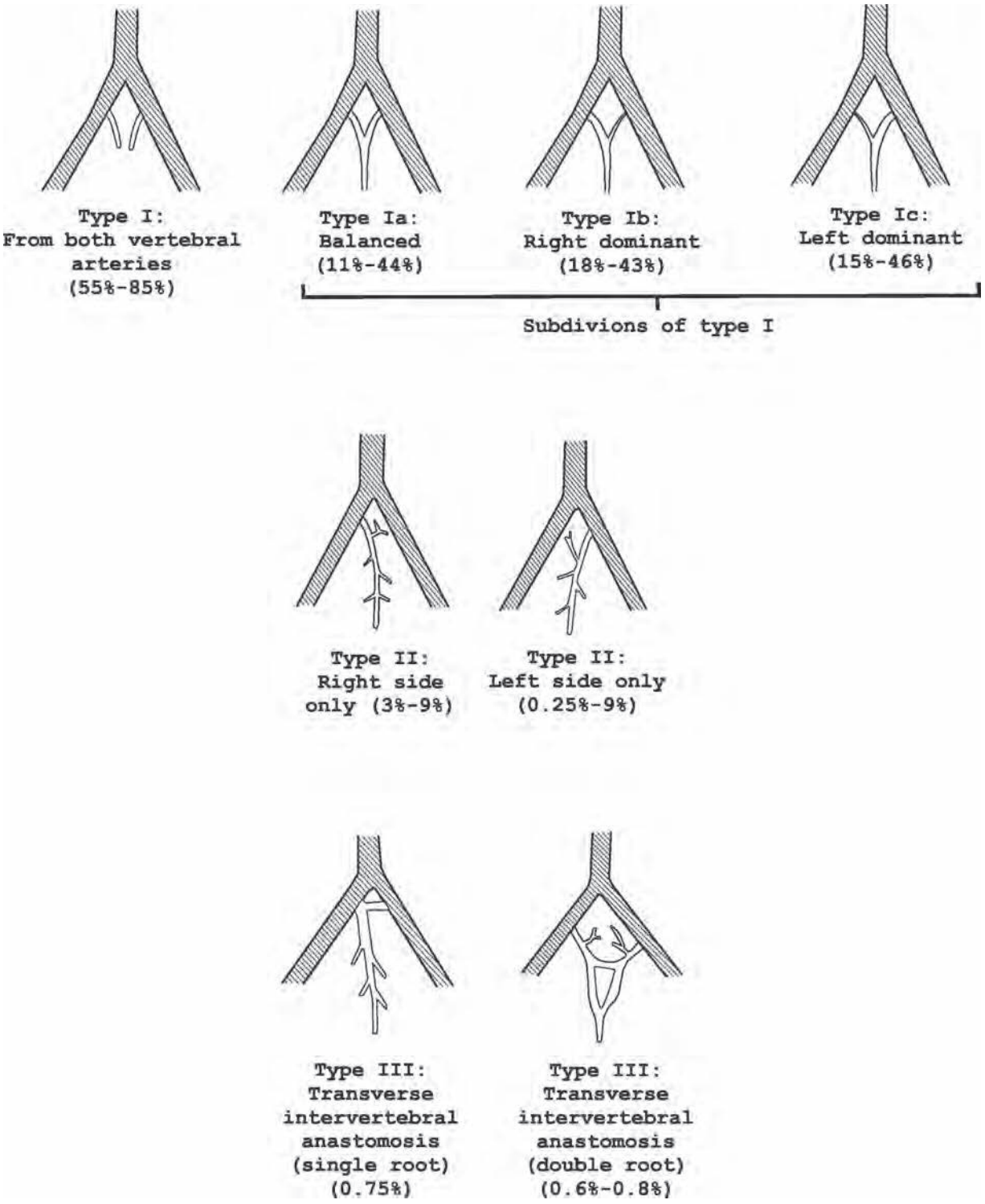

A

Figure 58.8 (a) Variations in the origin pattern of the anterior spinal artery.

(continued)

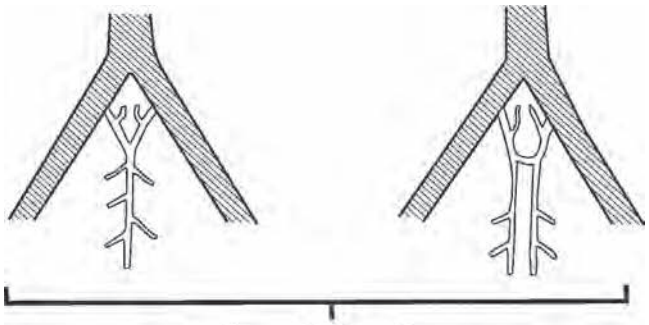

Normal level:
Lower end of
the olive
(73%)

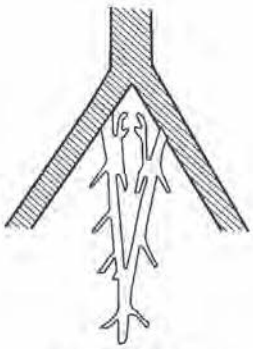

Low level:
At or below junction
between medulla oblongata
and spinal cord
(31%)

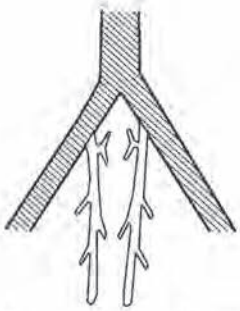

No communication:
Anterior spinal arteries
remain duplicated
(2.5-6%)

B

Figure 58.8 *(continued)* (b) Variations of the level of origin and/or connections of the anterior spinal artery.

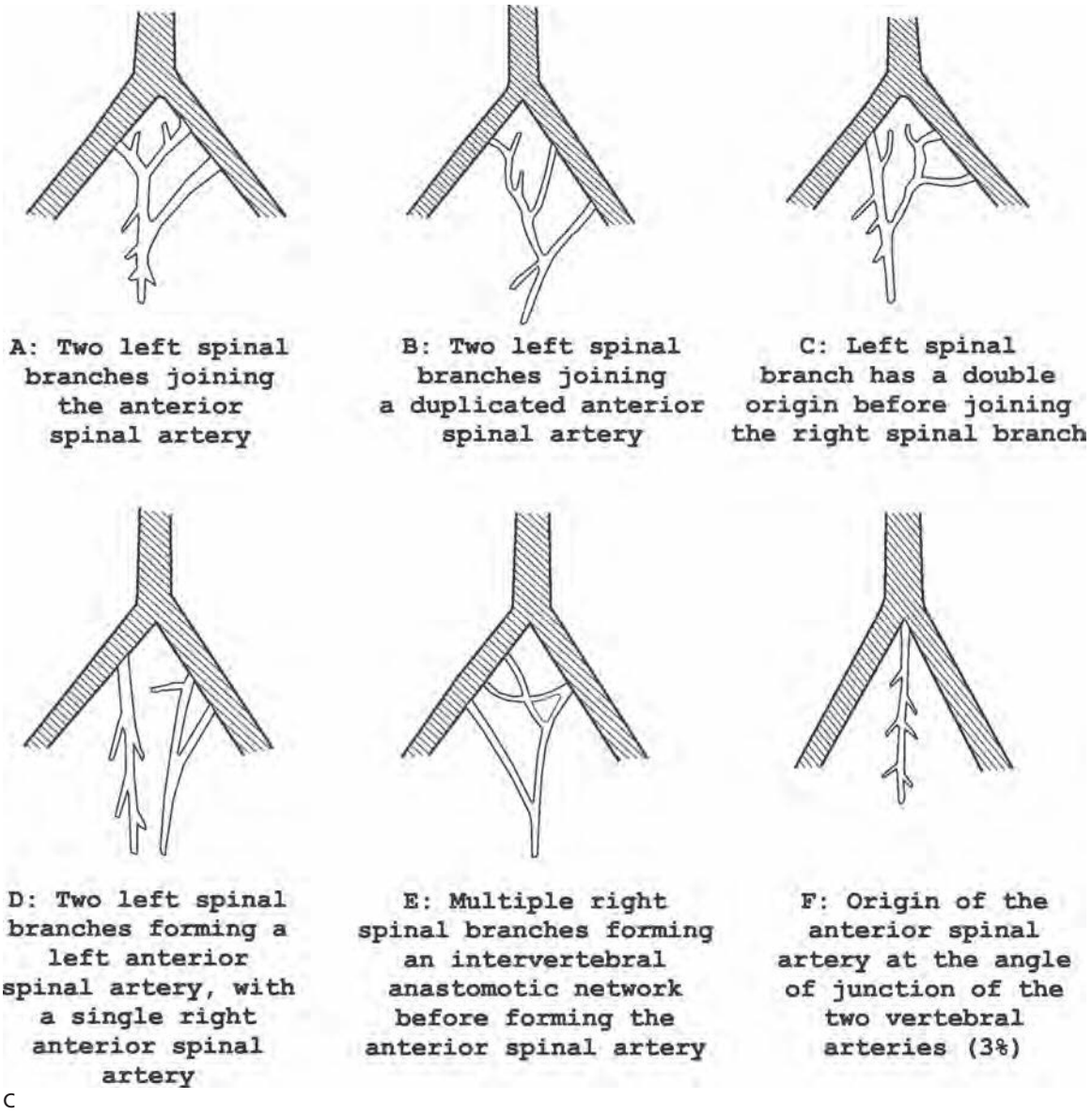

Figure 58.8 *(continued)* (c) Other reported variations of the anterior spinal artery in the cervical region. Adapted from Stopford (1916).

divide and deviate in their course, and many communications exist between the left and right artery at various levels along the spinal cord (Dommisse 1973). The vessel was found to be absent on one or both sides in a large percentage of cases, but because of difficulty retaining this vessel during dissection, it was impossible to provide reliable figures (Stopford 1916).

Dommisse (1973) examined the number of posterior radiculomedullary arteries in the cervicothoracic region and found that they were equal for both sides; the majority (16 of the 18 individuals) were found at level C6, 9 at levels C5 and T1 and 8 at level C6, with an average number of 2.8 arteries supporting the posterior spinal arteries. This corresponded to what had been reported prior to Dommisse's work (Table 1). During examination of the source of the posterior radiculomedullary arteries, he found that the majority of those that joined the posterior spinal arteries arose from the vertebral arteries. The exception was in the area of the thoracic inlet (levels C8 and T1), where the majority of posterior radiculomedullary arteries originated from branches of the costocervical trunk.

The source of the cervical anterior and posterior radiculomedullary arteries in Dommisse's sample can be summarized as follows. The vertebral artery supplied 77% of the anterior and 51% of the posterior radiculomedullary arteries. The

Table 58.1 Number and position of anterior radicular arteries in the cervical segment of the spinal cord.

References	Anterior radicular arteries	Posterior radicular arteries
Adamkiewicz 1881	Usually 3 (C3, C4, and C8)	1 or 2 (C6 or C7)
Kadyi 1889	Usually 2 (between C4 and C7, usually at C5 or C6)	1 or 2 (between C4 and C7)
Bolton 1939	Not reported	1 major, at C4
Suh and Alexander 1939	1–2 in lower and 1 in upper cervical region (between C3 and C6)	Not reported
Zülch 1954	1 or 2, usually at C6 or C7	Not reported
Woollam and Millen 1958	1 major (C6 or C7) and 3–5 minor (above C6)	1 at C2, 1–3 between C5 and C7
Gillilan 1958	At least 2; a major one at C5 or C6, and one at C3	Not reported
Perese and Fracasso 1959	1–5 (usually between C3 and C7)	Not reported
Chakrovorty 1971	2 or 3 (usually between C4 and C5), rarely at C8	1 or 2 (between C2 and C6, usually at C4)
Lazorthers et al. 1971	2–3 in the mid-cervical segment (levels not specified) and 1 in the lower segment	Not reported
Dommisse 1973	On average 3 (between C4 and C7)	On average between 2 and 3 (between C4 and T1)

Source: Dommisse (1973). Reproduced with permission from Department of Anatomy, University of Pretoria.

costocervical trunk and its two principle divisions supplied 20% of the anterior and 37% of the posterior radiculomedullary arteries. In the area of the thoracic inlet the costocervical trunk and proximal intercostal arteries provided 86% of the posterior radiculomedullary arteries joining the two posterior spinal arteries (Dommisse 1973).

A case was reported where the anterior spinal artery was not continuous, but was interrupted for a few millimeters between levels C6 and C7. Closer inspection revealed an adequate alternative blood supply to the region by four medium-sized (diameter 0.4–0.7 mm) tributaries between levels C5 and C7 (Romanes 1964).

Arterial supply to the midthoracic segment

The midthoracic segment corresponds approximately to vertebral levels T4–T8. Its vascularization is generally less abundant than the cervicothoracic and thoracolumbar regions and often comes from a single main source artery situated approximately at the level of T7 (Fig. 58.9; Lazorthes et al. 1971; Dommisse 1973).

When compared with the cervicothoracic segment, the latter has a ratio of 3:2 more radiculomedullary arteries supporting the longitudinal trunks (although this is mostly blood vessels joining the posterior spinal arteries). The average number of anterior radiculomedullary arteries for the 35 cadavers were only 2.3, while the average diameter was much less, an average of only 0.29 mm for a neonatal and 0.39 mm for an adult cadaver sample. There is also a predisposition for these arteries to the left side with a 4:1 ratio. Although more numerous than their anterior counterparts, with an average number of posterior radiculomedullary arteries of 5.3 arteries on levels T2–T9, the posterior arteries have a much lower average diameter of

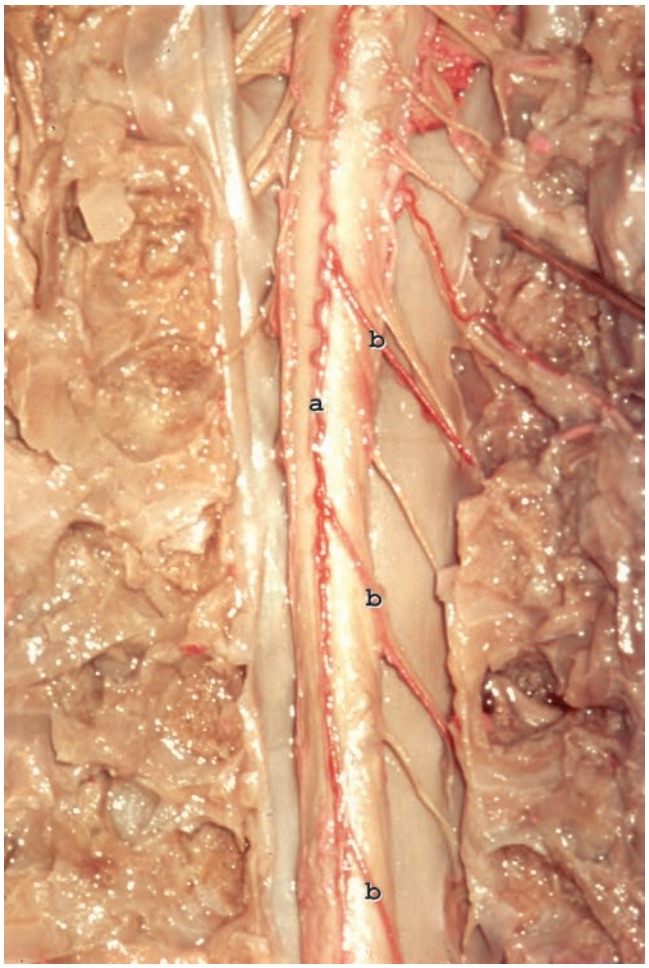

Figure 58.9 Anterior spinal artery (a) in the thoracic region and supplied by several small anterior radiculomedullary arteries (b). Source: Dommisse (1973). Reproduced with permission from Department of Anatomy, University of Pretoria.

only 0.15 mm. This is in contrast with the cervicothoracic and thoracolumbar segments of the spinal cord where the anterior spinal artery is, on average, fed by more anterior radiculomedullary arteries than its posterior counterparts (Dommisse 1973).

Highly selective angiography of the spinal cord of nine patients revealed extreme narrowing of the anterior spinal artery in the midthoracic segment of the spinal cord; in some cases, it even appeared to be interrupted (Gao et al. 2013). This coincides with what Dommisse (1973) found in 35 cadavers. He described the anterior spinal artery to be narrowest over a total of four to five spinal segments centered upon level T6, whereas Romanes (1965) stated that the smallest diameter (0.2 mm or less) of the artery was from levels T6 to T8 or even T10.

Similar to its anterior counterpart, the diameters of the posterior spinal arteries are the narrowest at the midthoracic segment, levels T2–T6 (down to 0.1 mm), and the widest at the lumbar enlargement (up to 1.2 mm) (Romanes 1965).

Arterial supply of the thoracolumbar segment

The thoracolumbar segment includes the last three or four thoracic segments of the spinal cord and the lumbar enlargement. Like the cervicothoracic segment, the thoracolumbar segment has a rich blood supply which has a few large radiculomedullary arteries supporting the distal anterior and posterior spinal arteries. A study of the anterior and posterior radiculomedullary arteries at this level revealed that the average number of arteries joining anterior and posterior longitudinal trunks was 2.3 and 2.1, respectively. These arteries also had a much larger diameter on average when comparing it to the midthoracic segment. The average diameter of the anterior radiculomedullary arteries were 0.3 mm: 0.25 mm in a neonatal sample and almost twice as much (0.44 mm) in an adult sample. The posterior radiculomedullary arteries were significantly smaller with an average diameter of only 0.15 mm (Dommisse 1973).

The rich vascularization of the thoracolumbar segment generally depends on a single large artery coming from one of the last posterior intercostal arteries or one of the first lumbar arteries. As early as 1882, this artery was described under the name of "magnus ramus radicularis anterior" (great anterior radicular artery; Adamkiewicz 1882). It is considered that this artery provides the main blood supply to the lumbar enlargement and is characterized by its large size, the "hairpin" bend it makes before joining the anterior spinal artery, and the significant enlargement of the anterior spinal artery below the point where the great anterior radicular artery joins the anterior spinal artery. It is even considered by some that the anterior spinal artery below the junction with the great anterior radicular artery is actually the descending branch of the latter. Another name for this artery is "arteria intumeseentia lumbalis" (artery of the lumbar enlargement; Lazorthes et al. 1958, 1971). The previous authors felt that the name was preferable because of its importance and fixity of its area of supply (the lumbar enlargement). A study of the different arrangements of this artery that may be encountered showed that it varied according to the artery's superior, middle, or inferior origin.

This artery is generally found in the vertebral canal between the levels of T9 and T12 in 75% and at levels L1 or L2 in 10% of cases. It can sometimes be found at higher levels, between levels T5 and T8 (15% of cases), although these vessels are more likely associated with supply to the midthoracic segment of the spinal cord, especially if a similar artery is present more distally. With the latter arrangement, a supplementary artery was observed below the "artery of the lumbar enlargement;" this was termed the "arteria conus medullaris" (artery of the conus medullaris; Lazorthes et al. 1971). The latter coincides with a report of two confirmed cases of a large radiculomedullary artery originating from level L4 (Lo et al. 2002). The authors stated that this had never before been reported, although this is contradicted by several studies where a low lumbar origin of the great anterior radicular artery was described (Suh & Alexander 1939; Romanes 1965; Dommisse 1973; Biglioli et al. 2000, 2004; Morishita et al. 2003). Regardless of its name, many studies have examined the great anterior radicular artery. These studies looked at level and artery of origin, course, and diameter (Table 58.2).

Using magnetic resonance angiography, the anterior spinal artery at the junction with the great anterior radicular artery was detected and classified into Type A (non-continuation of the anterior spinal artery above the junction of the great anterior radicular artery), Type B (continuation of the anterior spinal artery above and below the junction), or Type C (non-continuation of the anterior spinal artery below the junction). In their study the authors claim that the anterior spinal artery could be classified as Type A in 55% of cases, Type B in 20%, and Type C in 3% (Kawaharada et al. 2004). Possible difficulties in detecting the anterior spinal artery at its narrowest points, using imaging modalities such as magnetic resonance angiography, cannot be overlooked as several previous anatomical studies have demonstrated the continuation of the anterior spinal cord, with significant segmental narrowing, along its course (Romanes 1965; Dommisse 1973; Carmichael & Gloviczki 1999; Biglioli et al. 2000; Kudo et al. 2003; Morishita et al. 2003).

A statistically significant difference exists between the diameters of the anterior spinal artery above and below the junction with the great anterior radicular artery. It was found to be 0.5 mm and could be up to 1.2 mm, respectively (Romanes 1965; Biglioli et al. 2000; Morishita et al. 2003). However, in a sample of 55 dissected spinal cords, there were three cases where the diameter of the anterior spinal artery was significantly larger above the junction with the great

Table 58.2 Summary of studies that investigates the great anterior radicular artery. Adapted from Dommisse (1973).

Author(s)	Sample	Range of origin	Most common level of origin	On left side (%)	Diameter (mm)
Suh and Alexander 1939		T8–L4	–	–	–
Lazorthes et al. 1964		T5–L2	T5–T8, 15%; T9–T12, 75%; L1–L2, 10%	–	–
Romanes 1965	22 cadavers	T6–L3	T6, 5%; T7–T8, 18%; T9–T11, 59%; T12–L1, 14%; L2–L3, 5%	68	0.2–1.2
Djindjian and Faure 1967		T5–L2	T5–T8, 15%; T9–T12, 75%; L1–L2, 10%	–	–
Dommisse 1973	35 cadavers	T7–L4	T5–T6, 7%; T7–T8, 15%; T9–T11, 50%; T12–L1, 9%; L2–L4, 13%; L5–S5, 7%	77	0.45–0.8
Rodriguez-Baeza et al. 1991	30 cadavers	T8–L2	T8, 7%; T9–T11, 63%; T12–L1, 17%; L2, 13%	80	0.6–1.2
Alleyne et al. 1998	9 cadavers	T9–L1	T9–T11, 71%; T12–L1, 29%	78	0.7–1.2
Koshino et al. 1999	102 cadavers	T5–L1	T5–T6, 3%; T7–T8, 8%; T9–T11, 67%; T12–L1, 19%; L2, 3%	72	0.5–1.49
Biglioli et al. 2000	31 cadavers	T9–L5	T12–L3, 83.9%	68	0.73–1.33
Kieffer et al. 2002	480 patients	–	T8–L1, 86%	77	
Takase et al. 2002	63 MDCT scans	T7–L2	T7–T8, 10%; T9–T11, 55%; T12–L1, 27%; L2, 8%	69	–
Morishita et al. 2003	55 cadavers	T7–L4	T7–T8, 10%; T9–T11, 68%; T12–L1, 16%; L2–L4, 6%	78	–
Kudo et al. 2003	19 contrast enhanced MDCT scans (only 13 arteries were identified)	T10–L2	T10–T11, 69%; T12–L1, 23%; L2, 8%	69	–
Yoshioka et al. 2003	24 MRA and CTA scans	T7–T12	T7–T8, 11%; T9–T11, 85%; T12, 3%	81	–
Kawaharada et al. 2004	120 MRA scans	T7–L1	T7–T8, 4%; T9–T11, 85%; T12–L1, 11%	95	–
Biglioli et al. 2004	51 cadavers	T9–L5	T9–T11, 16%; T12–L1, 39%; L2–L4, 41%; L5, 4%	63	0.73–1.33
Boll et al. 2006	100 contrast enhanced MDCT scans	T8–L2	T8, 3%; T9–T11, 73%; T12–L1, 22%; L2, 2%;	63	1.0–2.8
Nijenhuis et al. 2007	60 MRA scans	T8–L2	T8, 3%; T9–T11, 77%; T12–L1, 20%	72	–
Backes et al. 2008	85 patients	T8–L2	–	68	–

anterior radicular artery. In all these cases, the latter and the lower lumbar artery supplied the lower lumbar spinal cord. The narrowing of the anterior spinal artery indicates that the blood supply to the lower spinal cord becomes progressively more dependent on the great anterior radicular artery (Morishita et al. 2003).

The radiculomedullary arteries were examined in 20 formalin-embalmed, latex-perfused cadavers. In the sample, a total of 72 anterior radiculomedullary arteries were found supporting the thoracolumbar segment of the spinal cord (average 3.6 per cadaver) while a much larger number of posterior radiculomedullary arteries were found, 177 for the total sample (average 8.9 per cadaver). The posterior radiculomedullary arteries were well developed in the thoracic region, arising from the intercostal arteries between levels T5 and T8 (67 of 177 observations). The lowest number of posterior radiculomedullary arteries was noted between levels L1 and L3 (20 of 177 observations) (Gao et al. 2013).

The great anterior radicular artery (of Adamkiewicz)

Studies have shown the great anterior radicular artery arises between levels T5 and L4 (see Table 58.2), but most commonly between levels T9 and L1 (Carmichael & Gloviczki 1999).

Suh and Alexander (1939) stated that the great anterior radicular artery can be identified at any segment between the levels of T8 and L4. When looking the blood supply of 22 spinal cords, Romanes (1965) found that the great anterior radicular artery joined the anterior spinal cord most commonly between the levels of T9 and T12 (64%). The range of origin varied between T6 and L3 and originated from the left side in 68% of cases. The diameter of the artery ranged between 0.2 mm and 1.2 mm.

In an early angiographic study of the great anterior radicular artery, it was reported that this artery originated from levels T9–T12 in 75%, levels T5–T8 in 15%, and levels L1 or L2 in 10% of cases. Similarly, it was more commonly found to originate from

the left side of the body. The thought behind this is simply that the aorta is a left-sided structure (Djindjian & Faure 1967).

Dommisse (1973) attempted to record the origin of the great anterior radicular artery in 35 cadavers, and found that the artery originated between the levels of T7 and L4 and was absent in two cases. It could be found originating at levels T9 and T11 in 64% of the time with T9 being the most common level of origin (27% of the sample). It originated more commonly from the left side in 77% of the sample, while it originated from the right side in only 17%. Variations that were recorded, and factors that made identification of the great anterior radicular artery difficult, included one case where there were two vessels of equal diameter, one originating at the level of T9 on the right (diameter 0.8 mm) and one originating at the level of L2 also on the right (0.75 mm). In a second case there were three possible arteries, two arising from the level of T7 and S2 on the left and one from the level of T9 on the right. The three arteries all had the same diameter (0.25 mm). Finally, there was another case where three large arteries supported the anterior spinal artery and supplied the lumbar enlargement. In this case the arteries originated from levels T9 and S3 on the right and L2 on the left. The arteries were 0.48 mm, 0.4 mm, and 0.45 mm in diameter, respectively (Dommisse 1973).

The great anterior radicular artery was dissected out on 30 spinal cords sourced from unfixed cadavers. The artery originated from levels T8 to L2 with the highest frequency at T9 (33%). In 80% of the cases it was located on the left side and its diameter ranged from 0.6 to 1.2 mm. In two-thirds of the cases the great anterior radicular artery was the last anterior radicular feeder artery to the thoracolumbar segment of the spinal cord, while in the remaining third there was a supplementary artery immediately below, which joined the anterior spinal artery more caudally (possibly the "artery of the conus medullaris," as termed by Lazorthes et al. 1971). In all these cases, except one, this artery originated from the left side with a diameter that ranged between 0.2 mm and 0.55 mm. The artery originated from levels T10 to L1, with the most common origin at the level of L1 (60%). In 23% of cases the great anterior radicular artery was the only artery to join and support the anterior spinal artery below level T6. The authors also found that in 63% of cases, the great anterior radicular artery had a posterior counterpart; however, this artery did not show any special distinguishing features with respect to other posterior radicular feeder arteries joining the posterior spinal arteries (Rodriguez-Baeza et al. 1991).

In an in-depth study of the vasculature of the spinal cord on 102 cadavers, mention was made of two or more great anterior radicular arteries found in 23 cadavers (26% of cases). The second generally originated between one and seven spinal cord segments more distal than the first artery. Of these duplications, the origin was unilateral in 57% of the cases and bilateral in 43%. A left-sided predominance was still present. The authors only classified a great anterior radicular artery if its diameter was 0.5 mm or greater (Koshino et al. 1999).

In another study, the origin of the great anterior radicular artery varied greatly from levels T9 to L5 and was most frequently found between levels T12 and L3, accounting for 83.9%. It originated from the left side in 67.7% of the cases. In all 31 cases the great anterior radicular artery constituted the lower radiculomedullary blood supply, based on the fact of its large diameter (0.73–1.33 mm) and because of its characteristic "hairpin" bend before joining the anterior spinal artery (Fig. 58.10; Biglioli et al. 2000).

On multi-detector helical CT (MDCT) scans of 63 patients, 78 great anterior radicular arteries were identified from their origin from the posterior intercostal or lumbar arteries until it joined the anterior spinal artery. The artery originated predominantly from the left side (69% of cases) between levels T7 and L2. It was found to originate most commonly from the level of T9 (24%) followed by T11 (22%). In 15 patients (24% of the cases), two great anterior radicular arteries were identified. The second vessel generally originated between one and five segmental

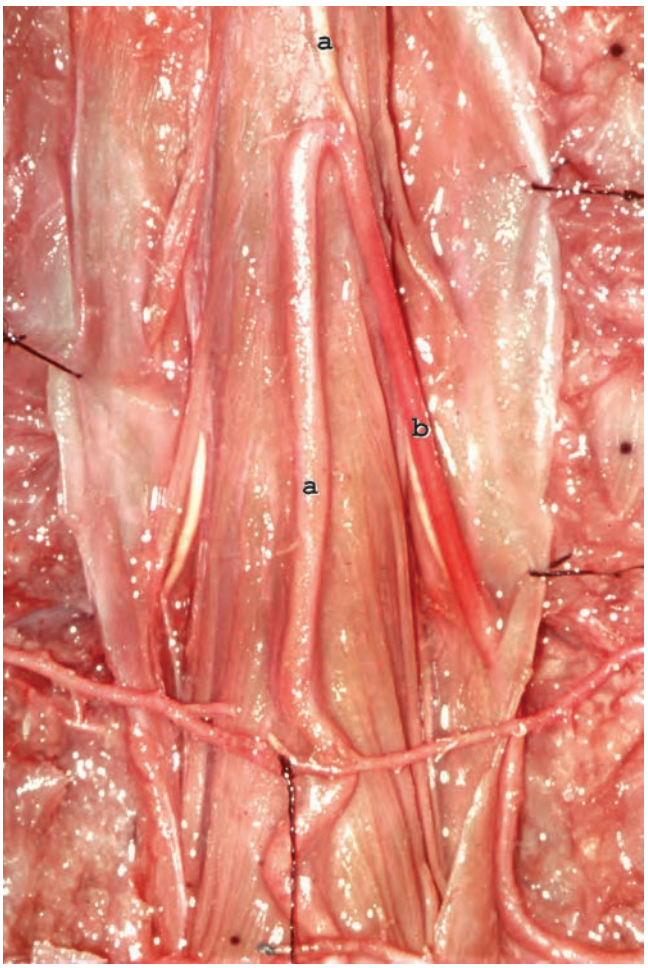

Figure 58.10 Anterior spinal artery (a) in the thoracolumbar segment of the spinal cord above and below the junction with the great anterior radicular artery (b) making a characteristic "hairpin" bend at the junction.

Source: Dommisse (1973). Reproduced with permission from Department of Anatomy, University of Pretoria.

levels caudal from the first. It is unclear what characteristics the authors used to classify the latter as a second great anterior radicular artery (similar to a study by Koshino et al. 1999) and not just another feeder artery found distal to the great anterior radicular artery (as was described by Rodriguez-Baeza et al. 1991) or, more specifically, the "artery of the conus medullaris" as referred to by Lazorthes et al. (1971) (Takase et al. 2002).

During examination of the arterial supply of the spinal cords of 55 formalin-fixed cadavers, the great anterior radicular artery originated from the levels T7–T8 in 10%, T9–T11 in 68%, T12–L1 in 16%, and L2–L4 in 6%. The artery originated from the left side in 43 (78%) of the cases (Morishita et al. 2003).

Magnetic resonance angiographic examination of the great anterior radicular artery of 120 patients revealed a single artery in 89% of cases. A second great anterior radicular artery was detected in the other 11% of patients, which originated unilaterally in 91% of the cases. In 95% of the cases the great anterior radicular artery originated from the left side, most commonly from the levels between T9 and T11 (85%) (Kawaharada et al. 2004).

The great anterior radicular artery was visualized in a sample of 100 patients undergoing high-resolution contrast-enhanced MDCT imaging. The authors state that, in their sample, the great anterior radicular artery originated from the left side of the body in 63% of the cases (37% on the right) with a segmental range from levels T8–L2 (34.6% of the cases at level T11). There was no statistical difference between the levels of origin between the sexes. The artery was measured to be 13.1–98.2 mm in length, spanned one to three vertebral segments, and had a diameter of 1.0–2.8 mm. Various forms of duplication of the great anterior radicular artery were found in 5% of cases. Ipsilateral duplication was observed originating from the same, and from adjacent segmental spinal arteries. Bilateral duplication with segmental skipping of the radiculomedullary artery was also encountered. Duplicated great anterior radicular arteries were observed in two men and three women (Boll et al. 2006).

The great anterior radicular artery was visualized preoperatively in 85 patients using magnetic resonance angiography of the spinal cord vasculature. The great anterior radicular artery was identified in all 85 patients and was found to originate from segmental medullary arteries between levels T8 and L2 and in 68% it derived from the left side. In 69% of the patients the connection between the great anterior radicular artery and the aorta was through a direct segmental supply. In the remaining 31% it had an indirect connection (i.e., via intersegmental collateral arteries) to a segmental spinal artery located one or two levels higher or lower (Backes et al. 2008). This collateral circulation was also examined on cadaveric specimens (Fig. 58.11; Dommisse 1973).

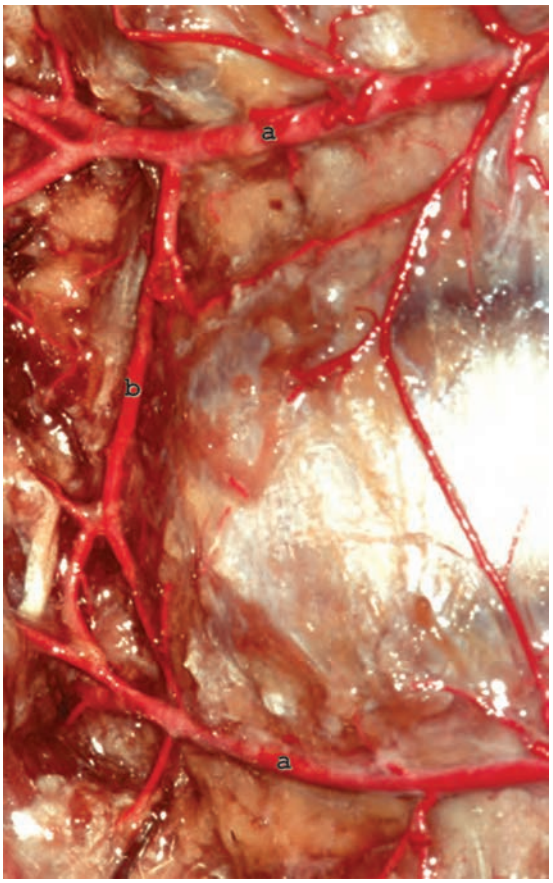

Figure 58.11 Branches of segmental spinal arteries (a) anastomose with branches of ipsi- and contralateral counterparts (b) over the vertebral bodies.

Source: Dommisse (1973). Reproduced with permission from Department of Anatomy, University of Pretoria.

Arterial anastomoses of the spinal cord

Svensson (1999) used the law of Hagen-Poiseuille to show that because of the narrowing of the anterior spinal artery prior to the junction with the great anterior radicular artery, if all the segmental spinal arteries were sacrificed blood would not be able to sufficiently flow down the anterior spinal artery through the narrowing. The blood flow through the narrow point will be so poor that ischemia could not be prevented. They theorized that, in such a situation, the blood supply to the lower segments of the spinal cord would be dependent on collateral circulation instead of the segmental spinal arteries and their branches. Although it is considered that most individuals have an adequate collateral circulation (see Fig. 58.11), an angiographic study of 480 patients with thoracic and thoracoabdominal aortic aneurysms revealed that only 25% of the sample had an adequate collateral circulation (Kieffer et al. 2002).

Collateral circulation was also displayed in a sample of 60 patients diagnosed with either a thoracic aortic aneurysm or thoracoabdominal aortic aneurysm undergoing preoperative magnetic resonance angiography. In the sample there were 24 cases (40%) where the segmental spinal artery, from which the great anterior radicular artery originated, was partially or completely occluded at its origin from the aorta. This study

demonstrated how, in cases such as these, the affected segmental spinal artery and therefore the great anterior radicular artery, was supplied indirectly through intersegmental collateral arteries from adjacent segmental spinal arteries. In 6 of the cases (10% of total sample) the segmental artery feeding the occluded artery through collateral circulation was separated by two vertebral levels, while only one level separated the remaining 18 cases (30% of total sample) (Nijenhuis et al. 2007).

At the distal end of the spinal cord around the conus medullaris, a constant anastomosis uniting the anterior spinal and the two posterior spinal arteries has regularly been described; this anastomosis is in the shape of a trident with an artery at each longitudinal arterial channel. These anastomoses have been called the "anastomotic loop of the conus medullaris" (Lazorthes et al. 1958) or the cruciate anastomosis (Dommisse 1973). Several patterns were identified and are displayed in Figure 58.12.

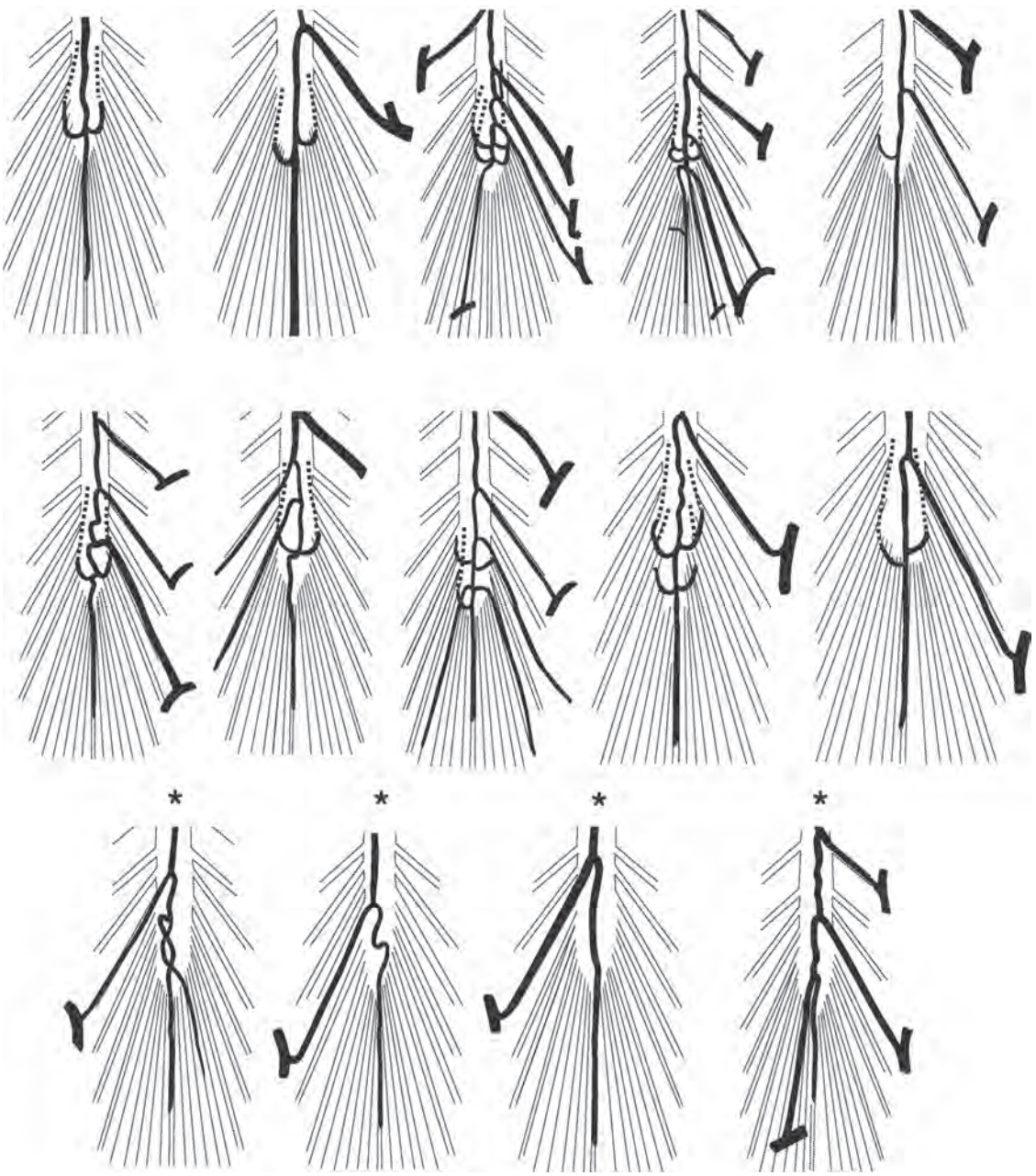

Figure 58.12 Vascular patterns of the cruciate anastomosis around the conus medullaris. Note four cases (*) where there were no clear connection between the three longitudinal arterial trunks.

Source: Dommisse (1973). Reproduced with permission from Department of Anatomy, University of Pretoria.

Summary of variations of the arteries to the spinal cord

Anterior spinal artery

This artery runs in the ventral median fissure of the spinal cord and is continuous throughout its course. A case was reported where the anterior spinal artery was interrupted for a few millimeters between levels C6 and C7 with four medium-sized (diameter 0.4–0.7 mm) tributaries, between levels C5 and C7, providing an adequate alternative blood supply to the region (Romanes 1965). Studies have also shown severe narrowing of this artery at segmental levels, most prominently over a total of four to five spinal segments centered upon level T6 (Dommisse 1973), whereas Romanes (1965) stated that the smallest diameter (0.2 mm or less) of the artery was from levels T6 to T8 or even T10. Highly selective angiography of the spinal cord of nine patients revealed extreme narrowing of the anterior spinal artery in the midthoracic segment of the spinal cord; in some cases, it even appeared to be interrupted (Gao et al. 2013). Using magnetic resonance angiography, the anterior spinal artery at the junction with the great anterior radicular artery was detected and classified into Type A (non-continuation of the anterior spinal artery above the junction of the great anterior radicular artery) in 55% of cases, Type B (continuation of the anterior spinal artery above and below the junction) in 20% of cases, or Type C (non-continuation of the anterior spinal artery below the junction) in 3% of cases (Kawaharada et al. 2004). Possible difficulties in detecting the anterior spinal artery at its narrowest points using imaging modalities such as magnetic resonance angiography should be taken into account. There is a statistically significant difference between the diameters of the anterior spinal artery above (mean 0.5 mm) and below (mean 1.2 mm) the junction with the great anterior radicular artery (Romanes 1965; Biglioli et al. 2013). Three cases were found where the diameter of the anterior spinal artery was significantly larger above this junction. In all these cases the great anterior radicular artery and a lower lumbar radiculomedullary artery supplied the lower lumbar spinal cord (Morishita et al. 2003).

The anterior spinal artery is often formed by two spinal branches joining to form the single longitudinal arterial trunk. This junction usually occurs intracranially or near the midline on the anterior aspect of the medulla oblongata, at the level of the olive (Tveten 1976; Rodriguez-Baeza et al. 1989; Gövsa et al. 1996). In 66.25% of cases the two spinal branches joined at the border between the medulla oblongata and spinal cord, while in 12.5% of cases it extended up to levels C2 and C3 of the cervical spinal cord before joining (Gövsa et al. 1996).

The origin of the anterior spinal artery pattern can be classified into three types as follows.

1. Type I: Left and right spinal branches originate from the vertebral arteries and join to form the anterior spinal artery in 85% (Stopford 1916), 54.6% (Miyadi-Tosihiko 1931), 80% (Lanz & Wachmuth 1979), 77.4% (Rodriguez-Baeza et al. 1989), and 75% (Gövsa et al. 1996) of cases. This pattern can be further subdivided into Type Ia (balanced): two spinal branches are of equal diameter (between 11% and 43.5% of cases); Type Ib (right dominant): diameter of the right spinal branch significantly larger than the left (between 17.5% and 43% of cases); and Type Ic (left dominant): diameter of the left spinal branch significantly larger than the right (between 15% and 46% of cases) (Stopford 1916; Rodriguez-Baeza et al. 1989; Gövsa et al. 1996).
2. Type II: Only one spinal branch, originating from the right vertebral artery in 3–8.8% of cases or the left vertebral artery in 0.25–9% of cases (Stopford 1916; Gövsa et al. 1996). Unilateral origin of the anterior spinal artery was previously reported in 9.7% of cases (Rodriguez-Baeza et al. 1989).
3. Type III: Anterior spinal artery originates from a transverse intervertebral anastomosis. The former originates from a single root in 0.75% of cases or a double root in 0.6% of cases (Gövsa et al. 1996). This type was previously reported in 12.9% of cases (Rodriguez-Baeza et al. 1989).

The level of origin of the right and left spinal branches is (1) at the extreme upper part of the vertebral artery (i.e., in the region of the cephalic extremity of the olivary eminence) in 51% and 59% of cases, respectively; (2) at the level of the mid-olivary region in 29% and 28%; and (3) at the level of the caudal extremity of, or slightly below, the olive in 20% and 13% (Stopford 1916).

Other variations of the origin of the anterior spinal artery

The anterior spinal artery arose from a single spinal branch that originated at the angle formed by the junction of the two vertebral arteries in 3% of cases (Stopford 1916).

The presence of two anterior spinal arteries on the ventral surface of the spinal cord was recorded when the left and right spinal branches failed to join. This was seen in 2.5–6% of cases (Stopford 1916; Gövsa et al. 1996). Often the duplicated anterior longitudinal arterial trunks will have communications, found at the normal level of junction between the two spinal branches (Stopford 1916), or with no communications between each other (although only the cervical region was examined) (Gövsa et al. 1996).

There was a double origin of the anterior spinal artery from the right side in one specimen and from the left side in two specimens (Stopford 1916).

Posterior spinal artery

The posterior spinal arteries are situated on the posterolateral aspect of the spinal cord, at the base of the dorsal nerve roots. Similar to the anterior spinal artery, both posterior spinal arteries are continuous throughout their course from its origin at the medulla oblongata to the conus medullaris. The two longitudinal arterial trunks frequently divide and deviate in their distal course with many communications, at various levels along the spinal cord, between the left and right artery (Dommisse 1973). The diameter of the posterior spinal arteries is narrowest in the midthoracic segment at levels T2–T6 (down to 0.1 mm) and

widest at the lumbar enlargement (up to 1.2 mm) (Romanes 1965).

The posterior spinal arteries originate from the posterior inferior cerebellar arteries in 73% of cases. The right posterior spinal artery originates from the ipsilateral vertebral artery in 20% of cases, while the left posterior spinal artery originates from the left vertebral artery in 18% of cases. In 9% of cases the right posterior spinal artery has a double origin from both the posterior inferior cerebellar artery and the vertebral artery, while it had a similar double origin in 7% of cases on the left (Stopford 1916).

Anterior and posterior radiculomedullary arteries

The anterior and posterior radiculomedullary arteries are branches of the segmental spinal arteries. The latter originates from vertebral, deep cervical, intercostal, lumbar, iliolumbar, and lateral sacral arteries and enters the vertebral canal through the intervertebral foramina. Unlike their radicular artery counterparts, not only do they supply the spinal nerve roots, but also continue to join the anterior and posterior spinal arteries. These arteries support and provide additional blood to the three longitudinal arterial trunks; they are variable in size, number, location, and even laterality of junction with the spinal arteries.

In an adult human, only about 6–8 radiculomedullary arteries are present and make functional connections with the anterior spinal artery, while 10–23 supply the posterior spinal arteries (Carmichael & Gloviczki 1999).

In the cervicothoracic segment there is an average of 3.4 anterior radiculomedullary arteries joining the anterior spinal artery, concentrated at the levels of C4–C7 with a right-sided predominance of 5:4 (Dommisse 1973). No difference in laterality has been reported (Romanes 1965). The number of anterior radiculomedullary arteries ranged between zero (one reported case) to eight cervical radiculomedullary feeders (three reported cases) with an average diameter of 0.3 mm (range 0.1–0.75 mm). An average of 2.8 posterior radiculomedullary arteries can be found on the dorsal aspect of the cervical spinal cord, with an equal distribution between left and right. The majority (89%) can be found at level C6, then C5 and T1 (50% of cases), and then at level C6 (44%). The number of posterior radiculomedullary arteries ranged between zero (one reported case) to seven cervical radiculomedullary feeders (one reported case) with an average diameter of 0.17 mm (range 0.03–0.3 mm) (Dommisse 1973).

The source of the cervical anterior and posterior radiculomedullary arteries in the cervicothoracic region can be summarized as follows: (1) the vertebral artery supplies 77% of the anterior and 51% of the posterior radiculomedullary arteries; and (2) the costocervical trunk and its two principle divisions supply 20% of the anterior and 37% of the posterior radiculomedullary arteries. In the area of the thoracic inlet, the costocervical trunk and proximal intercostal arteries provides 86% of the posterior radiculomedullary arteries joining the two posterior spinal arteries (Dommisse 1973).

When compared with the cervicothoracic segment, the midthoracic segment has a ratio of 3:2 more radiculomedullary arteries supporting the longitudinal trunks (although this is mostly blood vessels to the posterior spinal arteries). The average number of anterior radiculomedullary arteries is only 2.3 (range 2–5). The average diameter is 0.31 mm (range 0.15–0.8 mm). There exists a left-sided predisposition of 4:1. The posterior radiculomedullary arteries in the midthoracic segment are more numerous with an average number of 5.3 (range 3–10) arteries between levels T2 and T9 (with the majority at T5, T8, and then T7 and T9), but has a lower average diameter of only 0.15 mm (range 0.03–0.3 mm). There exists a right-sided predisposition of 3:2 (Dommisse 1973).

On average, 2.3–3.6 anterior and 2.1–8.9 posterior radiculomedullary arteries join anterior and posterior spinal arteries in the thoracolumbar segment (Dommisse 1973; Gao et al. 2013). They also have a much larger average diameter compared to the midthoracic segment. The average diameter of the anterior radiculomedullary arteries is 0.3 mm while the posterior radiculomedullary arteries are only about 0.15 mm (Dommisse 1973). The posterior radiculomedullary arteries are well developed in the thoracic region, arising from the intercostal arteries at levels T5–T8 (67 of 177 observations). The smallest number of posterior radiculomedullary arteries can be found between levels L1 and L3 (20 of 177 observations; Gao et al. 2013).

The great anterior radicular artery (of Adamkiewicz)

The blood supply to the ventral portion of the thoracolumbar segment is dependent on a single large anterior radiculomedullary artery, known as the great anterior radicular artery, joining the anterior spinal artery. In 23% of cases the great anterior radicular artery was the only artery to join and support the anterior spinal artery below level T6. In 63% of cases the great anterior radicular artery has a posterior branch, joining one of the posterior spinal arteries (Rodriguez-Baeza et al. 1991). In 69% of people, the connection between the great anterior radicular artery and the aorta is through a segmental spinal artery originating at the same level. In the remaining 31%, it has an indirect connection (via intersegmental collateral arteries) to a segmental spinal artery located one or two levels superior or inferior (Backes et al. 2008). The origin of the great anterior radicular artery can be anywhere between T5 and S5, but it most commonly arises between levels T9 and T12. It originates from the left side in 63–95% of cases and can have a diameter of 0.2–2.8 mm (Table 58.2).

A common phenomenon in the thoracolumbar segment of the spinal cord is multiple anterior radiculomedullary arteries all fitting the description of the great anterior radicular artery. This makes identification of the latter difficult. Several studies have reported this duplication and appear to be present in 5–26% of people. The second vessel generally originates between one and seven spinal cord segments distal to the first artery. Of these duplications, the origin is unilateral in 57–91%

of the cases and bilateral in 9–43% of the cases. A left-sided predominance still persists (Lazorthes et al. 1971; Dommisse 1973; Rodriguez-Baeza et al. 1991; Koshino et al. 1999; Takase et al. 2002; Kawaharada et al. 2004; Boll et al. 2006).

Arterial anastomoses of the spinal cord

The law of Hagen-Poiseuille shows that the blood supply to the thoracolumbar segment of the spinal cord is dependent on blood from the segmental spinal arteries. The narrowing of the anterior spinal artery, prior to the junction with the great anterior radicular artery, is too great to allow sufficient vascularization and prevent ischemia. In such cases, the vascularization of the lower spinal cord is dependent on a collateral circulation instead of the segmental spinal arteries and their branches (Svensson 1999). Unfortunately, in the absence of the segmental spinal arteries, an adequate collateral circulation is only present in approximately 25% of people (Kieffer et al. 2003).

Some segmental spinal arteries are connected by intersegmental collateral arteries. Two adjacent segmental spinal arteries are connected by an intersegmental collateral artery in 30% of cases, while the anastomosis between two segmental spinal arteries extend over two vertebral levels in 10% of cases (Nijenhuis et al. 2007).

At the distal end of the spinal cord, around the conus medullaris, a constant anastomosis uniting the anterior spinal and the two posterior spinal arteries is present and shaped like a trident, with an artery at each longitudinal arterial channel (anastomotic loop of the conus medullaris or the cruciate anastomosis) (Lazorthes et al. 1958; Dommisse 1973). Several patterns have been identified and can be seen in Figure 58.12.

Lastly, mention of the artery of Desproges-Gotteron is rarely found in the literature. This posterior radiculomedullary (radiculo-pial) artery, also known as the "cone artery," arises from the internal iliac artery or its branches (e.g., iliolumbar), courses alongside the L5 or S1 roots up to the conus medullaris, and anastomoses with the perimedullary network (conal basket). Desproges-Gotteron found that in approximately 15% of cases, the artery of Adamkiewicz was absent or originated higher than normal; in such cases, an artery that followed a lower lumbar nerve always contributed to blood supply to the lower cord (Desproges-Gotteron 1955).

References

Adamkiewicz A. 1882. Die Blutgefässe des menschlichen Rückenmarkes. II Tell. Die Gefässe der Rückenmarkoberfläche. *S B Heidelberg Akad Wiss* 85: 101–130 (article in German).

Alleyne CH, Cawley CM, Shengelaia GG, Barrow DL. 1998. Microsurgical anatomy of the artery of Adamkiewicz and its segmental artery. *J Neurosurg* 89: 791–795.

Backes WH, Nijenhuis RJ, Mess WH, Wilmink FA, Schurink GWH, Jacobs MJ. 2008. Magnetic resonance angiography of collateral blood supply to spinal cord in thoracic and thoracoabdominal aortic aneurysm patients. *J Vasc Surg* 48: 261–271.

Biglioli P, Spirito E, Roberto M, Grillo F, Cannata A, Parolari A, Maggioni M, Coggi G. 2000. The anterior spinal artery: The main arterial supply of the human spinal cord: a preliminary anatomic study. *J Thorac Cardiovasc Surg* 119: 376–379.

Biglioli P, Roberto M, Cannata A, Parolari A, Fumero A, Grillo F, Maggioni M, Coggi G, Spirito R. 2004. Upper and lower spinal cord blood supply: The continuity of the anterior spinal artery and the relevance of the lumbar arteries. *J Thorac Cardiovasc Surg* 127: 1188–1192.

Boll DT, Bulow H, Blackham KA, Aschoff AJ, Schmitz BL. 2006. MDCT Angiography of the spinal vasculature and the artery of Adamkiewicz. *AJR* 187: 1054–1060.

Bolton B. 1939. The blood supply of the human spinal cord. *J Neurol Psychiatry* 2: 137–148.

Bosman MC. 2008. *Neuroanatomy, second edition*. Pretoria: UPrinters.

Brugieres P, Djindjian M, Revel MP. 1990. Anterior cervical spinal artery originating from a right vertebral artery with a bifid origin. *Neuroradiology* 32: 506–507.

Carmichael SW, Gloviczki P. 1999. Anatomy of the blood supply to the spinal cord: the artery of Adamkiewicz. *Perspect Vasc Surg Endovasc Ther* 12: 113–122.

Chakrovorty BG. 1971. Arterial supply of the cervical spinal cord (with special reference to the radicular arteries). *Anat Rec* 170: 311–329.

Desproges-Gotteron R. 1955. *Contribution à l'Étude de la Sciatique Paralysante*. Paris: Bosc Frères.

Djindjian R, Faure C. 1967. Accidents médullaires de l'aortographie. *J Belg Radiol* 50: 207–213 (in French).

Dommisse GF. 1973. The vascular system of the human spinal cord. Thesis. University of Pretoria, South Africa.

Gao L, Wang L, Su B, Wang P, Ye J, Shen H. 2013. The vascular supply to the spinal cord and its relationship to anterior spine surgical approaches. *Spine J* 13(8): 966–973.

Gillilan LA. 1958. The arterial blood supply of the human spinal cord. *J Comp Neurol* 110: 75–103.

Gövsa F, Aktan ZA, Arisoy Y, Varol T, Özgür T. 1996. Origin of the anterior spinal artery. *Surg Radiol Anat* 18: 189–193.

Kadyi H. 1889. Über die Blutegefässe des mensehlichen Rückenmarkes. Lemberg: Gubrynowicz & Schmidt (in German).

Kawaharada N, Morishita K, Hyodoh H, Fujisawa Y, Fukada J, Hachiro Y, Kurimoto Y, Abe T. 2004. Magnetic resonance angiographic localization of the artery of Adamkiewicz for spinal cord blood supply. *Ann Thorac Surg* 78: 846–852.

Kieffer E, Fukui S, Chiras J, Koskas F, Bahnini A, Cormier E. 2002. Spinal cord arteriography: a safe adjunct before descending thoracic or thoracoabdominal aortic aneurysmectomy. *J Vasc Surg* 35: 262–268.

Koshino T, Murakami G, Morishita K, Mawatari T, Abe T. 1999. Does the Adamkiewicz artery originate from the larger segmental arteries? *J Thorac Cardiovasc Surg* 117: 898–905.

Kudo K, Terae S, Asano T, Oka M, Kaneko K, Ushikoshi S, Miyasaka K. 2003. Anterior spinal artery and artery of Adamkiewicz detected by using multidetector row CT. *AJNR* 24: 13–17.

Lanz I, Wachsmuth W. 1979. *Praktische Anatomie I* (eds Kopf I, Tell B). Berlin, Heidelberg, New York: Springer (in German).

Lasjaunias P, Vallee B, Person H, Ter Brugge K, Chiu M. 1985. The lateral spinal artery of the upper cervical spinal cord. Anatomy, normal variations, and angiographic aspects. *J Neurosurg* 63: 235–241.

Lazorthes G, Poulhès J, Bastide G, Roulleau J, Chaucholle A-R. 1958. La vascularisation artérielle de la moelle: recherches anatomiques et applications à la pathologie médullaire et à la pathologie aortique. *Neurochir* 4: 3–19.

Lazorthes G, Bastide G, Chancholle A, Zadeh O. 1964. Etude anatomique de l'artère du renflement lombaire. *C R Ass Anal* 120: 883–886.

Lazorthes G, Gouaze A, Zadeh JO, Santini JJ, Lazorthes Y, Burdin P. 1971. Arterial vascularization of the spinal cord. Recent studies of the anastomotic substitution pathways. *J Neurosurg* 35: 253–262.

Lo D, Vallee JN, Spelle L, Cormier E, Saillant G, Rancurel G, Chiras J. 2002. Unusual origin of the artery of Adamkiewicz from the fourth lumbar artery. *Neuroradiology* 44: 153–157.

Melissano G, Chiesa R. 2009. Advances in imaging of the spinal cord vascular supply and its relationship with paraplegia after aortic interventions. A review. *Eur J Vasc Endovasc Surg* 38: 567–577.

Melissano G, Bertoglio L, Civelli V, Moraes Amato AC, Coppi G, Civilini E, Calori G, De Cobelli F, Del Maschio A, Chiesa R. 2009. Demonstration of the Adamkiewicz artery by multidetector computed tomography angiography analysed with the open-source software OsiriX. *Eur J Vasc Endovasc Surg* 37: 395–400.

Miyadi-Tosihiko. 1931. Pri la angioj de la spinalmedolo ce japanaj. *Mitt Med Ges Tokio* 45: 1727–1753.

Morigaki R, Satomi J, Shikata E, Nagahiro S. 2012. Aneurysm of the lateral spinal artery: A case report. *Clin Neuro Neurosurg* 114: 713–716.

Morishita K, Murakami G, Fujisawa Y, Kawaharada N, Fukada J, Saito T, Abe T. 2003. Anatomical study of blood supply to the spinal cord. *Ann Thorac Surg* 76: 1967–1971.

Nijenhuis RJ, Jacobs MJ, Schurink GW, Kessels AGH, van Engelshoven JMA, Backes WH. 2007. Magnetic resonance angiography and neuromonitoring to assess spinal cord blood supply in thoracic and thoracoabdominal aortic aneurysm surgery. *J Vasc Surg* 45: 71–78.

Perese DM, Fracasso JE 1959. Anatomical considerations in surgery of the spinal cord: a study of vessels and measurements of the cord. *J Neurosurg* 16: 314–325.

Rodriguez-Baeza A, Muset-Lara A, Rodriguez-Pazos M, Domenech-Mateu JM. 1989. Anterior spinal arteries. Origin and distribution in man. *Acta Anatomica* 136: 217–221.

Rodriguez-Baeza A, Muset-Lara A, Rodriguez-Pazos M, Domenech-Mateu JM. 1991. The arterial supply of the human spinal cord: A new approach to the arteria radicularis magna of Adamkiewicz. *Acta Neurochir (Wien)* 109: 57–62.

Romanes GJ. 1965. The arterial blood supply of the human spinal cord. *Paraplegia* 2: 199–207.

Siclari F, Burger IM, Fasel JHD, Gailloud P. 2007. Developmental anatomy of the distal vertebral artery in relationship to variants of the posterior and lateral spinal arterial systems. *AJNR Am J Neuroradiol* 28: 1185–1190.

Soubeyrand M, Court C, Fadel E, Vincent-Mansour C, Mascard E, Vanel D, Missenard G. 2011. Preoperative imaging study of the spinal cord vascularization: Interest and limits in spine resection for primary tumors. *Eur J Radiol* 77: 26–33.

Stopford, JSB. 1916. The arteries of the pons and medulla oblongata. *J Anat Physiol* 50: 133–164.

Suh TH, Alexander L. 1939. Vascular system of the human spinal cord. *Arch Neurol Psychiat* 41: 659–677.

Svensson L. 1999. Commentary to the paper entitled "Does the Adamkiewicz artery originate from the larger segmental arteries?" *J Thorac Cardiovasc Surg* 117: 903–905.

Takase K, Sawamura Y, Igarashi K, Chiba Y, Haga K, Saito H, Takahashi S. 2002. Demonstration of the artery of Adamkiewicz at multidetector row helical CT. *Radiology* 223: 39–45.

Turnbull IM. 1971. Micro vasculature of the human spinal cord. *J Neurosurg* 35: 141–147.

Turnbull IM. 1972. Blood supply of the spinal cord. *Handbook Clin Neurol* 12: 478–491.

Turnbull IM, Brieg A, Hassler O. 1966. Blood supply of cervical spinal cord in man. *J Neurosurg* 24: 951–965.

Tveten L. 1976. Spinal cord vascularity. *Acta Radiol* 17: 257–283.

Woollam DHM, Millen JW. 1958. Discussion on vascular disease of the spinal cord. *Proc R Soc Med* 51: 540–550.

Yoshioka K, Niinuma H, Ohira A, Nasu K, Kawakami T, Sasaki M, Kawazoe K. 2003. MR Angiography and CT Angiography of the artery of Adamkiewicz: Noninvasive preoperative assessment of thoracoabdominal aortic aneurysm. *Radiographics* 23: 1215–1225.

Zülch KJ. 1954. Mangeldurchblutung an der Grenzzone zweier Gefäßgebiete als Ursache bisher ungeklärter Rückenmarksschädingungen. *Dtsch Z Nervenheilk* 172: 81–101 (in German).

59 Diploic veins

Satoshi Tsutsumi
Juntendo University Urayasu Hospital, Chiba, Japan

Introduction

The calvarial diploic veins (DVs) are distinct, intraosseously formed venous structures first described in 1928 (Jefferson and Stewart 1928). While the cranial emissary veins have been well investigated (Mortazavi et al. 2012), the DVs have been explored only sporadically and even today there is a lack of systematic knowledge. DVs have received little attention because they are visualized inconsistently and unclearly by conventional neuroimaging techniques and they present infrequently in association with dural arteriovenous fistulas (Benndorf and Lehmann 2004; Burger et al. 2005; Shim et al. 2011), tumorous pathologies (Ohigashi and Tanabe 2001; Tsutsumi et al. 2011), and sinus pericranii (Rizvi et al. 2010). Clinically, they can cause troublesome bleeds by trauma or at craniotomy, especially when the lesser wing of the sphenoid bone is drilled. There have been attempts to reveal the distribution of DVs radiographically (Hershkovitz et al. 1999) in corrosion cast models (San Millán Ruíz et al. 2004; Johnston et al. 2007), by cadaveric dissection (Tubbs et al. 2007; García-González et al. 2009), magnetic resonance (MR) imaging (Jivraj et al. 2009), or via experimental study (Toriumi et al. 2011). However, their detailed morphology and their relationships with the intracranial and extracranial venous systems are not well understood. To date, only an infusion study with corrosion casting material has demonstrated direct communications between the local DVs and the superior sagittal sinus (SSS) (Johnston et al. 2007). Recently we reported the peculiar architectures and the four major common pathways of the DVs as MR images (Tsutsumi et al. 2013).

The present chapter describes morphological variations of the DVs and associated arachnoid protrusions (APs), peculiar arachnoidal extensions appearing contiguous to DVs, and their potential role as cerebrospinal fluid pathways based on findings from high-resolution MR imaging, cadaveric dissection, and laboratory investigation.

A total of 400 patients (mean age of 52 years) with intact scalp, skull, dura mater, and dural sinuses were examined by MR imaging using a 3.0 T scanner. Patients with symptoms of increased intracranial pressure or intracranial hypotension were excluded. A coronal T2-weighted sequence involving the whole cranial vault was performed on 150 patients with the following parameters: repetition time (TR) 5598.69 ms; echo time (TE) 100.00 ms; slice thickness (ST) 1.00 mm; interslice gap (IG) 0.2 mm; matrix 230×230; field of view (FOV) 250 mm; flip (FA) angle 90°; and scan duration 6 min 40 s. The remaining 250 patients were examined using a coronal T2-weighted sequence focusing on the pterional region with the following parameters: TR 4038.35 ms; TE 90.00 ms; ST 2.00 mm; IG 0.2 mm; matrix 300×189; FOV 150 mm; FA 90°; and scan duration 4 min 25 s. A contrast study with an intravenous gadolinium infusion (0.1 mmol/kg), involving the whole cranial vault, was performed on 100 of the 400 patients. Three injected cadaveric heads were subjected to frontotemporal craniotomy to examine the interrupted routes of the DVs. APs and surrounding structures were observed microscopically in a fourth cadaveric head. Furthermore, both peripheral and diploic venous bloods were collected from 15 patients (6 males and 9 females; mean age 50 years) who had undergone surgical craniotomies. Albumin and cerebrospinal fluid-specific biomarkers, prostaglandin D synthase (PGDS), and cystatin C (CysC) were measured in these patients by enzyme-linked immunosorbent assay (ELISA).

MR imaging

Major DV pathways

MR imaging delineated the DVs in all 100 patients who underwent contrast examination. The DVs had irregular contours and peculiar branching patterns quite different from those of the cerebral cortical veins, which exhibit smooth branching and tubular lumens. The DVs could be divided into four major pathways: the pteriofrontoparietal (PFP); frontoorbital (FO); occipitoparietal (OP); and occipitocervical (OC) routes, depending on the topological differences in the calvaria.

The PFP connected the lateral edge of the sphenoparietal sinus to the superior sagittal sinus (SSS) in the parietal region; this was the most prominent type, found in 98% of both sides. The PFP route followed a nearly vertical, superoinferior course as a

Bergman's Comprehensive Encyclopedia of Human Anatomic Variation, First Edition. Edited by R. Shane Tubbs, Mohammadali M. Shoja and Marios Loukas.
© 2016 John Wiley & Sons, Inc. Published 2016 by John Wiley & Sons, Inc.

single trunk from the pterional region to the level of the frontal eminence, then changed direction posteriorly and divided into several branches which coursed toward the parietal SSS. The pattern of these branches in patients with well-developed DVs was racemose. Distal branches of the PFP communicated with the parietal SSS in 88% of sides.

The FO route consisted of two major distribution parts, orbital and pterional, and was found in 100% of both sides. The orbital part coursed downward as a single branch (63%) or a few branches (37%) in the supraorbital region, changed direction anteriorly at the level of the orbital roof, and drained extracranially into the subcutaneous vein through the outer table of the supraorbital rim. The PFP and FO parts fused proximally with the sphenoparietal sinus and descended as the middle meningeal vein, which coursed inferomedially along the middle cranial fossa, passed through the temporal base adjacent to the foramen ovale, and finally drained into the pterygoid plexus.

The OP route was found in 88% of both sides. It coursed in the superoinferior direction as a single trunk and connected the junction part of the transverse-sigmoid sinus to the SSS. This route arose as several tributaries from the parietal SSS, converged into a single trunk at the level of the parietal eminence, coursed inferiorly, and finally drained into the transverse-sigmoid junction.

The OC route was delineated as a unique, unpaired pathway and was found in 89%. It occurred as a single major channel coursing in the superoinferior direction in the median occipital bone, drained extracranially, passing through the lower part of the occipital bone, and finally joined the suboccipital venous channels. The OC was connected inferiorly to the parietooccipital SSS in 42%. Caudally, it communicated with the confluence of the sinuses (torcular herophili) via various sizes of channels in 84%. Small tributaries coursing in the occipital bone parallel to the transverse sinus and connecting to the OC or confluence were seen in 85% of sides. There was considerable inter-individual diversity in the degree of development of the PFP, FO, OP, and OC, and asymmetry within the same subject was common. The distribution of major DV pathways over the skull is summarized as a schema. The calvaria and contained diplöe were much thinner in pediatric patients aged less than 18 years than in adult subjects. The DVs were poorly developed in these pediatric patients and were found in limited regions in the skull.

APs and contiguous DVs

APs associated with the DVs were roughly classifiable into vesicular, tubular, and extensive types (Fig. 59.1). In the cerebral convexity, APs were commonly identified in the parasagittal region, connecting to either a linear or a branching architecture with variable thickness but following a consistent course in the diplöe. These APs were consistently distributed throughout the pterional region (Fig. 59.2 a, b), middle cranial fossa (MF) (Fig. 59.2 c), and posterior cranial fossa (PF) (Fig. 59.2 d); contiguous DVs followed characteristic courses in each cranial region. DVs

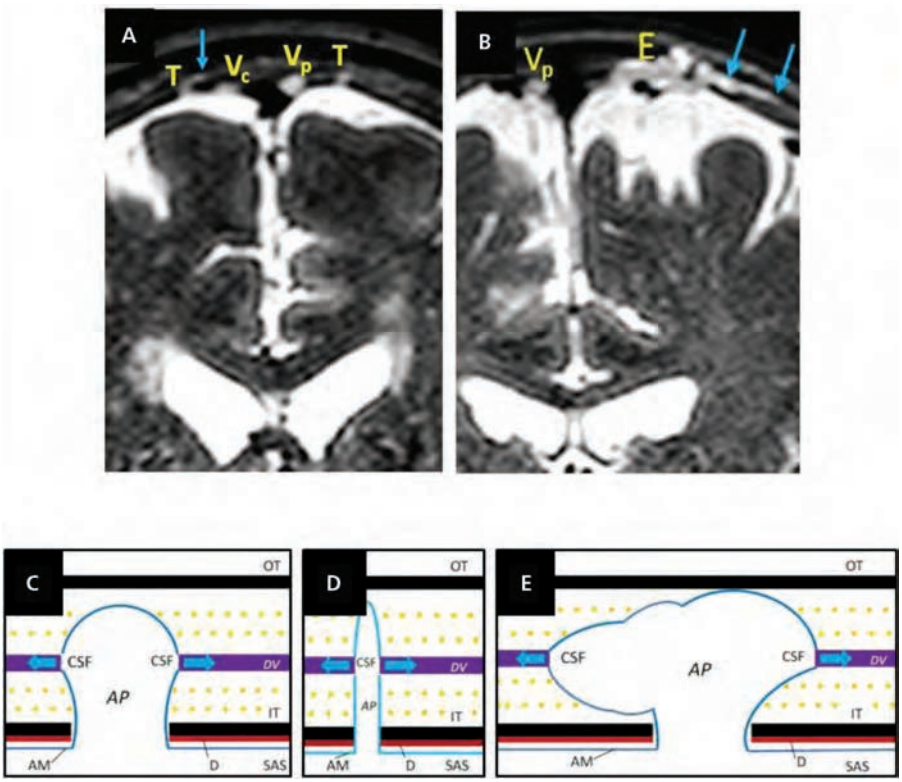

Figure 59.1 Coronal T2-weighted MR images illustrating various types of arachnoid protrusions (APs): (a) tubular (T); vesicular and located at convexity (V_c) or in the para-sinus region (V_p); and (b) extensive (E), with contiguous diploic veins (DVs) (arrows). (c) Vesicular, (d) tubular, and (e) extensive types of AP and DV. AM: arachnoid membrane, CSF: cerebrospinal fluid, IT: inner table, OT: outer table, SAS: subarachnoid space. Source: Tsutsumi et al. (2014).

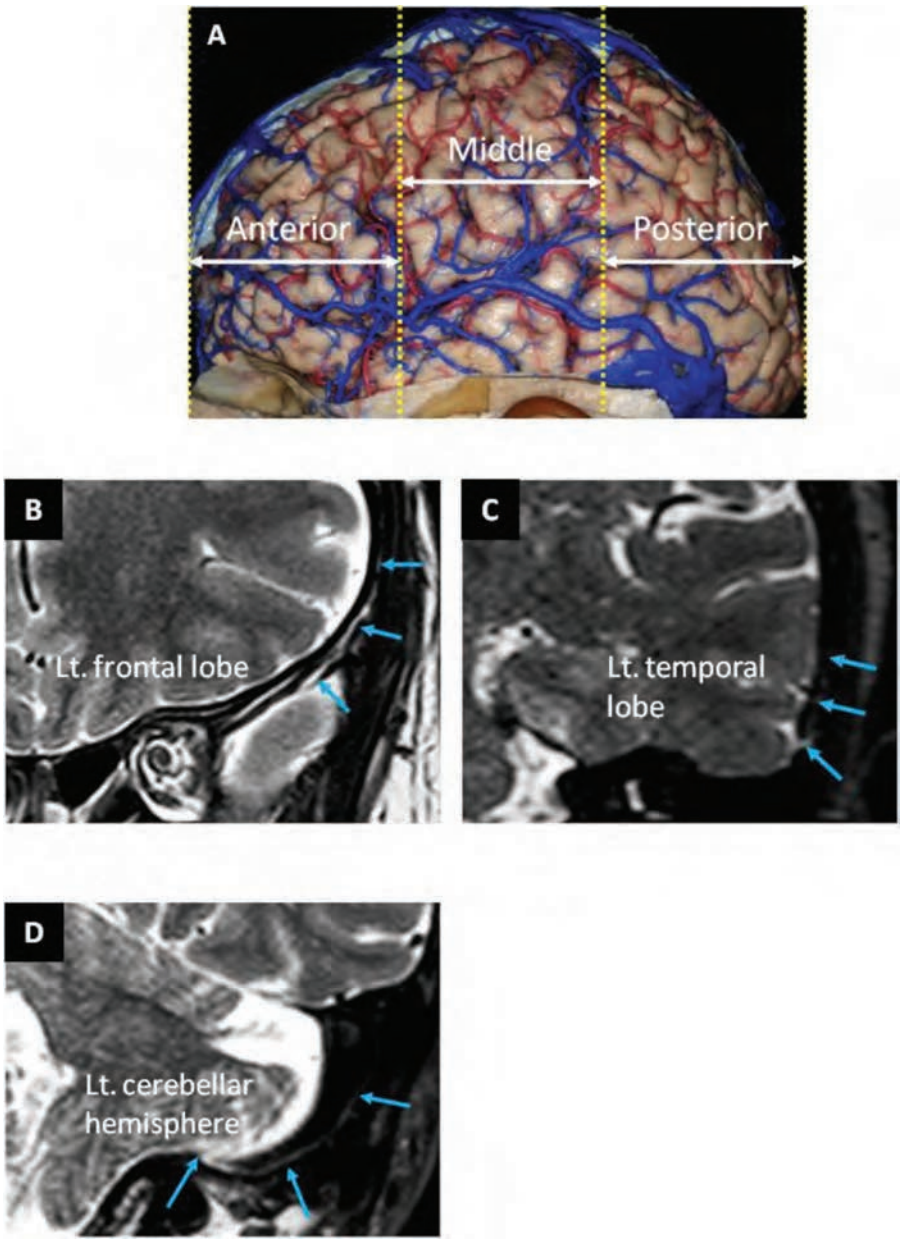

Figure 59.2 (a) Left lateral view of cadaveric cerebral hemisphere revealing three divisions into anterior, middle, and posterior third. Diploic veins (arrows) on coronal T2-weighted MR images at the mid-level of (b) anterior, (c) middle, and (d) posterior corresponding to panels. Source: Tsutsumi et al. (2014).

appeared with similar intensity to CSF on non-contrast sequence imaging, but had identical configurations to those delineated on contrast-enhanced images. Both techniques therefore seem to visualize the same DVs (Fig. 59.3). The results also indicate that DVs can appear both as fluid-filled channels and as venous structures on MR imaging.

In 150 patients, the total number of AP–DV pairings located in the cerebral convexity was 987: 489 on the right and 498 on the left. When the cerebral convexity was divided into anterior (A), middle (M), and posterior (P) thirds, 55% of the 987 pairings were found in M, 27% in P and 18% in A. The mean numbers of AP–DV pairings in one subject were 1.2 in A, 3.6 in M, and 1.7 in P. In total, an average of 6.6 pairings was found in each subject (6.9 in the population of subjects over 18 years of age and 2.3 in the population under 18 years of age). In the cerebral convexity, vesicular APs predominated and comprised 68% of the 987 pairings, followed by tubular (22%) and extensive AP types (10%).

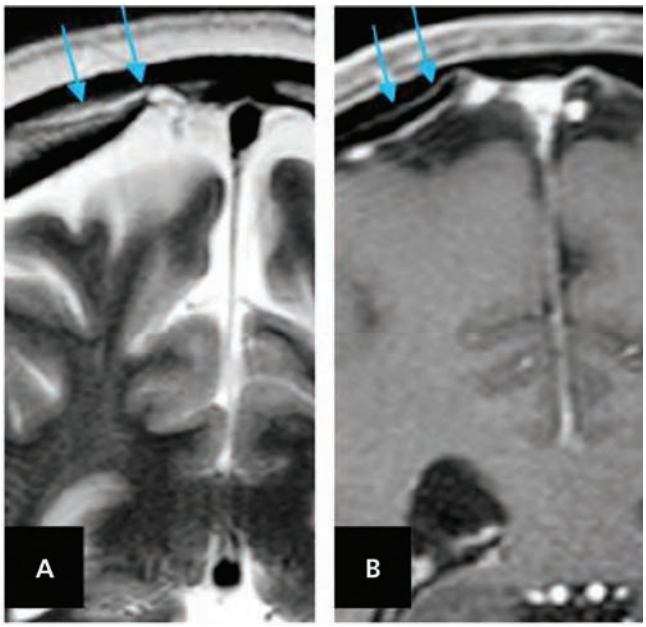

Figure 59.3 (a) Coronal T2-weighted and (b) post-contrast T1-weighted MR images at the same level demonstrate the diploic vein (arrows) appearing as a linear hyperintensity with similar configuration. Source: Tsutsumi et al. (2014).

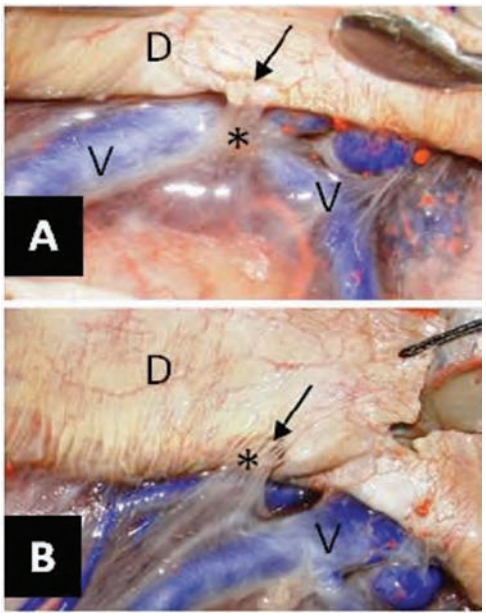

Figure 59.4 Cadaveric specimen revealing an arachnoid protrusion at the parasagittal cerebral convexity penetrating the dura mater (D) through (a) a smooth-contoured single defect (arrow) or (b) a mesh-like lacunae (arrow). Source: Tsutsumi et al. (2014).

The total number of AP–DV pairings distributed in the skull base was 375 in 150 patients, 159 on the right and 216 on the left. A total of 53% of these 375 pairings were located in the MF and 47% in the PF. Neither APs nor DVs were found in the anterior fossa. In the MF, AP–DV pairings were identified twice as often on the left side as on the right. The mean number of pairings in one subject was 1.3 in MF and 1.2 in PF. In total, an average of 2.5 pairings was found in each subject (2.6 in the population of subjects more than 18 years of age and 0.6 in the population less than 18 years of age). In the skull base, tubular APs predominated and comprised 61% of the pairings in MF and 94% in PF, followed by vesicular AP pairings. Extensive APs were not found. At least one arachnoid granulation was found in the SSS in 100% of the subjects studied, whereas in the transverse sinus was identified in 23% of subjects on the right and 37% of subjects on the left.

In the pterional region, AP–DV pairings were observed in 20% of 250 patients on the right and 29% on the left. The identification of these pairings did not depend on patient age. All of the identified APs were of the tubular type and were located at the lower surface of the lateral lesser sphenoid wing.

Cadaveric dissection

The FO and PFP predominated in all sides, and various distributions in the diplöe were observed through the outer table. These routes were consistently traversed by conventional frontotemporal craniotomy.

On microscopic inspection, APs were found to penetrate the dura mater through either a single defect (Fig. 59.4a) or mesh-like lacunae (Fig. 59.4b). These were observed throughout the cranial dura mater.

Laboratory investigation

Albumin, PGDS, and CysC levels were measured in the diploic and peripheral venous bloods of 15 patients who underwent craniotomy surgeries in various regions. CSF was also obtained intraoperatively from five of these patients. In all 15, the diploic vein/peripheral vein ratios of both PGDS and CysC were significantly above control values, at 2.43±1.99 (p=0.011) and 1.31±0.43 (p=0.023), respectively. These results were statistically significant (p<0.05). In contrast, there was no difference in albumin levels between the groups (Fig. 59.5).

The functional implications of the distribution of DVs in the human skull remain elusive. In the present investigation, calvarial DVs were consistently delineated on MR images and were classified into four major pathways. In addition, as in previous reports (García-González et al. 2009), the pterional, orbital, and asterional areas were identified as topographically pivotal centers for DVs. Our study also demonstrated that the midline suboccipital area could be an essential center for DVs that function as a conduit connecting to the suboccipital venous system.

Likewise, APs and contiguous DVs were consistently delineated on MR imaging throughout the cranium, with appearances characteristic of the different regions. Laboratory investigation

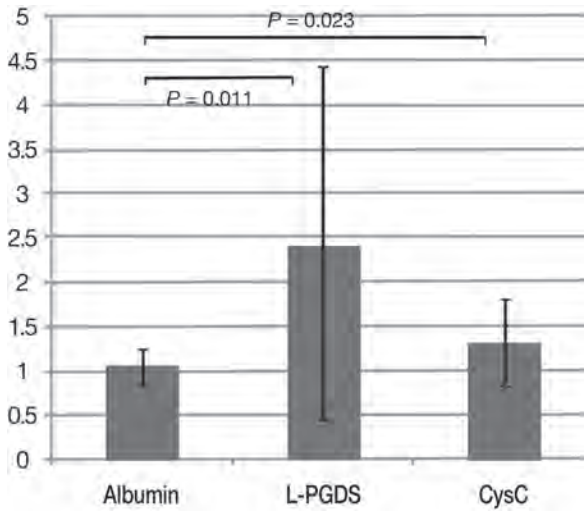

Figure 59.5 Bar graph of diploic vein/peripheral vein ratios for albumin, PGDS, and CysC. PDGS: prostaglandin D synthase; CysC: cystatin C. Source: Tsutsumi et al. (2014).

of PGDS and CysC suggested that CSF and dissolved, CSF-specific low-MW proteins could pass through APs into the DVs. We therefore considered that at least some of the intracranial CSF can permeate APs and enter the DVs.

As in the previous study (Jivraj et al. 2009), all pediatric patients aged less than 18 years in the present investigation only had diploic veins in limited regions of the skull, with much thinner calvaria and diplöe than the adult patients. Although the numbers are too small for definite conclusions, these findings could reveal age-related development of the DVs and APs.

References

Benndorf G, Lehmann TN. 2004. Bilateral diploic arteriovenous fistula causing scalp hematoma. *J Neurosurg* 100: 950–955.

Burger IM, Tamargo RJ, Broussard J, Gailloud P. 2005. Combined surgical and endovascular treatment of a spontaneous diploic arteriovenous fistula. Case report. *J Neurosurg* 103: 179–181.

García-González U, Cavalcanti DD, Agrawal A, Gonzalez LF, Wallace RC, Spetzler RF, Preul MC. 2009. The diploic venous system: surgical anatomy and neurosurgical implications. *Neurosurg Focus* 27: E2.

Hershkovitz I, Greenwald C, Rothschild BM, Latimer B, Dutour O, Jellema LM, Wish-Baratz S, Pap I, Leonetti G. 1999. The elusive diploic veins: anthropological and anatomical perspective. *Am J Phys Anthropol* 108: 345–358.

Jefferson G, Stewart D. 1928. On the veins of the diplöe. *Brit J Surg* 16: 70–88.

Jivraj K, Bhagava R, Aronyk K, Quateen A, Walji A. 2009. Diploic anatomy studied in-vivo by MRI. *Clin Anat* 22: 296–301.

Johnston KD, Walji AH, Fox RJ, Pugh JA, Aronyk KE. 2007. Access to cerebrospinal fluid absorption sites by infusion into vascular channels of the skull diplö. *J Neurosurg* 107: 841–843.

Mortazavi MM, Tubbs RS, Riech S, Verma K, Shoja MM, Zurada A, Benninger B, Loukas M, Cohen Gadol AA. 2012. Anatomy and pathology of the cranial emissary veins: A review with surgical implications. *Neurosurgery* 70: 1312–1319.

Ohigashi Y, Tanabe A. 2001. A huge frontal meningioma associated with intraoperative massive bleeding and severe brain swelling: case report. *J Clin Neurosci* 8(Suppl 1): 54–58.

Rizvi M, Behari S, Singh RK, Gupta D, Jaiswal AK, Jain M, Phadka RV. 2010. Sinus pericranii with unusual features: multiplicity, associated dural venous lakes and venous anomaly, and a lateral location. *Acta Neurochir (Wien)* 152: 2197–2204.

San Millán Ruíz D, Fasel JH, Rüfenacht DA, Gailloud P. 2004. The sphenoparietal sinus of breschet: does it exist? An anatomic study. *AJNR Am J Neuroradiol* 25: 112–120.

Shim JH, Yoon SM, Shim JJ, Kim RS. 2011. A case of intraosseous dural arteriovenous fistulas involving diploic vein treated with transarterial onyx embolization. *J Korean Neurosurg Soc* 50: 260–263.

Toriumi H, Shimizu T, Shibata M, Unekawa M, Tomita Y, Tomita M, Suzuki N. 2011. Developmental and circulatory profile of the diploic veins. *Microvasc Res* 81: 97–102.

Tsutsumi S, Yasumoto Y, Ito M. 2011. Case of calvarial fibrous dysplasia presenting with cyst degeneration. *No Shinkei Geka* 39: 163–168 (in Japanese).

Tsutsumi S, Nakamura M, Tabuchi T, Yasumoto Y, Ito M. 2013. Calvarial diploic venous channels: an anatomic study using high-resolution magnetic resonance imaging. *Surg Radiol Anat* 35: 935–941.

Tubbs RS, Salter EG, Wellons JC 3rd, Blount JP, Oakes WJ. 2007. The sphenoparietal sinus. *Neurosurgery* 60(2 Suppl 1): ONS9–12.

60 Dural venous sinuses

Shamfa C. Joseph[1], Elias Rizk[2] and R. Shane Tubbs[1,3,4]
[1]St George's University, School of Medicine, St Georges, Grenada
[2]Penn State, Hershey, Pennsylvania, United States
[3]Seattle Science Foundation, Seattle, Washington, United States
[4]University of Dundee, Dundee, United Kingdom

The dural venous sinuses are valveless venous channels found between the endosteal and meningeal layers of the dura mater. These venous channels are lined with endothelium and drain blood from the cranium into the internal jugular veins.

The network of dural venous sinuses usually comprises a superior sagittal sinus, an inferior sagittal sinus, a straight sinus, a confluence of sinuses (torcular Herophili), a pair of transverse sinuses, a pair of sigmoid sinuses, a pair of cavernous sinuses, an occipital sinus, a pair of intercavernous sinuses (anterior and posterior), a pair of superior petrosal sinuses, a pair of inferior petrosal sinuses, and a pair of sphenoparietal sinuses (Jinkins 2000). These venous sinuses develop from a widespread venous network, which allows for multiple variations (Streeter 1915). Insufficient knowledge of these variations can lead to misdiagnosis and can complicate interventional neurosurgical procedures. It is therefore important to understand not just the anatomy of the most consistent presentation of the dural sinuses, but also the variant anatomy. In this chapter, we will cover the anatomic variations of the dural venous sinuses.

Superior sagittal sinus

The diameter of the superior sagittal sinus varies from 3.0 to 4.5 mm (Bisaria 1985a). Its length varies from 24 to 27 cm in computed tomography venography, which carries a more accurate method of measurement than cadaveric dissection (Brockmann et al. 2012).

The superior sagittal sinus can be hypoplastic at its rostral end (Fig. 60.1). According to San Millan Ruiz et al. (2012), it is the most frequent variation of the superior sagittal sinus observed. In a study conducted by San Millan Ruiz et al. (2012), observing 100 patients, 7% of patients were found to have unilateral hypoplasia of the rostral end of the superior sagittal sinus with compensatory drainage through a large parasagittal superior frontal vein. Three percent of patients presented with a complete or bilateral hypoplastic rostral superior sagittal sinus. Browder and Kaplan (1976) found that the length of the zone of atresia of the sinus correlated with the caudomedial course of the veins. The longer the zone of atresia, the longer the caudomedial course (Browder and Kaplan 1976). The length of atresia ranges from 1 to 9 cm (Kaplan et al. 1972; Kaplan and Browder 1973a). This variation may be explained by failure or delay in the formation of the rostral segment of the sagittal plexus during development (San Millan Ruiz et al. 2012). Histological studies of the atretic regions disclosed non-functional, thin and irregularly shaped

Figure 60.1 Agenesis of the anterior one-third of the superior sagittal sinus and enlarged inferior sagittal sinus. Courtesy of J. K. Curé.

Bergman's Comprehensive Encyclopedia of Human Anatomic Variation, First Edition. Edited by R. Shane Tubbs, Mohammadali M. Shoja and Marios Loukas.
© 2016 John Wiley & Sons, Inc. Published 2016 by John Wiley & Sons, Inc.

endothelial-lined channels in the collagenous matrix (Kaplan and Browder 1973b). In these cases, veins of the frontal poles of the brain are directed medially and caudally forming a pair of large intradural parasagittal veins that join the origin and/or the course of the superior sagittal sinus close to the coronal suture at midline (Kaplan et al. 1972; Kaplan and Browder 1973b).

Occasionally, only a unilateral prominent parasagittal vein is developed (Kaplan and Browder 1973b), often associated with a contralateral small midline venous channel embedded in the falx cerebri and appearing as a smooth anterior continuation of the middle third of the superior sagittal sinus (San Millan Ruiz et al. 2012). This latter condition is defined as *unilateral hypoplastic rostral superior sagittal sinus* (San Millan Ruiz et al. 2012). The presence of these parasagittal veins is clinically important to differentiate this normal variation from thrombosis of the anterior third of the superior sagittal sinus (San Millan Ruiz et al. 2012). In other occasions, no intradural channels are observed and the cortical veins course irregularly over the cortex and then converge caudomedially to establish the lumen of the sinus (Kaplan and Browder 1973a). In longer atretic segments, tributaries from larger cortical surface, including the inferomesial poles, will course medially and caudally to form the sinus, with more striking change in venous patterns (Kaplan et al. 1972).

There have also been reports of complete absence of the superior sagittal sinus (Knott 1881; Bergman et al. 1988).

The primitive marginal sinus is an embryonic sinus that later develops into the superior sagittal sinus. Meila et al. (2012) reported cases of a persistent primitive marginal sinus with a frequency of 9.8% in children with vein of Galen malformation. Some of the presentations included the presence of:

- bilateral persistent primitive marginal sinus, transverse sinus, and fully developed superior sagittal sinus;
- the median vein of the prosencephalon draining directly through a small left primitive marginal sinus; or
- an absence of the left transverse sinus; a persistent primitive marginal sinus connected the superior sagittal sinus from its proximal third directly to the left sigmoid sinus.

Duplication of the superior sagittal sinus (Fig. 60.2) is uncommon, and may or may not be associated with encephalocele or other dural and bony defects (Otsubo et al. 1999; Tubbs and Loukas 2006; Neumann et al. 2010). It usually includes a small portion of the sinus, either the most rostral part (San Millan Ruiz et al. 2012) or the distal part near its termination. Near-complete duplication of the superior sagittal sinus is rare, and represents persistent left and right primordia of the superior sagittal sinus during fetal development (Tubbs and Loukas 2006). Woodhall (1936) reported two cases where it was doubled and Knott (1881) and Malacarne (1780) described an early bifurcation of the sinus into the transverse sinus. Curé et al. (1994) also reported that the superior sagittal sinus may become septated or partially duplicated and suggested that it occurred as a result of compression of overlapping lamboidal suture in infants. In a study of 50 children with developmental delays, Widjaja and Griffiths (2004) observed "high splitting" of the superior sagittal sinus in two patients. In another patient they also observed a shortened superior sagittal sinus, which was drained anteriorly by two prominent cortical veins. Bisaria (1985b) investigated the cranial cavities of adult cadavers and found splitting of the superior sagittal sinus into two channels with and without partition. Another variation observed by Bisaria (1985b), one which is rare, was the presence of the superior sagittal sinus dividing into three channels with two transverse sinuses on one side.

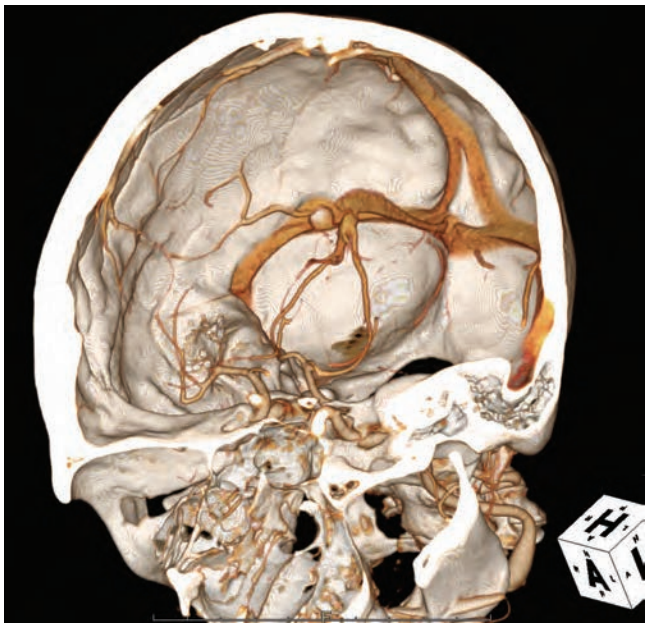

Figure 60.2 Splitting of the posterior terminal part of the superior sagittal sinus. Courtesy of J. K. Curé.

The superior sagittal sinus can drain into the torcular, jugular bulb, or left or right transverse sinuses (Fig. 60.3).

Bridging veins and lateral lacunae

Based on computed tomography venography (CTV) findings and cadaveric dissections, Brockmann et al. (2012) proclaimed that most bridging veins (BVs) empty within 3 cm rostral or caudal to the coronal suture. BVs that drain distal to the coronal suture either join first to become lacunae, or empty directly with a hairpin-shaped route. Both variants empty into the superior sagittal sinus in an antidrom direction. Although a similar structure might be found rostral to the coronal sutures, most veins empty directly in an orthodrom or perpendicular direction (Brockmann et al. 2012).

Ueyama et al. (1998) have divided the area between the superior surface of the cerebellum and tentorium cerebelli into two types: vermian/midline and hemispheric/lateral groups. The vermian bridging veins are present in the midline and empty into the confluence of sinuses. The hemispheric bridging veins

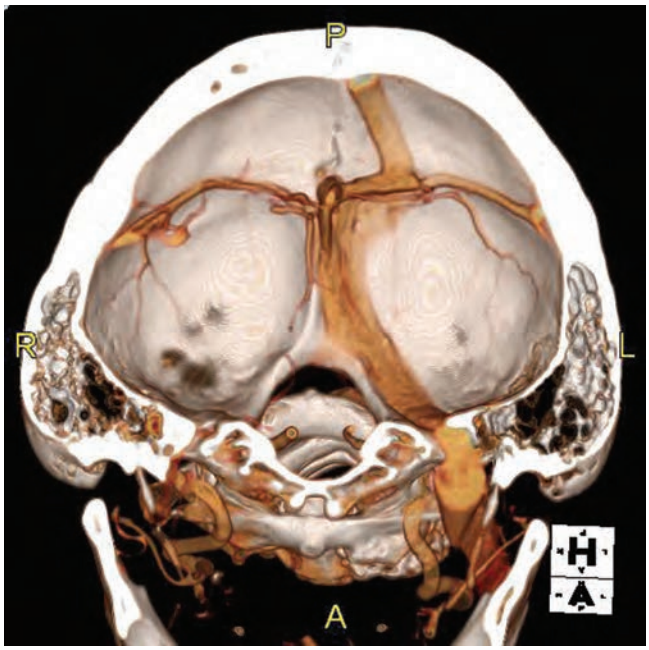

Figure 60.3 Superior sagittal sinus draining into the left transverse sinus and left oblique occipital sinus. Courtesy of J. K. Curé.

are found on the hemispheric surface of the tentorium cerebelli and empty into the tentorial sinuses. The hemispheric bridging veins were further classified into three types: type I, which is formed by the union of superior and inferior hemispheric veins; type II, which is formed by the union of superior hemispheric veins only; and type III, which is formed by the union of inferior hemispheric veins only (Mortazavi et al. 2013).

The lateral lacunae (of Trolard) are divided into frontal (small), parietal (large), and occipital (intermediate) lacunae (Standring 2008; Tubbs et al. 2008) The length of lacunae ranges between 1 and 6 cm, and the width ranges between 0.5 and 3.5 cm. Tubbs et al. (2008) found a mean of 1.9 lacunae (range 0–3) were found on right sides and a mean of 1.4 (0–3) lacunae were seen on left sides. Although there tended to be slightly more lacunae on right sides, this did not reach statistical significance. The average length of the lacunae was 3.2 cm (range 1.5–6 cm) for right sides and 2.0 cm (range 1.1–3.2 cm) for left sides. The mean width of these venous lakes was 1.5 cm for right sides (range 0.8–3.4 cm) and 0.8 cm for left sides (range 0.4–1.2 cm). Lacunae were variably positioned but tended to cluster near the vertex of the skull. No lacunae were identified posterior to the lambdoidal sutures and only five lacunae were found to lie anterior to the coronal suture, with four of these located on the right. When lacunae were identified anterior to the coronal suture, they were generally 5–6 cm from this structure. The vast majority of lacunae could be identified between the coronal and lambdoidal sutures and within 3 cm of the midline. Larger lacunae appear most consistently in the parietal and posterior frontal regions between the coronal and lambdoidal sutures and near the vertex of the skull. Nevertheless, they can be found anywhere along the superior sagittal sinus. Laterally, they usually lie within 3 cm of the midline (Tubbs et al. 2008), and can be as close as 1.1 cm (Tubbs et al. 2001). In older people, these lacunae tend to coalesce and form one elongated lacunae of each side (Standring 2008).

Whether or not the lacunae are the major draining site of the cortical veins and its clinical importance is a matter of debate (O'Connell 1934; Woodburne and Burkel 1978; Rhoton 2002a; Standring 2008). Rhoton (2002a) found that entering or occluding a lacuna during surgery does not necessarily result in the obstruction of adjacent cortical veins (Rhoton 2002a). However, Thuy et al. (2012) reported on a rare anatomic variation in which the superior anastomotic vein of Trolard communicates directly with a lateral lacuna of the superior sagittal sinus. The authors also suggest that, in such a variation, an occlusion of the lacunae may lead to a devastating cortical venous infarct if collateral venous drainage is not adequate (Thuy et al. 2012).

Crosby et al. (1962) stated that sometimes the sphenoparietal sinus continues laterally and superiorly, accompanying an anterior branch of the middle meningeal artery, to communicate with the superior sagittal sinus via the lacunae. Rhoton (2002a) found that the lacunae receive predominantly the drainage from the meningeal veins and, contrary to some authors (Le Gros Clark 1920), he did find sites of communication between cortical veins and the lacunae although these usually passed inferior to rather than emptying directly into the lacunae to reach the superior sagittal sinus. Additionally, some lacunae were found to share a common opening into the sinus with cortical veins. Interestingly, O'Connell (1934) observed that thrombus was never found in the lacunae at postmortem examination.

Topographically, Rhoton (2002a) found that the lacunae are largest and most constant in the parietal and posterior frontal regions and that smaller lakes are seen in the occipital and frontal regions; on occasion, separate lacunae are replaced by a single lacuna on each side of the superior sagittal sinus. This is in contrast to the descriptions of others, who found the lacunae as mostly related to the posterior part of the superior sagittal sinus (Gómez et al. 1981). This author further described the lacunae as extending as far as 3 cm lateral to the midline and spreading out over the upper extent of the precentral, central, and postcentral gyri.

Browder and Kaplan (1976) observed that there were three lacunae on either side of the superior sagittal sinus, differing in width. In old specimens, Browder and Kaplan (1976) found that the lacunae extended as a continuous structure in the parasagittal zone throughout the rostral 4/5th of the superior sagittal sinus. Browder et al. (1973) noted that there was a connection between the lateral border of the lacunae and the superior cerebral vein, as it traveled to the superior sagittal sinus in 10% of specimens.

Inferior sagittal sinus

This sinus is also known as the sinus longitudinal inferior. Anomalies of the inferior sagittal sinus are not very common. Figure 60.1 illustrates an extremely enlarged inferior sagittal sinus. From examining 449 specimens, Browder and Kaplan (1976) reported a case of an aneurysm of the inferior sagittal sinus without arterial components. Knott (1881) found variations in size and differences in the point of origin of the sinus. Knott (1881) also noted a very strange termination in one of the cases where the sinus turned upwards and terminated in the superior sagittal (longitudinal) sinus instead of passing through the straight sinus (sinus rectus) just above the level of the internal occipital protuberance. Saxena et al. (1974) reported completed absence of the inferior sagittal sinus in 1 of 76 cases. Browder and Kaplan (1976) observed that, in one of the cases that they examined, the inferior sagittal sinus was absent to the naked eye but was seen under histological view.

Confluences of sinuses (torcular Herophili)

The confluence of the venous sinuses of the dura mater is often described as the junction of the superior sagittal, straight, occipital, and the two transverse sinuses. Labbé (1883) quoted Hallet's first description of an absence of the torcular Herophili in one of his drawings. Multiple variations have been described. In this section, we present several classifications of the variations at the torcular Herophili.

Woodhall (1936) described five variations of the torcular Herophili. Essentially, he added one type to the previously described classification by Edwards (1931).

1. The plexiform type (56%): this type consists of several channels that provided adequate communication between the two sides.
2. The ipsilateral type (31%): the sagittal sinus runs toward one side and the straight sinus runs to the opposite side.
3. The common pool type (9%): the straight and superior sagittal sinuses merge and both lateral sinuses drain this junction.
4. The unilateral type (4%): both the sagittal sinus and straight sinus enter the same lateral sinus with absence of the contralateral sinus.
5. The occipital type: characterized by the persistence of a large single sinus or of a paired occipital sinus with a large marginal sinus.

Woodhall (1936) suggested different draining patterns of the transverse sinus with the various patterns of the confluence. In the plexiform type, the sagittal and straight sinuses can drain equally into both sides of the transverse sinus, or one draining solely into one side of the transverse sinus and the other draining into the other side of the transverse sinus.

Browning (1953) also described four types of patterns. These were based on the presence or absence of bifurcation of the superior sagittal and straight sinus without regard for their sizes, or for those involving the transverse sinus.

1. Type I (common pool, (36%): the superior sagittal and straight sinuses form an open confluence from which the two transverse sinuses arise.
2. Type II (double bifurcation, 24%): both the superior and the straight sinuses bifurcate with union of their right and left branches to form the corresponding transverse sinus.
3. Type III (straight sinus bifurcation, 24%): the superior sagittal sinus deviates to the right of the left transverse sinus while the straight sinus bifurcates into two branches. One branch joins the superior sagittal sinus while the other branch becomes the opposite transverse sinus.
4. Type IV (superior sagittal sinus bifurcation, 16%): this is similar to type III; however, the roles of the straight and sagittal sinuses are reversed. </nl>

Bisaria (1985b) described three types of variations of the confluence.

1. Type 1 (24.5%): includes specimens where the superior sagittal sinus drains into one lateral sinus and the straight sinus into the other separately.
2. Type 2 (9.1%): includes specimens in which the superior sagittal sinus and the straight sinus fork into the lateral sinuses.
3. Type 3 (57.3%): includes specimens in which a confluence of sinuses is present with varying degrees of partitioning.

Bisaria (1985a) also observed other rare variations, including: (1) doubled straight sinuses uniting near the internal occipital protuberance to form one sinus and then becoming continuous with the left transverse sinus; (2) the transverse sinus originating from a tentorial vein; (3) a circular defect in the roof of a transverse sinus; and (4) the drainage of the tentorial vein into the confluence of sinuses.

Fukusumi et al. (2010) noted several different configurations of the confluence with other venous sinuses. There were four different patterns of drainage of the superior sagittal sinus into the transverse sinus (note that the straight sinus can be classified in the same way).

1. Type I (20%): the superior sagittal sinus drains into the confluence, which bifurcates into two transverse sinuses.
2. Type II (26.7%): there are two superior sagittal sinus (right and left limbs) that both drain into the same side of the transverse sinus.
3. Type III (44.2%): the superior sagittal sinus drains completely into the right transverse sinus.
4. Type IV (9.2%): the superior sagittal sinus drains completely into the left transverse sinus.

Macroscopically examining the occipital bone of 160 cadavers in order to determine the sinus flow around the torcular Herophili, Singh et al. (2004) described the following four patterns of flow through the dural sinuses: <nl>

1. Confluence type (35%): the superior sagittal sinus drains into a common pool of venous sinuses.
2. Bifurcation type (14%): the superior sagittal sinus divides into bilateral transverse sinuses (Fig. 60.2).

3. Right-dominant type (41%): the superior sagittal sinus drains only into the right transverse sinus.
4. Left-dominant type (10%): the superior sagittal sinus drains only in the left transverse sinus. </nl>

Kobayashi et al. (2006) described the following different patterns of the confluence from observing contrast-enhanced 3D MRV of 549 patients.

1. Type I (32.7%): the superior sagittal sinus, straight sinus and transverse sinus merge at one point.
2. Type II: the superior sagittal sinus bifurcates into bilateral transverse sinus: (a) the superior sagittal sinus into the right transverse sinus (31.5%); and (b) the superior sagittal sinus in the left transverse sinus (6.2%).
3. Type III: the superior sagittal sinus and the straight sinus branch into the bilateral transverse sinus (18.9%).
4. Type IV: the straight sinus branches into bilateral transverse sinus: (a) into the right transverse sinus (3.1%); and (b) into the left transverse sinus (4.4%).
5. Type V: (a) the straight sinus branches into the occipital sinus (0.5%); and (b) the straight sinus communicates with veins other than occipital sinus via small anastomotic veins (0.4%).
6. Type VI: (a) the left transverse sinus was defective (0.4%); and (b) the right transverse was defective (0.9%).
7. Type VII: the straight sinus branches into bilateral transverse sinuses and the s.uperior sagittal sinus drains into the straight sinus and the left transverse sinus (0.2%).
8. Type VIII: the superior sagittal sinus branches into the bilateral transverse sinus and the straight sinus branches into the superior sagittal sinus and the left transverse sinus (0.4%).
9. Type IX: the superior sagittal sinus branches into the right transverse sinus and occipital sinus. The straight sinus drains into the left transverse sinus and occipital sinus and the superior sagittal sinus communicates with the straight sinus via the small anastomotic veins (0.4%).

Surendrababu et al. (2006) investigated 100 patients to observe the variations in the cerebral venous anatomy and found that 39% of the superior sagittal sinus drained into the right transverse sinus. Fifteen percent drained into the left transverse sinus (Fig. 60.3) and the remainder drained into the torcular Herophili.

The tendency for the majority of the observed superior sagittal sinus to drain into the right transverse sinus and the straight sinus to drain into the left transverse sinus is as a result of the absence of insufficient anastomosis between these sinuses at the confluence (Woodhall 1936). However, Baker (1955) stated that these systems were devoid of anastomoses in only 3% of cases. He further reported that in 20–30% of all cases, the straight sinus and the superior sagittal sinus drained into a common compartment, which gave rise to two transverse sinuses.

Another variation was noted by Curé et al. (1994) where the basal vein of Rosenthal drained into a pouch found above the torcular Herophili. The basal vein of Rosenthal may also drain into the torcular (Figs 60.4, 60.5).

Figure 60.4 Basal vein of Rosenthal draining into the torcular. Courtesy of J. K. Curé.

Browder and Kaplan (1976) found many variations in 93 of 123 specimens observed. In these cases, they reported the absence of a "true confluence" but found many of the following aberrations in that area:

- doubling of the caudal end of the superior sagittal sinus in 21 cases (Fig. 60.2);
- narrowing of the origin of transverse by a vascular pad projecting in the lumen in 40 cases;
- the origin of the transverse sinus was represented by small multiple connections between the sinus and the confluence of sinuses in 21 cases;
- complete atresia of a segment of the sinus or of its entire length in 11 cases;
- the straight sinus had multiple connections with the area of confluence and/or the proximal transverse sinus (sometimes, one of the branches may join the caudal part of the superior sagittal sinus and/or occipital sinus); and
- a single (or frequently doubled) occipital sinus was observed with multiple terminal connections to the major channels in the area of the confluence.

Browder and Kaplan (1976) also noted peculiar aberrations in eight specimens. They noted that some venous channels

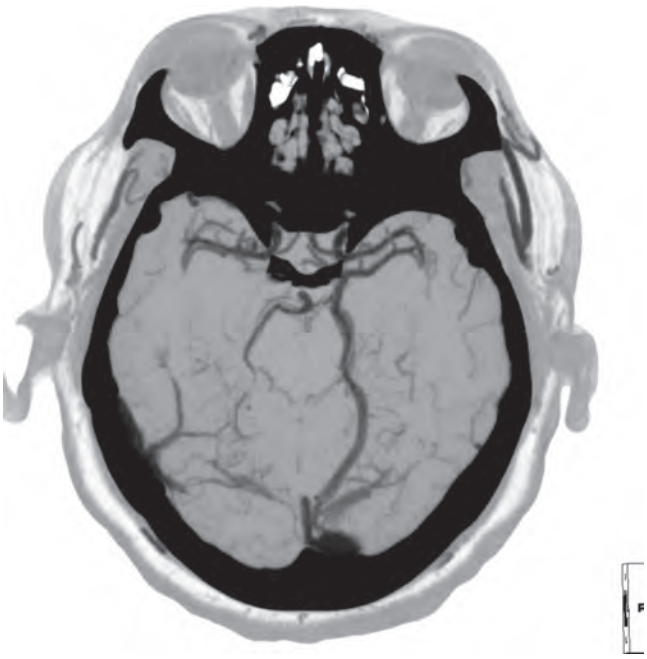

Figure 60.5 Basal vein of Rosenthal draining into the torcular. Courtesy of J. K. Curé.

formed triangular, figure-of-eight or circular configurations in the area of the confluence.

Bergman et al. (1988) also described variations of the confluence. They mentioned that the superior sagittal sinus and straight sinus can drain into a common pool or they can split into two channels with one branch joining the transverse sinuses. In 9 of the 42 cases reviewed by Bergman et al. (1988), the superior sagittal sinus joined the right transverse sinus. In two cases, the superior sagittal sinus joined the left transverse sinus. It was also observed that, in these cases, the straight sinus divided into a right and a left limb. Each limb entered into the corresponding transverse sinus. In the other 29 cases, in addition to the straight sinus bifurcating and entering the transverse sinus on the same side, the superior sagittal sinus also divided and opened along with the straight sinus into the ipsilateral transverse sinus.

Transverse sinus

According to Hollinshead (1968), the most clinically significant variation in the region of the confluence is the reduction or absence of a transverse sinus or a sigmoid sinus. It is important to identify these variations as they may cause false-positive results in a Tobey–Ayer test, leading to a false diagnosis of venous thrombosis (Hollinshead 1968).

Lower was the first to describe the right transverse sinus being slightly to moderately larger than the left transverse sinus (Knott 1881). This is secondary to the natural continuation of the sagittal sinus into the right side (Browder and Kaplan 1976; Woodhall 1936). The right transverse sinus is larger than the left (Fukusumi et al. 2010), especially in men (Singh et al. 2004). In almost all related studies, the right transverse sinus was the predominant sinus in four times more cases than the left transverse sinus (Fukusumi et al. 2010). The left transverse sinus has also been reported to be larger and longer than the right transverse sinus in some individuals (Surendrababu et al. 2006; Srijit and Shipra 2007). From the 31 cases examined by Woodhall (1936), six cases had a dominant transverse sinus on the right side while three cases had a dominant transverse sinus on the left side. Browder and Kaplan (1976) conducted a study of 215 specimens and found that 33% showed right-sided dominance; 16% showed equal dominance; 8% showed left-sided dominance; and the remainder had a variety of developmental aberrations. They also observed that in cases where there was doubling of the distal 1–3 cm of the superior sagittal sinus, the smaller channel was the origin of a small transverse sinus. They also found that, in some cases, the lumen of the transverse sinus was also narrowed by the presence of a vascular mesh. Another variation found by Browder and Kaplan (1976) was the presence of numerous connections joining the confluence of sinuses to the transverse sinus. As many as five openings were observed in some specimens. In these cases, it was found that the transverse sinus was usually smaller on that side.

Aplasia and hypoplasia of one transverse sinus might be seen, with the latter being more prevalent (Das and Hasan 1970). They are mainly noticed on the left side, but may also be seen in the right transverse sinus. In total aplasia, both the superior sagittal sinus and straight sinus drain into the contralateral transverse sinus, and the superior petrosal sinus is continued directly into the sigmoid sinus forming its starting point (Waltner 1944). In a rare occasion, the left transverse sinus was severely hypoplastic and the right was absent. In this case, the superior sagittal sinus and the straight sinus both drained via a very large occipital sinus into the marginal sinus and subsequently into the jugular bulbs (Hamnett et al. 2010).

An increase in frequency of an absent transverse sinus on magnetic resonance venography (MRV) may be associated with increasing age. In a study by Rollins et al. (2005), a transverse sinus was absent in 5% of patients less than 25 months of age and in 13% of patients older than 25 months. According to them, this may be due to alterations in posterior fossa venous flow patterns rather than structural involution of the transverse sinus.

Developmental abnormalities of the proximal transverse sinus were observed in 13 of 422 specimens studied by Browder and Kaplan (1976). There was narrowing on the right side in 5 cases; on the left side in 7 cases; and on both sides in 1 specimen. In the case with narrowing on both sides, it was observed that the superior sagittal sinus continued as a large occipital sinus that joined the marginal sinus. This joined with the small bullous segment of the distal transverse sinuses at the jugular foramina. Browder and Kaplan (1976) also observed atresia of a segment of one transverse sinus in 11 (7 on the right and 4 on

the left) of the 422 specimens studied. They also noted doubling of a part of the horizontal segment of the transverse sinus in 14 specimens (9 on the left side and 5 on the right side).

Bergman et al. (1988) reported that the horizontal segment of the transverse sinus can sometimes be absent. When this happens, it usually occurs on the left side. They also noted that the transverse sinus can occasionally communicate with the cavernous sinus or ophthalmic vein through an aberrant vein. Knott (1881) described two instances of complete absence of the right transverse sinus with only a small venous channel terminating at the mastoid foramen. Woodhall (1936) found three similar cases. Woodhall (1936) and Lieutaud (1742) each recorded a complete absence of the left transverse sinus. Knott (1881) and Browder and Kaplan (1976) described bilateral diminution of the transverse sinus, with the majority of the blood terminating in occipital and marginal sinuses.

The transverse sinus and the lateral sinus have been used to describe the combined transverse and sigmoid sinuses (Hollinshead 1968). Duplication of the lateral sinus section of the transverse sinus was described by Streit (1903). The absence of the lateral sinus, although uncommon, can occur. A few cases have been reported by Lieutaud (1742), Knott (1881), Woodhall (1936), Furstenberg (1937) and Browder and Kaplan (1976).

Malacarne (1780), Barkow (1851), Laff (1930), Hoople (1936) and Knott (1981) described unusual cases where most of the blood from the transverse sinus left the skull through the mastoid foramen. Hoople (1936) found that when this occurred, the jugular foramen is usually contracted and the sigmoid sinus is usually reduced or absent. In Knott's cases the transverse sinus was very small, measuring 1.5 mm in diameter. In Malacarne's case, the mastoid foramen was enlarged and a normal sized lateral sinus exited through it. Laff (1930) also observed this, but also noted the presence of other abnormalities including: a small jugular foramen; an absent jugular bulb; and the inferior petrosal sinus that emptied into a small jugular vein. Barkow (1851) observed that in addition to finding an enlarged mastoid foramen, the sigmoid sinus was absent. Hoople (1936) reported another variation where the right transverse and sigmoid sinuses were small and the sigmoid sinus ended blindly at the jugular foramen with its drainage entering through the sinuses of the middle cranial fossa. Furstenberg (1937) described a variation in the lateral sinus in which it was completely located outside the skull in the soft tissues. Williams (1930) reported a "thread-like lateral sinus."

Streit (1903) observed cases where the lateral sinus was doubled. In some of the cases, they observed that the channels were separated by a fibrous septum for a short or long distance or sometimes by a bony ridge.

In a study conducted by Ayanzen et al. (2000), 59% of the transverse sinuses observed were found to be right-dominant. Twenty-five percent were left-dominant and 16% were co-dominant. Thirty-one percent of patients with normal MRI had flow gaps. Ninety percent of them had a non-dominant transverse sinus and 10% had a co-dominant transverse sinus (Ayanzen et al. 2000). A similar observation was made by Surendrababu et al. (2006). They investigated 100 patients to observe the variations in the cerebral venous anatomy, and found that 59 patients had a right-dominant transverse sinus, 30 patients had a left-dominant sinus, and 10 patients had a co-dominant transverse sinus. They also found that the right transverse sinus was hypoplastic in 13 patients and the left transverse sinus was hypoplastic in 35 patients. However, in one patient, the transverse sinus was absent on the left side.

Alper et al. (2004) used time-of-flight MRV to observe the transverse sinuses in 105 people and found that 21 (20%) had aphasia of the left sinus; 41 (39%) had hypoplasia of the left sinus; 33 (31%) were symmetric; 6 (6%) showed hypoplasia of the right sinus; and 4 (4%) showed aphasia of the right sinus. In general, 62 (59%) had a larger right transverse sinus and 10 (9.5%) had a larger left transverse sinus. Twenty-four percent had flow gaps (aphasia) in right and left transverse sinuses.

Baker (1955) described a rare anomaly where both the superior sagittal sinus and the straight sinus drained into one transverse sinus and the other transverse sinus, which was much smaller in size, received blood from anterior tributaries.

Overlapping of the lamboidal sutures in infants may result in septation of the transverse sinus, usually at the proximal end (Curé et al. 1994). Some patients may have an aneurysm of the distal end of the transverse sinus, sigmoid sinus, or the jugular bulb (Curé et al. 1994).

Sigmoid sinus

There are fewer variations with the sigmoid sinus than the transverse sinus (Waltner 1944). The jugular bulb may be absent. Williams (1930) reported an apparent unilateral absence of the sigmoid sinus. He followed this with another observation in 1940 of a complete absence of the venous sinuses on the right including the sigmoid sinus (Williams and Hallberg 1941). Similarly, others have reported cases of complete absence of the sigmoid sinus (Waltner 1944; Deeb et al. 1981; Kiritsi et al. 2011).

Ruttin (1926) was the first to describe an outpouching or diverticulum of the sigmoid sinus superiorly. Furstenberg (1937) described a case of the sigmoid sinus ending in a blind pouch and draining through a large mastoid foramen.

Hypoplasia or total aplasia of the sigmoid sinus is mostly seen on the left side, but may also be found on the right side (Surendrababu et al. 2006). In these cases, the transverse sinus drains into an enlarged mastoid emissary foramen (although this might be observed with normal sigmoid sinus), and the inferior petrosal sinus empties into a small jugular vein. This is usually associated with underdeveloped peterous bone (Waltner 1944; Manjunath 2004). In other cases of total absence or hypoplasia of both the transverse sinus and sigmoid sinus, the large superior petrosal sinus may pass directly through the mastoid foramen, and a large inferior petrosal sinus might be seen (Williams 1930; Waltner 1944). In a study observing the cerebral venous

anatomy of 100 patients, Surendrababu et al. (2006) discovered a hypoplastic sigmoid sinus on the right in 6 patients and on the left in 19 patients. Two patients had an aplastic sigmoid sinus on the left.

Tomura et al. (1995) studied the temporal bones of 325 patients using HR-CT and observed that 1.6% of cases had an anteriorly located sigmoid sinus.

Due to the importance of the sigmoid sinus in mastoid surgeries, Sarmiento and Eslait (2004) have studied its location and relation to other structures forming the Trautmann's triangle. Trautmann's triangle is defined as the area limited posteriorly by the anterior border of the sigmoid sinus, superiorly by the petrous ridge, and anteriorly by a line connecting the jugular bulb to the petrous apex (Reis et al. 2007). They found three distinct anatomic variations in the location of the sigmoid sinus in the mastoid cavity: type 1 (22.3%), type 2 (57.5%), and type 3 (20.2%). In type 1, the location of the sigmoid sinus was posterior, enlarging Trautmann's triangle. In type 2, the sigmoid sinus was located anteriorly diminishing the size of Trautmann's triangle. In type 3, the sigmoid sinus was medially displaced which also reduced the area of Trautmann's triangle.

The relationship between the degree of pneumatization and the distance of the sigmoid sinus from the posterior border of the external acoustic meatus (EAM) is controversial (Shatz and Sade 1990; Turgut and Tos 1992; Ichijo et al. 1996; Dai et al. 2007). Most evidence indicates that this distance is significantly shorter, with the sigmoid sinus situated more medially in well-pneumatized temporal bone (Shatz and Sade 1990; Ichijo et al. 1996; Dai et al. 2007). These findings also apply to the distance between the transverse sinus and the EAC (Shatz and Sade 1990).

Regarding gender and side variations, Dai et al. (2007) found that the sigmoid sinus in males tends to be situated more laterally and posteriorly than compared to females. This is probably related to sexual difference of cranial base size. When compared to the left side, the sigmoid sinus on the right side tends to protrude more deeply with greater cross-sectional area and situated more laterally, regardless of the cranial width. This might be related to the right-side dominance of venous sinus drainage. In males, the right sigmoid sinus was situated more anteriorly than the left sigmoid sinus (Dai et al. 2007).

Duplication of the transverse sinus is more frequent than the sigmoid sinus. The two channels are sometimes separated by a bony ridge, but might also be separated by a fibrous septum or dural sheath dividing the lumen of the sinus for a shorter or a longer distance (Waltner 1944).

Contracted jugular foramen with small internal jugular vein is a rare phenomenon that mostly affects the left side, and is associated with significant enlargement of the contralateral vein. Occasionally, the affected side is associated with absent transverse sinus, sigmoid sinus, or both (Waltner 1944; Manjunath 2004).

On rare occasions, the vertical segment of the sigmoid sinus may have an unusual anterior course reaching up to the posterior wall of the external acoustic meatus (Gangopadhyay et al. 1996).

A case of sigmoid sinus ending in a blind pouch and draining through a large mastoid foramen has been reported (Furstenberg 1937). In a similar case, Ruttin (1926) reported on a small vein connecting the enlarged sigmoid sinus with the internal jugular vein, the superior petrosal sinus, and a thin transverse sinus emptying into the sigmoid sinus.

In certain conditions the left transverse sinus may begin as a tentorial vein, whereas the superior sagittal sinus and straight sinus are continuous with the right transverse sinus (Bisaria 1985a).

A 2-cm-long oblique sinus connecting the left and right transverse sinus has also been reported (Srijit and Shipra 2007).

Straight sinus (sinus rectus)

The straight sinus may be doubled or tripled (Saxena et al. 1973). Saxena et al. (1973) examined the straight sinus in 43 cadavers and found that 13.85% were doubled with 9.3% in the median position and 4.65% in the paramedian position. In 56 human cadavers, Magden (1991) found the straight sinus in 26.7% of cadavers to be doubled, being either median in position (one superior to the other; 17.8%) or paramedian (both lying on one side of the midline at the junction of the falx cerebri with the tentorium cerebella; 8.9%). In two cases (3.5%) the straight sinus was triple, being either median in position or paramedian.

The length of the straight sinus ranges between 4 and 7 cm, and its width at the terminal point ranges between 2 and 5 mm (Saxena et al. 1974).

In cases of absent inferior sagittal sinus, the straight sinus is formed by the continuation of the great cerebral vein. It may also communicate with the occipital sinus, the cavernous sinus through tentorial veins, and with the right transverse sinus (Saxena et al. 1974; Browder et al. 1976).

Double straight sinus is an infrequent anatomic variation that may be either median or paramedian. In median position, one straight sinus is superior and the other inferior. The superior straight sinus represents a continuation of the inferior sagittal sinus and the inferior of the great cerebral vein. The two straight sinuses may either drain into the same or contralateral transverse sinuses. In paramedian position, the sinuses lie on either side of the midline. In most instances, the left represents a continuation of the great cerebral vein and the right represents the continuation of the inferior sagittal sinus. Each paramedian straight sinus drains in the ipsilateral transverse sinus (Saxena et al. 1973, 1974; Browder et al. 1976; Magden 1991).

A triple straight sinus is rare and, when present, the sinuses are also described as median or paramedian. In both positions, a middle straight sinus is also found in addition to the superior and inferior or right and left straight sinus, which drains in either transverse sinuses (Magden 1991).

Partial duplication of the straight sinus may also be found. It usually includes the anterior part of the sinus extending to the junction with the vein of Galen. Duplication of posterior and middle parts and partial tripling has also been observed (Browder et al. 1976).

Hasegawa et al. (1991) examined the anatomic variations of the straight sinus in 108 control cases and 5 cases with a pineal region tumor. In 108 cases, the length of the straight sinus was 51±5.2 mm. The angle of the straight sinus to the nasion-tuberculum sellae line was 51±6.7°, the angle to the tuberculum sellae-inion line was 44±5.0°, and the angle the nasion-inion line was 47±5.0°. The straight sinus was placed into three groups based on the relationship with the corpus callosum.

- Type 1 (63%): the extended line of the slope of the straight sinus is tangential to the upper aspect of the splenium of the corpus callosum.
- Type 2 (high-angle, 26%): the extended line is far above the tangent line.
- Type 3 (low-angle, 11%): the extended line is far below the tangent line.

The straight sinus can also be completely or partially absent. Van den Bergh et al. (1984) described a case of congenital absence of the straight sinus in a patient with Aarskog syndrome (x-linked recessive syndrome). Knott (1881) also described one instance in which the sinus was completely absent. However, Hsu and Chalopka (2012) reported a case of a 16-year-old male with a midline persistent falcine sinus (connecting the vein of Galen and the posterior one-third of the superior sagittal sinus) with the absence of only the proximal end of the straight sinus (Fig. 60.6a, b). The distal end of the straight sinus drained the cortical veins of the occipital lobe and the superior cerebellum. Kim and Lee (2010) reported two cases of persistent falcine sinus with the complete absence of the straight sinus in a 60-year-old woman and an 11-year-old girl. Ryu (2010) examined the CTA of 586 patients and found that 12 patients had a falcine sinus with one associated with a dysplastic tentorium. Three patients had an absent straight sinus, eight patients had a rudimentary straight sinus andfour patients had a normal sinus.

Superior petrosal sinus

The superior petrosal sinus can be completely absent or enlarged, passing into the mastoid foramen in order to compensate for a small or absent transverse sinus (Knott 1881; Williams 1930; Waltner 1944). A communication between the ophthalmic vein and the superior petrosal sinus has been described (Knott 1881). Theile also noted an aberrant termination of the superior petrosal sinus into the foramen spinosum of the middle cranial fossa (Streit 1903). On rare occasions, the vein of Labbé may drain into the superior petrosal sinus; this can make surgical approaches at the skull base extremely difficult or impossible (Avci et al. 2011). Seven percent of the 14 fixed cadaver heads examined by Avci et al. (2011) showed the vein of Labbé draining directly into the superior petrosal vein. The superior petrosal sinus may be absent (Hyrtl 1862; Knott 1881).

Tubbs et al. (2013b) observed different arrangements of the superior petrosal sinus from studying the relationship between

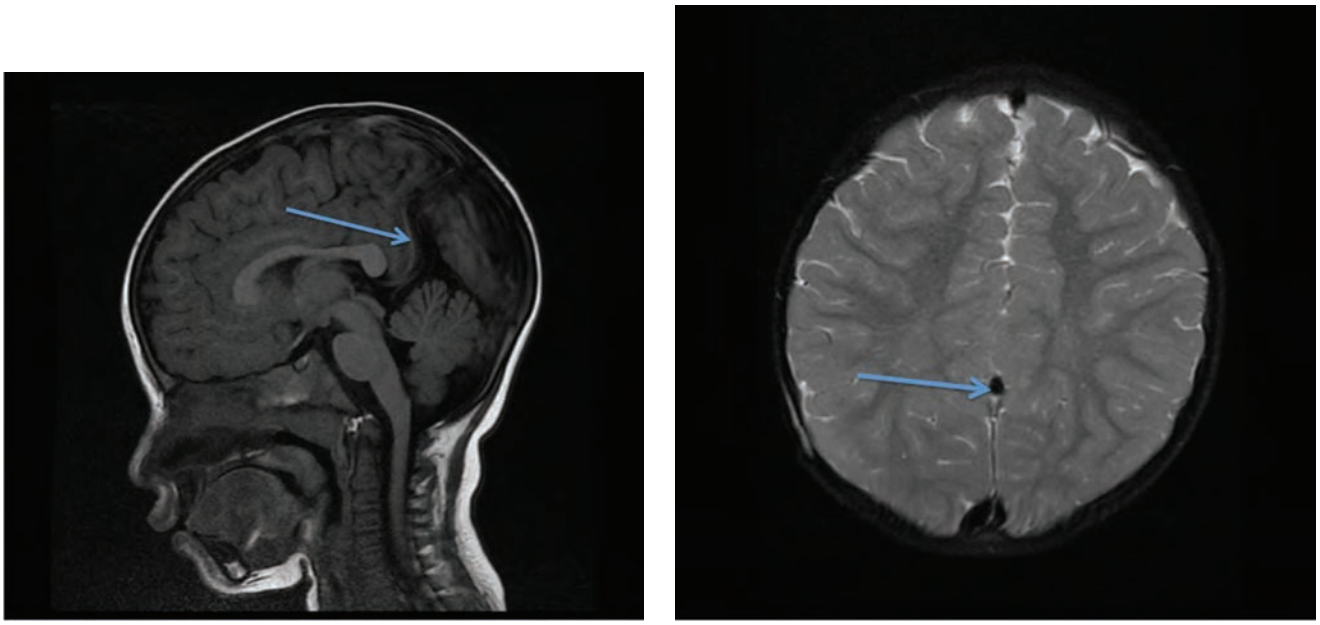

A B

Figure 60.6 (a) Mid-sagittal MRI illustrating a persistent falcine sinus (arrow) draining into the superior sagittal sinus with aplastic straight sinus; and (b) axial MRI of (a) noting the flow void of the persistent falcine sinus draining to the superior sagittal sinus (arrow).

the superior petrosal sinus and the porus trigeminus. In the 25 (50 sides) cadaver heads, 68% of the superior petrosal sinuses were superior to the opening of Meckel's cave; 18% were inferior; and 16% surrounded the opening of Meckel's cave. It was also observed that the superior petrosal sinuses that coursed inferiorly to the porus trigeminus were generally smaller than those that coursed superiorly or around the opening of Meckel's cave (Tubbs et al. 2013b).

Coates (1934) examined 31 cadavers (63 sinuses identified) to determine the relationship of the superior petrosal sinus to the trigeminal nerve. In eight specimens, both right and left sinuses passed over the cranial surface of the trigeminal nerve root. Both right and left sinuses passed under the trigeminal nerve root in three cases. The sinus divided on both sides in three cases, with some portions passing under the trigeminal root and others passing over the trigeminal nerve root.

On rare occasions, the basal vein of Rosenthal may drain into the superior petrosal sinus (Curé et al. 1994; Fig. 60.7).

Occasionally, the superior petrosal sinus may communicate with the superior ophthalmic veins through an aberrant vein termed the ophthalmo-petrosal sinus in up to 9% of the cases, according to Knott (Bergman et al. 1988). The foramen of the ophthalmo-petrosal sinus of Hyrtl is rarely seen in humans. The foramen may vary in size and may be found on one or both sides (Shapiro and Robinson 1967).

Tanoue et al. (2006) have classified the proximal communication of the superior petrosal sinus into three types. In Type A, most common, the superior petrosal sinus runs along the lesser sphenoid wing and connects with the anterior aspect of the cavernous sinus. In Type B, the superior petrosal sinus runs along the lesser sphenoid wing and connects with the foramen ovale venous plexus or the pterygoid venous plexus, in addition to the anterior aspect of the cavernous sinus. In Type C, a hypoplastic superior petrosal sinus connects with the anterior aspect of the cavernous sinus (Tanoue et al. 2006). In other occasions, the superior petrosal sinus communicates via an aberrant vein with the superior ophthalmic vein (Bergman et al. 1988). The superior petrosal sinus can be totally absent (Waltner 1944).

Figure 60.7 The left and right superior petrosal sinuses draining both basal veins of Rosenthal. Courtesy of J. K. Curé.

Middle petrosal sinus

For details of the middle petrosal sinus, the reader is referred to Bergman et al. (1988).

Inferior petrosal sinus

Major variations in the inferior petrosal sinus are extremely rare. Theile described drainage of this sinus into the superior thyroid vein (Streit 1903). Rubinstein et al. (1995) examined the anatomic variations in the course of the inferior petrosal sinus in relation to the glossopharyngeal nerve and found that, in 22 of the 25 specimens, the inferior petrosal sinus entered the foramen by passing inferior to the horizontally positioned and laterally coursing glossopharyngeal nerve. In the other three cases, the inferior petrosal sinus entered the foramen more inferiorly, heading inferiorly anteromedial or medial to the glossopharyngeal nerve as it descended into the foramen. In the jugular foramen of 16 of 20 specimens, the inferior petrosal sinus coursed inferiorly and laterally running between the descending portion of the glossopharyngeal nerve anteriorly, and the vagus and the accessory nerves posteriorly. In three specimens, the sinus remained medial to the nerves but passed medial to, and then posterior to, all three nerves in one specimen. The junction of the inferior petrosal sinus to the jugular venous system was also varied. In four of the cases, the junction was within the jugular foramen. In eight cases, it was found in the extracranial opening of the jugular foramen. In 15 cases, it was found below the skull base. In evaluating the anatomy and the normal variations of the craniocervical veins, Tanoue et al. (2010) reported two variations in the draining patterns of the inferior petrosal sinus.

- Type A (92%): the inferior petrosal sinus originated from the posterosuperior aspect of the cavernous sinus, coursed along the petroclival fissure, and drained into the medial portion of the jugular through the anterior edge of the jugular foramen.
- Type B (8%): the inferior petrosal sinus coursed along the petroclival fissure, penetrated the mid-portion of the petroclival fissure, and drained into the medial aspect of the jugular bulb.

Knott (1881) examined 11 skulls (22 sinuses) and found that the inferior petrosal sinus terminated near the lower margin of

the jugular foramen in eight sinuses; slightly above the jugular foramen in nine sinuses; and a little below in the remaining five sinuses. In two sinuses, it ended 3/8th of an inch below the skull.

Variations at the junction of the inferior petrosal sinus and the internal jugular vein (internal jugular vein) have been classified into four types. In Type I, the inferior petrosal sinus drains directly into the superior jugular bulb. In Type II, the inferior petrosal sinus drains into a communicating vein that links the superior jugular bulb to the deep cervical plexus. In Type III, the poorly formed inferior petrosal sinus is represented by a plexus of veins. In Type IV, the inferior petrosal sinus drains directly into the deep cervical venous plexus. An incomplete Type IV in which an extremely small channel links the internal jugular vein to the point of junction between the inferior petrosal sinus and the vertebral venous plexus vertebral venous plexus) was described. Inferior petrosal sinus communication with the vertebral venous plexus is via the anterior condylar vein (anterior condylar vein, mostly), lateral condylar vein, or both (Shiu et al. 1968; Miller et al. 1993; Ayeni et al. 1995; Gailloud et al. 1997; Mitsuhashi et al. 2007; Zhang et al. 2010a).

The inferior petrosal sinus can extend below the skull. Unilateral and bilateral extracranial extension of the inferior petrosal sinus may represent the most common type of inferior petrosal sinus termination. In these cases, the inferior petrosal sinus courses parallel to the internal jugular vein, separated by a variable distance of up to 100 mm (the longest reported) below the jugular foramen before joining it, reaching up to the level of C5. In other conditions the extracranial inferior petrosal sinus may divide into two branches, draining into the internal jugular vein at different levels before or after the confluence with the anterior condylar vein. One of these branches may also subdivide and join at a different level. A second division of the subdivided branches may also be seen. In the jugular foramen, the inferior petrosal sinus and the jugular bulb may be close enough to establish a small anastomosis *en passant* by direct contact with their walls (Ayeni et al. 1995; Gailloud et al. 1997; Mitsuhashi et al. 2007; Zhang et al. 2010b). The inferior petrosal sinus may also be valvular at this level.

Absence of the inferior petrosal sinus has been described but is not uncommon (Mitsuhashi et al. 2007). Mitsuhashi et al. (2007) classified the junction of the inferior petrosal sinus and internal jugular vein. In Type A, the inferior petrosal sinus drains into the superior jugular bulb. In Type B, the inferior petrosal sinus drains into the internal jugular vein at the level of the extracranial opening of the hypoglossal canal. In Type C, the inferior petrosal sinus drains into internal jugular vein at a lower extracranial level, either as a single route (C1) or with another upper venous route (C2). In Type D, the inferior petrosal sinus forms a plexus and has multiple junctions to the internal jugular vein around the jugular foramen. In Type E, the inferior petrosal sinus drains directly into the vertebral venous plexus with no connection to the internal jugular vein. Finally, in Type F the inferior petrosal sinus is absent (Mitsuhashi et al. 2007). Types D and E correspond to types III and IV, respectively, of the classifications of Shiu et al. (1968) and Miller et al (1993).

Zhang et al. (2010a) have subdivided the classification of Mitsuhashi et al. (2007) by adding the patterns of inferior petrosal sinus anastomosis with sigmoid sinus, anterior condylar vein, lateral condylar vein, and vertebral venous plexus. Type A is divided into: A1, inferior petrosal sinus directly drains into superior jugular bulb; and A2, inferior petrosal sinus has two branches after leaving the cranium to communicate with sigmoid sinus and superior jugular bulb. Type B is divided into: B1, inferior petrosal sinus drains into internal jugular vein at the level of hypoglossal canal; and B2, inferior petrosal sinus drains into internal jugular vein at the level of hypoglossal canal and has a communicating branch with sigmoid sinus. To type C, they added: C3, inferior petrosal sinus drains into internal jugular vein at a lower extracranial level either alone or with other higher branch, with a communicating branch with sigmoid sinus. Type D was divided into: D1, plexus-like inferior petrosal sinus drains into internal jugular vein near the jugular foramen; and D2, plexus-like inferior petrosal sinus drains into internal jugular vein near the jugular foramen and has a communicating branch with sigmoid sinus. In this study, a communicating branch between sigmoid sinus and inferior petrosal sinus was seen in 19% of the cases, especially in type B2 (Zhang et al. 2010a).

The diameter of the inferior petrosal sinus at its confluence with the internal jugular vein is 0.8–5.7 mm, and is usually larger on the right side (Zhang et al. 2010a, b).

In a rare case, the inferior petrosal sinus drained into the superior thyroid vein (Waltner 1944).

Tentorial sinuses

The first observation of cerebellar tentorial sinuses was described in a study on the torcular Herophili and lateral sinuses by Gibbs and Gibbs (1934). Huang et al. (1969), Babin and Megret (1973), Huang and Wolf (1974), Browder and Kaplan (1976), Bisaria (1985a) and Chung and Weon (2005) all commented on its presence in anatomical or radiographic studies. Duval et al. (1975) looked at 23 skulls and recorded the presence of the tentorial sinus in more than half of the cases. Matsushima et al. (1989) studied 26 sides of the cerebellar tentorium of 13 specimens and classified the tentorial sinuses into the following four groups:

- Group I (69.2%): the sinuses receive venous blood from the cerebral hemisphere through bridging veins.
- Group II (88.5%; which is further classified into five different subgroups): the sinuses are drained and formed by the terminal portions of the cerebellar hemispheric or vermian veins.
- Group III (42.3%): many small veins originating in the tentorium join to form a small sinus.
- Group IV (7.6%): the sinus is formed by a bridging vein from the cerebral hemisphere or brain stem to the tentorial free edge.

The variable position of the tentorial sinus may be explained during development. As the temporal lobe and the cranial fossae expand cranioventrally, the tentorial sinus is pulled into the dural mesenchyme. This process may be responsible for the difference in position of the tentorial sinus from a medial to lateral position on the middle cranial fossa floor.

Muthukumar and Palaniappan (1998) studied the anatomy of the tentorial venous sinuses in 80 cadavers and found that 86% had these sinuses. They observed three types of tentorial sinuses, as follows.

- Type I (25%): this type was the largest and was often found in the medial one-third of the tentorium cerebelli. They often had a branching staghorn appearance and usually drained into the straight sinus, the torcular Herophili, and the medial one-third of the transverse sinus.
- Type II (25%): this type was the smallest of the three types and was usually found in the lateral one-third of the tentorium cerebelli. They usually drained into the junction of the transverse sinus and the superior petrosal sinus, and into the lateral one-third of the transverse sinus.
- Type III (50%): the size of type III ranged from small to medium. They had a tendency to drain into the straight sinus, torcular Hereophili, and the medial one-third of the transverse sinus.

The tentorial sinus, located on each half of the tentorium, is divided into medial and lateral groups (Oka et al. 1985; Sakata et al. 2000; Rhoton et al. 2002b; Miabi et al. 2004). Miabi et al. (2004) reported variations in the lateral tentorial sinus in 104 of 110 lobes and classified them into 3 types.

- Type I (candelabra): found in 30 (28.8%).
- Type II (independent veins) found in 22 (21.1%).
- Type III (venous lakes): found in 37 (35.55).

The lateral tentorial sinus was indeterminate in 15 (14.4%) cases. Instead of draining into the vein of Galen, the basal vein of Rosenthal may drain into the tentorial sinus (Curé et al. 1994). The tentorial sinus may be absent. It can also have the occipital sinus and an accessory common internal cerebral vein as abnormal tributaries (Bergman et al. 1988). Occasionally, the tentorial sinuses are absent (Bergman et al. 1988).

Falcine venous plexus/sinus

A falcine sinus is a normal anatomic structure that usually involutes after birth. It is located within the falx cerebri, and is mostly seen posteriorly connecting the posterior part of the superior sagittal sinus with the straight sinus or the posterior part of the inferior sagittal sinus. Crosby et al. (1962) stated that the inferior sagittal sinus "begins in about the middle of the border of the falx with the convergence of the falcial plexus of veins." Kaplan et al. (1975) also acknowledged finding these channels in the falx. This venous plexus can communicate with the superior sagittal sinus. Rhoton (2003) noted that this connection could be large enough that the superior sagittal sinus will drain primarily into the straight and inferior sagittal sinus. Tubbs et al. (2007a) studied 27 adult specimens and found an extensive network of small tributaries within the falx cerebri in all the specimens. These channels were most prominent in the posterior one-third and within the inferior two-thirds of the falx cerebri. All the venous channels communicated with the inferior sagittal sinus. The authors further classified the venous channels based on their communication with the superior sagittal sinus.

- Type I (37%): no communication with the superior sagittal sinus.
- Type II (26%): limited communication with the superior sagittal sinus.
- Type III (37%): extensive communication with the superior sagittal sinus.

According to Curé et al. (1994), a falcine sinus may be seen in cases where there is an absent, small, or stenotic straight sinus (Fig. 60.6a). Falcine sinuses are often seen in patients who have vein of Galen malformations. It has also been suggested by Yokota et al. (1978) that the falcine sinus may actually be an "accessory straight sinus" seen in fetal specimens at 5 months, running upward within the falx between the vein of Galen and the superior sagittal sinus.

Hsu and Chalopka (2012) noted the presence of a midline persistent falcine sinus connecting the vein of Galen and the posterior one-third of the superior sagittal sinus in a 16-year-old male. Kim and Lee (2010) reported observing two cases of persistent falcine sinus in a 60-year-old woman and an 11-year-old girl. An anterior falcine sinus draining the paramedian cortical veins of the frontal lobes into inferior sagittal sinus has also been reported in a patient with agenesis of the anterior one-third of the superior sagittal sinus (Matouk et al. 2011). The falcine sinus is mostly seen in those with a congenitally absent straight sinus, which has the same embryonic origin with the falcine sinus, and is almost always associated with other anomalies including bifid cranium, vein of Galen malformation, arteriovenous malformation, agenesis of the corpus callosum, Apert syndrome, osteogenesis imperfecta, Chiari malformation type II, occipital encephalocele, acrocephalosyndactyly, absent tentorium cerebelli, and bilateral giant parietal foramina. Acquired lesions in association with persistent falcine sinus are uncommon and include venous sinus thrombosis or obstruction of the straight sinus by a mass lesion. A persistent falcine sinus with no associated anomalies is thought to be rare (Tubbs et al. 2007a; Cai et al. 2009). However, Ryu (2010) has reported this finding in 2.1% of 610 consecutive patients on computed tomography angiography.

Occipital sinus

The occipital sinus, the smallest of all venous sinuses, usually lies in the midline near the posterior attachment of the falx cerebelli. It starts caudally at the level of the foramen magnum where it communicates with the marginal sinus (when present)

anteriorly and the vertebral venous plexus inferiorly, and ends cranially at the confluence of sinuses (Adeeb et al. 2012). The length of the occipital sinus falls within the range 1.5–7 cm, its width is 1–19 mm near its termination (Das and Hasan 1970), and it is relatively wider in neonates (Widjaja and Griffiths 2004; Kopuz et al. 2010). The occipital sinus is sometimes quite large, and may even replace one of the sigmoid sinuses. This is especially true in cases of an absent transverse sinus. In such cases, the occipital sinus functions as the main drainage canal, and the marginal sinus would also be large (Hollinshead 1969; Widjaja and Griffiths 2004; Kopuz et al. 2010).

In most cases, a single occipital sinus is observed, but double occipital sinus and total absence of the sinus are not uncommon (Das and Hasan 1970; D'Costa et al. 2009; Kopuz et al. 2010). In other studies, however, an absent occipital sinus rather than its presence was the most common variation (San Millan Ruiz et al. 2002; Widjaja and Griffiths 2004) Triple occipital sinus is rare (Lang 1991), and in some conditions the OC is composed of a mesh of venous collaterals (Rollins et al. 2005). A single occipital sinus may be midline in position, right-sided, or left-sided. The median occipital sinus may occasionally divide into two or more divisions, either caudally or cranially (Das and Hasan 1970; Kopuz et al. 2010; Adeeb et al. 2012).

An age-related regression in the occipital sinuses may occur. In the MRV study by Rollins et al. (2005), the occipital sinus was found in 13% of patients who were 25 months of age but in only 2% of children older than 5 years.

This occipital sinus appears to be present with high frequency in anatomical studies (Knott 1881; Woodhall 1936, 1939; Woodhall and Seeds 1936; Gibbs and Gibbs 1934; Browning 1953; Balo 1950; Padget 1956). Knott (1881) detected its presence in 42 out of 44 specimens. Thirty-three specimens had a single occipital sinus. Eighteen of these originated above the torcular Herophili; seven opened into the left lateral sinus; five opened into the right lateral sinus; and three connected with the straight sinus quarter of an inch in front of the torcular Herophili. A bilateral sinus was found in the nine other specimens. In one of the nine cases, the occipital sinus was found lying beneath the dura mater on both sides of the internal occipital crest. Three cases had very small occipital sinuses that ended below the anastomosing network at the posterior lip of the margin of the foramen magnum. In two cases, the left occipital sinus continued on to form the marginal sinus to join the lateral sinus at the jugular foramen. A connection was made with the veins of the spinal canal. Browder and Kaplan (1976) noted the presence of a single occipital sinus in 75%, paired occipital sinuses in 8%, and absence in 15% of the specimens studied. In 2% of cases, the sinus served as a major draining pathway (Browder and Kaplan 1976). Das and Hasan (1970) looked at 200 adult cadavers and found the occipital sinus to be present in 129 specimens. They also noted a single midline occipital sinus in 35% of the specimens, a double sinus in 22.5% of the specimens, a single left-sided sinus in 4% of specimens, and a single right-sided sinus in 3% of specimens.

The size of the occipital sinus varies significantly. This can potentially cause great difficulty in posterior fossa surgical approaches (Hollinshead 1968). Hollinshead (1968) reported that sometimes the occipital sinus can be so large that it replaces the sigmoid sinus. The course of the occipital sinus may also deviate from the common presentation. Instead of passing in the midline, sometimes it deviates to one side and merges with the sigmoid sinus as it passes through the jugular foramen (Hollinshead 1968).

Tubbs et al. (2008) reported a larger than usual occipital sinus (1.5×6 cm) that drained directly into the jugular foramen and subsequently into the internal jugular vein instead of its normal drainage into the marginal sinus. An occipital sinus draining into the sigmoid sinus has been termed an oblique occipital sinus (Lang 1991). This is referred to as the oblique occipital sinus (Figs 60.8, 60.9; Tubbs et al. 2011). Another variation of the occipital sinus is where it drains directly into the bulb of the left lateral sinus with no drainage into the right lateral sinus (Tubbs et al. 2011).

The occipital sinus may be duplicated or absent. Variations of the ipsilateral lateral sinus have been observed when the occipital sinus was absent or drained into the jugular bulb. When the lateral sinus is rudimentary, the occipital sinus functions as the main drainage (Tubbs et al. 2011).

Baker (1955) described a huge occipital sinus receiving drainage from the straight and superior sagittal sinuses in 2% of cases. He also reported that in 25–30% of cases, the occipital sinus may be doubled or even absent in up to 3% of cases. D'Costa et al. (2009) studied the variations in the falx cerebelli in 52 cadavers

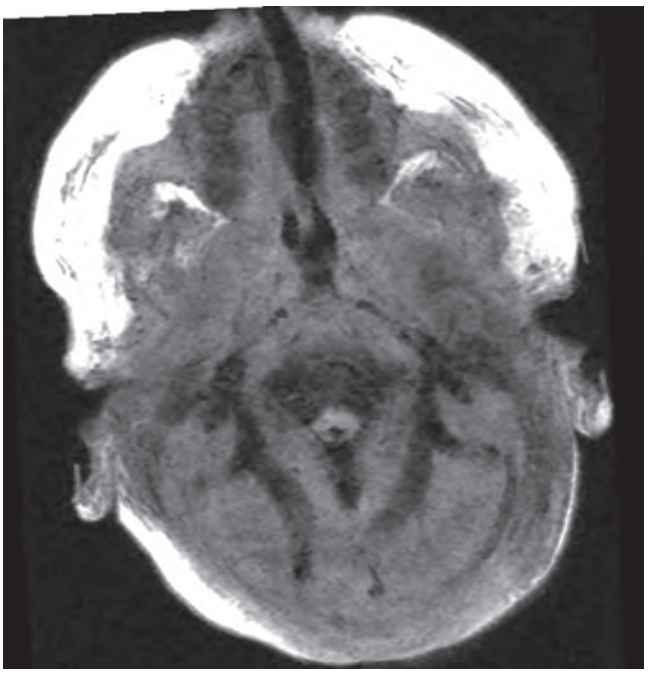

Figure 60.8 Large bilateral oblique occipital sinuses. Courtesy of J. K. Curé.

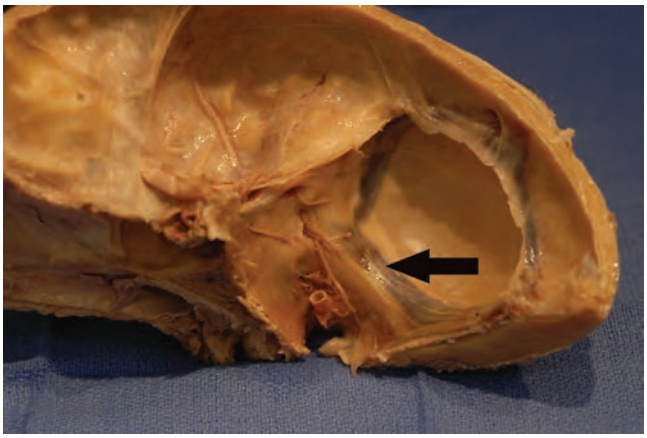

Figure 60.9 Cadaveric image of a right-sided oblique occipital sinus (arrow).

of South Indian origin and found a duplicated falx cerebelli with duplicated occipital venous sinuses in 8 cases (15.4%). No marginal sinus was found. Each of the falx cerebelli had a distinct occipital venous sinus attached to its border.

Shoja et al. (2007) described a rare variation of the occipital sinus, which they termed a "lateral occipital sinus," in a young male cadaver. The specimen examined had a duplicated falx cerebelli (right and left) and an accessory falx cerebelli attached to the underside of the tentorium cerebella 3.4 mm lateral to the base of the right falx cerebelli. There was an occipital sinus measuring 2.5 mm, which was found near the right posterolateral rim of the foramen magnum. No marginal sinus was observed. An additional venous sinus was discovered embedded within the dura mater and posterolateral to the foramen magnum at the right floor, which they referred to as a "lateral occipital sinus." The lateral occipital sinus traveled superiorly and posteromedially and divided into a medial and two lateral branches. The medial branch connected the right sigmoid sinus to the occipital sinus and the two lateral branches connected the right transverse sinuses.

Tanoue et al. (2010) used contrast-enhanced CT with a multidetector scanner to study the antomic variations of the veins at the craniocervial junction in 50 patients. The occipital sinus was seen on 18 cases. Four cases were the prominent-type occipital sinuses that originated from the torcular Herophili, coursed along the internal occipital crest, and drained into the right sigmoid sinus. Seven of the other types of the occipital sinus drained into the marginal sinus and three drained into the sigmoid sinus.

Termination of the superior sagittal, straight, transverse, and occipital sinuses

Termination of the superior sagittal sinus into the transverse sinus is the most common anatomic variation of the sinus. It ends into the right transverse sinus in most cases (right dominance), but may also end into the left transverse sinus (left dominance), and the confluence of sinuses (co-dominance). This pattern of dominance varies with patient age and is more similar to the adult pattern after 5 years of age. In children less than 2 years, the co-dominance pattern was reported to be the highest (Rollins et al. 2005). This termination usually occurs at the level of internal occipital protuberance, but may also occur above this level. In other cases, the superior sagittal sinus may fork and join with a forked straight sinus, and then becomes continuous with the transverse sinus. A partition of the dura mater may also be seen in the terminal portion of the sinus, dividing this part of the sinus into unequal channels. This dural partition may also extend and divide the confluence of sinuses, the straight sinus, or the transverse sinus. In rare occasions, the superior sagittal sinus may be divided into three channels with variant terminations. In one case, this termination included a superficial thread-like transverse sinus overlying a deeper transverse sinus.

Fukusumi et al. (2010) classified the drainage pattern of the superior sagittal sinus into the transverse sinus into four types. The same classification was also applied by Singh et al. (2004) based on the occipital bone impressions for dural venous sinuses around the confluence. They also added that type I was seen more commonly in females, while males mostly showed type III termination. Similarly, the straight sinus can also be classified in this way (Saxena et al. 1974; Fukusumi et al. 2010). The first two types are most commonly observed, and draining into the left transverse sinus is more common than draining into the right (Surendrababu et al. 2006).

In most cases, the occipital sinus terminates in the confluence of sinuses, but may also terminate into transverse sinus, superior sagittal sinus, or straight sinus (Das and Hasan 1970). In the latter condition, the occipital sinus is termed the oblique occipital sinus, and functions as the main drainage canal when the transverse sinus is rudimentary (Tubbs et al. 2011a). A more developed oblique occipital sinus was reported by Shoja et al. (2007) in association with other dural variations. In this case, the sinus was found posterolateral to the foramen magnum coursing superiorly and posteromedially and connecting the terminal portion of the right sigmoid sinus to the occipital and right transverse sinuses via one medial and two lateral branches, respectively (Shoja et al. 2007). On rare occasions, the occipital sinus may drain into the superior bulb of the internal jugular vein, in association with either normal, hypoplastic, or absent transverse sinus and sigmoid sinus (San Millan Ruiz et al. 2006).

Based on their findings, Kopuz et al. (2010) have classified the venous sinuses termination in the region of the confluence of sinuses in neonates into six types. In type I, the superior sagittal sinus is continuous with the right transverse sinus, and two occipital sinus are opened to the confluence. In type II the superior sagittal sinus is also continuous with the right transverse sinus but more than two occipital sinuses are seen opening into the confluence. Types III and IV are similar to types I and II, respectively, except that the superior sagittal sinus is

continuous with the left transverse sinus. In type V the superior sagittal sinus drains into the confluence, to which both transverse sinus and two occipital sinus are connected. In type VI, the superior sagittal sinus bifurcates before joining the transverse sinus (Kopuz et al. 2010).

Marginal sinus

The marginal sinus is an inconstant remnant of the embryonic posterior venous plexus. When present, it encircles the internal aspect of the foramen magnum and has a diameter within the range 7–15 mm, which tapers to 3–5 mm anteriorly and posteriorly. The marginal sinus connects anteriorly with the basilar venous plexus on the superior surface of the inferior clivus and with the occipital sinus posteriorly at the junction of the left and right posterior parts of the marginal sinus. However, the marginal sinus and occipital sinus may not be connected. Extracranially, it communicates with the internal vertebral venous plexus, paravertebral or deep cervical veins in the suboccipital region. Moreover, it may join the distal portions of the sigmoid sinus via small connections that pass across the intracranial surface of, and communicate with, the veins of the hypoglossal canal.

Knott (1881) described this sinus in two of the specimens studied. Similarly, Woodhall and Seeds (1936) and Browning (1953) also described them as large venous lakes at the foramen magnum region. Caruso et al. (1999) also detected this sinus on MR imaging of the craniocervical junction. Tubbs et al. (2006) examined the marginal sinus in 15 cadaveric specimens and found that 93% demonstrated drainage into the hypoglossal canal. Seventy-three percent (11 specimens) were pierced by the hypoglossal nerve root. Eighty percent (12 specimens) communicated with the basilar venous plexus and 100% communicated with the occipital venous sinus. All specimens had communication with the sigmoid sinus. In all left sides, the vertebral artery coursed through the marginal sinus as it pierced the posterior atlanto-occipital membrane. Eighty-seven percent ran through the marginal sinus on the right side. Browder and Kaplan (1976) and Hollinshead (1968) found that large occipital sinuses usually corresponded to large marginal sinuses.

Cavernous sinus

This sinus might be completely absent (Bergman et al. 1988). Knott (1881) noted a smaller than usual size of the cavernous sinus. The structures within the cavernous sinus also vary. According to Knott (1881) and Bergman et al. (1988), the cavernous sinus can receive a vein via the foramen rotundum.

Tanoue et al. (2006) evaluated 37 patients using 3D fast gradient echo MR imaging and discovered four different patterns of communication between the cavernous sinus and the superficial middle cerebral vein.

- Type A: the superficial middle cerebral vein connects with the proximal sphenoparietal sinus and flows into the frontal aspect of the cavernous sinus.
- Type B: the superficial middle cerebral vein connects with the lateral aspect of the cavernous sinus independently.
- Type C: the superficial middle cerebral vein turns downward and connects with the pterygoid venous plexus through the middle cranial fossa.
- Type D: the superficial middle cerebral vein runs across the pyramidal ridge and connects with the superior petrosal sinus or transverse sinus via the tentorial sinus.

Takahashi et al. (2007) classified the termination of the superficial middle cerebral vein into four groups.

1. Cavernous type (35.4%): the superficial middle cerebral vein enters the anterolateral aspect of the cavernous sinus.
2. Paracavernous type (10.4%): the superficial middle cerebral vein courses outside of the cavernous sinus and enters the foramen ovale or the superior petrosal sinus
3. Laterocavernous type (16.7%): the superficial middle cerebral vein runs between the two layers of the lateral wall of the cavernous sinus and enters the pterygoid venous plexus. The diameter of the superficial middle cerebral vein is smaller within the lateral wall.
4. Absent superficial middle cerebral vein (35.4%).

Controversy has arisen in the literature regarding the structure of the medial wall of the cavernous sinus, which at the same time forms the lateral part of the pituitary capsule. This is especially important in identifying the route of pituitary tumor extension. In a systematic review by Goncalves et al. (2012), four studies concluded that the medial wall of the cavernous sinus is composed of a loose, fibrous structure that might have small histological defects representing important sites of adenoma extension. On the other hand, ten studies presumed that the medial wall is formed by a single, thin layer of dura that may allow direct extension (Goncalves et al. 2012). Special attention should be given to the study of Diao et al. (2013) which has shown that the medial wall of the cavernous sinus consists of both the meningeal dura and web-like loose fibrous network, located at the anterosuperior and posteroinferior aspects of the sinus, respectively.

Sphenoparietal sinus

This sinus was first illustrated by Gilbert Breschet in the nineteenth century (Breschet 1829; San Millan Ruiz et al. 2004). The sphenoparietal sinus is around 3 mm in diameter and connects with the anterior and superior part of the cavernous sinus. Through its course, it receives veins from the temporal lobe and from the anterior temporal diploic vein, Sylvian vein, vein of Rosenthal, sphenoid emissary vein, anterior veins from the temporal lobe tip, and other small dural veins (San Millan Ruiz et al. 2004; Tubbs et al. 2007b). In other studies, this sinus may exit the cranium by joining

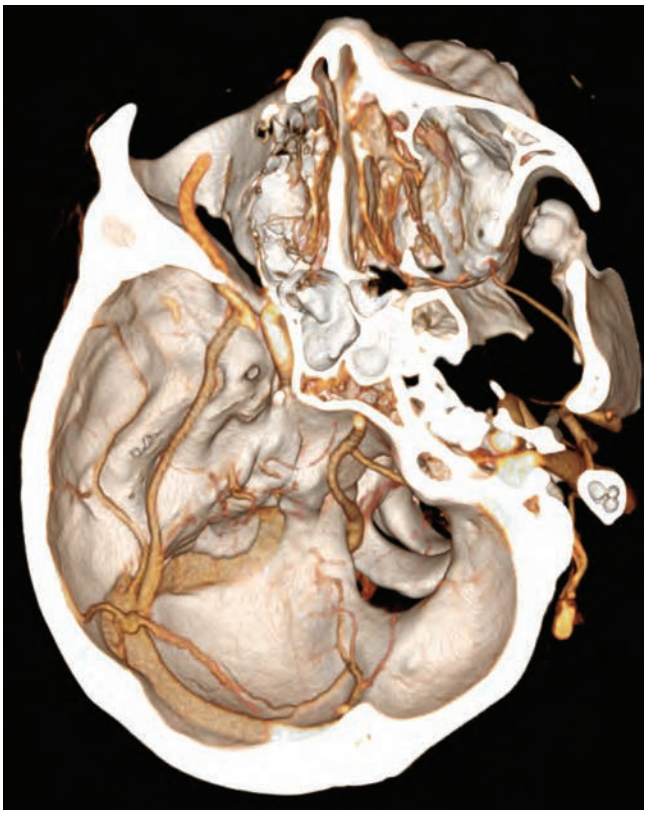

Figure 60.10 Sphenoparietal sinus draining to the ipsilateral transverse sinuse. Courtesy of J. K. Curé.

Figure 60.11 Sphenoparietal sinus draining to the ipsilateral transverse sinuse. Courtesy of J. K. Curé.

the sphenoidal emissary veins and the pterygoid venous plexus, where it is referred to as the sphenobasal sinus, and may course more posteriorly along the floor of the middle fossa to drain into the superior petrosal or transverse sinuses, where it is termed the sphenopetrosal sinus (Figs 60.10, 60.11) (Tubbs et al. 2007b).

Tanoue et al. (2006) evaluated 37 patients using 3D fast gradient echo MR imaging and noted three variations of the sphenoparietal sinus.

- Type A (72%): the sphenoparietal sinus courses along the lesser sphenoid wing and connects with the anterior aspect of the cavernous sinus.
- Type B (4%): the sphenoparietal sinus courses along the lesser sphenoid wing and connects with the foramen ovale venous plexus or the pterygoid venous plexus.
- Type C (14%): a hypoplastic sphenoparietal sinus enters the cavernous sinus.

Tubbs et al. (2007a) studied the sphenoparietal sinus of 15 cadavers and found that most sinuses began at the lateral tip of the lesser wing of the sphenoid bone and ended in the cavernous sinus near the passage of the ophthalmic nerve. No connection with the middle meningeal veins was observed in seven left sides and eight right sides. The sinus had a connection with the Sylvian vein in all except one specimen. They also observed that one sinus drained into the foramen rotundum rather than the cavernous sinus. Ten specimens had temporal veins from the anterior temporal tip that drained into the sphenoparietal sinus.

Suzuki and Matsumoto (2000) studied 500 superficial middle cerebral veins in 250 patients, and found that the superficial middle cerebral vein was present in 456 sides, 62% drained into the sphenoparietal sinus or the cavernous sinus, and 12% joined the emissary veins.

Knott (1881) noticed that the size of the canal varied greatly. He also observed that in cases where the sinus was inadequately represented, small veins were found. Cruveilhier (1852) described this venous sinus as draining diploic and meningeal veins and coursing between the middle and anterior parts of the base of the skull, occupying a transversally oriented gutter, and ending in the cavernous sinus. Trolard (1890) described a venous sinus that travels under the lesser wing of the sphenoid bone, and later named the sinus of the lesser sphenoid wing by Wolf et al. (1963). The sphenoid part of the sinus connects with the sphenoid's anterior branches of the middle meningeal veins and sits in the sphenoparietal sulcus (of Trolard), forming a distinct dural venous entity before these veins along the middle meningeal artery enter the parietal bone (parietal part) (San Millan Ruiz et al. 2004;

Tubbs et al. 2007b). According to Trolard and others, the parietal part of the sinus is actually a prolongation of the parietal part of the anterior branches of the middle meningeal veins (Trolard 1890; San Millan Ruiz et al. 2004).

Hédon (1888) noted that the superficial middle cerebral vein ends in this sinus under the lesser wing of sphenoid bone, and that it constitutes the sphenoparietal sinus. Later authors supported these findings, and added that the superficial middle cerebral vein could either join the sphenoparietal sinus or drain directly into the cavernous or paracavernous sinuses (Wolf et al. 1963; Hacker 1974; Bisaria 1985b; Oka et al. 1985). Nevertheless, San Millan Ruiz et al. (1999, 2004) denied the presence of this sinus even in cases where the superficial middle cerebral vein courses under the lesser sphenoid wing, and found that the superficial middle cerebral vein ends in the CV, paracavernous sinus, or laterocavernous sinus, or may be absent. They also added that if a dural venous sinus actually exists under the lesser sphenoid wing, it is not related to the superficial middle cerebral vein (San Millan Ruiz et al. 1999, 2004).

Ophthalmo-petrous/-petrosal sinus of Hyrtl

This sinus was first described by Hyrtl (1862). From the superior orbital fissure, this sinus passes backwards above the inner surface of the great wing of the sphenoid and the anterior surface of the temporal bone and ends in the transverse sinus (Hollinshead 1968). Knott (1881) was able to locate this sinus in 4 out of 44 specimens. When present, this sinus passes backwards from the sphenoidal fissure over the inner surface of the greater wing of the sphenoid and anterior surface of the petrous portion of the temporal bone, and terminates into the lateral portion of the transverse sinus (Knott 1881; Tubbs et al. 2007b). This sinus can also terminate by exiting through the middle meningeal vein (Hollinshead 1968) or anteriorly through the foramen ovale (Hollinshead 1968; Tubbs et al. 2007b). Both Knott (1981) and Hyrtl (1862) reported that in 8–9% of cases, the ophthalmo-petrosal sinus connected the superior petrosal or the lateral sinus.

Tubbs et al. (2007b) discovered a rare linear anteroposterior venous sinus when dissecting the cadaveric head of a 69-year-old male. The 5-mm-wide sinus ran from the sphenoparietal sinus into the middle meningeal veins.

Based on its anterolateral orientation, San Millan Ruiz et al. (2004) suggested that an orbital vein, one of the branches observed feeding the middle and the lateral one-third of the sinus of the lesser wing in a dissected specimen, could have been an ophthalmomeningeal vein of Hyrtl.

Basilar venous plexus

Tubbs et al. (2007b) examined 20 cadavers and found a basilar venous plexus in all of them. They observed that in 35%, the basilar venous plexus communicated with veins draining into the hypoglossal canal. In 60%, the basilar venous plexus communicated with the marginal sinus. In two specimens, a connection between the internal vertebral plexus and the basilar plexus was observed. They also noted that the concentration of the venous channels in the basilar plexus decreased as the structure descended inferiorly to a plane between the right and left jugular tubercles.

Aquini et al. (1994) studied 32 basilar plexuses. In 23 (71.8%) specimens, the basilar plexus was the widest intercavernous connection. The pattern of distribution varied. At the level of the dorsum sellae, the basilar plexus appeared as transverse, irregular vascular channels. In 24 cases, it did not have a well-defined vascular pattern.

Petrosquamous sinus

This sinus communicates with the deep temporal and middle meningeal veins and courses along the angle between the petrous and squamous portion of the temporal bone until it terminates in the transverse sinus or the posterior portion of the superior petrosal sinus (Hollinshead 1968). The petrosquamous sinus usually disappears during fetal development and is variably present in adults. It might be found unilaterally or bilaterally, and is more common on the left side (Conroy 1982; Marsot-Dupuch et al. 2001). It has been reported more commonly in women and in patients with severe, congenital inner ear anomalies, including aplasia of the semicircular canal, patients with hypoplasia of the internal jugular vein, and patients with other craniovertebral anomalies including sigmoid sinus hypoplasia/aplasia, facial nerve dehiscence, and craniostenosis (Marsot-Dupuch et al. 2001; An et al. 2011; Giesemann et al. 2011). A persistent petrosquamous sinus functions as an emissary vein that connects the intra- and extracranial venous networks. Nevertheless, it is often described as part of the dural venous sinuses. It arises from the dorsolateral portion of the transverse sinus at the junction with the sigmoid sinus and before the confluence of the transverse sinus with the superior petrosal sinus (Marsot-Dupuch et al. 2001). It may also arise from the sigmoid sinus (An et al. 2011) and, in a rare occasion, the origin was reported from a dilated mastoid emissary vein (Chauhan et al. 2011). It then courses along the junction of the squamous and petrous parts of temporal bone (the petrosquamosal suture), where it marks a groove that sometimes becomes a canal (canal of Vergi). It has two emptying pathways: one anteroinferiorly into the retromandibular vein via the retroarticular foramen; and one anteromedially into the pterygoid venous plexus via the foramen ovale or foramen spinosum. It ultimately drains into the external jugular vein (EJV), which marks the main drainage pathway of this sinus (Marsot-Dupuch et al. 2001; Wysocki 2002; San Millan Ruiz et al. 2006; Adeeb et al. 2012). San Millan Ruiz et al. (2006) reported one case in which the anterior portion of the petrosquamous sinus gave rise to two branches: the medial branch reaching the

foramen ovale; and a lateral branch connected extracranially with a deep temporal vein.

The petrosquamous sinus receives tributaries from the middle and superficial temporal veins, the masseteric veins, and the internal maxillary vein. It may also drain the posterior temporal diploic vein and the emissary veins of the cranial fossa. The diameter of the petrosquamous sinus is usually as small as that of a silk thread, but might reach a diameter of 2–4 mm and may have an irregular contour and tortuous course in the manner of a diploic vein (Marsot-Dupuch et al. 2001; San Millan Ruiz et al. 2006). Rarely, when the sigmoid sinus is absent or severely hypoplastic, the petrosquamous sinus may represent the major or the only drainage pathway of the transverse sinus, directing the venous blood to the EJV system. In such occasions, the EJV system becomes the major encephalic outflow pathway in the affected side (San Millan Ruiz et al. 2006).

Knott (1881) found this sinus present bilaterally in 7 out of 44 specimens and unilaterally in 19 specimens. Similarly, Vernieuwe (1921) found this sinus in 12 out of 60 specimens. Cheatle (1899), Streit (1903), and Laff (1930) all noted such a variation. Stewart (1929) reported that there was some association between the petrosquamous and the passage of infection from the middle ear to the brain. Small veins from the middle ear may drain through the petrosquamous fissure into this sinus (Hollinshead 1968). Cheatle (1899) described two cases where infection passed through the petrosquamous from the veins of the middle ear and entered the lateral sinus.

San Millan Ruiz et al. (2006) observed 13 cranial venous systems and found that a petrosquamous sinus was found in 5 of the 26 corrosion casts. In two of the five cases, a connection with the emissary veins of the foramen ovale was observed. The anterior portion of petrosquamous sinus in one of the cases divided into two branches: a medial and a lateral branch which connected extracranially to the deep temporal vein. The petrosquamous sinus had an irregular contour and a tortuous course in three cases. The other two cases had a smooth contour and were less tortuous. When the sigmoid sinus is absent or underdeveloped, the petrosquamous sinus may serve as the main outflow pathway of the transverse sinus (San Millan Ruiz et al. 2006). San Millan Ruiz et al. (2006) also described a large petrosquamous sinus found in a 7-year-old girl. On the left side, the petrosquamous sinus drained the transverse sinus. It had an anterolateral and anteromedial branch that connected it to the external jugular vein. The anterolateral branch communicated with the deep temporal veins and the anteromedial branch communicated with the emissary veins of the middle cranial fossa. The anterolateral branch left the skull through the postglenoid foramen located in the temporal squama. The sigmoid sinus and the internal jugular vein were absent. According to San Millan Ruiz et al. (2006), only the connection of the petrosquamous sinus with the middle meningeal vein and the transverse sinus persist in humans; the lateral connection with the deep temporal vein usually disappears.

Knott (1881) observed that this sinus was present on both sides in 7 of 44 cases. It was found only on one side in 19 cases. Of these 19 cases, 11 were found on the left side and 8 were found on the right side.

Accessory sinus of Kelch

When this sinus is present, it passes backward from the sphenoidal fissure crossing the upper border of the petrous portion of the temporal bone beneath the tentorium cerebelli and the superior petrosal sinus, ending into the lateral portion of the transverse sinus or into the superior petrosal sinus (Kelch 1813; Poirier 1898; Jones 1912; Stewart 1929; Hollinshead 1968). In his Doctor of Medicine thesis, Becker described this sinus in 23 out of 31 specimens. Sixteen of the 23 skulls showed it on both sides and the remainder showed it only on the left side (Stewart 1929). Knott (1881) observed this sinus in three cases.

Accessory sinus of Verga

This sinus communicates between the cavernous sinus or the ophthalmic vein anteriorly, and the left lateral sinus posteriorly (Knott 1881; Hollinshead 1968).

Petro-occipital sinus/vein

This sinus runs between the cavernous sinus and the jugular bulb passing through an opening in the petro-occipital suture. It runs along the inferior surface of the petro-occipital suture, making it one of a kind to be situated extra-cranially (Stewart 1929). Tubbs et al. (2014) proposed that, since this primarily extracranial vein communicates with intracranial sinuses, it should be considered an emissary vein.

Tubbs et al. (2014) identified the petro-occipital vein in 83.3% of 12 (24 sides) cadaveric heads. Contrary to the usual union of the internal carotid plexus to the superior jugular vein, in 10% of the sides the anterior part of the vein communicated directly with the cavernous sinus. In 15%, the posterior vein drained into sigmoid sinus. The size of the vein also varied. Sixty percent had a constant width. In 25%, the width tapered at the vein's last anterior 1–2 cm and in 15% it tapered at the vein's last posterior 1–2 cm. Venous connections were found through the bony partition between the inferior petro-occipital vein and the inferior petrosal sinus in 40% of sides. Tubbs et al. (2014) also made the following observations:

- the petro-occipital vein is larger on the side of a non-dominant transverse sinus;
- the size of the inferior petrosal sinus is always smaller in diameter when a petro-occipital vein is present;

- the posterior aspect of the vein communicated with the veins of the hypoglossal canal in 20% of sides; and
- diploic veins from the clivus drained into the inferior petro-occipital vein on one left and two right sides.

Anterior and posterior intercavernous sinuses/circular sinus

One or more transverse vessels cross the pituitary and connect the opposite sides. Browder and Kaplan (1976) found this to be present in all the specimens studied. On the other hand, Knott (1881) found this to be absent in 26 out of 44 specimens studied. Renn and Rhoton (1975) examined 50 adult sella and surrounding structures and found that 76% had an anterior intercavernous sinus and 32% had a posterior intercavernous sinus. They also noted that the anterior intercavernous sinuses were usually larger than the posterior intercavernous sinuses; however, either one or both can be absent. The anterior intercavernous sinuses were not wholly contained by the diaphragm but extended in front of the gland in 10% of cases. Tubbs et al. (2013a) studied the morphology of the anterior and posterior intercaverous sinuses in 35 cadavers and classified them into four types (Fig. 60.12).

- Type I (80%) have both an anterior and posterior intercavernous sinus.
- Type II (25% of type I) have a circular connection between the anterior and posterior intercavernous sinuses.
- Type III (17%) have only an anterior intercavernous sinus.
- Type IV (2.9%) have only a posterior intercavernous sinus.

Tubbs et al. (2013a) also found that in 80% of specimens, the anterior intercavernous sinus was larger than the posterior intercavernous sinus. In five specimens, the anterior intercavernous sinus occupied the entire anterior wall of the sella turcica. Six specimens had an inferior intercavernous sinus which was much smaller than the anterior or posterior intercavernous sinuses.

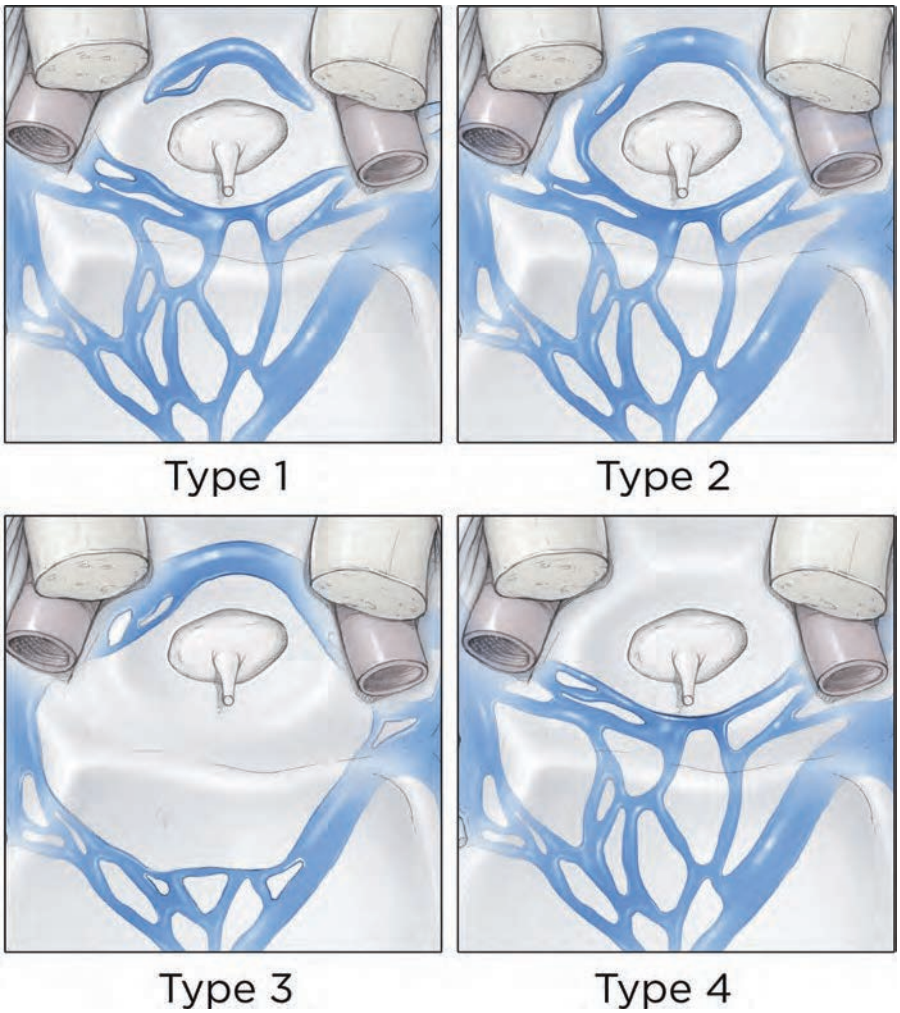

Figure 60.12 Variations of the intercavernous sinuses. Adapted from Tubbs et al. (2014).

Aquini et al. (1994) studied the intercavernous sinuses in 32 sphenoid bones using electrolytic decalcification techniques, vascular filling, x-rays and serial anatomic sections. They observed four venous sinuses interconnecting with the cavernous sinus. One hundred percent of cases had an anterior intercavernous sinus. It was the broadest intercavernous connection in three cases and occupied the entire sella turcica in 17 cases. In 22 cases, it had a curvilinear shape. In 10 cases, it ran at the level of the prechiasmatic groove. A posterior intercavernous sinus was also present in 100% of cases, and was the widest interconnection in one case.

Inferior intercavernous sinus

First described by Winslow, this sinus is located at the inferior surface of the pituitary body. Knott (1881) described this sinus in 6 out of 44 specimens. In 12 cases, instead of the circular sinus, Knott (1881) found a single intercavernous vein beneath the pituitary body. Eighty percent of the 35 cadaveric heads examined by Tubbs et al. (2013b) had both anterior and posterior intercavernous sinuses. Twenty-five percent of these cases had a circular connection between them. Aquini et al. (1994) observed the inferior intercavernous sinus in 96.9% by serial section and 75% in x-ray studies. Five specimens had the largest intercavernous connections. The inferior intercavernous sinus presented in three different ways on the sella turcica floor: the plexus-like type; venous lake; and the mixed type. A basilar plexus was found in 100% of cases (see section on "Basilar venous plexus").

Laterocavernous sinus

The lateral wall of the cavernous sinus is classically described as a double-layered structure. Whether or not it encloses a venous structure between its layers remains controversial. When present, the sinus appears as a slit-like venous sinus that runs parallel to the cavernous sinus, separated from it by the medial layer of the lateral wall of the cavernous sinus. It receives blood from the superficial middle cerebral vein in most cases and may also receive the deep middle cerebral vein. It has three draining pathways, either isolated or combined: the superior petrosal sinus (most common), pterygoid venous plexus, and the cavernous sinus (least common). In the latter case, the LS communicates with the cavernous sinus either through a large opening in the posterior aspect of the lateral wall of the cavernous sinus (most common) or through one or several secondary anastomoses with the cavernous sinus along its course. These are established either via small apertures in the medial layer of the cavernous sinus lateral wall or via small anastomotic channels at the skull base small (San Millan Ruiz et al. 1999; Gailloud et al. 2000; Lv et al. 2011).

Other variations

Srijit and Shipra (2007) reported an unusual 'oblique sinus'. The sinus was 2 cm wide and joined both left and right transverse sinuses. The superior sagittal sinus drained into the right transverse sinus, but at a higher angle than the left transverse sinus. The normal position of the confluence sinus was not seen. There was a greater indentation of the posterior lobe of the left cerebral hemisphere than on the right side.

Cavernous spaces in dural sinuses

Key and Retzius (1875) described the presence of peculiar lacunae in the dura mater. Further investigations have been conducted since then to determine the exact anatomy, histology, and function of these lacunae. Balo (1950) examined the dura mater of 100 individuals and mainly focused on the superior sagittal, straight, and the confluence of sinuses. He found that the posterior part of the superior sagittal sinus is surrounded by 1–3 mm tissue, which resembled a site of hemorrhage. On histological examination however, this spongy tissue had cavernous spaces similar to the corpora cavernosa of the penis. These cavernous tissues extend 1–2 cm along the wall of the sinus and alternate with areas without or with little cavernous tissues. It does not have a proper wall and presents within the collagenous fibers of the sinus wall. Similar structures were found along the wall of the straight sinus and the confluence of sinuses. The latter has a special form of these tissues, which extend into the lumen of the sinus in a pad-like structure. No similar structures were found in any other sinuses. The spaces of these cavernous tissues are either empty or completely filled with red blood cells. Fat globules may also be present between these blood cells, or scattered between the collagenous fibers (Balo 1950).

Chordae Willisii

Willis (1664) described the presence of many fibers or cords extending in the lumen in the dural sinuses, which he found resembling the cords extending in the ventricles of the heart, collectively known as the chordae Willisii (cords of Willis). Schmutz (1980) classified them into three types: (1) cord-like (trabecular); (2) longitudinal (lamellar or laminar), least common; and (3) valve-like (mixed or valvular), most common (Sharifi et al. 2004). Sharifi et al. (2004) found 432 chordae Willisii in 25 examined sinuses. The lowest number of them in a single sinus was 11 and the highest was 25, mean 17.2 (Sharifi et al. 2004). These fibrous structures are most commonly found at the site of cortical vein insertions into the venous sinuses, and that is why they are most commonly found in the middle third of the superior sagittal sinus. They are also found in the transverse sinus, straight sinus, and the confluence of sinuses. These structures are 1–5 in number, are usually thin (1–2 mm in diameter), extend from their broad-based attached site in the wail of the sinus, travel for 1–4 cm inside the sinus toward its tapering end, and divide the lumen into two or more channels.

Various functions have been attributed to these cords including structural tethers (which limit the expansion of the lumen), valvular structures (which limit the reflux of blood from the dural sinuses into the cortical veins), and structures that demarcate a vestibule and act as a baffle, directing the drainage of the blood delivered to the sinus from the cortical veins.

References

Avci E, Dagtekin A, Akture E, Uluc K, Baskaya MK. 2011. Microsurgical anatomy of the vein of Labbe. *Surg Radiol Anat* 33: 569–573.

Alper F, Kantarci M, Dane S, Gumustekin K, Onbas O, Durur I. 2004. Importance of anatomical asymmetries of transverse sinuses: An MR venographic study. *Cerebrovasc Dis* 18: 236–239.

An YH, JH Wee, Han KH, Kim YH. 2011. Two cases of petrosquamosal sinus in the temporal bone presented as perioperative finding. *Laryngoscope* 121: 381–384.

Aquini MG, Marrone ACH, Schneider FL. 1994. Intercavernous venous communications in the human skull base. *Skull Base Surg* 4: 145–150.

Ayanzen RH, Bird CR, Keller PJ, McCully FJ, Theobald MR, Heiserm JE. 2000. Cerebral MR venography: Normal anatomy and potential diagnostic pitfalls. *AJNR Am J Neuroradiol* 21: 74–78.

Ayeni SA, Ohata K, Tanaka K, Hakuba A. 1995. The microsurgical anatomy of the jugular foramen. *J Neurosurg* 83: 903–909.

Babin E, Megret M. 1973. Variations in the drainage of the basal vein. *Neuroradiology* 6: 154–161.

Baker AB. 1955. Clinical Neurology. Vol 3. New York: Hoeber-Harper.

Balo J. 1950. The dural venous sinuses. *Anat Rec* 106: 319–24.

Barkow JCL. 1851. *Anatomische Abhandlungen*. Breslau: F Hirt.

Bergman R, Thompson SA, Afifi AK, Saadeh FA. 1988. *Cardiovascular system. In: Compendium of Human Anatomic Variation* (ed. BergmanR). Baltimore, Munich: Urban & Schwarzenberg.

Bisaria KK. 1985a. Anatomic variations of venous sinuses in the region of the torcular Herophili. *J Neurosurg* 62: 90–95.

Bisaria KK. 1985b. The superficial sylvian vein in humans: With special reference to its termination. *Anat Rec* 212: 319–325.

Breschet G. 1829. *Recherches Anatomiques, Physiologiques et Pathologiques sur le Système Veineux et Spécialement sur les Canaux Veineux des Os*. Paris: Villeret et Rouen.

Brockmann C, Kunze SC, Schmiedek P, Groden C, Scharf J. 2012. Variations of the superior sagittal sinus and bridging veins in human dissections and computed tomography venography. *Clin Imaging* 36: 85–89.

Browder J, Kaplan H. 1976. *Cerebral Dural Sinuses and their Tributaries*. Illinois: Thomas C.

Browder J, Browder A, Kaplan HA. 1973. Anatomical relationships of the cerebral and dural venous systems in the parasagittal area. *Anat Rec* 176: 329–332.

Browder J, Kaplan HA, Krieger AJ. 1976. Anatomical features of the straight sinus and its tributaries. *J Neurosurg* 44: 55–61.

Browning H. 1953. The confluence of dural venous sinuses. *Am J Anat* 92: 307–329.

Cai CQ, Zhang QJ, Yang WD, Wang CX, Shen CH. 2009. Neuroimages of persistent falcine sinus in children. *World J Pediatr* 5: 63–64.

Caruso RD, Rosenbaum AE, Chang JK, Joy SE. 1999. Craniocervical junction venous anatomy on enhanced MR images: The suboccipital cavernous sinus. *AJNR Am J Neuroradiol* 20: 1127–1131.

Chauhan NS, Sharma YP, Bhagra T, Sud B. 2011. Persistence of multiple emissary veins of posterior fossa with unusual origin of left petrosquamosal sinus from mastoid emissary. *Surg Radiol Anat* 33: 827–831.

Cheatle AH. 1899. On the anatomy and pathological importance of the petrosquamosal sinus. *Lancet* 2: 611–612.

Chung JI, Weon YC. 2005. Anatomic variations of the deep cerebral veins, tributaries of basal vein of Rosenthal: Embryologic aspects of the regressed embryonic tentorial sinus. *Interv Neuroradiol* 11: 123–130.

Coates AE. 1934. A note on the superior petrosal sinus and its relation to the sensory root of the trigeminal nerve. *J Anat* 68: 428.

Conroy GC. 1982. The emissary foramina: Their value in platyrrhine systematics. *Am J Phys Anthropol* 57: 7–12.

Crosby E, Humphrey T, Lauer E. 1962. *Correlative Anatomy of the Nervous System*. New York: The Macmillan Company.

Cruveilhier J. 1852. *Traité d'Anatomie Descriptive: Angéologie*. Paris: Labbé.

Curé JK, Tassel PV, Smith MT. 1994. Normal and variant anatomy of the dural venous sinuses. *Seminars in Ultrasound, CT and MRI* 15: 499–519.

D'Costa S, Krishnamurthy A, Nayak SR, Madhyasta S, Prabhu LV, Jiji PJ, Ranade AV, Pai MM, Vadgaonkar R, Kumar CG, Rai R. 2009. Duplication of falx cerebelli, occipital sinus, and internal occipital crest. *Rom J Morphol Embryol* 50: 107–110.

Dai PD, Zhang HQ, Wang ZM, Sha Y, Wang KQ, Zhang TY. 2007. Morphological and positional relationships between the sigmoid sinus and the jugular bulb. *Surg Radiol Anat* 29: 643–651.

Das AC, Hasan M. 1970. The occipital sinus. *J Neurosurg* 33: 307–311.

Deeb ZL, Rotenberg D, Black FO. 1981. Aplasia of sigmoid sinus with high-lying jugular bulb. *AJNR Am J Neuroradiol* 2: 187–188.

Diao Y, Liang L, Yu C, Zhang M. 2013. Is there an identifiable intact medial wall of the cavernous sinus? Macro-microscopic anatomical study using sheet plastination. *Neurosurgery* 73: 106–109.

Duval JM, Latouche X, MOndine P, Robillard D. 1975. Sinus of the cerebellar tentorium. *Bull Assoc Anat (Nancy)* 59: 855–862.

Edwards EA. 1931. Anatomic variations of the cranial venous sinuses. Their relation to the effect of jugular compression in lumbar manometric test. *Arch Neurol and Psychia* 26: 801–814.

Fukusumi A, Okudera T, Takahashi S, Taoka T, Sakamoto M, Nakagawa H, Takayama K, Kichikawa K, Iwasaki S. 2010. Anatomical evaluation of the dural sinuses in the region of the torcular herophili using three dimensional CT venography. *Acad Radiol* 17: 1103–1111.

Furstenberg AC. 1937. Septic thrombophlebitis of the sigmoid sinus. *Trans Am Acad Ophtal* 42: 424.

Gailloud P, Fasel JH, Muster M, Desarzens F, Ruefenacht DA. 1997. Termination of the inferior petrosal sinus: An anatomical variant. *Clin Anat* 10: 92–96.

Gailloud P, San Millan Ruiz D, Muster M, Murphy KJ, Fasel JH, Rufenacht DA. 2000. Angiographic anatomy of the laterocavernous sinus. *AJNR Am J Neuroradiol* 21: 1923–1929.

Gangopadhyay K, McArthur PD, Larsson SG. 1996. Unusual anterior course of the sigmoid sinus: report of a case and review of the literature. *J Laryngol Otol* 110: 984–986.

Gibbs E, Gibbs F. 1934. The cross section areas of the vessels that form the torcular and the manner in which flow is distributed to the right and to the left lateral sinus. *Anat Rec* 59: 419–426.

Giesemann AM, Goetz GF, Neuburger J, Lenarz T, Lanfermann H. 2011. Persistent petrosquamosal sinus: High incidence in cases of complete aplasia of the semicircular canals. *Radiology* 259: 825–833.

Gómez DG, Di Bendetto AT, Pavese AM, Firpo A, Hershan DB, Potts DG. 1981. Development of arachnoid villi and granulations in man. *Acta Anat* 111: 247–258.

Goncalves MB, de Oliveira JG, Williams HA, Alvarenga RM, Landeiro JA. 2012. Cavernous sinus medial wall: Dural or fibrous layer? Systematic review of the literature. *Neurosurg Rev* 35: 147–153.

Hacker H. 1974. Normal supratentorial veins and dural sinuses. Radiology of the skull and brain: Angiography. In: *Radiology of the Skull and Brain: Angiography* (eds Newton T, Potts D). St Louis: Mosby. p 1851–1862.

Hamnett NT, Ogungbo B, Nahser H, Javadpour M. 2010. Anomalous cerebral venous sinus drainage. *Br J Neurosurg* 24: 497–498.

Hasegawa M, Yamashita J, Yamashima T. 1991. Anatomical variations of the straight sinus on magnetic resonance imaging in the infratentorial supracerebellar approach to pineal region tumors. *Surg Neurol* 36: 354–359.

Hédon C. 1888. Etude anatomique sur la circulation veineuse de l'encéphale. These Bordeaux.

Hollinshead WH. 1968. *Anatomy for Surgeons, second edition. Vol 1*. Maryland: Harper & Row.

Hoople GD. 1936. Anormaly of the lateral sinus: Report of a case. *Ann Otol Rhinol Laryngol* 45: 1019.

Hsu S, Chaloupka JC. 2012. Atretic parietal cephalocele associated with sinus pericranii: Embryological consideration. *Brain Dev* 34: 325–328.

Huang Y, Wolf B. 1974. Veins of the posterior fossa. In: *Radiology of the Skull and Brain* (eds Newton T, Ports D). St Louis: Mosby.

Huang YP, Wolf BS, Okudera T. 1969. Angiographic anatomy of the inferior vermian vein of the cerebellum. *Acta Radiol Diagn (Stockh)* 9: 327–344.

Hyrtl J. 1862. Der sinus opththalmo-petrosus. *Wien Med Wochenschr* 12: 290–291.

Ichijo H, Hosokawa M, Shinkawa H. 1996. The relationship between mastoid pneumatization and the position of the sigmoid sinus. *Eur Arch Otorhinolaryngol* 253: 421–424.

Jinkins RJ. 2000. *Venous Drainage of the Cranium. Atlas of Neuroradiologic Embryology, Anatomy and Variants*. Philadelphia: Lippincott Williams and Wilkins.

Jones FW. 1912. On the grooves upon the ossa perietellia, commonly said to be caused by the arteria meningea media. *J Anat Physiol* 46: 228–238.

Kaplan HA, Browder J. 1973a. Atresia of the rostral superior sagittal sinus: Substitute parasagittal venous channels. *J Neurosurg* 38: 602–607.

Kaplan HA, Browder J. 1973b. Venous aneurysm of the inferior sagittal sinus: Case report. *J Neurol* 39: 537–539.

Kaplan HA, Browder AA, Browder J. 1972. Atresia of the rostral superior sagittal sinus: Associated cerebral venous patterns. *Neuroradiology* 4: 208–211.

Kaplan HA, Browder J, Krieger AJ. 1975. Venous channels within the intracranial dural partitions. *Radiology* 115: 641–645.

Kelch BG. 1813. Beiträge zur pathol. *Anat* 13: 80–83.

Key A, Retzius MG. 1875. *Studien in der anatomie des nervensystems und des bindegewebes, book studien in der anatomie des nervensystems und des bindegewebes*. Stockholm: Norstad.

Kim MS, Lee GH. 2010. Two cases with persistent falcine sinus as congenital variation. *J Korean Neurosurg Soc* 48: 82–84.

Kiritsi O, Noussios G, Tsitas K, Chouridis P, Lappas D, Natsis K. 2011. Anatomical variants of the emissary veins: Unilateral aplasia of both the sigmoid sinus and the internal jugular vein and development of the petrosquamosal sinus. A rare case report. *Folia Morphol (Warsz)* 70: 305–308.

Knott JF. 1881. On the cerebral sinuses and their variations. *J Anat Physiol* 16: 27–42.

Kobayashi K, Matsui O, Suzuki M, Ueda F. 2006. Anatomical study of the confluence of the sinuses with contrast-enhanced magnetic resonance venography. *Neuroradiology* 48: 307–311.

Kopuz C, Aydin ME, Kale A, Demir MT, Corumlu U, Kaya AH. 2010. The termination of superior sagittal sinus and drainage patterns of the lateral, occipital at confluens sinuum in newborns: clinical and embryological implications. *Surg Radiol Anat* 32: 827–833.

Labbé C. 1883. Anomalies des sinus de la dure-mère. Dévelopment de ces sinus. Considérations sur la suppléance reciproque de ces canaux veineaux dans les cas d'absence de l'un d'eux description de quelque sinus peu connus. Archives de Physiologie Normale et Pathologique 3: 1–27.

Laff HJ. 1930. Unilateral absence of sigmoid sinus. *Arch Otolaryng* 11: 151.

Lang J. 1991. Clinical Anatomy of the Posterior Cranial Fossa and its Foramina. New York: Thieme.

Le Gross Clark WE. 1920. On the pacchionian bodies. *J Anat* 55: 40–48.

Lieutaud J. 1742. *Essais anatomiques*. Paris: P.M. Huart.

Lv X, Jiang C, Li Y, Liu L, Liu J, Wu Z. 2011. The laterocavernous sinus system: venous inflows, venous outflows, and clinical significance. *World Neurosurg* 75: 90–95.

Magden AO. 1991. Triple straight sinus: report of 2 cases. *Anat Anz* 173: 17–22.

Malacarne MV. 1780. Encefalotomia nuova universale. In Encefalotomia Nuova Universale. Torino: G. Biolo.

Manjunath KY. 2004. Anomalies of transverse and sigmoid sinuses associated with contracted jugular foramina. *Indian J Otolaryngol Head Neck Surg* 56: 108–114.

Marsot-Dupuch K, Gayet-Delacroix M, Elmaleh-Berges M, Bonneville F, Lasjaunias P. 2001. The petrosquamosal sinus: CT and MR findings of a rare emissary vein. *AJNR Am J Neuroradiol* 22: 1186–1193.

Matouk CC, Mandell DM, Krings T, Willinsky RA, Ter Brugge KG. 2011. Persistant anterior falcine sinus: Demonstration by CT angiography. *Can J Neurol Sci* 38: 760–761.

Matsushima T, Suzuki SO, Fukui M, Rhoton ALjr, de Oliveira E, Ono M. 1989. Microsurgical anatomy of the tentorial sinuses. *J Neurosurg* 71: 923–928.

Meila D, Paramasivam S, Niimi Y, Brassel F, Berenstein A. 2012. The persistent primitive marginal sinus: observations in children with Vein of Galen malformation. *Neuroradiology* 54: 1375–1379.

Miabi Z, Midia R, Rohrer SE, Hoeffner GE, Vandorpe R, Berk CM, Midia M. 2004. Delineation of lateral tentorial sinus with contrast-enhanced MR Imaging and its surgical implications. *AJNR Am J Neuroradiol* 25: 1181–1188.

Miller DL, Doppman JL, Chang R. 1993. Anatomy of the junction of the inferior petrosal sinus and the internal jugular vein. *AJNR Am J Neuroradiol* 14: 1075–1083.

Mitsuhashi Y, Nishio A, Kawahara S, Ichinose T, Yamauchi S, Naruse H, Matsuoka Y, Ohata K, Hara M. 2007. Morphologic evaluation of the caudal end of the inferior petrosal sinus using 3D rotational venography. *AJNR Am J Neuroradiol* 28: 1179–1184.

Mortazavi M, Denning M, Yalcin B, Shoja M, Loukas M, Tubbs RS. 2013. The intracranial bridging veins: A comprehensive review of their history, anatomy, histology, pathology, and neurosurgical implications. *Childs Nerv Syst* 29: 1073–1078.

Muthukumar N, Palaniappan P. 1998. Tentorial venous sinuses: An anatomic study. *Neurosurgery* 42: 363–371.

Neumann JO, Herweh C, Halatsch ME. 2010. Congenital duplication of the superior sagittal sinus and parietal encephalocele after vacuum extraction delivery. *Acta Neurochir (Wien)* 152: 713–716.

O'Connell JEA. 1934. Some observations of the cerebral veins. *Brain* 57: 484–503.

Oka K, Rhoton AL Jr, Barry M, Rodriguez R. 1985. Microsurgical anatomy of the superficial veins of the cerebrum. *Neurosurgery* 17: 711–748.

Otsubo Y, Sato H, Sato N, Ito H. 1999. Cephaloceles and abnormal venous drainage. *Childs Nerv Syst* 15: 329–332.

Padget DH. 1956. The cranial venous system in man in reference to development, adult configuration and relation to the arteries. *Am J Anat* 98: 307–355.

Poirier P. 1898. *Traite d'Anatomie Humaine. Vol 11*. Paris: Mason & Cie.

Reis CVC, Zabramski JM, Safavi-Abassi S, Deshmukh P, Spetzler RF, Preul MC. 2007. Trautmann's triangle and the transpetrosal approaches: An anatomical study. *Skull Base* 17: 79.

Renn W, Rhoton A. 1975. Microsurgical anatomy of the sellar region. *J Neurosurg* 43: 288–298.

Rhoton A. 2002a. The cerebral veins. *Neurosurgery* 51: 159–205.

Rhoton A. 2002b. The sellar region. *Neurosurgery* 51: 1–374.

Rhoton A. (ed.) 2003. Rhoton's Cranial Anatomy and Surgical Approaches. Schaumburg: Congress of Neurological Surgeons.

Rollins N, Ison C, Booth T, Chia J. 2005. MR venography in the pediatric patient. *AJNR Am J Neuroradiol* 26: 50–55.

Rubinstein D, Burton B, Walker A. 1995. The anatomy of the inferior petrosal sinus, glossopharyngeal nerve, vagus nerve, and accessory nerve in the jugular foramen. *AJNR Am J Neuroradiol* 16: 185–194.

Ruttin E. 1926. Kloaken und blindsackbildung am sinus sigmoideus. *Acta Otolaryngol* 9: 217–220.

Ryu CW. 2010. Persistent falcine sinus: Is it really rare? *AJNR Am J Neuroradiol* 31: 367–369.

Sakata K, Al-Mefty O, Yamamoto I. 2000. Venous consideration in petrosal approach: Microsurgical anatomy of the temporal bridging vein. *Neurosurgery* 47: 153–161.

San Millan Ruiz D, Gailloud P, de Miquel Miquel MA, Muster M, Dolenc VV, Rufenacht DA, Fasel JH. 1999. Laterocavernous sinus. *Anat Rec* 254: 7–12.

San Millan Ruiz D, Gailloud P, Rufenacht DA, Delavelle J, Henry F, Fasel JH. 2002. The craniocervical venous system in relation to cerebral venous drainage. *AJNR Am J Neuroradiol* 23: 1500–1508.

San Millan Ruiz D, Fasel JHD, Rüfenacht DA, Gailloud P. 2004. The sphenoparietal sinus of Breschet: does it exist? An anatomic study. *AJNR Am J Neuroradiol* 25: 112–120.

San Millan Ruiz D, Gailoud P, Yilmaz H, Perren F, Rathgeb J, Rufenacht CH, Fassel JHD. 2006. The petrosquamosal sinus in humans. *J Anat* 209: 711–720.

San Millan Ruiz D, Fasel JHD, Gailloud P. 2012. Unilateral hypoplasia of the rostral end of the superior sagittal sinus. *AJNR Am J Neuroradiol* 33: 286–291.

Sarmiento PB, Eslait FG. 2004. Surgical classification of variations in the anatomy of the sigmoid sinus. *Otolaryngol Head Neck Surg* 131: 192–199.

Saxena RC, Beg MA, Das AC. 1973. Double straight sinus: report of six cases. *J Neurosurg* 39: 540–542.

Saxena RC, Beg MA, Das AC. 1974. The straight sinus. *J Neurosurg* 41: 724–727.

Schmutz HK. 1980. The chordae Willisii in the superior sagittal sinus: Morphology and classification. *Acta Anat (Basel)* 108: 94–97.

Shapiro R, Robinson F. 1967. The foramina of the middle cranial fossa: A phylogenetic, anatomic and pathologic study. *Am J Roentgenol Radium Ther Nucl Med* 101: 779–794.

Sharifi M, Kunicki J, Krajewski P, Ciszek B. 2004. Endoscopic anatomy of the chordae willisii in the superior sagittal sinus. *J Neurosurg* 101: 832–835.

Shatz A, Sade J. 1990. Correlation between mastoid pneumatization and position of the lateral sinus. *Ann Otol Rhinol Laryngol* 99: 142–145.

Shiu PC, Hanafee WN, Wilson GH, Rand RW. 1968. Cavernous sinus venography. *Am J Roentgenol Radium Ther Nucl Med* 104: 57–62.

Shoja MM, Tubbs RS, Loukas M, Shokouhi G, Oakes WJ. 2007. A complex dural-venous variation in the posterior cranial fossa: A triplicate falx cerebelli and an aberrant venous sinus. *Folia Morphol (Warsz)* 66: 148–151.

Singh M, Nagashima M, Inoue Y. 2004. Anatomical variations of occipital bone impressions for dural venous sinuses around the torcular Herophili, with special reference to the consideration of clinical significance. *Surg Radiol Anat* 26: 480–487.

Srijit D, Shipra P. 2007. Unusual venous sinuses. *Bratisl Lek Listy* 108: 104–106.

Standring S. 2008. Gray's Anatomy: The Anatomical Basis of Clinical Practice, 40th edition. Philadelphia: Churchill Livingstone.

Stewart JP. 1929. The persistence of fetal blood sinuses and their relation to the middle ear spaces. *Arch Otolaryngol Head Neck Surg* 10: 266–275.

Streeter GL. 1915. The development of the venous sinuses of the dura mater in the human embryo. *Am J Anat* 18: 145.

Streit H. 1903. Ueber otologisch wichtige anormalien der hirnsinus, uber accessorische sinus und bedeutendere venenverbindungen. *Arch f Ohneuheilk* 58: 85–161.

Surendrababu N, Subathira, Livingstone RS. 2006. Variations in the cerebral venous anatomy and pitfalls in the diagnosis of cerebral venous sinus thrombosis: Low field MR experience. *Indian J Med Sci* 60: 135–142.

Suzuki Y, Matsumoto K. 2000. Variations of the superficial middle cerebral vein: Classification using three-dimensional CT angiography. *AJNR Am J Neuroradiol* 21: 932–938.

Takahashi S, Sakuma I, Otani T, Yashuda K, Tomura N, Watarai J, Yanagisawa T, Mizoi K. 2007. Venous anatomy of the sphenoparietal sinus: Evaluation by MR Imaging. *Interv Neuroradiol* 13: 84–89.

Tanoue S, Kiyosue H, Okahara M, Sagara Y, Hori Y, Kashiwagi J, Mori H. 2006. Para-cavernous sinus venous structures: Anatomic variations and pathologic conditions evaluated on fat-suppressed 3D fast gradient-echo MR images. *AJNR Am J Neuroradiol* 27: 1083–1089.

Tanoue S, Kiyosue H, Sagara Y, Hori Y, Okahara M, Kashiwagi J, Mori H. 2010. Venous structures at the craniocervical junction: Anatomical variations evaluated by multidetector row CT. *Br J Radiol* 83: 831–840.

Thuy MN, Ramesh R, Soh B, Drummond KJ. 2012. Cadaveric dissection identifying the left superior anastomotic vein of Trolard communicating indirectly with the superior sagittal sinus via a lateral lacuna. *J Clin Neurosci* 19: 286–288.

Tomura N, Sashi R, Kobayashi M, Hirano H, Hashimoto M, Watari J. 1995. Normal variations of the temporal bone on high-resolution CT: Their incidence and clinical significance. *Clin Radiol* 50: 144–148.

Trolard P. 1890. Les veines méningées moyennes. *Rev Sci Biol*: 485–499.

Tubbs RS, Loukas M. 2006. Duplication of the superior sagittal sinus. *Clin Anat* 19: 728.

Tubbs RS, Salter G, Elton S, Grabb PA, Oakes WJ. 2001. Sagittal suture as an external landmark for the superior sagittal sinus. *J Neurosurg* 94: 985–987.

Tubbs RS, Ammar K, Liechty P, Wellons III JC, Blount JP, Salter G, Oakes JW. 2006. The marginal sinus. *J Neurosurg* 104: 429–431.

Tubbs RS, Loukas M, Louis RGjr, Shoja MM, Acakpo-Satchivi L, Blount JP, Salter G, Oakes WJ, Wellons JCIII. 2007a. Anatomy of the falcine venous plexus. *J Neurosurg* 107: 155–157.

Tubbs RS, Salter EG, Wellons JC 3rd, Blount JP, Oakes WJ. 2007b. The sphenoparietal sinus. *Neurosurgery* 60: 9–12.

Tubbs RS, Loukas M, Shoja MM, Apaydin N, Ardalan MR, Oakes JW. 2008. Lateral lakes of Trolard: Anatomy, quantitation and surgical landmarks. *J Neurosurg* 108: 1005–1009.

Tubbs RS, Bosmia AN, Shoja MM, Loukas M, Curé JK, Cohen-Gadol AA. 2011. The oblique occipital sinus: A review of anatomy and imaging characteristics. *Surg Radiol Anat* 33: 747–749.

Tubbs RS, Griessenauer C, Loukas M, Cohen-Gadol AA. 2013a. The circular sinus: An anatomic study with neurosurgical and neurointerventional applications. *World Neurosurg* 12: 1341–1343.

Tubbs RS, Mortazavi MM, Krisnamurthy S, Verma K, Griessenauer CJ, Cohen-Gadol AA. 2013b. The relationship between the superior petrosal sinus and the porus trigeminus: An anatomical study/laboratory investigation. *J Neurosurg* 119(5): 1221–1225.

Tubbs RS, Watanabe K, Loukas M, Cohen-Gadol AA. 2014. Anatomy of the inferior petro-occipital vein and its relation to the base of the skull: Application to surgical and endovascular procedures of the skull base. *Clin Anat* 27(5): 698–701.

Turgut S, Tos M. 1992. Correlation between temporal bone pneumatization, location of lateral sinus and length of the mastoid process. *J Laryngol Otol* 106: 485–489.

Ueyama T, Al-Mefty O, Tamaki N. 1998. Bridging veins on the tentorial surface of the cerebellum: A microsurgical anatomic study and operative considerations. *Neurosurgery* 43: 1137–1145.

Van den Bergh P, Fryns JP, Wilms G, Piot R, Dralands G, Van den Bergh R. 1984. Anomalous cerebral venous drainage in Aarskog syndrome. *Clin Genet* 25: 288–294.

Vernieuwe S. 1921. The petrosquamus sinus. *Rev Laryngol* 53: 207.

Vitek JJ. 1989. Accessory meningeal artery: An anatomic misnomer. *AJNR Am J Neuroradiol* 10: 569–573.

Waltner J. 1944. Anatomic variations of the lateral and sigmoid sinuses. *Arch Otolaryngol Head Neck Surg* 39: 307–312.

Widjaja E, Griffiths PD. 2004. Intracranial MR venography in children: Normal anatomy and variations. *AJNR Am J Neuroradiol* 25: 1557–1562.

Williams HL. 1930. Apparent unilateral absence of sigmoid sinus noted at operation. *Arch Otolaryng* 12: 339–341.

Williams HL, Hallberg OE. 1941. Congenital absence of cranial venous sinuses on the right. *Arch Otolaryng* 33: 78.

Willis T. 1664. *Cerebri anatome cui accessit nervorum descriptio et usus, book cerebri anatome cui accessit nervorum descriptio et usus*. London: T. Roycroft.

Wolf BS, Huang YP, Newman CM. 1963. The superficial sylvian venous drainage system. *Am J Roentgenol Radium Ther Nucl Med* 89: 398–410.

Woodhall B. 1936. Variations of the cranial venous sinuses in the region of the torcular Herophili. *Arch Surg* 33: 297.

Woodhall B. 1939. Anatomy of cranial blood sinuses with particular reference to the lateral sinuses. *Laryngoscope* 49: 966–1010.

Woodhall B, Seeds AE. 1936. Cranial venous sinuses, correlation between skull markings and roentgenograms of the occipital bone. *Arch Surg* 33: 867–875.

Wysocki J. 2002. Morphology of the temporal canal and postglenoid foramen with reference to the size of the jugular foramen in man and selected species of animals. *Folia Morphol (Warsz)* 61: 199–208.

Yokota A, Oota T, Matsukado Y, Matsukado Y, Okudera T. 1978. Structures and development of the venous system in congenital malformations of the brain. *Neuroradiology* 16: 26–30.

Zhang W, Ye Y, Chen J, Wang Y, Chen R, Xiong K, Li X, Zhang S. 2010a. Study on inferior petrosal sinus and its confluence pattern with relevant veins by MSCT. *Surg Radiol Anat* 32: 563–572.

Zhang W, Ye YY, Chen JH, Chen R, Kuang LQ, Li X. 2010b. Imaging study of the long extracranial extension of the inferior petrosal sinus with MSCT. *Clin Anat* 23: 160–167.

Further reading

Bayrak A, Akay H, Ozmen C, Senturk S. 2009. Arachnoid granulations: Frequency and distribution in multi-detector row CT of dural sinuses. *Biotechnology & Biotechnological Equipment* 23: 1255–1258.

Browder J, Browder A, Kaplan HA. 1972. The venous sinuses of the cerebral dura mater. I. Anatomical structures within the superior sagittal sinus. *Arch Neurol* 26: 175–180.

Bykal L, Ceylan S, Akturk F, Dinc H, Kuzeyli K, Duru S, Soylev E. 1995. Unilateral transverse sinus aplasia: A case report. *Turkish Neurosurgery* 5: 73–75.

Choi JH, Woo HY. 2013. The neglected emissary vein in mastoidectomy; persistent petrosquamosal sinus in the laterally located sigmoid sinus. *Am J Otolaryngol* 34: 255–257.

Farb RI. 2007. The dural venous sinuses: Normal intraluminal architecture defined on contrast-enhanced MR venography. *Neuroradiology* 49: 727–732.

Gailloud P, Muster M, Khaw N, Martin JB, Murphy KJ, Fasel JH, Rufenacht DA. 2001. Anatomic relationship between arachnoid granulations in the transverse sinus and the termination of the vein of Labbe: An angiographic study. *Neuroradiology* 43: 139–143.

Gorbunov EN. 1967. Case of atresia of the sigmoid sinus. *Zh Ushn Nos Gorl Bolezn* 27: 104–105.

Grossman CB, Potts DG. 1974. Arachnoid granulations: Radiology and anatomy. *Radiology* 113: 95–100.

Grzybowski DM, Herderick EE, Kapoor KG, Holman DW, Katz SE. 2007. Human arachnoid granulations Part I: A technique for quantifying area and distribution on the superior surface of the cerebral cortex. *Cerebrospinal Fluid Res* 4: 6.

Gutierrez Y, Friede RL, Kaliney WJ. 1975. Agenesis of arachnoid granulations and its relationship to communicating hydrocephalus. *J Neurosurg* 43: 553–558.

Haroun AA, Mahafza WS, Al Najar MS. 2007. Arachnoid granulations in the cerebral dural sinuses as demonstrated by contrast-enhanced 3D magnetic resonance venography. *Surg Radiol Anat* 29: 323–328.

Harris F, Rhoton A Jr. 1976. Anatomy of the cavernous: A microsurgical study. *J Neurosurg* 45: 169–180.

Hassler W, Schlenker M. 1982. Double falx cerebelli. Case report. *Acta Neurochir (Wien)* 62: 265–269.

Hyrtl J. 1836. Neue beobachtungen aus dem gebiete der menschlichen und vergleichenden anatomie. *Med Jahrb Oesterreich Staates* 10: 457–466.

Ikushima I, Korogi Y, Makita O, Yamura M, Kawano H, Kohama M, Arikawa K, Takahashi M. 1999. MRI of arachnoid granulations

within the dural sinuses using a FLAIR pulse sequence. *Br J Radiol* 72: 1046–1051.

Kedzia A. 1987. The cerebral and meningeal venous valves during human ontogenesis. *Folia Morphol (Warsz)* 46: 197–206.

Kurata A, Suzuki S, Iwamoto K, Nakahara K, Sasaki M, Kijima C, Inukai M, Abe K, Niki J, Satou K, Fujii K, Kan S. 2011. Dural arteriovenous fistulas in the cavernous sinus: Clinical research and treatment. ISRN Neurol 2011, article ID: 453834, doi: 10.5402/2011/453834.

Larsen JL, Olsen KO. 1991. Radiographic anatomy of the distal dural sac. A myelographic investigation of dimensions and termination. *Acta Radiol* 32: 214–219.

Leach JL, Jones BV, Tomsick TA, Stewart CA, Balko MG. 1996. Normal appearance of arachnoid granulations on contrast-enhanced CT and MR of the brain: Differentiation from dural sinus disease. *AJNR Am J Neuroradiol* 17: 1523–1532.

Liang L, Korogi Y, Sugahara T, Ikushima I, Shigematsu Y, Takahashi M, Provenzale JM. 2002. Normal structures in the intracranial dural sinuses: Delineation with 3D contrast-enhanced magnetization prepared rapid acquisition gradient-echo imaging sequence. *AJNR Am J Neuroradiol* 23: 1739–1746.

Mamourian AC, Towfighi J. 1995. MR of giant arachnoid granulation, a normal variant presenting as a mass within the dural venous sinus. *AJNR Am J Neuroradiol* 16: 901–904.

Martin TJ, Troost BT, Ginsberg LE, Tegeler CH, Weaver RG. 1995. Left dural to right cavernous sinus fistula. A case report. *J Neuroophthalmol* 15: 31–35.

Paparella M, Sajjadi H. 1988. *The lateral sinus and Trautmann's triangle in Meniere's disease: Considerations of pathogenesis. Proceedings of the Second International Symposium on Menieres's Disease*. J Nadol Amsterdam, Kugler Publications.

Petroni S, Marrone AC. 1997. Study of the trabecular projections (Chordae Willisii) of the superior sagittal sinus. *Ital J Anat Embryol* 102: 155–163.

Ruge JR, Russell EJ, Levy RM. 1990. Mineralization of the falx cerebri simulating interhemispheric vascular anomalies on MR imaging. Report of three cases. *J Neurosurg* 72: 971–974.

San Millan Ruiz D. 2006. Systèmes veineux de la base du crâne et de la jonction cranio-cervicale: Anatomie macroscopique et radiologique et implications cliniques. Unpublished doctoral dissertation. Universite de Geneve.

Shohat M, Lachman R, Gruber HE, Rimoin DL. 1989. Brachyolmia: radiographic and genetic evidence of heterogeneity. *Am J Med Genet* 33: 209–219.

Shoja M, Tubbs RS, Shokouhi G, Ashrafian A, Oakes JW. 2006a. A triple dural-venous variation in the posterior cranial fossa: A duplicated plus accessory falx cerebelli and an aberrant venous sinus. 23rd Annual Meeting of the American Association of Clinical Anatomists, Milwaukee, Wisconsin.

Shoja MM, Tubbs RS, Khaki AA, Shokouhi G. 2006b. A rare variation of the posterior cranial fossa: duplicated falx cerebelli, occipital venous sinus, and internal occipital crest. *Folia Morphol (Warsz)* 65: 171–173.

Tubbs RS, Dockery SE, Salter G, Elton S, Blount JP, Grabb PA, Oakes WJ. 2002. Absence of the falx cerebelli in a Chiari II malformation. *Clin Anat* 15: 193–195.

Tubbs RS, Kelly DR, Lott R, Salter EG, Oakes WJ. 2006. Complete ossification of the human falx cerebri. *Clin Anat* 19: 147–150.

Tubbs RS, Loukas M, Shoja MM, Oakes WJ. 2007. Accessory venous sinus of Hyrtl. *Folia Morphol (Warsz)* 66: 198–199.

Tubbs RS, Hansasuta A, Loukas M, Louis RGJr, Shoja MM, Salter GE, Oakes J W. 2007. The basilar venous plexus. *Clin Anat* 20: 755–759.

Tubbs RS, Shoja MM, Loukas M. 2008. An unusual finding of the posterior cranial fossa: One case report. *Ital J Anat Embryol* 113: 83–86.

Tubbs RS, Loukas M, Shoja MM. 2009. Two cases of persistent falcine sinus. *World J Pediatr* 5: 234.

Tubbs RS, Denardo AJ, Cohen-Gadol AA. 2011. Intercavernous connection between the internal carotid arteries. *J Neurosurg Pediatr* 8: 625–627.

VandeVyver V, Lemmerling M, De Foer B, Casselman J, Verstraete K. 2007. Arachnoid granulations of the posterior temporal bone wall: Imaging appearance and differential diagnosis. *AJNR Am J Neuroradiol* 28: 610–612.

Watanabe A, Nagaseki Y, Ohkubo S, Ohhashi Y, Horikoshi T, Nishigaya K, Nukui H. 2003. Anatomical variations of the ten triangles around the cavernous sinus. *Clin Anat* 16: 9–14.

Wolpow ER, Schaumburg HH. 1972. Structure of the human arachnoid granulation. *J Neurosurg* 37: 724–727.

Zhang Z, Yang K, Wang C, Zhang C, Xie X, Tang J. 2013. Congenital pial arteriovenous fistula in the temporal region draining into cavernous sinus: A case report. *Korean J Radiol* 14: 497–500.

Zuckerkandl E. 1876. Zur anatomie der orbitalarterien. *Med Jahr* 6: 343.

61 Cerebral veins

Alireza Sadighi, Ulaş Cikla, Gregory C. Kujoth and Mustafa K. Başkaya
University of Wisconsin, Madison, Wisconsin, United States

The study of cerebral vein variations has received less attention than that of the cerebral arteries. The cerebral venous system is more variable than the arterial system in the size of vessels and the connections among them, so it has proved challenging to define a normal venous pattern (Rhoton 2002; Tatu et al. 2009). The cerebral venous system has some unique characteristics, including the absence of muscular tissue in the brain vein walls and the lack of valves in the vessels. It is estimated that about 70% of the whole cerebral blood volume is stored within the cerebral veins. Furthermore, most of the cerebral venous blood drains into the transverse and sigmoid sinuses of the skull base (Kılıç and Akakin 2008).

In principle, it is impossible to describe all variations of the cerebral venous system without studying the brain of every human being. However, familiarity with the known variations could elucidate the system. The clinical importance of these variations is highlighted by the neurosurgeons' need to select the approach that will sacrifice as few veins as possible during surgery and minimize the risk of permanent neurological sequelae after the operation. New vascular imaging modalities such as digital subtraction angiography and magnetic resonance (MR) venography have generated additional and more detailed data for a better understanding of cerebral venous anatomy.

Several surgical or angiographic classification schemes for the cerebral venous system have been proposed (Ono et al. 1984b; Oka et al. 1985; Yaşargil 1987; Lasjaunias et al. 2001; Rhoton 2007). Surgery-based classifications are generally regional rather than global because their definition criteria are based upon the approach to the target, whereas angiography-based classifications are influenced by the way in which the image is obtained (Nowinski 2012).

For the purposes of this chapter, the cerebral venous system is classified into (a) the superficial venous system and (b) the deep venous system. In the superficial venous system we discuss the Sylvian vein, the inferior anastomotic vein (vein of Labbé), and the superior anastomotic vein (vein of Trolard). The internal cerebral vein (ICV), the basal vein of Rosenthal (BVR), and the subependymal veins are discussed under the deep venous system.

Veins of the deep venous system

Basal vein of Rosenthal

Friedrich-Christian Rosenthal, a prominent German anatomist and surgeon, connected his name to the basal cerebral vein (Rosenthal 1824; Binder et al. 2006) after publishing "De intimis cerebri veins seu de venae magnae Galeni ramis" ("On the deep cerebral veins or the branches of the great vein of Galen") in 1824.

The basal vein of Rosenthal (BVR) is not one of the original pial veins but a secondary vessel formed by longitudinal anastomoses of three primitive veins during development: the telencephalic, diencephalic, and mesencephalic veins. In fact, it is a longitudinal anastomotic channel (Padget 1956, 1957). The BVR starts just anterior to the midbrain, below the anterior perforated substance. It passes laterally to the anterior perforated substance and courses posteriorly between the midbrain and the temporal lobe within the ambient cistern. It generally terminates in the vein of Galen; however, the straight sinus or the internal cerebral veins also occasionally receive its drainage (Wackenheim and Braun 1978; Suzuki et al. 2001; Chung and Weon 2005). During its course within the cistern, the posterior cerebral and superior cerebellar arteries and the trochlear nerve accompany the BVR (Tubbs et al. 2007). The BVR originates from the union of four major vessels: (1) the anterior cerebral vein, which is composed of the anterior limbic and pericallosal veins; (2) the deep middle cerebral vein (deep Sylvian vein); (3) the inferior striate veins; and (4) the medial and inferior frontal veins, including the olfactory vein (Huang and Wolf 1974a; Wackenheim and Braun 1978). Several other tributaries to the BVR have been mentioned in the literature: the hippocampal, inferior choroidal (occasionally large), inferior ventricular, posterior thalamic, peduncular, lateral mesencephalic, pontine, precentral, and quadrigeminal veins (Grand and Hopkins 1999; Tubbs et al. 2007). Many other variations of the BVR, in passage and drainage, have been reported in the literature and no classification system is considered complete; however, we will explain some of the most useful classifications of BVR variations (Padget 1956; Huang and Wolf 1974a; Ito 1986) in detail below.

Bergman's Comprehensive Encyclopedia of Human Anatomic Variation, First Edition. Edited by R. Shane Tubbs, Mohammadali M. Shoja and Marios Loukas.
© 2016 John Wiley & Sons, Inc. Published 2016 by John Wiley & Sons, Inc.

Three-dimensional computed tomography (3D CT) angiography imaging (Suzuki et al. 2001) of patients with diverse cerebral complaints due to cerebrovascular diseases, brain tumors, and other intracranial diseases has been considered for evaluation of the BVR, based upon its embryological development. Suzuki et al. used a prior anatomical classification of the BVR into three segments (Huang and Wolf 1974a) to evaluate the drainage pathways of this vein: (1) extension of the first segment from the union of the inferior striate, anterior cerebral, and deep middle cerebral veins to the anterior end of cerebral peduncle; (2) extension of the second segment to the union of the BVR and the lateral mesencephalic vein; and (3) drainage via the third segment into the vein of Galen or the internal cerebral vein. Five drainage pathways were considered for evaluation of the BVR: (1) into the vein of Galen; (2) into the cavernous sinus or sphenoparietal sinus; (3) into the superior petrosal sinus through the lateral mesencephalic vein; (4) into the superior petrosal sinus through the peduncular vein; and (5) into the transverse or straight sinus through the tentorium. Potential variations of the BVR can be classified according to these five drainage pathways and the anastomoses among the primary primitive veins (deep telencephalic, ventral diencephalic, dorsal diencephalic, and mesencephalic). Considering all these combinations, a myriad of variations (Fig. 61.1) can be expected (Huang and Wolf 1974a; Suzuki et al. 2001).

Using venous angiography, Watanabe et al. (2002) proposed a classification system for venous drainage of the BVR that identifies three major patterns: Type A, in which the main drainage of the BVR is into the vein of Galen; Type B, displaying anterior (uncal vein) and posterior (into the Galenic system) drainages of the BVR; and Type C, which has no BVR drainage into the Galenic venous system (Fig. 61.2). In this retrospective study, venograms of patients with either perimesencephalic nonaneurysmal subarachnoid hemorrhage (PN-SAH) or aneurysmal subarachnoid hemorrhage (A-SAH) were evaluated. No BVR anatomy in normal brains was studied in this evaluation and 13 BVR were excluded from the study due to motion artifacts or low-quality images. The authors found the following results from 191 BVR of A-SAH cases: 79 (41%) had type A variations; 70 (37%) type B variations; and 42 (22%) type C variations. Bilateral type A patterns were observed in 22 (22%) veins. The following variation patterns were observed among 12 BVRs in the PN-SAH group: three (25%) type A; two (17%) type B; and seven (58%) type C veins. No bilateral type A was found in this group and two (33%) BVRs drained into the tentorial sinus. These findings suggest that the BVR is more variable (type C, in 58%) in PN-SAH cases than in A-SAH (type C, in 22%) subjects, although the number of PN-SAH cases examined was much smaller. Of six cases (type C variants) in the PN-SAH group, the BVR drained into the tentorial sinus in two patients, main trunk agenesis of the BVR secondary to segmentation was found in two cases, and anterior drainage into the superior petrosal sinus and anterior pontomesencephalic vein was also revealed in two patients (Fig. 61.2).

Applying 3D CT angiography, variations of the BVR were classified by Chung and Weon (2005) into four groups on the

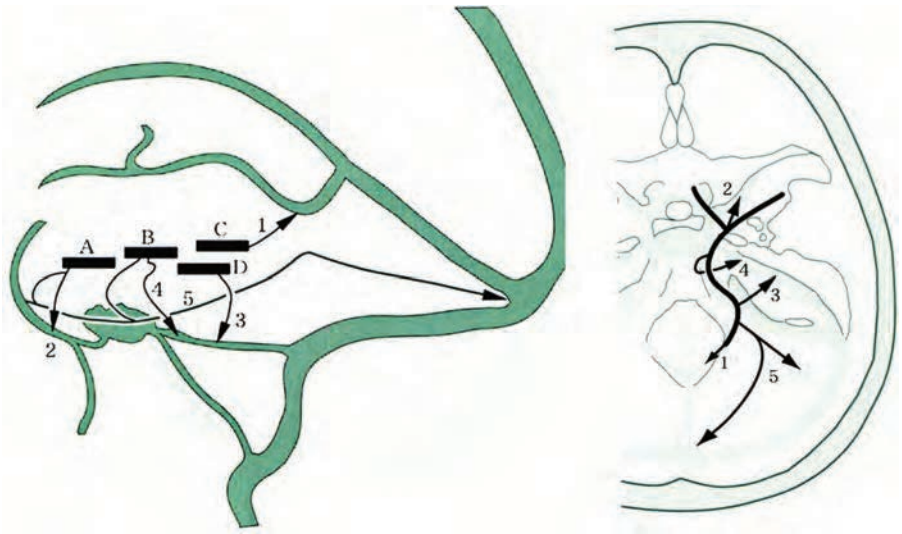

Figure 61.1 Left: In the 14–18 mm embryonic stage, development of the telencephalic, diencephalic, and mesencephalic vein components results in differentiation into the deep telencephalic vein (A), the ventral diencephalic vein (B), and the dorsal diencephalic vein (C). During the 60–80 mm embryonic stage (Padget), anastomoses among the abovementioned components and the mesencephalic vein (D) generates the BVR. For each of the primitive veins (four vessels) there are one or more drainage pathways (five routes). Combinations of the anastomoses and the drainage pathways lead to many variations. Right: The primitive veins and the drainage routes of the BVR join together longitudinally. The BVR is evaluated in terms of five drainage pathways: (1) to the great vein of Galen; (2) to the cavernous sinus or sphenoparietal sinus; (3) to the superior petrosal sinus via the lateral mesencephalic vein; (4) to the superior petrosal sinus via the peduncular vein; (5) to the transverse sinus or straight sinus via the tentorium.

Source: Suzuki et al. (2001). Reproduced with permission from American Society of Neuroradiology.

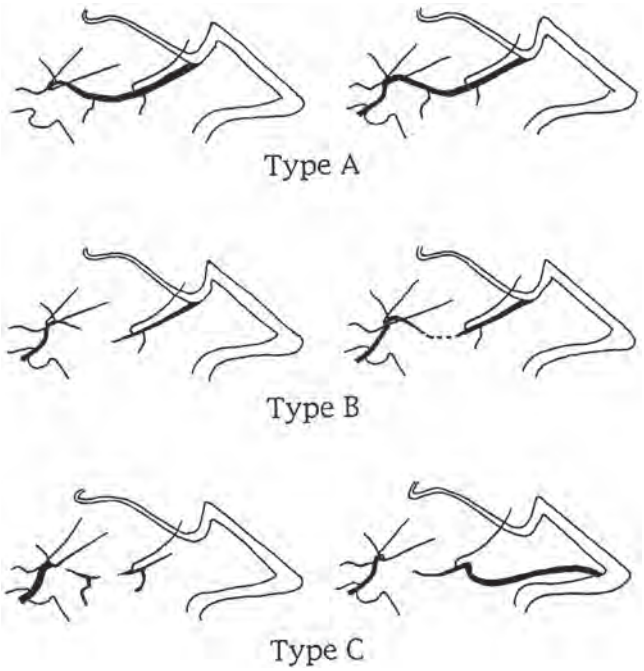

Figure 61.2 Variants of the basal vein of Rosenthal (BVR).

Source: Watanabe et al. (2002). Reproduced with permission from Springer Science and Business Media.

basis of the developmental alterations of the drainage pathways (Fig. 61.3): (a) telencephalic group (43%), composed of tributaries of the uncal, inferior frontal, anterior communicating, inferior striatal and the deep middle cerebral veins; (b) diencephalic group (35%), composed of the interior ventricular and peduncular veins; (c) tegmental bridging group (11%), involving anastomosis of the longitudinal lateromesencephalic vein (LMV) with the superior petrosal sinus; and (d) tectal group (6%), consisting of the superior vermian vein and the internal occipital vein in relation to the Galenic connection. In this study, 82 hemispheres were evaluated, of which four (5%) were unclassified and small basal tributaries of the BVR were found with no connection to the vein of Galen. In eight (10%) hemispheres, no Galenic connections were identified (Chung and Weon 2005).

In a cadaveric study, bilateral drainage of the BVR was observed more laterally into the pial veins of the temporal and occipital lobes instead of the Galenic system (Tubbs et al. 2007). There is also a report describing the drainage of the pineal veins into the BVR instead of the vein of Galen (Wackenheim and Braun 1978). Drainage of the veins of the medial occipital lobe into the caudal part of the BVR has also been reported (Browder and Kaplan 1976).

Venous variations of the subependymal veins

The striatum, the internal capsule, the corpus callosum, the septum, the fornix, and the deep white matter are drained through the subependymal veins, which travel below the ependyma of

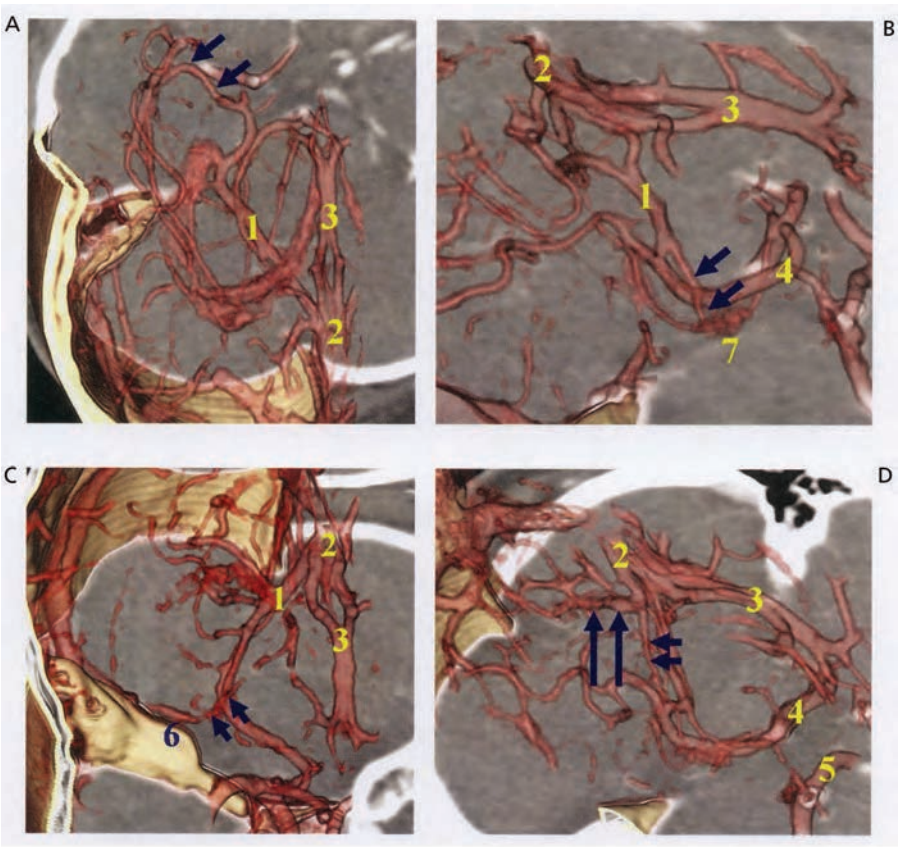

Figure 61.3 Basal vein of Rosenthal (BVR) classifications based on the developmental alterations of efferent pathways. (a) Telencephalic group, including tributaries of the inferior striatal, uncal, inferior frontal, anterior communicating, and deep middle cerebral (arrows) veins. (b) Diencephalic group, including tributaries of the peduncular and inferior ventricular (arrows) and posterior communicating veins. (C) Tegmental bridging group of lateromesencephalic vein (LMV) anastomosis (arrows) with the superior petrosal sinus. (D) Tectal group of superior vermian vein. This figure illustrates the Galenic connection of the small BVR constituting the superior vermian vein (short arrows) and adjacent posterosuperior cerebellar vein (long arrows). 1, basal vein of Rosenthal (BVR); 2, vein of Galen; 3, deep middle cerebral vein (DMCV); 4, inferior striatal vein; 5, inferior ventricular vein; 6, superior petrosal sinus; 7, choroid plexus

Source: Chung & Weon (2005). Reproduced with permission from SAGE.

the lateral ventricles (Ferner 1958; Hassler 1966; Stephens and Stilwell 1969; Sindou and Auque 2000). Subependymal veins are classified into two groups: medial and lateral. Veins of both groups are joined to the deep venous system of the cerebrum after crossing through the choroïdal fissure, the trigonal side of which hosts the medial group veins and the thalamic side of which hosts the lateral group (Wolf and Huang 1964). These veins are further classified by division of the ventricle through which they pass (Stein and Rosenbaum 1974). Table 61.1 details the classification of the subependymal veins and their final drainages.

The point at which the thalamostriate vein (TSV) joins the ICV has been named the "venous angle of the brain" (Krayenbühl and Richter 1952). In the past, using cerebral phlebography, the venous angle of the brain was used to locate the foramen of Monro; however, a false venous angle of the brain could be found in normal variations or tributaries of the ICV. The importance of differentiating the venous angle type (true or false) for detecting space-occupying lesions of brain had been highlighted in the pre-computerized brain scanning era (Curry and Culbreth 1951; Umbach 1952; Johanson 1954; Mokrohisky et al. 1956; Probst 1970).

Bilateral carotid angiograms of 200 normal cases have led to descriptions of normal anatomical variations of the deep cerebral veins among individuals and between the two hemispheres (Banna and Young 1970). In 130 (65%) cases in this study the anatomical appearances of the subependymal veins were similar in both hemispheres, whereas 70 (35%) appeared asymmetric between their hemispheres. The anatomically normal anterior septal vein (ASV) was described as reaching the ICV in the region near the foramen of Monro, although the ASV can also join the atrial vein (AV) or run ventrally to the interventricular foramen. The presence of more than one ASV has also been reported. In nearly all cases the TSV is seen as a single vein, although sometimes there are two TSVs of different sizes. The width and shape of the angle made by the junction between the TSV and ICV also vary. The atrial or posterior horn vein is generally a single vein with a medial and lateral ramification. Independent union of these two ramifications with the ICV has also been observed. Additionally, variations in the shape of the arch for the ICV can be seen using angiography.

The venous asymmetries between the two hemispheres observed in 70 (35%) cases in this study were attributed to variations of the ASV and TSV and the shape of the arch made by the ICV. The ASV can unite with the ipsilateral ICV at different anatomical points. Sometimes, two ASVs are visible in one side and just one in the opposite side; this pattern can also occur with the TSV.

The microsurgical anatomy of the deep venous system was studied in 20 cerebral hemispheres to describe its details and propose a new classification method (Ono et al. 1984b). In this classification, the deep venous system is divided into two groups: (1) ventricular, composed of the veins that join together on the walls of the lateral ventricle (the subependymal veins were placed in this group); and (2) cisternal, composed of the veins that drain the walls of the basal cisterns. In this study, the ASV and ICV were found in all of the evaluated hemispheres; however, the presence of the TSV was reported in just 90% (18). Evaluation of the transcortical approach to the third ventricle revealed 53% of cases with a traditional course for the TSV through the foramen of Monro; a dorsal curve of the TSV was reported in 39% of subjects, located behind the foramen of Monro in the medial side (Lang 1985).

An anatomical study by Türe et al. (1997) evaluated 20 cadaveric brain specimens for variations of the subependymal veins of the lateral ventricle in the foramen of Monro region. Four types of variations were described, characterizing the location of the ASV and ICV junction in relation to the foramen of Monro: Type IA, in which the junction of ASV to the ICV at the venous angle is close to the posterior margin of the foramen (this was the most common variation, observed in 52.5% of studied hemispheres); Type IB, in which the ASV, in the presence of a true venous angle, is connected to the main body of the ICV far from the foramen of Monro (found in 15% of hemispheres); Type IIA, in which a false venous angle receives the ASV beyond the foramen (observed in 25% of hemispheres); and Type IIB, in

Table 61.1 Classification of the subependymal veins and their final drainages

Part of ventricle	Draining vein	Anatomical location relative to lateral ventricle walls	Final major draining vein(s)
Frontal horn	Anterior septal vein (ASV)	Medial	Internal cerebral vein (ICV)
	Anterior caudate vein	Lateral	
Ventricular body	Posterior septal vein	Medial	
	Thalamo-striate vein (TSV)	Lateral	
	Thalamo-caudate vein	Lateral	
	Posterior caudate	Lateral	
Atrium and occipital horn	Medial atrial vein	Medial	Internal cerebral vein (ICV) and basal vein of Rosenthal (BVR)
	Lateral atrial vein	Lateral	
Temporal horn	Amygdalian vein	Medial	Basal vein of Rosenthal (BVR)
	Hippocampal vein	Medial	
	Inferior ventricular vein	Lateral	

which the main body of the ICV, located far from the foramen of Monro, receives the ASV in the presence of a false venous angle (reported in 7.5% of hemispheres).

Using MR time of flight (TOF) venography, Çimşit et al. (2003) studied the anatomical variations of the subependymal veins in the foramen of Monro region and the third ventricle. The ASV, TSV, and ICV courses in 50 healthy subjects, 10 patients with third ventricle tumors, and 4 patients with lateral ventricle tumors were evaluated. In this study, the method of Türe et al. (1997) was used to classify the foramen of Monro location and ASV-ICV junction. Of 128 studied hemispheres, 69 (53.9%) were type IA with the ASV-ICV junction located at the venous angle. In the remaining 59 (46.1%) sides, Type IB, IIA, and IIB patterns with the ASV-ICV junction located beyond the foramen of Monro were observed (Fig. 61.4). The distance of the ASV-ICV junction from the posterior margin of the foramen of Monro ranged from 2.5 to 14.1 mm (mean 6.9 mm) in types IB, IIA, and IIB.

Phase-sensitive MR imaging has been used to examine the anatomy of the ICV. In a study of 100 patients by Wang et al. (2010), 29 patients had symmetrical patterns of ICVs and their tributaries in both hemispheres; the remaining patients displayed asymmetries to various degrees. The junction of the TSV, septal vein (SV), and ICV was found in close proximity to the posterior margin of the foramen of Monro in 161 (80.5%) sides, but was on the further side of the foramen in 39 (19.5%) cases. There was no asymmetry between left and right hemispheres for any of the TSV-SV-ICV junction variants. Among 185 anterior caudate nucleus veins with one or several small veins originating from the head of the caudate nucleus, classic terminal drainage into the TSV was observed in 131 (70.8%) sides. The SV, TSV, and anterior caudate nucleus veins joined together to form the ICV in 40 (21.6%) hemispheres. Separate incorporation of the anterior caudate nucleus veins and TSV into the SV or ICV was found in 14 (7.6%) sides. The patterns of the anterior caudate nucleus drainage were strikingly different between the right and left sides, with drainage into the TSV being more common in the right. This was in contrast to the more frequent drainage of the left side anterior caudate nucleus veins into the SV or ICV. In hemispheres with the TSV-SV-ICV junction located in the posterior location, the anterior caudate nucleus veins drained most frequently into the SV or ICV.

Cerebral venous variations in the region of the third ventricle were also evaluated using phase-sensitive MR imaging in a study of 642 hemispheres (Fujii et al. 2010). The passage of the ASV, TSV, and ICV was classified according to the method of Türe et al. (1997) on the basis of ASV-ICV junction morphology and the existence of a true venous or false venous angle, as explained in detail earlier. The authors added a new group to the Türe et al. classification scheme, type III, which they defined as including any venous variations not placed in the other four groups. Among the evaluated cases, only one (0.2%) was designated type III and consisted of the joining of the ASV and medial atrial vein. Most hemispheres (407 cases, 63.4%), featured the type IA pattern of the ASV-ICV junction located at the venous angle. In 235 (36.6%) sides, the ASV-ICV junction was located far from the foramen of Monro and was classed into one of the other three groups as follows: type IB in 111 (17.3%) sides; type IIA in 106 (16.5%); and type IIB in 17 (2.6%). In this study, the incidence of false venous angles was lower than in previous studies (Tamaki et al. 1973; Türe et al. 1997); the authors suggested that the small population of hemispheres studied anatomically (40 hemispheres), and the difficulty of evaluating the phase-sensitive study images meticulously due to the extremely short distance between the venous junction and the foramen of Monro, could have contributed to this discrepancy.

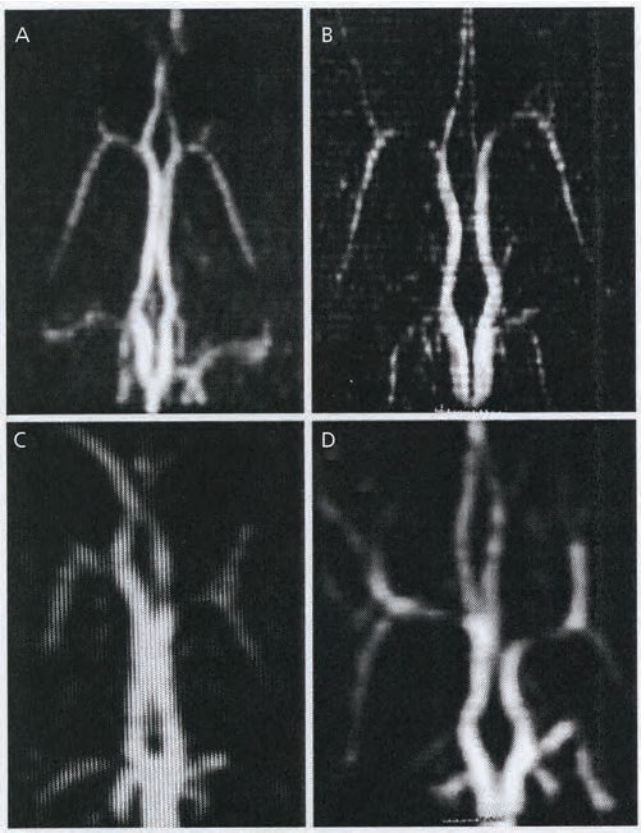

Figure 61.4 Visualization of the ASV-ICV junction by MR TOF venography: (a) Type IA; (b) Type IB; (c) Type IIA; and (d) Type IIB.

Source: Çimşit et al. (2003). Reproduced with permission from Springer Science and Business Media.

Veins of the pineal region

In the pineal region multiple veins join together on the great cerebral vein of Galen, and its complexity has represented a great challenge to neurosurgeons since the first years of the twentieth century (Dandy 1921, 1936; Giordano et al. 2007). Sir Victor Horsley (Macnalty 1957) was the first to attempt to reach the pineal region for tumor removal, and different types of approach have subsequently been described (Dandy 1921; Stein 1971; Rhoton et al. 1981; Ziyal et al. 1998). A neurosurgeon requires thorough knowledge of the possible venous variations in this area, as these can pose a great obstacle to approaching the pineal region surgically. The pineal body or "Habenula Trigone" is drained by the pineal vein (Tamaki et al. 1974; Yamamoto and Kageyama 1980).

There are other names for the pineal vein in the literature including the "epithalamic vein" (Schlesinger 1939), the "medial posterior thalamic vein" (Huang and Wolf 1974b) and the "latero epiphyseal vein" (Duvernoy 1975). In some studies, the pineal and posterior thalamic veins have been regarded as different (Giudicelli and Salamon 1970; Rosenbaum 1974), although it has been highlighted (Yamamoto and Kageyama 1980) that from an anatomical point of view it might be too difficult to distinguish them. Variations of the venous system of the pineal region are discussed here, although we should note that several such variations have been discussed earlier in the chapter, relating to BVR variations.

Unification of the two ICVs in the quadrigeminal cistern creates the vein of Galen (Yamamoto and Kageyama 1980). The average length of this vein is about 12 mm, ranging from 8 mm to 25 mm. In an anatomical study of the pineal region (Yamamoto and Kageyama 1980), the following veins were found to empty into the vein of Galen: the ICV (in 100% of specimens); the precentral cerebellar vein (86.4%); the internal occipital vein (77%); the BVR (51.7%); the posterior pericallosal vein (41.5%); the pineal vein (40.9%); the posterior mesencephalic vein (38.4%); and the posterior ventricular vein (6.7%). After traveling superoposteriorly under the splenium of the corpus callosum and incorporating the inferior sagittal sinus, the vein of Galen terminates in the straight sinus.

Three forms of variations of the pineal veins were described in an anatomical study by Tamaki et al. (1973). In the Type 1 pattern, veins of the superior and inferior surfaces of the pineal body join to form one or two main trunks and then travel posteriorly and superiorly in the quadrigeminal cistern before reaching the vein of Galen. In the Type 2 pattern, the inferior and superior surfaces of the pineal body are drained by veins from the proximal portion of the pineal body, creating one main venous trunk in the lateral side of the pineal body, before reaching the terminal portion of the ipsilateral ICV. However, in this study the Type 2 pattern was only observed in specimens with a very short vein of Galen. Finally, the Type 3 category displayed a combination of Type 1 and Type 2 attributes. The superior pineal veins draining the superior part of the pineal body travel superiorly and posteriorly before joining the vein of Galen; the inferior pineal veins draining the inferior part of the pineal body travel back and upward before reaching the terminal portion of the ICV separately. This type of variation was reported in just one brain.

In a recent 7 Tesla MR imaging study of the pineal gland (Cho et al. 2011), venous variations of this anatomical area were classified using the Tamaki et al. scheme (Tamaki et al. 1973). The results from 34 healthy volunteers are summarized in Figure 61.5 and Table 61.2.

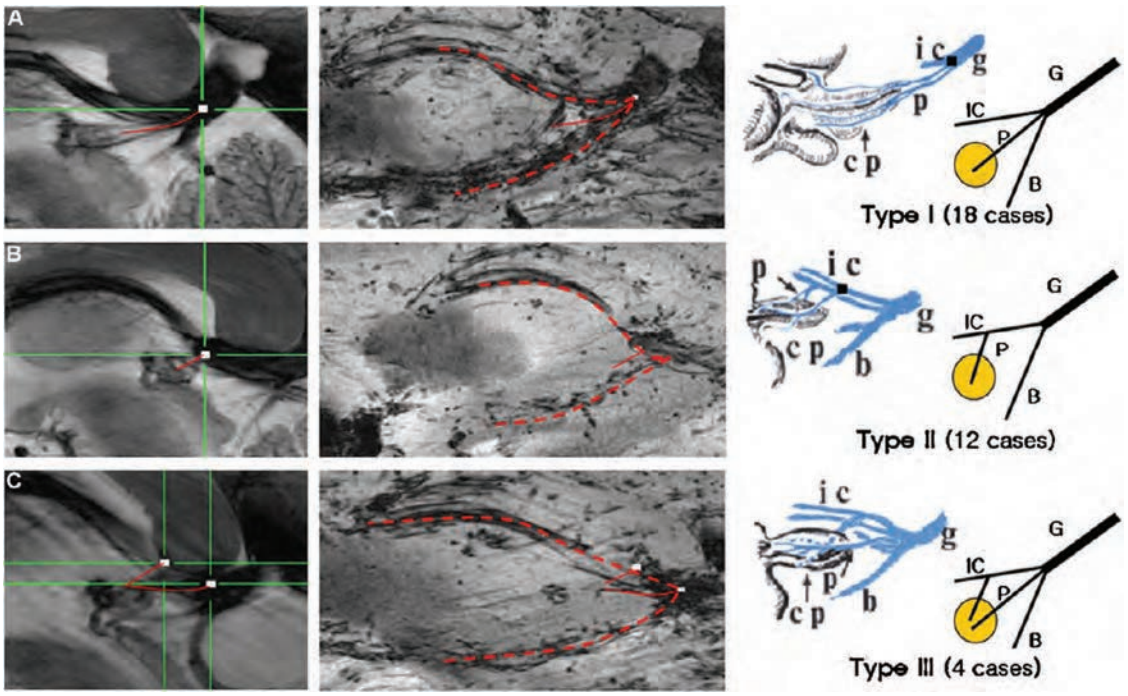

Figure 61.5 Images obtained by 7T MRI illustrating three types of pineal gland, classified on the basis of vascular distribution or structure: (a) Type I, direct drainage of the pineal vein into the great cerebral vein of Galen; (b) Type II, drainage of the pineal vein into the internal cerebral vein; and (c) Type III, drainage of the pineal vein into both the great cerebral vein of Galen and internal cerebral vein. Single-slice MR images of the pineal glands. Left: location of the pineal vein roots are indicated by the green bar and small white box. Middle: images at minimum-intensity projection of 17 slices each, thickness 2 mm, represent two landmark veins. The internal cerebral vein (upper) and the basal vein (lower) are indicated by the red dotted lines; thin solid red lines indicate the pineal veins (middle). Right: drawings of the three types of pineal veins (left) described by Tamaki et al. (1973) with modified images of Cho et al. (2011) (right). g: great cerebral vein of Galen; ic: internal cerebral vein; b: basal vein of Rosenthal; p: pineal vein; cp: corpus pineale.

Source: Cho et al. (2011). Reproduced with permission from Elsevier.

Table 61.2 Classification of the pineal gland using 7T MR imaging.

	Men (*n*)	Women (*n*)
Type 1	15	3
Type 2	5	7
Type 3	2	2
Total	22	12

Source: Cho et al. (2011). Reproduced with permission from Elsevier Masson SAS.

On average, 1.9 pineal veins (ranging from one to five) are joined into the Galenic system (Yamamoto and Kageyama 1980). The variant patterns of drainage of the pineal veins into the Galenic system have been classified into five types by Yamamoto and Kageyama (1980). The earlier, three-group anatomical classification of the pineal vein developed by Tamaki et al. (1973) could not be applied to all brains in this cadaveric study (Yamamoto and Kageyama 1980), so two additional groups were introduced for finer classification. In Type 1, the terminal portion of one of the ICVs receives the pineal vein, whereas in Type 2 the pineal veins drain into the terminal portions of both ICVs. In the Type 3 pattern, the vein of Galen receives the pineal veins directly, and in Type 4 one of the ICVs and the vein of Galen receive the pineal vein. Type 5 displays drainage of the pineal vein into the precentral cerebellar vein. It has been reported (Salamon and Huang 1976) that the medial posterior thalamic vein drainage is not limited to the ICV or the vein of Galen but also can occur into the BVR. In 40.9% of cases in the Yamamoto and Kageyama (1980) study, the pineal veins passed through both superior and inferior surfaces of the pineal body, whereas they passed through only the superior (31.8%) or only the inferior (27.3%) surface in the remainder.

The Galenic venous system was subjected to a comparative anatomical and imaging study in 10 cadavers of several age groups and in 10 age-matched living subjects (Kılıç et al. 2005). The vein of the Galen, ICV, BVR, and the internal occipital, occipitotemporal, precentral cerebellar, tectal, pineal, superior vermian (including superior cerebellar), and posterior pericallosal veins were studied. The anatomical evaluation results of this study are summarized in Table 61.3.

Anatomical information from this research highlights the uniqueness of the Galenic venous system in each studied case. Furthermore, it was found that the tributaries of a particular vessel can differ among subjects (interpersonal variations, Table 61.3). Right- and left-sided differences in each single subject were also reported (intrapersonal variations). Comparison of the adult and pediatric Galenic venous systems revealed the possibility of age-specific variations. For example, in two newborn cadavers, the vein of Galen followed a straight posteriorly oriented horizontal course after the unification of the two ICVs (Fig. 61.6). However, in eight adult cadaveric brains,

Table 61.3 Results of an anatomical study of the Galenic venous system.

Veins	Incidence in anatomical dissections	Origin of the vein	Destinations of the vein and their incidence
Vein of Galen	10/10 (100%); all single	Always originates from the unification of two internal cerebral veins in the quadrigeminal cistern	Straight sinus; 10/10 (100%)
Basal vein of Rosenthal	20/20 (100%); all single	Comes through ambient cistern to quadrigeminal cistern	GV 8/20 (40%); ICV 8/20 (40%); GV-ICV unification 4/20 (20%)
Internal cerebral vein	20/20 (100%); all single	Velum interpositum	GV 20/20 (100%)
Occipitotemporal vein	8/20 (40%); all single	Lingual gyrus	Internal occipital vein: 4/8; occipitotemporal veins (50%); BV: 4/8 occipitotemporal veins (50%)
Precentral cerebellar vein	10/10 (100%); 7/10 single; 3/10 double	Unification of bilateral superior cerebellar peduncular veins; comes to quadrigeminal cistern from the infratentorial space.	GV: 8/10 (80%); straight sinus: 2/10 (20%)
Superior cerebellar and Vermian veins	8/10 (80%); 1/8 single; 7/8 double or triple	Superior part of cerebellum and vermis	GV: 100% of all determined superior cerebellar vermian and superior cerebellar veins
Posterior pericallosal vein	12/20 (60%); all single	Originates from cingular gyrus and post part of corpus callosum	GV: 8/12 (66%); ICV: 2/12 (16%); internal occipital vein: 2/12 (16%)
Tectal veins	8/10 brains; all multiple	From inferior and superior colliculi	GV: 100%
Pineal veins	8/10 brains; all multiple	From pineal gland	GV: 100%
Internal occipital vein	16/20 hemispheres (80%); 10/16 single; 6/16 double	From medial-inferior part of occipital lobe	GV: 8/16 hemispheres (50%); ICV: 4/16 hemispheres (25%); BV: 4/16 hemispheres (25%)

Source: Kılıç et al. (2005). Reproduced with permission from Elsevier.

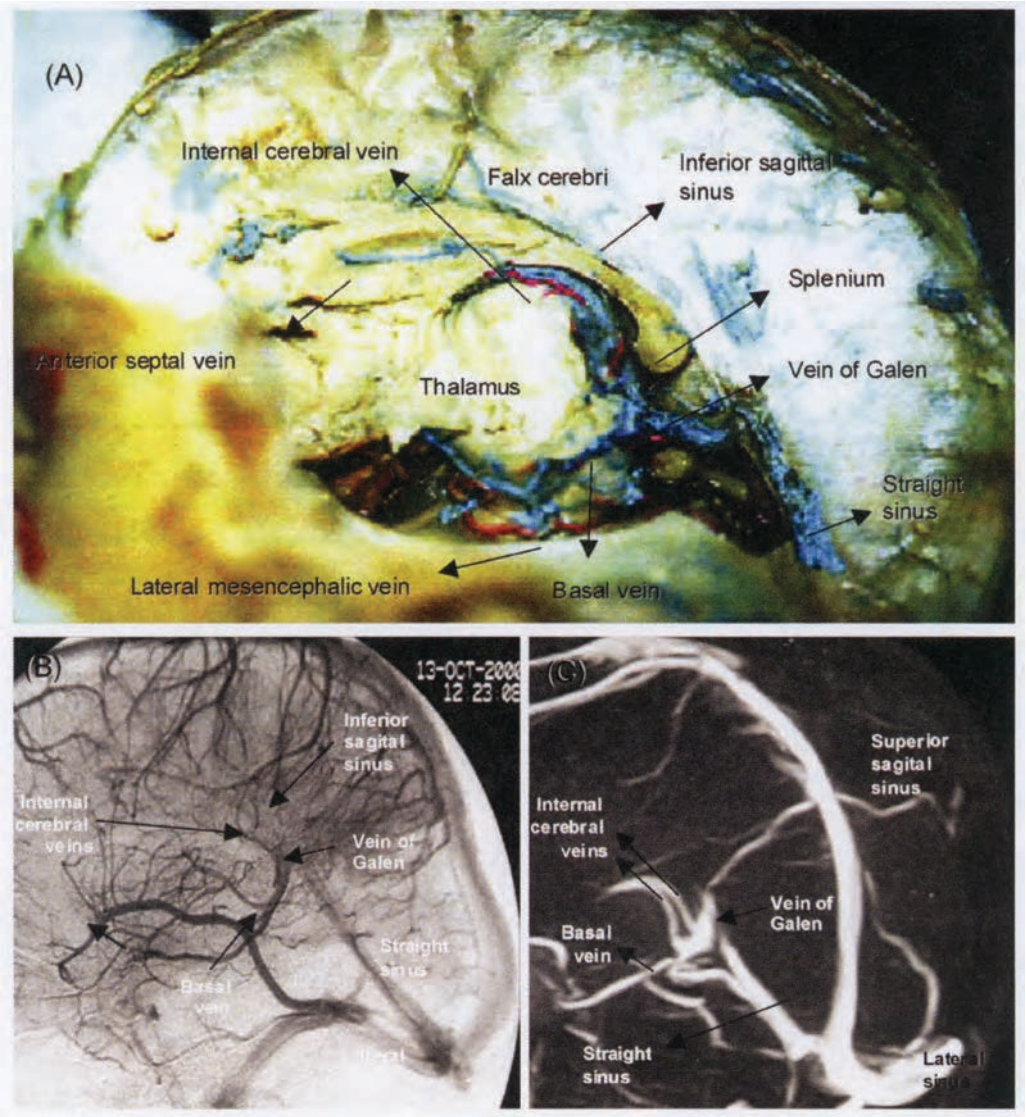

Figure 61.6 (a) Anatomical dissection; (b) venous phase of the DSA; and (c) MRV of the Galenic venous system in the newborn. A horizontal course of the vein of Galen is highlighted, directed posteriorly after unification of the two internal cerebral veins. To some extent, a level junction of the Galenic vein and straight sinus is also revealed.

Source: Kılıç et al. (2005). Reproduced with permission from Elsevier.

the left vein of Galen took a posterosuperior course to make an acute angle with the straight sinus (Fig. 61.7). Different growth specifications of the posterior fossa have been proposed to explain the change in the configuration of the vein of Galen (Ono et al. 1984a; Jeffery 2002). Earlier studies (Johanson 1954; Ono et al. 1984b) reported that if the falco-tentorial junction is located below the splenium, then the junction of the vein of Galen with the straight sinus can take a flat shape; these prior studies also identified an obtuse angle to this junction in 8% of adult subjects. In contrast, in the Kılıç et al. (2005) study, an obtuse angle was observed in both pediatric specimens but no adult brain displayed a similar variation.

Kılıç et al. (2005) also employed digital subtraction venography (DSV) and magnetic resonance venography (MRV) in their study of the Galenic venous system in five adults and five pediatric cases. These imaging techniques effectively revealed the large veins in the Galenic venous system, but smaller veins proved difficult to visualize (Table 61.4). The general sensitivities of DSV and MRV in the Galenic venous system study were about 45.5% and 32.5%, respectively. Wide interpersonal, intrapersonal, and age-related variations were reported among both the anatomical and imaging components of this study. These findings support the opinion that careful individualized study of the pineal region venous anatomy is warranted for each person in advance of a neurosurgical procedure in this region.

Using reconstructions from CT and MR imaging scans with navigation software, Giordano et al. (2007) studied the complex venous anatomy of the pineal region in 100 patients. On the basis of these findings, drainage of the last segment of the BVR was classified into five variants: Type 0, not present; Type 1,

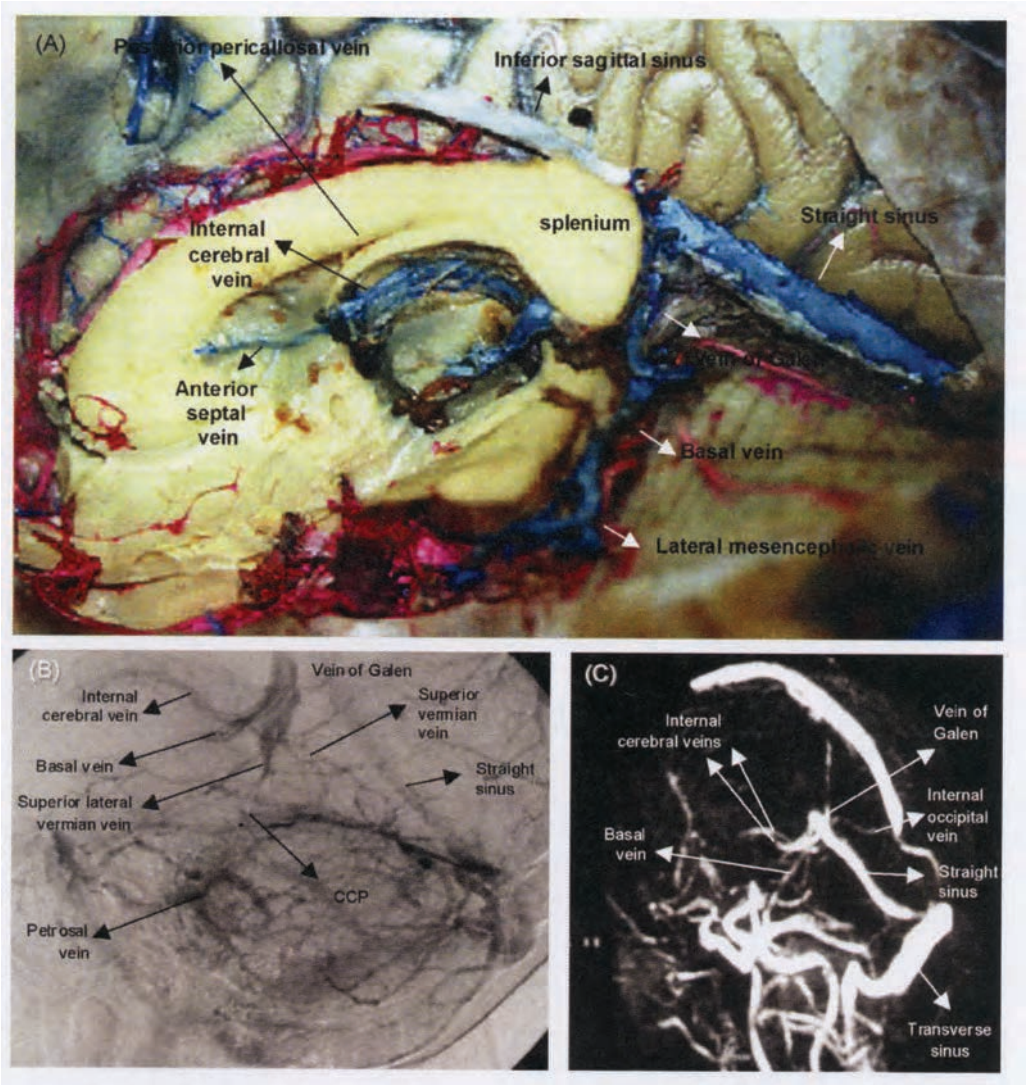

Figure 61.7 (a) Anatomical dissection; (b) venous phase of the DSA; and (c) MRV of the adult Galenic venous system. In contrast to the newborn specimen, the vein of Galen has a further posterosuperior passage to end in an acute angle with the straight sinus.

Source: Kılıç et al. (2005). Reproduced with permission from Elsevier.

Table 61.4 Demonstration of venous structures using anatomical dissection and imaging modalities. DSA: digital subtraction venography; MRV: magnetic resonance venography.

Evaluated vessel(s)	Observed in anatomical study	Observed in DSA	Observed in MRV
The vein of Galen	10 of 10 (100%)	10 of 10 (100%)	10 of 10 (100%)
Internal cerebral veins	20 of 20 (100%)	20 of 20 (100%)	18 of 20 (90%)
Basal vein of Rosenthal	20 of 20 (100%)	18 of 20 (90%)	12 of 20 (60%)
Internal occipital vein	16 of 20 (80%)	11 of 20 (55%)	7 of 20 (35%)
Occipitotemporal veins	8 of 20 (40%)	0 of 10	0 of 10
Precentral cerebellar veins	10 of 10 (100%)	5 of 10 (50%)	0 of 10
Tectal veins	8 of 10 (80%)	0 of 10	0 of 10
Pineal veins	8 of 10 (80%)	0 of 10	0 of 10
Superior vermian veins (including superior cerebellar veins)	8 of 10 (80%)	5 of 10 (50%)	2 of 10 (20%)
Posterior pericallosal veins	12 of 20 (60%)	6 of 10 (60%)	2 of 10 (20%)

Source: Kılıç et al. (2005). Reproduced with permission from Elsevier.

drainage into the ICV; Type 2, drainage at the union of the ICVs; Type 3, drainage into the vein of Galen; and Type 4, drainage into the straight sinus. No difference was found in terms of right and left side patterns or in comparisons between the CT and MR imaging-based reconstructions. However, there was a significant difference between male and female venous distributions in Types 0 and 3 (p=0.025). Interestingly, in one patient with the Type 1 pattern, the BVR drained into the contralateral ICV. In this patient, the left BVR traveled along its normal course in the ambient cistern, but then passed under the ipsilateral ICV and joined the right ICV.

The internal occipital vein drainage pathway in the pineal region was analyzed using a three-dimensional (3D) navigation technique in 100 living subjects (Giordano et al. 2009). In 39.4% of cerebral hemispheres the internal occipital vein (IOV) joined the BVR, whereas in 60.6% the vein of Galen received the internal occipital vein.

Veins of superficial venous system

Superficial Sylvian vein

The superficial Sylvian vein is centrally located between the superior and temporal cortical vessels; it generally originates from the posterior third of the Sylvian fissure and runs anteriorly and inferiorly in the superficial borders of the fissure (Wolf et al. 1963; Galligioni et al. 1969; Rhoton 2002). After its dural entrance in the pterional area, it passes through the lesser wing of the sphenoid bone to reach the anterior portion of the cavernous sinus at the medial end of the superior orbital fissure. This vein drains the parts of the brain close to the Sylvian fissure. The superficial Sylvian vein anastomoses with the deep venous system of brain through the uncal, insular, and basal veins and other superficial cerebral and dural veins (Galligioni et al. 1969). The superficial Sylvian vein also has connections with the extracranial vessels, such as the pterygoid plexus through the sphenoid emissaries, and with the facial veins through the orbital venous circulation.

In the absence of the superficial Sylvian vein, several alternative drainage pathways have been described (Wolf et al. 1963): (1) a wide cortical vein from the Sylvian fissure running forward to reach the anterior portion of the superior sagittal sinus; (2) a wide cortical vein originating from the Sylvian fissure running backward and upward to reach the posterior part of the superior sagittal sinus; (3) a wide cortical temporal vein running backward and downward from the Sylvian fissure to the superior region of the petrous pyramid, and then traveling backward in the angle between the petrous pyramid and the temporal squama to meet the transverse sinus, far from the back of the sigmoid sinus; and (4) a wide vessel starting in the horizontal part of the Sylvian fissure and traveling posteriorly in a circuitous manner backward and downward to meet the transverse sinus. In the two cases in this latter group, a long vein was observed under the temporal lobe starting close to the temporal lobe traveling into the tentorium at the apex of the petrous pyramid and then running back either laterally or medially to reach the transverse sinus. It was reported that this vessel could be related to the tentorial sinus (Padget 1957; Wolf et al. 1963) and to the accessory sinus reported by Kelch (Wolf et al. 1963).

Variations in which the convex portion of the superficial Sylvian vein is not remarkable but the basal drainage pathway is inconsistent with conventional descriptions have also been categorized. An uncommon variation entails failure of the vein, on its way to the pterion, to turn inside to reach the sinus along the lesser wing of the sphenoid bone; instead it travels directly backward along the inner aspect of the temporal squama, passing through the tentorium on the petrous pyramid and joining the transverse sinus. In a more common variation, the sinus of the lesser wing of the sphenoid bone receives the vein after its medial turn, but it fails to travel as a single channel along the entire length of the lesser wing. In the dura of the anterior wall of the middle fossa, the vein goes downward before reaching the cavernous sinus. It can then travel along the base of the middle fossa over the petrous pyramid before joining the superior petrosal sinus. It has been highlighted that a channel of this type could be related to the ophthalmopetrosal sinus of Hyrtl (Knott 1881). The angiographic findings of Wolf et al. (1963) indicate that, in addition to the common tributaries of the superficial Sylvian vein, there is a prominent vessel called the uncal vein on the medial side of the temporal lobe in front of the uncus. This could be part of the superficial Sylvian venous drainage pathway, considering its common connection with the medial end of the sinus of the lesser wing of the sphenoid bone or the adjacent cavernous sinus (Wolf et al. 1963).

In another angiographic study (Galligioni et al. 1969), the variations of the superficial Sylvian vein were classified into two broad region-based categories: (a) convex region variations and (b) basal region variations.

Convexity variations included: (1) a vein from the frontal area to the anterior portion of the superior sagittal sinus drains the superficial Sylvian vein region when no superficial Sylvian vein is present; (2) the superficial Sylvian vein area of drainage can be drained by a parietal vein; or (3) it can be drained by a temporal superficial vein reaching the transverse sinus. All three of these variations can coexist in different combinations, with one type dominant. Alternative routes of temporal lobe drainage can be observed in the complete absence of a superficial Sylvian vein or with a very thin superficial Sylvian vein; one example consists of a group of very thin, straight veins, partly in the dura, traveling in bundles before reaching the transverse sinus at different points. In some cases, along with Padget's "tentorial sinus", a lengthy vein travels inside the tentorium from the temporal pole, terminating in the tip of the petrous bone and the transverse sinus.

Basal region variations included: (1) part of the superficial Sylvian vein running on the convexity up to the pterion ridge is normal in its passage; the vein turns backward along the internal part of the temporal squama, inside the tentorium on the

petrous bone, before joining the transverse sinus; (2) in some cases, after its passage through the lesser wing of the sphenoid bone, the vein travels on the surface of the middle cranial fossa to reach the superior petrosal sinus; or (3) it runs directly toward the paracavernous sinus as a wide venous passage lateral to the cavernous sinus and reaches the pterygoid plexus through the sphenoid emissary veins; or (4) the uncal vein, described as a tributary of the superficial cerebral vein, runs on the medial part of the temporal lobe on the anterior edge of the uncus; the uncal vein highlights the medial part of the temporal lobe and can be considered an anastomotic vein between the superficial Sylvian vein and the deep group of middle cerebral veins (Wolf et al. 1963). Over its entire course, the superficial Sylvian vein can appear as two trunks or can be replaced by groups of different thin veins. Originating from the inferior part of the temporal region, several short thin veins reach the lower groups of thin veins. However, the upper groups are connected to the uncal vein and sometimes to an insular vein (Galligioni et al. 1969; Rhoton 2002).

Each of the abovementioned drainage variations of the superficial Sylvian vein can be found concurrently with the complex system of several superficial Sylvian veins (Galligioni et al. 1969). The superficial venous system was not compared systematically between the cerebral hemispheres in this angiographic study.

In an anatomical study of 230 patients with anterior circulation aneurysms (Aydin et al. 1996), the Sylvian vein and cistern were evaluated using a pterional approach and classified into four types on the basis of Sylvian vein branching and drainage patterns: Type I (45%, *n*=103), drainage of the fronto-orbital (frontosylvian), frontoparietal (parietosylvian) and anterior temporal (temporosylvian) veins into one Sylvian vein; Type II (29%, *n*=67), drainage of two superficial Sylvian veins with a separated basal vein into the sphenoparietal and basal vein of Rosenthal; Type III (15%, *n*=34), drainage of two superficial Sylvian veins into the sphenoparietal and the superior petrosal veins; and Type IV (11%, *n*=26), a hypoplastic superficial Sylvian vein with a deeper course. In 70% of the studied cases (*n*=160) the Sylvian vein passed through the temporal side, whereas in 19% (n=45) it passed through the frontal side; it exhibited deep coursing in 8% (*n*=18) of cases. A mixed course was observed in only 3% (*n*=7) of cases.

In a three-dimensional CT angiographic study (Suzuki and Matsumoto 2000), 250 cases were evaluated to classify superficial Sylvian venous drainage pathway variations according to the changes observed during embryo development, as defined by Padget (1957). In this study, seven types of drainage pathways were proposed as follows:

1. sphenoparietal (54%, *n*=271), with drainage of the superficial Sylvian vein into the sphenoparietal sinus;
2. cavernous (7%, *n*=36), where the anterior end of the cavernous sinus receives the drainage;
3. emissary (12%, *n*=62), in which the drainage pathway passes through the lesser wing of the sphenoid bone, travels inferiorly toward the floor of the middle cranial fossa to join the sphenoidal emissary veins, and leaves its floor to meet the pterygoid plexus;
4. superior petrosal (2%, *n*=9), where the drainage travels along the lesser wing of the sphenoid bone before reaching the cavernous sinus along the anterior inner wall of the middle fossa, goes downward and then travels along the medial side of its floor toward the foramen ovale to meet the superior petrosal sinus;
5. basal (2%, *n*=10), in which drainage passes through the lesser wing of the sphenoid bone, goes downward along the anterior wall of the middle cranial fossa, and travels along its floor lateral to the foramen ovale over the petrous pyramid to meet the transverse sinus through the lateral tentorial sinus or superior petrosal sinus;
6. squamosal (2%, *n*=12), where drainage runs directly back along the temporal squama and then travels posteriorly to reach the transverse sinus or lateral tentorial sinus; and
7. undeveloped (9%, *n*=44), in which there is no superficial Sylvian vein and its drainage is taken over by a large channel extending forward, upward and backward, or downward and backward into the superior sagittal sinus or transverse sinus.

In an anatomical study (Kazumata et al. 2003) on 82 patients (single hemispheres only), variations of the Sylvian vein were investigated during surgical exploration of the Sylvian fissure. These variations were classified on the basis of the branching and drainage patterns into three categories: superficial, intermediate, and basal components.

1. Superficial veins included the superficial Sylvian vein (SSV) or superficial middle cerebral vein. The fronto-orbital (fronto-SSV), frontoparietal (parieto-SSV), and anterior temporal (temporo-SSV) veins comprise the SSV. In this study, a single SSV was defined as an SSV with tributaries from both the frontal and temporal lobes draining into the dural sinus as a single trunk. At the entrance of the dural sinus, a double SSV was defined as one SSV with tributaries from the frontal lobe (fronto-SSV), and another with tributaries from the temporal lobe (temporo-SSV). A small vein at the anterior temporal region with tributaries from the middle and inferior temporal gyri was mentioned; this could be called the temporopolar vein but it was not studied further.
2. The intermediate category consists of insular veins. Four veins, including the insular veins of the anterior limiting sulcus, precentral sulcus, central sulcus, and posterior limiting sulcus have been described. Drainage of the common stem of the insular vein can be classified into either the classic pattern, in which a common stem travels to the BVR, or the nonclassic pattern, with a common stem joining the sphenoparietal sinus. The anastomosis between the common stem of the insular veins and the SSV was also evaluated. In its absence the common stem of the insular veins was primarily joined to the BVR.
3. The basal components consist of the olfactory vein, posterior fronto-orbital vein, anterior cerebral vein, and twigs from

the optic chiasm; all these veins are also components of the first section of the BVR. A small vein from the frontal base and draining into the sphenoparietal sinus was designated a frontobasal bridging vein (FBBV). It can drain into the sphenoparietal sinus in single trunk form, as a common stem with the SSV, or in the form of an anastomotic vein with the common stem of the insular veins (common vertical trunk).

In this same study, the drainage pattern of the SSV was also classified into three types: Type I, characterized by an absent or severely hypoplastic SSV (eight cases, 10%); Type II, displaying a single main SSV stem draining into the sphenoparietal sinus (38 cases, 46%); or Type III, in which two main stems (fronto-SSV and temporo-SSV) make up the SSV, draining into the sphenoparietal sinus (36 cases, 44%). Insular veins formed an anastomotic trunk and traveled toward the sphenoparietal sinus in 42 cases (51%). There was no anastomosis between the insular veins and the sphenoparietal sinus in 40 cases (49%). An FBBV was reported in 47 cases, and in 35 cases the first portion of the basal vein of Rosenthal consisted of the olfactory, posterior fronto-orbital, and anterior cerebral veins and twigs from the optic chiasm.

Kazumata et al. further classified the patterns of Type II branching into four subtypes: Type IIA, containing only the SSV, with no deep middle cerebral vein or FBBV, joined to the sphenoparietal sinus (three cases); Type IIB, drainage of the FBBV into the SSV, with SSV drainage into the sphenoparietal sinus (eight cases); Type IIC, in which the deep middle cerebral vein joined to the SSV and the SSV traveled toward the sphenoparietal sinus (10 cases); and Type IID, where the FBBV and deep middle cerebral vein both drained into the SSV and the SSV joined the sphenoparietal sinus (10 cases). Seven cases of the Type II category fell into none of the above subtypes. Similarly, four subtypes were defined for the Type III branching category. Type IIIA contained only the temporo-SSV and fronto-SSV, but no FBBV or deep middle cerebral vein, joined to the sphenoparietal sinus (seven cases); in Type IIIB, the deep middle cerebral vein joined to the fronto-SSV and the fronto-SSV and temporo-SSV drained into the sphenoparietal sinus (eight cases); in Type IIIC, the FBBV joined the fronto-SSV, and the fronto-SSV and temporo-SSV drained into the sphenoparietal sinus (10 cases); and in Type IIID, the FBBV and deep middle cerebral vein joined the fronto-SSV, and the fronto-SSV and temporo-SSV drained into the sphenoparietal sinus (nine cases). In two cases of Type III, the branching pattern met the criteria for none of the above subtypes.

In an earlier study of the drainage pathways of the SSV, Bisaria (1985) reported the following results: 68.2% of cases drained toward the sphenoparietal sinus; 21% exhibited direct drainage into the cavernous sinus; 10% to the middle meningeal vein; and the remaining cases split between draining into the superior petorsal sinus (0.71%) or the emissary vein in the foramen lacerum (0.71%).

MP-RAGE, a new method of MR imaging, was performed on 400 hemispheres to evaluate the major anastomotic veins including the superficial Sylvian vein, the vein of Trolard, and the vein of Labbé, and to examine the drainage pathways of the superficial Sylvian vein (Ikushima et al. 2006). In this study, the major anastomotic veins were classified into four types (Fig. 61.8) and the percentages and numbers of cases observed were: (a) the vein of Trolard as the dominant pathway (8%, *n*=33); (b) a dominant vein of Labbé (39%, *n*=155); (c) a dominant superficial Sylvian vein (35%, *n*=141); and (d) all three anastomotic veins are present but the veins of Labbé and Trolard are dominant (18%, *n*=71).

The drainage pathways of the superficial Sylvian vein characterized using MP-RAGE (Fig. 61.9) were observed at the following frequencies: (1) sphenoparietal type (57.5%, *n*=231); (2) cavernous type (19.5%, *n*=78); (3) emissary type (5.5%, *n*=21); (4) basal type (3.5%, *n*=15); (5) squamosal type (0.5%, *n*=3); (6) basal vein type (0.3%, *n*=1); and (7) undeveloped (16%, *n*=51). In this imaging study, the vein of Trolard and the superficial Sylvian vein predominated on the right side and the vein of Labbé predominated on the left.

San Millan Ruíz et al. (2006) have offered another classification system for the drainage pathways of the superficial Sylvian vein, based on which the sinus of the middle cranial fossa ultimately receives blood from it: (1) paracavernous; (2) laterocavernous; and (3) cavernous types. These authors have highlighted that the categorization of the superficial Sylvian vein drainage in the middle cranial fossa by Ikushima et al. (2006) into basal, squamosal, or emissary types could correspond to the paracavernous sinus. Since it is difficult to distinguish the laterocavernous and cavernous sinuses from each other in contrast-enhanced

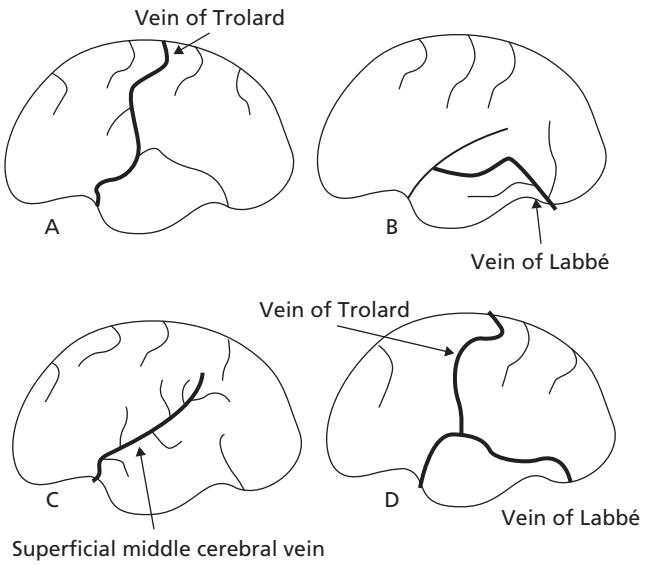

Figure 61.8 Different forms of the major superficial anastomotic veins. (a) Vein of Trolard is dominant; (b) vein of Labbé is dominant; (c) superficial Sylvian vein is dominant; and (d) all three anastomotic veins are present, but the veins of Labbé and Trolard are dominant.

Source: Ikushima et al. (2006). Reproduced with permission from Elsevier.

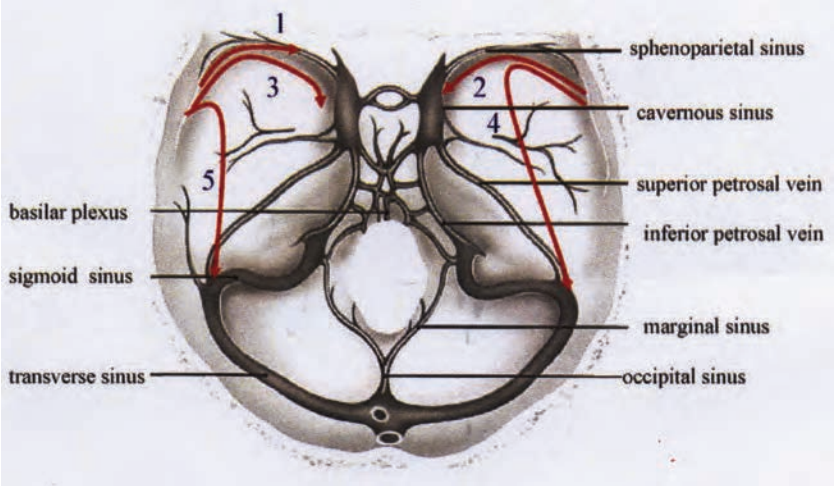

Figure 61.9 Drainage pathway classification for the superficial middle cerebral vein: 1, sphenoparietal type: the sphenoparietal sinus receives the SMCV and then the SMCV runs along the lesser wing of the sphenoid bone to reach the cavernous sinus; 2, cavernous type: the SMCV directly enters the anterior end of the cavernous sinus; 3, emissary type: the SMCV courses along the lesser wing, travels inferiorly to reach the floor of the middle cranial fossa, joins the sphenoidal emissary veins, and passes through the floor to meet the pterygoid plexus; 4, basal type: the SMCV travels along the lesser wing, turns downward along the anterior wall of the middle cranial fossa, then travels along its floor laterally to the foramen ovale over the petrous pyramid, possibly to join the transverse sinus through the lateral tentorial sinus or superior petrosal sinus; 5, squamosal type: the SMCV does not turn medially to reach the sinus along the lesser wing, but instead travels directly backward along the inner aspect of the temporal squama and runs posteriorly to join the transverse sinus or lateral tentorial sinus; 6, basal vein type: the SMCV enters the basal vein of Rosenthal; and 7, undeveloped type: the SMCV is absent.

Source: Ikushima et al. (2006). Reproduced with permission from Elsevier.

MP-RAGE (because of their close proximity), the sphenoparietal and cavernous types could be considered as a laterocavernous type (San Millan Ruiz et al. 2006).

Vein of Labbé

The man who gave his name to the vein of Labbé was born on 8 October 1851 in a small village in Normandy called Merlerault in the district of Orne. In 1879, Charles Labbé described the vein that bears his name in an article named "Note sur la circulation veineuse du cerveau et sur le mode de dévelopment des corpuscules de Pacchioni" published in the *Archives de Physiologie Normale et Pathologique* (Journal of Physiology (Paris)) (Labbé 1883; Bartels and van Overbeeke 1997). The vein of Labbé, also known as the inferior anastomotic vein, is the largest anastomotic channel (2–3 mm diameter) that crosses the temporal lobe between the Sylvian fissure and the transverse sinus. It originates from the middle section of the Sylvian fissure and travels posteriorly and inferiorly toward the anterior section of the transverse sinus. It is typically more evident on the surface of the dominant hemisphere and receives different numbers of superficial veins from the occipital and temporal lobes (Kaplan 1973; Kaplan et al. 1973; Kaplan and Browder 1974). It can pass through the temporal lobe as far back as the posterior border of the lobe or as far forward as the anterior third of the lateral surface (Bigelow et al. 1993; Rhoton 2002). Blood from the lateral surface of the temporal lobe or from the Sylvian fissure region passes through this anastomotic vein. In most earlier studies, the vein of Labbé was defined as a drainage system of venous canals instead of a single isolated vein, so the term "anastomotic vein" could be more appropriate (Perese 1960; Di Chiro 1962; Wolf et al. 1963; Kaplan and Browder 1974; Lang and Schneider 1989; Koperna et al. 1992).

An angiographic evaluation of 65 cases (Di Chiro 1962) revealed a frequent double vein of Labbé with anterior and posterior parts. The smaller posterior component derives from the unification of two branches, one from the supra-marginal and angular gyri and the other from the posterior external occipital surface. Venous drainage patterns in the two hemispheres differed in 56 cases, but 9 samples were similar in their angiographic appearance between hemispheres. Similarity between hemispheres in the vein of Labbé has also been reported in just one case in another study (Sakata et al. 2000).

Anatomical evaluation of 286 fresh cadaver specimens (Kaplan and Browder 1974) demonstrated multiple variations for the course of the vein of Labbé.

A separate anatomical study of 22 hemispheres (Koperna et al. 1992) revealed that the vein of Labbé was apparent in 82% of cases; the remaining 18% of samples had two veins with equal diameters from the temporal lobe. The vein of Labbé entered the dura mater in two different forms: (a) perforation of the dura connected to the bone by the vein, followed by its entrance into a lacuna superior to the transverse sinus; or (b) after crossing the transverse sinus the vein lay on the surface of the tentorium, loosely connected to it, and after its entrance to the tentorium it formed a tentorial sinus that connected to the transverse sinus. The vein of Labbé emptied into the transverse sinus through one

of the tentorial sinuses in 73% of the studied samples; a lacuna in the lateral skull wall of 27% of the samples connected this vein to the transverse sinus. In none of the samples was the vein of Labbé connected directly to the transverse sinus.

In this same study (Koperna et al. 1992), the distance between the confluence of sinuses and the crossing point of the superior petrosal sinus with the transverse sinus was divided into three equal parts. The entrance into the dura was observed within the anterior third in 75% of cases and within the middle third in the remaining 25%. In no sample was the dura observed within the posterior third segment. The distance between the veins entering the anterior third of the sinus and the superior petrosal sinus entrance point was not less than 7 mm. The section of the vein of Labbé attached to the tentorium varied in size from 3 mm to 23 mm. The maximum distance between the entrance point into the tentorium and the medial border of the transverse sinus was about 11 mm. The maximum distance between the entrance point into the dura of skull and the edge of the transverse sinus was 15 mm. In only one case did the vein of Labbé receive no further veins before turning into a tentorial sinus. It revealed no characteristic drainage in 9% of the studied samples; instead, the middle cerebral veins or the superior anastomotic vein (vein of Trolard) substituted for its drainage responsibility.

Evaluation of 40 temporal lobe specimens (Guppy et al. 1997) demonstrated a highly variable course for the vein of Labbé, so the term "lateral venous complex" was used instead. The lateral venous complex was one of four separate venous drainage complexes described by the authors. The other three were: (a) the anteroinferior complex; (b) the mediolnferior complex; and (c) the posteroinferior complex. Each was traced to the transverse and/or petrosal sinus. The geometry of the junction between these veins and the sinuses was designated the "venous configuration". The place at which the venous configuration reached the transverse sinus was called a "venous point" and the distance from the venous point to the sigmoid-transverse-superior petrosal (STP) junction was measured.

Three basic configuration types of the vein of Labbé were also described by these authors (Guppy et al. 1997): (a) unification of multiple veins creating one draining vein; (b) multiple independent draining veins; and (c) a venous lake in the tentorium before drainage into the sinuses. The lateral venous complex representing the classic vein of Labbé was reported in all studied specimens. A venous lake was found in only 12.5% of lateral venous complexes in this study, in contrast to reports of no venous lakes among 30 samples (Krisht et al. 1996) or of more frequent tentorial sinuses (about 73%) in a previous anatomical study (Koperna et al. 1992). These differences could be attributable to differences among the definitions used in these studies. The description of a vein star (Koperna et al. 1992) as a place where all veins reach a small sinus before their final passage to the transverse sinus resembles the description of the transverse sinus point by Krisht et al. (1996). A venous lake is defined as a channel between the leaflets of the tentorium, at a distance greater than 1 cm from its connection to the transverse sinus, to which one or more veins from various venous complexes join (Guppy et al. 1997).

In an anatomical study of 20 specimens (Sakata et al. 2000), the vein of Labbé was found at the level of the middle temporal vein in 9 samples and at the posterior temporal vein level in 12. Only one underdeveloped vein of Labbé was reported at the middle temporal vein level. In another study, the vein of Labbé was reported at the middle temporal vein in 12 specimens, at the posterior temporal vein in 6, and at the anterior temporal vein in 2 (Oka et al. 1985). The position of this vein has also been reported to be mid-temporal in 60%, posterior temporal in 30%, and anterior temporal in 10% of cases (Tubbs et al. 2012).

The venous drainage pattern of the temporal lobe has been classified into five types (Sakata et al. 2000) on the basis of the distribution of the venous entry complex. In Type IA (20%) the venous entry complex is located only at the transverse sinus area, whereas in Type IB (20%) it is only in the tentorial area. Type IIA (35%) exhibits entry in the petrosal and transverse sinus areas and Type IIB (5%) in the tentorial and transverse sinus areas. Finally, Type III (20%) consists of entry in all three areas. In 74% of specimens the vein of Labbé extended into the transverse sinus group; however, in 19% it reached the tentorial group. The superior petrosal sinus received the vein of Labbé directly in one specimen.

In a recent anatomical study (Avci et al. 2011) the vein of Labbé was found in 80% of the specimens, whereas in 20% two veins with almost equal diameters were reported. The vein of Labbé drained directly into the transverse sinus in 46.5% of the specimens, and indirectly into the transverse sinus through one of the tentorial sinuses (venous lake, lateral tentorial sinus) or the meningeal vein in the occipital dura in 46.5%. It drained close to the confluence of sinuses at the posterior one-third of tentorium in just one case (3.5%), and into a large meningeal vein in the occipital dura in one other specimen (3.5%). The superior petrosal sinus in two (7%) specimens received the vein of Labbé directly. The distance of the sigmoid-transverse-superior petrosal (STP) junction from the tentorial entrance of the vein of Labbé was about 13.1 mm; it traveled within the tentorium for various lengths over the range 2.8–24.5 mm, before reaching its final destination in the transverse sinus. The vein of Labbé entered the transverse sinus, either directly or through a tentorial venous lake, at an average distance of about 24.6 mm (range 11.7–56.7 mm) from the STP junction.

In a comparative study employing both cadaveric examination and commonly used venous neuroimaging modalities (DSA, CTV, MRV), Han et al. (2008) evaluated the dural entrance of the vein of Labbé in 184 specimens. The approximate average diameter of the vein of Labbé in the cadavers and neuroimages was 2.8 mm and direct drainage into the transverse sinus was found in 74% (137 of 184) of cases. In the other venous specimens, the veins of Labbé reached the sinus indirectly either: (a) through the tentorial sinus in 8% (15 of 184); (b) through the meningeal vein in the occipital dura in 9% (17 of 184); or (c) through the petrosal sinus in 8% (15 of 184). The dural entrance

of the vein of Labbé was more commonly distributed near the junction of the transverse, sigmoid, and petrosal sinuses. Using MP-RAGE imaging on 400 hemispheres the vein of Labbé was found to reach the transverse sinus in 80% of cases, whereas it joined the superior petrosal sinus in 4%. In 16% of the studied cases, the vein of Labbé was found to be undeveloped (Ikushima et al. 2006).

Vein of Trolard

From around a century ago, Jean Baptiste Paulin Trolard's name can be found in the medical literature due to his work on the anastomotic veins of the cerebral vasculature. He was born on 27 November 1842 in the town of Sedan (Ardennes), France and after years of contribution not only to neuroanatomy but also to humanitarian and environmental causes, he died in Saint-Eugène, Algeria, on 13 April 1910 (Loukas et al. 2010). The vein of Trolard, also known as the superior anastomotic vein, passes through the cortical surface of the frontal and parietal lobes as the largest anastomotic vein between the superior sagittal sinus and the Sylvian fissure. In a cadaveric study, it was found at a location related to the precentral, central, or (most commonly) postcentral vein (Rhoton 2002). It is usually seen as a single vein, although it can be split into two and is also predominant in the minor hemisphere (46–52% in the right; 18–24% in the left; Sindou and Auque 2000).

On the basis of an intraoperative study, Tanriverdi et al. (2009) found: (1) the most common predominant superficial anastomotic vein, regardless of sex, is the combination of the vein of Labbé and the superficial Sylvian vein; (2) the course of the vein of Trolard is more variable than the vein of Labbé and the superficial Sylvian vein; (3) the vein of Trolard is most frequently observed at the level of the central vein and the vein of Labbé at the level of the middle temporal vein; and (4) the superficial Sylvian vein predominates in the right hemisphere and the vein of Labbé in the left, and these patterns are independent of gender.

An evaluation of 117 normal and 117 pathological phlebograms (Matsubara and Nomura 1961) revealed variations in the superficial anastomotic veins in 30% of healthy cases; in most of these, the vein of Trolard was the dominant drainage pathway. Variations were found in 54% of the pathological phlebograms, and the superficial Sylvian vein and vein of Labbé were larger than in normal cases. In some pathological cases, abnormal drainage forms became normal following extensive lesion removal. This study revealed that dominant drainage through the vein of Trolard is more common in normal female cases aged 10–19 years in the right hemisphere and in the right hemisphere of males aged 20–29 years, highlighting that the differences between hemispheres in cerebral surface venous return can be related to the differences in functions of the two hemispheres in these age groups.

From phlebograms of 175 brains, the vein of Labbé was reported to be predominant on the left hemisphere in 42% of cases and on the right side in 21%; however, in 52% of right-sided and 24% of left-sided phlebograms, the vein of Trolard was dominant (Delmas et al. 1951). Evaluation of 180 normal carotid angiograms demonstrated that the vein of Labbé was predominant in 40% of subjects, while the vein of Trolard dominated in 32% (Di Chiro 1962). The veins of Trolard and Labbé were codominant in 11% of cases. An inverse relationship between the veins of Trolard and Labbé was also reported, such that predomination of one of these veins in one side is accompanied by diminution or absence of the other (Di Chiro 1962).

MR venography has revealed significant differences between right and left hemispheres with respect to the predominant superficial anastomotic veins. A study by Ayanzen et al. (2000) demonstrated that the vein of Trolard predominated in 37% and 34% of subjects in the right and left hemispheres, respectively. However, the vein of Labbé predominated on the right and left hemispheres in 91% and 96%, respectively. These findings are consistent with other MR studies of the cerebral surface veins (Ikushima et al. 2006; Surendrababu et al. 2006).

References

Avci E, Dagtekin A, Akture E, Uluc K, Baskaya MK. 2011. Microsurgical anatomy of the vein of Labbe. *Surg Radiol Anat* 33: 569–573.

Ayanzen RH, Bird CR, Keller PJ, McCully FJ, Theobald MR, Heiserman JE. 2000. Cerebral MR venography: normal anatomy and potential diagnostic pitfalls. *AJNR Am J Neuroradiol* 21: 74–78.

Aydin IH, Kadioglu HH, Tuzun Y, Kayaoglu CR, Takci E. 1996. The variations of Sylvian veins and cisterns in anterior circulation aneurysms. An operative study. *Acta Neurochir (Wien)* 138: 1380–1385.

Banna M, Young JR. 1970. Normal anatomical variation and asymmetry of the Galenic venous system. *Br J Radiol* 43: 126–131.

Bartels RH, van Overbeeke JJ. 1997. Charles Labbe (1851–1889). *J Neurosurg* 87: 477–480.

Bigelow DC, Hoffer ME, Schlakman B, Hurst RW, Smith PG. 1993. Angiographic assessment of the transverse sinus and vein of labbe to avoid complications in skull base surgery. *Skull Base Surg* 3: 217–222.

Binder DK, Clusmann H, Schaller C. 2006. Friedrich-Christian Rosenthal: surgeon and anatomist. *Neurosurgery* 59: 1328–1333.

Bisaria KK. 1985. The superficial sylvian vein in humans: with special reference to its termination. *Anat Rec* 212: 319–325.

Browder J, Kaplan HA. 1976. *Cerebral Dural Sinuses and their Tributaries*. Springfield, Ill.: CT Thomas.

Cho ZH, Choi SH, Chi JG, Kim YB. 2011. Classification of the venous architecture of the pineal gland by 7T MRI. *J Neuroradiol* 38: 238–241.

Chung JI, Weon YC. 2005. Anatomic variations of the deep cerebral veins,tributaries of Basal vein of rosenthal: embryologic aspects of the regressed embryonic tentorial sinus. *Interv Neuroradiol* 11: 123–130.

Çimşit NC, Türe U, Ekinci G, Necmettin Pamir M, Erzen C. 2003. Venous variations in the region of the third ventricle: the role of MR venography. *Neuroradiology* 45: 900–904.

Curry RW, Culbreth GG. 1951. The normal cerebral angiogram. *Am J Roentgenol Radium Ther* 65: 345–373.

Dandy W. 1921. An operation for the removal of pineal tumors. *Surg Gynecol Obstet* 33: 113–119.

Dandy W. 1936. Operative experience in cases of pineal tumor. *Arch Surg Forum* 33: 19–46.

Delmas A, Pertuiset B, Bertrand G. 1951. Veins of the temporal lobe. *Rev Otoneuroophtalmol* 23: 224–230.

Di Chiro G. 1962. Angiographic patterns of cerebral convexity veins and superficial dural sinuses. *Am J Roentgenol Radium Ther Nucl Med* 87: 308–321.

Duvernoy HM. 1975. *The Superficial Veins of the Human Brain; Veins of the Brain Stem and of the Base of the Brain*. Berlin, New York: Springer-Verlag.

Ferner H. 1958. The internal cerebral veins in man and their influx area. *Verh Anat Ges* 1958: 237–244.

Fujii S, Kanasaki Y, Matsusue E, Kakite S, Kminou T, Ogawa T. 2010. Demonstration of cerebral venous variations in the region of the third ventricle on phase-sensitive imaging. *AJNR Am J Neuroradiol* 31: 55–59.

Galligioni F, Bernardi R, Pellone M, Iraci G. 1969. The superficial sylvian vein in normal and pathologic cerebral angiography. *Am J Roentgenol Radium Ther Nucl Med* 107: 565–578.

Giordano M, Wrede KH, Stieglitz LH, Samii M, Ludemann WO. 2007. Identification of venous variants in the pineal region with 3D preoperative computed tomography and magnetic resonance imaging navigation. A statistical study of venous anatomy in living patients. *J Neurosurg* 106: 1006–1011.

Giordano M, Wrede KH, Stieglitz LH, Columbano L, Samii M, Luedemann WO. 2009. Depiction of small veins draining into the vein of galen using preoperative 3-dimensional navigation in living patients. *Neurosurgery* 64: 247–251.

Giudicelli G, Salamon G. 1970. The veins of the thalamus. *Neuroradiology* 1: 92–98.

Grand W, Hopkins LN. 1999. *Vasculature of the Brain and Cranial Base: Variations in Clinical Anatomy*. New York, NY: Thieme.

Guppy KH, Origitano TC, Reichman OH, Segal S. 1997. Venous drainage of the inferolateral temporal lobe in relationship to transtemporal/transtentorial approaches to the cranial base. *Neurosurgery* 41: 615–620.

Han H, Yao Z, Wang H, Deng X, Yu Fong AH, Zhang M. 2008. Dural entrance of the bridging vein into the transverse sinus provides a reliable measure for preoperative planning: an anatomic comparison between cadavers and neuroimages. Neurosurgery 62: ONS289–295.

Hassler O. 1966. Deep cerebral venous system in man. A microangiographic study on its areas of drainage and its anastomoses with the superficial cerebral veins. *Neurology* 16: 505–511.

Huang Y, Wolf B. 1974a. The basal cerebral vein and its tributaries. In *Radiology of the Skull and Brain* (eds THNewton, DGPotts). Saint Louis: Mosby, vol II, 2111–2154.

Huang Y, Wolf B. 1974b. Veins of the posterior fossa. In *Radiology of the Skull and Brain* (eds THNewton, DGPotts). Saint Louis: Mosby, vol II, 2155–2216.

Ikushima I, Korogi Y, Kitajima M, Yamura M, Yamashita Y. 2006. Evaluation of drainage patterns of the major anastomotic veins on the lateral surface of the cerebrum using three-dimensional contrast-enhanced MP-RAGE sequence. *Eur J Radiol* 58: 96–101.

Ito J. 1986. Supratentorial venous system. In *Neuroradiology* (eds IY Maki, H Kuru). Tokyo: Asakura Shoten: 443–484.

Jeffery N. 2002. Differential regional brain growth and rotation of the prenatal human tentorium cerebelli. *J Anat* 200: 135–144.

Johanson C. 1954. The central veins and deep dural sinuses of the brain; an anatomical and angiographic study. *Acta Radiol Suppl* 107: 8–184.

Kaplan HA. 1973. *The Blood Vessels of the Brain in 3-D, and a Synopsis of Cerebrovascular Anatomy and Clinical Syndromes*. Brooklyn: Stereo Publications.

Kaplan HA, Browder J. 1974. Importance of veins in partial cerebral lobectomy. *J Neurosurg* 41: 360–366.

Kaplan HA, Browder A, Browder J. 1973. Naasal venous drainage and the foramen caecum. *Laryngoscope* 83: 327–329.

Kazumata K, Kamiyama H, Ishikawa T, Takizawa K, Maeda T, Makino K, Gotoh S. 2003. Operative anatomy and classification of the sylvian veins for the distal transsylvian approach. *Neurol Med Chir (Tokyo)* 43: 427–434.

Kılıç T, Akakin A. 2008. Anatomy of cerebral veins and sinuses. *Front Neurol Neurosci* 23: 4–15.

Kılıç T, Ozduman K, Çavdar S, Özek MM, Pamir MN. 2005. The galenic venous system: surgical anatomy and its angiographic and magnetic resonance venographic correlations. *Eur J Radiol* 56: 212–219.

Knott JF. 1881. On the cerebral sinuses and their variations. *J Anat Physiol* 16: 27–42.

Koperna T, Tschabitscher M, Knosp E. 1992. The termination of the vein of "Labbe" and its microsurgical significance. *Acta Neurochir (Wien)* 118: 172–175.

Krayenbühl H, Richter HR. 1952. *Die Zerebrale Angiographie*. Stuttgart: Thieme.

Krisht A, Barrow D, Al-Mefty O, Dawson R, Shengelala G, Bonner G. 1996. Venous anatomy of the vein of Labbé complex. In *Surgery of the Intracranial Venous System: Embryology, Anatomy, Pathophysiology, Neuroradiology, Diagnosis, Treatment* (ed. A Hakuba). Tokyo, New York: Springer, pp. 36–42.

Labbé C. 1883. Anomalies des sinus de la dure–mère. Développement de ces sinus. Considérations sur la suppléance réciproque de ces canaux veineux dans les cas d'abscence de l'un d'eux. Description de quelques sinus peu connus. *Arch Physiol Norm Pathol* 3: 1–27.

Lang J. 1985. Surgical anatomy of the hypothalamus. *Acta Neurochir (Wien)* 75: 5–22.

Lang J, Schneider W. 1989. The superficial cerebral veins. *Gegenbaurs Morphol Jahrb* 135: 271–303.

Lasjaunias PL, Berenstein A, Brugge KGt. 2001. Surgical Neuroangiography: Clinical Vascular Anatomy and Variations. Berlin, New York: Springer.

Loukas M, Shea M, Shea C, Lutter-Hoppenheim M, Zand P, Tubbs RS, Cohen-Gadol AA. 2010. Jean Baptiste Paulin Trolard (1842–1910): his life and contributions to neuroanatomy. *J Neurosurg* 112: 1192–1196.

Macnalty A. 1957. Sir Victor Horsley: his life and work. *Br Med J* 1: 910–916.

Matsubara T, Nomura T. 1961. An observation on the superficial cerebral veins in cerebral phlebograms. *No To Shinkei* 13: 765–769.

Mokrohisky JF, Paul RE, Lin PM, Stauffer HM. 1956. The diagnostic importance of normal variants in deep cerebral phlebography, with special emphasis on the true and false venous angles of the brain and evaluation of venous angle measurements. *Radiology* 67: 34–47.

Nowinski WL. 2012. Proposition of a new classification of the cerebral veins based on their termination. *Surg Radiol Anat* 34: 107–114.

Oka K, Rhoton AL Jr, Barry M, Rodriguez R. 1985. Microsurgical anatomy of the superficial veins of the cerebrum. *Neurosurgery* 17: 711–748.

Ono M, Rhoton AL Jr, Barry M. 1984a. Microsurgical anatomy of the region of the tentorial incisura. *J Neurosurg* 60: 365–399.

Ono M, Rhoton AL Jr, Peace D, Rodriguez RJ. 1984b. Microsurgical anatomy of the deep venous system of the brain. *Neurosurgery* 15: 621–657.

Padget DH. 1956. The cranial venous system in man in reference to development, adult configuration, and relation to the arteries. *Am J Anat* 98: 307–355.

Padget DH. 1957. Development of cranial venous system in man, from view point of comparative anatomy (Carnegie Institution of Washington publication 611). *Contrib Embryol* 36: 79–140.

Perese DM. 1960. Superficial veins of the brain from a surgical point of view. *J Neurosurg* 17: 402–412.

Probst FP. 1970. Position of the "venous angle" in the median sagittal plane. A new topometric method. *Acta Radiol Diagn (Stockh)* 10: 271–288.

Rhoton AL. 2002. The cerebral veins. *Neurosurgery* 51: S159–205.

Rhoton AL. 2007. *Cranial anatomy and surgical approaches*. New York: Lippincott Williams & Wilkins.

Rhoton AL, Yamamoto I, Peace DA. 1981. Microsurgery of the third ventricle: Part 2. Operative approaches. *Neurosurgery* 8: 357–373.

Rosenbaum AE. 1974. Deep supratentorial veins. II. Abnormal supratentorial deep cerebral veins. In *Radiology of the Skull and Brain* (eds TH Newton, DG Potts). St Louis: Mosby, vol. II, pp. 1999–2110.

Rosenthal F. 1824. *De Intimis Cerebri Venis, seu de Venae Magnae Galeni Ramis*. Bonn: Weber.

Sakata K, Al-Mefty O, Yamamoto I. 2000. Venous consideration in petrosal approach: microsurgical anatomy of the temporal bridging vein. *Neurosurgery* 47: 153–160.

Salamon G, Huang YP. 1976. Radiologic Anatomy of the Brain. Berlin, New York: Springer-Verlag.

San Millan Ruiz D, Fasel JH, Gailloud P. 2006. Drainage pathways in the middle cranial fossa. *Eur J Radiol* 60: 40–41.

Schlesinger B. 1939. The venous drainage of the brain, with special reference to the Galenic system. *Brain* 62: 274–291.

Sindou M, Auque J. 2000. The intracranial venous system as a neurosurgeon's perspective. *Adv Tech Stand Neurosurg* 26: 131–216.

Stein BM. 1971. The infratentorial supracerebellar approach to pineal lesions. *J Neurosurg* 35: 197–202.

Stein RL, Rosenbaum AE. 1974. Deep supratentorial veins. Section I. Normal deep cerebral venous system. In *Radiology of the Skull and Brain* (eds TH Newton, DG Potts). Saint Louis: Mosby, vol 2, pp. 1903–1998.

Stephens RB, Stilwell DL. 1969. *Arteries and Veins of the Human Brain*. Springfield, Ill: Charles C. Thomas.

Surendrababu NR, Subathira, Livingstone RS. 2006. Variations in the cerebral venous anatomy and pitfalls in the diagnosis of cerebral venous sinus thrombosis: low field MR experience. *Indian J Med Sci* 60: 135–142.

Suzuki Y, Matsumoto K. 2000. Variations of the superficial middle cerebral vein: classification using three-dimensional CT angiography. *AJNR Am J Neuroradiol* 21: 932–938.

Suzuki Y, Ikeda H, Shimadu M, Ikeda Y, Matsumoto K. 2001. Variations of the basal vein: identification using three-dimensional CT angiography. *AJNR Am J Neuroradiol* 22: 670–676.

Tamaki N, Fujiwara K, Matsumoto S, Takeda H. 1973. Veins draining the pineal body. An anatomical and neuroradiological study of "pineal veins". *J Neurosurg* 39: 448–454.

Tamaki N, Fujiwara K, Matsumoto S. 1974. "Pineal veins"—-anatomy and angiography (author's transl). *No Shinkei Geka* 2: 379–387.

Tanriverdi T, Al-Jehani H, Poulin N, Olivier A. 2009. Superficial anastomotic veins: neurosurgical view depending on 251 craniotomies. *Can J Neurol Sci* 36: 65–71.

Tatu L, Vuillier F, Moulin T. 2009. Chapter 13 Anatomy of the circulation of the brain and spinal cord. *Handb Clin Neurol* 92: 247–281.

Tubbs RS, Loukas M, Louis RG, Jr., Shoja MM, Askew CS, Phantana-Angkool A, Salter EG, Oakes WJ. 2007. Surgical anatomy and landmarks for the basal vein of rosenthal. *J Neurosurg* 106: 900–902.

Tubbs RS, Louis RG, Jr., Song YB, Mortazavi M, Loukas M, Shoja MM, Cohen-Gadol AA. 2012. External landmarks for identifying the drainage site of the vein of Labbe: application to neurosurgical procedures. *Br J Neurosurg* 26: 383–385.

Türe U, Yaşargil MG, Al-Mefty O. 1997. The transcallosal-transforaminal approach to the third ventricle with regard to the venous variations in this region. *J Neurosurg* 87: 706–715.

Umbach W. 1952. Cerebral phlebography. *Fortschr Geb Rontgenstr* 77: 179–187.

Wackenheim A, Braun JP. 1978. *The veins of the posterior fossa: normal and pathologic findings*. Berlin, New York: Springer-Verlag.

Wang J, Sun J, Gong X. 2010. Evaluation of the anatomy and variants of internal cerebral veins with phase-sensitive MR imaging. *Surg Radiol Anat* 32: 669–674.

Watanabe A, Hirano K, Kamada M, Imamura K, Ishii N, Sekihara Y, Suzuki Y, Ishii R. 2002. Perimesencephalic nonaneurysmal subarachnoid haemorrhage and variations in the veins. *Neuroradiology* 44: 319–325.

Wolf BS, Huang YP. 1964. The subependymal veins of the lateral ventricles. *Am J Roentgenol Radium Ther Nucl Med* 91: 406–426.

Wolf BS, Huang YP, Newman CM. 1963. The superficial sylvian venous drainage system. *Am J Roentgenol Radium Ther Nucl Med* 89: 398–410.

Yamamoto I, Kageyama N. 1980. Microsurgical anatomy of the pineal region. *J Neurosurg* 53: 205–221.

Yasargil MG. 1987. Microneurosurgery. *Stuttgart*, New York: Georg Thieme Verlag, Thieme Medical Publishers.

Ziyal IM, Sekhar LN, Salas E, Olan WJ. 1998. Combined supra/infratentorial-transsinus approach to large pineal region tumors. *J Neurosurg* 88: 1050–1057.

62 Emissary veins

R. Shane Tubbs[1–3], Koichi Watanabe[4] and Marios Loukas[2]
[1]Seattle Science Foundation, Seattle, Washington, USA
[2]St George's University, School of Medicine, St Georges, Grenada
[3]University of Dundee, Dundee, UK
[4]Kurume University School of Medicine, Fukuoka, Japan

Emissary veins connect the veins outside the cranium with the intracranial venous sinuses (Mortazavi et al. 2012; Fig. 62.1). These structures are more commonly found in children, and not all of the various emissary veins are identified in every individual (Eckley 1903). These veins serve an important function of equalizing intracranial pressure, and can act as safety valves during cerebral congestion or in patients with lesions of the neck or skull such as obstruction of the internal jugular veins (Eckley 1903; Boyd 1930; Braun and Tournade 1977; Williams et al. 1989; Curé et al. 1994; Louis et al. 2009). The foramina for these vessels tend to be larger during childhood (Williams et al. 1989) and may communicate with the diploic veins (Curé et al. 1994). Louis et al. (2009) found that emissary veins act as the primary outflow route for venous drainage in the upright position, and may serve to cool venous blood circulating through the head.

Emissary veins can often be seen on MRI, CT, and angiograms, and the various types are named according to their positions on the skull (Boyd 1930; Hacker 1974; Louis et al. 2009). Interestingly, an enlarged emissary foramen does not necessarily transmit a large emissary vein (Boyd 1930), and fossil records indicate that there is an increasing frequency of some emissary veins such as the mastoid and parietal vessels in man (Falk 1986).

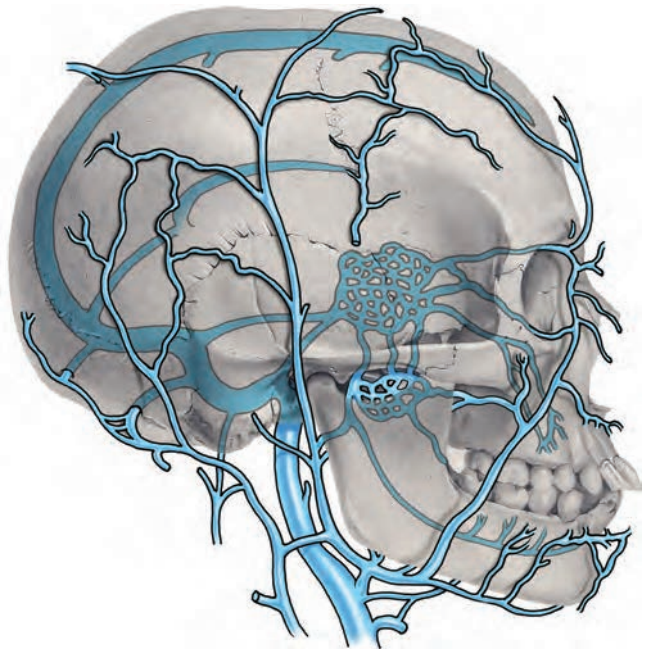

Figure 62.1 Schematic drawing of the major emissary veins and their internal connections.

Posterior condylar emissary vein

The posterior condylar emissary vein connects the lower end of the sigmoid, marginal, or occipital sinuses with the internal vertebral venous plexus (Pearson 1979; Falk 1986; Williams et al. 1989; Curé et al. 1994). Irmak et al. (2004) noted that a posterior condylar emissary vein may connect the sigmoid sinus with the suboccipital plexus of veins (Curé et al. 1994). Observations have shown that the posterior condylar foramen is usually the largest emissary foramen in the retromastoid region (Boyd 1930). Lang (1985) found that this vein joins the hypoglossal plexus in 3.84% and it joins the internal jugular vein below the jugular foramen in another 3.84%.

Mastoid emissary vein

The mastoid emissary vein passes through the mastoid canal and connects the transverse or sigmoid sinus to the posterior auricular or occipital veins, which then join the vertebral plexus of veins (Cheatle 1925; Boyd 1930; Falk 1986; Curé et al. 1994; Irmak et al. 2004; Standring 2005). Lang and Samii (1991)

Bergman's Comprehensive Encyclopedia of Human Anatomic Variation, First Edition. Edited by R. Shane Tubbs, Mohammadali M. Shoja and Marios Loukas.
© 2016 John Wiley & Sons, Inc. Published 2016 by John Wiley & Sons, Inc.

Figure 62.2 Left mastoid region noting several mastoid veins draining through a single mastoid foramen.

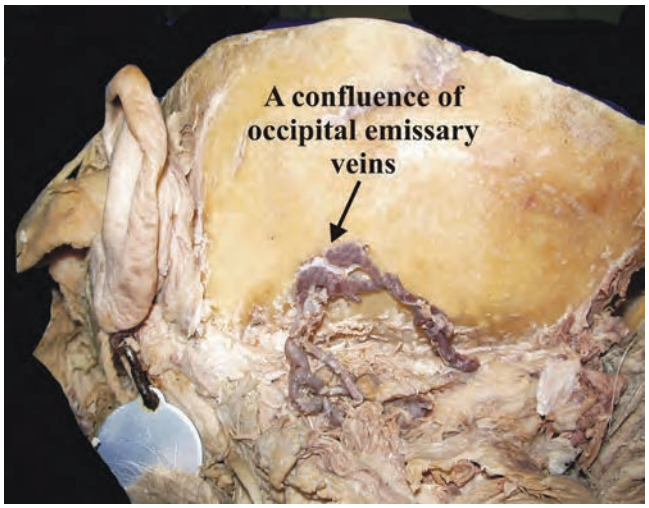

Figure 62.3 Two occipital veins entering a single occipital foramen on the left side.

observed that the mastoid emissary foramen exists less frequently in females than males, although the reason for this is unclear. It is controversial whether mastoid foramina are more common on right versus left sides (Louis et al. 2009). Cheatle (1925) noted an infrequent association between the mastoid emissary vein and the petrosquamosal sinus. Multiple emissary veins may converge toward one mastoid foramen (Fig. 62.2).

Occipital emissary vein

The occipital emissary vein connects the transverse sinus to the occipital vein, which then drains blood to the vertebral venous plexus (Falk 1986; Williams et al. 1989). On occasion, the occipital emissary vein joins the transverse-sigmoid sinus complex (Neuroangio 2013). Okudera et al. (1994) have reported that the occipital vein may drain to the confluence of sinuses. There may be several occipital veins that drain to one occipital foramen (Fig. 62.3).

Parietal emissary vein

The parietal emissary vein connects the superior sagittal sinus with the occipital vein that then joins the vertebral venous plexus (Falk 1986; Williams et al. 1989). Parietal emissary veins may also interact with the diploic veins.

Petrosquamosal sinus

Although it serves as the primary cerebral drainage site in many lesser primates and quadrupeds, the petrosquamosal sinus is a rare emissary vein in humans that typically disappears prior to birth in humans. The petrosquamosal sinus ranges from 2 to 4 mm in diameter and originates at the junction between the transverse and sigmoid sinuses, coursing laterally above the superior border of the temporal bone.

Ophthalmic veins

The ophthalmic veins are considered by some to be emissary veins as they may carry out a similar function by connecting the exterior with the interior skull (angular vein to cavernous sinus) and are valveless. The ophthalmic veins travel through the orbit and traverse the superior orbital fissure to reach the most anterior portion of the cavernous sinus (Dwight et al. 1913).

Sphenoidal emissary vein (Vesalius)

Sphenoidal emissary veins (Vesalian or Meckel's veins) connect the cavernous sinus with the pterygoid or pharyngeal plexuses (Dwight et al. 1913; Gray 1918; Hayashi et al. 2010). These veins are not constant and are only found in approximately one in three cases (Dwight et al. 1913). When present, the foramen for this vessel is found just medial to the foramen ovale.

Emissary veins of the foramen ovale

As for sphenoidal emissary veins, the emissary veins of the foramen ovale connect the cavernous sinus to the pterygoid plexus (Dwight et al. 1913; Gray 1918).

Internal carotid venous plexus

The internal carotid plexus of veins extends through the carotid canal and connects the cavernous sinus with the internal jugular vein (Gray 1918). This collection of veins is classified by some as emissary veins as it joins the intradural sinuses with extracranial veins (Ernst et al. 1999).

Emissary vein of the foramen cecum

The single emissary vein of the foramen cecum joins the superior sagittal sinus with veins of the nasal cavity and is unpaired (Gray 1918). This vessel is larger at birth than in the adult.

Emissary veins of the foramen lacerum

An inconsistent number of small veins may traverse the cartilage-filled foramen lacerum. Such emissary veins connect the cavernous sinus with the pterygoid venous plexus (Dwight et al. 1913).

Emissary veins of the clivus

Some have identified transclival emissary veins (Tubbs et al. 2007). If present, these structures connect the basilar venous plexus to veins on the inferior surface of the clivus adjacent to the pharynx.

Anterior condylar vein

The anterior condylar vein accompanies the hypoglossal nerve through the hypoglossal canal and joins the anterior condylar confluent (Chen et al. 2007).

Temporal emissary vein

This venous structure may connect the remnant of the petrosquamosal sinus with the deep temporal vein and likely represents the dorsal cerebral vein seen in some mammals.

Superficial petrosal emissary vein

This vein connects the vessel(s) traveling along the superficial petrosal vein in the middle cranial fossa to the vein traveling with the facial nerve within the stylomastoid foramen. Such vessels may be remnants of the primary head sinus.

Hoshi et al. (2000) reported a case of removal of a hypoglossal neurinoma where the condylar emissary veins were enlarged. Coagulation of these channels resulted in dural venous sinus thrombosis and cerebellar infarction, leading to the patient's death. Sphenoidal emissary veins and veins of the foramen ovale may hinder lateral extradural approaches to the skull base.

In the event of compromise of the internal jugular veins, emissary veins may increase in size and provide the primary venous outflow of the skull (Ginsberg 1994; Marsot-Dupuch et al. 2001). The main venous outflow of the posterior fossa venous sinuses may be via the occipital and mastoid emissary veins (Jeevan et al. 2008).

Tinnitus has been reported as a consequence of large posterior condylar veins (Lambert and Cantrell 1986; Forte et al. 1989; Chen et al. 2007). One case of tinnitus was alleviated after decreasing blood flow through the internal jugular vein via direct pressure on the neck, altering the flow within the posterior condylar emissary vein (Lambert and Cantrell 1986). Although rare, dural arteriovenous fistulas have been identified at the anterior condylar vein. Ernst et al. (1999) reported three cases of dural arteriovenous fistula involving this vein within the hypoglossal canal. In a cadaver, Moore et al. (2013) identified an anastomosis between the posterior condylar vein and the vertebral venous plexus.

An enlarged anterior condylar emissary vein has also been linked to unilateral tongue atrophy (Shiozawa et al. 1996). Sinus pericranii are dilated extracranial veins found under the scalp under or inside the periosteum (Ota et al. 1975) and are characterized by communication of pericranial varicosities with an underlying dural sinus (Carpenter et al. 2004). Such vessels may be sizable and may represent ectopic diploic veins. Emissary veins such as the parietal veins may connect these structures to the diploic venous system.

References

Boyd G. 1930. The emissary foramina of the cranium in man and the anthropoids. *J Anat* 65: 108–121.

Braun JP, Tournade A. 1977. Venous drainage in the craniocervical region. *Neuroradiol* 13: 155–158.

Carpenter JS, Rosen CL, Bailes JE, Gailloud P. 2004. Sinus pericranii: clinical and imaging findings in two cases of spontaneous partial thrombosis. *AJNR Am J Neuroradiol* 25: 121–125.

Cheatle A. 1925. The mastoid emissary vein and its surgical importance. *Proc R Soc Med* 18: 29–34.

Chen Z, Feng H, Zhu G, Wu N, Lin J. 2007. Anomalous intracranial venous drainage associated with basal ganglia calcification. *AJNR Am J Neuroradiol* 28: 22–24.

Curé JK, Van Tassel P, Smith MT. 1994. Normal and variant anatomy of the dural venous sinuses. *Semin Ultrasound CT MR* 15: 499–519.

Dwight T, Hamann C, McMurrich J, Piersol G. 1913. *Human Anatomy*. London: Lippincott Company.

Eckley W. 1903. Anatomic and physiological correspondences of child and the adult. *JAMA* 20: 1337.

Ernst R, Bulas R, Tomsick T, van Loveren H, Aziz KA. 1999. Three cases of dural arteriovenous fistula of the anterior condylar vein within the hypoglossal canal. *AJNR Am J Neuroradiol* 20: 2016–2020.

Falk D. 1986. Evolution of cranial blood drainage in hominids: Enlarged occipital/marginal sinuses and emissary foramina. *Am J Phys Anthropol* 70: 311–324.

Forte V, Turner A, Liu P. 1989. Objective tinnitus associated with abnormal mastoid emissary vein. *J Otolaryngol* 18: 232–235.

Ginsberg LE. 1994. The posterior condylar canal. *AJNR Am J Neuroradiol* 15: 969–972.

Gray H. 1918. Anatomy of the Human Body. Philadelphia: Lea & Febiger.

Hacker H. 1974. Emissary veins related to the transverse sinus, sigmoid sinus, and torcular herophili. In: *Radiology of the Skull and Brain* (eds TH Newton, DG Potts). St Louis: C.V. Mosby Company.

Hayashi N, Sato H, Tsuboi Y, Nagai S, Kuwayama N, Endo S. 2010. Consequences of preoperative evaluation of patterns of drainage of the cavernous sinus in patients treated using the anterior transpetrosal approach. *Neurol Med Chir (Tokyo)* 50: 373–377.

Hoshi M, Yoshida K, Ogawa K, Kawase T. 2000. Hypoglossal neurinoma: two case reports. *Neurol Med Chir (Tokyo)* 40: 489–493.

Irmak MK, Korkmaz A, Erogul O. 2004. Selective brain cooling seems to be a mechanism leading to human craniofacial diversity observed in different geographical regions. *Med Hypotheses* 63: 974–979.

Jeevan DS, Anlsow P, Jayamohan J. 2008. Abnormal venous drainage in syndromic craniosynostosis and the role of CT venography. *Childs Nerv Syst* 24: 1413–1420.

Lambert PR, Cantrell RW. 1986. Objective tinnitus in association with an abnormal posterior condylar emissary vein. *Am J Otol* 7: 204–207.

Lang J. 1985. Anatomy of the brainstem and the lower cranial nerves, vessels, and surrounding stuctures. Am J Otol Suppl Nov: 1–19.

Lang J Jr, Samii A. 1991. Retrosigmoidal approach to the posterior cranial fossa. An anatomical study. *Acta Neurochir (Wien)* 111: 147–153.

Louis RG Jr, Loukas M, Wartmann CT, Tubbs RS, Apaydin N, Gupta AA, Spentzouris G, Ysique JR. 2009. Clinical anatomy of the mastoid and occipital emissary veins in a large series. *Surg Radiol Anat* 31: 139–144.

Marsot-Dupuch K, Gayet-Delacroix M, Elmaleh-Bergès M, Bonneville F, Lasjaunias P. 2001. The petrosquamosal sinus: CT and MR findings of a rare emissary vein. *AJNR Am J Neuroradiol* 22: 1186–1193.

Moore G, Lenz R, DiLandro AC,Tubbs RS, Loukas M, Kozlowski PB, D'Antoni AV. 2013. Unique anastomosis between the condylar emissary vein and extracranial venous plexus: an anatomic and histologic case report. *Biomed Int J* 4: 95–99.

Mortazavi MM, Tubbs Rs, Riech S, Verma K, Shoja MM, Zurada A, Benninger B, Loukas M, Cohen Gadol AA. 2012. Anatomy and pathology of the cranial emissary veins: a review with surgical implicaitons. *Neurosurgery* 70: 1312–1318.

Neuroangio. 2013. Venous Anatomy of the Brain. Available at: http://neuroangio.org/venous-brain-anatomy/ (accessed 9 November 2015).

Okudera T, Huang YP, Ohta T, Yokota A, Nakamura Y, Maehara F, Utsunoiya H, Uemura K, Fukasawa H. 1994. Development of posterior fossa dural sinuses, emissary veins, and jugular bulb: Morphological and radiologic study. *AJNR Am J Neuroradiol* 15: 1871–1883.

Ota T, Waga S, Handa H, Nishimura S, Mitani T. 1975. Sinus pericranii. *J Neurosurg* 42: 704–712.

Pearson BW. 1979. Microsurgical anatomy of the approach to the base of the skull. *Clin Neurosurg* 26: 379–390.

Shiozawa Z, Koike G, Seguchi K, Shindo K, Sugita K. 1996. Unilateral tongue atrophy due to an enlarged emissary vein in the hypoglossal canal. *Surg Neurol* 45: 477–479.

Standring S. 2005. *Gray's Anatomy*, 39th edition. Elsevier, Churchill Livingstone.

Tubbs RS, Kelly DR, Humphrey ER, Chua GD, Shoja MM, Salter EG, Acakpo-Satchivi L, Wellons JC 3rd, Blount JP, Oakes WJ. 2007. The tectorial membrane: anatomical, biomechanical, and histological analysis. *Clin Anat* 20: 382–386.

Williams P, Warwick R, Dyson M, Bannister L. 1989. *Gray's Anatomy*, 37th edition. Edinburgh: Churchill Livingstone.

63 Veins of the neck

R. Shane Tubbs[1–3] and Koichi Watanabe[4]
[1]Seattle Science Foundation, Seattle, Washington, USA
[2]St George's University, School of Medicine, St Georges, Grenada
[3]University of Dundee, Dundee, UK
[4]Kurume University School of Medicine, Fukuoka, Japan

Common facial vein

The common facial vein may cross over the sternocleidomastoid muscle and open into the external jugular vein (Bertha and Suganthy 2011); open into the anterior jugular vein; run beneath the posterior belly of the digastric and stylohyoid muscles; or receive the lingual vein, a pharyngeal vein or the submental vein. The anterior facial vein may receive the angular, the posterior facial, and the lingual veins. Tubbs et al. (2002) found the common facial vein in only two-thirds of specimens. The vessel was also found to be –10 to 15 mm (mean 3.0 mm) above the bifurcation of the common carotid artery. The facial vein proper can open into the internal, external, or anterior jugular veins.

Anterior jugular vein

The anterior jugular may exist as two parallel vessels, one opening into the transverse cervical vein and one into the external jugular. One anterior jugular vein may open into the external jugular and the other into the subclavian vein. When the anterior jugular vein connects with the external vein, the so-called submandibular venous arch is formed (Lang 1993). The submandibular vein may drain into the anterior jugular vein (Chauhan et al. 2011). There may only be one anterior jugular vein or it may exist as multiples. Both anterior jugular veins, forming an inferior arch, may then drain via a single vein into the subclavian or internal jugular veins (Fig. 63.1).

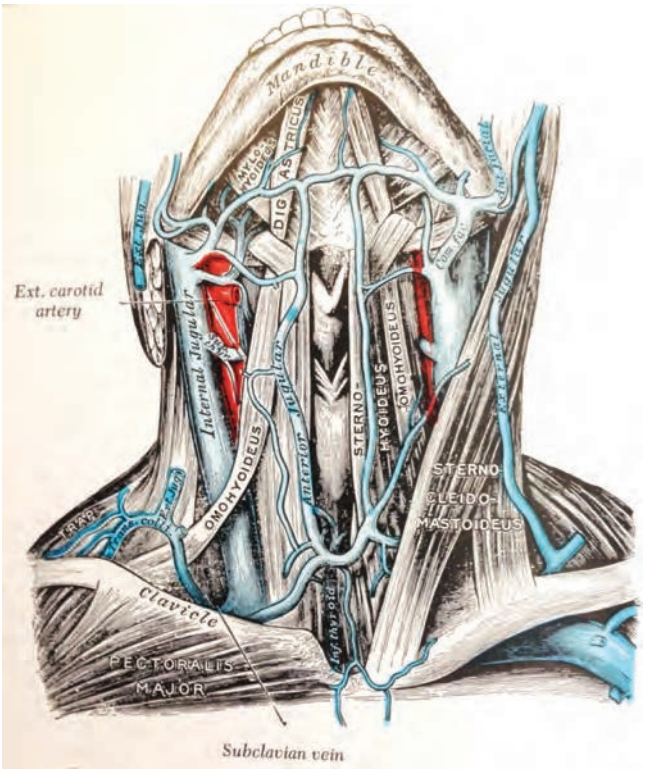

Figure 63.1 Illustration of the external jugular vein draining into the transverse cervical vein.

Source: Gray (1918).

External jugular vein

Both veins may be very small, or one may be much larger than the other. The external jugular may be missing on one or both sides; the veins that usually form it then open into the internal jugular vein. It may be formed solely by the posterior auricular or occipital veins (Lang 1995). In a cadaver study, Deslaugiers et al. (1994) found drainage into the external jugular vein to include: the transverse cervical vein in 88 cases (88%) (Fig. 63.1), usually opposite the intersection of the external jugular vein with the dorsal border of the sternocleidomastoid muscle;

Bergman's Comprehensive Encyclopedia of Human Anatomic Variation, First Edition. Edited by R. Shane Tubbs, Mohammadali M. Shoja and Marios Loukas.
© 2016 John Wiley & Sons, Inc. Published 2016 by John Wiley & Sons, Inc.

Figure 63.2 External jugular vein formed by the retromandibular and facial veins, which then drains into the internal jugular vein.

Source: Satishkumar et al. (2013). Reproduced with permission from International Journal of Anatomical Variations.

the suprascapular vein in 47 cases (47%); the anterior jugular vein in 46 cases (46%); and the cervical vein or anastomosis with the latter in 13 cases (13%). These authors found that the external jugular vein flowed: into the jugulosubclavian venous confluence in 60%; into the subclavian vein at a distance from its junction with the internal jugular vein in 36%; and into the trunk of the internal jugular vein in 4% (Fig. 63.2). The external jugular vein can drain into the transverse cervical vein, which may or may not unite with the suprascapular vein. The retromandibular vein may not divide and continue as the external jugular that then drains into the internal jugular vein (Satishkumar et al. 2013). On occasion it receives the facial, lingual, or the cephalic veins. It may pass over the clavicle and open into the cephalic, subclavian, or internal jugular veins. The vein is sometimes doubled (Shenoy et al. 2012). Rajanigandha et al. (2008) reported a left retromandibular vein that joined the facial vein to form the common facial vein. The short vein divided into anterior and posterior parts. The posterior part drained into the internal jugular vein via a connecting vein. The anterior part continued as a variant external jugular vein where it crossed the midline to drain into the right subclavian vein. The external jugular may descend posterior to the inferior belly of the omohyoid.

In some cases it forms a venous ring around the clavicle. The vein occasionally receives a lingual vein or an accessory external thoracic that ascends subcutaneously from the region of the nipple.

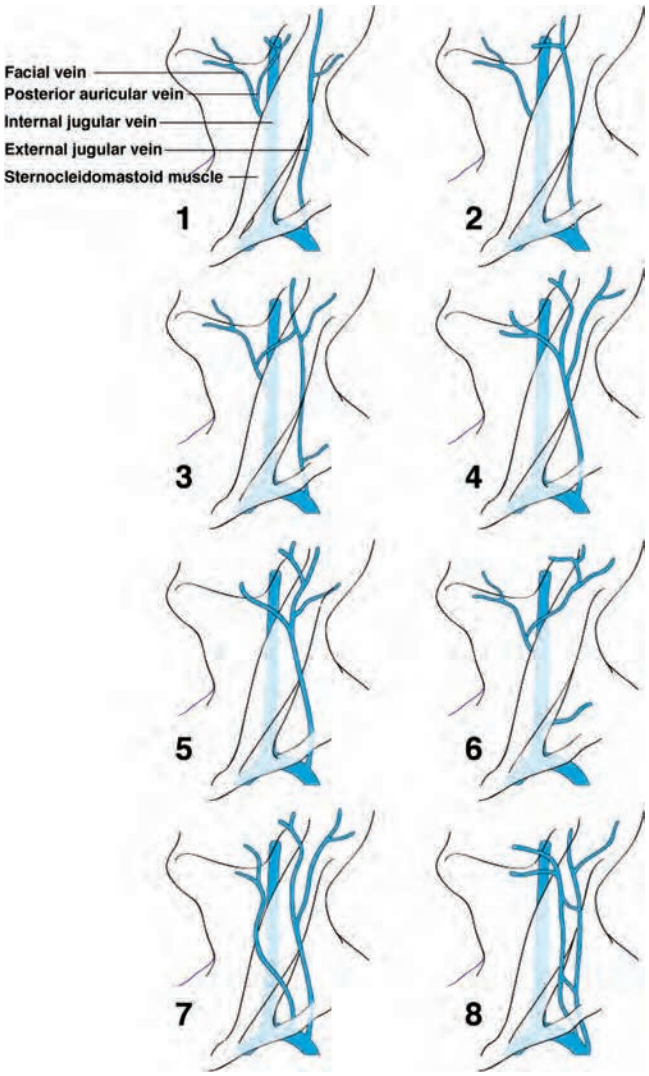

Figure 63.3 Variations in the formation of the external jugular vein. Adapted from Krmpotić-Nemanić et al. (1988).

Rao et al. (2009) reported a cadaver with the supraclavicular nerve forming a loop around the external jugular vein. Lang (1995) stated that the retromandibular vein can open separately into the internal jugular vein or into the external jugular vein. Figure 63.3 summarizes many of the more common variations of the external jugular vein.

Communicating vein

This vessel, also known as the vein of Kocher, is often a branch of the common facial vein. It usually drains into the anterior jugular vein and can be enlarged to compensate for deficiencies in the size of other regional veins, for example external jugular or anterior jugular veins.

Internal jugular vein

This vein may course in front of, or rarely behind, the common carotid artery. This vein may be duplicated unilaterally or bilaterally and this duplication may be partial or complete (Kapre and Mangalgiri 2012). The jugular bulb may lie exposed within the middle ear cavity. The vein may be absent or rudimentary, its blood return taken over by the external jugular. Unusual tributaries of the internal jugular include the supreme thoracic, bronchial, superior laryngeal, palatine, superficial cervical, vertebral, suprascapular, temporomaxillary, left superior intercostal, bronchial, suprascapular, and transverse cervical veins. The inferior petrosal sinus may drain into the extracranial internal jugular vein. In 70% of cases the nerve passes anterior to the vein, in 26.8% of cases the nerve passes behind the vein, and in 3.2% of cases the nerve passes through the internal jugular vein (Bergman 1996). The omohyoid has been reported to travel posterior to the internal jugular vein and the spinal accessory nerve may pierce the vein. The left and right internal jugular veins may communicate across the midline via their medial branches. In relation to the lower half of the sternocleidomastoid muscle, the IJV can be located at its anterior, middle, or posterior borders (Lang 1993). An accessory vein that arises from the junction of the IJV and subclavian vein and travels posteriorly is known as the posterior jugular vein of Walther.

Inferior thyroid vein

The two veins may form a transverse venous arch across the trachea. The inferior thyroid may receive bronchial or thymic veins. Wafae et al. (2008) found the inferior thyroid vein was constant (96.7%) and varied in number, with one (62.1%), two (27.6%) or even five occurring, and was formed by the confluence of two primary branches (78.6%) as a result of the abundance of anastomoses coming from the lower and medial parts of the gland. The number of terminations corresponded to the number of veins at the level of the 5th to 8th rings in 36.9%, of the 9th to 10th rings in 34.8%, and of the 11th to 14th rings in 28.3%, and occurred in the right brachiocephalic vein (26.1%), in the left brachiocephalic vein (60.9%), or into both veins (13.0%). Figure 63.4 summarizes many of the variations of the inferior thyroid veins.

Superior thyroid vein

This vein may receive the inferior petrosal vein (Bergman 1996). Wafae et al. (2008) found the superior thyroid vein to be constant, single on both sides (83.3%), with its termination (87.1%) at the internal jugular vein (97.2%), and either isolated (29.4%) or with other veins, mostly the lingual vein (52.1%). Figure 63.4 summarizes many of the variations of the inferior thyroid veins.

Middle thyroid vein

Wafae et al. (2008) found that the middle thyroid vein was a single vessel in 96.1% of their specimens but that it was not constant (43.3%). Dionigi et al. (2010) found the middle thyroid vein in 38% of dissected lobes and 62% of operated patients. These authors concluded that most veins arose from the mid region of the thyroid in 80%. Oszukowski and Kosinski (1996) found one fetus with a middle thyroid vein that drained into the vertebral vein. The middle thyroid vein is often absent and can drain into the brachiocephalic vein (Krmpotić-Nemanić et al. 1988).

Fourth thyroid vein

An additional thyroid vein may drain the thyroid gland. This vein (of Kocher) is found between the middle and inferior thyroid veins and drains into the internal jugular vein. When present, this vessel is found approximately 1 cm below the middle thyroid vein.

Posterior thyroid vein

This vessel may or may not represent the fourth thyroid vein. It is described as draining either into the internal jugular vein via the middle thyroid vein or into a posterior plexus on the posterior aspect of the gland (Krmpotić-Nemanić et al. 1988)

Vertebral veins

A vertebral vein may have two roots that encircle the corresponding subclavian vein. It may receive the upper intercostal veins as tributaries. It has been found passing in front of the clavicle. When an accessory vertebral vein is present, it arises from the venous plexus on the vertebral artery and descends through the seventh transverse foramen to join the brachiocephalic vein. Mears (1888) reported a vertebral vein that discharged itself by means of a sinus-like canal, a quarter of an inch in diameter, which passed horizontally backward between the posterior roots of the second and third cervical transverse processes to end on the semispinalis muscle by breaking up into similar smaller sinus-like branches among the muscles; one such branch, of crow-quill size, entered the spinal canal between the laminae of the second and third vertebrae. Miyake et al. (2010) classified the vertebral veins into four types as follows: Type A (80.6%), a vertebral vein that descended ventral to the subclavian artery (SA) and drained into the upper portion of the brachiocephalic vein (BCV); Type B (5.8%), a vertebral vein that descended dorsal to the SA and drained into the upper portion or the lower portion of the BCV; Type C (8.3%), a doubled vertebral vein that crossed both sides of

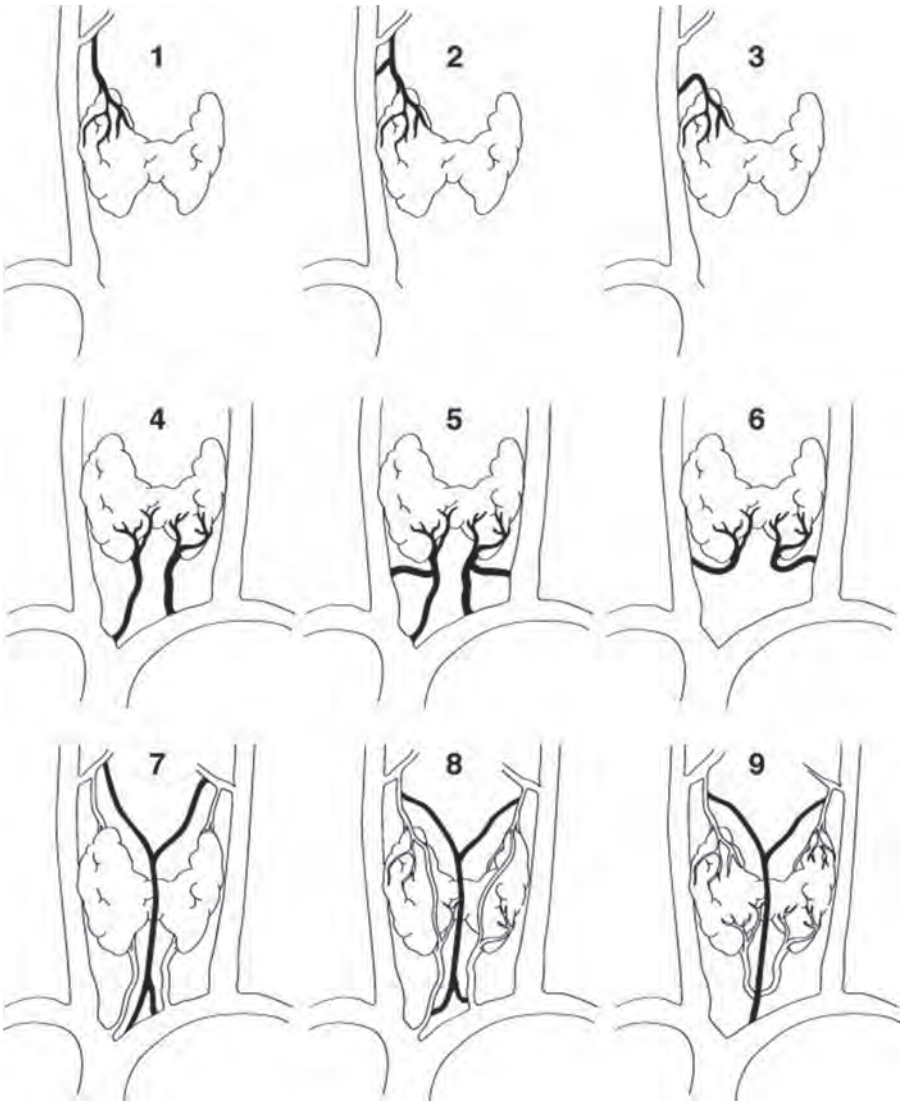

Figure 63.4 Various combinations of drainage of the superior, middle, and inferior thyroid veins. (1–3) Superior thyroid vein variations; (4–6) inferior thyroid vein variations; (7–9) variant combinations of the superior and inferior thyroid veins. Note the so-called "median" thyroid vein formed in (7–9). Adapted from Krmpotić-Nemanić et al. (1988).

the SA and drained into the upper portion of the BCV and formed a common trunk; and Type D (5.3%), a vertebral vein that descended ventral to the SA and drained into the upper portion of the BCV, with another vertebral vein dorsal to the SA which drained into the upper portion or the lower portion of the BCV.

References

Bergman R. 1996. *Catalog of Human Anatomic Variation*. Baltimore: Urban & Schwarzenberg.

Bertha A, Suganthy R. 2011. Anatomical variations in termination of common facial vein. *J Clin Diagn Res* 5: 24–27.

Chauhan NK, Rani A, Chopra J, Rani A, Srivastava AK, Kumar V. 2011. Anomalous formation of external jugular vein and its clinical implication. *Natl J Maxillofac Surg* 2: 51–53.

Deslaugiers B, Vaysse P, Combes JM, Guitard J, Moscovici J, Visentin M, Vardon D, Bécue J. 1994. Contribution to the study of the tributaries and the termination of the external jugular vein. *Surg Radiol Anat* 16: 173–177.

Dionigi G, Congiu T, Rovera F, Boni L. 2010. The middle thyroid vein: anatomical and surgical aspects. *World J Surg* 34: 514–520.

Gray H. 1918. *Anatomy of the Human Body*. Philadelphia: Lea & Febiger.

Kapre M, Mangalgiri AS. 2012. Clinical importance of duplication of the internal jugular vein. *Indian J Otolaryngol* 64: 386–388.

Krmpotić-Nemanić J, Draf W, Helms J. 1988. *Surgical Anatomy of Head and Neck*. Berlin: Springer-Verlag.

Lang J. 1993. *Clinical Anatomy of the Cervical Spine*. New York: Thieme.

Lang J. 1995. *Clinical Anatomy of the Masticatory Apparatus and Peripharyngeal Spaces*. New York: Thieme.

Mears WP. 1888. Abnormal distribution of arteries and veins in the neck. *J Anat Physiol* 22: 304–306.

Miyake H, Kiyosue H, Tanoue S, Goto Y, Mori H, Fujikura. 2010. Termination of the vertebral veins: Evaluation by multidetector row computed tomography. *Clin Anat* 23: 662–672.

Oszukowski P, Kosinski H. 1996. Opening of the middle thyroid vein into the vertebral vein in the fetus. *Przegl Lek* 53: 634–635.

Rajanigandha V, Rajalakshmi R, Ranade AV, Pai MM, Prabbu LV, Ashwin K, Jiji PJ. 2008. An anomalous left external jugular vein draining into right subclavian vein: a case report. *Int J Morphol* 26: 893–895.

Rao TR, Shetty P, Rao S. 2009. A rare case of looping of supraclavicular nerve branches around external jugular vein and transverse cervical artery. *IJAV* 2: 48–50.

Satishkumar S, Archana S, Deepak J. 2013. Variant formation of external jugular vein and branching pattern of external carotid artery. *IJAV* 6: 140–142.

Shenoy V, Saraswathi P, Raghunath G, Karthik JS. 2012. Double external jugular vein and other rare venous variations of the head and neck. *Singapore Med J* 53: 251–253.

Tubbs RS, Patwardhan RV, Oakes WJ. 2002. Ninth cranial nerve stimulation for epilepsy control. Part 2: surgical feasibility in humans. *Pediatr Neurosurg* 36: 244–247.

Wafae N, Hirose K, Franco C, Wafae GC, Ruiz CR, Daher L, Person OC. 2008. The anatomy of the human thyroid veins and its surgical application. *Folia Morphol* 67: 221–225.

Further reading

Brown S. 1941. The external jugular vein in American Whites and Negroes. *Am J Phys Anthropol* 28: 213–226.

Duval P. 1891. Veines jugulaires superficielles anormales. *Bull Mém Soc Anatomique Paris* 5: 222–223.

Gruber W. 1872. Anomalie der Vena jugularis anterior. *Arch Pathol Anat Physiol Klin Med* 54: 188.

Horner WE. 1818. A case of unusual arrangement in the ascending cava and in the external jugular veins of the human subject. *J Acad Nat Sci Phil* 1: 401–405.

64 Veins of the upper limb

Teresa Vazquez and Jose Sanudo
Complutense University of Madrid, Madrid, Spain

The veins of the upper limb are divided in two groups based on their relation to the investment fascia: deep and superficial. The superficial vein system is the first developed in the embryo and initially receives blood from the deep veins. However, with the development of the muscular mass, deep veins became the main system and the superficial veins then drain on the deep veins (Hochsteter 1891).

In the hand, the fetal pattern persists during the entire lifetime and the superficial veins are dominant; in the forearm, this pattern is comparable and in the arm and shoulder the deep veins are predominant (Charpy 1903).

Several techniques have been used for establishing the variable arrangement of superficial veins, such as dissection (Charles 1932) or by placing a tourniquet around the arm of an individual and then observing the pattern resulting as the veins become engorged (Berry and Newton 1908; Okamoto 1922). Ethnical variations were reported in these studies (Berry and Newton 1908; Okamoto 1922; Charles 1932).

Deep veins

The deep veins are smaller than the superficial veins because most of the blood of the upper limb drains in the latter. The deep veins generally occur in pairs (venae comitantes), with the exception of the axillar and subclavian veins that are single trunks, flanking the corresponding artery and connecting at intervals by anastomoses. However, there are some authors who consider that both brachial veins join into a single trunk in the upper third of the arm and that this represents the medial brachial, while the lateral vein exists as a collateral channel (Charpy 1903).

Deep veins are provided by a variable number of paired faced valves. There are 8–15 pairs for each radial or ulnar vein, 5–15 for each brachial vein, and 3 for the axillar vein. In the latter case, valves are located according to the main tributary draining levels; one pair is located in relation to the subclavian vein (Bardelebeen 1880; Charpy 1903; Paturet 1951).

Axillary vein

The origin of the axillary vein is variable. Normally it arises by joinning both (internal and external) brachial veins, but often it receives an important contribution from the basilic vein draining through the internal brachial vein (Charles 1932).

The length of this vein has been reported as variable based on the confluence level of the abovementioned veins, either distal to the axillary cavity, in the axillary cavity, or until just below the clavicle.

However, an accessory axillary vein has been described with an incidence of 56.7%. This accessory vein could originate from the lateral brachial vein (55.9%), from the common brachial (32.4%), or from the deep brachial vein (11.8%). It runs upward laterally to the axillary artery and brachial plexus, usually ending in the infraclavicullar portion of the axillary artery (79.4%; Gusmao and Prates 1992).

A similar collateral channel running in parallel with the axillary vein has been reported as a result of the anastomosis of both brachial circumflex veins before draining into the axillary vein (Charpy 1903).

Subclavian vein

The subclavian vein drains into the brachiocephalic trunk under the regulation of a pair of confronted valves. Only one of the seven comitantes veins of the subclavian system, the internal thoracic vein, drains into the subclavian vein. It also receives the anterior and external jugular veins (Fig. 64.1).

It has also been reported located with the artery and brachial plexus, behind the scalenus anterior muscle, and in some cases the artery in front of the muscle and the vein behind. Cases of two veins, one behind and another in front of the scalenus anterior muscle, have also been reported (Luschka 1862). Putz and Djedovic (2008) reported a venous ring around the subclavius muscle formed by the left suprascapular and subclavian veins. Codesido and Guerri-Guttenberg (2008) reported a right accessory phrenic nerve that pierced through an annulus of the subclavian vein.

Bergman's Comprehensive Encyclopedia of Human Anatomic Variation, First Edition. Edited by R. Shane Tubbs, Mohammadali M. Shoja and Marios Loukas.
© 2016 John Wiley & Sons, Inc. Published 2016 by John Wiley & Sons, Inc.

Figure 64.1 Dissection of the lateral view of the left neck showing the subclavian vein (sv) receiving its tributaries: anterior (aj) and external (ej) jugular veins; ij: internal jugular vein; th: thyroid gland.

Superficial veins

The superficial veins are more variable in number, location, and tributaries. We describe them regionally in the hand, forearm, arm, and axilla, using the names and definition as they appear in the *Terminologia Anatomica*. In this way, we distinguish two veins in the arm (the cephalic and the basilic veins), three main veins in the forearm (the antebrachial cephalic, antebrachial basilica, and the median antebrachial veins), and a complex dorsal venous network in the hand.

The caliber of these veins is directly related to the muscular mass; it is therefore considered that the caliber of superficial veins is smaller in females compared to males and in children compared to adults.

The superficial veins as well as the deep veins are provided with valves, but in smaller number (Paturet 1951). The cephalic and basilic antebrachial veins have 4–8 pairs, always constant in their draining level (Charpy 1903; Paturet 1951; Shima et al. 1992). The basilic antebrachial vein has 6–8 pairs, one always in the draining level of the axillary (Charpy 1903; Paturet 1951). The median cephalic and median basilic are frequently observed without valves (Charpy 1903; Paturet 1951).

Veins of the hand

In the hand, there is a poor palmar network of veins that drains by the capitular veins into the dorsal digital veins. Part of the network drains into the median antebrachial vein.

Dorsal digital veins

Dorsal digital veins are two veins coursing until the commissures of each digit where they join to make up small arcades from which the dorsal metacarpal veins arise proximally (Fig. 64.2).

Dorsal metacarpal veins

Dorsal metacarpal veins course between the interosseous spaces in a variable number (3–5). Anastomoses between veins make up an irregular dorsal network (30%) or, more frequently, an arch (70%; Okamoto 1922).

The main venous outlet of this network or arch is the ulnar side (53%; Berry and Newton 1908) and the position of the arch has been reported in the middle third or in the lower third of the hand (Berry and Newton 1908). After receiving the digital branch of the index finger and both digital branches of the thumb, the radial end terminates as the cephalic antebrachial vein (Fig. 64.2). After receiving the digital branch of the ulnar side of the little finger, the ulnar end of the branch terminates as the basilic antebrachial vein (Fig. 64.2). However, the ulnar end has also been reported as the origin of the antebrachial cephalic vein in 6% of cases (Okamoto 1922).

Ascendant vein

The ascendant vein is a variable vein reported with an incidence from 27.5% (Okamoto 1922) to 82% (Berry and Newton 1908; Fig. 64.2). It arises from the concavity of the dorsal venous arch and ascends to terminate in a variable way in the antebrachial cephalic vein (65%) or in the basilic vein (17%; Berry and Newton 1908).

Oblique vein

The oblique vein is a variable vein found in 41% (Okamoto 1922) to 47% (Berry and Newton 1908) of cases. It arises from the ulnar end of the dorsal arch and terminates in the antebrachial cephalic vein (Fig. 64.2).

Veins of the forearm and elbow

The main veins of the forearm are the cephalic antebrachial vein, the basilic antebrachial vein, and the median antebrachial vein (Fig. 64.3).

Cephalic antebrachial vein

After its origin in the dorsal region of the hand, the cephalic antebrachial vein winds round the lateral border of the forearm and passes proximally along the anterior surface of the forearm to reach the elbow, where it can adopt three different dispositions (Fig. 64.3): type 1 (19%): just before continuing its proximal course in the arm as the cephalic vein, it gives off the median cubital vein; type 2 (27%), it presents along its course

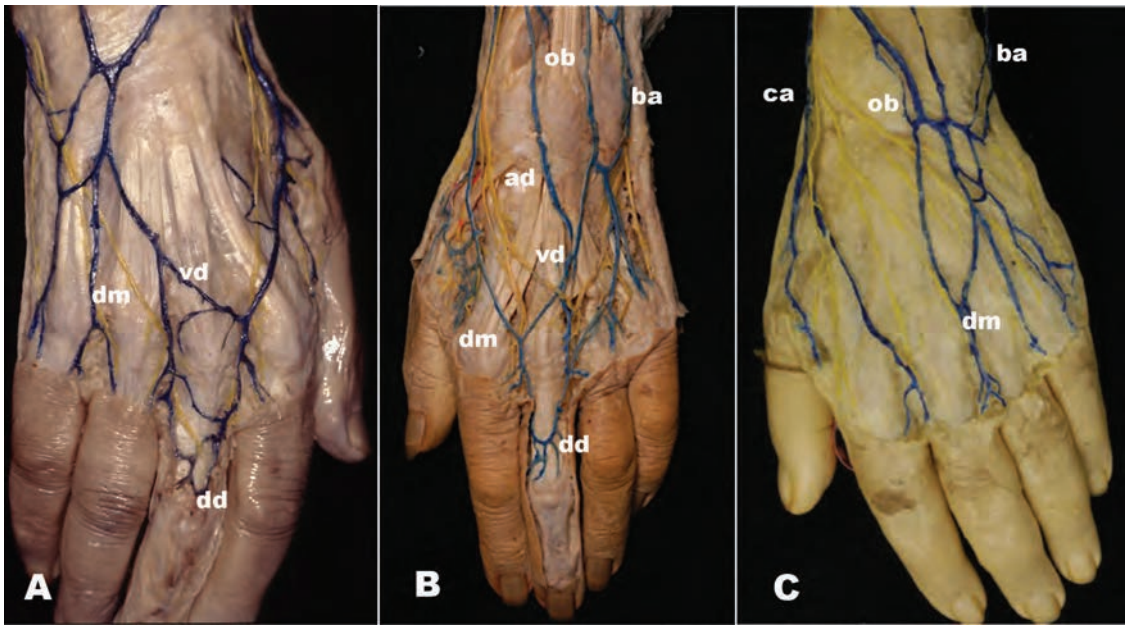

Figure 64.2 Dissections of the superficial dorsal regions of the hand. (a, b) Different arrangement of venous dorsal arches; and (c) absence of dorsal venous arch. ad: ascendent vein; ba: basilic antebrachial vein; ca: cephaloc antebrachial vein; dd: dorsal digital vein; dm: dorsal metacarpal vein; ob: oblique vein; vd: dorsal venous arch

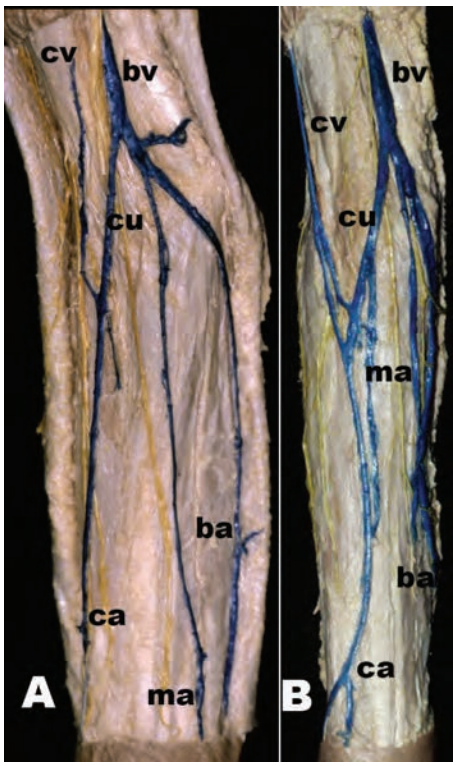

Figure 64.3 Dissections of the superficial anterior regions of the forearm and elbow: (a) slender cephalic vein; and (b) duplication of cephalic, median, and basilic antebrachial veins ba: basilic antebrachial vein; bv: basilic vein; ca: cephalic antebrachial vein; cu: medial cubital vein; cv: cephalic vein; ma: median antebrachial vein

a duplication "inselbildung"; and type 3 (43%), it receives an accessory cephalic vein (accesory radial vein of other authors) located laterally on the forearm, which opens into the cephalic antebrachial vein (Okamoto 1922) (Fig. 64.3). It has also been reported that the cephalic antebrachial vein terminates into the antebrachial basilic vein with a prevalence of less than 1% (Okamoto 1922). This last situation has been reported by some author as agenesia of the cephalic vein.

Finally, the duplication of the vein "inselbildung" with an incidence of 0.5–15% has also been reported (Okamoto 1922; Charles 1932; Fig. 64.3).

The existence of the accessory cephalic vein (radial accessory vein) has been reported with incidences ranging from 9% (Charles 1932) to 82% (Berry and Newton 1908). It has been described arising from small venous branches in the distal part of the dorsal surface of the forearm (39%), from the ulnar extremity of the dorsal venous arch (28%; Okamoto 1922), or from the antebrachial cephalic (16%; Berry and Newton 1908; Fig. 64.3). This vein could be duplicated Fig. (64.3).

The median cubital vein has been reported as a collateral branch of the cephalic antebrachial, connecting it with the basilic antebrachial vein at elbow level (Fig. 64.3). Its incidence has been reported as 85.5% (Okamoto 1922), and its absence reported in 8% of cases (Bertelli 1890), 14.5% (Okamoto 1922), and 29.5% of cases (Charles 1932). The duplication of the median cubital vein has been reported in 2.2% (Charles 1932), 8.5% (Okamoto 1932), or 16% of cases (Berry and Newton 1908) (Fig. 64.3).

Basilic antebrachial vein

The course of this vein is remarkably constant. It receives the median cubital vein before making up the basilic in 70.5% of cases (Charles 1932; Fig. 64.3). It also receives the median antebrachial directly in 27% of cases (Charles 1932), by one of its terminal divisions in 19.7%, or indirectly, draining previously into the median cubital vein, in 61% of cases (Charles 1932). Duplication of the vein has also been reported in 1% (Okamoto 1922) or 2.5% (Charles 1932) of cases. Accessory basilic veins have also been described coming from the dorsal region of the forearm (Fig. 64.3).

Median antebrachial vein

This vein is outstandingly variable in its origin, course, and termination (Fig. 64.3). It has been described as absent in 4% of cases and duplicated in 2% (Berry and Newton 1908; Okamoto 1922; Charles 1932). After an ascending course along the forearm, the vein terminates in the median cubital vein (43–54.5% of cases) or in the basilic vein (35–44% of cases), or divides into the median cephalic and median basilic (1–27.5% of cases; Berry and Newton 1908; Okamoto 1922; Charles 1932; Fig. 64.3). This vein has been described as finishing in a loop in the neighborhood of the median cubital in 13.5% of cases (Okamoto 1922).

Patterns of superficial veins in the cubital fossa

There have been many studies dedicated to the study of this topic, since it is an important level where several clinical procedures are carried out (intravenous injections, sampling blood, etc).

Classically, four different patterns associated with the form of different letters have been described (Paturet 1951). Paturet (1951) reports the M-type as the most frequent (60%), followed by the Y-type (30%), N-type (8%), and finally the W-type (2%; Fig. 64.4). However, the many other studies based on different ethnic samples report more types and propose different incidences (Sohier et al. 1964; Tewari et al. 1971; Singh 1982; Del Sol et al. 2007; Ukoha et al. 2013).

Veins of the arm and axilla

Veins of the arm and axillar cavity are remarkably constant structures.

Basilic vein

The basilic vein is larger than the cephalic vein. After its origin in the elbow, it pierces the investment fascia in the middle third of the arm to drain into the medial brachial vein and continues as the axillary vein without any clear line of demarcation, or courses upward to join the axillary vein just below the clavicle (7%; Charles 1932; Figs 64.3, 64.5). Its absence has not been reported, but a very weak basilic vein has been described in 1% of cases (Okamoto 1922). Accessory basilic veins have also been described (Charpy 1903).

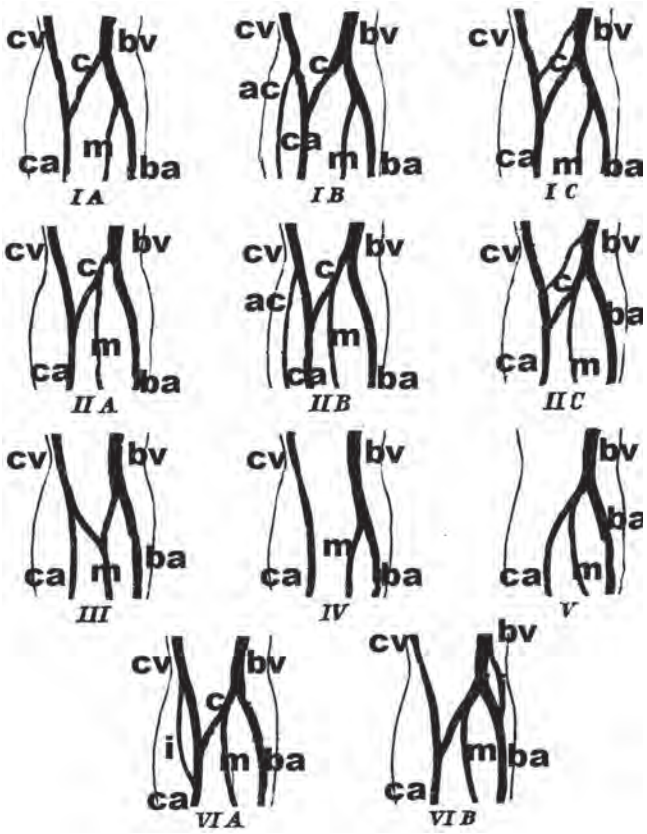

Figure 64.4 Anterior views (types IA to VIB) of the different venous types reported in the elbow. ac: accesory cephalic vein ba: basilic antebrachial vein; bv: basilic vein; c: medial cubital vein; ca: cephalic antebrachial vein cv: cephalic vein; m: median antebrachial vein; i: duplicated vein; Adapted from Charles (1932) with permission from John Wiley & Sons.

Cephalic vein

The cephalic vein is absent in 16% of cases (Bertelli 1890). In some cases it has been described draining into the antebrachial cephalic vein at the elbow level; this situation is reported as agenesis (Okamoto 1922; Figs 64.2, 64.3). In 4.5% of cases, a thin caliber of the vein has been described (Okamoto 1922; Fig. 64.6). It has been reported draining into the subclavian vein after passing over the clavicle (Quain 1844) or running between the clavicle and the subclavius muscle (Testut and Latarjet 1929). The cephalic vein may drain into the basilic, external, or internal jugular veins (Saaid and Drysdale 2008).

A more unfrequent anastomosis is named "jugulocephalic aanstomosis". It course over the clavicle connecting the cephalic vein previous its draining into the axillary vein and the external jugular vein located in the area V(Fig. 1.9.). This variation has been reported as nomal in human embryos and monkeys (Charpie, 1903). In two cases Thomson's report describe this anastomosis passing over, under (between the clavicle and the subclavius muscle) or divided into two branches, one over and

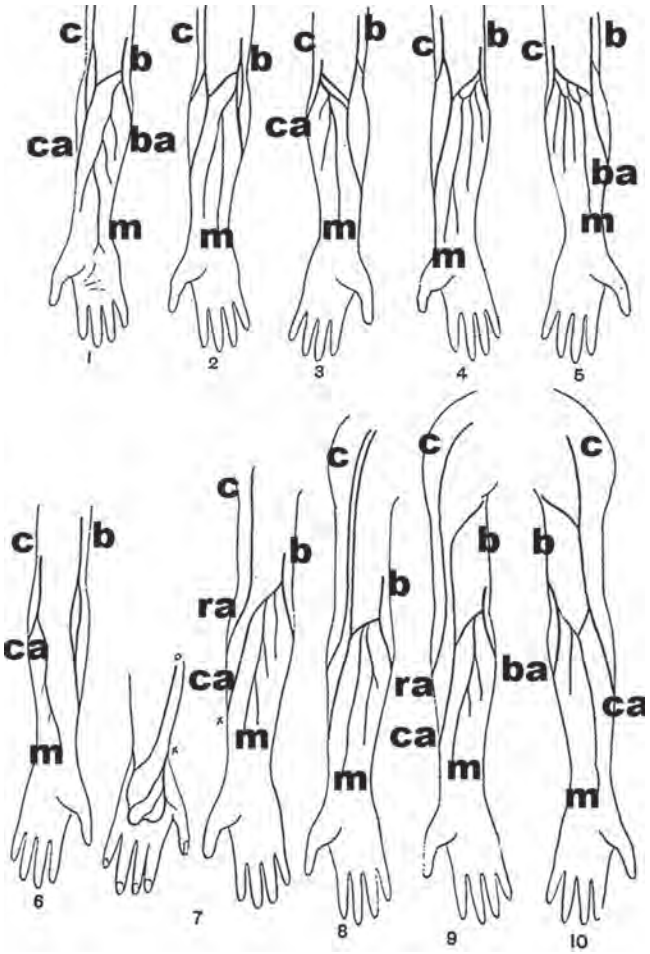

Figure 64.5 Anterior views (1–10) of the upper limb venous patterns in the forearm, elbow, arm, and shoulder. b: basilic vein; ba: basilic antebrachial vein; c: cephalic vein; ca: cephalic antebrachial vein; ra: accesory radial vein. Adapted from Okamoto (1922) with permission from John Wiley & Sons.

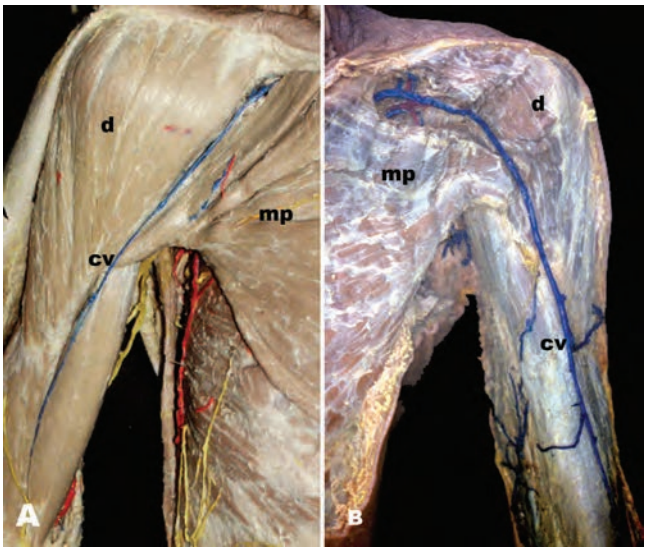

Figure 64.6 Dissections of the superficial regions of the arm and pectoral regions showing cephalic veins with (a) thin and (b) normal caliber. cv: cephalic vein; d: deltoid muscle; mp: major pectoral muscle.

another under the clavicle, for draining into the subclavian vein (Charpie, 1903). (Fig. 64.7)

Anastomosis

The superficial and deep venous systems are connected by anastomoses at different levels. The draining points of the basilic and cephalic veins into the deep veins (the medial brachial and the axillary veins, respectively) represent two of these.

Another constant point is located at elbow level and is represented by a large-caliber perforating vein that connects the middle point of the division of the median antebrachial vein just before dividing into the median cephalic and the median basilic veins with a brachial vein (generally the medial).

Other constant points of anastomoses are the connections between the dorsal (superficial system) and palmar (deep system)

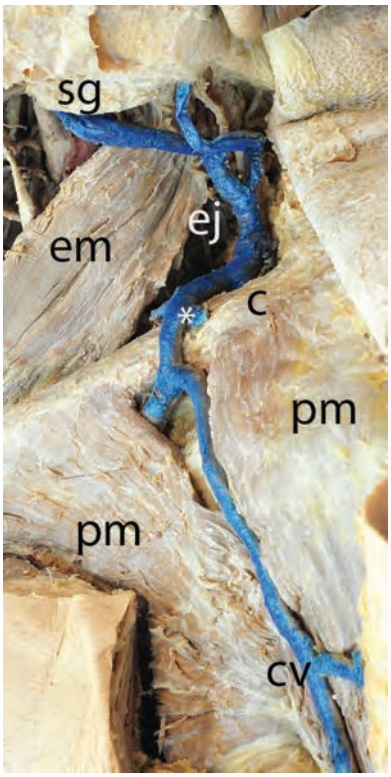

FIGURE 64.7. Dissection of the superficial left pectoral and neck regions showing the cephalic vein draining into the axilar vein with a previous anastomosis with the external jugular vein over the clavicle, named jugulocephalic anastomosis (*). c: clavicle; cv: cephalic vein; ej: external jugular vein; em: esternocleidomastoid muscle; pm: pectoralis major muscle; sg: submandibular gland.

metacarpal veins. Another such anastomoses is fou d at the level of the thenar and hypothenar eminences, where muscular veins of both regions drain into the superficial veins of the thumb and little finger.

An exceptional anastomosis has been described in the middle of the arm in the form of a chiasma between the brachial and basilic veins (Kumar et al. 2012). Not every anastomosis reported has valves.

As for venous valves, topographical relationships have an outstanding clinical relevance. Venipuncture, to collect venous blood and administer intravenous injections in the cubital fossa, requires accurate knowledge of the topographical region (Mikuni et al. 2013).

References

Berry RJA, Newton HAS. 1908. A study of the superficial veins of the superior extremity in 300 living subjects. *Anat Anz* 33: 591–602.

Bertelli D. 1890. Le sillon intermédiaire antérieur do la moélle humaine dans la premiere année de vie. *Arch Ital de Biol* 11: 1–10.

Charles CM. 1932. On arrangements of the superficial veinsof cubital fossa in American whites and American Negroes males. *Anat Rec* 54: 9–14.

Charpy A. 1903. Veines in particulier. In: *Traité d'Anatomie Humaine* (eds P Poirier, A Charpy). Paris: Masson et Cie Editeurs.

Codesido M, Guerri-Guttenberg RA. 2008. Right accessory phrenic nerve passing through an annulus of the subclavian vein. *Clin Anat* 21: 779–780.

Del Sol M, Lagos-Mardones M, Torres-Bustos E. 2007. Venous formation in the cubital fossa of Mapuche. Biscopy study. *Int J Morphol* 25: 885–894.

Gusmao C, Prates JC. 1992. An anatomical study on the accessory axillary vein. *Surg Radiol Anat* 14: 131–136.

Hochsteter. 1891. Ueber die entwicklung der extremitaetvenen. *Morphologie Jahrbuch* 12: 24–32.

Kumar N, Aithal AP, Rao MKG, Nayak SB. 2012. The venous chiasma between the basilic and the brachial vein: A case report. *J Clin Diagn Res* 6: 1539–1540.

Luschka H. 1862. *De Anatomie des Menschen*. Tubingen: Verlag.

Mikuni Y, Chiba S, Tonosaki Y. 2013. Topographical anatomy of superficial veins, cutaneous nerves, and arteries at venipuncture sites in the cubital fossa. *Anat Sci Int* 88: 46–57.

Okamoto K. 1922. A study of the superficial veins in the superior extremity of live Japanese. *Anat Rec* 23: 323–331.

Paturet G. 1951. *Traité d'Anatomie Humaine*. Vol II. Paris: Masson & Cie Editeurs.

Putz D, Djedovic G. 2008. Venous ring around the subclavius muscle: A rare variation. *Clin Anat* 21: 781–782.

Quain R. 1844. *Anatomy of the arteries of the human body*. London: Taylor and Walton.

Saaid A, Drysdale I. 2008. Unusual termination of the cephalic vein. *Clin Anat* 21: 786–787.

Shima H, Ohno K, Shimizu T. 1992. An anatomical study of the valves of the superficial veins of the forearm. *J Craniomazillofac Surg* 20: 305–309.

Singh JD. 1982. Patterns of superficial veins of the cubital fossa in Nigerian subjects. *Acta Anat* 1: 217–219.

Sohier HML, Fustec R, Laffont J, Le Guyader A. 1964. Veines superficialles du pli du coude chez Africain d'Afrique occidental. *Bull Assoc Anat (Nancy)* 720: 1230–1235.

Testut L, Latarjet A. 1929. *Traité d'Anatomie Humanine*. Vol II, eight edition. Pais: Gaston Doin & Cie Editeurs.

Tewari SP, Singh SP, Singh S. 1971. The arrangement of superficial vein in cubital fossa in Indian subjects. *J Anat Soc India* 20: 99–102.

Ukoha UU, Oranusi CK, Okafor JI, Ogugua PC, Obiaduo AO. 2013. Patterns of superficial venous arrangement in the cubital fossa of Adult Nigerians. *Niger J Clin Pract* 16: 104–109.

65 Intrathoracic veins

Jonathan D. Spratt
University Hospital of North Durham, Durham, United Kingdom

Azygos venous system

Introduction

The azygos system veins, draining the posterior walls of the thorax and upper abdomen into the superior vena cava (SVC), vary greatly in their mode of origin, course, tributaries, anastomoses, termination, and intrinsic morphology.

The system most commonly consists of a right-sided azygos vein, along with its left-sided tributaries, the hemiazygos and accessory hemiazygos veins. The azygos vein is so named because of its asymmetry. The Greek root zyg refers to a pair and "A-" means "not." "Azygos" therefore means unpaired.

The azygos vein is formed by the union of the ascending lumbar veins with the right subcostal veins at the level of T12, coursing superiorly in the posterior mediastinum, and arching over the right main bronchus posteriorly at the root of the right lung to join the posterior border of the SVC. This "arch of the azygos vein" (*arcus venae azygos*) is an important surgical landmark.

The arch may be displaced laterally in the floor of a pleural septum (azygos fissure), separating an azygos lobe from the remaining upper lobe of the right lung. Rarer variations include a double or absent azygos vein and reception of bronchial and gonadal veins. More widespread venous thorax anomalies exist due to interdependence of caval and azygos variants from shared embryogenesis.

Other regular recipients include the bronchial, pericardial, and right superior intercostal veins; the posterior right intercostal veins from the fifth to eleventh intercostal spaces; the superior phrenic, mediastinal, and esophageal veins; and the vertebral venous plexuses.

The hemiazygos venous system is a major tributary, a similar structure on the opposite side of the vertebral column, but is more variable and not unusually incompletely formed.

Sieb (1934) studied the azygos system in 200 cadavers and described three groups from 21 structural sets: double-column (D); transitional (T); and single-column (S) types (Fig. 65.1).

Clinical importance

Alongside the increasing complexity and volume of thoracic intervention in recent years, the wider availability of cross-sectional imaging has led to an expanding knowledge base of intrathoracic venous variation. The thoracic radiologist and surgeon must be aware of their potential to cause diagnostic misinterpretation and consequential inappropriate therapeutic intervention.

Some of the anatomical variants may complicate radiological assessment of trauma, mediastinal surgery, computed tomography (CT) cancer staging, and radiotherapy planning (Pilcher and Padhani 2001). Confusion with aneurysm, lymphadenopathy, and other abnormalities such as tumor on CT scanning may occur as can catastrophic hemorrhage at mediastinal surgery. The coexistence of a double superior vena cava with azygos and superficial jugular venous anomalies is also clinically important for central line placement and surgical approach. When performing selective venography (e.g., embolization and hormone sampling) and planning radiological therapeutic procedures (e.g., caval filtration), these variants become highly relevant.

Interpretation of the chest radiograph can be influenced by appreciation of the various appearances of the azygos lobe, fissure, and vein in the right upper zone. CT is sufficient for their demonstration, and in most cases there is no need for confirmation by more invasive methods such as cavography. The presence of valves in the azygos arch can hinder CT vascular diagnosis where present.

Variations in origin of azygos vein

The azygos vein originates in the thorax from a variable combination of lateral, intermediate, and/or medial roots at the level of the twelfth thoracic vertebra. The lateral azygos root, found in 85% of bodies, forms by union of the ascending and subcostal veins. The intermediate root, found in 34% of bodies, arises from the dorsal side of the inferior vena cava at the level of the second lumbar segmental vein, often as a common trunk with the segmental or right renal vein. The medial root, found in

Bergman's Comprehensive Encyclopedia of Human Anatomic Variation, First Edition. Edited by R. Shane Tubbs, Mohammadali M. Shoja and Marios Loukas.
© 2016 John Wiley & Sons, Inc. Published 2016 by John Wiley & Sons, Inc.

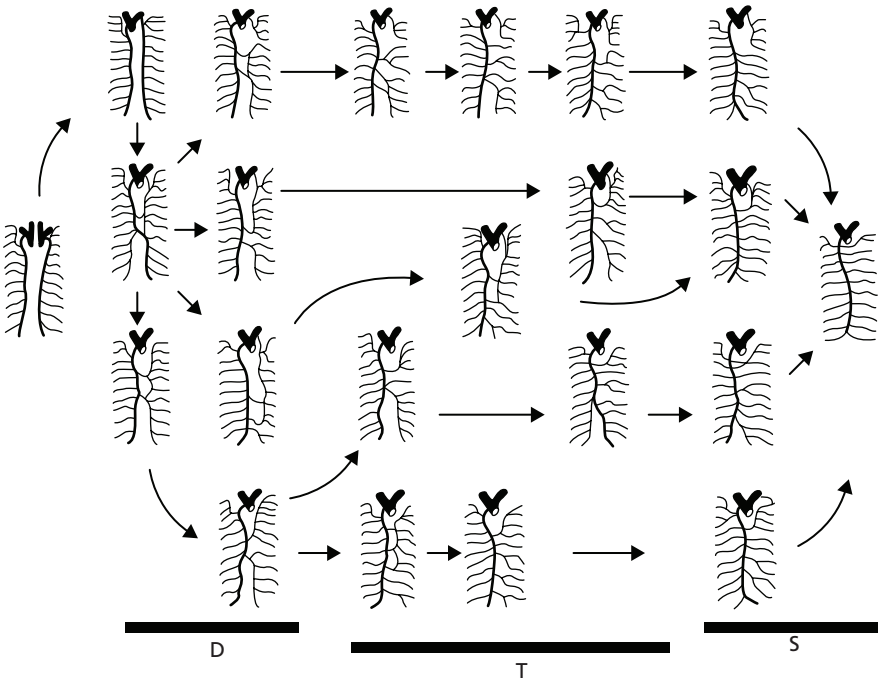

Figure 65.1 A diagrammatic presentation of different types of azygos system arrangement arranged in 3 structural sets, passing from the left to right, as indicated by arrows. D: double column types; T: transitional types; S: single column types.

Source: Sieb (1934). Reproduced with permission from John Wiley & Sons.

38% of bodies, is a small plexiform complex closely associated with the ventral side of the lumbar vertebral bodies dorsal to the aorta and its lumbar segmental branches.

Variation in course and termination of azygos vein

In one clinically significant variation, the azygos arch loses contact with the superior surface of the right main bronchus and grooves the right lung within the base of an accessory pleural fissure before entering the posterior wall of the superior vena cava. This creates an azygos lobe of the right lung (Fig. 65.2), with the azygos fissure consisting of four pleural layers (Fig. 65.3a–d). Present in 1% of bodies, this may be seen as an azygos fissure in 0.57% of chest radiographs (Fig. 65.4) as described in the analysis of 323,641 cases (Anson et al. 1940). More unusually, the azygos fissure is seen as an opaque azygos lobe medially in the right upper zone of the radiograph (Fig. 65.5). While often seen within the base of the azygos fissure at the edge of the mediastinal contour, the vein may be misinterpreted as a lung nodule (a "pseudonodule") if it comes to rest during its embryological relative descent more superolaterally within the fissure (Fig. 65.6). Recognition of its characteristic ovoid shape aligned with the fissure, described as an inverted teardrop, should obviate this interpretation error.

In the presence of an azygos lobe the SVC can sometimes be found in a more anterior position than is usual, and this can be confused as pathological mediastinal widening on a partial anomalous (PA) chest radiograph (Agrawal et al. 1995). CT has revealed that in the presence of an azygos lobe, the azygos arch is at a more cephalad position than normal and the axis of the SVC is oriented toward the left. The azygos lobe intrudes into the pretracheal and retrotracheal mediastinum contacting the anterior wall of the trachea, the medial wall of the superior vena cava, and most of the posterior wall of the trachea in the majority of patients. The presence of an azygos lobe significantly alters the contour of the right mediastinum and changes the relation of lung to the superior vena cava and trachea (Speckman et al. 1981).

The right brachiocephalic vein (RBV) has been reported to follow an extramediastinal and intrapulmonary course in the anterior portion of the azygos fissure (Arslan et al. 2000). CT scanning can easily demonstrate the variant mediastinal vascular anatomy and may differentiate from anomalous pulmonary venous return.

Rarely, the azygos vein passes through the aortic hiatus of the diaphragm. It may open directly into the right atrium (ascribed to the embryonic disappearance of the right common cardinal vein). The azygos occasionally opens into the right brachiocephalic or even the right subclavian veins (ascribed to an elongated embryonic right common cardinal vein).

Variations in tributaries of azygos vein

The azygos vein receives the hemiazygos vein on its left margin, as a side or double branch at T8 or T9 vertebral levels. In 40% of cases, the hemiazygos is continuous above with the accessory hemiazygos vein (a single trunk in 72% of bodies joining it at T6 or T7 levels). The accessory hemiazygos vein drains the left superior (supreme) intercostal vein in 57% of humans.

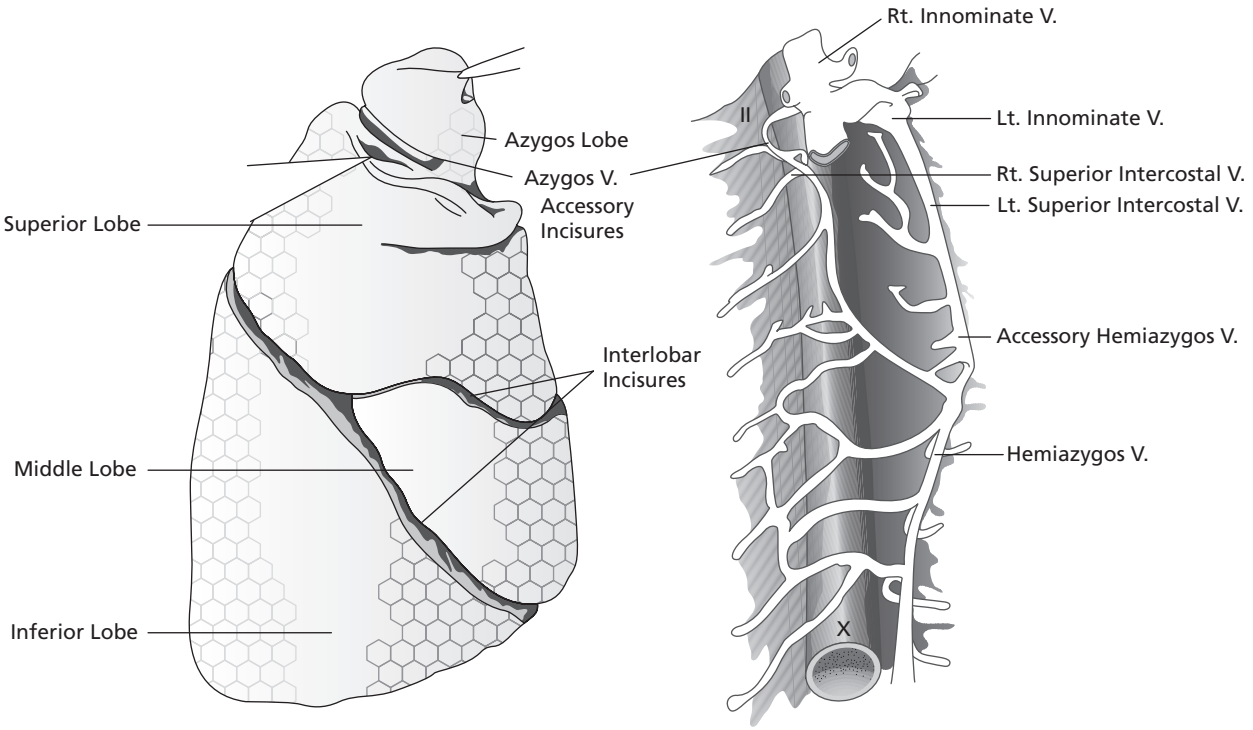

Figure 65.2 Pulmonary lobe of azygos vein. Adapted from Anson et al. (1940).

The hemiazygos and accessory hemiazygos veins are incompletely formed in 15% of bodies, and in this situation the posterior intercostal veins on the left side of the thorax may drain into the azygos vein independently when the azygos vein lies on the midline. Specific descriptions when the hemiazygos vein is absent include the posterior 8th, 9th, and 10th left intercostal veins uniting with their common trunk, crossing the vertebral column obliquely anterior to the aorta and posterior to the esophagus, and opening into the azygos vein at the level of T7–T8 vertebrae (Ozbek et al. 1999). The seventh left posterior intercostal vein also crossed the column anteriorly and joined the common trunk. These variable positions and courses of the veins related to the azygos system require extra caution during mediastinal surgery. Absence of the accessory hemiazygos vein has been reported with the left fourth, fifth, sixth, and seventh posterior intercostal veins terminating directly into azygos vein (Quadros et al. 2009).

A review of late nineteenth century papers (Poynter 1922) highlighted that Soloweilschik (1899) found 22% variation, many of a very minor nature. The cross-connections of the hemiazygos to the azygos are almost as frequent at the T8 or T9 levels and in 10% both are present. Three connections are maintained in 4% of cases and four or more connections are found in 2%. Zumstein (1895) described how the left spermatic and suprarenal veins joined the accessory hemiazygos in 2% of cases, while in 12% a branch from (or all of) the left renal opened into this vein. In 4% the accessory hemiazygos does not join the hemiazygos, but enters the coronary sinus. In 7%, the right and left systems did not connect; forming a separate system, the left flowed into the left brachiocepahalic vein (*vena anonyma*) (except in one case which entered a persistent left cava).

The azygos vein has been documented opening into the hemiazygos vein, and this in turn into the right atrium (Gruber 1864). Alternatively, if the hemiazygos vein is underdeveloped, its branches open directly into the azygos vein. Independent right and left azygos veins with hemiazygos absence have recently been reported on CT scanning (Keskin et al. 2013).

The azygos vein may receive either or both supreme intercostal veins and any combination of intercostal and lumbar veins. The left superior intercostal communicates with the azygos system in 57% of individuals. Unusual tributaries include the pulmonary, right internal thoracic, superior phrenic, bronchial, and gonadal veins. The testicular vein and, on the left side, the renal and suprarenal veins have been documented exhibiting azygos continuation.

Rarely, a hemiazygos vein draining the ninth to eleventh left posterior intercostal veins may pass anterior to the aorta at the level of T8, where it is joined by two separate continuations of the seventh and eighth left posterior intercostal veins. The resultant dilated vessel, termed the "interazygos vein" (Pyrzowski et al. 2007) opens into the azygos vein on the right side of the vertebral column. This "interazygos vein," passing

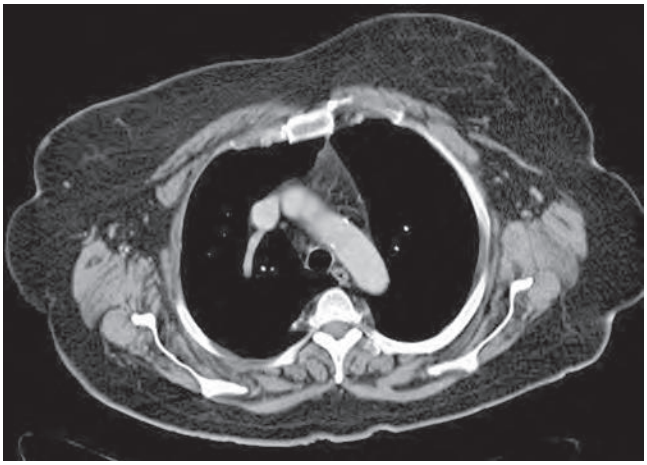

A

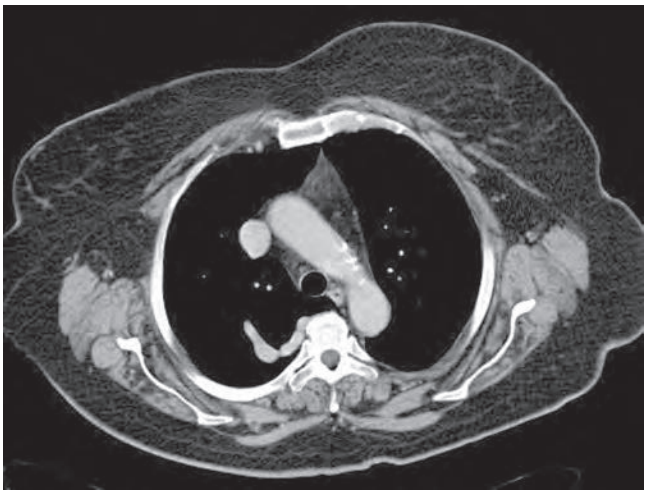

B

C

D

Figure 65.3 Azygos lobe and fissure on axial CTs: (a, b) soft tissue and (c, d) lung windows.

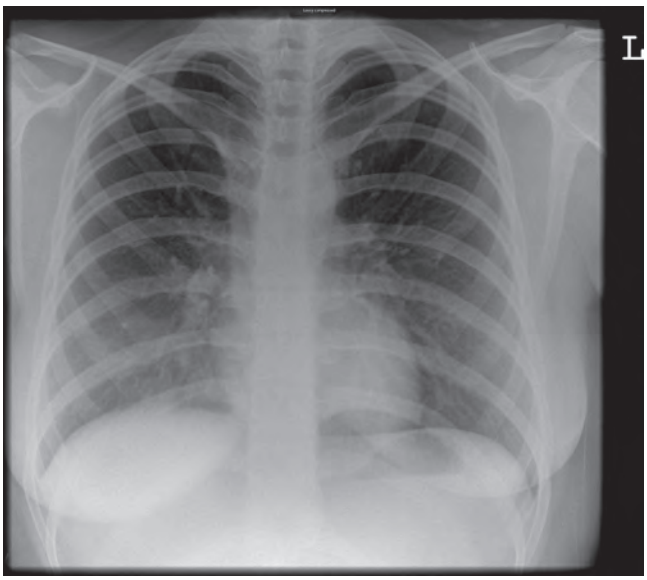

Figure 65.4 Azygos lobe on partial anomalous (PA) chest radiograph.

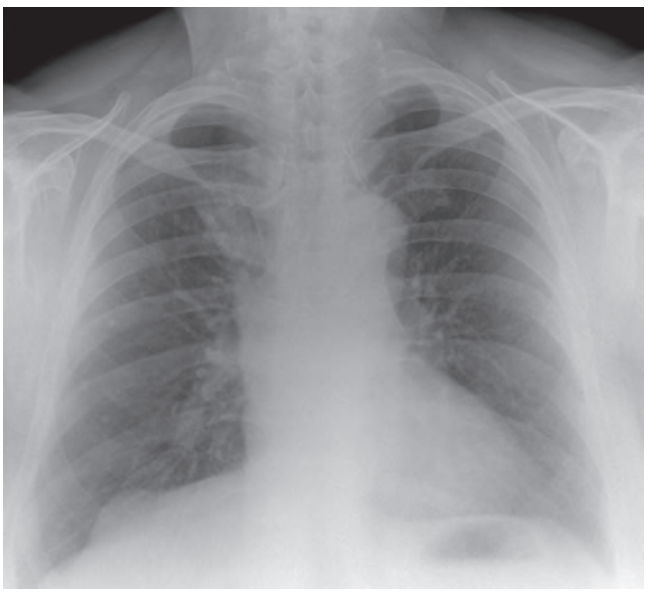

Figure 65.5 Opaque azygos lobe on PA chest radiograph.

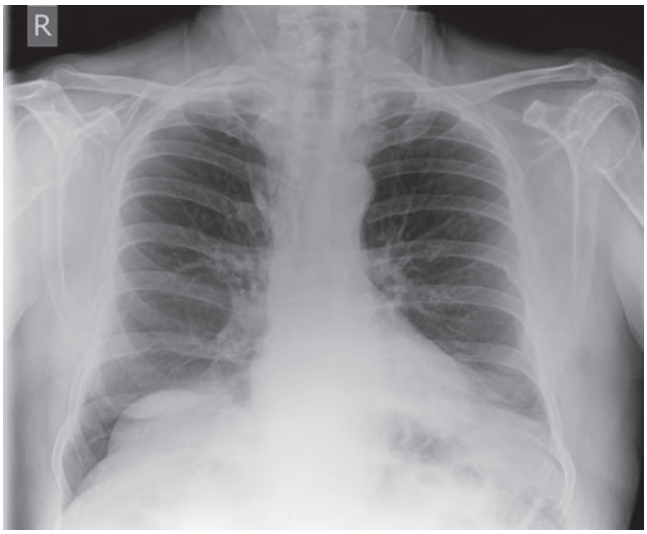

Figure 65.6 Azygos vein as "pseudonodule" within azygos fissure on PA chest radiograph.

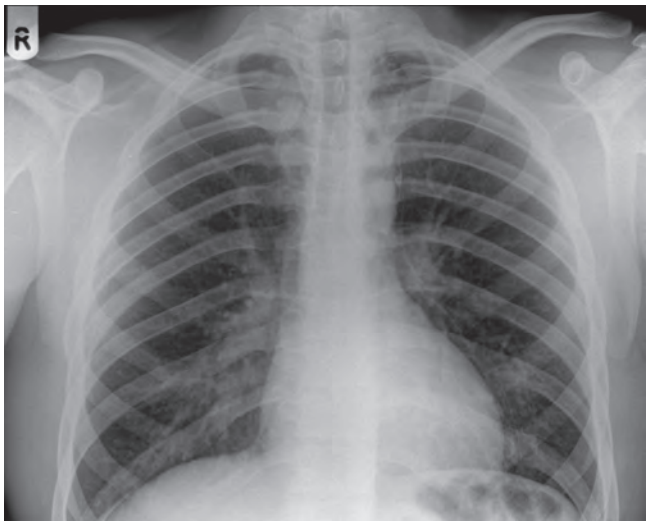

Figure 65.7 Left superior intercostal vein or "aortic nipple" on chest radiograph with small pneumomediastinum.

ventrally to the aorta, could mimic enlarged lymph nodes and cause misinterpretation on CT or, if accidentally damaged during mediastinal surgery, may lead to intraoperative hemorrhage (Celik et al. 1996).

Recently, the diameters and levels of the azygos, the hemiazygos, accessory hemiazygos, and left superior intercostal veins were investigated in 48 cadavers. Anson's system was used, which characterizes vertical and horizontal connections. The classification included primitive or embryological, transient, and unicolon types as three basic types and their eleven subgroups; 2.1% were Type I, 91.7% Type II, and 2.1% Type III. Although similar to the previous literature, 4.2% subjects did not fit in any otherwise defined groups and were named as an atypical group (Kutoglu et al. 2012).

Absence of the inferior segment of the azygos vein has been reported, associated with a dominant hemiazygos vein that drained the right and left intercostal veins from T10 to T6, which curved towards the right to reach the superior vena cava after having drained the right superior intercostal veins (Caggiati and Barberini 1996). The "aortic nipple" on a PA chest radiograph (Fig. 65.7) projecting a short left superior intercostal vein draining into the left brachiocephalic vein adjacent to the aortic arch is therefore associated with agenesis of the azygos vein.

Rarely, the azygos vein may be absent; this is associated with a double superior vena cava (Arslan et al. 1999).

Variability at the azygocaval junction

Variations of the diameter and level of the azygos vein at its opening into the SVC and the position of the azygos vein with respect to the vertebral column and carina have been examined by CT in 103 cases (Tatar et al. 2008). The diameter of the azygos vein at the opening into the SVC ranged between 4.3 mm and 16 mm with the azygos vein situated in the midline in 41 cases, with its arching and opening level at the fifth thoracic vertebra in most cases, most often at the same level as the carina. Hemiazygos veins were detected in 90 patients.

Associations with caval variations

Complex anomalies that concern the wider thoracic venous system merge variants of the vena cavae and azygos systems. Many have been described incidentally associated with a number of congenital cardiovascular, tracheobronchial, and other visceral malformations, as have left hepatic lobe agenesis and a hypertrophic right hepatic lobe, all in the healthy with no cardiac or other defects (Dietz and Reinheimer 1991).

The inferior vena cava may continue into the azygos vein, which becomes as large as the vena cava itself (Fig. 65.8a–e) with absence of the short retro hepatic segment of the vena cava (inferior vena caval "interruption") just below the central tendon of the diaphragm. This is very rarely an isolated phenomenon (Pillet et al. 1986). In one series of patients with situs ambiguus and left isomerism, 91% had interruption of the IVC with azygos continuation. Polysplenia with situs inversus is also an association (Fig. 65.9). In 73% the azygos continuation was to the left SVC, in one case to the right SVC, and in one case to both the left and right SVCs (Roguin et al. 1984).

Pathognomonic ultrasonographic features of this anomaly are easily demonstrated and include absence of the IVC at the level of the liver and independent drainage of the confluence of hepatic veins into the right atrium. Conventional venography can now be replaced by ultrasonic examination to establish this diagnosis (Garris et al. 1980). The confirmation of the azygos system anatomy is important in planning the surgical correction of patients with left isomerism.

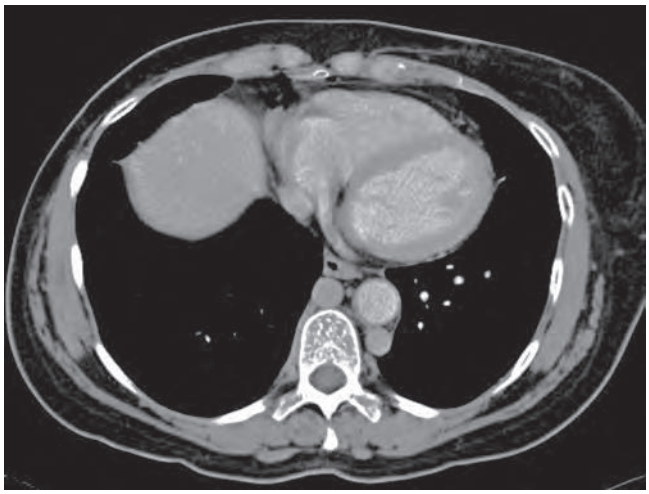

A

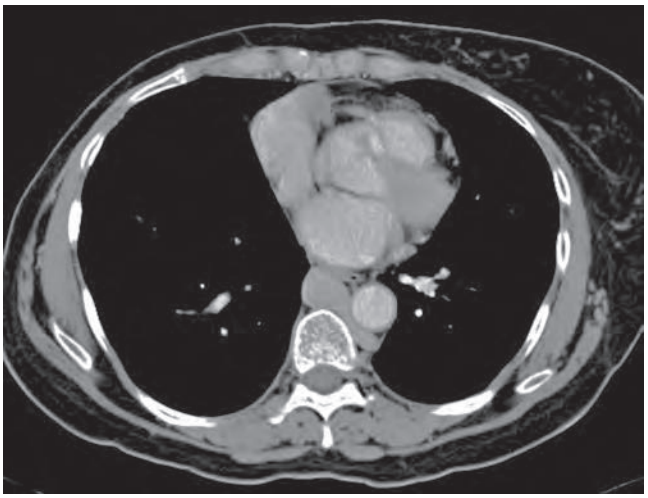

B

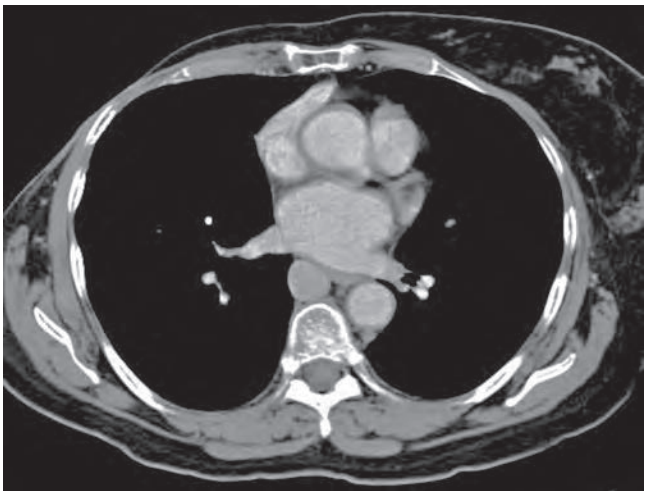

C

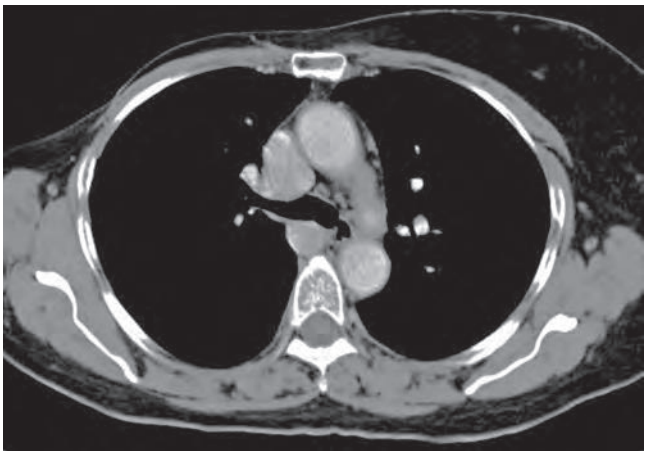

D

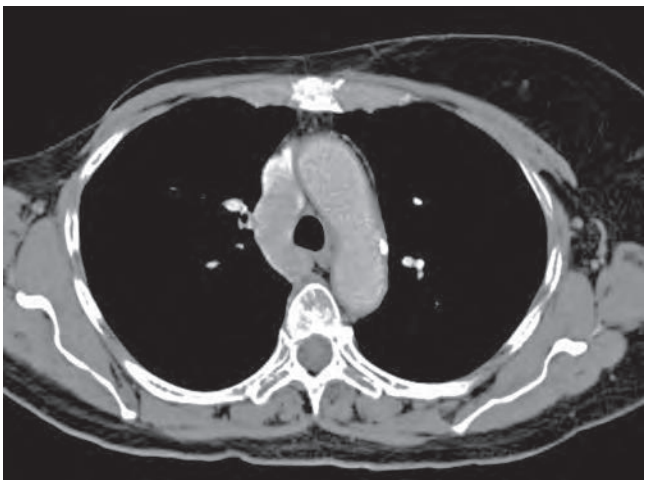

E

Figure 65.8 Axial CT series revealing azygos continuation of IVC at level of (a) coronary sinus; (b) interazygos vein; (c) left atrium; (d) right main bronchus; and (e) azygos arch.

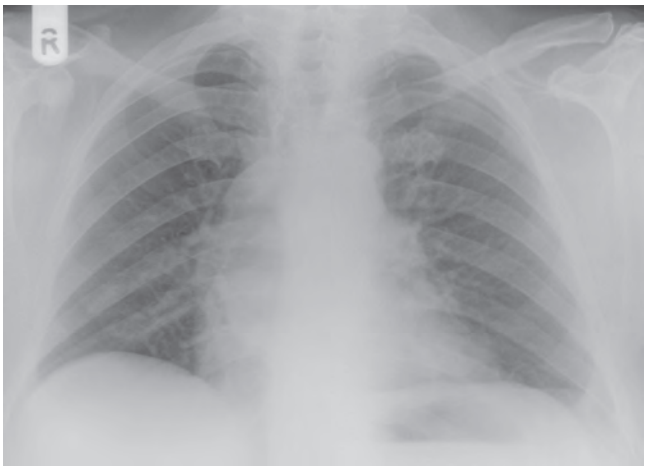

Figure 65.9 Axial CT scan of polysplenia with situs inversus associated with interruption of the IVC with azygos continuation.

A case of azygos/accessory hemiazygos continuation of the IVC mimicked the chest radiograph appearances of dissection of the aorta, a diagnosis suspected clinically (Evans 1993). Contrast-enhanced CT enabled the correct diagnosis to be made. Deviation of the venous blood into a prominent azygos vein can be seen on a PA chest film as an ovoid opacity in the right tracheobronchial angle corresponding to the azygos prominence (Alex et al. 1982) (Fig. 65.10). Knowledge of this variation will be a counter to the differential diagnosis for a dilated azygos vein on a chest radiograph, which includes congestive cardiac failure, posterior mediastinal tumor compression, IVC thrombosis, and the clinically (usually obvious) third trimester of pregnancy, when blood volume has increased by 30–40%.

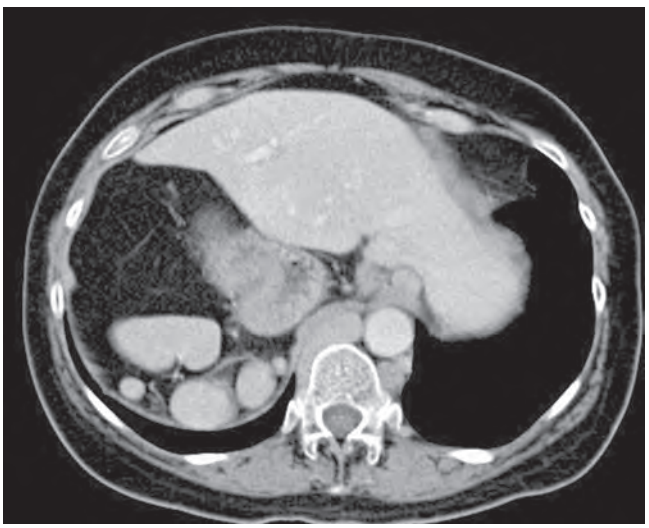

Figure 65.10 PA chest radiograph revealing enlarged azygos vein in tracheobronchial angle secondary to azygos continuation of an interrupted IVC.

Accessory hemiazygos continuation of a left IVC with communication to the left brachiocephalic vein through an enlarged left superior (highest) intercostal vein has caused diagnostic confusion as a widened mediastinum on chest radiography following blunt chest trauma (Sanchez et al. 1985).

Absence of the hepatic segment of the inferior vena cava with azygos continuation has also been reported with congenital absence of the SVC with two brachiocephalic veins draining separately in the absence of congenital anomalies of the remaining thoracoabdominal vasculature and viscera (Quraishi et al. 2010).

A left azygos vein with a left superior vena cava has been described where the left azygos vein received the bilateral intercostal veins and extended into the left superior vena cava, thought to be due to persistence of the proximal part of the left posterior cardinal vein (Uemura et al. 2009).

A left SVC has been noted on CT scanning sharing azygos continuation of the IVC, its varicose ascent along the left cardiac border boldly apparent, having coursed under the central tendon from an interrupted IVC (Fig. 65.11a–e).

An accessory hemiazygos vein has been described draining into the left SVC of a double SVC system without coronary sinus communication, therefore blood from the left SVC drained into the right SVC via the transverse anastomosis between the left and right azygos lines (Sakamoto et al. 1993).

Azygos variations in morphology and drainage are reported with a double SVC system. In a single patient, a right SVC terminated into the right atrium and received the right root of the azygos vein, and the left SVC received the left root of the azygos vein before entering the dilated coronary sinus. The azygos vein ascended in the right chest and, at the level of T3, it divided into the right and left roots which joined the respective superior vena cavae (Gesase et al. 2008). Left oblique and horizontal fissures demarcating left upper, middle, and lower lobes were noted and a neck dissection revealed abnormal connection of the superficial veins, illustrating coexisting variants in multiple systems.

Three new variants have been more recently described on CT scanning: a right double inferior vena cava with azygos continuation of the posteromedial vein; an agenesis of the superior vena cava with drainage through the azygos and hemiazygos veins to the inferior vena cava; and a double inferior vena cava with hemiazygos and azygos continuation of the left inferior vena cava (Minniti et al. 2002). Azygos continuation of both parts of a duplicated inferior vena cava has also been documented on CT scanning (Esposito et al. 1999) following six previous cadaveric case reports of the same findings. This is thought to be due to simultaneous altered development of both subcardinal and supracardinal venous channels. As with other more complex venous variations, this may be isolated or associated with other congenital malformations, most often splenic or cardiac.

Azygos system valves

In the most definitive study of azygos vein valves (Falla et al. 1963), 100 cadaveric specimens were evaluated and a rather

A

B

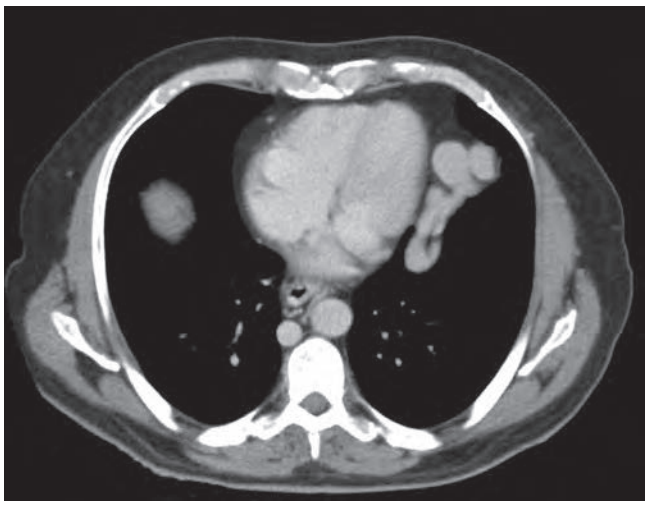

C

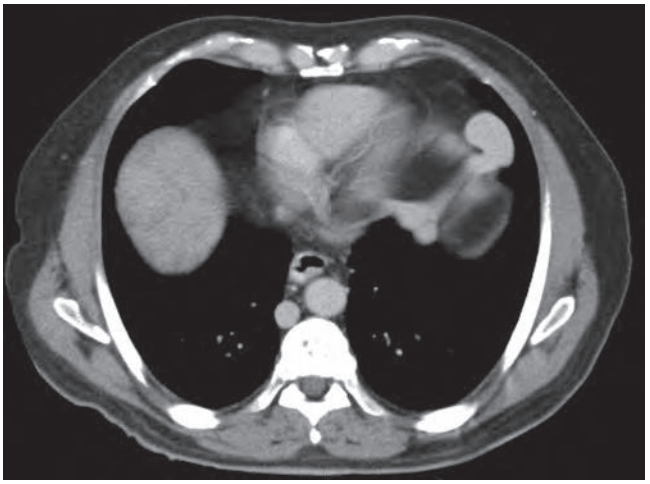

D

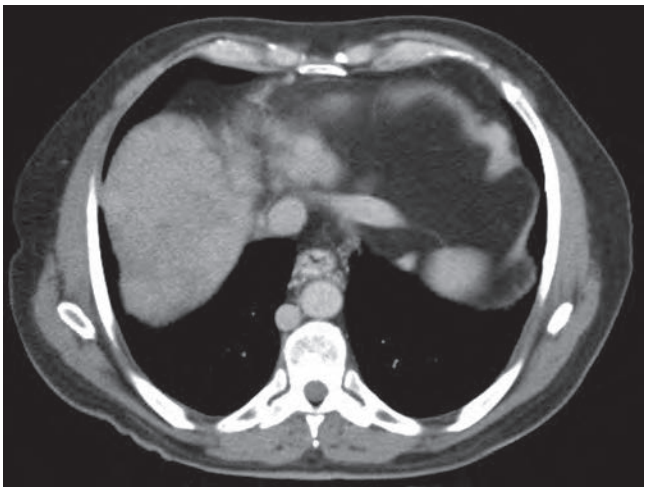

E

Figure 65.11 CT series: left SVC continuation of an interrupted IVC sharing azygos continuation with (a) coronal and (b–e) axial sections.

constant valve was found between the azygos and the SVC, but "prior dissections in most of these specimens prevented proper examination of the valve." Valves elsewhere in the azygos, hemiazygos, and vertebral veins were found to be inconstant, often occurring at junctions with horizontal veins, and were always incomplete in both form and function.

Authors of most azygos vessel imaging studies in the 1960s and 1970s either did not mention or denied the existence of valves in the azygos venous system, possibly due to the use of older technology and antegrade technique. A report of 50 retrograde catheter-based azygos venograms did not explicitly mention the presence of valves in the azygos arch, but did describe the tendency of the venography catheter to get "caught in the bend between the ascending and the transverse portions of the azygos vein," and also stressed the need to insert the catheter into the azygos vein at least "5 cm, since failure to do so may result in incomplete filling of the azygos vein, thus raising the question of an obstruction" (Ranniger 1968). Taken together, these reports support the more recent CT study that a valve is commonly found in the azygos arch within 4 cm of the SVC (Yeh et al. 2004).

Although the presence of a proximal azygos vein valve is not known to be of clinical importance, it is of relevance to radiodiagnosis as a cause of streak artefact obscuring the ascending aorta and more central pulmonary arteries hindering the diagnosis of aortic dissection and pulmonary embolism. Refluxed contrast material may appear as discrete collections of contrast material layering in the cusps of the azygos arch valve separate from the contrast material in the SVC. Radiologists should distinguish these contrast collections from other high-attenuating structures such as calcified lymph nodes, surgical clips, or tracheal calcifications (Yeh et al. 2004).

Embryological aspects

The embryology of these veins has not been determined for man, but Evans (1993) highlighted their origin from the posterior cardinal veins. Poynter (1922) also highlighted an explanation from the familiar figure of Ferdinand Hochstetter, professor of anatomy at the University of Vienna until 1928.

Internal thoracic vein

The internal thoracic vein drains the chest wall and breasts. Bilaterally, it arises from the superior epigastric vein, accompanies the internal thoracic artery along its course, and terminates in the brachiocephalic vein. Occasionally the internal thoracic vein receives the lateral thoracic veins, and it may drain into the vena cava or the azygos system.

The two internal thoracic veins may be connected across the sternum in each interspace and the connection with the usual circulatory pattern may be lost on one side, so that both sides terminate in a common trunk.

Superior intercostal vein

The left superior intercostal communicates with the azygos system in 57% of individuals, but its drainage path and termination are into the left brachiocephalic vein. The vein is found in 65% of humans and receives the second, third, and fourth posterior intercostal veins, which unite into a longitudinal trunk. An accessory superior intercostal vein can be present.

Supreme intercostal vein

The supreme intercostal may drain into the azygos on the right side and the hemiazygos on the left.

Brachiocephalic veins and superior vena cava

Brachiocephalic veins

Anomalous brachiocephalic vein (BV) is uncommon, accounting for approximately 0.2–1% of congenital cardiovascular anomalies (Curtil et al. 1999; Chen et al. 2005). Normal development of the BV encompasses persistence of the right common cardinal vein and precardinal anastomosis and regression of the middle and lower portions of the left common cardinal vein. The cause of an anomalous BV remains controversial. Abnormal regression of the precardinal anastomosis or development of the precardinal anastomosis in any pathway where there is the available space has been proposed (Chen et al. 2005).

The presence of double transverse precardinal anastomoses is proposed to explain three patterns of anomalous BV development: anomalous subaortic left BV (Fig. 65.12a–c); persistent left SVC with a hypoplastic left BV connecting to the right SVC; and double SVC with agenesis of the left brachiocephalic vein. Recognition of these anomalies of the brachiocephalic vein is important for avoiding misinterpretation as an enlarged lymph node and for unusual insertion course of a central venous catheter, cardiovascular intervention, and surgical planning, especially in establishment of a systemic-to-pulmonary venous anastomosis.

In another variation, a vein runs from the left brachiocephalic or from the left superior intercostal vein through the "vestigial fold" (of Marshall) of the pericardium to the vein of Marshall to the coronary sinus. When the coronary sinus is absent the blood flow is reversed.

A case of anomalous (subaortic) position of the left BV has been revealed on CT and MRI. Formed by the union of the left internal jugular and left subclavian veins, passing downward along the left lateral side of the aortic arch, entering the aortopulmonary window, descending in the mediastinum between the ascending aorta and the trachea, it joined with the right BV to form the SVC (Gülsün et al. 2003). No cardiac anomalies accompanied the subaortic left brachiocephalic vein in the case described.

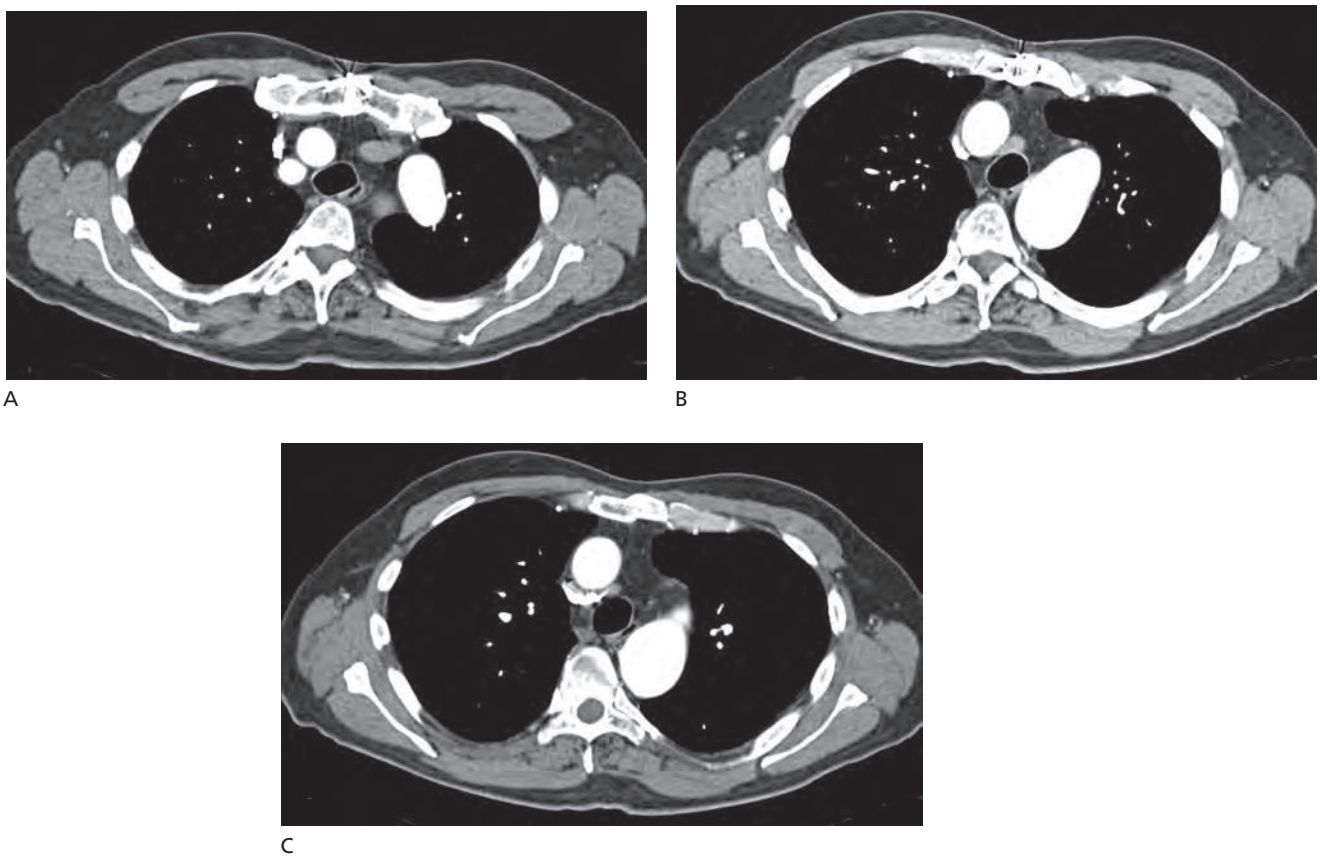

Figure 65.12 (a–c) Subaortic left brachiocephalic vein with cervical aortic arch (axial CT series).

Cooper (1832) and Gruber (1876) found that an innominate vein passed through the thymus gland in about 2% of their subjects. The left BV may cross over the thymus gland, and it is not unusual to receive cervical and/or accessory cervical veins or for bronchial veins to be tributaries of the BVs. They may pass behind the aorta, and Quain found them extending well up into the neck on the left side. The right and left BVs occasionally open into the right atrium separately.

The right BV has been reported to follow an extramediastinal and intrapulmonary course in the anterior portion of the azygos fissure (Arslan et al. 2000).

Unusual tributaries include the thyroidea ima, internal thoracic, accessory subclavian, and supreme intercostal veins. When an accessory vertebral vein is present, it arises from the venous plexus on the vertebral artery and descends through the seven transverse foramina to reach the brachiocephalic vein.

Chiene (1868) described a right brachiocephalic vein, which received the right inferior thyroid, superior intercostals, and the azygos veins, opened into the upper and back part of the right auricle in the usual position of the superior vena cava. The left brachiocephalic vein descended in front of the aortic arch and root of the left lung, disappeared behind the left auricular appendage, ran obliquely across the posterior wall of the left auricle to the auriculo-ventricular groove, and opened into the right auricle to the left of the orifice of the inferior vena cava, at the place where the coronary sinus terminates in a normal heart. There was no valve at its mouth. The vein was joined by the left inferior thyroid vein and left superior intercostal, the latter coming forward immediately above the root of the lung. It increased greatly in size when it reached the heart, where it received the great coronary vein and the middle and posterior cardiac veins. The two innominate veins were joined together by a slender transverse branch, which crossed obliquely.

Superior vena cava

Ancel and Villemin (1908) (see Poynter 1922) have classified the anomalies of the SVC as follows.

1. Double SVC without anastomoses. Persistence of the left duct of Cuvier and failure of development of the left BV.
2. Double SVC with small anastomoses, persistence of the left duct of Cuvier, and a small BV.
3. Double SVC with normal innominate vein.
4. Persistence of the left SVC without atrophy of the right SVC.

Double SVC

Doubled SVC has an incidence of 0.16% (a study of 3000 subjects). The left subclavian may join the left internal jugular vein to form a trunk that continues almost vertically downward over the arch of the aorta in front of the root of the left lung and opens into the coronary sinus of the heart. This variation is known as the persistent left SVC, and results from the retention of the embryonic arrangement. It occurs (all sources) in about 0.4% of cases. A persistent left superior vena cava may be associated with the presence of two azygos veins.

When a left superior vena cava is present, the accessory hemiazygos vein (the remnant of the anterior part of the left cardinal vein) may open into it by arching over the root of the left lung, in a way similar to that in which the azygos (the right cardinal vein) opens into the superior vena cava over the root of the right lung.

The usual left BV may be absent, quite small, or even rudimentary, and may receive anomalous pulmonary veins; the longest recorded living history of an individual with this "incompatible with life" variation is 42 years.

The left SVC may open into the left auricle (atrium) of the heart, coronary sinus (Fig. 65.13a–g), innominate vein, or right SVC. On occasion it communicates with a typical IVC by means of a channel that is a remnant of a persistent sinus venosus, which may drain an interrupted IVC alongside azygos continuation (Fig. 65.11a–e).

Persistent left SVC (PLSVC) is the most common thoracic venous anomaly (0.6%), and results when the left superior cardinal vein caudal to the innominate vein fails to regress. It is most commonly observed in isolation but can be associated with other cardiovascular abnormalities (*c.* 30%) including atrial septal defect, bicuspid aortic valve, coarctation of aorta, coronary sinus ostial atresia, and cor triatriatum with presentation via arrhythmias and cardiac conduction disturbances.

The presence of PLSVC is usually asymptomatic, but can render access to the right side of the heart challenging via the left subclavian approach (a common site of access utilized when placing pacemakers and Swan–Ganz catheters). This anomaly may be detected only by chest radiograph following placement of the catheter.

Incidental notation of a dilated coronary sinus on echocardiography should raise the suspicion of PLSVC (Goyal et al. 2008); this should be confirmed with MRI in order to rule out congenital heart disease (Gonzalez-Juanatey et al. 2004). The diagnosis should be confirmed by saline contrast echocardiography. A wide spectrum of clinicians should be aware of this anomaly, its variations, and possible complications (Uçar et al. 2010). PLSVC should not be regarded as a strict contraindication to infusion of chemotherapy or hyperosmolar nutritional solutions (Iovino et al. 2012).

Solitary left SVC

The right BV may cross the arch of the aorta to join a vertical left BV, forming a left SVC with an absent right SVC (Fig. 65.13a–h) which in this case drains into an enlarged coronary sinus (Fig. 65.13i, j). A left-sided central line can be seen within a solitary left SVC (Fig. 65.14a), and its position confirmed with contrast injection (Fig. 65.14b).

The arrangement of the azygos veins under these conditions may be reversed: a left azygos opens (over the root of the left lung) into the left SVC, and the now right hemiazygos and accessory veins are organized in a manner similar to the typical arrangement of the left hemiazygos veins. This arrangement of veins may occur independently of any general transposition of the viscera. There are other variations in the development of the great veins from the common cardinals, primitive jugular, and anterior and posterior cardinal veins.

Abnormal communications can coexist with the external jugular veins; see Figure 65.15 for an illustrated case of large communications anterior to the sternal notch and lower thyroid between the jugular system, and a double SVC complex with aberrant left SVC hemiazygos drainage.

Unusual tributaries of a right SVC

The right SVC is usually connected to the right atrium, but may be joined to the coronary sinus by a vein of substantial length and size. Unusual tributaries of the SVC include the internal thoracic on the right side, the right supreme intercostal, and the thyroidea ima vein.

When an accessory vertebral vein is present, it arises from the venous plexus on the vertebral artery and descends through the seven transverse foramina to join the subclavian vein.

In vivo normative values for SVC length and range level of the cavoatrial junction

A CT study of 100 patients (mean age 16 years) revealed that the true cavoatrial junction is located more inferiorly than commonly believed, and is not accurately estimated with commonly used imaging landmarks (Baskin et al. 2008). A point two vertebral body units below the carina enables the reliable estimate of the position of the cavoatrial junction. Catheter tip position can be most reliably described in vertebral body units below the carina, with use of the thoracic spine as an internal ruler on radiographic assessment of central line placement.

A more accurate understanding of SVC anatomy is essential for the correct interpretation of central venous access device position. The right tracheobronchial angle has been described as the most reliable landmark for the upper margin of the SVC on an MRI study (Aslamy et al. 1998). Venous catheters placed caudal to this landmark and cephalic to the right superior cardiac silhouette, or no more than 2.9 cm caudal to the tracheobronchial angle, result in catheter tips within the SVC.

Azygos lobe and SVC position

Mediastinal widening on a chest radiograph with an azygos lobe on further radiological investigation with CT and superior vena cavograms showed excessive anteriorization of the SVC (Agrawal et al. 1995). With an azygos lobe, the azygos arch is at

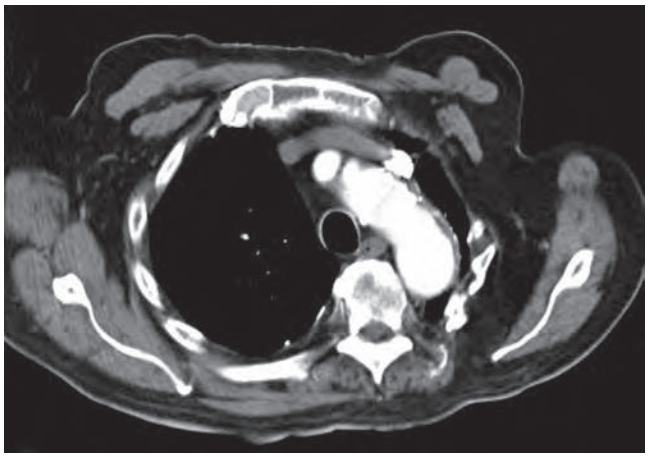
A

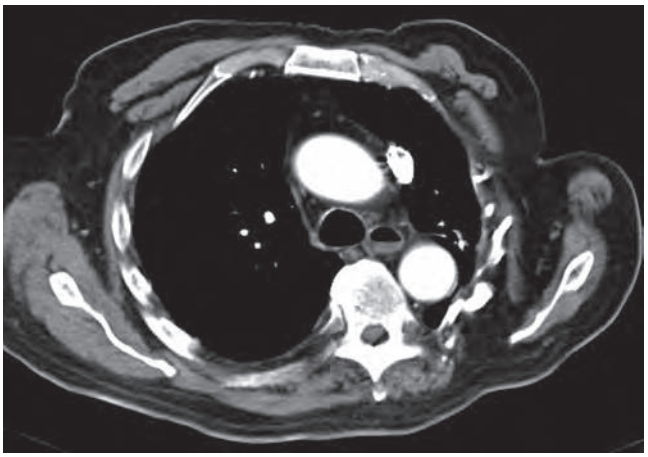
B

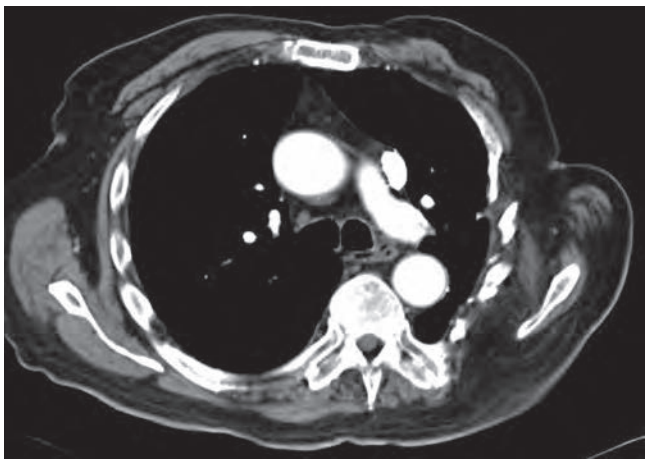
C

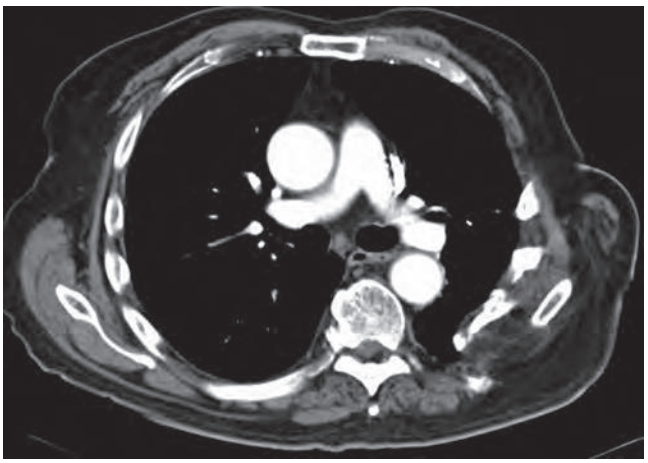
D

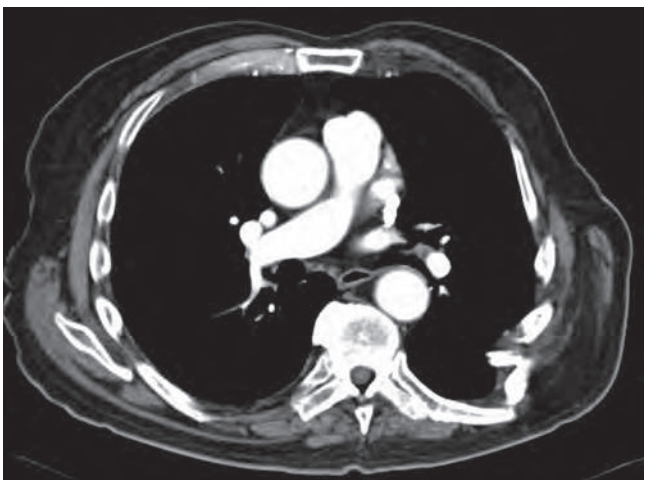
E

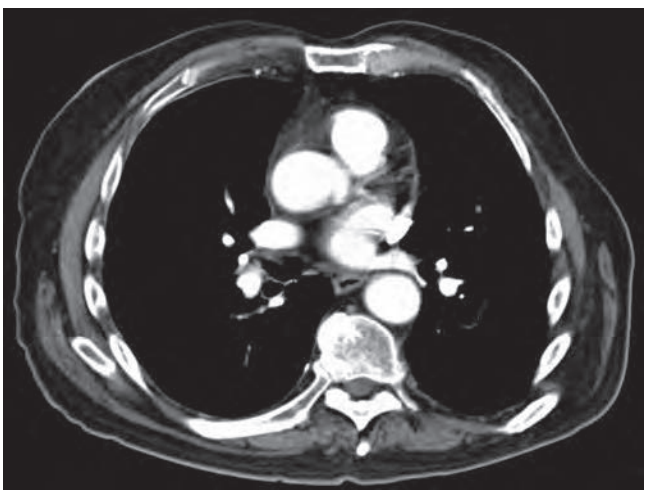
F

Figure 65.13 (a–j) Left SVC draining into enlarged coronary sinus (axial CT series).

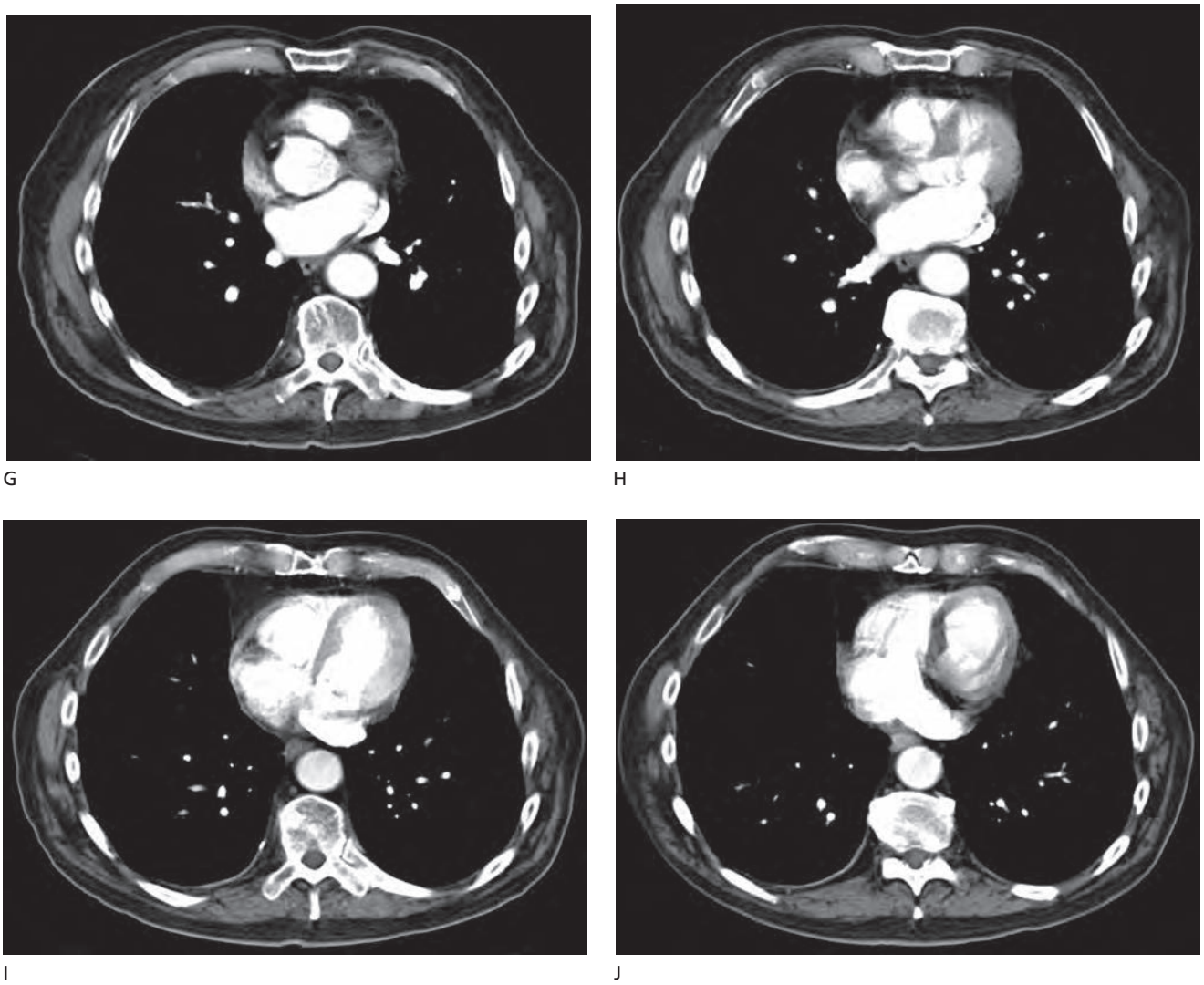

G H I J

Figure 65.13 (a–j) *(continued)*.

a more cephalad position than normal and the axis of the SVC is oriented toward the left. The azygos lobe intrudes into the pretracheal and retrotracheal mediastinum, contacting the anterior wall of the trachea, the medial wall of the SVC, and most of the posterior wall of the trachea in the majority of patients. The presence of an azygos lobe significantly alters the contour of the right mediastinum and changes the relation of lung to the SVC and trachea (Speckman et al. 1981).

Pulmonary veins

Pulmonary vein anomalies have a prevalence of 0.2% (Haramati et al. 2003) to 0.7% (Specht and Brown 1953). Anomalous connections between the pulmonary and systemic venous system were first recognized by Winslow who collected 106 cases (Winslow 1739). Partial anomalous connection of right pulmonary veins is 10 times more frequent than that of the left pulmonary veins (Snellen et al. 1968), the asymmetrical occurrence caused by frequent drainage of some of the right pulmonary veins into the junctional area between right atrium and SVC in the presence of normal left pulmonary veins, and the complete absence of isolated left pulmonary venous connection to the right atrium.

Abnormal connection of solitary pulmonary veins was always effected to the most proximal venous structure among the four possible derived from the main embryonic channels (SVC and IVC on the right side and left SVC and coronary sinus on the left side). Common pulmonary veins from one lung also drained in accordance with this proximity rule, if this may also be taken

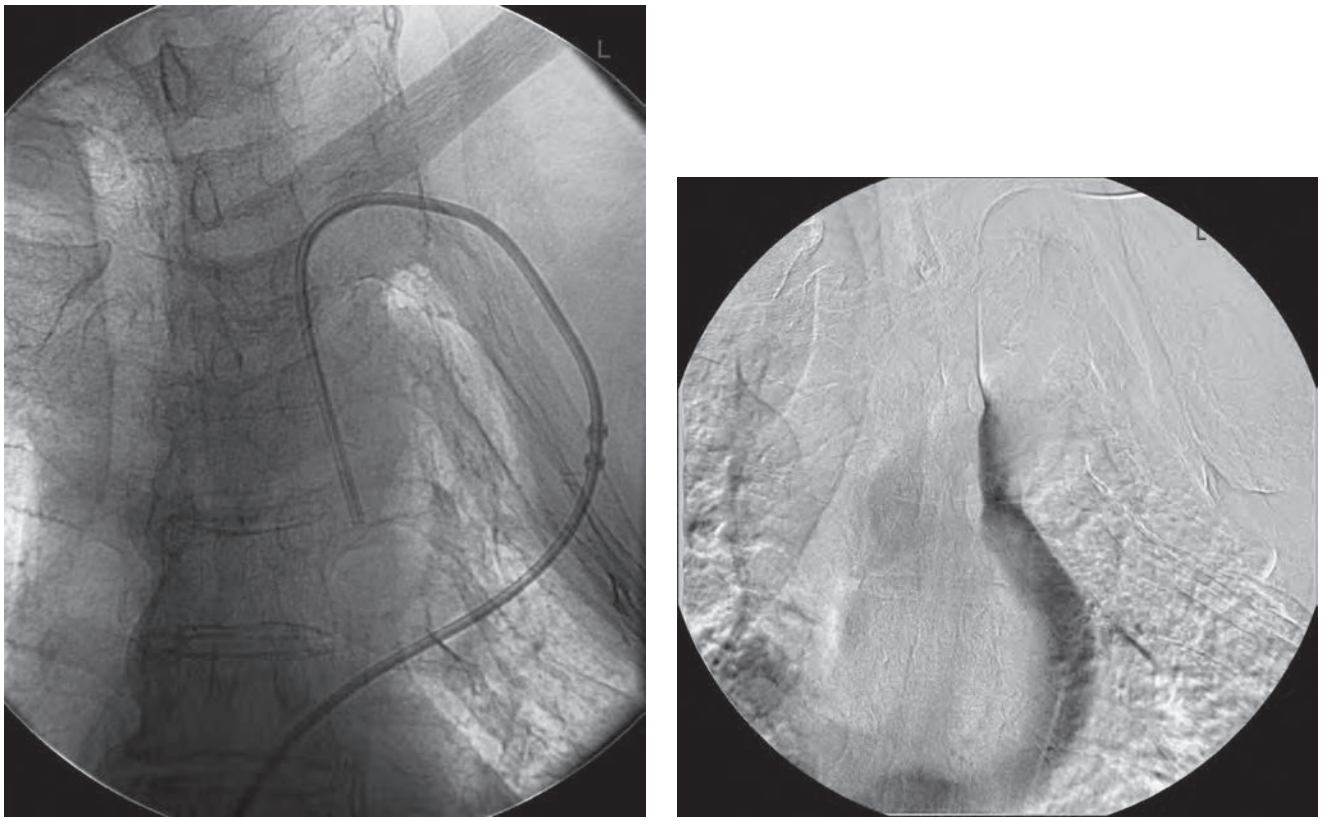

A B

Figure 65.14 Left-sided central line within left SVC: (a) pre-contrast spot film and (b) post-contrast spot film confirms location

Figure 65.15 Aberrant jugular notch veins communicating with left SVC, which also receives an enlarged hemiazygos vein (axial CT series).

to apply to the drainage of right pulmonary veins into the right atrium. The one exception was the drainage of all right pulmonary veins into the portal venous system (Snellen et al. 1968).

A series of 35 cases of anomalous pulmonary drainage was reported without cardiac anomalies (Parsons et al. 1952). In five cases the pulmonary vein was connected to the SVC, in five to the right auricle, in five to the left BV, in nine to the coronary sinus, in one to the IVC, in three to the portal vein, in five to a persistent left SVC, and in two to the ductus venosus. The pulmonary veins may also open into the azygos vein.

More recent intraoperative findings describe in detail an isolated partial anomalous pulmonary venous connection (PAPVC) of a left upper pulmonary vein, deviating from the usual course at the left pulmonary hilum taking on a cranial trajectory, running in parallel with the left phrenic nerve on the mediastinal surface of the left upper lobe, entering the mediastinum, and then draining into the left vein brachiocephalic vein (Savu et al. 2010). This variant is rarely discovered during upper left division segmentectomy for primary lung cancer, and caution is advised when performing lung resection with the potential for PAPVC in mind (Takamori et al. 1995; Miwa et al. 2004).

Pulmonary veins vary in number and size. There are reports of one or more pulmonary veins entering either the right atrium or the inferior or superior vena cava or azygos vein. In one case, a left pulmonary vein opened into the left brachiocephalic vein.

These unusual connections between the pulmonary veins and many adversely inappropriate neighbouring veins are explicable only on the basis of very early embryonic stages in which the developing foregut, trachea, and lung buds are supplied by

a common plexus of small channels that network in all directions through the loose mesenchyme, and communicate with the primitive cardinal veins in many places. With the development of certain channels in this primitive vascular bed to form the pulmonary veins leading to the left atrium, the primitive connections with the cardinal veins usually disappear. The unusual development of one or more of them, and its retention by the adult derivative of the particular part of the cardinal system involved, are most probably responsible for the occurrence of these unusual pulmonary connections.

Steinberg and Finby classified the congenital anomalies of the pulmonary circulation as listed in Table 65.1. Keith et al. (1954) reported on 58 cases of anomalous pulmonary drainage as described in Table 65.2.

Total anomalous pulmonary venous connection is an uncommon congenital cardiovascular anomaly, but one that occurs frequently in the asplenia syndrome. The left pulmonary veins have been described as uniting to form a common pulmonary vein, which crossed the mediastinum and then proceeded in an intrapulmonary fashion in the right lung, with a small pulmonary vein emerging from the right upper lobe draining into the right superior vena cava (Chung et al. 1997). Nine other cases have been reported, four also with asplenia and five with otherwise normal cardiac anatomy apart from an atrial septal defect. The incidence of pulmonary venous obstruction is high, at least 70%. Two cases, both with a normal heart, had corrective surgery. One with no pulmonary venous obstruction was repaired successfully. Embryologically, this type of total anomalous pulmonary venous connection represents a developmental error early in embryonic development before the venous connection between the two lungs and the cardinal vein involute (Chung et al. 1997).

An isolated anomalous pulmonary venous return of both left pulmonary veins to the innominate vein was recently described in a 16-year-old male with pulmonary hypertension after echocardiographic and CT evaluation (Providência et al. 2011).

A partial anomalous pulmonary venous connection was seen in 0.2% of adults in a recent series of 1825 CT cases (Haramati et al. 2003). In contrast to previous series focusing on children, the anomalous vein in adults was most commonly from the left upper lobe in women, and infrequently associated with atrial septal defects. A total of 79% had an anomalous left upper lobe vein connecting to a persistent left vertical vein (only 5% of whom had a left upper lobe vein in the normal location), 17% had an anomalous right upper lobe vein draining into the SVC (60% of whom also had a right upper lobe pulmonary vein in the normal location), and 3% had an anomalous right lower lobe vein draining into the suprahepatic IVC. Only 3% were diagnosed with a secundum atrial septal defect.

Table 65.1 Congenital anomalies of the pulmonary circulation.

A. Malformations of the pulmonary artery	
Primary Table 1 dilatation (aneurysm)	Requires no treatment
Valvular stenosis	Requires surgical treatment
B. Malformation of a branch of the pulmonary artery	
Absence of a main branch pulmonary artery	No treatment required; prognosis good
Absence of a lung (agenesis)	Compatible with normal life
C. Pulmonary arteriovenous fistulas	Requires surgical treatment
D. Alteration of pulmonary circulation	
Patent ductus arteriosus	May require surgery
Reversal of blood flow	Requires surgical treatment
Anomalous insertions of pulmonary veins	May be asymptomatic (with one lung involved)
Partial	Requires surgical treatment
Total	Requires surgical treatment
Anomalous aortic circulation to the lung	May require surgery

Source: Steinberg and Finby (1956). Reproduced with permission from Sage.

Table 65.2 Variations of the pulmonary venous drainage.

Cases	Drainage site	% of cases
25	Left superior vena cava (or left innominate vein)	43
11	Coronary sinus	19
8	Right auricle	14
7	Right superior vena cava	12
4	Portal vein	6.9
2	Ductus venosus	3.4
0	Inferior vena cava	0
1	Superior vena cava and right auricle	1.7

Source: Keith et al. (1954). Produced with permission from Elsevier.

Sinus venosus syndrome

Sinus venosus syndrome should be regarded as an anomalous venous connection, with an interatrial communication outside the confines of the atrial septum in the unfolding wall that normally separates the left atrium from either caval vein. It results in overriding of the caval veins across the intact atrial septum and partial pulmonary vein anomalous drainage. It should be differentiated from posterior atrial septal defect without overriding or anomalous venous connections (Oliver et al. 2002).

Levoatriocardinal vein

The levoatriocardinal vein is a pulmonary-systemic connection that provides an alternative egress for pulmonary venous blood in left-sided obstructive lesions. It is thought to result from the persistence of anastomotic channels that connect the capillary plexus of the embryonic foregut to the cardinal veins. Only

12 cases of levoatriocardinal vein have been reported since its first description in 1926. In patients with left ventricular inflow obstruction, a levoatriocardinal vein is thought to form when the atrial septum fails to provide an alternate egress for left atrial blood. However, when a septal defect or alternative shunt occurs in conjunction with a levoatriocardinal vein, the clinical presentation may be postponed. Echocardiography provides a rapid, noninvasive modality for identifying the pulmonary-systemic connection, which may masquerade as the vertical vein in anomalous pulmonary venous connection or act as an unexpected source of left to right shunting in patients undergoing surgery for hypoplastic left heart syndrome (Bernstein et al. 1995).

Scimitar syndrome and variant

Scimitar syndrome is a relatively rare variety of congenital heart disease characterized by partial or complete anomalous pulmonary venous connection of the right lung into the IVC causing a left to right shunt. The anomalous vein is visible roentgenographically as a crescentic shadow of vascular density along the right border of the cardiac silhouette. Scimitar syndrome is suspected clinically because of dextroversion, and diagnosed by color Doppler echocardiography when a scimitar vein was detected entering the IVC. CT can confirm the diagnosis in all patients (Fig. 65.16a–e), and the illustrated case reveals associated IVC interruption with azygos continuation, illustrating the common theme of coexisting venous variant complexes.

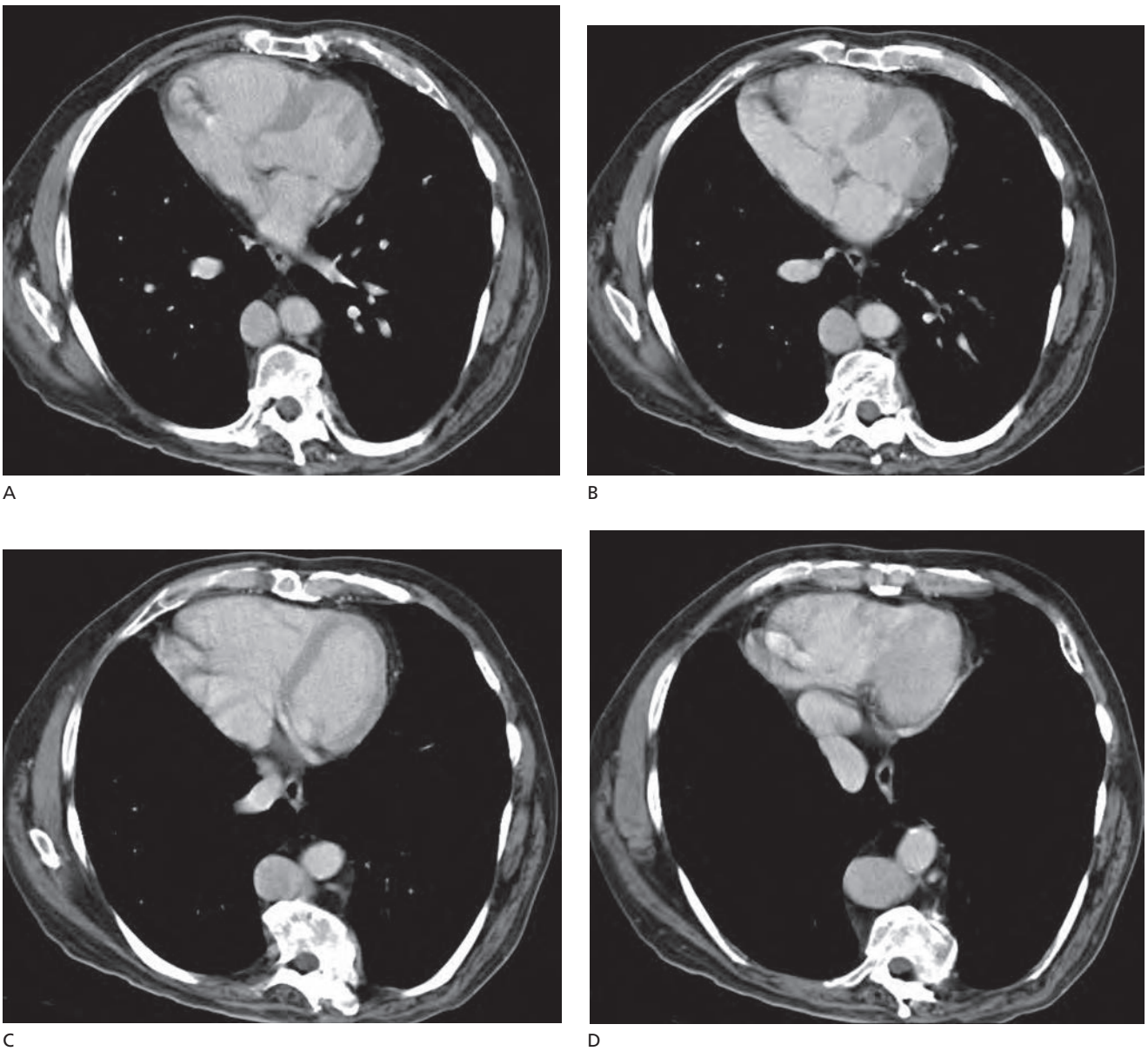

Figure 65.16 (a–d) Scimitar vein draining into supradiaphragmatic IVC with coexisting azygos continuation of IVC interruption (axial CT series).

Horseshoe lung, unilobar or hypoplastic right lung, and hypoplastic right lower lobe are all associations and most have pulmonary arterial hypertension. All presented with lower respiratory tract infections, volume loss of the right lung, a normal or hyperinflated left lung, dextroversion of the heart, and scimitar arteries from the descending aorta (Baskar et al. 2009). Strong association with anatomical or functional absence of the right pulmonary artery has been noted accompanying pulmonary hypoplasia with systemic arteries from the abdominal aorta supplying the right lung (Dupuis et al. 1995).

Two scimitar veins have been reported uniting into a common trunk immediately before their confluence into the IVC (Tsitouridis et al. 2006).

Meandering pulmonary vein

A meandering pulmonary vein that followed a circuitous course through the right lung, and came into close proximity to the IVC before draining the entire right lung to the left atrium, has also been described (Salazar-Mena et al. 1999; Tsitouridis et al. 2006). A case is reported in which a meandering right pulmonary vein connecting to the left atrium is associated with hypoplasia of the right lung, horseshoe lung, abnormal pulmonary lobation, and abnormal branching of the pulmonary arteries (Yoo et al. 2006).

References

Agrawal GG, Gandhi MS, Gandhi SD. 1995. Excessive anteriorisation of the superior vena cava associated with an azygos lobe. *Surg Radiol Anat* 17: 173–175.

Alex JF, Girodet B, Van Straaten L, Maréchal C. 1982. Continuation of the azygos vein with agenesis of the inferior vena cava. *Rev Fr Mal Respir* 10: 277–284.

Ancel P, Villemin F. 1908. Sur la persistance de la veine cave supérieure gauche chez l'homme. *J de la Anat et de la Physiol Normales et Pathologiques* 44: 46–62.

Anson BJ, Siekert RG, Richmond TE, Bishop WE. 1940. The accessory pulmonary lobe of the azygos vein. *Q Bull NW Uni Med School* 24: 285–290.

Arslan G, Ozkaynak C, Cubuk M, Sindel T, Lüleci E. 1999. Absence of the azygos vein associated with double superior vena cava: a case report. *Angiology* 50: 81–84.

Arslan G, Cubuk M, Ozkaynak C, Sindel T, Lüleci E. 2000. Intrapulmonary right brachiocephalic vein associated with azygos lobe. *Clin Imaging* 24: 84–85.

Aslamy Z, Dewald CL, Heffner JE. 1998. MRI of central venous anatomy: Implications for central venous catheter insertion. *Chest* 114: 820–826.

Baskar KR, Saldanha R, Sahadevan MR, Rao SK, Vakamudi M, Rajagopal BK. 2009. Scimitar syndrome: experience with 6 patients. *Asian Cardiovasc Thorac Ann* 17: 266–271.

Baskin KM, Jimenez RM, Cahill AM, Jawad AF, Towbin RB. 2008. Cavoatrial junction and central venous anatomy: Implications for central venous access tip position. *J Vasc Interv Radiol* 19: 359–365.

Bernstein HS, Moore P, Stanger P, Silverman NH. 1995. The levoatriocardinal vein: Morphology and echocardiographic identification of the pulmonary-systemic connection. *J Am Coll Cardiol* 26: 995–1001.

Caggiati A, Barberini F. 1996. Partial agenesis of the azygos vein: A case report. *Anat Anz* 178: 273–275.

Celik HH, Sargon MF, Aldur MM, Cumhur M. 1996. An anomalous course of the interazygos vein. *Surg Radiol Anat* 18: 61–62.

Chen SJ, Liu KL, Chen HY, Chiu IS, Lee WJ, WU MH, Li YW, Lue HC. 2005. Anomalous brachiocephalic vein: CT, embryology, and clinical implications. *AJR Am J Roentgenol* 184: 1235–1240.

Chiene J. 1868. On a case in which the innominate veins opened separately into the right auricle, and in which the intestines were misplaced; with remarks on the development of the parts. *J Anat Physiol* 2: 13–18.

Chung JH, Suh YL, Lee HJ, Kang IS, Choe YH, Ree HJ. 1997. Rare variant of total anomalous pulmonary venous connection: Intrapulmonary drainage of one lung by the other: a case report and review of the literature. *Pediatr Pathol Lab Med* 17: 133–140.

Cooper A. 1832. *The Anatomy of the Thymus Gland*. London: Longman.

Curtil A, Tronc F, Champsaur G, Bozio A, Sassolas F, Carret JP, Vallée B. 1999. The left retro-aortic brachiocephalic vein: Morphologic data and diagnostic ultrasound in 27 cases. *Surg Radiol Anat* 21: 251–254.

Dietz R, Reinheimer G. 1991. CT diagnosis of inferior vena cava anomalies. The azygos continuation. *Radiologe* 31: 352–354.

Dupuis C, Remy J, Remy-Jardin M, Rey C, Brevière GM, Kerkoub A. 1995. Scimitar syndrome with anatomical or functional absence of the right pulmonary artery. Apropos of 4 cases. *Arch Pediatr* 2: 347–352.

Esposito S, Mansueto G, Amodio F, Meccariello R, Galasso L, Salzano A, Vallone G. 1999. Duplication of the vena cava inferior with a continuation into the vena azygos. A report of a rare case. *Minerva Chir* 54: 261–265.

Evans AJ. 1993. Case report: Azygos/accessory hemiazygos continuation of the inferior vena cava mimicking dissection of the aorta. *Clin Radiol* 48: 207–209.

Falla A, Preston F, Anson B. 1963. Classification and calibration of the azygos venous system in 100 specimens. *Surg Gynecol Obstet* 116: 405–412.

Garris JB, Kangarloo H, Sample WF. 1980. Ultrasonic diagnosis of infrahepatic interruption of the inferior vena cava with azygos (hemiazygos) continuation. *Radiology* 134: 179–183.

Gesase AP, Fabian FM, Ngassapa DN. 2008. Double superior vena cava presenting with anomalous jugular and azygous venous systems. *Indian Heart J* 60: 352–358.

Gonzalez-Juanatey C, Testa A, Vidan J, Izquierdo R, Garcia-Castelo A, Daniel C, Armesto V. 2004. Persistent left superior vena cava draining into the coronary sinus: Report of 10 cases and literature review. *Clin Cardiol* 27: 515–518.

Goyal SK, Punnam SR, Verma G, Ruberg FL. 2008. Persistent left superior vena cava: A case report and review of literature. Cardiovasc Ultrasound 6: 50.

Gruber W. 1864. Über einen fall von einmündung der vena hemiazyga in das atrium dextrum cordis beim menschen. *Arch Anat Physiol Wissen Med* 13: 729–740.

Gruber W. 1876. Verlauf der vena anonyma sinistra vor der thymus. *Arch Pathol Anat Physiol Klin Med* 66: 462–463.

Gülsün M, Gökoğlu A, Ariyürek M, Demirkazik FB, Hazirolan T. 2003. Subaortic left brachiocephalic vein: Computed tomography and magnetic resonance angiography findings. *Surg Radiol Anat* 25: 335–338.

Haramati LB, Moche IE, Rivera VT, Patel PV, Heyneman L, McAdams HP, Issenberg HJ, White CS. 2003. Computed tomography of partial anomalous pulmonary venous connection in adults. *J Comput Assist Tomogr* 27: 743–749.

Iovino F, Auriemma PP, Viscovo LD, Scagliarini S, De Napoli M, De Vita F. 2012. Persistent left superior vena cava: A possible contraindication to chemotherapy and total parenteral nutrition in cancer patients. *Oncol Lett* 4: 759–762.

Keith JD, Rowe RD, Vlad P, O'Hanley JH. 1954. Complete anomalous pulmonary venous drainage. *Am J Med* 16: 23–38.

Keskin S, Keskin Z, Sekmenli N. 2013. The independent right and left azygos veins with hemiazygos absence: A rare case presentation. Case Rep Vasc Med, doi: 10.1155/2013/282416.

Kutoglu T, Turut M, Kocabiyik N, Ozan H, Yildirim M. 2012. Anatomical analysis of azygos vein system in human cadavers. *Rom J Morphol Embryol* 53: 1051–1056.

Minniti S, Visentini S, Procacci C. 2002. Congenital anomalies of the venae cavae: Embryological origin, imaging features and report of three new variants. *Eur Radiol* 12: 2040–2055.

Miwa K, Takamori S, Hayashi A, Fukunaga M, Ikeda K, Shirouzu K. 2004. Incidental partial anomalous pulmonary venous connection in left lung cancer. *Jap J Thorac Cardiovasc Surg* 52: 189–190.

Oliver JM, Gallego P, Gonzalez A, Dominguez FJ, Aroca A, Mesa JM. 2002. Sinus venosus syndrome: atrial septal defect or anomalous venous connection? A multiplane transoesophageal approach. *Heart* 88: 634–638.

Ozbek A, Dalçik C, Colak T, Dalçik H. 1999. Multiple variations of the azygos venous system. *Surg Radiol Anat* 21: 83–85.

Parsons HG, Purdy A, Jessup B. 1952. Anomalies of the pulmonary veins and their surgical significance. *Pediatrics* 9: 152–166.

Pilcher JM, Padhani AR. 2001. Problem in diagnostic imaging: Mediastinal venous anomalies. *Clin Anat* 14: 218–226.

Pillet J, Mercier P, Cronier P, Moreau P, Lescalie F, Chevalier JM, Enon B, Jaeger JF, Caron Poitreau C, Rieux D. 1986. Isolated azygos continuation of the inferior vena cava. (Absence of the retrohepatic segment of the inferior vena cava). *Bull Assoc Anat (Nancy)* 70: 69–74.

Poynter CWM. 1922. *Congenital Anomalies of the Arteries and Veins of the Human Body with Bibliography*. Lincoln: University of Nebraska. Vol 22. p 1–106.

Providência R, Botelho A, Mota P, Catarino R, Abecassis M, Leitão-Marques A. 2011. Multidetector CT of rare isolated partial anomalous pulmonary venous return. BMJ Case Rep, doi: 10.1136/bcr.10.2010.3381.

Pyrzowski J, Spodnik JH, Lewicka A, Popławska A, Wójcik S. 2007. A case of multiple abnormalities of the azygos venous system: A praeaortic interazygos vein. *Folia Morphol (Warsz)* 66: 353–355.

Quadros LS, Potu BK, Guru A, Pulakunta T, Ray B, D'Silva SS, Sequeira S, Thomas H. 2009. Anomalous azygos venous system in a south Indian cadaver: A case report. Cases J 14: 6746.

Quraishi MB, Mufti O, Wase A. 2010. Absent left and right superior vena cava and azygos continuation of inferior vena cava: A rare anomaly of systemic venous return. *J Invasive Cardiol* 22: 159–161.

Ranniger K. 1968. Retrograde azygography. *Radiology* 90: 1097–1104.

Roguin N, Hammerman H, Korman S, Riss E. 1984. Angiography of azygos continuation of inferior vena cava in situs ambiguus with left isomerism (polysplenia syndrome). *Pediatr Radiol* 14: 109–112.

Sakamoto H, Akita K, Sato K, Sato T. 1993. Left superior vena cava continuing to the accessory hemiazygos without anastomosis with the coronary sinus. *Surg Radiol Anat* 15: 151–154.

Salazar-Mena J, Salazar-Gonzalez J, Salazar-Gonzalez E. 1999. Meandering right pulmonary vein: A case of scimitar variant. *Pediatr Radiol* 29: 578–580.

Sanchez FW, Greer CF, Thomason DM, Vujic I. 1985. Hemiazygos continuation of a left inferior vena cava: Misleading radiographic findings in chest trauma. *Cardiovasc Intervent Radiol* 8: 140–142.

Savu C, Petreanu C, Cadar G, Matache R, Galie N. 2010. Pulmonary vein anomaly in a patient with pulmonary aspergillosis. *Chirurgia (Bucur)* 105: 275–278.

Sieb GA. 1934. The azygos system of veins in American White and American Negroes, including observations on the inferior caval venous system. *Am J Physiol Anthrop* 19: 39–163.

Snellen HA, van Ingen HC, Hoefsmit EC. 1968. Patterns of anomalous pulmonary venous drainage. *Circulation* 38: 45–63.

Soloweilschink L. 1899. *Etude sur la Situation Sociale et Economique des Ouvriers Juifs*. Brux: Tibideaux.

Specht HD, Brown AF. 1953. Drainage of pulmonary veins into ductus venosus with other anomalies. *AMA Arch Intern Med* 92: 148–151.

Speckman JM, Gamsu G, Webb WR. 1981. Alterations in CT mediastinal anatomy produced by an azygos lobe. *AJR Am J Roentgenol* 137: 47–50.

Sperino G. 1887. Polmone destro bilobato con lingula sopraannumeraria in corrispondenza dell'apice – Decorso anormale della grande vena azigos. *Giornale della Accademia di Medicina di Torino* 35: 265–263.

Steinberg I, Finby A. 1956. Clinical and angiocardiographic features of congenital anomalies of the pulmonary circulation: A classification and review. *Angiology* 7: 378–395.

Takamori S, Hayashi A, Nagamatsu Y, Tayama K, Kakegawa T. 1995. Left partial anomalous pulmonary venous connection found during a lobectomy for lung cancer: report of a case. *Surg Today* 25: 982–983.

Tatar I, Denk CC, Celik HH, Oto A, Karaosmanoglu DA, Ozdemir BM, Surucu SH. 2008. Anatomy of the azygos vein examined by computerized tomography imaging. *Saudi Med J* 29: 1585–1588.

Tsitouridis I, Tsinoglou K, Morichovitou A, Stratilati S, Siouggaris N, Kontaki T. 2006. Scimitar syndrome versus meandering pulmonary vein: Evaluation with three-dimensional computed tomography. *Acta Radiol* 47: 927–932.

Uemura M, Takemura A, Ehara D, Yasumitsu H, Ohnishi Y, Suwa F. 2009. Left superior vena cava with left azygos vein. *Okajimas Folia Anat Jap* 86: 55–60.

Uçar O, Paşaoğlu L, Ciçekçioğlu H, Vural M, Kocaoğlu I, Aydoğdu S. 2010. Persistent left superior vena cava with absent right superior vena cava: A case report and review of the literature. *Cardiovasc J Afr* 21: 164–166.

Winslow J. 1793. *Exposition Anatomique de la Structure du Corps Humain*. Amsterdam: Aux Depens de Compagnie.

Yeh BM, Coakley FV, Sanchez HC, Wilson MW, Reddy GP, Gotway MB. 2004. Azygos arch valves: Prevalence and appearance at contrast-enhanced CT. *Radiology* 230: 111–115.

Yoo SJ, Al-Otay A, Babyn P. 2006. The relationship between scimitar syndrome, so–called scimitar variant, meandering right pulmonary vein, horseshoe lung and pulmonary arterial sling. *Cardiol Young* 16: 300–304.

Zumstein J. 1895. Zur anatomie und entw der nervensystems des menschen. *Anat Heite* 6: 570–580.

Further reading

Adachi B. 1928. *Anatomie der Japaner. Verlag der Kaiserlich–Japanischen Universität zu Kyoto*. Kyoto: Maruzen Co.

Alfke H, Wagner HJ, Klose KJ. 1995. A case of an anomalous pulmonary vein of the right middle lobe. *Cardiovasc Intervent Radiol* 18: 406–409.

Andreassi G. 1941–1942. Über die Verbindung zwischen dem oberen und unteren Hohlvenensystem in hinblick auf die laterale und mediale Wurzel der Vena Azygos und der Vena hemiazygos. *Anat Anz* 92: 240–245.

Anson BJ. (ed.) 1966. *Morris' Human Anatomy*, 12th edition. New York: McGraw-Hill Book Company.

Appelton AB. 1945. The arteries and veins of the lungs. 1. Right upper lobe. *J Anat* 79: 97–120.

Atwell WJ, Zoltowski P. 1938. A case of a left superior vena cava without a corresponding vessel on the right side. *Anat Rec* 70: 525– 532.

Aüer J. 1948. The development of the human pulmonary vein and its major variations. *Anat Rec* 101: 581–594.

Baroni B. 1925. Un caso di persistenza dell vena cava superiore sinistra in un cuore di uomo adulto. *Monitore Zool Ital* 36: 66–68.

Barth. 1853. Oblitération de la veine cave supérieur. *Bull Mem Soc Anatomique Paris* 28: 2–6.

Bassiano T. 1881. Otto vene polmonari nell'orecchietta sinistra del cuore. *Annali Universali di Medicina e Chirurgia* 6: 403–408.

Bastien. 1859. Anomalie de la veine azygos droite. *Soc Biol Comptes Rendus Séances Mém* 11: 204.

Basu BN. 1932. Persistent "left superior vena cava," "left duct of Cuvier" and left horn of the sinus venosus. *J Anat* 66: 628–270.

Beattie J. 1931. The importance of anomalies of the superior vena cava in man. *Canad Med Assoc J* 25: 281–284.

Bedart. 1892. Veine cave supérieure située à gauche. *Bull de la Soc d'Anthrop de Paris* 1892: 379.

Bergman RA, Thompson SA, Afifi AK, Saadeh FA. 1988. *Compendium of Human Anatomic Variation: Catalog, Atlas and World Literature*. Baltimore and Muchich: Urban & Schwarzenberg.

Beyerlein K. 1914. Die persistierende vena cava superior sinistra als abflussrohr für das coronarvenenblut. *Frankfurter Z Pathologie* 15: 327–332.

Boyden EA. 1946. The anatomical hazards of lingulectomy. *Surgery* 20: 828–829.

Boyden EA. 1961. The nomenclature of the bronchopulmonary segments and their blood supply. *Chest* 39: 1–6.

Boyden EA, Scannell JG. 1948. An analysis of variations in the bronchovascular pattern of the right upper lobe of 50 lungs. *Am J Anat* 82: 27–73.

Boyden EA, Hamre CJ. 1951. An analysis of variations in the bronchovascular patterns of the middle lobe in fifty dissected and twenty injected lungs. *J Thoracic Surg* 21: 172–188.

Brantigan OC. 1947. Anomalies of the pulmonary veins. Their surgical significance. *Surg Gynecol Obstet* 84: 653–658.

Brody H. 1942. Drainage of the pulmonary veins into the right side of the heart. *Arch Pathol* 33: 221–240.

Brooks HStJ. 1885. Vena azygos major ascending on the left side, and the bearing of this anomaly on the development of the azygos bloodvessels. *Trans Acad Med Ireland* 3: 450–452.

Butler H, Balankura K. 1952. Preaortic thoracic duct and azygos vein. *Anat Rec* 113: 409–419.

Butler H. 1952a. Abnormal disposition of the pulmonary veins. *J Anat* 86: 485–486.

Butler H. 1952b. An abnormal disposition of the pulmonary veins. *Thorax* 7: 249–254.

Cameron J. 1911. Persistence of the left posterior cardinal vein. *J Anat Physiol* 45: 416–419.

Cameron J. 1915. A specimen showing complete remains of the left superior vena cava, with a description of a venule, which represents the "lost" extrapericardiac portion of the left duct of Cuvier. *J Anat Physiol* 49: 140–147.

Carpentier C, Bertaux A. 1888a. Anomalie des systèmes de la veine cave inférieure et des veines azygos. *Archives de Physiologie Normale et Pathologique* 20: 79–89.

Carpentier C, Bertaux A. 1888b. Anomalie des systèms de la veine cave inferieure et des veines azygos, observée chez un homme adulte. *Soc Biol, Comptes Rendus Hebdomadaires de Séances et Mémoires* 40: 339–340.

Charles JJ. 1889. Notes of a case of persistent left superior vena cava, the right superior vena cava being in great part a fibrous cord. *J Anat Physiol* 23: 649–650.

Cheselden W. 1713. Some anatomical observations. *Philos Trans R Soc Lond B Biol Sci* 28: 282.

Chiari H. 1880. Einmündung der rechtsseitigen pulmonalvenen in der rechten vorhof. Defect im septum atriorum. Excentrische hypertophie der rechten herzhälfte. Dilitation der arteria pulmonalis. Bei einem jährigen knaben. *Jahrbuch Kinderheilkunde Physische Erziehung* 15: 319–334.

Chouke KS. 1939. A case of bilateral superior vena cava in an adult. *Anat Rec* 74: 151–157.

Collins EW. 1874. Accessory pulmonary lobe of the vena azygos. *Dublin J of Med Sci* 58: 252–254.

Compere DE, Forsyth HF. 1944. Anomalous pulmonary veins. *J Thoracic Surg* 13: 63–66.

Conn LC, Calder J, MacGregor JW, Shaner RF. 1942. Report of a case in which all the pulmonary veins from both lungs drain into the superior vena cava. *Anat Rec* 83: 335–340.

Cooke FN, Evans JM, Kistin AD, Blades B. 1951. An anomaly of the pulmonary veins. *J Thoracic Surg* 21: 452–459.

Cooper CM. 1900. A pericardial sac in which the large azygos vein pierced the sac before opening into the superior vena cava. *J Anat Physiol* 34: 426.

Cordier G, Cabol C. 1953. Les veines du poumon gauche. Caractères généraux et systématisation. *Assoc Anatomistes, Comptes Rendus* 40: 627–638.

Cordier P, Devos L, Delcroix A. 1938. Essai de classification des variations du systèm azygos intrathoracique (interprétation embryologique. *Assoc Anatomistes, Comptes Rendus* 33: 100–118.

Cords E. 1921. Ein fall von teilweiser Erhaltung der V. cava sup. sin. zusammen mit einer Anomalie der Vv. pulmonalis. *Anat Anz* 54: 491–495.

Daser P. 1902. Űber eine seltene Lage: Anomalie der vena anonyma sinistra. *Anat Anz* 20: 535–555.

Davis FAG. 1935–1936. Unusual course of vena hemiazygos. *J Anat* 70: 321.

Delmas A, Heffez A. 1952. Sur l'abouchement des veines pulmonaires dans l'oreillette gauche (nombre et calibre). *Assoc Anatomistes, Comptes Rendus* 39: 777–783.

Dévé MF. 1899. Le lobule de la veine azygos ou "lobule de Wrisberg." *Bull Mém Soc Anatomique de Paris* 74: 489–514.

Dionis du Séjour. Lobe surnuméraire du poumon droit. Lobe de la veine azygos. *Bull Mém Soc Anatomique de Paris* 6: 132–135.

Donadio N. 1924–1925. Ein fall von verdoppelung der vena cava superior. *Anat Anz* 59: 321–327.

Dotter CT, Hardesty NM, Steinberg I. 1949. Anomalous right pulmonary vein entering the inferior vena cava: Two cases diagnosed during life by angiocardiography and cardiac catheterization. *Am J Med Sci* 218: 31–36.

Douglass R. 1948. Anomalous pulmonary vessels. *J Thoracic Surg* 17: 712–716.

Edwards JE. 1953. Pathologic and developmental considerations in anomalous pulmonary venous connection. *Staff Meetings Mayo Clinic* 28: 441–452.

Edwards JE, DuShane JW. 1950. Thoracic venous anomalies. *Arch Path* 49: 517–537.

Edwards JE, DuShane JW, Alcott DL, Burchell HB. 1951. Thoracic venous anomalies. *Arch Path* 51: 446–460.

Findlay CW Jr, Maier HC. 1966. Anomalies of the pulmonary vessels and their surgical significance. *Surgery* 29: 604–641.

Fisher E. 1899. Seltener Verlauf der Vena azygos (Abspaltung eines Lungenlappens). *Anat Anz* 15: 476–481.

Fitzgerald DP. 1909. The study of developmental abnormalities as an aid to that of human embryology, based on observations on a persistent left superior vena cava. *Dublin J Med Sci* 127: 14–18.

Fraser RS, Dvorkin J, Rossall RE, Eidem R. 1961. Left superior vena cava. A review of associated congenital heart lesions, catherization data and roentgenologic findings. *Am J Med* 31: 711–716.

Friedman SM. 1945. Report of two unusual venous anomalies. (Left postrenal inferior vena cava; post-aortic left innominate vein). *Anat Rec* 92: 71–76.

Gegenbaur C. 1880. Ein fall von einmündung der oberen rechten Lungenvene in die obere Hohlvene. *Morphologisches Jahrbuch* 6: 315–317.

Ghon A. 1916. Ein beitrag zu den anomalien der pulmonalvenen. *Beiträge Pathol Anat Allg Pathol* 62: 175–193.

Graf G. 1938. Infarto emorragico di un lobo azigos polmonare in un neonato di tre settimane, portatore di una complessa cardioppatia congenita (transposizione corretta die grossi; vasi, pervietà die setti interventricolare ed interatriale). *Pediatria* 46: 740–751.

Greenfield WS. 1876. Persistence of the left vena cava superior, with absence of right. *Trans Pathol Soc Lond* 27: 120–124.

Grishman A, Brahms SA, Gordon A, King FH. 1951. Aberrant insertion of the pulmonic veins. *J Mount Sinai Hospital* 17: 336–343.

Grishman A, Poppel MH, Simpson RS, Sussman ML. 1949. The roentgenographic and angiographic aspects of (1) aberrant insertion of pulmonary veins associated with interatrial defect and (2) congenital arteriovenous aneurysm of the lung. *Am J Roentgenol* 62: 500–508.

Gruber W. 1864. Duplicität der vena cava superior. *Mem Acad Imp Sci St Petersbourg* 7: 45–82.

Gruber W. 1865. Rudimentäre vena cava superior sinistra bei einem erwachsenen. *Arch Pathol Anat Klin Med* 32: 114–117.

Gruber W. 1866. Weitere falle von einmündung der vena hemiazyga in das atrium dextrum cordis beim menschen. *Arch Anat Physiol Wissen Med* 23: 224–230.

Gruber W. 1876a. Ein all von einmundung der vena pulmonalis dextra superior in die vena cava superior. Arch Pathol Anat Physiol Klin Med 68: 284.

Gruber W. 1876b. Verlauf der vena anonyma sinistra vor der thymus. *Arch Pathol Anat Physiol Klin Med* 66: 462–463.

Gruber W. 1880a. Verlauf der vena anonyma sinistra vor der thymusdruse. *Arch Pathol Anat Physiol Klin Med* 82: 475.

Gruber W. 1880b. Duplicität der vena cava superior, mit vorkommen zweier venae azygae und einer sufficienten valvula an der mündung der vena azygos sinistra. *Arch Pathol Anat Physiol Klin Med* 81: 462–465.

Gruber W. 1880c. Vorkommen einer vena cava superior sinistra (bei Abwesenheit der V. cava superior der norm). *Arch Pathol Anat Physiol Klin Med* 81: 458–462.

Gruber W. 1881. Duplicität der vena cava superior mit vorkommen zweier transversaler communicationäste und zweier venae azygae. *Arch Pathol Anat Physiol Klin Med* 86: 38–41.

Gruber W. 1885. Duplicität der vena cava superior (11. Fall eigener Beobachtung) bei verschluss der mindüng der vena cava superior sinistra in das atrium dextrum und deren auftreten als abfuhrungskanal der herzvenen in die vena anonyma sinistra (sicherer 1. Fall). *Arch Pathol Anat Physiol Klin Med* 99: 492–497.

Gruber W. 1885. Einmündung der vena pulmonalis dextra superior in die vena cava superior. *Arch Pathol Anat Physiol Klin Med* 102: 3–5.

Grzybiak M, Szostakiewicz–Sawicka H, Treder A. 1975. Remarks on pathways of drainage from the left upper intercostal spaces in man. *Folia Morphol (Warsz)* 34: 301–313.

Hafferi A. 1923–1924. Ein fall von abnormen verlauf des ductus thoracicus und der V. hemiazygos. *Anat Anz* 57: 373–378.

Halbertsma HJ. 1862. Ontleedkundige aanteekeningen. *Nederlandsch Tijdschrift Geneeskunde* 6: 609–612.

Halpert B. 1927. Complete situs inversus of the vena cava superior. *Anat Rec* 35: 38.

Halpert B, Coman F. 1930. Complete situs inversus of the vena cava superior. *Am J Pathol* 6: 191–197.

Harris HA, Lewis I. 1940. Anomalies of the lungs, with special reference to the dangers of abnormal vessels in lobectomy. *J Thoracic Surg* 9: 667–671.

Hart-Smith T. 1895. Abnormal left innominate vein. *J Anat Physiol* 29: 24–26.

Healey JE Jr. 1952. An anatomic survey of anomalous pulmonary veins: Their clinical significance. *J Thoracic Surg* 23: 433–444.

Heitzman ER, Scrivani JV, Martino J, Moro J. 1971. The azygos vein and its pleural reflections. *Radiology* 101: 249–266.

Heller A. 1900. Anomalien der vena azygos. *Verhandlungen-Deutsche Pathologische Gesellschaft* 12: 248.

Hickman. 1869. Malformation of the heart. 1) Transposition of auricles and of the aorta; absence of pulmonary artery; patent foramen ovale; communicating ventricles; with lateral transposition of principal viscera; cyanosis. 2) Transposition of viscera. Malformation of heart; pulmonary veins from right lung entering left auricle and from left lung entering right auricle. *Trans Pathol Soc Lond* 20: 88–98.

Holtby JRD. 1915. A pleural fold containing the vena azygos. *J Anat Physiol* 69: 236–239.

Horner WE. 1818. A case of unusual arrangement in the ascending cava and in the external jugular veins of the human subject. *J Acad Nat Sci Phila* 1: 401–405.

Howden R. 1887. Case of double superior vena cava with left-sided arrangement of the azygos vein. *J Anat Physiol* 21: 72–75.

Huffmire AP, Bower GC. 1919–1920. A case of persistence of the left superior vena cava in an aged adult. *Anat Rec* 17: 127–129.

Hughes CW, Rumore PC. 1944. Anomalous pulmonary veins. *Arch Pathol* 37: 364–366.

Hurley LE, Coates AE. 1927. A case of right-sided aortic arch and persistent left superior vena cava. *J Anat* 61: 333–339.
Huu N. 1956. Veine cave supërieure gauche et pathologic cardiovasculaire moderne. *Assoc Anatomistes, Comptes Rendus* 43: 619–635.
Ingalls NW. 1932. Anomalous pulmonary vessels. *Anat Rec* 53: 269–281.
Johnston TB. 1915. A rare vascular anomaly: opening of the upper left pulmonary vein into a persistent left superior vena cava. *J Anat Physiol* 69: 182–186.
Kadyi H. 1881. Ueber einige abnormitäten des gefässsystemes. *Medizinische Jahrbücher* 1881: 37–44.
Keyes DC, Keyes HC. 1925. A case of persistent left superior vena cava with reversed azygos system. *Anat Rec* 31: 23–26.
Klob J. 1859. Einige venen–anomalien. Zeitschr. *der Gesellschaft der Aerzte in Wien* 737–738.
Kodama K. 1930. Fortbestand der V. supracardinalis dextra und sinistra bei einem Japaner. *Okajimas Folia Anat Jap* 9: 72–76.
Kodama K. 1932. Persistenz des ductus cuvieri sinister bei einem Japaner. *Okajimas Folia Anat Jap* 9: 365–369.
Kolesnikow N. 1932. Ein seltener fall der mindüng der vena pulmonalis in die vena cava superior. *Anat Anz* 74: 233–237.
Kretschny F. 1877. Verschliessung der vena anonyma dextra durch eine struma substernalis. *Wein Med Wochenschr* 27: 3–6.
Krishnamurti A. 1964. Double left innominate vein in a Chinese cadaver. *J Anat Soc India* 13: 100–102.
Krizan Z, Herman O, Dzidrov V. 1958. Teilweiser fortbestand des supracardinalsystems neben der normalen vena cava inferior beim menschen. *Acta Anat* 34: 312–325.
Kuhlenbeck H. 1930. Teilweise erhaltene linke vena supracardinalis, fensterbildung im beriche der rechten vena iliaca communis und akzessoriche nierengefässe bei einem erwachsenen menschen. *Anat Anz* 19: 117–122.
Lachi P. 1879. Di alcune varietà anatomiche. *L'Imparziale* 19: 365–372.
Lacroix C. 1844. Cas remarquable d'anatomie anormale. *J Soc Méd–Pratique Montpellier* 7: 199–216.
Latarjet A. 1948. *Testut's Traite d'Anatomie Humaine, ninth edition*. Paris: G Doin and Cie.
Lindsay HC. 1925. An abnormal vena hemiazygos. *J Anat* 59: 438.
Little TE. 1880. Abnormality of the great cardiac vessels. Absence of the superior vena cava. *Dublin J Med Sci* 60: 443–445.
Looten J, Ruyssen G. 1910. Anomalie de la veine pulmonaire. *Bibliographie Anatomique* 20: 219–223.
Lucien M. 1954. Considérations sur le developpment de la veine cava supérieure chez l'homme. Assoc Anatomistes, Comptes Rendus. 41: 977–981.
Marchessaux L. 1838. Transposition compléte des organes: Division du tronc brachio-céphalique gauche immédiatement après sa naissance, simulant deux troncs isolés; existence de deux veinescaves supérieures. *Archives Générales de Médecine* 1: 346–348.
Marshall J. 1850. On the development of the great anterior veins in man and mammalia; including an account of certain remnants of foetal structures found in the adult, comparative view of these great veins in different mammalia, and an analysis of their occasional pecularities in the human subject. *Philos Trans R Soc Lond B Biol Sci* 140: 133–170.
McCotter RE. 1914–1915. Demonstration of three human hearts showing double superior venae cavae. *Michigan Uni Clin Soc Trans* 6: 120–122.
McCotter RE. 1915. Demonstration of three human hearts showing double superior vena cavae. *Michigan State Medical Society* 14: 479–481.
McCotter RE. 1915–1916. Three cases of the persistence of the left superior vena cava. *Anat Rec* 10: 371–383.
McManus JFA. 1941. A case in which both pulmonary veins emptied into a persistent left superior vena cava. *CMAJ* 46: 261–264.
Michaelsohn A. 1920. Einmündung aller lungenvenen in die persisterende Vena cava superior sinistra und cor biloculare bei einem 21 jährigen manne. *Frankfurter Z Pathol* 23: 222–246.
Mönckeberg JG. 1921. Das verhalten des sinusknotens bei fehlen der vena cava superior dextra und persistenz der vena cava superior sinistra. *Beitr Pathol Anat Allg Pathol* 69: 537–548.
Mori M. 1929. Ein fall von verdoppelter Vena cava inferior. *Igaku-Kenkiu* 3: 1343–1345.
Morison BG. 1879. The arrangement of the azygos and superior intercostal veins in the thorax. *J Anat Physiol* 13: 346–349.
Morton WRM. 1948. Pre-aortic drainage of the hemiazygos veins. Report of two cases. *Anat Rec* 101: 187–191.
Motti E. 1893. Anomalie degli organi interni nei malati di menti. Rara anomalia polmonale. *Giornale Internazionale della Scienze Mediche* 15: 881–892.
Nabarro D. 1903. Two hearts showing peculiarities of the great veins. *J Anat Physiol* 37: 382–391.
Nakano K. 1931. Uber die persistierenden Vv. supracardinales als Verdopplung der V. cava inferior. *Hokkaidô-Igaku-Zasshi* 9: 1089–1096.
Nandy K, Blair CB Jr. 1965. Double superior venae cavae with completely paired azygos veins. *Anat Rec* 15: 1–9.
Nathan H. 1960. Anatomical observations on the course of the azygos vein. *Thorax* 15: 229–232.
Neil CA. 1956. Development of the pulmonary veins with reference to the embryology of anomalies of pulmonary venous return. *Pediatrics* 18: 880–887.
Odgers PNB. 1928. A case of bilateral superior vena cava in the adult. *J Anat* 62: 221–223.
O'Malley TS. 1917. An anomalous vena pulmonalis within the lung. *Anat Rec* 12: 173–175.
Papez JW. 1937–38. Two cases of persistent left superior vena cava in man. *Anat Rec* 70: 191–198.
Papilian V, Rubin R. 1923–24. Der zusammenhang des sinus venosus mit der vena cava sinistra. *Anat Anz* 57: 276–277.
Peele TL. 1932. A case of closed coronary sinus and left superior vena cava. *Anat Rec* 54: 83–86.
Petersson O. 1868. Menniskohjerta med vena cava superior sinistra. *Upsala Lakareforening Forhandlingar* 3: 697–705.
Pozzi S. 1872. Note sur les lobes surnuméraires du poumon droit de l'homme et en particulier sur une anomalie réversive (existence d'un lobus impar). *Revue d'Anthropologie* 1: 413–451.
Prows MS. 1942. Two cases of bilateral superior vena cavae, one draining a closed coronary sinus. *Anat Rec* 87: 99–106.
Quain J, Schafer EA, Sharpey W, Thompson A. 1878. *Quain's Elements of Anatomy*. New York: William Wood and Co.
Reed AF. 1938–39. A left superior vena cava draining the blood from a closed coronary sinus. *J Anat* 73: 195–197.
Regen FP. 1927. The supposed homology of the vena azygos and vena cava inferior considered in light of new facts concerning their development. *Anat Rec* 35: 129–148.
Rex H. 1882. Über einen fall von duplicität der vena cava superior. *Prager Medicinische Wochenschrift* 7: 341–342.
Ring J. 1805. A singular case of malformation of the heart. *London Med Phys J* 13: 120–121.

Rozel A. 1966. Über die anomalie der arteria subclavia dextra und die persistenz der vena cava superior sinsistra. *Anat Anz* 118: 348–367.

Sahinoglu K, Cassell MD, Miyauchi R, Bergman RA. 1994. Human persistent left superior vena cava with doubled coronary sinus. *Anat Anz* 176: 451–454.

Sanders JM. 1946. Bilateral superior vena cavae. *Anat Rec* 94: 657–662.

Schaefer EA, Symington J, Bryce TH. (eds) 1915. Quain's Anatomy, 11th edition. London: Longmans, Green and Co.

Schröder R. 1911. Über anomalien der pulmonalvenen, zugleich ein beitrag zum cor biloculare. *Arch Pathol Anat Physiol* 205: 122–138.

Schütz H. 1914. Einige fälle von entwicklungsanomalie der vena cava superior (Persistenz des linken Ductus Cuvieri). *Arch Anat Physiol Klin Med* 216: 35–45.

Schütz J. 1913. A vena cava superior (fejödési rendellenességének néhány esete). *Orvosi Hetilap* 57: 845–849.

Severeano G. 1904. Réunion des veines pulmonaires droites dans un seul tronc. *Bibliographie Anatomique* 13: 237–241.

Shattock SG. 1885. Specimen of double vena cava (persistent left duct of Cuvier) the vessel of the left side being larger. *Trans Pathol Soc Lond* 35: 130–131.

Singh B, Ahuja VK. 1963. Double superior vena cava with double vena azygos. *J Anat Soc India* 12: 33–35.

Smith JH. 1919–1920. Description of a case of persistent left duct of Cuvier in man. *Anat Rec* 17: 131–133.

Smith WC. 1916. A case of left superior vena cava without a corresponding vessel on the right side. *Anat Rec* 11: 191–198.

Steinberg I, Dubilier W Jr, Lukas DS. 1953. Persistence of the left superior vena cava. *Dis Chest* 24: 479–488.

Sylwanowicz W. 1931. Sur les valvules du systéme des azygos. *Assoc Anatomistes, Comptes Rendus* 26: 503–506.

Tadokoro H. 1930. Ein fall von linksseitiger vena cava inferior, welcher beginnt mit den Zusammenfluss der V. hypogastrica communis (V.iliaca int. comm.) und der beiden Vv. *iliacae externae. Kaibôgaku – Zasschi* 2: 1029–1036.

Taguchi K. 1901. Über die varietäten der vena cava inferior beim Menschen. *Juntendô-Iji-Kenkiukwai-Zasshi* 343: 1–17.

Taruffi C. 1880. Sulle anomalie delle vene azigos ed emiazigos. *Mem Accad Sci Istituto di Bologna S* 4: 675–681.

Thompson IM. 1929. Venae cavae superiores dextra et sinistra of equal size in an adult. *J Anat* 63: 496–497.

Tichomiroff M. 1895. Ein fall von congenitalem mangel der linken lunge mit persistenz der linken oberen hohlvene bei einem erwachsenen. *Internationale Monatsschrift für Anatomie und Physiologie* 12: 37–45.

Tichomiroff M. 1898. Verdoppelung der unteren hohlvenen bei dem menschen. *Internatl Monatsschrift für Anatomie und Physiol* 15: 143–144.

Toldt C. 1928. *An Atlas of Human Anatomy for Students and Physicians, second edition*. New York: Macmillan Co.

Troyer JR. 1961. A multiple anomaly of the human heart and great veins. *Anat Rec* 139: 509–513.

Vaket L, Poppelier G, Vermeire P. 1958. Sur un case d'anomalie combinée de la veine cave supérieure et du systèm azygos. *Acta Anat* 32: 235–239.

Valentin S. 1791. Double viene azigos. *J Médecine, Chirurgie, Pharmacie* 86: 238–239.

Valleix A. 1835. Transposition irrégulière des organs, de droite a gauche; absence de la closion inter-auriculaire du coeur; ventricule pulmonaire rudimentaire, et ne communiquant pas avec les oreilletes; closion inter-ventriculaires incomplète deux veines cave supérieures… *Arch Gén Méd* 8: 78–91.

Van Cleave CD. 1931. A multiple anomaly of the great veins and intratrial septum in a human heart. *Anat Rec* 50: 45–51.

Versari R. 1906. Rare anomalie de la valvule d'Eustache chez un homme adulte avec double veine cave supérieure. *Arch Ital Biol* 46: 298.

Villemin G, Dufour R, Rigaud A, Gouaze A. 1952. A propos d'une disposition peu fréquente de persistence de la veine cave supérieure gauche chez l'homme. *Assoc Anatomistes, Comptes Rendus* 39: 178–182.

Voyer G. 1888. Cas rare de malformation congénitale du coeur. *Gazette Méd Nantes* 6: 53–54.

Wallraff J. 1938–1939. Ein fall von linker vena cava superior ohne entsprechende vene auf der rechten seite. *Anat Anz* 87: 305–311.

Walsham WJ. 1880. A left superior vena cava. *St Bartholomews Hosp Rep* 16: 93–97.

Weigert C. 1881. Über einen fall von links verlaufender vena cava superior, mutmasslich bedingt durch frühzeitige synostosis der sutura mastoidea dextra. *Arch Pathol Anat Physiol Klin Med* 84: 184–188.

Wennerstrand JR. 1963. A case with a vena cava superior on both sides. *Anat Anz* 112: 338–343.

Wilde IC. 1740. Obserfationes anatomicae rariores. Obseruatio III. Devena azygos trunco duplici. *Comentarii Academiae Scientiarvm Imperialis Petropolitanae* 12: 318–320.

Wutzer CW. 1834. Einmündung des ductus thoracicus in die vena azygos. *Arch Anat Physiol Wissen Med* 1834: 311–318.

Zaaijer T. 1869. Vena cava superior dextra et sinistra. Afwijking in de samenstelling der vena cava inferior. *Nederlandsch Tijdschrift voor Geneeskunde* 13: 157–160.

Zaaijer T. 1872. Observations Anatomiques. Veines caves supérieures droite et gauche. *Archives Neerlandaises des Sciences Exactes et Naturelles* 7: 449–459.

Zoltowsky P, Atwell W. 1938. A case of a left superior vena cava without a corresponding vessel on the right side. *Anat Rec* 70: 525–532.

66 Cardiac veins

Horia Muresian
Cardiovascular Surgery, San Donato Milan, Italy; University Hospital of Bucharest, Bucharest, Romania

In contrast to the coronary arterial system, the venous drainage of the heart consists of different types of conduits exhibiting notable anatomical variability (Loukas et al. 2009). The components of the cardiac venous system (CVS) are more difficult to classify and denominate than their arterial counterparts. The CVS comprises (Fig. 66.1): the greater or major CVS (M-CVS), the smaller or minor CVS (m-CVS), and the compound CVS. In this chapter the term "major" will be used in preference to "greater," avoiding confusion with "the great cardiac vein" (i.e., the anterior interventricular vein and its continuation). Similarly, the term "minor" will be used instead of "smaller" to avoid confusion with "the small cardiac vein," the collector of the anterior cardiac veins.

The compound CVS refers to structures draining through both systems. Tributaries of the M-CVS and m-CVS communicate. The general pattern of venous drainage is that the external two-thirds of the ventricular wall drains through the M-CVS and the internal one-third through the m-CVS. The left ventricle (LV), part of the right ventricle (RV), and the left atrium (LA), are drained by the coronary sinus (CS) system. Most of the RV and LA and right atrium (RA) are drained by non-CS tributaries. Almost all veins of the M-CVS eventually drain into the RA (Fig. 66.2). Epicardial veins are generally superficial to the epicardial coronary arterial main trunks and their branches. In humans the veins do not always parallel the arterial branches, except those located in the coronary sulcus or interventricular sulci.

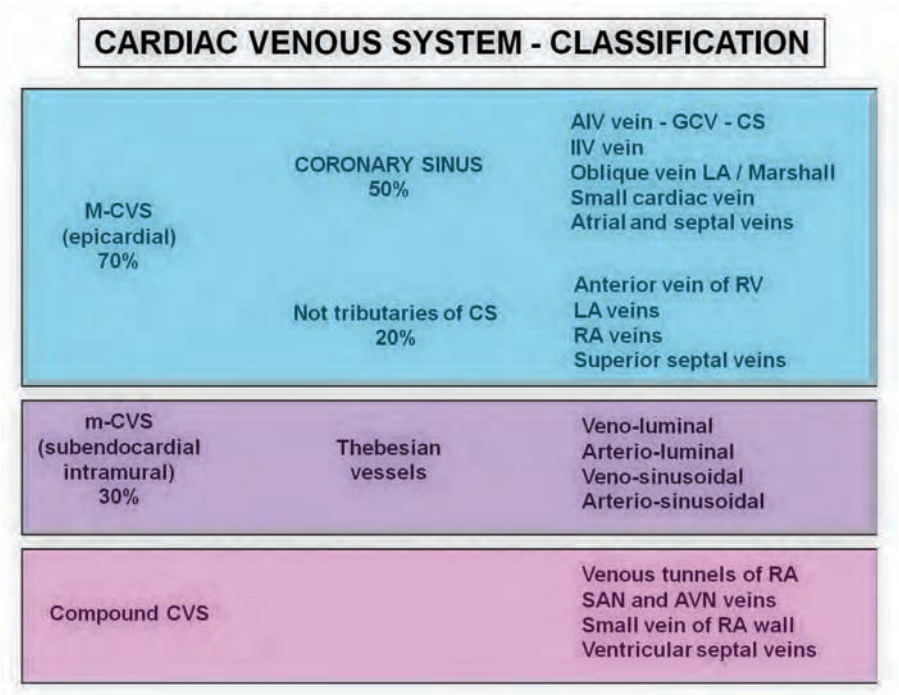

Figure 66.1 Classification of the cardiac venous system of the human heart. AIV: anterior interventricular vein (great cardiac vein); AVN: atrioventricular node; CS: coronary sinus; GCV: great cardiac vein; IIV: inferior interventricular vein (middle cardiac vein); M-CVS: major ("greater") cardiac venous system; m-CVS minor ("smaller") cardiac venous system; SAN: sinu-atrial node.

Bergman's Comprehensive Encyclopedia of Human Anatomic Variation, First Edition. Edited by R. Shane Tubbs, Mohammadali M. Shoja and Marios Loukas.
© 2016 John Wiley & Sons, Inc. Published 2016 by John Wiley & Sons, Inc.

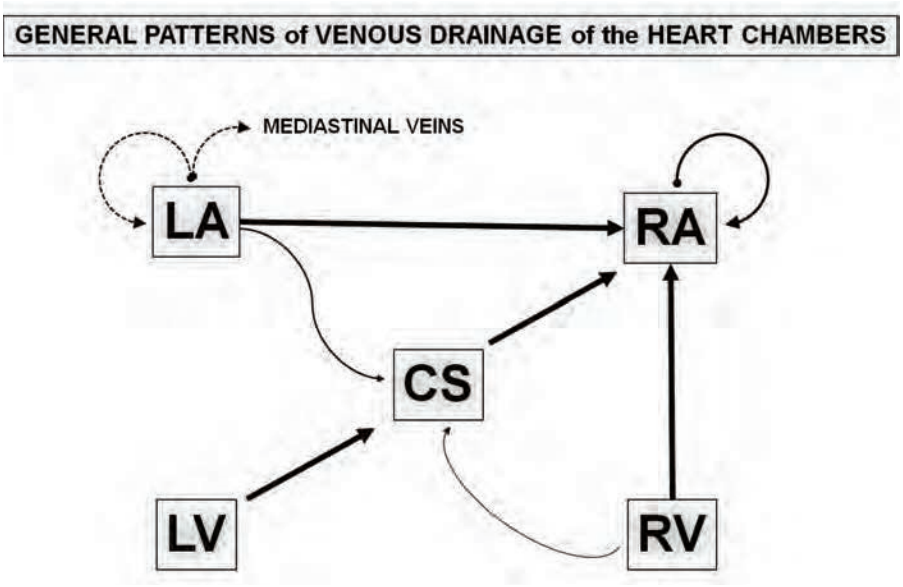

Figure 66.2 General patterns of venous drainage of the heart chambers. A schematic representation of the major pathways followed by the veins draining the four cardiac chambers. The left ventricle (LV) is drained by veins eventually terminating directly or indirectly in the CS. The right ventricle (RV) drains only partially into the CS; the greater part is drained by veins emptying into the right atrium (RA). Most if not all RA veins drain into the RA itself. Some veins of the left atrium (LA) drain into the CS but most of them drain into the RA. Some LA veins drain directly into the LA, the superior right pulmonary vein, or posterolateral veins (as the oblique vein of Marshall) eventually terminating in the CS. Some veins of the LA "roof" anastomose with mediastinal veins.

The coronary sinus and its tributaries

The CS system begins as the anterior interventricular vein (AIV) at the level of the anterior interventricular sulcus (AIVS) at either the apex, the distal one-third or the distal one-half of the AIVS. The AIV crosses the bifurcation of the left coronary artery (LCA), changing direction and joining the left coronary sulcus as the great cardiac vein (GCV). After being joined by the oblique vein of the LA (Marshall) it becomes the coronary sinus (CS). It then proceeds, winding around the mitral annulus to reach the area of apposition between the LA and RA (not the true interatrial septum). It goes deeper and opens into the RA (Fig. 66.3) under the fossa ovalis (actually the true septum). The CS shares an intimate relationship with the circumflex branch of the LCA, being located superior to the latter. Apart from the GCV, the major tributaries of the CX are:

- the left marginal vein (LMV) of the LV;
- the left posterior vein (LPV) of the LV;
- the middle cardiac vein or inferior interventricular vein (IIV);
- the oblique vein (OV) of the LA (Marshall); and
- the small cardiac vein (SCV).

Other epicardial veins can drain the inferior/posterior LV wall, located either between the LMV and LPV or between the LPV and IIV (Fig. 66.4; white arrows).

The various patterns of venous drainage of the inferior/posterior LV wall are presented in Figure 66.4. Only veins with diameters of 1 mm or more and epicardial lengths of 2 cm or more are generally considered (Baroldi and Scomazzoni 1967). There are frequent communications at the peripheral level among the epicardial veins (and their tributaries); nevertheless, obstruction of the major venous collectors such as the CS is not well tolerated and leads to venous infarction.

The great cardiac vein (GCV)

The CS is actually the continuation of the anterior interventricular/great cardiac vein system (AIV/GCV). The correct denomination is "great cardiac vein;" it has an anterior interventricular portion also known as "the anterior interventricular vein". The AIV begins at the level of the anterior interventricular sulcus (AIVS) at either the apical level, the distal third, or the distal half. It then proceeds alongside the LAD, although their reciprocal relationship is variable. This can create difficulties in coronary bypass grafting and especially during procedures on the beating heart. Upon reaching the left coronary sulcus, the continuation of the AIV is called the GCV. It usually crosses superficial to the branches of the division of the LCA (i.e., the LAD and Cx) although deeper locations have been noted and, in some instances, arterial compression causes aneurysmal dilatation of the GCV (Bates 2004; Loukas et al. 2007; Saremi et al. 2010). Aberrant drainage of the GCV into the RA or SVC has also been described (von Lüdinghausen 1989; Williams et al. 2013). Myocardial bridges can be encountered over the GCV or one of its tributaries (Saremi et al. 2010). The GCV drains the interventricular septum and the anterior surfaces of both the RV and the LV including the apical region of the heart (von Lüdinghausen 2003; Kawashima et al. 2003). The LMV usually drains into the GCV before its continuation into the CS. One or more veins coursing obliquely over the anterior surface of the LV, following a pattern similar to the diagonal arterial branches of the LAD, also join the GCV. Their disposition, length, and diameter are all extremely variable.

The left marginal vein (LMV)

The LMV is present in most cases, draining much of the LV myocardium; it usually courses superficial to the obtuse marginal artery, terminating in the GCV or CS.

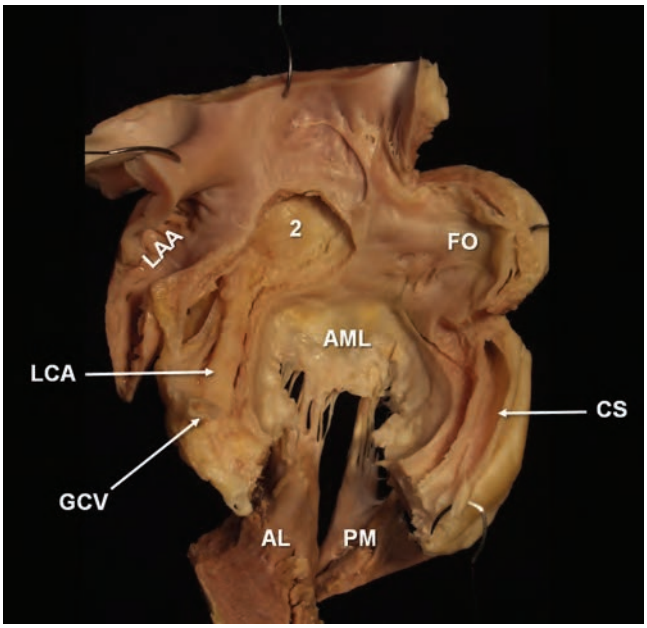

Figure 66.3 The general disposition of the coronary sinus. The coronary sinus (CS) is the direct continuation of the great cardiac vein (GCV). In this specimen, the GCV is seen crossing over the left coronary artery (LCA) while gaining its position in the left coronary sulcus. The CS winds around the mitral "annulus" in correspondence with the posterior mitral leaflet (partially cut in this specimen, in order to demonstrate the subvalvar apparatus of the mitral valve, with the anterolateral (AL) and the posteromedial (PM) papillary muscles). The CS goes deeper beneath the fossa ovalis (FO), which represents the true atrial septum, and terminates in the RA. In order to perform pecutaneous mitral annuloplasty (PMA) for treating mitral regurgitation and dilated ischemic or non-ischemic cardiomyopathy, a double-anchor device is implanted into the GCV-CS at the level of the mitral commissures. The length of the CS-GCV and the diameters at the anchor locations of the PMA must be accurately determined. The distance between the CS and mitral annulus increases secondary to LA enlargement. Ischemic complications can also occur if the Cx or distal branches of the RCA traveling the coronary sulcus around the mitral annulus are distorted during the PMA procedure. AML: anterior leaflet of the mitral valve; 2: aortic sinus #2 (i.e., left-facing aortic sinus) with the origin of the LCA; LAA: left atrial appendage.

The left posterior (posterolateral) vein (LPV)

The epicardial area between the left (obtuse) margin of the LV and the inferior interventricular sulcus is drained by one or more conspicuous branches of variable diameter and length. The LPV usually begins close to the posterior apical region and follows an oblique course over the LV inferior wall, terminating in the CS. When short (or absent), it is replaced by smaller branches draining into the LMV or IIV (Fig. 66.4).

Both the LMV and the LPV are relevant for electrophysiological procedures such as LV pacing and cardiac resynchronization therapy (CRT). Their diameter, length, and course are important particulars that either allow or preclude these procedures. The relationship with the left phrenic nerve is also clinically significant: the nerve can be inadvertently stimulated if the electrode comes into too close contact with it because of the anatomical variations of the epicardial veins.

The LMV can be absent in patients with previous posterolateral myocardial infarction; this has important clinical implications for the selection of patients for CRT (van de Veire et al. 2006; Saremi et al. 2012).

The inferior interventricular (middle cardiac) vein (IIV)

The IIV drains the adjacent inferior walls of the RV and LV including the apical area and the posterior septum. Contributing branches from the anterior apical portion of the heart frequently drain into the IIV. The vein is a constant landmark and terminates in the CS at about 1 cm from the CS ostium. The following are among its notable variations:

- duplicated IIV with an additional RV vein from the posterior RV wall (Fig. 66.5a);
- duplicated IIV with an additional LV vein from the posterior LV (Fig. 66.5b);
- oblique disposition of the IIV (which actually becomes interventricular only in proximity to the confluence with the CS (Fig. 66.5c);
- fusiform aneurysmal dilatation (twice the normal diameter) of the venous confluence IIV-CS; his is the most common location for bulbous enlargement of the cardiac veins (Saremi et al. 2010, 2012; Fig. 66.5d);
- IIV formed by two equally sized apical tributaries (Fig. 66.5e);
- varicoid IIV (Fig. 66.5f); or
- angled IIV-CS confluence (Fig. 66.5g).

Variations in the number of tributaries and the position, diameter, length, etc. of the epicardial veins can all be identified and quantified easily using cardiac computed tomographic venous mapping (Saremi et al. 2012).

The oblique vein (OV) of the LA (Marshall)

The OV represents a remnant of the left superior vena cava. In the adult heart it is positioned between the left atrial appendage (LAA) and the left pulmonary veins. It can be obliterated either in its superior part (more frequently) or over its entire length (more rarely). It usually originates below the left inferior pulmonary vein. The muscle sleeve of the OV (the Marshall bundle) is connected to the musculature surrounding the CS or the left pulmonary veins and is recognized as a source of activation in atrial tachyarrhythmias (Chauvin et al. 2000; Hwang et al. 2000; Hsu et al. 2004; Tan et al. 2006; Cabrera et al. 2008).

The OV can persist as a patent left superior vena cava (see the section on "Coronary sinus variations and anomalies" below). It is one of the landmarks used to locate the origin of the CS, as well as the valve of Vieussens and the extension of the muscular sleeve over the CS. However, these landmarks are not all at the same level and are usually located within a 10 mm interval (Ortale et al. 2001)

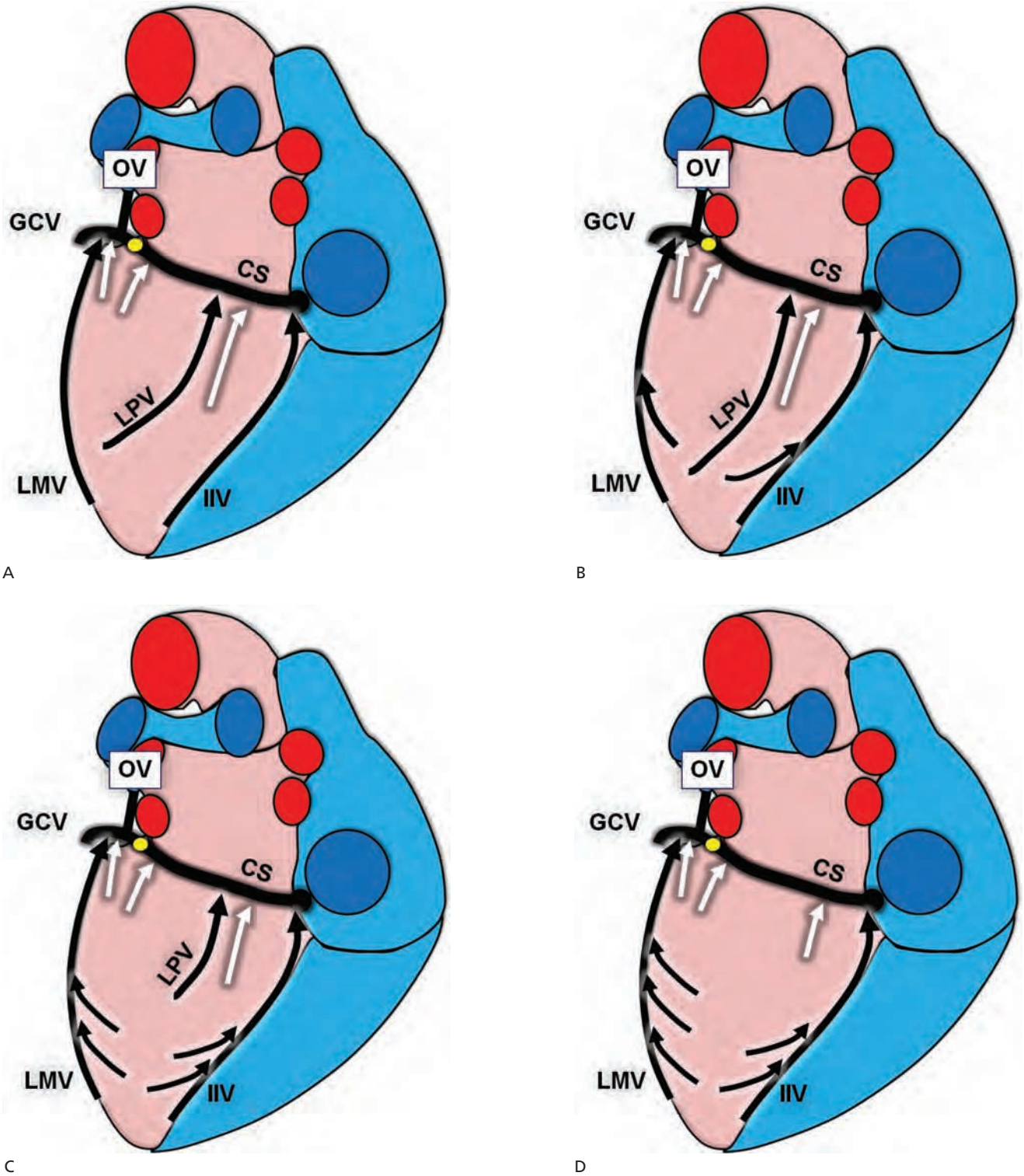

Figure 66.4 Patterns of drainage of the posterior inferior wall of the left ventricle. CS: coronary sinus; GCV: great cardiac vein; IIV: inferior interventricular vein (middle cardiac vein); LMV: left marginal (obtuse marginal) vein; LPV: posterior vein of the LV; OV: oblique vein of the left atrium (Marshall). White arrows indicate other veins of the posterior inferior wall of the LV of variable length and diameter. The yellow dot indicates the approximate position of the valve of Vieussens. The heart chambers are colored accordingly: blue: right heart chambers, caval veins and pulmonary trunk; red: left heart chambers, pulmonary veins and aorta. (a) LMV, LPV, and IIV are well developed and can be paralleled by one or more conspicuous additional posterior LV veins. (b) The LMV and the IIV depict more tributaries from the apical level. (c) LPV is shorter; some of the apical tributaries drain directly into the LMV or IIV while other portions of the posterior LV in proximity to the coronary sulcus are drained by additional veins (white arrows). (d) Absent LPV. Tributaries from the apex and apical third of the LV drain into the LMV and IIV. The remainder of the posterior LV is drained through smaller additional veins (white arrows). The presence or absence of the LPV or LMV and the development of additional posterior LV veins, including diameter and epicardial length, all represent important particulars of electrophysiological relevance (e.g., CRT, LV pacing).

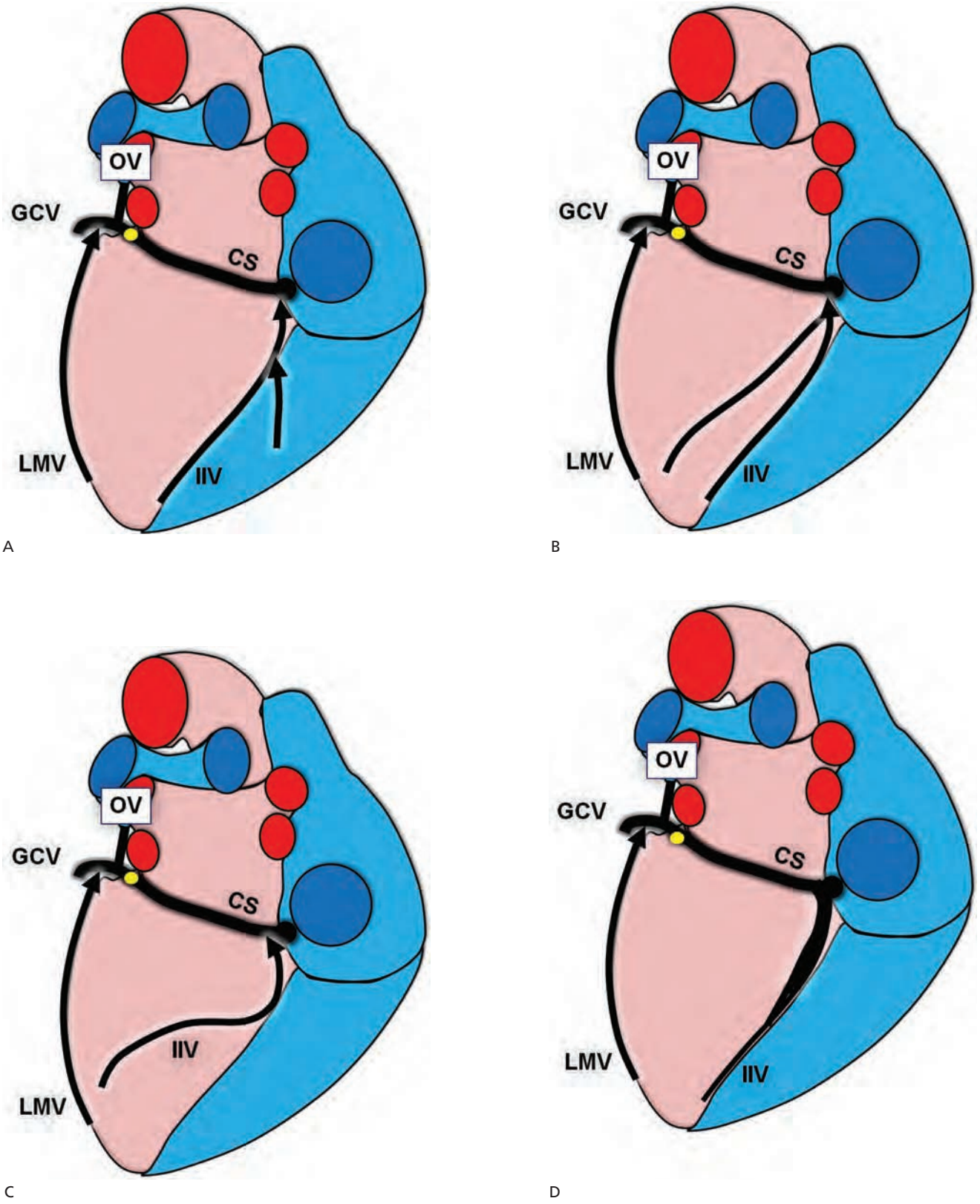

Figure 66.5 Variations of the inferior interventricular vein: duplicated IIV with additional tributary from the (a) posterior RV wall and (b) posterior LV wall; (c) IIV with oblique disposition over the posterior LV wall (the IIV gains the inferior interventricular sulcus close to the crux cordis); (d) aneurysmal (fusiform) dilatation of the IIV-CS confluence.

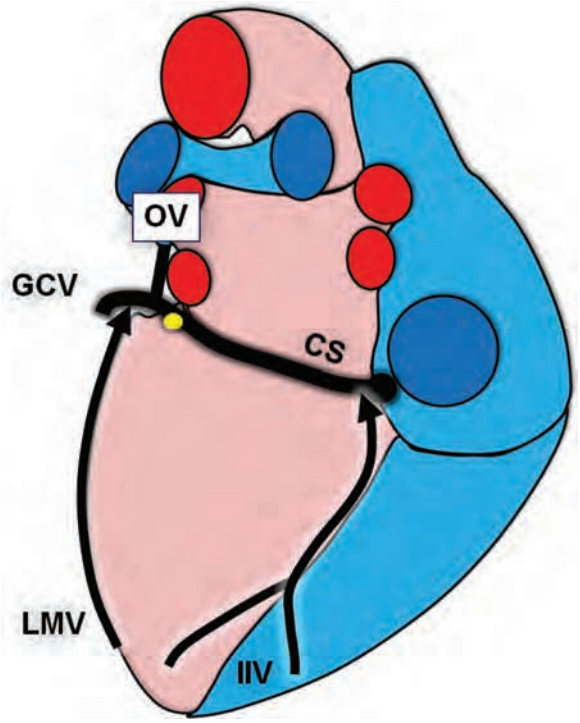

E

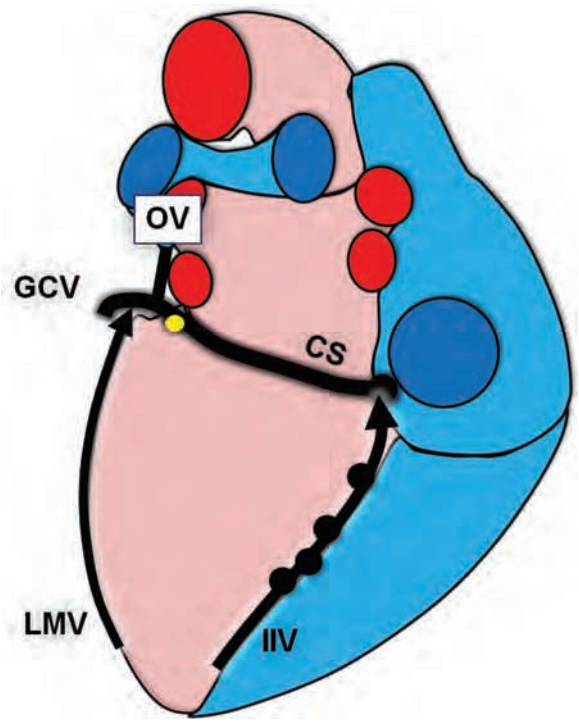

F

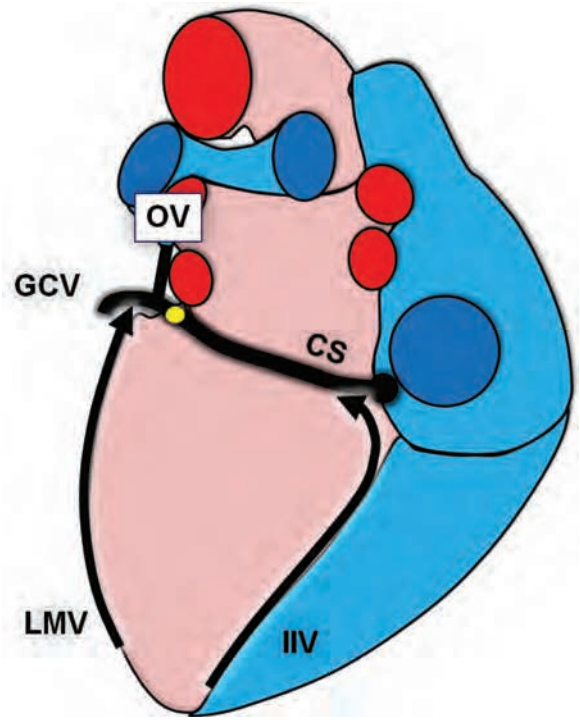

G

Figure 66.5 *(continued)* (e) the IIV is formed by the confluence of two equally sized apical tributaries (from the posterior walls of the RV and LV respectively); (f) varicoid IIV; (g) angled IIV-CS confluence, the IIV following an almost recurrent tract. Such variations are significant when visualization and/or selective catheterization of the IIV is contemplated.

The small (right coronary) vein (SCV)

The SCV is an inconstant venous collector at the level of the right coronary sulcus that drains into the CS, the IIV (rarely), or directly into the RA (Parsonnet 1953; Baroldi and Scomazzoni 1967). The variations of the SCV are illustrated in Figures 66.6–66.9. It drains most of the anterior wall of the RV so it will be discussed in the following section along with the right cardiac venous system (Cendrowska-Pinkosz 2004).

Anterior cardiac or right cardiac venous system

The veins draining the RV and originating on its anterolateral surface constitute the anterior or right cardiac venous system (anterior cardiac veins, ACV) and usually number three to six (Baroldi and Scomazzoni 1967). The right marginal (acute marginal) vein is the most constant collector. Four types of venous drainage are described:

- Type I (33%): The SCV is absent and the ACVs drain directly into the RA either separately (Fig. 66.6a), through a common ostium shared with the RMV (Fig. 66.6b), or adopting an intermediate pattern. One ACV joins the same opening as the RMV while the others drain separately into the RA (Fig. 66.6c).
- Type II (30%): The SVC opens into the CS but is rudimentary (having a diameter of 1–2 mm) and has very few and slender tributaries. The RMV and the ACVs drain independently into the RA (Fig. 66.7a) or share common ostia (Fig. 66.7b).
- Type III (30%): The SCV begins at the level of the anterior surface of the RV (beyond the acute margin) and has a more conspicuous caliber. Only the RMV joins the SCV at an acute angle; the ACVs can drain independently into the RA through separate openings (Fig. 66.8a) or sometimes share a common ostium (Fig. 66.8b). In other cases, all but one or two of the ACVs join the SCV in a similar fashion to the RMV (Fig. 66.8c). In all cases, the SCV can share direct openings into the RA as well as the terminal opening into the CS (black dots in Fig. 66.8).
- Type IV: The SCV is a larger collector (Fig. 66.9) and terminates in the RA (without joining the CS); additional openings can be present throughout the course (black dots in Fig. 66.9). The RMV and most, if not all, of the ACVs join the SCV. The SCV is sometimes replaced by the venous tunnel of the RA (see the following section).

Venous drainage of particular regions of the heart

For a comprehensive approach to the various types of venous conduits and their variability, it is convenient to describe the drainage of some particular regions and structures of the heart. However, these veins are of small caliber and are difficult to individualize by diagnostic imaging techniques. Moreover, their clinical significance can vary. In some forms of congenital heart disease, anastomotic venous channels offer alternative routes for venous blood flow (e.g., the veins of the left atrium can anastomose with some mediastinal veins such as azygos, bronchial, etc.). In other cases the multiple venous channels can be freely interrupted without adverse effects (e.g., the Cox maze procedure, cardiac transplantation, and bi-atrial and transseptal approaches in various cardiac surgical procedures).

Veins draining the LA walls

For veins draining the LA walls (Fig. 66.10), the following patterns have been described (Saremi et al. 2012; von Lüdinghausen et al. 1995).

- The left and posterior walls of the LA (including the veins of the LAA) empty into the GCV or CS.
- The veins of the septal aspect of the LA drain into the RA through the septum; the most numerous and conspicuous are located superior to the fossa ovalis. These veins are similar to the veins of the left lateral and posterior LA walls; the greater part of the interatrial septum is formed by infolding of the adjacent LA and RA walls (Anderson et al. 2006), so the veins of the right lateral wall of the LA become "septal veins." The pattern of their drainage is similar to that of the small veins of the RA wall, opening directly into the RA chamber (the m-CVS).
- The veins of the posterior and superior aspects of the LA ("the roof" of the LA) drain into the LA itself, via the left superior pulmonary vein or indirectly into other LA veins such as the OV.

Veins draining the RA walls

Almost all of the veins draining the RA walls terminate in the RA and consequently belong to the m-CVS. Following their location, the RA veins are classified as follows.

- The small intramural veins with diameters of 0.5–1 mm drain directly into the RA chamber after an intramural course of a few millimeters. The veins that drain the RAA have no connection with the epicardial veins and also belong to the m-CVS. They usually number between two and seven.
- In some cases an intra-atrial venous tunnel is identified winding around and 1–2 cm superior to the tricuspid valve; the tunnel begins at the right lateral wall of the RA and terminates in the RA chamber at the level of the posterior wall (von Lüdinghausen 2003). Some of the veins of the m-CVS drain into this tunnel (previously named "the coronary sinus of the right atrium"). The SCV can also drain into the tunnel.
- Small veins and sinusoids also belonging to the m-CVS in the region of the sinus node drain into the RA. Numerous small venous channels are found at this level; they could in principle offer a "protective" role for the vascularization of the sinus area, especially when the arterial supply is injured or interrupted by surgery. However, due to the multiplicity of arterial sources in the sinus node area, this remains a conjecture.

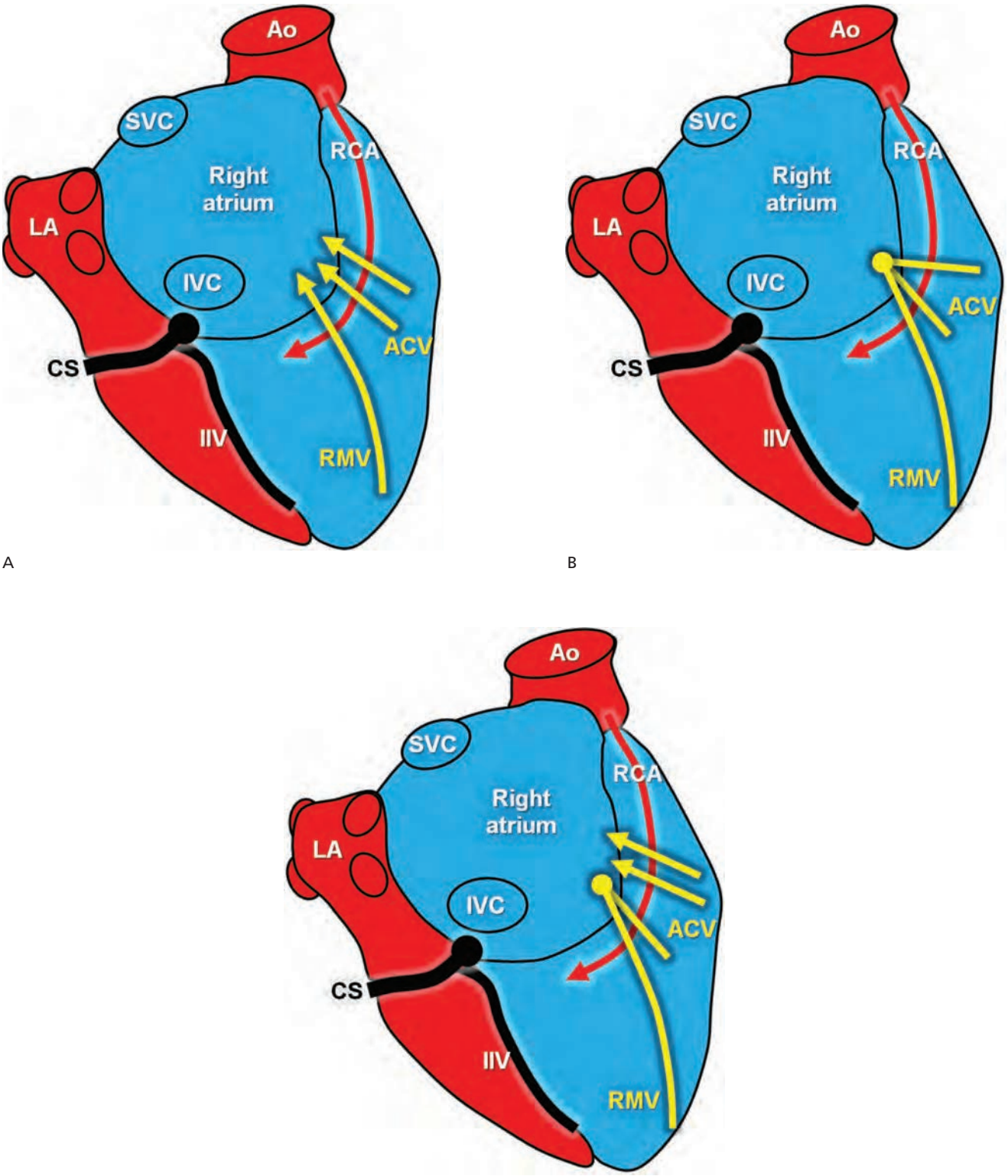

Figure 66.6 The anterior cardiac (right cardiac) venous system and patterns (types) of drainage. Various patterns (types) of venous drainage of the anterior and right aspects of the RV are presented. ACV: anterior cardiac veins (depicted in yellow); RMV: right marginal vein (the acute marginal vein of the right ventricle); SCV: small cardiac vein. The veins usually cross superficially over the right coronary artery (RCA) or its major branches. Type I: absent SCV. (a) The ACVs and the RMV all drain separately into the RA. (b) The ACVs drain into the RA through a common opening shared with the RMV. (c) The ACVs drain separately into the RA. One or more ACVs join the RMV to drain into the RA through a common ostium.

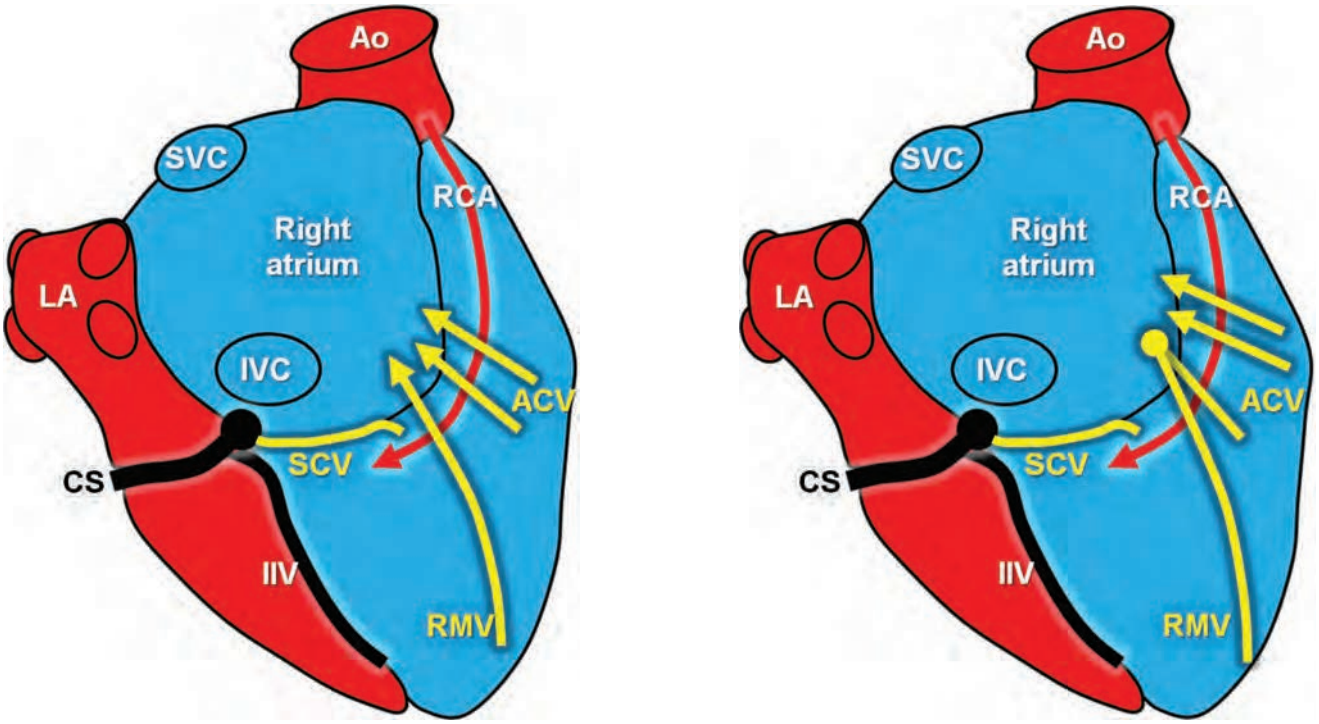

Figure 66.7 As for Figure 66.6. Type II: the SCV is present but of reduced caliber and length. (a) The venous drainage is through the ACVs and RMV which (a) open independently into the RA; or (b) terminate either separately or by sharing common openings into the RA.

- The region of the atrioventricular node and adjacent elements (base of the interatrial septum, bundle of His) are drained in a similar manner by small veins that can terminate directly in the RA chamber (close to the CS ostium) or in the CS. Due to their variable disposition and diameters, they can be mistaken for some forms of atrial septal defects.

The general pattern of the venous drainage of the LA and RA walls is summarized in Table 66.1.

Veins of the (sub)pulmonary infundibulum

These veins also belong to the m-CVS and drain directly into the RA, usually crossing over the right coronary artery and its branches.

Venous circulation of the interventricular septum

The veins draining the ventricular septum are similar in disposition to the septal arteries; however, the venous tributaries, especially those of small caliber, are more numerous than the corresponding arterial branches. The number of venous branches with diameters of 1 mm or more is almost equal to the number of arterial branches of equal diameter (Baroldi and Scomazzoni 1967). In most cases, the anterior two-thirds of the septum are drained by the anterior venous branches into the AIV/GCV system; the remaining one-third drains through the posterior branches into the IIV. Some authors have reported that the anterior branches drain the proximal anterior part of the septum while the posterior branches drain the distal posterior part (Aho 1950). The number of anterior septal veins ranges from 4 to 22 (average 10) and posterior septal veins from 0 to 24 (average 10.6). The superior third of the septum (the distal portion, in correspondence to the ventricular outflow tracts) is drained by a right and a left superior septal vein. The left superior septal vein is the longest and widest venous channel, reaching 2–3 mm in diameter (Saremi et al. 2012); it runs along the main arterial septal branch.

Venous anastomotic circulation

Anastomoses between tributaries of the intramural and epicardial veins are numerous, as evidenced in various anatomical studies. However, the collateral venous circulation is extremely variable and no particular pattern can be identified. Intersystemic anastomoses have been identified between the CS and the SCV systems of veins. Anastomoses between secondary branches of the same system have also been demonstrated (homosystemic/intrasystemic anastomoses). Other types of anastomoses include "terminal," when two tributaries continue directly one into the other, and "lateral," in which collateral vessels are arranged along the course of two contiguous veins

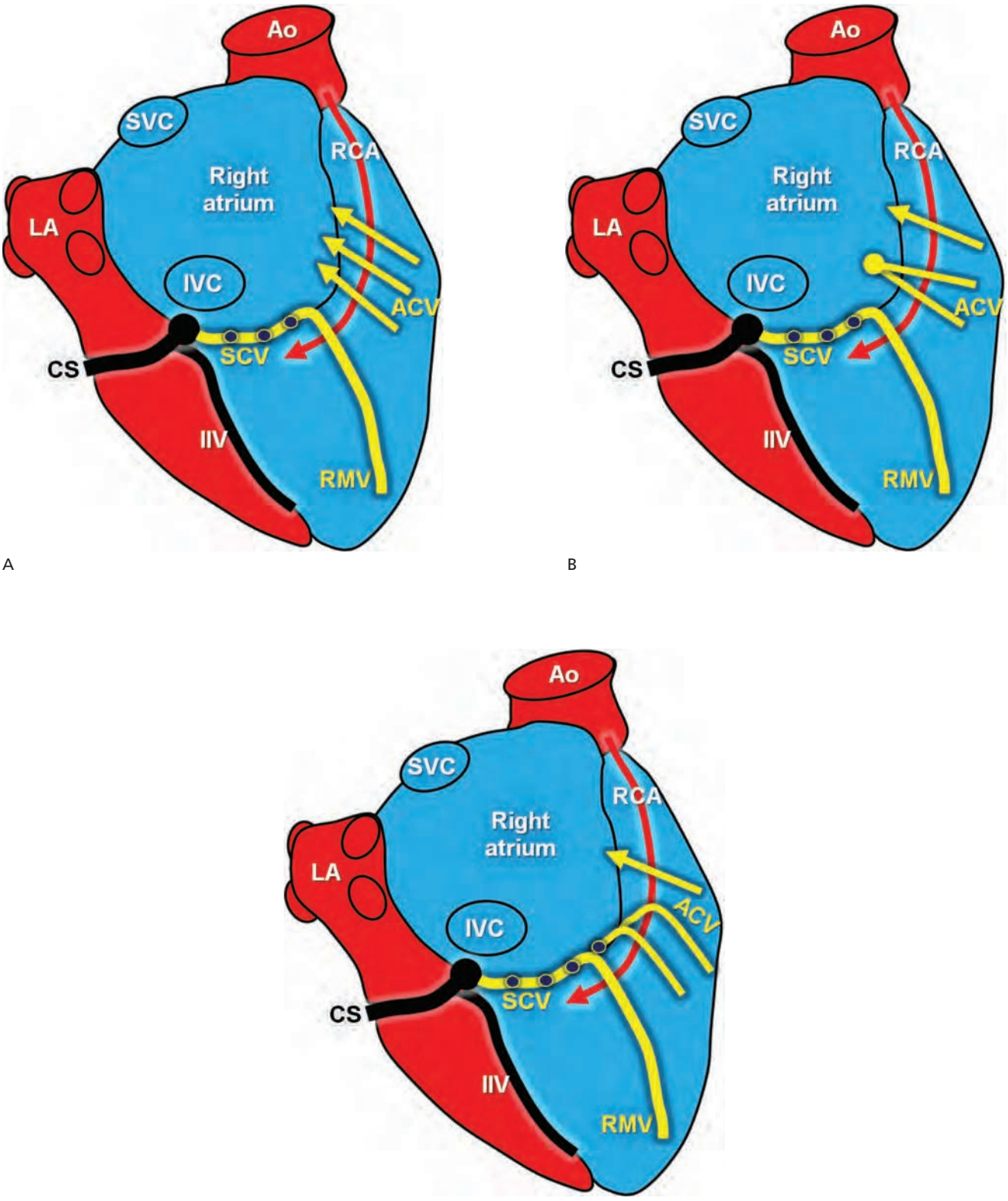

Figure 66.8 As for Figure 66.6. (a) Type III: the SCV is present and of considerable length and caliber. Only the RMV joins the SCV, while the ACVs open separately into the RA. The SCV also presents one or more direct openings into the RA along its tract (black dots). (b) Type III: the SCV is present and, as above, is joined by the RMV at an acute angle. Some of the ACVs open separately into the RA or by sharing a common ostium. (c) Type III: the SCV is present and larger; it is joined by the RMV and most of the ACVs with one or two exceptions.

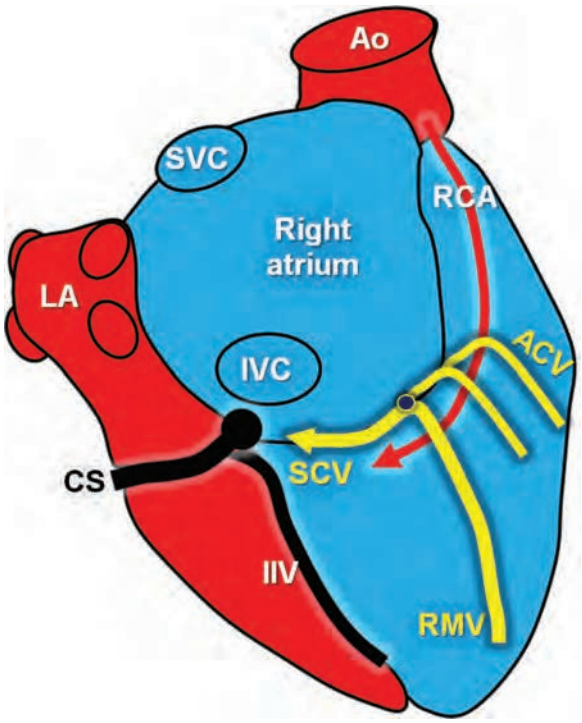

Figure 66.9 As for Figure 66.6. Type IV: the SCV is a large venous collector draining all the ACVs and the RMV. As in the types depicted in Figures 66.6–66.8, the SCV has one or more additional openings into the RA (black dot).

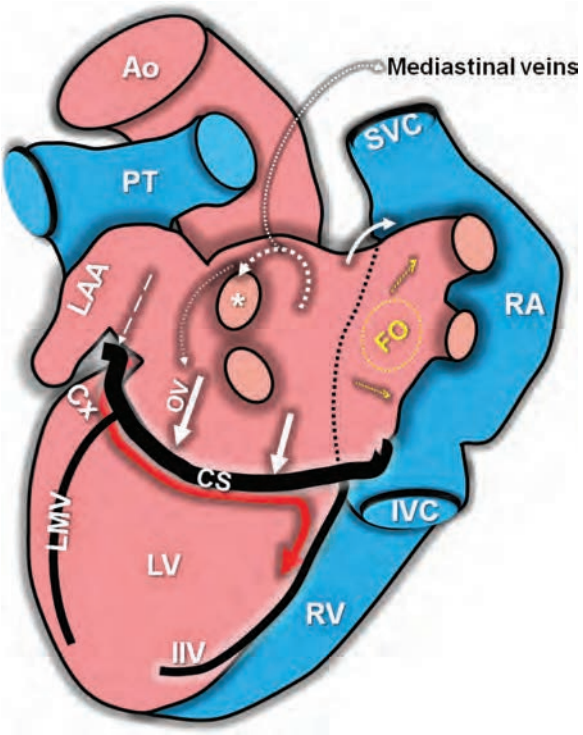

Figure 66.10 The venous drainage of the left atrium. The CS and its major tributaries (LMV and IIV) are depicted in black. The left and posterior walls of the LA are drained by veins emptying into the CS (white arrows), including the oblique vein of the LA (OV). The septal wall is drained by veins coursing superior to the fossa ovalis (FO) and terminating into the RA (yellow arrows). The veins of the suepriro and posterior aspects of the LA (LA roof) drain directly into the LA, into the left superior pulmonary vein (white dotted arrow) or into one of the tributaries of the CS (e.g., the OV). These latter veins can also anastomose with some of the mediastinal veins.

(Baroldi and Scomazzoni 1967). Some areas of the heart contain prominent anastomoses: the cardiac apex; the interior/posterior surface; and the anterior surface of the heart. Not least, anastomoses with extracardiac veins should be noted in view of their significance as alternative routes.

Table 66.1 Patterns of venous drainage of the atrial walls

Type of vein/territory drained	Termination site
Left atrium	
Anteroseptal, posteroseptal and inferoseptal veins	RA
Posterior and oblique veins of the LA	CS
Left lateral and auricular veins	GCV
Non-coronary proper veins of the LA	LA
Non-coronary proper veins of the LA	Pulmonary veins, terminal part
Non-coronary extracardiac veins of the LA	Mediastinal veins
Right atrium	
Anterior cardiac veins and some small (minor) RA veins	Intramural tunnels leading to RA cavity
Cava-atrial veins*	SVC, IVC near ostia

*Thin subepicardial or intramyocardial veins at the junction of the SVC and IVC with the RA

The consequences of obstruction of blood flow in a given vein are difficult to predict. Similarly, the pattern of retrograde delivery of a cardioplegic solution can vary, especially in diseased hearts. In particular, the parallel m-CVS and the particular conduits (Thebesian vessels, sinusoids, venoluminal vessels) in which blood flow is or can become bidirectional render the clinical and physiological picture even more complex (Ansari 2001).

Valves of the cardiac veins

The valves can in principle impede the advancement of catheterization devices or pacing leads. However, they are usually unicuspid and incomplete at the ostium. The larger epicardial veins (AIV, GCV, IIV, LPV) have an average of 2.5–3 valves/vein, while the LMVs have an average of 0.8 valves/vein (Ratajczyk-Pakalska et al. 1991; Anderson et al. 2008).

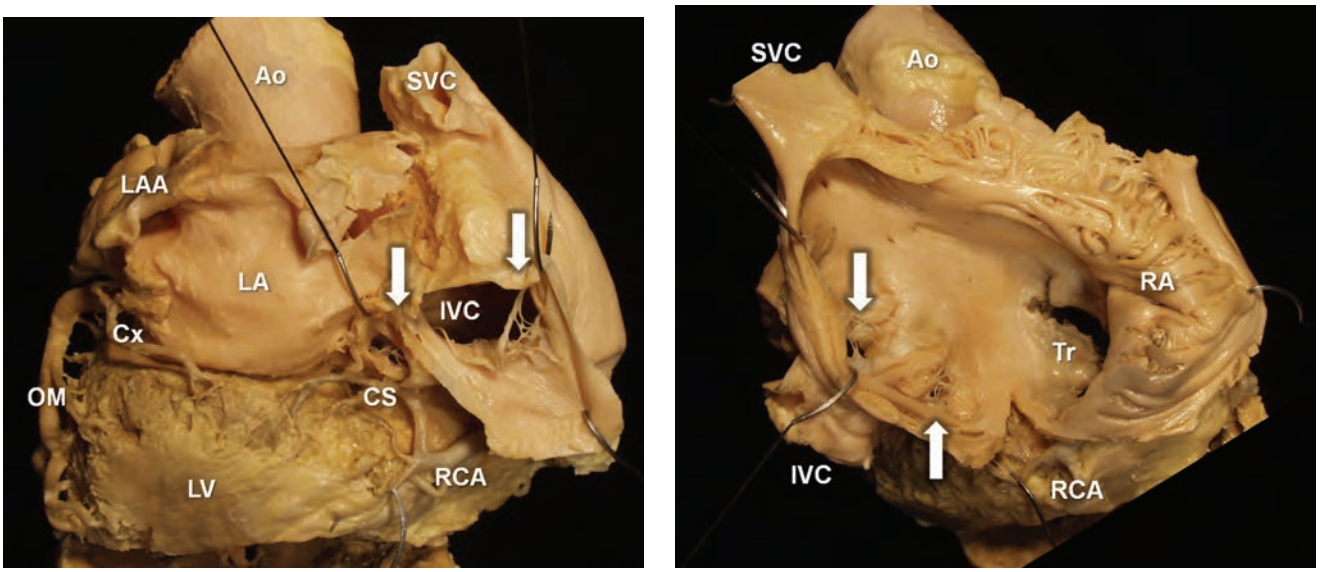

Figure 66.11 The Chiari network. (a) Posterior aspect of a heart specimen in which a Chiari network is visible over both the IVC and the CS ostium (white arrows). The remainder of the CS was deliberately excised in order to demonstrate the arterial branches vascularizing the area of the CS ostium. (b) Heart specimen with widely opened RA (right aspect), demonstrating the presence of a Chiari network over the IVC and CS ostium (white arrows). The difference between the morphology of the right atrial appendage and the right atrium proper is evident. The septal leaflet of the tricuspid valve is also evident (Tr).

Particular anatomical dispositions of the CS ostial valve or adjacent structures can interfere with or impede catheterization of the vein: a large Eustachian valve or ridge or cyst (Cho et al. 2012); a deep sub-Thebesian recess; a hypoplastic CS ostium; an unusually large or a circular Thebesian valve; an absent, thread-like, bridging, or fenestrated valve; a Eustachian valve cyst (Cho et al. 2012); or the presence of a Chiari network (Bhatnagar et al. 2006; Fig. 66.11). Additional valves in the CS can also impede the advancement of catheters or guidewires (Fig. 66.12).

Pathological persistence of sinus valves

This represents a very uncommon lesion. Due to exaggerated development of the derivatives of the right valves of the sinus venosus (Eustachian and Thebesian valves), various degrees of subdivision of the RA occur; this condition is called "cor triatriatum dexter." The SVC, IVC, and CS (or any combination of these) can be excluded from the true RA. This can cause obstruction to the systemic (or CS) venous return or channeling of the systemic blood flow into the LA.

Various forms of pathological persistence of sinus valves have been described as follows.

- A septum-like membrane extends across the RA from the terminal crest toward the septal wall of the RA, and from the SVC to a point below the CS ostium. The RA is consequently divided into two chambers, the sinus venarum (sinus of the caval veins) and the RA proper (including its appendage); the latter communicates with the RV through the tricuspid valve.

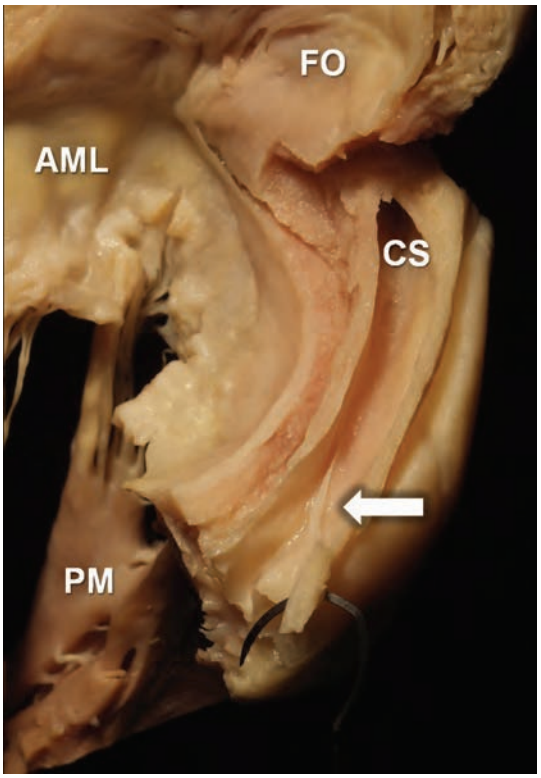

Figure 66.12 Valve of the coronary sinus. A close-up of the same specimen as in Figure 66.3, demonstrating the presence of an additional unicuspid valve of the CS (not the valve of Vieussens). Such additional valvular structures can impede the advancement of guidewires or catheters.

The two chambers communicate through various openings in the membrane.

- The membrane covers only the orifices of the SVC and IVC but not the CS ostium.
- The membrane covers only the IVC.
- Only the CS ostium is excluded from the RA by the membrane.
- The IVC and CS are excluded from the RA.
- A fibrous sac forms, resembling a closed windsock, and is stretched forward by the current of blood (Bankl 1977).

Associated cardiac anomalies include atrial septal defect (or patent foramen ovale) and hypoplastic right syndrome.

Coronary sinus variations and anomalies

The morphology of the CS is presented in Table 66.2 (Saremi et al. 2012). Some major anomalies of the CS are as follows (Bankl 1977).

- Absence of the CS. This is associated with persistence of a left superior vena cava (LSVC).
- Isolated congenital absence of the CS without LSVC (Foale et al. 1979). The cardiac veins drain separately into the RA and LA. Such cases are extremely rare (Fig. 66.13).
- Hypoplasia of the CS. One or more of the cardiac veins fail to join the CS and drain into the atria via Thebesian vessels.
- Atresia or stenosis of the CS ostium (von Lüdinghausen and Lechtleuthner 1988). This can be an isolated anomaly or can be associated with other anomalies (Fig. 66.14). Four types are described: (1) LSVC retrogradely draining into the brachiocephalic vein (Prows 1942); (2) gross connection with the LA (unroofed CS); (3) multiple connections via Thebesian vessels to both atria; and (4) with levoatrio-cardinal connection (Gerlis et al. 1984; Ito et al. 2000). Caution should be exercised when a LSVC is ligated in case it is draining a closed CS (Harris 1960).

Table 66.2 Coronary sinus morphology. Adapted from Saremi et al. (2012).

Size	Large	Acquired	Ventricular systole; heart failure; cardiomyopathy; AF; AVNRT
L = 2–5 cm ø = 6–14 mm		Congenital	Persistent LSVC; CAVF; CS-ASD
	Small	Acquired	Atrial systole; lipomatosis; small heart; CS stenosis; women
		Congenital	CS atresia; CS hypoplasia; unroofed CS; congenital heart disease: TOF, Ebstein, cc-TGA
Shape	Windsock (40%); tubular (50%); filiform (10%)		
Course	Straight (16%); gently curved (62%); high-riding (22%)		

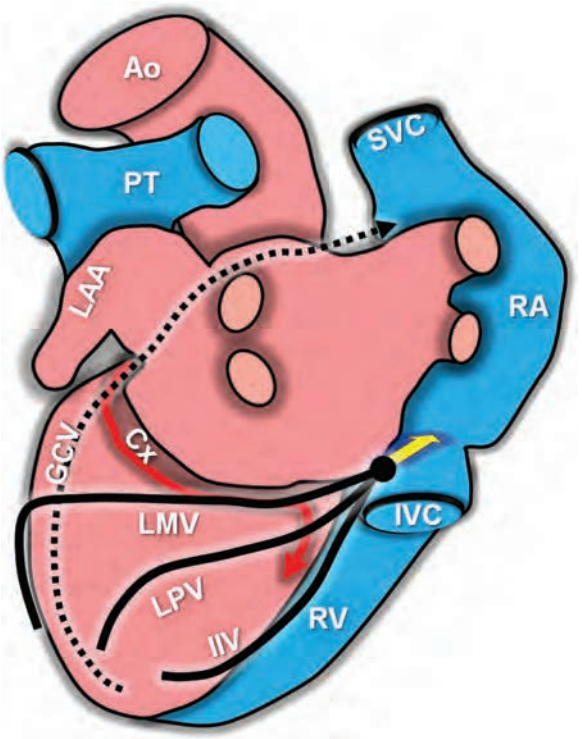

Figure 66.13 Absence of the coronary sinus without a persistent left superior vena cava. The LMV, LPV, and IIV drain directly into the RA (by a shared ostium or separately), highlighted by yellow arrow. The GCV also drains aberrantly into the SVC (or RA), highlighted by black dotted arrow.

- Enlargement of the CS due to persistence of the LSVC (Nathani et al. 2011).
- Enlargement of the CS in total or partial anomalous pulmonary venous connection.
- Communication of the CS with both atria.
- Connection of the CS to the inferior vena cava. The CS is normally located but joins the IVC just before its junction with the RA.
- Partial anomalous hepatic-venous connection to the CS. The CS is normal but continues to receive a left hepatic vein. This is evidence that it once functioned as the left horn of the sinus venosus (Bankl 1977; van der Horst et al. 1971; Steding et al. 1990).
- Left hepatic vein and persistent LSVC drainage into the CS (Buehler et al. 2011).
- Coronary arteriovenous fistula.
- Aneurysm of the CS. Association with pre-excitation due to accessory sino-ventricular connections has been described (Gerlis et al. 1985).
- Congenital diverticulum of the heart arising from the CS (Di Segni et al. 1986).
- Association between CS atresia and CAVF (Patel et al. 2011).
- Giant CS and persistent LSVC and absent right superior vena cava (Chan and Abdulla 2000).

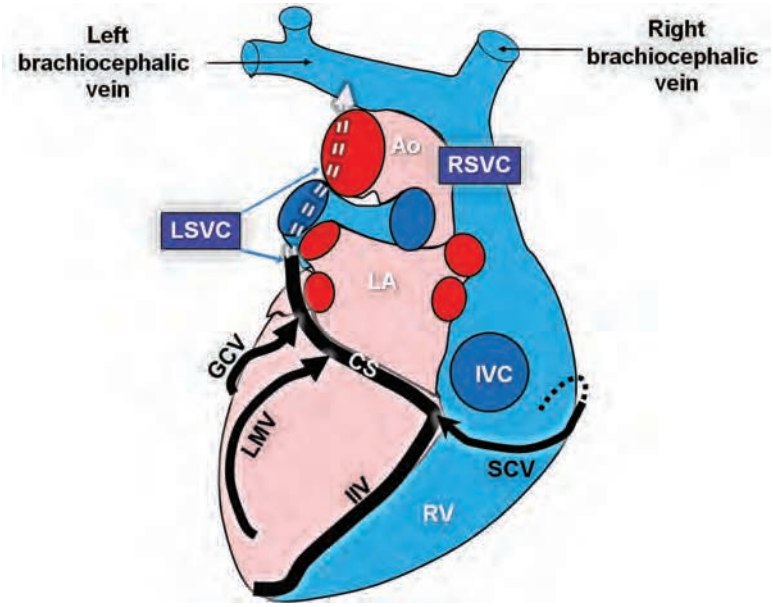

Figure 66.14 Atresia or stenosis of the coronary sinus ostium. The figure illustrates the pattern of drainage when the CS ostium is absent. The flow of blood is retrograde through the CS, which empties either through a persistent LSVC, directly into the LA (unroofed CS), through enlarged Thebesian vessels with both atria, or by means of a levoatrio-cardinal vein.

- Hemiazygous continuation to the CS with normal left brachiocephalic vein (Benrey et al. 1975).
- Persistent LSVC to an unroofed CS (Heng and De Giovanni 1997). There are four types of unroofed CS, which are classified as follows: (1) completely unroofed CS with LSVC; (2) completely unroofed CS without LSVC; (3) partially unroofed CS in its midportion; and (4) partially unroofed CS in its terminal portion (Raj et al. 2010).
- High insertion of the CS (Saremi et al. 2012).

The clinical significance of such anomalies and variations is evident, especially when catheterization of the CS is contemplated for cardiac resynchronization therapy or percutaneous mitral annuloplasty of retrograde delivery of a cardioplegic solution (Saremi et al. 2012). The main particulars that must be identified or clarified before a planned CRT procedure include:

- variants of CS morphology such as hypoplasia, absence of the CS, duplication, presence of any diverticulum;
- high insertion of the CS;
- anatomical barriers;
- size of the CS (for balloon occlusion);
- distance of the target vein from the CS ostium and the angle of confluence of the target vein with the CS; and
- diameter and length of the target vein, taking into account that the chosen vein must lead to the desired target territory and that it must have a diameter of >1.5 mm (allowing the smallest pacing leads, i.e., 4F, to pass).

The muscular connections (CS-LA muscle connections) should also be included among the variations of the CS. The CS is surrounded by a myocardial sleeve (van den Berg and Moorman 2009, 2011), which can also extend over the OV (Kim et al. 2000); this sleeve can be a continuation of the RA musculature. Some fibers originating from this sleeve connect to the LA myocardium along the inferior mitral annulus (Chauvin et al. 2000; Saremi et al. 2011), providing the second-largest electrical continuity between atria. Along with the Bachman bundle (the anterosuperior interatrial muscle bridge), these muscular connections between the RA and LA ensure rapid interatrial conduction leading to physiological biatrial contraction (von Lüdinghausen et al. 1992; Chauvin et al. 2000). Connections between the CS and the ventricular musculature have also been reported (Sun et al. 2002).

The general pattern and characteristics of the epicardial veins are listed in Table 66.3.

Final remarks

There are numerous individual variations in the cardiac venous system of the human heart; a thorough knowledge of the general disposition of the venous conduits is mandatory for understanding both the normal physiology and the modifications encountered in disease. New diagnostic and therapeutic approaches focus on the study of the cardiac venous circulation, while the data are somewhat more difficult to interpret than those from the arterial segment. Numerous paths are opened for future research and for a better understanding of this unparalleled circulatory system.

Table 66.3 Characteristics of the epicardial veins. Adapted from Saremi et al. (2012).

Vein	Origin	Territory	Ostial Ø (mm)	Prevalence (%)	Termination site	Number	Variations	Ostial valve (%)
CS	GCV	Left coronary sulcus	4–14 (10)	99	RA	1 (duplication is rare)	Absence (see text for details)	80
AIV-GCV	Apex; apical 1/3 or apical 1/2	Anterior septum, anterior surface of RV and LV, LA (partially); cardiac apex	AIV 0.9–4.4 (2–7); GCV 1.2–6.3 (3.9)	100	CS (99%) Other sites: SVC, RA	1 (98%) (duplication is rare 3%)	Drainage into the SVC or RA (1%), aneurysm of the GCV, MB (2–8%); myocardial belt (6%)	85
IIV	Apex	RV and LV posterior walls, apex, posterior third of the septum	2–5.3 (3.6)	100	CS RA (2.5%)	1 (75%) 2 (24%)	Aneurysm (8%), varicoid, duplicated, MB (2.5%)	60
LPV	LV posterior wall	Inferior and lateral LV walls	1–5.5 (2.4)	95	CS (37–77%) GCV (13%)	1 (63%) 2 (23%) Multiple small (9%) Absent (5%)	Bulbar aspect (5%) MB (2%)	30
LMV	Posterolateral wall of LV	Most of the LV myocardium (apical, lateral, inferior)	1–3 (2.2)	70–85	GCV (80%) CS (20%)	1	Absence is common (may be replaced by smaller LV inferiro veins)	30
OV	Junction of GCV-CS	Between LAA and left pulmonary veins (2–3 cm in length)	0.4–1.8	85–95	CS	1	Drainage into persistent LSVC	NA
SCV	Right coronary sulcus	Diaphragmatic surface of RV	<1	30–50	CS (85%) IIV (12%)	1	May receive the RMV (10%)	NA
RMV	Apex of RV and acute margin of RV	Anterior and inferior RV walls	0.5–3	13–80	SCV (30%) RA Venous tunnel of RA	1	Large draining into a vertical RA tunnel	NA
ACV	Anterior RV	Anterior and anterolateral RV	0.5–1	90	RA (30%) Venous tunnel of RA (66%) SCV	1 (24–57%) 2 (33–48%) 3 (9–28%) or minute branches (up to 15 in number)	Large infundibular vein or AIV draining into ACV	12

List of abbreviations

ACAOS: abnormal coronary artery (origin) from the opposite (aortic) sinus
ACxPA: abnormal circumflex from the pulmonary artery
ACV: anterior cardiac vein(s)
AIV: anterior interventricular vein
AIVS: anterior interventricular sulcus
AL: anterolateral papillary muscle of the mitral valve
ALADPA: abnormal LAD from the pulmonary artery
ALCAPA: abnormal left coronary artery from the pulmonary artery
AML: anterior mitral leaflet
Ao: aortic root
AOCAP: abnormal origin of both coronaries from the pulmonary trunk
APOC: abnormal pulmonary origin of the coronaries
ARCAPA: abnormal right coronary artery from the pulmonary artery
ATO-Cx: acute take-off of the circumflex branch
AVN: atrioventricular node
CAA: coronary artery anomalies and variations
CALM: congenital atresia/absence of the left main vein
CAn: coronary aneurysm and ectasia
CAVF: coronary arteriovenous fistula
COSA: congenital coronary ostial stenosis or atresia
CS: coronary sinus
CVS: coronary (cardiac) venous system
Cx: circumflex branch of the left coronary artery
$D_{1,2}$ etc.: diagonal branches of the LAD
D_{RV}: diagonal branch of the right ventricle
FO: fossa ovalis
GCV: great cardiac vein
IIV: inferior interventricular vein (middle cardiac vein)
IVC: inferior vena cava
LA: left atrium
LAA: left atrial appendage
LAD: left anterior descending artery (the correct term is "anterior interventricular branch")
LAD_L: long LAD (in cases with dual LAD)
LAD_S: short LAD (in cases with dual LAD)
LCA: left coronary artery ("left main trunk")
L-COSA: congenital coronary ostial stenosis or atresia of the left coronary artery
LMV: left marginal vein (vein of the obtuse margin of the left ventricle)
LPA: left pulmonary artery
LPV: left posterior vein (posterior vein of the left ventricle)
LV: left ventricle
LVOT: left ventricular outflow tract
MB: myocardial bridging/muscular bridging
M-CVS: major cardiac venous system
m-CVS: minor cardiac venous system
NF: non-facing sinus (of the aortic or pulmonary root)
OV: oblique vein of the left atrium (Marshall)
PDA: posterior descending artery (the correct term is "inferior interventricular artery")
PL: posterior (posteromedial) papillary muscle of the mitral valve
PT: pulmonary trunk
R-COSA: congenital coronary ostial stenosis or atresia of the right coronary artery
RI: ramus intermedius (intermediate branch of the left coronary artery)
RMV: right marginal vein (vein of the acute margin of the right ventricle)
RPA: right pulmonary artery
RV: right ventricle
RVOT: right ventricular outflow tract
S: septal branch (generic term)
$S_{1,2}$ etc.: septal branches (of the LAD)
SAN: sinuatrial node
SCV: small cardiac vein
SEC: subendocardial coronary course
Sinus #1: right-facing sinus (of the aortic or pulmonary root)
Sinus #2: left-facing sinus (of the aortic or pulmonary root)
SVC: superior vena cava
TA: anterior papillary muscle of the tricuspid valve
TM: medial papillary muscle group of the tricuspid valve
Tr: tricuspid valve

References

Aho A. 1950. On the venous network of the human heart and its arteriovenous anastomoses. *Ann Med Exper Biol Fenniae* (suppl I) 29: 1–90.

Anderson RH, Brown NA, Moorman AF. 2006. Development and structures of the venous pole of the heart. *Dev Dyn* 235(1): 2–9.

Anderson SE, Quill JL, Iaizzo PA. 2008. Venous valves within left ventricular cardiac veins. *J Interv Card Electrophysiol* 23(2): 95–99.

Ansari A. 2001. Anatomy and clinical significance of ventricular Thebesian veins. *Clin Anat* 14(2): 102–110.

Bankl H. 1977. *Congenital malformations of the heart and great vessels. Synopsis of pathology, embryology and natural history*. Baltimore, Munich: Urban & Schwarzenberg.

Baroldi G, Scomazzoni G. 1967. *Coronary circulation in the normal and the pathologic heart. Office of the Surgeon General*. Department of the Army. Washington DC, pp. 61–85.

Bates GS. 2004. Great cardiac vein variations. *Clin Anat* 17(5): 436–443.

Benrey J, Williams RL, Reul GJ. 1975. Hemiazygos continuation to coronary sinus with normal left innominate vein. *Cardiovasc Dis Bull Texas Heart Inst* 2(3): 325–330.

Bhatnagar KP, Nettleton GS, Campbell FR, Wagner CE, Kubawara N, Muresian H. 2006. Chiari anomalies in the human right atrium. *Clin Anat* 19: 510–516.

Buehler M, Abdullah A, Lewis T. 2011. Left hepatic vein and persistent left superior vena cava drainage into the coronary sinus with subaortic valve stenosis. *Int J Angiol* 20: 243–246.

Cabrera JA, Ho SY, Climent V, Sánchez-Quintana D. 2008. The architecture of the left lateral atrial wall: a particular anatomic region with implications for ablation of atrial fibrillation. *Eur Heart J* 29(3): 356–362.

Cendrowska-Pinkosz M. 2004. The variability of the small cardiac vein in the adult human heart. *Folia Morphol (Warsz)* 63(2): 159–162.

Chan K-L, Abdulla A. 2000. Giant coronary sinus and absent right superior vena cava. *Heart* 83: 702–704.

Chauvin M, Shah DC, Haïssaguerre M, Marcellin L, Brechenmacher C. 2000. The anatomic basis of connections between the coronary sinus musculature and the left atrium in humans. *Circulation* 101(6): 647–652.

Cho HJ, Jung JI, Kim HW, Lee KY. 2012. Intracardiac Eustachian valve cyst in an adult detected with other cardiac anomalies: usefulness of multidetector CT in diagnosis. *Korean J Radiol* 13(4): 500–504.

Di Segni E, Siegal A, Katzenstein M. 1986. Congenital diverticulum of the heart arising from the coronary sinus. *Br Heart J* 56: 380–384.

Foale RA, Baron DW, Rickards AF. 1979. Isolated congenital absence of coronary sinus. *British Heart J* 42: 355–358.

Gerlis LM, Gibbs JL, Williams GJ, Thomas GDH. 1984. Coronary sinus orifice atresia and persistent left superior vena cava. A report of two cases, one associated with atypical coronary artery thrombosis. *Br Heart J* 52: 648–653.

Gerlis LM, Davies MJ, Boyle R, Williams GJ, Scott H. 1985. Pre-excitation due to accessory sinoventricular connections. *Br Heart J* 53(3): 314–322.

Harris WG. 1960. A case of bilateral superior venae cavae with a closed coronary sinus. *Thorax* 15: 172–173.

Heng JT, De Giovanni JV. 1997. Occlusion of persistent left superior vena cava to unroofed coronary sinus using vena cava filter and coils. *Heart* 77: 579–580.

Hsu LF, Jaïs P, Keane D, Wharton JM, Deisenhofer I, Hocini M, Shah DC, Sanders P, Scavée C, Weerasooriya R, Clémenty J, Haïssaguerre M. 2004. Atrial fibrillation originating from persistent left superior vena cava. *Circulation* 109(7): 828–832.

Hwang C, Wu TJ, Doshi RN, Peter CT, Chen PS. 2000. Vein of Marshall cannulation for the analysis of electrical activity in patients with focal atrial fibrillation. *Circulation* 101(13): 1503–1505.

Ito H, Tamura H, Ito Y. 2000. Coronary sinus ostial atresia with persistent left superior vena cava connected with atrial septal defect. *Heart* 84: 289.

Kawashima T, Sato K, Sato F, Sasaki H. 2003. An anatomical study of the human cardiac veins with special reference to the drainage of the great cardiac vein. *Ann Anat* 185(6): 535–542.

Kim DT, Lai AC, Hwang C, Fan LT, Karagueuzian HS, Chen PS, Fishbein MC. 2000. The ligament of Marshall: a structural analysis in human hearts with implications for atrial arrhythmias. *J Am Coll Cardiol* 36(4): 1324–1327.

Loukas M, Tubbs RS, Jordan R. 2007. Aneurysm of the great cardiac vein. *Surg Radiol Anat* 29(2): 166–172.

Loukas M, Bilinsky S, Bilinsky E, El-Sedfy A, Anderson RH. 2009. Cardiac veins: a review of the literature. *Clin Anat* 22(1): 129–145.

Nathani S, Parakh N, Chaturvedi V, Tyagi S. 2011. Giant coronary sinus. *Tex Heart Inst J* 38(3): 310–311.

Ortale JR, Gabriel EA, Iost C, Márquez CQ. 2001. The anatomy of the coronary sinus and its tributaries. *Surg Radiol Anat* 23(1): 15–21.

Parsonnet V. 1953. The anatomy of the veins of the human heart with special reference to normal anastomotic channels. *J Med Soc NJ* 50(10): 446–452.

Patel SM, McLeod CJ, Friedman PA, Liu XK, Asirvatham SJ. 2011. Successful ablation of a left-sided accessory pathway in a patient with coronary sinus atresia and arteriovenous fistula: clinical and developmental insights. *Indian Pacing and Electrophysiol J* 11(2): 43–49.

Prows MS. 1942. Two cases of bilateral superior venae cavae, one draining a closed coronary sinus. *Anat Rec* 87: 99–106.

Raj V, Joshi S, Ho YC, Kilner P. 2010. Case report: completely unroofed coronary sinus with a left superior vena cava draining into the left atrium studied by cardiovascular magnetic resonance. *Indian J Radiol Imaging* 20(3): 215–217.

Ratajczyk-Pakalska E, Bloch P, Kulig A. 1991. Angioarchitectonics of the venous vessels and morphological changes in coronary heart disease. *Basic Res Cardiol* 86(6): 554–560.

Saremi F, Channual S, Sarlaty T, Tafti MA, Milliken JC, Narula J. 2010. Coronary venous aneurysm in patient without cardiac arythmia as detected by MDCT: an anatomic variant or a pathologic entity. *JACC Cardiovasc Imaging* 3(3): 257–265.

Saremi F, Thonar B, Sarlaty T, Shmayevich I, Malik S, Smith CW, Krishnan S, Sánchez-Quintana D, Narula N. 2011. Posterior interatrial muscular connection between the coronary sinus and left atrium: anatomic and functional study of the coronary sinus with multidetector CT. *Radiology* 260(3): 671–679.

Saremi F, Muresian H, Sanchez-Quintana D. 2012. Coronary veins: comprehensive CT-anatomic classification and review of variants and clinical implications. *Radiographics* 32: E1–E32.

Steding G, Xu JW, Seidl W, Männer J, Xia H. 1990. Developmental aspects of the sinus valves and the sinus venosus septum of the right atrium in human embryos. *Anat Embryol (Berl)* 181(5): 469–475.

Sun Y, Arruda M, Otomo K, Beckman K, Nakagawa H, Calame J, Po S, Spector P, Lustgarten D, Herring L, Lazzara R, Jackman W. 2002. Coronary sinus-ventricular accessory connections producing posteroseptal and left posterior accessory pathways: incidence and electrophysiological identification. *Circulation* 106(11): 1362–1367.

Tan AY, Chou CC, Zhou S, Nihei M, Hwang C, Peter CT, Fishbein MC, Chen PS. 2006. Electrical connections between left superior pulmonary vein, left atrium, and ligament of Marshall: implications for mechanisms of atrial fibrillation. *Am J Physiol Heart Circ Physiol* 290(1): H312–H322.

van de Veire NR, Schuijf JD, de Sutter J, Devos D, Bleeker GB, de Roos A, van der Wall EE, Schalij MJ, Bax JJ. 2006. Non-invasive visualization of the cardiac venous system in coronary artery disease patients using 64-slice computed tomography. *J Am Coll Cardiol* 48(9): 1832–1838.

van den Berg G, Moorman AFM. 2009. Concepts of cardiac development in retrospect. *Pediatr Cardiol* 30: 580–587.

van den Berg G, Moorman AFM. 2011. Development of the pulmonary vein and the systemic sinus venosus: an interactive 3D overview. *PLoSONE* 6(7): e22055, doi: 10.1371/journal.pone.0022055.

van der Horst RL, Winship WS, Gotsman MS. 1971. Drainage of left hepatic vein into coronary sinus associated with other systemic venous anomalies. *British Heart J* 33: 164–166.

von Lüdinghausen M. 1989. Aberrant course of the anterior interventricular part of the great cardiac vein in the human heart. *Gegenbaurs Morphol Jahrb* 135(3): 475–478.

von Lüdinghausen M. 2003. The venous drainage of the human myocardium. *Adv Anat Embryol Cell* Biol 168: I–VIII, I–104.

von Lüdinghausen M, Lechleuthner A. 1988. Atresia of the right atrial ostium of the coronary sinus. *Acta Anat (Basel)* 131(1): 81–83.

von Lüdinghausen M, Ohmachi N, Boot C. 1992. Myocardial coverage of the coronary sinus and related veins. *Clinc Anat* 5(1): 1–15.

von Lüdinghausen M, Ohmachi N, Besch S, Mettenleiter A. 1995. Atrial veins of the human heart. *Clin Anat* 8: 169–189.

Williams V, Bartanuszova M, Rahimi OB, Moore CM. 2013. A rare variant of the great cardiac vein. *IJAV* 6: 112–114.

67 Pulmonary veins

Yutthaphan Wannasopha and Juntima Euathrongchit
Chiang Mai University, Chiang Mai, Thailand

The pulmonary veins are the channels that carry arterialized blood from the lungs. They have no intraluminal valves, in contrast to other veins. They originate from the capillary networks in the alveolar walls and empty into the upper posterolateral surfaces of the left atrium of the heart.

Most individuals have four pulmonary veins and four independent ostia, two on each side (Fig. 67.1). In each lobe of the (bilateral) lungs there is a single trunk of pulmonary venous drainage supplied by smaller intra- and inter-segmental tributary veins. However, the right middle lobar and superior lobar veins from each lower lobe usually join before they drain into the left atrium. As a result, two pulmonary veins – superior and inferior – usually emerge from each lung (Standring 2008). The bilateral superior pulmonary veins pierce the mediastinum downward and anterior to the accompanying pulmonary arteries, whereas the inferior pulmonary veins penetrate upward and are situated inferior to their homonymous bronchi (Ghaye et al. 2003). The inferior pulmonary veins follow a horizontal course centrally and a vertical course distally. The left superior pulmonary vein is longer than the right.

To clarify our understanding of how the pulmonary veins vary, the focus should be on their embryological development. The exact origin of the pulmonary vein remains controversial and its development is very complicated. It canalizes from a mid-pharyngeal strand and drains into the atrium between the ridges of the dorsal mesocardial connection at about six weeks of development in humans (Anderson et al. 2006). To begin with, a single orifice forms near the atrioventricular junction and a primitive common pulmonary vein begins as an outpouching sac from the dorsal wall of the left atrium (Anderson et al. 2006; Dillman et al. 2009). Subsequently, the common pulmonary vein connects with the part of the splanchnic plexus that receives blood flowing from the lungs (Dillman et al. 2009). By 30–32 days, the connections of the splanchnic plexus have disappeared and the common pulmonary vein has developed to form separate entrances at the four corners of the roof of the left atrial body (Fig. 67.2; Agarwal et al. 2004; Anderson et al. 2006; Dillman et al. 2009). If the common pulmonary vein fails to incorporate properly, variations in the pulmonary venous anatomy result. Both under- and overincorporation of the common pulmonary vein into the left dorsal atrium during gestation lead to anatomical variations in the number, branching patterns, and lengths of its preostial portions (Ghaye et al. 2003).

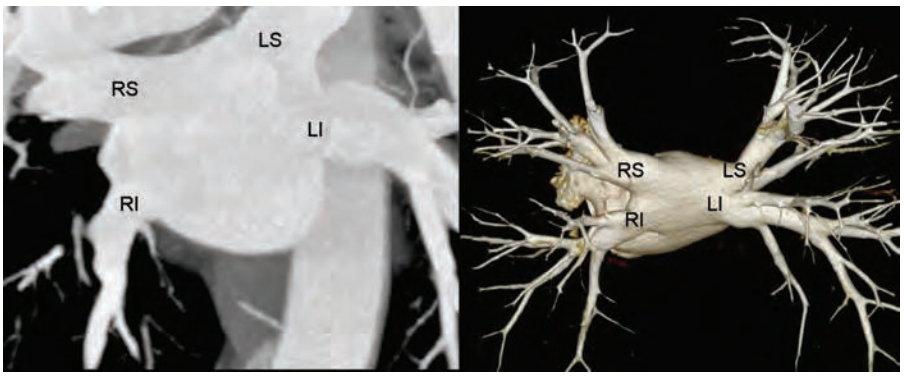

Figure 67.1 Thick-slab coronal oblique MPR image and 3DVR image show four pulmonary veins and four independent ostia, two on each side. RS: right superior; RI: right inferior; LS: left superior; and LI: left inferior.

Bergman's Comprehensive Encyclopedia of Human Anatomic Variation, First Edition. Edited by R. Shane Tubbs, Mohammadali M. Shoja and Marios Loukas.
© 2016 John Wiley & Sons, Inc. Published 2016 by John Wiley & Sons, Inc.

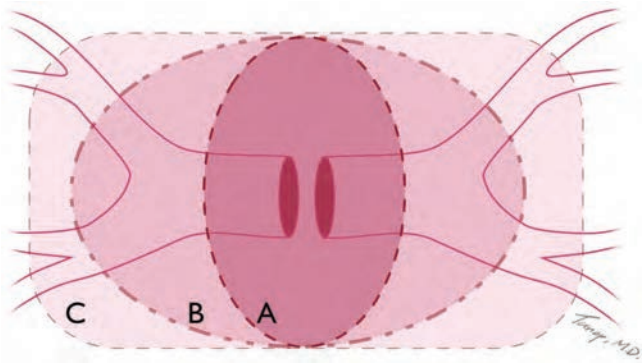

Figure 67.2 Modified drawing of three variant configurations of the atrial-venous junction. The pulmonary veins are the branching lines and the oval (A, B) and rectangular (C) shapes represent the left atrium. A normal pulmonary venous drainage pattern is demonstrated in image B, which has two ostia on each side. Under-incorporation and over-incorporation of the pulmonary veins into the left atrium are displayed in A and C, respectively. Adapted from Ghaye et al. (2003).

Underincorporation of the pulmonary venous system can entail either symmetrical or asymmetrical bilateral involvement, or can involve only one side. Underincorporation is responsible for a single ostium draining into the left atrium; this is more common on the left side. A rarer instance of underincorporation involves the persistence of the common pulmonary vein, resulting in a narrowing of the common cavity opening into the left atrium, the cor triatriatum sinister (Ghaye et al. 2003). This condition is also known as a triatrial heart and has an estimated incidence of 0.1% of all congenital cardiac malformations (Joe et al. 2003). In cor triatriatum sinister, the left atrium is divided by a membrane or fibromuscular septum into a superior-posterior chamber that receives the four pulmonary veins and an inferior-anterior chamber that connects to the left ventricle. These two chambers are connected through an opening that demonstrates various degrees of stenosis (Fig. 67.3).

Supernumerary or accessory pulmonary veins with independent ostia emptying into the left atrium are caused by overincorporation beyond the first branching division. This type of variation tends to occur on the right side.

There are many pulmonary venous drainage variation patterns. Marom et al. (2004) developed a system for classifying pulmonary venous anatomy on the basis of cross-sectional images, as shown in Figure 67.4. The categorization is based on both the drainage patterns of the pulmonary veins and the number of venous ostia on each side. Each pattern contains two or three alphanumeric characters. The first letter indicates the side of drainage (L: left; R: right), the number denotes the number of venous ostia, and the last letter specifies a particular variation of that pattern.

Most of the general population has two right pulmonary venous ostia: the right middle lobe vein drains into the right superior pulmonary vein in approximately 53–88% of cases and into the right inferior pulmonary vein in about 2–12%. Another variation on the right side is direct drainage of the right middle lobe vein into the left atrium with an independent ostium, resulting in three venous ostia; this has been reported in about 2–27% of the population (Fig. 67.5; Ghaye et al. 2003; Marom et al. 2004; Rajeshwari and Ranganath 2012; Wannasopha et al. 2012). Rare instances of more than three pulmonary venous ostia on the right side have been described in the literature. This is estimated to occur in approximately 0.5–4% of individuals (Fig. 67.6; Marom et al. 2004; Throning et al. 2011; Wannasopha et al. 2012).

The left pulmonary venous drainage pattern demonstrates less anatomical variability than the right. Most people (86–91%) have two left venous ostia for the upper and lower lobe veins, whereas a single left common trunk has been found in approximately 8–14% of the population (Marom et al. 2004; Throning et al. 2011). In contrast, Wannasopha et al. (2012) studied anatomical variations in the pulmonary venous drainage among Thai people and found a slightly higher percentage with a single left common trunk (59%) than with two left venous ostia (41%; Fig. 67.7). Supernumerary or accessory pulmonary veins are very rare on the left side; they were observed in approximately 0.5% in one series (Throning et al. 2011).

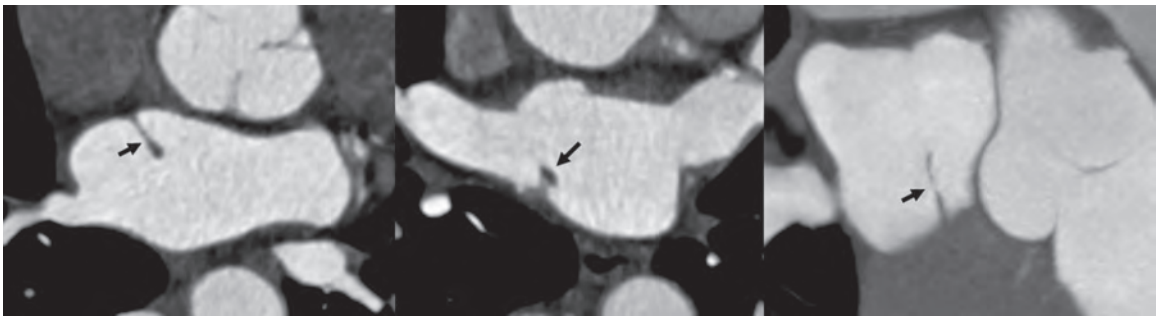

Figure 67.3 Contrast-enhanced axial MDCT scan and thick-slab coronal oblique MPR images of a 66-year-old man shows a thin incomplete membrane in the left atrium (arrow) which separates the left atrium into the proximal and distal chambers, representing cor triatriatum sinister.

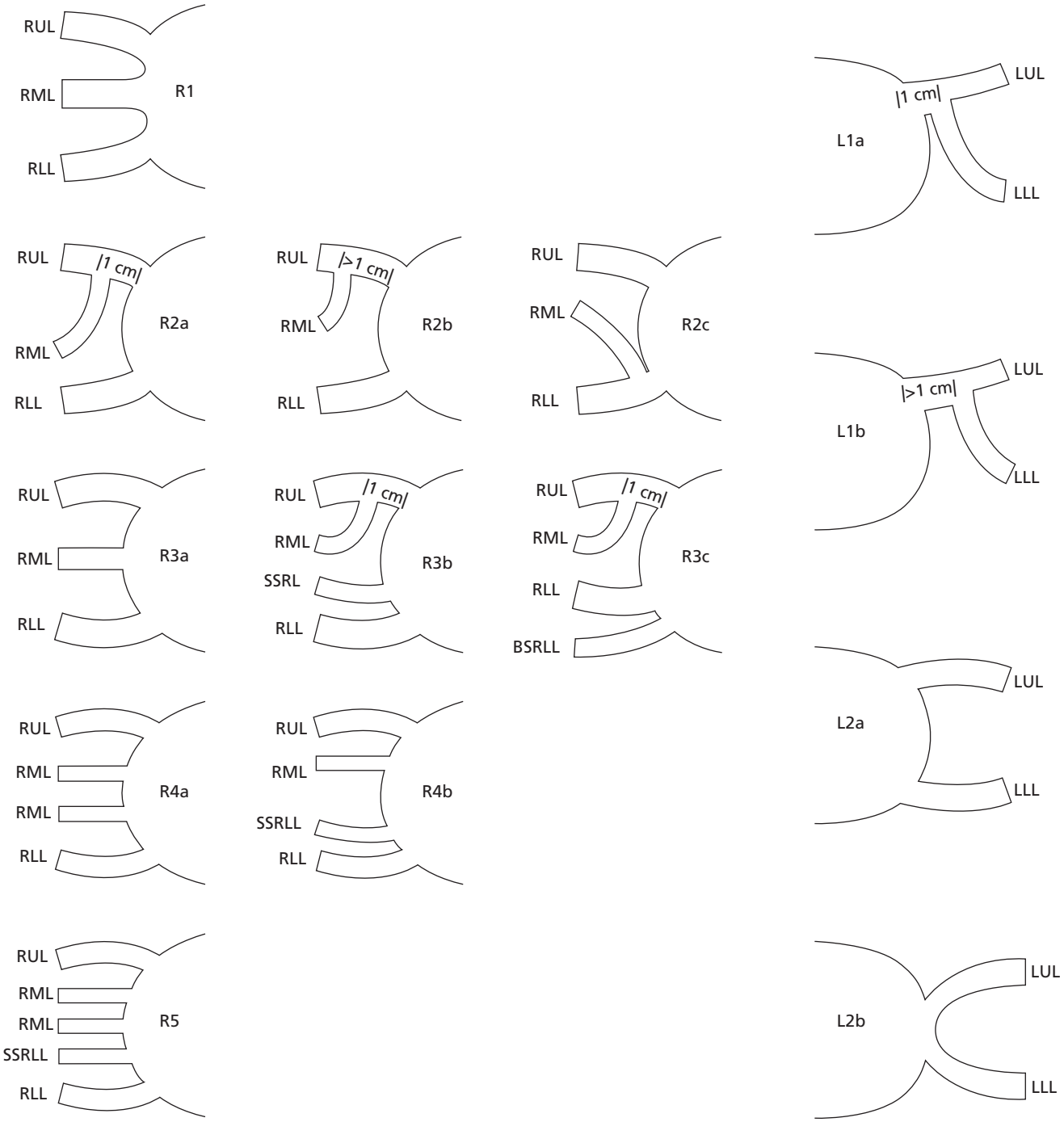

Figure 67.4 Modified drawing of pulmonary venous drainage classification pattern. RUL: right upper lobe; RML: right middle lobe; RLL: right lower lobe; LUL: left upper lobe; LLL: left lower lobe; SSRLL: superior segment right lower lobe; BSRLL: basilar segment right lower lobe. Distance from the ostium 1 cm. Adapted from Marom et al. (2004).

Other anatomical variants differing from Marom's classification have also been proposed. One of the most notable variants is the right top pulmonary vein, first described by von Haller (Arslan et al. 2008). This is a small vein arising from the left atrial roof adjacent to the right superior pulmonary vein and extending upward and posteriorly, passing behind the bronchus intermedius. It receives mainly from the posterior part of the right upper lobe but also drains a few subsegmental branches

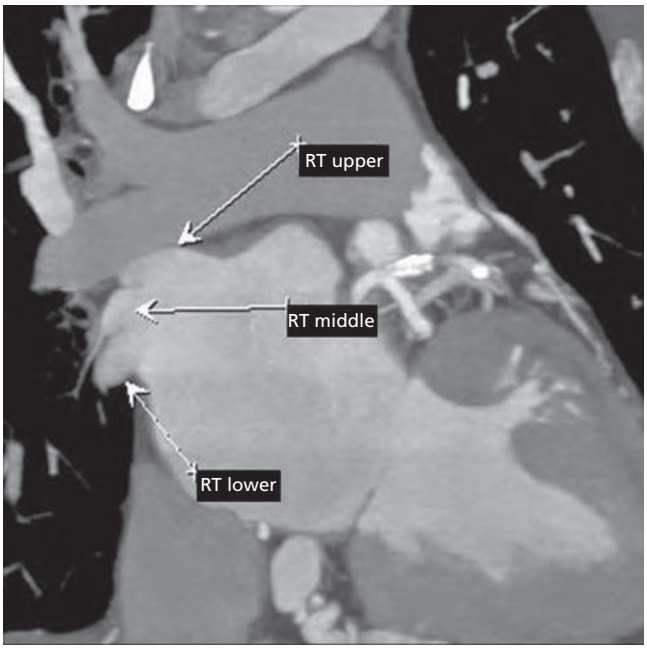

Figure 67.5 Thick-slab coronal oblique MPR image of a 72-year-old woman, showing three right atrial venous ostia for the upper, middle, and lower pulmonary veins.

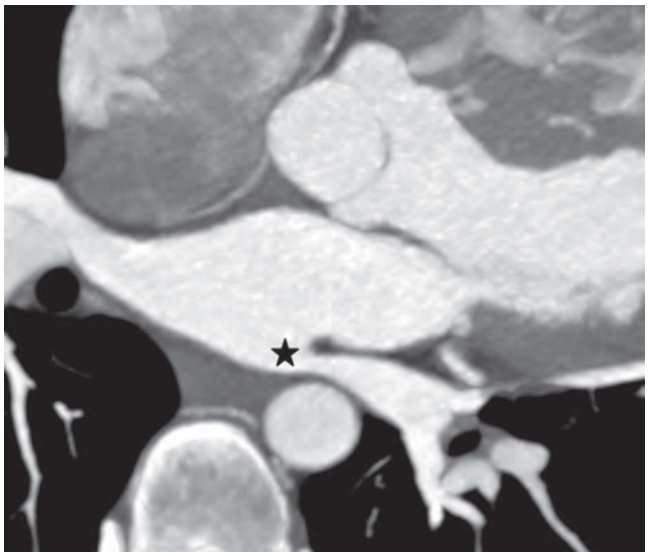

Figure 67.7 Contrast-enhanced axial MDCT scan image of a 60-year-old-man, showing a single left common pulmonary venous trunk draining the left lung to the left atrium via the solitary venous ostium (star).

of the superior segment of the right lower lobe (Fig. 67.8). The right top pulmonary vein is an infrequent anatomical variation, which has an incidence of 2.2–3.3% (Arslan et al. 2008).

Another pulmonary venous drainage variation incompatible with Marom's classification is an anomalous midline common ostium of the left and right inferior pulmonary veins. This variation has been reported in only a few cases. The features include single right and left superior pulmonary veins, but there is a large common ostium in the mid-posterior-inferior part of the left atrium, directly over the esophagus, draining both the right and left inferior pulmonary veins (Fig. 67.9).

Wannasopha et al. (2012) found other pulmonary venous variations that are incompatible with Marom's classification. One case has two right pulmonary ostia for the upper and lower lobe veins and two middle lobe veins; one branch joins the proximal upper lobe vein while the other joins the lower lobe vein (Fig. 67.10). The other case has four right pulmonary ostia for the upper, posterior segment of the upper lobe, superior segment of the lower lobe and lower lobe veins (Fig. 67.11; Wannasopha et al. 2012). Shepherd (1889) reported a right pulmonary vein that drained into the azygos vein.

Pulmonary veins are the principal source of ectopic atrial depolarization, usually initiating paroxysmal atrial fibrillation.

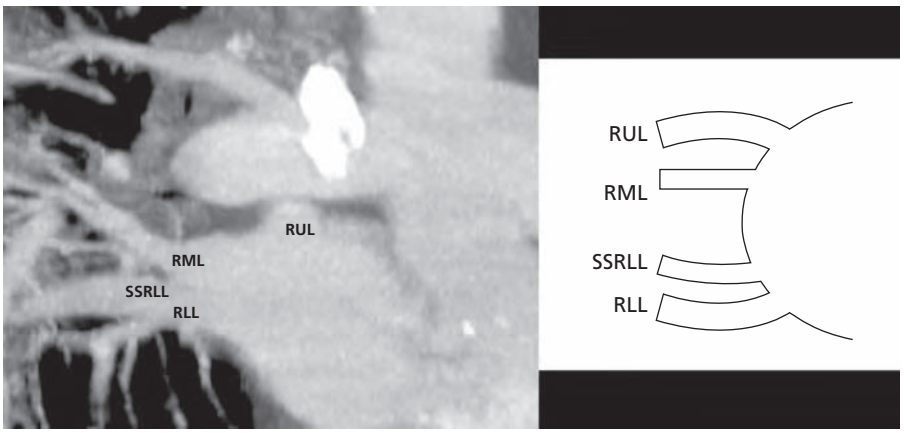

Figure 67.6 Thick-slab coronal oblique MPR image and diagram of a 78-year-old man, showing four atrial venous ostia for the right upper lobe (RUL), right middle lobe (RML), superior segment right lower lobe (SSRLL), and right lower lobe pulmonary veins.

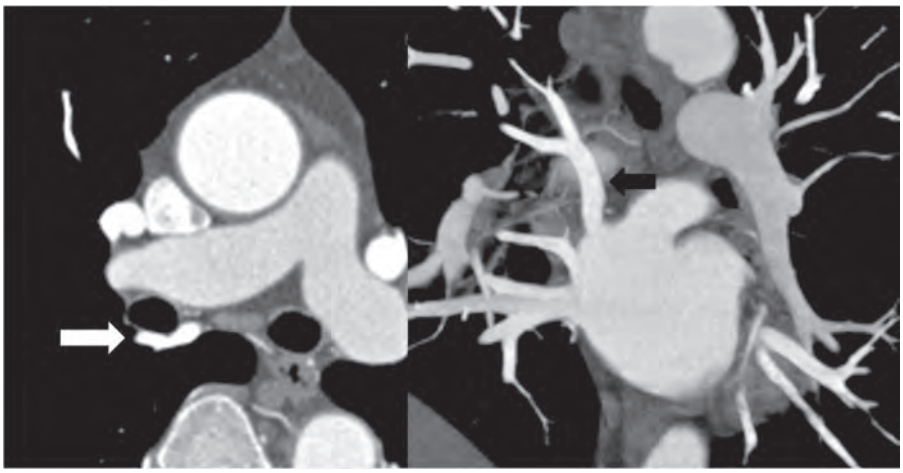

Figure 67.8 Contrast-enhanced axial MDCT scan and coronal view images of a 48-year-old woman, showing a right top pulmonary vein passing behind the intermediate bronchus and draining into the left atrial roof (arrow).

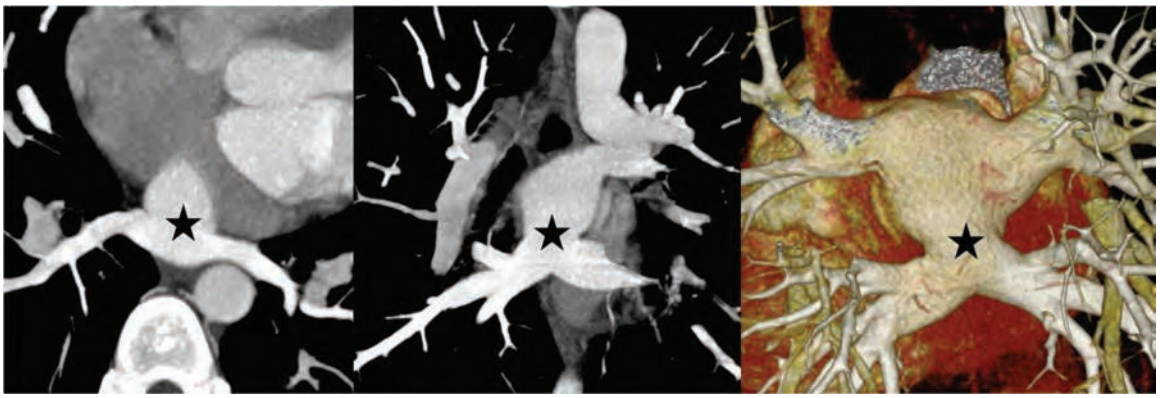

Figure 67.9 Contrast-enhanced axial MDCT scan, thick-slab coronal MPR and 3DVR images of a 19-year-old man, showing that bilateral inferior pulmonary veins connect to the left atrium by a large common ostium located mid posterior-inferior to the left atrium (star), compatible with anomalous midline common ostium of the left and right inferior pulmonary veins.

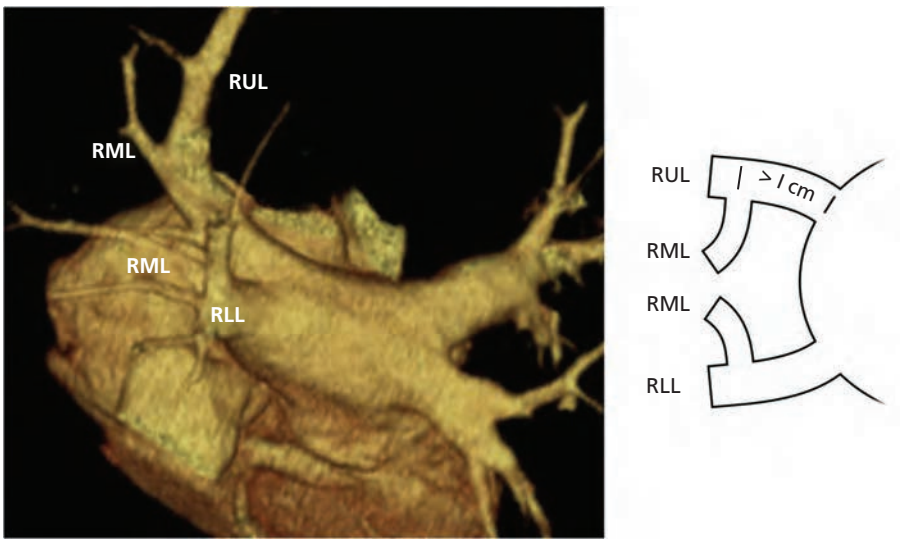

Figure 67.10 3DVR image and diagram of a 56-year-old woman, showing two right pulmonary venous ostia for the upper (RUL) and lower lobe (RLL) veins. One middle lobe vein joins the proximal upper lobe vein and another one joins the lower lobe vein.

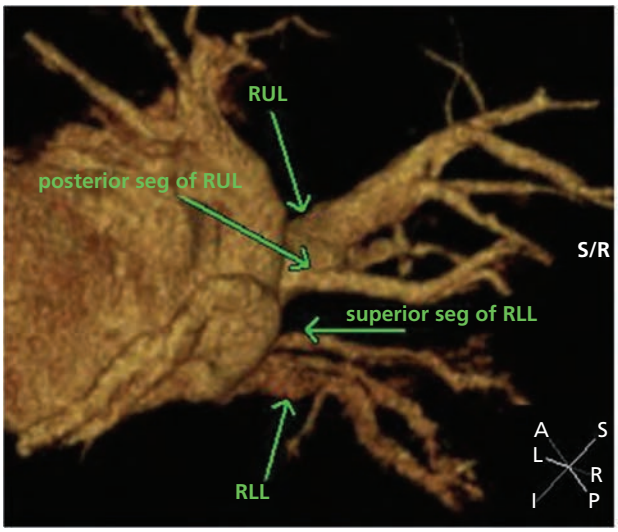

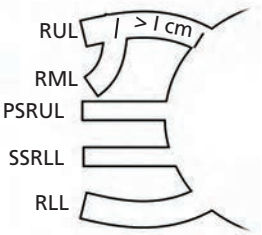

Figure 67.11 3DVR image and diagram of a 63-year-old man, showing four right pulmonary venous ostia for the upper (RUL), posterior segment right upper lobe (PSRUL), superior segment right lower lobe (SSRLL), and lower lobe (RLL) veins.

Selective radiofrequency catheter ablation of these arrythmogenic triggers has emerged as a realistic treatment strategy for patients with refractory atrial fibrillation (Marom et al. 2004; Throning et al. 2011). Variability in pulmonary venous anatomy could considerably alter the success rates of radiofrequency ablation. Knowledge of pulmonary venous drainage variations and the relationships between the pulmonary veins and the left atrium is essential for guidance during ablation procedures, and also for facilitating safe catheter ablation to isolate a pulmonary vein. Moreover, information about pulmonary venous variations can prevent misinterpretation of pulmonary venous angiographic findings and preclude perioperative bleeding in video-assisted thoracoscopic surgery (VATS).

References

Agarwal PP, Seely JM, Matzinger FR. 2004. MDCT of anomalous unilateral single pulmonary vein. *Am J Roentgenol* 183: 1241–1243.

Anderson RH, Brown NA, Moorman AFM. 2006. Development and structures of the venous pole of the heart. *Dev Dynam* 235: 2–9.

Arslan G, Dincer E, Kabaalioglu A, Ozkaynak C. 2008. Right top pulmonary vein: Evaluation with 64 section multidetector computed tomography. *Eur J Radiol* 67: 300–303.

Dillman JR, Yarram SG, Hernandez RJ. 2009. Imaging of pulmonary venous developmental anomalies. *Am J Roentgenol* 192: 1272–1285.

Ghaye B, Szapiro D, Dacher JN, Rodriguez LM, Timmermans C, Devillers D, Dondelinger RF. 2003. Percutaneous ablation for atrial fibrillation: The role of cross-sectional imaging. *Radiographics* 23: 19–33.

Joe BN, Poustchi-Amin M, Woodard PK. 2003. Case 56: Cor triatriatum dexter. *Radiology* 226: 701–705.

Marom EM, Herndon JE, Kim YH, McAdams HP. 2004. Variations in pulmonary venous drainage to the left atrium: Implications for radiofrequency ablation. *Radiology* 230: 824–829.

Rajeshwari MS, Ranganath P. 2012. Variations in draining of right pulmonary veins at the hilum and an anatomical classification. *ISRN Pulmonology* 2012: 1–4.

Shepherd FJ. 1889. Some vascular anomalies observed during the session 1888-89. *J Anat Physiol* 24: 69–71.

Standring S. 2008. *Gray's Anatomy: The Anatomy Basis of Clinical Practice*, 40th edition. Edinburgh: Churchill Livingstone.

Throning C, Hamady M, Liaw JVP, Juli C, Lim PB, Dhawan R, Peters NS, Davies DW, Kanagaratnam P, O'Neill MD, Wright AR. 2011. CT evaluation of pulmonary venojus variation in patients undergoing catheter ablation for atrial fibrillation. *Clin Imag* 35: 1–9.

Wannasopha Y, Oilmungmool N, Euathrongchit J. 2012. Anatomical variations of pulmonary venous drainage in Thai people: Multidetector CT study. *Biomed Imaging Interv J* 8: 4.

68 Inferior vena cava, portal and hepatic venous systems

Jonathan D. Spratt
University Hospital of North Durham, Durham, United Kingdom

Inferior vena cava

Introduction

Due to advances in non-invasive vascular imaging, anatomic variants and anomalies of the inferior vena cava (IVC) have become more commonly recognized in routine practice. Congenital anomalies of the IVC and its tributaries occur in roughly 4% of the population and have been known to anatomists since 1793, when Abernethy described a congenital mesocaval shunt and azygos continuation of the IVC in a 10-month-old infant with polysplenia and dextrocardia.

Anomalies of the IVC have been described more frequently (0.6–2%) in those with other cardiovascular defects, and less frequently in otherwise healthy individuals (Anderson et al. 1961). Their embryological basis is incompletely understood with the aetiology of infrarenal interrupted IVC being particularly controversial, thought most likely to be the result of perinatal IVC thrombosis.

Clinical application

Familiarity with these variations will prevent personal litigation from such a wide spectrum of clinical scenarios, from avoidance of erroneous radiodiagnosis of retroperitoneal mass, or lymphadenopathy causing over-staging of malignancy, to enabling pre-interventional identification that could prevent morbidity for the aortic and renal surgeon and vascular radiologist. Familiarity could provide explanation for recurrent pulmonary embolus (PE) post-IVC filter placement, prevent surprises during multivisceral recovery surgery on deceased donors (where preoperative cross-sectional imaging is usually not available), enable the prescription of the most appropriate investigation to elucidate the cause of deep vein thrombosis (DVT) and PE in younger adults, particularly active males, and elucidate the cause of symptomatic pelvic varicosities in younger women and otherwise unexplained haematochezia in young adults. The association with renal atrophy/agenesis and congenital cardiac disease is self-evident.

Embryogenesis

The embryogenesis of the IVC is a complex process involving the formation of several anastomoses between three paired embryonic veins with numerous variations in the basic venous plan. Our limited understanding mainly derives from developmental study in the domestic cat (Huntington and McLure 1920). A classification system for IVC anomalies was based on abnormal regression or abnormal persistence of various embryonic veins, and up to 14 theoretical variations in the anatomy of the infrarenal IVC were suggested with 11 of the 14 variants previously observed in the domestic cat or in humans.

The IVC is composed of four segments, namely hepatic, suprarenal, renal, and infrarenal. The hepatic segment is derived from the vitelline vein. The right subcardinal vein develops into the suprarenal segment by formation of the subcardinal-hepatic anastomosis. The renal segment develops from the right supra-subcardinal and postsubcardinal anastomoses. It is controversially accepted that the infrarenal segment derives from the right supracardinal vein. In the abdomen, the postcardinal veins are progressively replaced by the subcardinal and supracardinal veins but persist in the pelvis as the common iliac veins.

Left IVC

A left IVC results from regression of the right supracardinal vein with persistence of the left supracardinal vein; prevalence is 0.2–0.5% (Phillips 1969). Typically, the left IVC joins the left renal vein which crosses anterior to the aorta in the normal fashion, uniting with the right renal vein to form a normal right-sided prerenal IVC (Fig. 68.1). The major clinical significance of this anomaly is the potential for misdiagnosis as left-sided paraaortic adenopathy (Siegfried et al. 1983). In addition, spontaneous rupture of an abdominal aortic aneurysm into a left IVC has been reported (Davachi 1965). Transjugular access to the infrarenal IVC for placement of an IVC filter may be difficult.

When part of a visceral transposition (in 0.2–0.5%), the IVC may lie on the left side of the aorta. It may also lie to the left of the aorta without visceral transposition, crossing to the right

Bergman's Comprehensive Encyclopedia of Human Anatomic Variation, First Edition. Edited by R. Shane Tubbs, Mohammadali M. Shoja and Marios Loukas.
© 2016 John Wiley & Sons, Inc. Published 2016 by John Wiley & Sons, Inc.

Figure 68.1 Coronal CT double IVC complex with no interruption of suprahepatic portion.

beneath the diaphragm to gain the caval opening or, alternatively, crosses over after receiving the left renal vein.

Compression of a left IVC may be a rare cause of the "nutcracker syndrome," left renal venous hypertension and hematuria. Just as in the more common cause from left renal vein compression, superior mesenteric artery transposition and division of the fibrous bundle at its origin may be curative (Yang et al. 2012).

Double IVC

Several variants of duplicated IVC exist; the most common of which is two distinct IVCs that arise from each iliac vein without a normal confluence. Duplication of the IVC results from persistence of both supracardinal veins; prevalence is 0.2–3% (Phillips 1969). The left IVC typically ends at the left renal vein, which crosses anterior to the aorta in the normal fashion to join the right IVC (Fig. 68.1). This may be associated with retroaortic right renal vein, hemiazygos continuation of the IVC, significant asymmetry in the sizes of the left and right veins, and a communication between the right and left IVC in the position of the normal left common iliac vein.

Double IVC should be suspected in cases of recurrent pulmonary embolism following placement of an IVC filter (Phillips 1969). As with left IVC, misdiagnosis of the aberrant vessel as lymphadenopathy should be avoided.

The embryologic basis of double IVC with retroaortic right renal vein and hemiazygos continuation of the IVC is persistence of the left lumbar and thoracic supracardinal vein and the left suprasubcardinal anastomosis, together with failure of formation of the right subcardinal-hepatic anastomosis. In addition, the right renal vein and right IVC meet and cross posterior to the aorta to join the left IVC and continue cephalad as the hemiazygos vein (Fig. 68.1). There is therefore also persistence of the dorsal limb of the renal collar and regression of the ventral limb. In the thorax, the hemiazygos vein crosses posterior to the aorta at approximately T8 or T9 to join the rudimentary azygos vein. Alternate collateral pathways for the hemiazygos vein include: (1) cephalad continuation to join the coronary vein of the heart via a persistent left SVC; and (2) accessory hemiazygos continuation to the left brachiocephalic vein (Haswell and Berrigan 1976).

In both of these alternate pathways, the aberrant vessel may simulate a left mediastinal mass (Haswell and Berrigan 1976). In addition, with accessory hemiazygos continuation, the aberrant vessel may mimic an aortic dissection (Cohen et al. 1984). More importantly, perioperative death following inadvertent ligation of hemiazygos-to-azygos continuation of a left IVC during thoracic surgery has been reported (Effler et al. 1951).

As discussed below in the section on "Azygos continuation of the IVC," when the subcardinal-hepatic anastomosis fails to form, the hepatic segment of the IVC ordinarily drains independently directly into the right atrium. However, there has been one case report of a patient with Budd–Chiari syndrome in whom the bulk of systemic venous drainage from the liver was via the right renal vein to a hemiazygos continuation of a left IVC (Sakamoto et al. 1997). With cross-sectional imaging, misdiagnosis of vessels as masses may be less likely due to the presence of MRI flow voids or flow-related contrast CT enhancement in the aberrant venous structures.

A double IVC with continuous suprahepatic IVC and preaortic left renal vein is shown on multiplanar CT (Figs 68.1–68.7). The IVCs are noted to be continuous with their respective common iliac veins. Another variant complex is a double IVC with a retroaortic left renal vein and azygos continuation of the IVC. This results from persistence of the left supracardinal vein and the dorsal limb of the renal collar with regression of the ventral limb and failure of formation of the subcardinal-hepatic anastomosis. It has been demonstrated that azygos continuation of the IVC can be predicted with ultrasonography by identifying the right renal artery crossing abnormally anterior to the IVC (Geley et al. 1999).

Azygos continuation of the IVC

Azygos continuation of the IVC has also been termed absence of the hepatic segment of the IVC with azygos continuation (Ginaldi et al. 1980); prevalence is 0.6%. The embryonic event is theorized to be failure to form the right subcardinal-hepatic anastomosis, with resulting atrophy of the right subcardinal vein. Consequently, blood is shunted from the suprasubcardinal anastomosis through the retrocrural azygos vein, which is partially derived from the thoracic segment of the right supracardinal vein. The renal portion of the IVC receives blood return from both kidneys and passes posterior to the diaphragmatic

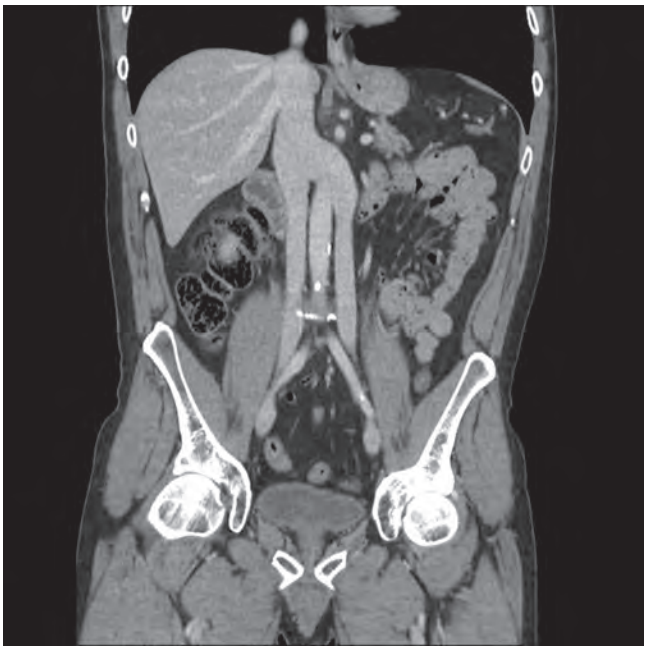

Figure 68.2 Coronal CT double IVC complex with no interruption of suprahepatic portion.

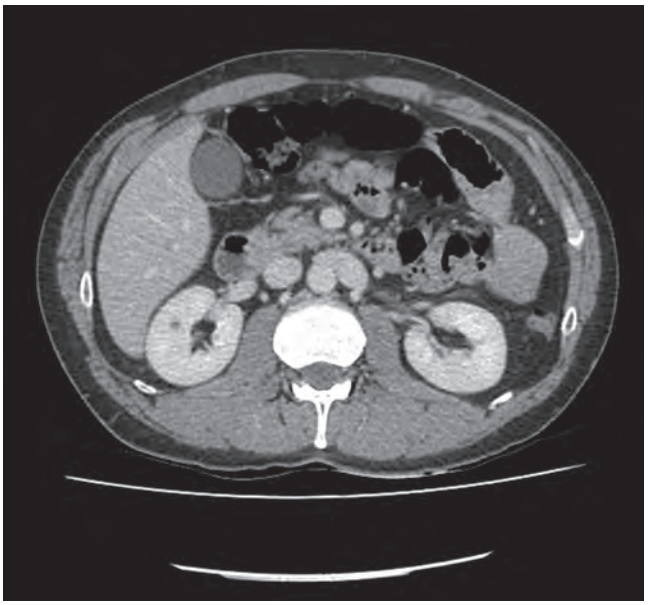

Figure 68.4 Axial CT of renal venous connections of double IVC complex.

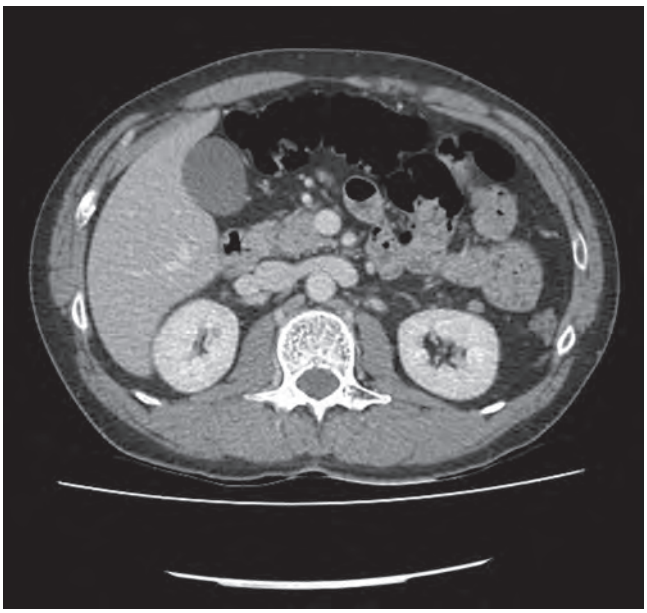

Figure 68.3 Axial CT of renal venous connections of double IVC complex.

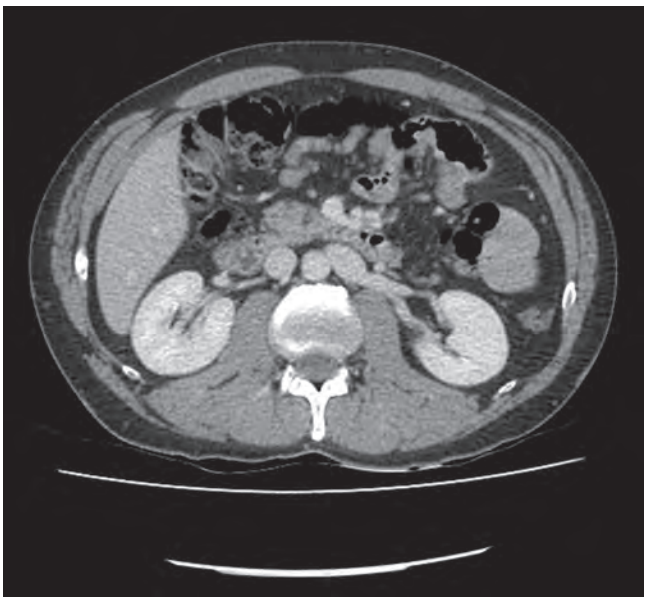

Figure 68.5 Axial CT of renal venous connections of double IVC complex.

crura to enter the thorax as the much-enlarged azygos vein (see Chapter 65) which joins the SVC at the normal location. The hepatic segment (often termed the posthepatic segment) is ordinarily not truly absent; rather, it drains directly into the right atrium. Since the postsubcardinal anastomosis does not contribute to formation of the IVC, each gonadal vein drains to the ipsilateral renal vein (Huntington and McLure 1920).

Formerly thought to be predominantly associated with severe congenital heart disease and asplenia or polysplenia syndromes, azygos continuation of the IVC has become increasingly recognized in otherwise asymptomatic patients since the advent of cross-sectional imaging (Schultz et al. 1984) and ultrasound (Mihmanli et al. 2001). Situs inversus with interrupted IVC without splenic syndrome has also been described as an

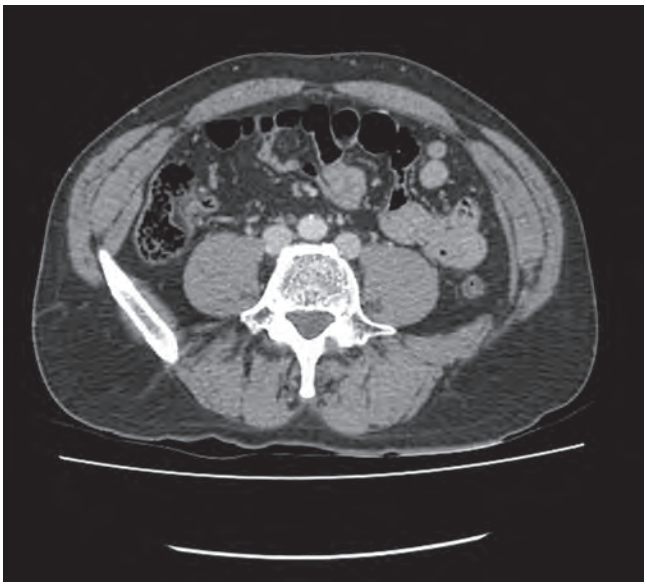

Figure 68.6 Axial CT of common iliac vein continuation into respective IVC.

uncommon cadaveric anatomic variant (Loukas et al. 2009). An interrupted IVC and a left-sided subrenal (postrenal) IVC with azygos or hemiazygos continuation are very rare anomalies (Vijayaraghavan et al. 2003).

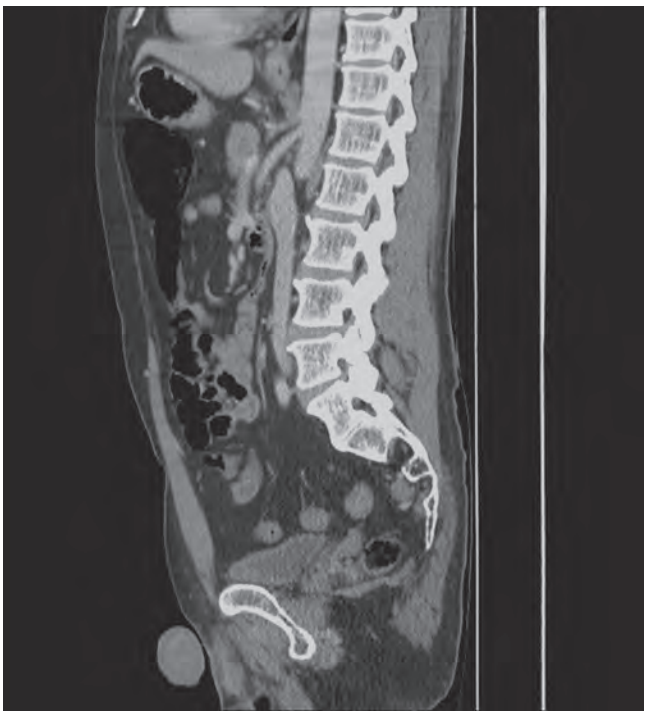

Figure 68.7 Left parasagittal CT demonstrating left IVC in continuity with left common iliac vein.

It is important to recognize the enlarged azygos vein at the confluence with the SVC and in the retrocrural space to avoid misdiagnosis as a right-sided paratracheal mass or retrocrural adenopathy. Preoperative knowledge of the anatomy may be important in planning cardiopulmonary bypass and to avoid difficulties in catheterizing the heart (Mazzucco et al. 1990).

Rare symmetrical drainage pattern

An atypical variant of duplicated IVC has recently been reported in a multi-trauma patient where the right and left iliac veins shared a normal confluence, but two IVCs drained independently into renal veins before reuniting into a single structure (Pineda et al. 2013). Most unusually, filters could be placed into both IVCs via a single puncture in the groin.

Partial or total absence of the IVC

The absence of the IVC is one among infrequent subtypes of IVC abnormalities that are rarely seen in general population, involving either that of entire IVC or that of its infrarenal segment. These two entities are relatively similar but their etiopathogeneses are still controversial. The absence of the entire IVC is thought to be a result of an embryologic disorder, whereas perinatal thrombosis is hypothesized to lead to the development of absent infrarenal IVC; the latter is therefore a developmental disorder. With absence of the IVC, as in pathological obstruction, venous blood from the inferior part of the body returns through four major pathways: deep (e.g., paraspinal-extravertebral and retroperitoneal); intermediate (e.g., left gonadal vein to the left renal vein); superficial (abdominal wall collaterals); and portal (e.g., the internal iliac vein to the hemorrhoidal plexus through the inferior mesenteric vein).

Several reports have described the absence of the entire IVC (Milner and Marchan 1980; Debing et al. 1993; Dougherty et al. 1996) or absence of the infrarenal IVC with preservation of the suprarenal segment (d'Archambeau et al. 1990; Bass et al. 1999).

Absence of the entire posthepatic IVC suggests that all three paired venous systems failed to develop properly. Absence of the infrarenal IVC implies failure of development of the posterior cardinal and supracardinal veins. Since it is difficult to identify a single embryonic event that can lead to either of these scenarios, there is controversy as to whether these conditions are true embryonic anomalies or the result of perinatal IVC thrombosis (Milner and Marchan 1980; d'Archambeau et al. 1990; Bass et al. 1999). The common iliac veins may be absent (Bass et al. 2000). The external and internal iliac veins join to form enlarged ascending lumbar veins, which convey blood return from the lower extremities to the azygos and hemiazygos veins via anterior paravertebral collateral veins. A normal suprarenal IVC is formed by confluence of the renal veins.

Patients with absent IVC may present with symptoms of lower-extremity venous insufficiency or idiopathic DVT (Chee et al. 2001; Ruggeri et al. 2001) and the collateral circulation may simulate a paraspinal mass (Milner and Marchan 1980). A congenitally or acquired absent IVC is associated with long-term

venous disease. Approximately 5% of individuals younger than 30 years with idiopathic DVT show IVC absence on CT. Almost 10% of such patients with a coexisting thrombophilia have congenital absence of the IVC.

Idiopathic DVT in a relatively young person with a past history of chronic leg ulceration or varicose veins should be investigated by MR scan of the abdomen (or CT scan if MR is contraindicated or not tolerated). Collateral veins in the abdominal wall may be patent or partially thrombosed on ultrasound if there is concomitant iliofemoral vein thrombosis. There is a male predilection for IVC agenesis, revealed by proximal DVT following major physical exertion (Lambert et al. 2010) and has been diagnosed at up to 54 years of age (Iqbal and Nagaraju 2008).

IVC absence in patients with DVT is underdiagnosed because of the limitation of ultrasonographic technique for reliable visualization of the retroperitoneum due to the combined effect of bowel gas interposition and poor beam penetration from patient habitus, as well as lack of awareness by the typical sonographer. Knowledge of the association of other anomalies in those with an absent IVC such as renal atrophy or agenesis is crucial, and can themselves be of significant clinical importance (Iqbal and Nagaraju 2008).

Other presentations may include chronic pelvic pain caused by parauterine and paraovarian pelvic varicosities (Wax et al. 2007) and haematochezia from perirectal haemorrhoidal-portal collateral veins (Koc et al. 2007).

It is important to note that an absent infrarenal IVC may be acquired as well as congenital, attributable to thrombosis and fibrosis after central venous and cardiac catheterizations during infancy (Tharumenthiran et al. 2001).

Infrarenal IVC and common iliac vein absence has been reported clinically presenting with extensive varicose collateral circulation on the thoracoabdominal wall, right varicocele, and severe varices on lower limbs; calcifications of adrenal glands indicated a hematologic disorder during perinatal period (Alicioglu et al. 2009).

IVC tributary variation

The IVC may receive the left spermatic vein, and rarely receives a left accessory renal vein that passes behind the aorta which may in turn receive the usual tributaries of the left renal vein. Up to seven accessory renal veins may be received on each side. The lumbar veins may enter the IVC on one or both sides as a common trunk. Note that any venous channel returning blood through the aortic hiatus of the diaphragm is referred to as a "persistent posterior cardinal vein."

Intrahepatic IVC course variation

Usually the IVC courses through the liver posteriorly and drains into the right atrium. An extremely rare case of the anterior intrahepatic course of the IVC has been described on a CT scan of a healthy 26-year-old female. The anterior intrahepatic segment was bridged to the posteroinferior portion of the IVC by an oblique segment. Associated renal and arterial anomalies were also observed (Abdullah et al. 2011).

Portal and hepatic veins

Introduction

Knowledge of the anatomic variants of the portal and hepatic veins is of prime importance for precise lesion localization, insertion of a transjugular intrahepatic portosystemic shunt (TIPS), and in planning liver transplantation, where it is essential for preoperative work-up and postoperative follow-up of the recipient as well as for assessment of potential donors.

Transhepatic portal vein embolization is gaining acceptance as a method to induce contralateral liver hypertrophy in patients with small future remnant livers. To perform embolization safely and efficaciously, the interventional radiologist must have an understanding of variant anatomy. Embolizing a nontargeted sector or segment in this patient population can make potentially resectable anatomy unresectable.

Ultrasound has been the method of choice for many years in delineating these variants, but the latest generation of cross-sectional scanners has highlighted the weakness in sonographic detection of intrasegmental vessels (portal branches, arterial branches, accessory hepatic veins) and there is now a strong case for the routine performance of 3D CT and MR angiography on every patient in anticipation of hepatobiliary surgery or intervention.

Portal vein

The portal vein often receives the left gastric vein and may also receive accessory splenic vein, inferior phrenic, pancreaticoduodenal, pulmonary, or right gastroepiploic veins.

The main portal vein is among the most constant of all blood vessels, only reported absent twice (Altavilla and Cusatelli 1998), rarely doubled and very rarely lying anterior in the portal triad (Marks 1969). A prepancreatic portal vein is frequently associated with situs inversus and other congenital malformations (Parisato and Pataro 1965).

In congenital agenesis of the right hepatic lobe, the right portal vein, right hepatic duct, and right hepatic vein are not identified (Radin et al. 1987; Chou et al. 1998). A retrohepatic gallbladder, posterolateral interposition of the right colic flexure, and superior migration of the right kidney are shared features of both congenital agenesis and severe atrophy of the right lobe. Agenesis of the left hepatic lobe is indicated by absence of hepatic parenchyma to the left of the gallbladder fossa and absence of a recognizable ligamentum teres and left portal vein (Belton and VanZandt 1988).

The presence of a rudimentary left portal vein favors the diagnosis of atrophy of the left hepatic lobe. Common features of both agenesis and atrophy of the left lobe are a superior location of the gallbladder just beneath the diaphragm, an abnormal U-shaped configuration of the stomach, and an abnormally

high duodenal bulb on images from an upper gastrointestinal series (Yamamoto et al. 1988; Kakitsubata et al. 1991).

Branching pattern

Variant portal vein branching anatomy is nearly as common as variant hepatic artery anatomy. The complexity of hepatic interventions now performed by interventional radiologists and surgeons, including portal vein embolization, anatomic resection, and transplantation, make recognition and understanding of normal and variant portal vein anatomy increasingly important (Covey et al. 2004).

Reported since 1957, variants of intrahepatic portal venous branching are now recognized to occur in increasing frequency at approximately 20% in series from the 1990s (Fraser-Hill et al. 1990; Atri et al. 1992; Couinaud 1999) and up to 35% in a more recent large CT series (Covey et al. 2004). The most common patterns include trifurcation of the main portal vein (7.8–10.8%), right posterior segmental branch arising from the main portal vein (4.7–5.8%), and right anterior segmental branch arising from the left portal vein (2.9–4.3%) (Fraser-Hill et al. 1990; Atri et al. 1992; Chevallier et al. 2000).

An absence of branching has been reported in which a single portal vein enters the right liver and courses into the left, giving only segmental branches along its course. Absence of branching of the portal vein is the most frequently reported congenital anomaly and should be differentiated from acquired atrophy of the hepatic lobes (Radin et al. 1987; Belton and VanZandt 1988; Yamamoto et al. 1988; Kakitsubata et al. 1991; Ozgun and Warshauer 1992; Chou et al. 1998). This is thought to be secondary to failure of the right and left portal veins to develop (Radin et al. 1987) or a congenital agenesis from thrombosis of the affected lobe or segment during embryologic growth (Ozgun and Warshauer 1992).

A spectrum of branching variants of the portal vein associated with malposition of the gallbladder has been described (Maetani et al. 1998; McNulty and Khosa 1999). Findings comprise an abnormal course of the horizontal portion of the left portal vein and an abnormal umbilical portion that is located above the gallbladder fossa. The gallbladder is deviated to the left and may lie to the left of or astride the ligamentum teres. The Cantlie line does not serve as a boundary between the right and left lobes in these cases (Fig. 68.8). The theory proposed to explain these findings is abnormal regression of the left umbilical vein with persistence of the right umbilical vein. The persistent right umbilical vein would form a right umbilical portion of the left portal vein. Since a whole spectrum of this variant has been reported (Maetani et al. 1998; McNulty and Khosa 1999), it has as yet to be established whether all anomalous umbilical portions originate from a right umbilical vein.

In a more contemporary retrospective review of 200 patients who underwent preoperative hepatic CT portography (Covey et al. 2004), 35% had variant portal vein anatomy, which is significantly greater than the 10–15% described in earlier published sonography literature described above. A total of 22% of patients had either trifurcation (type 2, Fig. 68.9) or Z (type 3) anatomy. Fourteen patients (7%) had a single posterior segment branch (types 4 and 5) arising as the first branch of the right portal vein. Other variants were seen in 6%. Those of the left

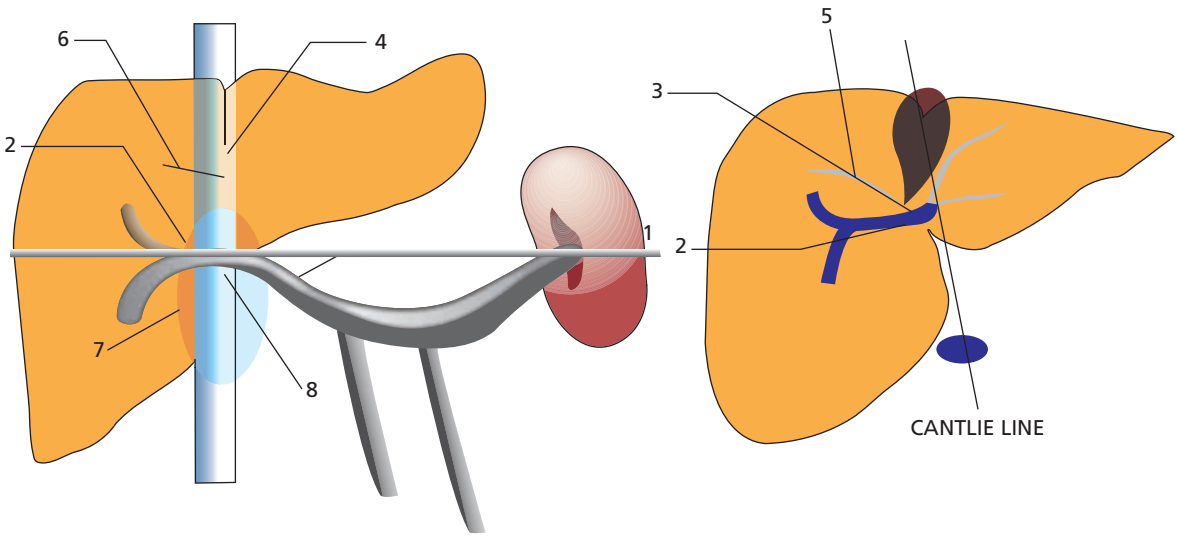

Figure 68.8 Portal vein anomaly associated with malposition of the gallbladder. Coronal (left) and axial (right) diagrams show that the first branch to split off is the right posterior portal vein. The main portal vein (1) then courses superiorly, giving off the right anterior portal vein and a small, ascending umbilical portion of the left portal vein (4). The gallbladder (7) is located astride the umbilical ligament and does not serve as a boundary between the right and left lobes. 2, right portal vein; 3, horizontal portion of the left portal vein; 5, branch to segment IV; 6, lig teres.

Source: Gallego et al. (2002).

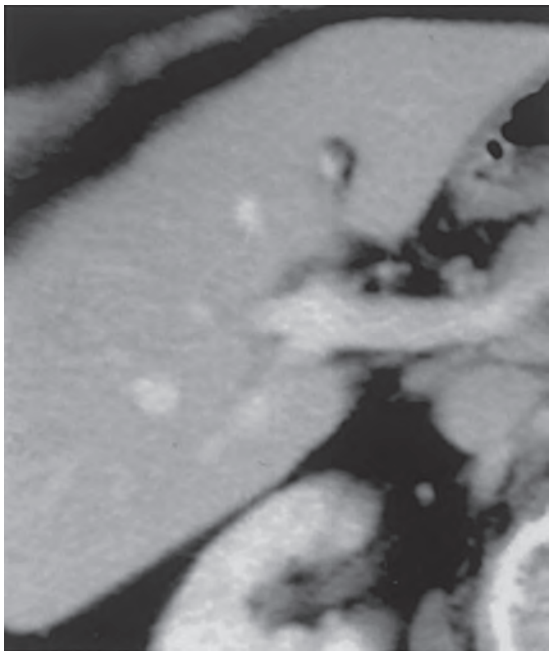

Figure 68.9 Main portal vein trifurcation (type 2) shown with contrast-enhanced axial CT scan.

Source: Gallego et al. (2002).

portal vein were rare: in only one patient did the segment-4 portal vein arise anomalously from the right anterior portal vein. None of the 200 patients in this study had congenital duplication or absence of the portal vein.

These findings are consistent with previous studies. A series of 24 patients who underwent MR angiography, conventional portal vein anatomy was detected in 76% (Carr et al. 2003). Four patients (16%) had trifurcation and an additional two (8%) had Z-type anatomy (type 3).

In a previous series where 200 patients underwent conventional arterioportography, 65% had standard portal vein anatomy; 7% of patients were determined to be unsuitable candidates, or to potentially require a more technically challenging surgery such as a venous graft because of variant portal vein anatomy (Cheng et al. 1997).

Formation of portal vein

Branches forming the portal vein are variable (Figs 68.10, 68.11), and accessory splenic veins have been reported. The splenic vein may anastomose with the renal or with the superior mesenteric vein. The superior mesenteric vein has been reported opening into the renal vein.

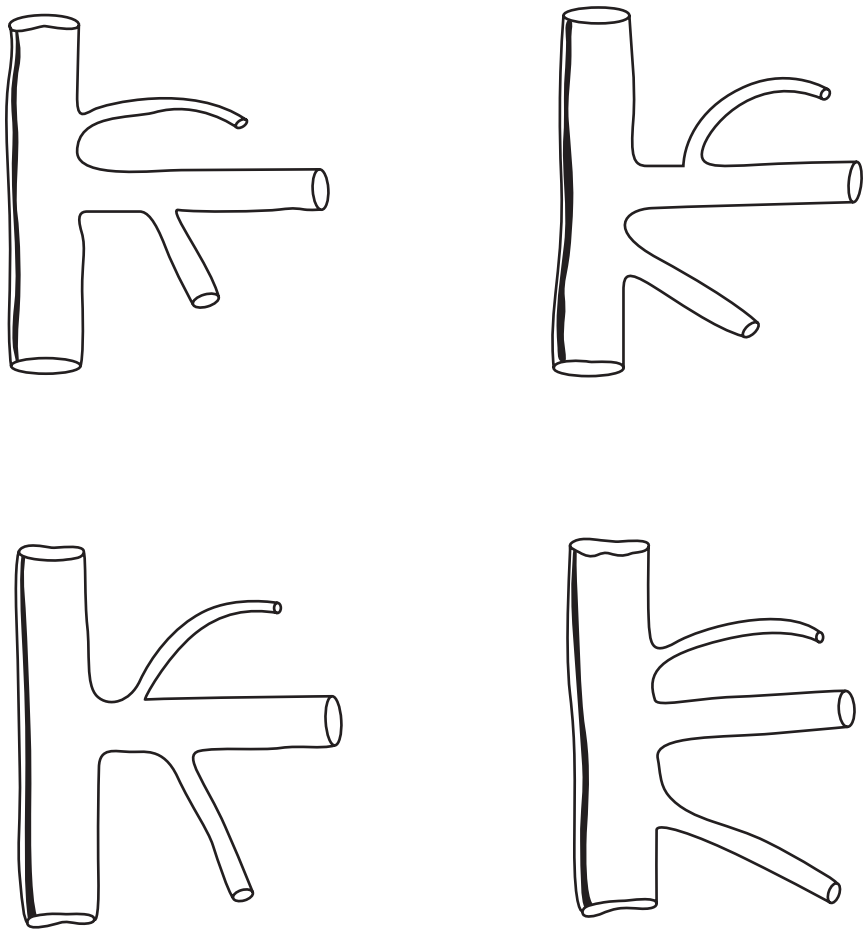

Figure 68.10 Upper left (Fig. 1): the usual arrangement; the inferior mesenteric enters the splenic vein, while the left gastric enters the portal vein. Upper right (Fig. 2): in this case, the left gastric enters the splenic vein while the inferior mesenteric enters the portal vein. Lower left (Fig. 3): the left gastric and the inferior mesenteric both join the portal vein. Lower right (Fig. 4): the left gastric, splenic, and inferior mesenteric enter the portal vein directly.

Source: Thompson (1890).

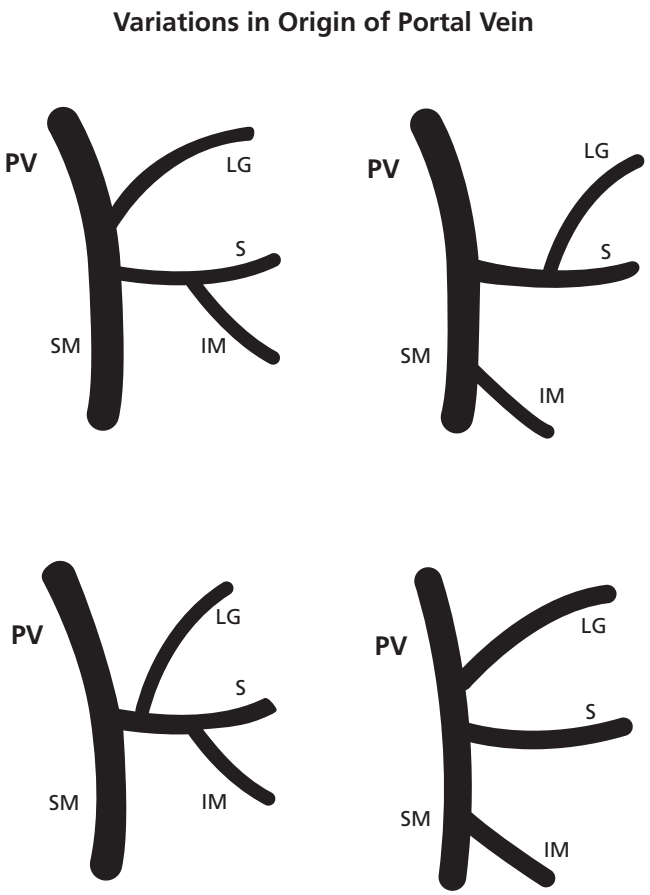

Figure 68.11 Variations in origin of the portal vein. PV: portal vein; IM: inferior mesenteric; LG: left gastric; S: splenic; SM: superior mesenteric.

Source: D'Alessandro and Bergman (www.anatomyatlases.org).

Clinical application

Some of these variants are subtle and may be easily overlooked with important clinical consequences. If the segment 6 or 7 portal vein arises alone as the first branch of the main portal vein (types 4 and 5), a left trisegmentectomy may inadvertently leave a single viable liver segment as the entire remnant liver, potentially resulting in liver failure and death.

Failure to recognize a Z-type portal vein variant (type 3) during a left liver resection, or when harvesting a living donor liver transplant, may result in loss of perfusion to the right anterior sector and may lead to necrosis of more than 80% of the liver (Maetani et al. 1998; McNulty and Khosa 1999).

Trifurcation of the portal vein (type 2) may require two separate anastomoses when the right liver is transplanted to an adult donor.

TIPS placement often depends on the blind canalization of the portal vein by a puncture originating from the hepatic vein and its predictable position relative to the hepatic vein accounts for high success rates. Although success typically depends on hepatic vein anatomy, variant portal vein anatomy can cause technical difficulties. The portal vein puncture site created during a TIPS placement can be acute if the portal vein trifurcates (type 2) and is therefore difficult to stent. Other portal venous variants may preclude successful access using a standard approach. Some authors have advocated the compulsory use of cross-sectional imaging before or during the TIPS procedure to assess the venous anatomy.

Hepatic veins

The most frequent hepatic anatomic variants are those involving the systemic veins. The impact of hepatic venous anatomic variations on hepatic resection and transplantation is the least-understood aspect of liver surgery. Knowing the variations of hepatic veins before surgery is useful during both partial hepatectomy and donor operations for living related liver transplantation.

Preoperative delineation of this complex venous anatomy is of paramount importance because the hepatic veins have to be transected in the cutting plane of the liver. The location of this plane is determined by the optimal graft volume required, and both the graft and the remnant liver have to retain perfect function. The venous anatomy would change the cutting plane in the living donor and the surgical method of anastomosis for the recipient.

Familiarity with the hepatic venous variants is essential for accurate surgical planning to avoid the postoperative complication of venous congestion.

Any clinically important hepatic vein variation detected on presurgical imaging should be carefully recorded in the radiology report (Barbaro et al. 2013). The most common is characterized by the presence of one or more accessory vessels that drain separately into the vena cava. This usually involves an accessory right inferior hepatic vein (52%) that drains the posteroinferior segments 6 and 7 of the right hemiliver directly into the IVC (Fig. 68.12).

Less frequent variants include the presence of two accessory hepatic veins (12%) or accessory veins that drain the caudate lobe in 12%. Supernumerary hepatic veins are also common (30%). There may be two left hepatic veins (19%), two right hepatic veins (8%), and/or two middle hepatic veins (3%). An inferior accessory hepatic vein can be used as an anatomic marker for the right adrenal vein for adrenal vein sampling (Trerotola et al. 2011).

Rarely, the right inferior hepatic vein may dominate over the right superior vein as an extra-wide constant channel, close to the visceral aspect of the liver. Its appropriate territory is segment 6, but it may encroach somewhat on adjacent segments. Clinically, the existence of an extrawide right inferior hepatic vein, as detected by MRI and located by intraoperative ultrasonography, allows performance of a subtotal hepatectomy leaving only segment 6 (Champetier et al. 1993). In certain pathologic conditions, an extra-wide right inferior hepatic vein may contribute to a compensatory circulation towards the right atrium, due to the development of anastomoses between the hepatic veins.

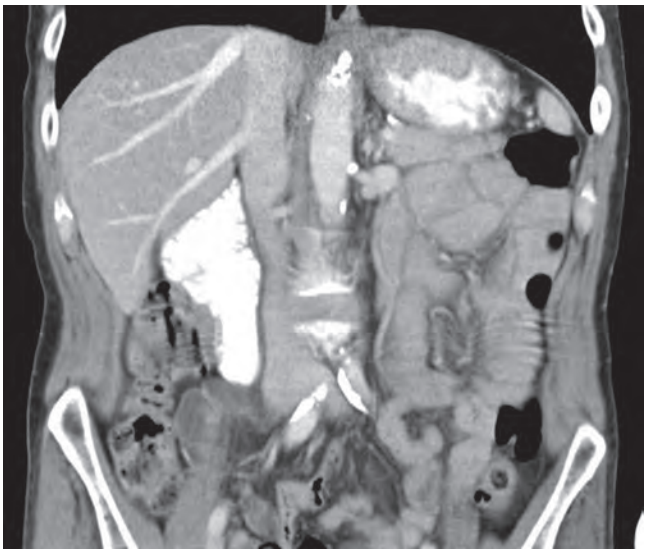

Figure 68.12 Coronal CT accessory right inferior hepatic vein.

Source: D'Souza (www.radpod.org). Reproduced with permission from D. D'Souza.

A rare variant that is important from a surgical point of view is characterized by the precocious division of the vein that drains the right superoanterior segment (8) in the middle hepatic vein.

Variations of the middle hepatic vein (MHV) and left hepatic vein (LHV) in 200 patients with normal liver function were analyzed using ultrasonography to clarify the feasibility of resecting the left lobe or left lateral segment in living subjects for living related hepatic transplantation (Cheng et al. 1996). The MHV and LHV were found to form a common trunk in 70% of cases, but drained independently into the IVC in 30%. In 7% of cases the left median vein (LMV) drained into the MHV, and in 32% of cases the anterior superior segmental vein (ASSV) draining segment 8 flowed into the MHV. The distance between the two confluence points (LHV into MHV/IVC and LMV into MHV) ranged from 0.3 to 2.5 cm, averaging 0.75 cm. The diameter of the LMV at the point that flows into MHV fell within the range 0.3–0.9 cm, averaging 0.61 cm. The distance from the IVC to the confluence of the MHV and LHV fell within the range 0–3.5 cm, averaging 1.5 cm in the cases where the MHV and LHV presented as common trunks.

A very recent prospective three-dimensional CT study, undertaken on 200 consecutive Chinese subjects with normal livers, revealed that the prevailing pattern of the three hepatic veins in these subjects was a right hepatic vein (RHV) and a common trunk for the MHV and LHV (61%). The remaining patients had the RHV, MHV, and LHV draining independently into the IVC (Fang et al. 2012). In 39% of patients, the RHV was small and was compensated by a large right inferior hepatic vein (IRHV; 21%), an accessory RHV (8.5%), or a well-developed MHV (6.5%). The presence of an enlarged IRHV facilitated the isolated resection of segment 8, even when the RHV must be ligated and divided without harming the drainage of inferior segments (Steinbrück et al. 2013). A segment 4 vein was seen in 51.5% of patients which joined the LHV (26%), the MHV (17.5%), or the IVC (8%). An umbilical vein and a segment 4 vein were seen in 3.5% of patients. These two veins joined either the LHV (2.0%) or the MHV (1.5%) (Fang et al. 2012).

Variation in extrahepatic course of hepatic veins

The right hepatic vein may pass through the caval diaphragmatic opening before joining the IVC. One of the hepatic veins has been shown draining directly into the right ventricle. A case has been described in which an accessory vein that contained valves, arising from three roots from the right lobe of the liver, coursed adjacent to the inferior vena cava to enter the right ventricle. A common hepatic vein may be formed that empties into the right atrium.

References

Abdullah A, Williamson K, Lewis T, Elsamaloty H. 2011. Variant ventral intrahepatic course of inferior vena cava: Volume-rendering and maximum intensity projection CT findings. *Br J Radiol* 84: 135–137.

Alicioglu B, Kaplan M, Ege T. 2009. Absence of infrarenal inferior vena cava is not a congenital abnormality. *Bratisl Lek Listy* 110: 304–306.

Altavilla G, Cusatelli P. 1998. Ultrastructural analysis of the liver with portal vein agenesis: A case report. *Ultrastruct Pathol* 22: 477–483.

Anderson RC, Adams P, Burke B. 1961. Anomalous inferior vena cava with azygos continuation (infra-hepatic interruption of the inferior vena cava). *J Pediatr* 59: 370–383.

Atri M, Bret PM, Fraser-Hill MA. 1992. Intrahepatic portal venous variations: Prevalence with US. *Radiology* 184: 157–158.

Barbaro B, Soglia G, Alvaro G, Vellone M, Giuliante F, Nuzzo G, Bonomo L. 2013. Hepatic veins in presurgical planning of hepatic resection: What a radiologist should know. *Abdom Imaging* 38: 442–460.

Bass JE, Redwine MD, Kramer LA, Harris JH Jr. 1999. Absence of the infrarenal inferior vena cava with preservation of the suprarenal segment as revealed by CT and MR venography. *AJR Am J Roentgenol* 172: 1610–1612.

Bass JE, Redwine MD, Kramer LA, Huynh PT, Harris, JH Jr. 2000. Spectrum of congenital anomalies of the inferior vena cava: Cross-sectional imaging findings. Radiographics 639–652.

Belton RL, VanZandt TF. 1988. Congenital absence of the left lobe of the liver: A radiologic diagnosis. *Radiology* 147: 184.

Carr JC, Nemcek AA Jr, Abecassis M, Abecassis M, Blei A, Clarke L, Pereles FS, McCarthy R, Finn JP. 2003. Preoperative evaluation of the entire hepatic vasculature in living liver donors with the use of contrast-enhanced MR angiography and true fast imaging with steady-state precession. *J Vasc Interv Radiol* 14: 441–449.

Champetier J, Haouari H, Le Bas JF, Létoublon C, Alnaasan I, Farah I. 1993. Large inferior right hepatic vein. Clinical implications. *Surg Radiol Anat* 15: 21–29.

Chee YL, Dominic J, Watson CG, Watson HG. 2001. Inferior vena cava malformation as a risk factor for deep venous thrombosis in the young. *Br J Haematol* 114: 878–880.

Cheng YF, Huang TL, Chen CL, Chen TY, Huang CC, Ko SF, Lee TY. 1996. Variations of the left and middle hepatic veins: application in living related hepatic transplantation. *J Clin Ultrasound* 24: 11–6.

Cheng YF, Huang TL, Chen CL, Sheen-Chen SM, Lui CC, Chen TY, Lee TY. 1997. Anatomic dissociation between the intrahepatic bile duct and portal vein: risk factors for left hepatectomy. *World J Surg* 21: 297–300.

Chevallier P, Oddo F, Baldini E, Peten EP, Diaine B, Padovani B. 2000. Agenesis of the horizontal segment of the left portal vein demonstrated by magnetic resonance imaging including phase-contrast magnetic resonance venography. *Eur Radiol* 10: 365–367.

Chou CK, Mak CW, Lin MB, Tzeng WS, Chang JM. 1998. CT of agenesis and atrophy of the right hepatic lobe. *Abdom Imaging* 23: 603–607.

Cohen MI, Gore RM, Vogelzang RL, Rochester D, Neiman HL, Clampton AR. 1984. Accessory hemiazygous continuation of left inferior vena cava: CT demonstration. *J Comput Assist Tomogr* 8: 777–779.

Couinaud C. 1999. Liver anatomy: Portal (and suprahepatic segmentation) or biliary segmentation. *Dig Surg* 16: 459–467.

Covey AM, Brody LA, Getrajdman GI, Sofocleous CT, Brown KT. 2004. Incidence, patterns, and clinical relevance of variant portal vein anatomy. *AJR Am J Roentgenol* 183: 1055–1064.

d'Archambeau O, Verguts L, Myle J. 1990. Congenital absence of the inferior vena cava. *J Belge Radiol* 73: 516–517.

Davachi AA. 1965. Acute spontaneous rupture of an arteriosclerotic aneurysm into an isolated left sided inferior vena cava. *Am J Cardiol* 15: 416.

Debing E, Tielemans Y, Jolie E, Van den Brande P. 1993. Congenital absence of inferior vena cava. *Eur J Vasc Surg* 7: 201–203.

Dougherty MJ, Calligaro KD, DeLaurentis DA. 1996. Congenitally absent inferior vena cava presenting in adulthood with venous stasis and ulceration: A surgically treated case. *J Vasc Surg* 23: 141–146.

Effler DB, Greer AE, Sifers EC. 1951. Anomaly of the vena cava inferior: Report of fatality after ligation. *JAMA* 146: 1321–1322.

Fang CH, You JH, Lau WY, Lai EC, Fan YF, Zhong SZ, Li KX, Chen ZX, Su ZH, Bao SS. 2012. Anatomical variations of hepatic veins: three-dimensional computed tomography scans of 200 subjects. *World J Surg* 36: 120–124.

Fraser-Hill MA, Atri M, Bret PM, Aldis AE, Illescas FF, Herschorn SD. 1990. Intrahepatic portal venous system: Variations demonstrated with duplex and color Doppler US. *Radiology* 177: 523–526.

Gallego C, Velasco M, Marcuello P, Tejedor D, De Campo L, Friera A. 2002. Congenital and acquired anomalies of the portal venous system. *Radiographics* 22: 141–159.

Geley TE, Unsinn KM, Auckenthaller TM, Fink CJ, Gassner I. Azygos continuation of the inferior vena cava in pediatric patients: Sonographic demonstration of the renal artery ventral to the azygos vein as a clue to diagnosis. *AJR Am J Roentgenol* 172: 1659–1662.

Ginaldi S, Chuang VP, Wallace S. 1980. Absence of hepatic segment of the inferior vena cava with azygous continuation. *J Comput Assist Tomogr* 4: 112–114.

Haswell DM, Berrigan TJ, Jr. 1976. Anomalous inferior vena cava with accessory hemiazygos continuation. *Radiology* 119: 51–54.

Huntington GS, McLure CFW. 1920. The development of the veins in the domestic cat (felis domestica) with especial reference, 1) to the share taken by the supracardinal vein in the development of the postcava and azygous vein and 2) to the interpretation of the variant conditions of the postcava and its tributaries, as found in the adult. *Anat Rec* 20: 1–29.

Iqbal J, Nagaraju E. 2008. Congenital absence of inferior vena cava and thrombosis: A case report. *J Med Case Reports* 2: 46.

Kakitsubata Y, Nakamura R, Mitsuo H, Suzuki Y, Kakitsubata S, Watanabe K. 1991. Absence of the left lobe of the liver: US and CT appearance. *Gastrointest Radiol* 16: 323–325.

Koc Z, Ulusan S, Oguzkurt L, Serin E. 2007. Symptomatic interrupted inferior vena cava: Report of a case presenting with haematochezia. *Br J Radiol R* 80: 122–124.

Lambert M, Marboeuf P, Midulla M, Trillot N, Beregi J, Mounier-Vehier C, Hatron P, Jude B. 2010. Inferior vena cava agenesis and deep vein thrombosis: 10 patients and review of the literature. *Vasc Med* 15: 451–459.

Loukas M, Strike DR, Tubbs RS, Tarneja N, Shoja MM. 2009. An interrupted inferior vena cava in a situs inversus. Case report and review of the literature. *Folia Morphol (Warsz)* 68: 184–187.

Maetani Y, Itoh K, Kojima N, Tabuchi T, Shibata T, Asonuma K, Tanaka K, Konishi J. 1998. Portal vein anomaly associated with deviation of the ligamentum teres to the right and malposition of the gallbladder. *Radiology* 207: 723–728.

Marks C. 1969. Developmental basis of the portal venous system. *Am J Surg* 117: 671–681.

Mazzucco A, Bortolotti U, Stellin G, Galucci V. 1990. Anomalies of the systemic venous return: A review. *J Card Surg* 5: 122–133.

McNulty JG, Khosa G. 1999. Absence of bifurcation of the portal vein (letter). *Radiology* 211: 589–590.

Mihmanli I, Bulakbasi N, Kantarci F, Adaletli I, Pabuscu Y. 2001. The value of ultrasonography in interrupted inferior vena cava with azygos continuation. *Eur J Ultrasound* 14: 179–182.

Milner LB, Marchan R. 1980. Complete absence of the inferior vena cava presenting as a paraspinous mass. *Thorax* 35: 798–800.

Ozgun B, Warshauer DM. 1992. Absent medial segment of the left hepatic lobe: CT appearance. *J Comput Assist Tomogr* 16: 666–668.

Parisato FO, Pataro EF. 1965. Vena porta: anomalía. *Angiología* 17: 119–123.

Phillips E. 1969. Embryology, normal anatomy, and anomalies. In: *Venography of the Inferior Vena Cava and its Branches* (eds Ferris EJ, Hipona FA, Kahn PC, Phillips E, Shapiro JH). Baltimore: Williams and Wilkins.

Pineda D, Moudgill N, Eisenberg J, DiMuzio P, Rao A. 2013. An interesting anatomic variant of inferior vena cava duplication: Case report and review of the literature. *Vascular* 21: 163–167.

Radin R, Colletti PM, Ralls PW, Boswell WD, Halls JM. 1987. Agenesis of the right lobe of the liver. *Radiology* 164: 639–642.

Ruggeri M, Tosetto A, Castaman G, Rodeghiero F. 2001. Congenital absence of the inferior vena cava: A rare risk factor for idiopathic deep-vein thrombosis. *Lancet* 357: 441.

Sakamoto N, Koizumi K, Asahina Y, Tazawa J, Maeda M, Marumo F, Sato C. 1997. Primary Budd-Chiari syndrome due to complex venous anomalies. *Abdom Imaging* 22: 499–501.

Schultz CL, Morrison S, Bryan PJ. 1984. Azygous continuation of the inferior vena cava: demonstration by NMR imaging. *J Comput Assist Tomogr* 8: 774–776.

Siegfried MS, Rochester D, Bernstein JR, Milner JW. 1983. Diagnosis of inferior vena cava anomalies by computerized tomography. *Comput Radiol* 7: 119–123.

Steinbrück K, Fernandes R, Bento G, Vasconcelos R, Stoduto G, Auel T, Pacheco-Moreira LF. 2013. Inferior right hepatic vein: A useful anatomic variation for isolated resection of segment VIII. *Case Rep Surg*, doi: 10.1155/2013/371264.

Tharumenthiran R, Hughes TMD, Richardson AJ. 2001. Perinatal inferior vena cava thrombosis and absence of the infrarenal inferior venacava. *J Vasc Surg* 33: 1097–1099.

Thompson WH. 1890. Formation of the portal vein. Collective investigation in the anatomical department of Trinity college, Dublin. *Trans Roy Acad Med Ireland* 8: 516–519.

Trerotola SO, Smoger, DL, Cohen DL, Fraker DL. 2011. The inferior accessory hepatic vein: An anatomic landmark in adrenal vein sampling. *J Vasc Interv Radiol* 22: 1306–1311.

Vijayaraghavan SB, Raja V, Chitra TV. 2003. Interrupted inferior vena cava and left-sided subrenal inferior vena cava: Prenatal diagnosis. *J Ultrasound Med* 22: 747–752.

Wax J, Pinette M, Fife J, Blackstone J, Cartin A. 2007. Absent infrarenal inferior vena cava: An unusual cause of pelvic varices. *J Ultrasound Med* 26: 699–701.

Yamamoto S, Kojoh K, Saito I, Yamamoto R, Ideguchi S, Ohmoto K, Ohumi T, Hino K, Yamamoto M, Wada A. 1988. Computer tomography of congenital absence of the left lobe of the liver. *J Comput Assist Tomogr* 12: 206–208.

Yang BZ, Li Z, Wang ZG. 2012. Nutcracker syndrome due to left-sided inferior vena cava compression and treated with superior mesenteric artery transposition. *J Vasc Surg* 56: 816–818.

Further reading

Abernethy J. 1793. Account of two instances of uncommon formation in the viscera of the human body. *Philos Trans R Soc* 83: 59–66.

Abernethy J. 1809. An account of two instances of uncommon formation in the viscera of the human body. *Philos Trans Roy Soc Lond* 17: 292.

Adachi B. 1937–38. Statistik der varietät der V. cava caudalis bei den Japanern. *Anat Anz* 85: 215–223.

Alten H von. 1913. Über linksseitige lage der Vena cava inferior. *Anat Anz* 43: 337–348.

Andreassi G. 1941–1942. Über die verbindung zwischen dem oberen und unteren hohlvenensystem in hinblick auf die laterale und mediale wurzel der vena azygos und der vena hemiazygos. *Anat Anz* 92: 240–245.

Anson BJ. (ed.) 1966. Morris' Human Anatomy, 12th edition. New York: McGraw-Hill.

Augier M. 1910. Disposition embryonnaire de la veine cave inférieure dans son segment sous–rénal par persistance des veines cardinales inférieures. *Biblio Anat* 19: 135–144.

Banner RL, Brasfield RD. 1958. Surgical anatomy of the hepatic veins. *Cancer* 1: 22–23.

Becker FF. 1962. A singular left sided inferior vena cava. *Anat Rec* 143: 117–120.

Benigni E. 1905. Persistenza della vena ombellicale nell adulto. *Gazzetta degli Ospedali e delle Cliniche* 25: 894–895.

Bergman RA, Thompson SA, Afifi AK, Saadeh FA. 1988. *Compendium of Human Anatomic Variation: Catalog, Atlas and World Literature*. Baltimore and Munich: Urban & Schwarzenberg.

Blasingame FJL, Burge CH. 1937. A case of left postrenal inferior cava without transposition of the viscera. *Anat Rec* 69: 465–470.

Boyden EA. 1932. Description of a horseshoe kidney associated with left inferior cava and disc–shaped suprarenal glands, together with a note on the occurrence of horseshoe kidneys in human embryo. *Anat Rec* 51: 187–211.

Boyer CC. 1953. Anomalous inferior vena cava formed from supracardinal complexex. *Anat Rec* 117: 829–839.

Cabanié H, Perruchio P, Soutoul J, Dejussieu J. 1958. Sur un cas d'absence du segment sous-rénal de la veine cave inferieure. *Assoc Anatomistes Comptes Rendus* 45: 219–225.

Calas F, Couppie G, Martin R, Bouchet Y. 1958. Étude des affluents et de la formation de la veine porte. *Assoc Anatomistes, Comptes Rendus* 45: 254–271.

Calori L. 1888. Sulle communicazioni della vena porta con le vene generali dell corpo. *Mem R Accad Sci Istituto di Bologna* 9: 461–469.

Carpentier, B. 1888. Anomalie des systems de la veine cave inferieure et des veines azygos, observée chez un homme adulte. *Soc Biol, Comptes Rendus Hebdomadaires Séances Mém* 40: 339–340.

Chalier A. 1907. Persistance de la veine cardinale inférieur gauche. *Lyon Méd* 3: 1065–1066.

Champneys F. 1872. Communication between the external iliac and portal veins. *J Anat Physiol* 6: 417–419.

Civalleri A. 1899. Note sur un cas d'oblitération de la veine cave inferieure avec circulation collaterale donnée par les azygos. *Arch Ital Biol* 32: 459.

Corsy F. 1920. Anomalie dans de système veine cave inferieure. Fautil maintenir le schéma classique du développement de ce système? *Soc Biol, Comptes Rendus Hebdomadaires Séances Mém* 83: 365–366.

Davis RA, Milloy FJ, Anson BJ. 1958. Lumbar, renal, and associated parietal and visceral veins based upon a study of 100 specimens. *Surg Gynecol Obstet* 107: 1–22.

Derbes VJ, Dial WA. 1936. Postcaval ueter. *J Urol* 36: 226–233.

Doehner GA. 1968. The hepatic venous system. Its normal roentgen anatomy. Its pathologic roentgen anatomy. *Radiology* 90: 1119–1131.

Douglass BE, Baggenenstross AH, Hollinshead WH. 1950. The anatomy of the portal vein and its tributaries. *Surg Gynecol Obstet* 91: 562–575.

Edwards EA. 1951. Clinical anatomy of lesser variations of the inferior vena cava; and a proposal for classifying the anomalies of this vessel. *Angiology* 2: 85–99.

Ferris EJ, Hipona FA, Kahn PC, Phillipps E, Shapiro JH. 1973. *Venography of the Inferior Vena Cava and its Branches*. Huntington: Krieger.

Filly RA, Laing FC. 1978. Anatomic variation of the portal venous anatomy in the porta hepatis: Ultrasonographic evaluation. *J Clin Ultrasound* 6: 83–89.

Fraenkel W. 1910. Linksseitige vena cava inferior. *Anat Anz* 37: 240–241.

Fraser J, Brown AK. 1944. A clinical syndrome associated with a rare anomaly of the vena portae system. *Surg Gynecol Obstet* 78: 520–524.

Friedman SM. 1945. Report of two unusal venous anomalies. (Left postrenal inferior vena cava; post-aortic left innominate vein). *Anat Rec* 92: 71–76.

Geipel P. 1903. Weitere beiträge zum situs transversus und zur lehre von den transpositionen der grossen gefässe des herzens. *Arch Kinderheilk* 35: 112–145.

Gérard G. 1907. Anomalie exceptionnelle de la veine cave inférieure. Absence complète du segment sous-rénal de la veine cardinale droite. Persistance du segment sous-rénal de la veine cardinale gauche formant une veine cave inférieure gauche. *Biblio Anat* 17: 227–233.

Gérard G. 1914. Duplicité apparente de la veine cave inférieure. Persistance de la veine cardinale gauche. *Biblio Anat* 24: 137–142.

Gilfillan RS. 1950. Anatomic study of the portal vein and its main branches. *Arch Surg* 61: 449–461.

Gladstone RJ. 1910. A case in which the right ureter passed behind the inferior vena cava: With a short note upon a case in which the left

renal vein passed behind the abdominal aorta, and the bearing of these abnormalities on the development of abdominal veins. *J Anat Physiol* 45: 225–231.

Gladstone RJ. 1912. A case of the left inferior vena cava occurring in a female subject in whom the left superior intercostal vein joined the vena azygos major, and the twelfth ribs were absent. *J Anat Physiol* 46: 220–227.

Gladstone RJ. 1929. Development of the inferior vena cava in light of recent research, with especial reference to certain abnormalities, and current descriptions of the ascending lumbar and azygos veins. *J Anat* 64: 70–93.

Guerrier Y, Rapp PE. 1953. La veine porte extra et intrahépatique. 1. Le mode de division extra-hépatique. *Assoc Anatomistes, Comptes Rendus* 40: 272–274.

Hardy KJ. 1972. The hepatic veins. *Aust NZ J Surg* 42: 1.

Heller A. 1904. Mangel der vena cava inferior. *Münchener Med Wochenschr* 51: 1666.

Horner WE. 1818. A case of unusual arrangement in the ascending cava and in the external jugular veins of the human subject. *J Acad Nat Sci Phila* 1: 401–405.

Huseby RA, Boyden EA. 1941. Absence of the hepatic portion of the inferior vena cava with bilateral retention of the supracardinal system. *Anat Rec* 81: 537–544.

Jeffray J. 1828. Account of a singular distribution of the venous system. *The Glasgow Medical Journal* 1: 1–4.

Johnston TB. 1913. Anomaly of the vena cava inferior; with a note on the relationships which help to determine the nature of anomalies of some of the abdominal veins. *J Anat Physiol* 47: 235–245.

Knight HO. 1921. An anomalous portal vein and its surgical dangers. *Ann Surg* 74: 697–699.

Kollmann J. 1893. Abnormitäten im bereich der vena cava inferior. *Anat Anz* 8: 75–80, 97–116.

Kosir V. 1922. Persisterende kardinalvenen und fehlende V. cava inferior. *Anat Anz* 55: 365–368.

Kowalski E, Pawlaczyk J. 1969. Venous blood vessels of rare shape in the liver. *Folia Morphol (Warsz)* 28: 497–501.

Krizan Z, Herman O, Dzidrov V. 1958. Teilweiser fortbestand des supracardinalsystems neben der normalen vena cava inferior beim menschen. *Acta Anat* 34: 312–325.

Kubota K, Noguchi I, Narita M, Nakano T, Nakagawa R. 1958. A case of collateral circulation between the portal and systemic veins through the left para-umbilical and left inferior epigastric vein in man. *Okajimias Folia Anat Jap* 30: 341–342.

Lander HH, Lyman RY, Anson BJ. 1941. An anatomical consideration of the structure in the hepatic pedicle. A study of 100 consecutive cadavers. *Q Bull NW University Medical School* 15: 103–109.

Last RJ. 1972. Anatomy: *Regional and Applied*, fifth edition. Baltimore: Williams and Wilkins Company.

Latimer HB, Virden HN. 1944. A case of complete absence of the inferior vena cava. *J Kansas Med Soc* 45: 346–347.

Lauber H. 1901. Ein fall von teilweiser persistenz der hinteren cardinalvenen beim menschen. *Anat Anz* 19: 590–594.

Laux G, Rapp PE. 1953. Le dispositif veineux du lobe de Spigel. *Assoc Anatomistes, Comptes Rendus* 40: 264–271.

Laverdiere JT, Laor T, Benacerraf B. 1995. Congenital absence of the portal vein: Case report and MR demonstration. *Pediatr Radiol* 25: 52–53.

Lawrence TWP, Nabarro D. 1902. A case of congenital malformation of the heart, with abnormalities of the abdominal viscera: Absence of spleen, absence of hepatic section of inferior vena cava. *J Anat Physiol* 36: 63–75.

Lee DB. 1880. Case of malformation of the heart, with transposition of the aorta and pulmonary artery. *Trans Pathol Soc Lond* 31: 58–62.

Lize I. 1969. Double inferior vena cava. *Folia Morphol (Warsz)* 28: 241–243.

Lucas MF. 1917. A case of double inferior vena cava. *J Anat Physiol* 51: 69–70.

Makowski A, Sierocinski W. 1975. A variation of the inferior vena cava in man. *Folia Morphol (Warsz)* 34: 103–108.

Marois D, van Heerden JA, Carpenter HA, Sheedy PF. 1979. Congenital absence of the portal vein. *Mayo Clinic Proc* 54: 55–59.

Masselot R, Leborgne J. 1978. Anatomical study of the hepatic veins. *Anatomia Clinica* 1: 109–125.

Maxwell EV, Erwin GS. 1928. Four cases of anomalous inferior vena cava with an explanation of their developmental origin. *J Anat* 62: 184–197.

McClure CFW, Butler EG. 1925. The development of the vena cava in man. *Am J Anat* 35: 331–383.

McWhinnie AM. 1840. Case of transposition of the thoracic and abdominal viscera, accompanied with an unusual variety in the venous system. *London Medical Gazette* 26: 31–36.

Milloy FJ, Anson BJ, Cauldwell EW. 1962. Variations in the inferior caval veins and in their renal and lumbar communications. *Surg Gynecol Obstet* 115: 131–142.

Mori M. 1929. Ein fall von verdoppelter vena cava inferior. *Igaku-Kenkiu* 3: 1343–1345.

Mouchet A. 1910. Persistance du segment sous-renal de la veine cardinale gauche. *Biblio Anat* 20: 29–34.

Nakano K. 1931. Uber die persistierenden Vv. supracardinales als verdopplung der V. cava inferior. *Hokkaidô-Igaku-Zasshi* 9: 1089–1096.

Neuberger H. 1913. Ein fall vollkommener persistenz der linken vena cardinalis posterior bei fehlender vena cava inferior. *Anat Anz* 43: 65–80.

Nowak M. 1963. A rare variation of the tributaries of the inferior vena cava in man. *Folia Morphol (Warsz)* 22: 144–152.

Obel W. 1975. Morphology of the trunk of the portal vein in man in various periods of life. *Folia Morphol (Warsz)* 34: 85–101.

Obel W. 1981. Initial branches of the portal vein in the developmental aspect in man. *Folia Morphol (Warsz)* 39: 327–340.

Otulakowski B, Wozniak W. 1975. A case of origin of the testicular artery from the renal artery, and course of the testicular artery behind the inferior vena cava. *Folia Morphol (Warsz)* 34: 349–351.

Patten C. 1909. Persistence of the embryonic arrangement of the post-renal part of the cardinal veins. *Anat Anz* 34: 189–191.

Powell EDU, Mullaney JM. 1960. The Chiari network and the value of the inferior vena cava. *Br Heart J* 22: 579–584.

Poynter CWM. 1992a. Congenital anomalies of the arteries and veins of the human body with bibliography. *Uni Stud Uni Nebraska* 22: 1–106.

Poynter CWM. 1922b. The azygos system of veins in American whites and American Negroes, including observations on the inferior caval venous system. *Am J Phys Anthrop* 19: 39–163.

Rao GRKH. 1959. Double inferior vena cava. *J Anat Soc India* 8: 30–31.

Raza S, Farid S, Reddy M, Ahmad N. 2011. Duplication of the inferior vena cava. *J Surg Case Rep* 2011: 10.

Reagen FP. 1927. The supposed homology of vena azygos and vena cava inferior considered in the light of new facts concerning their development. *Anat Rec* 35: 129–148.

Reis RH, Esenther G. 1959. Variations in the pattern of renal vessels and their relations to the type of posterior vena cava in man. *Am J Anat* 104: 295–318.

Retterer É. 1894. De l'histoire des rapports de l'artère hépatique et de la veine porte. *J l'Anat Physiol Norm Pathol l'Homme Animaux* 33: 133–140.

Rischbieth H. 1914. Anomaly of the inferior vena cava: Duplication of the post-renal segment. *J Anat Physiol* 48: 287–292.

Saito M, Sano N, Kaneda I, Arakawa M, Ishida S, Takahashi S, Sakamoto K. 1995. Multisegmental anomaly of the inferior vena cava with thrombosis of the left inferior vena cava. *Cardiovasc Intervent Radiol* 18: 410–413.

Sappey C, Dumontpallier. 1861. Note sur un cas d'oblitération de la veine cave inférieure avec circulation collatérale, suive de faits analogues demontrant gu'il existe trois principales variétes d'oblitération de cette veine. *Soc Biol, Comptes Rendus Séances Mém* 13: 135–155.

Schmidt GP. 1975. Über eine besondere Form der doppelseitigen V. cava. *Anat Anz* 137: 200–206.

Segall H. 1923. The blood and bile channels of the liver with special reference to the compensatory arterial circulation of the liver in its relation to surgical ligation of the hepatic artery. Report of a case of arteriosclerotic aneurism of the gastroduodenal artery. *Surg Gynecol Obstet* 37: 152–178.

Seib GA. 1934. The azygos system of veins in American Whites and American Negroes, including observations on the inferior caval system. *Am J Phys Anthropol* 19: 39–163.

Shepherd FJ. 1882. On some anatomical variations: Common iliac arteries. *Ann Anat Surg* 6: 172.

Skamnakis SN. 1931–1932. Eine anomalie der vena cava inf. undabnormer verlauf des rechten ureters. *Anat Anz* 73: 50–56.

Sledzinski Z, Tyzkiewicz T. 1975. Hepatic veins of the right part of the liver in man. *Folia Morphol (Warsz)* 34: 315–322.

Soltes GD, Fisher RG, Whigham CJ Jr. 1992. Placement of dual bird's nest filters in an unusual case of duplicated inferior vena cava. *J Vasc Interv Radiol* 3: 709–711.

Sperino G. 1879. Nuove anastomosi tra il sistema della vena porta ed il sistema venoso generale. *Giornale Acad Med Torino* 26: 116–125.

Tadokoro H. 1930. Ein fall von linksseitiger vena cava inferior, welcher beginnt mit den zusammenfluss der V. hypogastrica communis (V.iliaca int. comm.) und der beiden Vv. iliacae externae. *Kaibôgaku-Zasschi* 2: 1029–1036.

Taguchi K. 1901. Über die varietäten der vena cava inferior beim Menschen. *Juntendô-Iji-Kenkiukwai-Zasshi* 343: 1–17.

Walsham WJ. 1881. Anatomical variations: An account of some of the more interesting abnormalities that have been met with in the dissecting-rooms during the session 1880–1881; with remarks. *Saint Bartholomews Hospital Reports* 17: 77.

Waring HF. 1894. Left vena cava inferior. *J Anat Physiol* 28: 46–50.

Waterston D. 1913. Duplication of the post-renal segment of the vena cava inferior. *J Anat Physiol* 47: 433–435.

Wermuth EG. 1939. Anastomoses between the rectal and uterine veins forming a connexion between the somatic and portal venous system in the recto-uterine pouch. *J Anat* 74: 116–126.

White WH. 1884. Left inferior vena cava. *Trans Pathol Soc Lond* 35: 131.

Wicke A. 1927. Über einen fall von inselbildung im bereiche der hinteren hohlvene (Vena cava posterior) und durchtrift des recten harnleiters beim erwachsenen. *Zeitschr für Anat Entwicklungsges* 84: 524–533.

Wilde JC. 1740. Observationes anatomicae rariores. Observatio 1 de vena cava duplici ascendente. *Commentarii Academiae Scientiarum Imperialis Petropolitanae* 12: 312–326.

Zagorsky P. 1822. De singularitate venae cavae inferioris et Quo. Rundam ramorum arteriae aortae. *Mém l'Acad Imp Sci St Pétersbourg* 8: 289–292.

Zhang JS, Wang YP, Wang MQ, Yang L, Zing CC, Yu M, Cui Z. 1996. Diagnosis of an accessory portal vein and its clinical implications for portosystemic shunts. *Cardiovasc Intervent Radiol* 19: 239–241.

Zientarski B. 1982a. Dimensions of the inferior vena cava in humans. *Folia Morphol (Warsz)* 41: 307–314.

Zientarski B. 1982b. Topography of hepatic veins in man. *Folia Morphol (Warsz)* 41: 419–428.

69 Adrenal, renal, gonadal, azygos, hemiazygos, lumbar, and ascending lumbar veins

Marios Loukas[1], R. Shane Tubbs[1-2]
[1]St George's University, School of Medicine, St Georges, Grenada
[2]Seattle Science Foundation, Seattle, Washington, USA
University of Dundee, Dundee, UK

Adrenal veins

The adrenal veins may present with a multitude of anatomical variants which surgeons must be aware of when performing adrenalectomies. The adrenal veins originate during the formation of the prerenal inferior vena cava and are remnants of the caudal portion of the subcardinal veins, cranial to the subcardinal sinus in the embryo. The many communications between the posterior cardinal, supracardinal, and subcardinal veins of the primordial venous system provide a high likelihood for variable anatomy. Most commonly, one central vein drains each adrenal gland. The long left adrenal vein joins the inferior phrenic vein and drains into the left renal vein, while the short right adrenal vein drains immediately into the inferior vena cava.

There is a vast amount of variation reported in the renal venous complex and, consequently, iatrogenic injury may occur during procedures such as AVS and adrenalectomy. For example, the short right adrenal vein can be difficult to cannulate and aspirate from during AVS. In addition, the vein's proximity to the inferior vena cava on the right, as well as the likely presence of collaterals and accessory veins on both sides, requires careful dissection during adrenalectomy.

The left adrenal vein is longer (2–4 cm) and passes downward inferomedially and posterior to the body of the pancreas. It receives the left inferior phrenic vein before entering the superior border of the left renal vein 3–5 cm from the inferior vena cava. The left gonadal vein drains into the inferior aspect of the left renal vein laterally to this. The left adrenal vein may be doubled and receive tributaries other than the inferior phrenic.

The right adrenal vein is very short, just 1–6 mm in length. Exiting anteriorly near the apex of the adrenal gland, the right adrenal vein courses transversely to directly enter the inferior vena cava posterolaterally, 3–5 cm superior to the right renal vein. Pearl (2008) suggested this occurs at the twelfth thoracic level, although Anson (1966) reported the confluence at the first lumbar level. Iwasaki et al. (2013) showed this occurred between the upper portions of thoracic level eleven and lumbar level one in most subjects. This was further supported by Kahn and Angle (2010) who observed similar results. Iwasaki et al. (2013) found that subjects with significantly greater body mass index had a right adrenal vein entering the inferior vena cava at a higher level. The right adrenal vein is rarely doubled and does not usually receive any tributaries.

Minute, superficial capsular veins, draining the surrounding fat from the glandular surface, and retroperitoneal veins communicate with both adrenal veins. These communications drain into small hepatic veins on the right and into the azygos or hemiazygos veins on the left. Jhingan et al. (2002) also described posterior hepatic veins contributing to the right adrenal vein. Avisse et al. (2000) reported each adrenal vein as having multiple accessory veins forming a network of collaterals creating a portal or caval shunt; an observation also reported by Scholten et al. (2013) despite evidence suggesting that there is only one large (5 mm diameter) central vein draining each gland. Pearl (2008) suggested these veins are necessary in maintaining blood flow to the adrenals in the event of adrenal vein obstruction. The morphology described above is believed to be the most common. However, Loukas et al. (2005) reported that the left inferior phrenic vein contributes to the left adrenal vein in only 34% of specimens studied. Many others have reported variations, for the left adrenal veins in particular and for the right although less numerous.

Other anatomical variations

As discussed in the previous section, many communications exist between the subcardinal, posterior cardinal, and supracardinal veins at the level of the kidney prior to the seventh week of development, leading to the possibility of variations in venous drainage. Many have reported variations in the gross appearance of the adrenal veins and their accompanying renal veins. It is therefore not possible to describe the variations in the venous drainage of the adrenal glands independently.

Anson and McVay (1971) illustrated numerous variations based on the adrenal and renal vein configurations and combinations. The left adrenal vein can enter the renal vein without

Bergman's Comprehensive Encyclopedia of Human Anatomic Variation, First Edition. Edited by R. Shane Tubbs, Mohammadali M. Shoja and Marios Loukas.
© 2016 John Wiley & Sons, Inc. Published 2016 by John Wiley & Sons, Inc.

receiving the inferior phrenic. This variant was first described by Cade (1954), but has also been seen in studies by Loukas et al. (2005) and Scholten et al. (2013). The "normal" configuration of the left adrenal vein, where it is joined by the inferior phrenic vein before entering the renal, can also be seen in combination with a gonadal vein draining directly opposite, instead of lateral, to this common trunk into the renal, or may drain into one of two renal veins. This "normal" configuration may be somewhat modified by an additional inferior phrenic that enters the gland before joining the adrenal vein, a variant also noted by Cade (1954). The left adrenal can be bifid and join the renal vein independently of the inferior phrenic. Double adrenal veins (with the inferior phrenic contributing to only one), draining into a single renal vein or one of the double renal veins was observed by Scholten et al. (2013). The adrenal vein may be joined by one of doubled gonadal veins and join the renal vein independently of the inferior phrenic. Stack et al. (2001) reported the left adrenal vein draining directly into the inferior vena cava. Jyothsna et al. (2012) reported a case where the left gonadal vein and second left lumbar vein joined the left adrenal vein to form a trunk, which together entered the left renal vein. Johnstone (1957) performed a cadaveric study to examine the anatomy of the adrenal veins. All ten subjects had a single left adrenal vein. One subject had two left inferior phrenic veins that merged with the left adrenal vein. Another subject had a small collateral venule from the spleen join the left inferior phrenic vein. Another subject had no inferior phrenic vein, but a retrocaval venule instead.

Pearl (2008) discussed communication between the right adrenal vein and small hepatic veins. Matsuura et al. (2008) observed this communication in 8% of their 104 patients undergoing multidetector computed tomography for vascular disease. A study by Johnstone (1957) showed a single right adrenal vein in eight out of ten subjects. From the eight, half drained into the inferior vena cava and half into a right hepatic vein. There were two right adrenal veins in one subject and three in another; both variations were observed by Scholten et al. (2013) in their laparoscopic study of 546 patients. In a study of 142 laparoscopic adrenalectomy patients, Parnaby et al. (2008) discovered two patients with two right adrenal veins. In the first, both adrenal veins directly drained into the inferior vena cava. In the second, the inferior vena cava and the right renal vein received tributary. Another variation with regards to the right adrenal-renal venous complex was noted in a cadaveric dissection by the authors. In one of the cadavers, it was noted that the right adrenal vein drained directly into the inferior vena cava, while the renal vein was found to be doubled. The inferior renal vein was noted to receive the right gonadal vein.

Renal veins

The renal veins show less variation than the renal arteries. One study found multiple renal veins to be rare on the left side (1%) and common on the right side (28%). In another study, the right renal vein was found to have one to three accessories (18% of 203 cases) and the left renal vein to have one or two accessories (9% of 203 cases). Poynter (1922) pointed out that the renal veins show a tendency to form two or more trunks as the arteries do, but in the veins the frequency is only about 7%. In about 2% of cases, the left renal vein may be retroaortic or even circumaortic (either a single vessel, or doubled with one limb anterior and the other posterior to the aorta with a reported frequency of 1.5–4.4% of all abdominal CT scans), or it may form a circumaortic renal venous collar (reported frequency 1.5–8.7%). In an MRI study, Dill et al. (2012) found total left renal vein variations, retroaortic left renal vein and circumaortic left renal veins in 2.68%, 1.66%, and 1.02%, respectively. In cases with a retroaortic left renal vein, the numbers of males and females with their correspondent percentages were 19/44 (43.2%) and 25/44 (56.8%), respectively. In cases with a circumaortic left renal vein, the numbers of males and females with their correspondent percentages were 13/27 (48.1%) and 14/27 (51.9%), respectively.

The right renal vein may be doubled, even though the left renal vein is usually single. The left renal may anastomose with the splenic vein and also receive lumbar veins. The renal and testicular veins show many irregularities when the left inferior vena cava persists.

Communication between the vena cava and accessory renal veins is not unusual, nor is an anastomosis between the splenic and left renal veins. The left azygos (hemiazygos) vein communicates with the left renal vein in the majority of individuals.

Li et al. (2011) described the renal vein variations seen in 61 cases of left donor nephrectomy. Seven types of posterior lumbar tributaries were seen, including: a reno-hemi-azygo-lumbar trunk in 16.4% (10/61 cases); no posterior lumbar tributaries in 16.4% (10/61 cases); one lumbar vein in 47.5% (29/61 cases); two lumbar veins in 32.8% (20/61 cases); and three lumbar veins in 3.3% (2/61 cases).

Lumbar veins

Any one lumbar vein may be absent or a single vein may be formed by multiple tributaries. Davis et al. (1958) found that the fifth lumbar vein was most frequently absent and that the lumbar veins usually took one of four courses to their drainage: (1) separately into the inferior vena cava; (2) separately into venous channels other than the vena cava but in the lumbar and renal regions; (3) as channels terminating into bone, intervertebral disc or prevertebral connective tissues; or (4) two to four veins combining to enter the inferior vena cava as a single trunk.

Ascending lumbar veins

In 100 cadavers Davis et al. (1958) found that the source vessel for the ascending lumbar vein was the common iliac vein, with the exception of 8 instances in which the vessel of origin was either the inferior vena cava or the external iliac vein. The ascending lum-

bar was often variable in its course from pelvic origin to thoracic termination; it was either a single, large, uninterrupted structure in 149 sides, or a less prominent connection between segmental lumbar veins, lacking at one segment and present at another. There were 13 examples of interruption in the ascending lumbar vein, the majority of which occurred at the third lumbar level. The origin of the ascending lumbar vein on the right was at the level of the fifth lumbar vertebra in 41 cases and at the first sacral vertebra in 59 instances; on the left, this origin was opposite the fifth lumbar in 32 cases and opposite the first sacral in 68 cases.

Gonadal veins

Zumstein (1895) reported that the right testicular opened into the right renal vein four times in 220 observations. In a case of doubled inferior vena cava, a left ovarian was found draining into the left inferior vena cava. Both testicular veins may drain into the left renal.

The gonadal vein may be represented by several vessels or may form a plexus. The veins may be partially divided into two parts, permitting passage of the gonadal arteries through the cleft vessels. Poynter (1922) reported a spermatic vein consisting of a number of intercommunicating trunks, some of which opened into the common iliac vein.

The gonadal vein may receive a duodenal or a suprarenal vein. The testicular vein has been reported forming an anastomosis with the splenic vein. Connections to the testicular vein from the capsular and subcostal veins have been reported.

Azygos veins

The azygos vein originates in the thorax at the level of the twelfth thoracic vertebra. It arises from lateral, intermediate, and/or medial roots or from any combination of the three. The lateral azygos root is found in 85% of bodies and arises by union of the ascending vein and subcostal vein. The intermediate root occurs in 34% of individuals. This root arises from the dorsal side of the vena cava near the level of the second lumbar segmental vein and often as a common trunk with the segmental or right renal vein. The medial root occurs in 38% of subjects. They are small plexiform veins closely associated with the ventral side of the lumbar vertebral bodies, dorsal to the aorta and its lumbar segmental branches.

The azygos vein receives the hemiazygos vein on its left margin, as a side or double branch at about the eighth and ninth vertebra. Slightly higher, at the sixth or seventh thoracic vertebra, it receives the accessory hemiazygos vein as a single trunk in 72% of individuals. The hemiazygos and accessory hemiazygos veins are incompletely formed in 15% of individuals. When this occurs, the posterior intercostal veins on the left side of the thorax may drain into the azygos vein independently. In this case the azygos vein lies on the midline.

In one clinically significant variation, the azygos curves over and grooves the right lung before entering the superior vena cava, just before it enters the heart. This is called the azygos lobe of the lung. In a study of 200 bodies, the azygos vein showed variation in 26%. The cross connections of the hemiazygos to the azygos occurred with almost equal frequency at the eight or ninth vertebra. At least two cross connections were present in 100%, three cross connections occurred in 4%, and four or more in 6%.

Rarely, the azygos vein passes through the aortic hiatus of the diaphragm. It may open directly into the right atrium (ascribed to the embryonic disappearance of the right common cardinal vein).

The azygos occasionally opens into the right brachiocephalic or even the right subclavian (believed to be caused by an elongated embryonic right common cardinal vein). If the hemiazygos is underdeveloped, its branches open directly into the azygos vein. The azygos may receive either or both supreme intercostal veins and any combination of intercostal and lumbar veins. The left superior intercostal communicates with the azygos system in 57% of individuals. The azygos may drain into the hemiazygos, which in turn drains into the right atrium (Gruber). The pulmonary veins have been found opening into the azygos vein. The azygos vein may be absent or doubled.

Unusual tributaries include the right internal thoracic, superior phrenic, bronchial, and gonadal veins.

The inferior vena cava has been seen continued into the azygos vein, which is then of course extremely large. The testicular vein and (on the left side) the renal and suprarenal veins have been seen terminating in the same manner.

A study of 200 bodies showed 26% variation; many of these are of a very minor nature. The cross connections of the hemiazygos to the azygos are almost as frequent at the eighth as at the ninth vertebra and in 10%, both are present. In 4%, three connections are maintained. In 12 bodies, 4 or more connections are found. In 4 bodies the left spermatic and suprarenal veins joined the accessory hemiazygos, while in 12% a branch from or all of the left renal opened into this vein (Zumstein 1895). In 4%, the accessory hemiazygos does not join the hemiazygos but enters the coronary sinus.

Gruber (1881) saw a case in which the azygos opened into the hemiazygos, and this in turn into the right atrium. "The azygos may curve from the fourth or fifth vertebra, grooving the lung to enter the superior vena cava just before it enters the heart" (Poynter 1922). In 84 cadavers, Bales (2014) found that approximately 5% of azygos veins ascended on the right side (classical) position; roughly 30% did not cross the midline; approximately 70% included part or all of their course left of the midline; and about 14% reached the extreme left side.

References

Anson BJ. 1966. *Morris' Human Anatomy*, 12th edition. New York: McGraw-Hill.

Anson BJ, McVay CB. 1971. *Surgical Anatomy*, fifth edition, Vol 1. Philadelphia: WB Saunders Co.

Avisse C, Marcus C, Patey M. 2000. Surgical anatomy and embryology of the adrenal glands. *Surg Clin North Am* 80: 403–415.
Bales G. 2014. A semi-quantitative approach to variation of the azygos vein course. *Clin Anat* 27(7): 1030–1037.
Cade S. 1954. Adrenalectomy for hormone dependent cancers: breast and prostate. *Ann R Coll Surg Engl* 15: 71–107.
Davis RA, Milloy FJ, Anson BJ. 1958. Lumbar, renal, and associated parietal and visceral veins based upon a study of 100 specimens. *Surg Gynecol Obstet* 107: 1–22.
Dill A, Ayaz UY, Karabacak OR, Tatar IG, Hekimoglu B. 2012. Study of the left renal variaitons by means of magnetic resonance imaging. *Surg Radiol Anat* 34: 267–270.
Gruber W. 1881. Duplicität der vena cava superior mit vorkommen zweier transversaler communicationäste und zweier venae azygae. *Arch Pathol Anat Physiol Klin Med* 86: 38–41.
Iwasaki T, Kurisu S, Mitsuba N. 2013. Effect of body mass index on the location of the right adrenal vein in patients with primary aldosteronism. *J Renin Angiotensin Aldosterone Syst* 14: 156–160.
Jhingan V, Sahni D, Chawla YK. 2002. Hepatic veins in northwest Indian subjects. *Trop Gastroenterol* 23: 176–180.
Johnstone FRC. 1957. The suprarenal veins. *Am J Surg* 94: 615–620.
Jyothsna P, Mohandas Rao KG, Somayaji SN, Ashwini LS. 2012. Multiple vascular anomalies involving testicular, suprarenal arteries and lumbar veins. *N Am J Med Sci* 4: 154–156.
Kahn SL, Angle JF. 2010. Adrenal vein sampling. *Tech Vasc Interventional Rad* 13: 110–125.
Li G, Dong J, Lu JS, Zu Q, Yang SX, Li HZ, Ma X, Zhang X. 2011. Anatomical variation of the posterior lumbar tributaries of the left renal vein in retroperitoneoscopic left living donor nephrectomy. *Int J Urol* 18: 503–509.
Loukas M, Louis RG, Hullet J. 2005. An anatomical classification of the variations of the inferior phrenic vein. *Surg Radiol Anat* 27: 566–574.
Matsuura T, Takase K, Ota H. 2008. Radiologic anatomy of the right adrenal vein: preliminary experience with MDCT. *Am J Roentgenol* 191: 402–408.
Parnaby CN, Galbraith N, O'Dwyer PJ. 2008. Experience of identifying the venous drainage of the adrenal gland during laparoscopic adrenalectomy. *Clin Anat* 21: 660–665.
Pearl M. 2008. *Image-Guided Interventions: Abdominal Aorta and the Inferior Vena Cava*. Philadelphia: Saunders.
Poynter CWM. 1922. Congenital anomalies of the arteries and veins of the human body with bibliography. *University Studies University Nebraska* 22: 1–106.
Scholten A, Cisco RM, Vriens MR. 2013. Variant adrenal venous anatomy in 546 laparoscopic adrenalectomies. *JAMA Surg* 148: 378–383.
Stack SP, Rösch J, Cook DM, Sheppard BC, Keller FS. 2001. Anomalous left adrenal venous drainage directly into the inferior vena cava. *J Vasc Interv Radiol* 12: 385–387.
Zumstein J. 1895. Zur anatomic und entw. der venensystems des menschcn. *Anat Hefte* 6: 570–580.

Further reading

Anson BJ, Siekert RG, Richmond TE, Bishop WE. 1940. The accessory pulmonary lobe of the azygos vein. *Q Bull Northwestern Univ Med School* 24: 285–290.
Bergman RA, Thompson SA, Afifi AK, Saadeh FA. 1988. *Compendium of Human Anatomic Variation: Catalog, Atlas and World Literature*. Baltimore and Munich: Urban & Schwarzenberg.
Brooks H. 1885. Vena azygos major ascending on the left side, and the bearing of this anomaly on the development of the azygos blood-vessels. *Trans Acad Med Ireland* 5: 450–452.
Butler H, Balankura K. 1952. Preaortic thoracic duct and azygos vein. *Anat Rec* 113: 409–419.
Brödel M. 1901. The intrinsic blood vessels of the kidney and their significance in nephrology. *Bull Johns Hop Hosp* 12: 10–13.
Gillaspie C, Miller L, Baskin M. 1916. Anomalous renal vessels and their surgical significance. *Anat Rec* 11: 77–86.
Horner WE. 1818. A case of unusual arrangement in the ascending cava and in the external jugular veins of the human subject. *J Acad Nat Sci Phil* 1: 401–405.
Kosinski H. 1976. The veins of the kidneys. *Folia Morphol* 35: 277–285.
Macalister A. 1868. Irregularity of the spermatic vein. *Med Press Circul* 5: 404–405.
Milloy FJ, Anson BJ, Cauldwell EW. 1962. Variations in the inferior caval veins and in their renal and lumbar communications. *Surg Gynecol Obstet* 115: 131–142.
Morison BG. 1879. The arrangement of the azygos and superior intercostal veins in the thorax. *J Anat Physiol* 13: 346–349.
Morison DM. 1926. A study of the renal circulation with special reference to its finer distribution. *Am J Anat* 37: 53–93.
Nandy K, Blair CB. 1965. Double superior venae cavae with completely paired azygos veins. *Anat Rec* 15: 1–9.
Nathan H. 1960. Anatomical observations on the course of the azygos vein. *Thorax* 15: 229–232.
Regen FP. 1927. The supposed homology of the vena azygos and vena cava inferior considered in light of new facts concerning their development. *Anat Rec* 35: 129–148.
Reis RH, Esenther G. 1959. Variations in the pattern of renal vessels and their relations to the type of posterior vena cava in man. *Am J Anat* 104: 295–318.
Rupert RR. 1913. Irregular kidney vessels found in fifty cadavers. *Surg Gynecol Obstet* 17: 580–585.
Rupert RR. 1915. Further study of irregular kidney vessels as found in one hundred eighteen cadavers. *Surg Gynecol Obstet* 21: 471–480.
Schaefer EA, Symington J, Bryce TH. 1915. *Quain's Anatomy*, 11th edition. London: Longmans, Green and Co.
Sieb GA. 1934. The azygos system of veins in American White and American Negroes, including observations on the inferior caval venous system. *Am J Physiol Anthrop* 19: 39–163.
Smith GT. 1963. The renal vascular patterns in man. *J Urol* 89: 275–288.
Smithuis T. 1956. The problem of renal segmentation in connection with modesof ramification of the renal artery and vein. *Arch Chir Neerl* 8: 227–241.
Sykes D. 1963. Some aspects of the blood supply of the human kidney. *Symp Zool Soc* 11: 49–58.
Walsham WJ. 1880. A double left renal vein. *St Bartholomews Hosp Rep* 16: 99.
Weinstein BB, Countiss EH, Derbes VJ. 1940. The renal vessels in 203 cadavers. *Urol Cutan Rev* 44: 137–139.
Weinstein BB, Countiss EH, Derbes VJ. 1940. Retroaortic renal vein. *Urol Cutan Rev* 46: 17–19.
Wozniak W. 1965. A case of termination of the ileocolic vein in the right renal vein associated with accessory renal blood vessels. *Folia Morphol* 24: 195–200.
Yelin G. 1940. Retroaortic renal vein. *J Urol* 44: 406–410.

70 Iliac veins

Deepali Onkar
NKP Salve Institute of Medical Sciences and Research Centre, Nagpur, India

Introduction

Variations of the iliac veins result from maldevelopment of the posterior cardinal veins during early embryogenesis. They have a wide spectrum and are commonly presented in the literature as case reports. They have also been described in cadaveric, venographic and, recently, multidetector computed tomography (CT) scan studies. These variations can be isolated or associated with malformations of the deep veins of the lower limb, such as in Klippel-Trenaunay syndrome. In 559 patients with Klippel-Trenaunay syndrome, Servelle (1985) observed variations of the iliac veins in 19 (3.3%) cases; these included agenesis in seven (36.8%) and hypoplasia in 12 (63.1%). Venieratos et al. (2012) studied 59 cadavers and demonstrated variations in the major pelvic veins in nine (15.3%). Detailed knowledge of normal iliac venous anatomy and its variations is essential during retroperitoneal surgery (Oto et al. 2003).

Common iliac vein

The common iliac vein is formed by the union of the external and internal iliac veins, anterior to the sacroiliac joints. It ascends obliquely up to the right side of the fifth lumbar vertebra where it joins the contralateral vein to form the inferior vena cava at an acute angle (Fig. 70.1). The right common iliac vein is shorter and nearly vertical, lying posterior and then lateral to its adjacent artery. The left common iliac vein is longer and more oblique and is first medial, then posterior, to its adjacent artery. These veins are valveless (Standring 2008).

Duplication

Either common iliac vein can be doubled in part or throughout its length (Edwards 1951; Sperling et al. 1975; Lotz and Seeger 1982; Bergman et al. 1988; Mayer 1998; Figs 70.2, 70.3). The duplicated channel can rejoin distal to the origin of the inferior vena cava, or one of the trunks can drain into the inferior vena cava and the other into the opposite common iliac vein (Lotz and Seeger 1982; Fig. 70.4).

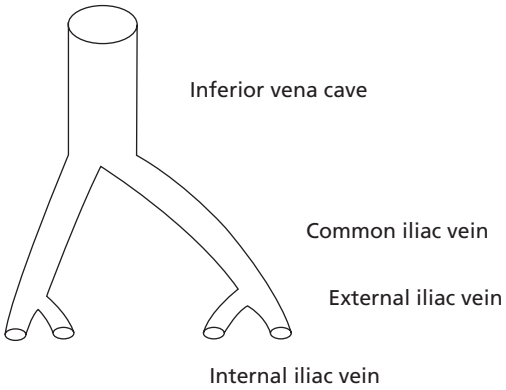

Figure 70.1 Normal iliac vein anatomy.

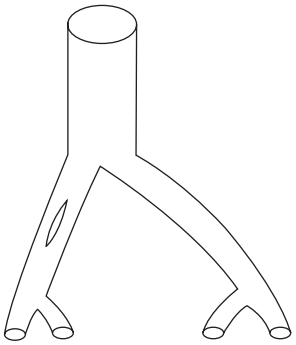

Figure 70.2 Partial duplication of the right common iliac vein.

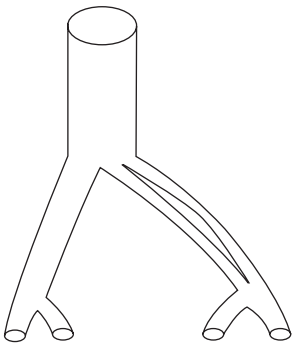

Figure 70.3 Complete duplication of the left common iliac vein.

Bergman's Comprehensive Encyclopedia of Human Anatomic Variation, First Edition. Edited by R. Shane Tubbs, Mohammadali M. Shoja and Marios Loukas.
© 2016 John Wiley & Sons, Inc. Published 2016 by John Wiley & Sons, Inc.

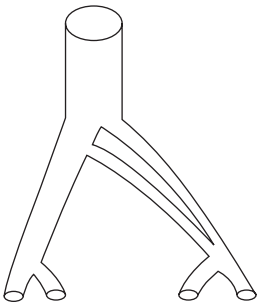

Figure 70.4 One of the duplicated trunks of the left common iliac vein draining into the inferior vena cava and another into the right common iliac vein.

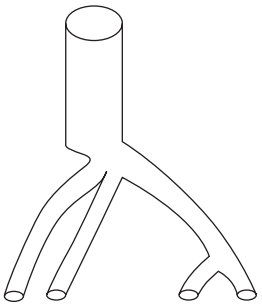

Figure 70.6 Agenesis of the right common iliac vein. Right external and internal iliac veins join the opposite common iliac vein to form the inferior vena cava.

Agenesis

Unilateral aplasia of the common iliac vein has been reported (Edwards 1951; Servelle et al. 1965; Babini et al. 1966; Martorell et al. 1978; Thomas and Posniak 1984; Servelle 1985; Bergman et al. 1988; Kutsal et al. 1999; Surucu et al. 2001; Spencer and Quarmby 2007; Yahyayev et al. 2013). In these cases, the external and internal iliac veins can drain separately into the origin of the inferior vena cava (Edwards 1951; Fig. 70.5). Sometimes, the external and internal iliac veins join the opposite common iliac vein to form the inferior vena cava (Bergman et al. 1988; Spencer and Quarmby 2007; Fig. 70.6) or the external iliac can drain into inferior vena cava and the internal iliac into the opposite common iliac vein (Surucu et al. 2001; Fig. 70.7). Cases of bilateral agenesis have also been reported (Mudler and deBoer 1972; Chandrasekar et al. 2012). Bilateral absence of the common iliac vein can be associated with the absence of the external iliac, internal iliac, and part of the "common" femoral vein on one side (Fig. 70.8). In such cases, the external and internal iliac veins on the normal side may drain into retroperitoneal collateral veins (Chandrasekar et al. 2012).

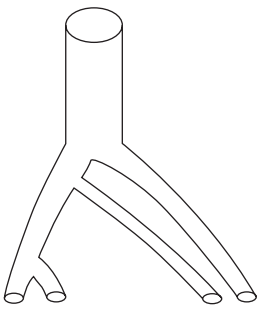

Figure 70.7 Agenesis of the left common iliac vein. Left external iliac vein draining into the inferior vena cava and left internal iliac vein into the right common iliac vein.

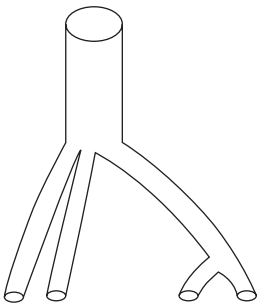

Figure 70.5 Agenesis of the right common iliac vein. Right external and internal iliac veins draining separately into the origin of the inferior vena cava.

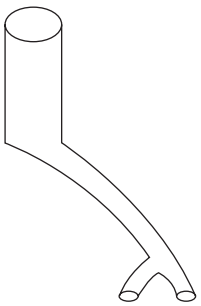

Figure 70.8 Agenesis of the right common, external, and internal iliac veins.

High junction

The external and internal iliac veins can join at a higher level, forming a short common iliac vein (Lotz and Seeger 1982; Morita et al. 2007). Formation of the left common iliac vein at a higher level was seen in 7.9% by Morita et al. (2007) (Fig. 70.9).

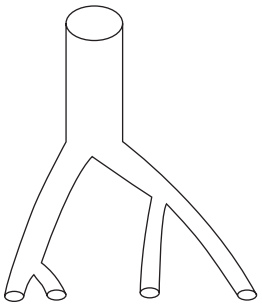

Figure 70.9 Left external and internal iliac veins joining at a higher level than normal.

Variations due to drainage patterns of the internal iliac veins

The common iliac vein can receive the contralateral internal iliac vein (Johnston 1913; Oto et al. 2003; Cardinot et al. 2006). It is usually the right internal iliac vein that opens into the left common iliac (Johnston 1913; Oto et al. 2003; Fig. 70.10). Sometimes, the common iliac vein receives a separate internal iliac vein or a common trunk formed by bilateral accessory internal iliac veins (Morita et al. 2007).

The right and left internal iliac veins occasionally unite and open as a common trunk at the confluence of the right and left external iliac veins to form the vena cava (Bergman et al. 1988; Fig. 70.11). Sometimes, two anomalous channels communicate between the two internal iliac veins and form a common trunk. Such trunks drain into the inferior vena cava, in addition to the original common iliac veins (Krishnamurthy et al. 2007; Fig. 70.12). An anastomotic vein may connect the right internal and left common iliac veins (Lotz and Seeger 1982; Venieratos et al. 2012; Fig. 70.13). Venieratos et al. (2012) identified this variation in 1.7%.

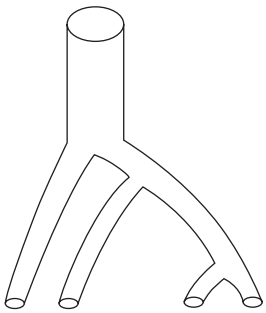

Figure 70.10 Left common iliac vein receiving the right internal iliac vein.

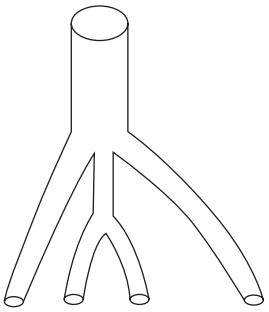

Figure 70.11 Right and left internal iliac veins forming a common trunk and draining into the inferior vena cava.

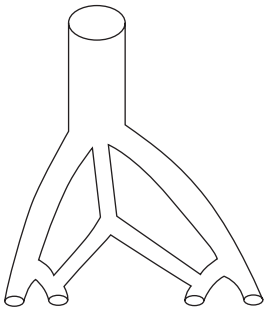

Figure 70.12 Both internal iliac veins are joined by a connecting vein forming a common trunk and draining into the inferior vena cava.

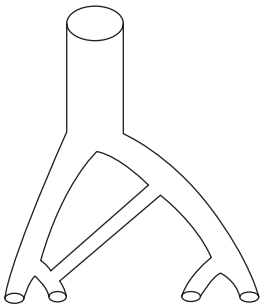

Figure 70.13 An anastomotic vein connecting the right internal iliac and left common iliac veins.

Other rare variations

The middle sacral trunk vein can divide with one branch opening into the right and the other into the left common iliac vein (Bergman et al. 1988). The common iliac vein occasionally receives an accessory renal vein or even the entire renal vein drainage (Bergman et al. 1988; Belsare et al. 2002; Jetti et al. 2008). A connection between the hepatic portal and right common iliac has also been reported (Bergman et al. 1988). The left ovarian vein can drain into the left common iliac vein (Belsare et al. 2002). The left common iliac vein can ascend left of the

aorta to the level of the left renal vein, where it crosses anterior to the aorta to join the inferior vena cava. Sometimes, each common iliac vein receives a lateral sacral vein. The right and left medial sacral veins, which unite to form a single trunk, can end at the common iliac junction (Standring 2008). A valve may be present in the common iliac vein (Le Page et al. 1991).

Internal iliac vein

The internal iliac vein is formed by the convergence of several veins above the greater sciatic foramen. It ascends posteromedial to the internal iliac artery. Its tributaries include the gluteal, internal pudendal, obturator, lateral sacral, middle rectal, vesical, uterine, and vaginal veins (Standring 2008).

Morita et al. (2007) conducted a study of 63 patients using multidetector computed tomography and reported internal iliac vein anomalies in 30.2%. These were more common in females, with a female/male ratio of 1.7:1. The incidence of separated trunks of the internal iliac vein was 22.2%, whereas it was 27% in a cadaveric study by Le Page et al. (1991).

Morita et al. (2007) observed that the right separated internal iliac vein drained into a central right common iliac vein in 1.6% (Fig. 70.14) while a separated left internal iliac vein drained into a central left common iliac vein in 4.8% (Fig. 70.15). In 11.1%, the right separated internal iliac vein drained into a central left common iliac vein (Fig. 70.16) and separated bilateral internal iliac veins drained into a central left common iliac vein in 4.8% (Fig. 70.17).

The internal iliac vein can be absent on one side (Chandrasekar et al. 2012). It is sometimes doubled (Lotz and Seeger 1982; Le Page et al. 1991; Venieratos et al. 2012). A duplicated internal iliac vein was seen in 1.7% (Venieratos et al. 2012). Duplicated channels can be interconnected by one or more veins (Lotz and Seeger 1982; Figs 70.18, 70.19).

An internal iliac vein can form an annulus around the internal iliac artery. It can receive an unusual vessel representing a confluence of the internal pudendal, obturator, gluteal, and sciatic veins (Bergman et al. 1988). It can also receive an accessory renal vein (Belsare et al. 2002).

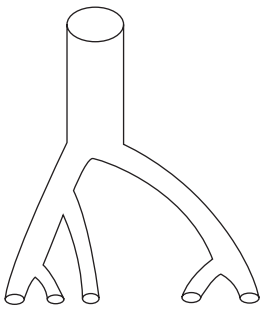

Figure 70.14 Right common iliac vein receiving separated right internal iliac veins more centrally.

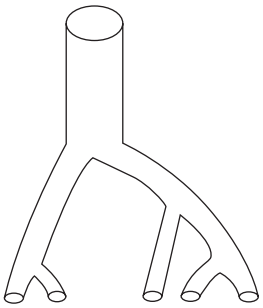

Figure 70.15 Left common iliac vein receiving separated left internal iliac vein more centrally.

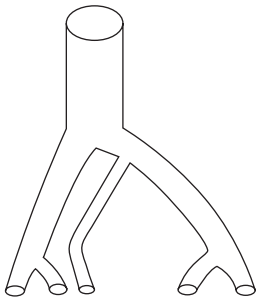

Figure 70.16 Left common iliac vein receiving separated right internal iliac vein at a higher level.

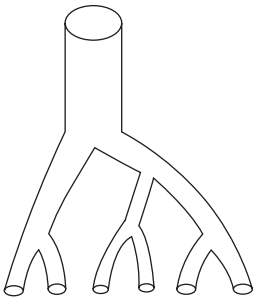

Figure 70.17 Left common iliac vein receiving a common trunk formed by bilateral accessory internal iliac veins.

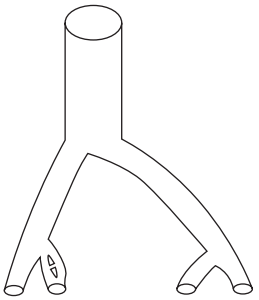

Figure 70.18 Duplication of right internal iliac vein. Duplicated veins are interconnected by a vein.

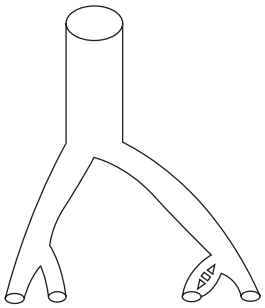

Figure 70.19 Duplication of left internal iliac vein. Duplicated veins are interconnected by two veins.

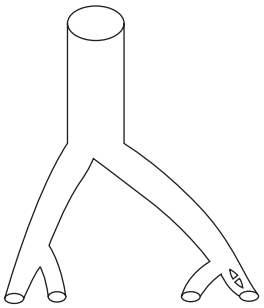

Figure 70.21 Duplicated left external iliac vein. Duplicated veins are interconnected by a vein.

External iliac vein

The external iliac vein is the proximal continuation of the femoral vein. On the right side, it lies medial to the external iliac artery and gradually inclines behind it as it ascends. On the left it is wholly medial. Its tributaries are the inferior epigastric, deep circumflex iliac, and pubic veins (Standring 2008). Variations of the external iliac vein are less frequent than those of the internal iliac vein. Unilateral aplasia has been reported (Servelle et al. 1965; Babini et al. 1966; Martorell et al. 1978; Dogan et al. 2003; Koplay and Kantarci 2007; Chandrasekar et al. 2012). Bilateral aplasia is rare (Mudler and deBoer 1972; Onkar et al. 2013). In cases of isolated bilateral external iliac vein aplasia, the veins of the lower limb can drain into the upper limb veins through the superficial veins of the abdomen (Onkar et al. 2013).

The external iliac vein can be duplicated (Sperling et al. 1975; Bergman et al. 1988; Djedovic et al. 2006) (Fig. 70.20). The duplicated veins can join to form one or more loops (Fig. 70.21) or a venous annulus around the external iliac artery (Djedovic and Putz 2006). The external iliac vein can be connected with the opposite common femoral vein (Koplay and Kantarci 2007).

The external iliac vein can lie lateral to the external iliac artery. It can receive a gonadal or obturator vein (Bergman et al. 1988; Nayak and Soumya 2009) or an accessory or separated internal iliac vein, if present (Le Page et al. 1991). An ascending lumbar vein was seen draining into the external iliac vein in 27.8% (Venieratos et al. 2012).

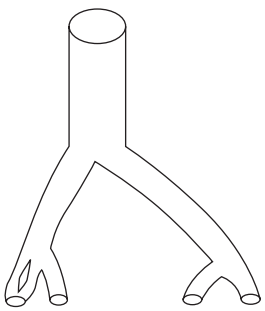

Figure 70.20 Duplicated right external iliac vein.

Although iliac veins are normally valveless (Standring 2008), a study of the valvular anatomy of the iliac veins in 42 human cadavers demonstrated that the external iliac vein had one valve in 26.2% of specimens. This vein had three times as many valves on the right side as on the left (39.6% v. 14.6%; Le Page et al. 1991).

References

Babini L, Birarelli B, Caprotti M. 1966. Raro caso di anomalia venosa dell'arto inferiore e del bacino. *Minerva Cardioangiol* 14: 306–310.

Belsare SM, Chimmalgi M, Vaidya SA, Sant SM. 2002. Ectopic kidney and associated anomalies: A case report. *J Anat Soci Ind* 51: 236–238

Bergman RA, Thompson SA, Afifi AK, Saadeh FA. 1988. *Compendium of Human Anatomic Variations*. Baltimore: Urban & Schwarzenberg.

Cardinot TM, Aragao AH, Babinski MA, Favorito LA. 2006. Rare variation in course and affluence of internal iliac vein due to its anatomical and surgical significance. *Surg Radiol Anat* 28: 422–425.

Chandrasekar VS, Kaliyaperumal V, Alfred D. 2012. Absence of infrarenal segment of inferior vena cava with anomalous right renal vein. *J Surg Case Rep* 7: 14.

Djedovic G, Putz D. 2006. Case report: description of a venous annulus of the external iliac vein. *Ann Anat* 188: 451–453.

Dogan R, Dogan OF, Oc M, Akata D, Gumus B, Balkanci F. 2003. A rare vascular malformation, Klippel-Trenaunay syndrome. Report of a case with deep vein agenesis and review of the literature. *J Cardiovasc Surg (Torino)* 44: 95–100.

Edwards EA. 1951. Clinical anatomy of lesser variations of the inferior vena cava; and the proposal for classifying the anomalies of the vessel. *Angiology* 2: 85–99.

Jetti R, Jevoor PS, Vollala VR, Potu BK, Ravishankar MV, Virupaxi RD. 2008. Multiple variations of the urogenital vascular system in a single cadaver: a case report. *Cases Journal* 1: 344.

Johnston TB. 1913. Anomaly of the vena cava inferior; with a note on relationships which help to determine the nature of anomalies of some of the abdominal systemic veins. *J Anat Physiol* 47: 235–245.

Koplay M, Kantarci M. 2007. Absence of left external iliac vein and an unusual venous connection between the right external iliac vein and the left main femoral vein. *Clin Anat* 20: 992–993.

Krishnamurthy A, Nayak SR, Khan S, Latha V, M Mangala, Pai, Vadgaonkar R. 2007. Anamolous channel draining the internal iliac veins: embryological and clinical significance. *Romanian J Morphol Embryol* 48: 71–73.

Kutsal A, Lampros TD, Cobanoglu A. 1999. Right iliac vein agenesis, varicosities, and widespread hemangiomas: report of a rare case. *Tex Heart Inst J* 26: 149–151.

Le Page PA, Villavicencio JL, Gomez ER, Sheridan MN, Rich NM. 1991. The valvular anatomy of the iliac venous system and its clinical implications. *J Vasc Surg* 14: 678–683.

Lotz PR, Seeger JF. 1982. Normal variation in iliac venous anatomy. *AJR* 138: 735–738.

Martorell F, Martorell A, Sanpons C, Monserrat J. 1978. Sindrome de Klippel-Trenaunay por aplasia de la vena iliaca. *Angiologia* 30: 49–53.

Mayer DR, Andresen R, Friedrich M. 1998. Right-sided double inferior vena cava and common iliac vein. *Aktuelle Radiol* 8: 148–150.

Morita S, Saito N, Mitsuhasi N. 2007. Variations in internal iliac veins detected using multidetector computed tomography. *Acta Radiol* 48: 1082–1085.

Mudler JW, deBoer GWGJ. 1972. Agenesie van de vena iliaca. *Ned Tijdschr Geneeskd* 116: 226–229.

Nayak BS, Soumya KV. 2009. Variant obturator vessels. *Int J Anat Var* 2: 111–112.

Onkar D, Onkar P, Mitra K. 2013. Isolated bilateral external iliac vein aplasia. *Surg Radiol Anat* 30: 85–87.

Oto A, Akpinar E, Surucu HS, Denk CC, Celik HH. 2003. Right internal iliac vein joining the left common iliac vein: case report demonstrated by CT angiography. *Surg Radiol Anat* 25: 339–341.

Servelle M. 1985. Klippel and Trenaunay's syndrome: 768 operated cases. *Ann Surg* 201: 365–373.

Servelle M, Zolotas E, Soulie J, Andrieux J, Cornu C. 1965. Syndrome de Klippel et Trenaunay malformation des veines iliaques, femorale et poplitee. *Arch Mal Coeur* 58: 1187–1197.

Spencer L, Quarmby JW. 2007. Klippel-Trenaunay syndrome with left iliac vein agenesis. *Euro J Vasc Endovasc Surg* 33: 505–506.

Sperling M, Winter G, Weiland W. 1975. Duplication of the external and common iliac veins with a venous trunk anterior to the artery (author's transl). *MMW Munch Med Wochenschr* 117: 1547–1550.

Standring S. 2008. *Gray's Anatomy*, 40th edition. New York: Churchill Livingstone, pp. 1089–1090.

Surucu HS, Erbil KM, Tastan C, Yener N. 2001. Anomalous veins of the retroperitoneum: clinical considerations. *Surg Radiol Anat* 23: 443–445.

Thomas ML, Posniak HV. 1984. Agenesis of the iliac veins. *J Cardiovasc Surg* 25: 64–66.

Venieratos D, Panagouli E, Lolis E. 2012. Variations of the iliac and pelvic venous system with special attention to the drainage patterns of the ascending lumbar and iliolumbar veins. *Ann Anat* 194: 396–403.

Yahyayev A, Bulakci M, Yilmaz E, Ucar A, Sayin OA, Yekeler E. 2013. Absence of right iliac vein and an unusual connection between both common femoral veins. *Phleb* 28: 162–164.

71 Veins of the lower limb

Santosh K. Sangari
Weill Cornell Medical College, New York, New York, United States

The veins of lower limb can be divided into superficial and deep veins. The superficial veins are present in the superficial fascia under the skin, whereas the deep veins are accompanied by the arteries of the lower limb, deep to the deep fascia. The perforating veins connect the superficial to the deep veins. In most veins of the lower limb except the foot, blood flows from superficial to deep veins directly and through the perforating veins. Both superficial and deep veins have valves, which prevent the reverse of blood flow.

There is symmetry between the veins of the two sides in 14% of cases, the main areas of asymmetry being 32% in the popliteal vein and 48% in the femoral vein (Quinlan et al. 2003).

An international interdisciplinary committee was formed in 2001 to address the non-uniform terminology that had been applied to the veins of the lower limb, which was creating problems for treating diseases of these veins. The committee refined and updated the nomenclature, which is followed in this chapter (Caggiati et al. 2002, 2005).

Developmental venous anomalies

During development, the distal arches in the lower extremities and their tributaries form the dorsal venous arch of the foot in adults. The preaxial vein of the lower limb becomes the great saphenous vein, which continues proximally to the cardinal portion of the common iliac, external iliac, and proximal femoral veins. The postaxial vein becomes the small saphenous vein, which originally continued as the popliteal veins and inferior gluteal veins to the posterior cardinal vein. During embryonic life, the sciatic vein is the main vein accompanying the sciatic nerve and drains blood from the deep structures of the lower limb. The venae comitantes of the arteries of the lower limb develop secondarily and become connected to the preaxial vein (Cunningham 1918).

1. Cardoso et al. (2010) observed bilateral persistent sciatic veins in one of 16 cadavers dissected.
2. Another well-recognized example of the persistence of an embryonic axial vein is the anterior accessory saphenous vein (older names include the anterolateral vein of thigh and lateral superficial femoral cutaneous vein), either terminating in the profunda femoris vein or continuing up the sciatic notch to join the internal iliac vein (Fig. 71.1). In this case the anomalous veins can take over the function of normal major veins, and it can be catastrophic to remove them (Tibbs et al. 1997).
3. There may be multiple sponge-like communications between a series of large arteries and veins, leading to arteriovenous fistulas (Fig. 71.2) in the lower limb, arterial bruits and pulsatile flow in the veins (Tibbs et al. 1997).

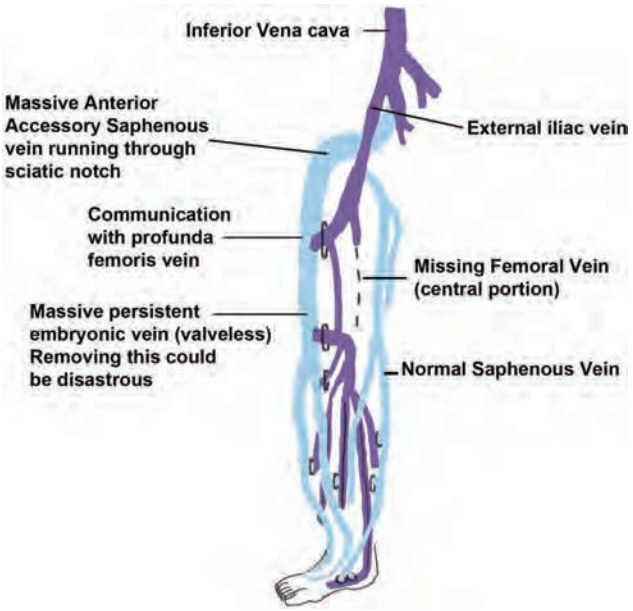

Figure 71.1 Anomalous development of veins of lower limb. Adapted from Tibbs et al. (1997).

Bergman's Comprehensive Encyclopedia of Human Anatomic Variation, First Edition. Edited by R. Shane Tubbs, Mohammadali M. Shoja and Marios Loukas.
© 2016 John Wiley & Sons, Inc. Published 2016 by John Wiley & Sons, Inc.

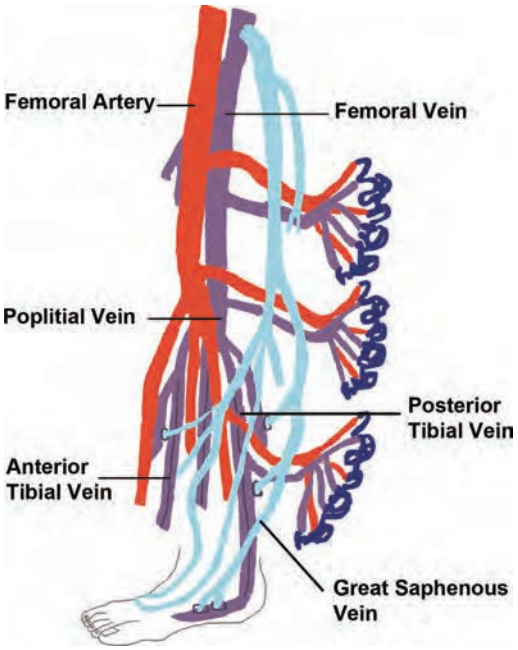

Figure 71.2 Multiple congenital arteriovenous fistulas. Adapted from Tibbs et al. (1997).

Superficial veins of the lower limb

The great and small saphenous veins and their tributaries form the superficial veins.

Great saphenous vein

This begins as a medial continuation of the dorsal venous arch on the dorsum of the foot in front of the medial malleolus and ascends up the medial surface of the leg. It ascends behind the knee on the anteromedial side of the thigh and passes through the saphenous opening, a short distance below the inguinal ligament, to drain into the femoral vein.

Variations in the great saphenous vein are as follows (Dwight et al. 1907):

1. The great saphenous vein can perforate the fascia lata some distance below the saphenous opening.
2. It can occasionally be double.
3. It can be replaced by a network of veins in which no special main stem can be recognized.

Patterns of the great saphenous vein

Cavezzi et al. (2006) investigated the veins of the lower limb using duplex ultrasound and revealed five anatomical patterns of the great saphenous vein in the thigh and at the knee. In the thigh, these patterns are as follows:

1. The great saphenous vein lies in the saphenous compartment with no large parallel tributary.
2. The great saphenous vein comprises two parallel veins in the saphenous compartment.
3. A single great saphenous vein lies in the saphenous compartment with a large subcutaneous tributary joining it at a variable level in the thigh.
4. The great saphenous vein and an anterior accessory saphenous vein come together just before the saphenofemoral junction.
5. There is a single great saphenous vein in the proximal thigh and a large distal subcutaneous tributary joins it at a variable distance along the thigh.

At the knee, the patterns are:

1. One great saphenous vein with no large tributary.
2. A great saphenous vein with one of more tributaries below the knee, typically a posterior arch vein or a Leonardo vein.
3. A great saphenous vein with one large tributary above the knee.
4. The great saphenous vein pierces the saphenous fascia about the midcalf to become a subcutaneous tributary, and is not demonstrable for some distance above or below the knee. It again pierces the saphenous fascia in the distal thigh to become the great saphenous vein.
5. Similar to (4) but the non-demonstrable portion of the great saphenous vein at the level of the knee is very small.

Tributaries of the great saphenous vein

The tributaries draining into the great saphenous vein, depicted in Figure 71.3, are remarkably variable (Bergman et al. 1988). The following refers to parts (A)–(S) of Figure 71.3:

- **A.** The superficial circumflex iliac and superficial epigastric form a common stem to drain into the great saphenous vein, whereas the superficial external pudendal vein drains independently, before the great saphenous vein passes through the saphenous opening. Figure 71.3A is a "textbook" diagram of venous drainage at the saphenous opening. Incidence 37%.
- **B.** The anterior and posterior accessory saphenous veins are multiple, have small lumens, and all open into the great saphenous vein independently. Incidence 6%.
- **C.** The anterior accessory saphenous vein is large and drains into the saphenous opening. An inconstant thoracoepigastric vein connects the superficial epigastric vein and drains into the great saphenous vein instead of the femoral vein. Incidence 2%.
- **D.** The anterior and posterior accessory saphenous veins enter the saphenous opening. Incidence 2%.
- **E.** The superficial external pudendal vein and the posterior accessory saphenous vein form a common stem before joining the great saphenous vein. Incidence 6%.
- **F.** The anterior accessory saphenous, superficial circumflex iliac, and superficial epigastric veins form a common stem and drain into the great saphenous vein. Incidence 9%.
- **G.** The anterior accessory saphenous vein and superficial circumflex iliac veins form a common stem and drain into the saphenous opening. Incidence 9%.
- **H.** The anterior accessory saphenous vein is large. The superficial epigastric and superficial external pudendal veins form a common stem. Incidence 2%.

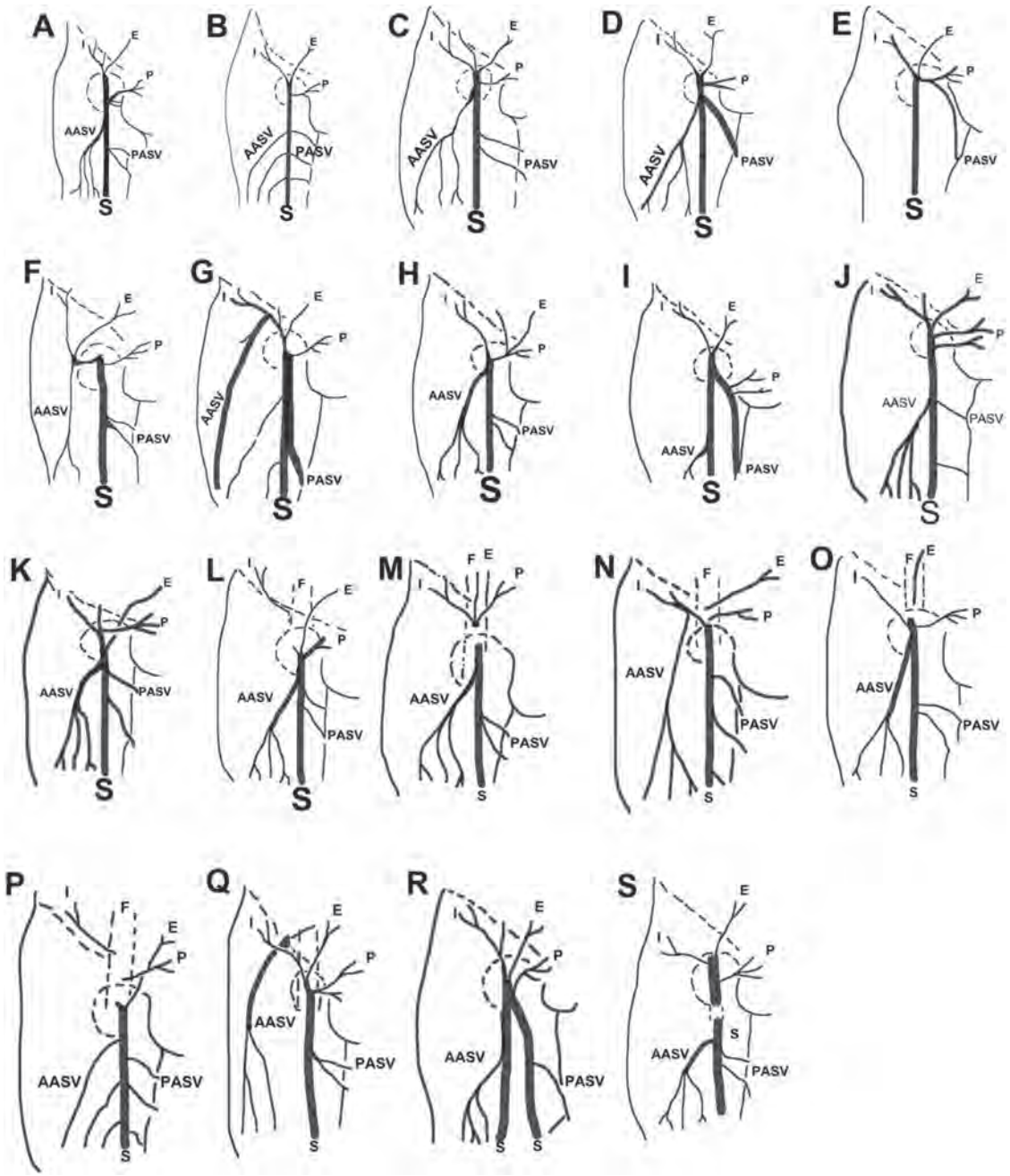

Figure 71.3 The drainage of veins in the great saphenous vein. I: superficial circumflex iliac vein; E: superficial epigastric vein; P: superficial external pudendal vein; AASV: anterior accessory saphenous vein; PASV: posterior accessory saphenous vein; SS: double saphenous vein; S: great saphenous vein; F: femoral vein. Adapted from Bergman et al. (1988) and Glasser (1943).

I. There are two superficial external pudendal veins, and a large posterior accessory saphenous vein is present. Incidence 1%.

J. The two superficial external pudendal veins drain into the saphenous opening. Incidence 3%.

K. The superficial epigastric vein drains into the great saphenous vein below the saphenous opening. Incidence 3%.

L. The superficial circumflex iliac vein opens into the femoral vein instead of the great saphenous vein. Incidence 1%.

M. The superficial circumflex iliac, superficial external pudendal, and superficial epigastric veins drain directly into the femoral vein. Incidence 6%.

N. The anterior accessory saphenous vein and the superficial circumflex iliac vein form a common stem. The superficial

external pudendal and superficial epigastric veins drain directly into the femoral vein. Incidence 1%.

O. The superficial epigastric vein drains directly into the femoral vein, whereas the anterior accessory saphenous vein passes into the saphenous opening. Incidence 6%.

P. The anterior and posterior accessory saphenous veins have small lumens. The superficial circumflex iliac and the superficial external pudendal veins drain into the femoral vein directly. Incidence 1%.

Q. The anterior accessory saphenous vein drains into the femoral vein directly. Incidence 1%.

R. There are two great saphenous veins, which join at the saphenous opening. Incidence 3%.

S. The great saphenous vein pierces the fascia lata about 1 inch (2.54 cm) below the saphenous opening to drain into the femoral vein. Incidence 1%.

Small saphenous vein

The small saphenous vein begins posterior to the lateral malleolus as a lateral continuation of the dorsal venous arch. It pierces the deep fascia of the upper half of the calf and runs between the two heads of the gastrocnemius to terminate in the popliteal vein. Giacomini (1873) described the thigh extension of the small saphenous vein, which was confirmed by Georgiev et al. (2003) in 95% of limbs.

1. The mode of ending of the small saphenous vein is variable (Standring 2008): (a) a communication branch from the small saphenous vein can ascend medially to terminate in the accessory saphenous vein or can be the main continuation of the small saphenous vein; (b) it can join the great saphenous vein in the proximal thigh; (c) it can bifurcate: one branch joins the great saphenous vein and the other drains into popliteal vein or profunda femoris vein (Fig. 71.4); or (d) sometimes it ends distal to the knee in the great saphenous vein or in the deep sural muscular veins.
2. The small saphenous vein can continue up the thigh with or without a small communication with the popliteal or profunda femoris vein, and can enter the pelvis with the sciatic nerve to drain into the internal iliac vein (Dwight et al. 1907).

Deep veins of the lower limb

The deep veins comprise the femoral, popliteal, anterior tibial, posterior tibial, and peroneal veins and the medial and lateral plantar veins and their tributaries. Variations in the venous anatomy of the lower limb are common and have important implications for diagnostic venogram imaging of deep vein thrombosis.

Femoral vein

The femoral vein accompanies the femoral artery in the femoral triangle and in the adductor canal. It begins as a continuation of the popliteal vein at the adductor hiatus and ends as the external iliac vein posterior to the inguinal ligament.

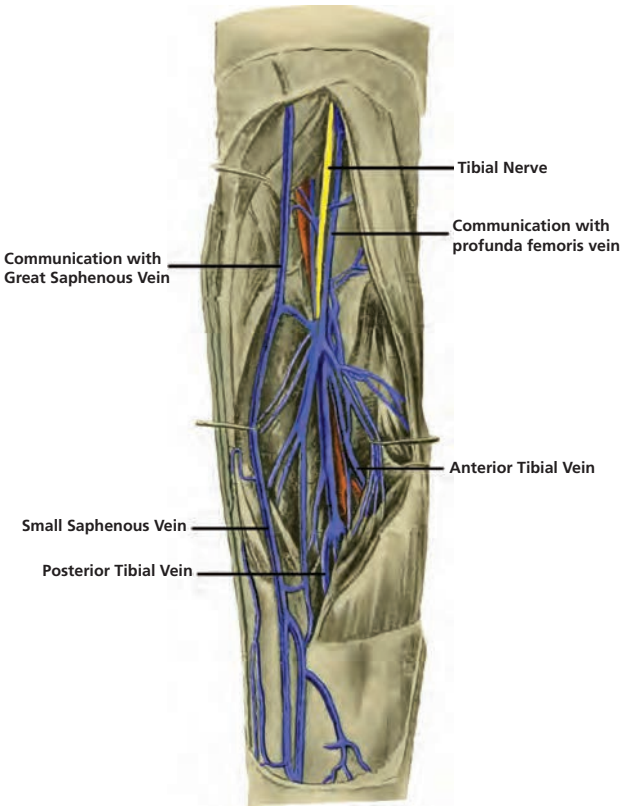

Figure 71.4 Veins in the popliteal fossa. Adapted from Dwight et al. (1907) with permission from Wolters Kluwer Health.

The term "superficial femoral vein" should be abandoned as the femoral comes under the category of deep veins. The word "superficial" can be misleading and can create fatal consequences in terms of treatment for deep vein thrombosis (Bundens et al. 1995; Hammond 2003).

The femoral vein has many muscular tributaries. The profunda femoris vein drains into it about 4–12 cm distal to the inguinal ligament.

1. The femoral vein can be double for part of or throughout its extent. Quinlan et al. (2003) observed multiple femoral veins in 32.5% of limbs, most of which were duplicated (253 out of 265), while 1.5% were triplicated or more complex. Patients with multiple femoral veins have a higher incidence of deep vein thrombosis than patients with single femoral veins. A decrease in blood flow velocity and subsequent pooling of blood in the duplicated vein could promote the formation of thrombi (Liu et al. 1986).
2. The femoral vein can split into two and encircle the femoral artery or lie posterior to it (Dwight et al. 1907).
3. False negative ultrasound diagnosis of deep vein thrombosis is higher in patients with duplicated femoral veins than in patients with single femoral veins (Screaton et al. 1998).
4. Occasionally the femoral vein lies anterior to the femoral artery throughout its extent (Dwight et al. 1907).

5. The femoral vein can take the form of a plexus of veins (Bergman et al. 1988).
6. The obturator vein can drain into the femoral vein (Bergman et al. 1988).
7. The femoral vein occasionally passes through the adductor magnus above the adductor hiatus, where it is normally perforated by one of the perforating veins. This arrangement is apparently due to enlargement of the profunda femoris vein, and the anastomosis between the perforating veins and the femoral vein can take the form of small venae comitantes or be reduced in size (Dwight et al. 1907).
8. The femoral vein can pierce the adductor magnus at the lesser trochanter and run with the sciatic nerve. In such cases the inferior gluteal artery is the primary vessel of the thigh and the femoral artery is very small (Bergman et al. 1988).

Profunda femoris vein/deep vein of the thigh

Normally the profunda femoris vein accompanies the profunda femoris artery and drains into the femoral vein in the femoral triangle. Through its tributaries, the profunda femoris vein connects distally with the popliteal vein and proximally with the inferior gluteal vein. The profunda femoris vein has many muscular tributaries. The medial and lateral circumflex femoral veins can terminate in the profunda femoris vein or the femoral vein. The terminations of the medial and lateral circumflex femoral veins can be classified into four types, as illustrated in Figure 71.5 (Bergman et al. 1988):

- Class I: The medial and lateral circumflex veins drain into the femoral vein directly (86.14% of 541 observations).
- Class II: The lateral circumflex femoral vein drains into the profunda femoris vein, whereas the medial circumflex femoral vein terminates in the femoral vein directly (5.18%).
- Class III: The medial circumflex femoral vein drains into the profunda femoris vein, whereas the lateral circumflex femoral vein terminates in the femoral vein directly (6.28%).
- Class IV: Both medial and lateral circumflex femoral veins drain directly into the profunda femoris vein (1.85%).

Most textbooks describe the circumflex femoral veins as terminating in the profunda femoris vein (class IV). In the above series, only 1.85% of the veins ended in that manner. This contrasts with Class I, in which the circumflex veins terminate directly in the femoral (86.14% of the 541 observations).

Class I has six subtypes:

- Type IA (64.87%) has single medial and lateral circumflex femoral veins terminating in the femoral vein, the medial circumflex femoral vein being the more proximal.
- Type IB (12.57%) has two lateral circumflex femoral veins which drain into the femoral vein distal to a single medial circumflex femoral vein.
- Type IC (3.70%) has two medial circumflex femoral veins lying proximal to a single lateral circumflex femoral vein.
- Type ID (14.98%) has two medial circumflex femoral veins and two lateral circumflex veins. Each medial circumflex femoral is proximal to its corresponding lateral circumflex femoral vein, although both the medial circumflex femoral veins are not necessarily proximal to the two lateral circumflex femoral veins.
- Type IE (2.96%) has the lateral circumflex femoral vein proximal to the medial circumflex femoral vein.
- Type IF (0.92%) has no medial circumflex femoral vein.

In subtypes IA, IB, and IC, the termination of the medial circumflex femoral vein is proximal to that of the lateral circumflex femoral vein. The termination of the medial circumflex femoral is proximal to that of the lateral circumflex femoral vein in the large majority of cases.

Class II (5.18%) has two types: In both subtypes, the medial circumflex femoral vein is characteristically proximal to the lateral circumflex femoral vein.

- Type IIA (4.07%) has a single medial circumflex emptying into the femoral vein and a single lateral circumflex femoral emptying into the profunda femoris vein.
- Type IIB (1.11%) has an accessory lateral circumflex femoral vein ending in the femoral, just distal to the medial circumflex femoral vein.

Class III (6.28%) has four subtypes:

- Type IIIA (3.51%) has a single medial circumflex femoral terminating in the profunda femoris vein, while the lateral circumflex terminates superiorly in the femoral.
- Type IIIB (1.56%) has an accessory medial circumflex femoral vein emptying into the femoral itself, proximal to the lateral circumflex vein.
- Type IIIC (0.74%) has two adjacent lateral circumflex femoral veins rather than a single vein.
- Type IIID (0.37%) has duplicate lateral circumflex veins emptying into the femoral and a single medial circumflex emptying into the profunda femoris vein.

In Class IV (1.85%), both the lateral and medial circumflex femoral veins end in the profunda femoris vein.

- Type IVA is more common and has a single medial circumflex femoral and a single lateral circumflex femoral, both emptying into the profunda femoris vein.
- Type IVB has an accessory medial circumflex femoral ending in the femoral.

Popliteal vein

Normally the popliteal vein runs with the popliteal artery and begins at the lower border of the popliteus by the union of the anterior and posterior tibial veins. The popliteal vein ascends through the floor of the popliteal fossa and pierces the adductor hiatus with the popliteal artery to continue as the femoral vein. The formation of the popliteal vein can be classified into three groups according to the number of popliteal veins at the level of the knee (Williams 1953):

- Group 1 (Fig. 71.6a): one popliteal vein. This group conforms to the usual description: the peroneal vein drains into the posterior tibial vein and the posterior tibial vein joins the anterior tibial vein to form the popliteal vein.
- Group 2 (Fig. 71.6b–d): two popliteal veins. This is the largest group, comprising two-thirds of cases. Of the two popliteal veins, one is much smaller than the other. The smaller trunk could

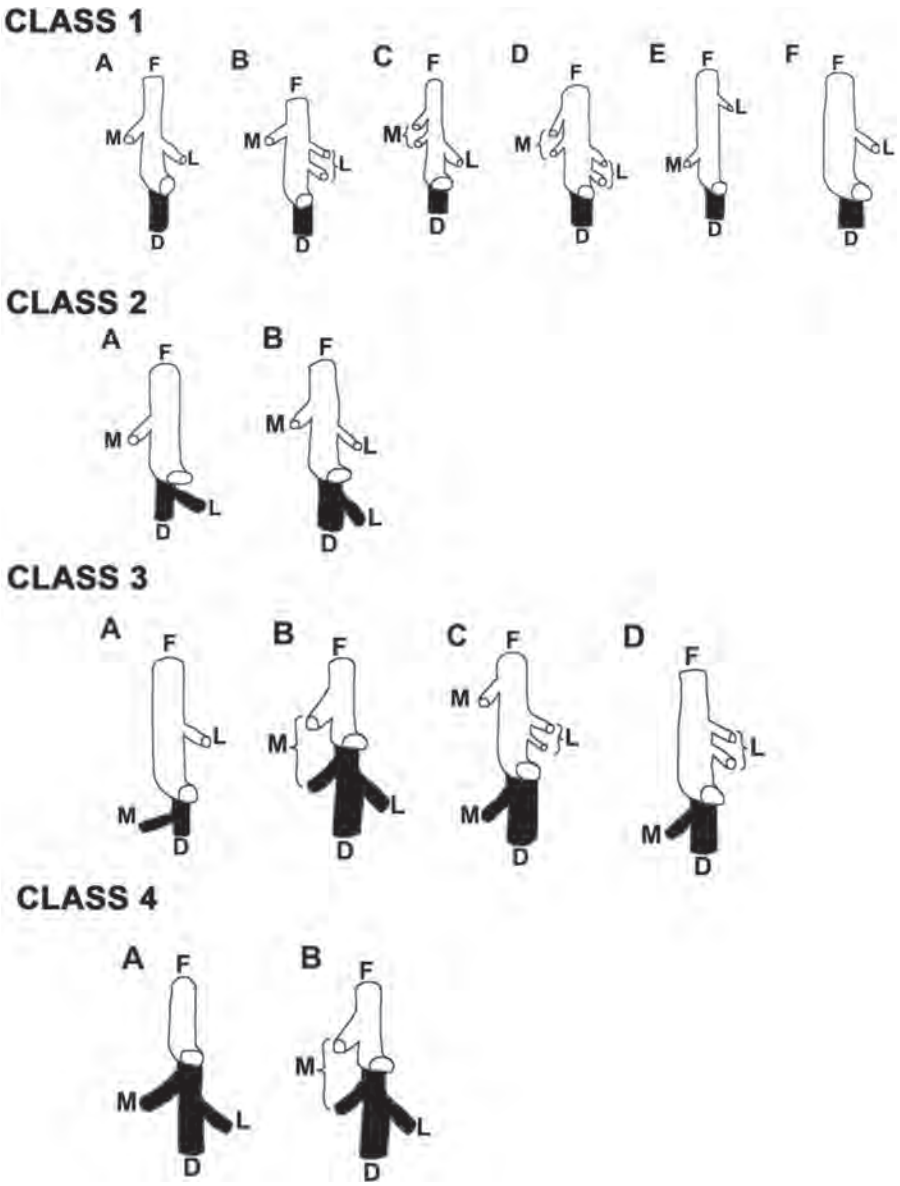

Figure 71.5 Various terminations of lateral and medial circumflex femoral veins. F: femoral vein; D: profunda femoris vein: M: medial circumflex femoral vein; L: lateral circumflex femoral vein. Adapted from Bergman et al. (1988).

be just one of the venae comitantes of the anterior tibial vein (Fig. 71.6b). The two popliteal veins can stay separate throughout their extent and they join to form the femoral vein above the knee (Fig. 71.6c), or the popliteal vein collateral is formed by branches of the anterior tibial and peroneal veins (Fig. 71.6d).

- Group 3 (Fig. 71.6e): three popliteal vein divisions formed individually by the anterior tibial, posterior tibial and peroneal veins. They join in different ways above the knee to form the femoral vein.

A wide range of variations of the popliteal vein have been described (Dwight et al. 1907).

1. Sometimes the communications of the popliteal vein with the profunda femoris vein become so large that the popliteal vein bifurcates. One branch becomes continuous with the femoral vein and the other with the profunda femoris vein.
2. The popliteal vein can be considerably shorter than usual.
3. It can be duplicated throughout its extent. Quinlan et al. (2003) observed duplication of the popliteal vein in 42% of limbs, of which 5% were true duplicated popliteal veins.
4. It can occasionally lie anterior to the popliteal artery.
5. Occasionally the popliteal vein ascends along the back of the thigh, either uniting with the tributaries of the profunda femoris vein or continuing into the pelvis with the sciatic nerve to become a tributary of the internal iliac vein. This anomaly is occasionally presented by the sciatic artery.
6. The popliteal artery and vein can be trapped in the medial head of the gastrocnemius and a variant vein may connect the popliteal to the profunda femoris or femoral vein in the adductor hiatus (Fig. 71.7).

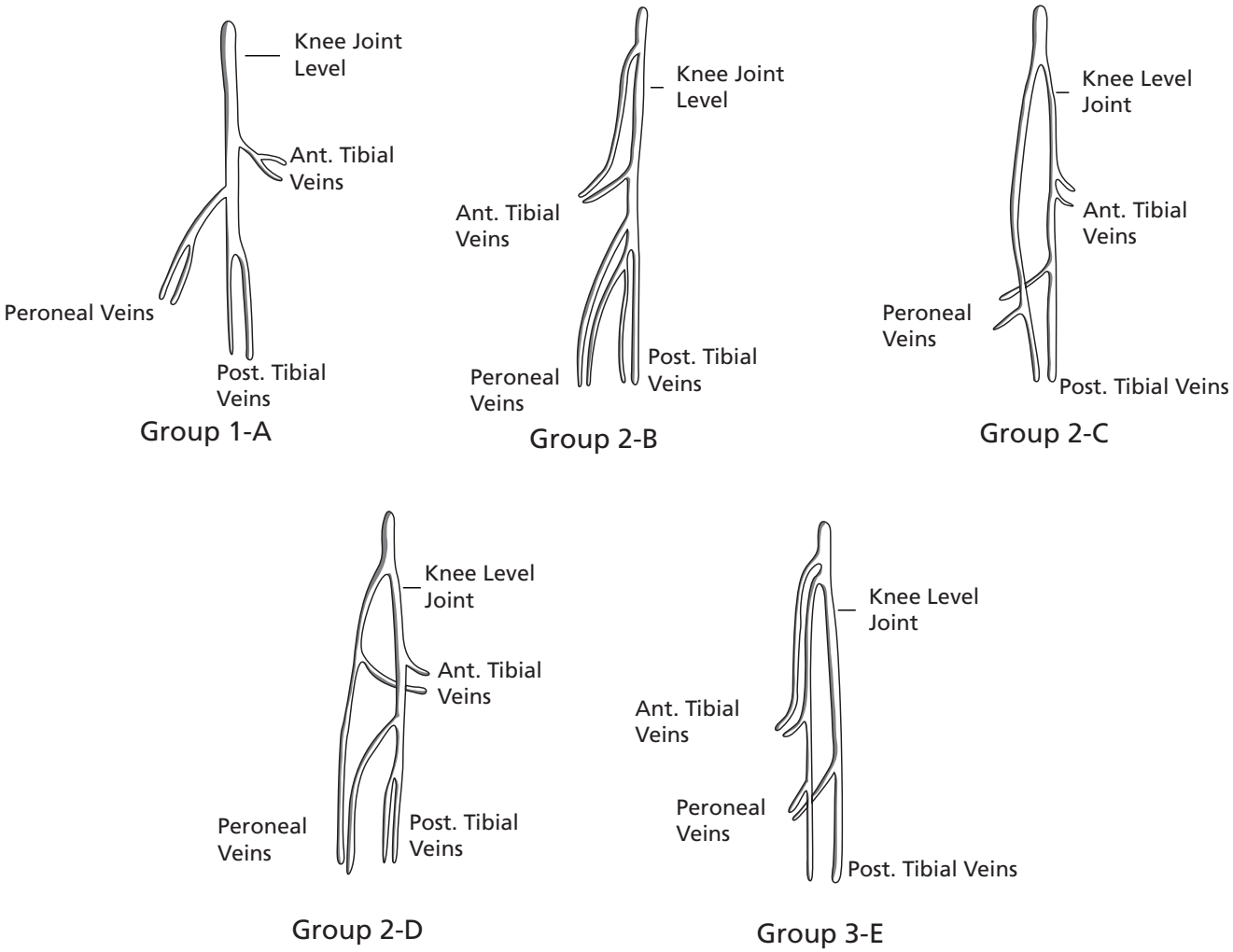

Figure 71.6 Variations in formation of popliteal vein. Adapted from Williams (1953) with permission from the Journal of the American College of Surgeons.

7. Occasionally, the third head of the gastrocnemius can entrap the tibial nerve and/or popliteal vessels and their branches; this causes no impairment of function in some individuals but can lead to impairment of the blood circulation in leg and foot or to muscle weakness in others (Bergman et al. 1988).

Deep veins of leg and foot

The deep veins of the foot form two divisions: plantar and dorsal. The plantar digital veins in the toes drain into the plantar metatarsal veins, which form the medial and lateral plantar veins. The body weight pressing against the ground with each step and contraction of the muscles of the feet provide a substantial pumping mechanism (muscle pump) for draining the capacious venous plexus of the sole of the foot. The medial and lateral plantar veins join to form the posterior tibial veins, which run with the posterior tibial artery.

The posterior tibial veins drain all the muscles of the posterior compartment of the leg. The big tributaries of the posterior tibial veins include the peroneal or fibular veins. There is considerable variation in venous drainage of the calf muscles. Irregular smaller plexuses of veins inside the soleus join to form the intramuscular soleal venous plexus (soleal pump). These veins form one to several main trunks to drain into the posterior tibial veins or peroneal veins in different ways. There can be one common venous trunk from the soleus muscle, which terminates in the posterior tibial or peroneal veins. Alternatively, terminal veins from the soleus muscle can form multiple intramuscular connections with the posterior tibial or peroneal veins at different levels in the leg.

The intramuscular venous plexus in the gastrocnemius muscle comprises 2–12 veins draining each head of the gastrocnemius and forming a characteristic pattern of termination. Eighty-seven percent of these drain into the popliteal vein, while the

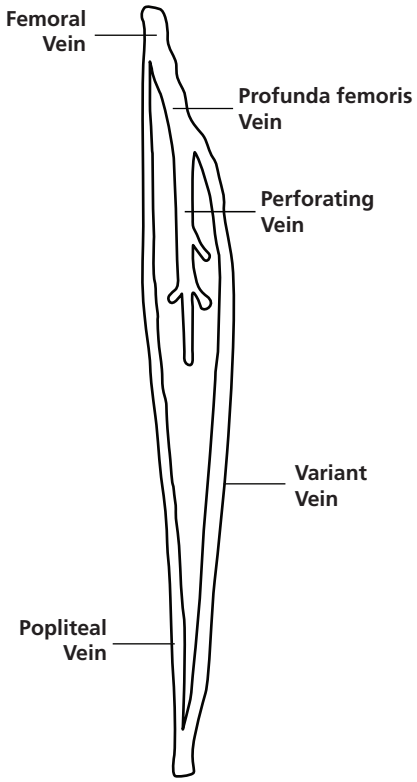

Figure 71.7 A variant vein duplicating the popliteal vein. Adapted from Bergman et al. (1988) and Arnold (1968).

other 13% drain into the posterior tibial vein or peroneal vein. The veins emerging from each head of the gastrocnemius can drain into each gastrocnemius trunk, or smaller veins from the gastrocnemius can drain into collateral veins to empty into the gastrocnemius trunk (Aragão et al. 2006).

On the dorsum of the foot, the dorsalis pedis veins drain the dorsal metatarsal veins formed from the deep dorsal digital veins of the toes. The dorsalis pedis veins become the anterior tibial veins in the anterior compartment of the leg.

Most of the anterior tibial (68%), posterior tibial (76%), and peroneal (76%) veins are paired. Single anterior tibial veins are seen in 32%, posterior tibial in 17%, and peroneal veins in 6%. Three or more peroneal veins are seen in 8% of patients. The peroneal veins drain into the trifurcation 59%, into the posterior tibial 32%, and into the anterior tibial veins 8% of the time. Variable numbers of gastrocnemius veins (1–6) are visualized (Quinlan et al. 2003).

There are approximately 9–11 valves in the anterior tibial vein, 9–19 in the posterior tibial vein, 7 in the peroneal vein, 1 in the popliteal vein, and 3 in the femoral vein. More than five valves in the deep veins between the popliteal fossa and ischial spine can lead to a higher incidence of deep vein thrombosis (35%) than in cases with five or fewer valves (13%) ($p<0.001$) (Liu et al. 1986).

Perforating veins/perforators

There are as many as 150 perforators in the lower limb, but only few of them are clinically important. The perforating veins are very variable in arrangement, size, and distribution.

Delis (2005) reported the highest prevalence of incompetent perforator veins in the middle third of the medial calf (29.8%), the lower third of the medial calf (15.3%), the middle third of the medial thigh (13.2%), and the middle third of the posterior calf (9.7%). The incidence of valvular incompetence increases significantly with the severity of chronic venous disease with incompetent perforating veins.

Perforators have been named by an international interdisciplinary consensus (Caggiati et al. 2002, 2005).

Perforators of foot and ankle

About half the perforators of the foot and ankle have valves and always face toward the superficial vein, allowing the blood to flow from deep to superficial veins. This is in contrast to the perforating veins of the leg and thigh in which the valves face the deep vein system, allowing the blood to flow from superficial to deep veins under normal conditions. The other half of the perforating veins are valveless. It is therefore assumed that blood flows through these perforators freely in both directions (Kuster et al. 1968).

Perforators of the foot (Figs 71.8, 71.9) include: dorsal (intercapitular veins); medial; lateral; and plantar foot perforators. Ankle perforators (Figs 71.8, 71.9) include: medial; anterior; and lateral ankle perforators.

Perforator 1 (Fig. 71.8) connects the great saphenous vein with the dorsalis pedis vein and has no valves. Most of the perforators are located below the malleoli, on the medial and lateral

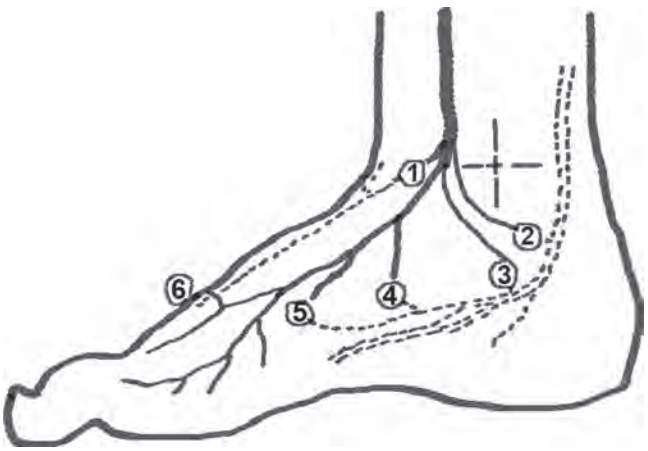

Figure 71.8 Perforating veins connecting great saphenous vein with the deep veins of the foot. The circled numbers indicate the locations at which the perforating veins pierce the deep fascia. Adapted from Kuster et al. (1968) with permission from the Journal of the American College of Surgeons.

side of the ankle and the foot. The medial perforators (2–5; Fig. 71.8) connect the great saphenous vein with the medial plantar veins. Perforators 2 and 5 are inconstant. Perforator 6 (Fig. 71.8) is on the dorsum of the foot connecting the dorsalis pedis vein with the dorsal venous arch.

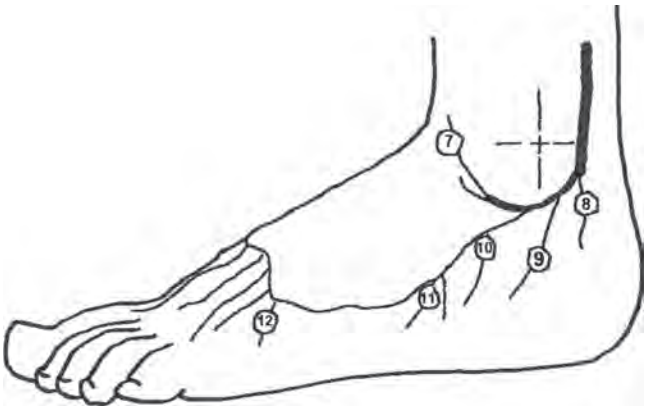

Figure 71.9 Perforating veins connecting small saphenous vein with the deep veins of the foot. The circled numbers indicate the locations at which the perforating veins pierce the deep fascia. Adapted from Kuster et al. (1968) with permission from the Journal of the American College of Surgeons.

The lateral perforators (8–12; Fig. 71.9) connect the small saphenous vein with the lateral plantar veins. Perforators 9–12 are inconstant (Kuster et al. 1968).

Leg perforators

Leg perforators (Fig. 71.10) are classified into four main groups:

1. Medial leg perforators have two subtypes: (a) Paratibial perforators connect the main trunk/tributaries of the great saphenous vein to the posterior tibial vein. These are known as Sherman perforators in the lower and mid leg and Boyd perforators in the upper leg. (b) Posterior tibial perforators, known as Cocket perforators, connect the posterior arch vein with the posterior tibial veins (upper, middle and lower Cocket perforators).
2. Anterior leg perforators connect the anterior tributaries of the great saphenous vein with the anterior tibial veins.
3. Lateral leg perforators connect veins of the lateral venous plexus with the fibular veins.
4. Posterior leg perforators include: medial gastrocnemius perforators; lateral gastrocnemius perforators; intergemellar perforators which connect the small saphenous vein with the calf veins (mid-calf perforators of May); and para-Achillean perforators which connect the small saphenous vein with the fibular veins (perforator of Bassi).

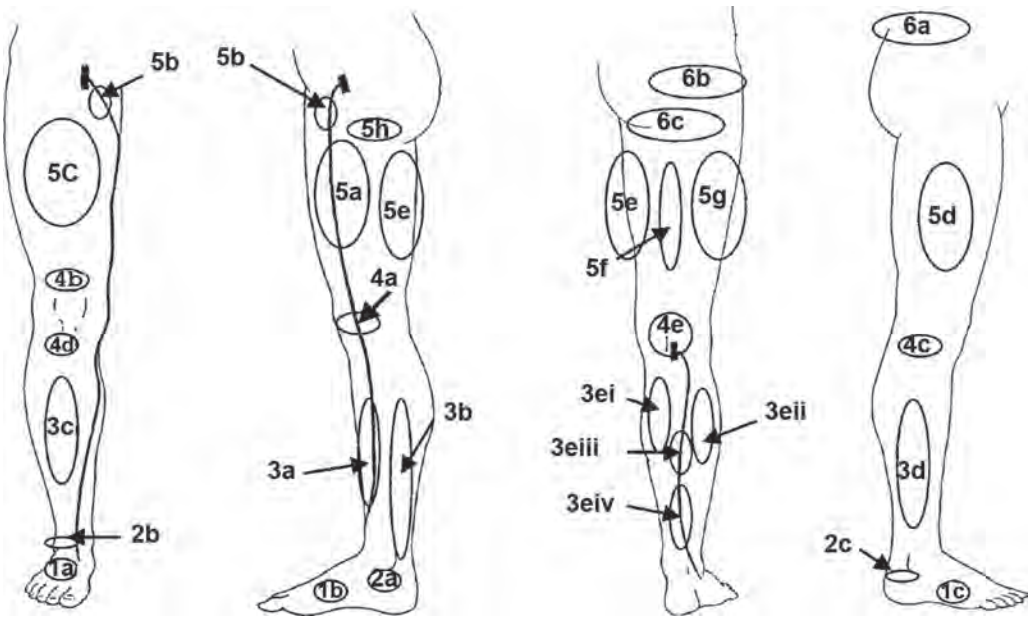

Figure 71.10 Topography of perforating veins (PVs) of lower limb. Foot perforating veins: 1a, dorsal foot PVs; 1b, medial foot PVs; 1c, lateral foot PVs. Ankle perforating veins: 2a, medial ankle PVs; 2b, anterior ankle PVs; 2c, lateral ankle PVs. Leg perforating veins: 3a, paratibial PV; 3b, posterior tibial PV; 3c, anterior leg PV; 3d, lateral leg PV; 3ei, medial gastrocnemius PVs; 3eii, lateral gastrocnemius PVs; 3eiii, intergemellar PVs; 3eiv, para-Achillean PVs. Knee perforating veins: 4a, medial knee PVs; 4b, suprapatellar PVs; 4c, lateral knee PVs; 4d, infrapatellar PVs; 4e, popliteal fossa PVs. Thigh perforating veins: 5a, PV of femoral canal; 5b, inguinal PVs; 5c, anterior thigh PVs; 5d, lateral thigh PVs; 5e, posteromedial PVs; 5f, sciatic PVs; 5g, posterolateral thigh PVs; 5h, pudendal PVs. Gluteal perforating veins: 6a, superior gluteal PVs; 6b, midgluteal PVs; 6c, lower gluteal PVs. Adapted from Caggiati et al. (2002) with permission from Elsevier.

Perforators of the knee

Perforators of the knee (Fig. 71.10) include: medial; lateral; infrapatellar; and popliteal fossa perforators.

Perforators of thigh

Perforators of the thigh (Fig. 71.10) include:

- Medial thigh perforators: femoral canal perforators (Dodd) and inguinal perforators connect the great saphenous vein or its tributaries with the femoral vein in the groin.
- Anterior thigh perforators, which pierce the quadriceps femoris.
- Lateral thigh perforators.
- Posterior thigh perforators, including posteromedial, posterolateral (perforators of Hach), sciatic, and pudendal perforators.
- Perforators of the gluteal muscles, including superior, middle, and lower gluteal perforators.

References

Aragão JA, Reis FP, Pitta GBB, Miranda Jr F, de Figueiredo P. 2006. Anatomical study of the gastrocnemius venous network and proposal for a classification of the veins. *Eur J Vasc Endovasc Surg* 31: 439–442.

Arnold G. 1968. Seltene Gefass, und muskalanomalien am bein. *Anat Anz* 123: 471–475.

Bergman RA, Thompson SA, Afifi AK, Saadeh FA. 1988. Commendium of Human Anatomical Variation. Baltimore, Munich: Urban and Schwarzenberg.

Bundens WP, Bergan JJ, Halasz NA, Murray J, Drehobl M. 1995. The superficial femoral vein. A potentially lethal misnomer. *JAMA* 274(16): 1296–1298.

Caggiati A, Bergan JJ, Gloviczki P, Jantet G, Wendell-Smith CP, Partsch H. 2002. Nomenclature of the veins of lower limb: An International Interdisciplinary consensus statement. *J Vasc Surg* 36: 416–422.

Caggiati A, Bergan JJ, Gloviczki P, Eklof B, Allegra C, Partsch H. 2005. Nomenclature of the veins of lower limb: Extensions, refinements, and clinical application. An international interdisciplinary consensus committee on venous anatomical terminology. *J Vasc Surg* 41: 719–724.

Cardoso BB, Alvarenga CO, Miyahara MDS, Burihan MC, Raphaella M, Lima QAD, Kuwahara C, Silva RCM. 2010. Persistent sciatic vein. *J Vasc Bras* 9(3): 137–140.

Cavezzi A, Labropoulos N, Partsch H, Ricci S, Caggiati A, Myers K, Nicolaides A, Smith PC. 2006. Duplex ultrasound investigation of the veins in chronic venous disease of the lower limbs: UIP consensus document. Part II. Anatomy. *Eur J Vasc Endovasc Surg* 31: 288–299.

Cunningham DJ. 1918. *Cunningham's Textbook of Anatomy, fifth edition*. New York: William Wood and Company.

Delis KT. 2005. Leg perforator vein incompetence: Functional anatomy. *Radiology* 235: 327–334.

Dwight T, McMurrich JP, Hamann CA, Piersol GA, White JW, Heisler JC. 1907. *Human Anatomy, Including Structure and Development and Practical Considerations*. Philadelphia and London: J.B. Lippincott Company.

Georgiev M, Myers KA, Belcaro G. 2003. The thigh extension of lesser saphenous vein: from Giacomini's observations to ultrasound scan imaging. *J Vasc Surg* 37(3): 558–563.

Giacomini C. 1873. Osservazioni anatomiche per servire allo studio della circolazione venosa delle estremita inferiori: Parte I: Delle vene superficiali dell'arto addominale e principalmente della saphena sterna. *Giornale della Reale Accademia di Medicina di Torino* 14: 109–215.

Glasser ST. 1943. An anatomic study of venous variations at the fossa ovalis. *Arch Surg* 46: 289–295.

Hammond I. 2003. The superficial femoral vein. *Radiology* 229(2): 604–606.

Kuster G, Lofgren EP, Hollinshead WH. 1968. Anatomy of veins of foot. *Surg Gyn Obstet* 24: 817–823.

Liu GC, Ferris EJ, Reifsteck JR, Baker ME. 1986. Effect of anatomic variations on deep venous thrombosis of the lower extremity. *AJR* 146: 845–848.

Quinlan DJ, Alikhan R, Gishen P, Sidhu PS. 2003. Variations in lower limb venous anatomy: Implications for US diagnosis of deep vein thrombosis. *Radiology* 228: 443–448.

Screaton NJ, Gillard JH, Berman LH, Kemp PM. 1998. Duplicated superficial femoral veins: a source of error in the sonographic investigation of deep vein thrombosis. *Radiology* 206(2): 397–401.

Standring S. 2008. Gray's Anatomy: The Anatomical Basis of Clinical Practice, 40th edition. Edinburgh: Churchill-Livingstone, Elsevier.

Tibbs DJ, Sabiston DC, Davies MG, Mortimer PS, Scurr JH. 1997. Varicose Veins, Venous Disorders, and Lymphatic Problems in the Lower Limbs. Oxford: Oxford University Press.

Williams AF. 1953. The formation of popliteal vein. *Surg Gyn Obstet* 99: 769–772.

72 Venous drainage of the spinal cord

Joel Raborn[1], Christoph J. Griessenauer[1], Mohammadali M. Shoja[2], and R. Shane Tubbs[3]
[1]University of Alabama at Birmingham, Birmingham, Alabama, United States
[2]Tuberculosis and Lung Disease Research Center, Tabriz University of Medical Sciences, Tabriz, Iran
[3]Seattle Science Foundation, Seattle, Washington, USA
St George's University, School of Medicine, St Georges, Grenada
University of Dundee, Dundee, UK

The venous system of the spine and spinal cord can be divided into intrinsic, extrinsic, and extradural components.

Intrinsic system

Axially oriented intrinsic venous system

In the central section of the spinal cord, capillaries from the medial parts of both sides drain into axially oriented, ventral (medial and anteromedial), and dorsal (medial and posteromedial) sulcal veins (Lasjaunias and Berenstein 1990). The ventral sulcal veins collect blood from nearby structures including the medial portion of the anterior horns, the anterior commissure, and white matter from the anterior funniculus (Santillan et al. 2012). The number of ventral sulcal veins varies over the length of the spinal cord. There are 4–8 ventral sulcal veins per centimeter in the cervical and upper thoracic areas, with a diameter of 100–200 μm. In the lower third of the thoracic cord and the lumbosacral area, their number density increases to 6–8 cm^{-1} and 8–12 cm^{-1}, respectively (Moes and Maillot 1981; Thron and Rossberg 1988; Lasjaunias and Berenstein 1990). The dorsal sulcal veins are similar in diameter (100–300 μm) and found at a number density of 4–6 cm^{-1} in the cervical cord (Moes and Maillot 1981; Thron and Rossberg 1988), 2–3 cm^{-1} in the upper thoracic cord, and 1–4 cm^{-1} in the thoracolumbar area (Moes and Maillot 1981; Thron and Rossberg 1988). The ventral dominance observed in the arterial system is therefore only partially present in the venous system of the thoracolumbar region (Lasjaunias and Berenstein 1990).

In the peripheral section, capillaries from peripheral gray matter and white matter travel toward the periphery forming radial veins (Lasjaunias and Berenstein 1990). Once these radial veins reach the spinal surface, they form a venous ring that continues to the extrinsic venous system (Santillan et al. 2012). This intrinsic system has an intricate network of anastomoses uniting the radial and sulcal veins and central and peripheral sections. This is most prominent in the thoracic region (Thron and Rossberg 1988). Transmedullary anastomotic veins span between the ventral and dorsal surface of the cord and are larger in caliber (100–700 μm) than sulcal veins and less concentrated (1–2 cm^{-1}), particularly in the lower thoracic and lumbar regions (Moes and Maillot 1981; Thron and Rossberg 1988; Lasjaunias and Berenstein 1990). They do not seem to collect drainage from smaller veins and travel horizontally through the midline of the spinal cord while also ascending or descending obliquely and longitudinally at the gray commissure (Thron and Rossberg 1988; Lasjaunias and Berenstein 1990).

Longitudinally oriented intrinsic venous system

In addition to highly prevalent axial anastomosis, the spinal cord has highly variable longitudinal intrinsic anastomosis present in the gray and white matter linking axial anastomosis (Lasjaunias and Berenstein 1990). The ventral and especially dorsal sulcal veins are joined via multimyelomeric ventro-dorsomedial or ventro-dorsolateral anastomoses. In the periphery, radial veins have longitudinal "intersegmental bridges" linking them. These bridges are considered part of the extrinsic venous system (Lasjaunias and Berenstein 1990).

Extrinsic system

The extrinsic system begins at the level of the spinal pia and includes the pial venous networks, the longitudinally oriented extrinsic venous system, and radicular veins (Santillan et al. 2012).

Pial venous networks

Pial venous collectors receive sulcal veins while intersegmental bridges link radial collectors that eventually drain into the anterior and posterior median veins, part of the longitudinally

Bergman's Comprehensive Encyclopedia of Human Anatomic Variation, First Edition. Edited by R. Shane Tubbs, Mohammadali M. Shoja and Marios Loukas.
© 2016 John Wiley & Sons, Inc. Published 2016 by John Wiley & Sons, Inc.

oriented extrinsic venous system, and its derivatives. Such connectors that are located laterally on the spinal cord are short and less prominent. The pial network is slightly more prominent ventrally, with one transverse vein occurring every 1–3 cm in the cervical and upper thoracic cord. The lumbosacral area is also rich in ventral transverse pial veins. Dorsal pial veins are most frequently found in the high cervical region around C2 and at the upper and lower extents of the thoracic region at approximately T1–2 and T9, respectively. The diameter of the pial collectors is around 400–500 μm, comparable to the size of the anterior and posterior median veins (Moes and Maillot 1981; Thron and Rossberg 1988; Lasjaunias and Berenstein 1990).

Longitudinally oriented extrinsic venous system

While the pial venous network has some axial components, the extrinsic system (for the most part) follows a longitudinal orientation. Longitudinal collectors at ventral and dorsal surfaces in the midline of the spinal cord represent the dominant venous channel of this system. In the dorsal cervical and lumbosacral regions there is usually a single ventral and dorsal collector, referred to as the anterior (ventral) and posterior (dorsal) median veins. The diameter of this single vessel can reach 500 μm in the cervical and up to 2000 μm in the lumbosacral region (Moes and Maillot 1981; Thron and Rossberg 1988; Lasjaunias and Berenstein 1990).

The anterior median vein accompanies the anterior spinal artery on the anteromedial surface of the spinal cord and continues to become the vein of the filum terminale (Gillilan 1970; Thron and Rossberg 1988; Lasjaunias and Berenstein 1990; Goshgarian 2003). In the ventral cervical and upper thoracic regions, up to three ventromedial venous channels are present. Three anterior cervical and upper thoracic longitudinal channels converge in the lower thoracic area, continue as a duplication, and unite proximal to the lumbosacral area (Moes and Maillot 1981; Thron and Rossberg 1988; Lasjaunias and Berenstein 1990). On the dorsal surface of the cord, there is triplection in the thoracic region and the vessels converge at the cervicothoracic and thoracolumbar junctions (Moes and Maillot 1981; Thron and Rossberg 1988; Lasjaunias and Berenstein 1990). The largest and most prominent veins (diameter up to 850 μm) travel on the posteromedial surface, while the other two veins follow the two posterior spinal arteries on the posterolateral surface of the spinal cord and are also referred to as the posterolateral spinal veins (Moes and Maillot 1981).

This redundancy at the thoracic level, as well as the number of transmedullary anastomoses, results in a decrease in flow and renders the cord susceptible to venous stasis and engorgement (Moes and Maillot 1981; Lasjaunias and Berenstein 1990; Goshgarian 2003). The posterior median vein also receives blood from radial veins and venous rings (Moes and Maillot 1981; Thron and Rossberg 1988; Lasjaunias and Berenstein 1990; Brockstein et al. 1994; Goshgarian 2003; Santillan et al. 2012). Secondary venous networks may exist that contribute to or replace these longitudinal venous channels at various segments (Santillan et al. 2012).

Radicular veins

The anterior and posterior venous segments collect blood over an equal territory, unlike the arterial system that exhibits more anterior dominance (except for the thoracolumbar region, where ventral sulcal veins are more prominent compared to their dorsal counterparts; Lasjaunias and Berenstein 1990). Radicular veins, veins that connect the extrinsic to the extradural systems, are therefore almost equally as common on the ventral and dorsal roots (Fig. 72.1). These veins are analogous to radiculomedullary arteries and, to be precise, are named radiculomedullary veins since they drain the spinal cord. They receive blood from the anterior or posterior median veins (Santillan et al. 2012).

There are numerous ventral (anterior) and dorsal (posterior) radiculomedullary veins, and their number ranges from 8–20 and 5–10, respectively (Gillilan 1970; Thron and Rossberg 1988; Lasjaunias and Berenstein 1990; Santillan et al. 2012). One important vein is the great anterior radiculomedullary vein (GARV); with a diameter of up to 2 mm, it travels with either the anterior or posterior nerve roots between T11 and L3. It can be mistaken for the artery of Adamkiewicz (AKA) because of its size and location in the thoracolumbar region. One distinguishable characteristic is the greater obtuse angle between GARV and the anterior or posterior median veins, referred to as the "coat hook" configuration, as opposed to the AKA that forms a sharper "hairpin" junction (Bowen et al. 1996). Furthermore, the AKA and GARV almost never enter or exit at the same level (Lasjaunias and Berenstein 1990).

The level at which the radiculomedullary veins exit through the dura, either with the nerve root (60% of cases) or a separate

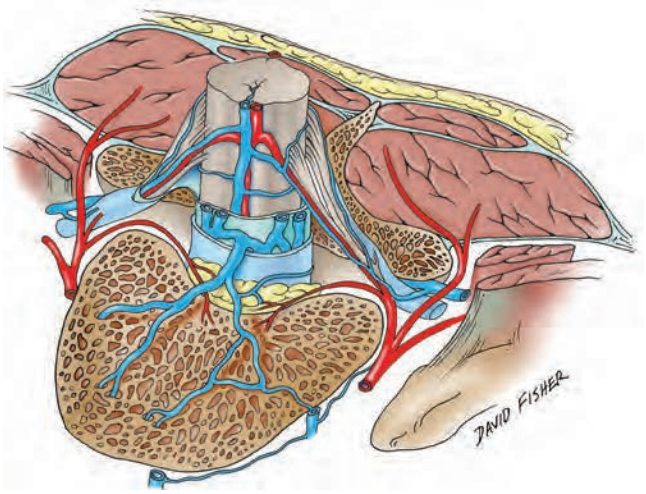

Figure 72.1 Drawing of the anterior spinal cord and its ventral and dorsal rootlets. Note the radicular and basivertebral veins.

Source: Griessenauer et al. (2015). Reproduced with permission from John Wiley & Sons.

foramen between two spinal nerves (40% of cases; Lasjaunias and Berenstein 1990), typically differs from the corresponding arterial supply. The radiculomedullary veins merge and receive drainage from the spinal nerve roots via superficial nerve root veins (Jinkins 2000). Within the nerve root, longitudinal veins receive blood from the venules surrounding the neural axons and empty into draining branch veins that then exit the nerve root dura, and subsequently empty into the superficial nerve root veins. This system of venous drainage of the spinal nerve root contains transverse coils in the venules, longitudinal veins, and draining branch veins that allow for compensation of extra blood volume (Jinkins 2000). The radiculomedullary veins drain into the epidural vertebral venous plexus via the spinal nerve venous channels (Lasjaunias and Berenstein 1990; Santillan et al. 2012). Commonly, there are two veins superior and inferior to the spinal nerve (Lasjaunias and Berenstein 1990).

Extradural system

Vertebral venous plexus

The vertebral venous plexus or plexus of Batson has been divided into three intercommunicating divisions: the internal and external vertebral and the basivertebral plexuses (Dommisse 1975; Lasjaunias and Berenstein 1990; Goshgarian 2003; Groen et al. 2004; Santillan et al. 2012). Angiographically, this system has a diamond-shaped appearance on an anteroposterior view (Lasjaunias and Berenstein 1990). The anterior and posterior internal vertebral venous plexuses, located epidurally within the vertebral canal, continue superiorly to communicate with the suboccipital venous system including the basilar and hypoglossal plexuses, marginal and occipital sinuses, and vertebral veins (Tubbs et al. 2007). The internal plexus includes four longitudinal veins, two in the anterior and two in the posterior internal plexus, and drains from all surrounding structures (Abrams 1957). The anterior plexus lies on either side of the posterior longitudinal ligament, and is connected to the basivertebral plexus via transverse branches. The posterior plexus is anterior to the ligamenta flava and connects to the posterior external plexus through perforating branches. The anterior (front of the vertebral bodies) and posterior (surrounding the posterior elements) external vertebral venous plexus surrounds the vertebral column, while the final division is the basivertebral veins that run horizontally within the vertebral body (Fig. 72.1).

Extraspinal efferents

Cervical, thoracic, lumbar, and sacral intervertebral veins connect the external and internal vertebral venous plexuses and communicate with various extraspinal longitudinal veins, including the vertebral veins, azygos system, and ascending lumbar veins, that eventually drain into the superior or inferior vena cavae (Abrams 1957; Santillan et al. 2012). Drainage of these extraspinal longitudinal veins depends on the specific vertebral level (Abrams 1957). At the cervical level, drainage occurs via the vertebral, deep cervical, and jugular veins, eventually into the superior vena cava (Lasjaunias and Berenstein 1990). Venous drainage from thoracic and lumbar intervertebral veins is accomplished through the azygos system and ascending lumbar veins. The right ascending lumbar vein continues with the azygos vein, while the left continues with the hemiazygos vein which crosses the vertebral column at either T8 or T9 to join the azygos vein. The accessory hemiazygos receives upper thoracic intervertebral veins and connects to the left superior intercostal vein above and the hemiazygos below (Abrams 1957). In the thoracic region, intervertebral veins on the left drain into either the accessory hemiazygos vein from T3–T8 and the hemiazygos vein below T8, while veins on the right drain into the azygos vein (Lasjaunias and Berenstein 1990). The azygos vein drains into the superior vena cava. In the lumbosacral level, the ascending lumbar veins communicate with the inferior vena cava via usually four horizontal, lumbar segmental veins. The first and second lumbar segmental veins usually converge prior to draining into the inferior vena cava (Lolis et al. 2011). Some spinal venous drainage into the left renal vein and vein of the crus of the diaphragm occurs through connections with the hemiazygos, subcostal, and ascending lumbar venous network (Gillot and Aaron 1968). The sacral veins empty into the lateral sacral vein, the sacral equivalent of the azygos and ascending lumbar veins, and into the internal iliac vein (Lasjaunias and Berenstein 1990). Numerous variations in the extraspinal venous system exist and demonstrate compensatory venous drainage through other pathways. If the inferior vena cava is occluded or congenitally absent, blood from the lower extremities enters the heart through the paravertebral and azygos systems into the superior vena cava (Dommisse 1975).

References

Abrams H. 1957. The vertebral and azygos venous systems, and some variations in systemic venous return. *Radiology* 69: 508–526.

Bowen B, DePrima S, Pattany P, Marcillo A, Madsen P, Quencer R. 1996. MR angiography of normal intradural vessels of the thoracolumbar spine. *AJNR Am J Neuroradiol* 17: 483–494.

Brockstein B, Johns L, Gewertz B. 1994. Blood supply to the spinal cord: anatomic and physiologic correlations. *Ann Vasc Surg* 8: 394–399.

Dommisse G. 1975. *The Arteries and Veins of the Human Spinal Cord from Birth.* New York: Churchill Livingstone, pp. 81–96.

Gillilan L. 1970. Veins of the spinal cord. *Neurology* 20: 860–868.

Gillot C, Aaron C. 1968. On the course of the branches of the left renal vein. *Arch Anat Pathol* 16: A196–202.

Goshgarian H. 2003. Blood supply of the spinal cord. In: *Spinal Cord Medicine: Principles and Practice* (eds Lin V, Cardenas D, Cutter N, Frost F, Hammond M, Lindblom L, Perkash I, Waters R, Woolsey R). New York: Demos Medical Publishing.

Griessenauer CJ, Raborn J, Foreman P, Shoja MM, Loukas M, Tubbs RS. 2015. Venous drainage of the spine and spinal cord: A comprehensive

review of its history, embryology, anatomy, physiology, and pathology. *Clin Anat* 28(1): 75–87.

Groen R, du Toit D, Phillips F, Hoogland P, Kuizenga K, Coppes M, Muller C, Grobbelaar M, Mattyssen J. 2004. Anatomical and pathological considerations in percutaneous vertebroplasty and kyphoplasty: a reappraisal of the vertebral venous system. *Spine* 29: 1465–1471.

Jinkins J. 2000. Spinal Vasculature. In: *Atlas of Neuroradiologic Embryology, Anatomy, and Variants* (eds JohnJ, BrownB, SeigafuseS, PalumboR). Philadelphia: Lippincott Williams & Wilkins, pp. 563–578.

Lasjaunias P, Berenstein A. 1990. *Surgical Neuroangiography: Functional Vascular Anatomy of Brain, Spinal Cord, and Spine*. New York: Springer-Verlag.

Lolis E, Panagouli E, Venieratos D. 2011. Study of the ascending lumbar and iliolumbar veins: surgical anatomy, clinical implications and review of the literature. *Ann Anat* 193: 516–529.

Moes P, Maillot C. 1981. Superficial veins of the human spinal cord. An attempt at classification. *Arch Anat Histol Embryol* 64: 5–110.

Santillan A, Nacarino V, Greenberg E, Riina H, Gobin Y, Patsalides A. 2012. Vascular anatomy of the spinal cord. *J NeuroIntervent Surg* 4: 67–74.

Thron A, Rossberg C. 1988. *Vascular Anatomy of the Spinal Cord: Neuroradiological Investigations and Clinical Syndromes*. New York: Springer.

Tubbs RS, Hansasuta A, Loukas M, Louis RG, Jr., Shoja MM, Salter EG, Oakes WJ. 2007. The basilar venous plexus. *Clin Anat* 20: 755–759.

73 Thymus

Ivan Varga
Comenius University in Bratislava, Bratislava, Slovakia

The thymus is a central lymphoid organ with important endocrine functions located in the superior mediastinum, but in newborns it extends caudally to the anterior mediastinum. Inside the thymus the T-lymphocytes proliferate, are selected, and mature. The size of the thymus is variable and depends on the age of the individual. It attains its maximum size at the time of birth and during the first few months of life, when it also has the greatest relative weight. Age-related thymic involution begins during or soon after the first postnatal year and continues progressively throughout the entire life span (Bodey et al. 1997). However, remnants of thymic tissue with lymphocyte populations are preserved beyond 100 years of age (Steinmann 1986). Thymic morphology varies greatly even in the same age group. For instance, in young adults the organ is typically bilobed and V-shaped, with two small processes extending into the neck; however, it can also be unilobed, trilobed, or shaped like a letter X or inverted letter V (Nasseri and Eftekhari 2010).

To understand the anatomical variations of the thymus we must first review its embryonic development. In humans, the paired thymic primordia are derived together with the inferior parathyroid glands from the third pharyngeal pouches. The rapid growth of the embryo during the seventh and eighth weeks of development causes the thymic and parathyroid primordia to descend and separate from the wall of the embryonic pharynx. The connection with the third pouch is then lost, although sometimes a solid cellular cord persists. Over the following days the paired thymic primordia approach each other ventrally to the future pericardium and great vessels (Bodey et al. 2004; Varga et al. 2008, 2011a). According to some authors (Van Dyke 1941; Gasser 1975), part of thymus also develops from the fourth pharyngeal pouches. Anomalies of thymic shape and size are explained by disrupted formation of the thymic primordia and/or of their descent from the embryonic pharynx to the mediastinum.

Thymic anatomical variations

The most common thymic anatomical anomalies include the following.

- *Anomalies in number of thymic lobes*. Varga et al. (2011b) found this anatomical variation of the thymus three times during ultrasonographic examination of a group of 212 full-term newborns. Two of the newborns examined had a cranial accessory lobe, which stretched to the neck. In one case, the left lobe was completely absent. These anomalies had no clinical significance.
- *Ectopic thymus*. A very rarely diagnosed developmental anomaly in children, the ectopic thymus is most often located in the midline neck and no thymic tissue is located in the normal position in the mediastinum (Shashiraj and Aggarwal 2005). Diagnosis of ectopic thymus is important as its treatment requires no medication or operation unless it causes symptoms. Because the thymus is important for the development of the immune system total thymectomy should be avoided early in life, especially if the aberrant ectopic thymus is the only functioning thymic tissue in the body (Liu et al. 2006). An ectopic thymus located in the neck is often called "*thymus cervicalis*."
- *Accessory thymic tissue*. This reflects failed migration of all the thymic primordia from the third pharyngeal pouches. It can be found at any level of the pathway of normal thymic descent, from the angle of the mandible to the superior mediastinum. Various authors have reported values for the prevalence of foci of accessory thymic tissue from 1.8% (when cadavers are studied macroscopically) to more than 50% (histological studies of adipose tissue from the neck and mediastinum; Table 73.1).
- *Aplasia of the thymus* and *thymoparathyroid aplasia (DiGeorge syndrome)*. One of the genetically determined consequences of disrupted formation of the embryonic pharyngeal region is most often caused by deletion of

Bergman's Comprehensive Encyclopedia of Human Anatomic Variation, First Edition. Edited by R. Shane Tubbs, Mohammadali M. Shoja and Marios Loukas.
© 2016 John Wiley & Sons, Inc. Published 2016 by John Wiley & Sons, Inc.

Table 73.1 Prevalence of accessory thymic tissue (from the lowest to the highest value) according to several authors

Reference	Description of the evaluated group	Prevalence of accessory thymic tissue
Yamashita et al. (1983)	657 patients with Basedow's disease (only macroscopic examination)	In the neck in 1.8%
Tabatabaie et al. (2007)	90 patients with thyroid disorders (histologically)	4.45%
Jaretzki and Wolff (1988)	50 patients with myasthenia gravis who underwent maximal thymectomy	32.0% in the neck and 98% in the mediastinum
Ashour (1995)	40 patients with myasthenia gravis who underwent maximal thymectomy	39.5%
Fukai et al. (1991)	Adipose tissue from the mediastinum was histologically examined in 27 autopsy subjects	In the anterior mediastinal fat in 44.4%, in the retrocarinal fat in 7.4%
Zieliński et al. (2004)	Histological examination of adipose tissue of 58 patients with myasthenia gravis after extended transsternal thymectomies	56.9% in the fat of the neck and the mediastinum

chromosome 22q11.2. DiGeorge syndrome is the most common microdeletion syndrome in humans and is characterized by cardiovascular, thymic and parathyroid, and craniofacial anomalies (Wurdak et al. 2006). The defects in thymus development and in development of the parathyroid glands, heart, and face are believed to be caused by impaired migration of neural crest cells into the embryonic pharyngeal apparatus. Immunodeficiency is a key feature of DiGeorge syndrome, and is secondary to thymic aplasia or hypoplasia with consequently impaired T-lymphocyte development (Gennery 2012).

Ectopic thymus

There is much controversy in the current literature about the terms used to classify thymic anomalies (Table 73.2). Most recent articles use the phrase "ectopic thymus" in a confusing way because they also use it to denote cervical extension of the thymus, accessory cervical lobes of the thymus, or accessory thymic tissue. A "genuine" ectopic thymus is a distinct entity from accessory thymic tissue located in the neck. The term "ectopic thymus" should be reserved for cases in which only ectopic thymic tissue is present, none being located in

Table 73.2 Some mistaken uses of the terms "ectopic" or "cervical" thymus in the current literature in cases when the thymus was located in the normal position

Reference	Short description of the case	Conclusion
Park et al. (2006)	A 2-month-old boy with asymptomatic left-sided submandibular neck mass. The patient underwent complete excision of the mass.	The pathological report confirmed the mass was thymic tissue. Chest X-ray revealed the thymus in the superior mediastinum, but the authors used the term "ectopic cervical thymus."
De Foer et al. (2007)	A 3-month-old boy with a right-sided painless soft submandibular mass lesion since birth. After a through-cut biopsy, no further therapy was required.	Pathological examination revealed thymic tissue. Sonographic evaluation of the superior mediastinum revealed a normally located thymus, but the authors used the term "ectopic cervical thymus."
Clark and Johnson (2009)	A 2-month-old boy presented with an asymptomatic left neck mass that increased in size for several weeks. The mass was surgically removed.	Pathological analysis confirmed that the mass was thymic tissue. Magnetic resonance revealed normal-appearing thymus in the superior mediastinum, but the authors described their case as "cervical ectopic thymus."
Wang et al. (2011)	A 4-month-old boy presented with a painless mass in the right upper neck region. The mass was surgically excised.	Histological diagnosis was "cervical ectopic thymus," but the presence of normal thymus in the mediastinum was confirmed by chest radiography.
Jiang et al. (2011)	A 6-month-old boy coughing for two weeks without wheezing, fever, respiratory difficulties, and restlessness. A posterior mediastinal mass was found by chest X-ray. Thoracotomy was performed.	Histological study revealed normal thymic tissue. The posterior mediastinal thymic tissue communicated with a normally positioned thymus, but the authors used the term "ectopic thymus."

the normal, mediastinal position. These two entities are also differentiated according to the recommendation of the Terminologia Embryologica (*ectopia thymi* versus *textus thymicus accessorius*).

Accessory thymic tissue

Jaretzki (1997) found foci of accessory thymic tissue or accessory thymic lobes in the mediastinal fat in 32%, the cervical fat in 22%, the aortopulmonary window in 24%, the retrothyroid position in 6%, and behind the innominate vein in 3% of patients with myasthenia gravis. This knowledge is extremely important when maximal surgical thymectomy is to be performed for myasthenia gravis (Anastasiadis and Ratnatunga 2007; Shrager 2008). Jaretzki (1997) defined these accessory thymic tissues as a "variation" of normal and not "ectopic." An intrathyroidal location of accessory thymic tissue, which can mimic benign or malignant thyroid lesions, can be clinically important (Durmaz et al. 2012; Sapthavee et al. 2013). According to Kim et al. (2012), on the basis of neck and thyroid ultrasonography findings from a group of 3195 children, the prevalence of intrathyroid thymic tissue was 0.4%.

Cervical accessory thymic tissue (Fig. 73.1) is often discovered incidentally and mistaken for an infection or neoplasm (Nolder et al. 2013). The literature contains a few records concerning anomalies in ectopic location of accessory thymic tissue. About 100 clinically important cases have been described in the literature, 10% of them in neonates (Table 73.2). This anomaly has a male predominance and occurs more commonly on the left side (Park et al. 2006). An ectopic thymus is usually located anteriorly and deep to the middle third of the sternocleidomastoid muscle, adhering posteriorly to the carotid sheath and often extending into the retropharyngeal space. Approximately 50% of all cervical thymic masses are continuous with the mediastinal thymus by direct extension or by connection to a vestigial remnant or a solid cord (Saggese et al. 2002). This anomaly is usually manifested as a neck tumor or swelling suggesting lymphadenopathy; it must also be differentiated from more frequently occurring cervical cysts, angiomas, or malignant neoplasms (Mizia-Malarz et al. 2009). Ectopic thymic tissue does not usually cause severe clinical symptoms; an estimated 80–90% of these anomalies are asymptomatic. If some symptoms are present when accessory thymic tissue is located in the cervical region, they most often arise from compression of structures in the neck (Rezzani et al. 2014). The most severe clinical symptoms of ectopic cervical thymic tissue include:

- severe dyspnea, stridor, or dysphagia (Bistritzer et al. 1985; Shah et al. 2001);
- mimicking thyroid gland enlargement (Conwell and Batch 2004) or a subglottic mass (Pai et al. 2005); or
- snoring (Prasad et al. 2006).

Another unusual location for ectopic thymic tissue is the posterior mediastinum; fewer than 20 cases have been described in the literature (Jiang et al. 2011).

Figure 73.1 Magnetic resonance demonstrates left-sided cervical extension (accessory thymic lobe or tissue) of the normally located thymus in the mediastinum in a case of a 7-year-old boy.

Cystic accessory thymic tissue

A cystic version of accessory thymic tissue located in the neck is called "congenital cervical thymic cyst." The cystic version of aberrant thymic tissue is more abundant than the "classical" solid form. Surgical removal and histological examination is often the only way to prove the diagnosis (Cigliano et al. 2009; Felgentreff et al. 2009; Meyer et al. 2010; Nasseri and Eftekhari 2010). The exact origin of cystic spaces inside thymic tissue is unknown. These cysts are lined by thymic epithelial cells; inside, cholesterol crystals and multinucleated giant macrophages are present (Figs 73.2, 73.3).

A thymopharyngeal duct cyst is another special and extremely rare variant of cystic accessory thymic tissue. About five cases have been described in the literature (Burton et al. 1995). From the embryological point of view, a thymopharyngeal duct cyst is probably a remnant of a transient duct-like structure during separation of the thymic primordia from the wall of the embryonic pharynx (Zarbo et al. 1983; Varga et al. 2011c). Another hypothesis for thymopharyngeal duct cyst formation is cystic degeneration of Hassall's corpuscles inside the accessory cervical thymic tissue (Kaufman et al. 2001). The differential diagnosis between a congenital thymic cyst and a thymopharyngeal duct cyst is controversial and in some described cases these two entities can be the same.

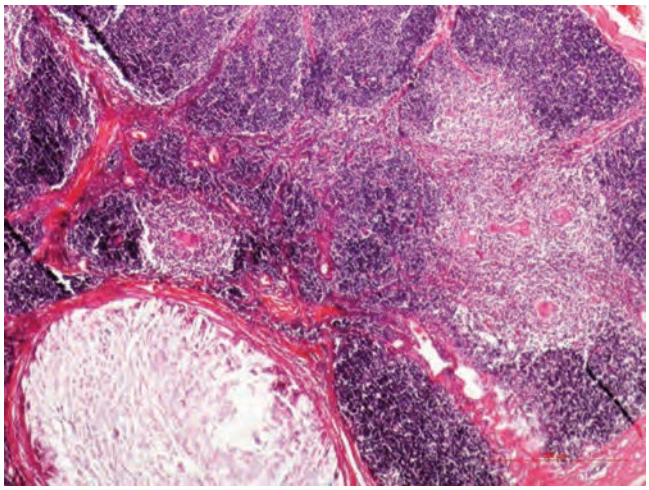

Figure 73.2 Microphotograph of a cystic version of accessory thymic tissue located in the neck of a 7-year-old boy. Within the thymic tissue with normal appearance is a large cystic space filled with cholesterol crystals and lined with thymic epithelial cells (staining with hematoxylin and eosin, magnification 40×).

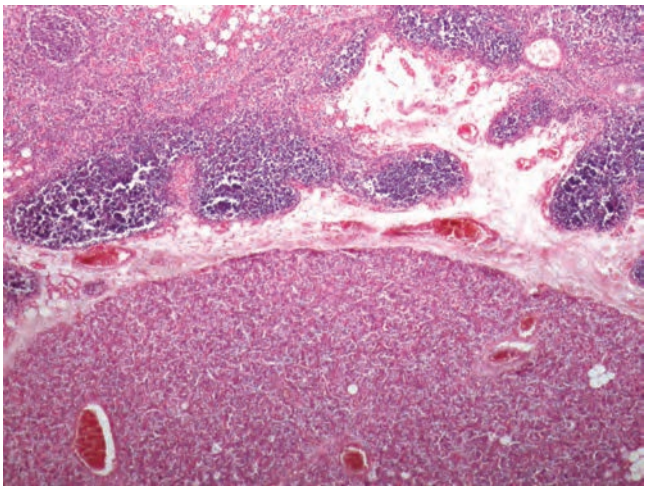

Figure 73.4 Microphotograph of an ectopic parathyroid gland (the lower half of the picture) within the thymic tissue (the upper half of the figure), an incidental finding during histological examination of thymic remnants from a 65-year-old man (staining with hematoxylin and eosin, magnification 40×).

Other variations

A relatively common and asymptomatic anatomical variation is fusion of the thymus with one or more parathyroid glands, much more often with the inferior because of the common embryonic origin of the two organs (Fig. 73.4; Noussios et al. 2012). According to Hojaij et al. (2011) the prevalence of ectopic occurrence of the parathyroid within the thymus or in the mediastinum is 19.6%.

Harman (1901) described a very interesting case in which a cephalic prolongation was continuous with the main thoracic thymus. This extension increased in size lateral to the thyroid gland and then ended at the level of the hyoid bone. Harman termed this finding the "socia thyme cervicalis."

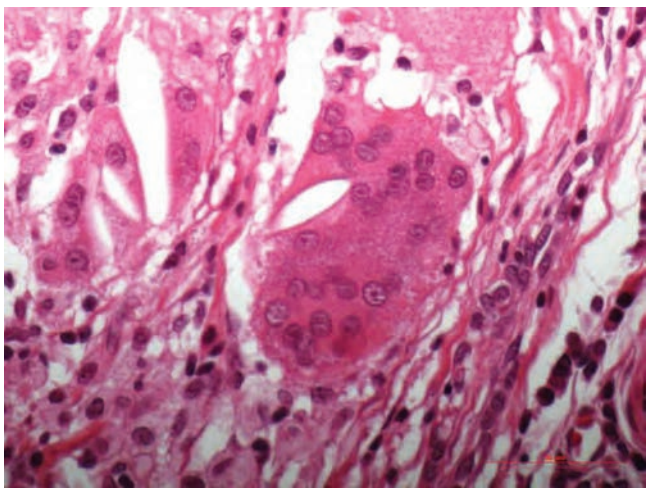

Figure 73.3 Detail of large, multinucleated macrophages from the thymic cyst (staining with hematoxylin and eosin, magnification 400×).

References

Anastasiadis K, Ratnatunga C. (eds) 2007. *The Thymus Gland. Diagnosis and Surgical Treatment*. Berlin: Springer-Verlag.

Ashour M. 1995. Prevalence of ectopic thymic tissue in myasthenia gravis and its clinical significance. *J Thorac Cardiovasc Surg* 109(4): 632–635.

Bistritzer T, Tamir A, Oland J, Varsano D, Manor A, Gall R, Aladjem M. 1985. Severe dyspnea and dysphagia resulting from an aberrant cervical thymus. *Eur J Pediatr* 144: 86–87.

Bodey B, Bodey B Jr, Siegel SE, Kaiser HE. 1997. Involution of the mammalian thymus, one of the leading regulators of aging. *In Vivo* 11(5): 421–440.

Bodey B, Siegel SE, Kaiser HE. 2004. Embryology of the mammalian thymus. *In Immunological Aspects Of Neoplasia: The Role Of The Thymus* (eds Bodey B, Siegel SE, Kaiser HE). Dordrecht: Kluwe Academic Publishers, pp. 5–14.

Burton EM, Mercado-Deane MG, Howell CG, Hatley R, Pfeifer EA, Pantazis CG, Chung C, Lorenzo RL. 1995. Cervical thymic cysts: CT appearance of two cases including a persistent thymopharyngeal duct cyst. *Pediatr Radiol* 25: 363–365.

Cigliano B, Baltogiannis N, De Marco M, Faviou E, Antoniou D, De Luca U, Soutis M, Settimi A. 2007. Cervical thymic cysts. *Pediatr Surg Int* 23(12): 1219–1225.

Clark JJ, Johnson SM. 2009. Solid cervical ectopic thymus in an infant. *J Pediatr Surg* 44(7): e19–21.

Conwell LS, Batch JA. 2004. Aberrant cervical thymus mimicking a cervical mass. *J Paediatr Child Health* 40: 579–580.

De Foer B, Vercruysse JP, Mariën P, Colpaert C, Pilet B, Pouillon M, Smet MH, Casselman JW, Breysem L. 2007. Cervical ectopic thymus presenting as a painless neck mass in a child. *JBR-BTR* 90(4): 281–283.

Durmaz E, Barsal E, Parlak M, Gurer I, Karaguzel G, Akcurin S, Bircan I. 2012. Intrathyroidal ectopic thymic tissue may mimic thyroid cancer: a case report. *J Pediatr Endocrinol Metab* 25(9–10): 997–1000.

Felgentreff K, Schupp W, Otten JE, Rückauer KD, Uhl M, Jüttner E, Superti-Furga A, Pohl M. 2009. Inspiratory stridor and dysphagia in two newborn infants caused by ectopic thymus tissue. *Eur J Pediatr* 168(9): 1141–1145.

Fukai I, Funato Y, Mizuno T, Hashimoto T, Masaoka A. 1991. Distribution of thymic tissue in the mediastinal adipose tissue. *J Thorac Cardiovasc Surg* 101(6): 1099–1102.

Gasser RF. 1975. *Atlas of Human Embryos*. Hagerstown: Harper & Row.

Gennery AR. 2012. Immunological aspects of 22q11.2 deletion syndrome. *Cell Mol Life Sci* 69(1): 17–27.

Harman NB. 1901. "Socia thyme cervicalis," and thymus accessories. *J Anat Physiol* 36: 47–53.

Hojaij F, Vanderlei F, Plopper C, Rodrigues CJ, Jácomo A, Cernea C, Oliveira L, Marchi L, Brandão L. 2011. Parathyroid gland anatomical distribution and relation to anthropometric and demographic parameters: a cadaveric study. *Anat Sci Int* 86(4): 204–212.

Jaretzki A 3rd. 1997. Thymectomy for myasthenia gravis; analysis of controversies regarding technique and results. *Neurology* 48(Suppl. 5): S52–S63.

Jaretzki A 3rd, Wolff M. 1988. "Maximal" thymectomy for myasthenia gravis. Surgical anatomy and operative technique. *J Thorac Cardiovasc Surg* 96(5): 711–716.

Jiang L, Sun B, Zheng Y, Du L. 2011. Posterior mediastinal thymus: case report and literature review. *Iran J Pediatr* 21(3): 404–408.

Kaufman MR, Smith S, Rothschild MA, Som P. 2001. Thymopharyngeal duct cyst: an unusual variant of cervical thymic anomalies. *Arch Otolaryngol Head Neck Surg* 127: 1357–1360.

Kim HG, Kim MJ, Lee MJ. 2012. Sonographic appearance of intrathyroid ectopic thymus in children. *J Clin Ultrasound* 40(5): 266–271.

Liu D, Kitajima M, Awai K, Nakayama Y, Tamura Y, Suda H, Asonuma K, Inomata Y, Yamashita Y. 2006. Ectopic cervical thymus in an infant. *Radiat Med 2006* 24(6): 452–455.

Meyer E, Mulwafu W, Fagan JJ, Brown RA, Taylor K. 2010. Ectopic thymic tissue presenting as a neck mass in children: a report of 3 cases. *Ear Nose Throat J* 89(5): 228–231.

Mizia-Malarz A, Sobol G, Maldyk J, Stolpa W, Szyszka A, Wos H. 2009. Cervical ectopic thymus in a 9–month–old girl: diagnostic difficulties. *J Pediatr Hematol Oncol* 31(8): 599–601.

Nasseri F, Eftekhari F. 2010. Clinical and radiologic review of the normal and abnormal thymus: pearls and pitfalls. *Radiographics* 30(2): 413–428.

Nolder AR, Agarwal A, Howard E, Richter GT. 2013. Ectopic thymus presenting as a retropharyngeal mass: surgical approach. *Ear Nose Throat J* 92(1): 41–43.

Noussios G, Anagnostis P, Natsis K. 2012. Ectopic parathyroid glands and their anatomical, clinical and surgical implications. *Exp Clin Endocrinol Diabetes* 20(10): 604–610.

Pai I, Hegde V, Wilson PO, Ancliff P, Ramsay AD, Daya H. 2005. Ectopic thymus presenting as a subglottic mass: diagnostic and management dilemmas. *Int J Pediatr Otorhinolaryngol* 69(4): 573–576.

Park JJ, Kim JW, Kim JP, Ahn SK, Jeong JH, Jeon SY. 2006. Two cases of ectopic cervical thymus: case reports and a review of the literature. *Auris Nasus Larynx* 33(1): 101–105.

Prasad TRS, Chui CH, Ong CL, Meenakshi A. 2006. Cervical ectopic thymus in an infant. *Singapore Med J* 47: 68–70.

Rezzani R, Nardo L, Favero G, Peroni M, Rodella LF. 2014. Thymus and aging: morphological, radiological, and functional overview. *Age (Dordr)* 36(1): 313–351.

Saggese D, Ceroni Compadretti G, Cartaroni C. 2002. Cervical ectopic thymus: a case report and review of the literature. *Int J Pediatr Otorhinolaryngol* 66: 77–80.

Sapthavee A, Kulbersh B, Maddalozzo J, Bogard A. 2013. Pathology quiz case 1: ectopic intrathyroidal thymic tissue. *JAMA Otolaryngol Head Neck Surg* 139(1): 87–88.

Shah SS, Lai SY, Ruchelli E, Kazahaya K, Mahboudi S. 2001. Retropharyngeal aberrant thymus. *Pediatrics* 108: 94–97.

Shashiraj, Aggarwal A. 2005. Undescended thymus presenting as midline neck swelling. *Indian J Pediatr* 72(1): 86.

Shrager JB. 2008. Surgical anatomy of the thymus gland. In: *Thymus Gland Pathology* (eds Lavini C, Moran CA, Morandi U, Schoenhuber R). Milan: Springer-Verlag Italia, pp. 133–136.

Steinmann GG. 1986. Changes in the human thymus during aging. In The Human Thymus. Histophysiology and Pathology (ed. Müller-Hermelink HK). Berlin: Springer-Verlag, pp. 43–88.

Tabatabaie SA, Hashemi SM, Sanei B, Sanei MH. 2007. The frequency of ectopic thymic tissue in the necks of patients without any thymic disease. *Med Sci Monit* 13(6): CR283–285.

Van Dyke JH. 1941. On the origin of accessory thymic tissue, thymus IV: the occurrence in man. *Anat Rec* 79: 179–209.

Varga I, Pospisilova V, Gmitterova K, Galfiova P, Polak S, Galbavy S. 2008. The phylogenesis and ontogenesis of the human pharyngeal region focused on the thymus, parathyroid, and thyroid glands. *Neuro Endocrinol Lett* 29(6): 837–845.

Varga I, Pospisilova V, Jablonska-Mestanova V, Galfiova P, Polak S. 2011a. The thymus: picture review of human thymus prenatal development. *Bratisl Lek Listy* 112(7): 368–376.

Varga I, Uhrinova A, Toth F, Mistinova J. 2011b. Assessment of the thymic morphometry using ultrasound in full-term newborns. *Surg Radiol Anat* 33(8): 689–695.

Varga I, Galfiova P, Jablonska-Mestanova V, Polak S, Adamkov M. 2011c. Some aspects of early development of the thymus: embryological basis for ectopic thymus and thymopharyngeal duct cyst. *Rev Arg de Anat Clin* 3(1): 22–31.

Wang J, Fu H, Yang H, Wang L, He Y. 2011. Clinical management of cervical ectopic thymus in children. *J Pediatr Surg* 46(8): e33–36.

Wurdak H, Ittner LM, Sommer L. 2006. DiGeorge syndrome and pharyngeal apparatus development. *Bioessays* 28(11): 1078–1086.

Yamashita H, Murakami N, Noguchi S, Noguchi A, Yokoyama S, Moriuchi A, Nakayama I. 1983. Cervical thymoma and incidence of cervical thymus. *Acta Pathol Jap* 33(1): 189–194.

Zarbo RJ, McClatchey KD, Areen RG, Baker SB. 1983. Thymopharyngeal duct cyst: a form of cervical thymus. *Ann Otol Rhinol Laryngol* 92: 284–289.

Zieliński M, Kuzdzal J, Szlubowski A, Soja J. 2004. Comparison of late results of basic transsternal and extended transsternal thymectomies in the treatment of myasthenia gravis. *Ann Thorac Surg* 78: 253–258.

74 Tonsils

R. Shane Tubbs[1-3] and Marios Loukas[3]
[1]Seattle Science Foundation, Seattle, Washington, USA
[2]University of Dundee, Dundee, UK
[3]St George's University, School of Medicine, St Georges, Grenada

Small, localized aggregations of lymphoid tissue can occur in the oral cavity, especially in the soft palate, the floor of the mouth, and the ventral surface of the tongue (Correll et al. 1983; Patel et al. 2004). Accessory tonsils have been reported (Paslin 1980). Tonsils may be congenitally absent (Datta et al. 2012).

Palatine tonsil

The palatine tonsil can be ectopic or doubled (Gniazdowski and Trybuś 1974; Sahov and Hieu 1959). The left and right tonsils are often asymmetrical in size. Palatine tonsils exist as two types: pedunculated or buried. The pedunculated type is nearly spherical and attached by a small base to a shallow tonsillar sinus. The buried type is attached by a broad base to a deep sinus. If the buried type is abnormally enlarged the condition may be obscured by tonsillar folds. Sinha and Singh (1978) reported ipsilateral absence of the palatine tonsil in a patient with microtia. The patient was also found to have an ectopic salivary gland. Grewal et al. (1985) also reported absence of the palatine tonsil and, in their patient, there was malformation of the external ear. A supernumerary palatine tonsil was reported by Laretus (1994) in which the tonsil simulated a pharyngeal tumor. Sprenger (1968) reported a uvula-like pharyngeal tonsil in the mesopharynx. Wise et al. (2005) reported a patient with ectopic salivary tissue involving the palatine tonsil.

Basak et al. (1999) reported a 48-year-old woman presented with dysphagia. On examination of the pharynx, a mass was visible behind and adjacent to the right palatine tonsil. It was excised and proved to be ectopic thyroid tissue.

Pharyngeal tonsil

Donnelly et al. (2002) performed sagittal midline cine MR imaging in 148 asymptomatic children (mean age of 3.4 years) referred for MR imaging of the brain who required sedation. The largest transverse diameter of the adenoids was recorded. The adenoid tonsils were considered enlarged in 64 patients (43%), and the palatine tonsils were considered enlarged in 29 patients (20%). The mean size of the enlarged adenoid tonsils was 11.6 mm and of the nonenlarged adenoid tonsils was 6.2 mm.

Prescott (1995) reported a child in which the soft palate was fused to the posterior pharyngeal wall. Instead of there being facial pillars, a muscular band on either side extended from the base of the tongue to the lateral pharyngeal walls. There was neither tonsil nor adenoid tissue present. The epiglottis was tethered to the posterior pharyngeal wall by bands from its lateral aspects. The right arytenoid mound was tethered to the posterior wall of the hypopharynx. The author postulated that these arose from a failure of development of the second branchial pouch. Beltramello et al. (1998) reported an adult female found to have pharyngeal tonsillar tissue in the fossa navicularis at the skull base and anterior to the pharyngeal tubercle.

Tubal tonsil

The tubal tonsil (TT) may be found in the inferior, posterior, and anterior walls of the auditory tube. In newborns the TT is presented as a diffuse lymphoid tissue (Sapin and Muragzamova 1989).

References

Başak S, Başak O, Odabaşi O, Düzcan E. 1999. Pharyngeal thyroid: a case report. Br J Oral Maxillofac Surg 37: 61–63.

Beltramello A, Puppini G, El-Dalati G, Girelli M, Cerini R, Sbarbati A, Pacini P. 1998. Fossa navicularis magna. *AJNR Am J Neuroradiol* 19: 1796–1798.

Correll RW, Wescott WB, Jensen JL. 1983. Asymptomatic, nonulcerated, freely movable nodule in the anterior floor of the mouth. *J Am Dent Assoc* 106: 853–854.

Bergman's Comprehensive Encyclopedia of Human Anatomic Variation, First Edition. Edited by R. Shane Tubbs, Mohammadali M. Shoja and Marios Loukas.
© 2016 John Wiley & Sons, Inc. Published 2016 by John Wiley & Sons, Inc.

Datta PG, Saha KL, Roy JS, Biswas AK, Das PP. 2012. Congenital absence of one tonsil without any other congenital abnormality: a rare presentation. *Bangladesh Med Res Counc Bull* 38: 39–40.

Donnelly LF, Casper KA, Chen B. 2002. Correlation on cine MR imaging of size of adenoid and palatine tonsils with degree of upper airway motion in asymptomatic sedated children. *AJR Am J Roentgenol* 179: 503–508.

Gniazdowski R, Trybuś L. 1974. Case of double palatal tonsil. *Otolaryngol* Pol 28: 243–244.

Grewal DS, Hiranandani NL, Kalgutkar JS. 1985. Congenital absence of the palatine tonsil associated with congenital malformation of the external ear. A congenital anomaly. *J Laryngol Otol* 99: 285–258.

Laretus VF. 1994. Retention polycystosis of a supernumerary palatine tonsil simulating a pharyngeal tumor. *Vestn Otorinolaringol*: 52–53.

Paslin DA. 1980. Accessory tonsils. *Arch Dermatol* 116: 720–721.

Patel K, Ariyaratnam S, Sloan P, Pemberton MN. 2004. Oral tonsils (ectopic oral tonsillar tissue). *Dent Update* 31: 291–292.

Prescott CA. 1995. Pharyngeal and pharyngolaryngeal bands: report of an unusual combination of congenital anomalies. *Ann Otol Rhinol Laryngol* 104: 653–654.

Sahov V, Vu Huu Hieu. 1959. A case of unusual anomaly of the palatine tonsil: *left ectopic tonsil. Ann Otolaryngol* 76: 958–959.

Sapin MR, Muragzamova GM. 1989. Age-related aspects of the anatomy and topography of the human tubal tonsil. *Arkh Anat Gistol Embriol* 96: 68–72.

Sinha SN, Singh AK. 1978. Ipsilateral absence of tonsil and microtia with ectopic salivary gland. A case report. *J Laryngol Otol* 92: 1147–1149.

Sprenger F. 1968. Uvula-like pharyngeal tonsil in mesopharynx. *HNO* 16: 349–50.

Wise JB, Sehgal K, Guttenberg M, Shah UK. 2005. Ectopic salivary tissue of the tonsil: a case report. *Int J Pediatr Otorhinolaryngol* 69: 567–71.

75 Thoracic duct, cisterna chyli, and right lymphatic duct

Young-Bin Song
Children's of Alabama, Birmingham, Alabama, United States

Cisterna chyli

The cisterna chyli does not show a constant and typical anatomy, but instead shows numerous variations. Although many anatomists agree that one of the main characteristics that define the cisterna chyli is the dilated sac (Jossifow 1906; Hollinshead 1971; Skandalakis et al. 2004; Loukas et al. 2007), they seem to differ on the measurement of the dilated sac. For example, Jossifow (1906), who was one of the earliest to study the detailed anatomy of the cisterna chyli, following the results that the cisterna chyli was present in only 40–50% of his specimens saw that most of his observed specimens failed to demonstrate a dilatation. On the other hand, Van Pernis (1949) did not define the cisterna chyli and observed it in all of his 1081 cadavers. According to Hollinshead (1971), these variations of prevalence depend on the definition of dilation, specifically, how much dilation is required to be considered a cisterna chyli. Perhaps this is why the prevalence of cisterna chyli is so variable.

Lee McGregor's Synopsis of Surgical Anatomy (Decker and du Plessis 1986) states that it is present in 50% of cases, whereas Jacobsson's (1972) and Loukas' studies (2007) report 52% and 83.3% prevalence of the cisterna chili, respectively. Kubik's (1995) study observed 14 of 70 dissections with cisterna chyli, while Propst-Proctor et al. (1983) only observed 12 of 1000 patients that had cisterna chyli. After the wide range in origin of the thoracic duct, other publications define the cisterna chyli as an "abdominal confluence of the lymphatic trunks" (Williams et al. 1995) or "confluence of lymphatic trunks that may form a sac" (Skandalakis et al. 2004). Currently, to the best of our knowledge, the study by Loukas et al. (2007) is the first attempt where specific criteria were used to define the cisterna chyli, stating that the mean dilation forming the cisterna chyli is 200% of the diameter of the thoracic duct.

The study by Loukas et al. (2007) also explored and categorized different patterns of lymphatic tributaries into four types, designated I–IV. After examining 100 human cadavers, their results are as follows (see Fig. 75.1).

- Type I: the most common configuration, in 45% or 45/100. The cisterna chyli was formed when the left lumbar trunk and the intestinal trunk joined together. Right lumbar trunks were attached to the intestinal trunk proximal to the cisterna chyli in 40% (18), and right lumbar trunks were attached to the left lumbar trunk proximal to the cisterna chyli in 60% (27).
- Type II: the second most common configuration, in 30% or 30/100. The intestinal trunks, right and left lumbar trunks, retroaortic nodes, and branches from the intercostal lymphatics all joined together in a variable manner to form the cisterna chyli.
- Type III: the third most common configuration, in 20% or 20/100. The cisterna chyli was formed when the right lumbar trunk and intestinal trunk joined together. Left lumbar trunks were shown to attach to the intestinal trunks proximal to the cisterna chyli in 20% (4), and left lumbar trunks were shown to attach to the right lumbar trunks proximal to the cisterna chyli in 80% (16).
- Type IV: the least common configuration showed a variable pattern of junction between lymphatic trunks that could not be clearly classified.

The most common configuration that Jossifow (1906) observed resembles the Type I configuration reported by Loukas et al. (2007), observed in 70% of specimens. Other authors have noted that in the region of the cisterna chyli there is widening of each of the two lumbar trunks, with and without anastomoses between them (55% and 5% respectively; Bartels 1909). A much elongated widening of the two lumbar trunks was observed due to the two trunks growing together in 10% of the cases (Bartels 1909). An intestinal trunk joining the left lumbar trunk was also observed when the two lumbar trunks were apart from each other (Bartels 1909). In addition, multiple sacculations could be observed near the contributing vessels, but not after the convergence with the cisterna chyli (Skandalakis et al. 2004).

Bergman's Comprehensive Encyclopedia of Human Anatomic Variation, First Edition. Edited by R. Shane Tubbs, Mohammadali M. Shoja and Marios Loukas.
© 2016 John Wiley & Sons, Inc. Published 2016 by John Wiley & Sons, Inc.

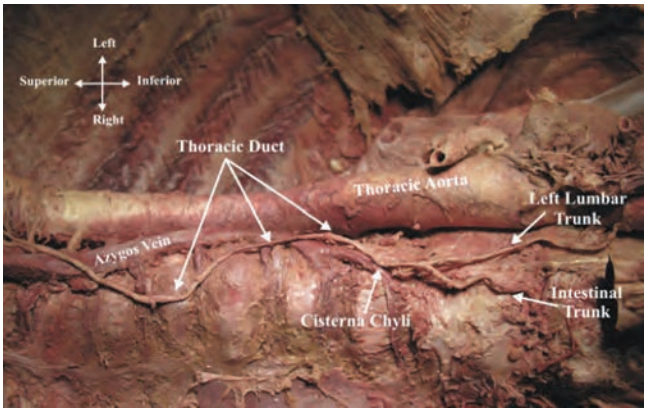

A

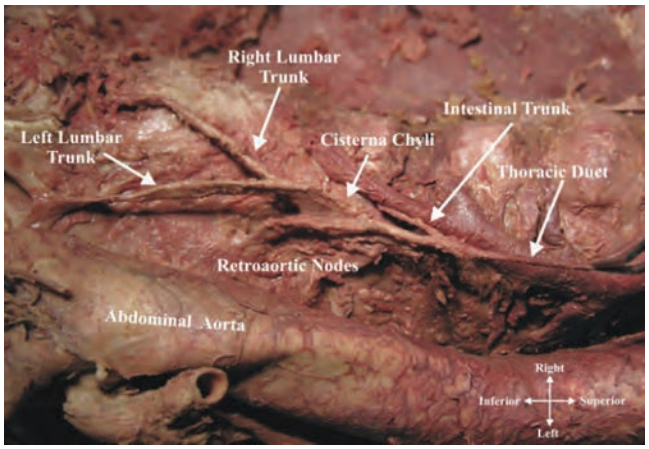

C

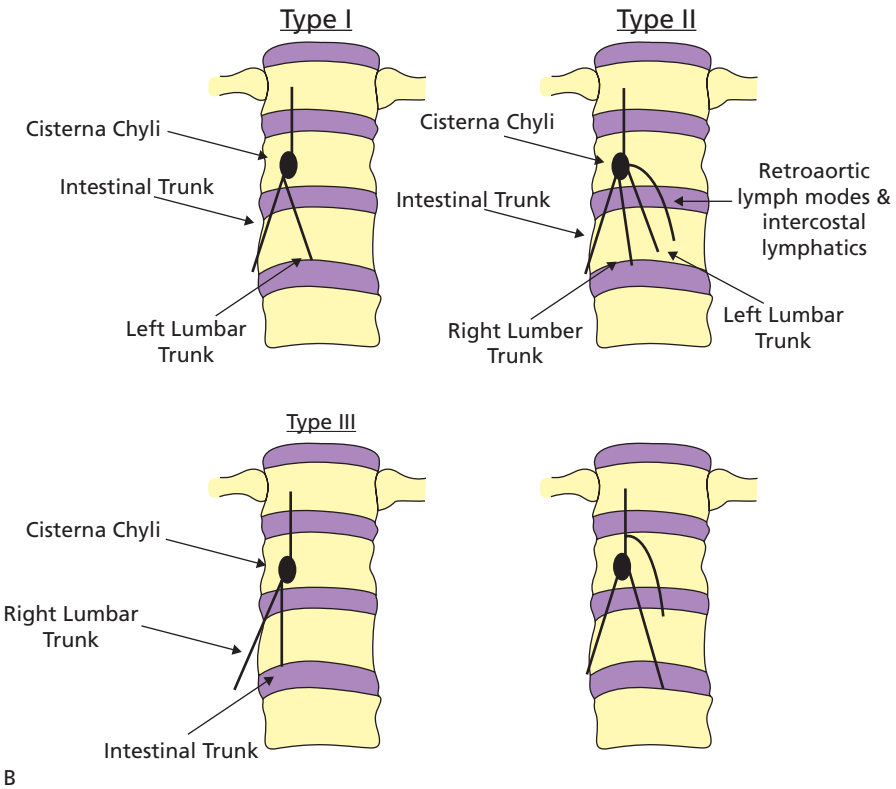

B

Figure 75.1 (a) Cisterna chyli: Types I, II, and III. (b) Schematic diagrams. Type II cisterna chyli, in which the intestinal trunk drained into the thoracic duct and the right lumbar trunk, left lumbar trunk, and retroaortic nodes joined to form the cisterna chyli. (c) Dissection of the thoracic duct and Type I cisterna chyli. The cisterna chyli was formed by the joining of the left lumbar trunk with the intestinal trunk. The thoracic aorta has been retracted to the right.

Source: Loukas et al. (2007). Reproduced with permission from John Wiley & Sons.

While the shape of the cisterna chyli is most often described as a dilated sac, other shapes have also been described. Loukas et al. (2007) found 42% of their specimens to be a shape of a fusiform, while 58% of the specimens were lobulated or saccular shape. It can also be globular (Kausel et al. 1957). The length of cisterna chyli can be 0.8–3.1 cm according to Loukas et al. (2007), of mean length of 1.69 cm with a standard deviation of ±0.33 cm according to Akcali et al. (2006), or 3–4 cm according to Kausel et al. (1957). The diameter is usually shorter than the length, but it still shows a wide range of variation:

- Kausel et al. (1957): 2–3 cm;
- Jacobsson (1972): mean 0.67 cm with a range of 0.4–1.4 cm;
- Akcali et al. (2006): mean of 0.71 cm with a range of 0.51–0.91 cm; and
- Loukas et al. (2007): mean of 1.2 cm with a range of 0.7–2.1 cm.

The location of the cisterna chyli with respect to the vertebral column also shows considerable variation, although the frequency of the variation decreases as it is discovered further from the L1–L2. Compared to L2 and L1 (56% and 33% respectively, from 1081 specimens), Van Pernis (1949) observed only 10% of cisterna chyli at the level of T12. Kausel et al. (1957) also found similar results, although he additionally found one instance where it extended from T12 to L3. Akcali et al. (2006) also noted similar findings where the cisterna chyli was extended to the inferior endplate of the L3. Loukas et al. (2007) groups the locations into five groups as follows: Type A, L1–L2 in 63%; Type B, T12–L1 in 21%; Type C, T11–T12 in 8%; Type D, T10–T11 in 5%; and Type E, T9–T10 in 3%.

There is one case where twin cisterna chyli were observed (Davis 1915). Two dilated lumbar trunks formed the twin cisterna chyli, which then emptied into the thoracic duct.

Thoracic duct

The thoracic duct typically arises from the cisterna chili; it carries lymph superiorly and drains it to the junction of the left internal jugular and subclavian veins. It is subject to wide variation, from the abdominal region where it originates to the cervical region where it terminates. In fact, Figure 75.2 by Anson and McVay (1971) shows many different variations of the thoracic duct, in form and vertebral relations. Smith and Birmingham (1889) reported complete absence of the thoracic duct in a premature fetus.

While the thoracic duct is typically 45 cm in length (Smith et al. 2013), Van Pernis (1949) and Celis and Porter (1952) observed more variation ranging from 36 to 45 cm. The diameter is not constant throughout the course, varying in size between different regions. Jacobsson (1972) found that the diameter is usually greatest in the cervical region and smallest in the lower thoracic region, and the external diameter fluctuated between 1.5 mm and 8 mm. Akcali et al. (2006) also measured the diameter of the thoracic duct and found that, at the levels of T5, T9, and T12, mean diameters were 2.3 mm, 2.6 mm, and 3.3 mm respectively. In addition, it seems to show an elastic property, being able to dilate to several times the normal width depending on the amount of lymph flow (Smith et al. 2013). See section on "Caliber and diameter" below.

Abdominal part of the thoracic duct

In the retroperitoneum, the abdominal part of the thoracic duct begins at the formation of the cisterna chyli and tracks superiorly through the aortic hiatus into the thorax (Bartels 1909). As observed by Jdanov (1959), cisterna chyli is not always present at the start of the thoracic duct. When Jdanov did not observe the cisterna chyli, many of his cadavers showed a simple fusion of the tributaries or a plexus, while some showed a sac-like dilatation of one or both lumbar trunks (Jdanov 1959). Jacobsson (1972) also observed the dilatation of lumbar trunks and plexiform system, while observing cisterna chyli in half of the specimens. Fifty-five percent of the specimens showed that the thoracic duct formed after the connection of lumbar trunks, while one or several branches of intestinal trunk emptied into the thoracic duct, one or both lumbar trunks, or into all three systems (Jacobsson 1972). Plexus formation at the beginning of the thoracic duct was observed in 24% of the specimens, while the confluence of the lumbar and intestinal trunks was observed in 20% of the specimens (Jacobsson 1972). In one instance, a plexiform system continued upward with the thoracic duct (Jacobsson 1972).

Both Rouvière (1938) and Jossifow (1906) classify the location of the thoracic duct's origin into two types: (1) low origin at the level of the first to second lumbar vertebrae; and (2) high origin at the level of the eleventh to twelfth thoracic vertebrae. If the origin is low, the inferior end of the thoracic duct is dilated and may be elongated to a length of 8 cm and a diameter of 0.6 cm (Rouvière 1938). If the origin is high, the lumbar trunks can be sac-like or dilated with an absence of cisterna chyli (Jossifow 1906; Rouvière 1938). On a rare instance, the thoracic duct can arise directly from intercostal lymph nodes that are part of an abnormal network of efferent lymph vessels (Rouvière 1938).

Thoracic part of the thoracic duct

The thoracic part of the thoracic duct is between an area where it courses after the aortic hiatus, between the aorta and azygos vein, to the superior thoracic aperture (Bartels 1909). It ascends through the posterior mediastinal cavity, anterior to the vertebral column, and varies between the right and the left from the midline. Variations in this region mainly concern branching and doubling of the duct and how it courses up to the superior thoracic region.

Thoracic ducts in the thoracic region often show branching or doubling trunks, connected by cross anastomoses that usually resolve to a single trunk. The plexus formation that was described in the abdominal part of the thoracic duct also continues through the thoracic part (Jacobsson 1972). Sometimes, the duct can communicate with the plexus of lymphatics around the aorta, at the level of the seventh and eighth thoracic vertebrae (Celis and Porter 1952). In addition, it can also connect with small plexus of lymphatic capillaries around the aorta and esophagus (Celis and Porter 1952). Elliot and Thompson (2013) reported a thoracic duct that crossed the descending thoracic aorta in its ascent (Fig. 75.3).

According to Jacobsson (1972), there are two more characteristics of branching of the thoracic duct. One is an insulae ("insular doubling"; Rouvière 1938), in which the thoracic duct divides into two or more branches and eventually reunites. Occasionally, these two branches show different pathways; one branch shows a normal course while the other shows "a most unexpected course" (Rouvière 1938). Celis and Porter (1952) described how 4% of their total cadavers (50 total) showed division of the thoracic duct into two equal vessels, which then reunited at the level of the fourth thoracic vertebra. A second characteristic

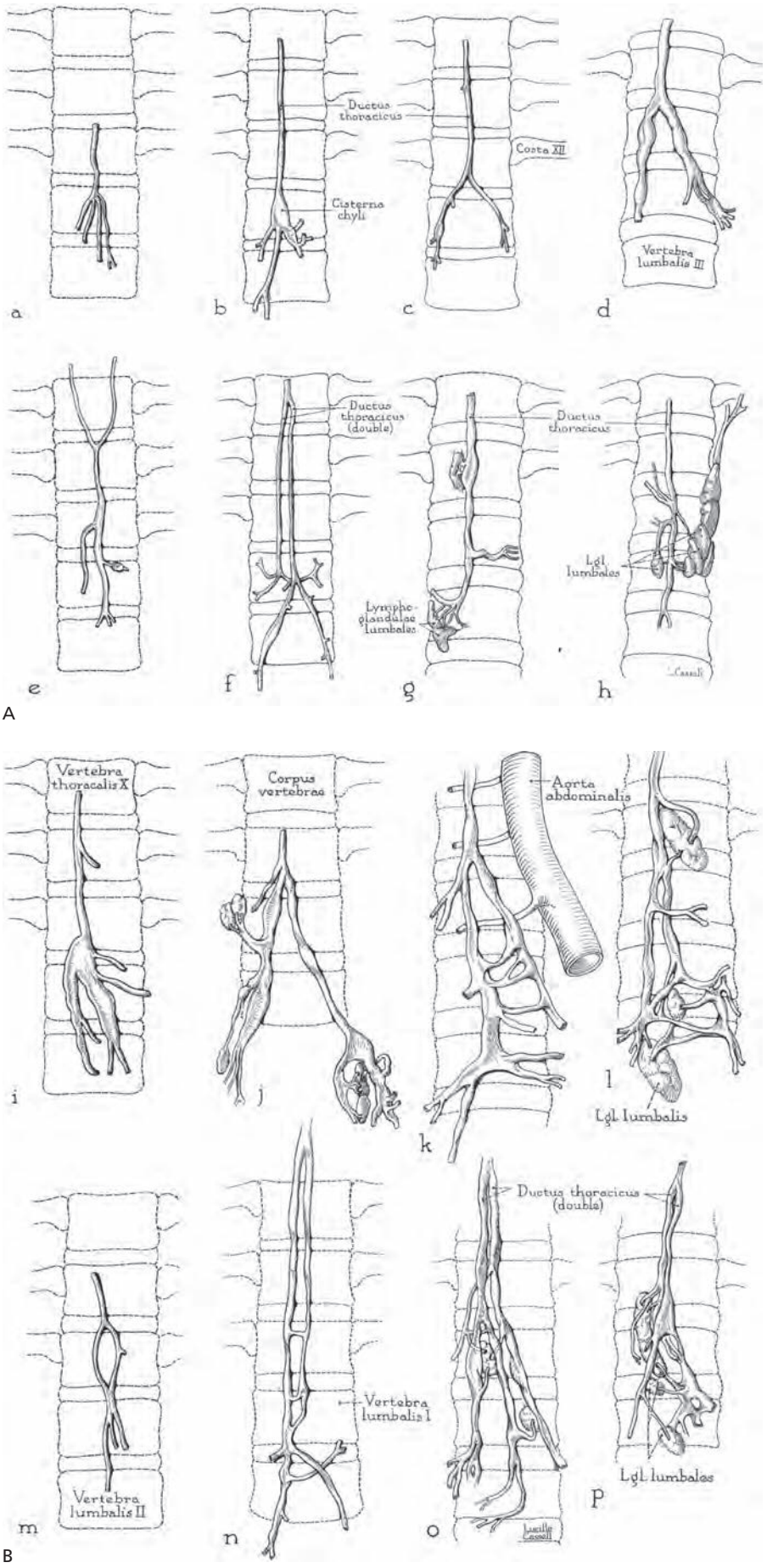

Figure 75.2 (a) An example of a duct formed by four confluent channels, none of them with a cistern-like sacculation. (b) Numerous tributaries confluent upon a true cisterna. (c) Bifid duct, one side with a small cisterna. (d) A pattern generally similar, but with a series of sacculations on each of the tributaries. (e) A duct divided cranially (thoracic level). (f) Doubling, through an area of four vertebrae, in one of two parallel channels. (g, h) Single channels closely related to lymphatic glands and receiving prevertebral tributaries. (i) An example of capacious cisterna. (j) Bifid duct, with the arms of the inverted Y widened to form a total of five sacculations (cisternae) of varying shape and size. (k, l) Examples of ducts with familiar form of an inverted Y, but with unusually rich sets of cross connections. (m) A duct with a short looped segment at diaphragmatic level. (n) Bilateral tributaries forming an elongate loop stretching over the area of five vertebrae, yet lacking sacculations. (o, p) Examples of trifid duct with sacculations forming lesser cisternae, the latter receiving tributaries from closely related lymph glands.

Source: Anson and McVay (1971). Reproduced with permission from Elsevier.

Figure 75.3 The preaortic course of the thoracic duct.

Source: Elliott and Thompson (2013). Reproduced with permission from International Journal of Anatomical Variations.

variation is an intermediate form, which resemblances a cross between the plexiform and insular form (Jacobsson 1972). Although Jacobsson (1972) observed more insular than plexiform configuration (24% and 8%, respectively), these duct divisions only accounted for 32% of the total specimens. In addition, the embryologic basis for the presence of insulae and plexiform divisions have been described in which, during embryologic development, numerous anastomoses between two thoracic ducts sometimes do not completely dissolve away, leaving residual communications that result in the formation of insulae or plexiform (Davis 1915; Jacobsson 1972).

The lymph vessels have been seen to join the thoracic duct along its thoracic part, coming from the intercostal spaces, para-aorta, and mediastinal lymph nodes (Jacobsson 1972). Some lymph vessels can pass through the aortic hiatus from the abdominal region to join into the lower thoracic region of the duct (Jacobsson 1972). Others can discharge independently to the great cervical veins (Rouvière 1938).

As the thoracic duct ascends towards the cervical region, it starts out from the right side of the median plane and crosses to the left side. Van Pernis (1949) observed two sites of crossover from right to left. After dissecting 1081 cadavers, 44.4% (480) of the specimens crossed at the level of the fifth thoracic vertebral body and 55.6% (601) of the specimens crossed at the level of the sixth thoracic vertebral body (Van Pernis 1949).

In rare cases of duplication of the thoracic duct, the origination of the doubling can be observed in the thoracic part of the duct (Shafiroff and Kau 1959). When the origination is below the thoracic region, in cases of complete bilateral thoracic ducts both ducts pass through the aortic hiatus (Chen et al. 2006).

Cervical part of the thoracic duct

When the thoracic duct reaches the superior thoracic aperture, it arrives at the cervical area. It forms an arch at the roof of the neck, passes posterior to the left common carotid artery, vagus nerve and internal jugular vein, and finally terminates into the junction of the left subclavian and internal jugular vein (Bartels 1909; Kaur et al. 2012). There is a great deal of variation in this region, especially regarding the termination of the duct.

The vertebral level where it arches laterally has shown different measurements. In addition, the height at which the duct reaches in the neck before descending towards the termination shows variations (Clark 1953). The most cranial part of the arch was reported to be between the first thoracic and sixth cervical vertebra by Lissitzyn (1924) and Rouvière (1938), whereas Jdanov (1959) observed this location to be between the upper border of the first thoracic and middle of the seventh cervical vertebrae. The height of the arch, which is measured from the clavicle, varies over the range 0.5–5 cm (Gray 1942; Baldridge and Lewis 1948; Van Pernis 1949; Kinnaert 1973). In addition, sometimes when the duct divided into two vessels, two arches have been observed (Celis and Porter 1952).

Greenfield and Gottlieb (1956) saw variations in the coursing of the thoracic duct in the roof of the neck. All but one duct (from 75 cadavers) passed the left innominate vein posteriorly to reach the roof of the neck; in 45 of those cases, however, the duct coursed posterior to the left common carotid artery and in 25 cases the duct was anterior to the internal jugular vein (Greenfield and Gottlieb 1956). In addition, Van Pernis (1949) observed that many of the thoracic ducts (92%) crossed the subclavian artery anteriorly, while only 8% of the ducts crossed posteriorly. In some cases, there was an absence of the classical arch altogether (Kinnaert 1973).

Thoracic duct termination

When the thoracic duct reaches the termination site, it demonstrates many different variations regarding pattern and site of termination. The greatest number of variations is found in the overall structure of the duct. In fact, Jacobsson (1972) identified 9 different types of cervical thoracic duct, classifying them by number of branches and the presence of insula or plexus. Shimada and Sato (1997) also classified the termination of the duct, by its location and number of branches, as four different types, each with multiple subtypes (see Fig. 75.4). Kausel et al. (1957) divided the variations into five different types according to drainage sites and branching (see Fig. 75.5).

One of the most documented variations of the thoracic duct involves the location of the termination. The most frequent location of the termination is at the left internal jugular vein, followed by the junction of the left internal jugular and subclavian veins (venous angle) and left subclavian vein. As shown in Table 75.1, the ranges for each of these three termination sites are wide, indicating that results are not consistent from one research group to another. Less common and rare termination sites include the external jugular vein (Greenfield and Gottlieb 1956; Jacobsson 1972; Zorzetto et al. 1977; Shimada and Sato 1997), the brachiocephalic vein (Davis 1915; Rouvière 1938; Greenfield and Gottlieb 1956; Jdanov 1959; Shafiroff and Kau 1959), the transverse cervical vein (Kinnaert 1973), the

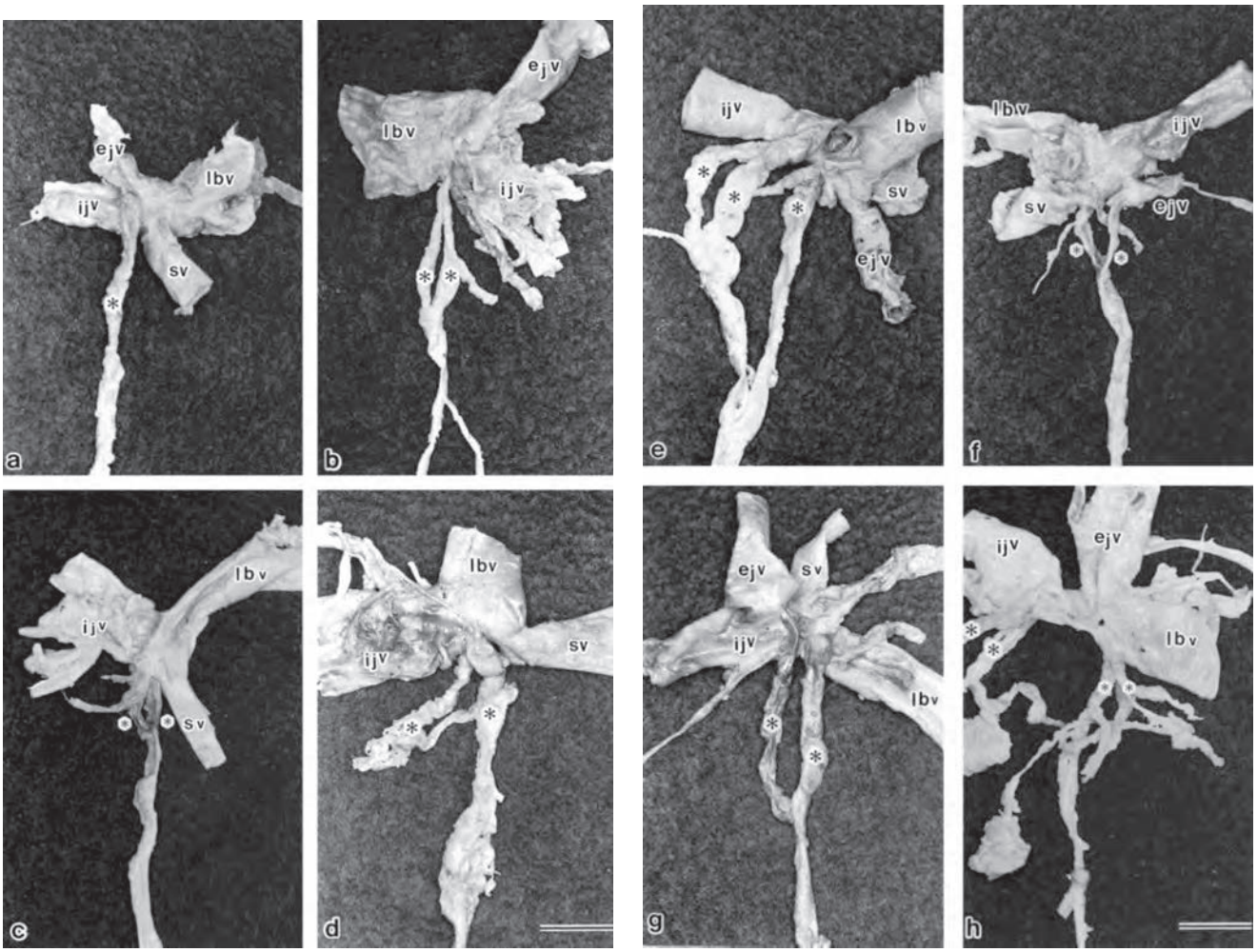

Figure 75.4 Photographs of the various types of endings of the trunk of the thoracic duct. (a) Type A-1; the duct is directly inserted into the venous angle. (b) Type A-2; the duct separates into two trunks before and after running below the left brachiocephalic vein. (c) Type A-3; the duct has two trunks, one extending to the beginning of the subclavian vein and the other to the venous angle. (d) Type B-1; the duct with two trunks runs directly to the internal jugular vein. (e) Type B-2; the duct separates into three trunks after running below the left brachiocephalic vein; one trunk runs to the internal jugular vein and the others (two branches) to the subclavian vein. (f) Type C-1; one trunk is inserted into the external jugular vein and the other into the subclavian vein. (g) Type C-2; ne trunk is inserted into the external jugular vein and the other into the internal jugular vein. (h) Type D; there are four trunks inserted into the beginning of the internal and external jugular veins and into the subclavian vein. ejv: external jugular vein; ijv: internal jugular vein; lbv: left brachiocephalic vein; sv: subclavian vein.

Source: Shimada and Sato (1997). Reproduced with permission from John Wiley & Sons.

suprascapular vein (Zorzetto et al. 1977), and the vertebral vein (Zorzetto et al. 1977).

The thoracic duct can join the venous system indirectly, by terminating into the lymph nodes that are part of the cervical lymphatic chain, or cervical lymph nodes can join the terminal ampulla (see Fig. 75.6; Zorzetto et al. 1977). The cervical lymphatic channels have been observed to join the thoracic duct near its termination, but can also drain independently or form a common trunk by joining with a horizontal lymphatic vessel (Kinnaert 1973).

The point of termination within each vessel can vary from the anterior and lateral surfaces to the posterior surface. When the single duct terminates into the left internal jugular vein, it most often terminates into lateral surfaces, followed by anterior surfaces (Greenfield and Gottlieb 1956). Additionally, it terminates into the posterior surfaces (dorsal aspect) least often (Greenfield and Gottlieb 1956; Jacobsson 1972). For the venous angle and subclavian vein, termination to the frontal aspect is least common (Jacobsson 1972). In addition, while the termination to the left subclavian vein is mainly between the internal and

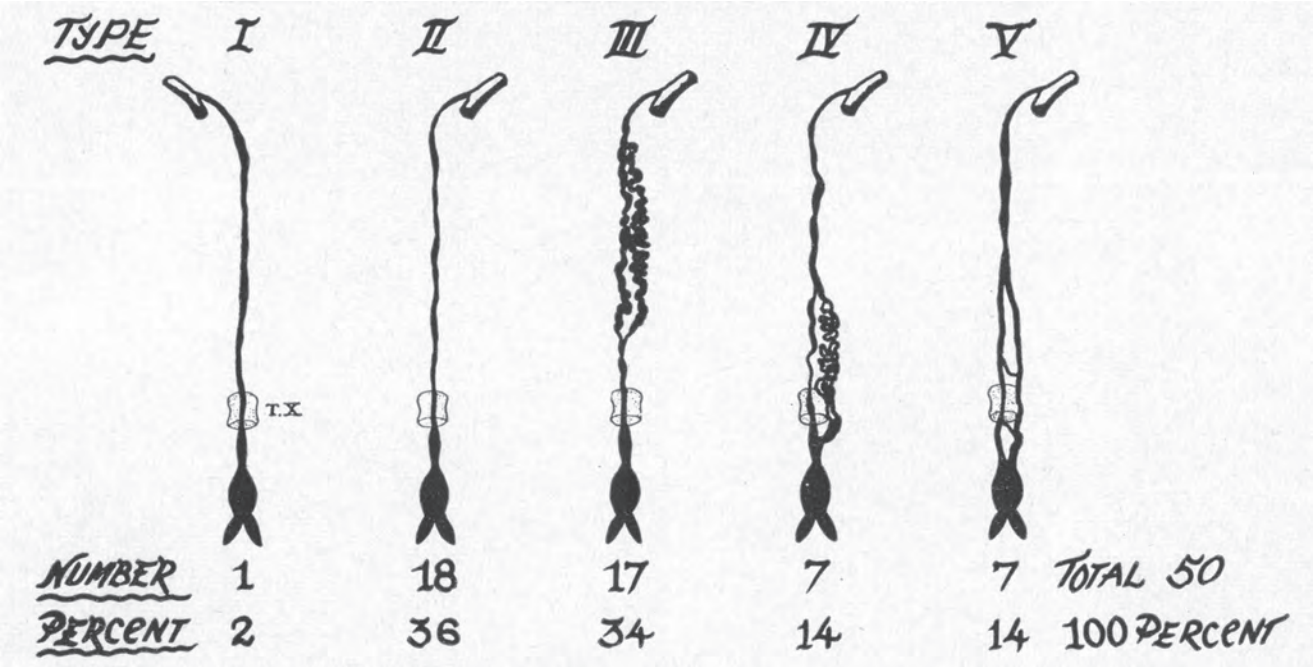

Figure 75.5 Anatomy of the thoracic duct. Chart demonstrating five major gross anatomic variations observed and their rate of occurrence.

Source: Kausel et al. (1957). Reproduced with permission from Elsevier.

external jugular veins, Greenfield and Gottlieb (1956) found one instance where the termination was lateral to the junction of the external jugular vein.

Another most documented variation involves the branching of the duct. Similar to the thoracic region, when the duct divides into multiple channels they reunite and form a common trunk or duct (Parsons and Sargent 1909; Rouvière 1938; Rocca-Rossetti 1961; Archimbaud et al. 1969; Jacobsson 1972; Kinnaert 1973; Zorzetto et al. 1977; Shimada and Sato 1997; Seeger et al. 2009). The incidence of reuniting into a common duct varies greatly among different authors however, ranging from 7% to 66%. Although some authors note that the majority of the branching results in merging into a common trunk, other studies have shown opposite results. For example, Zorzetto et al. (1977) found that 15.69% of the cases demonstrated multiple channels reuniting to form a single ending branch, whereas Kinnaert's (1973) study demonstrated the much higher rate of 65.90% in 47 studied cases. In addition, radiologic technique using a high-resolution ultrasonographic (US) examination was performed by Seeger et al. (2009). It was demonstrated that, in most cases where the branching occurred, multiple channels merged to a single lumen; channels terminated separately at different locations only in 21 of 155 cases.

There has also been research performed to show that the branches do not reunite but instead stay separate and terminate independently. Previous research has shown that 10–41% of the cadavers studied have multiple channels that terminate separately (Parsons and Sargent 1909; Davis 1915; Correia 1926; Van Pernis 1949; Greenfield and Gottlieb 1956; Shafiroff and Kau 1959; Rocca-Rossetti 1961; Archimbaud et al. 1969; Jacobsson 1972; Kinnaert 1973; Zorzetto et al. 1977). The branches can be double, triple, or even multiple vessels, which can terminate in many different combinations of veins (Rouvière 1938; Jdanov 1959; Tesauro 1966; Shimada and Sato 1997; Seeger et al. 2009; Kaur et al. 2012). However, as the number of branches increases, the prevalence rate decreases (Parsons and Sargent 1909; Davis 1915; Greenfield and Gottlieb 1956; Jdanov 1959; Jacobsson 1972). Nevertheless, regardless of whether the branches reunite or terminate separately, the frequency of the branching is much more prevalent in the cervical region, compared to the thoracic region (Jacobsson 1972).

Right-sided termination

Not all thoracic ducts terminate on the left side. Many research projects have shown that a percentage of the duct terminate on the right side. As shown in Table 75.2, the general prevalence of the thoracic duct terminating into the right venous system is 1–11%. In addition, similar to the variation on the left side, the termination endings can be single or multiple where it terminates into the right internal jugular vein (Watson, 1872; Davis 1915; Greenfield and Gottlieb 1956; Kausel et al. 1957; Peña and Zuñiga 2009), right venous angle (Rouvière 1938; Nathan and Gitlin 1968; Okumura and Fujimoto 1974; Van der Putte and van Limborgh 1980; Wirth and Kubik 1980; Nathan and

Table 75.1 Site of the termination of the thoracic into the left venous system.

Location of thoracic duct endings	Jdanov 1959	Kinnaert 1973	Zorzetto et al. 1977	Shimada and Sato 1997	Shafiroff and Kau 1959	Greenfield and Gottlieb 1956	Davis 1915	Archimbaud et al. 1969	Parsons and Sargent 1909	Rocca-Rossetti 1961	Celis and Porter 1952	Total
Single ending												
Internal jugular vein	48	14	15	16	18	19	1	6	34	5	1	177
Venous angle	35	16	18	28	3	19	5	10	3	7		111
Subclavian vein	9	7	2		7	18	12	18		1	24	98
External jugular vein						7						7
Angle of internal jugular and external posterior jugular vein			5									5
Angle of internal jugular and vertebral vein			1									1
Cervical lymphatic chain			2									2
Junction between internal jugular and brachiocephalic vein						7						7
Multiple endings												
Internal jugular veins		3										3
Subclavian vein		1										1
Transverse cervical veins		1										1
Venous angle and internal jugular vein		1					1					2
Venous angle and subclavain vein		4	4	10								18
Venous angle and suprascapular vein			1									1
Internal jugular vein and subclavian vein			1	11					3		1	16
Internal jugular vein and brachiocephalic vein			1									1
Internal jugular vein and suprascapular vein			1									1
External jugular vein and subclavian vein				12								12
External jugular vein and internal jugular vein				16								16
Internal jugular vein and vertebral vein							1					1
Internal jugular and subclavain and external jugular angle								2				2
Internal jugular and subclavain and venous angle										1		1
Complex configuration				7								7
Total	100	47	51	100	30	71	21	36	40	14	26	536

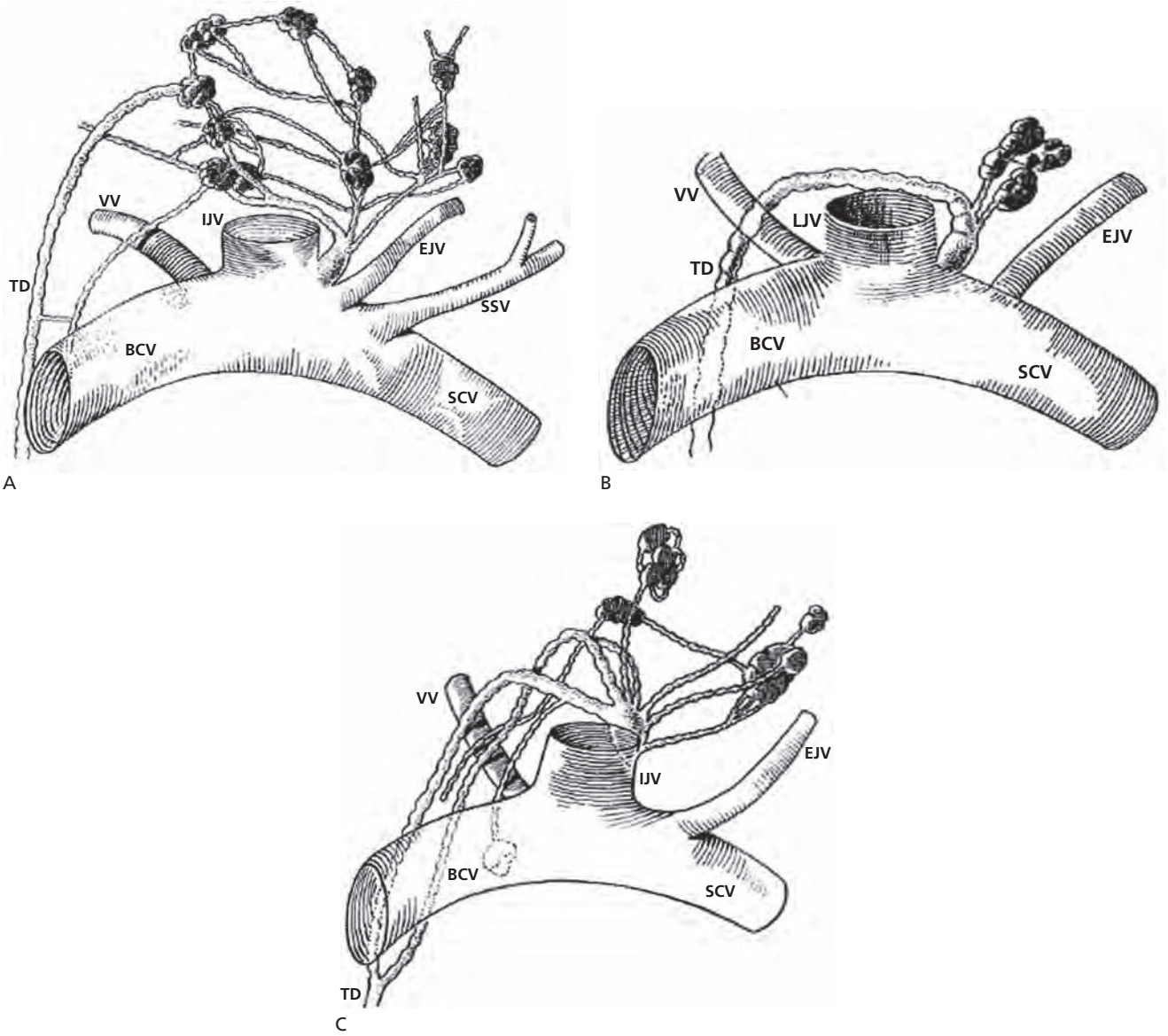

Figure 75.6 (a) Thoracic duct ending in lymph nodes of the cervical lymphatic chain; three branches from the lymphatic chain are into a single trunk that ends by an ampulla in the angle formed by internal jugular vein and external jugular vein. (b) Single thoracic ending in a terminal ampulla that receives vessels from cervical lymph nodes. (c) Multiple lymphoid channels (stippled) ending in an ampullar dilatation of a thoracic duct that ended in the internal jugular vein. Cross-hatched structures are lymph nodes. TD: thoracic duct; BCV: brachiocephalic vein; VV: vertebral vein; IJV: internal jugular vein; SCV: subclavian vein; EJV: external jugular vein; SSV: suprascapular vein.

Source: Zorzetto et al. (1977). Reproduced with permission from John Wiley & Sons.

Siedel 1983; Epstein and Debord 2002; Chen et al. 2006; Seeger et al. 2009), or right subclavian vein (Celis and Porter 1952; Clark 1953).

There are three main forms of variations that can terminate into the right side; Lane and Todd (1847) developed one of the earliest classification systems as follows.

- I: Bilateral thoracic ducts may exist, with one terminating into the left and the other into the right venous angle.
- II: A single thoracic duct may bifurcate, with one branch terminating at the left venous angle and another branch at the right venous angle.
- III: A single duct may drain into the right venous angle.

It is difficult to estimate the prevalence for each classification because the publications that have reported right-sided termination of the thoracic duct did not specify whether it was due to bilateral duct system, bifurcation, or a single duct system.

Table 75.2 Prevalence rate of right-sided termination

Authors	Number of cases	Percent
Davis 1915	1 in 22	4.5
Minkin 1925	1 in 102	1.0
Van Pernis 1949	61 in 1081	5.6
Celis and Porter 1952	1 in 50	2
Greenfield and Gottlieb 1956	1 in 75	1.3
Kausel et al. 1957	1 in 50	2
Lachapèle et al. 1964	1 in 60	1.7
Werner 1965	2 in 79	2.5
Archimbaud et al. 1969	2 in 38	5.3
Jacobsson 1972	5 in 122	4.1
Van der Putte and van Limborgh 1980	2 in 40	5
Seeger et al. 2009	63 in 564	11.2

However, some findings seem to suggest that a single duct terminating at the right venous angle is less prevalent than bilateral termination (Wirth and Kubik 1980; Seeger et al. 2009). In addition, a left-sided thoracic duct is less likely to be present if the thoracic duct is right-sided (Watson 1872).

There have been a few reports where a thoracic duct terminating at the right venous angle is associated with venous malformation, such as aberrant retroesophageal right subclavian artery (RRSA; Orts Llorca 1936; Nathan and Gitlin 1968; Nathan and Siedel 1983). When the thoracic duct is in the superior mediastinum, its normal path can be disrupted by the anomalous right subclavian artery. Instead of ascending toward the left side, it can track the artery until it terminates into the right venous angle (Nathan and Siedel 1983). In one case, the thoracic duct branched into two while tracking the inferior surface of the right subclavian artery, which reunited into one common trunk just before the venous angle termination (Nathan and Gitlin 1968). From 29 cases where RRSA was observed, thoracic ducts following the artery to the right were observed in 24 cases (Orts Llorca 1936). It is important to note that not all endings at the right venous angle are accompanied by anomalous large arteries, and the extent to which an RRSA is associated with a right-sided termination is not known and requires further research (Nathan and Gitlin 1968; Nathan and Siedel 1983). In addition to the association between the RRSA and the right-sided venous angle termination, there can be in very rare cases a third association relating to the truncus bicaroticus, although the authors did not elaborate further (Nathan and Gitlin 1968). Lastly, Ranade et al. (2006) reported a rare case of lymphatico-venous communication, where a left branch from the duplicated thoracic duct terminated into the inferior vena cava at the level of the lower border of L3 vertebra.

Duplication of the thoracic duct

As noted in previous sections, rare cases of duplication of the thoracic duct have been reported where branches terminate on both the right and left side (Davis 1915; Yamada 1932; Rouvière 1938; Van Pernis 1949; Celis and Porter 1952; Shafiroff and Kau 1959; Lachapèle et al. 1964; Jacobsson 1972; Chen et al. 2006; Ranade et al. 2006). The ducts can be partially duplicated, which often show interconnected network of anastomoses between the two partially duplicated ducts (Davis 1915). When it duplicates, the site of duplication is often in the upper part of the thoracic course, which can be located in both the thorax and the neck (Shafiroff and Kau 1959; Okumura and Fujimoto 1974). Van Pernis (1949) found that the right thoracic ducts joined the left thoracic duct at the levels between the second and third thoracic vertebra. Similarly, Jacobsson (1972) noted that the branch left the main trunk just above the aortic arch to terminate into the right side of the neck. Contrastingly, a case report by Ranade et al. (2006) revealed a Y-shaped bifurcation at the level of T12 vertebra without the presence of cisterna chyli. The lengths of the two branches were significantly different, measuring 8.5 cm and 12.5 cm for right and left branches, respectively (Ranade et al. 2006).

In one case, Akcali et al. (2006) observed two different lymphatic drainage systems, where it covered the vertebral bodies between the seventh and the twelfth thoracic vertebrae (see Fig. 75.7). Left ascending branches formed the main duct while inferior and right tributaries formed the right ascending trunk, eventually joining with the main duct near

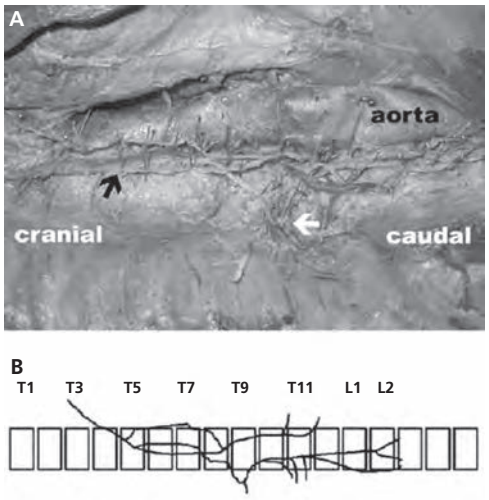

Figure 75.7 (a) Photograph and (b) schematic diagram of the double lymphatic drainage system. White arrow in (a) indicates the thick branch originating from the posterior chest wall. Black arrow indicates one of the main trunks, which was damaged during dissection. Note that the lymphatic system covers the inferior thoracic spine.

Source: Akcali et al. (2006). Reproduced with permission from Springer Science and Business Media.

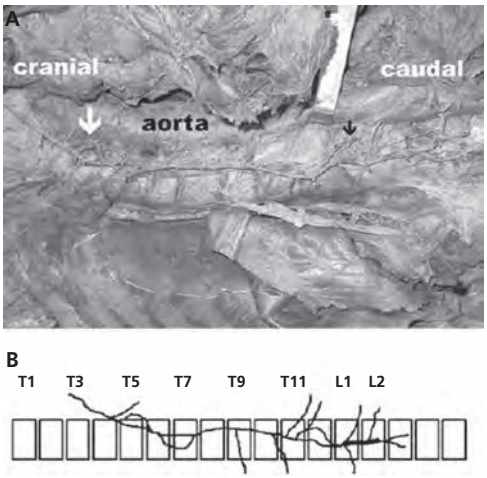

Figure 75.8 The thoracic duct with ring formation and its tributaries can be seen in the (a) photograph and (b) diagram. White and black arrows in (a) show the lymphatic network at the upper and lower thoracic segments.

Source: Akcali et al. (2006). Reproduced with permission from Springer Science and Business Media.

the fifth thoracic vertebrae (Akcali et al. 2006). In another case, the thoracic duct twice formed a ring shape by looping itself around the vertebrae, once at the upper thoracic region and another at the thoracolumbar junction (see Fig. 75.8; Akcali et al. 2006).

In extremely rare circumstances, completely bilateral thoracic ducts have been reported (Yamada 1932; Chen et al. 2006). In one particular case reported by Chen et al. (2006), bilateral thoracic ducts were accompanied by a persistent left superior vena cava (SVC) (see Fig. 75.9). From the both sets of cisterna chyli, the left and right thoracic ducts began at the level of the first lumbar vertebra and entered the thoracic region via aortic hiatus, ascending together until being separated at the level of fifth thoracic vertebra (Chen et al. 2006). An anastomotic branch was present between the two at the level of the tenth thoracic vertebra, and the two eventually terminated at their corresponding right and left venous angles (Chen et al. 2006).

As mentioned earlier regarding the association between the right-sided termination and venous malformation, coexistence of venous and lymphatic variations is common. In addition to association between the right-sided termination and aberrant retroesophageal right subclavian artery, Yamada (1932) reported complete double thoracic ducts with a right-sided aortic arch. In addition, coexistence of double persistent left superior vena cava and bilateral thoracic ducts has been discovered, although this incidence is very rare (Chen et al. 2006).

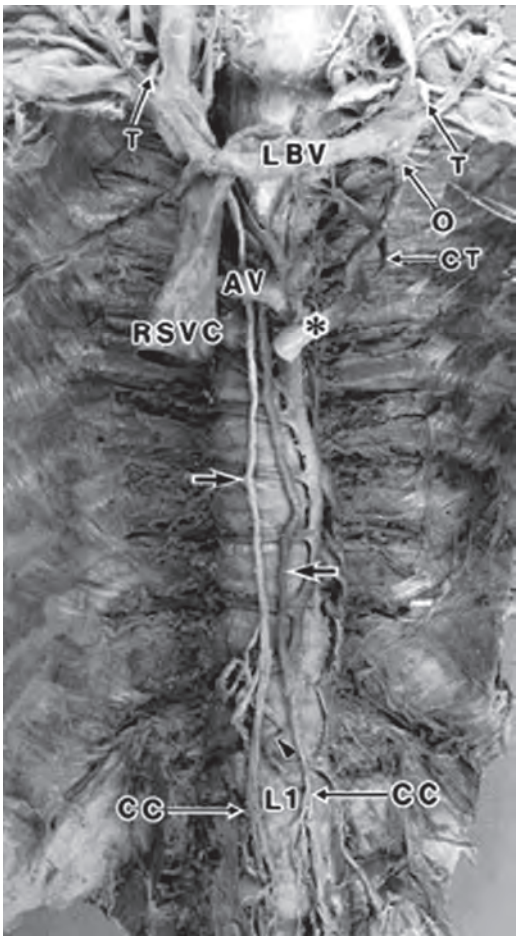

Figure 75.9 Posterior and superior mediastinum showing bilateral thoracic ducts and coexistent double SVC. AV: azygos vein; CC: cisterna chyli; CT: common trunk of accessory hemiazygos and left superior intercostal vein; L1: the first lumbar vertebra; LBV: left brachiocephalic vein; O: point of origin of the left superior vena cava; RSVC: right superior vena cava; T: termination points of the left and right thoracic ducts; arrowhead: anastomotic branch between the left and right thoracic ducts; arrows: bilateral thoracic ducts; *: left superior vena cava.

Source: Chen et al. (2006). Reproduced with permission from John Wiley & Sons.

Tributaries

The cervical lymph trunks, which consist of jugular, bronchomediastinal, and subclavian lymph trunks, usually join the thoracic duct near the termination. However, this is not always the case. Due to the variations of the tributaries, the lymph from the thoracic duct, left upper extremity, and left side of the head and neck do not always drain together. The cervical lymph trunks can terminate into a number of vessels independently – including venous angle, internal jugular vein, subclavian vein, and transverse cervical vein – without joining the thoracic duct (Lane and Todd 1847; Davis 1915; Kinnaert 1973). In one instance, the cervical lymph trunk joined the horizontal lymphatic vessel and formed a common trunk, which then terminated into the jugular vein (Kinnaert 1973). In addition, of the three lymph trunks the

left bronchomediastinal trunk is least likely to join the thoracic duct directly; instead, it often joins at the venous angle (Kwon et al. 2002; Langford 2002).

Valves

Valves are present throughout the course of the thoracic duct. They can vary in size, number, type, and the characteristics of the cusps, depending on the location in the thoracic duct. Jacobsson (1972) came up with six different types of valves in the thoracic duct, where different types are location specific. For example, type A is more usually present in the abdominal and cervical parts, whereas type B is more commonly present in the thoracic part of the duct (Jacobsson 1972). In addition, type D valves are most common at the junction with the venous system at the terminal endings, especially when the termination is at an oblique angle (Jacobsson 1972). Although most of the valves are bicuspid (Bartels 1909; Rouvière 1938; Gray 1942; Jacobsson 1972; Seeger et al. 2009), tricuspid valves have also been discovered (Jacobsson 1972).

The number of valves that are present throughout the course of the thoracic duct varies. The valves become more numerous as the duct reaches the termination site. On average, Jacobsson (1972) has found 4.6 valves below the diaphragm, 5.9 valves between the diaphragm and the aortic arch, and 11.1 valves between the aortic arch and its termination site. However, ultrasonographic examinations revealed that, in rare cases, 2 of 564 subjects showed no valves in the cervical part of the thoracic duct (Seeger et al. 2009). In addition, if the duct divided into one or several branches, valves were more likely to appear inferior to the division (Jacobsson 1972).

Specifically, terminal valves have been studied in detail, showing that terminal valves are more constant in position and number compared to rest of the valves in the thoracic duct (Van Pernis 1949). The majority of the terminal valves are found at the junction with the venous system or within 1 cm from the junction (Van Pernis 1949; Jacobsson 1972). Sometimes attachments of the valves were present without cusps, which the author termed a "moat-like constriction" (Jacobsson 1972).

Caliber and diameter

Similar to the valves, the diameter of the thoracic duct changes depending on the location throughout the course. When the thoracic duct reaches the thoracic area the diameter noticeably narrows; this marks the smallest external diameter, and gradually becomes wider as it ascends toward its termination (Jacobsson 1972). In the cervical area, the duct continues to widen until it reaches the widest point near the termination (Jacobsson 1972). Overall, the thoracic duct is widest at the cervical region and narrowest at the thoracic region (Correia 1926; Jacobsson 1972).

The diameters measured by different authors show variable results. Van Pernis (1949) measured the external diameter to be 2–4 mm. Using lymphangiography, Nusbaum et al. (1964) and Hidden and Florent (1966) measured the diameter to be 2–6 mm and 0.5–5 mm, respectively. Shafiroff and Kau (1959) measured the widths to be 5–12 mm. Kinnaert (1973) observed that when there were single duct terminations the diameters were 2–5 mm; when the multiple channels ended in a short common duct, the diameters were 0.5–3 mm. Akcali et al. (2006) showed that at levels of T5, T9, and T12, mean diameters were 2.3 mm, 2.6 mm, and 3.3 mm, respectively. The mean diameter of 2.5 mm was found in US imaging (Seeger et al. 2009). Finally, a rare incidence of double thoracic ducts showed that the caliber of each duct was measured to be about 3 mm (Chen et al. 2006).

A dilatation (or an ampulla) is common, especially in the terminal side of the thoracic duct (Correia 1926; Jacobsson 1972; Kinnaert 1973; Zorzetto et al. 1977; Seeger et al. 2009). Kinnaert (1973) noted that of the 47 patients studied, 10 patients showed an ampulla at the extremity of the thoracic duct, sometimes associated with lymph nodes. In addition, Jacobsson (1972) observed that an ampullary dilatation is often present before the terminal valves, especially when the duct terminated into jugular, subclavian, or bronchomediastinal trunks. Zorzetto et al. (1977) observed an ampullar dilatation at the final portion of the thoracic duct in 20 of 51 cases.

Right lymphatic duct

Uunlike the thoracic duct, the right lymphatic duct is less distinguished in size and characteristics, usually 1–2 cm in length (Skandalakis et al. 2007; Standring et al. 2008). Although the right lymphatic duct originates from the right jugular, bronchomediastinal, and subclavian lymphatic trunks, it may not form into a single trunk; instead, these individual lymphatic trunks terminate separately (Davis 1915; Smith et al. 2013). In fact, Standring et al. (2008) note that these three lymphatic trunks terminating independently is a norm. Instead, it is rare for these lymphatic trunks to join together to form a right lymphatic duct (Standring et al. 2008). Sometimes, the formation of a right lymphatic duct is partial, when any combination of terminals from subclavian and jugular trunks is fused (Standring et al. 2008).

The right lymphatic duct does not always resemble a single trunk and it collects lymph from the right side of the head, neck, and thorax and the right upper limb (Bartels 1909; Anson and McVay 1971). It reaches the ventral aspect of the right venous junction by crossing the medial border of the scalenus anterior, where it terminates into the junction of the right subclavian and internal jugular veins (Skandalakis et al. 2007; Standring et al. 2008). However, its termination sites can show numerous variations where tributaries can enter into the right lymphatic duct, fully or partially (Skandalakis et al. 2007). In addition, when the thoracic duct shows Lane's type II classification, one of the branches that terminate on the right side can join the right lymphatic duct near the termination site (Lane and Todd 1847). When it shows type III, an equivalent structure of the right lymphatic trunk can be present on the left side (Smith et al. 2013).

References

Akcali O, Kiray A, Ergur I, Tetik S, Alici E. 2006. Thoracic duct variations may complicate the anterior spine procedures. *Eur Spine J* 15: 1347–1351.

Anson BJ, McVay C. 1971. Thoracic cavity and its contents. In: *Surgical Anatomy*. Vol 1. Philadelphia: W.B. Saunders, pp. 442–446.

Archimbaud JP, Bansillon V, Bernhardt J, Bonnet P, Saubier EC. 1969. Quarante dissections du canal thoracique. Sa terminaison chez l'homme vivant. *Lyon Medical* 30: 211–214.

Baldridge RR, Lewis RV. 1948. Traumatic chylothorax. *Ann Surg* 128: 1056–1078.

Bartels P. 1909. Das Lymphgefässsystem. In Bardeleben's Handbuch der Anatomie des Menschen. Jena: Gustav Fischer, pp. 85–99.

Celis A, Porter JK. 1952. Lymphatics of the thorax; an anatomic and radiologic study. Acta Radiol 38: 461–470.

Chen H, Shoumura S, Emura S. 2006. Bilateral thoracic ducts with coexistent persistent left superior vena cava. *Clin Anat* 19: 350–353.

Clark ER. 1953. The lymphatic system and the spleen. In: Morris' Human Anatomy, 11th edition (ed. SchaefferJP) New York: The Blakiston Division, McGraw-Hill Book Company, pp. 864–867.

Correia M. 1926. Le canal thoracique chez l'homme. *Folia Anatomica Universitatis Conimbrigensis* 1: 1–20.

Davis HK. 1915. A statistical study of the thoracic duct in man. *Am J Anat* 17: 211–244.

Decker GAG, du Plessis DJ. (eds) 1986. Lee McGregor's Synopsis of Surgical Anatomy, 12th edition. Bristol: Wright.

Elliott GE, Thompson KL. 2013. A previously undocumented pre-aortic pathway of the thoracic duct. A case report. *IJAV* 6: 221–224.

Epstein DA, Debord JR. 2002. Abnormalities associated with aberrant right subclavian arteries: a case report. *Vasc Endovascular Surg* 36: 297–303.

Gray H. 1942. *Anatomy of the Human Body (Gray's Anatomy), 24th edition*. Philadelphia: Lea and Febiger.

Greenfield J, Gottlieb MI. 1956. Variations in the terminal portion of the human thoracic duct. *AMA Arch Surg* 73: 955–959.

Hidden G, Florent J. 1966. Radio-anatomical study of the opacified thoracic duct by segmental lymphography. *J Chir* 91: 373.

Hollinshead WH. 1971. *Anatomy for Surgeons*. Vol 2. New York: Hoeber-Harper.

Jacobsson SI. 1972. *Clinical Anatomy and Pathology of the Thoracic Duct: An Investigation of 122 Cases*. Stockholm: Almqvist and Wiksell.

Jdanov DA. 1959. Anatomie du canal thoracique et des principaux collecteurs lymphatiques du tronc chez l'homme. *Acta Anat* 37: 20–47.

Jossifow GM. 1906. Der anfang des ductus thoracicus und dessen erweiterung. *In Arch Anat Physiol, Anat Entwickelungsgeschichte* (ed. WaldeyerW). Leipzing: VeitandComp, pp. 68–76.

Kaur D, Jain M, Dhall U, Singh K. 2012. An unusual course of the thoracic duct in relation to the vertebral vessels. *Singapore Med J* 1: e1–2.

Kausel HW, Reeve TS, Stein AA, Alley RD, Stranahan A. 1957. Anatomic and pathologic studies of the thoracic duct. *J Thorac Surg* 34: 631–641.

Kinnaert P. 1973. Anatomical variations of the cervical portion of the thoracic duct in man. *J Anat* 115: 45–52.

Kubik S. 1995. Cardiovascular system. In: *Gray's Anatomy, 38th edition* (eds Williams PL, Bannister LH, Berry MM). New York: Churchill Livingstone, pp. 1610.

Kwon SS, Falk A, Mitty HA. 2002. Thoracic duct injury associated with left internal jugular vein catheterization: anatomic considerations. *J Vasc Interv Radiol* 13: 337–339.

Lachapèle AP, Hughes A, Lagarde C. 1964. De l'ètude anatomo-radiologique du canal thoracique d'apres 60 opacifications sur l'etre humain vivant. *J Radiol Electrol Med Nucl* 45: 1–10.

Lane S, Todd RB. (eds) 1847. *The Cyclopaedia of Anatomy and Physiology*. London: Sherwood, Gilbert and Piper.

Langford RJ. 2002. Valves in the subsidiary lymph trunks in the neck. *J Craniomaxillofac Surg* 30: 121–124.

Lissitzyn MS. 1924. Ductus thoracicus. *Arch Klin Chir* 128: 213–215.

Loukas M, Wartmann CT, Louis RG Jr, Tubbs RS, Salter EG, Gupta AA, Curry B. 2007. Cisterna chyli: a detailed anatomic investigation. *Clin Anat* 20: 683–688.

Minkin A. 1925. Zur frage des rechtsseitigen verlaufes des ductus thoracicus. *Anat Anz* 60: 314–318.

Nasbaum M, Baum S, Hedges RC, Blakemore WS. 1964. Roentgenographic and direct visualization of thoracic duct. *Arch Surg* 88: 105–113.

Nathan H, Gitlin G. 1968. Thoracic duct terminating on the right side associated with aberrant retro-oesophagal right subclavian artery and truncus bicaroticus. *Thorax* 23: 266–270.

Nathan H, Seidel MR. 1983. The association of a retroesophageal right subclavian artery, a right-sided terminating thoracic duct, and a left vertebral artery of aortic origin: Anatomical and clinical considerations. *Acta Anat* 117: 362–373.

Okumura K, Fujimoto T. 1974. A case of anomalous right subclavian artery passing behind the esophagus with a rare variation of the thoracic duct. *Acta Anat Jpn* 49: 179–183.

Orts Llorca F. 1936. Über den rechtsseitigen Verlauf des Ductus thoracicus bei erhaltener rechter Aortenwurzel. *Anat Anz* 81: 283–290.

Parsons FG, Sargent PWG. 1909. On the termination of the thoracic duct. *The Lancet* 173: 1773–1774.

Peña E, Zuñiga J. 2009. An anatomical variation: the aberrant termination of the thoracic duct. *Biomedica* 29: 204–208 (in Spanish).

Propst-Proctor SL, Rinsky LA, Bleck EE. 1983. The cisterna chyli in orthopaedic surgery. *Spine* 8: 787–792.

Ranade AV, Rai R, Prabhu LV, Kumaran M. 2006. A rare lymphaticovenous communication associated with duplication of thoracic duct. *Int J Morphol* 2: 155–158.

Rocca-Rossetti S, Aresu R, Liguori G. 1961. Ricerche sulla composizione della linfa umana. I. Anatomia chirurgica del dotto toracico al collo e tecnica del cateterismo. *Rassegna Medica Sarda* 63: 651–656.

Rouvière H. 1938. *Anatomie des Lymphatiques de l'Homme*. Paris: Masson.

Seeger M, Bewig B, Günther R, Schafmayer C, Vollnberg B, Rubin D, Hoell C, Schreiber S, Fölsch UR, Hampe J. 2009. Terminal part of thoracic duct: high-resolution US imaging. *Radiology* 252: 897–904.

Shafiroff BG, Kau QY. 1959. Cannulation of the human *thoracic lymph duct. Surgery* 45: 814–819.

Shimada K, Sato I. 1997. Morphological and histological analysis of the thoracic duct at the jugulo-subclavian junction in Japanese cadavers. *Clin Anat* 10: 163–172.

Skandalakis JE, Colborn GL, Weidman TA, et al. 2004. *Lymphatic system. In: Surgical Anatomy*, Vol 2 (ed. SkandalakisJE). Athens: Paschalidis Medical Publications, Ltd, pp. 1648–1659.

Skandalakis JE, Skandalakis LJ, Skandalakis PN. 2007. Anatomy of the lymphatics. *Surg Oncol Clin N Am* 16: 1–16.

Smith AJ, Birmingham A. 1889. Absent thoracic duct causing oedema of a foetus. *J Anat Physiol* 23: 531–536.

Smith ME, Riffat F, Jani P. 2013. The surgical anatomy and clinical relevance of the neglected right lymphatic duct: review. *J Laryngol Otol* 8: 1–6.

Standring S, Borley NR, Collins P, Crossman AR, Gatzoulis MA, Healy JC, Johnson D, Mahadevan V, Newell RLM, Wigley CB. 2008. *Neck. In Gray's Anatomy, 40th edition*. Edinburgh: Elsevier, Churchill Livingstone, pp. 435–466.

Tesauro B. 1966. Anatomical aspects of the thoracic duct after ligation. *Bull Soc Int Chir* 25: 602–607.

Van der Putte SC, van Limborgh J. 1980. The embryonic development of the main lymphatics in man. *Acta Morphol Neerl Scand* 18: 323–335.

Van Pernis PA. 1949. Variations of the thoracic duct. *Surgery* 26: 806–809.

Watson M. 1872. Note on the termination of the thoracic duct on the right side. *J Anat Physiol* 6: 427–428.

Werner B. 1965. Thoracic duct cannulation in man. I. Surgical technique and a clinical study on 79 patients. *Acta Chir Scand Suppl* 353: 1–32.

Williams PL, Bannister LH, Berry MM. (eds) 1995. *Gray's Anatomy, 38th edition*. New York: Churchill Livingstone, pp. 327–328, 1609–1611.

Wirth W, Kubik S. 1980. Lymphographic roentgen anatomy. In: *Atlas of Lymphography* (eds Viamonte M, Rüttimann A, Agbaba M). Stuttgart: Thieme-Verlag, pp. 71–89.

Yamada G. 1932. A case of right sided aortic arch. *Acta Anat Jap* 5: 783–793.

Zorzetto NL, Ripari W, De Freitas V, Seullner G. 1977. Anatomical observations on the ending of the human thoracic duct. *J Morphol* 3: 363–369.

Further reading

Baumeister RGH. 1989. Surgical anatomy of the lymphatic system. In: *Vascular Surgery* (eds HebererG, van DongenRJAM). Berlin, Heidelberg: Springer-Verlag.

Crumley RL, Smith JD. 1976. Postoperative chylous fistula prevention and management. *Laryngoscope* 86: 804–813.

Gladstone RJ, Wakeley CPG. 1915. Two cases, considered from the developmental standpoint, in which the right subclavian arose from the arch of the aorta beyond the origin of the left subclavian artery; with a note on the relation of the subclavian veins to the cardinal system. *J Anat Physiol* 49: 362–375.

Kihara T, Adachi B. 1953. Der ductus thoracicus der Japaner. In: *Lymphgefäßsystem der Japaner Das* (eds Kihara T, Adachi B). Kyoto: Kenkyusha, pp. 44–49.

76 Lymphatics of the lower limb

Shun Yamazaki[1], Hiroo Suami[2], Nobuaki Imanishi[1], Sadakazu Aiso[1], Minoru Yamada[1], Masahiro Jinzaki[1], Sachio Kuribayashi[1], David W. Chang[2] and Kazuo Kishi[1]

[1]Keio University, Tokyo, Japan

[2]The University of Texas MD Anderson Cancer Center, Houston, Texas, United States

The capillary vessels of the superficial lymphatic system in the lower extremities originate in the dermis, and those of the deep lymphatic system originate in the fascia, periosteum, perichondrium, aponeurosis, and articulation. In essence, the deep fascia divides the superficial and deep lymphatic systems. In the dermis, the lymph capillary vessels initially form a two-dimensional network just beneath the papillary layer and are absent from the epidermis. They originate near the blood capillaries, penetrating into the papillae of the dermis, and have diameters of 20–70 μm (Wenzel-Hora et al. 1987). These vessels drain into the precollectors (Sacchi et al. 1997) and then into the subcutaneous lymph-collecting vessels. The vessels of the superficial lymphatic system, running above the deep fascia, do not follow the course of the blood vessels and nerves. However, they have a distribution similar to the cutaneous veins. In contrast, the lymph-collecting vessels belonging to the deep lymphatic system originate in the tissues under the deep fascia and accompany the blood vessels in those tissues (Kutsuna 1968).

Lymph nodes

The two main types of lymph nodes in the lower extremities are the regional and interval nodes. Nodes that are normally present and receive lymph directly from vessels, in particular tissues and organs, are known as regional lymph nodes. Those that are infrequently found between the lymph-collecting vessels and the regional lymph node basins are called interval lymph nodes (Bartels 1909). Importantly, regional lymph nodes are associated with cancer metastasis and are targets for lymph node dissection, a surgical treatment for superficial cancers.

Regional lymph node

There are two types of regional lymph nodes in the lower extremities: inguinal and popliteal. There are many reports that popliteal nodes are important sentinel lymph nodes for skin cancers of the lower leg (Thompson et al. 2000; Menes et al. 2004; Morcos and Al-Ahmad 2011). Although some authors regard popliteal lymph nodes as interval nodes (Sumner et al. 2002), they meet the above definition of the regional type. We therefore class them as regional lymph nodes.

Inguinal lymph node

Superficial inguinal lymph nodes are found in front of the deep fascia of the thigh, in the groin area. Daseler et al. (1948) mentioned that during inguinal node dissection, most superficial lymph nodes are found in the quadrangular area that runs parallel to, and 1 cm above, the inguinal ligament. A 20-cm-long vertical line running through the superior anterior iliac spine represents the lateral boundary, and a 15-cm-long vertical line running through the pubic tubercle represents the medial boundary (Daseler et al. 1948). There are seven–ten (average nine) superficial inguinal lymph nodes. Two or three of the large ones are drained by the great saphenous lymph vessels (see section on "Great saphenous lymph vessels" below), which carry most of the lymph in the superficial lower extremities.

There are one–three *deep* inguinal lymph nodes found subfascially in the iliopectineal fossa. They are normally present just beneath the junction of the great saphenous and femoral veins. Rosenmüller lymph nodes (also called Cloquet's nodes or Pirogoff's nodes) are another type of deep inguinal nodes, present in approximately 40% of people and located in the femoral ring.

Popliteal lymph node

Popliteal lymph nodes are classified as either superficial or deep. Typically, there is only one *superficial* popliteal lymph node, although there can be as many as three. Located beneath the deep fascia, the superficial popliteal lymph node(s) is/are nevertheless regional nodes associated with the small saphenous vessels that belong to the superficial lymphatic system. This node is drained by the small saphenous lymph vessels, described in "Small saphenous lymph vessels" below.

On average there are two *deep* popliteal lymph nodes (range two–five). They are distributed along the popliteal artery and

Bergman's Comprehensive Encyclopedia of Human Anatomic Variation, First Edition. Edited by R. Shane Tubbs, Mohammadali M. Shoja and Marios Loukas.
© 2016 John Wiley & Sons, Inc. Published 2016 by John Wiley & Sons, Inc.

vein and are regional nodes of the deep lymphatic system of the foot. They receive lymph from the superficial popliteal lymph nodes and the deep lymph-collecting vessels in the leg.

Interval lymph nodes

Interval lymph nodes are inconsistently found in conjunction with arteries and vessels.

- Anterior tibial lymph node is present in 38% of cases alongside the anterior tibial artery, typically present at the junction of this artery with the anterior tibial recurrent artery.
- Posterior tibial lymph node is present in 46% of cases alongside the posterior tibial artery, typically present at the junction of this artery with the fibular artery.
- Fibular lymph node is present in 35% of cases, anywhere along the fibular artery (Kutsuna 1968).

Lymph vessels

Lymph vessels in the lower extremities are divided into superficial vessels that run above the deep fascia and deep vessels that run beneath the deep fascia. These vessels are described in greater detail in the following sections.

Superficial lymph vessels

Great saphenous lymph vessels (anteromedial bundle, ventromedial bundle)

The great saphenous lymph vessels drain a large area of skin and subcutaneous tissue in the thigh and lower leg. Lymph vessels originating from the toes converge to the medial frontal aspect of the ankle, and those originating from the medial frontal part of the foot join the vessels from the first toe. Some of the vessels originating from the medial posterior part of the foot join the vessels from the toes, and others ascend the leg, parallel to the great saphenous vein. Similarly, some of the vessels originating from the lateral frontal part of the foot join vessels from the little toe, whereas others ascend along the posterior aspect of the external malleolus and converge at the medial aspect of the knee. In the lower leg, most of the great saphenous lymph vessels converge in the medial posterior aspect of the knee along with the great saphenous vein. Several lymph vessels also run through the lateral aspect of the knee toward the thigh. The lateral posterior aspect of the foot (lateral heel) is part of the small saphenous lymph vessel basin.

Small saphenous lymph vessels (dorsolateral bundle, ventromedial bundle)

The small saphenous lymph vessels drain a small area of skin and subcutaneous tissue from the lateral heel and part of the posterior lower leg, around the small saphenous vein. These vessels originate in the lateral heel and travel near the small saphenous vein to drain into the superficial popliteal lymph node.

Deep lymph vessels

The deep lymph vessels originate in the deep fascia, fascia, periosteum, perichondrium, aponeurosis, and articulation, accompanying each deep artery and vein. They comprise the anterior tibial, posterior tibial, fibular, popliteal, and femoral lymph vessels. Anatomical variations in the deep lymph-collecting vessels are discussed in the following section.

Anatomical variations of the lymphatic system

This section describes the anatomical variations in the lymphatic system of the lower extremities. Knowledge of such variations is important for understanding the pathway of skin cancer metastasis in the peripheral lower extremities (Yamazaki et al. 2013). There are at least three types of anatomical variations in the lymphatic pathway including lymph-collecting vessels and regional lymph nodes.

- Type 1 (60%): The great saphenous lymph-collecting vessels drain into the superficial lymph nodes, and the small saphenous lymph-collecting vessels drain into the superficial popliteal lymph node. The efferent lymph-collecting vessels from the superficial popliteal node pass through the deep popliteal nodes and run to the deep layer, converging with the deep lymph-collecting vessels that accompany the femoral artery and vein. Most of the deep lymph-collecting vessels drain into the deep inguinal lymph nodes but some drain directly into the external iliac nodes, bypassing the deep inguinal nodes (Yamazaki et al. 2013).
- Type 1a: There are no connecting vessels between the small saphenous and the great saphenous lymph-collecting vessels.
- Type 1b: Some lymph-collecting vessels arise from the small saphenous and join the great saphenous lymph-collecting vessels.
- Type 2 (15%): The great saphenous lymph-collecting vessels drain into the superficial lymph nodes, and the small saphenous lymph-collecting vessels drain into the superficial popliteal node. However, the efferent lymphatic vessel from the superficial popliteal node does not run deep but turns toward the medial side of the knee and joins the great saphenous lymph vessels. In this case, the small saphenous vein converges with the great saphenous vein via the Giacomoni vein.
- Type 2a: There are no connecting vessels between the small saphenous and the great saphenous lymph collecting vessels.
- Type 2b: Some lymph-collecting vessels arise from the small saphenous vessels and join the great saphenous lymph-collecting vessels.
- Type 3 (15%): Most of the great saphenous lymph-collecting vessels drain into the superficial lymph nodes, but some diverge before reaching those nodes and converge with the superficial popliteal nodes around the popliteal fossa. The small saphenous lymph-collecting vessels divide into two

pathways: one converging with the great saphenous lymph-collecting vessels and the other draining into the superficial popliteal nodes. The efferent lymph-collecting vessels from the superficial popliteal lymph node run as Type 1 to the deep layer and drain into the deep inguinal or external iliac lymph nodes.

Lymph drainage territories in the lower extremities

The drainage areas of the lower extremities are divided into two territories. One involves the small saphenous lymph vessels and covers the area from the lateral heel to the posterior thigh. The second involves the great saphenous lymph vessels and covers the balance of the lower extremities.

Except for Type 3, the flow from the great saphenous lymph vessel territory drains into the superficial lymph nodes; in Type 3 it drains into the superficial inguinal and popliteal lymph nodes, and eventually reaches the deep inguinal or external iliac lymph nodes.

The flow from the small saphenous lymph vessel territory drains into the superficial inguinal lymph node in Types 1a and 2a. In other types, the flow from this territory drains into the superficial inguinal and superficial popliteal lymph nodes. In Type 2, the lymph flow drains into the superficial inguinal lymph nodes, while in other types the drainage can sometimes be into the superficial inguinal, deep inguinal, or external iliac lymph nodes.

Anatomical changes to the lymphatics in lymphedematous lower extremities

Lymphedema is a condition of lymph stasis in the skin and subcutaneous tissue caused by chronic inflammation with accompanying morphological changes in the lymphatic system. It is categorized as either primary or secondary. Primary lymphedema is probably the result of a lymphatic developmental error, whereas secondary lymphedema is caused by destruction of lymphatic function, frequently resulting from lymph node dissection during surgical treatment of a malignant tumor.

Patients with primary lymphedema

Primary lymphedema is a condition of lymph stasis caused by cryptogenic hypoplasia and dysfunction of the lymph vessels and lymph nodes. The dysfunction can be categorized as congenital, praecox, or lymphedema tarda (Kinmonth et al. 1957). In primary lymphedema, the morphological changes in the lymphatic system are wide-ranging and can include partial defects in the great saphenous lymph vessels as well as some regional lymph nodes.

Patients with secondary lymphedema

Anatomical changes to the lymphatics after pelvic lymphadenectomy have been well described. In the first stage, the lymph-collecting vessels are dilated shortly after the dissection, and those passing through the lateral knee can be visualized by lymphoscintigraphy. In the second stage, fibrosis of the lymph vessels gradually progresses (Koshima et al. 1996; Suami et al. 2007) and backflow of lymph into the precollectors and lymph capillaries (called dermal back flow, DBF) can occur because of valvular dysfunction. DBF spreads from the inguinal to the proximal medial thigh region and subsequently to the lower leg. In some cases, lymph vessels bypass the great saphenous vessels and connections to the small saphenous lymph vessels can be seen. In the final stage, no lymph-collecting vessels can be demonstrated by lymphoscintigraphy, due to the diffuse fibrosis (Kubik 2006; Maegawa et al. 2010; Yamamoto et al. 2011).

References

Bartels, P. 1909. Das Lymphgefässsystem. In *Bardeleben's Handbuch der Anatomie des Menschen*. Jena: Gustav Fischer, pp. 85–99.

Daseler EH, Anson BJ, Reimann AF. 1948. Radical excision of the inguinal and iliac lymph glands. A study based on 450 anatomical dissections and upon supportive clinical observations. *Surg Gynecol Obstet* 87: 679–694.

Kinmonth JB, Taylor GW, Tracy GD, Marsh JD. 1957. Primary lymphoedema; clinical and lymphangiographic studies of a series of 107 patients in which the lower limbs were affected. *Br J Surg* 45: 1–9.

Koshima I, Kawada S, Moriguchi T, Kajiwara Y. 1996. Ultrastructural observations of lymphatic vessels in lymphedema in human extremities. *Plast Reconstr Surg* 97: 397–405.

Kubik S. 2006. Lymphatic system of the lower extremities. In: *Földi's Textbook of Lymphology*, second edition (eds FöldiM, FöldiM). Munich: Urban & Fischer.

Kutsuna M. 1968. *The Anatomy of the Lymphatic System in the Japanese*. Tokyo: Kanehara Shuppan in Japanese).

Maegawa J, Mikami T, Yamamoto Y, Satake T, Kobayashi S. 2010. Types of lymphoscintigraphy and indications for lymphaticovenous anastomosis. *Microsurgery* 30: 437–442.

Menes TS, Schachter J, Steinmetz AP, Hardoff R, Gutman H. 2004. Lymphatic drainage to the popliteal basin in distal lower extremity malignant melanoma. *Arch Surg* 139: 1002e6.

Morcos B, Al-Ahmad F. 2011. Metastasis to the popliteal lymph nodes in lower extremity melanoma and their management. *Surg Oncol* 20: e119–22.

Sacchi G, Weber E, Agliano M, Raffaelli N, Comparini L. 1997. The structure of superficial lymphatics in the human thigh: pre- collectors. *Anat Rec* 247: 53–62.

Suami H, Pan WR, Taylor GI. 2007. Changes in the lymph structure of the upper limb after axillary dissection: radiographic and anatomical study in a human cadaver. *Plast Reconstr Surg* 120: 982–991.

Sumner III WE, Ross MI, Mansfield PF, Lee JE, Prieto VG, Schacherer W. 2002. Implications of lymphatic drainage to unusual sentinel lymph node sites in patients with primary cutaneous melanoma. *Cancer* 95: 354e60.

Thompson JF, Hunt JA, Culjak G, Uren RF, Howman-Giles R, Harman CR. 2000. Popliteal lymph node metastasis from primary cutaneous melanoma. *Eur J Surg Oncol* 26: 172e6.

Wenzel-Hora BI, von Berens Rautenfeld D, Majewski A, Lubach D, Partsch H. 1987. Scanning electron microscopy of the initial lymphatics of the skin after use of the indirect application technique with glutaraldehyde and MERCOX as compared to clinical findings. *Lymphology* 20: 126–144.

Yamamoto T, Matsuda N, Doi K, Oshima A, Yoshimatsu H, Todokoro T, Ogata F, Mihara M, Narushima M, Iida T, Koshima I. 2011. The earliest finding of indocyanine green lymphography in asymptomatic limbs of lower extremity lymphedema patients secondary to cancer treatment: the modified dermal backflow stage and concept of subclinical lymphedema. *Plast Reconstr Surg* 128: 314e–321e.

Yamazaki S, Suami H, Imanishi N, Aiso S, Yamada M, Jinzaki M, Kuribayashi S, Chang DW, Kishi K. 2013. Three-dimensional demonstration of the lymphatic system in the lower extremities with multidetector-row computed tomography: a study in a cadaver mode. *Clin Anat* 26: 258–266.

77 Forebrain

R. Shane Tubbs[1-3], Mohammadali M. Shoja[4], and Marios Loukas[2]
[1]Seattle Science Foundation, Seattle, Washington, United States
[2]St George's University, School of Medicine, St Georges, Grenada
[3]University of Dundee, Dundee, United Kingdom
[4]Tuberculosis and Lung Disease Research Center, Tabriz University of Medical Sciences, Tabriz, Iran

The septum pellucidum may be absent. Agenesis of the septum pellucidum is often associated with agenesis of the corpus callosum, but either condition may occur without the other. The septum may also be perforated. The corpus callosum can be thinned, missing sections, or completely absent. The anterior commissure and fornix can be absent. The massa intermedia can be absent or duplicated. Its area ranges from 9.8 to 205 mm^2 (Davie and Baldwin 1967) and its shape is very variable. An additional commissure of the third ventricle can be seen above the optic chiasm and between the columns of the fornix, and this commissure itself can be doubled.

The pituitary gland can be duplicated (Ginat et al. 2013). Rarely, the gland is absent. One of its parts, for example the neurohypophysis, can be absent. The anterior lobe can be retained in a persistent craniophyarngeal duct. Ectopic pituitary tissue can be found along the craniopharyngeal canal and in the nasopharynx or sphenoid sinus. Accessory pituitary on the inferior surface of the sphenoid bone is known as the phyaryngeal hypophysis of Erdheim.

The pineal gland can be hypoplastic or, rarely, absent. Ectopic ganglion cells have been seen along the gland.

Midline cysts occur in the interhemispheric region of the brain and have a circular or elliptical shape. Anterior midline intracranial cysts are most often found in one of three forms: cavum septum pellicidum, cavum vergae, and cavum velum interpositum. Even though most of these fluid collections are benign, there can be pathologic effects in some patients depending on the size of the cavities.

Cavum velum interpositum

The velum interpositum space is the subarachnoid space between the connected fornix and its respective choroid plexus, and the choroid forming the roof of the third ventricle inferiorly. It is an anterior extension of the quadrigeminal plate cistern, located superior to the pineal gland. If this potential space is dilated, then it is known as the cavum velum interpositum. The differential diagnosis of these midline cystic brain lesions includes an enlarged third ventricle, a vein of Galen aneurysm, an interhemispheric cyst in relation to the agenesis of the corpus callosum, and a suprasellar arachnoid cyst.

Most cases of cavum velum interpositum occur in newborns. A typical axial MRI or CT scan will display a triangular-shaped CSF space between the lateral ventricles. On sagittal images, a cavum velum interpositum appears like a slit with collections of CSF behind the foramen of Monro, below the fornices, and above the tela choroidea of the third ventricle.

During the early fetal stages, a continuous layer of pia mater encloses the prosencephalon and diencephalon. As the brain slowly develops, the growing and covered cerebral vesicles of the forebrain overlap the pia mater of the third ventricle. This causes double layering of the tela choroidea, or velum interpositum, of the roof of the third ventricle. The anterior aspect of the tela choroidea is closed and is at the foramen of Monro where the pia mater folds on itself. When the posterior end remains open, the formation of the cavum velum interpositum occurs. The potential space between the double layers of the tela choroidea creates the cavum velum interpositum that interacts with the quadrigeminal cistern. The internal cerebral veins are situated between the two layers of the cavum velum interpositum, as is the posterior medial choroidal artery. On axial imaging, the cavum velum interpositum has a distinct triangular appearance with an apex directed anteriorly toward the forniceal columns. An enlarged cavum velum interpositum displaces the internal cerebral veins inferiorly and laterally.

Cavum septum pellucidum

When a septum pellucidum has a separation between its two leaflets, this is termed a cavum septum pellucidum. This cavity is sagittally oriented and has a concentration of CSF that filters

Bergman's Comprehensive Encyclopedia of Human Anatomic Variation, First Edition. Edited by R. Shane Tubbs, Mohammadali M. Shoja and Marios Loukas.
© 2016 John Wiley & Sons, Inc. Published 2016 by John Wiley & Sons, Inc.

from the ventricles through the septal laminae. Cavum septum pellucidum is bounded on all sides: anteriorly by the genu of the corpus callosum; superiorly by the body of the corpus callosum; posteriorly by the anterior limb and pillars of the fornix; inferiorly by the anterior commissure and the rostrum of the corpus callosum; and laterally by the leaflets of the septum pellucidum. Since it is an enclosed space, it is not a part of the ventricular system and does not communicate with the subarachnoid space. The cavum septum pellucidum is lined with glial, neuronal, and ependymal cells.

There are many variants of cavum septum pellucidum, but the most common type is non-communicating. Cavum septum pellucidum is present in all fetuses, but over 85% of them fuse around 3–6 months after birth. This structure may persist in up to 20% of adults.

The cavum septum pellucidum's embryological development explains why it is so pervasive in infants. The cavum septum pellucidum is found in the caudal portion of the interhemispheric fissure. During the fifth month of the embryonic period, the corpus callosum closes superiorly and the forceps minor enlarges to the frontal lobes while the fornix stays in its initial position. The corpus callosum forms from anterior to posterior, except for the rostrum which connects the genu and the lamina terminalis. Because of this, the leaflets of the septum pellucidum are pulled toward the lamina terminalis, sealing the cavum from the posterior fornix to the rostrum of the corpus callosum, due to the frontalization of fibers in the genu portion by the seventh month. When the gap is not closed, the condition remains.

Cavum vergae

The third related intracranial midline cyst is a cavum vergae, first described by Verga and sometimes referred to as Verga's ventricle. Cavum vergae is an extension of a cavum septum pellucidum posteriorly past the columns of the fornix and foramina of Monro. This structure is present in up to 30% of newborns, but persists into adulthood in less than 1% of individuals. The posterior floor of a cavum vergae is, therefore, the commissure of the fornix. This condition takes place when there is a separation of the leaflets of the septum pellucidum with posterior extension to the splenium of the corpus callosum. The anterior columns of the fornix separate the anterior cavum septum pellucidum and the posterior cavum vergae. Historically these cavities, cavum septum pellucidum and cavum vergae, were considered fifth and sixth ventricles, respectively. This argument was refuted since they do not contain choroid plexus. The cavum vergae is bordered anteriorly by the posterior border of the cavum septi pellucidum, inferiorly by the body of the fornix, and superiorly and posteriorly by the corpus callosum. Anatomically speaking, these two cavities are not separated; however, a cavum septum pellucidum may exist without a cavum vergae. Some have described the passage between these two cavities as Verga's aqueduct.

Ectopic brain tissue

Brain tissue may occur at an aberrant location within its organ of origin (central nervous system) and should be referred to as a heterotopia. If this tissue is outside of the central nervous system, then it is referred to as ectopic brain tissue. This entity most commonly occurs in the nasal region and is often referred to as a nasal glioma. Up to 25% of these nasal gliomas have fibrous connections to the intracranial space. Non-nasal locations for misplaced central nervous system tissue are rare with locations previously described in the lip, lung, middle ear, orbit, tongue, palate, pharynx, cornea, back, subpleurally, retroperitoneally, and scalp.

Nasal gliomas share similar characteristics to ectopic brain tissue; however, non-nasal ectopias show more advanced and mature differentiation into various neural components such as ependymal and choroids plexus cells. Some have opined that ectopic brain tissue has a separate embryologic genesis and is therefore not related to nasal gliomas. Many favor the theory that early neuroectoderm is displaced early in embryogenesis, and that multipotential cells mature ectopically. Nevertheless, the true mechanism for the development of ectopic brain tissue remains unclear. Parenthetically, our case with normal intracranial anatomy supports the theory of multipotential cells maturing distal to the central nervous system.

The cerebral hemispheres may be asymmetric. The brain may be incompletely or imperfectly divided into two hemispheres.

Sylvian fissure

The caudal extremity of the sylvian (lateral) fissure may be forked (41%), forming ascending and descending branches. The ascending branch is the most constant and is regarded as the true continuation of the fissure. The ascending branch forms the axis of the supramarginal gyrus. Triradiate termination of the sylvian fissure has been reported.

According to Cunningham, the anterior rami of the sylvian fissure may assume different configurations: they may be Y-shaped where the two rami, enclosing the triangular frontal gyrus, join the sylvian fissure by a common stem (32% of hemispheres); the two rami may join the sylvian fissure separately, and they may be V- or U-shaped (37% of hemispheres); or a single ramus may join the fissure (30% of hemispheres). Less frequently, there are more than two rami, or the two rami are reduced to one (taking the position of either one of them) or are intermediate in position. In one study, two rami were observed in 85% of Brains, one ramus in 12%, and three rami in 3%.

The length of the anterior ascending ramus varies over the range 10–30 mm, and of the anterior horizontal 10–25 mm.

The sylvian fissure is frequently longer on the left hemisphere than on the right.

Other Sulci/Fissures

The postcentral sulcus may be formed by up to four different segments

The intraparietal sulcus may be formed by various combinations of its three phylogenetic components: a rostral vertical component, the postcentral inferior and superior sulci; a middle horizontal component, the intraparietal proper; and a caudal component, the paroccipital. The inferior and superior postcentral components may separate from the intraparietal sulcus proper and join the postcentral sulcus. The inferior postcentral sulcus may terminate in a forked fashion with the anterior branch directed toward the lower concavity of the central sulcus. Occasionally, the inferior postcentral sulcus gives rise below the bifurcation to the sulcus retrocentralis (postcentralis) transversus. The development of the transverse retrocentral (postcentral) sulcus bears an inverse relationship to the development of the subcentral posterior sulcus situated close to the sylvian fissure. The transverse postcentral and the subcentral sulci may join the sylvian fissure.

The relationship of the horizontal component (intraparietal sulcus proper) to the superior and inferor postcentral sulci has been described under five categories: in category 1, all three sulci are separate; in category 2, the horizontal component is continuous with the inferior postcentral component; in category 3, the superior and inferior postcentral sulci are confluent and are separate from the intraparietal sulcus proper; in category 4, all three components are continuous with other; and in category 5, the horizontal component is continuous with the superior postcentral component.

The intraparietal sulcus proper may have one or two dorsal branches extending into the superior parietal lobule and continuous with one or more of its sulci. One or more short ventral branches may also extend into the inferior parietal lobule. One of these branches, the intermedius primus or anterior, marks the boundary between the supramarginal and angular gyri. The intermedius primus or anterior may be continuous with the superior temporal sulcus. Another branch, the sulcus angularis, may be axial to the angular gyrus and may be continuous with the superior temporal sulcus. The sulcus intermedius posterior is very variable and represents another inferior branch of the intraparietal sulcus proper. An accessory obique sulcus of the cuneus may be present and is known as the sulcus of Brissaud.

The superior temporal sulcus is usually a continous sulcus but is occasionally separated into two or three sections, especially in the left hemisphere. The sulcus may encroach on the territory of the middle temporal sulcus. The terminal portion of the sulcus may be forked. This sulcus may separate into two–six parts. It may interdigitate with the superior temporal sulcus.

In its simplest form, this sulcus is triradiate with an anterior branch (orbitalis anterior) and two posterior branches (orbitalis posterior and lateralis). The two posterior branches form a U-shaped furrow with a caudally directed concavity. A second anterior branch (orbitalis anterior lateralis) may be present lateral to the orbitalis anterior branch. The orbitalis anterior lateralis may join with the U-shaped furrow and with the orbitalis anterior, forming an H-shaped configuration. The two longitudinal arms of the H-shaped pattern may separate to form two distinct sagittal furrows.

This sulcus usually bends medially at its rostral extremity, but it occasionally bends laterally. Its caudal extremity usually forks: the medial branch is short, while the lateral is usually long and bends anteriorly to hook around or anastomose with the posterior orbital sulcus.

The central sulcus usually presents two anterior convexities, but occasionally four or five may occur. The upper half of the sulcus may turn sharply backward. The upper end of the sulcus usually cuts the dorsal border of the brain and turns caudally; rarely, it ends as much as 1 cm from the dorsal border. The upper third of the sulcus is frequently separated from the rest of the sulcus. The lower part of the sulcus may be directed forward and may unite with the subcentral anterior sulcus. In some cases, the central sulcus may be interrupted, doubled, or absent; when doubled, the sulci are separated by the rolandic gyrus.

The precentral sulcus may be composed of two or three parts: precentral inferior, precentral medius, precentral superior. In about 17% of brains, the precentral sulcus does not show discontinuity into separate parts.

The upper extremity of the precentral inferior sulcus may be located anterior to the lower end of the precentral superior sulcus or may unite with the latter forming a continuous sulcus. Occasionally, a horizontal ramus extends from the precentral inferior sulcus above the inferior frontal sulcus; this horizontal ramus may be confluent with the middle or superior frontal sulci.

A separate precentral medius sulcus may be present. Most frequently, it is derived from the upper part of the precentral inferior sulcus or the posterior part of the horizontal ramus. The precentral superior sulcus may give rise to the superior frontal sulcus. A posterior ramus of the precentral superior sulcus is sometimes present and may appear as an extension of the superior frontal sulcus. A superior precentral sulcus may cut or reach the superomedial border of the frontal lobe, but in most cases it fails to reach that border.

The inferior frontal sulcus may be attached to the precentral inferior sulcus, or it may be interrupted. It sometimes terminates in a bifurcation. The anterior part of the sulcus may be separated from the rest of the sulcus; the separated part is referred to as the lateral frontomarginal sulcus. This may form a continuous furrow or be broken up into several parts. It is more constant than the inferior frontal sulcus. The posterior end of the sulcus may be connected with the superior precentral sulcus.

The middle frontal sulcus is rarely uninterrupted. Its posterior end may be free or may join the middle or lower segment of the precentral sulcus. An accessory sulcus of the middle frontal gyrus can be present and is known as the rostral sulcus of Eberstaller.

The cingulate sulcus may show partial or complete interruption in 28–50% of brains. The subcallosal portion of the sulcus

may be doubled or tripled. In some cases the marginal ramus passes upward over the superomedial border to the dorsolateral surface.

The parieto-occipital fissure may take a straight course or may assume a simple or S-shaped curve.

The calcarine fissure may be hook-like. Its anterior part may show one or several side branches pointing backward and downward, and its posterior part may be interrupted or may extend to the dorsolateral surface of the hemisphere.

The anterior end of the collateral fissure may be continuous with the rhinal fissure or with the anterior segment of the inferior temporal sulcus. The posterior end of the collateral fissure occasionally bifurcates into Y- or T-shaped branches.

References

Davie JC, Baldwin M. 1967. Radiographic anatomical study of the massa intermedia. *J Neurosurgery* 26: 483–487.

Ginat DT, Holbrook EH, Faquin W, Curtin HD. 2013. Nasal hamartoma associated with duplicated pituitary. *J Comput Assist Tomogr* 37: 369–370.

78 Cerebral ventricles

Martin M. Mortazavi[1], Nimer Adeeb[2], Mohammad Jaber[2] and R. Shane Tubbs[3-5]
[1]University of Washington School of Medicine, Seattle, Washington, United States
[2]Children's of Alabama, Birmingham, Alabama, United States
[3]Seattle Science Foundation, Seattle, Washington, United States
[4]St George's University, School of Medicine, St Georges, Grenada
[5]University of Dundee, Dundee, United Kingdom

The ventricular system of the brain consists of four freely communicable, cerebrospinal fluid (CSF) -filled cavities: the two lateral ventricles, the third ventricle, and the fourth ventricle (Mortazavi et al. 2013). The size and shape of the ventricles vary widely and are discussed in detail. The overall volume of the ventricular system falls within the range 8667–50,183 mm^3 (Liu et al. 2009).

Lateral ventricles

Size

The mass of the brain increases dramatically with age, reaching a weight five times greater than that at birth by 15 years and attaining maximum weight around the age of 19. However, the most rapid increase in brain weight occurs during the first three years of life. After the age of 45–50, brain weight progressively declines, reaching its lowest mass after 86 years (about 11% less than the maximum). Brain weight is about 9.8% higher in males than females (Dekaban 1978).

These changes in the overall mass of the brain and the associated loss of white and gray matter are directly reflected in the lateral ventricles, which are inversely related in size to their surrounding neural tissues (Lemaitre et al. 2005). Age-related decrease in brain volume is therefore followed by an approximately constant increase in ventricular volume during each decade of life. Moreover, decrease in brain tissue, mainly of gray matter, is more rapid in males than females (Good et al. 2001).

Variation in ventricle size in neonates and infants

Variations in the size of the lateral ventricles in term and preterm neonates and infants have been extensively studied to determine an age-related reference range; there are also published studies of variations related to gender, ventricular asymmetry, and the effect of the mode of delivery in this age group. This is particularly important for assigning a specific cut-off point to define ventricular dilatation in cases of hydrocephalus or intraventricular hemorrhage. These studies have been reviewed by Brouwer et al. (2010) and updated reference values and curves were proposed by the same authors using more sophisticated equipment (Brouwer et al. 2012). They found that cross-sectional reference values for the ventricular index and thalamo-occipital distance increased with maturity, whereas the anterior horn width remained constant. According to them, these new cross-sectional and longitudinal reference curves could allow for early identification and quantification of ventriculomegaly due to either posthemorrhagic ventricular dilation or periventricular white matter loss (Brouwer et al. 2012).

Variations in size in adults

Volumetric measurement of the lateral ventricle using high-resolution magnetic resonance imaging (MRI) by Allen et al. (2002) revealed site- and gender-related variations. In both males and females, the right lateral ventricle was significantly larger than the left. Range and mean were also generally greater in males than females. However, this gender difference was, according to the authors, statistically insignificant (Allen et al. 2002). Similarly, Erdogan et al. (2004) reported no significant relationship between gender and the size of the lateral, third, or fourth ventricles. Trimarchi et al. (2013) also found larger right ventricles in all three of the types of lateral ventricle they proposed. On the other hand, and using the same method of high-resolution MRI, Yotsutsuji et al. (2003) detected larger left lateral ventricles and significant gender-related variation, with larger ventricles in males. Similar findings were reported by Goldstein et al. (2001) using MRI and by Chance et al. (2003) using postmortem MRI. However, some authors (Skullerud 1985; Allen et al. 2002) considered postmortem studies unreliable for measuring brain areas, due to changes associated with treatment of the specimens after death and shrinkage or expansion during preservation. Their findings are listed in Table 78.1.

Bergman's Comprehensive Encyclopedia of Human Anatomic Variation, First Edition. Edited by R. Shane Tubbs, Mohammadali M. Shoja and Marios Loukas.
© 2016 John Wiley & Sons, Inc. Published 2016 by John Wiley & Sons, Inc.

Table 78.1 Gender and site variations in the mean volume (cm^3) of the lateral ventricles by chronologic order

		Male		Female	
Study	**Type**	**Right**	**Left**	**Right**	**Left**
Goldstein et al. (2001)	MRI	17.9		13.3	
Allen et al. (2002)	High-resolution MRI	2.2–22.3 (mean 6.8)	2.3–25.3 (mean 7.1)	2.1–9.1 (mean 4.8)	1.1–11.1 (mean 4.5)
Chance et al. (2003)	Postmortum MRI	10.6	11.9	8.5	9.6
Yotsutsuji et al. (2003)	High-resolution MRI	7.8	9.8	6.1	7.2

Torkildsen (1934) measured the lengths of the lateral ventricles from the tip of frontal horn to the atrium on postmortem ventriculographs and ventricular casts. Using the ventricular cast method, the lengths of left and right lateral ventricles fell within the range 7.5–8.1 cm (left mean 7.85 cm, right mean 7.9 cm). Using ventriculographs, the length of the left lateral ventricle taken at the same distance fell within the range 7.9–10 cm (mean 8.7 cm) and the right 8–10.5 cm (mean 8.9 cm) (Torkildsen 1934). However, neither method is as reliable as recent imaging techniques, since some shrinkage of the ventricle in association with brain preparation is expected in both. Moreover, in ventriculography, the measurements are only reliable when the portion of the ventricle in question is completely filled (Torkildsen 1934).

Dias Medora and Prashant (2007) measured the same distance using computed tomography (CT) scanning. In males, the mean length was 7.09 cm on the left and 6.96 cm on the right. In females, the mean length was 6.73 cm on the left and 6.57 cm on the right (Dias Medora and Prashant 2007). In both studies, the length of occipital horn was not included because its presence is inconsistent.

In their review on heritability of lateral ventricle size in monozygotic and dizygotic twins, Kremen et al. (2012) concluded that genetic as well as environmental factors are major contributors to ventricular size and expansion. Heritability increases with age from childhood (32–35%) to at least late middle age (75%). These findings indicate smaller size and volume variations in twins, more so in monozygotic than dizygotic twins (Gerig et al. 2001). This represents a major exception to the common trend of inter-individual variations of ventricular size.

Asymmetry in the lateral ventricles

Asymmetry between the two lateral ventricles is relatively common, found in 5–12% of the population. Such asymmetry can be expected when there are underlying pathological conditions, but in the absence of identified pathology it raises many questions; its exact cause is still obscure (Kiroglu et al. 2008; Mortazavi et al. 2013). The occipital horn usually represents the first and maybe the only portion of the lateral ventricle to enlarge under pathological conditions, so its variations have received most attention in the literature (Reeder et al. 1983).

Kiroglu et al. (2008) studied the association between asymmetry of the lateral ventricle and clinical and structural pathologies, and concluded that asymmetric lateral ventricles represent a normal anatomical variation. Mild or moderate degrees of asymmetry without septal deviation or diffuse enlargement entail relatively low risk for accompanying disorders. However, severe asymmetries and septal deviation or diffuse enlargement should not be considered normal.

Asymmetry and age

Asymmetries in different areas of the human brain including the ventricular system have been identified during the fetal, perinatal, and adult periods at the gross and microscopic levels (Kiroglu et al. 2008).

In a sonographic examination of the brains of 66 human neonates with gestational ages of 28–44 weeks, Horbar et al. (1983) reported asymmetry in the body of the lateral ventricle. This asymmetry could be found as early as the first postnatal day in infants with a gestational age as low as 28 weeks. The body of the left lateral ventricle was larger in 31.8% of the neonates, whereas the right body was larger in only 6.1%. According to these authors, this asymmetry could result from intrauterine or postnatal compression of the skull (Horbar et al. 1983). Asymmetry in the overall size of the lateral ventricle in neonates has been reported in more recent studies, but none have succeeded in detecting a specific etiology (Ichihashi et al. 2002).

Strauss and Fitz (1980) studied the occipital horns of 75 subjects aged five months to 18 years. They found that in 29 of the cases (38.7%) the left occipital horn was longer than the right, while the right was longer in 13 (17%). They also reported an association between this asymmetry and brain lesions during the first year of life, mainly in cases of longer right occipital horn, where 85% had histories of brain injury in early life compared to 46% of those with longer left horns (Strauss and Fitz 1980).

Asymmetry and handedness

Although opposed by some authors (Chiu and Damasio 1980), the effect of handedness on brain tissue asymmetry has been

extensively studied. It is now well established that certain areas in the occipital and frontal lobes (Strauss and Fitz 1980; Herve et al. 2006) and visual cortical areas (Erdogan et al. 2002) are larger in dominant hemispheres, the gray matter being more affected than the white matter (Herve et al. 2006). More extensive brain tissue was expected to correlate with smaller ventricles, but this was not consistent in all studies.

The earliest reference to the relationship between ventricular asymmetry and handedness was by McRae et al. (1968). They found that the left occipital horn was longer than the right in 57% and the right occipital horn was longer in 13%. According to the authors, this is related to brain dominance in most cases as the left occipital horn is longer in right-handed adults and the right is longer in left-handers (McRae et al. 1968). These findings were opposed by authors such as Zipursky et al. (1990), who found no effect of handedness on lateral ventricle size and reported that the left lateral ventricles are significantly larger than the right in both right- and left-handed subjects. More recently, Erdogan et al. (2004) studied the effects of gender and handedness on the size and asymmetry of the lateral, third, and fourth ventricles. They stated that both handedness and the gender-handedness interaction (handedness in both genders) were significant influences on the volumes of the right and left lateral, third, and fourth ventricles, though gender alone had no significant effect (Erdogan et al. 2004). However, their findings were the opposite of those by McRae et al. (1968). They found that the right lateral and third ventricles had significantly larger volumes in right-handers than left-handers (9.8 versus 5.7 cm^3), but the mean volumes of the left-lateral and fourth ventricles exhibited no significant handedness difference. Nevertheless, no study has reported the effect of brain dominance alone on ventricular asymmetry in groups with similar hand dominance. The degree and character of right-to-left asymmetry also changes in cases of various diseases and abnormalities. For instance, highly localized reductions in volume in the left frontal and occipital horns of the lateral ventricles have been reported in patients with autism (McRae et al. 1968).

These diverse findings suggest that handedness *per se* and its effect on brain tissue mass is less likely to be the prominent determinant of ventricular asymmetry.

Shape of the lateral ventricles

Trimarchi et al. (2013) classified the lateral ventricles on the basis of their morphology into three types.

- Type I is seen in 33% of subjects. In this type the body of the lateral ventricles has an irregular but almost rectangular shape. It continues anteriorly with two asymmetrical frontal horns, inferiorly with two temporal horns, and posteriorly with two occipital horns. The occipital horns in this type delineate a concavity turned posteriorly and medially, shrinking gradually and ending with a rounded extremity. Type I has the largest total ventricle volume of around 14,000 mm^3.
- Type II is also seen in 33% of subjects. In this type the body has a more regular rectangular shape. The occipital horn finishes with an external direction and presents a pointed extremity. This type has a mean volume of around 12,500 mm^3.
- Type III is found in 34% of subjects. In this type the lateral ventricles are triangular, with the apex formed by the two frontal horns and the base by the two occipital horns. The temporal horns extend and curve anteromedially, shrinking gradually and finishing in pointed ends. This type is found mostly and with equal frequency in young and elderly subjects, and has characteristics intermediate between the other two types. It also has the lowest total volume of all types of around 11,000 mm^3 (Trimarchi et al. 2013) (Table 78.2).

Table 78.2 Morphology of the lateral ventricle by Trimarchi et al. (2013).

Type	Description
I	The body is irregular rectangular. The occipital horns have a medial concavity ending with a rounded end. The anterior horns are asymmetrical.
II	The body is rectangular. The occipital horns have a slight lateral concavity ending with a pointed end.
III	The lateral ventricular system has a triangular shape with the frontal horns as the apex and the occipital horns as the base. The temporal horns have a medial concavity ending with a pointed end.

The volumes of all three types of lateral ventricle increase linearly with age after the fourth decade, reaching a maximum in the 51–69 years group with mean values between 11,000 and 14,000 mm^3. Although the right ventricle increased slightly more with age, this was not statistically significant. Due to their earlier and steeper decrease in brain tissue mass, males tend to undergo a greater increase in ventricle size with age than females of age 40–69 years (Trimarchi et al. 2013), though females exhibit a rapid increase in ventricular volume during this period due to brain tissue reduction resulting from decreased estrogenic hormone levels during menopausal and postmenopausal ages (Low et al. 2006; Lord et al. 2008; Goto et al. 2011). This underlines the importance of gender in age-associated progressive ventricular enlargement.

Occipital horn (OH)

Presence and size of the OH

The OH is the most inconsistent part of the lateral ventricles. It was absent in 2 out of 11 cases (18.2%) studied by ventricular casts and in 5 out of 13 (38.5%) studied by ventriculography (Torkildsen 1934).

When present, the OH is of length 0.3–3.6 cm and is slightly longer on the right than the left side (mean 1.45 cm vs 1.39 cm on ventricular cast and 1.3 cm vs 1.0 cm on ventriculography; Torkildsen 1934). In another study using a high-intensity-based segmentation method, the length fell within the range 1–5 cm (Liu et al. 2009).

The mean volume of the left OH was measured in one study as 2.8 cm^3 and of the right as 2.2 cm^3 in males. In females it was 1.9 cm^3 on the left and 1.6 cm^3 on the right (Yotsutsuji et al. 2003). It is therefore larger in males and on the left side.

Constriction and atresia in OH

Occasionally, in cases where the calcarine fissure is deeply located, it can cut in far enough to obliterate the posterior horn and separate it from the lateral ventricle (Torkildsen 1934). In other cases, there is a constriction in the middle part of the OH, rendering the posterior portion of the horn considerably wider than the middle. It can also be completely constricted with a cavity posterior to the obstruction (Torkildsen 1934).

Accessory medial prominence

In most individuals, the medial wall of the OH exhibits two prominent elevations: the upper prominence (bulb of the OH) is formed by splenial fibers running posteromedially into the occipital lobes, constituting the major forceps; and the lower prominence (calcar avis), which varies greatly in size, is formed from an indentation of the anterior segment of the calcarine sulcus (Vandewalle et al. 2003).

In almost 40% of specimens there is a third elevation at the junction between the medial wall and floor of the OH lying ventrorostral to the calcar avis. This accessory elevation is formed by a splenial fiber bundle emerging in the OH at the angle between the tail of the hippocampus and the bulb of the OH. The rostral part of the bundle fans out inferolaterally over the collateral trigone, and is directed toward the caudal parahippocampal gyrus. The larger posterior part protrudes into the medial wall, curves posterolaterally along the ventral border of the calcar avis to the tip of the occipital horn, and ends in the white matter overlying the lingual gyrus (Vandewalle et al. 2003).

Similar fibers from the splenium were also found in specimens lacking an accessory elevation. In these cases, the authors (Vandewalle et al. 2003) concluded that the depth of penetration of the calcarine sulcus (and prominence of calcar avis) into the medial wall of the OH is a major determinant of the presence of this accessory elevation. That is, when the calcar avis is more prominent, it pushes the overlying splenial fibers, resulting in a more prominent elevation (Vandewalle et al. 2003).

Temporal horn (TH)

Using ventricular casting, the length of the TH fell within the range 2.5–5 cm and was larger on the left than the right side (mean 4.08 cm vs 3.97 cm). Using ventriculography, it was of length 2.5–5.6 cm and was larger on the right than the left (mean 3.7 cm vs 3.6 cm). The TH appears shorter on ventriculography because of incomplete filling with air during examination. The height of the TH was measured to be 0.4–1 cm (mean 0.7 cm), with no significant difference between right and left sides (Torkildsen 1934).

The mean volume of the TH in males was 0.69 cm^3 on the left and 0.85 cm^3 on the right side according to Chance et al. (2003), and 0.53 cm^3 on the left and 0.47 cm^3 on the right according to Yotsutsuji et al. (2003). In females, the mean volume was 0.64 cm^3 on the left and 0.54 cm^3 of the right side according to Chance et al. (2003), and 0.33 cm^3 on the left and 0.37 cm^3 on the right according to Yotsutsuji et al. (2003). In the first study (Chance et al. 2003), the right TH was larger than the left in males and the left was larger in females. The opposite was reported in the second study (Yotsutsuji et al. 2003). In both studies the size of the TH and the entire ventricle increased with age. This was further supported by Mu et al. (1999), who found that the size of the TH increased from around 0.1 cm^3 at the age of 40–60 years to around 0.4 cm^3 at 81–90 years. However, they found no significant side- or gender-related differences (Mu et al. 1999).

Frontal horn (FH)

The mean length of the FH in males was 2.78 cm on the left and 2.74 cm on the right. In females it was 2.58 cm on the left and 2.55 cm on the right (Dias Medora and Prashant 2007). This study revealed a larger size on the left than the right, both horns being larger in males than females.

In contrast, Shapiro et al. (1986) found that in 89.7% of cases both FH were symmetrical in length. There was asymmetry in the other 10.3%. In 67.7% of the asymmetrical cases, the right FH was longer than the left. In the remaining 32.3% the left FH was longer than the right (Shapiro et al. 1986).

The height of the FH ranged from 1.5 to 2.1 cm using ventricular casting and was slightly larger on the right than the left (mean 1.94 cm vs 1.88 cm). Using ventriculography the height ranged from 1 to 2 cm with no significant side difference. The height of the FH was smaller, by almost 0.5 cm in some cases, using ventriculography than ventricular casting. This is probably because the lowest portion of the anterior horn is narrow and not always well filled with air (Torkildsen 1934).

In males, the mean volume of the left FH was 3.2 cm^3 and the right FH 2.6 cm^3. In females, the mean volume of the left FH was 2.5 cm^3 and the right FH 2.1 cm^3 (Yotsutsuji et al. 2003). The FH is therefore usually larger in males and on the left side.

Body

Size

Using ventricular casting, the anteroposterior length of the lateral ventricle body fell within the range 1.5–2.1 cm and was slightly larger on the left side (mean 1.97 cm vs 1.91 cm). Using this method, the height of the body was 0.5–1.2 cm in the middle part and 0.5–1 cm in the posterior part, being slightly larger on the right side (Torkildsen 1934). Using ventriculography the length was 1–2 cm and was slightly larger on right side (mean 1.5 cm vs 1.4 cm). The height fell within the range 0.7–1.6 cm in the middle part and 0.8–1.5 cm in the posterior

Table 78.3 Types of the body of the lateral ventricle by Torkildsen (1934).

Type	Description
A	The body continues smoothly posteriorly with the occipital horn
B	The posterior wall of the body forms a mild angle between the body and the occipital horn
C	The posterior wall of the body forms a acute angle between the body and the occipital horn

part, and was also slightly larger on the right side (Torkildsen 1934).

The mean volume of the body in males was 3.3 cm^3 on the left side and 2.5 cm^3 on the right. In females it was 2.5 cm^3 on the left side and 2.1 cm^3 on the right. The body was larger on the left side in both genders and was generally larger in males (Yotsutsuji et al. 2003).

Shape

The posterior portion of the lateral ventricle body was classified into three types on the basis of its shape. The difference in appearance of this portion of the ventricle depends upon the splenium of the corpus callosum, which forms the posterior wall. In type A the body runs smoothly into the OH. In types B and C the body joins the OH at an angle, which is slight in type B and acute in type C (Torkildsen 1934; Table 78.3).

Foramen of Monro

Some anatomists describe the foramen on Monro as one Y-shaped foramen, while others describe it as right and left foramina that communicate with the third ventricle (Glastonbury et al. 2011).

The size and shape of the foramina of Monro depend on the size of the ventricles: if the ventricles are small, each foramen is a crescent-shaped opening bounded anteriorly by the concave curve of the fornix and posteriorly by the convex anterior tubercle of the thalamus. As the ventricles enlarge, the foramen on each side becomes larger and rounder (Rhoton 2002; Mortazavi et al. 2013).

The diameter of the foramen of Monro in one study ranged from 3 to 4 mm (Rhoton 2002). In another more descriptive study, it ranged from 0.7 to 3.0 mm × 0.8 to 2.6 mm (mean 1.6 × 1.5 mm; Duffner et al. 2003). In some cases, the foramen of Monro is not as enlarged as expected in patients with longstanding hydrocephalus, which can affect access to the third ventricle (Rohde and Gilsbach 2000). A similar finding was reported in cases of aqueductal stenosis (Javadpour et al. 2001).

Congenital atresia of the foramen of Monro with associated unilateral hydrocephalus has rarely been reported in the literature (Wilberger et al. 1983).

Third ventricle

There are rare reports of congenital fusion of the thalami resulting in third ventricular atresia accompanied by other midline malformations and lateral ventricular dilatation (Kepes et al. 1969; Arvanitis et al. 2010).

As for the lateral ventricles, the third ventricle changes in size with age, especially in the elderly where it balloons as the brain tissue regresses. This has been attributed mainly to regression of the median nuclei of the thalami and a progressive diminution of the massa intermedia that joins them (LeMay 1984). Meshram and Hattangdi (2012) also reported decreases in all dimensions of the diencephalon with aging, associated with increased third ventricular volume. On the other hand, no systematic increase in third ventricular size during the first 20 years of life was recorded by Mathew (2012).

The mean width of the third ventricle in various studies fell within the range 0.39–0.92 cm (Gawler et al. 1975, 1976; Brinkman et al. 1981; Soininen et al. 1982; Dias Medora and Prashant 2007). Gawler et al. (1976) reported a maximal width of 0.3–0.6 cm (mean 0.46 cm). Duffner et al. (2003) reported an almost similar maximal width of 0.18–0.75 cm (mean 0.33 cm). Dias Medora and Prashant (2007) found that the width was significantly larger in males than females (mean 0.45 cm vs 0.39 cm). Considering different age groups, Mathew (2012) found that the mean width of the third ventricle anterior to the interthalamic junction ranged from 0.38 to 0.57 cm. Posterior to the interthalamic junction the mean width ranged from 0.41 to 0.61 cm. It was generally larger after 20 years and during 10–14 years, and in males than females (Mathew 2012). Benedict et al. (2006) reported similar results regarding the widths anterior and posterior to the interthalamic junction. In contrast to previous studies they found larger values in females. Meshram and Hattangdi (2012) measured the third ventricular width in different age groups. In individuals of 20–60 years of age, the maximal width fell within the range 0.2–1.45 cm (mean 0.57 cm) in males and 0.32–1.3 cm (mean 0.73 cm) in females. In individuals older than 60 years the maximal width was 0.51–1.38 cm (mean 0.8 cm) in males and 0.53–1.29 cm (mean 0.84 cm) in females (Meshram and Hattangdi 2012). Similar to the findings of Mathew (2012), Meshram and Hattangdi (2012) reported greater widths in females.

The mean anteroposterior length measured by Mathew (2012) ranged from 2.3 to 3.1 cm. It is generally larger in males and between 6 and 9 years. Similar results were reported by Brinkman et al. (1981), with almost similar values in both genders. According to Meshram and Hattangdi (2012), the maximal anteroposterior length in individuals between 20 and 60 years of age ranged from 1.44 to 3.26 cm (mean 2.42 cm) in males and from 1.28 to 3.16 cm (mean 2.42 cm) in females. In individuals more than 60 years of age, the maximal length was 1.8–3.21 cm (mean 2.52 cm) in males and 1.98–3.18 cm (mean 2.53 cm) in females (Meshram and Hattangdi 2012).

The mean height measured by Mathew (2012) fell within the range 2–2.5 cm and was generally larger in males and for ages 3–5 years. The maximal height measured by Duffner et al. (2003) was 1.44–2.55 cm (mean 1.86 cm). According to Meshram and Hattangdi (2012), the maximal height in individuals 20–60 years of age was within the range 1.5–2.5 cm (mean 1.99 cm) in males and 1.5–2.5 cm (mean 2.01 cm) in females. In individuals more than 60 years of age, the maximal height was 1.5–2 cm (mean 1.88 cm) in males and 1.5–2.5 cm (mean 1.94 cm) in females (Meshram and Hattangdi 2012).

The mean volume of the third ventricle according to two studies was within the range 1–1.6 cm^3 in males and 0.7–1 cm^3 in females (Goldstein et al. 2001; Yotsutsuji et al. 2003).

Floor

Dimensions

In a study by Aydin et al. (2009), the mean anteroposterior diameter (between the infundibulum and intermamillary region) and the widest transverse diameter of the floor of the third ventricle were 5.69 and 3.35 mm, respectively. The mean distance between the basilar apex and the center of the floor was 6.54 mm. The center of the floor at the junction of the transverse and anteroposterior diameters was in an area where the floor was thinnest on histological sections, at the posterior third of the anteroposterior diameter. The surface area of the floor was 9.63 mm^2 (Aydin et al. 2009).

Rohde and Gilsbach (2000) identified different anatomical variations encountered during endoscopic third ventriculostomy (ETV). These variations were found in 9 out of 25 patients (36%). Six (24%) of the variations were identified at the floor of the third ventricle. In four (16%) cases with longstanding hydrocephalus the floor was not thin and translucent, as would be expected in such patients, and could not be identified on preoperative MRI (Rohde and Gilsbach 2000). Similar findings have occasionally been reported in other studies (Riegel et al. 2001). In such cases, floor perforation is more difficult and time consuming and it is usually not possible to identify the basilar artery before opening the basilar cistern, which increases the risk of injury (McLaughlin et al. 1997; Vandertop 1998; Rohde and Gilsbach 2000). Similarly, failure to identify the oculomotor nerve increases the risk of nerve palsy (Buelens et al. 2011). It can also be associated with increased stretching of the floor and walls of the third ventricle and the hypothalamic structures, and bleeding from the small arteries of the tuber cinereum (Rohde and Gilsbach 2000; Iaccarino et al. 2009). The thickness of the floor did not correlate with the duration of hydrocephalus (Iaccarino et al. 2009). A similarly opaque, non-translucent floor has been reported in individuals with no brain pathology, and is estimated to occur in 84% of individuals compared to 16% with translucent floors (Romero Adel et al. 2011). Buelens et al. reported an incidence of 86% compared to 14%, and Scholz et al. (2007) reported a 100% incidence of opaque floors. This finding therefore represents the most common variation of the third ventricular floor. The incidence of translucent floor increased above 80 years of age, but an opaque floor can also be present at this age (Romero Adel et al. 2011).

In normal individuals, the floor of the third ventricle slopes downward from the mamillary bodies into the infundibular recess (McLone 2004). In 2 out of 25 cases (8%), Rohde and Gilsbach (2000) found that this downward slope was steep. Perforation of the floor is again more difficult and time consuming in such cases, as it is usually associated with slipping of the perforation catheter during the process. This can result in insufficient opening and inadequate CSF draining. It is also occasionally harder to inspect beneath the floor in such cases. In both cases in this study, it was necessary to place a shunt to achieve relief. Unlike the thickened floor, this variant could be identified on preoperative MRI (Rohde and Gilsbach 2000). Other abnormal anatomical findings of the third ventricle in longstanding hydrocephalic patients included a small third ventricle and narrowed foramen of Monro (Rohde and Gilsbach 2000).

Recesses of the third ventricle

In the sagittal plane the third ventricle has a fish-like shape created by two anterior and two posterior recesses and a curving roof and floor. The anterior "fish mouth" shape of the third ventricle is created by the optic recess superiorly and the infundibular recess inferiorly (Glastonbury et al. 2011).

The shape and size of these anterior recesses and hence their distance from the sella turcica vary widely (Bull 1956). Persistent infundibular recess, or empty sella syndrome extending and displacing the pituitary gland, is a rare congenital anomaly caused by failed cellular proliferation; the distal aspect of the embryonic infundibular recess is normally obliterated early in gestation. However, this is considered a pathological abnormality rather than an anatomical variant (Steno et al. 2009; Glastonbury et al. 2011).

A normal variant in which an enlarged infundibular recess forming a diverticulum that extends inferiorly into the pituitary stalk to the approximate level of the diaphragma sellae was reported by Shibata and Maravilla (1994). It has no clinical implications.

Dilatation of the posterior suprapineal recess is held to be the most common variation in the third ventricle (Krokfors et al. 1967), occurring in 2–4% of individuals (Robertson 1957; Glastonbury et al. 2011). In most cases, the suprapineal recess represents a small cavity in the posterosuperior part of the third ventricle above the pineal body and the habenular commissure, extending posteriorly near the corpus callosum to the vicinity of the quadrigeminal cistern. It is usually 2–3 mm in height and length. Occasionally, one or both measurements exceeds 1 cm and the length can even reach 4 cm. Although the incidence of this condition was higher in craniocerebral traumas and epileptic patients, it had no pathological significance (Glastonbury et al. 2011).

Table 78.4 Types of the intermamillary space by Iaccarino et al. (2009).

Type	Description
"Kissing type"	No measurable distance between the mamillary bodies is present
"Split type"	A measurable distance between the mamillary bodies is present

Intermamillary distance (IMD) and thickened floor

The distance between the mamillary glands represents a fundamental anatomical landmark for the ETV, providing indirect information about the conformation of the floor of the third ventricle (Iaccarino et al. 2009). Iaccarino et al. (2009) classified the IMD into two types (Table 78.4). In type I (kissing type), which is more common, there was no measurable distance between the mamillary bodies. This type was found in 85–89% of cases (Iaccarino et al. 2009; Romero Adel et al. 2011). In type II (split type), less common, the distance was measurable. This type was found in 11–15% of cases (Iaccarino et al. 2009; Romero Adel et al. 2011), most commonly in patients more than 60 years of age and with some degree of age-related brain atrophy. However, in patients above 60 years of age, 56% had the kissing type and 44% the split type, with IMD in the range 0.09–0.55 cm. In patients with hydrocephalus, the split type was more commonly associated with a thickened floor and could be a good indicator of the condition on preoperative MRI (Iaccarino et al. 2009). In patients with thick floors the mean IMD was 0.55 cm, while in patients with thin floors it was 0.27 cm (Iaccarino et al. 2009). On the other hand, Romero Adel et al. (2011) found that the third ventricular floor tends to be less translucent with decreased IMD (Romero Adel et al. 2011).

Relationship to the oculomotor nerve

Due to the potential for direct mechanical injury to the oculomotor nerve during third ventriculostomy, Buelens et al. (2011) studied variations in the relationship of this nerve to the floor of third ventricle. The interpeduncular part of the oculomotor nerve (at risk of injury) could be seen in 14% of cases and was located inferior (16 mm on average) and lateral (8–11 mm away from the midline) to the midpoint of the floor of the ventricle. The authors reported that the angle at which the oculomotor nerve could be injured was more oblique (at least 12° greater) than the normal angle of approach, so there should be no risk in most cases (Buelens et al. 2011).

Safety triangle

The safety triangle on the third ventricular floor for ventriculocisternostomy is demarcated by two straight lines that connect the mamillary bodies and the infundibular recess on each side and another straight line that connects the extremes of the mamillary bodies. The area of perforation was recommended as halfway between the infundibular recess and the mamillary bodies in the midline. The safety triangle was measured by Romero Adel et al. (2011) and was within the range 1.21–10.52 mm^2 (mean 3.69 mm^2).

Massa intermedia (MI)

Presence and location

Absence of the MI was reported in 24% of cases by Yamamoto et al. (1981). Other studies reported a range of 13–33% of cases (Carpenter 1991; Nopoulos et al. 2001; Kiernan and Barr 2009). The presence and size of the MI exhibit sexual dimosphism; it is present more often and is substantially larger in females (Allen and Gorski 1991; Nopoulos et al. 2001). In a study by Nopoulos et al. (2001), the MI was absent in around 33% of males compared to around 13% of females, which represents the largest gender-related difference among studies of this structure (Allen and Gorski 1991). Allen and Gorski (1991) found that when the MI was present (78% in females vs 68% in males), it was an average of 53.3% or 17.5 mm^2 larger in females. When present, it is usually located 2.5–6.0 mm (mean 3.9 mm) posterior to the foramen of Monro (Yamamoto et al. 1981).

Duplicated MI

In rare cases, the MI might be duplicated (Malobabic et al. 1987; Tubbs et al. 2004a). This variation was illustrated for the first time by Tubbs et al. (2004a).

Aqueduct of Sylvius

On the basis of his histological studies, Gerlach (1858) subdivided the Sylvian aqueduct into three parts and claimed that its shape differs from site to site on cross sections. On the other hand, Turkewitsch (1935, 1936) recognized five portions, namely: the aditus ad aquaeductum or aditus aquaeducti; anterior part; ampulla; genu; and posterior part. Woollam and Millen (1953) considered this subdivision too elaborate and suggested a division into three parts: pars anterior; ampulla; and pars posterior (Flyger and Hjelmquist 1957; Mortazavi et al. 2013).

According to Flyger and Hjelmquist (1957), the cross-sectional area of the aqueduct differs among individuals and from site to site over the range 0.40–9.84 mm^2. They added that the size of the duct increases with age (Flyger and Hjelmquist 1957). This contradicts the earlier findings of Spiller (1916), who reported that the aqueductal lumen continues to decrease in size with age much like the central canal of the spinal cord.

Krogness introduced the A:B ratio as a reliable method for measuring the position of the cerebral aqueduct in two age groups: 2–62 years (Krogness 1975) and 0–22 months (Krogness 1976). This method relies on the pneumoencephalogram to measure two distances: A, from the surface of the skull to the aqueduct; and B, from the surface to the dorsum sellae. In both

age groups the ratio was within the range 0.68–0.75 (mean 0.72). This means that the A:B method is independent of age and skull dimensions, and is sensitive to variations in the position of the aqueduct. Any measurement less than the lower limit of 0.68 indicates pathological dorsal displacement of the cerebral aqueduct (Krogness 1976).

Congenital occlusion of the aqueduct has been reported and usually affects the proximal part (Glastonbury et al. 2011). This condition can be associated with lateral and third ventricular enlargement or isolated lateral ventricular enlargement (Bickers and Adams 1949; Ang et al. 2006). It can also be associated with other anomalies including Chiari malformation (Ang et al. 2006).

Fourth ventricle

Gawler et al. (1976) found that the height of the fourth ventricle was within the range 0.6–1.5 cm (mean 1.08 cm). According to Duffner et al. (2003), the height ranged from 3.34 to 4.43 cm (mean 3.83 cm). In the study of Dias Medora and Prashant (2007), the mean height was 1.18 cm in males and 1.11 cm in females.

The width of the fourth ventricle was within the range 1.02–1.64 cm (mean 1.25 cm) (Duffner et al. 2003). The mean width according to Dias Medora and Prashant (2007) was 1.31 cm in males and 1.21 cm in females.

The mean ventricular volume was measured by Goldstein et al. (2001) as 1.8 cm^3 in males and 1.7 cm^3 in females.

Foramen of Magendie

The presence of the foramen of Magendie as a normal opening between the fourth ventricle and the subarachnoid space has been a matter of debate since the earliest description by Magendie (1828), although it is mostly accepted today (Hewitt 1960). In his book, François Magendie reported the presence of an opening in the midline of the lower part of the roof of the fourth ventricle that is variable in size and wide enough to admit the point of the finger; it was later named after him (Tubbs et al. 2008). The presence of this opening was confirmed by later authors including Luschka (1855) and Key and Retzius (1875), and by more recent authors (Hewitt 1960; Ciolkowski et al. 2011). However, it was denied by others (Todd 1847; Virchow 1854; Reichert 1861). Rogers (1931) documented this controversy and confirmed the presence of the aperture, but stated that it is not a normal foramen but rather a deformity in the roof of the ventricle. However, he believed that his finding did not contradict Magendie, who did not claim the aperture to be a normal opening.

According to the early description by Key and Retzius (1875), the width of the foramen of Magendie ranges from 5 to 8 mm. The width as measured by Ciolkowski et al. (2011) was 4.0–9.4 mm (mean 6.53 mm). Its width from left to midline was 2.0–5.8 mm (mean 3.57 mm) and from right to midline 0.8–4.6 mm (mean 2.95 mm) (Ciolkowski et al. 2011).

In 30 of 38 brains (78.9%) examined by Hewitt (1960), the roof of the fourth ventricle was prolonged at the upper part of the foramen of Magendie as a triangular fold containing the lower part of the chorioid plexus and attached to the pia over the anterior end of the inferior vermis. When present, this triangular fold converted the foramen into a funnel-shaped opening. In the remaining specimens, the fold was absent and the vertical limbs of the choroid plexus were continued beyond the margin of the aperture and adherent to the pia over the tonsil of the cerebellum (Hewitt 1960).

In view of the principal role of this aperture as a conduit for CSF flow from the ventricular into the subarachnoid space, its congenital absence (or atresia) has been strongly correlated to the development of hydrocephalus since the early literature (Hilton 1877; Barr 1948; Alexander and Fowler 1956; Rifkinson-Mann et al. 1987). It was also reported in association with syndromes such as Chiari malformation, Dandy-Walker syndrome, tuberous sclerosis, spina bifida, platybasia, achondroplasia, basilar impression, and atlanto-occipital fusion (Brodal and Hauglie-Hanssen 1959; Rifkinson-Mann et al. 1987). Congenital absence was reported in 4% of the brains examined by Barr (1948).

Arachnoid veils obstructing the foramen of Magendie and blocking CSF flow were described by Tubbs et al. (2004b). These structures were distinguished from scar tissue and were not caused by inflammatory processes. They were found in 7% of patients with Chiari I malformation, but whether they were the cause of syringomyelia in such patients was not concluded (Tubbs et al. 2004b).

Foramen of Luschka

Barr (1948) reported a congenital bilaterally imperforate foramina of Luschka in 20% of otherwise healthy individuals. In a study by Sharifi et al. (2009), the foramina of Luschka were congenitally occluded by an arachnoid-like membrane in 6 out of 80 specimens (7.5%). A similar arachnoid-like membrane was reported to occlude the foramina in 2.5% of cases by Retzius and 14% of cases by Suzuki (Sharifi et al. 2009).

Similar to the foramen of Magendie, congenital occlusion of the foramina of Luschka (which tends to be bilateral) has been associated with obstructive hydrocephalus and other diseases including Dandy-Walker syndrome (Dandy 1921; Alexander and Fowler 1956; Brodal and Hauglie-Hanssen 1959; Rifkinson-Mann et al. 1987; Sharifi et al. 2009).

In the study of Sharifi et al. (2009), the height of the foramen on the left side fell within the range 0.6–7 mm (mean 3.98 mm) and on the right side 2–7 mm (mean 3.92 mm). The width on the left side was 0.8–3.6 mm (mean 1.88 mm) and on the right side 1–4 mm (mean 1.8 mm) (Sharifi et al. 2009).

Relationship to the surrounding vessels

The distance between the anterior inferior cerebellar artery (AICA) and the foramina of Luschka ranges from 1.4 to 10 mm (mean 3.9 mm) on the left side and from 1.2 to 8.8 mm (mean 3.89 mm) on the right. The distance between the posterior inferior cerebellar artery (PICA) and the foramina of Luschka ranges from 1.2 to 17 mm (mean 5.81 mm) on the left and from 1.2 to 15.2 mm (mean 7.08 mm) on the right (Sharifi et al. 2009).

Relationship to the surrounding cranial nerves

The distances between the foramina of Luschka and the abducens (CN VI), facial (CN VII), and vesibulocochlear (CN VIII) rootlets on the right side was within the range 4.2–19.8 mm (mean 9.15 mm), 1.6–7.4 mm (mean 3.94 mm), and 1–7.2 mm (mean 3.52 mm), respectively. On the left side, they fell within the range 6–13 mm (mean 9.15 mm), 0.6–6 mm (mean 3.32 mm), and 0.8–7 mm (mean 2.76 mm), respectively (Sharifi et al. 2009).

Occasionally, a tortuous vertebral artery occupies the cerebellopontine angle and further complicates the region, or can compress or block the entrance of the foramina of Luschka (Sharifi et al. 2009).

References

Alexander E Jr, Fowler FD. 1956. Atresia of the foramina of Luschka and Magendie; a cause of obstructive internal hydrocephalus. *AMA J Dis Child* 92(2): 131–137.

Allen JS, Damasio H, Grabowski TJ. 2002. Normal neuroanatomical variation in the human brain: an MRI-volumetric study. *Am J Phys Anthropol* 118(4): 341–358.

Allen LS, Gorski RA. 1991. Sexual dimorphism of the anterior commissure and massa intermedia of the human brain. *J Comp Neurol* 312(1): 97–104.

Ang BT, Steinbok P, Cochrane DD. 2006. Etiological differences between the isolated lateral ventricle and the isolated fourth ventricle. *Childs Nerv Syst* 22(9): 1080–1085.

Arvanitis LD, Sgantzos MN, Kotrotsios A, Vassiou KG. 2010. Congenital fusion of the thalami (atresia of the third ventricle) associated with parietooccipital meningocele. *Pediatr Dev Pathol* 13(5): 419–422.

Aydin S, Yilmazlar S, Aker S, Korfali E. 2009. Anatomy of the floor of the third ventricle in relation to endoscopic ventriculostomy. *Clin Anat* 22(8): 916–924.

Barr ML. 1948. Observations on the foramen of Magendie in a series of human brains. *Brain* 71(3): 281–289.

Benedict RH, Bruce JM, Dwyer MG, Abdelrahman N, Hussein S, Weinstock-Guttman B, Garg N, Munschauer F, Zivadinov R. 2006. Neocortical atrophy, third ventricular width, and cognitive dysfunction in multiple sclerosis. *Arch Neurol* 63(9): 1301–1306.

Bickers DS, Adams RD. 1949. Hereditary stenosis of the aqueduct of Sylvius as a cause of congenital hydrocephalus. *Brain* 72(2): 246–262.

Brinkman SD, Sarwar M, Levin HS, Morris HD 3rd. 1981. Quantitative indexes of computed tomography in dementia and normal aging. *Radiology* 138(1): 89–92.

Brodal A, Hauglie-Hanssen E. 1959. Congenital hydrocephalus with defective development of the cerebellar vermis (Dandy-Walker syndrome) clinical and anatomical findings in two cases with particular reference to the so-called atresia of the foramina of Magendie and Luschka. *J Neurol Neurosurg Psychiatry* 22(2): 99–108.

Brouwer MJ, de Vries LS, Pistorius L, Rademaker KJ, Groenendaal F, Benders MJ. 2010. Ultrasound measurements of the lateral ventricles in neonates: why, how and when? A systematic review. *Acta Paediatr* 99(9): 1298–1306.

Brouwer MJ, de Vries LS, Groenendaal F, Koopman C, Pistorius LR, Mulder EJ, Benders MJ. 2012. New reference values for the neonatal cerebral ventricles. *Radiology* 262(1): 224–233.

Buelens E, Wilms G, van Loon J, van Calenbergh F. 2011. The oculomotor nerve: anatomic relationship with the floor of the third ventricle. *Childs Nerv Syst* 27(6): 943–948.

Bull J. 1956. The normal variations in the position of the optic recess of the third ventricle. *Acta radiol* 46(1–2): 72–80.

Carpenter M. 1991. *Core Text of Neuroanatomy*, vol. 4. Baltimore: Williams & Wilkins.

Chance SA, Esiri MM. Crow TJ. 2003. Ventricular enlargement in schizophrenia: a primary change in the temporal lobe? *Schizophr Res* 62(1–2): 123–131.

Chiu HC, Damasio AR. 1980. Human cerebral asymmetries evaluated by computed tomography. *J Neurol Neurosurg Psychiatry* 43(10): 873–878.

Ciolkowski M, Sharifi M, Tarka S, Ciszek B. 2011. Median aperture of the fourth ventricle revisited. *Folia Morphol (Warsz)* 70(2): 84–90.

Dandy W. 1921. The diagnosis and treatment of hydrocephalus due to occlusions of the foramina of Magendie and Luschka. *Surg Gynec Obstet* 32: 112–124.

Dekaban AS. 1978. Changes in brain weights during the span of human life: relation of brain weights to body heights and body weights. *Ann Neurol* 4(4): 345–356.

Dias Medora D, Prashant N. 2007. Morphometric study of the ventricular system of brain by computerised tomography. *J Anat Soc India* 56(1): 19–24.

Duffner F, Schiffbauer H, Glemser D, Skalej M, Freudenstein D. 2003. Anatomy of the cerebral ventricular system for endoscopic neurosurgery: a magnetic resonance study. *Acta Neurochir (Wien)* 145(5): 359–368.

Erdogan AR, Ozdikici M, Aydin MD, Aktas O, Dane S. 2002. Right and left visual cortex areas in healthy subjects with right- and left-eye dominance. *Int J Neurosci* 112(5): 517–523.

Erdogan AR, Dane S, Aydin MD, Ozdikici M, Diyarbakirli S. 2004. Sex and handedness differences in size of cerebral ventricles of normal subjects. *Int J Neurosci* 114(1): 67–73.

Flyger G, Hjelmquist U. 1957. Normal variations in the caliber of the human cerebral aqueduct. *Anat Rec* 127(2): 151–162.

Gawler J, Bull JD, Du Boulay GH, Marshall J. 1975. Computerized axial tomography: the normal EMI scan. *J Neurol Neurosurg Psychiatry* 38(10): 935–947.

Gawler J, Du Boulay GH, Bull JD, Marshall J. 1976. Computerized tomography (the EMI Scanner): a comparison with pneumoencephalography and ventriculography. *J Neurol Neurosurg Psychiatry* 39(3): 203–211.

Gerig G, Styner M, Jones D, Weinberger D, Lieberman J. 2001. Shape analysis of brain ventricles using SPHARM. IEEE Workshop on Mathematical Methods in Biomedical Image Analysis District of Columbia, USA. *IEEE Computer Society.*

Gerlach J. 1858. *Mikroskopische Studien aus dem Gebiete der Menschlichen Morphologie*. Enke: Erlangen.

Glastonbury CM, Osborn AG, Salzman KL. 2011. Masses and malformations of the third ventricle: normal anatomic relationships and differential diagnoses. *Radiographics* 31(7): 1889–1905.

Goldstein JM, Seidman LJ, Horton NJ, Makris N, Kennedy DN, Caviness VS Jr, Faraone SV, Tsuang MT. 2001. Normal sexual dimorphism of the adult human brain assessed by in vivo magnetic resonance imaging. *Cereb Cortex* 11(6): 490–497.

Good CD, Johnsrude IS, Ashburner J, Henson RN, Friston KJ, Frackowiak RS. 2001. A voxel-based morphometric study of ageing in 465 normal adult human brains. *Neuroimage* 14(1): 21–36.

Goto M, Abe O, Miyati T, Inano S, Hayashi N, Aoki S, Mori H, Kabasawa H, Ino K, Yano K, Iida K, Mima K, Ohtomo K. 2011. 3 Tesla MRI detects accelerated hippocampal volume reduction in postmenopausal women. *J Magn Reson Imaging* 33(1): 48–53.

Herve PY, Crivello F, Perchey G, Mazoyer B, Tzourio-Mazoyer N. 2006. Handedness and cerebral anatomical asymmetries in young adult males. *Neuroimage* 29(4): 1066–1079.

Hewitt W. 1960. The median aperture of the fourth ventricle. *J Anat* 94: 549–551.

Hilton J. 1877. *On Rest and Pain*. London: George Bell & Sons.

Horbar JD, Leahy KA, Lucey JF. 1983. Ultrasound identification of lateral ventricular asymmetry in the human neonate. *J Clin Ultrasound* 11(2): 67–69.

Iaccarino C, Tedeschi E, Rapana A, Massarelli I, Belfiore G, Quarantelli M, Bellotti A. 2009. Is the distance between mammillary bodies predictive of a thickened third ventricle floor? *J Neurosurg* 110(5): 852–857.

Ichihashi K, Iino M, Eguchi Y, Uchida A, Honma Y, Momoi M. 2002. Difference between left and right lateral ventricular sizes in neonates. *Early Hum Dev* 68(1): 55–64.

Javadpour M, Mallucci C, Brodbelt A, Golash A, May P. 2001. The impact of endoscopic third ventriculostomy on the management of newly diagnosed hydrocephalus in infants. *Pediatr Neurosurg* 35(3): 131–135.

Kepes JJ, Clough C, Villanueva A. 1969. Congenital fusion of the thalami (atresia of the third ventricle) and associated anomalies in a 6-month-old infant. *Acta Neuropathol* 13(1): 97–104.

Key A, Retzius M. 1875. *Studien in der Anatomie des Nervensystems und des Bindegewebes*. Stockholm: Samson & Wallin.

Kiernan J, Barr J. 2009. *The Human Nervous System: an Anatomical Viewpoint*. Philadelphia: Lippincott Williams & Wilkins.

Kiroglu Y, Karabulut N, Oncel C, Yagci B, Sabir N, Ozdemir B. 2008. Cerebral lateral ventricular asymmetry on CT: how much asymmetry is representing pathology? *Surg Radiol Anat* 30(3): 249–255.

Kremen WS, Panizzon MS, Neale MC, Fennema-Notestine C, Prom-Wormley E, Eyler LT, Stevens A, Franz CE, Lyons MJ, Grant MD, Jak AJ, Jernigan TL, Xian H, Fischl B, Thermenos HW, Seidman LJ, Tsuang MT, Dale AM. 2012. Heritability of brain ventricle volume: converging evidence from inconsistent results. *Neurobiol Aging* 33(1): 1–8.

Krogness KG. 1975. Normal position of the aqueduct of Sylvius. Part 1: significance of aqueduct to dorsum sellae measurements. *J Neurosurg* 42(5): 499–502.

Krogness KG. 1976. Normal position of the aqueduct of sylvius in infancy. *Pediatr Radiol* 4(4): 221–222.

Krokfors G, Katila O, Taalas J. 1967. Enlarged suprapineal recess of the third ventricle. *Acta Neurol Scand* 43(5): 607–615.

Lemaitre H, Crivello F, Grassiot B, Alperovitch A, Tzourio C, Mazoyer B. 2005. Age- and sex-related effects on the neuroanatomy of healthy elderly. *Neuroimage* 26(3): 900–911.

LeMay M. 1984. Radiologic changes of the aging brain and skull. *AJR Am J Roentgenol* 143(2): 383–389.

Liu J, Huang S, Nowinski WL. 2009. Automatic segmentation of the human brain ventricles from MR images by knowledge-based region growing and trimming. *Neuroinformatics* 7(2): 131–146.

Lord C, Buss C, Lupien SJ, Pruessner JC. 2008. Hippocampal volumes are larger in postmenopausal women using estrogen therapy compared to past users, never users and men: a possible window of opportunity effect. *Neurobiol Aging* 29(1): 95–101.

Low LF, Anstey KJ, Maller J, Kumar R, Wen W, Lux O, Salonikas C, Naidoo D, Sachdev P. 2006. Hormone replacement therapy, brain volumes and white matter in postmenopausal women aged 60–64 years. *Neuroreport* 17(1): 101–104.

Luschka H. 1855. *Die Adergeflechte des Menschlichen Gehirnes: eine Monographie*. Berlin: Reimer.

Magendie F. 1828. *Mémoire Physiologique sur le Cerveau*. France: Royal Academy of Sciences.

Malobabic S, Puskas L, Blagotic M. 1987. Size and position of the human adhaesio interthalamica. *Gegenbaurs Morphol Jahrb* 133(1): 175–180.

Mathew L. 2012. Assessment of Third Ventricle with MRI: Morphological Variations Among Different Gender and Age Group. *Webmed Central Anatomy* 3(5), doi: 10.9754/journal.wmc.2012.003370.

McLaughlin M R, Wahlig JB, Kaufmann AM, Albright AL. 1997. Traumatic basilar aneurysm after endoscopic third ventriculostomy: case report. *Neurosurgery* 41(6): 1400–1404.

McLone DG. 2004. The anatomy of the ventricular system. *Neurosurg Clin N Am* 15(1): 33–38.

McRae DL, Branch CL, Milner B. 1968. The occipital horns and cerebral dominance. *Neurology* 18(1): 95–98.

Meshram P, Hattangdi S. 2012. The morphometric study of third ventricle and diencephelon by computerised tomography. *Indian J Appl Basic Med Sci* 14(19): 8.

Mortazavi M, Adeeb N, Bavarsad R, Tamargo R, Tubbs RS. 2013. The ventricular system of the brain: A comprehensive review of history, anatomy, histology, embryology and surgical considerations. *Childs Nervous System* 30(1): 19–35.

Mu Q, Xie J, Wen Z, Weng Y, Shuyun Z. 1999. A quantitative MR study of the hippocampal formation, the amygdala, and the temporal horn of the lateral ventricle in healthy subjects 40 to 90 years of age. *AJNR Am J Neuroradiol* 20(2): 207–211.

Nopoulos PC, Rideout D, Crespo-Facorro B, Andreasen NC. 2001. Sex differences in the absence of massa intermedia in patients with schizophrenia versus healthy controls. *Schizophr Res* 48(2–3): 177–185.

Reeder JD, Kaude JV, Setzer ES. 1983. The occipital horn of the lateral ventricles in premature infants. An ultrasonographic study. *Eur J Radiol* 3(2): 148–150.

Reichert K. 1861. *Der Bau des Menschlichen Gehirns*. Leipzig: Engelmann.

Rhoton AL Jr. 2002. The lateral and third ventricles. *Neurosurgery* 51(4 Suppl): S207–271.

Riegel T, Alberti O, Hellwig D, Bertalanffy H. 2001. Operative management of third ventriculostomy in cases of thickened, non-translucent third ventricular floor: technical note. *Minim Invasive Neurosurg* 44(2): 65–69.

Rifkinson-Mann S, Sachdev VP, Huang YP. 1987. Congenital fourth ventricular midline outlet obstruction. Report of two cases. *J Neurosurg* 67(4): 595–599.

Robertson E. 1957. *Pneumoencephalography*. Springfield: Charles C. Thomas.

Rogers L. 1931. The Foramen of Magendie. *J Anat* 65(4): 457–467.

Rohde V, Gilsbach JM. 2000. Anomalies and variants of the endoscopic anatomy for third ventriculostomy. *Minim Invasive Neurosurg* 43(3): 111–117.

Romero Adel C, Aguiar PH, Borchartt TB, Conci A. 2011. Quantitative ventricular neuroendoscopy performed on the third ventriculostomy: anatomic study. *Neurosurgery* 68(2 Suppl Operative): 347–354.

Scholz M, Mielke D, Fricke B, Pechlivanis I, Engelhardt M, Schmieder K, Harders AG. 2007. Individualized ventriculostomy in hydrocephalus: an intravital anatomical study. *Neurol India* 55(4): 355–362.

Shapiro R, Galloway SJ, Shapiro MD. 1986. Minimal asymmetry of the brain: a normal variant. *Am J Roentgenol* 147(4): 753–756.

Sharifi M, Ungier E, Ciszek B, Krajewski P. 2009. Microsurgical anatomy of the foramen of Luschka in the cerebellopontine angle, and its vascular supply. *Surg Radiol Anat* 31(6): 431–437.

Shibata DK, Maravilla KR. 1994. Diverticulum of the third-ventricle infundibulum: a normal variant simulating an abnormality of the pituitary stalk on MR images. *AJR Am J Roentgenol* 163(2): 423–424.

Skullerud K. 1985. Variations in the size of the human brain. Influence of age, sex, body length, body mass index, alcoholism, Alzheimer changes, and cerebral atherosclerosis. *Acta Neurol Scand Suppl* 102: 1–94.

Soininen H, Puranen M, Riekkinen PJ. 1982. Computed tomography findings in senile dementia and normal aging. *J Neurol Neurosurg Psychiatry* 45(1): 50–54.

Spiller W. 1916. Syringomyelia. Syringoencephalomyelia. *Nerv Ment Dis* 44: 395–414.

Steno A, Popp AJ, Wolfsberger S, Belan V, Steno J. 2009. Persisting embryonal infundibular recess. *J Neurosurg* 110(2): 359–362.

Strauss E, Fitz C. 1980. Occipital horn asymmetry in children. *Ann Neurol* 8(4): 437–439.

Todd R. 1847. *The Cyclopedia of Anatomy and Physiology*. London: Longman.

Torkildsen A. 1934. The Gross Anatomy of the Lateral Ventricles. *J Anat* 68(4): 480–491.

Trimarchi F, Bramanti P, Marino S, Milardi D, Di Mauro D, Ielitro G, Valenti B, Vaccarino G, Milazzo C, Cutroneo G. 2013. MRI 3D lateral cerebral ventricles in living humans: morphological and morphometrical age-, gender-related preliminary study. *Anat Sci Int* 88(2): 61–69.

Tubbs RS, Smyth MD, Oakes WJ, Blount JP. 2004a. Duplication of the massa intermedia in a child. *Pediatr Neurosurg* 40(1): 42–43.

Tubbs RS, Smyth MD, Wellons JC 3rd, Oakes WJ. 2004b. Arachnoid veils and the Chiari I malformation. *J Neurosurg* 100(5 Suppl Pediatrics): 465–467.

Tubbs RS, Loukas M, Shoja MM, Shokouhi G, Oakes WJ. 2008. Francois Magendie (1783–1855) and his contributions to the foundations of neuroscience and neurosurgery. *J Neurosurg* 108(5): 1038–1042.

Turkewitsch N. 1935. Die entwicklung des aquaeductus cerebri des menschen. *Morphol Jahrb* 76: 421–447.

Turkewitsch N. 1936. Die entwicklung des subkommissuralen organs beim bind (bos taurua L.). *Morphol Jahrb* 77: 573–586.

Vandertop PW. 1998. Traumatic basilar aneurysm after endoscopic third ventriculostomy: case report. *Neurosurgery* 43(3): 647–648.

Vandewalle G, Beuls E, Vanormelingen L, Vandersteen M. 2003. Accessory intraventricular prominence of the occipital horn of the lateral ventricle. *J Neurosurg* 99(1): 151–155.

Virchow R. 1854. *Handbuch der Speziellen Pathologie und Therapie*. Berlin: Verlag.

Wilberger JE Jr, Vertosick FT Jr, Vries JK. 1983. Unilateral hydrocephalus secondary to congenital atresia of the foramen of Monro. Case report. *J Neurosurg* 59(5): 899–901.

Woollam DH, Millen JW. 1953. Anatomical considerations in the pathology of stenosis of the cerebral aqueduct. *Brain* 76(1): 104–112.

Yamamoto I, Rhoton AL Jr, Peace DA. 1981. Microsurgery of the third ventricle: Part I. Microsurgical anatomy. *Neurosurgery* 8(3): 334–356.

Yotsutsuji T, Saitoh O, Suzuki M, Hagino H, Mori K, Takahashi T, Kurokawa K, Matsui M, Seto H, Kurachi M. 2003. Quantification of lateral ventricular subdivisions in schizophrenia by high-resolution three-dimensional magnetic resonance imaging. *Psychiatry Res* 122(1): 1–12.

Zipursky RB, Lim KO, Pfefferbaum A. 1990. Volumetric assessment of cerebral asymmetry from CT scans. *Psychiatry Res* 35(1): 71–89.

79 Pons, medulla oblongata and cerebellum

Dylan Goodrich[1], Jennifer Yang[2], Joseph H. Miller[2], and W. Jerry Oakes[3]
[1]St George's University, School of Medicine, St Georges, Grenada
[2]University of Alabama at Birmingham, Birmingham, Alabama, United States
[3]Children's of Alabama, Birmingham, Alabama, United States

The rhombencephalon is an embryological term for the hindbrain structures that consist of the pons, medulla oblongata and cerebellum. Its structures are located within the posterior fossa12/07/2015 7:31:00 AM. The hindbrain serves many essential functions and is therefore the most phylogenetically conserved portion of the brain. Most notably, the pons plays an important role in vision, sleep, arousal, and sensorimotor integration with the cerebellum. The medulla is vitally important for respiratory and circulatory control and acts as a conduit for both sensory and motor pathways between the brain and spinal cord. The cerebellum is important for balance and motor control and has gained attention for its role in higher functions (Middleton and Strick 1994; Riva and Giorgi 2000).

Major anatomic variations in the hindbrain often result in stillbirth; however, normal variations are known and may remain asymptomatic or unknown during life. Injury to these structures can result in significant morbidity or mortality. Understanding the variant anatomy of the rhombencephalon is clinically important. This chapter focuses mainly on variations within the pons, medulla, and cerebellum, and the common anatomical variants that are compatible with post-fetal life and remain asymptomatic.

Embryology

Developmentally, the rhombencephalon forms the hindbrain. During the three-vesicle stage at approximately 4 weeks gestational age, there is the prosencephalon (forebrain), mesencephalon (midbrain), and rhombencephalon (hindbrain). During the five-vesicle stage (sixth week gestational age), the rhombencephalon divides into metencephalon (pons, cerebellum; the upper part of the fourth ventricle) and myelencephalon (medulla; the lower part of the fourth ventricle).

The hindbrain contains eight developmental segments similar to the developing spinal cord called rhombomeres for sensory and motor innervation of the head through cranial nerve projections. These rhombomeres are connected to the developing mesencephalon (midbrain) via the isthmus, a rhombomere that becomes part of the pons. The pons and the medulla are formed in the lateromedial direction in neural tube development (in the cell columns fan out laterally from midline due to an expanding fourth ventricle). However, unlike the spinal cord, the compartmentalization of the rhombomeres is obscured due to the maturation of neural connections in the hindbrain. The cerebellum forms from rhombomere 1 in the region of the developing dorsolateral pons. Migrating neurons from the floor plate play a critical role. The Hox genes encode many transcription factors that are critical for neural development, including rhombomere patterning (Wang and Zoghbi 2001). Mutations in specific Hox genes are implicated in certain abnormal hindbrain-related functions in conditions such as autism (Raznahan et al. 2012).

Pons

The pons plays several major relay functions between the cerebral cortex, cerebellum, and the rest of the brainstem. The pontine nuclei forms relays between the cortex and cerebellum and functions to control fine movements. The pons also plays a critical role in respiratory function. Additionally, the pons hosts the nuclei of cranial nerves V, VI, VII, and VIII, their respective tracts, and descending cortical tracts (Martin 2003). Normal anatomic variants in the pons are poorly characterized, although variations that lie on the disease continuum are more commonly found in the literature.

The facial colliculi located on the dorsal pons on the floor of the fourth ventricle within the rhomboid fossa may vary and this has clinical significance for surgery. Bogucki et al. (1997) noted in a cadaver study that in 37.5% of specimens the facial colliculi were not readily visible in patients without evidence of pathology. It was hypothesized that, if unable to be seen in such a high of proportion of postmortem studies, then surgical infiltration into this area would have even less adequate visualization. Since the facial colliculi are often used as markers for

Bergman's Comprehensive Encyclopedia of Human Anatomic Variation, First Edition. Edited by R. Shane Tubbs, Mohammadali M. Shoja and Marios Loukas.
© 2016 John Wiley & Sons, Inc. Published 2016 by John Wiley & Sons, Inc.

making microsurgical incisions to infiltrate and treat lesions of the pons (Strauss et al. 1997), this may pose a problem and further require the need for electrophysiological monitoring. This technique is often used in order to infiltrate the pons without disrupting critical fibers coursing through (Katsuta et al. 1993; Asaad et al. 2010). The facial colliculi are also known to vary in distance from their lower border to the obex over the range 11.5–18 mm (mean 14.2 mm), further adding to their anatomic variability (Lang et al. 1991). Position of the facial colliculi is also analyzed morphometrically for safe surgery (Bogucki et al. 2000).

The striae medullares have been found to have varying numbers and orientations. Cadaver studies have found that striae medullares are absent in 14–30% of specimens (Lang et al. 1991; Bogucki et al. 1997; Quester and Schröder 1999). Twenty-two rhomboid fossae analyzed by Lang et al. (1991) exhibited 0–9 striae on the left side (mean 2.8) and 0–8 on the right side (mean 2.6). Striae were oriented in either a transverse or oblique fashion with a ratio of 62:38 respectively on the left side and 80:20 on the right. Oblique striae may run a course from the middle area of the rhomboid fossa outward and forward or may run from the lateral area of the rhomboid fossa anteriorly and medially.

The locus coeruleus was also found to show notable variations with regard to size and position within the pons. In a stereotactic study (Fernandes et al. 2012), the measured locus coeruleus was found to vary in length over the range 12–17 mm (mean 14.5 mm). Its center can vary anywhere over the range 15–20.5 mm above the pontomedullary junction (mean 18.5 mm), but its distance from the midline showed much a lower variation with a range of 2.6–3.7 mm. Variations of distance from the center of the locus coeruleus to the midline were much greater at its extremities with distances at the caudal end varying over the range 6.1–14.8 mm (mean 10.4 mm) and the rostral end 2.7–6.7 mm (mean 4.3 mm). Localization of the locus coeruleus gains importance when considering microsurgical procedures.

Medulla

The medulla oblongata is critical for the brainstem's control of homeostatic functions, including blood pressure and autonomic responses. Possibly due to its critical physiological role, medullary structure and anatomy is phylogenetically preserved; little variation exists among mammalians and normal anatomic variants of the medulla are poorly characterized in the literature.

The rostral medulla contains the inferior olivary nucleus ventrally, which communicates with the cerebellum through the inferior cerebellar peduncle for motor coordination. The nucleus ambiguous lies dorsal to the olive and contains the preganglionic parasympathetic neurons for the glossopharyngeal and vagus nerves. The spinal nucleus and tract for the trigeminal nerve also lie laterally and dorsally. Also on the dorsal side are the vestibular nuclei, which houses the descending vestibulospinal tract that is important for the maintenance of posture. Medially, the rostral medulla also contains the medial longitudinal fasciculus, the tectospinal tract, and the medial lemniscus. The sulcus limitans are grooves that separate the medial and lateral compartments of the dorsal medulla and terminate caudally at the obex.

Anatomically, the various nuclei medulla are organized similarly to that of the spinal cord. The caudal medulla contains the major dorsal column nuclei: the nucleus gracilis and cuneate nucleus. Here, the ascending dorsal column fibers synapse and cross via arcuate fibers and ascend into the thalamus as the medial lemniscus. Lateral to the dorsal column nuclei on either side is the spinal tract of CN V, which conveys pain and temperature from the ipsilateral side. More ventral to the spinal tract of CN V is the ascending fibers from the spinothalamic tract. The hypoglossal nucleus is located centrally, and the roots of the hypoglossal nerve exit ventrally to innerve the tongue. The nucleus for the spinal accessory nerve (CN XI) is located ventrally lateral to the decussation of the pyramids. The ventral medulla contains the decussation of the pyramids ventrally, the site where the descending corticospinal tract cross before entering the spinal cord (Martin 2003).

The medulla is continuous with the spinal cord through the foramen magnum. An MRI study of 200 patients in China measured the cervicomedullary angle (CMA) and found that there is very little variation based on age and gender, making it a reliable surgical parameter (Wang et al. 2009). Marshall (1892) found that the weight of the pons and medulla ranged from 0.83 to 1.1 ounces. There may be schisis of the lower medulla.

Measurements of the medulla show slight variability anatomically. Akar et al. (1995) performed measurements on 11 cadaveric specimens and found that vertical dimensions of the pyramid were longer on average on the right side with an average length of 19.7 mm (range 16–22 mm) compared to the left side with an average length of 18.5 mm (range 13–21 mm). This exhibits not only variation between contralateral sides but variation within each side itself between specimens. The olives showed similar asymmetry with the right side measuring 11.7 mm on average (range 9–15 mm) and the left measuring 10.8 mm on average (range 10–15 mm).

Tracts

There are many numerous variations that have been found in the ventral medulla regarding axonal fiber tracts. Aberrant pyramidal fibers are rather commonly seen with Nyberg-Hansen and Rinvik (1963) going so far as to say "these bundles are so common that we are inclined to consider them as normal components of the pyramidal tract." Typically these consist of corticobulbar fibers that deviate from the main pyramidal fasciculi and often cross the medial lemniscus. Larger bundles of corticobulbar fibers called Pick's bundles may be found entirely out of place after separating from the tract as high up as the internal capsule, or may even course upward if they separate at a lower level (Rasmussen 1955; Nyberg-Hansen and Rinvik 1963). Circumolivary bundles (or fascicles) are commonly found. They

are made of fibers leaving the pyramids and coursing laterally, passing under the ipsilateral olive, turning rostrally and typically disappearing into the restiform body (Swank 1934). They are thought to be corticobulbar fibers that are destined for motor nuclei or corticopontobulbar fibers (Rasmussen 1955). In a study on 85 brain stems, Swank (1934) found these fascicles bilaterally in four specimens and unilaterally in five. In addition, 30 incidences of circumolivary striae which were deemed to be smaller in size compared to the fascicles, yet followed the same route, were also reported.

Decussation of pyramidal fibers also shows unique variability and manifestations in the medulla. A total of 73% of specimens analyzed by Kertesz and Geschwind (1971) showed that the uppermost decussations occurred from the left to right side with 17% from the right to left and no preference for the final 10%. This may contribute to asymmetry commonly exhibited in the pyramids. Outright anomalies of pyramid decussation may also be observed where decussation does not occur within the normal area and, instead, fibers decussate throughout the spinal cord (Rasmussen 1955). If this occurs unilaterally then it is common to see the ipsilateral pyramid appearing larger than normal while the contralateral pyramid is smaller.

An additional aberrant tract known as the conductor sonorous may also be present (Barnand and Spann 1946; Rasmussen 1955). Its course is rather elaborate: first starting at the chief sensory nucleus of the trigeminal nerve, it runs caudally and medially toward the midline before passing through the medulla to the ventral side, where it courses under the pyramids and olives to the inferior cerebellar peduncle. In a study specifically analyzing this tract, it was found grossly in 3 of 50 analyzed cadavers (Barnand and Spann 1946).

Cerebellum

The cerebellum functions as a regulator of motor function, coordination, and posture. It extends dorsally from the base of the brain at the level of the pons, and is separated from the overlying cerebrum by the cerebellar tentorium. In the axial plane, it is divided into the medial vermis and flanking lateral hemispheres, and in the sagittal plane it is divided into three lobes: anterior, posterior, and flocculonodular. The major pathways to and away from the cerebellum mainly traverse through three peduncles, which lie deep to the hemispheres. The superior cerebellar peduncle contains the main output pathway, the dentatorubrothalamic tract, and the afferent ventral spinocerebellar tract. The middle cerebellar tract contains afferent pontocerebellar fibers. The inferior cerebellar tract is mainly afferent, housing the dorsal spinocerebellar tract, cuneocerebellar tract, and olivocerebellar tract from the contralateral inferior olivary nucleus. The primary fissure divides the anterior lobe from the posterior lobe, and the posterolateral fissure divides the flocculonodular lobe from the posterior lobe (Martin 2003).

The individual embryological timeline of the cerebellum may indicate why it more commonly varies in structure than other members of the rhombencephalon. Its early differentiation in development combined with its relatively late maturation may predispose it to what Wang and Zoghbi (2001) described as a "special susceptibility to disruptions." It has been found that phylogenetically recent portions of the cerebellum may mature later in life than other regions of the cerebellum (Tiemeier et al. 2009). Although many researchers look to determine genetic and molecular causes of pathological processes, asymptomatic variants have been increasingly studied to increase the understanding of cerebellum development.

Hemispheres

Cerebellar hypoplasia is the most common variant described in literature with regard to symptomatic processes. Cerebellar hypoplasia may be degenerative, as is frequently seen in alcoholics, or congenital. As previously mentioned, the cerebellum forms from rhombomere 1 (r1) and any aberration in this process may result in cerebellar hypo- or aplasia. Hypoplasia may sometimes be asymptomatic, but it is rare (deSouza et al. 1994).

Hemiagenesis is possible where there is a complete unilateral agenesis of the cerebellum that may rarely be symptomless. It is worth noting that unilateral agenesis and hypoplasia are distinct; if the components of the hemisphere are present but significantly smaller, it should be considered hypoplasia and not agenesis (Erskine 1950). Due to agenesis there is a deficiency in corticopontine, central tegmental tracts, and cerebellopontine tracts contralaterally. This results in associated contralateral hypoplasia of the inferior olives, nuclei pontis and red nucleus in the brain stem (Rasmussen 1955).

Age effects on the cerebellar hemispheres have been noted with decreased volume being significantly correlated with increased adulthood age as a normal sign of atrophy (Raz et al. 1998). Andersen et al. (2003) conducted a stereological study on cadavers to analyze cerebellar changes with age and found a significant percent decrease in white matter in the whole cerebellum (27%), particularly in the flocculonodular lobe (59%). Mean purkinje cell perikaryon volume was found to be decreased in 33% of cases and total cerebellar volume was decreased in 16%; this was actually determined not significant, but was close (p=0.06).

Sexual dimorphisms have been analyzed with respect to the cerebellar hemispheres and total cerebellum. Marshall (1892) found that the average weight of the total cerebellum in individuals with no signs of neurological dysfunction differed between sexes from 4.66 oz in females to 5.06 oz in males. However, when correcting for height, the sizes were determined nearly equal. Males typically have on average larger volumes of the hemispheres compared to females when corrected for height; however, the effect observed was not equivalent in both hemispheres (Raz et al. 1998). Other instances of morphometric analysis have exhibited no increase in cerebellar hemisphere volume when corrected for age and intracranial volumes

(Fan et al. 2010). Males and females were also noted to have differences in symmetry in different sections of the cerebellum. Longitudinal findings demonstrated that total cerebellum volume follows an inverted "U" shape with peaks occurring at an average age of 11.8 years in females and 15.6 years in males, with males exhibiting a 10–13% larger volume depending on age (Tiemeier et al. 2009). A longitudinal study of cerebellar volume via 3D ultrasound of 27 fetuses from 20 to 40 weeks of gestation showed that the volume of the left hemisphere is larger than the right at a given time (Rutten et al. 2009).

Vermis

The cerebellar vermis is the middle portion of the cerebellum that lies between the two attached hemispheres. In most people the paravermian sulcus forms the limit of the vermis laterally in the anterior lobe, but may not always be present (Andersen et al. 2003).

Hypoplasia of the inferior vermis is one of the most common variants in the cerebellum, which may be associated with Joubert's syndrome or occasionally asymptomatic (deSouza et al. 1994). Agenesis of the vermis has been known to occur in symptomless patients where there are parts of the vermis or fastigial nuclei missing or the vermis can be divided in half and connected by a thin membrane (Rasmussen 1955). Rhombencephalosynapsis occurs from complete absence of the cerebellar vermis with complete fusion of the two hemispheres and has been known to be asymptomatic; however, this is rarely seen in these individuals (Scroop et al. 2000; Boltshauser 2004).

Normal variations of the cerebellar vermis that are less explicit than hypoplasia may be determined in vivo from MRI studies. Males have been found to have a larger vermis area on average even after correcting for height, with the posterior lobules having no statistically significant differences and the anterior lobules showing significantly larger areas. Age is also correlated with significant shrinkage of vermal area (Raz et al. 1998). Size of vermal sulci, associated with vermal atrophy, was shown to increase in older subjects with most significant changes occurring after the fifth decade of life (Raininko et al. 1994).

The cerebellar vermis contains 8 lobules, some which have been identified as having normal variations. Its central lobule, or second lobule of the upper portion, has been shown by Bispo et al. (2010) to vary in the contents of the folia: 80% had one folium; 17.5% had two folia of different sizes; and 2.5% had two folia of equal size. Further findings by their group revealed that the folium of the vermis emerged from the central white matter in 47.5%, with 42.5% emerging from the tuber and 5% from the declive. No description was given regarding the other 5%.

Tonsils

Cerebellar tonsil herniation through the foramen magnum is an uncommon finding defined as Chiari Type I malformation when it extends >5 mm below the foramen magnum. This most often results in a pathological state (not discussed here). However, tonsil herniation is also an asymptomatic variant that may extend beyond the defined cut-off. Up to 30% of patients with herniations of 5–10 mm may be asymptomatic (Elster and Chen 1992) and a range of 7–25 mm has been seen based on MRI (Meadows et al. 2000). Due to the fact that MRI observations may not be made of asymptomatic individuals, the rate of ectopia of the cerebellar tonsils may be significantly higher than typically thought.

A large study by Smith et al. (2013) examined 2378 randomly selected patient MRIs retrospectively to analyze cerebellar tonsil position in those who were not diagnosed with Chiari Type 1 malformation. The study highlighted many variants and also how selected variables affected tonsil position. A total of 3% of patients exhibited cerebellar tonsil position greater than 5 mm below the foramen magnum, with a female to male ratio of 47 to 27. Of this group of patients, only 51% of tonsils were symmetric with respect to left or right. This differed significantly from the overall symmetry percentage of 84% encountered in the entire study population. Morphology analysis showed that 97% of patients had rounded tonsils, 1% had pegged tonsils, and the remaining 2% had an intermediate morphology. Of those 74 patients with herniation greater than 5 mm, only 54% had a rounded configuration. Overall, females were shown to have lower mean tonsil position. Patients in the first decade of life had a high position of tonsils with a few extreme outliers exhibiting low position, but in adult cohorts tonsil position rose higher with age.

Nuclei

The dentate nucleus has a highly complex and inconsistent structure, with Kozlova (1984) going so far as to claim "it is impossible to classify its individual variability." Measurements have to be in clearly defined planes and performed consistently, which may not be true from one study to another. Using a median sagittal plane, Kozlova (1984) measured the width of the dentate nucleus as within the range 9–20 mm; using a horizontal plane through the apex of the roof of the fourth ventricle, the height of the dentate nucleus was measured as 8–20 mm; and using a frontal plane passing through apex of the roof of the fourth ventricle, the length of the dentate nucleus was measured as 13–23 mm. Using the same planes for the nucleus emboliformis, nucleus globosus, and tegmental nucleus, the following measurement variations were found:

- nucleus emboliformis: width 3–8 mm; height 2–6 mm; and length 4–11 mm;
- nucleus globosus: width 1–4 mm; height 2–5 mm; and length 2–6 mm; and
- tegmental nucleus: width 4–6 mm; height 2–5 mm; and length 3–7 mm.

Nuclei of the cerebellum therefore exhibit variation that may have an impact for surgeons attempting to treat lesions of these areas. Further variation has been discovered with respect to location of these nuclei compared to the outer surface of the

cerebellum and other landmarks (Kozlova 1984), including the cerebellar peduncles (Ramos et al. 2011). These variations will also have increased significance when looking to correct pathologies of the cerebellum that do or do not involve these locations.

References

Akar ZC, Dujovny M, Gomez-Tortosa E, Slavin KV, Ausman JI. 1995. Microvascular anatomy of the anterior surface of the medulla oblongata and olive. *J Neurosurg* 82: 97–105.

Andersen BB, Gundersen HJG, Pakkenberg B. 2003. Aging of the human cerebellum: a stereological study. *J Comp Neurol* 466: 356–365.

Asaad WF, Walcott BP, Nahed BV, Ogilvy CS. 2010. Operative management of brainstem cavernous malformations. *Neurosurg Focus* 29: E10.

Barnand JW, Spann JL. 1946. An aberrant trigemino-cerebellar tract in the human brain. *J Comp Neurol* 85: 171–176.

Bispo RFM, Ramalho AJC, Gusmão LCB, Cavalcante APH, Rocha AAC, Sousa-Rodrigues CF. 2010. Cerebellar vermis: topography and variations. *Int J Morphol* 28: 439–443.

Bogucki J, Gielecki J, Czernicki Z. 1997. The anatomical aspects of a surgical approach through the floor of the fourth ventricle. *Acta Neurochir (Wien)* 139: 1014–1019.

Bogucki J, Czernicki, Gielecki J. 2000. Cytoarchitectonic basis for safe entry into the brainstem. *Acta Neuorchir (Wien)* 142: 383–387.

Boltshauser E. 2004. Cerebellum - Small brain but large confusion: a review of selected cerebellar malformations and disruptions. *Am J Med Genet A* 126A: 376–385.

deSouza N, Chaudhuri R, Bingham J, Cox T. 1994. MRI in cerebellar hypoplasia. *Neuroradiology* 36: 148–151.

Elster AD, Chen MYM. 1992. Chari I malformations: clinical and radiologic reappraisal. *Radiology* 183: 347–353.

Erskine CA. 1950. Asymptomatic unilateral agenesis of the cerebellum. *Mschr Psychiat Neurol* 119: 321–339.

Fan L, Tang Y, Sun B et al. 2010. Sexual dimorphism and asymmetry in human cerebellum: an MRI-based morphometric study. *Brain Res* 1353: 60–73.

Fernandes P, Regala J, Correia F, Gonçalves-Ferreira AJ. 2012. The human locus coeruleus 3-D stereotactic anatomy. *Surg Radiol Anat* 34: 879–885.

Katsuta T, Morioka T, Fujii K, Fukui M. 1993. Physiological localization of the facial colliculus during direct surgery on an intrinsic brain stem lesion. *Neurosurgery* 32: 861–863.

Kertesz A, Geschwind N. 1971. Patterns of pyramidal decussation and their relationship to handedness. *Arch Neurol* 24: 326–332.

Kozlova GP. 1984. Individual anatomical variations in cerebellar nuclei. *Neurosci Behav Physiol* 14: 63–67.

Lang J Jr, Ohmachi N, Lang J Sr. 1991. Anatomical landmarks of the rhomboid fossa (floor of the 4th ventricle), its length and width. *Acta Neurochir (Wien)* 113: 84–90.

Marshall J. 1892. On the relations between the weight of the brain and its parts, and the stature and mass of the body, in man. *J Anat Physiol* 26: 445–500.

Martin J. 2003. *Neuroanatomy: Text and Atlas*, third edition. New York: McGraw-Hill.

Meadows J, Kraut M, Guarnieri M, Haroun RI, Carson BS. 2000. Asymptomatic chiari type I malformations. *J Neurosurg* 92: 920–926.

Middleton FA, Strick PL. 1994. Anatomical evidence for cerebellar and basal ganglia involvement in higher cognitive function. *Science* 266: 458–461.

Nyberg-Hansen R, Rinvik E. 1963. Some comments on the pyramidal tract, with special reference to its individual variations in man. *Acta Neurol Scand* 39: 1–30.

Quester R, Schröder R. 1999. Topographic anatomy of the cochlear nuclear region at the floor of the fourth ventricle in humans. *J Neurosurg* 91: 466–476.

Raininko R, Autti T, Vanhanen SL, Ylikoski A, Erkinjuntti T, Santavuori P. 1994. The normal brain stem from infancy to old age. A morphometric MRI study. *Neuroradiology* 36: 364–368.

Ramos A, Chaddad-Neto F, Doria-Netto HL, Campos-Filho JM, Oliveira E. 2012. Cerebellar anatomy as applied to cerebellar microsurgical resections. *Arg Neuropsiquiatr* 70: 441–446.

Rasmussen AT. 1955. Anomalies of the nervous system. In: *Clinical Neurology*, Volume 3 (ed. BakerAB). New York: Hoeber-Harper, pp. 1675–1680.

Raz N, Dupuis JH, Briggs SD, McGavran C, Acker JD. 1998. Differential effects of age and sex on the cerebellar hemispheres and vermis: a prospective study. *Am J Neuroradiol* 19: 65–71.

Raznahan A, Lee Y, Vaituzis C et al. 2012. Allelic variation within the putative autism spectrum disorder risk gene homeobox A1 and cerebellar maturation in typically developing children and adolescents. *Autism Res* 5: 93–100.

Riva D, Giorgi C. 2000. The cerebellum contributes to higher functions during development: evidence from a series of children surgically treated for posterior fossa tumours. *Brain* 123: 1051–1061.

Rutten MJ, Pistorius LR, Mulder EJH, Stoutenbeek PH, de Vries LS, Visser GHA. 2009. Fetal cerebellar volume and symmetry on 3-D ultrasound: volume measurement with multiplanar and vocal techniques. *Ultrasound Med Biol* 35: 1284–1289.

Scroop R, Sage M, Yoyvodic F. 2000. Rhombencephalosynapsis. *Australas Radiol* 44: 225–227.

Smith BW, Strahle J, Bapuraj JR, Muraszko KM, Garton HJL, Maher CO. 2013. Distribution of cerebellar tonsil position: implications for understanding chiari malformation. *J Neurosurg* 119: 812–819.

Strauss C, Lütjen-Drecoll E, Fahlbusch R. 1997. Pericollicular surgical approaches to the rhomboid fossa. Part I. Anatomical basis. *J Neurosurg* 87(6): 893–899.

Swank RL. 1934. The relationship between the circumolivary pyramidal fascicles and the pontobulbar body in man. *J Comp Neurol* 60: 309–317.

Tiemeier H, Lenroot RK, Greenstein DK, Tran L, Pierson R, Giedd JN. 2009. Cerebellum development during childhood and adolescence: a longitudinal morphometric MRI study. *Neuroimage* 49: 63–70.

Wang S, Wang C, Passias PG, Li G, Yan M, Zhou H. 2009. Interobserver and intraobserver reliability of the cervicomedullary angle in a normal adult population. *Eur Spine J* 18: 1349–1354.

Wang VY, Zoghbi HY. 2001. Genetic regulation of cerebellar development. *Nat Rev Neurosci* 2: 484–491.

80 Subarachnoid space

Martin M. Mortazavi[1], Nimer Adeeb[2], Fareed Rizq[2] and R. Shane Tubbs[3]
[1]University of Washington School of Medicine, Seattle, Washington, United States
[2]Children's of Alabama, Birmingham, Alabama, United States
[3]Seattle Science Foundation, Seattle, Washington, USA
St George's University, School of Medicine, St Georges, Grenada
University of Dundee, Dundee, UK

Subarachnoid space size

Cerebral subarachnoid space

Variations the size of the subarachnoid space have been revealed by ultrasonographic (US) measurements mainly in neonates, infants, and children (Libicher and Troger 1992; Frankel et al. 1998; Lam et al. 2001; Narli et al. 2006; Sabouri et al. 2011; Okur et al. 2013); computed tomography (CT) and magnetic resonance (MR) studies have also been conducted. The width of the subarachnoid space correlates positively with weight, height, and head circumference; there is no significant gender difference (Narli et al. 2006; Sabouri et al. 2011). The width also correlates positively with age, peaking at 7 (Lam et al. 2001) or 13 (Okur et al. 2013) months and declining thereafter. This has been related to the development of the arachnoid villi and improved cerebrospinal fluid (CSF) drainage at 6–18 months of age (Sabouri et al. 2011). A wide subarachnoid space is therefore considered an anatomical variation during the first year of life. The site of measurement is also important: the craniocortical (CC) distance (between the cranium and cerebral hemisphere), sinocortical (SC) area (between the cerebral hemisphere and the superior sagittal sinus), or interhemispheric (IH) area (between the two hemispheres), measured from the narrowest to the widest point (Lam et al. 2001) (Fig. 80.1). Libicher and Troger (1992) reported the upper limits of the normal range as 3, 4, and 6 mm at the CC, SC, and IH respectively. Sabouri et al. (2011) reported higher upper limits: 5, 5.8, and 8 mm at the CC, SC, and IH, respectively. These authors also suggested that race, socioeconomic conditions, and dietary regime could affect the width of the subarachnoid space. Okur et al. (2013) reported the narrowest CC width of the subarachnoid space, over the range 0.5–6 mm (Okur et al. 2013). Frankel et al. (1998) and Sabouri et al. (2011) reported narrower ranges of 1.9–5.7 mm and 1–4 mm, respectively. However, measurement of the subarachnoid space to ventricular width ratio (SAS:VW ratio) could be a more accurate method for determining a normal value; the ratio between the shortest CC width of the subarachnoid space and the shortest width of the anterior horn of the lateral ventricle at the foramen of Monro are calculated (Okur et al. 2013).

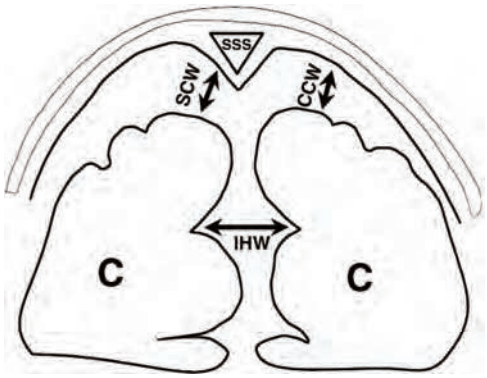

Figure 80.1 Anatomic landmarks and sonographic variables of the subarachnoid space in the coronal plane. C = cerebral cortex; SSS = superior sagittal sinus; CCW = craniocortical width; IHW = interhemispheral width; SCW = sinocortical width.

Source: Lam et al. (2001)

Spinal subarachnoid space

The subarachnoid space dimensions measured between the arachnoid and the pia on the anterior and posterior sagittal diameters and the right and left transverse diameters are symmetrical between the right and left sides. In contrast, they are asymmetrical and vary widely on the anterior and posterior sides over the range 1–5 mm, and are larger on the posterior side. These measurements also vary and decrease monotonically from the cervical to the lumbar spine (Zaaroor et al. 2006).

Others

The subarachnoid space can be absent in locations where the brain is in close proximity or adherent to the arachnoid, and where the nerves and blood vessels exit the brain (Adeeb et al. 2013).

Bergman's Comprehensive Encyclopedia of Human Anatomic Variation, First Edition. Edited by R. Shane Tubbs, Mohammadali M. Shoja and Marios Loukas.
© 2016 John Wiley & Sons, Inc. Published 2016 by John Wiley & Sons, Inc.

Hodges (1970) denied the presence of a sheet-like subarachnoid space over the cerebral hemispheres and considered the arachnoid to be in direct contact with the gyri. Instead, he believed this space to be formed where the arachnoid bridges over the sulci, creating a space within each sulcus about 1–2 mm across and 5–10 mm deep (Hodges 1970).

Subarachnoid cisterns

The basilar cisterns underlie and partially surround the structures on the floor of the skull, and are named according to the major anatomical structures they bathe. The first detailed description and naming of most cisterns was provided by Key and Retzius (1875) and the cisterns have received more attention since. In the following text, deviations from the normal anatomy of the subarachnoid cisterns will be described.

Chiasmatic cistern

The location of the chiasmatic cistern in relation to the sellae can vary. It usually overlies the diaphragma sella and the sella turcica, but it sometimes lies more posterior over the dorsum sella (post-fixed chiasm) or, less commonly, more anterior over the tuberculum sella (prefixed chiasm) (Gulsen et al. 2010). In cases of incompetent diaphragma sella, the chiasmatic cistern can extend into the sella turcica (Yaşargil 1984).

Subdiaphragmatic cistern

The size of this cistern is determined by the length of the subdiaphragmatic portion of the pituitary stalk, which can be completely supradiaphragmatic in cases where the opening of the diaphragma sellae is huge and the pituitary dome herniates upwards, resulting in a large cistern. It also varies according to: (1) the shape of the diaphragma sellae (flat, concave, or convex); (2) the size of the sellar cavity; (3) the size of the pituitary gland; (4) the location of the pituitary stalk; and (5) the size of the pituitary stalk (Di Ieva et al. 2012).

Lamina terminalis (LT) cistern

The anteroposterior (AP) length of the cistern's floor ranges from 14.0 to 28.0 mm. Its anterior boundary can extend as far as 5.0 mm anterior to the limbus sphenoidalis. Occasionally there is no significant anterior boundary, and the LT cistern communicates directly with the interhemispheric cistern (Wang et al. 2011a).

The LM cistern can also extend inferoanteriorly to form a tent-shaped recess above the interspace anterior to the OC, with an AP length of 4.0–12.0 mm. Its superolateral wall is formed by the pia mater under the gyrus rectus (GR), and its inferior wall by the arachnoid between the optic nerves (ON). There are sometimes dividing membranes within this recess (Yaşargil 1984; Wang et al. 2011a).

In some cases, the lateral walls partially adhere to each other in the middle part of the cistern (Wang et al. 2011a).

The origin of the frontopolar arteries and the median artery of the corpus callosum (CC) (Yaşargil 1984; Wang et al. 2011a), and several (15–40) small subcallosal arteries, might be found within the lamina terminalis cistern in addition to its normal content. The subcallosal arteries have diameters of 0.1–0.3 mm and can arise from the anterior communicating artery (ACoA), the A2 segment of the anterior cerebral artery (ACA), or the median artery of the CC (Wang et al. 2011a).

Carotid cistern

The medial wall of the carotid cistern can be absent, unilaterally or bilaterally. In such cases the cistern communicates freely with the chiasmatic cistern. In other cases, the arachnoid membranes separating the carotid, interpeduncular, and crural cisterns are absent, creating a confluent area through which cerebrospinal fluid can pass easily via the posterior part of the carotid cistern (Yaşargil 1984; Brasil and Schneider 1993; Froelich et al. 2008).

Olfactory cistern

The anterior part of this cistern is usually high and broad. Its highest point reaches 3.0–4.0 mm above the olfactory bulb and its most lateral point extends 2.0–3.0 mm beyond the bulb. Its posterior part is usually wide, reaching a maximal width of 1 cm (Wang et al. 2008). There may be a slit-like extension of the olfactory cistern (5–13 mm) if the olfactory sulcus is deep (Yaşargil 1984; Wang et al. 2008).

The size of the cistern's cavity also varies. It can be very narrow, with walls attaching to the olfactory structures and insufficient communication with the surrounding subarachnoid space (Wang et al. 2008).

There are usually openings at the inferior wall of the olfactory cistern through which it communicates with the adjacent carotid and sylvian cisterns. They might be big (reaching up to 5 mm in diameter), small (less than 0.1 mm in diameter), or absent (Wang et al. 2008).

There can also be up to four small olfactory arterial branches, 0.1–0.35 mm in diameter. They arise from the main olfactory artery, anterior olfactory artery, posterior olfacorty artery (most common), or recurrent artery of Heubner (least common). The latter does not usually enter the cistern but the small arterial branches do. The course of these branches within the cistern depends on their origin, since they can begin anteriorly or posteriorly if they arise from the anterior or posterior olfactory artery, respectively. Infrequently, the arterial branches are derived from the orbital artery; these often have a more anterior origin and divide repeatedly within the cistern. Olfactory veins within the cistern are usually 1–3 in number and 0.3–0.5 mm in diameter. They drain into the frontopolar vein or the origin of the superior sagittal sinus (Wang et al. 2008).

Sylvian cistern

The size and shape of this cistern depends on the relationship between the frontal and temporal lobes. In most cases it narrows superiorly as the frontal and temporal lobes approach each other

over a length of 15–20 mm. At this level, the width of the cistern is usually about 0.5–1.0 cm. Occasionally, the frontal and temporal lobes are closely apposed and cover the substance of the cistern. In other cases, part of the frontal lobe herniates into the adjacent temporal lobe or vice versa, distorting the structure of the cistern. In rare cases the cistern is clearly visible on the surface (Yaşargil 1984).

In view of the above variations in the size and characteristics of the investing arachnoid trabeculae and membranes, the Sylvian cistern has been categorized into four types: type 1: large cistern, transparent and fragile arachnoid; type 2: small cistern, transparent and fragile arachnoid; type 3: large cistern, thickened and tough arachnoid; type 4: small cistern, thickened and tough arachnoid. The difficulty of microsurgical dissection of the Sylvian cistern increases from type 1 to type 4 (Yaşargil 1984).

Some anatomists divide the cistern into anterior (sphenoidal) and posterior compartments in relation to the limen insulae. The anterior compartment extends from the origin of the middle cerebral artery laterally to the insula medially. It is limited superiorly by the posterior part of the orbital gyri and the lateral part of the anterior perforated substance, and inferiorly by the planum temporalis on the superior surface of the temporal lobe. The posterior compartment is located behind the limen insula and opens into the lateral cerebral surface. It is further subdivided into medial and lateral parts by the intermediate Sylvian membrane, which spans the interval between the upper and lower walls of the posterior compartment of the Sylvian fissure. The medial part is located between the medial parts of the opposing surfaces of the frontoparietal and temporal operculae, and extends into the insular cleft located between the insula and the insular surface of the opercula, its floor being formed by the upper surface of the temporal lobe. The lateral part is located in the lateral part of the cleft between the operculae. Its medial wall is formed by the intermediate Sylvian membrane, its lateral wall by the outer arachnoid membrane, and its superior and inferior walls by the lateral part of the opposing operculae (Inoue et al. 2009) (Fig. 80.2).

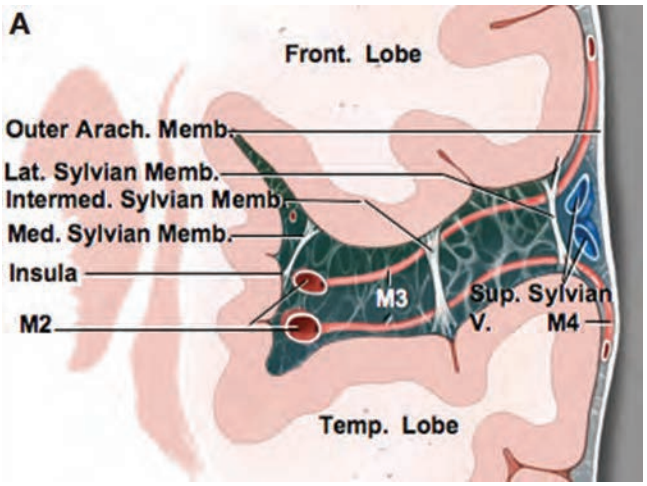

Figure 80.2 Anterior view of a drawing of a coronal section extending through the left sylvian fissure showing the lateral, intermediate, and medial sylvian membranes. The outer arachnoidal membrane forms the outer wall of the sylvian cistern and fissure. The lateral sylvian membrane spans the lateral part of the sylvian fissure and extends from the frontoparietal to the temporal operculum deep to the superficial sylvian veins. The intermediate sylvian membrane spans the interval between the medial part of the frontoparietal operculum above and the medial side of the superior temporal and Heschl's gyrus below. The medial sylvian membrane extends downward from the medial edge of the frontoparietal operculum and attaches to the insula on the medial side of the M2 segment of middle cerebral artery.

Source: Inoue et al. (2009)

Pericallosal cistern

Some authors have subdivided the pericallosal cistern into three compartments: inferior, anterior, and superior. The inferior compartment is positioned above the lamina terminalis cistern and below the rostrum of the corpus callosum, and is bounded anteriorly by the outer arachnoid membrane and laterally by the paraterminal and paraolfactory gyri. The anterior compartment is bounded anteriorly by the outer arachnoid membrane, posteriorly by the genu of the corpus callosum, and laterally by the cingulate gyri. The superior compartment is located between the body of the corpus callosum inferiorly, and the outer arachnoid membrane spanning the interval between the paired cingulated sulci superiorly. It narrows posteriorly and ends on the superior surface of the splenium. There are no distinct divisions between the three compartments (Inoue et al. 2009).

Other authors divide this cistern into anterior and posterior portions separated by arachnoid trabeculae at the branching of the callosomarginal and pericallosal arteries, but with no distinct division (Yaşargil 1984).

Interpeduncular cistern

Lu and Zhu (2005a) have described the presence of two distinct arachnoid membranes within and dividing the interepeduncular cistern: the basilar artery (BA) bifurcation membrane and the posterior perforated membrane.

The BA bifurcation membrane attaches caudally to the anterior walls of the BA bifurcation and the proximal segments of the posterior cerebral artery (PCA) and/or superior cerebellar artery (SCA). It spreads obliquely forward and upward and attaches to the anterior edge of the mamillary bodies and the diencephalic leaf of the Liliequist membranes. Laterally, it attaches via the arachnoid trabeculae to the diencephalic-mesencephalic leaflets of Liliequist's membrane. It can appear as an intact membrane (most common), a porous and sparse network, or a dense and porous network (least common). It divides the cistern into two portions: a deep part, which communicates with the ambient cistern; and a superficial part which communicates with the oculomotor cistern. The superficial portion contains only the upper part of the basilar artery. The deep portion contains the bifurcation of the BA, the proximal portions of the PCA and the SCA, the oculomotor nerves, the posterior communicating artery (PCoA), the perforating branches of the

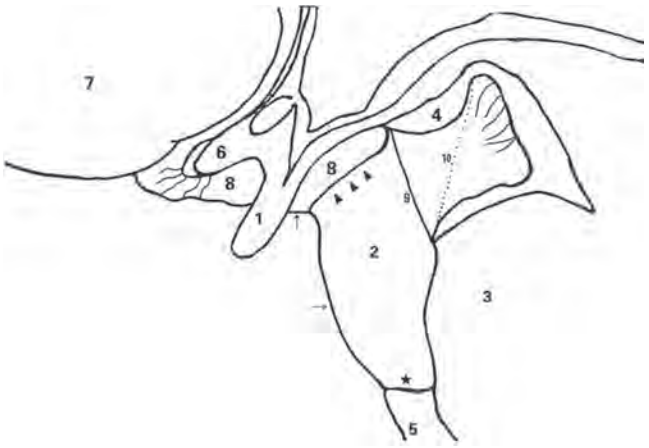

Figure 80.3 Drawing demonstrating the sagittal view of the Liliequist membrane and the interpeduncular cistern. The arrows indicate the mesencephalic leaf and the arrowheads the diencephalic leaf of the Liliequist membrane; the star marks the medial and the lateral pontomesencephalic membrane. 1 = infundibulum and pituitary stalk; 2 = interpeduncular cistern; 3 = pons; 4 = mammillary bodies; 5 = prepontine cistern; 6 = optic chiasm; 7 = frontal lobe; 8 = chiasmatic cistern; 9 = BA bifurcation membrane; 10 = posterior perforated membrane.

Source: Lu and Zhu (2005).

arteries, the posterior perforated substance, and the posterior perforated membrane (Lu and Zhu 2005a).

The posterior perforated membrane attaches caudally to the apex of the BA and the superior wall of the proximal segments of the PCA, and rostrally to the posterosuperior margins of both mamillary bodies. Laterally, it attaches to the diencephalic-mesencephalic leaflets of the Liliequist membrane by arachnoid trabeculae. This membrane subdivides the deep portion of the cistern into anterior and posterior parts. The anterior part contains only mamillary bodies and the perforating arteries that supply them; the posterior part houses all the other contents (Lu and Zhu 2005a) (Fig. 80.3).

Ambient cistern

In contrast to the previous descriptions, Qi et al. (2011a) considered the ambient cistern as extending from the posterior edge of the oculomotor nerve anteriorly to the ascending part of the posterior mesencephalic membrane posteromedially (Qi et al. 2011a). The anterior and posterior perimesencephalic membranes of the ambient cistern are mostly discontinuous and are connected by sparse arachnoid trabeculae. However, a complete, intact perimesencephalic membrane (previously known as the superior cerebellar membrane) can sometimes be found (Qi et al. 2011a).

In contrast to Yaşargil (1984) and Yaşargil et al. (1976), who divided the ambient cistern into supra- and infratentorial compartments, Qi et al. (2011a) considered that the ambient cistern is the compartment extending above rather than across the level of the tentorial incisura, and further divided it into anterior and posterior parts. According to them, this exclusion of the infratentorial compartment is justified by the presence of a perimesencephalic membrane, arising at the level of the tentorial incisura and creating a relatively intact separation between the supra- and infratentorial compartments. In contrast, there was no complete membrane except for scattered arachnoid trabeculae in the infratentorial compartment, which was defined as the cerebellopontine cistern anteriorly and the cerebellomesencephalic cistern posteriorly.

The anterior part of the supratentorial compartment is located anterolaterally to the cerebral peduncle and superiorly to the anterior perimesencephalic membrane. The lateral wall is formed by the medial surface of the temporal lobe and the superior wall by the pia covering the lateral surface of the upper peduncle, the optic tract, and the uncus. The posterior compartment is located posterolaterally to the midbrain tegmentum and superiorly to the posterior perimesencephalic membrane. The lateral wall is formed by the medial occipital lobe and the superior wall by the pia covering the midbrain tegmentum, the lateral geniculate body, and the medial occipital lobe (Qi et al. 2011a) (Fig. 80.4, Fig. 80.5).

On the basis of this description, Qi et al. (2011a) excluded the superior cerebellar artery and the trochlear nerve (which are infratentorial) from the contents of the ambient cistern. They also reported the P2 and P3 segments of the anterior choroidal artery and their branches as among the contents (Qi et al. 2011a).

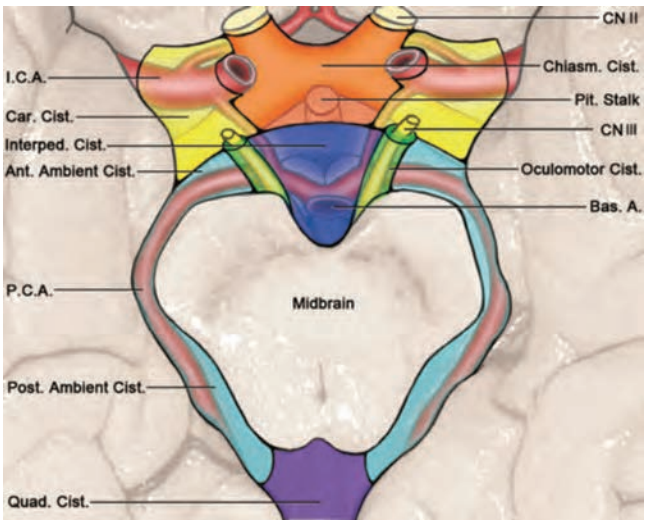

Figure 80.4 The ambient cistern and adjacent cisterns (inferior view). The anterior ambient cistern (light blue) communicates with the carotid cistern (yellow) anteriorly, the interpeduncular cistern (dark blue) medially, the cerebellopontine cistern inferiorly, and the oculomotor cistern (green) inferomedially. The posterior ambient cistern (light blue) borders the cerebellomesencephalic cistern inferiorly and the quadrigeminal cistern (purple) posteromedially. Car. = carotid; Chiasm. = chiasmatic; Interped. = interpeduncular.

Source: Qi et al. (2011).

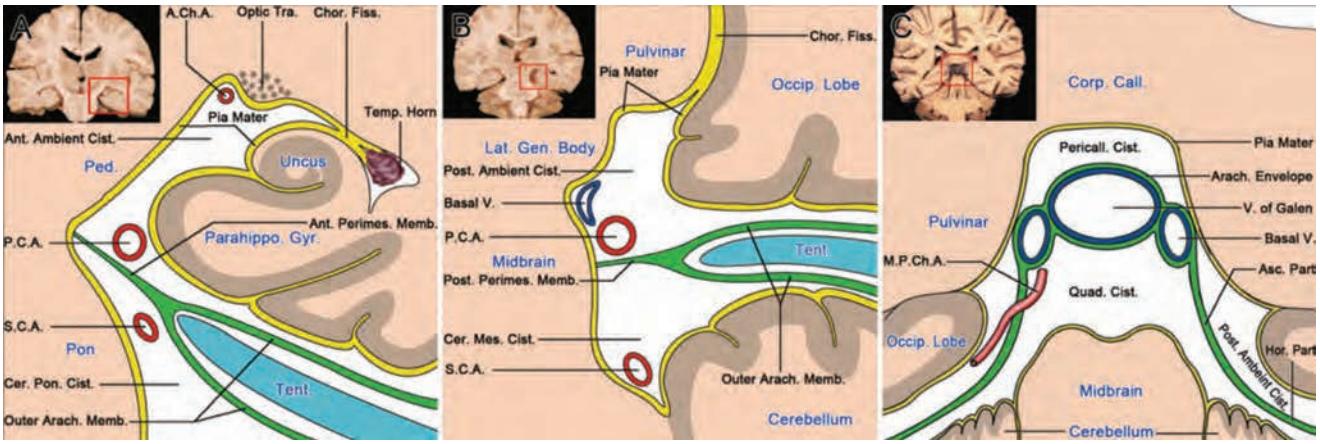

Figure 80.5 A–C: Coronal schematic diagrams of the anterior and posterior ambient cisterns. A: Anterior ambient cistern. Its superior wall is formed by the pial layers covering the lateral surface of the peduncle, optic tract, and uncus, which merge to form a reflection before entering the choroid fissure. The inferior wall is formed by the anterior perimesencephalic membrane, the medial wall by the lateral surface of the peduncle, and the lateral wall by the parahippocampal gyrus. The anterior ambient cistern is separated from the cerebellopontine cistern inferiorly by the lateral part of the anterior perimesencephalic membrane. B and C: Posterior ambient cistern. Its superior wall is formed by the pial convergence of the midbrain tegmentum, the lateral geniculate body, and the medial occipital lobe. The inferior wall is formed by the posterior perimesencephalic membrane, the medial wall by the upper midbrain tegmentum, and the lateral wall by the medial occipital lobe. The posterior ambient cistern borders the cerebellomesencephalic cistern inferiorly through the horizontal part of the posterior perimesencephalic membrane and the quadrigeminal cistern medially by the ascending part. The medial posterior choroidal artery (PChA) usually passes through the ascending part and enters the quadrigeminal cistern. P.C.A. = posterior cerebral artery; S.C.A: superior cerebellar artery; A.Ch. A: anterior choroidal artery; Call. = callosum; Cer. Mes. = cerebellomesencephalic; Cer. Pon. = cerebellopontine; Chor. = choroidal; Corp. = corpus; Fiss. = fissure; Gen. = geniculate; Gyr. = gyrus; Parahippo. = parahippocampal; Pericall. = pericallosal; Quad. = quadrigeminal; Tra. = tract.

Source: Qi et al. (2011).

Crural cistern

The crural cistern was considered by Qi et al. (2011a) as part of the anterior ambient cistern rather than a separate cistern. This is because there is no definite border or separation between them except for infrequent sparse arachnoid trabeculae (Qi et al. 2011a). It is occasionally divided into upper and lower parts by an intracrural membrane, extending between the posterior segment of the uncus and the cerebral peduncle (Inoue et al. 2009).

Prepontine cistern

The lower part of the anterior pontine membrane is occasionally absent, and in such cases the anterior inferior cerebellar artery exits the prepontine cistern to the cerebellopontine cistern by passing below (rather than through) the anterior pontine membrane (Matsuno et al. 1988).

Cerebellomedullary cistern (cisterna magna)

The cistern magna has a variable expansion dorsally (behind the vermis) depending on the degree of development of the falx cerebelli. It usually ends near the lobulus pyramis of the vermis but can extend all the way up the tentorium, mainly in cases of absent or small falx cerebelli (Yaşargil 1984; Matsuno et al. 1988).

Occasionally, a median arachnoid sheet divides the cistern into two sagittal compartments. Another two paramedian sheets can extend into the dorsal spinal subarachnoid space, dividing it into separate compartments (Yaşargil 1984).

Arachnoid trabeculae

The arachnoid fibers and trabeculae that bridge the subarachnoid space and basilar cisterns usually have fine structures. Nevertheless, they tend to be thicker and tougher where the arteries and nerves pass through the trabeculated wall from one cisternal compartment to another. In most individuals, the three cisterns in which the arachnoid trabeculae and membranes are densest and present the greatest obstacles during operations are the interpeduncular and quadrigeminal cisterns and the cisterna magna (Matsuno et al. 1988).

Variable arachnoid trabeculae that differ in their strength and density are also seen in other subarachnoid cisterns and elsewhere in the subarachnoid space. They usually enclose small blood vessels and adhere to the surface of larger blood vessels and nerves in the subarachnoid space (Yaşargil 1984).

Arachnoid membranes

The arachnoid membranes vary greatly in appearance and configuration. Some are reticulated and porous, such as the basilar artery bifurcation membrane; some are intact and dense without foramina, such as the diencephalic leaf of Liliequist's membrane; and others are plexiform or band-shaped or cord-shaped, such as the anterior cerebral membrane and

the anterior choroidal membrane. Some trabecular arachnoid membranes differ in appearance and configuration among specimens, such as the basilar artery bifurcation membrane, which may be intact, porous, and sparse, or porous and dense (Lu and Zhu 2005b).

Arachnoid Liliequist membrane

The membrane that is today known as Liliequist's membrane (LM) was first described and illustrated by Key and Retzius (1875). In his pneumoencephalographic studies of the subarachnoid space and cisterns, Liliequist (1956, 1959) provided the first detailed anatomical description of this membrane, which was subsequently named after him. With the advance of neuroendoscopic and microscopic techniques, interest in studying the LM and other subarachnoid membranes and cisterns increased again, pioneered by Yaşargil's studies (Yaşargil et al. 1976). It was reported that failure to open the LM during third ventriculostomy could result in failure of the procedure (Buxton et al. 1998), which further increased the importance of identifying this membrane. However, since the earliest descriptions, controversy regarding the structure of the LM has continued. We therefore provide a detailed review of the various descriptions of it, including variations.

Presence of LM

The LM is found in most individuals, mainly separating the interpeduncular, prepontine, and chiasmatic cisterns. However, it was reported to be absent in 2 out of 13 cadavers (15.4%) studied by Froelich et al. (2008), and in 15 out of 35 cadavers (43%) studied by Zhang and An (2000). In such cases, free communication among the interpeduncular, prepontine, and chiasmatic cistern is expected, forming one large cistern. A carotid-interpeduncular wall separating the interpeduncular and carotid cisterns was added by Brasil and Schneider (1993), which can be absent unilaterally or bilaterally. However, this seems to contradict the description of Froelich et al. (2008), who stated that the interpeduncular cistern communicates anterolaterally with the carotid cistern along the posterior communicating artery. These authors added that in cases of single LM (see "Single membrane" below), the prepontine cistern can communicate with the carotid cistern anterolaterally around the posterolateral free border of the LM, and with the ambient cistern laterally along the course of the posterior cerebral artery and across the posterolateral free border of the LM (Froelich et al. 2008). Moreover, Brasil and Schneider (1993) described free communication between the carotid and crural cisterns superolateral to the free margin of the LM. Matsuno et al. (1988) also reported communication with the ambient and crural cisterns.

Types of LM

On the basis of the various descriptions, the LM has been divided into three types. In type A it is composed of two leaves, diencephalic (DL) and mesencephalic (ML), which originate at the dorsum sellae. In type B it appears as one leaf anteriorly and two leaves posteriorly, the LM arising as a single membrane and then splitting into DL and ML. In type C, the most common, the LM appears as a single (diencepahlic) membrane (Froelich et al. 2008) (Fig. 80.6).

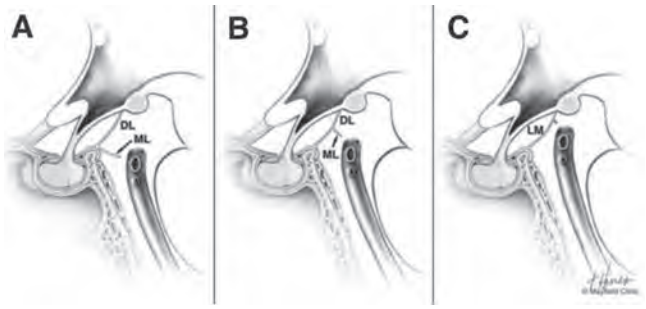

Figure 80.6 variations of Liliequist's membrane (LM). A, the diencephalic leaf (DL) and mesencephalic leaf (ML) originate along the dorsum sellae and course separately toward the diencephalon and basilar bifurcation, respectively. B, with two posterior leaves including the diencephalic leaf attached to the diencephalon and mesencephalic leaf toward the basilar bifurcation. C, as a single membrane attached posterosuperiorly to the diencephalon between the infundibulum and mamillary bodies.

Source: Froelich et al. (2008).

Single membrane (Type C)

The classic description by Liliequist (1956, 1959) was of a single membrane with forward convexity, extending from the dorsum sellae to the anterior edge of the mamillary bodies (Type C). Brasil and Schneider (1993) gave a similar description. Yaşargil (1984) and Yaşargil et al. (1976) added that this well-developed membrane stretches like a curtain from one mesial temporal surface to another. A full description of the type C LM would therefore be of a single, non-fenestrated membrane that arises inferiorly from the basilar arachnoid membrane, covering the dorsum sellae and the posterior clinoid processes, curving anteriorly and attaching superiorly to the pia of the hypothalamus just anterior the mamillary bodies, posterior to the infundibulum. Laterally, it attaches to the pia of the mesial surface of the temporal uncus (Vinas and Panigrahi 2001). This lateral extension (at the carotid-interpeduncular wall) is perforated by the oculomotor nerve and the posterior communicating artery (Brasil and Schneider 1993).

Lateral extension

Other authors disagree on the extent of the lateral extension. Epstein (1965) described the LM as a semilunar transverse membrane stretching obliquely between the oculomotor nerves, which is similar to the description by Matsuno et al. (1988). Such a termination would render the LM a continuous, unperforated membrane. On the other hand, Fox (1989) accepted both types of lateral extension and added that it can also end just before (medial to) the oculomotor nerve, to which it is then connected via arachnoid trabeculae. Similar results were reported by Anik

et al. (2011) and Fushimi et al. (2003). Froelich et al. (2008) described the different relationships with the oculomotor nerve. In 6 out of 13 specimens (46%) the nerve was surrounded by the lateral aspect of the ML, creating a separate oculomotor cistern. In two specimens (15.4%) it ran between two lateral leaves of the ML. The superior leaf was attached to the pia of the mesial surface of the temporal lobe, and the inferior leaf was continuous with the arachnoid above and below the level of the incisura. In three specimens (23%) the nerve was above the mesencephalic leaf and connected to it by an arachnoidal ring (Froelich et al. 2008). Zhang et al. (2012) agreed that the ventral wall of the oculomotor cistern is partly formed by the lateral extension of the LM (and partly by the basal arachnoid mater), but they regarded the dorsal membrane (oculomotor membrane) as a different entity and differentiated it from the temporal membrane, which they described as the lateral extension of the DL (Zhang et al. 2012).

Superior extension

Regarding its superior attachment, Vinas and Panigrahi (2001) added that as well as the premamillary attachment described above there can also be a retromamillary attachment. This is surgically important, as in these patients it is less important to fenestrate the LM during third ventriculostomy because the third ventricle will be opened into the interpeduncular cistern following fenestration of the floor (Vinas and Panigrahi 2001). Similar findings were also described by Matsuno et al. (1988) regarding the attachment of the DL. Inoue et al. (2009) also reported both types of superior attachments of the DL; they found that it was attached to the posterior edge of the mamillary bodies (retromamillary) in 47% of brains, the apex of the mamillary bodies in 33%, and the anterior edge of the mamillary bodies (premamillary) in 20%. On the other hand, Anik et al. (2011) reported that direct attachment to the mamillary bodies was the most common type, found in 17 out of 24 specimens (70.8%). Lu and Zhu (2003) described a more anterior superior-attachment of the DL on the posterior surface of the infundibulum all over its course, found in four out of eight cadavers (50%). In the other four (50%) the DL had a superior attachment that was 1.96–4.92 mm posterior to the infundibulum (premamillary) (Lu and Zhu 2003).

Free border

Brasil and Schneider (1993) divided the single LM into three parts (or walls) on the basis of its cisternal relationships: two carotid-interpeduncular walls laterally and a chiasmatic-interpeduncular wall medially. Each of these walls could be selectively absent. They also added that, besides its classic superior attachment, the LM attaches to the pia of the inferior surface of the optic tracts. There is a free margin between the inferolateral border of the optic tracts and the uncus. Superolateral to this free margin there is free communication between the carotid and crural cisterns (Brasil and Schneider 1993). The same free margin was also reported by Lu and Zhu (2003) in the DL of the LM. On the other hand, Zhang et al. (2012) observed this free lateral border of the DL between the inferolateral border of the optic tracts and the oculomotor sheath in only 4 out of 24 specimens (16.7%; Zhang et al. 2012).

Agreeing about the lateral extension of the LM, Epstein (1965) and Fox (1989) described the presence of free border lateral to or at (medial to) the oculomotor nerve, respectively. Froelich et al. (2008) described the free border as located posterolaterally between the central attachment to the diencephalon and tentorial edge in type C and in the DL of types A and B, and at the posterior end of the ML in front of the basilar bifurcation in types A and B. Zhang and An (2000) claimed that the free border of the LM is located on its superoposterior part. All these authors agree that the free border becomes attached to the surrounding structures via arachnoid trabeculae. With some exceptions, these trabeculae are not considered part of the LM; they also render it otiose to identify the border of an irregular arachnoid trabecular network because it varies greatly and could be the cause of variations in gross anatomical findings. This was also supported by the findings of Anik et al. (2011), who claimed that various free edges were found in the ML in 7 out of 24 specimens (29.2%) while it was totally closed in 12 (50%).

The carotid-chiasmatic walls

Brasil and Schneider (1993) contradicted the previous descriptions by Epstein (1965), Fox (1989), and Yaşargil (1984), indicating that the LM can surround the infundibulum to create a "hypophyseal cistern." They suggested that these surrounding membranes represent the carotid-chiasmatic walls (or chiasmatic membrane) and added that the LM is always located posterior to the infundibulum (Brasil and Schneider 1993). The same description was offered by Vinas and Panigrahi (2001) who added that, although the chiasmatic membranes arise from the LM, they represent a different entity.

These controversies were further clarified by Zhang and An (2000). Using a modified E12 sheet plastination method, cadaveric dissections, and electron microscopy, these authors concluded that the arachnoid membrane-like LM has an architecture significantly different from that of the arachnoid trabeculated carotid-chiasmatic walls. The LM appears thicker, unperforated, and with a cleaner surface, and is composed of two layers of arachnoid mater (presumed to be the DL and ML described in other studies) that are better visualized in the middle portion. However, no double layers could be found in 15 out of 35 cadavers (43%). On the other hand, the carotid-chiasmatic walls are composed of accumulated, irregularly oriented arachnoid trabeculae that extend from the LM to the pia mater covering the surface of the optic chiasm. Unlike the LM, these walls have openings of various sizes and are penetrated by perforating arteries from the posterior communicating and internal carotid arteries, giving them a vascularized appearance. This is surgically important as it suggests that the most suitable site for opening the LM and approaching the interpeduncular cistern is

the part of the LM between the carotid-chiasmatic wall and the oculomotor nerve (Zhang and An 2000), with careful attention to the posterior communicating artery and its branches (Lu and Zhu 2003).

Regarding the lateral extension and free border, Zhang and An (2000) stated that the free border of the LM is located on its superoposterior part and continues along the entire length, and can be grossly visualized. At this free border, the LM is connected via arachnoid trabeculae to the surrounding structures including the infundibulum and mamillary bodies. Laterally, it attaches to neither the uncus nor the oculomotor nerve. Instead, it fans out near the free edge of the tentorium and continues with the arachnoid mater covering the tentorium below and above the tentorial notch. Zhang and An (2000) did not comment on the anterior attachment of the LM, but regarded the membrane as continuous anteroinferiorly with the arachnoid mater covering the tentorium, the dorsum sellae, and the clivus (Fig. 80.7).

Double membranes (Types A, B)

The LM was first described as double membranes by Matsuno et al. (1988). Other authors including Inoue et al. (2009) have given similar descriptions. The classic description is of an arachnoid membrane arising from the arachnoid covering of the dorsum sellae and the posterior clinoid processes (some also add the arachnoid covering of the posterior petroclinoid and adjacent tentorial edge; Froelich et al. 2008), extending between the oculomotor nerve and then splitting into two leaves, the DL and ML (type B). According to these authors, the previous description of a single membrane by Liliequist was of the DL; this can be visualized by the pneumatograph due to its unperforated nature, in contrast to the perforated ML (see section "The mesencephalic" below) which was visualized in later cadaveric studies (Matsuno et al. 1988) (Fig. 80.8).

The diencephalic

The DL is a thicker and mostly unperforated membrane that attaches to the posterior or anterior edge or to the tips of the mamillary bodies, separating the interpeduncular and chiasmatic cisterns. At its superior end, the DL sends many arachnoid trabeculae to attach to the surrounding structures, including the infundibulum and mamillary bodies (Matsuno et al. 1988; Froelich et al. 2008; Inoue et al. 2009). The DL is thick in most cases (54%: Anik et al. 2011; 75%: Lu and Zhu 2003), but can be thin (25%: Lu and Zhu 2003; 46%: Anik et al. 2011). It is also mostly semitransparent (83.3%: Anik et al. 2011; 87.5%: Lu and Zhu 2003) but can be opaque (12.5%: Lu and Zhu 2003; 16.7%: Anik et al. 2011). It can also be a largely porous trabeculated membrane (Wang et al. 2011b; Zhang et al. 2012), and in these cases it may have only a small crescent-shaped dense non-porous part in its anteroinferior attachments (Zhang et al. 2012). The Dl was reported to be absent in 3 out of 24 cadavers (12.5%) by Anik et al. (2011), 6 out of 24 cadavers (25%) by Zhang et al. (2012), and 5 out of 15 cadavers (26.7%) by Wang et al. (2011b). In these cases, the chiasmatic and interpeduncular cisterns merge into one (Wang et al. 2011b).

As expected from the description of an unperforated DL, the lateral attachment of the LM is related to the arachnoid sheath surrounding the oculomotor nerve, with numerous trabeculae extending from the oculomotor nerve to the uncus and tentorium (Matsuno et al. 1988; Inoue et al. 2009). Lu and Zhu (2003) reported a case with a unilateral window in the DL connecting the posterior communicating cistern with the interpeduncular cistern (Lu and Zhu 2003).

The length of the DL from the inferior to the superior edge is within the range 5.0–13.0 mm (mean 10.8 mm). The width at the inferior edge is 10.0–28 mm (mean 19.9 mm), and the width at the superior edge is 5.0–14.0 mm (mean 9.5 mm) (Wang et al. 2011b).

The mesencephalic

The ML is a thinner membrane, mostly perforated (by the basilar artery), that extends backward and attaches to the pontomesencephalic junction, separating the interpeduncular and prepontine cisterns (Matsuno et al. 1988; Froelich et al. 2008; Inoue et al. 2009). Lu and Zhu (2003) described a different course and termination of the ML (see below). Other authors have reported a free posterior border of the ML connected to the basilar bifurcation and surrounding structures by arachnoid trabeculae (Froelich et al. 2008). Occasionally, the ML is thick (or equal in thickness to the DL) and has small perforations. It can also form a tight cuff around the basilar artery, but more commonly it has a large opening through which the basilar artery ascends (Matsuno et al. 1988; Inoue et al. 2009).

The length of the ML from the anterior to the posterior end is over the range 2.5–10.8 mm (mean 4.8 mm). The width at its posterior attachment is 2.5–10.8 mm (mean 4.8 mm). In cases of type A LM, the width of the anterior edge of the ML is similar to that of the inferior edge of the DL. In cases of type B, the width of the anterior edge of the ML is 3.0–22.0 mm (mean 12.6 mm; Wang et al. 2011b).

Findings of Froelich et al.

In the cadaveric study of Froelich et al. (2008), the LM was identified in 11 out of 13 cadavers (85%). When present, it consisted of either one leaf (type C, most common) or two leaves (type A, B). Type A was found in two specimens (15.4%) and, in addition to the classic description, the authors reported a lateral attachment of the DL to the paramedian perforating substance and of the ML to the pia of the parahippocampal gyri (mesial surface of the temporal lobe). Type B was also found in two specimens (15.4%) where the LM arose as a single membrane and then split into two leaves, DL and ML, with connections similar to those in type A. The authors described the free borders of these two types as located in the posterior end of the ML, in front of the basilar bifurcation, but occasionally covering part of the basilar tip. Type C was found in seven specimens (53.8%), with a posterolaterally located free

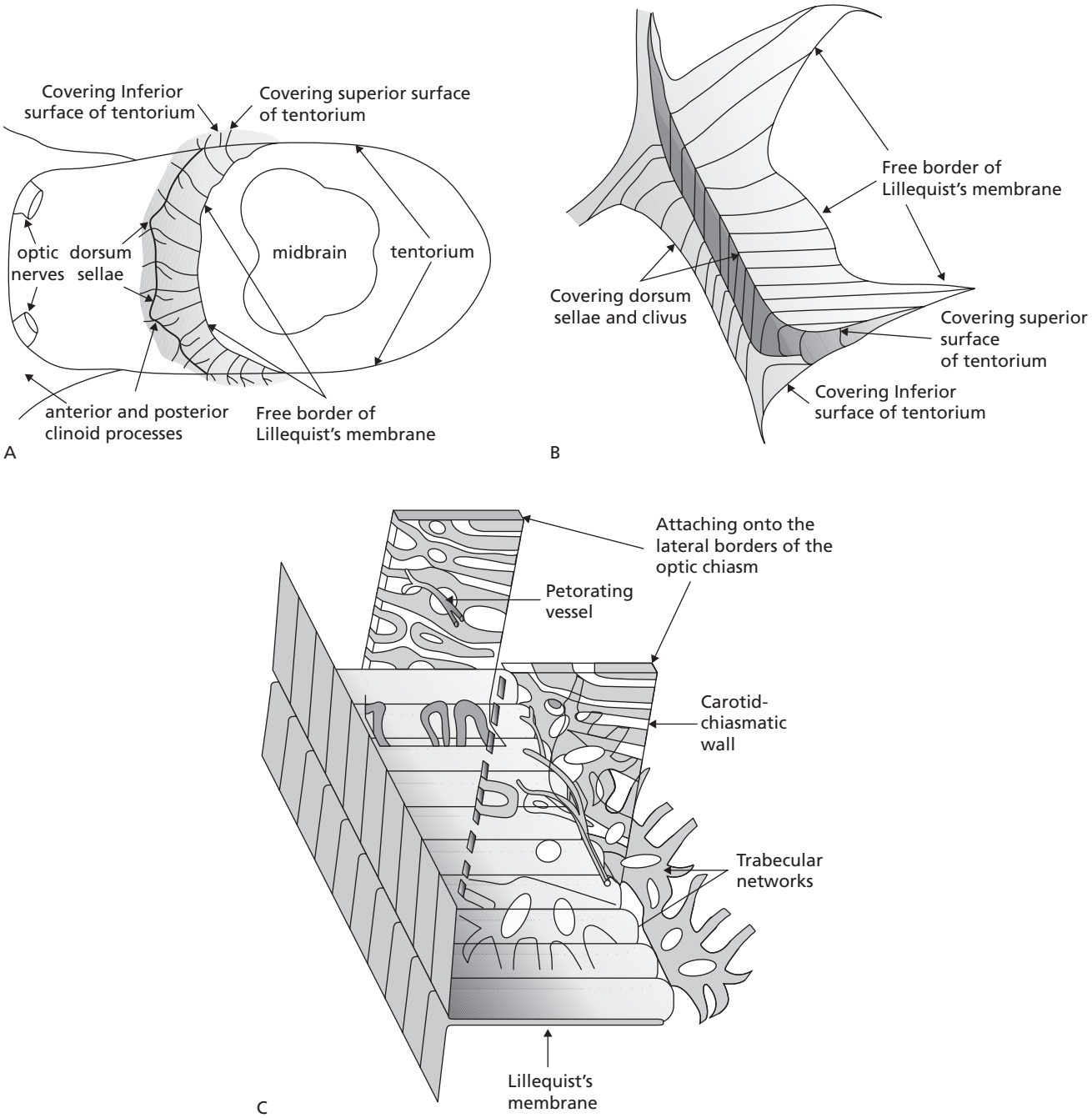

Figure 80.7 Major arachnoid trabeculae within the subarachnoid cisterns. (a) Superior view of the sellar area and tentorial notch. The shaded area represents Liliequist's membrane and its anteroinferior and lateral attachments. (b) Diagrammatic representation of Liliequist's membrane. The free border surrounds the anterior aspect of the brainstem and extends posteriorly to the roots of the trigeminal nerves. (c) Relationship between Liliequist's membrane and the carotidchiasmatic walls. The carotid-chiasmatic walls are arachnoid trabecular networks that continue with loose and irregular arachnoid trabecular networks on the surface and along the free border of Liliequist's membrane.

Source: Zhang and An (2000).

border between the central diencephalic attachment and the tentorial edge. This free border allowed the prepontine and carotid cisterns to communicate with each other (Froelich et al. 2008).

The authors added that the LM is continuous with the arachnoid covering the temporal fossa floor and the superior aspect of the tentorium, above the tentorial edge. Below the tentorial edge the membrane was continuous with the arachnoid

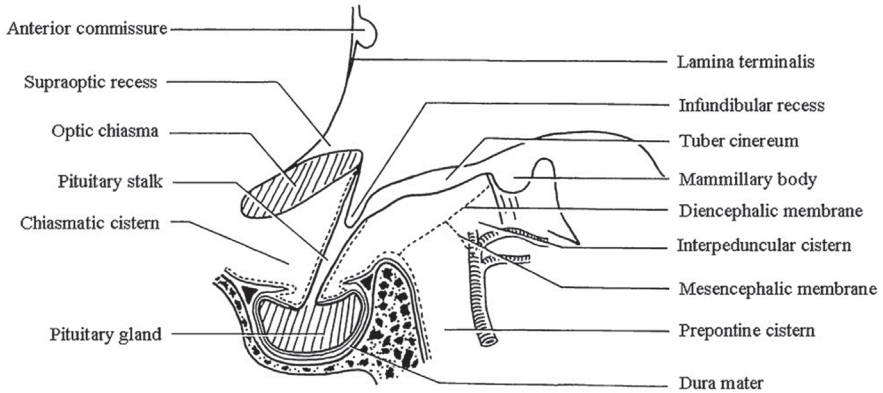

Figure 80.8 Side view of Liliequist's membrane.

Source: Wang et al. (2011b).

covering the inferior aspect of the tentorium and posterior fossa dura (Froelich et al. 2008). They also agreed with other authors that the LM is continuous laterally with the lateral pontomesencephalic membrane (Matsuno et al. 1988), which separates the ambient cistern from the cerebellopontine cistern, and with the caudal oculomotor membrane (Vinas et al. 1994, 1996a, b), as they share a common embryological origin (Froelich et al. 2008).

Relation with the posterior communicating artery

Froelich et al. (2008) also described the different relationships of the LM with the posterior communicating artery. In specimens with a single membrane (type C) and a posterolateral free border, the posterior communicating artery coursed above the membrane and crossed the free border to join the posterior cerebral artery. In specimens with a DL and ML, the artery coursed between those leaves (Froelich et al. 2008) (Fig. 80.9). Zhang et al. (2012) stated that, in all cases, the posterior communicating artery courses lateral to the lateral border of the DL. On the other hand, Lu and Zhu (2003) stated that the artery penetrates the DL to enter the interpeduncular cistern. They also reported one specimen where a unilateral posterior communicating artery penetrated the DL at its inferior border, coursed within the leaf, and left via the superior border to enter the deep part of the interpeduncular cistern (Lu and Zhu 2003).

Zhang et al. (2012) found the LM to be composed of two layers of arachnoid mater, named the basal and attaching layers; this was similar to the description by Zhang and An (2000). The basal layer arises from the basal arachnoid mater covering the dorsum sellae and posterior clinoid processes, which multiplies into several cellular layers at the basal attachments of the LM, then extends superoposteriorly and folds upon itself to form the uninterrupted basal layer of the LM. This basal layer extends as the inferior part of the DL (no comments were made on the ML) and extends laterally beyond the oculomotor nerve to continue with the arachnoid mater covering the tentorium below and above the tentorial notch. In the midsagittal plane, the basal part constituted more than half the entire length of the LM in two out of four specimens (50%) and less than 20% of the length in one (25%). The attaching layer spreads from the posterior border of the basal layer to attach on the surrounding structures. The diencephalic part of this layer (attaching the DL to the mamillary bodies) is composed of accumulated arachnoid trabeculae. In contrast to previous studies (see above), Zhang et al. (2012) therefore considered these arachnoid trabeculae as a part of the LM.

Regarding the gross lateral extension, Zhang et al. (2012) described a triangular membrane, found in 14 out of 24 specimens (58.3%), that spread from the lateral free border of the diencephalic membrane to the mesial temporal uncus. They termed it the temporal membrane and considered it to be part of the DL. This membrane separates the carotid from the ambient cistern and sends variable arachnoid trabeculae to attach to the

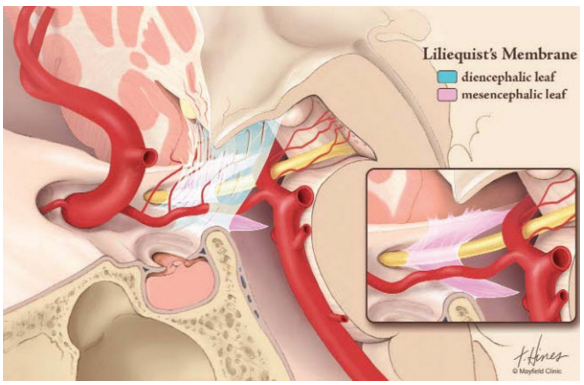

Figure 80.9 Three-dimensional illustration (sagittal cut, oblique view) of Liliequist's membrane composed of two separate diencephalic (aqua) and mesencephalic (pink) leaves that originate at the dorsum sellae (Type A). Note the posterior communicating artery coursing above the mesencephalic leaf. Inset, with removal of the diencephalic leaf, the mesencephalic leaf can be seen surrounding the oculomotor nerve and reflecting onto the tentorial edge.

Source: Froelich et al. (2008)..

arachnoid sheath surrounding the oculomotor nerve. In contrast to the DL, the temporal membrane is usually porous and trabeculated, and is occasionally sheet-like with small openings. When this membrane is present, the posterior communicating artery always courses above it (Zhang et al. 2012).

The ML was divided by Zhang et al. (2012) into three parts, one medial ML and two lateral ML. The medial ML extends between the oculomotor nerves and was referred to as the ML in previous studies, separating the interpeduncular and prepontine cisterns (Zhang et al. 2012). A similar division was used by Qi et al. (2011a), who also used the name "anterior perimesencephalic membrane" to describe the ML.

The relationships between the DL and the medial ML are the types described earlier as A, B, or C (the classical classification of the LM). However, Zhang et al. (2012) found type B to be the most common, followed by type A then C. When the DL is absent, the medial mesencephalic membrane is defined as the combination of an anteriorly located crescent-shaped dense non-porous part, which attaches to the basal arachnoid membrane (exactly the same as that of the DL) and courses between the oculomotor nerves (to which it attaches laterally), and a posteriorly located porous trabeculated part that extends to the caudal end of the medial ML (Zhang et al. 2012) (Fig. 80.10).

According to Zhang et al. (2012), regardless of the type of medial ML, its caudal end can be above, at, or below the level of the terminal basilar bifurcation. The lateral ML is equivalent to the lateral pontomesencehalic membrane. It separates the ambient and cerebellopontine cisterns and communicates medially with the DL and medial ML below the oculomotor nerve (the part of the LM that forms part of the ventral sheath of the oculomotor), and attaches to the anterior tentorial edge laterally. Anteriorly it attaches to the basal arachnoid mater covering the posterior border of the oculomotor trigone, and posteriorly it sends out variable arachnoid trabeculae to attach to the anterolateral pontomesencephalic junction. The size of the non-porous sheet-like portion of this membrane varies, and is inversely proportional to the non-porous sheet-like portion of the DL (or ML when the DL is absent). When the non-porous sheet-like part of the DL or ML is prominent the counterpart of the lateral ML is smaller, and vice versa (Zhang et al. 2012).

On the basis of these findings, Zhang et al. (2012) proposed another classification of the LM according to presence (type I) or absence (type II) of the DL. In type I, most common, the LM appears similar to that previously described as being divided into types A, B, and C. In type II only the medial and lateral ML are present, with a course similar to that described above and with no separation between the interpeduncular cistern and the chiasmatic cistern (Zhang et al. 2012).

Regarding the oculomotor membrane, Zhang et al. (2012) distinguished it from the temporal membrane and described three coronal configurations based on its relationship to the carotid membrane: inverted Y-shaped (most common); inverted V-shaped; and inverted U-shaped (least common). In the inverted Y-shaped configuration, the lateral carotid membrane constitutes the upper arm of the inverted Y and attaches superiorly on the mesial temporal uncus near the attachment of the temporal membrane. In the inverted V-shaped configuration, the lateral carotid membrane is absent and the apex of the inverted V attaches directly to the mesial temporal uncus near the attachment of the temporal membrane. In the inverted U-shaped configuration, the dome of the oculomotor membrane adheres to the dorsal surface of the oculomotor nerve and can be connected to the mesial temporal uncus by scattered arachnoid trabeculae, which represents a less well-developed lateral carotid membrane. According to the authors, the LM can attach to the mesial temporal uncus either directly by its temporal membrane or indirectly by the oculomotor membrane (Zhang et al. 2012).

Triple membranes

Diencephalic-mesencephalic membrane (DML)

The LM was first described as comprising three leaves by Lu and Zhu (2003). These leaves were the DL, ML, and the diencephalic-mesencephalic leaf (DML). These authors described the ML (but not the DL) differently from others. In their study of eight cadavers, Lu and Zhu stated that the ML represents an intact, thick, dense, and unperforated membrane that forms the anterioinferior wall of the interpeduncular cistern. According to them, the ML intersects with the DL at the dorsum sellae and posterior clinoid processes rather than originating from this point. Rostrally, it spreads along the surface of the diaphragma sellae and attaches to the posterior surface of the infundibulum, 1.48–3.98 mm above its inferior bottom, and fuses with the basal chiasmatic membrane (the arachnoid covering the floor of the chiasmatic cistern). In most cases (seven out of eight specimens) the ML was totally above the diaphragma sellae and did not enter the intrasellar region. In

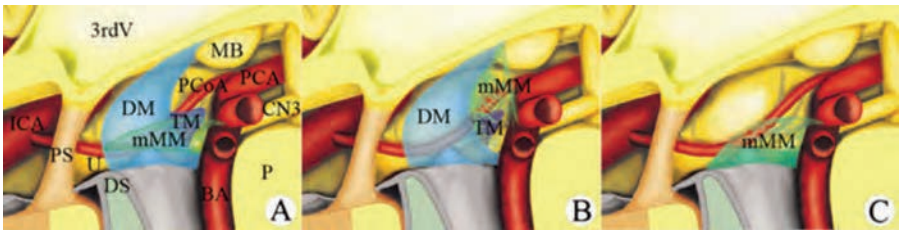

Figure 80.10 Schematic drawing of (a, b) type I and (c) type II of Liliequist's membrane.

Source: Zhang et al. (2012).

the remaining specimen it turned downward around the infundibulum through the opening of the diaphragma sellae along with the chiasmatic membrane to encircle the pituitary gland. Caudally, the ML ends at the junction of the superior one-third and the inferior two-thirds of the basilar artery or the midpoint of the basilar artery and the ventral surface of the pons at this level; in contrast to the classical description, it does not attach to the pons directly or form a cuff around the basilar artery, but only parallels the anterior wall of the basilar artery and the ventral surface of the pons. The authors added that it is not the ML but the medial pontomesencephalic membrane that separates the interpeduncular and prepontine cisterns and is penetrated by the basilar artery. This medial pontomesencephalic membrane was also found to join the ML to the pons in most cases (seven out of eight specimens), but the ML had a free posterior border in the remaining specimen, similar to that described by Froelich et al. Laterally, the ML attaches to the mesial surface of the temporal lobe but also encircles the oculomotor nerve for variable distance (2.72–4.98 mm) through the cavernous sinus (Lu and Zhu 2003).

Anik et al. (2011), who regarded the LM as a single, double, or triple membrane, gave an almost similar description but considered that the posterior end of the ML to the basilar bifurcation could also course toward the vertebrobasilar junction through the prepontine cistern. They also reported one specimen in which two ML were identified, one splitting from the anterior portion and attached to the basilar artery at the level of the vertebral artery bifurcation, and the other splitting from the posterior portion of the LM and attached to the basilar artery bifurcation. However, they did not comment on the anterior extension of ML described by Lu and Zhu, but considered the ML to be in direct continuation anteriorly with the basal arachnoid membrane (Anik et al. 2011). In contrast, Fushimi et al. (2003) recognized the anterior extension as a distinct part of the LM, named the sellar part. This part could be identified in most cases, but sometimes could not be visualized.

In the study by Anik et al. (2011), the ML continues caudally as the medial and lateral pontomesencephalic membrane. The medial pontomesencephalic membrane (MPMM) courses anterolaterally, medial to the trigeminal and abducens nerves. The lateral pontomesencephalic membrane (LPMM) courses posterolaterally, lateral to the trigeminal and abducens nerves. Both membranes are connected between these two nerves. The LPMM joins the formation of a ring that covers the third nerve, attaching to the DL on the distal posterior surface of the nerve and to the mesial temporal surface coursing lateral to the uncus. Both the MPMM and LMPMM continue inferiorly as the medial and lateral pontomedullary membranes respectively. They continue as a single membrane through the prepontine and premedullary areas as the prepontine and premedullary membranes, respectively. They attach to the dura covering the superior aspects of the cranial nerves laterally (Anik et al. 2011). According to Matsuno et al. (1988) and Lu and Zhu (2007), the medial pontomedullary membrane is located at the medial part of the pontomedullary sulcus and separates the prepontine and premedullary cisterns, and the lateral pontomedullary membrane is located at the lateral pontomedullary sulcus and separates the cerebellopontine and cerebellomedullary cisterns.

The DML is a pair of parallel leaflets connecting the DL to the ML. It represents a triangular or quadrilateral membrane that is dense and intact in most cases (seven out of eight specimens) but can also be composed of sparse networks (Lu and Zhu 2003). In the study of Anik et al. (2011) the DML was not consistently present but was seen in 17 out of 24 specimens (70.8%). The DML is located ventral to the cerebral peduncles and medial to the oculomotor nerves, separating the interpeduncular and oculomotor cisterns; along with the other LM leaves it participates in the formation of the oculomotor sheath. It attaches to the DL anterosuperiorly, the lateral margin of the mamillary bodies superiorly, the ML anteroinferiorly, the medial or lateral pontomesencephalic membranes inferiorly (representing the direct continuation of the ML), and has a free posterior border (between the attachment to the lateral margin of the mamillary body and the attachment to the ML). The space between the posterior margin of the DML and the cerebral peduncles allow the interpeduncular cistern to communicate with the crural and ambient cisterns. The authors stated that absence of the DML in previous studies is probably due to this leaf being fragile, thin, and easily destroyed. They stated that it is often overlooked or described as arachnoid trabeculae joining the LM to the oculomotor nerves (Lu and Zhu 2003).

Hypothalamic membrane

In their study of 15 cadavers, Wang et al. (2011b) divided the LM into three parts (or leaflets): the DL, ML, and hypothalamic leaflets. Beside the previously described superior attachment of the DL, Wang et al. added that it can be attached to the anterior, middle, or posterior edge of the tuber cinereum. Laterally, it attaches to the oculomotor nerve and is continued with the inferior oculomotor sheath. Between the superior attachment and the oculomotor nerve, a free border forms a cuff around the posterior cerebral artery. The authors also found that the posterior communicating artery only rarely penetrates the DL, as a small branch of the basilar artery can also do. Many arachnoid trabeculae were also found extending from the DL to the posterior communicating and posterior cerebral arteries and from the superior end of the DL to the surrounding structures (Wang et al. 2011b).

Similar to the findings of Matsuno et al. (1988), the ML in the study of Wang et al. (2011b) extended to the pontomesencephalic junction but could also reach up to 5.0 mm (mean 2.5 mm) above the junction. Beside the classical A and B types of ML origin, the authors reported the ML arising from the hypothalamic leaflet (HL) in 3 out of 15 specimens (20%) and having a free anterior edge in one (6.7%). The lateral attachment of the ML was mostly to the oculomotor sheath, but was also occasionally seen with the posterior cerebral arteries or the superior

cerebellar arteries. Free lateral borders were also observed in some specimens. Many arachnoid trabeculae were also found extending from the ML to the surrounding neurovascular structures (Wang et al. 2011b).

Between the sellar segment of the DL, the anterior part of the ML, and the posterior part of the superior clivus, a space could be found anteroinferior to the interpeduncular cistern; Wang et al. (2011b) called this the post-dorsum cistern. There is no arachnoid mater separating the post-dorsum from the prepontine cistern; when the DL is absent, all the space beneath the ML becomes the prepontine cistern and the ML constitutes its superior wall (Wang et al. 2011b).

The HL described by Wang et al. (2011b) were pairs of triangular or quadrangle membranes that extend upwards from the oculomotor nerve and/or the lateral part of the DL (or ML) to attach to the lateral edge of the hypothalamus. In most cases, these membranes were thin and trabeculated, with many scattered holes. Only rarely did they develop into complete net-like shapes. In two specimens with absent DL, the HL was developed so well that it seemed to replace the DL. Inferiorly, each HL is mostly attached to the superomedial or inferomedial edge of the oculomotor nerve. They can also be attached to superior wall of the oculomotor nerve sheath, the lateral part of the DL, or the lateral part of the ML (when the DL is absent). The HL can extend laterally above the oculomotor nerve attaching to the temporal lobe, with an attaching line ranging from 1.5 to 8 mm. Inferoanteriorly, it is attached to the arachnoid membrane covering the diaphragma sellae, the dorsum sellae, or the superior wall of the cavernous sinus by some fibrous trabeculae. Superiorly, it attaches mostly to the inferolateral surface or the lateral edge of the tuber cinereum. It can also attach to the lateral edge of the median eminence area or the side of the infundibulum, the paramedian area below the optic chiasm/tract, or extend to the inferolateral surface of the mamillary bodies. The length of the superior edge falls within the range 6–20 mm (mean 10 mm), and the distance between the upper attaching edges is 2–8 mm. The anterior edge of the HL is mostly attached to the dorsum sellae or the posterior clinoid process. It can also be continuous with the carotid–chiasmatic walls (which indicates that they represent distinct structures), connected to the fibrous trabecular network in the chiasmatic cistern, attached to the anterior edge of the DL or ML, or completely free. Mostly, the posterior edge adheres in multiple places to the posterior communicating artery or its branches, which course through the HL to supply the tuber cinereum and the mamillary bodies. It can also be completely free, surrounding the posterior cerebral artery in a cuff-like shape and connected via arachnoid trabeculae to the tuber cinereum, the mamillary bodies, or the cerebral peduncle. Like the DL and ML, the HL can also send many arachnoid trabeculae to the surrounding structures, including the posterior cerebral artery or its branches. It was also found to separate the superolaterally located posterior communicating cistern from the interpeduncular cistern (Wang et al. 2011b).

Arachnoid membranes over the pineal region

In contrast to Lu and Zhu (2005b), who described the arachnoid envelope over the pineal region (AEPG) as being formed by the cerebellar precentral membrane (CPM), Qi et al. (2011b) believed that this membranous covering of the vein of Galen and surrounding structures (forming a closed, non-communicating compartment) is formed by the confluence of the supratentorial and infratentorial outer arachnoid membranes at the tentorial apex. They added that the CPM, which is a trabecular arachnoid membrane separating the quadrigeminal from the supracerebellar cistern, has part of its superior attachments on the ventral surface of the posterior AEPG but does not envelope the vein of Galen. The other difference from the description of Lu and Zhu (2005b) was that the AEPG does not end at the origin of the vein of Galen but extends anteriorly to enclose the suprapineal recess, and can also enclose the pineal gland and distal segment of the internal cerebral veins (Qi et al. 2011b).

The AEPG is divided into two parts by a perpendicular plane crossing the origin of the vein of Galen: a tuciform posterior part envelopes the vein of Galen and the terminal segments of its tributaries, and the trumpet- or funnel-shaped anterior part envelopes the suprapineal recess, the pineal gland, and the distal segments of the internal cerebral veins. Occasionally, a significant prominent suprapineal recess extends into the posterior AEPG over the vein of Galen. In these cases, the arachnoid cuff may be enlarged, and through it the tip of the suprapineal recess can protrude out of the posterior AEPG and reach the tentorial apex (Qi et al. 2011b).

The posterior AEPG

As viewed laterally, the posterior end of the posterior AEPG, also called the arachnoid cuff, is divided into two types according to its relationship with the tentorial dura mater overlying the posterior end of the vein of Galen, to which it attaches. In type I, the arachnoid cuff is totally covered by the tentorium, and the posterior segment of the vein of Galen cannot be seen because of the overlapping of the arachnoid envelope and dural coverage. In type II, more common, a crescent-shaped segment of the vein of Galen can be seen between the tentorial edge and the arachnoid cuff as a result of the forward convexity of the lateral edges of the arachnoid cuff (Qi et al. 2011b).

Below the junction of the vein of Galen and the straight sinus, the arachnoid membrane at the ventral edge of the arachnoid cuff becomes thickened with marked variations, forming intrasinus arachnoid structures. In most cases, oval or round nodular arachnoid clusters (or granulations) bulge into the inferior wall of the vein of Galen, narrowing its lumen. In other cases, similar structures can be incorporated into the venous wall at the junction of the vein of Galen, rather than protruding into the lumen. Least commonly, the thickened membrane causes gentle elevation without compressing the vein of Galen, and no changes in the vein of Galen and its junction can be seen (Qi et al. 2011b).

The anterior AEPG

The anterior end of the anterior AEPG is attached to the dorsal surface of the suprapineal recess superiorly and the lateral surfaces of the suprapineal recess laterally; inferiorly, it can be attached on either the inferior or the superior surface of the pineal gland. When the whole pineal gland is enclosed in the anterior AEPG, the inner surface of its inferior wall can either be smooth or (more commonly) have a crescent-shaped arachnoid ridge between the inferior wall of the suprapineal recess and the posterosuperior surface of the pineal gland (Qi et al. 2011b).

Others

The fibrous pedicle that connects the tip of the suprapineal recess and the outer surface of the vein of Galen near its origin can be either thick and long in cases of a small suprapineal recess (and longer distance), or short and thin in cases of a large suprapineal recess (and shorter distance) (Qi et al. 2011b).

The relationship between the AEPG and the internal cerebral veins (ICV) can be classified into two types based on the site of entrance of the ICV. In type I (more common), the ICV enter through the lateral wall of the anterior AEPG at any point from the anterior to the posterior portion. In type II, the ICV enter at the junction of the anterior and posterior AEPG; the compartments of the anterior and posterior AEPG (which are otherwise connected) are separated by the arachnoid septum located between the posterior ends of the ICV (Qi et al. 2011b).

Other arachnoid membranes

According to Lu and Zhu (2005b), arachnoid membranes that can be either unilaterally or bilaterally absent include the basilar artery bifurcation membrane, lateral carotid membrane, posterior communicating membrane, anterior choroidal membrane, basilar artery bifurcation membrane, posterior perforated membrane, medial pontomesencephalic membrane, basilar membrane, medial pontomedullary membrane, superior cerebellar membrane, posteroinferior cerebellar artery membrane, and dorsal vermian membrane (Lu and Zhu 2005b). Liliequist's membrane was not reported absent by Lu and Zhu (2005b) but other authors have reported it either wholly or partly absent. The lateral lamina terminalis membrane and the intracrural membrane were also reported occasionally absent by Inoue et al. (2009).

The superior margin of the posterior communicating membrane (PCM) can be free or joined to the anterior choroidal membrane or the inferior aspect of the diencephalon by arachnoid trabeculae. The PCM can also be absent; in such cases the carotid cistern and the posterior communicating cistern merge into one (Lu and Zhu 2007).

The chiasmatic membrane almost always lies above the diaphragma sellae, but in one specimen reported by Lu and Zhu (2003), this membrane, along with the anterior extension of the ML of the LM, turned downward around the infundibulum through the opening of the diaphragma sellae to encircle the pituitary gland (Lu and Zhu 2003).

Subarachnoid space within the Fallopian canal

Gacek (1998) described variations in the subarachnoid space within the Fallopian canal (FC). On the basis of the lateral limits of the arachnoid membrane within the FC, the subarachnoid space is divided into three categories. In type I, most common, it terminates at or proximal to the lateral end of the petrosal FC and its junction with the tympanic FC. In type II, it extends beyond the medial aspect of the geniculate ganglion and penetrates into the substance of the geniculate ganglion and surrounding facial nerve fascicles. The subarachnoid space displaces fascicles of the facial nerve and portions of the geniculate ganglion by dissecting between the perineural membrane covering these neural structures. In type III, least common, it extends beyond the tympanic facial nerve. This configuration is separated from the middle ear space by the fibrous tissue sheath of the nerve and the bony FC wall. The subarachnoid space reaches this lateral position in the FC by extending the dorsal cul-de-sac over the geniculate ganglion. In types II and III, the laterally extended subarachnoid space can present clinically as an asymptomatic enlargement of the canal by computed tomography or as cerebrospinal fluid otorrhea (Gacek 1998).

References

Adeeb N, Deep A, Griessenauer CJ, Mortazavi MM, Watanabe K, Loukas M, Tubbs RS, Cohen-Gadol AA. 2013. The intracranial arachnoid mater : a comprehensive review of its history, anatomy, imaging, and pathology. *Childs Nerv Syst* 29(1): 17–33.

Anik I, Ceylan S, Koc K, Tugasaygi M, Sirin G, Gazioglu N, Sam B. 2011. Microsurgical and endoscopic anatomy of Liliequist's membrane and the prepontine membranes: cadaveric study and clinical implications. *Acta Neurochir (Wien)* 153(8): 1701–1711.

Brasil AV, Schneider FL. 1993. Anatomy of Liliequist's membrane. *Neurosurgery* 32(6): 956–960.

Buxton N, Vloeberghs M, Punt J. 1998. Liliequist's membrane in minimally invasive endoscopic neurosurgery. *Clin Anat* 11(3): 187–190.

Di Ieva A, Tschabitscher M, Matula C, Komatsu F, Komatsu M, Colombo G, Sherif C, Galzio RJ. 2012. The subdiaphragmatic cistern: historic and radioanatomic findings. *Acta Neurochir (Wien)* 154(4): 667–674.

Epstein BS. 1965. The role of a transverse arachnoidal membrane within the interpeduncular cistern in the passage of pantopaque into the cranial cavity. *Radiology* 85(5): 914–920.

Fox JL. 1989. *Atlas of Neurosurgical Anatomy: The Pterional Perspective*. New York: Springer-Verlag.

Frankel DA, Fessell DP, Wolfson WP. 1998. High resolution sonographic determination of the normal dimensions of the intracranial extraaxial compartment in the newborn infant. *J Ultrasound Med* 17(7): 411–418.

Froelich SC, Abdel Aziz KM, Cohen PD, van Loveren HR, Keller JT. 2008. Microsurgical and endoscopic anatomy of Liliequist's membrane: a complex and variable structure of the basal cisterns. *Neurosurgery* 63(1 Suppl 1): ONS1–9.

Fushimi Y, Miki Y, Ueba T, Kanagaki M, Takahashi T, Yamamoto A, Haque TL, Konishi J, Takahashi JA, Hashimoto N. 2003. Liliequist membrane: three-dimensional constructive interference in steady state MR imaging. *Radiology* 229(2): 360–365.

Gacek RR. 1998. Anatomy and significance of the subarachnoid space in the Fallopian canal. *Am J Otol* 19(3): 358–365.

Gulsen S, Dinc AH, Unal M, Canturk N, Altinors N. 2010. Characterization of the anatomic location of the pituitary stalk and its relationship to the dorsum sellae, tuberculum sellae and chiasmatic cistern. *J Korean Neurosurg Soc* 47(3): 169–173.

Hodges FJ. 1970. Anatomy of the ventricles and subarachnoid spaces. *Seminars in Roentgenology* 5(2): 101–121.

Inoue K, Seker A, Osawa S, Alencastro LF, Matsushima T, Rhoton AL Jr. 2009. Microsurgical and endoscopic anatomy of the supratentorial arachnoidal membranes and cisterns. *Neurosurgery* 65(4): 644–665.

Key A, Retzius M. 1875. *Studien in der Anatomie des Nervensystems und des Bindegewebes*. Stockholm: Samson & Wallin.

Lam WW, Ai VH, Wong V, Leong LL. 2001. Ultrasonographic measurement of subarachnoid space in normal infants and children. *Pediatr Neurol* 25(5): 380–384.

Libicher M, Troger J. 1992. US measurement of the subarachnoid space in infants: normal values. *Radiology* 184(3): 749–751.

Liliequist B. 1956. The anatomy of the subarachnoid cisterns. *Acta Radiol* 46(1–2): 61–71.

Liliequist B. 1959. The subarachnoid cisterns. An anatomic and roentgenologic study. *Acta Radiol Suppl* 185: 1–108.

Lu J, Zhu XL. 2003. Microsurgical anatomy of Liliequist's membrane. *Minim Invasive Neurosurg* 46(3): 149–154.

Lu J, Zhu XL. 2005a. Microsurgical anatomy of the interpeduncular cistern and related arachnoid membranes. *J Neurosurg* 103(2): 337–341.

Lu J, Zhu XL. 2005b. Characteristics of distribution and configuration of intracranial arachnoid membranes. *Surg Radiol Anat* 27(6): 472–481.

Lu J, Zhu XL. 2007. Cranial arachnoid membranes: some aspects of microsurgical anatomy. *Clin Anat* 20(5): 502–511.

Matsuno H, Rhoton AL Jr, Peace D. 1988. Microsurgical anatomy of the posterior fossa cisterns. *Neurosurgery* 23(1): 58–80.

Narli N, Soyupak S, Yildizdas HY, Tutak E, Ozcan K, Sertdemir Y, Satar M. 2006. Ultrasonographic measurement of subarachnoid space in normal term newborns. *Eur J Radiol* 58(1): 110–112.

Okur A, Küçük O, Karaçavuş S, Yıldırım A, Erdoğan Y, Serin H. 2013. A novel index in healthy infants and children – subarachnoid space: ventricle ratio. *Folia Morphol (Warsz)* 72(2): 142–146.

Qi ST, Fan J, Zhang XA, Pan J. 2011a. Reinvestigation of the ambient cistern and its related arachnoid membranes: an anatomical study. *J Neurosurg* 115(1): 171–178.

Qi ST, Zhang XA, Fan J, Huang GL, Pan J, Qiu BH. 2011b. Anatomical study of the arachnoid envelope over the pineal region. *Neurosurgery* 68(1 Suppl Operative): 7–15.

Sabouri S, Khatami A, Shahnazi M, Tonekaboni SH, Momeni A, Mehrafarin M. 2011. Ultrasonographic measurement of subarachnoid space and frontal horn width in healthy Iranian infants. *Iranian J Child Neurol* 5(1).

Vinas FC, Panigrahi M. 2001. Microsurgical anatomy of the Liliequist's membrane and surrounding neurovascular territories. *Minim Invasive Neurosurg* 44(2): 104–109.

Vinas FC, Dujovny M, Fandino R, Chavez V. 1994. Microsurgical anatomy of the supratentorial arachnoidal trabecular membranes and cisterns. *Neurol Res* 16(6): 417–424.

Vinas FC, Dujovny M, Fandino R, Chavez V. 1996a. Microsurgical anatomy of the arachnoidal trabecular membranes and cisterns at the level of the tentorium. *Neurol Res* 18(4): 305–312.

Vinas FC, Dujovny M, Fandino R, Chavez V. 1996b. Microsurgical anatomy of the infratentorial trabecular membranes and subarachnoid cisterns. *Neurol Res* 18(2): 117–125.

Wang SS, Zheng HP, Zhang X, Zhang FH, Jing JJ, Wang RM. 2008. Microanatomy and surgical relevance of the olfactory cistern. *Microsurgery* 28(1): 65–70.

Wang SS, Zheng HP, Zhang FH, Wang RM. 2011a. The microanatomical structure of the cistern of the lamina terminalis. *J Clin Neurosci* 18(2): 253–259.

Wang SS, Zheng HP, Zhang FH, Wang RM. 2011b. Microsurgical anatomy of Liliequist's membrane demonstrating three-dimensional configuration. *Acta Neurochir (Wien)* 153(1): 191–200.

Yaşargil MG. 1984. *Microsurgical Anatomy of the Basal Cisterns and Vessels of the Brain: Diagnostic Studies, General Operative Techniques and Pathological Considerations of the Intracranial Aneurysms*. New York: Thieme.

Yaşargil MG, Kasdaglis K, Jain KK, Weber HP. 1976. Anatomical observations of the subarachnoid cisterns of the brain during surgery. *J Neurosurg* 44(3): 298–302.

Zaaroor M, Kosa G, Peri-Eran A, Maharil I, Shoham M, Goldsher D. 2006. Morphological study of the spinal canal content for subarachnoid endoscopy. *Minim Invasive Neurosurg* 49(4): 220–226.

Zhang M, An PC. 2000. Liliequist's membrane is a fold of the arachnoid mater: study using sheet plastination and scanning electron microscopy. *Neurosurgery* 47(4): 902–909.

Zhang XA, Qi ST, Huang GL, Long H, Fan J, Peng JX. 2012. Anatomical and histological study of Liliequist's membrane: with emphasis on its nature and lateral attachments. *Childs Nerv Syst* 28(1): 65–72.

81 Meninges

Nimer Adeeb[1], Martin M. Mortazavi[2] and R. Shane Tubbs[3]
[1]Children's of Alabama, Birmingham, Alabama, United States
[2]University of Washington School of Medicine, Seattle, Washington, United States
[3]Seattle Science Foundation, Seattle, Washington, USA
St George's University, School of Medicine, St Georges, Grenada
University of Dundee, Dundee, UK

Dura mater

Anatomical variations in the main dural sheath are extremely rare. Sargon et al. (2002) reported a multilayered dura mater in a 55-year-old male cadaver. The endosteal layer of the dura mater covering the left cerebral hemisphere was formed from five layers with a normal meningeal layer. This variation was associated with agenesis of the corpus callosum and septum pellucidum, representing a unique anatomical entity (Sargon et al. 2002).

Dural folds

Falx cerebri

Height

Frequent and marked variation in the height of the falx cerebri has been reported at three levels of measurement:

1. line A, between the tuberculum sellae and bregma;
2. line B, from the tuberculum sellae and the internal surface of the skull forming an angle of 30° posterior to line A; and
3. line C, between the tuberculum sellae and the internal surface of the skull along a line crossing the proximal end of the vein of Galen.

The height of the falx cerebri ranged over 2.8–4.8 cm (mean 3.58 cm), 4.1–6.2 cm (mean 5.19 cm), and 4.0 cm to 6.2 cm (mean 5.27 cm) along lines A, B, and C, respectively (Galligioni et al. 1969).

Falcine ossification

Ossification/calcification of the falx cerebri is an uncommon accidental finding. The prevalence of this entity varies widely. Sands et al. (1987) reported 12 cases with falcine ossification out of 3000 patients (0.4%), studied with magnetic resonance imaging. Ohela and Teir (1956) reported 11 cases with ossification in 100 cadaveric autopsies (11%). Lee et al. (1988) claimed a 7% prevalence of this benign condition. This anatomical variant usually involves only a small part of the falx and includes a compacted cortical bone surrounding a complete medullary cavity with bony trabeculae and marrow (Ohela and Teir 1956; Batnitzky et al. 1974; Sands et al. 1987; Lee et al. 1988; Rao et al. 2007; Debnath et al. 2009). Complete ossification of the falx cerebri has also been reported in the literature (Tubbs et al. 2006). Mineralization of the falx does not seem to correlate with increasing age (Bruyn 1963) and is not necessarily associated with any underlying medical disorder (Tubbs et al. 2006; Rao et al. 2007).

Diseases such as endocrine disorders, basal cell nevus syndrome, Maroteaux type brachyolmia, hypertelorism, pseudoxanthoma elastrium, and myotonic dystrophy can entail a higher rate of ossification (Satoh et al. 1977; Shohat et al. 1989; Cohen et al. 1995; Miaux et al. 1997; Dorenbeck et al. 2002; Tubbs et al. 2006).

Diagnostic confusion with interhemispheric vascular lesions, myelometaplasia, falcine osteosarcoma, dural metastases, and leukemic infiltration is possible on brain imaging (Wang et al. 1986; Ruge et al. 1990; Tubbs et al. 2006).

The newly formed bony tissue acts like any other bone in the body and can be a site of primary or secondary bone lesions (Tubbs et al. 2006; Rao et al. 2007).

Absent, duplicated, and fenestrated falx cerebri

Absent falx cerebri has been reported in patients with holoprosencephaly associated with absence of the interhemispherical fissure (Chang 2003).

A rare case of accessory falx cerebri was reported by Krauss et al. (1990) in a 12-year-old boy. This dural septum spanned the temporo-occipital base upward to the lower parietal area in the direction of the corona, and was supplied by a small leptomeningeal artery. A small venous sinus was also seen within its layers (Krauss et al. 1990).

The falx cerebri may have fenestrations within it (Fig. 81.1).

Bergman's Comprehensive Encyclopedia of Human Anatomic Variation, First Edition. Edited by R. Shane Tubbs, Mohammadali M. Shoja and Marios Loukas.
© 2016 John Wiley & Sons, Inc. Published 2016 by John Wiley & Sons, Inc.

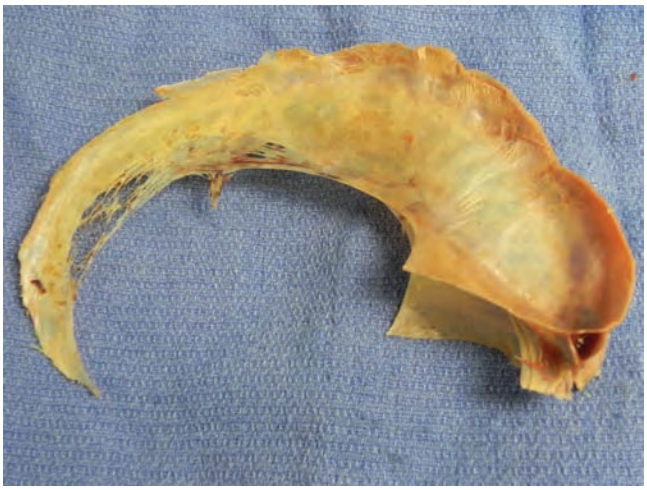

Figure 81.1 Falx cerebri and associated fenestrated anterior portion.

Tentorium cerebelli

Tentorial notch

Variations in the structure of the tentorial notch and its correlation with intracranial pathologies and transtentorial herniation have put it at the center of a detailed anatomical study and classification system. Adler and Milhorat (2002) reported that among 100 adult human autopsy cases the maximal notch length (MNL) measured from the superoposterior edge of the dorsum sellae to the apex of the notch ranged over 44–70 mm (mean 57.7 mm). The posterior tentorial length, measured as the shortest distance between the apex of the notch and the most anterior part of the confluence of the sinuses, ranged over 35–63 mm (mean 48.3 mm). The maximal notch width (MNW) in the axial plane ranged over 24.5–39.0 mm (mean 29.6 mm). The anterior notch width in the axial plane through the posterior aspect of the dorsum sellae ranged over 21.0–34.0 mm (mean 26.6 mm). On the basis of these measurements of the MNL and the MNW, a classification system has been proposed for anatomical description. The MNW is classed as narrow (less than or equal to 27.0 mm), typical (27.1–31.9 mm), or wide (greater than or equal to 32.0 mm). The MNL is classed as short (less than or equal to 53.5 mm), typical (53.6–61.9 mm), or long (greater and equal to 62.0 mm). Notches that are both wide and long are labeled large, those that are narrow and short are labeled small, and notches that are either wide and short or narrow and long are labeled mixed (Adler and Milhorat 2002). Large notches contain more neural tissue than small notches (Tables 81.1, 81.2).

Variations in the tentorial inclination and curvature of the tentorial free edge seen in lateral view were also found to correlate with the length of the tentorial notch. Short tentorial notches tend to have a steeper inclination and greater curvature of the tentorial edge. On the other hand, long notches are flattened, exposing more notch contents to the supratentorial compartment (Adler and Milhorat 2002).

Table 81.1 Classification of the tentorial notch by Adler and Milhorat (2002).

	Maximal notch width (MNW)		
Maximal notch length (MNL)	**Narrow (≤27.0 mm)**	**Typical (27.1–31.9 mm)**	**Wide (≥32.0 mm)**
Short (≤53.5 mm)	Small	Short	Mixed
Typical (53.6–61.9 mm)	Narrow	Typical	Wide
Long (≥62.0 mm)	Mixed	Long	Large

On the basis of these anatomical variations, large notches have more propensity for transtentorial herniation of cerebellar or cerebral parenchyma in a rostral or caudal direction, respectively.

Calcification of tentorial cerebelli

Tentorial ossification/calcification is a rare entity that can be found in humans as physiological calcification. It can be seen as single or multiple foci of mineralization (Daghighi et al. 2007; Makariou and Patsalides 2009; Uduma et al. 2012). Complete ossification has never been reported. Humans with this finding would probably be less able to mobilize brain tissue with unilateral increases in intracranial pressure as seen in subfalcine herniation, since bone would be less giving than the softer unossified falx cerebri (Tubbs et al. 2006). However, this has not been clinically proven.

Falx cerebelli

The length of the tentorium cerebelli falls within the range 2.8–4.5 cm and its thickness 1–13 mm. These measurements differ in cases with duplicated falx cerebelli (Lang 1991; Shoja et al. 2006, 2007).

Duplicated falx cerebelli

Duplication of the falx cerebelli is seldom reported in the literature (Hassler and Schlenker 1982; Shoja et al. 2006; D'Costa et al. 2009). In autopsies of 52 adult cadavers, D'Costa et al. (2009) reported eight cases of this variation. Hasan and Das (1969) also found duplicated falx cerebelli in 76 (76%) of 100 cadavers (Hasan and Das 1969). Each falx cerebelli is

Table 81.2 Variations in the measurements (mm) of tentorial notch by Adler and Milhorat (2002).

Measurement	Value (mean)
Maximal notch length	44.0–70 (57.7)
Posterior tentorial length	35.0–63.0 (48.3)
Maximal notch width	24.5–39.0 (29.6)
Anterior notch width	21.0–34.0 (26.6)

separately attached to the tentorium at its base and courses for a different length over a distinct internal occipital crest arising and diverging inferiorly near the posterolateral borders of the foramen magnum. The distance between the two falces falls within the range 3–30 mm, and the length of each falx 2.5–5 cm; the maximum width can be 25 mm (Shoja et al. 2006, 2007; D'Costa et al. 2009). This variation is often associated with duplicated occipital sinus, each falx possessing a distinct occipital venous sinus on each attached border draining into its respective transverse sinus (Shoja et al. 2006; D'Costa et al. 2009). Other intracranial variations including a Menelfe type 1 accessory middle cerebral artery, a duplicated anterior communicating artery, and a persistent intracranial olfactory artery can also be associated with this entity (Shoja et al. 2006). Shoja et al. (2007) reported a unique case of a triplicate falx cerebelli associated with a single occipital venous sinus. However, an additional dural venous sinus was found posterolateral to the foramen magnum coursing superiorly and posteromedially and connecting the terminal portion of the right sigmoid sinus to the occipital and right transverse sinuses via one medial and two lateral branches, respectively (Shoja et al. 2007).

Absent, hypoblastic, and fenestrated falx cerebelli

These rare anatomical variations were first reported in association with Chiari II malformation (Naidich et al. 1980; Tubbs et al. 2002) and vermian agenesis (Michaud et al. 1982). The only case of absent falx cerebelli in an otherwise anatomically normal brain was reported by Mavridis et al. (2013) in 91-year-old female cadaver.

Diaphragma sellae

Dimensions of the diaphragma sellae and its foramen

Variations in the size and shape of the diaphragma sellae and its foramen are not uncommon. The diaphragma is usually concave (Sage et al. 1982; Rhoton 2002; Ongeti et al. 2012) but can be convex (Gulsen et al. 2010). Its foramen is round in most cases and elliptical in others (Rhoton 2002; Ju et al. 2010; Ongeti et al. 2012). The latter can be further classified as sagittal elliptical or, more commonly, coronal elliptical (Ongeti et al. 2012). The diaphragma diameter ranges over 4–15 mm and the diameter of the foramen 3–14 mm, with larger coronal than sagittal dimension (Nomura et al. 2002; Campero et al. 2008; Ongeti et al. 2012), and with ethnic (Bergland et al. 1968; Campero et al. 2008; Ongeti et al. 2012) and gender variations as it is usually wider in Africans and in females (Ongeti et al. 2012). However, another study revealed larger dimensions in males rather than females (Won et al. 2010). Campero et al. (2008) proposed a threefold classification of the diaphragma sellae based on the diameter of its opening:

- Group A: the diameter of the opening is less than 4 mm;
- Group B: it is 4–8 mm; and
- Group C: it is more than 8 mm (Campero et al. 2008).

Table 81.3 Classification of topographic relation between the foramen of the diaphragm sellae and the optic chiasm by Won et al. (2010). The classification is based on dividing the suprasellar region into anterior, right, left, and posterior parts by two diagonal lines along both optic nerves, and the relation of the foramen to these parts.

Type	Description
I	In the midline
Ia	In the anterior part
Ib	In the anterior, right, and left parts
Ic	In all four parts
II	In the anterior and left part
III	In the anterior and right part

This classification could represent an effective predictive value for tumor expansion and should be considered during instrumentation in the hypophyseal fossa. Moreover, a wide diaphragma sellae foramen, as well as a functionally incompetent diaphragma, is an important contributor to the empty sellae syndrome.

Diaphragma sellae foramen and the optic chiasm

Won et al. (2010) studied the topographical relationship between the foramen of the diaphragm sellae and the optic chiasm, upon which they proposed a classification system. They divided the suprasellar region into anterior, right, left, and posterior sections by two diagonal lines along both optic nerves. The foramen was classified on the basis of its relationship to these four parts into the following types: type I (on the midline, most common); type II (in the anterior and left part); and type III (in the anterior and right part). Type I could be further subdivided into: type Ia (in the anterior part); type Ib (in the anterior, right, and left parts, most common); and type Ic (in all four parts) (Won et al. 2010). This classification could predict the route of an expanding pituitary tumor and the site of subsequent optic pathway compression (Table 81.3).

Dural sac (DS)

Shape of the dural sac

Park et al. (1996) divided the DS into five types according to shape: Type I (pointed), tapering contour with a "rat tail" appearance; Type II (ovoid), tapering smoothly with round end; Type III (round), not tapering, with round end; Type IV (pointed ovoid), ending in papillae; and Type V (round pointed), ending in papillae. The most common type was Type I followed by Type II.

Termination of the dural sac

In most individuals, the level of termination of the DS is at the upper (Scharf et al. 1998; Binokay et al. 2006) or middle

(Macdonald et al. 1999) third of S2. The widest range was reported by Soleiman et al. (2005) in MR imaging of 635 patients, where the level of DS termination ranged from the lower third of L3 to the upper third of S5 (Soleiman et al. 2005). However, other studies have demonstrated a consistently narrower range, with no termination higher than the L5–S1 intervertebral disc (Larsen and Olsen 1991; Scharf et al. 1998; Macdonald et al. 1999; Binokay et al. 2006) or lower than the upper one-third of S3 (Scharf et al. 1998; Binokay et al. 2006). This suggests a much lower incidence of DS termination outside this range. Only a few studies in the literature have reported gender, age, or racial variations. Binokay et al. (2006) attributed the variations in termination to racial differences. Macdonald et al. (1999) reported slight gender differences, with lower termination seen in males. Soleiman et al. (2005) recorded a U-shaped correlation between age and DS termination; levels of termination were lower in individuals of age 20–39 years and 60–80 years than in those 40–59 years old (Scharf et al. 1998). No comparable results were reported in other studies.

The level of DS termination moved cranially when changing from the natural extended position to a flexed position. In a study by Koo et al. (2009) the median level of termination changed from the middle third of S2 to the upper third of S2 after flexion.

Dural sac diameter

In one study, the DS diameter varied with change in body posture (Hirasawa et al. 2007). At all spinal levels, the mean DS cross-sectional area in the supine position was significantly smaller than in the standing and sitting positions. This could be due to a gravity-related increase in hydrostatic CSF pressure in standing and sitting positions; no significant differences were noticed between those two positions. However, at one level (L5–S1) the cross-sectional area was largest in the sitting-with-extension position. Similar results were reported regarding the anterior-posterior (AP) diameter. Moreover, at the L3–L4 and L4–L5 levels, the mean AP DS diameter in the sitting-extended position was significantly shorter than in the sitting flexed position. This could be because in flexed position the dura is held at the ventral and the dorsolateral sides by the corresponding meningovertebral ligaments, changing its shape to a triangle (Hirasawa et al. 2007).

Thickness of dural sac

Inter- and intra-individual variations in dural sac thickness were reported by Reina et al. (1999) They found that the mean thickness of the DS was 0.322 mm. No significant variations were recorded in the thickness of the anterior zones, with mean thickness 0.353 mm. In the posterior zones, the mean thickness was 0.295 mm with significant variations. The posterior zone was also found to be significantly thinner than the anterior zone after the space between the second and third lumbar roots (Reina et al. 1999).

Duplication of the dural sac

Loughenbury et al. (2005, 2010) reported an adult cadaver with duplication of the dura mater from C2 to L5. Anteriorly, the dura mater was firmly attached to the PLL and spinal nerve sheaths, particularly in the lower thoracic and lumbar regions. The dural sheath consisted of two layers adherent throughout their length, both layers completely enveloping the spinal cord and nerve roots and merging caudally with the filum terminale. Each layer was of similar thickness, but the external layer tended to be thicker anteriorly and less consistent in thickness posteriorly, particularly above the level of T10. From the most cranial point observed (C2) to the level of the T10–T11 intervertebral disc, the outer layer of the dura mater was strongly adherent to the deep layer of the PLL in the midline: below this level the attachment was largely by loose fibrous tissue. The deep and superficial layers of the PLL, as well as the peridural membrane anterior to the PLL, had the usual morphology.

Previous reports of duplication of the ventral aspect of the spinal dura, which were observed during intra-operative dissection, linked it with idiopathic herniation of the spinal cord. Oe et al. (1990) presented a case of idiopathic herniation of the spinal cord associated with ventral duplication of the dura and a dorsal subarachnoid cyst, which was present at the level of dural duplication. The additional dural layer was resected but the patient did not improve clinically. Nakazawa et al. (1993) reported two patients with Brown-Séquard syndrome, which both clinically and radiologically was consistent with a ventral arachnoid cyst. Intra-operative dissection demonstrated idiopathic spinal cord herniation accompanied by localized duplication of the ventral dura mater, which in one patient extended from C6 to T5.

Arachnoid mater

The arachnoid is thicker at the basal part, between the temporal lobes, and at the anterior surface of the pons. With age, the arachnoid of the superior surface can become white and opaque, mainly near the midline (Snell 2010).

Arachnoid granulations (AG)

The presence of AG is considered a normal anatomical variation. They have been reported in 10–90% of people depending on the study technique, and are better detected using a three-dimensional (3D) MP-RAGE or 3D MRV (Leach et al. 1996; Ikushima et al. 1999; Gailloud et al. 2001; Liang et al. 2002; Haroun et al. 2007; Bayrak et al. 2009; Adeeb et al. 2013a). Although they play the most significant role in cerebrospinal fluid (CSF) absorption, they usually present as small protrusions (aracnoid villi) that do not grow to a grossly detectable size within the dural sinuses (Adeeb et al. 2013a). The number of AG in each individual ranges over 0–6, and the size of each AG ranges over 2–22 mm (Ikushima et al. 1999; Haroun et al. 2007; Bayrak et al. 2009). The size and number of AG increase with age (Ikushima et al. 1999; Haroun et al. 2007; Adeeb et al. 2013a)

and peak during the sixth decade (Ikushima et al. 1999). In the study by Haroun et al. (2007), the mean size of AG was 6 mm for patients aged less than 45 years and 8 mm for older patients (Haroun et al. 2007). They usually become detectable around 18 months of age due to the negative pressure created in the dural sinuses when the person attains the upright position, and thus a suction force causes the AG to enlarge and bulge into the lumen (Adeeb et al. 2013a). In contrast, a study by Bayrak et al. (2009) involving 140 patients reported an inverse relationship between age and AG. No gender variation has been reported (Ikushima et al. 1999; Haroun et al. 2007; Bayrak et al. 2009). The AG may be round (most common), oval, or lobulated (least common) and with regular or, less commonly, irregular outlines (Haroun et al. 2007).

Location

The SSS is the most common location for the AG, mostly found in the lateral lacunae and the middle third of the floor of the sinus. Their protrusion into the lateral lacunae in most cases leads to the inference that the TS is a more common location than the SSS. When found within the TS, they mostly occur in the middle and lateral parts and more on the left side. Other locations include StS, SS, CS, SPS, ShPS, the confluence of sinuses, and the vein of Galen (le Gros Clark 1920; Grossman and Potts 1974; Leach et al. 1996; Ikushima et al. 1999; Farb 2007; Grzybowski et al. 2007; Haroun et al. 2007; Bayrak et al. 2009).

Aberrant locations of the AG have been reported, including the anterior and middle cranial fossa, and less frequently the posterior temporal bone. In the middle fossa, AG are mostly found (in decreasing frequency) in or near the middle meningeal vein, ShPS, lateral foramen rotundum, and CS. Granulations of these aberrant locations entail high CSF pressure due to lack of proper communication with the venous sinuses. This pressure can cause bone erosion and, depending on its site, otorrhea or rhinorrhea (VandeVyver et al. 2007; Schuknecht et al. 2008; Chen et al. 2011).

Other

Regarding the relation of the AG and the wall of the dural sinuses and lateral lacunae, various assumptions have been made. le Gros Clark (1920) stated that these granulations, irrespective of their size, are attached to the undersurface of the dura mater; if this attachment is removed, a small aperture can be noticed at the site (le Gros Clark 1920). Wolpow and Schaumburg (1972) demonstrated two types of granulations in humans: one that is totally invested with dura mater and one that, in addition, is fused with the dura mater. In the latter type, removal of the granulation leaves a tear in the wall of the sinus (Wolpow and Schaumburg 1972). Jayatilaka (1969) also mentioned two major types: one protruding into the dural sinuses and the other in the subdural space.

Occasionally, the AG has a larger diameter (up to 3 cm) and fills the lumen of the dural sinus causing local dilation. The TS is usually involved. They are found mostly in patients older than 45 years, but have also been reported in children (Mamourian and Towfighi 1995; Chin et al. 1998).

Calcification of the AG (mainly affecting their central parts) has been reported by Roche and Warner (1996). Subtotal and total agenesis of the AG has also been reported, the latter being associated with impaired CSF absorption and consequent hydrocephalus (Gutierrez et al. 1975).

Pia mater

Denticulate (DL) ligaments

The numbers of DL on each side of the spinal cord vary between 18 and 22. DL are usually present in the cervical and thoracic areas and less frequently in the lumbar area (Tubbs et al. 2001; Ceylan et al. 2012). Unilateral absence and asymmetry in the number of the DL have also been reported (Tubbs et al. 2011). The apices of these ligaments can be single or duplicated, and DL can extend into their dural attachments for distances that vary among individuals and between spinal cord levels, shortest in the upper cervical area and increasing caudally. The distance from the dural attachment site to the intervertebral foramen was estimated as between 10 mm in the cervical area and 20 mm in the lower thoracic area in a study by Ceylan et al. (2012). Moreover, these authors found that the attachment is facilitated by fibrous bands in both the cervical and lower thoracic areas, but is direct in the upper thoracic area. This variation was related by these authors to the mobility of the cervical and lower thoracic vertebrae, the DL in that region allowing the necessary motion of the cervical and lower thoracic portions of the spinal cord within the canal (Ceylan et al. 2012). Occasionally, the DL have a free lateral margin (Nicholas and Weller 1988).

Intrathecal ligaments (ITL)

Kershner and Binhammer (2002) described discrete round bands of tissue located internal to the arachnoid and randomly binding some dorsal roots to the lateral aspect of the dura in a manner similar to the attachment of a DL; they can join the ventral and dorsal roots. The number of these ITL ranges between 8 and 27 per specimen. They are found anywhere between the first lumbar vertebra and the second sacral intervertebral foramen, mostly between the intervertebral disks of L4–L5 and L5–S1. The ITL ranges over 0.13–0.35 μm in thickness and 3–3.5 cm in length. Histological examination revealed a fibrous core consisting mainly of collagen bundles and, to a lesser degree, elastin. Fibroblasts were scattered along the length of the ligament and were denser near sites of attachment. This core was surrounded by leptomeningeal cells that became continuous with the pia mater of the spinal roots. The broad-based attachments at both sides, along with their histological characteristics, partly explain why the ITL need more force to disrupt the arachnoid. According to the authors, the similarities between these ligaments and the DL suggest that the ITL represent remnants from fetal development of the DL (Kershner and Binhammer 2002; Adeeb et al. 2013b).

Filum terminale (FT)

In most individuals the FT starts at the L1 level, ranging at any point from the lower one-third of the T11 to the L2–L3 intervertebral space (Pinto et al. 2002). The fusion between the FT and dura mater of the DS marks the distinction between the intradural and extradural compartments of the FT. This commonly occurs at the S2 vertebral body level, but can occur at any level between L5 and S3. In most cases, the FT joins the dorsal midline of the dura. On other occasions it fuses either to the right or left of midline (Hansasuta et al. 1999). The length of the intradural segment of the FT ranges over 112.8–211.1 mm (mean 156.4 mm). The thickness at the starting point ranges over 0.4–2.5 mm (mean 1.38 mm), and at the midpoint 0.1–1.55 mm (mean 0.76 mm) (Pinto et al. 2002). The length of the extradural part (filum terminal externum; coccygeal ligament) ranges between over 7–10.5 cm (mean 8 cm) and its mean width is 1 mm (Tubbs et al. 2005). Smooth muscle cells are sometimes found in the extradural part of the filum terminale.

References

Adeeb N, Deep A, Griessenauer CJ, Mortazavi MM, Watanabe K, Loukas M, Tubbs RS, Cohen-Gadol AA. 2013a. The intracranial arachnoid mater: a comprehensive review of its history, anatomy, imaging, and pathology. *Childs Nerv Syst* 29(1): 17–33.

Adeeb N, Mortazavi MM, Deep A, Griessenauer CJ, Watanabe K, Shoja MM, Loukas M, Tubbs RS. 2013b. The pia mater: a comprehensive review of literature. *Childs Nerv Syst.* 29(10): 1803–1810.

Adler DE, Milhorat TH. 2002. The tentorial notch: anatomical variation, morphometric analysis, and classification in 100 human autopsy cases. *J Neurosurg* 96(6): 1103–1112.

Batnitzky S, Powers JM, Schechter MM. 1974. Falx "calcification"—-does this exist? *Neuroradiology* 7(5): 255–260.

Bayrak A, Akay H, Ozmen C, Senturk S. 2009. Arachnoid granulations: frequency and distribution in multi-detector row CT of dural sinuses. *Biotechnol & Biotechnolog Equip* 23(2): 1255–1258.

Bergland RM, Ray BS, Torack RM. 1968. Anatomical variations in the pituitary gland and adjacent structures in 225 human autopsy cases. *J Neurosurg* 28(2): 93–99.

Binokay F, Akgul E, Bicakci K, Soyupak S, Aksungur E, Sertdemir Y. 2006. Determining the level of the dural sac tip: magnetic resonance imaging in an adult population. *Acta Radiol* 47(4): 397–400.

Bruyn GW. 1963. Calcification and ossification of the cerebral falx and superior longitudinal sinus. *Psychiatr Neurol Neurochir* 66: 98–119.

Campero A, Martins C, Yasuda A, Rhoton AL Jr. 2008. Microsurgical anatomy of the diaphragma sellae and its role in directing the pattern of growth of pituitary adenomas. *Neurosurgery* 62(3): 717–723.

Ceylan D, Tatarli N, Abdullaev T, Seker A, Yildiz SD, Keles E, Konya D, Bayri Y, Kilic T. Cavdar S. 2012. The denticulate ligament: anatomical properties, functional and clinical significance. *Acta Neurochir (Wien)* 154(7): 1229–1234.

Chang LH. 2003. Alobar holoprosencephaly: report of two cases with unusual findings. *Chang Gung Med J* 26(9): 700–706.

Chen F, Deng XF, Liu B, Zou LN, Wang DB, Han H. 2011. Arachnoid granulations of middle cranial fossa: a population study between cadaveric dissection and in vivo computed tomography examination. *Surg Radiol Anat* 33(3): 215–221.

Chin SC, Chen CY, Lee CC, Chen FH, Lee KW, Hsiao HS, Zimmerman RA. 1998. Giant arachnoid granulation mimicking dural sinus thrombosis in a boy with headache: MRI. *Neuroradiology* 40(3): 181–183.

Cohen MM Jr, Richieri-Costa A, Guion-Almeida ML, Saavedra D. 1995. Hypertelorism: interorbital growth, measurements, and pathogenetic considerations. *Int J Oral Maxillofac Surg* 24(6): 387–395.

D'Costa S, Krishnamurthy A, Nayak SR, Madhyasta S, Prabhu LV, J JP, Ranade AV, Pai MM, Vadgaonkar R, Ganesh Kumar C, Rai R. 2009. Duplication of falx cerebelli, occipital sinus, and internal occipital crest. *Rom J Morphol Embryol* 50(1): 107–110.

Daghighi MH, Rezaei V, Zarrintan S, Pourfathi H. 2007. Intracranial physiological calcifications in adults on computed tomography in Tabriz, Iran. *Folia Morphol (Warsz)* 66(2): 115–119.

Debnath J, Satija L, George RA, Vaidya A, Sen D. 2009. Computed tomographic demonstration of unusual ossification of the falx cerebri: a case report. *Surg Radiol Anat* 31(3): 211–213.

Dorenbeck U, Leingartner T, Bretschneider T, Kramer BK, Feuerbach S. 2002. Tentorial and dural calcification with tertiary hyperparathyroidism: a rare entity in chronic renal failure. *Eur Radiol* 12(3): S11–13.

Farb RI. 2007. The dural venous sinuses: normal intraluminal architecture defined on contrast-enhanced MR venography. *Neuroradiology* 49(9): 727–732.

Gailloud P, Muster M, Khaw N, Martin JB, Murphy KJ, Fasel JH, Rufenacht DA. 2001. Anatomic relationship between arachnoid granulations in the transverse sinus and the termination of the vein of Labbe: an angiographic study. *Neuroradiology* 43(2): 139–143.

Galligioni F, Bernardi R, Mingrino S. 1969. Anatomic variation of the height of the falx cerebri. Its relationship to displacement of the anterior cerebral artery in frontal space-occupying lesions. *Am J Roentgenol Radium Ther Nucl Med* 106(2): 273–278.

Grossman CB, Potts DG. 1974. Arachnoid granulations: radiology and anatomy. *Radiology* 113(1): 95–100.

Grzybowski DM, Herderick EE, Kapoor KG, Holman DW, Katz SE. 2007. Human arachnoid granulations. Part I: a technique for quantifying area and distribution on the superior surface of the cerebral cortex. *Cerebrospinal Fluid Res* 4: 6.

Gulsen S, Dinc AH, Unal M, Canturk N, Altinors N. 2010. Characterization of the anatomic location of the pituitary stalk and its relationship to the dorsum sellae, tuberculum sellae and chiasmatic cistern. *J Korean Neurosurg Soc* 47(3): 169–173.

Gutierrez Y, Friede RL, Kaliney WJ. 1975. Agenesis of arachnoid granulations and its relationship to communicating hydrocephalus. *J Neurosurg* 43(5): 553–558.

Hansasuta A, Tubbs RS, Oakes WJ. 1999. Filum terminale fusion and dural sac termination: study in 27 cadavers. *Pediatr Neurosurg* 30(4): 176–179.

Haroun AA, Mahafza WS, Al Najar MS. 2007. Arachnoid granulations in the cerebral dural sinuses as demonstrated by contrast-enhanced 3D magnetic resonance venography. *Surg Radiol Anat* 29(4): 323–328.

Hasan M, Das A. 1969. A note on the falx cerebelli. *Acta Anatomica* 74: 624–628.

Hassler W, Schlenker M. 1982. Double falx cerebelli. Case report. *Acta Neurochir (Wien)* 62(3–4): 265–269.

Hirasawa Y, Bashir WA, Smith FW, Magnusson ML, Pope MH, Takahashi K. 2007. Postural changes of the dural sac in the lumbar spines of asymptomatic individuals using positional stand-up magnetic resonance imaging. *Spine (Phila Pa 1976)* 32(4): E136–140.

Ikushima I, Korogi Y, Makita O, Yamura M, Kawano H, Kohama M, Arikawa K, Takahashi M. 1999. MRI of arachnoid granulations within the dural sinuses using a FLAIR pulse sequence. *Br J Radiol* 72(863): 1046–1051.

Jayatilaka A. 1969. Arachnoid granulations and arachnoid villi in mammals. *Ceylon J Med Sci* 18(1): 25–30.

Ju KS, Bae HG, Park HK, Chang JC, Choi SK, Sim KB. 2010. Morphometric study of the korean adult pituitary glands and the diaphragma sellae. *J Korean Neurosurg Soc* 47(1): 42–47.

Kershner DE, Binhammer RT. 2002. Lumbar intrathecal ligaments. *Clin Anat* 15(2): 82–87.

Koo BN, Hong JY, Kim HE, Kil HK. 2009. The effect of flexion on the level of termination of the dural sac in paediatric patients. *Anaesthesia* 64(10): 1072–1076.

Krauss J, Sorensen N, Lang J. 1990. A case of "accessory falx cerebri". *Childs Nerv Syst* 6(5): 275–276.

Lang J. 1991. *Clinical Anatomy of the Posterior Cranial Fossa and its Foramina*. New York: Thieme.

Larsen JL, Olsen KO. 1991. Radiographic anatomy of the distal dural sac. A myelographic investigation of dimensions and termination. *Acta Radiol* 32(3): 214–219.

le Gros Clark WE. 1920. On the pacchionian bodies. *J Anat* 55(1): 40–48.

Leach JL, Jones BV, Tomsick TA, Stewart CA, Balko MG. 1996. Normal appearance of arachnoid granulations on contrast-enhanced CT and MR of the brain: differentiation from dural sinus disease. *AJNR Am J Neuroradiol* 17(8): 1523–1532.

Lee DH, Larson TC 3rd, Norman D. 1988. Falx ossification: MR visualization. *Can Assoc Radiol J* 39(4): 260–262.

Liang L, Korogi Y, Sugahara T, Ikushima I, Shigematsu Y, Takahashi M, Provenzale JM. 2002. Normal structures in the intracranial dural sinuses: delineation with 3D contrast-enhanced magnetization prepared rapid acquisition gradient-echo imaging sequence. *AJNR Am J Neuroradiol* 23(10): 1739–1746.

Loughenbury P, Wadhawani S, Soames RW. 2005. Unusual variant of the spinal dural sheath: a case report. In Proceedings of 23rd Annual Meeting of the American Association of Clinical Anatomists and the British Association of Clinical Anatomists, New York.

Loughenbury P, Wadhwani S, Soames R. 2010. Double spinal dural sheath: a cadaveric case report. *IJAV* 3: 41–43.

Macdonald A, Chatrath P, Spector T, Ellis H. 1999. Level of termination of the spinal cord and the dural sac: a magnetic resonance study. *Clin Anat* 12(3): 149–152.

Makariou E, Patsalides A. 2009. Intracranial calcifications. *Appl Radiol* 38(11): 48–60.

Mamourian AC, Towfighi J. 1995. MR of giant arachnoid granulation, a normal variant presenting as a mass within the dural venous sinus. *AJNR Am J Neuroradiol* 16(4 Suppl): 901–904.

Mavridis IN, Lontos K, Anagnostopoulou S. 2013. Absent falx cerebelli: report of a rare case. *Anat Sci Int* 88(3): 181–182.

Miaux Y, Chiras J, Eymard B, Lauriot-Prevost MC, Radvanyi H, Martin-Duverneuil N, Delaporte C. 1997. Cranial MRI findings in myotonic dystrophy. *Neuroradiology* 39(3): 166–170.

Michaud J, Mizrahi EM, Urich H. 1982. Agenesis of the vermis with fusion of the cerebellar hemispheres, septo-optic dysplasia and associated anomalies. Report of a case. *Acta Neuropathol* 56(3): 161–166.

Naidich TP, Pudlowski RM, Naidich JB, Gornish M, Rodriguez FJ. 1980. Computed tomographic signs of the Chiari II malformation. Part I: Skull and dural partitions. *Radiology* 134(1): 65–71.

Nakazawa H, Teyama Y, Satomi K, Fujimore Y, Hirabayashi K. 1993. Idiopathic spinal cord herniation: report of two cases and review of the literature. *Spine* 18: 2138–2141.

Nicholas DS, Weller RO. 1988. The fine anatomy of the human spinal meninges. A light and scanning electron microscopy study. *J Neurosurg* 69(2): 276–282.

Nomura M, Tachibana O, Yamashima T, Yamashita J, Suzuki M. 2002. MRI evaluation of the diaphragmal opening: using MRI parallel to the transsphenoidal surgical approach. *J Clin Neurosci* 9(2): 175–177.

Oe T, Hoshino Y, Kurokawa T. 1990. A case of idiopathic herniation of the spinal cord associated with duplicated dura mater and with an arachnoid cyst. *J Jap Orthop Assoc* 84: 43–49.

Ohela K, Teir H. 1956. Calcification of dura mater; medico-legal aspects of a case. *Dtsch Z Gesamte Gerichtl Med* 45(6): 488–491.

Ongeti K, El-Busaidy H, Fundi N. 2012. Reappraisal of the dimensions of the diaphragma sellae. *Anatomy Journal of Africa* 1(1): 24–27.

Park S, Choi W, Kim E, Oh J, Yoon Y. 1996. Normal variation of lumbosacral thecal sac on MR. *J Korean Radiol Soc* 34(5): 565–569.

Pinto FC, Fontes RB, Leonhardt Mde C, Amodio DT, Porro F, Machado J. 2002. Anatomic study of the filum terminale and its correlations with the tethered cord syndrome. *Neurosurgery* 51(3): 725–730.

Rao S, Rao T, Ovchinnikov N, McRae A, Rao A. 2007. Unusual isolated ossification of falx cerebri: a case report. *Neuroanatomy* 8: 54–55.

Reina MA, Lopez Garcia A, de Andres JA, Sellers F, Arrizabalaga M, Mora MJ. 1999. Thickness variation of the dural sac. *Rev Esp Anestesiol Reanim* 46(8): 344–349.

Rhoton AL Jr. 2002. The sellar region. *Neurosurgery* 51(4): S331–374.

Roche J, Warner D. 1996. Arachnoid granulations in the transverse and sigmoid sinuses: CT, MR, and MR angiographic appearance of a normal anatomic variation. *AJNR Am J Neuroradiol* 17(4): 677–683.

Ruge JR, Russell EJ, Levy RM. 1990. Mineralization of the falx cerebri simulating interhemispheric vascular anomalies on MR imaging. Report of three cases. *J Neurosurg* 72(6): 971–974.

Sage MR, Blumbargs PC, Mulligan BP, Fowler GW. 1982. The diaphragma sellae: its relationship to the configuration of the pituitary gland. *Radiology* 145(3): 703–708.

Sands SF, Farmer P, Alvarez O, Keller IA, Gorey MT, Hyman RA. 1987. Fat within the falx: MR demonstration of falcine bony metaplasia with marrow formation. *J Comput Assist Tomogr* 11(4): 602–605.

Sargon M, Brohi R, Ozeksi P, Tonak A, Cumhur M. 2002. Agenesis of the corpus callosum and septum pellucidum together with a multiple layered duramater. *Neuroanatomy* 1(1): 2–4.

Satoh M, Fukazawa H, Yagawa K, Endo H, Suzuki A. 1977. Two cases of nevoid basal cell carcinoma syndrome. *Acta Pathol Jap* 27(5): 713–727.

Scharf CB, Paulino AC, Goldberg RN. 1998. Determination of the inferior border of the thecal sac using magnetic resonance imaging: implications on radiation therapy treatment planning. *Int J Radiat Oncol Biol Phys* 41(3): 621–624.

Schuknecht B, Simmen D, Briner HR, Holzmann D. 2008. Nontraumatic skull base defects with spontaneous CSF rhinorrhea and arachnoid herniation: imaging findings and correlation with endoscopic sinus surgery in 27 patients. *AJNR Am J Neuroradiol* 29(3): 542–549.

Shohat M, Lachman R, Gruber HE, Rimoin DL. 1989. Brachyolmia: radiographic and genetic evidence of heterogeneity. *Am J Med Genet* 33(2): 209–219.

Shoja MM, Tubbs RS, Khaki AA, Shokouhi G. 2006. A rare variation of the posterior cranial fossa: duplicated falx cerebelli, occipital venous sinus, and internal occipital crest. *Folia Morphol (Warsz)* 65(2): 171–173.

Shoja MM, Tubbs RS, Loukas M, Shokouhi G, Oakes WJ. 2007. A complex dural-venous variation in the posterior cranial fossa: a triplicate falx cerebelli and an aberrant venous sinus. *Folia Morphol (Warsz)* 66(2): 148–151.

Snell RS. 2010. *Clinical Neuroanatomy*, seventh edition. Philadelphia: Wolters Kluwer Lippincott Williams & Wilkins.

Soleiman J, Demaerel P, Rocher S, Maes F, Marchal G. 2005. Magnetic resonance imaging study of the level of termination of the conus medullaris and the thecal sac: influence of age and gender. *Spine (Phila Pa 1976)* 30(16): 1875–1880.

Tubbs RS, Salter EG, Grabb PA, Oakes WJ. 2001. The denticulate ligament: anatomy and functional significance. *J Neurosurg* 94(2 Suppl): 271–275.

Tubbs RS, Dockery SE, Salter G, Elton S, Blount JP, Grabb PA, Oakes WJ. 2002. Absence of the falx cerebelli in a Chiari II malformation. *Clin Anat* 15(3): 193–195.

Tubbs RS, Murphy RL, Kelly DR, Lott R, Salter EG, Oakes WJ. 2005. The filum terminale externum. *J Neurosurg Spine* 3(2): 149–152.

Tubbs RS, Kelly DR, Lott R, Salter EG, Oakes WJ. 2006. Complete ossification of the human falx cerebri. *Clin Anat* 19(2): 147–150.

Tubbs RS, Mortazavi MM, Loukas M, Shoja MM, Cohen-Gadol AA. 2011. The intracranial denticulate ligament: anatomical study with neurosurgical significance. *J Neurosurg* 114(2): 454–457.

Uduma FU, Pius F, Mathieu M. 2012. Computed tomographic pattern of physiological intracranial calcifications in a city in central Africa. *Glob J Health Sci* 4(1): 184–191.

VandeVyver V, Lemmerling M, De Foer B, Casselman J, Verstraete K. 2007. Arachnoid granulations of the posterior temporal bone wall: imaging appearance and differential diagnosis. *AJNR Am J Neuroradiol* 28(4): 610–612.

Wang AM, Fitzgerald TJ, Lichtman AH, Power TC, Zamani AA, Haykal HA, Rumbaugh CL. 1986. Neuroradiologic features of primary falx osteosarcoma. *AJNR Am J Neuroradiol* 7(4): 729–732.

Wolpow ER, Schaumburg HH. 1972. Structure of the human arachnoid granulation. *J Neurosurg* 37(6): 724–727.

Won HS, Han SH, Oh CS, Lee JI, Chung IH, Kim SK. 2010. Topographic variations of the optic chiasm and the foramen diaphragma sellae. *Surg Radiol Anat* 32(7): 653–657.

Further reading

Adeeb N, Mortazavi MM, Tubbs RS, Cohen-Gadol AA. 2012. The cranial dura mater: a review of its history, embryology, and anatomy. *Childs Nerv Syst* 28(6): 827–837.

Alkhazali T. 2009. Anatomical variation in the course, branches, and metrical measurement of the grooves, of the middle meningeal artery inside the skull. *Tikrit Medical Journal* 15(2): 38–41.

Alper F, Kantarci M, Dane S, Gumustekin K, Onbas O, Durur I. 2004. Importance of anatomical asymmetries of transverse sinuses: an MR venographic study. *Cerebrovasc Dis* 18(3): 236–239.

An YH, Wee JH, Han KH, Kim YH. 2011. Two cases of petrosquamosal sinus in the temporal bone presented as perioperative finding. *Laryngoscope* 121(2): 381–384.

Ayanzen RH, Bird CR, Keller PJ, McCully FJ, Theobald MR, Heiserman JE. 2000. Cerebral MR venography: normal anatomy and potential diagnostic pitfalls. *AJNR Am J Neuroradiol* 21(1): 74–78.

Ayeni SA, Ohata K, Tanaka K, Hakuba A. 1995. The microsurgical anatomy of the jugular foramen. *J Neurosurg* 83(5): 903–909.

Balo J. 1950. The dural venous sinuses. *Anat Rec* 106(3): 319–324.

Bergman R, Thompson S, Afifi A. 1988. Compendium of Human Anatomic Variation: Text, Atlas, and World Literature. Berlin, Munich: Urban & Schwarzenberg.

Bisaria KK. 1985a. Anatomic variations of venous sinuses in the region of the torcular Herophili. *J Neurosurg* 62(1): 90–95.

Bisaria KK. 1985b. The superficial sylvian vein in humans: with special reference to its termination. *Anat Rec* 212(3): 319–325.

Breschet G. 1829. *Recherches Anatomiques Physiologiques et Pathologiques sur le Système Veineux et Spécialement sur les Canaux Veineux des Os*. Paris: Villeret et Rouen.

Brockmann C, Kunze SC, Schmiedek P, Groden C,. Scharf J. 2012. Variations of the superior sagittal sinus and bridging veins in human dissections and computed tomography venography. *Clin Imaging* 36(2): 85–89.

Browder J, Browder A, Kaplan HA. 1972. The venous sinuses of the cerebral dura mater. I. Anatomical structures within the superior sagittal sinus. *Arch Neurol* 26(2): 175–180.

Browder J, Kaplan HA, Krieger AL. 1976. Anatomical features of the straight sinus and its tributaries. *J Neurosurg* 44(1): 55–61.

Bruner E, Sherkat S. 2008. The middle meningeal artery: from clinics to fossils. *Childs Nerv Syst* 24(11): 1289–1298.

Bykal L, Ceylan S, Akturk F, Dinc H, Kuzeyli K, Duru S, Soylev E. 1995. Unilateral transverse sinus aplasia: a case report. *Turkish Neurosurgery* 5: 73–75.

Cai CQ, Zhang QJ, Yang WD, Wang CX, Shen CH. 2009. Neuroimages of persistent falcine sinus in children. *World J Pediatr* 5(1): 63–64.

Chandler SB, Derezinski CF. 1935. The variations of the middle meningeal artery within the middle cranial fossa. *Anat Rec* 62(3): 309–319.

Chauhan NS, Sharma YP, Bhagra T, Sud B. 2011. Persistence of multiple emissary veins of posterior fossa with unusual origin of left petrosquamosal sinus from mastoid emissary. *Surg Radiol Anat* 33(9): 827–831.

Choi JH, Woo HY. 2013. The neglected emissary vein in mastoidectomy; persistent petrosquamosal sinus in the laterally located sigmoid sinus. *Am J Otolaryngol.* 34(3): 255–257.

Conroy GC. 1982. The emissary foramina: Their value in platyrrhine systematics. *American Journal of Physical Anthropology* 57(1): 7–12.

Cruveilhier J. 1852. *Traité d'Anatomie Descriptive: Angéologie*. Paris, Labé.

Curnow J. 1873. Two instances of irregular ophthalmic and middle meningeal arteries. *J Anat Physiol* 8(1): 155–156.

Dai PD, Zhang HQ, Wang ZM, Sha Y, Wang KQ, Zhang TY. 2007. Morphological and positional relationships between the sigmoid sinus and the jugular bulb. *Surg Radiol Anat* 29(8): 643–651.

Das AC, Hasan M. 1970. The occipital sinus. *J Neurosurg* 33(3): 307–311.

Diao Y, Liang L, Yu C, Zhang M. 2013. Is there an identifiable intact medial wall of the cavernous sinus? Macro-/microscopic anatomical study using sheet plastination. *Neurosurgery* 73: 106–110.

Duncan IC, Dos Santos C. 2003. Accessory meningeal arterial supply to the posterior nasal cavity: another reason for failed endovascular treatment of epistaxis. *Cardiovasc Intervent Radiol* 26(5): 488–491.

Fukusumi A, Okudera T, Takahashi S, Taoka T, Sakamoto M, Nakagawa H, Takayama K, Kichikawa K, Iwasaki S. 2010. Anatomical evaluation of the dural sinuses in the region of the torcular herophili using three dimensional CT venography. *Acad Radiol* 17(9): 1103–1111.

Furstenberg A. 1937. Septic thrombophlebitis of the sigmoid sinus. *Trans Am Acad Ophthalmol* 42: 424–431.

Gailloud P, Fasel JH, Muster M, Desarzens F, Ruefenacht DA. 1997. Termination of the inferior petrosal sinus: an anatomical variant. *Clin Anat* 10(2): 92–96.

Gailloud P, San Millan Ruiz D, Muster M, Murphy KJ, Fasel JH, Rufenacht DA. 2000. Angiographic anatomy of the laterocavernous sinus. *AJNR Am J Neuroradiol* 21(10): 1923–1929.

Gangopadhyay K, McArthur PD, Larsson SG. 1996. Unusual anterior course of the sigmoid sinus: report of a case and review of the literature. *J Laryngol Otol* 110(10): 984–986.

Giesemann AM, Goetz GF, Neuburger J, Lenarz T, Lanfermann H. 2011. Persistent petrosquamosal sinus: high incidence in cases of complete aplasia of the semicircular canals. *Radiology* 259(3): 825–833.

Giuffrida-Ruggeri V. 1904. Proposta di uno studio delle ramificazinoi dell'arteria meningea media nei degenerati. Comunicazioni al XII Congresso della Società Freniatica Italiana.

Goncalves MB, de Oliveira JG, Williams HA, Alvarenga RM, Landeiro JA. 2012. Cavernous sinus medial wall: dural or fibrous layer? Systematic review of the literature. *Neurosurg Rev* 35(2): 147–153.

Hacker H. 1974. Normal supratentorial veins and dural sinuses. In *Radiology of the Skull and Brain: Angiography* (eds T Newton, D Potts). St Louis: Mosby, pp. 1851–1862.

Hamnett NT, Ogungbo B, Nahser N, Javadpour M. 2010. Anomalous cerebral venous sinus drainage. *Br J Neurosurg* 24(4): 497–498.

Hollinshead W. 1969. *Anatomy for Surgeons. Vol. 1. The Head and Neck*. New York: Harper and Row.

House H P, Patterson ME. 1964. Persistent stapedial artery: report of two cases. *Trans Am Acad Ophthalmol Otolaryngol* 68: 644–646.

Hyrtl J. 1836. Neue beobachtungen aus dem gebiete der menschlichen und vergleichenden anatomie. Med Jahrb Oesterreich Staates(10): 457–466.

Ichijo H, Hosokawa M, Shinkawa H. 1996. The relationship between mastoid pneumatization and the position of the sigmoid sinus. *Eur Arch Otorhinolaryngol* 253(7): 421–424.

Kanavel A, Davis L. 1922. Surgical anatomy of the trigeminal nerve. Surg Gynecol Obstetr 34: 357–366.

Kaplan HA, Browder J. 1973. Atresia of the rostral superior sagittal sinus: substitute parasagittal venous channels. *J Neurosurg* 38(5): 602–607.

Kaplan HA, Browder AA, Browder J. 1972. Atresia of the rostral superior sagittal sinus: associated cerebral venous patterns. *Neuroradiology* 4(4): 208–211.

Kaplan HA, Browder J, Krieger AJ. 1975. Venous channels within the intracranial dural partitions. *Radiology* 115(3): 641–645.

Kedzia A. 1987. The cerebral and meningeal venous valves during human ontogenesis. Folia Morphol (Warsz) 46(3–4): 197–206.

Komiyama M, Kitano S, Sakamoto H, Shiomi M. 1998. An additional variant of the persistent primitive trigeminal artery: accessory meningeal artery-antero-superior cerebellar artery anastomosis associated with moyamoya disease. *Acta Neurochir (Wien)* 140(10): 1037–1042.

Kopuz C, Aydin ME, Kale A, Demir MT, Corumlu U, Kaya AH. 2010. The termination of superior sagittal sinus and drainage patterns of the lateral, occipital at confluens sinuum in newborns: clinical and embryological implications. *Surg Radiol Anat* 32(9): 827–833.

Kresimir Lukic I, Gluncic V, Marusic A. 2001. Extracranial branches of the middle meningeal artery. *Clin Anat* 14(4): 292–294.

Kumar S, Mishra NK. 2012. Middle meningeal artery arising from the basilar artery: report of a case and its probable embryological mechanism. *J Neurointerv Surg* 4(1): 43–44.

Lv X, Jiang C, Li Y, Liu L, Liu J, Wu Z. 2011. The laterocavernous sinus system: venous inflows, venous outflows, and clinical significance. *World Neurosurg* 75(1): 90–95.

Magden AO. 1991. Triple straight sinus: report of 2 cases. *Anat Anz* 173(1): 17–22.

Manjunath K. 2001. Anomalous origin of the middle meningeal artery: a review. *J Anat Soc India* 50(2): 179–183

Manjunath KY. 2004. Anomalies of transverse and sigmoid sinuses associated with contracted jugular foramina. *Indian J Otolaryngol Head Neck Surg* 56(2): 108–114.

Marsot-Dupuch K, Gayet-Delacroix M, Elmaleh-Berges M, Bonneville F, Lasjaunias P. 2001. The petrosquamosal sinus: CT and MR findings of a rare emissary vein. *AJNR Am J Neuroradiol* 22(6): 1186–1193.

Matouk CC, Mandell DM, Krings T, Willinsky RA, Ter Brugge KG. 2011. Persistant anterior falcine sinus: demonstration by CT angiography. *Can J Neurol Sci* 38(5): 760–761.

Matsushima T, Suzuki SO, Fukui M, Rhoton AL Jr, de Oliveira E, Ono M. 1989. Microsurgical anatomy of the tentorial sinuses. *J Neurosurg* 71(6): 923–928.

Miller DL, Doppman JL, Chang R. 1993. Anatomy of the junction of the inferior petrosal sinus and the internal jugular vein. *AJNR Am J Neuroradiol* 14(5): 1075–1083.

Mitsuhashi Y, Nishio A, Kawahara S, Ichinose T, Yamauchi S, Naruse H, Matsuoka Y, Ohata K, Hara M. 2007. Morphologic evaluation of the caudal end of the inferior petrosal sinus using 3D rotational venography. *AJNR Am J Neuroradiol* 28(6): 1179–1184.

Mortazavi M, Denning M, Yalcin B, Shoja M, Loukas M, Tubbs RS. 2013. The intracranial bridging veins: a comprehensive review of their history, anatomy, histology, pathology, and neurosurgical implications. *Childs Nerv Syst* 29(7): 1073–1078.

Neumann JO, Herweh C, Halatsch ME. 2010. Congenital duplication of the superior sagittal sinus and parietal encephalocele after vacuum extraction delivery. *Acta Neurochir (Wien)* 152(4): 713–716.

O'Connell JEA. 1934. Some observations on the cerebral veins. *Brain* 57(4): 484–503.

Ohata K, Nishio A, Takami T, Goto T. 2006. Sudden appearance of transdural anastomosis from middle meningeal artery to superior cerebellar artery during preoperative embolization of meningioma. *Neurol India* 54(3): 328.

Oka K, Rhoton AL Jr, Barry M, Rodriguez R. 1985. Microsurgical anatomy of the superficial veins of the cerebrum. *Neurosurgery* 17(5): 711–748.

Omeis I, Crupain M, Tenner M, Murali R. 2006. Anomalous origin of the middle meningeal artery from the petrous segment of the internal carotid artery associated with multiple cerebrovascular abnormalities. *Internet J Radiol* 4(2).

Otsubo Y, Sato H, Sato aN, Ito H. 1999. Cephaloceles and abnormal venous drainage. *Childs Nerv Syst* 15(6–7): 329–332.

Paparella M, Sajjadi H. 1988. The lateral sinus and Trautmann's triangle in Meniere's disease: considerations of pathogenesis. Proceedings of the Second International Symposium on Menieres's Disease. J. Nadol. Amsterdam: Kugler Publications.

Petroni S, Marrone AC. 1997. Study of the trabecular projections (Chordae Willisii) of the superior sagittal sinus. *Ital J Anat Embryol* 102(3): 155–163.

Reis CVC, Zabramski JM, Safavi-Abassi S, Deshmukh P, Spetzler RF, Preul MC. 2007. Trautmann's triangle and the transpetrosal approaches: an anatomical study. *Skull Base* 17(S 2): A079.

Rhoton AL Jr. 2002. The cerebral veins. *Neurosurgery* 51(4): S159–205.

Rollins N, Ison C, Booth T, Chia J. 2005. MR venography in the pediatric patient. *AJNR Am J Neuroradiol* 26(1): 50–55.

Ruttin E. 1926. Kloaken- und blindsackbildung am sinus sigmoideus. *Acta Otolaryng* 9: 217–220.

Ryu CW. 2010. Persistent falcine sinus: is it really rare? *AJNR Am J Neuroradiol* 31(2): 367–369.

San Millan Ruiz D, Gailloud P, de Miquel Miquel MA, Muster M, Dolenc VV, Rufenacht DA, Fasel JH. 1999. Laterocavernous sinus. *Anat Rec* 254(1): 7–12.

San Millan Ruiz D, Gailloud P,. Rufenacht DA, Delavelle J, Henry F, Fasel JH. 2002. The craniocervical venous system in relation to cerebral venous drainage. *AJNR Am J Neuroradiol* 23(9): 1500–1508.

San Millan Ruiz D, Fasel JH, Rufenacht DA, Gailloud P. 2004. The sphenoparietal sinus of breschet: does it exist? An anatomic study. *AJNR Am J Neuroradiol* 25(1): 112–120.

San Millan Ruiz D, Gailloud P, Yilmaz H, Perren F, Rathgeb JP, Rufenacht DA, Fasel JH. 2006. The petrosquamosal sinus in humans. *J Anat* 209(6): 711–720.

San Millan Ruiz D, Fasel JH, Gailloud P. 2012. Unilateral hypoplasia of the rostral end of the superior sagittal sinus. *AJNR Am J Neuroradiol* 33(2): 286–291.

Sarmiento PB, Eslait FG. 2004. Surgical classification of variations in the anatomy of the sigmoid sinus. *Otolaryngol Head Neck Surg* 131(3): 192–199.

Saxena RC, Beg MA, Das AC. 1973. Double straight sinus. Report of six cases. *J Neurosurg* 39(4): 540–542.

Saxena RC, Beg MA, Das AC. 1974. The straight sinus. *J Neurosurg* 41(6): 724–727.

Schmutz HK. 1980. The chordae Willisii in the superior sagittal sinus: morphology and classification. *Acta Anat (Basel)* 108(1): 94–97.

Shah QA, Hurst RW. 2007. Anomalous origin of the middle meningeal artery from the basilar artery: a case report. *J Neuroimaging* 17(3): 261–263.

Sharifi M, Kunicki J, Krajewski P, Ciszek B. 2004. Endoscopic anatomy of the chordae willisii in the superior sagittal sinus. *J Neurosurg* 101(5): 832–835.

Shatz A, Sade J. 1990. Correlation between mastoid pneumatization and position of the lateral sinus. *Ann Otol Rhinol Laryngol* 99(2 Pt 1): 142–145.

Shiu PC, Hanafee WN, Wilson GH, Rand RW. 1968. Cavernous sinus venography. *Am J Roentgenol Radium Ther Nucl Med* 104(1): 57–62.

Singh M, Nagashima M, Inoue Y. 2004. Anatomical variations of occipital bone impressions for dural venous sinuses around the torcular Herophili, with special reference to the consideration of clinical significance. *Surg Radiol Anat* 26(6): 480–487.

Srijit D, Shipra P. 2007. Unusual venous sinuses. *Bratisl Lek Listy* 108(2): 104–106.

Standring S. 2008. *Gray's Anatomy: The Anatomical Basis of Clinical Practice*. 40th edition. Philadelphia: Churchill Livingstone.

Surendrababu N, Subathira R, Livingstone RS. 2006. Variations in the cerebral venous anatomy and pitfalls in the diagnosis of cerebral venous sinus thrombosis: low field MR experience. *Indian J Med Sci* 60(4): 135–142.

Tanoue S, Kiyosue H, Okahara M, Sagara Y, Hori Y, Kashiwagi J, Mori H. 2006. Para-cavernous sinus venous structures: anatomic variations and pathologic conditions evaluated on fat-suppressed 3D fast gradient-echo MR images. *AJNR Am J Neuroradiol* 27(5): 1083–1089.

Thuy MN, Ramesh R, Soh B, Drummond KJ. 2012. Cadaveric dissection identifying the left superior anastomotic vein of Trolard communicating indirectly with the superior sagittal sinus via a lateral lacuna. *J Clin Neurosci* 19(2): 286–288.

Trolard P. 1890. Les veines méningées moyennes. Rev Sci Biol: 485–499.

Tubbs RS, Loukas M. 2006. Duplication of the superior sagittal sinus. *Clin Anat* 19(8): 728.

Tubbs RS, Salter EG, Elton S, Grabb PA, Oakes WJ. 2001. Sagittal suture as an external landmark for the superior sagittal sinus. *J Neurosurg* 94(6): 985–987.

Tubbs RS, Ammar K, Liechty P, Wellons JC 3rd, Blount JP, Salter EG, Oakes WJ. 2006. The marginal sinus. *J Neurosurg* 104(3): 429–431.

Tubbs RS, Loukas M, Louis RG Jr, Shoja MM, Acakpo-Satchivi L, Blount JP, Salter EG, Oakes WJ Wellons JC 3rd. 2007a. Anatomy of the falcine venous plexus. *J Neurosurg* 107(1): 155–157.

Tubbs RS, Salter EG, Wellons JC 3rd, Blount JP, Oakes WJ. 2007b. The sphenoparietal sinus. *Neurosurgery* 60(2 Suppl 1): ONS9–12.

Tubbs RS, Loukas M, Shoja MM, Apaydin N, Ardalan MR, Oakes WJ. 2008. Lateral lakes of Trolard: anatomy, quantitation, and surgical landmarks. Laboratory investigation. *J Neurosurg* 108(5): 1005–1009.

Tubbs RS, Bosmia AM, Shoja MM, Loukas M, Cure JK, Cohen-Gadol AA. 2011. The oblique occipital sinus: a review of anatomy and imaging characteristics. *Surg Radiol Anat* 33(9): 747–749.

Turgut S, Tos M. 1992. Correlation between temporal bone pneumatization, location of lateral sinus and length of the mastoid process. *J Laryngol Otol* 106(6): 485–489.

Ueyama T, Al-Mefty O, Tamaki N. 1998. Bridging veins on the tentorial surface of the cerebellum: a microsurgical anatomic study and operative considerations. *Neurosurgery* 43(5): 1137–1145.

Vitek JJ. 1989. Accessory meningeal artery: an anatomic misnomer. *AJNR Am J Neuroradiol* 10(3): 569–573.

Waltner JG. 1944. Anatomic variations of the lateral and sigmoid sinuses. *Archives of Otolaryngology* 39(4): 307–312.

Watanabe A, Nagaseki Y, Ohkubo S, Ohhashi Y, Horikoshi T, Nishigaya K, Nukui H. 2003. Anatomical variations of the ten triangles around the cavernous sinus. *Clin Anat* 16(1): 9–14.

Widjaja E, Griffiths PD. 2004. Intracranial MR venography in children: normal anatomy and variations. *AJNR Am J Neuroradiol* 25(9): 1557–1562.

Williams HJR. 1930. Apparent unilateral absence of the sigmoid sinus noted at operation. *Archives of Otolaryngology* 12(3): 339–341.

Wolf BS, Huang YP, Newman CM. 1963. The superficial sylvian venous drainage system. *Am J Roentgenol Radium Ther Nucl Med* 89: 398–410.

Woodburne R. 1978. Essentials of Human Anatomy. New York: Oxford University Press.

Wysocki J. 2002. Morphology of the temporal canal and postglenoid foramen with reference to the size of the jugular foramen in man and selected species of animals. *Folia Morphol (Warsz)* 61(4): 199–208.

Zhang WG, Ye YY, Chen JH, Wang Y, Chen R, Xiong K, Li X, Zhang S. 2010a. Study on inferior petrosal sinus and its confluence pattern with relevant veins by MSCT. *Surg Radiol Anat* 32(6): 563–572.

Zhang WG, Ye YY, Chen JH, Chen R, Kuang LQ, Li X. 2010b. Imaging study of the long extracranial extension of the inferior petrosal sinus with MSCT. *Clin Anat* 23(2): 160–167.

Zuckerkandl E. 1876. Zur Anatomie der Orbitalarterien. *Med Jahr*(6): 343.

82 Spinal cord and associated structures

Shoko M. Yamada[1], Daniel J. Won[1], Pedro B. Nava[1], R. Shane Tubbs[2] and Shokei Yamada[1]
[1]Loma Linda University School of Medicine, Riverside, California, United States
[2]Seattle Science Foundation, Seattle, Washington, USA
St George's University, School of Medicine, St Georges, Grenada
University of Dundee, Dundee, UK

Overview of the spinal cord

The spinal cord is a long cylindrical viscoelastic structure contained in the vertebral canal as a caudal extension of the brain stem. It is divided into five vertical regions: cervical, thoracic, lumbar, sacral, and coccygeal. They are named relative to their nerve roots exiting through the corresponding vertebral foramina. The spinal cord parenchyma is extremely soft, easily compressible and extensible, and is surrounded by three layers of meninges: the pia mater, arachnoid mater, and dura mater.

The curvature of the spine and spinal cord

To accommodate the natural curvature of the spine, cervical lordosis, thoracic kyphosis, and lumbosacral lordosis, the spinal cord follows similar curvatures. Abnormal curvatures of the spinal column include scoliosis, rotational scoliosis, hyperkyphosis, and hyperlorodsis. These are associated with various disorders such as trauma, destructive tumors, degenerative osteoarthritic spondylosis, spondylolisthesis, idiopathic scoliosis, tethered cord syndrome (TCS), and split spinal cord. The scoliosis associated with TCS requires untethering of the spinal cord, usually by sectioning the inelastic filum, before the corrective spine surgery for scoliosis is performed. Decompressive laminectomy in the osteoarthritic narrow canal is sometimes needed to prevent the neurological deficits secondary to correction of scoliosis.

Cerebrospinal fluid relative to spinal cord position

The subarachnoid space is filled with cerebrospinal fluid (CSF), protecting the spinal cord from direct injuries exerted by external forces and from the compressive effects of mass lesions, and from toxicity from any source. The cervical and lumbosacral cord segments are located rather posteriorly close to the posterior arachnoid membrane, while the thoracic segments are located anteriorly close to the anterior arachnoid. These curvatures are maintained in the supine, prone, and recumbent positions.

In normal individuals the posterior roots cover the lower S2 through coccygeal cord segments and filum (2.5–3.0 cm in length). Exposure of these segments requires lateral retraction of the posterior roots.

Spinal cord surgery is usually performed with the patient in the prone position. After laminectomy, the dura and arachnoid are incised to gain access to the spinal cord. As soon as the CSF is drained outside the subarachnoid space, the spinal cord sinks toward the anterior arachnoid membrane. This positional change indicates that the subarachonoid space is now completely vented to the atmosphere, in contrast to the closed craniospinal cavity which is incompletely vented. In the latter condition, the spinal cord is semi-floating in CSF and does not touch the anterior or posterior arachnoid membrane. However, in patients with TCS, the conus medullaris and filum are posteriorly exposed to contact the posterior arachnoid membrane, as demonstrated by MRI (Yamada and Lonser 2000) and intrathecal endoscopy (Woods et al. 2010).

Meninges

The three meningeal layers protect the spinal cord to maintain its structural and physiological integrity and are composed of fibrous tissue with different amounts of fibroblasts and collagen. The pia mater ("tender mother" in Latin), the innermost meningeal layer, is closely connected to the soft spinal cord parenchyma and maintains the cylindrical form. The subpial tissue has abundant elastin and contributes to the viscoelasticity of the spinal cord. The medial layer is the arachnoid mater, a thin, fibrous, elastic membrane. Between the pia and arachnoid extends a fine fibrous network like a spider's web. This network is similar to the arachnoid trabeculations connecting the cerebral arachnoid and the pia, and is more closely distributed in the lumbosacral than the cervical and thoracic subarachnoid space. The lumbosacral spinal cord and cauda equina are fastened quite tightly but elastically to the arachnoid membrane

Bergman's Comprehensive Encyclopedia of Human Anatomic Variation, First Edition. Edited by R. Shane Tubbs, Mohammadali M. Shoja and Marios Loukas.
© 2016 John Wiley & Sons, Inc. Published 2016 by John Wiley & Sons, Inc.

by this network. The lumbosacral cord is gently supported by these trabeculations, since there is no dentate ligament at the lumbosacral level.

In addition, there is an intermediate arachnoid membrane under the arachnoid mater, and the trabeculations are more crowded between this membrane and the pia than under the arachnoid proper. Furthermore, in patients with an elongated cord, these trabeculations are more extensive than in individuals with a normal lumbosacral cord length. In patients with an elongated (lumbosacral) cord, they cover the spinal cord more extensively than in a lumbosacral cord of normal length.

The dura mater is the outer meningeal layer and consists of fibroblasts and collagen. Fibroadipose tissue is mixed with richly entwined veins and connects the outer layer of the dura and the periosteum of the vertebrae. As in the subdural space, the inner layer of the dura can be loosely connected to the arachnoid, probably by fibroblastic tissue (Haines et al. 1993).

Dentate ligaments

The dentate ligaments bridge the pia and dura and support the spinal cord vertically and horizontally. There are 20–22 pairs of dentate ligaments reported in *Cunningham's Textbook of Anatomy* (Romanes 1983). The most cephalic pair is located between the occiput and the first vertebra, namely at the junction between the medulla oblongata and the first spinal cord segment. The second cervical pair is attached to the lower C1 cord and upper C2 cord segments, and the ninth pair to the lower C8 and the upper T1 cord segments. The number of dentate ligaments varies depending on the level of the lowest pair of ligament attachments to the spinal cord, for example 20 pairs for the lowest ligaments at T11–T12 cord segments (Fig. 82.1), and 21 for the T12–L1 lowest, respectively. The authors have not encountered the 22nd dentate ligament from studies of 12 cadavers and 135 surgical cases, although this ligament has been reported (RS Tubbs, personal communication, 2012).

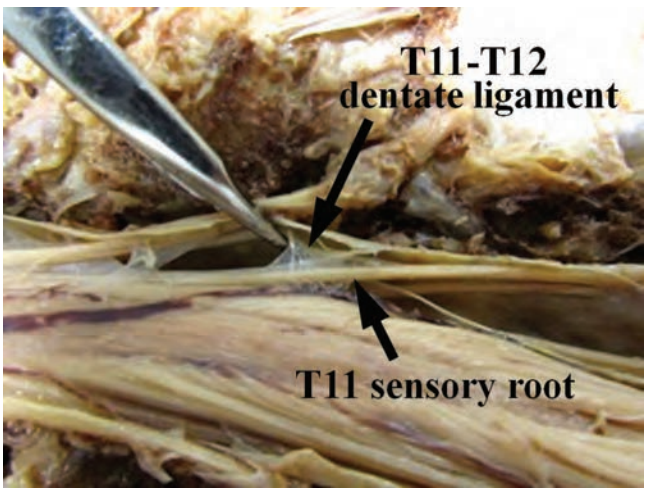

Figure 82.1 The 20th dentate ligament is the lowest in this cadaver. It separates the T11 motor and sensory nerve roots.

The correlation of spinal cord segments with bony anatomy

The number of cord segments is counted by the number of nerve roots. The C1 spinal nerve leaves the spinal cord between the occiput and the C1 vertebra, which makes the center of the C1 cord segment slightly higher than that of the C1 vertebral body. The C8 cord segment is approximately opposite the T1 thoracic vertebra. Each cord segment below T2 is opposite the vertebra of the same number plus 2. The T12 and L1 spinal cord segments are therefore located at the T10 vertebra, the L2 and L3 segments at the T11 vertebra, L3 and L4 at T12, L5, the S1 cord at the L1 vertebra, and S2 through the coccygeal segments at the L2 vertebra (Yamada et al. 1976). Reimann and Anson (1944) studied variations of the caudal end of the spinal cord relative to the vertebral levels in cadavers (see the section "Variation of the caudal end of the spinal cord and the diameter of the filum").

Lengths of L1 through coccygeal cord segments

The authors' interest in spinal cord length is focused on the lumbosacral cord because it varies depending on cord level. The lengths of sacral and coccygeal cord segments in adults fall within the range 55–63 mm. Measurement of the segments in a normal individual is based on the general belief that the caudal end of the normal spinal cord is located at the L1–L2 interspace or above (Tubbs and Oakes 2010), or at the L2–L3 interspace or above (Yamada and Lonser 2000). The lengths of the lumbosacral spinal cord segments vary. If maximally elongated, the lumbosacral cord fills in the entire caudal dural canal in the L1 through S2 vertebrae. The S2 through coccygeal cord segments measure 55±5 mm, equal to the length of the S1–S2 spinal canal.

The entire length of the lower S2 cord segment through the coccygeal segments and the filum is completely covered by the posterior nerve roots, part the cauda equina (Fig. 82.2). This portion of the spinal cord is 2.5–3.0 cm long and difficult to measure by the current resolution of MRI.

In contrast, the lumbosacral cord segments and filum in patients with TCS are located posteriorly and exposed medioposterior to the posterior roots. Those segments are conjectured to be under excessive tension exerted by the inelastic filum and take the shortest course along the concave side of the lumbosacral lordotic canal, thus minimizing the tension (Yamada et al. 2010). Apparently, during the embryological period

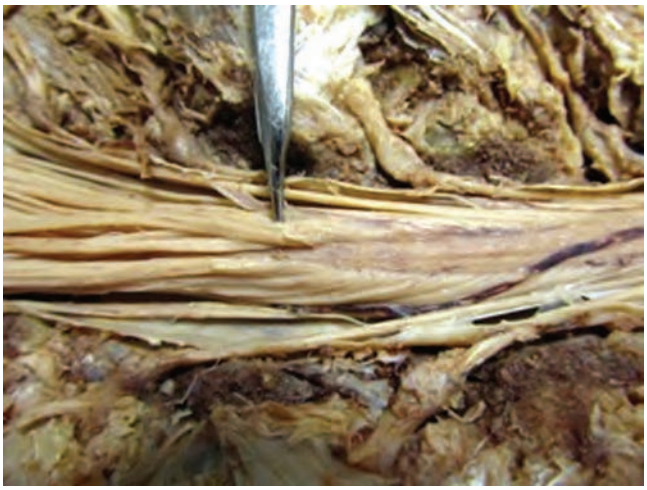

Figure 82.2 Normally the group of the lower S2 cord segment and the S3, S4, S5, and coccygeal segments are completely covered by the posterior nerve roots, which form part of the cauda equina. The tip of the forceps points to the middle of the S2 cord segment.

the posterior roots were not allowed to grow over these cord segments (Conus medullaris).

Diameter of L1–S1 cord segments

The distances from dorsal midline to central canal and the widths of gray matter through the central canal depend on the spinal cord level. The purpose of these measurements was to perform coronal longitudinal myelotomy accurately to control mass spasms in the lower limbs caused by an upper motor lesion secondary to trauma or other diseases above the lumbosacral cord. They are also useful for anterior commissural myelotomy for pain control in the lumbaosacral area (Yamada et al. 1976).The width of gray matter ranges from 4.0 mm at the L1 cord segment to 6.0 mm at the S1 segment. The diameter of the lower end of the spinal cord and the filum is 1.2±2 mm in the coronal dimension and 1.0–1.2 mm in the anteroposterior dimension.

Changing orientation of spinal cord segments relative to the vertebral levels during development

During the 9th week of gestation, the permanent spinal cord is formed with the coccygeal cord segments filling the entire coccygeal canal. Each of the spinal cord segments is approximately opposite the vertebra with the corresponding number. Each nerve root travels horizontally from its own cord segment to the exit through the foramen. This anatomical relationship between the cord segments, nerve roots, and vertebral levels is also seen in adults, and most of them develop TCS some time in their lives.

From the 9th week onwards the spinal column grows faster than the spinal cord, and the latter moves gradually in the rostral direction away from the corresponding vertebrae. By the time of birth the caudal end of the conus medullaris reaches the L3 vertebral level; it reaches the L1 or L2 vertebra by three months of age and remains at the same level in adults. Accordingly, the spinal cord segments are higher than their foramenal exits in the upper thoracic through the lumbar canal, each nerve root traveling in the caudal direction toward its foramen.

In some individuals, often in TCS patients, the caudal end of an elongated spinal cord remains in the lower end of the sacral dural sac. This anatomical relationship suggests that the lumbosacral cord never ascended from the embryonic stage. An additional abnormality is noted in these patients: the lower sacral nerve rootlets travel upwards (cephalad) and join the higher rootlets of the same cord segment, exiting through the same foramen. This anomalous finding probably indicates that the lower sacral vertebrae grow in the caudal direction in the embryo and pull the sacral cord downward (caudad). Another example of caudad extension of the sacral cord was seen in a patient with caudal lipomyelomeningocele (LMMC). The S2–S5 cord segments extended into the lipomatous sac outside the spinal canal and the nerve roots arising from those segments ascended back into the spinal canal and joined the S1 nerve root, exiting through the S1–S2 foramen. This anomalous nerve root arrangement is likely to have resulted from downward growth of the lower sacral cord, as the lipomatous mass grew in the same direction. As a compensatory mechanism to the developmental failure of the S2–S5 vertebrae, the S2–S5 roots found the S1–S2 foramen. In this patient, incontinence developed at the age of 4 years as a sign of TCS.

The relationship between the age of patients with TCS and the location of the spinal cord tip is as follows. The cord tip locations are crowded at the L5, S1, and S2 levels in children, and at L2, L3, and L4 levels in adults. Although these data were collected from patients after the condition had developed in adulthood, they were considered normal individuals for several months or years before the diagnosis was made.

The volume of the spinal cord

According to Barry et al. (1957), the volume of the cervical and lumbar enlargements is greater than the thoracic and sacral cord segments. The spinal cord at the myeloschisis level in dysraphic patients is much greater in volume than any cord segment. In addition, Barry et al. (1957) found rapid growth of the thoracic cord above the myeloschisis to prevent the traction effect of the anomaly to the cervical cord and brain stem.

Embryologically, the secondary neurulation of the spinal cord follows the vacuolization of the caudal end of the lumbosacral

cord and corresponds to the period of coccygeal cord formation (Kunitomo 1978). During this week, the caudal coccygeal cord transforms to the filum terminale and the coccygeal medullary vestige begins to form at its caudal end. By the 11th week the vestige is isolated from the spinal cord. Since it is surrounded by the mesodermal tissue (Kunitomo 1978), failure of the vestige to separate from the filum terminale probably results in fibrosis of the filum at a later date (Yamada and Iacono 1995). This is considered to be the mechanism causing TCS associated with an inelastic filum.

Variation of the caudal end of the spinal cord and the diameter of the filum

Variation of the diameter of the filum terminale and the caudal end of the spinal cord was considered important for the diagnosis of TCS (Pang 1986; Tubbs and Oakes 2010; Yamada et al. 2004). A statistical analysis of 104 adult patients with TCS was published (Yamada et al. 2004), and the data from a further 27 cases were accumulated for measuring the diameter of the filum.

Variation of the caudal end of the spinal cord

The location of the caudal end of the spinal cord is variable in normal individuals and in patients with TCS (Table 82.1). A conus tip at the T12, L1, or L2 vertebra is considered normal in location; at L4, L5, or S1 it is considered to be abnormally low, because the latter are often seen in TCS patients associated with fibrosis of the filum, lipoma, myelomeiningocele, and other anomalies associated with the caudal end of the spinal cord. Whether the conus tip at L3 should be considered abnormally low is debatable.

Reimann and Anson (1944) studied the caudal end of the spinal cord relative to the vertebral levels in cadavers, and found that the spinal cord terminates mostly between T12 and L2 vertebrae and at L3 only in 0.7%. The latter location is considered abnormal only if the patient is symptomatic for TCS and the filum is fibrosed. However, the origin of the coccygeal nerve (100 μm in diameter) is the landmark for determining the conus-filum junction. Because of the current limitation on resolution, MRI studies do not allow for accurate localization of the conus tip relative to the vertebral level.

Diameter of the filum terminale

A filum diameter equal to or above 2 mm was claimed to be one of the diagnostic criteria for tethered spinal cord in children (Pang 1985). However, authors from the same institution reported that the diameter of TCS patients could be 1 mm (Hochhouser et al. 1985). Selden et al. (2003) reported that the diameters of the pediatric patients were greater than 1.5 mm but less than 2 mm. According to Yamada et al. (2004), the diameter ranged from 0.5 mm to 5 mm in adult and late teenage patients with TCS; the normal diameter is 1.0±0.5 mm (Fig. 82.3).

These patients were considered normal individuals before they developed signs and symptoms. However, from the authors' experience, the patient who was operated on for an intraspinal disorder without signs of TCS had a 3 mm thick filum. On stretch testing, the filum elongated more than 50%, whereas in every TCS patient the filum elongates 10% or less no matter whether its diameter is 2 mm or less. The filum may contain adipose tissue.

Table 82.1 Variation in locations of the caudal end of the spinal cord is in TCS patients.

Spinal cord tip opposite vertebra	Number of patients	Percentage
L1	9	9
L2	47	33
L3	48	38
L4	19	15
L5	4	3
S1	4	2
Total	131	100
Regional segments	**Number of patients**	**Percentage**
L1 and L2	56	42
L3	48	38
L4, L5, and S1	27	20
Total	131	100

Source: Yamada et al. (1980).

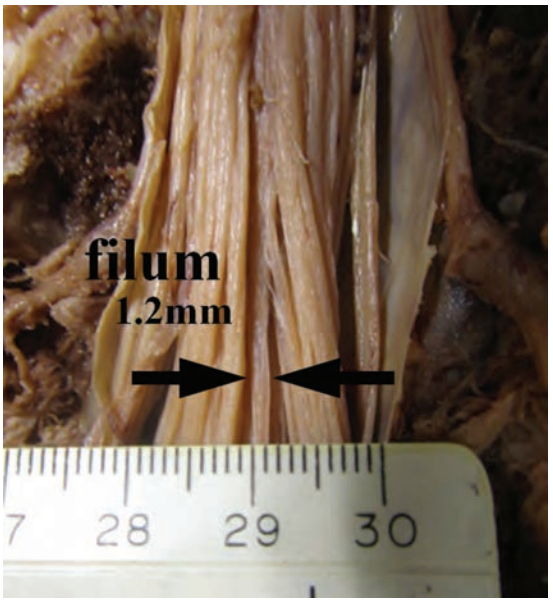

Figure 82.3 The filum in a normal individual (cadaver) measures 1.2 mm (1 mm scale), which is within normal limits.

Other

Sweet (1976) found that corticospinal tract was crossed and uncrossed in 71.5%, only crossed in 13.2%, crossed and uncrossed on one side and only crossed contralaterally in 11.8%, uncrossed bilaterally in 2.8%, and was uncrossed on one side and crossed contralaterally in 0.7%. The pyramidal decussation is often asymmetric.

In general, the spinal cord can be asymmetric on cross-section. Groups of nerves cells (i.e., heterotopias) may be displaced some distance into the white matter, usually into the dorsal columns. Large cells at the apex of the dorsal horns are not unusual. The spinal cord may be incompletely developed, termed atelomyelia. If the pyramidal tracts are aplastic, the sulcus of Flechsig can be seen in the dorsal part of the lateral funiculus, due to the absence of the lateral corticospinal tract.

References

Barry A, Pattern BM, Stewart BH. 1957. Possible factors in the development of the Arnold–Chiari malformation. *J Neurosurg* 14(3): 285–301.

Haines DE, Harkey HL, Al-Mefty O. 1993. The "subdural" space: a new look at an outdated concept. *Neurosurgery* 32(1): 111–120.

Hochhouser L, Chaung L, Harwood-Nash DS, Armstrong D, Savoie J. 1985. The tethered cord syndrome revisited (abstract). *Am J Neuroradiol* 7: 543.

Kunitomo K. 1978. The development and reduction of the tail and of the caudal end of the spina cord. *Contrib Embryol Carnegie Inst* 8: 127–138.

Pang D. 1986. Tethered cord syndrome. In *Advances in Neurosurgery*, Vol 1(1) (ed. HH Hoffman). New York: Springer, pp. 45–79.

Reimann AF, Arson BJ. 1944. Vertebral level of termination of the spinal cord with a report of a sacral cord. *Anat Rec* 88: 127–138.

Romanes GJ. 1983. *The central nervous system. In Cunningham's Textbook of Anatomy* (ed. JG Momanes). London: Oxford University Press pp. 553–683.

Selden NR, Nixon RR, Skog SR, Ashley DB. 2003. Minimal tethered cord syndrome associated with thickening of the filum terminale. *J Neurosurg* 19: 314–218.

Sweet WH. 1976. Recent observations pertinent to improving anterolateral cordotomy. *Clin Neurosurg* 23:80–95.

Tubbs SR, Oakes WJ. 2010. The normal position of the conus medullaris does not exclude a tethered spinal cord. In *Tethered Cord Syndrome in Children and Adults* (ed. S.Yamada). New York: Thieme, pp. 190–195.

Woods KM, Colohan ART, Yamada S, Yamada SM, Won DJ. 2010. Intrathecal endoscopy to enhance the diagnosis of tethered cord syndrome. *J Neurosurg* 13: 477–483.

Yamada S, Iacono RP. 1995. Tethred cord syndrome. In *Disorders of the Pediatric Spine* (ed. D Pang). New York: Raqaven Press, pp. 159–173.

Yamada S, Lonser RR. 2000. Adult tethered cord syndrome. *J Spinal Disord* 13: 319–323.

Yamada S, Perot PL, Ducker TB, Lockard I. 1976. Myelotomy for control of mass spasms in paraplegia. *J Neurosurg* 45: 681–683.

Yamada S, Won DJ, Colohan ART. 1980. Tethered cord syndrome in adults. Presented at the Western Neurosurgical Society Meeting on 19–21 August 1980.

Yamada S, Won DJ, Yamada SM, Hadden A, Javed Siddiqi. 2004. Adult tethered cord syndrome relative to spinal cord length and filum thickness. *Neurol Res* 26(10):732-734.

Yamada S, Lonser RR, Colohan ART, Yamada CT. 2010. Tethered cord syndrome in adults and teenage patients without spinal dysraphism. In *Tethered Cord Syndrome in Children and Adults* (ed. S Yamada). New York, NY: Thieme, pp. 162–179.

Further reading

Cragie EH. 1983. Vascular supply. In *The Spinal Cord*, third edition (ed. GM Austin). New York: Igaku-Shoin, pp. 47–69.

Lemire RG, Loesser JD, Leech RW. 1975. Normal and Abnormal Development of the Human Nervous System. New York: Harper & Row.

Tureen LL. 1928. Circulation of the spinal cord and the effect of vascular occlusion. *A Res Nerv Ment Dis Proc* 18: 394–437.

Yamada S. 1983. Microsurgery. In *The Spinal Cord*, third edition (ed. GMAustin). New York: Igaku-Shoin, pp. 415–444.

Yamada S, Lonser RR, Iacono RP. 1997. Bridge bypass coaptation for cervical root avulsion. In Neurosurgical Operative Atlas, Vol 6 (ed. SS Rengachary). Park Ridge, IL: American Association of Neurological Surgeons (AANS) Publications, pp. 43–50.

Yamada S, Won DJ, Kido DD. 2001. Adult tethered cord syndrome: New classification correlated with symptomatology, imaging and pathophysiology. *Neurosurg Quart* 11: 260–275.

83 Cranial nerves *N*-VI

Jenna R. Voirol[1], Kelley A. Strothmann[1], Anthony Zandian[2], and Joel A. Vilensky[1]
[1]Indiana University, Fort Wayne, Indiana, United States
[2]St George's University, School of Medicine, St Georges, Grenada

In the minds of most anatomists, veins are most variable, arteries are moderately variable, and nerves are the least variable. That is, nerves are considered markedly less variable than veins and arteries. We suggest that this perception is based on peripheral nerves, although it is difficult to reconcile this view when the brachial and lumbar plexuses are considered. Regardless, upon compiling the variability in the first seven cranial nerves (including the terminal nerve, or nerve *N*), we were struck by how variable these nerves could appear. The perplexing aspect of many neurological conditions that affect the head and neck, such as trigeminal neuralgia, may in part be due to variability in the course and composition of the nerves involved.

Nerve N: terminal nerve

Vilensky (2014) presented a recent review on the anatomy of this nerve in human. Briefly, the Terminal Nerve (NT) is a cranial nerve that appears to exist anatomically in all vertebrates. It is certainly functional in some and perhaps all, including humans. However, in many mammals including humans, the NT is very small and has been more or less overlooked and not considered among the cranial nerves. The filaments of this nerve arise anterior and are distinct from the olfactory nerve and tract. The NT fibers are unmyelinated and contain ganglia. The fibers pass through the cribriform plate medial to those of the olfactory nerve. The fibers end in the nasal mucosa and probably contain autonomic as well as neuromodulatory neurons. The nerve appears to play a role in reproductive behavior, perhaps in modulating the reception and recognition of pheromones. Whether there is significant variation in the size and function of this nerve in humans remains to be determined.

Olfactory nerve (CN I)

Two studies found bilateral absence of the bulb, tract, and sinus with the brain specimen showing deep olfactory sulci. The dura surrounding the anterior cranial fossa was not perforated in these specimens where the olfactory nerve would normally course through (Stewart 1939; Morton 1947). Unilateral absence of the olfactory bulb, tract, and trigone was noted in one study (Shoumura et al. 1985).

Five studies found bilateral absence of the olfactory both and tract. Of the variations of the olfactory nerve, bilateral absence of the olfactory bulb and tract was noted to be the most common variation (Di Rienzo 2002). Unilateral absence of the olfactory bulb and tract was noted in four separate studies (Valenti 1910; Mirsalis 1929; Horowitz 1935–36; Roback and Conway 1940). One such clinical presentation included a 35-year-old male with impaired judgment, defective sense of smell, and deafness (Valenti 1910).

Regarding defects limited to the olfactory bulb, three studies found bilateral absence of the bulb (Roback and Conway 1940; Rombaux et al. 2007; Shoumura et al. 1985). Unilateral absence was noted in one study (Shoumura et al. 1985). One patient has been reported with a cystic dilated right olfactory bulb (Roy et al. 1987).

Optic nerve (CN II)

Three studies found complete aplasia of the optic nerve, tract, chiasm, and disc (Scott et al. 1997; Bergman 2006; Sanjari et al. 2006). One case noted penetration of the internal carotid artery by the nerve (Jea et al. 2003). Three studies found double optic nerves with unilateral doubled optic discs and retinal blood supply (Donoso et al. 1981; Lamba 1969; Taylor 2007). Another study found variations in the intracisternal length (4.8–15.1 mm) and intracranial length of the optic nerve (Lang and Reiter 1984). Accessory optic nerves where stray fibers occur in the ciliary body and pigmented layer of the retina have been reported. The optic nerve can be hyperpigmented. Unilateral and bilateral hypoplasia of the optic nerve was also noted (Sadun and Wang 2011; Taylor 2005, 2007). With bilateral aplasia, the presentation was typically blindness, roving eye movements, and sluggish pupillary reaction to light. Unilateral hypoplasia presented with strabismus, afferent pupil

Bergman's Comprehensive Encyclopedia of Human Anatomic Variation, First Edition. Edited by R. Shane Tubbs, Mohammadali M. Shoja and Marios Loukas.
© 2016 John Wiley & Sons, Inc. Published 2016 by John Wiley & Sons, Inc.

defect, unsteady fixation: see-saw nystagmus. Complete aplasia of the optic nerve including the central retinal vessels may be unilateral or bilateral, with unilateral aplasia being more common (Hotchkiss and Green 1979; Margo et al. 1992; Chat et al. 2002; Mosin et al. 2004; Taylor 2005, 2007; Sadun and Wang 2011). Unilateral aplasia of the optic nerve was associated with normal brain development. However, bilateral aplasia was associated with other congenital CNS malformations. Additionally, one study found the optic nerve traveling in the floor of the sphenoid sinus (Girguis-Bucher and Schiegal Wagner 2013).

Variations of the optic tract included unequal length and conjoined optic tract to the peduncles cerebri (Bergman et al. 2006). Variations in the mean cross-sectional area to the right hemisphere (5.1–11.33 mm) and left hemisphere (5.7–10.8 mm) were observed by one study (Andrews et al. 1997). Unilateral and bilateral absence of the optic tract has been reported (Taylor 2007). Variations in the length from the optic chiasm to the lateral geniculate body in females ranged over 25–48 mm and in males 22.5–52 mm (Lang and Reiter 1984).

The optic chiasm varied in length over the range 2–10 mm (Lang and Reiter 1984). The so-called spur may be present on the chiasm. One study noted an asymmetrical optic chiasm, possibly due to optic nerve aplasia (Taylor 2005). Unilateral or bilateral absence of the optic chiasm presented as one of three types, where nasal-retinal fibers would not decussate to the contralateral hemisphere (Taylor 2005, 2007; Brown et al. 2006; Biega et al. 2007). These were classified as the following: type 1: reduced decussation, normal appearing optic nerves; type 2: reduced decussation chiasmal hypoplasia, midline defects (septo-optic dysplasia); and type 3: reduced decussation, chiasmal hypoplasia, clefts, and agenesis of corpus callosum. There also exist variations in the relationship of the chiasm to the sella turcica, which is prefixed in 7.5%, centered over the diaphragm sella in 85%, and postfixed in 7.5% (Griessenauer et al. 2014). A variation in the relationship to the sulcus chiasmatis and hypophysis cerebri exist, with the chiasma resting on the sulcus/hypophysis in 5%, resting on the diaphragm in 12%, projecting backward onto dorsum sellae in 79%, and lying on and behind dorsum sellae in 4% (Whitnall 1979). The papillomacular bundle can be absent.

Variations limited to the optic disc included variations in size (Taylor 2007; Sadun and Wang 2011), absence of missing retinal vessels and poor vision (Taylor 2005), unilateral duplication with decreased visual acuity (Fig. 83.1) (Donoso et al. 1981; Islam et al. 2005), and dysplasia (Sadun and Wang 2011). Coloboma in the inferonasal portion of the disc was noted in two studies (Taylor 2007; Sadun and Wang 2011). Multiple holes, or pits, of the optic nerve head were noted in two studies and were associated with visual field defects (Taylor 2007; Sadun and Wang 2011). Morning Glory Disc or a funnel-shaped staphylomatous excavation of peripapillary retina was noted in two studies (Taylor 2007; Sadun and Wang 2011). Tilted disc syndrome was noted in three studies (Taylor 2007; Witmer et al. 2010; Sadun and Wang 2011). This represents an obliquely placed optic disc with rotations around the AP axis (Fig. 83.2). Tilted disc syndrome presents in 0.4–3.5% of the general population and is bilateral in 80% of the cases. This usually presents with myopia, astigmatism, visual field loss, deficient color vision, and retinal abnormalities (Witmer et al. 2010). Situs inversus of the disc may occur where there is reversal in position of the macula and papilla, so that the central retinal vessels are directed toward the nasal side. The retina can be hyperpigmented. The macula can be excessively large.

Figure 83.1 Unilateral duplication of the optic disc.

Source: Donoso et al. (1981). Reproduced with permission from Elsevier.

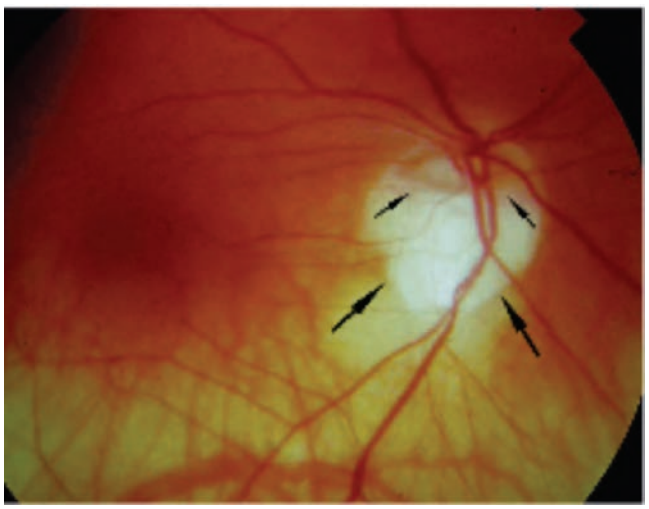

Figure 83.2 Obliquely placed optic disc.

Source: Witmer et al. (2010).

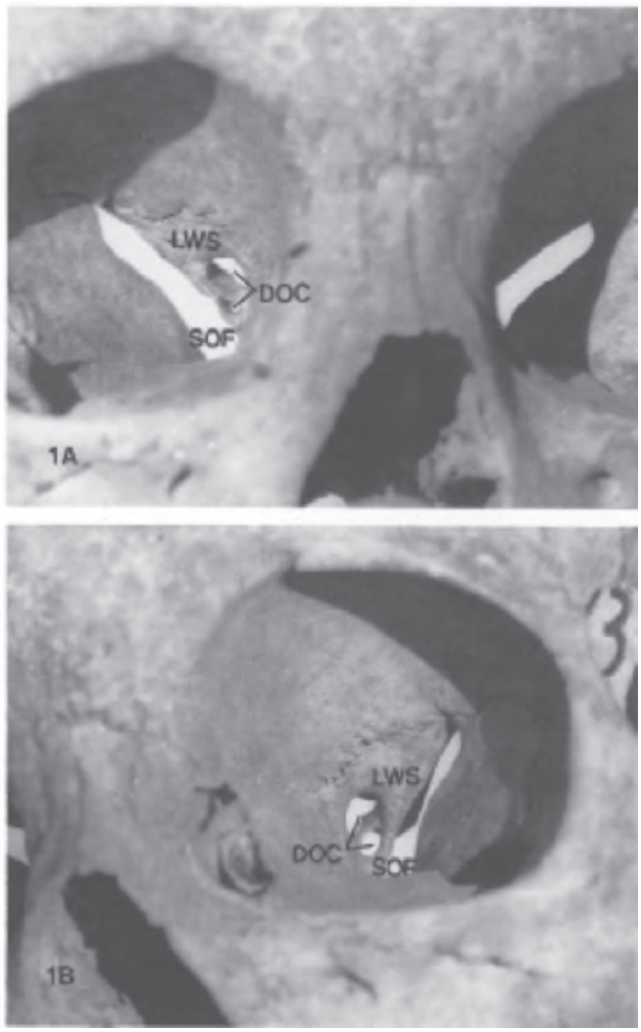

Figure 83.3 Duplication of the optic canal: (a) right side; and (b) left side. LWS: lesser wing of sphenoid; DOC: duplicated optic canal; SOF: superior orbital fissure

Source: Orhan Magden and Kaynak (1996). Reproduced with permission from Elsevier.

Defects limited to the optic canal included bilateral or unilateral duplication (Fig. 83.3). These duplicated canals extend from the orbit to the middle cranial fossa and penetrated the layer of bone between the optic nerve and ophthalmic artery (Orhan Magden and Kaynak 1996; Math et al. 2010; Patil et al. 2011).

Similar to the variation in the olfactory nerve, most of the reported variations in the optic nerve pertain to aplasia and hypoplasia. In addition, for the nerve, there is notable variation in sizes and lengths of its component parts. The most interesting variation relative to its path is that reported by Girguis-Bucher and Schlegel-Wagner (2013), in which the nerves are described as traveling in the floor of the sphenoid sinus.

Oculomotor nerve (CN III)

For the oculomotor nerve there is variation in the location of its origin and in the number of originating rootlets. Along the path of the nerve there is variation in its branching pattern, of its innervation of the extraocular muscles, and its branches to the ciliary ganglion. The nerve may innervate variant muscles and it may communicate with branches of V_1.

The roots of the oculomotor nerve can vary in their mode of emergence. 21% had one root; 71% had two roots; and 8% had two roots which formed a structure that embraced the medial part of the crus cerebri (Tschabitscher and Hocker 1991). One study used MRI to reveal absence of CN III exiting the midbrain in a patient with congenital inferior oculomotor palsy (Kau et al. 2007).

Variations to the nerve itself have been described in eight studies, which have noted a branch to the lateral rectus with or without CN VI and have been associated with Duane Radial Ray and Mobius syndromes (Schafer and Symington 1909; Piersol 1918; Hoyt and Nachtigaller 1965; Warwick 1976; Whitnall 1979; Miller et al. 1982; Demer et al. 2007; Wu et al. 2013). Another possibility includes a communication of CN III with CN IV, VI, and V in the cavernous sinus (Shafer and Symington 1909; Busacca 1925; Warwick 1976; Whitnall 1979; Gottlob et al. 2002; Kassem and Kodsi 2009). Such a communication between CN III and V can lead to Marcus-Gunn jaw-winking syndrome (Fig. 83.4). Typical features include bilateral ptosis and convergent squint on upward gaze. Tooth brushing may cause one eye to become elevated beyond the midline and the eyelid to cover part of the right pupil. Furthermore, it has been observed that CN III can make a communication with CN VI in the orbit (Hoyt and Nachtigaller 1965). One study found a perforated CN III by the posterior cerebral artery with possible compression, and in another example a branch to the pterygopalatine ganglion (Whitnall 1979). Four studies found an aberrant innervation of the superior oblique muscle in the absence of CN IV (Schafer and Symington 1909; Piersol 1918; Whitnall 1979; Kaeser et al. 2012). The lack of hypotrophy of the superior oblique muscle and lack of motor deficit during upward and downward gaze suggest aberrant innervation by CN III. Finally, two studies were able to identify unilateral and bilateral hypoplasia of the subarachnoid portion of CN III (Lim et al. 2007; Kim and Hwang 2009). This hypoplasia was associated with fibrosis of the extraocular muscles and may correlate with ptosis of the upper eyelid. Aplasia of CN III has also been identified using MR imaging of patients with congenital oculomotor nerve palsy, Duane retraction syndrome, and congenital fibrosis syndromes.

The superior division of CN III can be absent and can result in congenital fibrosis of the extraocular muscles that it innervates (Engle 1997). Another study found the nerve innervating an anomalous ocular muscle originating from the belly or proximal part of the levator palpebrae superioris and inserting on the sclera, trochlea, and surrounding tissues (Isomura

Figure 83.4 Eye deviation during tooth brushing.

Source: Gottlob et al. (2002). Reproduced with permission from Elsevier.

1977). Innervation of this muscle originated from two prominent medial branches from the superior branch of CN III. These branches united into a common loop that then supplied the levator palpebrae superioris and the anomalous ocular muscle (Isomura 1977). A communication between CN III and the nasocilliary nerve was also noted in three separate studies (Shafer and Symington 1909; Warwick 1976; Whitnall 1979). If a retractor bulbi muscle is present, it is supplied by the CN III.

The inferior division of CN III was found to be absent in one study, causing limited elevation, adduction, and depression of the eye ipsilateral to the region of loss (Lim et al. 2007). One study found the inferior division innervating the levator palpebri superioris, causing constant elevation of the eyelid whenever the ipsilateral medial rectus was contracted (Martyn 1919). One study found a communication between the inferior division of CN III and CN V leading to Marcus Gunn jaw-winking syndrome (Kassem and Kodsi 2009). Another study found an unusually small branch from the inferior division to the ciliary ganglion, causing the ganglion to become fixed to the nerve and the inferior oblique muscle (Warwick 1976). A separate study characterized the inferior division giving off a branch to the medial rectus with variant innervation of the levator palpebri superioris by this branch (Whitnall 1979). Branching to the inferior oblique muscle was especially varied. Several studies characterized two branches to the inferior rectus and inferior oblique (Shafer and Symington 1909; Whitnall 1979). Another variant traversed the inferior rectus to perforate the ciliary ganglion before reaching the inferior rectus (Shafer and Symington 1908; Piersol 1918; Whitnall 1979). Finally, the entrance of the nervous branch to the inferior oblique could occur on the orbital, ocular, or posterior surfaces of the muscle (Ahmad and Das 2011; Kumar et al. 2011). If CN VI is absent, CN III will innervate the lateral rectus muscle. CN III may innervate the superior oblique muscle.

Branching of the inferior division of CN III was found to be one of five types (Erdogmus 2007).

1. Type 1 has the inferior division splitting in half, the first branch leading towards the medial rectus, and the second branch dividing into two additional branches. This first branch supplies the inferior rectus and inferior oblique. The second branch ended in the ciliary ganglion. Type 2 divides the inferior division into two thick branches: the first branch to the medial rectus, and the second branch divides into three additional branches. Individual branches would then supply the inferior rectus, inferior oblique, and ciliary ganglion.
2. Type 3 has the inferior division dividing into two branches: the first branch ends at the medial rectus, and the second branch then divides into two additional branches. Of these, the first branch ends at the inferior rectus and the second branch further divides into two additional branches. The first branch end in the inferior oblique and the second branch terminates on the ciliary ganglion.
3. Type 4 has the inferior division dividing into three branches. The first branch supplies the medial rectus; the second branch supplies the inferior rectus and inferior oblique; and the third branch supplies the ciliary ganglion.
4. Type 5 has the inferior division splitting into four branches, supplying the medial rectus, inferior oblique, inferior rectus, and the ciliary ganglion.

Trochlear nerve (CN IV)

Unilateral or bilateral absence of the trochlear nerve was found in three studies. Symptoms include hypoplasia of the superior oblique, head tilt, increased hypertropia on ipsilateral gaze, and an association with Brown syndrome (Kaeser et al. 2012).

Variation in the number of roots was also noted. One to six additional roots were observed, with two being the most common (Tschabitscher and Hocker 1991). The trochlear nerve was also observed either exiting from the brainstem at the level of decussation at the dorsal side of the velum (Bergman et al. 2006). The individual fibers composing the trochlear nerve also varied, with numbers ranging from 16 to 24; 4–8 of these fibers were observed entering the nerve uncrossed (Kidd 1922). One study found the trochlear nerve in contact with the superior cerebellar artery where the trochlear nerves are located under the incisura tentoria, forming a plane roughly horizontal and limited laterally by the tentorial edges. The same study found the trochlear nerve crossed by the posterior ethmoidal artery within the orbit. The trochlear nerve may also pierce the levator palpebri superioris *en route* to the superior oblique (Schafer and Symington 1909; Whitnall 1979). The trochlear nerve may also end on the medial or superior border of the superior oblique.

Branching patterns of the trochlear nerve include variations with 1–3 trunks and 6–12 branches. It may innervate the orbicularis oculi, branch to the frontal nerve, communicate with the supratrochlear nerve, communicate with the infratrochlear nerve, or communicate with the nasal nerve (Schafer and Symington 1909; Whitnall 1979). The trochlear nerve may also communicate with the nasociliary or lacrimal nerves (Whitnall 1979).

One study observed numerous variations of the site where the trochlear nerve enters the dura (Figs 83.5–83.10; Bisaria 1988). One such variation has the trochlear nerve entering at small aperture hidden under or behind the free margin of tentorium cerebelli. Another variation includes the nerve piercing the dura in the lateral angle between the attached and free margins of the tentorium cerebelli. The trochlear nerve may also pierce the inner stratum of the dura below the free border of the tentorium cerebelli under the posterior clinoid process.

At the level where the trochlear nerve is inside the cavernous sinus, it may further vary as follows (Bisaria 1988): it may be embedded in the lateral wall of the cavernous sinus; it may run through the septum deep to the superficial dural layer; or it may be found on the lateral wall composed of two dural layers through which the trochlear nerve travels. It may lie between the lateral wall and endothelium, or run in the deep dural layer of the lateral wall. The diameter of the trochlear nerve was also found to vary as it ran through the cavernous sinus from its entrance to the superior orbital fissure (Bisaria 1988). The trochlear nerve may also divide into two branches inside the cavernous sinus; one case was found where the trochlear nerve then reunited with the inferior root that was adherent to V2 (Bisaria 1988).

Tubbs and Oakes (1998) performed a study in which they measured the length and distance of CN IV to various anatomical landmarks. They found variation in the cisternal length of CN IV, which fell in the range of 24–45 mm in length. The relationship of the anterior and posterior clinoid processes to the dural entrance of CN IV was measured as 16–26 mm and

Figure 83.5 CN IV piercing tentorium cerebelli under free margin.

Source: Bisaria (1988). Reproduced with permission from John Wiley & Sons.

Figure 83.6 CN IV piercing tentorium cerebelli under free margin.

Source: Bisaria (1988). Reproduced with permission from John Wiley & Sons.

Figure 83.7 CN IV (T) running between superficial and deep layers of dura.

Source: Bisaria (1988). Reproduced with permission from John Wiley & Sons.

Figure 83.9 CN IV (T) running between superficial and deep layers of dura.

Source: Bisaria (1988). Reproduced with permission from John Wiley & Sons.

Figure 83.8 CN IV (T) running between superficial and deep layers of dura.

Source: Bisaria (1988). Reproduced with permission from John Wiley & Sons.

Figure 83.10 Branching (B) of CN IV (T) in cavernous sinus.

Source: Bisaria (1988). Reproduced with permission from John Wiley & Sons.

11–20 mm, respectively. The midpoint of the lateral midbrain to CN IV was measured to be 0–6 mm in length. Tubbs and Oakes also noted the relationship of CN IV to vascular structures such as SCA and basal vein of Rosenthal to be 0–12 mm and 2–11 mm, respectively.

Ophthalmic nerve, the trigeminal nerve roots, the trigeminal ganglion, and the ciliary ganglion (V_1)

The trigeminal nerve roots and ganglion showed moderate variability. Complete unilateral aplasia was noted resulting in corneal hypoesthesia, some loss of facial sensation, and diminished use of the muscles of mastication (Villanueva et al. 2005). Unilateral aplasia at the level of the brainstem resulted in anesthesia of CN V distribution including corneal and facial anesthesia or hypoesthesia, which may lead to hypoplasia of the muscles of mastication (Aleksic et al. 1975; Villanueva et al. 2005; Becker et al. 2008). The trigeminal ganglion was found to give a branch arising directly from the ganglion, which traveled through a special foramen between the foramina rotundum and ovale (Turner 1868).

The frontal nerve was found to give rise to an infratrochlear branch instead of the normal nasociliary branch (Warwick 1976; Whitnall 1979). The frontal nerve may also give sensory branches to the superior oblique muscle (Warwick 1979; Whitnall 1979). The frontal nerve may also be undivided in the orbit (Bergman et al. 2006).

The supraorbital nerve was found to exit the skull through foramen, notch, or both (Fig. 83.11). Vascular compression is possible at these points, and may be a potential source of migraine headaches (Falluco et al. 2012). The nerve may also communicate with the auriculotemporal nerve, which provides a possible explanation of extended anesthesia to the temporoparietal region after nerve block (Andersen et al. 2000). The supraorbital nerve may also communicate with the ipsilateral supratrochlear nerve, leading to possible anesthesia to the supratrochlear region. Incomplete anesthesia to this region during nerve block may also require additional injections (Andersen et al. 2000). The supratrochlear nerve may also exit through two separate foramina or exit as two branches through one foramen, leading to possible unsuccessful forehead anesthesia, surgical trauma, and post-operative nerve lesions resulting in pain or permanent anesthesia (Anderson et al. 2000).

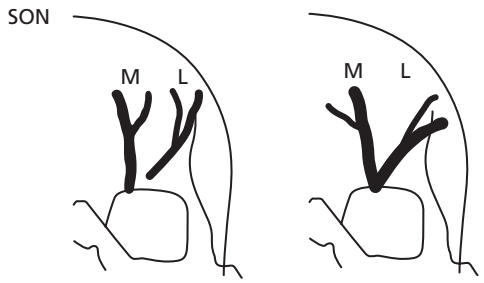

Figure 83.11 Variations of supraorbital nerve (SON) exit. M: medial branch; L: lateral branch.

Source: Fallucco et al. (2012). Reproduced with permission from Walters Kluwer Health.

The supratrochlear nerve has been noted to exit the skull as one or multiple branches (Anderson et al. 2000). Furthermore, it may arise from a branch of the supraorbital nerve (Whitnall 1979) or be duplicated (Whitnall 1979; Andersen et al. 2000).

The lacrimal nerve may replace or become replaced by the zygomaticotemporal nerve (Evans 1959; Warwick 1976; Whitnall 1979). The lacrimal nerve may furthermore increase in size over its course due to contributions from the zygomaticotemporal nerve (Evans 1959). Branches from the lacrimal nerve to the ciliary nerve with concurrent filaments feeding into the lacrimal nerve from the root of the ciliary ganglion have been noted (Whitnall 1979). Doubling of the lacrimal nerve is possible, as well as communications between CN IV, the frontal nerve, and the nasociliary nerve (Whitnall 1979).

The nasociliary nerve may give off sensory branches to the superior rectus, medial rectus, and levator palpebri superioris (Warwick 1976). The nasociliary nerve may also give rise to a filament coursing under CN II and above the inferior rectus, further communicating with CN III and the carotid plexus forming an arch from which several ciliary branches pierce the outer layer of the sclera (Hallet 1847). Another variation includes a filament coursing over CN II or communicating with CN III and the carotid plexus forming an arch, which embraced CN II (Hallet 1847). The nasociliary nerve may also contain a small ganglion that sends fibers to CN III and CN VI (Warwick 1976).

In one study, the long ciliary nerve was found to consist of three nerves instead of two (Hallet 1847).

In three separate studies, the infratrochlear nerve was found to be absent with the supratrochlear nerve occupying its place (Warwick 1976; Whitnall 1979). In a separate example, the internal nasal nerve was found to be absent or passing through the posterior ethmoid canal. This lack of internal nasal nerves may result in diminished sensory supply to the anterior part of the lateral nasal septum (Whitnall 1979).

The anterior ethmoidal nerve may give branches to the frontal and ethmoidal sinuses in the anterior ethmoidal foramen (Warwick 1976). Other observed variations include branches to the levator palpebri superioris, CN II, CN VI, and mucous membranes of the frontal sinus. The presumed sensory fibers carried to these muscles are not likely to be clinically significant (Warwick 1979). The anterior ethmoidal nerve may also be limited to the nasal cavity. The lack of an external nasal nerve may result in absence of sensation on the tip of the nose (Bergman et al. 2006).

The ciliary ganglion can have marked variability, including variations in size, shape, and morphology of the roots of the ganglion. These variations include oval, quadrilateral, rectangular, egg, or irregular-shaped ganglia (Hallet 1847; Siessere et al. 2008). Doubling and tripling of the ganglion has also been noted bilaterally (Hallet 1847; Whitnall 1979). Small or absent

ciliary ganglia have been noted (Warwick 1976; Whitnall 1979). Accessory ganglia may also be present on the medial side of the optic nerve (Whitnall 1979). Additional roots may also enter the ganglion from branches of the pterygopalatine ganglion, CN VI, oculomotor, trochlear, or lacrimal nerves (Schafer and Symington 1909; Warwick 1976; Whitnall 1979). In one study, the ciliary ganglion was perforated by a branch of the ciliary artery (Whitnall 1979). The ciliary ganglion may have connections with CN IV or CN VI (Warwick 1976). Finally, the ciliary ganglion may be fused with sympathetic roots that enter the ganglion (Whitnall 1979).

The sympathetic root of the ciliary ganglion expressed variability of its own. In one study, it was found fused with the sensory root before entering the ganglion (Whitnall 1979). The sympathetic root may also enter the ganglion separately, as part of the sensory root to the ganglia, or it may enter the ganglia with CN III (Hamel et al. 2012). Complete absence of the sympathetic root was also noted as a result of a forward retro-orbital connection between the internal carotid plexus and the ophthalmic nerve within the cavernous sinus (Hamel et al. 2012).

The sensory root of the ciliary ganglion may have absent or multiple roots, which could result in sensory impulses traveling through the long ciliary nerve instead of the ganglion (Schafer and Symington 1909; Warwick 1976; Whitnall 1979). Various origins of the sensory root of the ciliary ganglion exist, including origins from the semilunar ganglion, ophthalmic nerve, supraorbital nerve, and lacrimal nerve (Whitnall 1979). Separate sensory and sympathetic roots can also form a common trunk for the sensory root of the ciliary ganglion (Warwick 1976).

The parasympathetic root of the ciliary ganglion can be doubled (Sinnreich and Nathan 1981) or absent, resulting in the ciliary ganglion becoming attached to the inferior branch of CN III or nerve to the inferior oblique. This may be a possible explanation as to why postganglionic mydrasis can occur following blowout orbital fracture or surgical repair of this type of fracture (Schafer and Symington 1909; Warwick 1976; Sinnreich and Nathan 1981; Hamel et al. 2012).

The short ciliary nerves of the ciliary ganglion have been found to enter the medial aspect of the eyeball after crossing inferior to the optic nerve (Sinnreich and Nathan 1981; Hamel et al. 2012). The short ciliary nerves may also originate from motor or sensory roots (Sinnreich and Nathan 1981). Finally, the short ciliary nerves may have connections with the long ciliary nerves (Sinnreich and Nathan 1981).

The motor root of the ciliary ganglion can either be absent, doubled, multiplied, bifurcate before entering the ciliary ganglion, or arise from the trunk of CN III or CN VI (Whitnall 1979).

Maxillary nerve (V_2)

The maxillary nerve itself expressed moderate variability. Bifid maxillary nerve was noted in one study (Somayaji and Rao 2012). Another study found a ciliary ganglion root (Liu 2005). One final study found branches joining the lacrimal nerve, CN VI, and the vidian nerve (Evans 1959).

The pterygopalatine ganglion can have two extra communications: a posterior nerve traversing the cavernous sinus and orbit to join the ophthalmic nerve; and one anterior nerve coursing in the direction of CN VI. This communication is a possible explanation for how orbital pain is relieved when the pterygopalatine ganglion is blocked (Oomen et al. 2011). The pterygopalatine ganglion may also be divided into a superior branch adjacent to the maxillary nerve, and an inferior branch at the origin of the greater palatine nerve. This may explain failure in ablation procedures of the pterygopalatine ganglion. For example, recurrent trigeminal neuralgia attacks may be explained even after injection treatment blocks one segment (Rusu et al. 2009). The pterygopalatine ganglion may also give branches to CN II, CN VI, and the ciliary nerves (Somayaji and Rao 2012). Finally, reversal of left and right nasopalatine nerves through the foramen of Scarpa has been noted, with the left nerve passing through the posterior foramen and the right nerve passing anterior to the foramen (Bergman et al. 2006).

The zygomaticotemporal nerve can vary in its course. It can travel in an intramuscular path through the temporalis muscle and exits through the deep temporal fascia. Clinically, different intramuscular pathways may lead to an increased risk of developing migraine headaches due to nerve entrapment (Janis et al. 2010). The zygomaticotemporal nerve may also travel in an extramuscular course, between the temporalis muscle and the lateral orbital rim (Janis et al. 2010). Double branches of the zygomaticotemporal nerve either exit through two foramina or arborize in the temporal fossa after exiting from bone or the temporalis muscle. This is clinically important in nerve decompression, where recurrent postoperative pain can be due to incomplete surgical release of the nerve (Janis et al. 2010). Another variation includes a branch of the zygomaticotemporal nerve passing through a small canal in the sphenozygomatic suture. This branch originates either from the main zygomatic nerve or as a communication between the lacrimal nerve and zygomatic nerve. This branch may be implicated in zygomatic or retro-orbital pain, entrapment, tension neuropathy, or compression from narrow canals (Akita et al. 2002).

A branch of the infraorbital nerve can replace the zygomaticofacial nerve. The only other documented variation of the zygomaticofacial nerve includes double or multiple branches, which could possibly complicate surgery in this region (Warwick 1976).

The infraorbital nerve may pass within a septum in the anterosuperior portion of the maxillary sinus (Fig. 83.12). This variant occurs both unilaterally and bilaterally and does not follow the inferior orbital wall to the orbital ridge. Surgeons should be aware of this variant during functional endoscopic sinus surgery. Removal of the septum would result in infraorbital palsy leading to pain and paraesthesia (Mailleux et al. 2010). Dehiscence of bone overlying the infraorbital nerve has been observed, which may cause issues during anesthetic injections introduced into the

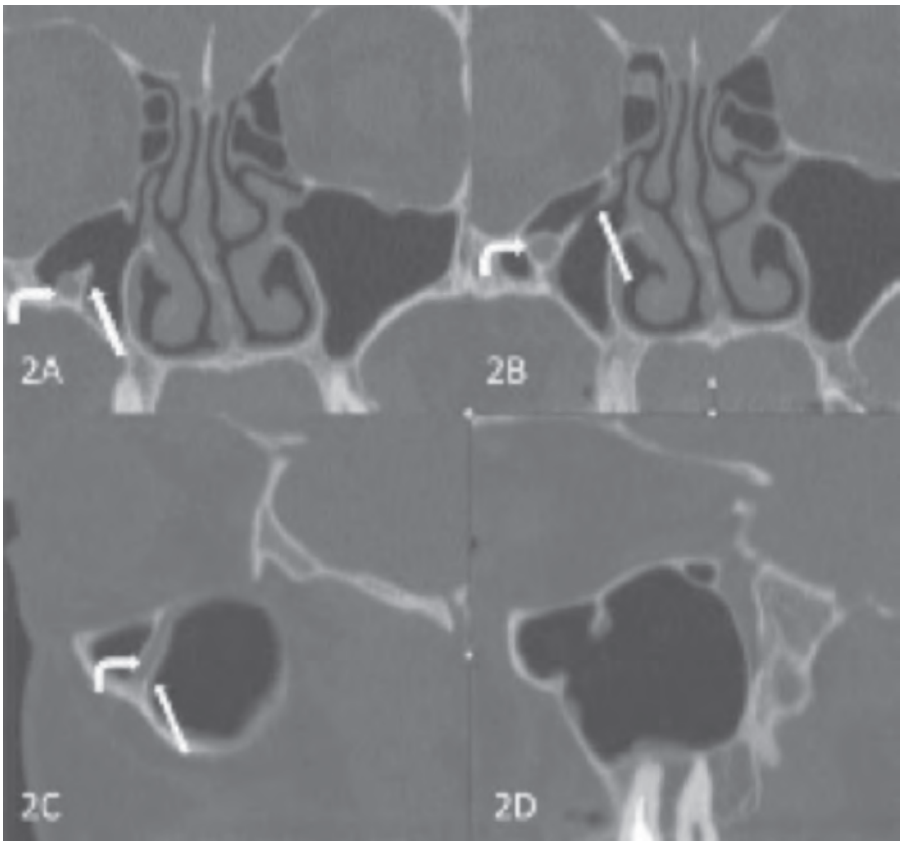

Figure 83.12 Septum, straight arrows; orbital nerve, curved arrow.

Source: Mailleux et al. (2010). Reproduced with permission from Belgian Society of Radiology.

maxillary sinus during nerve block (Mailleux et al. 2010; Tubbs et al. 2010). The infraorbital nerve may also traverse the lumen of the maxillary sinus within the lamella of the infraorbital ethmoid cells. This may cause nerve damage during a Caldwell-Luc procedure when the surgeon enters the sinus (Chandra et al. 2004). The infraorbital nerve may also run in a more lateral fashion than normal, allowing the nerve to pass through the junction of the maxillary and zygomatic bones (Jordan 1967; Tubbs et al. 2010). Unilaterally doubled infraorbital nerves have been observed dividing near the maxillary nerve trunk and orbit with one normal branch and one smaller accessory branch. Neither is completely encased in body canals, and each exit through a separate foramen (Jordan 1967).

The infraorbital nerve may also be divided in the infraorbital canal as equal-sized branches. Each branch was observed encased in separate bony canals and exited through separate foramen. The medial branch was observed exiting 1 cm higher than the lateral branch. The medial branch traveled to the external nasal surface. The lateral branch traveled to the external nasal surface, superior upper lip, and had a communication with CN VII (Leo et al. 1995). A separate variation includes 1-5 branches exiting a single foramen (Leo et al. 1995). Unilateral bifurcation distal to the entrance of the maxillary nerve to the orbit is also possible (Fig. 83.13). These branches enter separate bony canals. The smaller branch of the medial nerve traveled through the lateral foramen. This is clinically significant when dealing with maxillary nerve blocks for trigeminal neuralgia or midface cancer pain treatment. Blockage of one branch could result in inadequate pain relief (Tubbs et al. 2010). Finally, the size of the infraorbital foramen can vary up to 14 mm inferior to the inferior orbital rim. This can put the nerve at risk of surgical trauma when elevating a facial flap during plastic surgery (Somayaji and Rao 2012).

The posterior superior alveolar nerve has been observed passing through canaliculi in the lateral wall of the maxillary sinus or under the mucosa of the sinus (Somayaji and Rao 2012). The posterior superior alveolar nerve may also present single or multiple branches into the zygomatic region (Somayaji and Rao 2012). The posterior superior alveolar nerve can also innervate areas normally supplied by the long buccal nerve (Somayaji and Rao 2012).

The middle superior alveolar nerve can run in the posterior, lateral, or anterior walls of the maxillary antrum after arising from the infraorbital nerve (Fitzgerald 1956). The middle superior alveolar nerve may also exhibit premature origin from the maxillary trunk and pierce the bone a few millimeters lateral to the infraorbital groove (Fitzgerald 1956). The middle superior alveolar nerve can also originate from the anterior superior

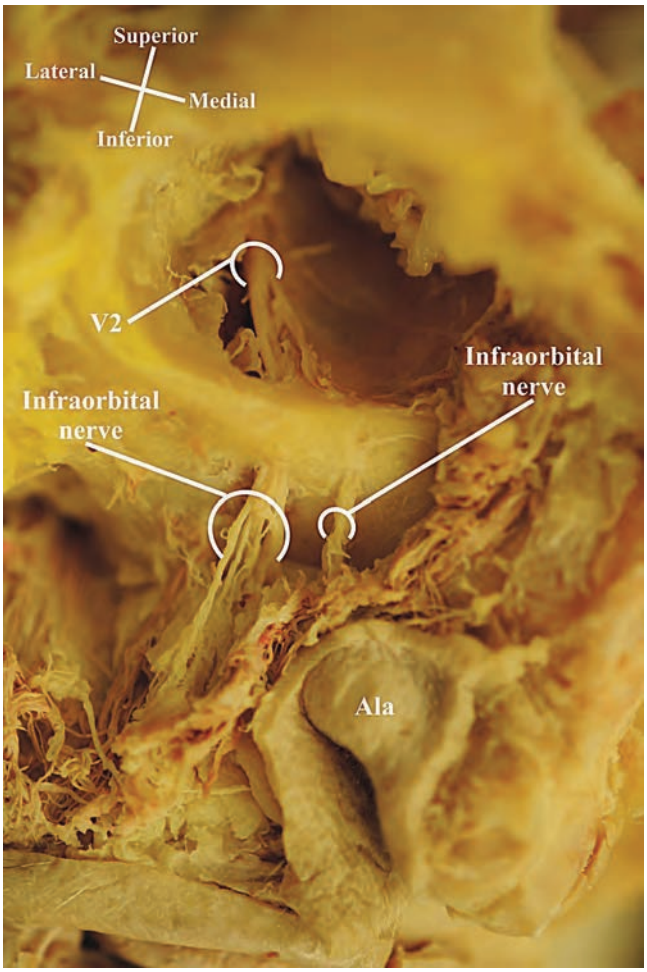

Figure 83.13 Variations between maxillary artery and inferior alveolar nerve.

Source: Tubbs et al. (2010). Reproduced with permission from Walters Kluwer Health.

alveolar nerve due to delayed separation from the infraorbital nerve (Fitzgerald 1956). The middle superior alveolar nerve may also be completely absent, with the anterior alveolar nerve supplying the premolar region. Clinically, vague maxillary pain in the premolar region can be due to sinus injection putting pressure on a variant branch of the anterior superior alveolar nerve (Fitzgerald 1956; Somayaji and Rao 2012).

The anterior superior alveolar nerve can present as a single trunk, as a diffuse plexus (de Oliveira-Santos et al. 2012), or with a canalis sinuous seen at the upper canine tooth and theorized to be a direct palatine extension of the nerve (de Oliveira-Santos et al. 2012). The anterior superior alveolar nerve may present with an accessory bilateral canal seen in the anterior maxilla region. It extends from the lateral nasal wall to an accessory foramen in the hard palate, coursing from the lingual to maxillary lateral incisors. Trauma of this variant nerve can result in non-integration of a dental implant and sensory impairment (Neves et al. 2012). Additional foramina for the anterior superior alveolar nerve have been seen in the anterior palate near the incisive foramen, connected superiorly to the nasopalatine canal (de Oliveira-Santos et al. 2012). Finally, canals associated with additional foramina of the anterior palate had an oblique path toward the anterior portion of the nasal floor. This may represent branches of the nasopalatine nerve or anterior superior alveolar nerve. This final variant suggests varying degrees of anastomoses between the nasopalatine and anterior superior alveolar nerves (de Oliveira-Santos et al. 2012).

Mandibular nerve (V_3)

The mandibular nerve and its branches exhibit the greatest variation of the cranial nerves discussed in this chapter. Starting with the mandibular division, unilateral and bilateral accessory foramina ovale have been observed. From these accessory foramina, branches of the mandibular division travel directly to the pterygoid muscles, tensor veli palatini, and tensor tympani. Unilateral accessory foramina are more common. Clinically, these foramina are a concern in surgical procedures involving the trigeminal nerve and trigeminal ganglion (Krmpotic-Nemanic et al. 2001). An accessory meningeal artery can split the mandibular nerve or one of its branches. This artery can be located medial, lateral, rostral, or split between the inferior alveolar nerve and lingual nerve (Fig. 83.14) (Baumel and Beard 1961). The mandibular division may be bifid, resulting in dental problems when the bifurcation is before the mandibular canal. Inferior alveolar nerve blocks may be unsuccessful in blocking stimuli completely. It may be more effective to use Gow-Gates or high inferior alveolar nerve block procedures (DeSantis and Liebow 1996). Additionally, the mandibular division can create anterior and posterior divisions separated by the pterygosphenoid ligament or bone (Bergman et al. 2006; Schafer and Symington 1909). The final observed variation in the mandibular division results in an aberrant branch to the medial rectus, resulting in the muscle becoming co-activated during contraction of the lateral pterygoid muscle (Lewis and Zee 1993).

The otic ganglion can vary in location, 0–4 mm from the anterior section of the mandibular nerve (Siessere et al. 2008). The otic ganglion may also send branches to the medial pterygoid muscle, sympathetic plexus of the middle meningeal artery, the lesser petrosal nerve, and the auricotemporal nerve (Siessere et al. 2008). The otic ganglion can also be completely absent unilaterally or bilaterally. In unilateral absence, the contralateral ganglion will present with a small thickening. In bilateral absence, a nerve plexus containing ganglion cells sometimes replaces the otic ganglia (Weigner 1898; Siessere et al. 2008).

The submandibular ganglion can vary in morphology, presenting as a triangular-, egg-, or plexiform-shaped mass (Siessere et al. 2008). The ganglion can also be fused with or free from the lingual nerve (Siessere et al. 2008).

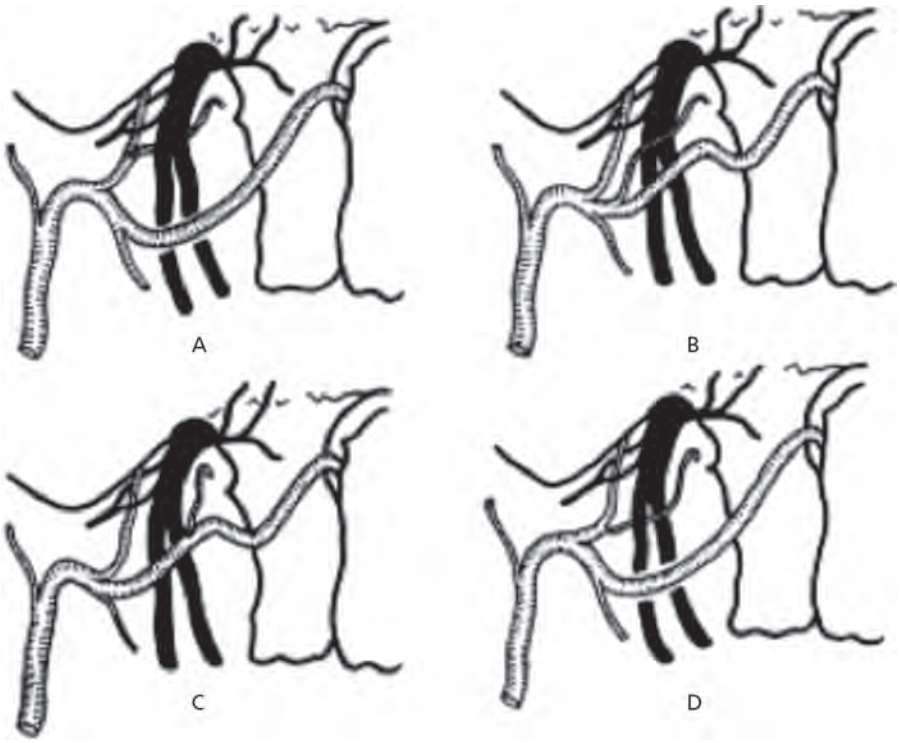

Figure 83.14 Accessory meningeal artery.

Source: Baumel and Beard (1961). Reproduced with permission from John Wiley & Sons.

The "long" buccal nerve may vary from its origin at the maxillary nerve in the spheno-maxillary fossa with no appreciable branches from the mandibular nerve (Turner 1868). The long buccal nerve can also arise separately from the maxillary nerve and mandibular nerve with branches innervating the buccinators (Turner 1868). The long buccal nerve may also arise from the posterior alveolar nerve (Bergman et al. 2006), or from the inferior alveolar nerve (Schafer and Symington 1909). The long buccal nerve can also arise directly from the trigeminal ganglion and pass through a special aperture between the foramen rotundum and foramen ovale (Schafer and Symington 1909). The long buccal nerve can be divided at the foramen ovale with one branch connected to the trigeminal ganglion and a second branch connected to a fasciculus from which the temporal and masseteric nerves arise (Turner 1868). Two separate roots of the long buccal nerve can also fuse together distal to the origin (Gulekon et al. 2005). Another variation includes a unilateral origin from the inferior alveolar nerve within the ramus of the mandible (via a narrow, anterosuperiorly oriented retromolar canal (Jablonski et al. 1985). Additional variants of the long buccal nerve include accessory innervation of the molars through the retromolar foramen (DeSantis and Liebow 1996), direct passage through the temporal muscle (Bergman et al. 2006), and complete absence (Bergman et al. 2006). Accessory innervation can cause difficulty in giving successful local anesthesia of the mandibular molars. Direct introduction of anesthetics into the retromolar area may bypass this problem (DeSantis and Liebow 1996).

The auricotemporal nerve has a wide variability; it may have one branch, divide into smaller branches, or may present a diffuse branching pattern (Andersen et al. 2000). There may exist single, double, triple, or quadruple roots (Baumel et al. 1971; Gulekon et al. 2005). With a single root, the auricotemporal nerve arose near the foramen ovale and followed the same course as the upper root of a two-rooted nerve. With a double root, one root would arise below the mandibular nerve and lay medial to the middle meningeal artery, then loop forward, and pass lateral to the artery to join the second root. Two roots may also subdivide to produce additional roots. Triple roots can present with varying degrees of length. Quadruple roots are commonly associated with a ganglion-like structure nearby. These roots can then go on to supply branches to the temporomandibular joint, external acoustic meatus, zygoma, and parotid gland.

Additionally, the auricotemporal nerve may present with a connecting branch running between the upper and lower nerve roots (Gulekon et al. 2005). The auricotemporal nerve can also vary regarding its relationship to the middle meningeal artery (Baumel et al. 1971; Gulekon et al. 2005). A single root can be medial or lateral to the middle meningeal artery. Double roots can present lateral or medial to the middle meningeal artery. Triple roots present with either upper two roots lateral to the middle meningeal artery or lower two roots medial to the middle meningeal artery. With quadruple roots, the first root is lateral to the middle meningeal artery, the second and third roots are medial to the middle meningeal artery, and the fourth root

is medial to the maxillary artery (Baumel et al. 1971; Gulekon et al. 2005).

Other variations of the auricotemporal nerve include communication with the lesser occipital nerve (Andersen et al. 2000), communication with temporal branch of CN VII (Baumel et al. 1971; Andersen et al. 2000), communication with the supraorbital nerve leading to unexpected supraorbital nerve block during anesthesia to the temporoparietal region (Andersen et al. 2000), and communication with the inferior alveolar nerve (Baumel et al. 1971; Racz et al. 1981; Khaledpour 1984; Gulekon et al. 2005). Five to nine terminal branches were observed in one study (Baumel et al. 1971).

The lingual nerve may present with plexiform roots (Racz et al. 1981) or can be formed from two roots, a posterior root originating from the mandibular nerve and an anterior root from a common trunk originating from the mandibular nerve, which is separated by the maxillary artery (Racz et al. 1981). A communication between the inferior alveolar nerve and the lingual nerve has been observed with one, two, or even three branches. These sensory fibers from the inferior alveolar nerve can be distributed to other regions providing excess innervation in the paralingual area. The parasympathetics to the inferior alveolar nerve may explain secretion of lower labial salivary glands in the absence of efferent input from the otic ganglion to the inferior alveolar nerve (Racz et al. 1981; Khaledpour 1984; Sandoval et al. 2009). The lingual nerve can also present with a communication with the inferior alveolar nerve split by the maxillary artery (Sandoval et al. 2009). In a separate case, the maxillary artery pierced the inferior alveolar nerve deep to the buccal nerve (Sandoval et al. 2009). Other variations include communication with CN XII intramuscularly with one, two, or three connections (Fitzgerald and Law 1958).

Fitzgerald and Law (1958) found lateral or medial communications with CN XII relative to the hypoglossal muscle. The medial communication was found to occur either proximally along lateral fibers of the genioglossus muscle or distally along the tip of the tongue. The lingual nerve may also send branches to the lateral and medial pterygoid muscle and palatoglossal muscle (Racz et al. 1981). The lingual nerve may be divided by a pterygospinous bony bridge, where the anterior fibers lay between the tensor veli palatini and bridge making the nerve vulnerable to compression (Erdogmus et al. 2009). The lingual nerve can be located above the lingual bony plate in the third molar region (Bergman et al. 2006). Finally, a small sublingual ganglion has been observed arising from the lingual nerve (Bergman et al. 2006).

The mylohyoid nerve presents with several types of communications, such as communication (transmylohyoid anastomose of Sappey) with the lingual nerve at the intermediate tendon of the digastric muscle which can help the lingual nerve regain function if injured during a third molar extraction. This abovementioned branch may innervate the tongue (Potu et al. 2009). The nerve to mylohyoid may also communicate with the lingual nerve at the lateral sulcus of the tongue (Racz et al. 1981) or communicate with a dental branch of the inferior alveolar nerve (Carter and Keen 1971). In one instance, the nerve to mylohyoid originated from the lingual nerve (Jablonski et al. 1985). The nerve to mylohyoid may give branches to the depressor anguli oris, platysma, the skin below the chin, and the submandibular gland (Bergman et al. 2006). The mylohyoid nerve can also be doubled with an accessory foramen on the lingual aspect of the mandible. This variation may result in unsuccessful anesthesia during a conventional inferior alveolar block. It may produce accessory innervation of the mandibular teeth and requires specific "high mandibular block" (DeSantis and Liebow 1996). The mylohyoid may give rise to accessory branches that supply the incisors, gingivae, or communicate with the incisive nerve proper (Anderson et al. 1991; DeSantis and Liebow 1996). The nerve to mylohyoid can also run through a canal in the mandible instead of a groove.

The inferior alveolar nerve has been observed to exhibit extensive variations. It may originate from two roots separated by a section portion of the maxillary artery (Sandoval et al. 2009). The inferior alveolar nerve can undertake a plexus arrangement after its origin from the mandibular nerve (Roy et al. 2002). The inferior alveolar nerve may also possess two long roots originating from the posterior mandibular nerve, which then later unite (Roy et al. 2002). Accessory roots of the inferior alveolar nerve can originate directly from the trigeminal ganglion only to join after entering the dental canal (Schafer and Symington 1909). The maxillary artery can also pierce the inferior alveolar nerve shortly after its origin. The artery passes lateral to the lingual nerve and medial to the buccal nerve. The maxillary artery can travel deep to the lingual and buccal nerve (Roy et al. 2002). The inferior alveolar nerve may also form from a common trunk with the lingual nerve, again being pierced by the maxillary artery, and ultimately running deep to the buccal nerve (Roy et al. 2002). The inferior alveolar nerve can also communicate with the nerve to the lateral pterygoid muscle (Sandoval et al. 2009).

A communication and anastomosis between the mandibular, the inferior alveolar, the auriculotemporal, and lingual nerves was seen in one specimen (Khaledpour 1984). The inferior alveolar nerve may divide into one large branch through the mental foramen, and one small branch forming a dental plexus (Anderson et al. 1991). The inferior alveolar nerve can also form one large main trunk and two smaller trunks (Anderson et al. 1991).

The inferior alveolar nerve can form one structure with short direct branches to molar roots, which terminate in a mental arborization (Carter and Keen 1971; Anderson et al. 1991). Furthermore, the inferior alveolar nerve may be situated lower in the mandible, with dental branches traveling in a more posterior and oblique fashion (Carter and Keen 1971). The inferior alveolar nerve may also be situated inferiorly with branches to molar roots arranged in a plexus (Carter and Keen 1991). The inferior alveolar nerve may be associated with the mandibular canal, running from lingual to second and third molar roots, subjacent to first molar roots, buccal, and premolar roots (Anderson et al. 1991). The inferior alveolar nerve can also travel from

the mandibular canal to buccal to apices of the second molar and lingual to apices of the first molar (Anderson et al. 1991). The inferior alveolar nerve can also travel from the mandibular canal to buccal to third molars (Anderson et al. 1991). Finally, the inferior alveolar nerve can be doubled in its course from the mandibular canal unilaterally or bilaterally. This variation usually indicated the presence of accessory nerves (Anderson et al. 1991; Buch and Agnihotri 2012; DeSantis and Liebow 1996).

The inferior alveolar nerve may travel through bifid mandibular canals that rejoin in the ramus of the mandible both unilaterally and bilaterally (Buch and Agnihotri 2012). A trifid mandibular canal has been observed in one study (de Oliveira-Santos et al. 2012). The incisive nerve from the inferior alveolar nerve can also travel through a canal or vacuoles of spongy bone (Anderson et al. 1991). The inferior alveolar nerve may run in a recurrent path vertical and posterior to the third molar region in the retromolar canal. This distributes to the temporalis tendon, buccinator muscle, posterior zone of the alveolar process, and third molar pulp. Ramus frame implants can produce paraesthesia due to damage of the nerve within the retromolar canal (Anderson et al. 1991).

A recurrent branch of the inferior alveolar nerve can supply the upper head of the lateral pterygoid muscle. The normal nerve supplying the lateral pterygoid is present in this variation (Buch and Agnihotri 2012). Another type of recurrent branch may course superficial or deep to the lower head of the lateral pterygoid muscle (Buch and Agnihotri 2012). Further variation includes a recurrent branch communicating with the anterior division of the mandibular nerve arising just below the origin of the mylohyoid nerve (Buch and Agnihotri 2012). One final variation includes a recurrent branch of the inferior alveolar nerve communicating with the posterior division of the mandibular nerve and rejoining with the proximal inferior alveolar nerve or auricotemporal nerve (Buch and Agnihotri 2012).

The mental nerve can have accessory nerves (Hanihara and Ishida 2001).

Abducent nerve (CN VI)

The abducent nerve can be absent unilaterally or bilaterally with branches of CN III supplying the lateral rectus. It can innervate the superior rectus in addition to communicating with a branch of CN III (Phillips et al. 1932; Tillack and Winer 1962; Whitnall 1979). The abducent nerve may vary in the number of roots emerging from the brainstem. One such variation included two roots emerging from the cavernous sinus only to unite shortly thereafter (Tillack and Winer 1962; Whitnall 1979). Another variation includes origins 8 mm above the inferior border of the pons, or an origin from the olive (Tilack and Winer 1962; Whitnall 1979).

The nerve may also be doubled or tripled unilaterally or bilaterally (Fig. 83.15). These additional branches originating in the cavernous sinus may pass over or under the petrosphenoidal ligament (Faik Ozveren et al. 2003; Romero et al. 2009; Ozer et al. 2010). The length of the abducens nerve in its subarachnoid segment was found to range from 12.8 mm to 19.1 mm (Joo et al. 2012). The relationship of the abducent nerve to the AICA in the anterior pontine segment was found to be ventral in 85% of specimens, and dorsal in 15% of specimens (Joo et al. 2012).

Figure 83.15 Duplication of the left abducens nerve.

Source: Dr Anna Zurada.

The branching patterns of the abducent nerve include branches to the superior rectus with or without CN III (Tilack and Winer 1962). Branches either to the nasocilliary nerve or the ciliary ganglion have been observed (Tilack and Winer 1962; Whitnall 1979). The abducent nerve may also receive branches from the otic or pterygopalatine ganglia (Tillack and Winer 1962). The abducent nerve may enter the orbit outside the common tendinous ring of Zinn (Tillack and Winer 1962). Aberrant and recurrent branches of the abducent nerve may also occur (Whitnall 1979).

References

Ahmad F, Das S. 2011. Innervation of the inferior oblique muscle: Anatomical facts. *Chang Gung Med J* 34: 548–549.

Akita K, Shimokawa T, Tsunoda A, Sato T. 2002. Nervous branch passing through accessory canal in the sphenozygomatic suture: the temporal branch of the zygomatic nerve. *Surg Radiol Anat* 24: 113–116.

Aleksic S, Budzilovich G, Reuben R, Feigin I, Finegold M, McCarthy J, Aston S, Converse JM. 1975. Congenital trigeminal neuropathy in oculoauriculovertebral dysplasia-hemifacial microsomia (Goldenhar-Gorlin syndrome). *J Neurol Neurosurg Psych* 38: 1033–1035.

Andersen NB, Bovim G, Sjaastad O. 2000. The frontotemporal peripheral nerves. Topographic variations of the supraorbital, supratrochlear and auriculotemporal nerves and their possible clinical significance. *Surg Radiol Anat* 23: 97–104.

Anderson LC, Kosinski TF, Mentag PJ. 1991. A review of the intraosseous course of the nerves of the mandible. *J Oral Implantol* 17: 394–403.

Andrews TJ, Halpern SD, Purves D. 1997. Correlated size variations in human visual cortex, lateral geniculate nucleus, and optic tract. *J Neurosci* 17: 2859–2868.

Baumel JJ, Beard DY. 1961. The accessory meningeal artery of man. *J Anat* 95: 386–402.

Baumel JJ, Vanderheiden JP, McElenney JE. 1971. The auriculotemporal nerve of man. *Am J Anat* 130: 431–440.

Becker M, Kohler R, Vargas MI, Viallon M, Delavell J. 2008. Pathology of the trigeminal nerve. *Neuroimag Clin N Am* 18: 283–307.

Bergman RA, Afifi AK, Miyauchi R. 2006. Illustrated Encyclopedia of Human Anatomic Variation. Available at: http://www.anatomyatlases.org/AnatomicVariants/AnatomyHP.shtml (accessed 17 November 2015).

Biega TJ, Khademian ZP, Vezina G. 2007. Isolated absence of the optic chiasm: A rare cause of congenital nystagmus. *AJNR* 26: 392–393.

Bisaria KK. 1988. Cavernous portion of the trochlear nerve with special reference to its site of entrance. *J Anat* 159: 29–35.

Brown MC, Souther CL, Anbarasu A, Kaye SB, Fischer AC, Hagan RP, Newman WD. 2006. Congenital absence of optic chiasm: demonstration of an uncrossed visual pathway using monocular flash visual evoked potentials. *Doc Ophthalmol* 113: 1–4.

Buch HA, Agnihotri RG. 2012. A recurrent variant branch of the inferior alveolar nerve: Is it unique? *Clin Anat* 25: 437–443.

Busacca A. 1925. Les anastomoses des nerfs moteurs dans la region du sinus caverneux. *Arch Italiennes Biol* 75: 145–146.

Carter RB, Keen EN. 1971. The intramandibular course of the inferior alveolar nerve. *J Anat* 108: 433–440.

Chandra RK, Kennedy DW. 2004. Surgical implications of an unusual anomaly of the infraorbital nerve. *Ear Nose Throat J* 83: 766–767.

Chat L, Hertz-Pannier L, Roche O, Boddaert N, Baraton J, Brunelle F. 2002. Value of MRI in the diagnosis of unilateral optic nerve aplasia: a case report. *J Radiolog* 83: 1853–1855.

de Oliveira-Santos C, Rubira-Bullen IRF, Monteiro SAC, Leon JE, Jacobs R. 2012. Neurovascular anatomical variations in the anterior palate observed on CBCT images. *Clin Oral Impl* 0: 1–5.

Demer JL, Clark RA, Lim KH, Engle EC. 2007. Magnetic resonance imaging of innervation and extraocular muscle abnormalities in Duane-Radial syndrome. *Integrative Ophthal Vis Sci* 48: 5505–5511.

DeSantis JL, Liebow C. 1996. Four common mandibular nerve anomalies that lead to local anesthesia failures. *JADA* 127: 1081–1086.

Di Rienzo L, Artuso A, Colosimo C. 2002. Isolated congenital agenesis of the olfactory bulbs and tracts in a child without Kallmann's syndrome. *Ann Otol Rhinol Laryngol* 111: 657–660.

Donoso LA, Magargal LE, Eiferman RA, Meye D. 1981. Ocular anomalies simulating double optic discs. *Can J Ophthal* 16: 84–87.

Engle EC, Goumnerov BC, McKeown CA, Schatz M, Johns DR, Porter JD, Beggs AH. 1997. Oculmotor nerve and muscle abnormalities in congenital fibrosis of the extraocular muscles. *Am Neurol Assoc* 41: 314–325.

Erdogmus S, Govsa F, Celik S. 2007. Innervation features of the extraocular muscles. *J Craniofac Surg* 18: 1439–1446.

Erdogmus S, Pinar Y, Celik S. 2009. A cause of entrapment of the lingual nerve: ossified pterygospinous ligament: a case report. *Neuroanatomy* 8: 43–45.

Evans TH. 1959. Unlisted nerve branches of the maxillary division of the trigeminal nerve (fifth cranial) which are related to nerve association of the lacrimal and salivary systems. *Am J Ophth* 47: 225–226.

Faik Ozveren M, Sam B, Akdemir I, Alkan A, Tekdemir I, Deda H. 2003. Duplication of the abducens nerve at the petroclival region: An anatomic study. *Neurosurgery* 52: 645–652.

Fallucco M, Janis JE, Hagan RR. 2012. The anatomical morphology of the supraorbital notch: clinical relevance to the surgical treatment of migraine headaches. *Plast Reconstr Surg* 130: 1227–1233.

Fitzgerald MJT. 1956. The occurrence of a middle superior alveolar nerve in man. *J Anat* 90: 520–522.

Fitzgerald MJT, Law ME. 1958. The peripheral connexions between the lingual and hypoglossal nerves. *J Anat* 92: 178–188.

Girguis-Bucher A, Schlegel-Wagner C. 2013. Anatomical variation of the extracranial course of the optic nerve in the floor of the sphenoid sinus: first reported case. *J Laryngol Otol*: 1–3.

Griessenauer CJ, Raborn J, Mortazavi MM, Tubbs RS, Cohen-Gadol AA. 2014. Relationship between the pituitary stalk angle in prefixed, normal, and postfixed optic chiasmata: an anatomic study with microsurgical application. *Acta Neurochir (Wien)* 156: 147–151.

Gottlob I, Jain S, Engle EC. 2002. Elevation of one eye during tooth brushing. *Am J Ophthalmol* 134: 459–460.

Gulekon N, Anil A, Poyraz A, Peker T, Turgut HB, Karakose M. 2005. Variations in the anatomy of the auriculotemporal nerve. *Clin Anat* 18: 15–22.

Hallet CH. 1847. Anomalies of the ciliary ganglion. *Med Times* 16: 392–393.

Hamel O, Corre P, Ploteau S, Armstrong O, Rogez JM, Robert R, Hamel A. 2012. Ciliary ganglion afferents and efferents variations: a possible explanation of postganglionic mydriasis. *Surg Radiol Anat* 34: 897–902.

Hanihara T, Ishida H. 2001. Frequency variations of discrete cranial traits in major human populations. IV. Vessel and nerve related variations. *J Anat* 199: 273–287.

Horowitz E. 1935–36. Uber einen fall von einseitiger aplasie des nervus olfctorius. *Anat Anz* 81: 353–359.

Hotchkiss ML, Green WR. 1979. Optic nerve aplasia and hypoplasia. *J Pediatr Ophthal Strabismus* 16: 225–240.

Hoyt WF, Nachtigaller H. 1965. Anomalies of ccular motor nerves: neuroanatomic correlates of paradoxical innervation in Duane's Syndrome and related congenital ocular motor disorders. *Am J Ophth* 60: 443–448.

Islam N, Best J, Mehta JS, Sivakumar S, Plant GT, Hoyt WF. 2005. Optic disc duplication or coloboma? *Br J Ophthalmol* 89: 26–29.

Isomura G. 1977. Nerve supply for anomalous ocular muscles in man. *Anat Anz* 142: 255–265.

Jablonski NG, Cheng CM, Cheng LC, Cheung HM. 1985. Unusual origins of the buccal and mylohyoid nerves. *Oral Surg Oral Med Oral Pathol* 60: 487–488.

Janis JE, Hatef DA, Thakar H, Reece EM, McCluskey PD, Schaub TA, Theivagt C, Guyuron B. 2010. The zygomaticotemporal branch of the trigeminal nerve: Part II. Anatomical variations. *Plast Reconstr Surg* 126: 435–442.

Jea A, Baskaya MK, Morcos JJ. 2003. Penetration of the optic nerve by an internal carotid artery-ophthalmic artery aneurysm case report and literature review. *Neurosurgery* 53: 996–1000.

Joo W, Yoshioka F, Funaki T, Rhoton AL. Jr. 2012. Microsurgical anatomy of the abducens nerve. *Clin Anat* 25: 1030–1042.

Jordan J. 1967. Double infraorbital nerve in man. *Folia Morphologica* 26: 405–407.

Kaeser PF, Kress B, Rohde S, Kolling G. 2012. Absence of the fourth cranial nerve in congenital Brown syndrome. *Acta Ophthalmol* 90: 310–313.

Kassem IS, Kodsi SR. 2009. Marcus gunn jaw winking with trigemino-oculomotor synkinesis of the inferior divison of the oculomotor nerve. *J AAPOS* 13: 315–316.

Kau HC, Tsai CC, Ortube M, Demer J. 2007. High-resolution magnetic resonance imaging of the extraocular muscles and nerves demonstrates various etiologies of third nerve palsy. *Am J Ophthalmol* 143: 280–287.

Khaledpour VC. 1984. An anatomic variant of the inferior alveolar nerve in man. *Anat Anz* 156: 403–406.

Kidd LJ. 1922. The fourth cranial nerve. *British J Ophth* 6: 49–55.

Kim JH, Hwang JM. 2009. Magnetic resonance imaging in three patients with congenital oculomotor nerve palsy. *Br J Ophthalmol* 93: 1266–1267.

Krmpotic-Nemanic J, Vinter I, Jalsovec D. 2001. Accessory oval foramen. *Ann Anat* 183: 293–295.

Kumar V, Devika P, Nair N, Pai SR, Pulakunta T, Naveen NS. 2011. An anatomical study of the inferior oblique muscle with emphasis on its nerve entry. *Chang Gung Med J* 34: 293–297.

Lamba PA. 1969. Doubling of the papilla. *Acta Ophthalmologica* 47: 4–9.

Lang J, Reiter U. 1984. Uber die intrazisternale lange von hirnbahnund nervenstrecken der hirnnerven I–IV. *Neurochirurgia* 27: 125–128.

Leo JT, Cassel MD, Bergman RA. 1995. Variation in human infraorbital nerve, canal and foramen. *Ann Anat* 177: 93–95.

Lewis RF, Zee DS. 1993. Abnormal spatial localization with trigeminal-oculomotor synkinesis. Evidence for a proprioceptive effect. *Brain* 116: 1105–1118.

Lim KH, Engle EC, Demer JL. 2007. Abnormalities of the oculomotor nerve in congenital fibrosis of the extraocular muscles and congenital oculomotor palsy. *Invest Ophth Vis Sci* 48: 1601–1606.

Liu GT. 2005. *The Trigeminal Nerve and its Central Connections*. Philadelphia, PA: Lippincott Williams and Wilkins.

Mailleux P, Desgain O, Ingabire MI. 2010. Ectopic infraorbital nerve in maxillary sinus septum: another potentially dangerous variant for sinus surgery. *JBR-BTR* 93: 308–309.

Margo CE, Hamed LM, Fang E, Dawson WW. 1992. Optic nerve aplasia. *Arch Ophthamol* 110: 1610–1613.

Martyn HS. 1919. Notes on a case of anomalous innervation of the levator palpebrae superioris. *Brit J Opthamol* 3: 310–313.

Math SC, Kulkarni SR, Jatti VKB, Shobha. 2010. Study of duplication of the optic canals in human adult skulls of North Karnataka. Indian J Foren Med Tox 4.

Miller NR, Kiel SM, Green WR, Clark AW. 1982. Unilateral Duane's retraction syndrome (Type 1). *Arch Ophth* 100: 1468–1472.

Mirsalis T. 1929. Ein neue fall von arhinecephalie. *Anat Anz* 67: 353–360.

Morton WR. 1947. Arhinencephaly and multiple developmental anomalies occurring in a human full-term foetus. *Anat Rec* 98: 45–58.

Mosin IM, Vasil'eva OIu, Pykov MI, Shuleshko OV, Sheianov NG. 2004. Isolated aplasia of the optic nerve. *Vestn Oftalmol* 120: 47–51.

Neves FS, Crusoé-Souza M, Franco LC, Caria PH, Bonfim-Almeida P, Crusoé-Rebello I. 2012. Canalis sinuosus: a rare anatomical variation. *Surg Radiol Anat* 34: 563–566.

Oomen KP, Ebbeling M, Ru JA, Hordijk GJ, Bleys RL. 2011. A previously undescribed branch of the pterygopalatine ganglion. *Am J Rhinol Allergy* 25: 50–53.

Orhan Magden A, Kaynak S. 1996. Bilateral duplication of the optic canals. *Ann Anat* 178: 61–64.

Ozer E, Icke C, Arda N. 2010. Microanatomical study of the intracranial abducens nerve: clinical interest and surgical perspective. *Turk Neurosurg* 20: 449–456.

Patil GV, Kolagi S, Padmavathi G, Rairam GB. 2011. The duplication of the optic canals in human skulls. *J Clin Diagn Res* 5: 536–537.

Phillips WH, Dirion JK, Graves GO. 1932. Congenital bilateral palsy of the abducens. *Arch Ophthalmol* 8: 355–364.

Piersol G.A. 1918. *Piersol's Human Anatomy*, sixth edition. Philadelphia, PA: L.B. Lippincott Company.

Potu BK, Pulakunta T, Ray B, Rao MS, Bhat KMR, D'Silva SS, Nayak SR. 2009. Unusual communication between lingual nerve and mylohyoid nerves in South Indian male cadaver: its clinical significance. *Rom J Morphol Embryol* 50: 145–146.

Racz L, Maros T, Seres-Sturm L. 1981. Anatomical variations of the nervus alveolaris inferior and their importance for Practice. *Anat Anz* 149: 329–332.

Roback HN, Conway MW. 1940. Agenesis of olfactory tracts: report of two cases. *Northw Med* 39: 264–265.

Rombaux P, Mouraux A, Bertrand B, Duprez T, Hummel T. 2007. Can we smell without an olfactory bulb? *Am J Rhinol* 21: 548–550.

Romero FR, Ramos JG, Chaddad-Neto F, Bethencourt JMA, de Oliveira E. 2009. Microsurgical anatomy and injuries of the abducens nerve. *Arq Neuropsiquiatr* 67: 96–101.

Roy EP, Frost JL, Schochet SS. 1987. Persistent olfactory bulb ventricle. *Clinical Neuropathol* 6: 86–87.

Roy TS, Sarkar AK, Panicker HK. 2002. Variation in the origin of the inferior alveolar nerve. *Clin Anat* 15: 143–147.

Rusu MC, Pop F, Curca GC, Podoleanu L, Voinea LM. 2009. The pterygopalatine ganglion in humans: A morphological study. *Ann Anat* 191: 196–202.

Sadun AA, Wang MY. 2011. Abnormalities of the optic disc. *Handbook Clin Neurol* 102: 117–157.

Sandoval MC, Lopez FB, Suazo FI. 2009. An unusual relationship between the inferior alveolar nerve, lingual nerve and maxillary artery. *Int J Odontostomat* 3: 51–53.

Sanjari MS, Ghasemi Falavarjani K, Parvaresh MM, Kharazi HH, Kashkooli MB. 2006. Bilateral aplasia of the optic nerve, chiasm, and tracts in an otherwise healthy infant. *Br J Ophth* 90: 513–514.

Schafer EA, Symington J. 1909. *Quain's Elements of Anatomy*. New York, NY: Longmans, Green and Co.

Scott IU, Warman R, Altman N. 1997. Bilateral aplasia of the optic nerves, chiasm, and tracts in an otherwise healthy infant. *Am J Ophth* 124: 409–410.

Shoumura K, Imai H, Nakaoka T, Isono H, Shoumura S, Deura S. 1985. Absence of olfactory bulbs and hypoplasia of olfactory tracts: a case report. *Kaibogaku Zasshi* 60: 630–639.

Siessere S, Vitti M, Gustavo de Sousa L, Semprini M, Iyomasa MM, Regalo SCH. 2008. Anatomic variation of cranial parasympathetic ganglia. *Braz Oral Res* 22: 101–105.

Sinnreich Z, Nathan H. 1981. The ciliary ganglion in man (anatomical observations). *Anat Anz* 150: 287–297.

Somayaji K, Roa M. 2012. Anatomy and clinical applications of the maxillary nerve in Dentistry: a literature review. *Dental Update* 39: 727–730, 733–735.

Stewart RM. 1939. Arhinencephaly. *J Neurol Psych* 2: 303–312.

Taylor D. 2005. Optic nerve axons: life and death before birth. *Eye* 19: 499–527.

Taylor D. 2007. Developmental abnormalities of the optic nerve and chiasm. *Eye* 21: 1271–1284.

Tillack TW, Winer JA. 1962. Anomaly of the abducens nerve. *Yale J Biol Med* 34: 620–624.

Tschabitscher VM, Hocker K. 1991. The spot and mode of emergence of cranial nerves III, IV, VI. *Anat Anz* 173: 45–49.

Tubbs RS, Oakes WJ. 1998. Relationships of the cisternal segment of the trochlear nerve. *J Neurosurg* 89: 1015–1019.
Tubbs RS, Loukas M, May WR, Cohen-Gadol AA. 2010. A variation of the infraorbital nerve: Its Potential clinical consequence especially in the treatment of trigeminal neuralgia: Case Report Open Neurosurg 67.
Turner WM. 1868. Notes on variations in the origin of the long buccal branch of the fifth cranial nerve. *Roy Soc Lon* 16: 456–457.
Valenti G. 1910. Un cas d'absence unilateral de l'appariel olfactif. *Arch Italiennes Biol* 54: 457.
Vilensky JA. 2014. The neglected cranial nerve: Nervus terminalis (cranial nerve N). *Clin Anat* 27(1): 46–53.
Villanueva O, Atkinson DS, Lambert SR. 2005. Trigeminal nerve hypoplasia and aplasia in children with Goldenhar Syndrome and corneal hypoesthesia. *J AAPOS* 9: 202–204.
Warwick R. 1976. *Eugene Wolff's Anatomy of the Eye and Orbit*, seventh edition. Philadelphia, PA: W.B. Saunders Company.
Weigner C. 1898. Le ganglion otique. *Bibliog Anat* 6: 302–306.
Whitnall S. 1979. *Anatomy of the Human Orbit and Accessory Organs of Vision*. Huntington, NY: Robert E. Kreiger Publishing Company.
Witmer WT, Margo CE, Drucker M. 2010. Tilted optic disks. *Survey Ophthal* 55: 403–428.
Wu SQ, Man FY, Jiao YH, Xian JF, Wang YD, Wang ZC. 2013. Magnetic resonance imaging findings in sporadic Mobius syndrome. *Chin Med J* 126: 2304–2307.

Further reading

Balcer LJ, Prasad S. 1988. Abnormalities of the optic nerve and retina. Neuro–Ophthalmol 183–196.
Burr HS, Robinson GB. 1925. An anatomical study of the gasserian ganglion, with particular reference to the nature and extent of Meckel's cave. *Anat Rec* 29: 269–282.
Carswell A, Whinney D, Hollings N, Flanagan P. 2008. Isolated olfactory nerve agenesis. *Brit J Hosp Med* 69: 474.
Cushing H. 1904. The sensory distribution of the fifth cranial nerve. *Bull Johns Hop Hosp* 15: 213–232.
Daimi SR, Siddiqui AU, Vyas VR, Sheikh. 2013. Unique presentation of maxillary artery, lingual nerve, and inferior alveolar nerve complex. *Int J App Basic Med Res* 1: 125–126.
Dixon F. 1895. On the development of the branches of the fifth cranial nerve in man. *Proceed Royal Soc Lon* 57: 488–490.
Doty RL. 2009. The olfactory system and its disorders. *Semin Neurol* 29: 74–81.
Frank VE. 1956. Two special cases of the lingual nerve. *Anat Anz* 103: 187–191.
Han SK, Shin YW, Kim WK. 2004. Anatomy of the external nasal nerve. *Plast Reconstr Surg* 114: 1055–1059.
Ho TP, Carrie S. 2001. Congenital anosmia. *Inter J Clin Prac* 55: 418–419.
Issajew PO. 1932. Ein fall der abwesenheit des n. olfactorius. *Anat Anz* 74: 398–400.
Krishnaraj Somayajo S, Rashmi Acharya S, Mohandas Rao KG, Venkataramana V. 2012. Anatomy and clinical applications of the mandibular nerve. *Bratisl Lek Listy* 113: 431–440.
Liss L, Gomez F. 1958. The nature of senile changes of the human olfactory bulb and tract. *AMA Arch Otolaryngol* 67: 167–171.
Loizeaux AD, Devos BJ. 1981. Inferior alveolar nerve anomaly. *J Hawaii Den Assoc* 12: 10–11.
Petty PG. 1965. Absence of olfactory bulbs and tracts with an associated bilobed pineal body. *Med J Austral* 2: 492–494.
Pia Majo B. 1934. Contribucion al estudio del ojal nervioso del auriculotemporal. *Arquivo Anat Antropolog* 16: 233–244.
Starkie C, Steward D. 1931. The intra-mandibular course of the inferior dental nerve. *J Anat* 65: 319–323.
Tubbs RS, Salter EG, Oakes WJ. 2006. Bony anomaly of meckel's cave. *Clin Anat* 19: 75–77.
Wollman F. 1942. Zum verlauf des nervus maxillaries auf grun einer varietatbeobachtung. *Anat Anz* 93: 129–132.
Wyatt WM. 1996. Accessory mandibular canal: Literature review and presentation of an additional variant. *Quintessence Internat* 27: 111–113.

84 Facial nerve

Mohammadali M. Shoja[1] and R. Shane Tubbs[2]
[1]Tuberculosis and Lung Disease Research Center, Tabriz University of Medical Sciences, Tabriz, Iran
[2]Seattle Science Foundation, Seattle, Washington, USA
St George's University, School of Medicine, St Georges, Grenada
University of Dundee, Dundee, UK

The anatomy of the facial nerve is subject to variations, and knowledge of these is of particular interest for surgeons operating on the posterior and middle cranial fossa, temporal bone, middle ear, and upper neck and parotid regions. This chapter describes some of the important variations of the facial nerve described in the literature.

After taking origin from the lateral part of the pontomedullary sulcus, the motor and sensory parts of the facial nerve course together along with the vestibulocochlear nerve in the cerebellopontine angle (CPA) to arrive at the porus of the internal acoustic meatus (IAM). The facial nerve travels inside the canal above and slightly anterior to the vestibulocochlear nerve to enter the opening of facial (Fallopian) canal located at the anterosuperior quadrant of the fundus (or lateral end) of the IAM. From there, it courses laterally and rather horizontally between the vestibule posteriorly and cochlea anteriorly to reach the medial wall of the epitympanic recess, where it make a sharp backward turn (known as the first or proximal external genu). It then courses in a backward direction on the medial wall of the tympanic cavity parallel and below the protrusion of the lateral (horizontal) semicircular canal and above the oval window and stapes footplate. Here, the nerve makes another bend (second genu), albeit blunted and downward, and is positioned on the posterior wall of the tympanic cavity (Schaeffer 1953). The facial nerve then exits the skull through the stylomastoid foramen situated in a niche bounded by the mastoid and styloid processes and lower wall of the external acoustic meatus (Botman and Jongkees 1955). Seven segments are discernible along the course of the facial nerve from the brainstem to the stylomastoid foramen:

1. Cisternal segment: extends laterally and posteriorly from the lateral pontomedullary sulcus to the porus of the IAM. This segment is accompanied by the vestibulocochlear nerve and is surrounded by an arachnoid layer.
2. Canalicular or meatal segment: extends from the porus of the IAM medially to the beginning of the facial canal, meatal opening, located at the anterosuperior quadrant of the IAM fundus laterally. This segment is accompanied by the vestibulocochlear nerve inside a dural-arachnoid sheath.
3. Labyrinthine or petrosal segment: length varies from 2.5 to 6 mm, and extends from the meatal opening medially to the geniculate ganglion laterally at the medial wall of the epitympanic recess. This segment comprises 10–18% of the endotemporal length of the facial nerve (Kudo and Nori 1974).
4. First or proximal external genu or geniculate segment: the main motor part and minor part (intermediate nerve of Wrisberg) of the facial nerve usually unite here, where the geniculate ganglion is also situated. The geniculate ganglion is pyramidal in shape with a length of 1–2 mm and occupies the anterior third of the first genu (Dobozi 1975; Nawar et al. 1980). The apex of the pyramid is anterolaterally oriented and marks the origin of the greater petrosal nerve. The dimensions of the ganglion are rather constant, with only slight variations among individuals (Dobozi 1975).
5. Tympanic or horizontal segment: its length varies over the range 8–11 mm and extends from the first to the second genu backward, often in a slightly lateral and inferior direction. This segment comprises 31–45% of the endotemporal length of the facial nerve (Kudo and Nori 1974).
6. Second or distal genu: length varies over the range 2–6 mm. This segment projects laterally and indents into the tympanic cavity (Botman and Jongkees 1955).
7. Mastoid, vertical or descending segment: length varies over the range 9–12 mm (Botman and Jongkees 1955). This segment comprises 37–54% of the endotemporal length of the facial nerve (Kudo and Nori 1974).

The labyrinthine, tympanic, and mastoid segments with the intervening genu of the facial nerve travel inside the bony canal within the temporal bone knows as facial canal or aqueduct of Fallopius. The tympanic surface of the facial canal is thinner over the tympanic (horizontal) segment of the nerve than it is over the mastoid segment (Botman and Jongkees 1955).

Bergman's Comprehensive Encyclopedia of Human Anatomic Variation, First Edition. Edited by R. Shane Tubbs, Mohammadali M. Shoja and Marios Loukas.
© 2016 John Wiley & Sons, Inc. Published 2016 by John Wiley & Sons, Inc.

Intermediate nerve of Wrisberg

This nerve contains sensory and preganglionic parasympathetic (secretomotor) fibers. The origin of the intermediate nerve varies in terms of its exact location and the number of rootlets and roots. In a study of 50 brainstems (100 sides), the intermediate nerve was noted to arise by 225 rootlets that joined together to form one to five root(s) on each side *en route* to the IAM (one root was observed in 58% of sides, two in 26%, three in 12%, four and five roots in 2% each; Oh et al. 2003). The origins of the rootlets (Fig. 84.1) were as follows:

1. from the pons halfway between the facial and vestibulocochlear nerves (*n*=72, 31.9%);
2. from the pons close to the motor part of the facial nerve (*n*=9, 4%);
3. from the pons close to the vestibulocochlear nerve (*n*=15, 6.6%);
4. from the pons with a common origin with the vestibulocochlear nerve (*n*=65, 28.8%);
5. from the proximal stem of the vestibulocochlear nerve (*n*=36, 15.9%);
6. from the pons with a common origin with the motor part of the facial nerve (*n*=23, 10.2%); or
7. from the proximal stem of the motor part of the facial nerve (*n*=6, 2.6%).

The intermediate nerve may adhere to the vestibular part of the vestibulocochlear nerve along its cisternal course in 22% of cases, making it impossible to identify in the CPA separately in these instances (Rhoton et al. 1968a). The majority of the sensory ganglion cells are located in the geniculate ganglion at the first genu and the parasympathetic ganglion cells in the pterygopalatine and otic ganglia. The intermediate nerve may unite with the main motor part of the facial nerve while within the IAM (Schaeffer 1953). According to Piersol (1918), the intermediate nerve may communicate with both the motor part of the facial nerve and the eighth cranial nerve within the IAM. Sachs (1968) reported a patient with facial neuralgia in whom sectioning of the intermediate nerve did not relieve the pain. Stimulation of the eighth cranial nerve resulted in facial pain, and neuralgia subsided subsequent to its resection. He concluded that the anastomoses, which existed between the intermediate nerve and eighth cranial nerve within IAM, allowed sensory impulses from the facial nerve distribution to bypass this nerve into the eighth cranial nerve.

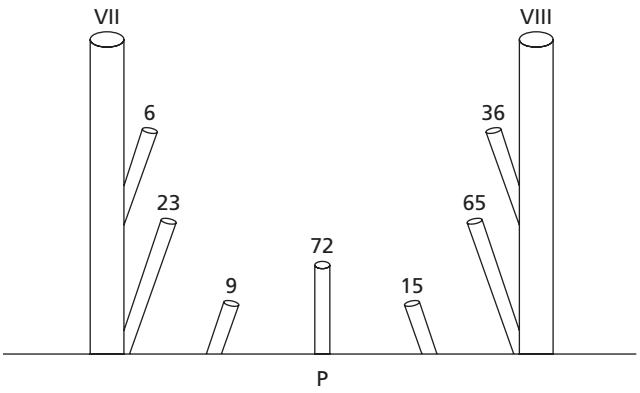

Figure 84.1 The origins of the rootlets of the intermediate nerve (225 rootlets in 50 brainstem specimens). P, pons; VII, facial nerve; VIII, vestibulocochlear nerve.

Source: Oh et al. (2003). Reproduced with permission from Springer Science and Business Media.

Cisternal segment

Spatial relationship to the vestibulocochlear nerve

Near the brainstem, the facial nerve is usually situated anterior to the vestibulocochlear nerve, but it may course anterosuperior or anteroinferior to it (Kim et al. 1998). Along the cisternal course, the two nerves keep a similar spatial relationship except for in about 20% of cases, where the vestibulocochlear nerve tends to shift below the facial nerve. Here, the gross segmentation of the vestibulocochlear nerve into its divisions is not clear.

Relationship to the arteries

Matsushima et al. (1990) investigated the arteries in contact with the cisternal segment of the facial nerve in 35 CPAs. The number of nerve–artery contact points varied: 10 nerves had one artery–nerve contact point; 20 nerves had two artery–nerve contact points; 4 nerves had three contact points; and one nerve had no contact with the artery.

The arteries may contact the facial nerve anywhere, either proximally at the root exit zone or more distally in the cisternal segment. Matsushima et al. (1990) found one artery–nerve contact at the facial nerve root exit zone in 19 of 35 cases (54%) and two such contacts in five cases (14%), comprising a total of 29 contact points. The culprit artery was the anterior inferior cerebellar artery (AICA) or its branch in 24 of the contacts points (83%), the posterior inferior cerebellar artery (PICA) in 2 (7%), and the vertebral artery in 3 (10%).

Relationship of the facial nerve to the anterior inferior cerebellar artery (AICA)

After taking origin from the basilar or vertebral arteries, AICA usually courses posteriorly, laterally, and then medially to reach its target areas. Along its course, AICA comes into close proximity to the facial and vestibulocochlear nerves within the CPA, and has to cross or pass through this nerve complex *en route* to the cerebellum. Due to inconsistency in the origin and course of AICA, this artery shows variable relationships with the facial and vestibulocochlear nerves in the CPA. This anatomy becomes even more complicated when AICA is duplicated or bifurcates along its course.

Yurtseven et al. (2004) investigated the CPA nerve–artery relationship in the dissection of 20 cadavers (40 sides) and 3D

Table 84.1 The course of AICA in relation to the facial-vestibulocochlear nerve complex (according to Yurtseven et al. 2004).

	Ventral to the nerve complex	Dorsal to the nerve complex	Between the nerves
Dissection (*n*=40)	13 (32.5%)	14 (35%)	13 (32.5%)
Imaging[1] (*n*=148)	48 (32.4%)	45 (30.4%)	51 (34.5%)

[1]Note AICA was not identified in the imaging of 4 sides.

FT-CISS MRI of 74 adults (148 sides). The following variants were noted: (1) AICA ventral to the facial-vestibulocochlear nerve complex; (2) AICA dorsal to the facial-vestibulocochlear nerve complex; and (3) AICA passing between the facial nerve superiorly and the vestibulocochlear nerve inferiorly. Table 84.1 lists the prevalence of different variants reported by Yurtseven et al. (2004).

Several authors (Martin et al. 1980; Kim et al. 1990) have attempted to illustrate the spatial relationship between the AICA and the facial–vestibulocochlear nerve complex by (1) dividing the course of AICA into three "nerve-related" segments (namely premeatal, meatal, and postmeatal) based on its relations with the facial–vestibulocochlear nerve complex and porus of the IAM (Fig. 84.2), and (2) dividing the CPA into nine arbitrary partitions in relation to the porus of the IAM (Fig. 84.3). The spatial nerve–artery relationships within

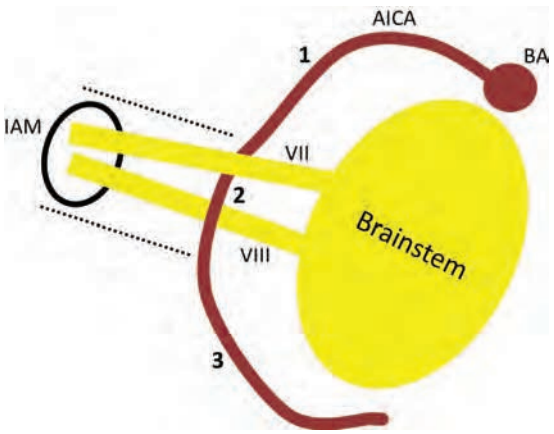

Figure 84.2 Classic course of the anterior inferior cerebellar artery (AICA) through the cerebellopontine angle. Three arterial segments are discernible: (1) premeatal segment, from its origin to the vicinity of facial (VII)-vestibulocochlear (VIII) nerve complex up to the plane of the ventral edge of the porus of the internal acoustic meatus (IAM); (2) meatal segment, situated caudal to the premeatal segment between the planes of the ventral and dorsal edges of the porus; and (3) postmeatal segments, situated caudal to the meatal segment. Note premeatal segment courses laterally toward the porus and postmeatal segment courses medially. The meatal segment usually forms a laterally convex loop (Kim et al. 1990).

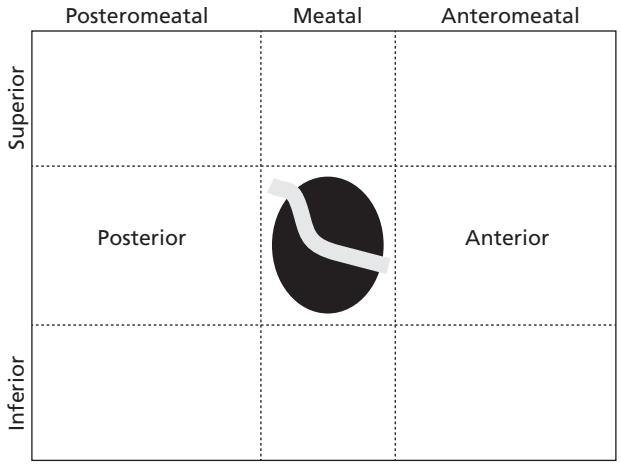

Figure 84.3 Cerebellopontine angle (CPA) partitioning in relation to porus of the internal acoustic meatus. Facial (VII)-vestibulocochlear (VIII) nerve complex, in the middle, represents the region of the porus. The planes of ventral, dorsal, superior and inferior edges of porus have been used to divide the CPA into nine partitions.

the CPA have been described in terms of the position of each nerve-related segment in theses partitions. In the study of 50 CPAs, Grant et al. (1979) reported that the premeatal segment was anteroinferior to the facial nerve in 83%. The following configurations of different arterial segments were described by Kim et al. (1990):

- Premeatal segment: (1) anteroinferior to the nerves (50 of 56); (2) inferior to the nerves (3 of 56); (3) anterosuperior to the nerves (1 of 56); (4) anterior to the nerves (1 of 56); and (5) posteroinferior to the nerves (1 of 56).
- Meatal segment: (1) between the nerves (31 of 69); (2) inferior to the nerves (23 of 69); and (3) superior to the nerves (15 of 69).
- Postmeatal segment: (1) posteroinferior to the nerves (24 of 65); (2) superior to the nerves (11 of 65); (3) posterosuperior to the nerves (10 of 65); (4) anterosuperior to the nerves (7 of 65); (5) anteroinferior to the nerves (6 of 65); (6) anterior to the nerves (4 of 65); (7) inferior to the nerves (2 of 65); and (8) posterior to the nerves (1 of 65).

Another variant configuration of AICA in relation to the facial–vestibulocochlear nerve complex is in regard to the lateral extent of its meatal loop along the nerve complex (Fig. 84.4). This loop may pass above, below, or between the facial and vestibulocochlear nerves (Martin et al. 1980; Kim et al. 1990). The meatal loop is usually located medial to the porus, but it may reach the porus or extend into the IAM. It rarely extends more than half the length of the IAM (Kim et al. 1990).

Rarely, AICA may pierce and pass through a cleft in the facial nerve (Liu and Fagan 2001). Internal auditory or labyrinthine branch/branches of the AICA may course between the facial and vestibulocochlear nerves or above these nerves (Kim et al. 1990).

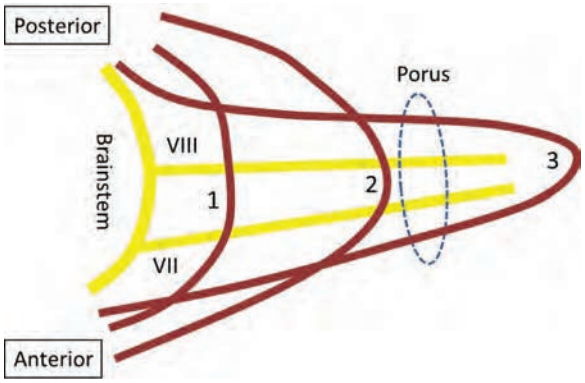

Figure 84.4 Extent of meatal loop of AICA along the facial-vestibulocochlear nerve complex. The meatal loop is usually located (1) medial to the porus, but it may (2) reach the porus or (3) extend into the internal acoustic meatus.

Relationship of the facial nerve to the posterior inferior cerebellar artery (PICA)

After branching off the vertebral or basilar arteries, the proximal part of the PICA (lateral medullary segment) may make a loop superiorly and/or laterally, bringing it into close contact with the anterior, inferior, or anteroinferior aspect of the facial–vestibulocochlear nerve complex in the CPA (Saylam et al. 2007a; Fig. 84.5). This variant, distorting the facial and/or vestibulocochlear nerve roots, has been observed by Saylam et al. (2007a) in 8 of 40 cases (20%) and by Lister et al. (1982) in 6 of 50 cases (12%). Matsushima et al. (1990) also observed instances where high-origin PICAs looped upward to contact the root exit zone of the facial nerve. A shifted (kinked) distal portion of the vertebral artery may also reach the root exit zone of the facial nerve (Matsushima et al. 1990).

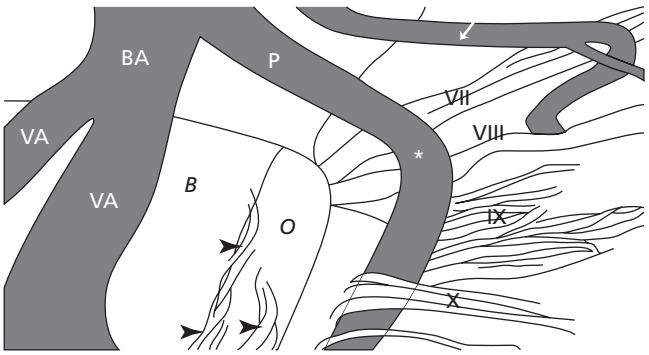

Figure 84.5 Schematic drawing of the anterior view of the cerbellopontine angle. The posterior inferior cerebellar artery (P) originates from the basilar artery (BA), courses laterally to press against the roots of facial (VII) and vestibulocochlear (VIII) nerves, before turning down to pass between the glossopharyngeal nerve (IX) posteriorly and vagus (X) anteriorly. Note the loop of the posterior inferior cerebellar artery (*) and anterior inferior cerebellar artery (white arrow). B, brainstem; O, medullary olive; VA, vertebral artery.

Source: Saylam et al. (2007a). Reproduced with permission from John Wiley & Sons.

Canalicular segment

Spatial relationship to cochlear and superior and inferior vestibular nerves

The relationship between facial and vestibulocochlear nerves varies along their cisternal and canalicular courses; at a given point, this relationship also varies among individuals (Kim et al. 1998). Between the porus and midportion of the IAM, the gross segmentation of the vestibulocochlear nerve into superior and inferior vestibular and cochlear nerves become more or less obvious, and the spatial relationship between each of them and the facial nerve can be readily described. At the porus, the facial nerve is usually situated anterior to the shallow groove of the vestibulocochlear nerve (Kim et al. 1998). In the midportion of the IAM, the classic relationship between the four nerves (i.e., facial, cochlear, and superior and inferior vestibular nerves in the anterosuperior, anteroinferior, posterosuperior, and posteroinferior quadrants, respectively) is established in about 90% of cases (Kim et al. 1998). Figures 84.6 and 84.7 show the spatial relationship between these nerves at the porus and midportion of the IAM.

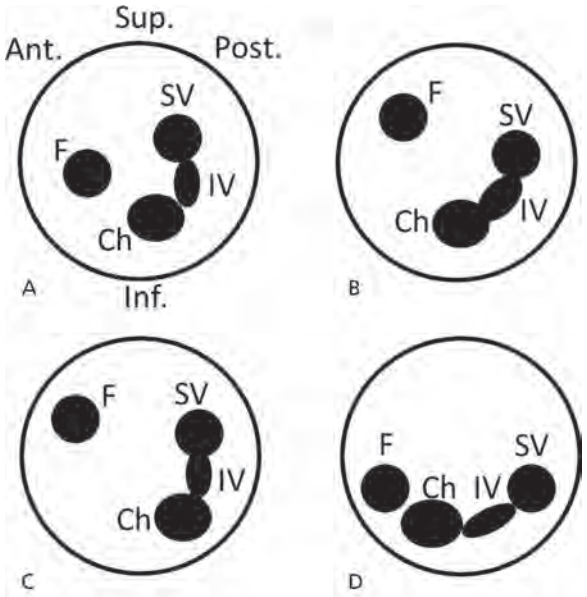

Figure 84.6 Relationship between the facial and vestibulocochlear nerves at the porus of the internal auditory meatus. (a) Most common form. F, Facial nerve; Ch, cochlear nerve; SV, superior vestibular nerve; IV, inferior vestibular nerve. Note directions: Ant., anterior; Post., posterior; Sup., superior. Adapted from Kim et al. (1998) with permission from American Society of Neuroradiology.

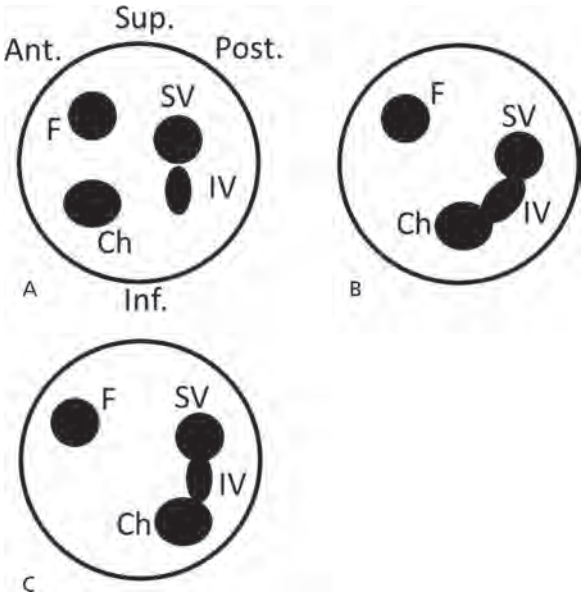

Figure 84.7 Relationship between the facial and vestibulocochlear nerves at the midportion of the internal auditory meatus. (a) Most common form. Abbreviations as for Figure 84.6. Adapted from Kim et al. (1998) with permission from American Society of Neuroradiology.

Anastomoses of the facial nerve with the vestibulocochlear nerve

The interconnection of the facial and vestibulocochlear nerves within the IAM has been noted by Cruveilhier (1851). Consistent anastomoses exist between the intermediate and vestibular nerves as well as between the genu of the facial nerve and vestibular ganglion (Shoja et al. 2014a). The anastomoses between facial and superior vestibular nerves are not uncommon findings during vestibular neurectomy (Fisch 1973). Özdogmus et al. (2004) reported anastomosis between the superior vestibular and facial nerves, but no anastomosis between the cochlear and facial nerves. In 14 of 17 specimens, Nageris et al. (2000) observed the anastomoses between the facial and either superior or inferior vestibular nerves, albeit without a consistent pattern.

Relationship to the arterial branches

A loop of AICA may extend into the IAM as mentioned earlier. The arterial system of the IAM, composed of the labyrinthine (or internal auditory) artery/arteries, shows a variable pattern of branching into the arteriae nervi, arteria vestibuli anterior, arteria vestibulocochlearis, arteria ganglii vestibularis, and arteria cochleae propria (Fisch 1973).

Facial nerve sensory ganglia

Despite the classical concept that the facial nerve sensory ganglia are located in the geniculate ganglion, two (geniculate and meatal) ganglia exist in most individuals. Duality of the facial nerve ganglia is explained by the nerve's dual developmental origin from the epibrachial placode and neural crest cells (Gacek 1998a).

Dobozi (1975) noted that in some cases few ganglion cells are scattered along the labyrinthine or meatal segment of facial nerve. In histopathological study of 11 temporal bones, Rupa et al. (1992) reported:

1. In 9 of 11 specimens (81.8%), the neurons aggregated at the apex of the genu close to the origin of the greater petrosal nerve.
2. In one specimen, ganglion cells extended into the labyrinthine segment of the facial nerve.
3. In one specimen, there was a paucity of ganglion cells in the geniculate segment.

In his seminal work, Gacek (1998a) studied 100 adult temporal bones to quantify the number of the ganglion cells and their pattern of distribution along the facial nerve segments. He observed two histological types (large lightly stained and small dark) of neurons.

1. Ganglion cell bodies were found in the geniculate and meatal segments in all specimens, in the labyrinthine segment in one-third of the specimens and none in the tympanic segment.
2. The cells in the geniculate segment were aggregated into a geniculate ganglion, while those in the meatal segment were scattered along the intermediate nerve – within or surrounding the nerve – into small or medium-size clusters of the meatal ganglia (collectively referred to as meatal ganglion).
3. In the majority of specimens, a larger fraction of sensory neurons was situated in the geniculate ganglion and smaller fraction in the meatal ganglia. The total number of ganglion cells was over the range 539–4017, and those in the geniculate and meatal ganglia 66–4017 and 0–2764, respectively.
4. In 88% of individuals, the geniculate ganglion contained the majority of neurons.
5. In 4% of specimens, the distribution of the neurons was equal in both ganglia.
6. In 8% of specimens, meatal ganglion contained the majority of neurons.
7. The geniculate ganglion was absent or remarkably reduced in two cases (2%), where all neurons were situated in the meatal ganglion.
8. The meatal ganglion was absent or remarkably reduced (containing less than 5% of neurons) in 12 cases (12%).

Endotemporal variations of the facial nerve

The endotemporal variations of the facial nerve include the following.

1. *Facial canal dehiscence with or without prolapse or displacement of the facial nerve*: the nerve may be exposed in the middle ear by lacking a bony cover (Bergman et al. 2006). The facial nerve may be displaced or prolapse in such cases,

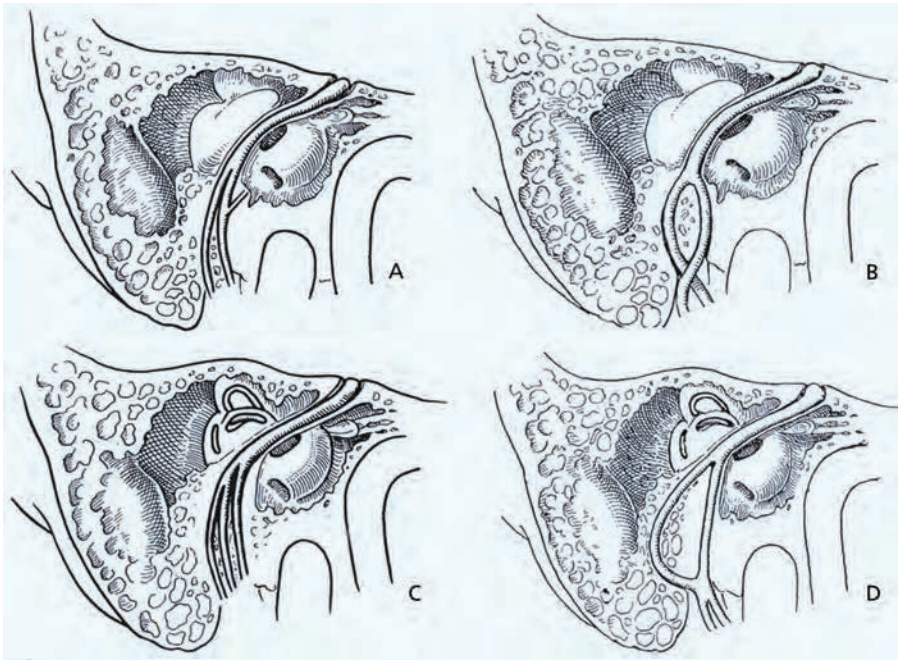

Figure 84.8 Endotemporal (a–c) division or (d) duplication of the facial nerve. Adapted from Fowler (1961) with kind permission from John Wiley & Sons.

overlying or running over the niche of the oval window, stapes, or promontory. Facial canal dehiscence arises from the failure of its cartilaginous analge to ossify (Leek 1974), and often involves the tympanic segment of the nerve.

2. *Duplication or fenestration of the facial nerve* (Fig. 84.8d): the canalicular, labyrinthine, tympanic and mastoid segments of facial nerve may be duplicated (Celin et al. 1991; Glastonbury et al. 2003; Jakkani et al. 2013).
3. *Endotemporal division of the facial nerve* (Fig. 84.8a–c): the nerve may be divided endotemporally with its branches coursing in the separate bony canals.
4. *Aberrant course of the facial nerve and canal* (Fig. 84.9): the facial nerve may have an unusual course through the temporal bone (Bergman et al. 2006). Such aberrancy may involve the labyrinthine, tympanic, and/or mastoid segments of the nerve.

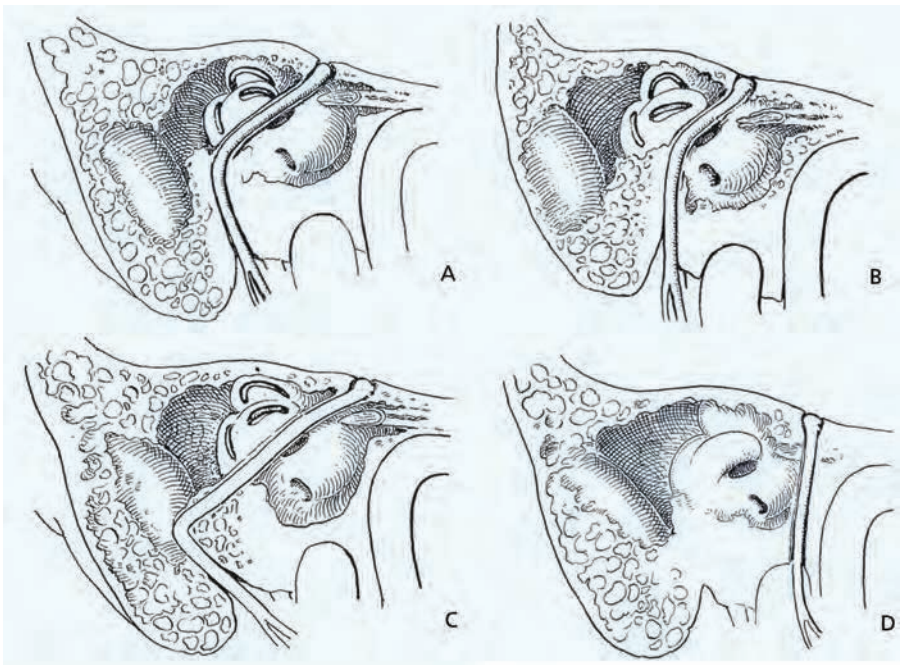

Figure 84.9 Course variations in the tympanic and mastoid segments of the facial nerve according to Folwer (1961). (a) The second genu is slightly displaced backward and downward. The tympanic segment is obliquely oriented (rather than horizontally), assuming a more anterior course in relation to the lateral semicircular canal. The mastoid segment is obliquely oriented. (b) The second genu is more obtuse (note Fowler described this variant as "nerve running straight down"). (c) The second genu is displaced backward and is situated posterior to the semicircular canal. (d) Facial nerve descending anterior to the promontory and oval and round windows. There was ipsilateral microtia in this case.

Source: Fowler (1961). Reproduced with permission from John Wiley & Sons.

It is worth mentioning that endotemporal variations of the facial nerve may coexist with congenital ear malformations, including middle ear or ossicular chain anomalies (Jakkani et al. 2013). Such associations can be explained by the common embryonic origin of these structures, as the facial nerve originates from the second branchial arches and the ossicular chain from the from the first and second branchial arches.

Labyrinthine segment

The labyrinthine segment is the shortest and thinnest segment of the facial nerve, which extends from the fundus of the IAM to the geniculate ganglion at the first external genu of the facial nerve within the facial canal (May 2000). Due to its proximity to the basal turn of the cochlea, the labyrinthine segment of the facial nerve is cautiously dissected out during the middle cranial fossa approaches to the IAM and facial nerve. In a histopathologic study of 48 temporal bones from subjects aged 6–76 years, the distance of the labyrinthine segment of the facial nerve to the basal turn of the cochlea fell within the range 0.06–0.8 mm; in 75% of cases, this distance was <0.5 mm (Redleaf and Blough 1996).

In the horizontal plane the labyrinthine segment is often convex laterally, but it may infrequently be straight (Kudo and Nori 1974). The labyrinthine segment of the facial nerve has been reported to take an aberrant course lateral to the labyrinthine bone, emerging behind and lateral to the posterior semicircular canal (Helms 1981). The facial nerve then ran anteriorly to the geniculate ganglion below the lateral semicircular canal, with its remaining course from the geniculate ganglion to the stylomastoid foramen being normal.

In individuals with an atretic IAM and intact facial nerve function, the facial nerve takes an aberrant course to the geniculate ganglion as follows (Giesemann et al. 2011).

1. The cisternal segment takes a ventral and superior course, travelling just beneath and lateral to the trigeminal nerve.
2. At the point where the trigeminal nerve enters the Gasserian ganglion, the aberrant facial nerve takes a sharp lateral turn, entering a minute canal within the anterior part of the petrous temporal, and courses in a lateral and inferior direction to reach the geniculate ganglion.

The subarachnoid space may extend into facial canal with CSF surrounding the facial nerve. In a histopathological study of 163 adult human temporal bones by Gacek (1998b), the subarachnoid space extended perineurally into the labyrinthine segment of the canal in 144 cases (type I, 88%) or intraneurally into the tympanic or geniculate part of the facial nerve (therefore separating the nerve fascicles) in 13 cases (type II, 8%). In 6 cases (type III, 4%), the subarachnoid spaced extended lateral to the geniculate and tympanic parts of the facial nerve by evagination of the superior cul-de-sac of the subarachnoid space over the geniculate ganglion, sometimes toward the bony roof of the middle ear. The subarachnoid space may also extend around the greater petrosal nerve. Gacek (1998b) postulated that when CSF pressure is high, the subarachnoid space extend laterally along the facial canal, although only 7 and 4 of type II and III specimens, respectively, had intracranial pathologies associated with elevated intracranial pressure. This probably implies that all three types mentioned above may be encountered under normal conditions.

Geniculate segment

The angle between the labyrinthine and mastoid segments of the facial nerve at the geniculate segment varies widely over the range 19–107° (Kudo and Nori 1974).

The geniculate segment of the facial nerve and proximal part of the greater petrosal nerve are usually situated within their own bony canals. During the ossification of this region, only a small hiatus remains for the exit of the greater petrosal nerve (Ge and Spector 1981). The ossification of the dural surface of the geniculate segment of the facial canal may be incomplete and the bone over the geniculate ganglion/segment may be absent (a form of facial canal dehiscence), leaving the ganglion denuded and exposed to the middle cranial fossa. In a study of 100 adult human temporal bones, Rhoton et al. (1968b) observed: in 2% of cases, the entire geniculate ganglion and genu were exposed; in 13% of cases, part of the geniculate ganglion and genu were not covered by bone; in 15% of cases, the ganglion was completely covered by bone, but the greater petrosal nerve was exposed; and in 70% of cases, the geniculate segment and proximal part of the greater petrosal nerve were covered by bone.

The anterior part of the geniculate ganglion was denuded in 5 of 24 cases (20%) examined by Dobozi (1975). In 2 of 10 adult temporal bones examined by Ge and Spector (1981), the bony roof of the canal was thin enough to allow visualization of the pinkish-yellow discoloration of the geniculate ganglion through it.

Tympanic and mastoid segments

Facial canal dehiscence with or without displacement or prolapse of the facial nerve

Despite differences among reports concerning its prevalence, the facial canal dehiscence, leaving facial nerve denuded or exposed, is probably the most common variation involving the anatomy of the facial nerve. In such cases, there are regional gaps in the thin layer of the bone covering the facial nerve (facial canal wall). It may involve any segment of the facial canal, leaving the denuded nerve exposed to the middle cranial fossa (covered with dura) or middle ear or mastoid air cells (covered with mucosa). Facial canal dehiscence was reported by Dietzel in 57% of 211 temporal bones (cf. Kettel 1963), by Baxter in 55% of 535 bones (cf. Nager and Proctor 1982), by Beddard and

Saunders in 25% of 52 dissections (cf. Hoogland 1977) and by Kaplan in 7 of 100 patients undergoing stapes mobilization procedure (cf. Hoogland 1977). In a study of 1000 temporal bones, at least one facial canal dehiscence was noted in 56% of cases, most often in the vicinity of the oval window area and horizontal segment of the facial nerve canal (Moreano et al. 1994). In another study, dehiscence was found in 6.4% of cases (23 of 357) intraoperatively, and in 19.7% of the autopsied temporal bones (59 of 300) specimens (Di Martino et al. 2005). Facial canal dehiscence may account for transient facial palsy following local anesthesia during middle ear surgeries. The bony facial canal is thicker at the mastoid segment. However, a ventral dehiscence at this segment into the tympanic cavity and posterior dehiscence into the mastoid air cells may still occur (Botman and Jongkees 1955). Fowler (1961) mentioned instances where the facial canal had "no outer bone sheath at all." Sammut (cf. Johnsson and Kingsley 1970) observed that the bony covering of the facial canal was solid in 63% of cases, thin in 22%, transparent in 9% and dehiscent in 6%. Nager and Proctor (1982) stated that the facial canal dehiscence is less common and smaller in the well-pneumatized temporal bones.

Although some degree of facial canal dehiscence and slight displacement of the facial nerve are not uncommon, significant prolapse or displacement of the dehiscent facial nerve coursing over the bony promontory, overlying or running inferior to the oval window, is rare; Huang (1997) observed such instances in three patients with congenital deafness and ossicular anomalies undergoing middle ear surgery. He counted almost 50 similar cases prior to his report, the first being described by Henner in 1960.

The facial nerve has been observed to herniate as a tumor-like mass through a round dehiscence in the tympanic segment of the facial nerve with the fibrous remnant of the stapedial artery connecting it to the promontory (Johnsson and Kingsley 1970). Nager and Proctor (1982) stressed that "inferior sagging" (or prolapse) of the facial nerve through a dehiscent canal should not be confused with aberrant facial nerves that course in an ectopic, often dehiscent, canal. Prolapse or herniation of the facial nerve may account for inadvertent facial nerve injury during middle ear surgeries such as stapedectomy (Leek 1974). The association of facial canal dehiscence with otosclerosis is controversial (Hoogland 1977; Tange and de Bruijn 1997).

Endotemporal division of the facial nerve

Splitting of the tympanic and mastoid segments of the facial nerve has been reported (Botman and Jongkees 1955; Djerić and Savić 1987). Most such cases involve the mastoid segment below the second genu (Fig. 84.8). The subsequent branches then take variable course within distinct canals in the mastoid temporal and exit through distinct foramina. In a survey of 400 temporal bone specimens, Djerić and Savić (1987) noted bifurcation of the mastoid segment in two cases (with a prevalence of 0.5%). Basek (1962) found endotemporal division in 3 out of 500 (0.6%) otherwise normal temporal bone specimens. Some of the reported variants of the endotemporal branching are as follows.

1. The mastoid segment divided into anterior and posterior branches. The anterior branch had the usual diameter of the facial nerve, and coursed laterally and downward to reach the stylomastoid foramen. The posterior branch was thinner and entered a bony canal in the mastoid process (Djerić and Savić 1987).
2. The facial nerve divided into two branches at the level of second genu, the anterior branch being larger than the posterior. Both nerves coursed vertically in distinct canals within the mastoid process and exited the temporal bone through separate foramina (Djerić and Savić 1987).
3. The facial nerve divided below the second genu into a thicker anterolateral branch that descended obliquely, giving rise to the chorda tympani and a thinner posteromedial branch that was straight in one case and curvy in another (Basek 1962).
4. In a specimen from a 34-week-old fetus, Basek observed the facial nerve splitting just at the level of the second genu into thicker lateral and thinner medial branches coursing in parallel 2 mm apart.
5. The mastoid segment divided into three branches just below the second genu (Botman and Jongkees 1955). The branches were laterally positioned (superficial in the mastoid temporal), diverged laterally and backward, coursed within separate bony canals, and exited the temporal bone through different foramina at the anterior surface of the mastoid process. The anterior branch was thicker, more or less at the normal position of the mastoid segment but slightly superficial, and gave rise to the chorda tympani.
6. A facial nerve has been observed to give rise to a small division (or minor trunk) in its mastoid portion, which then joins the distal zygomaticotemporal (upper) division of the facial nerve and departs from it as the buccal nerve (Katz and Catalano 1987).
7. The temporofacial and cervicofacial rami may emerge separately through the petrotympanic fissure and stylomastoid foramen (Kilic et al. 2010).
8. The bifurcated horizontal segment or second genu may surround the oval window and footplate (Phelps and Lloyd 1981).
9. According to Terrahe (cf. Phelps and Lloyd 1981), bifurcation of the mastoid segment is more common with congenital ear malformations.

A congenital mesodermal abnormality may sometimes present as an osseous ridge parallel to and pedicled on the mastoid segment of facial nerve, mimicking a facial nerve bifurcation (Neely and MacRae 1979; Sigari et al. 2007).

Variations in the course of the facial nerve

Aberrancies in the facial nerve course may occur with or without associated bony canal dehiscence. Significant variations are infrequently observed in an otherwise normal temporal bone. However, it is not unusual to find them in association with subtle abnormalities (such as ossicular or stapedial abnormalities),

gross dysplasia of the temporal bone, or outer, middle, and inner ear malformations. For example, a downward displacement of the tympanic segment of the facial nerve, either with dehiscent or intact canal, is a relatively common form of aberrant facial nerve. If such a displacement occurs during the fifth to sixth weeks of gestation, the contact between the stapes blastema and otic capsule – which is crucial for the normal development – is disrupted, resulting in various ossicular abnormalities such as absence or dysplasia of the stapes and other ossicles (Reiber and Schwaber 1997; Ballester et al. 2000). According to Durcan et al. (1967), if the development of Richert's cartilage is altered, the facial canal may not develop normally and the nerve may tend to course anterior to the derivatives of the arch cartilage. Notably, Phelps and Lloyd (1981) postulated that even with severe labyrinthine abnormalities, the facial nerve tends to course normally providing that the external and middle ears are normal.

In the following section, we describe the aberrancies of the facial nerve course irrespective of the abnormalities of the ear, as such anatomical knowledge is particularly useful for the surgeons operating on or around the facial nerve and the temporal bone. Whenever applied, the mention of associated gross malformations is made.

The tympanic segment of the facial nerve may be straight or convex laterally, superiorly, or superolaterally (Kudo and Nori 1974). The lateral semicircular canal projects laterally over the facial canal in 90% of cases; the distance between these two structures varies over the range 0.1–1 mm anteriorly and 2–3 mm posteriorly (Botman and Jongkees 1955). Kudo and Nori (1974) reported that the lateral margin of the facial nerve lies 0.5–2.6 mm medial to the prominent point of the lateral semicircular canal. At the second genu of the facial nerve, the facial canal and nerve projecting laterally may sometimes become even more prominent than the prominence of the lateral semicircular canal (Leek 1974). Fowler (1961) referred to this as "hump anomaly," and believed that a dorsal hump posterior and inferior to the lateral semicircular canal is the most common facial nerve course variation in otherwise normal temporal bones (Fig. 84.10). The unusual lateral projection or hump of the facial nerve course may involve the horizontal segment anteriorly, below the lateral semicircular canal.

In a series of 25 normal-appearing temporal bones, there was one case with a facial canal hump at the second genu (4%) and one with canal overhang in the oval window region (4%); these two were the only gross variations observed other than three cases (12%) with dehiscent facial canal (Kharat et al. 2009). Durcan et al. (1967) reported a series of 29 temporal bones with unusual facial nerve courses as follows:

1. nerve with gross overhang (or lateral hump with slight downward displacement partially obscuring the superior or posterosuperior edge of the oval window niche) in the stapes area (17 cases);
2. facial nerve bifurcation around the stapedial crura (4 cases);
3. nerve coursing over the promontory (3 cases); and
4. facial nerve with reduplicated chorda tympani (4 cases).

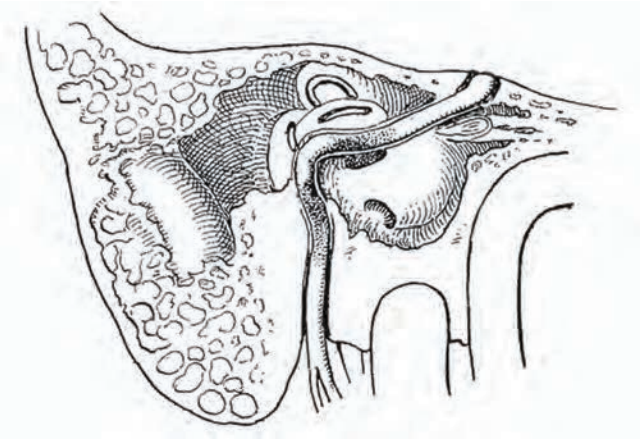

Figure 84.10 "Hump anomaly," the most common facial nerve course variation according to Fowler 1961. The second genu projects laterally and presents as a prominence or hump posterior and lateral to the horizontal semicircular canal.

Source: Fowler (1961). Reproduced with permission from John Wiley & Sons.

In a series of 31 cases with congenital ear malformation with or without atresia of the external ear canal, a marked overhanging of the facial nerve ridge with absent or blunted second genu was the second most common anomaly after facial canal dehiscence (Phelps and Lloyd 1981). Hoogland (1977) described an aberrant facial nerve coursing over the oval window region (oval window was absent or completely obscured by the overlying nerve). The stapedial crura had no connection with the footplate.

Fowler (1961) described a facial nerve coursing between the oval and round windows (low-lying horizontal segment) in a patient with persistent stapedial artery and congenital stapes footplate fixation. Mayer and Crabtree (1976) reported three cases in which the dehiscent facial nerve coursed inferior to the oval window. These authors found nine similar reports in the literature and noted that:

1. The majority of cases had normal pinnae, external ear canal, and tympanic membrane;
2. all the patients had congenital conductive hearing loss;
3. facial nerves were dehiscent in all cases, were normal-appearing in nine cases, and appeared as a "boggy mass" in three cases; and
4. 10 of the 12 patients had ossicular (stapedial) abnormalities.

Dickinson et al. (1968) reported a facial nerve coursing in a bony canal located vertically across the promontory and anterior to the oval and round window. Hoogland and Marres (1977) reported a similar aberrancy in a patient with congenital ossicular malformation where the nerve, after leaving the geniculate ganglion, ran straightly downward over the promontory and anterior to a persistent stapedial artery.

Ballester et al. (2000) observed aberrant facial nerve courses in relation to the oval window – typically associated with

stapes abnormalities – in 40 of 595 (6.7%) stapedotomy cases as follows.

1. Partial displacement or prolapse (*n*=32), in which the facial nerve partially obscured the oval window. The varieties were: with intact facial canal (*n*=26); with completely or partially dehiscent facial canal (*n*=5); and with facial nerve duplicated around the oval window (*n*=1).
2. Total displacement or prolapse (*n*=8), in which the facial nerve obscured the oval window rather completely. The varieties were: with intact facial canal (*n*=5); and with complete dehiscent facial canal (*n*=3).

In one case the dehiscent nerve, covering the lower part of the oval window, also passed over the promontory (i.e., dehiscence and displacement simultaneously involving the proximal and distal parts of the tympanic segment). In one case the dehiscent nerve fanned out into several fascicles over the promontory and oval window.

Helms (1981) illustrated the aberrancies of the tympanic and mastoid segments of the facial nerve, and outlined the following variants.

1. Elongation of the tympanic segment with posterior displacement of the second genu (Fig. 84.11(2)).
2. Posterior and inferior displacement of the second genu (Fig. 84.11(3)). The displaced second genu may be located on the surface of the sigmoid sinus (Fig. 84.11(4); note that the sinus is not shown in the figure).
3. Blunting of the second genu with the facial nerve overlying the niche of the oval window or stapes (Fig. 84.11(5)).
4. Absence of pars tympani and vertical descent of the facial nerve from the geniculate ganglion (Fig. 84.11(6)). The nerve courses over the promontory anterior to the oval and round windows.
5. Facial nerve overlying the stapes footplate (Fig. 84.11(7)).
6. Facial nerve coursing through the crura of the stapes (Fig. 84.11(8)). The nerve may be hypoplastic (Altman cf. Hoogland 1977) or the crura may have no contact with the stapes footplate (Rohrt and Lorentzen cf. Hoogland 1977).
7. Prolapse or protrusion of the axon bundle of the facial nerve out of the dehiscent facial canal and epineurium anterior and posterior to the stapes footplate (Fig. 84.11(9)).
8. Partial duplication (or fenestration) of the tympanic segment coursing anteriorly and posteriorly of the stapes (Fig. 84.11(10)).
9. Duplication (or fenestration) of the mastoid segment (Fig. 84.11(11)).
10. Endotemporal branching of the facial nerve with bifurcation or trifurcation of the mastoid segment. The endotemporal branches exit the mastoid temporal through distinct foramina (Fig. 84.11(12–14)).

In a series of seven cases with various ossicular abnormalities and some with features of Treacher-Collins, DiGeorge and CHARGE syndromes (Song et al. 2012), the following aberrancies of the facial nerve were observed: horizontal segment coursing inferior to the oval window; vertical segment abruptly turning anteriorly; vertical segment anteriorly or anteromedially displaced; and bifurcated horizontal or vertical segment.

The angle between the mastoid and tympanic segments has been reported to vary over the range 95–120° (Kharat et al. 2009). The mastoid segment of the facial nerve usually tends to orient laterally, and may have a vertical (most common), forward, or backward course (Salame et al. 2002). It may course straightly or be slightly concave anteriorly (Hollinshead 1969). In all the specimens (46 sides) examined by Salame et al. (2002), the facial nerve trunk invariably exited the skull through the stylomastoid foramen. There may be fibrous or bony narrowing of the stylomastoid foramen (Fowler 1961).

The external projection of the mastoid segment usually corresponds to the frontal plane passing through the tympanomastoid suture, but the nerve may lie posterior or anterior to this plane (Hollinshead 1969). Kettel (1946) cited Hawley as describing four cases (from 300 dissections) where the facial nerve was displaced 3–4 mm behind this plane and one case in which the nerve ended in a blind pouch, sending only a thin fiber in the normal path (facial nerve hypoplasia).

Kettel (1946) observed the mastoid segment of the facial nerve lying behind the frontal plane of the tympanomastoid suture in 7 out of 125 (5.6%) facial nerve operations.

1. In three cases (2.4%), the distal part of the mastoid segment coursed normally along the plane of the tympanomastoid suture, but the proximal part made a posteriorly convex curve behind this plane. The most prominent point of this convexity was just below the most prominent point of the lateral semicircular canal.
2. In three cases (2.4%), the entire mastoid segment was displaced posteriorly and situated medial to the mastoid air cells between the sigmoid sinus and posterior wall of the bony external ear canal.
3. In one case (0.8%), posterior displacement of the mastoid segments involved both proximal and, more frequently, distal parts in a way that the proximal half made a further posteriorly convex curve behind the already displaced distal part. This variant had the features of the previous two forms combined.

Schwatze (cf. Botman and Jongkees 1955) distinguished three different courses of the mastoid segment: (1) a steep course where the nerve lies inside a sagittal plane midway through the tympanic annulus; (2) a flat course when the nerve crosses this plane and runs laterally; and (3) an oblique course when the nerve follows a course in between the above two forms.

Sendulski (cf. Botman and Jongkees 1955) described three positions of the mastoid segments in relation to the sagittal plane passing midway through the tympanic annulus: medial to this plane (55%); along this plane (29%); and lateral to this plane (16%).

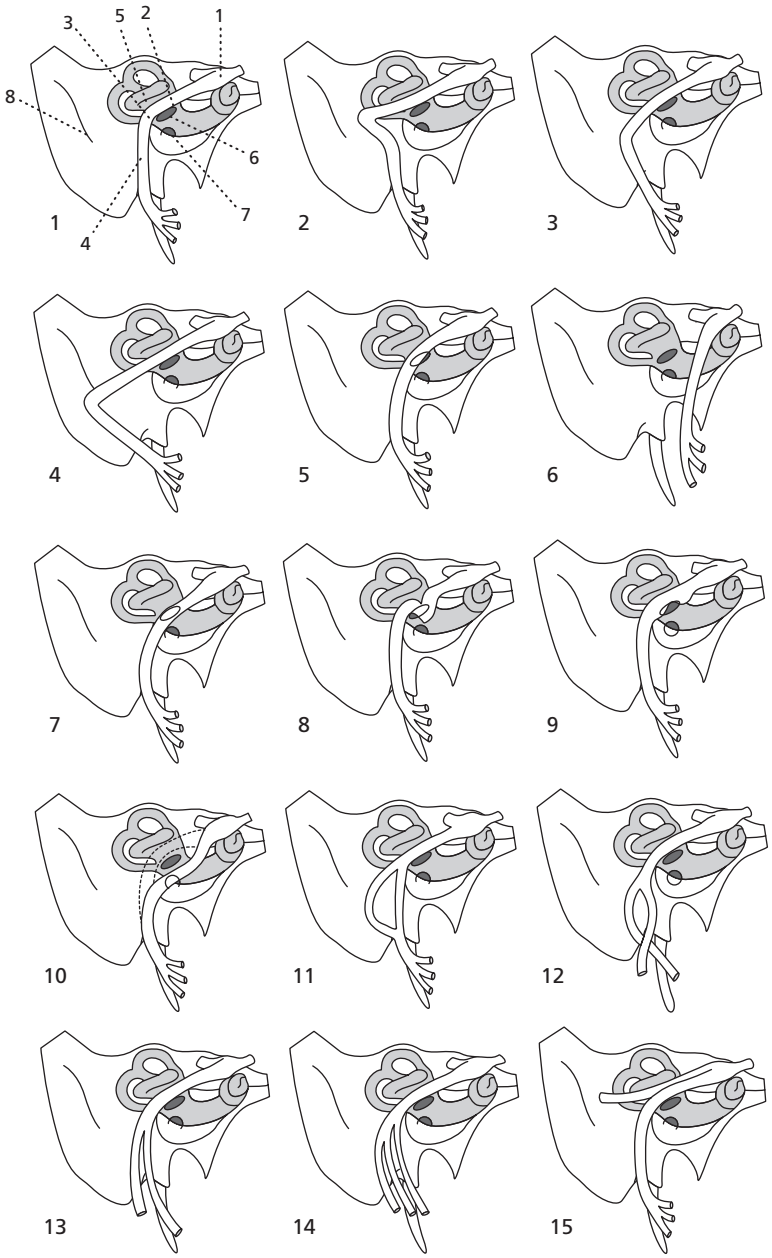

Figure 84.11 Variations of the course of the tympanic and mastoid segments of the facial nerve. 1, first external genu of the facial nerve harboring the geniculate ganglion; 2, tympanic segment; 3, second external genu; 4, mastoid segment; 5, lateral or semicircular; 6, oval window (location of stapes); 7, round window; 8, mastoid region of the temporal bone.

Source: Helms (1981). Reproduced with permission from Springer Science and Business Media.

The mastoid segment may be laterally displaced and positioned more superficially within the mastoid temporal. In a study of 37 temporal bone specimens, Adad et al. (1999) noted that the facial nerve coursed lateral to the plane of tympanic annulus in 70% of instances and medial to it in the remaining cases (30%). According to Streita (cf. Botman and Jongkees 1955), a very steep tympanic membrane is accompanied by a far lateral course of the facial nerve. In hypoplastic mastoids, the facial nerve may exit from the bone laterally without a descending segment (Terrahe cf. Phelps and Lloyd 1981). The facial nerve may lie in the wall of mastoid antrum and emerge from the mastoid process (Tubbs et al. 2013). It may also emerge from the lateral surface of the mastoid process (Nager and Proctor 1982).

The mastoid segment may be displaced ventrally (or ventrolaterally), being in close proximity to the external bony ear canal. Greisen (1975) observed such a variant (intraoperatively in a patient with cholesteatoma and ruptured tympanic membrane) in which the facial nerve also arched forward and pierced the posterior wall of the external ear canal 2–3 mm lateral to the tympanic membrane. The nerve coursed for a length of 7–8 mm in the external bony ear canal under the

skin. In a patient with congenital conductive hearing loss and stenotic meatus but normal-appearing pinna, Kuo and Wang (2012) reported a similar aberrancy in the course of the facial nerve where the mastoid segment was situated right behind the tympanic membrane and next to the medial edge of the posterior wall of the external canal. Fowler (1961) cited a personal communication with Angell-James on a variant facial nerve that ran through the anterior edge of the bony external ear canal.

Phelps and Lloyd (1981) reported a rare facial nerve course in cases with congenital ear malformation: (1) the inferior part of the mastoid segment may cover the round window; (2) the nerve may cross the eardrum turning forward in the floor of the external ear canal; and (3) the nerve may exit the temporal bone through the floor of the tympanic cavity.

Other rare variations of the tympanic and mastoid segments of the facial nerve include:

1. The facial nerve may pass through the center of the superior semicircular canal and bypass the tympanic cavity *en route* to the stylomastoid foramen (Dworacek cf. Nager and Proctor 1982).
2. Unusual muscle fibers may exist in the facial canal along with the facial nerve (Bergman et al. 2006).
3. An accessory cavity of the tympanum (posterior tympanic recess) may extend medial to the tympanic segment of the facial canal, separating it from the bony labyrinthine (Proctor and Nager 1982).
4. The mastoid segment may be concave anteriorly (in 12 of 24 cases reported by Kudo and Nori 1974), or medially (in 1 of 24 cases).
5. Haynes (1955) stated that in the well-pneumatized mastoid temporal, a group of air cells may be found situated directly over the facial nerve about the posterior end of the lateral semicircular canal.
6. The mastoid segment may be entirely surrounded by air cells, and the wall between the cells and the nerve may be thin or dehiscent (Phelps and Lloyd 1981).
7. The relationship between the mastoid segment of the facial nerve and jugular vein varies with the distance between them ranging from 1.5 to 10 mm (Saleh et al. 1995). The arbitrary plane of the mastoid segment passes through the jugular bulb at its anterior third (40%), middle (30%), or posterior third (30%) (Saleh et al. 1995).

In their comprehensive review, Proctor and Nager (1982) illustrated 25 aberrancies in the course of the facial nerve. Some of the rare variants not mentioned above are:

1. facial nerve coursing superior to the lateral semicircular canal;
2. facial nerve turning forward at the middle of horizontal segment and following the course of chorda tympani;
3. facial nerve descending over the promontory and coursing posteriorly inferior to the round window *en route* to the stylomastoid foramen; and
4. S-shaped course of the mastoid segment.

Variations in the branches of the main facial nerve trunk

Chorda tympani

The chorda tympani usually originates from the mastoid segment of the facial nerve within the facial canal. After branching off, it may accompany the facial nerve for a distance of 1–8 mm before entering its own specific canal (Kulczyński and Woźniak 1978). In a study of 200 temporal bones (Djerić 1993), chorda tympani originated from the mastoid segment of the facial nerve at its midportion (70% of cases), proximal third (20%), and distal third (10%). Chorda tympani may have an extracranial origin from the facial nerve. This was noted by McManus et al. (2012) in 6 of 40 (15%) specimens. In another series of 30 dissections on Chinese adult temporal bones, chorda tympani had an extratemporal origin in 53.3% of instances (Low 1999). The intraosseous length of the chorda tympani shows a greater inter-individual variability compared to its extraosseous length (Bartsch et al. 1991). Muren et al. (1990) found the point of origin of the chorda tympani within 10 mm above the stylomastoid foramen, and within a range of 7–19 mm below the lower border of the lateral semicircular canal. The point of origin may rarely be located as high as the second genu (Cawthorne cf. Muren et al. 1990). Haynes (1955) also observed a chorda tympani nerve originating at the level of the semicircular canal. Fowler (1961) depicted a variant chorda tympani originating from the anterior part of the horizontal segment of the facial nerve in an individual with deformed ossicles and persistent stapedial artery.

In a series of 24 dissections, Kudo and Nori (1974) observed the following variations in the chorda tympani.

1. The point of origin was 1–8.7 mm above the stylomastoid foramen.
2. In one case, the origin of chorda tympani was outside the stylomastoid foramen, without the nerve reaching the temporal bone.
3. In one case, the proximal portion of the chorda tympani ran downward and then turned upward (convexity downward) before attaining its usual course.

Kulczyński and Woźniak (1978) reported the following variations of the chorda tympani.

1. In 38 of 74 cases, it originated from the facial nerve within the first 2 mm above the stylomastoid foramen. In 4 cases in this group, its origin was at the level of the stylomastoid foramen.
2. In 32 of 74 cases, it originated 3–7 mm above the foramen.
3. In 4 of cases, it originated >8 mm above the foramen.
4. In 4 of cases, it originated below the foramen. The chorda tympani then accompanied the facial nerve upward and entered the tympanic cavity.

Minnigerode (1965) reported a sizable lateral branch of the chorda tympani in the tympanic cavity that supplied the posterosuperior quadrant of the tympanic membrane. In half of the specimens dissected by Kulczyński and Woźniak (1978), a branch from the chorda tympani was observed to arise at the

level of sphenoid spine and run toward the cartilaginous part of the external ear canal.

The chorda tympani may travel in a sulcus on the posterior wall of the external ear canal (seen in 8 of 74 specimens by Kulczyński and Woźniak 1978). It most often joins the lingual nerve 24–27 mm below the skull base (Trost et al. 2011). However, after exiting from the iter chordae anterius at the medial end of the petrotympanic fissure, it may run independently of the lingual nerve (Bergman et al. 2006). The chorda tympani may also attach to the inferior alveolar nerve for a distance before re-emerging to join the lingual nerve *en route* to the tongue (Bergman et al. 2006).

The chorda tympani has been observed to emerge from the stylomastoid foramen along with the facial nerve, communicate with it and, after an extratemporal course of 5 mm, turn back to re-enter the facial canal through the stylomastoid foramen (Salame et al. 2002; seen in 1 of 46 dissections). The chorda tympani communicated with the lesser petrosal nerve in 28 and with otic ganglion in 19 of 74 cases (Kulczyński and Woźniak 1978).

Sensory auricular branch of the facial nerve

Eshraghi et al. (2002) have described a sensory auricular branch of the facial nerve originating from its mastoid segment above the chorda tympani in all 10 specimens they examined; the sensory branch was of variable size and direction. After its origin, the sensory nerve either coursed superiorly or laterally before turning inferiorly to pass posterior to the chorda tympani; in one case, it passed anterior to the chorda tympani. The sensory branch has been postulated to supply the posteroinferior aspect of external ear canal at the level of bone–cartilage junction.

Extracranial or extratemporal branches of the facial nerve

These branches can be classified into two groups: (1) pre-parotid branches arising from the facial nerve trunk somewhere between the stylomastoid foramen and the parotid gland; and (2) intra-parotid branches within the parotid gland, including the terminal branches of the facial nerve. In a study of 46 sides, the number of pre-parotid branches varied from two to four (Salame et al. 2002). In the majority of instances (72%), only two branches (posterior auricular nerve and nerve to the digastric muscle) exited. In 24% of cases, three distinct branches (posterior auricular nerve and nerves to the digastric and stylohyoid muscles) were present. Four branches (communicating branch to the glossopharyngeal nerve, posterior auricular nerve, and nerves to the digastric and stylohyoid muscles) were noted in 4% of cases.

Pre-parotid branches

The posterior auricular nerve most often originates from the facial nerve trunk after it exits through the stylomastoid foramen. The distance of posterior auricular nerve origin from the stylomastoid foramen varies over the range 1.90–4.38 mm (Salame et al. 2002) and 1.6–11.1 mm (Smith and Ross 2012) in different studies. Although the posterior auricular nerve was the most constant first extratemporal branch of the facial nerve in the 46 sides examined by Salame et al. (2002), this nerve may very rarely arise from the facial nerve before it exits from the stylomastoid foramen (Bergman et al. 2006). In a study of 11 head sides, Smith and Ross (2012) found three variants of the posterior auricular nerve. In type I (5 of 11 cases), the nerve had a single trunk. In types II (4 of 11) and III (2 of 11), the nerve had a common trunk with one and two other branches, respectively. The other branches noted in types II and III passed into the parotid gland. The posterior auricular nerve may course medial to the mastoid process (most common), over the mastoid, or within the substance of the parotid gland below the mastoid process before appearing posterior to the external ear canal.

The communicating branch to the glossopharyngeal nerve was the first extratemporal branch of the facial nerve trunk in 2 of 46 sides dissected by Salame et al. (2002). The nerve to the digastric muscle is a constant branch of the facial nerve trunk that supplies the posterior belly of the digastric muscle. The nerve to stylohyoid muscle usually has a common stem with the nerve to the digastric muscle, but it may directly arise from the facial nerve trunk in about a quarter of specimens (Salame et al. 2002). Twigs from the stylohyoid branch may supply the lower surface of the anterior belly of the digastric muscle (Kawai et al. 2003). It has also been observed that twigs from the stylohyoid and marginal mandibular branches supplied the anterior belly of the digastric muscle along with, and while anastomosing with, the mylohyoid nerve branches (Asami et al. 2006). The nerve to the digastric muscle may send branches to the styloglossus and sternocleidomastoid muscles (Bergman et al. 2006). An aberrant branch from the facial nerve has been observed to partly supply the sternocleidomastoid muscle (Cvetko 2013).

Schaeffer (1953) noted an inconsistent branch of the facial nerve, first described by Cruveilhier as the lingual branch, supplying the root of the tongue and palate. It originated below the stylohyoid branch, descended along the anterior border of the stylopharyngeus muscle, and pierced the superior constrictor muscle to appear behind the anterior palatine arch.

Facial nerve and its terminal branches in relation to the parotid gland

The facial nerve passes through the parotid gland *en route* to the muscles of facial expression. The relationship between the facial nerve and parotid gland tissue, its superficial and deep parts, had been a subject of extensive debate in the anatomical and surgical literature over the last century, with one group even believing that the nerve under normal situation does not pass through the gland, but deep to and outside of it. It is beyond the scope of this chapter to discuss the historical aspects of such discourse; however, interested readers are referred to the elegant paper of Davis et al. (1956).

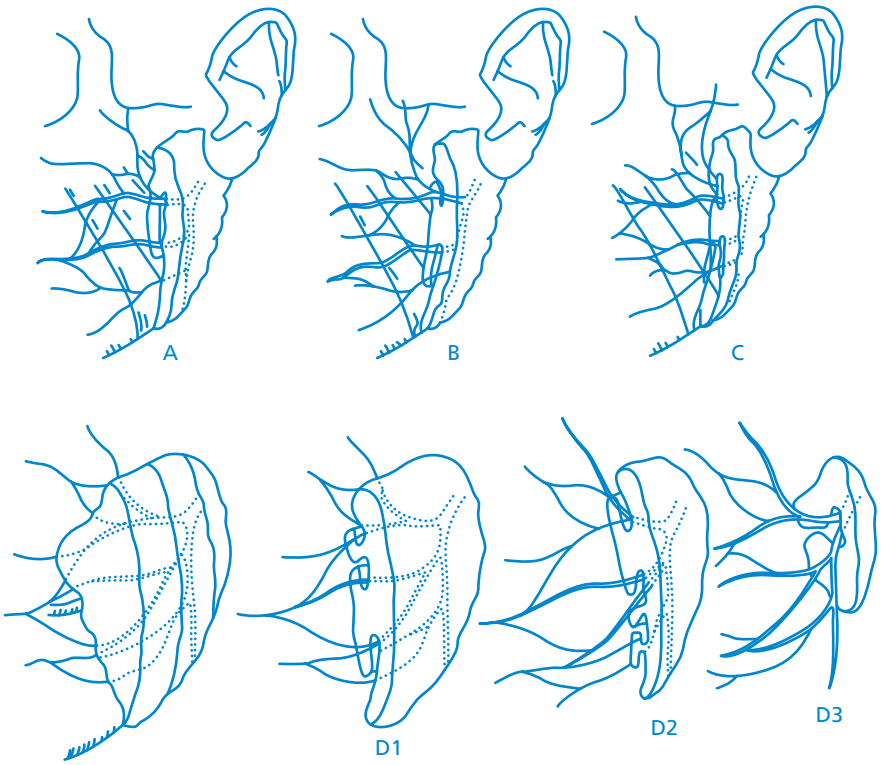

Figure 84.12 Relations of the facial nerve with the parotid gland according to different authors. (a) Grégoire; (b) McWhorter; (c) Rouvière and Cordier; (d1–3) McKenzie's concept.

Source: McKenzie (1948). Reproduced with permission from John Wiley & Sons.

According to Bergman et al. (2006), the parotid gland is variably divided by the facial nerve and its branches, and the classic description of the superficial and deep lobes remains arbitrary. Figure 84.12 shows the configuration of the parotid gland in relation to the facial nerve according to four different authorities (cf. McKenzie 1948).

1. Grégoire (1912) described the gland as having superficial and deep lobes, which are separated by the facial nerve and united above with the connecting isthmus superior to the nerve.
2. McWhorter (1917) described the gland as having superficial and deep lobes, with the connecting isthmus passing between the two main divisions of the facial nerve.
3. Rouvière and Cordier (1934) described the gland as having superficial and deep lobes, with mixed configurations of Grégoire and McWhorter.
4. McKenzie (1948) advocated a more comprehensive anatomical model to explain what he had observed, "each specimen had something different to show in the way of detailed distribution of the gland around the nerve." He maintained that the superficial and deep parts of the parotid variably connect together through the gaps between the branches of the facial nerve and parotid tissue wraps itself around the facial nerve branches, attaining a unique morphology at any given coronal plane.

The facial nerve has been observed to pass deep to the parotid gland and divide into its terminal branches outside the gland (Rai et al. 2011), but such a variant is exceptionally rare.

Variations in facial nerve terminal branching and their anastomoses

A clear separation of the nerve into five main terminal branches (temporal, zygomatic, buccal, mandibular, and cervical) may be difficult or impossible (Bergman et al. 2006). The terminal division of the facial nerve shows significant variations. The number of the main divisions or trunks may vary. Bifurcation and trifurcation of the facial nerve within the parotid gland has been reported. In 350 facial specimens dissected by Davis et al. (1956), the main trunk of the facial nerve invariably divided into two trunks: temporofacial and cervicofacial. In 13.3% of specimens from Korean cadavers dissected by Kwak et al. (2004), the facial nerve terminated within the parotid by trifurcation. In a series of 46 dissections (Salame et al. 2002), the facial nerve was found bifurcated before entering the parotid gland in 6 cases (13%), bifurcated within the gland in 39 cases (85%), and trifurcated within the gland in 1 case (2%).

Upon entering the parotic gland, the facial nerve may already have a major and a minor trunk as a result of endotemporal division or division just before entering the gland. In the study of Kwak et al. (2004), 26.7% of cases had an additional minor trunk; the minor trunk coursed below the major trunk and joined the cervical branch after sending a small communication to the cervicofacial division. Katz and Catalano (1987) observed an additional minor trunk in 3% of their cases; the minor trunk coursed superior to the major trunk, transiently joined the temporofacial division, and departed from it as the buccal branch.

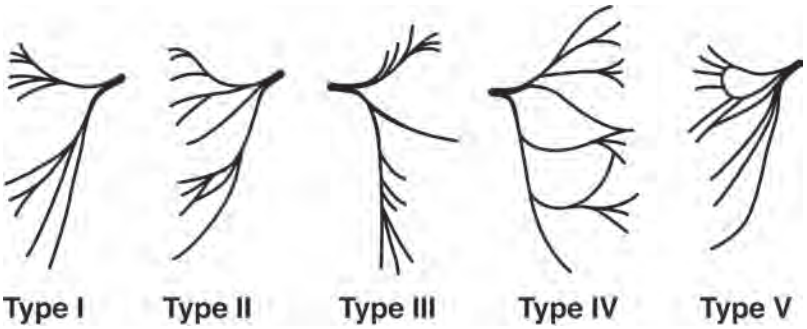

Figure 84.13 Facial nerve branching pattern within the parotid gland.

Source: Dargent and Duroux (1946).

Lineaweaver et al. (1997) observed a varying number (9–19) of the facial nerve branches at the anterior border of the parotid gland: (1) temporal: 1–3 branches, average 2; (2) zygomatic: 1–4 branches, average 3; (3) buccal: 3–7 branches, average 4; (4) marginal mandibular: 1–3 branches, average 2; and (5) cervical: 0–4 branches, average 1.

Several authors have attempted to classify the terminal division pattern of the facial nerve. Dargent and Duroux (1946) dissected 68 facial nerves from within the parotid gland. They identified two major "classes" and five "variants" (Fig. 84.13) of intra-parotid facial nerve branching from 59 of 68 dissections as follows (cf. Bergman et al. 2006).

1. Class 1 (n=35): facial nerve without anastomoses among the terminal branches. This class was composed of three variants: (1) classical variety (15 cases); (2) with precocious branching (11 cases); and (3) rare, with ladder-like branching (9 cases).
2. Class 2 (n=24): facial nerve with anastomoses between the terminal branches, forming an intra-glandular plexus. This class comprised two variants: (4) with long anastomotic loops (13 cases); and (5) with short anastomotic loops between branches of the temporofacial and cervicofacial division (11 cases).

In their classic paper, Davis et al. (1956) classified the facial nerve division pattern into six types (Fig. 84.14) based on the anastomoses between the terminal branches of the temporofacial and cervicofacial trunks (i.e., temporal, zygomatic, buccal, marginal mandibular and cervical branches).

- Type I, where no anastomoses, including side-anastomoses, between the terminal branches exist.
- Type II, where branches of the temporofacial division anastomose with each other. The first variant of this type has two (upper and lower) zygomatic branches that join together before supplying the facial muscles in the zygomatic and buccal areas. There is a distinct buccal branch, originating from the cervicofacial division, which courses independently. In another variant, the anastomoses may exist between the temporal and zygomatic branches, with the buccal branch yet coursing independently. Alternatively, there may be anastomoses among the three temporal, zygomatic, and buccal branches. The latter variant is considered a type II if the buccal branch is from the temporofacial division.
- Type III, where there is a single anastomosis between a branch of the temporofacial division and a branch of the cervicofacial division. There are several variants of this type with respect to the arrangement of the buccal branch. In one variant the buccal branch, arising from the cervicofacial trunk, sends a small anastomotic twig to the zygomatic branch, and the main buccal branch courses forward to supply the muscles in the buccal region. In another variant, the buccal branch, arising from the cervicofacial trunk, forms an anastomotic loop with the zygomatic branch, and twigs of this anastomotic loop supply the zygomatic and buccal regions.
- Type IV is the combination of type II and III, where the branches of the temporofacial division anastomose with each other plus there is a single anastomosis between a branch derived from the temporofacial division and a branch from the cervicofacial division. In a typical variant of this type, there are: (1) an anastomotic loop formed between the temporal and zygomatic branches; (2) an anastomotic loop between two (upper and lower) zygomatic branches of the temporofacial division (similar to the first variant of type II noted above); and (3) an anastomotic loop between the buccal branch (of the cervicofacial division) and the zygomatic branch.
- Type V, where two anastomoses occur between the branches of the temporofacial and cervicofacial divisions. The zygomatic branch may be double. In a typical variant, a distinct branch from the cervicofacial division (an accessory buccal branch) joins the zygomatic branch. The (main) buccal branch, arising from the cervicofacial division distal to the latter branch, sends an anastomotic twig to the zygomatic branch. In this way, an anastomotic loop is formed between the zygomatic, accessory, and main buccal branches.
- Type VI, where multiple neuroanastomoses exist between the branches of the temporofacial and cervicofacial divisions. There is a transverse, plexiform anastomotic strand – zygomatic and buccal in distribution – that receives multiple communicating branches from the temporofacial and cervicofacial divisions, as well as their zygomatic, buccal, and marginal mandibular branches.

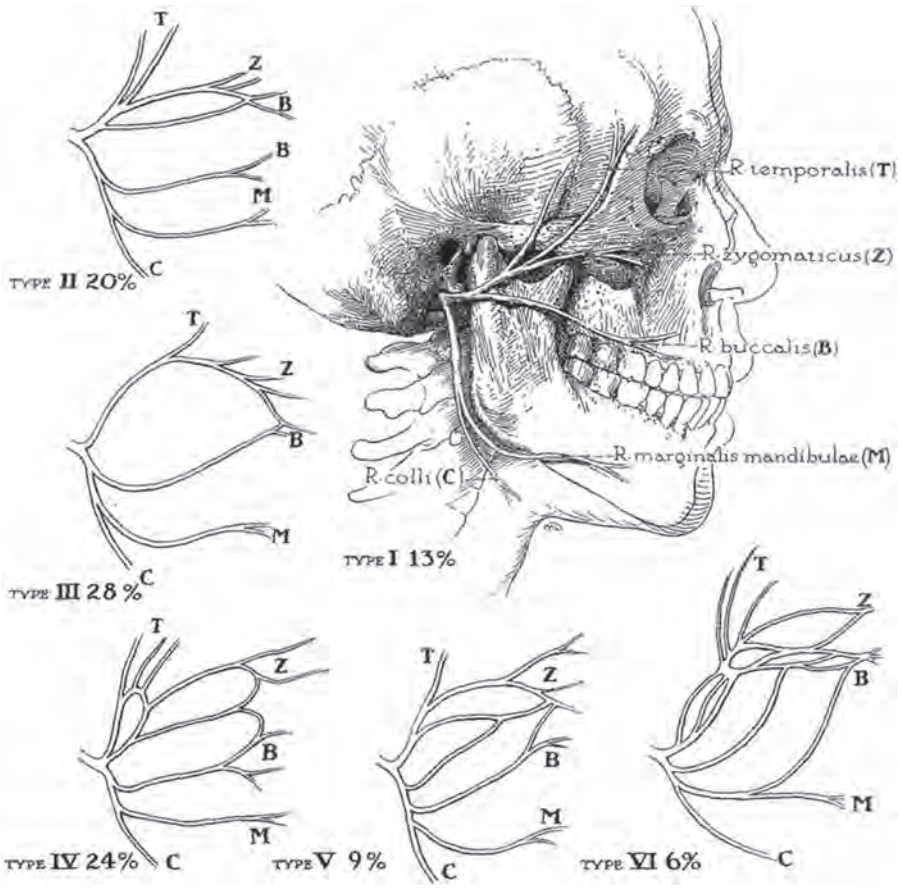

Figure 84.14 The classification of the facial nerve branching according to Davis et al. (1958). This classification is essentially based on an earlier classification introduced by McCormack et al. (1945).

Source: Davis et al. (1958).

A note on the classification of Davis and colleagues

The classification of Davis et al. (1956) has been adopted by many anatomists (Table 84.2). As mentioned above, this classification is based on the presence or absence of the anastomoses between the terminal branches of the facial nerve. Although the classification simplifies this complex anatomy, it does not fully take into consideration the variations in the number and origin of the various terminal branches of the facial nerve. This is particularly notable in the case of buccal branch which, not uncommonly, is multiple and may variably originate from the temporofacial or cervicofacial divisions. Identification and labeling of the terminal branches sometimes prove to be difficult. For example, the first variant of type II mentioned by Davis et al. (1956) had two zygomatic branches that formed an anastomotic loop (aka zygomatic loop) supplying the zygomatic and buccal

Table 84.2 The terminal branching pattern of the facial nerve according to the classification of Davis et al. (1956.)

Type	Davis et al. 1956	Bernstein and Nelson 1984	Park and Lee 1997	Myint et al. 1992	Weerapanta et al. 2010
I	44 (13%)	3 (9%)	7 (56.3%)	9 (11.4%)	1 (1%)
II	71 (20%)	3 (9%)	15 (13.5%)	12 (15.2%)	10 (10%)
III	99 (28%)	8 (25%)	37 (33.4%)	27 (34.2%)	20 (20%)
IV	82 (24%)	7 (19%)	26 (23.4%)	15 (19%)	18 (18%)
V	32 (9%)	8 (22%)	7 (6.3%)	6 (7.6%)	29 (29)
VI	22 (6%)	6 (16%)	19 (17.1%)	10 (12.7%)	21 (21%)
Total N	350	35	111	79	100

areas. The lower zygomatic branch that Davis and colleagues noted can alternatively be regarded as an accessory buccal branch arising from the temporofacial division. Similarly, the typical variant of type IV may be viewed as having an accessory buccal branch arising from the temporofacial division, which then anastomosed with both zygomatic and main buccal nerves. Type V may be seen as having an accessory buccal branch with double root origin – one from the temporofacial division and one from the cervicofacial division – that receives anastomotic twigs from both the zygomatic and main buccal nerve.

The classification of Davis and colleagues was modified by Katz and Catalano (1987) in a study of 100 patients undergoing parotidectomy. Their new classification of the intra-parotid facial nerve branching pattern was based on: (1) the anastomoses between the terminal branches; (2) the origin of the buccal branch; and (3) the number of facial nerve main trunks within the parotid gland (in some cases there were two trunks, major and minor). They classified the pattern of the facial nerve terminal branching into five main categories. Types I–IV (97%) had a single facial nerve trunk within the parotid gland, which divided into two main divisions (i.e., upper, temporofacial, or temporozygomatic and lower, cervicofacial, or cervicomandibular divisions). Type V, comprising 3% of cases, had a minor and a major facial nerve trunk. The types and variants reported by Katz and Catalano were as follows.

- Type I (24%): with only a side-anastomosis in either zygomatic or marginal mandibular branch. A side-anastomosis is a kind of neuroanastomosis in which the anastomotic twigs originate from a nerve proximally and re-join the same nerve distally. Type I had two variants. In type IA (18%), the buccal branch originated from the cervicofacial division and the zygomatic branch, arising from the temporofacial division, had a side-anastomosis. This variant resembles type II pattern in the classification of Davis and colleagues. In type IB (6%), the buccal branch originated from the temporofacial division and the marginal mandibular nerve had a side-anastomosis. This variant with side-anastomosis was not mentioned by Davis and colleagues.
- Type II (14%): had an anastomotic loop formed between the zygomatic and buccal branches. This variant corresponds to the type II pattern in the classification of Davis and colleagues.
- Type III (44%): had a major connection between the buccal branch and zygomatic or marginal mandibular nerves. There were three variants. In type IIIA (25%), the buccal branch originated from the cervicofacial division and received an anastomotic branch from the zygomatic nerve *en route* to the buccal region. In type IIIB (13%), the buccal branch originated from the marginal mandibular nerve and received an anastomotic branch from the zygomatic nerve. In type IIIC (6%), the buccal branch originated from the temporofacial division and received an anastomotic branch from the marginal mandibular nerve. This variant also corresponds to the type III pattern in the classification of Davis and colleagues.
- Type IV (14%): the so-called "multiple-loop pattern," had multiple anastomotic loops between the zygomatic, buccal, and marginal mandibular branches. In type IVA (10%), the buccal branch originated from the cervicofacial division. In type IVB (4%), the buccal branch originated from both the temporofacial and cervicofacial divisions. According to Katz and Catalano (1987), this class corresponds to types IV, V, and VI mentioned by Davis and colleagues.
- Type V (3%): had a major and minor facial nerve trunk within the parotid gland. The major trunk bifurcated into upper and lower divisions. The minor (probably arising from the facial nerve endotemporally or before entering the parotid) coursed superior to the major trunk, transiently joined the temporofacial division and then departed from it as the buccal branch. There were no anastomoses among the terminal branches. This variant was not mentioned by Davis and colleagues.

Kopuz et al. (1994) dissected 50 specimens to investigate the facial nerve branching pattern according to the Katz-Catalano classification (Table 84.3, Fig. 84.15). Type IV branching pattern (multiple-loop) was the most common pattern, although the original study of Katz and Catalano notes that type III branching pattern (the so-called buccal loop) was the most common pattern. Kopuz et al. found two additional variants with double main trunks, as follows.

1. In one case (2%), the major trunk constituted the upper (temporofacial) division and the minor trunk constituted the lower (cervicofacial) division. The buccal branch originated from the minor trunk and received a communicating twig from the major trunk. In this way, both major and minor trunks contributed to the formation of buccal branches.
2. In two cases (3%), the major trunk bifurcated into upper and lower divisions. The minor trunk united with the lower division. Upper buccal branches were derived from the upper division and lower buccals from the lower division.

Table 84.3 Prevalence of various branching patterns of the facial nerve according to Katz-Catalano classification.

	IA	IB	II	IIIA	IIIB	IIIC	IVA	IVB	V
Katz and Catalano 1987	18 (18%)	6 (6%)	14 (14%)	25 (25%)	13 (13%)	6 (6%)	10 (10%)	4 (4%)	3 (3%)
Kopuz et al. 1994	6 (12%)	6 (12%)	6 (12%)	3 (6%)	1 (2%)	3 (6%)	1 (2%)	18 (36%)	6 (12%)

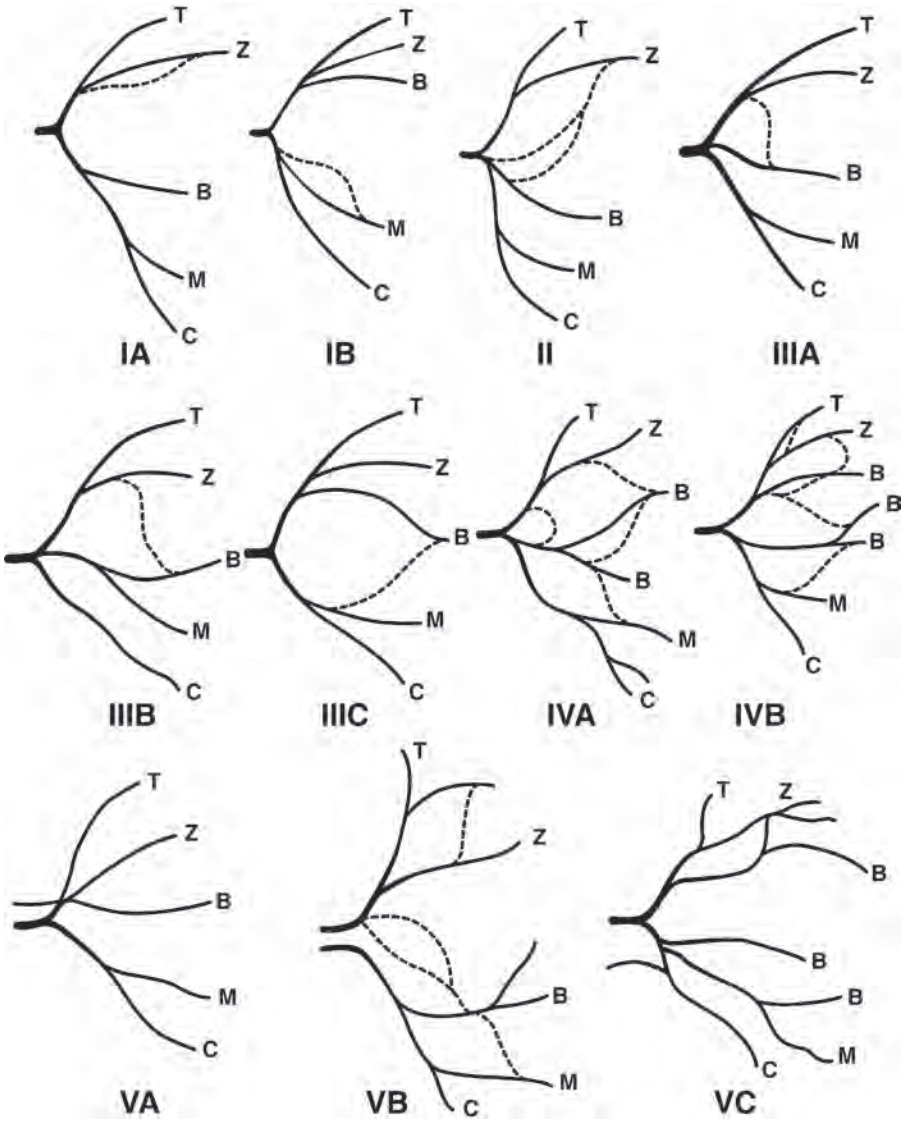

Figure 84.15 Classification used by Kopuz et al. (1994). This is essentially based on the Katz-Catalano classification, with the only exception being type V includes two additional variants (VB and VC). Adapted from Kopuz et al. (1994).

Inter-observer differences in the facial nerve branching patterns

Several factors may contribute to the observed differences in the prevalence of facial nerve branching patterns among studies.

1. Dissection methods: the facial nerve branches progressively divide along their courses, and smaller branches have ample opportunity to anastomose. Depending on the anterior limit of the dissection, various branching pattern and anastomoses can be observed. For example, dissection of Davis et al. (1956) extended to the anterior border of the masseter and that of Bernstein and Nelson (1984) to under the labio-buccal muscles, possibly revealing a greater number of anastomoses. Retrieval of small anastomotic branches may be difficult in the embalmed versus fresh specimens. Application of microscopic dissection may yield more tiny branches and neural interconnections.
2. Ethnic variations: it is not unlikely that the facial nerve branching patterns somehow differ among various ethnic groups.
3. Sample size: smaller samples are less likely to represent the general population of the study, and the results are more likely to deviate from the actual patterns. To date, the largest study was by Davis et al. (1956), making it the most credible study yet.
4. Nomenclature and identifying branches: proper identification and naming of the branches may require tracking them distally toward the destination.

Due to extensive variations in the facial nerve branching pattern, the classic textbook description of its division into five branches may be encountered in a minority of cases (see Davis' type I pattern in Table 84.2). A variant facial nerve has been reported with six terminal branches and has been erroneously

suggested to be a novel variant (see the report by Smith and Ross 2013); a careful re-examination of the supporting image revealed that it represented a class 1/variant III of Dargent and Duroux.

Temporal branch of the facial nerve

After exiting the superior border of the parotid gland, the temporal branch pierces the parotidomasseteric fascia below the zygomatic arch and divides into anterior, middle, and posterior rami (Ammirati et al. 1993; Pekar et al. 2004). The anterior ramus supplies the orbicularis oculi and corrugator supercilli, the middle ramus supplies the frontalis muscle, and the posterior ramus supplies the anterior and superior auricular and tragus muscles (Ammirati et al. 1993). The frontal ramus usually courses within the subgaleal space to reach the frontalis muscle. Occasionally, a twig from the frontal ramus enters the interfascial space (between the superficial and deep layers of the superficial temporal fascia) *en route* to the frontalis muscle (Ammirati et al. 1993).

Two to six temporal braches may be encountered along the line drawn from the superior border of the external ear to the lateral canthus (Lineaweaver et al. 1997). Gosain et al. (1997) found 2–4 branches crossing the inferior aspect of the zygomatic arch: the anterior ramus was located a median of 12 mm anterior to the articular eminence; the middle ramus was located a median of 4 mm anterior to the articular eminence; and the posterior ramus was located in distance between 10 mm posterior to 7 mm anterior to the articular eminence.

In a study of 18 hemifacial specimens, Babakurban and colleagues (2010) found a varying number of temporal branch twigs crossing the zygomatic arch: one in 14.3%; two in 57.1%; three in 14.3%; and four in 14.3%.

Zygomatic branch of the facial nerve

A twig from the zygomatic branch has been observed to descend and pierce risorius and/or platysma at the mid-cheek (Tohma et al. 2004).

Buccal branch of the facial nerve

The buccal branch of the facial nerve is highly variable, and its variability is responsible for much of the complexity observed in the pattern of facial nerve terminal branching. The main buccal nerve may originate from the upper or lower main division of the facial nerve, or may have a common stem with the marginal mandibular or zygomatic branch (Katz and Catalano 1987; Namking et al. 1994). Additional buccal branches and offshoots may come from zygomatic or marginal mandibular nerves. The buccal branch itself may communicate with the zygomatic or marginal mandibular branches of the facial nerve (Tzafetta and Terzis 2010). The buccal branch may be single, double, or triple; in the latter two instances, the branches anastomose together or with the branches from the zygomatic or marginal mandibular nerves. The buccal branch may originate as two roots, one from the temporofacial and one from the cervicofacial division, which then join together to form a single buccal nerve or a loop. A variant buccal nerve (3%) has been reported in which it directly originated from the facial nerve main trunk (probably endotemporally) and, *en route* to its destination, joined the upper division (zygomaticotemporal or temporofacial branch) of the facial nerve (Katz and Catalano 1987). In a dissection of 20 specimens, Pogrel et al. (1995) observed the following variants of the buccal nerve in relation to the parotid duct: (1) 75%: as the buccal nerve leaves the parotid gland, it is single and courses below the parotid duct; (2) 10%: as the buccal nerve leaves the parotid gland, it is single and courses above the parotid duct; and (3) 15%: two buccal nerves exit from the anterior border of the parotid gland, one passing superior to the parotid duct and one passing below it.

In a Chinese study, the buccal branch was found to course within a distance between 10.7 mm superior and 9.3 mm inferior to the parotid duct (Liu et al. 2007). According to Pogrel et al. (1996), the buccal branch runs in parallel to the parotid duct in 75% of cases. In 25% of instances, the nerve crosses the duct 1–2 mm (mean 2.3 mm) ventral to the anterior border of the parotid gland. A superior buccal nerve (located above the duct after emergence from the parotid) is more likely to cross the duct.

Saylam et al. (2006) also investigated the relationship between the buccal branches and parotid duct in 60 hemifacial dissections. They distinguished four main categories.

1. Type 1 (n=21, 35%): A single buccal branch coursed below the duct and, after exiting the anterior border of the parotid, divided into two (n=10) or three (n=11) branches. In two cases, the superior branch crossed over the duct.
2. Type 2 (n=15, 25%): A single buccal branch coursed above the duct and, after exiting the anterior border of the parotid, divided into two branches. In ten cases, the main buccal branch divided above the duct and its inferior branch crossed over the duct. In five cases, the main buccal branch divided after crossing over the duct.
3. Type 3 (n=16, 26.7%): Buccal branches formed a buccal plexus. The buccal plexus received communicating branches from the zygomatic branch in four cases and from both zygomatic and marginal mandibular branches in two cases.
4. Type 4 (n=8, 13.3%): Two buccal branches, one above the duct and one below it, exited from the parotid gland. Both upper and lower buccal branches divided into superior and inferior divisions.

In a study of 30 hemifaces from Korean adult cadavers, Kwak et al. (2004) classified the branching pattern of the facial nerve according to the anatomy of the buccal branch. In two cases (6.8%), one buccal branch originated from either of the two main (temporofacial or cervicofacial) divisions. In such cases, the buccal branch anastomosed with the zygomatic or marginal mandibular nerves. In 93.2% of cases two buccal branches originated, one from the temporofacial and one from the cervicofacial division. The two branches anastomosed peripherally to

make a loop. Kwak et al. (2004) further categorized the double-rooted buccal nerve into the following classes.

1. Type I (13.8%): neither upper nor lower buccal branch had a connection with any other facial nerve branches.
2. Type II (44.7%): the upper buccal branch communicated with the zygomatic branch.
3. Type III (17.3%): the lower buccal branch communicated with the marginal mandibular nerve.
4. Type IV (17.3%): the upper buccal branch communicated with the zygomatic branch, and the lower buccal branch communicated with the marginal mandibular nerve.

Anastomoses of the buccal branch occur at the posterior aspect of the buccal fat pad (anterior to the masseter) and/or under the labio-buccal muscles overlying the anterior part of the buccal fat (Bernstein and Nelson 1984).

Marginal mandibular nerve

The variations of the marginal mandibular nerve involve: (1) the number of branches and its division pattern from the facial nerve trunk; (2) relationship to the retromandibular vein; (3) relationship to the angle and inferior border of the mandible; (4) relationship to the facial artery; (5) anastomoses with other nerves; and (6) muscular innervation

The marginal mandibular nerve may have one to four rami. The rami may separate within the parotid gland or outside of it. As the nerve progressively undergoes branching, the number of branches reasonably varies based on the level of dissection (e.g., inside the parotid, or at the angle or inferior border of the mandible).

The marginal mandibular nerve ran above the inferior border of the mandible posterior to the facial artery in 74% of specimens dissected by Saylam et al. (2007b) and in 81% of specimens studied by Dingman and Grabb (1962). In a series of 202 patients who underwent neck dissection for treatment of head and neck cancers (Balagopal et al. 2012), 80% of cases had a single trunk that crossed the facial artery below the inferior border of mandible (60%), at the inferior border of mandible (26%), or above the inferior border of mandible (14%). Weerapanta et al. (2010) observed that: (1) posterior to the facial artery, the marginal mandibular nerve passed above the inferior border of the mandible in 57% of cases and below it in 43% of cases; and (2) anterior to the facial artery, the nerve was above the inferior border of the mandible.

In a series of 85 facial halves, Kim et al. (2009) noted that, upon leaving the parotid gland, the marginal mandibular nerve had one trunk in 28% of cases, two trunks in 52%, three in 18%, and four trunks in 2% of cases. Most branches of the marginal mandibular nerve crossed the facial artery superficially (75% of branches) and some (20%) passed deep to the artery. Some branches (5%) did not cross the facial artery, but ran in parallel to it. The branches of the marginal mandibular nerve may form a plexus around the facial artery (Savary et al. 1997). Kim et al. (2009) classified the marginal mandibular nerve into: (1) six different categories based on its anastomoses with other facial nerve branches (Fig. 84.16, left), and (2) four categories based on its relationship with the retromandibular nerve (Fig. 84.16, right).

- Type Ia (most common variety): No anastomoses.
- Type Ib: No anastomosis. The cervical branch originated from the marginal mandibular nerve.
- Type IIa: Anastomosis between the buccal and marginal mandibular branches.
- Type IIb: Anastomosis between the marginal mandibular and cervical branches.
- Type IIc: Segmental duplication (or side-anastomosis) of the marginal mandibular nerve.
- Type IId: Duplicated marginal mandibular nerve anastomosing with the buccal branch.

The division of the cervicofacial trunk into buccal, marginal mandibular, and cervical branches may occur after (most common) or before the nerve crosses the vein either laterally (most common) or medially (Kim et al. 2009).

In a series of 50 dissections, the marginal mandibular nerve coursed above, below, and at the level of the angle of mandible in 8 (16%), 16 (32%), and 26 (52%) cases, respectively (Batra et al. 2010). There was one branch at the exit from the parotid in 44 cases (88%), and two branches in the remaining (12%). Anterior to the facial artery, the nerve coursed above the inferior border of the mandible in all cases similar to the results of Dingman and Grabb (1962). Posterior to the artery, it coursed along the inferior border of the mandible in 26 cases (52%). There were anastomoses with the buccal branch in 12% of cases and with the mental nerve in 28% (Batra et al. 2010).

The marginal mandibular branches usually course within a distance between 13.4 mm superior and 4.8 mm inferior to the inferior border of the mandible (Liu et al. 2007). In a series of 100 dissections, fine branches of the marginal mandibular nerve were noted in many cases, travelling up to 2 cm below the inferior border of the mandible to supply the upper part of the platysma (Dingman and Grabb 1962).

Cervical branch of the facial nerve

Important variations of the cervical branch involve: (1) pattern and level of origin from the lower division of the facial nerve; (2) the number of branches at a given level; (3) anastomoses with other facial nerve branches and cutaneous cervical nerves; and (4) muscular innervations.

In a series of 20 Sihler-stained facial halves, Salinas et al. (2009) observed that the cervical branch separated from the cervicofacial trunk within the parotid in 16 cases. In three cases, the common stem of the cervical and marginal mandibular branches divided outside the gland and in one case, they separated just upon emerging from the gland. Salinas et al. (2009) also noted the following.

1. A single cervical branch in three cases, two branches in eleven and three branches in six cases.
2. All cervical branches coursed posterior to the angle of mandible by a variable distance of 1–15 mm.

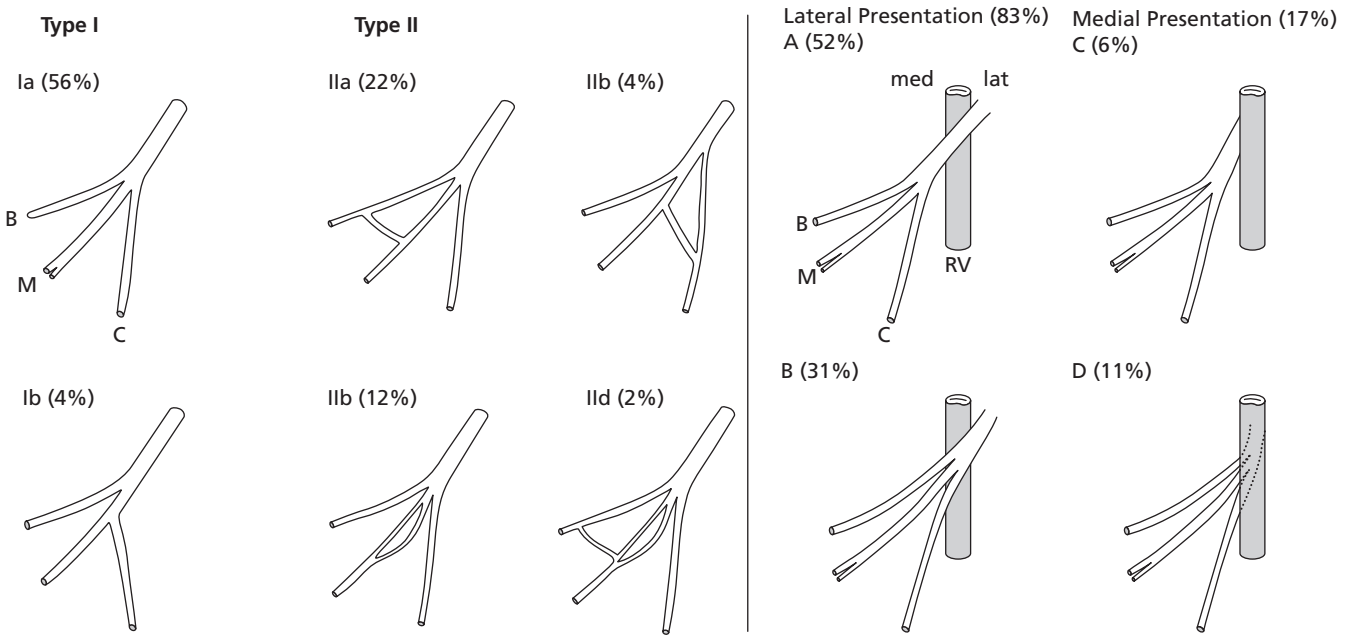

Figure 84.16 Two different classification of the anatomy of the marginal mandibular nerve. Left: the classification is based on its anastomoses with other nerves. Type Ia, no neuroanastomoses; Type Ib, no neuroanastomoses and the cervical branch originates from the marginal mandibular branch; Type IIa, neuroanastomosis between the lower buccal and marginal mandibular nerves; Type IIb, neuroanastomosis between the marginal mandibular and cervical branches; Type IIc, segmental split or division of the marginal mandibular nerve; Type IId, a segmentally split or divided marginal mandibular nerve makes connection with the buccal branch. B, buccal branch; M, marginal mandibular nerve; C, cervical branch. Right: the classification is based on the origin of the marginal mandibular nerve from the cervicofacial division in relation to the retromandibular vein.

Source: Kim et al. (2009). Reproduced with permission from John Wiley & Sons.

3. Anastomosis with marginal mandibular nerve in seven cases (six extramuscular and one intramuscular), a single anastomosis with the transverse cervical nerve in twelve cases and double anastomoses in eight cases.
4. Anastomosis with great auricular nerve in three cases. In one case, the communicating branches from the great auricular and transverse cervical nerve united, and then communicated with the cervical branch.
5. In one case, a sizable ascending rami from the cervical branch supplied depressor anguli oris muscle.

Anastomoses among the terminal branches of the facial nerve

Many studies have been conducted on the matter of anastomoses between the facial nerve branches because of its potential significance in various facial procedures. In 27% of the cases examined by Kitamura and Yamazaki (1958), no communication was found between the branches of the facial nerve.

Bernstein and Nelson (1984) classified the anastomoses of the buccal branches in 35 dissections in the following categories: buccal-buccal anastomoses (19%), where buccal branches unite; zygomatic-buccal anastomoses (72%), where zygomatic and buccal branches unite; and buccal-zygomatic-marginal mandibular anastomoses (9%), where the marginal mandibular nerve anastomoses with the zygomatic and buccal branches, resembling type VI of Davis et al. (1956).

In a study of 17 specimens, Lineaweaver et al. (1997) observed the following prevalence of anastomoses among the terminal branches.

- Temporal-zygomatic anastomoses: within the parotid gland in 14 cases (82%) and outside the gland in 15 cases (88%)
- Zygomatic-buccal anastomoses: within the parotid gland in 11 cases (65%) and outside the gland in 8 cases (47%)
- Buccal-mandibular anastomoses: within the parotid gland in 13 cases (76%) and outside the gland in 15 cases (88%)
- Marginal mandibular-cervical anastomoses: within the parotid gland in 10 cases (59%) and outside the gland in 13 cases (76%).

Numerous anastomoses may exist between the twigs of the temporal branch above the zygomatic arch (Gosain et al. 1997). In a microscopic dissection of three facial specimens, Tohma et al. (2004) noted multiple vertical anastomoses between the upper buccal, lower buccal, and marginal mandibular branches in addition to a main anastomosis between the lower zygomatic and upper buccal branches. Katz and Catalano (1987) reported that the marginal mandibular nerve may send a communicating branch to the buccal branch in 10% of cases and may receive a communicating branch from it in 10% of cases. In a series of 30 facial halves, Schwember and

Rodríguez (1988) observed buccal-zygomatic anastomoses in 24 cases, buccal-marginal mandibular in 14, and zygomatic-marginal mandibular in 8.

Relationship of facial nerve and terminal branches to the parotid region superficial veins

In a dissection of 132 parotid glands, Touré and Vacher (2010) found the facial nerve passing lateral to the retromandibular vein (65% of cases), medial to it (13%), or between the superficial and deep divisions of the vein (7%). The facial nerve trunk has also been observed to pass between the maxillary and superficial temporal veins (Astik et al. 2011). Terminal branches may also pass through the clefts in superficial veins or they may form nerve loops through which superficial veins pass (Bergman et al. 2006). Dingman and Grabb (1962) studied 100 facial halves and noted that retromandibular nerve passes medial to the mandibular branch of the facial nerve in 98% of cases and lateral to it in 2%.

In a study of 54 parotid regions, Laing and McKerrow (1988) found the retromandibular vein in 52 cases and classified its relationship with the facial nerve in the following manner (Fig. 84.17).

1. The vein was in direct contact and deep to the upper and lower divisions of the facial nerve (*n*=37, 68.5%).
2. The vein was deep to the upper and lower divisions of the facial nerve, with a small piece of parotid tissue intervening between the vein and lower division of the facial nerve (*n*=11 20.4%). The upper division was in direct contact with vein.
3. The branches of the upper division of the facial nerve coursed superficial and deep to the vein tributaries, and the lower division was superficial to the vein (*n*=5, 9.3%). The confluence of the maxillary and superficial temporal veins to the retromanduibular vein was low-lying.
4. The vein was in direct contact, deep to the upper division, and superficial to the lower division of the facial nerve (*n*=1, 1.8%).

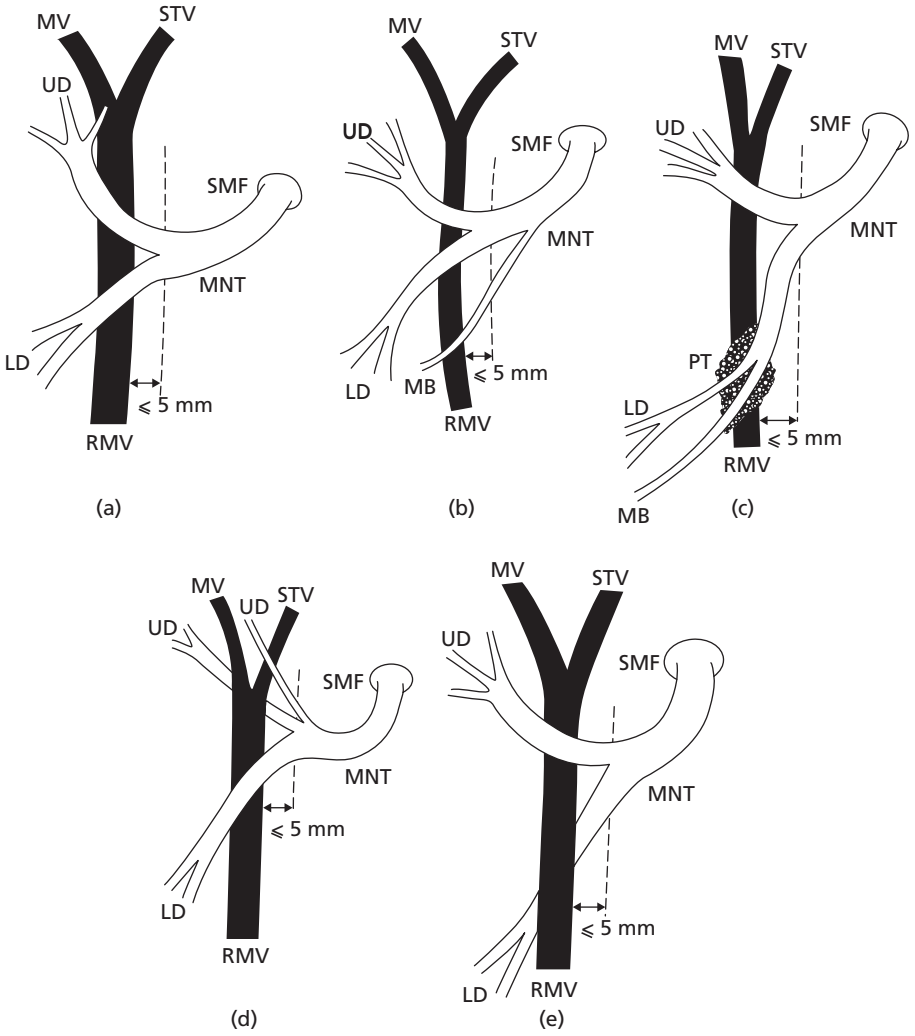

Figure 84.17 Relationship of the upper (UD) and lower (LD) divisions of the facial nerve with the retromandibular vein. MNT, main nerve trunk; RMV, retromandibular vein; STV, superficial temporal vein; MV, maxillary vein; PT, parotid tissue; SMF, stylomastoid foramen. The vein-nerve crossing line was ≤5 mm distal to the plane of the nerve bifurcation in all variants.

Source: Laing and McKerrow (1988). Reproduced with permission from John Wiley & Sons.

Kopuz et al. (1995) observed the following relationships in a dissection of 50 parotid regions:

1. The retromandibular vein crossed the upper and lower divisions of the facial nerve medially (n=45, 90%).
2. The retromandibular vein crossed the upper division medially and the lower division laterally (n=5, 10%).
3. In four cases (8.8%), the vein crosses the lower division after it branched. In all such cases, the vein crossed the main root of the upper division (before it branched).
4. The nerve was in direct contact with (adherent to) the vein. The vein-nerve crossing line was 2.3–5.1 mm apart from (distal to) the facial nerve bifurcation point. In one case, the nerve passed immediately through the angle of facial nerve bifurcation.

Anastomoses of the facial nerve and its branches with other nerves

The facial nerve and its branches variably communicate with the other nerves in the vicinity. Some of these anastomoses are rather constant and common while other are inconstant and less frequent. This subject has been reviewed by Diamond and colleagues (2011) and Shoja and colleagues (2014a, b). Following are some of the known anastomoses.

1. Facial nerve with the superior or inferior vestibular nerve.
2. Geniculate ganglion or main trunk with the lesser petrosal nerve.
3. Geniculate ganglion with the sympathetic plexus around the middle meningeal artery.
4. Greater petrosal nerve with the lesser petrosal nerve.
5. Greater petrosal nerve with the deep petrosal nerve (to form Vidian nerve). The greater petrosal nerve communicates with the maxillary nerve at the level of pterygopalatine ganglion.
6. A twig from the endotemporal main facial trunk with the tympanic plexus.
7. Main facial nerve trunk with the main trunk of glossopharyngeal nerve.
8. Main facial nerve trunk or its digastric, styloid, or stylohyoid branch with a communicating branch form the glossopharyngeal nerve (aka ramus communicans nervi facialis cum nervo glossopharyngeo).
9. Cervical branch of the facial nerve with a branch from the glossopharyngeal nerve.
10. Stylohyoid branch with the ascending branch of the stylopharyngeal or tonsillar branches of the glossopharyngeal nerve.
11. Main facial nerve trunk with the auricular branch of the vagus nerve.
12. Greater petrosal nerve with the sphenoidal (ascending) branch of the otic ganglion.
13. Posterior auricular nerve with the auricular branch of the vagus nerve.
14. Chorda tympani with the tympanic plexus.
15. Chorda tympani with the lingual nerve from mandibular nerve.
16. Chorda tympani with the otic ganglion.
17. Chorda tympani with the greater auricular nerve.
18. Temporofacial division with auriculotemporal nerve of mandibular nerve.
19. Temporal branch with temporal branch of the zygomaticotemporal nerve (a branch of maxillary nerve).
20. Temporal branch with the auriculotemporal nerve.
21. Zygomatic branch with zygomatic branch of the zygomaticotemporal nerve (a branch of maxillary nerve).
22. Zygomatic and buccal branches with long buccal nerve (from mandibular nerve).
23. Marginal mandibular branch with mental nerve (from inferior alveolar nerve).
24. Zygomatic and/or buccal branches with infraorbital nerve (a branch of maxillary nerve).
25. Temporal branch with supraorbital nerve (from the ophthalmic nerve).
26. A terminal branch with external nasal nerve (from anterior ethmoidal nerves, a branch of the ophthalmic nerve).
27. Cervicofacial division with great auricular nerve.
28. Mandibular branch with great auricular nerve.
29. Cervical branch with great auricular nerve.
30. Posterior auricular branch with great auricular nerve of the facial nerve.
31. Posterior auricular branch with lesser occipital nerve.
32. Cervical branch with transverse cervical nerve.

It is beyond the scope of this chapter to give a detailed account of all these anastomoses. However, the anatomy and prevalence of some of the important variants are described in the following sections.

Anastomoses with trigeminal nerve branches

Auriculotemporal nerve

The facial nerve often receives communicating branches from the auriculotemporal nerve. These anastomoses are among the most constant and strong connections between the facial and trigeminal nerves (Baumel 1974). In a study on Korean cadavers, this anastomosis existed in 93.3% of cases (Kwak et al. 2004). The communicating branches (aka communicating auriculotemporal nerves) varied in number from two to four (with three rami in *c.* 47% of cases), were intra-parotid in location, and connected the proximal portion of the auriculotemporal nerve with the upper division of the facial nerve at the posterior border of the masseter (Kwak et al. 2004).

Bernstein and Nelson (1984) noted two–four communicating auriculotemporal nerves to the main facial trunk or its temporal or zygomatic branches in their dissection. They observed that Davis' type IV, V, and VI facial nerve-branching patterns were associated with three–four such communications.

In a study of 55 facial sides from Thai cadavers, Namking et al. (1994) observed communicating auriculotemporal nerves in all the specimens. The communicating branches originated from the auriculotemporal nerve near its origin, crossed the superficial temporal artery anteriorly (most common) or

posteriorly, and coursed laterally to join the upper division of the facial nerve or its branches deep in the parotid gland. The terminal fibers (probably proprioceptive in nature) distributed to the upper facial muscles (especially orbicularis oculi). No communication was found with the lower division of the facial nerve. The authors distinguished the following types of anastomoses.

- Type 1: One communicating branch existed (*n*=11, 20%). The variants were: (1) a single communicating branch to the main root of the upper division (*n*=1); (2) the communicating branch bifurcated, one offshoot to the common stem of the lower temporal and upper zygomatic nerves and the other offshoot to the common stem of the lower zygomatic nerves (*n*=5); and (3) the communicating branch bifurcated, one offshoot to the common stem of the lower zygomatic nerve and the other offshoot to the root of upper buccal nerve (*n*=5).
- Type 2: Two communicating branches existed (*n*=32, 58%). The variants were: (1) one communicating branch to the common stem of the lower temporal, zygomatic, and upper buccal nerves, and the other branch to the root of upper division of the facial nerve (*n*=8); (2) one communicating branch to the common stem of the lower temporal and zygomatic nerves, and the other branch to the common stem of the lower temporal, zygomatic, and upper buccal nerves (*n*=17); (3) the first communicating branch bifurcated with one offshoot to the common stem of the lower temporal and upper zygomatic nerves and another offshoot to the common stem of the two lower zygomatic nerves, and the second communicating branch to the common stem of the lower temporal, zygomatic, and upper buccal nerves (*n*=2); (4) the first communicating branch to the common stem of the lower temporal and zygomatic nerves, and the second trifurcated into three offshoots to the common stem of the lower temporal and zygomatic nerves, root of the upper buccal nerves, and upper division of the facial nerve (*n*=3); and (5) both communicating branches joined the root of upper division of the facial nerve (*n*=2).
- Type 3: Three communicating branches existed (*n*=10, 18%). The variants were: (1) the first communicating branch to the common stem of the lower zygomatic nerves, the second to the common stem of the lower temporal and zygomatic nerves, and the third bifurcated into offshoots to the common stem of the upper buccal nerves, and the common stem of the lower zygomatic and upper buccal nerves (*n*=5); and (2) the first communicating branch to the common root of the two upper temporal nerves, the second to the common stem of two lower zygomatic branches, and the third to the common stem of the lower temporal, zygomatic, and upper buccal nerves (*n*=5).
- Type 4: According to Namking et al. (1994), this unusual type (*n*=2) involved offshoots from the communicating branches that ran parallel to one to two terminal facial nerve branches for variable distances.

Sensory buccal nerve (branch of trigeminal nerve)

The buccal branch of the facial nerve variably anastomoses with the sensory buccal nerve to form a buccal plexus.

Mental nerve

Terminal twigs from the marginal mandibular nerve anastomose with the angular and inferior labial lateral branches of the mental nerve close to mental foramen, and twigs from the cervical branch anastomose with the inferior labial medial branch of the mental nerve within platysma (Won et al. 2014).

Other branches

Yang et al. (2013) observed the following periorbital neuroanastomoses in a series of 14 Sihler-stained specimens:

1. descending twigs from the supraorbital nerve with the temporal branch of the facial nerve superolateral to the orbit (12 of 14 cases);
2. twigs from the supratrochlear nerve with the temporal branch of the facial (8 cases);
3. twigs of the infratrochlear nerve with the long twigs of the buccal branch of the facial nerve at the nasion (12 cases);
4. twigs of the supratrochlear nerve with the long twigs of the buccal branch of the facial nerve (7 cases);
5. twigs of the zygomaticofacial nerve with the zygomatic branch of the facial nerve (12 cases);
6. twigs of the zygomaticotemporal nerve with the temporal branch of the facial nerve (2 cases, uncertain anastomoses);
7. twigs of the infraorbital nerve with the buccal branch of the facial nerve at the nasion (12 cases); and
8. twigs of the infraorbital nerve with the zygomatic branch of the facial nerve at the nasion (4 cases).

In another study, anastomoses between the zygomaticotemporal nerve and twigs of the temporal branch of the facial nerve were found in 14 out of 17 cases located 36 mm lateral to the lateral canthus; 9 cases had 1 anastomosis and 5 had 2 anastomoses (Odobescu et al. 2012).

With the glossopharyngeal nerve

Direct communication between the facial and glossopharyngeal nerve trunks and indirect communications through their branches may exist. A direct communicating branch to the glossopharyngeal nerve may arise from the trunk of the facial nerve immediately after it exits the stylomastoid foramen; this branch has been noted by Salame et al. (2002) in 2 of 46 sides (4%) and was found to originate from the facial nerve before the origin of the posterior auricular nerve. This inconstant and direct connection between the two nerve trunks is sometimes referred to as the ansa of von Haller (Fig. 84.18), which forms a loop in front of the internal jugular vein (Testut 1902; Gould 1904).

In a study of 490 head sides, Kawai et al. (1989) distinguished various types of facial nerve–glossopharyngeal nerve communication at the posterior digastric region in 18.8% of neck sides.

1. In the majority of cases (88%), the anastomotic loop or ansa pierced the posterior belly of the digastric muscle and partly

travelled within this muscle before re-emerging; this neural communication is the Haller-Sappey ansa mentioned by Henle in 1871.

2. In the remaining 12% of neck sides, the ansa either travelled medial (8.7%) or lateral (5.4%) to the posterior digastric belly. These authors also made other interesting observations.
   1. In only a portion of specimens, the intramuscular ansa supplied motor branches to the posterior digastric belly. This indicated that the ansa does not solely serve to supply motor innervation to the posterior digastric belly.
   2. After travelling medial, lateral, or within the posterior digastric belly, the communicating branch joined with either stylohyoid or digastric branches *en route* to the facial nerve and sometimes with the nerve trunk directly.
   3. In all cases, the communication between the facial and glossopharyngeal nerves originated from the latter. The fibers traversing the communication ultimately entered the facial nerve and were distributed through two facial nerve branches destined to the posterior auricular region.
   4. In addition to the above-mentioned anastomoses at the region of the posterior belly of the digastric muscle, Kawai et al. (1989) also noted more distally located communications between the cervical branch of the facial nerve and a glossopharyngeal nerve branch coursing lateral to the posterior digastric belly. The distal anastomosis was present in a very small percentage of specimens (1%) with or without an associated proximal anastomosis (Kawai et al. 1989). Ultimately, these authors concluded that the facial nerve–glossopharyngeal nerve anastomosis in fact represents the auricular branch of the glossopharyngeal nerve (Kawai et al. 1989).

Müller and Rude (2000) described an anastomosis between the facial and glossopharyngeal nerves near the skull base that was formed by an ascending branch of the stylopharyngeal or tonsillar branches of the glossopharyngeal nerve and a branch from the stylohyoid branch of the facial nerve. Notably, concomitant anastomoses were also found between the ascending branch of the glossopharyngeal nerve and the sympathetic plexus around the internal carotid artery (Müller and Rude 2000).

With the vagus nerve

The auricular branch of the vagus nerve (known as Arnold's nerve) is a cutaneous nerve, which originates from the jugular ganglion of the vagus and receives a twig from the inferior ganglion of the glossopharyngeal nerve within the jugular foramen (Landois 1904; Tekdemir et al. 1998; Merchant and Nadol 2010). Arnold's nerve enters the mastoid canaliculus on the lateral wall of the jugular foramen, and passes transversely and posterolaterally through this canaliculus to emerge within the mastoid portion of the facial canal. Within the facial canal, Arnold's nerve crosses the facial nerve posteriorly and gives off two branches; superior and inferior (Merchant and Nadol 2010). The superior branch joins the facial nerve. The inferior branch receives a twig from the facial nerve and ultimately leaves the temporal bone through the tympanomastoid fissure. Outside the skull, Arnold's nerve travels between the external ear canal and mastoid process in close proximity to the posterior auricular branch of the facial nerve and sends a communicating branch to it, which ultimately provides proprioceptive innervation of the striated muscles supplied by the posterior auricular nerve (Landois 1904; Sharpey-Schäfer et al. 1909). Arnold's nerve supplies the auricle and external ear canal. Aronld's nerve may completely fuse with the facial nerve trunk, and its fibers are then distributed via the branches of the posterior auricular nerve (Sharpey-Schäfer et al. 1909).

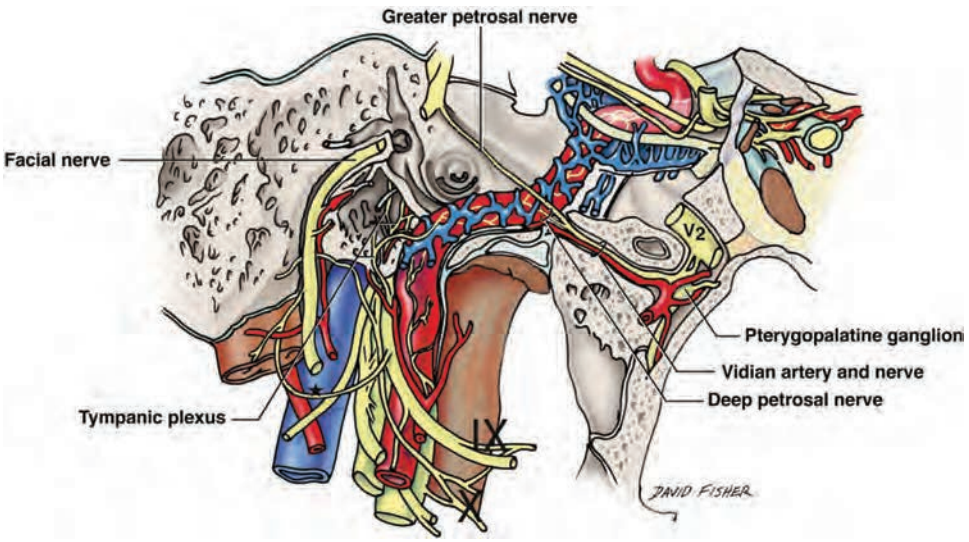

Figure 84.18 Connections between cranial nerves VII, IX, and X and some of their branches. Notable here is the loop-shaped connection (*) between the proximal portions of the facial and glossopharyngeal nerve trunks, known as ansa of von Haller.

Source: Shoja et al. (2014b). Reproduced with permission from John Wiley & Sons.

References

Adad B, Rasgon BM, Ackerson L. 1999. Relationship of the facial nerve to the tympanic annulus: a direct anatomic examination. *Laryngoscope* 109: 1189–1192.

Ammirati M, Spallone A, Ma J, Cheatham M, Becker D. 1993. An anatomicosurgical study of the temporal branch of the facial nerve. *Neurosurgery* 33: 1038–1043.

Asami Y, Kawai K, Kanoh T, Koizumi M, Honma S, Tokiyoshi A, Kodama K. 2006. Double innervation of the anterior belly of the digastric muscle. *Anat Sci Int* 81: 130–133.

Astik RB, Dave UH, Gajendra KS. 2011. Variant position of the facial nerve in parotid gland. *Int J Anat Var* 4: 3–4.

Babakurban ST, Cakmak O, Kendir S, Elhan A, Quatela VC. 2010. Temporal branch of the facial nerve and its relationship to fascial layers. *Arch Facial Plast Surg* 12: 16–23.

Balagopal PG, George NA, Sebastian P. 2012. Anatomic variations of the marginal mandibular nerve. *Indian J Surg Oncol* 3: 8–11.

Ballester M, Blaser B, Häusler R. 2000. Stapedotomy and anatomical variations of the facial nerve. *Rev Laryngol Otol Rhinol (Bord)* 121: 181–186 (in French).

Bartsch C, Wagner A, Miehe B, Kowalewski R. 1991. The emergence of the chorda tympani from the tympanic cavity and its course until its entry into the lingual nerve. *Anat Anz* 173: 243–246 (in German).

Basek M. 1962. Anomalies of the facial nerve in normal temporal bones. *Ann Otol Rhinol Laryngol* 71: 382–390.

Batra AP, Mahajan A, Gupta K. 2010. Marginal mandibular branch of the facial nerve: An anatomical study. *Indian J Plast Surg* 43: 60–64.

Baumel JJ. 1974. Trigeminal-facial nerve communications. Their function in facial muscle innervation and reinnervation. *Arch Otolaryngol* 99: 34–44.

Bergman RA, Afifi AK, Miyauchi R. 2006. Illustrated Encyclopedia of Human Anatomic Variation. Available at: http://www.anatomyatlases.org/AnatomicVariants/AnatomyHP.shtml (accessed 18 November 2015).

Bernstein L, Nelson RH. 1984. Surgical anatomy of the extraparotid distribution of the facial nerve. *Arch Otolaryngol* 110: 177–183.

Botman JW, Jongkees LB. 1955. Endotemporal branching of the facial nerve. *Acta Otolaryngol* 45: 111–114.

Celin SE, Wilberger JE, Chen DA. 1991. Facial nerve bifurcation within the internal auditory canal. *Otolaryngol Head Neck Surg* 104: 389–393.

Cruveilhier J. 1851. *Traite d'Anatomie Descriptive*, 3rd edition. Paris: G. Doin & Cie.

Cvetko E. 2013. Sternocleidomastoid muscle additionally innervated by the facial nerve: case report and review of the literature. Anat Sci Int. PMID: 24347311.

Dargent M, Duroux PE. 1946. Donnés anatomiques concernant la morphologie et certains rapports du facial intra-parotiden. *La Presse Médicale* 37: 523–524.

Davis RA, Anson BJ, Budinger JM, Kurth LR. 1956. Surgical anatomy of the facial nerve and parotid gland based upon a study of 350 cervicofacial halves. *Surg Gynecol Obstet* 102: 385–412.

Di Martino E, Sellhaus B, Haensel J, Schlegel JG, Westhofen M, Prescher A. 2005. Fallopian canal dehiscences: a survey of clinical and anatomical findings. *Eur Arch Otorhinolaryngol* 262: 120–126.

Diamond M, Wartmann CT, Tubbs RS, Shoja MM, Cohen-Gadol AA, Loukas M. 2011. Peripheral facial nerve communications and their clinical implications. *Clin Anat* 24: 10–18.

Dickinson JT, Srisomboon P, Kamerer DB. 1968. Congenital anomaly of the facial nerve. *Arch Otolaryngol* 88: 357–359.

Dingman RO, Grabb WC. 1962. Surgical anatomy of the mandibular ramus of the facial nerve based on the dissection of 100 facial halves. *Plast Reconstr Surg Transplant Bull* 29: 266–272.

Djerić DR. 1993. Anatomical variations of the chorda tympani nerve. *Med J Islamic Republic of Iran* 7: 7–8.

Djerić D, Savić D. 1987. Endotemporal branching of the facial nerve. *Acta Anat (Basel)* 129: 10–11.

Dobozi M. 1975. Surgical anatomy of the Geniculate ganglion. *Acta Otolaryngol* 80: 116–119.

Durcan DJ, Shea JJ, Sleeckx JP. 1967. Bifurcation of the facial nerve. *Arch Otolaryngol* 86: 619–631.

Eshraghi AA, Buchman CA, Telischi FF. 2002. Sensory auricular branch of the facial nerve. *Otol Neurotol* 23: 393–396.

Fisch UP. 1973. Excision of the Scarpa's ganglion. *Arch Otolaryngol* 97: 147–149.

Fowler EP Jr. 1961. Variations in the temporal bone course of the facial nerve. *Laryngoscope* 71: 937–946.

Gacek RR. 1998a. On the duality of the facial nerve ganglion. *Laryngoscope* 108: 1077–1086.

Gacek RR. 1998b. Anatomy and significance of the subarachnoid space in the fallopian canal. *Am J Otol* 19: 358–365.

Ge XX, Spector GJ. 1981. Labyrinthine segment and geniculate ganglion of facial nerve in fetal and adult human temporal bones. *Ann Otol Rhinol Laryngol Suppl* 90: 1–12.

Giesemann AM, Neuburger J, Lanfermann H, Goetz F. 2011. Aberrant course of the intracranial facial nerve in cases of atresia of the internal auditory canal (IAC). *Neuroradiology* 53: 681–687.

Glastonbury CM, Fischbein NJ, Harnsberger HR, Dillon WP, Kertesz TR. 2003. Congenital bifurcation of the intratemporal facial nerve. *AJNR Am J Neuroradiol* 24: 1334–1337.

Gosain AK, Sewall SR, Yousif NJ. 1997. The temporal branch of the facial nerve: how reliably can we predict its path? *Plast Reconstr Surg* 99: 1224–1233.

Gould GM. 1904. *The Student's Medical Dictionary*, 11th edition. Philadelphia: P. Blackiston's Son & Company.

Grant JL, Martin R, Rhoton AL Jr. 1979. Anatomical relationship of anterior inferior cerebellar artery and VIIth and VIIIth cranial nerves. *Surg Forum* 30: 429–431.

Grégoire R. 1912. Le nerf facial et la parotide. *J Anat Paris* 48: 437–447.

Greisen O. 1975. Aberrant course of the facial nerve. *Arch Otolaryngol* 101: 327–328.

Haynes DR. 1955. The relations of the facial nerve in the temporal bone. *Ann R Coll Surg Engl* 16: 175–185.

Helms J. 1981. Variations of the course of the facial nerve in the middle ear and mastoid. In: *The Cranial Nerves* (eds M.Samii, P. J.Jannetta). Berlin: Springer, pp. 391–393.

Henner R. 1960. Congenital middle ear malformations. *AMA Arch Otolaryngol* 71: 454–458.

Hollinshead WH. 1969. *Anatomy for Surgeons: The Head and Neck*, third edition. New York: Harper and Row.

Hoogland GA. 1977. The facial nerve coursing across the oval window area. *ORL J Otorhinolaryngol Relat Spec* 39: 148–154.

Hoogland GA, Marres EH. 1977. The facial nerve coursing across the promontory with a persistent stapedial artery. *ORL J Otorhinolaryngol Relat Spec* 39: 338–341.

Huang TS. 1997. Anomalously coursing facial nerves above and below the oval window: three case reports. *Otolaryngol Head Neck Surg* 116: 438–441.

Jakkani RK, Ki R, Karnawat A, Vittal R, Kumar AD. 2013. Congenital duplication of mastoid segment of facial nerve: A rare case report. *Indian J Radiol Imaging* 23: 35–37.

Johnsson LG, Kingsley TC. 1970. Herniation of the facial nerve in the middle ear. *Arch Otolaryngol* 91: 598–602.

Katz AD, Catalano P. 1987. The clinical significance of the various anastomotic branches of the facial nerve. Report of 100 patients. *Arch Otolaryngol Head Neck Surg* 113: 959–962.

Kawai K, Kodama K, Okamoto K. 1989. Proximal communication between the glossopharyngeal and facial nerves. *Acta Anat* 134: 151–155.

Kawai K, Koizumi M, Honma S, Tokiyoshi A, Kodama K. 2003. Derivation of the anterior belly of the digastric muscle receiving twigs from the mylohyoid and facial nerves. *Ann Anat* 185: 85–90.

Kettel K. 1946. Abnormal course of the facial nerve in the Fallopian canal. *Arch Otolaryngol* 44: 406–408.

Kettel K. 1963. Surgery of the facial nerve. *Arch Otolaryngol* 77: 327–341.

Kharat RD, Golhar SV, Patil CY. 2009. Study of intratemporal course of facial nerve and its variations – 25 temporal bones dissection. *Indian J Otolaryngol Head Neck Surg* 61: 39–42.

Kilic C, Kirici Y, Kocaoglu M. 2010. Double facial nerve trunk emerged from the stylomastoid foramen and petrotympanic fissure: a case report. *J Korean Med Sci* 25: 1228–1230.

Kim DI, Nam SH, Nam YS, Lee KS, Chung RH, Han SH. 2009. The marginal mandibular branch of the facial nerve in Koreans. *Clin Anat* 22: 207–214.

Kim HN, Kim YH, Park IY, Kim GR, Chung IH. 1990. Variability of the surgical anatomy of the neurovascular complex of the cerebellopontine angle. *Ann Otol Rhinol Laryngol* 99: 288–296.

Kim HS, Kim DI, Chung IH, Lee WS, Kim KY. 1998. Topographical relationship of the facial and vestibulocochlear nerves in the subarachnoid space and internal auditory canal. *AJNR Am J Neuroradiol* 19: 1155–1161.

Kitamura T, Yamazaki H. 1958. Distribution of the facial nerve in the parotid gland. *Jap J Otol* 61: 141–114.

Kopuz C, Turgut S, Yavuz S, Ilgi S. 1994. Distribution of facial nerve in parotid gland: analysis of 50 cases. *Okajimas Folia Anat Jap* 70: 295–299.

Kopuz C, Ilgi S, Yavuz S, Onderoğlu S. 1995. Morphology of the retromandibular vein in relation to the facial nerve in the parotid gland. *Acta Anat (Basel)* 152: 66–68.

Kudo H, Nori S. 1974. Topography of the facial nerve in the human temporal bone. *Acta Anat (Basel)* 90(3): 467–480.

Kulczyński B, Woźniak W. 1978. Variation of the origin and course of the chorda tympani. *Folia Morphol (Warsz)* 37: 237–241.

Kuo CY, Wang CH. 2012. Aberrant facial nerve exposed behind the eardrum. *Otolaryngol Head Neck Surg* 147: 1158–1159.

Kwak HH, Park HD, Youn KH, Hu KS, Koh KS, Han SH, Kim HJ. 2004. Branching patterns of the facial nerve and its communication with the auriculotemporal nerve. *Surg Radiol Anat* 26: 494–500.

Laing MR, McKerrow WS. 1988. Intraparotid anatomy of the facial nerve and retromandibular vein. *Br J Surg* 75: 310–312.

Landois L. 1904. *Textbook of Human Physiology, including Histology and Microscopical Anatomy with especial reference to the Practice of Medicine*. Philadelphia: P. Blakiston's.

Leek JH. 1974. An anomalous facial nerve: the otologist's albatross. *Laryngoscope* 84: 1535–1544.

Lineaweaver W, Rhoton A, Habal MB. 1997. Microsurgical anatomy of the facial nerve. *J Craniofac Surg* 8: 6–10.

Lister JR, Rhoton AL Jr, Matsushima T, Peace DA. 1982. Microsurgical anatomy of the posterior inferior cerebellar artery. *Neurosurgery* 10: 170–199.

Liu AT, Jiang H, Zhao YZ, Yu DZ, Dang RS, Zhang YF, Zhang JL. 2007. Anatomy of buccal and marginal mandibular branches of facial nerve and its clinical significance. *Zhonghua Zheng Xing Wai Ke Za Zhi* 23: 434–437 (in Chinese).

Liu R, Fagan P. 2001. Unusual course of the anterior inferior cerebellar artery through the facial nerve in the cerebellopontine angle. *Otolaryngol Head Neck Surg* 124: 479.

Low WK. 1999. Surgical anatomy of the facial nerve in Chinese mastoids. *ORL J Otorhinolaryngol Relat Spec* 61: 341–344.

Martin RG, Grant JL, Peace D, Theiss C, Rhoton AL Jr. 1980. Microsurgical relationships of the anterior inferior cerebellar artery and the facial-vestibulocochlear nerve complex. *Neurosurgery* 6: 483–507.

Matsushima T, Inoue T, Fukui M. 1990. Arteries in contact with the cisternal portion of the facial nerve in autopsy cases: microsurgical anatomy for neurovascular decompression surgery of hemifacial spasm. *Surg Neurol* 34: 87–93.

May M. 2000. Anatomy of Clinician. In: *The Facial Nerve*, second edition (eds M May, BM Schaitkin). New York: Thieme, pp. 19–56.

Mayer TG, Crabtree JA. 1976. The facial nerve coursing inferior to the oval window. *Arch Otolaryngol* 102: 744–746.

McCormack LJ, Cauldwell EW, Anson BJ. 1945. The surgical anatomy of facial nerve with special reference to the parotid gland. *Surg Gynecol Obstet* 80: 620–630.

McKenzie J. 1948. The parotid gland in relation to the facial nerve. *J Anat* 82: 183–186.

McManus LJ, Dawes PJ, Stringer MD. 2012. Surgical anatomy of the chorda tympani: a micro-CT study. *Surg Radiol Anat* 34: 513–518.

McWhorter GL. 1917. The relations of the superficial and deep lobes of the parotid gland to the ducts and to the facial nerve. *Anat Rec* 12: 149–154.

Merchant SN, Nadol JB. 2010. *Schuknecht's Pathology of the Ear*. Shelton: People's Medical Publishing House.

Minnigerode B. 1965. Intratympanic aurzweigung der chorda tympani, ein seltene anatomische verlaufsvariante. *Acta Otolaryngol* 59: 20–22.

Moreano EH, Paparella MM, Zelterman D, Goycoolea MV. 1994. Prevalence of facial canal dehiscence and of persistent stapedial artery in the human middle ear: a report of 1000 temporal bones. *Laryngoscope* 104: 309–320.

Müller T, Rude J. 2000. On a complex anastomosis of the glossopharyngeal nerve in humans. *Kaibogaku Zasshi* 75: 345–348.

Muren C, Wadin K, Wilbrand HF. 1990. Anatomic variations of the chorda tympani canal. *Acta Otolaryngol* 110: 262–265.

Myint K, Azian AL, Khairul FA. 1992. The clinical significance of the branching pattern of the facial nerve in Malaysian subjects. *Med J Malaysia* 47: 114–121.

Nager GT, Proctor B. 1982. The facial canal: normal anatomy, variations and anomalies. II. Anatomical variations and anomalies involving the facial canal. *Ann Otol Rhinol Laryngol Suppl* 97: 45–61.

Nageris B, Braverman I, Kalmanowitz M, Segal K, Frenkiel S. 2000. Connections of the facial and vestibular nerves: an anatomic study. *J Otolaryngology* 29: 159–161.

Namking M, Boonruangsri P, Woraputtaporn W, Güldner FH. 1994. Communication between the facial and auriculotemporal nerves. *J Anat* 185: 421–426.

Nawar NN, Mikhail Y, Ibrahim KA. 1980. Quantitative and histomorphological studies on the geniculate ganglion of the facial nerve in man. *Acta Anat (Basel)* 106: 57–62.

Neely JG, MacRae DL. 1979. Congenital mesodermal mass (normal variant) contiguous with the mastoid segment of the facial nerve. A report of five cases. *Am J Otol* 1: 80–84.

Odobescu A, Williams HB, Gilardino MS. 2012. Description of a communication between the facial and zygomaticotemporal nerves. *J Plast Reconstr Aesthet Surg* 65: 1188–1192.

Oh CS, Chung IH, Lee KS, Tanaka S. 2003. Morphological study on the rootlets comprising the root of the intermediate nerve. *Anat Sci Int* 78: 111–113.

Özdogmus O, Sezen O, Kubilay U, Saka E, Duman U, Şan T, Çavdar S. 2004. Connections between the facial, vestibular and cochlear nerve bundles within the internal auditory canal. *J Anat* 205: 65–75.

Park IY, Lee ME. 1977. A morphological study of the parotid gland and the peripheral branches of the facial nerve in Koreans. *Yonsei Med J* 18: 45–51.

Pekar L, Bláha M, Schwab J, Melechovský D. 2004. Craniotomy and the temporal branch of the facial nerve. *Rozhl Chir* 83: 205–208 (in Czech).

Phelps PD, Lloyd GA. 1981. Course of the facial nerve in congenital ear deformities. Tomographic demonstration. *Acta Radiol Diagn (Stockh)* 22: 475–483.

Piersol GA. 1918. *Human Anatomy*, 6th edition. Philadelphia: J. B. Lippincott.

Pogrel MA, Schmidt B, Ammar A. 1996. The relationship of the buccal branch of the facial nerve to the parotid duct. *J Oral Maxillofac Surg* 54: 71–73.

Proctor B, Nager GT. 1982. The facial canal: normal anatomy, variations and anomalies. I. Normal anatomy of the facial canal. *Ann Otol Rhinol Laryngol Suppl* 97: 33–44.

Rai AR, Rai R, Bhat K, Rai R. 2011. Anomalous location of facial nerve deep to parotid gland. *J Craniofac Surg* 22: 652–653.

Redleaf MI, Blough RR. 1996. Distance from the labyrinthine portion of the facial nerve to the basal turn of the cochlea. Temporal bone histopathologic study. *Ann Otol Rhinol Laryngol* 105: 323–326.

Reiber ME, Schwaber MK. 1997. Congenital absence of stapes and facial nerve dehiscence. *Otolaryngol Head Neck Surg* 116: 278.

Rhoton AL Jr, Kobayashi S, Hollinshead WH. 1968a. Nervus intermedius. *J Neurosurg* 29: 609–618.

Rhoton AL Jr, Pulec JL, Hall GM, Boyd AS Jr. 1968b. Absence of bone over the geniculate ganglion. *J Neurosurg* 28: 48–53.

Rouvière, H, Cordier G. 1934. Sur le developpement de la glande parotide et les connexions qui existent entre les deux lobes de cette glande. *Ann Anat Path Med–Chir* 11: 622–624.

Rupa V, Weider DJ, Glasner S, Saunders RL. 1992. Geniculate ganglion: anatomic study with surgical implications. *Am J Otol* 13: 470–473.

Sachs E Jr. 1968. The role of the nervus intermedius in facial neuralgia. *J Neurosurg* 28: 54–60.

Salame K, Ouaknine GE, Arensburg B, Rochkind S. 2002. Microsurgical anatomy of the facial nerve trunk. *Clin Anat* 15: 93–99.

Saleh E, Naguib M, Aristegui M, Cokkeser Y, Sanna M. 1995. Lower skull base: anatomic study with surgical implications. *Ann Otol Rhinol Laryngol* 104: 57–61.

Salinas NL, Jackson O, Dunham B, Bartlett SP. 2009. Anatomical dissection and modified Sihler stain of the lower branches of the facial nerve. *Plast Reconstr Surg* 124: 1905–1915.

Savary V, Robert R, Rogez JM, Armstrong O, Leborgne J. 1997. The mandibular marginal ramus of the facial nerve: an anatomic and clinical study. *Surg Radiol Anat* 19: 69–72.

Saylam C, Ucerler H, Orhan M, Ozek C. 2006. Anatomic landmarks of the buccal branches of the facial nerve. *Surg Radiol Anat* 28: 462–467.

Saylam C, Ucerler H, Orhan M, Cagli S, Zileli M. 2007a. The relationship of the posterior inferior cerebellar artery to cranial nerves VII–XII. *Clin Anat* 20: 886–891.

Saylam C, Ucerler H, Orhan M, Uckan A, Ozek C. 2007b. Localization of the marginal mandibular branch of the facial nerve. *J Craniofac Surg* 18: 137–142.

Schaeffer JP. (ed.) 1953. *Morris' Anatomy*, 11th edition. New York: The Blackston Company.

Schwember G, Rodríguez A. 1988. Anatomic surgical dissection of the extraparotid portion of the facial nerve. *Plast Reconstr Surg* 81: 183–188.

Sharpey-Schäfer EA, Symington J, Bryce TH. (eds) 1909. *Quain's Elements of Anatomy*, Volume 3, part 2, 11th edition. New York: Longmans, Green and Co.

Shoja MM, Oyesiku NM, Griessenauer CJ, Radcliff V, Loukas M, Chern JJ, Benninger B, Rozzelle CJ, Shokouhi G, Tubbs RS. 2014a. Anastomoses between lower cranial and upper cervical nerves: A comprehensive review with potential significance during skull base and neck operations, Part I: Trigeminal, facial, and vestibulocochlear nerves. *Clin Anat* 27: 118–130.

Shoja MM, Oyesiku NM, Shokouhi G, Griessenauer CJ, Chern JJ, Rizk EB, Loukas M, Miller JH, Tubbs RS. 2014b. A comprehensive review with potential significance during skull base and neck operations, Part II: glossopharyngeal, vagus, accessory, and hypoglossal nerves and cervical spinal nerves 1–4. *Clin Anat* 27: 131–144.

Sigari F, Mhoon E, Montag A, Redleaf M. 2007. Pseudobifurcation of the vertical facial nerve in a temporal bone laboratory. *Otolaryngol Head Neck Surg* 137: 513–514.

Smith OJ, Ross GL. 2012. Variations in the anatomy of the posterior auricular nerve and its potential as a landmark for identification of the facial nerve trunk: a cadaveric study. *Anat Sci Int* 87: 101–105.

Smith OJ, Ross GL. 2013. A branching pattern of the facial nerve trunk with six initial branches: possible implications for parotid surgery? *J Plast Reconstr Aesthet Surg* 66: 288–289.

Song JJ, Park JH, Jang JH, Lee JH, Oh SH, Chang SO, Kim CS. 2012. Facial nerve aberrations encountered during cochlear implantation. *Acta Otolaryngol* 132: 788–794.

Tange RA, de Bruijn AJ. 1997. Dehiscences of the horizontal segment of the facial canal in otosclerosis. *ORL J Otorhinolaryngol Relat Spec* 59: 277–279.

Tekdemir I, Aslan A, Elhan A. 1998. A clinic-anatomic study of the auricular branch of the vagus nerve and Arnold's ear-cough reflex. *Surg Radiol Anat* 20: 253–257.

Testut L. 1902. *Tratado de Anatomia Humana, tomo tercero*, sexta edicion. Barcelona: Salvat.

Tohma A, Mine K, Tamatsu Y, Shimada K. 2004. Communication between the buccal nerve (V) and facial nerve (VII) in the human face. *Ann Anat* 186: 173–178.

Touré G, Vacher C. 2010. Relations of the facial nerve with the retromandibular vein: anatomic study of 132 parotid glands. *Surg Radiol Anat* 32: 957–961.

Trost O, Rouchy RC, Teyssier C, Kazemi A, Zwetyenga N, Malka G, Cheynel N, Trouilloud P. 2011. CT-scan imaging of iron marked chorda tympani nerve: anatomical study and educational perspectives. *Surg Radiol Anat* 33: 515–521.

Tubbs RS, Steck DT, Mortazavi MM, Cohen-Gadol AA. 2013. The nervus intermedius: a review of its anatomy, function, pathology, and role in neurosurgery. *World Neurosurg* 79: 763–767.

Tzafetta K, Terzis JK. 2010. Essays on the facial nerve: Part I. Microanatomy. *Plast Reconstr Surg* 125: 879–889.

Weerapanta E, Bunaprasertb T, Chokrungvaranontc P, Chentanezd V. 2010. Anatomy of the facial nerve branching patterns, the marginal mandibular branch and its extraparotid ramification in relation to the lateral palpebral line. *Asian Biomedicine* 4: 603–608.

Won SY, Yang HM, Woo HS, Chang KY, Youn KH, Kim HJ, Hu KS. 2014. Neuroanastomosis and the innervation territory of the mental nerve. *Clin Anat* 27(4): 598–602.

Yang HM, Won SY, Kim HJ, Hu KS. 2013. Sihler staining study of anastomosis between the facial and trigeminal nerves in the ocular area and its clinical implications. *Muscle Nerve* 48: 545–550.

Yurtseven T, Savaş R, Koçak A, Turhan T, Aktaş EO, Işlekel S. 2004. Relationship between anterior inferior cerebellar artery and facial-vestibulocochlear nerve complex: an anatomical and magnetic resonance images correlation study. *Minim Invasive Neurosurg* 47: 306–311.

85 Vestibulocochlear nerve

Mohammadali M. Shoja[1] and R. Shane Tubbs[2]
[1]Tuberculosis and Lung Disease Research Center, Tabriz University of Medical Sciences, Tabriz, Iran
[2]Seattle Science Foundation, Seattle, Washington, USA
St George's University, School of Medicine, St Georges, Grenada
University of Dundee, Dundee, UK

The cisternal and canalicular segments of the facial nerve and the vestibulocochlear nerve are invested in a common arachnoid sheath. The variations in the relationship of the facial–vestibulocochlear nerve complex with the structures in the cerebellopontine angle and within the internal acoustic meatus have already been mentioned in the previous chapter on the variations of the facial nerve (Chapter 84). Some of the important gross variations of the vestibulocochlear nerve are as follows:

1. Proximal stem of the vestibulocochlear nerve, close to the pons, may give rise to the rootlets of the intermediate nerve of Wrisberg (Oh et al. 2003).
2. In 22% of cases, the intermediate nerve adheres to the vestibular part of the vestibulocochlear nerve along its cisternal course (Rhoton et al. 1968).
3. The anterior inferior cerebellar artery (AICA) may cross the vestibulocochlear nerve inferiorly, posteriorly, anteriorly, or between it and the facial nerve (Kim et al. 1990; Yurtseven et al. 2004). The meatal loop of AICA establishes a variable relationship with the vestibulocochlear nerve.
4. The gross segmentation of the vestibulocochlear nerve into its division is not clear in the cisternal segment, but this becomes evident beginning from the porus or midportion of the internal acoustic meatus (Kim et al. 1998). The relationship between facial nerve and vestibulocochlear nerve subdivisions may vary along the meatal segment (see Chapter 84).
5. The lateral or superior loop of a high-lying posterior inferior cerebellar artery (PICA) or a kinked vertebral artery may come into close contact with the proximal cisternal part of the vestibulocochlear nerve (Matsushima et al. 1990).
6. The vestibular nerve may communicate with the intermediate nerve and/or the geniculate ganglion of the facial nerve (Piersol 1918).
7. The vestibular and cochlear nerves may communicate with each other. The communication between the vestibular and cochlear nerves is known as von Oort's anastomosis (Shoja et al. 2014). This anastomosis usually occurs within the internal acoustic meatus and rarely within the cerebellopontine angle (Ozdoğmuş et al. 2004; Tian et al. 2008; Unel et al. 2012). Labrousse et al. (2004) found this anastomosis to have an average diameter of 0.5 mm and average length of 0.5–1 mm at the bottom of the internal acoustic meatus in 7out of 10 specimens (70%). Tian et al. (2008) described the vestibulocochlear anastomoses as a single connecting branch or a brush-like nerve fiber bundle in 24 out of 30 cadaveric specimens (80%). In a magnetic resonance imaging study, these connections were noted in 31 out of 138 ears (*c.* 22%); in the majority of cases, these were located in the midportion of the internal acoustic meatus. Using scanning electron microscopy, Ozdoğmuş et al. (2004) revealed that Oort's anastomosis specifically connects the inferior vestibular nerve with the cochlear nerve.

References

Kim HN, Kim YH, Park IY, Kim GR, Chung IH. 1990. Variability of the surgical anatomy of the neurovascular complex of the cerebellopontine angle. *Ann Otol Rhinol Laryngol* 99: 288–296.

Kim HS, Kim DI, Chung IH, Lee WS, Kim KY. 1998. Topographical relationship of the facial and vestibulocochlear nerves in the subarachnoid space and internal auditory canal. *AJNR Am J Neuroradiol* 19: 1155–1161.

Labrousse M, Cucherousset J, Avisse C, Delattre JF, Chays A. 2004. Anatomohistologic study of von Oort's vestibulocochlear anastomosis. *Ann Otolaryngol Chir Cervicofac* 121: 205–512 (in French).

Matsushima T, Inoue T, Fukui M. 1990. Arteries in contact with the cisternal portion of the facial nerve in autopsy cases: microsurgical anatomy for neurovascular decompression surgery of hemifacial spasm. *Surg Neurol* 34: 87–93.

Bergman's Comprehensive Encyclopedia of Human Anatomic Variation, First Edition. Edited by R. Shane Tubbs, Mohammadali M. Shoja and Marios Loukas.
© 2016 John Wiley & Sons, Inc. Published 2016 by John Wiley & Sons, Inc.

Oh CS, Chung IH, Lee KS, Tanaka S. 2003. Morphological study on the rootlets comprising the root of the intermediate nerve. *Anat Sci Int* 78: 111–113.

Ozdoğmuş O, Sezen O, Kubilay U, Saka E, Duman U, Şan T, Çavdar S. 2004. Connections between the facial, vestibular and cochlear nerve bundles within the internal auditory canal. *J Anat* 205: 65–75.

Piersol GA. 1918. *Human Anatomy, sixth edition*. Philadelphia: J. B. Lippincott.

Rhoton AL Jr, Kobayashi S, Hollinshead WH. 1968. Nervus intermedius. *J Neurosurg* 29: 609–618.

Shoja MM, Oyesiku NM, Griessenauer CJ, Radcliff V, Loukas M, Chern JJ, Benninger B, Rozzelle CJ, Shokouhi G, Tubbs RS. 2014. Anastomoses between lower cranial and upper cervical nerves: A comprehensive review with potential significance during skull base and neck operations, Part I: Trigeminal, facial, and vestibulocochlear nerves. *Clin Anat* 27: 118–130.

Tian GY, Xu DC, Huang DL, Liao H, Huang MX. 2008. The topographical relationship and anastomosis of the nerves in the human internal auditory canal. *Surg Radiol Anat* 30: 243–247.

Unel S, Yilmaz M, Albayram S, Işk Z, Ceyhan E, Isildak H, Teixido M, Savas Y, Kiris A. 2012. Anastomoses of the vestibular, cochlear, and facial nerves. *J Craniofac Surg* 23: 1358–1361.

Yurtseven T, Savaş R, Koçak A, Turhan T, Aktaş EO, Işlekel S. 2004. Relationship between anterior inferior cerebellar artery and facial-vestibulocochlear nerve complex: an anatomical and magnetic resonance images correlation study. *Minim Invasive Neurosurg* 47: 306–311.

86 Glossopharyngeal nerve

Mohammadali M. Shoja[1], Marios Loukas[2] and R. Shane Tubbs[2–4]
[1]Tuberculosis and Lung Disease Research Center, Tabriz University of Medical Sciences, Tabriz, Iran
[2]St George's University, School of Medicine, St Georges, Grenada
[3]Seattle Science Foundation, Seattle, Washington, USA
[4]University of Dundee, Dundee, UK

Origin from the brain stem

Glossopharyngeal nerve (GN) rootlets originate from the upper part of the post-olivary groove just above the rootlets of the vagus and 2–4 mm dorsal to the olive (Rhoton and Buza 1975). The intracranial (cisternal) length of the GN varied over the range 15–21 mm in one study (Rhoton and Buza 1975) and 11–18 mm in another study (Ozveren et al. 2003). Its diameter after union of the rootlets was 0.4–1.1 mm (Rhoton and Buza 1975).

The following variations in the arrangement of GN rootlets were observed by Rhoton and Buza (1975) in 50 specimens they examined:

1. In 27 specimens, one or two rootlets originated ventral to the dorsal root/rootlet component. The ventral rootlets were smaller and motor in nature. The dorsal root/rootlet component was larger and sensory in nature.
2. In 23 specimens, the ventral rootlet was not observed and there was only a single root/rootlet component corresponding to the main dorsal root/rootlet component of the previous variant.

In the majority of the specimens, the dorsal component was composed of a single root originating from the medulla, except: (1) in one of the specimens, the GN had two rootlets of rather equal size from the medulla that remained separate intracranially; and (2) in another specimen, the GN had two rootlets from the medulla that united before entering the jugular foramen.

Ozveren et al. (2003) reported 3–5 GN rootlets originating from the medulla.

Intracranial course

Relationship to posterior inferior cerebellar artery (PICA) and anterior inferior cerebellar artery (AICA)

The PAIC has a variable and tortuous (with multiple loops) course within the posterior cranial fossa; such variability accounts for the variable relationship that cranial nerves (CN) IX to XII establish with the PICA. Most often, the PICA originates from the vertebral artery and has its first loop upward. The upper limit of the loop of PICA may extend up to and even slightly above the rootlets of the GN; this variant (i.e., high-lying PICA loop) has been noted in 14% of the specimens dissected by Rhoton and Buza (1975). The following variations in the relationship between the GN rootlets and the proximal and distal limbs of the high-lying loop of PICA have been reported.

1. The proximal and distal limbs may pass ventral to the GN rootlets. This variant has been reported by Rhoton and Buza (1975) in 2% of the specimens they studied.
2. The proximal and distal limbs may pass dorsal to the GN rootlets. This variant has been reported by Rhoton and Buza (1975) in 12% of the specimens they studied.
3. The loop of PICA may turn backward above the GN rootlets. In such cases, the proximal limb of the PICA loop is ventral to the GN rootlets, and the distal limb dorsal to it. This variant has been reported by Rhoton and Buza (1975) in 2% of the specimens they studied.

Macchi et al. (2004) reported the following variants in the 80 specimens they examined:

1. The PICA passed above the GN in 22 cases, through the GN rootlets in 4 specimens and between the GN and the vagus in 8 specimens.
2. The relationship between PICA and GN was related to the level of the origin of PICA, as follows: (1) when the origin of PICA was from the basilar artery (18 out of 80 specimens; 22.5%), the artery passed above the GN in 12 specimens, through the GN rootlets in 4 specimens and between the GN and the vagus in 2 specimens; (2) when the origin of the PICA was from the lateral medullary portion of the vertebral artery (34 specimens), it coursed above the GN in 8 cases; and (3) when the origin of the PICA was from the premedullary segment of the vertebral artery (26 specimens), it coursed between the GN and the vagus in 8 cases and above the GN in 2 cases.

Bergman's Comprehensive Encyclopedia of Human Anatomic Variation, First Edition. Edited by R. Shane Tubbs, Mohammadali M. Shoja and Marios Loukas.
© 2016 John Wiley & Sons, Inc. Published 2016 by John Wiley & Sons, Inc.

Jugular foramen

The GN passes through the anteromedial part of the jugular foramen. Variation of GN within the jugular foramen entails its relationship with the surrounding septa and bony structures, inferior petrosal sinus, and cranial nerves X and XI.

In a study of 45 cadavers (Saleh et al. 1995), the jugular foramen compartments and their contents were as follows.

1. In 70% of specimens (*n*=28), the foramen was divided into two compartments by a bony or a fibrous septum.
2. In 67.5% of the specimens (*n*=27), the GN passed through the anterior compartment and CN X and XI and jugular bulb through the posterior compartment.
3. In one of the specimens (2.5%), the GN and cranial nerves X and IX passed through the anterior compartment and the jugular bulb through the posterior compartment.
4. In 25% of specimens (*n*=10), there was no compartmentalization.
5. In 5% (*n*=2), the foramen was divided into three compartments by bony septa: the anterior compartment contained the GN; the middle contained CN X and XI; and the posterior contained the jugular bulb.

In the same study (Saleh et al. 1995), the following relationships with the inferior petrosal sinus (IPS) were observed. In 85% of the specimens, IPS coursed in the same compartment with the GN. In 15% of the specimens (*n*=6), the IPS coursed in a same compartment with the CN X and XI. The IPS traverses the anterior part of the jugular foramen anteroposteriorly before joining the jugular bulb (or occasionally the internal jugular vein). The foraminal course of IPS is oblique and inclined inferiorly and laterally. The IPS has a close relationship to the cranial nerves IX to XI. The following configurations were noted.

1. In most cases, the GN was superior to the IPS. CN X and XI were inferior to the IPS.
2. In 20% of the cases, the GN and CN X and XI were all superior and lateral to the IPS.
3. In 7.5% of the cases, the GN and CN X and XI were all inferior and medial to the IPS.
4. In cases where the IPS traversed the entire height of the jugular foramen to enter the internal jugular vein, the GN was always lateral to the sinus and CN X and XI medial to it.

Lang and Weigel (1983) reported the following relationship between the IPS and CN IX to XI at their entrance into the jugular foramen.

1. In 48% of the specimens, the IPS passed between the CN IX and CN X; the GN was superior (and slightly lateral) to the IPS.
2. In 30% of the specimens, the IPS entered the jugular foramen anterior to the GN; the GN was posterior (or medial/inferior) to the IPS.
3. In 16% of the specimens, the IPS entered to the jugular foramen medial to the vagus nerve; the GN along with the vagus was superior and lateral to IPS.
4. In 6% of cases, the IPS passed between the vagus and accessory nerves.

Extracranial course

The GN pierces the stylopharyngeus muscle in 12% of cases; this variation is more common on the left side of the neck compared to the right side (Lang 1995).

In a histological study, sympathetic and parasympathetic ganglion cells were found along the lingual branch of the GN in 9 of 12 specimens examined (Oda et al. 2013). These ganglia are situated in the superolateral side of the tonsillar tissue, and vary in number from 2 to 25.

Tympanic branch

The tympanic nerve (or nerve of Jacobson) arises from the glossopharyngeal nerve most often at the level of the inferior ganglion and occasionally at a higher level (Donaldson 1980). The tympanic nerve may arise from two roots, one of which may come from the vagus nerve (Cruveilhier 1853).

A hypotympanic branch of the tympanic nerve was found by Porto et al. (1978) in 10 out of 20 specimens (50%); nine of them coursed anterosuperiorly and one of posteriorly.

Donaldson (1980) observed five variants of the tympanic nerve as follows:

1. a single nerve without hypotympanic branch (26/50, 52%);
2. a single nerve with one anterior hypotympanic branch (17/50, 34%);
3. a single nerve with two anterior hypotympanic branches (5/50, 10%);
4. two tympanic nerve branches travelling through separate inferior tympanic canaliculi (1/50, 2%); the two branches were parallel to each other over the promontory; and
5. a single nerve travelling through an abnormally positioned tympanic canaliculus (1/50, 2%); the nerve travelled anteromedially in the bony septum separating the internal jugular vein and internal carotid artery, and entered the tympanic cavity along with a caroticotympanic branch of the internal carotid sympathetic plexus.

Carotid branch

The carotid sinus is innervated by branches from the GN, vagus and cervical sympathetic. In rare instances, a branch from the hypoglossal nerve may also contribute to this innervation. The main nerve to the carotid sinus arises from the GN or one of its branches (Boyd 1937; Sheehan et al. 1941); it is variably referred to as "carotid sinus nerve proper (CSNP)" (Boyd 1937; Sheehan et al. 1941), carotid sinus nerve, Hering's nerve, intercarotid nerve of De Castro or ramus caroticus glossopharyngei of Braeucker (Shoja et al. 2014). The CSNP is a constant branch of the GN. This nerve was absent along with the common carotid artery in only 1 out of 59 hemi-necks dissected by Boyd. The length of this nerve varied over the range 2–7 cm in one study (Sheehan et al. 1941) and

4–8.8 cm in another study (Toorop et al. 2009), depending on its origin from the GN and the level of common carotid artery bifurcation.

Origin of the CSNP from the GN

In the study of Boyd (1937), the mode of origin of CSNP from the GN was as follows:

- From the glossopharyngeal nerve trunk: (1) by one root (4/58); (2) by two roots (33/58); (3) by three roots (7/58); or (4) by four roots (1/58).
- From the pharyngeal branches of the GN: (1) by one root (6/58); or (2) by two roots (2/58).
- From the nerve to stylopharyngeus: by one root (2/58).

In all the specimens (n=33) dissected by Sheehan et al. (2041), the CSNP directly branched from the GN. They reported the variations in the point of origin of the CSNP from the main trunk of the GN as follows: in 19 specimens, the point of origin was within 1 cm of the base of the skull; in 12 specimens, the point of origin was 1–3 cm from the base of the skull; and in 2 specimens, the point of origin was as far as 4 cm from the base of the skull.

Sheehan et al. (1941) concluded that the high origin of the CSNP from the GN is a constant feature. They also observed the following variations:

1. in more than 50% of the specimens, the origin of the CSNP from the GN was double, and the two roots united 1–3 cm distally;
2. in 2 specimens out of 33, a complete double CSNP was observed; and
3. in the remaining specimens, the CSNP was a single nerve at origin (irrespective of its communications with other nerves).

Relationship of the CSNP to the internal carotid artery

The CSNP may descend anterior to the internal carotid artery, anterolateral, or anteromedial to it. Table 86.1 lists the incidence of these variants reported in the literature.

Neural communications of the CSNP

The CSNP receives communicating branches from the adjacent nerves. Several authors have explored this anatomy. Cordier and Coulouma (1932) noted an anastomosis with the vagus nerve in 93% of cases and an additional anastomosis with the cervical sympathetic in 16% of cases. In the study of Boyd (1937) of 58 CSNP specimens, the observed neural communications were as follows: with the pharyngeal branch of the vagus in 26 cases; with the cervical sympathetic in 18 cases; with the superior laryngeal nerve in 11 cases; with the vagus nerve trunk in 3 cases; with the hypoglossal nerve in 2 cases; and with the descendens hypoglossi in 1 case.

Sheehan et al. (1941) noted that, most often (in 24 out of 33 specimens), the CSNP received communicating branches from the nodose ganglion or pharyngeal branch of the vagus. There was no communicating loop with the superior cervical sympathetic ganglion. A communicating loop between the CSNP and the superior cervical sympathetic ganglion was observed in seven cases. There was no communicating loop from the vagus. Finally, in two cases, a communicating loop with the vagus coexisted with another loop from the superior cervical sympathetic ganglion (Sheehan et al. 1941).

Toorop et al. (2009) reported the following anastomoses of the CSN: with the vagus nerve trunk in 3 out of 12 specimens; with the pharyngeal branch of the vagus in 6 out of 12 specimens; with the sympathetic trunk in 2 out of 12 specimens; and with the superior cervical sympathetic ganglion in 2 out of 12 specimens.

Table 86.1 The course of the CSNP along the internal carotid artery.

	Anterior	Anterolateral	Anteromedial
Sheehan et al. 1941	18/33	9/33	6/33
Toorop et al. 2009	1/12	5/12	6/12

Pharyngeal branches

The formation of the pharyngeal plexus - into which the pharyngeal branches of the GN makes substantial contribution - has been described in Chapter 87. The pharyngeal plexus has been reported to give a slender branch: the middle laryngeal nerve (Bergman et al. 2006). It supplies the cricothyroid muscle and then pierces the cricothyroid membrane to supply the mucous membrane of the lower part of the larynx.

Muscular branches

The GN may give rise to the mylohyoid nerve supplying the mylohyoid muscle and anterior belly of the digastric (Schaefer et al. 1915). Through the branches of the pharyngeal plexus, the GN may additionally provide some motor innervation to the superior constrictor muscle (Goodwin 1993).

Lingual division and its branches

After giving rise to the pharyngeal branches the main trunk of the GN continues as the lingual division (abbreviated LBGN), comprising a significant proportion of the fibers in the GN. From the LBGN, smaller lingual branches arise and supply sensory fibers to the tongue and tonsillar bed. The LBGN enters the base of the tongue just posterior to the hypoglossal nerve (Touré et al. 2005). It then takes a short ventral and medial course to divide into its terminal intralingual (anterior and posterior)

branches. The anterior branch runs anterolaterally and divides into branches that anastomose with the branches of the lingual and hypoglossal nerve. The posterior branch runs posteromedially and further divides into anterior, lateral, and posterior divisions. The anterior division of the posterior branch of the LBGN supplies the root of tongue and its lateral and posterior division reaches the lateral glossoepiglottic groove (Touré et al. 2005).

The LBGN may pass immediately outside (lateral to) the tonsillar capsule. This variation may make patients with tonsillitis prone to glossopharyngeal neuralgia (Khan and Iyer 2007). Ohtsuka et al. (2002) examined 107 specimens to explore the relationship between the LBGN and the palatine tonsil. They noted that the depth of LGBN from the tonsil and their relationships was related to the muscle composition of the tonsillar bed. They distinguished three variants as follows:

- Type A (classic textbook description): the superior constrictor muscle covered most of the tonsillar bed, and the gap between the superior and middle constrictor muscles were extremely narrow. The LBGN was separated from the tonsillar capsule by the superior constrictor muscle. This variant (deep LBGN) was observed in 23.4% of the specimens.
- Type B: There was a gap between the superior and middle constrictor muscles. The LBGN was separated from the tonsillar capsule by blood vessels, loose connective tissue, and minor bundles of the stylopharyngeus and palatopharyngeus muscles. This variant (intermediately deep LBGN) was observed in 55.5% of the specimens.
- Type C: There was a large gap between the superior and middle constrictor muscles, and the tonsillar bed lacked a muscular cover over a large area. The LGBN adhered to the tonsillar tissue through a thin layer of loose connective tissue. This variant (shallow LBGN) was observed in 21.5% of the specimens.

Anastomotic branches

Anastomoses exist between the main trunk and branches of the GN and other adjacent nerve trunks and branches. These neuroanastomoses are variable, and their incidences have been investigated in few studies. Some of the following anastomoses are rare: main glossopharyngeal nerve trunk with the main trunk of the facial nerve; main glossopharyngeal nerve trunk with the main trunk of the vagus nerve (located intracranially, at the level of jugular foramen or extracranially); petrous ganglion of the glossopharyngeal nerve with the superior (jugular) ganglion of the vagus nerve; pharyngeal branch of the glossopharyngeal nerve with the pharyngeal branch of the vagus nerve (forming pharyngeal plexus); carotid sinus nerve with a branch from the main trunk of the vagus nerve (forming the superficial carotid ansa); carotid sinus nerve with a branch from the pharyngeal branch of the vagus nerve; or carotid sinus nerve with the branches from pharyngeal branches of the glossopharyngeal nerve. The glossopharyngeal may receive fibers from the hypoglossal nerve just distal to the hypoglossal canal.

In a study of six Sihler-stained tongues, the following anastomoses were observed in all specimens (Touré et al. 2005).

1. The posterior division of the posterior branch of the LBGN anastomoses with a branch of the vagus within the lateral glossoepiglottic groove.
2. The right and left posterior terminal branches of the LBGN anastomose across the midline to form the pre-epiglottic neural arcade.
3. The anterior branch of the LBGN anastomoses with the branches of the lingual and hypoglossal nerves within the substance of the tongue.

References

Bergman RA, Afifi AK, Miyauchi R. 2006. Illustrated Encyclopedia of Human Anatomic Variation. Available at: http://www.anatomyatlases.org/AnatomicVariants/AnatomyHP.shtml (accessed 17 November 2015).

Boyd JD. 1937. Observations on the human carotid sinus and its nerve supply. *Anat Anz* 84: 386–399.

Cordier P, Coulouma M. 1932. Recherches sur les nerfs du sinus carotidien et sur leurs variations. *Compt Rendus Assoc Anat* 27: 161–178.

Cruveilhier J. 1853. *The Anatomy of the Human Body*. New York: Harper.

Donaldson I. 1980. Surgical anatomy of the tympanic nerve. *J Laryngol Otol* 94: 163–168.

Goodwin WJ Jr, Arnold D, Wachholz J. 1993. Surgical anatomy of the glossopharyngeal nerve. *Laryngoscope* 103: 1302–1304.

Khan NU, Iyer A. 2007. Glossopharyngeal neuralgia associated with anomalous glossopharyngeal nerve. *Otolaryngol Head Neck Surg* 136: 502–503.

Lang J. 1995. *Clinical Anatomy of the Masticatory Apparatus and Peripharyngeal Spaces*. Berlin: Thieme.

Lang J, Weigel M. 1983. Nerve-vessel relations in the region of the jugular foramen. *Anat Clin* 41–56.

Macchi V, Porzionato A, Parenti A, De Caro R. 2004. The course of the posterior inferior cerebellar artery may be related to its level of origin. *Surg Radiol Anat* 26: 60–65.

Oda K, Takanashi Y, Katori Y, Fujimiya M, Murakami G, Kawase T. 2013. A ganglion cell cluster along the glossopharyngeal nerve near the human palatine tonsil. *Acta Otolaryngol* 133: 509–512.

Ohtsuka K, Tomita H, Murakami G. 2002. Anatomy of the tonsillar bed: topographical relationship between the palatine tonsil and the lingual branch of the glossopharyngeal nerve. *Acta Otolaryngol Suppl* 546: 99–109.

Ozveren MF, Türe U, Ozek MM, Pamir MN. 2003. Anatomic landmarks of the glossopharyngeal nerve: a microsurgical anatomic study. *Neurosurgery* 52: 1400–1410.

Porto AF Jr, Whicker J, Proud GO. 1978. An anatomic study of the hypotympanic branch of Jacobson's nerve. *Laryngoscope* 88: 56–60.

Rhoton AL Jr, Buza R. 1975. Microsurgical anatomy of the jugular foramen. *J Neurosurg* 42: 541–550.

Saleh E, Naguib M, Aristegui M, Cokkeser Y, Sanna M. 1995. Lower skull base: anatomic study with surgical implications. *Ann Otol Rhinol Laryngol* 104: 57–61.

Schaefer EA, Symington J, Bryce TH. 1915. *Quain's Anatomy, 11th edition*. London: Longmans, Green, and Co.

Sheehan D, Mulholland JH, Shafiroff B. 1941. Surgical anatomy of the carotid sinus nerve. *Anat Rec* 80: 431–442.

Shoja MM, Oyesiku NM, Shokouhi G, Griessenauer CJ, Chern JJ, Rizk EB, Loukas M, Miller JH, Tubbs RS. 2014. A comprehensive review with potential significance during skull base and neck operations, Part II: Glossopharyngeal, vagus, accessory, and hypoglossal nerves and cervical spinal nerves 1–4. *Clin Anat* 27: 131–144.

Toorop RJ, Scheltinga MR, Moll FL, Bleys RL. 2009. Anatomy of the carotid sinus nerve and surgical implications in carotid sinus syndrome. *J Vasc Surg* 50: 177–182.

Touré G, Bicchieray L, Selva J, Vacher C. 2005. The intra-lingual course of the nerves of the tongue. *Surg Radiol Anat* 27: 297–302.

87 Vagus, accessory, and hypoglossal nerves

Mohammadali M. Shoja[1], Christoph J. Griessenauer[2], Marios Loukas[3] and R. Shane Tubbs[3–5]

[1]Tuberculosis and Lung Disease Research Center, Tabriz University of Medical Sciences, Tabriz, Iran
[2]University of Alabama at Birmingham, Birmingham, Alabama, USA
[3]St George's University, School of Medicine, St Georges, Grenada
[4]Seattle Science Foundation, Seattle, Washington, USA
[5]University of Dundee, Dundee, UK

The last three cranial nerves demonstrate variability in their branches and relationships with other structures along their courses. These variations are relatively well appreciated in the literature. Less well appreciated among them are the vast and variable anastomoses that these nerves or their branches make with each other or other nearby nerves. In this chapter, we review the anastomoses of the vagus, accessory, and hypoglossal nerves. This chapter is based on a review article previously published by our group (Shoja et al. 2014).

Vagus to glossopharyngeal nerve anastomoses

The anastomoses between the glossopharyngeal and vagus nerves can be divided into two classes: (1) direct communications involving the main trunks or ganglia; and (2) indirect connections involving their branches. These anastomoses exist intracranially, at the level of the jugular foramen, or extracranially. A study found direct intracranial anastomoses in 2.5% of specimens (Tubbs et al. 2011). These authors distinguished two types of direct intracranial anastomoses: in type I, the connecting branch passed more vertically with respect to the longitudinal axes of the nerve trunks; and in type II, it coursed obliquely (so was therefore longer). The first indirect glossopharyngeal-vagus anastomosis, which conveys sensory fibers, is formed by the joining of a twig from the glossopharyngeal nerve with the auricular branch of the vagus (Arnold's nerve) within the jugular foramen (Kawai et al. 1989; Brown et al. 2000). Through this communication, the general somatic afferent fibers enter the glossopharyngeal nerve (see the section "Auricular branch of the vagus and its communications" below for more discussion). Additionally, the inferior (petrous or Andersch's) ganglion of the glossopharyngeal nerve may also directly communicate with the jugular ganglion of the vagus within the jugular foramen (Jackson 1921); this anastomotic twig is variable and inconstant (Cruveilhier 1844). Some authors have also noted a direct anastomosis between the trunks of the glossopharyngeal and vagus nerves just below the jugular foramen (Testut 1902; Toldt 1907; Jackson 1921). This communicating branch enters the glossopharyngeal nerve at the level of or slightly below Andersch's ganglion (Testut 1902). The incidence of this direct extracranial anastomosis has yet to be investigated. Testut (1902) cited Cruveilhier as stating that this anastomosis conveys accessory nerve fibers from the vagus to the glossopharyngeal nerve.

The pharyngeal, intercarotid, and carotid sinus plexuses

The pharyngeal, intercarotid, and carotid sinus plexuses are neural networks mainly composed of fibers originating from the glossopharyngeal and vagus nerves and cervical sympathetics (Fuse 1950; De Castro 2009; Toorop et al. 2009). The intercarotid plexus, located in the triangular space between the internal and external carotid arteries (Fuse 1950), is linked to the pharyngeal plexus medially and supplies the carotid sinus and carotid body inferiorly. Fuse (1950) described the intercarotid plexus as being composed of three main trunks (superficial, intermediate, and deep) with variable interconnections (Fig. 87.1). One of the main constituents of the intercarotid plexus is the carotid sinus nerve (Hering's nerve, intercarotid nerve of De Castro or ramus caroticus glossopharyngei of Braeucker), which is a branch of the glossopharyngeal nerve and usually originates when the latter crosses over the internal carotid artery. Although it is known that the carotid sinus nerve often receives communicating branches from the pharyngeal branch of the vagus nerve, vagus nerve trunk, sympathetic trunk, or superior cervical sympathetic ganglion (Toorop et al. 2009), the true anatomy of such communications is more complex; in fact, these nerves establish a plexus within the intercarotid triangle.

Bergman's Comprehensive Encyclopedia of Human Anatomic Variation, First Edition. Edited by R. Shane Tubbs, Mohammadali M. Shoja and Marios Loukas.
© 2016 John Wiley & Sons, Inc. Published 2016 by John Wiley & Sons, Inc.

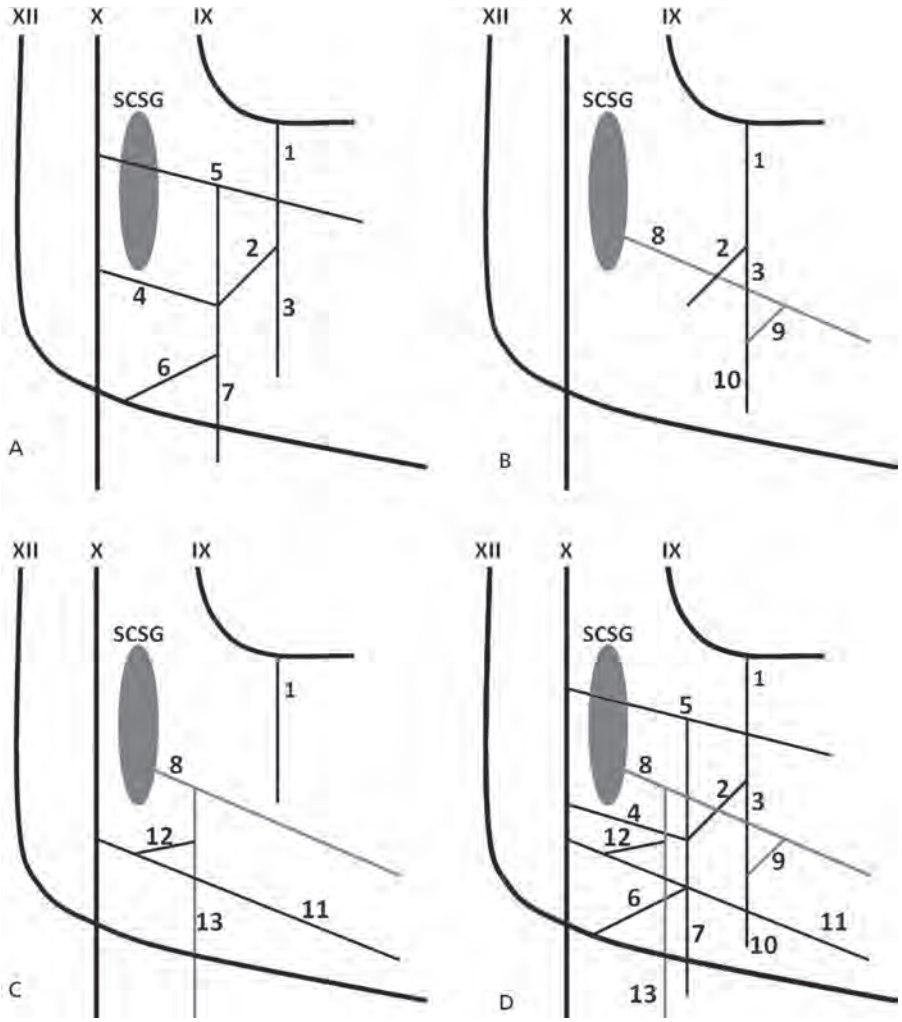

Figure 87.1 The intercarotid plexus and its main trunks. (a) Formation of the superficial trunk; (b) formation of the intermediate trunk; (c) formation of the deep trunk; and (d) superimposition of (a–c). 1, carotid sinus nerve; 2, superficial branch of the carotid sinus nerve; 3, deep branch of the carotid sinus nerve; 4, carotid branch of the vagus nerve; 5, pharyngeal branch of the vagus nerve with its carotid branch; 6, carotid branch of the hypoglossal nerve; 7, superficial trunk of the intercarotid plexus; 8, inferior branch of the SCSG (the superior cervical sympathetic ganglion); 9, the communicating sympathetic branch to the deep branch of the carotid sinus nerve; 10, intermediate trunk of the intercarotid plexus; 11, superior laryngeal nerve; 12, the communicating branch of the superior laryngeal nerve to the sympathetic; 13, deep trunk of the intercarotid plexus.

Source: Shoja et al. (2014). Reproduced with permission from JohnWiley & Sons.

The carotid sinus nerve descends along the internal carotid artery overlying the medial border of the artery or on the anterior surface of the artery (Toorop et al. 2009), and it soon divides into two main superficial and deep branches (Fuse 1950). The anatomy of the intercarotid plexus has been elegantly studied by Fuse (1950): the superficial branch of the carotid sinus nerve anastomoses with the carotid branch of the vagus nerve to form the so-called superficial carotid ansa on the outer surface of the internal carotid artery, from which the superficial trunk of the intercarotid plexus is derived (superficial carotid ansa). The superficial carotid ansa further receives communications from the hypoglossal nerve as well as the pharyngeal branch of the vagus nerve. The deep branch of the carotid sinus nerve receives a communicating branch from the inferior branch of the superior cervical sympathetic ganglion to form the intermediate trunk of the intercarotid plexus (Fig. 87.1). Another branch of the inferior branch of the superior cervical sympathetic ganglion forms the deep trunk of the intercarotid plexus after receiving a communicating branch from the superior laryngeal nerve (Fig. 87.1). The intermediate and/or deep trunk of the intercarotid plexus as described by Fuse (1950) may be absent in *c.* 7% of specimens. The carotid sinus nerve itself can be duplicated in about one-third of subjects, implying a significant inter-individual variability in the topography and composition of the intercarotid plexus. Direct branches originating from the vagus nerve trunk below the inferior (nodose) ganglion may partially supply the wall of the common carotid artery bifurcation and proximal internal carotid artery in *c.* 83% of cases (Fuse 1950). The terminal branches of the intercarotid plexus and its trunks innervates the carotid sinus and carotid body, which participate in the regulation of blood pressure and respiration through the mediation of baroreceptor (in the carotid sinus) and chemoreceptor (in the carotid body) reflexes. The carotid sinus plexus sits within the adventitia of the carotid sinus. Notably, earlier texts have considered the carotid sinus nerve as one of the pharyngeal branches of the glossopharyngeal nerve (Sharpey-Schäfer et al. 1909). Such a designation is not far from accurate as the intercarotid and carotid sinus

plexuses can be viewed topographically as the lateral extension of the pharyngeal plexus.

Auricular branch of the vagus and its communications

The auricular branch of the vagus nerve (known as Arnold's nerve) is a cutaneous nerve, which originates from the jugular ganglion of the vagus and receives a twig form the inferior ganglion of the glossopharyngeal nerve within the jugular foramen (Landois 1904; Tekdemir et al. 1998; Merchant and Nadol 2010). Cruveilhier (1844) has referred to the auricular branch of the vagus nerve as the branch of the jugular fossa. Arnold's nerve enters the mastoid canaliculus on the lateral wall of the jugular foramen, and passes transversely and posterolaterally through this canaliculus to emerge within the mastoid portion of the facial canal. Within the facial canal, Arnold's nerve crosses the facial nerve posteriorly and gives off two branches: superior and inferior (Merchant and Nadol 2010). The superior branch joins the facial nerve. The inferior branch receives a twig from the facial nerve and ultimately leaves the temporal bone through the tympanomastoid fissure. Outside the skull, Arnold's nerve travels between the external auditory meatus and mastoid process in close proximity to the posterior auricular branch of the facial nerve and sends a communicating branch to it, which ultimately provides proprioceptive innervation of the muscles supplied by the posterior auricular nerve (Landois 1904; Sharpey-Schäfer et al. 1909). Arnold's nerve supplies the auricle and external ear canal. Very rarely, Aronld's nerve completely fuses with the facial nerve trunk, and its fibers are then distributed via the branches of the posterior auricular nerve (Sharpey-Schäfer et al. 1909). Stimulation of Arnold's nerve by mechanical irritation of the external ear canal can result in a vagal visceral reflex manifesting as cough (known as Arnold's ear-cough reflex), vomiting and, less commonly, bradycardia (Gupta et al. 1986; Landois 1904; Canning 2006).

Vagovagal anastomoses

Branches of the vagus nerves communicate with each other in the neck and thoraco-abdominal regions. Mentioned earlier was the communicating branch from the superior laryngeal nerve to the pharyngeal plexus, which connects with twigs of the pharyngeal branches of the vagus nerve at the level of this plexus.

Galen's anastomosis or ansa of Galen

Beneath the laryngopharyngeal (hypopharyngeal) mucosa in the paraglottic space, a neural communication between the dorsal or inferior descending branch of the internal laryngeal nerve, one of the two terminal divisions of the superior laryngeal nerve, and the posterior division of the recurrent laryngeal nerve exists (Sañudo et al. 1999; Naidu et al. 2012). Known as Galen's anastomosis or ansa of Galen, this anastomosis has been reported with variable prevalence in the anatomical literature. Although earlier studies have found this anastomosis in about 15–25% of their specimens (cf. Naidu et al. 2012), some authors have noted it in all their cases (Sañudo et al. 1999). However, the majority of reports in the literature have mentioned a frequency of 70–90% (Furlan et al. 2002; Naidu et al. 2012). This anastomosis can be a single or double trunk and may infrequently present with a plexiform pattern of neural interconnection. Galen's anastomosis is primarily thought to be sensory in nature (Song et al. 2009). However, its branches have been observed to supply the posterior crico-arytenoid muscle on 13% of neck sides (Naidu et al. 2012).

Vagus to accessory nerve anastomoses

At the level of jugular foramen, the accessory nerve is connected to the vagus nerve, mostly to its superior ganglion, via its internal ramus or pars vagalis (Lang 1989; Katsuta et al. 1997). Such branches, historically, have been considered as taking cranial accessory nerve fibers to the vagus nerve to be distributed via its recurrent laryngeal nerve branch. These small cross-links may simply be considered as proximal interconnections between the vagus and accessory nerves. Notably, the two or three thin connections between the superior ganglion of the vagus nerve and the accessory nerve are sometimes referred to as Lobstein's anastomoses (Olry 1995). The much larger external ramus (of the spinal accessory nerve) travels inferiorly to innervate the trapezius and sternocleidomastoid muscles. Small ganglia can be found along the spinal portion of the accessory nerve and are known as the ganglia of Laruelle.

Vagus to hypoglossal nerve anastomoses

The extra-cranial part of the hypoglossal nerve may receive one or more communicating branches as large as 2 mm in diameter from the vagus nerve. Although most of such vagal communications come from between the superior and inferior vagal ganglia, occasionally they arise directly from the inferior ganglion, or even intracranially from above the superior vagal ganglion (Saraswathi 2003). Such anastomoses may serve as afferent and efferent loops for tongue reflexes as the inferior vagal ganglion may potentially harbor the cell bodies of afferent hypoglossal fibers (Saraswathi 2003). Likewise, efferent vagal parasympathetic fibers may be conveyed to the hypoglossal nerve for distribution to the sublingual glands (Saraswathi 2003).

von Luschka (1867) described a 1–2 mm thick lingual branch of the vagus nerve, which in fact did not arise from the trunk of the vagus but from its pharyngeal branch. The lingual branch of the vagus, according to von Luschka, receives a communication from the pharyngeal branch of the glossopharyngeal nerve and joins the hypoglossal nerve where it turns around the occipital artery (Fig. 87.2). This description has been cited by several authors following von Luschka. Although the functional

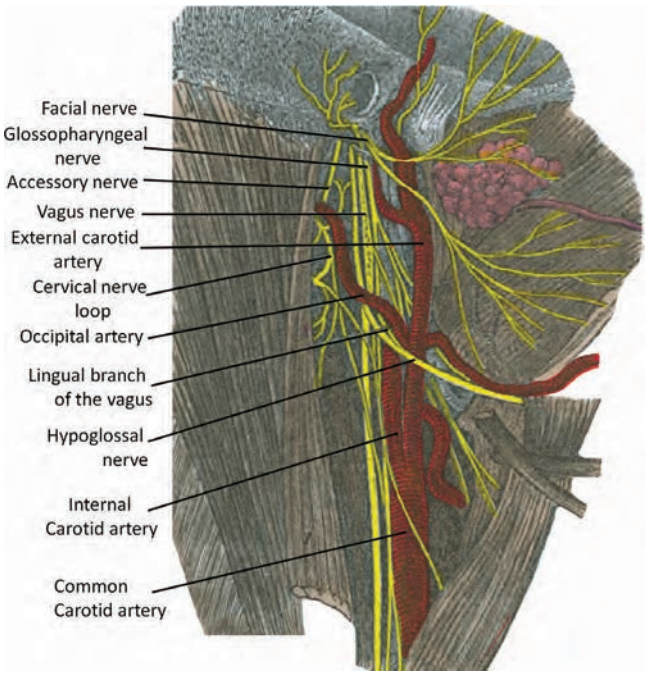

Figure 87.2 Lingual branch of the vagus nerve.

Source: Shoja et al. (2014). Reproduced with permission from JohnWiley & Sons. Adapted from von Luschka (1867).

significance of this anastomosis remains uncertain, it has been posited that it provides proprioceptive innervation to the muscles supplied by the hypoglossal nerve (Landois 1904).

Vagus to cervical nerve anastomoses and vagocervical complex

Although it is known that the inferior (nodose) ganglion of the vagus receives communication(s) from the loop between the ventral rami of the C1 and C2 spinal nerves (Jackson 1921) and/or from the ventral rami of C2 (Hovelacque 1927), the functional significance of such anastomoses is yet to be fully understood. The vagocervical complex (Fig. 87.3) is a rare variant neural anastomosis between the vagus nerve or a direct branch of it and the branches of the upper cervical spinal nerves that replaces the ansa cervicalis (Rath and Anand 1994; Vollala et al. 2005). At least two variants of the vagocervical complex have been reported; both innervate the infrahyoid muscles. In one variant, the ansa cervicalis is totally absent, the upper cervical spinal nerve fibers join the vagus nerve and then they exit the vagus distally to innervate the infrahyoid muscles. The vagal branch to the infrahyoid muscles, the so-called descending branch of the vagocervical complex, is a long nerve which pierces the carotid sheath and supplies the infrahyoid muscles

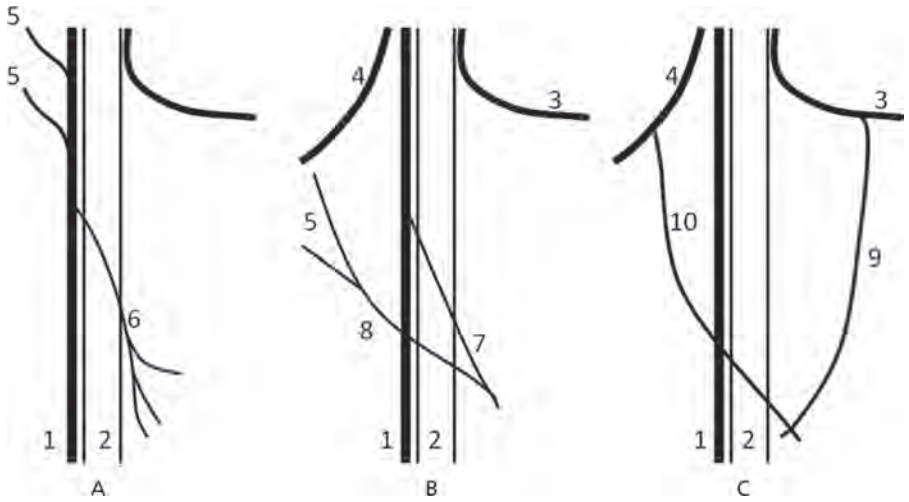

Figure 87.3 Three possible variant neural anastomoses replacing the classical ansa cervicalis. 1, vagus nerve; 2, common carotid artery, which is continued proximally as internal carotic artery; 3, hypoglossal nerve; 4, spinal accessory nerve; 5, branches from the upper cervical spinal nerves; 6, descending branch of the vagocervical complex; 7, aberrant superior root of ansa cervicalis coming from the vagus nerve (descendens vagi); 8, classic inferior root of ansa cervicalis coming from the branches of the upper cervical spinal nerves; 9, descendens hypoglossi (the classic superior root of the ansa cervicalis); 10, aberrant inferior root of ansa cervicalis coming from the spinal accessory nerve. The ansa cervicalis can be replaced by (a, b) two different types of vagocervical complex and (c) spinal accessory-hypoglossal nerve anastomosis. Note that several other very rare variants – not shown in this drawing – also exist.

Source: Shoja et al. (2014). Reproduced with permission from JohnWiley & Sons.

close to their inferior insertions (Fig. 87.3a). Notably, the term "vagocervical complex" was used to indicate the communicating branches of C1 and C2 to the vagus nerve, vagal branch to the infrahyoid muscles, and intervening portion of the vagus nerve (Rath and Anand 1994). Bilateral presence of vagocervical complex with absence of the ansa cervicalis has been reported (Abu-Hijleh 2005). In another variant, the ansa cervicalis-like neural loop is present, but the superior root originates from the vagus nerve trunk (descendens vagi) instead of originating from the hypoglossal nerve. The descendens vagi then joins the inferior root composed of the branches from the upper cervical spinal nerves (Fig. 87.3b).

Hypoglossal nerve and its anastomoses

A number of variations in the course and branches of the hypoglossal nerve have been reported. Horner mentioned a variable number of rootlets (4–8) through which the hypoglossal nerve originates from the medulla oblongata; these rootlets join to form two or three trunks before leaving the skull base. These rootlets have been reported to pierce the intracranial vertebral artery (de Caro et al. 1995). The hypoglossal nerve may have a dorsal root bearing a ganglion and it may also exit from the posterior surface of the medulla oblongata (Bergman et al. 2006). The hypoglossal nerve can innervate the mylohyoid, digastric, or stylohyoid muscles. Outside the skull, the hypoglossal nerve may fuse to form a common trunk with the vagus soon after exiting the skull base; it then separates from the vagus en route to the tongue (Ghanbari et al. 2007). This variant is not an uncommon finding during carotid endarterectomy (Schauber et al. 1997); however, its prevalence needs to be identified in postmortem studies. There is an intraoperative report of a patient who had a supernumerary hypoglossal nerve (Islam et al. 2012). The supernumerary nerve was located superior and ventral to the "true" hypoglossal nerve; both of these nerves supplied the tongue and there were several interconnections between them.

The proximal portion of the hypoglossal nerve (immediately after exiting the skull base) is most often located medial to the internal jugular vein (Salame et al. 2006). Salame and colleagues (2006) dissected 46 neck sides and observed quite a few variations in the course of the horizontal segment of the hypoglossal nerve. The horizontal segment of the hypoglossal nerve was located superior to the intermediate tendon of the digastric muscle in 21 (45.7%) neck sides and inferior or directly deep to the tendon in 25 (54.3%) neck sides. The horizontal segment of the hypoglossal nerve crossed the lingual artery in 33 dissections (72%), whereas it was inferior to the origin of the lingual artery from the external carotid artery (EAC) in the other 13 dissections (28%). The diameter of the hypoglossal nerve before entering the submandibular triangle ranged over 1.9–3.8 mm (mean 2.7 mm). After giving rise to the descendens hypoglossi, the hypoglossal nerve may give rise to 1–5 extra-lingual branches; there were two branches in 48% of instances, three in 26%, one in 17%, and four or five in the remaining. Of direct branches of the hypoglossal nerve, the nerve to the geniohyoid muscle was identified in 78% of cases and nerve to the thyrohyoid muscle in 37%.

Relationship of hypoglossal nerve to the external and internal carotid arteries

The hypoglossal nerve often crosses the internal and external carotid arteries approximately 2–4 cm above the carotid bifurcation (Schauber et al. 1997). Occasionally, it may pass as low as the level of carotid bifurcation (low-lying variant). Shin and colleagues (2012) dissected 29 neck sides from Korean adult cadavers. These authors noted that the distance from the common carotid bifurcation to the point that the hypoglossal nerve crossed the ventral and dorsal borders of the internal and external carotid arteries varied over the range 8.7–34.1 mm (mean 18.5 mm) and 7.5–28.1 mm (mean 15.5 mm), respectively. There were no statistically significant differences in these measurements with respect to gender or neck side.

The hypoglossal nerve (Fig. 87.4) communicates with the sympathetic trunk, the pharyngeal plexus, the loop between the first cervical ventral ramus, and the ascending branch of the second cervical ventral ramus in the cervical plexus and the lingual, glossopharyngeal, and vagus nerves (Saraswathi 2003; Bergman et al. 2006). A peripheral anastomosis may also exist between the two hypoglossal nerves. Alternatively termed the hypoglossal transverse arch, transmedian anastomosis of the hypoglossal nerves, suprahyoid loop of the hypoglossal nerve, or Hyrtl's ansa suprahyoidea hypoglossi, the interhypoglossal anastomosis connecting the terminal parts of the hypoglossal nerve trunks is located anterior to the hyoid bone and the genioglossus muscles superiorly and geniohyoid muscles inferiorly, and may be established as early as 60 days gestation (Platzer 1959; Gonzalez-Compta and Domenech-Mateu 1996; Bergman et al. 2006). The first description of such an anastomotic loop was made by Scarpa (cf. Gonzalez-Compta and Domenech-Mateu 1996). Hyrtl reported a similar anastomosis in 1 out of 10 adult cadavers (cf. Gonzalez-Compta and Domenech-Mateu 1996). An incidence of 8–10% has also been reported in the literature (Bergman et al. 2006).

After exiting the skull and near the atlas, the hypoglossal nerve is joined by branches from the superior cervical sympathetic ganglion and then a filament from the loop between the first and second cervical nerves (Chhetri and Berke 1997; Indrasingh et al. 1999). The latter connection, which occurs distal to a vagohypoglossal anastomosis, leaves the hypoglossal nerve as the descendens hypoglossi (or superior root of the ansa cervicalis), the nerve to the thyrohyoid, and the nerve to the geniohyoid (Indrasingh et al. 1999; Khaki et al. 2006). Rarely, a branch from the descendens hypoglossi may pass into the thorax and join the sympathetic trunk or vagus nerve. In such cases, the aberrant branch can be traced back superiorly into either of these two latter nerves (Piersol 1911). The descendens hypoglossi may supply the C3 root to the phrenic nerve, which travels via

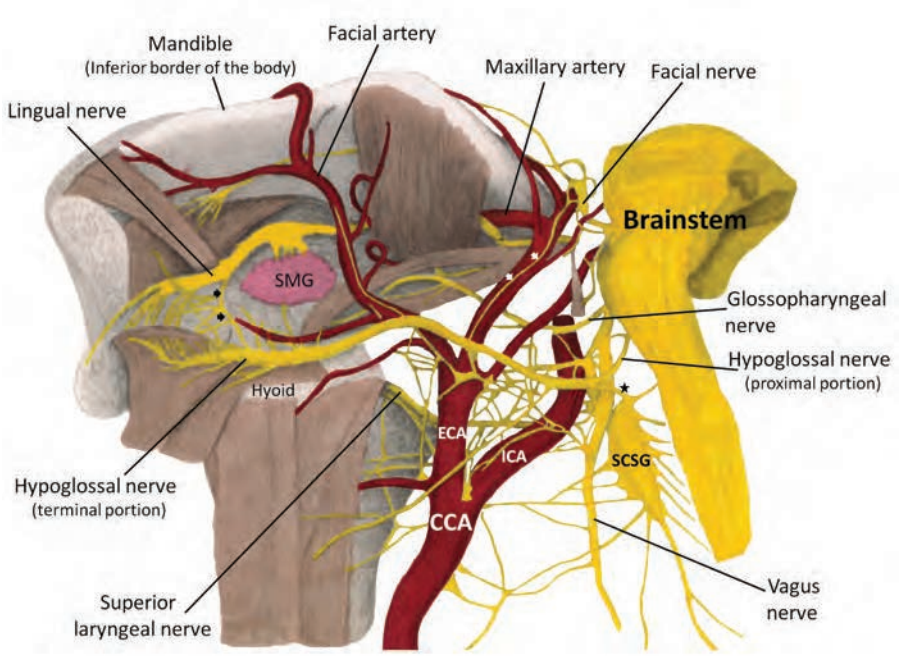

Figure 87.4 Hypoglossal nerve and its peripheral anastomoses. The mandible has been cut in the midline and retracted upward to uncover the submandibular region and the structures of the deep upper neck. There is a connection (star) between the superior cervical sympathetic ganglion (SCSG) and hypoglossal nerve as the latter turns forward at the level of the hyoid bone. The terminal portions of the lingual and hypoglossal nerves anastomose with each other in the suprahyoid region (black arrows). The extensive network of neural connections between the SCSG, glossopharyngeal and vagus nerves and their branches represents a part of the pharyngeal plexus and pericarotid plexus in the neck. These two plexuses are continuous. The hypoglossal nerve is also connected to them through fine branches. Note a neural strand (white arrows) running upward over the external carotid artery (EAC) and connecting the facial nerve with the pericarotid sympathetic plexus. CCA, common carotid artery; ICA, internal carotid artery; SMG, submandibular gland.

Source: Shoja et al. (2014). Reproduced with permission from JohnWiley & Sons. Adapted from Swan (1834).

the inferior root of the ansa cervicalis (Turner 1893). The thin communicating branch between descendens hypoglossi, ansa cervicalis, or its branch to sternothyroid and the phrenic nerve is called anastomosis of Valentin and was found in 2 out of 80 (2.5%) neck sides in a series (Caliot et al. 1986).

The descendens hypoglossi anastomoses with a branch from the C2–4 ventral rami over the anterior wall of the carotid sheath to form a neural loop referred to as the ansa cervicalis or ansa hypoglossi (Chhetri and Berke 1997). The ansa cervicalis nerve is an efferent and partially afferent nerve that provides a source of multi-segmental innervation for the infrahyoid muscles to ensure laryngeal stability and excursion during phonation and deglutition (Chhetri and Berke 1997; Khaki et al. 2006). Branches from the ansa cervicalis may occasionally descend into the thorax and join the cardiac and phrenic nerves, and therefore participate in the innervation of the heart, pericardium, and diaphragm (Paviraev and Chernikov 1967). Although the nature of these neural fibers has not been explored, they most likely represent postganglionic sympathetic fibers that have joined ansa cervicalis or its roots proximally. The ansa cervicalis may also communicate with the trunk of the vagus nerve or provide an accessory phrenic nerve (Indrasingh et al. 1999). The superior root may rarely originate from the vagus nerve or sympathetic trunk (Piersol 1911). The inferior root is subject to considerable variation in its origin, composition, and course (Caliot et al. 1986; Khaki et al. 2006). Despite the asymmetry of the right and left ansa cervicalis, Caliot et al. (1986) distinguished seven morphologic forms of this loop with respect to the composition of the inferior root from the primary cervical ventral rami, with the most common form being a C2–3 composite (74%). Absence of the inferior root has been reported with a frequency of 3% (Chhetri and Berke 1997). The course and location of the ansa cervicalis along the great vessels of the neck, as well as its regional branching pattern, also show extensive variations (Chhetri and Berke 1997). The ansa cervicalis may also send branches to the spinal accessory nerve in the neck (Brown 2002).

In cases with a vagocervical complex where the proper ansa cervicalis is not seen, the branches from the vagus nerve are found to supply the infrahyoid muscles and can be traced back into the cervical nerve roots. In contrast, despite resembling and replacing the ansa cervicalis, a pseudo ansa cervicalis does not

send muscular branches to the infrahyoid muscles (Indrasingh et al. 1999). Rarely, the inferior root of the ansa cervicalis may be replaced by long fibers from the extra-cranial part of the spinal accessory nerve (Khaki et al. 2006; Fig. 87.3c). The superior root may originate from the vagus nerve rather than the hypoglossal nerve (Vollala et al. 2005). Figure 87.3 shows three possible variants of neural connections replacing the classic ansa cervicalis.

Accessory nerve to cervical nerve anastomoses

Intradural part

As the spinal accessory nerve ascends intradurally through the vertebral canal, it is located in the vicinity of the anterior and posterior rootlets of the upper four cervical nerves (Kumaki 1970; Moriishi et al. 1989; Weigner 1901). Four types of intradural communication between the first cervical nerve rootlets/root and the spinal accessory nerve have been described by Ouaknine and Nathan (1973) and Hagenah et al. (1983). Collectively, type I constituted 57/250 of cases in which the posterior C1 root is absent and the spinal accessory nerve is occasionally connected to the anterior C1 rootlets/root. Type II variant (39/250) has no communication with the posterior C1 nerve root. In type III (84/250), anastomosis occurs between the accessory and the posterior C1 rootlets/root either at their crossing point or through a posterior C1 rootlet/root anastomotic branch. In type IV variant (70/250), the accessory nerve anastomoses with a posterior C1 root that has no connection with the spinal cord. In the type I and IV variants, sensory fibers from the posterior C1 root travel caudally through the spinal accessory nerve rootlet to enter the spinal cord through the posterior C2 rootlets (Ouaknine and Nathan 1973). While the sensory fibers have to course centrally through the posterior C1 root in type II variants, in type III variants these may pass through either the spinal accessory nerve or the posterior C2 rootlets. Surprisingly, the anastomosis between the accessory nerve and the posterior C1 nerve rootlets/root has been reported to be more frequent in patients with spasmodic torticollis (Freckmann and Hagenah 1986).

Although cervical dorsal nerve rootlet/root connections to the intradural accessory nerve are well described, very rarely, spinal accessory nerve rootlets may replace an absent cervical dorsal nerve root at upper cervical spinal levels. Such variants may reflect a focal developmental alteration in the pathway of neural crest cells (Streeter 1904; Wetmore and Elde 1991).

Extradural part

The extradural communications between the spinal accessory nerve and the cervical plexus have been investigated by Brown et al. (2000). In addition to interlacing with the C2 and C3 branches before or within the sternocleidomastoid muscle, these authors found that the spinal accessory nerve receives, in all specimens, a communicating branch from the great auricular nerve upon its emergence from the posterior border of this muscle. The term "spinal accessory nerve plexus" has been used to denote the communications between the spinal accessory nerve and branches from other lower cranial and upper cervical nerves (Brown et al. 1988; Brown 2002). Such a contribution of the C2–3 nerve roots to the spinal accessory nerve plexus also occurs within the posterior triangle of the neck (Williams and Warwick 1990). Branches from the brachial plexus, phrenic, and transverse cervical nerves may likewise join the spinal accessory nerve before entering the underside of the trapezius muscle (Brown et al. 1988, 2000; Brown 2002). The spinal accessory nerve may occasionally be absent, in which case the trapezius muscle is solely supplied by the cervical spinal nerve branches (Piersol 1911).

Autonomic anastomoses to lower cranial nerves

Brown (2002) reported branches of the stellate ganglion that join the cervical nerves in a network including the spinal accessory nerve. The deep petrosal nerve consists of postsynaptic sympathetic fibers derived from neuronal cell bodies found in the superior cervical ganglion. Just posterior to the sphenoid bone, the deep petrosal nerve travels through the cartilage (it travels superior to this cartilage, according to Piersol 1911) filling the foramen lacerum to join with the greater petrosal nerve to form the nerve of the pterygoid canal (vidian nerve), which traverses the pterygoid canal (vidian canal).

The jugular nerve is a communicating branch between the superior cervical ganglion of the sympathetic nerve, the superior ganglion of the vagus nerve, and the inferior ganglion of the glossopharyngeal nerve (Rouvière 1959; Pegington 1986). The hypoglossal nerve may occasionally communicate with the cervical sympathetic chain, vagus, lingual, or phrenic nerves (Bourgery and Jacob 1831; Gray 1918; Drummond 1988; Lang 1989; Abu-Hijleh 2005).

References

Abu-Hijleh MF. 2005. Bilateral absence of ansa cervicalis replaced by vagocervical plexus: case report and literature review. *Ann Anat* 187: 121–125.

Bergman RA, Afifi AK, Miyauchi R. 2006. Illustrated Encyclopedia of Human Anatomic Variation. Available at: http://www.anatomyatlases.org/AnatomicVariants/AnatomyHP.shtml (accessed 19 November 2015).

Bourgery JM, Jacob NH. 1831. *Atlas of Human Anatomy and Surgery (Atlas d'Anatomie Humaine et de Chirurgie)*. London: Taschen.

Brown H. 2002. Anatomy of the spinal accessory nerve plexus: relevance to head and neck cancer and atherosclerosis. *Exp Biol Med* 227: 570–578.

Brown H, Burns S, Kaiser CW. 1988. The spinal accessory nerve plexus, the trapezius muscle, and shoulder stabilization after radical neck cancer surgery. *Ann Surg* 208: 654–661.

Brown H, Hidden G, Ledroux M, Poitevan L. 2000. Anatomy and blood supply of the lower four cranial and cervical nerves: Relevance to surgical neck dissection. *Proc Soc Exp Biol Med* 223: 352–361.

Caliot P, Dumont D, Bousquet V, Midy D. 1986. A note on the anastomoses between the hypoglossal nerve and the cervical plexus. *Surg Radiol Anat* 8: 75–79.

Canning BJ. 2006. Anatomy and neurophysiology of the cough reflex: ACCP evidence-based clinical practice guidelines. *Chest* 129(1Suppl): 33–47.

Chhetri DK, Berke GS. 1997. Ansa cervicalis nerve: review of the topographic anatomy and morphology. *Laryngoscope* 107: 1366–1372.

Cruveilhier J. 1844. *The Anatomy of the Human Body*. New York: Harper & Brothers.

de Caro R , Parenti A, Munari PF. 1995. Course of the caudal hypoglossal rootlet through the vertebral artery. *J Anat* 187 (Pt 2): 499–501.

De Castro F. 2009. The discovery of sensory nature of the carotid bodies. In *Arterial Chemoreceptors: Volume 648 of Advances in Experimental Medicine and Biology* (eds C Gonzalez, CA Nurse, C Peers). London: Springer, pp. 1–18.

Drummond PD. 1988. Autonomic disturbances in cluster headache. *Brain* 111: 1199–1209.

Freckmann N, Hagenah R. 1986. Relationship between the spinal accessory nerve and the posterior root of the first cervical nerve in spasmodic torticollis and common autopsy cases. *Zent bl Neurochir* 47: 134–138.

Furlan JC, Brandão LG, Ferraz AR. 2002. Prevalence of Galen's anastomosis: an anatomical and comparative study. *J Laryngol Otol* 116: 823–825.

Fuse S. 1950. On the so-called intercarotid plexus; a macroscopical study on 56 Japanese cadavers. *Folia Psychiatr Neurol Jap* 4: 1–11.

Ghanbari AA, Ayoubian A, Niknafs B, Khaki AA. 2007. A case report of hypoglossal and vagus nerves constituted a common trunk in the sheath of carotid. *Medical Journal of Gilan University of Medical Sciences* 16: 120–124.

Gonzalez-Compta X, Domenech-Mateu JM. 1996. Anastomosis between both hypoglossal nerves in a 30 mm human embryo. *Anat Embryol (Berl)* 193: 205–207.

Gray H. 1918. *Anatomy of the Human Body*. Philadelphia: Lea & Febiger.

Gupta D, Verma S, Vishwakarma SK. 1986. Anatomic basis of Arnold's ear-cough reflex. *Surg Radiol Anat* 8: 217–220.

Hagenah R, Kosak M, Freckmann N. 1983. Anatomic topographical relationship of the intraspinal accessory root to the upper cervical roots and to the vessels of the cranial cervical region. *Acta Anat* 115: 158–167.

Hovelacque A. 1927. *Anatomie des Nerfs Craniens et Rachidiens et du Systéme Grand Sympatique chez l'Homme, volume 1*. Paris: Gaston Doin et Cie Editeurs.

Indrasingh I, Abraham S, Vettivel S, Chandi G. 1999. A rare vagal origin of the superior root of ansa cervicalis: a case report. *J Anat Soc India* 48: 6–8.

Islam S, Walton GM, Howe D. 2012. Aberrant anatomy of the hypoglossal nerve. *J Laryngol Otol* 126: 538–40.

Jackson CM. 1921. *Morris's Human Anatomy: A Complete Systematic Treatise by English and American Authors, sixth edition*. Philadelphia: P. Blakiston's Son & Co.

Katsuta T, Rhoton AL Jr, Matsushima T. 1997. The jugular foramen: microsurgical anatomy and operative approaches. *Neurosurgery* 41: 149–201.

Kawai K, Kodama K, Okamoto K. 1989. Proximal communication between the glossopharyngeal and facial Nerves. *Acta Anat* 134: 151–155.

Khaki AA, Shokouhi G, Shoja MM, Farahani RM, Zarrintan S, Khaki A. 2006. Ansa cervicalis as a variant of spinal accessory nerve plexus: a case report. *Clin Anat* 19: 540–543.

Kumaki K. 1970. The cervical and the spinal accessory nerves. An account by means of fibre analysis. *Acta Anat Nippon* 45: 311–344.

Landois L. 1904. *Textbook of Human Physiology, including Histology and Microscopical Anatomy with especial reference to the Practice of Medicine*. Philadelphia: P. Blakiston's.

Lang J. 1989. *Clinical anatomy of the nose, nasal cavity and paranasal sinuses*. Stuttgart: Georg Thieme Verlag.

Merchant SN, Nadol JB. 2010. *Schuknecht's pathology of the Ear. Shelton*: People's Medical Publishing House.

Moriishi J, Otani K, Tanaka K, Inoue SI. 1989. The intersegmental anastomoses between spinal nerve roots. *Anat Rec* 224: 110–116.

Naidu L, Ramsaroop L, Partab P, Satyapal KS. 2012. Galen's "anastomosis" revisited. *Clin Anat* 25: 722–728.

Olry R. 1995. *Dictionary of Anatomical Eponyms*. New York: Verlag.

Ouaknine G, Nathan H. 1973. Anastomotic connections between the eleventh nerve and the posterior root of the first cervical nerve in humans. *J Neurosurg* 38: 189–197.

Paviraev NP, Chernikov YF. 1967. Anatomy of the ansa cervicalis. *Excerpta Medica* 21: 219.

Pegington J. 1986. *Clinical Anatomy in Action. 2: The Head and Neck*. Edinburgh: Churchill Livingstone.

Piersol GA. 1911. *Human Anatomy*. Philadelphia: J.B. Lippincott.

Platzer W. 1959. Eine transmediane Anastomose der beiden Nn. hypoglossi. *Arch Psychiatr Z Ges Neurol* 199: 372–376.

Rath G, Anand C. 1994. Vagocervical complex replacing an absent ansa cervicalis. *Surg Radiol Anat* 16: 441–443.

Rouvière H. 1959. *Anatomie Humaine. Nerfs de la tête et du cou, eighth edition*. Paris: Masson et Cie.

Salame K, Masharawi Y, Rochkind S, Arensburg B. 2006. Surgical anatomy of the cervical segment of the hypoglossal nerve. *Clin Anat* 19: 37–43.

Sañudo JR, Maranillo E, León X, Mirapeix RM, Orús C, Quer M. 1999. An anatomical study of anastomoses between the laryngeal nerves. *Laryngoscope* 109: 983–987.

Saraswathi P. 2003. Communication between the vagus and hypoglossal nerves. *Eur J Anat* 7: 131–134.

Schauber MD, Fontenelle LJ, Solomon JW, Hanson TL. 1997. Cranial/cervical nerve dysfunction after carotid endarterectomy. *J Vasc Surg* 25: 481–487.

Sharpey-Schäfer EA, Symington J, Bryce TH. (eds) 1909. *Quain's Elements of Anatomy, Volume 3,* Part 2, 11th edition. New York: Longmans, Green and Co.

Shin DS, Bae HG, Shim JJ, Yoon SM, Kim RS, Chang JC. 2012. Morphometric study of hypoglossal nerve and facial nerve on the submandibular region. *J Korean Neurosurg Soc* 51: 253–261 (in Korean).

Shoja MM, Oyesiku NM, Shokouhi G, Griessenauer CJ, Chern JJ, Rizk EB, Loukas M, Miller JH, Tubbs RS. 2014. A comprehensive review with potential significance during skull base and neck operations, Part II: glossopharyngeal, vagus, accessory, and hypoglossal nerves and cervical spinal nerves 1–4. *Clin Anat* 27: 131–144.

Song P, Schwartz JS, Gacek RR, Malmgren LT, Blitzer A. 2009. Peripheral laryngeal motor innervation. In: *Neurologic Disorders of the Larynx* (eds A Blitzer, MF Brin, LO Ramig). New York: Thieme.

Streeter GL. 1904. The development of the cranial and spinal nerves in the occipital region of the human embryo. *Am J Anat* 4: 83–116.

Swan J. 1834. *A Demonstration of the Nerves of the Human Body*. London: Longman.

Tekdemir I, Aslan A, Elhan A. 1998. A clinic-anatomic study of the auricular branch of the vagus nerve and Arnold's ear-cough reflex. *Surg Radiol Anat* 20: 253–257.

Testut L. 1902. *Tratado de Anatomia Humana, Tomo Tercero, Sexta Edicion*. Barcelona: Salvat.

Toldt C. 1907. *Anatomischer Atlas für Studierende und Ärzte, Volum 6*. Berlin/Wien: Urban & Schwarzenberg.

Toorop RJ, Scheltinga MR, Moll FL, Bleys RL. 2009. Anatomy of the carotid sinus nerve and surgical implications in carotid sinus syndrome. *J Vasc Surg* 50: 177–182.

Tubbs RS, Mortazavi MM, Loukas M, Shoja MM, Cohen-Gadol AA. 2011. Intraoperative and anatomical descriptions of intracranial connections between the glossopharyngeal and vagus nerves: clinical implications. *J Neurosurg* 115: 179–181.

Turner W. 1893. A phrenic nerve receiving a root of origin from the descendens hypoglossi. *J Anat Physiol* 27: 427.

Vollala VR, Bhat SM, Nayak S, Raghunathan D, Samuel VP, Rodrigues V, Mathew JG. 2005. A rare origin of upper root of ansa cervicalis from vagus nerve: a case report. *Neuroanatomy* 4: 8–9.

von Luschka H. 1867. *Die Anatomie des Menschlichen Kopfes in Rücksicht auf die Bedürfnisse der Praktischen Heilkunde. Tübingen*: Verlag Der H.H. Laupp'schen Buchhandlung.

Weigner K. 1901. Beziehungen des nervus accessorius zu den proximalen spinalnerven. *Arb Anat Inst Wiesbaden* 17: 549–587.

Wetmore C, Elde R. 1991. Detection and characterization of a sensory microganglion associated with the spinal accessory nerve: a scanning laser confocal microscopic study of the neuron and their processes. *J Comp Neurol* 305: 148–163.

Williams PL, Warwick R. 1990. *Gray's Anatomy*, 36th edition. Churchill, Livingstone: Oxford.

Further reading

Brennan PA, Al Gholmy M, Ounnas H, Zaki GA, Puxeddu R, Standring S. 2010. Communication of the anterior branch of the great auricular nerve with the marginal mandibular nerve: A prospective study of 25 neck dissections. *Br J Oral Maxillofac Surg* 48: 431–433.

Buchanan AM. 1917. *Human Anatomy, volume 3*, 3rd edition. St. Louis: Mosby.

Foerster O. 1933. The dermatomes in man. *Brain* 56: 1–39.

Freeman W. 1935. Motor and sensory overlap in the spinal roots. *Ann Surg* 101: 133–137.

Hansen JT, Benninger B, Brueckner JK, Carmichael SW, Granger NA, Tubbs RS. 2011. *Netter's Atlas of Human Anatomy, fifth edition*. Philadelphia: Saunders.

Kierner AC, Zelenka I, Burian M. 2001. How do the cervical plexus and the spinal accessory nerve contribute to the innervation of the trapezius muscle? As seen from within using Sihler's stain. *Arch Otolaryngol Head Neck Surg* 127: 1230–1232.

Kopf-Maier P. (ed) 2004. Wolf-Heidegger's Color Atlas of Human Anatomy. New York: Sterling Publishing Company, Inc.

Morris H, Lond MB. (eds) 1893. *Human Anatomy*. Philadelphia: P. Blakiston, Son & Co.

Pearson AA. 1937. The spinal accessory nerve in human embryos. *J Comp Neurol* 68: 243–266.

Quain R, Sharpey W. (eds) 1849. *Quain's Human Anatomy, Volume 2*. Philadelphia: Lea and Blanchard.

Reichman EF, Simon RR. 2004. *Emergency Medicine Procedures*. New York: McGraw-Hill.

Sappey PC. 1872. *Traité d'Anatomie Descriptive, Volume 3: Névrologie-Organes des Sens*. Paris: Delahaye.

Sobotta J. 1907. *Atlas and Text-book of Human Anatomy, Volume 3*. Philadelphia and London: W.B. Saunders Company.

Standring S. 2005. *Gray's Anatomy*, 39th edition. London: Churchill Livingstone.

Tubbs RS, Loukas M, Yalçin B, Shoja MM, Cohen-Gadol AA. 2009. Classification and clinical anatomy of the first spinal nerve: surgical implications. *J Neurosurg Spine* 10: 390–394.

Tubbs RS, Shoja MM, Loukas M, Lancaster J, Mortazavi MM, Hattab EM, Cohen-Gadol AA. 2011. Study of the cervical plexus innervation of the trapezius muscle. *J Neurosurg Spine* 14: 626–629.

Tubbs RS, Mortazavi MM, Loukas M, D'Antoni AV, Shoja MM, Cohen-Gadol AA. 2011. Cruveilhier plexus: an anatomical study and a potential cause of failed treatments for occipital neuralgia and muscular and facet denervation procedures. *J Neurosurg* 115: 929–933.

88 Autonomic nervous system

Paul Anthony Irwin[1], R. Isaiah Tubbs[1] and R. Shane Tubbs[2]
[1]Children's of Alabama, Birmingham, Alabama, United States
[2]Seattle Science Foundation, Seattle, Washington, USA
St George's University, School of Medicine, St Georges, Grenada
University of Dundee, Dundee, UK

Sympathetic trunk

The sympathetic trunk commonly has communications with lower cranial nerves at the skull base, but rarely communicates with the glossopharyngeal nerve. Communicating branches between the cervical sympathetic trunk and the ansa cervicalis are variable. In one study, the following patterns were noted. Communicating branches were found (a) between the superior cervical ganglion and superior root of the ansa cervicalis; (b) joining C2 and C3; and (c) variably joining the connecting loop between C2 and C3. The sympathetic chain on the left side may split and encircle the subclavian artery. The two sympathetic trunks may communicate across the midline, especially in the lumbar region. The sympathetic chain has been found terminating at the level of the second sacral nerve (Fawcett 1895). In the region of the middle cervical ganglion, the trunk may lie posterior to the inferior thyroid artery and bifurcated in this region with the inferior thyroid artery lying between the two parts (Piersol 1916). Caliot (1984) reported that the sympathetic and recurrent laryngeal nerve anastomoses occurred in 63% of specimens (19 out of 30) on the right side. Among those, the anastomoses are direct and form an ansa around the subclavian artery in 23% (7 out of 30) of the specimens. More frequently (40%, 12 out of 30), the anastomoses occur superior to the arch of the subclavian artery and in close relationship to the common carotid artery. Among those, in 4 samples the connection originates from the sympathetic chain and the other 8 samples originated from the inferior cervical ganglion. On the left side the anastomoses occurred in 60% of the specimens (18 out of 30); none of them formed loops around the subclavian artery due to a separated origin of the common carotid and subclavian arteries. Most of the anastomoses are located superior to the subclavian artery on the left side and originate from the inferior cervical ganglion (57%, 17 out of 30). In 2 out of 30 cases, the anastomoses originated from the ansa subclavia and were located inferior to the subclavian artery. In addition, Caliot (1984) also described how a direct anastomosis occurs at a low frequency (8%, 5 out of 60) between the trunk of the vagus nerve and ansa subclavia and cervical sympathetic trunk at the level of the subclavian artery. The chain may communicate with the phrenic nerve in up to 47% of the cases (Caliot 1984). Gandhi et al. (2013) found that the sympathetic trunk traversed dorsal to the crus of diaphragm in 72.6% of cases; in 13.3%, it entered dorsal to the medial arcuate ligament.

Sympathetic ganglia

The ganglia of the sympathetic trunk vary in size over the range 6 mm to 6 cm (Hollinshead 1956). Kiray et al. (2005) found the superior, middle, and inferior (or cervicothoracic) ganglia in 20.8% of specimens; superior and inferior (or cervicothoracic) ganglia in 45.8%; superior, middle, vertebral, and inferior (or cervicothoracic) ganglia in 12.5%; and superior, vertebral, and inferior (or cervicothoracic) ganglia in 20.8% of specimens. The superior ganglion was observed in all specimens, and the middle ganglion and vertebral ganglion were each observed in 33.3%. In one fetus, Than and Dharap (1996) found only two cervical ganglia on left and right sides. All cervical ganglia may be fused as a long slender ganglionic mass.

Superior cervical ganglion

The superior cervical ganglion may be fused with the middle cervical ganglion (Bhatnagar et al. 2003). The internal carotid nerve may connect to the glossopharyngeal nerve (Müller and Rude 2000). Lang (1989) mentioned that the

Bergman's Comprehensive Encyclopedia of Human Anatomic Variation, First Edition. Edited by R. Shane Tubbs, Mohammadali M. Shoja and Marios Loukas.
© 2016 John Wiley & Sons, Inc. Published 2016 by John Wiley & Sons, Inc.

superior cervical ganglion can be duplicated and that there may be ganglion cells along twigs extending intracranially from this structure.

Inferior cervical ganglion

The inferior cervical ganglion is irregular in shape and usually larger than the middle ganglion. It is frequently combined with the first thoracic and is named the stellate (cervicothoracic) ganglion. A direct communication to the phrenic nerve is often derived from the inferior ganglion, less frequently from the middle cervical ganglion. The inferior cervical ganglion may fuse not only with the first thoracic but also the second thoracic ganglia (Pick and Sheehan 1946).

Stellate ganglion

The inferior part of the stellate ganglion is in close contact with the cervical pleura and may connect with the phrenic nerve. This phrenic-stellate anastomosis, varying in size, often doubled or tripled and sometimes plexiform, is situated between the subclavian artery and the anterior side of the pleural dome. This classic description of multiple anastomosis between the phrenic nerve and stellate ganglion is contradicted by Caliot's (1984) study, in which 47% of specimens displayed the phrenic-stellate anastomosis where the majority of them have only single nerve cord. In Caliot's (1984) report, only 30% (18 out of 60) of connections fit the classic description in which the anastomosis courses underneath the subclavian artery and forms a loop around it. In the other 28% (17 out of 60), it traveled superior to the subclavian artery.

Middle cervical ganglion

The sympathetic plexus in the region of the middle cervical ganglion may be posterior to the inferior thyroid artery or may be bifurcated, with the artery lying between the two trunks. The middle cervical ganglion may be absent, in which case the middle cardiac nerves are carried in the interganglionic chain. When there are two ganglia, the upper (usually smaller) part is called the middle cervical ganglion of Arnold (or Luschka) or the thyroid ganglion of Krause, and the larger lower part is called the middle cervical ganglion of Swan (or Krause) or the inferior cervical ganglion of Arnold (Luschka or Rüdinger). The middle cervical ganglion may communicate with the phrenic nerve. According to Allan (1958), in cases of retroesophageal right subclavian artery, the sympathetic (middle and inferior) cardiac nerves follow the vessel in its course to reach the cardiac plexus. Thompson (1884) recorded a case of right retro-esophageal subclavian artery, where the right middle cervical ganglion formed a ring of ganglioniform enlargements through which the vertebral artery traversed prior to entering the transverse foramen of the fourth cervical vertebra.

Thoracic sympathetic ganglia

Adjacent thoracic ganglia may fuse (Pick and Sheehan 1946). Thoracic ganglia may give off two–three or, rarely, four branches to each corresponding nerve. The ganglia may provide a branch to the next inferior spinal nerve (Pick and Sheehan 1946). Additional ganglia of the thoracic sympathetic chain may be present. The first thoracic ganglion is usually larger than the others and is variable in shape (ovoid or semilunar). It may be fused with the inferior cervical (stellate) or second thoracic ganglion.

Singh et al. (2005) found that the second thoracic ganglion was commonly located (92.5%) in the second intercostal space at the level of the intervertebral disc between the second and third thoracic vertebrae. Fused ganglia between the second thoracic and first thoracic (5%) and stellate (5%) ganglia were noted.

Lumbar sympathetic ganglia

Although there are usually four lumbar ganglia, the number may vary from three to eight. The most constant and usually largest of these ganglia is the ganglion located on the second lumbar vertebra. When there are fewer than four ganglia they tend to be larger than usual. There may be up to six lumbar ganglia. The ganglia may all fuse to form a single elongated ganglionic mass (Pick and Sheehan 1946).

Sacrococcygeal sympathetic ganglia

The sacral ganglia vary greatly in size and number, but there are usually four. Variations in size and number of ganglia are greater in the sacral region than in the thoracic and lumbar regions. The number of sacral ganglia usually ranges between three and five (Fawcett 1895). A single median terminal ganglion (ganglion impar or coccygeal ganglion) is often found at the distal end of the sympathetic chain of ganglia on the proximal part of the coccyx. Fawcett (1895) reported this ganglion in 60% of cases. A study by Oh et al. (2004) revealed variable locations of the ganglion impar along the midline of the coccyx, with some ganglia lying in front of the sacrococcygeal junction and others only 10 mm from the tip of the coccyx. Furthermore, Agarwal-Kozlowski et al. (2009) reported that only 18% of these ganglia lie at the level of the sacrococcygeal junction. The shape and size of the ganglion impar have been found to be variable. Oh et al. (2004) reported the two most common shapes as oval (26%) and irregular (20%). Other shapes included triangular

(14%), elongated (10%), rectangular (8%), and U-shaped (8%). In the remaining 14%, the two caudal ends of the sympathetic chains converged with no discernable ganglion. In addition, the diameters of all shapes excluding the elongated ganglia ranged over 0.7–4.2 mm, with the average elongated ganglia measuring 4.4 mm in length (Oh et al. 2004).

Small "intermediate" ganglia have been reported on the ventral roots and rami communicantes (Mitchell 1953; Pick and Sheehan 1946). These are most commonly identified on gray rami in the cervical and lower lumbar regions. For nerves, they are most commonly found on the third and fourth cervical nerves and the rami attached to them. The peak region where these ganglia are found is in the upper lumbar region. The ganglia may be micro- or macroscopic.

Ansa subclavia

The ansa is usually single on the left side but on the right side it is most often composed of two–five filaments. Caliot et al. (1984) reported that the ansa subclavia existed in 83% of 60 cadeveric specimens. In 32% (19 out of 60) of specimens a single cord existed, in 28% of specimens a double cord existed, and in 13% and 10% of specimens triple and quadruple cords existed, respectively. On the left side, 57% of the ansa subclavia (17 out of 30) contained more than two nerve cords compared to 47% of the ansa subclavia on the right side (14 out of 30). The right side has more nerve cords in total compared to the left sides (54 vs 47).

In addition to the anatomical heterogeneity of the number of cords in the ansa subclavia, there appears to be variation in the origin and termination of the loops. Paturet (1965) classified three types of variations according to the origin and termination of the loop: (1) a short loop on the nerve devoid of the middle cervical ganglion; (2) a short loop with a middle cervical ganglion situated more or less low down; (3) a long loop originating from the superior cervical sympathetic ganglion or form the immediately adjacent sympathetic chain.

Rami communicans

The upper two cervical nerves received two or three and occasionally four rami from the superior cervical ganglion. The ramus to C3 often forms a loop with a lower ramus from the sympathetic chain, and from this loop fine branches may pass to C3 and sometimes to C4. In about half the cases, C8 was omitted from the distribution of the superior cervical ganglion and forms its only connection with the cervical sympathetic chain lower down; it may receive no apparent sympathetic connection at all (Pick and Sheehan 1946). The middle cervical ganglion may give off two–three rami to adjacent spinal nerves. The inferior cervical/stellate ganglion may give off two–eight rami to adjacent nerves.

Superior cardiac nerve

The superior cardiac nerve (a branch from the superior cervical ganglion) may be absent, particularly on the right side. In such cases, it is replaced by a branch from the vagus or from the external laryngeal nerve. The nerve may not have a separate course, but may be a part of another cardiac nerve from one of the other cervical ganglia. A pretracheal branch arising from the communication between the superior cardiac nerve and the recurrent laryngeal nerve has been reported. It descends on the trachea and terminates in the pericardium and anterior pulmonary plexus.

Cardiac plexus

The nerves that supply the heart usually converge anteriorly toward the lower part of the trachea but may be followed separately to the heart. Cardiac ganglia, varying in size and number, may occur along the cervicothoracic nerves that supply the aorta, pulmonary trunk, and arteries as well as the heart. Pather et al. (2003) found that the superior cervical cardiac ramus originated from the superior cervical ganglion in 53% of cases. The middle cervical ganglion gave rise to the middle cervical cardiac ramus in 88% of cases. The cervicothoracic ganglion gave rise to the cervicothoracic cardiac ramus in 84% of cases.

Splanchnic nerves

Greater splanchnic nerve

The greater splanchnic is usually formed from the seventh, eighth, and ninth thoracic ganglia, but the upper and lower limits are variable. Edwards and Baker (1940) found that the nerve arises symmetrically in only 12% of bodies (100 cadavers). So-called normal nerves (T7–T9) occurred in 23%; only 9% of these were symmetric bilaterally. A study of six adult and 14 fetal cadavers by Naidoo et al. (2001) looked further at the anatomical variation of the splanchnic nerves. They reported the greater splanchnic nerve to be present in all cases, with an origin between T6 and T9 73% of the time. In addition to frequency and origin of the greater splanchnic nerve, these authors noted that the number of roots contributing to the nerve varied between three and ten, with the widest example being from T4–T11 and the narrowest from T5–T7. Stone and Chauvin (1990) reported that 36.8% of greater splanchnic nerves originated above the T5 ganglion. Groen et al. (1987) found the greater splanchnic nerve arising from one–four large branches, most frequently from the T8–T9 ganglia and as high as T6. The group also reported the lowest contribution from T11, initially proposed by Hollinshead (1956) to be as low as the T12 ganglia. The roots of the greater thoracic splanchnic nerve rarely converge all at once,

but instead the upper roots tend to converge before joining the lower roots.

Lesser splanchnic nerve

The nerve may be absent (7% on the right side, 2% on the left, and 2% bilaterally). It is usually formed from the tenth and eleventh thoracic ganglia. The nerve arises symmetrically in 35% of bodies (Edwards and Baker 1940). "Normal" nerves (T10–T11) occurred in 14% of subjects; only 1% of these were symmetric bilaterally. Naidoo et al. (2001) found the lesser splanchnic nerve present in 92% of cases, with an origin from T10–T11 29% of the time. Edwards and Baker (1940) noted the origin of the lesser splanchnic nerve as high as T7, albeit commonly originating between T10 and T11. Reed (1943) reported that the majority of lesser splanchnic nerves originate from T9–T12. Furthermore, Reed documented the least splanchnic nerve arising from the T11, T12 or both ganglia at the same time, while Jit and Mukerjee (1960) found the least splanchnic nerve arising from a single nerve root in 37% of cases.

It is not uncommon for the fibers of the lower splanchnic nerve to join the greater splanchnic nerve and travel as one bundle through the diaphragm and into the abdomen. At the junction of its roots, the lesser splanchnic nerve may contain a ganglion known as the ganglion of Sperino.

Least (lowest) splanchnic nerve

This nerve may be absent (11% on the right side and 4% on the left side). The splanchnicus imus usually arises from the twelfth thoracic ganglion. It may be absent bilaterally in 2% of bodies. When absent, the lesser splanchnic supplies the renal plexus. The nerve arises symmetrically in 79% of bodies. "Normal" nerves were found in 92% of bodies and were symmetric in 77% of the specimens examined by Edwards and Baker (1940). Naidoo et al. (2001) found the least splanchnic nerve present in 55% of cases, with an origin from T11–T12 in 14%. This nerve may join the lesser splanchnic nerve.

Accessory splanchnic nerve

A fourth or accessory splanchnic nerve may be found in 4% of cases with a course and termination similar to the least splanchnic nerve. This may or may not be the same nerve as the nerve of Sousa Pereira.

Supreme splanchnic nerve

Wrisberg observed a supreme splanchnic nerve eight times in a "large number" of bodies. It was described as being formed by branches from cardiac nerves, and from lower cervical and upper thoracic ganglia.

The phrenic plexus, a collection of nerves derived from branches of the celiac ganglia and vagus nerves, travels with the inferior phrenic arteries and is disseminated by these vessels to the diaphragm, parietal peritoneum, adrenal gland, inferior vena cava, and esophagus and gastroesophageal junction. The right phrenic plexus communicates at the foramen for the vena cava with the right phrenic nerve and a small ganglion may be seen at this location. Some of the lumbar splanchnics, especially the more inferior branches, have a propensity to travel posterior to the common iliac arteries.

Celiac ganglion

Ward et al. (1979) examined 20 autopsied adult bodies and found that the celiac ganglia vary in diameter over the range 0.5–4.5 cm, in number from one to five, and in location from the middle of L2 to the intervertebral disc between T12 and L1. Zhang et al. (2006) reported that celiac ganglia were at the level of T12 or L1 in 94% of the 65 cadavers studied.

External carotid plexus

A ganglion (so-called temporal ganglion) is sometimes found as a part of the external carotid artery plexus near the point of origin of the posterior auricular artery. It may be about 2 mm in length. It has been reported to receive nerve fibers from the stylohyoid branch of the facial nerve. An intercarotid ganglion known as Arnold's ganglion may be found.

Parasympathetic ganglia

Some comments regarding the parasympathetic ganglia are made in Chapter 83 devoted to the cranial nerves. The autonomic fibers within these nerves are covered separately in this dedicated chapter.

Ciliary ganglion

This ganglion contains preganglionic nerves and postganglionic neurons of the oculomotor nerve. The ciliary ganglion is small and flat, about the size of a pinhead. It may be significantly diminished in size (Pearson and Pytel 1978). This ganglion may also be oval shaped, quadrilateral shaped, of irregular form, egg-shaped, or rectangular. It can measure 1–3 mm in diameter (Siéssere et al. 2008).

The following variations in the size and roots of this ganglion have been reported. It may be absent grossly, in which case its constituent neurons are scattered among the nerve fibers associated with the ganglion. The ganglion may be doubled or even tripled. An accessory ganglion along the inferior division of the oculomotor nerve is termed Antonelli's ganglion; other ectopic ganglia have been named after Axenfeld. An accessory ciliary ganglion located inferior to the optic nerve is known as the ganglion of Svitzer. The motor root, branch of the oculomotor nerve to the inferior oblique muscle, sometimes bifurcates before reaching the ganglion. The sympathetic root may enter

the ganglion separately or as part of the sensory root, or it may accompany the oculomotor nerve. Additional roots entering the ganglion have been described; these arise from the superior division of the oculomotor, trochlear, lacrimal, and abducens nerves and from the pterygopalatine ganglion. Girijavallabhan and Bhat (2008) found the ganglion located between the optic nerve and medial rectus muscle, and lateral to the ophthalmic artery.

The sensory root (branch of the ophthalmic nerve) may (a) be absent or multiple, in which case the sensory fibers from the nasociliary nerve are probably carried by the long ciliary nerves to the eyeball; or (b) arise directly from the semilunar (trigeminal) ganglion, the trunk of the ophthalmic nerve, or the supraorbital or lacrimal nerves. The ciliary ganglion has been found to be perforated by a ciliary artery.

Otic ganglion

Siéssere et al. (2008) found that the otic ganglion was an oval structure, measuring 3.5–4.5 mm in length, 3 mm in width, and 1.5 mm in depth. It was observed that the otic ganglion was present in 18 infratemporal fossae (10 cadavers), having a structure similar to that of the classical description. In 13 ganglia, a connecting branch to the medial pterygoid muscle was evident and, in nine other ganglia, a small ramus to the sympathetic plexus of the middle meningeal artery was noted. In most infratemporal fossae, the ganglionic form was seen bilaterally (eight cadavers), although in two instances this form was seen unilaterally and only a small thickening was found on the contralateral side. This thickening on the medial aspect of the mandibular nerve was seen in two additional infratemporal fossae in two other cadavers.

The lesser petrosal nerve receives a communicating branch composed of fibers from the nervus intermedius and Arnold's nerve, from either the facial nerve at the geniculate ganglion (geniculotympanic nerve), distal to the geniculate ganglion, or from the greater petrosal nerve (Vidić and Young 1967). Ganglion cells may be found along the lesser petrosal nerve (Ogawa and Rutka 1999). The junction of the communicating branch with the lesser petrosal nerve has been observed to have three different patterns. A single communicating branch from the facial nerve distal to the geniculate ganglion, composed of fibers from the nervus intermedius and Arnold's nerve, is the predominate pattern observed. Two communicating branches to the lesser petrosal nerve, with the nervus intermedius branching from the geniculate ganglion and Arnold's nerve branching distal to the geniculate ganglion and joining the lesser petrosal nerve proximal to the nervus intermedius, is observed less frequently than the pattern described above. The third pattern is observed infrequently and is characterized by the same single communicating branch described above joining a meningeal branch of the mandibular division of the trigeminal nerve before the tympanic branch of the glossopharyngeal nerve joins to form the lesser petrosal nerve (Kakizawa et al. 2007). The geniculate ganglion may be connected to the tympanic branch of the glossopharyngeal nerve (Vidić 1968).

Pterygopalatine ganglion

The pterygopalatine ganglion may be rhomboidal, pear-shaped, semi-lunar, triangular, or fusiform in shape and has a length of 5–7 mm. Siéssere et al. (2008) found that the pterygopalatine ganglion was flat and had a diameter of 3–5 mm. The ganglion may be much diminished in size (Pearson and Pytel 1978). Rusu et al. (2009) found four morphological types of the pterygopalatine ganglion were defined macroscopically: A (10%): partitioned pterygopalatine ganglion, the upper partition receiving the vidian nerve; B (55%): single, the upper part (base) receiving the vidian nerve; C (15%): single, but the vidian nerve reaches the lower part (tip) of the ganglion; D (20%): partitioned, the lower partition receiving the vidian nerve. These authors concluded that the pterygopalatine ganglion can present either as a single ganglion or as a partitioned one, with distinct superior and inferior components. Furthermore, microganglia may be found along the branches of the pterygopalatine ganglion.

Submandibular ganglion

The submandibular ganglion has been found to be triangular, egg-shaped, or plexiform in shape. Siéssere et al. (2008) found that the ganglion was a fusiform structure 2–3 mm in diameter. These authors also found that, in 46.9% of specimens, the lingual nerve and the submandibular ganglion were fused. An accessory submandibular ganglion has been described as the ganglion of Langley.

Other

There may be a ganglion at this junction between the greater and deep petrosal nerves that is most likely parasympathetic in nature (Lang 1989). Ganglion cells may be found along the lesser petrosal nerve (Ogawa and Rutka 1999). Ganglion cells may also be found near the origin of the ophthalmic nerve and are known as the ganglia of Takeda. An accessory sympathetic ganglion has been found behind the external carotid artery as it gives rise to the posterior auricular artery, known as Scarpa's ganglion.

Pelvic splanchnic nerves

The pelvic splanchnics or nervi erigentes (erotic) are seen soon after their emergence from the anterior sacral foramina (S2–S4) and branch number varies over the range 3–10.

According to He et al. (2010), these parasympathetic nerve fibers of the pelvic plexus are most often derived from the S3 spinal nerve. Baader and Herrmann (2003) identified the pelvic splanchnic nerves originating primarily from the ventral ramus of S3 in 44 of 85 (52%) hemipelves; from the ventral ramus of S4 in 27 of 85 (32%) hemipelves; from S2 in 11 of 85 (12%); and primarily from the ventral ramus of S5 in 3 of 85 (4%) of hemipelves. According to Baader and Herrmann (2003), the contributions of the pelvic splanchnic nerves to the inferior hypogastric plexus were slightly different in females, with their origins mainly from either ventral ramus S3 (60%, 21 of 35 hemipelves) or S4 (37%, 13 of 35 hemipelves). The pelvic splanchnic nerve may run ventrally, horizontally, and even inferiorly, contrasting with the usual observations from dissection studies that described a ventrosuperior course of the pelvic splanchnic nerve along the sacrum (Tamakawa et al. 2003).

References

Agarwal-Kozlowski K, Lorke DE, Habermann CR, Esch JS, Beck H. 2009. CT-guided blocks and neuroablation of the ganglion impar (Walther) in perineal pain: anatomy, technique, safety, and efficacy. *Clin J Pain* 25: 570–576.

Allan FD. 1958. An analysis of the cervicothoracic visceral branches of the vagus and the sympathetic trunk in the presence of an anomalous right subclavian artery. *Anat Rec* 132: 71–80.

Baader B, Herrmann M. 2003. Topography of the pelvic autonomic nervous system and its potential impact on surgical intervention in the pelvis. *Clin Anat* 16: 119–130.

Bhatnagar KP, Nettleton GS, Kuwabara N, Wagner CE, Campbell FR. 2003. A case of bilateral ectopic superior cervical ganglia in man. *Ann Anat* 185: 149–152.

Caliot P. 1984. The nerve loops crossing below the subclavian artery and their anatomical variations. *Anatomia Clinica* 6: 209–213.

Edwards LF, Baker RC. 1940. Variations in the formation of the splanchnic nerves in man. *Anat Rec* 77: 335–342.

Fawcett E. 1895. An unusual mode and site of termination of the right sacral sympathetic cord. *J Anat Physiol* 29: 329.

Gandhi KR, Verma VK, Chavan SK, Joshi SD, Joshi SS. 2013. The morphology of lumbar sympathetic trunks in humans: a cadaveric study. *Folia Morphol* 72: 217–222.

Girijavallabhan V, Bhat KMR. 2008. Positional variation of the ciliary ganglion and its clinical relevance. *Neuroanatomy* 7: 38–40.

Groen GJ, Baljet B, Boekelaar AB, Drukker J. 1987. Branches of the sympathetic trunk in the human foetus. *Anat Embryol* 176: 401–411.

He JH, Wang Q, Cai QP, Dang RS, Jiang EP, Huang HL. 2010. Quantitative anatomical study of male pelvic autonomic plexus and its clinical potential in rectal resection. *Surg Radiol Anat* 32: 783–790.

Hollinshead WH. 1956. Anatomy for Surgeons: *The Thorax, Abdomen, and Pelvis, Vol 2*. New York: Hoeber Harper.

Jit I, Mukerjee RN. 1960. Observations of the anatomy of the human thoracic sympathetic chain and its branches; with an anatomical assessment of operations for hypertension. *J Anat Soc India* 9: 55–82.

Kakizawa Y, Abe H, Fukushima Y, Hongo K, El-Khouly H, Rhoton A. 2007. The course of the lesser petrosal nerve on the middle cranial fossa. *Neurosurgery* 61: 15–23.

Kiray A, Arman C, Naderi S, Guvencer M, Korman E. 2005. Surgical anatomy of the cervical sympathetic trunk. *Clin Anat* 18: 179–185.

Lang J. 1989. *Clinical Anatomy of the Nose, Nasal Cavity and Paranasal Sinuses*. Stuttgart: Georg Thieme Verlag.

Mitchell GAG. 1953. *Anatomy of the Autonomic Nervous System*. Edinburgh: E & S Livingstone LTD.

Müller T, Rude J. 2000. On a complex anastomosis of the glossopharyngeal nerve in humans. *Acta Anat Nippon* 75: 345–348.

Naidoo N, Partab P, Pather N, Moodley J, Singh B, Satyapal KS. 2001. Thoracic splanchnic nerves: implications for splanchnic denervation. *J Anat* 199: 585–590.

Ogawa T, Rutka J. 1999. The presence of ganglion cells in the human middle ear: a histological survey. *Acta Otolaryngol* 540: 38–41.

Oh CS, Chung IH, Ji HJ, Yoon DM. 2004. Clinical implications of topographic anatomy on the ganglion impar. *Anesthesiology* 101: 249–250.

Pather N, Partab P, Singh B, Satyapal KS. 2003. The sympathetic contributions to the cardiac plexus. *Surg Radiol Anat* 25: 210–215.

Paturet G. 1964. *Traite d'Anatomie Humaine*. Paris: Masson et Cie.

Pearson J, Pytel B. 1978. Quantitative studies of ciliary and sphenopalatine ganglia in familial dysautonomia. *J Neurol Sci* 39: 123–130.

Pick J, Sheehan D. 1946. Sympathetic rami in man. *J Anat* 80: 12–20.

Piersol D. 1916. *Human Anatomy*. Philadelphia: JB Lippincott.

Reed AF. 1943. The origins of the splanchnic nerves. *Anat Rec* 109: 341.

Rusu MC, Pop F, Curcă GC, Podoleanu L, Voinea LM. 2009. The pterygopalatine ganglion in humans: a morphological study. *Ann Anat* 191: 196–202.

Siéssere S, Vitti M, de Sousa LG, Semprini M, Mizusaki Iyomasa M, Cecílio Hallak Regalo S. 2008. Anatomic variation of cranial parasympathetic ganglia. *Braz Oral Res* 22: 101–105.

Singh B, Ramsaroop L, Partab P, Moodley J, Satyapal KS. 2005. Anatomical variations of the second thoracic ganglion. *Surg Radiol Anat* 27: 119–122.

Stone HH, Chauvin EJ. 1990. Pancreatic denervation for pain relief in chronic alcohol associated pancreatitis. *Br J Surg* 77: 303–305.

Tamakawa M, Murakami G, Takashima K, Kato T, Hareyama M. 2003. Fascial structures and autonomic nerves in the female pelvis: A study using macroscopic slices and their corresponding histology. *Anat Sci International* 78: 228–242.

Than M, Dharap AS. 1996. Variations in the formation of the cardiac plexus. A study in human foetuses. *Z Morphol Anthropol* 81: 179–188.

Thompson A. 1884. Variations of the thoracic duct associated with abnormal arterial distribution. *J Anat Physiol* 18: 416–425.

Vidić B. 1968. The origin and the course of the communicating branch of the facial nerve to the lesser petrosal nerve in man. *Anat Rec* 162: 511–516.

Vidić B, Young PA. 1967. Gross and microscopic observations on the communicating branch of the facial nerve to the lesser petrosal nerve. *Anat Rec* 158: 257–261.

Ward EM, Rorie DK, Nauss LA, Bahn RC. 1979. The celiac ganglion in man: Normal anatomic variations. *Anesth Analg* 58: 461–465.

Zhang XM, Zhao QH, Zeng NL, Cai CP, Xie XG, Li CJ, Liu J, Zhou JY. 2006. The celiac ganglia: Anatomic study using MRI in cadavers. *AJR* 186: 1520–1523.

Further reading

Anson BJ. 1950. *Atlas of Human Anatomy*. Philadelphia: W.B. Saunders Co.

Anson BJ. 1966. *Morris' Human Anatomy*, 12th edition. New York: The Blakiston Division, McGraw-Hill Book Company.

Ashley FL, Anson BJ. 1946. The pelvic autonomic nerves in the male. *Surg Gynecol Obstet* 82: 598–608.

Beck TS. 1847. On the structure and functions of the sympathetic nervous system. *Lancet* 1: 615–617.

Becker RF, Grunt JA. 1957. The cervical sympathetic ganglia. *Anat Rec* 127: 1–14.

Cotte G, Noel R. 1928. Sure l'existence de ganglion sympathiques dans le nerf présacré. *Assoc Anatomistes Comptes Rendus* 23: 99.

Ellison JP, Williams TH. 1969. Sympathetic nerve pathways to the human heart and their variations. *Am J Anat* 124: 149–162.

Gardiner E, Gray DJ, O'Rahilly R. 1969. *Anatomy*, 3rd edition. Philadelphia: W.B. Saunders Co.

Harman NB.1899. The pelvic splanchnic nerves: An examination into their range and character. *J Anat Physiol* 33: 386–399.

Huber GC. 1930. *Piersol's Human Anatomy*, ninth edition. Philadelphia: L.B. Lippincott.

Jackson CM. 1933. *Morris' Human Anatomy*, ninth edition. Philadelphia: P. Blakiston's Son & Co.

Kirgis HD, Kuntz A. 1942. Inconstant sympathetic neural pathways. Their relations to sympathetic denervation of the upper extremity. *Arch Surg* 44: 95–102.

Kopsch F. 1908. *Rauber's Lehrbuch der Anatomie des Menschen*. Leipzig: Georg Thieme.

Królikowska M, Zawodniak R. 1979. Variation of origin of major, minor and lowest splanchnic nerves in man. *Folia Morphol (Warsaw)* 38: 341–346.

Monteiro H, Rodrigues A. 1931. Sur les variations du nerf vertebral. *Assoc Anatomistes Comptes Rendus* 26: 406–419.

Rodrigues A. 1930. Communicating branches between the cervical sympathetic and the descendens cervicalis. *J Anat* 64: 308–318.

Schaefer EA, Symington J, Bryce TH. (eds) 1915. *Quain's Anatomy*, 11th edition. London: Longmans, Green, and Co.

Siwe SA. 1931. The cervical part of the gangliated cord, with special reference to its connections with the spinal nerves and certain cerebral nerves. *Am J Anat* 48: 479–497.

Skoog T. 1947. Ganglia in the communicating rami of the cervical sympathetic trunk. *Lancet* 2: 457–460.

Whitnall SE. 1932. *The Anatomy of the Human Orbit*, second edition. London: Oxford University Press.

Wrete, M. The anatomy of the sympathetic trunks in man. *J Anat* 93: 448–459.

89 Spinal nerves

R. Shane Tubbs
Seattle Science Foundation, Seattle, Washington, USA
St George's University, School of Medicine, St Georges, Grenada
University of Dundee, Dundee, UK

C1 dorsal root, ganglion, and ramus

When present, the dorsal root of C1 is smaller than its corresponding ventral root. Some have found that the dorsal root of C1 is absent in approximately 8% of individuals (Williams 1995) while others (Rhoton 2003) have found that this root is "infrequently present" or never present (April 1997). This absence may be found bilaterally (Crosby et al. 1962).

The dorsal root ganglion of C1 may be absent. Crosby et al. (1962) have also stated that, when present, the C1 ganglia may be rudimentary or may even share a ganglion with the spinal accessory nerve. It lies within the vertebral canal, although Grant (1940) stated that this potential ganglion can rest on the posterior arch of the atlas. Standring (2005) stated that the spinal root of the spinal accessory nerve "usually passes through the first cervical dorsal root ganglion." Small aberrant ganglia may occur on the upper cervical dorsal roots interposed between the dorsal root ganglia and spinal cord (Williams 1995).

As a rule, the dorsal primary ramus of the first cervical nerve (suboccipital nerve) does not divide into medial and lateral branches. A filament of the branch of the suboccipital nerve to the inferior oblique muscle may join the second dorsal ramus. A meningeal branch of the C1 spinal nerve as well as an articular branch to the atlanto-occipital joint have been described (Ouaknine and Nathan 1973).

Tubbs et al. (2007) identified the C1 and C2 spinal nerves in 100% of the specimens examined. No cutaneous branch of the C1 spinal nerve was observed in any specimen. In 46.6% of the specimens the C1 spinal nerve received a mean of two dorsal rootlets (range of one–five rootlets). In the remaining specimens, C1 did not receive any dorsal rootlets. In the specimens found to receive C1 dorsal rootlets, 28.5% were found to have a distinct dorsal root ganglion present. In 50% specimens, the spinal accessory nerve joined with dorsal rootlets of C1. In these case, C1 did not possess a dorsal root ganglion.

C1 dorsal roots

The first cervical dorsal root can be absent (Hollinshead 1982). Lang (1993) identified 1–10 dorsal rootlets (mean 3) for the first cervical nerve. This author has also reported that these rootlets are absent in 5% and 9% of right and left sides, respectively. Rhoton (2003) found 15 dorsal roots from 25 spinal cords without commenting as to whether any of these were ipsilateral or bilateral. Lang (1993) found that the spinal accessory nerve joins with the rootlets of C1 in 82% and 52% of right and left sides, respectively, and that often there is a swelling at the point of this connection. Some have opined that this swelling represents the dorsal root ganglion of C1 (discussed in the following section; Kazzander 1891). However, others have posited that these swellings contain tension receptors for the sternocleidomastoid and trapezius muscles and some concluded that they represent connective tissue hyperplasia or accumulation of amyloid bodies (Lang 1993). Ouaknine and Nathan (1973) found a defined dorsal root of C1 in 46% of their specimens. These authors classified the relationships between the C1 roots and the spinal accessory nerve as: Type I, with no connections between these two nerves (12%); Type II, with a communication between the spinal accessory nerve and the dorsal root at a midpoint between its entrance into the cord and fusion with the ventral roots (24%); Type III, with a dorsal root that communicates to the dorsal spinal cord via the spinal accessory nerve (44%); and Type IV, in which there were no posterior roots of C1 and therefore no connection to the spinal accessory nerve (20%). Oh et al. (2002) have studied the relationships between the spinal accessory nerve and the dorsal root of the first cervical nerve in 100 sides. In the most common type of connection (38%), either: a branch from the C1 dorsal root was seen to course cranially and join the spinal accessory nerve; or the dorsal root and accessory nerve fused as they coursed orthogonal to one other. In the second most common type (36%), the accessory nerve connected with a posterior C1 root that had no direct connection with the spinal cord; the nerve fibers of the posterior root were observed in stained samples to course caudally along

Bergman's Comprehensive Encyclopedia of Human Anatomic Variation, First Edition. Edited by R. Shane Tubbs, Mohammadali M. Shoja and Marios Loukas.
© 2016 John Wiley & Sons, Inc. Published 2016 by John Wiley & Sons, Inc.

the accessory nerve and join the posterior C2 root. In the least common type (6%), no connection was observed between the accessory nerve and the dorsal C1 root. In the next least common type (20% of cases), the posterior C1 root was absent and a connecting branch was sometimes observed between the accessory nerve and the ventral C1 root. Tubbs et al. (2007) found that 50% of their specimens with dorsal roots had communications with the spinal accessory nerve.

Interestingly, Kuntz (1942) stated that every spinal nerve is attached to the spinal cord by a dorsal and ventral root. Lang (1992) found a connection between the dorsal root of C1 and C2 on 29% of right and 24% of left sides. Embryologically, the hypoglossal nerve lies in series with the roots of the spinal nerves, and represents the fused ventral roots of four precervical or spino-occipital nerves whose dorsal roots have disappeared (Williams 1995).

C1 dorsal root ganglion

Froriep's ganglion (August von Froriep 1849–1917), which is a vestigial dorsal root ganglion, deteriorates to give rise to the motor neuron elements of the hypoglossal nerve (Kuratani et al. 1988). This ganglion may remain as an inconstant dorsal root ganglion on the posterior aspect of the hypoglossal nerve (Kuratani et al. 1988).

Tubbs et al. (2007) found that 28.5% of specimens had a dorsal root ganglion associated with the C1 root when present. The spinal accessory nerve may perforate the dorsal root ganglion of C1 (Ouaknine and Nathan 1973).

C1 dorsal ramus

Some have reported that, occasionally, after the dorsal ramus of C1 (suboccipital nerve) courses between the vertebral artery and posterior arch of the atlas to innervate the suboccipital muscles and semispinalis capitis, it extends as a cutaneous branch (accessory occipital nerve, Ouaknine and Nathan 1973) to the skin of the upper part of the posterior neck and the inferior part of the scalp traveling with the occipital artery (Schaeffer 1953; Strandring 2005). This would necessitate both a dorsal root ganglion and dorsal root system. This cutaneous branch is said to connect with the greater and lesser occipital nerves and may also communicate with the spinal accessory nerve (Strandring 2005). Abouleish (1996) stated that the C1 dorsal ramus does not have a dermatomal distribution. Others have also stated that the dorsal ramus of C1 does not have a cutaneous branch (Grant 1940). Parenthetically, Dubuisson (1995) has performed C1–C3 dorsal rhizotomy for medically refractory occipital neuralgia in 11 patients with the preservation of scalp sensation in all cases. Tubbs et al. (2007) found a suboccipital nerve in all of their specimens but did not observe a cutaneous branch in any.

Sometimes, the dorsal ramus of C1 joins the second and third cervical dorsal rami to form a communicating loop known as Cruveilhier's cervical plexus (Goss 1955). Although the dorsal ramus of C1 was not directly implicated, Parke and Valsamis (1967) have described neural input to the so-called ampulloglomerular organ located at the site where the suboccipital nerve courses between the vertebral artery and posterior arch of the atlas. These authors suggested that this structure, which is perhaps similar to the coccygeal gland, may have some chemoreceptive role for this region.

Connections between dorsal rootlets

Scant studies have reported occasional intradural communications between adjacent rootlets. These are most concentrated in the cervical followed by the lumbar regions and are rare in the thoracic region. Additionally, such communications are primarily between the dorsal rootlets; ventral root intercommunications are rarely reported. Schwartz (1956) reported such connections between cervical nerve roots, which he associated with the variation in the "normal" dermatome distribution. Such variations may be of neurosurgical significance during such procedures as dorsal rhizotomy for the relief of pain.

The least to greatest number of interconnections between adjacent dorsal roots was found between T1 and T2, C1 and C2, C8 and T1, C2 and C3, C3 and C4, C4 and C5, C7 and C8, C6 and C7, and C5 and C6. In this same order, the percent of total connections for each of these levels was 0%, 0.8%, 2%, 7%, 13%, 15%, 16%, 20%, and 25%. A total of 73 and 61 interconnections were identified for left and right sides, respectively.

For dorsal rootlet connections, Schwartz found that the most frequent communications in his group of dissections were between C7 and C6 and that none of the connections extended further than one segment. Pallie and Manuel (1968) found that these connections occurred at varying frequencies ranging from 3 to 8 in any given case and that they were best developed in the superior cervical region, essentially absent from the thoracic region, and then present again in lumbosacral regions. Marzo et al. (1987) also found that no connection extended more than one level, that the most frequent level of intercommunication was between C5 and C6, and the least common site was between C8 and T1. For dorsal rootlets, Moriishi et al. (1989) found connections between C4 and C5, C5 and C6, C6 and C7, C7 and C8, and C8 and T1 in 31%, 56%, 53%, 31%, and 11%, respectively. Lang (1993) reported that dorsal interconnections for left sides were the most common between C2 and C3 and least common between C8 and T1; for right sides, dorsal interconnections were less common between C1 and C2 and most common between C6 and C7. For comparison, we found the number of interconnections between adjacent dorsal roots (from least to greatest) to be: 0% between T1 and T2; 0.8% between C1 and C2; 2% between C8 and T1; 7% between C2 and C3; 13% between C3 and C4; 15% between C4 and C5; 16% between C7 and C8; 20% between C6 and C7; and 25% between C5 and C6.

Efferent fibers may be found traveling in the dorsal nerve roots (Mitchell 1953). Dorsal roots or the dorsal root ganglion

may send fibers to the meninges directly or these fibers may arise from the ventral root, all in the absence of a recurrent meningeal branch.

Greater occipital nerve

The greater occipital nerve has been reported to send a branch to the auricle. The greater and lesser occipital nerves complement each other, with each one compensating for any deficiency in the nerve supply of another. The external (lateral) branch of the second cervical nerve may have a cutaneous branch in addition to its usual muscular branches; it may also supply the suboccipital superior oblique muscle in addition to its usual supply to the semispinalis cervicis, inferior oblique, semispinalis cervicis, and multifidus spinae muscles. It may send a branch to the auricle (Piersol 1916). The external branch may give off a cutaneous filament or may supply the superior oblique muscle (Piersol 1916).

Ducic et al. (2009) found that the greater occipital nerve had an average diameter of 3.8±1.6 mm (range 2.1–6.1 mm). As it traverses from its medial origin, it emerges from the semispinalis capitis muscle an average of 14.9±4.5 mm lateral to the midline and 30.2±5.1 mm inferior to the occipital protuberance, and from the trapezius muscle 37.8±4.6 mm from the occipital protuberance (range 24–49 mm). In 1.5% of patients the nerve did not traverse the semispinalis muscle. Overall, in 56.1% of measured individuals, the course of the greater occipital nerve was symmetric between the left and right sides; in the remaining 43.9%, the courses of the nerves were asymmetric.

Lesser occipital nerve

The lesser occipital nerve may be very small and distributed only to the skin of the neck. In such cases, the greater occipital nerve supplies the areas usually supplied by the lesser occipital. In some cases, instead of its usual dorsal and upward course beneath the deep fascia along the posterior border of the sternocleidomastoid muscle, the lesser occipital nerve passes directly backward, piercing the trapezius muscle near its upper border before reaching the scalp (Piersol 1916). The auricular branch of the lesser occipital nerve may be derived from the greater occipital. It usually arises from the second and third cervical nerves or from the loop between them.

Ducic et al. (2009) found that the lesser occipital nerve had an average diameter of 1.2±1.6 mm. In 85% of individuals, it was located along the posterior border of the sternocleidomastoid muscle, at a reference point 3 cm inferior to the occipital protuberance. In the remaining 15% the location varied considerably, ranging from the midsuperficial surface of the sternocleidomastoid muscle to within 1 cm of the greater occipital nerve.

The sixth, seventh, and eighth cervical nerves may give rise to cutaneous branches of considerable size (Piersol 1916).

The cutaneous branches of the fifth and sixth cervical nerves may be very small or completely absent.

Communications between cervical dorsal rami

Cruveilhier (1844) stated that "as the posterior branch of the third cervical nerve emerges from the posterior intervertebral foramen, it gives off an ascending branch, which forms an anastomotic arch with the descending branch of the second nerve: the succession of arches formed by the anastomoses of the first, second, and third nerves, and the very numerous branches which arise from their convexities, constitute a plexus, which may be called the posterior cervical plexus." Today, Cruveilhier's name lives on eponymously with this plexus of nerves.

On the majority (86.7%) of the sides (apart from 1 left and three right sides, all from male cadavers), at least one communicating branch was identified between the upper cervical dorsal rami and specifically between their medial branches. This series of looping nerve communications always occurred deep to the semispinalis capitis muscle and near the posterior bony elements of the vertebrae, and never spanned more than one segment. The majority of loops were observed to have a curvilinear form with their convexity usually directed laterally. For the C1 dorsal ramus (suboccipital nerve), a communicating loop was found joining the medial branch of the dorsal ramus of C2 (greater occipital nerve) on 65.4% of sides. This branch joined the C1 dorsal ramus at its emergence between the posterior arch of the atlas and the horizontal segment of the vertebral artery within the suboccipital triangle, and descended to attach to the medial division of the C2 dorsal ramus usually at its course below the obliquus capitis inferior muscle. On 29.4% of sides, however, this loop pierced the obliquus capitis inferior muscle before joining C2. On 54% of sides, a communicating loop was found joining the medial branches of the dorsal rami of C2 and C3 (third occipital nerve); on 15.4%, a communicating loop was found joining the medial branches of the dorsal rami of C3 and C4. Connections between C2, C3, and C4 occurred between the semispinalis capitis posteriorly and the anteromedial semispinalis cervicis muscle (i.e., inferior to the suboccipital triangle). Connecting branches between C2 and C4 occurred near the origin of the dorsal rami at these levels. No specimen was found to have communicating branches between the dorsal rami of cervical nerves C5–C8. Articular branches were noted to arise from the deep surface of these interneural connections as they crossed the adjacent facet joint on 34.6% of sides. These facet branches were most commonly seen originating from the communicating loop connecting C2 to C3 (66.7%), less commonly from the loop connecting C1 and C2 (33.3%), and never from loops connecting C3 and C4. Also, 35% of loops were found to have fibers emanating from them that terminated in surrounding musculature (e.g., semispinalis capitis). Branches usually, but not always, arose from the convexity of the anastomosing

loops. The mean diameter of these anastomosing loops was 1.1 mm (range 0.8–1.2 mm) with the connections between C2 and C3 typically being the larger of these. Of all the communicating loops, those joining C1 to C2 were the longest and, on average, were 21 mm in length (range 15–25 mm).

Thoracic, lumbar, sacrococcygeal roots, and nerves

The anterior or posterior root (or both) of these nerves is sometimes absent in one or more thoracic spinal nerves. The sixth, seventh, and eighth thoracic nerves may give off cutaneous branches. The first thoracic nerve may have no cutaneous branch (Piersol 1916). The lateral cutaneous branch of T12 may be absent (Griffin 1890). A lateral cutaneous branch of the T1 may be present. On the right side, Turner (1871) found that dorsal rami of T2 and T3 pierced the vertebral aponeurosis, gave branches to the lower fibers of the rhomboid major, and then pierced the lower part of the trapezius. On the left side, the external branch of the dorsal ramus of T3 terminated in the lower fibers of the rhomboid major. Redundant nerve roots have been reported by Cressman and Pawl (1968) and Schut and Groff (1968).

The dorsal or ventral roots or spinal nerve of any thoracic nerve can be absent. The first thoracic nerve may fail to contribute to the formation of the posterior cord of the brachial plexus or it may be the sole source of the medial cord of the plexus. The first and second thoracic nerves are occasionally joined by a connecting branch.

The lateral branch of the second thoracic, the intercostobrachial nerve, may divide into an anterior and posterior division. The anterior division may be absent. The lateral branch anastomoses with the medial brachial cutaneous, usually with the lateral branch of the third intercostal, and rarely with the lateral branch of the first intercostal if it is present.

The size of the intercostobrachial cutaneous nerve and the extent of its distribution are reportedly inversely proportional to the size of the other cutaneous nerves of the arm, especially the medial brachial cutaneous nerve. When the medial brachial cutaneous nerve is absent, it is replaced by the intercostobrachial nerve.

The sixth, seventh, and eighth thoracic nerves can provide cutaneous branches from both their lateral and medial branches. Thoracic spinal nerves can supply the sternalis muscle.

The dorsal root ganglia associated with any one of the lumbar or upper sacral spinal nerves may be doubled. Ganglia aberrantia (small detached portions of spinal ganglia) may be found along the posterior roots of the upper cervical, lumbar, and sacral spinal nerves.

In the lumbar region, two pairs of nerve roots may originate from a single dural sleeve or a dural sleeve may arise from a low position on the dural sac (Bogduk 1997). In the latter case, the variant root does not hug the undersurface of its adjacent pedicle, but rather the superior surface of the pedicle below. The incidence of these types of lumbar nerve variations has been found to be 8.5% (Hasner et al. 1952). Intradural anastomoses between adjacent lumbar nerve roots have an incidence of 11–30% (d'Avella and Mingrino 1979). The number of roots in an intervertebral foramen may vary or there may be no nerve at any particular foramen. For the latter, the intervertebral foramen superior or inferior to it may contain two sets of nerves. Extradural anastomoses between adjacent lumbar nerves may occur (Bogduk 1997). Various lumbar roots may be absent.

In fetuses, the L2 lateral cutaneous branch becomes cutaneous in 90%, the L3 branch in 70%, and the L4 branch in 40% (Pearson et al. 1966). In adults, L1 and L2 both become cutaneous in about 27% and L1–L3 all supply cutaneous branches in only 13% of cases (Bogduk 1997). Cutaneous branches from L4 appear to be uncommon. A variable number of branches of the lumbar dorsal rami may innervate the facet joints (Bogduk 1997). Occasionally, an articular branch may arise from the dorsal ramus proper and innervate the ventral aspect of the adjacent joint.

In the coccygeal region, anterior roots may be completely absent or increased in number (one, two, or more). This is usually associated with an unusual number or arrangement of vertebrae. The greatest variation in nerve numbers per region occurs in the coccygeal region where there may be no coccygeal nerves or one–two additional nerves. Traces of rudimentary nerves may be found along the filum terminale (Piersol 1916). The spinal ganglion and sensory root of the coccygeal nerves may be absent; the same may occur to a lesser degree in other spinal nerves. Occasionally, rudimentary anterior roots are found in the filum terminale. One or two additional coccygeal nerves may be present bilaterally or only on one side. The ganglia of the fifth lumbar and first four sacral lie within the vertebral canal, but these are also extradural. The fifth sacral and the coccygeal nerves (when present) are located within the dural cavity.

Cluneal nerves

In a cadaveric study (Tubbs et al. 2010), an intermediate superior cluneal nerve and lateral superior cluneal nerve were not identified on 4 (20%) and 5 sides (25%), respectively. When one of the superior cluneal nerves was absent, its territory was simply covered by the existing two superior cluneal nerves. The diameter of the superior cluneals ranged over 0.8–2.1 mm (mean 1.1 mm) and their average length was 17 cm (range 14.5–20 cm). The lateral superior cluneal nerve tended to be the largest of the three superior cluneal nerves and occupied a more superficial plane. From the midpoint of the PSIS, the superior cluneal branches passed at means of 5 cm (range 4–5.8 cm), 6.5 cm (range 4–8.2 cm), and 7.3 cm (range 5.5–8.5 cm) laterally on the iliac crest. The superior lateral cluneal nerve often extended distally to the level of the greater trochanter of the femur. These nerves traveled from their origin to termination in

a more or less oblique course from medial to lateral and, more often than not, anastamosed with one another in their distal course inferior to the iliac crest. For the middle cluneal nerves, the S2 branch was found on 14 sides (70%) and the S3 branch was found on 9 sides (45%). The diameter of the middle cluneal nerves measured 0.5–1 mm (mean 0.8 mm). At their origin, the middle cluneal nerves had mean distances of 2 cm superior to the PSIS (range 1.2–2.3 cm), at the PSIS (range 0.8 cm superior to 0.5 cm inferior) and 1.5 cm inferior to the PSIS (0.5–2.2 cm). The middle cluneal nerves, especially the superior branches, were often found to communicate with the medial superior cluneal nerve.

References

Abouleish EI. 1996. The C1 nerve does not have a dermatomal distribution. *Reg Anesth* 21: 167–168.

April EW. 1997. *Clinical Anatomy, third edition*. Baltimore: Williams & Wilkins.

Bogduk N. 1997. *Clinical Anatomy of the Lumbar Spine and Sacrum*. New York: Churchill Livingstone.

Cressman MR, Pawl RP. 1968. Serpentine myelographic defect caused by a redundant nerve root. *J Neurosurg* 28: 391–393.

Crosby EC, Humphrey T, Lauer EW. 1962. *Correlative Anatomy of the Nervous Sytem*. New York: The Macmillan Company.

Cruveilhier J. 1844. *The Anatomy of the Human Body*. New York: Harper & Brothers.

D'Avella D, Mingrino S. 1979. Microsurgical anatomy of lumbosacral spinal roots. *J Neurosurg* 51: 819–823.

Dubuisson D. 1995. Treatment of occipital neuralgia by partial posterior rhizotomy at C1–3. *J Neurosurg* 82: 581–586.

Ducic ID, Moriarty M, Al-Attar A. 2009. Anatomical variaitons of the occipital nerves: implications for the treatment of chronic headache. *Plast Reconstr Surg* 123: 859–863.

Goss CM. 1955. *Gray's Anatomy*, 26th edition. Philadelphia: Lea & Febiger.

Grant JCB. 1940. *A Method of Anatomy: Descriptive and Deductive*, second edition. Baltimore: Williams and Wilkins.

Griffin M. 1890. Some varieties of the last dorsal and first lumbar nerves. *J Anat Physiol* 2: 48–55.

Hasner E, Schalintzek M, Snorrason E. 1952. Roentgenological examination of the function of the lumbar spine. *Acta Radiol* 37: 141–149.

Hollinshead WH. 1982. *Anatomy for Surgeons: The Head and Neck, third edition*. Philadelphia: J.B. Lippincott Company.

Kazzander G. 1891. Sulla radice dorsale del nervo ipiglosso nell'uomo e nei mammiferi domestici. *Anat Anz* 6: 444–450.

Kuntz A. 1942. *A Textbook of Neuroanatomy, third edition*. Philadelphia: Lea & Febiger.

Kuratani S, Tanaka S, Ishikawa Y, Zukeran C. 1988. Early development of the hypoglossal nerve in the chick embryo as observed by the whole-mount nerve staining method. *Am J Anat* 182: 155–168.

Lang J. 1992. *Suboccipital Approach (and other Approaches) to Aneurysms at the Craniocervical Junction*. Stuttgart: F.K. Schattauer Verlagsgesellschaft.

Lang J. 1993. *Clinical Anatomy of the Cervical Spine*. New York: Thieme.

Marzo JM, Simmons EH, Kallen F. 1987. Intradural connections between adjacent cervical spinal roots. *Spine* 12: 964–968.

Mitchell GAG. 1953. *Anatomy of the Autonomic Nervous System*. Edinburgh: E & S Livingstone.

Moriishi J, Otani K, Tanaka K, Inoue S. 1989. The intersegmental anastomoses between spinal nerve roots. *Anat Rec* 224: 110–116.

Oh CS, Chung IH, Koh KS, Kim HJ, Nam KI. 2002. Morphologic study of the connections between the accessory nerve and the posterior root of the first cervical nerve. *Clin Anat* 15: 267–270.

Ouaknine G, Nathan H. 1973. Anastomotic connections between the eleventh nerve and the posterior root of the first cervical nerve in humans. *J Neurosurg* 38: 189–197.

Pallie W, Manuel JK. 1968. Intersegmental anastomoses between dorsal spinal rootlets in some vertebrates. *Acta Anat (Basel)* 70: 341–351.

Parke WW, Valsamis MP. 1967. The ampulloglomerular organ: an unusual neurovascular complex in the suboccipital region. *Anat Rec* 159: 193–198.

Pearson AA, Sauter RW, Buckley TF. 1966. Further observations on the cutaneous branches of the dorsal rami of the spinal nerves. *Am J Anat* 119: 891–904.

Piersol GA. 1916. *Human Anatomy*. Philadelphia: JB Lippincott Company.

Rhoton AL. 2003. *Rhoton's Anatomy*. Philadelphia: Lippincott Williams and Wilkins.

Schaeffer JP. 1953. *Morris' Human Anatomy: a Complete Systematic Treatise*, 11th edition. New York: The Blakiston Company.

Schut L, Groff RA. 1968. Redundant roots as a cause of complete myelographic block. *J Neurosurg* 28: 394–395.

Schwartz HG. 1956. Anastomoses between cervical nerve roots. *J Neurosurg* 13: 190–194.

Standring S. 2005. *Gray's Anatomy*, 39th edition. Edinburough: Elsevier.

Tubbs RS, Loukas M, Slappey JB, Shoja MM, Oakes WJ, Salter EG. 2007. Clinical anatomy of the C1 dorsal root, ganglion, and ramus: a review and anatomical study. *Clin Anat* 20: 624–627.

Tubbs RS, Levin MR, Loukas M, Potts EA, Cohen-Gadol AA. 2010. Anatomy and landmarks for the superior and middle cluneal nerves: application to posterior iliac crest harvest and entrapment syndromes. *J Neurosurg Spine* 13: 356–359.

Turner P. 1871. Some additional variations in the distribution of the nerves of the human body. *J Anat Physiol* 6: 101–106.

Williams PL. 1995. *Gray's Anatomy. The Anatomical Basis of Medicine and Surgery*, 38th edition. New York: Churchill Livingstone.

Further reading

Clemente CD. 1985. *Articulations of the upper extremity. In Gray's Anatomy*, 30th edition. Baltimore: Williams & Wilkins, pp. 367.

Koch D, Wakhloo AK. 1992. CT-guided chemical rhizotomy of the C1 root for occipital neuralgia. *Neuroradiology* 34: 451–452.

McKenzie KG. 1955. The surgical treatment of spasmodic torticollis. *Clin Neurosurg* 2: 37–43.

90 Cervical plexus

Necdet Kocabiyik
Gulhane Military Medical Academy, Ankara, Turkey

There are fewer variations in the nervous system than in any other organ system. This is undoubtedly because the nervous system more or less controls the functions of all the other organs (Henle 1868; Schaefer et al. 1915; Jackson 1933; Cordier et al. 1936; Latarjet 1948).

The cervical plexus consists of three loops. A large part of the anterior primary division of the first cervical nerve joins the hypoglossal or cervical loop. The rest supplies the cervical plexus, thus forming the first loop. From the first loop of the plexus, two branches of the first cervical nerve usually enter the sheath of the hypoglossal nerve and descend with it to supply the hypoglossal or cervical loop. The first cervical nerve departs from the hypoglossal (or vagus) as the descendens cervicalis or hypoglossi and later contributes to the communicans cervicalis, which develops from the second and third cervical nerves; this concludes the hypoglossal or cervical loop, the location of which varies. The cervical loop is generally observed between the sheaths of the sternocleidomastoid and carotid artery superficial to the internal jugular vein, but it can be situated between the carotid artery and the internal jugular instead or, more rarely, posterior to both artery and vein. It can be extended, ending below the level of the thyroid cartilage, or short, ending at the level of the hyoid bone. The descendens hypoglossi (or cervicalis) lengthens distally on the sheaths of the great vessels, or is sometimes situated within one of these sheaths. The second cervical nerve supplies the first and second loops of the cervical plexus. The third cervical merges with the second and fourth cervical to complete the lower loops of the plexus (Henle 1868; Schaefer et al. 1915; Jackson 1933; Cordier et al. 1936; Latarjet 1948).

Ansa cervicalis

The inferior root of the ansa cervicalis, which is the ramus descendens cervicalis, is formed by the combination of a branch from the second with another from the third cervical ramus. It descends on the lateral side of the internal jugular vein, crosses that vein a little below the middle of the neck, and continues forward to join the superior root, the ramus descendens hypoglossi, anterior to the common carotid artery. It forms the ansa cervicalis, which is the ansa hypoglossi, by which all infrahyoid muscles except the thyrohyoid are supplied. The inferior root comes from the second and third cervical ventral rami in 75% of cases, from the second to fourth in 15%, and from the third alone in 5%. Occasionally, it is derived from either the second alone or from the first to the third (Standring 2008). Rao et al. (2007) reported a duplicated ansa cervicalis.

The ramus descendens hypoglossi can be subsitituted by the vagus (CN X). The innervation of the infrahyoid muscles arises directly from C2 and C3 by branches when no ansa is present. The nerve to the thyrohyoid can develop as a branch of the ramus descendens hypoglossi, and the descendens hypoglossi can contribute to the phrenic nerve. In addition to these, various connections with the cervical sympathetic trunk have been reported and the communicating branch from the fourth cervical nerve can join the descending cervical nerve in the ansa cervicalis (Turner 1893; Lippmann 1910; Schaefer et al. 1915; Rodrigues 1930; Wischnewsky 1930; Langsam 1941; Winckler 1955).

The most inferior aspect of the ansa cervicalis extends no lower than the lowest point of the cervical part of the hypoglossal nerve in 18% and touches the intermediate tendon of the omohyoid muscle in 6.5% (Lang 1993).

Great auricular nerve

The mastoid or posterior branch of the great auricular nerve can arise independently of the cervical plexus, in which case it passes upward between the lesser occipital and great auricular nerves to reach its destination. The great auricular nerve can arise solely from the third or from both the third and fourth cervical nerves (Henle 1868; Schaefer et al. 1915; Jackson 1933; Cordier et al. 1936; Latarjet 1948). An anatomical variant has been reported in which the anterior branch joins the marginal mandibular branch of the facial nerve on its deep surface in the submandibular triangle (Brennan et al. 2010).

There are conflicting opinions about the exact anatomical course of the great auricular nerve. Zohar et al. (2002) aimed

Bergman's Comprehensive Encyclopedia of Human Anatomic Variation, First Edition. Edited by R. Shane Tubbs, Mohammadali M. Shoja and Marios Loukas.
© 2016 John Wiley & Sons, Inc. Published 2016 by John Wiley & Sons, Inc.

to study the pathway of the anterior branch and endings of this nerve in relation to the parotid gland. Nineteen fresh adult cadavers whose causes of death were not due to pathology in the parotid region were studied, including the parotid gland at the site of termination of the anterior branch of the nerve. There was no evidence of well-organized fibers of the great auricular nerve inside the parotid gland in most cases (21/37=57%). In a few (5/37=13%), nerve fibers were observed to penetrate the interlobular septa; in others (11/37=30%), nerve bundles were found deep in the gland alongside small ducts and close to thin-walled blood vessels. These findings prove that there are anatomical variations of the endings of the anterior branch of the great auricular nerve. Zohar et al. (2002) suggested that the significance of nerve bundles deep in the gland along ducts and near vessels should be explored in the future. The great auricular nerve may ascend as high as the lateral canthus of the eye.

Lesser occipital nerve

Occasionally, the lesser occipital nerve pierces through the sternocleidomastoid muscle. It is sometimes very small and distributed only to the skin of the neck. In such cases, the greater occipital nerve supplies the areas usually supplied by the lesser occipital. This branch also communicates with the posterior branch of the great auricular nerve and is occasionally derived from the great occipital nerve.

In some cases, instead of its usual dorsal and upward course beneath the deep fascia along the posterior border of the sternocleidomastoid muscle, the lesser occipital nerve passes directly backward, piercing the trapezius muscle near its upper border before reaching the scalp. Its auricular branch can derive from the greater occipital. It usually arises from the second and third cervical nerves or from the loop between them (Henle 1868; Schaefer et al. 1915; Jackson 1933; Cordier et al. 1936; Latarjet 1948). Duplication and triplication of the lesser occipital nerves have been noted.

Phrenic nerve

The phrenic nerve can be absent, and absence of both phrenic nerves is exceedingly rare. The phrenic nerve can receive additional roots from one or more of the following nerves: nerve to subclavius; nerve to sternohyoid; second, or rarely sixth, cervical nerve; descendens cervicalis; ansa cervicalis; and brachial plexus. It can also receive a branch from CN XII (hypoglossal) and may communicate with CN XI (spinal accessory). It can arise exclusively from the nerve to the subclavius; on occasion, it supplies a branch to the subclavius muscle. It sometimes passes along the lateral border of the anterior scalene muscle or pierces that muscle. It might not be consolidated into a single trunk until it enters the thorax, where the size of the nerve can differ bilaterally. Instead of descending behind the subclavian vein, the phrenic nerve can pass anterior to it or even through a ring or annulus formed by the vein. An accessory phrenic nerve can also arise from the fifth or fifth and sixth cervical nerves and pass in front of or behind the subclavian vein to join the main trunk of the phrenic nerve at the root of the neck or within the thorax. Yano (1925) found an accessory phrenic nerve in 75% of 309 cases studied. The phrenic nerve can supply a branch to the scalenus anterior and can descend in contact with the posterior surface of the sternocleidomastoid, cross in front of the subclavian and right brachiocephalic veins, and lie about 1.5 cm in front of the scalenus anterior muscle and subclavian artery. In one case, Yano (1925) found that the right phrenic passed through an annulus of the subclavian vein (Ziemessen 1882; Larkin 1889; Turner 1893; Wernicke 1897; Haro 1907; Sauerbruch 1913; Schaefer et al. 1915; Felix 1922a, b; Kiss and Ballon 1925; Oliver et al. 1926; Ruhemann 1926; Yano 1928; Bertelli 1933–34; Ono 1934–35; Greenfield and Curtis 1942; Kelley 1950; Van der Stricht 1950; Fontes 1955; Prioton and Thevenet 1957; Jaya 1960; Minne et al. 1989). Loukas et al. (2006) described the various sources of an accessory phrenic nerve. The accessory phrenic nerve is composed of fibers from the fifth cervical ventral ramus that runs in a branch of the nerve to the subclavius. This lies lateral to the phrenic nerve and descends posterior (occasionally anterior) to the subclavian vein. The accessory phrenic nerve usually joins the phrenic nerve near the first rib but sometimes joins it near the pulmonary hilum or beyond. It can derive from the fourth or sixth cervical ventral rami or from the ansa cervicalis (Standring 2008).

The full length of the phrenic nerve was 24.6±1.7 cm on the right side and 30.6±1.8 cm on the left (Jiang et al. 2011). Prakash et al. (2007) observed variations only on the right side during routine dissection of a 30-year-old male cadaver. In its early course close to its origin, the phrenic nerve gave a communicating branch to the C5 root of the brachial plexus. At the level of the root of the neck, just before entering the thorax, it was located in front of the subclavian vein; it is more usually located posteriorly, between the subclavian vein and artery. The authors concluded that variations of the phrenic nerve made it highly vulnerable to injury during subclavian catheterization for vascular access (Prakash et al. 2007).

Loukas et al. (2006) reported phrenic nerve injury in 10–85% of patients after cardiac operations, emphasizing the importance of accurate anatomical description of the innervation of the diaphragm in order to reduce iatrogenic injury, length of hospitalization, and associated costs. They dissected 80 adult formalin-fixed cadavers, resulting in 160 nerve specimens. All nerves contributing to the phrenic nerve after crossing the anterior scalene were considered as accessory phrenic nerves. The phrenic nerve was present in all specimens, and 61.8% also had an accessory phrenic nerve. The accessory phrenic nerve arose from the nerve to the subclavius in 60.6%, ansa cervicalis in 12.1%, and nerve to the sternohyoid in 7%. It joined the phrenic nerve in the thorax anterior to the subclavian vein in 45.5% specimens and posterior to it in 22.2%. A phrenic-accessory phrenic nerve

loop was found around the subclavian vein in 45 specimens and around the internal thoracic artery in 38. In conclusion Loukas et al. (2006) suggested that, in order to reduce injuries to the diaphram, the possible presence of an accessory phrenic nerve should be considered before mobilization and skeletonization of the internal thoracic artery above the second rib.

Williams et al. (1995) claimed that the phrenic nerve originated from nerve root C4. Normally, it arises chiefly from the fourth cervical nerve with a few filaments from the third and a communicating branch from the fifth. Codesido and Guerri-Guttenberg (2008) found this case really interesting because the right accessory phrenic nerve went through a transient division of the subclavian vein before joining the phrenic nerve. They explained that in this case the nerve originated from nerve root C5, its least-frequent origin. It reached the anterior surface of the subclavian vein where it ran through an annulus located 1 cm away from the jugulo-subclavian junction. From there, it emerged from the posterior surface of the vein to join the phrenic nerve in the thorax. This was the first time this variation had been reported in the literature. The authors believed that these variations could predispose to complications during subclavian venous catheterization, since the lumen of the subclavian vein was transiently divided by the accessory phrenic nerve (Codesido and Guerri-Guttenberg 2008).

Canella et al. (2010) conducted a study demonstrating that in normal subjects the cervical course of the phrenic nerve could be depicted using ultrasonography. They suggested that the anterior scalene muscle was an easily identified landmark, as were the transverse cervical and cervical ascending arteries.

The phrenic nerve is frequently anesthetized when an interscalene block is performed, which is not surprising as the roots of the cervical plexus are often anesthetized with this block (Bigeleisen 2003). Nevertheless, it was also frequently anesthetized (36–67%) when a supraclavicular block was performed (Knoblanche 1979; Farrar et al. 1981; Lanz et al. 1983), which surprised Lanz et al. (1983) since the cervical roots are seldom blocked by this technique. Moreover, Urmey et al. (1991) observed that the quality of phrenic nerve block differed between the supraclavicular and interscalene approaches. They suggested that when an interscalene block was used there was a 100% incidence of diaphragmatic hemiparesis accompanied by a 25% reduction in forced vital capacity. However, a supraclavicular block caused diaphragmatic paresis in only 50% of patients and there was no reduction in forced vital capacity (Neal et al. 1998). Clemente (1985) suggested that further review would clarify the issue. They claimed that, since the phrenic nerve usually arises predominantly from the root of C4 with contributions from C3 and C5, it is formally considered part of the cervical plexus.

Bergman et al. (1988), who described many variations of the phrenic nerve, assumed that in most cases it descends along the anterior surface of the scalenius anticus muscle and enters the thorax sandwiched between the subclavian artery and vein. Moreover, they determined that the phrenic nerve can also pass anterior to the subclavian vein rather than descending behind it. They added that an accessory phrenic nerve could arise from roots C5 and C6 or from the nerve to the subclavius muscle, which was present in up to 75% of cadavers.

Neal et al. (1998) suggested that the phrenic nerve can receive branches from the cervical or brachial plexus or arise entirely from the latter. Cranial nerves XI or XII can also contribute branches, arising in close proximity to the site where supraclavicular blocks are performed. These authors therefore considered the possibility of anesthetizing only part of the phrenic nerve with a supraclavicular block when account was taken of the relatively high frequency of an accessory phrenic nerve or a branch from the brachial plexus itself. Bigeleisen (2003) claimed that this situation could lead to a partial block of the ipsilateral hemidiaphragm and was consistent with the outcomes of the study by Neal et al. (1998), particularly the preservation of forced vital capacity under supraclavicular block, even in patients who had evidence of hemiparesis. In such patients, the needle tip was likely to be placed near one of the posterior divisions of the plexus that gave rise to the radial nerve and all or part of the phrenic nerve. Stimulation would have caused contraction of the supinator and brachioradialis muscles, a paresthesia in the thumb, and a motor response in the diaphragm consistent with the phrenic nerve variations (Bigeleisen 2003).

In the general population, Bigeleisen (2003) assumed that more distal blocks, such as a low interscalene or supraclavicular blocks, could also give rise to a partial phrenic nerve block even if phrenic nerve anatomy was standard. In this instance, less local anesthetic might bathe the phrenic nerve roots, resulting in a partial phrenic block. This scenario was also consistent with the work of Neal et al. (1998). By way of summary, Bigeleisen (2003) reported a case of simultaneous diaphragmatic and brachial plexus stimulation resulting in a successful nerve block. The qualitative difference in phrenic nerve block between interscalene and supraclavicular blocks was explained on the basis of known anatomical variations. The case demonstrated the need for a thorough knowledge of anatomical variations and standard anatomy for the safe, efficient practice of regional anesthesia.

Rao et al. (2007) reported a left-sided phrenic nerve that formed a loop around a common arterial trunk from the subclavian artery, which gave rise to the inferior thyroid, suprascapular, and internal thoracic arteries. After this loop, the nerve rejoined and traveled distally in a normal manner.

The phrenic nerve can pierce the anterior scalene muscle.

Transverse cervical nerve

Instead of a single nerve, the superficial cervical can have two or more branches arising from the cervical plexus. This nerve can arise solely from the third or from both the third and fourth cervical nerves. In its course in the neck, it sometimes passes through an annulus in the external jugular (Henle 1868; Schaefer et al. 1915; Bautzmann 1930; Jackson 1933; Cordier et al. 1936;

Latarjet 1948). One study commented on the communication of the ascending branch with the marginal mandibular branch of the facial nerve instead of the cervical branch (Salinas et al. 2009).

Supraclavicular nerves

The following variations have been reported in these nerves. A branch to the phrenic nerve can pass down into the thorax over the subclavian artery or vein before joining the phrenic nerve. An additional bundle from the fifth cervical nerve can join this branch. A branch to the rhomboid muscles can pass through the trapezius muscle on its way to the skin close to the midline, at the level of the spinous processes of the fifth and sixth thoracic vertebrae. In 10 of 254 cases, the clavicle was perforated by the middle branch of the supraclavicular nerves (Papadatos 1980). They traversed the bone in intraclavicular canals and were visible on X-ray films (Henle 1868; Kopsch 1908; Schaefer et al. 1915; Oliver et al. 1926; Latarjet 1948; Anson 1966).

Tubbs et al. (2006) reported a male cadaver with the right intermediate branch of the supraclavicular nerve piercing the clavicle. No other anomalies were found in this specimen. Following a review of the literature, it appeared that symptoms related to this finding were rare but most commonly involved the intermediate branch of the supraclavicular nerve. Symptoms could be alleviated by surgical decompression of the entrapped nerve. Although this condition is rare, clinicians should include entrapment of the supraclavicular nerve within the clavicle in differential diagnosis of shoulder pain (Tubbs et al. 2006).

Since the definition of supraclavicular nerve entrapment syndrome by Gelberman et al. (1975) a number of clinical cases of this specific neuropathy have been reported. In all these cases, the nerve injury was attributed to the location of the supraclavicular nerve branch in a narrow canal in the clavicle. However, in the anatomical literature, variations in the course of the supraclavicular nerves have been ascribed not only to bony canals but also to abnormal fibrous and muscular structures. Since a narrow site with rigid walls along the course of a nerve is necessary for an entrapment neuropathy to develop, the study by Jelev and Surchev (2007) examined all the variant anatomical structures that could be involved in supraclavicular nerve entrapment. They described three groups of structures closely related to the course of the supraclavicular nerve: transclavicular canals, fibrous bands, and unusual muscular structures (supraclavicularis proprius muscle, cleido-occipitalis muscle, etc.). In view of the characteristics of the variations found, they suggested for the first time that (in addition to the bony canals through the clavicle) certain fibrous, muscular structures could also be an anatomical basis for supraclavicular nerve entrapment syndrome.

Despite the rarity of this syndrome, it should be considered among the causes of anterior shoulder girdle pain. It is usually related to anatomical variants (involving the bone structures, fibrous bands, or muscles and tendons). Computed tomography is the most useful investigation. Medications used to treat neuropathic pain can provide relief. Otherwise, a local glucocorticoid injection or even surgical decompression should be considered (Douchamps et al. 2012).

Because the supraclavicular nerve lies close to the clavicle it is particularly vulnerable to injury in cases of clavicle fracture and during surgical treatment of these fractures. The development of painful neuromas after iatrogenic transection and symptomatic nerve entrapment in fracture callus after healing have been described previously. Also, in a case of acute supraclavicular nerve entrapment and tension after fracture of the clavicle, significant pain relief, fracture fixation, and nerve decompression were essential (O'Neill et al. 2012). Rao et al. (2009) reported a supraclavicular nerve that looped around the external jugular vein and the transverse cervical artery.

Cervical rami communicantes

Communicating branches between the cervical sympathetic trunk and descendens cervicalis are variable. In one study, communicating branches were found (a) between the superior cervical ganglion and descendens cervicalis; (b) joining C2 and C3; and (c) variably joining the connecting loop between C2 and C3 (Rodrigues 1930).

Cervical plexus connections to accessory nerve

Lee et al. (2009) conducted a total of 181 neck dissections prospectively enrolled in their study. The relationships between the spinal accessory nerve and adjacent structures (internal jugular vein, sternocleidomastoid muscle, cervical plexus) and the number of lymph nodes in level IIb were investigated. The cervical plexus contributed to the spinal accessory nerve from C2 in 96 cases, C2 and C3 in 69, and C3 in 16. In some cases the spinal accessory nerve ran along the inner surface of the sternocleidomastoid muscle without penetration (44.5%), and there was a variety of cervical plexus contributions along its course. Lee et al. recommended awareness of these anatomical variations and meticulous dissection to minimize the risk of injuring the spinal accessory nerve.

Kierner et al. (2001) assumed that their research was the first to demonstrate that the spinal accessory nerve and the trapezius branches of the cervical plexus merge and pass together to the transverse as well as the ascending part of the trapezius muscle. However, the descending part of the muscle is innervated solely by a single fine branch of the spinal accessory nerve. Furthermore, these authors demonstrated that the so-called segmental branches did not branch within the trapezius muscle and were obviously identical to the cutaneous nerves arising from the posterior division of the cervical nerve, which were thought

to be purely afferent. Apart from the well-known innervation of the trapezius muscle by the spinal accessory nerve and the rami trapezi of the cervical plexus, no other nerve supply could be found. This contrasts with the findings of Soo et al. (1990), Krause et al. (1993) and Niemeyer and Ludolph (1987). Furthermore, Kierner et al. (2001) found no branches other than that arising from the spinal accessory nerve that passed toward the descending part of the muscle, indicating dual innervation as stated by Krause et al. (1991). However, purely cervical innervation of the descending part, as suggested by Haas and Sollberg (1962), seems even more unusual and has never been proven. On the basis of more recent work by Karuman and Soo (1996) and Kierner et al. (2001), the authors strongly disagreed with Weitz et al. (1982), who claimed that the whole trapezius muscle had a dual innervation and inferred surgical consequences. On the other hand, on the basis of their clinical experience Fahrer et al. (1974) had already pointed out that a purely cervical supply to the upper part of the trapezius muscle, as suggested by Rosenstein (1935), could not be accepted as a rule. These authors found no evidence that the trapezius muscle could be supplied by cervical fibers only. It must be stressed that the aforementioned studies were all based on clinical experience, gross dissection, and/or electromyography, which leaves a shade of doubt about the reliability of their findings (Kierner et al. 2001).

References

Anson BJ. (ed.) 1966. *Morris' Human Anatomy, twelth edition*. New York: McGraw-Hill Book Company.

Bautzmann H. 1930. Verlauf des nervus cutaneous colli durch eine ınsel der vena jugularis externa. *Anat Anz* 70: 516–519.

Bergman RA, Thompson SA, Afifi AK, Saddeh FA. 1988. *Copendium of Human Anatomical Variation*. Baltimore: Urban and Schwarzenburg.

Bertelli D. 1933–34. Distribuzione dei nervi frenici nel diaframma dei Mammiferi. *Arch Ital Anat Embriol* 32: 110–148.

Bigeleisen PE. 2003. Anatomical variations of the phrenic nerve and its clinical implication for supraclavicular block. *Br J Anaesth* 91: 916–917.

Brennan PA, Al Gholmy M, Ounnas H, Zaki GA, Puxeddu R, Standring S. 2010. Communication of the anterior branch of the great auricular nerve with the marginal mandibular nerve: a prospective study of 25 neck dissections. *Br J Oral Maxillofac Surg* 48: 431–433.

Canella C, Demondion X, Delebarre A, Moraux A, Cotten H, Cotten A. 2010. Anatomical study of phrenic nerve using ultrasound. *Eur Radiol* 20: 659–665.

Clemente CD. (ed.) 1985. *Anatomy of the Human Body*. Philadelphia: Lea & Febiger.

Codesido M, Guerri-Guttenberg RA. 2008. Right accessory phrenic nerve passing through an annulus of the subclavian vein. *Clin Anat* 21: 779–780.

Cordier P, Coulouma P, Delcroix D. 1936. Contribution a l'étude de la constitution du plexus cervical chez l'homme et quelques primates. *Assoc Anat Comptes Rendus* 31: 114–123.

Douchamps F, Courtois AC, Bruyère PJ, Crielaard JM. 2012. Supraclavicular nerve entrapment syndrome. *Joint Bone Spine* 79: 88–89.

Fahrer H, Ludin HP, Mumenthaler M, Neiger M. 1974. The innervation of the trapezius muscle. An electrophysiological study. *J Neurol* 207: 183–188.

Farrar MD, Scheybani M, Nolte H. 1981. Upper extremity block, effectiveness and complications. *Reg Anesth* 6: 133–134.

Felix W. 1922a. Anatomische, experimentelle und klinische untersuchungen über den n. phrenicus und über die zwerchfellinnervation. *Deutsche Z Chir* 171: 283–397.

Felix W. 1922b. Über den nervus phrenicus und die zwerchfellinnervation. *Zentralbl Chir* 49: 1832.

Fontes V. 1955. Les origines du nerf phrénique. *Assoc Anat Comptes Rendus* 42: 518–526.

Gelberman RH, Verdeck WN, Brodhead WT. 1975. Supraclavicular nerve-entrapment syndrome. *J Bone Joint Surg Am* 57: 119.

Greenfield J, Curtis GM. 1942. The "sniff test" in thoracic surgery. With a review of 119 phrenic nerve interruptions. *J Thoracic Surg* 12: 79–85.

Haas E, Sollberg G. 1962. Research on the function of the shouder girdle after section of the accessory nerve. *Z Laryngol Rhinol Otol* 41: 669–677.

Haro S. 1907. Ueber einige klinisch sehr wichtige verlaufsanomalien des n. phrenicus. *Tokyo J Med Sci* 21: 21–29.

Henle J 1868. *Handbuch der Systematischen Anatomie des Menschen*. Braunschweig: von Friedrich Vieweg und Sohn.

Jackson CM. (ed.) 1933. *Morris' Human Anatomy, ninth edition*. Philadelphia: P. Blakiston's Son & Co.

Jaya Y. 1960. Liver as a content of the right sided diaphragmatic hernia: A case report. *J Anat Soc India* 9: 37–38.

Jelev L, Surchev L. 2007. Study of variant anatomical structures (bony canals, fibrous bands, and muscles) in relation to potential supraclavicular nerve entrapment. *Clin Anat* 20: 278–285.

Jiang S, Xu WD, Shen YD, Xu JG, Gu YD. 2011. An anatomical study of the full-length phrenic nerve and its blood supply: Clinical implications for endoscopic dissection. *Anat Sci Int* 86: 225–231.

Karuman PM, Soo KC. 1996. Motor innervation of the trapezius muscle: A histochemical study. *Head Neck* 18: 254–258.

Kelley WO. 1950. Phrenic nerve paralysis. Special considerations of the accessory phrenic nerve. *J Thoracic Surg* 19: 923–928.

Kierner AC, Zelenka I, Burian M. 2001. How do the cervical plexus and the spinal accessory nerve contribute to the innervation of the trapezius muscle? As seen from within using Sihler's stain. *Arch Otolaryngol Head Neck Surg* 127: 1230–2332.

Kiss F. Ballon HC. 1925. Contribution to the nerve supply of the diaphragm. *Anat Rec* 41: 285–298.

Knoblanche GE. 1979. The incidence and aetiology of phrenic nerve blockade association with supraclavicular brachial plexus block. *Anaesth Intensive Care* 7: 346.

Kopsch F. 1908. *Rauber's Lehrbuch der Anatomie des Menschen*. Leipzig: Georg Thieme.

Krause HR, Bremerich A, Herrmann M. 1991. The innervation of the trapezius muscle in connection with radical neck-dissection. An anatomical study. *J Craniomaxillofac Surg* 19: 87–89. Erratum in: J Craniomaxillofac Surg 19: 231.

Krause HR, Kornhuber A, Dempf R. 1993. A technique for diagnosing the individual patterns of innervation of the trapezius muscle prior to neck dissection. *J Craniomaxillofac Surg* 21: 102–106.

Lang J. 1993. *Clinical Anatomy of the Cervical Spine*. New York: Thieme.

Langsam CLM. 1941. Omohyoideus in American Whites and Negroes. *Am J Phys Anthropol* 28: 249–259.

Lanz E, Theiss D, Jankovic D. 1983. The extent of blockade following various techniques of brachial plexus block. *Anesth Analg* 62: 55–58.
Larkin FC. 1889. Accessory phrenic nerve. *J Anat Physiol* 23: 340.
Latarjet A. 1948. *Testut's Traité d'Anatomie Humaine, ninth edition*. Paris: G. Doin & Co.
Lee SH, Lee JK, Jin SM, Kim JH, Park IS, Chu HR, Ahn HY, Rho YS. 2009. Anatomical variations of the spinal accessory nerve and its relevance to level IIb lymph nodes. *Otolaryngol Head Neck Surg* 141: 639–644.
Lippmann R Von. 1910. Abnormer ursprung des ramus descendens n. hypoglossi aus dem n. vagus. *Anat Anz* 37: 1–4.
Loukas M, Kinsella CR Jr, Louis RG Jr, Gandhi S, Curry B. 2006. Surgical anatomy of the accessory phrenic nerve. *Ann Thorac Surg* 82: 1870–1875.
Minne J, Senneville A, Guyot A. 1949. Remarques sur la division et les branches terminales du nerf phrenique droit. *Assoc Anatomistes Comptes Rendus* 36: 484–491.
Neal JM, Moore JM, Kopacz DJ, Liu SS, Kramer DJ, Plorde JJ. 1998. Quantitative analysis of respiratory, motor, and sensory function after supraclavicular block. *Anesth Analg* 86: 1239–1244.
Niemeyer K, Ludolph A. 1987. The importance of the subfascial branches of the cervical plexus for the motor innervation of the trapezius muscle. Results of electromyographic studies of the trapezius muscle following radical neck dissection. *Dtsch Z Mund Kiefer Gesichtschir* 11: 356–360.
O'Neill K, Stutz C, Duvernay M, Schoenecker J. 2012. Supraclavicular nerve entrapment and clavicular fracture. *J Orthop Trauma* 26: e63–65.
Oliver E, Rocquet M. 1926. La traversée diaphragmatique du nerf phrénique droit et ses variations. *Assoc Anat Comptes Rendus* 21: 441–444.
Ono N. 1934–35. Untersuchungen und studien über die ursprungszellen des n. phrenicus. *Jap J Med Sci* 5: 1–34.
Papadatos D. 1980. Supraclavicular nerves piercing the clavicle: A study of 10 cases. *Anat Anz* 147: 371–381.
Prakash, Prabhu LV, Madhyastha S, Singh G. 2007. A variation of the phrenic nerve: Case report and review. *Singapore Med J* 48: 1156–1157.
Prioton JB. Thevenet A. 1957. La distribution intra-diaphragmatique des nerfs phréniques. *Assoc Anatomistes Comptes Rendus* 44: 635–645.
Rao TR, Kumar B, Shetty P, Rao SR. 2007. Variaiton in the course of the left phrenic nerve: a case report. *Neuroanatomy* 6: 24–25.
Rao TR, Shetty P, Rao S. 2009. A rare case of looping of supraclavicular nerve branches around external jugular vein and transverse cervical artery. *IJAV* 2: 48–50.
Rodrigues A. 1930. Le descendens cervicalis chez l'homme et chez le mammifères (quelques notes sur son évolution phylogénique). *Assoc Anat Comptes Rendus* 25: 267–282.
Rosenstein A. 1935. Anatomie der peripheren nerven. In *Handbuch der Neurologie (eds O Bumke, O Foerster)*. Berlin: Springer Verlag.
Ruhemann E. 1926. Die topographie des nervus phrenicus unter abnormen verhältnissen. *Arch Klin Chirurgie* 139: 557–562.
Salinas NL, Jackson O, Dunham B, Bartlett SP. 2009. Anatomical dissection and modified Sihler stain of the lower branches of the facial nerve. *Plast Reconstr Surg*, 124: 1905–1915.
Sauerbruch F. 1913. Die beeinflussung von lungenerkrankungen durch künstliche lähmung des zwerchfells (phrenikotomie). *Münch Med Wochenschr* 60: 625–626.
Schaefer EA, Symington J, Bryce TH. (eds) 1915. *Quain's Anatomy, 11th edition*. London: Longmans, Green, and Co.
Soo KC, Guiloff RJ, Oh A, Della Rovere GQ, Westbury G. 1990. Innervation of the trapezius muscle: A study in patients undergoing neck dissections. *Head Neck* 12: 488–495.
Standring S. 2008. *Gray's Anatomy, 40th edition*. Edinburgh: Churchill Livingstone.
Tubbs RS, Salter EG, Oakes WJ. 2006. Anomaly of the supraclavicular nerve: Case report and review of the literature. *Clin Anat* 19: 599–601.
Turner W. 1893. A phrenic nerve receiving a root of origin from the descendens hypoglossi. *J Anat Physiol* 27: 427.
Urmey WF, Talts KH, Sharrock NE. 1991. One hundred percent incidence of hemidiaphragmatic paresis associated with interscalene brachial plexus anesthesia as diagnosed by ultrasonography. *Anesth Analg* 72: 498–503.
Van der Stricht J. 1950. A propos d'une anomalie du nerf phrénique. *Assoc Anatomistes Comptes Rendus* 37: 478–484.
Weitz JW, Weitz SL, McElhinney AJ. 1982. A technique for preservation of spinal accessory nerve function in radical neck dissection. *Head Neck Surg* 5: 75–78.
Wernicke. 1897. Insuffizienz der nervi phrenici. *Monatsschar Psych Neurol* 2: 200.
Williams PL, Bannister LH, Berry MM, Collins P, Dyson M, Dussek JE, Ferguson MWJ. 1995. *Anatomía de Gray*, 38th edition. Madrid: Hart-Court.
Winckler G. 1955. A propros des relations que relations que existent entre le plexus cervical et le nerf grand hypoglosse. *Assoc Anatomistes Comptes Rendus* 42: 1415–1419.
Wischnewsky AS. 1930. Die aufbautypen des ramus descendens nervi hypoglossi. *Z Anat Entwicklungs* 92: 551–564.
Yano K. 1925. Zur anatomie des nervus pherincus und nebenphrenicus. *Folia Anatomica Japonica* 3: 95–106.
Yano K. 1928. Zur anatomie und histologie des nervus phrenicus und sogenannten nebenphrenicus, nebst bemerkungen uber ihre verbindung mit sympathicus. *Folia Anat Jap* 6: 247–290.
Ziemessen H. 1882. Erregbarkeit des n. phrenicus. *Arch Klin Med* 30: 270.
Zohar Y, Siegal A, Siegal G, Halpern M, Levy B, Gal R. 2002. The great auricular nerve; does it penetrate the parotid gland? An anatomical and microscopical study. *J Craniomaxillofac Surg* 30: 318–321.

Further reading

Anson BJ, McVay CB. 1971. *Surgical Anatomy, fifth edition*. Philadelphia: WB Saunders.
Cunningham D. 1888. The musculus sternalis. *J Anat Physiol* 22: 391–407.
Huber GC. (ed.) 1930. *Piersol's Human Anatomie, ninth edition*. Philadelphia: L.B. Lippincott.
Krause HR. 1994. Reinnervation of the trapezius muscle after radical neck dissection. *J Craniomaxillofac Surg* 22: 323–329.
Li Y, Zhang J, Yang K. 2013. Evaluation of the efficacy of a novel radical neck dissection preserving the external jugular vein, greater auricular nerve, and deep branches of the cervical nerve. *Onco Targets Ther* 10: 361–367.
Oberländer W. 1975. Beobachtung eines sensiblen astes aus dem ramus dorsalis des 1. cervicalsegmentes. *Anat Anz* 138: 26–28.
Wimmer A. 1958. Einige, darunter seltene nervenvariationen des halsgebietes. *Anat Anz* 105: 391–396.

91 Nerves of the upper extremity

Mark A. Mahan[1] and Robert J. Spinner[2]
[1]University of Utah, Salt Lake City, Utah, USA
[2]Mayo Clinic, Rochester, Minnesota, USA

Variation in the nerves of the upper extremity is profound and relevant to diagnostic and operative success. Nerve variability can produce unexpected clinical manifestations, confusing diagnostic findings, and seemingly incoherent injury patterns if patterns of variation are not appreciated. Surgical exploration for amelioration of neurologic loss or pain may be misguided if the spectrum of variation is not appreciated, dooming surgical outcomes to failure. As an example, many patients with intrinsic muscle atrophy and clawing at the metacarpophalangeal joints in association with posterior interosseous nerve injury have undergone surgical exploration of the ulnar nerve although the injury is due to a known, but infrequent, variation known as the Bichat-Froment-Rauber anastomosis. These variations in nerve distribution and destination are particularly vexing and may prompt an incorrect diagnosis, confuse the surgeon, and create therapeutic failures.

Furthermore, variation in adjacent structures may contribute to the development and clinical variability of neuropathy. Nerves pass through muscle compartments, travel around joints and directly pass through muscles, which provide ample opportunity for the entrapment and consequent injury to nerves. For example, variant muscles or fibrous bands appear to relate to the development of neuropathies and pain syndromes, either by compression or restriction of nerve movement. Understanding the complex regional relationships, zones of anatomic constriction, and the variability of innervation can provide the clinician with the framework to thoughtfully approach complex problems that do not fit textbook norms.

Nerves may intersect and communicate fibers between themselves, creating variant neural pathways. The nerves of the upper extremity arise from the brachial plexus, a complex region of neural intersection where the ventral rami of the cervical and upper thoracic nerves are progressively sorted into bundles for terminal branching. The sorting process is carried out during development; any errors or variation in proximal sorting may lead to correction in the distal regions. Aberrant plexus sorting may therefore underlie the appearance of peripheral communicating branches that intersect between nerves, allowing nerve fibers to arrive at their originally intended destinations. Injury to the nerve proximal to a communicating branch may create confusingly large or little neurological loss, suggesting multiple nerve injuries or injuries at disparate locations.

Variations of the nerves of the upper extremity can be categorized as: relationships with adjacent structures, such as muscles, arteries, and tendons; variation in origin of the nerve; or variation in distribution and target of the nerve; these categories form the basic structure of this chapter. Consideration of the variations related to nerve entrapment and intraneural communications are considered independently, as these topics span multiple domains and sections. Clinical correlations of nerve variation are outside the scope of this chapter, but are covered by Mahan and Spinner (2015).

Variations in the human may resemble the normal structures of other animals, and may therefore represent vestiges of common embryonic vessels and nerves. The early proponents of this principle were Bayer (1893), Zuckerkandl (1894), and de Vriese (1902). In studying the comparative biology and embryologic development of brachial plexus (Miller 1934; Miller and Detwiler 1936), Miller noted an important reciprocal relationship between vessels and nerves that occurs during development, specifically that variation in one may influence variation in the other. Miller asserted that the intrinsic arrangement of the brachial plexus is determined by the origin and course of the subclavian and axillary artery (Miller 1939; Fig. 91.1a, b). Among her lines of evidence, she noted that a sixth segmental artery appeared to relate to the merger of the middle trunk with the inferior trunk. She also found that a brachial plexus, that is associated with a ninth segmental artery, remains a compact structure with short trunks and cords.

Wherever reasonable, we have indicated possible association between anatomic variations in man and normal anatomy in other mammals as it may be that the nature of nerve variation may arise as a combination of embryological and evolutionary processes.

Bergman's Comprehensive Encyclopedia of Human Anatomic Variation, First Edition. Edited by R. Shane Tubbs, Mohammadali M. Shoja and Marios Loukas.
© 2016 John Wiley & Sons, Inc. Published 2016 by John Wiley & Sons, Inc.

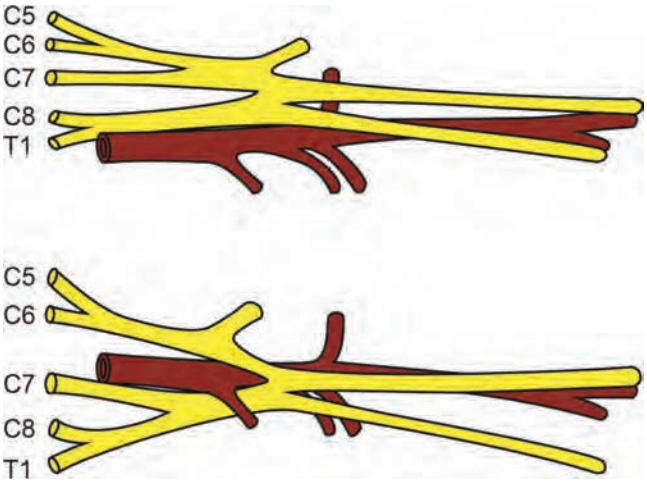

Figure 91.1 Variation of the brachial plexus in relationship to variation of the subclavian artery. Note that a sixth segmental artery appears to lead to fusion of the middle trunk with the lower trunk. Adapted from Miller (1939). Reproduced with permission from the Department of Neurosurgery, University of Utah.

Overview

One perspective that helps to simplify the organization of the brachial plexus and nerves of the upper extremity is to view the organization from the origin of the nerve fibers. For example, the motor neurons that form the fifth cervical root generally serve shoulder movement. Similarly, the sixth cervical root supplies elbow flexion; the seventh cervical root supplies elbow extension; and the eighth cervical and first thoracic root supply hand function. While this is an oversimplification, the segmental architecture of the spinal cord is translated into functional control of specific movements. In essence, the rostrocaudal organization of the spinal cord mirrors the rostrocaudal pattern of the upper extremity.

In addition to this rostrocaudal organization, there is a dorsoventral organization. The ventral muscles are primarily internal rotators at the shoulder and flexors of the forearm, wrist, and fingers. In contrast, the dorsal muscles are shoulder abductors and external rotators and extensors of the forearm, wrist, and fingers. Generally, nerves that supply the ventral muscles are derived primarily from the anterior divisions, whereas dorsal muscles are supplied by the posterior divisions. There are notable exceptions however, such as the brachioradialis muscle which receives primary innervation from the radial nerve.

Another simplification is that the terminal nerves supply specific regions of the limb. In modest approximation, the musculocutaneous nerve supplies the anterior (flexor) arm with motor nerves and the lateral aspect of the forearm with sensory nerves. The median nerve supplies most of the flexor forearm and the thenar part of the hand with motor and sensory nerves. The ulnar nerve supplies some forearm muscles (one and a half) and most of the intrinsic hand muscles. Branches of the posterior cord and the radial nerve supply the scapular and shoulder region and all the extensor muscles of the arm and forearm. Lastly, the large muscles that insert on the thorax, such as the pectoralis major and the latissimus dorsi muscles, generally receive supply from multiple spinal levels, which are formed from proximal branches from the brachial plexus.

The brachial plexus serves to route nerve fibers with a similar function into the proper terminal nerves, such as grouping extensors into the posterior divisions. Errors in distribution usually occur and are corrected distally in the arm, forearm, or hand, such as with the Martin-Gruber anastomoses. As a result of the complexity of the task, the brachial plexus can be extremely variable in form.

Typical brachial plexus

The brachial plexus is usually formed by the ventral primary rami of the fifth to eighth cervical nerves and the greater part of the first thoracic nerve (Fig. 91.2). Branches from the fourth cervical and second thoracic nerves may also contribute.

The fifth through eighth cervical nerves pass dorsal to the vertebral artery and between the anterior and posterior portions of the intertransverse muscles. The nerves course under a fascial cover through the posterior triangle of the neck, usually between the anterior and middle scalenes. At this point, the fifth and sixth nerves receive a gray (unmyelinated) ramus from the middle cervical sympathetic ganglion. The seventh and eighth nerves usually receive their gray rami from the inferior cervical sympathetic ganglion. The first thoracic (and second, if present) receives both gray (sympathetic) and white (ventral primary) rami from the first (and second, if present) thoracic sympathetic ganglia. The first thoracic contribution to the brachial plexus courses upward laterally, crosses the neck of the first rib ventrally, becoming dorsal to the apex of the pleural sac, and finally enters the region of the posterior triangle to join the cervical portion of the plexus.

The ventral primary rami of the fifth and sixth cervical nerves unite to form the upper trunk, the seventh cervical nerve alone forms the middle trunk, and the eighth cervical and first thoracic nerves unite to form the lower trunk. Each of the three trunks divides to form an anterior and a posterior division. Three cords are formed from these divisions. The lateral (outer) cord is formed by the union of the anterior division of the upper and middle trunks (anterior primary division of the fifth, sixth, and seventh cervical nerves). The medial (inner) cord is formed by the union of the eighth cervical and first thoracic nerve. The posterior cord is commonly formed by the posterior divisions of all three trunks containing nerve fibers from all contributions to the plexus.

The lateral cord terminally divides into the musculocutaneous and lateral root of the median nerve, as well as a small branch that merges with the medial root of the median nerve and the ulnar nerve. The posterior cord terminally divides into the

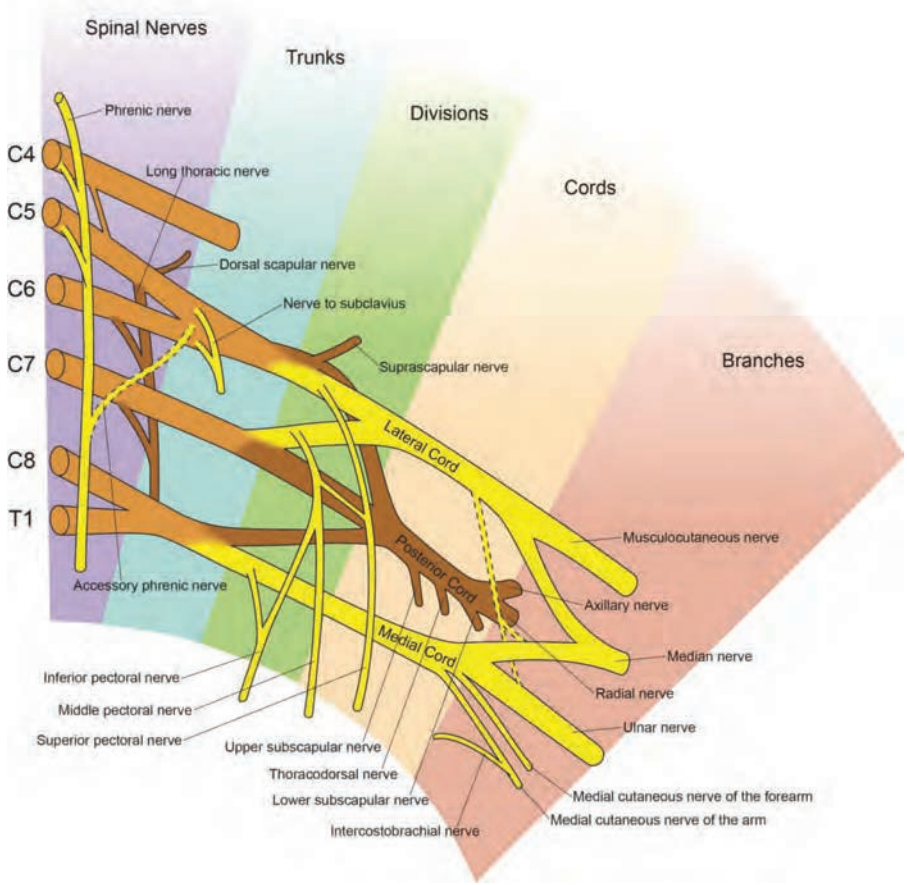

Figure 91.2 Depiction of the brachial plexus with important variations and delineation of the posterior and anterior divisions. In contrast to other depictions of the brachial plexus (Standring 2008), this artistic representation includes the majority of repeatedly described and high-frequency variations, including the accessory phrenic nerve, the fourth cervical and second thoracic nerve contributions, and the lateral cord branch to the medial root of the median nerve. Other anatomical findings that are not well depicted in classic brachial plexus representations, such as the origin of the suprascapular nerve from the posterior division of the upper trunk and the origins and formations of the pectoral plexus, have been detailed. Reproduced with permission from the Department of Neurosurgery, University of Utah.

radial and axillary nerves. The medial cord terminally divides into the medial root of the median nerve and the ulnar nerve. Motor innervation to the musculature of the thoracic wall and scapula typically arises directly from the brachial plexus, including the dorsal scapular nerve, long thoracic nerve, nerve to the subclavius, suprascapular nerve, medial and lateral pectoral nerves (ansa pectoralis or the pectoral plexus), upper and lower subscapular nerves, and thoracodorsal nerve.

Regional relationships

The brachial plexus extends from its medial origin from the spinal nerves, as they exit their respective transverse processes, to the lower border of pectoralis major, where the three cords divide to form their terminal branches. On its medial aspect, the brachial plexus is bound anteriorly by the anterior scalene, posteriorly by the middle scalene, and inferiorly by the first thoracic rib, forming the interscalene triangle. This region is often referred to as the thoracic outlet. This space also contains the subclavian artery, whereas the subclavian vein is anterior to the anterior scalene. Further laterally, in the posterior triangle of the neck, the brachial plexus is covered by the supraclavicular fat pad and is crossed by the external jugular vein, the transverse cervical and suprascapular veins, the transverse cervical and suprascapular arteries, and the posterior belly of the omohyoid muscle. The dorsal scapular artery may pass through or above the plexus, depending on the site of origin of the dorsal scapular artery.

At the level of the coracoid, the cords of the brachial plexus are arranged around the axillary artery. The lateral cord lies lateral to the artery, the medial cord medial to the artery, and the posterior cord is deep to the artery. In this region, the plexus lies on fat and subscapularis. The brachial plexus is covered anteriorly by pectoralis major and minor and the coracoclavicular fascia.

Variations

Cervical ribs, rudimentary cervical ribs, elongated transverse processes, and fibrous bands extending laterally from transverse processes may intersect the brachial plexus. The incidence of a cervical rib is approximately 0.05% (Steiner 1943) to 3% (Gulekon and Turgut 1999) of individuals, with an accepted frequency of 1–2% (Pollack 1980; Brewin et al. 2009; Viertel et al. 2012), although the incidence of elongated transverse processes is likely higher (Brewin et al. 2009). The presence of fibrous bands and accessory muscles at the thoracic outlet is highly variable (33%, Roos 1976; 63%, Juvonen et al. 1995). A scalenus minimus muscle (of Albinus, scalenus pleuralis, petit scalene, scalenus accessorius, scalenus anticus minor, Sibson's muscle), which originates on the seventh cervical transverse process and inserts on the inner margin of the first thoracic rib, passes anterior to the brachial plexus and posterior to the subclavian artery. This muscle may be present in 4–100% of specimens: 4% (Natsis et al. 2013), 10% (Cordier and Devos 1938), 25% (Hafferl 1939), 30% (Daseler and Anson 1959), 33% (Boyd 1934), 34% (Telford and Mottershead 1948), 43% (Macalister 1864), 47% (Gaughran 1964), 54% (Stott 1928), 61% (Gage and Parnell 1947), 72% (Zuckerkandl 1894), or 100% (Le Double 1897). Accessory scalene muscles may also be interpreted as a scalenus minimus, which may artificially inflate the incidence (Paraskevas et al. 2007). The scalenus minimus may be normal in some simian species (Law 1920).

Fibrous bands may extend from the pleural fascia to the cervical vertebral bodies or to the first rib (Sibson's fascia or the ligament costo-pleuro-vertebralis of Zuckerkandl) (Fig. 91.3). There is much disagreement on the precise composition of these fascial attachments between the pleural apex and structures at the root of the neck, as summarized by Gaughran (1964) (Fig. 91.4). The variation and disagreement in dissection is too large a topic to address here; succinctly summarized, three common findings regarding apical pleural membranes include: (1) an expanse that runs from the vertebral bodies to the pleural apex and first rib; (2) a band that runs transversely underneath the lower trunk and a band that passes anteriorly over the lower trunk to connect to the seventh cervical transverse process; and (3) a band that runs anteriorly to posteriorly along the first rib, from which the first thoracic nerve passes underneath to exit laterally. This second structure is very similar to the arrangement of the scalenus minimus, and they may be variations of the same structure, as first noted by Sibson in 1846: "The pleural scalenus [scalenus minimus] arises from the transverse process of the seventh cervical vertebra, becomes tendinous and aponeurotic, and is inserted by a funnel-like tendinous web into the whole circuit of the first rib" (Sibson 1846; Fig. 91.3). These bands have been re-categorized by later authors (Roos 1976) into a numbered system without acknowledgement of prior anatomical studies, suggesting independent and identical observation of such variant suprapleural and muscular bands.

The upper trunk may have a variable emergence from the anterior scalene (13% of specimens, Natsis et al. 2006; 37%, Harry et al. 1997). Common variations include passage of the fifth cervical nerve superficial to the anterior scalene (2% of specimens, Matejcik 2005; 3%, Natsis et al. 2006; 3%, Harry et al. 1997)

Figure 91.3 Fascial bands arising from the pleural membrane.

Source: Poirier and Charpy (1901).

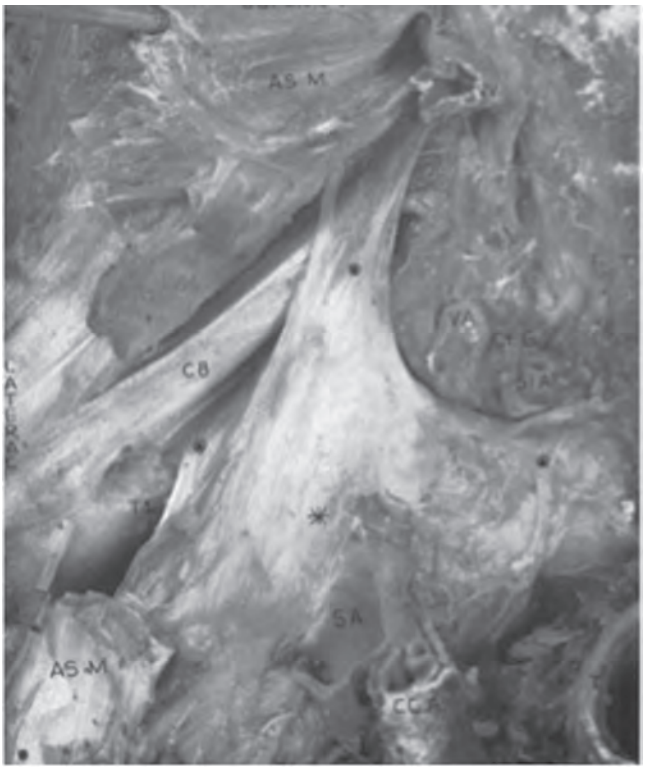

Figure 91.4 Depiction of suprapleural membranes.

Source: Gaughran (1964). Reproduced with permission from John Wiley & Sons.

or piercing the muscle (1% of specimens, Natsis et al. 2006; 13% Harry et al. 1997), the upper trunk superficial to the anterior scalene (2% of specimens, Natsis et al. 2006) or perforating the muscle (6% of specimens, Natsis et al. 2006; 15%, Harry et al. 1997), and the fifth cervical and sixth cervical nerves independently perforating the muscle (6% of specimens, Harry et al. 1997). Telford and Mottershead (1948) noted that the insertion of the upper and middle scalene muscles may be overlapping or falciform, which may compress the brachial plexus.

The dorsal scapular artery (descending scapular artery or deep branch of the transverse cervical artery) may pass over the brachial plexus or pierce the brachial plexus in its dorsal trajectory, which has been found to correlate with the origin of the artery. When the dorsal scapular artery arises directly from the subclavian artery (31% of specimens, Chaijaroonkhanarak et al. 2014; 69%, Huelke 1958; 75%, Reiner and Kasser 1996), it pierced the brachial plexus. When the dorsal scapular artery arose from the thyrocervical trunk, which is the other origin (23% of specimens, Reiner and Kasser 1996; 30%, Huelke 1958; 69%, Chaijaroonkhanarak et al. 2014) the dorsal scapular artery passed over the brachial plexus and did not pierce between the nerves. The most common location of the dorsal scapular artery to pierce the brachial plexus is between the upper and middle trunks (46% of specimens, Huelke 1958; 63%, Chaijaroonkhanarak et al. 2014; 69%, Reiner and Kasser 1996). Between the middle and lower trunks is the second most common location (18% of specimens, Chaijaroonkhanarak et al. 2014; 31%, Reiner and Kasser 1996; 44%, Huelke 1958) where the dorsal scapular artery pierced the brachial plexus (Fig. 91.5).

Origins

The brachial plexus is primarily composed of the anterior primary divisions of the fifth, sixth, seventh, and eighth cervical and first thoracic nerves. It may also receive variable branches from the fourth cervical and second thoracic nerves. The contribution of the roots to the brachial plexus as well as their pattern of muscle innervation comes from three lines of evidence: human anatomical studies, human electrophysiologic studies, and analogy to animal studies.

Multiple authors have noted a variable shift of the predominant source of the brachial plexus. Historically, descriptions have typically categorized plexuses as prefixed (cephalic or high) brachial plexus versus postfixed (caudal or low) brachial plexus based on the contributions of the adjacent spinal nerves. A prefixed plexus is one in which the fourth cervical nerve contributes a large branch to the formation of the plexus, whereas the contribution from the first thoracic nerve is small. A postfixed plexus receives little or no contribution from the fourth cervical nerve, whereas the first thoracic branch is large and the second thoracic nerve supplies a branch to the plexus. Other authors have noted contributions of the fourth cervical and second thoracic levels independent of a prefixed or postfixed pattern, including both intradural and extrathoracic communications. Additionally, different authors have defined the criteria determining pre- and postfixed differently, which has the effect of increasing the variability of prevalence without true differences in anatomy (Pellerin et al. 2010).

The incidence of fourth cervical nerve contribution to the brachial plexus commonly ranges over 22–63% (22%, Lee et al. 1992; 23%, Yan and Horiguchi 2000; 26%, Loukas et al. 2007b; 28%, Tubbs et al. 2009b; 41%, Bonnel and Rabischong 1980; 41%, Senecail et al. 1979; 63%, Kerr 1918; Table 91.1). Several authors have found intradural communications between adjacent dorsal and ventral rootlets in the cervical spine, with one or more such connection found in most specimens (Schwartz 1956; Marzo et al. 1987). Even in plexuses without prefixation at the roots of the plexus, 17–36% of specimens had an intradural connection between the fourth cervical and fifth cervical levels (17%, Tubbs et al. 2009b; 21%, Marzo et al. 1987; 23%, Tubbs et al. 2008; 31–36%, Tanaka et al. 2000). However, interconnections are uncommon between the first and second

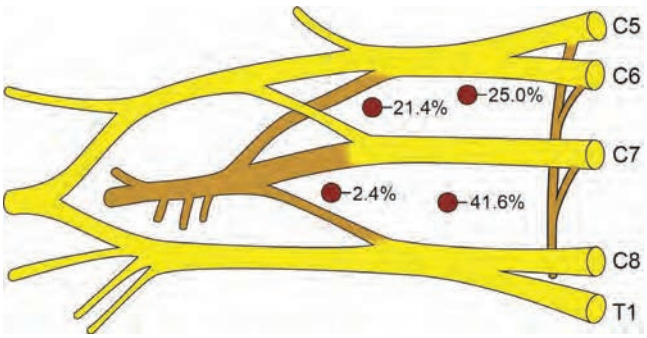

Figure 91.5 Frequency map detailing the locations where the dorsal scapular artery pierced the brachial plexus, when the dorsal scapular artery arose directly from the subclavian artery. Adapted from Huelke (1958). Reproduced with permission from the Department of Neurosurgery, University of Utah.

Table 91.1 Specimens with prefixed and postfixed brachial plexuses.

Reference	Sample size	Prefixed brachial plexus (%)	Postfixed brachial plexus (%)
Bonnel and Rabischong 1980	100	41	4
Fazan et al. 2003	54	24	6
Kerr 1918	175	63	7
Lee et al. 1992	152	22	1
Loukas et al. 2007b	214	26	4
Matejcik 2003	110	24	1
Tubbs et al. 2009b	60	28	5
Tubbs et al. 2008	60	15	0
Uysal et al. 2003	200	2	3
Yan and Horiguchi 2000	48	23	0

thoracic levels (Marzo et al. 1987; Tubbs et al. 2009b). The fourth cervical nerve may also provide fibers to the long thoracic nerve (Ramamurthy et al. 1990) or the suprascapular nerve (Lee et al. 1992), independent of plexal connections.

Postfixed plexuses are less common. The frequency of a postfixed brachial plexus has commonly ranged over 1–24% (3%, Uysal et al. 2003; 4%, Loukas et al. 2007b; 5%, Tubbs et al. 2009b) of specimens, which may depend largely on the definition of postfixation. However, absence of postfixation does not indicate that the second thoracic nerve does not participate in the formation of the brachial plexus. Cunningham (1877) noted that 73% of plexuses had a contribution from the second thoracic nerve. Other early anatomists found similarly frequent contributions from the second thoracic nerve (30% of specimens, Kerr 1918; 33%, Paterson 1896; 58%, Harman 1900). Recently, Loukas and colleagues studied the contribution of the second thoracic nerve in non-prefixed, non-postfixed specimens, as defined by the spinal level of the first contributing nerve. In this group, they found that 17% of specimens had an intrathoracic contribution from the second thoracic nerve and a communication from the second thoracic nerve occurred extrathoracically in 86% of these specimens. They concluded that even in so-called "'typical" plexuses, 100% had communications with the second thoracic nerve. However, it should be noted that there is an intimate and variable relationship between the first and second thoracic nerves and the neighboring sympathetic ganglia, such as the nerve of Kuntz (Fig. 91.6), which might confuse dissections (Harman 1900).

Sympathetic innervation of the upper arm derives from the intermediolateral cell column of the upper thoracic spinal cord. It has been found that the fibers from the second to eighth thoracic levels may participate in the sympathetic innervation of the upper extremity, although a narrow number of thoracic levels has also been suggested (Cho et al. 2005; Zhang et al. 2009). A variant communication from the second thoracic level to the brachial plexus, commonly referred to as the nerve of Kuntz (1927), may exist in 12–68% of individuals (12%, Marhold et al. 2008; 34%, Ramsaroop et al. 2001; 67%, Marhold et al. 2008; 68%, Chung et al. 2002), which has been found less commonly in intraoperative series (Marhold et al. 2008).

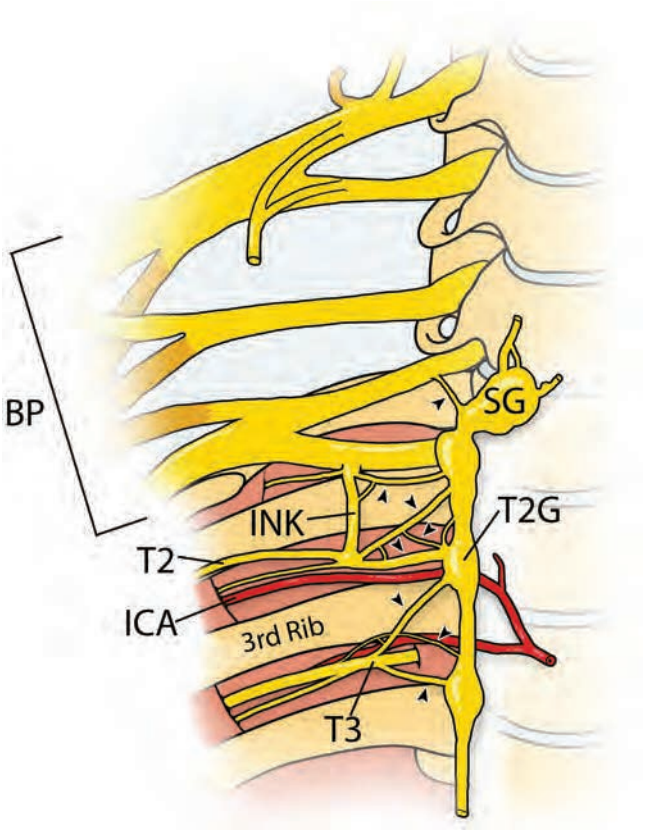

Figure 91.6 Depiction of the intercostal nerve of Kuntz. INK, intercostal nerve of Kuntz; BP, brachial plexus; ICA, intercostal artery; RC, ramus communicans; SG, stellate ganglion; ST, sympathetic trunk. Arrowheads indicate the ramus communicans. Adapted from Chung et al. (2002). Reproduced with permission from the Department of Neurosurgery, University of Utah.

Variation in morphology and targets

The form, branching, and composition of nerves are extremely variable; as many as 38 distinct patterns of variations have been cataloged (Kerr 1918). Kerr placed brachial plexus variations into two categories: one in which proximal patterns were different but the terminal branches were composed of fibers from the same spinal nerves as the usual pattern; and one in which the distribution of fibers from the spinal nerves was different from the common pattern. This primarily occurred when the fibers of the seventh or eighth cervical nerves went to the medial cord or the lateral cord, respectively.

In consideration of this second group, several authors have identified a branch to the medial head of the median nerve that may arise from the anterior division of the middle trunk, the lateral cord, or the lateral head of the median nerve. A similar branch from the upper plexus may also be found to contribute to the medial cord or the ulnar nerve proper. Walsh (1877) considered this thin branch, which he noted arising from the lateral cord, a constant (Fig. 91.7). Other authors have reported it infrequently. One may well consider this branch, due to reports of both great variability and consistency, as a communication between the medial and lateral cords, as Linell (1921a) did (54% of specimens). It is described below in both the sections on "Division variation" and "Cord variation".

Trunk variations

Most commonly, when the fourth cervical nerve contributes to the brachial plexus, it joins the fifth cervical nerve proximal to the fifth cervical nerve's juncture with the sixth cervical nerve (Walsh 1877; Kerr 1918). On occasion however, the upper trunk may form from the fourth and fifth cervical nerves. In this case, the sixth cervical nerve continues independently to divide into

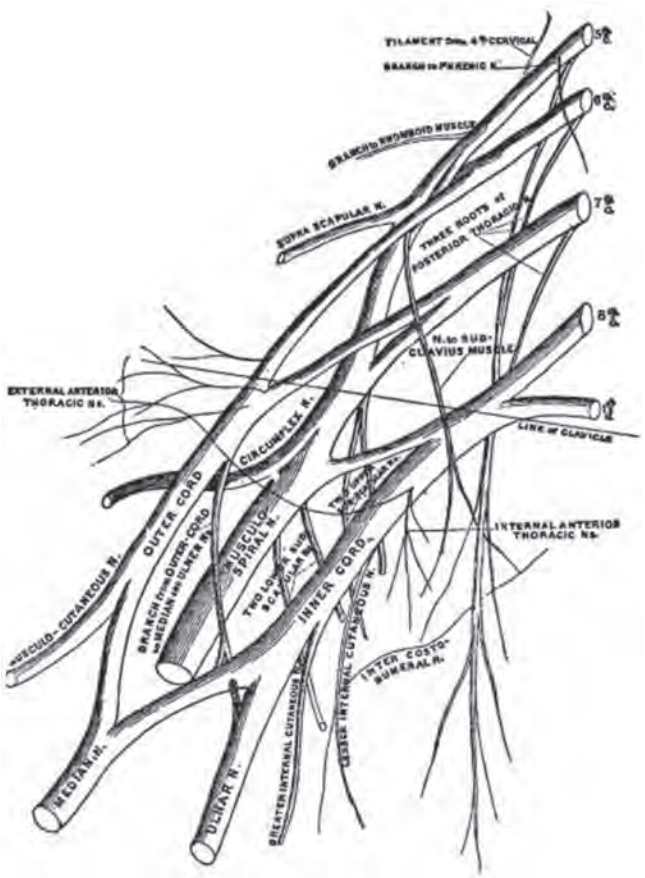

Figure 91.7 The brachial plexus; note the presence of the communication from the lateral (outer) cord to the medial (inner) cord.

Source: Walsh (1877).

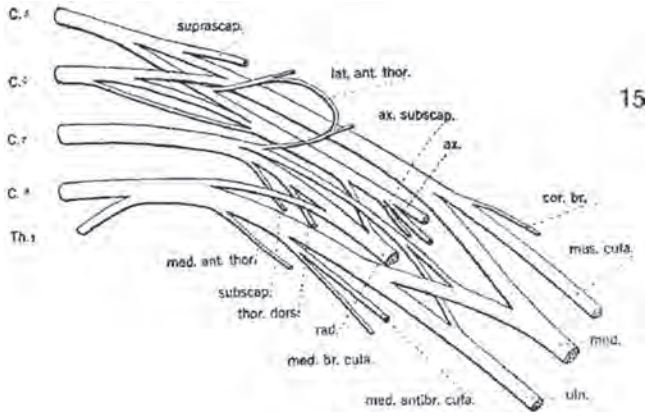

Figure 91.8 Brachial plexus demonstrating three brachial plexus variations: (1) the absence of an upper trunk; (2) the absence of a posterior cord; and (3) the contribution of a branch from the middle trunk to the medial head of the median nerve and the ulnar nerve.

Source: Kerr (1918). Reproduced with permission from John Wiley & Sons.

anterior and posterior branches which join the lateral cord and the posterior cord, respectively (Uysal et al. 2003).

Occasionally, spinal nerves will not combine to form formal trunks. The fifth and sixth cervical nerves may not join (1%, Uysal et al. 2003; 3%, Matejcik 2003; 10%, Kerr 1918) to form the upper trunk. Most commonly, each spinal nerve then branches into two independent anterior and posterior branches which then join to form the lateral and posterior cords, respectively (Fig. 91.8) (Kerr 1918; Singla et al. 2011). In contrast to the low frequency of this pattern by others, Walsh (1877) concluded that a simultaneous merging and dispersion of the fifth and sixth cervical nerve into the anterior and posterior divisions of the upper trunk, that is to say, no definite upper trunk, was the most consistent arrangement of the upper trunk. Infrequently, the upper trunk and middle trunk may merge into one bundle prior to dividing into the anterior and posterior divisions (2%, Kerr 1918; 4%, Matejcik 2003).

The inferior trunk may not form in 1–10% (Uysal et al. 2003) of brachial plexuses (1%, Matejcik 2003; 5%, Chaudhary et al. 2012; 5%, Kerr 1918; 9%, Uysal et al. 2003; 10%, Uysal et al. 2003). In these cases, the eighth cervical nerve is divided into two or three branches, where one merged with the posterior cord and the others joined to form the medial cord or also give a branch to the lateral cord (Chaudhary et al. 2012). In these cases, the first thoracic nerve did not provide a branch to the posterior cord; instead, it unites with the anterior branch of the eight cervical nerve to form the medial cord (Kerr 1918; Uysal et al. 2003). In several cases, the second thoracic nerve sends fibers to the first thoracic nerve which may be interpreted as a "lower trunk" formed from the first and second thoracic nerves. Similar to the situation with the upper trunk, the middle trunk may merge with the lower trunk prior to ramification into the divisions (3%, Matejcik 2003). Occasionally, the inferior trunk does not send a branch to the posterior division (1%, Matejcik 2003; 9%, Fazan et al. 2003). The eighth cervical nerve or the lower trunk may send a branch to the middle trunk, lateral cord, or lateral head of the median nerve (4%, Kerr 1918).

As a final consideration, many authors have noted that trunk level variations may be created through dissection techniques; specifically, whether more or less connective tissue is removed (Walsh 1877; Kerr 1918) (Fig. 91.9). Caution must be advised in the interpretation of incidence and variety of trunk level anomalies.

Division variations

A branch from the anterior division of the middle trunk may join the medial head of the median nerve, the medial cord, or directly to the ulnar nerve (Kerr 1918; Linell 1921a; Huber 1936; Bonnel and Rabischong 1980) in 3% (Kerr 1918), 4% (Walsh 1877), or 5% (Uysal et al. 2003) of specimens).

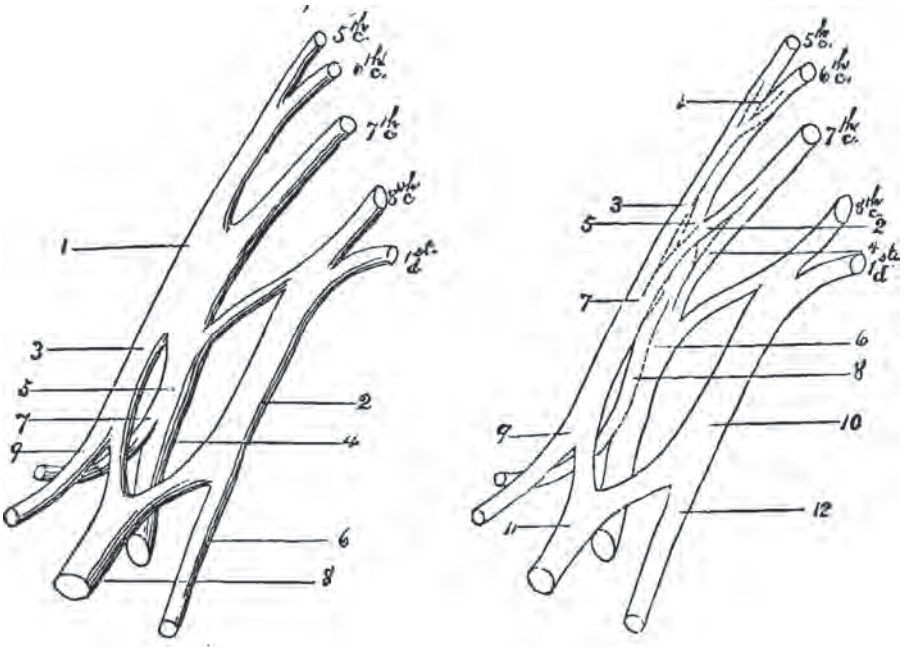

Figure 91.9 Depiction of pseudo-variation. The plexus on left has "fascial envelope" intact, whereas the plexus on the right has the "fascial envelope" removed. Removal of this fascia accounts for Walsh's assertions that a single upper trunk and a definitive posterior cord do not exist.

Source: Walsh (1877).

Cord variations

Kerr (1918) found that the lateral cord develops strictly from the anterior divisions of the upper and middle trunks in only 82% of specimens. The lateral cord may receive contributions from the lower trunk or the eighth cervical nerve in 2% (Matejcik 2003) or 3% (Kerr 1918) of specimens. The lateral cord may not receive contributions from the middle trunk in 3% (Uysal et al. 2003) or 4% (Kerr 1918) of specimens, and therefore does not receive contributions from the seventh cervical nerve. This may be called an absence of the lateral cord, as the origin of the musculocutaneous and lateral head of the median appears to be from the anterior division of the upper trunk. In this pattern, a branch from the anterior division of the middle trunk contributes directly to the median nerve. As described above, the medial head of the median nerve may receive contribution from the lateral cord, from the anterior division of the middle trunk or from a trifurcation of the middle trunk. Whereas some authors found a branch from the lateral cord to the medial head of the median nerve to be essentially constant (86%, Harris 1904; 91%, Walsh 1877; 100%, Matejcik 2003), it has not been mentioned by a number of authors or is an infrequent observation (1%, Pandey and Shukla 2007; 5%, Uysal et al. 2003). The lateral head of the median nerve may arise from the anterior division of the middle trunk, rather than the lateral cord (Matejcik 2003). Likewise, there may be two lateral heads from the lateral cord to the median nerve (4%, Walsh 1877). The lateral cord may fail to divide into a musculocutaneous and median nerve (Le Minor 1990; Nakatani et al. 1997b); it was reported as being rare (0%, Fazan et al. 2003) or merely infrequent (15%, Linell 1921a), as described in the section on "Communications between the musculocutaneous and median nerves".

The medial cord forms from the anterior division of the lower trunk; variation may occur when the eighth cervical nerve divides into anterior and posterior branches prior to merging with the first thoracic nerve (3%, Kerr 1918). Infrequently, the medial cord may be "absent" where the medial cord and lower trunk are identical and the posterior division arises from the medial head to the median nerve (Kerr 1918).

A formal posterior cord may not exist in some individuals (3%, Matejcik 2003; 4%, Pandey and Shukla 2007; 20%, Kerr 1918; 71%, Bonnel and Rabischong 1980); Walsh went even further to state "There is no true posterior cord, such as, for instance, Gray, Quain, Sappey, Cruveilhier, Henlé and Hyrtl describe it" (Walsh 1877). When a posterior cord does not form, the axillary nerve branches from the posterior division of the upper trunk or upper and middle trunks. Likewise, the radial nerve forms from the fusion of two heads, a cephalic and a caudal head, derived from the posterior divisions (20%, Kerr 1918). There are two configurations of the two heads. In the first, the posterior divisions of the upper and middle trunks merge to form a cephalic head of the radial nerve, which then joins a caudal head derived from the posterior division of the lower trunk (11%, Kerr 1918). In the second, the posterior division of the middle trunk joins the posterior division of the lower trunk to form a caudal head of the radial nerve, which then joins a cephalic head formed from the posterior division of the upper trunk (6%, Kerr 1918). The posterior cord may infrequently provide branches to the median and ulnar nerves (Matejcik 2003; Pandey and Shukla 2007). The posterior cord may divide around the subscapular artery to then reunite and continue as the radial nerve (Bhat and Girijavallabhan 2008).

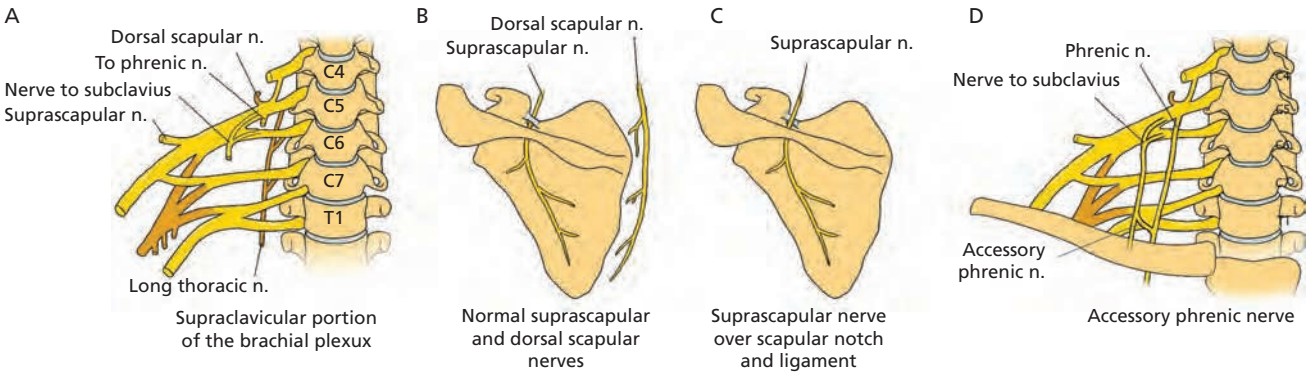

Figure 91.10 (a–c) Depiction of the common anatomy of the nerves arising from the supraclavicular brachial plexus, and (d) a variant origin of an accessory phrenic nerve. Adapted from Bergman et al. (1988). Reproduced with permission from the Department of Neurosurgery, University of Utah.

Nerves arising from the supraclavicular brachial plexus

There are generally six nerves that arise from the supraclavicular portion of the brachial plexus; four from the spinal nerves and two from the trunks (Fig. 91.10; Table 91.2).

Dorsal scapular nerve

The most cranial branch is the dorsal scapular nerve. It usually arises from the fifth cervical nerve and frequently has a contribution from the fourth. It courses downward and dorsally, crossing the middle scalene and passing beneath the anterior border of levator scapulae. The nerve parallels the medial border of the scapula and supplies the lower portion of levator scapulae and both rhomboideus minor and major muscles successively.

Regional relationships

The dorsal scapular nerve may pierce levator scapulae instead of passing deep to the muscle.

Table 91.2 Nerves arising from the supraclavicular brachial plexus.

Branches	Nerve origins
From spinal nerves	
Nerves to scaleni and longus colli	C5–8
Branch to phrenic nerve	C5
Dorsal scapular nerve	C5
Long thoracic nerve	C5, 6 (7)
From trunks	
Nerve to subclavius	C5, 6
Suprascapular nerve	C5, 6

Origins

In a study of 20 cadaveric specimens, one dorsal scapular nerve derived innervation from the fifth and sixth cervical nerves, whereas the remainder received exclusive contribution from the fifth cervical nerve. In a study of 152 plexuses, the dorsal scapular nerve arose from the upper trunk 9% of cases, from the fourth cervical and fifth cervical ventral rami in 8% of specimens, from the fifth cervical and sixth cervical ventral rami in 8%, and from the fifth cervical ventral ramus in 76% (Lee et al. 1992).

Targets

One cadaveric study found that the dorsal scapular nerve supplied the levator scapula in only 11 of 35 specimens (Frank et al. 1997).

Long thoracic nerve

The long thoracic nerve that supplies serratus anterior arises usually from three cervical nerves: the fifth, sixth, and seventh. Fibers from two cervical nerves, the fifth and sixth, pierce and pass through the middle scalene. The seventh passes ventrally or in front of the middle scalene muscle and joins the long thoracic on the lateral border of the scalenes. The long thoracic nerve lies deep to the suprascapular nerve. Branches of the fifth and sixth cervical nerves supply the upper digitations of serratus anterior and may exist as a distinct upper branch of the long thoracic nerve (Bertelli and Ghizoni 2005). Distally, all branches join to form a common trunk. The trunk passes downward and behind the brachial plexus and the first part of the axillary artery, but lies superficially on the axillary surface of the muscle, supplying each digitation of the muscle.

Regional relationships

Infrequently, the long thoracic nerve does not pass through the middle scalene muscle, and the nerve trunk is formed over the first rib. The nerve is usually composed of fibers from the fifth,

sixth, and seventh cervical nerves; the fifth and sixth may pierce the middle scalene while the seventh passes in front of that muscle and behind the anterior scalene muscle. The fibers from the fifth and sixth cervical nerves may either fully penetrate the middle scalene (and therefore course between the middle and posterior scalene muscles), partially penetrate, or not penetrate the middle scalene (and therefore course anterior to the middle scalene muscle) (Tubbs et al. 2006b).

Origins

The long thoracic nerve has been reported to receive a contribution from the fourth cervical and fifth cervical nerves, which may not join the main trunk of the long thoracic nerve but pass directly to the upper digitations of serratus anterior. The nerve may receive a branch from the eighth cervical nerve and, with equal frequency, the branch from the seventh cervical nerve is absent (Thomas Horwitz and Tocantins 1938). Some authors have noted a frequent innervation of the lower serratus by intercostal nerves (Erdogmus and Govsa 2005).

Targets

A separately formed branch from the fifth cervical nerve may separately innervate the upper serratus anterior.

Suprascapular nerve

The suprascapular nerve supplies both supraspinatus and infraspinatus muscles. The nerve is derived from the fifth and sixth cervical nerves. The suprascapular nerve is classically described as originating from the upper trunk, but may commonly arise from the posterior division of the upper trunk. The nerve passes distally and dorsally and parallels the dorsal scapular nerve. It lies initially at the upper border of the posterior belly of omohyoid, lateral but dorsal to that muscle. It passes beneath trapezius and reaches the superior scapular notch to join the suprascapular artery. Usually, the two structures are separated by the superior transverse scapular ligament with the artery passing above the ligament and nerve. After entering the supraspinous fossa, the nerve branches and supplies the muscle from its deep side and also sends a branch to the shoulder joint. It then descends to pass around the notch of the scapular neck (great scapular notch) to supply infraspinatus, also from branches on the deep side of the muscle (Fig. 91.10b, c).

Regional relationships

The relationship between the suprascapular nerve and the superior transverse scapular ligament is highly variable. The suprascapular nerve may pass above along with the artery, or both may pass below the ligament. In some cases, the nerve divides into two parts. The upper branch may pass through or above the transverse ligament of the scapular notch, and the lower branch has been found passing through a foramen in the scapula below the notch. The entire nerve may pass above the ligament instead of taking its usual course below the ligament.

The superior transverse scapular ligament may be partially or completely ossified; complete ossification creates a neuroforamen. Complete ossification may narrow the nerve passage, compared with non-ossified specimens (Tubbs et al. 2013b).

There are many variations in the superior transverse scapular ligament, including variations with multiple bands (Ticker et al. 1998).

Origins

In 50% of individuals, the fourth cervical nerve also contributes to the nerve. The suprascapular may arise solely from the fifth cervical nerve.

Walsh (1877) identified the origin of the suprascapular nerve as the posterior division of the upper trunk, which had largely been neglected in anatomy texts. Arad et al. (2014) reviewed 100 cadaveric specimens and found the origin of the suprascapular nerve from the posterior division of the upper trunk in 66%, from the upper trunk proper in 29%, and from the nerves in the remainder.

Targets

The suprascapular nerve may provide branches to teres minor, the upper part of subscapularis, the scapula and its periosteum, and the acromioclavicular articulation.

Phrenic nerve and nerves to subclavius, scalenus, and longus colli

A branch from the fifth cervical nerve contributes to the formation of the phrenic nerve, which arises from the third and fourth cervical nerves. The phrenic nerve courses anterior to the anterior scalene muscle and anterior to the subclavian artery. An accessory phrenic nerve is a frequent variation, often carrying fibers from the fifth cervical nerve to the diaphragm through the nerve to subclavius or third cervical nerve through the ansa cervicalis.

The nerve to subclavius is usually a small branch from the fifth cervical nerve, but the fourth and sixth cervical nerves may also contribute. It runs distally, anterior to the lower portion of the brachial plexus and the subclavian artery (third portion). It pierces the clavipectoral fascia and enters the subclavius at its inferior deep border. The nerve may innervate the clavicular part of the sternocleidomastoid muscle (Turner 1872).

Nerves from the sixth, seventh, eighth and, occasionally, the fifth cervical nerves supply the scalene and longus colli muscles.

Regional relationships

The accessory phrenic nerve may join the main trunk of the phrenic nerve either distal or proximal to the subclavian vein (Fig. 91.10d). The accessory phrenic nerve may pass beneath the vein along with the main trunk of the phrenic, or it may loop over the vein to join the main trunk at some inconstant point within the thorax. In an overwhelming majority of cases, the accessory phrenic nerve lies lateral to the phrenic nerve.

Origins

The incidence of an accessory phrenic nerve ranges over 18–80% (Nayak et al. 2008), with the most frequent estimates of 50–65%. In a study of 160 cadaveric specimens (Loukas et al. 2006a), an accessory phrenic nerve arose from the nerve to subclavius in 61%, ansa cervicalis in 12%, and nerve to sternohyoid in 7%. Other common sources include the upper trunk, supraclavicular nerve, spinal accessory nerve, hypoglossal nerve, and independently from the third, fourth, or fifth cervical nerve.

Targets

The right phrenic nerve descends immediately lateral or posterolateral to the inferior vena cava, although it may occasionally be anterolateral. The left phrenic nerve descends over the anterolateral angle of the pericardial base to reach the diaphragm. Both nerves always divide into a variable number of branches, from two to seven (Botha 1957). There remains much debate as to whether there is intercostal innervation to the diaphragm.

Nerves arising from the lateral cord of the brachial plexus

The nerves that arise from the lateral cord (Fig. 91.11a; Table 91.3) include the lateral pectoral nerve(s), the nerve to the coracobrachialis, and the musculocutaneous nerve. The lateral

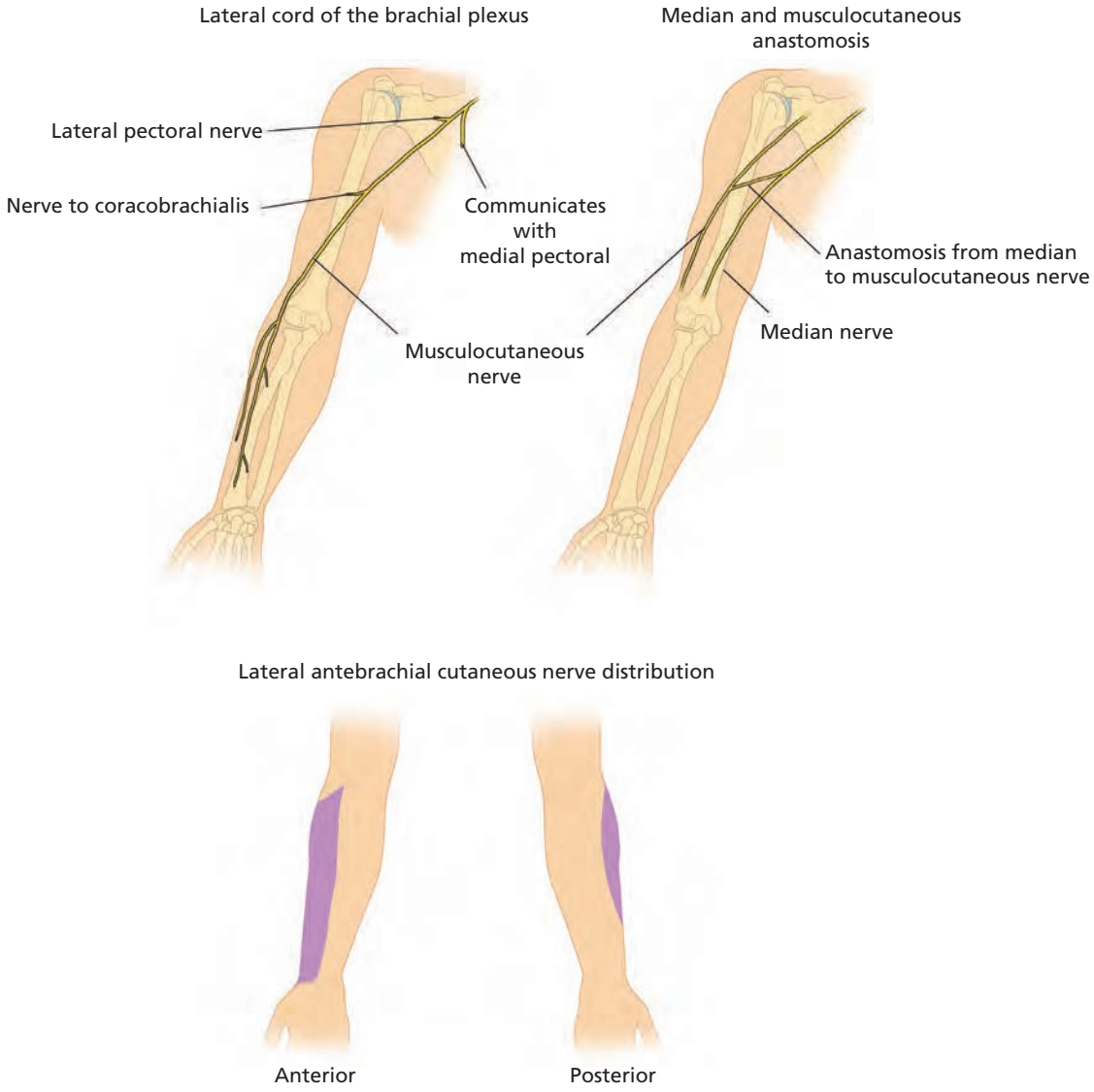

Figure 91.11 Depiction of the common anatomy of the nerves arising from the lateral cord of the brachial plexus, including (upper, right) the most common configuration of a median and musculocutaneous communication and (lower) the cutaneous distribution of the lateral antebrachial cutaneous nerve. Adapted from Bergman et al. (1988). Reproduced with permission from the Department of Neurosurgery, University of Utah.

Table 91.3 Nerves arising from the lateral cord of the brachial plexus.

Branches from lateral cord	Nerve origins
Lateral pectoral branches	C5–6
Nerve to coracobrachialis	C5–7
Musculocutaneous nerve	C5–7

cord provides a contribution to the median nerve, which is discussed in the section on "Nerves arising from the medial cord of the brachial plexus".

The separation of lateral cord fibers destined to form the median nerve is imperfectly achieved at the terminus of the lateral cord. Frequently, there are communicating branches between the musculocutaneous and median nerves. This topic is discussed in a separate "Communications" section below.

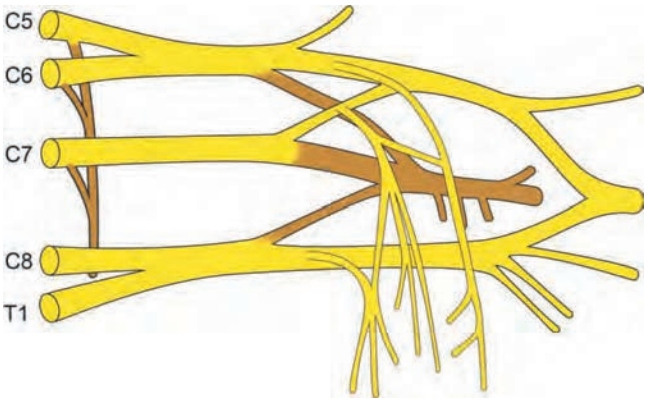

Figure 91.12 Generalized relationship of the pectoralis nerves. Adapted from Lee (2007a). Reproduced with permission from the Department of Neurosurgery, University of Utah.

Pectoral branches

The pectoralis major is somewhat unique in that it commonly receives innervation from all five spinal nerves that form the brachial plexus (fifth cervical nerve through first thoracic nerve), which means it receives fibers from the outflow of the upper, middle, and lower trunks. The branch pattern is currently undergoing reclassification.

Classic anatomic descriptions describe the innervation of the pectoralis muscles as arising from a lateral pectoral nerve and a medial pectoral nerve, the naming of which reflects the origin of the nerves from the medial or lateral cord and not anatomical position. However, many recent reports have identified a consistent superior pectoral nerve (or branch) in addition to the classically described two-nerve depiction, and hence renamed the pectoral nerves as superior, middle, and inferior (Aszmann et al. 2000). Our review of the original descriptions of the pectoral nerves suggests that the classic two-nerve description of pectoral innervation potentially oversimplifies those early descriptions (Kerr 1918), and that multiple branches from the brachial plexus may contribute to pectoralis innervation. Adding further confusion, some authors have called this nerve complex the subpectoral plexus (Lee 2007a) (Fig. 91.12).

Further complicating the naming and description of the pectoral nerves, the lateral pectoral nerve (or superior and middle pectoral nerves) rarely arises from the lateral cord. Rather, it commonly arises from the anterior division of the upper and middle trunks. Similarly, the medial pectoral nerve more commonly arises from the anterior division of the lower trunk, rather than the medial cord proper (Aszmann et al. 2000; Porzionato et al. 2012). One should be aware that the anterior division of the lower trunk and the medial cord is a continuous structure; this is a difference in naming convention and not anatomy. Various authors define the distinction between the anterior division of the lower trunk and the medial cord differently (Linell 1921a; Loukas et al. 2006b).

Some of the nerve fibers from the lateral pectoral nerve unite with fibers from the medial pectoral nerve, forming a loop that lies anterior to the first part of the axillary artery (ansa pectoralis). The lateral pectoral nerve innervates the upper and medial portions of pectoralis major, as well as parts of the shoulder and the acromioclavicular joints. The medial pectoral nerve primarily innervates the pectoralis minor and lower portions of the pectoralis major muscles.

Regional relationships

The ansa pectoralis usually encircles the thoracoacromial artery, with one origin from the lateral cord or anterior divisions of the upper and middle trucks and the other origin from the medial cord, as the lateral cord lies on the superficial aspect of the axillary artery and the medial cord is deep to the axillary artery. The presence of the ansa pectoralis has been reported as variable in some series (Macchi et al. 2007), but uniform in others (Aszmann et al. 2000; Loukas et al. 2006b; Sefa Ozel et al. 2011). The origin and destination of the ansa pectoralis are variable; the most frequent origin is the deep branch of the lateral pectoral nerve or middle pectoral nerve. Similarly, one study identified that the ansa pectoralis crossed the axillary artery at the second segment, specifically, distal to the thoracoacromial artery, in 90% of cases (Loukas et al. 2006b).

The medial pectoral nerve may pass on the lateral aspect of the pectoralis minor, through the muscle, or as a variable number of branches that may do either.

Origins

Classic anatomical descriptions indicate that the pectoralis minor muscle is innervated by cervical spinal nerves six through eight (Standring 2008). However, the spinal root contribution to the pectoral nerves may vary. In 30 brachial plexuses studied

for spinal nerve contributions, only half of the lateral pectoral nerves received contributions from the fifth cervical nerve (Lee 2007a). Similarly, one quarter of the medial pectoral nerves did not receive contributions from the first thoracic nerve.

As indicated above, the origin of the fibers from the upper and middle trunks to the pectoralis muscles has been described as a common lateral pectoral trunk (classic description) or as independent superior and middle branches.

Targets

The lateral pectoral nerve is often described as innervating the upper pectoralis major, whereas the medial pectoral nerve innervates the pectoralis minor and lower pectoralis major. The superior branches of the pectoral nerve typically innervate the most rostral aspect of the pectoralis, specifically the lateral and clavicular areas of the muscle.

Cutaneous branches of the lateral pectoral may provide branches to the axillary and mammary regions.

The medial pectoral nerve may supply branches to the clavicular head of deltoid and to the acromioclavicular articulation.

Nerve to coracobrachialis

Many anatomy texts describe the origin of the nerve to the coracobrachialis muscle as arising from the musculocutaneous nerve. However, the origin of the nerve to the coracobrachialis muscle may be variable and has been noted to arise independently from the lateral cord.

Regional relationships

The nerve to the coracobrachialis arises from the musculocutaneous nerve proximal to the passage of the musculocutaneous nerve through the coracobrachialis muscle (Flatow et al. 1989). Typically, the nerve to the coracobrachialis entered the muscle 3 cm below the coracoid process, whereas the musculocutaneous nerve enters the muscle at least 5–6 cm below the coracoid process and often much further distally (Flatow et al. 1989; Clavert et al. 2009; Pianezza et al. 2012).

Origins

The nerve to the coracobrachialis arose from the musculocutaneous nerve in 50% of Kerr's series (Kerr 1918). The nerve to the coracobrachialis usually consists of several small branches that leave the main trunk of the musculocutaneous nerve, near its origin.

Anatomical texts have described the origins of the nerve fibers to the coracobrachialis as arising from the fifth to seventh cervical nerves (Mancall et al. 2011) or limited to the sixth to seventh cervical nerves (Lindner 1989). Woo et al. (2010) found that only the sixth and seventh cervical nerves contributed to the nerve to the coracobrachialis, with no contribution from the fifth cervical nerve in 45 specimens. Furthermore, the nerve fibers from the seventh cervical nerve have been found to pass independently to supply the muscle on multiple occasions.

Targets

The nerve to the coracobrachialis may ramify into multiple branches prior to the insertion on the coracobrachialis muscle, with two-thirds having two to three branches (Clavert et al. 2009).

Musculocutaneous nerve

The musculocutaneous nerve supplies the flexors of the arm, including the coracobrachialis, biceps brachii, and brachialis muscles, and the skin of the anterolateral forearm via the lateral antebrachial cutaneous nerve, which is the distal-most branch of the musculocutaneous nerve.

Initially, the nerve lies close to the axillary artery but then usually pierces the coracobrachialis muscle and passes laterally and obliquely to lie between biceps brachii and brachialis. Here it supplies motor branches to both muscles and also provides a sensory branch to the elbow joint. Below the last branch to brachialis, the musculocutaneous nerve becomes the lateral antebrachial cutaneous nerve (Fig. 91.11a).

As the lateral antebrachial cutaneous nerve continues distally and pierces the deep fascia at the lateral side of biceps and its tendon, it divides into anterior and posterior branches just above the cubital fossa. The anterior branch of the lateral cutaneous nerve supplies the skin of the lateral and anterior part of the forearm and terminates in the skin over the middle part of the thenar eminence. The smaller posterior branch runs distally and backward in front of the lateral epicondyle of the humerus, and supplies the skin on the lateral and posterior side of the forearm as far as the wrist. The nerve may have communications distally with the posterior cutaneous nerve of the forearm, superficial branch of the radial nerve, and palmar cutaneous branch of the median nerve.

Regional relationships

The relationship with the musculocutaneous nerve and the coracobrachialis muscle is variable, with a range of locations and varying patterns of nerve passing through the muscle. The most common variation (10–22%, Kervancioglu et al. 2011) is where, instead of piercing coracobrachialis, the musculocutaneous nerve runs with the median nerve a variable distance down the arm and then, either as a single branch or as several branches, passes between the biceps brachii and brachialis to supply the biceps brachii, brachialis, and coracobrachialis muscles. Alternatively, in some cases only the muscular branch or only the cutaneous branch of the nerve follows its usual course and pierces the coracobrachialis. In infrequent cases, the lateral cord may pierce the coracobrachialis and then divide into the musculocutaneous nerve and the lateral head of the median nerve (see "Communications" section below).

As described in the paragraph above, the musculocutaneous nerve may pass through the coracobrachialis muscle at a range of locations along the muscle. This point has been found from 3 cm to 12.5 cm distal to the coracoid process (Flatow et al. 1989; Pianezza et al. 2012).

Aberrancy in the development of the biceps brachii muscle, such as supernumerary or absent heads, has been associated with abnormal branching patterns of the musculocutaneous nerve (Kosugi et al. 1992; Abu-Hijleh 2005; Mehta et al. 2009; Pacholczak et al. 2011).

The lateral antebrachial cutaneous nerve runs parallel to the cephalic vein in the forearm, but may run dorsal (deep) or volar (superficial) to the vein (Beldner et al. 2005).

Origins

The musculocutaneous nerve primarily arises from the fifth and sixth cervical nerves (Mancall et al. 2011); in 50–80% (Kerr 1918) of individuals, the fourth and seventh cervical nerves may also contribute. The eighth cervical nerve contributes infrequently. The musculocutaneous nerve most commonly arises solely from the lateral cord (89%, Kerr 1918), but may also receive a contribution from the posterior cord or the medial cord, such as from a fusion with the median nerve (after it receives the medial root from the lower trunk); this was noted in 7% (Kerr 1918), 6% (Testut 1884), and 5% (Choi et al. 2002) of specimens.

Communications between the musculocutaneous and median nerves

Failure of nerve fibers to segregate within the brachial plexus into the common anatomic form often leads to distal communicating fibers or abnormal branch patterns. The re-routing between the musculocutaneous and the median nerve exists in three patterns: (1) median nerve innervating musculocutaneous nerve territory, that is, branches of the median nerve innervating elbow flexor muscles typically innervated by the musculocutaneous nerve; (2) musculocutaneous nerve innervating median nerve territory, that is, branches of the musculocutaneous nerve innervated forearm flexor and/or pronator muscles typically innervated by the median nerve; or (3) communicating branches between the musculocutaneous and median nerves.

The first two are relatively infrequent (4 of 112 in one series; Chiarapattanakom et al. 1998), including cases of complete absence of the musculocutaneous (1.4–8% in five anatomical series; Prasada Rao and Chaudhary 2001; Guerri-Guttenberg and Ingolotti 2009). However, the incidence of communicating branches is much higher (10–54%, Guerri-Guttenberg and Ingolotti 2009), with large series such as Kerr (1918) reporting 28% and Testut (1884) reporting 36%. In about three-quarters of cases, a branch of the musculocutaneous joined to the median (Fig. 91.11c); contributions from the median nerve to the musculocutaneous nerve are less frequent.

In one study investigating the origins and destinations of the fibers contained in the communicating branches, the fibers were exclusively from the sixth and seventh cervical nerves (Maeda et al. 2009). The authors found that there was an orderly expansion in the range of innervation; specifically, all fibers innervated the thenar muscles and proper digital nerves, a subset also innervated the pronator teres muscle, a smaller subset also innervated the flexor carpi radialis and lumbricals, and so on, with the smallest subset innervating all of the muscles typically innervated by the median nerve.

The absence of the musculocutaneous nerve in man may be an ontological remnant during embryogenesis. The musculocutaneous nerve is absent in lower vertebrates such as amphibians, reptiles, and birds; in these species, all motor branches to the flexor muscles of the arm originate from the median nerve. Anatomical studies of embryos suggest that the musculocutaneous nerve is derived from the median nerve (Iwata 1960).

Targets

The biceps brachii muscle is most frequently innervated by one nerve branch, in roughly 60% of specimens (Chiarapattanakom et al. 1998; Kervancioglu et al. 2011), which ramifies into two sub-branches to innervate the distinct head of the biceps brachii muscle. In a third of cases, there are two branches, usually within 2 cm of each other. Rarely, there are three branches to the biceps brachii muscle, which has been associated with a supernumerary head of the biceps brachii (Kosugi et al. 1992). Similarly, the brachialis muscle is most frequently innervated by a single branch in roughly 75–90% of specimens (Chiarapattanakom et al. 1998; Kervancioglu et al. 2011). The brachialis muscle frequently receives dual innervation from the radial nerve. Rarely, the musculocutaneous nerve may supply muscles typically innervated by the radial nerve, such as the brachioradialis and extensor carpi radialis muscles (Yogesh et al. 2011).

Significant variations may arise in the musculocutaneous nerve with respect to the median nerve, such as incomplete sorting of fibers within the lateral cord. Aberrant proximal sorting may lead to possible distal interconnections between the two nerves as well as apparent anomalous innervation by either nerve (see "Communications" section below).

The lateral antebrachial cutaneous nerve may give rise to a recurrent branch to provide sensibility to the skin over the distal third of the anterolateral surface of the upper arm (Horiguchi 1981). The anterior division of the lateral antebrachial cutaneous nerve travels with the radial nerve beyond the wrist where they may often communicate. There may not be a sensory deficit when the radial nerve is sectioned above the lower third of the forearm.

Nerves arising from the medial cord of the brachial plexus

Five nerves arise from the medial cord of the brachial plexus, including the medial (or inferior) pectoral branches, medial brachial cutaneous nerve, medial antebrachial cutaneous nerve, median nerve, and ulnar nerve (Fig. 91.13; Table 91.4). The medial root of the median nerve, as well as the ulnar nerve, may commonly receive a branch from the lateral cord (described previously in "Cord variations"). The presumed purpose of this

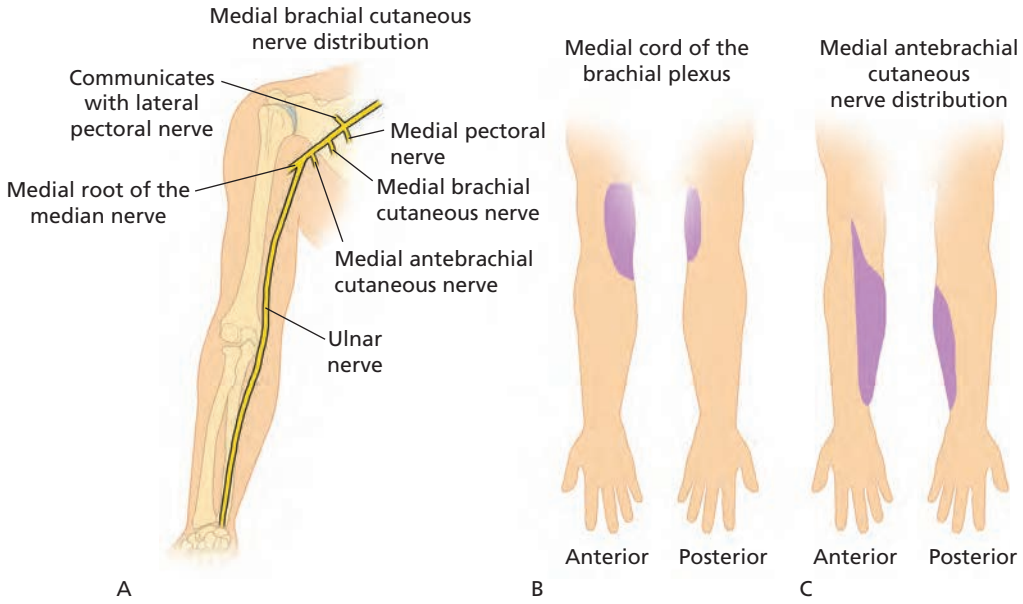

Figure 91.13 Depiction of (a) the common anatomy of the nerves arising from the medial cord of the brachial plexus, including (b) the cutaneous distribution of the medial brachial cutaneous nerve and (c) the medial antebrachial cutaneous nerve. Adapted from Bergman et al. (1988). Reproduced with permission from the Department of Neurosurgery, University of Utah.

branch is to supply fibers from the seventh cervical nerve to the ulnar nerve for innervation of the flexor carpi ulnaris (Iwamoto et al. 1980; Chuang et al. 1998).

The separation of lateral cord fibers destined to form the median nerve may be imperfectly achieved at the terminus of the lateral cord. Frequently, there are communicating branches between the musculocutaneous and median nerves (see "Communications between the musculotaneous and median nerves" above). Similarly, the separation of fibers between the ulnar and median nerves may be incomplete at the level of the cords. Redistribution of hand fibers may therefore occur distally, often referred to as a Martin-Gruber anastomosis (see "Communications between the median and ulnar nerves" below).

Medial pectoral nerve

The medial pectoral nerve (medial anterior thoracic nerve) is composed of nerve fibers from the eighth cervical and first thoracic nerves. The nerve passes between the second division of the axillary artery and the axillary vein. Some of the fibers may join with those of the lateral pectoral nerve to form a loop or ansa anterior to the axillary artery. Other fibers pass below and to the lateral part of pectoralis minor; these fibers usually pierce the muscle and supply pectoralis major, which overlies pectoralis minor. Both muscles are supplied by both the medial and lateral pectoral nerves.

See the earlier "Pectoral branches" section for a full discussion of the relevant anatomical variations.

Table 91.4 Nerves arising from the medial cord of the brachial plexus.

Branches from medial cord	Nerve origins
Medial pectoral branches	C8–T1
Medial brachial cutaneous nerve	C8–T1
Medial antebrachial cutaneous nerve	C8–T1
Median nerve	C(5)6–C8 (T1)
Ulnar nerve	C8–T1

Medial brachial cutaneous nerve

The medial brachial cutaneous nerve (or lesser internal cutaneous nerve or nerve of Wrisberg) is primarily composed of fibers from the eighth cervical and first thoracic nerves (Fig. 91.13b). The nerve courses distally on the medial side of the axillary vein. It pierces the deep fascia near the bend of the elbow at the middle of the arm, where it turns dorsally to supply the skin that covers the olecranon process.

In the axilla, the medial brachial cutaneous nerve may have one or two communicating loops with the intercostobrachial nerve.

Regional relationships

Most dissections describe the passage of the medial brachial cutaneous nerve as occurring along or posterior to the basilic vein; little academic work has focused on the variation with respect to the venous structures that the medial brachial cutaneous nerve accompanies.

Origins

Although the medial brachial cutaneous nerve is typically composed of fibers from the eighth cervical and first thoracic nerves (90–95% of specimens); it may also be composed exclusively of fibers from the first thoracic nerve (5–10% of specimens). However, the medial brachial cutaneous nerve frequently communicates with the intercostobrachial nerve, which is part of the sensory afferent of the second thoracic nerve. This communication has been found to occur in approximately 50–60% of specimens (Kerr 1918; Race and Saldana 1991). The connection between the intercostobrachial nerve may be multiplied (two or more communicating branches), forming a plexus at the posterior boundary of the axillary space. This plexus may include branches to the lateral cutaneous branch of the third intercostal nerve.

The medial brachial cutaneous nerve may arise as a single branch or as multiple branches; Kerr (1918) found that 83% arose as a single branch and the remainder were multiple branches with plexiform connections to the medial antebrachial cutaneous nerve and the intercostobrachial nerve. In this series, of those specimens where the medial brachial cutaneous nerve arose as a single nerve, it arose from the lower trunk or medial cord in two-thirds. The remainder arose from the ulnar nerve, directly from the eighth cervical or first thoracic nerves. In between one-fifth (Kerr 1918) and one-half (Masear et al. 1989) of all specimens, it was found that the medial brachial cutaneous nerve and the medial antebrachial cutaneous nerve had a common trunk, arising either from the medial cord or from the lower trunk. Uniquely, Turner (1872) described the ulnar nerve as giving off a branch that joined the medial brachial cutaneous nerve in the axilla.

Targets

The extent of cutaneous innervation subserved by the medial brachial cutaneous nerve is quite variable, particularly when the medial brachial cutaneous nerve communicates with other cutaneous nerves such as the medial antebrachial cutaneous nerve, intercostobrachial nerve, or posterior cutaneous nerve of the arm. Race and Saldana noted that the medial brachial cutaneous nerve was at the medial epicondyle in 80% of specimens (Race and Saldana 1991). Other scholarly work depicted two consistent arborization points of the medial brachial cutaneous nerve at 7 cm and 15 cm proximal to the medial epicondyle (Chowdhry et al. 2010). This correlates with the findings of Masear et al. (1989) who had noted that if the medial brachial cutaneous nerve arose from the medial antebrachial cutaneous nerve, there were two arborization points.

Medial antebrachial cutaneous nerve

The medial antebrachial cutaneous nerve is composed of fibers from the eighth cervical and first thoracic nerves (Fig. 91.13c). This nerve is associated closely with the ulnar nerve at its origin. The nerve may initially be found on the medial side of the axillary artery, but it becomes superficial and then lies between the artery and vein. In the upper part of the arm, the nerve lies anterior to the medial side of the brachial artery; in this region or above, it provides a small branch that pierces the superficial fascia to supply the skin of along the biceps and elbow flexion crease. Near the upper part of the lower third of the arm, the nerve and the basilic vein together pierce the fascia, and the nerve divides into anterior (volar) and posterior (ulnar) branches (Fig. 91.14). The anterior branch is the larger of the two branches. It passes anterior or posterior to the median basilic vein, divides into several smaller branches, runs down the forearm, and finally supplies the skin that covers the anteriomedial (palmomedial) aspects of the forearm as far distally as the wrist. The terminal branches communicate with the palmar cutaneous branches of the ulnar and median nerves in the hand. The terminal branches of the posterior branch cross the ulnar nerve proximal and distal to the medial epicondyle. Terminal branches supply the skin of the posteromedial (dorsomedial) part of the forearm and join the dorsal cutaneous branch of the ulnar nerve.

Regional relationships

The anterior and posterior branches separate at 7–22 cm (average 14.5 cm) proximal to the medial epicondyle (Masear et al. 1989). The anterior branch divides into two to five terminal branches and the posterior branch divides into one to four terminal branches, yielding a total arborization of five to eight branches (Masear et al. 1989; Race and Saldana 1991). Race and Saldana noted that three to seven fine branches crossed the ulnar nerve to innervate the skin of the olecranon. These posterior branches cross posteriorly between 6 cm proximal and 4–6 cm distal to the medial epicondyle (Dellon and Mackinnon 1985; Masear et al. 1989). Intraoperatively, Lowe et al. (2004) found one to four branches crossing the ulnar nerve during surgical decompression at the cubital tunnel; the most common configuration had branches at 2 cm proximal to the medial epicondyle and 3 cm distal to the medial epicondyle.

The medial antebrachial cutaneous nerve has been classically depicted as coursing anterior and lateral to the basilic vein. One study noted that the medial antebrachial cutaneous nerve coursed deep to the basilic vein in all specimens (40 arms; Race and Saldana 1991); whereas another study found the medial antebrachial cutaneous nerve deep to the basilic vein in only half of specimens, with the other half crossing superficial to the vein (50 arms; Masear et al. 1989).

Origins

The intercostobrachial nerve may infrequently contribute to the medial antebrachial cutaneous nerve (Race and Saldana 1991). The medial antebrachial cutaneous nerve may communicate with the ulnar nerve (Masear et al. 1989).

The medial antebrachial cutaneous nerve and the medial brachial cutaneous nerve may arise from a common trunk, occurring in approximately one-fifth (Kerr 1918) to one-half (Masear et al. 1989) of all specimens and whose origin is either from the

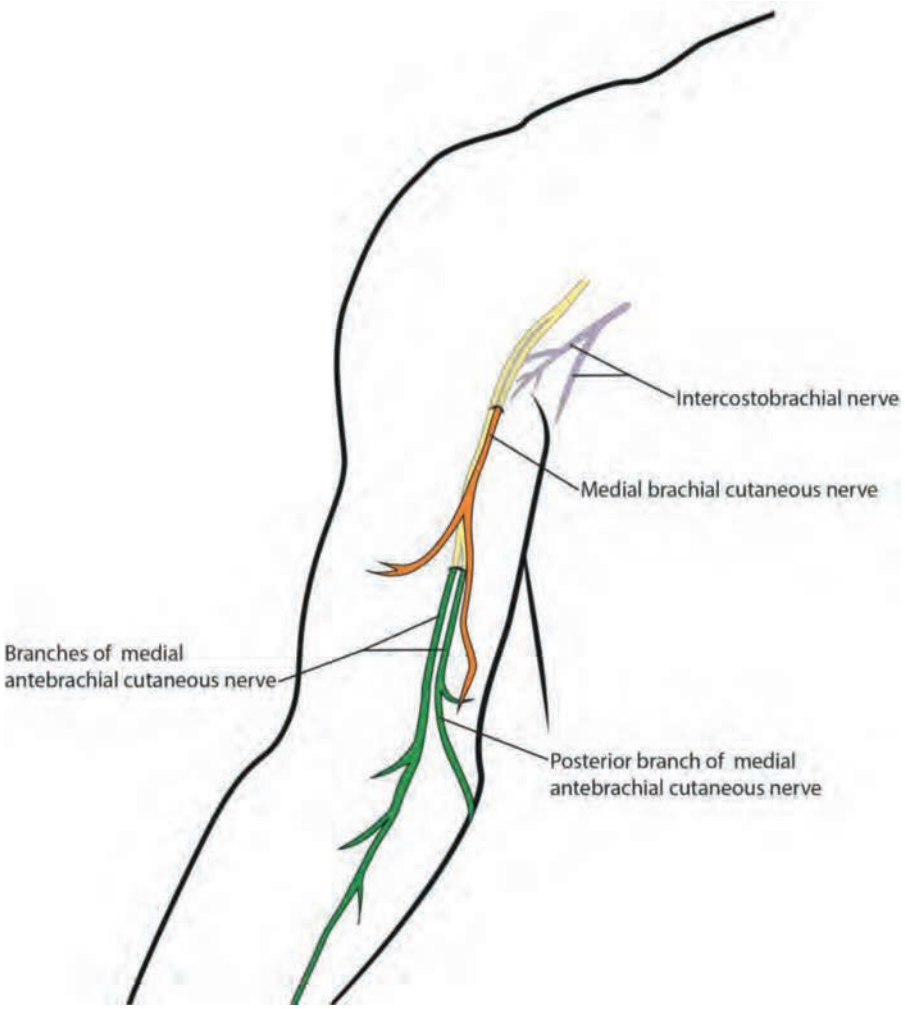

Figure 91.14 Relationship of the cutaneous nerves of the arm, including lateral antebrachial cutaneous nerve, medial brachial cutaneous nerve, and medial antebrachial cutaneous nerve. Reproduced with permission of the Department of Neurosurgery, University of Utah.

medial cord or lower trunk. A common trunk including the medial pectoral nerve, the medial brachial cutaneous nerve, and the medial antebrachial cutaneous nerve has been described multiple times (Masear et al. 1989).

The posterior division of the medial antebrachial cutaneous nerve may arise separately from the posterior branch of the lower trunk of the brachial plexus.

Targets

The cutaneous distribution of the medial antebrachial cutaneous nerve is the anteromedial forearm distally, the medial antecubital fossa, and about the olecranon. The variety of branching patterns is considerable in this region.

As is the case with many cutaneous nerves, the medial antebrachial cutaneous nerve may communicate with other nerves of the region. Proximally, the medial antebrachial cutaneous nerve and the medial brachial cutaneous nerve overlap in the distal third of the arm. The anterior branch may join with the palmar cutaneous branches of the ulnar and median nerves in the hand, although one study found no such communication in 50 arms (Masear et al. 1989). The posterior branch may join with the dorsal cutaneous branch of the ulnar nerve or replace it entirely.

The medial antebrachial cutaneous nerve frequently has articular branches to the elbow, which may arise from either the anterior or posterior branches (Masear et al. 1989).

Median nerve

The median nerve is composed of fibers from the sixth, seventh, and eighth cervical nerves. As with most other nerves, the median nerve may receive contributions from the fifth cervical nerve above or, on occasion, from the first thoracic nerve below.

The median nerve is formed by the fusion of two large branches, one each from the lateral and medial cords (Fig. 91.15a). These two branches, alternatively called the medial and lateral roots, radices (singular, radix), or heads, unite slightly below the level of pectoralis minor, anterior or anterolateral to the third of the axillary artery and lateral to the coracobrachialis muscle. This is equivalent to the surgical neck of the humerus when the arm is abducted to 90°.

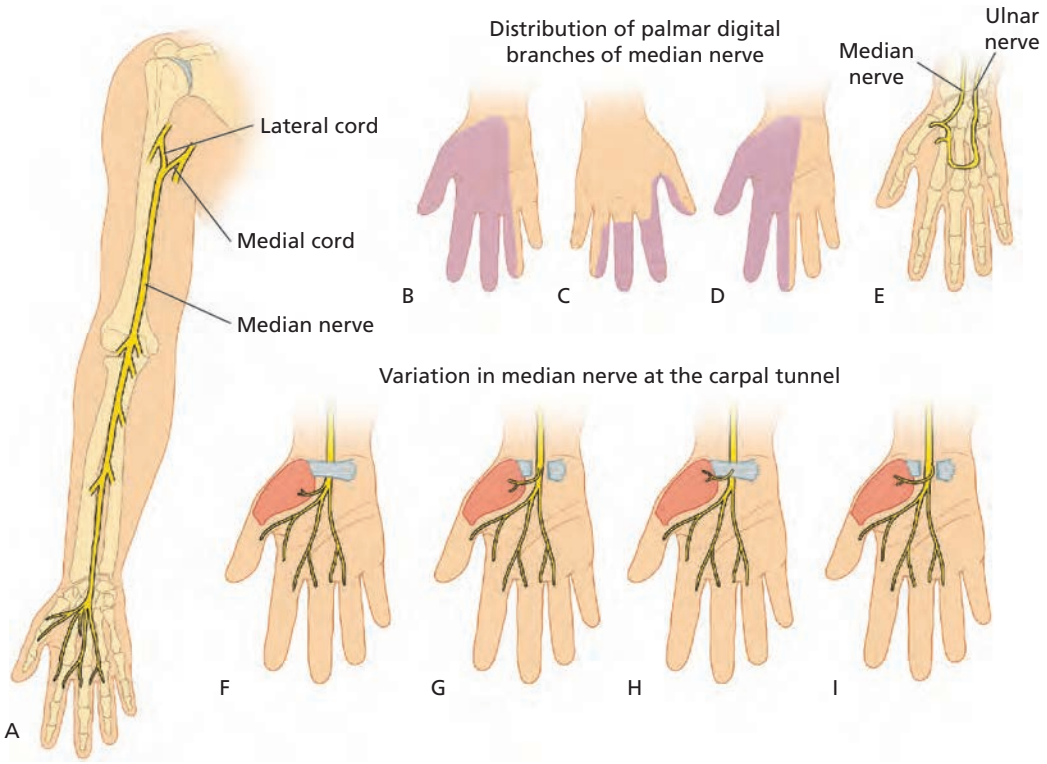

Figure 91.15 (a) Depiction of the common anatomy of the median nerve arising from the fusion of the medial and lateral roots arising from the medial and lateral cords, respectively. (b, c) Common cutaneous distribution of the median nerve, including (d) restricted distribution of the median nerve. (e) Distal communication between the median and ulnar nerves at the thenar muscles (Riche-Cannieu). (f–i) Variable origin and course of the thenar motor branch of the median nerve, including (f) common anatomy, (g) early ventral branch, (h) transligamentous branch, and (i) branch from the ulnar side of the median nerve. Adapted from Bergman et al. (1988). Reproduced with permission from the Department of Neurosurgery, University of Utah.

In the axillary fossa, the median nerve lies lateral to the axillary artery, a position it also maintains with the brachial artery in the upper arm. At the middle of the arm, approximately the level of the insertion of coracobrachialis muscle, the median nerve passes anterior to the brachial artery to lie on its medial side in the cubital fossa. The median nerve innervates no muscles in the arm; however, it provides fibers to innervate the brachial artery and its branches (Siegel and Gelberman 1991; Standring 2008).

At the elbow, the nerve supplies articular fibers to the elbow joint (Gardner 1948a). While in the cubital fossa, the median nerve provides three or four branches to supply the muscles of the flexor–pronator group; these branches innervate the pronator teres, flexor carpi radialis, palmaris longus and, by way of the branches to the flexor carpi radialis and palmaris longus, the proximal portion of the flexor digitorum superficialis.

When the median nerve leaves the cubital fossa, it passes between the two heads of pronator teres and is therefore superficial and medial to the ulnar artery, separated by the deep head of pronator teres. After passing through the pronator teres, the median nerve passes deep to the tendinous arch of the flexor digitorum superficialis. At this point it provides approximately three branches to the distal flexor digitorum superficialis. The median nerve then continues distally between flexor digitorum profundus and flexor digitorum superficialis. In the distal third of the forearm, the nerve becomes more superficial and is located between flexor carpi radialis on the radial side and flexor digitorum superficialis tendons on the ulnar side, with the inconstant palmaris longus above. Thompson (1923) reported the median nerve piercing the radial head of the flexor digitorum superficialis and then piercing its distal tendon at the wrist.

The anterior interosseous nerve arises from the median nerve at the level of the tuberosity of the radius. This is equivalent to the midportion of the pronator teres (Tubbs et al. 2006a) or just proximal to the tendinous edge of the flexor digitorum superficialis. The nerve courses along the interosseous membrane, along with the anterior interosseous artery, and passes beneath pronator quadratus in the distal part of the forearm. In its course through the forearm, it supplies flexor pollicis longus, the lateral parts of flexor digitorum profundus, and pronator quadratus. Sensory nerve fibers from the wrist joint and sympathetic fibers to the anterior interosseous artery are also found in this nerve.

The palmar cutaneous branch of the median nerve is the last major branch of the median nerve in the forearm. It is located above the flexor retinaculum and passes between the tendons of

the flexor carpi radialis and palmaris longus muscles (Chaynes et al. 2004). The branch arises off the radial side of the median nerve along the radial edge of the flexor digitorum superficialis, 5–7 cm proximal to the wrist crease (Bonnel et al. 1980). It then associates with the sheath of the flexor carpi radialis tendon 1–1.5 cm proximal to the distal volar wrist crease (Taleisnik 1973; Matloub et al. 1998). The nerve enters the subcutaneous layer of the palm approximately 8 mm from the distal volar wrist crease (Bezerra et al. 1986). Sensation from the skin of the thenar eminence and the lateral part of the palm are carried by this nerve; branches to the lunate and scaphoid bones may also be present (Matloub et al. 1998).

Under the flexor retinaculum, the median nerve divides into three common palmar digital nerves that enter the palm deep (dorsal) to the superficial palmar (arterial) arch.

1. The first common palmar digital nerve supplies the abductor pollicis brevis, the opponens pollicis, and the superficial head of flexor pollicis brevis through the recurrent branch of the median nerve. The common digital nerve divides into three proper palmar digital nerves. The first proper palmar digital branch, and the most lateral of these nerves, passes obliquely across the tendon of flexor pollicis longus, runs along the radial border of the thumb, and carries sensation from the thumb pad and the matrix of the thumbnail. The second proper palmar digital branch supplies the medial side of the palmar surface of the thumb and also the matrix of the thumbnail. The third proper palmar digital branch carries sensation from the radial side of the second digit and supplies motor nerve fibers to the first lumbrical muscle.
2. The second common palmar digital nerve supplies the second lumbrical with its motor nerve and then divides near the metacarpophalangeal articulation into two proper palmar digital branches, which diverge to supply adjacent sides of the second and third digits (Fig. 91.15b, c).
3. The third common palmar digital nerve divides into two proper palmar digital branches, which carry sensation from adjacent sides of the third and fourth digits where some fibers from the median nerve mingle with fibers from the ulnar nerve.

Regional relationships

The fusion of the two roots from the medial and lateral cords most commonly occurs superficial (anterior) to the axillary artery. Miller categorized variations associated with both abnormal compositions of the median nerve and pattern of the axillary artery, as the artery and nerve have been found to develop in concerted relationship (Nakatani et al. 1997a; Schoenwolf 2009). In this study of 480 brachial plexuses, conjoined arterial and neural variations existed in 8% of specimens. Of these, the most common variation was that the axillary artery was superficial to the median nerve (3.5%), which is the most common configuration in non-human primates (82%, Miller 1939). The remainder included perforation of a nerve by a vessel (2% of plexuses) and numerous patterns of communicating branches in relationship to anomalous vessel branching or location. Pandey confirmed this relationship between aberrant artery location and variant median nerve formation, noting that abnormal vessel location often heralded a communicating branch (Pandey and Shukla 2007).

In cases of high division of the brachial artery, when the resulting radial and ulnar arteries lie side by side in the arm, the median nerve will lie between the two vessels. One or the other artery will become superficial to the nerve. The median nerve may be perforated by the median artery. A persistent median artery may accompany the median nerve in the carpal tunnel in approximately 2–2.5% of cases (McCormack et al. 1953; Barfred et al. 1985).

The course of the median nerve has significant variation. The median nerve may pass through the coracobrachialis, similar to the normal course of the musculocutaneous nerve (Nakatani et al. 1998; El-Naggar and Al-Saggaf 2004). The median nerve usually passes between the two heads of pronator teres; however, it may pass superficial or deep to the two heads, or it may pierce the humeral head. The median nerve may lie on the superficial surface of flexor digitorum superficialis instead of its deep surface.

The thenar motor branch of the median nerve may arise in variable relationship to the transverse carpal ligament. The typical pattern is for the branch to arise distal to the ligament and then travel recurrent to arrive at the thenar musculature (termed extraligamentous). The thenar motor branch may arise within the carpal tunnel, underneath the transverse carpal ligament (termed subligamentous). Lastly, the thenar motor branch may pass through the transverse carpal ligament (term transligamentous). In a study of 100 cadaver hands, Poisel (1974) found 46% to be extraligamentous, 31% subligamentous, and 23% transligamentous. However, surgical series have found a much lower incidence of transligamentous branches over the range 1–15% (Tountas et al. 1987; Amadio 1988).

Variations causing median nerve entrapment

The axillopectoral muscle (axillary arch or Langer's muscle), a variant muscle, can cause neurovascular compression and consequent neuropathy of the median nerve (Van Hoof et al. 2008). This muscle arises from the latissimus dorsi tendon, crosses the axillary neurovascular bundle, and inserts on the pectoralis major tendon. It may also span from the coracoid process to the tendinous insertion of the long head of the triceps (Turgut et al. 2005). This muscle may be present in approximately 7% of the general population, although a varying incidence ranging from 0.25% to 27% has been reported (Besana-Ciani and Greenall 2005). This muscle may be the vestigial remnant of the panniculus carnosus, which is well developed in rodents and lower mammals (Bergman et al. 2015).

A variant osseoligamentous complex, known as the supracondylar process and associated ligament of Struthers, may entrap the median nerve or brachial artery above the elbow (Struthers 1854; Laha et al. 1977; Al-Qattan and Husband 1991). The supracondylar process is a spur-like ossification from the anteromedial aspect of the distal humerus, located

approximately 6 cm proximal to the medial epicondyle. The process is the attachment for an anomalous ligament (the ligament of Struthers), which runs between the supracondylar process and medial epicondyle, forming a fibroosseous tunnel (also called the end epitrochlear foramen or supratrochlear foramen (Anonymous 1906). The ligament is frequently associated with a high origin of the pronator teres muscle (Crotti et al. 1981; McCulloch et al. 2010). This complex may be present in 0.4–2.8% of limbs (Terry 1921; Natsis 2008; Aydinlioglu et al. 2010) and is common in lower mammals such as dogs, but lost in apes (Al-Qattan and Husband 1991; Richmond et al. 1998). The ancient pharaoh Tutankhamun was noted to have an epitrochlear foramen on x-ray (Mahdy 2001).

Pronator syndrome is a form of median neuropathy that may develop from entrapment of the median nerve due to anatomical variation of the pronator teres. Variations of the pronator teres include absence of the ulnar (deep) head (6–12%: Dellon and Mackinnon 1987; Nebot-Cegarra et al. 1991), fibrous or tendinous arch to either head, high origin of the humeral head (19% with origin more than 2 cm proximal to the medial epicondyle), insertion of the ulnar (deep) head on the superficialis arch, or passage of the median nerve through the humeral (superficial) head (3%).

In the cubital fossa, the median nerve may be entrapped by a thickened lacertus fibrosus (Hagert 2013) or accessory tendons of the biceps brachii (Spinner et al. 1991).

The median nerve may be compressed along its course by variant muscles, including anomalous palmaris longus, palmaris profundus (Pirola et al. 2009), anomalous flexor digitorum superficialis, anomalous lumbricals, flexor carpi radialis brevis (Van Meir and De Smet 2003), and accessory flexor pollicis longus (Ganzter's muscle). Similarly, the anterior interosseous nerve has been documented to be compressed by Gantzer's, palmaris profundus, and flexor carpi radialis brevis muscles.

In the carpal tunnel, the median nerve may be compressed by accessory muscles such as abnormal or hypertrophied lumbricals, flexor digitorum superficialis, and palmaris muscles (Fig. 91.16) (De Smet 2002).

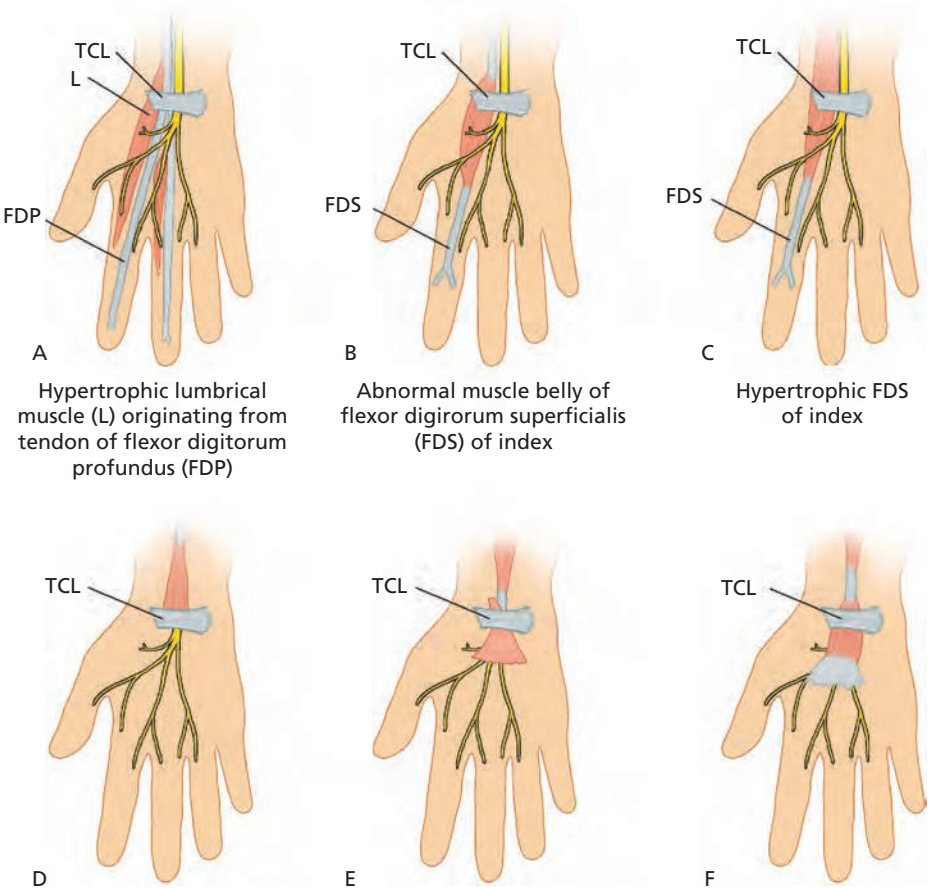

Figure 91.16 (a–f) Variant muscles compressing the median nerve at the carpal tunnel. Adapted from De Smet (2002). Reproduced with permission of the Department of Neurosurgery, University of Utah.

Origins

Variant formation of the cords leads to the aberrant origin of the median nerve. The typical formation of the median nerve by the fusion of the medial and lateral roots along the anterior surface of the third division of the axillary artery occurs in approximately 85% of specimens (86%, Kerr 1918; 86% Pandey and Shukla 2007)). The most common variation seen in Kerr's series relates to early branching of the middle trunk prior to the typical formation of the anterior division. Often these communicating branches of the middle trunk fuse with the medial cord, which may give the appearance of duplicated lateral root. The lateral cord may continue independently when it does not receive fibers from the seventh cervical nerve. An infrequent variation was a complete fusion of the medial and lateral cords forming a common origin of the musculocutaneous, median, and ulnar nerves. Common stems of the median and musculocutaneous nerves and median and ulnar nerves may also occur.

The median nerve may be bifid in the forearm, alternatively described as a high division, first described by Gruber and found in approximately 3% of cases by multiple authors (Hartmann 1888; Winkelman and Spinner 1973; Amadio 1988).

The median nerve, or the anterior interosseous nerve, may connect with the other principal nerves of the forearm, most commonly the ulnar nerve. These two nerves may frequently pass fibers from one to the other, similar to the relationship of the median providing fibers to the musculocutaneous nerve described above. This is detailed in the section "Communications between the median and ulnar nerves." Interestingly, there are no significant motor connections between the median and radial nerves. The established communications, described by multiple independent authors, between the median nerve and the radial nerve are limited to: (1) communications between the anterior interosseous nerve and the posterior interosseous nerve; and (2) communications between the palmar cutaneous branch of the median nerve and the superficial branch of the radial nerve (branch of Lejars) (Le Nen et al. 1991; Chaynes et al. 2004).

Targets

Fibers that are usually destined to the distribution of the musculocutaneous nerve may course within the median nerve (see "Communications between the musculocutaneous and median nerves" above). The median nerve may therefore share communicating branches with the musculocutaneous, may provide branches to the flexor muscles of the arm, or may replace the entire musculocutaneous nerve.

The branching pattern of the median nerve is quite variable. The branches arising from the median nerve can be categorized into the following groups: branches above the separation of the anterior interosseous nerve; branches from the anterior interosseous nerve; branches in the forearm distal to the anterior interosseous nerve branch; and branches within the hand. Individual branches from the median nerve and anterior interosseous nerve may innervate multiple muscles in the forearm, defying simple classification (Gunther et al. 1992).

The branches proximal to the anterior interosseous nerve innervate the muscles of the flexor-pronator group, including pronator teres, flexor carpi radialis, palmaris longus, and flexor digitorum superficialis. Commonly the pronator teres receives a branch that bifurcates into two branches to the superficial and deep heads. Equally common is to have two or more distinct branches to the pronator teres (Sunderland and Ray 1946; Dellon and Mackinnon 1987; Gunther et al. 1992). In contrast, the flexor carpi radialis usually only has one branch (Sunderland and Ray 1946; Blair and Joos 1982). The flexor digitorum superficialis may receive up to seven branches and often (in 30% of specimens) receives branches from the anterior interosseous nerve (Sunderland and Ray 1946). However, the majority of these branches arise as a common stem with fibers destined to other median innervated muscles, most commonly flexor carpi radialis.

The anterior interosseous nerve primarily innervates the radial half of the flexor digitorum profundus, the flexor pollicis longus, and the pronator quadratus. The flexor digitorum profundus is commonly innervated by multiple branches from the anterior interosseous nerve, ranging from one to six branches. The flexor digitorum profundus may also receive branches directly from the median nerve, which commonly occur above or at the origin of the anterior interosseous nerve from the median nerve. Similarly, the flexor pollicis longus receives one to six branches from the anterior interosseous nerve and may also receive branches directly from the median nerve (30% of specimens; Sunderland and Ray 1946). The anterior interosseous nerve may innervate the entirety of the flexor digitorum profundus (21% of patients; Sunderland 1945). However, a spectrum from complete ulnar innervation to complete median has been reported (Marinacci 1964a, b), with noted dual innervation of the middle, ring, and little finger bellies of flexor digitorum profundus (Sunderland 1945).

The branches of the median nerve in the forearm distal to the anterior interosseous nerve comprise multiple branches to the flexor digitorum superficialis and the palmar cutaneous branch(es). The flexor digitorum superficialis is innervated by multiple branches from the median nerve, both above and below the origin of the anterior interosseous nerve. There are commonly three to four branches to the flexor digitorum superficialis below the origin of the anterior interosseous nerve (Gunther et al. 1992).

The palmar cutaneous branch of the median nerve is uniformly present in all major series (Chaynes et al. 2004), but there may be two branches (15%, Matloub et al. 1998). The precise course of this nerve is a matter of significant investigation, as well as its relationship to the palmar cutaneous nerve of the ulnar nerve. The origin ranged over 3–21.5 cm proximal to the distal wrist crease (Bezerra et al. 1986; Naff et al. 1993; Dowdy et al. 1994; Watchmaker et al. 1996; Matloub et al. 1998; Chaynes et al. 2004). The palmar cutaneous branch of the median nerve

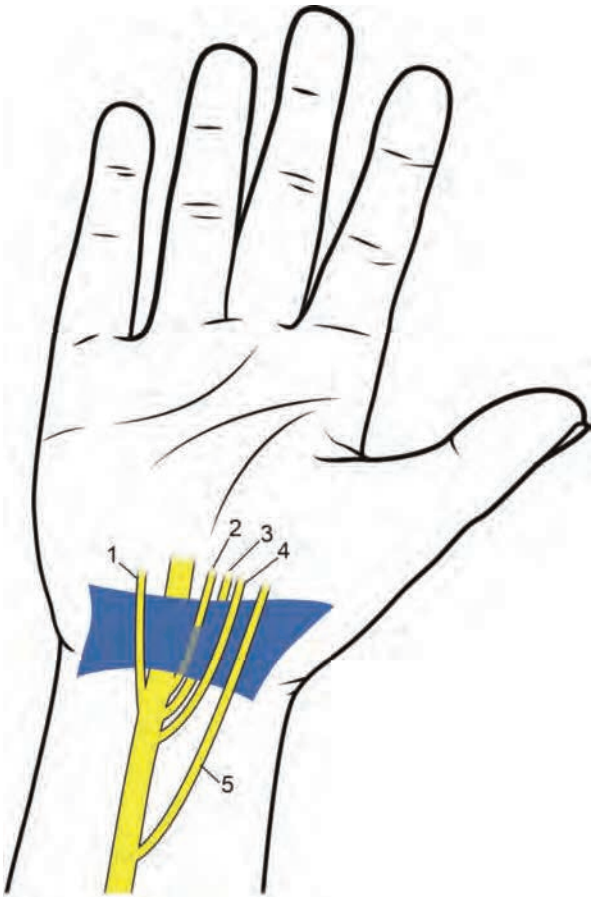

Figure 91.17 Variation on course of palmar cutaneous branch of the median nerve. 1, Origin from the ulnar-side of the median nerve, most uncommon; 2, trans-ligamentous, through the transverse carpal ligament; 3, deep to the transverse carpal ligament; 4, passing superficial to the transverse carpal ligament; 5, proximal origin, often associated with duplicated branches. Adapted from Das and Brown (1976) with permission from Elsevier. Reproduced with permission of the Department of Neurosurgery, University of Utah.

commonly pierces through the transverse carpal ligament through a separate canal and exits above the fibers of the palmar aponeurosis (Taleisnik 1973; Naff et al. 1993), although some branches may not penetrate the transverse carpal ligament or pass entirely through the carpal tunnel and recurrently innervate the skin of the thenar eminence (Fig. 91.17). The palmar cutaneous branch of the median nerve may also pass through the tendon of the palmaris longus, 1–1.5 cm from the tendon's insertion into the palmar aponeurosis (5–7.5% when the palmaris longus is present; Dowdy et al. 1994; Matloub et al. 1998). There may be communicating branches between the cutaneous branch of the median nerve and the superficial branch of the radial nerve, also known as the branch of Lejars (Le Nen et al. 1991; Chaynes et al. 2004), or the palmar cutaneous branch of the ulnar nerve, also known as the Berrettini branch (Ferrari and Gilbert 1991; Tubbs et al. 2011b). Additionally, the palmar cutaneous branch may be absent, replaced by branches of the lateral antebrachial cutaneous nerve, superficial branch of the radial nerve, branch of the ulnar palmar cutaneous nerve, or combinations of these branches (Lejars 1890).

There is significant variability in the pattern of innervation of the intrinsic hand muscles, and with apparent contradiction among authors. For example, Spourgitis (1895) stated that flexor pollicis brevis was primarily median innervated, whereas Riche (1897) found that it was primarily ulnar innervated. It is now well appreciated that there is frequent dual innervation, particularly of flexor pollicis brevis (Brooks 1886). Similar to the pattern of innervation of the flexor digitorum profundus, the intrinsic muscles of the hand exhibit a spectrum ranging from all-median to all-ulnar innervation (Marinacci 1964a, b; Rowntree 1949), with dual innervation being common (Brooks 1887; Mannerfelt 1966). Studying paralysis of the hand resulting from median nerve and ulnar nerve injuries, Rowntree found that the pattern of innervation described in standard anatomy texts was present in only one-third of cases (Rowntree 1949).

While reports of the so-called "all-median hand" are somewhat rare, innervation of the third lumbrical and first dorsal interosseous are among the most common anomalous patterns. For example, the third common palmar digital nerve occasionally gives a small branch to the third lumbrical, providing dual innervation from both the ulnar and the median nerves (Sunderland and Ray 1946). Kimura and Ayyar (1984) found that median nerve innervation to first dorsal interosseus and abductor digiti minimi occurred in 43% and 16% of cases, respectively. Sunderland (1945) suggested that the pattern of innervation of the individual slips of the flexor digitorum profundus correlated with the innervation of the corresponding lumbricals; it was however noted that this was not a constant relationship.

Sensory nerve distribution to the fingers is equally variable, as described in "Ulnar nerve/Targets" below.

Ulnar nerve

The ulnar nerve, the largest branch of the medial cord, is composed of nerve fibers from the eighth cervical and first thoracic nerves. The nerve begins as the terminal branch of the medial cord at the point where the medial cord provides the medial root to the median nerve, approximately at the level of the inferior border of pectoralis minor. The ulnar nerve runs distally in the axilla between the axillary artery and vein.

The ulnar nerve has a unique course where it passes from the flexor side of the arm to the extensor side, thereby passing posterior to the axis of rotation at the elbow, and then back again into the flexor side of the forearm. In the upper half of the arm, it can be found on the medial side of the brachial artery. At about the level of the insertion of coracobrachialis, it runs dorsally at an acute angle and, accompanied by the superior ulnar collateral artery, pierces the medial intermuscular septum. A fascial band from the coracobrachialis, known as the internal brachial ligament, may accompany the ulnar nerve in passage through the medial intermuscular septum. It passes distally in a groove

in the medial head of triceps brachii to the space between the olecranon process and the medial epicondyle of the humerus. The nerve is bound tightly to triceps by deep fascia in this part of its course through the arm.

At the elbow, the ulnar nerve travels in a fibroosseus channel that can be divided into three parts. At the entrance, when the nerve is in the olecranon groove of the medial epicondyle, the ulnar nerve provides articular branches to innervate the joint capsule. At the second part, the nerve enters a fascial arcade, passing superficial to the joint capsule and ulnar (medial) collateral ligament complex and deep to the cubital retinaculum (also known as Osborne's ligament). Usually the nerve provides two branches to the flexor carpi ulnaris: one to the humeral head and another to the ulnar head. In the third part, the ulnar nerve enters the flexor side of the forearm, passing anteriorly underneath the flexor carpi ulnaris and entering the enveloping fascia of the flexor digitorum profundus and flexor digitorum superficialis (Inserra and Spinner 1986). At about the distal end of the proximal third of the forearm, the nerve is joined by the ulnar artery, which lies on its radial side.

In the forearm, the ulnar nerve provides motor branches to the flexor carpi ulnaris and the ulnar side of the flexor digitorum profundus, as well as sensory branches including the palmar cutaneous branch (also described as the nerve of Henle) and the dorsal (posterior) cutaneous branch. The palmar cutaneous branch of the ulnar nerve leaves the main trunk in the middle of the forearm and passes anterior to the ulnar artery into the palm of the hand. It contains sensory fibers from the skin of the hypothenar eminence and medial part of the palm. The dorsal or posterior cutaneous branch of the ulnar nerve arises about 6–7 cm above the wrist joint and passes under the cover of the flexor carpi ulnaris to terminate on the posterior or dorsal medial aspect of the wrist; it then divides to supply the hand and fingers, primarily on the medial side. This nerve divides into five branches known as the dorsal digital nerves (Fig. 91.18), which usually distribute to the dorsal surface of the ulnar side of the third, fourth, and fifth digits and to the radial side of the fourth and fifth digits. These nerve branches usually extend as far as the base of the terminal phalanx on the fifth digit and as far as the base of the second phalanx on the fourth digit.

The main trunk of the ulnar nerve continues to the wrist where, on the radial side of the pisiform bone, it divides into a superficial and a deep branch. The superficial branch supplies palmaris brevis and the skin that overlies the hypothenar

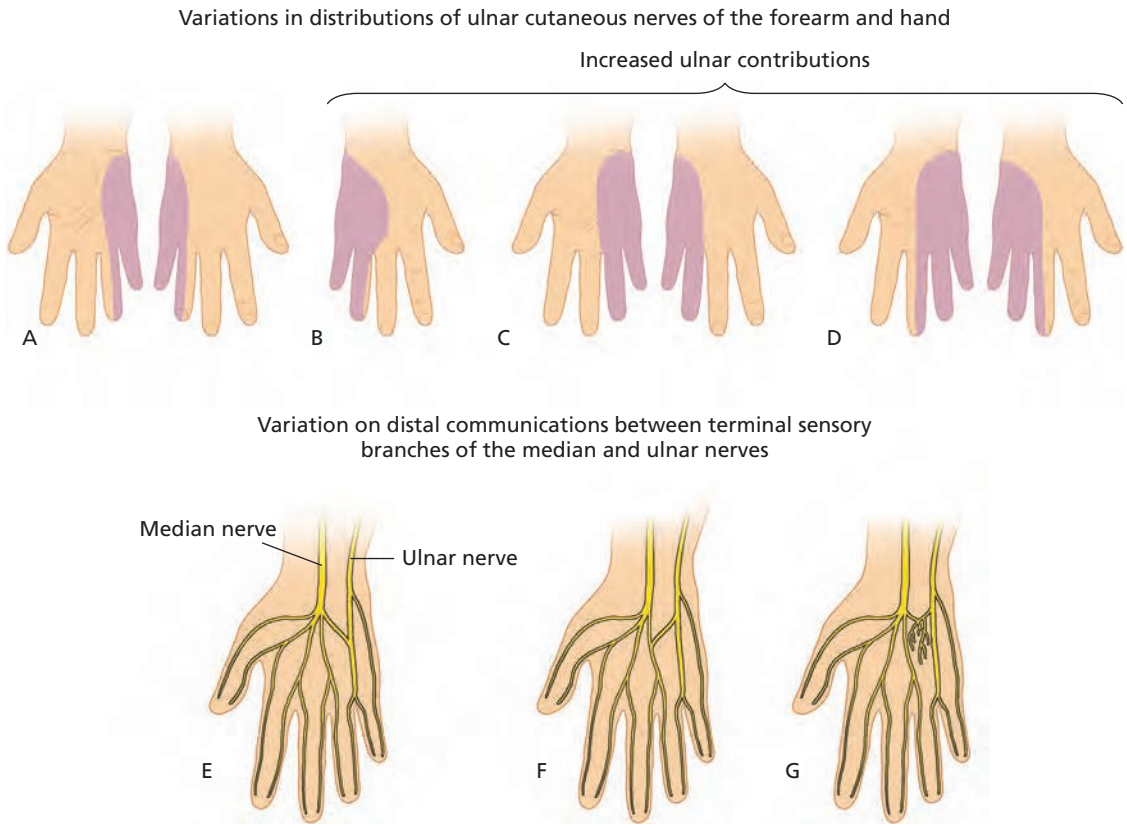

Figure 91.18 (a–d) Depiction of the common cutaneous distribution of the ulnar nerve, including (b–d) expanded distribution of the ulnar nerve. (e–g) Variations on the distal communication (ramus communicans) between the terminal sensory branches of median and ulnar nerves. Adapted from Bergman et al. (1988). Reproduced with permission from the Department of Neurosurgery, University of Utah.

eminence in the palm. The superficial branch continues and divides into common palmar digital nerves, which run distally and then divide into proper digital branches, which run to the medial side of the fifth digit and the adjacent sides of the fifth and fourth digits (one and one half digits on the medial side). This nerve also supplies the dorsal surface of the second and third phalanges of the fourth and fifth fingers.

The deep branch of the ulnar nerve accompanies the deep branch of the ulnar artery into a space between the abductor digiti minimi and the flexor digiti minimi brevis muscles. It passes through the fibers of the opponens digiti minimi to lie on the deep surface of the long flexor tendons of the palm. The nerve also supplies the abductor and opponens digiti minimi, the flexor digiti minimi brevis, the third and fourth lumbricals, all the dorsal and palmar interossei, the adductor of the thumb, and the medial head and, occasionally, the lateral head or flexor pollicis brevis. The remaining muscles are innervated by the median nerve, including the first two lumbricals and the intrinsic hand muscles of the thumb, although there may be significant variation.

Regional relationships

As the ulnar nerve passes from the anterior to the posterior muscle compartment of the arm it may travel through a myofibrous or fasciomyofibrous tunnel, often referred to as the arcade of Struthers (not to be confused with the rare ligament of Struthers or supracondylar spur, as described in "Median nerve/Variations causing median nerve entrapment"). A fibrous tunnel surrounding the ulnar nerve at the transition between compartments is a relatively constant feature, found in 67–100% in several anatomic series (Kane et al. 1973; Amadio 1986; Al-Qattan and Murray 1991; Gonzalez et al. 2001; Wehrli and Oberlin 2005; Tubbs et al. 2011a). Others have concluded differently however, finding that the ulnar nerve crossed from the anterior to posterior without passing through the medial intermuscular septum or that the passage had a non-constraining "roof" (Dellon 1986; Won et al. 2011). Others have disagreed with the term arcade and favored naming the constraining myofascial band as the internal brachial ligament, which is an aponeurotic continuation of the brachialis muscle (Wehrli and Oberlin 2005).

Normal fascial passageways at the elbow may entrap the ulnar nerve, causing an ulnar neuropathy known as cubital tunnel syndrome. Several surgical cases have reported the entrapment of the distal ulnar nerve near the wrist by the tendon of the flexor carpi ulnaris (O'Hara and Stone 1988; Al-Qattan and Duerksen 1992). In some cases, both the nerve and the tendon are split with a portion of the nerve passing through an opening in the flexor carpi ulnaris tendon (Zook et al. 1988; Kang et al. 1996). The branches in these reports are not related to the dorsal cutaneous branch of the ulnar nerve, unlike the Kaplan's anomalous branch.

The ulnar nerve within Guyon's canal at the wrist bifurcates into a superficial and a deep branch. The deep branch passes deep to the abductor and flexor digiti minimi. A fibrous arcade may exist on the proximal edge of these muscles (40–60% of hand specimens; Dellon and Mackinnon 1988; Konig et al. 1994; Bozkurt et al. 2005) and is conceived as a potential zone for compression of the deep branch.

Variations causing ulnar nerve entrapment

The ulnar nerve may be compressed along its course by anomalous muscles, including epitrochleoanconeus (anconeus epitrochlearis), accessory flexor digiti minimi, accessory abductor digiti minimi, and palmaris longus (Still and Kleinert 1973; Lahey and Aulicino 1986; De Smet 2002).

An anconeus epitrochlearis runs obliquely across the ulnar nerve, spanning the medial epicondyle of the humerus to the olecranon. It may be either tendinous or fleshy in composition. Anatomical studies suggest an incidence of 11–27% (Gruber 1866; Dellon and Mackinnon 1986). On MRIs of asymptomatic individuals, this muscle has been found in 23% of elbows (Husarik et al. 2009).

Variant muscles may enter into Guyon's canal with the ulnar nerve. The most common muscles are the accessory abductor digiti minimi, which may arise from the palmaris longus or the antebrachial fascia of the forearm, and the accessory flexor digiti minimi. The distinction between an abnormal palmaris longus and an accessory abductor digiti minimi may not be clear, as the abnormal palmaris longus may insert on the abductor digiti minimi (Fig. 91.19). Anatomical studies suggest the incidence of these muscles falls within the range 16–22% of specimens; when present, a high percentage of specimens had bilateral anomalous muscles (46%) (Dodds et al. 1990; Bozkurt et al. 2005). A similar incidence (25%) of anomalous muscles within Guyon's canal were found in MRIs of asymptomatic volunteers, also noting a high preponderance of bilateral findings (67%, Zeiss et al. 1992).

Origins

The ulnar nerve may receive fibers of the seventh cervical nerve through a lateral root (or head) of the ulnar nerve, forming an ulnar loop at the edge of the subscapularis (not to be confused with the medial and lateral roots of the median nerve, as described in the section "Median nerve/Origins"). Kerr (1918) found this in 43% of 175 plexus specimens, and Walsh (1877) found this in 91% of 290 specimens when care was taken to identify this branch; Fuss (1989) found this variant to be present in 56% of 158 specimens and suggested this as a "normal variation" and not a "variety." This lateral root may also provide branches to the medial root of the median nerve or pass through the medial root of the median nerve (Kerr 1918). Alternatively, the ulnar nerve may receive a branch directly from the seventh cervical nerve (Walsh 1877).

Communications between the median and ulnar nerve are common in both the forearm and hand, which are described in the section "Communications between the median and ulnar nerves" below. The patterns of crossing fibers are most commonly median to ulnar, usually to provide innervation of muscles typically innervated by the ulnar nerve. As such, this

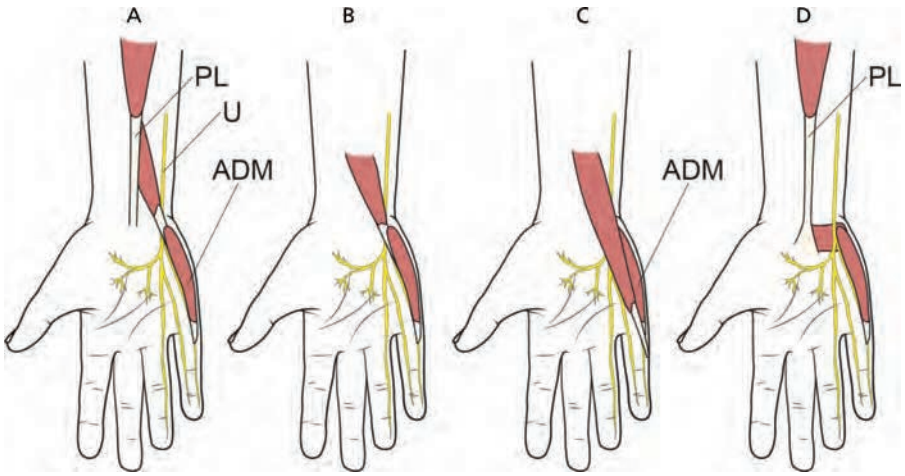

Figure 91.19 (a–d) Variant muscles at Guyon's canal. Adapted from De Smet (2002). Reproduced with permission of the Department of Neurosurgery, University of Utah.

communication could be considered a distal sorting of motor fibers that failed to enter the ulnar nerve from the medial cord.

Proximal communicating branches from the radial nerve to the ulnar nerve in the arm have been reported frequently (Oluyemi et al. 2007; Ozguner et al. 2010). This branch is known as the ulnar collateral branch and may contain fibers destined to innervate the medial head of the triceps, which is described in the section "Communications between the ulnar and radial nerves" below. There are also frequent communications between the posterior cutaneous branch of the ulnar nerve and the superficial branch of the radial nerve.

Targets

The medial antebrachial cutaneous nerve may arise from the ulnar nerve rather than the medial cord, lower trunk, or first thoracic nerve (Kerr 1918; Race and Saldana 1991).

Several authors have described ulnar nerve innervation of the medial head of the triceps, which was first observed in the mid-eighteenth century by Schaarschmidt (1750) (Bekler et al. 2009; Loukas et al. 2013; Pascual-Font et al. 2013). Anatomical series found 28–61% of specimens had one or more branches from the ulnar nerve to the triceps (Bekler et al. 2009; Loukas et al. 2013). Other authors disagree with these descriptions, finding that all branches to the medial triceps originated from the radial nerve (Cruveilhier 1836; Krause 1864; Linell 1921b). One anatomic dissection and literature review identified these ulnar-like branches as the classically described ulnar collateral branches of the radial nerve, which may join the ulnar nerve proximally and give the impression of direct ulnar innervation of the triceps (Pascual-Font et al. 2013), see "Communications between the ulnar and radial nerves" below.

When an anconeus epitrochlearis muscle (see "Variations causing ulnar nerve entrapment" above) is present, it receives a branch from the ulnar nerve.

In the upper portion of the forearm, the flexor carpi ulnaris is innervated by two to four branches. These branches are typically terminal branches, although a few may provide a very small branch to flexor digitorum profundus (Sunderland and Hughes 1946). The flexor digitorum profundus is most commonly innervated by a single branch, as Sunderland found in 80% of cases (Sunderland and Hughes 1946). In some cases, the ulnar nerve may not innervate the flexor digitorum profundus at all (creating the so-called "all-median hand"; Rowntree 1949; Marinacci 1964a, b). The ulnar nerve may send fibers to the flexor pollicis longus (Sunderland and Hughes 1946), flexor digitorum superficialis, first and second lumbricals (Bonnel and Vila 1985), and the entire thenar musculature (Brooks 1887); in about 2% of cases noted by Rowntree (1949), all hand intrinsics were innervated by the ulnar nerve.

Considerable debate exists regarding the relationship of the palmar cutaneous branch of the ulnar nerve to the nerve of Henle. The nerve of Henle is a variably identifiable nerve to the ulnar artery that may continue to the skin of the palm, first noted by Bourgery (1844), described in detail by Henlé (1868), and reported by Pick (1958). It is described to arise in the mid-forearm, approximately 14–16 cm proximal to the wrist (Martin et al. 1996; McCabe and Kleinert 1990). Anatomic series describe identification of a mid-forearm vascular branch of the ulnar nerve in 40% (Martin et al. 1996), 45% (McCabe and Kleinert 1990), and 58% (Balogh et al. 1999) of specimens. The nerve of Henle may communicate with the medial antebrachial cutaneous nerve (13% of specimens; Balogh et al. 1999). This nerve has been shown to consist only of sympathetic and sensory fibers (Balogh et al. 1999). McCabe and Kleinert (1990) noted that the presence of a nerve of Henle was associated with the absence of a palmar cutaneous branch. The palmar cutaneous branch of the ulnar nerve is described to arise proximal to the wrist, with anatomic descriptions noting it arising 11–13 cm proximal to the pisiform (Engber and Gmeiner 1980) or 8–19 cm in length (Tubbs et al. 2011b), entirely consistent with the same description of the nerve of Henle. The presence of a palmar cutaneous branch of the ulnar nerve has ranged from 14% (Engber and

Gmeiner 1980) or 16% (Martin et al. 1996) to 90% (Tubbs et al. 2011b) in anatomic series. Based on these studies, it appears that the terms "nerve of Henle" and the "palmar cutaneous branch of the ulnar nerve" are descriptors of the same branch of the ulnar nerve; this provides branches that form the nervi vasorum of the ulnar artery, terminates in the palm, and contains both sympathetic and sensory fibers.

The dorsal cutaneous branch of the ulnar nerve usually arises from the ulnar or medial aspect of the ulnar nerve at an average distance of 6.4 cm from the distal aspect of the head of the ulna (Botte et al. 1990). The number of branches ranges from three to nine, with an average of five branches (Botte et al. 1990). This branch is at risk in surgeries involving the ulnar head, the ulnocarpal joint, and the triangular fibrocartilage complex. The dorsal branch has been reported completely absent, with cutaneous sensibility supplied by the radial nerve (Learmonth 1919) (see "Communications between the ulnar and radial nerves" below) or the posterior cutaneous nerve of the forearm.

A branch of the dorsal cutaneous branch may return to the volar hand, frequently joining the superficial branch of the ulnar nerve. This was first identified by Kaplan (1963) in dissection, and has become known as a Kaplan's anomalous branch. In joining the superficial branch, a Kaplan's anomalous branch makes a loop around the pisiform; Kaplan surmised this loop to be a source for persistent pisiform pain. Several case reports note various patterns to the Kaplan accessory branch (McCarthy and Nalebuff 1980; Wulle 1988; Hoogbergen and Kauer 1992; Hankins and Flemming 2005). Incidence of a Kaplan's anomalous branch varies; one study found one case in 25 specimens (Hoogbergen and Kauer 1992), another found one case in 50 specimens (Bonnel and Vila 1985), and yet another found no cases in 58 specimens (Dodds et al. 1990). Several internally anastomotic loops around the hamate have also been described (Lassa and Shrewsbury 1975; McCarthy and Nalebuff 1980; Dodds et al. 1990).

The ulnar nerve may trifurcate in Guyon's canal, instead of the typical bifurcation into the superficial and deep branches of the ulnar nerve. Bonnel found this pattern in 11 of 50 specimens, where the trifurcation yielded a deep motor branch and two superficial sensory branches (one forming the medial proper digital nerve to the fifth digit, and the other forming the common digital nerve to the fourth interspace; Bonnel and Vila 1985).

The motor branch of the ulnar nerve has been reported to divide into a median division running in the normal course and a lateral division passing deep to the hook of the hamate. A variant deep branch such as this may produce only partial loss of ulnar motor function (Auerbach et al. 1994). This variation should also be considered when performing decompression of Guyon's canal or excision of an ununited hook of the hamate (Ay et al. 2005; Aydinlioglu et al. 2010).

The sensory field of the ulnar nerve is variable. Linell found 80% of specimens demonstrated ulnar sensory branches consistent with the classic palmar sensory pattern of both sides of the fifth digit and the ulnar side of the fourth digit, whereas 15% had two and one-half fingers and 5% had two complete fingers innervated by the ulnar sensory branches. In 8% of Bonnel's series, the ulnar nerve provided branches to the ulnar and radial sides of the palmar aspect of the fourth digit (Bonnel and Vila 1985).

Communications between the median and ulnar nerves

In the forearm: Martin-Gruber anastomosis and Marinacci communication

Frequently, the median nerve or anterior interosseous nerve will send motor fibers to the ulnar nerve, where fibers destined to join the ulnar nerve travel with the proximal median nerve. This communication was described as early as 1763 by the Swedish anatomist Martin (1763) and later by Gruber 1870. The passage of fibers can create clinically confusing scenarios where proximal median nerve lesions above the anastomosis share features of ulnar nerve injury, suggesting potential localization of the injury to the spinal cord, lower trunk, or dual nerve injury. Rarely, the ulnar nerve will send fibers to the median. Communications from the ulnar nerve to the median nerve have been called a Marinacci communication (Marinacci 1964a, b), although they may also be grouped among the Martin-Gruber anastomoses. The preponderance of cases suggest that the fibers are predominantly motor (Leibovic and Hastings 1992), although sensory communications have been reported (Ranschburg 1917). The communicating branch primarily contains fibers destined for hand intrinsic muscles (see the following section), but may also contain fibers for flexor digitorum profundus.

The diagnosis of a Martin-Gruber anastomosis can be made by electrodiagnostic studies (Gutmann 1993). The compound muscle action potential (CMAP) in the thenar muscles after stimulation of the median nerve at the elbow is larger than median nerve stimulation at the wrist; conversely, CMAPs are lower for ulnar nerve stimulation at the elbow than ulnar nerve stimulation at the wrist. The diagnosis is confirmed by recording CMAPs in normally ulnar-innervated muscles resulting from median nerve stimulation, such as the first dorsal interosseous or hypothenar muscles. The consideration of a Martin-Gruber anastomosis is essential in electrodiagnostic studies as the reduction in CMAPs along the median or ulnar nerve, if considered in isolation, may suggest a focal conduction block, prompting misdiagnosis and unnecessary treatment (Marras and Midroni 1999).

The incidence of the anastomosis varies slightly based on method of diagnosis, over the range 5–40% in electrophysiologic studies (Mannerfelt 1964; Crutchfield and Gutmann 1980; Sonck et al. 1991; Gutmann 1993; van Dijk and Bouma 1997) and 10–30% in anatomic studies (Curtis 1886; Gruber 1870; Nakashima 1993; Taams 1997; Shu et al. 1999; Rodriguez-Niedenfuhr et al. 2002b), with an average estimate of 17% in all arms (Leibovic and Hastings 1992). The communication is usually in the form of a branch that leaves the median in common

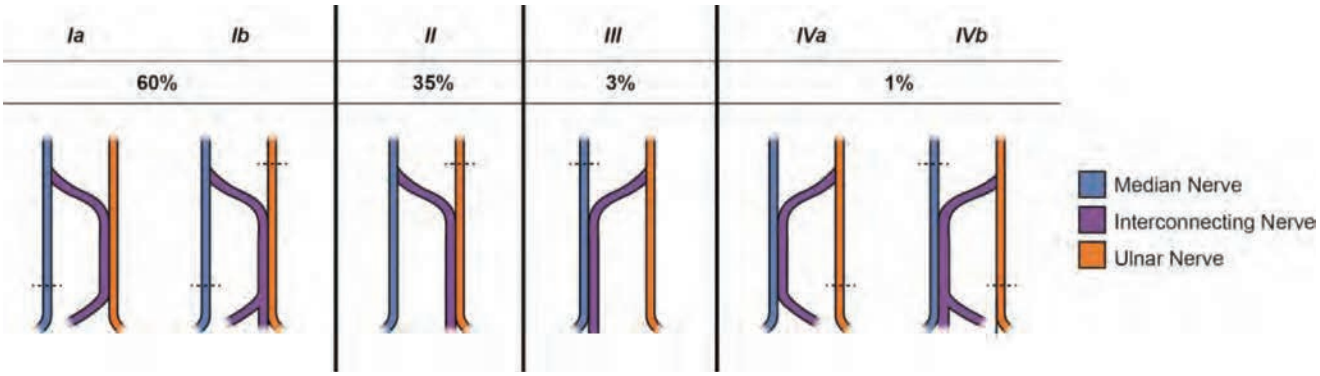

Figure 91.20 Martin-Gruber anastomoses as categorized by Leibovic and Hastings (1992). The frequency is listed below the category title. Nerve lesions at sites marked by bars may be minimally symptomatic or clinically silent on motor examination. Reproduced with permission of the Department of Neurosurgery, University of Utah.

either with muscular branches at the elbow or with the anterior interosseous nerve, and joins the ulnar nerve at about the middle of the forearm. Less frequently, the connection is between branches from the median and ulnar nerves to the flexor digitorum profundus, forming a loop (ansa) or small plexus, some of which may be intramuscular (Verchere 1883; Nakashima 1993; Rodriguez-Niedenfuhr et al. 2002a).

Multiple classification schemes have been developed, based largely on the origin of the communicating branch (e.g., whether it arose from the anterior interosseous nerve, the median nerve proper, or a muscular branch, such as those to flexor digitorum profundus; Thomson 1893; Shu et al. 1999). Rodriguez-Niedenfuhr amalgamated results from multiple cadaveric studies and demonstrated little consistency between authors on the origins of the communicating branch (Rodriguez-Niedenfuhr et al. 2002b). Leibovic proposed a classification system of forearm anastomosis between the median and ulnar nerves (Fig. 91.20) based on the distribution of nerve fibers, as extracted from case reports (Leibovic and Hastings 1992). Many of the patterns imply anomalous innervation within the hand, such as thenar innervation carried primarily through the distal ulnar nerve (Fig. 91.20a).

Communications between the median and ulnar nerves are relatively uniform in the proximal forearm in non-human primates (Hepburn 1892). Interestingly, there may be an autosomal dominant inheritance pattern within some families with electrophysiologic evidence of a Martin-Gruber anastomosis (Crutchfield and Gutmann 1980).

Within the hand: the Riche-Cannieu anastomosis

Several communications between the median and ulnar nerves in the hand have been described, including a motor communication between the thenar (recurrent) motor branch of the median nerve and the deep branch of the ulnar nerve (referred to as the Riche-Cannieu anastomosis, thenar loop, or thenar ansa), and a sensory communication (referred to as the ramus communicans or Berrettini branch) between the third and fourth common digital nerves (Fig. 51.21).

The Riche-Cannieu anastomosis is a communication in the depth of thenar eminence between the thenar motor branch of the median nerve to the superficial head of the flexor pollicis brevis and the deep ulnar branch to the deep head of the flexor pollicis brevis. The anastomotic branch passes between the two heads of the adductor pollicis and runs recurrently to the tendon of the flexor pollicis longus on either its medial or lateral side, forming an ansa. Harness and Sekeles (1971) reported finding that half of these anastomoses were according to the description of Cannieu (1897), in that the anastomotic ansa circled around the lateral side of the tendon of flexor pollicis longus. The percentage of cases or specimens demonstrating dual innervation of the flexor pollicis brevis has ranged over 15–100% in anatomical studies (Brooks 1886; Cannieu 1897; Day and Napier 1961; Mannerfelt 1966; Harness and Sekeles 1971; Homma and Sakai 1992), 89% in clinical studies of nerve lesions (Highet 1943) (results from Rowntree 1949 excluded due to methodology), and 38–68% in electromyographic studies (Forrest 1967; Belson et al. 1976).

Variations within the thenar ansa have been recorded, including incorporation of the digital nerve of the thumb, the branch of the adductor pollicis coming from the deep branch of the ulnar nerve, and an anastomosis passing through the first lumbrical, which then receives its innervation from the deep branch of the ulnar nerve. Other muscles of the thenar eminence may receive dual innervation from the median and ulnar nerves (Harness et al. 1974).

The ramus communicans (Berrettini branch, after the eighteenth-century artist; Berrettini 1741) is a communicating branch between the third common digital nerve of the median nerve and the fourth common digital nerve of the ulnar nerve, superficial to the tendons of the flexor digitorum superficialis

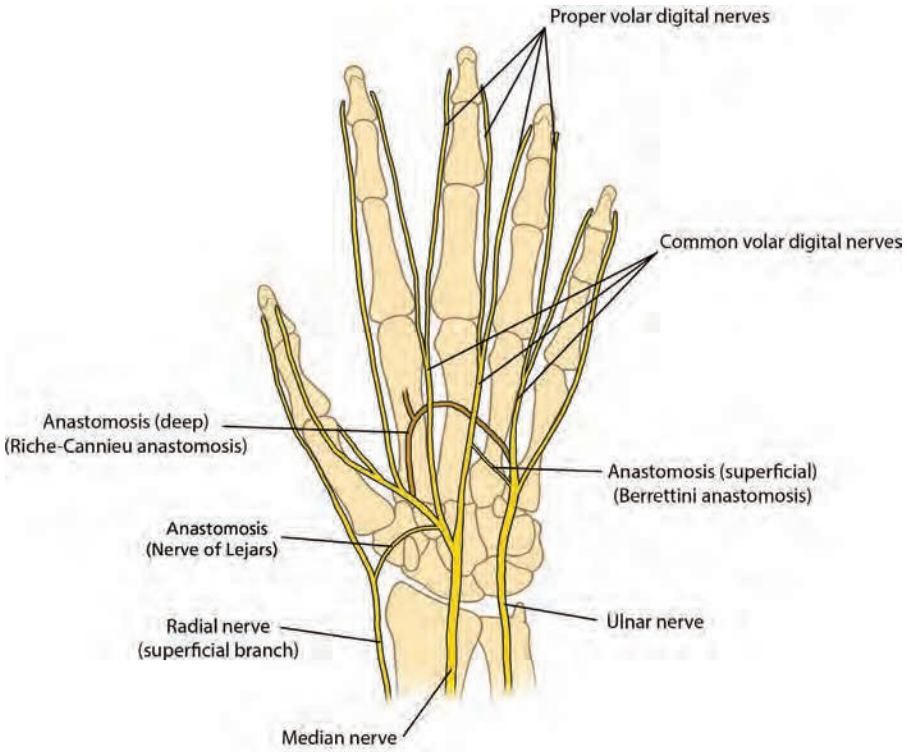

Figure 91.21 Median and ulnar communications within the hand, including the Riché-Cannieu anastomosis, nerve of Lejars, and the Berrettini anastomosis. Reproduced with permission of the Department of Neurosurgery, University of Utah.

and flexor digitorum profundus. It has been categorized into four types by Ferrari and Gilbert (1991), based on the location from the transverse carpal ligament as well as the number of communicating branches. Various anatomical studies have suggested a high incidence of this branch (81–100%; Ferrari and Gilbert 1991; Stancic et al. 1999; Don Griot et al. 2000; Loukas et al. 2007a), prompting some authors to consider the communication an anatomical constant rather than a variation (Bonnel and Vila 1985).

Nerves arising from the posterior cord of the brachial plexus

The branches from the posterior cord of the brachial plexus have been categorized into five named nerves (Table 91.5; Fig. 91.22). As with other muscular branches arising directly off the brachial plexus, there is variation in the number and pattern of the subscapular nerves. Classically, the subscapular nerves are divided into an upper and a lower subscapular nerve (Kerr 1918); however, there are often more than two distinct nerves to the subscapular muscle (McCann et al. 1994; Ouattara et al. 2006), with the attendant confusion among anatomists regarding classification (Walsh 1877). Because the upper and lower subscapular nerves have the same target and similar origins, their variations are presented in relationship to each other.

Table 91.5 Nerves arising from the posterior cord of the brachial plexus.

Branches from posterior cord	Nerve origins
Upper and lower subscapular nerves	C5–C6
Thoracodorsal nerve	(C5–C6) C7–C8
Axillary nerve	C5–C6
Radial nerve	C5–C8 (T1)

Upper and lower subscapular nerves

Within anatomic studies that looked solely at the innervation of the subscapularis muscle, Walsh noted three to five nerves; McCann et al. (1994) noted 82% had three nerves, 16% had four nerves, and only 2% had two nerves; Herringham (1886) noted up to four nerves; and Kato (1989) found that 90% of specimens had at least three nerves. Although there are commonly more than two nerves to the subscapularis, those nerves whose origin is proximal to the thoracodorsal nerve retain the term upper subscapular nerves; similarly, those nerves to the subscapularis whose origin is distal to the thoracodorsal nerve are described as the lower subscapular nerves. Furthermore, there is evidence that the structure of the muscle changes along the rostrocaudal axis (Paterson 1911), and the pattern of electrophysiologic data suggests independent activation of portions of the muscle based upon shoulder position (Kadaba et al. 1992).

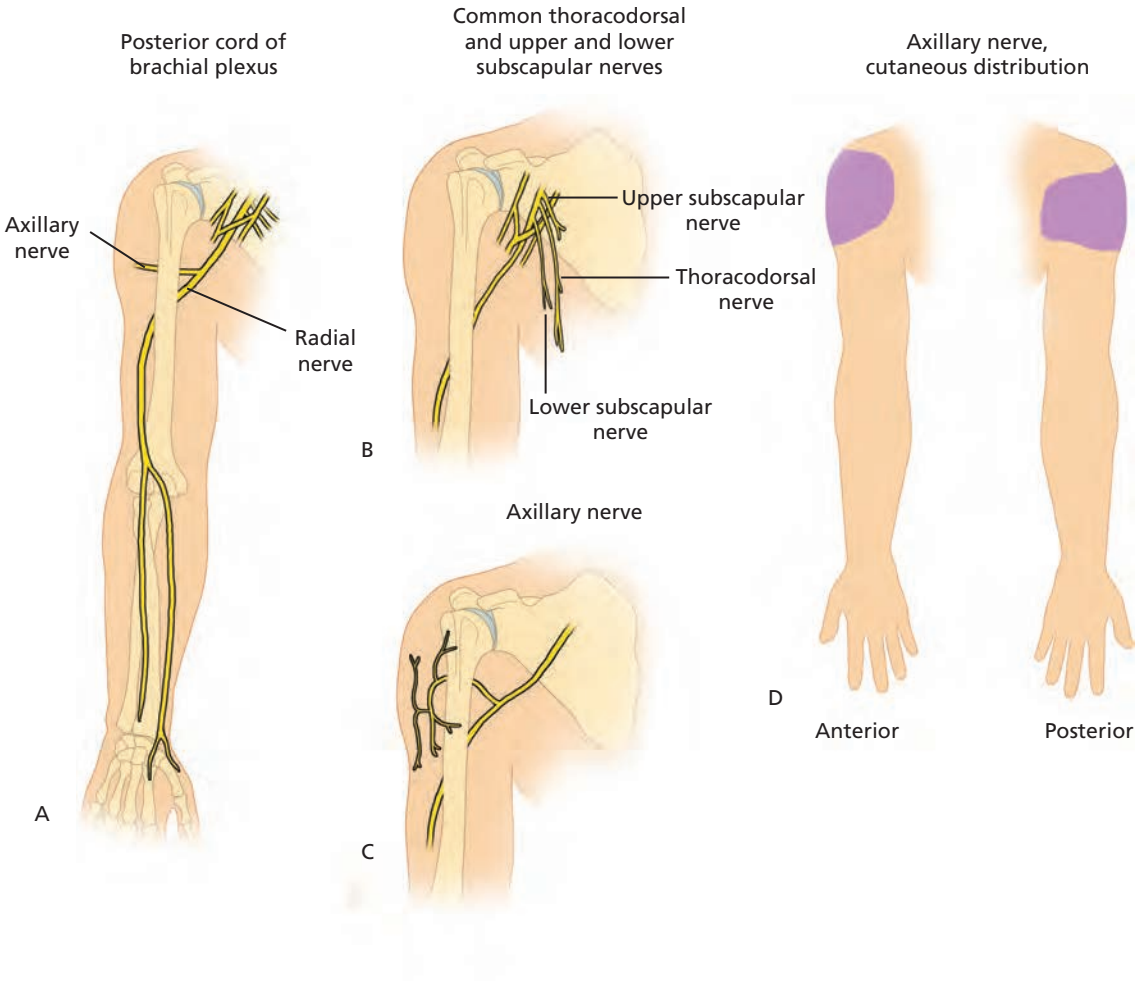

Figure 91.22 (a–c) Depiction of the common anatomy of the nerves arising from the posterior cord of the brachial plexus, including (d) the sensory distribution of the axillary nerve. Adapted from Bergman et al. (1988). Reproduced with permission of the Department of Neurosurgery, University of Utah.

The upper or short subscapular nerves are composed of the fifth and sixth cervical nerves. The nerves lie in the upper axillary fossa and supply only the rostral portion of the subscapularis muscle.

The lower (axillary, inferior) subscapular nerves are composed of fibers from the fifth and sixth cervical nerves. The nerve passes behind the subscapular artery, distal to its circumflex scapular branch, and supplies teres major and the lower portion of subscapularis.

Regional relationships

The lower subscapular and axillary nerves may traverse the subscapularis muscle deep to an accessory subscapularis (subscapularis minor; subscapulo-capsular or subscapulo-humeral muscle, Macalister 1867; simply the additional slip, Paterson 1911; or the accessory subscapularis-teres-latissimus muscle, Kameda 1976a) muscle, which may be largely tendinous in composition and a source for potential entrapment (Breisch 1986). The paucity of reports suggests that the incidence of this muscle is probably rare. A report found this variant configuration in one of 222 specimens (Yoshinaga et al. 2008), whereas another found the presence of the muscle in ten of 380 specimens (Kameda 1976a); it should be noted that in the ten variant specimens, the muscles identified as an accessory subscapularis included variations that had origins on the latissimus dorsi, which may be considered an axillary arch by other authors (Turgut et al. 2005). The described innervation of this anomalous muscle has included upper subscapular (Takafuji et al. 1991), lower subscapular (Kameda 1976a), branch of the radial (Yoshinaga et al. 2008) or thoracodorsal (Kameda 1976a).

Origins

The upper subscapular nerve typically receives fibers from the fifth and sixth cervical nerve (Kato 1989). The upper subscapular

nerve may arise directly from the fifth cervical nerve or from the middle trunk, suggestive of receiving fibers from the seventh cervical nerve alone (Kerr 1918). Kerr (1918) noted a large number of specimens (65%) with contributions from the fourth cervical nerve.

The upper subscapular nerve may arise from the posterior (dorsal) division of the upper (cephalic) trunk or from the posterior cord. In his summary of 350 plexuses, Walsh (1877) stated that the upper subscapular nerve arose from the posterior division. Kerr (1918) noted that at least one upper subscapular nerve arose from the posterior division in 57% of specimens; McCann et al. (1994) noted that the most superior subscapular nerve arose from the posterior division in 56%. Although these numbers are similar, the naming convention is different and the denominators for the percentages are therefore potentially different. In contrast, Tubbs et al. (2007) reported no instances of the upper subscapular nerve arising from the posterior division and Chen et al. (2013) only noted 9% of upper subscapular nerves arising from the posterior division.

The upper subscapular nerve frequently comprises two or more nerves (Herringham 1886), sometimes with a common origin (Walsh 1877). In the studies that specified the number of independent nerves arising as upper subscapular nerves, the number of specimens with two or more upper scapular nerves ranged over 10–67% (see Table 91.6).

The lower subscapular nerves primarily receive fibers from the sixth cervical nerve, with variable contributions from the fifth and seventh cervical nerves (Kato 1989). The lower subscapular nerve comprised exclusively fifth through seventh cervical nerves in the majority of specimens (63%, Kato 1989; 77%, Kim et al. 2008; 97%, Chen et al. 2013).The remainder were formed from the sixth through seventh cervical nerves (Kato 1989; Kim et al. 2008), and rarely fifth and sixth cervical nerves (Chen et al. 2013). It may also receive contributions from the fourth cervical nerve (Kerr 1918), although few other anatomical works support this finding (Kim et al. 2008; Chen et al. 2013).

The lower subscapular nerves may arise from the posterior cord, posterior divisions of the upper or middle trunks, axillary nerve, or as a common trunk with the thoracodorsal nerve. Kerr found that the origin of 75% of the lower subscapular nerves was the elements of the posterior cord; the remainder came from elements arising from the posterior divisions of the upper and middle trunks, for example, a lower subscapular nerve branching from an axillary nerve arising from the posterior divisions of the upper and middle trunks. The most common origins of the lower subscapular nerves are directly from the posterior cord and the axillary nerve. The incidence of the lower subscapular nerves arising from the axillary nerve has varied among studies from 17% (Chen et al. 2013), to 21% (Tubbs et al. 2007), to 54% (Kerr 1918). There may be multiple branches from the lower subscapular nerve to the subscapularis muscle (Table 91.7).

Table 91.6 Variation in the number of nerves arising from the upper subscapular nerve.

	Kerr 1918	Tubbs et al. 2007	Chen et al. 2013
Number of specimens	157	62	33
One nerve	54%	90%	33%
Two nerves	41%	8%	61%
Three nerves	6%	2%	6%

Table 91.7 Variation in the number of branches from the lower subscapular nerve to the subscapularis muscle.

	Kerr 1918	Tubbs et al. 2007	Chen et al. 2013
Number of specimens	41	62	33
One nerve	51%	94%	89%
Two nerves	37%	6%	8%
Three nerves	12%	–	3%

Targets

The upper subscapular nerves appear to exclusively innervate the subscapularis muscle; there are no case series reporting the upper subscapular nerves innervating other muscles.

The lower subscapular nerves typically innervate the lower edge (axillary portion) of the subscapularis muscle and the teres major. The lower subscapular nerves may infrequently send branches to the latissimus dorsi (Kerr 1918; Chen et al. 2013). The branch to teres major may also arise from the axillary nerve (Kerr 1918).

Thoracodorsal nerve

The thoracodorsal nerve (middle subscapular or long subscapular nerve) is composed of fibers from the seventh and eighth cervical nerves, but has also been found to contain fibers from the sixth cervical. The nerve crosses the axillary artery dorsally, is accompanied by the subscapular artery along the axillary margin of subscapularis, and terminates in the latissimus dorsi muscle (Fig. 91.22b).

Regional relationships

An accessory subscapularis-teres-latissimus muscle was found very infrequently to overlie the thoracodorsal nerve (2 of 380 specimens) (Kameda 1976b).

Origins

The thoracodorsal nerve receives the majority of fibers from the seventh and eighth cervical nerves (Kato 1989). Fibers from the seventh cervical nerve are universally present in several studies; fibers from the eighth cervical nerve are present in 85% (Lee 2007b). The sixth cervical nerve contributes fibers to the

thoracodorsal nerve in 25% (Kato 1989; Lee 2007b) to 35% of specimens (Inserra and Spinner 1986).

Different authors found the origins of the thoracodorsal either very consistent or fairly variable. Tubbs et al. (2007) reported always finding a single thoracodorsal nerve that in all but 1 of 62 specimens arose from the posterior cord (98.5% of specimens). In contrast, Kerr (1918) found this pattern in 58% of 161 specimens. In the remainder, the thoracodorsal formed from the axillary nerve, the radial nerve, and the posterior divisions of the upper and middle trunks. In the ten cases with variant subscapular muscles listed by Kameda (1976b), none of the thoracodorsal nerves arose from the posterior cord. Major classical authors on the brachial plexus, including Herringham, Harris, Linell, and Walsh, provided little comment on the variation of the origins of the thoracodorsal nerve.

Targets

The thoracodorsal nerve divides into two branches upon entering the latissimus dorsi, which separately innervate the medial and lateral portions of the muscle (Bartlett et al. 1981; Tobin et al. 1981; Theeuwes et al. 2011). The thoracodorsal nerve at the neurovascular pedicle to the latissimus dorsi demonstrated a bifurcation (in 94% of 115 specimens), and in a small minority (6% of 115 specimens) where the nerve arborized into three or four branches (Tobin et al. 1981).

The thoracodorsal nerve is among the most common sources for innervation of a variant axillary arch muscle, along with the pectoral nerves (Turgut et al. 2005).

Axillary nerve

The axillary nerve (circumflex nerve) is composed of fibers from the fifth and sixth cervical nerves (Fig. 91.22c). After traveling along the anteroinferior aspect of the subscapularis muscle, the axillary nerve provides a branch to the shoulder joint and passes through the quadrangular (quadrilateral, lateral axillary hiatus) space (of Velpeau), wrapping around the surgical neck of the humerus posteriorly with the posterior circumflex humeral vessels. Around the quadrangular space, the axillary nerve divides into two parts: an anterior branch (lateral division) and a posterior (medial division) branch. The anterior branch innervates the anterior two-thirds of the deltoid muscle (Fig. 91.22d). The posterior branch innervates both teres minor and the lower and posterior portions of the deltoid muscle. The nerve continues as the posterior (or upper) lateral brachial cutaneous nerve, and is composed of sensory fibers that supply the skin over the lower portion of the deltoid muscle.

Regional relationships

The lower subscapular and axillary nerves may traverse the subscapularis muscle deep to an accessory subscapularis – either the subscapularis minor, subscapulo-capsular or subscapulo-humeral muscle (Macalister 1867), simply the additional slip (Paterson 1911), or the accessory subscapularis-teres-latissimus muscle (Kameda 1976a) muscle – which may be largely tendinous in composition and a source of potential entrapment (Breisch 1986). An accessory subscapularis is commonly described as located on the superior aspect of the subscapularis; in addition, the axillary nerve may pass under a muscle slip of the lower margin of the subscapularis (Duparc et al. 1997).

The axillary nerve passes through an anatomic hiatus known as the quadrangular (quadrilateral, lateral axillary hiatus) space (of Velpeau), traveling medial to the humerus, inferior to the teres minor, superior to the teres major, and lateral to the long head of the triceps. Some authors believe that this musculoskeletal confine predisposes the axillary nerve to injury at this proximal location or possible nerve entrapment (McKowen and Voorhies 1987; Francel et al. 1991; Millett et al. 2013), with the consequent development of an axillary nerve mononeuropathy. The constellation of deltoid weakness, posterior axillary numbness, and pain at the quadrangular space is sometimes referred to as the quadrilateral space syndrome, first described by Bateman in 1955 (Tubbs et al. 2005). It is commonly associated with compression of the posterior circumflex humeral artery, and provocative angiogram has been utilized as a criterion for diagnosis (Cahill and Palmer 1983). Variant fibrous bands may account for idiopathic versions of this syndrome (Tubbs et al. 2005; McClelland and Paxinos 2008).

The axillary nerve most commonly bifurcates into the anterior and posterior branches within or posterior to the quadrangular space in 55% (Gelber et al. 2006), 87% (Uz et al. 2007), and 100% (Tubbs et al. 2005) of specimens. Uz et al. (2007) found the point of bifurcation proximal to the quadrangular space in 13%, whereas Gelber et al. (2006) found this arrangement in 38% of specimens.

Origins

The axillary nerve may be derived solely from the fifth cervical nerve, as the contribution from the sixth cervical may be insignificant or absent altogether.

The axillary nerve is most commonly one of two terminal branches of the posterior cord, as found in 80% of 173 specimens by Kerr (1918). Of the remaining 20%, half arise from the posterior divisions of the upper and middle trunks and the other half from the posterior division of only the upper trunk.

Communications between the axillary and radial nerves

In contrast to the number of communicating branches between the nerves of the anterior (volar) side of the arm, such as the Martin-Gruber anastomoses, reported communications on the posterior (dorsal) side are decidedly less frequent. In a review of electronically searchable records, only two studies were identified that reported on nerve communications in the posterior arm. One study found eight communicating branches between the axillary nerve and the radial nerve in 602 specimens (Koizumi et al. 1999). The authors found that the communicating branches from the axillary nerve supplied proximal radially innervated muscles. Another study found one such branch in 100 specimens (Darji et al. 2013).

Table 91.8 Locations of the articular branches from the axillary nerve to the glenohumeral joint.

	Uz et al. 2007	Gelber et al. 2006	Duparc et al. 1997	Loukas et al. 2009
Main axillary nerve	30%	30%	100%	–
Anterior branch of axillary nerve	16%	–	–	100%
Posterior branch of axillary nerve	33%	66%	–	–

Targets

The axillary nerve may be the origin for the lower subscapular nerve, as was found in 55% of specimens (Kerr 1918); branches to the lower margin of the subscapularis muscle; a branch to teres major; a branch to the coracobrachialis (Duparc et al. 1997); or the origin of the thoracodorsal nerve (Gelber et al. 2006).

The axillary nerve provides sensory branches to the glenohumeral joint that have been found to arise from multiple locations along the axillary nerve, although there is considerable variation between observations amongst authors (Duparc et al. 1997; Gelber et al. 2006; Uz et al. 2007). There are commonly multiple articular branches from the axillary nerve to the shoulder capsule (Table 91.8). Duparc et al. (1997) noted that multiple articular branches from the axillary nerve to the joint capsule fixated the nerve, which may predispose the axillary nerve to injury. The radial, suprascapular, and subscapular nerves may also provide articular branches to the glenohumeral joint (Gardner 1948b; Gelber et al. 2006).

The precise location of the branch to the teres minor is disputed. The branch to the teres minor is most commonly described as arising from the posterior branch of the axillary nerve (100% of specimens, Gelber et al. 2006; Uz et al. 2007; Loukas et al. 2009). The teres minor branch has also been described as arising from proximal axillary nerve (100% of specimens, Duparc et al. 1997). The branch to the teres minor may then divide to provide the posterior brachial cutaneous nerve (three of 32 specimens, Duparc et al. 1997). In a similar percentage of specimens, the posterior brachial cutaneous nerve may be absent (4 of 32 specimens, Duparc et al. 1997).

The anterior branch of the axillary nerve primarily innervates the anterior two-thirds of the deltoid, commonly referred to as the anterior and middle deltoid. The posterior deltoid is most frequently innervated by the posterior branch, with occasional exclusive innervation by the anterior branch (3.3% of specimens, Uz et al. 2007; 10%, Loukas et al. 2009). The middle deltoid segment may receive additional innervation from a branch of the posterior branch (38% of specimens, Loukas et al. 2009). Similarly, the posterior deltoid may receive branches from both the anterior and posterior branches (18%, Loukas et al. 2009; 27%, Uz et al. 2007).

Radial nerve

The radial nerve (musculospiral nerve) is composed of fibers from the sixth, seventh, and eighth cervical nerves. It may also receive contributions from the fourth and fifth cervical nerves and from the first thoracic nerve. It is the largest branch of the posterior cord of the brachial plexus. The nerve is first named radial at the lower border of pectoralis major. It passes distally in the axillary fossa and laterally to the axillary artery and courses anterior to subscapularis, latissimus dorsi, and teres major. It enters the arm and lies initially on the medial side of the upper part of the humerus, dorsal to the brachial artery, and anterior to the long head of triceps. The radial nerve then runs obliquely and laterally behind the humerus in the radial groove or sulcus and then between the lateral and medial heads of triceps. The nerve is accompanied at this point by the deep (profunda) brachial artery. At the upper end of the lower third of the humerus, the nerve is located on the lateral side of the arm where it pierces the lateral intermuscular septum. The radial nerve continues distally and anteriorly between brachioradialis and extensor carpi radialis longus laterally and brachialis medially. The radial nerve terminates just above the capitulum of the humerus by dividing into superficial and deep terminal branches.

In the axillary fossa, the radial nerve provides a motor branch to the long head of triceps and other branches to the medial head of triceps. One of the branches occasionally accompanies the ulnar nerve before it enters the medial head of triceps; it is called the ulnar collateral branch, although it is not of ulnar nerve origin. The posterior brachial cutaneous nerve arises from the radial nerve, crosses the tendon of latissimus dorsi, and pierces the superficial fascia to supply the skin of the middle of the back of the arm below the deltoid muscle insertion.

In the radial groove, the radial nerve supplies the lateral and medial heads of triceps as well as the small anconeus muscle and the elbow joint. The posterior antebrachial cutaneous nerve is distributed distally between the lateral and medial heads of triceps and then divides, near the elbow, into upper and lower branches. These nerves pierce the lateral head of triceps. The smaller upper branch, the lower lateral brachial cutaneous nerve, supplies the skin over the lower half of the lateral and anterior aspects of the arm. The larger lower branch of the nerve supplies the skin over the dorsum of the forearm as far as the wrist (Fig. 91.23a–c).

After the radial nerve perforates the lateral intermuscular septum, it supplies motor nerves to the brachioradialis and extensor carpi radialis longus, and sensory nerves to the elbow joint. The radial nerve may also supply extensor carpi radialis brevis, which is also commonly innervated by a branch from the

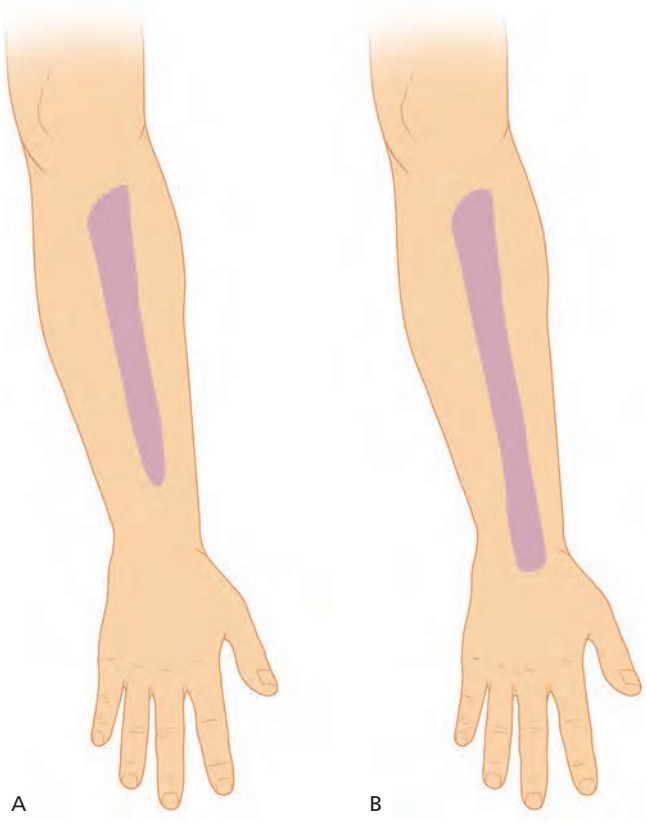

Figure 91.23 (a, b) Variable distribution of sensory loss after division of the posterior antebrachial cutaneous. Adapted from Stopford (1918). Reproduced with permission of the Department of Neurosurgery, University of Utah.

terminal sensory division of the radial nerve in the forearm, the superficial branch of the radial nerve.

The deep terminal branch of the radial nerve passes distally between brachialis and extensor carpi radialis longus to lie anterior to the lateral part of the elbow joint. It continues distally, passes dorsally through the belly of the supinator muscle and enters a space between the superficial and deep muscles on the extensor or dorsal side of the forearm. The deep branch now becomes the posterior interosseous nerve of the forearm. The nerve is accompanied by the posterior interosseous artery and lies on the interosseous membrane and the dorsal aspect of the radius. It passes in a groove at the wrist with extensor digitorum communis and extensor indicis, and carries sensory nerve fibers from the carpal joints. The posterior interosseous nerve of the forearm supplies extensor carpi radialis brevis, supinator, extensor digitorum communis, extensor digit minimi, extensor carpi ulnaris, extensor indicis, extensor pollicis longus, extensor pollicis brevis, and abductor pollicis longus.

The superficial terminal branch of the radial nerve is primarily sensory. It courses distally beneath brachioradialis and passes anterior to the elbow joint. It runs lateral to the radial artery, which it parallels in the proximal end of the forearm. At the inferior border of pronator teres, it turns dorsally to lie on the deep surface of the tendon of brachioradialis and then emerges near the dorsal surface of the forearm. It proceeds distally to the back of the wrist and then divides into its terminal cutaneous branches. The most lateral branch carries sensation from the radial part of the thenar eminence. The most medial branch of this nerve is overlapped by branches from the ulnar nerve and is called the ulnar anastomotic branch. The other branches, which carry sensation from the skin over the digits, are called the dorsal digital nerves. These nerves supply the skin on the back of the first digit, on both sides of the second digit, and on the radial side of the third digit (Fig. 91.24d–g). These cutaneous nerves usually extend to the base of the nail of the first digit, to the distal interphalangeal joint of the second, before the proximal interphalangeal joint of the third, and to the metacarpophalangeal joint of the fourth digit.

Regional relationships

The radial nerve may accompany the axillary (circumflex) nerve through the quadrangular space. Decompression of the quadrangular space may improve radial nerve sensory neuropathy (Brown and Chung 1999).

The radial nerve passes through the lateral intermuscular septum at the distal end of the nerve's transit along the posterior margin of the humerus, also known as the spiral groove. Authors disagree whether the radial nerve rests within a true

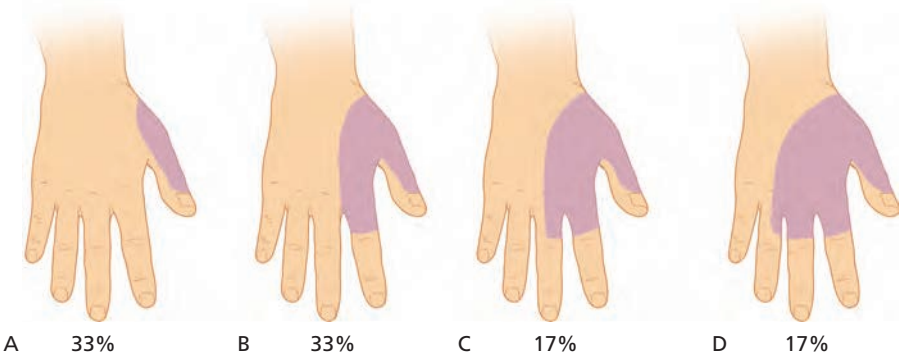

Figure 91.24 (a–d) Range in the distribution of sensory loss after division of the distal radial nerve. Percentages shown below the figure reflect the frequency of patients reporting the highlighted area of sensory loss after traumatic division of the radial nerve. Adapted from Stopford (1918). Reproduced with permission of the Department of Neurosurgery, University of Utah.

osseous groove of the humerus (Sunderland 1946; Whitson 1954; Carlan et al. 2007), with some suggesting that the radial nerve passes over the medial head of the triceps and not the humerus. Furthermore, it has been suggested that the spiral groove is the consequence of the insertion of the brachialis, and the radial nerve lies outside the groove (Whitson 1954). The location where the radial nerve pierced the lateral intermuscular septum was found to be 8–12 cm (mean of 10 cm) above the lateral epicondyle in 20 specimens (Sunderland 1946). The posterior brachial cutaneous branch may or may not pierce the lateral intermuscular septum; from 0% (MacAvoy et al. 2006; Carlan et al. 2007) to 85% (Tubbs et al. 2009a) of specimens were found to have the posterior brachial cutaneous branch piercing the lateral intermuscular septum.

The radial nerve may bifurcate into the deep and superficial branches of the radial nerve proximal to the lateral epicondyle. This may occur in as many as 40% of specimens (Linell 1921b), although other authors have not found bifurcations above the epicondyle (Abrams et al. 1997; Sunderland 1946).

The proximal edge of the supinator may have a ligamentous arch known as the arcade of Frohse (Frohse and Frankel 1908). The leading edge of the supinator may be membranous (20%, Ozkan et al. 1999; 68%, Thomas et al. 2000; 70%, Spinner 1968) or tendinous (30%, Spinner 1968; 32%, Thomas et al. 2000; 80%, Ozkan et al. 1999). The posterior interosseous nerve may pass over instead of piercing the supinator muscle (Tountas and Bergman 1993). The posterior interosseous nerve may enter the supinator as a single nerve or as two equally sized branches (Tubbs et al. 2013a). The posterior interosseous nerve commonly enters the supinator at the proximal edge of the muscle, but may exit the muscle either from within the muscle belly or from underneath the distal margin (50% of specimens at each site, Seradge et al. 2000).

The superficial branch of the radial nerve may pierce the brachioradialis tendon, instead of emerging from the lateral side of the muscle, in 10% of specimens (Abrams et al. 1992). However, this variation is not frequently reported in some major surgical series (Dellon and Mackinnon 1986). The tendon of the brachioradialis may be split in 6% of specimens (Turkof et al. 1994), with the superficial branch of the radial nerve emerging within this split in half of the cases (3% of specimens, Turkof et al. 1994). This variation was found in 5% of patients who underwent surgical exploration for entrapment of the superficial branch of the radial nerve (Turkof et al. 1995). Some authors have suggested that the exit of the superficial branch of the radial nerve between the tendons of the brachioradialis and the extensor carpi radialis longus may facilitate neuroma formation (Dellon and Mackinnon 1984).

Variations causing radial nerve entrapment

The radial nerve may be entrapped by variant myofascial structures at multiple locations along its course. The passage of the radial nerve through the lateral intermuscular septum places the nerve within a fibro-osseous tunnel, which may constrain the radial nerve during arm movement. Several reports have implicated triceps use with either transient (Lotem et al. 1971; Streib 1992) or sustained radial neuropathy (Manske 1977). These cases have been correlated with an accessory slip of the lateral head of the triceps below the radial nerve or the passage of the radial nerve through a tendinous arch of the lateral head of the triceps, rather than the lateral intermuscular septum alone, which may compress the nerve during activity (Lotem et al. 1971; Nakamichi and Tachibana 1991). Despite the fibro-osseous tunnel, reports on compression of the radial nerve at the lateral intermuscular septum are relatively sparse (Eversmann 1983).

In contrast, entrapment of the radial nerve in the proximal forearm, the so called "radial tunnel syndrome" (Roles and Maudsley 1972), is much more frequently diagnosed and treated (Lawrence et al. 1995; Sotereanos et al. 1999). Five anatomical zones of the radial tunnel have been described: (1) fibrous bands anterior to the radial head; (2) a vascular leash supplying the brachioradialis and the extensor carpi radialis longus which overlies the radial nerve; (3) tendinous margin of the extensor carpi radialis brevis; (4) the arcade of Frohse, a ligamentous band at the proximal edge of the supinator (Eversmann 1983); and (5) within the supinator muscle. These sites have been associated with posterior interosseous nerve syndrome (a neuropathy) or radial tunnel syndrome (a pain syndrome).

The superficial branch of the radial nerve may be independently entrapped (cheiralgia paresthetica or Wartenberg's syndrome; Wartenberg 1932) by fibrous bands that may exist where the nerve emerges from beneath the brachioradialis (Eversmann 1983), or if the nerve emerges directly through or between slips of the brachioradialis tendon (Abrams et al. 1992). However, many surgical series have not found specific anatomic variations (Dellon and Mackinnon 1986; Turkof et al. 1995). The more common cause of the painful, neuropathic radiation in the distribution of the superficial branch of the radial nerve is however extrinsic compression of the nerve, for example, from watches (Stopford 1922) or jewelry and the so-called "handcuff palsy" (Massey and Pleet 1978).

Origins

The radial nerve is commonly described as receiving contribution from the fifth through eighth cervical nerves, with variable contribution from the first thoracic (Standring 2008). Herringham (1886) noted a small contribution from the first thoracic nerve in only 13%; similarly, Wichmann (1900) found only 18% of radial nerves derived from the first thoracic nerve. However, Harris (1904) found that the first thoracic contributed to the formation of the radial nerve in 82% of specimens; similarly, Kerr (1918) noted that the first thoracic nerve was part of 98% of his specimens.

The radial nerve commonly develops as the terminal continuation of the posterior cord after the origin of the axillary nerve. However, the radial nerve may form from the union of the posterior divisions of the upper, middle, and lower trunks (20% of

specimens, Kerr 1918). The posterior division of the upper and middle trunks may merge to form a cephalic head of the radial nerve (11% of specimens); conversely, the posterior division of the middle trunk may join the posterior division of the lower trunk to form a caudal head of the radial nerve (6% of specimens, Kerr 1918).

Communications between the medial antebrachial cutaneous and radial nerves

The medial brachial cutaneous nerve may provide fibers to the radial nerve at the radial nerve's origin (Kerr 1918). Distally, the medial antebrachial cutaneous nerve may share communicating branches with the superficial branch of the radial nerve (Kerr 1918; Marathe et al. 2010). Presumably, the frequency of these communications is decidedly rare as they are not found in many dissection series (Masear et al. 1989; Race and Saldana 1991).

Communications between the lateral antebrachial cutaneous and radial nerves

The cutaneous distributions of the lateral antebrachial cutaneous nerve and the superficial branch of the radial nerve partially overlap in variable extent (Mackinnon and Dellon 1985; Dellon and Mackinnon 1986). The formation of plexiform communications between the lateral antebrachial cutaneous nerve and the superficial branch of the radial nerve has been found to occur in 32% (Mackinnon and Dellon 1985) to 35% (Abrams et al. 1992) of specimens, and 27% of cases at surgical exploration for neuromas or entrapment neuropathy of the dorsolateral forearm (Mackinnon and Dellon 1985). Stopford (1918) noted that division of the superficial branch of the radial nerve at the wrist produced a larger region of anesthesia than at the forearm, indicating the effect of communications from the lateral antebrachial cutaneous nerve to the superficial branch of the radial nerve.

Communications between the median and radial nerves

The anterior interosseous branch of the median nerve may receive a contribution from the posterior interosseous nerve through a foramen in the interosseous membrane, as first noted by Rauber (1865; see also Doyle and Botte 2003). Both the distal anterior interosseous nerve and posterior interosseous nerve innervate the wrist joint (Grafe et al. 2005); however, this communication has been suggested as a pathway for innervation of hand intrinsic muscles (Spinner 1978).

The superficial branch of the radial nerve may communicate with the palmar cutaneous branch of the median nerve. The incidence of the communication ranges from 4% to 40% (4%, Bezerra et al. 1986; 25%, Kuhlmann and Meyer-Otetea 1976; 40%, Kuhlmann et al. 1978).

Communications between the ulnar and radial nerves

There are classic descriptions of proximal interconnections between the radial and ulnar nerves, known as the ulnar collateral branch (of Krause) (Gruber 1867; Krause 1864, 1868; Ramstrom 1918–19; Linell 1921a). The branch arises from the radial nerve proximal to the spiral groove and may either join or accompany the ulnar nerve in the axilla. These branches are believed to be composed primarily of motor fibers and provide innervation to the medial head of the triceps (Pascual-Font et al. 2013). Incidence of this branch has ranged from 0.63% to 100% (Pascual-Font et al. 2013). Most authors have argued that the ulnar collateral branch is simply a branch from the radial nerve to the medial head of the triceps and can be separated at dissection (Harris 1904; Linell 1921b), whereas others suggest a true fascicular interconnection. Several authors have noted a precise correlation between the presence of an ulnar collateral branch with apparent branches of the ulnar nerve to the medial head of the triceps, implying the function of this proximal communication (Cruveilhier 1836; Krause 1864; Ramstrom 1918–19).

The posterior interosseous nerve may provide innervation to the dorsal interosseous muscles, ranging from solely the first dorsal interosseous to the first through third dorsal interossei. Spinner referred to the anomaly as the Froment-Rauber nerve (Spinner 1978), as it was first described by Froment (1846) as well as by Rauber (1865, 1868). Bichat (1802) noted communication between the terminal branches of the posterior interosseous nerve and the deep branch of the ulnar nerve in the dorsal interosseous muscles of the hand that was independent of direct innervation. Although it was described by Bichat (1802), the communication is commonly referred to as the Froment-Rauber anastomosis (although Spinner suggested adding Bichat's name; Spinner 1978). Lesions of the radial nerve have produced wasting of the first webspace (Kamerath et al. 2013) or clawing of the third through fifth digits (Guo et al. 2011).

The dorsum of the hand is innervated by two primary branches, the dorsal cutaneous branch of the ulnar nerve and the superficial branch of the radial nerve, which may share a communicating branch similar to the ramus communicans (Berrettini branch) between the median and ulnar common digital nerves (see "Communications between the median and ulnar nerves" above). The incidence of this branch has ranged from 4% to 60% (4%, Botte et al. 1990; 15%, Auerbach et al. 1994; 60%, Loukas et al. 2008).

Targets

The radial nerve may provide articular branches to the glenohumeral joint, in addition to the branches provided by the axillary and suprascapular nerves to the joint (Gelber et al. 2006). The thoracodorsal nerve may arise from the radial nerve, as frequently as 5.5% in one large series, which was equal to the frequency of the thoracodorsal originating from the axillary nerve (Kerr 1918).

The radial nerve branches to the triceps are numerous and highly variable; one well respected author found that variability was too overwhelming to delineate (Sunderland 1946). Linell categorized the branches into one of four categories: branches to the long head, branches to the ulnar collateral nerve, branches to

the lateral head, and branches to the medial head (Linell 1921b). Sunderland noted that the branches to the long head appeared first, originating high in the axilla, followed by the branches to the ulnar collateral, then branches to the lateral head, and finally to the medial head, whose branches may originate as distal as the humeral groove, as confirmed by other authors (Sunderland 1946; Carlan et al. 2007). In addition, a branch to the lateral head may also supply the medial head, but such multiple innervation was not seen in branches to the long head.

The lateral brachial cutaneous nerve usually arises from the radial nerve, but it may also come from the posterior brachial cutaneous nerve.

The radial nerve may supply a portion of the lateral (radial) part of brachialis (Jones 1919; Hollinshead 1958; Ip and Chang 1968; Mahakkanukrauh and Somsarp 2002; Oh et al. 2009), which is usually supplied by the musculocutaneous nerve. The reported incidence of the radial nerve innervating the brachialis muscle has varied from 50% to 100% (50% of specimens, Abrams et al. 1997; 67%, Blackburn et al. 2007; 82%, Mahakkanukrauh and Somsarp 2002; 90%, Sunderland 1946; 100%, Oh et al. 2009). Abrams et al. (1997) noted one to three branches to the brachialis. Oh et al. (2009) observed that the branch to the brachialis originated from the fifth and sixth cervical nerves in 95% of specimens and that all fibers were routed through the posterior divisions, which implied that the branch was not anterior division fibers inappropriately sorted within the brachial plexus. They also noted that the fibers to the brachialis were proximally associated with the bundle that supplied the brachioradialis; both muscles produce elbow flexion (Oh et al. 2009). The elbow flexion with the brachialis has been noted in severe proximal injury to the musculocutaneous nerve (Jones 1919); similarly, brachialis contraction has been found with radial nerve stimulation (Hollinshead 1958), although Linell observed that direct intraoperative stimulation of this nerve yielded no visible contraction (Linell 1921b).

The order of motor branches from the radial and posterior interosseous nerve in the forearm, from proximal to distal, is most commonly brachialis, extensor carpi radialis longus, supinator, extensor carpi radialis brevis, extensor digitorum communis, extensor carpi ulnaris, extensor digiti minimi, abductor pollicis longus, extensor pollicis longus, extensor pollicis brevis, and extensor indicis proprius; this order is however quite variable (Sunderland 1946; Spinner 1978; Abrams et al. 1997; Doyle and Botte 2003; Ay et al. 2005). For example, the brachioradialis may rarely receive a branch prior to those to brachialis. The most consistent segment of radial nerve branching in the forearm is at the elbow, where the extensor carpi radialis longus is innervated prior to supinator, which is then most commonly followed by branches to extensor carpi radialis brevis (Abrams et al. 1997). The origin of the branches from the posterior interosseous nerve may arise as individual branches from a common trunk or resemble a cauda equina.

The extensor carpi radialis brevis may derive innervation from multiple sources; it may receive branches directly from the radial nerve trunk or the radial nerve bifurcation (24–55%), from the posterior interosseous nerve (2–60% of specimens), or from the superficial branch of the radial nerve (16–43%) (Abrams et al. 1997).

The posterior interosseous nerve may supply anconeus, extensor carpi radialis longus (Linell 1921a), first dorsal interosseous (Dumitru et al. 1988), and opposed surfaces of the middle and index fingers. One study found that the first dorsal interosseous and the adductor pollicis received motor branches (choline acetyltransferase staining) from either the superficial branch of the radial nerve or the posterior interosseous nerve in 30% of specimens (Okwueze et al. 2007) (see "Communications between the ulnar and radial nerves" above).

The radial nerve may supply the entire dorsum of the hand including the dorsal aspect of all the fingers (Learmonth 1919). The radial nerve may send dorsal digital branches to the little finger and to the ulnar side of the ring finger instead of the ulnar nerve. The radial nerve may also supply the middle and index fingers through its posterior interosseous branches. The radial nerve provides variable sensation to the palmar side of the thumb, with most cases providing significant innervation of the palmar aspect of the thumb (Fetrow 1970).

While the superficial branch of the radial nerve may send branches widely, lesions of the radial nerve rarely produced large regions of anesthesia; as noted by Stopford (1918), "this nerve rarely appears to supply the extensive area of skin usually supposed" (see Fig. 91.14). Furthermore, Stopford noted that the posterior antebrachial cutaneous nerve provided a considerable amount of innervation to the dorsum of the hand in a majority of cases, that is, injury above the origin of the posterior antebrachial cutaneous nerve produced a larger region of anesthesia on the dorsal hand than injury to the superficial branch of the radial nerve alone (Stopford 1918). In accounting for lesions of the ulnar nerve, Stopford (1918) noted that 20% of ulnar nerve lesions had dorsal sensory loss greater than the typical ulnar-sided one and a half digits, implying restricted distribution of the superficial branch of the radial nerve.

Cases have been reported in which the radial sensory nerve branches are absent (Appleton 1911), and branches from the musculocutaneous nerve (lateral antebrachial cutaneous for the thumb) and the ulnar nerve (for the remainder of the digits) compensate for the deficiency.

Conclusion

Variation of nerves of the upper extremity is considerable. We have organized well-described variations under the rubrics of regional anatomy, origin, and targets, providing an anatomical context for comprehension of the sometimes overwhelming range of variation. There are often communicating branches, particularly between major mixed motor-sensory nerves. Lastly, variations in regional anatomy may predispose certain nerves to entrapment, and may progress into a clinical neuropathy.

Appreciation of the rich amount of variation within the upper extremity will allow the diagnostician and surgeon to avoid potential pitfalls and problems in treating patients with nerve disorders. Indeed, frequently it is variation that is the paramount factor in clinical problems.

References

Abrams RA, Brown RA, Botte MJ. 1992. The superficial branch of the radial nerve: An anatomic study with surgical implications. *J Hand Surg* 17: 1037–1041.

Abrams RA, Ziets RJ, Lieber RL, Botte MJ. 1997. Anatomy of the radial nerve motor branches in the forearm. *J Hand Surg Am* 22: 232–237.

Abu-Hijleh MF. 2005. Three-headed biceps brachii muscle associated with duplicated musculocutaneous nerve. *Clin Anat* 18: 376–379.

Al-Qattan M, Husband J. 1991. Median nerve compression by the supracondylar process: a case report. *J Hand Surg Br* 16: 101–103.

Al-Qattan MM, Duerksen F. 1992. A variant of flexor carpi ulnaris causing ulnar nerve compression. *J Anat* 180(1): 189–190.

Al-Qattan MM, Murray KA. 1991. The arcade of Struthers: an anatomical study. *J Hand Surg Br* 16: 311–314.

Amadio PC. 1986. Anatomical basis for a technique of ulnar nerve transposition. *Surg Radiol Anat* 8: 155–161.

Amadio PC. 1988. Anatomic variations of the median nerve within the carpal tunnel. *Clin Anat* 1: 23–31.

Anonymous. 1906. *Epitrochlear foramen. In: The Century Dictionary and Cyclopedia* (ed. WD Whitney). New York: The Century.

Appleton AB. 1911. A case of abnormal distribution of the n. musculocutaneus, with complete absence of the ramus cutaneus n. radialis. *J Anat Physiol* 46: 89–94.

Arad E, Li Z, Sitzman TJ, Agur AM, Clarke HM. 2014. Anatomic sites of origin of the suprascapular and lateral pectoral nerves within the brachial plexus. *Plast Reconstr Surg* 133: 20e–27e.

Aszmann OC, Rab M, Kamolz L, Frey M. 2000. The anatomy of the pectoral nerves and their significance in brachial plexus reconstruction. *J Hand Surg Am* 25: 942–947.

Auerbach DM, Collins ED, Kunkle KL, Monsanto EH. 1994. The radial sensory nerve. An anatomic study. Clin Orthop Relat Res: 241–249.

Ay S, Apaydin N, Acar H, Akinci M, Piskin A, Tekdemir I, Elhan A. 2005. Anatomic pattern of the terminal branches of posterior interosseous nerve. *Clin Anat* 18: 290–295.

Aydinlioglu A, Gumrukcuoglu F, Koyun N. 2010. The prevalence of supracondyloid process in the living: a radiographic study. *W Indian Med J* 59: 545–548.

Balogh B, Valencak J, Vesely M, Flammer M, Gruber H, Piza-Katzer H. 1999. The nerve of Henle: an anatomic and immunohistochemical study. *J Hand Surg Am* 24: 1103–1108.

Barfred T, Hojlund AP, Bertheussen K. 1985. Median artery in carpal tunnel syndrome. *J Hand Surg Am* 10: 864–867.

Bartlett SP, May JW, Jr., Yaremchuk MJ. 1981. The latissimus dorsi muscle: a fresh cadaver study of the primary neurovascular pedicle. *Plast Reconstr Surg* 67: 631–636.

Bayer L. 1893. Beitrag zur vergleiehenden Anatoinie der Oberarmarterien. *Morph Jahrb* 19: 1–41.

Bekler H, Wolfe VM, Rosenwasser MP. 2009. A cadaveric study of ulnar nerve innervation of the medial head of triceps brachii. *Clin Ortho Rel Res* 467: 235–238.

Beldner S, Zlotolow DA, Melone CP Jr, Agnes AM, Jones MH. 2005. Anatomy of the lateral antebrachial cutaneous and superficial radial nerves in the forearm: a cadaveric and clinical study. *J Hand Surg Am* 30: 1226–1230.

Belson P, Smith LK, Puentes J. 1976. Motor innervation of the flexor pollicis brevis: an electromyographic study. *Am J Phys Med* 55: 122–138.

Bergman RA, Thompson SA, Afifi AK, Saadeh FA. 1988. *Compendium of Human Anatomic Variation: Catalog, Atlas and World Literature*. Baltimore and Munich: Urban & Schwarzenberg.

Bergman R, Afifi A, Ryosuke M. 2015. Panniculus Carnosus. Opus I: Muscolar System. Illustrated Encyclopedia of Human Anatomic Variation. Available from: http://www.janela1.com/vh/docs/v0000978.htm (accessed 13 December 2015).

Berrettini P. 1741. *Tabulae anatomicae*. Rome: F Amidei.

Bertelli JA, Ghizoni MF. 2005. Long thoracic nerve: anatomy and functional assessment. *J Bone Joint Surg* 87: 993–998.

Besana-Ciani I, Greenall MJ. 2005. Langer's axillary arch: anatomy, embryological features and surgical implications. *Surgeon* 3: 325–327.

Bezerra AJ, Carvalho VC, Nucci A. 1986. An anatomical study of the palmar cutaneous branch of the median nerve. *Surg Radiol Anat* 8: 183–188.

Bhat KMR, Girijavallabhan V. 2008. Variaiton in the branching pattern of posterior cord of brachial plexus. *Neuroanatomy* 7: 10–11.

Bichat X. 1802. *Traite d'Anatomie Descriptive*. Paris: Brosson and Gabon.

Blackburn SC, Wood CP, Evans DJ, Watt DJ. 2007. Radial nerve contribution to brachialis in the UK Caucasian population: position is predictable based on surface landmarks. *Clin Anat* 20: 64–67.

Blair WF, Joos K. 1982. The innervation of flexor carpi radialis. An interfascicular dissection. *Arch Neurol* 39: 647–649.

Bonnel F, Rabischong P. 1980. Anatomie et systématisation du plexus brachial de l'adulte. *Anatomia Clinica* 2: 289–298.

Bonnel F, Vila RM. 1985. Anatomical study of the ulnar nerve in the hand. *J Hand Surg Br* 10: 165–168.

Bonnel F, Mailhe P, Allieu Y, Rabischong P. 1980. Bases anatomiques de la chirurgie fasciculaire du nerf médian au poignet. *Ann Chir* 34(9): 707–710.

Botha GM. 1957. The anatomy of phrenic nerve termination and the motor innervation of the diaphragm. *Thorax* 12: 50–56.

Botte MJ, Doyle JR. 2003. *Surgical Anatomy of the Hand and Upper Extremity*. Philadelphia: Lippincott Williams & Wilkins.

Botte MJ, Cohen MS, Lavernia CJ, von Schroeder HP, Gellman H, Zinberg EM. 1990. The dorsal branch of the ulnar nerve: an anatomic study. *J Hand Surg Am* 15: 603–607.

Bourgery M. 1844. *Traite Complet de l'Anatomie de l'Homme*. Paris: C. A. Delaunay.

Boyd G. 1934. Abnormality of subclavian artery associated with presence of the scalenus minimus. *J Anat* 68: 280.

Bozkurt MC, Tagil SM, Ozcakar L, Ersoy M, Tekdemir I. 2005. Anatomical variations as potential risk factors for ulnar tunnel syndrome: a cadaveric study. *Clin Anat* 18: 274–280.

Breisch EA. 1986. A rare human variation: the relationship of the axillary and inferior subscapular nerves to an accessory subscapularis muscle. *Anat Rec* 216: 440–442.

Brewin J, Hill M, Ellis H. 2009. The prevalence of cervical ribs in a London population. *Clin Anat* 22: 331–336.

Brooks HS. 1886. Variations in the nerve supply of the flexor brevis pollicis muscle. *J Anat Physiol* 20: 641–644.

Brooks HS. 1887. Variations in the nerve supply of the lumbrical muscles in the hand and foot, with some observations on the innervation of the perforating flexors. *J Anat Physiol* 21: 575–585.

Brown DL, Chung KC. 1999. Quadrangular space syndrome associated with superficial radial sensory neuropathy. *Ann Plast Surg* 43: 207–210.

Cahill BR, Palmer RE. 1983. Quadrilateral space syndrome. *J Hand Surg Am* 8: 65–69.

Cannieu A. 1897. Recherches sur une anastomose entre la branche profunde du cubital et le median. *Bull Soc Physiol Norm Pathol* 17: 339–342.

Carlan D, Pratt J, Patterson JM, Weiland AJ, Boyer MI, Gelberman RH. 2007. The radial nerve in the brachium: an anatomic study in human cadavers. *J Hand Surg Am* 32: 1177–1182.

Chaijaroonkhanarak W, Kunatippapong N, Ratanasuwan S, Amarttayakong P, Umka J, Prachaney P, Namking M, Pannangrong W. 2014. Origin of the dorsal scapular artery and its relation to the brachial plexus in Thais. *Anat Sci Int* 89: 65–70.

Chaudhary P, Singla R, Kalsey G, Arora K. 2012. A four trunked brachial plexus and a post fixed brachial plexus: A conjunction or a coincidence?: Report of three cases. *Clin Anat* 25: 593–600.

Chaynes P, Becue J, Vaysse P, Laude M. 2004. Relationships of the palmar cutaneous branch of the median nerve: a morphometric study. *Surg Radiol Anat* 26: 275–280.

Chen LZ, Chen L, Zhu Y, Gu YD. 2013. Semiquantifying of fascicles of the C7 spinal nerve in the upper and lower subscapular nerves innervating the subscapularis and its clinical inference in Erb's palsy. *Clin Anat* 26: 470–475.

Chiarapattanakom P, Leechavengvongs S, Witoonchart K, Uerpairojkit C, Thuvasethakul P. 1998. Anatomy and internal topography of the musculocutaneous nerve: the nerves to the biceps and brachialis muscle. *J Hand Surg Am* 23: 250–255.

Cho HM, Lee DY, Sung SW. 2005. Anatomical variations of rami communicantes in the upper thoracic sympathetic trunk. *Eur J Cardiothorac Surg* 27: 320–324.

Choi D, Rodriguez-Niedenfuhr M, Vazquez T, Parkin I, Sanudo JR. 2002. Patterns of connections between the musculocutaneous and median nerves in the axilla and arm. *Clin Anat* 15: 11–17.

Chowdhry S, Elston JB, Lefkowitz T, Wilhelmi BJ. 2010. Avoiding the medial brachial cutaneous nerve in brachioplasty: an anatomical study. *Eplasty* 10: e16.

Chuang DC-C, Cheng S-L, Wei F-C, Wu C-L, Ho Y-S. 1998. Clinical evaluation of C7 spinal nerve transection: 21 patients with at least 2 years' follow-up. *Br J Plastic Surg* 51: 285–290.

Chung IH, Oh CS, Koh KS, Kim HJ, Paik HC, Lee DY. 2002. Anatomic variations of the T2 nerve root (including the nerve of Kuntz) and their implications for sympathectomy. *J Thorac Cardiovasc Surg* 123: 498–501.

Clavert P, Lutz JC, Wolfram-Gabel R, Kempf JF, Kahn JL. 2009. Relationships of the musculocutaneous nerve and the coracobrachialis during coracoid abutment procedure (Latarjet procedure). *Surg Radiol Anat* 31: 49–53.

Cordier P, Devos L. 1938. Le dome pleural. Aspect Endothoracique. *Ann d'Anat Path* 15: 465–488.

Crotti F, Mangiagalli E, Rampini P. 1981. Supracondyloid process and anomalous insertion of pronator teres as a source of median nerve neuralgia. *J Neurosurg Sci* 25: 41–44.

Crutchfield CA, Gutmann L. 1980. Hereditary aspects of median-ulnar nerve communications. *J Neurol Neurosurg Psychiatry* 43: 53–55.

Cruveilhier J. 1836. *Traité d'Anatomie Descriptive*. Paris: Bechet Jeune.

Cunningham DJ. 1877. Note on a connecting twig between the anterior divisions of the first and second dorsal nerves. *J Anat Physiol* 11: 539–540.

Curtis F. 1886. L'anastomose du médian et du cubital. *Int Monatschrift für Anat Hist (Leipzig)* 3: 309–324.

Darji AP, Chauhan HM, Khatri H, Aterkar S, Pensi CA. 2013. Variations in branching pattern of Brachial Plexus: A cadaveric study. *Int J Biomed Adv Res* 4: 174–178.

Das SK, Brown HG. 1976. In search of complications in carpal tunnel decompression. *Hand* 8: 243–249.

Daseler EH, Anson BJ. 1959. Surgical anatomy of the subclavian artery and its branches. *Surg Gynecol Obstet* 108: 149.

Day MH, Napier JR. 1961. The two heads of flexor pollicis brevis. *J Anat* 95: 123–130.

De Smet L. 2002. Median and ulnar nerve compression at the wrist caused by anomalous muscles. *Acta Orthop Belg* 68: 431–438.

De Vriese B. 1902. Recherches sur l'évolution des vaisseaux sanguins des membres chez l'homme. *Arch Biol* 18: 665–721.

Dellon AL. 1986. Musculotendinous variations about the medial humeral epicondyle. *J Hand Surg Br* 11: 175–181.

Dellon AL, Mackinnon SE. 1984. Susceptibility of the superficial sensory branch of the radial nerve to form painful neuromas. *J Hand Surg Br* 9: 42–45.

Dellon AL, Mackinnon SE. 1985. Injury to the medial antebrachial cutaneous nerve during cubital tunnel surgery. *J Hand Surg Br* 10: 33–36.

Dellon AL, Mackinnon SE. 1986. Radial sensory nerve entrapment in the forearm. *J Hand Surg Am* 11: 199–205.

Dellon AL, Mackinnon SE. 1987. Musculoaponeurotic variations along the course of the median nerve in the proximal forearm. *J Hand Surg Br* 12: 359–363.

Dellon AL, Mackinnon SE. 1988. Anatomic investigations of nerves at the wrist: II. Incidence of fibrous arch overlying motor branch of ulnar nerve. *Ann Plast Surg* 21: 36–37.

Dodds GA 3rd, Hale D, Jackson WT. 1990. Incidence of anatomic variants in Guyon's canal. *J Hand Surg Am* 15: 352–355.

Don Griot JP, Zuidam JM, van Kooten EO, Prose LP, Hage JJ. 2000. Anatomic study of the ramus communicans between the ulnar and median nerves. *J Hand Surg Am* 25: 948–954.

Dowdy PA, Richards RS, McFarlane RM. 1994. The palmar cutaneous branch of the median nerve and the palmaris longus tendon: a cadaveric study. *J Hand Surg Am* 19: 199–202.

Doyle JR, Botte MJ. 2003. *Surgical anatomy of the hand and upper extremity*. Philadelphia: Lippincott Williams & Wilkins.

Dumitru D, Walsh N, Visser B. 1988. Congenital hemihypertrophy associated with posterior interosseous nerve entrapment. *Arch Phys Med Rehabil* 69: 696–698.

Duparc F, Bocquet G, Simonet J, Freger P. 1997. Anatomical basis of the variable aspects of injuries of the axillary nerve (excluding the terminal branches in the deltoid muscle). *Surg Radiol Anat* 19: 127–132.

El-Naggar MM, Al-Saggaf S. 2004. Variant of the coracobrachialis muscle with a tunnel for the median nerve and brachial artery. *Clin Anat* 17: 139–143.

Engber WD, Gmeiner JG. 1980. Palmar cutaneous branch of the ulnar nerve. *J Hand Surg Am* 5: 26–29.

Erdogmus S, Govsa F. 2005. Distal variations of the neurovascular pedicle of the serratus anterior muscle as a flap. *Surg Radiol Anat* 27: 100–107.

Eversmann Jr WW. 1983. Compression and entrapment neuropathies of the upper extremity. *J Hand Surg* 8: 759–766.

Fazan VPS, Amadeu AdS, Caleffi AL, Rodrigues Filho OA. 2003. Brachial plexus variations in its formation and main branches. *Acta Cirurgica Brasileira* 18: 14–18.

Ferrari GP, Gilbert A. 1991. The superficial anastomosis on the palm of the hand between the ulnar and median nerves. *J Hand Surg Br* 16: 511–514.

Fetrow KO. 1970. Practical and important variations in sensory nerve supply to the hand. *Hand* 2: 178–184.

Flatow EL, Bigliani LU, April EW. 1989. An anatomic study of the musculocutaneous nerve and its relationship to the coracoid process. Clin Orthop Relat Res: 166–171.

Forrest WJ. 1967. Motor innervation of human thenar and hypothenar muscles in 25 hands: a study combining electromyography and percutaneous nerve stimulation. *Can J Surg* 10: 196–199.

Francel TJ, Dellon AL, Campbell JN. 1991. Quadrilateral space syndrome: diagnosis and operative decompression technique. *Plast Reconstr Surg* 87: 911–916.

Frank DK, Wenk E, Stern JC, Gottlieb RD, Moscatello AL. 1997. A cadaveric study of the motor nerves to the levator scapulae muscle. *Otolaryngol Head Neck Surg* 117: 671–680.

Frohse F, Frankel M. 1908. *Die Muskeln des menschlichen Armes*. Jena: Fischer.

Froment J. 1846. *Traite d'Anatomie Humaine*. Paris: Mequignon-Marvis.

Fuss FK. 1989. The lateral root of the ulnar nerve. *Acta Anat (Basel)* 134: 199–205.

Gage M, Parnell H. 1947. Scalenus anticus syndrome. *Am J Surg* 73: 252–268.

Gardner E. 1948a. The innervation of the elbow joint. *Anat Rec* 102: 161–174.

Gardner E. 1948b. The innervation of the shoulder joint. *Anat Rec* 102: 1–18.

Gaughran GR. 1964. Suprapleural membrane and suprapleural bands. *Anat Rec* 148: 553–559.

Gelber PE, Reina F, Monllau JC, Yema P, Rodriguez A, Caceres E. 2006. Innervation patterns of the inferior glenohumeral ligament: anatomical and biomechanical relevance. *Clin Anat* 19: 304–311.

Gonzalez MH, Lotfi P, Bendre A, Mandelbroyt Y, Lieska N. 2001. The ulnar nerve at the elbow and its local branching: an anatomic study. *J Hand Surg Br* 26: 142–144.

Grafe MW, Kim PD, Rosenwasser MP, Strauch RJ. 2005. Wrist denervation and the anterior interosseous nerve: anatomic considerations. *J Hand Surg* 30: 1221–1225.

Gruber W. 1866. Über die muskel epitrochleo-anconeus des menschen und den Saugethieren. Mem Imp Acad Sci St Petersbourg: 1–26.

Gruber W. 1867. The anomalous course of the ulnar nerve in front of the medial epicondyle. *Arch Anat Physiol Wissen Med* 1867: 560–564 (in German).

Gruber W. 1870. Uber die verbindung des nervus medianus mit dem nervus ulnaris am unterarme des menschen und der saugetiere. *Arch Anat Physiol Med Lezpzig* 37: 501–522.

Guerri-Guttenberg RA, Ingolotti M. 2009. Classifying musculocutaneous nerve variations. *Clin Anat* 22: 671–683.

Gulekon I, Turgut H. 1999. The prevalence of cervical rib in Anatolian population. Gazi Med J: 149–152.

Gunther SF, DiPasquale D, Martin R. 1992. The internal anatomy of the median nerve in the region of the elbow. *J Hand Surg Am* 17: 648–656.

Guo BY, Ayyar DR, Grossman JA. 2011. Posterior interosseus palsy with an incidental Froment-Rauber nerve presenting as a pseudoclaw hand. *Hand (NY)* 6: 344–347.

Gutmann L. 1993. AAEM minimonograph #2: important anomalous innervations of the extremities. *Muscle Nerve* 16: 339–347.

Hafferl A. 1939. *Die Muskulatur Die Anatomie der Pleurakuppel*. Berlin: Julius Springer Verlag.

Hagert E. 2013. Clinical diagnosis and wide-awake surgical treatment of proximal median nerve entrapment at the elbow: a prospective study. *Hand (NY)* 8: 41–46.

Hankins CL, Flemming S. 2005. A variant of Kaplan's accessory branch of the dorsal cutaneous branch of the ulnar nerve: a case report and review of the literature. *J Hand Surg Am* 30: 1231–1235.

Harman NB. 1900. The anterior limit of the cervico-thoracic visceral efferent nerves in man. *J Anat Physiol* 34: 359–380.

Harness D, Sekeles E. 1971. The double anastomotic innervation of thenar muscles. *J Anat* 109: 461–466.

Harness D, Sekeles E, Chaco J. 1974. The double motor innervation of the opponenes pollicis muscles: an electromyographic study. *J Anat* 117: 329–331.

Harris W. 1904. The true form of the brachial plexus, and its motor distribution. *J Anat Physiol* 38: 399.

Harry WG, Bennett JD, Guha SC. 1997. Scalene muscles and the brachial plexus: anatomical variations and their clinical significance. *Clin Anat* 10: 250–252.

Hartmann H. 1888. Etude de quelques anastomoses elliptiques des nerfs du member supérior. Leur importance du point de vue de la conservation des functions sensitive–motrices aprés une section nerveuse. *Bull Mem Soc Anat Paris* 1888(2): 151–165.

Henlé J. 1868. *Handbuch der Systematischen Anatomie des Menschen*. Braunschweig: Druck und Verlag Von Friedrich Vieweg and Sohn.

Hepburn D. 1892. The comparative anatomy of the muscles and nerves of the superior and inferior extremities of the anthropoid apes: Part I. *J Anat Physiol* 26: 149–186.

Herringham W. 1886. The minute anatomy of the brachial plexus. Proc Roy Soc London: 423–441.

Highet W. 1943. Innervation and function of the thenar muscles. *The Lancet* 241: 227–230.

Hollinshead W. 1958. *Anatomy for Surgeons*. London: Cassell and Co.

Homma T, Sakai T. 1992. Thenar and hypothenar muscles and their innervation by the ulnar and median nerves in the human hand. *Acta Anat (Basel)* 145: 44–49.

Hoogbergen MM, Kauer JM. 1992. An unusual ulnar nerve-median nerve communicating branch. *J Anat* 181(3): 513–516.

Horiguchi M. 1981. The recurrent branch of the lateral cutaneous nerve of the forearm. *J Anat* 132: 243–247.

Huber G. 1936. *The peripheral nervous system. In: Piersol's Human Anatomy*, 9th ed. London, England: J.B. Lippincott, pp. 1292–1314.

Huelke DF. 1958. A study of the transverse cervical and dorsal scapular arteries. *Anat Rec* 132: 233–245.

Husarik DB, Saupe N, Pfirrmann CW, Jost B, Hodler J, Zanetti M. 2009. Elbow nerves: MR findings in 60 asymptomatic subjects—-normal anatomy, variants, and pitfalls. *Radiology* 252: 148–156.

Inserra S, Spinner M. 1986. An anatomic factor significant in transposition of the ulnar nerve. *J Hand Surg Am* 11: 80–82.

Ip MC, Chang KS. 1968. A study on the radial supply of the human brachialis muscle. *Anat Rec* 162: 363–371.

Iwamoto G, Haber L, Dixon J, Gonyea W. 1980. Anatomical distribution of flexor carpi radialis and flexor carpi ulnaris motor nuclei in the cat spinal cord. *Neurosci Lett* 20: 25–30.

Iwata H. 1960. Studies on the development of the brachial plexus in Japanese embryo. *Republic Department Anatomy Mie Prefect University School of Medicine* 13: 129–144.

Jones FW. 1919. Voluntary muscular movements in cases of nerve lesions. *J Anat* 54: 41–57.

Juvonen T, Satta J, Laitala P, Luukkonen K, Nissinen J. 1995. Anomalies at the thoracic outlet are frequent in the general population. *Am J Surg* 170: 33–37.

Kadaba MP, Cole A, Wootten ME, McCann P, Reid M, Mulford G, April E, Bigliani L. 1992. Intramuscular wire electromyography of the subscapularis. *J Orthop Res* 10: 394–397.

Kameda Y. 1976a. An anomalous muscle (accessory subscapularis-teres-latissimus muscle) in the axilla penetrating the brachial plexus in man. *Acta Anat (Basel)* 96: 513–533.

Kameda Y. 1976b. An anomalous muscle (accessory subscapularis-teres-latissimus muscle) in the axilla penetrating the brachial plexus in man. *Cells Tissues Organs* 96: 513–533.

Kamerath JH, Epstein DK, Fitzpatrick KF. 2013. The Froment-Rauber nerve: a case report and review. *Muscle Nerve* 47: 768–771.

Kane E, Kaplan EB, Spinner M. 1973. Observations of the course of the ulnar nerve in the arm. *Ann Chir* 27: 487–496.

Kang HJ, Yoo JH, Kang ES. 1996. Ulnar nerve compression syndrome due to an anomalous arch of the ulnar nerve piercing the flexor carpi ulnaris: a case report. *J Hand Surg Am* 21: 277–278.

Kaplan EB. 1963. Variation of the ulnar nerve at the wrist. *Bull Hosp Joint Dis* 24: 85–88.

Kato K. 1989. Innervation of the scapular muscles and its morphological significance in man. *Anat Anz* 168: 155–168.

Kerr AT. 1918. The brachial plexus of nerves in man, the variations in its formation and branches. *Am J Anat* 23: 285–395.

Kervancioglu P, Orhan M, Kilinc N. 2011. Patterns of motor branching of the musculocutaneous nerve in human fetuses and clinical significance. *Clin Anat* 24: 168–178.

Kim DI, Lee KS, Kim HJ, Chae HK, Yu KH. 2008. The spinal root origins and clinical implications of the lower subscapular nerve. *Clin Anat* 21: 416–419.

Kimura I, Ayyar DR. 1984. The hand neural communication between the ulnar and median nerves: electrophysiological detection. *Electromyogr Clin Neurophysiol* 24: 409–414.

Koizumi M, Kawai K, Maeda S, Okamoto K, Kodama K. 1999. Communication between the axillary and radial nerves in the human upper arm. *Ann Anat* 181: 213–221.

Konig PS, Hage JJ, Bloem JJ, Prose LP. 1994. Variations of the ulnar nerve and ulnar artery in Guyon's canal: a cadaveric study. *J Hand Surg Am* 19: 617–622.

Kosugi K, Shibata S, Yamashita H. 1992. Supernumerary head of biceps brachii and branching pattern of the musculocutaneus nerve in Japanese. *Surg Radiol Anat* 14: 175–185.

Krause W. 1864. Contributions to the systematic neurology of the human arm. *Arch Anat Physiol Wissen Med* 1864: 349–357 (in German).

Krause W. 1868. On the ulnar collateral nerve of the radial nerve. *Arch Anat Physiol Wissen Med* 1868: 134–136 (in German).

Kuhlmann N, Meyer-Otetea G. 1976. The cutaneous branches of the palm (author's transl). *Ann Chir* 30: 859–865.

Kuhlmann N, Tubiana R, Lisfranc R. 1978. Contribution of anatomy to the understanding of carpal tunnel compression syndromes and sequelae of decompression operations. *Rev Chir Orthop Reparatrice Appar Mot* 64: 59–70.

Kuntz A. 1927. Distribution of the sympathetic rami to the brachial plexus: its relation to sympathectomy affecting the upper extremity. *Arch Surg* 15: 871.

Laha RK, Dujovny M, DeCastro SC. 1977. Entrapment of median nerve by supracondylar process of the humerus: case report. *J Neurosurg* 46: 252–255.

Lahey MD, Aulicino PL. 1986. Anomalous muscles associated with compression neuropathies. *Orthop Rev* 15: 199–208.

Lassa R, Shrewsbury MM. 1975. A variation in the path of the deep motor branch of the ulnar nerve at the wrist. *J Bone Joint Surg Am* 57: 990–991.

Law AA. 1920. Adventitious ligaments simulating cervical ribs. *Ann Surg* 72: 497–499.

Lawrence T, Mobbs P, Fortems Y, Stanley J. 1995. Radial tunnel syndrome: A retrospective review of 30 decompressions of the radial nerve. *J Hand Surg Br* 20: 454–459.

Le Double A-F. 1897. Traité des Variations du Système Musculaire de l'Homme: et de leur Signification au point de vue de l'Anthropologie Zoologique: Paris: Schleicher Frères.

Le Minor JM. 1990. A rare variation of the median and musculocutaneous nerves in man. *Arch Anat Histol Embryol* 73: 33–42.

Le Nen D, Poureyron Y, Chardel P, Beal D, Lefevre C, Sénécail B, Courtois B. 1991. Anatomical basis of neurotisation of the median nerve in the hand by the radial nerve. *Surg Radiolog Anat* 13: 271–275.

Learmonth JR. 1919. A variation in the distribution of the radial branch of the musculo-spiral nerve. *J Anat* 53: 371–372.

Lee HY, Chung IH, Sir WS, Kang HS, Lee HS, Ko JS, Lee MS, Park SS. 1992. Variations of the ventral rami of the brachial plexus. *J Korean Med Sci* 7: 19–24.

Lee KS. 2007a. Anatomic variation of the spinal origins of lateral and medial pectoral nerves. *Clin Anat* 20: 915–918.

Lee KS. 2007b. Variation of the spinal nerve compositions of thoracodorsal nerve. *Clin Anat* 20: 660–662.

Leibovic SJ, Hastings H 2nd. 1992. Martin-Gruber revisited. *J Hand Surg Am* 17: 47–53.

Lejars F. 1890. L'innervation de l'eminence thenar. *Bull Mem Soc Anat Paris IV* 5: 433–437.

Lindner H. (ed.) 1989. *Clinical Anatomy*. Connecticut: Appleton & Lange.

Linell E. 1921a. The distribution of nerves in the upper limb, with reference to variabilities and their clinical significance. *J Anat* 55: 79–112.

Linell E. 1921b. The distribution of nerves in the upper limb, with reference to variabilities and their clinical significance. *J Anat* 55: 79–112.

Lotem M, Fried A, Levy M, Solzi P, Najenson T, Nathan H. 1971. Radial palsy following muscular effort. A nerve compression syndrome possibly related to a fibrous arch of the lateral head of the triceps. *J Bone Joint Surg Br* 53: 500–506.

Loukas M, Kinsella CR Jr, Louis RG Jr, Gandhi S, Curry B. 2006a. Surgical anatomy of the accessory phrenic nerve. *Ann Thoracic Surg* 82: 1870–1875.

Loukas M, Louis RG Jr, Fitzsimmons J, Colborn G. 2006b. The surgical anatomy of the ansa pectoralis. *Clin Anat* 19: 685–693.

Loukas M, Louis RG Jr, Stewart L, Hallner B, DeLuca T, Morgan W, Shah R, Mlejnek J. 2007a. The surgical anatomy of ulnar and median nerve communications in the palmar surface of the hand. *J Neurosurg* 106: 887–893.

Loukas M, Louis RG Jr, Wartmann CT. 2007b. T2 contributions to the brachial plexus. Neurosurgery 60: ONS13–18.

Loukas M, Louis RG Jr, Wartmann CT, Tubbs RS, Turan-Ozdemir S, Kramer J. 2008. The clinical anatomy of the communications between the radial and ulnar nerves on the dorsal surface of the hand. *Surg Radiol Anat* 30: 85–90.

Loukas M, Grabska J, Tubbs RS, Apaydin N, Jordan R. 2009. Mapping the axillary nerve within the deltoid muscle. *Surg Radiol Anat* 31: 43–47.

Loukas M, Bellary SS, Cankara N, Shoja MM, Tubbs RS, Spinner RJ. 2013. Ulnar nerve innervation of the medial head of the triceps brachii muscle: A cadaveric study. *Clin Anat* 26(8): 1028–1030.

Lowe III JB, Maggi SP, Mackinnon SE. 2004. The position of crossing branches of the medial antebrachial cutaneous nerve during cubital tunnel surgery in humans. *Plast Reconst Surg* 114: 692–696.

Macalister A. 1864. Notes on muscular anomalies in human anatomy. Proc Roy Irish Acad IX: 444–467.

Macalister A. 1867. Notes on an instance of irregularity in the muscles around the shoulder joint. *J Anat Physiol* 1: 316–319.

MacAvoy MC, Rust SS, Green DP. 2006. Anatomy of the posterior antebrachial cutaneous nerve: practical information for the surgeon operating on the lateral aspect of the elbow. *J Hand Surg Am* 31: 908–911.

Macchi V, Tiengo C, Porzionato A, Parenti A, Stecco C, Mazzoleni F, De Caro R. 2007. Medial and lateral pectoral nerves: course and branches. *Clin Anat* 20: 157–162.

Mackinnon SE, Dellon AL. 1985. The overlap pattern of the lateral antebrachial cutaneous nerve and the superficial branch of the radial nerve. *J Hand Surg Am* 10: 522–526.

Maeda S, Kawai K, Koizumi M, Ide J, Tokiyoshi A, Mizuta H, Kodama K. 2009. Morphological study, by teasing examination, of the communication from the musculocutaneous to median nerves. *Anat Sci Int* 84: 41–46.

Mahakkanukrauh P, Somsarp V. 2002. Dual innervation of the brachialis muscle. *Clinical Anatomy* 15: 206–209.

Mahan MA, Spinner RJ. 2015. Clinical importance of anatomic variation of the nerves of the upper extremity In: *Nerves and Nerve Injuries: Vol 1: History, Embryology, Anatomy, Imaging, and Diagnostics* (eds RS Tubbs, E Rizk, MM Shoja, M Loukas, N Barbaro, RJ Spinner). Waltham, Mass: Academic Press, pp. 589–605.

Mahdy CE. 2001. Tutankhamun: The Life and Death of the Boy-King. New York: St Martin's Press.

Mancall EL, Brock DG, Gray H. 2011. *Gray's Clinical Neuroanatomy: The Anatomic Basis for Clinical Neuroscience*. Philadelphia: Saunders.

Mannerfelt L. 1964. *Studies on an Anastomosis between the Median and Ulnar Nerves in the Forearm*. Lund: CWK Gleerup.

Mannerfelt L. 1966. Studies on the hand in ulnar nerve paralysis. A clinical-experimental investigation in normal and anomalous innervation. *Acta Orthop Scand* 87: 81.

Manske PR. 1977. Compression of the radial nerve by the triceps muscle: a case report. *J Bone Joint Surg Am* 59: 835–836.

Marathe R, Mankar S, Joshi M, Sontakke Y. 2010. Communication between radial nerve and medial cutaneous nerve of forearm. *J Neurosci Rural Pract* 1: 49–50.

Marhold F, Izay B, Zacherl J, Tschabitscher M, Neumayer C. 2008. Thoracoscopic and anatomic landmarks of Kuntz's nerve: implications for sympathetic surgery. *Ann Thorac Surg* 86: 1653–1658.

Marinacci AA. 1964a. Diagnosis of "All Median Hand". *Electromyography* 4: 85–93.

Marinacci AA. 1964b. The problem of unusual anomalous innervation of hand muscles. the value of electrodiagnosis in its evaluation. *Bull Los Angel Neuro Soc* 29: 133–142.

Marras C, Midroni G. 1999. Proximal Martin-Gruber anastomosis mimicking ulnar neuropathy at the elbow. *Muscle Nerve* 22: 1132–1135.

Martin CH, Seiler JG 3rd, Lesesne JS. 1996. The cutaneous innervation of the palm: an anatomic study of the ulnar and median nerves. *J Hand Surg Am* 21: 634–638.

Martin R. 1763. *Tal om Nervers Allmonna Egenskaper i Manniskans Kropp*. Stockholm: Lars Salvius.

Marzo JM, Simmons EH, Kallen F. 1987. Intradural connections between adjacent cervical spinal roots. *Spine (Phila Pa 1976)* 12: 964–968.

Masear VR, Meyer RD, Pichora DR. 1989. Surgical anatomy of the medial antebrachial cutaneous nerve. *J Hand Surg Am* 14: 267–271.

Massey EW, Pleet AB. 1978. Handcuffs and cheiralgia paresthetica. *Neurology* 28: 1312–1312.

Matejcik V. 2003. Aberrant formation and clinical picture of brachial plexus from the point of view of a neurosurgeon. *Bratisl Lek Listy* 104: 291–299.

Matejcik V. 2005. Variations of nerve roots of the brachial plexus. *Bratisl Lek Listy* 106: 34–36.

Matloub HS, Yan JG, Mink Van Der Molen AB, Zhang LL, Sanger JR. 1998. The detailed anatomy of the palmar cutaneous nerves and its clinical implications. *J Hand Surg Br* 23: 373–379.

McCabe SJ, Kleinert JM. 1990. The nerve of Henle. *J Hand Surg Am* 15: 784–788.

McCann PD, Cordasco FA, Ticker JB, Kadaba MP, Wootten ME, April EW, Bigliani LU. 1994. An anatomic study of the subscapular nerves: A guide for electromyographic analysis of the subscapularis muscle. *J Shoulder Elbow Surg* 3: 94–99.

McCarthy RE, Nalebuff EA. 1980. Anomalous volar branch of the dorsal cutaneous ulnar nerve: a case report. *J Hand Surg Am* 5: 19–20.

McClelland D, Paxinos A. 2008. The anatomy of the quadrilateral space with reference to quadrilateral space syndrome. *J Shoulder Elbow Surg* 17: 162–164.

McCormack LJ, Cauldwell EW, Anson BJ. 1953. Brachial and antebrachial arterial patterns; a study of 750 extremities. *Surg Gynecol Obstet* 96: 43–54.

McCulloch RA, MacLean SBM, Dhaliwal J, Simons AW. 2010. Median nerve compression secondary to a high insertion of pronator teres. *Shoulder & Elbow* 2: 124–126.

McKowen HC, Voorhies RM. 1987. Axillary nerve entrapment in the quadrilateral space. Case report. *J Neurosurg* 66: 932–934.

Mehta V, Yadav Y, Arora J, Kumar H, Suri RK, Rath G. 2009. Clinico-embryological perspective of a rare accessory brachial muscle with possible musculocutaneous nerve compression. *Morphologie* 93: 27–29.

Miller RA. 1934. Comparative studies upon the morphology and distribution of the brachial plexus. *Am J Anat* 54: 143–175.

Miller RA. 1939. Observations upon the arrangement of the axillary artery and brachial plexus. *Am J Anat* 64: 143–163.

Miller RA, Detwiler S. 1936. Comparative studies upon the origin and development of the brachial plexus. *Anat Rec* 65: 273–292.

Millett PJ, Schoenahl JY, Allen MJ, Motta T, Gaskill TR. 2013. An association between the inferior humeral head osteophyte and teres minor fatty infiltration: evidence for axillary nerve entrapment in glenohumeral osteoarthritis. *J Shoulder Elbow Surg* 22: 215–221.

Naff N, Dellon AL, Mackinnon SE. 1993. The anatomical course of the palmar cutaneous branch of the median nerve, including a description of its own unique tunnel. *J Hand Surg Br* 18: 316–317.

Nakamichi K-I, Tachibana S. 1991. Radial nerve entrapment by the lateral head of the triceps. *J Hand Surg* 16: 748–750.

Nakashima T. 1993. An anatomic study on the Martin-Gruber anastomosis. *Surg Radiol Anat* 15: 193–195.

Nakatani T, Mizukami S, Tanaka S. 1997a. A rare case: the medical cord of the brachial plexus sandwiched between the axillary and superficial brachial arteries. *Kaibogaku Zasshi* 72: 151–154.

Nakatani T, Tanaka S, Mizukami S. 1997b. Absence of the musculocutaneous nerve with innervation of coracobrachialis, biceps brachii, brachialis and the lateral border of the forearm by branches from the lateral cord of the brachial plexus. *J Anat* 191(3): 459–460.

Nakatani T, Tanaka S, Mizukami S. 1998. Bilateral four-headed biceps brachii muscles: The median nerve and brachial artery passing through a tunnel formed by a muscle slip from the accessory head. *Clin Anat* 11: 209–212.

Natsis K. 2008. Supracondylar process of the humerus: study on 375 Caucasian subjects in Cologne, Germany. *Clin Anat* 21: 138–141.

Natsis K, Totlis T, Tsikaras P, Anastasopoulos N, Skandalakis P, Koebke J. 2006. Variations of the course of the upper trunk of the brachial plexus and their clinical significance for the thoracic outlet syndrome: a study on 93 cadavers. *Am Surg* 72: 188–192.

Natsis K, Totlis T, Didagelos M, Tsakotos G, Vlassis K, Skandalakis P. 2013. Scalenus minimus muscle: overestimated or not? An anatomical study. *Am Surg* 79: 372–374.

Nayak SR, Krishnamurthy A, Prabhu LV, Ramanathan L, Pai MM, Potu BK, Das S. 2008. Incidence of accessory phrenic nerve and its clinical significance: a cadaveric study. *Acta Medica (Hradec Kralove)* 51: 181–184.

Nebot-Cegarra J, Perez-Berruezo J, Reina de la Torre F. 1991. Variations of the pronator teres muscle: predispositional role to median nerve entrapment. *Arch Anat Histol Embryol* 74: 35–45.

O'Hara JJ, Stone JH. 1988. Ulnar neuropathy at the wrist associated with aberrant flexor carpi ulnaris insertion. *J Hand Surg Am* 13: 370–372.

Oh CS, Won HS, Lee KS, Chung IH. 2009. Origin of the radial nerve branch innervating the brachialis muscle. *Clinical Anatomy* 22: 495–499.

Okwueze MI, Cardwell NL, Wolfort SL, Nanney LB. 2007. Unexpected motor axons in the distal superficial radial and posterior interosseous nerves: A cadaver study. *Clinical Anatomy* 20: 790–794.

Oluyemi K, Adesanya O, Ofusori D, Okwuonu C, Ukwenya V, Odion B. 2007. Abnormal pattern of brachial plexus formation: an original case report. *Internet J Neurosurg* 4: 1–7.

Ouattara D, Berton C, Wavreille G, Fontaine C. 2006. Contribution to subscapularis nerve supply. 18 dissections. *Morphologie* 90: 175–179.

Ozguner G, Desdicioglu K, Albay S. 2010. Connection between radial and ulnar nerves at high humeral level. *Int J Anat Var* 3: 49–50.

Ozkan M, Bacakoglu AK, Gul O, Ekin A, Magden O. 1999. Anatomic study of posterior interosseous nerve in the arcade of Frohse. *J Shoulder Elbow Surg* 8: 617–620.

Pacholczak R, Klimek-Piotrowska W, Walocha JA. 2011. Absence of the musculocutaneous nerve associated with a supernumerary head of biceps brachii: a case report. *Surg Radiol Anat* 33: 551–554.

Pandey SK, Shukla VK. 2007. Anatomical variations of the cords of brachial plexus and the median nerve. *Clinical anatomy* 20: 150–156.

Paraskevas G, Ioannidis O, Papaziogas B, Natsis K, Spanidou S, Kitsoulis P. 2007. An accessory middle scalene muscle causing thoracic outlet syndrome. *Folia Morphol (Warsz)* 66: 194–197.

Pascual-Font A, Vazquez T, Marco F, Sanudo JR, Rodriguez-Niedenfuhr M. 2013. Ulnar nerve innervation of the triceps muscle: real or apparent? An anatomic study. *Clin Orthop Relat Res* 471: 1887–1893.

Paterson AM. 1896. A discussion of some points in the distribution of the spinal nerves. *J Anat Physiol* 30: 530–538.

Paterson AM. 1911. The subscapularis muscle. *J Anat Physiol* 46: 11.

Pellerin M, Kimball Z, Tubbs RS, Nguyen S, Matusz P, Cohen-Gadol AA, Loukas M. 2010. The prefixed and postfixed brachial plexus: a review with surgical implications. *Surg Radiol Anat* 32: 251–260.

Pianezza A, Salces y Nedeo A, Chaynes P, Bickler PE, Minville V. 2012. The emergence level of the musculocutaneous nerve from the brachial plexus: implications for infraclavicular nerve blocks. *Anesth Analg* 114: 1131–1133.

Pick J. 1958. The innervation of the arteries in the upper limb of man. *Anat Rec* 130: 103–123.

Pirola E, Hebert-Blouin MN, Amador N, Amrami KK, Spinner RJ. 2009. Palmaris profundus: one name, several subtypes, and a shared potential for nerve compression. *Clin Anat* 22: 643–648.

Poirier P, Charpy A. 1901. *Trait d'Anatomie Humaine*. Vol. 4. Paris: Masson and Cie.

Poisel S. 1974. The origin and course of the ramus muscularis of the nervus digitalis palmaris communis I (n. medianus). *Ursprung und Verlauf des Ramus Muscularis des Nervus Digitalis Palmaris Communis I (N. Medianus)* 18: 471–474.

Pollack E. 1980. Surgical anatomy of the thoracic outlet syndrome. *Surg Gynecol Obstet* 150: 97–103.

Porzionato A, Macchi V, Stecco C, Loukas M, Tubbs RS, De Caro R. 2012. Surgical anatomy of the pectoral nerves and the pectoral musculature. *Clin Anat* 25: 559–575.

Prasada Rao PV, Chaudhary SC. 2001. Absence of musculocutaneous nerve: two case reports. *Clin Anat* 14: 31–35.

Race CM, Saldana MJ. 1991. Anatomic course of the medial cutaneous nerves of the arm. *J Hand Surg Am* 16: 48–52.

Ramamurthy S, Hickey R, Maytorena A, Hoffman J, Kalantri A. 1990. Long thoracic nerve block. *Anesth Analg* 71: 197–199.

Ramsaroop L, Partab P, Singh B, Satyapal KS. 2001. Thoracic origin of a sympathetic supply to the upper limb: the 'nerve of Kuntz' revisited. *J Anat* 199: 675–682.

Ramstrom M. 1918–19. Investigations on the innervation of the medial head of the triceps brachii muscle. *Anat Anz* 51: 420–431 (in German).

Ranschburg P. 1917. Uber die anastomosen der nerven der oberen extremitat des menschen mit rucksicht auf ihre neurologische undnervenchirurgische bedeutung. *Neurol Zentralbl* 13: 521–534.

Rauber A. 1865. Vater'sche Korper der Bander und Periostnerven. Inaugural Dissertation, Munich.

Rauber A. 1868. *Ueber die Nerven der Knochenhaut, und Knochen des Vorderaremes und Unterschenkeis*. Munchen: C. Fritsch.

Reiner A, Kasser R. 1996. Relative frequency of a subclavian vs. a transverse cervical origin for the dorsal scapular artery in humans. *Anat Rec* 244: 265–268.

Riche P. 1897. Le nerf cubital et les muscles de l'eminence thenar. *Bull Mem Soc Anat Paris* 5: 251–252.

Richmond BG, Fleagle JG, Kappelman J, Swisher CC 3rd. 1998. First hominoid from the Miocene of Ethiopia and the evolution of the catarrhine elbow. *Am J Phys Anthropol* 105: 257–277.

Rodriguez-Niedenfuhr M, Vazquez T, Ferreira B, Parkin I, Nearn L, Sanudo JR. 2002a. Intramuscular Martin-Gruber anastomosis. *Clin Anat* 15: 135–138.

Rodriguez-Niedenfuhr M, Vazquez T, Parkin I, Logan B, Sanudo JR. 2002b. Martin-Gruber anastomosis revisited. *Clin Anat* 15: 129–134.

Roles NC, Maudsley RH. 1972. Radial tunnel syndrome: resistant tennis elbow as a nerve entrapment. *J Bone Joint Surg Br* 54: 499–508.

Roos DB. 1976. Congenital anomalies associated with thoracic outlet syndrome: anatomy, symptoms, diagnosis, and treatment. *Am J Surg* 132: 771–778.

Rowntree T. 1949. Anomalous innervation of the hand muscles. *J Bone Joint Surg Br* 31B: 505–510.

Schaarschmidt A. 1750. *Neurological Tables*. Berlin, Germany: Johann Jacob Schuz (in German).

Schoenwolf GC. 2009. *Larsen's Human Embryology*, fourth edition. Philadelphia: Churchill Livingstone/Elsevier.

Schwartz HG. 1956. Anastomoses between cervical nerve roots. *J Neurosurg* 13: 190–194.

Sefa Ozel M, Ozel L, Toros SZ, Marur T, Yildirim Z, Erdogdu E, Kara M, Titiz IM. 2011. Denervation point for neuromuscular blockade on lateral pectoral nerves: a cadaver study. *Surg Radiol Anat* 33: 105–108.

Senecail B, Delmas A, Quereux P. 1979. Morphologic and biometric data on the constitution of the brachial plexus in man. *Bull Assoc Anat (Nancy)* 63: 513–525.

Seradge H, Tian W, Baer C, Seradge A. 2000. Anatomical variation of the posterior interosseous nerve: a cadaver dissection study. *Orthopedics* 23: 1195–1196.

Shu HS, Chantelot C, Oberlin C, Alnot JY, Shao H. 1999. Martin-Gruber communicating branch: anatomical and histological study. *Surg Radiol Anat* 21: 115–118.

Sibson F. 1846. On the mechanism of respiration. *Philos Trans R Soc Lond* 136: 501–550.

Siegel D, Gelberman R. 1991. Median nerve: applied anatomy and operative exposure. In: *Operative Nerve Repair and Reconstruction* (ed. RH Gelberman). Philadelphia: JB Lippincott, pp. 365–378.

Singla RK, Mahajan R, Sharma R, Sharma T. 2011. Bilateral non-formation of upper trunk of the brachial plexus with a unilateral communication between the musculocutaneous nerve and the median nerve: a case report. *J Clin Diag Res* 5: 1637–1640.

Sonck WA, Francx MM, Engels HL. 1991. Innervation anomalies in upper and lower extremities: potential clinical implications. How to identify with electrophysiologic techniques. *Electromyogr Clin Neurophysiol* 31: 67–80.

Sotereanos DG, Varitimidis SE, Giannakopoulos PN, Westkaemper JG. 1999. Results of surgical treatment for radial tunnel syndrome. *J Hand Surg* 24: 566–570.

Spinner M. 1968. The arcade of Frohse and its relationship to posterior interosseous nerve paralysis. *J Bone Joint Surg Br* 50: 809–812.

Spinner M. 1978. *Injuries to the Major Branches of Peripheral Nerves of the Forearm*, 2nd edition. Philadelphia: WB Saunders.

Spinner RJ, Carmichael SW, Spinner M. 1991. Partial median nerve entrapment in the distal arm because of an accessory bicipital aponeurosis. *J Hand Surg Am* 16: 236–244.

Spourgitis J. 1895. Sur un rameau musculaire très rare fourni par le nerf cubital. *Bull Mem Soc Anat Paris* 9: 410–411.

Stancic MF, Micovic V, Potocnjak M. 1999. The anatomy of the Berrettini branch: implications for carpal tunnel release. *J Neurosurg* 91: 1027–1030.

Standring S. 2008. Gray's Anatomy. Philadelphia: Elsevier.

Steiner HA. 1943. Roentgenologic manifestations and clinical symptoms of rib abnormalities 1. *Radiology* 40: 175–178.

Still JM Jr, Kleinert HE. 1973. Anomalous muscles and nerve entrapment in the wrist and hand. *Plast Reconstr Surg* 52: 394–400.

Stopford J. 1918. The variation in distribution of the cutaneous nerves of the hand and digits. *J Anat* 53: 14–25.

Stopford J. 1922. Neuritis produced by a wristlet watch. *Lancet* 199: 993–994.

Stott C. 1928. A note on the scalenus minimus muscle. *J Anat* 62: 359.

Streib E. 1992. Upper arm radial nerve palsy after muscular effort: report of three cases. *Neurology* 42: 1632–1634.

Struthers J. 1854. On some points in the abnormal anatomy of the arm. *Br Foreign Med Chir Rev* 14: 170–179.

Sunderland S. 1945. The innervation of the flexor digitorum profundus and lumbrical muscles. *Anat Rec* 93: 317–321.

Sunderland S. 1946. Metrical and non-metrical features of the muscular branches of the radial nerve. *J Comp Neurol* 85: 93–111.

Sunderland S, Hughes ES. 1946. Metrical and non-metrical features of the muscular branches of the ulnar nerve. *J Comp Neurol* 85: 113–125.

Sunderland S, Ray LJ. 1946. Metrical and non-metrical features of the muscular branches of the median nerve. *J Comp Neurol* 85: 191–203.

Taams KO. 1997. Martin-Gruber connections in South Africa. An anatomical study. *J Hand Surg Br* 22: 328–330.

Takafuji T, Igarashi J, Kanbayashi T, Yokoyama T, Moriya A, Azuma S, Sato Y. 1991. A very rare and anomalous accessory subscapularis muscle occurring in the axilla of a Japanese adult. *J Med Kyorin Soc* 22: 397–403.

Taleisnik J. 1973. The palmar cutaneous branch of the median nerve and the approach to the carpal tunnel. An anatomical study. *J Bone Joint Surg Am* 55: 1212–1217.

Tanaka N, Fujimoto Y, An HS, Ikuta Y, Yasuda M. 2000. The anatomic relation among the nerve roots, intervertebral foramina, and intervertebral discs of the cervical spine. *Spine (Phila Pa 1976)* 25: 286–291.

Telford ED, Mottershead S. 1948. Pressure at the cervico-brachial junction; an operative and anatomical study. *J Bone Joint Surg Br* 30B: 249–265.

Terry R. 1921. A study of the supracondyloid process in the living. *Am Phys Anthropol* 4: 129–139.

Testut L. 1884. *Les Anomalies Musculaires chez l'Homme: Expliquées par l'Anatomie Comparée leur Importance en Anthropologie*: Paris: G. Masson.

Theeuwes HP, Gosselink MP, Bruynzeel H, Kleinrensink GJ, Walbeehm ET. 2011. An anatomical study of the length of the neural pedicle after the bifurcation of the thoracodorsal nerve: implications for innervated free partial latissimus dorsi flaps. *Plast Reconstr Surg* 127: 210–214.

Thomas SJ, Yakin DE, Parry BR, Lubahn JD. 2000. The anatomical relationship between the posterior interosseous nerve and the supinator muscle. *J Hand Surg Am* 25: 936–941.

Thomas Horwitz M, Tocantins LM. 1938. An anatomical study of the role of the long thoracic nerve and the related scapular bursae in the pathogenesis of local paralysis of the serratus anterior muscle. *Anat Rec* 71: 375–385.

Thompson IM. 1923. Anomaly of median nerve and flexor digitorum sublimis muscle. *J Anat Physiol* 23: 375–379.

Thomson A. 1893. Third annual report of the committee of collective investigation of the Anatomical Society of Great Britain and Ireland for the year 1891–1892. *J Anat* 27: 183–194.

Ticker JB, Djurasovic M, Strauch RJ, April EW, Pollock RG, Flatow EL, Bigliani LU. 1998. The incidence of ganglion cysts and other variations in anatomy along the course of the suprascapular nerve. *J Shoulder Elbow Surg* 7: 472–478.

Tobin GR, Schusterman M, Peterson GH, Nichols G, Bland KI. 1981. The intramuscular neurovascular anatomy of the latissimus dorsi muscle: the basis for splitting the flap. *Plast Reconstr Surg* 67: 637–641.

Tountas CP, Bergman RA. 1993. *Anatomic Variations of the Upper Extremity*. New York: Churchill Livingstone.

Tountas CP, Bihrle DM, MacDonald CJ, Bergman RA. 1987. Variations of the median nerve in the carpal canal. *J Hand Surg Am* 12: 708–712.

Tubbs RS, Tyler-Kabara EC, Aikens AC, Martin JP, Weed LL, Salter EG, Oakes WJ. 2005. Surgical anatomy of the axillary nerve within the quadrangular space. *J Neurosurg* 102: 912–914.

Tubbs RS, Custis JW, Salter EG, Wellons JC, 3rd, Blount JP, Oakes WJ. 2006a. Quantitation of and superficial surgical landmarks for the anterior interosseous nerve. *J Neurosurg* 104: 787–791.

Tubbs RS, Salter EG, Custis JW, Wellons III JC, Blount JP, Oakes WJ. 2006b. Surgical anatomy of the cervical and infraclavicular parts of the long thoracic nerve. *Journal of Neurosurgery* 104: 792–795.

Tubbs RS, Loukas M, Shahid K, Judge T, Pinyard J, Shoja MM, Slappey JB, McEvoy WC, Oakes WJ. 2007. Anatomy and quantitation of the subscapular nerves. *Clin Anat* 20: 656–659.

Tubbs RS, Loukas M, Shoja MM, Ardalan MR, Apaydin N, Myers C, Shokouhi G, Oakes WJ. 2008. Contributions of the fourth spinal nerve to the brachial plexus without prefixation. *J Neurosurg Spine* 8: 548–551.

Tubbs RS, Apaydin N, Uz A, Sullivan A, Loukas M, Shoja MM, Cohen Gadol AA. 2009a. Anatomy of the lateral intermuscular septum of the arm and its relationships to the radial nerve and its proximal branches. Laboratory investigation. *J Neurosurg* 111: 336–339.

Tubbs RS, El-Zammar D, Loukas M, Comert A, Cohen-Gadol AA. 2009b. Intradural cervical root adjacent interconnections in the normal, prefixed, and postfixed brachial plexus. *J Neurosurg Spine* 11: 413–416.

Tubbs RS, Deep A, Shoja MM, Mortazavi MM, Loukas M, Cohen-Gadol AA. 2011a. The arcade of Struthers: An anatomical study with potential neurosurgical significance. *Surg Neurol Int* 2: 184.

Tubbs RS, Rogers JM, Loukas M, Comert A, Shoja MM, Cohen-Gadol AA. 2011b. Anatomy of the palmar branch of the ulnar nerve: application to ulnar and median nerve decompressive surgery. *J Neurosurg* 114: 263–267.

Tubbs RS, Mortazavi MM, Farrington WJ, Chern JJ, Shoja MM, Loukas M, Cohen-Gadol AA. 2013a. Relationships between the posterior interosseous nerve and the supinator muscle: application to peripheral nerve compression syndromes and nerve transfer procedures. *J Neurol Surg A Cent Eur Neurosurg* 74: 290–293.

Tubbs RS, Nechtman C, D'Antoni AV, Shoja MM, Mortazavi MM, Loukas M, Rozzelle CJ, Spinner RJ. 2013b. Ossification of the suprascapular ligament: A risk factor for suprascapular nerve compression? *Int J Shoulder Surg* 7: 19–22.

Turgut HB, Peker T, Gulekon N, Anil A, Karakose M. 2005. Axillopectoral muscle (Langer's muscle). *Clin Anat* 18: 220–223.

Turkof E, Puig S, Choi MS, Schilhan R, Millesi H, Firbas W. 1994. Superficial branch of the radial nerve emerging between two slips of a split brachioradialis muscle tendon: a variation of possible clinical relevance. *Acta Anat (Basel)* 150: 232–234.

Turkof E, Puig S, Choi SS, Zoch G, Dellon AL. 1995. The radial sensory nerve entrapped between the two slips of a split brachioradialis tendon: a rare aspect of Wartenberg's syndrome. *J Hand Surg Am* 20: 676–678.

Turner P. 1872. Further examples of variations in the arrangement of the nerves of the human body. *J Anat Physiol* viii: 297–299.

Uysal II, Seker M, Karabulut AK, Büyükmumcu M, Ziylan T. 2003. Brachial plexus variations in human fetuses. *Neurosurgery* 53: 676–684.

Uz A, Apaydin N, Bozkurt M, Elhan A. 2007. The anatomic branch pattern of the axillary nerve. *J Shoulder Elbow Surg* 16: 240–244.

van Dijk JG, Bouma PA. 1997. Recognition of the Martin-Gruber anastomosis. *Muscle Nerve* 20: 887–889.

Van Hoof T, Vangestel C, Forward M, Verhaeghe B, Van Thilborgh L, Plasschaert F, De Muynck M, Vanderstraeten G, D'Herde K. 2008. The impact of muscular variation on the neurodynamic test for the median nerve in a healthy population with Langer's axillary arch. *J Manipulative Physiol Ther* 31: 474–483.

Van Meir N, De Smet L. 2003. Carpal tunnel syndrome in children. *Acta Orthop Belg* 69: 387–395.

Verchere F. 1883. Note sur l'innervation des muscles flechisseurs communs des doigts. Anastomose du nerf median et du nerf cubital. *Union Medicale* 35: 205–207.

Viertel VG, Intrapiromkul J, Maluf F, Patel NV, Zheng W, Alluwaimi F, Walden MJ, Belzberg A, Yousem DM. 2012. Cervical ribs: a common variant overlooked in CT imaging. *AJNR Am J Neuroradiol* 33: 2191–2194.

Walsh J. 1877. The anatomy of the brachial plexus. *Am J Med Sci* 74: 387–399.

Wartenberg R. 1932. Cheiralgia paraesthetica. (Isolierte Neuritis des Ramus superficialis nervi radialis.). *Zeitschr Gesamte Neurolog Psychiat* 141: 145–155.

Watchmaker GP, Weber D, Mackinnon SE. 1996. Avoidance of transection of the palmar cutaneous branch of the median nerve in carpal tunnel release. *J Hand Surg Am* 21: 644–650.

Wehrli L, Oberlin C. 2005. The internal brachial ligament versus the arcade of Struthers: an anatomical study. *Plast Reconstr Surg* 115: 471–477.

Whitson RO. 1954. Relation of the radial nerve to the shaft of the humerus. *J Bone Joint Surg Am* 36A: 85–88.

Wichmann R. 1900. *The Spinal Nerves and their Segment Covers (Die Rückenmarksnerven und ihre Segmentbezüge ein Lehrbuch der Segmental–Diagnostik der Rückenmarkskrankheiten)*. Berlin: Salle.

Winkelman N, Spinner M. 1973. A variant high sensory branch of the median nerve to the third web space. *Bull Hosp Joint Diseases* 34: 161.

Won HS, Han SH, Oh CS, Chung IH, Kim SM, Lim SY. 2011. Topographic relationship between the medial intermuscular septum and the ulnar nerve in the upper arm. *J Neurosurg* 114: 1534–1537.

Woo JS, Shin C, Hur MS, Kang BS, Park SY, Lee KS. 2010. Spinal origins of the nerve branches innervating the coracobrachialis muscle: clinical implications. *Surg Radiol Anat* 32: 659–662.

Wulle C. 1988. Kaplan's anastomosis in the little finger. *Handchir Mikrochir Plast Chir* 20: 285–287.

Yan J, Horiguchi M. 2000. The communicating branch of the 4th cervical nerve to the brachial plexus: the double constitution, anterior and posterior, of its fibers. *Surg Radiol Anat* 22: 175–179.

Yogesh A, Marathe R, Pandit S. 2011. Musculocutaneous nerve substituting for the distal part of radial nerve: A case report and its embryological basis. *J Neurosci Rural Pract* 2: 74–76.

Yoshinaga K, Kawai K, Tanii I, Imaizumi K, Kodama K. 2008. Nerve fiber analysis on the so-called accessory subscapularis muscle and its morphological significance. *Anat Sci Int* 83: 55–59.

Zeiss J, Jakab E, Khimji T, Imbriglia J. 1992. The ulnar tunnel at the wrist (Guyon's canal): normal MR anatomy and variants. *AJR Am J Roentgenol* 158: 1081–1085.

Zhang B, Li Z, Yang X, Li G, Wang Y, Cheng J, Tang X, Wang F. 2009. Anatomical variations of the upper thoracic sympathetic chain. *Clin Anat* 22: 595–600.

Zook EG, Kucan JO, Guy RJ. 1988. Palmar wrist pain caused by ulnar nerve entrapment in the flexor carpi ulnaris tendon. *J Hand Surg Am* 13: 732–735.

Zuckerkandl E. 1894. Zur Anatomie und Entwicklungsgeschichte der Arterien des Vorderarmes. *Anatomy and Embryology* 4: 1–98.

92 Lumbosacral plexus

Nihal Apaydin
Ankara University Faculty of Medicine, Ankara, Turkey

Variations in the formation and distribution of the lumbosacral plexus and its branches have been the subject of several investigations. One of the first detailed descriptions of the anatomy of the lumbosacral plexus was provided by a French anatomist and pathologist with particular interest in the nervous system: Cruveilhier (1844). The classical definitions and common classifications were formulated in late 1800s and early 1900s. Eisler (1892) studied variations in the lumbosacral plexus extensively, paying particular attention to the thickness and number of different spinal nerves entering into the formation of its individual branches. Paterson (1893) defined the separation of the nerves into dorsal and ventral groups, documenting the ordinary pattern of formation of the lumbosacral plexus. He also introduced the term "nervus furcalis." Sherrington (1892) introduced the terms "prefixed" and "postfixed" for cases in which the plexus originated more superiorly (rostrally) for prefixed or more inferiorly (caudally) for postfixed plexuses than the more usual pattern. Bardeen and Elting (1901) used the terms "proximal" and "distal" in much the same way as Sherrington used "prefixed" and "postfixed." They suggested that the distal limit of the lumbar plexus is less definite than the proximal limit and portions of more distal lumbar nerves join with the sacral nerves to form the sacral plexus. They also concluded that race, sex, and side of the body have little or no relationship to variations in the lumbosacral plexus. Severeano (1904) studied 50 bodies bilaterally and divided the formation of the lumbar plexus into three types: ordinary (formation normale), prefixed (formation supérieure) and postfixed (formation inférieure) (Webber 1961).

The descriptions in the current literature and the variations identified in case reports rely mainly on these early publications. Variations in the formation of the lumbosacral plexus have long been a source of diagnostic confusion, as well as atypical clinical and electromyographic findings. It is also important to know that muscle innervation can change independently of the number of the root entering the plexus because the connections between the plexus roots vary.

The lumbosacral plexus provides the nerve supply to the pelvis and lower limbs; in addition, it provides the autonomic supply to the pelvic organs. It is formed by the union of the anterior primary divisions of the lumbar, sacral, and coccygeal nerves. For convenience of description and because of the differences in position and course of some of the nerves arising from it, the lumbosacral plexus is subdivided into four parts: lumbar, sacral, pudendal, and coccygeal. It must be remembered that these plexuses overlap and that there is no definite line of demarcation between their origins and distributions. The distribution of the nerves in the limbs is not typically segmental and is interrupted by the overlapping of the areas of distribution (Hollinshead 1956; Bergman et al. 1984, 1988; Williams 2005; Mahadevan 2008).

Lumbar plexus

The lumbar plexus is located in the posterior abdominal wall, in front of the transverse processes of the lumbar vertebrae and deep inside or posterior to the psoas major muscle. Variations in the position of the plexus are usually accompanied by variations in the vertebral column itself. While the origin of the various branches of the lumbar plexus varies according to whether the plexus is prefixed, ordinary, or postfixed, it is typically formed by the union of the anterior rami of the first three lumbar nerves and usually a part of the fourth lumbar nerve, and projects laterally and caudally from the intervertebral foramina. A communicating branch from T12, also known as the subcostal nerve, often joins the first lumbar nerve. The range of variations in the formation of the lumbar plexus is summarized in Table 92.1 (Hollinshead 1956; Bergman et al. 1984, 1988; Williams 2005; Mahadevan 2008).

The lumbosacral plexus is usually bilaterally asymmetric. In its usual form, the L2–L4 ventral rami first bifurcate into anterior and posterior primary divisions. The L1 nerve splits into cranial and caudal branches after receiving a contribution from T12. The cranial branch is thicker and bifurcates into the iliohypogastric and ilioinguinal nerves, the former also formed by the subcostal nerve in people where this nerve contributes to the

Bergman's Comprehensive Encyclopedia of Human Anatomic Variation, First Edition. Edited by R. Shane Tubbs, Mohammadali M. Shoja and Marios Loukas.
© 2016 John Wiley & Sons, Inc. Published 2016 by John Wiley & Sons, Inc.

Table 92.1 Range of variation of lumbar plexus.

Nerve	Prefixed plexus (high form)	Usual pattern	Postfixed plexus (low form)
Lateral femoral cutaneous	L1, L2	L2, L3	L3, L4
Femoral	T12, L4	L1, L4	L1, L5
Obturator	L1, L4	L2, L3	L2, L5
Furcal	L3, L4	L4	L4, L5

Source: Bardeen and Elting (1901).

lumbar plexus. The caudal branch of the L1 nerve unites with the anterior division of L2 to form the genitofemoral nerve. The anterior divisions of the L2–L4 roots form the obturator nerve. The posterior divisions of L2 and L3 further split into two. The thinner branches unite to form the lateral femoral cutaneous nerve; the thicker branches together with a contribution from the posterior division of L4 join to create the femoral nerve. The psoas major and quadratus lumborum are innervated by the T12 and L1 nerves and the L2–L4 anterior primary divisions (Hollinshead 1956; Urbanowicz and Zaluska 1969; Bergman et al. 1984, 1988; Williams 2005; Mahadevan 2008). The anterior division of L4 is commonly divided between the lumbar and sacral plexuses, hence it is called the furcal (meaning forked) nerve (Paterson 1894). Fibers from the anterior division of L4 join the anterior division of L5 and create the lumbosacral trunk to join the sacral plexus. Eisler found the furcal nerve to be formed by L5 in 19 out of 22 variations noted in the formation of the lumbar plexus; in only two cases was it formed by L3. The proportion of L4 contributing to the sacral plexus is also variable. The common formation of the lumbar plexus is the manner of division of this nerve: in a postfixed plexus it contributes all or most of its fibers to the lumbar plexus, while in a prefixed plexus it contributes few or none. More rarely, an appreciable part of the twelfth thoracic or a part of the fifth lumbar nerve participates in the formation of prefixed and postfixed plexuses, respectively (Hollinshead 1956; Urbanowicz and Zaluska 1969; Bergman et al. 1984, 1988).

Matejik (2010) reported the variations of the lumbosacral plexus in 50 cadavers and found the prefixed type in 19 cases and postfixed in five, the rest being the ordinary form. He also reported that the Th12 and L1 roots are thicker in the prefixed type. In this type, the L4 root contributes more significantly to the sacral plexus and the S3 and S4 roots are absent. If the L4 root does not contribute to the sacral plexus or contributes only minimally, the L5 root is also thinner, S1–S3 are thicker and S4 is also present. As expected, in the postfixed type the L5 root is the largest contributor to the sacral plexus. These variations at the level of neural root formation are reported to be the most common variations of the lumbosacral plexus (Matejcík 2010). Erbil et al. (1998) described a rare variation: occurrence of the prefixed type on one side and the postfixed type on the other.

The lumbosacral trunk, either a single trunk formed by the union of L4 and L5 or two parallel but non-united trunks, also appears medial to the psoas muscle, usually within the pelvis itself, on the anterior surface of the sacrum. It lies medial and posterior to the obturator nerve and is usually not visible from the abdomen, since it is covered first by the psoas muscle and then by the hypogastric vessels. The iliolumbar artery typically passes between the lumbosacral trunk and the obturator nerve (Hollinshead 1956). Urbanowicz (1981) studied the connections between the lumbar and the sacral plexus bilaterally in 122 subjects. The plexuses were joined by a single nervus furcalis in 91.8% of subjects and by a doubled nervus furcalis in 0.8%. The single furcal nerve was formed by the abdominal nerve L4 in 80% and L5 in 7.7%. The doubled furcal nerve arose from L3 and L4 in 0.4% of cases and from L4 and L5 in 0.4%. The major part of the furcal nerve arising from L4 usually went to the lumbar plexus, and from L5 to the sacral plexus. In 7.4% of cases no connection between the plexuses could be found (Urbanowicz 1981). In a series of 20 fetal specimens, Yasar et al. (2014) observed a single furcal nerve which only originated from the L4 spinal nerve. Lane (1886) described a sixth lumbar nerve that contributed to the sacral plexus. A branch of L3 has been reported by Thompson traveling through the psoas major behind the femoral vessels, to terminate in the adductor longus muscle.

The nerves contributing to the formation of the branches of the lumbosacral trunk in prefixed, postfixed and ordinary types are summarized in Table 92.1. Branches of the lumbar plexus are described in the following sections.

Iliohypogastric nerve

The iliohypogastric nerve usually originates from the ventral ramus of the L1 spinal nerve. It emerges from the upper lateral border of the psoas major, crossing obliquely behind the lower renal pole and in front of the quadratus lumborum. Above the iliac crest, it enters the posterior part of the transversus abdominis. Between the transversus abdominis and internal oblique it divides into lateral and anterior cutaneous branches. The lateral cutaneous branch runs through the internal and external oblique above the iliac crest, a little behind the iliac branch of the T12 spinal nerve. It is distributed to the posterolateral gluteal skin. The anterior cutaneous branch runs between the internal oblique and transversus abdominis and innervates both muscles. It runs through the internal oblique approximately 2 cm medial to the anterior superior iliac spine and through the external oblique aponeurosis approximately 3 cm above the superficial inguinal ring, and is then distributed to the suprapubic skin supplying sensory branches. The iliohypogastric nerve usually gives communicating branches to the subcostal and ilioinguinal nerves (Williams 2005; Mahadevan 2008). The iliac branch of the iliohypogastric nerve can be absent, replaced by the lateral cutaneous branch of the twelfth thoracic nerve. The hypogastric branch can supply the pyramidalis muscle and be joined with the twelfth thoracic nerve. The iliohypogastric

nerve is sometimes derived from the twelfth thoracic nerve and can also receive a root from the eleventh (Hollinshead 1956; Bergman et al. 1984, 1988). Anloague and Huijbregts (2009) demonstrated the absence of the iliohypogastric nerve in 20.6% of the lumbar plexuses they investigated. Sometimes its anterior branch is replaced by the ilioinguinal nerve just before the former exits from the external inguinal ring (Aasar 1947).

Ilioinguinal nerve

The ilioinguinal nerve is usually smaller than the iliohypogastric nerve and arises with it from the first lumbar ventral ramus. It emerges from the lateral border of the psoas major, with or just inferior to the iliohypogastric nerve. It passes obliquely across the quadratus lumborum and the upper part of the iliacus and enters the transversus abdominis near the anterior end of the iliac crest. Here, it sometimes connects with the iliohypogastric nerve. It pierces the internal oblique lower than the iliohypogastric, supplies it and then traverses the inguinal canal below the spermatic cord. Sometimes it passes deep to the inguinal ligament (Aasar 1947). It emerges with the cord from the superficial inguinal ring and supplies the proximal medial skin of the thigh and the skin over the root of the penis and upper part of the scrotum in males. In females it innervates the skin covering the mons pubis and the adjoining labium majus. The ilioinguinal and iliohypogastric nerves are reciprocal in size. The ilioinguinal is occasionally very small and ends by joining the iliohypogastric, a branch of which then takes its place (Williams 2005; Mahadevan 2008).

This nerve can be small and terminate near the iliac crest by joining the iliohypogastric nerve as they exit through the psoas major muscle. In this case the iliohypogastric nerve sends branches to replace the absent terminal part of the ilioinguinal nerve. The ilioinguinal nerve can be entirely absent, its distribution being taken over by the genital branch of the genitofemoral nerve; the iliohypogastric nerve supplies its territory. The ilioinguinal nerve can also be replaced by either the genital (more commonly) or femoral branches of the genitofemoral nerve. The ilioinguinal can provide a lateral cutaneous or iliac branch to supply the skin in the region of the anterior superior iliac spine. It can partially or completely replace the genital branch of the genitofemoral nerve or the lateral femoral cutaneous nerve. It sometimes arises from L2 instead of L1 (Griffin 1891). Sometimes it gives a communicating branch to the lateral femoral cutaneous nerve. If such a branch is present, it pierces the external oblique aponeurosis near the anterior superior iliac spine and joins the nerve in that vicinity (Aasar 1947; Hollinshead 1956; Bergman et al. 1984, 1988).

The ilioinguinal and iliohypogastric nerves sometimes arise as a common trunk, usually separating between the transversus and internal oblique muscles. The ilioinguinal nerve can be derived from the last thoracic nerve (T12), from a loop between the L2 and L3 nerves, or even from the L2 and L3 nerves directly. It can also supply branches to the rectus abdominis muscle. In a study of 200 cadavers, the ilioinguinal nerve was reported to arise from the lumbar plexus in 72.5% and by a common trunk with the iliohypogastric nerve in 25%; it was absent in 2.5%. It was formed from one root in 92.5% and from two roots in about 5% of cases. In 86%, it carried fibers from one spinal nerve (primarily from L1) and in 11% from two (T12–L1, L1–L2, or L2–L3). Within the inguinal canal, the nerve usually lies ventral to the spermatic cord (60% of cases) but it can lie posterior the cord or within it. It usually leaves the superficial inguinal ring medially but sometimes through its lateral aspect. In some cases, the nerve runs outside the inguinal ring (Aasar 1947; Hollinshead 1956; Bergman et al. 1984, 1988).

Genitofemoral nerve

The genitofemoral nerve is formed within the substance of the psoas major, originating from the L1 and L2 ventral rami. It descends obliquely through the muscle to emerge on its medial border, opposite the third or fourth lumbar vertebra. It then descends beneath the peritoneum on the psoas major, crosses obliquely behind the ureter and divides above the inguinal ligament into genital and femoral branches; it often divides close to its origin, in which case its branches emerge separately from the psoas major. The genital branch innervates the genital area. It crosses the lower part of the external iliac artery, entering the inguinal canal by the deep ring. It supplies the cremaster and the skin of the scrotum in males. In females, it accompanies the round ligament and ends in the skin of the mons pubis and labium majus. The femoral branch provides sensory innervation of the medial upper thigh and the skin over the femoral vessels. It descends lateral to the external iliac artery, passing behind the inguinal ligament. It then enters the femoral sheath lateral to the femoral artery. It pierces the anterior layer of the femoral sheath and fascia lata and supplies the skin anterior to the upper part of the femoral triangle. It connects with the femoral intermediate cutaneous nerve and supplies the femoral artery (Williams 2005; Mahadevan 2008).

Some authors consider this to be the most variable nerve of the lumbar plexus. Its genital and femoral branches can arise separately from the lumbar plexus. Either of them can be derived entirely from the L1 or L2 nerves. It occasionally arises from L3. The genital branch sometimes receives fibers from the T12 nerve. The genitofemoral or either of its branches (genital or femoral) can be absent. In such cases the ilioinguinal nerve replaces the genital branch while the lateral cutaneous or the anterior femoral nerve replaces the femoral branch. The branches of the genitofemoral can replace the ilioinguinal nerve or communicate with it. The genital branch can bypass the deep inguinal ring running superficial to it in the aponeurosis of the external abdominal oblique muscle. The femoral branch can replace or join the lateral or middle cutaneous nerve. Occasionally, the femoral branch has an extensive cutaneous distribution to the upper two-thirds of the thigh. The genital branch can supply the lower fibers of the internal oblique and transversalis muscles. Occasionally, the nerve divides within the substance of the psoas muscle and its terminal branches emerge separately

from the anterior surface of that muscle. In a study of 200 cadavers, the genitofemoral nerve arose as a single trunk in 80% and as two separate branches (genital and femoral) in 20%. The single trunk can arise from L1, L2, or L3. The two separate trunks can arise from L1 and L2 or L1, L2, and L3. In this study, L2 contributed to the nerve in all cases but L3 in only 0.75%. The level of division into terminal branches is also highly variable (Aasar 1947; Hollinshead 1956; Bergman et al. 1984, 1988). Anloague and Huijbregts (2009) reported variations of the genitofemoral nerve in 47.1% of the cases they dissected. The most common variation included a split of this nerve into genital and femoral branches within the substance of the psoas muscle (26.5%). In 20.6%, this bifurcation occurred at the upper rather than middle portion of the anterior surface of the psoas. Sim and Webb (2004) also found that the nerve divided into genital and femoral branches prior to emergence from the psoas major in only 5 of 60 plexuses (8.3%).

Lateral femoral cutaneous nerve

This is an exclusively sensory nerve. Several variations in its formation, course, and branches have been reported. In its usual form it arises from posterior divisions of L2 and L3, but it can arise in a "high form" (prefixed) from L1 and L2 or in a "low form" (postfixed) from L3 and L4. It can also arise from the femoral nerve or as an independent branch of the lumbar plexus. It emerges from the lateral border of the psoas major and crosses the iliacus obliquely towards the anterior superior iliac spine, parallel to the iliac crest. It supplies sensory fibers to the parietal peritoneum in the iliac fossa. The right nerve passes posterolateral to the cecum, separated from it by the fascia iliaca and peritoneum. The left nerve passes behind the lower part of the descending colon. It supplies the parietal peritoneum in the iliac fossa. Both nerves pass behind or through the inguinal ligament approximately 1 cm medial to the anterior superior iliac spine and anterior to, or through, the sartorius into the thigh.

The nerve can be absent on one side and be replaced by a branch of the anterior femoral cutaneous nerve or by the ilioinguinal nerve (Bergman et al. 1984, 1988). Carai et al. (2009) reported that the lateral femoral cutaneous nerve was wholly absent in 13 (8.8%) of 148 patients who received surgical intervention for meralgia paresthetica. The nerve usually passes behind or through the inguinal ligament, variably medial to the anterior superior iliac spine (commonly 1 cm) and anterior or posterior to or through the sartorius into the thigh. It can pass beneath the inguinal ligament at a point midway between the anterior superior iliac spine and the femoral artery. It is sometimes associated with the anterior femoral cutaneous nerve until it passes distal to the inguinal ligament (Bergman et al. 1984, 1988). Then it divides into anterior and posterior branches. The anterior branch becomes superficial approximately 10 cm distal to the anterior superior iliac spine and supplies the skin of the anterior and lateral thigh as far as the knee. It contributes to the formation of the peripatellar plexus, connecting with the cutaneous branches of the anterior division of the femoral nerve and the infrapatellar branch of the saphenous nerve. The posterior branch pierces the fascia lata higher than the anterior branch, and divides to supply the skin on the lateral surface from the greater trochanter to about halfway along the thigh. It can also supply the gluteal skin. In some cases, the posterior branch emerges from beneath the inguinal ligament about 5 cm medial to the anterior superior iliac spine and can be replaced by a branch of the genitofemoral nerve (Bergman et al. 1984, 1988).

Anloague and Huijbregts (2009) reported variation in the lateral femoral cutaneous nerve in 17.6% of the cases they dissected. In its variant form it arose either from the L1 and L2 nerve roots or solely from L2. Another variation included a bifurcation of the lateral femoral nerve within the pelvic cavity prior to its exit near the anterior superior iliac spine. Such bifurcations normally occur after the nerve exits the pelvis (Anloague and Huijbregts 2009).

De Ridder et al. (1999) reported that in 24 of 200 cadavers they dissected, the lateral femoral cutaneous nerve arose from L1 and L2 and even solely from L2 and L3. Sim and Webb (2004) reported that in 22 of 60 plexuses (36.7%) the lateral femoral cutaneous nerve arose from the first two lumbar nerves. In only one plexus (1.7%) the nerve arose solely from the L2 ventral ramus, and in six plexuses (10%) it derived directly from the femoral nerve, yielding a total of 48.3% variation for this nerve. Erbil et al. (1998) reported a patient where the right lateral femoral cutaneous nerve was derived from the anterior divisions of the L2 and L3 nerve roots. Webber (1961) classified the neural contribution to the lateral femoral cutaneous nerve in eight distinct patterns in the 50 plexuses they examined. Grothaus et al. (2005) found that it bifurcated into additional branches before crossing the inguinal ligament in 27.6% of 29 cadavers. Carai et al. (2009) also reported early nerve bifurcation in 37.8% of 148 cases. Erbil et al. (1998) reported similar bifurcations of this nerve into either two or three branches in two of 56 plexuses (3.5%). Rosenberger et al. (2000) found that in 23% of 53 cadavers the lateral femoral cutaneous nerve gave rise to two branches.

Anatomical variations of the nerve were found in about 25% of the patient population in a study by De Ridder et al. (1999). Kosiyatrakul et al. (2010) examined its location in relation to the anterior superior iliac spine and the iliac crest in 96 cadaveric specimens, and revealed that 18.8% passed lateral to the anterior superior iliac spine. Dimitropoulos et al. (2011) demonstrated that the nerve was absent under the inguinal ligament in one patient. In contrast, it was found crossing the iliac crest at a distance of 2 cm laterally to the anterior superior iliac spine. Mischkowski et al. (2006) described a case of a lateral femoral cutaneous nerve that crossed at a distance less than 5 mm superolaterally from the most anterior point of the spine. Erbil et al. (2002) observed two variations out of 28 cadavers they examined. In one of these specimens the ventral rami of the S1–S2 spinal nerves were united and then divided into four branches: the obturator, femoral, and two lateral femoral cutaneous nerves. In another case they noted three lateral femoral

cutaneous nerves, all piercing the psoas major muscle anterolaterally. Two of these nerves united by a communicating branch anterior to the iliacus muscle (Erbil et al. 2002).

Femoral nerve

This is a motor and sensory nerve derived from the posterior divisions of the ventral rami of the L2–L3–L4 spinal nerves. It is located lateral to the psoas muscle, in the cleavage between the psoas and iliacus. In its course to the thigh, the femoral nerve can pierce the iliacus. It is covered by the iliac fascia, which separates it from the main vessels. Here, it gives off branches that supply the iliacus and pectineus and sends sensory fibers to the femoral artery. Posterior to the inguinal ligament it lies lateral to the femoral artery and is separated from it by part of the psoas major. Under the inguinal ligament, the femoral nerve lies lateral to the femoral artery and vein (vein-artery-nerve or VAN from medial to lateral). However, it has also been reported to enter the thigh between the femoral artery and vein. It has anterior and posterior divisions. The anterior division has two sensory branches that supply the anteromedial thigh and two muscular branches that supply the sartorius and pectineus muscles. The posterior division has one sensory branch, the saphenous nerve, and muscular branches to the quadriceps. The muscular branch to the rectus femoris also supplies the hip joint while the muscular branches to the three vasti muscles also supply the knee joint (Williams 2005; Mahadevan 2008).

In *Gray's Anatomy* (Mahadevan 2008), the femoral nerve is classically described as having three main divisions: nerve to the pectineus, anterior division, and posterior division. The anterior division gives the intermediate and medial cutaneous nerve of the thigh and the nerve to the sartorius. The posterior division gives the saphenous nerve and muscular branches to the quadriceps femoris. There are also unnamed vascular branches, which travel along the femoral artery and its branches.

Anloague and Huijbregts (2009) reported variations of the femoral nerve in 35.3% of investigated lumbar plexuses. In those cases the nerve was observed to bifurcate into two and sometimes three separate slips within the mid-substance of the psoas major. Spratt et al. (1996) reported that 3 out of 136 plexuses (2.2%) contained a variant slip of the iliacus and psoas major muscles that split the femoral nerve. In a case report, Jelev et al. (2005) noted similar variations of the iliacus and psoas muscles splitting the femoral nerve.

The anterior cutaneous branch can arise from the beginning of the femoral nerve or directly from the lumbar plexus. It can partly or completely replace the femoral branch of the genitofemoral nerve. The posterior branch of the medial cutaneous nerve is sometimes very small or absent, in which case the obturator or saphenous nerves provide its usual area of supply. The saphenous nerve can end at the knee and be replaced in the leg by a branch of the tibial nerve. The patellar branch of the saphenous nerve can arise from the nerve to the vastus medialis. The saphenous sometimes provides the medial dorsal digital nerve to the great toe. Branches from the femoral nerve to the tensor fasciae latae and adductor longus have also been reported. A branch was also found passing behind the femoral artery and vein, joining an accessory obturator nerve, and supplying part of the obturator muscle. The portion of the nerve arising from L4 can run a separate course. Leaving the pelvis with the superior gluteal nerve it can pass under the fascia lata to supply the rectus femoris and vastus lateralis (Bergman et al. 1984, 1988).

The intermediate cutaneous nerve of the thigh has a separate origin from the lumbar plexus. This nerve sometimes arises from the lumbar plexus or from the beginning of the femoral nerve, and partially or totally replaces the femoral branch of the genitofemoral nerve (Aasar 1947).

Saphenous nerve

This is a sensory nerve that originates from the posterior division of the femoral nerve (L3–L4) in the inguinal region. It is the largest and longest cutaneous branch of the femoral nerve. It descends lateral to the femoral artery in the femoral triangle and enters the adductor canal, where it crosses in front of the artery to lie medial to it. At the distal end of the canal it leaves the artery and emerges through the aponeurotic covering of the vastoadductor membrane with the saphenous branch of the descending genicular artery. As it leaves the adductor canal, it gives off an infrapatellar branch that contributes to the peripatellar plexus. It then pierces the fascia lata between the tendons of the sartorius and gracilis, becoming subcutaneous to supply the prepatellar skin. It descends along the medial tibial border with the long saphenous vein. It passes in front of the medial malleolus in the ankle before terminating around the base of the first metatarsal on the medial side of the foot. It divides distally into a branch that continues along the tibia to the ankle and one that passes anterior to the ankle to supply the skin on the medial side of the foot, often as far as the first metatarsophalangeal joint. It can connect with the medial branch of the superficial fibular nerve (Bergman et al. 1984, 1988; Williams 2005; Mahadevan 2008).

Obturator nerve

The obturator is the nerve of the medial compartment of the thigh. It arises from the anterior divisions of the second to fourth lumbar ventral rami. It can have additional roots from the first or fifth lumbar nerve. It can arise in a "high form" from L1, L2, L3, and L4 (very rarely from L1, L2, and L3), or in a "low form" from L2, L3, L4, and L5. In its usual form, the branch from the third is the largest while that from the second is often very small. The second lumbar nerve does not always contribute to it. The obturator descends through the psoas major and emerges from its medial border at the pelvic brim running down between this muscle and the lumbar vertebral column. It crosses the sacroiliac joint behind the common iliac artery and lateral to the internal iliac vessels, running along the lateral pelvic wall medial to the obturator internus, anterosuperior to the obturator vessels. It can run in a bony canal prior to entering the obturator foramen (Varricchio et al. 2013). Tubbs et al.

(2005) reported this nerve to appear at a mean distance of 5 cm inferior to the supracristal plane on a vertical line through the ASIS and having a mean distance of 3 cm lateral to the midline. It enters the thigh through the upper part of the obturator foramen. Near the foramen it divides into anterior and posterior branches, which are separated at first by part of the obturator externus and more distally by the adductor brevis. One study found that the nerve divided within the pelvis in 23.22%, in the obturator canal in 51.78%, and in the thigh in 25% (Anloague and Huijbregis 2009). The branch from the main trunk of the nerve to the obturator externus muscle can pass to the lateral (instead of the medial) side of the obturator nerve. It gives articular branches to the hip and knee and can supply the skin on the medial thigh and leg. The anterior sensory branch is frequently missing, and in these cases the femoral nerve also supplies the medial thigh. The highly variable distribution of the cutaneous branch of the obturator nerve has contributed to the confusion about how much of the medial thigh and the obturator nerve innervates the knee. Branches to the following structures have also been reported: the obturator internus and pectineus muscles, obturator artery, and periosteum of the pelvic surface of pubis (Bergman et al. 1984, 1988, Williams 2005; Mahadevan 2008). Locher et al. (2008) noted substantial anatomical variation in the location of the branches, which were not all the same in the cadaveric specimens they dissected.

The anterior branch of the obturator leaves the pelvis anterior to the obturator externus and descends in front of the adductor brevis, deep to the pectineus and adductor longus. It can pass posterior to the adductor brevis muscle. The anterior branch innervates the gracilis, adductor brevis, and adductor longus, and sometimes the pectineus. It can communicate with the accessory obturator nerve (when this nerve is present). It also gives articular branches to the hip joint. On occasions it supplies the skin of the medial side of the thigh. It can communicate with the medial cutaneous and saphenous branches of the femoral nerve to form the subsartorial plexus. The contribution of the obturator nerve to this plexus is highly variable. When its communicating branch is large and reaches the leg, the posterior branch of the medial cutaneous nerve is small. Occasionally the communicating branch to the medial femoral cutaneous and saphenous branches continues as a cutaneous branch to the thigh and leg. When this occurs, the nerve emerges from the distal border of the adductor longus to descend along the posterior margin of the sartorius to the knee. Here, it pierces the deep fascia and connects with the saphenous nerve to supply the skin on the medial side of the leg.

The posterior branch of the obturator nerve has a short trajectory. It usually pierces the obturator externus anteriorly and passes beneath the adductor brevis to the front of the adductor magnus. It can also pass posterior to the adductor brevis muscle. The posterior branch gives branches to the obturator externus, adductor magnus, and adductor brevis when the latter is not supplied by the anterior division. It gives branches to the knee joint and popliteal artery.

Accessory obturator nerve

An accessory obturator nerve has a reported incidence of 30% (Hollinshead 1956), 29% (of 120 cases; Eisler 1892), 11% (Sim and Webb 2004), 8% (Webber 1961) and 3% (Akkaya et al. 2008). In contrast, Tubbs et al. (2005) reported finding not a single accessory obturator nerve in 22 plexuses. When present, it arises from the L3 or more commonly the L3 and L4 nerves between the roots of the femoral and obturator nerves. It can also arise from L2, L3, and L4; only from L2 and L3; only from L3; or from the obturator nerve (Bergman et al. 1984, 1988). In a series of 1000 specimens from 500 embalmed adult human cadavers, the accessory obturator nerve was reported to be present in 13.2% (13.3% of the males and 12.9% of the females) with predominance on the left side of the body (Katritsis et al. 1980). Sim and Webb (2004) also noted that it occurred more frequently on the left side and in females. Katritsis et al. (1980) found it to be formed by roots from the anterior primary divisions of L3 and L4 (63.6%); from L2, L3, and L4 (10.6%); from L2 and L3 (7.6%); from L3 (6.1%); or from the trunk of the obturator nerve (12.1%).

The accessory obturator nerve usually courses medial and posterior to the obturator nerve and is usually not visible from the abdomen, since it is covered first by the psoas muscle and then by the hypogastric vessels. It courses with the obturator nerve to the level of the brim of the pelvis, but is sometimes closely related to the femoral nerve. Instead of passing through the obturator foramen in the same way as the obturator nerve, it descends along the medial border of the psoas muscle, crosses over the superior ramus of the pubic bone, passes beneath the pectineus, and terminates in three branches, which are also variable. These terminal branches usually replace the femoral branch to the pectineus and supply the muscle and the hip joint. It can also give branches to the adductor muscles by rejoining the obturator nerve. However, sometimes these only supply the pectineus or make a significant contribution to the innervation of the adductor muscles (Hollinshead 1956; Bergman et al. 1984, 1988).

Accessory nerve of Jamieson

Occasionally, L2 and L3 ventral rami supply a cutaneous nerve. This nerve is destined for the anterior thigh (Jamieson 1903).

Sacral plexus

The sacral and coccygeal plexuses are formed by the ventral rami of the sacral and coccygeal spinal nerves. The sacral plexus lies against the posterior pelvic wall anterior to the piriformis, posterior to the internal iliac vessels and ureter, and behind the sigmoid colon on the left. The sacral plexus is formed by the lumbosacral trunk, the first to third sacral ventral rami, and part of the fourth sacral ventral ramus (the remainder of which joins the coccygeal plexus). The upper four sacral ventral rami enter the pelvis by the anterior sacral foramina, the fifth between the

sacrum and coccyx; the ventral ramus of the coccygeal nerve curves forwards below the rudimentary transverse process of the first coccygeal segment. The first and second sacral ventral rami are large, the third to fifth diminish progressively, and the coccygeal is the smallest. Each receives a gray ramus communicans from a corresponding sympathetic ganglion. Visceral efferent rami leave the second to fourth sacral rami as the pelvic splanchnic nerves, containing parasympathetic fibers to minute ganglia in the walls of the pelvic viscera. The origins of the nerves forming the sacral plexus are highly variable depending on whether the plexus is prefixed, postfixed, or has the usual pattern. The range of these variations was extensively defined by Eisler (1892), providing the basis for different classification systems that are still used today (Table 92.2).

Branches of the sacral plexus are described in the following sections.

Nerve to quadratus femoris (and gemellus inferior)

This arises from the ventral branches of the L4–S1 ventral rami. It leaves the pelvis via the greater sciatic foramen below the piriformis, descends on the ischium deep to the sciatic nerve, the gemelli and the tendon of the obturator internus, and innervates the gemellus inferior, quadratus femoris, and the hip joint (Williams 2005; Mahadevan 2008). Wilson (1889) was probably the first to report an abnormal distribution of the nerve to the quadratus femoris, in which the nerve was longer than usual and entered the anterior aspect of the adductor magnus supplying it. Bergman also noted this nerve to give branches to the upper part of the adductor magnus and superior gemellus. Bardeen and Elting (1901) suggested there could be numerous communicating branches between the nerve and the quadratus femoris, obturator internus, and piriformis because of their close positional relationship. The branch to the superior gemellus is sometimes this muscle's only nerve supply (Aasar 1947; Bergman et al. 1984, 1988). Kikuchi (1987) described the superior gemellus as supplied not only by the nerve to the obturator internus (obturator internus nerve) but also by that to the quadratus femoris (quadratus femoris nerve). He inferred that the superior gemellus has two different embryological origins. Honma et al. (1998) reported a communication between a branch to the inferior gemellus from the quadratus femoris nerve and a branch of the obturator internus nerve within the obturator internus muscle, and recognized these muscles as part of the same muscle mass. Aung et al. (2001) reported in their series of 101 specimens that the quadratus femoris nerve arose from the ventral surface of L4, L5, and S1 in 79.4%. This nerve and the nerve to the obturator internus can be united in their early course (Piersol 1916).

Nerve to obturator internus (and gemellus superior)

The nerve to the obturator internus and gemellus superior arises from the L5–S1 and S2 ventral rami. It leaves the pelvis via the greater sciatic foramen below the piriformis. It gives a branch to the upper posterior surface of the gemellus superior, crosses the ischial spine, and then re-enters the pelvis via the lesser sciatic foramen running on the pelvic surface of the obturator internus. Aung et al. (2001) examined the innervation patterns of the obturator internus, superior and inferior gemelli, and quadratus

Table 92.2 Range of variation of sacral plexus.

Nerve	Prefixed plexus (high form)	Usual pattern	Postfixed plexus (low form)
Lumbosacral trunk	L4	L4	L4
Nerve to quadratus femoris	L4, L5	L4, L5, S1	L5, S1
Nerve to obturator internus	L4, L5, S1, S2	L5, S1, S2	S1,S2, S3
Tibial	L3, L4, L5, S1, S2	L4, L5, S1, S2, S3	L5, S1, S2, S3, S4
Superior gluteal	L4, L5, S1	L4, L5, S1, S2	L5, S1, S2
Inferior gluteal	L4, L5, S1	L5, S1, S2	(L5), S1, S2
Nerve to piriformis	L5, S1, S2	S1, S2	S1,S2, S3
Common fibular	L3, L4, L5, S1	L4, L5, S1, S2	L5, S1, S2, S3
Posterior femoral cutaneous	L5, S1, S2	S1,S2, S3	S2, S3, S4
Pudendal	L5, S1, S2, S3	S1, S2, S3, S4	S1, S2, S3, S4
Extreme range of variations			
Lumbosacral trunk	L3 or L3, L4	L4	L4, L5 or L5
Common fibular	L3, L4, L5, S1, S2	L4, L5, S1, S2	L4, L5, S1, S2, S3, S4
Tibial	L3, L4, L5, S1, S2	L4, L5, S1, S2, S3	L4, L5, S1, S2, S3, S4
Posterior femoral cutaneous	L5, S1, S2, S3	L5, S1, S2, S3, S4	L5, S1, S2, S3, S4

Source: Eisler (1892).

femoris muscles in 101 pelvic halves of 60 human cadavers and found that the quadratus femoris and obturator internus nerves formed a common trunk in 84.6%. There was also frequently communication between the obturator internus and quadratus femoris nerves. The obturator internus nerve arose from the ventral surface of L5, S1, S2, and S3 in 84.6% (Aung et al. 2001).

Nerve to piriformis

The nerve to the piriformis usually arises from the dorsal branches of the S1–S2 ventral rami and enters the anterior surface of the piriformis. It sometimes arises from only the S2 ventral ramus (Bergman et al. 1984, 1988, Williams 2005; Mahadevan 2008). It can be a single or doubled nerve. An additional branch can arise from the superior gluteal nerve (Piersol 1916).

Superior gluteal nerve

The superior gluteal nerve arises from the dorsal branches of the L4–L5 and S1–S2 ventral rami. It is accompanied by the superior gluteal vessels and leaves the pelvis via the greater sciatic foramen above the piriformis. It then divides into superior and inferior branches. The superior branch accompanies the upper branch of the deep division of the superior gluteal artery and innervates the gluteus medius and occasionally the gluteus minimus. The inferior branch runs with the lower ramus of the deep division of the superior gluteal artery across the gluteus minimus and innervates the gluteus medius and minimus. It then ends in the tensor fasciae latae (Williams 2005; Mahadevan 2008). This nerve can receive fibers from the S2 spinal nerve. A branch to the piriformis can arise from the lowest root of this nerve (Bergman et al. 1984, 1988).

The branching pattern and the course of the superior gluteal nerve (SGN) was classified into two types by Jacobs and Buxton (1989): (1) transverse neural trunk pattern, in which the branches arose separately in parallel to each other; and (2) spray pattern, in which the SGN had branches that fanned out along the intermuscular plane between the gluteus medius and minimus. In most of their cases (80%) they observed the spray pattern. However, a more recent study by Apaydin et al. (2013) revealed the "transverse neural trunk pattern" in 85.7% of the specimens and the "spray pattern" in 14.3%.

Inferior gluteal nerve

The inferior gluteal nerve arises from the dorsal branches of the L5, S1, and S2 ventral rami. It leaves the pelvis via the greater sciatic foramen below the piriformis and divides into branches that enter the deep surface of the gluteus maximus (Williams 2005; Mahadevan 2008). It can also be joined with the nerve to the short head of the biceps femoris. The inferior gluteal nerve frequently provides a communicating branch that joins the posterior femoral cutaneous nerve (Bergman et al. 1984, 1988). The motor branches of the inferior gluteal nerve, after branching from the main trunk, spread in a large area curving medially and dorsally and entering the deep surface of the gluteus maximus (Apaydin et al. 2009a).

Perforating cutaneous nerve

When present, the perforating cutaneous nerve usually arises from the posterior aspects of the S2 and S3 ventral rami. It pierces the sacrotuberous ligament, curves round the inferior border of the gluteus maximus, and supplies the skin over the inferomedial aspect of this muscle. Instead of piercing the sacrotuberous ligament, it sometimes accompanies the pudendal nerve or passes between the ligament and the gluteus maximus. It can arise from the pudendal nerve or be absent, in which case it can be replaced by a branch from either the posterior femoral cutaneous nerve or the third and fourth, or fourth and fifth, sacral ventral rami. It is sometimes joined with the pudendal nerve at its origin. Its prevalence has been reported as 64% (Aasar 1947; Bergman et al. 1984, 1988).

Posterior femoral cutaneous nerve

This is also known as the posterior cutaneous nerve of the thigh. It is not a branch of the sciatic nerve. Its branches are all cutaneous and are distributed to the gluteal region, perineum and the flexor aspect of the thigh and leg. It arises from the dorsal branches of S1, S2, and the ventral branches of S2, S3. It typically leaves the pelvis via the greater sciatic foramen below the piriformis, first medial and then superficial to the sciatic nerve. It descends under the gluteus maximus with the inferior gluteal vessels, lying posterior or medial to the sciatic nerve. It runs down superficial to the long head of the biceps femoris, deep to the fascia lata. It pierces the deep fascia behind the knee and becomes superficial, accompanying the short saphenous vein. Its terminal twigs connect with the sural nerve. Three or four gluteal branches curl around the lower border of the gluteus maximus to supply the skin over the inferolateral portion of the muscle. The perineal branch supplies the superomedial skin in the thigh. It communicates with the inferior rectal and posterior scrotal or labial branches of the perineal nerve, and gives numerous branches to the skin of the back and medial sides of the thigh, the popliteal fossa, and the proximal part of the back of the leg (Williams 2005; Mahadevan 2008).

A number of variations in the course and distribution of this nerve have been reported. It can originate as two trunks from the common fibular and tibial nerves after they separate from the sciatic nerve. In such cases, the ventral trunk accompanies the tibial nerve below the piriformis and provides the perineal and medial femoral branches of the posterior femoral cutaneous nerve. The dorsal trunk accompanies the common peroneal nerve beneath the piriformis and provides the gluteal and femoral branches of the posterior femoral cutaneous nerve. The posterior femoral cutaneous nerve can be joined with a branch from the sciatic nerve. A perineal branch sometimes pierces the sacroiliac ligament. In some cases, the posterior femoral cutaneous ends behind the knee and can be replaced in the leg by a branch from the sural nerve (Bergman et al. 1984,

1988). The communicating branches from the sciatic nerve to the posterior femoral cutaneous nerve can innervate the long head of the biceps femoris (Aasar 1947). Two posterior femoral cutaneous nerves may be present (Huban et al. 2012).

Tubbs et al. (2009) reported the perineal branch of the posterior cutaneous nerve to arise directly from the posterior femoral cutaneous nerve in 55% of sides and from the inferior cluneal nerve in 30%. It was absent in 15%. It was found to pierce the sacrotuberous ligament and give two–three branches to the medial thigh that continued on to the scrotum or labia major. Communications between this branch and the perineal branch of the pudendal nerve were common. Tunali et al. (2011) reported a communicating branch between the posterior femoral cutaneous nerve and the sciatic nerve, 11 cm below the infrapiriform foramen.

Sciatic nerve

This is the largest nerve in the body. It is almost 2 cm wide at its origin near the sacral plexus. It originates from the ventral rami of spinal nerves L4–L5, S1–S3. The greater part of S2 and S3 converge on the inferomedial aspect of the lumbosacral trunk in the greater sciatic foramen to form the sciatic nerve. The ventral and dorsal divisions of the nerve do not separate physically from each other, but their fibers remain separate within the rami. The ventral and dorsal divisions of each contributing root join within the sciatic nerve. The fibers of the dorsal divisions go on to form the common fibular nerve and those of the ventral division form the tibial nerve. The sciatic nerve occasionally divides into common fibular and tibial nerves inside the pelvis. In these cases the common fibular nerve usually runs through the piriformis. The sciatic nerve typically comes out of the pelvis through the greater sciatic foramen, entering the gluteal region anterior to the piriformis muscle. After reaching the lateral aspect of the ischial tuberosity, it turns vertically downward to run between the ischium medially and the greater trochanter laterally. For most of its trajectory in the gluteal region it runs parallel to the midline. Superiorly it lies deep to gluteus maximus, resting first on the posterior ischial surface with the nerve to the quadratus femoris between them. It then crosses posterior to the obturator internus, gemelli and quadratus femoris, separated by the latter from the obturator externus and the hip joint. The posterior femoral cutaneous nerve and the inferior gluteal artery usually accompany it medially. The nerve then enters the thigh behind the adductor magnus and is crossed posteriorly by the long head of the biceps femoris. It corresponds to a line drawn from just medial to the midpoint between the ischial tuberosity and greater trochanter to the apex of the popliteal fossa. It gives articular branches to the posterior aspect of the hip joint. These branches are sometimes derived directly from the sacral plexus. Muscular branches are distributed to the biceps femoris, semitendinosus, semimembranosus, and the ischial part of the adductor magnus.

The sciatic nerve has two main terminal branches: the tibial nerve and the common peroneal (fibular) nerve. The tibial nerve arises from its medial side, being derived from the anterior divisions of the ventral rami of L4–L5, S1–S3, and the common peroneal nerve arises from its lateral side, being derived from the posterior divisions of the ventral rami of L4–L5, S1–S2. However, the point of division of the sciatic nerve into its major components (tibial and common fibular) is very variable. The most common site is at the junction of the middle and lower thirds of the thigh, near the apex of the popliteal fossa, but the division can occur at any level above this point, or more rarely below it. It is also possible for these components to leave the sacral plexus separately, in which case the common fibular component usually passes through the piriformis at the greater sciatic notch while the tibial passes below the muscle (Bergman et al. 1984, 1988, Williams 2005; Mahadevan 2008).

The tibial and common peroneal components can easily be identified as two separate nerves throughout their trajectory in about 11% of cases. However, even in those cases a common sheath of connective tissue surrounds the two components. The sciatic nerve can be readily divided artificially back to the spinal nerves. It is therefore important not to confuse this with a true separation of the components, which generally takes place in the popliteal fossa. Upon entering the popliteal fossa, the two nerve components (peroneal and tibial) finally diverge from each other, having never mixed their fibers. The tibial nerve continues to run posteriorly in the direction of the main trunk, at the center of the popliteal fossa. The common peroneal component turns laterally to run just medial to the biceps tendon.

A number of variations in the course and distribution of the sciatic nerve have been reported. The main variations concern the relationship of the nerve to the piriformis. Beaton and Anson classified variations in the relationship of the sciatic nerve and its subdivisions to the piriformis muscle in 120 specimens in 1937, and in 240 specimens in 1938. Their classification, known as the Beaton & Anson classification, is as follows:

- Type 1: undivided nerve below undivided muscle;
- Type 2: divisions of nerve between and below undivided muscle;
- Type 3: divisions above and below undivided muscle;
- Type 4: undivided nerve between heads;
- Type 5: divisions between and above heads; and
- Type 6: undivided nerve above undivided muscle.

Patel et al. (2011) reported two other types, which were not previously defined by Beaton and Anson. These were a sciatic nerve: (1) already divided in the pelvis, its two divisions traveling out below the piriformis; and (2) already divided in the pelvis, its two divisions leaving the pelvis differently (the common fibular nerve coming out after piercing the piriformis and the tibial nerve coming out below the piriformis). Additionally, Arifoglu et al. (1997) reported a case with a double superior gemellus and double piriformis associated with a high dividing sciatic nerve, which passed between the two piriformis muscles in the same lower extremity. Carare and Goodwin (2008) observed the common peroneal nerve and the tibial nerve to originate independently from the lumbosacral plexus in one

Table 92.3 Incidence of the six types of Beaton and Anson's classification, regarding the anatomical relationship between the piriformis muscle and sciatic nerve.

		Beaton & Anson classification (%)						
Authors	**Number of cases**	**Type I**	**Type II**	**Type III**	**Type IV**	**Type V**	**Type VI**	**Other (%)**
Beaton & Anson (1938)	120 cadavers	84.2	11.7	3.3	0.8	–	–	
Beaton (1938)	240 cadavers	90	7.1	2.1	0.8	–	–	
Pećina (1979)	130 extremities	78.4	20.8	0.8	–	–	–	
Ugrenović et al. (2005)	200 cadavers	96	2.5	1.5	–	–	–	
Patel et al. (2011)	86 extremities	91.8	–	–	–	–	–	8.2
Fishman and Zybert (1992)	918 patients (1014 legs)	85.5	–	–	–	–	–	14.5
Pokorny et al. (2006)	91 extremities	79.1	–	–	14.3	4.4	2.2	14.3
Natsis et al. (2014)	294 extremities	93.6	4.1	0.3½	0.3	–	0.3	1.4

case. Furthermore, in their case, the two roots of the common peroneal nerve joined only at the inferior end of the piriformis muscle, after one of the roots pierced the muscle. The results of recent studies are presented in Table 92.3.

The sacral nerve can bifurcate into its two major divisions (common peroneal and tibial) anywhere between the sacral plexus and the lower part of the thigh. The two terminal branches can arise directly from the sacral plexus (Santanu et al. 2013). The division into terminal branches has been reported to occur below the popliteal space. The nerve to the short head of the biceps femoris sometimes arises directly from the sacral plexus. In one study of 420 limbs, the sciatic nerve passed beneath the piriformis in 87.5%, through it in 12% (peroneal division), and above it in 0.5%. In another study of 138 subjects, the sciatic passed beneath the piriformis in 118 cases (85.5%), the peroneal division passed through it in 17 (12.3%), and the entire sciatic passed through it in 3 (2.2%) (Bergman et al. 1984, 1988). Babinski et al. (2003) described another anatomical variation in which the common fibular nerve passed superior, and the tibial nerve inferior, to the superior gemellus muscle. Pokorny et al. (2006) examined 91 cadavers and found an atypical relationship in 19 cases (20.9%).

Natsis et al. (2014) dissected 294 limbs and noted the typical relationship between the common fibular and tibial nerve in 275 (93.6%), demonstrating four additional variations (1.4%) not described in the Beaton and Anson classification. In one of these, the common fibular nerve passed between the superficial and the deep muscle bellies of a doubled piriformis muscle, while the tibial nerve passed below the muscle. In another, the piriformis muscle had three bellies. The common fibular nerve passed between the superficial and intermediate muscle bellies while the tibial nerve passed through the deep muscle. The other variation presented a bilateral supernumerary muscle located just superior to the piriformis in the suprapiriform foramen. The sciatic nerve ran below the piriformis muscle. Mas et al. (2002) reported a sciatic nerve where the tibial component traveled inferior to the superior gemellus muscle and the common peroneal part left the pelvis below the piriformis muscle.

The sciatic nerve may innervate the gluteus maximus (Huban et al. 2012).

Common fibular (peroneal) nerve

The common fibular nerve (common peroneal nerve) is derived from the dorsal branches of the L4, L5 and S1, S2 ventral rami. It is approximately half the size of the tibial nerve. It descends obliquely along the lateral side of the popliteal fossa to the fibular head, medial to the biceps femoris. It lies between the bicipital tendon and the lateral head of the gastrocnemius. It then passes into the anterolateral compartment of the leg through a tight opening in the thick fascia overlying the tibialis anterior. It curves lateral to the fibular neck, deep to the fibularis longus, and divides into superficial and deep fibular nerves. The course of the common fibular nerve can be indicated by a line drawn from the apex of the popliteal fossa, passing distally, medial to the biceps tendon, to the back of the head of the fibula, where it can be rolled against the bone. In the gluteal region, Santanu et al. (2013) reported the common peroneal part of the sciatic nerve as innervating the gluteus maximus muscle.

It innervates the anterolateral part of the knee joint capsule and the proximal tibiofibular joint via three articular branches. Two of these branches accompany the superior and inferior lateral genicular arteries and can arise together. The third branch is known as the recurrent articular nerve; it arises near the termination of the common fibular nerve. It ascends with the anterior recurrent tibial artery through the tibialis anterior and supplies it. Watt et al. (2014) supported the use of the term "anterior tibial recurrent nerve (ATRN)" for the branch innervating the tibialis anterior and reported four major branching patterns of the common fibular nerve as follows: Type 1, neither the deep fibular nerve nor the ATRN branch before piercing the anterior intermuscular septum; Type 2, the ATRN branches before piercing the anterior intermuscular septum; Type 3, the

deep fibular nerve branches before piercing the anterior intermuscular septum; and Type 4, both the deep fibular nerve and the ATRN branch before piercing the anterior intermuscular septum.

The nerve usually gives off two cutaneous branches, the lateral sural and sural communicating nerves. The lateral sural nerve (lateral cutaneous nerve of the calf) supplies the skin on the anterior, posterior, and lateral surfaces of the proximal leg. The sural communicating nerve arises near the head of the fibula and joins the sural nerve crossing over the lateral head of gastrocnemius. It can descend separately as far as the heel (Bergman et al. 1984, 1988, Williams 2005; Mahadevan 2008). Occasionally, the sural nerve arises purely from the tibial nerve and, even less commonly, it is purely peroneal (lateral sural cutaneous nerve).

The sciatic usually divides into the common peroneal and tibial nerves at the level of the lower thigh. These two nerves usually arise separately from the sacral plexus. They can be separated in the greater sciatic foramen by the piriformis and pass into the thigh as continuous but separate structures. Huelke (1958) examined 198 adult lower extremities and reported that the peroneal communicating nerve arose directly from the common peroneal nerve in 54.7%, usually as a branch separate from the lateral sural cutaneous nerve (41.5%). The peroneal communicating nerve gave rise to the lateral sural cutaneous branches in 13.2% of sides studied. The peroneal communicating nerve was a terminal branch of the lateral sural cutaneous nerve in one-third of the sides, and arose from a trunk common to it and to the lateral sural cutaneous nerve in 12%. The peroneal communicating nerve was absent in 19.7% of the 198 sides, so no sural nerve was formed in these cases. When this occurs, it is usually the medial sural cutaneous nerve that passes on to the dorsum of the foot as the lateral dorsal cutaneous nerve. Only 58.6% of the cadavers had the same type of origin of the peroneal communicating nerve in both legs. There were no significant differences between the right and left sides, between sexes, or the place where the peroneal communicating or sural nerves arose. The union between the peroneal communicating and medial sural cutaneous nerves was seen on 159 sides (80.3%). This union was more often located in the lower half of the leg (75%) (Bergman et al. 1984, 1988).

Deep fibular (peroneal) nerve

This nerve begins at the bifurcation of the common fibular nerve, between the fibula and the proximal part of the fibularis longus. It passes obliquely forwards deep to the extensor digitorum longus to the front of the interosseous membrane. Here, it gives muscular branches to the tibialis anterior, extensor hallucis longus, extensor digitorum longus, and fibularis tertius. In the anterior compartment it accompanies the anterior tibial artery in the proximal third of the leg. It descends with this artery to the ankle, where it divides into lateral and medial terminal branches. As it descends, the nerve is first lateral to the artery, then anterior, and finally lateral again at the ankle. It is usually divided into medial and lateral branches. It also gives an articular branch to the ankle joint. The lateral terminal branch crosses the ankle deep to the extensor digitorum brevis and supplies that muscle. It also gives three very small interosseous branches, which supply the tarsal and metatarsophalangeal joints of the middle three toes. The medial terminal branch runs distally on the dorsum of the foot lateral to the dorsalis pedis artery, and connects with the medial branch of the superficial fibular nerve in the first interosseous space. It divides into two dorsal digital nerves, which supply adjacent sides of the great and second toes. Before dividing it gives off an interosseous branch, which supplies the first metatarsophalangeal joint. The deep fibular nerve can end as three terminal branches instead of two. A number of variations in the digital distribution of the nerve have been reported. It can supply the medial side of the great toe, adjacent sides of the second and third toes, or the lateral three-and-one-half toes. It sometimes has no digital branches at all. Absence of the cutaneous part of the superficial peroneal nerve and the deep peroneal nerve and its branch to the extensor digitorum brevis has been reported. In this case the nerves were replaced by the saphenous and sural nerves (Bergman et al. 1984, 1988).

Superficial fibular (peroneal) nerve

The superficial fibular nerve (SFN or superficial peroneal nerve) begins at the bifurcation of the common fibular nerve. It lies at first deep to the fibularis longus, then passes anteroinferiorly between the fibularis longus and brevis and the extensor digitorum longus and pierces the deep fascia in the distal third of the leg. It divides into a large medial dorsal cutaneous nerve and a smaller, more laterally placed, intermediate dorsal cutaneous nerve, usually after piercing the crural fascia. Sometimes it divides while it is still deep to the fascia. Solomon et al. (2001) reported the superficial fibular nerve to branch into the medial dorsal cutaneous nerve of the foot and the intermediate dorsal cutaneous nerve of the foot before piercing the crural fascia in 24 out of 68 cases (35%). Apaydin et al. (2008a) investigated the compartmental anatomy of the superficial fibular nerve and defined three particular types in its course. In 71% of cases the SFN coursed entirely within the lateral compartment of the leg (Type I). In 23.7% it penetrated the anterior intermuscular septum, 12.7 cm inferior to the apex of the head of fibula, and coursed in the anterior compartment (Type II). In the remaining 5.3% of the specimens the SFN had branches in both the anterior and lateral compartments (Type III). Prakash et al. (2010) examined 60 specimens for the location and course of the superficial fibular nerve and found it was located in the anterior compartment of the leg in 28.3%. In 8.3% it branched before piercing between the fibularis longus and extensor digitorum longus muscles, whereas in 11.7% it branched after piercing them. In 41 out of 60 specimens the sensory division of the superficial peroneal nerve branched into the medial dorsal cutaneous and the intermediate dorsal cutaneous nerve distal to its emergence from the deep fascia.

As the nerve lies between the muscles of the lateral compartment of the leg, it supplies the fibularis longus, fibularis brevis, and the skin of the lower leg. The course, compartmental location, and peripheral digital distribution of the superficial fibular nerve are subject to considerable variation. For example, Browne and Morris (2007) described an adult female cadaver where the superficial fibular nerve bifurcated into two equal-caliber branches 3 cm distal to the fibular head. The two branches remained in the lateral compartment of the leg and passed between the fibularis longus and brevis muscles. The anterior branch pierced the lateral intermuscular septum and then pierced the crural fascia to continue as the medial dorsal cutaneous nerve of the foot. The posterior branch pierced the crural fascia to continue as the intermediate dorsal cutaneous nerve of the foot. Variation in the distribution of the cutaneous nerves of the dorsum of the foot was reported in a series of 229 feet in 1892 by the Committee of Collective Investigation of the Anatomical Society of Great Britain and Ireland: 12 patterns of termination of the dorsal nerves were described, which are known as Kosinski's variants (Kosinski 1926; Solomon et al. 2001). Great variability was described in both the deep course (Kosinski 1926; Von Reinman 1984; Blair and Botte 1994; Benjamin et al. 1995) and the peripheral toe distribution (Brodie et al. 1892; Kosinski 1926) of the sural and superficial fibular nerves. Solomon et al. (2001) described five types additional to Kosinski's variants in their series of 68 feet. Adkinson et al. (1991) reported that 14% of 85 legs had the superficial fibular nerve located in the medial compartment, while in 12% this nerve divided deep to the deep fascia in the lateral compartment and then the medial dorsal cutaneous nerve of the foot passed into the anterior compartment.

Another variant of the superficial fibular nerve with more practical implications in the approach to the lateral malleolus was described by Blair and Botte (1994). These authors reported that in 16% of 25 cases the nerve branched deep and the medial dorsal cutaneous nerve of the foot pierced the fascia anterior to the lateral malleolus, while the intermediate dorsal cutaneous nerve of the foot pierced the fascia posterior to the lateral malleolus and then crossed the bone to follow its course towards the dorsum of the foot.

The medial dorsal cutaneous nerve typically passes in front of the ankle joint and divides into two dorsal digital branches, one of which supplies the medial side of the hallux and the other supplies the adjacent side of the second and third toes. It communicates with the saphenous and deep fibular nerves. The intermediate branch traverses the dorsum of the foot laterally. It divides into dorsal digital branches that supply the contiguous sides of the third to fifth toes and the skin of the lateral aspect of the ankle, where it connects with the sural nerve. Some of the lateral branches of the superficial fibular nerve are frequently absent and are replaced by sural branches (Bergman et al. 1984, 1988, Williams 2005; Mahadevan 2008).

Accessory fibular nerves

An accessory superficial fibular nerve and an accessory deep fibular nerve have been described as variant branches of the superficial fibular nerve; both are probably the products of atypical branching of the main nerve deep to the crural fascia. The accessory deep peroneal nerve was reported to be a common variant branch of the superficial peroneal nerve. It participates in the innervation of the extensor digitorum brevis muscle, which can interfere with the differential diagnosis of peroneal nerve lesions (Tzika et al. 2012). Rayegani et al. (2011) found the accessory deep fibular nerve to be present in 28 out of 230 patients (12%). In another study, Prakash et al. (2010) demonstrated the accessory deep peroneal nerve as an additional branch from the sensory division of the superficial fibular nerve in 20 out of 60 specimens. The course of this nerve lay in the anterior compartment of the leg and then passed deep to the extensor retinaculum and supplied the ankle and the dorsum of the foot. Paraskevas et al. (2013) also reported an accessory superficial fibular nerve, which arose from the superficial fibular nerve 0.89 cm proximal to its penetration of the crural fascia.

Tibial nerve

The tibial nerve is the larger component of the sciatic nerve, and is derived from the anterior divisions of the L4–L5 and S1–S3 ventral rami. It descends along the back of the thigh and popliteal fossa to the distal border of the popliteus. It then passes anterior to the arch of the soleus with the popliteal artery and continues into the leg. In the thigh it is overlapped proximally by the hamstring muscles but it becomes more superficial in the popliteal fossa, where it is lateral to the popliteal vessels. At the level of the knee the tibial nerve becomes superficial to the popliteal vessels and crosses to the medial side of the artery. In the distal popliteal fossa the junction of the two heads of the gastrocnemius overlaps it. In its distal third it is covered only by skin and fasciae, overlapped sometimes by the flexor hallucis longus. It lies on the tibialis posterior for most of its course except distally, where it adjoins the posterior surface of the tibia.

It gives articular branches to the knee joint forming a plexus with a branch from the obturator nerve. The branches that innervate the gastrocnemius, plantaris, soleus, and popliteus arise proximally either independently or by a common trunk. Apaydin et al. (2008b) examined the course and branching pattern of the tibial nerve in the deep posterior compartment of the leg and defined three particular types: Type I (55.6%): separate branches to each of the muscles in the deep posterior compartment of the leg; Type II (30.6%): two main branches of the tibial nerve that provide motor branches; and Type III (13.8%): one main branch, giving rise to separate motor branches to each of the muscles. In 61.1% of their cases, the proximal and distal branches of the tibial nerve innervated the flexor hallucis longus. In 38.9%, this muscle was innervated only by one proximal branch. In all of their cases the tibialis posterior was innervated by both the proximal and distal branches and the flexor digitorum longus was innervated only distally (Apaydin et al. 2008b).

The branch to the flexor hallucis longus accompanies the fibular vessels. It has an interosseous branch that descends near the fibula to reach the distal tibiofibular joint. It also gives off the medial calcaneal nerve, which perforates the flexor retinaculum to supply the skin of the heel and medial side of the sole. The medial calcaneal nerve can have two sets of branches, which reunite to form the rest of the nerve (Aasar 1947).

The tibial nerve ends under the flexor retinaculum by dividing into the medial and lateral plantar nerves. Bareither et al. (1990) dissected 126 human cadaver lower extremities to determine the level of division of the tibial nerve into medial and lateral plantar nerves. They reported a considerable amount of variance in the level of division, documenting a higher incidence of division proximal to the usual description. This is deep to the flexor retinaculum between the calcaneus and medial malleolus.

The medial plantar nerve is the larger terminal division of the tibial nerve. The medial plantar artery accompanies it laterally. It originates under the flexor retinaculum and passes deep to the abductor hallucis. Between the abductor hallucis and flexor digitorum brevis it gives off a medial proper digital nerve to the hallux, and divides near the metatarsal bases into three common plantar digital nerves. Its cutaneous branches pierce the plantar aponeurosis between the abductor hallucis and flexor digitorum brevis to supply the skin of the sole of the foot.

Muscular branches supply the abductor hallucis, flexor digitorum brevis, flexor hallucis brevis, and the first lumbrical. The former two arise near the origin of the nerve and enter the deep surfaces of the muscles. The branch to the flexor hallucis brevis is from the hallucal medial digital nerve, and that to the first lumbrical from the first common plantar digital nerve. Articular branches supply the joints of the tarsus and metatarsus. Three common plantar digital nerves pass between the slips of the plantar aponeurosis, each dividing into two proper digital branches. The first supplies adjacent sides of the hallux and second toe and the second supplies adjacent sides of the second and third toes; the third supplies adjacent sides of the third and fourth toes, and also connects with the lateral plantar nerve. The first gives a branch to the first lumbrical. Each proper digital nerve has cutaneous and articular branches: near the distal phalanges a dorsal branch supplies structures around the nail, and the termination of each nerve supplies the ball of the toe.

The lateral plantar nerve supplies the skin of the fifth toe, the lateral half of the fourth toe, and most of the deep muscles of the foot. It has superficial and deep branches. Before division, it supplies the flexor digitorum accessorius and abductor digiti minimi and gives rise to small branches that pierce the plantar fascia to supply the skin of the lateral part of the sole. The superficial branch splits into two common plantar digital nerves: the lateral supplies the lateral side of the fifth toe, the flexor digiti minimi brevis and the two interossei in the fourth intermetatarsal space; the medial connects with the third common plantar digital branch of the medial plantar nerve and divides into two to supply the adjoining sides of the fourth and fifth toes. The deep branch accompanies the lateral plantar artery deep to the flexor tendons and adductor hallucis and supplies the second to fourth lumbricals, adductor hallucis and all the interossei (except those of the fourth intermetatarsal space). Branches to the second and third lumbricals pass distally deep to the transverse head of the adductor hallucis and curl round its distal border to reach them. The first and second lumbricals can receive branches from both the lateral and medial plantars. The branch of the lateral nerve to the second lumbrical courses forward beneath the transversus (adductor hallucis), then turns backward over the transversus to reach the lumbrical muscle. Cruveilhier (1844) described a branch of the lateral plantar that pierced the transversus to reach the third lumbrical. The lateral nerve rarely provides a branch to the lateral head of the flexor hallucis brevis (Bergman et al. 1984, 1988).

Hallopeau's nerve is a branch of the lateral plantar nerve that supplies the flexor hallucis brevis muscle while also forming an anastomosis with the medial plantar nerve. In a study by Chou et al. (2008) this neural anastomosis was found in 4 out of 26 specimens.

Sural nerve

The sural nerve is typically formed by the union of the lateral and medial sural communicating nerves, which originate from the common fibular and tibial nerves. After its formation, the sural nerve descends between the heads of the gastrocnemius, piercing the deep fascia proximally in the leg. It is not uncommon for the medial sural communicating branch to be joined at a variable level by the lateral sural communicating branch of the common fibular nerve after piercing the deep fascia. The sural nerve descends lateral to the calcaneal tendon, near the short saphenous vein, to the region between the lateral malleolus and the calcaneus, and supplies the posterior and lateral skin of the distal third of the leg. It then passes distal to the lateral malleolus along the lateral side of the foot and little toe, supplying the overlying skin. It connects with the posterior femoral cutaneous nerve in the leg and with the superficial fibular nerve on the dorsum of the foot. The surface marking at the ankle is a line parallel to the calcaneal tendon halfway between the tendon and the lateral malleolus. Its position is variable, however (Webb et al. 2000; Apaydin et al. 2009b). Apaydin et al. (2009b) demonstrated that in 95.5% of their specimens the sural nerve was initially medial to the lateral border of the CT proximally and intersected with the lateral border of the CT at 55% of the mid-tendon line.

Several variations have been reported in the formation and distribution of branches of these nerves. The point of union of the two branches of the sural nerve is subject to wide variation. It can be high in the popliteal space or sometimes there is no union at all. The union can occur 3 cm below the origin of the peroneal communicating nerve. The two branches of the sural nerve can arise 3 cm apart about 10 cm above the knee, and pierce the medial head of the gastrocnemius muscle before joining the peroneal communicating nerve. In some cases the two branches do not rejoin. The sural nerve sometimes supplies the dorsal

Table 92.4 Formation of sural nerve.

Author	Number of cases	Typical sural nerve formation (%)	MSCN as SN (%)	LSCN as SN (%)
Bardeen (1907)	76	59.2	39.4	1.3
Catania (1924)	100	65	29	6
Kosinski (1926)	118	40.2	53.8	6
Andreassi (1931)	144	63.9	34.7	1.4
Ssokolow (1933)	500	52.6	43.8	3.6
Mogi (1938)	180	83.3	16.7	–
P'an (1939)	286	81.5	13.3	5.2
Williams (1954)	257	83.7	16.0	0.4
Huelke (1957)	352	80.7	19.0	0.3
Huelke (1958)	198	80.3	19.2	0.5

Source: Huelke (1958). Reproduced with permission from John Wiley & Sons. MSCN: medial sural cutaneous nerve; LSCN: lateral sural cutaneous nerve; SN: sural nerve.

cutaneous area of the lateral two-and-one-half toes. It can terminate at the lateral border of the foot without providing any digital branches. When the medial sural cutaneous nerve is joined by the peroneal communicating nerve, the combined nerve is termed the sural nerve (Bergman et al. 1984, 1988). The incidence of the sural nerve and the innervation pattern when it is absent were summarized in a table by Huelke (1958) (Table 92.4).

Eid and Hegazi (2011) examined 24 specimens and noted a sural communicating nerve connected with the sural nerve in 87.5%. In 62%, the predominant site of union between these two nerves was in the lower one-third of the leg and ankle region. There were four types of pattern of innervation of the toes by the sural nerve. The predominant pattern was type I (45.8%), where the lateral side of the little toe was supplied by the sural nerve alone. The second most common pattern was type IV (29.2%), where the lateral two-and-a-half toes were supplied by the sural nerve alone (Eid and Hegazi 2011). Madhavi et al. (2005) determined the cutaneous pattern of distribution of the sural nerve on the dorsum of the foot in 260 Indian feet and demonstrated 6 patterns of innervation of the toes. The reported types did not differ from those reported by Kosinski in 1926. There was no association between the innervation pattern and side or sex. Two cases of anomalous innervation of the abductor digiti quinti muscle of the foot via the sural nerve have been described (Ragno and Santoro 1995). Amoiridis et al. (1997) reported motor fibers from the sural nerve innervating the abductor digiti minimi in 13 out of 207 individuals. The sural nerve may have an intramuscular course through the gastrocnemius muscle (Shankar and Veeramani 2008).

Pudendal plexus

This is generally considered a part of the sacral plexus, so its branches are considered to be branches of the sacral plexus. If it is formed as a separate plexus, it generally arises from the ventral rami of S2–S4 and is located on the anterior surface of the piriformis. The sacral visceral and sacral muscular branches are also considered to arise from this plexus. The origins of the nerves forming the pudendal plexus are subject to variations. These variations depend on whether the plexus is prefixed, postfixed, or has usual pattern. The range of variations was extensively defined by Eisler (1892), providing the basis for different classification systems that are still used today (Table 92.5).

Pudendal nerve

The pudendal nerve arises from the ventral divisions of the S2–S4 ventral rami and is formed just above the superior border

Table 92.5 Range of variation of pudendal plexus.

Nerve	Prefixed plexus (high form)	Usual pattern	Postfixed plexus (low form)
Pudendal.	S2, S3	S2, S3, S4	S3, S4
Extreme range of variation			
Pudendal	L5, S1, S2, S3, S4, S5	S1, S2, S3, S4	S2, S3, S4, S5

Source: Eisler (1892).

of the sacrotuberous ligament and the upper fibers of the ischiococcygeus. It leaves the pelvis via the greater sciatic foramen between the piriformis and ischiococcygeus. It enters the gluteal region and crosses the sacrospinous ligament close to its attachment to the ischial spine, medial to the internal pudendal vessels. It accompanies the internal pudendal artery through the lesser sciatic foramen into the pudendal (Alcock's) canal on the lateral wall of the ischio-anal fossa. It travels ventrally through the pudendal canal and in the posterior part of the canal it gives rise to their main branches: the inferior rectal nerve, the perineal nerve, and the dorsal nerve of the penis or clitoris. The inferior rectal nerve was previously known as the hemorrhoidal nerve. It arises from S3, S4, and occasionally S2. It can arise from the sacral plexus directly rather than being one of the aforementioned three terminal branches of the pudendal nerve (Aasar 1947; Hollinshead 1956; Bergman et al. 1984, 1988). Mahakkanukrauh et al. (2005) reported that 15 inferior rectal nerves out of 73 specimens originated independently from S4.

Several variations have been reported in the formation of the pudendal nerve and the course of its branches. Its roots can arise from both the S4 and S5 spinal nerves. Piersol (1916) reported a possible contribution from either the L5 or S1 spinal nerves. The inferior rectal branch can pierce the sacrospinous ligament on its course to the perineum. The lateral superficial perineal branch of the pudendal sometimes pierces the sacrotuberous ligament (Aasar 1947; Bergman et al. 1984, 1988). Yi and Itoh (2010) reported an "accessory pudendal nerve" that originates primarily from the rami of S2, receiving contributions from the adjacent roots of S1 and S3. The accessory nerve had two branches: the main branch supplied the dorsum of the clitoris, and another thin branch joined to supply the area of the posterior femoral cutaneous nerve. Mahakkanukrauh et al. (2005) investigated the branching of the pudendal nerve in relation to the sacrospinous ligament in 73 sides of 37 cadavers and grouped the branching patterns as follows: Type I: one trunk (56.2%); Type II: two trunks (11%); Type III: two trunks, one being an inferior rectal nerve piercing through the sacrospinous ligament (11%); Type IV: two trunks, one being inferior rectal nerve not piercing through the sacrospinous ligament (9.5%); and Type V: three trunks (12.3%).

Sacral visceral branches

Visceral branches, the pelvic splanchnic nerves, arise from the second to fourth sacral ventral rami and innervate the pelvic viscera.

Sacral muscular branches

Several muscular branches arise from the S4 ventral ramus to supply the superior surface of the levator ani and the upper part of the external anal sphincter. The levator ani can be supplied by S2, S3, or S4 spinal nerves. The branches to the levator ani enter the pelvic surface of the muscle while the branch to the external anal sphincter (perineal branch of the S4) reaches the ischio-anal fossa by running either through the ischiococcygeus or between the ischiococcygeus and iliococcygeus. It supplies the skin between the anus and coccyx via its cutaneous branches. The nerve to the external sphincter ani can pass between the coccygeus and levator ani instead of piercing the coccygeus (Bergman et al. 1984, 1988; Williams 2005; Mahadevan 2008).

Coccygeal plexus

The coccygeal plexus is typically formed by the S5 and coccygeal ventral rami and usually receives a small descending branch from S4. It is usually regarded as a subdivision of the pudendal plexus. The S5 ventral ramus emerges from the sacral hiatus, curves around the lateral margin of the sacrum below its cornu, and pierces the ischiococcygeus from below to reach its pelvic surface. Here it is joined by a descending branch of the S4 ventral ramus and the coccygeal ventral ramus, which emerges from the sacral hiatus. The small trunk that is formed in this way is the coccygeal plexus. Anococcygeal nerves arise from it and form a few fine filaments, which pierce the sacrotuberous ligament to supply the adjacent skin (Bergman et al. 1984, 1988; Williams 2005; Mahadevan 2008).

References

Aasar YH. 1947. *Anatomical Anomalies*. Cairo: Fouad I University Press, pp. 92–101.

Adkinson DP, Bosse MJ, Gaccione DR, Gabriel KR. 1991. Anatomical variations in the course of the superficial peroneal nerve. *J Bone Joint Surg* 73A: 112–114.

Akkaya T, Comert A, Kendir S, Acar HI, Gumus H, Tekdemir I, Elhan A. 2008. Detailed anatomy of accessory obturator nerve blockade. *Minerva Anestesiol* 74: 119–122.

Amoiridis G, Schols L, Ameridis N, Przuntek H. 1997. Motor fibers in the sural nerve of humans. *Neurology* 49: 1725–1728.

Andreassı G. 1931. Osservazioni intorno all'origine, comportainento e distribuzione dei riervi cataneo mediale della sura, ranlo anastomotico peoniero e cutaneo laterale del h sura nell'uomo. *Ricerelie di Morfolog* 11: 83–100.

Anloague PA, Huijbregts P. 2009. Anatomical variations of the lumbar plexus: A descriptive anatomy study with proposed clinical implications. *J Man Manip Ther* 17: e107–e114.

Apaydin N, Basarir K, Loukas M, Tubbs RS, Uz A, Kinik H. 2008a. Compartmental anatomy of the superficial fibular nerve with an emphasis on fascial release operations of the leg. *Surg Radiol Anat* 30(1): 47–52.

Apaydin N, Loukas M, Kendir S, Tubbs RS, Jordan R, Tekdemir I, Elhan A. 2008b. The precise localization of distal motor branches of the tibial nerve in the deep posterior compartment of the leg. *Surg Radiol Anat* 30(4): 291–295.

Apaydin N, Bozkurt M, Loukas M, Tubbs RS, Esmer AF. 2009a. The course of the inferior gluteal nerve and surgical landmarks for its localization during posterior approaches to hip. *Surg Radiol Anat* 31(6): 415–418.

Apaydin N, Bozkurt M, Loukas M, Vefali H, Tubbs RS, Esmer AF. 2009b. Relationships of the sural nerve with the calcaneal tendon: an

anatomical study with surgical and clinical implications. *Surg Radiol Anat* 1(10): 775–780.

Apaydin N, Kendir S, Loukas M, Tubbs RS, Bozkurt M. 2013. Surgical anatomy of the superior gluteal nerve and landmarks for its localization during minimally invasive approaches to the hip. *Clin Anat* 26(5): 614–620.

Arifoglu Y, Sürücü HS, Sargon MF, Tanyeli E, Yazar F. 1997. Double superior gemellus together with double piriformis and high division of the sciatic nerve. *Surg Radiol Anat* 19(6): 407–408.

Aung HH, Sakamoto H, Akita K, Sato T. 2001. Anatomical study of the obturator internus, gemelli and quadratus femoris muscles with special reference to their innervation. *Anat Rec* 263(1): 41–52.

Babinski MA, Machado FA, Costa WS. 2003. A rare variation in the high division of the sciatic nerve surrounding the superior gemellus muscle. *Eur J Morphol* 41(1): 41–42.

Bardeen CR. 1907. Development and variations of the nerves and musculature of the inferior extremity and of the neighboring regions of the trunk in man. *Am J Anat* 6: 259–390.

Bardeen CR, Elting AW. 1901. A statistical study of the variations in the formation and position of the lumbosacral plexus in man. *Anat Anz* 19: 124–128, 209–232.

Bareither DJ, Genau JM, Massaro JC. 1990. Variation in the division of the tibial nerve: application to nerve blocks. *J Foot Surg* 29(6): 581–583.

Beaton LE. 1938. The sciatic nerve and piriform muscle: Their interrelationa possible cause of coccgodynia. *J Bone Joint Surgery Am* 20: 686–688.

Beaton LE, Anson BJ. 1938. The relation of the sciatic nerve and its subdivisions to the piriformis muscle. *Anat Rec* 70: 1–5.

Benjamin AC, Tuma Jr P, Grillo MA, Ferreira MC. 1995. Surgical anatomy of the sural nerve. *Revista do Hospital das Clinicas Faculdade de Medicina de Sao Paulo* 50: 25–29.

Bergman RA, Thompson, SA, Afifi AK. 1984. Catalogue of Human Variations. Baltimore and Munich: Urban & Schwarzenberg, pp. 158–161.

Bergman RA, Thompson SA, AWW AK, Saddeh FA. 1988. Compendium of Human Anatomical Variations. Baltimore: Urban and Schwarzenburg, pp. 143–148.

Blair JM, Botte MJ. 1994. Surgical anatomy of the superficial peroneal nerve in the ankle and foot. *Clinical Orthop Rel Res* 305: 229–238.

Brodie G, Shaw EH, Macload P, Harris WA, Fawcett E. 1892. Collective investigation on the distribution of cutaneous nerve of the dorsum of the foot. *J Anat Physiol* 26: 89–90.

Browne JA, Morris MJ. 2007. Variant superficial fibular (peroneal) nerve anatomy in the middle third of the lateral leg. *Clin Anat* 20: 996–997.

Carai A, Fenu G, Sechi E, Crotti FM, Montella A. 2009. Anatomical variability of the lateral femoral cutaneous nerve: Findings from a surgical series. *Clin Anat* 22: 365–370.

Carare RO, Goodwin M. 2008. A unique variation of the sciatic nerve. *Clin Anat* 21(8): 800–801.

Catania V. 1924. Il comporta mento dei nervi cutanei dorsali piede. *Arch Ital Anat Embriol* 21: 295–331.

Chou LB, Choi LE, Ramachandra T, Ma G. 2008. Variation of nerve to flexor hallucis brevis. *Foot Ankle Int* 29(10): 1042–1044.

Cruveilhier J. 1844. *The Anatomy of the Human Body*. Harper & Brothers, New York.

De Ridder VA, de Lange S, Popta JV. 1999. Anatomical variations of the lateral femoral cutaneous nerve and the consequences for surgery. *J Orthop Trauma* 13: 207–211.

Dimitropoulos G, Schaepkens van Riempst J, Schertenleib P. 2011. Anatomical variation of the lateral femoral cutaneous nerve: a case report and review of the literature. *J Plast Reconstr Aesthet Surg* 64(7): 961–962.

Eid EM, Hegazy AM. 2011. Anatomical variations of the human sural nerve and its role in clinical and surgical procedures. *Clin Anat* 24(2): 237–245.

Eisler P. 1892. *Der Plexus lumbosacralis des Menschen*. Berlin: Halle.

Erbil K, Onderoglu S, Basar R. 1998. Unusual branching in lumbar plexus. Case report. *Folia Morphol (Warsz)* 57: 377–381.

Erbil KM, Sargon FM, Sen F, Oztürk H, Taşcioğlu B, Yener N, Ozozan VO. 2002. Examination of the variations of lateral femoral cutaneous nerves: report of two cases. *Anat Sci Int* 77(4): 247–249.

Fishman LM, Zybert PA. 1992. Electrophysiologic evidence of piriformis syndrome. *Arch Phys Med Rehabil* 73: 359–364.

Griffin M. 1891. Some variations of the last dorsal and first lumbar nerves. *J Anat Physiol* 26: 48–55.

Grothaus MC, Holt M, Mekhail AO, Ebraheim NA, Yeasting RA. 2005. Lateral femoral cutaneous nerve: An anatomic study. *Clin Orthop* 437: 164–168.

Hollinshead WH. 1956. *Anatomy for Surgeons. Volume 2. The Thorax, Abdomen and Pelvis*. London: Cassell & Co. Ltd., pp. 636–638.

Honma S, Jun Y, Horiguchi M. 1998. The human gemelli muscles and their nerve supplies. *Kaibogaku Zasshi* 73: 329–335.

Huban TR, Nayak VS, D'Souza AS. 2012. A rare variation in the innervation of the gluteus maximus muscle. A case report. Proceed Anat Assoc Thai 1: 12.

Huelke DF. 1957. A study of the formation of the sural nerve in adult man. *Am J Phys Anthropol* 15: 137–147.

Huelke DF. 1958. Origin of the peroneal communicating nerve in adult man. *Anat Rec* 132: 81–92.

Jacobs LGH, Buxton RA. 1989. The course of the SGN in the lateral approach to the hip. *J Bone Joint Surg (Am)* 71A: 1239–1243.

Jamieson EB. 1903. Some anomalies in nerves arising from the lumbosacral plexus, and a bilaminar musculus pectineus in a foetus; and on variations in the nerve supply in man and in some other mammals. *J Anat Physiol* 37: 266–286.

Jelev L, Shivarov V, Surchev L. 2005. Bilateral variations of the psoas major and the iliacus muscles and presence of an undescribed variant muscle-accessory iliopsoas muscle. *Ann Anat* 187: 281–286.

Katritsis E, Anagnostopoulou S, Papadopoulos N. 1980. Anatomical observations on the accessory obturator nerve (based on 1000 specimens). *Anat Anz* 148(5): 440–445.

Kikuchi T. 1987. A macroscopical observation of the nerves to the pelvic floor muscles, the obturator internus, the quadratus femoris and the gemelli (in Japanese with English abstract). *Sapporo Med J* 56: 319–332.

Kosinski C. 1926. The course, mutual relations and distribution of the cutaneous nerves of the metazonal region of the leg and foot. *J Anat Physiol* 60: 274–297.

Kosiyatrakul A, Nuansalee N, Luenam S, Koonchornboon T, Prachaporn S. 2010. The anatomical variation of the lateral femoral cutaneous nerve in relation to the anterior superior iliac spine and the iliac crest. *Musculosckelet Surg* 94: 17–20.

Lane WA. 1886. Some variations in the human skeleton. *J Anat Physiol* 20: 388–404.

Locher S, Burmeister H, Böhlen T, Eichenberger U, Stoupis C, Moriggl B, Siebenrock K, Curatolo M. 2008. Radiological anatomy of the obturator nerve and its articular branches: basis to develop a method of

radiofrequency denervation for hip joint pain. *Pain Med* 9(3): 291–298.

Madhavi C, Isaac B, Antoniswamy B, Holla SJ. 2005. Anatomical variations of the cutaneous innervation patterns of the sural nerve on the dorsum of the foot. *Clin Anat* 18(3): 206–209.

Mahadevan V. 2008. Pelvic girdle and lower limb. In: Gray's Anatomy, 40th edition. (ed. S Standring). New York: Elsevier, pp. 1327–1429.

Mahakkanukrauh P, Surin P, Vaidhayakarn P. 2005. Anatomical study of the pudendal nerve adjacent to the sacrospinous ligament. *Clin Anat* 18: 200–205.

Matejcík V. 2010. Anatomical variations of lumbosacral plexus. *Surg Radiol Anat* 32: 409–414.

Mas N, Ozeksi P, Ozdemir B, Kapakin S, Sargon MF, Celik HH, Yener N. 2002. A case of bilateral high division of the sciatic nerves, together with a unilateral unusual course of the tibial nerve. *Neuroanatomy* 2: 13–15.

Mischkowski RA, Selabch I, Neugebauer J, Koebke J, Zöller JE. 2006. Lateral femoral cutaneous nerve and iliac crest bone graftsanatomical and clinical considerations. *Int J Oral Maxillofac Surg* 35: 366–372.

Mogi E. 1938. Uber die sensiblen wandennerven bei den Japanischen zmillingen. *Okaj Folia Anat Jap* 16: 229–274.

Natsis K, Totlis T, Konstantinidis GA, Paraskevas G, Piagkou M, Koebke J. 2014. Anatomical variations between the sciatic nerve and the piriformis muscle: a contribution to surgical anatomy in piriformis syndrome. *Surg Radiol Anat* 36(3): 273–280.

P'an M. 1939. Formation of the sural nerve in the Chinese. *Am J Phys Anthrop* 25: 311–321.

Paraskevas GK, Natsis K, Tzika M, Ioannidis O. 2013. Potential entrapment of an accessory superficial peroneal sensory nerve at the lateral malleolar area: a cadaveric case report and review of the literature. *J Foot Ankle Surg* 52: 92–95.

Patel S, Shah M, Vora R, Zalawida A, Rathod SP. 2011. A variation in the high division of the sciatic nevre and its relation with piriformis syndrome. *National J Med Res* 1(2): 27–30.

Paterson AM. 1893. The origin and distribution of nerves to the lower limb. *J Anat Physiol* 28(1): 84–95.

Pećina M. 1979. Contribution to the etiological explanation of the piriformis syndrome. *Acta Anat (Basel)* 105(2): 181–187.

Piersol GA. 1916. Human Anatomy. Philadelphia: Lippincott Company.

Pokorny D, Jahoda D, Veigl D, Pinskerova V, Sonsa A. 2006. Topographic variations of the relationship of the sciatic nerve and the piriformis muscle and its relevance to palsy after total hip arthroplasty. *Surg Radiol Anat* 28: 88–91.

Prakash, Bhardwaj AK, Singh DK, Rajini T, Jayanthi V, Singh G. 2010. Anatomic variations of superficial peroneal nerve: clinical implications of a cadaver study. *Ital J Anat Embryol* 115(3): 223–228.

Ragno M, Santoro L. 1995. Motor fibers in human sural nerve. *Electromyogr Clin Neurophysiol* 35(1): 61–63.

Rayegani SM, Daneshtalab E, Bahrami MH, Eliaspour D, Raeissadat SA, Rezaei S, Babaee M. 2011. Prevalence of accessory deep peroneal nerve in referred patients to an electrodiagnostic medicine clinic. *J Brachial Plex Peripher Nerve Inj* 6(1): 3.

Rosenberger RJ, Loeweneck H, Meyer G. 2000. The cutaneous nerves encountered during laparoscopic repair of inguinal hernia: New anatomical findings for the surgeon. *Surg Endoscop* 14: 731–735.

Santanu B, Pitbaran C, Sudeshna M, Hasi D. 2013. Different neuromuscular variations in the gluteal region. *IJAV* 6: 136–139.

Severeano G. 1904. Du plexus lombaire. *Biblio Anatomique* 12: 299–313.

Shankar N, Veeramani R. 2008. An unusual origin and intramuscular course of the sural nerve: a case report. *Neuroanatomy* 7: 79–82.

Sherrington CS. 1892. Notes on the arrangement of some motor fibers in the lumbosacral plexus. *J Physiol (London)* 13: 621–772.

Sim IW, Webb T. 2004. Anatomy and anaesthesia of the lumbar somatic plexus. *Anaesth Intensive Care* 32: 178–187.

Solomon LB, Ferris L, Tedman R, Henneberg M. 2001. Surgical anatomy of the sural and superficial fibular nerves with an emphasis on the approach to the lateral malleolus. *J Anat* 199: 717–723.

Spratt JD, Logan BM, Abrahams PH. 1996. Variant slips of psoas and iliacus muscles, with splitting of the femoral nerve. *Clin Anat* 9: 401–404.

Ssokolow P. 1933. Zur Anatomie des N. suralis beim Menschen und Affen. *Z Ges Anat* 100: 194–217.

Tubbs RS, Salter EG, Wellons JC III, Blount JP, Oakes WJ. 2005. Anatomical landmarks for the lumbar plexus on the posterior abdominal wall. *J Neurosurg Spine* 2: 335–338.

Tubbs RS, Miller J, Loukas M, Shoja MM, Shokouhi G, Cohen-Gadol AA. 2009. Surgical and anatomical landmarks for the perineal branch of the posterior femoral cutaneous nerve: implications in perineal pain syndromes. Laboratory investigation. *J Neurosurg* 111(2): 332–335.

Tunali S, Cankara N, Albay S. 2011. A rare case of communicating branch between the posterior femoral cutaneous and the sciatic nerves. *Rom J Morphol Embryol* 52(1): 203–205.

Tzika M, Paraskevas GK, Kitsoulis P. 2012. The accessory deep peroneal nerve: a review of the literature. *Foot (Edinb)* 22(3): 232–234.

Ugrenović S, Jovanović I, Krstić V, Stojanović V, Vasović L, Antić S, Pavlović S. 2005. The level of the sciatic nerve division and its relations to the piriform muscle. *Vojnosanit Pregl* 62: 45–49.

Urbanowicz Z. 1981. Connections between the lumbar and the sacral plexus in man. *Folia Morphol (Warsaw)* 40: 271–279.

Urbanowicz Z, Zaluska S. 1969. Formation of the lumbar plexus in man and macaca. *Folia Morphol (Warsaw)* 28: 256–271.

Varricchio P, Pinhal-Enfield G, Melovitz-Vasan C. 2013. Uncommon course of obturator nerve through an osseous tunnel: Clinical relevance. *IJAV* 6: 133–135.

Von Reinman R. 1984. Uberzählige nervi peronei beim menschen. *Accessory peroneal nerves in the human. Anat Anz* 155: 257–267.

Watt T, Hariharan AR, Brzezinski DW, Caird MS, Zeller JL. 2014. Branching patterns and localization of the common fibular (peroneal) nerve: an anatomical basis for planning safe surgical approaches. *Surg Radiol Anat* 36(8): 821–828.

Webb J, Moorjani N, Radford M. 2000. Anatomy of the sural nerve and its relation to the Achilles Tendon. *Foot Ankle Int* 21: 475–477.

Webber RH. 1961. Some variations in the lumbar plexus of nerves in man. *Acta Anat* 44: 336–345.

Williams A. 2005. *Pelvic girdle and lower limb. In: Gray's Anatomy*, 39th edition (ed. S.Standring). New York: Elsevier, pp. 1456–1499.

Williams D. 1954. A study of the human fibular communicating nerve. *Anat Rec* 120: 533–544.

Wilson JT. 1889. Abnormal distribution of the nerve to the quadratus femoris in man, with remarks on its significance. *J Anat Physiol* 23(3): 354–357.

Yasar S, Kaya S, Temiz C, Tehli O, Kural C, Izci Y. 2014. Morphological structure and variations of lumbar plexus in human fetuses. *Clin Anat* 27(3): 383–388.

Yi SQ, Itoh M. 2010. A unique variation of the pudendal nerve. *Clin Anat* 23(8): 907–908.

93 Facial asymmetry

Senem T. Ozdemir[1], Marios Loukas[2] and R. Shane Tubbs[2–4]
[1]Uludag University, Bursa, Turkey
[2]St George's University, School of Medicine, St Georges, Grenada
[3]Seattle Science Foundation, Seattle, Washington, USA
[4]University of Dundee, Dundee, UK

Perfect symmetry in the bilateral features of the body is a theoretical concept that is rarely observed in biology. Mild asymmetries occur in the normal growth and development of the body, including the face (Burke and Healy 1993; Ferrario et al. 1995, 2001; Shaner et al. 2000). Interestingly, the human form is generally, externally symmetrical and internally asymmetrical. However, in normal individuals there are small differences between the dimensions of the left and right halves of the face, which alone do not normally result in an esthetically unpleasing appearance (Ferrario et al. 1995, 2001). The human face is an organ that is unique to an individual with its dental, skeletal, and soft tissue structures and has a harmony and a balance in itself. Facial asymmetry can be defined as simply one side being larger than the other (Smith 2000). Exact measurements of facial asymmetry are necessary to differentiate between patients whose asymmetry is within the normal range for the population. It is therefore important to know the reference values of facial asymmetry in different populations.

Although many investigators have also found asymmetry as a normal facial feature, there is no consensus in the literature regarding the degree, side, and spatial localization of facial asymmetry (Ferrario et al. 1995, 2001; Shaner et al. 2000). Shaner et al. (2000) have pointed out that normal limits of soft tissue asymmetry in the measurements taken from the upper and middle regions of the face did not exceed 5 mm in males and 6 mm in females as a general rule. In the same study, it has been stated that measurements that involved lower regions of the face had a much higher normal variability, with the differences between the two parts being 6 mm or greater. Ferrario et al. (2001) indicated that the differences between the most symmetric and the most asymmetric groups were less than 2.5 mm.

The left side of the face has been found to be more dominant in some studies (Vig and Hewitt 1975; McIntyre and Mossey 2002); in contrast, the right side has been shown to be more dominant in other studies (Farkas and Cheung 1981; Ferrario et al. 1994, 1995, 2001; Shaner et al. 2000). McIntyre and Mossey (2002) evaluated facial asymmetry and found size asymmetry characterized by a wider left side of the face and a shorter vertical dimension on the right side. Ferrario et al. (1994) showed that the right side of the face was larger than the left side.

Different results have been reported to be related to sex and age regarding the dominant part of the face. Smith (2000) stated that while the right side of the face was larger in females than in males, the left sides of the face is larger in males than the females. In another study, where three different age groups were evaluated, maximum normal asymmetry was found slightly more often in females than in males (Ferrario et al. 2001). In their study, they indicated that the right side of the face was greater in size than the left side except for adolescent females. As the growth stage proceeds, right-sided dominance becomes less frequent, whereas left-side dominance becomes more frequent (Haraguchi et al. 2008).

In the literature, significant differences regarding the degree of facial asymmetry between the different regions of the face have been reported. Farkas and Cheung (1981) carried out a study on 308 normal Caucasian children in order to evaluate the degree of subtle asymmetry using anthropometrics. In their study, the most asymmetric part of the face (69.2%) was the upper third. Ferrario et al. (1994) showed that there was a certain degree of soft tissue facial asymmetry both in individuals and in global populations and that this was especially evident in the middle (tragus) and lower (gonion) thirds of the face. Shaner et al. (2000) stated that measurements that involve the tragion and gonion to the mouth and chin regions had a much greater normal variability. According to Ercan et al. (2008), in both sexes the most asymmetric part of the face was the middle third of the face (maxillary bone, zygomatic corner, and lower orbital border). However, asymmetry in the lower facial third, which is seen especially in females, has been accepted as a result of the functional adaptation of this part. In several studies, it has been reported that asymmetry in the lower third

Bergman's Comprehensive Encyclopedia of Human Anatomic Variation, First Edition. Edited by R. Shane Tubbs, Mohammadali M. Shoja and Marios Loukas.
© 2016 John Wiley & Sons, Inc. Published 2016 by John Wiley & Sons, Inc.

of the face was greater than the middle and the upper thirds (Shaner et al. 2000; Haraguchi et al. 2002; Severt and Proffit 1997; Huang et al. 2013). Huang et al. reported that facial asymmetry is more obvious when moving downward on the face. They reported that the maximal asymmetry allowed in the menton and cheilion can be as high as 6.5 mm. Furthermore, Farkas (1994) found that the facial asymmetry that occurs in normal people is lower than 2% for the eye and orbital region, lower than 7% for the nasal region, and approximately 12% for the oral region. Response of functional adaptation to asymmetrical masticatory activity is mentioned in the literature as the main cause of asymmetries in the lower part of the face (Vig and Hewitt 1975).

In recent years, a range of 3D measurements have been suggested for facial asymmetry evaluation and until recently landmark-based methods have dominated the field (Ercan et al. 2008; Ferrario et al. 1994, 2001; Shaner et al. 2000; Huang et al. 2013; Alqattan et al. 2015). Change in the form (size and shape) of organisms and morphometrics can also be defined as the quantitative analysis of biological form. Statistical shape analysis has recently become more important in the medical and biological sciences. Most studies in medicine are related to the examination of geometrical properties of an organ or the organism (Ercan et al. 2012; Sigirli and Ercan 2013). Ercan et al. (2008) used the landmark-based method for facial asymmetry and found that the number of significantly asymmetric linear distances between the two halves of the face was greater in females than in males. In females, 33% (91/280) of distances between the left and right sides of the face demonstrated asymmetry. In this group, 86% (78/91) of asymmetric linear distances were larger on the left side and 14% (13/91) were larger on the right side. Asymmetric linear distances between the two sides of face were found more commonly at the middle third of the face (maxillary bone, zygomatic corner, and lower orbital border) in both sexes. Alqattan et al. (2015) used a landmark-based 3D analysis method, and reported that the lowest asymmetry index was found for the pronasale in males and the highest for the cheilion in females.

As with the cerebral hemispheres, the facial hemi-sides are functionally asymmetric; this is not surprising given the morphogenetic link between the brain and craniofacial appearance. Differential activity of the two hemifaces in relation to the contralateral hemispheres was thought to result in differential muscular development of the two hemifaces, hence facial asymmetry (Smith 2000). The control of the facial musculature is complex, with different patterns of neural innervation present for the upper versus lower face. It depends on the nature of neurological control of the two sides of the face by the two cerebral hemispheres. Mobility of facial expression also exhibits facial asymmetry (Haraguchi et al. 2008). Most studies suggested that the left side of the face is more expressive of emotions: an asymmetry that probably stems from the right hemisphere dominance of emotional expression (Borod et al. 1998; Haraguchi et al. 2002; Nicholls et al. 2004). Such a functional asymmetry in facial expression may have some relationship to the dimensional balance between the left and the right hemiface (Haraguchi et al. 2008).

Differential hemispheric cognitive activity may influence the two sides of the face (Smith 2000). Smith (1998) reported that humanities faculty members were predominantly right-face dominant due to their dominant verbal activity. However, mathematicians and physicists were predominantly left-face dominant due to their visuospatial activities. In addition, Hennessy et al. (2004) indicated that variation in facial shape and asymmetry reflected variation in adult brain function.

References

Alqattan M, Djordjevic J, Zhurov AI, Richmond S. 2015. Comparison between landmark and surface-based three-dimensional analyses of facial asymmetry in adults. *Eur J Orthod* 37(1): 1–12.

Borod JC, Koff E, Yecker S, Santschi C, Schmidt JM. 1998. Facial asymmetry during emotional expression: gender, valence, and measurement technique. *Neuropsychol* 36: 1209–1215.

Burke PH, Healy MJ. 1993. A serial study of normal facial asymmetry in monozygotic twins. *Ann Hum Biol* 20: 527–534.

Ercan I, Ozdemir ST, Etoz A, Sigirli D, Tubbs RS, Loukas M, Guney I. 2008. Facial asymmetry in young healthy subjects evaluated by statistical shape analysis. *J Anat* 213: 663–669.

Ercan I, Ocakoglu G, Sigirli D, Ozkaya G. 2012. Statistical shape analysis of and usage in medical sciences: Review. *Turkiye Klinikleri J Biostat* 4: 27–35.

Farkas LG. 1994. *Anthropometry of the Head and Face*, second edition. New York: Raven Press Ltd.

Farkas LG, Cheung G. 1981. Facial asymmetry in healthy North American caucasians. *Angle Orthodontist* 51: 70–77.

Ferrario VF, Sforza C, Poggio CE, Tartaglia G. 1994. Distance from symmetry: a three-dimensional evaluation of facial asymmetry. *J Oral Maxillofac Surg* 52: 1126–1132.

Ferrario VF, Sforza C, Miani A, Serrao G. 1995. A three-dimensional evaluation of human facial asymmetry. *J Anat* 186: 103–110.

Ferrario VF, Sforza C, Ciusa V, Dellavia C, Tartaglia GM. 2001. The effect of sex and age on facial asymmetry in healthy subjects: a cross-sectional study from adolescence to mid-adulthood. *J Oral Maxillofac Surg* 59: 382–388.

Haraguchi S, Takada K, Yasuda Y. 2002. Facial asymmetry in subjects with skeletal Class III deformity. *Angle Orthod* 72: 28–35.

Haraguchi S, Iguchi Y, Takada K. 2008. Asymmetry of the face in orthodontic patients. *Angle Orthodontist* 78: 421–426.

Hennessy RJ, Lane A, Kinsella A, Larkin C, O'Callaghan E, Waddington JL. 2004. 3D morphometrics of craniofacial dysmorphology reveals sex-specific asymmetries in schizophrenia. *Schizophrenia Res* 67: 261–268.

Huang CS, Liu XQ, Chen YR. 2013. Facial symmetry index in normal young adults. *Orthodontics and Craniofacial Research* 16: 97–104.

McIntyre GT, Mossey PA. 2002. Asymmetry of the parental craniofacial skeleton in orofacial clefting. *J Orthod* 29: 299–305.

Nicholls ME, Ellis BE, Clement JG, Yoshino M. 2004. Detecting hemifacial asymmetries in emotional expression with three-dimensional computerized image analysis. *Proc Biol Sci* 271: 663–668.

Severt TR, Proffit WR. 1997. The prevalence of facial asymmetry in the dentofacial deformities population at the University of North Carolina. *Int J Adult Orthodon Orthognath* 12: 171–176.

Shaner DJ, Peterson AE, Beattie OB, Bamforth JS. 2000. Assessment of soft tissue facial asymmetry in medically normal and syndrome-affected individuals by analysis of landmarks and measurements. *Am J Med Genet* 93: 143–154.

Sigirli D, Ercan I. 2013. Growth and allometry in modern morphometrics: Review. *Turkiye Klinikleri J Biostat* 5: 42–48.

Smith WM. 1998. Hemispheric and facial asymmetry: Faces of Academe. *J Cogn Neurosci* 10: 663–665.

Smith WM. 2000. Hemispheric and facial asymmetry: Gender differences. *Laterality* 5: 251–258.

Vig PS, Hewitt AB. 1975. Asymmetry of the human facial skeleton. *Angle Orthod* 45: 125–129.

Further reading

Baudouin JY, Tiberghien G. 2004. Symmetry, averageness, and feature size in the facial attractiveness of women. *Acta Psychol (Amst)* 117: 313–332.

Burrows AM, Richtsmeier JT, Mooney MP, Smith TD, Losken HW, Siegel MI. 1999. Three-dimensional analysis of craniofacial form in a familial rabbit model of nonsyndromic coronal synostosis using Euclidean distance matrix analysis. *Cleft Palate Craniofac J* 36: 196–206.

Cole TM III, Richtsmeier JT. 1998. A simple method for visualization of influential landmarks when using Euclidean distance matrix analysis. *Am J Phys Anthropol* 107: 273–283.

DeLeon VB. 2007. Fluctuating asymmetry and stress in a medieval Nubian population. *Am J Phys Anthropol* 132: 520–534.

Ferrario VF, Sforza C, Pizzini G, Vogel G. 1993. Sexual dimorphism in the human face assessed by euclidean distance matrix analysis. *J Anat* 183: 593–600.

Hennessy RJ, McLearie S, Kinsella A, Waddington JL. 2006. Facial shape and asymmetry by three-dimensional laser surface scanning covary with cognition in a sexually dimorphic manner. *J Neuropsych Clin Neurosci* 18: 73–80.

Kane AA, DeLeon VB, Valeri C, Becker DB, Richtsmeier JT, Lo LJ. 2007. Preoperative osseous dysmorphology in unilateral complete cleft lip and palate: A quantitative analysis of computed tomography data. *Plast Reconstr Surg* 119: 1295–1301.

Mutsvangwa T, Douglas T. 2007. Morphometric analysis of facial landmark data to characterize the facial phenotype associated with fetal alcohol syndrome. *J Anat* 210: 209–220.

Rossi M, Ribeiro E, Smith R. 2003. Craniofacial asymmetry in development: An anatomical study. *Angle Orthodontist* 73: 381–385.

Sengupta M, Karmakar B. 2007. Genetics of anthropometric asymmetry in an Indian endogamous population: Vaidyas. *Am J Hum Biol* 19: 399–408.

Weinberg SM, Neiswanger K, Richtsmeier JT, Maher BS, Mooney MP, Siegel MI, Marazita ML. 2008. Three-dimensional morphometric analysis of craniofacial shape in the unaffected relatives of individuals with nonsyndromic orofacial clefts: A possible marker for genetic susceptibility. *Am J Med Genet A* 15: 409–420.

Zaidel DW, Cohen JA. 2005. The face, beauty, and symmetry: perceiving asymmetry in beautiful faces. *Intern J Neurosci* 115: 1165–1173.

94 Eyelids, eyelashes, and eyebrows

Candace R. Wooten and Marios Loukas
St George's University, School of Medicine, St Georges, Grenada

The eyelids play an important role in the function of the eyes; they protect the eye by shielding the cornea and controlling the entry of light. Major abnormalities in the structure of the eyelids not only alter the appearance of the eye, they can also alter its function and create significant medical problems. A minor variation in the structure of the eyelid may be an uncommon anomaly or a feature commonly seen in the normal population. For example, Bravo et al. (2013) found that of the 204 patients studied 184 (90.2%) had some degree of lower lid asymmetry. Most (118; 64.13%) presented with the right lower eyelid at a more inferior position than the left, while 66 (35.87%) presented with the right lower eyelid at a higher position than the left, a difference that was highly significant.

Abnormal distance between the eyes: telecanthus

Telecanthus is an increased distance between the inner canthi due to abnormally long medial canthal tendons (Hoyt and Taylor 2013; Kanski and Bowling 2013). This anomaly is often confused with hypertelorism (wide separation of the orbits) (Hoyt and Taylor 2013). There are two classifications: primary and secondary. Primary telecanthus presents with increased distance between the inner canthi, normally spaced outer canthi, and normal interpupillary measurement (Hoyt and Taylor 2013). Secondary telecanthus also presents with increased inner canthi distance, but is associated with ocular hypertelorism (Hoyt and Taylor 2013).

Telecanthus is a common feature in many different syndromes including BPES, the telecanthus-hypospadias syndrome, Waardenburg syndrome, Noonan syndrome, Robinow syndrome, Möbius syndrome, Treacher Collins, Rubinstein-Taybi, Barber-Say syndrome, and Turner syndrome (Stevens and Wilroy 1988; Allen and Rubin 2008; Kanski and Bowling 2011).

The telecanthus-hypospadias syndrome (BBB syndrome, Opitz syndrome, hypertelorism-hypospadias syndrome) is described in the literature as an X-linked condition with examples of possible autosomal dominant inheritance (Stevens and Wilroy 1988). Telecanthus is a defining feature in this syndrome. Additional features include hypospadias, cranial abnormalities, cleft lip/palate, congenital heart defect, and mental retardation (Stevens and Wilroy 1988).

Telecanthus is a prominent feature in Waardenburg's syndrome (WS) type 1 and type 3 (Pingault et al. 2010). This is an autosomal dominant disorder due to a mutation in the PAX3 gene. The term dystopia canthorum (lateral displacement of the inner canthus) is used to describe the appearance of telecanthus present in this syndrome. The main features of the disorder are dystopia canthorum with a broad nasal root, a white forelock, heterochromia irides, and sensorineural hearing loss (Pingault et al. 2010).

Blepharophimosis-ptosis-epicanthus inversus syndrome (BPES) is an autosomal dominant systemic syndrome due to a mutation of the FOXL2 gene (Allen and Rubin 2008). Telecanthus is frequently seen in association with this condition. It presents at birth with narrowed horizontal palpebral aperture, bilateral ptosis, telecanthus, bilateral epicanthus inversus, poorly developed nasal bridge, and hypoplasia of the superior orbital rims (Allen and Rubin 2008; Kanski and Bowling 2011Other associated ocular anomalies are ectropion, euryblepharon, strabismus, microphthalmos, lacrimal drainage apparatus abnormality, and optic disc coloboma (Allen and Rubin 2008). Extraocular features include premature ovarian failure, seen only in Type 1 BPES. Premature ovarian failure is not present in Type 2 BPES (Allen and Rubin 2008).

Major eyelid malformations

Cryptophthalmos

Cryptophthalmos (Greek for "hidden eye") is a congenital absence of the palpebral fissure (Francois 1969). There are three classifications: complete, incomplete, and abortive (Francois 1969). Each form can present as bilateral or unilateral (Howard et al. 1979; Egier et al. 2005).

The most common form of cryptophthalmos is the complete form. The skin of the forehead is continuous with the skin of the

Bergman's Comprehensive Encyclopedia of Human Anatomic Variation, First Edition. Edited by R. Shane Tubbs, Mohammadali M. Shoja and Marios Loukas.
© 2016 John Wiley & Sons, Inc. Published 2016 by John Wiley & Sons, Inc.

cheek, creating a complete absence of lid structures (Stevenson and Hall 2006). Due to a nonexistent conjunctival sac, the posterior aspect of the overlying skin is fused to the cornea. Beneath the skin is a micropthalmic globe. The eyebrows, eyelashes, meibomian glands, lacrimal glands, and lacrimal puncta are either absent or underdeveloped (Stevenson and Hall 2006).

The incomplete (atypical, partial) form presents with an underdeveloped eyelid (Stevenson and Hall 2006). The medial aspects of the upper and lower lids are fused together, but the lateral aspect develops normally (Egier et al. 2005). The conjunctival sac is usually present in this form, and the globe is microphthalmic (Stevenson and Hall 2006).

The abortive form (congenital symblepharon) can present with a malformed upper eyelid and normal lower lid (Hoyt and Taylor 2013). The skin of the forehead fuses onto the upper portion of the cornea and continues over the cornea as an epidermal membrane (Stevenson and Hall 2006). The lower lid forms normally, although the lacrimal punctum may be absent. The globe is usually of normal size (Stevenson and Hall 2006).

A fourth type of cryptophthalmos (autosomal dominant variant) presents with fully formed eyelids complete with accessory structures, but the lid is displaced inferiorly close to the inferior orbital rim (Saal et al. 1992; Stevenson and Hall 2006). The conjunctival sac is underdeveloped and the globe is not visible (Saal et al. 1992). Ocular anomalies associated with this form are micropthalmia, Peter's anomaly, and optic nerve hypoplasia (Egier et al. 2005).

Cryptophthalmos can occur alone (isolated) or in combination with multiple extraocular anomalies (syndromic).

Isolated cryptophthalmos is a very rare occurrence. Although the exact etiology is unknown, isolated cryptopthalmos is believed to be of autosomal recessive inheritance (Thomas et al. 1996). Some rare cases of autosomal dominant inheritance (nonsyndromal cryptophthalmos) have been documented (Saal et al. 1992; Egier et al. 2005). Isolated cryptophthalmos is not accompanied by cognitive impairment or systemic malformations, but other ocular malformations such as micropthalmia, central dimpling overlying the globes, hypoplastic optic nerve, Peter's anomaly, and eyelid coloboma can be observed (Dinno et al. 1974; Saal et al. 1992; Egier et al. 2005).

Cryptophthalmos is commonly observed in patients with the autosomal recessive Fraser's syndrome (cryptophthalmos-syndactyly syndrome, cryptophthalmos syndrome, syndromic cryptophthalmos; Saal et al. 1992). This syndrome has been linked to mutations in the FRAS1 and FRAS2 genes (Hoyt and Taylor 2013). Thomas et al. (1996) divided diagnostic criteria for this syndrome into major and minor criteria. Major criteria include cryptophthalmos, syndactyly, abnormal genitalia, and a family history of siblings with Fraser's syndrome (Thomas et al. 1996). Minor criteria includes congenital malformation of the nose, congenital malformation of the ears, congenital malformation of the larynx, cleft lip and/or palate, skeletal defects, umbilical hernia, renal agenesis, and mental retardation (Thomas et al. 1996). They further proposed that diagnosing Fraser's syndrome required the following: two major criteria, one minor criteria, or one major and four or more minor criteria. The presence of cryptophthalmos is not necessary for the diagnosis of Fraser syndrome (Thomas et al. 1996).

Cryptophthalmos is also associated with a rare disorder known as Manitoba-oculo-trichoanal (MOTA) syndrome (Mitter et al. 2012). It is an autosomal recessive disorder caused by a mutation in the FREM1 gene. Other ocular manifestations include eyelid coloboma and anophthalmia/microphthalmia. It also presents with abnormal hair growth from scalp to eyebrow, bifid or broad nasal tip, and gastrointestinal anomalies including omphalocele and anorectal malformations (Mitter et al. 2012).

Ablepharon

Ablepharon (ablepharia) is the congenital absence of the eyelids (Hoyt and Taylor 2013). This does not present as an isolated event; rather, it is a key feature in multiple syndromes.

Ablepharon-macrostomia syndrome is a rare congenital syndrome with equal occurrence in males and females (Stevens and Sargent 2002). It was previously believed to be of autosomal recessive inheritance, but new cases of possible autosomal dominant inheritance have recently appeared in the literature (Rohena et al. 2011). Ablepharon is a defining characteristic of this syndrome. Other ocular anomalies include microblepharon, corneal opacity, corneal ulceration, and hypertelorism (Stevens and Sargent 2002; Rohena et al. 2011). It also presents with macrostomia, ear anomalies, sparse or absent hair including eyebrows and eyelashes, absent/faint nipples, absent zygomatic arches, camptodactyly, umbilical abnormalities, abnormal genitalia, and redundant skin. Functional impairments include visual impairment, hearing loss, dry skin, growth impairment, and developmental delay (Stevens and Sargent 2002; Rohena et al. 2011).

Neu-Laxova syndrome is a rare congenital syndrome with autosomal recessive inheritance (Manar and Asma 2010). The exact etiology is still unknown, but ablepharon is a common occurrence in this syndrome (Martín et al. 2006). Other ocular anomalies include proptosis with ectropion and hypertelorism (Manning et al. 2004; Manar and Asma 2010). Patients also present with microcephaly, abnormal facial features including flattened nose and malformed ears, shortened neck, ichthyosis, central nervous system (CNS) anomalies, limb deformities, hypoplastic lungs, generalized edema, and marked intrauterine growth restriction (IUGR) (Manning et al. 2004; Manar and Asma 2010).

Microblepharon

Microblepharon is a congenitally shortened vertical length of the eyelids (Jordan et al. 2000). Severe microblepharon may approach true ablepharon and is seen in association with the ablepharon-macrostomia syndrome (see ablepharon) (McCarthy and West 1977).

Microblepharon is associated with multiple ocular malformations including ectropion, absence of the puncta, and tetrastichiasis (Merriam 1988).

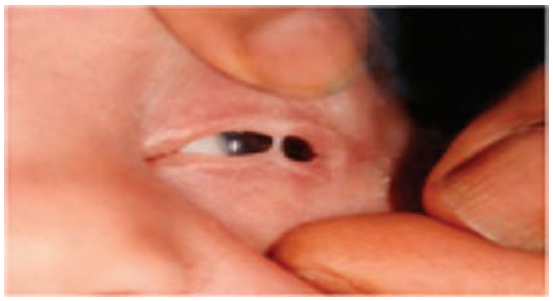

Figure 94.1 Ankyloblepharon in an infant.

Source: Ioannides and Georgakarakos (2011). Reproduced with permission from Macmillan.

Ankyloblepharon

Ankyloblepharon (Fig. 94.1) is defined as partial or complete adhesion of the ciliary margins of the upper and lower eyelids (Hoyt and Taylor 2013). The congenital presentation of this malformation is known as ankyloblepharon filiforme ad natum. It presents as single or multiple thin bands of fibrous tissue connecting the upper and lower eyelids (Hoyt and Taylor 2013). It can present either unilaterally or bilaterally (Ioannides and Georgakarakos 2011; Cizmeci et al. 2013).

Ankyloblepharon filiforme ad natum may appear as an isolated malformation, associated with other malformations, or it may be associated with an ectodermal dysplasia syndrome.

The isolated form of ankyloblepharon is the most common presentation (Ioannides and Georgakarakos 2011). The etiology of this form is currently unknown (Cizmeci et al. 2013). Congenital isolated ankyloblepharon may be more common, but it is important to check for other anatomic malformations. Ophthalmic associations of ankyloblepharon filiforme ad natum include iridogoniodysgenesis with juvenile glaucoma (Scott et al. 1994). Systemic malformations to look for are cleft lip and palate, hydrocephalus, meningomyelocoele, imperforate anus, cardiac defects, and syndactyly (Akkermans and Stern 1979).

Congenital ankyloblepharon is associated with a distinct group of ectodermal dysplasia syndromes. These syndromes of autosomal dominant inheritance belong to a group of disorders characterized by a TP53 gene mutation (Celik et al. 2011). The variant most often associated with congenital ankyloblepharon is called Hay-Wells syndrome (ankyloblepharon-ectodermal dysplasia clefting syndrome or AEC). Ankyloblepharon is a defining feature of this disorder. It commonly presents with cleft lip/palate, hypohidrosis, limb malformations, scalp dermatitis with erosions, alopecia, eczematous changes, coarse wiry hair, and tooth and nail anomalies (Celik et al. 2011). Genitourinary defects, hearing impairment, and mammary anomalies have also been documented. Recent literature on congenital ankyloblepharon links the anomaly with the other variants in this group of TP53 mutations, including ectrodactyly-ectodermal dysplasia-clefting syndrome (EEC) and Rapp-Hodgkin syndrome (RHS) (Clements et al. 2010; Chiu et al. 2011).

A very rare form of ectodermal dysplasia called CHANDS (acronym for curly hair, ankyloblepharon, nail dysplasiais) is of autosomal recessive inheritance (Toriello et al. 1979). Congenital ankyloblepharon filiforme ad natum is a defining feature. Hypoplastic nails and restricted hair growth appear later in life (Toriello et al. 1979).

Congenital ankyloblepharon is also featured in popliteal pterygium syndrome (PPS, popliteal web syndrome, facio-genito-popliteal syndrome) (Ioannides and Georgakarakos 2011). This syndrome was previously believed to be of autosomal dominant inheritance caused by mutations in the IRF6 gene (Akkermans and Stern 1979; Qasim and Shaukat 2012). Recent literature now links it to a lethal autosomal recessive form known as Bartsocas-Papas syndrome (Kalay et al. 2012). Ankyloblepharon appears to be the only ocular anomaly (Qasim and Shaukat 2012). Other features of this syndrome include popliteal pterygia, cleft palate, cleft lip, lower lip pits or sinuses, syndactyly, genitourinary anomalies, nail anomalies, syngnathia, talipes, and digital reduction defects (Qasim and Shaukat 2012).

Although it is not classified as an ectodermal dysplasia syndrome, cases of Edward's syndrome (Trisomy 18) have presented with ankyloblepharon filiforme ad natum (Evans et al. 1990).

Coloboma

Eyelid coloboma is defined as a clefting or notching of the eyelids (Hoyt and Taylor 2013). Colobomas present as a triangular- or quadrilateral-shaped defect at the lid margin (Stevenson and Hall 2006; Hoyt and Taylor 2013). The most common location is the nasal portion of the upper lid (Hoyt and Taylor 2013). When present on the lower lid, the defect is seen on the temporal portion (Stevenson and Hall 2006).

Colobomas can have unilateral and bilateral presentations, as well as multiple colobomas in same lid (Hoyt and Taylor 2013).

Eyelid colobomas can occur as an isolated event, in association with other ocular malformations, or as a part of a systemic syndrome.

The etiology of isolated eyelid colobomas is unknown (Hoyt and Taylor 2013). Isolated eyelid colobomas unrelated to other congenital anomalies is seen in the literature (Adegbehingbe et al. 2005). In other cases, additional ocular malformations are present. These ocular malformations include symblepharon, corneal opacities, iris and retinal colobomas, microphthalmos, and anophthalmos (Shrestha et al. 2012; Hoyt and Taylor 2013).

Eyelid colobomas are associated with multiple defined syndromes. They can be categorized by their involvement with the upper lid, lower lid, or both.

Upper eyelid syndromes

Upper eyelid colobomas are present in two distinct syndromes: Goldenhar's Syndrome and MOTA syndrome. Goldenhar's Syndrome (oculo-auriculo-vertebral dysplasia syndrome) is a craniofacial syndrome with no clear mode of inheritance

(Copel et al. 2012). Ocular anomalies include upper eyelid coloboma, epibulbar dermoids, lipodermoids, and microphthalmia (Copel et al. 2012). Other anomalies include ear malformations, microstomia, macrostomia, cleft palate/lip, mandibular hypoplasia, anomalies of the spine, radial anomalies, and cardiac defects. Functional deficits include visual impairment, hearing loss, and dysphagia (Copel et al. 2012). Manitoba oculotrichoanal (MOTA) syndrome is also associated with eyelid colobomas. It is a rare autosomal recessive disorder linked to mutations in the FREM1 gene (Mitter et al. 2012; Slavotinek et al. 2012). Ocular manifestations include upper eyelid coloboma, cryptophthalmos, anophthalmia/microphthalmia, abnormal hair growth from scalp to eyebrow, bifid or broad nasal tip, and gastroinstestinal anomalies including omphalocele and anorectal malformations (Mitter et al. 2012; Slavotinek et al. 2012).

Lower eyelid syndromes

Colobomas of the lower lid are present in several systemic syndromes: three craniofacial syndromes and two acrofacial syndromes.

Lower lid colobomas are seen in Treacher-Collins syndrome, a craniofacial dysplasia syndrome involving the middle and lower thirds of the face (Neligan 2012; Hoyt and Taylor 2013). The proposed etiology is a mutation in the TCOF1 gene transmitted via autosomal dominant inheritance, but several instances of probable spontaneous mutations are seen in the literature (Hing et al. 2006; Neligan 2012; Hoyt and Taylor 2013). There are several malformations seen with the eyelids including coloboma of the lower lids, antimongoloid obliquity of the palpebral fissures, dystopia of the lateral canthi, shortening of the palpebral fissure, absence of the eyelashes, and notching of eyebrows (Neligan 2012). Malformations of the orbit include absent inferior portion of the lateral wall and inferior migration of the superolateral portion of the frontal bone (Neligan 2012). Other cranial manifestations include hypoplastic or absent malar bone, absent zygomatic arch, narrow and underprojected maxilla, high and narrow palate, hypoplastic mandible, class III malocclusion with anterior open bite, long and protruded chin, protruded nose with a broad base, flattened frontonasal angle, narrow pharynx, microtia, macrostomia, and ear deformities (Neligan 2012).

Lower lid colobomas are also seen in the craniofacial syndrome oculo-oto-facial dysplasia (OOFD). This is a very rare autosomal recessive disorder seen in a geographically isolated Native Alaskan community (Hing et al. 2006). Cranial manifestations include lower eyelid coloboma, malar and mandibular hypoplasia, orofacial clefting, choanal atresia, and external ear malformation with preauricular tags. Extra-cranial findings include atrioseptal defect, renal dysplasia, and imperforate anus (Hing et al. 2006).

Burn-McKeown syndrome is a very rare disorder associated with lower eyelid coloboma. Ocular manifestations include lower lid coloboma and narrow palpable fissures (Malik et al. 2014). Other anomalies include choanal atresia, congenital heart defect, cleft lip, and prominent ears. Hearing loss was also described (Malik et al. 2014).

Lower lid colobomas are also associated with two distinct acrofacial defects (mandibulofacial dysostosis and limb defects): Nager syndrome (preaxial acrofacial dysostosis) and Miller syndrome (postaxial acrofacial dysostosis) (Hing et al. 2006).

Nager syndrome

Nager syndrome involves malformation of the face, limb, and skeleton (Malik et al. 2014). The etiology is unknown, but the mode of inheritance has been linked to both autosomal dominant and autosomal recessive inheritance (Hing et al. 2006). Ocular manifestations of this syndrome include colobomas on the inner aspect of lower eyelids, widely separated downward slanting eyes, absence of eyelashes, and ptosis of the upper eyelids (Malik et al. 2014). It also presents with malformations of the external ear, preauricular skin tags, malar hypoplasia, high nasal bridge, cleft palate/lip, soft palate anomalies, laryngeal defects, and temporomandibular joint fibrosis (McDonald and Gorski 1993). Functional deficits include bilateral conductive hearing loss. Pre-axial limb malformations are seen in both the upper and lower limbs, and skeletal malformations are seen in the axial skeleton (McDonald and Gorski 1993).

Miller syndrome

Miller Syndrome (Genee-Wiedemann syndrome) also involves malformations of the face, limb, and skeleton (Rainger et al. 2012). It is an autosomal recessive mutation of the (DHODH) gene. It presents with ocular manifestations including coloboma of the lower eyelid, aplasia of the medial lower lid eyelashes, and lower eyelid ectropion (Rainger et al. 2012). Other cranial manifestations include micrognathia, orofacial clefts, malar hypoplasia, cleft lip/palate, cup-shaped ears. Limb, gastrointestinal, and cardiac anomalies have also been reported (Hing et al. 2006).

Both upper and lower eyelids

Colobomas of both the upper and lower lids are present in at least two distinct syndromes: amniotic band syndrome and nasopalpebral lipoma-coloboma syndrome.

Amniotic band syndrome (amniotic deformity, adhesions, mutilations (ADAM), complex, amniotic band sequence, congenital constriction bands and pseudoainhum) manifests due to entrapment of fetal parts (usually a limb or digits) in fibrous amniotic bands while in utero (Hollsten and Katowitz 1990). Ocular anomalies such as colobomas, ptosis, and ectropion are seen (Hollsten and Katowitz 1990).

Nasopalpebral lipoma-coloboma syndrome is an extremely rare craniofacial disorder transferred via autosomal dominant inheritance (Chacon-Camacho et al. 2013). Coloboma are seen in the upper and lower eyelids. Other ocular manifestations include upper eyelid and nasopalpebral lipomas, displaced or aplastic lacrimal punctae, persistent epiphora, aberrant eyelashes, conjunctival hyperemia, corneal and lens opacities,

telecanthus, and divergent strabismus (Chacon-Camacho et al. 2013). It also presents with broad forehead, widow's peak, flaring of medial eyebrows, and maxillary hypoplasia (Chacon-Camacho et al. 2013).

Epitarsus

Congenital epitarsus presents as an apron-like fold of conjunctiva attached to the inner surface of the upper lid (Hoyt and Taylor 2013). It occurs primarily in the upper lid, but cases of lower lid epitarsus are recorded in the literature (Khurana et al. 1986).

Congenital epitarsus is extremely rare; it is more often seen as an acquired condition due to conjunctivitis (Nema et al. 1965). There are several presumed etiologies for congenital epitarsus. These include primary congenital deformity of the conjunctiva, adhesions of the amniotic bands to the epithelial covering of the eyeball, and persistence of a hypertrophic plica semilunaris (Khurana et al. 1986).

Palpebral fissures and folds

Epicanthus

Epicanthus (epicanthal fold, eye fold, plica palpebronasalis, palpebronasal fold) is a common variation of the eyelids where bilateral, vertical cutaneous folds extend from the upper or lower lids toward the medial canthi. There are four classifications: palpebralis, tarsalis, inversus, and superciliaris (Kanski and Bowling 2013).

1. Epicanthus palpebralis presents with a vertical cutaneous fold arising from the nasal root and directed toward the internal part of the upper lids (Hoyt and Taylor 2013). The skin folds are equally prominent between the upper and lower lids (Kanski and Bowling 2013). This form is the most common type among those of Caucasian origin.
2. The most common form of epicanthal fold is epicanthus tarsalis (Vaughan et al. 2008). In this form, the cutaneous folds originate in the medial aspect of the upper lids and extend medially before dissipating (Kanski and Bowling 2011). They are most prominent superiorly. This form is the most common type among those of oriental and central Asian origin (Kanski and Bowling 2011).
3. Epicanthus inversus presents with cutaneous folds that begin inferiorly and extend upward to the medial canthal area (Hoyt and Taylor 2013). This form occurs in blepharophimosis syndrome (see section on "Blepharoptosis" below).
4. Epicanthus superciliaris presents with cutaneous folds arising above the brow and extending downward toward the lateral border of the nose (Kanski and Bowling 2011).

The exact etiology of these eyelid variations is not yet established. Lai et al. (2012) noted that a palpable and lengthy medial canthal ligament was present in many cases of epicanthal fold corrective surgery. These patients also presented with an excess of orbicularis muscle and fibrofatty tissues underlying the fold (Lai et al. 2012).

Epicanthal folds are present, to some degree, in children of all races (Vaughan et al. 2008). They are very common in young children with a flat nasal bridge (Hoyt and Taylor 2013).

Epicanthal folds are a common feature in several syndromes including BPES, Down's Syndrome, Zellweger syndrome, fetal alcohol syndrome, Noonan Syndrome, and Turner Syndrome (da Cunha and Moreira 1996; Stromland and Pinazo-Duran 2002; Steinberg et al. 2006; Brunnerova et al. 2007; Allen and Rubin 2008; Demir et al. 2010; Hoyt and Taylor 2013).

Down's Syndrome (Trisomy 21) is a chromosome abnormality that is closely associated with congenital ocular anomalies. Epicanthal folds are one of the most common ocular findings in this syndrome (da Cunha and Moreira 1996). Other ocular anomalies include upward slanting of the palpebral fissure, astigmatism, iris abnormalities, strabismus, lacrimal system obstruction, blepharitis, retinal abnormalities, hyperopia, amblyopia, nystagmus, cataracts, and myopia (da Cunha and Moreira 1996).

Orientation and length of the palpebral fissures

There are several variations in the orientation and length of the palpebral fissures. The literature describes four common variations: upslanted, downslanted, long, and short.

While the lateral canthus is normally 1–2 mm higher than the medial canthus, the normal orientation varies depending on ethnic origin (Vaughan et al. 2008). The palpebral fissures are defined as upslanted when the lateral canthus is positioned higher than usual (Hoyt and Taylor 2013). This variation is associated with several distinct syndromes. One of the most recognizable associations is Down Syndrome (Trisomy 21) (Hoyt and Taylor 2013). Upslanted palpebral fissures are the most common ocular malformation in this syndrome (Hoyt and Taylor 2013).

The palpebral fissures are defined as downslanted when the lateral canthus is positioned lower than usual (Hoyt and Taylor 2013). This variation is associated with hypoplastic malar bones. Many other syndromes also feature this condition. First or second brachial arch malformations, such as Treacher-Collins syndrome, commonly present with downslanted palpebral fissures (Hoyt and Taylor 2013). Other syndromes featuring this malformation are Marfan syndrome, Rubinstein Taybi syndrome, Noonan syndrome, and Coffin Lowry syndrome (Dollfus and Verloes 2004).

The palpebral fissures may vary in length. Euryblepharon is defined as a horizontal enlargement of the palpebral fissure (Kanski and Bowling 2011). This condition presents with an outward and downward displacement of the lateral canthus and a downward displacement of the lower lid (Hoyt and Taylor 2013). Associated ocular findings include lateral displacement of the proximal lacrimal drainage system, a double row of meibomian gland orifices, telecanthus, and strabismus (Kanski and Bowling 2011). Euryblepharon may occur as an isolated event or be associated with a defined syndrome such as Trisomy 21, Kabuki syndrome, and other craniofacial dystosis (Hoyt and Taylor 2013).

Figure 94.2 Distichiasis in two patients.

Source: Patil et al. (2004). Reproduced with permission from Macmillan.

Blepharophimosis refers to a horizontal and vertical shortening of the palpebral aperture (Fig. 94.2) (Tyers 2011). This shortening occurs due to an associated condition known as telecanthus, an increased distance between the medial canthi.

Blepharophimosis can be isolated or part of a syndrome. According to the literature, blepharophimosis is a feature in over 100 syndromes, including BPES, fetal alcohol syndrome, and Ohdo's syndrome (Biesecker 1991; Stromland and Pinazo-Duran 2002; Tyers 2011). Biesecker (1991) further classified these syndromes by identifying a group that included both blepharophimosis and mental retardation.

Fetal alcohol syndrome frequently presents with ocular anomalies. Typical features of this syndrome include blepharophimosis, blepheroptosis, telecanthus, and epicanthus (Stromland and Pinazo-Duran 2002). It is one of the most common causes of blepharophimosis.

A widely documented syndrome featuring this anomaly is blepharophimosis-ptosis-epicanthus inversus syndrome (BPES). It is an autosomal dominant systemic syndrome caused by a mutation in the FOXL2 gene (Allen and Rubin 2008; Kanski and Bowling 2011). It presents at birth with narrowed horizontal palpebral aperture, bilateral ptosis, telecanthus, bilateral epicanthus inversus, poorly developed nasal bridge, and hypoplasia of the superior orbital rims (Allen and Rubin 2008; Kanski and Bowling 2011).

Abnormal position of eyelid

Blepharoptosis

Congenital blepharoptosis ("ptosis") is an abnormally low-lying upper eyelid margin while the eye is in primary gaze (Kanski and Bowling 2011). It presents with reduced movement of the lid on upgaze and lid lag on downgaze (Vaughan et al. 2008). An absent or diminished upper lid crease is seen in the ptotic eye (Kanski and Bowling 2013). In bilateral cases, the patient will compensate by elevating the chin to allow for binocular vision (Hoyt and Taylor 2013; Kanski and Bowling 2013).

Congenital blepharoptosis is most frequently associated with an idiopathic dystrophy of the levator palpebrae superioris muscle (Hou et al. 2013; Hoyt and Taylor 2013; Kanski and Bowling 2013). Other theories propose absent muscle development due to a failure of neuronal migration as the cause behind the ptosis (McMullan and Tyers 2001).

The congenital form of blepharoptosis can be an isolated event, associated with other ocular anomalies, or associated with a syndrome.

Isolated cases of blepharoptosis can present unilaterally or bilaterally (McMullan and Tyers 2001). Several patterns of inheritance for isolated cases are described in the literature, including autosomal recessive and autosomal dominant. McMullan and Tyers (2001) introduced a new case of congenital isolated bilateral ptosis with an X-linked dominant inheritance pattern.

Several ocular defects can coexist with congenital blepharoptosis. These include lagophthalmos, astigmatism, strabismus, epicanthus, or blepharophimosis (Friedman and Keiser 2007). If the ptosis is left untreated, amblyopia often develops (Kanski and Bowling 2011). Vaughan et al. (2008) found that at least 25% of cases of congenital blepharoptosis were associated with superior rectus muscle dystrophy. This presents as a defective upward gaze due to muscle weakness (Hoyt and Taylor 2013).

Congenital blepharoptosis is associated with multiple defined syndromes.

Noonan syndrome is an autosomal dominant congenital disorder that is frequently associated with ocular anomalies. These include eyelid ptosis, hypertelorism, epicanthal folds, proptosis, strabismus, and nystagmus (Demir et al. 2010). Extra ocular malformations include pulmonary artery stenosis, cardiomyopathy, short stature, webbing of the neck, pectus excavatum, and cryptorchidism (Demir et al. 2010; Hoyt and Taylor 2013).

Saethre-Chotzen syndrome (Acrocephalosyndactyly type III) is an autosomal dominant syndrome associated with an asymmetric craniosynostosis (Hoyt and Taylor 2013). Severe ptosis

of the eyelids is just one of several craniofacial anomalies present (Kress et al. 2006). Other features include a low-set frontal hairline, subnormal ear length, dilated parietal foramina, interdigital webbing, and hallux valgus or broad great toe with bifid distal phalanx (Kress et al. 2006). Mental delay and sensorineural hearing loss may also be present (Kress et al. 2006).

Lymphedema-distichiasis syndrome is an autosomal dominant mutation of the FOXC2 gene (Hoyt and Taylor 2013). Defining characteristics include lower limb lymphedema and distichiasis (Fabretto et al. 2010). Eyelid ptosis is not a defining feature, but it is associated with this disorder. Other complications include cardiac defects, varicose veins, cleft palate, spinal extradural cysts, diabetes, and photophobia (Fabretto et al 2010).

Rubinstein-Taybi syndrome (broad thumb-hallux syndrome, Rubinstein syndrome) is an autosomal dominant mutation of the CREBBP gene (Hoyt and Taylor 2013). Key features of this syndrome include growth retardation, skeletal abnormalities, and mental retardation. It involves several facial anomalies, including eyelid ptosis and downward slanting palpebral fissures (Bartholdi et al. 2007; Hoyt and Taylor 2013).

Congenital fibrosis of the extraocular muscles (CFEOM) includes eyelid ptosis and external ophthalmoplegia as its identifying features; McMullan and Tyers 2001). The condition is caused by a congenitally absent central caudal third nerve subnucleus (McMullan and Tyers 2001). This leads to a failure of the superior division of the oculomotor nerve to develop and innervate the levator palpebrae superioris muscle (McMullan and Tyers 2001).

Eyelid ptosis is also associated with the skin disease congenital cutis laxa (Shah-Desai et al. 1999). This rare generalized inherited elastosis frequently exhibits ocular manifestations including excess skin in the eyelids, ptosis, lower lid ectropion, and entropion of the lids (Shah-Desai et al. 1999).

Ectropion

Congenital ectropion of the eyelid is an outward rotation of the eyelid margin (Hoyt and Taylor 2013). When it occurs congenitally, the patient presents at birth with an eversion of the lid along with lid swelling, conjunctival prolapse, and chemosis (Adeoti et al. 2010; Hoyt and Taylor 2013). It may occur in the upper or lower lid, but congenital cases are seen most often in the lower lid (Miletić et al. 2010; Hoyt and Taylor 2013). It is usually present bilaterally, but may appear unilaterally (Adeoti et al. 2010). It is frequently associated with African origin (Maheshwari and Maheshwari 2006).

The congenital form of ectropion can be of two types: the primary type is associated with other eyelid abnormalities; and the secondary type is associated with ocular, orbital, or skin disease (Miller et al. 1988).

An acute presentation of eyelid eversion that presents shortly after birth has been documented (Hoyt and Taylor 2013). It is caused by orbicularis muscle spasms; usually after intense crying spells. The acute form of ectropion is often a self-limiting phenomenon, but some cases require surgical intervention (Hoyt and Taylor 2013).

The exact etiology of congenital ectropion of the eyelids is unknown (Maheshwari and Maheshwari 2006).

Isolated congenital ectropion is a rare anomaly (Hoyt and Taylor 2013). It is more often associated with other ocular anomalies or defined syndromes (Maheshwari and Maheshwari 2006).

The primary form of ectropion is associated with several ocular malformations including a supernumerary rows of lashes, tarsal aplasia and hypoplasia, absence of the Meibomian glands, tight orbital septum, microblepharon, megaloblepharon, euryblepharon, laxity of the lateral canthal ligaments, lateral displacement of the lateral canthus, and partial coloboma of the lower lid (Miller et al. 1988). This form is also associated with several syndromes including mandibulofacial dystosis, blepharophimosis-ptosis-epicanthus inversus syndrome, and Trisomy 21 (Miller et al. 1988).

The secondary form of ectropion is associated with microphthalmos, buphthalmos, orbito-palpebral cysts, and primary skin diseases (Miller et al. 1988). Eyelid ectropion is frequently seen in cases of the skin disease lamellar ichthyoses (collodion babies, harlequin fetus) (Cruz et al. 2000; Hoyt and Taylor 2013). This autosomal recessive disease presents at birth with an inelastic membrane covering the fetus (Cruz et al. 2000). This membrane soon dries, fissures, and develops into large, dark skin scales that cover the entire body (Cruz et al. 2000). The most common eyelid abnormality reported in association with this condition is ectropion of the eyelid (Cruz et al. 2000). Eyelid ectropion is also associated with the skin disease congenital cutis laxa (Shah-Desai et al. 1999). This rare generalized inherited elastosis frequently exhibits ocular manifestations including excess skin in the eyelids, ptosis, lower lid ectropion, and entropion of the lids (Shah-Desai et al. 1999).

Ectropion of the eyelid is also associated with several very rare systemic syndromes. Kabuki syndrome is a rare systemic syndrome associated with eyelid ectropion, due to a mutation in the KMT2D gene (Bögershausen and Wollnik 2013). The prominent features of this disorder are craniofacial anomalies including lower eyelid ectropion, euryblepharon, long palpebral fissures, long dense eyelashes and arched eyebrows, cleft palate, fingertip pads, cardiac defects, urogenital anomalies, growth and developmental delay, feeding problems, and repeated infections (Bögershausen and Wollnik 2013).

Another rare systemic syndrome related to eyelid ectropion is Neu-Laxova syndrome, an autosomal recessive disorder characterized by multiple anomalies including ichthyosis, marked intrauterine growth restriction (IUGR), microcephaly, short neck, central nervous system (CNS) anomalies, limb deformities, hypoplastic lungs, edema, and abnormal facial features including severe proptosis with ectropion, ablepharon, hypertelorism, micrognathia, flattened nose, and malformed ears (Manning et al. 2004; Manar and Asma 2010; Hoyt and Taylor 2013).

Say-Barber syndrome is another very rare condition featuring eyelid ectropion (Dinulos and Pagon 1999). Other features include hypertrichosis, fragile, atrophic skin, eyelid ectropion, and macrostomia (Dinulos and Pagon 1999).

Miller Syndrome (Genee-Wiedemann syndrome) also involves eyelid ectropion (Rainger et al. 2012), an autosomal recessive mutation of the (DHODH) gene. Other ocular manifestations include coloboma of the lower eyelid and aplasia of the medial lower lid eyelashes. Extraocular manifestations include micrognathia, orofacial clefts, malar hypoplasia, cleft lip/palate, cup-shaped ears, limb, gastrointestinal, and cardiac anomalies (Hing et al. 2006; Rainger et al. 2012).

Entropion

Congenital entropion of the eyelid is an inward rotation of the eyelid margin (Hoyt and Taylor 2013). Both upper and lower lids can be involved, but inversion of the lower lid is more common (Fig. 94.3; Hoyt and Taylor 2013). The congenital form is very rare, and it more commonly presents as an acquired condition (Tost 2013). Congenital entropion has a high prevalence among those of Oriental origin (Nakauchi and Mimura 2012).

Congenital tarsal kink is a rare form of upper eyelid entropion caused by a horizontal kink in the upper tarsal plate, leading to inward rotation of the eyelid margin (Naik et al. 2007). It is seen both unilaterally and bilaterally. The literature shows this malformation presenting at birth, although one case presented as late as 44 weeks of age (Naik et al. 2007).

When evaluating a patient with suspected entropion, the diagnosis must be distinguished from other ocular anomalies. Congenital entropion is often mistaken for the less severe, more common epiblepharon. It is important to distinguish between these anomalies as congenital entropion requires immediate surgical intervention to prevent corneal ulceration (Soylev et al. 2005; Hoyt and Taylor 2013). Congenital retraction of the eyelid, trichiasis, and distichiasis may also simulate congenital entropion (Maman and Taub 2011).

Figure 94.3 Entropion in a child.

Source: Awan et al. (2009). Reproduced with permission from Macmillan.

The exact etiology of congenital entropion of the lids is unknown (Hoyt and Taylor 2013). It is proposed that the tarsal plate loses its upright position and becomes inverted (Soylev et al. 2005). Other theories include hypertrophy of the marginal portion of the orbicularis muscle and anomalous insertion of the levator muscle on the tarsal plate (Zak 1984; Hoyt and Taylor 2013).

Microphthalmos and enophthalmos are ocular malformations that have a close association with entropion. It has been proposed that these anomalies create a lack of support of the posterior border of the eyelid, causing the eyelid to easily invert at the margin (Hoyt and Taylor 2013).

The literature also links congenital entropion of the lids to several systemic anomalies. These include cardiovascular, musculoskeletal, and central nervous system anomalies (Zak 1984; Hiles and Wilder 1969). There are also cases of entropion in patients with delays in mental development (Hiles and Wilder 1969). Eyelid entropion is also associated with the skin disease congenital cutis laxa (Shah-Desai et al. 1999). This rare generalized inherited elastosis frequently exhibits ocular manifestations including excess skin in the eyelids, ptosis, lower lid ectropion, and entropion of the lids (Shah-Desai et al. 1999).

Retracted lid

Congenital eyelid retraction presents in a newborn with the resting position of the upper lid above the superior limbus or the resting position of the lower lid resting below the inferior limbus. Congenital cases usually involve the upper lid (Hoyt and Taylor 2013).

The etiology of congenital eyelid retraction is currently unknown, but several theories are proposed in the literature (Hoyt and Taylor 2013). They include an increase in the number and size of the levator muscle fibers, thickened or shortened levator aponeurosis, and thickened or shortened orbital septum (Hoyt and Taylor 2013). Its presentation in preterm infants has been attributed to an immature myelination of vertical eye movement systems and immaturity of extrageniculocalcarine visual pathways (Bartley 1995).

Congenital retraction of the lid can present as a benign, isolated event, but the most common cause of lid retraction is an underlying systemic disease such as thyroid disease, dorsal midbrain syndrome, or hydrocephalus (Collin et al. 1990; Bartley 1995; Spierer and Bourla 2004; Maman and Taub 2011).

Epiblepharon

Epiblepharon is a congenital anomaly in which the pretarsal orbicularis muscle and excess skin covering the lid overrides the lid margin (Katowitz and Katowitz 2009; Kanski and Bowling 2013). The lashes are tilted in a vertical direction and are pressed inward, against the globe. (Katowitz and Katowitz 2009). When the extra skin is pulled down, the lashes turn out away from the globe and the lid resumes a normal position (Kanski and Bowling 2011). It can be observed in the upper or lower lids, but it is more commonly seen in the lower eyelid. When observed

in the upper lid, it is commonly confused with ptosis of the lid (Katowitz and Katowitz 2009).

When evaluating a patient with suspected epiblepharon, the diagnosis must be distinguished from other ocular anomalies. Congenital entropion is often mistaken for the less severe epiblepharon, a more common malformation (Soylev et al. 2005; Hoyt and Taylor 2013). It is important to distinguish between these anomalies as congenital entropion requires immediate surgical intervention to prevent corneal ulceration (Soylev et al. 2005; Hoyt and Taylor 2013). Epiblepharon usually resolves within the first two years of life as the facial bones grow and mature. Surgery is rarely indicated (Hoyt and Taylor 2013).

There are several proposals behind the etiology of congenital lower lid epiblepharon (Kakizaki et al. 2013). One theory attributes this anomaly to a hypertrophied orbicularis oculi muscle. Kakizaki et al. (2013) proposed that an overriding of a normal-sized orbicularis oculi muscle causes lower lid epiblepharon. Upper eyelid epiblepharon is likely due to the effect of gravity on the eyelid skin.

Congenital epiblepharon is frequently associated with Asian origin (Katowitz and Katowitz 2009). The condition is usually not related to other eyelid abnormalities (Sung et al 2010). Sung et al. (2010) described one rare occurrence of congenital epiblepharon associated with congenital eyelid retraction.

Meibomian glands

There may be 30–40 Meibomina glands in the upper lid and 20–30 in the lower lid, which open directly into the inner margin of the eyelids.

Eyelashes and eyebrows

Absent eyelashes/eyebrows

Absent/sparse eyebrows and eyelashes can occur as an isolated condition or associated with other anomalies (Hoyt and Taylor 2013). Absence of the eyebrows and eyelashes is also featured in several syndromes, including alopecia universalis congenital, GAPO syndrome, Setleis' syndrome, Parry-Romberg syndrome, Nager syndrome, and many ectodermal dysplastic syndromes such as EEC syndrome (Hoyt and Taylor 2013; Malik et al. 2014).

Alopecia universalis congenital (congenital atrichia, universal alopecia) is the complete absence of hair on the body (Nöthen et al. 1998). This universal absence of hair at birth is linked to an autosomal recessive mode of inheritance, and eyelashes and eyebrows are absent in these cases (Nöthen et al. 1998).

White eyelashes/eyebrows

Depigmented eyelashes and eyebrows are seen in association with two distinct conditions: oculocutaneous albinism and poliosis (Hoyt and Taylor 2013). Oculocutaneous albinism is a group of autosomal recessive conditions caused by a defect in melanin synthesis that affects the skin, eyes, ears, and hair (Calonje et al. 2012). Poliosis is defined as white brows or lashes in an otherwise normally pigmented individual (Hoyt and Taylor 2013).

Ectopic eyelashes

Distichia is a congenital condition featuring ectopic cilia on the upper eyelid. These accessory rows of eyelashes emerge at or behind the meibomian gland orifices (Kanski and Bowling 2013). Distichia is seen as an isolated event or associated with a syndrome.

Lymphedema-distichiasis syndrome is an autosomal dominant mutation of the FOXC2 gene (Hoyt and Taylor 2013). Defining characteristics include lower limb lymphedema and distichiasis (Fabretto et al. 2010). Other complications include cardiac defects, varicose veins, cleft palate, spinal extradural cysts, diabetes, eyelid ptosis, and photophobia (Fabretto et al 2010).

Setleis' syndrome (focal facial dermal dysplasia) is an autosomal recessive mutation of the TWIST2 gene (Tukel et al. 2010). Distichia is a common feature in this disorder (Hoyt and Taylor 2013). Other features include absent eyelashes, coarse facial features, and bilateral temporal skin defects resembling forceps marks (Hoyt and Taylor 2013).

Thick eyelashes

Trichomegaly is defined as an increased length, thickness, and pigmentation of the eyelashes (Paul et al. 2012). The congenital form of this condition can present as a benign familial trait; although this is very rare (Paul et al. 2012). Trichomegaly is most often seen in association with a syndrome. It is a defining feature of Oliver-McFarlane syndrome and Cornelia de Lange syndrome (Paul et al. 2012). Trichomegaly is also seen in many rare conditions including Hermansky-Pudlak syndrome, Aghaei-Dastgheib syndrome, cone-rod dystrophy, Goldstein-Hutt syndrome, Phylloid hypomelanosis, and cases of congenital heart disease (Paul et al. 2012).

Thick eyebrows

Heavy and thick eyebrows occur in several metabolic disorders. These disorders, such as mucopolysaccharidoses, mucolipidoses, and fucosidosis, are often associated with coarse facial features (Hoyt and Taylor 2013).

Rubinstein-Taybi syndrome also features thickened, arched eyebrows. Other ocular features include prominent eyelashes, down-slanting palpebral fissures, and eyelid ptosis (Hoyt and Taylor 2013).

Synophrys is a distinct condition affecting both the thickness and position of the eyebrows. It presents with the two eyebrows meeting in the midline. Synophrys can occur in association with a defined syndrome, but it is also a common feature in naturally hairy persons (Hoyt and Taylor 2013). It is a distinct feature in Cornelia de Lange syndrome, Waardenburg's syndrome, and other facial malformation syndromes (Mehta et al. 2004; Hei et al. 2012; Hoyt and Taylor 2013).

Cornelia de Lange syndrome (CdLS) is a disorder of unknown etiology. The main facial features in this condition are synophrys, thickened, long and curved eyelashes, and long prominent philtrum (Hei et al. 2012). Also seen are multi-system malformations including growth and developmental retardation, esophagogastric reflex, and hypophalangism (Hei et al. 2012).

References

Adegbehingbe BO, Olabanji JK, Adeoye AO. 2005. Isolated bilateral upper lid coloboma: a case report. *Niger J Med* 14: 224–226.

Adeoti C, Ashaye A, Isawumi M, Raji R. 2010. Non-surgical management of congenital eversion of the eyelids. *J Ophthalmic Vis Res* 5: 188–192.

Akkermans CH, Stern LM. 1979. Ankyloblepharon filiforme adnatum. *Br J Ophthalmol* 63: 129–131.

Allen C, Rubin P. 2008. Blepharophimosis-ptosis-epicanthus inversus syndrome (BPES): clinical manifestation and treatment. *Int Opht Clin* 48: 15.

Awan MA, Chadha V, Gonzalez P, Diaper CJ, Cauchi P, Kemp EG. 2009. Small tarsal plates causing recurrent lower lid entropion in a young adult. *Eye* 23(11): 2129–2130.

Bartholdi D, Roelfsema JH, Papadia F, Breuning MH, Niedrist D, Hennekam RC, Schinzel A, Peters DJ. 2007. Genetic heterogeneity in Rubinstein–Taybi syndrome: delineation of the phenotype of the first patients carrying mutations in EP300. *J Med Genet* 44: 327–333.

Bartley GB. 1995. The differential diagnosis and classification of eyelid retraction. *Trans Am Ophthalmol Soc* 93: 371–389.

Biesecker LG. 1991. The Ohdo blepharophimosis syndrome: a third case. *J Med Genet* 28: 131–134.

Bögershausen N, Wollnik B. 2013. Unmasking Kabuki syndrome. *Clin Genet* 83: 201–211.

Bravo FG, Kufeke M, Pascual D. 2013. Incidence of lower eyelid asymmetry: an anthropometric analysis of 204 patients. *Aesthet Surg* 33(6): 783–788.

Brunnerova R, Lebl J, Krasny J, Pruhova S. 2007. Ocular manifestations in Turner's Syndrome. *Cesk Slov Oftalmol* 63: 176–184.

Calonje E, Brenn T, Lazar A. 2012. Disorders of pigmentation. In *McKee's Pathology of the Skin*, Fourth Edition (eds JE Calonje, T Brenn, AJ Lazar, PH McKee). China: Elsevier Saunders, pp. 912–934.

Celik TH, Buyukcam A, Simsek–Kiper PO, Utine GE, Ersoy-Evans S, Korkmaz A, Yntema HG, Bodugroglu K, Yurdakok M. 2011. A newborn with overlapping features of AEC and EEC syndromes. *Am J Med Genet Part A* 155: 3100–3103.

Chacon-Camacho OF, Lopez-Martinez MS, Vázquez J, Nava-Castañeda A, Martin-Biasotti F, Piña-Aguilar RE, Iñiguez-Soto M, Acosta-García J, Zenteno JC. 2013. Nasopalpebral Lipoma-Coloboma syndrome: Clinical, radiological, and histopathological description of a novel sporadic case. *Am J Med Genet* 161A: 1470.

Chiu YE, Drolet BA, Duffy KJ, Holland KE. 2011. A case of ankyloblepharon, ectodermal dysplasia, and cleft lip/palate syndrome with ectrodactyly: are the p63 syndromes distinct after all? *Pediatr Dermatol* 28: 15.

Cizmeci MN, Kanburoglu MK, Akelma AZ. 2013. Stitched eye in the newborn: ankyloblepharon filiforme adnatum. *J Pediatr* 162: 211–212.

Clements SE, Techanukul T, Holden ST, Mellerio JE, Dorkins H, Escande F, McGrath JA. 2010. Rapp-Hodgkin and Hay-Wells ectodermal dysplasia syndromes represent a variable spectrum of the same genetic disorder. *Br J Dermatol* 163: 624–629.

Collin JR, Allen L, Castronuovo S. 1990. Congenital eyelid retraction. *Br J Ophthalmol* 74: 542–544.

Copel J, D'Alton M, Gratacós E, Platt L, Tutschek B, Feltovich H, Odibo A. 2012. Syndromes. In *Obstetric Imaging* (ed. J Copel). Philadelphia: Elsevier Saunders, pp. 600–603.

Cruz A, Menezes F, Chaves R, Coelho RP, Velasco E, Kikuta H. 2000. Eyelid abnormalities in lamellar ichthyoses. *Ophthalmology* 107: 1895–1898.

da Cunha RP, Moreira JB. 1996. Ocular findings in Down's syndrome. *Am J Ophthalmol* 122: 236–244.

Demir K, Yntema H, Altincik A, Böber E. 2010. A mother and son with Noonan syndrome resulting from a PTPN11 mutation: first report of molecularly proven cases from Turkey. *Turk J Pediatr* 52: 321.

Dinno, ND, Edwards WC, Weiskopf B. 1974. The Cryptophthalmos-syndactyly syndrome. Description, manner of inheritance, and notes on the eye lesions. *Clin Pediatr* 13: 219.

Dinulos MB, Pagon RA. 1999. Autosomal dominant inheritance of Barber-Say syndrome. *Am J Med Genet* 86: 54–56.

Dollfus H, Verloes A. 2004. Dysmorphology and the orbital region: a practical clinical approach. *Surv Ophthalmol* 49: 547–561.

Egier D, Orton R, Allen L, Siu VM. 2005. Bilateral Complete isolated cryptopthalmos, a case report. *Ophthal Genet* 26: 185–189.

Evans DG, Evans ID, Donnai D, Lindenbaum RH. 1990. Ankyloblepharon filiforme adnatum in trisomy 18 Edwards syndrome. *J Med Genet* 27: 720–721.

Fabretto A, Shardlow A, Faletra F, Lepore L, Hladnik U, Gasparini P. 2010. A case of lymphedema-distichiasis syndrome carrying a new de novo frameshift FOXC2 mutation. *Ophthal Genet* 31: 98–100.

Francois J. 1969. Syndrome malformatif avec cryptophtalmie. *Acta Genet Med Gemellol* 18: 18–50.

Friedman N, Kaiser P. 2007. Lids and adnexa. In *Essentials of Ophthalmology* (eds N Friedman, P Kaiser). China: Elsevier Saunders, pp. 125–147.

Hei MY, Chen J, Wu LQ, Yu B, Tan YJ, Zhao LL. 2012. Cornelia de Lange syndrome: report of a case and the review of literature on 17 cases. *Zhonghua Er Ke Za Zhi* 50: 606–611.

Hiles DA, Wilder LW. 1969. Congenital entropion of the upper lids. *J Pediatr Ophthalmol Strabismus* 6: 157.

Hing A, LeBlond C, Sze R, Starr J, Monks S, Parisi M. 2006. A novel oculo-oto-facial dysplasia in a native Alaskan community with autosomal recessive inheritance. *Am J Med Genet* 140A: 804–812.

Hollsten DA, Katowitz JA. 1990. The ophthalmic manifestations and treatment of the amniotic band syndrome. *Ophthal Plast Reconstr Surg* 6: 1–15.

Hou D, Li G, Fang L, Li B. 2013. Frontalis muscle flap suspension for the correction of congenital blepharoptosis in early age children. PLoS One 8: e53185.

Howard RO, Fineman RM, Anderson B Jr., Moseley N, Gilman M, Rothman S. 1979. Unilateral cryptophthalmia. *Am J Ophthalmo* 87: 556–560.

Hoyt C, Taylor D. 2013. Developmental anomalies of the lids. In *Pediatric Ophthalmology and Strabismus: Expert Consult – Online and Print*, Fourth Edition (eds C Hoyt, D Taylor). London, New York: Elsevier Limited, pp. 147–164.

Ioannides A, Georgakarakos ND. 2011. Management of ankyloblepharon filiforme adnatum. *Eye* 25: 823.

Jordan DR, Hwang IP, Pashby R. 2000. Microblepharon: a case report. *Ophthalmic Surg Lasers* 31: 502–505.

Kakizaki H, Takahashi Y, Kang H, Ikeda H, Iwaki M, Selva D, Leibovitch I. 2013. No histological evidence of orbicularis oculi muscle hypertrophy in congenital epiblepharon. *Clin Exp Ophthalmol* 41: 167.

Kalay E, Sezgin O, Chellappa V, Mutlu M, Morsy H, Kayserili H, Kreiger E, Cansu A, Toraman B, Abdalla EM, Aslan Y, Pillai S, Akarsu NA. 2012. Mutations in RIPK4 cause the autosomal-recessive form of popliteal pterygium syndrome. *Am J Hum Genet* 90: 76–85.

Kanski J, Bowling B. 2011. Eyelids. In *Clinical Ophthalmology: A Systematic Approach*, Seventh Edition (eds J Kanski, B Bowling). China: Elsevier Saunders, pp. 1–63.

Kanski J, Bowling B. 2013. Eyelids. In *Synopsis of Clinical Ophthalmology*, Third Edition (eds J Kanski, B Bowling). China: Elsevier Saunders, pp. 1–31.

Katowitz WR, Katowitz JA. 2009. Congenital and developmental eyelid abnormalities. *Plast Reconstr Surg* 124: 93e–105e.

Khurana AK, Ahluwalia BK, Mehtani VG. 1986. Primary epitarsus: a case report. *Br J Ophthalmol* 70: 931–932.

Kress W, Schropp C, Lieb G, Petersen B, Büsse-Ratzka M, Kunz J, Reinhart E, Schäfer WD, Sold J, Hoppe F, Pahnke J, Trusen A, Sörensen N, Krauss J, Collmann H. 2006. Saethre-Chotzen syndrome caused by TWIST 1 gene mutations: functional differentiation from Muenke coronal synostosis syndrome. *Eur J Hum Genet* 14: 39–48.

Lai CS, Lai CH, Wu YC, Chang KP, Lee SS, Lin SD. 2012. Medial epicanthoplasty based on anatomic variations. *J Plast Reconstr Aesthet Surg* 65: 1182.

Maheshwari R, Maheshwari S. 2006. Congenital eversion of upper eyelids: Case report and management. *Indian J Ophthalmol* 54: 203–204.

Malik R, Goel S, Aggarwal S. 2014. Limbal dermoid in Nager syndrome acrofacial dysostosis: A rare case report. *Indian J Ophthalmol* 62(3): 339–341.

Maman D, Taub P. 2011. Congenital entropion. *Ann Plast Surg* 66: 351–353.

Manar AL, Asma B. 2010. Neu-Laxova syndrome: A new patient with detailed antenatal and post natal findings. *Am J Med Genet* 152A: 3193–3196.

Manning MA, Cunniff CM, Colby CE, El-Sayed YY, Hoyme HE. 2004. Neu-Laxova syndrome: detailed prenatal diagnostic and post-mortem findings and literature review. *Am J Med Genet* 125A: 240–249.

Martín A, Eguiluz I, Barber MA, Medina N, Plasencia W, García-Alix A, García-Hernández JA. 2006. A rare cause of polyhydramnios: Neu-Laxova. *J Matern Fetal Neonatal Med* 19: 439–442.

McCarthy GT, West CM. 1977. Ablepharon-macrostomia syndrome. *Dev Med Child Neurol* 19: 659–672.

McDonald MT, Gorski JL. 1993. Nager acrofacial dysostosis. *J Med Genet* 30: 779–782.

McMullan TFW, Tyers AG. 2001. X-linked dominant congenital isolated bilateral ptosis: the definition and characterisation of a new condition. *Br J Ophthalmol* 85: 70–73.

Mehta M,Kavadu P, Chougule S. 2004. Waardenburg syndrome. *Indian J Otolaryngol Head Neck Surg* 56: 300–302.

Miletić D, Elabjer BK, Bosnar D, Busić M. 2010. Our approach to operative treatment of lower lid ectropion. *Acta Clin Croat* 49: 283–287.

Miller R, Martin F, Allen H. 1988. A case of congenital ectropion in Down's syndrome. *Aust N Z J Ophthalmol* 16: 119.

Mitter D, Schanze D, Sterker I, Muller D, Till H, Zenker M. 2012. MOTA Syndrome: molecular genetic confirmation of the diagnosis in a newborn with previously unreported clinical features. *Mol Syndromol* 3: 136–139.

Morax S, Gatinel D. 1996. Primary congenital ectropion. Apropos of 2 cases. *J Fr Ophtalmol* 19: 415–422.

Naik M, Honavar S, Bhaduri A, Linberg J. 2007. Congenital horizontal tarsal kink : a single-center experience with 6 cases. *Ophthalmology* 114: 1564–1568.

Nakauchi K, Mimura O. 2012. Fish-tail resection for treating congenital entropion in Asians. *Clin Ophthalmol* 6: 831–836.

Neligan P. 2012. Pediatric plastic surgery. In *Plastic Surgery: 6-volume set*, third edition (ed. P Neligan). Philadelphia: Elsevier, pp. 828–836.

Nema HV, Nath K, Ahuja OP, Shukla BR. 1965. Accessory conjunctival folds: so-called epitarsus. *Br J Ophthalmol* 49: 148–153.

Nöthen MM, Cichon S, Vogt IR, Hemmer S, Kruse R, Knapp M, Höller T, Faiyaz ul Haque M, Haque S, Propping P, Ahmad M, Rietschel M. 1998. A gene for universal congenital alopecia maps to chromosome 8p21–22. *Am J Hum Genet* 62: 386–390.

Paul LJ, Cohen PR, Kurzrock R. 2012. Eyelash trichomegaly: review of congenital, acquired, and drug-associated etiologies for elongation of the eyelashes. *Int J Dermatol* 51: 631–646.

Patil BB, Bell R, Brice G, Jeffery S, Desai SP. 2004. Distichiasis without lymphoedema? *Eye* 18(12): 1270–1272.

Pingault V, Ente D, Dastot-Le Moal F, Goossens M, Marlin S, Bondurand N. 2010. Review and update of mutations causing Waardenburg syndrome. *Hum Mutat* 31: 391–406.

Qasim M, Shaukat M. 2012. Popliteal pterygium syndrome: a rare entity. *APSP J Case Rep* 3: 5.

Rainger J, Bengani H, Campbell L, Anderson E, Sokhi K, Lam W, Riess A, Ansari M, Smithson S, Lees M, Mercer C, McKenzie K, Lengfeld T, Gener Querol B, Branney P, McKay S, Morrison H, Medina B, Robertson M, Kohlhase J, Gordon C, Kirk J, Wieczorek D, Fitzpatrick DR. 2012. Miller (Genee-Wiedemann) syndrome represents a clinically and biochemically distinct subgroup of postaxial acrofacial dysostosis associated with partial deficiency of DHODH. *Hum Mol Genet* 21: 3969–3983.

Rohena L, Kuehn D, Marchegiani S, Higginson J. 2011. Evidence for Autosomal dominant inheritance of ableharon-macrostomia syndrome. *Am J Med Genet* 155A: 850–854.

Saal HM, Traboulsi EI, Gavaris P, Samango-Sprouse CA, Parks M. 1992. Dominant syndrome with isolated cryptophthalmos and ocular anomalies. *Am J Med Genet* 43: 785.

Scott MH, Richard JM, Farris BK. 1994. Ankyloblepharon filiforme adnatum associated with infantile glaucoma and iridogoniodysgenesis. *J Pediatr Ophthalmol Strabismus* 31: 93–95.

Shah-Desai S, Collins A, Tyers AG. 1999. Surgical correction of entropion and excess upper eyelid skin in congenital cutis laxa: a case report. *Orbit* 18: 53–58.

Shrestha JB, Shrestha GS, Joshi N, Karmacharya PC. 2012. Congenital isolated bilateral upper lid coloboma. *Nepal J Ophthalmol* 4: 194–196.

Slavotinek AM, Baranzini SE, Schanze D, Labelle-Dumais C, Short KM, Chao R, Yahyavi M, Bijlsma EK, Chu C, Musone S, Wheatley A, Kwok PY, Marles S, Fryns JP, Maga AM, Hassan MG, Gould DB, Madireddy L, Li C, Cox TC, Smyth I, Chudley AE, Zenker M. 2012. Manitoba-oculo-tricho-anal (MOTA) syndrome is caused by mutations in FREM1. *J Med Genet* (0022–2593) 48: 375.

Soylev MF, Kocak N, Ozkan SB, Durak I, Aktunc T. 2005. Congenital upper eyelid entropion. *AAPOS* 9: 64–65.

Spierer A, Bourla N. 2004. Primary congenital upper eyelid retraction in infants and children. *Ophthal Plast Reconstr Surg* 20: 246–248.

Steinberg S, Dodt G, Raymond G, Braverman N, Moser A, Moser H. 2006. Peroxisome biogenesis disorders. *BBA Mol Cell Res* 1763: 1733.

Stevens C, Sargent L. 2002. Ablepharon-macrostomia syndrome. *Am J Med Genet* 107: 30–37.

Stevens C, Wilroy RS. 1988. The telecanthus-hypospadias syndrome. *J Med Genet* 25: 536–542.

Stevenson RE, Hall JG. 2006. Craniofacial structures. In *Human Malformations and Related Anomalies* (eds RE Stevenson, JG Hall). New York: Oxford University Press.

Stromland K, Pinazo-Duran MD. 2002. Opthalmic involvement in the fetal alcohol syndrome: clinical and animal model studies. *Alcohol Alcohol* 37: 2–8.

Sung MS, Lee MJ, Choung HK, Kim NJ, Khwarg SI. 2010. Lower eyelid epiblepharon associated with lower eyelid retraction. *Korean J Ophthalmol* 24: 4–9.

Thomas IT, Frias JL, Felix V, Sanchez de Leon L, Hernandez RA, Jones MC. 1986. Isolated and syndromic cryptophthalmos. *Am J Med Genet* 25: 85–98.

Toriello HV, Lindstrom JA, Waterman DF, Baughman FA. 1979. Re-evaluation of CHANDS. *J Med Genet* 16: 316–317.

Tost F. 2013. Surgical treatment of upper lid entropion – selected aspects. *Klin Monbl Augenheilkd* 230: 28–35.

Tukel T, Šošić D, Al-Gazali LI, Erazo M, Casasnovas J, Franco HL, Richardson JA, Olson EN, Cadilla CL, Desnick RJ. 2010. Homozygous nonsense mutations in TWIST2 cause Setleis syndrome. *Am J Hum Genet* 87: 289–296.

Tyers A. 2011. The blepharophimosis-ptosis-epicanthus inversus syndrome (BPES). *Orbit* 30: 199.

Vaughan D, Asbury T, Riordan-Eva P, Whitcher J. 2008. Lids, lacrimal apparatus, and tears. In *Vaughan & Asbury's General Ophthalmology*. New York: Lange Medical Books/McGraw-Hill Medical Publication Division, pp. 79–97.

Zak TA. 1984. Congenital primary upper eyelid entropion. *J Pediatr Ophthalmol Strabismus* 21: 69–73.

Further reading

Bedran EG, Pereira MV, Bernardes TF. 2010. Ectropion. *Semin Ophthalmol* 25: 59–65.

Fung AT, Martin P, Petsoglou C, Kourt G. 2009. Repair of isolated abortive crypophthalmos with lower eyelid switch flap amniotic membrane graft. *Ophthal Plast Reconstr Surg* 25: 158–161.

Merriam, J C. 1988. Reconstruction of the lids of a child with microblepharon and multiple congenital anomalies. *Trans Am Ophthalmol Soc* 86: 55.

95 Eye and lacrimal apparatus

Frederic J. Bertino
St George's University, School of Medicine, St Georges, Grenada
Emory University, School of Medicine, Atlanta, Georgia, USA

Although small, the eye and lacrimal apparatus may contain many structural variations. These variations may have links to genetic and physiologic changes that ultimately result in a different structural anatomy to the normal phenotype without producing pathology. A knowledge of the anatomical variations in this region could prove helpful in differential diagnosis, as in the case of ectopic lacrimal gland tissue when considering the possibility of intraocular tumors for example, or when considering the cause of a patient's myopia.

Globe protrusion

An ethnic difference exists between Caucasians and those of African ancestry, as the latter group tends to show globe protrusion at the upper limits of normal compared to their Caucasian counterparts (Blake et al. 2003; Table 95.1).

Refractive error

Normal variances in corneal curvature, axial length, and lens power – the three anatomical parameters that collectively have an impact on visual acuity – have been specifically correlated to differences in the observed visual acuities of different ethnic groups. Axial length was originally thought to be the primary determinant of visual acuity, as there exists a positive correlation between axial length and myopia in Asian and Caucasian school children (Blake et al. 2003). However, it was realized that axial length was not the sole contributor to nearsightedness; the radii of corneal curvature of Chinese subjects was smaller (with a lesser degree of hyperopia) than African-American and Caucasian subjects with no observed variance in axial length (Blake et al. 2003). Similarly, Inuit subject groups tend to show more hyperopia with flatter (larger) corneal radii and longer axial lengths than African, Chinese, and Caucasian subjects (Wojciechowsky et al. 2003).

Table 95.1 Degree of globe protrusion (mm) across different reviews.

	Caucasians		African-Americans	
Study	**Means ± SD**	**Ranges**	**Means ± SD**	**Ranges**
Migliori and Gladstone (1984)				
Male, $p<0.025$	16.5±2.58	11.3–21.7	18.5±3.08	12.3–24.7
Female, $p<0.025$	15.4±2.33	10.7–20.8	17.8±2.57	12.6–23.0
Dunsky (1992)				
Male	–	–	18.2±2.97	12.3–24.1
Female	–	–	17.5±2.64	12/2–22.7
Barretto and Mathog (1999)				
Male, $p<0.025$	17.0±2.65	11.7–22.3	18.23±2.26	13.7–22.8
Female, $p<0.01$	15.98±2.22	11.5–20.4	17.27±1.44	14.4–20.2

Source: Blake et al. (2003). Reproduced with permission from Wolters Kluwer Health.

Bergman's Comprehensive Encyclopedia of Human Anatomic Variation, First Edition. Edited by R. Shane Tubbs, Mohammadali M. Shoja and Marios Loukas.
© 2016 John Wiley & Sons, Inc. Published 2016 by John Wiley & Sons, Inc.

Table 95.2 Prevalence of myopia of various ages and races across several studies.

Study	Race	Age (years)	Prevalence (%)
Zadnik et al. (1993)	Asian	6–14	27.3
	Caucasian	6–14	8.8
Sperduto et al. (1983)	African-American	12–54	13.0
	Caucasian	12–54	26.2
Wang et al. (1995) (Beaver Dam Eye Study)	Caucasian	48–84	26.2
Lam and Goh (1991) (Hong Kong Schools)	Asian	6–17	55.0

Source: Blake et al. (2003). Reproduced with permission from Wolters Kluwer Health.

When examining myopic trends across ethnic groups independent of axial length, corneal curvature, and lens power, it becomes clear that certain ethnic groups display higher prevalence of the refractive error more commonly than others. Caucasians have a consistently higher prevalence of myopia than African subjects across all age groups; Chinese subjects have a higher degree of myopia than Indians and Malays (Blake et al. 2003). A large study in Singapore showed that Chinese subjects have the highest prevalence of myopia in the 100,000 person sample size, followed by Eurasians, Indians, and Malays respectively (Au Eong et al. 1993). In fact, data indicate that since 1930, Far East Asian populations tend to have a higher prevalence of myopia than their western counterparts (Blake et al. 2003).

The reasons for these ethnic correlations in myopia are not entirely clear; however, a strong correlation exists between the degree of myopia and time spent in education. A different study among Singaporean residents of Chinese, Indian, and Malay recently showed that the degree of myopia was highest in Chinese subjects (−2.75D) followed by Indian (−1.13D) and Malay (−0.88D). These results were positively correlated with time in education (Wu et al. 2001; Table 95.2).

Cornea

Corneal curvature can be used to determine degree of myopia (along with axial length and lens power). There also exists variance in corneal thickness determined by ethnicity, diurnal variation, female reproductive cycle, and level of hydration.

Ethnic variations in the human cornea

African-Americans tend to have a thinner central corneal thickness (CCT) compared to their Caucasian counterparts and, similarly, patients with thinner corneas have higher intraocular pressures (IOP) (Blake et al. 2003). The Ocular Hypertension Treatment Study showed African-American CCT to be 555.7±40.0 μm, 23 μm thinner than Caucasian subjects (579.0±37.0 μm) (Brandt et al. 2001).

There are inconsistent findings in CCT readings in Japanese and Hong Kong Chinese populations, but a few studies have shown similar results with the CCT readings in the two groups being 552.0±36 μm and 555±35 μm, respectively. Other studies on these populations have showed much thicker CCT in Hong Kong Chinese populations without gender difference (Blake et al. 2003). Finally, Mongolian populations were found to have the thinnest recordings of CCT among other Asian populations, with slight discrepancies between right (495.0±32 μm) and left (514±32 μm) eyes (Blake et al. 2003).

In keeping with racial variation, a positive correlation exists between CCT and IOP in Malay children. The CCT and subsequently IOP were found to be significantly less than for other ethnic groups (Table 95.3; Heidary et al. 2011).

The correlation between IOP and CCT supports the hypothesis that there are clear ocular anatomical variations among different ethnic groups and that, specifically, a small CCT may have implications in the diagnosis of glaucoma as it underestimates the IOP of a specific patient.

In comparing corneal diameter, a statistically significant difference exists not between Asian and Caucasian eyes, but between genders. Corneal diameter could be flatter (as hypothesized) in Asians (v. their Caucasian counterparts), which may indicate a greater rate of corneal flattening (with increased diameter). This may be the reason why Far East populations have a higher incidence of myopia than western/Caucasian populations, and may require special consideration in the production of corrective contact lenses for specific ethnic markets or regions (Blake et al. 2003).

Finally, corneal endothelial density is greater in Japanese populations compared to American subjects over the age range 10–70 years. This anatomical finding may indicate a lower incidence of aphakic bullous keratopathy in Japanese populations than in Americans (Blake et al. 2003).

Diurnal variations in corneal thickness

Axial length is described as the distance between the anterior cornea and retina. This distance is known to undergo significant diurnal variation (Read et al. 2008). It is thought that similar changes in IOP correspond to changes in axial length and may account for the axial length change; however, the exact role of these intraocular pressure changes and their relation to axial length is still unclear (Read et al. 2008).

Corneal thickness and anterior chamber depth also undergo significant diurnal change, an association discovered in a study of healthy young men and women. Table 95.4 lists the variations observed in axial length, intraocular pressure, ocular pulse amplitude, central corneal thickness, anterior chamber depth, and anterior chamber volume (Read et al. 2008).

Central corneal thickness, axial length, IOP, and ocular pulse amplitude were found to be at their highest levels after waking and at their lowest levels in the evening/late afternoon.

Table 95.3 Mean central corneal thickness (CCT) and intraocular pressure (IOP) values obtained from the literature.

Study	Age group	Ethnicity	CCT (μm)	CCT instrument	IOP (mm Hg)	IOP instrument
Haider et al. (2008)	7 months–8 years	African-American	535±35	Ultrasound Pachymeter (USP)	16±4	Tono-Pen
		White	559±38		15±4	
Hussein et al. (2004)	6 months–14 years	Caucasian	551±48	USP	–	–
		Hispanic	550±34			
		African-American	532±48			
Hikoya et al. (2009)	8 months–18 months	Japanese	36.9±544.3	USP	13.9±2.4	Tono-Pen
Muir et al. (2004)	5–17 years	African	537±36	USP	19.3±6.0	Goldmann applanation and Tono-Pen
		Caucasian	564±28		17.7±4.2	
Yildirim et al. (2007)	Mean 10.1±1.6 years	Turkish	564.92±32	USP	16.7±2	Noncontact tonometer
					17.9±2	Tono-Pen
Muir et al. (2006)	9 months–17 years	Caucasian	562±35	USP	–	–
		African	543±37			
Sahin et al. (2008)	7–12 years	Turkish	561.37±33	USP	17.47±2.7	Tono-Pen
					16.81±3.1	Rebound tonometer
Muller et al. (2000)	5–11 years	Caucasian	529±36	USP	15.4±2.4	Noncontact tonometer
Tong et al. (2004)	9–11 years	Chinese	546.0±31.8	Noncontact optical pachymeter	–	–
		Non-Chinese (Malay, Indian)	536.6±31.5			
Dai and Gunderson (2006)	1–18 years	African-American	523±40	USP	–	–
		Caucasian	563±36			
		Hispanic	568±44			
Osmera et al. (2009)	7–17 years	Czech	554±33	USP	14.5±2.6	Goldmann applanation tonometry
Herse and Yao (1993)	5–20 years	New Zealand	540±33	Optical pachometry	–	–
Coste et al. (2008)	3–16 years	White European Caucasian + North African	529.30±32.53	Specular microscopy	–	–
Lee et al. (2004)	9–11 years	Chinese	–	–	16.6±2.7	Noncontact tonometry
Doughty et al. (2002)	5–15 years	Caucasian	529±34	USP and specular microscopy	16.8±2.9	Noncontact tonometry
Lim et al. (2009)	Mean 13.97±0.90 years	Singaporean (Chinese, Malay, Indian)	578.76±34.47	Ocular response analyzer	15.12±2.84	Ocular response analyzer

Source: Heidary et al. (2011). Reproduced under the terms of the Creative Commons CC-BY Licence.

Anterior chamber depth was highest at night and lowest in the evening (Harper et al. 1996; Read et al. 2008). Minor differences in results across studies on the topic occur because of the age of the patients examined; however, all studies suggest the same trending diurnal variation.

Significant associations exist between axial length and intraocular pressure measured by DCT (direct contour tonometry). This association is in agreement with the hypothesis that passive expansion and contraction of the globe in response to variations of IOP result in variances in axial length. These

Table 95.4 Variations observed in axial length (AL), intraocular pressure (IOP), ocular pulse amplitude (OPA), central corneal thickness (CCT), anterior chamber depth (ACD), and anterior chamber volume (ACV).

Variable	Mean ± SD	Mean amplitude of change ± SD
AL (mm)	23.77±0.7	0.046±0.022
IOP (mm Hg)	14.49±1.17	3.12±0.94
OPA (mm Hg)	2.10±0.79	1.27±0.44
CCT (mm)	0.532±0.029	0.018±0.008
ACD (mm)	3.16±0.27	0.073±0.037
ACV (mm^3)	187.1±30.1	15.10±6.95

Source: Read et al. (2008).

anatomical changes are now shown to occur in response to normal physiological variations (diurnal cycling).

Corneal thickness variation and the female reproductive cycle

A positive correlation exists between urine estrogen level and increasing corneal thickness, corresponding to the physiological rhythm of the menstrual cycle. At high levels of measured urine estrogen in women not on oral contraceptives, corneal thickness is maximal with a decreased degree of curvature (from corneal swelling). This is possibly due to the fluid retention that occurs with elevated levels of estrogen at the peaks just before ovulation, and the second lower peak at progesterone's elevation after ovulation. Increased tissue fluid makes the cornea edematous and increases thickness while decreasing the level of curvature (Kiely et al. 1983).

At menses, constant progesterone and estrogen show stable readings in corneal thickness (CT). In the first days after menses, increases in corneal thickness are observed in conjunction with slight increases in urine estrogen. This is followed by a transient decrease in CT, then a plateau, then an increase in CT at ovulation. The maximal increase in CT occurs 4 days after ovulation at the first estrogen peak. The second estrogen peak (occurring with the maximum progesterone peak) causes an increase in CT, but not as large as the previous. Increases in CT occur just before the hormone decline, 6–7 days before menses occurs again. A decrease in CT with corresponding decrease in estrogen then follows and, paradoxically, a sharp decrease in urine estrogen and progesterone yields one final CT increase on the last day of the cycle (Kiely et al. 1983). Similar trends were noted across several related studies (Goldich et al. 2011).

Corneal thickness variation with hydration

A nonlinear negative relationship exists between refractive index and level of corneal hydration, an association discovered by variances in corneal thickness with level of hydration (Kim et al. 2004). Increasing corneal tissue hydration increases the geometric thickness of the cornea and subsequently decreases the refractive index.

The trend between corneal thickness, IOP, and refractory index in accordance with hydration, diurnal, ovulatory, and racial differences between various groups points to the correlation that increased corneal thickness leads to an increase in corneal diameter (or radius) and yields a flatter cornea. Flatter corneas have been linked to decreases in refractive index as a function of corneal thickening, and subsequent myopia in various racial groups.

These changes are very minimal and do not impact the outcome, or imply contraindication to women looking to undergo LASIK (laser-assisted in situ keratomileusis) surgery (Seymenoglu et al. 2011). However, corneal thickness also underestimates IOP, which may impede a proper diagnosis of glaucoma in patients with thinner corneas.

In June 2013, a new layer of the human cornea was described by Dua et al. (2013). Dua's layer is a circular, pre-Descemet, acellular corneal layer abundant in collagen and described in 19 adult (average age 77 years) male and female subjects. The layer is impervious to air and develops independently to Descemet's membrane contrary to previous thought. Dua's layer's mean thickness is reported to be 10.15±3.6 μm with a range of 6.3–15.83 μm.

This discovery will have benefit in corneal surgeries, Dua's layer acting as a "splint" to prevent Descemet layer-rolling for endothelial transplant insertion. It is also believed that this new layer may provide further insight into posterior corneal pathology such as acute hydrops in keratoconus and pre-Descemet dystrophies. Dua's layer has not yet been demonstrated in the eyes of younger patients, but is hypothesized to be present based on clinical observation in clinical procedures for keratoconus.

Conjunctiva

Two major variations have been observed within the realm of the human conjunctiva: a diurnal variation in the fluctuation of the redness and temperature correlated with blood flow; and normally occurring non-pathological extraocular pigmentations that may extend into the sclera.

The bulbar conjunctiva possesses a diurnal cycle in that the period of highest blood flow to the tissue occurs just after waking (07:00), and is minimal from the mid-morning throughout the middle of the day (09:00–15:00). Similarly, redness and temperature of the bulbar conjunctiva is highest (34.5°C) at waking and lowest at the middle of the day (Duench et al. 2007).

Three normal, non-malignant variations of conjunctival and scleral pigmentation may occur among certain ethnic groups. These pigmentations are generally stationary; they normally occur in childhood, but may present as early as birth (Henkind and Friedman 1971).

Episcleral melanosis and pigmented spots are frequently seen in East Asian and African patients. In Caucasians it resembles melanosis oculi, an abnormal pathological pigmentation consisting of a bluish mottled episcleral discoloration with

an overall increase in ocular pigment. Episcleral melanosis is more commonly seen in eyes with darker irides. It appears as a bilateral brown-black or gray-blue pigmentation on the episclera. The conjunctiva may be moved over the pigmented areas (Henkind and Friedman 1971).

Intrascleral nerve loops (Axenfeld) are found in any patient independent of ethnicity, although these may appear more commonly in darker-skinned races (Blake et al. 2003). These nerve loops originate as long ciliary nerve roots or anterior perforating ciliary vessels associated with uveal melanocytes that appear as single or multiple circumscribed, raised, pigmented spots appearing underneath the conjunctiva approximately 3–4 mm from the limbus. They are unrelated to UV light exposure, as the location of these nerve loops is usually under the eyelid and receives no exposure to UV light. Axenfeld nerve loops may be tender on palpation (Henkind and Friedman 1971). Episcleral pigment spots with radiations to scleral canal emissaries are more common among Inuit populations and less common among Japanese populations; they are least common among Northern Europeans (Blake et al. 2003).

Anterior chamber

There exists five points (Fig. 95.1) at which the iris can join (insert into) the sclera at the inner side of the globe forming the posterior border of the anterior chamber (Oh et al. 1994). These insertion points from anterior to posterior are:

A. Into/anterior to Schwalbe's line (outermost limit to the corneal epithelium, the termination of Descemet's membrane).
B. Anterior to the posterior trabecular meshwork.
C. The scleral spur (the attachment site for type I tendons of the ciliary muscle), a site of attachment less commonly seen in Caucasians but more common for African-Americans and Asians.
D. Anterior portion of the ciliary body, the most common insertion point for all racial groups.
E. Posterior portion of the ciliary body (Oh et al. 1994).

The point at which the iris joins the scleral wall occurs more anteriorly in Asians, more posteriorly in African-Americans, and most posteriorly in Caucasians. This anatomical difference further suggests the ethnic incidence of angle-closure glaucoma, occurring least commonly in Caucasians, more commonly in African-Americans, and most commonly in Asians (Oh et al. 1994). Similarly, hyperopic eyes, female gender, and increasing age all contribute to a narrower anterior chamber in all ethnic groups. Refractive error is significantly related to the width of the angle of iris insertion (Oh et al. 1994).

Variations in the anterior chamber depth have been correlated to the incidence of primary angle-closure glaucoma (PACG) in different racial groups (Blake et al. 2003). Inuit groups have shallower anterior chamber angles than other races, and subsequently have an increased incidence of PACG in that population. The angle in this group was also found to be smaller than Caucasian, African, and East Asian groups. These factors all contribute to a shallower anterior chamber and increased incidence of PACG.

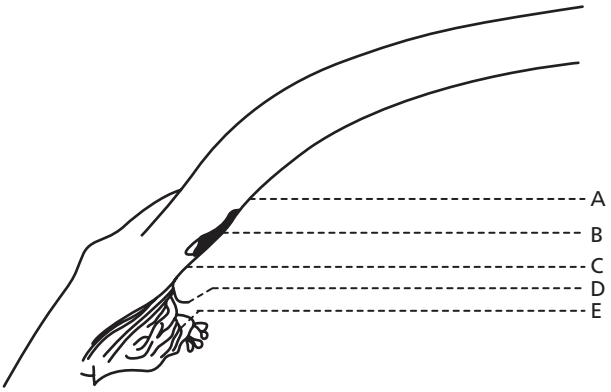

Figure 95.1 Illustration of the various points at which the iris may attach to the inner side of the globe.

Source: Oh et al. (1994).

In studying the East Asian population, it was found that though the anterior chamber angles were deeper than those of the white population, the presence of myopia and PACG was increased in this population almost ten-fold compared to the Caucasian counterpart. It is suggested that this phenomenon exists because the Asian group had a more anterior iris root insertion than the posterior iris insertion found in the Caucasian group (Oh et al. 1994). This led to a difference in angle configuration and could therefore be the reason for the variation.

The increased incidence of PACG among Chinese groups is thought to occur because the Chinese group had a smaller radius of corneal curvature compared to Caucasian and African groups. Smaller corneal curvature radius implies a smaller volume of the anterior chamber with increased crowding. This "creeping angle closure" over time could also explain the increased incidence of PACG in the group from near-sighted working conditions (education etc.) (Blake et al. 2003).

Canal of Schlemm and the ocular drainage apparatus

Two main variations – the diameter of the flow pathway and the rate of humoral flow – are observed when assessing the canal of Schlemm and the ocular drainage apparatus. Measurements of the diameters of the ocular drainage apparatus among various ethnic groups have been recorded (Table 95.5) and, although the findings of the spatial relationship between Schlemm's canal, its location from the angle insertion, and location from the limbus is unknown, there is a significant variation in these factors between different ethnic groups. It is thought that knowledge of these variations in diameter and associated anatomical

Table 95.5 Ultrasound measurements of the diameter and location of the Canal of Schlemm from the angle of insertion and limbus. PSK: pseudophakic eye.

Variable	No. of patients	Canal diameter (μm)	Distance from angle (μm)	Distance from limbus (μm)
Age (years)				
≤40	37	120±47	334±93	645±73
>40	57	122±46	314±96	636±84
Gender				
Female	54	128±50	329±106	633±85
Male	40	113±37	313±77	648±71
Race				
Caucasian	47	117±44	338±104	624±73
African	34	128±52	314±87	659±92
Asian	8	124±39	268±56	626±43
Hispanic	5	110±32	308±83	680±68
Refractive error				
Myopia	44	122±45	342±100	638±89
Hyperopia	6	180±69	281±46	613±53
Plano	44	113±37	309±91	649±72
Lens				
Phakic	75	123±46	318±84	640±80
PSK	19	116±43	339±130	636±80
IOP (mm Hg)				
≤21	88	121±47	322±96	641±81
>21	6	125±34	323±89	618±60
Pachymetry (μm)				
≤555	15	106±36	287±66	625±85
>555	18	124±48	263±84	702±61

Source: Irshad et al. (2010). Reproduced with permission from Elsevier.

measurements may prove beneficial in ocular surgery for landmark approximation (Irshad et al. 2010).

The canal of Schlemm is most posteriorly located in Hispanic and African groups compared to their Asian and Caucasian counterparts when considering the canal's distance from the location of the limbus. With respect to the angle of iris insertion, the canals in the eyes of Asian groups suggest a more anterior displacement than other ethnic groups (Irshad et al. 2010).

Another study suggested that the canal of Schlemm was significantly smaller in cross- sectional area, perimeter, inner wall length, and number of endothelial nuclei in eyes with primary open-angle glaucoma compared to normal eyes that subsequently results in an increasing canal resistance to flow. The hypothesized ramification of the increased resistance could suggest a propensity for anterior canal collapse, leading to a markedly elevated intraocular pressure (Allingham et al. 1996).

The aqueous humor flow rate is 2.75±0.63 μm/min in normal individuals in readings taken during the daytime. The normal range for flow may be between 1.8 and 4.3 μm/min (Brubaker 1991). Flow rates vary normally with circadian rhythm and tend to be highest in the morning with slightly lower rates in the afternoon. During sleep, the rates drop to approximately half that of the morning hour rates. A slight decline in aqueous humor flow rate occurs after age 10 by approximately 3.2% every decade (Brubaker 1991).

Iris

Although not completely understood, the most familiar anatomical variation of the human iris is its color. Six single nucleotide polymorphisms (SNPs) have been shown to most accurately predict normal variations in human eye color in a recent forensic study (in descending order): HERC2 rs12913832, OCA2 rs1800407, SLC24A4 rs12896399, SLC45A2 rs16891982, TYR rs1393350, and IRF4 rs12203592. These six SNPs are thought to encode the variations found in brown, intermediate green/hazel, and blue eye color (Liu et al. 2013).

For example, previous studies suggest that the G allele of the HERC2 rs12913832 SNP is associated with blue iris color (Edwards et al. 2012). This polymorphism was found significantly more often in European populations than a comparative South Asian population. However, the blue-intermediate-brown spectrum is too concrete to classify eyes as patterns of heterochromasia. Varying degrees of brightness, yellow, blue, and red contrast change the original two-dimentional linear spectrum into a three-dimensional color palate (Fig. 95.2) where the L^* axis corresponds to color brightness; a^* the red-green spectrum; and b^* the blue-yellow spectrum (Edwards et al. 2012). Although exact correspondence between SNP identification and specific eye color is not accurately known, the proposed spectrum of a 3D model by Edwards et al. (2012) suggests a new method for mapping a genetically directed normal anatomic variation.

It is clear that certain ethnic variations in iris color occur as a rule through a generational reproducibility of phenotypic traits. Blue irides are more commonly found among Caucasian races, appearing as such because of the lack of pigmentation by melanocytes in the anterior surface of the iris. This contrasts the increased pigmentation as seen in darker eyes, and there exists no difference in the physical number of melanocytes in the iris tissue (Blake et al. 2003).

Gray eyes occur because of a combination of an increased density of the stroma that scatters light in a similar manner as blue irides and a diminished melanocyte density.

Lack of melanin pigment allows for more visualization of the vasculature underlying the iris, which tends to yield a blue-gray iris color (Blake et al. 2003). Additionally, there is a correlation between blue and hazel eye color and macular degeneration among Caucasian patients (Blake et al. 2003).

Lens and pupil

Oscillations in pupil size are common and referred to as "hippus." These perpetual changes in size often make the exact measurement of the pupil difficult to obtain by photographic snapshots of the structure (Winn et al. 1994). However, aside from normal hippus, autonomic function stimulated by emotional, luminescent, and accommodation stimuli all affect variations in pupillary size (Winn et al. 1994).

When measuring for variations in pupillary size (keeping independent variations induced by autonomic stimuli), pupil size does decrease with increasing age, irrespective of gender, refractive index, or iris color (Winn et al. 1994). At three different luminescent readings with refractive index corrected, it was found that patients in a 25-year-old study group showed pupillary sizes of approximately 5.75, 3.75, and 3.00 mm in diameter at 9, 220, and 4400 cd m^{-2} respectively. At the same luminescent readings, the 67-year-old group had pupillary diameters of 4.50, 3.50, and 2.25 mm, respectively, indicating a negative correlation between age and pupillary size (Winn et al. 1994).

No evidence in the literature exists to support a clear ethnic difference in lens size to account for ethnic predisposition, however some studies found some minor variations in certain groups of people (Blake et al. 2003). African patients in one study were found to have thinner lenses than Danish (Caucasian) patients, and this difference may explain the lower incidence of acute closure attacks in some African populations.

Inuit populations with higher incidence of anterior chamber angle closure had significantly thicker lenses than that of their Chinese, Caucasian, and African counterparts (Blake et al. 2003). Aside from these minor correlations, no true racial anatomical difference in lens size or shape currently exists.

Sclera

Two important anatomical variations occur within the human sclera: the scleral thickness, and hydraulic conductivity. Differences in scleral thickness are a common variation throughout the general population, and may decrease in thickness in glaucomatous eyes. Similarly, knowledge of the hydraulic conductivity of the sclera can predict the entrance of medication and fluid into the eye.

Scleral thickness and dimensions

The thickness of the human sclera in a population of 11 eyes was 670±80 μm, with a mean SD range of 564–832 μm. Maximum thickness was observed at the posterior pole of the eye with a mean thickness of 996±181 μm. The thinnest part of the sclera occurred at the equator (491±91 μm; Norman et al. 2010). Glaucomatous eyes suggest that the dimensions of optic nerve head canal diameter, axial length, and posterior sclera were decreased, lengthened, and thinned respectively, with increases in IOP (Norman et al. 2010). The significant variances in scleral thickness in the 11 eyes studied also suggest that there exists a wide variance in scleral size in the greater population (Norman et al. 2010).

This association is in agreement with other research on the topic (Vurgese et al. 2012). It is of note that scleral thickness was found to be statistically independent of glaucoma presence (beyond an axial length of 26 mm and the correlated thinning of the posterior sclera), age, and gender (Vurgese et al. 2012).

Hydraulic conductivity of the sclera

There exists a significant decrease in hydraulic conductivity (HC) with increasing age and decreasing scleral thickness (Jackson et al. 2006). HC is important because it is related to the ability for fluid and medications to enter and drain through the sclera. Uveoscleral outflow, intraocular pressure, and trans scleral fluid dynamics are all functions of HC. There was no significant variation in scleral topographic relationship to HC and certain areas of the sclera are not thought to have heightened or decreased HC compared to other areas of the sclera (Jackson et al. 2006).

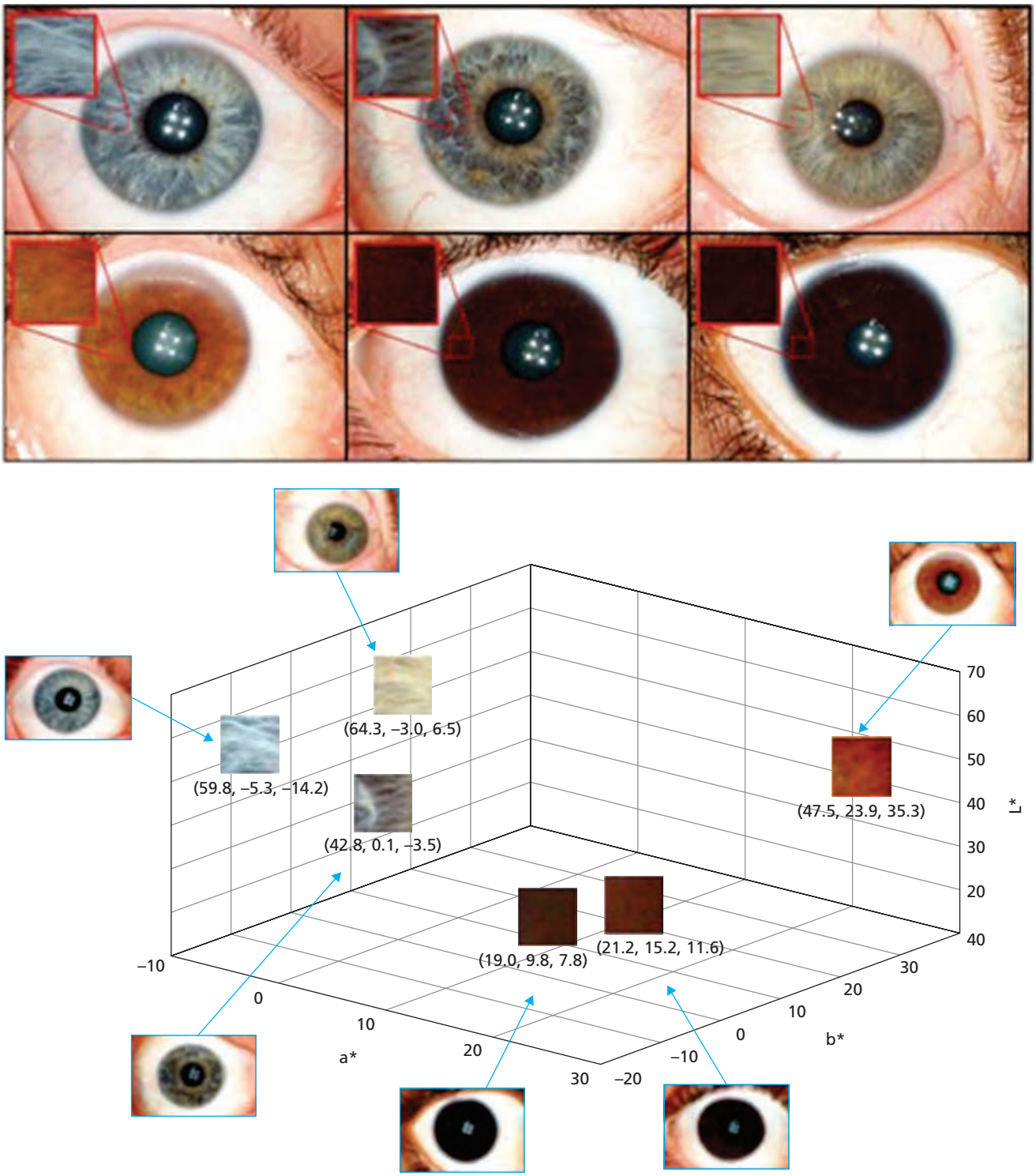

Figure 95.2 A three-dimensional spectrum created by Edwards et al. (2012), demonstrating the varieties of iris color. The L^* axis corresponds to color brightness; a^* the red-green spectrum; and b^* the blue-yellow spectrum.

Source: Edwards et al. (2012). Reproduced with permission from John Wiley & Sons.

Lacrimal apparatus

Variant dimensions of typical lacrimal glands

The typical lacrimal gland consists of two lobes: a larger orbital lobe and smaller mobile palpebral lobe that forms a C-shaped exocrine gland that wraps around the levator palpebrae superioris aponeurosis. The orbital lobe rests on the superior surface and the palpebral lobe lies inferior to the aponeurosis, resting on Tenon's capsule. The two lobes are joined temporally, separated by an interlobar gap formed by the aponeurosis, and the gland sits in a superior-temporal location within the orbit. It is the only human exocrine gland to be fully encased in a small bony chamber (Lorber 2007). There are approximately 20–40 accessory lacrimal glands (of Krause) located in the conjunctival fornix and along the superior tarsal border in the upper eyelid (glands of Wolfring). Half the number of accessory glands in the upper eyelid usually exists in the lower (Lorber 2007).

The lacrimal gland is divided into two lobes. The larger orbital lobe ranges over 20–25 mm in length on its long axis and 10–15 mm on its short axis. Its thickness is 3–5 mm (Lorber 2007). The smaller palpebral lobe may be 9–15 mm in length on the long axis and approximately 8 mm on its short axis. The palpebral lobe thickness is approximately 2 mm. The gland in its entirety is approximately 15–20 mm on the long axis, 10–12 mm on the short axis, and 5 mm thick. It may weigh anywhere between 500 mg and 1.5 g, with an approximate average of about 780–940 mg (Lorber 2007). The larger orbital lobe may weigh between 670 and 720 mg and the smaller palpebral lobe about 220 mg. Smaller lacrimal gland sizes may correspond to atrophy or incomplete specimen removal (Lorber 2007).

The lacrimal gland has a gender dimorphism. Lacrimal glands from men weigh 0.2–0.45 g and from women 0.14–0.40 g (Lorber 2007). Being smaller than 0.5 g, these specimens were deemed as atrophic; however, in a comparison of glands larger than 0.5 g, a clear size difference between genders exists. The gender difference may be explained by the fact that the bony orbital space in females may be smaller than males, and therefore must accommodate a smaller gland (Lorber 2007). Charpy and Nicholas described in 1912 how the maximal peak weight of the lacrimal gland occurs during ages 8–10 and atrophies with increasing age (Lorber 2007). This finding is especially noted in males where significant gland atrophy occurred in two groups of men aged 51–60 and 61–80 years (Lorber 2007).

Hypofunction of the lacrimal gland is more common in postmenopausal women than in men or younger women (Lorber 2007). High prolactin levels or relative androgen decrease, along with a 63% smaller acinar area than the male gland, means postmenopausal women have a higher likelihood of gland hypofunction. The larger mass in males serves as an adequate buffer to maintain functional gland integrity. Glandular hypofunction based on age and gender may be due to the shorter lifespan of men and the inability to reach advanced age as often as women. This may be why the prevalence of hypofunction is higher in the older female age group.

Typical lacrimal ducts

The number of lacrimal ducts may be variable (Cohen et al. 2006; Lorber 2007). The orbital lobe may contain anywhere between <6 and >14 ducts. The palpebral lobe has been reported to contain anywhere from 5–12 ducts. All ducts (orbital and palpebral) exit through the palpebral lobe. A single lacrimal gland will generally contain 6–12 lobes; however, there are glandular variations containing more than 12 total ducts. Most of the ducts empty into the superior fornix approximately 4–5 mm above the tarsus, though it is not unheard of for some of them to open into the inferior fornix. Palpebral ducts also open into the superior fornix irrespective of the orbital ducts (Cohen et al. 2006; Lorber 2007).

Atypical lacrimal glands

Three gross atypical variants of the human lacrimal gland have been described (Lorber and Vidic 2006). They include the subencapsulated variant, the bilayered variant, and the macrovariant. With the typical lacrimal gland included, the organ has four acknowledged normal anatomical variants.

Subencapsulated lacrimal gland

The subencapsulated variant is covered widely in a connective tissue or fibro-adipose tissue on its deep surface (Lorber and Vidic 2009). This contrasts the typical gland that possesses an interlobar gap formed by the passage of the aponeurosa between the two lobes. The additional tissue in the subencapsulated variant narrows the interlobar gap superiorly and interrupts it inferiorly (Lorber and Vidic 2009). This limits the movement of the palpebral lobe significantly. Distinguishing between the two lobes in the subencapsulated variant is difficult due to the presence of this new layer. The capsule tissue is separate from Tenon's Capsule and is not penetrated by blood vessels or muscles (Lorber and Vidic 2009). This variant is not uncommon, appearing in 18.2% of the 22 male and 34.8% of the female specimen glands examined (Lorber and Vidic 2009).

Bilayered lacrimal gland

The bilayered variant lacrimal gland is described as ovoid with the convex orbital lobe superiorly attached to the upper portion of the central part of a significantly larger palpebral lobe (Lorber and Vidic 2009). The orbital lobe in this case does not contribute significantly to overall gland dimensions. The anterior borders of both lobes are parallel, though separated by approximately 7 mm due to the large palpebral lobe protrusion. The free border of the orbital lobe does not extend deeply and covers only the temporal ridge of the levator palpebrae superioris aponeurosa (Lorber and Vidic 2009). This is somewhat analogous to the subencapsulated variant and, even more similarly, the palpebral lobe has a dense connective tissue covering in the bilayered variant. This variant is reported to have no gender dimorphism as it was described equally in just over 21–22% of the male and

female subjects by Lorber and Vidic (2009). The bilayered variant least resembles the normal anatomy of the typical gland among its other variant counterparts (Lorber and Vidic 2009).

In men, typical glands were found to be both thicker overall than their subencapsulated counterparts, and with thicker orbital lobes than both the subencapsulated and bilayered variants (Lorber and Vidic 2009). Men with typical glands had thinner palpebral lobes than the subencapsulated variants (Lorber and Vidic 2009). Females with bilayered gland variants have significantly wider palpebral lobes than those women with typical and subencapsulated glands.

Macrovariant lacrimal gland

Of the lacrimal variants described so far, the macrovariant lacrimal gland is the least commonly seen in clinical observation; it appeared in only one specimen out of 23 females and zero in 22 males (Lorber and Vidic 2009). The macrovariant resembles the typical lacrimal gland in that the lobes extend transversely to the aponeurosa. The interlobar gap is abnormally enlarged, much more than the previous three variants (including the typical gland) (Lorber and Vidic 2009). The gaping space prevents overlap by the deeply posterior orbital lobe and the palpebral lobe, making gland width and depth extensive. Because of the depth of the orbital lobe, it is possible that it may be located above the globe posteriorly. Finally, both surfaces of the macrovariant gland have a thick fibroadipose coat (Lorber and Vidic 2009).

Canaliculus

The canaliculus drains fluid from the punctum and may range over 8–10 mm in length and 0.5–1.0 mm in diameter (Cohen et al. 2006). There may be supernumerary (two to four) puncta. Duplication of the canaliculus is rare (1:60,000). The puncta are occasionally imperforate. Diverticula of sinuses in the lacrimal duct may occur, or the nasolacrimal duct may be doubled. In most individuals (more than 90%), a common canaliculus forms from the fusion of the superior and inferior canaliculi before entering the nasolacrimal sac (Cohen et al. 2006). In a study it was found that 94% of subjects showed this most common configuration, with 4% demonstrating a variation where the upper and lower canaliculi joined at the lacrimal sac without a common canaliculus. The remaining 2% of individuals possessed completely separate drainage of both canaliculi into the lacrimal sac. Other anatomical studies on the canalicular drainage apparatus have shown similar results (Cohen et al. 2006).

Nasolacrimal sac, nasolacrimal duct, and canal

The nasolacrimal sac ranges over 12–15 mm vertically and 4–8 mm anteroposteriorly (Cohen et al. 2006). The fundus of the sac may extend 3–5 mm superior to the medial canthal tendon, and the body of the sac is approximately 10 mm in height (Cohen et al. 2006). A gender dimorphism exists in that the nasolacrimal fossa and duct (specifically the middle and lower regions) are narrower in females, which may explain the higher frequency of nasolacrimal obstruction in females resulting in dacryocystocele (Cohen et al. 2006). Similarly, a racial variation exists in that the nasolacrimal canal containing the nasolacrimal duct is wider in Asian and African-American populations, suggesting a higher incidence in nasolacrimal obstruction in Caucasians than other ethnic groups (Cohen et al. 2006).

Multiple variations of the mucosal folds that surround the canalicular/lacrimal sac junction have been described. They include variants such as anterior 180, posterior 180, 360 valve, inferior 180, superior 180, anterior 270, and no valve. The "no valve" type was the most commonly reported finding; the next-most commonly reported variation was the "360 valve", followed by the "anterior 180" variant. These variants are more commonly mutually exclusive, and the variation (if one exists) is more likely to be unilateral than bilateral (Table 95.6; Zoumalan et al. 2011). The two most common variants were found to be more commonly right sided than left sided (Zoumalan et al. 2011). The left orbit contained a higher incidence of the posterior 180 variant and was less likely to contain canalicular/lacrimal sac mucosal fold than the right (Zoumalan et al. 2011). The presence of these one-way valvular variants may create an obstruction to flow and a higher incidence of dacryocystocele that can be relieved by manual compression, inferior or superior canaliculitis, and dacryocystitis (Zoumalan et al. 2011).

In addition to the variations in valve opening at mucosal folds, there are also variations in the angles that exist between the long axis of the lacrimal sac and the nasolacrimal duct (Narioka et al. 2007). This angle may be the source of false passage during nasolacrimal intubation, balloon dacryocystoplasty, and polyurethane stents in the correction of ductal stenosis or obstruction (Narioka et al. 2007).

Narioka et al. (2007) define "false passage" as "perforation of the lacrimal probe or tubing through the lumen of the nasolacrimal drainage system." The angle between the lacrimal sac and nasolacrimal duct can be approximated from facial measurements of nasal length, height, and depth (Narioka et al. 2007).

The long axes of the lacrimal sac and nasolacrimal duct were bent posteriorly in the sagittal plane in Narioka's study of 46 right and left Japanese specimens. The anterior and posterior directed angles between the lacrimal sac and nasolacrimal duct in the sagittal plane have been described. In the anterior type, the inclination of the lacrimal sac was larger than the nasolacrimal duct (+8.9±5.0° from 0–19° of horizontal). In the posterior type, the inclination of the lacrimal sac was smaller than that of the nasolacrimal duct (–12.3±9.0° from –2 to –26° of horizontal) (Narioka et al. 2007).

In the coronal plane, the long axes of the lacrimal sac are bent laterally in all subjects from the same study, with mean angle measuring 24.7±7.9° (Narioka et al. 2007). Similarly, two angles are also described in this plane: inward (10.2±4.5°) and outward

Table 95.6 The prevalence of the variant mucosal folds of the canaliculus/lacrimal sac and variations in the mucosal folds based on laterality (right v. left orbital orientation). Adapted from Zoumalan et al. (2011) with permission from Wolters Kluwer Health.

	n = 124		No. in indicated orbit	
Valve type	**Prevalence (no.)**	**Percentage (%)**	**Right**	**Left**
Anterior 180	20	16.2	14	6
Posterior 180	13	10.5	4	9
360 valve	36	29	28	8
Inferior 180	1	0.81	1	0
Superior 180	1	0.81	0	1
Anterior 270	3	2.4	2	1
No valve	50	40.3	24	26
Total	124	100	73	51

(7.6±4.1°) from the sagittal line (Narioka et al. 2007). The long axis of the nasolacrimal duct was always bent inwardly from that of the lacrimal sac; the lateral angle of the nasolacrimal duct therefore never exceeded that of the lacrimal sac (Narioka et al. 2007). The mean angle created by the junction of the lacrimal sac and nasolacrimal duct was found to be 28.3±12.2°. Female subjects were found to have larger inclinations of the lacrimal sac than their male counterparts (Narioka et al. 2007).

There is a strong negative correlation between nasal depth and the angle of the lacrimal sac and nasolacrimal duct in the anterior-posterior plane, and a strong negative correlation in the coronal plane between nasal breadth, height, and length and the lacrimal sac/nasolacrimal duct angle (Narioka et al. 2007).

The opening of the nasolacrimal duct may: be at or near the superior vault of the inferior meatus; be at the lateral wall of the nose and extending to the floor of the nose lateral to the nasal mucosa; be midway down the lateral wall of the inferior meatus without an opening into it; end very superior to the inferior meatus with bony obstruction; end blindly in the anterior aspect of the inferior concha; end blindly in the medial wall of the maxillary sinus; or be encased in bone up to the floor of the lateral wall of the nose with no opening into the inferior meatus (Hurwitz 1996).

Ectopic lacrimal tissue

Ectopic lacrimal gland tissue is a rare clinical finding. However, when it does occur, it is most frequently described in the orbit or anywhere in the ocular adnexa. This region includes the eyelid, tarsal plate, conjunctiva, cornea, and under the nasal mucosa. Even more rarely are cases of ectopic lacrimal tissue within the globe (Jung et al. 2006). The most common areas for ectopic lacrimal tissue tend to be within the bulbar conjunctiva and limbal area (Pfaffenroth and Green 1971).

Theories on the formation of ectopic lacrimal tissue include: (1) early abnormal implantation of progenitor cells programmed to become lacrimal tissue; (2) the implantation of lacrimal tissue with surface epithelium during lens development; (3) closing of the choroidal fissure, thus pinching off lacrimal gland buds when the glandular tissue is in propinquity to the choroid (especially in developmental delay of the region); (4) pre-existing scleral defects allowing intraocular extension of the glandular tissue; and (5) growth-factor-induced (FGF-10) stimulation of conjunctival epithelium to stimulate lacrimal gland proliferation in an epithelial-mesenchymal interaction (Jung et al. 2006).

Intraocular lacrimal tissue would most likely present in children whose parents report an abnormal-looking eye. It is important to consider ectopic intraocular lacrimal tissue when considering other eye pathology in a young patient (i.e., retinoblastoma, other neoplasms). Glands of Manz are among normally occurring lacrimal glands that were originally described in pigs, but may be present in humans (Kessing 1968). These accessory glands were found in the same anatomical location in humans as described in the pigs originally studied. They occur in the bulbar area, nasal to the cornea and approximately 0.5 mm in diameter. Kessing (1968) has suggested that this aberrant gland of Manz occurs in approximately 12% of the population.

In addition to the rarely occurring glands of Manz, additional accessory lacrimal glands have been described and are normally occurring in the human population (Kessing 1968). These are known as the glands of Krause. Krause glands appear to occur most frequently in the upper fornical area, and are adjacent to the palpebral lobe of the lacrimal gland proper when temporally located (Kessing 1968). There are approximately 40–45 glands of Krause in the upper fornix, and approximately 6–8 in the lower fornix (Pfaffenbach and Green 1971). Figure 95.3 is a drawn schematic of the conjunctiva and the relative frequencies of occurrence of accessory submucous lacrimal glands (Kessing 1968).

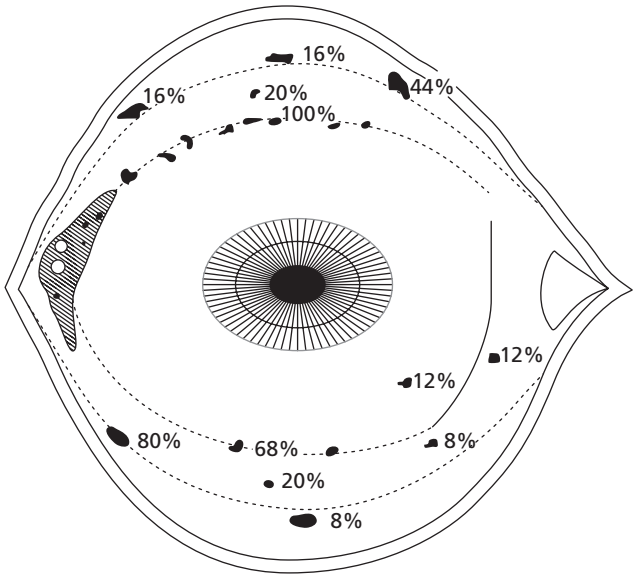

Figure 95.3 Illustrated schematic of the right eye and conjunctiva with the relative frequencies of occurrence of submucosal lacrimal glands.

Source: Kessing (1968). Reproduced with permission from John Wiley & Sons.

References

Allingham RR, DeKater AW, Ethier CR. 1996. Schlemm's canal and primary open angle glaucoma: correlation between Schlemm's canal dimensions and outflow facility. *Exp Eye Res* 62: 101–109.

Au Eong KG, Tay TH, Lim MK. 1993. Race, culture and myopia in 110236 young Singaporean males. *Singapore Med J* 34: 29–32.

Barretto RL, Mathog RH. 1999. Orbital measurement in black and white populations. *Laryngoscope* 109: 1051–1054.

Blake R, Lai W, Edward D. 2003. Racial and ethnic differences in ocular anatomy. *Int Ophthalmol Clin* 43: 9–25.

Brandt JD, Beiser JA, Kass MA, et al. 2001. Central corneal thickness in the ocular hypertension treatment study. *Ophthalmology* 108: 1779–1788.

Brubaker R. 1991. Flow of aqueous humor in humans (the Friedenwald lecture). *Invest Ophth Vis Sci* 32: 3145–3166.

Cohen AJ, Mercandetti M, Brazzo BG. 2006. *The Lacrimal System Diagnosis, Management, and Surgery*. New York: Springer Science+Business Media, Inc. pp. 11–17; 20–23.

Coste R, Cornand E, Denis D. 2008. Central corneal thickness in a pediatric population using a noncontact specular microscope: a study of 405 cases. *J Fr Ophtalmol* 31: 273–278.

Dai E, Gunderson CA. 2006. Pediatric central corneal thickness variation among major ethnic populations. *J Aapos* 10: 22–25.

Doughty MJ, Laiquzzaman M, Muller A, Oblak E, Button NF. 2002. Central corneal thickness in European (white) individuals, especially children and the elderly, and assessment of its possible importance in clinical measures of intra- ocular pressure. *Ophthalmic Physiol Opt* 22: 491–504.

Dua HS, Faraj LA, Said D, Gray T, Lowe J. 2013. Human corneal anatomy redefined; a novel pre-Descemet's layer (Dua's layer). *Ophthalmology* 120(9): 1778–1785.

Duench S, Simpson T, Jones L, Flanagan J, Fonn D. 2007. Assessment of variation in bulbar conjunctival redness, temperature, and blood flow. *Optometry Vision Sci* 84: 511–516.

Dunsky IL. 1992. Normative data for Hertel's exophthalmometry in a normal adult black population. *Optom Vis Sci* 69: 562–564.

Edwards M, Gozdzik A, Ross K, Miles J, Parra E. 2012. Technical note: quantitative measures of iris color using high resolution photographs. *Am J Phys Anthropol* 147: 141–149.

Goldich Y, Barkana Y, Pras E, Fish A, Mandel Y, Hirsh A, Tsur N, Morad Y, Avni I, Zadok D. 2011. Variations in corneal biomechanical parameters and central corneal thickness during the menstrual cycle. *J Cataract Refract Surg* 37: 1507–1511.

Haider KM, Mickler C, Oliver D, Moya FJ, Cruz OA, et al. 2008. Age and racial variation in central corneal thickness of preschool and school-aged children. *J Pediatr Ophthalmol Strabismus* 45: 227–233.

Harper CL, Boulton ME, Bennett D, Marcyniuk, B, Jarvis-Evans JH, Tullo AB, Ridgeway AE. 1996. Diurnal variations in human corneal thickness. *Brit J Ophthalmol* 80: 1068–1072.

Heidary F, Gharebaghi R, Wan Hitam WH, Naing NN, Wan-Arfah N, Shatriah I. 2011. Central corneal thickness and intraocular pressure in Malay children. *PLoS ONE* 6(10): e25208.

Henkind P, Friedman AH. 1971. External ocular pigmentation. *Int Ophthalmol Clin* 11: 92.

Herse P, Yao W. 1993. Variation of corneal thickness with age in young New Zealanders. *Acta Ophthalmol (Copenh)* 71: 360–364.

Hikoya A, Sato M, Tsuzuki K, Koide YM, Asaoka R, et al. 2009. Central corneal thickness in Japanese children. *Jap J Ophthalmol* 53: 7–11.

Hurwitz JJ. 1996. Embryology of the lacrimal drainage system. In *The Lacrimal System* (ed. JJ Hurwitz). Philadelphia: Lippincott–Raven.

Hussein MA, Paysse EA, Bell NP, Coats DK, Brady McCreery KM, et al. 2004. Corneal thickness in children. *Am J Ophthalmol* 138: 744–748.

Irshad F, Mayfield M, Zurakowski D, Ayyala R. 2010. Variation in Schlemm's canal diameter location by ultrasound biomicroscopy. *Ophthalmology* 117: 916–920.

Jackson T, Hussain A, Hodgetts A, Morley A, Hillencamp J, Sullivan P, Marshall J. 2006. Human scleral hydraulic conductivity: age-related changes, topographical variation, and potential scleral outflow facility. *Invest Ophth Vis Sci* 47: 4942–4946.

Jung JY, Kim JH, Kim ST, Kim HJ, Weon Y-C. 2006. MR features of intraocular ectopic lacrimal tissue. *Am J Neuroradiol* 27: 2196–2198.

Kessing SV. 1968. Ectopic lacrimal gland tissue at the corneal limbus (gland of Manz?). *Acta Ophthalmol* 46: 398–403.

Kiely P, Carney L, Smith G. 1983. Menstrual cycle variations of corneal topography and thickness. *Am J Optom Phys Opt.* 60: 822–829.

Kim Y, Walsh J, Golstick T, Glucksberg M. 2004. Variation of corneal refractive index with hydration. *Phys Med Biol* 49: 859–868.

Lam CSY, Goh WSH. 1991. The incidence of refractive errors among school children in Hong Kong and its relationship with the optical components. *Clin Exp Optom* 74: 97–103.

Lee AJ, Saw SM, Gazzard G, Cheng A, Tan DT. 2004. Intraocular pressure associations with refractive error and axial length in children. *Br J Ophthalmol* 88: 5–7.

Lim L, Cheung N, Gazzard G, Chan YH, Wong TY, et al. 2009. Corneal biomechanical properties and retinal vascular caliber in children. *Invest Ophthalmol Vis Sci* 50: 121–125.

Liu F, Wen B, Keyser M. 2013. Colorful DNA polymorphisms in humans. *Semin Cell Dev Biol* 24(6–7): 562–575.

Lorber M, Vidic B. 2009. Measurements of lacrimal glands from cadavers, with descriptions of typical glands and three gross variants. *Orbit* 28: 137–146.

Lorber M. 2007. Gross characteristics of normal human lacrimal glands. *Ocul Surf* 5: 13–22.

Migliori ME, Gladstone GJ. 1984. Determination of the normal range of exophthalmometric values for black and white adults. *Am J Ophthalmol* 98: 438–442.

Muir KW, Jin J, Freedman SF. 2004. Central corneal thickness and its relationship to intraocular pressure in children. *Ophthalmology* 111: 2220–2223.

Muir KW, Duncan L, Enyedi LB, Freedman SF. 2006. Central corneal thickness in children: Racial differences (black vs. white) and correlation with measured intraocular pressure. *J Glaucoma* 15: 520–523.

Muller A, Doughty MJ, Wright L. 2000. Reassessment of the corneal endothelial cell organisation in children. *Br J Ophthalmol* 84: 692–696.

Narioka J, Matsuda S, Ohashi Y. 2007. Correlation between anthropometric facial features and characteristics of nasolacrimal drainage system in connection to false passage. *Clin Exp Ophthalmol* 35: 651–656.

Norman R, Flanagan J, Rausch S, Sigal I, Tertinegg I, Eilaghi A, Portnoy S, Sled J, Ethier R. 2010. Dimensions of the human sclera: Thickness measurement and regional changes with axial length. *Exp Eye Res* 90: 277–284.

Oh YG, Minelli S, Spaeth GL. 1994. The anterior chamber angle is different in different racial groups: a gonioscopic study. *Eye* 8: 104–108.

Osmera J, Filous A, Hlozanek M. 2009. Central corneal thickness, intraocular pressure and their correlation in healthy Czech children aged 7–17 years. *Cesk Slov Oftalmol* 65: 19–23.

Pfaffenbach DD, Green WR. 1971. Ectopic lacrimal gland. *Int Ophthalmol Clin* 11: 149–159.

Read S, Collins M, Iskander, D. 2008. Diurnal variation of axial length, intraocular pressure, and anterior eye biometrics. *Invest Ophth Vis Sci* 49: 2911–2918.

Sahin A, Basmak H, Yildirim N. 2008. The influence of central corneal thickness and corneal curvature on intraocular pressure measured by tono-pen and rebound tonometer in children. *J Glaucoma* 17: 57–61.

Seymenoglu G, Baser E, Zerdeci N, Guljan C. 2011. Corneal biomechanical properties during the menstrual cycle. *Curr Eye Res* 36(5): 399–403.

Sperduto RD, Seigel D, Roberts J, Rowland M. 1983. Prevalence of myopia in the United States. *Arch Ophthalmol* 101: 405–407.

Tong L, Saw SM, Siak JK, Gazzard G, Tan D. 2004. Corneal thickness determination and correlates in Singaporean schoolchildren. *Invest Ophthalmol Vis Sci* 45: 4004–4009.

Vurgese S, Panda-Jonas S, Jonas JB. 2012. Scleral thickness in human eyes. *PLoS ONE* 7(1): e29692.

Wang Q, Klein BEK, Klein R, et al. 1995. Refractive status in the Beaver Dam Eye Study. *Invest Ophthalmol Vis Sci* 35: 4344–4347.

Winn B, Whitaker D, Elliott DB, Phillips NJ. 1994. Factors affecting light-adapted pupil size in normal human subjects. *Invest Ophthalmol Vis Sci* 35: 1132–1137.

Wu HM, Seet B, Yap EPH, et al. 2001. Does education explain ethnic differences in myopia prevalence? A population-based study of young adult males in Singapore. *Optom Vis Sci* 78: 234–239.

Wojciechowski R, Congdon N, Anninger W, Broman AT. 2003. Age, gender, biometry, re- fractive error, and the anterior chamber angle among Alaskan Eskimos. *Ophthalmology* 110: 365–375.

Yildirim N, Sahin A, Basmak H, Bal C. 2007. Effect of central corneal thickness and radius of the corneal curvature on intraocular pressure measured with the Tono-Pen and noncontact tonometer in healthy schoolchildren. *J Pediatr Ophthalmol Strabismus* 44: 216–222.

Zadnik K, Mutti DO, Friedman NE, et al. 1993. Initial cross-sectional results from the Orinda Longitudinal Study of Myopia. *Optom Vis Sci* 70: 750–758.

Zoumalan CI, Joseph JM, Lelli GJ, Segal KL, Adeleye A, Kazim M, Lisman RD. 2011. Evaluation of the canalicular entrance into the lacrimal sac: an anatomical study. *Ophthal Plast Reconstr Surg* 27: 298–303.

96 Lateral nasal wall and paranasal sinuses

Amr E. El-Shazly
Liège University Hospital, Liège, Belgium

The anatomy of the lateral nasal wall is highly variable and a sound knowledge of its variants is mandatory for performing endoscopic nasal surgery safely. Although some of these anatomical variations are associated with rhinosinusitis, the aim of this chapter is to highlight them without focusing on the associated clinical picture.

Variations of the nasal turbinates

The nasal turbinates are usually three but can sometimes be four in number. They are bony projections from the lateral nasal wall covered by pseudostratified ciliated columnar respiratory epithelium. The inferior turbinate is a separate bone while the middle and superior turbinates arise from the ethmoid bone. Variations of these structures include pneumatization, secondary turbinate, accessory turbinate, paradoxical turbinate, agenesis/hypogenesis, and bifid turbinate (Ozcan et al. 2008).

Variations of the inferior turbinate

Bifid inferior turbinate

In this anomaly, two inferior turbinate appear with a single root (Lee and Koh 2011; Lee et al. 2012). It might be a form of severe medial displacement and inferior rotation of the uncinate process, since cases reported in the literature have been associated with absence of the uncinate process (Spear et al. 2003; Selcuk et al. 2008). Some authors have termed this variation "accessory inferior turbinate."

Pneumatization of inferior turbinate

Pneumatization in the inferior turbinate, inferior concha bullosa (presence of air cell inside the turbinate), is less common than in the middle turbinate (concha bullosa). It is a radiological diagnosis and pneumatization of several turbinates in the same patient has been reported (Sagit et al. 2008; Pittore et al. 2011; Ozturan et al. 2013). These can exist unilaterally or bilaterally (Aydin et al. 2001; Christmas and Merrell 2004). In a radiological study by Ozturk et al. (2005), pneumatization of inferior turbinate (PIT) was found in one of 250 cases. The authors suggested that most PIT cases could result from defects in articulation between the maxillary process of the palatine bone and the maxillary bone. In such a situation, the maxillary process of the palatine bone and the nasal process of the maxillary bone, which form the medial wall of the maxillary sinus at the inferior turbinate level, can attach separately to the inferior turbinate. Kharoubi (2010) reviewed the incidence of this variation in the literature and found 25 reported cases of inferior concha bullosa.

Paradoxical inferior turbinate

The inferior turbinate convexity is directed medially, but as an anatomical variation the convexity can be directed laterally, that is, paradoxical inferior turbinate. In the literature there is a single case report of a giant paradoxical curvature of the bony part of the inferior turbinate (Naiboglu et al. 2011). This anomaly is less common than paradoxical middle turbinate.

Agenesis of inferior turbinate

Agenesis of the inferior turbinate is rare. It is usually unilateral (Caylakli et al. 2008; Waldhera et al. 2010). In a cadaver dissection study, hypogenesis on one side and agenesis on the other has been reported (Gumusalan 1977). As a personal experience the author came across five cases of unilateral hypogenesis of the inferior turbinate during septoplasty procedures. In all these cases there was significant deviation of the anterior part of the nasal septum (cartilaginous part) towards the hypoplastic concha, resulting in significant unilateral nasal obstruction (unpublished data).

Variations of the middle turbinate

The morphogenesis and anatomical structure of the ethmoid sinus reveal that it is formed from several ethmoid ridges (Rice 1995; Arredondo de Arreola et al. 1996). The first permanent ethmoturbinal ridge forms the middle turbinate, the second forms the superior turbinate, and the third forms the supreme turbinate (variably present). The supporting bony attachments for the freely hanging portions of the turbinates are called lamellae (Stammberger and Kennedy 1995): the lamellae of the uncinate process and the ethmoid bulla, the basal lamellaae of the middle and superior turbinates, and the lamella of the supreme turbinate, if present.

Bergman's Comprehensive Encyclopedia of Human Anatomic Variation, First Edition. Edited by R. Shane Tubbs, Mohammadali M. Shoja and Marios Loukas.
© 2016 John Wiley & Sons, Inc. Published 2016 by John Wiley & Sons, Inc.

Secondary and accessory middle turbinates

During embryological development, secondary evaginations and invaginations emerge from the lateral nasal wall, resulting in extra turbinates. When viewed by nasal endoscopy, these anomalies give the appearance of a double middle turbinate (Fig. 96.1). However, there is controversy regarding the incidence of the secondary middle turbinate. Estimates of its incidence range from 0.8% to 14.3% (Khanobthamchai et al. 1991 a; Aykut et al. 1994; Kantarci et al. 2004). It is a bony structure covered by mucosa and originating from the lateral wall of the middle meatus, as illustrated in Figure 96.2 c. Several origins have been described including the lateral wall of

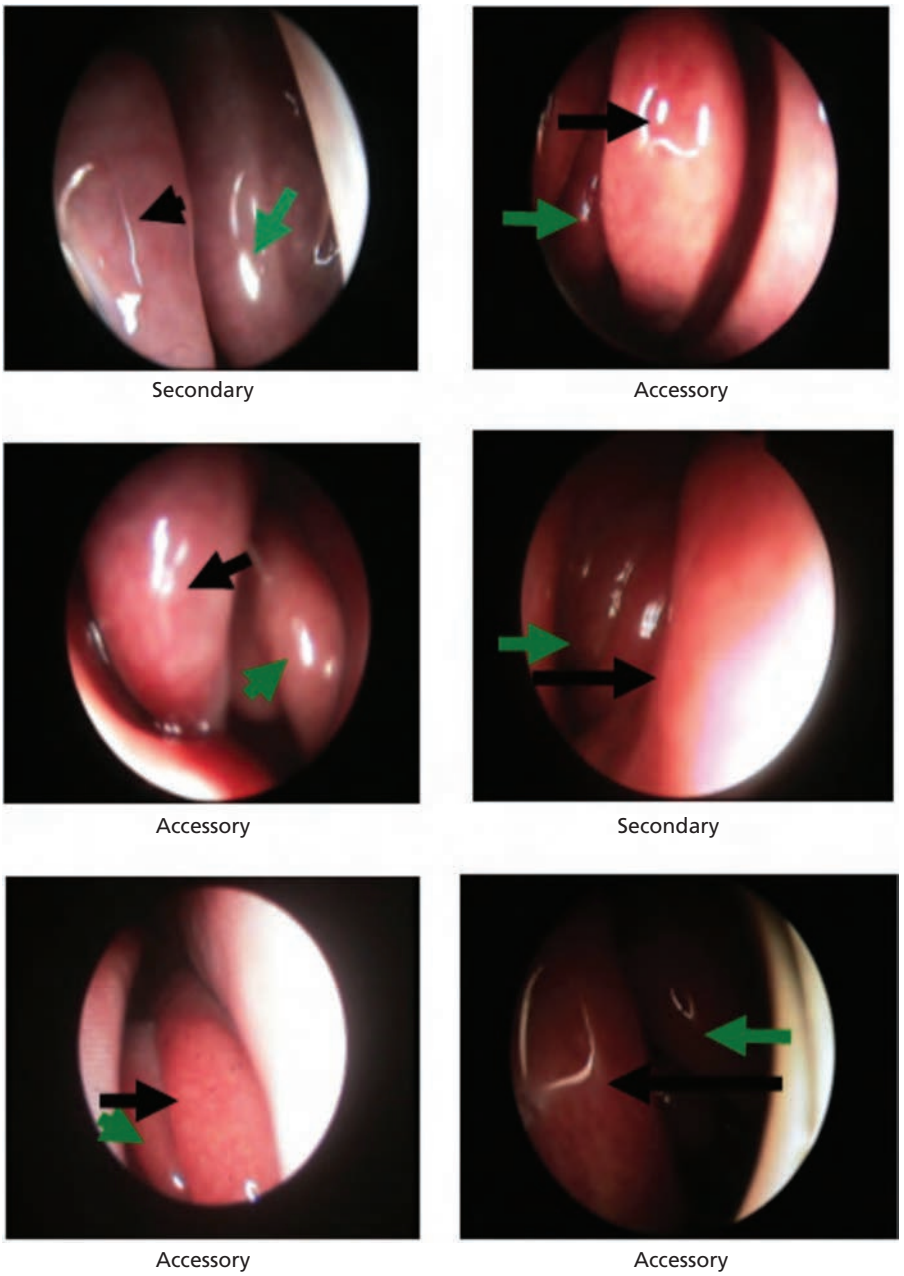

Figure 96.1 Endoscopic view of the middle meatus after application of a diluted adrenaline pack to the middle meatus. Black arrows represent the middle turbinate while green arrows represent the extra turbinate (accessory or secondary). Photos are from different patients presenting mainly with refractory frontal headache and blocked nose. Note that the endoscopic view cannot differentiate between the accessory and the secondary middle turbinates.

Source: El-Shazly et al. (2012). Reproduced with permission from John Wiley & Sons.

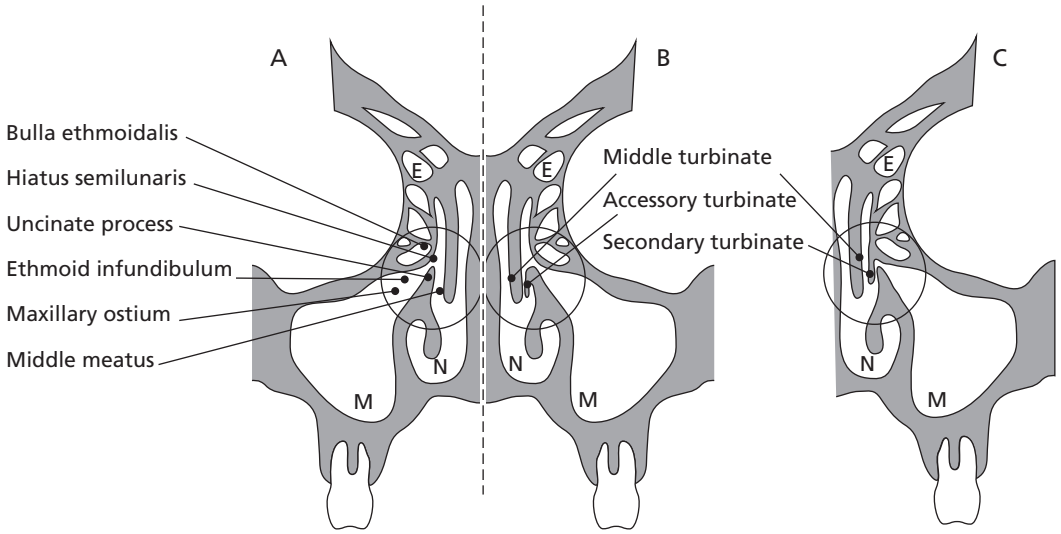

Figure 96.2 (a–c) Schematic illustration of the coronal view of a normal rhinosinusal anatomy, demonstrating the relationship between the maxillary sinus (M), ethmoid (E), and nasal fossae (N). The ostiomeatal unit (in circle) is composed of the middle turbinate, the bulla ethmoidalis, and the uncinate process. These structures define the middle meatus, the hiatus semilunaris, the ethmoid infundibulum, and the maxillary ostium.

Source: El-Shazly et al. (2012). Reproduced with permission from John Wiley & Sons.

the ethmoid bulla or the lamina papyracea (Aouad and Strong 2010). This extra turbinate can extend in a superomedial or inferomedial direction (Khanobthamchai et al. 1991 a; Apaydin et al. 2002), as seen in Figure 96.3 a. It is usually bilateral and is not associated with sinusitis, since it does not compromise the ostiomeatal complex (Khanobthamchai et al. 1991 a; Aykut et al. 1994). Another variation giving the same endoscopic appearance as a secondary middle turbinate is the accessory middle turbinate. This is regarded as a medially bent uncinate process, as illustrated in Figures 96.1b and 96.3b. Isobe et al. (1998) dissected 136 hemi-sectioned heads investigating the variations of the uncinate process. The authors detected only three cases of a medially curved uncinate process, all of which were classified as type (N), that is, free process with no articulation with the surrounding structures except for the ethmoid bone at the base of the uncinate process. El-Shazly et al. (2012) studied the incidence of the secondary and accessory middle turbinates over a two-year period in a rhinology clinic practice and found it to be present in 2% of patients seen for refractory rhinological symptoms. These variations affected males more than females of various ethnic origins, and were more striking in black Africans. They could exist unilaterally, bilaterally, or both in the same patient. Associated anomalies included concha bullosa, large

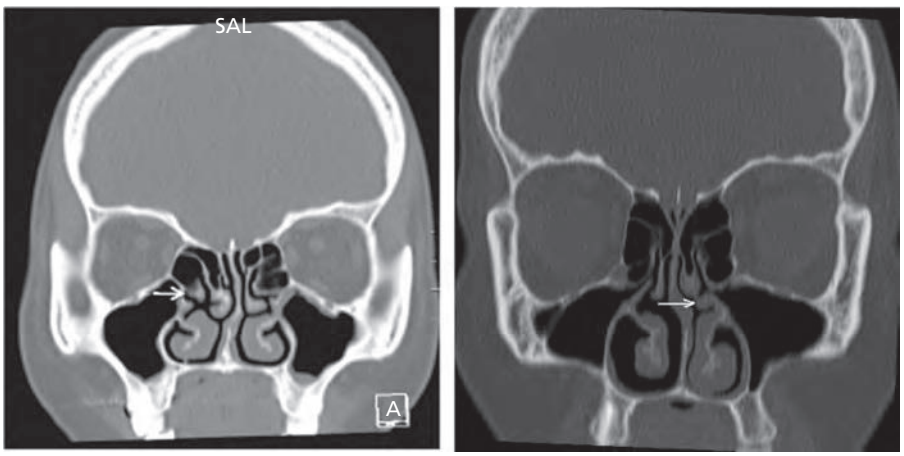

Figure 96.3 CT-Scan coronal cuts revealing (a) a secondary middle turbinate originating from the lateral wall of the middle meatus and projecting into the middle meatus in a inferior and medial direction (arrow), and (b) a left accessory middle turbinate protruding above the inferior turbinate (arrow).

Source: El-Shazly et al. (2012). Reproduced with permission from John Wiley & Sons.

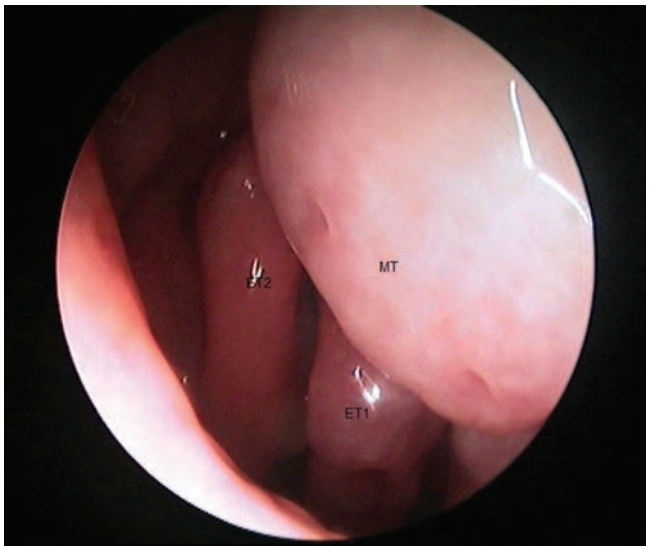

Figure 96.4 Endoscopic nasal view illustrating the triple middle turbinate anomaly. MT: middle turbinate; ET: extra turbinate.

prominent bulla ethmoidalis, paradoxical middle turbinate, and ethmomaxillary sinus.

Trifurcate and triple middle turbinate

Another variation of this structure is the trifurcate middle turbinate, in which the middle turbinate seems to have a single root (Eweiss et al. 2008). The real incidence of this variation is not clear. The present author detected only one unilateral case of triple middle turbinate during nasal endoscopic examinations (Fig. 96.4). The patient presented with unilateral nasal obstruction without obstruction of the ostiomeatal complex or associated sinusitis.

Figure 96.5 Coronal CT-scan view illustrating bilateral paradoxical curvature of the middle turbinate.

Aberrant middle turbinate

This is a very rare variation of the middle turbinate. Only one case report is found in the English literature (Lee et al. 2008). Here the middle turbinate is straightened anteriorly, curves posteromedially around the posterior free edge of the nasal septum, and extends into the nasopharynx. This is unilateral with no other associated anomalies.

Paradoxical middle turbinate

Paradoxical curvature of the middle turbinate refers to convex curvature on the lateral side of the structure (Fig. 96.5). Reports about the incidence of this variation differ. In one study of 200 CT scans, it was detected in 3% (Arslan et al. 1999). Another study of 133 CT scans detected this variation in 5.3% (Lerdlum and Vachiranubhap 2005). Another study looked at the incidence of the paradoxical middle turbinate in relation to ethnic origin by comparing a cohort of 100 Caucasian patients undergoing endoscopic sinus surgery in London and 100 Chinese patients treated in Hong Kong. The paradoxical middle turbinate was more common in Caucasians (Badia et al. 2005).

Pneumatization of the middle turbinate (concha bullosa)

Pneumatization of the middle turbinate is a frequent variation with an estimated incidence of 14–53.6%, being more common in Caucasians. Concha bullosa invading the maxillary sinus has recently been reported (Ozturan and Degirmenci 2013). In a recent study investigating the anatomical characteristics and variations of three segments of middle turbinate bones using tri-planar computed tomographic (CT) projections obtained from 200 bones of 100 normal adult Chinese subjects, 48 bones of the vertical segment were pneumatized on both sides, 14 were pneumatized on one side and 21 had paradoxical curvature. The distribution of pneumatized concha bullosa bones (based on shape) was as follows: 41 lamellar, five bulbous, and seven extensive types (Wu et al. 2014). Concha bullosa is a radiological diagnosis and can exist without rhinological symptoms. However, if the pneumatization of the middle turbinate is very large, it can present with headache, compromise the ostiometal unit, and predispose to the development of sinusitis.

Variations of the superior turbinate

The reported variation of this structure is the pneumatized superior turbinate. The anomaly can exist alone or rarely in conjunction with pneumatization of other turbinates (Clerico 1996). Few reports have demonstrated pneumatization of all six turbinates in the same patient (Sagit et al. 2008; Ozturan et al. 2013). This anomaly can contribute to endonasal contact point headache.

Variations of the maxillary sinus

Several anomalies of the maxillary sinus have been reported. These include hypoplasia/aplasia, atelectic maxillary sinus, septated maxillary sinus, and sinus with accessory ostium for drainage.

Hypoplasia and aplasia

The maxillary sinus is the largest of all paranasal sinuses. It is present at birth as rudimentary air cells and develops throughout childhood. Normally both sides develop at similar rates, and this is reflected in the symmetry of facial morphology. However, anomalies such as hypoplasia to aplasia can occur. These variations affect the maxillary and frontal sinuses more than other sinuses. Sometimes this hypoplasia is associated with segmental odontomaxillary dysplasia (Gonzalea-Arriagada et al. 2010). Maxillary hypoplasia is usually unilateral but bilateral cases have been reported (Celebi et al. 2012). Combined aplasia of several sinuses can also occur. For example, Guven et al. (2010) reported combined aplasia of the sphenoid, frontal, and maxillary sinuses with hypoplatic ethmoid cells with no systemic or skeletal disease.

Maxillary sinus atelectasis

Maxillary bone loss and atelectasis of the sinus walls can be associated with chronic clinical or subclinical maxillary sinusitis (Antonelli et al. 1992; Hourany et al. 2005). Ostial obstruction and inflammation-mediated osteopenia have been proposed as responsible mechanisms. The condition results in cosmetic facial deformity, and possibly descent of the orbital contents and the development of diplopia due to enophthalmos when the sinus orbital floor is affected (Fig. 96.6). When the condition is recognized in association with sinusitis, a middle meatal antrostomy is indicated to prevent further atelectasis.

Maxillary sinus septa

A septated maxillary sinus can complicate endoscopic sinus surgery and should be differentiated from the ethmomaxillary sinus (see "Ethmomaxillary sinus" below). Rosano et al. (2012) performed a Medline search limited to studies published in English from 1980 to January 2009, and found 22 articles. The prevalence of maxillary sinus septa ranged over 14.3–33.3%. There was no specific geographical distribution within the sinuses. The mean heights of septa ranged over 2.8–8.1 mm.

Accessory maxillary sinus ostia

The maxillary sinus ostium for drainage is located high anterosuperiorly on the medial wall of the maxillary sinus and opens into the hiatus semilunaris of the lateral nasal cavity either posteriorly or inferiorly to the free edge of the uncinate process. There is sometimes an extra opening into the maxillary sinus. Prasanna and Mamatha (2010) studied 40 cadavers and found accessory maxillary ostia (of Giraldes) in nearly 75% of them, each opening into a membranous meatus inferior to the uncinate process. The present author also noticed this variation in some patients presenting with accessory middle turbinates (unpublished data).

Variations of ethmoidal air cells

The bony ethmoidal labyrinth is pyramidal in shape, about 4–5 cm in width and 2.5–3 cm in height, and is composed of 7–11 air cells. The sigmoid attachment of the middle turbinate to the lateral nasal wall (basal lamella) represents the boundary between the anterior and posterior ethmoidal cells. The most posterior ethmoid air cell is a pyramidal sinus with

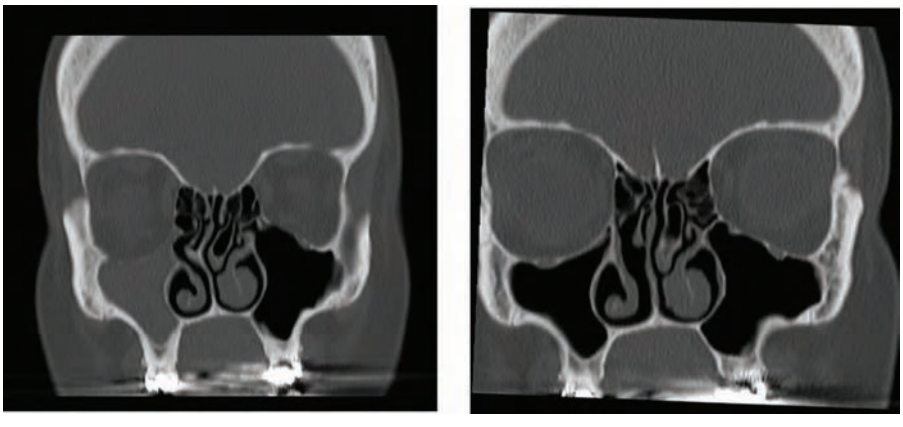

A B

Figure 96.6 CT-scan coronal views. (a) Right atelectasis with maxillary sinusitis. The atelectasis affected the orbital floor with dehesicence in the inferomedial orbital rim. This patient presented with vertigo and symptoms of maxillary sinusitis associated with enophthalmos and diplopia. Associated variations included nasal septum deviated towards the right with left concha bullosa of the middle turbinate. (b) Same patient six months post-operatively (middle meatal antrostomy and septoplasty, with complete aeration of the maxillary sinus and straight septum).

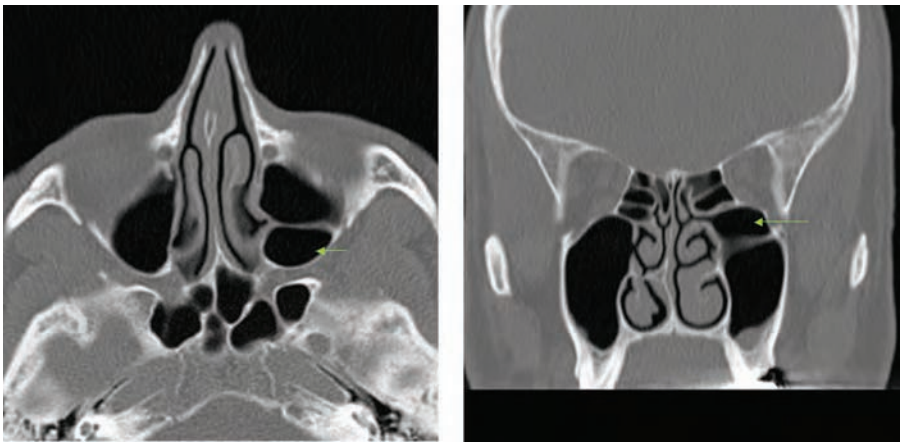

A B

Figure 96.7 The ethmomaxillary sinus indicated by the arrows: (a) axial view; and (b) coronal view.

its apex directed posterolaterally within the lateral wall of this sinus; the bony canal of the optic nerve runs towards its apex. The posterior reach of this sinus is often lateral to and behind the anterior face of the sphenoid sinus and is referred to as the sphenoethmoidal cell (Onodi cell). Drainage of the anterior group of cells is in the middle meatus while the posterior group of cells drains into the superior meatus at its anterior recess. Variations of the ethmoidal air cells are described in the following sections.

Onodi cells

Onodi cells are the posterior-most ethmoid air cells that lie superior to and pneumatize into the sphenoid sinus. Identification of these cells is essential prior to endoscopic sinus and skull base surgery due to their relationship to the optic nerves and carotid arteries. The incidence of Onodi cells ranges over 7–24%, but in a recent study of high-resolution computed tomography scans from 170 adult patients, Tomovic et al. (2012) reported an overall prevalence of Onodi cells of 65.3%. Onodi cell prevalence was equivalent among males and females. Sandulescu et al. (2011) reported a unilateral sphenoethmoid cell (SEC), Onodi-positive, overriding not only the superior aspect of the sphenoid but also its lateral side, being intimately related to the maxillary nerve.

Haller cells

These are infraorbital ethmoid cells resulting from extensions of ethmoid air cells into the areas of the floor of the orbit or into the roof of the maxillary sinus. They originate from either the anterior or the posterior ethmoidal cells and are seen in 40% of patients. These cells can occur unilaterally or bilaterally. They can be excessively pneumatized and therefore contribute to obstruction of the ostiomeatal complex area. Rarely, there is mucocele of the Haller cell (Luxenberger et al. 1999). Haller cells can push the natural ostium of the maxillary sinus downward and anteriorly causing difficulties during surgery. If this condition is not recognized preoperatively, the risk of orbital complications during surgery increases.

Agger Nasi cells

The Agger Nasi air cells, also called the nasoturbinal concha and the nasal ridge, are the most anterior ethmoidal air cells, lying anterolateral and inferior to the frontoethmoidal recess and anterior and above the attachement of the middle turbinate. The reported incidence of these cells varies from one study to another (10–98%); overall, they are identified in approximately 90% of patients. The orbit, the lacrimal sac, and the nasolacrimal duct are its lateral relations. Agger Nasi cell pneumatization with narrowing of the frontal sinus outflow tract is a significant cause of persistent frontoethmoid pain and chronic frontal sinusitis. Hypoplasia or absence of Agger Nasi cells is closely associated with hypoplastic frontal sinuses (Earwaker 1993).

Ethmomaxillary sinus

The ethmomaxillary sinus is an enlarged posterior ethmoidal air cell within the maxillary sinus that drains in the superior meatus (Khanobthamchai et al. 1991b), as demonstrated in Figure 96.7. Its incidence ranges over 0.7–1.9%, and reports differ concerning the percentages of unilateral or bilateral cases and associated anatomical variations (Sirikçi et al. 2004; El-Shazly et al. 2012). This anomaly could make endoscopic anatomical orientation difficult during endoscopic surgery, giving the impression of a septate maxillary sinus. Entry into it can be mistaken for the maxillary sinus, especially if the ethmomaxillary sinus is large. Preoperative identification of this anomaly by CT scanning is therefore mandatory for reducing the incidence of surgical complications.

Variations of the uncinate process

The uncinate process is a thin bony structure arising from the posteromedial border of the nasolacrimal duct. It is a very important landmark in functional endoscopic sinus surgery. Variations of the uncinate process include hypoplasia/aplasia, hypertrophy, pneumatization, deviation, and variations of the attachment. Hypoplasia and aplasia of the uncinate process are closely linked to hypoplasia of the maxillary sinus (Bolger et al. 1990; Okur et al. 2001). Excessive hypertrophy of the uncinate process can necessitate osteotomy during dacryocystorhinostomy (Mehta and Puri 2008). Pneumatization of the uncinate process if large enough can compromise the drainage of the anterior group of sinuses (frontal sinus, anterior ethmoid air cells, and the maxillary sinus). Inflammation involving a pneumatized uncinate with formation of a mucocele could present a challenge to clinical diagnosis (Burrows 2011). A deviation of the uncinate process, if it is bent medially, can project into the middle meatus resulting in an accessory middle turbinate (El-Shazly et al. 2012). Lateral deviation of the uncinate process can compromise sinuses drainage and result in sinusitis.

Variations of the superior attachment of the uncinate process were studied by CT-scan images and classified into six types by Landsberg and Friedman (2001): type 1, insertion into the lamina papyracea (52%); type 2, insertion into the posterior wall of the Agger Nasi cell (18.5%); type 3, insertion into the lamina papyracea and junction of the middle turbinate with the cribriform plate (17.5%); type 4, insertion into the junction of the middle turbinate with the cribriform plate (7%); type 5, insertion into the skull base (3.6%); and type 6, insertion into the middle turbinate (1.4%). On the basis of this classification, another study (Liu et al. 2010) of the incidence of these variations in 264 sides of 132 patients with identifiable superior attachments of the uncinate process (UP) in a Taiwanese population found that a single insertion of the UP into the lamina papyracea was the most common type (70.4%). The other types of UP superior attachment had the following distribution: 10.2% into the middle turbinate; 7.6% into the lamina papyracea and the skull base; 6.1% into the skull base; 4.9% into the lamina papyracea and the middle turbinate; and 0.8% into the middle turbinate and the skull base. This could also reflect ethnospecific incidences of the type of superior attachment of the uncinate process.

Isobe et al. (1998) studied the morphology of the UP and nasal fontanelle in 119 human cadaver specimens. The authors described the uncinate attachment as follows. Type I: The infero-posterior tip of the UP is articulated to the inferior turbinate. This was the most frequently observed type. Subtype I-b: The UP adheres to the inferior turbinate along the antero-inferior margin. Type N: The tip of the UP has no articulation and forms a free edge. Type S: The tip articulates to the superior structures, such as the bulla ethmoid, medial orbital wall, tegument of the maxillary sinus, and basal area of the ethmoid sinus. Type P: The tip articulates with the perpendicular plate of the palatine bone.

Frontal and sphenoid sinuses pneumatization

These sinuses can be pneumatized to various extents. Pneumatization of the sphenoid sinuses involves fusion of several ossification centers during intrauterine life (Cope 1917; Van Alayea 1951; Peele 1975). Pneumatization recesses to the greater sphenoid wing or laterally to the smaller sphenoid wing and anterior clinoid process can occur. The sphenoid sinus may be absent or have air extension into the dorsum sellae, posterior clinoid processes, or pterygoid plates. Pneumatization extensions into the greater wing are usually in a downward direction towards the pterygoid base. The lateral pneumatization extension into the lesser wing of sphenoid may be in an anterolateral direction above the optic nerve or in a posterolateral direction below the optic nerve.

Earwaker (1993) evaluated CT scans of 800 patients prior to endoscopic nasal surgery. He reported the presence of inferolateral recesses in 114 cases, and in 13 cases there was a further anterolateral extension into the posterior aspect of the lateral orbital wall. On the other hand, bilateral absence or hypoplasia of the sphenoid sinsues (Orhan 1996) are also variations of pneumatization. In a recent study utilizing cone beam tomography (Guldner et al. 2012) the authors studied 580 patients and were able to describe different variants of pneumatization: type I, absent or hypoplastic sinus; type II, the posterior wall of the sphenoid sinus is in front of the anterior wall of the sella; type III, the posterior wall is between the anterior and posterior walls of the sella; type Iva, the posterior wall is behind the posterior wall of the sella without air dorsal to the sella; and type IVb, similar to type IVa but with air dorsal to the sella.

Pneumatization of the frontal sinuses results from extensions from the anterior ethmoidal air cells. These extension-variations include aplastic, hypoplastic, or asymmetrical sinuses on both sides. Recesses related to the frontal sinus can be observed toward the lamina of the frontal bone, crista galli, or anterior ethmoidal air cells.

References

Antonelli PJ, Duvall AJ, Teitelbaum SL. 1992. Maxillary sinus atelectasis. *Ann Otol Rhinol Laryngol* 101: 977–981.

Aouad RK, Strong EB. 2010. Secondary middle turbinate. *Otolaryngol Head Neck Surg* 142: 140–141.

Apaydin FD, Duce MN, Yildiz A, Egilmez H, Ozer C, Talas US. 2002. Inferomediallyprojecting pneumatised secondary middle turbinate. *Eur J Radiol* 43: 42–44.

Arredondo de Arreola G, Lopez Serna N, De Hoyos Parra R. 1996. Morphogenesis of the lateral nasal wall from 6 to 36 weeks. *Otolaryngology Head Neck Syrg* 114: 54–60.

Arslan H, Aydinlioglu A, Bozkurt M, Egeli E. 1999. Anatomic variations of the paranasal sinuses: CT examination for endoscopic sinus surgery. *Auris Nasus Larynx* 26: 39–48.

Aydin O, Ustundag E, Ciftci E, Keskin G. 2001. Pneumatization of the inferior turbinate. *Auris Nasus Larynx* 28: 361–363.

Aykut M, Gumusburun E, Muderris S, Adiguzel E. 1994. The secondary nasal middleconcha. *Surg Radiol Anat* 16: 307–309.

Badia L, Lund VJ, Wei W, Ho WK. 2005. Ethnic variation in sinonasal anatomy on CT-scanning. *Rhinology* 43: 210–214.

Bolger WE, Woodruff WW, Morehead J, Parsons DS. 1990. Maxillary sinus hypoplasia/classification and description of associated uncinated process hypoplasia. *Otolaryngol Head Neck Surg* 103: 759–765.

Burrows SA. 2011. Mucocele of a pneumatized uncinate process: first reported case. *J Laryngol Otol* 125: 635–637.

Caylakli F, Yilmaz I, Hurcan C, Ozer C, Ozluoglu L. 2008. Unilateral inferior turbinate agenesis: a case report. *Ear Nose Throat J* 87: 26–27.

Celebi S, Taskin U, Altin F, Ozkul MH. 2012. Bilateral aplasia of paranasal sinuses. *Eur Arch Otorhinolaryngol* 269: 1055–1057.

Christmas DA, Merrell RA. 2004. Pneumatized inferior turbinatea; report of three cases. *Ear Nose Throat J* 83: 152–153.

Clerico DM. 1996. Pneumatized superior turbinate as a cause of referred migrane headache. *Laryngoscope* 106: 874–879.

Cope VZ. 1917. The internal structure of the sphenoid sinus. *J Anat* 51: 125–136.

Earwaker J. 1993. Anatomic variants in sinonasal CT. *Radiographics* 13: 381–415.

El-Shazly AE, Poirrier AL, Cabay J, Lefebvre PP. 2012. Anatomical variations of the lateral nasal wall: The secondary and accessory middle turbinates. *Clin Anat* 25: 340–346.

Eweiss A, Khatwa MM, Zeiton H. 2008. Trifurcate middle turbinate: an unusual anatomical variation. *Rhinology* 46: 246–248.

Gonzalea-Arriagada WA, Vargas PA, Fuentens-Cortes R, Nasi-Toso M., Lopes MA. 2010. Segmental odontomaxillary dysplasia: report of 3 cases and literature review. *Head Neck Pathol* 6: 171–177.

Guldner C, Pistorius SM, Diogo I, Bien S, Sesterhenn A, Werner JA. 2012. Analysis of pneumatization and neurovascular structures of the sphenoid sinus using cone-beam tomography (CBT) *Acta Radiol* 53: 214–219.

Gumusalan Y. 1977. Coincidence of bilateral hypogenesis and unilateral agenesis of the turbinates (conchae nasales) in man. *J Otolaryngol* 26: 392–395.

Guven DG, Yilmaz S, Ulus S, Subasi B. 2010. Combined aplasia of sphenoid, frontal, and maxillary sinuses accompanied by ethmoid sinus hypoplasia. *J Craniofac Surg* 21: 1431–1433.

Hourany R, Aygun N, Charley C. Della Santina CC, Zinreich SJ. 2005. Silent sinus syndrome: an acquired condition. *AJNR Am J Neuroradiol* 26: 2390–2392.

Isobe M, Murakami G, Kataura A. 1998. Variations of the uncinate process of the lateral nasal wall with clinical implications. *Clin Anat* 11: 295–303.

Kantarci M, Karasen RM, Alper F, Onbas O, Okur A, Karaman A. 2004. Remarkable anatomic variations in paranasal sinus region and their clinical importance. *Eur J Radiol* 50: 296–302.

Khanobthamchai K, Shankar L, Hawke M, Bingham B. 1991 a. The secondary middle turbinate. *J Otolaryngol* 20: 412–413.

Khanobthamchai K, Shankar L, Hawke M, Bingham B. 1991b. Ethmomaxillary sinus and hypoplasia of maxillary sinus. *J Otolaryngol* 20: 425–427.

Kharoubi S. 2010. Pneumatization (concha bullosa) of the inferior turbinate: *Case report and literature review Rev Laryngol Otol Rhinol (Bor)* 131: 321–324.

Landsberg R, Friedman M. 2001. A computer-assisted anatomical study of the nasofrontal region. *Laryngoscope* 111: 2125–2130.

Lee JH, Koh SH. 2011. A variant form of bifid inferior turbinate. *Ear Nose Throat J* 90: E33–34.

Lee PH, Lee AS, Bhadelia RA. 2008. Aberrant middle turbinate masquerading as a nasopharyngeal mass. *Am J Neuroradiol* 29: 1564–1565.

Lee SY, Bae KE, Lee HB, Cho WH, Kim JH, Cho HS, Lee JH. 2012. Bilateral accessory inferior turbinates and secondary middle turbinates. *Jap J Radiol* 30: 530–532.

Lerdlum S, Vachiranubhap B. 2005. Prevalence of anatomic variation demonstrated on screening sinus computed tomography and clinical correlation. *J Med Assoc Thai* 88(4): S110–115.

Liu SC, Wang CH, Wang HW. 2010. Prevalence of the uncinate process, agger nasi cell and their relationship in a Taiwanese population. *Rhinology* 48: 239–244.

Luxenberger W, Anderhuber W, Stammberger H. 1999. Mucocele in an orbitoethmoidal (Haller's) cell (accidentally combined with acute contralateral dacryocystitis). *Rhinology* 37: 37–39.

Mehta A, Puri N. 2008. An unusual variation in the anatomy of the uncinate process in external dacryocystorhinostomy. *Indian J Ophthalmol* 56: 413–416.

Naiboglu B, Yaylaci A, Oysu C. 2011. Paradoxical giant inferior concha. *Ear Nose Throat J* 90: E18–19.

Okur E, Okur N, Aksungur EH, Kiroglu M, Inal M, Soyupak S. 2001. Aplasia of bilateral uncinate processes with bilateral nasomaxillary cavity. *Eur J Radiol* 38: 47–49.

Orhan M, Govsa F, Saylam C. 1996. A quite rare condition: absence of sphenoidal sinuses. *Laryngoscope* 106: 874–879.

Ozcan KM, Selcuk A, Ozcan I, Akdogan O, Dere H. 2008. Anatomical variations of nasal turbinates. *J Craniofac Surg* 19: 1678–1682.

Ozturan O, Degirmenci N. 2013. Pneumo-concha dilatans; middle concha growing in anterior and lateral directions. *J Craniofac Surg* 24: 444–446.

Ozturan O, Yenigun A, Degirmenci N, Yilmaz F. 2013. Conchae bullosis: a rare case with bilateral triple turbinate Pneumatizations. *J Laryngol Otol* 127: 73–75.

Ozturk A, Alatas N, Ozturk E, San I, Sirmatel O, Kat N. 2005. Pneumatization of the inferior turbinates: incidence and radiologic appearance. *J Comput Assist Tomogr* 29: 311–314.

Peele JC. 1975. Unusual anatomical variations of the sphenoid sinuses. *Laryngoscope* 67: 208–237.

Pittore B, Al Safi W, Jarvis SJ. 2011. Concha bullosa of the inferior turbinate: an unusual cause of nasal obstruction. *Acta Otorhinolaryngol Ital* 31: 47–49.

Prasanna LC, Mamatha H. 2010. The location of maxillary sinus ostium and its clinical application. *Indian J Otolaryngol Head Neck Surg* 62: 335–337.

Rice D. 1995. Embryology. In: *The Sinuses* (eds PJ Donald, JL Gluckman, DHRice). New York: Raven Press, pp. 15–24.

Rosano G, Gaudy JF, Chaumanet G, Del Fabbro M, Taschieri S. 2012. Maxillary sinus septa. Prevalence and anatomy. *Rev Stomatol Chir Maxillofac* 113: 32–35.

Sagit M, Saka C, Kuran G, Akin I. 2008. An unusual pneumatization of turbinates. *B-ENT* 4: 101–103.

Sandulescu M, Rusu MC, Ciobanu IC, Lie A, Jianu AM. 2011. More actors, different play: sphenoethmoid cell intimately related to the maxillary nerve canal and cavernous sinus apex. *Rom J Morphol Embryol* 52: 931–935.

Selcuk A, Ozcan KM, Ozcan I, Dere H. 2008. Bifid inferior turbinate: a case report. *J Laryngol Otol* 122: 647–649.

Sirikçi A, Bayazit YA, Bayram M, Kanlikama M. 2004. The ethmomaxillary sinus: a particular anatomic variation of the paranasal sinuses. *Eur Radiol* 14: 281–285.

Spear SA, Brietzke SE, Winslow C. 2003. Bilateral bifid inferior turbinates. *Ann Otol Rhinol Laryngol* 112: 195–196.

Stammberger HR, Kennedy DW. 1995. Paranasal sinuses: anatomic terminology and nomenclature. The Anatomic Terminology Group. *Ann Otol Rhinol Laryngol Suppl* 167: 7–16.

Tomovic S, Esmaeili A, Chan NJ, Choudhry OJ, Shukia PA, Liu JK, Eloy JA. 2012. High resolution computed tomography analysis of the prevalemce of onodi cells. *Laryngoscope* 122: 1470–1473.

Van Alayea OE. 1951. *Nasal Sinuses: An Anatomic and Clinical Consideration*. Baltimore, MD: Williams and Wilkins.

Waldhera R, Garg A, Gulati SP, Ghai A, Kalra V. 2010. Extremely rare anatomical anomalies of turbinates: sagittally clefted middle turbinate and inferior turbinate agenesis. *Pakistan J Otolaryngol* 26: 32–33.

Wu HB, Yuan HS, Zhu L. 2014. Tri-planar computed tomographic projection of three segments of the middle turbinate in a Chinese population. *Eur Arch Otorhinolaryngol* 271(3): 511–518.

97 Ear

Aman Deep[1], Martin M. Mortazavi[2] and Nimer Adeeb[1]
[1]Children's of Alabama, Birmingham, Alabama, USA
[2]University of Washington School of Medicine, Seattle, Washington, USA

Anatomical observations are very important for determining the shape, position, and variations of the ear. An anatomical variation can be an isolated anomaly or part of a syndrome and its effect can range from no defect to complex hearing loss. The ear has a very complex structure and careful observations can help in the diagnosis of anomalies and syndromes. The purpose of this chapter is to describe anatomical variations of the ear.

Variations of the external ear

Various classifications are used in the literature to describe anomalies of the external ear. Recently, Hunter and Yotsuyanagi (2005) published a classification modified from the Weerda classification (Table 97.1). They divided the anomalies into three grades of dysplasia. Grade I anomalies entail minor variations that do not warrant the use of skin and cartilage to repair the structural defect. The category includes macrotia, anomalies of the pinna (protruding ear, cryptotia, Darwin's tubercle, satyr ear, Stahl ear, shell ear, Mozart ear, and lop ear), absent helical cleft, and anomalies of the lobule and tragus. Grade II dysplasia or second-degree microtia includes anomalies where some normal ear features are detectable and reconstruction requires the use of additional skin and cartilage. This grade covers severely deformed cup ear and mini ear. In Grade III dysplasia, no normal ear features are detectable and complete reconstruction is required. This category includes microtia (unilateral or bilateral) with external acoustic meatus atresia, and anotia or complete absence of the ear.

Table 97.1 Classification of anomalies of external ear. Adapted from Hunter and Yotsuyanagi (2005).

Grade of dysplasia	Types
Grade I	1. Enlarged ear 2. Anomalies of pinna: cryptotia, protruding ear, satyr ear, Stahl ear, Darwin's tubercle, Shell ear, Mozart ear, lop ear Lop ear is divided into mild and moderate malformation: 1. Mild anomalies: helical folding lies above the Darwin tubercle: (a) hiding helix; and (b) constricted helix type IV A 2. Moderate anomalies: helical folding lies above the Darwin tubercle: (a) absence of helix or cleft in helix; (b) anomalies of lobule; and (c) anomalies of tragus
Grade II	1. Cup ear 2. Mini ear
Grade III	1. Microtia (unilateral or bilateral) with external canal atresia 2. Anotia

Microtia

Microtia is a congenital anomaly where the pinna is underdeveloped (Luquetti et al. 2012). It ranges from mild structural abnormality to absence of the ear/anotia (Fig. 97.1). Terminologies ranging from "microtia"/"microtia/anotia" to "microtia-anotia" are used in the literature. It can occur as an isolated anatomical anomaly or as part of a syndrome. Sufferers are predominantly male. Microtia is unilateral in 77–93% of cases with 60% involvement of the right ear. The incidence is 0.8–2.4 per 10,000 live births. Hispanics and Asians have a higher prevalence than African Americans and Europeans. The highest incidence of 8.3 per 10,000 live births has been reported in Navajo Indians (Luquetti et al. 2012).

Various risk factors have been reported including maternal diabetes mellitus, low birth weight, advanced maternal age, exposure to thalidomide, retinoic acid derivatives, and mycophenolate mofetil. There is some association of microtia with autosomal trisomies (18, 21, and 22) and trisomy 13 and 18 mosaicism. Single-gene disorders, for example *SIX1* and *EYA1* and chromosomal translocation 6p24, are also reported to be associated with microtia.

Herman Marx (1926) proposed the first and most frequently used classification system for the condition. He divided microtia

Bergman's Comprehensive Encyclopedia of Human Anatomic Variation, First Edition. Edited by R. Shane Tubbs, Mohammadali M. Shoja and Marios Loukas.
© 2016 John Wiley & Sons, Inc. Published 2016 by John Wiley & Sons, Inc.

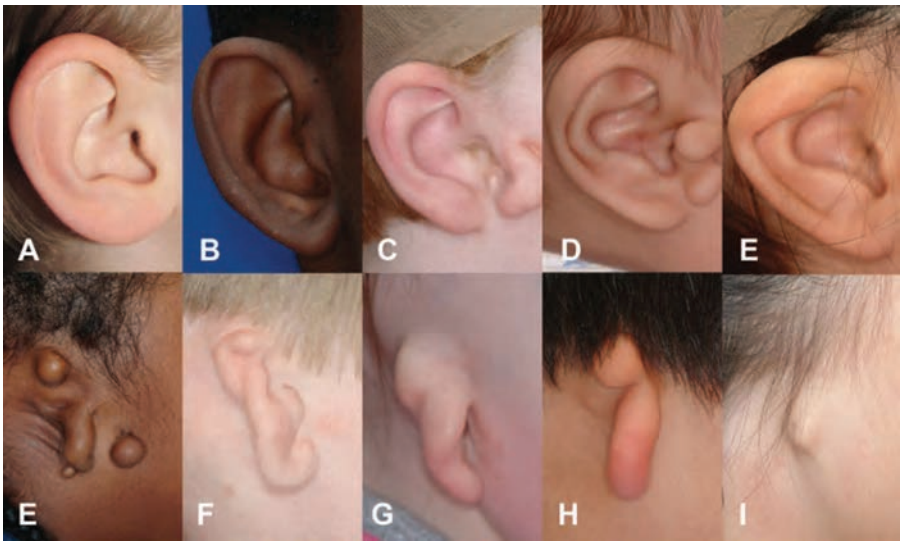

Figure 97.1 Variations of microtia: (a) typical ear; (b–d) first-degree dysplasia; (e) second-degree dysplasia; and (f–i) third-degree dysplasia.

Source: Luquetti et al. (2012). Reproduced with permission from John Wiley & Sons.

into three grades based on identification of auricular landmarks. Rogers (1968) added grade IV microtia (anotia) to the existing Marx classification. Tanger (1978) published a surgical approach-based classification system, and Weerda (1988) modified both of these systems and developed a new one. His classification was based on embryological variations and surgical classification as well as other external ear deformities and minor anomalies. Hunter and Yotsuyanagi (2009) recently published a classification to standardize the terminologies referring to the external ear (Table 97.2).

Table 97.2 Classifications of microtia. Adapted from Luquetti et al. (2012).

Grade/type	Description	Grade/degree	Description
Herman Marx Classification		*Weerda Classification*	
Grade I	Auricle is abnormal but all landmarks are identifiable	Grade I First-degree Malformations	Macrotia, prominent ear, and cryptotia; Scaphoid ear, transverse cleft(coloboma), Stahl ear; Satyr ear; Darwin tubercle, defromed tragus and antitragus, helix crus absence; Lobular deformities: aplastic, hypoplastic and hyperplastic lobe, lobular fixation and lobular cleft; Deformity of cup ear I, IIa, IIb.
Grade II	Auricle is abnormal and few landmarks are identifiable	Grade II Second-degree malformations	Deformity of cup ear III; Microtia: hypopastic upper pinna, hypoplastic middle pinna, and hyoplastic or aplastic lower pinna
Grade III	Anotia	Grade III Third-degree Malformations	Grade III unilateral or bilateral microtia; Anotia
Tanger Classification		*Hunter Classification*	
Type I	Complete absence of ear (anotia)	Microtia First-degree	All normal ear components are present and the median longitudinal length of ear is greater than two standard deviations below the mean
Type II	Complete hypoplasia of ear with and without external acoustic meatus atresia (microtia)	Microtia Second-degree	Presence of few normal ear components and median longitudinal length of ear is greater than two standard deviations below the mean
Type III	Hypoplastic middle third of auricle	Microtia Second-degree	Some auricular structures are present but these structures do not conform to recognized ear component
Type IV	Hypoplastic superior third of auricle, cup and lop ear and cryptotia	Anotia	Ear is completely absent
Type V	Prominent ear		

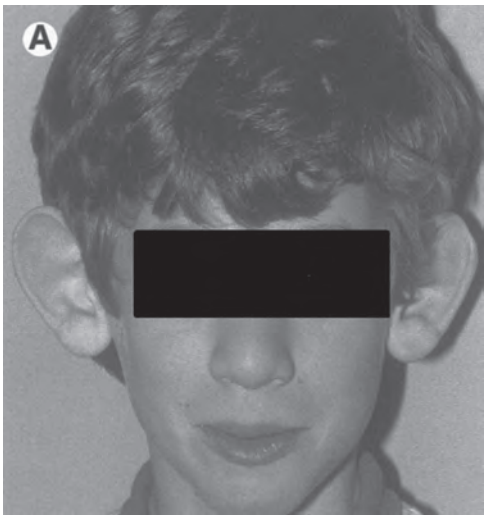

Figure 97.2 Macrotia.

Source: Bauer (1997). Reproduced with permission from Elsevier.

Figure 97.3 Protruding ear.

Source: Hunter and Yotsuyanagi (2005). Reproduced with permission from John Wiley & Sons.

Macrotia

Macrotia is an abnormal enlargement of the pinna (Fig. 97.2): an ear with length for age measurement above the 97th percentile. An adult ear has a width range of 3–4.5 cm and length range of 5.5–7 cm, and the term macrotia is used when the ear measures more than these values. Feingold and Bossert (1974) proposed a gold standard measurement. The curves were based on the measurements they made of Caucasian children in Boston. According to Feingold and Bossert, the ear grows about 10% of its length and 40% of its height between the ages of 6 and 14 years. The ear can be divided into three parts:

1. Upper third: the part of the ear above inferior crus, which comprises 33% of the total height of the ear.
2. Middle third: inferior crus to incisura, which comprises 43% of the height of the ear.
3. Lower third: incisura to the tip, which comprises 23% of the total height.

In true macrotia, the upper third of the ear is most commonly enlarged.

Protruding ear

Protruding ear is one of the most common anatomical variations. It is defined as an ear with a >40 degree angle in relation to the mastoid bone (Fig. 97.3). According to Carey (1993), the gap between the mastoid bone and the helix in protruding ear is greater than 2 cm. Driessen et al. (2011) found a sex difference in protrusion of the ear. In males, for an ear to be prominent, the protrusion should be greater than 21.5 mm for the upper or 20.0 mm for the lower part of the ear. In females, the protrusion in the upper ear should exceed 17.5 mm and the lower ear 15.5 mm. The auricular length is greater in males and correlates with age in both sexes. The most commonly used method to assess protrusion is to measure the gap between the rim of the helix and a point on the mastoid perpendicular to the helix rim. Any variation in shape or position of the mastoid can influence the measurement; this is the biggest drawback of the method. Another widely used method is to measure the auriculocephalic angle. If this is greater than 30–40 degrees, various authors regard it as indicating protrusion. In the auriculocephalic angle method any variation of temporal bone convexity or soft tissue above the bone can change the measurement, so it is not foolproof. Smith (1978) described the protruding ear as a result of a developmental defect in the posterior auricular muscle. One role of the posterior auricular muscle is to draw the pinna towards the skull, and dysfunction of this muscle causes the pinna to protrude. According to the author, the protruding pinna should be considered a part of the neuromuscular defect and not articular cartilage dysmorphogenesis. Association of protruding ears with myotonic dystrophy and congenital muscular dystrophy has been frequently reported in the literature. Anencephaly, trisomy 8 syndromes, 18p syndrome, 4p syndrome, and Langer-Giedion syndrome are also associated with protruding ears.

Cryptotia

In cryptotia, the upper pole of helix cartilage is buried under the fold of the skin which results in loss of the auriculocephalic sulcus (Fig. 97.4). This is more common in the Japanese than the Caucasian population; its incidence in the former is about 1 in 400 births. The term cryptotia was introduced by Sercer (1934). Altmann (1955) used the phrase "pocket ear" for this anomaly. Gosserez and Piers (1959) called it "congenital invagination" of external ear. There is no clear pathology underpinning it, although various hypotheses have been published. Wreden (1879) reported this anomaly and proposed that abnormal insertion of the superior auricular muscle into

Figure 97.4 Cryptotia.

Source: Hunter and Yotsuyanagi (2005). Reproduced with permission from John Wiley & Sons.

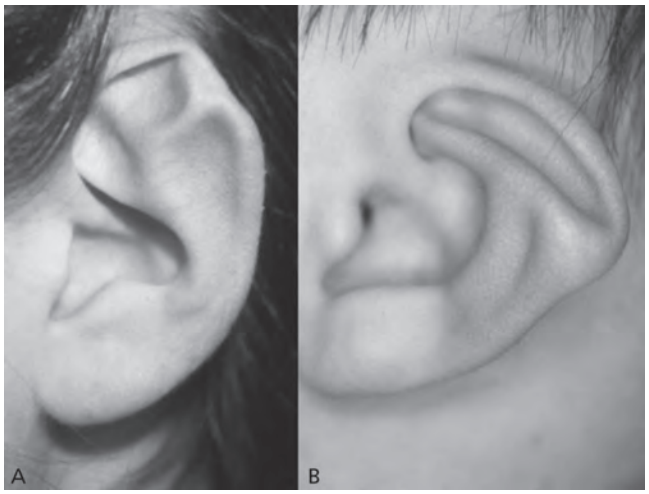

Figure 97.5 Stahl ear: (a) typical Stahl ear and (b) variant of Stahl ear.

Source: Hunter and Yotsuyanagi (2005). Reproduced with permission from John Wiley & Sons.

the upper part of the helix instead of the eminentia triangularis is the cause. Marx (1926) described this anomaly as a result of pressure from the umbilical cord over the auricle/vascular changes in the auricle. Sercer (1934) attributed it to a cartilage developmental defect. Gosserez and Piers (1959) reported a series of 21 cases. Hirose et al. (1985) conjectured that the cause was a defect in the intrinsic musculature. Hayashi et al. (1993) described familial cases of cryptotia and described its X-linked inheritance. They also suggested neuromuscular abnormality as a cause of cryptoptia.

Stahl ear

In Stahl's ear, there is an abnormal cartilage fold extension to the helix margin from the crus anthelix through the scaphoid fossa (Fig. 97.5). This abnormality predominantly involves the superior crus of the antihelix. There is also helix narrowing, scaphoid broadening, and superior crus antihelix hypoplasia or absence. In Stahl's ear, some cases present as an abnormal inferior crus position while in others there is an extra crus, sometimes called a "third crus." Yamada and Fukuda (1980) published a case series of 38 patients (21 males and 17 females) and classified this anomaly into four subdivisions:

1. Posteriosuperior extension of the third crus from the crura antihelix. The shape of the ridge is sharp.
2. Posteriorosuperior extension of the third crus from the crura antihelix with rounded ridge.
3. Posteriorosuperior extension of the third crus, which is wider and has two ridges.
4. Posterioinferior extension of the third crus from the crura antihelix.

In the nineteenth century, Stahl divided auricular variations/malformations into three subtypes: helix transversus spleniformis; crus antihelicis trifurcata; and crus superius turgidum. Stahl's ear comes under the second classification, that is, crus antihelicis trifurcate. There are various hypotheses regarding the development of this variation but the most widely held is an error in embryonic development during the third month when the helix and scaphoid are formed (Aki et al. 2000).

Shell ear

In Shell ear the superior antihelix crus is absent (Fig. 97.6). The inferior crus is horizontal and wider. "Snail ear" and "shell ear" are other names used in the literature (Hunter and Yotsuyanagi 2005).

Question mark ear

In cases of question mark ear, the lower third of the ear is affected (Fig. 97.7). It involves the cleft between the helix and

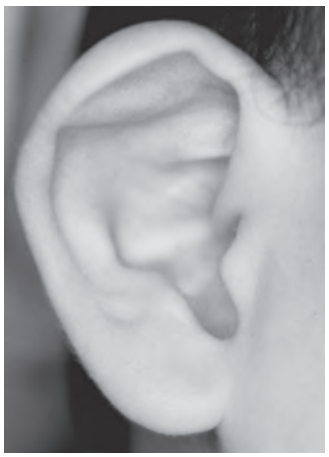

Figure 97.6 Shell ear.

Source: Hunter and Yotsuyanagi (2005). Reproduced with permission from John Wiley & Sons.

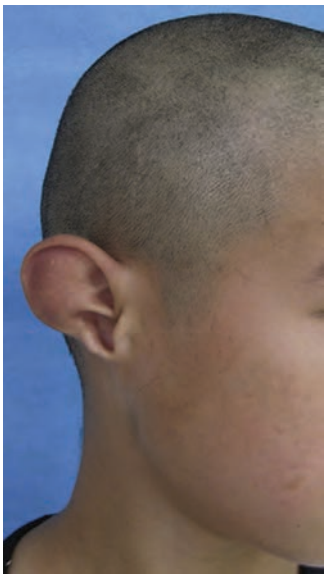

Figure 97.7 Question mark ear.

Source: Pan et al. (2010). Reproduced with permission from Elsevier.

the lobe of the ear. It can also present with a shallow dimple on the skin involving the posterior ear, absence or prominence of the upper helix or ear lobe, and antitragus transposition. It can occur as an isolated anomaly or as part of a syndrome. In this anomaly the scapha is absent and the ear protrudes from the affected site. It is a male-predominant anomaly with a 2:1 sex ratio and can present as a unilateral or bilateral defect. Its association with auriculo-condylar syndrome (ACS) and its autosomal dominant inheritance have been reported. Pan et al. (2010) published a 32-case series which included 30 sporadic cases and two of familial origin. They divided the ear defect into moderate and severe types depending on the anatomical characteristics. In the moderate type the lobule and inferior part of the helix presented with a cleft, and in the severe type the lobule and inferior part of the helix were absent. Question mark ear involves the first and second arches. Auriculo-condylar syndrome (ACS), Townes-Brocks syndrome, Treacher-Collins syndrome, and oculoauriculo-vertebral spectrum also involve the first and second arches. Question mark ear is closely associated with ACS, which is characterized by the presence of auricular clefts, microstomia, hypoplasia of the mandibular condyle, micrognathia, temporomandibular joint abnormalities, and round face with prominent cheeks. Masotti et al. (2008) conducted a genome-wide search and linked ACS to the 1p21.1–q23.3 gene. Due to the occurrence of question mark ear in ACS and its similar inheritance mode, allelism could be plausible.

Mirror ear/polyotia

Polyotia or mirror ear is characterized by presence of an accessory ear (Fig. 97.8). It has a comparable size and can be considered an extra auricle. There is no clear-cut etiology of this condition. Abnormal migration of neural crest cells (NCC) has been reported as the potential cause. It can occur as an isolated anomaly or a part of a syndrome complex. Its association with Brachmann-de Lange syndrome, Treacher-Collins syndrome and Goldenhar syndrome has been reported in the literature. Lammer (1991) proposed that retinoic acid embryopathy (RAE) is responsible for abnormal migration of NCC. In a retrospective study, he described a case series in which patients exposed to retinoic acid during pregnancy had newborns with external ear defects including partial duplication of the ears.

Mozart ear

In Mozart ear, the anterosuperior auricular margin has a bulging appearance. The cavum conchae protrudes convexly and the external auditory meatus has a slit-like opening (Fig. 97.9). In other words, the superior pinna margin bulges because of the two-crura fusion of the antihelix and crus helix. The other characteristics of this anomaly are a smaller tragus, absent or poorly developed ear lobe, cavum cochae and crus helicus fusion, non-prominent antihelix lower half, crus helicus with horizontal ridge, and absence of the antitragus. In the literature the terms "lower conchal stria" or "convex conchae" are also used. Paton et al. (1986) published an article on Mozart ears. They carried out surveys among the patients attending ENT clinics in Birmingham (1185 patients) and medical clinics in London (1092 patients) and found only two cases. Yamashita et al. (2011) reported a case of a female patient with Mozart ears.

Lop ears

Lop ear is an anomaly of the superior one-third of the pinna (Fig. 97.10). It involves over-folding of the scapha and helix, absence or smaller size of antihelix superior crus, smaller scapha, and an auricle that is shorter in vertical height. In Caucasian, African-descent and Japanese populations the reported incidences are 2–5%, 10–15%, and 38%, respectively. Lop ear can occur as an isolated anomaly or as part of an autosomal dominant inherited disorder such as familial blepharophimosis, scalp-ear-nipple syndrome, oto-facio-cervical, tricho-rhino phalangeal, brachio-oto-renal and lacrimal-auricular-dental-digital syndromes, Kabuki syndrome, and Townes-Brock syndrome. It can also occur in association with Fraser and Mengel syndrome which exhibits autosomal recessive inheritance, and also in Trisomy 21 and 4q deletion syndrome (Carey et al. 2006).

Davis (1987) described hillock 3 hypoplasia as a major factor in the pathogenesis of lop ears. According to him, hillock 3 hypoplasia results in forward displacement of the helix to bridge the gap and the resultant pull causes the superior one-third of the pinna to over-fold. Karmody and Annino (1995) described lop ear as an anomaly of the cartilage. Manigila and Maniglia (1981) ascribed it to failure of unfolding of the helix during the 12–16th weeks of intrauterine life. Carey et al. (2006) reported the cause of transient lop ear to be pressure on the fetal auricle from the brim of the maternal pelvis. Interestingly, in the Japanese population the incidence of lop ear at birth is 38% and

Figure 97.8 Polyotia.

Source: Gore et al. (2006). Reproduced with permission from Elsevier.

Figure 97.9 Mozart ear.

Source: Paton et al. (1986). Reproduced with permission from BMJ Publishing Group.

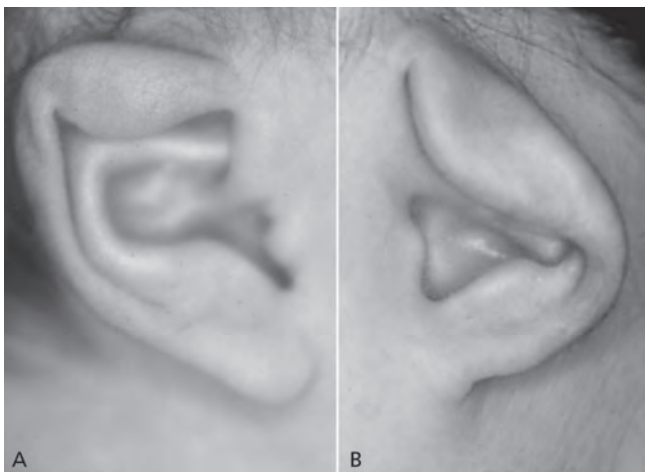

Figure 97.10 Lop ear: (a) milder; and (b) severe form.

Source: Hunter and Yotsuyanagi (2005). Reproduced with permission from John Wiley & Sons.

at 1 year of age has decreased to only 6%. This could indicate correction of a transient lop ear initially caused by intrauterine compression.

Hunter and Yotsuyanagi (2005) subclassified lop ear into a milder form and a moderate form. The milder form includes an anomaly limited to helix folding above Darwin's tubercle. In the moderate form of lop ear, the folding of the helix extends below Darwin's tubercle.

Upper auricular detachment

In upper auricular detachment, there is no attachment between the crus helix and the anterior or ascending helix. The root of the helix and the distant lower end are also detached. The only site of attachment is to the mastoid area. In the literature, congenital amniotic bands and absence of mesenchymal fusion among the mandibular and hyoid arch hillocks are described as a potential cause of this anomaly (Hunter and Yotsuyanagi 2005).

Ear lobe indentations/pits

Ear lobe pits occur most commonly in patients with Wiedmann-Beckwith syndrome (WBS). Various terminologies such as dimples, creases, pits, and indentations are used in the literature (Fig. 97.11). Irving (1967) published a series of 11 cases and described the occurrence of semi-horizontal linear grooves in the ear lobe. Kosseff et al. (1972) described the bilateral focal occurrence of 1–2 mm indented areas that were well demarcated on the posterior helix rims in a patient with WBS. There is no clearly defined cause of this anomaly. Best (1991) suggested that an infarction or localized degeneration could cause posterior helical bits. Embryonic exposure to retinoic acid has also been suggested as a cause.

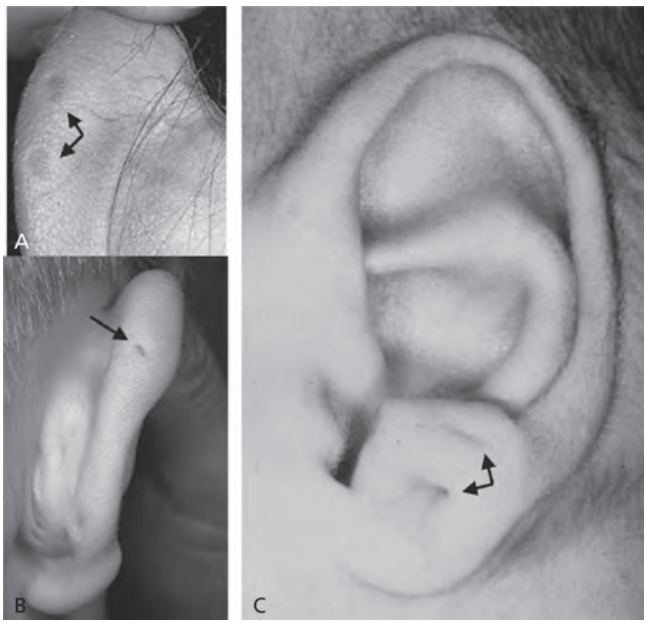

Figure 97.11 (a) Ear pits and (b) indentations. (c) Horizontal lobular grooves in patient with Beckwith-Weidemann syndrome.

Source: Hunter and Yotsuyanagi (2005). Reproduced with permission from John Wiley & Sons.

Figure 97.12 Darwin's tubercle.

Source: Hunter and Yotsuyanagi (2005). Reproduced with permission from John Wiley & Sons.

Darwin's tubercle

Darwin tubercle is a small blunt projection from the helix. Davis (1987) described it as a site of fusion between hillocks 4 and 5. Carey (1993) suggested that a Kossef tubercle persists in embryos up to seven weeks of age; after that it disappears. No association with any syndrome or other anomalies has been reported in the literature (Fig. 97.12).

Cup ears

There is much confusion regarding the difference between cup ears and lop ears. Rogers (1968) described it as a deformity with features of both protruding ears and lop ears. In cup ears the protrusion results from overdevelopment of the concave concha. A shorter helix and faulty antihelix are a few of the common features it shares with lop ears. Due to the forward cupping of the lobule, the vertical height of the ear from the superior pole to the lobule bottoms is less than in a normal ear. Peterson and Schminke (1968) published a study of a family with 12 members from five generations with cup-shaped ears. In addition to cup ears, the proband had Pierre Robin syndrome.

Variations of the auditory meatus

Aural atresia

Aural atresia is a congenital anomaly involving failure of development of the external acoustic meatus. Depending on severity, it can involve the tympanic membranes, middle ear ossicles, mastoid cells, and cochlea. The incidence of this anomaly is

1:10,000–20000 live births. It is male-predominant. The incidence of unilateral atresia is 3–5 times higher than bilateral atresia, and in unilateral atresia the right ear is more commonly involved. The anomaly is usually sporadic but an autosomal recessive mode of inheritance is also known. The association of aural atresia with Pierre Robin, CHARGE, Treacher-Collins, Crouzon's, Goldenhar's, Mobius, Klippel-Feil, Fanconi's, DiGeorge, and VATER syndromes has been reported in the literature. It also coexists with cleft palate, hemifacial microsomia, posterior cranial hypoplasia, hydrocephalus, and genitourinary abnormalities.

There are various classifications of aural atresia (Table 97.3):

Altmann (1955) divided atresia into three degrees depending on severity:

1. First-degree: The external acoustic meatus is mildly deformed, the tympanic cavity has normal or hypoplastic characteristics, the ossicles are deformed, and the mastoid is well aerated.
2. Second-degree: This includes intermediate deformities. The external acoustic meatus either ends blindly or is absent, the tympanic cavity is narrow, the ossicles are either deformed or fixed, and the mastoid cells are poorly pneumatized.
3. Third-degree: This includes severe deformities. The external acoustic meatus is absent, the middle ear is hypoplastic, the ossicles are deformed, and there is no mastoid cell pneumatization.

De la Cruz and Teufert (2010) modified Altmann's classification into minor and major malformations:

- Minor malformations: Mastoid cell pneumatization is normal, inner ear is normal, oval window footplate, and normal facial nerve course in relationship to it are found.
- Major malformation: Mastoid cell has poor pneumatization, oval window/footplate is either abnormal or absent, facial nerve course in relationship to the footplate and inner ear are abnormal.

Schuknecht (1989) introduced another classification based on surgical techniques and intraoperative findings:

- Type A: Atresia involves cartilaginous external acoustic meatus, corrected with meatoplasty.
- Type B: Cartilaginous and bony parts of external acoustic meatus are narrow, with small tympanic membrane and mildly deformed malleus and incus. Correction involves canalplasty with or without ossicular chain reconstruction.
- Type C: Complete atresia of the external acoustic meatus. Mastoid cell and middle ear have normal pneumatization.
- Type D: Complete atresia of external acoustic meatus with poorly pneumatized middle ear.

Jahrsdoerfer et al. (1992) introduced a point-based classification system using radiological findings of the temporal bone obtained from high resolution CT scans. A total of 10 points can be awarded on the basis of anatomical findings. Open oval window, normal middle ear space, normal course of facial nerve, presence of malleus-incus complex, well-pneumatized mastoid cells, normal incus–stapes connection, normal round window, and normal appearance of external ear are each awarded one point. Presence of stapes scores two points. A score of 10 = excellent, 9 = very good, 8 = good, 7 = fair, 6 = marginal and less than 5 counts as poor post-surgical prognosis. A score of 8 corresponds to an 80% success rate in hearing restoration to normal or near normal level. A score of less than 5 is not considered for surgical intervention. Siegert et al.

Table 97.3 Classifications of aural atresia. Data from Altmann (1995) and De la Cruz and Teufert (2010).

Altman Classification		*De la Cruz Classification*	
Degree	**Description**	**Malformation**	**Description**
First	External acoustic meatus has mild deformity, tympanic cavity with normal or hypoplastic characteristics, ossicles deformity and well aerated mastoid	Minor	Mastoid cell has normal pneumatization, normal inner ear, oval window footplate and normal facial nerve course in relationship to the footplate
Second	Includes intermediate deformities. External acoustic meatus either ends blindly or is absent, tympanic cavity is narrow, ossicles are either deformed or fixed, and poorly pneumatized mastoid cells	Major	Mastoid cell has poor pneumatization, oval window/ footplate is either abnormal or absent, abnormal facial nerve course in relationship to the footplate and abnormal inner ear
Third	Includes severe deformities. External acoustic meatus is absent, hypoplasia of middle ear, deformed ossicles, and absence of mastoid cell pneumatization	–	–
Schuknecht Classification			
Type	Description		
A	Atresia involves cartilaginous external acoustic meatus, corrected with meatoplasty		
B	Cartilaginous and bony part of external acoustic meatus is narrow, small tympanic membrane and mildly deformed malleus and incus. Correction involves canalplasty with or without ossicular chain reconstruction procedure		
C	Complete atresia of external acoustic meatus. Mastoid cell and middle ear has normal pneumatization		
D	Complete atresia of external acoustic meatus with poorly pneumatized middle ear		

Table 97.4 Twenty-eight point-based prognostic scale for aural atresia surgical outcome. Adapted from Siegert et al. (1996).

Entity	Points
External auditory meatus: bone atresia; soft tissue atresia; normal	0; 1; 2
Mastoid cell aeration: absent; fair; excellent	0; 1; 2
Middle ear space: absent; medium; large	0; 1; 2
Middle ear aeration: absent; minor; major	0; 1; 2
Facial nerve: major variation; minor variation; normal	0; 2; 4
Vessels: major variation; minor variation; normal	0; 1; 2
Malleus and incus: absent; deformed; normal	0; 1; 2
Stapes: absent; deformed; normal	0; 2; 4
Oval window: obliterated; open	0; 4
Round window: obliterated; open	0; 4

(1996) introduced a more extensive 28-point-based prognostic rating scale. In a patient with bilateral malformation, a score greater than or equal to 15 is recommended for middle ear reconstruction and in a unilateral malformation the cutoff is 20 points (Table 97.4).

Colman (1974) classified aural atresia patients with conductive hearing loss into three groups:

- Group I: Consists of minor anomalies, meatus is narrow but open, ossicular fixation involves stapes.
- Group II: Pinna is deformed, external meatus is completely closed, and middle ear has complex abnormalities.
- Group III: Severe deformity of the pinna and the middle ear. Mastoid cell pneumatization is absent and there are cochlear deformities.

Group I had excellent post-surgical results and group II had variable results. Group III had poor outcomes.

Variations of the internal auditory canal

Narrow internal auditory canal

Narrowing of the internal auditory canal coexists with anomalies of the external middle and inner ear. The normal diameter of the internal auditory is 4 mm with a range of 2–8 mm. The canal is considered narrow when the diameter is less than 2 mm. It contributes to 12% of temporal bone defects. Vestibulocochlear nerve has a trophic influence on the growth of the internal auditory canal and hypoplasia or aplasia of the vestibulocochlear nerve results in abnormal development of the canal and therefore causes narrowing. Another hypothesis is that a mechanical obstruction caused by bony stenosis results in aplasia or hypoplasia of the vestibulocochlear nerve. This hypothesis is less likely to be the cause because most cases reported in the literature have normal facial function (Demir et al. 2005).

Duplication of internal auditory canal

Duplication of the internal auditory canal is a rare anomaly. It mostly occurs unilaterally, but bilateral occurrences have been reported. According to Weissman et al. (1991), the facioacoustic primordium separates abnormally in this condition, which causes the fibers of the vestibulocochlear and facial nerves to follow aberrant courses and results in duplication. According to Curtin and May (1986), chondrification of the internal auditory canal's mesenchymal precursor is delayed, which causes the facial nerve to follow a course away from the vestibulocochlear nerve. The wide gap between the two nerves results in abnormal ossification and therefore duplication.

Variations of the facial nerve

The two most common facial nerve anatomical variations encountered in the middle ear are displacement of the facial nerve and absence of the bony sheath due to dehiscence or absence of the fallopian canal. Dehiscence of the fallopian canal exposes the facial nerve due to lack of the bony sheath. The nerve has only a thin layer of fibrous membrane and is vulnerable to herniation into the tympanic cavity. Fallopian canal dehiscence occurs during ontogenetic development. During this period the ossification process closes the facial nerve sulcus. Malformation of Reichert's cartilage precludes closure of the sulcus and results in dehiscence or complete absence of the bony canal. There are various hypothetical explanations of the facial nerve displacement. One is based on the failure of late fusion between the second brachial arch and otic capsule, which prevents anterior migration of the facial nerve (Al-Mazrou et al. 2003).

Exposure of the facial nerve in the middle ear can be divided into three degrees:

- First-degree: Severe fallopian canal dehiscence without facial nerve displacement.
- Second-degree: The facial nerve is completely herniated from the fallopian canal and lies on the oval window with minimal or no attachment to the stapes.
- Third-degree: The facial nerve lies over the promontory.

Rohrt and Lorentzen (1976) divided the facial nerve displacement into four groups (Table 97.5):

- Group I: Stapes footplate is partially obliterated by the facial nerve.
- Group II: Facial nerve bifurcation.
- Group III: Oval window and stapes are deformed and the facial nerve lies on the footplate.
- Group IV: Facial nerve lies on the promontory.

Jahrsdoerfer (1981) published a case series of facial nerve anomalies and divided them into three categories based on anatomical variation and ease of surgical correction (Table 97.5): (1) facial nerve overlies the stapes and oval window; (2) displacement of the facial nerve along with presence of the oval window; or (3) displacement of the facial nerve along with absence of the oval window.

Table 97.5 Classification of facial nerve's variations in the middle ear. Data from Rohrt and Lorentzen (1976) and Jahrsdoerfer (1981).

Rohrt Classification		*Jahrsdoerfer Classification*	
Group	Description	Category	Description
I	Stapes footplate is partially obliterated by the facial nerve	I	Facial nerve overlies on the stapes and oval window
II	Facial nerve bifurcation	II	Displacement of facial nerve along with presence of oval window
III	Oval window and Stapes are deformed and facial nerve lies on the footplate	III	Displacement of facial nerve along with absence of oval window
IV	Facial nerve lies on the promontory	–	–

Vascular variations

Vascular variations of the middle ear are of great surgical importance. The most commonly encountered include an aberrant internal carotid artery, dehiscence of the carotid artery canal, a high jugular bulb, dehiscence of the high jugular bulb, and a persistent stapedial artery. The incidence of aberrant internal carotid artery is less than 1%, dehiscence of high jugular bulb has an incidence of 1%, and the incidence of high jugular bulb ranges over 6–22%.

An aberrant internal carotid artery is a very important vascular anomaly in terms of surgical significance as bleeding from it can be life-threatening. It is caused by agenesis of the first embryonic segment of the internal carotid artery. It can present as pulsatile tinnitus, hearing loss, or serous otitis media. On a high-resolution CT scan it presents as a retrotympanic mass with enlarged inferior tympanic canaliculus, absence of bony plate and the vertical segment of the internal carotid artery canal. Various hypotheses regarding the cause of this anomaly have been presented in the literature. A persistent stapedial artery during embryogenesis can cause traction on the internal carotid artery and displace it into the tympanic cavity, and the displacement can also be caused by bony carotid canal agenesis.

A high jugular bulb is the most common anomaly in the middle ear. It is mostly unilateral with a right side to left side ratio of 2:1, but bilateral cases have been reported. High jugular bulbs can be medial or lateral. A lateral high jugular bulb protrudes into the middle ear cavity and a medial jugular bulb lies superior and medial to the cochlea. The condition usually presents as a pulsatile tinnitus.

Dehiscent jugular bulb, as the name suggests, is dehiscence of the sigmoid plate and jugular bulb that extends superolaterally into the middle ear cavity. It has great surgical importance as it has only a thin layer of mucosa and could cause catastrophic bleeding in the event of accidental intraoperative injury. It can present as a bluish discolored mass behind the tympanic cavity.

A persistent stapedial artery (PSA) is a rare vascular anomaly of the middle ear. The incidence of PSA is 0.2–4.8 per thousand adults. It usually presents as pulsatile tinnitus and conductive hearing loss due to ankylosis of the stapes. It can also present as sensorineural hearing loss by eroding against the otic capsule. It can occur as an isolated anomaly or in combination with an aberrant internal carotid artery and stapes and facial nerve anomalies. Association with Paget's disease, thalidomide exposure, otosclerosis and trisomy 13 has been reported in the literature. Normally, the stapedial artery originates from the hyoid artery during the fifth week of embryonic life. From its origin it travels intracranially via the stapes obturator foramen. It divides into dorsal and ventral branches. The middle meningeal artery arises from its dorsal branch. The ventral branch gives rise to the infraorbital and inferior alveolar arteries extracranially after its exit via the foramen spinosum. The ventral branches further anastomose with the developing external carotid artery. During the tenth week of gestation, the stapedial artery degenerates through reversal of blood flow at the foramen spinosum and separates the internal from the external carotid artery. The presence of a stapedial artery in postnatal life indicates the absence of its passage through the foramen spinosusm so the anastomosis between the internal carotid and middle meningeal arteries persists and results in PSA (Lau et al. 2004).

Variations of the round and oval windows

Round window atresia mostly occurs as part of a syndrome complex, for example mandibulofacial dysostosis, cretinism, stapes ankylosis, mondini anomaly, and extensive otosclerosis. Its occurrence as an isolated anomaly has also been reported in the literature. It can present both unilaterally and bilaterally. The round window develops during the eleventh week of gestation. It first appears as an embryonic connective tissue condensation between the fossula of the cochlear fenestra and the scala tympani. During otic capsule ossification, the presence of a cartilage ring prevents ossification of the round window opening. In the absence of the cartilaginous ring, ossification obliterates the opening and causes congenital atresia. In congenital absence of the oval window there is no connection between the otic capsule bone and the vestibule. There is complete closure of the oval window by a thick bony plate or a concentric narrowing. The foot plate and anular ligament are absent (de Alarcon et al. 2007).

Variations of the Eustachian tube

Anomalies of the Eustachian tube (ET) are not common and mostly occur as part of a syndrome complex. Anatomical variations can involve the bony or more commonly the cartilaginous part. ET anomalies are reported to be associated with cleft palate deformities, Down syndrome, the oculoauriculovertebral spectrum, and Klippel-Feil syndrome. The normal width of the ET is 1.5 mm; enlargement of its bony portion is rare. The oculoauriculovertebral spectrum is characterized by mandibular hypoplasia, vertebral anomalies, microtia and epibulbar dermoids and lipodermoids. Haginomori et al. (2003) reported a case of enlargement of the bony part of the Eustachian tube in a patient with oculoauriculovertebra spectrum; the diameter of the ET was 7 mm. Jovankovičová et al. (2012) described a case of Klippel-Feil syndrome with an enlarged right-sided ET with a width of 5.5 mm.

Variations of the inner ear

There are various classifications to describe inner ear malformations. The most commonly used classification was introduced by Jackler et al. (1987) and was based on radiographic appearances. This was further modified by Marangos (2002) and Sennaroglu and Saatci (2002). Jackler et al. divided the malformations into two categories, A and B. Category A entailed congenital anomalies with an absent or malformed cochlea, and category B entailed congenital malformations with a normal cochlea.

The radiological classification was based on radiographic appearances with the following size reference ranges: the cochlea was considered small if it was less than 7 mm measured vertically (normal size 8–10 mm); and a vestibule greater than 5 mm in vertical measurement was considered enlarged. The intraosseous portion of the vestibular aqueduct with diameter greater than 2 mm was categorized as enlarged. Internal auditory canals with greater than 10 mm vertical diameter and less than 3 mm vertical diameter were considered enlarged and narrowed, respectively (Table 97.6).

Marangos (2002) modified Jackler's classification and divided inner ear variations into four categories. Category A entailed malformations with deficient embryonic development, category B included aberrant embryonic development, category C included isolated malformations, and category D included syndromic malformations (Table 97.7).

Sennaroglu and Saatci (2002) further categorized cochleovestibular malformations into five subdivisions based on cochlear, vestibular, semicircular canal, internal auditory canal, and vestibular cochlear aqueduct defects. They also proposed a categorization of cochlear malformations based on embryonic developmental arrest: Michel deformity caused by developmental arrest at the third week, aplasia of the cochlea by late third week arrest, common cavity malformation during fourth week arrest, cystic cochleovestibular malformation/incomplete partition type I by fifth week arrest, hypoplasia of the cochlea during sixth week arrest, Mondini deformity/incomplete partition type II by seventh week arrest, and normal development (Table 97.8).

Table 97.6 Classification of inner ear anomalies. Adapted from Jackler et al. (1987).

Category A (aplasia or cochlear malformations)	
Complete aplasia of labyrinth	Absence of inner ear development
Aplasia of cochlea	Deveopmental absence of cochlea, vestibule and semicircular canals are normal or malformed
Hypoplastic cochlea	Small cochlea, vestibule and semicircular canal are normal or malformed
Incoplete partition of cochlea	Cochlea small and incomplete, vestibule and semicircular canals are normal or malformed
Common cavity	Common cavity formation between cochlea and vestibule with absence of internal architecture, semicircular canal is either normal or deformed.
Category B (normal cochlea)	
Vestibule and lateral semicircular canal dysplasia	Vestibule is enlarged and lateral. Semicircular canal is short and dilated.
Enlarged vestibular aqueduct	Vestibular aqueduct is enlarged with normal semicircular canal.

Variations of the cochlea

According to Sennaroglu and Saatci (2002), cochlear malformations can be subdivided into Michel anomaly/complete

Table 97.7 Classification of inner ear anomalies. Adapted from Marangos (2002).

Category	Types
A: incomplete embryonic development	Michel deformity/completely aplastic inner ear; common cavity; cochlear aplasia or hypoplasia with normal development of posterior layrinth; posterior labyrinth aplasia or hypoplasia with normal development of cochlea; completely hypoplastic labyrinth; dysplasia mondini type
B: aberrant embryonic development	Vestibular aqueduct enlargement; internal auditory canal narrowing; longer lengthed crista transeversa; tripartitus of internal auditory canal; cochlea and meatus incompletely separated
C: hereditary malformations of isolated origin	Hearing loss of X-linked origin
Category D	Malformations with syndromic association

Table 97.8 Classification of inner ear anomalies. Adapted from Sennaroglu and Saatci (2002).

Category	Types
Malformations of cochlea	Michel deformity: complete aplasia of inner ear structures
	Aplasia of cochlea: complete absence of cochlea
	Common cavity malformation
	Hypoplastic cochlea
	Incomplete partition I; II
Malformations of vestibule	Hypoplastic, dilated or absent vestibule, common cavity and Michel deformity
Malformations of semicircular canal	Absence, hypoplasia or enlargement of semicircular canal
Malformations of internal auditory canal	Absence, narrowing or enlargement of internal auditory canal
Malformations of vestibular and cochlear aqueduct	Vestibular and cochlear aqueduct, either normal or enlarged

labyrinthine aplasia, cochlear aplasia, common cavity, cochlear hypoplasia, and incomplete partition types I and II on the basis of anatomical features and the time of arrest of development during intrauterine life.

Michel anomaly/complete labyrinthine aplasia

A Michel anomaly is characterized by complete aplasia of the labyrinthine structure, where there is complete absence of inner ear structure. It accounts for 1% of the congenital anomalies of the inner ear. It is generally bilateral but unilateral cases have also been reported. Congenital absence of inner ear structure is due to otic placode arrest before the third week of embryonic development. Michel (1863) described this anomaly in an autopsy report of a 12-year-old male with the bilateral defect.

Cochlear aplasia

In this anomaly there is complete absence of the cochlea. The vestibule and semicircular canal can be normal, dilated, or hypoplastic. It can occur as a bilateral or unilateral anomaly. On examination of the anterior part of the internal auditory canal, it presents as a dense otic bone. The absence of the cochlea results in anterior displacement of the labyrinthine segment of the facial canal from its usual course. This anomaly should be differentiated from common cavity and cochlear ossification. In cochlear ossification there is bulge in the promontory caused by the basal turn of the cochlea, which is absent in cochlear aplasia. It can be differentiated from common cavity by the absence of a cavity in the cochlear location, anteroinferior location of the internal auditory canal in relation to the malformed cavity, and bony sclerosis at the location of the absent cochlea (Sennaroglu and Saatci 2002).

Common cavity

Common cavity malformation results from arrested development during the fourth week of intrauterine life. In this anomaly there is no differentiation between the cochlea and vestibule and a common cavity forms. The internal auditory canal dimensions are abnormal and vary among patients, as described by Sennaroglu and Saatci (2002). Enlarged internal auditory canals were found in patients with large common cavities, and small dimensions were present in patients with small common cavities.

Incomplete partition type I

This anomaly, also known as cystic cochleovestibular malformation, is characterized by cystic dilatation of the cochlea and vestibule. The cochlea is empty. The cochlea and vestibule have normal dimensions but lack internal structures. The cochlea lacks the modiolus and cribriform areas, so the cystic cavity is empty. The cause is arrest of development at the fifth week of intrauterine life (Sennaroglu and Saatci 2002).

Cochleovestibular hypoplasia

This anomaly is believed to result from developmental arrest at the sixth week of intrauterine life. The cochlea is hypoplastic/smaller in size and the vestibule is either hypoplastic or absent. The dimensions of the internal auditory canal vary from normal to smaller (Sennaroglu and Saatci 2002).

Incomplete partition type II

This anomaly, also known as Mondini malformation, results from developmental arrest later than type I because the cochlea and vestibule have normal size and their internal structures are better developed. The vestibule has minimal dilatation. It contributes to 50% of cochlear deformities, and is believed to be a result of arrested development at the seventh week of intrauterine life. The cochlea has 1.5 turns and its apex between the middle and apical turns has an interscalar defect. The basal part of the modiolus is developed in the cochlea so there are more nerve endings and spiral ganglia than in the incomplete partition type I malformation (Sennaroglu and Saatci 2002).

Variations of the semicircular canal

Aplasia of semicircular canal

Aplasia of the semicircular canal can present as an isolated anomaly or part of a syndrome. The patient usually presents with sensorineural hearing loss. It is a common associated anomaly in patients with CHARGE syndrome. The association of aplastic semicircular canals with CHARGE syndrome was first reported by Guyot et al. (1987) in a study based on histopathological findings of temporal bones. Its association with Noonan syndrome has also been reported. Superior semicircular canal development is usually complete at the 19th week of intrauterine life and the horizontal semicircular canal by 22 weeks. The semicircular canal can develop any time up to 24 weeks. In Noonan syndrome, patients usually present with mixed-type bilateral severe hearing loss. The literature reports 20% low-frequency and 50% high-frequency hearing loss.

Variations of the vestibular and cochlear aqueduct

Enlargement of vestibular aqueduct (VA)

This is the most common radiologically detected anomaly in children affected by sensorineural hearing loss. It is a bilateral anomaly with normal to mild impairment of hearing in childhood and it deteriorates with age. Almost 40% of patients develop sensory hearing loss. Valvassori and Clemis (1978) defined the enlarged VA using hypocycloidal polytomography. According to them the aqueduct should have dimensions greater than 1.5 mm at the midpoint.

Arenberg et al. (1984) first proposed a classification of the VA on the basis of radiological findings. They divided the VA into five types (Table 97.9): type I, the VA measures 1–2 mm in the distal one-third of its course; type II measures less than 1 mm in the distal two-thirds of the aqueduct course; type III VA is greater than 2 mm in the distal one-third and in close proximity to the external aperture; in type IV the external aperture measures 1–2 mm; type V lacks an external aperture.

Dewan et al. (2009) recently proposed new "Cincinati criteria" based on CT findings from children with normal hearing. According to these criteria, a vestibular aqueduct with a 1.0 mm midpoint and 2.0 mm opercular width, greater than the 95 percentile, is regarded as enlarged. They compared the Cincinnati criteria with the Valvassori criteria. According to their study, the Cincinnati criteria identified enlargement of the vestibular aqueduct in 44% patients and the Valvassori criteria identified it in only 16%. Among those patients, 45% had unilateral and 55% bilateral anomaly with the Cincinnati criteria, and 64% were unilaterally affected and 36% bilaterally with the Valvassori criteria. According to Dewan et al. (2009), the Cincinnati criteria were superior to the Valvassori criteria in identifying patients with enlargement of the vestibular aqueduct.

Enlargement of cochlear aqueduct

Controversy exists regarding the existence of enlargement of the cochlear aqueduct (CA). Jackler and De la Cruz (1993) published a study based on the CT appearance of the CA. They divided the CA into four parts: (1) the lateral orifice segment, which has a narrow bony aqueduct opening into the cochlear basal turn; (2) the segment of the labyrinthine capsule with the CA running medially through it; (3) petrous apex segment; and (4) medial orifice segment.

Table 97.9 Classification of vestibular aqueduct. Adapted from Arenberg et al. (1984).

Type	Description
I	VA measures 1–2 mm in dimension in the distal one-third of its course
II	VA measures less than 1 mm in distal two-thirds of the aqueduct course
III	VA is greater than 2 mm in distal one-third and in close proximity to the external aperture
IV	The external aperture measures 1–2 mm in size
V	Absence of external aperture

Table 97.10 Classification of cochlear aqueduct based on CT findings. Adapted from Migirov and Kronenberg (2005).

Type	Description
I	Basal turn of cochlea and its opening into subarachnoid space is clearly visible
II	Cochlear aqueduct defined in the medial two-thirds
III	Only medial third and/or external aperture can be defined
IV	Undefined CA

According to the study, the CA diameter is not consistent and is cochlear-segment specific. The petrous and labyrinthine segments with diameters up to 2 mm were considered normal by Jackler and De la Cruz (1993). The median orifice segment has a variable diameter in the range 0–11 mm with mean 4.5 mm. Migirov and Kronenberg (2005) published a classification of the cochlear aqueduct based on CT findings (Table 97.10). They divided the CA into four types: (I) basal turn of cochlea and its opening into subarachnoid space is clearly visible; (II) cochlear aqueduct defined in the medial two-thirds; (III) only the medial third and/or external aperture can be defined; and (IV) undefined CA.

In the literature, Mukherji et al. (1998) described a case of enlargement of the cochlear aqueduct in an 18-month-old patient with severe bilateral hearing loss. The mid-portion diameter was 1.2 mm and was considered enlarged. To justify their findings, the author examined 50 temporal bones radiologically using 1-mm-thick contiguous axial CT sections. The diameter of the mid-otic segment of the CA was 0.56±0.26 mm. Stimmer (2010) published a report of radiological findings from 400 temporal bones using spiral CT. A diameter greater than 1 mm in the whole otic capsule segment was considered enlarged. However, they found no diameter greater than 1 mm.

References

Aki FE, Kaimoto CL, Katayama ML, Kamakura L, Ferreira MC. 2000. Correction of Stahl's ear. *Aesthetic Plast Surg* 24(5): 382–385.

Al-Mazrou KA, Alorainy IA, Al-Dousary SH, Richardson MA. 2003. Facial nerve anomalies in association with congenital hearing loss. *Int J Pediatr Otorhinolaryngol* 67(12): 1347–1353.

Altmann F. 1955. Congenital aural atresia of the ear in men and animals. *Ann Otol Rhinol Laryngol* 64: 824–858.

Arenberg IK, Dupatrocinio I, Dreisbach JM, Seibert C. 1984. Radiographic classification of the vestibular and cochlear aqueducts: the paired correlation between normal and abnormal vestibular aqueduct and cochlear aqueduct anatomy. *Laryngoscope* 94(10): 1325–1333.

Bauer BS. 1997. Correction of macrotia. *Oper Tech Plast Reconst Surg* 4(3): 134–140.

Best LG. 1991. Familial posterior helical ear pits and Wiedemann-Beckwith syndrome. *Am J Med Genet* 40(2): 188–195.

Carey JC. 1993. External ear: 5.12 Protruding ear. In: *Human Malformations and Related Anomalies* (eds RE Stevenson, JG Hall, RM Goodman). New York: Oxford University Press.

Carey JC, Park AH, Muntz HR. 2006. Lop/cup ear anomaly. In: *Human Malformations and Related Anomalies* (eds RE Stevenson, JG Hall, KK Sulik, E Gilbert-Barness, KK Buchanan). Oxford: Oxford University Press, pp. 344–346.

Colman BH. 1974. Congenital atresia of the ear: the otological problem. *Proc R Soc Med* 67(12 Pt 1): 1203–1204.

Curtin H, May M. 1986. Double internal auditory canal associated with progressive facial weakness. *Am J Otol* 7(4): 275–281.

Davis J. 1987. *Surgical embryology. In: Aesthetic and Reconstructive Otoplasty* (ed. J Davis). New York: Springer Verlag, pp. 93–125.

de Alarcon A, Jahrsdoerfer RA, Kesser BW. 2008. Congenital absence of the oval window: diagnosis, surgery, and audiometric outcomes. *Otol Neurotol* 29(1): 23–28.

De la Cruz A, Teufert KB. 2010. Reconstruction of the auditory canal and tympanum. In: *Cummings Otolaryngology Head and Neck Surgery, fifth edition (eds PW Flint, BH Haughey, VJ Lund, et al.)* Philadelphia, PA: Elsevier Mosby, pp. 2752–2760.

Demir OI, Cakmakci H, Erdag TK, Men S. 2005. Narrow duplicated internal auditory canal: radiological findings and review of the literature. *Pediatr Radiol* 35(12): 1220–1223.

Dewan K, Wippold FJ 2 nd, Lieu JE. 2009. Enlarged vestibular aqueduct in pediatric sensorineural hearing loss. *Otolaryngol Head Neck Surg* 140(4): 552–558.

Driessen JP, Borgstein JA, Vuyk HD. 2011. Defining the protruding ear. *J Craniofac Surg* 22(6): 2102–2108.

Feingold M, Bossert WH. 1974. Normal values for selected physical parameters: an aid to syndrome delineation. *Birth Defects Orig Artic Ser* 10(13): 1–16.

Gore SM, Myers SR, Gault D. 2006. Mirror ear: a reconstructive technique for substantial tragal anomalies or polyotia. *J Plast Reconstr Aesthet Surg* 59(5): 499–504.

Gosserez M, Piers JH. 1959. Congenital invagination of the external ear. *Ann Chir Plast* 4(2): 143–151.

Guyot JP, Gacek RR, DiRaddo P. 1987. The temporal bone anomaly in CHARGE association. *Arch Otolaryngol Head Neck Surg* 113: 321–324.

Haginomori S, Nonaka R, Hoshijima H, Higashikawa M, Takenaka H, Uesugi Y, Narabayashi I. 2003. Enlarged bony portion of the eustachian tube in oculoauriculovertebral spectrum. *Otol Neurotol* 24(6): 961–962.

Hayashi R, Matsuo K, Hirose T. 1993. Familial cryptotia. *Plast Reconstr Surg* 91(7): 1337–1339.

Hirose T, Tomono T, Matsuo K, Katohda S, Takahashi N, Iwasawa M, Satoh R. 1985. Cryptotia: Our classification and treatment. *Br J Plast Surg* 38: 352–360.

Hunter AG, Yotsuyanagi T. 2005. The external ear: more attention to detail may aid syndrome diagnosis and contribute answers to embryological questions. *Am J Med Genet A* 135(3): 237–250.

Irving IM. 1967. Exomphalos with macroglossia: a study of eleven cases. *J Pediatr Surg* 2(6): 499–507.

Jackler RK, Luxford WM, House WF. 1987. Congenital malformations of the inner ear: a classification based on embryogenesis. *Laryngoscope* 97: 2–14.

Jahrsdoerfer RA. 1981. The facial nerve in congenital middle ear malformations. *Laryngoscope* 91(8): 1217–1225.

Jahrsdoerfer RA, Yeakley JW, Aguilar EA, Cole RR, Gray LC. 1992. Grading system for the selection of patients with congenital aural atresia. *Am J Otol* 13(1): 6–12.

Jovankovičová A, Jakubíková J, Durovčíková D. 2012. A case of Klippel Feil syndrome with congenital enlarged Eustachian tube. *Int J Pediatr Otorhinolaryngol* 76(4): 596–600.

Karmody CS, Annino DJ J. 1995. Embryology and anomalies of the external ear. *Facial Plast Surg* 11(4): 251–256.

Kosseff AL, Hermann J, Opitz JM. 1972. The Wiedemann-Beckwith syndrome: genetic considerations and a diagnostic sign. *Lancet* 1: 844.

Lammer E. 1991. Preliminary observations on isotretinoin-induced ear malformations and pattern formation of the external ear. *J Craniofac Genet Dev Biol* 11(4): 292–295.

Lau CC, Oghalai JS, Jackler RK. 2004. Combination of aberrant internal carotid artery and persistent stapedial artery. *Otol Neurotol* 25(5): 850–851.

Luquetti DV, Heike CL, Hing AV, Cunningham ML, Cox TC. 2012. Microtia: epidemiology and genetics. *Am J Med Genet A* 158: 124–139.

Maniglia AJ, Maniglia JV.1981. Congenital lop ear deformity. *Otolaryngol Clin North Am* 14(1): 83–93.

Marangos N. 2002. Dysplasia of the inner ear and inner ear canal. *HNO* 50(9): 866–880.

Marx H. 1926. *Die missbildungen des ohres. Handbuch der spez path Anatomie Histologie*. Berlin: Springer, pp. 620–625.

Masotti C, Oliveira KG, Poerner F, Splendore A, Souza J, Freitas Rda S, Zechi-Ceide R, Guion-Almeida ML, Passos-Bueno MR. 2008. Auriculo-condylar syndrome: mapping of a first locus and evidence for genetic heterogeneity. Eur *J Hum Genet* 16(2): 145–152.

Michel P. 1863. Mémoire sur les anomalies congénitales de l'oreille interne. *Gazette Méd de Strasbourg* 23: 55–58.

Migirov L, Kronenberg J. 2005. Radiology of the cochlear aqueduct. *Ann Otol Rhinol Laryngol* 114(11): 863–866.

Mukherji SK, Baggett HC, Alley J, Carrasco VH. 1998. Enlarged cochlear aqueduct. *AJNR Am J Neuroradiol* 19(2): 330–332.

Pan B, Jiang H, Zhao Y, Lin L, Guo D, Zhuang H. 2010. Clinical analysis, repair and aetiology of question mark ear. *J Plast Reconstr Aesthet Surg* 63(1): 28–35.

Paton A, Pahor AL, Graham GR. 1986. Looking for Mozart ears. *Br Med J (Clin Res Ed)* 293(6562): 1622–1624.

Peterson DM, Schimke RN. 1968. Hereditary cup-shaped ears and the Pierre Robin syndrome. *J Med Genet* 5(1): 52–55.

Rogers BO. 1968. Microtic, lop, cup and protruding ears: four directly inheritable deformities? *Plast Reconstr Surg* 41(3): 208–231.

Rohrt T, Lorentzen P. 1976. Facial nerve displacement within the middle ear (report on 3 cases). *J Laryngol Otol* 90(12): 1093–1098.

Schuknecht HF. 1989. Congenital aural atresia. *Laryngoscope* 99(9): 908–917.

Sennaroglu L, Saatci I. 2002. A new classification for cochleovestibular malformations. *Laryngoscope* 112(12): 2230–2241.

Sercer A. 1934. Beitrag zur Kenntnis der Formanomalien des äusseren Ohres. *Acta Otolaryngol* 20: 59.

Siegert R, Weerda H, Mayer T, Bruckmann H. 1996. Hochauflösende computertomographie fehlgebildeter mittelohren. *Laryngo-Rhino-Otol* 75: 187–194.

Smith DW. 1978. Protruding auricle: A neuromuscular sign. *Lancet* 1(8067): 747–749.

Stimmer H. 2010. Enlargement of the cochlear aqueduct: does it exist? *Eur Arch Otorhinolaryngol* 268(11): 1655–1661.
Tanger RC. 1978. Microtia: a long-term follow-up of 44 reconstructed auricles. *Plast Reconstr Surg* 61(2): 161–166.
Valvassori GE, Clemis JD. 1978. The large vestibular aqueduct syndrome. *Laryngoscope* 88(5): 723–728.
Weerda H. 1988. Classification of congenital deformities of the auricle. *Facial Plast Surg* 5(5): 385–388.
Weissman JL, Arriaga M, Curtin HD, Hirsch B. 1991. Duplication anomaly of the internal auditory canal. *AJNR Am J Neuroradiol* 12(5): 867–869.
Wreden R. 1879. Zur Casuistik de angeborenen Missbildungen des Ohres. *Monatsschrift der Ohrenheilkinde* 4: 21.
Yamada A, Fukuda O. 1980. Evaluation of Stahl's ear, third crus of antihelix. *Ann Plast Surg* 4(6): 511–515.
Yamashita K, Yotsuyanagi T, Saito T, Isogai N, Mori H, Itani Y. 2011. Mozart ear: diagnosis, treatment, and literature review. *Ann Plast Surg* 67(5): 547–550.

Further reading

Abdel-Aziz M. 2013. Congenital aural atresia. *J Craniofac Surg* 24(4): e418–422.
Agrawal P. 2009. Congenital upper auricular detachment: Report of two unusual cases. *Indian J Plast Surg* 42(2): 265–268.
Baik HW, Yu H, Kim KS, Kim GH. 2008. A narrow internal auditory canal with duplication in a patient with congenital sensorineural hearing loss. *Korean J Radiol* 9: S22–25.
Bartel-Friedrich S, Wulke C. 2007a. Classification and diagnosis of ear abnormalities. *Laryngorhinootologie* 86(l): S77–95.
Bartel-Friedrich S, Wulke C. 2007b. Classification and diagnosis of ear malformations. GMS Curr Top Otorhinolaryngol Head Neck Surg 6: Doc05.
Bendor-Samuel RL, Tung TC, Chen YR. 1995. Polyotia. *Ann Plast Surg* 34(6): 650–652.
Borrmann A, Arnold W. Non-syndromal round window atresia: an autosomal dominant genetic disorder with variable penetrance? *Eur Arch Otorhinolaryngol* 264(9): 1103–1108.
Casselman JW, Offeciers FE, Govaerts PJ, Kuhweide R, Geldof H, Somers T, D'Hont G. 1997. Aplasia and hypoplasia of the vestibulocochlear nerve: diagnosis with MR imaging. *Radiology* 202(3): 773–781.
De Alarcon A, Jahrsdoerfer RA, Kesser BW. 2008. Congenital absence of the oval window: diagnosis, surgery, and audiometric outcomes. *Otol Neurotol* 29(1): 23–28.
Di Martino E, Sellhaus B, Haensel J, Schlegel JG, Westhofen M, Prescher A. 2005. Fallopian canal dehiscences a survey of clinical and anatomical findings. *Eur Arch Otorhinolaryngol* 262(2): 120–126.
Gado MH, Arenberg IK. 1975. Radiological visualization of the vestibular aqueduct. Technique and morphological features. *Radiology* 117(3 Pt 1): 621–626.
Guala A, Guarino R, Sparago A, Riccio A, Franceschini P. 2007. Familial posterior helical ear pits. *Am J Med Genet A 143* A(23): 2832–2834.
Hitier M, Zhang M, Labrousse M, Barbier C, Patron V, Moreau S. 2013. Persistent stapedial arteries in human: from phylogeny to surgical consequences. *Surg Radiol Anat* 35(10): 883–891.
Ho S, Lee D, Yellon R. 2000. *Cryptotia.Otolaryngol Head Neck Surg* 123(3): 339.
Jackler RK, De la Cruz A. 1989. The large vestibular aqueduct syndrome. *Laryngoscope* 99(12): 1238–1242.
Jackler RK, Hwang PH. 1993. Enlargement of the cochlear aqueduct: fact or fiction? *Otolaryngol Head Neck Surg* 109(1): 14–25.
Jain R, Gandhi D, Gujar S, Mukherji SK. 2004. Case 67: Persistent stapedial artery. *Radiology* 230(2): 413–416.
Kantu K, Aretsky PJ, Polisar IA. 1972. Cryptotia. *Laryngoscope* 82(2): 161–165.
Kontorinis G, Goetz F, Giourgas A, Lanfermann H, Lenarz T, Giesemann AM. 2013. Aplasia of the cochlea: radiologic assessment and options for hearing rehabilitation. *Otol Neurotol* 34(7): 1253–1260.
Leung AK, Kong AY, Robson WL, McLeod DR. 2007. Dominantly inherited lop ears. *Am J Med Genet A* 143 A(19): 2330–2333.
Lin YY, Wang CH, Liu SC, Chen HC. 2012. Aberrant internal carotid artery in the middle ear with dehiscent high jugular bulb. *J Laryngol Otol* 126(6): 645–647.
Linthicum FH Jr. 2001. Scheibe (cochleosaccular) dysplasia. *Otol Neurotol* 22(5): 708.
Maisels DO. 1974. The surgery of abnormalities of the external ear excluding agenesis. *Proc R Soc Med* 67(12 Pt 1): 1201–1203.
Martin C, Tringali S, Bertholon P, Pouget JF, Prades JM. 2002. Isolated congenital round window absence. *Ann Otol Rhinol Laryngol* 111(9): 799–801.
Muderris T, Bercin S, Sevil E, Cetin H, Kiris M. 2013. A potentially catastrophic anatomical variation: aberrant internal carotid artery in the middle ear cavity. *Case Rep Otolaryngol* 2013: 743021.
Sampaio AL, Cureoglu S, Schachern PA, Kusunoki T, Paparella MM, Oliveira CA. 2004. Cochleosaccular dysplasia: a morphometric and histopathologic study in a series of temporal bones. *Otol Neurotol* 25(4): 530–535.
Satar B, Mukherji SK, Telian SA. 2003. Congenital aplasia of the semicircular canals. *Otol Neurotol* 24(3): 437–446.
Scheibe A. 1892. A case of deaf-mutism, with auditory atrophy and anomalies of development in membranous labyrinth in both ears. *Arch Otol* 21: 12–22.
Scheibe A. 1895. Anomalies of development in the inner ear of a deaf-mute. *Z Ohrenheil* 27: 95–99 (in German).
Shkalim V, Eliaz N, Linder N, Merlob P, Basel-Vanagaite L. 2008. Autosomal dominant isolated question mark ear. *Am J Med Genet* A 146 A(17): 2280–2283.
Suzuki C, Balaban C, Sando I, Sudo M, Ganbo T, Kitagawa M. 1998. Postnatal development of Eustachian tube: a computer-aided 3-D reconstruction and measurement study. *Acta Otolaryngol* 118(6): 837–843.
Welling DB, Glasscock ME 3rd, Gantz BJ. 1992. Avulsion of the anomalous facial nerve at stapedectomy. *Laryngoscope* 102(7): 729–733.
Weon YC, Kim JH, Choi SK, Koo JW. 2007. Bilateral duplication of the internal auditory canal. *Pediatr Radiol* 10: 1047–1049.
Yuen A, Coombs CJ. 2006. Reduction otoplasty: correction of the large or asymmetric ear. *Aesthetic Plast Surg* 30(6): 675–678.
Zheng Y, Schachern PA, Cureoglu S, Mutlu C, Dijalilian H, Paparella MM. 2002. The shortened cochlea: its classification and histopathologic features. *Int J Pediatr Otorhinolaryngol* 63(1): 29–39.

98 Salivary glands and ducts

Louise Wing[1] and Tarik F. Massoud[2]
[1]John Radcliffe Hospital, Oxford, UK
[2]Stanford University School of Medicine, Stanford, California, USA

All major and minor salivary glands arise by ingrowth of the oral epithelium into the underlying mesenchyme (Little and Rickles 1967). The parotid, submandibular, and sublingual salivary glands are known as the "major" salivary glands. These paired glands are intimately related to the mandible, and each gland type is histologically distinct. Their function is to produce saliva of variable composition, which is secreted into the oral mucosa via a ductal system.

Variations in anatomy most commonly arise in relation to the size and shape of the glands and their ductal systems. These variations have traditionally been described from the practice of cadaveric dissection; however, an increasing proportion are now being described from clinical imaging on account of the ever-improving resolution of radiological technique, such as digital subtraction sialography (DSS), MR sialography, and volumetric CT. Documentation and knowledge of detailed anatomical and morphometric variations of the salivary glands and ducts should be useful in the clinical management and therapeutic planning of patients undergoing salivary gland surgery, as well as luminal procedures on the salivary ducts including sialography, sialoendoscopy, interventional maneuvers and therapies, and lithotripsy. The various salivary glands may also be deficient. For example, Yan et al. (2012) reported a child with bilateral aplasia of all of the major salivary glands. Pham et al. (2010) reported agenesis of all major salivary glands in a case.

Parotid glands

The parotid glands are the largest of the three major salivary glands. Each forms an inverted apex with its superficial and deep components intimately related to the mandibular ramus. The gland is bounded inferiorly by the stylomastoid membrane, which may demonstrate points of weakness through which parotid tissue may herniate (Abdullah et al. 2013). Although usually bordered superficially by skin, anteromedially by the masseter and pterygoid muscles, and posteromedially by the sternocleidomastoid muscle and mastoid process, reports of variation in location and morphology exist. For example, the parotid gland has been found to lie at the anterior border of the masseter muscle with absent retromandibular and facial portions (Boulgakow 1926). The gland may extend to the mandibular ramus to cover the buccinator muscle. Banquer (1975) identified parotid gland tissue within the mandible.

Parotid glandular volume ranges from 9.8 cm^3 to 60 cm^3 (Ericson and Hedin 1970; Ono et al. 2006). Absence of the parotid gland is rare; more cases of bilateral absence exist in the literature than of unilateral absence (Martín-Granizo and Garca-González 2004). These cases are often associated with ectopic salivary tissue or form part of a clinical syndrome. In the case of unilateral agenesis, compensatory hypertrophy of the contralateral gland is common.

A common anatomical variant is that of an accessory parotid gland (Fig. 98.1). Although it has historically been stated that accessory parotid glands are present in approximately 20% of the population (Frommer 1977), higher rates of up to 68% have been reported in more recent literature (Toh et al. 1993; Horsburgh and Massoud 2013a); this high rate of accessory gland and duct depiction may be due to the inherent capability of high-resolution DSS images to detect small glandular tissue collections along the main parotid duct. Accessory parotid glands are usually located cranial to the parotid duct, with only one excretory accessory duct entering the main parotid duct. Multiple accessory glands have been reported in approximately 16% of cases by Som and Brandwein (2003) and in 31% of those with accessory glands by Horsburgh and Massoud (2013a); each gland has its own primary drainage into the main parotid duct.

Parotid ducts

The caliber of the salivary ducts is of clinical relevance, since it can indicate pathological processes (Zenk et al. 1998). It is important therefore to be aware of variations in baseline normal anatomy and morphometry. Moreover, an exact knowledge of the range in dimensions of the excretory salivary ducts is of

Bergman's Comprehensive Encyclopedia of Human Anatomic Variation, First Edition. Edited by R. Shane Tubbs, Mohammadali M. Shoja and Marios Loukas.
© 2016 John Wiley & Sons, Inc. Published 2016 by John Wiley & Sons, Inc.

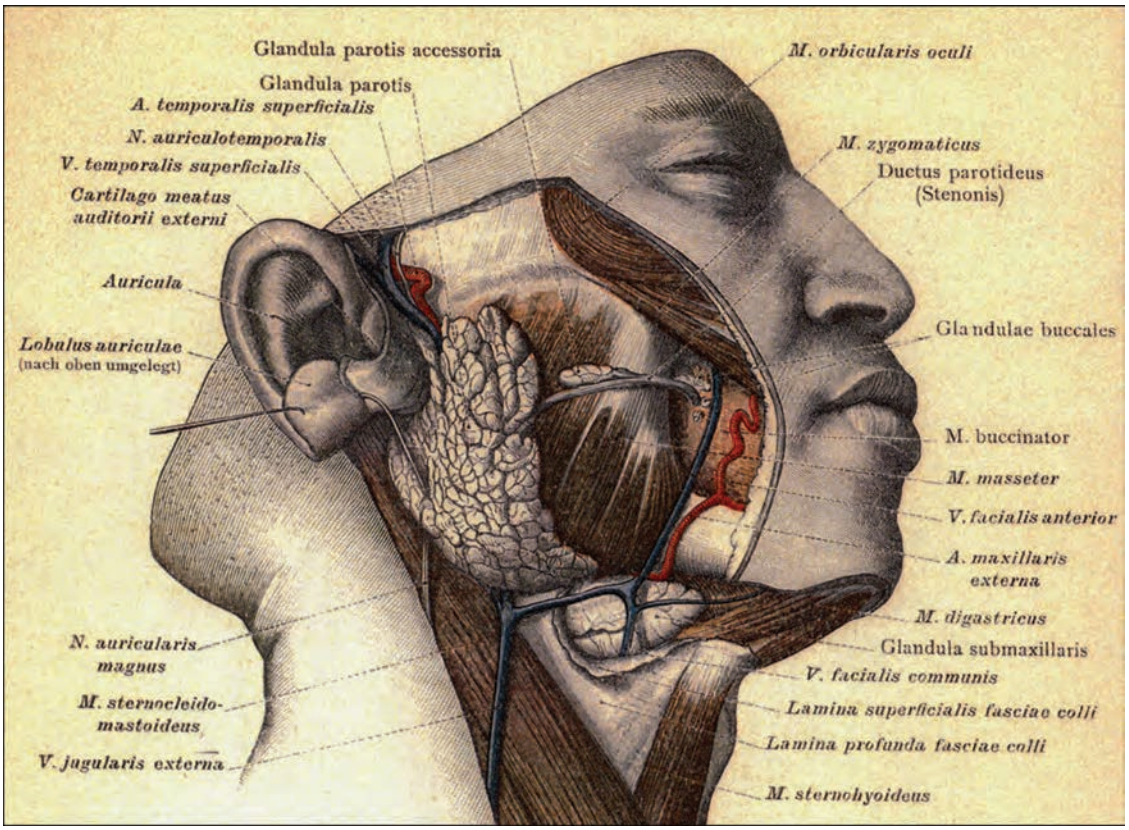

Figure 98.1 Accessory parotid gland (small green structure) lying superior to parotid duct as it passes over the masseter, prior to piercing the buccinators.

Source: Toldt (1919).

prime importance regarding to further development of salivary duct instrumentation for diagnostic and minimally invasive interventional therapies (Drage et al. 2000).

Niels Stensen (1638–1686) was an eminent Danish anatomist and geologist (Perrini et al. 2010). The parotid duct (Stensen's duct) continues to bear his name. Two main tributaries within the anterior part of the parotid gland unite to form the parotid duct. It exits the anterior border of the upper part of the parotid gland, passes horizontally across the lateral surface of the masseter muscle, and takes a right-angle turn medially at its anterior edge. It then passes through the buccal fat, buccopharyngeal fascia, and buccinator muscle. Here the parotid duct then runs obliquely forward for a short distance between buccinator and the oral mucosa, before it penetrates the oral mucosa at a small papilla in the buccal vestibule opposite the maxillary second molar.

The mean total length of the parotid duct as demonstrated recently on DSS is 52 mm (range 23–73 mm) (Horsburgh and Massoud 2013a, b). This is in agreement with previous reports, where the duct is described as being 5 cm long (Warwick and Williams 1973), although Som and Brandwein (2003) and Martinez-Madrigal and Micheau (1989) stated that it is 6–7 cm long.

The mean width of the proximal, mid, and distal segments of the parotid duct are 1.8 mm, 1.1 mm, and 1.6 mm, respectively (Horsburgh and Massoud 2013a). In 1968, Hettwer and Folsom examined 35 parotid ducts in healthy volunteers. The mean width of the ducts was 1.7 mm. On the other hand, Ericson found the mean width of the parotid duct to be 2 mm. It is believed that the submucosal passage of the distal parotid duct serves as a valvular mechanism preventing inflation of the gland with raised intraoral pressures. Alternatively, the buccinator may act as a valve that prevents inflation of the duct during blowing. Consequently, Kilpinen (1978) sialographically examined the parotid duct among wind musicians and reported parotid duct widths varying from 1.8 mm to 2.2 mm; this is in general agreement with findings in other studies. He therefore concluded that playing a wind instrument does not affect the width of the parotid duct. However, in common with the findings of Horsburgh and Massoud (2013a), Kilpinen (1978) noted that the middle of the parotid duct narrows to a mean value of 1.3 mm as it is projected on the anterior edge of the ramus of the mandible and as it lies over buccinator.

Unilateral duplication of the parotid duct is rare (Aktan 2001; de Souza Fernandes et al. 2009; Fig. 98.2); despite the paucity

Figure 98.2 Right cadaveric dissection noting a duplicated parotid duct. For reference, note the latex injected facial vein and artery anterior to the duplicated duct.

Source: de Souza Fernandes et al. (2009).

of case reports, the prevalence of these duplications has been reported as 7% (Bailey 1971). In such cases, superior and inferior parotid ducts of very similar caliber (2.5–3 mm) merge just prior to the opening at the oral cavity. Only one case of bilateral duplication of the parotid duct has been described (Astik and Dave 2011). In all described cases, duplicated parotid ducts are shorter than standard single parotid ducts, measuring 26.5–37.3 mm. The opening of the parotid duct may be imperforate (Watts 1988).

Although the parotid duct orifice is traditionally described as located at the level of the upper second molar, there is a degree of individual variation in the positioning of the parotid duct orifice, between the first and second maxillary molars (Suzuki et al. 2009).

An accessory parotid duct may join the parotid duct as the latter passes over the masseter muscle. The angle of confluence of the accessory parotid duct with the main parotid duct is usually quite acute (mean of 53°); however, there can be a wide variation with a range of 23–122° (Horsburgh and Massoud 2013a).

Submandibular glands

The submandibular gland varies in size over the range 1.6–22.5 cm^3 (Ono 2006) and lies below the body of the mandible within submandibular triangle (formed inferiorly by the two bellies of digastric muscles). The submandibular gland may be absent (unilaterally or bilaterally) as well as duplicated (Sperino 1903). Supernumerary submandibular gland lobes have been reported (Sukekawa and Itoh 2007). Carney et al. (1996) identified a submandibular gland located 2 cm inferior to the mandible. Accessory submandibular glands have been rarely described. One such case demonstrated circumferential narrowing of the mid portion of the submandibular duct on DSS, caused by accessory salivary gland tissue, proven on histology (Köybaşioğlu et al. 2000; Fig. 98.3). Two other case reports describe accessory glands lying anterior to the submandibular gland (Jafek and Strife 1973; Bryan et al. 2013). Rarely, a small inclusion of submandibular gland may occur in the body of the mandible, known as a Stafne defect. The prevalence of this is thought to range over 0.48–1.5% (de Courten et al. 2002). Submandibular gland aplasia is thought to be rarer than parotid gland aplasia. Both bilateral (Ahmed et al. 2009) and unilateral (Nayak and Ayyar 1927) absences have been reported.

Submandibular ducts

The submandibular duct begins by numerous branches that exit the deep surface of the gland. It bends sharply at the posterior margin of mylohyoid muscle to form the genu of the submandibular duct. It then runs forward lateral to hyoglossus and genioglossus muscles and medial to the attachment of mylohyoid muscle to the mandible, along the lower edge of the mylohyoid muscle, before running forward and slightly upward along the medial side of the sublingual gland more anteriorly. At the anterior border of the hyoglossus muscle it is crossed laterally by the lingual nerve. It opens by a narrow orifice on the summit of

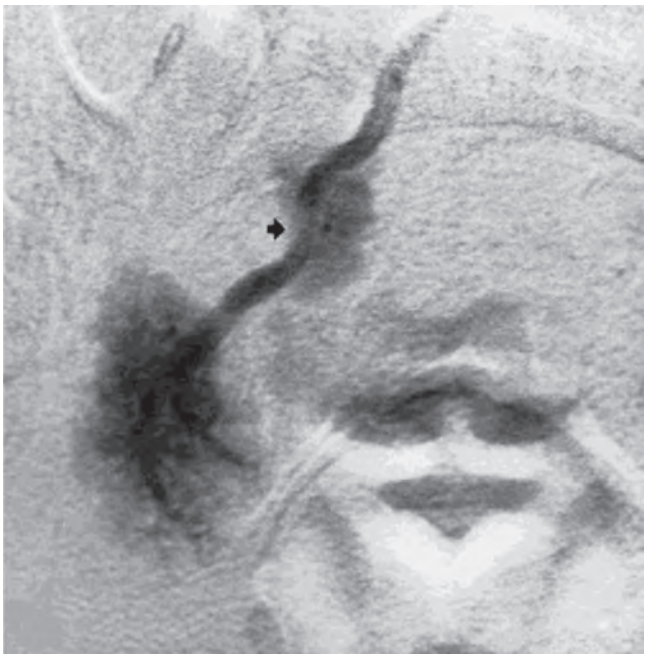

Figure 98.3 Accessory submandibular gland on digital substraction sialography, compressing Wharton's duct (arrow).

Source: Köybaşioğlu et al. (2000). Reproduced with permission from John Wiley & Sons.

the sublingual papilla. In 1659 Thomas Wharton was the first to describe the submandibular glands and their ducts more accurately than had previously been done, having researched their nature and function via dissection and experiment (Freer 1996). The submandibular duct may bifurcate (Rose 1932), duplicate (Ahmed et al. 2007), or triplicate (Gaur et al. 1994). Ellegård and Kjellmer (2010) reported atresia of the submandibular orifices.

As for the parotid ducts, it has been suggested that anatomical and morphometric features of the submandibular duct may be etiological factors in the formation of sialoliths and sialadenitis since these morphological characteristics may contribute to stagnation of saliva (Drage et al. 2002). It is therefore essential to clearly establish the normal variant features of these salivary ducts before an attempted understanding of their potential etiological role in salivary disease, as well as in planning of therapeutic luminal procedures on the salivary ducts.

The mean length of the submandibular duct has been described recently by Horsburgh and Massoud (2013a, b) using DSS as 58 mm (range 42–76 mm). The length had been described previously as being approximately 5 cm long (Carlson 2000; Yousem 2000; Drage et al. 2002; Som and Brandwein 2003), but Stimec et al. (2006) found a mean submandibular duct length of only 37.2 mm when using postmortem sialography.

The mean width of the submandibular ducts has also been described recently by Horsburgh and Massoud (2013a) on DSS as 2.0 mm in the proximal third, 2.7 mm in the middle third, and 2.1 mm in the distal third of the ducts. Hettwer and Folsom (1968) examined 35 parotid and submandibular duct sialograms on healthy volunteers. The mean width of the submandibular ducts was 2.7 mm. However, Zenk et al. (1998) have argued that the values of the diameters obtained by sialography likely differ considerably from their data obtained by postmortem histomorphometry: their mean width of submandibular duct was only 1.5 mm. They believe that the elasticity of the excretory ducts in particular seems to influence radiologically determined duct diameters, that is, the ducts are non-physiologically dilated by contrast media. This behavior may be due to elastic fibers within the submucosa of the duct epithelium. Using postmortem sialography, Stimec et al. (2006) found the mean width of the proximal submandibular duct to be 1.73 mm, its mid portion 1.82 mm, and the distal submandibular duct 1.77 mm.

The genu of the submandibular duct is defined as the angle between the main duct and the main intraglandular duct; it depicts the change in angulation as the submandibular duct turns around the posterior free margin of mylohyoid (Nahlieli et al. 2001). Drage et al. (2002) found the mean angle of the normal genu in the lateral projection to be 102.7° on sialography. However, using postmortem sialography Stimec et al. (2006) found the mean angle of the genu to be 114.4°, with no differences in measurements of the right and left submandibular ducts. Recently, Horsburgh and Massoud (2013a, b) found this angle to be a mean of 115° with a range of 80–144° on DSS.

A submandibular duct kink is defined as a complete narrowing that is only corrected by excessive forward stretching of the duct (Nahlieli et al. 2001). Occasionally, this may be revealed as retention of contrast medium in the duct on post-evacuation radiographs of a DSS. These kinks may be present in the hilar region of the gland at or a few millimeters from the genu. After sialoliths and pathological strictures, kinks are the most common cause of obstruction. Kinks may be produced by the angulation at the genu, and also the herniation of the surrounding tissue (i.e., fat, usually at the site of a large perforating branch of the submental artery) under the submandibular duct through the mylohyoid muscle or loosening of the muscle itself. Nahlieli et al. (2001) observed a kink in seven submandibular ducts (and two similar configurations in parotid ducts) amongst 220 obstructed salivary ducts. In the recent series by Horsburgh and Massoud (2013a), they viewed two possible kinks in the submandibular ducts; they did not have sialoendoscopic corroboration of this however, which would also be required to make this diagnosis by ruling out the presence of a pathological stricture.

Duplication and triplication anomalies of the submandibular duct are rare (Fig. 98.4). By 2007, only nine such cases had been reported (Gadodia et al. 2007). No attempt has been made to quantify the prevalence of these variants (Mori 1986; Gaur 1994). They result from inadequate development of the terminal segment of the submandibular duct, with invagination in two places or premature ventral branching. The resulting accessory submandibular duct is usually smaller and runs to a variable length in parallel with the main submandibular duct.

Figure 98.4 Duplicated submandibular ducts. Yellow arrow: submandibular duct; pink arrow, orifice. The red arrow points to the submandibular gland.

Source: Zhang et al. (2010). Reproduced with permission from Elsevier.

Sublingual glands and ducts

The sublingual glands are the last of the major salivary glands to appear, are the smallest (weighing approximately 2 g) and, uniquely, do not acquire long ducts as they migrate during development (Sumi et al. 1999; Tucker 2007). The sublingual gland has a variable relation to the mandible and may be absent or hypertrophied. They are best considered in the context of their relation to the submandibular glands. They sit on the mylohyoid muscle, beneath the mucous membrane of the floor of the mouth. The sheet-like mylohyoid muscle lies superior and medially to the submandibular gland, separating the majority of it from the sublingual gland although a deep portion of the submandibular gland lies adjacent to the sublingual gland (Otonari-Yamammoto et al. 2010). Indeed, fusion of the two glands has been reported (Sperino 1903; Rad 2003). Defects may arise within the mylohyoid containing "boutons" of salivary gland tissue, with equal proportions of submandibular and sublingual tissue (Engel et al. 1987). This variation is reasonably common with prevalence quoted as 37–63% (Gaughran 1963; White et al. 2001).

Accessory sublingual glands are known as the glands of Stöhr or the glandulae sublinguales minors. There ducts are termed the canals of Walther.

Anatomically, each sublingual gland is subdivided into anterior and posterior parts, and each part has a different drainage system. The major sublingual ducts were first described by Caspar Bartholin the Younger (Secundus, born 1655, died 1738) in 1685 (Hill 2007). The smaller ducts described by Augustus Quirinus Rivinus (born 1652, died 1723), are 8–20 in number, originate from the posterior part of each sublingual gland, and empty in the floor of the mouth at the sublingual folds (plica fimbriata or sublingualis) formed by the gland and located on either side of the lingual frenulum. The ducts from each anterior sublingual gland may unite to form a larger sublingual duct of Bartholin, which either joins the submandibular duct or drains into the floor of the mouth at the sublingual papilla (caruncle). The exact microanatomic relations between the ducts at the caruncle were investigated in detail by Zhang et al. (2010). In 60 bilateral cadaveric dissections those investigators found that 14 (23.3%) submandibular ducts opened directly at the sublingual caruncle separate from the Bartholin ducts and that 24 (40%) ducts joined and opened together at the caruncle. In 22 (36.7%) of the dissections the Bartholin duct was absent; instead, there appeared to be drainage via multiple ducts of Rivinus opening at the mucous membrane of the oral floor. These authors did not comment on symmetry or asymmetry of the arrangement of these salivary ducts. The Bartholin ducts may be demonstrated at DSS during submandibular DSS (Horsburgh and Massoud 2013c).

Heterotopic and minor salivary glands

Heterotopic salivary gland tissue (i.e., salivary gland tissue lying outside of the typical anatomical distribution) is reported in the literature. There is debate over the most common site, with some authors stating that it is within the upper third of the neck (Ferlito et al. 1999) and others at the base of the neck (Barbuscia et al. 2011), although it is usually found along the medial edge of the sternocleidomastoid muscle. Ectopic salivary tissue has been reported in various areas including the tonsillar fossa, parathyroid glands, lower neck, larynx, anus, tongue, within the maxilla and mandible, soft palate, hard palate, cheeks, lips, and external and middle ear. During the neck dissection of a male cadaver, Sanli et al. (2010) found that large heterotopic submandibular glands were encountered bilaterally in the upper neck. They were symmetrical, capsulated, and lay deep to the superficial lamina of the superficial cervical fascia. Both glands were located in the submandibular and carotid triangles. The somewhat smaller orthotopic submandibular glands and the sublingual glands were in their normal anatomic location. The duct of

the heterotopic gland united with the corresponding orthotopic submandibular gland's duct on each side and ended on the ipsilateral sublingual caruncle. Histopathologic examination of the heterotopic glands revealed seromucous (mainly serous) tissue.

Aberrant salivary ducts may drain to the skin or pharynx (McFerran and Phillips 1993). Nanson (1979) has reported salivary gland drainage into the thyroglossal duct from an intralingual ectopic salivary gland.

The minor glands (namely labial, buccal, palatine, glossopalatine, lingual, and sublingual; although tonsillar, supraglottic, and paranasal sinus glands may also occur) are small collections of mucous secreting glands measuring up to 5 mm in size, located throughout the upper aerodigestive tract and paranasal sinuses. The majority either open directly onto the buccal mucosa or, less commonly, have very primitive ductal systems; the most developed ducts which may occur are the von Ebner ducts of the posterior lingual glands (Hand et al. 1999). Sublingual accessory salivary glands near the apex of the tongue are variably referred to as the glands of Suzanne, Blandin, Bauhin, or Nuhn. Accessory salivary glands near the lateral borders of the tongue are referred to as Weber's glands.

References

Abdullah A, Rivas FF, Srinivasan A. 2013. Imaging of the salivary glands. *Semin Roentgenol* 48: 65–74.

Ahmed M, Strauss M, Kassaie A, Shotelersuk V, DeGuzman R. 2009. Bilateral submandibular gland aplasia with clinico–radiological mass due to prolapsing sublingual salivary tissue through mylohyoid boutonniere: a case report and review. *Dentomaxillofac Radiol* 38: 121–124.

Ahmed S, Al-Jawad H, Al-Sayyari A, Khan AN. 2007. Congenital duplication of submandibular ducts. *Saudi Med J* 28: 1293–1294.

Aktan ZA, Bilge O, Pinar YA, Ikiz AO. 2001. Duplication of the parotid duct: a previously unreported anomaly. *Surg Radiol Anat* 23: 353–354.

Astik RB, Dave UH. 2011. Embryological basis of bilateral double parotid ducts: a rare anatomical variation. *IJAV* 4: 141–143.

Bailey L. 1971. *Short Practice of Surgery*, 15th edition. London, Lewis.

Banquer E. 1975. Parotid tissue embedded in the mandible. Bibliographic review and presentation of a case of this unusual ectopia.*Trib Odontol (B Aires)* 59: 106–111.

Barbuscia MA, Caizzone A, Vecchio DA, Mirone S, Putortì A, Cingari EA, Scardigno MR, Ilaqua A, Cavallari V. 2011. Ectopic parotid: case report. *G Chir* 32: 429–433.

Bataskis JG. 1986. Pathology consultation; Heterotopic and accessory salivary tissues. *Ann Head Neck Med Surg* 95: 434–435.

Boulgakow B. 1926. A Case of maldevelopment of the right parotid gland. *J Anat* 60: 341.

Bryan S, Bodner L, Manor E, Brennan PA. 2013. Pleomorphic adenoma occurring outside the submandibular gland: a case report of an accessory submandibular gland. *J Oral Maxillofac Surg* 71: 1703–1705.

Carlson GW. 2000. The salivary glands. Embryology, anatomy, and surgical applications. *Surg Clin North Am* 80: 261–273.

Carney AS, Sharp JF, Cozens NJ. 1996. Atypically located submandibular gland diagnosed by Doppler ultrasound. *J Laryngol Otol* 110: 1171–1172.

de Courten A, Küffer R, Samson J, Lombardi T. 2002. Anterior lingual mandibular salivary gland defect (Stafne defect) presenting as a residual cyst. *Oral Surg Oral Med Oral Pathol Oral Radiol Endod* 94: 460–464.

de Souza Fernandes AC, Lima GR, Rossi AM, Aguiar CM. 2009. Parotid gland with double duct: An anatomic variation description. *Int J Morphol* 27(1): 129–132.

Drage NA, Brown JE, Escudier MP, McGurk M. 2000. Interventional radiology in the removal of salivary calculi. *Radiology* 214: 139–142.

Drage NA, Wilson RF, McGurk M. 2002. The genu of the submandibular duct: is the angle significant in salivary gland disease? *Dentomaxillofac Radiol* 31: 15–18.

Ellegård E, Kjellmer I. 2010. Atresia of the submandibular duct orifices: an unusual cause of feeding problems and failure to thrive in an infant. *Acta Paediatr* 99: 1100–1101.

Engel JD, Harn SD, Cohen DM. 1987. Mylohyoid herniation: gross and histologic evaluation with clinical correlation. *Oral Surg Oral Med Oral Pathol* 63: 55–59.

Ericson S, Hedin M. 1970. A clinical roentgenologic method of calculating the volume of the parotid gland. *Oral Surg Oral Med Oral Pathol* 29: 536–543.

Ferlito A, Bertino G, Rinaldo A, Mannarà GM, Devaney KO. 1999. A review of heterotopia and associated salivary gland neoplasms of the head and neck. *J Laryngol Otol* 113: 299–303.

Freer S. 1996. *Thomas Wharton's Adenographia. First published in London in 1656*. Oxford: Clarendon Press.

Frommer J. 1977. The human accessory parotid gland: its incidence, nature, and significance. *Oral Surg Oral Med Oral Pathol* 43: 671–676.

Gadodia A, Seith A, Neyaz Z, Sharma R, Thakkar A. 2007. Magnetic resonance identification of an accessory submandibular duct and gland: an unusual variant. *J Laryngol Otol* 121: e18.

Gaughran GR. 1963. Mylohyoid boutonnière and sublingual bouton. *J Anat* 97: 565–568.

Gaur U, Choudhry R, Anand C, Choudhry S. 1994. Submandibular gland with multiple ducts. *Surg Radiol Anat* 16: 439–440.

Hand AR, Pathmanathan D, Field RB. 1999. Morphological features of the minor salivary glands. *Arch Oral Biol* 44: S3–10.

Hettwer KJ, Folsom T. 1968. The normal sialogram. *Oral Surg Oral Med Oral Pathol* 26: 790–799.

Hill RV. 2007. The contributions of the Bartholin family to the study and practice of clinical anatomy. *Clin Anat* 20: 113–115.

Horsburgh A, Massoud TF. 2013a. The salivary ducts of Wharton and Stenson: analysis of normal variant sialographic morphometry and a historical review. *Ann Anat* 195: 238–242.

Horsburgh A, Massoud TF. 2013b. The role of salivary duct morphology in the aetiology of sialadenitis: statistical analysis of sialographic features. *Int J Oral Maxillofac Surg* 42: 124–128.

Horsburgh A, Massoud TF. 2013c. Lessons learned from unintended sublingual sialography: imaging anatomy, technical considerations, and diagnostic implications. *AJR Am J Roentgenol* 200: 879–883.

Jafek BW, Strife JL. 1973. Accessory lobe of the submandibular gland. *Radiology* 109: 75–77.

Kilpinen E. 1978. Width of the main duct of the parotid gland in wind instrument musicians. *Dentomaxillofac Radiol* 7: 79–81.

Köybaşioğlu A, Ileri F, Gençay S, Poyraz A, Uslu S, Inal E. 2000. Submandibular accessory salivary gland causing Warton's duct obstruction. *Head Neck* 22: 717–721.

Little JW, Rickles NH. 1967. The histogenesis of the branchial cyst. *Am J Pathol* 50: 533–547.

Martín-Granizo R, Garca-González D. 2004. Unilateral agenesis of the parotid gland: a case report. *Oral Surg Oral Med Oral Pathol Oral Radiol Endod* 98: 712–714.
Martinez-Madrigal F, Micheau C. 1989. Histology of the major salivary glands. *Am J Surg Pathol* 13: 879–899.
McFerran DJ, Phillips RR. 1993. Case report: congenital fistula between the submandibular gland and the oropharynx. *Br J Radiol* 66: 561–562.
Mori S, Wada T, Harada Y, Toyoshima S. 1986. Accessory duct in the submandibular gland. *Oral Surg Oral Med Oral Pathol* 62: 607–608.
Nahlieli O, Shacham R, Yoffe B, Eliav E. 2001. Diagnosis and treatment of strictures and kinks in salivary gland ducts. *J Oral Maxillofac Surg* 59: 484–490.
Nanson EM. 1979. Salivary gland drainage into the thyroglossal duct. *Surg Gynecol Obstet* 149: 203–205.
Nayak UV, Ayyar AA. 1927. Anomalies in the development of salivary glands. *J Anat* 61: 261–262.
Ono K, Morimoto Y, Inoue H, Masuda W, Tanaka T, Inenaga K. 2006. Relationship of the unstimulated whole saliva flow rate and salivary gland size estimated by magnetic resonance image in healthy young humans. *Arch Oral Biol* 51: 345–349.
Otonari-Yamamoto M, Nakajima K, Tsuji Y, Otonari T, Curtin HD, Okano T, Sano T. 2010. Imaging of the mylohyoid muscle: separation of submandibular and sublingual spaces. *AJR Am J Roentgenol* 194: W431–438.
Perrini P, Lanzino G, Parenti GF. 2010. Niels Stensen (1638–1686): scientist, neuroanatomist, and saint. *Neurosurgery* 67: 3–9.
Pham Dang N, Picard M, Mondié JM, Barthélémy I. 2010. Complete congenital agenesis of all major salivary glands: a case report and review of the literature. *Oral Surg Oral Med Oral Pathol Oral Radiol Endod* 110: e23–7.
Rad S. 2003. Unusual communication of the salivary glands. *Arch Iran Med* 6: 299–300.
Rose B. 1932. Bifurication of the submaxillary duct. *Am J Surg* 17: 257–258.
Sanli EC, Oztürk NC, Polat A, Oztürk H. 2010. Bilateral and symmetrical heterotopic submandibular glands in the upper neck: case report. *Surg Radiol Anat* 32: 979–982.
Som PM, Brandwein MS. 2003. Salivary glands: anatomy and pathology. In: *Head and Neck Imaging* (eds PM Som, HDCurtin). Mosby, St Louis: Elsevier, pp. 2005–2133.
Sperino G. 1903. Absence congenitale de la glande submaxillaris dans sa place normale; sa transposition au-dessus du m. mylo-hyoideus; fusion partielle de cette glande avec la glandula sublingualis. *Arch Ital Biol* 40: 318.
Stimec B, Nikolic S, Rakocevic Z, Bulajic M. 2006. Symmetry of the submandibular glands in humans: a postmortem study assessing the linear morphometric parameters. *Oral Surg Oral Med Oral Pathol Oral Radiol Endod* 102: 391–394.
Sukekawa R, Itoh I. 2007. Rare case of supernumerary submandibular gland lobes forming a complex with the sublingual gland. *Kaibogaku Zasshi* 82: 93–97.
Sumi M, Izumi M, Yonetsu K. 1999. Sublingual gland: MR features of normal and diseased states. *AJR* 172: 717–722.
Suzuki A, Watanabe S, Ono Y, Ohashi H, Pai C, Xing X, Wang X. 2009. Influence of the location of the parotid duct orifice on oral clearance. *Arch Oral Biol* 54: 274–278.
Toh H, Kodama J, Fukuda J, Rittman B, Mackenzie I. 1993. Incidence and histology of human accessory parotid glands. *Anat Rec* 236: 586–590.
Toldt C. 1919. *An Atlas of Human Anatomy for Physicians and Students*. New York: Rebman Company.
Tucker AS. 2007. Salivary gland development. *Semin Cell Dev Biol* 18: 237–244.
Warwick R, Williams PL. 1973. Gray's Anatomy, 35th edition. Edinburgh: Longman.
Watts KD. 1988. Congenital imperforate parotid duct openings: a case report. *Br J Oral Maxillofac Surg* 26: 341–343.
White DK, Davidson HC, Harnsberger HR, Haller J, Kamya A. 2001. Accessory salivary tissue in the mylohyoid boutonnière: a clinical and radiologic pseudolesion of the oral cavity. *AJNR Am J Neuroradiol* 22: 406–12.
Yan Z, Ding N, Liu X, Hua H. 2012. Congenital agenesis of all major salivary glands and absence of unilateral lacrimal puncta: a case report and review of the literature. *Acta Otolaryngol* 132: 671–675.
Yousem DM, Kraut MA, Chalian AA. 2000. Major salivary gland imaging. *Radiology* 216: 19–29.
Zenk J, Hosemann WG, Iro H. 1998. Diameters of the main excretory ducts of the adult human submandibular and parotid gland: a histologic study. *Oral Surg Oral Med Oral Pathol Oral Radiol Endod* 85: 576–580.
Zhang L, Xu H, Cai Z, Mao C, Wang Y, Peng X, Zhu ZH, Yu GY. 2010. Clinical and anatomic study on the ducts of the submandibular and sublingual glands. *J Oral Maxillofac Surg* 68: 606–610.

Further reading

Bailey H. 1948. Surgical anatomy of the parotid gland. *Brit M J* 2: 245–248.
Brünner H. 1962. Zur makroskopischen Form der Glandula parotis. *Anat Anz* 110: 327–335.
Gasser RF. 1970. The early development of the parotid gland around the facial nerve and its branches in man. *Anat Rec* 167: 63–77.
Giannelli L, Lahgi A, Quercioli V. 1899. Recherches sur le canal de sténon. *Arch Ital Biol* 32: 460.
Hurford FR. 1946. The surgical anatomy of the parotid glands. *Brit J Surg* 34: 186–187.
López P, Cortón D, Uroz J, Antón L, Tracchia R. 1990. Congenital atresia of the parotid duct. *Cir Pediatr* 3: 136–137.
McCormack LJ, Cauldwell EW, Anson BJ. 1945. The surgical anatomy of the facial nerve. With special reference to the parotid gland. *Surg Gyn Obst* 80: 620–630.
McKenzie J. 1948. The parotid gland in relation to the facial nerve. *J Anat* 82: 183–196.
McWhorter GL. 1917. The relations of the superficial and deep lobes of the parotid gland to the ducts and to the facial nerve. *Anat Rec* 12: 149–154.
McWhorter GL. 1927. Operation on two cases of secondary carcinoma and one case of primary cystadenoma of the parotid gland. Relation of the parotid to the facial nerve. *Surg Clin N America* 7: 489–505.
Najwer K, Jaszkin-Grudzinska J. 1982. A case of two-lobar parotid gland. *Folia Morphol (Warsaw)* 41: 335–337.
Parsons FG. 1911. On the form of the parotid gland. *J Anat Physiol* 45: 239–241.
Polayes IM, Rankow RM. 1979. Cysts, masses, and tumors of the accessory parotid gland. *Plast Reconstr Surg* 64: 17–23.
Sun L, Sun Z, Ma X. 2013. Congenital parotid ectopia in accessory maxilla and facial cleft anomalies: three cases report. *In J Pediatr Otorhinolaryngol* 77: 608–612.

99 Thyroid gland

Bulent Yalcin
Gulhane Military Medical Academy, Ankara, Turkey

Anatomy

The thyroid gland, brownish-red and highly vascular, is located anteriorly in the lower neck, level with the fifth cervical to the first thoracic vertebrae. It is ensheathed by the pretracheal layer of the deep cervical fascia and consists of right and left lobes connected by a narrow, median isthmus. It usually weighs 25 g, but this varies. The lobes of the thyroid gland are approximately conical. Their ascending apices diverge laterally to the level of the oblique lines on the laminae of the thyroid cartilage, and their bases are level with the fourth or fifth tracheal cartilage. Each lobe is usually 5 cm long, its maximum transverse and anteroposterior measurements being 3 cm and 2 cm, respectively. The isthmus connects the lower parts of the two lobes, although occasionally it is absent. It measures 1.25 cm transversely and vertically and is usually anterior to the second and third tracheal cartilages, though often higher or sometimes lower because its site and size are very variable (Standring 2008).

The thyroid gland is supplied by the superior and inferior thyroid arteries and sometimes by an arteria thyroidea ima from the brachiocephalic trunk or aortic arch. The arteries are large and their branches frequently anastomose both on and inside the gland, ipsilaterally and contralaterally. The superior thyroid artery, which is closely related to the external laryngeal nerve, pierces the thyroid fascia and then divides into anterior and posterior branches. The anterior branch supplies the anterior surface of the gland and the posterior branch supplies the lateral and medial surfaces. The inferior thyroid artery approaches the base of the thyroid gland and divides into superior (ascending) and inferior thyroid branches to supply the inferior and posterior surfaces of the gland. The superior branch also supplies the parathyroid glands. The venous drainage from the thyroid is usually via the superior, middle, and inferior thyroid veins. The superior thyroid vein emerges from the upper part of the gland and runs with the superior thyroid artery towards the carotid sheath: it drains into the internal jugular vein. The middle thyroid vein collects blood from the lower part of the gland: it emerges from the lateral surface of the gland and also drains into the internal jugular. The inferior thyroid veins arise in a glandular venous plexus, which also connects with the middle and superior thyroid veins. These veins form a pretracheal plexus, from which the left inferior vein descends to join the left brachiocephalic vein and the right descends obliquely across the brachiocephalic artery to join the right brachiocephalic vein at its junction with the superior vena cava. The inferior thyroid veins often open via a common trunk into the superior vena cava or left brachiocephalic vein. They drain the esophageal, tracheal, and inferior laryngeal veins and have valves at their terminations.

Thyroid lymphatic vessels communicate with the tracheal plexus and pass to the prelaryngeal nodes just above the thyroid isthmus and to the pretracheal and paratracheal nodes; some also drain into the brachiocephalic nodes related to the thymus in the superior mediastinum. Laterally, the gland is drained by vessels lying along the superior thyroid veins to the deep cervical nodes. Thyroid lymphatics can drain directly, with no intervening node, into the thoracic duct.

The thyroid gland is innervated from the superior, middle, and inferior cervical sympathetic ganglia. Postganglionic fibers from the inferior cervical ganglion form a plexus on the inferior thyroid artery that accompanies the artery to the thyroid gland and communicates with the recurrent and external laryngeal nerves, the superior cardiac nerve, and the plexus on the common carotid artery (Standring 2008).

Embryology

Among all the endocrine glands, the thyroid is the first to appear during embryonic development in humans (Devi et al. 2009); its development begins by the third week of gestation and ends by the eleventh week. Reports in the literature suggest that chromosome 22 could have a role in the process (Gangbo et al. 2004). The primordium of the medial part of the thyroid gland appears during the third week of gestation as an epithelial proliferation in the floor of the pharynx immediately caudal to the tuberculum impar at the border between the first and second pharyngeal pouches (Sadler and Langman 2006). It appears as a duct-like invagination of the endoderm in the floor of the pharynx. This point of origin of the thyroid gland is later called the foramen cecum. This midline structure undergoes enlargement,

Bergman's Comprehensive Encyclopedia of Human Anatomic Variation, First Edition. Edited by R. Shane Tubbs, Mohammadali M. Shoja and Marios Loukas.
© 2016 John Wiley & Sons, Inc. Published 2016 by John Wiley & Sons, Inc.

bifurcation, lobulation, and detachment from the pharynx. By the end of the seventh week of gestation, the thyroid has descended from the floor of the pharynx in front of the hyoid bone and the lingual cartilage and reached its final position anterior to the trachea (Hoyes and Kershaw 1985). The lateral thyroid primordia originate from the fourth and fifth pharyngeal pouches and descend to join the medial primordium by the fifth week of gestation, contributing up to 30% of the weight of the gland (Organ and Organ 2000). The lateral thyroid anlage arises from the neural crest cells and provides the parafollicular C cells that produce calcitonin (Sugiyama 1971). By the seventh week, the gland consists of a median isthmus and two lateral lobes (Sadler and Langman 2006).

During its migration the thyroid remains connected to the tongue by the thyroglossal duct, which usually disappears between the fifth and tenth gestational weeks and atrophies, and is sometimes represented by a strip of fibrous or muscular tissue. The lingual part of the thyroglossal duct can remain identifiable until late in fetal life (Hoyes and Kershaw 1985). A thyroglossal duct cyst due to incomplete degeneration of the duct can occur at any point along the migratory path of the thyroid gland near the midline of the neck (Mohebati and Shaha 2012). Remnants of the duct within the tongue are referred to as Bochdalek's canal.

Any deviation from the normal development of the thyroid gland, including the descent of the median thyroid diverticulum from the foramen cecum at the tongue to its adult position between the fifth cervical and first thoracic vertebrae and partial persistence of the thyroglossal duct or tract, results in the formation of structures such as a pyramidal lobe or levator glandulae thyroidea or in partial or total agenesis of thyroid gland, absence of isthmus, or ectopic and accessory thyroid tissue (Prakash et al. 2012).

Otto (1994) questioned whether the thyroid descends. His account claims that the embryonic thyroid develops near the heart and has to ascend to the neck. A secondary epithelial cord connects the thyroid to the tongue (thyroglossal duct). It contains two different types of epithelial tissue, one coming from the oral cavity and the other from the thyroid. In the sixth week the two types of epithelium usually separate and regress. Any disturbance of this process can cause thyroid anomalies containing either thyroid tissue (accessory thyroid glands, pyramidal lobes) or only epithelial tissue arising from the oral cavity (median cervical cysts or sinuses).

Variations of the thyroid gland

Pyramidal lobe

Most variations of the thyroid gland are due to partial persistence of the median or thyroglossal duct (Melnick and Stemkowski 1981). The most obvious example of this persistence is the pyramidal lobe. The pyramidal lobe (lobus pyramidalis, Lalouette's pyramid, Morgagni's appendix) is a vestigial remnant of the distal part of the thyroglossal duct. A conical pyramidal lobe often ascends towards the thyroid cartilage or the hyoid bone from the isthmus or the adjacent part of either lobe (more often the left). It varies in shape and position as well as appearance and size (Standring 2008). A wide variety of forms have been described: pyramidal, triangular, string, or flat (Zivic et al. 2011). Rarely, a high separation of the thyroglossal duct can generate two independent thyroid lobes and pyramidal lobes with no isthmus (Chaithra Rao et al. 2012).

Since Lalouette gave this entity its name in 1749, diverse statements have been made about the variations and frequencies of the pyramidal lobe (cited by Zivic et al. 2011). The alleged frequencies are summarized in Table 99.1: cadaveric studies give incidences of 28.9–76.8% (Marshall 1895; Gardner 1966; Kitagawa 1993; Won and Chung 2002; Harjeet et al. 2004; Braun

Table 99.1 Incidence of the pyramidal lobe in the literature.

Authors	Examination method	Frequency (%)
Marshall 1895	Cadaveric	43
Gardner 1966	Cadaveric	40
Hunt et al. 1968	Surgical	41
Izenstark et al. 1969	Radiologic-scintigraphy	35
Blumberg 1981	Surgical	60–65
Levy et al. 1982	Radiologic-scintigraphy	43
Savage et al. 1984	Radiologic-scintigraphy	25
Siraj et al. 1989	Radiologic-scintigraphy	41
Kitagawa 1993	Cadaveric (fetus)	48.6
Wahl et al. 1997	Radiologic-scintigraphy	81
Spencer et al. 1997	Radiologic-scintigraphy	36
Won and Chung 2002	Cadaveric	76.8
Filho et al. 2004	Surgical	50.7
Harjeet et al. 2004	Cadaveric	28.9
Çicekbaşı et al. 2007	Cadaveric (fetus)	18.3
Braun et al. 2007	Radiologic-scintigraphy	13
Braun et al. 2007	Cadaveric	55
Sturniolo et al. 2008	Surgical	25.5
Ranade et al. 2008	Cadaveric	58
Sultana et al. 2008	Cadaveric	50
Geraci et al. 2008	Surgical	12
Joshi et al. 2010	Cadaveric	37.8
Zivic et al. 2011	Surgical	61
Tanriover et al. 2011	Cadaveric	57.8
Ozgur et al. 2011	Cadaveric	65
Prakash et al. 2012	Cadaveric	35.7
Park et al. 2012	Radiologic-CT	41.2
Kim et al. 2013	Radiologic-CT	44.6

et al. 2007; Ranade et al. 2008; Sultana et al. 2008; Joshi et al. 2010; Tanriover et al. 2011; Ozgur et al. 2011; Prakash et al. 2012) and surgical studies 12–65% (Hunt et al. 1968; Blumberg 1981; Filho et al. 2004; Geraci et al. 2008; Sturniolo et al. 2008; Zivic et al. 2011). Among radiological studies, scintigraphy and computed tomography (CT) give frequencies of 13–81% (Izenstark et al. 1969; Levy et al. 1982; Savage et al. 1984; Siraj et al. 1989; Wahl et al. 1997; Spencer et al. 1997; Braun et al. 2007) and 41.2–44.6% (Park et al. 2012; Kim et al. 2013), respectively. Kitagawa (1993) and Çicekbaşı et al. (2007) observed the pyramidal lobe in 48.6% and 18.3% of fetuses, respectively. The pyramidal lobe is present in 22.2–62% of females and 33.9–62% of males (Table 99.2) (Spencer et al. 1997; Braun et al. 2007; Sultana et al. 2008; Zivic et al. 2011; Tanriover et al. 2011; Park et al. 2012; Prakash et al. 2012). There is no gender difference in frequency or in the age at which the pyramidal lobe is detected (Park et al. 2012).

The pyramidal lobe arises from different parts of the thyroid gland (Table 99.2): in 15–96% from the left lateral lobe, in 0–49% from the isthmus, and in 4–44.4% from the right lateral lobe (Fig. 99.1) (Spencer et al. 1997; Wahl et al. 1997; Won and Chung 2002; Harjeet et al. 2004; Braun et al. 2007; Geraci et al. 2008; Joshi et al. 2010; Zivic et al. 2011; Tanriover et al. 2011; Park et al. 2012). It most commonly originates from the left side of the thyroid gland; the difference between the sides is statistically significant (Park et al. 2012). It extends to different structures (Table 99.3): to the thyroid cartilage in 27.5–91.9% of cases (Marshall 1895; Harjeet et al. 2004; Braun et al. 2007; Ozgur et al. 2011; Park et al. 2012); to the hyoid bone in 17–65.4% (Marshall 1895; Bergman et al. 1988; Harjeet et al. 2004; Braun et al. 2007; Ozgur et al. 2011; Park et al. 2012); to the median thyrohyoid ligament in 3–31.8% (Harjeet et al. 2004; Ozgur et al. 2011; Park et al. 2012); and to the tongue in 0.7% (Park et al. 2012) (Fig. 99.2). Because of these differences its length ranges over 1.8–50 mm (Filho et al. 2004; Braun et al. 2007; Geraci et al. 2008; Sultana et al. 2008; Zivic et al. 2011; Tanriover et al. 2011; Park et al. 2012; Kim et al. 2013). The mean length has been reported as 20.8 mm (Kim et al. 2013), 20.1 mm (Zivic et al. 2011; Tanriover et al. 2011), 24.1 mm (Braun et al. 2007), and 25 mm (Park et al. 2012); it has been measured at 24.3 mm (Park et al. 2012) and 29 mm (Braun et al. 2007) in females and at

Table 99.2 Incidence (%) of the pyramidal lobe in both genders and its origin point from the part of the thyroid gland.

Authors	In female	In male	Left lobe	Isthmus	Right lobe
Wahl et al. 1997			53	8	39
Spencer et al. 1997	32	46	47.2	8.3	44.4
Won and Chung 2002			48.8	21.7	26.4
Harjeet et al. 2004			40.6	34.5	21.2
Braun et al. 2007	48.2	62	50	28.1	21.8
Geraci et al. 2008			96	0	4
Sultana et al. 2008	41.7	52.1	usually		
Joshi et al. 2010			47	20.6	32.6
Zivic et al. 2011	62	50	15	49	36
Tanriover et al. 2011	60	57.3	40.3	27.1	32.6
Prakash et al. 2012	22.2	40.3	usually		
Park et al. 2012	44.7	33.9	54	19.2	25.1

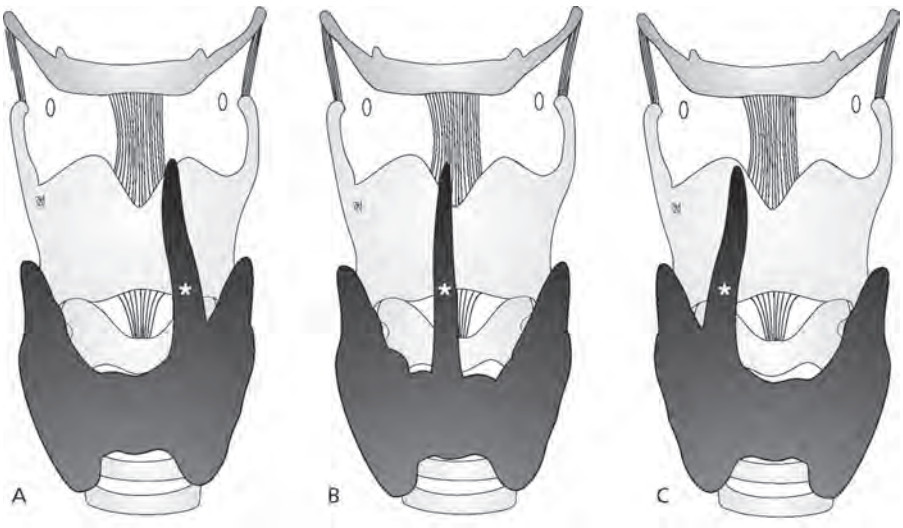

Figure 99.1 The pyramidal lobe (white asterisk) arises: (a) from the left lateral lobe of the thyroid gland; (b) from the isthmus; or (c) from the right lateral lobe of the thyroid gland.

Table 99.3 Incidence (%) of the pyramidal lobe reaching to different structures.

Authors	Hyoid bone	Thyroid cartilage	Median thyrohyoid ligament	Tongue
Marshall 1895	65.4	34.6		
Bergman et al. 1988	52.8			
Harjeet et al. 2004	5.5	91.9	3	
Braun et al. 2007	18.8	31.25		
Ozgur et al. 2011	17.5	27.5	30	
Park et al. 2012	17	50.3	31.8	0.7

14 mm (Braun et al. 2007) and 26 mm (Park et al. 2012) in males. Park et al. (2012) reported no gender difference. The thickness of the pyramidal lobe is 1.3–19 mm (Sultana et al. 2008) and its mean volume is 129.4 cm^3 (142.7 cm^3 in females, 92.9 cm^3 in males) (Park et al. 2012).

The pyramidal lobe originates unilaterally from the thyroid gland and attaches to the corresponding side of the points mentioned above. In 3.3% (Harjeet et al. 2004) or 22.5% (Ozgur et al. 2011) of cases however, it originates unilaterally and then crosses over to the opposite side (Fig. 99.3). Although it is continuous with the main thyroid gland in most cases, it is separate from it in 9.2% (Kim et al. 2013) or 12.5% (Park et al. 2012).

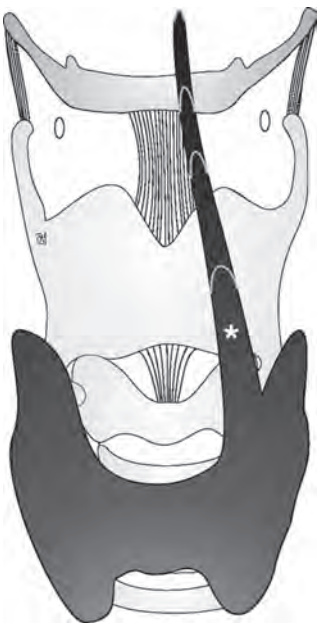

Figure 99.2 The pyramidal lobe (white asterisk) extents to the thyroid cartilage, to the median thyrohyoid ligament, to the hyoid bone, or to the tongue. Interrupted lines indicate the reaching points of the pyramidal lobe.

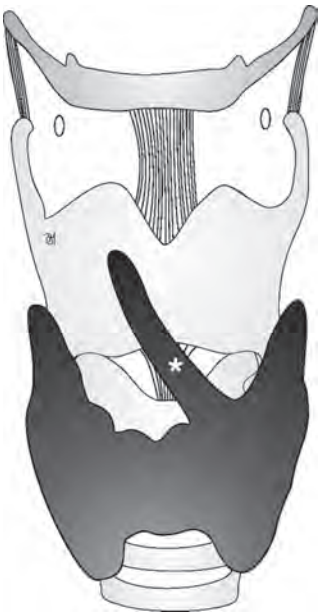

Figure 99.3 The pyramidal lobe (white asterisk) originates unilaterally and then crosses over to the opposite side.

In 1–10% cases two pyramidal lobes originate from two separated lateral lobes of the thyroid gland (Fig. 99.4a) (Harjeet et al. 2004; Joshi et al. 2010; Ozgur et al. 2011). They unite cranially in 0.1–2.5% of cases (Fig. 99.4b) (Harjeet et al. 2004; Ozgur et al. 2011).

Thyroid cells in the pyramidal lobe are usually inactive but become activated if the functioning thyroid tissue is removed. This explains why scintigraphy seldom reveals a pyramidal lobe, even when one is present (Braun et al. 2007). Savage et al. (1984) suggested that scintigraphic images might not truly reflect the anatomical origin of the pyramidal lobe.

The levator glandulae thyroidea muscle

The levator glandulae thyroidea muscle is a fibrous or fibromuscular band, the levator of the thyroid gland, which sometimes descends from the body of the hyoid to the isthmus or pyramidal lobe (Standring 2008).

Keyes (1940) and Lehr (1979) suggested that the levator glandulae thyroidea muscle is an embryological derivative of the cricothyroid. According to those authors, the thyroid gland can displace the muscle fibers of origin with the superior laryngeal nerve of the fourth brachial arch during its passage through the mesoderm (Keyes 1940; Lehr 1979). However, the embryological mechanism responsible for the development of the levator glandulae thyroidea remains largely unknown. Watanabe and Suda (1962) proposed that the presence of this muscle is entirely genetic. Petterson et al. (1979) claimed a genetic association with trisomy 13.

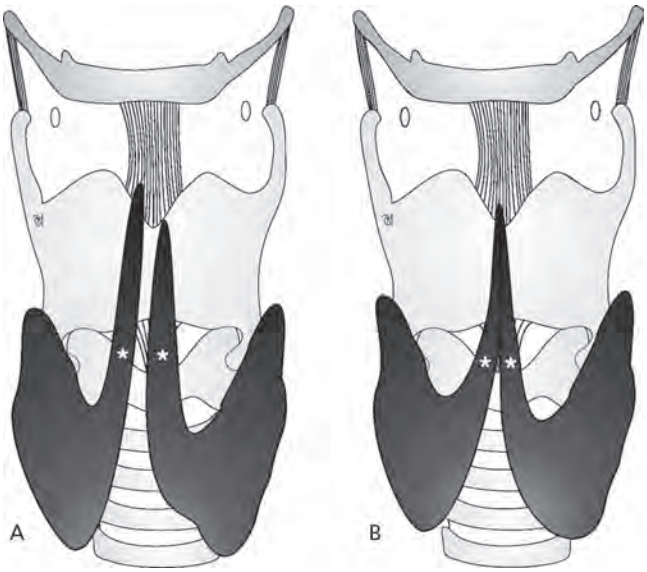

Figure 99.4 (a) Two pyramidal lobes (white asterisks) originate from two separated lateral lobes of the thyroid gland. (b) They united cranially in some cases.

This accessory muscle, first described by Winslow (1743) and initially named the thyro-adénoidïen, runs from the inferior pharyngeal constrictor muscle to the thyroid gland. Sömmerring (1794) introduced the muscle and named it the levator glandulae thyroidea. It was described as an accessory muscle that ran from the hyoid bone to insert partly on the thyroid cartilage and partly on the isthmus of the thyroid gland. Sömmerring's muscle is the same as the hyo-thyroglandulaire of Pointe, the levator glandulae thyroidea superficialis medius et longus of Krause (1879), and the musculus thyroideus of Merkel (1913); its usual full name in the literature is the levator glandulae thyroidea of von Sömmerring (Ranade et al. 2008).

Merkel (1913) stated that it was constant and glandular, though usually surrounded by muscle fibers. Huschke (1845) spoke of the structure only as glandular, mentioning nothing about muscle (cited by Ranade et al. 2008). The structure is described in textbooks as a fibrous or fibromuscular band (Standring 2008). Skandalakis (2004) called this fibrous band the suspensory ligament of the thyroid gland. Kulkarni et al. (2012) reported a fibrous, fibromuscular, and predominantly muscular levator glandulae thyroid. Kumar et al. (2005) stated that it has ligamentous and muscular parts: near the thyroid gland the structure appeared ligamentous; near the thyrohyoid it became muscular. Godart (1847) proved it to be muscular in one case by conducting a nitric acid test. In recent reports it has been described as muscular (Gregory and Guse 2007; Loukas et al. 2008). Chaithra Rao et al. (2012) and Kulkarni et al. (2012) wrote of a bilaterally fibromuscular and predominantly muscular levator glandulae thyroidea, respectively.

Eisler (1900) classified the muscle according to its innervation and based this on its proposed embryonic origins. The anterior levator glandulae thyroidea muscle, derived from the cricothyroid, is innervated by the external laryngeal branch of the superior laryngeal nerve. The lateral levator glandulae thyroidea muscle, derived from the thyrohyoid muscles or from the infrahyoid muscle group as a whole and attached to the hyoid bone, is innervated by the ansa cervicalis. Finally, the posterior levator glandulae thyroidea muscle is innervated similarly to the anterior by the superior laryngeal branch of the vagus, and is apparently derived from the inferior constrictor of the pharynx. Kim et al. (2010) reported a case with a levator glandulae throidea muscle and claimed that its embryological origin might be similar to that of the omohyoid muscle.

Articles about the vascular and nerve supplies to this muscle are very rare. It was stated in a textbook (Sinnatamby 2006) that the muscle is innervated by a branch of the external laryngeal nerve. In a case report by Loukas et al. (2008) the muscle was said to be supplied by muscular branches of the superior thyroid artery, innervated by branches of the ansa cervicalis, and derived from the infrahyoid muscles. In another case report, Kumar et al. (2005) stated that it could be derived from the thyroyhoid or infrahyoid muscles and innervated by a branch of the ansa cervicalis.

Mori (1964) studied 510 cadavers and found the levator glandulae thyroidea muscle in 210 (41.17%). He classified the muscle into the following types on the basis of a gross anatomical analysis of the origin and insertion of each variant:

- The thyreoglandularis is the most common variant (54.7%), arising from the thyroid cartilage and inserting onto the sheath of the thyroid gland.
- The hyopyramidalis is the second most common variant (25.2%), arising from the hyoid bone and inserting onto the tip of the pyramidal lobe of the thyroid gland.
- The hyoglandularis (13.3%) arises from the hyoid bone and inserts onto the sheath of the thyroid gland.
- The tracheoglandularis (3.3%) arises from the upper end of the trachea and inserts onto the capsule of the isthmus of the thyroid gland.
- The thyreopyramidalis arises from the thyroid cartilage and inserts onto the tip of the pyramidal lobe of the thyroid gland. Note that Mori (1964) gave the frequency of this type in his article as 0.8%. When the frequencies of his other types are considered, the frequency should be 3.3% (7 of 210 cadavers).

The prevalence of the levator glandulae thyroid muscle as quoted in the literature ranges over 0.5–85.7% (Table 99.4) (Watanabe and Suda 1962; Mori 1964; Lehr 1979; Harjeet et al. 2004; Ranade et al. 2008; Sultana et al. 2009; Joshi et al. 2010; Ozgur et al. 2011; Kulkarni et al. 2012; Prakash et al. 2012). It is found in 10.6–27.8% of females and 22.9–96.1% of males (Table 99.4) (Harjeet et al. 2004; Ranade et al. 2008; Prakash et al. 2012). Measurements of the muscle were: length 5.8–49 mm; breadth 3–12 mm, and thickness 1–3.2 mm (Harjeet et al. 2004; Loukas et al. 2008; Ozgur et al. 2011).

Table 99.4 Incidence (%) of the levator glandulae thyroidea muscle in the literature.

Authors	In both gender	In female	In male
Watanabe and Suda 1962	85.7		
Mori 1964	41.2		
Lehr 1979	0.5		
Harjeet et al. 2004	19.5	10.6	22.9
Ranade et al. 2008	49.5	11.8	96.1
Sultana et al. 2009	43.3		
Joshi et al. 2010	30		
Ozgur et al. 2011	15		
Kulkarni et al. 2012	30		
Prakash et al. 2012	38.3	27.8	34.6

Table 99.5 The levator glandulae thyroidea muscle arises from the parts of the thyroid gland.

Authors	Lateral lobe of the thyroid gland	Isthmus of the thyroid gland	Pyramidal lobe
Winslow 1743	x		
Mori 1964	x (68.1%)	x (3.3%)	x (28.3%)
Bergman et al. 1988	x	x	x
Saadeh et al. 1996	x		
Kumar et al. 2005		x	
Gregory and Guse 2007	x		
Loukas et al. 2008			x
Sultana et al. 2009		x (15.3%)	x (84.7%)
Kim et al. 2010		x	
Chaithra Rao et al. 2012	x		
Kulkarni et al. 2012			x

The muscle arises from different parts of the thyroid gland (Table 99.5): from the right or left lateral lobe (Fig. 99.5a) (Winslow 1743; Mori 1964; Bergman et al. 1988; Saadeh et al. 1996; Gregory and Guse 2007; Chaithra Rao et al. 2012); from the isthmus (Fig. 99.5b) (Mori 1964; Bergman et al. 1988; Kumar et al. 2005; Sultana et al. 2009; Kim et al. 2010); or from the pyramidal lobe (Fig. 99.5c) (Mori 1964; Bergman et al. 1988; Loukas et al. 2008; Sultana et al. 2009; Kulkarni et al. 2012). It also extends different structures (Table 99.6): to the hyoid bone (Marshall 1895; Eisler 1900; Mori 1964; Bergman et al. 1988; Harjeet et al. 2004; Kumar et al. 2005; Loukas et al. 2008; Sultana et al. 2009; Joshi et al. 2010; Ozgur et al. 2011; Chaithra Rao et al. 2012); to the thyroid cartilage (Marshall 1895; Mori 1964; Bergman et al. 1988; Harjeet et al. 2004; Gregory and Guse 2007; Loukas et al. 2008; Sultana et al. 2009; Kim et al. 2010; Joshi et al. 2010); to the inferior pharyngeal constrictor muscle (Winslow 1743); to the upper trachea (Mori 1964); to the mastoid process (Saadeh et al. 1996; Faysal et al. 1996); to the median cricothyroid ligament (Loukas et al. 2008); and to the median thyrohyoid ligament (Harjeet et al. 2004). It is stated that the muscle extends generally to the hyoid bone in 17.5–92% of cases (Marshall 1895; Mori 1964; Harjeet et al. 2004; Sultana et al. 2009; Joshi et al. 2010, Ozgur et al. 2011) and to the thyroid cartilage in 8–58.1% (Marshall 1895; Mori 1964; Harjeet et al. 2004; Sultana et al. 2009; Joshi et al. 2010).

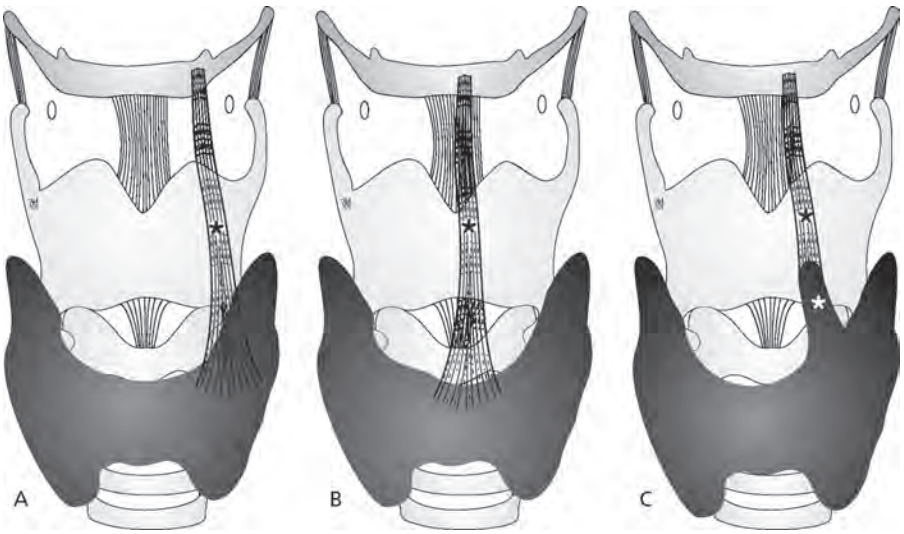

Figure 99.5 The levator glandulae thyroidea muscle (black asterisk) arises: (a) from the right or left lateral lobe of the thyroid gland; (b) from the isthmus; or (c) from the pyramidal lobe (white asterisks).

Table 99.6 The levator glandulae thyroidea muscle extends to different structures.

Authors	Hyoid bone	Thyroid cartilage	Upper trachea	Mastoid process	Median cricothyroid ligament	Median thyrohyoid ligament	Inferior pharyngeal constrictor muscle
Winslow 1743							x
Marshall 1895	x (28.3%)	x (15%)					
Eisler 1900	x						
Mori 1964	x (38.3%)	x (58.1%)	x (3.3%)				
Bergman et al. 1988	x	x					
Faysal et al. 1996				x			
Saadeh et al. 1996				x			
Harjeet et al. 2004	x (53.2%)	x (34%)				x (10.8%)	
Kumar et al. 2005	x						
Gregory and Guse 2007		x					
Loukas et al. 2008	x	x			x		
Sultana et al. 2009	x (92%)	x (8%)					
Kim et al. 2010		x					
Joshi et al. 2010	x (66.7%)	x (33.3%)					
Ozgur et al. 2011	x (17.5%)						
Chaithra Rao et al. 2012	x						

Thyroglossal duct cyst

Thyroglossal duct remnants are the most common midline neck masses in childhood (Tunkel and Domenech 1998). About 7% of the adult population has these remnants (Ellis and van Nostrand 1977). Embryologically, the thyroid analog arises from the foramen cecum and descends, reaching its final position in the seventh or eighth week of development. The remaining thyroglossal duct can become obliterated or be a cyst, a duct, or ectopic tissue.

The cyst originates from persistent epithelial remnants of the thyroglossal duct that are present during the descent of the thyroid gland from the foramen cecum to its final position in the anterior neck (Mondin et al. 2008). There are different terms in the literature to denote a lump arising from the thyroglossal tract remnant, for example: "thyroglossal duct cyst," "thyroglossal tract cyst," "thyroglossal cyst," "thyroglossal tract remnant," and "thyroglossal duct remnant." "Thyroglossal duct cyst" is the most commonly used term in the recent literature (Mondin et al. 2008).

The cyst is observed in more than 75% of congenital midline neck masses (Tunkel and Domenech 1998). It accounted for 54.6% of all congenital cervical cysts (Hsieh et al. 2003). In a retrospective analysis of 236 patients under 20 years of age, eight (3.38%) were diagnosed with a thyroglossal duct cyst (Jain and Pathak 2010). It has been observed in 31.5–38.1% of children and in 61.9–68.5% of adult patients (Allard 1982; Brousseau et al. 2003; Lin et al. 2008). Although female predominance has been reported (Gross and Connerly 1940; Türkyilmaz et al. 2004), the male:female (M:F) ratio quoted in the literature varies as follows: 32:30 (Brousseau et al. 2003); 49:16 (Lin et al. 2008); 117:64 (Hsieh et al. 2003); 5:9 (Mondin et al. 2008). Lin et al. (2008) stated that there is no significant sex difference between children and adults with the cyst.

The thyroglossal duct cyst is observed at the midline in 35–82.6% of patients and off the midline in 10–37.5% (Pollock 1966; Wadsworth and Siegel 1994; Ahuja et al. 1999; Ahuja et al. 2000; Brousseau et al. 2003; Kutuya and Kurosaki 2008; Lin et al. 2008). Its location has been reported as infrahyoid/thyrohyoid (between the hyoid bone and the thyroid gland) in 25–87.5% (Pounds 1981; Allard 1982; Ghaneim and Atkins 1997; Ahuja et al. 1999, 2000; Brousseau et al. 2003; Sauvageau et al. 2006; Mondin et al. 2008; Kutuya and Kurosaki 2008; Lin et al. 2008; Narayana Moorthy and Arcot 2011), hyoid/overhyoid in 12.5–75% (Pounds 1981; Wadsworth and Siegel 1994; Ahuja et al. 2000; Brousseau et al. 2003; Kutuya and Kurosaki 2008; Lin et al. 2008), suprahyoid in 4.4–25% (Pounds 1981; Allard 1982; Wadsworth and Siegel 1994; Ghaneim and Atkins 1997; Ahuja et al. 1999, 2000; Brousseau et al. 2003; Sauvageau et al. 2006; Kutuya and Kurosaki 2008; Mondin et al. 2008; Lin et al. 2008; Narayana Moorthy and Arcot 2011), suprasternal in 12.9–13% (Allard 1982; Ghaneim and Atkins 1997; Sauvageau et al. 2006), submental in 10% (Brousseau et al. 2003), and lingual in 1–2.1% (Allard 1982; Ghaneim and Atkins 1997; Sauvageau et al. 2006) (Table 99.7). Intra-thyroid (Hatada et al. 2000; Roy et al. 2003; Johnston et al. 2003; Pérez-Martínez et al. 2005), intra-hyoid (Tas et al. 2003; Bist et al. 2007), intra-laryngeal (Loh et al. 2006; Kurien and Michael 2012), and mediastinal (Chon et al. 2007; Granato et al. 2011) cases have also been reported (Fig. 99.6).

Thyroglossal duct cysts range over 0.5–8 cm in diameter (Wadsworth and Siegel 1994; Dedivitis et al. 2002; Pérez-Martínez et al. 2005; Kutuya and Kurosaki 2008; Lin et al. 2008; Mondin et al. 2008; Valentino et al. 2012; Sarmento et al. 2013). Their shape is unilocular in 88–100% and multilocular in 0–13.9% (Ahuja et al. 1999, 2000; Kutuya and Kurosaki 2008).

Table 99.7 Incidence (%) of location of the thyroglossal duct cyst in the literature

Authors	Infrahyoid/thyrohyoid	Hyoid/overhyoid	Suprahyoid	Suprasternal	Submental	Lingual
Pounds 1981	25–65	15-50	20–25			
Allard 1982	60.9		24.1	12.9		2.1
Wadsworth and Siegel 1994		75	25			
Ghaneim and Atkins 1997	60		24	13		2
Ahuja et al. 1999	83	12.5	5			
Ahuja et al. 2000	47.8	47.8	4.4			
Brousseau et al. 2003	27	48	13		10	
Sauvageau et al. 2006	60		24	13		1
Kutuya and Kurosaki 2008	38.9	44.4	16.7			
Mondin et al. 2008	78.6		21.4			
Lin et al. 2008	57	25	17.9			
Narayana Moorthy and Arcot 2011	87.5		12.5			

Posterior enhancement is present in 56.5–87.5% and absent from 12.5–43.5% (Wadsworth and Siegel 1994; Ahuja et al. 1999, 2000; Kutuya and Kurosaki 2008). They have a variable ultrasonographic appearance: anechoic in 13–41.7%; homogeneously hypoechoic in 0–18%; pseudosolid in 0–56.5%; and heterogeneous in 28–41.7% of patients (Wadsworth and Siegel 1994; Ahuja et al. 1999, 2000; Kutuya and Kurosaki 2008).

Agenesis/hemiagenesis of thyroid gland

Developmental defects of the thyroid gland, including aplasia (absent gland), hypoplasia (small gland), and ectopia (unusual location), are collectively referred to as thyroid dysgenesis (Satoshi et al. 2010). The incidence of agenesis of the thyroid gland is about 0.8%, but hemiagenesis reaches 16% (Letonturier et al. 1979; Jain et al. 2010; Kirmızibekmez et al. 2012).

Embryological development of the thyroid gland begins from an invagination of the endoderm in the primitive pharynx. This invagination grows ventrally while remaining attached to the pharyngeal floor. The thyroid rudiment will migrate to its correct anatomical position anterior to the pharynx and only then will it begin to grow laterally to create the bilobed "thyroid gland" (Maiorana et al. 2003). Presumably, failure of the cells to migrate laterally results in agenesis of part of the gland (Sari et al. 2000). The etiology remains unclear but could have a genetic component, as this rare condition has been documented in monozygotic twins (Cakir et al. 2009).

The first case of hemiagenesis of the thyroid gland was reported by Handfield-Jones (1866). Its prevalence as observed in many subsequent studies is in the range 0.05–16% (Table 99.8) (Marshall 1895; Hamburger and Hamburger 1970; Harada et al. 1972; Letonturier et al. 1979; Melnick and Stemkowski 1981; Sari et al. 2000; Shabana et al. 2000; Maiorana et al. 2003; Jain and Pathak 2010; Kirmızibekmez et al. 2012). Hemiagenesis of the left lobe is most common (Fig. 99.7; Table 99.8) (Hamburger and Hamburger 1970; Harada et al. 1972; Letonturier et al. 1979; Melnick and Stemkowski 1981; Shabana et al. 2000; Maiorana et al. 2003; Jain and Pathak 2010). This variation is up to eight times more common in

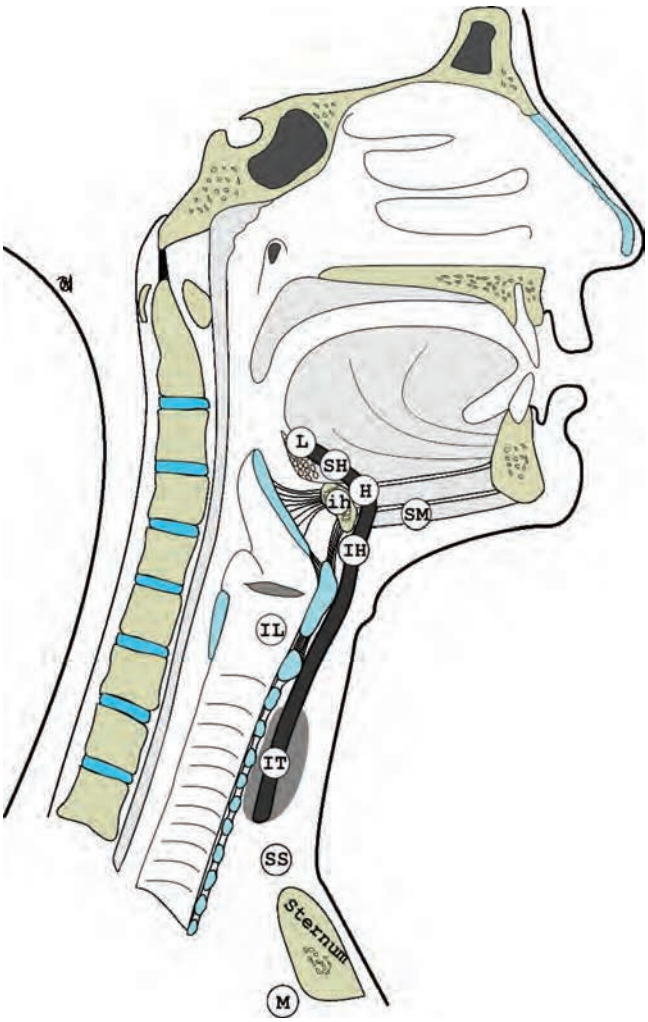

Figure 99.6 The thyroglossal duct cyst is located in different places such as the lingual (L), suprahyoid (SH), hyoid/overhyoid (H), intra-hyoid (ih), submental (SM), infrahyoid/thyrohyoid (IH), intra-laryngeal (IL), intra-thyroid (IT), suprasternal (SS), or mediastinal (M). Black thick line indicates the route of the thyroglossal duct.

Table 99.8 Incidence (%) and side of hemiagenesis of the thyroid gland in the literature

Authors	Frequency	Right lobe	Left lobe
Marshal 1895	1.66	100	0
Hamburger and Hamburger 1970	0.06	25	75
Harada et al. 1972	0.06	0	100
Letonturier et al. 1979	16	25	75
Melnick and Stemkowski 1981	0.5	25	75
Sari et al. 2000	0.5	50	50
Shabana et al. 2000	0.21	0	100
Maiorana et al. 2003	0.05	0	100
Jain and Pathak 2010	0.4	0	100
Kirmızibekmez et al. 2012	5.1	58	42

females (Harada et al. 1972; Letonturier et al. 1979; Melnick and Stemkowski 1981; McHenry et al. 1995; Sari et al. 2000; Shabana et al. 2000; Berker et al. 2010; Wu et al. 2012).

Agenesis of thyroid isthmus

Agenesis of the thyroid isthmus is a rare anomaly (Fig. 99.8). It can be explained as an anomaly of embryological development (Chaithra Rao et al. 2012). The caudal end of the thyroglossal duct bifurcates and forms the thyroid lobes and isthmus. A high division of the thyroglossal duct can result in two independent thyroid lobes and no isthmus (Kulkarni et al. 2012).

The isthmus can be absent in amphibians, birds, and (among mammals) monotremes, certain marsupials, cetaceans, carnivores, and rodents. In rhesus monkeys (*Macacus rhesus*) the thyroid glands are normal in position but lack an isthmus. In most tetrapod species there are two paired thyroid glands, that is, the right and left lobes are not joined together (Chaithra Rao et al. 2012). The underlying etiology of isthmus agenesis has not been well defined. Genetic factors and defects in embryological development seem to be important; mutations in the genes responsible for the development of the thyroid could be implicated, especially TITF1-2 genes (Devi et al. 2012) and chromosome 22 (Gangbo et al. 2004).

Thyroid isthmus agenesis does not cause clinical symptoms by itself and the diagnosis is mostly incidental to the existence of other thyroid pathologies (Schanaider and de Oliveira 2008). The absence of an isthmus can be associated with other types of dysorganogenesis, such as absence of a lobe or presence of ectopic thyroid tissue (Duh et al. 1994).

The first specimen of an abnormal thyroid gland seems to have been described by Gow (1884), who found the isthmus and left lobe of the gland to be absent in the cadaver of a female aged 60–70 years. According to the literature the isthmus is absent in 0.01–33% of cases (Table 99.9) (Marshall 1895; Williams et al. 1989; Sagiroglu 1997; Mikosch et al. 1999; Won and Chung 2002; Harjeet et al. 2004; Braun et al. 2007; Ranade et al. 2008; Dixit et al. 2009; Berker et al. 2010; Joshi et al. 2010; Tanriover et al. 2011; Ozgur et al. 2011; Prakash et al. 2012). It is absent in 2.5–47% of females and 9.6–30.6% of males (Sagiroglu 1997; Ranade et al. 2008; Dixit et al. 2009; Prakash et al. 2012).

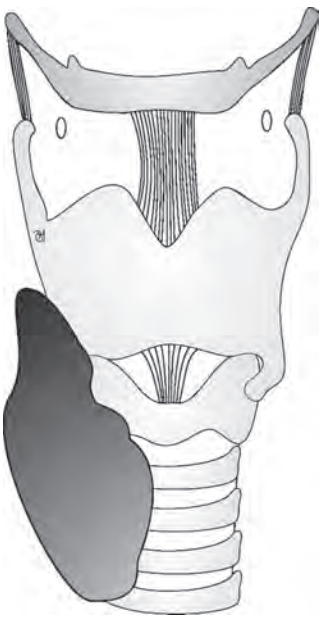

Figure 99.7 Hemiagenesis of the left lobe of the thyroid gland is most common. Prevalence of the hemiagenesis of the thyroid gland ranges over 0.05–16% in the literature.

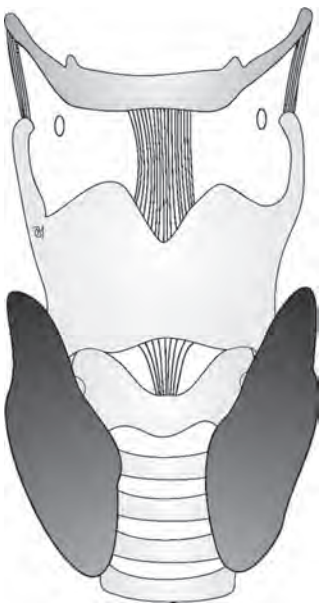

Figure 99.8 Agenesis of thyroid isthmus is a developmental anomaly. Its prevalence ranges over 0.01–33% in the literature.

Table 99.9 Incidence of agenesis (%) of the isthmus of the thyroid gland in the literature

Authors	In both gender	In female	In male
Marshal 1895	10		
Williams et al. 1989	0.02		
Sagiroglu 1997	28	38.4	16.6
Mikosch et al. 1999	0.01		
Won and Chung 2002	3		
Harjeet et al. 2004	7.9		
Braun et al. 2007	6.9		
Ranade et al. 2008	33	47	30.6
Dixit et al. 2009	14.6	2.5	13.5
Berker et al. 2010	30		
Joshi et al. 2010	16.6		
Tanriover et al. 2011	2.2		
Ozgur et al. 2011	12,5		
Prakash et al. 2012	8.5	5.6	9.6

Ectopic/accessory thyroid gland

Thyroid gland ectopia is rare. It is defined as the presence of fully functional thyroid tissue in an aberrant location along the embryological line of descent of the gland (Radkowski et al. 1991). Such tissue can be found not only along the route of thyroglossal duct but also in mediastinum and subdiaphragmatic organs. Accessory thyroid tissue is defined as the persistence of thyroid tissue and remnants of the thyroglossal duct (Hollander et al. 2004). It can be found anywhere from the base of the tongue to the thyroid isthmus, with most of the functional thyroid gland in the normal pretracheal location.

The midline ectopic thyroid along the migration path from foramen cecum to the mediastinum can be explained by the failure of part of the thyroid anlage to descend. Some authors suggest that this phenomenon is likely to be related to developmental defects other than abnormal migration of the thyroid bud (Huang and Chen 2007).

Its prevalence is about 1 per 100,000–300,000 people, rising to 1 per 4000–8000 patients with thyroid disease (Di Benedetto 1997; Babazade et al. 2009). However, in autopsy studies, the prevalence ranges over 7–10% (Kousta et al. 2005; Bersaneti et al. 2011). In scintigraphic and ultrasonic studies it has been observed in 1.6% and 1.7% of cases (Jain and Pathak 2010; Kirmızibekmez et al. 2012). In 70–90% of cases it is the only thyroid tissue present (Di Benedetto 1997; Kousta et al. 2005; Yoon et al. 2007; Babazade et al. 2009; Gopal et al. 2009; Bersaneti et al. 2011).

The most frequent location of ectopic thyroid tissue is at the base of tongue (lingual thyroid), especially in the region of the foramen cecum (Noussios et al. 2011). Since 1869, when Hickmann (1869) first reported lingual thyroid in a newborn who was suffocated 16 hours after birth because of the mass causing upper airway obstruction, several reports of ectopic thyroid tissue have been published. The lingual thyroid accounts for about 90% of the reported cases (Larochelle et al. 1979; Pintar and Dominique 1991; Tunkel and Domenech 1998; Basaira et al. 2001), although lower rates (47%) have been reported (Gopal et al. 2009; Yoon et al. 2007). The mean age at presentation is about 40.5 years, ranging from birth to 83 years. In 70–75% of cases, lingual thyroid is the only thyroid tissue present (Neinas et al. 1973; Batsakis et al. 1996). Approximately 30% of patients with a lingual thyroid have a normal pretracheal thyroid (Montgomery 1935). Around 70% will have subclinical hypothyroidism, often becoming clinical during periods of physiological stress such as puberty and pregnancy (Larochelle et al. 1979).

Apart from the foramen cecum, ectopic thyroid has been described at numerous other sites, between the base of the tongue and its final pretracheal position and in the mediastinum and distant subdiaphragmatic areas (Noussios et al. 2011). Rare locations reported in the literature include the submandibular region (Helidonis et al. 1980; Alsop et al. 1986; Rubenfeld et al. 1988; Aguirre et al. 1991; Latimer and Lindsay 1995; Morgan et al. 1995; Hansen and Christensen 1996; Sambola-Cabrer et al. 1996; Sironi et al. 1996; Di Benedetto 1997; Akoz et al. 1998; Temmel et al. 1998; Feller et al. 2000; Kumar et al. 2001; Maino et al. 2004; Mehboob et al. 2005; Babazade et al. 2009; Bersaneti et al. 2011); the submental region (Richards et al. 2004); the carotid bifurcation (Rubenfeld et al. 1988; Hollander et al. 2004); the sella turcica (Ruchti et al. 1987; Malone et al. 1997); cervical lymph nodes (Cheren'ko 1990); the subisthmic region (Bhatnagar et al. 1997); intrathymic (Spinner et al. 1994); in the larynx (Richardson and Assor 1971; Braun et al. 2007); the trachea (Randolph et al. 1963; Myers and Pantangco 1975; Donegan and Wood 1985; Muysoms et al. 1997; Hari et al. 1999; Yang et al. 2010); the mediastinum (Salvatore and Gallo 1975; De Andrade 1977; deSouza and Smith 1983; Arriaga and Myers 1988; Sand et al. 1996; Guimarães et al. 2009); the lung (Simon and Baczako 1989; Bando et al. 1993; Weng et al. 2000); intrapericardial (Willis 1953); intracardiac (Rogers and Kesten 1962; Shemin et al. 1985; Pollice and Caneso 1986; Kantelip et al. 1986; Doria et al. 1989; Richmond et al. 1990; Fujioka et al. 1996; Casanova et al. 2000; Ruberg et al. 2006); the aorta (Kampmeier 1937; Williams et al. 2002); the pharynx (Epstein and Loeb 1955); the esophagus (Postlethwait and Detmer 1975; Whale 1987); the liver (Strohschneider et al. 1993; Jamshidi et al. 1998); the gall bladder (Curtis and Sheahan 1969); the groin (Rahn 1959); the adrenal gland (Shiraishi et al. 1999); the ovarium (Kempers et al. 1970; Kim et al. 2002; Ciccarelli et al. 2004; Yoo et al. 2008); the uterus (Yılmaz et al. 2005); and the vagina (Kurman and Prabha 1973). Supernumerary thyroid lobules just around the aortic arch are termed the glands of Wölfler.

It is very uncommon for two ectopic foci to be present simultaneously. In most cases, the first lesion is lingual or sublingual and the second is subhyoid (in most cases), infrahyoid, or suprahyoid (Chawla et al. 2007). Dual ectopic thyroid glands in the porta hepatis and the tongue have also been described.

Figure 99.9 Classification of the Zuckerkandl tubercle (ZT). (a) Grade 0 (unrecognizable); (b) grade 1 (only a thickening of the lateral edge of the thyroid lobe); (c) grade 2 (<1 cm); and (d) grade 3 (>1 cm). Data from Pelizzo et al. (1998).

Primary thyroid carcinomas arising from ectopic thyroid tissue are uncommon and have been reported in cases of lingual thyroid, thyroglossal duct cyst, lateral aberrant thyroid tissue, mediastinal, and struma ovarii (Shah et al. 2007). Scintigraphy using Tc-99m, I-131, or I-123 is the most important diagnostic tool for detecting ectopic thyroid tissue, and demonstrates the absence or presence of the thyroid in its normal location. A thyroid scan can also reveal additional sites of thyroid tissue (Noussios et al. 2011).

Ectopic thyroid tissue that is partially separated from the main gland is referred to as Barraya's gland.

The Zuckerkandl tubercle

The Zuckerkandl tubercle (ZT) is a lateral or posterior projection from the lateral thyroid lobe, which indicates the point of embryological fusion of the ultimobranchial body and principal median thyroid process (Gauger et al. 2001). In 1902, Emil Zuckerkandl referred to the tubercle as "processus posterior glandulae thyroideae" (Zuckerkandl 1902). It is considered an anatomical landmark for locating the inferior laryngeal nerve and parathyroid glands (Pelizzo et al. 1998; Gauger et al. 2001). Pelizzo et al. (1998) classified the tubercle as: grade 0 (unrecognizable); grade 1 (only a thickening of the lateral edge of the thyroid lobe); grade 2 (smaller than 1 cm); or grade 3 (larger than 1 cm) (Fig. 99.9). They observed grade 0 in 23%, grade 1 in 8.6%, grade 2 in 53.8%, and grade 3 in 14.4% of Italian patients during lobectomy. Hisham and Aina (2000) found grades 0 and 1 in 19.8%, grade 2 in 25%, and grade 3 in 55.2% of Malaysian patients. Gauger et al. (2001) found grade 0 in 37%, grades 1 and 2 in 18%, and grade 3 in 45% of Australian patients. Yalcin et al. (2006) observed grade 0 in 11.3%, grade 1 in 20%, grade 2 in 56.3%, and grade 3 in 12.5% of Turkish cadavers.

Arterial variations of the thyroid gland

The thyroid and suprarenal glands are each said to have the most abundant blood supply of any organ in the body for their size (Hollinshead 1968). The thyroid gland is a very vascular structure, being supplied by four main arteries: the two superior and two inferior thyroid arteries.

The superior thyroid artery is generally considered to be constant and the first branch of the external carotid artery. It has been reported as originating from the external carotid artery in 24–87.9% of cases, from the bifurcation of the common carotid artery in 0–70%, and from the common carotid artery in 2.1–47.5% (Adachi 1928; Poisel and Golth 1974; Lippert and Pabst 1985; Lucev et al. 2000; Hayashi et al. 2005; Zümre et al. 2005; Delic et al. 2008; Ozgur et al. 2009; Vázquez et al. 2009; Sanjeev et al. 2010; Natsis et al. 2011; Ongeti and Ogeng'o 2012; Anagnostopoulou and Mavridis 2013; Bergman et al. 2013). The superior thyroid artery arises separately, but in 0–7.3% of cases it originates from a common trunk with the lingual artery (the thyrolingual trunk) or from a common trunk with the lingual and facial arteries (the thyrolinguofacial trunk) in 0–12.3% of cases (Adachi 1928; Poisel and Golth 1974; Lucev et al. 2000; Hayashi et al. 2005; Zümre et al. 2005; Delic et al. 2008; Ozgur et al. 2009; Vazquez et al. 2009; Sanjeev et al. 2010; Natsis et al. 2011; Ongeti and Ogeng'o 2012; Anagnostopoulou and Mavridis 2013).

The inferior thyroid artery usually (85–90.5%) originates from the thyrocervical trunk (Lippert and Pabst 1985; Bergman et al. 2013). It also originates directly from the subclavian artery in 1.2–33% of cases (Lippert and Pabst 1985; Bergman et al. 2013); from the common carotid artery in 1% (Lippert and Pabst 1985); from a common stem with the vertebral artery in 0.5–1% (Lippert and Pabst 1985; Bergman et al. 2013); from a common stem with the internal thoracic artery in 1%; from a common stem with the suprascapular artery in less than 1%; from a common stem with the ascending cervical, transverse cervical, and suprascapular arteries in 60.5–96.6% (Bergman et al. 2013); from a common stem with the ascending cervical and suprascapular arteries in 0.9–3.1% (Bergman et al. 2013); from a common stem with the ascending cervical and transverse cervical arteries in 8.2–8.6% (Bergman et al. 2013); from a common trunk with the transverse cervical and suprascapular arteries in 0.5–0.9% (Bergman et al. 2013); from a common trunk with the transverse cervical, ascending cervical, suprascapular and internal thoracic arteries in 3.8–7.4% (Bergman et al. 2013); from a common trunk with the ascending cervical, transverse cervical, and internal thoracic arteries in 0.9–1% (Bergman et al. 2013); and from a common trunk with the ascending cervical in

1.6–5.7% (Bergman et al. 2013). Absence of the inferior thyroid artery is reported to differ among populations: 0.2–2.2% in English; 1.6% in Italians; 2.3% in Americans; 3.6% in Swiss; 3.8% in Germans; 5.9% in Japanese; 0.9% in Bulgarians (cited by Jelev and Surchev 2000). When it is absent its place is usually taken by a branch from the superior thyroid artery of the same side, from the inferior thyroid artery of the other side, or, less frequently, by a thyroidea ima artery (Hollinshead 1968).

The thyroidea ima artery is occasionally present as either accessory to or replacing the inferior thyroid artery (Hollinshead 1968). Its incidence as quoted in the literature ranges over 0.4–12.2% (Hollinshead 1968; Bergman et al. 2013). The artery usually arises from the brachiocephalic artery (43.3%). It also originates from the common carotid (2–17.7%), the aortic arch (0.3–13.3%), or more rarely the internal thoracic (6.6%), subclavian (3.3%), inferior thyroid (1.1%), transverse scapular (1.1%), or pericardiophrenic arteries or either thyrocervical trunk (Hollinshead 1968; Bergman et al. 2013). The thyroidea ima artery usually arises from the right side.

References

Adachi B. 1928. *Das Arteriendystem der Japaner*. Kyoto: Maruzen.

Aguirre A, de la Piedra M, Ruiz R, Portilla J. 1991. Ectopic thyroid tissue in the submandibular region. *Oral Surg Oral Med Oral Pathol* 71(1): 73–6.

Ahuja AT, King AD, King W, Metreweli C. 1999. Thyroglossal duct cysts: sonographic appearances in adults. *AJNR Am J Neuroradiol* 20(4): 579–582.

Ahuja AT, King AD, Metreweli C. 2000. Sonographic evaluation of thyroglossal duct cysts in children. *Clin Radiol* 55(10): 770–774.

Akoz T, Erdogan B, Ayhan M, Cinar F. 1998. Ectopic submandibular thyroid tissue. Rev Laryngol Otol Rhinol (Bord) 119(5): 323–325.

Allard RH. 1982. The thyroglossal cyst. *Head Neck Surg* 5(2): 134–146.

Alsop JE, Yerbury PJ, O'Donnell PJ, Heyderman E. 1986. Signet-ring cell microfollicular adenoma arising in a nodular ectopic thyroid. A case report. *J Oral Pathol* 15(10): 518–519.

Anagnostopoulou S, Mavridis I. 2013. Emerging patterns of the human superior thyroid artery and review of its clinical anatomy. *Surg Radiol Anat* 36(1): 33–38.

Arriaga MA, Myers EN. 1988. Ectopic thyroid in the retroesophageal superior mediastinum. *Otolaryngol Head Neck Surg* 99(3): 338–340.

Babazade F, Mortazavi H, Jalalian H, Shahvali E. 2009. Thyroid tissue as a submandibular mass: a case report. *J Oral Sci* 51(4): 655–657.

Bando T, Genka K, Ishikawa K, Kuniyoshi M, Kuda T. 1993. Ectopic intrapulmonary thyroid. *Chest* 103(4): 1278–1279.

Basaria S, Westra WH, Cooper DS. 2001. Ectopic lingual thyroid masquerading as thyroid cancer metastases. *J Clin Endocrinol Metab* 86(1): 392–395.

Batsakis JG, El-Naggar AK, Luna MA. 1996. Thyroid gland ectopias. *Ann Otol Rhinol Laryngol* 105(12): 996–1000.

Bergman RA, Thompson SA, Afifi AK, Saadeh FA. 1988. *Compendium of Human Anatomic Variation*. Baltimore, Munich: Urban and Schwarzenberg.

Bergman RA, Afifi AK, Miyauchi R. 2013. Anatomy Atlases. Available at http://www.anatomyatlases.org/AnatomicVariants/Cardiovascular/Directory/Alphabetical/T.shtml (accessed 26 November 2015).

Berker D, Ozuguz U, Isik S, Aydin Y, Ates Tutuncu Y, Akbaba G, Guler S. 2010. A report of ten patients with thyroid hemiagenesis: ultrasound screening in patients with thyroid disease. *Swiss Med Wkly* 140(7–8): 118–121.

Bersaneti JA, Silva RD, Ramos RR, Matsushita Mde M, Souto LR. 2011. Ectopic thyroid presenting as a submandibular mass. *Head Neck Pathol* 5(1): 63–66.

Bhatnagar KP, Nettleton GS, Wagner CE. 1997. Subisthmic accessory thyroid gland in man: a case report and a review of thyroid anomalies. *Clin Anat* 10(5): 341–344.

Bist SS, Bisht M, Varshney S, Gupta N, Bhatia R. 2007. Thyroglossal duct cyst in hyoid bone: Unusual location. *Indian J Otolaryngol Head Neck Surg* 59(4): 366–368.

Blumberg NA. 1981. Observations on the pyramidal lobe of the thyroid gland. *S Afr Med J* 59(26): 949–950.

Braun EM, Windisch G, Wolf G, Hausleitner L, Anderhuber F. 2007. The pyramidal lobe: clinical anatomy and its importance in thyroid surgery. *Surg Radiol Anat* 29(1): 21–27.

Brousseau VJ, Solares CA, Xu M, Krakovitz P, Koltai PJ. 2003. Thyroglossal duct cysts: presentation and management in children versus adults. *Int J Pediatr Otorhinolaryngol* 67(12): 1285–1290.

Cakir M, Gonen S, Dikbas O, Ozturk B. 2009. Thyroid hemiagenesis with Graves' disease, Graves' ophthalmopathy and multinodular goiter. *Intern Med* 48(12): 1047–1049.

Casanova JB, Daly RC, Edwards BS, Tazelaar HD, Thompson GB. 2000. Intracardiac ectopic thyroid. *Ann Thorac Surg* 70(5): 1694–1696.

Chaithra Rao BR, Sunkeswari S, Kulkarni MN, Kalghatgi RN. 2012. Bilateral levator glandulae thyroidea with agenesis of isthmus of thyroid gland – a case report. *Anatomica Karnataka* 6(2): 81–84.

Chawla M, Kumar R, Malhotra A. 2007. Dual ectopic thyroid: case series and review of the literature. *Clin Nucl Med* 32(1): 1–5.

Cheren'ko MP. 1990. The so-called goiter of the accessory thyroid glands. *Klin Khir* (12): 1–4.

Chon SH, Shinn SH, Lee CB, Tae K, Lee YS, Jang SH, Paik SS. 2007. Thyroglossal duct cyst within the mediastinum: an extremely unusual location. *J Thorac Cardiovasc Surg* 133(6): 1671–1672.

Ciccarelli A, Valdes-Socin H, Parma J, Khoo SK, Schoumans J, Colao A, Hamoir E, Beckers A. 2004. Thyrotoxic adenoma followed by atypical hyperthyroidism due to struma ovarii: clinical and genetic studies. *Eur J Endocrinol* 150(4): 431–437.

Cicekcibasi AE, Salbacak A, Seker M, Ziylan T, Tuncer I, Buyukmumcu M. 2007. Developmental variations and clinical importance of the fetal thyroid gland. A morphometric study. *Saudi Med J* 28(4): 524–528.

Curtis LE, Sheahan DG. 1969. Heterotopic tissues in the gallbladder. *Arch Pathol* 88(6): 677–683.

De Andrade MA. 1977. A review of 128 cases of posterior mediastinal goiter. *World J Surg* 1(6): 789–797.

Dedivitis RA, Camargo DL, Peixoto GL, Weissman L, Guimarães AV. 2002. Thyroglossal duct: a review of 55 cases. *J Am Coll Surg.* 194(3): 274–277.

Delic J, Bajtarevic A, Isakovic E. 2008. Variations of arteria thyroidea superior researched by MR angiography. *Acta Medica Sal* 37: 47–50.

deSouza FM, Smith PE. 1983. Retrosternal goiter. *J Otolaryngol* 12(6): 393–396.

Devi SK, Sharmila BP, Susan PJ, Gajendra K. 2009. Agenesis of isthmus of thyroid gland with bilateral glandulae thyroideae. *Int J Anat Var* 2: 29–30.

Devi SK, Sharmila BP, Bapuji P. 2012. Agenesis of isthmus of thyroid gland with embryological and clinical basis. *NMJ* 1(1): 32–34.

Di Benedetto V. 1997. Ectopic thyroid gland in the submandibular region simulating a thyroglossal duct cyst: a case report. *J Pediatr Surg* 32(12): 1745–1746.

Dixit D, Shilpa MB, Harsh MP, Ravishankar MV. 2009. Agenesis of isthmus of thyroid gland in adult human cadavers: a case series. *Cases J* 2: 6640.

Donegan JO, Wood MD. 1985. Intratracheal thyroid-familial occurrence. *Laryngoscope* 95(1): 6–8.

Doria E, Agostoni P, Fiorentini C. 1989. Accessory thyroid tissue in the right ventricle. *Chest* 96(2): 424–425.

Duh QY, Ciulla TA, Clark OH. 1994. Primary parathyroid hyperplasia associated with thyroid hemiagenesis and agenesis of the isthmus. *Surgery* 115(2): 257–263.

Eisler P. 1900. Der M. levator glandulae thyroidea und verwandte praelaryngeale Muskelbildungen. *Anat Anz* 17 183–189.

Ellis PD, van Nostrand AW. 1977. The applied anatomy of thyroglossal tract remnants. *Laryngoscope* 87(5 Pt 1): 765–770.

Epsteın HC, Loeb WJ. 1955. Thymic tumor of the pharynx. *J Pediatr* 47(1): 105–108.

Faysal SA, Sami KH, Fuad HA, Jihad HS. 1996. An unusual levator glandulae thyroidea: a case report and literature review. *J Anat Soc India* 45: 125–128.

Feller KU, Mavros A, Gaertner HJ. 2000. Ectopic submandibular thyroid tissue with a coexisting active and normally located thyroid gland: case report and review of literature. *Oral Surg Oral Med Oral Pathol Oral Radiol Endod* 90(5): 618–623.

Filho VJ, Moyses RA, Moyses NA, Ferraz AR. 2004. Pyramidal lobe of the thyroid: intra-operative anatomic study. *Rev Bras Cir* 33: 35–37.

Fujioka S, Takatsu Y, Tankawa H, Yamanaka K, Ando F. 1996. Intracardiac ectopic thyroid mass. *Chest* 110(5): 1366–1368.

Gangbo E, Lacombe D, Alberti EM, Taine L, Saura R, Carles D. 2004. Trisomy 22 with thyroid isthmus agenesis and absent gall bladder. *Genet Couns* 15(3): 311–315.

Gardner WU. 1966. The endocrine glands and unclassified organs. In: Morris' Human Anatomy, 12th edition (ed. BJ Anson). London: McGraw-Hill, pp. 1547.

Gauger PG, Delbridge LW, Thompson NW, Crummer P, Reeve TS. 2001. Incidence and importance of the tubercle of Zuckerkandl in thyroid surgery. *Eur J Surg* 167(4): 249–254.

Geraci G, Pisello F, Li Volsi F, Modica G, Sciumè C. 2008. The importance of pyramidal lobe in thyroid surgery. *G Chir* 29(11–12): 479–482.

Ghaneim A, Atkins P. 1997. The management of thyroglossal duct cysts. *Int J Clin Pract* 51(8): 512–513.

Godart J. 1847. Muscle de la glande thyroide, muscle de Duvernoi, musculus levator glandulae thyreoideae. (Exemple du Sömmerring.) *Bull Soc Anat Paris* 22: 202–205.

Gopal RA, Acharya SV, Bandgar T, Menon PS, Marfatia H, Shah NS. 2009. Clinical profile of ectopic thyroid in Asian Indians: a single-center experience. *Endocr Pract* 15(4): 322–325.

Gow WJ. 1884. Total absence of the left lobe of the thyroid body. *J Anat Physiol* 18: 118.

Granato F, Roberts F, West D. 2011. A thyroglossal duct cyst of the anterior mediastinum. *Ann Thorac Surg* 92(3): 1118–1120.

Gregory JK, Guse DM. 2007. Unique variant of levator glandulae thyroidea muscle. *Clin Anat* 20(8): 966–967.

Gross RE, Connerly ML. 1940. Thyroglossal cysts and sinuses: a study and report of 198 cases. *N Engl J Med* 223: 616–624.

Guimarães MJ, Valente CM, Santos L, Baganha MF. 2009. Ectopic thyroid in the anterior mediastinum. *J Bras Pneumol* 35(4): 383–387.

Hamburger JI, Hamburger SW. 1970. Thyroidal hemiagenesis. Report of a case and comments on clinical ramifications. *Arch Surg* 100(3): 319–320.

Handfield-Jones C. 1866. Primary hyperparathyroidism with thyroid hemi-agenesis. In: *Handbuch der SystematischenAnatomie des Menschen* (ed. J Henle). Sohn: Friedrich Vlewig und Braunschweig.

Hansen LT, Christensen PH. 1996. Ectopic thyroid gland in the submandibular region. *Ugeskr Laeger* 158(23): 3324–3325.

Harada T, Nishikawa Y, Ito K. 1972. Aplasia of one thyroid lobe. *Am J Surg* 124(5): 617–619.

Hari CK, Brown MJ, Thompson I. 1999. Tall cell variant of papillary carcinoma arising from ectopic thyroid tissue in the trachea. *J Laryngol Otol* 113(2): 183–185.

Harjeet A, Sahni D, Jit I, Aggarwal AK. 2004. Shape, measurements and weight of the thyroid gland in northwest Indians. *Surg Radiol Anat* 26(2): 91–95.

Hatada T, Ichii S, Sagayama K, Ishii H, Sugihara A, Terada N, Yamamura T. 2000. Intrathyroid thyroglossal duct cyst simulating a thyroid nodule. *Tumori* 86(3): 250–252.

Hayashi N, Hori E, Ohtani Y, Ohtani O, Kuwayama N, Endo S. 2005. Surgical anatomy of the cervical carotid artery for carotid endarterectomy. *Neurol Med Chir (Tokyo)* 45(1): 25–30.

Helidonis E, Dokianakis G, Papazoglou G, Pantazopoulos P, Thomopoulou H. 1980. Ectopic thyroid gland in the submandibular region. *J Laryngol Otol* 94(2): 219–224.

Hickmann W. 1869. Congenital tumor of the base of the tongue, pressing down the epiglottis on the larynx and causing death by suffocation sixteen hours after birth. *Trans Pathol Soc Lond* 20: 160–161.

Hisham AN, Aina EN. 2000. Zuckerkandl's tubercle of the thyroid gland in association with pressure symptoms: a coincidence or consequence? *Aust N Z J Surg* 70(4): 251–253.

Hollander EJ, Visser MJ, van Baalen JM. 2004. Accessory thyroid gland at carotid bifurcation presenting as a carotid body tumor: case report and review of the literature. *J Vasc Surg* 39(1): 260–262.

Hollinshead WH. 1968. *Anatomy for Surgeons: Head and Neck*, Vol. 1, second edition. New York: Harper & Row.

Hoyes AD, Kershaw DR. 1985. Anatomy and development of the thyroid gland. *Ear Nose Throat J* 64(7): 318–333.

Hsieh YY, Hsueh S, Hsueh C, Lin JN, Luo CC, Lai JY, Huang CS. 2003. Pathological analysis of congenital cervical cysts in children: 20 years of experience at Chang Gung Memorial Hospital. *Chang Gung Med J* 26(2): 107–113.

Huang TS, Chen HY. 2007. Dual thyroid ectopia with a normally located pretracheal thyroid gland: case report and literature review. *Head Neck* 29(9): 885–888.

Hunt PS, Poole M, Reeve TS. 1968. A reappraisal of the surgical anatomy of the thyroid and parathyroid glands. *Br J Surg* 55(1): 63–66.

Huschke E. 1845. *Traité de splanchnologie et des organes des sens. In: Encyclopedie Anatomique*. Vol V. Paris: JB Bailliere.

Izenstark JL, Forsaith AL, Horwitz NH. 1969. The pyramidal lobe in thyroid imaging. *J Nucl Med* 10(8): 519–524.

Jain A, Pathak S. 2010. Rare developmental abnormalities of thyroid gland, especially multiple ectopia: A review and our experience. *Indian J Nucl Med* 25(4): 143–146.

Jamshidi M, Kasirye O, Smith DJ. 1998. Ectopic thyroid nodular goiter presenting as a porta hepatis mass. *Am Surg* 64(4): 305–306.

Jelev L, Surchev L. 2001. Lack of inferior thyroid artery. *Ann Anat* 183(1): 87–90.

Johnston R, Wei JL, Maddalozzo J. 2003. Intra-thyroid thyroglossal duct cyst as a differential diagnosis of thyroid nodule. *Int J Pediatr Otorhinolaryngol* 67(9): 1027–1030.

Joshi SD, Joshi SS, Daimi SR, Athavale SA. 2010. The thyroid gland and its variations: a cadaveric study. *Folia Morphol (Warsz)* 69(1): 47–50.

Kampmeier OF. 1937. Origin and development of the mediastinal and aortic thyroids and the periaortic fat bodies. *Univ Illinois Bull (Illinois Med Dent Monogr 2)*: 35(12): 1–82.

Kantelip B, Lusson JR, De Riberolles C, Lamaison D, Bailly P. 1986. Intracardiac ectopic thyroid. *Hum Pathol* 17(12): 1293–1296.

Kempers RD, Dockerty MB, Hoffman DL, Bartholomew LG. 1970. Struma ovarii-ascitic, hyperthyroid, and asymptomatic syndromes. *Ann Intern Med* 72(6): 883–893.

Keyes EL. 1940. Demonstration of the nerve to the levator glandulae thyroidea muscle. *Anat Rec* 77: 293–295.

Kim DI, Kim HJ, Park JY, Lee KS. 2010. Variation of the infrahyoid muscle: duplicated omohyoid and appearance of the levator glandulae thyroidea muscles. *Yonsei Med J* 51(6): 984–986.

Kim DW, Jung SL, Baek JH, Kim J, Ryu JH, Na DG, Park SW, Kim JH, Sung JY, Lee Y, Rho MH. 2013. The prevalence and features of thyroid pyramidal lobe, accessory thyroid, and ectopic thyroid as assessed by computed tomography: a multicenter study. *Thyroid* 23(1): 84–91.

Kim SJ, Pak K, Lim HJ, Yun KH, Seong SJ, Kim TJ, Lim KT, Jung HW, Park IS, Shim JU, Park CT, Lee KH. 2002. Clinical diversity of struma ovarii. *Korean J f Obstetr Gynecol* 45: 748–752.

Kirmızibekmez H, Güven A, Yildiz M, Cebeci AN, Dursun F. 2012. Developmental defects of the thyroid gland: relationship with advanced maternal age. *J Clin Res Pediatr Endocrinol* 4(2): 72–75.

Kitagawa W. 1993. Arterial supply of the thyroid gland in the human fetuses. *Nihon Ika Daigaku Zasshi* 60(3): 140–155.

Kousta E, Konstantinidis K, Michalakis C, Vorias M, Sambalis G, Georgiou M, Theodoropoulos GE. 2005. Ectopic thyroid tissue in the lower neck with a coexisting normally located multinodular goiter and brief literature review. *Hormones (Athens)* 4(4): 231–234.

Krause W. 1879. Handbuch der menschlichen Anatomie. Durchaus nach eigenen Untersuchungen, und mit besonderer Rücksicht auf das Bedürfnis der Studirenden, der praktischen Ärzte und Wundärzte und der Gerichtsärzte. Third edition, Bd 2. Hannover: Hahn'sche Buchhandlung.

Kulkarni V, Sreepadma S, Deshpande SK. 2012. Morphological variations of the thyroid gland. *Medica Innıvatica* 1(2): 35–38.

Kumar R, Sharma S, Marwah A, Moorthy D, Dhanwal D, Malhotra A. 2001. Ectopic goiter masquerading as submandibular gland swelling: a case report and review of the literature. *Clin Nucl Med* 26(4): 306–309.

Kumar TA, Lekha DS, Kolla S, Rao N, Jothi SS. 2005. Levator glandulae thyroidea: a case report. *J Anat Soc India* 54, 347–350.

Kurien R, Michael R. 2012. Subglottic thyroglossal duct cyst: a rare intralaryngeal presentation. *Ear Nose Throat J* 91(7): E15–19.

Kurman RJ, Prabha AC. 1973. Thyroid and parathyroid glands in the vaginal wall: report of a case. *Am J Clin Pathol* 59(4): 503–507.

Kutuya N, Kurosaki Y. 2008. Sonographic assessment of thyroglossal duct cysts in children. *J Ultrasound Med* 27(8): 1211–1219.

Larochelle D, Arcand P, Belzile M, Gagnon NB. 1979. Ectopic thyroid tissue: a review of the literature. *J Otolaryngol* 8(6): 523–530.

Latimer J, Lindsay KA. 1995. Case report: lingual thyroid in association with a lateral ectopic thyroid mass. *Clin Radiol* 50(7): 501–502.

Lehr RP Jr. 1979. Musculus levator glandulae thyroidea: an observation. *Anat Anz* 146(5): 494–496.

Letonturier P, Hazard J, Tourneur R, Perlemuter L, Angel R. 1979. Thyroid hemiagenesis (single thyroid lobe). 8 cases (author's transl). *Nouv Presse Med* 8(15): 1227–1229.

Levy HA, Sziklas JJ, Rosenberg RJ, Spencer RP. 1982. Incidence of a pyramidal lobe on thyroid scans. *Clin Nucl Med* 7(12): 560–561.

Lin ST, Tseng FY, Hsu CJ, Yeh TH, Chen YS. 2008. Thyroglossal duct cyst: a comparison between children and adults. *Am J Otolaryngol* 29(2): 83–87.

Lippert H, Pabst R. 1985. *Arterial Variations in Nan*. New York: Springer.

Loh WS, Chong SM, Loh KS. 2006. Intralaryngeal thyroglossal duct cyst: implications for the migratory pathway of the thyroglossal duct. *Ann Otol Rhinol Laryngol* 115(2): 114–116.

Loukas M, Merbs W, Tubbs RS, Curry B, Jordan R. 2008. Levator glandulae thyroidea muscle with three slips. *Anat Sci Int* 83(4): 273–276.

Lucev N, Bobinac D, Maric I, Drescik I. 2000. Variations of the great arteries in the carotid triangle. *Otolaryngol Head Neck Surg* 122(4): 590–591.

Maino K, Skelton H, Yeager J, Smith KJ. 2004. Benign ectopic thyroid tissue in a cutaneous location: a case report and review. *J Cutan Pathol* 31(2): 195–198.

Maiorana R, Carta A, Floriddia G, Leonardi D, Buscema M, Sava L, Calaciura F, Vigneri R. 2003. Thyroid hemiagenesis: prevalence in normal children and effect on thyroid function. *J Clin Endocrinol Metab* 88(4): 1534–1536.

Malone Q, Conn J, Gonzales M, Kaye A, Coleman P. 1997. Ectopic pituitary fossa thyroid tissue. *J Clin Neurosci* 4(3): 360–363.

Marshall CF. 1895. Variations in the form of the thyroid gland in man. *J Anat Physiol* 29: 234–239.

McHenry CR, Walfish PG, Rosen IB, Lawrence AM, Paloyan E. 1995. Congenital thyroid hemiagenesis. *Am Surg* 61(7): 634–639.

Mehboob M, Babar KM, Khan JA; Abdullah Al-Angari. 2005. Accessory thyroid nodule in sub-mandibular region. *J Coll Physicians Surg Pak* 15(9): 564–565.

Melnick JC, Stemkowski PE. 1981. Thyroid hemiagenesis (hockey stick sign): a review of the world literature and a report of four cases. *J Clin Endocrinol Metab* 52(2): 247–251.

Merkel FS. 1913. *Die Anatomie des Menschem mit Hinweisen aufdie arztliche Praxis, Abt. 3*. Wiesbaden: JF Bergman.

Mikosch P, Gallowitsch HJ, Kresnik E, Molnar M, Gomez I, Lind P. 1999. Thyroid hemiagenesis in an endemic goiter area diagnosed by ultrasonography: report of sixteen patients. *Thyroid* 9(11): 1075–1084.

Mohebati A, Shaha AR. 2012. Anatomy of thyroid and parathyroid glands and neurovascular relations. *Clin Anat* 25(1): 19–31.

Mondin V, Ferlito A, Muzzi E, Silver CE, Fagan JJ, Devaney KO, Rinaldo A. 2008. Thyroglossal duct cyst: personal experience and literature review. *Auris Nasus Larynx* 35(1): 11–25.

Montgomery ML. 1935. Lingual thyroid: a comprehensive review. *Western J Surg* 43: 661–669.

Morgan NJ, Emberton P, Barton RP. 1995. The importance of thyroid scanning in neck lumps: a case report of ectopic tissue in the right submandibular region. *J Laryngol Otol* 109(7): 674–676.

Mori M. 1964. Statistics on the musculature of the Japanese. *Okajimas Folia Japan* 40: 195–300.

Muysoms F, Boedts M, Claeys D. 1997. Intratracheal ectopic thyroid tissue mass. *Chest* 112(6): 1684–1685.

Myers EN, Pantangco IP Jr. 1975. Intratracheal thyroid. *Laryngoscope* 85(11 pt 1): 1833–1840.

Narayana Moorthy S, Arcot R. 2011. Thyroglossal duct cyst: more than just an embryological remnant. *Indian J Surg* 73(1): 28–31.

Natsis K, Raikos A, Foundos I, Noussios G, Lazaridis N, Njau SN. 2011. Superior thyroid artery origin in Caucasian Greeks: A new classification proposal and review of the literature. *Clin Anat* 24(6): 699–705.

Neinas FW, Gorman CA, Devine KD, Woolner LB. 1973. Lingual thyroid. Clinical characteristics of 15 cases. *Ann Intern Med* 79(2): 205–210.

Noussios G, Anagnostis P, Goulis DG, Lappas D, Natsis K. 2011. Ectopic thyroid tissue: anatomical, clinical, and surgical implications of a rare entity. *Eur J Endocrinol* 165(3): 375–382.

Ongeti KW, Ogeng'o JA. 2012. Variant origin of the superior thyroid artery in a Kenyan population. *Clin Anat* 25(2): 198–202.

Organ GM, Organ CH Jr. 2000. Thyroid gland and surgery of the thyroglossal duct: exercise in applied embryology. *World J Surg* 24(8): 886–890.

Otto HD. 1994. Teratogenic and clinical aspects of abnormalities of the head and neck region. *Eur Arch Otorhinolaryngol Suppl* 1: 15–100.

Ozgur Z, Govsa F, Celik S, Ozgur T. 2009. Clinically relevant variations of the superior thyroid artery: an anatomic guide for surgical neck dissection. *Surg Radiol Anat* 31(3): 151–159.

Ozgur Z, Celik S, Govsa F, Ozgur T. 2011. Anatomical and surgical aspects of the lobes of the thyroid glands. *Eur Arch Otorhinolaryngol* 268(9): 1357–1363.

Park JY, Kim DW, Park JS, Kang T, Kim YW. 2012. The prevalence and features of thyroid pyramidal lobes as assessed by computed tomography. *Thyroid* 22(2): 173–177.

Pelizzo MR, Toniato A, Gemo G. 1998. Zuckerkandl's tuberculum: an arrow pointing to the recurrent laryngeal nerve (constant anatomical landmark). *J Am Coll Surg* 187(3): 333–336.

Pérez-Martínez A, Bento-Bravo L, Martínez-Bermejo MA, Conde-Cortes J, de Miguel-Medina C. 2005. An intra-thyroid thyroglossal duct cyst. *Eur J Pediatr Surg* 15(6): 428–430.

Pettersen JC, Koltis GG, White MJ. 1979. An examination of the spectrum of anatomic defects and variations found in eight cases of trisomy 13. *Am J Med Genet* 3(2): 183–210.

Pintar JE, Dominique CTA. 1991. Normal development of the hypothalamic-pituitary-thyroid axis. In: *Werner and Jugbar's The Thyroid, sixth edition* (eds LE Braverman, RD Utiger). Philadelphia, Pa Lippingcott, pp. 11–14.

Poisel S, Golth D. 1974. Variability of large arteries in the carotid trigone. *Wien Med Wochenschr* 124(15): 229–232.

Pollice L, Caneso G. 1986. Struma cordis: ectopic thyroid goiter in the right ventricle. *Arch Pathol Lab Med* 110: 452–453.

Pollock WF. 1966. Cysts and sinuses of the thyroglossal duct. *Am J Surg* 122: 225–229.

Postlethwait RW, Detmer DE. 1975. Ectopic thyroid nodule in the esophagus. *Ann Thorac Surg* 19(1): 98–100.

Pounds LA. 1981. Neck masses of congenital origin. *Pediatr Clin North Am* 28(4): 841–844.

Prakash, Rajini T, Ramachandran A, Savalgi GB, Venkata SP, Mokhasi V. 2012. Variations in the anatomy of the thyroid gland: clinical implications of a cadaver study. *Anat Sci Int* 87(1): 45–49.

Radkowski D, Arnold J, Healy GB, McGill T, Treves ST, Paltiel H, Friedman EM. 1991. Thyroglossal duct remnants. Preoperative evaluation and management. *Arch Otolaryngol Head Neck Surg* 117(12): 1378–1381.

Rahn J. 1959. An unusual heterotopia of thyroid gland tissue. *Zentralbl Allg Pathol* 99(1–2): 80–86.

Ranade AV, Rai R, Pai MM, Nayak SR, Prakash, Krisnamurthy A, Narayana S. 2008. Anatomical variations of the thyroid gland: possible surgical implications. *Singapore Med J* 49(10): 831–834.

Randolph J, Grunt JA, Vawter GF. 1963. The medical and surgical aspects of intratracheal goiter. *N Engl J Med* 268: 457–461.

Richards PS, Ahuja AT, King AD. 2004. Clinics in diagnostic imaging (101): Multinodular accessory thyroid tissue. *Singapore Med J* 45(11): 542–546.

Richardson GM, Assor D. 1971. Thyroid tissue within the larynx. Case report. *Laryngoscope* 81(1): 120–125.

Richmond I, Whittaker JS, Deiraniya AK, Hassan R. 1990. Intracardiac ectopic thyroid: a case report and review of published cases. *Thorax* 45(4): 293–294.

Rogers WM, Kesten HD. 1962. Embryologic bases for thyroid tissues in the heart. *Anat Rec* 142: 323.

Roy D, Roy PG, Malik VK, Seenu V. 2003. Intrathyroidal thyroglossal duct cyst presenting as a thyroid nodule. *Int J Clin Pract* 57(7): 637–638.

Rubenfeld S, Joseph UA, Schwartz MR, Weber SC, Jhingran SG. 1988. Ectopic thyroid in the right carotid triangle. *Arch Otolaryngol Head Neck Surg* 114(8): 913–915.

Ruberg FL, McDonnell ME, Trabb J, Shemin RJ, Hoyt RF Jr, Braverman LE, Balady GJ. 2006. An intracardiac accessory thyroid gland. *Am J Cardiol* 97(6): 926–928.

Ruchti C, Balli-Antunes M, Gerber HA. 1987. Follicular tumor in the sellar region without primary cancer of the thyroid. Heterotopic carcinoma? *Am J Clin Pathol* 87(6): 776–780.

Saadeh FA, Kawas SH, Haikal FA, Hawi JS. 1996. An unusual levator glandulae thyroidea: A case report and literature review. *J Anat Soc India* 45: 125–128.

Sadler TW, Langman J. 2006. *Langman's Medical Embryology*, 10th edition. Philadelphia, PA: Lippincott Williams & Wilkins.

Sagiroglu AO. 1997. Gross anatomical study on anomalies of the thyroid gland. *Gazi Med J* 8: 33–39.

Salvatore M, Gallo A. 1975. Accessory thyroid in the anterior mediastinum: case report. *J Nucl Med* 16(12): 1135–1136.

Sambola-Cabrer I, Fernández-Real JM, Ricart W, Barbas JF, Ollé M, Teruel J. 1996. Ectopic thyroid tissue presenting as a submandibular mass. *Head Neck* 18(1): 87–90.

Sand J, Pehkonen E, Mattila J, Seppänen S, Salmi J. 1996. Pulsating mass at the sternum: a primary carcinoma of ectopic mediastinal thyroid. *J Thorac Cardiovasc Surg* 112(3): 833–835.

Sanjeev IK, Anita H, Ashwini M, Mahesh U, Rairam GB. 2010. Branching pattern of external carotid artery in human cadavers. *J Clin Diagnos Res* 4: 3128–3133.

Sari O, Ciftçi I, Törü M, Erbaş B. 2000. Thyroid hemiagenesis. *Clin Nucl Med* 25(10): 766–768.

Sarmento DJ, Araújo PP, da Silveira EJ, Germano AR. 2013. Double thyroglossal duct cyst involving the floor of the mouth and sublingual gland region. *J Craniofac Surg* 24(2): e116–119.

Satoshi N, Koji M, Yumi A, Masanori A, Tomonobu H. 2010. Transcription factor mutations and congenital hypothyroidism: systematic genetic screening of a population–based cohort of Japanese patients. *J Clin Endocrinol Metab* 95: 1981–1985.

Sauvageau A, Belley-Côté EP, Racette S. 2006. Fatal asphyxia by a thyroglossal duct cyst in an adult. *J Clin Forensic Med* 13(6–8): 349–352.

Savage PE, Khan O, Grover S, Ott R, McCready VR. 1984. The appearance of the pyramidal lobe on thyroid scintigraphy. *Nucl Med Commun* 5(3): 163–168.

Schanaider A, de Oliveira PJ Jr. 2008. Thyroid isthmus agenesis associated with solitary nodule: A case report. *Cases J* 1(1): 211.

Shabana W, Delange F, Freson M, Osteaux M, De Schepper J. 2000. Prevalence of thyroid hemiagenesis: ultrasound screening in normal children. *Eur J Pediatr* 159(6): 456–458.

Shah BC, Ravichand CS, Juluri S, Agarwal A, Pramesh CS, Mistry RC. 2007. Ectopic thyroid cancer. *Ann Thorac Cardiovasc Surg* 13(2): 122–124.

Shemin RJ, Marsh JD, Schoen FJ. 1985. Benign intracardiac thyroid mass causing right ventricular outflow tract obstruction. *Am J Cardiol* 56(12): 828–829.

Shiraishi T, Imai H, Fukutome K, Watanabe M, Yatani R. 1999. Ectopic thyroid in the adrenal gland. *Hum Pathol* 30(1): 105–108.

Simon M, Baczako K. 1989. Thyroid inclusion in the lung. Metastasis of an occult papillary carcinoma or ectopia? *Pathol Res Pract* 184(2): 263–270.

Sinnatamby CS. 2006. *Last's Anatomy*, 11th edition. China: Churchill Livingstone, Elsevier.

Siraj QH, Aleem N, Inam-Ur-Rehman A, Qaisar S, Ahmad M. 1989. The pyramidal lobe: a scintigraphic assessment. *Nucl Med Commun* 10(9): 685–693.

Sironi M, Assi A, Andruccioli M, Spreafico G. 1996. Submandibular ectopic thyroid gland. *Clin Nucl Med* 21(7): 585.

Skandalakis JE. 2004. *Respiratory System in Skandalakis' Surgical Anatomy*. Athens: Paschalidis Medical Publications.

Sömmerring ST. 1794. De muscularis, tendinibus ET buris mucosis. Frankfurt is Main. Clossius ET Schreger, pp 128.

Spencer RP, Scholl RJ, Erbay N. 1997. Tc-99m pertechnetate thyroid images in hyperthyroidism. Size, distribution, and presence of a pyramidal lobe. *Clin Nucl Med* 22(8): 519–522.

Spinner RJ, Moore KL, Gottfried MR, Lowe JE, Sabiston DC Jr. 1994. Thoracic intrathymic thyroid. *Ann Surg* 220(1): 91–96.

Standring S. 2008. *Head and Neck. In: Gray's Anatomy*, 40th edition. Spain: Churchill Livingstone, Elsevier, pp. 462–465.

Strohschneider T, Timm D, Worbes C. 1993. Ectopic thyroid gland tissue in the liver. *Chirurg* 64(9): 751–753.

Sturniolo G, Bonanno L, Gagliano E, Tonante A, Taranto F, Mamo M, De Salvo G, Sturnioloa G. 2008. The thyroid pyramidal lobe: frequency, morphological features and related diseases. *Chir Ital* 60(1): 41–46.

Sugiyama S. 1971. The embryology of the human thyroid gland including ultimobranchial body and others related. *Ergeb Anat Entwicklungsgesch* 44: 3–111.

Sultana S, Mannan S, Ahmed M, Rahman M, Khan M, Khalil M. 2008. An anatomical study on pyramidal lobe of thyroid gland in Bangladeshi people. *Mymensingh Med J* 17(1): 8–13.

Sultana SZ, Khalil M, Khan MK, Shamim R, Parveen S, Ara ZG. 2009. Morphological study of levator glandulae thyroidea in Bangladeshi cadaver. *Mymensingh Med J* 18(2): 179–183.

Tanriover O, Comunoglu N, Eren B, Comunoglu C, Turkmen N, Bilgen S, Kaspar EC, Gündogmus UN. 2011. Morphometric features of the thyroid gland: a cadaveric study of Turkish people. *Folia Morphol (Warsz)* 70(2): 103–108.

Tas A, Karasalihoglu AR, Yagiz R, Doğanay L, Guven S. 2003. Thyroglossal duct cyst in hyoid bone: unusual location. *J Laryngol Otol* 117(8): 656–657.

Temmel AF, Baumgartner WD, Steiner E, Kletter K, Franz P, Kautzky-Willer A. 1998. Ectopic thyroid gland simulating a submandibular tumor. *Am J Otolaryngol* 19(5): 342–344.

Tunkel DE, Domenech EE. 1998. Radioisotope scanning of the thyroid gland prior to thyroglossal duct cyst excision. *Arch Otolaryngol Head Neck Surg* 124(5): 597–601.

Türkyilmaz Z, Sönmez K, Karabulut R, Demirgoullari B, Sezer C, Basaklar AC, Kale N. 2004. Management of thyroglossal duct cysts in children. *Pediatr Int* 46(1): 77–80.

Valentino M, Quiligotti C, Villa A, Dellafiore C. 2012. Thyroglossal duct cysts: Two cases. *J Ultrasound* 15(3): 183–185.

Vázquez T, Cobiella R, Maranillo E, Valderrama FJ, McHanwell S, Parkin I, Sañudo JR. 2009. Anatomical variations of the superior thyroid and superior laryngeal arteries. *Head Neck* 31(8): 1078–1085.

Wadsworth DT, Siegel MJ. 1994. Thyroglossal duct cysts: variability of sonographic findings. *AJR Am J Roentgenol* 163(6): 1475–1477.

Wahl R, Müh U, Kallee E. 1997. Hyperthyroidism with or without pyramidal lobe Graves' disease or disseminated autonomously functioning thyroid tissue? *Clin Nucl Med* 22(7): 451–458.

Watanabe S, Suda M. 1962. On the musculus levator glandulae thyroidea of the Ainu. *Saporro Igacu Zasshi* 21: 115–120.

Weng LP, Kaiser A, Koch HH, Wünsch PH. 2000. Multilocular thyroid gland ectopy. *Dtsch Med Wochenschr* 125(14): 421–424.

Whale HL. 1987. Esophageal tumor of thyroid tissue. *BMJ* 2: 1921.

Williams ED, Toyn CE, Harach HR. 1989. The ultimobranchial gland and congenital thyroid abnormalities in man. *J Pathol* 159(2): 135–141.

Williams RJ, Lindop G, Butler J. 2002. Ectopic thyroid tissue on the ascending aorta: an operative finding. *Ann Thorac Surg* 73(5): 1642–1643.

Willis RA. 1953. *Pathology of Tumors*. London: Butterworth.

Winslow JB. 1743. *Exposition Anatomique de la Structure du Corps Humain*. Amsterdam: Wetstein.

Won HS, Chung IH. 2002. Morphologic variations of the thyroid gland in Korean Adults. *Korean J Phys Anthrop* 15(2): 119–125.

Wu YH, Wein RO, Carter B. 2012. Thyroid hemiagenesis: a case series and review of the literature. *Am J Otolaryngol* 33(3): 299–302.

Yalcin B, Tagil SM, Kocabiyik N, Ozan H. 2006. Incidence and morphology of the zuckerkandl's tubercle: An anatomic dissection study. *SDU Tip Dergisi* 13(2): 1–4.

Yang Y, Li Q, Qu J, Xiang Y, Pan Y, Liao Z, Zhang X. 2010. Ectopic intratracheal thyroid. *South Med J* 103(5): 467–470.

Yılmaz F, Uzunlar AK, Sögütçü N. 2005. Ectopic thyroid tissue in the uterus. *Acta Obstet Gynecol Scand* 84(2): 201–202.

Yoo SC, Chang KH, Lyu MO, Chang SJ, Ryu HS, Kim HS. 2008. Clinical characteristics of struma ovarii. *J Gynecol Oncol* 19(2): 135–138.

Yoon JS, Won KC, Cho IH, Lee JT, Lee HW. 2007. Clinical characteristics of ectopic thyroid in Korea. *Thyroid* 17(11): 1117–1121.

Zivic R, Radovanovic D, Vekic B, Markovic I, Dzodic R, Zivaljevic V. 2011. Surgical anatomy of the pyramidal lobe and its significance in thyroid surgery. *S Afr J Surg* 49(3): 110, 112, 114.

Zuckerkandl E. 1902. *Nebst Bemerkangen uber die Epithelkorperchen des Menschen*. Anat Hefte LXI: 61.

Zümre O, Salbacak A, Ciçekcibaşi AE, Tuncer I, Seker M. 2005. Investigation of the bifurcation level of the common carotid artery and variations of the branches of the external carotid artery in human fetuses. *Ann Anat* 187(4): 361–369.

100 Parathyroid glands

Bulent Yalcin
Gulhane Military Medical Academy, Ankara, Turkey

Anatomy

The parathyroid glands are small, yellowish-brown, ovoid, or lentiform structures, usually lying between the posterior lobar borders of the thyroid gland and its capsule. They are commonly 6 mm long, 3–4 mm across, and 1–2 mm from back to front, each weighing about 50 mg. Typically, there are two on each side, superior and inferior, but there can be more; alternatively, there may only be three or many minute parathyroid islands scattered in connective tissue near the usual sites. Very occasionally an occult gland follows a blood vessel into a groove on the surface of the thyroid. Normally the inferior parathyroids migrate only to the inferior thyroid poles, but they sometimes descend with the thymus into the thorax or are sessile and remain above their normal level near the carotid bifurcation. The anastomotic connection between the superior and inferior thyroid arteries that occurs along the posterior border of the thyroid gland usually passes very close to the parathyroids and is a useful aid to identifying them (Standring 2008).

The superior parathyroid glands are more constant in location than the inferior and are usually located midway along the posterior borders of the thyroid gland, although they can be higher. The inferior pair are more variably situated (depending on their embryological development) and can be within the fascial thyroid sheath, below the inferior thyroid arteries and near the inferior lobar poles; outside the sheath, immediately above an inferior thyroid artery; or in the thyroid gland near its inferior pole. These variations are surgically important (Standring 2008).

Both the superior and inferior parathyroid glands are usually supplied by the inferior thyroid arteries; the superior parathyroid can be supplied by the superior thyroid artery, or from anastomoses between the superior and inferior thyroid arteries in 10–15% cases. The glands drain into the plexus of veins on the anterior surface of the thyroid. Lymph vessels are numerous and are associated with those of the thyroid and thymus glands. The nerve supply is sympathetic, either direct from the superior or middle cervical ganglia or via a plexus in the fascia on the posterior lobar aspects. Parathyroid activity is controlled by variations in blood calcium level: it is inhibited by a rise and stimulated by a fall. The nerves are believed to be vasomotor but not secretomotor (Standring 2008).

Embryology

The parathyroid glands develop at six weeks and migrate caudally at eight weeks (Smith and Oates 2004). They originate from the endoderm and develop from the dorsal wing of the third and fourth pharyngeal pouches (Mohebati and Shaha 2012). There are typically four glands in humans, usually located on the upper two-thirds of the posterior surface of the thyroid gland. The superior parathyroid glands develop from the fourth pharyngeal pouch while the inferior derive from the third; after losing their attachments to the pharyngeal wall, they follow the descending route of the thyroid gland (Fancy et al. 2010; Mohebati and Shaha 2012). While the dorsal wing of the third pharyngeal pouch gives rise to the inferior parathyroids, the ventral wing gives rise to the thymus which migrates to its final position in the mediastinum. The descending pathway of the thymus is also followed by the inferior parathyroids, and this explains their unusual location in the mediasinum (Fancy et al. 2010; Mohebati and Shaha 2012). In contrast, the superior parathyroids share a common embryological origin with the lateral thyroid; consequently, they are usually located at the posterior part of the cricothyroid junction, less commonly behind the upper pole, and rarely behind the lower pharyngeal and upper esophageal junction in the midline (Wang 1976). They usually lie above the intersection between the recurrent laryngeal nerve and the inferior thyroid artery (Akerström et al. 1984). The inferior parathyroids are usually located at an anterior or a lateroposterior surface of the lower thyroid pole and in the thymic tongue (Wang 1976).

Number of parathyroid glands

Although there are typically four parathyroid glands in humans, more than four (and rarely fewer than four) have been also described in the literature (Table 100.1).

Bergman's Comprehensive Encyclopedia of Human Anatomic Variation, First Edition. Edited by R. Shane Tubbs, Mohammadali M. Shoja and Marios Loukas.
© 2016 John Wiley & Sons, Inc. Published 2016 by John Wiley & Sons, Inc.

Table 100.1 Incidence (%) of supernumerary of the parathyroid gland and its number in the literature.

Authors	Supernumerary	Number of the parathyroid glands					
		1	2	3	4	5	6
MacCallum 1906				16			
Gilmour 1938	6.5		0.2	6.1	87	6	0.5
Wang 1976	2.5				97.5	1.8	0.6
Akerström et al. 1984	13			3	84		
Cordeiro 1987				31			
Hooghe et al. 1992				17.6			
Numano et al. 1998	16.5						
Pattou et al. 2000	30						
Gough 2006	10						
Gomes et al. 2007	14.3			5.7	80		
Hojaij et al. 2011	10.7	3.6	1.8	5.4	78.6	8.9	1.8

Previous studies have reported a total of four glands in 78.6–97.5% of cases (Gilmour 1938; Wang 1976; Akerström et al. 1984; Gomes et al. 2007; Hojaij et al. 2011). Different percentages of cases with fewer than four glands are described in the literature. Three glands have been observed in 3–31% of cases (MacCallum 1906; Gilmour 1938; Akerström et al. 1984; Cordeiro 1987; Hooghe et al. 1992; Gomes et al. 2007; Hojaij et al. 2011). Two glands have been reported in 0.2–1.8% (Gilmour 1938; Hojaij et al. 2011), and even a single gland occurs in 3.6% (Hojaij et al. 2011).

More than four glands have also been reported. These supernumerary glands are frequently associated within a lobule of thymic tissue, which suggests derivation from the same primordium as the thymus after multiple divisions during embryological descent (Wang 1976). The percentage of supernumerary glands has been reported in 2.5–30% of cases (Gilmour 1938; Wang 1976; Akerström 1984; Numano et al. 1998; Pattou et al. 2000; Gough 2006; Gomes et al. 2007; Hojaij et al. 2011). Fifth and sixth supernumerary glands have been reported in 1.8–8.9% (Gilmour 1938; Wang 1976; Hojaij et al. 2011) and 0.5–1.8% (Gilmour 1938; Wang 1976; Hojaij et al. 2011) of cases, respectively.

Ectopia of the parathyroid glands

Ectopic parathyroid glands have been attributed to abnormal migration during embryogenesis. At 26 days of embryo development, five pairs of pharyngeal pouches are formed. The third pair proliferates into the inferior parathyroid glands and the thymus, and the fourth proliferates into the superior parathyroid glands and the lateral angle of the thyroid gland. From their origin, the inferior parathyroid glands migrate a variable distance with the thymus. Because the inferior parathyroid glands undergo more extensive migration during embryogenesis, they are more likely to be found in ectopic locations (Phitayakorn and McHenry 2006).

An ectopic superior parathyroid gland is defined as a gland in a location other than juxtacricothyroidal posteriorly or within the capsule of the posterior surface of the superior pole of the thyroid gland. An ectopic inferior parathyroid gland is defined as a gland in a location other than on or immediately adjacent to the anterior or posteriolateral surface of the inferior pole of the thyroid gland (Phitayakorn and McHenry 2006). Ectopic inferior parathyroid glands are due to abnormal migration during embryogenesis, whereas ectopic superior parathyroid glands are more likely to be due to pathological displacement from a normal anatomical position (Phitayakorn and McHenry 2006).

The most common site for an ectopic inferior parathyroid gland is intrathymic; for an ectopic superior parathyroid gland it is in the tracheoesophageal groove (Phitayakorn and McHenry 2006). Although uncommon, ectopic parathyroids constitute an important diagnostic challenge for the surgeon. Their prevalence ranges over 28–42.8% in autopsy series (Nanka et al. 2006; Hojaij et al. 2011), although much lower rates (2%) have been reported (Wang 1976). Data from surgical and cadaveric studies revealed a prevalence of 6.3–52% of cases (Gough 2006; Phitayakorn and McHenry 2006; Gomes et al. 2007; Mendoza et al. 2010; Hamidi et al. 2006; Hojaij et al. 2011; Roy et al. 2013). Ectopic parathyroid glands were superior in 38% and inferior in 62% of patients (Phitayakorn and McHenry 2006).

The location of ectopic and supernumerary parathyroid glands is variable and classified as: intrathymic in 14.8–80% (Wang 1976; Shen et al. 1996; Numano et al. 1998; Pattou et al. 2000; Gough 2006; Phitayakorn and McHenry 2006; Gomes et al. 2007; Roy et al. 2013); intrathyroidal in 5.4–38.4% (Shen

et al. 1996; Gough 2006; Phitayakorn and McHenry 2006; Gomes et al. 2007; Hojaij et al. 2011; Roy et al. 2013); mediastinal in 6–26% (Shen et al. 1996; Gough 2006; Phitayakorn and McHenry 2006; Gomes et al. 2007; Hojaij et al. 2011; Roy et al. 2013); in the thyrothymic ligament, defined as the area between the inferior pole of thyroid gland and the thymus, in 10.8–18.5% (Phitayakorn and McHenry 2006; Gomes et al. 2007); within the tracheoesophageal groove in 16.2% (Phitayakorn and McHenry 2006); para/retroesophageal in 7.4–31% (Shen et al. 1996; Phitayakorn and McHenry 2006; Gomes et al. 2007; Roy et al. 2013); in the carotid sheath in 2.7–9% (Shen et al. 1996; Gough 2006; Phitayakorn and McHenry 2006; Gomes et al. 2007; Roy et al. 2013); at the base of the skull in 7.6% (Gough 2006); undescended/submandibular in 4–5.4% (Phitayakorn and McHenry 2006; Roy et al. 2013); retropharyngeal in 3.7% (Gomes et al. 2007); lateral to the thyroid gland in 3.7% (Gomes et al. 2007); and at the carotid bifurcation in 1.8% (Wang 1976).

Other rare locations reported in the literature include: the supraclavicular region (Galloway et al. 1996); dorsolateral to the common carotid artery (Libánský et al. 2008); at the posterior triangle of the neck (Udekwu et al. 1987; Herrera et al. 1993; Raffaelli et al. 2000); beside the recurrent laryngeal nerve (Gomes et al. 2007); in the vagus nerve sheath (Nguyen 1999; Yousef et al. 2007); at the hypoglossal nerve (Karvounaris et al. 2010); and in the mucosa of the pyriform sinus (Joseph et al. 1982), the aortopulmonary window (McHenry et al. 1988; Obara et al. 1990; Arnault et al. 2010), the pericardium (Nguyen 1999; Yadav et al. 2010), and the diaphgragm (Saky et al. 2001).

References

Akerström G, Malmaeus J, Bergström R. 1984. Surgical anatomy of human parathyroid glands. *Surgery* 95(1): 14–21.

Arnault V, Beaulieu A, Lifante JC, Sitges Serra A, Sebag F, Mathonnet M, Hamy A, Meurisse M, Carnaille B, Kraimps JL. 2010. Multicenter study of 19 aortopulmonary window parathyroid tumors: the challenge of embryologic origin. *World J Surg* 34(9): 2211–2216.

Cordeiro AC. 1987. Contribuicao para o estudo da morfologia macroscopica das paratireoides em cirurgia e necropsia. Tese de Livre-Docencia, Faculdade de Medicina da Universidade de Sao Paulo, Sao Paulo, p 57.

Fancy T, Gallagher D 3rd, Hornig JD. 2010. Surgical anatomy of the thyroid and parathyroid glands. *Otolaryngol Clin North Am* 43: 221–227.

Galloway A, Jarmer S, Moinuddin S. 1996. Fine needle aspiration cytology of an ectopic parathyroid adenoma: a case report. *Acta Cytol* 40(2): 315–318.

Gilmour JR. 1938. The gross anatomy of the parathyroid glands. *J Pathol Bacteriol* 46: 133.

Gomes EM, Nunes RC, Lacativa PG, Almeida MH, Franco FM, Leal CT, Patrício Filho PJ, Farias ML, Gonçalves MD. 2007. Ectopic and extranumerary parathyroid glands location in patients with hyperparathyroidism secondary to end stage renal disease. *Acta Cir Bras* 22(2): 105–109.

Gough I. 2006. Reoperative parathyroid surgery: the importance of ectopic location and multigland disease. *ANZ J Surg* 76: 1048–1050.

Hamidi S, Soltani A, Hedayat A, Kamalian N. 2006. Primary hyperparathyroidism: a review of 177 cases. *Med Sci Monit* 12(2): CR86–89.

Herrera MF, Reza A, Graeff A, López-Graniel CM, López LH, Angeles A. 1993. Ectopic parathyroid adenoma in the posterior triangle of the neck. *Rev Invest Clin* 45(6): 589–591.

Hojaij F, Vanderlei F, Plopper C, Rodrigues CJ, Jácomo A, Cernea C, Oliveira L, Marchi L, Brandão L. 2011. Parathyroid gland anatomical distribution and relation to anthropometric and demographic parameters: a cadaveric study. *Anat Sci Int* 86(4): 204–212.

Hooghe L, Kinnaert P, Van Geertruyden J. 1992. Surgical anatomy of hyperparathyroidism. *Acta Chir Belg* 92(1): 1–9.

Joseph MP, Nadol JB, Pilch BZ, Goodman ML. 1982. Ectopic parathyroid tissue in the hypopharyngeal mucosa (pyriform sinus). *Head Neck Surg* 5(1): 70–74.

Karvounaris DC, Symeonidis N, Triantafyllou A, Flaris N, Sakadamis A. 2010. Ectopic parathyroid adenoma located inside the hypoglossal nerve. *Head Neck* 32(9): 1273–1276.

Libánský P, Astl J, Adámek S, Nanka O, Pafko P, Spacková J, Foltán R, Sedý J. 2008. Ectopic parathyroid adenoma in child. *Prague Med Rep* 109(2–3): 200–203.

MacCallum WG. 1906. The surgical relations of the parathyroid glands. *Br M J* 2: 1282–1286.

McHenry C, Walsh M, Jarosz H, Henkin R, Tope J, Lawrence AM, Paloyan E, Clark O, Wheeler M, Proye C, Kaplan E. 1988. Resection of parathyroid tumor in the aortopulmonary window without prior neck exploration. *Surgery* 104 (6): 1090–1094.

Mendoza V, Ramírez C, Espinoza AE, González GA, Peña JF, Ramírez ME, Hernández I, Mercado M. 2010. Characteristics of ectopic parathyroid glands in 145 cases of primary hyperparathyroidism. *Endocr Pract* 16(6): 977–981.

Mohebati A, Shaha AR. 2012. Anatomy of thyroid and parathyroid glands and neurovascular relations. *Clin Anat* 25(1): 19–31.

Nanka O, Libánsky P, Sedý J, Pozniak J, Adámek S. 2006. Surgical-anatomical study as a part of operative treatment of primary hyperparathyroidism. *Rozhl Chir* 85(12): 618–623.

Nguyen BD. 1999. Parathyroid imaging with Tc-99m sestamibi planar and SPECT scintigraphy. *Radiographics* 19(3): 601–616.

Numano M, Tominaga Y, Uchida K, Orihara A, Tanaka Y, Takagi H. 1998. Surgical significance of supernumerary parathyroid glands in renal hyperparathyroidism. *World J Surg* 22(10): 1098–1103.

Obara T, Fujimoto Y, Tanaka R, Ito Y, Kodama T, Yashiro T, Kanaji Y, Yamashita T, Fukuuchi A. 1990. Mid-mediastinal parathyroid lesions: preoperative localization and surgical approach in two cases. *Jpn J Surg* 20(4): 481–486.

Pattou FN, Pellissier LC, Noël C, Wambergue F, Huglo DG, Proye CA. 2000. Supernumerary parathyroid glands: frequency and surgical significance in treatment of renal hyperparathyroidism. *World J Surg* 24(11): 1330–1334.

Phitayakorn R, McHenry CR. 2006. Incidence and location of ectopic abnormal parathyroid glands. *Am J Surg* 191(3): 418–423.

Raffaelli M, Defechereux T, Lubrano D, Sadoul JL, Henry JF. 2000. Intravagal parathyroid ectopia. *Ann Chir* 125(10): 961–964.

Roy M, Mazeh H, Chen H, Sippel RS. 2013. Incidence and localization of ectopic parathyroid adenomas in previously unexplored patients. *World J Surg* 37(1): 102–106.

Saky MT, Hasinski S, Rose LI. 2001. Ectopic primary hyperparathyroidism. *Endocr Pract* 7(4): 272–274.

Shen W, Düren M, Morita E, Higgins C, Duh QY, Siperstein AE, Clark OH. 1996. Reoperation for persistent or recurrent primary hyperparathyroidism. *Arch Surg* 131(8): 861–869.

Smith JR, Oates ME. 2004. Radionuclide imaging of the parathyroid glands: patterns, pearls, and pitfalls. *Radiographics* 24(4): 1101–1115.

Standring S. 2008. Head and neck. In: *Gray's Anatomy*, 40th edition. Spain: Churchill Livingstone, Elsevier, pp. 462–465.

Udekwu AO, Kaplan EL, Wu TC, Arganini M. 1987. Ectopic parathyroid adenoma of the lateral triangle of the neck: report of two cases. *Surgery* 101(1): 114–118.

Wang C. 1976. The anatomic basis of parathyroid surgery. *Ann Surg* 183(3): 271–275.

Yadav R, Mohammed TL, Neumann DR, Mihaljevic T, Hoschar A. 2010. Case of the season: ectopic parathyroid adenoma in the pericardium: a report of robotically assisted minimally invasive parathyroidectomy. *Semin Roentgenol* 45(1): 53–56.

Yousef GM, Denic N, Wadhwa J, Chandracanth SA, Smith T, Elms F, Diamandis EP. 2007. Intravagal ectopic parathyroid presenting as vocal cord paralysis: case report and review of the literature. *J Otolaryngol* 36(6): E93–95.

101 Laryngeal cartilages

Arán Pascual-Font and Jose Sanudo
Complutense University of Madrid, Madrid, Spain

This chapter is divided into three sections: the first is dedicated to variations in the major cartilages of the larynx; the second to variations in the supernumerary cartilages; and the third to ossification of the laryngeal cartilages.

Major cartilages

Thyroid cartilage

A very common variation is the foramen thyroideum (Fig. 101.1a). It is situated in the posterosuperior portion of the thyroid lamina, below the superior thyroid tubercle. Its incidence has been reported to be 31% (León et al. 1997). It can appear either unilaterally or bilaterally, and contains vessels and/or nerves passing through the gap (León et al. 1997).

The two halves of the thyroid cartilage can be asymmetric. Most frequently they differ in length or curvature (Fig. 101.1a); less frequent is unilateral agenesis (absence of the superior horn) (Fig. 101.1b) (Maue and Dickson 1971; Garcia-Tapia Urrutia and Fernandez Gonzalez 1999). Asymmetries are not uncommon in the thyroid notch and the craniocaudal dimension of the isthmus, or in the length of the inferior horn.

Greater prominence of the inferior thyroid tubercle has also been described (Keen and Wainwright 1958; Maue and Dickson 1971; Garcia-Tapia Urrutia and Fernandez Gonzalez 1999).

Bilateral asymmetry and poorly defined boundaries are extremely common in the facets (Maue and Dickson 1971). The cricothyroid facets of the thyroid cartilage are absent on at least one side in approximately 20%. In 25%, the facets are flat bilaterally and in 20% they are slightly oval bilaterally. Accessory thyrohyoid ligaments may occur.

The thyroid cartilage can be joined to the hyoid bone by a rigid cartilaginous or bony bridge (8%), making the tip of its superior horn directly continuous with the hyoid bone (Keen and Wainwright 1958).

The thyroid lamina in the infant larynx forms a semicircle, and during growth it becomes angulated. The angle formed

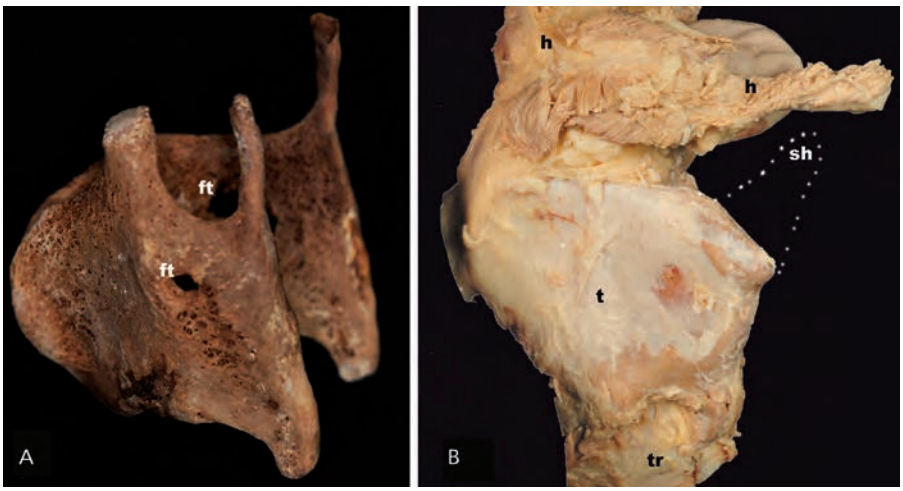

Figure 101.1 A. Lateral view of the thyroid cartilage showing the foramen thyroideum in both sides of the thyroid lamina (ft). B. Lateral view of the larynx showing the unilateral absence of the left superior horn (sh) of the thyroid cartilage (t). Abbreviattions: h, hyoid bone; ft; foramen thyroid; tr, trachea; sh, superior horn.

Bergman's Comprehensive Encyclopedia of Human Anatomic Variation, First Edition. Edited by R. Shane Tubbs, Mohammadali M. Shoja and Marios Loukas.
© 2016 John Wiley & Sons, Inc. Published 2016 by John Wiley & Sons, Inc.

by the union of the lamina is the same in the young male and female populations, but it is bigger in female adults than male adults (Kahane 1978).

During the pubertal period, the cartilaginous structure of the thyroid cartilage grows considerably, making the male thyroid eminence markedly different between adults and young people (Kahane 1978). It is common for one of the superior horns to be shorter than the other, and also common for one to be absent (more frequently on the left side). The vocal cords may be duplicated (Frank and Malev 1939). Hong and Yang (2003) reported a patient with agenesis of the epiglottis and false vocal cords.

Cricoid cartilage

The configuration and arrangement of the posterior lamina is often asymmetrical in orientation and size. This is also true of the position of the superior and lateral facets which can be asymmetric in size or orientation, resulting in anomalous arrangements of the arytenoid cartilages with important functional modifications (Garcia-Tapia Urrutia and Fernandez Gonzalez 1999).

The angle formed by the intersection of lines drawn through the longitudinal axes of the cricoarytenoid facets is very variable (Maue and Dickson 1971). The cricothyroid facets are also variable in size, shape, configuration, and even presence (Maue and Dickson 1971).

A bridge of cartilage joining the lower border of the cricoid cartilage to the first ring of the trachea has been reported on both the right side (20%) and the left side (7%) of the cricotracheal joint (Luschka 1871; Keen and Wainwright 1958).

At birth, the lower border of the cricoid cartilage is located at a level between the second and the third cervical vertebrae. Immediately after birth the larynx descends because of the growth of the vertebral column. At the age of five years, the lower border of the cricoid cartilage is located at the level of the sixth cervical vertebra, reaching the seventh between the ages of 15 and 20 years (Zemlin 1998).

The cricoid cartilage may be bifid posteriorly. Such clefting may be partial or include the posterior cervical trachea (Benjamin 1989).

Arytenoid cartilages

An extraordinary degree of similarity of the human arytenoid cartilages has been described, with noticeable symmetry between right and left sides and in relation to the distances from the apex to the vocal and muscular processes (Maue and Dickson 1971).

The arytenoid cartilages are proportionally larger in the infant than in the adult larynx (Zemlin 1998).

Epiglottis

Asymmetries in the degree of transverse concavity are very frequent. When the depression is very marked its shape resembles the Greek letter omega, omega denoting the epiglottis, very characteristic of the infant's larynx (Garcia-Tapia Urrutia and Fernández González 1999). The epiglottic cartilage may be rudimentary, with duplication of the mucosa substituting for cartilage. A high-rising epiglottis has been described (Alamri and Stringer 2011). The epiglottis may be retroverted (Agada et al. 2007) or bifid (Tsurumi et al. 2010).

Supernumerary cartilages

Cuneiform cartilages (Wrisberg)

They are not always present but when they occur they appear in the quadrangular lamina, the aryepiglottic ligament (Harrison 1995). They are two small elongated pieces of elastic fibrocartilage (Ajmani et al. 1980). They are more common in females (24%) than males (15%) and present frequent changes in their arrangement and size (Ajmani et al. 1980; Garcia-Tapia Urrutia and Fernández González 1999).

They are never present in newborns. They can be identified only after six months of life (Harrison 1995).

Corniculate cartilages (Santorini)

They appear articulated with the apex of the arytenoid cartilage as a conical nodule of elastic fibrocartilage (Ajmani et al. 1980; Harrison 1995). They are not always present, being absent more often in males than females (Ajmani et al. 1980).

Triticeal cartilages

This is not constant, being present more often in females (9.5%) than in males (7%) (Ajmani et al. 1980). Tubbs et al. (2010) identified triticeal cartilages in 51% of specimens and found it to be hyaline in nature. The cartilages may be ossified (Grossman 1945). The triticeal cartilage was located in the upper, middle, and lower third of the thyrohyoid membrane in 14%, 66%, and 20% of sides, respectively. Regardless of the position of the triticeal cartilage within the thyrohyoid membrane, the internal laryngeal nerve crossed directly over the triticeal cartilage on 59% of sides. Di Nunno et al. (2004) identified triticial cartilages in 12 (30%), they were bilateral in 7 (17.5%), and monolateral in 5 (12.5%). These cartilages were more frequent in men (8 out of 26, 31%) than in women (4 out of 14, 28.5%).

Interarytenoid cartilage

This cartilage can be rarely found between the two arytenoid cartilages inside the ligament and is termed jugal or interarytenoid, extending between the superior border of the cricoid and the two arytenoid cartilages (Luschka 1871). This cartilage may be the same as the cartilage of Seiler.

Posterior sesamoid cartilages

These cartilages appear irregularly in both males and females. They are located in the prolongation of the vocal process of the arytenoid cartilage inside the vocal ligament (Luschka 1871).

Anterior sesamoid cartilages

They appear irregularly as a cartilaginous nodule, variable in size, at the anterior end of the vocal folds related to the anterior commissure (Luschka 1871).

Ossification of the laryngeal cartilages

Ossification within the human larynx is often considered a degenerative process of the hyaline cartilage associated with age (Harrison 1995). Ossification has been described in the thyroid, cricoid, arytenoids, and triticeal cartilages, with higher frequency in males than in females (Roncallo 1948; Keen and Wainwright 1958; Ajmani et al. 1980; Munir and Hogg 1993; Strek et al. 1993). The areas where ossification begins are near the points subject to particular loads (Roncallo 1948; Strek et al. 1993).

Thyroid ossification invariably begins at the posterior border near the root of the inferior horn, then spreads to the midline and extends upward to the upper and posterior part of the thyroid lamina; some windows of unossified cartilage remain (Keen and Wainwright 1958; Ajmani et al. 1980; Munir and Hogg 1993; Harrison 1995).

Cricoid ossification begins at the upper border of the posterior plate, spreads along the superior margin and reaches the anterior part of the arch (Keen and Wainwright 1958; Ajmani et al. 1980; Munir and Hogg 1993; Harrison 1995).

Ossification of the arytenoids starts in the muscular process and spreads to the base (Keen and Wainwright 1958; Ajmani et al. 1980; Munir and Hogg 1993; Harrison 1995).

Ossification of the laryngeal cartilages commences between the ages of 25 and 40 years in the thyroid cartilage, then in the cricoid and in the arytenoids (Keen and Wainwright 1958). The cartilages can be completely converted to bone by the age of 65 years (Ajmani et al. 1980).

References

Agada FO, Coatesworth AP, Grace AR. 2007. Retroverted epiglottis presenting as a variant of globus pharyngeus. *J Laryngol Otol* 121: 390–392.

Ajmani ML, Jain SP, Saxena SK. 1980. A metrical study of laryngeal cartilages and their ossification. *Anat Anz* 148: 42–48.

Alamri Y, Stringer MD. 2011. A high-rising epiglotis: a benign anatomical variant. *Clin Anat* 24: 652–654.

Benjamin B. 1989. Minor congenital laryngeal clefts: diagnosis and classification. *Ann Otol Rhinol Laryngol* 98: 417–420.

Di Nunno N, Lombardo S, Costantinides F, Di Nunno C. 2004. Anomalies and alterations of the hyoid–larynx complex in forensic radiographic studies. *Am J Forensic Med Pathol* 25: 14–19.

Frank DI, Malev M. 1939. Double vocal cords Arch. *Otolaryngol* 29: 713–729.

Garcia-Tapia Urrutia R, Fernandez Gonzalez S. 1999. Anatomía y fisiologia del sistema fonatorio. In Suarez C, Gil-Carcerdo LM, Medina J, Ortega P, Trinidad J. Tratado de Otorrinolaringologia y Cirugia de Cabeza y Cuello. Madrid: Proyectos Medicos SL, pp. 1801–1835.

Grossman JW. 1945. The triticeous cartilages. *Am J Roentgenol Radium Ther* 53: 166–170.

Harrison DFN. 1995. *The Anatomy and Physiology of the Mammalian Larynx*. Cambridge University Press, Cambridge, pp. 56–87.

Hong KH, Yang YS. 2003. Agenesis of the epiglottis and false vocal cords with maxillary hypoplasia in an adult. *J laryngol Otol* 117: 895–898.

Kahane J. 1978. A morphological study of the human prepubertal and pubertal larynx. *Am J Anat* 151: 11–20.

Keen JA, Wainwright J. 1958. Ossification of the thyroid, cricoid and arytenoid cartilages. *S Afr J Lab Clin Med* 4: 83–108.

León X, Maranillo E, Mirapeix RM, Quer M, Sañudo JR. 1997. Foramen thyroideum: a comparative study in embryos, fetuses, and adults. *Laryngoscope* 107: 1146–1150.

Luschka H. 1871. *Der Kehlkopf des Menschen*. Tübingen: H. Laupp, pp. 63–89.

Maue WM, Dickson DR. 1971. Cartilages and ligaments of the adult human larynx. *Arch Otolaryngol* 94: 432–439.

Munir L, Hogg DA. 1993. Age changes in the human laryngeal cartilages. *Clin Anat* 6: 154–162.

Roncallo P. 1948. Researches about ossification and conformation of the thyroid cartilage in men. *Acta Otolaryngol* 36: 110–34.

Strek P, Skawina A, Petri M, Olszewski E, Nowogrodzka-Zagórska M, Waloch J. 1993. The investigations of mechanical properties of ossificating thyroid cartilages of the human larynx. *Folia Morphol(Warsz)* 52: 39–46.

Tsurumi H, Ito M, Ishikura K, Hataya H, Ikeda M, Honda M, Nishimura G. 2010. Bifid epiglottis: syndromic constituent rather than isolated anomaly. *Pediatr Int* 52: 723–728.

Tubbs RS, Dixon JF, Loukas M, Shoja MM, Cohen-Gadol AA. 2010. Relationship between the internal laryngeal nerve and the triticeal cartilage: a potentially unrecognized compression site during anterior cervical spine and carotid endarterectomy operations. *Neurosurgery* 66: 187–190.

Zemlin WR. 1998. *Speech and Hearing Science: Anatomy and Physiology*, fourth edition. Needham Heights, MA: Allyn and Bacon.

102 Trachea

Koichi Watanabe
Kurume University School of Medicine, Fukuoka, Japan

Morphological variations of the trachea may be congenital or acquired. Various degrees of congenital deficits of the trachea have been reported. Absence of the trachea involves a defect of a certain length of the trachea and is considered to be caused by a deficit of the entire tracheal ring. However, tracheal stenosis does not involve a deficit of the trachea, but is characterized by a narrowing of the trachea secondary to a defect of the membranous wall and is considered to be a partial deficit of the tracheal wall. The tracheal bronchus, a positional abnormality of a bronchus, has also been reported. The tracheal bronchus may be classified as a supranumerary or displaced bronchus. In addition, the congenital tracheal diverticulum is considered to be a vestigial supranumerary bronchus. One type of acquired tracheal diverticulum results from increased intratracheal pressure.

Absence of the trachea

Various degrees of congenital aplasia of the trachea have been reported. The first case of tracheal agenesis was reported by Payne in 1900. Holinger estimated the incidence of tracheal agenesis to be approximately 1 in 50,000 live births among patients admitted to a hospital (Holinger et al. 1952; Haben et al. 2002). The male:female ratio is 2:1 (Weil 1991; Haben et al. 2002). In 2000, van Veenendaal et al. reported that at least 86 cases had been described in the literature until the year 2000, and he added three cases to his article. The most commonly used classification was proposed by Floyd et al. in 1962, who classified tracheal agenesis into the following three types:

- Type 1 is agenesis of the proximal trachea with a normal short segment of the distal trachea and the presence of a tracheoesophageal fistula.
- Type 2 is agenesis of the entire trachea with normal main bronchi fused at the midline of the carina.
- Type 3 is complete agenesis of the trachea with the bilateral main bronchi arising separately from the esophagus.

Among them, type 2 is the most frequently occurring type. The incidence of each type is 13%, 65%, and 22%, respectively (Koltai and Quiney 1992). However, some anomalies do not fit into this classification (Faro et al. 1979) (Fig. 102.1). Type 2 tracheal agenesis without tracheoesophageal communication (Milles and Dorsey 1950; Mar and Essex 1997) and total tracheopulmonary agenesis (Morrison 1949; Devi and Moore 1966) have also been reported. Based on these unclassified cases, Faro et al. (1979) reported a new classification system comprising six types (types A–G). Furthermore, Fraser et al. (2005) reported extremely rare cases of tracheal agenesis with laryngeal atresia, a tracheoesophageal fistula at the proximal end of the trachea, and an interposing distal trachea and bronchi between a divided esophagus. Most of these patients died a short time after birth.

Tracheal agenesis is usually associated with other anomalies. Up to 94% of patients with tracheal agenesis reportedly have other congenital anomalies (Evans et al. 1999; Van Veenendaal et al. 2000; Felix et al. 2006). Cardiovascular anomalies are the most frequently associated, with an incidence of 69% (Felix et al. 2006). The respiratory tract distal to the trachea (47–50%), the gastrointestinal tract (47–50%), the genitourinary tract (35–49%), the musculoskeletal system (19–38%), and the nervous system (7%) have also been reported to be associated with tracheoesophageal fistulas (Evans et al. 1999; Van Veenendaal et al. 2000; Felix et al. 2006). Moreover, tracheoesophageal fistulas may be associated with VACTERL, which includes vertebral defects, anal atresia, cardiac anomalies, tracheoesophageal fistula, renal anomalies, and limb defects (Milstein et al. 1985), or TACRAD (tracheal agenesis or laryngotracheal atresia, cardiac abnormalities, radial ray defects, and duodenal atresia) (Evans et al. 1985; Diaz et al. 1989; Hiyama 1994; Van Veenendaal et al. 2000).

Congenital tracheal stenosis

Congenital tracheal stenosis is a rare anomaly, and fewer than 70 cases had been described up to 1994 (Hoffer et al. 1994). The incidence in the general population is unclear, but Benjamin et al. reported 21 cases among 70,000 patients admitted to the hospital (Benjamin et al. 1980; Phipps et al. 2006). Several

Bergman's Comprehensive Encyclopedia of Human Anatomic Variation, First Edition. Edited by R. Shane Tubbs, Mohammadali M. Shoja and Marios Loukas.
© 2016 John Wiley & Sons, Inc. Published 2016 by John Wiley & Sons, Inc.

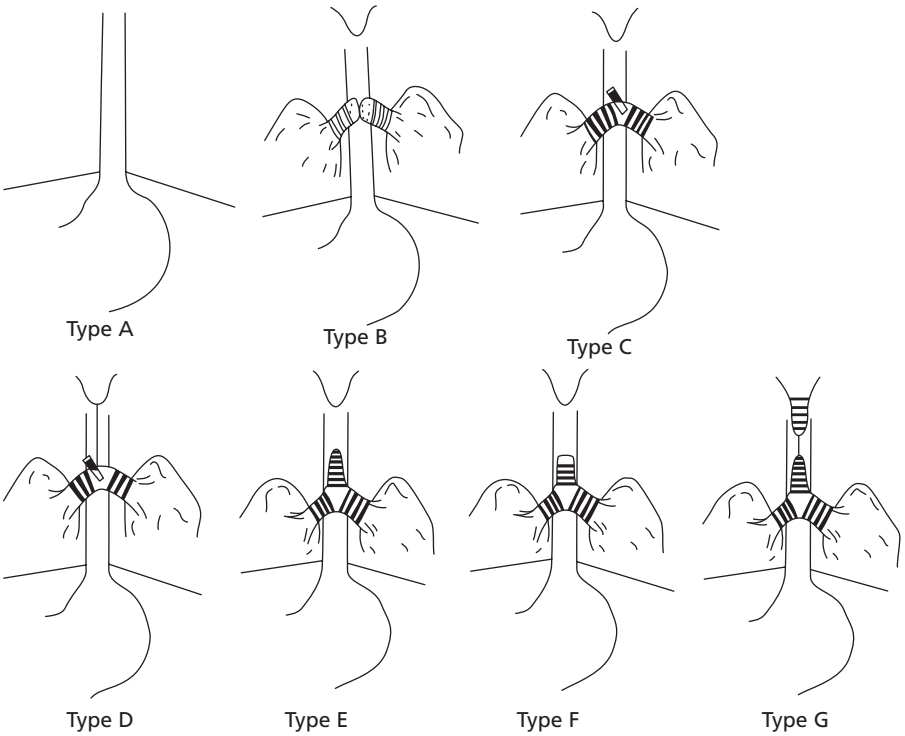

Figure 102.1 Classification of tracheal agenesis: Type A, total pulmonary agenesis; Type B, tracheal agenesis in which the main bronchi arise directly from the esophagus (corresponding to Type III in Floyd's classification); Type C, tracheal agenesis in which there are fused main bronchi with bronchoesophageal fistula (corresponding to Type II in Floyd's classification); Type D, tracheal agenesis in which the larynx is joined to the distal trachea through an atretic strand and a tracheoesophageal fistula is present; Type E, upper tracheal agenesis in which there is a direct tracheoesophageal communication (corresponding to Type I in Floyd's classification); Type F, tracheal agenesis in which there is a blind bronchial bifurcation and no esophageal communication; and Type G, short segment tracheal agenesis.

Source: Faro et al. (1979). Reproduced with permission from Elsevier.

classifications have been proposed. As a representative classification, Wolman (1941) classified congenital tracheal stenosis into two groups: type A, characterized by a short segment of stenosis comprising one or two cartilages; and type B, characterized by stenosis involving the larger part of the trachea. In addition, Cantrell and Guild (1964) classified congenital tracheal anomaly into three morphological types: generalized hypoplasia; funnel-like stenosis; and segmental stenosis (Fig. 102.2). Generalized hypoplasia is defined by narrowing of the entire trachea with cartilaginous rings. In funnel-like stenosis, the upper portion of the trachea is normal but becomes narrower toward the level of the carina. The membranous wall of the trachea is partially absent with fusion of the tracheal cartilage in a portion of the stenotic area. In segmental stenosis, a portion of the trachea at any level is narrowed in an hourglass fashion. The cartilage forms complete rings at the site of the stenosis. The length of the stenosis varies over the range 1–5 cm; most cases are approximately 2 cm.

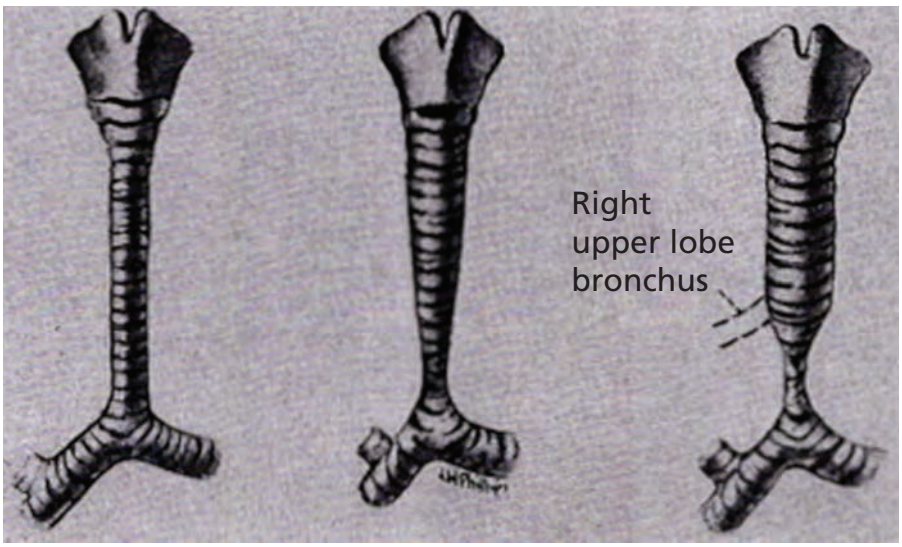

Figure 102.2 Classification of congenital tracheal stenosis. Congenital tracheal stenosis was classified into three types: generalized hypoplasia, funnel-like stenosis, and segmental stenosis.

Source: Cantrell and Guild (1964). Reproduced with permission from Elsevier.

Two major causes of tracheal stenosis have been reported. It usually occurs for no obvious reason, but in some cases it results from the external force produced by a congenital cardiovascular anomaly. In particular, it has been reported that an aberrant pulmonary artery (pulmonary artery sling) running between the esophagus and trachea may cause tracheal stenosis and was observed in 30–50% of patients (Cohen and Landing 1976; Berdon et al. 1984; Hoffer et al. 1994; Koopman et al. 2004; Phipps et al. 2006).

Other associated anomalies, such as pulmonary, cardiovascular, and gastrointestinal anomalies, have also been reported (Cantrell and Guild 1964). Pulmonary anomalies including an unusual origin of the major bronchi (Evans 1949), the entire right bronchial tree arising from the left main bronchus (Holinger et al. 1950), aplasia of the right lung (Putney and Baltzell 1952), and abnormal lobulation (Weber 1952; Cantrell and Guild 1964) have been reported. Reported cardiovascular anomalies include ventricular septal defect (Montandon 1944), persistent truncus arteriosus (Holinger et al. 1950), and atrial septal defect (Houston and Mackie 1961). Anomalies of the extremities include clubfoot (Guisez 1927), congenital absence of the thumb (Haardt 1938), and pectus excavatum. Finally, gastrointestinal anomalies may include Meckel's diverticula (Haardt 1938), intestinal stenosis (Lerro 1935), imperforate anus (Houston and Mackie 1961), and abnormal lobulation of the liver (Haardt 1938).

Tracheal diverticulum

A tracheal diverticulum is defined as a sac that protrudes outward from the trachea. It was first described by Rokitansky in 1838. The incidence is reportedly about 1–3.7% in autopsy studies and among image diagnoses (MacKinnon 1953; Goo et al. 1999; Buterbaugh and Erly 2007). Clinically, it is diagnosed as a paratracheal air cyst and it contains cysts both with and without tracheal communication. Approximately 98% of tracheal air cysts are located in the right paratracheal region. Tracheal communications were found in 8–35% of cases on imaging diagnosis (Goo et al. 1999; Buterbaugh and Erly 2007). Both congenital and acquired factors affect the occurrence, location, and form of tracheal diverticula, and the wall compositions differ among the types of diverticula (Soto-Hurtado et al. 2006).

Congenital diverticula are very rare and generally occur in the right part of the trachea 4–5 cm below the vocal cords or a few centimeters above the carina. They are small, and communication with the trachea is narrow. The wall of the diverticula includes all layers of the normal tracheal wall: respiratory epithelium, smooth muscle, and cartilage. It is presumed that the diverticular wall is a remnant of supernumerary lung tissues (Frenkiel et al. 1979). Associations with bronchomalacia (Early and Bothwell 2002) and cystic adenomatoid malformation of the lung (Restrepo 2004) have been reported.

Acquired diverticula may be observed at any level of the trachea. However, they are more common in the posterolateral region of the trachea at the thoracic inlet (Soto-Hurtado et al. 2006). Acquired diverticula are larger than congenital diverticula and have a wide opening to the trachea. The wall consists of respiratory epithelia only and lacks smooth muscle and cartilage. It is generally said that increases in the intraluminal pressure caused by chronic coughing or chronic obstructive pulmonary disease result in the development of acquired diverticula (Frenkiel et al. 1979; Goo et al. 1999).

Tracheal bronchus

A tracheal bronchus is defined as an abnormal bronchus arising directly from the lateral wall of the trachea. Sandifort first described the tracheal bronchus in 1785 (Aoun et al. 2004). The incidence of the tracheal bronchus is reportedly 0.001–2% in bronchoscopic, autopsy, and radiographic examinations (Doolittle and Mair 2002). It is more common in male than female patients (Aoun et al. 2004). The tracheal bronchus is usually observed in the right wall of the trachea 2 cm above the carina. However, it can be located anywhere between the cricoid cartilage and the carina, and cases of a tracheal bronchus arising from the left wall of the trachea have also been reported (Ghaye et al. 2001). However, the tracheal bronchus occurs in the right wall of the trachea in most cases.

The tracheal bronchus is classified as either supranumerary or displaced (Fig. 102.3). A supranumerary tracheal bronchus is an extra bronchus, despite the fact that the lung contains normal bronchi and lobes. Congenital tracheal diverticula and cysts, which are thought to be remnants of supranumerary bronchi,

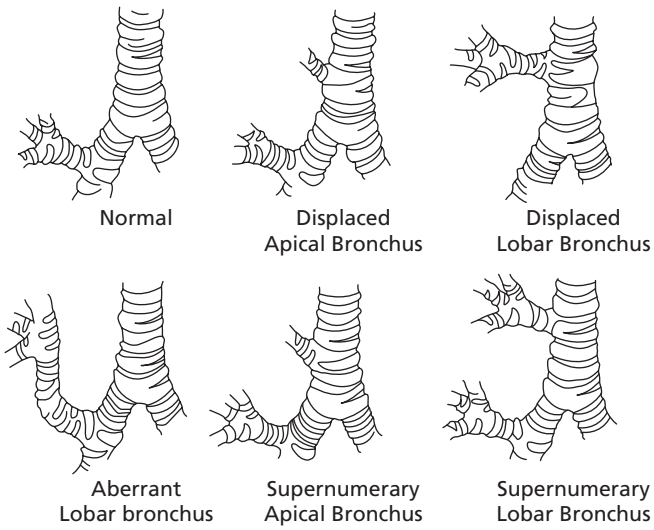

Figure 102.3 Anatomical variations of right upper lobe bronchus.

Source: McLaughlin et al. (1985). Reproduced with permission from Elsevier.

were also recently assigned to this category. Supranumerary tracheal bronchi can be either extralobar or intralobar, depending on whether they share pleura with the upper lobe.

A displaced bronchus arises from the trachea and aerates a normal lung lobe or segment. A displaced bronchus that aerates the whole right upper lobe is called a true tracheal bronchus and occurs at an incidence of 0.2% (Ghaye et al. 2001). The apical lobe is most frequently associated with a tracheal bronchus that aerates a lung segment and is called an apical tracheal bronchus (Barat and Konrad 1987).

The tracheal bronchus is often associated with other anomalies such as rib anomalies, vertebral anomalies, Down syndrome, duodenal webs, laryngeal webs, pectus excavatum, esophageal atresia, VATER associations, Klippel-Feil syndrome, and hypoplastic lungs (McLaughlin et al. 1985; Aoun et al. 2004).

References

Aoun NY, Velez E, Kenney LA, Trayner EE. 2004. Tracheal bronchus. *Resp Care* 49: 1056–1058.

Barat M, Konrad HR. 1987. Tracheal bronchus. *Am J Otolaryngol* 8: 118–122.

Benjamin B, Pitkin J, Cohen D. 1980. Congenital tracheal stenosis. *Ann Otol Rhinol Laryngol* 90(4 Pt 1): 364–371.

Berdon WE, Baker DH, Wung JT, Chrispin A, Kozlowski K, De Silva M, Alford B. 1984. Complete cartilage-ring tracheal stenosis associated with anomalous left pulmonary artery: the ring-sling complex. *Radiol* 152: 57–64.

Buterbaugh JE, Erly WK. 2008. Paratracheal air cysts: a common finding on routine CT examinations of the cervical spine and neck that may mimic pneumomediastinum in patients with traumatic injuries. *AJNR* 29: 1218–1221.

Cantrell JR, Guild HG. 1964. Congenital stenosis of the trachea. *Am J Surg* 108: 297–305.

Cohen SR, Landing BH. 1976. Tracheostenosis and bronchial abnormalities associated with pulmonary artery sling. *Ann Otol Rhinol Laryngol* 85: 582.

Devi B, More JRS. 1966. Total tracheopulmonary agenesis associated with asplenia, agenesis of umbilical artery and other anomalies. *Acta Paediatr Scand* 55: 107–116.

Diaz EM Jr, Adams JM, Hawkins HK, Smith RJ. 1989. Tracheal agenesis: a case report and literature review. *Arch Otolaryngol Head Neck Surg* 115: 741.

Doolittle AM, Mair EA. 2002. Tracheal bronchus: classification, endoscopic analysis, and airway management. *Otolaryngol Head Neck Surg* 126: 240–243.

Early EK, Bothwell MR. 2002. Congenital tracheal diverticulum. *Otolaryngol Head Neck Surg* 127: 119–121.

Evans JA, Reggin J, Greenberg C, Opitz JM, Reynolds JF. 1985. Tracheal agenesis and associated malformations: a comparison with tracheoesophageal fistula and the VACTERL association. *Am J Med Gen* 21: 21–34.

Evans JA, Greenberg CR, Erdile L. 1999. Tracheal agenesis revisited: analysis of associated anomalies *Am J Med Genet* 82: 415–422.

Evans WA Jr. 1949. Congenital obstructions of the respiratory tract; tracheal malformations. *Am J Roentgenol Rad Ther* 62: 167–176.

Faro RS, Goodwin CD, Organ CH, Hall RT, Holder TM, Ashcraft KW, Amoury RA. 1979. Tracheal agenesis. *Ann Thorac Surg* 28: 295–299.

Felix JF, van Looij MA, Pruijsten RV, de Krijger RR, de Klein A, Tibboel D, Hoeve HL. 2006. Agenesis of the trachea: phenotypic expression of a rare cause of fatal neonatal respiratory insufficiency in six patients. *Internatiol J Pediatr Otorhinolaryngol* 70: 365–370.

Floyd J, Campbell Jr DC, Dominy DE. 1962. Agenesis of the trachea. *Am Rev Resp Dis* 86: 557.

Fraser N, Stewart RJ, Grant J, Martin P, Gibbin KP, Padfield CJH. 2005. Tracheal agenesis with unique anatomy. *J Pediatr Surg* 40: e7–e10.

Frenkiel S, Assimes IK, Rosales JK. 1979. Congenital tracheal diverticulum. A case report. *Ann Otol Rhinol Laryngol* 89: 406–408.

Ghaye B, Szapiro D, Fanchamps JM, Dondelinger RF. 2001. Congenital bronchial abnormalities revisited. *Radiographics* 21: 105–119.

Goo JM, Im JG, Ahn JM, Moon WK, Chung JW, Park JH, Han MC. 1999. Right paratracheal air cysts in the thoracic inlet: clinical and radiologic significance. *AJR* 173: 65–70.

Haardt W. 1938. Ueber angeborene Enge der Luftröhre. *Wien Kiln Webnscbr* 51: 657.

Haben CM, Rappaport JM, Clarke KD. 2002. Tracheal agenesis. *J Am Coll Surg* 194(2): 217–222.

Hiyama E, Yokoyama T, Ichikawa T, Matsuura Y. 1994. Surgical management of tracheal agenesis. *J Thorac Cardiovas Surg* 108: 830.

Hoffer ME, Tom LW, Wetmore RF, Handler SD, Potsic WP. 1994. Congenital tracheal stenosis: the otolaryngologist's perspective. *Arch Otolaryngol Head Neck Surg* 120: 449.

Holinger PH, Johnston KC, Basinger CE. 1950. Benign stenosis of the trachea. *Ann Otol Rhinol Laryngol* 59: 837–859.

Holinger PH, Johnston KC, Parchet VN, Zimmermann AA. 1952. Congenital malformations of the trachea, bronchi and lung. *Trans Ann Meet Am Bronchoesophagol Assoc* 58: 67–88.

Houston IB, Mackie DG. 1961. Congenital tracheal stenosis. *Thorax* 16: 94–96.

Koopman JP, Bogers AJJC, Witsenburg M, Lequin MH, Tibboel D, Hoeve LJ. 2004. Slide tracheoplasty for congenital tracheal stenosis. *J Pediatr Surg* 39: 19–23.

Guisez J. 1927. Malformation congénitale de la trachée. *Bull d'Oto-Rhino-Laryngol* 25: 289.

Koltai PJ, Quiney R. 1992. Tracheal agenesis. *Ann Otol Rhinol Laryngol* 101: 560–566.

Lerro E. 1935. Un caso di stridore congenito da stenosi tracheale. *Pediatria* 43: 440.

MacKinnon D. 1953. Tracheal diverticula. *J Pathol Bacteriol* 65: 513–517.

Mar S, Essex C. 1997. Type 2 tracheal agenesis without tracheoesophageal fistula. *Int J Pediatr Otorhinolaryngol* 39: 159–161.

McLaughlin FJ, Strieder DJ, Harris GBC, Vawter GP, Eraklis AJ. 1985. Tracheal bronchus: association with respiratory morbidity in childhood. *J Pediatr* 106: 751–755.

Milles G, Dorsey DB. 1950. Intra-uterine respiration-like movements in relation to development of the fetal vascular system: a discussion of intra-uterine physiology based upon cases of congenital absence of the trachea, abnormal vascular development, and other anomalies. *Am J Pathol* 26: 411–425.

Milstein JM, Lau M, Bickers RG. 1985. Tracheal agenesis in infants with VATER association. *Arch Pediatr Adol Med* 139: 77.

Montandon A. 1944. Sténose congénitale de la trachée et malformations associées. *Practica Oto Rhino Laryngol* 6: 179–191.

Morrison JE. 1949. Congenital malformation in one of monozygotic twins. *Arch Dis Child* 24: 214.

Payne WA. 1900. Congenital absence of the trachea. *Brooklyn Med J* 14: 568.

Phipps LM, Raymond JA, Angeletti TM. 2006. Congenital tracheal stenosis. *Crit Care Nurse* 26: 60–69.

Putney FJ, Baltzell WH. 1952. Agenesis of the lung with tracheal stenosis; case report. *The Ann Otol Rhinol Laryngol* 61: 677–680.

Restrepo S, Villamil MA, Rojas IC, Lemos DF, Echeverri S, Triana G, Angarita M. 2004. Association of two respiratory congenital anomalies: tracheal diverticulum and cystic adenomatoid malformation of the lung. *Pediatr Radiol* 34: 263–266.

Soto-Hurtado EJ, Peñuela-Ruíz L, Rivera-Sánchez I, Torres-Jiménez J. 2006. Tracheal diverticulum: a review of the literature. *Lung* 184: 303–307.

Van Veenendaal MB, Liem KD, Marres HAM. 2000. Congenital absence of the trachea. *Europ J Pediatr* 159: 8–13.

Weber HW. 1952. Uber kongenitale trachealstenosen. *Zentralbl Allg Path* 89: 148.

Weil RJ. 1991. Pathologic quiz case 1. Tracheal agenesis (TA) (Floyd's type II). *Arch Otolaryngol Head Neck Surg* 117: 804.

Wolman IJ. 1941. Congenital stenosis of the trachea. *Arch Pediatr Adol Med* 61: 1263.

103 Lungs

Koichi Watanabe
Kurume University School of Medicine, Fukuoka, Japan

Two types of anatomical variations of lung fissures have been identified: morphological variation of normal lung fissures (right horizontal fissure and bilateral oblique fissures); and supernumerary fissures that do not exist normally. The depth of normal lung fissures varies widely from complete to less than half separation in some cases. Supernumerary fissures such as the superior accessory fissure, the medial basal fissure, the left horizontal fissure, and the azygos fissure form supernumerary lobes.

Developmental arrest causes hypoplasia or aplasia of the lung. It occurs in various degrees from hypoplasia of a lobe to agenesis of entire bilateral lungs. Cardiovascular anomalies are often associated with this and can be lethal.

Lung sequestration describes part of lung which is separated from the normal bronchial tree and has an anomalous blood circulation system. Lung sequestration is classified into either extralobar or intralobar types, whether abnormal tissue is separated from the surrounding lung parenchyma or not.

The bronchial tree also has many variations. Most of the lobar and segmental bronchi have varied branching patterns. In addition, supernumerary or lack of bronchus is also observed occasionally.

Horizontal (minor) and oblique (major) fissures

Many classifications of the degree of lung fissure have been reported. Medlar (1947) observed 1200 pairs of lungs and classified the condition of fissures into three levels: complete, over half complete, and less than half complete to no fissure. Another comprehensive review by Yamashita (1978) investigated 140 specimens and reported a more detailed classification system. Lung fissures were classified by considering the shape and rates of fixed parts. For example, the right horizontal fissure was classified into 10 patterns (Fig. 103.1a), the right oblique fissure was classified into 13 patterns (Fig. 103.1b), and the left oblique fissure was classified into 12 patterns (Fig. 103.1c).

According to Medlar (1947), the proportion of the right oblique fissure was: complete 69.6%, over half complete 25.6%, and less than half complete 4.8%. The proportion of the right horizontal fissure was: complete 37.7%, over half complete 17.1%, and less than half complete 45.2%.The proportion of the depth of the left oblique fissure was: complete 82.1%, over half complete 10.6%, and less than half complete 7.3%. These results showed that bilateral oblique fissures occurred with a high rate (left 82%, right 69%) of complete separation, whereas right horizontal fissures accounted for approximately 40% of complete separation.

Supernumerary fissures

Supernumerary fissures form supernumerary lobes, which are found incidentally and often do not cause symptoms (Fig. 103.2). The superior accessory fissure can be observed in either the right or left lower lobe and forms a dorsal lobe (superior accessory lobe). A medial basal fissure observed in the right or left lower lobe forms a cardiac lobe. A left horizontal fissure observed in the left upper lobe forms a left middle lobe, similar to the right lung. This lobe is sometimes associated with asplenia. However, the azygos lobe is formed by extrinsic vessels (abnormal azygos vein), and can be observed in the right and/or left upper lobe.

Superior accessory fissure (dorsal lobe, superior accessory lobe)

This fissure divides the superior segment of the right or left lower lobe from the remaining lower lobe, and forms a supernumerary lobe called the "dorsal lobe." It is also called the "dorsal lobe of Nelson" or "lobe of Nelson and Fowler" or "superior accessory lobe." According to a report by Dévé (1900), this lobe was observed on the right in 22%, on the left in 8.7%, and bilaterally in 7% of the general population. Langlois and Henderson (1980) reported that this fissure was present on the right in 17.5% and on the left in 2% of cases. In both reports, the frequency of both sides of the fissure was somewhat different, but that of the right lung was higher than the left lung. Boyden (1955) reported that this fissure did not necessarily correspond to intersegmental planes. Ferry and Boyden (1951) reported a case where the

Bergman's Comprehensive Encyclopedia of Human Anatomic Variation, First Edition. Edited by R. Shane Tubbs, Mohammadali M. Shoja and Marios Loukas.
© 2016 John Wiley & Sons, Inc. Published 2016 by John Wiley & Sons, Inc.

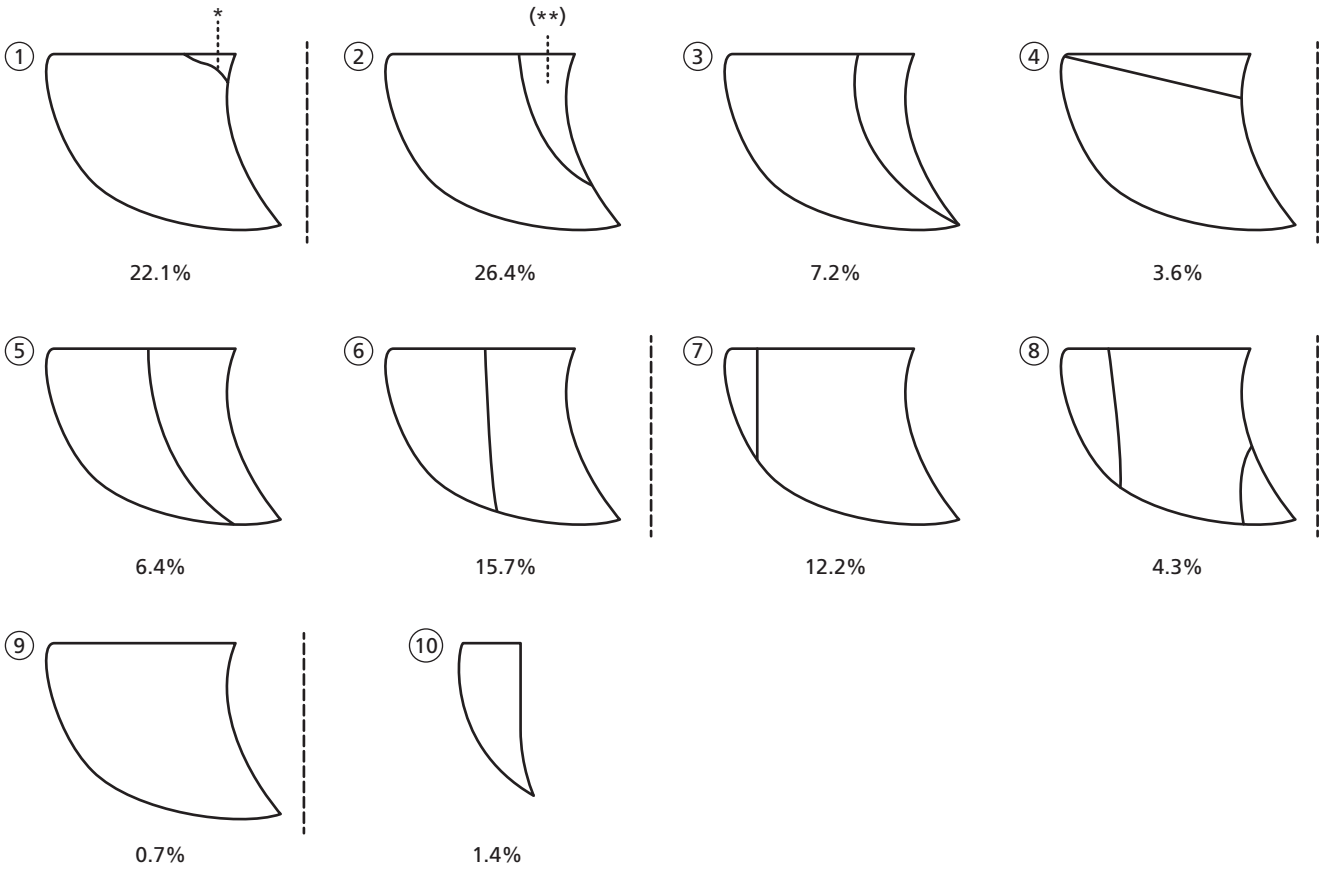

Figure 103.1 Classification of the fissure. (a) Degree of right horizontal fissure. *Root of bronchovascular trees of the middle lobe; **site of fusion with the right upper lobe.

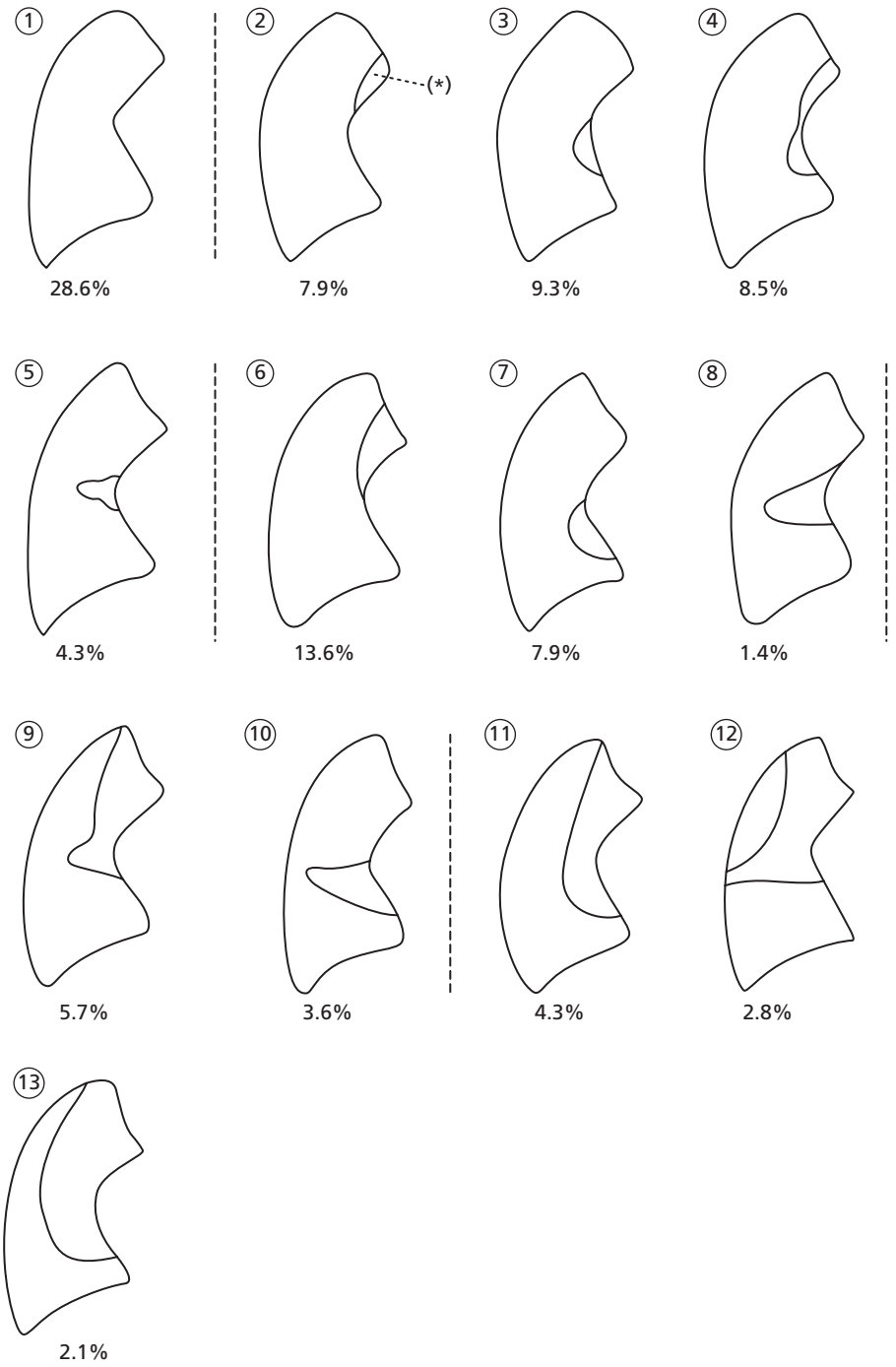

Figure 103. (b) Degree of right oblique fissure. *Site of fusion with the right upper and middle lobes.

(continued)

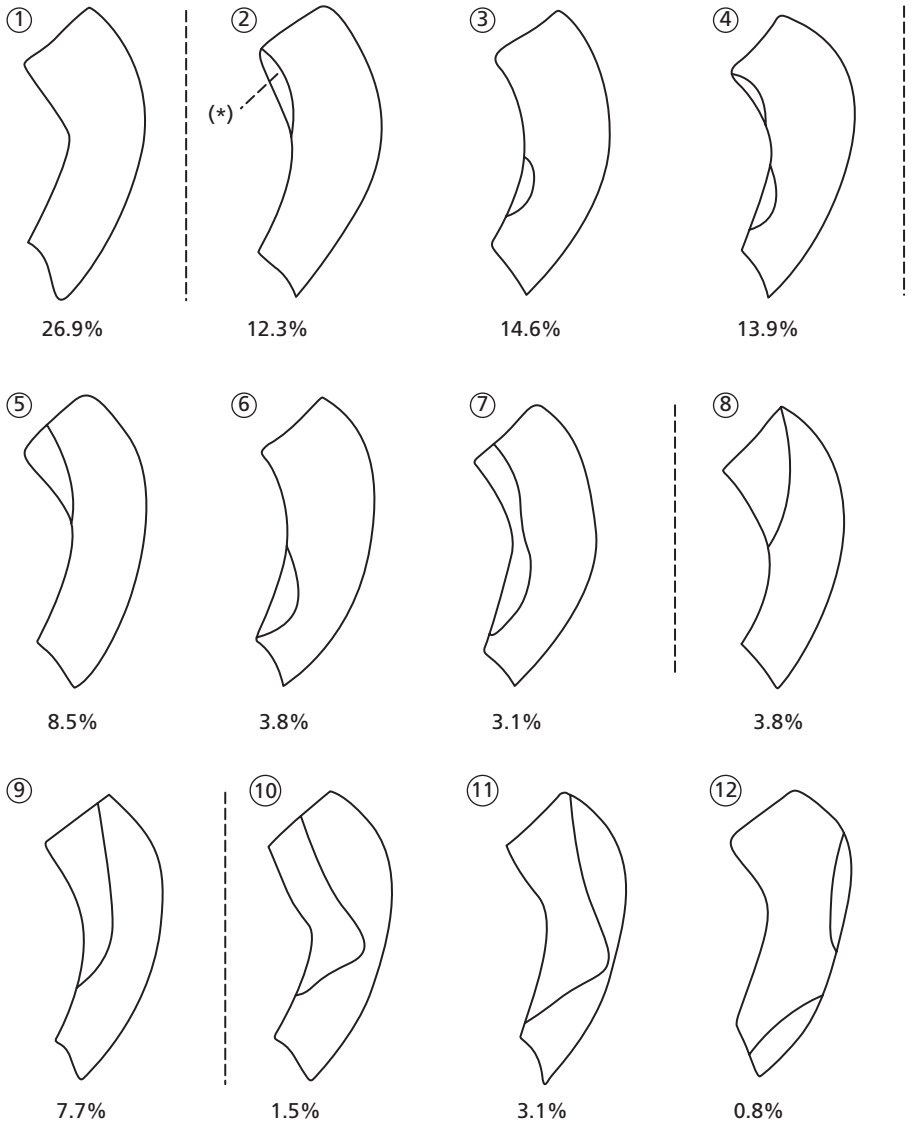

Figure 103.1 *(continued)* (c) Degree of left oblique fissure. *Site of fusion with the left upper lobe.

Source: Yamashita (1978).

fissure developed not between superior and sub-superior segments but between sub-superior and lateral basal zones.

Medial basal fissure (cardiac lobe, infracardiac lobe)

The medial basal fissure is located between the medial basal segment (B8) and anterior basal segment (B7) of the lower lobe, and divides the media basal segment from the remaining lower lobe. This divided segment is called the "cardiac lobe" or "infracardiac lobe." The frequency of this fissure has been reported as 10–45% (Schaffner 1898; Dévé 1900; Smith and Boyden 1949; von Hayak 1960). It was reported that this lobe is normally observed in animals. This fissure is often observed in the right lung; however, it may also be rarely found in the left lung. Trapnell (1973) reported a frequency in the left side of 0.3% and a frequency in the right side of 11%. A study by Langlois and Henderson (1980) reported that the fissure frequency was 10% for the right side and 18.3% for the left side.

Left horizontal fissure (left middle lobe)

This fissure subdivides the left upper lobe into two portions, with the lower part termed the "left middle lobe." Boyden (1955) classified the left middle lobe divided by this fissure into four types: (1) a true middle lobe separating normal upper and lower division segments; (2) a compressed lingular; (3) an expanded lingular; and (4) an ectopic pulmonary type that always separates the sector of an eparterial bronchus from the left upper lobe. The frequency of this lobe varies between reports and

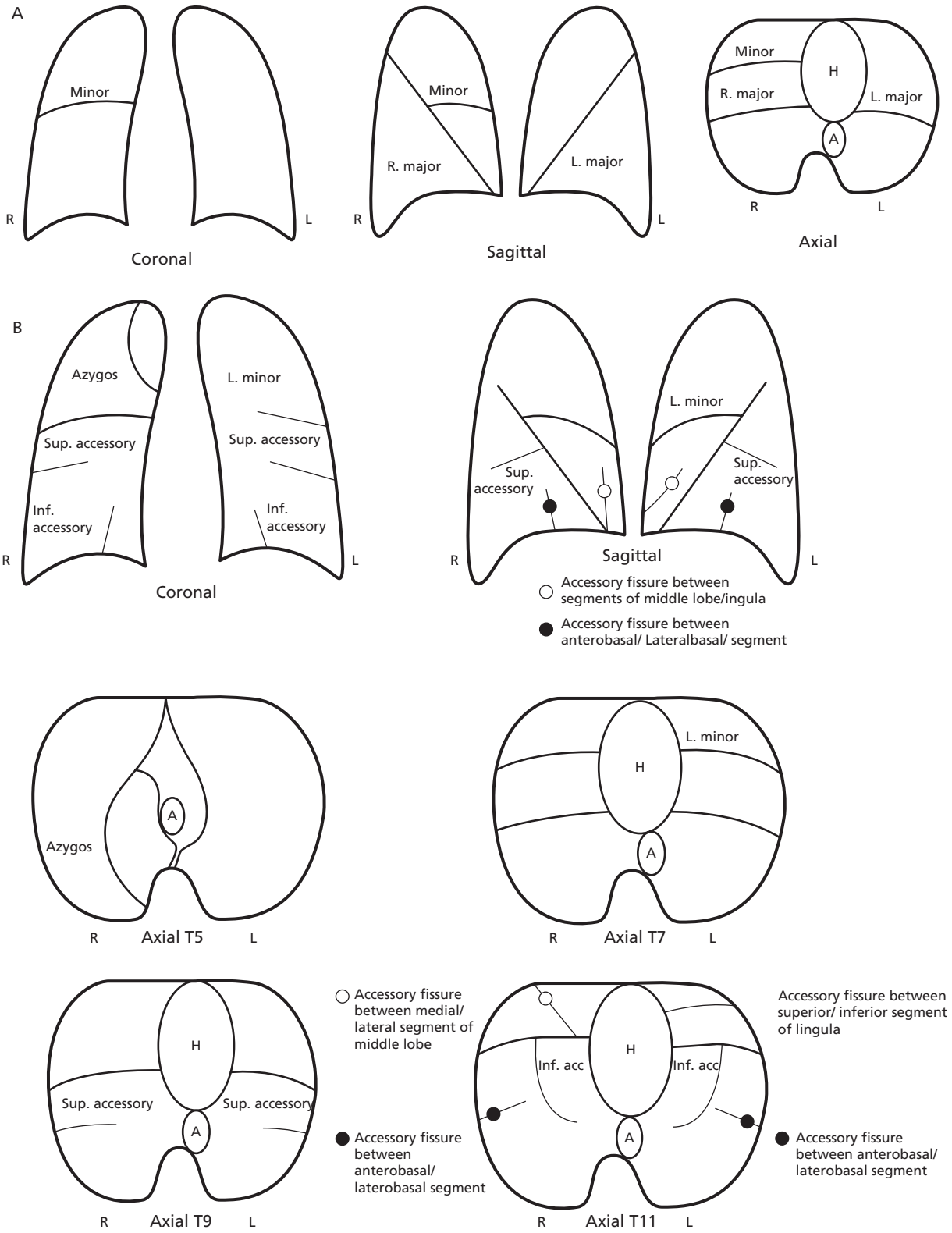

Figure 103.2 The normal lung fissures and accessory lung fissures: (a) in coronal, sagittal, and axial projections; and (b) most frequent accessory fissures (left minor fissure, superior accessory fissure, inferior accessory fissure, accessory fissure between medial and lateral segment of middle lobe, accessory fissure between superior and inferior segment of lingual, accessory fissure between anterobasal and laterobasal segment of the lower lobe, and azygos fissure) in coronal, sagittal and axial projections (at the T5, T7, T9, and T11 vertebral body levels).

Source: Cronin et al. (2010). Reproduced with permission from Elsevier.

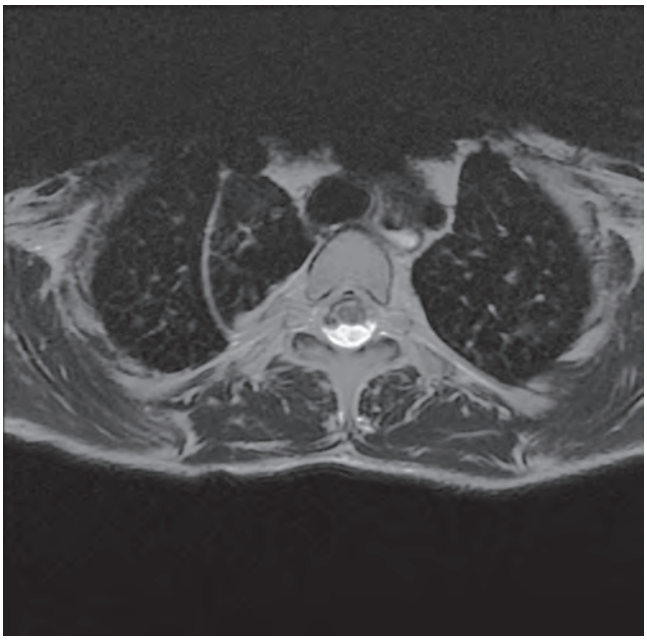

Figure 103.3 Horizontal section of MRI image of azygos vein lobe. Image courtesy of Dr R Shane Tubbs, Pediatric Neurosurgery Children's of Alabama.

was reported to be between 0.17% and 15% (Medlar 1947; Langlois and Henderson 1980). This type of anomaly is sometimes associated with asplenia.

Azygos fissure (azygos lobe)

The azygos lobe is defined as part of the upper lobe split by the azygos vein that has an abnormal course and forms another lobe (Fig. 103.3). This anomalous lobe was first reported by Wrisberg in 1778, found in the cadaver dissection of a three-year-old boy. Azygos lobes were present in both lungs (Boyden 1952). The majority of azygos lobe cases are observed in the right lung. However, some cases were observed in the left lung or in both lungs (Chiba et al. 1990). In addition, a rare case of two accessory fissures in the right upper lobe and a presumed double azygos lobe was reported (Tüzün and Hekimoglu 2004).

The free margin of the fold is concave and contains the azygos vein between two parietal pleura. The pleural fold and azygos vein are related, similar to the mesentery and a portion of the small intestine. The fold is termed the "meso-azygos" (Bluntschli 1905; Hjelm and Hulten 1928). The location of the fissure varies between cases. Stibb (1919) proposed a classification of the position of the fissure as follows: (a) more or less horizontal and cutting the outer (lateral) surface of the lung at some point between the apex and a point two inches below the apex; (b) nearly vertical and dividing the apex of the lung into lateral halves; and (c) vertical and cutting off a small tongue-shaped lobe from the inner (mediastinal) surface, the pedicle being attached to the upper margin of the root of the lung (Stibb 1919).

The frequency of this fissure was reported to be 0.01–2.6% in the general population (Chiba et al. 1990). The cause of the azygos lobe is presumed to be genetic, as familial cases of azygos lobe have been reported (Pipkin et al. 1952; Postmus et al. 1986). Pipkin et al. (1952) claimed the azygos lobe appeared to be dependent upon an autosomal dominant gene.

Agenesis, aplasia, and hypoplasia of the lung

The lung can undergo various degrees of developmental arrest. Over 400 cases of developmental arrest of the lung were reported up to 1968 (Schechter 1968). The earliest report of the congenital absence of the lung was by de Pozzi in 1674. Other early reports include Riviere in 1679 and Morgagni in 1762. Haberlein and Klinz are usually credited with the first adequate description (Oyamada 1953). The incidence of agenesis has been estimated to be 1 in 10,000–15,000 autopsies (Ellis 1917; Olcott and Dooley 1943; Krivchenya et al. 2007). Borja et al. (1970) reported four cases among 114,569 admissions (1in 28,642) in a hospital over 19 years. The difference between genders was 3:2 (males to females) (Marioni 1962), and the right to left ratio was 1:3 (Ingram et al. 1950).

The exact cause of the developmental arrest of the lung is unknown; however, vitamin A deficiency (Wilson and Warkany 1949), viral infections (Heerup 1927), genetic factors, neural crest injuries during embryogenesis (Osborne et al. 1989), and a decrease of amniotic fluid volume have been proposed as causative factors.

Schneider and Schwalbe (1913) proposed a classification of developmental defects of the lung: lung agenesis, lung aplasia, and lung hypoplasia. This classification is still widely used in articles of lung agenesis (Table 103.1). Schechter refined the classification of Schneider and proposed a new classification in 1968 (Schechter 1968) with four categories: aplasia, dysplasia, hypoplasia, and ectoplasia. These categories are divided into further subcategories (Table 103.2).

The incidence of associated anomalies was 50–60% of cases (Wexels 1951; Schaffer and Rider 1957; Sbokos and

Table 103.1 Classification of the developmental arrest of the lung. Data from Boyden (1955).

Group	Name	Description
1	Lung agenesis	No formed bronchus or lung is observed; carina, bronchi, pulmonary vessels, and lung parenchyma are absent
2	Lung aplasia	No lung tissue, or slight presence of lung tissue; main bronchus stump is present with well-formed bifurcation; pulmonary artery and parenchyma are absent
3	Hypoplasia	The main bronchus is incompletely developed; marked hypoplasia of one or both lungs

Table 103.2 Classification by Schechter.

Class	Name	Description
1	(Pulmonary) bronchopneumonic aplasia	Unilateral or bilateral absence (of formation) of the entire lung. In pulmonary aplasia, both components (bronchial and alveolar tissue) of the whole lung are missing.
2	(Pulmonary) bronchopneumonic dysplasia	Interrupted formation of one of the lung components (bronchial tree), with omission of the other (alveoli). In dysplasia, some vestiges of the air-conducting system are present.
3	(Pulmonary) bronchopneumonic hypoplasia	Qualitative or quantitative reduction in pulmonary mass. Includes all situations in which both bronchial and alveolar elements are present, regardless of their structural integrity or functional capacity.
4	(Pulmonary) bronchopneumonic ectoplasia	All or part of a lung is joined to the upper digestive system by a track. This category is an extremely rare condition.

Source: Schechter (1968). Reproduced with permission from Elsevier.

McMillan 1977). Anomalies of pulmonary vessels in the diseased side were found in all cases with lung anomalies. The degree of pulmonary vessel anomalies varied from a complete absence of the hemi-side of pulmonary vessels to minor abnormalities in size, number, and relation of each vessel (Sbokos and McMillan 1977). Associated cardiac anomaly has also been reported. Patent ductus arteriosus, patent foramen ovale, abnormal origin of great vessels, a vascular ring produced by a right aortic arch, and other cardiovascular and non-cardiovascular anomalies have also been reported (Valle 1955; Pallie et al. 1967; Maltz and Nadas 1968; Sbokos and McMillan 1977).

The mortality of children with lung aplasia is 33% during the first year of life and 50% in the first five years of life (Wexels 1951; Nicks 1957). Lethal outcomes are usually the result of infection of the single lung and concomitant severe heart and vessel malformations. However, several patients were diagnosed in their fourth and fifth decades and at least one lived to the age of 72 (Heerup 1927; Devi and Moore 1966; Nelson et al. 1967).

Bilateral agenesis of the lungs

Over ten cases of bilateral agenesis of lungs have been reported to date. In this anomaly, bilateral lungs lack agenesis or, in some cases, have primitive bronchial buds (Allen 1925; Tuynman and Gardner 1952; DeBuse and Morris 1973) and the trachea ends blindly at various levels in almost all cases. In two reported cases, the trachea was absent (Roderer 1754; Oyamada et al. 1953; Devi and Moore 1966). In another two cases, the trachea was connected to the esophagus and formed a tracheo-esophageal fistula (Schmit 1893; DeBuse and Morris 1973).

Related to bilateral lung agenesis, heart and great vessel anomalies are also observed. Usually, the pulmonary artery joins the aorta at the site of the ductus arteriosus and pulmonary veins are absent. The left atrium receives no vessel or anomalous left superior vena cava or inferior vena cava. With regards to heart anomalies, patients develop patent foramen ovale (Schmit 1893; Allen 1925; Ostor et al. 1978), atrial septal defect (Devi and Moore 1966), or ventricular septal defect (Devi and Moore 1966).

The bilateral agenesis of the lungs may be associated with other anomalies including absent spleen (Devi and Moore 1966), accessory spleen (Tuynman 1952 and Gardner; Ostor et al. 1978), renal tubular cysts (Ostor et al. 1978), unilateral agenesis of the kidney (Ostor et al. 1978), unilateral hypoplasty of the kidney (DeBuse and Morris 1973), anal imperforate (DeBuse and Morris 1973; Ostor et al. 1978), and absence of the diaphragm (Toriello et al. 1985a, b).

Horseshoe lung

Horseshoe lung is an anomaly in which parts of the right and left lungs are fused together by a tongue of parenchyma postero-inferior to the pericardial reflection at the cardiac apex (Freedom et al. 1986). It is usually associated with scimitar syndrome, which consists of partial anomalous pulmonary venous drainage of the right lung, right lung hypoplasia, dextroposition of the heart, and anomalous systemic arterial supply from the aorta to the right lung. However, according to Frank et al. (1986), cases without scimitar syndrome have been observed only rarely (Cipriano et al. 1975; Purcaro et al. 1976; Currarino and Williams 1985; Čičak et al. 2010). Although a similar malformation was described in the nineteenth century (Morestin and Porregaux 1894), it was first described in detail by Spencer in 1962 (Frank 1985). Up to 2001, Männer et al. (2001) described that almost 40 cases had been reported in the literatures since the first report by Spencer (1977). Regarding the fused part of these two lungs, two patterns have been reported: one in which the fusion was within the isthmus, and the other in which the fused tissue was separated by a fissure-like layer of visceral pleura (Freedom et al. 1986). The right lung has often been reported as hypoplastic and lacking normal identifiable fissure and lobes, whereas the left lung has usually had a more normal appearance (Freedom et al. 1986). Regarding the bronchial pattern, the abnormality has also been observed on the right side. Arterial supply to the right lung is provided both by the mediastinal right pulmonary artery and by an anomalous arterial supply originating from the descending aorta. The so-called "horseshoe part" is supplied by a branch of the right pulmonary artery and contributions from the left pulmonary artery (Freedom et al. 1986). Some variation cases of horseshoe lung, such as those with left lung hypoplasia (Ersöz et al. 1992; Oguz et al. 2009; Jeewa et al. 2010; Salerno et al. 2010; Yildiz et al. 2012), diaphragmatic herniation of the liver (Čičak et al. 2010), and facio-auriculo-vertebral sequence (D'Alessandro et al. 2006) have also been reported recently. Moreover, Männer et al. (2001) described a rare case with the fused part of both lungs in the apical region instead of the usual postero-inferior part.

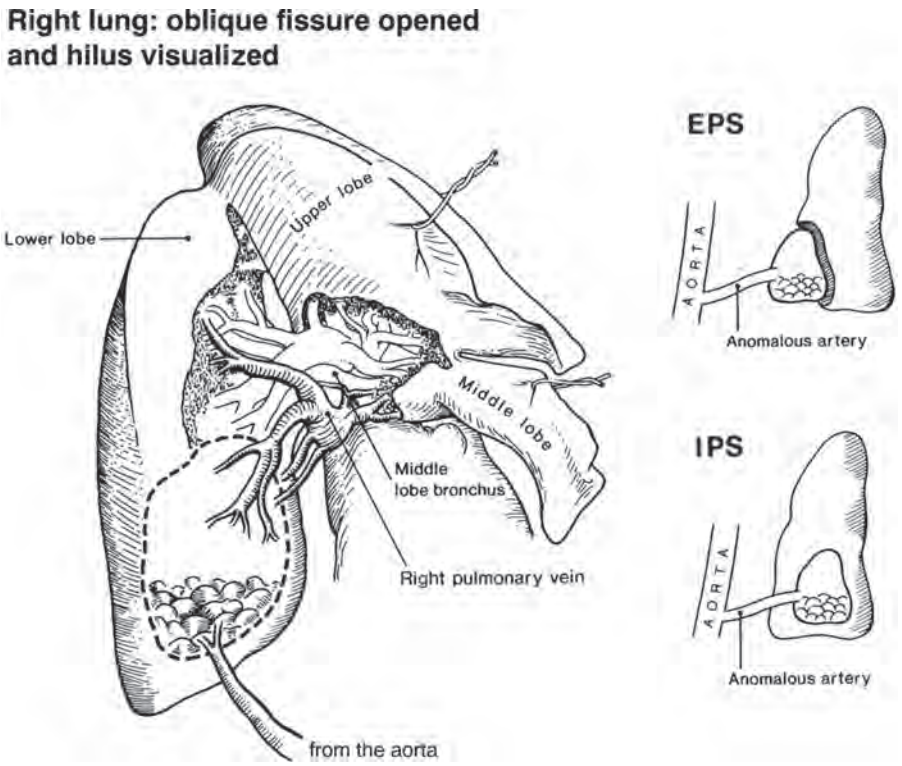

Figure 103.4 Intralobar sequestration: the large anomalous artery supplying the basal area of the intralobar pulmonary sequestration and four efferent veins draining into the pulmonary vein are shown. Also depicted is the difference between intralobar pulmonary sequestration (IPS) and extralobar pulmonary sequestration (EPS).

Source: Samuel and Burge (1999). Reproduced with permission from BMJ Publishing Group.

Pulmonary sequestration

Pulmonary sequestrations are defined as regions of lung parenchyma that lack a normal connection to the tracheobronchial tree and possess an anomalous systemic blood supply (Samuel and Burge 1999). This anomaly is commonly observed in the left side above the diaphragm; incidence was reported to be 0.15–1.70% in the general population. This anomaly was first described by Rokitansky (1861). Peyce (1946) introduced the term "sequestration." There are two types of pulmonary sequestrations: intralobar and extralobar types. Intralobar sequestration is a condition where abnormal tissue is contained within the normal lung. Extralobar sequestration describes a condition where sequestration of the lung is completely separate from the normal pulmonary lobe and has its own pleural investment.

Intralobar sequestration

Intralobar sequestration is previously termed "bronchogenic cyst with aberrant blood supply" (Tosatti and Gravel 1951; Wyman and Eyler 1952; Bressler and Wiener 1954; Mannix and Haight 1955). In most cases, the sequestrated portion is located in the posterobasal segment of the lower lobe (Fig. 103.4). However, rare cases found in the upper lobe and in the right middle lobe have also been reported (Warner et al. 1958; Savić et al. 1979). The proportion of cases with left or right lower lobes was 7:4 (deParedes et al. 1970). In addition, a case with intralobar sequestration in bilateral lower lobes (Gerle et al. 1968) and cases with intra- and extralobar sequestrations (Kafka and Beco 1960; Savić et al. 1979) were reported. Regarding blood supply, sequestrations are usually supplied from one or more arteries from the aorta via branches of the lower thoracic aorta arising immediately above the diaphragm (deParedes et al. 1970). In addition, branches from the abdominal aorta or intercostal arteries often supply the sequestration. Cases involving the intercostal artery (Ravitch and Hardy 1949) and the liver (Talalak 1960) have also been reported. Venous drainage is usually to the inferior pulmonary vein (deParedes et al. 1970). However, the involvement of other drainage veins including the hemiazygos vein (Harris and Lewis 1940; Simopoulos et al. 1959; Cooley 1962), vena cava inferior, azygos vein, intercostal vein, or vena cava superior have also been reported (Savić et al. 1979). Different from extralobar sequestration, this type of sequestration is not usually associated with other congenital anomalies (deParedes et al. 1970).

Extralobar sequestration

Extralobar sequestration was previously termed "lower accessory lung" (Cockayne and Gladstone 1917; Davies and Gunz 1944; DeBakey et al. 1950; Boyden et al. 1962) or "Rokitansky's lobe" (St Raymond et al. 1956). The majority of cases (80–90%) of extralobar sequestrations occur on the left side (Smith 1956; Savić et al. 1979). Extralobar sequestration is usually located in the posterior costodiaphragmatic angle adjacent to the lower esophagus (deParedes et al. 1970) and above the diaphragm (Fig. 103.5). However, in rare cases extralobar sequestration is observed below the diaphragm (Valle and White 1947). The

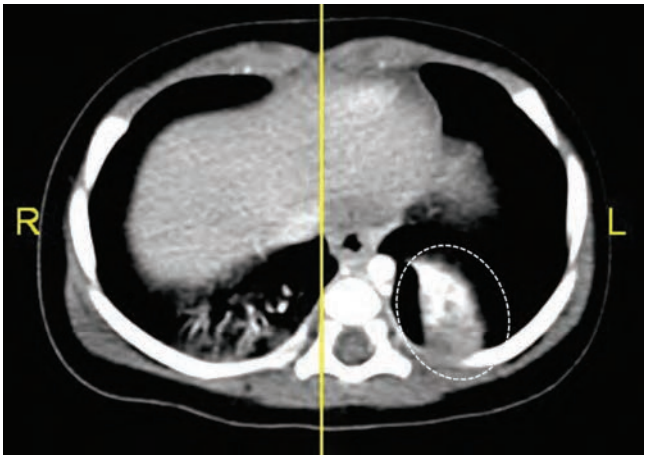

A

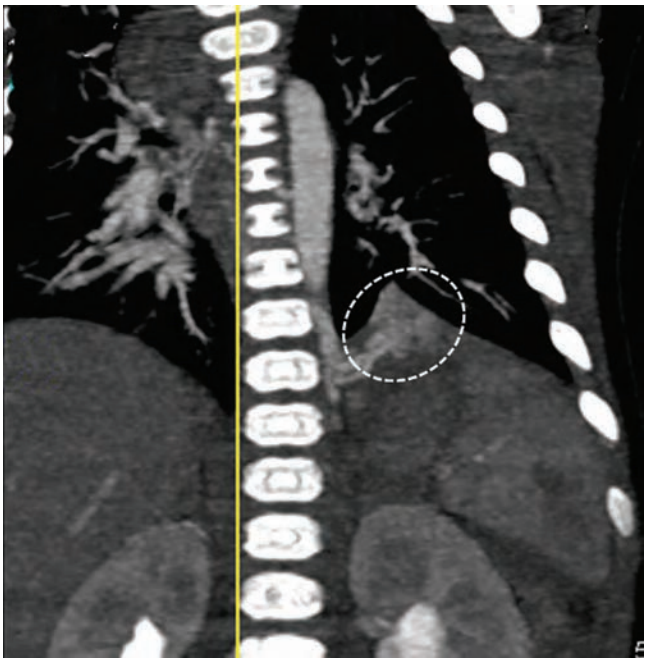

B

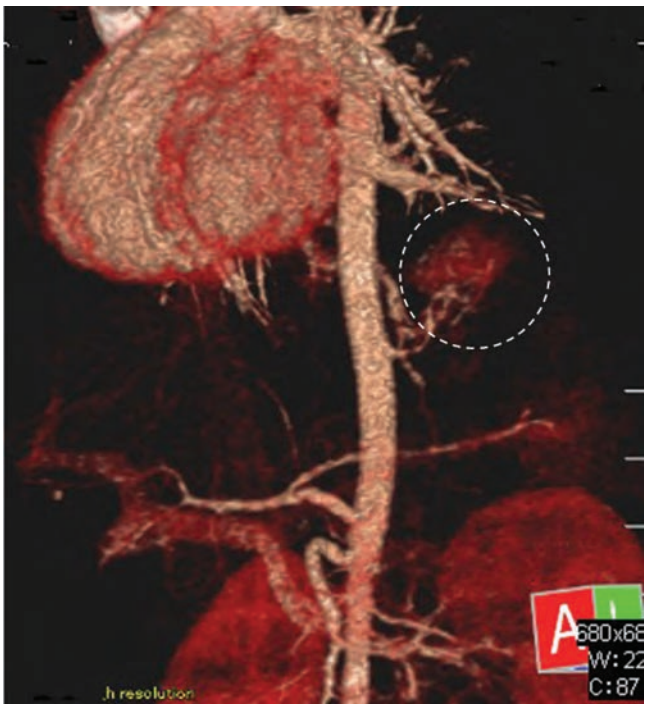

C

Figure 103.5 Case of extralobar sequestration. The extralobar pulmonary sequestration is located in the posterior aspect of the left lung immediately above the diaphragm and supplied by thoracic aorta. Dotted circle indicates the extralobar sequestration. (a) Horizontal section of CT image; (b) coronal section of CT image; and (c) 3D reconstructed CT image.

Source: Dr Kimio Asagiri, Department of Pediatric Surgery, Kurume University School of Medicine.

arterial supply of the sequestration originates from the lower thoracic or upper abdominal aorta (deParedes et al. 1970), such as the left gastric artery (Gerle et al. 1968), left renal artery (Shuford and Sybers 1969), and intercostal arteries (Davies and Gunz 1944). These veins drain to the neighboring systemic veins, such as the hemiazygos vein (deParedes et al. 1970). In some cases, the vein drains to the portal system (St Raymond et al. 1956; Shuford and Sybers 1969). Extralobar sequestration is associated with diaphragmatic defects in 29.7–58.0% of cases (Valle and White 1947; deParedes et al. 1970).

Anatomical variations of the bronchial pattern

Bronchial trees have many variations. Most of the lobar and segmental bronchi have branching pattern variations. The lung area is occasionally supplied by a displaced bronchus arising from another part of the bronchial tree instead of the proper bronchus. This bronchus is called the X bronchus and is sometimes observed in 1b sub-segment (BX1b). Surplus (supernumerary) or a lack of bronchus is also occasionally observed. For example, pre-eparterial bronchus is sometimes supernumerary. The left bronchus equivalent to the right B7 is often absent. The branch supplying the zone between the two normal zones can also be absent. The sub-superior and accessory sub-superior bronchi are in this category, and these branches supply the middle level of the posterior costal surface of the lower lobe.

Numbering of the bronchus

Numbering of the bronchus can be confusing when reading old literature, especially pre-1950, because the new lung segment number system is different from the old system.

Jackson and Huber (1943) reviewed the terminologies of lung lobes and segments used previously and proposed new terminology of the lobes and segments of the lung. In the classification, the right lung was divided into three lobes: upper, middle, and lower. The left lung was divided into two lobes – upper and lower – and the upper lobe was divided into two divisions: upper division and lower (lingual) division. Regarding the segments, the right upper lobe consists of three segments: apical, posterior, and anterior. The right middle lobe consists of two segments – lateral and medial – and the right lower lobe consists of five segments: superior, medial basal, anterior basal, lateral basal, and posterior basal. The upper division of the left upper lobe consists of two segments: apical-posterior and anterior. The lower (lingular) division of the left upper lobe consists of two segments – superior and inferior – and the left lower lobe consists of five segments: superior, anterior-medial, basal, lateral basal, and posterior basal segments.

Following this classification, Boyden (1945) proposed a numbering of the bronchus based on Jackson and Huber's classification. This numbering was accepted widely, and many authors used this classification in their articles (Rigler 1948).

A meeting in 1949 established a standard nomenclature of the bronchus that was accepted as standard (Boyden 1953). The numbering system for the bronchus was adopted, but some points were changed from Boyden's original numbering. The two main different points were as follows: B2 and B3 were interchanged (posterior segment was B3 and anterior segment was B2 in Boyden's system, whereas the posterior segment is B2 and the anterior segment is B3 in the current nomenclature). Another change was that B7 was deleted from the left lung.

Bridging bronchus

Gonzalez-Crussi et al. (1976) first reported a female infant case of bridging bronchus, which was described as follows. The trachea was positioned normally and divided into right and left main-stem bronchi in the normal way. One centimeter beyond its origin, the left main-stem bronchus in turn divided into two large branches: a left wide branch that penetrated the ipsilateral lung parenchyma, and a narrower branch that coursed to the right, bridged the mediastinum, and entered the contralateral (right) lung, where it divided into the middle and lower lobes (Gonzalez-Crussi et al. 1976). Wells et al. (1988) classified the sling left pulmonary artery into four types and the bridging bronchus was classified into two subtypes (Fig. 103.6). One type (II-A) has a normal trachea and bilateral main bronchi; the right main bronchus supplies exclusively the right upper lobe; and the bridging bronchus emerges from the left main bronchus at the level of the interspace between the sixth and seventh thoracic vertebrae, goes through the mediastinum, and supplies the right middle and lower lobes. In the other type (II-B), the right main bronchus ends blindly without supplying any lobe or is absent, and the bridging bronchus arises from the left main bronchus at the level of the interspace between the sixth and the seventh thoracic vertebrae, and supplies the right middle and lower lobes. In this type, the right lung is frequently hypoplastic (Baden et al. 2008). However, some variant cases that did not match these two types have also been reported. In a case reported by Starshak et al. (1981), the bridging bronchus arising from the left main bronchus supplied only the left lower lobe and the right main bronchus supplied the right upper and middle lobes. Rishavy et al. (2003) reported a case of bridging bronchus arising from the anterior aspect of carina and heading to the right lower lobe. This anomaly is extremely rare and Rishavy et al. (2003) commented that only eight cases had been reported up to 2001 since the report of Gonzalez-Crussi et al. (1976). The bridging bronchus is associated with other congenital anomalies. Sling left pulmonary artery is often observed in patients with bridging bronchus, which is an aberrant left pulmonary artery arising from the proximal right pulmonary artery, passing posterior over the proximal right bronchus, and coursing between the trachea and esophagus to the left hilum. Stenosis of the trachea or left main bronchus has also been observed (Medina-Escobedo and Lopez-Corella 1992; Topcu et al. 2006). Other associated anomalies, such as cardiovascular, skeletal, genitourinary, and abdominal malformations which occur in the VATER

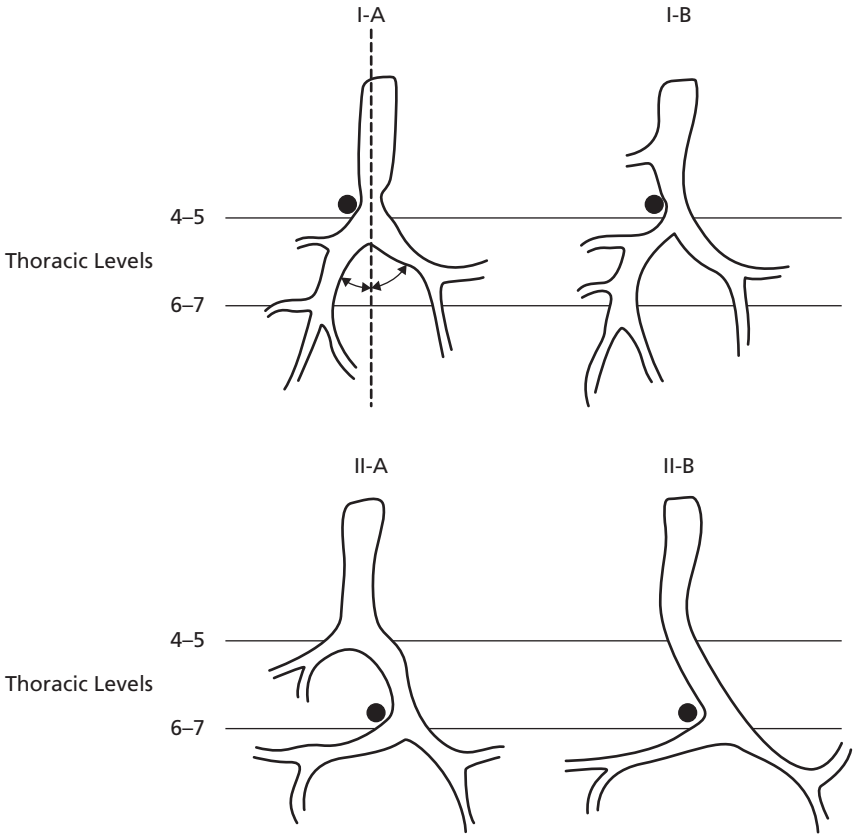

Figure 103.6 Tracheobronchial tree in the various forms of sling left pulmonary artery. In this classification bridging bronchus corresponds to II-A and II-B, and the bridging bronchus (pseudocarina) is located at thoracic vertebral levels 6–7.

Source: Wells et al. (1988). Reproduced with permission from Elsevier.

association, have been reported (Starshak et al. 1981; Medina-Escobedo and Lopez-Corella 1992; Baden et al. 2008).

Braided bronchus

Wheeler et al. (1998) reported a female infant case of braided bronchus, the only known case to have been reported (to the best of the author's knowledge). In that case, the trachea and left main bronchus were normal; however, the right main bronchus branched into four bronchi. The first supplied a large retro-cardiac lobe and extended into the left chest; the second supplied additional right lower lung tissue; the third supplied the right lateral upper and middle lung fields; and the fourth crossed beneath the third bronchus on a path to the region of the right heart border. In addition, a subsegmental branch arising from the second bronchus traveled behind the fourth bronchus to subtend the right lung apex, giving rise to a unique "braided" appearance.

Bronchial isomerism

Isomerism can be defined as the absence of the normal lateralizing features that distinguish right- and left-sided organs such as the lungs (Anderson et al. 1998). Regarding the lungs, right and left bronchial isomerism has been reported (Fig. 103.7). Right bronchial isomerism is characterized by two tri-lobed lungs each with a short main bronchus; left bronchial isomerism is characterized by two bi-lobed lungs each with a long main bronchus (Bush 1999). These two isomerisms are known to be related to other anomalies. Right bronchial isomerism is associated with congenital asplenia and cardiac abnormalities. Asplenia causes immune insufficiency with susceptibility to pneumococcal sepsis. These associated anomalies are said to correspond to Ivemark syndrome. On the contrary, left bronchial isomerism is associated with polysplenia, malrotation of the gut, and cardiovascular malformation. Mohan et al. (1983) described four types of bronchial isomerism when considering these associated anomalies.

1. Type 1 is predominant in males, consists of bilateral tri-lobed lungs, and is associated with asplenia, gut malrotation, and congenital cardiovascular anomalies that include transposition of the great vessels, atrial and ventricular septal defects, and right-sided aortic arches.
2. Type 2 consists of anisosplenia associated with the other features of type 1 isomerism.
3. Type 3 combines bilateral bi-lobed lungs with polysplenia, gut malrotation, and congenital heart disease, and appears to have no sex predilection.
4. Type 4 occurs more often in females and includes bi-lobed lobes with gut malrotation, anisosplenia, and a double outlet from the right ventricle.

The frequency of these two forms of bronchial isomerism in the general population has not been reported. However, the incidence of right bronchial isomerism in patients with asplenia

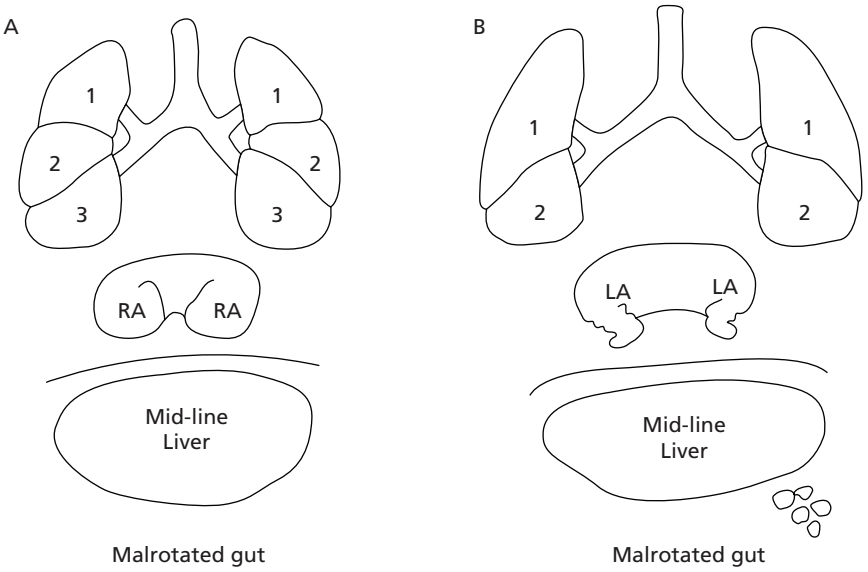

Figure 103.7 Morphology of right and left bronchial isomerism: (a) bilateral tri-lobed lungs, each with a short main bronchus; and (b) bilateral bi-lobed lungs, each with a long main bronchus, respectively. RA: right atrium; LA: left atrium. Adapted from Bush (1999) with permission from John Wiley & Sons.

has been reported as 70%, whereas the incidence of left bronchial isomerism in patients with polysplenia syndrome has been reported as 60% (Gutgesell 1990).

Right upper lobe bronchus

The right main bronchus branches the right upper lobe bronchus initially and becomes the truncus intermedius, which divides into the right middle lobe bronchus and the right lower lobe bronchus. The right upper lobe bronchus has three segmental bronchi: apical (B1); posterior (B2); and anterior (B3). According to Bloomer et al. (1960), the proportion of the branching patterns was 52% with a trifurcation pattern and 48% with a successive or double bifurcation pattern. In other reports, the trifurcation pattern was 46% (Boyden and Scannell 1948) and 38% (Foster-Carter 1942), and the bifurcation pattern was 54% (Boyden and Scannell 1948). Boyden and Scannell (1948) described a quadrivial type of branching that occurred in 16% of cases. Foster-Carter (1942) and Appleton (1945) also reported the quadrivial type of branching. Occasionally, an X branch that arises as an additional or accessory branch of a segmental bronchus to supply a territory usually served by the ramus of another segmental bronchus is observed. BX1b, a branch that supplies the 1b area although it arises from another branch as an accessory branch, is the most commonly observed X branch. The frequency of BX1b was reported to be 28% by Boyden and Scannell (1948) and 14% by Bloomer et al. (1960).

Pre-eparterial bronchus

The pre-eparterial bronchus is an anomaly in which a bronchus arises from a central rather than upper lobe bronchus. This anomaly may vary in degree from a partial splitting of the parent bronchus to a displaced apical bronchi arising from the trachea (Boyden 1952). The partial splitting of the parent bronchus is quite common, although cases where the anomalous bronchus originates at the level of the bifurcation of the trachea are rare.

This anomaly includes two types: displaced and supernumerary bronchi (Chiari 1889; Boyden 1952). A displaced bronchus is a normal branch arising in an abnormal position. In this case, the apical bronchus (B1) usually arises from the upper lobe bronchus and displaces upward. The "supernumerary bronchus" is an excessive bronchus observed in addition to normal bronchi.

A bronchoscopic study by Gonlugur et al. (2005) demonstrated that the frequency of pre-eparterial bronchus was 7.5% in cases with major variations and 0.2% in the general population.

Post-eparterial bronchus

In some cases, an upper lobe bronchus may originate at a lower level. For example, the right anterior bronchus (B3) may arise from the middle lobe stem. Similar to the pre-eparterial bronchus, this anomaly is not only supernumerary but also merely a displaced portion of the upper lobe bronchus since it distributes to the territory of B3 in that lobe (Boyden 1955).

Right middle bronchus

The right middle lobe bronchus has two segmental bronchi: lateral (B4) and medial (B5). These segmental bronchi have two subsegmental bronchi; B4a, B4b; and B5a, B5b. Bloomer et al. (1960) reported the division pattern of the middle bronchus with a bifurcation pattern in 96% of cases and a trifurcation pattern in 4% of cases. According to Boyden and Hamre (1951), bifurcation was observed in 98% of cases and trifurcation in 2% of cases.

Moreover, the bifurcation pattern has three types of branching pattern: (1) the prevailing lateral-medial type; (2) the modified lateral-medial type; and (3) the superior-inferior type. The most common pattern is the prevailing lateral-medial type bifurcating into B4 and B5, and the frequency was reported to be 70% by Bloomer et al. (1960) and 62% by Boyden and Hamre (1951).

The modified lateral-medial pattern describes the middle lobe bronchi bifurcating into the lateral and medial branches, although the subsegmental branch arises from another segmental branch (X branch). The major pattern of this modified lateral-medial pattern is a middle bronchus bifurcation into B4a and B5+BX4b as described by Boyden and Hamre (1951), and B5a and B4+B5b by Bloomer et al. (1960).

The superior-inferior pattern might be caused by a displacement and a rotation of the bronchi on the lobar stem. In this pattern, one or two subsegmental branches arise superiorly, and the remaining subsegmental branches arise inferiorly. The frequency of this type was shown to be 18% by Boyden and Hamre (1951) and 12% by Bloomer et al. (1960).

Right lower bronchus

The right lower bronchus branches into the right superior segmental bronchus (B6) and becomes the basal trunk. The basal trunk has four bronchi: the medial basal (B7), the anterior basal (B8), the lateral basal (B9), and the (B10) bronchi. In the right lower bronchus, the sub-superior bronchus, accessory subsuperior bronchus, and paravertebral bronchus are sometimes observed. An accessory ramus of the left posterior basal bronchus is known as the internal marginal ramus of Lucien.

Superior segmental bronchus (B6)

The superior segmental bronchus (B6) has three subsegmental branches: medial (B6a); superior (B6b); and lateral (B6c) bronchi. The major branching pattern of the B6 bronchus is a bifurcation type, usually arising from one stem and dividing into B6a+b and B6c. The frequency of the bifurcation type was reported to be 74% by Bloomer et al. (1960) and 94% by Smith and Boyden (1949). Other branching patterns include trifurcation (B6a, B6b, and B6c) with a frequency of 16% by Bloomer et al. (1960) and 6% by Smith and Boyden (1949), and two separate stem patterns with a frequency 8% (Bloomer et al. 1960). According to Smith and Boyden (1949), a segment supplied by the accessory branch of the subsuperior bronchus (B*) or directly by a branch from the basal stem had a frequency of 10%.

Sub-superior and accessory sub-superior bronchus

The sub-superior bronchus (B*) arises beneath the superior bronchus (B6) from the posterior aspect of the basal trunk. The branch arising from the upper portion of the posterior basal bronchus is called the accessory sub-superior bronchus (BX*) and is distributed to the middle level of the posterior costal surface of the lower lobe. According to Smith and Boyden (1949), one or more sub-superior or accessory sub-superior bronchi are observed in all specimens with frequencies as follows: subsuperior bronchus (62%), accessory sub-superior bronchus (86%), and in both bronchi (48%).

Paravertebral bronchi

The dorsal rami bronchus is not classifiable because of its origin from the medial side of the bronchus and because its distribution is different from the sub-superior region. These bronchi are called paravertebral bronchi (Smith and Boyden 1949).

Medial basal segmental bronchus (B7)

The medial basal segment bronchus arises as an independent bronchus with a frequency of 80%. The B7 bronchus usually divides into two rami: B7a and B7b. In 14–18% of cases, B7 does not arise as an independent stem from the common basal bronchus (Smith and Boyden 1949).

Anterior basal segmental bronchus (B8)

The anterior basal segmental bronchus (B8) is the second of the basal bronchi and arises slightly below B7 from the anterolateral aspect of the basal trunk. The anterior basal bronchus (B8) arises independently from the basal trunk in 78% of cases and divides into two rami: B8a and B8b. They occur in common with B7 or 7a in 16–18% of cases, and with B9 in 2–4% of cases (Smith and Boyden 1949).

Lateral basal segmental bronchus (B9)

B9 arises from a common trunk with B10 in most cases. Smith and Boyden (1949) reported that B9 was absent in 8% of cases. Bloomer et al. (1960) reported that B9 arose from a common trunk with the anterior basal segmental bronchus (B8) in 4% of cases. The lateral basal segmental bronchus (B9) divides into two rami: lateral (B9a) and basal (B9b) rami. Lateral ramus (B9a) had a frequency of 86%. In 14% of cases, the ramus was absent and was replaced by B* or B8a. The basal ramus (B9b) was absent in 8% of cases (Smith and Boyden 1949).

Posterior basal segmental bronchus (B10)

Typically, B10 divides into three major branches: BX*, B10a, and B10b. The highest branch is the accessory sub-superior bronchi BX* observed in 77–86% of specimens (Smith and Boyden 1949).

Left upper bronchus

The left upper bronchus forms two divisions: the upper and lower divisions. Two types of bronchial patterns were reported: a bifurcate type and trifurcate type. The bifurcate type was reported in 86% of cases by Bloomer et al. (1960) and 74% of cases by Boyden and Hartmann (1946). The trifurcate type was reported in 14% of cases by Bloomer et al. (1960) and 26% of cases by Boyden and Hartmann (1946).

The upper division is further divided into two bronchi: the apico-posterior (B1+B2) and anterior (B3) bronchi. The lower

division divides into two bronchi: superior (B4) and inferior (B5). The lower division is also called the lingular division.

The upper division bronchus divides into two in 82% of cases, and the most common pattern was a bifurcating type into the apical-posterior (B1+2) and anterior (B3) bronchi. The trifurcate pattern was reported in 18% of cases.

B3a is absent in 40% of cases and, in this situation, BX3a from the lingual division is replaced in 10% of cases or B4a or B2b expands and compensates for B3a. According to Bloomer et al. (1960), in 4% of cases with the bifurcation form B3 arises from the common trunk of B4+B5 (Bloomer et al. 1960).

The lower division bronchi have few variations. They usually bifurcate into two segments: superior (B4) and inferior (B5) segmental bronchi. The proportion of bifurcation is 78–84%. In 22% of cases, the common lingular stem gives off a posterior ramus that heads to B4a or BX3 before dividing into B4 and B5.

Left lower bronchus

The left lower bronchus usually divides into two bronchi: superior segmental bronchus (B6) and basal bronchus. The basal bronchi consist of three bronchi: the antero-medial basal (B8); the lateral basal (B9); and the posterior basal (B10) bronchi. On the left side, the medial basal segment (B7) is absent in the current classification of lung segments. Prior to the established current classification, Berg et al. (1949) claimed the B7 branch arose in common with the anterior basal branch (B8) and was distributed to the inferior portion of the anterior surface.

Superior segmental bronchus (B6)

The superior segmental bronchus has three rami: the medial branch (B6a); the superior branch (B6b); and the lateral branch (B6c), similar to the right side. It bifurcates in 85% of cases and trifurcates in 15% of cases (Berg et al. 1949; Bloomer et al. 1960). In contrast to the right side, the most common branching pattern of the left superior segmental bronchus is a division into B6a and B6b+c, which occurs in 43% of cases (Berg et al. 1949; Bloomer et al. 1960). As for other patterns, bifurcations into B6b and B6a+c were reported in 27% of cases and bifurcations into B6c and B6a+c were reported in 10% of cases. However, B6 usually bifurcates into B6c and B6a+b on the right lung (Bloomer et al. 1960).

Sub-superior bronchus (B*)

The sub-superior (B*) or the accessory sub-superior (BX*9 or BX*10) bronchi occupy a zone between the superior and basal territories known as the sub-superior zone, present in 100% of specimens (Bloomer et al. 1960). The sub-superior bronchus (B*) arises from the stem bronchus between the first dorsal or superior bronchus (B6) and the origin of B9. This bronchus (B*) occurs less frequently on the left (29%) than on the right side (62%). When the sub-superior bronchus (B*) is absent, the sub-superior segment joins the accessory sub-superior bronchi that arises as the uppermost branch of B9 (BX*(9)) or B10 (BX*(10)). On the right lung, these branches supply the lateral sector of the costal surface, but the left bronchus usually supplies the posterolateral sector (Bloomer et al. 1960).

Anterior basal segmental bronchus (B8)

The anterior basal segment is the first branch of the basal bronchi and divides into two sub-segmental bronchi: B8a and B8b (Bloomer et al. 1960).

Lateral basal segmental bronchus (B9)

The lateral basal segmental bronchus was absent in 10% of specimens observed, and is represented by displaced rami arising as accessory branches of an adjacent bronchi: B8 or B10 (Bloomer et al. 1960).

Posterior basal segmental bronchus (B10)

The posterior basal segmental bronchus is the largest of the basal bronchi and has two main rami: lateral (B10a) and posterior (B10b). This branch has one or two accessory sub-superior bronchi (BX*) and paravertebral branches before its bifurcation in 30% of specimens observed (Bloomer et al. 1960).

References

Allen A. 1925. Congenital absence of both lungs. *Surg Gynecol Obstet* 41: 375–376.

Anderson RH, Webb S, Brown NA. 1998. Defective lateralisation in children with congenitally malformed hearts. *Cardiol Young* 8: 512–531.

Appleton AB. 1945. The arteries and veins of the lungs: I. Right upper lobe. *J Anat* 79(3): 97.

Baden W, Schaefer J, Kumpf M, Tzaribachev N, Pantalitschka T, Koitschev A, Hofbeck M. 2008. Comparison of imaging techniques in the diagnosis of bridging bronchus. *Euro Respir J* 31(5): 1125–1131.

Berg RM, Boyden EA, Smith FR. 1949. An analysis of variations of the segmental bronchi of the left lower lobe of 50 dissected, and ten injected lungs. *J Thorac Surg* 18(2): 216.

Bloomer WE, Liebow AA, Hales MR. 1960. *Surgical Anatomy of the Bronchovascular Segments*. Springfield, Illinois: CC Thomas.

Bluntschli H. 1905. Bemerkungen über einen abnormen Verlauf der Vena azygos in einer den Oberlappen der rechten Lunge durchsetzenden Pleurafalte. *Morph Jb* 33: 562.

Borja AR, Ransdell HT, Villa S. 1970. Congenital developmental arrest of the lung. *The Ann Thorac Surg* 10(4): 317–326.

Boyden EA. 1945. The intrahilar and related segmental anatomy of the lung. *Surgery* 18: 706.

Boyden EA. 1952. The distribution of bronchi in gross anomalies of the right upper lobe, particularly lobes subdivided by the azygos vein and those containing pre-eparterial bronchi. *Radiology* 58(6): 797–807.

Boyden EA. 1953. A critique of the international nomenclature on bronchopulmonary segments. *CHEST J* 23(3): 266–269.

Boyden EA. 1955. Developmental anomalies of the lungs. *Am J Surg* 89(1): 79–89.

Boyden EA, Hartmann JF. 1946. An analysis of variations in the bronchopulmonary segments of the left upper lobes of fifty lungs. *Am J Anat* 79(3): 321–360.

Boyden EA, Scannell JG. 1948. An analysis of variations in the bronchovascular pattern of the right upper lobe of fifty lungs. *Am J Anat* 82(1): 27–73.

Boyden EA, Hamre CJ. 1951. An analysis of variations in the bronchovascular patterns of the middle lobe in fifty dissected and twenty injected lungs. *J Thorac Surg* 21(2): 172.

Boyden EA, Bill Jr AH, Creighton SA. 1962. Presumptive origin of a left lower accessory lung from an esophageal diverticulum. *Surgery* 52: 323.

Bressler S, Wiener D. 1954. Bronchiogenic cyst associated with an anomalous pulmonary artery arising from the thoracic aorta. *Surgery* 35(5): 815.

Bush A. 1999. Left bronchial isomerism, normal atrial arrangement and bronchomalacia mimicking asthma: a new syndrome? *Euro Respir* J 14(2): 475–477.

Chiari H. 1889. Uber das Vorkommen eines doppelen eparteriellen Seitenbronchus an dem rechten Stammbronchus des Menschen. *Prag Med Wchnschr* 12: 560.

Chiba S, Suzuki T, Takahashi D, Kasai T. 1990. An autopsy case of azygos lobe and the extra-pulmonary course of the bronchial veins in man. *Okajimas Folia Anat Jap* 66(6): 313.

Čičak B, Mihatov-Štefanović I, Vrsalović R, Babić N, Markičević-Ružičić K. 2010. Horseshoe lung associated with diaphragmatic herniation of the liver. *Acta Clinica Croatica* 49(4): 445–451.

Cipriano P, Sweeney LJ, Hutchins GM, Rosenquist GC. 1975. Horseshoe lung in an infant with recurrent pulmonary infections. *Arch Pediatr Adol Med* 129(11): 1343.

Cockayne EA, Gladstone RJ. 1917. A case of accessory lungs associated with hernia through a congenital defect of the diaphragm. *J Anat* 52(1): 64.

Cooley JC. 1962. Intralobar bronchopulmonary sequestration: a report of three cases. *CHEST J* 42(1): 95–99.

Cronin P, Gross BH, Kelly AM, Patel S, Kazerooni EA, Carlos RC. 2010. Normal and accessory fissures of the lung: evaluation with contiguous volumetric thin-section multidetector CT. *Euro J Radiology* 75(2): e1–e8.

Currarino G, Williams B. 1985. Causes of congenital unilateral pulmonary hypoplasia: a study of 33 cases. *Pediatr Radiol* 15(1): 15–24.

D'Alessandro L, Kovesi T, Massoud S, Lougheed J, Hunter A, Reisman J. 2006. Horseshoe lung and facio-auriculo-vertebral sequence: A previously unreported association. *Pediatr Pulmon* 41(6): 592–596.

Davies DV, Gunz FW. 1944. Two cases of lower accessory lung in the human subject. *J Pathol Bacteriol* 56(3): 417–427.

DeBakey M, Arey JB, Brunazzi R. 1950. Successful removal of lower accessory lung. *J Thorac Surg* 19(2): 304.

DeBuse PJ, Morris G. 1973. Bilateral pulmonary agenesis, oesophageal atresia, and the first arch syndrome. *Thorax* 28(4): 526–528.

deParedes CG, Pierce WS, Johnson DG, Waldhausen JA. 1970. Pulmonary sequestration in infants and children: a 20-year experience and review of the literature. *J Pediatr Surg* 5(2): 136–147.

Dévé MF. 1900. Les lobes surnuméraires du poumon. *Bull Mem Soc Anat Paris* 75: 341–367.

Devi B, More JRS. 1966. Total tracheopulmonary agenesis associated with asplenia, agenesis of umbilical artery and other anomalies. *Acta Paediat* 55(1): 107–116.

Ellis AG. 1917. Congenital absence of lung. *Am J Med Sci* 154(1): 33–38.

Ersöz A, Soncul H, Gökgöz L, Kalaycioğlu S, Tunaoğlu S, Kaptanoğlu M, Yener A. 1992. Horseshoe lung with left lung hypoplasia. *Thorax* 47(3): 205–206.

Ferry Jr RM, Boyden EA. 1951. Variations in the bronchovascular patterns of the right lower lobe of fifty lungs. *J Thorac Surg* 22(2): 188.

Foster-Carter AF. 1942. The anatomy of the bronchial tree. *Brit J Tuberc* 36(1): 19–39.

Frank JL, Poole CA, Rosas G. 1986. Horseshoe lung: clinical, pathologic, and radiologic features and a new plain film finding. *Am J Roentgenol* 146(2): 217–226.

Freedom RM, Burrows PE, Moes CA. 1986. "Horseshoe" lung: report of five new cases. *Am J Roentgenol* 146(2): 211–215.

Gerle RD, Jaretzki III A, Ashley CA, Berne AS. 1968. Congenital bronchopulmonary-foregut malformation: pulmonary sequestration communicating with the gastrointestinal tract. *New Engl J Med* 278(26): 1413–1419.

Gonlugur U, Efeoglu T, Kaptanoglu M, Akkurt I. 2005. Major anatomical variations of the tracheobronchial tree: bronchoscopic observation. *Anat Sci Int* 80(2): 111–115.

Gonzalez-Crussi F, Padilla LM, Miller JK, Grosfeld JL. 1976. "Bridging bronchus": a previously undescribed airway anomaly. *Arch Pediatr Adol Med* 130(9): 1015.

Gutgesell HP. 1990. *Cardiac Malposition and Heterotaxy. The Science and Practice of Pediatric Cardiology*. Philadelphia: Lea & Febiger.

Harris HA, Lewis I. 1940. Anomalies of the lungs with special reference to the danger of abnormal vessels in lobectomy. *J Thorac Surg* 9: 666.

Heerup L. 1927. Case of absence of left lung. *Hospitalstidende* 70: 1165.

Hjelm R, Hulten O. 1928. Rontgenologische Studien uber den Lobus der Vena Azygos. *Acta Radiolog* 9(2): 126–135.

Ingram Jr MD, Hudson GW, Davis TJ. 1950. Aplasia of the lung with angiocardiographic demonstration of anomalous pulmonary circulation. *Am J Roentgenol Radium Ther* 64(3): 409.

Jackson CL, Huber JF. 1943. Correlated applied anatomy of the bronchial tree and lungs with a system of nomenclature. *CHEST J* 9(4): 319–326.

Jeewa A, Culham JG, Human DG. 2010. A case of horseshoe lung and complex congenital heart disease in a term newborn. *Pediatr Radiol* 40(2): 206–209.

Kafka V, Beco V. 1960. Simultaneous intra- and extrapulmonary sequestration. *Arch Dis Child* 35(179): 51.

Krivchenya DU, Rudenko EO, Lysak SV, Dubrovin AG, Khursin VN, Krivchenya TD. 2007. Lung aplasia: anatomy, history, diagnosis and surgical management. *Euro J Pediatr Surg* 17(4): 244–250.

Langlois SLP, Henderson DW. 1980. Variant pulmonary location. *Australas Radiol* 24(3): 255–261.

Maltz DL, Nadas AS. 1968. Agenesis of the lung: presentation of eight new cases and review of the literature. *Pediatr* 42(1): 175–188.

Männer J, Jakob C, Steding G, Füzesi L. 2001. Horseshoe lung: report on a new variant – "inverted" horseshoe lung – with embryological reflections on the formal pathogenesis of horseshoe lungs. *Ann Anat (Anat Anz)* 183(3): 261–265.

Mannix Jr EP, Haight C. 1955. Anomalous pulmonary arteries and cystic disease of the lung. *Medicine* 34(2): 193–231.

Marioni P. 1962. Agenesis of the lung review and report of three cases. *CHEST J* 41(2): 232–236.

Medina-Escobedo G, Lopez-Corella E. 1992. Sling left pulmonary artery, bridging bronchus, and associated anomalies. *Am J Med Genet* 44(3): 303–306.

Medlar EM. 1947. Variations in interlobar fissures. *Am J Roentgenol Rad Ther* 57(6): 723.

Mohan KK, Kramer NEIL, Margolis ML, Steiner RM, Cohn HE. 1983. Intralobar pulmonary sequestration in conjunction with bronchial isomerism. *Thorax* 38(1): 77–79.

Morestin J, Porregaux G. 1894. Ectopie du poumon. *Bull SOC Anat Paris* 69: 968–983.

Nelson CS, McMillan IKR, Bharucha PK. 1967. Tracheal stenosis, pulmonary agenesis, and patent ductus arteriosus. *Thorax* 22(1): 7–12.

Nicks R. 1957. Agenesis of the lung with persistent ductus arteriosus. *Thorax* 12(2): 140–141.

Oguz B, Alan S, Ozcelik U, Haliloglu M. 2009. Horseshoe lung associated with left-lung hypoplasia, left pulmonary artery sling and bilateral agenesis of upper lobe bronchi. *Pediatr Radiol* 39(9): 1002–1005.

Olcott CT, Dooley SW. 1943. Agenesis of lung in an infant. *Arch Pediatr Adol Med* 65(5): 776.

Osborne J, Masel J, McCredie J. 1989. A spectrum of skeletal anomalies associated with pulmonary agenesis: possible neural crest injuries. *Pediatr Radiol* 19(6–7): 425–432.

Ostor AG, Stillwell R, Fortune DW. 1978. Bilateral pulmonary agenesis. *Pathology* 10(3): 243–248.

Oyamada A, Gasul BM, Holinger PH. 1953. Agenesis of the lung report of a case, with a review of all previously reported cases. *AMA Am J Dis Child* 85(2): 182–201.

Pallie W, Alhady SMA, Din OB. 1967. Agenesis of the right lung: an unusual presentation. *Thorax* 22(4): 368–374.

Peyce DM. 1946. Lower accessory pulmonary artery with intralobar sequestration of lung: a report of seven cases. *J Pathol Bacteriol* 58(3): 457–467.

Pipkin SB, Kegel R, Pipkin AC. 1952. Inheritance of the accessory lobe of the azygos vein. *J Heredity* 43(6): 260–262.

Postmus PE, Kerstjens JM, Breed A, Jagt E. 1986. A family with lobus venae azygos. *CHEST J* 90(2): 298–299.

Purcaro A, Caruso L, Ciampani N, Inglese L. 1976. Polmane a ferro di cavallo malposizione cardiaca. Ed. Anomalie vascoliari polmonari: una sindrome caratteristica. *G Ital Cardiol* 6(2): 312–316.

Ravitch MM, Hardy JB. 1949. Congenital cystic disease of the lung in infants and in children. *Arch Surg* 59(1): 1–6.

Rigler LG. 1949. Segmental anatomy of the lung. *Radiology* 52(4): 582–583.

Rishavy TJ, Goretsky MJ, Langenburg SE, Klein MD. 2003. Anterior bridging bronchus. *Pediatr Pulmonol* 35(1): 70–72.

Roderer GJ. 1754. Fetus parasitici descripto. Commentarii *Soc Regiae Scient Gottingensis* 4: 113.

Rokitansky C. 1861. *Lehrbuch Derpathologischen Anatomic, third edition*. Vienna: Braumiller.

Salerno T, Guccione P, Malena S, Cutrera R. 2010. Horseshoe lung associated with unique left pulmonary vein: An unreported association. *Pediatr Cardiol* 31(6): 905–907.

Samuel M, Burge DM. 1999. Management of antenatally diagnosed pulmonary sequestration associated with congenital cystic adenomatoid malformation. *Thorax* 54(8): 701–706.

Savić B, Birtel FJ, Knoche R, Tholen W, Schild H. 1979. *Pulmonary sequestration. In Advances in Internal Medicine and Pediatrics/ Ergebnisse der Inneren Medizin und Kinderheilkunde*. Berlin Heidelberg: Springer, pp. 57–92.

Sbokos CG, McMillan IKR. 1977. Agenesis of the lung. *Brit J Dis Chest* 71: 183–197.

Schaffer AJ, Rider RV. 1957. A note on the prognosis of pulmonary agenesis and hypoplasia according to the side affected. *Trans Am Clin Climatol Assoc* 68: 25.

Schaffner G. 1898. Ueber den Lobus inferior accessorius der menschlichen lunge. *Virchows Archiv* 152(1): 1–25.

Schechter DC. 1968. Congenital absence or deficiency of lung tissue: the congenital subtractive bronchopneumonia malformations. *Ann Thorac Surg* 6(3): 286–313.

Schmit H. 1893. Ein fall von vollständiger agenesie beider lungen. *Virchows Archiv* 134(1): 25–32.

Schneider P, Schwalbe E. 1913. *Die Morphologie der Missbildungen des Menschen und der Tiere*. Jena: Gustav Fischer.

Shuford WH, Sybers RG. 1969. Bronchopulmonary sequestration with venous drainage to the portal vein. *Am J Roentgenol* 106(1): 118–120.

Simopoulos AP, Rosenblum DJ, Mazumdar H, Kiely B. 1959. Intralobar bronchopulmonary sequestration in childrendiagnosis by intrathoracic aortography. *AMA J Dis Child* 97(6): 796–804.

Smith FR, Boyden EA. 1949. An analysis of variations of the segmental bronchi of the right lower lobe of 50 injected lungs. *J Thorac Surg* 18(2): 195.

Smith RA. 1956. A theory of the origin of intralobar sequestration of lung. *Thorax* 11(1): 10–24.

Spencer H. 1977. *Pathology of the Lung, third edition*. Oxford: Pergamon Press.

St Raymond Jr AH, Hardy JD, Robbins SG. 1956. Lower accessory lung communicating with the esophagus and associated with congenital diaphragmatic hernia. *J Thorac Surg* 31(3): 354–358.

Starshak RJ, Sty JR, Woods G, Kreitzer FV. 1981. Bridging bronchus: a rare airway anomaly. *Radiology* 140(1): 95–96.

Stibbe EP. 1919. The accessory pulmonary lobe of the vena azygos. *J Anat* 53(4): 305.

Talalak P. 1960. Pulmonary sequestration. *Arch Dis Child* 35(179): 57–60.

Topcu S, Liman ST, Sarisoy HT, Babaoglu A, Ozker E. 2006. Stenotic bridging bronchus: a very rare entity. *J Thorac Cardiovasc Surg* 131(5): 1200–1201.

Toriello HV, Higgins JV, Jones AS, Radecki LL. 1985a. Pulmonary and diaphragmatic agenesis: report of affected sibs. *Am J Med Genet* 21(1): 87–92.

Toriello HV, Bauserman SC, Opitz JM, Reynolds JF. 1985b. Bilateral pulmonary agenesis: association with the hydrolethalus syndrome and review of the literature from a developmental field perspective. *Am J Med Genet* 21(1): 93–103.

Tosatti E, Gravel JA. 1951. Two cases of bronchiogenic cyst associated with anomalous arteries arising from the thoracic aorta. *Thorax* 6(1): 82–88.

Trapnell DH. 1973. The differential diagnosis of linear shadows in chest radiographs. *Radiol Clin North Am* 11: 77–92.

Tuynman PE, Gardner LW. 1952. Bilateral aplasia of the lung. *AMA Arch Pathol* 54(3): 306.

Tüzün M, Hekimoglu B. 2004. Double accessory fissures in the upper lobe of the right lung (double azygos fissures?): high resolution computed tomography appearance. *Acta Radiologica* 45(1): 109–110.

Valle AR. 1955. Agenesis of the lung. *Am J Surg* 89(1): 90–100.

Valle AR, White ML. 1947. Subdiaphragmatic aberrant pulmonary tissue (case report). *CHEST J* 13(1): 63–68.

von Hayak H. 1960. *The Human Lung*. New York: Hafner.

Warner CL, Britt RL, Riley Jr. HD 1958. Bronchopulmonary sequestration in infancy and childhood. *J Pediatr*, 53(5): 521–528.

Wells TR, Gwinn JL, Landing BH, Stanley P. 1988. Reconsideration of the anatomy of sling left pulmonary artery: the association of one form with bridging bronchus and imperforate anus. Anatomic and diagnostic aspects. *J Pediatr Surg* 23(10): 892–898.

Wexels P. 1951. Agenesis of the lung. *Thorax* 6(2): 171–192.

Wheeler DS, Poss WB, Cocalis M, Krumwiede G, Gaston B. 1998. Braided bronchus: a previously undescribed airway anomaly. *Pediatr Pulmonol* 25(5): 348–351.

Wilson JG, Warkany J. 1949. Aortic-arch and cardiac anomalies in the offspring of vitamin A deficient rats. *Am J Anat* 85(1): 113–155.

Wyman SM, Eyler WR. 1952. Anomalous pulmonary artery from the aorta associated with intrapulmonary cysts (intralobar sequestration of lung): its roentgenologic recognition and clinical significance. *Radiology* 59(5): 658–667.

Yamashita H. 1978. *Roentgenologic Anatomy of the Lung*. Tokyo: Igaku-Shoin, pp. 49–53.

Yildiz AE, Oguz B, Haliloglu M. 2012. Horseshoe lung associated with left lung hypoplasia and single left pulmonary vein; a rare combination. *Clin Radiol* 67(1): 86–88.

104 Heart

Maira du Plessis and Marios Loukas
St George's University, St George, Grenada

Pericardium

The pericardium is a strong fibrous (outer) and smooth serous (inner) sac covering the heart. The serous consists of two layers, one lining the internal aspect of the fibrous (parietal) and the other (visceral) closely adhered to the surface of the heart. A thin layer of pericardial fluid provides a smooth gliding surface between the two. The three layers are separate although closely opposed, but fuse to the outer cuff (adventitia) of the great vessels where they enter or leave the heart (Standring 2009). For all but the inferior vena cava, the pericardium extends for a short distance covering the vessel before it fuses to its wall. It is reported to be attached to the sternum anteriorly and diaphragm inferiorly; however, the extent of these ligaments is widely debated (Standring 2009). Absence of the pericardium has been reported.

Heart dimensions (weight, length, position)

The heart is typically positioned in the middle mediastinum with a third of its size located on the right of the midline and the remainder two-thirds on the left. On average the heart apex and base are 12 cm apart, 8–9 cm in width at its widest and 6 cm in its anteroposterior dimensions. It typically weighs 300 g in males (range 280–340 g) and 250 g in females (range 230–280 g). It is deemed to be approximately 0.45% and 0.40% of body weight in males and females, respectively (Standring 2009).

Situs inversus/situs ambiguous/bifid apex

The apex of the heart may be positioned to the right (dextrocardia), left (levocardia), or the middle (mesocardia) (Loukas et al. 2009a). Situs inversus (mirror image) occurs in about 0.01% of the population and is congenital in nature (Fulcher and Turner 2002; Loukas et al. 2009a). Situs inversus is usually associated with dextrocardia, but has been reported with levocardia in which only the heart is in its normal position. Situs ambiguous, also known as heterotaxy syndrome (polysplenia or asplenia syndrome), is characterized by the major organs being misplaced from their normal position but not in a mirrored fashion (Loukas et al. 2009a). As a result there is no clear lateralization of the organs and is usually associated with cardiac malformations.

Atrial appendages (left and right)

The right appendage (auricle) is large and triangular with a broad base; the left is more tube-like with a narrow base where it joins the rest of the atrium (Ho et al. 2002; Standring 2009). The right appendage overlies the root of the aorta, as well as the anterior wall of the right atrium. The left appendage is located more superiorly and points toward the aortic root; it often overlies the main trunk of the left coronary artery with its tip reaching the pulmonary trunk (Ho et al. 2002). The morphology of the atrial appendages varies among species (Ho et al. 2002). In the right atrium the terminal sulcus marks the separation between the appendage and the venous inflow; this does not happen for the left (Ho et al. 2002). The right auricle contains pectinate muscle that extends from the main chamber. In some cases, Chiari formations formed by inadequate regression of the Eustachian valve may extend into the right auricle creating a web-like net (Le Count 1901–1903). The left atrial appendage contains pectinate muscle and is confined to the small appendage (Ho et al. 2002).

Foramen/fossa ovalis

The fossa ovalis (Fig. 104.1) is found on the right-sided atrial septal wall; the rim (limbus) is a prominent ridge most distinctly in its superior aspect. The fossa ovalis shows a great deal of variation in shape, area, thickness, and permeability. The shape of the fossa is oval in 78% of individuals while in the remainder it is round. The area showed a range of 18–45.32 mm^2, which is larger in males than in females in a study by Reig et al. (1997). The anterior limbus is thicker than the posterior limbus and the foramen was shown to be permeable in 22%

Bergman's Comprehensive Encyclopedia of Human Anatomic Variation, First Edition. Edited by R. Shane Tubbs, Mohammadali M. Shoja and Marios Loukas.
© 2016 John Wiley & Sons, Inc. Published 2016 by John Wiley & Sons, Inc.

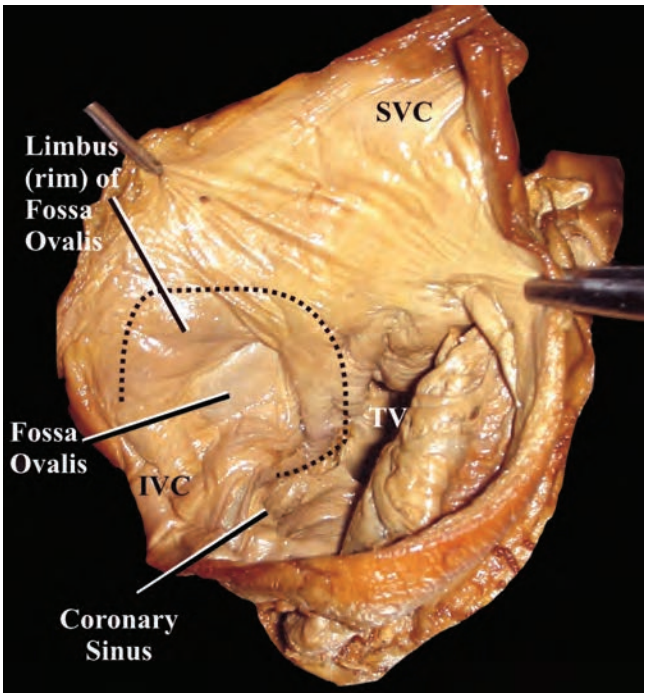

Figure 104.1 Right atrial view after perpendicular incision on the main axis of the intervenous area, in the direction of the vertical line connecting the long axis of the two venae cavae. Notice the prominent elevation of the limbus (rim) of the fossa ovalis demarcated with dotted lines. TV, tricuspid valve; SVC, superior vena cava; IVC, inferior vena cava.

Source: Loukas et al. (2012). Reproduced with permission from John Wiley & Sons.

(Reig et al. 1997). This is referred to as a patent foramen ovale and has a wide range of sizes (Standring 2009). The fossa ovalis may be covered with a membrane, which may be significantly thicker than the surrounding fossa, and the patent foramen may or may not produce symptoms. There appears to be a connecting channel in the interatrial septum regardless of patency of the foramen ovalis (Sweeney and Rosenquist 1979). Ferreira et al. (1992) found that in 17% of specimens with patent foramen ovale studied, it was not accompanied by deficiency of the flap valve. In 12 of these specimens the defect was 50% or larger than the fossa itself (Ferreira et al. 1992). Absence of the anterior or posterior lip of the fossa has also been reported (Ferreira et al. 1992). The fossa ovalis represents nearly 30% of the total septal surface area in normal hearts (Sweeney and Rosenquist 1979).

Pectinate muscle (tenia sagitalis/ crista terminalis)

The junction between the embryological sinus venosus (venous) and the muscular (true atrial) part of the right atrium is marked internally by the crista terminalis (terminal crest) (Fig. 104.2). A smooth muscular ridge extending normally

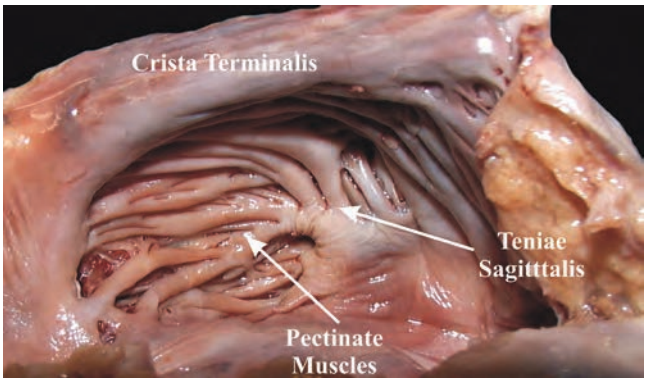

Figure 104.2 A type III PM, in which PM exist with uniform spacing and no trabeculation with fibers oriented parallel to CT.

Source: Loukas et al. (2008b). Reproduced with permission from Elsevier.

from the upper part of the septal surface, anterior to the superior vena cava, then passes its right side to attach to the right of the inferior vena cava orifice (Loukas et al. 2008b; Standring 2009). The pectinate muscles arise from the terminal crest running anterolaterally and are subject to many variations (Loukas et al. 2008b). They typically extend into the auricle where they form trabeculations (Standring 2009). A prominent and the largest slip of pectinate muscle forming the bridge of the crista terminalis is termed the "taenia sagittalis" or sagittal worm (Loukas et al. 2008b; Fig. 104.2). Variations of the pectinate muscles in the right atrium described by Loukas et al. (2008b) are:

1. fibers run parallel to each other with uniform spacing between them, attaching perpendicular to the crista terminalis (Fig. 104.3);
2. fibers arranged haphazardly with many cross-overs and trabeculations (Fig. 104.4);

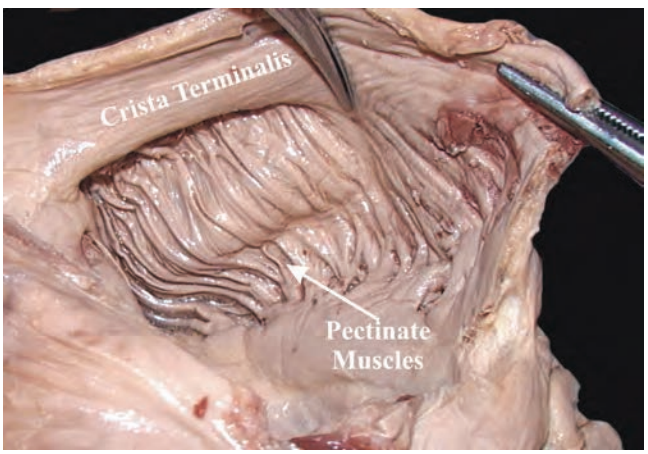

Figure 104.3 Type I PM oriented perpendicular to crista terminalis.

Source: Loukas et al. (2008b). Reproduced with permission from Elsevier.

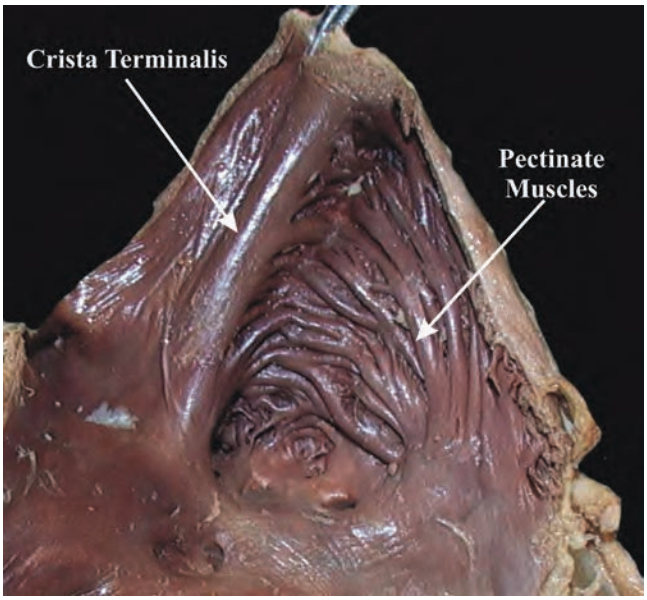

Figure 104.4 Type II PM, in which non-uniform PM are organized in a haphazard, trabecular fashion with numerous cross-overs.

Source: Loukas et al. (2008b). Reproduced with permission from Elsevier.

3. fibers with uniform spacing and no trabeculations, but run parallel to the crista terminalis instead of perpendicular (Fig. 104.5);
4. pectinate muscle fibers branch out from a solitary common trunk (Fig. 104.6);
5. fibers criss-cross running both perpendicular and parallel to the crista terminalis; and

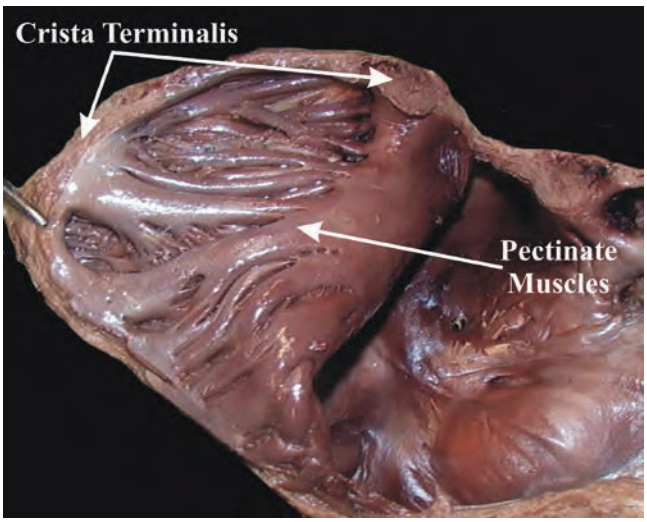

Figure 104.5 PM (of Type V) with uniform spacing and no trabeculation with fibers oriented parallel to the CT, but with more than one common muscular trunk.

Source: Loukas et al. (2008b). Reproduced with permission from Elsevier.

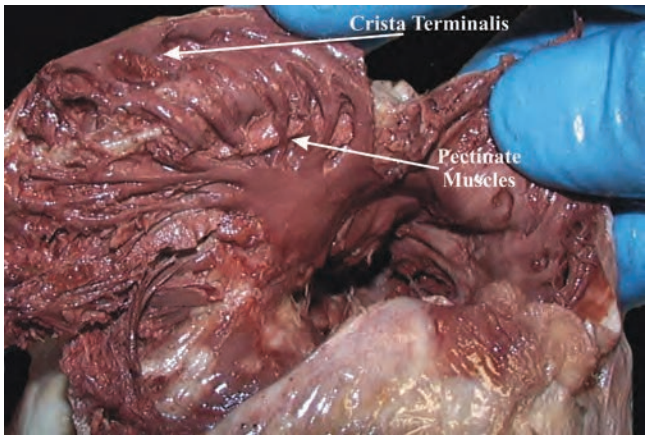

Figure 104.6 Arborizing PM of type IV originating from a common muscular trunk (solitary trunk). Fibers oriented both perpendicular and parallel to CT.

Source: Loukas et al. (2008b). Reproduced with permission from Elsevier.

6. prominent muscular column with velamentous (sheet or veil-like) pectinate muscle (Fig. 104.7).

The pectinate muscles may also display a combination of these features, as seen in Figure104.8.

Tenia sagitallis is also subject to variation and is absent in 15% of specimens studied, and it may be single or multiple (Loukas et al. 2008b). It ranges in both thickness (0.2–0.6 mm) and length (4–15 mm). The measurements of the crista terminalis were 0.5–11 mm in thickness and 40–62 mm in length (Loukas et al. 2008b). There does not appear to be any significant difference between race, gender, or age in any of the measured dimensions.

The pectinate muscles of the left atrium are confined to the left atrial appendage.

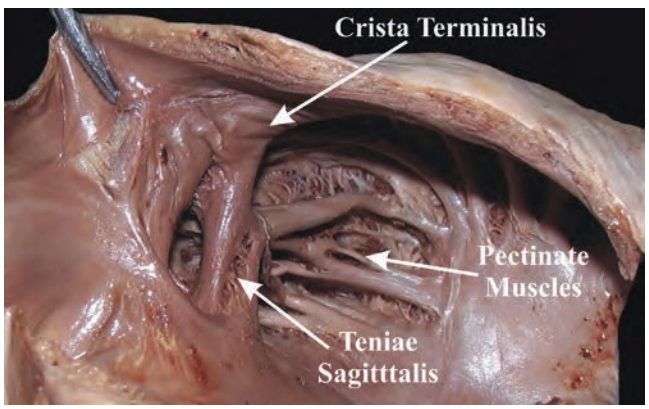

Figure 104.7 A prominent muscular column, the TS, with velamentous PM (Type VI) having potential clinical implications in cardiac catheterization procedures.

Source: Loukas et al. (2008b). Reproduced with permission from Elsevier.

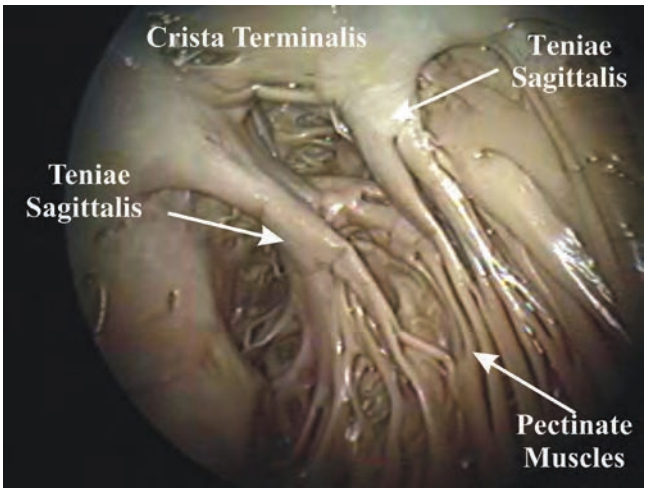

Figure 104.8 An endoscopic view of the right atrium. Note two prominent muscular columns (the TS) with velamentous PM (Type VI) having potential clinical implications in cardiac catheterization procedures.

Source: Loukas et al. (2008b). Reproduced with permission from Elsevier.

Tendon of Todaro

The tendon of Todoro can be seen as an endomyocardial prominence inside the right atrium (Domènech-Mateu et al. 1994). It is a round subendocardial tendon composed of collagen that is easily palpable. Located between the attachment of the Eustachian valve and the coronary sinus ostium (Standring 2009), it forms the roof of the last portion of the sinus venosus, and lies between the Eustachian and Thebesian valves (Domènech-Mateu et al. 1994). It forms part of the cardiac skeleton of the heart (Domènech-Mateu et al. 1994). The tendon of Todaro marks the superior border of the triangle of Koch, where the atrioventricular node may be identified. It has been shown that the tendon of Todaro can be single, double, triple, or absent.

Eustachian valve

The Eustachian valve is found anterior to the opening of the inferior vena cava into the right atrium. It is a flap-like fold of endocardium enclosing a small amount of muscle fibers, varies in size, and can be located on the lateral or right margins of the vein. The Eustachian valve runs into the sinus septum inferiorly and becomes continuous with the valve of the coronary sinus before inserting into the crista terminalis laterally (Standring 2009). While it is constantly large in the fetus, size varies greatly in the adult. It may be filamentous, cribriform, or even entirely absent but may leave a prominent recess posteroinferiorly to the coronary sinus opening (Standring 2009). The valve is said to disappear during childhood and, although it regresses, it does not disappear entirely in all individuals. When persisting, it has a variety of appearances and sizes. It has also been demonstrated in association with patent foramen ovale and may be seen extending from the posteroinferior lip of the fossa. It was described by Bell and Bell (1816) as having an anterior horn running from the inferior vena cava and connecting via a posterior horn to the left of the isthmus. If the valve is not adequately absorbed, it may form a fibrous network called the Chiari network (Iaizzo 2010; Loukas et al. 2010b). It may persist very large and divide the right atrium into two cavities. The Eustachian valve when present may send several bands of tissue to various structures of the right atrium. It is usually associated with the superior attachment of the Thebesian valve and without any cardiac abnormalities (Chairi 1897). The Eustachian valve variations described by Yater (1928) are: (1) absent; (2) simple flap not fenestrated, crescent shaped; (3) fenestrated, usually thin band; (4) a network of threads; (5) fused to Thebesian valve; and (6) Chiari's network.

Thebesian valve

The Thebesian valve is located directly below the Eustachian valve. It is usually attached to the lower end of the interatrial septum and covers the coronary ostium. It can be large and broad, fenestrated, consist of variable numbers of fibrous strands, or may even be absent (Chairi 1897; Yater 1928). It may lie anterior or posterior to the orifice and lie vertically or transversely across the coronary sinus orifice (Yater 1928). Yater (1928) classified the valve variations as follows (Fig. 104.9): (1) absence; (2) simple non-fenestrated, either crescent-shaped, semilunar, or triangular in shape; (3) simple fenestrated, ranged between small crescent shape to broad fold covering orifice; (4) simple fold with accessory threads; (5) simple vertical bar; (6) threads only; (7) U-shaped folds on limbs on either side of orifice; (8) complicated membranes passing vertically over orifice; (9) a single fold with the Eustachian valve; or (10) miscellaneous types not fitting in other categories (inverted U-shape; crescent-shaped fold with strands anterior to orifice; cresent-shaped fold with a branch; network over the sinus orifice; large fenestrated veil; or triangular fold with one fenestra attached to inferior rim of orifice).

The position of the flap may be vertical or horizontal and may have a variable number of branches and fenestrae (Yater 1928).

Papillary muscles and chorda tendinae

The papillary muscles and their tendinous cords vary greatly in terms of number, shape, and location (Loukas et al. 2008a). The chorda tendinae are classified based on their length, or the distance between the papillary muscle and leaflet. Further classifications are single, free-edge, deep, and basal (Standring 2009) and false when they do not attach to leaflets at all (Loukas et al. 2007a; Loukas et al. 2008a). Right ventricular papillary muscles were classified by Wafae et al. (1990) based on their position: posterior (posterolateral or posteromedial); anterior; or septal (infundibular or septal inferior).

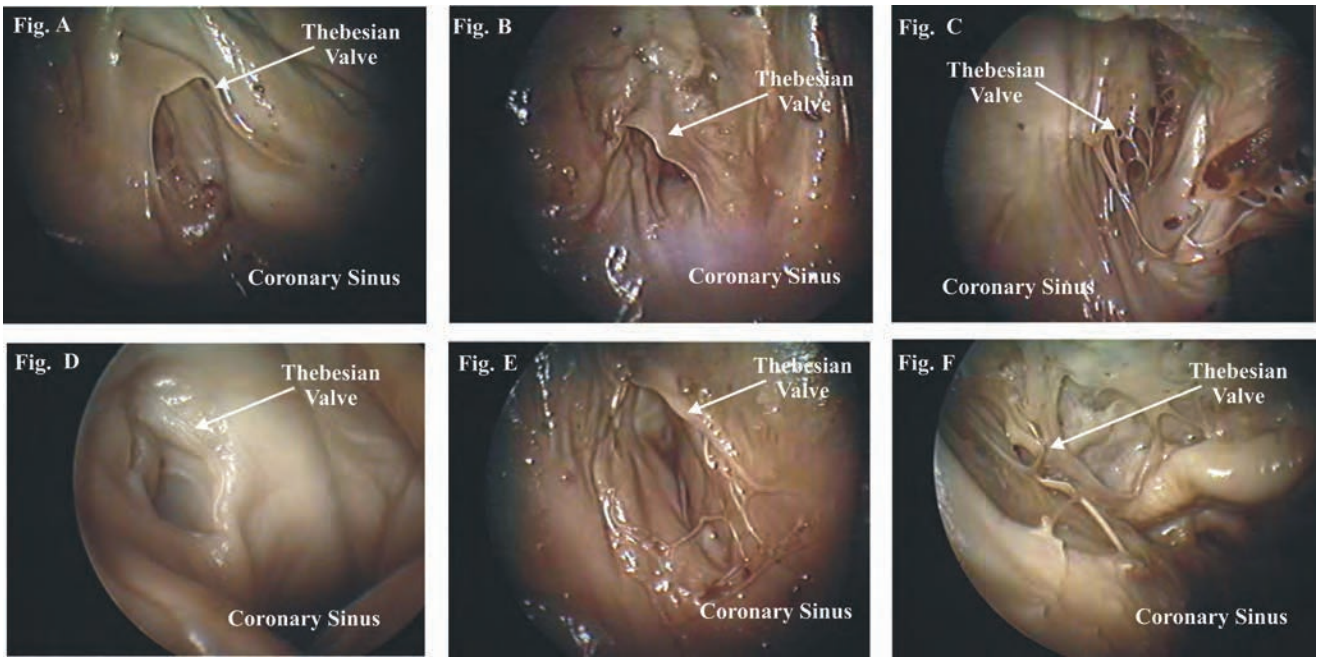

Figure 104.9 The different types of Thebesian valves as seen with an endoscope: (a, b) folds at different locations; (c) an example of a fenestrated valve; (d) a small fold; (e) an example of a branching valve; and (f) a valve with branches.

Source: Loukas et al. (2009c). Reproduced with permission from John Wiley & Sons.

They also stated that four (46%) or even five papillary muscles were often found instead of the usual three (Wafae et al. 1990).

Normally only two papillary muscles are present in the left ventricle. There may however be three components, and the size and degree of separation of these differ (Treder-Mentuch 1984). Typically, there are two parietal and one internal (Treder-Mentuch 1984).

Papillary muscle complex

Many authors have questioned the gross anatomy of the septal papillary muscle of the conus, also known as the papillary muscle complex (PMC), during the past century. According to Loukas et al. (2009) the PMC was present in 82% of hearts, while in the remaining 18% of specimens it was replaced by tendinous chords (Fig. 104.10). The PMC was connected with the septal (59.7%), anterior (20.7%), or both septal and anterior leaflets (19.5%) with single (29.8%) or multiple chordae tendinae (70.1%). The PMC was also found to be present as a single papilla (51.8%), double papilla (32.9%) (Fig. 104.11), or triple papilla (15.2%) (Fig. 104.12). In addition to the PMC, accessory single septal papillary muscles were present in 42 specimens, double septal papillary muscles 32 specimens (Fig. 104.13), and triple septal papillary muscles in 26 specimens. In the right ventricular inflow tract, the location of the PMC was consistently found to be in a position below the junction of the anterior and septal leaflets of the tricuspid valve. In the right ventricular outflow tract, in 73 specimens the PMC was located at the junction formed superiorly by the inferior border of the subpulmonary infundibulum and inferiorly by the superolateral border of the septal band, extending into the region of the subpulmonary infundibulum. In the remaining 27%, the PMC was located primarily at the area occupied by the superolateral border of the septal band without extending to the subpulmonary infundibulum.

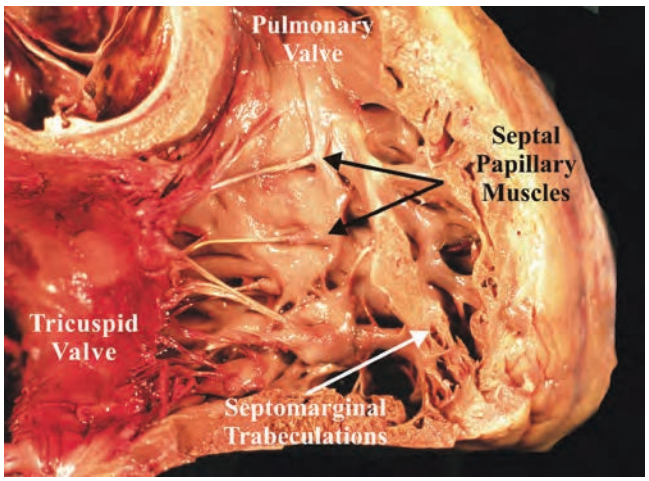

Figure 104.10 The papillary muscle of the conus (PMC) is absent. The characteristic papilla is absent and the chordae tendinae originate from the septal wall.

Source: Loukas et al. (2009b). Reproduced with permission from Springer Science and Business Media.

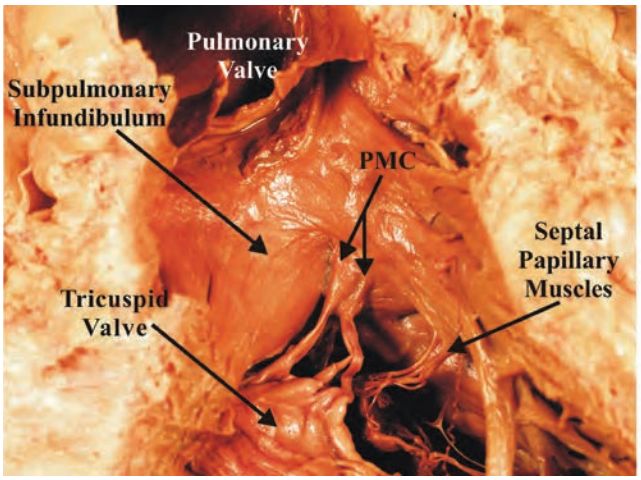

Figure 104.11 A papillary muscle of the conus (PMC) is evident, exhibiting double papillae from which the chordae tendinae arise.

Source: Loukas et al. (2009b). Reproduced with permission from Springer Science and Business Media.

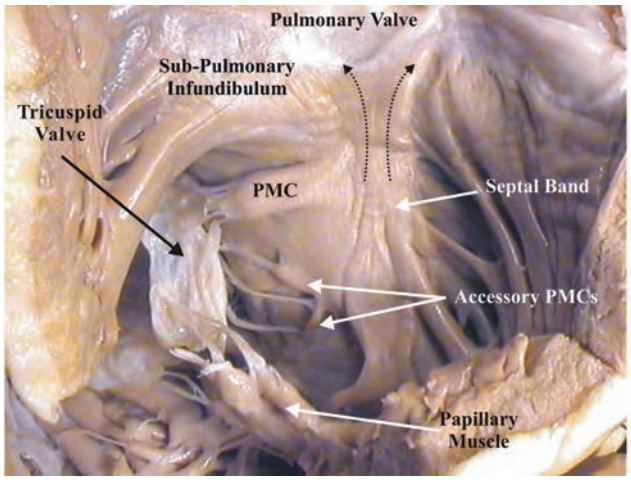

Figure 104.13 A papillary muscle of the conus (PMC) is evident; in addition, two accessory septal papillary muscles are evident, presenting a characteristic papillae-type morphology.

Source: Loukas et al. (2009b). Reproduced with permission from Springer Science and Business Media.

Moderator band

The moderator band shows a great deal of morphological variation in both appearance and dimensions (Loukas et al. 2010a). The appearance of the band varies with length (11.3–24.3 mm) and thickness (1.3–8.4 mm) and forms a variety of combinations of the two. The band has different points of origin which is based on the distance to three landmarks: the septal and inferior leaves of the tricuspid valve (19.2–39.7 mm); the apex of the heart (25.2–48.3 mm); and the base of the pulmonary valve (36.3–57.8 mm). The attachment was noted by Brown to be sufficiently low in some individuals that it resembles an ordinary ventricular trabeculation (Davies 1890). It may detach from the septum entirely, producing a free muscular trabeculation (Wittkampf et al. 1995) and may be sufficiently large to produce a double-chambered right ventricle (Wu et al. 2009; Loukas et al. 2013). Figures 104.14–104.17 show the extent of this variation as well as the relationships with the apex and papillary muscles in each case.

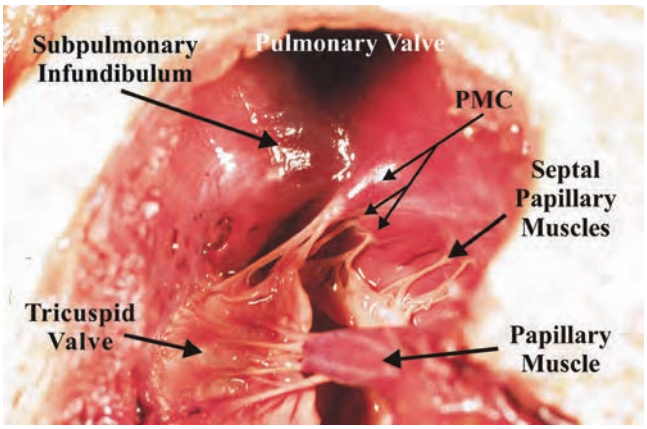

Figure 104.12 A papillary muscle of the conus (PMC) is evident, exhibiting triple papillae from which the chordae tendinae arise.

Source: Loukas et al. (2009b). Reproduced with permission from Springer Science and Business Media.

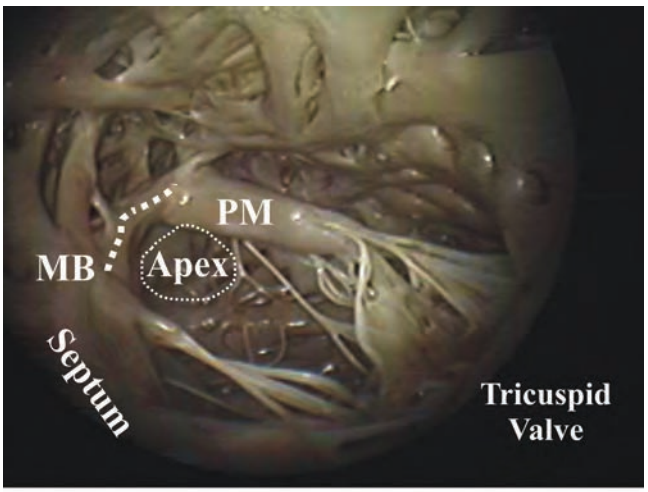

Figure 104.14 Endoscopic picture taken through the tricuspid valve, identifying a short and thick moderator band. MB, moderator band; PM, papillary muscle.

Source: Loukas et al. (2010a). Reproduced with permission from John Wiley & Sons.

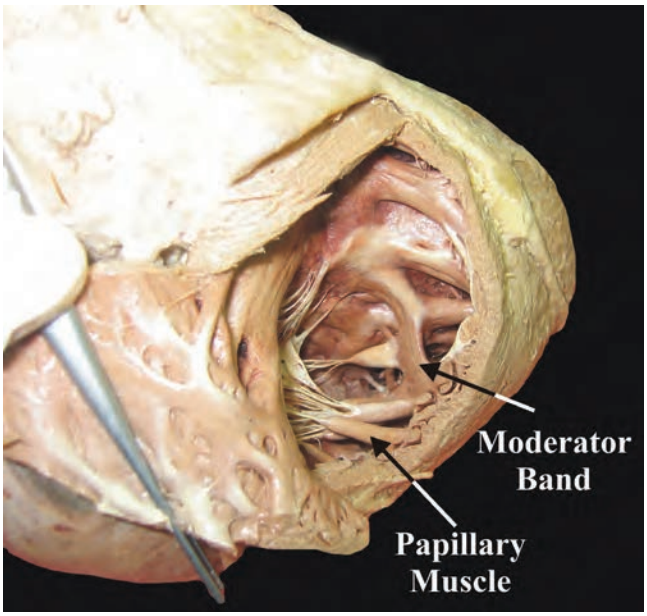

Figure 104.15 Moderator band forms a long and thick band.

Source: Loukas et al. (2010a). Reproduced with permission from John Wiley & Sons.

Tricuspid valve

Normally the tricuspid valve is described as having three leaflets: anterior, septal, and posterior (Wafae et al. 1990). There may be supernumerary leaflets either by duplication or subdivision (Wafae et al. 1990). Wafae et al. (1990) reported in 72% of 50 hearts the valve was formed by less (two) or more (four, five or six) leaflets (Wafae et al. 1990). With four being the most common (52%), this was termed the anterolateral leaflet due to its favored position between the anterior and posterior leaflets. They also reported commissural leaflets in 64% with a range of one to four leaflets, with one being the most common (78.1%; Wafae et al. 1990). The commissural leaflets were located between the anterior and septal or the posterior and septal leaflets. There does not appear to be a correlation between supernumerary leaflets and the presence or number of commissural leaflets (Wafae et al. 1990). Proposed naming of the leaflets was based on their radians on the valve opening: anterior (0–140°); posterior (140–220°); septal (220–360°); anterolateral (100–180°); posteromedial (110–160°); and posterolateral (120–140°).

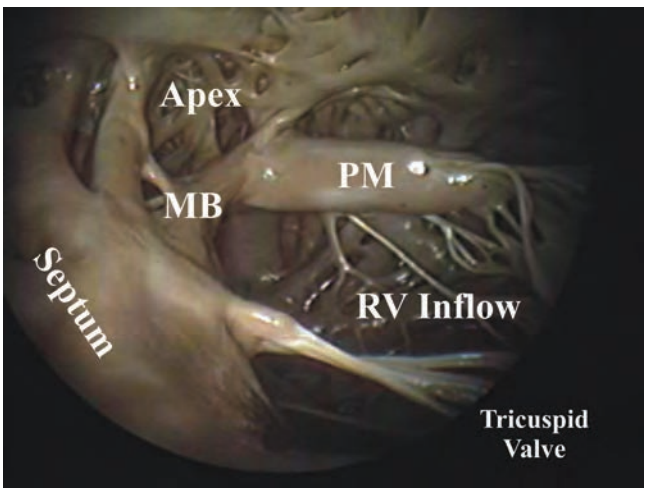

Figure 104.16 Endoscopic picture taken through the tricuspid valve, identifying a long and thin moderator band. MB, moderator band; PM, papillary muscle.

Source: Loukas et al. (2010a). Reproduced with permission from John Wiley & Sons.

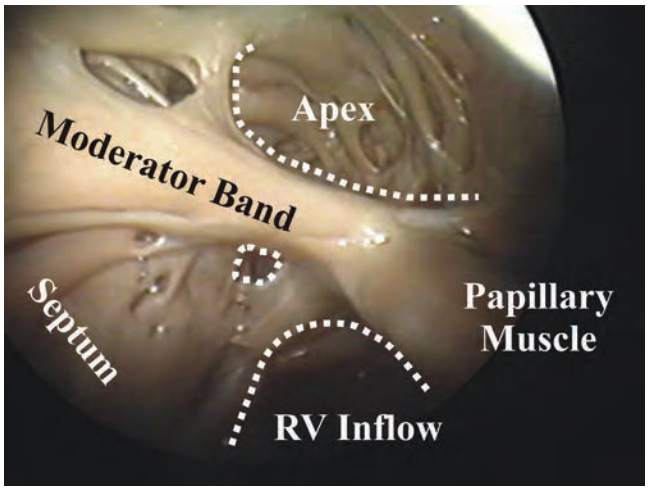

Figure 104.17 Endoscopic picture taken through the tricuspid valve, identifying a short and thick moderator band.

Source: Loukas et al. (2010a). Reproduced with permission from John Wiley & Sons.

Mitral valve

The mitral valve consists of a continuous flap attaching around the periphery of the ostium (Ranganathan et al. 1970). The free edge of this veil-like structure shows various indentations, two of which are regular, dividing the flap into anterior and posterior leaves (Ranganathan et al. 1970). The chorda tendinae, which attach the flaps to the papillary muscles, attach to thickened areas between the two leaves called commissures. The arrangement of the attachments does however vary (Ranganathan et al. 1970). Other names for the anterior leaflet are: aortic, septal, greater, or anteromedial. It is the larger of the two and either triangular or semicircular in shape. The free margins of the anterior leaflet have no indentations (Ranganathan et al. 1970). The posterior leaflet also carries the names ventricular, mural, smaller, or posterolateral leaflet. It is smaller and contains numerous indentations along its free edge. Ranganathan et al. (1970) therefore suggested the rejection of multiple cups

based on this morphology; they suggest instead that the posterior leaflet is subdivided into three smaller areas. Others have named the components of the leaf separately, but maintain that it a single structure. The valve can be duplicated.

Pulmonary valve

The pulmonary valve displays a very similar anatomy as the aortic valve, but does not have any vessels branching from it. The leaflets are positioned in different orientations to the aortic (Loukas et al. 2014). The leaflet size of the pulmonary valve shows inequality among the different leaflets (Vollebergh and Becker 1977). It has been noted that the pulmonary valve may exhibit two cusps instead of the usual three (Fig. 104.18).

Aortic valve

The aorta contains three leaflets or leaves that hang off the edge of the wall, two of which have the ostia of the coronary arteries. Power (1850) reported a specimen with five semilunar valves and quoted Hunter who stated that he found a specimen with only two valves. The leaflets of the aortic valve may be of unequal size. The aortic valve typically consists of three leaflets; the left and right each contain the ostium for the two coronary arteries and the non-coronary leaflet, respectively. Other names for the non-coronary leaflet which have been proposed are posterior and facing (Loukas et al. 2014). Vollebergh and Becker (1977) showed that the three leaflets are rarely equal in size, and can be classified in seven different ways based on this classification. Age-related thickening of the leaflet borders has also been noted (Vollebergh and Becker 1977).

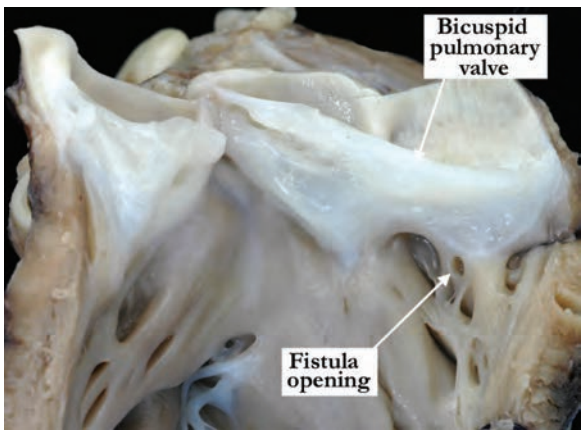

Figure 104.18 Cut section of the pulmonary trunk, showing a bicuspid valve instead of the usual tree cusps.

Source: D Spicer.

Tendon of the infundibulum

Tendon of the infundibulum (conus ligament) is a band of collagen extending from between the pulmonary infundibulum and the root of the aorta (Standring 2009). However, Loukas et al. (2001) demonstrated that this "tendon" could not be found in the vast majority of the hearts studied. Instead were multiple fascial bands (a finding supported by many authors) that passed between the structures in an unorganized and non-uniform manner (Loukas et al. 2007b).

False tendons

Left

False tendons as defined by Kervangcioglu et al. (2003) are single or multiple, fibromuscular or fibrous bands traversing the ventricle without attaching to the leaflets. False tendons are essentially false chorda tendinae consisting of cardiac myocytes and connective tissue. They may contain varying amounts of conductive tissue within them, depicted in Figure 104.19 using various staining methods. Alternative attachments are connecting the two papillary muscles (22%) or even parts of the ventricular wall (Loukas et al. 2007a; Loukas et al. 2008a). They are located in the left ventricle, found in more than 50% of hearts, and often show multiple tendons in the same individual. Luetmer et al. (1986) reported false tendons in 55% of hearts studied of which 38% had multiple tendons. In a study by Loukas et al. (2007a) on the false tendons of the left ventricle it was shown that, in 62% of hearts studied, 39% displayed the presence of multiple tendons. These tendons were found attaching the ventricular septum to the posteromedial (92%) and anterolateral (16.5%) papillary muscles and the free ventricular wall (12.5%). The remainder (11.6%) of tendons attached to three or more points in a web-like fashion (Loukas et al. 2007a). The variations and different types of false tendons based on their attachments are depicted in Figures 104.20–104.22.

Right

These false tendons may also be found on the right (Loukas et al. 2008a). The right ventricle can show as many as five false tendons. Loukas et al. (2008a) classified the RFT according to their attachments:

1. between the ventricular septum and the anterior papillary muscle (Fig. 104.23);
2. between the ventricular septum and the posterior papillary muscle;
3. anterior leaflet of the tricuspid valve to the right ventricular free wall;
4. connecting the posterior papillary muscle to the right ventricular free wall; or
5. anterior papillary muscle to the ventricular wall.

The length of the tendons ranged over 6–48 mm, and had a diameter at midpoint of 1.1–2.0 mm. Less than half (41.6%) of RTFs carry conduction fibers.

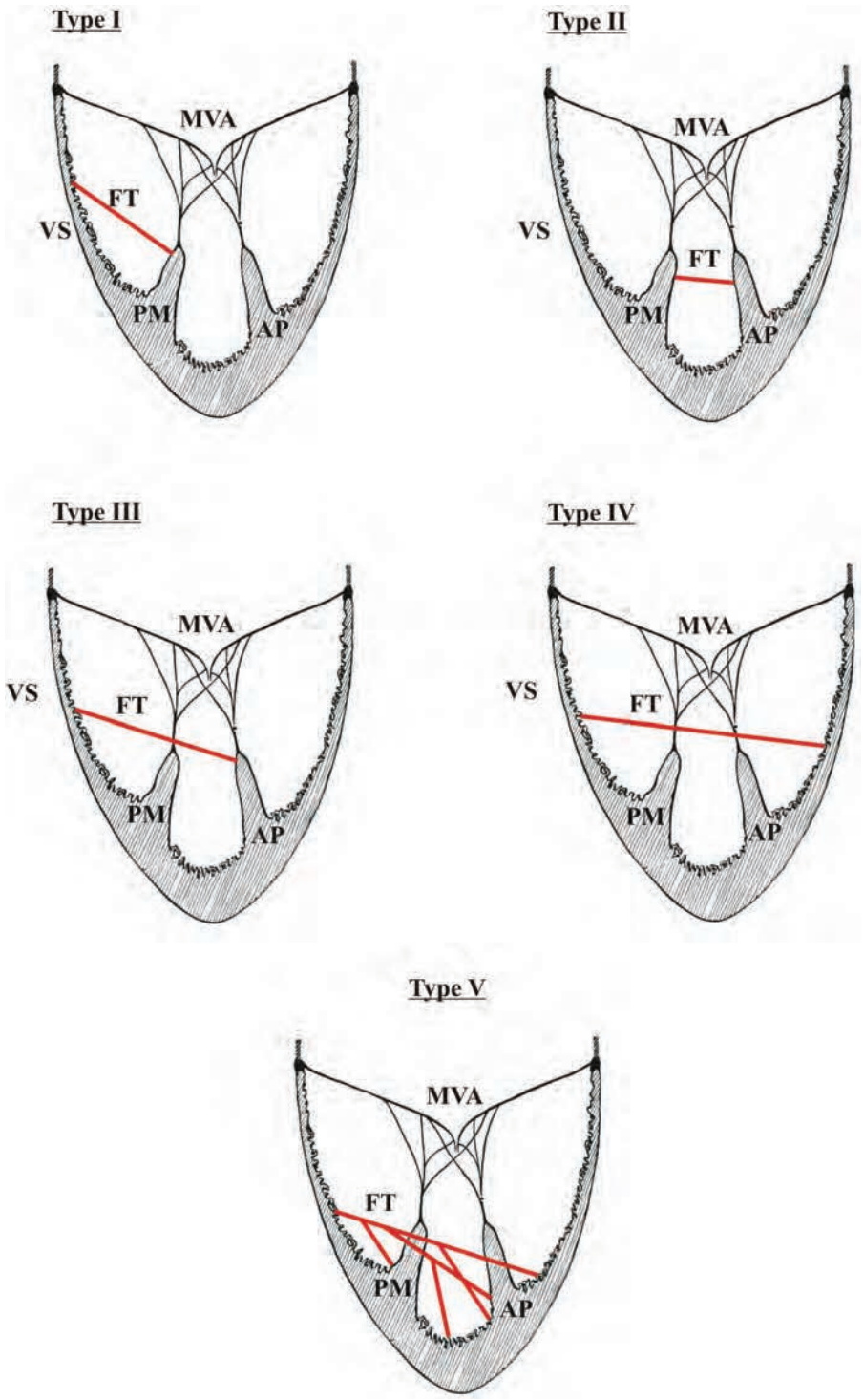

Figure 104.19 Five types of false tendon topography within the left ventricle based on attachment points.

Source: Loukas et al. (2007a). Reproduced with permission from John Wiley & Sons.

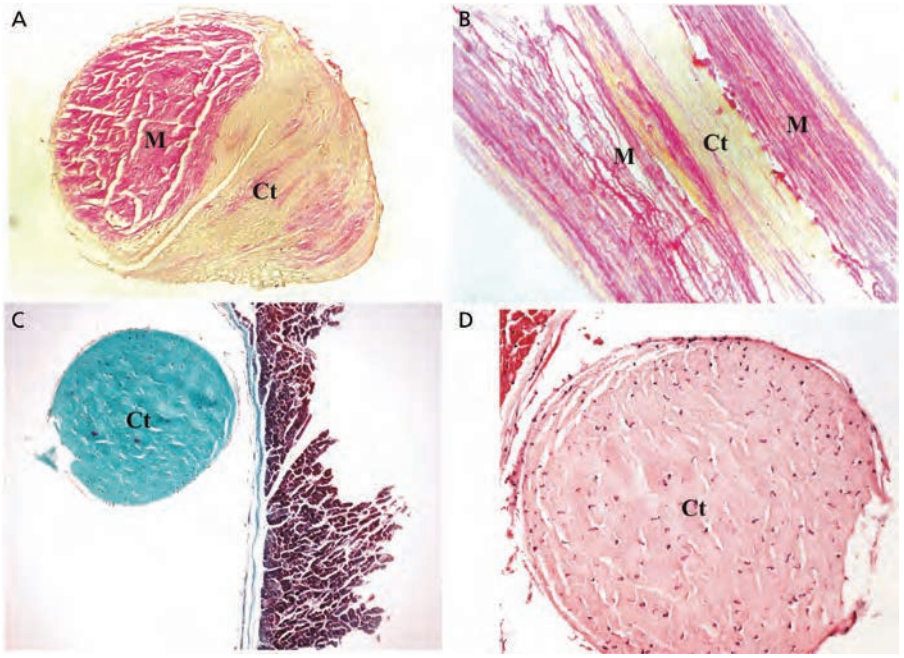

Figure 104.20 Histologic sections of FTs stained with (a, b) Van Geisson; (c) Masson Trichrome; and (d) eosin–hematoxylin. M, muscle tissue; Ct, connective tissue.

Source: Loukas et al. (2007a). Reproduced with permission from John Wiley & Sons.

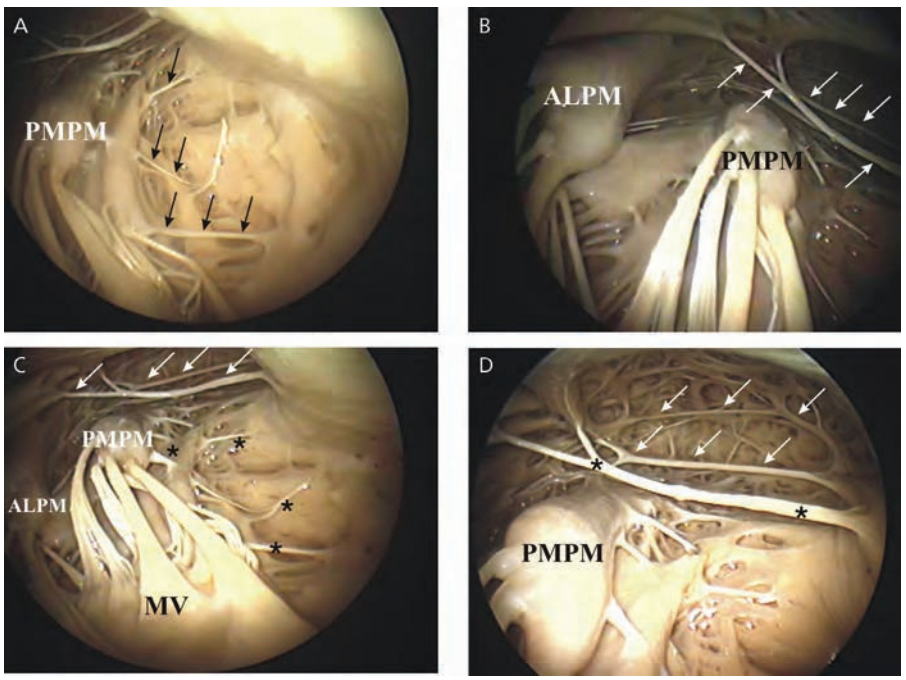

Figure 104.21 Endoscopic images of multiple FTs within one specimen: (a) three examples of FT type I (arrows); (b) example of a FT type IV (arrows); (c) examples of FT types I (asterisks) and III (arrows); and (d) examples of FT types III (asterisks) and V (arrows). MV, mitral valve; PMPM, posteromedial papillary muscle; ALPM, anterolateral papillary muscle.

Source: Loukas et al. (2007a). Reproduced with permission from John Wiley & Sons.

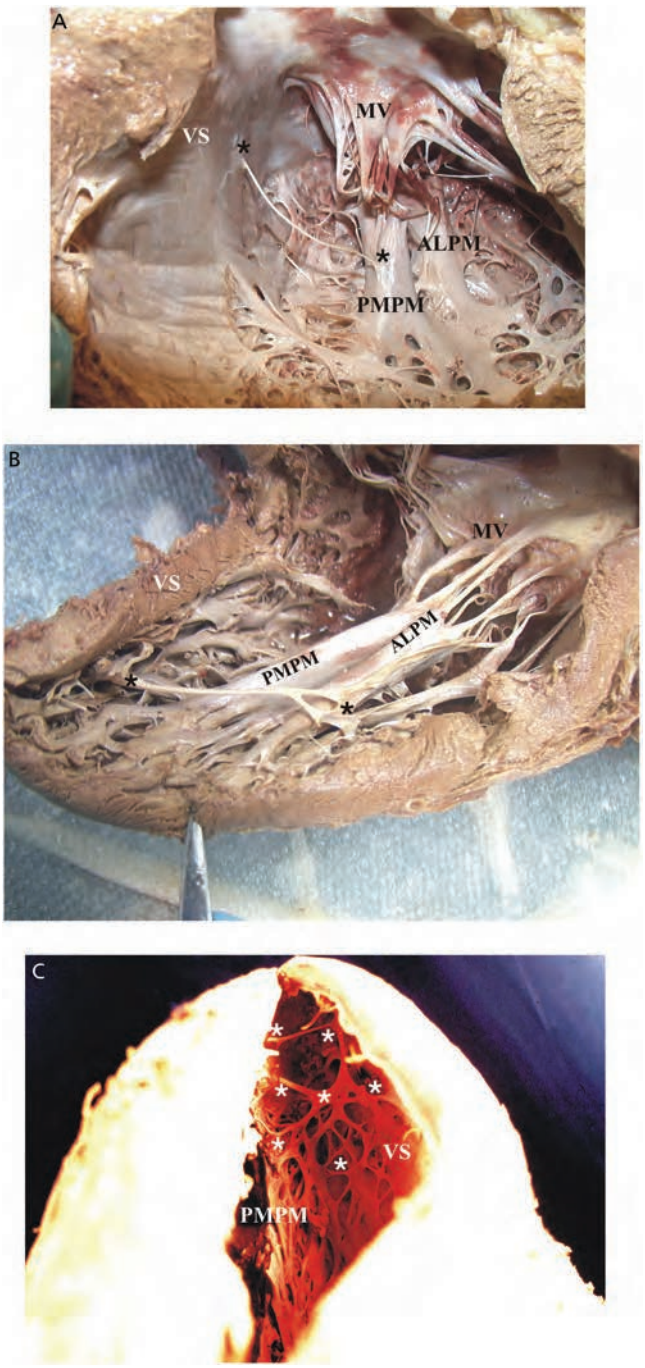

Figure 104.22 Gross dissections of FTs. Example of (a) type I; (b) type III; and (c) type V. The asterisks indicate the points of attachment. MV, mitral valve; PMPM, posteromedial papillary muscle; ALPM, anterolateral papillary muscle; VS, ventricular septum.

Source: Loukas et al. (2007a). Reproduced with permission from John Wiley & Sons.

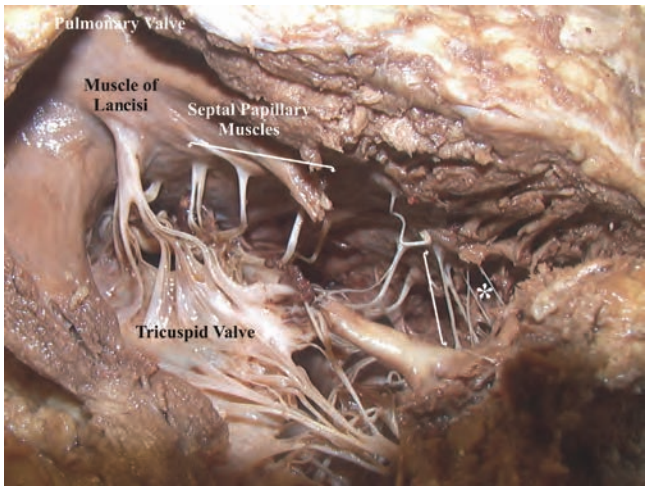

Figure 104.23 An example of type I RFTs. The asterisk indicates the accessory false tendons arising distally from the ventricular septum to the anterior papillary muscle. In addition, the septal papillary muscles are also indicated for comparison to the right ventricular false tendons.

Source: Loukas et al. (2008a). Reproduced with permission from Springer Science and Business Media.

Sinu-atrial node

The sinu-atrial node (SA node) is located in the superior part of the terminal sulcus and extends downward to the opening of the superior vena cava, where it lies inferolateral to it (Standring 2009). The SA node may be found histologically at the junction between the right atrial appendage and the anterior wall of the superior vena cava (Meridith and Titus 1968). The cells of the SA node are arranged radially and do not display intercalated discs (Meridith and Titus 1968).

Atrioventricular node

The atrioventricular (AV) node is situated in a triangular area at the inferior aspect of the interatrial septum, marking the apex of the triangle of Koch. The sides of the triangle are formed by the tendon of Todaro and the tricuspid annulus, with its base at the orifice of the coronary sinus (McGuire et al. 1992). The AV node penetrates the fibrous body at the apex of this triangle to form the bundle of His. The triangle has been described by some as uniform in size (McGuire et al. 1992). However, other studies have shown it to be different among individuals; this has also been suggested in response to the variable size of the AV node itself (Inoue and Becker 1998a). The AV node of the heart has been shown to have both posterior and anterior extensions (Inoue and Becker 1998b). The AV node may be identified as a pale circular structure located just above the fibrous ring of the tricuspid valve. The cells of the AV node are arranged in a network and are smaller than those of the SA node (Meridith and Titus 1968). An accessory atrioventricular bundle (of Paladino and Kent) may exist.

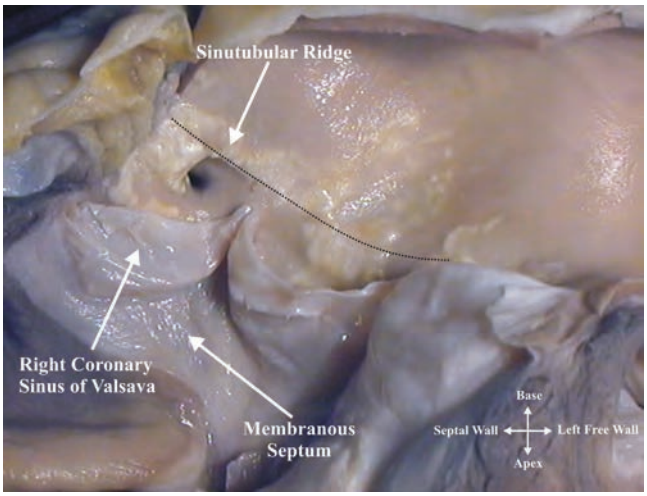

Figure 104.24 Gross anatomical demonstration of the sinutubular junction (SJ; dotted line). The sinutubular ridge is developed at the zones of opposition in an adult specimen. The membranous septum and the right coronary sinus of Valsalva are indicated for orientation.

Source: Loukas et al. (2009d). Reproduced with permission from Springer Science and Business Media.

Sinutubular junction

The sinutubular is the junction between the ascending aorta and the left ventricular outflow, and can be seen just superior to the attachment sites of the aortic leaflets. The area is said to form a ridge in some individuals (62%), but is absent in fetal and neonatal hearts (Figs 104.24, 104.25). It appears that the ridge increases in thickness as individuals age, as indicated by Loukas et al. (2009d) by $p = 0.043$; in addition to the ridge formation, the junction is subject to age-related atherosclerotic changes (Loukas et al. 2009d).

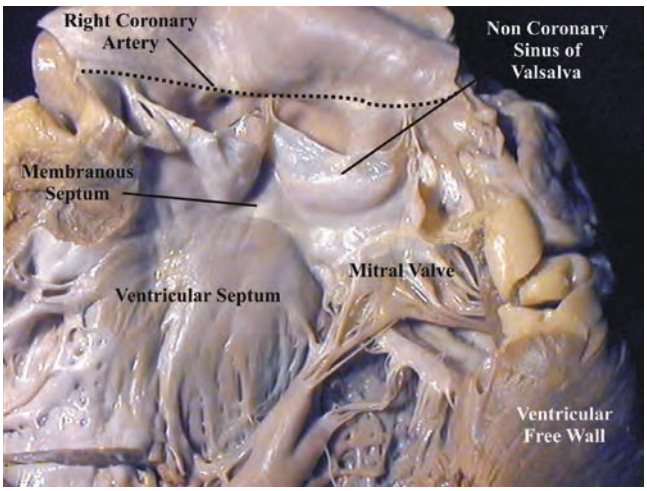

Figure 104.25 The SJ (dotted line) in relationship to right coronary artery, mitral valve, ventricular septum, membranous septum, and aortic sinus of Valsalva.

Source: Loukas et al. (2009d). Reproduced with permission from Springer Science and Business Media.

References

Bell J, Bell C. 1816. *The Anatomy of the Human Body*, second edition, vol 2. London: TN Longman, pp. 473–474.

Chairi H. 1897. Reticulum formation in the right atrium of the heart. *Beitr Path Anat* 22: 1–6.

Davies FA. 1890. *Circulatory system. Annual of the Universal Medical Sciences*. Vol 5. Atlanta: Cambridge.

Domènech-Mateu JM, Martínez-Pozo A, Arnó-Palau A. 1994. Development of the tendon of todaro during the human embryonic and fetal periods. *Anat Rec* 238: 374–382.

Ferreira SMAG, Ho SY, Anderson RH. 1992. Morphological study of defects of the atrial septum within the oval fossa: implications for transcatheter closure of left to right shunt. *Br Heart J* 67: 316–320.

Fulcher A, Turner M. 2002. Abdominal manifestations of situs anomalies in adults. *Radiographics* 22: 1439–1456.

Ho SY, Anderson RH, Sanchez-Quintana D. 2002. Gross structure of the atriums: More than an anatomic curiosity? *PACE* 25: 342–350.

Iaizzo PA. 2010. *Handbook of Cardiac Anatomy, Physiology, and Devices*. Minnesota: Springer.

Inoue S, Becker AE. 1998a. Koch's triangle sized up: Anatomical Landmarks in perspective of catheter ablation procedures. *PACE* 21: 1553–1557.

Inoue S, Becker AE. 1998b. Posterior extensions of the human compact atrioventricular node. *Circulation* 97: 188–193.

Kervangcioglu M, Ozbag D, Kervancioglu P, Hatipoglu ES, Kilinc M, Yilmaz F, Deniz M. 2003. Echocardiographic and morphologic examination of left ventricular false tendons in human and animal hearts. *Clin Anat* 16: 389–395.

Le Count ER. 1901–1903. Network formations in the right auricle, with demonstration of a specimen. *Tr Chicago Path Soc* 5: 309.

Loukas M, Dimopoulos C, Bartczak A, Kordula J, Wagner T, Fudalej M. 2001. The anatomy of the tendon of infundibulum. *Folia Morphol* 60: 281–284.

Loukas M, Louis RG JR, Black B, Pham D, Fudalej M, Sharkees M. 2007a. False tendons: An endoscopic cadaveric approach. *Clin Anat* 20: 163–169.

Loukas M, Tubbs RS, Bright JL, Fudalej M, Wagner T, Anderson RH. 2007b. The anatomy of the tendon of the infundibulum revisited. *Folia Morphol (Warsz)* 66: 33–38.

Loukas M, Wartmann CT, Tubbs RS, Apaydin N, Louis RG Jr, Black B, Jordan R. 2008a. Right ventricular false tendons, a cadaveric approach. *Surg Radiol Anat* 30: 317–322.

Loukas M, Tubbs RS, Tongson JM, Polepali S, Curry B, Jordan R, Wagner T. 2008b. The clinical anatomy of the crista terminalis, pectinate muscles and tenia sagittalis. *Ann Anat* 190: 81–87.

Loukas M, Strike DRG, Tubbs RS, Tarneja N, Shoja MM. 2009a. An interrupted inferior vena cava in a situs inversus: a case report and review of the literature. *Folia Morphol* 68: 184–187.

Loukas M, Tubbs RS, Louis RG Jr, Apaydin N, Bartczak A, Huseng V, Alsaiegh N, Fudalej M. 2009b. An endoscopic and anatomical approach to the septal papillary muscle of the conus. *Surg Radiol Anat* 31: 701–706.

Loukas M, Bilinsky S, Bilinsky E, El-Sedfy A, Anderson. 2009c. Cardiac veins: a review of the literature. *Clin Anat* 22: 129–145.

Loukas M, Wartman CT, Tubbs RS, Apaydin N, Louis RG Jr. Easter L, Black B, Jordan R. 2009d. The clinical anatomy of the sinutubular junction. *Anat Sci Int* 84: 27–33.

Loukas M, Klaassen Z, Tubbs RS, Derderian T, Paling D, Chow D, Patel S, Anderson RH. 2010a. Anatomical observations of the moderator band. *Clin Anat* 23: 443–450.

Loukas M, Sullivan A, Tubbs RS, Weinhaus AJ, DerDerian T, Hanna M. 2010b. Chiari's network: review of the literature. *Surg Radiol Anat* 32: 895–901.

Loukas M, El-Zammar D, Tubbs RS, Birungi J, Jacob J, Shoja MM, Anderson RH. 2012. Intervenous tubercle of Lower: true tubercle or normal interatrial fold? *Clin Anat* 25: 729–736.

Loukas M, Housman B, Blaak C, Kralovic S, Tubbs RS, Anderson RH. 2013. Double-chambered right ventricle: a review. *Cardiovasc Pathol* 22: 417–423.

Loukas M, Bilinsky E, Bilinsky S, Blaak C, Tubbs RS, Anderson RH. 2014. The anatomy of the aortic root. *Clin Anat* 27(5), 748–756.

Luetmer PH, Edwards WD, Seward JB, Tajik AJ. 1986. Incidence and distribution of left ventricular false tendons: an autopsy study of 483 normal human hearts. *J Am Coll Cardiol* 8: 179–183.

McGuire MA, Johnson DC, Robotin M, Richards DA, Uther JB, Ross DL. 1992. Dimensions of the triangle of Koch in humans. *Am J Cardiol* 70: 829–830.

Meridith J, Titus JL. 1968. The anatomic atrial connections between sinus and A-V node. *Circulation* 37: 566–579.

Power JH. 1850. *Surgical Anatomy of the Arteries and Descriptive Anatomy of the Heart by the Late Valentine Flood, M.D*. Dublin: Fannin and Co.

Ranganathan N, Lam JHC, Wigle ED, Silver MD. 1970. Morphology of the human mitral valve II. The valve leaflets. *Circulation* 41: 459–467.

Reig J, Mirafeix R, Jornet A, Petit M. 1997. Morphologic characteristics of the fossa ovais as an anatomic basis for transeptal catheterization. *Surg Radiol Anat* 19: 279–282.

Standring S. 2009. *Gray's Anatomy*, 40th edition. Philadelphia: Elsevier.

Sweeney LJ, Rosenquist GC. 1979. The normal anatomy of the atrial septum in the human heart. *Am Heart J* 98: 194–199.

Treder-Mentuch A. 1984. The papillary muscles of the left ventricle in human heart. *Folia Morphol (Warsz)* 43: 115–120.

Vollebergh FEMG, Becker AE. 1977. Minor congenital variations of cusp size in tricuspid aortic valves, possible link with isolated aortic stenosis. *Brit Heart J* 39: 1006–1011.

Wafae N, Hayashi H, Gerola LR, Vieira MC. 1990. Anatomical study of the human tricuspid valve. *Surg Radiol Anat* 12: 37–41.

Wittkampf FHM, Ector H, van Hemel NM. 1995. The Pacemaker Clinic of the 90s: Essentials in Brady-Pacing. Philadelphia: Kluwer.

Wu MC, Ku PM, Chou MC, Huang TY. 2009. Usefulness of 64-slice computed tomography for evaluation of double-chambered right ventricle combined with atrial and ventricular septal defects. *Tex Heart Inst J* 36: 74–75.

Yater WM. 1928. Variations and anomalies of the venous valves of the right atrium of the heart. *Arch Pathol* 7: 418–440.

Further reading

Acar C, Périer, Fontaliran F, Deloche A, Carpentier. 1990. Anatomical study of the tricuspid valve and its variations. *Surg Radiol Anat* 12: 229–233.

Anderson RH. 2000. Atrial structure in the presence of visceral heterotaxy. *Cardiol Young* 10: 299–302.

Anderson RH, Ho SY, Becker AE. 2000. Anatomy of the human atrioventricular junctions revisited. *Anat Rec* 260: 81–91.

Corno AF, Bron C, von Segesser LK. 1999. Divided right atruim. Diagnosis by echocardiography, and considerations on the functional role of the eustachian valve. *Cardiol Young* 9: 427–429.

Helwig FC. 1931. The frequency of anomalous retinacula in the right atrium of the human heart "Chiari network." *Am J Path* 8: 73–79.

McDonald PC, Wilson JE, McNeil S, Gao M, Spinelli JJ, Rosenberg F, Wiebe H, McManus BM. 2002. The challenge of defining normality for human mitral and aortic valves: geometrical and compositional analysis. *Cardiovasc Pathol* 11: 193–209.

Schwinger ME, Gindea AJ, Freedberg RS, Kronzon I. 1990. The anatomy of the interatrial septum: A transesophageal echocardiographic study. *Am Heart J* 119: 1401–1405.

Shirani J, Zafari AM, Roberts WC. 1995. Morphologic features of fossa ovalis membrane aneurysm in the adult and its clinical significance. *JACC* 26: 466–471.

Steding G, Jinwen X, Seidl W, Männer J, Xia H. 1990. Developmental aspects of the sinus valves and the sinus venosus septum of the right atrium in human embryos. *Anat Embryol* 181: 496–475.

Wartmann CT, Kinsella CR Jr, Tubbs RS, Loukas M. 2011. A rare case of a complete left inferior vena cava associated with the symptoms of Dunbar syndrome. *Clin Anat* 24: 262–265.

105 Esophagus

Koichi Watanabe
Kurume University School of Medicine, Fukuoka, Japan

The majority of anatomical variations of the esophagus are congenital. They usually occur at the time of separation of the esophagus and trachea from the primitive foregut in the third to seventh weeks of intrauterine life. Congenital esophageal anomalies sometimes involve the trachea. Esophageal stenosis, atresia, tracheoesophageal fistula, duplication cyst, and failure of separation are included in this category. On the other hand, an esophageal diverticulum is a typical example of an acquired anomaly.

In terms of variations in the muscles of the esophagus, striated muscle may be found infrequently in the distal segment (Bergman 1996). Pleuroesophageal and bronchoesophageal muscles are also rarely observed (Cunningham 1876; Bilge et al. 2013). A thyroesophagus muscle was reported by Gruber (1877).

Pleuroesophageal muscle

The pleuroesophageal muscle connects the left pleura and left boundary of the esophagus, passing over the thoracic aorta. It was first reported by Hyrtl in 1844 (Hyrtl 1844; Cuningham 1876; Bilge et al. 2013). This muscle and the bronchoesophageal muscle depicted later are rarely described in current anatomical textbooks and atlases (Bilge et al. 2013). However, Cunningham claimed that he was able to find a pleuroesophageal slip or slips in 13 of his 14 special dissections, and 10 of them included muscle tissue. In terms of the muscle size, Cunningham stated that the width was 0.25–0.5 inch (6.4–12.7 mm) in the majority of the cases, and the largest muscle was 1.25 inch (31.8 mm) wide and 1.5 inch (38.1 mm) long. Bilge described a pleuroesophageal muscle 8.5–10.5 mm wide, 37.6 mm long, and 1–2.5 mm thick. Histologically, all articles reported that this muscle comprises smooth muscle fibers (Hyrtl 1844; Cunningham 1876; Bilge et al. 2013). Bilge assessed the muscle histologically and embryologically, and concluded that it originates from the esophagus at an early stage of fetal development and not from the pleura. Cunningham (1876) depicted the function of this muscle as supporting the esophagus at fixed points upon which it can contract more readily in the process of swallowing. Bilge et al. (2013) also stated that the muscle is an anchoring structure of the esophagus. In another view, Henle (1866) claimed that this muscle protects the esophageal vessels from pressure and friction (Cunningham 1876).

Bronchoesophageal muscle

The bronchoesophageal muscle connects the esophagus and trachea (or bronchus). This muscle was first reported by Hyrtl in 1844, as was the above-described pleuroesophageal muscle. This muscle has also rarely been described in anatomical textbooks, atlases, and articles. However, Cunningham (1876) reported its relatively high frequency of occurrence (10 out of 14 cases). He described the details of the muscle as follows. It is generally double and represented by two slips springing from the posterior aspect of the bronchus, expanding as they pass downward and backward. Their constituent fibers mingle with the longitudinal muscular fibers on the anterior surface of the esophagus (Cunningham 1876). The function of this muscle has not yet been completely explained. However, in a recent report, it was presumed that these muscles play a role in anchoring the esophagus along with the pleuroesophageal muscle (Bilge et al. 2013).

Esophageal diverticulum

An esophageal diverticulum is a sac that protrudes from the esophageal wall and usually occurs in three locations: pharyngoesophageal (cricopharyngeal diverticulum); parabronchial (midesophageal diverticulum); or supradiaphragmatic (epiphrenic diverticulum). Onset may be either congenital or acquired. However, congenital diverticula are rare and probably classified as esophageal duplication. The cause of development of an esophageal diverticulum differs according to location. Cricopharyngeal and epiphrenic diverticula are categorized as pulsion diverticula and develop secondary to increased intraesophageal pressure during deglutition. Midesophageal diverticula are categorized as traction diverticula and develop secondary to an external force to the esophageal wall.

Bergman's Comprehensive Encyclopedia of Human Anatomic Variation, First Edition. Edited by R. Shane Tubbs, Mohammadali M. Shoja and Marios Loukas.
© 2016 John Wiley & Sons, Inc. Published 2016 by John Wiley & Sons, Inc.

Cricopharyngeal diverticulum (Zenker's diverticulum)

Zenker's diverticulum was first described by Zenker and Von Ziemssen in 1878 as a diverticulum that occurs at the point at which the hypopharynx meets the esophagus (Fig. 105.1a). This diverticulum occurs in Killian's dehiscence, the weak zone between the inferior constrictor muscle and cricopharyngeal muscle in the posterior hypopharynx (Delahunty et al. 1971; Zaninitto et al. 1996). Zenker's diverticulum usually lacks a muscle layer in the sack and is therefore classified as a pseudodiverticulum. The size varies from small to large. Borrie reported a 4×8 cm sac that filled the thoracic inlet and extended down to the aortic arch (Borrie and Wilson 1980). Affected patients are usually past middle age; patients under 40 years of age are rare (Van Overbeek 2003). The incidence of Zenker's diverticulum is reportedly quite different according to geographical region. It is not rare in the United States, Canada, or Australia, but is very uncommon in Japan and Indonesia (Van Overbeek 2003). It is generally believed that incomplete upper esophageal sphincter opening during deglutition secondary to fibrotic changes in the cricopharyngeal muscle causes the development of this diverticulum (Cook et al. 1992; Shaw et al. 1996; Zaninitto et al. 1996; Venturi et al. 1997; Bonavina et al. 2007).

Midesophageal diverticulum (Rokitansky's diverticulum)

A midesophageal diverticulum was first reported by Rokitansky in 1840. This diverticulum is extremely rare, and it is assumed that fewer than a dozen cases have been reported (Palotás et al. 2004). Its size is usually 3 cm or smaller. However, a case in which the diverticulum extended caudally for 7 cm was also reported (Hadi and Rameh 2007). Historically, it was assumed that inflammation of the mediastinal lymph nodes caused by tuberculosis or histoplasmosis caused adhesion between the esophageal wall and mediastinal lymph nodes, resulting in the development of a midesophageal diverticulum. It was therefore called a traction diverticulum (Kragh 1922; Borrie and Wilson 1980). However, recent studies have suggested that esophageal motor dysfunction could cause this diverticulum (Kaye 1974; Borrie and Wilson 1980). In contrast to cricopharyngeal and epiphrenic diverticula, midesophageal diverticula usually have a muscle layer in the sac.

Epiphrenic diverticulum

An epiphrenic diverticulum was first described by Mondiere in 1833. It is a rare anomaly that comprises less than 10% of all esophageal diverticula (Borrie and Wilson 1980). It occurs in the lower third of the esophagus, usually within the distal 10–15 cm, and usually projects into the right thoracic cavity (Clark et al. 1995) (Fig. 105.1b). Epiphrenic diverticula are usually observed in middle-aged and elderly men. In early research, it was assumed that increased intraluminal pressure due to hypertrophy of the muscle just beneath the diverticulum or the lower esophageal constrictor might cause this diverticulum (Kay 1953; Effler et al. 1959). However, recent studies have indicated that esophageal motility disorders cause this diverticulum (Debas et al. 1980; Nehra et al. 2002). It has been reported that hiatal hernia, esophageal spasm, or achalasia are often associated with epiphrenic diverticula (Rasmussen et al. 1988).

Esophageal duplication cyst

Esophageal duplication cysts comprise 10–15% of all alimentary tract duplications, representing the second most common duplication of the gastrointestinal tract (Whitaker et al. 1980; Hocking and Young 1981; Gupta et al. 2010). The incidence is estimated as one in 8200 and predominant in male (Arbona et al. 1984). They may be located in the esophageal wall or paraesophageal region with attachment to the esophageal wall (Fig. 105.2). The cyst communicates with the esophageal lumen in 10% of cases (Market et al. 1996). Approximately 60% of duplications are located in the lower esophagus, and the remaining 40% are equally distributed in the upper and middle esophagus (Whitaker et al. 1980). Because the esophagus, trachea, and bronchi develop in close proximity to one another during the embryonic stage, esophageal duplication cysts and bronchogenic cysts are sometimes difficult to distinguish from each other. Esophageal duplication cysts are usually diagnosed circumstantially by the facts that they are located close to the esophagus, have two smooth muscle layers and no cartilage, and are lined with columnar, cuboidal, stratified, squamous, or ciliated epithelium.

Esophageal duplication cysts are sometimes associated with other anomalies such as small intestinal duplication, esophageal atresia, and vertebral and spinal abnormalities.

Esophageal atresia

Both the esophagus and trachea arise from the primitive foregut. At the stage in which the foregut divides to form the esophagus and trachea, failure of separation or developmental errors may occur. Esophageal atresia, which results from a developmental error, is often associated with tracheoesophageal fistulas. Numerous variations of esophageal atresia exist. Several classifications have even been proposed; however, the classification by Gross (1953) is currently accepted (Fig. 105.3). The most frequently occurring type of esophageal atresia is type C in Gross's classification, which accounts for 70–90% of all cases. Its configuration is characterized by a blind ending of the upper esophagus and opening of the lower esophagus into the trachea (Holden and Wooler 1970). In addition to the major types of anomaly listed in the classification, many types of unclassified esophageal atresia exist (Holden and Wooler 1970). For example, atresia secondary to a membranous diaphragm with or without a tracheoesophageal fistula as well as the absence of a large segment of the esophagus have been

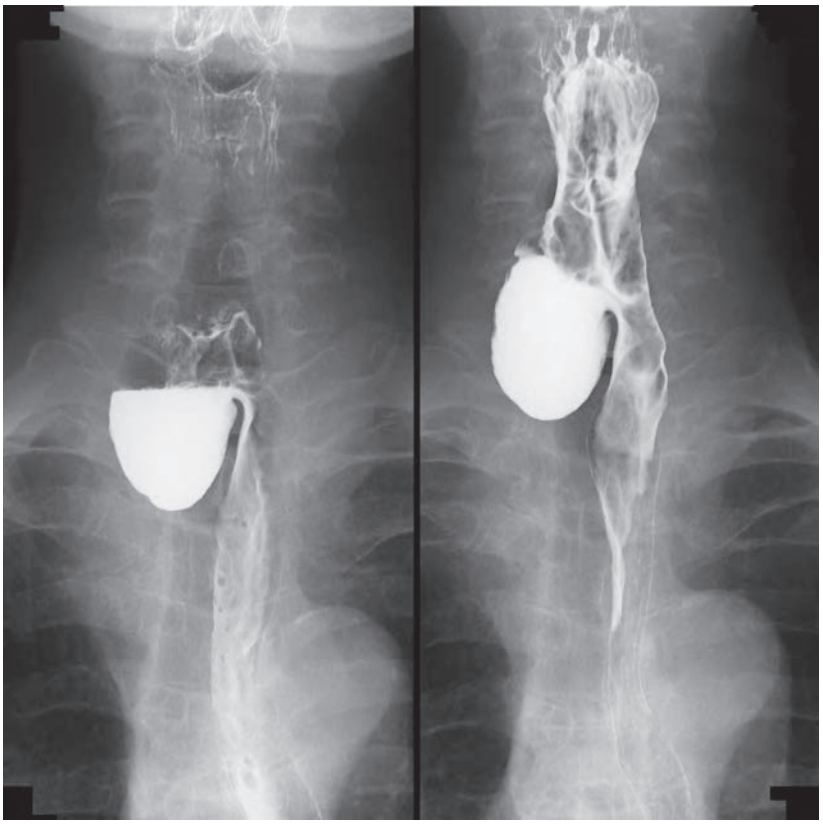

A

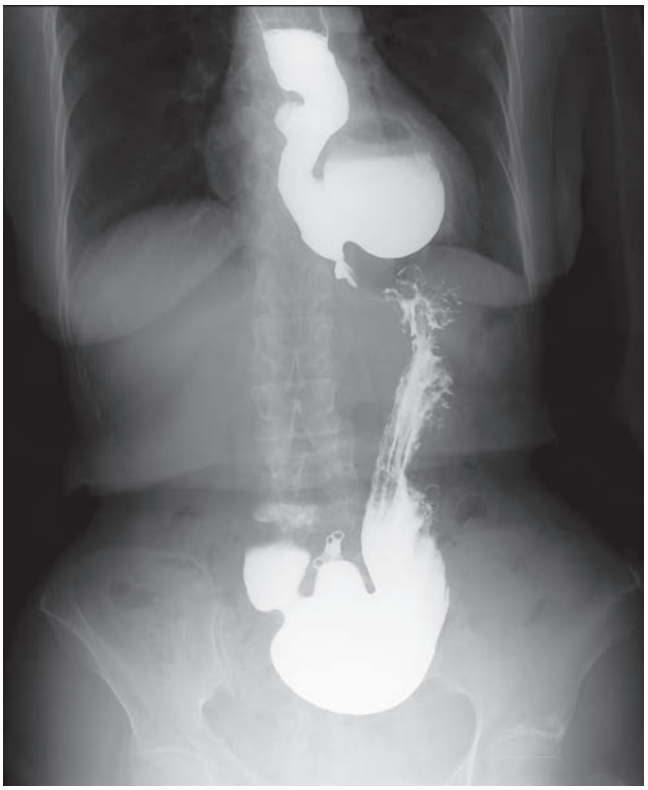

B

Figure 105.1 A contrast radiography of (a) cricopharyngeal diverticulum and (b) epiphrenic diverticulum.

Source: Dr Noriyuki Koga, Department of Plastic Surgery, Kurume University School of Medicine.

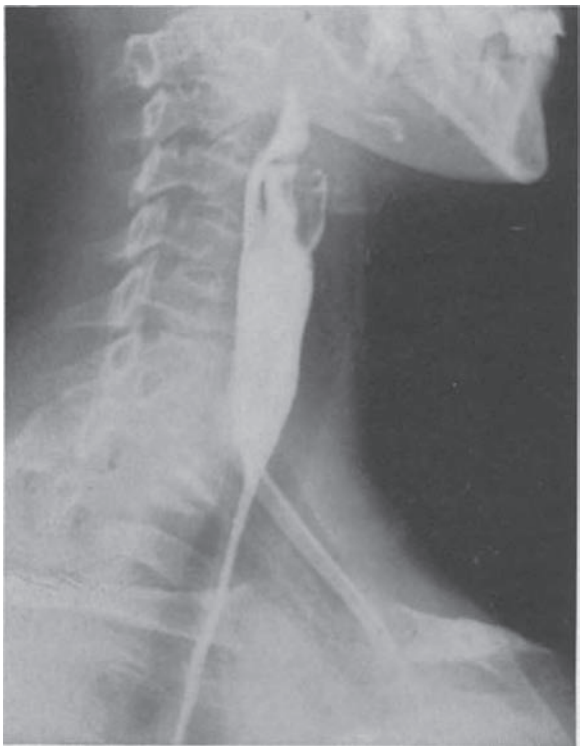

A

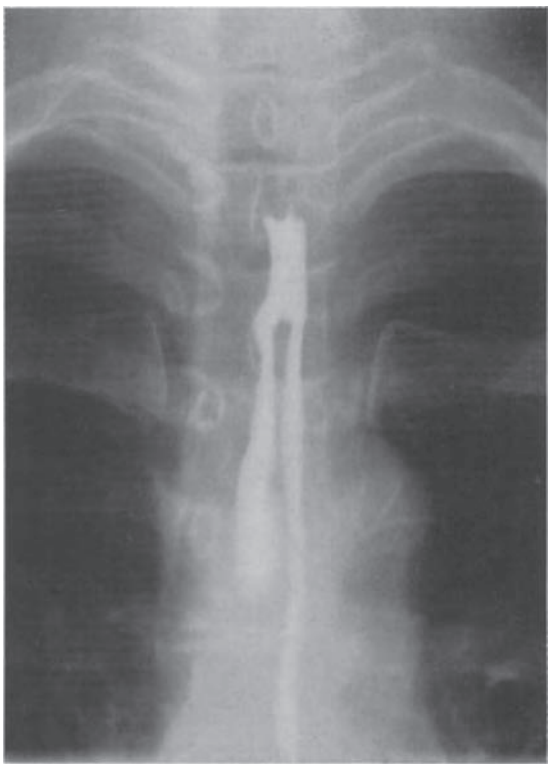

B

Figure 105.2 Esophageal duplication cyst: (a) lateral view and (b) frontal view.

Source: Maier (1957). Reproduced with permission from Wolters Kluwer Health.

reported. The incidence of esophageal atresia is reported as 1 in every 2500–4500 live births (Pinheiro et al. 2012). The incidence among twins is 2.56 times higher than that among single births (Pinheiro et al. 2012).

Esophageal atresia is often associated with other congenital anomalies at an estimated frequency of more than 50% (Pinheiro et al. 2012). Anomalies of the cardiovascular system are the anomalies most commonly associated with esophageal atresia and are observed in 20–30% of cases. Other associated anomalies include musculoskeletal malformations, anorectal and intestinal malformations, genitourinary malformations, head and neck anomalies, mediastinal anomalies, and chromosomal anomalies (Engum et al. 1995; Pinheiro et al. 2012). VACTERL (vertebral, anal, cardiac, tracheal, esophageal, renal, and limb anomalies) association, CHARGE (coloboma, heart defect, atresia choanae, retarded growth and development, genital hypoplasia, and ear deformities) association, Potter's syndrome (bilateral renal agenesis, pulmonary hypoplasia, and typical dysmorphic facies), cerebral hypoplasia, and chromosomal anomalies may also be associated with esophageal atresia.

Failure of separation of the trachea and esophagus

When the foregut separates into the esophagus and trachea, various degrees of failure of separation may remain. This phenomenon was first described by Richter in 1792. The incidence was reported as 1 in 10,000–20,000 births (Pezzettigotta et al. 2008). These separation failures usually occur only in the larynx and comprise almost half of all separation failures (Zachary and Emery 1961). Several classifications of laryngotracheoesophageal clefts have been proposed. Among them, the most prevailing classification was proposed by Benjamin, who separated the laryngotracheoesophageal cleft into four types (types 1–4) (Benjamin and Inglis 1989; Geller et al. 2010) (Fig. 105.4). Type 1 is a supraglottic interarytenoid cleft that is located above the level of the vocal cords. Type 2 is a partial cricoid cleft that extends below the level of the vocal cords, and partly but not completely penetrates the posterior lamina of the cricoid cartilage. Type 3 is a total cricoid cleft that completely extends through the cricoid cartilage with or without further extension into part of the cervical tracheoesophageal wall. Type 4 is a laryngoesophageal cleft that involves a major part of the intrathoracic tracheoesophageal wall. The most severe case, a so-called esophagotracheal cleft formed by complete failure of separation from the carina to the larynx, has also been reported (Zachary and Emery 1961; Roggini et al. 2000).

As in terms of associated anomalies, relationships to VATER association, tracheoesophageal fistulas, and G syndrome have been identified (Optiz and Reynolds 1987; Benjamin and Inglis 1989; DuBois et al. 1990; Chitkara et al. 2003).

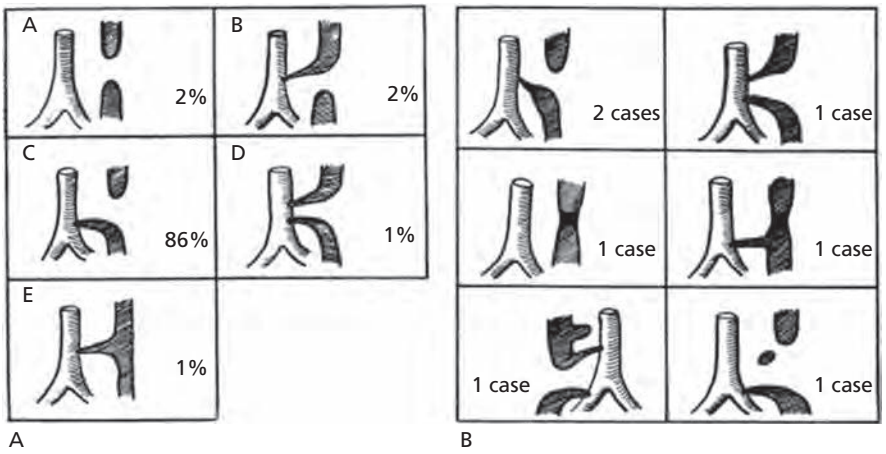

Figure 105.3 Classification of esophageal atresia with or without tracheoesophageal fistula.

Source: Holden and Wooler (1970). Reproduced with permission from BMJ Publishing Group.

Congenital esophageal stenosis

Congenital esophageal stenosis is defined as an intrinsic stenosis of the esophagus caused by congenital malformation of the esophageal wall architecture (Nihoul-Fékété et al. 1987). The incidence of congenital esophageal stenosis is 1 in 25,000–50,000 live births. There are three major causes of congenital esophageal stenosis: fibromuscular thickening of the esophageal wall; membranous web formation; and intramural tracheobronchial remnants. Tracheobronchial remnants reportedly result from failed separation of the respiratory system from the foregut. Amae et al. (2003) presumed that membranous webs result from disturbances in recanalization. Congenital esophageal stenosis is often associated with other anomalies such as congenital esophageal atresia, intestinal atresia, anorectal malformations, and chromosomal anomalies (Deiraniya 1974; Nishina et al. 1981; Nihou-Fékété et al. 1987). The incidence of such associations is reportedly 17–33% (Nishina et al. 1981; Nihoul- Fékété et al. 1987; Gupta et al. 1989; Amae et al. 2003).

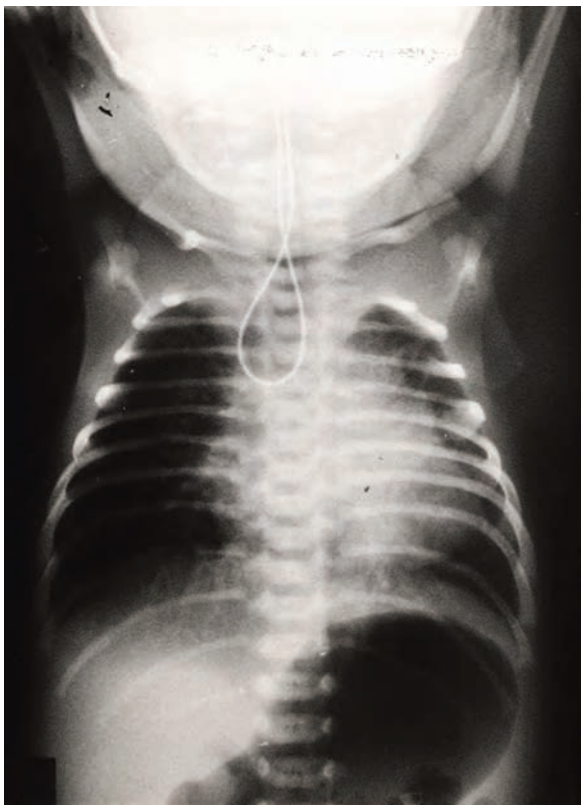

Figure 105.4 A case of congenital atresia. Observe the coiled-up sign, which is a naso-gastric tube turned up at the blind-ended upper esophagus.

Source: Dr Kimio Asagiri, Department of Pediatric Surgery, Kurume University School of Medicine.

References

Amae S, Nio M, Kamiyama T, Ishii T, Yoshida S, Hayashi Y, Ohi R. 2003. Clinical characteristics and management of congenital esophageal stenosis: a report on 14 cases. *J Pediatr Surg* 38: 565–570.

Arbona JL, Fazzi JG, Mayoral J. 1984. Congenital esophageal cysts: case report and review of literature. *Am J Gastroenterol* 79: 177.

Benjamin B, Inglis A. 1989. Minor congenital laryngeal clefts: Diagnosis and classification. *Ann Otol Rhinol Laryngol* 98: 417–420.

Bergman RA. 1996. Anatomy Atlas. Available at http://www.anatomyatlases.org/ (accessed 1 December 2015).

Bilge O, Servet C, Aktug H. 2013. The pleura-esophageal muscle: a disregarded anatomical structure. *Anat Sci Int* 2: 1–4.

Bonavina L, Bona D, Abraham M, Saino G, Abate E. 2007. Long-term results of endosurgical and open surgical approach for Zenker diverticulum. *World J Gastroenterol* 13: 2586.

Borrie J, Wilson RL. 1980. Oesophageal diverticula: principles of management and appraisal of classification. *Thorax* 35: 759–767.

Chitkara AE, Tadros M, Kim HJ, Harley EH. 2003. Complete laryngotracheoesophageal cleft: complicated management issues. *Laryngoscope* 113: 1314–1320.

Clark SC, Norton SA, Jeyasingham K, Ridley PD. 1995. Oesophageal epiphrenic diverticulum: an unusual presentation and review. *Ann Royal Coll Surg Engl* 77: 342.

Cook IJ, Gabb M, Panagopoulos V, Jamieson GG, Dodds WJ, Dent J, Shearman DJ. 1992. Pharyngeal (Zenker's) diverticulum is a disorder of upper esophageal sphincter opening. *Gastroenterology* 103: 1229–1235.

Cunningham DJ. 1876. Notes on the broncho-oesophageal and pleuraoesophageal muscles. *J Anat Physiol* 10: 320.

Debas HT, Payne WS, Cameron AJ, Carlson HC. 1980. Physiopathology of lower esophageal diverticulum and its implications for treatment. *Surg Gynecol Obst* 151: 593.

Deiraniya AK. 1974. Congenital oesophageal stenosis due to tracheobronchial remnants. *Thorax* 29: 720–725.

Delahunty JE, Margulies SI, Alonso WA, Knudson DH. 1971. The relationship of reflux esophagitis to pharyngeal pouch (Zenker's diverticulum) formation. *Laryngoscope* 81: 570–577.

DuBois JJ, Pokorny WJ, Harberg FJ, Smith RJ. 1990. Current management of laryngeal and laryngotracheoesophageal clefts. *J Pediatr Surg* 25:855–860.

Effler DB, Barr D, Groves LK. 1959. Epiphrenic diverticulum of the esophagus: surgical treatment. *Arch Surg* 79: 459.

Engum SA, Grosfeld JL, West KW, Rescorla FJ, Scherer LR. 1995. Analysis of morbidity and mortality in 227 cases of esophageal atresia and/or tracheoesophageal fistula over two decades. *Arch Surg* 130: 502.

Geller K, Kim Y, Koempel J, Anderson KD. 2010. Surgical management of type III and IV laryngotracheoesophageal clefts: the three-layered approach. *Inter J Pediatr Otorhinolaryngol* 74: 652.

Gross RE. 1953. *The Surgery of Infancy and Childhood*. Philadelphia: WB Saunders Co.

Gruber W. 1877. Über das neur anheftungsbündel des oesophagus an die glandula thyreoidea-musculus threo-oesophagus. *Arch Pathol Anat Physiol Lkin Med* 69: 396–398.

Gupta B, Meher R, Raj A, Agarwal S. 2010. Duplication cyst of oesophagus: a case report. *J Paediatr Child Health* 46: 134–135.

Gupta R, Daie Parizi MH, Tabrizche H. 1989. Intranural tracheobronchial remnants: A misdiagnosed cause of congenital esophageal stenosis. *Med J Islamic Repub Iran (MJIRI)* 3: 97–101.

Hadi U, Rameh C. 2007. Giant midesophageal diverticulum presenting as food impaction: case report and review of the literature. *Am J Otolaryngol* 28: 122–125.

Henle J. 1866. Systematischen Anatomie Des Menschen. 2. Band. Braunschweig: Friedrich Vieweg und Sohn, pp. 159–162.

Hocking M, Young DG. 1981. Duplications of the alimentary tract. *Brit J Surg* 68: 92–96.

Holden MP, Wooler GH. 1970. Tracheo-oesophageal fistula and oesophageal atresia: results of 30 years' experience. *Thorax* 25: 406–412.

Hyrtl J. 1844. *Lehrbuch der Anatomie des Menschen*. Prague: Timileaux.

Kay EB. 1953. The inferior oesophageal disease. *J Thoracic Surg* 25: 1–13.

Kaye MD. 1974. Oesophageal motor dysfunction in patients with diverticula of the mid-thoracic oesophagus. *Thorax* 29: 666–672.

Kragh J. 1922. Tuberculous diverticula of the oesophagus (so-called traction diverticula). *Acta Otolaryngologia* 4: 49.

Maier HC. 1957. Intramural duplication of the esophagus. *Ann Surg* 145: 395.

Market DJ, Grumbach K, Haney PJ. 1996. Thoracoabdominal duplication cyst: prenatal and postnatal imaging. *J Ultrasound Med* 15: 333–336.

Mondiere JT. 1833. Notes sur quelques maladies de l'oesophage. *Arch Gen Med Paris* 3: 28–65.

Nehra D, Lord RV, DeMeester TR, Theisen J, Peters JH, Crookes PF, Bremner CG. 2002. Physiologic basis for the treatment of epiphrenic diverticulum. *Ann Surg* 235: 346.

Nihoul-Fékété C, De Backer A, Lortat-Jacob S, Pellerin D. 1987. Congenital esophageal stenosis. *Pediatr Surg Intern* 2: 86–92.

Nishina T, Tsuchida Y, Saito S. 1981. Congenital esophageal stenosis due to tracheobronchial remnants and its associated anomalies. *J Pediatr Surg* 16: 190–193.

Opitz JM, Reynolds JF. 1987. G syndrome (hypertelorism with esophageal abnormality and hypospadias, or hypospadias-dysphagia, or "Opitz-Frias" or "opitz-G" syndrome): perspective in 1987 and bibliography. *Am J Med Gen* 28: 275–285.

Palotás A, Lázár G, Paszt A, Szentpáli K. 2004. Alkali ingestion predisposes to developing giant mid-esophageal pulsion diverticulum: a report of a medical rarity. *Med Hypoth* 62: 931–934.

Pezzettigotta SM, Leboulanger N, Roger G, Denoyelle F, Garabédian EN. 2008. Laryngeal cleft. *Otolaryngologic Clin North Am* 41: 913–933.

Pinheiro PFM, Silva ACS, Pereira R M. 2012. Current knowledge on esophageal atresia. *World J Gastroenterol* 18: 3662.

Rasmussen PC, Jensen BS, Winther A. 1988. Oesophageal achalasia combined with epiphrenic diverticulum: a case report. *Scand Cardiovascular J* 22: 81–82.

Roggini M, Carbone I, Bosco S, Cozzi DA, Andreoli G, Capocaccia P. 2000. Persisten esophagotrachea: description of case. *Europ Rev Med Pharmacol Sci* 4: 95–98.

Rokitansky C. 1840. Spinderformige: erweiterung der speiserohre. Medicinische Jahrebucher des k.k. *Osterreichischen Staates* 21: 219.

Shaw DW, Cook IJ, Jamieson GG, Gabb M, Simula ME, Dent J. 1996. Influence of surgery on deglutitive upper oesophageal sphincter mechanics in Zenker's diverticulum. *Gut* 38: 806–811.

Van Overbeek JJ. 2003. Pathogenesis and methods of treatment of Zenker's diverticulum. *Ann Otol Rhinol Laryngol* 112: 583–593.

Venturi M, Bonavina L, Colombo L, Antoniazzi L, Bruno A, Mussini E, Peracchia A. 1997. Biochemical markers of upper esophageal sphincter compliance in patients with Zenker's diverticulum. *J Surg Res* 70: 46–48.

Whitaker JA, Deffenbaugh LD, Cooke AR. 1980. Esophageal duplication cyst. Case report. *Am J Gastroenterol* 73: 329.

Zachary RB, Emery JL. 1961. Failure of separation of larynx and trachea from the esophagus: persistent esophagotrachea. *Surgery* 49: 525.

Zaninotto G, Costantini M, Boccu C, Anselmino M, Parenti A, Guidolin D, Ancona E. 1996. Functional and morphological study of the cricopharyngeal muscle in patients with Zenker's diverticulum. *Brit J Surg* 83: 1263–1267.

Zenker FA, Von Ziemssen H. 1878. Dilatations of the esophagus. *Cyclopedia Pract Med* 3: 46–48.

106 Stomach

Koichi Watanabe
Kurume University School of Medicine, Fukuoka, Japan

Anatomical variations of the stomach are either congenital or acquired. Congenital anomalies include microgastria, atresia, duplication, and heterotopic pancreatic tissue. These occur during embryonic development of the stomach from the foregut. In contrast, hourglass stomach, double pylorus, and muscular defect were once believed to have both a congenital and an acquired onset, but congenital causes are not currently considered. Diverticulum of the stomach has both congenital and acquired types, and each has different characteristics.

Microgastria

The first case of microgastria was reported by Dide in 1894, and was observed as an abnormally small stomach in a necropsy study of an epileptic woman (Aintablian et al. 1987). Schulz described this anomaly as a new syndrome in 1971, which was associated with skeletal abnormalities (Schultz 1971; Anderson and Guzzetta 1983). Microgastria is an extremely rare anomaly, and Jones commented that only 59 cases have been reported as of 2007 (Jones and Cohen 2007; Vasas et al. 2011). The morphological findings of microgastria are characterized by a small tubular stomach with a compensatory dilated esophagus (Fig. 106.1) (Hochberger and Swoboda 1974). It is believed that this anomaly is caused by arrested development of the stomach from the foregut, especially the greater curvature of the stomach, during the fourth–fifth week of embryonic development (Simstein 1986).

Microgastria is often associated with other congenital anomalies such as malrotation, asplenia, skeletal anomaly, cardiac anomaly, renal anomaly, and tracheoesophageal anomaly (Aintablian et al. 1987; Kroes and Festen 1998). Asplenia most frequently accompanies microgastria because both the stomach and the spleen are derived from the same tissue, embryonic dorsal mesogastrium (Vasas et al. 2011). The association of microgastria with skeletal, cardiac, renal, and tracheoesophageal anomaly has been attributed to the failure of mesodermal development (Vasas et al. 2011).

Most patients with this anomaly have postprandial vomiting, recurrent aspiration pneumonia, and growth impairment (Anderson and Guzzetta 1983; Kroes and Festen 1998) with many cases requiring surgery during childhood.

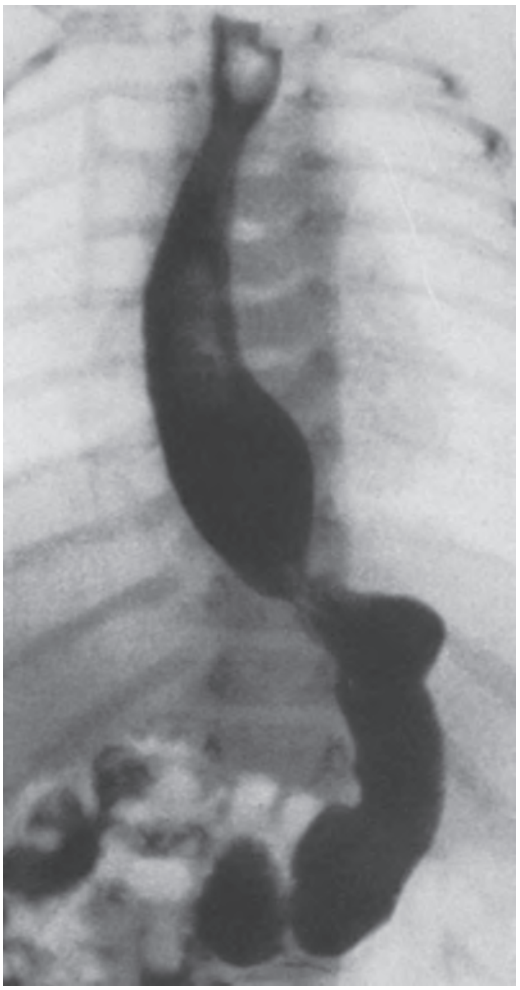

Figure 106.1 Fluoroscopic findings of microgastria. Dilated esophagus and tube-like stomach with cascade in the fornix were observed.

Source: Hochberger and Swoboda (1974). Reproduced with permission from Springer Science and Business Media.

Bergman's Comprehensive Encyclopedia of Human Anatomic Variation, First Edition. Edited by R. Shane Tubbs, Mohammadali M. Shoja and Marios Loukas.
© 2016 John Wiley & Sons, Inc. Published 2016 by John Wiley & Sons, Inc.

Atresia of the stomach

Atresia of the stomach is the lack of continuity of the stomach. Brown and Hertzler (1959) reported three types of gastric obstruction on the basis of the anatomical findings of obstruction: (1) by the diaphragm; (2) due to an area of mucosal atresia; and (3) due to complete segmental aplasia of the gastrointestinal tract. Lorenzat examined 140 cases and reported a similar classification: type A: pyloric membrane; type B: pyloric canal is replaced by a solid core of tissue; and type C: atretic pylorus with a gap between the stomach and the duodenum (Lorenzat and Morger 1987; Okoye et al. 2000).

Obstruction by the diaphragm is usually called pre-pyloric diaphragm or antral diaphragm. The obstruction consists of mucosal and submucosal tissue causing various degrees of obstruction occurring in the antrum at variable distances from the pylorus, including complete obstruction; complete obstruction with small aperture; and partial obstruction (web-like lesion). Lorenzat and Morger (1987) reported that this type of atresia occurred in 57% of all gastric atresias.

Brown and Hertzler (1959) reported two cases of segmental aplasia with more extensive obstructions than with membranous obstructions. These cases had continuity between the stomach and the duodenum, but with complete occlusion or severe stenosis by pre-pyloric lesions in some sections. Lorenzat reported a frequency of this type of atresia of 34% (Lorenzat and Morger 1987; Okaye et al. 2000).

For cases with a gap between the stomach and the duodenum corresponding to type 3 in Brown's classification and type C in Lorenzat's classification, Lorenzat reported a frequency of 9%. Previous cases have also been reported (Neale 1884; Holladay 1946).

Rare cases have been reported with double pre-pyloric membranes forming a cystic structure between the two membranes (Metz et al. 1941) or a non-obstructive antral web with hypertrophic pyloric stenosis (Rowling 1959b; Bell et al. 1977; Mandell 1978).

This anomaly is found in newborns, infants, children, and sometimes in middle-aged adults. Mandell suggested two possible explanations for the development of an antral web: an excess of local endodermal proliferation and redundancy. Another possible cause is secondary mucosal development due to a more distal obstruction such as a duodenal ulcer or congenital pyloric stenosis (Mandell 1978). Two hypotheses explain the adult-onset form. One is that the stomach becomes hypertrophied and decompensates after many years of extra effort forcing food through the aperture (Schwartz and Shepard 1956). Another is that age-related decreased mastication increases the stomach's burden, leading to symptoms (Banks et al. 1967).

Several anomalies have been associated with pyloric stenosis. Chen and Emil (2008) summarized these cases and categorized them into three groups: (1) pyloric atresia as an isolated abnormality; (2) pyloric atresia in association with other intestinal atresias; (3) pyloric atresia in association with other disorders including the esophagus (Müller et al. 1990; Centikursun et al. 1955; Okoye et al. 2000); duodenum (Haller and Cahill 1968; Al-Salem 1999; Chen and Emil 2008); and the jejunum, rectum, and colon (Guttman et al. 1973; Puri et al. 1985; Al-Salem et al. 1997). Other disorders including dermal pathological conditions such as epidermolysis bullosa and aplasia cutis congenita have been reported; these are known as Carmi syndrome (Lestringant et al. 1992) and Bart syndrome (Maman et al. 1998; Morrell et al. 2000; Bart and Lussky 2005) respectively.

Hourglass stomach

This deformity occurs when the stomach divides into two chambers by annular construction and forms an hourglass shape (Fig. 106.2). Hourglass stomach was initially assumed to have both congenital and acquired onsets; however, this deformity is currently considered to result from acquired causes. Meckel considered that a congenital hourglass stomach might result from an imperfection of development (Moynihan 1904). However, Moynihan investigated previous cases that were assumed to have a congenital onset, and concluded that no existing records showed evidence of congenital hourglass stomach. Rowlands (1931) asserted that the hourglass contraction is almost always due to a particularly chronic gastric ulcer. He experienced seven cases of hourglass stomach and only one of the seven cases was

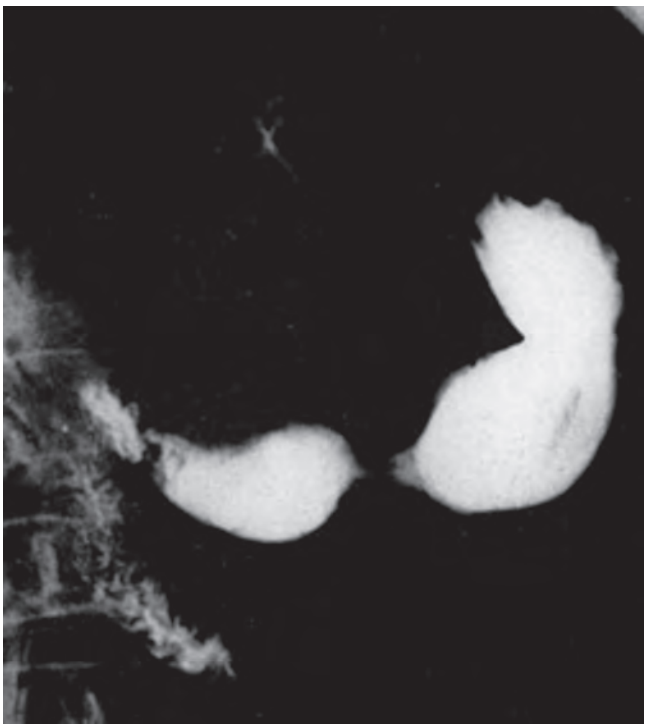

Figure 106.2 Fluoroscopic findings of an hourglass stomach.

Source: Schroeder (1949). Reproduced with permission from Wolters Kluwer Health.

considered a congenital deformity. Other authors stated that the constriction in hourglass stomach is always of pathological origin (Primrose 1914). However, a case that was assumed to have a congenital onset was presented by Schroeder in 1949. His case was an hourglass deformity in a 74-year-old man and the stomach was resected surgically. The specimen showed normal mucosa with no ulcers or scars, and histopathological annular hypertrophy of the submucosa and musculature. He concluded his case had a congenital onset (Schroeder 1949). No known congenital cases have been reported since Schroeder's case, to the best of the author's knowledge.

Congenital (or infantile) hypertrophic pyloric stenosis

Congenital (or infantile) hypertrophic pyloric stenosis occurs when the pyloric portion of the stomach becomes abnormally thickened causing narrowing and elongation of the pyloric channels. It was first described by Hirschsprung in 1888 (Hirschsprung 1888; Ranells et al. 2011). This disease usually develops in 3- to 5-week-old infants with projectile non-bilious vomiting after feeding and palpation of the hypertrophied pyloric muscle feels like an olive (Fig. 106.3) (Spicer 1982). The reported frequency of this anomaly is in the range of 1–2 per 1000 infants. Babies born to white and non-Hispanic mothers have a higher risk than babies born to black and Asian mothers (Carter and Powell 1954; Ranells et al. 2011). The prevalence is the highest in the first-born baby and boys have a three to five times higher rate than that of girls (MacMahon 2006; Ranells et al. 2011). The cause of this anomaly is still unclear; however, abnormalities of the sphincter control system including the enteric nervous system, gastrointestinal hormones, and interstitial cells of Cajal, are assumed to cause hypertrophic pyloric stenosis. Environmental factors may play a role; an association between congenital hypertrophic pyloric stenosis and medicating infants with erythromycin was recently reported (Honein 1999; Mahon et al. 2001). Other drugs such as thalidomide, hydantonins, and trimethadione have also been reported as increasing the risk of infantile hypertrophic pyloric stenosis (Ranells et al. 2011).

Duplication of the stomach

The alimentary tract has rare duplications of various degrees. Duplication of the ilium is the most common and that of the stomach is relatively rare, accounting for 3.8% of all alimentary tract duplications (Silverman et al. 1971). Usually, the gastric duplication is evident by the first year of life with symptoms such as vomiting or abdominal pain; however, some adult cases have been reported. Lewis reported the age proportions of this anomaly and reviewed 39 cases; 25 cases (64%) were children and 14 cases (36%) were adults (Lewis et al. 1961). The frequency of female patients is twice that of male patients. Rowling defined the diagnostic criteria of this anomaly as follows: (1) the wall of the cyst is continuous with the stomach wall; (2) the cyst is surrounded by smooth muscle that is continuous with the muscle of the stomach; and (3) the inner wall of the cyst is lined by alimentary epithelium (Rowling 1959a; Wieczorek et al. 1984).

Usually, gastric duplications are discovered as spherical cystic structures that do not communicate with the inner lumen of the stomach. However, rarely, they form tubular structures contiguous with the inner cavity of the stomach. Duplications can communicate with the duodenum (Cashion 1934; Young 1965) or Meckel's diverticulum (McCutchen and Josey 1951; Bartels 1967). Cysts are most commonly 3–6 cm in diameter, but cysts less than 3 cm or more than 6 cm in diameter have also been observed (Wieczorek et al. 1984). Duplications are located in the greater curvature in half of the reported cases, sometimes in the lesser curvature, anterior wall, or posterior wall (Fig. 106.4).

Other anomalies associated with gastric duplication have been observed in nearly half of the reported cases. The most major associated anomaly is duplication of the esophagus, and vertebral abnormalities are also occasionally observed (Wieczorek et al. 1984).

Diverticula

Diverticulum of the stomach was first reported by Baillie in 1793 (Lay Martin 1936; Brown et al. 1949). According to Brown et al., gastric diverticulum is a rare disease with only one case in 2000 X-ray examinations of the stomach (0.05%) in his research, and a frequency range of 1 in 833–3600 cases (0.027–0.12%). The frequency of gastric diverticula in autopsy studies is less than that of X-ray studies; this is because patients undergoing X-ray examination are usually symptomatic and the data do not represent that of the total population.

Gastric diverticulum is classified into two types: true diverticulum and false diverticulum. True gastric diverticulum has a congenital onset and its wall consists of all layers of the stomach wall. False diverticulum is acquired and usually lacks the proper muscularis in its wall.

True diverticulum is usually found in adults from their 20s to 60s, and is most frequently observed in the 40s. However, cases of young children have also been reported. There appears to be no significant difference in frequency between genders (Palmer 1951b). Interestingly, the majority of true diverticula have occurred in a specific location, on the posterior wall and 2 cm below the esophagogastric junction and 3 cm from the neighboring lesser curvature. Palmer stated that 76% (259 in 342 cases) of true diverticula occurred in this location (Palmer 1951b). It is assumed that this part of the stomach has an innate anatomical weakness of the gastric wall (Cunha 1935; Miskovitz and Steinberg 1982). The other 24% of true diverticula

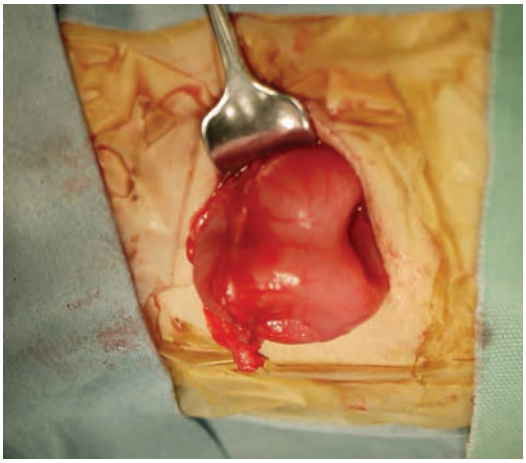

A

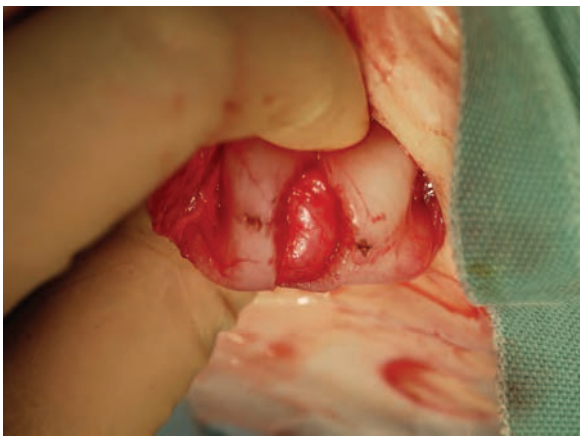

B

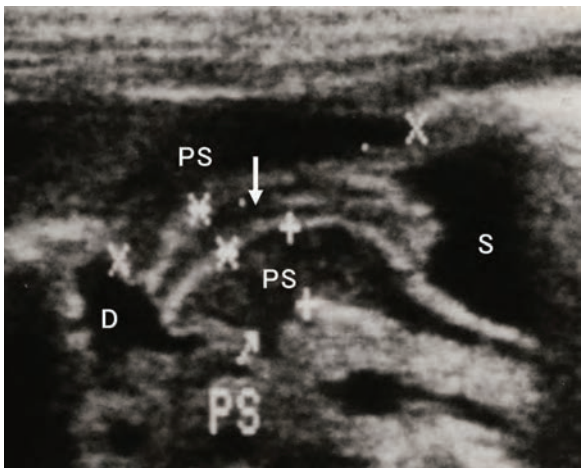

C

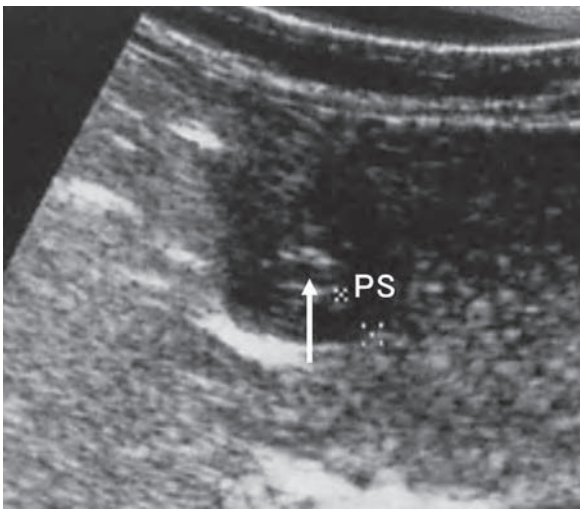

D

E

Figure 106.3 A case of congenital hypertrophic pyloric stenosis. (a, b) Operative findings. Pyloric sphincter was cut longitudinally (Heineke-Mikulicz pyloroplasty). (c) ultrasonography (longitudinal section); (d) ultrasonography (cross-section). Arrow, pyloric channel; D, duodenum; S, stomach; PS, pyloric sphincter muscle. (e) Fluoroscopy.

Source: Dr Kimio Asagiri, Department of Pediatric Surgery, Kurume University.

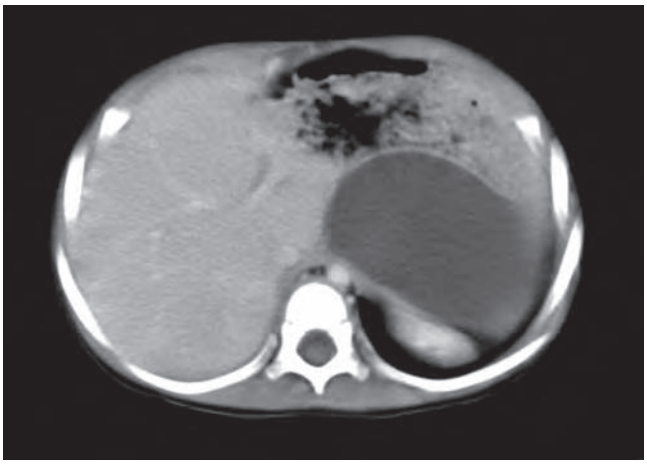

A

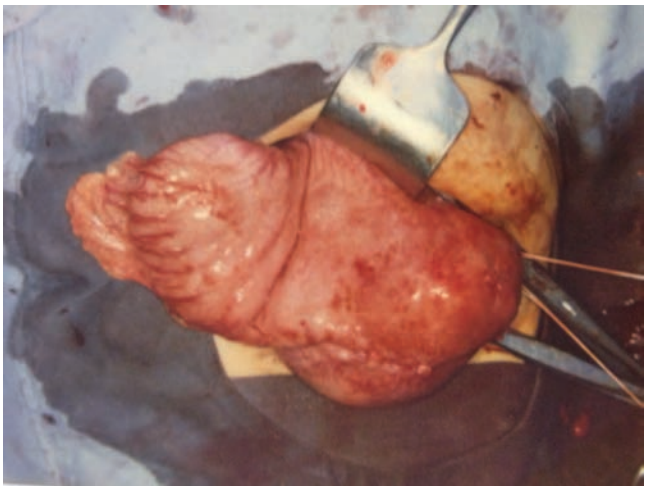

B

Figure 106.4 A case of duplication of the stomach: (a) CT and (b) operative findings. Source: Dr Kimio Asagiri, Department of Pediatric Surgery, Kurume University.

occurred in various areas of the stomach. True gastric diverticulum occurs as a single lesion in most cases and the size usually ranges over 0.3–5 cm. The most frequent size range is over 1.1–2 cm as the largest diameter and the largest reported true diverticulum was 11 cm (Moses 1946). True diverticula have normal mucosa in half of the cases in microscopic examinations of surgery or autopsy cases and gastritis is found in most of the other cases. Some cases have carcinoma or precancerous change.

False diverticula are caused, in some cases, by mesodermal and ectodermal intramural tumors such as schwannoma. The formation of diverticula is assumed to occur when the intramural tumor forms a central ulceration, which then becomes necrotic and creates an excavation. Sarcoma, carcinoma, and syphilis also cause false diverticula (Palmer 1951b). A gastric ulcer that penetrates the gastric wall causes false diverticula by inflammatory adhesion between the ulcer base and the serosa. Contracture after gastric surgery may also produce false diverticula near the suture line.

Congenital muscular defect

Congenital muscular defect of the stomach is assumed to be a cause of gastric perforation in newborn infants, which usually happens with abdominal distension and free intra-peritoneal space in the very early days after birth. The first report of gastric perforation in the neonatal period was made by Siebold in 1825 (Inouye and Evans 1964). Since then, several cases of gastric perforation in the neonatal period have been reported. The causes of neonatal gastric rupture include peptic ulcer (Smythe 1934; Bird et al. 1941; Rosenberg and Heath 1946); trauma (related to the resuscitation machine; Musser 1956; Darke and Bloomfield 1975); nasogastric tube (Dunham and Goldstein 1934; Kunz 1952; Potter 1952; Wagner et al. 1952); delivery (Pendergrass and Booth 1946); and musculature defect of the stomach. Recently, intestinal ischemia induced by asphyxia (Touloukian 1972), lack of C-KIT^{+} mast cells (Yamataka et al. 1999), and abnormal distribution of intestinal pacemaker cells (Ohshiro et al. 2000) have all been proposed as possible causes.

Brody (1940) illustrated the first case of the congenital absence of gastric musculature. In 1943, Herbut encountered an infant case having three musculature defects in the mid-portion of the greater curvature (Herbut 1943). The microscopic findings in the musculature defect parts revealed that the muscle of the wall ended abruptly in the surrounding tissue and no muscle was found in the defective section. Herbut asserted that gastric musculature defect caused the gastric rupture in his case. Herbut also discussed spontaneous rupture in the adult cases that Wolf reported previously, and mentioned the possibility of the existence of a congenital small muscular defect in these adult cases (Herbut 1943). Although the majority of the cases of gastric rupture were considered to be secondary to gastric ulceration (Smythe 1934; Bird et al. 1941; Rosenberg and Heath 1946) or tube feeding (Dunham and Goldstein 1934; Kunz 1952; Potter 1952; Wagner et al. 1952), Braunstein asserted that some gastric rupture cases with pyloric atresia and cases of perforation after tube feeding were the result of gastric musculature defects based on histological examinations (Braunstein 1954). MacGillivray et al. (1956) also reported one case of gastric rupture which it was assumed resulted from the musculature defect, although nasogastric tubes had been placed in the stomach. It was claimed that the nasogastric tube itself was too soft to perforate the stomach wall without a musculature defect.

Some authors have doubted the existence of congenital musculature defect (Musser 1956). They claim that the finding of the muscular defect is merely the separation of the muscle fibers as a result of severe dilation of the stomach. However, there have been cases in which the mechanism of the rupture is explained only by the congenital musculature defect.

Heterotopic pancreatic mucosa

Heterotopic pancreas occurs when the pancreas tissue exists in a distant organ outside the original position of the pancreas without anatomic or vascular connection between the two (Martinez et al. 1958; Armstrong et al. 1981). It was first reported by Schultz in 1727 as a gross appearance and the first histological report was written by Klobin in 1859 (Martinez et al. 1958). Heterotopic pancreas is observed in the stomach, duodenum, jejunum, and Meckel's diverticula, and rarely observed in the esophagus, gallbladder, common bile duct, spleen, mesentery, mediastinum, and uterine tubes. Von Heinrich (1909) proposed a classification system: type 1: typical pancreatic tissue with acini, ducts, and islets; type 2: pancreatic tissue with ducts and acini (endocrine elements are absent); and type 3: pancreatic tissues consisting of numerous ducts (absence of islet cells, rare acini).

Most gastric heterotopic pancreas lesions have been found in the pylorus and antrum with a frequency range of 0.5–13.7% in autopsy studies and 0.5% in upper abdominal surgeries (De Castro Barbosa 1946; Feldman and Weinberg 1952; Herold and Kraft 1995). Most lesions are within 5 cm in diameter. According to Yamagiwa et al. (1977), the diameter of this lesion was in the range of 0.3–4.7 cm; approximately 80% of the lesions were within 3 cm. Martinez et al. (1958) stated that 59% of the masses were in the range of 1–2 cm in diameter and the largest was 4.5 cm. Palmer (1951a) stated that 73% are submucosal, 17% are muscular, and 10% are subserosal. Yamagiwa et al. (1977) reported that 42% of the lesions are in the submucosa; 25% in the muscularis; 18% in the submucosal to muscular layer; 12% in the subserosal layer; and 13% in the muscular to subserosal layers. The gross appearances depends on the layer in which the lesions exists. Lesions in the submucosal to muscular layers usually present with a nipple-like appearance, and those in the muscular to subserosal layers have a flat appearance or thickening of the wall.

Double or triple pyloric antrum or pylorus

Double pylorus is a relatively rare abnormality, first described by Smith and Tuttle (1969). The frequency was reported at 0.02–0.08% in endoscopic examinations. The ratio of male to female is approximately 2:1 (Hegedus et al. 1978; Kothandaraman et al. 1983) and two types of double pylorus occur: congenital and acquired. Most of the cases of double pylorus are the acquired type, developing secondary to gastric ulcer. Lesions are usually located on the lesser curvature of the gastric antrum and the fistula continues to the duodenal bulb.

In contrast, congenital double pylorus is extremely rare and very few cases have been reported (Rohde et al. 1975; Jorge and Diaz 1976; Sufian et al. 1977; Naidoo and Singh 2012). Double pylorus cases with normal histology of both pyloric channels and no evidence of ulcer are diagnosed as congenital. Some authors doubt the existence of congenital double pylorus because the findings in some cases that were reported as congenital were extremely similar to the acquired form (Jamshidnejad et al. 1978). However, cases in which a congenital onset could not be disproven have also been reported. The representative case was reported by Sufian et al. (1977); this case had quite different findings from other cases, with a long accessory channel on the greater curvature with normal mucosal holds. It is still uncertain whether congenital double pylorus truly exists.

References

Aintablian NH, Slim MS, Antoun BW. 1987. Congenital microgastria. *Pediatr Surg Int* 2: 307–310.

Al-Salem AH. 1999. Pyloric atresia associated with duodenal and jejunal atresia and duplication. *Pediatr Surg Int* 15: 512–514.

Al-Salem AH, Qaissaruddin S, Varma KK. 1997. Pyloric atresia associated with intestinal atresia. *J Pediatr Surg* 32: 1262–1263.

Anderson KD, Guzzetta PC. 1983. Treatment of congenital microgastria and dumping syndrome. *J Pediatr Surg* 18: 747–750.

Armstrong CP, King PM, Dixon JM, Macleod IB. 1981. The clinical significance of heterotopic pancreas in the gastrointestinal tract. *Brit J Surg* 68: 384–387.

Banks PA, Waye JD, Waitman AM, Cornell A. 1967. Mucosal diaphragm of the gastric antrum. *Gastroenterology* 52: 1003.

Bart BJ, Lussky RC. 2005. Bart syndrome with associated anomalies. *Am J Perinatol* 22: 365–369.

Bartels RJ. 1967. Duplication of the stomach. Case report and review of the literature. *Am Surg* 33: 747–752.

Bell MJ, Ternberg, JL, McAlister W, Keating JP, Tedesco FJ. 1977. Antral diaphragm: a cause of gastric outlet obstruction in infants and children. *J Pediatr* 90: 196–202.

Bird CE, Limper MA, Mayer JM. 1941. Surgery in peptic ulceration of stomach and duodenum in infants and children. *Ann Surg* 114: 526.

Braunstein H. 1954. Congenital defect of the gastric musculature with spontaneous perforation: Report of five cases. *J Pediatr* 44: 55–63.

Brody H. 1940. Ruptured diverticulum of the stomach in a newborn infant, associated with congenital membrane occluding the duodenum. *Arch Path* 29: 125.

Brown CH, Bissonnette RP, Albee RD. 1949. Diverticula of the stomach; a report of 30 cases and a review of the literature. *Gastroenterol* 12: 10.

Brown RP, Hertzler JH. 1959. Congenital prepyloric gastric atresia: a report of two cases. *Arch Pediatr Adol Med* 97: 857.

Carter CO, Powell BW. 1954. Two-generation pyloric stenosis. *Lancet* 266: 746–748.

Cashion WA. 1934. Supernumerary stomach with duodenal bulb associated with diaphragmatic hernia. *Med Bull* 11: 61.

Centikursun S, Ozturk H, Celasun B. 1955. Epidermolysis bullosa associated with pyloric, esophageal and anal atresia: A case report. *J Pediatr Surg* 30: 1477–1478.

Chen T, Emil S. 2008. Closed loop foregut obstruction in a premature neonate. *J Pediatr Surg* 43: e11–e14.

Cunha F. 1935. Diverticula of upper end of stomach. *Am J Surg* 27: 252–266.

Darke SG, Bloomfield E. 1975. Case of complete gastric rupture complicating resuscitation. *Brit Med J* 3: 414.

De Castro Barbosa JJ. 1946. Pancreatic heterotopia: review of the literature and report of 41 authenticated surgical cases, of which 25 were clinically significant. *Surg Gynecol Obstet* 82: 527–542.

Dunham EC, Goldstein RM. 1934. Rupture of the stomach in newborn infants: Report of two cases. *J Pediatr* 4: 44–50.

Feldman M, Weinberg T. 1952. Aberrant pancreas: a cause of duodenal syndrome. *J Am Med Assoc* 148: 893–898.

Guttman FM, Braun P, Garance, PH, Blanchard H, Collin PP, Dallaire L, Perreault G. 1973. Multiple atresias and a new syndrome of hereditary multiple atresias involving the gastrointestinal tract from stomach to rectum. *J Pediatr Surg* 8: 633–640.

Haller JA, Cahill JL. 1968. Combined congenital gastric and duodenal obstruction: pitfalls in diagnosis and treatment. *Surgery* 63: 503.

Hegedus V, Poulsen PE, Reichardt J. 1978. The natural history of the double pylorus. *Radiology* 126: 29–34.

Herbut PA. 1943. Congenital defect in the musculature of the stomach with rupture in a newborn infant. *Arch Pathol* 36: l–94.

Herold G, Kraft K. 1995. Adenocarcinoma arising from ectopic gastric pancreas: two case reports with a review of the literature. *Zeitschrift für Gastroenterologie* 33: 260.

Hirschsprung H. 1888. Falle von angeborener Pylorusstenose, beobachtet bei Sauglingen. *Jahrb Kinderheik* 27: 61.

Hochberger O, Swoboda W. 1974. Congenital microgastria. *Pediatr Radiol* 2: 207–208.

Holladay LJ. 1946. Case report of congenital aplasia of the pylorus. *J Indiana Med Assoc* 39: 350.

Honein MA, Paulozzi LJ, Himelright IM, Lee B, Cragan JD, Patterson L, Erickson JD. 1999. Infantile hypertrophic pyloric stenosis after pertussis prophylaxis with erythromycin: a case review and cohort study. *The Lancet* 354: 2101–2105.

Inouye WY, Evans G. 1964. Neonatal gastric perforation: a report of six cases and a review of 143 cases. *Arch Surg* 88: 471.

Jamshidnejad JAV, AD, Koehler RE, Narayan D. 1978. Double channel pylorus. *Am J Roentgenol* 130: 1047–1050.

Jones VS, Cohen RC. 2007. An eighteen year follow–up after surgery for congenital microgastria: case report and review of literature. *J Pediatr Surg* 42: 1957–1960.

Jorge AD, Diaz M. 1976. Double pylorus and esophageal achalasia. *Endoscopy* 8: 208–211.

Kothandaraman KR, Kutty KP, Hawken KA, Barrowman JA. 1983. Double pylorus: in evolution. *J Clin Gastroenterol* 5: 335–338.

Kroes EJ, Festen C. 1998. Congenital microgastria: a case report and review of literature. *Pediatr Surg Int* 13: 416–418.

Kunz HW. 1952. Paraffin-tipped polyethylene tubing for feeding of premature babies, infants, and children. *J Pediatr* 41: 84–85.

Lay Martin MD. 1936. Diverticula of the stomach. *Ann Int Med* 10: 447.

Lestringant GG, Akel SR, Qayed KI. 1992. The pyloric atresia-junctional epidermolysis bullosa syndrome: report of a case and review of the literature. *Arch Dermatol* 128: 1083.

Lewis PL, Holder T, Feldman M. 1961. Duplication of the stomach: report of a case and review of the English literature. *Arch Surg* 82: 634.

Lorenzat CA, Morger R. 1987. Betrag Zur Kongenitalen Pylorus Atresia. Inaugural Dissertation, Universitat Zurich.

MacGillivray PC, Stewart AM, MacFarlane A. 1956. Rupture of the stomach in the newborn due to congenital defects in the gastric musculature. *Arch Dis Child* 31: 56–58.

MacMahon B. 2006. The continuing enigma of pyloric stenosis of infancy: a review. *Epidemiology* 17: 195–201.

Mahon BE, Rosenman MB, Kleiman MB. 2001. Maternal and infant use of erythromycin and other macrolide antibiotics as risk factors for infantile hypertrophic pyloric stenosis. *J Pediatr* 139: 380–384.

Maman E, Maor E, Kachko L, Carmi R. 1998. Epidermolysis bullosa, pyloric atresia, aplasia cutis congenita: histopathological delineation of an autosomal recessive disease. *Am J Med Genet* 78: 127–133.

Mandell GA. 1978. Association of antral diaphragms and hypertrophic pyloric stenosis. *Am J Roentgenol* 131: 203–206.

Martinez NS, Morlock CG, Dockerty MB, Waugh JM, Weber HM. 1958. Heterotopic pancreatic tissue involving the stomach. *Ann Surg* 147: 1.

McCutchen GT, Josey RB. 1951. Reduplication of the stomach. *J Pediatr* 39: 216–220.

Metz AR, Householder R, DePree JF. 1941. Obstruction of the stomach due to congenital double septum with cyst formation. *Trans West Surg Assoc* 50: 242.

Miskovitz PF, Steinberg H. 1982. Diverticula of the gastrointestinal tract. *Disease-a-Month*, 29: 5–61.

Morrell DS, Rubenstein DS, Briggaman RA, Fine JD, Pulkkinen L, Uitto J. 2000. Congenital pyloric atresia in a newborn with extensive aplasia cutis congenita and epidermolysis bullosa simplex. *Brit J Dermatol* 143: 1342–1343.

Moses WR. 1946. Diverticula of the stomach. *Arch Surg* 52: 59.

Moynihan BG. 1904. Remarks on hour-glass stomach. *Brit Med J* 1: 413.

Müller M, Morger R, Engert J. 1990. Pyloric atresia: report of four cases and review of the literature. *Pediatr Surg Int* 5: 276–279.

Musser HH. 1956. The etiology of rupture of the stomach in the newborn. *J Ohio State Med Assoc* 52: 838.

Naidoo R, Singh B. 2012. Congenital double pylorus. *Case Rep Gastrol Med* 1: 1–2.

Neale. 1884. Case of malformation of stomach. *Lancet* 1: 227.

Ohshiro K, Yamataka A, Kobayashi, H Hirai, S, Miyahara, K, Sueyoshi N, Miyano T. 2000. Idiopathic gastric perforation in neonates and abnormal distribution of intestinal pacemaker cells. *J Pediatr Surg* 35: 673–676.

Okoye BO, Parikh DH, Buick RG, Lander AD. 2000. Pyloric atresia: five new cases, a new association, and a review of the literature with guidelines. *J Pediatr Surg* 35: 1242–1245.

Palmer ED. 1951a. Benign intramural tumors of the stomach: a review with special reference to gross pathology. *Medicine* 30: 81–182.

Palmer ED. 1951b. Gastric diverticula. *Int Abst Surg* 92: 417.

Pendergrass EP, Booth RE. 1946. Report of a case of ruptured stomach in an infant 3 days old. *Am J Roentgenol Radium Ther* 56: 590–593.

Potter EL. 1952. Pathology of the Fetus and the Newborn. Chicago: Year Book Publishers.

Primrose A. 1914. Hour-glass contraction of the stomach with report of three cases. *Can Med Assoc J* 4: 776.

Puri P, Guiney EJ, Carroll R. 1985. Multiple gastrointestinal atresias in three consecutive siblings: observations on pathogenesis. *J Pediatr Surg* 20: 22–24.

Ranells JD, Carver JD, Kirby RS. 2011. Infantile hypertrophic pyloric stenosis: epidemiology, genetics, and clinical update. *Adv Pediatr* 58: 195–206.

Rohde H, Troidl H, Fischer M. 1975. Antral duodenal fistula following penetration and perforation of a prepyloric ulcer into the duodenal bulb. *Gastro Endos* 22: 99–101.

Rosenberg AA, Heath MH. 1946. Acute gastric ulcer with perforation in one of premature twins: Report of a case. *J Pediatr* 28: 93–95.

Rowlands RP. 1931. A clinical lecture on hour-glass contraction of the stomach. *Brit Med J* 2: 50–52.

Rowling JT. 1959a. Some observations on gastric cysts. *Brit J Surg* 46: 441–445.

Rowling JT. 1959b. The prepyloric septum: a rare anomaly. *Brit J Surg* 47: 162–166.

Schroeder CM. 1949. Hourglass stomach caused by annular muscular hypertrophy: report of a case. *Ann Surg* 130: 1085.

Schulz RD. 1971. Congenital microgastria. *Annales de Radiologie* 14: 285.

Silverman A, Roy CC, Cozzetto FJ. 1971. Pediatric Clinical Gastroenterology. St Louis: CV Mosby.

Simstein NL. 1986. Congenital gastric anomalies. *Am Surg* 52: 264–268.

Smith VM, Tuttle KW. 1969. Gastroduodenal (pyloric) band. *Gastroenterology* 56: 331–336.

Smythe FW. 1934. Gastric ulcers in the premature newborn: Report of two cases. *Am J Surg* 24: 818–827.

Spicer RD. 1982. Infantile hypertrophic pyloric stenosis: a review. *Br J Surg* 69: 128–135.

Sufian S, Ominsky S, Matsumoto T. 1977. Congenital double pylorus. A case report and review of the literature. *Gastroenterology* 73: 154.

Swartz WT, Shepard RD. 1956. Congenital mucosal diaphragm of the pyloric antrum. *J Kentucky Med Assoc* 54: 149.

Touloukian RJ. 1973. Gastric ischemia: the primary factor in neonatal perforation. *Clin Pediatr* 12: 219.

Vasas P, Mudan SS, Akle CA. 2011. Congenital microgastria with limb defect combined with megaduodenum: case report and review of literature. *Indian J Sur* 73: 122–124.

Von Heinrich H. 1909. Ein beitrag zur histologie des sogen. akzessorischen pankreas. *Virchows Archiv* 198: 392–401.

Wagner EA, Jones DV, Koch CA, Smith GD. 1952. Polyethylene tube feeding in premature infants. *J Pediatr* 41: 79–83.

Wieczorek RL, Seidman I, Ranson JH, Ruoff M. 1984. Congenital duplication of the stomach: case report and review of the English literature. *Am J Gastroenterol* 79: 597.

Yamagiwa, H, Ishihara, A, Sekoguchi T, Matsuzaki O. 1977. Heterotopic pancreas in surgically resected stomach. *Gastroenterologia Japonica* 12: 380–386.

Yamataka A, Yamataka T, Kobayashi H, Sueyoshi N, Miyano T. 1999. Lack of C–KIT^{+} mast cells and the development of idiopathic gastric perforation in neonates. *J Pediatr Surg* 34: 34–38.

Young GB. 1965. Duplication of the stomach. *Brit J Radiol* 38: 853–856.

107 Gallbladder and extrahepatic bile ducts

Mark D. Stringer
Wellington Hospital & University of Otago, Wellington, New Zealand

Anatomical variations in the gallbladder, extrahepatic bile ducts and related vascular supply are critically important in clinical practice. This is particularly so for general and transplant surgeons, interventional radiologists, and gastroenterologists performing endoscopic retrograde cholangiopancreatography. In the United States alone, gallstone disease affects more than 20 million adults (Everhart et al. 1999), results in approximately 750,000 cholecystectomies each year, and incurs an estimated annual cost of more than six billion dollars (Shaffer 2006). Removal of the gallbladder (cholecystectomy) consistently features among the top ten most frequent surgical procedures performed each year in highly developed healthcare systems. Clinically significant anatomical variants are noted at 15–20% of laparoscopic cholecystectomies (Talpur et al. 2010; Hasan et al. 2013). These are mostly accounted for by variations in the cystic artery (approximately 10%), cystic duct (approximately 4%), right hepatic artery (approximately 3%), and gallbladder (approximately 2%). Anatomical variants are an important factor in the etiology of inadvertent bile duct injuries, a potentially life-threatening complication of cholecystectomy (De Werra et al. 2013). Anatomical variations in the extrahepatic biliary tree are also important in liver transplantation, bile duct surgery, and endoscopic or percutaneous procedures on the biliary tract.

This chapter documents anatomical variations in the gallbladder, extrahepatic bile ducts, and cystic artery.

Development of the gallbladder and extrahepatic bile ducts

The development of the gallbladder and extrahepatic bile ducts is key to understanding many of the congenital anatomical variants described in this chapter and therefore merits a brief review.

In the human embryo, the first anlage of the extrahepatic bile ducts and developing liver is the hepatic diverticulum or liver bud, which appears around 18 days after fertilization. The gallbladder develops from the caudal portion of this hepatic foregut diverticulum (pars cystica) and is first visible at about 29 days after fertilization, with the cystic duct recognizable at about 34 days (Roskams and Desmet 2008). The gallbladder elongates and is tubular in shape until the eleventh week of gestation, following which it enlarges and becomes saccular. The fetal gallbladder becomes embedded within a fossa in the liver (Wang et al. 2012) and remains intrahepatic until about 17 weeks gestation, after which it normally protrudes below the inferior surface of the liver (Haffajee 2000).

The extrahepatic biliary tree develops in the embryo (between the third and eighth weeks after fertilization) by lengthening of the caudal part of the hepatic diverticulum. Contrary to earlier descriptions, the extrahepatic bile ducts in humans are patent throughout development (Tan and Vijayan 2001; Roskams and Desmet 2008). The hepatic duct and extrahepatic segments of the right and left hepatic ducts develop from the cranial part (pars hepatica) of the hepatic diverticulum, whereas the proximal segments of the hilar ducts are derived from the intrahepatic ductal plates. As the duodenum rotates to the right at about the fifth week of gestation, the developing common bile duct becomes displaced to its normal position dorsal to the duodenum. A localized outgrowth from the distal common bile duct forms the ventral pancreas. The common bile duct retains its connection to the foregut at the major duodenal papilla, which opens into the second part of the duodenum. In this region, the terminal common bile duct unites with the terminal pancreatic duct to form a short common pancreaticobiliary channel.

Gallbladder

Anatomical variations in the gallbladder may affect its volume, attachments, shape, number, position, and wall.

Gallbladder volume

In the fasting state, the adult gallbladder is usually 7–10 cm long with a resting volume of about 25–30 mL and a capacity of up to 50 mL (Di Ciaula et al. 2012). These dimensions are variable.

Gallbladder attachments

The gallbladder usually lies in a shallow fossa on the visceral surface of the right lobe of the liver covered by peritoneum extending from the surface of the liver. Disruption of the normal embedding and re-exposure of the gallbladder during early

Bergman's Comprehensive Encyclopedia of Human Anatomic Variation, First Edition. Edited by R. Shane Tubbs, Mohammadali M. Shoja and Marios Loukas.
© 2016 John Wiley & Sons, Inc. Published 2016 by John Wiley & Sons, Inc.

development may result in anomalous peritoneal attachments to the liver.

Intrahepatic gallbladder

The gallbladder is almost completely buried within the liver, representing persistence of its early fetal position (Guiteau et al. 2009). A small portion of the neck of the gallbladder may be visible, part of the fundus may protrude through the anterior surface of the liver, or a bridge of liver parenchyma may cover the body of the organ.

Mesenteric attachment of the gallbladder

There are two anatomical variants, both of which increase the mobility of the gallbladder and predispose it to torsion (Gupta et al. 2009). In the first, the whole gallbladder is suspended from the liver by a peritoneal mesentery, which may be congenital or acquired (in the elderly). In the second, only the cystic duct and artery are connected to the under surface of the liver by a mesentery and the gallbladder hangs freely without attachment to the gallbladder fossa. Both variants are sometimes described as a "floating" or "hanging" gallbladder. In such cases, the fundus of the gallbladder may extend as far inferiorly as the iliac fossa or pelvis (Tzardinoglou et al. 1996). The true incidence of a floating gallbladder is unknown but more than 500 cases of gallbladder torsion secondary to this anomaly have been reported.

Cystoduodenal ligament

The gallbladder is connected to the first part of the duodenum by a lateral extension of the lesser omentum, the cystoduodenal ligament (Ashaolu et al. 2011). The cystic duct and artery lie between the two peritoneal layers of the ligament. The free edge of the lesser omentum that forms the anterior boundary of the epiploic foramen is displaced to right. A peritoneal fold extending inferiorly from the cystoduodenal ligament and running across the duodenum to the hepatic flexure has also been described (Pamidi et al. 2008).

Gallbladder shape

The normal gallbladder has a fundus, body, and neck. The bulbous fundus lies at the lateral end of the body and usually projects below the inferior border of the liver lying in contact with the anterior abdominal wall behind the ninth costal cartilage. However, its position is variable (Mirjalili et al. 2012). The neck of the gallbladder may have a localized dilatation just proximal to the cystic duct; this is not a true anatomical variant but an acquired dilatation associated with gallstone disease, known as "Hartmann's pouch" (Hartmann 1891; Stringer 2009).

Phrygian cap

The fundus is folded back upon the body of the gallbladder, producing a so-called Phrygian cap appearance because of its resemblance to an ancient conical cap with the top flopped forwards worn by the inhabitants of Phrygia (now in central Turkey) (Boyden 1935) (Fig. 107.1). The folding may be concealed within the peritoneal covering of the gallbladder but more commonly involves the overlying serosa (Edell 1978). Most authors have regarded this as a congenital variant (Boyden 1935; van Kamp et al. 2013) but some have suggested that it is more often acquired (Gross 1936). The incidence has been estimated to be up to 4% (Edell 1978) but this figure may be inflated by publication bias and variable definitions. The deformity has no pathological significance but may be mistaken for pathology or a septate gallbladder.

Septate gallbladder

A septate gallbladder is characterized by the presence of a septum or septae that partially or completely divides the gallbladder into two or more chambers drained by a single cystic duct. The septum may be longitudinal or transverse. The latter produces an hourglass constriction but this appearance may also be acquired from inflammation or other gallbladder pathology. St-Vil et al. (1992) described a gallbladder divided transversally by a windsock-type diaphragm, isolating the fundus from the rest of the biliary tree. These authors believed this to be the first isolated case of a congenital hourglass gallbladder.

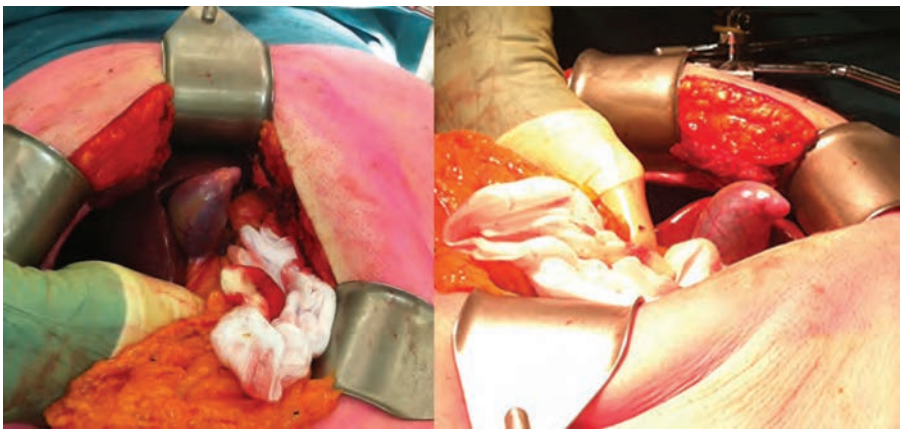

Figure 107.1 Phrygian cap appearance of the gallbladder.

Source: Dr Marie-Janne van Kamp, Medisch Spectrum Twente, Enschede, The Netherlands.

The development of a septate gallbladder has been ascribed to incomplete resolution of a solid stage of gallbladder development (Patel et al. 2008) but the human gallbladder is normally patent throughout development (Tan and Vijayan 2001) and septae must therefore represent disordered sacculation of the initially tubular embryonic gallbladder.

Bilobed gallbladder

The fundus and body of the gallbladder are separated to a variable extent by an external cleft giving the organ a 'V' shape (Gross 1936). The two cavities fuse at the neck of the gallbladder and drain by a single cystic duct. This variant is sometimes classified within the spectrum of "double gallbladder" (Patel et al. 2008).

Gallbladder diverticulum

A diverticulum projects from the surface of the gallbladder anywhere along its length and typically measures 1–5 cm long. A gallbladder diverticulum may be congenital or acquired. It may be associated with acalculous or calculous cholecystitis and carcinoma of the gallbladder. The prevalence reported in the literature varies widely, but most studies cite a figure of less than 0.2% for congenital diverticula. However, one study of 100 cadavers documented a solitary gallbladder diverticulum (considered to be congenital) in 9 (Rajguru et al. 2013) (Fig. 107.2).

Gallbladder number

Gallbladder agenesis

Complete absence of the gallbladder in the presence of normal hepatic and common bile ducts is a rare anatomical variant. After excluding cases where gallbladder agenesis is part of a pathological disorder such as biliary atresia, the estimated incidence of this variant is approximately 0.01–0.07% (Monroe 1959; Singh et al. 1999). In such cases the gallbladder fossa may be marked by a shallow groove (Gross 1936). Gallbladder agenesis is probably caused by failure of the outpouching from the hepatic diverticulum that normally gives rise to the cystic duct and gallbladder. A few familial cases have been recorded (Wilson and Deitrick 1986). An absent gallbladder (Fig. 107.3) may be asymptomatic but some affected individuals develop biliary symptoms, which have been attributed to biliary dyskinesia or calculi. Ultrasound imaging often fails to make the correct diagnosis and consequently some affected patients undergo unnecessary and potentially dangerous surgery (Joliat et al. 2013). If gallbladder agenesis is suspected, magnetic resonance cholangiography appears to be an effective modality for confirming the diagnosis.

Figure 107.2 Diverticulum of the gallbladder in a cadaver.

Source: Rajguru et al. (2013). Reproduced with permission from Journal of Clinical and Diagnostic Research.

Accessory gallbladder

Although frequently also referred to as a "double gallbladder," some authors have drawn a distinction between true duplication with a fused single cystic duct and an accessory gallbladder with separate cystic ducts (Lamah et al. 2001). The numerous variations have been classified by several authors (Boyden 1926; Gross 1936; Harlaftis et al. 1977). The commonest arrangement is two separate gallbladders in an orthotopic location draining via a single or separate cystic ducts into an extrahepatic bile duct (Figs 107.4–107.6). Occasionally, an accessory gallbladder drains into an intrahepatic duct (Weibel et al. 2001). Hassan et al. (2012) described a unique case of a woman with an accessory gallbladder in whom separate cystic ducts drained into the right and left hepatic ducts, respectively.

The two gallbladders may be enclosed within a single peritoneal envelope or have separate peritoneal coats. Rarely, an accessory gallbladder lies in an ectopic location (e.g., intrahepatic or left-sided) and drains independently into an extrahepatic bile duct. The accessory gallbladder can be of variable size and can contain heterotopic gastric mucosa or pancreatic tissue (Bailie et al. 2003).

Human autopsy studies have estimated the incidence of an accessory gallbladder to be 0.03% (Boyden 1926). The variant is understood to arise from duplication of the outpouching from the hepatic diverticulum that normally forms the cystic duct and gallbladder (Boyden 1926).

Triple gallbladder

A further variant on the theme of an accessory gallbladder is a triple gallbladder. Approximately 12 cases have been reported (Khadim et al. 2011). Each gallbladder may drain into the common bile duct through a separate cystic duct or two or all three of the gallbladders may share a cystic duct (Alicioglu 2007). One or more of the gallbladders may be ectopic (e.g., intrahepatic).

Figure 107.3 Magnetic resonance cholangiogram showing absence of the gallbladder and cystic duct.

Source: Joliat et al. (2013). Reproduced with permission from Elsevier.

Gallbladder position

Floating gallbladder

See "Mesenteric attachment of the gallbladder" above.

Left-sided gallbladder

The gallbladder is located to the left of the falciform and round ligaments, usually on the undersurface of the left lobe of the liver but occasionally intrahepatic (Makni et al. 2012; Strong et al. 2013) (Fig. 107.7). A left-sided gallbladder associated with situs inversus is not considered part of this category of anatomical variants. The cystic duct from a left-sided gallbladder usually passes posterior to the falciform ligament and anterior to the common hepatic duct before joining the right side of the common hepatic duct; occasionally, it joins the left side of the common hepatic duct or drains into the left hepatic duct (Gross 1936; Strong et al. 2013). A left-sided gallbladder is usually

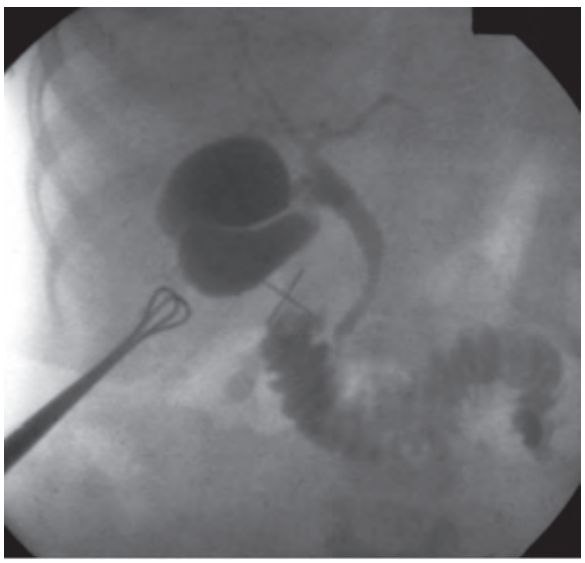

Figure 107.4 Operative cholangiogram of a double gallbladder with two separate cystic ducts in a child.

Source: Bailie et al. (2003). Reproduced with permission from Elsevier.

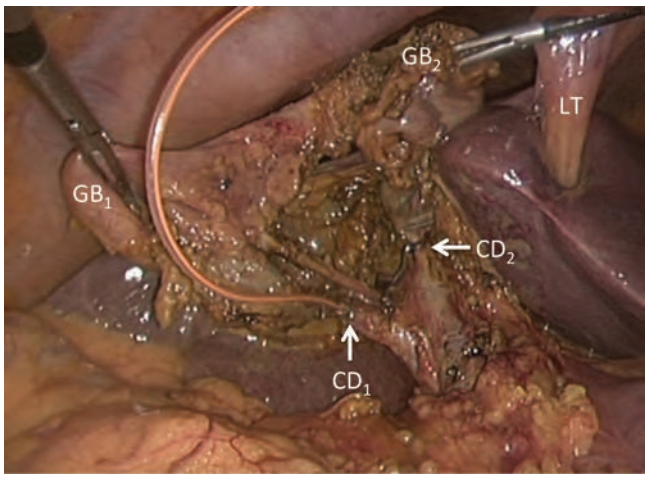

Figure 107.5 Laparoscopic view of a double gallbladder with separate cystic ducts in an adult. LT: ligamentum teres; GB: gallbladder; CD: cystic duct. There is a catheter in CD_1 and CD_2 has been clipped.

Source: Dr Amin Makni, Dept of General Surgery, La Rabta hospital, Tunis, Tunisia

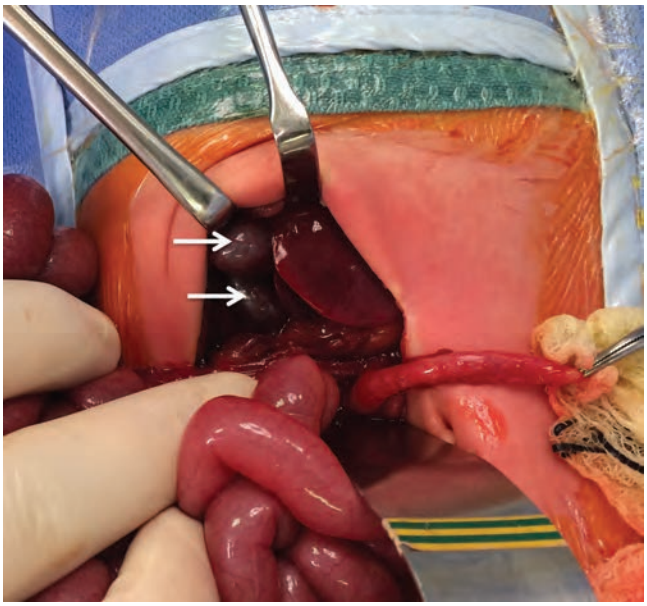

Figure 107.6 Operative view of a double gallbladder (arrows) in a neonate with colonic atresia. The microcolon beyond the site of the atresia is seen on the right of the image.

supplied by a cystic artery arising from the right hepatic artery and passing anterior to the common hepatic duct (Strong et al. 2013). Fewer than 200 cases of a left-sided gallbladder have been reported, although the incidence may be as high as 0.4% (Strong et al. 2013). The diagnosis can be missed using ultrasound and is often made at operation. A left-sided gallbladder increases the risk of bile duct injury during laparoscopic cholecystectomy, and may complicate hepatic resection and liver transplantation (Strong et al. 2013).

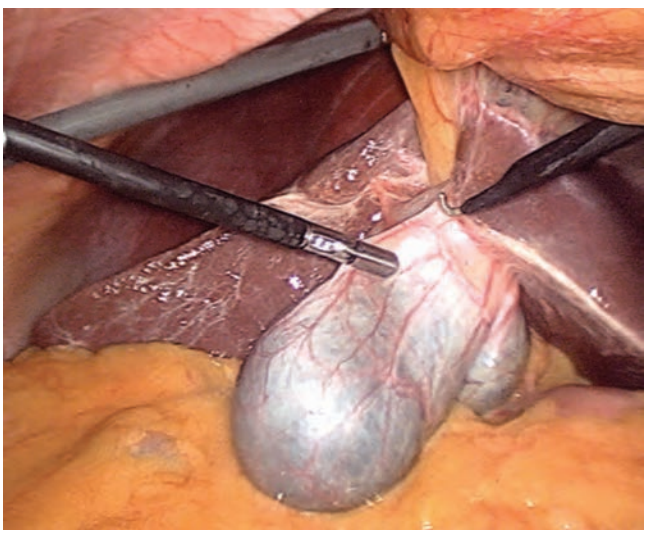

Figure 107.7 Left-sided gallbladder.

Source: Strong et al. (2013). Reproduced with permission from Elsevier.

The developmental origin of a left-sided gallbladder is controversial. When the cystic duct from a left-sided gallbladder joins the common hepatic duct from its right side the variation has been regarded as arising from abnormal migration of the gallbladder; if the cystic duct merges with the common hepatic duct on its left side or drains into the left hepatic duct, left-sided budding of the gallbladder/cystic duct anlage in the embryo has been proposed (Iskandar et al. 2013). To complicate matters, some authors have considered that a left-sided gallbladder arises as a result of a poorly developed quadrate lobe (segment IV) (Lucidarme et al. 2006) while others have attributed it to a right-sided round ligament (from persistence of the right umbilical vein rather than the normal left umbilical vein) (Nagai et al. 1997; Shindoh et al. 2012; Strong et al. 2013). With the latter, the ligamentum teres connects to the portal vein in the right medial sector of the liver and intrahepatic portal venous anatomy may therefore also be abnormal (Shindoh et al. 2012). Iskandar et al. (2013) state that a true left-sided gallbladder is one in which the gallbladder is located to the left of a normally sited round ligament.

Retrohepatic gallbladder

The gallbladder lies in the retroperitoneum adjacent to the inferior vena cava or vertebral column. It may occur in association with atrophy or distortion of the right lobe of the liver (Gross 1936; Principe et al. 1979; Chowbey et al. 2004).

Other ectopic gallbladder sites

Single case reports of other ectopic gallbladder positions have been reported. These include the lesser omentum, falciform ligament (Nelson et al. 1953), transverse mesocolon (Saygun et al. 2004), suprahepatic immediately below the diaphragm (Agarwal et al. 2011), abdominal wall (Alawaneh 1979), retrorenal (Lamah et al. 2001), left lower abdomen (Lamah et al. 2001) and intrathoracic (Labitzke 1991).

Absent, accessory, floating, and multiseptate gallbladders have been reported more commonly in females (Gross 1936; Singh et al. 1999; Cho et al. 2005; Faure et al. 2008).

Gallbladder wall

Ectopic tissue is rarely found within or attached to the wall of the gallbladder. Ectopic liver (Karaman et al. 2012), pancreas (Foucault et al. 2012), and gastric tissue (Hayama et al. 2010) have been reported, often forming a nodule or mass within the wall of the gallbladder.

Cystic duct

Variations in cystic duct anatomy are of considerable importance during surgical excision of the gallbladder (cholecystectomy). Cystic duct variations may be classified according to the following scheme.

Length, diameter, and internal structure

The normal cystic duct in adults has a variable length (5–90 mm) and luminal diameter (2.6±0.7 mm) (Lichtenstein and Ivy 1937; Castelain et al. 1993). It is typically 2–4 cm long. There is one report of isolated saccular dilatation of the duct (Champetier et al. 1987).

The mucous membrane of the cystic duct typically has 2–10 crescentic folds projecting into its lumen collectively referred to as the spiral "valve" of Heister (Dasgupta and Stringer 2005). The folds are arranged more or less spirally and usually run in a clockwise direction down the duct, interdigitating with folds on the opposite wall of the duct (Mentzer 1926). In about 2% of autopsies with no history of biliary tract pathology, the spiral folds are totally absent. At the other extreme, as many as 22 folds have been recorded in the healthy cystic duct (Mentzer 1926).

Tortuosity and course

The cystic duct is frequently tortuous but other variants are described. In a series of 612 autopsy specimens, Mentzer (1926) found that 19 cystic ducts were S-shaped, 41 were curved with acute flexures, and 5 were straight. In about 17% of individuals the cystic duct spirals around the common hepatic duct and in another 10% it runs parallel to it before the two ducts unite (Thompson 1933; Shaw et al. 1993).

Ectopic termination

In most individuals, the junction between the cystic and common hepatic ducts lies in the middle third of their the combined lengths of the common hepatic and common bile ducts. In a radiologic study of 524 patients in the US with suspected biliary tract disease, the cystic duct joined the right lateral aspect of the common hepatic duct in 50%, the medial aspect in 20%, and anteriorly or posteriorly in 30% (Shaw et al. 1993) (Fig. 107.8). In this same study, the cystic duct junction was in the distal third of the combined common hepatic/bile duct segment in 10% (Shaw et al. 1993). In a recent MRI study of 590 patients in Turkey medial entry of the cystic duct was recorded in 17% (Onder et al. 2013). Rarely, the cystic duct drains into a more proximal duct such as the right hepatic duct, right intrahepatic sectoral duct, or even the left hepatic duct (Lamah and Dickson 1999) (Fig. 107.9). Very rarely, it empties directly into the duodenum or stomach.

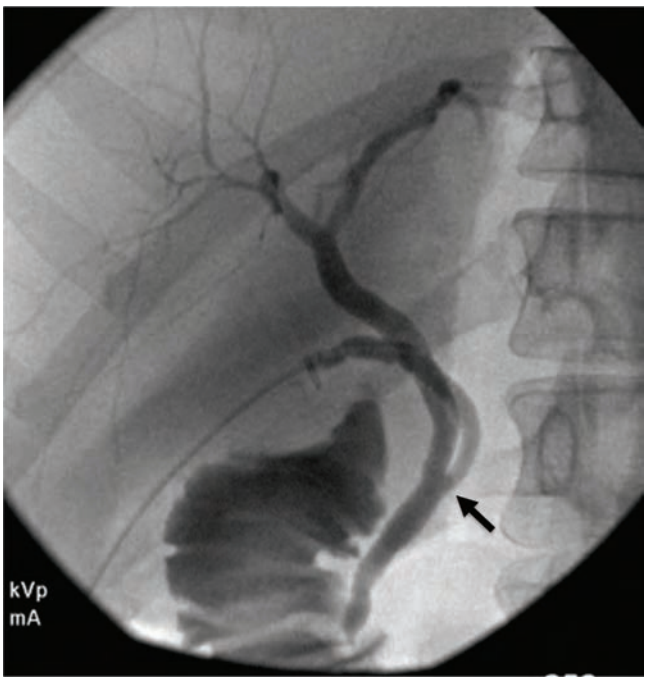

Figure 107.8 Operative cholangiogram (via catheter in cystic duct) showing a left-sided (medial) insertion of the cystic duct (arrow).

Source: Professor John McCall, Dunedin, New Zealand.

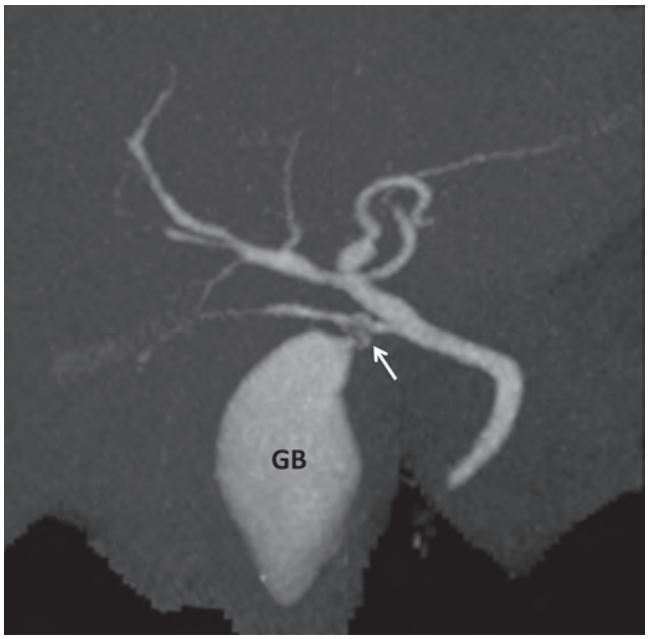

Figure 107.9 CT cholangiogram showing the cystic duct (arrow) draining into an aberrant segmental bile duct. GB: gallbladder.

Source: Professor John McCall, Dunedin, New Zealand.

Absent

The cystic duct may be absent such that the neck of the gallbladder empties directly into the bile duct (Adam and Metcalf 1966).

Duplication

Duplication of the cystic duct from a single gallbladder has been reported (Lobo et al. 2000).

Hepatic ducts

The right and left hepatic ducts exit the liver and unite at the porta hepatis to form the common hepatic duct. The common hepatic duct normally descends for a few centimeters before being joined obliquely on its right side by the cystic duct to form the common bile duct. The diameter of the normal adult

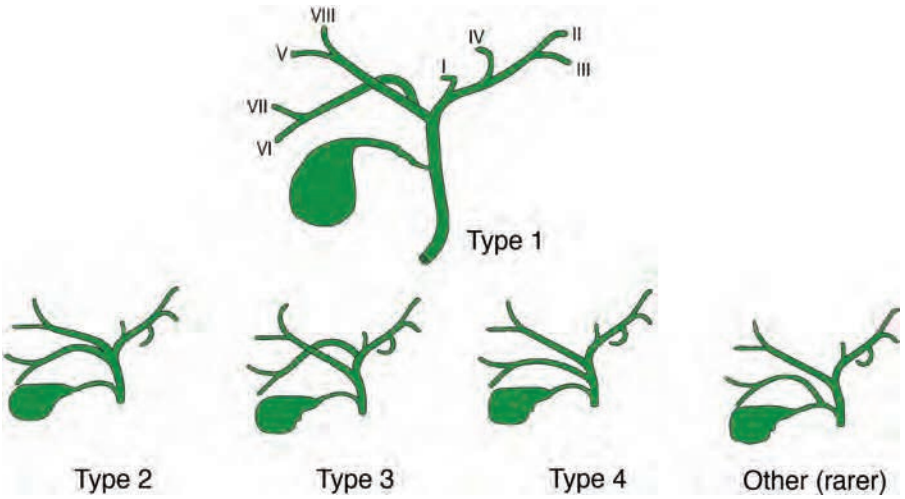

Figure 107.10 Intrahepatic bile duct variation affecting the extrahepatic bile ducts. Type 1: normal; type 2: absence of right hepatic duct (trifurcation pattern); type 3: right posterior sectoral duct draining into the left hepatic duct; type 4: low drainage of the right posterior sectoral duct into the common hepatic duct. Other (rarer): right posterior sectoral duct draining into the cystic duct. Roman numerals refer to liver segments.

Source: Stringer (2009).

common hepatic duct is variable but is less than 5 mm when measured by ultrasound.

Intrahepatic bile duct variants involving the extrahepatic bile ducts

The right hepatic duct and its branches are more often subject to variation than the left ductal system (Cucchetti et al. 2011; Chaib et al. 2014). Most of these variations affect the intrahepatic bile ducts exclusively but they may in turn alter the arrangement of the extrahepatic bile ducts. The variations have been classified into several main types (Figs 107.10, 107.11) and their approximate frequency is shown in Table 107.1. Left intrahepatic ductal variations largely concern the arrangement of the segment IV bile duct, which usually drains into the left hepatic duct but may open into the segment II or III bile duct, the right anterior sectoral duct, or even the common hepatic duct (Chaib et al. 2014). The bile ducts draining the caudate lobe (segment I) usually join the origin of the left hepatic duct or the hilar ductal confluence but may drain into both hepatic ducts.

A small bile duct from segment V of the liver that traverses the gallbladder fossa is often known as Luschka's duct (Luschka 1863; Spanos and Syrakos 2006; Kocabiyik et al. 2009). It joins the right hepatic duct or its anterior sectoral branch, the common hepatic duct, or rarely the cystic duct. Autopsy studies have identified such a duct in up to 30% of individuals but many are small and relatively insignificant; if only larger ducts (1–2 mm) are considered, the prevalence is nearer 5% (Ko et al. 2006). This ductal variant may be injured during cholecystectomy, resulting in a postoperative bile leak.

Contrary to some reports, Luschka did not describe an intrahepatic bile duct draining directly from the liver into the gallbladder. This has been referred to in the literature as a cholecystohepatic duct (or a cystohepatic duct when it drains directly into the cystic duct; Champetier et al. 1991). Anomalous intrahepatic bile ducts that drain directly into the gallbladder or cystic duct are almost always from right lobe liver segments and are found in up to 1% of individuals (Turner and Fulcher 2001).

Hepaticocystic duct

In this rare anatomical variant, the common bile duct is absent and both the right and left hepatic ducts drain into the gallbladder, which empties via the cystic duct into the duodenum

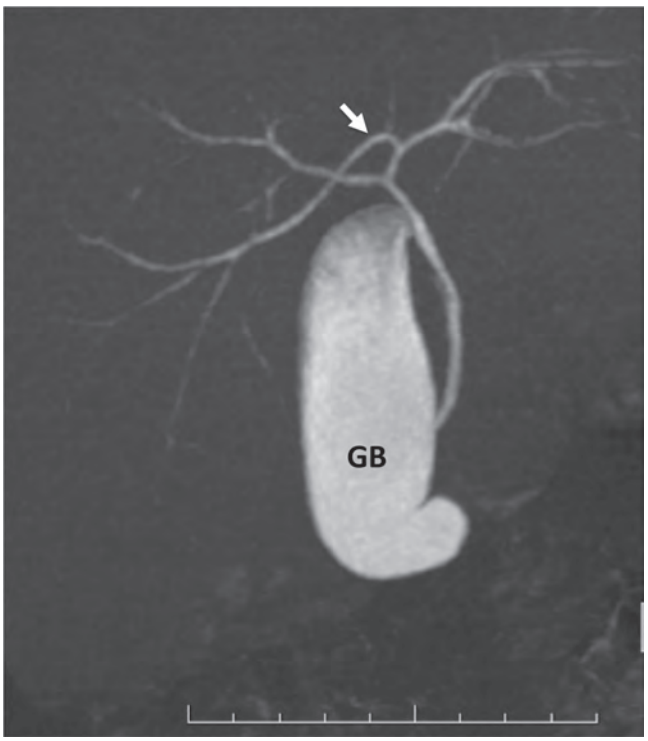

Figure 107.11 Magnetic resonance cholangiogram showing the right posterior sectoral duct (arrow) draining into the left hepatic duct. GB: gallbladder.

Source: Professor John McCall, Dunedin, New Zealand.

Table 107.1 Major variations of the intrahepatic bile ducts involving the extrahepatic bile ducts. Based on data from Cucchetti et al. (2011) and Chaib et al. (2014).

Type	Approximate percentage of population	Description
1	60*	Normal anatomy
2	15	Absence of right hepatic duct. Common hepatic duct is formed by the union of right anterior, right posterior, and left hepatic ducts (trifurcation).
3	15	One of the right sectoral ducts (usually the posterior) joins the left hepatic duct.
4	10	Low drainage of one the right sectoral ducts (usually the posterior) into the common hepatic duct.
Rarer types	<5	The segment V duct or right posterior sectoral duct drains into the cystic duct or gallbladder.

*Slightly greater in men and lower in women. The percentages of different types vary between populations and are approximate values.

(Losanoff et al. 2002). The right and left hepatic ducts can drain independently into the gallbladder or via a common hepatic duct or via multiple smaller ducts.

Among 590 patients, Onder et al. (2013) found that 233 (39.5%) showed anatomic variations at different levels in the intra- and extrahepatic biliary tracts. Among these variations, a right posterior hepatic duct insertion into the left hepatic duct at the level of the bifurcation was observed in 71 patients (12.1%), a trifurcation was observed in 30 patients (5.1%), and aberrant insertion of the right hepatic duct into the main hepatic duct was noted in 18 patients (3.1%).

Common bile duct

Length and diameter

In healthy adults, the common bile duct is usually 6–8 cm long and its diameter measured by ultrasound is no more than 7 mm. Mean diameter increases slightly with advancing age from 3.6 mm below 60 years to 4 mm after 80 years (Perret et al. 2000).

Absent

Agenesis of the common bile duct is discussed above ("Hepaticocystic duct").

Double

There have been several reports of a double common bile duct (Boyden 1932; Bernard et al. 2001). The two ducts may run in parallel separated by a septum and open into the duodenum or they may branch in such a way that one of the ducts has an ectopic termination (Bernard et al. 2001). In some reports the position of the cystic duct has not been clearly documented (Ravaioli et al. 2011), making it difficult to distinguish a double parallel common bile duct from a low confluence of the right and left hepatic ducts.

Ectopic termination

The common bile duct rarely drains into the stomach or main pancreatic duct (Kanematsu et al. 1992). Gastric drainage can be via a solitary common bile duct or via one limb of a double common bile duct, with the other limb draining normally into the duodenum (Bernard et al. 2001). Other rare terminations of the common bile duct have been reported, but the anatomy of some of these cases (Bernard et al. 2001) calls into question whether the term "common bile duct" is appropriate.

Pancreaticobiliary junction

The common bile duct usually enters the duodenal wall where it unites with the pancreatic duct in a 'Y' configuration, forming a short common channel measuring 2–10 mm in length. This opens onto the medial wall of the second part of the duodenum at the major duodenal papilla. This configuration is found in 60–80% of individuals (DiMagno et al. 1982; Flati et al. 1994). In most other instances, the two ducts unite in a 'V' configuration forming a short common channel less than 2 mm in length or they remain entirely separate and drain independently at the major duodenal papilla. Occasionally, the common bile duct and pancreatic duct unite outside the duodenal wall to form an abnormally long common channel (Kamisawa and Okamoto 2008) or they empty into the major and minor duodenal papilla, respectively (DiMagno et al. 1982; Flati et al. 1994).

Cystic artery

The hepatobiliary triangle formed by the cystic duct, the common hepatic duct and the inferior surface of segment V of the liver (often mistakenly referred to as Calot's triangle; Stringer 2009) is an important landmark during cholecystectomy since it usually contains the cystic artery as it runs from the right branch of the hepatic artery to the gallbladder (Suzuki et al. 2000). It may occasionally contain an accessory bile duct.

The cystic artery usually arises from the right branch of the hepatic artery, and most often passes posterior to the common hepatic duct within the hepatobiliary triangle where it lies anterosuperior to the cystic duct. There are anatomical variations in the number, origin, and course of the cystic artery (Fig. 107.12). One or more variants are present in up to 20% of individuals (Mlakar et al. 2003; Molmenti et al. 2003; Saidi et al. 2007).

The most common variant is an origin from the hepatic artery proper, when the cystic artery often crosses anterior

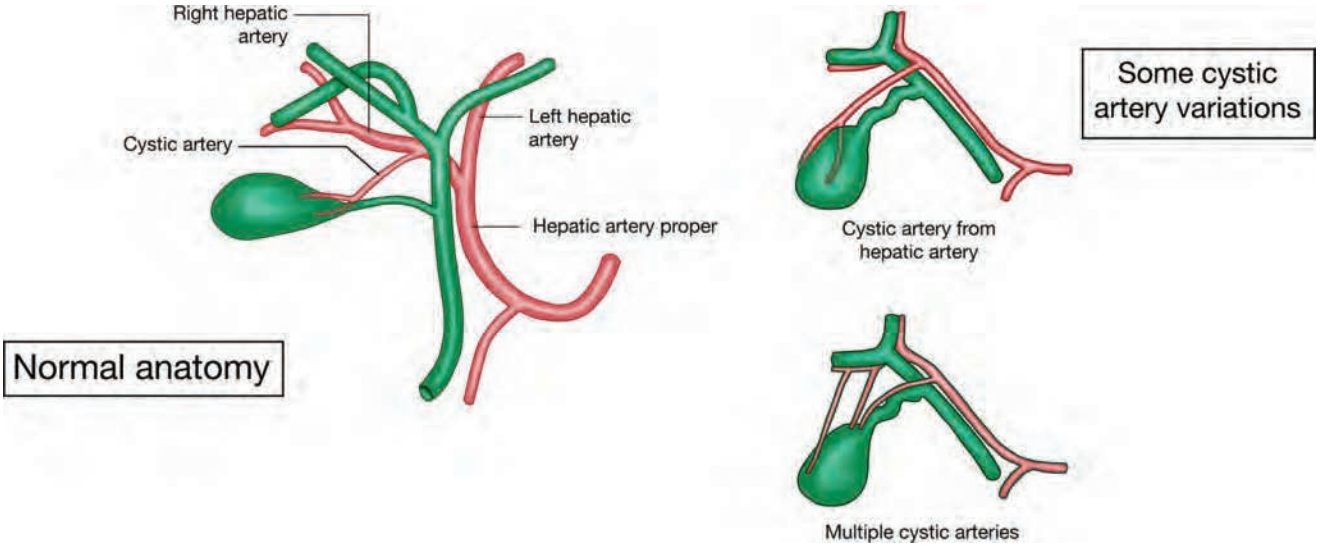

Figure 107.12 Normal arrangement of the cystic artery and two of the more common variants.

Source: Stringer (2009).

to the common hepatic duct or common bile duct to reach the gallbladder (Fig. 107.13). Rarely, it may arise from the left hepatic, gastroduodenal, superior pancreaticoduodenal, coeliac, right gastric, or superior mesenteric artery (Molmenti et al. 2003), when it may not traverse the hepatobiliary triangle. The cystic artery frequently bifurcates close to its origin, giving rise to two vessels. In about 10% of individuals, one or more accessory cystic arteries are present arising from the hepatic artery or one of its branches (Molmenti et al. 2003; Saidi et al. 2007). There appear to be ethnic variations in the frequency of different cystic artery variants (Chen et al. 2000; Saidi et al. 2007) In a recent literature review of 9800 individuals, the cystic artery originated from the right branch of the hepatic artery in 79%, passing through the hepatobiliary triangle in 82% (Andall et al. 2015). It coursed anterior to the common hepatic or common bile duct in 18% and 5% of persons, respectively, and was located inferior to the cystic duct in another 5%. Multiple cystic arteries were present in 9%..

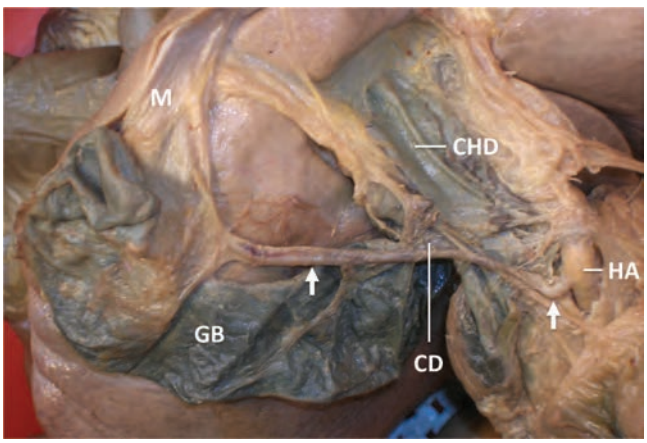

Figure 107.13 Cadaver dissection showing a cystic artery (arrows) arising from the hepatic artery proper and passing to a gallbladder suspended on a mesentery. GB: gallbladder; M: mesentery; CHD: common hepatic duct; HA: hepatic artery.

References

Adam Y, Metcalf W. 1966. Absence of the cystic duct: a case report, the embryology and a review of the literature. *Ann Surg* 164: 1056–1058.

Agarwal V, Pande S, Garg SK, Jangid DR. 2011. Anomalously placed suprahepatic gall-bladder: A case detected on F-18 FDG PET/CT. *Indian J Nucl Med* 26: 120–122.

Alawaneh I. 1979. Anomaly of the gallbladder lying extraperitoneally in the internal oblique muscle: report of an unusual case. *Int Surg* 64: 45–47.

Alicioglu B. 2007. An incidental case of triple gallbladder. *World J Gastroenterol* 13: 2004–2006.

Andall RG, Matusz P, du Plessis M, Ward R, Tubbs RS, Loukas M. The clinical anatomy of cystic artery variations: a review of over 9800 cases. Surg Radiol Anat. 2015 [Epub ahead of print] PubMed PMID: 26698600

Ashaolu JO, Ukwenya VO, Adenowo TK. 2011. Cystoduodenal ligament as an abnormal fold and the accompanying anatomical and clinical implications. *Surg Radiol Anat* 33: 171–174.

Bailie AG, Wyatt JI, Sheridan MB, Stringer MD. 2003. Heterotopic gastric mucosa in a duplicate gallbladder. *J Pediatr Surg* 38: 1401–1403.

Bernard P, Le Borgne J, Dupas B, Kohnen-Shari N, Raoult S, Hamel A. 2001. Double common bile duct with ectopic drainage into the stomach. Case report and review of the literature. *Surg Radiol Anat* 23: 269–272.

Boyden EA. 1926. The accessory gall-bladder: an embryological and comparative study of aberrant biliary vesicles occurring in man and the domestic mammals. *Am J Anat* 38: 177–231.

Boyden EA. 1932. The problem of double ductus choledochus. *Anat Rec* 55: 71–93.

Boyden EA. 1935. The Phrygian cap in cholecystography: a congenital anomaly of the gallbladder. *Am J Radiol* 33: 589.

Castelain M, Grimaldi C, Harris AG, Caroli-Bosc FX, Hastier P, Dumas R, Delmont JP. 1993. Relationship between cystic duct diameter and the presence of cholelithiasis. *Dig Dis Sci* 38: 2220 –2224.

Chaib E, Kanas AF, Galvão FH, D'Albuquerque LA. 2014. Bile duct confluence: anatomic variations and its classification. *Surg Radiol Anat* 36: 105–109.

Champetier P, Partensky C, Ponchon T. 1987. Cystic malformations of the cystic duct. *Surg Radiol Anat* 9: 287–291.

Champetier J, Létoublon C, Alnaasan I, Charvin B. 1991. The cystohepatic ducts: surgical implications. *Surg Radiol Anat* 13: 203–211.

Chen TH, Shyu JF, Chen CH, Ma KH, Wu CW, Lui WY, Liu JC. 2000. Variations of the cystic artery in Chinese adults. *Surg Laparosc Endosc Percutan Tech* 10: 154–157.

Cho YP, Kim HJ, Jung SM, Kang GH, Han MS, Jang HJ, Kim YH, Lee SG. 2005. Torsion of the gallbladder: report of a case. *Yonsei Med J* 46: 862–865.

Chowbey PK, Wadhwa A, Sharma A, Khullar R, Soni V, Baijal M. 2004. Ectopic gallbladder: laparoscopic cholecystectomy. *Surg Laparosc Endosc Percutan Tech* 14: 26–28.

Cucchetti A, Peri E, Cescon M, Zanello M, Ercolani G, Zanfi C, Bertuzzo V, Di Gioia P, Pinna AD. 2011. Anatomic variations of intrahepatic bile ducts in a European series and meta-analysis of the literature. *J Gastrointest Surg* 15: 623–630.

Dasgupta D, Stringer MD. 2005. Cystic duct and Heister's "valves". *Clin Anat* 18: 81–87.

De Werra C, Del Giudice R, Di Micco R, Aloia S, Bracciano L, Cervotti M, Galloro G, Bucci L. 2013. Biliary duct injuries in the laparoscopic era: our experience. *G Chir* 34: 59–63.

Di Ciaula A, Wang DQ, Portincasa P. 2012. Gallbladder and gastric motility in obese newborns, pre-adolescents and adults. *J Gastroenterol Hepatol* 27: 1298–1305.

DiMagno EP, Shorter RG, Taylor WF, Go VL. 1982. Relationships between pancreaticobiliary ductal anatomy and pancreatic ductal and parenchymal histology. *Cancer* 49: 361–368.

Edell S. 1978. A comparison of the "phrygian cap" deformity with bistable and gray scale ultrasound. *J Clin Ultrasound* 6: 34–35.

Everhart JE, Khare M, Hill M, Maurer KR. 1999. Prevalence and ethnic differences in gallbladder disease in the United States. *Gastroenterology* 117: 632–639.

Faure JP, Doucet C, Scepi M, Rigoard P, Carretier M, Richer JP. 2008. Abnormalities of the gallbladder, clinical effects. *Surg Radiol Anat* 30: 285–290.

Flati G, Flati D, Porowska B, Ventura T, Catarci M, Carboni M. 1994. Surgical anatomy of the papilla of Vater and the biliopancreatic ducts. *Am Surg* 60: 712–718.

Foucault A, Veilleux H, Martel G, Lapointe R, Vandenbroucke-Menu F. 2012. Heterotopic pancreas presenting as suspicious mass in the gallbladder. *JOP* 13: 700–701.

Gross R. 1936. Congenital anomalies of gallbladder. A review of one hundred and forty-eight cases with a report of double gallbladder. *Arch Surg* 32: 131–162.

Guiteau JJ, Fisher M, Cotton RT, Goss JA. 2009. Intrahepatic gallbladder. *J Am Coll Surg* 209: 672.

Gupta V, Singh V, Sewkani A, Purohit D, Varshney R, Varshney S. 2009. Torsion of gall bladder, a rare entity: a case report and review article. *Cases J* 2: 193.

Haffajee MR. 2000. The fetal gallbladder: morphology and morphometry by microdissection. *Surg Radiol Anat* 22: 261–270.

Harlaftis N, Gray SW, Skandalakis JE. 1977. Multiple gallbladders. *Surg Gynecol Obstet* 145: 928–934.

Hartmann H. 1891. Quelques points l'anatomie et de la chirurgie des voies biliaires. *Bull Soc Anat Paris* 5: 480–500.

Hasan MM, Reza E, Khan MR, Laila SZ, Rahman F, Mamun MH. 2013. Anatomical and congenital anomalies of extra hepatic biliary system encountered during cholecystectomy. *Mymensingh Med J* 22: 20–26.

Hassan S, Young AL, Farooq M, Pai D, Gough M. 2012. Accessory gallbladder: a new anatomical variation arising from both left and right hepatic ducts. *Ann R Coll Surg Engl* 94: e204–205.

Hayama S, Suzuki Y, Takahashi M, Hazama K, Fujita M, Kondo S, Katoh H. 2010. Heterotopic gastric mucosa in the gallbladder: report of two cases. *Surg Today* 40: 783–787.

Iskandar ME, Radzio A, Krikhely M, Leitman IM. 2013. Laparoscopic cholecystectomy for a left-sided gallbladder. *World J Gastroenterol* 19: 5925–5928.

Joliat GR, Shubert CR, Farley DR. 2013. Isolated congenital agenesis of the gallbladder and cystic duct: report of a case. *J Surg Educ* 70: 117–120.

Kamisawa T, Okamoto A. 2008. Pancreatographic investigation of pancreatic duct system and pancreaticobiliary malformation. *J Anat* 212: 125–134.

Kanematsu M, Imaeda T, Seki M, Goto H, Doi H, Shimokawa K. 1992. Accessory bile duct draining into the stomach: case report and review. *Gastrointest Radiol* 17: 27–30.

Karaman K, Teke Z, Ercan M, Keklik TT, Bostanci EB, Akoglu M. 2012. Ectopic liver (choristoma) attached to the gallbladder wall. *ANZ J Surg* 82: 948.

Khadim MT, Ijaz A, Hassan U, Gulzar S, Mushtaq S. 2011. Triple gallbladder: a rare entity. *Am J Gastroenterol* 106: 1861–1862.

Ko K, Kamiya J, Nagino M, Oda K, Yuasa N, Arai T, Nishio H, Nimura Y. 2006. A study of the subvesical bile duct (duct of Luschka) in resected liver specimens. *World J Surg* 30: 1316–1320.

Kocabiyik N, Yalcin B, Kilbas Z, Karadeniz SR, Kurt B, Comert A, Ozan H. 2009. Anatomical assessment of bile ducts of Luschka in human fetuses. *Surg Radiol Anat* 31: 517–521.

Labitzke R. 1991. Congenital intrathoracic ectopic gallbladder – a currently unreported developmental disorder. Attempt at a classification of abnormal gallbladder sites. *Chirurg* 62: 755–758.

Lamah M, Dickson GH. 1999. Congenital anatomical abnormalities of the extrahepatic biliary duct: a personal audit. *Surg Radiol Anat* 21: 325–327.

Lamah M, Karanjia ND, Dickson GH. 2001. Anatomical variations of the extrahepatic biliary tree: review of the world literature. *Clin Anat* 14: 167–172.

Lichtenstein ME, Ivy AC. 1937. The function of the "valves" of Heister. *Surgery* 1: 38–52.

Lobo EJ, Herbella FA, Goldenberg A, Kobata MH, Triviño T. 2000. Laparoscopic cholecystectomy in a patient with a duplicated cystic duct. *Surg Laparosc Endosc Percutan Tech* 10: 326–328.

Losanoff JE, Jones JW, Richman BW, Rangnekar NJ. 2002. Hepaticocystic duct: a rare anomaly of the extrahepatic biliary system. *Clin Anat* 15: 314–315.

Lucidarme O, Taboury J, Savier E, Cadi M, Hannoun L, Grenier PA. 2006. Fusion of the midplane with the left intersectional plane: a liver anatomical variation revisited with multidetector-row CT. *Eur Radiol* 16: 1699–1708.

Luschka H. 1863. *Die anatomie des menschlichen bauches*. Tubingen: Verlag der H Lauppschen, Buchhandlung.

Makni A, Magherbi H, Ksantini R, Rebai W, Safta ZB. 2012. Left-sided gallbladder: an incidental finding on laparoscopic cholecystectomy. *Asian J Surg* 35: 93–95.

Mentzer SH. 1926. The valves of Heister. *Arch Surg* 13: 511–522.

Mirjalili SA, McFadden SL, Buckenham T, Wilson B, Stringer MD. 2012. Anatomical planes: are we teaching accurate surface anatomy? *Clin Anat* 25: 819–826.

Mlakar B, Gadzijev EM, Ravnik D, Hribernik M. 2003. Anatomical variations of the cystic artery. *Eur J Morphol* 41: 31–34.

Molmenti EP, Pinto PA, Klein J, Klein AS. 2003. Normal and variant arterial supply of the liver and gallbladder. *Pediatr Transplant* 7: 80–82.

Monroe SE. 1959. Congenital absence of the gallbladder: a statistical study. *J Int Coll Surg* 32: 369–373.

Nagai M, Kubota K, Kawasaki S, Takayama T, Bandai Y, Makuuchi M. 1997. Are left–sided gallbladders really located on the left side? *Ann Surg* 225: 274–280.

Nelson PA, Schmitz RL, Perutsea S. 1953. Anomalous position of the gallbladder within the falciform ligament. *Arch Surg* 66: 679.

Onder H, Ozdemir MS, Tekbas G, Ekici F, Gumus H, Bilici A. 2013. 3-T MRI of the biliary tract variations. *Surg Radiol Anat* 35: 161–167.

Pamidi N, Nayak S, Vollala VR. 2008. Cystogastrocolic fold and associated atrophy of the gallbladder. *Singapore Med J* 49: e250–251.

Patel NR, Joshipura VP, Haribhakti SP, Soni HN. 2008. Septate gallbladder in the laparoscopic era. *J Minim Access Surg* 4: 20–22.

Perret RS, Sloop GD, Borne JA. 2000. Common bile duct measurements in an elderly population. *J Ultrasound Med* 19: 727–730.

Principe A, Spangaro M, Lapilli A, Vecchi R, Volta L, De Lorenzi P. 1979. Congenital anomalies of the gallbladder. A case of retrohepatic gallbladder contained in the coronary ligament. *Minerva Chir* 34: 879–884.

Rajguru J, Jain S, Khare S, Fulzele RR, Ghai R. 2013. Embryological basis and clinical correlation of the rare congenital anomaly of the human gall bladder: – "the diverticulum" – a morphological study. *J Clin Diagn Res* 7: 2107–2110.

Ravaioli M, Ercolani G, Cescon M, Del Gaudio M, Cucchetti A, Ramacciato G, Francioni G, Pinna AD. 2011. Double common bile duct: a pitfall during liver transplantation and cholecystectomy. *Surgery* 150: 139–140.

Roskams T, Desmet V. 2008. Embryology of extra- and intrahepatic bile ducts, the ductal plate. *Anat Rec (Hoboken)* 291: 628–635.

Saidi H, Karanja TM, Ogengo JA. 2007. Variant anatomy of the cystic artery in adult Kenyans. *Clin Anat* 20: 943–945.

Saygun O, Aydinuraz K, Daphan C, Akkus A, Ağalar F. 2004. Case report: intramesocolic malposition of the gallbladder. *Turk J Med Sci* 34: 281–282.

Shaffer EA. 2006. Epidemiology of gallbladder stone disease. *Best Pract Res Clin Gastroenterol* 20: 981–996.

Shaw MJ, Dorsher PJ, Vennes JA. 1993. Cystic duct anatomy: an endoscopic perspective. *Am J Gastroenterol* 88: 2102–2106.

Shindoh J, Akahane M, Satou S, Aoki T, Beck Y, Hasegawa K, Sugawara Y, Ohtomo K, Kokudo N. 2012. Vascular architecture in anomalous right-sided ligamentum teres: three-dimensional analyses in 35 patients. *HPB (Oxford)* 14: 32–41.

Singh B, Satyapal KS, Moodley J, Haffejee AA. 1999. Congenital absence of the gall bladder. *Surg Radiol Anat* 21: 221–224.

Spanos CP, Syrakos T. 2006. Bile leaks from the duct of Luschka (subvesical duct): a review. *Langenbecks Arch Surg* 391: 441–447

Stringer MD. 2009. *Eponyms in Surgery and Anatomy of the Liver, Bile Ducts and Pancreas*. London: Royal Society of Medicine Press Ltd.

Strong RW, Fawcett J, Hatzifotis M, Hodgkinson P, Lynch S, O'Rourke T, Slater K, Yeung S. 2013. Surgical implications of a left-sided gallbladder. *Am J Surg* 206: 59–63.

St-Vil D, Luks FI, Hancock BJ, Garel L, Brochu P, Blanchard H, Bensoussan AL. 1992. Diaphragm of the gallbladder: a case report. *J Pediatr Surg* 27: 1301–1303.

Suzuki M, Akaishi S, Rikiyama T, Naitoh T, Rahman MM, Matsuno S. 2000. Laparoscopic cholecystectomy, Calot's triangle, and variations in cystic arterial supply. *Surg Endosc* 14: 141–144.

Talpur KA, Laghari AA, Yousfani SA, Malik AM, Memon AI, Khan SA. 2010. Anatomical variations and congenital anomalies of extra hepatic biliary system encountered during laparoscopic cholecystectomy. *J Pak Med Assoc* 60: 89–93.

Tan CE, Vijayan V. 2001. New clues for the developing human biliary system at the porta hepatis. *J Hepatobiliary Pancreat Surg* 8: 295–302.

Thompson IM. 1933. On the arteries and ducts in the hepatic pedicle. *Univ Calif Pub Anat* 1: 55–59.

Turner MA, Fulcher AS. 2001. The cystic duct: normal anatomy and disease processes. *Radiographics* 21: 3–22.

Tzardinoglou E, Prousalidis J, Apostolidis S, Katsohis C, Aletras H. 1996. Hanging noncalculous gallbladder. *HPB Surg* 9: 137–139.

van Kamp MJ, Bouman DE, Steenvoorde P, Klaase JM. 2013. A phrygian cap. *Case Rep Gastroenterol* 7: 347–351.

Wang BJ, Kim JH, Yu HC, Rodríguez-Vázquez JF, Murakami G, Cho BH. 2012. Fetal intrahepatic gallbladder and topographical anatomy of the liver hilar region and hepatocystic triangle. *Clin Anat* 25: 619–627.

Weibel D, Kaufmann M, Reidtmann-Klee HJ. 2001. Accessory gallbladder originating from the right hepatic duct. *Surg Endosc* 15: 519.

Wilson JE, Deitrick JE. 1986. Agenesis of the gall bladder: case report and familial investigation. *Surgery* 99: 106–109.

Further reading

Beckingham IJ. 2001. ABC of diseases of liver, pancreas, and biliary system: gallstone disease. *Br Med J* 322: 91–94.

Singh B, Ramsaroop L, Allopi L, Moodley J, Satyapal KS. 2006. Duplicate gallbladder: an unusual case report. *Surg Radiol Anat* 28(6): 654–657.

Todani T, Watanabe Y, Narusue M, Tabuchi K, Okajima K. 1977. Congenital bile duct cysts: Classification, operative procedures, and review of thirty-seven cases including cancer arising from choledochal cyst. *Am J Surg* 134: 263–269.

108 Liver

Koichi Watanabe
Kurume University School of Medicine, Fukuoka, Japan

Of the morphological variations of the liver, accessory hepatic grooves are the most frequently observed anomaly with a reported incidence of approximately 30% of the population. These grooves are often found on the liver's diaphragmatic surface and appear to be caused by some type of acquired force.

Hypoplasia or agenesis of the liver is congenital and has been observed in both the right and the left lobes. Conversely, accessory liver lobes can be congenital or acquired. Accessory lobes arising from the superior liver surface represent a congenital anomaly, as do some cases of accessory lobes arising from the inferior surface. In contrast, Riedel's lobe, which arises from the inferior liver surface and protrudes downward, occurs as a secondary change induced by abdominal inflammation. Extremely rare cases of morphological variation that have been reported include a liver without any lobar division (Bergman et al. 1995) and a liver with 16 lobes (Moser 1898).

Ectopic liver tissue represents a congenital anomaly; it can be found in association with various organs in the abdominal and thoracic cavities.

Accessory hepatic grooves

Accessory grooves are sometimes found on the liver's diaphragmatic surface (Fig. 108.1). Several hypotheses have been proposed as to the origin of these grooves. Early reports from the nineteenth century generally claimed that accessory fissures occurred as a result of external compression by the diaphragm and the ribs (Schafer and Dymington 1896; Cullen 1925). Some authors have considered the grooves to be related to the lobulations of the liver, while others have assessed them as acquired changes caused by the external force from other organs (Schafer and Dymington 1896; Baxter 1953), clothes (Okudaira 1995), or coughing (Sherlock and Dooley 2008). Conversely, Ono proposed that the grooves formed during a late stage of diaphragmatic growth after establishment of the basic segmental configuration of the liver (Ono et al. 2000).

Accessory grooves of the liver are not a rare anomaly; they are found in approximately 30–40% of autopsies (Newell and Morgan-Jones 1993). Auh et al. (1984) reported that the incidence of the grooves increases with aging. In his study, the incidence of accessory grooves was 13% in patients aged 17–60 years, but it increased to 33% in patients aged 61–84 years. The incidence for ages 81–84 years was extremely high at 71% (Auh et al. 1984). These results imply that accessory grooves are acquired after birth.

Agenesis or hypoplasia of the right lobe of the liver

Agenesis of the right lobe of the liver was first reported by Heller in 1870 (Champetier et al. 1985), and approximately 30 cases had been reported in the literature as of 2008 (Fields et al. 2008). The incidence in men is slightly higher than in women (Radin 1987; Fields et al. 2008). The left and caudate liver lobes usually become hypertrophied in compensation for the absence of the right lobe (Fig. 108.2). The middle hepatic vein is typically preserved, and the gallbladder is often located on the right side of the liver (Champetier et al. 1985). However, some variations exist. Cases of a hypoplastic left medial section and a hyperplastic left lateral section have also been observed. Moreover, the

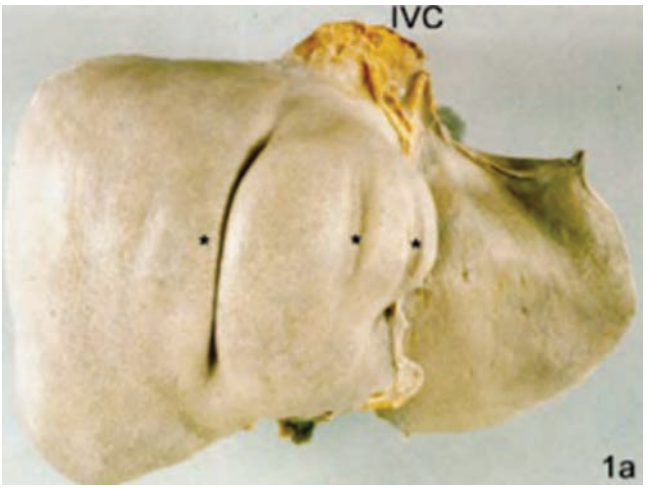

Figure 108.1 A case of an accessory hepatic grooves. Asterisks indicate hepatic sulci on the diaphragmatic surface.

Source: Macchi et al. (2003). Reproduced with permission from John Wiley & Sons.

Bergman's Comprehensive Encyclopedia of Human Anatomic Variation, First Edition. Edited by R. Shane Tubbs, Mohammadali M. Shoja and Marios Loukas.
© 2016 John Wiley & Sons, Inc. Published 2016 by John Wiley & Sons, Inc.

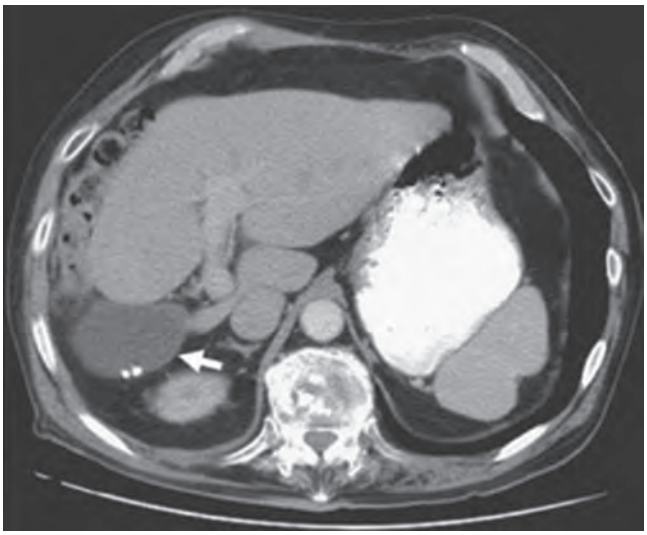

Figure 108.2 Computed tomography scan image of a case of agenesis of the right lobe of the liver. The image shows complete agenesis of the right liver and the unusual position of the gallbladder arrow.

Source: Fields et al. (2008). Reproduced with permission from Springer Science and Business Media.

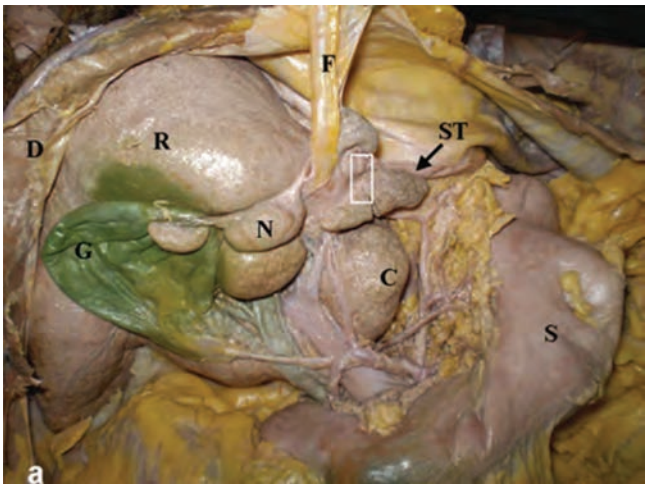

Figure 108.3 Dissection findings of agenesis of the left lobe of the liver. D: diaphragm; R: right lobe liver; F: falciform ligament; G: gall bladder; N: accessory nodule liver; C: caudate process; ST: suspected remnant of septum transversum; S: stomach.

Source: Prithishkumar and Kanakasabapathy (2010). Reproduced with permission from John Wiley & Sons.

caudate lobe is absent in about half of the cases (Fields et al. 2008). In cases not associated with left lobe hypertrophy, portal hypertension may be found (Bertrand et al. 1962; Negre et al. 1962; Renkes et al. 1995). As for other associated anomalies, partial or complete diaphragmatic defects (Kovarik and Jenson 1969; Merab et al. 1971) and intestinal malrotation (Kovarik and Jenson 1969) have been reported.

Agenesis or hypoplasia of the left lobe of the liver

Agenesis or hypoplasia of the left lobe of the liver was first reported by Arnold (1932). This anomaly is rare, and approximately 20 cases had been reported as of 2004. Suzuki et al. (1996) described three possible causes of left lobe hypoplasia: (1) dysgenesis of the hepatic primordium during development; (2) an anomaly of the umbilical vein; or (3) insufficient growth or thrombo-embolism of the left branch of the portal vein (Suzuki et al. 1996).

Anatomical findings associated with left lobe hypoplasia have not yet been comprehensively reviewed. However, Lee et al. (2004) reviewed four cases of left lobe hypoplasia. According to this report, it is presumed that a remnant of the left lobe usually exists in these cases and that the left hepatic vein drains from it (Fig. 108.3). The territory of the anterior section of the right lobe S5 and S8 usually expands in compensation.

As for associated anomalies, intestinal malrotation (Ahmed et al. 1988; Champetier et al. 1985; Banerjee and Harrison 1989) and absence of the gallbladder (Saigusa et al. 2001) have been reported.

Accessory lobes of the liver

Accessory liver lobes have occasionally been observed in the superior and anterior aspects of the liver. Accessory lobes found in the superior aspect usually push up against the diaphragm; this diaphragmatic deformity can be recognized on a chest X-ray. Rarely, the accessory lobe can pierce the diaphragm and be exposed in the thoracic cavity. An accessory lobe protruding from the anterior aspect of the liver is called a Riedel's lobe. It is hypothesized that most of these cases occur as a secondary change due to abdominal inflammation. An accessory lobe located in the inferior aspect of the liver has also been reported (Fraser 1952) along with ectopic liver tissue not connected with the liver proper.

Accessory lobes of the superior aspect of the liver

An abnormal lobe arising from the superior aspect of the right lobe was first reported by Choule (1932). Following that report, additional cases were described (Friedman et al. 1947; Hardisty et al. 1948; Katz and Williams 1952; Richman and Barry 1954). However, as these cases were diagnosed by chest X-ray, it was not possible to identify whether the accessory lobe was located inferior or superior to the diaphragm (Rendina et al. 1989). Hansbrough and Lipin (1957) reported the first case of a supra-diaphragmatic accessory lobe, an accessory lobe piercing the diaphragm and lying in the right thoracic cavity. Since that report, fewer than 20 cases have been published in the literature (Choi et al. 2008). Rendina et al. (1989) reviewed the nine cases reported previously. According to this review, the accessory lobes were located

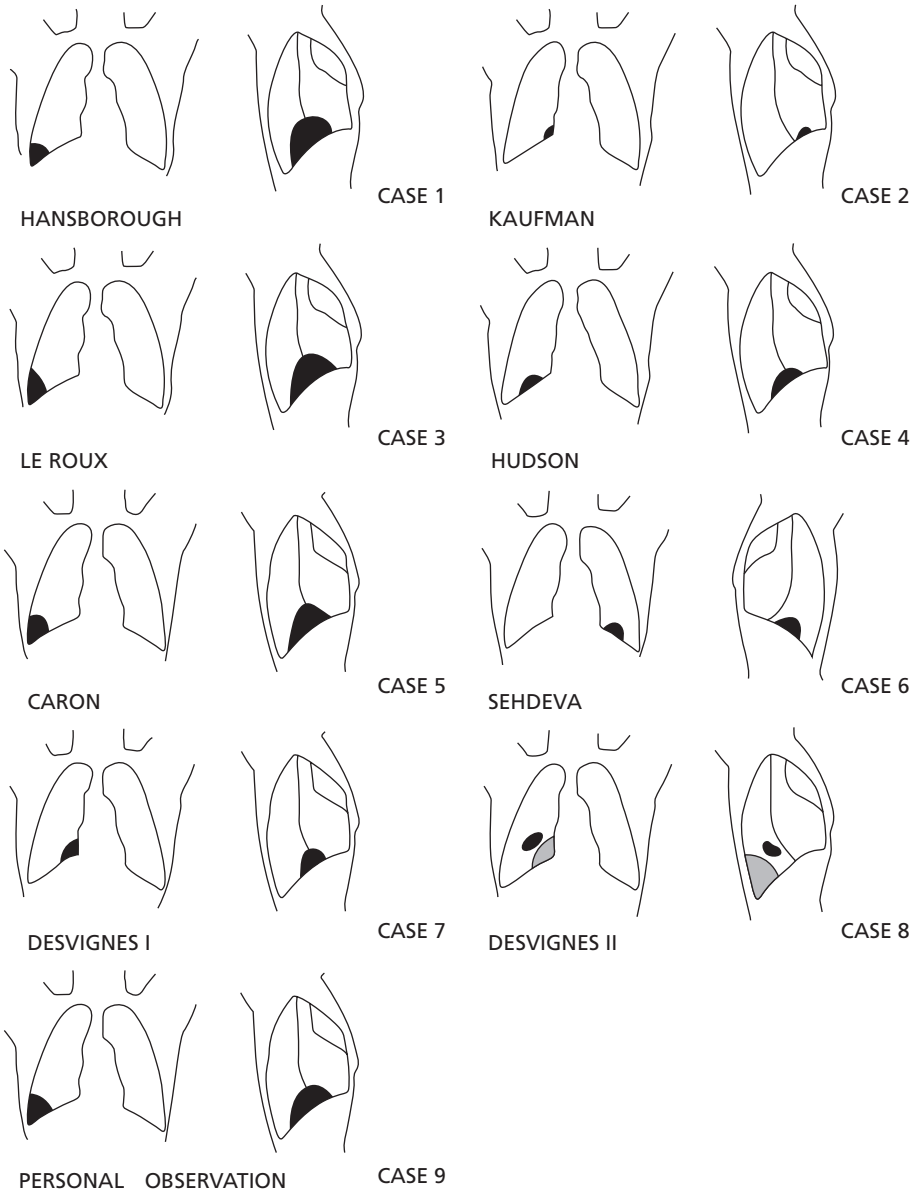

Figure 108.4 Appearance of intrathoracic accessory lobe of the superior aspect of the liver previously reported Personal observation case 9 is the case reported by Rendina.

Source: Rendina et al. (1989). Reproduced with permission from Oxford University Press.

as follows: four cases in the right costo-phrenic angle; two in the right cardio-phrenic angle; and three cases in the right diaphragmatic dome, the parenchyma of the right lower lobe, and the left diaphragmatic dome (Fig. 108.4). The accessory lobes varied in size over the range 3–12 cm in diameter (Rendina et al. 1989).

The supra-diaphragmatic accessory lobe is usually asymptomatic. However, it can sometimes cause thoracic pain. As for specific cases, Mulla and Weintraub (1955) reported a case with an accessory liver lobe in the thorax in which the right lung was absent. Sehdeva and Logan (1971) depicted a case of an accessory lobe located on the left side of the diaphragm. Finally, Choi et al. (2008) reported a case with a supra-diaphragmatic accessory liver lobe and simultaneous pulmonary sequestration in the same right lung.

Riedel's lobe

Riedel's lobe is an accessory lobe that protrudes downward from the right liver lobe (Fig. 108.5). This variant was first described by Riedel in 1888 as a "tongue-shaped projection descending from the anterior surface of the anterior margin of the right lobe of the liver to below the umbilicus" (Riedel 1888; Dick 1951). Some authors have claimed that this variation is a congenital anomaly (Reitmeier et al. 1958; Farmer et al. 1969; Sham et al. 1978). Indeed, some cases have been found in young children (Dick 1951). Leaf stated that these lobes were frequently

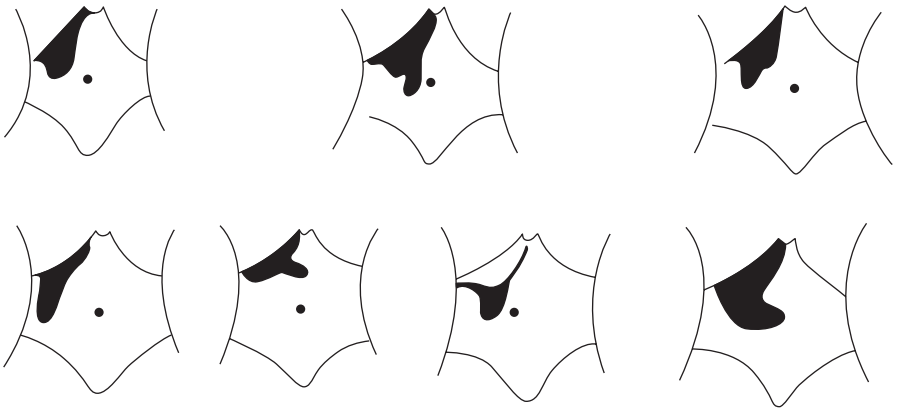

Figure 108.5 Illustration of the cases of Riedel's lobe.

Source: Dick (1951). Reproduced with permission from King's College London.

observed in monkeys, which reinforced the hypothesis (Leaf 1898–99).

However, as Riedel himself stated, Riedel's lobe almost always coexists with gallbladder disease (Riedel 1888; Lockwood 1903; Reitmeier et al. 1958). Cases associated with appendicitis (Cullen 1925) or hepatic tumors (Lane 1966) have also been reported. It is therefore currently speculated that Riedel's lobe occurs secondary to inflammation of the surrounding tissues rather than as a congenital anomaly.

The incidence of Riedel's lobe has been reported to be in the range of 3.3–31% of the general population (Sham et al. 1978; Baum et al. 1982; Gillard et al. 1998). Concerning gender association, Riedel and some previous authors have stated that this variation is more common in women than in men. However, in a more recent report using computed tomography, a significant difference between genders was not observed (Gillard et al. 1998).

A Riedel-like lobe, which protrudes downward from the left liver lobe instead of the right lobe, has also been reported (Dick 1951; Van Der Reis et al. 1956) (Fig. 108.6).

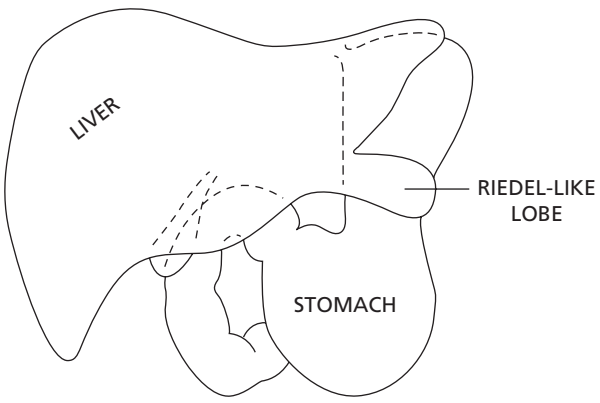

Figure 108.6 Illustration of a case of a Riedel-like lobe.

Source: Dick (1951). Reproducede with permission from King's College London.

Other accessory lobes of the liver and ectopic liver tissue

Fraser (1952) reported a case of an accessory lobe located on the inferior aspect of the liver; it was located near the gallbladder and attached to the liver and gallbladder by a pedicle that included a hepatic artery, hepatic vein, portal vein, and bile duct. Johnstone (1965) reported an extremely rare case of an accessory lobe projecting from the anterior superior border of the liver and through a hiatus in the upper abdominal wall.

Ectopic liver tissue lacks a connection to the liver and is most commonly attached to the gallbladder (Cullen 1925; Bassis and Izenstark 1956; Hamdani and Baron 1994; Sato et al. 1998; Lundy et al. 2005). The size of the mass has been reported to be in the range of microscopic to 3 cm in diameter (Lundy et al. 2005). Ectopic liver tissue has also been reported in association with the adrenal glands (Cullen 1925; Buck and Koss 1988), pancreas (Davies 1946; Cardona et al. 2007), spleen (Heid and von Haam 1948), umbilicus (Shaw and Pierog 1969), umbilical cord (Preminger et al. 2001), thoracic cavity (Lasser and Wilson 2006), and pericardium (Kinnunen et al. 1997), or with an omphalocele (Fock 1968).

References

Ahmed AF, Bediako AK, Rai D. 1988. Agenesis of the left hepatic lobe with gastric volvulus. New York *State Med J* 88: 327–328.

Arnold M. 1932. A note on a case of complete absence of the left love of the liver in man. *Anat Rec* 53: 169–172.

Auh YH, Rubenstein WA, Zirinsky K, Kneeland JB, Pardes JC, Engel IA, Kazam E. 1984. Accessory fissures of the liver: CT and sonographic appearance. *AJR* 143: 565–572.

Banerjee B, Harrison DC. 1989. Radiologic diagnosis of absent left lobe of the liver. *AJR* 152: 894–895.

Bassis ML, Izenstark JL. 1956. Ectopic liver: its occurrence in the gall bladder. *Arch Surg* 73: 204.

Baum S, Locko RC, d'Avignon MB. 1982. Functional anatomy and radionuclide imaging: Riedel's lobe of the liver. *Anatomia Clinica* 4: 121–123.

Baxter JS. 1953. *Frazer's Manual of Embryology*. London: Bailliere, Tindall and Cox.

Bergman RA, Afifi AK, Miyauchi R. 1995. Liver. Available at http://www.anatomyatlases.org/AnatomicVariants/OrganSystem/Text/Liver.shtml (accessed 14 December 2015).

Bertrand L, Janbon M, Negre E, Bertrand A. 1962. Agenesia of the right lobe of the liver. Hemorrhages caused by manifesting portal hypertension: 2 observations. *Lyon Médical* 94: 419.

Buck FS, Koss MN. 1988. Heterotopic liver in an adrenal gland. *Fetal Pediatr Pathol* 8: 535–540.

Cardona D, Grobmyer S, Crawford JM, Liu C. 2007. Hepatocellular carcinoma arising from ectopic liver tissue in the pancreas. *Virchows Arch* 450: 225–229.

Champetier J, Yver R, Letoublon C, Vigneau B. 1985. A general review of anomalies of hepatic morphology and their clinical implications. *Anatomia Clinica* 7: 285–299.

Choi SU, Kim HK, Kim J. 2008. Heterotopic supradiaphragmatic liver combined with intralobar pulmonary sequestration. *Ann Thorac Surg* 85: 1809–1810.

Choule KS. 1932. Note on Anomalous lobe of the liver. *Anat Rec* 53: 177.

Cullen TS. 1925. Accessory lobes of the liver and accessory hepatic lobe springing from the surface of the gallbladder. *Arch Surg* 11: 718–764.

Davies JNP. 1946. An accessory liver in an African. *Brit Med J* 2: 736.

Dick J. 1951. Riedel's lobe and related partial hepatic enlargements. *Guy's Hospital Reports* 1003: 270.

Farmer RG, Hermann RE, Sullivan BH. 1969. Congenital hepatic fibrosis of Riedel's lobe causing portal hypertension Report of a Case. *Clev Clin Quart* 36: 143–148.

Fields RC, Heiken JP, Strasberg SM. 2008. Biliary injury after laparoscopic cholecystectomy in a patient with right liver agenesis: case report and review of the literature. *J Gastroin Surg* 12: 1577–1581.

Fock G. 1963. Ectopic liver in omphalocele. *Acta Paediatr* 52: 288–292.

Fraser CG. 1952. Accessory lobes of the liver. *Ann Surg* 135: 127.

Friedman PS, Solis-Cohen L, Levine S. 1947. Accessory lobe of the liver and its significance in roentgen diagnosis. *Am J Roentgenol Rad Ther* 57: 601.

Gillard JH, Patel MC, Abrahams PH, Dixon AK. 1998. Riedel's lobe of the liver: Fact or fiction? Clin Anat 11: 47–49.

Hamdani SD, Baron RL. 1994. Ectopic liver simulating a mass in the gallbladder wall: imaging findings. *AJR Am J Roentgenol* 162: 647–648.

Hansbrough ET, Lipin RJ. 1957. Intrathoracic accessory lobe of the liver. *Ann Surg* 145: 564.

Hardisty NM, Kearney EA, Brooks FP. 1948. Report of a case of an anomalous lobe of the liver. *Am J Roentgenol Rad Ther* 60: 486.

Heid G, von Haam E. 1948. Hepatic heterology in the splenic capsule. *Arch Path* 46: 377–379.

Johnstone G. 1965. Accessory lobe of liver presenting through a congenital deficiency of anterior abdominal wall. *Arch Dis Child* 40: 541–544.

Katz HJ, Williams AJ. 1952. Accessory lobes of liver and their significance in roentgen diagnosis. *Ann Int Med* 36: 880.

Kinnunen P, Kulmala P, Kaarteenaho-Wiik R, Vuopala K. 1997. Ectopic liver in the human pericardium. *Histopathol* 30: 277–279.

Kovarik JL, Jensen NK. 1969. Congenital aplasia of the right hepatic lobe with right-sided diaphragmatic hernia and intestinal malrotation. *Intern Surg* 51: 499.

Lane D. 1966. Masses in the right hypochondrium and Riedel's lobe. *Med J Aust* 1: 896–899.

Lasser A, Wilson GL. 1975. Ectopic liver tissue mass in the thoracic cavity. *Cancer* 36: 1823–1826.

Leaf CH. 1898–99. An accessory lobe, tongue-shaped, on the right surface of the liver with enlargement of the right lobe. *J Anat Physiol* 33: 18.

Lee UY, Murakami G, Han SH. 2004. Left lobe hypoplasia of the human liver: a report of two cases. *Surg Radiol Anat* 26: 417–423.

Lockwood CB. 1903. Hepatectomy for the removal of Riedel's lobe. *Lancet* 2: 223–224.

Lundy J, Johnson E, Edwards K, Rivera D. 2005. Laparoscopic management of gallbladder-associated ectopic liver. *J Soc Laparoendoscopic Surg* 9: 485–487.

Macchi V, Feltrin G, Parenti A, De Caro R. 2003. Diaphragmatic sulci and portal fissures. *J Anat* 202: 303–308.

Merab A, Nasr B, Khouri KN, Saade B. 1971. Agenesis of the right liver lobe with agenesis of the right hemidiaphragm. *J Méd Libanais* 24: 287.

Moser W. 1898. A liver with sixteen lobes. *Med Rec* 53: 671–672.

Mulla N, Weintraub S. 1955. Accessory liver with double gall bladder. *Arch Surg* 71: 202.

Negre E, Pujol H, Thevenet A. 1962. Portal hypertension in agenesis of the right lobe of the liver. *La Presse Médicale* 70: 2501.

Newell RL, Morgan-Jones R. 1993. Grooves in the superior surface of the liver. *Clin Anat* 6: 333–336.

Okudaira M. 1995. *Kanzo Byori Liver Pathology*. Tokyo: Igaku-shoin Ltd, pp. 12–13.

Ono ML, Murakami G, Sato TJ, Sawada K. 2000. Hepatic grooves and portal segmentation. *Kaibogaku Zasshi* 75: 517–523.

Preminger A, Udassin R, Pappo O, Arad I. 2001. Ectopic liver tissue within the umbilical cord. *J Pediatr Surg* 36: 1085–1086.

Prithishkumar IJ, Kanakasabapathy I. 2010. Agenesis of the left lobe of liver-A rare anomaly with associated hepatic arterial variations. *Clin Anat* 23: 899–901.

Radin DR, Colletti PM, Ralls PW, Boswell WD, Halls JM. 1987. Agenesis of the right lobe of the liver. *Radiology* 164: 639–642.

Reitemeier RJ, Butt HR, Baggenstoss AH. 1958. Riedel's lobe of the liver. *Gastroenterol* 34: 1090.

Rendina EA, Venuta F, Pescarmona EO, Martelli M, Ricci C. 1989. Intrathoracic lobe of the liver. Case report and review of the literature. *Eur J Cardio-Thoracic Surg* 3: 75.

Renkes P, Blum A, Claviere C, Bazin C, Bigard MA, Regent D, Gaucher P. 1995. Agenesis of the right lobe of the liver and portal hypertension. *Gastroentérologie Clin Biol* 19: 309.

Richman S, Barry Jr WF. 1954. Localized bulge of the right diaphragm simulating neoplasms. *Am J Roentgenol Rad Ther Nuc Med* 72: 22.

Riedel I. 1888 Uber den zungenformigen fortsatz des rechten leberlappens und seine pathognostische bedeutung fur die erkrankung der gallenblase nebst bemerkungen uber gallensteinsperationem. *Berl Kim Wschr* 25: 577–602.

Saigusa K, Aoki Y, Horiguchi M. 2001. Hypoplasia of the left lobe of the liver. *Surg Radiol Anat* 23: 345–347.

Sato S, Watanabe M, Nagasawa S, Niigaki M, Sakai S, Akagi S. 1998. Laparoscopic observations of congenital anomalies of the liver. *Gastro Endo* 47: 136–140.

Schafer E, Dymington J. 1896. *Quain's Elements of Anatomy*, 10th edition. London: Longmans, Green and Co.

Sehdeva JS, Logan WD. 1971. Heterotopic supradiaphragmatic liver. *Ann Thorac Surg* 11: 468–471.

Sham R, Sain A, Silver, L. 1978. Hypertrophic Riedel's lobe of the liver. *Clin Nucl Med* 3: 79–81.

Shaw A, Pierog S. 1969. "Ectopic" liver in the umbilicus: an unusual focus of infection in a newborn infant. *Pediatrics* 44: 448–450.

Sherlock S, Dooley J. 2008. Diseases of the Liver and Biliary System. New Jersey: John Wiley & Sons.

Suzuki T, Sakurabayashi S, Yoshino K, Yamamoto Y, Nishimura S, Abe K, Yamada F. 1996. A case of the hypoplasia of the hepatic left lobe complicated with cholangiocarcinoma. *Nihon Shokakibyo Gakkai Zasshi* 93: 276.

Van Der Reis L, Clark AG, McPhee VG. 1956. Congenital hepatomegaly: report of a case. *Cal Med* 85: 41.

Further reading

Large AM. 1963. Left-sided gallbladder and liver without situs inversus. *Arch Surg* 87: 982.

Southam JA. 1975. Left-sided gallbladder: calculous cholecystitis with situs inversus. *Ann Surg* 182: 135.

109 Pancreas

Koichi Watanabe
Kurume University School of Medicine, Fukuoka, Japan

Anatomical variations of the pancreas are relatively rare. Agenesis of the pancreas and annular pancreas occur during fusing of the dorsal and ventral pancreatic buds. A bifid tail of the pancreas is an extremely rare anomaly. Anatomical variation of the uncinate process surrounding the portal vein is called a portal annular pancreas, and this variation is significant for pancreaticoduodenectomy.

Agenesis or hypogenesis of the pancreas

The pancreas consists of two parts embryologically: the dorsal pancreatic primordium and the ventral pancreatic primordium. The dorsal pancreas, which has a long duct continuing from the accessory pancreatic papilla to the tail, develops into the upper part of the head, body, and tail of the pancreas. The ventral pancreas, which has a short main pancreatic duct connected to the common bile duct, develops into the lower part of the pancreatic head. The ventral pancreas, which is situated to the right side of the duodenum initially, rotates to the left side just beneath the dorsal pancreas and these two elements then fuse to form the pancreas.

Agenesis of the pancreas occurs when either or both of these two primordia stop developing. This anomaly is relatively rare and approximately 50 cases have been reported (Schnedl et al. 2009). Three types of agenesis have been reported: complete, ventral, and dorsal agenesis. Complete agenesis occurs when both pancreatic buds stop developing and only five cases have been reported (Dourov and Buyl-Stroevens 1969; Mehes et al. 1976; Topke and Menzel 1976; Lemons et al. 1979; Wildling et al. 1993; Voldsgaard et al. 1994). Complete agenesis appears to be a lethal condition. All reported cases were diagnosed with intrauterine growth restriction (IUGR) during pregnancy, hyperglycemia without ketonemia after birth, and died within 2 weeks after birth (Voldsgaard et al. 1994).

Agenesis of the ventral pancreas is also extremely rare and lethal. Only one case has been described (Theodor 1909). The patient underwent laparotomy at 2 weeks of age because of jaundice, and died during the operation. The postmortem pathological examination showed that the pancreas was 2.5 cm long and only 3 mm in breadth; the head was absent and the tail tapered off toward the head (Theodor 1909; Howard and Hess 2002).

Agenesis of the dorsal pancreas is the most common form of pancreatic agenesis with approximately 50 cases reported in the literature (Schnedl et al. 2009). It is classified into two types: complete and partial agenesis of the dorsal pancreas. Complete agenesis of the dorsal pancreas results in an absence of body, tail, and the dorsal duct system. Partial agenesis of the dorsal pancreas usually affects the accessory papilla, the terminal end of the main dorsal duct, or the pancreatic body. The islet cells that secrete insulin are located mainly in the pancreatic tail. In agenesis of the dorsal pancreas, patients therefore often have diabetes mellitus. Schnedl et al. (2009) examined 53 previously reported cases and 28 (53%) had hyperglycemia.

Annular pancreas

Annular pancreas occurs when a part of the pancreas surrounds a portion of the duodenum (Fig. 109.1). Tiedemann reported the first case of annular pancreas in 1818 and approximately 740 cases have been reported in the English literature (Tiedemann 1818; Kiernan et al. 1980; Zyromski et al. 2008). The frequency of this anomaly is reported as 1 in 1000 in endoscopic and imaging method studies (Chevillotte et al. 1984; Fogel et al. 2006; Zyromski et al. 2008), and 3 in 20,000 in autopsy and surgical series (Ravitch and Woods 1950; Theodorides 1964; Zyromski et al. 2008). Annular pancreas is more common in females.

Although many hypotheses attempt to explain the formation of this anomaly, the most convincing and currently supported theory was advocated by Lecco (Lecco 1910; Kiernan et al. 1980). The pancreas consists of two pancreatic buds: dorsal and ventral. The ventral pancreatic bud, which is located on the right side of the duodenum with Wirsung's duct and the common bile duct, rotates to the left side and forms the normal pancreas. An annular pancreas forms when the ventral pancreas bud rotates as a part of it remains attached to the anterior wall of the duodenum. This theory has been proven by dissection findings, showing that a branch of the ventral pancreatic duct surrounds and passes through the duodenum. However, other dissection

Bergman's Comprehensive Encyclopedia of Human Anatomic Variation, First Edition. Edited by R. Shane Tubbs, Mohammadali M. Shoja and Marios Loukas.
© 2016 John Wiley & Sons, Inc. Published 2016 by John Wiley & Sons, Inc.

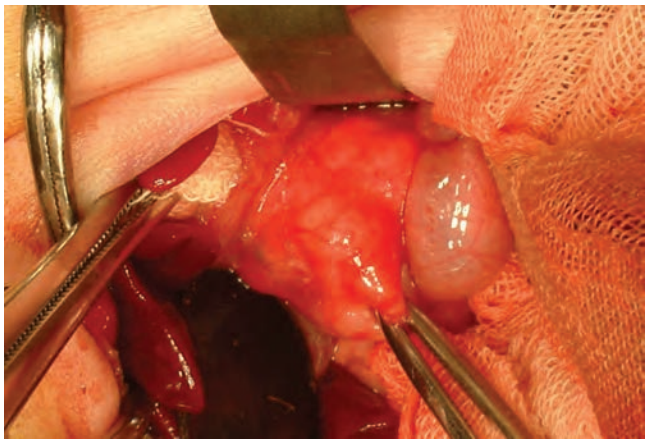

Figure 109.1 Operative finding of an annular pancreas.

Source: Dr Kimio Asagiri, Department of Pediatric Surgery, Kurume University School of Medicine.

cases have shown different findings, including Erimoglu and Theodorides' case, which had four small pancreatic ducts in the ring part of the annular pancreas (Erimoglu 1952; Theodorides 1964). In this case, the authors presumed that small aberrant pancreatic tissues formed the annular pancreas. Another type has been reported where the annular part of the duct began from the posterior aspect of the duodenum, ran from the right side, the anterior side, and to Santorini's duct, surrounding the duodenum (Erimoglu 1952; Theodorides 1964).

An annular pancreas is often associated with other anomalies and Down syndrome is the most frequent (Torfs and Christianson 1998; Zyromski et al. 2008). Other anomalies such as cardiac defects, intestinal atresia, biliary anomalies, and tracheoesophageal fistula are also associated with an annular pancreas.

Portal annular pancreas

Portal annular pancreas occurs when the uncinate process of the pancreas extends and fuses to the dorsal surface of the body by surrounding the portal vein (Karasaki et al. 2009). This anomaly was first reported by Sugiura et al. (1987) and very few cases have been reported. (Sugiura et al. 1987; Karasaki et al. 2009; Joseph et al. 2010; Jang et al. 2012; Kobayashi et al. 2012; Muto et al. 2012; Matsumoto et al. 2013). Karasaki et al. (2009) examined 700 multi-detector computed tomography (MDCT) images and reported that the frequency of this anomaly was estimated at 1.14% and the male-to-female ratio was 1:7. They classified this anomaly into three types: suprasplenic vein type, infrasplenic vein type, and mixed type (Fig. 109.2). The suprasplenic vein type occurs when the uncinate process of the pancreas surrounds the portal vein cranial to the splenoportal confluence. In the infrasplenic type, the fusion between the uncinate process and the pancreatic body occurs caudal to the splenoportal confluence. The mixed type occurs when the pancreas covers both the superior mesenteric vein and the portal vein. This anomaly does not have any symptoms, but it becomes important when performing pancreaticoduodenectomy. In this case, the surgeon must dissect the pancreatic parenchyma from the portal vein more than for a normal pancreas, increasing the risk of pancreatic duct leakage after surgery.

Heterotopic pancreas

Heterotopic pancreas occurs when pancreatic tissue exists in a distant organ outside the orthotopic pancreas without anatomic or vascular connection between the pancreatic tissues. It was first reported by Schultz in 1727 as the gross appearance and the first histological report was by Klob in 1859 (Ugelli 1934; Martinez et al. 1958). This lesion has been observed in the stomach, duodenum, and jejunum, Meckel's diverticulum, and rarely in the esophagus, gallbladder, common bile duct, spleen, mesentery, mediastinum, and uterine tubes. The most commonly used classification was proposed by Von Heinrich in 1909, who categorized heterotopic pancreas into three types: type 1: all of the components of the pancreas including ducts, acini, and endocrine islets; type 2: ducts with acini; and type 3: ducts with a few acini or dilated ducts only (adenomyoma) (Von Heinrich 1909).

Bifid tail of the pancreas

Bifid tail of the pancreas is an extremely rare anomaly and only two cases have been reported (Kikuchi et al. 1983; Dinter et al. 2005). Kikuchi's case was a 49-year-old man, and the pancreas anomaly was found by computed tomography during a series of examinations of a gastric cancer. The pancreas had an extra tail that arose from the pancreas body and headed to the posterior wall of the stomach, and the pancreatic duct had an extra branch at the body of the pancreas (Kikuchi et al. 1983). Dinter's case was a 51-year-old woman in whom a bifid tail of the pancreas was found during systemic examinations of lung cancer (Dinter et al. 2005). Similar to Kikuchi's case, the pancreas had a bifurcated body and the duct had duplication in the body of the pancreas with a pseudocyst in the ventral part of the duplicated pancreas. The cause of bifid tail of the pancreas anomaly has not been completely determined.

Pancreatic ducts

A sphincteric arrangement of the muscle tissue at the end of the accessory pancreatic duct has been described. The accessory duct may be rudimentary or (rarely) absent. Similar variations occur in the pancreatic duct. Rarely, the pancreas may open into the duodenum by three ducts. Abnormalities of the pancreas are often associated with duodenal diverticula. Other studies of variations in the pancreatic ducts indicate that in as many as 40% of

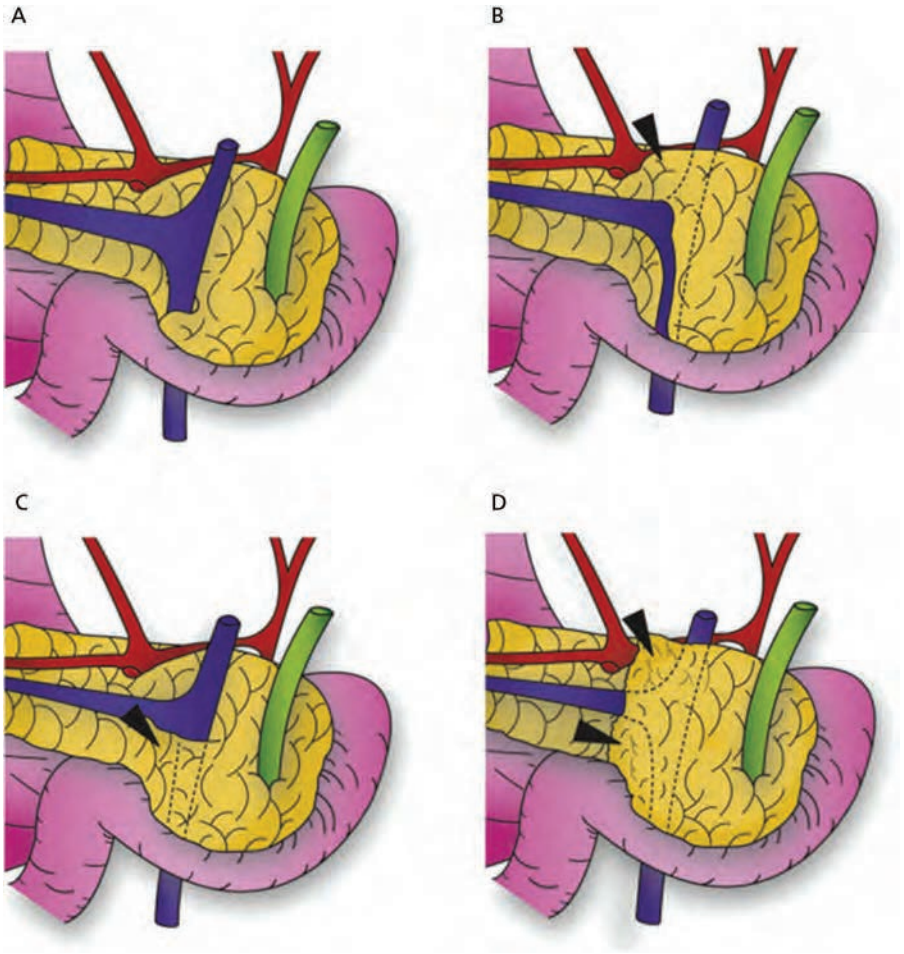

Figure 109.2 Classification of portal annular pancreas: (a) normal pancreas; (b) duprasplenic vein type, the lingual projection from the uncinate process fused to the body of the pancreas by surrounding the portal vein cranial of the splenoportal confluence; (c) infrasplenic vein type in which fusion occurs caudal to the confluence; (d) mixed type, where the fused pancreas covers both portal trunk and superior mesenteric vein. Arrowhead indicates the fusion between the lingual projection and the body of the pancreas.

Source: Karasaki et al. (2009). Reproduced with permission from Elsevier.

adults the accessory (Bernard's or Santorini's) duct is not functionally joined to the chief or primary pancreatic duct. In 15% of cases there is a dual drainage from both ducts, in 7% there is a dual drainage and a functional connection between the two ducts, and in 2% the accessory duct does not drain into the duodenum but into the primary duct. Reinhoff and Pickrell (1945) found no connection between the pancreatic and bile ducts in 73 of 250 specimens (about 29%), each entering the duodenum contiguously or at separate points. In 92 specimens (37%) the two ducts were contiguous with the dividing septum terminating about 2 mm from the apex.

In 81 instances (30%) the duct emptied into a common ampulla, which extended 3–14 mm from the apex of the duodenal orifice. In four specimens the length of the diverticulum exceeded 10 mm. In four instances the pancreatic duct was reduced to a fibrous cord, and the accessory duct drained the entire gland.

Based on the combined studies of Dawson and Langman (1961) and Singh (1956) of 100 specimens, 63 belonged to type I, 30 to type II, and 7 to type III. In one case classified as type II the duct of Santorini was larger than the duct of Wirsung. In 63 cases belonging to type I, the hepatopancreatic duct varied in length from 1 mm to 14.5 mm. The three types are classified as follow:

- Type I: the bile duct and the duct of Wirsung join together in the duodenal wall to form the hepatopancreatic duct and open through it into the duodenum.
- Type II: the two ducts are separated throughout their extent by a septum and open separately at the summit of the major duodenal papilla.
- Type III: the whole pancreas is drained by the duct of Santorini. The duct of Wirsung is either reduced to a fibrous cord or is absent.

References

Chevillotte G, Sahel J, Raillat A, Sarles, H. 1984. Annular pancreas. *Dig Dis Sci* 29: 75–77.

Dawson W, Langman J. 1961. An anatomical-radiological study on the pancreatic duct pattern in man. *Anat Rec* 139: 59–68.

Dinter D, Löhr JM, Neff KW. 2007. Bifid tail of the pancreas: benign bifurcation anomaly. *Am J Roentgenol* 189: W251–W253.

Dourov N, Buyl-Stroevens ML. 1969. Agénésie du pancréas. *Arch Fr Pediatr* 26: 641–650.

Erimoglu C. 1952. A case of pancreas annulare. *Proc Kon Nederl Akad Wet* 55: 18.

Fogel EL, Zyromski N, Mchenry L, Watkins JL, Schmidt S, Lazzell-Pannell L, Lehman GA. 2006. Annular pancreas (AP) in the adult: experience at a large pancreatobiliary endoscopy center. *Gastro Endo* 63: 308.

Howard JM, Hess W. 2002. *History of the Pancreas: Mysteries of a Hidden Organ*. New York: Springer.

Jang JY, Chung YE, Kang CM, Choi SH, Hwang HK, Lee WJ. 2012. Two cases of portal annular pancreas. *Korean J Gastroenterol* 60: 52–55.

Joseph P, Raju RS, Vyas FL, Eapen A, Sitaram V. 2010. Portal annular pancreas. A rare variant and a new classification. *J Pancreas* 11: 453–455.

Karasaki H, Mizukami Y, Ishizaki A, Goto J, Yoshikawa D, Kino S. Kasai S. 2009. Portal annular pancreas, a notable pancreatic malformation: frequency, morphology, and implications for pancreatic surgery. *Surgery* 146: 515–518.

Kiernan PD, ReMine SG, Kiernan PC, ReMine WH. 1980. Annular pancreas: Mayo Clinic experience from 1957 to 1976 with review of the literature. *Arch Surg* 115: 46.

Kikuchi K, Nomiyama T, Miwa M, Harasawa S, Miwa T. 1983. Bifid tail of the pancreas: a case presenting as a gastric submucosal tumor. *Am J Gastroenter* 78: 23–27.

Kobayashi S, Honda G, Kurata M, Okuda Y, Tsuruta K. 2012. Pancreaticoduodenectomy in portal annular pancreas: report of a case. *Surg Today* 43(8): 1–4.

Lecco TM. 1910. Zur morphologie des pankreas annulare. *Sitzungsb Wien Akad Wiss* 119: 391–406.

Lemons JA, Ridenour R, Orsini EN. 1979. Congenital absence of the pancreas and intrauterine growth retardation. *Pediatrics* 64: 255–257.

Martinez NS, Morlock CG, Dockerty MB, Waugh JM, Weber HM. 1958. Heterotopic pancreatic tissue involving the stomach. *Ann Surg* 147: 1.

Matsumoto I, Shinzeki M, Fukumoto T, Ku Y. 2013. An extremely rare portal annular pancreas for pancreaticoduodenectomy with a special note on the pancreatic duct management in the dorsal pancreas. *Surgery* 153(3): 434–436.

Mehes K, Vamos K, Goda M. 1976. Agenesis of pancreas and gall-bladder in an infant of incest. *Acta Paediatrica Hungarica* 17: 175–176.

Muto J, Mano Y, Harada N, Uchiyama H, Yoshizumi T, Taketomi A, Maehara Y. 2012. Additional resection of the pancreas body prevents postoperative pancreas fistula in patients with portal annular pancreas who undergo pancreaticoduodenectomy. *Case Reports Gastroenterol* 6: 131–134.

Ravitch MM, Woods AC. 1950. Annular pancreas. *Ann Surg* 132: 1116.

Reinhoff WF, Pickrell WL. 1945. Pancreatitis. An anatomic study of the pancreatic and extrahepatic biliary systems. *Arch Surg* 51: 205–219.

Schnedl WJ, Piswanger-Soelkner C, Wallner SJ, Reittner P, Krause R, Lipp RW, Hohmeier HE. 2009. Agenesis of the dorsal pancreas and associated diseases. *Dig Dis Sci* 54: 481–487.

Singh I. 1956. Observations on the mode of termination of the bile and pancreatic ducts: Anatomical factors in pancreatitis. *J Anat Soc India* 5: 54–60.

Sugiura Y, Shima S, Yonekawa H. 1987. The hypertrophic uncinate process of the pancreas wrapping the superior mesenteric vein and artery: a case report. *Jap J Surg* 17: 182–185.

Theodor F. 1909. Angeborene aplasie der gallenwege verbunden mit lebercirhose, durch operation behandelt. *Arch Kinderheild* 49: 358.

Theodorides T. 1964. Annular pancreas. *J de Chirurgie* 87: 445.

Tiedemann F. 1818. Uber die verschiedenheiten des ausftihrungsganges der bauchspeicheldrtise bei den menschen und saugetieren. *Dtsch Arch Physiol* 4: 403.

Topke B, Menzel K. 1976. Die pankreasagenesie des neugebohrenen einsetenes, klinisch aber characteristisches krankheitsbild. *Acta Paediatr Acad Sci Hung* 17: 175–176.

Torfs CP, Christianson RE. 1998. Anomalies in Down syndrome individuals in a large population-based registry. *Am J Med Gen* 77: 431–438.

Ugelli L. 1934. I pancreas accessori e loro importanza chirurgica. *Policlinico* 41: 424.

Voldsgaard P, Kryger-Baggesen N, Lisse I. 1994. Agenesis of pancreas. *Acta Paediatrica* 83: 791–793.

Von Heinrich H. 1909. Ein beitrag zur histologie des sogen: akzessorichen pankreas. *Virchows Arch A Pathol Anat Histopathol* 198: 392–401.

Wildling R, Schnedl WJ, Reisinger EC, Schreiber F, Lipp RW, Lederer A, Krejs GJ. 1993. Agenesis of the dorsal pancreas in a woman with diabetes mellitus and in both of her sons. *Gastroenterology* 104: 1182–1182.

Zyromski NJ, Sandoval JA, Pitt HA, Ladd AP, Fogel EL, Mattar WE, Grosfeld JL. 2008. Annular pancreas: dramatic differences between children and adults. *J Am Coll Surg* 206: 1019–1025.

110 Spleen

Koichi Watanabe
Kurume University School of Medicine, Fukuoka, Japan

The majority of anatomical variations of the spleen occur during the embryonic period. Splenic lobulations and clefts are remnants of the fetal spleen. An accessory spleen represents heterotopic splenic tissue and is also formed during the embryonic period. It does not typically cause symptoms and is usually found incidentally. In contrast, asplenia (congenital absence of the spleen) and polysplenia are often associated with cardiovascular malformations, and the associated heart disease can be lethal. A wandering spleen results from abnormalities of the ligaments that normally fix the spleen in place; this causes the spleen to move to an unusual position. This condition can be congenital or acquired.

Splenic lobulations and clefts (notches)

Lobulations are sometimes observed along the medial part of the spleen. In rare cases, the resulting lobule can be located partially posterior to the upper pole of the left kidney and can displace it anteriorly (Dodds et al. 1990; Gayer et al. 2001). Although the fetal spleen has lobulations, they usually disappear after birth. Splenic lobulations are therefore remnants of the fetal splenic lobulations.

Conversely, clefts (or notches) are typically observed on the diaphragmatic surface of the spleen (Fig. 110.1). There are usually two clefts, but in some cases as many as five or more can be seen (Shepherd 1902). They can be sharp in appearance and are occasionally as deep as 2–3 cm. They are also remnants of the fetal splenic lobulations (Dodds et al. 1990; Gayer et al. 2001).

Accessory spleen

An accessory spleen is heterotopic splenic tissue located adjacent to the spleen (Fig. 110.2). It is usually round or oval in shape and resembles an enlarged lymph node. An accessory spleen is most commonly observed near the splenic hilum or next to the pancreatic tail, but it is occasionally found along the splenic vessels or in association with the gastrosplenic ligament, splenorenal ligament, stomach wall, bowel, greater omentum,

A B

Figure 110.1 (a, b) Splenic fissure. An unusual fissure was observed on the diaphragmatic surface of the spleen.

Source: Kumar et al. (2012). Reproduced with permission from International Journal of Anatomical Variations.

Bergman's Comprehensive Encyclopedia of Human Anatomic Variation, First Edition. Edited by R. Shane Tubbs, Mohammadali M. Shoja and Marios Loukas.
© 2016 John Wiley & Sons, Inc. Published 2016 by John Wiley & Sons, Inc.

Figure 110.2 Axial CT image of accessory spleen An accessory spleen is located in the tail of the pancreas measuring 1.6 cm in diameter with similar enhancement as the spleen.

Source: Tozbikian et al. (2007). Reproduced with permission from Elsevier.

mesentery, pelvis, or scrotum. The incidence has been reported to be 10–30% of the population (Dodds et al. 1990; Freeman et al. 1993; Gayer et al. 2001). There is typically only one accessory spleen. However, less than ten accessory spleens have been reported (Curtis and Movitz 1946; Halpert 1959; Wadham et al. 1981). They are generally 10–20 mm in diameter (Halpert 1959; Wadham et al. 1981; Dodds et al. 1990; Mortelé et al. 2004). However, an enlarged accessory spleen 5 cm in diameter has been reported. An accessory spleen does not usually cause symptoms and is of no clinical significance in most patients. However, it is sometimes confused with an enlarged lymph node in diagnostic imaging (Gayer et al. 2001).

The occurrence of many splenic nodules (42–400 have been reported) needs to be distinguished from the presence of accessory spleens. This condition is called "splenosis," and it is caused by the scattered transplantation of splenic fragments on the peritoneum; this can result from splenectomy or splenic rupture due to trauma (Curtis and Movitz 1946).

Wandering spleen

Wandering spleen is the condition in which the spleen moves to an unusual location with its vascular pedicle due to incomplete fixation or laxity of the ligaments supporting the spleen: the gastro-splenic and spleno-renal ligaments. It was first described by Van Horne in 1667, and 238 cases had been reported in the literature by 2005 (Soleimani et al. 2007). The incidence is presumed to be less than 0.2% of the population (Fujiwara et al. 1995).

This condition can be congenital or have an acquired onset. Congenital cases are found in children and occur because the ligaments fail to develop. Acquired cases are caused by loosening of the splenic ligaments due to abdominal wall laxity (Bollinger and Lorentzen 1990), the hormonal effects of pregnancy (Sheflin et al. 1984; Herman and Siegel 1991), or splenomegaly; these cases are most commonly found in women aged 20–40 years (Raissaki et al. 1998). A wandering spleen can cause symptoms such as abdominal discomfort, intestinal obstruction, and pain; it can cause an acute abdomen if torsion of the pedicle occurs. Surgical treatment such as splenectomy or splenopexy is generally necessary.

Congenital absence of the spleen (asplenia, splenic agenesis)

Congenital absence of the spleen is an extremely rare anomaly. It was first reported by Martin in 1826; 36 cases (26 cases in infants and 10 cases in adults) had been found up to 1952 (Polhemus and Schafer 1955). It is also called congenital asplenic syndrome or Ivemark syndrome (Freedom 1972). In most cases, this anomaly is associated with severe congenital heart malformations such as pulmonary stenosis, pulmonary atresia, anomaly of the great vessels, and atrioventricularis communis. Approximately half of the reported cases have had partial or total situs inversus. In congenital asplenic patients, findings in the peripheral blood are similar to those found after splenectomy; erythrocytes contain Howell-Jolly and Heinz bodies and normoblastemia, target cells, and siderocytes are observed (Bush and Ainger 1955; Nihoyannopoulos et al. 1956; Gilbert et al. 1958).

Polysplenia

Polysplenia is defined as the presence of multiple small splenic nodules instead of a normal spleen (Griffiths and Marshall 1984). The splenic nodules are usually equal in size, and two or more will be present. They range in size from 1 to 6 cm in diameter (Gayer et al. 2001). It is reported that the frequency is about 2.5 in 100,000 live births, but only 5% of these patients survive beyond 5 years of life (Winer-Muram 1995). Polysplenia, as with the congenital absence of the spleen, is associated with heart and visceral anomalies. However, the associated anomalies are less severe than with congenital asplenic syndrome, and some cases not associated with cardiac anomalies have been reported. The splenic nodules are usually located in the left upper quadrant along the greater curvature of the stomach. In the case of situs inversus, the nodules are located on the right side (Peoples et al. 1983).

References

Bollinger B, Lorentzen T. 1990. Torsion of a wandering spleen: ultrasonographic findings. *J Clin Ultrasound* 18: 510–511.

Bush J A, Ainger LE. 1955. Congenital absence of the spleen with congenital heart disease. *Pediatrics* 15: 93–100.

Curtis GM, Movitz D. 1946. The surgical significance of the accessory spleen. *Ann Surg* 123: 276.

Dodds WJ, Taylor AJ, Erickson SJ, Stewart ET, Lawson TL. 1990. Radiologic imaging of splenic anomalies. *AJR Am J Roentgenol* 155: 805–810.

Freedom RM. 1972. The asplenia syndrome: a review of significant extracardiac structural abnormalities in 29 necropsied patients. *J Pediatr* 81: 1130–1133.

Freeman JL, Jafri SZ, Roberts JL, Mezwa DG, Shirkhoda A. 1993. CT of congenital and acquired abnormalities of the spleen. *Radiographics* 13: 597–610.

Fujiwara T, Takehara Y, Isoda H, Ichijo K, Tooyama N, Kodaira N, Kawaguchi K. 1995. Torsion of the wandering spleen: CT and angiographic appearance. *J Comput Assist Tom* 19: 84–86.

Gayer G, Zissin R, Apter S, Atar E, Portnoy O, Itzchak Y. 2001. CT findings in congenital anomalies of the spleen. *Brit J Radiol* 74: 767–772.

Gilbert EF, Nishimura K, Wedum BG. 1958. Congenital malformations of the heart associated with splenic agenesis with a report of five cases. *Circulation* 17: 72–86.

Griffiths JD, Marshall VC. 1984. Torsion of the spleen in the polysplenia syndrome. *Austral New Zeal J Surg* 54: 571–573.

Halpert B. 1959. Lesions observed in accessory spleens of 311 patients. *Am J Clin Pathol* 32: 165–168.

Herman TE, Siegel MJ. 1991. CT of acute splenic torsion in children with wandering spleen. *AJR Am J Roentgenol* 156: 151–153.

Kumar V, Kumar N, Jetti R. 2012. Unusual fissure on the diaphragmatic surface of the spleen: a case report. *IJAV* 5: 96–98.

Mortelé KJ, Mortelé B, Silverman SG. 2004. CT features of the accessory spleen. *Am J Roentgenol* 183: 1653–1657.

Nihoyannopoulos J, Zannos L, Oeconomou-Mavrou C, Statherou E. 1956. Report of a case with congenital absence of the spleen and laevocardia. *J Clin Pathol* 9: 323.

Peoples WM, Moller JH, Edwards JE. 1983. Polysplenia: a review of 146 cases. *Pediatr Cardiol* 4: 129–137.

Polhemus DW, Schafer WB. 1955. Congenital absence of the spleen. *Pediatrics* 16: 495–497.

Raissaki M, Prassopoulos P, Daskalogiannaki M, Magkanas E, Gourtsoyiannis N. 1998. Acute abdomen due to torsion of wandering spleen: CT diagnosis. *Europ Radiol* 8: 1409–1412.

Sheflin JR, Lee CM, Kretchmar KA. 1984. Torsion of wandering spleen and distal pancreas. *Am J Roentgenol* 142: 100–101.

Shepherd RK. 1902. The form of the human spleen. *J Anat Physiol* 37: 50.

Soleimani M, Mehrabi A, Kashfi A, Fonouni, H, Büchler, MW Kraus TW. 2007. Surgical treatment of patients with wandering spleen: report of six cases with a review of the literature. *Surg Today* 37: 261–269.

Tozbikian G, Bloomston M, Stevens R, Ellison EC, Frankel WL. 2007. Accessory spleen presenting as a mass in the tail of the pancreas. *Ann Diag Pathol* 11: 277–281.

Wadham BM, Adams PB, Johnson MA. 1981. Incidence and location of accessory spleens. *NEJM* 304: 1111.

Winer-Muram HT. 1995. Adult presentation of heterotaxic syndromes and related complexes. *J Thorac Image* 10: 43–57.

111 Small intestines, appendix, and colon

Koichi Watanabe
Kurume University School of Medicine, Fukuoka, Japan

Midgut rotation

The primitive gut has three regions: the foregut, midgut, and hindgut. The midgut is the portion of the intestine that is supplied by the superior mesenteric artery and eventually forms the intestinal section from the duodenum to the transverse colon. At the end of the fifth gestational week, the midgut forms a U-shaped loop toward the umbilical cord. The cranial part of the loop is termed the cranial limb, postarterial limb, or duodenojejunal loop and eventually forms the duodenum, jejunum, and ileum. The caudal part of the loop is termed the caudal limb, prearterial limb, or ileocecal loop and eventually forms the colon. The yolk stalk, which continues to the yolk sac, is attached to the apex of the loop. There is not enough room in the peritoneal cavity for growth of the midgut at this point in time of gestational development, so it develops in the extraembryonic coelom which is inside the proximal part of the umbilical cord and outside the abdominal cavity. The first rotation is a 90-degree counterclockwise rotation of the midgut loop around the axis of the superior mesentery artery. The cranial limb elongates to form the jejunum and ileum during this rotation. In the abdominal cavity, the hindgut lies on the left side and the small intestine elongates behind the superficial mesenteric artery. At the 10th–11th week of gestation, the intestinal tract abruptly returns to the peritoneal cavity. The cranial limb (small intestine) returns to the abdominal cavity first, and the caudal limb (cecum and colon) returns next with a further 180-degree counterclockwise rotation. The extents of the first and second rotations differ among the literature. Some authors have stated that the first rotation is 180 degrees counterclockwise and that the second rotation is 90 degrees counterclockwise (Gray and Skandalakis 1972). The colon passes anterior to the superior mesenteric artery and moves to the right side of the abdominal cavity. After completing the total 270-degree rotation, the cecum descends from the right upper quadrant to its normal position, and the ascending and descending colon attaches to the posterior abdominal wall by fusion and anchoring of the mesentery.

Frazer and Robbins (1915) first described the development of the midgut as occurring in three stages as a more optimal interpretation of the congenital anomalies of the midgut. The first stage comprises the first 10 weeks of gestation, during which the midgut protrudes and prolapses to the extraembryonic coelom. Failure of this stage causes exomphalos and malrotation of the duodenum. The second stage occurs between the 10th and 11th weeks of gestation, during which the midgut returns to the abdomen. Failure of this stage causes nonrotation, incomplete rotation, paraduodenal hernia formation, or reverse rotation. The third stage comprises the 12th week of gestation to birth; during this stage, the mesentery becomes attached to the posterior abdominal wall. Failure of this stage causes the formation of a mobile cecum, subhepatic cecum, or retrocecal appendix.

Exomphalos

Exomphalos results from failure of the intestine, which grows outside of the abdominal cavity, to return to the abdominal cavity in the first stage.

Malrotation

The incidence of malrotation or nonrotation of the midgut is presumed to be approximately 1 in 500 live births (Stewart et al. 1976; Torres and Zigler 1993). Two-thirds of cases are diagnosed during the newborn period. The male:female ratio is reportedly 2:1 in this age group. However, male patients comprise approximately 20% of cases that occur after 1 year of age (Torres and Zigler 1993).

Malrotation of the midgut is often associated with other congenital anomalies including intestinal atresia, omphalocele formation, congenital diaphragmatic hernia formation, or Hirschsprung's disease (Ford et al. 1992).

Nonrotation

Nonrotation of the intestine is considered to occur in the second stage of midgut rotation. In nonrotation of the intestine, the midgut is only rotated to 90 degrees instead of the normal 270 degrees (Fig. 111.1). As the midgut returns to the abdomen, the caudal limb (cecum and colon) enters the abdomen first and lies on the left side of the abdomen while the cecum localizes on the midline; the cranial limb (small intestine) then enters the abdomen and lies on the right (Gray and Skandalakis 1972).

Bergman's Comprehensive Encyclopedia of Human Anatomic Variation, First Edition. Edited by R. Shane Tubbs, Mohammadali M. Shoja and Marios Loukas.
© 2016 John Wiley & Sons, Inc. Published 2016 by John Wiley & Sons, Inc.

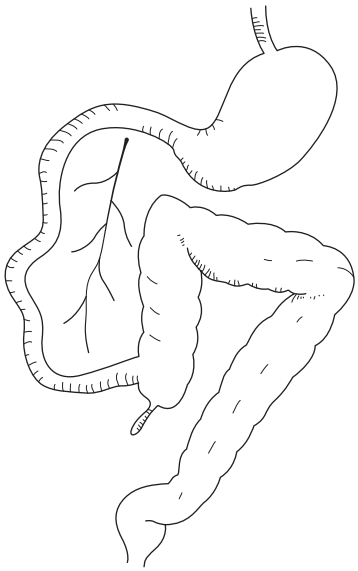

Figure 111.1 Nonrotation. Colon and cecum lie on the left side of the abdomen and small intestine lies on the right.

Nonrotation is the most common form of midgut malrotation (Bill 1979; Kawashima et al. 2001). Most cases are symptomatic and diagnosed in infancy and childhood (Fig. 111.2). However, adult cases have also been reported.

Mixed rotation, partial rotation, or incomplete rotation

Mixed, partial, or incomplete rotation may result when rotation of the midgut stops in the second stage. The degrees of rotation vary from nonrotation (90 degrees) to normal (270 degrees); rotation usually stops at 180 degrees. As a result, the duodenum is usually fixed on the right and the cecum is located in the left upper quadrant or close to the midline, just below the pylorus. The cecum is fixed to the retroperitoneum by a peritoneal band called Ladd's ligament, which forms when the cecum and ascending colon attach to the abdominal wall during the third stage of midgut rotation (Fig. 111.3). This band constrains the duodenum and frequently causes duodenal obstruction in infancy. Berdon et al. (1970) illustrated two types of the attachment of Ladd's band to the large intestine (Fig. 111.4). The variety of the attachment of Ladd's band is considered to result from the degrees of midgut rotation.

Reverse rotation

This type of malrotation is extremely rare and comprises only 4% of all malrotation cases (Aldridge 1961). Reverse rotation may be found in patients of any age from newborn to adult. Adult cases comprise approximately 75% of all cases; this differs from other types of malrotation, which are usually diagnosed in infancy. Reverse rotation is twice as common in female as in male patients (Scobie 1969). In this condition, the first 90-degree counterclockwise rotation of the midgut takes place; however, the subsequent 180-degree rotation occurs in the clockwise direction instead of in the normal counterclockwise direction (Dott 1923).

Estrada and Gurd (1962) classified reverse rotation of the midgut into two types according to the sequence of which limb, the cranial or caudal limb, re-enters the abdominal cavity first. The type of reverse rotation in which the caudal limb re-enters first is termed "retroarterial colon type"; the colon lies behind

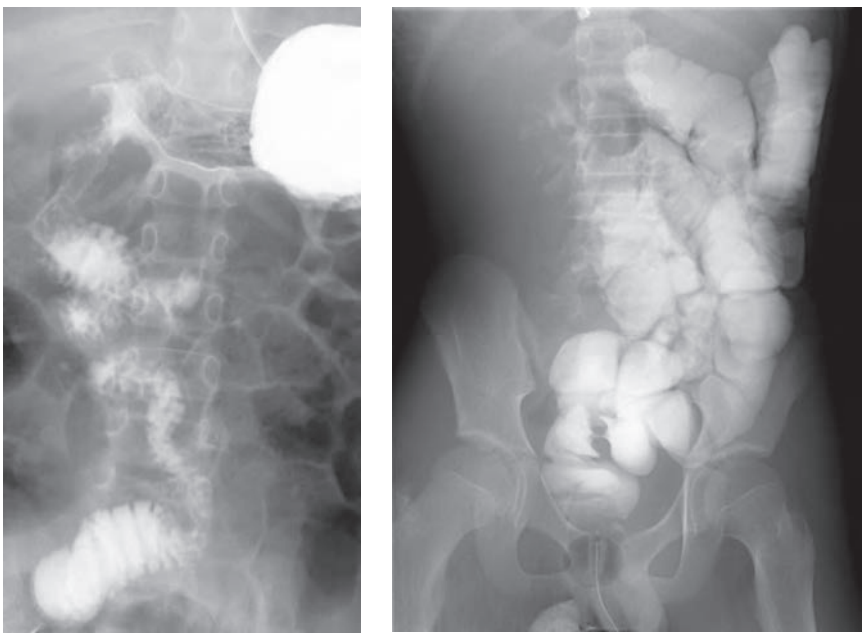

A B

Figure 111.2 X-ray examination of nonrotation. (a) Upper gastro-intestinal X-ray study; the small intestine is located on the right side of the abdomen. (b) Barium enema X-ray study; the large intestine is located on the left side of the abdomen.

Source: Dr Kimio Asagiri, Department of Pediatric Surgery, Kurume University School of Medicine.

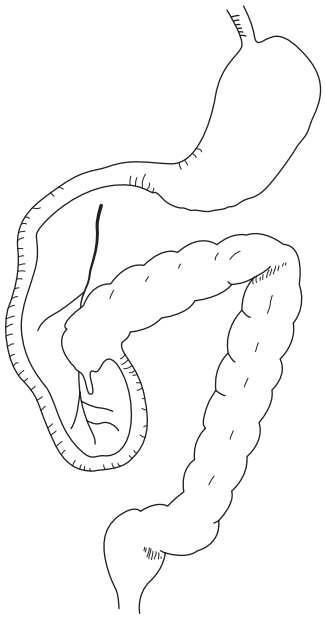

Figure 111.3 Mixed rotation. The duodenum is usually fixed on the right and the cecum is located in the left upper quadrant or close to the midline.

the superior mesenteric artery, and the small intestine is ventral to the colon and the artery (Gray and Skandalakis 1972). The majority of reported cases of reverse rotation of the midgut are of the latter type, and Gray and Skandalakis (1972) depicted that some 30 cases have been described since 1883.

Reverse rotation is usually asymptomatic, but eventually causes intestinal obstruction. Davies et al. (1955) reviewed 21 previously reported cases in the literature and found that the obstructive symptoms were chiefly caused by the following three conditions: obstruction of the transverse colon due to compression by the superior mesenteric artery; volvulus of the mobile right colon or the entire midgut; or duodenal-jejunal obstruction.

Another type of reverse rotation is termed "liver and entire colon ipsilateral type" and is extremely rare. In this type, the cranial limb re-enters the abdomen first, the small intestine lies in front of the superior mesenteric artery and occupies the left side of the abdominal cavity, and the colon lies to the right with the cecum on the midline (Gray and Skandalakis 1972).

Amir-Jahed (1968) reported a more detailed classification (Fig. 111.5). All patients with reverse rotation had the common feature of the duodenum passing anteriorly to the superior mesenteric artery. However, the distal midgut, especially the transverse colon, was described as one of two types depending on whether it passed anteriorly (prearterial type) or posteriorly (retroarterial type) to the superior mesenteric artery. With respect to the final orientation of the midgut loop, this is reflected as the cecum localizing on the right or left side of the abdominal cavity. The authors therefore classified reverse rotation into four types.

- Type 1 is the prearterial right-sided cecum type. This type involves very little actual reverse rotation with the exception of the first part of the jejunum. The rest of the midgut remains stationary. This type is very similar to nonrotation and is the type of reverse rotation most often mistaken for it.
- Type 2 is the prearterial left-sided cecum type. This type is characterized by a 180-degree reverse rotation of the distal midgut loop with mislocation of the splenic flexure.
- Type 3 is the retroarterial right-sided cecum type. In this type, it is considered that the caudal limb re-enters the abdomen first, as in the retroarterial colon type described by

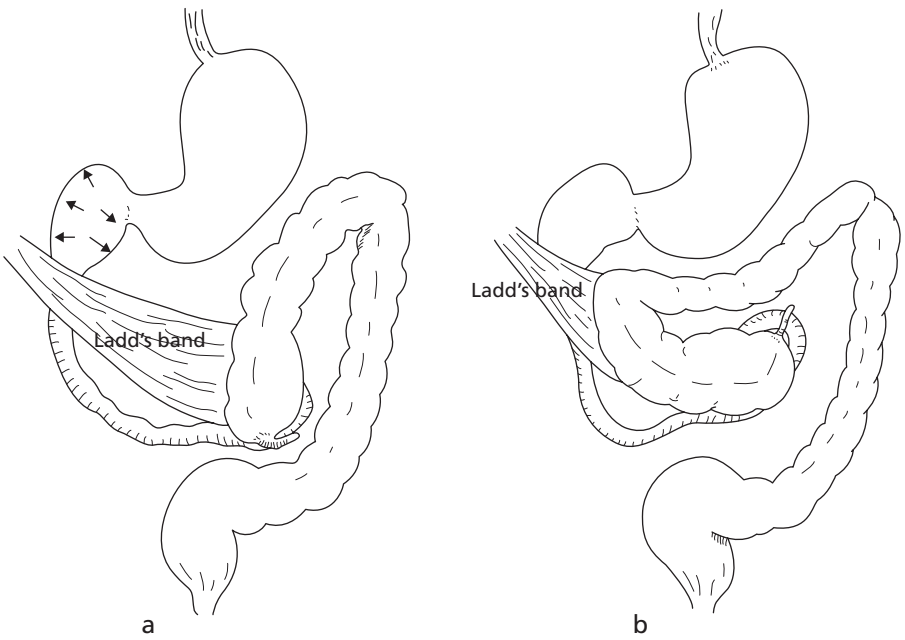

Figure 111.4 Two types of Ladd's bands reported by Berdon et al. (1970): (a) Ladd's bands extend from the cecum; (b) Ladd's bands extend from the ascending colon.

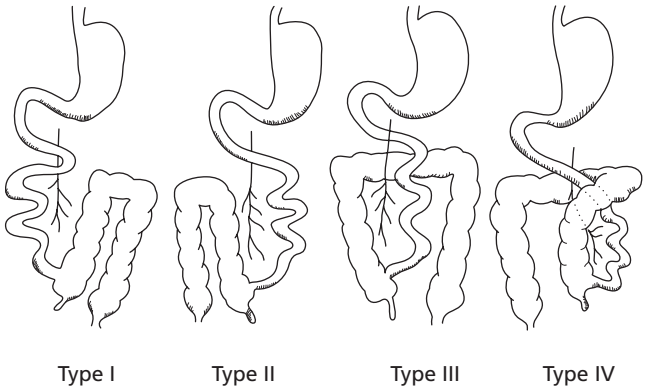

Figure 111.5 The classification of the reverse rotation reported by Amir-Jahed (1968): type I: prearterial right-sided cecum; type II: prearterial left-sided cecum; type III: retroarterial right-sided cecum; and type IV: retroarterial left-sided cecum.

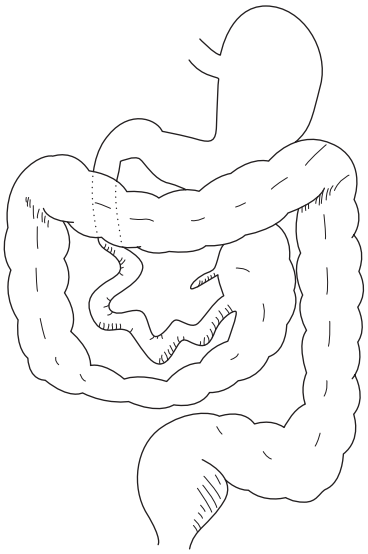

Figure 111.6 Hyperrotation. The cecum is extended and located in the left lumbar region instead of the right pelvic region.

Estranda and Gurd (1962), and it is presumed that the caudal limb rotates and localizes normally but that the cranial limb rotates 90 degrees in a clockwise direction.

- Finally, type 4 is the retroarterial left-sided cecum type. This category applies to the cases reported by Guttierez (1934) and Haller and Morgenstern (1964). In this type, the caudal limb re-enters the abdomen first at a 180-degree clockwise rotation with mislocation of the splenic flexure, and the transverse colon and cecum are secondarily folded from their retroarterial position to a partial prearterial position.

However, some cases that did not completely fit this classification have also been reported. In the cases reported by Aldridge (1961) and Scobie (1969), the duodenum passed anterior to the superior mesenteric artery but underneath the mesentery at its left border of it, the cecum was located on the left side while the ascending colon passed obliquely upward and to the right, and the transverse colon passed posterior to the superior mesenteric artery. This is similar to the type 2 reverse rotation described by Amir-Jahad with an additional 180-degree clockwise rotation from the jejunum to the ascending colon.

Hyper-rotation (hyperdescent of the cecum)

This type of abnormal midgut rotation is extremely rare, and only two cases (Low and Hilderman 1940; Pellatt and Evans 1982) have ever been reported according to our investigation. In both cases, the general intestinal pattern was almost normal with the exception of the cecum and ascending colon. The cecum was located in the left lumbar region instead of the right pelvic region, just beneath the left side of the transverse colon. The ascending colon extended its length and ran downward from the cecum, passed the midline, touched the sigmoid colon, and turned upward to the hepatic flexure (Fig. 111.6). In the case described by Low and Hilderman (1940), the hepatic flexure was normally positioned; in the case described by Pellatt and Evans (1982) however, it was located at a lower position because of the relatively large liver. The total rotation of the midgut was approximately 400 degrees, in contrast with the normal 270 degrees (Low and Hilderman 1940). Low and Hilderman (1940) presumed the cause of hyper-rotation to be supernormal growth of the ascending colon because the position of the anastomosis between the right and left colic arteries was normal. In contrast, the hypothesis put forward by Pellatt and Evans (1982) was based on an embryological explanation not commonly accepted (Harris et al. 1976). When the midgut re-enters the peritoneal cavity, the liver is much larger than the volume of the cavity. The cecum is positioned in the right iliac fossa instead of the normal embryological location of the right upper quadrant. The ascending colon then grows upward as the liver recedes. In such cases, when a larger-than-usual liver occupies the majority of a longer-than-usual peritoneal cavity, the cecum is forced from the right iliac fossa to another site by extension of the ascending colon. Finally, it moves to the left side (Pellatt and Evans 1982).

Encapsulated small intestine

This anomaly involves coverage of the whole small intestine by an avascular sac that has no communication with the abdominal cavity (Gray and Skandalakis 1972). It usually results from a chronic inflammatory disease such as tuberculosis, appendicitis, or cholecystitis. Other recently reported causes include peritoneal dialysis, the beta-blocker practolol, ventriculoperitoneal shunting, peritoneovenous shunting, sarcoidosis, and systemic lupus erythematosis (Chew et al. 2006). However, cases considered to be congenital have very rarely been reported (Costantinides et al. 1998). The first congenital case of an encapsulated small intestine was reported by Cleland in 1868, and approximately 20 cases have been reported in the

English-language literature since then (Mordehai et al. 2001). The small intestine is usually the only organ covered by the sac. However, a case in which the sac covered both the ascending colon and small intestine has been reported (Hosokawa and Nakajima 1962). With respect to the origin of the sac, Gray and Skandalakis (1972) stated that the sac originates from the extraembryonic coelom, which lines the umbilical cord and enters the abdominal cavity with the small intestine at time of midgut re-entrance. However, in the case in which the sac covered both the ascending colon and small intestine, the origin of the sac may have differed from the other reported cases. Hosokawa and Nakajima (1962) concluded that the sac was derived from the mesocolon of the ascending colon in his case.

Duodenum

Anatomical variations within the normal range of the duodenum have seldom been reported. However, the position of the duodenum reportedly undergoes considerable changes with age. Katz et al. (1987) stated that the duodenojejunal flexure is positioned on the right side across the midline in 92.3% of individuals aged 0–4 months, in 66.7% of individuals aged 4 months to 4 years, and in 0.0% of individuals aged 4–18 years. Katz et al. (1987) considered that increasing muscle tone and growth causes the duodenum to take the position of that in the normal adult. Anson (1963) visually depicted eight duodenal types according to the specific form and position of the duodenum. However, the exact definition of each type is ambiguous because the author did not describe each type in words, but only in pictures. Myles (1937) reported four types of duodenal ptosis in an X-ray study. The first type is general ptosis, which is usually a part of general visceral ptosis and is characterized by accentuation of the normal mobility of the duodenum. The second type is ptosis of the duodenal cap itself, which is accompanied by ptosis of the stomach. The third type is undue mobility or ptosis of the junction between the cap and the descending portion of the duodenum. This type is also called a dropped loop. It results in the formation of an abnormal mesentery of the upper segment of the duodenal arc. Finally, the fourth type is ptosis of the descending segment. Ballooning or even stasis of the lowest portion of the duodenal loop occurs. An accessory duodenal recess lying below the horizontal part of the duodenum is called the mesentericoparietal recess of Broesire.

Duodenal stenosis or atresia

A variety of intrinsic and extrinsic congenital lesions may cause congenital duodenal obstruction. Intrinsic factors include atresia, septum formation, and webbing. Extrinsic factors include abnormal fixation of the duodenum, persistence of the hepaticoduodenocolic ligament, annular pancreas, and vascular anomalies. Other causes of duodenal obstruction include prenatal mesenteric cysts, tumor or cysts of the liver or pancreas, and malrotation of the intestine (Marlock and Gray 1943). Congenital duodenal obstruction is usually symptomatic and diagnosed in the neonatal period.

Various degrees of intrinsic duodenal atresia and stenosis have been reported. Duodenal webbing and diaphragm formation with an aperture cause stenosis. Kaddah et al. (2006) reported a 17% rate of duodenal diaphragm formation among all causes of the duodenal obstruction. Gray and Skandalakis (1972) classified intestinal atresia into three types: in type 1, a diaphragm of the mucosa develops; in type 2, a segment of the intestine is reduced to a solid cord without a lumen; and in type 3, there is complete segmental absence of a portion of the intestine. Although this classification applies to all portions of the intestine, it also applies to duodenal atresia.

Louw (1966) examined the type and site of obstruction in all portions of the intestine and found that the duodenum was the most frequent site of obstruction, accounting for approximately 40% (88 of 138 cases). The types of obstruction were as follows: stenosis, 44% (24 of 55 cases); type 1 atresia, 35% (19 cases); type 2 atresia, 22% (12 cases); and type 3 atresia, 0% (no cases). Similar rates have been reported in other studies (Nixon and Tawes 1971; Schnauffer 1991); a stenosis:atresia ratio of 2:3 or 2:2 has also been reported (Kaddah et al. 2006). Moreover, Boyden et al. (1967) reviewed previously reported articles and concluded that the most frequent location of duodenal obstruction was around the papilla in the second portion, and that obstruction occurred in 83% of cases of duodenal stenosis and atresia.

Duodenal diverticulum

Duodenal diverticulum is a relatively common anomaly and is classified into two types: extramural and intramural. Most duodenal diverticula are acquired and of the extramural type. This type is presumed to develop due to herniation of the mucosa through a defect of the muscle layer of the weak part of the duodenum. Extramural diverticula are often associated with biliary tract disease (Afridi et al. 1991). The incidence of biliary tract stones is reported to be significantly higher in patients with juxtapapillary diverticula. This theoretical relationship presumes that dysfunction of the papilla Vater and overgrowth of bacteria due to the diverticulum cause an ascending infection of the biliary tract. The infection in turn causes the formation of calcium bilirubinate stones (Løtveit et al. 1988; et al. Afridi 1991). The intramural type is rare and congenital in onset. Yang et al. (1974) claimed that the presence of an incomplete duodenal diaphragm results in the development of an intramural diverticulum under the force of peristalsis. This type of duodenal diverticulum is known to be frequently associated with other abnormalities such as choledochocele, annular pancreas, intestinal malrotation, situs inversus, superior mesenteric artery syndrome, imperforate anus, Hirschsprung's disease, congenital heart disease, hypoplastic kidney, extrophy of the bladder, and duplication of the papilla of Vater (Karoll et al. 1983; Afridi et al. 1991; D'Alessio 2005). The frequency of coexisting anomalies in patients with intramural diverticula is reportedly 40% (Afridi et al. 1991).

Ackermann (1943) reviewed previous reports and found that the incidence of duodenal diverticula was 3–22% among autopsy cases and 0.016–5.19% among X-ray examinations. The rate among X-ray examinations is much lower than that among autopsy studies, but these X-ray study reports were so old that they may have been associated with accuracy, technique, and X-ray equipment problems. An incidence similar to that among the autopsy examinations was recently reported among endoscopic retrograde cholangiopancreatography examinations (Rosetti et al. 2013).

Most authors have stated that the second and third portions of the duodenum are the most frequent locations of diverticula. Mendelson et al. (1984) reported that diverticula usually occur on the medial aspect of the second portion and within 2.5 cm of the ampulla of Vater. Occurrence on the lateral aspect of the second portion is rare (Scudamore et al. 1982; Mendelson et al. 1984). However, Ackermann (1943) reported no diverticula in the first portion, but approximately equivalent frequencies of diverticula in the second, third, and fourth portions (36%, 5 of 14 cases; 36%, 5 of 14 cases; and 21%, 3 of 14 cases, respectively) and a frequency of 7% (1 of 14 cases) between the second and third portions.

With respect to the shape of duodenal diverticula, most are globular and some are funnel-shaped or cylindrical (Ackermann 1943).

Duodenal duplication

Duodenal duplication is a rare congenital anomaly of the gastrointestinal tract. It usually occurs in the distal ileum and is sometimes observed in the esophagus, colon, and jejunum. It represents 2–12% of all gastrointestinal tract duplications. Most duodenal duplication cysts are located in the first and second portions of the duodenum on the mesenteric side of the anterior wall (Inouye et al. 1965). However, cysts located in other portions of the duodenum have also been reported. Such duplication cysts usually exist in contact with the duodenal wall but do not communicate with the lumen of the duodenum, and a smooth muscle layer is present within the cyst wall. A few cases of duodenal duplication communicating with the pancreatic duct (either the duct of Wirsung or duct of Santorini) have also been reported (Shimada et al. 1984; Ogura 1998). These cysts are usually 2–12 cm in diameter (Inouye et al. 1965).

Duodenal duplication is usually diagnosed during infancy and childhood. However, adult cases have also been reported. There are no sex differences (Inouye et al. 1965). Common symptoms are abdominal pain, nausea, and vomiting.

Suspensory ligament of the duodenum

A suspensory ligament of the duodenum was first described by Treitz in 1853, who stated the suspensory ligament of the duodenum had two segments. One is the so-called suspensory ligament of the duodenum, which is usually described as a ligament that arises from the duodenojejunal flexure and a part of the inferior transverse portion of the duodenum, and inserts into the connective tissue surrounding the stems of the superior mesenteric artery and celiac artery. The other is a strip of muscle called the Hilfsmuskel, which arises from the right border of the esophageal opening of the diaphragm and extends to the termination of the suspensory muscle of the duodenum (Costacurta 1972; Jit and Grewal 1977; Kim et al. 2008). However, the Hilfsmuskel is considered to be a different structure from the suspensory ligament of the duodenum.

Costacurta (1972) reviewed the rate of appearance of the suspensory ligament of the duodenum and found that it has been reported at rates of 13.4% (Le Double 1897) to 100.0% (Shaar 1927; Costacurta 1972). However, this rate was approximately 70–90% in most reports (Low 1907; Crymble 1910; Haley and Perry 1949), and the rate of 13.4% reported by Le Double (1897) seems extremely low compared with that in other reports.

Jit and Grewal (1977) examined 100 cadavers and reviewed the variations of the ligament. With respect to the cranial attachment, the suspensory muscle was attached to the stem of both the superior mesenteric artery and celiac artery in 78% of cases, only to the superior mesenteric artery in 17%, and to the celiac artery in 5%. Costacurta (1972) examined 100 dissection cases and also found that the suspensory muscle was attached in the region of the superior mesenteric artery and/or celiac artery in 99% of cases (Costacurta 1972; Jit and Grewal 1977).

Akin et al. (1976) classified the variations of the caudal attachment to the duodenum into four types (Fig. 111.7). In type A, the muscle attaches to the third and fourth portions of the duodenum and the duodenojejunal flexure. In type B, the muscle divides into multiple bands. In type C, the muscle attaches to the third and fourth portions of the duodenum only. Finally, in type D, the muscle attaches to the duodenojejunal flexure only. Meyers (1995) reviewed previously reported articles, and the most frequent pattern was type A (40–61%), followed by type C (31–53%). Type D was rare at 0–8%. Jit and Grewal (1977) reported that the muscle was attached to the third and fourth portions of the duodenum (corresponding to type C in Akin's classification) in 53% of cases; to the third and fourth portions of the duodenum and the duodenojejunal flexure (corresponding to type A in Akin's classification) in 40% of cases; only to the third portion of the duodenum in 4% of cases; to the fourth part of the duodenum and duodenojejunal flexure in 2% of cases; and to the second, third, and fourth portions of the duodenum in 1% of cases (Jit and Grewal 1977). However, Haley and Peden (1943) and Haley and Perry (1949) reported that the most frequent pattern of caudal attachment of the suspensory ligament of the duodenum was to the third and fourth portions of the duodenum and to the duodenojejunal flexure at a rate of 61%. The second most frequent pattern of caudal attachment was to the third and fourth portions of the duodenum at a rate of 15.6% (Haley and Perry 1949; Jit and Grewal 1977). Argeme et al. (1970) stated that the muscle was attached to the third and fourth portions of the duodenum in all cases and reached the

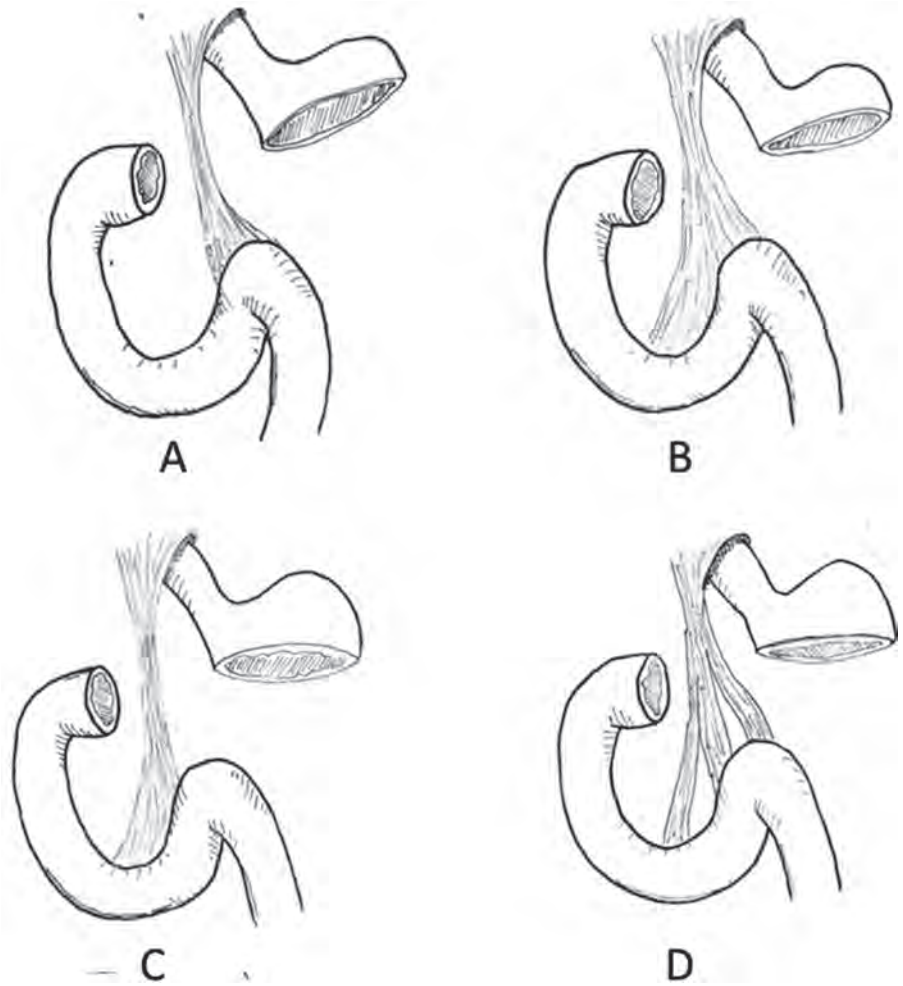

Figure 111.7 The variation of caudal attachment of duodenal suspensory ligament reported by Akin et al. (1976). Type A: the muscle attaches to the third and fourth portions of the duodenum and the duodenojejunal flexure. Type B: the muscle divides into multiple bands. Type C: the muscle attaches to the third and fourth portions of the duodenum only. Type D: the muscle attaches to the duodenojejunal flexure only.

duodenojejunal flexure in 60% of them (Argeme et al. 1970; Jit and Grewal 1977). Costacurta (1972) reported that the muscle was attached to the flexure and fourth portion of the duodenum in 74% of cases and to the flexure and third and fourth portions in 26% (Costacurta 1972; Jit and Grewal 1977).

Ileum and jejunum

The length of the small intestine changes with age. In adults, the mean length is approximately 600 cm. Weser (1983) stated that the length is usually about 600 cm, with a range of 260–800 cm (Weser 1983; Hasosah et al. 2008). Weaver et al. (1991) described a length of about 550 cm with a range of 350–700 cm. The average length of the small intestine in newborns has been reported as 240 cm (Reiquam et al. 1965), 248 cm (Benson et al. 1960), and 305 cm (Potts 1955). The length increases with age; in Weaver's (1991) series, the mean length was 275 cm at term, 380 cm at 1 year, 450 cm at 5 years, 500 cm at 10 years, and 575 cm at 20 years of age. Short bowel syndrome has been reported as a congenital anomaly associated with the length of the small intestine. It was first reported by Hamilton in 1969; since then, about 40 cases have been reported (Hasosah et al. 2008). It is often associated with malrotation, and the length of the small intestine has been reported as 20 cm (Chu et al. 2004) to 237 cm (Kern et al. 1990). The average length of the anomaly is reportedly 57 cm (Hasosah et al. 2008).

Peyer's patches have been included in research on the structure of the intestinal wall. According to standard anatomical textbooks, Peyer's patches are usually oval or round in shape and approximately 1 cm wide, and they extend along the intestine opposite the mesenteric attachment of the ileum or occasionally in the jejunum (Clemente and Grey 1984). The number of patches is usually reported as 20–30. Cornes (1965) examined Peyer's patches using a specific chemical for cadaver preservation and obtained results somewhat different than the standard description. The Peyer's patches were usually oval or rectangular in shape and situated along the antimesenteric border. The patches in the duodenum, terminal ileum, and occasionally in the proximal jejunum were randomly situated throughout the

wall. Bizarrely shaped patches were also observed in the proximal jejunum and around the ileocecal valve. In most cases, the ileum was the most frequently observed site of Peyer's patches, but in some specimens the jejunum contained more patches than the ileum. The number of Peyer's patches varies from early fetal life to puberty. The mean number of patches varied in Cornes' report from 59 before 30 weeks of gestation to 239 at puberty. These numbers are much higher than the 20–30 reported in standard anatomical textbooks. However, cases of more than 70 patches (Sappy 1877; Passow 1885; Gundobin 1892) and 246 patches (Hellmann 1921) have also been reported. Cornes (1965) presumed that postmortem changes or chemical preservation made the Peyer's patches shrink and more difficult to observe.

Intestinal atresia and stenosis

Various degrees of congenital obstruction of the small intestine have been reported. Louw (1967) classified intestinal obstruction into four types of stenosis and three types of atresia. Stenosis is a narrowing of a portion of the intestine, but not complete obstruction of the intestinal lumen. Stenosis is rare and extrinsic factors such as annular pancreas, ligaments, and blood vessels have been cited as causes. Perforated diaphragmatic atresia (type 1 intestinal atresia) also causes stenosis.

Atresia is classified into three types according to the organic degree of obstruction. Type 1 is characterized by closure of the intestine by the diaphragmatic mucosa. In type 2, the proximal and distal portions of the intestine end blindly and are joined by a solid cord. In type 3, both portions of the intestine end blindly and are disconnected. Type 1 is atresia caused by diaphragmatic mucosa within the lumen. Histologically, the diaphragm usually consists of mucosa and submucosa. It sometimes contains openings of various degrees; in some such cases, food is still able to pass through the intestines and the condition is categorized as stenosis. A perforated diaphragm may also cause a diverticulum to form (Heilbrum and Boyden 1964; Gray and Skandalakis 1972). If an opening exists, it may be 2–10 mm in diameter and is usually located off-center (Gray and Skandalakis 1972). In type 2 atresia, the intestine ends blindly at the site of the atresia, and both ends are connected by a fibrous cord that lies along the edge of the intact mesentery (Gray and Skandalakis 1972). In type 3 atresia, the intestine ends blindly as in type 2 but there is no connecting fibrous cord and the mesentery between the blind ends of the intestine is sometimes absent.

In a study by Louw (1967), the most frequent site affected by intestinal obstruction was the duodenum and ileum above Meckel's diverticulum. The frequency of obstruction (both stenosis and atresia) at each site was as follows: duodenum, 40% (55/138); ileum, 25% (35/138); jejunum, 15% (21/138); colon, 4% (6/138); and multiple sites, 15% (21/138). In cases of stenosis alone, the duodenum was affected in 75% of cases (24/32), the ileum in 19% (6/32), and the jejunum in 6% (2/32). In cases of atresia alone, the duodenum was the most frequently affected site at 30% (32/106); involvement of the ileum occurred in 27% of cases (29/106), jejunum in 18% (19/106), colon in 6% (6/106), and multiple sites in 20% (21/106). The type of atresia was dependent upon the site. Atresia in the duodenum comprised both type 1 and 2, and type 1 was the more frequent type. Atresia in the jejunum, ileum, and colon comprised all three types; the most frequent type was type 3, and the second most frequent type was type 2. In another study (DeLorimier et al. 1969) that focused on the jejunum and ileum, the rate of atresia at each site was as follows: proximal jejunum, 31%; distal jejunum 20%; proximal ileum, 13%; distal ileum, 36%; and multiple sites, 6%. The most frequent site of obstruction was the distal ileum, and the second most frequent site was the proximal jejunum. The frequency of stenosis alone at each site was as follows: proximal jejunum 20% (5/25); distal jejunum, 16% (4/25); proximal ileum, 16% (4/25); and distal ileum, 40% (10/25). The types of obstruction were: stenosis, 4% (25/559); type 1 atresia 19% (104/559); type 2 atresia, 31% (172/559); and type 3 atresia, 46% (258/559). Recently, the classification was modified in some points (Martin and Zerella 1976). Type 1 and type 2 are as for the classical description. However, type 3 was divided into two: type 3a and 3b. Type 3a is as for the traditional type 3 (the intestine ends blindly, there is no connecting fibrous cord, and the mesentery between the blind ends of the intestine is sometimes absent). Type 3b comprises a proximal jejunal atresia, the absence of large part of the small intestine, and distal ileum coils the supplying artery. It is often associated with malrotation. This type is also called "apple-peel" or "Christmas-tree" deformity because of the shape of the distal ileum. The distal small bowel receives its blood supply from a single ileocolic or right colic artery because the large part of the superior mesenteric artery is absent. Type 4 is multiple atresia of type 1, 2, and 3 (Fig. 111.8). In latest statistics reported by Stollman et al. (2009), stenosis was 7%; type 1 atresia, 16%; type 2 atresia, 21%; type 3a, 24%; type 3b, 10%; type 4, 22%.

Duplication of the small intestine

Duplication of the alimentary tract is a rare congenital anomaly. The frequency of this anomaly was reported as 1 in every 4500 individuals in an autopsy study. It was reported as 1 in every 18,000 live births (Potter 1961). Duplication of the small intestine is the most frequent type throughout the digestive tract and accounts for approximately 40% of cases (Iyer and Mahour 1995). Duplication tends to occur more in the ileum than in the jejunum; the ileum:jejunum ratio of duplication has been reported as 2:1 (Bower et al. 1978; Holcomb et al. 1989). Duplication cysts are usually classified into three types: saccular (spherical) cysts, small intramural cysts, and tubular cysts. Most duplication cysts are saccular in shape (80–90%). Small intramural cysts have been found at or near the ileocecal valve and cause obstruction. Tubular-shaped cysts have also been observed as occurring in the colon (Wardell and Vidican 1990; Macpherson 1993; Karnak et al. 2000). The cyst size varies among cases. In most cases, the length of the duplicated segment is <10 cm. However, cases of very long tubular duplications (>70 cm) have

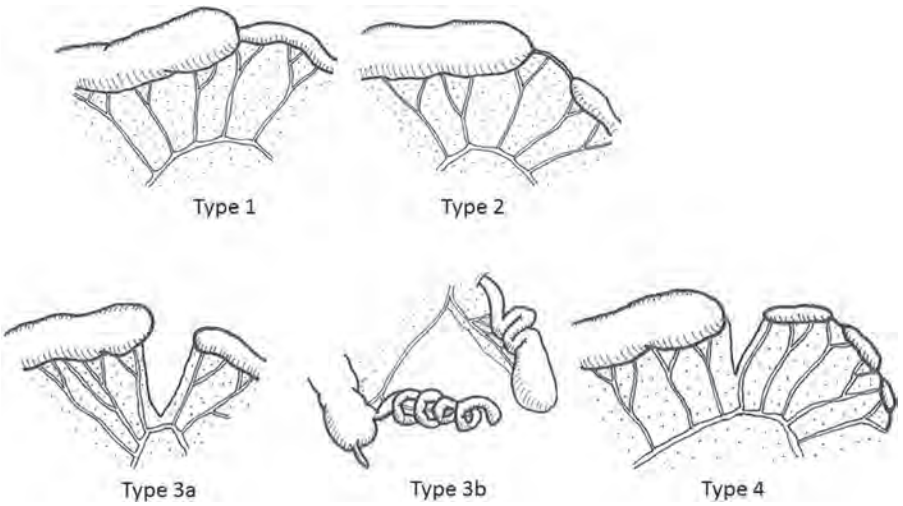

Figure 111.8 The classification of intestinal atresia. Type 1: atresia caused by diaphragmatic mucosa within the lumen. Type 2: the proximal and distal portions of the intestine end blindly and are joined by a solid cord. Type3a: the intestine ends blindly, there is no connecting fibrous cord, and the mesentery between the blind ends of the intestine is sometimes absent. Type 3b ("apple-peel" or "Christmas-tree" deformity): a proximal jejunal atresia, absence of large part of the small intestine, and distal ileum coils the supplying artery. Type 4: multiple atresia of type 1, 2, and 3. Adapted from Louw (1959). Also adapted from Grosfeld et al. (1970) with permission from Elsevier.

also been reported (Schwartz et al. 1980; Balén et al. 1993; Sham et al. 2010; Khan et al. 2012). The duplication involves all layers of the wall of the small intestine including the mucosa, submucosa, muscle, and serosa. The cyst is usually attached to the mesenteric border of the small intestine and has a common blood supply with the adjacent gastrointestinal tract (Bower et al. 1978). This differs from Meckel's diverticulum, which receives a separate blood supply derived from the vitelline arteries. The smooth muscle of the duplication cyst often shares a blood supply with the contiguous intestinal tract, and the inner lumen of the cyst may or may not communicate with the inner lumen of the intestine. A duplication involving communication of the inner lumen of the cyst with the intestinal tract usually becomes tubular in shape; in contrast, a duplication without inner luminal communication tends to become cystic in shape (Gray and Skandalakis 1972). The duplication may contain gastric mucosa in about half of cases. Gastrointestinal bleeding due to peptic ulceration sometimes occurs.

Non-Meckelian jejunal and ileal diverticula

Diverticula in the small intestine are classified as either Meckel's diverticula or non-Meckelian diverticula. Meckel's diverticulum is a remnant tissue of the omphalomesenteric duct and the wall comprises all layers of the small intestine; it is therefore categorized as a true diverticulum.

A non-Meckelian diverticulum is a pseudo-diverticulum and is usually located on the mesenteric border of the jejunum. The wall comprises mucosa and submucosa and lacks a smooth muscle layer. These features are quite different from Meckel's diverticulum. A non-Meckelian diverticulum was first reported by Soemmering in 1794 (Makris et al. 2009). This is a rare condition, and the incidence of jejunal diverticula has been reported as 0.02–0.42% in roentgenographic studies, 2.0–2.3% in enteroclysis studies, and 0.06–4.6% in an autopsy study (Makris et al. 2009). With respect to sex differences, it is generally reported that the incidence in males is twice that in females (Gray and Skandalakis 1972; Makris et al. 2009). However, some reports have claimed an opposite ratio (Lee and Finby 1958; Makris et al. 2009). Because most of these diverticula are acquired, the incidence increases with age. Although pediatric cases have rarely been reported, individuals in their sixth decade are most frequently affected (Gray and Skandalakis 1972; Chow et al. 1997).

These diverticula are more frequent in the jejunum than in the ileum. Chiu et al. (2000) reported that about 80% occurred in the jejunum, 15% occurred in the ileum, and 5% occurred in both. With respect to the number of diverticula, although both single and multiple lesions have been reported, about one-half to two-thirds are multiple (Benson et al. 1943; Baskin and Mayo 1952; Altemeier et al. 1963; Williams et al. 1981; Wilcox and Shatney 1988; Makris et al. 2009). Multiple lesions most commonly occur in the jejunum. The diameter varies from <1 to >10 cm (Lee and Finby 1958). The average was 1–4 cm in the report of Benson et al. (1943), but often reached >5 cm (Tsiotos et al. 1994; Mekris et al. 2009). However, the symptoms do not correlate with the diameter.

Non-Meckelian diverticula are known to be associated with diverticula in other organs. They are often observed in the colon and duodenum. Diverticula in the esophagus, stomach, and urinary bladder are also known to be associated with non-Meckelian diverticula (Makris et al. 2009).

Meckel's diverticulum and relevant anomaly

Meckel's diverticulum is a true diverticulum that usually occurs in the distal ileum. It is the most common congenital anomaly of the gastrointestinal tract. The incidence has been reported as 0.3–4.0% of the population in autopsy studies (Soderlund 1959; DeBartolo and van Heerden 1976; Turgeon and Barnett 1990). The incidence is approximately equal in both sexes; however, males are more frequently affected than females

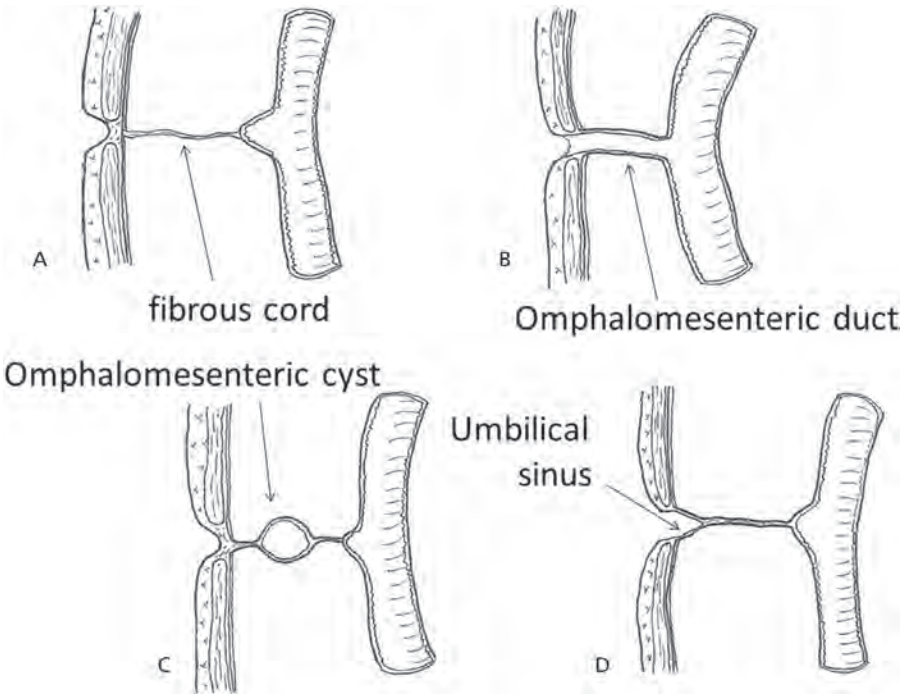

Figure 111.9 Variations of Meckel's diverticulum. (a) Meckel's diverticulum with fibrous cord; (b) patent omphalomesenteric duct (umbilicoileal fistula); (c) omphalomesenteric duct (umbilical) cyst; and (d) omphalomesenteric duct (umbilical) sinus.

Source: Adapted from Skandalakis et al. (1982). Also adapted from Debartolo and van Heerden (1976) with permission from Wolters Kluwer Health.

among symptomatic patients (DeBartolo and van Heerden 1976). This anomaly was first reported by Fabricuis Hildanus in 1598, and Johann Friedrich Meckel described its developmental origin and morphological variations in 1809 (Turgeon and Barnett 1990; Uppal et al. 2011). Embryologically, the yolk sac provides nutrition to the embryo through the yolk stalk (also called the vitelline duct or omphalomesenteric duct) in early fetal life; this role ends after the placenta develops. The yolk sac and yolk stalk normally disappear by the seventh to eighth week of gestation. During this decline, the remnant tissue of the yolk stalk may remain between the umbilicus and intestine to various degrees, potentially forming Meckel's diverticulum, a patent omphalomesenteric duct (umbilicoileal fistula), an omphalomesenteric duct (umbilical) sinus, an omphalomesenteric duct (umbilical) cyst, an umbilical mucosal polyp, or a fibrous cord connecting the ileum to the umbilicus (Fig. 111.9). Among these omphalomesenteric duct anomalies Meckel's diverticulum is the most common, occurring in 2–3% of all infants.

Omphaloileal fistula

An omphaloileal fistula develops between the umbilicus and ileum when the yolk stalk remains without withdrawing (Fig. 111.10). It is an extremely rare condition with a reported incidence of 0.0063–0.0670% of all anomalies of the omphalomesenteric duct (Rao et al. 1979). The fistula is usually open to the ileum; however, cases involving the appendix (Crymble 1922; Singleton and King 1951; Eckstein 1963; Sandborn and Schafer 1967; Kadzombe and Currie 1988; Crankson et al. 1998) or colon have also been reported (Crankson et al. 1998). Gastric mucosa has been observed in 33% of complete fistulas (Soderlund 1959; Gray and Skandalakis 1972).

The ileum may prolapse to the outside of the body through the fistula to various degrees. The ileum prolapsed in 20% of fistulas in Kittle's study (Kittle et al. 1947; Gray and Skandalakis 1972). Complete prolapse of the intestine may occur in cases involving a fistula of shorter length (Kling 1968).

Omphalomesenteric duct cyst

Cysts are rarely observed in the umbilical cord (Fig. 111.11). These umbilical cord cysts have been classified into three types: true cyst, amnion inclusion cyst, and pseudocyst. The pseudocyst, which is not lined by epithelium, is the most common type; the true cyst is rare (Ratan et al. 2007). Omphalomesenteric cysts are true cysts, and the wall includes all layers of the bowel wall. The mucosa is usually gastric or ileac, but colonic mucosa and pancreatic tissue have also been observed (Heifetz and Rueda-Pedraza 1983). The cyst results from the failure of yolk stalk withdrawal and occurs in the intermediate portion of the omphalomesenteric duct. The inner cavity of the cyst communicates with neither the inner lumen of the small intestine nor the outside of the body. The cyst most commonly presents as an abdominal mass (Kutin et al. 1979). When it is located within the abdominal cavity, it may cause intestinal obstruction due to bowel compression. When it is located close to the bowel, it is similar to a duplication cyst.

Umbilical sinus and umbilical polyp

Umbilical sinuses and polyps are remnants of the omphalomesenteric duct on the umbilical side, opposite to Meckel's

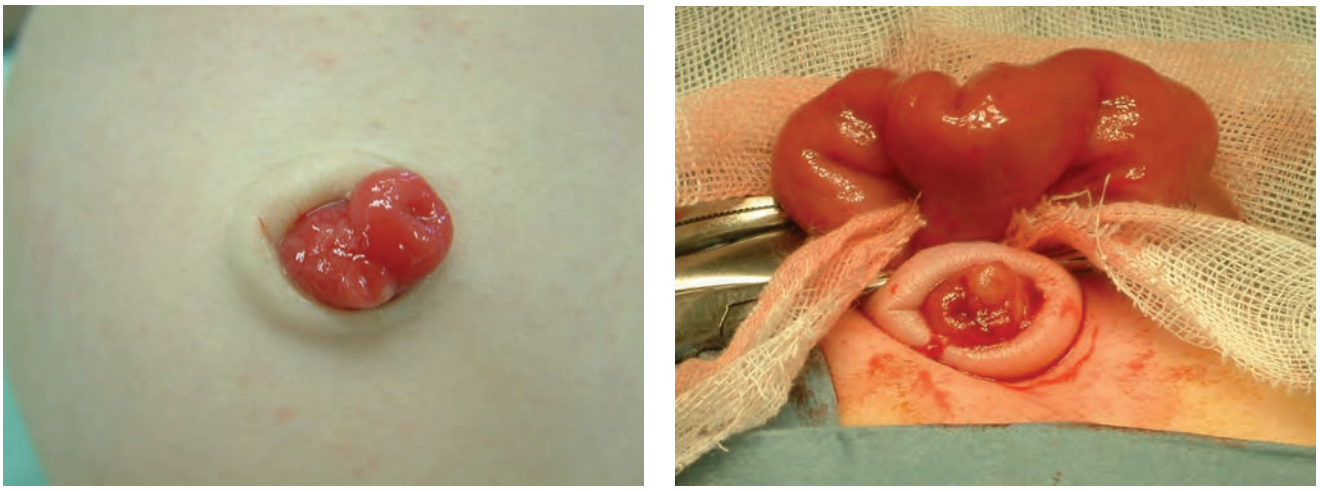

A B

Figure 111.10 A case of omphalo ileal fistula: (a) a part of ileum prolapsed from the umbilicum; and (b) operation findings (small gauze passed under the fistula).

Source: Dr Kimio Asagiri, Department of Pediatric Surgery, Kurume University School of Medicine.

diverticulum, which is a remnant on the ileal side. An umbilical sinus develops when the remnant sinks inward to the ileum, while an umbilical polyp develops when the remnant protrudes outward. The depth of the sinus varies and continues to the fibrous cord connected to the ileum. Histologically, the mucosa may be either ileac or gastric. However, colonic mucosa and pancreatic tissue (Kondoh et al. 1994; Pacilli et al. 2007) have also been reported (Heifetz and Rueda-Pedraza 1983). These sinuses are usually found in the neonatal period; however, they have also been found in older children (Luna et al. 1987; Magee and Hebert 1990; Pacilli et al. 2007) and adults (Kondoh et al. 1994; Pacilli et al. 2007).

Meckel's diverticulum

Meckel's diverticulum comprises all layers of the intestinal wall (mucosa, submucosa, muscle, and serosa) and is classified as a true diverticulum. It typically arises along the antimesenteric border of the small intestine and receives its own blood supply

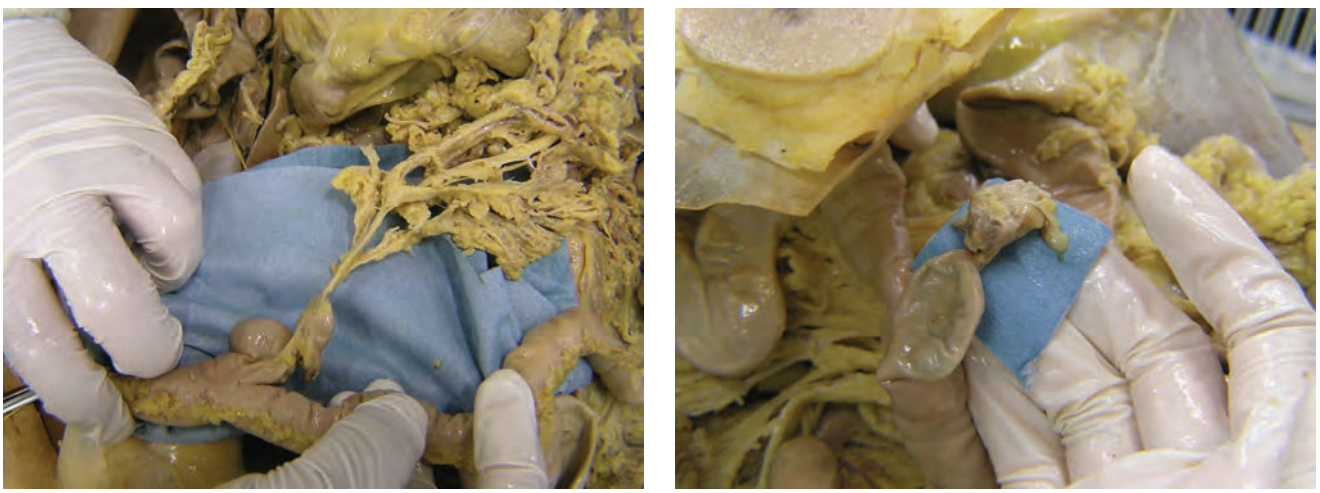

A B

Figure 111.11 A case of omphalomesenteric duct cyst found in a anatomical dissection course. (a) Meckel's diverticulum and the cyst were supplied by the vitelline artery originating from the superior mesenteric artery. (b) Cyst located near Meckel's diverticulum.

Source: Dr Tsuyoshi Saga, Department of Anatomy, Kurume University School of Medicine.

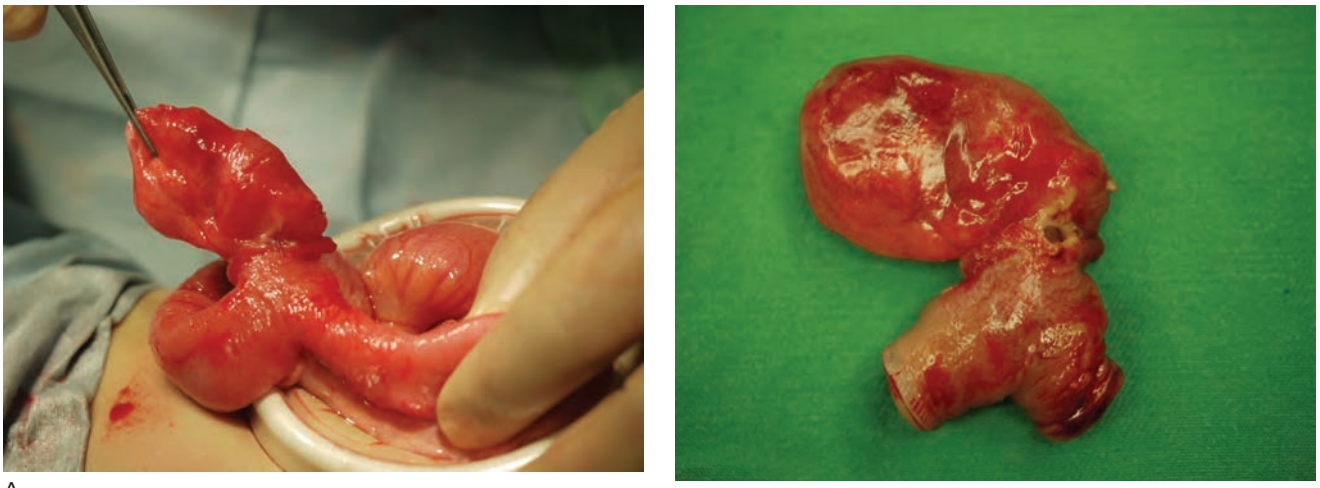

A B

Figure 111.12 A case of Meckel's diverticulum: (a) Meckel's diverticulum held by forceps; and (b) removed specimen of Meckel's diverticulum.

Source: Dr Kimio Asagiri, Department of Pediatric Surgery, Kurume University School of Medicine.

from the vitelline arteries, which continue from the superior mesenteric artery embryologically (Fig. 111.12) (Gray and Skandalakis 1972). It is attached to the umbilicus or another part of the body wall by a fibrous band in approximately 25% of cases (Fig. 111.13).

Atypical cases of Meckel's diverticulum have been described in which the diverticulum was located on the mesenteric border, but contained other features characteristic of Meckel's diverticulum (Segal et al. 2004; Sarioglu-Buke et al. 2008; Uppal et al. 2011).

Figure 111.13 A case of the intestinal ischemia due to fibrous band.

Source: Dr Kimio Asagiri, Department of Pediatric Surgery, Kurume University School of Medicine.

DeBartolo and van Heerden (1976) reported that the size of Meckel's diverticulum varies over the range 1–56 cm in length and 1–50 cm in diameter. A diverticulum of >60 cm in length was recently reported (Yochum et al. 2013). However, Meckel's diverticulum is generally 3–6 cm long and 2 cm in diameter (Gray and Skandalakis 1972). Gray and Skandalakis (1972) commented that very long ileal diverticula are not Meckel's diverticula, but giant diverticula (dorsal enteric remnant) that result from failure of the endoderm of the gut to separate from the overlying neural tube. With respect to other unusual cases, double Meckel's diverticula have also been reported (Tauro et al. 2009; Emre et al. 2013).

Meckel's diverticulum is usually located within 100 cm of the ileocecal valve. Mackey and Dineen (1983) reported a mean distance of 34 cm from the ileocecal valve to the diverticulum; this distance was 34 cm in children under 2 years of age, 46 cm in those 3–21 years of age, and 67 cm in adults over 21 years of age (Turgeon and Barnett 1990). The distance appears to become longer with age. Diverticula located in the proximal jejunum, appendix, colon, and rectum have also been reported (DeBartolo and van Heerden 1976; Uppal et al. 2011). Floating or wandering diverticula were reported in two patients (Hoelzel et al. 2007; Wu and Kao 2010). However, apparent floating diverticula are scintigraphic findings caused by positional changes associated with urination or a long and mobile mesentery; such findings do not indicate that the position of the diverticulum is actually moving in the intestine.

Heterotopic tissues are sometimes observed within the diverticulum. Gastric mucosa and pancreatic mucosa are the representative tissues. The frequency of gastric mucosa in diverticula is much higher than that of pancreatic tissue. DeBartolo and van Heerden (1976) found ratios of aberrant tissue to normal

mucosa of 1:10 to 2:3 for gastric mucosa and 1:170 to 1:10 for pancreatic mucosa. These aberrant tissues are usually situated in the diverticular apex (Curd 1936; Elliott and Evans 1953). Other aberrant mucosae in Meckel's diverticula have also been reported, including duodenal, jejunal, colonic, bile duct, and endometrial mucosae (Gray and Skandalakis 1972; DeBartoro and van Heerden 1976; Uppal et al. 2011). Tumors have also occasionally been found in Meckel's diverticula. Carcinoid tumors (Nies et al. 1992; Anderson 2000) occur most frequently. Sarcomas (Moses 1947; Yamaguchi et al. 1978), adenocarcinomas (Yamaguchi et al. 1978; Kusumoto et al. 1992), leiomyomas, lipomas, fibromas, neurofibromas, and angiomas have also been reported (DeBartolo and van Heerden 1976; Turgeon et al. 1990; Uppal et al. 2011).

Vermiform appendix

Collins (1932) examined 4680 of his own cases and reviewed 25 previous reports from 1861 to 1929 concerning the size of the vermiform appendix. The average length of the vermiform appendix ranged over 6–10 cm, and the average diameter 0.3–1.0 cm (Collins 1932). The appendix of males was longer than that of females by an average of approximately 1 cm. Another study showed that the appendix of children is longer than that of adults (Bakheit and Warille 1999). With respect to racial differences, Dock (1892) stated that the average length of the vermiform appendix in Africans is greater than that in Caucasians (Collins 1932). Some cases of nearly 30-cm-long appendices have been reported (Kelly and Hurdon 1905; Lake 1920; Royster 1927). The longest reported appendix was 33 cm (Kelly and Hurdon 1905). In contrast, shorter appendices of <1 cm also have been reported; 0.3 cm (Collins 1932) appears to be the shortest reported appendix.

Position of the vermiform appendix

The position of the vermiform appendix is usually classified as retrocecal, pelvic, paracecal, preileal, or postileal, and the proportion of each position differs among various reports (Fig. 111.14). Ahmed et al. (2007) reviewed previous reports and found that the retrocecal and pelvic positions were the most frequently reported among the five abovementioned positions. Wakeley (1933) examined the highest number of cases (n=10,000) and found that 65.3% of vermiform appendices were in the retrocecal position. The author claimed that: the cecum undergoes helicoidal torsion during its development; both the appendicocecal junction and appendix are displaced upward, backward, and to the left; and the appendix is ultimately positioned behind the cecum. In contrast, in the second largest study (4680 cases) reported by Collins (1932), 78.5% of appendices were in the pelvic position. Based on this deviation, Ahmed et al. (2007) suggested that the pelvic appendix has a high incidence in infants and neonates and that the incidence of the retrocecal appendix is high in adults. This theory remains controversial, but Ahmed et al. (2007) presumed that lateral growth of the cecum in the postpartum period is responsible for this difference in position with age. In an extremely rare case, an appendix located in the cecal wall without the presence of its proper peritoneum was reported (Abramson 1983).

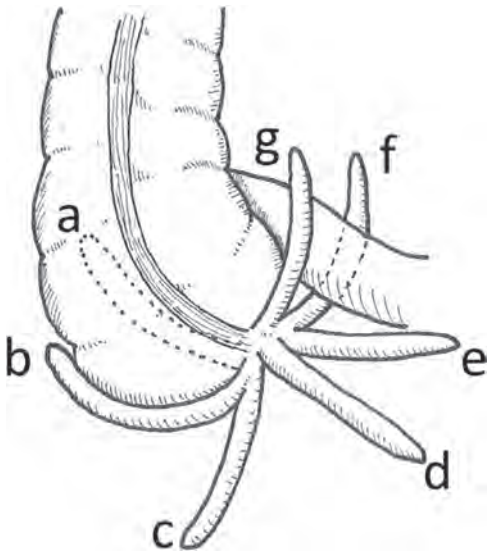

Figure 111.14 Position of the vermiform appendix. a, retrocecal position; b, paracecal position; c, subcecal position; d, pelvic position; e, subileal position; f, postileal; g, preileal position.

The vermiform appendix usually possesses its proper mesentery, the mesoappendix. The mesoappendix is usually triangular in shape and extends to the tip of the appendix. It is derived from the posterior layer of the mesentery of the ileum. The appendicular artery, which is a branch of the ileocecal artery, supplies the appendix. However, some variations in the extent of the mesoappendix have also been reported. Treves (1885) showed that the mesoappendix may reach the tip of the appendix in the fetus, but it often reaches one-half to two-thirds of the length of the appendix in adults. A relationship between the degree of extension of the mesoappendix and the position of the appendix has also been reported. A two-thirds extension of the mesoappendix is more common in appendices located in the pelvic cavity, and a one-half extension is more common in appendices located in the retrocecal position (Bakheit and Warille 1999; Bergmann 2000; Rahman et al. 2009). In contrast to the descriptions in standard anatomical textbooks, some reports have claimed that extension of the mesoappendix to the tip of the appendix is not the most common variation. In Khalil's series (2009), a two-thirds extension was the most common variation and occurred in 45% of cases (45/100). Banerjee et al. (2012) reported that the mesoappendix extended to the tip in only 4 of 25 cases and that the mesoappendix did not reach the tip in the remaining 21 cases. Complete absence of the mesoappendix has also been described. Lockwood and Rolleston (1891) stated that the mesoappendix is occasionally absent. A

case involving the absence of the mesoappendix throughout the length of the appendix was recently reported (Kaleemuddin et al. 2014).

Appendicular diverticulum

Two types of diverticula of the vermiform appendix have been reported: congenital and acquired. Congenital diverticula are rare, and Majeski (2003) found that approximately 50 cases had been reported up to 2003. This type of diverticulum is categorized as a true diverticulum and contains all layers of the intestinal wall, including a well-developed tunica muscularis. Acquired diverticula are more common than congenital. Acquired diverticula are actually pseudodiverticula that result from outward prolapse of the mucosa through a smooth muscle defect. They are located on the mesenteric border of the appendix and usually in the distal one-third of the appendix. In contrast to a true diverticulum, the tunica muscularis is absent. These diverticula are usually small and single, reportedly ranging over 3–5 mm in diameter. They are more common in males. Diverticula of the vermiform appendix cause diverticulitis, the symptoms of which are similar to those of appendicitis.

Duplication of the vermiform appendix

The incidence of duplication of the alimentary tract has been reported as 1 in 5000 live births. Duplication of the vermiform appendix is even rarer, with a reported incidence of about 1 in 12,500 individuals (Collins 1955). The most generally accepted classification was reported by Cave (1936) and Wallbridge (1962) and divides duplication of the appendix into three types. Type A is described as incomplete duplication in which both appendices have a common base. Duplication may vary from nearly complete (double-barreled appendix) to involving a distal bifurcation. Type A duplication is not associated with other congenital anomalies. Type B is described as complete duplication with a single cecum. It is further divided into two subtypes: B1 and B2. Subtype B1 is the "avian" type in which both appendices are located symmetrically on either side of the ileocecal valve. This avian type is normally found in birds and is associated with intestinal and genitourinary tract anomalies. Subtype B2 is the "teniae-colic" type. The first appendix arises from the normal position where the three teniae coli connect, and the second appendix arises from another location in the colon along the teniae coli. Type B duplication is not associated with other anomalies. In type C, which is characterized by complete duplication of the cecum, each cecum has its own appendix. This type is known to be associated with other anomalies such as those involving the ileum, colon, anus, genitourinary tract, and lower vertebral column. Type B duplication is the most common of these three types, accounting for about 60% of all cases (Wallbridge 1962). Some aspects of this classification were recently modified. The horseshoe appendix, which was identified by Mesko et al. (1989), is characterized by one appendix with two openings into a common cecum and was added as type D (Fig. 111.15).

However, atypical cases difficult to apply to this classification system have also been reported. Kim and McClenathan (2001) reported a case of a duplicated appendix in which the first appendix arose from the normal position and the second appendix arose from the midpoint of the first appendix and ended as a muscular structure about 5 cm in diameter. Triple appendices have also been reported (Tinckler 1968; Uriev et al. 2006). In Tinckler's case the triple appendix was associated with external deformities, namely a complete ectopia vesicae with a double penis and complete failure of fusion of the symphysis pubis, resulting in marked outward rotation of each half of the pelvis. The case of Uriev et al. (2006) involved one appendix that had a normal appearance but contained three tiny mucosa-lined lumens.

Agenesis of the vermiform appendix

Congenital absence of the vermiform appendix is extremely rare and was first described by Morgani in 1718 (Zetina-Mejia et al. 2008). Collins found an incidence of agenesis of the vermiform appendix of 1 in 104,066 cases among laparotomies for suspected appendicitis (Chèvre et al. 2000). Collins (1951) found that 60 cases of agenesis of the vermiform appendix had been reported up to 1951. Agenesis of the appendix seems to be associated with cecum agenesis. Collins (1951) proposed a classification system for agenesis of the cecum and appendix (Zetina-Mejia et al. 2008). This classification system contains five types: type I, complete absence of the appendix and cecum; type II, the presence of a rudimentary cecum and absence of the appendix; type III, the presence of a normal blind cecum without an appendix; type IV, the presence of a plain, blind rudimentary appendix; and type V, the presence of a blind giant cecum without an appendix. The most common type is type III (Collins 1951). The exact cause of this anomaly remains unknown. However, it has been reported that jejunal atresia or short gut syndrome may be associated with agenesis of the appendix (Woywodt et al. 1998). Thalidomide has also been reported to affect the development of the fetal appendix and result in agenesis (Shand and Bremner 1977).

Atresia of the vermiform appendix

Atresia of the vermiform appendix is an extremely rare anomaly. De la Fuente (1985) described the first 25 cases of previously undescribed complete and incomplete septae of the appendix, which corresponded to type 1 atresia of the small intestine. Both complete and incomplete septae were observed among these cases, and the number of septae varied from one to four or five per appendix. As in other types of atresia, only one case each of type 2 and type 3 has been reported as far as is known (Woywodt et al. 1998; Yaylak et al. 2013). The case corresponding to type 2 atresia was reported by Woywodt et al. (1998). A 4-day-old boy developed vomiting and failure to pass meconium. Multiple atresias of the proximal jejunum, jejunal diverticulum, and type 2 atresia of the appendix were found at surgery. The appendix was swollen and 16 mm in length with a fibrous atretic

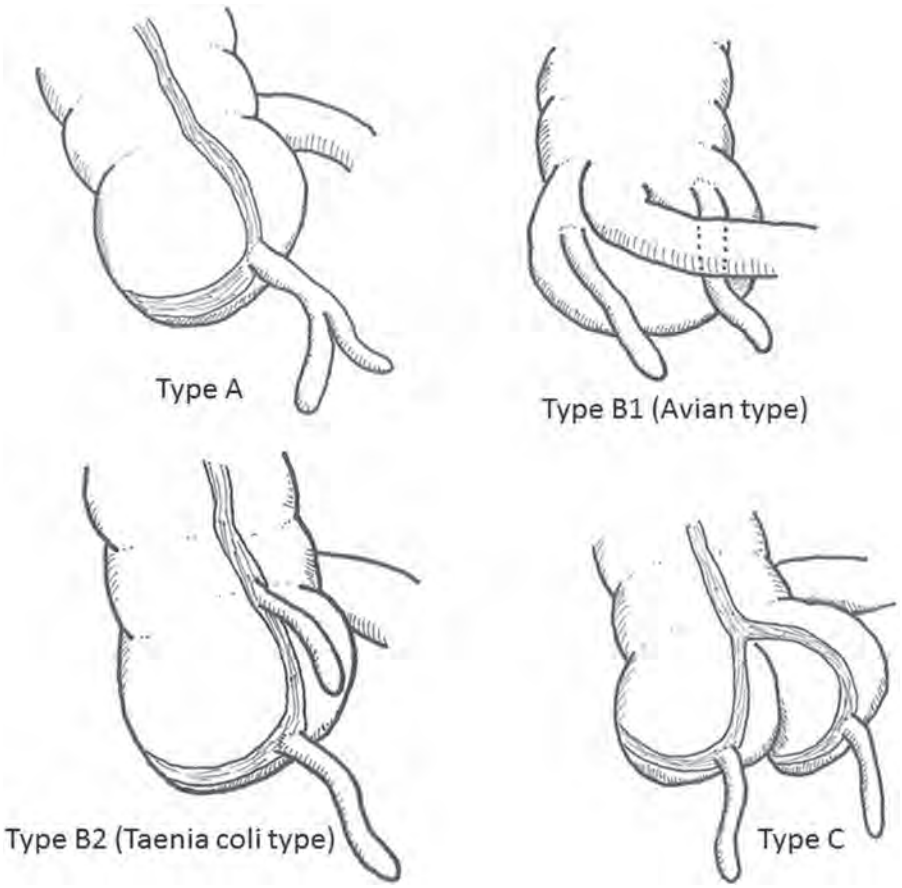

Figure 111.15 Classification of duplication of the vermiform appendix. Type A: incomplete duplication in which both appendices have a common base. Type B1 ("avian" type or "bird-like" type): both appendices are located symmetrically on either side of the ileocecal valve. Type B2 (teniae-colic type): the first appendix arises from the normal position and the second appendix arises from another location in the colon along the teniae coli. Type C: complete duplication of the cecum and each cecum has its own appendix.

portion close to its origin (Woywodt et al. 1998). The case corresponding to type 3 atresia was reported by Yaylak et al. (2013). This case involved a 59-year-old man with acute abdomen, and atresia of the appendix was confirmed at surgery. The mass was located approximately 10 cm proximal to the ileocecal valve and had a free tip without connection to the cecum. It was supplied by the ileocecal artery (Yaylak et al. 2013).

Umbilical appendix

Nearly 10 cases of umbilical appendix have been reported (Crymble 1922; Singleton and King 1951; Eckstein 1963; Sandburn and Schafer 1967; Biagtan et al. 1980; Kadzombe and Currie 1988; Borgna-Pignatti et al. 1995; Zaidenstein et al. 1995; Crankson et al. 1998; Fuijkschot et al. 2006; Salah et al. 2009). This condition is usually found in association with an incurable granulation or discharge in the umbilicus, as are omphalomesenteric fistulas and umbilical sinuses, and is associated with the remnant of the vitelline duct. There are two possible theories of formation of an umbilical appendix. One is that the omphalomesenteric duct develops in the appendix. The omphalomesenteric duct is usually located in the distal ileum; however, cases in the colon (Crankson et al. 1998) and appendix have also been reported. The other theory is failure of the appendix to re-enter the peritoneal cavity. When the midgut re-enters the peritoneal cavity from the extraembryonic coelom, the appendix fails to re-enter the peritoneal cavity, as does the omphalocele. The herniation of the appendix remains in the umbilical cord after birth, and the fistula develops secondary to clamping of the umbilical cord.

Ileocecal valve

The ileocecal valve comprises two segments: the labium superius and labium inferius. These two segments coalesce and continue as a narrow membranous ridge termed the frenula (Clemente and Gray 1985). Although these labia vary in size, the labium superius is usually larger than the labium inferius. Buirge (1943) reported that the mean height of the labium superius was 1.5 cm with a range of 0.4–2.5 cm (Salem and McGee 1959). Rosenberg and DiDio (1970) stated that the valve projected 2–3 cm into the inner lumen of the colon. Hinkel (1952) stated that a normal valve may be up to 4 cm in diameter. In one endoscopic study, the mean height of the valve was 1.7 cm (range 0.7–3.7 cm) and the mean width was 2.8 cm (range 1.1–6.0 cm) (El-Amin et al. 2003). Variations of the frenulum have also been reported.

According to Salem and McGee (1959), the medial frenulum (anterior side) was absent in 22% of cases, the lateral frenulum (posterior side) was absent in 2%, and both were absent in 2%. Rosenberg and DiDio (1970) reported that the appearance of the terminal ileum changes rapidly after death. In a cadaver study, 60% of cases demonstrated the bilabial configuration that is usually described in anatomical textbooks, while 40% demonstrated a papillary appearance in which the terminal ileum projected into the colon as a nipple. This papillary appearance is infrequent in cadavers but is the most frequent type in living humans. With the recent development of imaging diagnostic techniques, the diagnosis of an ileocecal valve has been achieved by endoscopy or computed tomography (CT) (two- or three-dimensional). In an endoscopic study by El-Amin et al. (2003), the valve had a smooth contour in 85% of cases and a lobulated contour in 15%; additionally, the two lips were symmetrical in 88% of cases and asymmetrical in 12%. The morphological appearance of the ileocecal valve is clinically classified as: labial, which has a slit-like opening; papillary, which has a dome-shaped opening; or lipomatous, which has a substantial deposit of fat within the lips. Regge et al. (2004) examined the appearance of the ileocecal valve on CT colonography and reported that the most frequently observed type was labial (76%), followed by papillary (21%) and lipomatous (3%).

The terminal ileum generally opens into the medial aspect of the large intestine. In a recent study, El-Amin et al. (2003) depicted the location of the ileocecal valve in a double-contrast X-ray study as the medial aspect in 74% of cases, the lateral aspect in 14%, and the posterior aspect in 3%. However, 79% of the lateral cases involved a mobile cecum. In contrast, most of the medial cases (96%) and all of the posterior cases involved a fixed cecum.

The ileocecal valve is reportedly located at the level of the first haustrum of the colon in 33% of cases, the second haustrum in 66%, and as distal as the third haustrum in 2% (Rubesin and Furth 2000; El-Amin et al. 2003; O'Connor et al. 2006; Jelbert et al. 2008).

Hunter (1934) described two positional relationships between the terminal ileum and the cecum (Fig. 111.16). In one, the terminal ileum was directed at nearly a right angle to the medial wall of the cecum and formed a "horse-neck" shape. In the other, the ileum passed from the pelvis obliquely upward and to the right, and the terminal ileum was flattened against the cecum. In an X-ray study, Fleishner and Bernstein (1950) also described the relationship between the terminal ileum and colon. The reverse S-shaped ascending terminal ileal loop was the most common, accounting for about 95% of cases. The ileum approached the colon in the horizontal plane in a few cases. Rarely, the ileum approached the colon from above.

Cecum

Banerjee et al. (2012) reviewed the size of the cecum in various anatomy textbooks and found mean lengths of 56 mm (Treves 1885), 60 mm (Morris 1942; Woodburne 1961; Standring 1995; Romanes 2000), and 62.5 mm (Jones and Buchanan 1950). Moore (1992) reported a range of 50–70 mm. The mean overall width was 75 mm (Banerjee et al. 2012). In Banerjee's study of 25 adult cadavers, the mean length and width of the cecum was 63±9.9 mm and 68±16 mm, respectively; this width was relatively less than that reported by previous authors.

Treves (1885) proposed the most broadly accepted classification of the appearance of the cecum, which divides the appearance into four types. The first type is the conical (or infantile) type and accounts for 2% of cases. In this type, the cecum is conical in shape and the appendix rises from its apex. The three teniae start from the appendix and are the same length. The second type is the quadrate (or childhood) type and accounts for 3% of cases. The cecum becomes quadrate in appearance because a saccule grows out on either side of the anterior teniae. These saccules are of equal size, and the appendix hangs from between them instead of from the apex of a cone. The third type is the normal (or adult) type and accounts for 90% of cases. In this type, the two saccules located on both sides of the anterior teniae grow at unequal rates (the right more quickly than the left) and the appendix consequently hangs between the anterior and posterolateral teniae. Finally, the fourth type is the

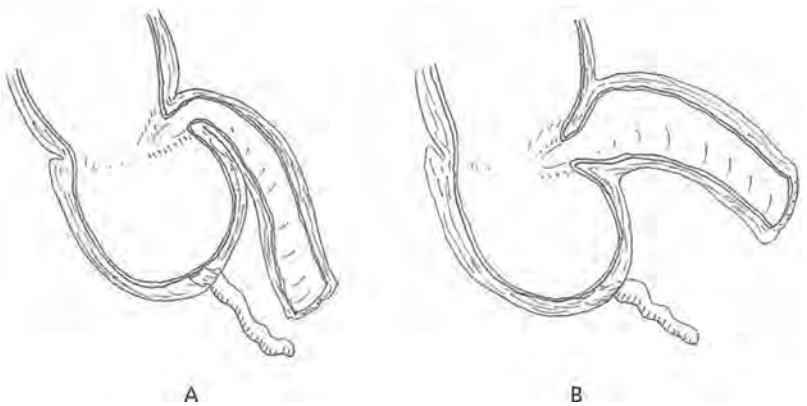

Figure 111.16 Variation of positional relationship between the terminal ileum and the cecum. (a) The terminal ileum is directed at almost a right angle to the medial wall of the cecum and forms a "horse-neck" shape. (b) The ileum passes from the pelvis obliquely upward and to the right, and the terminal ileum is flattened against the cecum.

Source: Hunter (1934).

ampullary exaggerated (or geriatric) type and accounts for 4% of cases. The right saccule is larger and the left saccule becomes atrophied, causing the apex of the cecum with the vermiform appendix to be located close to the ileocecal junction.

Pavlov and Petrov (1968) also reported a classification system for the shape of the cecum. He examined 126 patients and categorized the cecum into three types: infantile type (13%), adult type (78%), and intermediate type (9%) (Weidman 2004).

The position of the cecum changes with the body position. Anatomically, it is usually situated in the right iliac fossa. It also lies on the iliacus muscles. In the erect living body, it is located in the right iliac fossa. In a cadaveric study by Banerjee et al. (2012), the cecum was in the right iliac fossa in 96% (23/24) of cases and in a subhepatic position in 4% (1/24). In a study of living humans in the supine position, the position of the lower pole of the cecum was iliac in 12% of subjects, inguinal in 37%, and pelvic in 51% (Karim et al. 1990). Rarely, because of malrotation of the midgut, the cecum is found in an unusual position such as the left iliac fossa, umbilical region, rectouterine pouch, subhepatic region, or right lumbar region. The peritoneum is reflected at the posterior surface of the cecum. Weidman (2004) and Anson (1963) classified the morphological variations into six types and several subtypes with respect to cecal fixation: type 1, almost complete dorsal fixation; type 2, medial fixation; types 3 and 4, free of dorsal attachment; type 5, nonfixation with continuing mobility of the greater part of the ascending colon; and type 6, complete absence of dorsal attachment. In the present series 19.6% of cases were characterized by attachment of almost the entire posterior surface of the cecum to the posterior abdominal wall. In a study by Weidman (2004), 24% of cases were characterized by complete unattachment of the cecum to the posterior wall. In the series of Wolfer et al. (1942), only 5.6% of cases demonstrated complete fusion of the cecum to the posterior wall while 20.0% were characterized by peritoneal attachment above the ileocecal junction (Balthazar 1977). The incidence of a mobile cecum is assumed to be approximately 25% of the general population (Hasbahceci et al. 2012).

Colon

According to some studies, the length of the large intestine has been reported to be about 150–200 cm. A difference in this length between males and females has also been reported, and usually the large intestine is longer in males than in females. Hirsch et al. (1956) reported a large intestinal length of 91–125 cm and Bergman (2000) reported a length of about 2 m. With respect to sex-specific length, Treves (1885) reported a length of 142.2 cm (4 feet 8 inches) in males and 137.2 cm (4 feet 6 inches) in females. Underhill (1955) reported a length of 180.34 cm (5 feet 11 inches) in males and 157.48 cm (5 feet 2 inches) in females. In contrast to these major reports, Sadahiro et al. (1992) reported that the large intestine was longer in females than in males. The mean length in both sexes was 129.54±15.94 cm, in males 125.87±15.42 cm, and in females 132.83±15.69 cm. The authors considered the possibility of a race-specific cause of this result. Furthermore, the length increased with age. The physical dimensions (height and body weight) of females tended to affect the increase in length. Sadahiro et al. (1992) reported the length, diameter, and surface area of six colon segments (cecum, ascending colon, transverse colon, descending colon, sigmoid colon, and rectum) and their sex differences. The cecum, ascending colon, transverse colon, and rectum in females were longer than those in males. There were no significant differences in the descending colon or sigmoid colon between the two sexes. The diameter of the descending colon, sigmoid colon, and rectum was larger in males than in females. There were no significant differences in the cecum, ascending colon, or transverse colon between the two sexes. Finally, the surface area of the ascending colon and transverse colon was larger in females than in males, whereas that of the descending colon, sigmoid colon, and rectum was larger in males than in females. There was no significant difference in the surface area of the cecum between the two sexes. These results require verification in other races.

Mesocolon of the ascending colon

The ascending colon does not usually have a mesentery, but is fused to the posterior wall of the abdomen, and its anterior surface is covered with peritoneum. However, there are various degrees of incomplete fixation of the ascending colon. Skandalakis et al. (1983) described three types of attachment of the ascending colon to the abdominal wall: A, normal retroperitoneal location of the colon; B, paracolic gutter (deep paracolic groove but does not form mesentery); and C, mobile colon mesentery. The frequency of persistent right mesocolon was reported to range over 11–37% in the literature (Weidman 2004). Absence of the mesocolon of the ascending colon is often associated with a mobile cecum. In one study, 55 of 87 cases demonstrated a mobile cecum alone, and 5 of 87 demonstrated a mobile cecum with the ascending colon (Skandalakis et al. 1983). A membrane termed Jackson's veil, which envelopes the ascending colon, is sometimes observed. This membrane was first reported by Jackson in 1911 and is also called the prececocolic fascia. This membrane may or may not be vascularized. It is most frequently observed in the ascending colon, and it may involve the cecum or hepatic flexure (Carslaw 1928). This membrane is considered to be congenital in origin; however, its specific origin remains unknown (Weidman 2004).

Duplication of the colon

Gastrointestinal duplication is a rare anomaly and was observed in approximately 1 in 4500 cases in an autopsy study. The most frequently involved site is the ileum, with an incidence of 60%. Duplication of the colon constitutes approximately 15% of all alimentary tract duplications. The duplication is often located in the cecum (Holcomb et al. 1989; Puligandla et al. 2003; Fotiadis et al. 2005) and is associated with duplication of the vermiform appendix (i.e., type C). Both cystic and

tubular types have been observed. In the tubular type, duplication extending throughout the entire colon has also been described. Such cases of entire colon duplication are known to be frequently associated with lower urinary tract and/or genital tract duplication (Kottra and Dodds 1971). Kottra and Dodds (1971) reported on the classification of duplication of the colon according to the appearance of colon duplication and other associated duplications. He classified colon duplication as type 1 and type 2. In type 1, the duplication is limited to the alimentary tract. In type 2, the duplication is associated with duplication of the urinary or genital tract. In addition, type 2 is reportedly associated with other anomalies, such as imperforate anus, rectal fistula, situs inversus, intestinal malrotation, duplication of the terminal ileum, Meckel's diverticulum, double appendix, duplication of the lumbar spine, butterfly vertebrae, lumbar meningomyelocele, sacral agenesis, diastasis recti, pubic separation, omphalocele, and bladder extrophy (Kottra and Dodds 1971).

Diverticulum of the colon

Diverticulum of the colon is a relatively common condition. The incidence is estimated to be about 2–10% and has increased during the past few decades. The incidence reportedly increases with aging, from <10% in individuals younger than 40 years to 50–66% in those older than 80 years. No sex difference has been reported (Stollman and Roskin 2004). Wagner and Zollinger (1961) reviewed previous reports on the distribution of diverticula in the colon and found that about 80% were located in the sigmoid colon and descending colon, 4% were located in the rectum, 10% were located in the transverse colon, 4% were located in the ascending colon, and 2% were located in the cecum (Wagner and Zollinger 1961). In Hughes's (1969) series, the distribution of diverticula was reported as follows: fewer than five diverticula in the sigmoid colon, 15%; more than five diverticula in the sigmoid colon, 26%; left colon, 39%; total colon, 16%; cecum only, 5%; and irregular type, 4%. Differences in the distribution among races have been recognized; the left colon is predominant in European races, while the right colon is predominant in Asians (Stollman and Raskin 2004). The diverticula occur in parallel rows between the teniae coli at the site of penetration of the vasa recta. The number of diverticula varies from single to multiple, and they are typically 5–10 mm in diameter (Stollman and Raskin 2004); however, cases of giant diverticula have also been reported (Melamed and Pantone 1960; Gallagher and Welch 1979; Kricun et al. 1980). Pathologically, the majority of diverticula of the colon are false diverticula; they occur in the weak part of the intestinal wall, as do diverticula of the small intestine. However, true diverticula also rarely occur in the colon, especially in the ascending colon and cecum (Gray and Skandalakis 1972).

Atresia of the colon

Atresia of the colon is an extremely rare anomaly, accounting for 1.8–15.0% of all gastrointestinal atresias (Vecchia et al. 1998; Ruggeri et al. 2008). The incidence has been estimated to be about 1 in 1948 births and about 1 in 66,000 births (Etensel et al. 2005). Etensel et al. (2005) reviewed the previously reported literature and found that the location of atresia of the colon was identified in 208 cases: 122 atresias were present in the right colon, and 48 were present in the left colon. In contrast, Karnak et al. (2001) reported that atresia of the colon occurs more frequently in distal than proximal locations and the frequency occurred in the order of sigmoid colon, descending colon, and ascending colon (Karnak et al. 2001). Etensel et al. (2005) reported that type 3 atresia was the most frequent (113 of 187 cases, 60.4%), followed by type 2 (28 cases), type 1 (27 cases), and type 4 (19 cases). In other reports, type 3 atresia was also the most frequently reported type (Chadha et al. 2006; Oldham et al. 2006). Additionally, the right side was the predominantly reported side among cases of type 3 atresia; however, the left side was more frequently reported in cases of type 1 and 2 atresia. In most cases of type 4 atresia, the atresia involved the entire colon (Etensel et al. 2005).

The incidence of associated anomalies is much lower than that of other gastrointestinal atresias. Two-thirds of colonic atresias are reportedly isolated anomalies. Deficient mesenteric fixation, other atresias, and abdominal wall defects have often been associated with colonic atresia. Rarely, cases associated with Hirschsprung's disease (Hyde and De Lorimier 1968; Haffner and Schistad 1969; Williams and Burrington 1993; Kim et al. 1995) or gastroschisis (Synder et al. 2001; Komuro et al. 2003) have also been reported.

References

Abramson DJ. 1983. Vermiform appendix located within the cecal wall. *Dis Colon Rectum* 26(6): 386–389.

Ackermann W. 1943. Diverticula and variations of the duodenum. *Ann Surg* 117: 403.

Afridi SA, Fichtenbaum CJ, Taubin H. 1991. Review of duodenal diverticula. *Am J Gastroenterol* 86: 935.

Ahmed I, Asgeirsson KS, Beckingham IJ, Lobo DN. 2007. The position of the vermiform appendix at laparoscopy. *Surg Radiol Anat* 29(2): 165–168.

Akin JT, Gray SW, Skandalakis JE. 1976. Vascular compression of the duodenum: presentation of ten cases and review of the literature. *Surgery* 79(5): 515–522.

Aldridge RT. 1961. Intestinal malrotation in the adult. *NZ Med J* 60: 420.

Altemeier WA, Bryant LR, Wulsin JH. 1963. The surgical significance of jejunal diverticulosis. *Arch Surg* 86(5): 732–745.

Amir-Jahed AK. 1968. Classification of reversed intestinal rotation. *Surgery* 64(6): 1071.

Anderson DJ. 2000. Carcinoid tumor in Meckel's diverticulum: laparoscopic treatment and review of the literature. *JAOA* 100(7): 432–434.

Anson BJ. 1963. *An Atlas of Human Anatomy*, second edition. Philadelphia and London, W.B. Saunders Company.

Argeme M, Mambrini A, Lebreuil G, Guérinel G. 1970. Dissection of the muscle of Treitz. *Comptes Rendus Assoc Anat* 147: 76.

Bakheit MA, Warille AA. 1999. Anomalies of the vermiform appendix and prevalence of acute appendicitis in Khartoum. *East African Med J* 76(6): 338–340.

Balén EM, Hernández-Lizoáin J, Pardo F, Longo JM, Cienfuegos JA, Alzina V. 1993. Giant jejunoileal duplication: prenatal diagnosis and complete excision without intestinal resection. *J Pediatr Surg* 28(12): 1586–1588.

Balthazar EJ. 1977. Congenital positional anomalies of the colon: Radiographic diagnosis and clinical implications. *Gastrointest Radiol* 2(1): 49–56.

Banerjee A, Kumar IA, Tapadar A, Pranay M. 2012. Morphological variations in the anatomy of caecum and appendix: a cadaveric study. *Nat J Clin Anat* 1(1): 30–35.

Baskin RH Jr, Mayo CW. 1952. Jejunal diverticulosis; a clinical study of 87 cases. Surg Clin North Am Aug: 1185–1196.

Benson CD, Lloyd JR, Smith JD. 1960. Resection and primary anastomosis in the management of stenosis and atresia of the jejunum and ileum. *Pediatrics* 26(2): 265–272.

Benson RE, Dixon CF, Waugh JM. 1943. Nonmeckelian diverticula of the jejunum and ileum. *Annals Surg* 118(3): 377.

Berdon WE, Baker DH, Bull S, Santulli TV. 1970. Midgut malrotation and volvulus: which films are most helpful? *Radiology* 96(2): 375–383.

Bergman J. 2000. Do any vestigial structures exist in humans. *Creation Ex Nihilo Tech J*, 14: 95–98.

Biagtan J, Rosenfeld W, Salazar D, Velcek F. 1980. Herniation of the appendix through the umbilical ring following umbilical artery catheterization. *J Pediatr Surg* 15(5): 672–673.

Bill AH. 1979. Malrotation of the intestine. *Pediatric Surg* 2: 912–923.

Borgna-Pignatti C, Andreis IAB, Bettili G, Zamboni G. 1995. Delayed separation of an appendix-containing umbilical stump. *J Pediatr Surg* 30(12): 1717–1718.

Bower RJ, Sieber WK, Kiesewetter WB. 1978. Alimentary tract duplications in children. *Annals Surg* 188(5): 669.

Boyden EA, Cope JG, Bill AH Jr. 1967. Anatomy and embryology of congenital intrinsic obstruction of the duodenum. *Am J Surg* 114: 190–202.

Buirge RE. 1943. Gross variations in the ileocecal valve a study of the factors underlying incompetency. *Anat Rec* 86(3): 373–385.

Carslaw RB. 1928. Right-sided visceroptosis: An estimate of the importance of abnormal mobility and prolapse of the ascending colon and cæcum in the causation of various abdominal conditions, based on observations in a series of 242 cases treated by right colopexy. *Brit J Surg* 15(60): 545–604.

Cave AJE. 1936. Appendix vermiformis duplex. *J Anat* 70(Pt 2): 283.

Chadha R, Sharma A, Roychoudhury S, Bagga D. 2006. Treatment strategies in the management of jejunoileal and colonic atresia. *J Indian Assoc Pediatr Surg* 11(2): 79–84.

Chèvre F, Gillet M, Vuilleumier H. 2000. Agenesis of the vermiform appendix. *Surg Laparosc Endosc Percutan Tech* 10(2): 110–112.

Chew MH, Sophian Hadi I, Chan G, Ong HS, Wong WK. 2006. A problem encapsulated: the rare peritoneal encapsulation syndrome. *Singapore Med J* 47(9): 808–810.

Chiu EJ, Shyr YM, Wu CW, Lui WY. 2000. Diverticular disease of the small bowel. *Hepato-Gastroenterol* 47(31): 181–184.

Chow DC, Babaian M, Taubin HL. 1997. Jejunoileal diverticula. *Gastroenterolog* 5(1): 78–84.

Chu SM, Luo CC, Chou YH, Yen JB. 2004. Congenital short bowel syndrome with malrotation. *Chang Gung Med J* 27(7): 548–550.

Clemente CD, Gray H. (eds). 1985. *Gray's Anatomy*, 30th edition. Philadelphia: Lea and Febiger.

Collins DC. 1932. The length and position of the vermiform appendix: a study of 4,680 specimens. *Annals Surg* 96(6): 1044.

Collins DC. 1951. Agenesis of the vermiform appendix. *Am J Surg* 82(6): 689–696.

Collins DC. 1955. A study of 50,000 specimens of the human vermiform appendix. *Surg Gynecol Obstetr* 101(4): 437.

Cornes JS. 1965. Number, size, and distribution of Peyer's patches in the human small intestine: Part I The development of Peyer's patches. *Gut* 6(3): 225–229.

Costacurta L. 1972. Anatomical and functional aspects of the human suspensory muscle of the duodenum. *Cells Tissues Organs* 82(1): 34–46.

Costantinides F, Di Nunno N, Bernasconi P, Jonjic N, Melato M. 1998. A new type of peritoneal encapsulation of the small bowel. *Am J Surg Pathol* 22(10): 1297–1298.

Crankson SJ, Ahmed GS, Palkar V. 1998. Patent omphalomesenteric duct of the vermiform appendix in a neonate: congenital appendicoumbilical fistula. *Pediatr Surg Int* 14(3): 229–230.

Crymble P. 1910. The muscle of Treitz and the plica duodeno-jejunalis. *Br Med J* 2(2598): 1156–1159.

Crymble P. 1922. A case of persistent vitelline duct to vermiform appendix. *Br J Surg* 19: 304–305.

Curd HH. 1936. A histologic study of Meckel's diverticulum: with special reference to heterotopic tissues. *Arch Surg* 32(3): 506.

D'Alessio MJ, Rana A, Martin JA, Moser AJ. 2005. Surgical management of intraluminal duodenal diverticulum and coexisting anomalies. *J Am Coll Surg* 201: 143–148.

Davies O, Johansen R, Goldman L. 1955. Reversed rotation of the bowel causing acute intestinal obstruction. *Annals Surg* 142(5): 875.

De la Fuente AA. 1985. Septa in the appendix: a previously undescribed condition. *Histopathol* 9(12): 1329–1337.

DeBartolo HM Jr, van Heerden JA. 1976. Meckel's diverticulum. *Annals Surg* 183(1): 30.

DeLorimier AA, Fonkalsrud EW, Hays DM. 1969. Congenital atresia and stenosis of the jejunum and ileum. *Surgery* 65(5): 819.

Dock G. 1892. Notes on the appendix vermiformis: anatomical and clinical. Med Age x: 397–402.

Dott NM. 1923. Anomalies of intestinal rotation: their embryology and surgical aspects: with report of five cases. *Br J Surg* 11(42): 251–286.

Eckstein HB. 1963. Exomphalos, a review of 100 cases. *Br J Surg* 50(222): 405–410.

El-Amin LC, Levine MS, Rubesin SE, Shah JN, Kochman ML, Laufer I. 2003. Ileocecal valve: spectrum of normal findings at double–contrast barium enema examination. *Radiology* 227(1): 52–58.

Elliott GB, Evans HS. 1953. Peptic perforation of Meckel's diverticulum. *Annals Surg* 138(1): 127.

Emre A, Akbulut S, Yilmaz M, Kanlioz M, Aydin BE. 2013. Double Meckel's diverticulum presenting as acute appendicitis: a case report and literature review. *J Emerg Med* 44(4): e321–e324.

Estrada RL, Gurd FN. 1962. Surgical correction of reversed rotation of the midgut loop. *Surg Gynecol Obstetr* 114: 707.

Etensel B, Temir G, Karkiner A, Melek M, Edirne Y, Karaca İ, Mir E. 2005. Atresia of the colon. *J Pediatr Surg* 40(8): 1258–1268.

Fleischner FG, Bernstein C. 1950. Roentgen-anatomical studies of the normal ileocecal valve. *Radiology* 54(1): 43–58.

Ford EG, Senac MO Jr, Srikanth MS, Weitzman JJ. 1992. Malrotation of the intestine in children. *Annals Surg* 215(2): 172.

Fotiadis C, Genetzakis M, Papandreou I, Misiakos EP, Agapitos E, Zografos GC. 2005. Colonic duplication in adults: report of two cases presenting with rectal bleeding. *World J Gastroenterol* 11(32): 5072.

Frazer JE, Robbins RH. 1915. On the factors concerned in causing rotation of the intestine in man. *J Anat Physiol* 50(1): 75.

Fuijkschot J, Wijnen RMH, Gerrits GPJM, Dubois SV, Rieu PNMA. 2006. A neonate with an intact congenital umbilical appendix: an alternative theory on the etiology of the appendico-umbilical fistula. *Pediatr Surg Int* 22(8): 689–693.

Gallagher JJ, Welch JP. 1979. Giant diverticula of the sigmoid colon: a review of differential diagnosis and operative management. *Arch Surg* 114(9), 1079.

Gray SW, Skandalakis JE. 1972. *Embryology for Surgeons: The Embryological Basis for the Treatment of Congenital Defects*. Philadelphia: Saunders, pp. 417–422.

Grosfeld JL, Ballantine TV, Shoemaker R. 1979. Operative management of intestinal atresia and stenosis based on pathological findings. *J Pediatr Surg* 14: 368.

Gundobin N. 1892. Uber den bau des darmkanals bei kindern. *Jb Kinderheilk* 33: 439–473.

Guttierez A. 1934. Anomalia en la torsion del intestine medio. *Rev Brasil Cir* 13: 232.

Haffner JFW, Schistad G. 1969. Atresia of the colon combined with Hirschsprung's disease A case report. *J Pediatr Surg* 4(5): 560–562.

Haley JC, Peden JK. 1943. The suspensory muscle of the duodenum. *Am J Surg* 59(3): 546–550.

Haley JC, Perry JH. 1949. Further study of the suspensory muscle of the duodenum. *Am J Surg* 77(5): 590–595.

Haller JD, Morgenstern L. 1964. Anomalous rotation and fixation of the left colon: Embryogenesis and surgical management. *Am J Surg* 108(3): 331–338.

Harris PF, Jones PRM, Robertson CS. 1976. A radiological study of morphology and growth in the human fetal colon. *Br J Radiol* 49(580): 316–320.

Hasbahceci M, Basak F, Alimoglu O. 2012. Cecal volvulus. *Indian J Surg* 74(6): 476–479.

Hasosah M, Lemberg DA, Skarsgard E, Schreiber R. 2008. Congenital short bowel syndrome: a case report and review of the literature. *Canadian J Gastroenterol* 22(1): 71.

Heifetz SA, Rueda-Pedraza ME. 1983. Omphalomesenteric duct cysts of the umbilical cord. *Fetal Pediatr Pathol* 1(3): 325–335.

Heilbrun N, Boyden EA. 1964. Intraluminal duodenal diverticula. *Radiology* 82(5): 887–894.

Hellmann TJ. 1921. Studien uber das lymphoide Gewebe. IV. Zur Frage des Status lymphaticus. Untersuchungenuber die menge des lymphoiden gewebes, besonders des darmes beim menschen mittels einer quantitative bestimmungsmethode. *Z Menschel Vererb Konstit Lchre* 8: 191–219.

Hinkel CL. 1952. Roentgenological examination and evaluation of the ileocecal valve. *Am Roentgenol Rad Ther Nucl Med* 68(2): 171.

Hirsch J, Ahrens EH, Blankenhorn DH. 1956. Measurement of the human intestinal length in vivo and some causes of variation. *Gastroenterol* 31: 274–84.

Hoelzel C, Gillitzer C, Kotzerke J. 2007. The floating Meckel. *Clin Nucl Med* 32(10): 810–811.

Holcomb GW, Gheissari A, O'Neill JA Jr, Shorter NA, Bishop HC. 1989. Surgical management of alimentary tract duplications. *Ann Surg* 209(2): 167.

Hosokawa H, Nakajima Y. 1962. A peritoneal sac enclosing the small intestine. *Okajimas Folia Anat Jap* 38: 175.

Hughes LE. 1969. Postmortem survey of diverticular disease of the colon. I. Diverticulosis and diverticulitis. *Gut* 10(5): 336.

Hunter RH. 1934. The ileo-caecal junction. *J Anat* 68(Pt 2), 264.

Hyde GA Jr, De Lorimier AA. 1968. Colon atresia and Hirschsprung's disease. *Surgery* 64(5): 976–978.

Inouye WY, Farrell C, Fitts WT Jr, Tristan TA. 1965. Duodenal duplication: case report and literature review. *Ann Surg* 162: 910.

Iyer CP, Mahour GH. 1995. Duplications of the alimentary tract in infants and children. *J Pediatr Surg* 30(9): 1267–1270.

Jelbert A, Swinson S, Atkin K, Bhalerao S, Babu S. 2008. Imaging of the ileocaecal valve. *Tech Coloproctol* 12(2): 87–92.

Jit I, Grewal SS. 1977. The suspensory muscle of the duodenum and its nerve supply. *J Anat* 123(Pt 2): 397.

Jones FW, Buchanan AM. 1950. *Buchanan's Manual of Anatomy*. Bailliere: Tindall Ltd, pp. 758–790.

Kaddah SN, Bahaa-Aldin KH, Aly HF, Hassan HS. 2006. Congenital duodenal obstruction. *Ann Pediatr Surg* 2: 130–135.

Kadzombe E, Currie ABM. 1988. Neonatal fistula from the appendix to the umbilicus. *J Pediatr Surg* 23(11): 1059–1060.

Kaleemuddin M, Shaik N, Vamshi Krishna K, Satish Kumar D, Uddin Ansari A, Ahmed S. 2014. Missing mesoappendix: a rare case. *History* 4(10): 5–7.

Karim OM, Boothroyd AE, Wyllie JH. 1990. McBurney's point: fact or fiction? *Ann Roy Coll Surg Engl* 72(5): 304.

Karnak I, Ocal T, Senocak, ME, Tanyel FC, Büyükpamukçu N. 2000. Alimentary tract duplications in children: report of 26 years' experience. *Turk J Pediatr* 42(2): 118.

Karnak I, Ciftci AO, Şenocak ME, Tanyel FC, Büyükpamukçu N. 2001. Colonic atresia: surgical management and outcome. *Pediatr Surg Int* 17(8): 631–635.

Karoll MP, Ghahremani GG, Port RB, Rosenberg JL. 1983. Diagnosis and management of intraluminal duodenal diverticulum. *Dig Dis Sci* 28: 411–416.

Katz ME, Siegel MJ, Shackelford GD, McAlister WH. 1987. The position and mobility of the duodenum in children. *Am J Roentgenol* 148(5): 947–951.

Kawashima K, Ishihara S, Amano K, Hirakawa K, Adachi K, Fukuda R, Kinoshita Y. 2001. Nonrotation of the midgut with appendiceal mucocele in an adult. *J Gastroenterol* 36(1): 44–47.

Kelly HA, Hurdon E. 1905. *The Vermiform Appendix and its Diseases*. Philadelphia, London: WB Saunders.

Kern IB, Leece A, Bohane T. 1990. Congenital short gut, malrotation, and dysmotility of the small bowel. *J Pediatr Gastroenterol Nutr* 11(3): 411–415.

Khan MA, Ahmed S, Ali SR, Bawany F. 2012. Giant ileal duplication with extensive gastric heterotopia. *JCPSP* 22(10): 679–680.

Kim CW, Superina RA, Ein S. 1995. Colonic atresia combined with Hirschsprung's disease: a diagnostic and therapeutic challenge. *J Pediatr Surg* 30(8): 1216–1217.

Kim EP, McClenathan JH. 2001. Unusual duplication of appendix and cecum: extension of the Cave-Wallbridge classification. *J Pediatr Surg* 36(9): e18.

Kim SK, Cho CD, Wojtowycz AR. 2008. The ligament of Treitz (the suspensory ligament of the Duodenum): anatomic and radiographic correlation. *Abdom Imag* 33(4): 395–397.

Kittle CF, Jenkins HP, Dragstedt LR. 1947. Patent omphalomesenteric duct and its relation to the diverticulum of Meckel. *Arch Surg* 54(1): 10–36.

Kling S. 1968. Patent omphalomesenteric duct: a surgical emergency. *Arch Surg* 96(4): 545.

Komuro H, Watanabe M, Matoba K, Kaneko M. 2003. Gastroschisis with omphalomesenteric artery remnant, colonic atresia and arthrogryposis multiplex congenita. *Euro J Pediatr Surg* 13(5): 334–336.

Kondoh S, Taniki T, Umemoto A, Kajikawa A, Sogame M, Tanaka K, Monden Y. 1994. A case of umbilical polyp with aberrant pancreas and small intestinal mucosa—-analysis of cases of umbilical polyp reported in Japan. *Nihon Geka Gakkai Zasshi* 95(10): 786.

Kottra JJ, Dodds WJ. 1971. Duplication of the large bowel. *Am J Roentgenol* 113(2): 310–315.

Kricun R, Stasik JJ, Reither RD, Dex WJ. 1980. Giant colonic diverticulum. *Am J Roentgenol* 135(3): 507–512.

Kusumoto H, Yoshitake H, Mochida K, Kumashiro R, Sano C, Inutsuka S. 1992. Adenocarcinoma in Meckel's diverticulum: report of a case and review of 30 cases in the English and Japanese literature. *Am J Gastroenterol* 87(7): 910.

Kutin ND, Allen JE, Jewett TC. 1979. The umbilical polyp. *J Pediatr Surg* 14(6): 741–744.

Lake GB. 1920. Report of an extremely long vermiform appendix. Jour Am Med Assoc lxxv, November 6, p. 1269.

Le Double AF. 1897. Traite des Variations du Systeme Musculaire de l'Homme et de leur Signification au Point de Vue de l'Anthropologie, Zoologique (Vol. 2). Paris: Schleicher Frères.

Lee RE, Finby N. 1958. Jejunal and ileal diverticulosis. *Arch Int Med* 102(1): 97.

Lockwood CB, Rolleston HD. 1891. The fossæ round the cæcum, and the position of the vermiform appendix, with special reference to retro-peritoneal hernia. *J Anat Physiol* 26(Pt 1): 130.

Løtveit T, Skar V, Osnes M. 1988. Juxtapapillary duodenal diverticula. *Endoscopy* 20(1): 175–178.

Louw JH. 1959. Congenital intestinal atresia and stenosis in the newborn observations on its pathogenesis and treatment. *Ann R Coll Surg Engl* 25: 209–234.

Louw JH. 1966. Jejunoileal atresia and stenosis. *J Pediatr Surg* 1(1): 8–23.

Louw JH. 1967. Resection and end-to-end anastomosis in the management of atresia and stenosis of the small bowel. *Surgery* 62(5): 940.

Low A. 1907. A note on the crura of the diaphragm and the muscle of Treitz. *J Anat Physiol* 42(1): 93.

Low FN, Hilderman WC. 1940. A case of hyper-rotation of the colon. *Anat Rec* 77(1): 27–30.

Luna ML, Cicini V, Herrera A, Casas JG, Magnin PH. 1987. Umbilical polyps. *Pediatric Dermatol* 4(4): 341–343.

Mackey WC, Dineen P. 1983. A fifty year experience with Meckel's diverticulum. *Surg Gynecol Ostetr* 156(1): 56–64.

Macpherson RI. 1993. Gastrointestinal tract duplications: clinical, pathologic, etiologic, and radiologic considerations. *Radiographics* 13(5): 1063–1080.

Magee KL, Hebert AA. 1990. Umbilical lesion in a young child. *Arch Dermatol* 126(12): 1643.

Majeski J. 2003. Diverticulum of the vermiform appendix is associated with chronic abdominal pain. *Am J Surg* 186(2): 129–131.

Makris K, Tsiotos GG, Stafyla V, Sakorafas GH. 2009. Small intestinal nonmeckelian diverticulosis. *J Clin Gastroenterol* 43(3): 201–207.

Marlock CG, Gray HK. 1943. Congenital duodenal obstruction. *Annals Surg* 118(3): 372–376.

Martin LW, Zerella JT. 1976. Jejunoileal atresia: a proposed classification. *J Pediatr Surg* 11(3): 399–403.

Melamed M, Pantone A. 1960. Giant diverticula of the colon. *Arch Surg* 81(5): 723–725.

Mendelson RM, Shepherd HA, Mitchell A. 1984. "Inverted" diverticulum mimicking an ulcerated duodenal tumour. *Br J Radiol* 57(677): 426–430.

Mesko TW, Lugo R, Breitholz T. 1989. Horseshoe anomaly of the appendix: a previously undescribed entity. *Surgery* 106(3): 563–566.

Meyers MA. 1995. Treitz redux: the ligament of Treitz revisited. *Abdominal Imag* 20(5): 421–424.

Moore KL. 1992. *Clinically Oriented Anatomy*. Baltimore: Williams and Wilkins, pp. 203–205.

Mordehai J, Kleiner O, Kirshtein B, Barki Y, Mares AJ. 2001. Peritoneal encapsulation: a rare cause of bowel obstruction in children. *J Pediatr Surg* 36(7): 1059–1061.

Morris H. 1942. *Human Anatomy*, 10th edition. Philadelphia: The Blakiston Company.

Moses WR. 1947. Meckel's diverticulum: report of two unusual cases. *New Engl J Med* 237(4): 118–122.

Myles RB. 1937. Anatomical variations of the stomach and duodenum within the abdominal cavity. *Br J Radiol* 10(111): 237–260.

Nies C, Zielke A, Hasse C, Rüschoff J, Rothmund M. 1992. Carcinoid tumors of Meckel's diverticula. *Dis Colon Rectum* 35(6): 589–596.

Nixon HH, Tawes R. 1971. Etiology and treatment of small intestinal atresia: analysis of a series of 127 jejunoileal atresias and comparison with 62 duodenal atresias. *Surgery* 69(1): 41.

O'Connor SD, Summers RM, Yao J, Pickhardt PJ, Choi JR. 2006. CT colonography with computer-aided polyp detection: volume and attenuation thresholds to reduce false-positive findings owing to the ileocecal valve. *Radiology* 241(2): 426–432.

Ogura Y, Kawarada Y, Mizumoto R. 1998. Duodenal duplication cyst communicating with an accessory pancreatic duct of Santorini. *Hepato-Gastroenterol* 45(23): 1613.

Oldham K, Colombani PM, Foglia RP, Foglia MA. 2006. *Principles and Practice of Pediatric Surgery*. Philadelphia: Lippincott Williams & Wilkins.

Pacilli M, Sebire NJ, Maritsi D, Kiely EM, Drake DP, Curry JI, Pierro A. 2007. Umbilical polyp in infants and children. *Euro J Pediatr Surg* 17(06): 397–399.

Passow A. 1885. Ueber das quantitative Verhalten der Solitärfollikel und Peyer'schen Haufen des Dünndarms. *Virchows Archiv* 101(1): 135–155.

Pavlov S, Petrov V. 1968. Sur l'anse sous-claviere de l'atrere sous-claviere droite retro-oesophagienne. Folia Med Plovdiv 1010: 73–78.

Pellatt A, Evans A. 1982. A further case of hyperrotation of the colon. *Anat Rec* 204(3): 289–293.

Potter EL. 1961. *Pathology of the Fetus and Infant*. Chicago: Year Book Medical Publishers.

Potts WJ. 1955. Pediatric surgery. *J Am Med Assoc* 157(8): 627–630.

Puligandla PS, Nguyen LT, St-Vil D, Flageole H, Bensoussan AL, Nguyen VH, Laberge JM. 2003. Gastrointestinal duplications. *J Pediatr Surg* 38(5): 740–744.

Rahman MM, Khalil M, Khalil M, Sultana SZ, Mannan S, Nessa A, Siddiquee FS. 2009. Extent of mesoappendix of vermiform appendix in Bangladeshi people. *J Bangladesh Soc Physiol* 4(1): 20–23.

Rao PLNG, Mitra SK, Pathak IC. 1979. Patent vitello intestinal duct. *Indian J Pediatr* 46(6): 215–218.

Ratan SK, Rattan KN, Kalra R, Maheshwari J, Parihar D, Ratan J. 2007. Omphalomesenteric duct cyst as a content of omphalocele. *Indian J Pediatr* 74(5): 500–502.

Regge D, Gallo TM, Nieddu G, Galatola G, Fracchia M, Neri E, Bartolozzi C. 2004. Ileocecal valve imaging on computed tomographic colonography. *Abdom Imag* 30(1): 20–25.

Reiquam CW, Allen RP, Akers DR. 1965. Normal and abnormal small bowel lengths: an analysis of 389 autopsy cases in infants and children. *Am J Dis Child* 109(5): 447–451.

Romanes GT. 2000. *Cunningham's Manual of Practical Anatomy: Abdomen*. 15th edition. New York: Oxford University Press, pp. 142–153.

Rosenberg JC, DiDio LJA. 1970. Anatomic and clinical aspects of the junction of the ileum with the large intestine. *Dis Colon Rectum* 13: 220–224.

Rosetti A, Christian BN, Pascal B, Stephane D, Philippe M. 2013. Perforated duodenal diverticulum, a rare complication of a common pathology: A seven-patient case series. *World J Gastroint Surg* 5(3): 47.

Royster HA. 1927. *Appendicitis*. New York: D. Appleton and Co.

Rubesin SE, Furth EE. 2000. *Other Tumors of the Colon. Textbook of Gastrointestinal Radiology*, second edition. Philadelphia: Saunders, pp. 1049–1074.

Ruggeri G, Libri M, Gargano T, Pavia S, Pasini L, Tani G, Lima M. 2008. Congenital colonic stenosis: a case of late-onset. *Med Surg Pediatr* 31(3): 130–133.

Sadahiro S, Ohmura T, Yamada Y, Saito T, Taki Y. 1992. Analysis of length and surface area of each segment of the large intestine according to age, sex and physique. *Surg Radiol Anat* 14(3): 251–257.

Salah SD, Almushly RM, Eltayeb K, Elgaili E. 2009. Case report: congenital umbilical appendix. *Sudan Med J* 45(2): 70–74.

Salem MH, McGee HH. 1959. Hypertrophy of ileocecal valve: plastic repair. *Arch Surg* 78(6): 928.

Sandborn WD, Shafer AD. 1967. Appendiceal–umbilical fistula. *J Pediatr Surg* 2(5): 461–463.

Sappey PC. 1877. Traité d'Anatomie Descriptive, Vol. 4. Paris: Adrien Dalahaye.

Sarioglu-Buke A, Corduk N, Koltuksuz U, Karabul M, Savran B, Bagci S. 2008. An uncommon variant of Meckel's diverticulum. *Canadian J Surg* 51(2): E46.

Schnaufer L. 1991. Duodenal Atresia, Stenosis and Annular Pancreas: Pediatric Surgery. Chicago: Year Book, pp. 829–837.

Schwartz DL, Becker JM, Schneider KM, So HB. 1980. Tubular duplication with autonomous blood supply: resection with preservation of adjacent bowel. *J Pediatr Surg* 15(3): 341–342.

Scobie WG. 1969. A case of reversed rotation presenting as duodenal ileus. *Br J Surg* 56(9): 709–711.

Scudamore CH, Harrison RC, White TT. 1982. Management of duodenal diverticula. *Canadian J Surg* 25(3): 311.

Segal SD, Albretch DS, Belland KM, Elster EA. 2004. Rare mesenteric location of Meckel's diverticulum, a forgotten entity: a case study aboard USS Kitty Hawk. Yokosuka: Yokosuka (Japan) Medical Dept.

Shaar PJ. 1926. *De musculus suspensorius duodeni van Treitz en Het Duodenum*. Zutphen, the Netherlands: Nauta & Co.

Sham M, Phadke D, Singh D. 2010. Bowel conservation in a case of giant jejuno-ileal duplication. *J Indian Assoc Pediatr Surg* 15(3): 104.

Shand JEG, Bremner DN. 1977. Agenesis of the vermiform appendix in a thalidomide child. *Br J Surg* 64(3): 203–204.

Shimada H, Nakgawara G, Nakano A, Kudo T, Monta S. 1984. A duodenal duplication cyst communicating with an accessory pancreatic duct. *Jap J Surg* 14: 32–36.

Singleton AO Jr, King WB. 1951. Persistent vitelline duct continuous with the appendix; case report. *Surgery* 29(2): 278.

Skandalakis JE, Gray SW, Rowe JS. 1983. *Anatomical Complications in General Surgery*. New York: McGraw-Hill.

Snyder CL, Miller KA, Sharp RJ, Murphy JP, Andrews WA, Holcomb III GW, Gittes GK, Ashcraft KW. 2001. Management of intestinal atresia in patients with gastroschisis. *J Pediatr Surg* 36(10): 1542–1545.

Soderlund S. 1959. Meckel's diverticulum. A clinical and histologic study. Acta Chirur Scandinavica, Supplementum 1.

Standring S. 1995. *Gray's Anatomy*, 38th edition. New York: Churchill Livingstone.

Stewart DR, Colodny AL, Daggett WC. 1976. Malrotation of the bowel in infants and children: a 15 year review. *Surgery* 79(6): 716.

Stollman N, Raskin JB. 2004. Diverticular disease of the colon. *Lancet* 363(9409): 631–639.

Stollman TH, de Blaauw I, Wijnen MH, van der Staak FH, Rieu PN, Draaisma JMT, Wijnen RM. 2009. Decreased mortality but increased morbidity in neonates with jejunoileal atresia; a study of 114 cases over a 34-year period. *J Pediatr Surg* 44(1): 217–221.

Tauro LF, Martis JJ, Shenoy HD. 2009. Double Meckel's diverticulum. *J Indian Med Assoc* 107(3): 174–175.

Tinckler LF. 1968. Triple appendix vermiformis: a unique case. *Br J Surg* 55(1): 79–81.

Torres AM, Zigler MM. 1993. Malrotation of the intestine. *World J Surg* 17(3): 326–331.

Treves F. 1885. Lectures on the anatomy of the intestinal canal and peritoneum in man. *Br Med J* 1: 527–530.

Tsiotos GG, Farnell MB, Ilstrup DM. 1994. Nonmeckelian jejunal or ileal diverticulosis: an analysis of 112 cases. *Surgery* 116(4): 726.

Turgeon DK, Barnett JL. 1990. Meckel's diverticulum. *Am J Gastroenterolog* 85(7): 777–781.

Underhill BM. 1955. Intestinal length in man. *Br Med J* 2(4950): 1243.

Uppal K, Tubbs RS, Matusz P, Shaffer K, Loukas M. 2011. Meckel's diverticulum: a review. *Clin Anat* 24(4): 416–422.

Uriev L, Maslovsky I, Mnouskin Y, Ben-Dor D. 2006. Triple-barreled type of appendiceal triplication. *Annals Diagn Path* 10(3): 160–161.

Vecchia LK, Grosfeld JL, West KW, Rescorla FJ, Scherer LR, Engum SA. 1998. Intestinal atresia and stenosis: a 25-year experience with 277 cases. *Arch Surg* 133(5): 490–497.

Wagner DE, Zollinger RW. 1961. Diverticulitis of the cecum and ascending colon. *Arch Surg* 83(3): 436–443.

Wakeley CP. 1933. The position of the vermiform appendix as ascertained by an analysis of 10,000 cases. *J Anat* 67(2): 277.

Wallbridge PH. 1962. Double appendix. *Br J Surg* 50(221): 346–347.

Wardell S, Vidican DE. 1990. Ileal duplication cyst causing massive bleeding in a child. *J Clin Gastroenterol* 12(6): 681–684.

Weaver LT, Austin S, Cole TJ. 1991. Small intestinal length: a factor essential for gut adaptation. *Gut* 32(11): 1321–1323.

Weidman TA. 2004. *Skandalakis' Surgical Anatomy*. New York: McGraw-Hill Companies.

Weser E. 1979. Nutritional aspects of malabsorption: short gut adaptation. *Am J Med* 67(6): 1014–1020.

Wilcox RD, Shatney CH. 1988. Surgical implications of jejunal diverticula. *South Med J* 81(11): 1386–1391.

Williams MD, Burrington JD. 1993. Hirschsprung's disease complicating colon atresia. *J Pediatr Surg* 28(4): 637–639.

Williams RA, Davidson DD, Serota AI, Wilson SE. 1981. Surgical problems of diverticula of the small intestine. *Surg Gynecol Obstetr* 152(5): 621.

Wolfer JA, Beaton LE, Anson BJ. 1942. Volvulus of the cecum. Anatomical factors in its etiology. Report of a case. *Surg Gynecol Obstet* 74: 882–894.

Woodburne RT. 1961. *Essentials of Anatomy*, second edition. Oxford: Oxford University Press.

Woywodt A, Verhaart S, Kiss A. 1998. Atresia of the appendix. *J Pediatr Surg* 33(9): 1423–1425.

Wu YC, Kao CH. 2010. The 'wandering' Meckel diverticulum: an unusual scintigraphic finding. *Pediatr Radiol* 40: 103–103.

Yamaguchi M, Takeuchi S, Awazu S. 1978. Meckel's diverticulum: investigation of 600 patients in Japanese literature. *Am J Surg* 136(2): 247–249.

Yang TS, Greenspan A, Farber M, Richter RM, Bryk D, Levowitz BS. 1974. Intraluminal duodenal diverticulum. *Arch Surg* 109(1): 113.

Yaylak F, Algin MC, Gungor Y, Korkmaz M. 2013. Atresia of the appendix vermiformis: A rare case of developmental abnormality. *World J Gastroenterol* 19(1): 122.

Yochum AM, Bonic EE, Yochum TR, Kettner NW. 2013. Giant Meckel diverticulum with enteroliths: a case report of a patient presenting with low back and episodic right lower quadrant pain. *J Chiropractic Med* 12(3): 207–211.

Zaidenstein L, Freud E, Schwartz M, Zer M. 1995. Clinical presentation of rare appendiculo-omphalic anomalies. *J Pediatr Surg* 30(12): 1702–1703.

Zetina-Mejia CA, Alvarez-Cosio JE, Quillo-Olvera J. 2008. Congenital absence of the cecal appendix. Case report. *Cirugia Cirujanos* 77(5): 407–410.

112 Sigmoid colon, rectum, and anus

Thandinkosi E. Madiba and Mohammad R. Haffajee
University of KwaZulu-Natal, Durban, South Africa

Normal anatomy

In the fetal period, the right two-thirds of the transverse colon are derived from the midgut while the left third of the transverse colon derives from the hindgut. The midgut loop is suspended from the dorsal abdominal wall by an elongated mesentery.

Left colic flexure

The transverse colon turns inferiorly at the left colic flexure (splenic flexure) to become the descending colon. The left colic flexure is more superior, more acute, and less mobile than the right colic flexure (hepatic flexure). It lies anterior to the inferior part of the left kidney and its superoposterior relation is the spleen. A number of ligaments attach the left colic flexure to the structures closely related to it, namely the phrenocolic, lienorenal, splenocolic, and the gastrocolic ligaments (Moore and Dalley 1999).

Descending colon

The descending colon passes retroperitoneally from the left colic flexure into the left iliac fossa, where it is continuous with the sigmoid colon. Peritoneum covers the colon anteriorly and laterally and binds it to the posterior abdominal wall as its mesentery fuses with the peritoneum on the left posterior abdominal wall (Moore and Dalley 1999). As it descends the colon passes anterior to the lateral border of the left kidney (Moore and Dalley 1999). As with the ascending colon, the descending colon has a paracolic gutter on its lateral aspect (Moore and Dalley 1999). The descending colon has a mesocolon of 10 cm or more in length.

Sigmoid colon

The sigmoid colon links the descending colon and the rectum. It is characterized by its S-shaped loop of variable length (usually 40 cm) and extends from the iliac fossa to the third sacral vertebra where it joins the rectum (Williams et al. 1989; Moore and Dalley 1999). The sigmoid colon usually has a long mesentery and therefore has considerable freedom of movement, especially its middle part (Moore and Dalley 1999).

The mesentery of the sigmoid colon (sigmoid mesocolon) in the embryo originally has a midline dorsal attachment (Last 1978). During intrauterine development, it hinges to the left and becomes partially fused with the parietal peritoneum of the posterior abdominal and pelvic wall. The sigmoid colon retains its mesentery during the postnatal period. This is thought to be due to imperfect blending of the primitive mesentery with the posterior parietal peritoneum (Williams et al. 1989). The sigmoid mesocolon is folded on itself and, at the apex of the attachment of the root of this mesentery, it forms an inverted V-shaped hooded recess called the intersigmoid recess. This generally lies at about the bifurcation of the left common iliac vessels with its "mouth" pointing inferiorly and to the left, under which is found the left ureter (Skandalakis and Gray 1994; Moore and Dalley 1999). The V-shaped attachment of the sigmoid mesocolon is described as constant (Johnson 1981). The left ureter and the division of the left common iliac artery lie retroperitoneally posterior to the apex of the intersigmoid recess (Moore and Dalley 1999).

Rectosigmoid junction and rectum

The rectosigmoid junction occurs at the level of the third sacral vertebra, approximately 15 cm from the anal verge. A number of structural changes occur as the sigmoid colon changes to rectum at the rectosigmoid junction: the sigmoid mesentery terminates; the omental appendices (appendices epiploicae), which are long in the sigmoid colon, disappear; and the tineae coli disappear as the longitudinal muscle in the wall of the colon broadens to form a complete layer in the rectum (Moore and Dalley 1999).

The rectum is the fixed terminal part of the large intestine and is continuous with the sigmoid colon at the level of third sacral vertebra (Moore and Dalley 1999). The junction is at the lower end of the mesentery of the sigmoid colon. The rectum is continuous inferiorly with the anal canal (Moore and Dalley 1999).

Bergman's Comprehensive Encyclopedia of Human Anatomic Variation, First Edition. Edited by R. Shane Tubbs, Mohammadali M. Shoja and Marios Loukas.
© 2016 John Wiley & Sons, Inc. Published 2016 by John Wiley & Sons, Inc.

Anatomic variations

Variations in the colon are of importance for medical practice, especially radiological and surgical applications. The principal colonic variations probably result from irregular or defective development leading to mild embryologic abnormalities of bowel rotation and fixation (Moore and Dalley 1999; Faure et al. 2001; Oyar et al. 2003; Unal et al. 2004; Indrajit et al. 2012). Examples are malrotation and abnormal fixations of the colon, shortened or absent mesocolon, or decreased retroperitoneal fat (Oyar et al. 2003; Unal et al. 2004).

Splenic flexure and descending colon

Mobile splenic flexure is one of the more common colonic variations, occurring in 20% of cases (Saunders et al. 1995). Pancreatico-gastric interposition of the splenic flexure and descending colon occurs in approximately 0.2% of cases (Unal et al. 2004). Anterolateral hepato-diaphragmatic interposition of the distal transverse colon and splenic flexure occurs in 1.3–3% of individuals (Unal et al. 2004). Interposition of the colon between the spleen and diaphragm (cephalo-diaphragmatic or retrosplenic interposition) has been described in 0.03–0.3% of cases and may represent a benign anatomical variation that can be recognized on CT images (Oldfield and Wilbur 1993; Oyar et al. 2003). When this occurs, the left colic flexure and distal part of transverse colon have been shown to be situated in the retroperitoneal space and sometimes between the kidney and psoas muscle (Pinto et al. 1996; Oyar et al. 2003).

Although retroperitoneal, the descending colon has a short mesentery in approximately 33% of people (Moore and Dalley 1999), especially in the iliac fossa; this is not usually long enough to cause volvulus of this part of the colon, however (Moore and Dalley 1999). A redundant loop of descending colon may occur which crosses the great vessels of abdomen to present itself, sometimes with the sigmoid colon on the right side of abdomen (Moore and Dalley 1999; Oyar et al. 2003; Indrajit et al. 2012). In malrotation an abnormal arrest in midgut rotation after the first 90° of rotation occurs, rendering the descending colon to lie anterior to the kidneys rather than lateral to them (Ramachandran et al. 2009).

Interposition of the descending colon between psoas muscle and kidney (retrorenal position), which can be partial or complete, has been reported to occur in 0.7–10%, and tends to occur more frequently in young women and individuals with less intra-abdominal fat (Prassopoulos et al. 1994; Faure et al. 2001; Unal et al. 2004; Eiref et al. 2010; Atar et al. 2013).

Sigmoid colon

Variations in the level of origin of the sigmoid colon from the descending colon have been shown to occur and can be described as low-level, mid-level, or high-level (Madiba and Haffajee 2010). In a low-level origin the descending colon comes all the way down to the left iliac fossa and the sigmoid colon turns medially at any level below the left iliac crest. In subjects with a high-level origin of the sigmoid colon, the origin occurs high in the descending colon close to its origin from the transverse colon above the level of the lower margin of the left rib cage, rendering the descending colon proper very short. A mid-level origin lies between the two (Madiba and Haffajee 2010; Fig. 112.1). A persistence of the primitive loop has also been described in which (1) there is no clear demarcation between the descending colon and the sigmoid colon, and (2) the combined length of the descending and sigmoid colon is displaced medially, taking an oblique and usually tortuous (but occasionally a straight) course from the splenic flexure towards the pelvis (Madiba and Haffajee 2010). This is demonstrated in Figure 112.2a. Figure 112.2b shows other variants of the position of the sigmoid colon.

Although some authorities contend that the intersigmoid recess is commonly present in infancy and tends to disappear later in life, the literature describes the inverted V shape of the intersigmoid recess as common or even constant (Johnson 1981). A study from South Africa has demonstrated this anatomical variability with the V shape occurring in only 18%, the U shape in 37%, and the straight shape in 45% (Madiba and Haffajee 2010). These variations seem to be population based, with specific deviations from the normal level of origin of the sigmoid colon being more pronounced in one population group. This is well demonstrated in Figures 112.3 and 112.4.

Variations on the length and shape of the sigmoid colon have been demonstrated by a number of authors. Madiba and Haffajee (2011) demonstrated varying length, shape, and position of the sigmoid colon accompanied by varying length and width of the sigmoid mesocolon. These differences were shown to be population based, with some population groups showing a tendency for elongated sigmoid colon with the resultant predisposition to sigmoid volvulus. The shape of the elongated sigmoid colon was further shown to be long-and-narrow or broad, with the former more predisposed to sigmoid volvulus than the latter. The differences in the shape were more gender based and would explain the male preponderance of sigmoid volvulus (Madiba and Haffajee 2011). These differences are shown in Figures 112.5 and 112.6.

Bhatnagar et al. (2004) further expanded on the elongated colon, showing two varieties of the elongated sigmoid colon. In the more common variation, the sigmoid mesocolon is vertically longer than wide (dolicho-mesocolic) and the sigmoid loop has its maximum convexity located just a little proximal to the apex. The other pattern is where the width of the mesocolon was greater than the vertical length (brachy-mesocolic) (Bhatnagar et al. 2004). The gender analysis in that study showed that the sigmoid mesocolon of the female tended to be brachy-mesocolic, whereas that of the male tended to be dolicho-mesocolic (Bhatnagar et al. 2004).

Megacolon

Hirschsprung disease is a developmental disorder of the enteric nervous system that is characterized by the absence of ganglion cells in the myenteric and submucosal plexuses of the distal

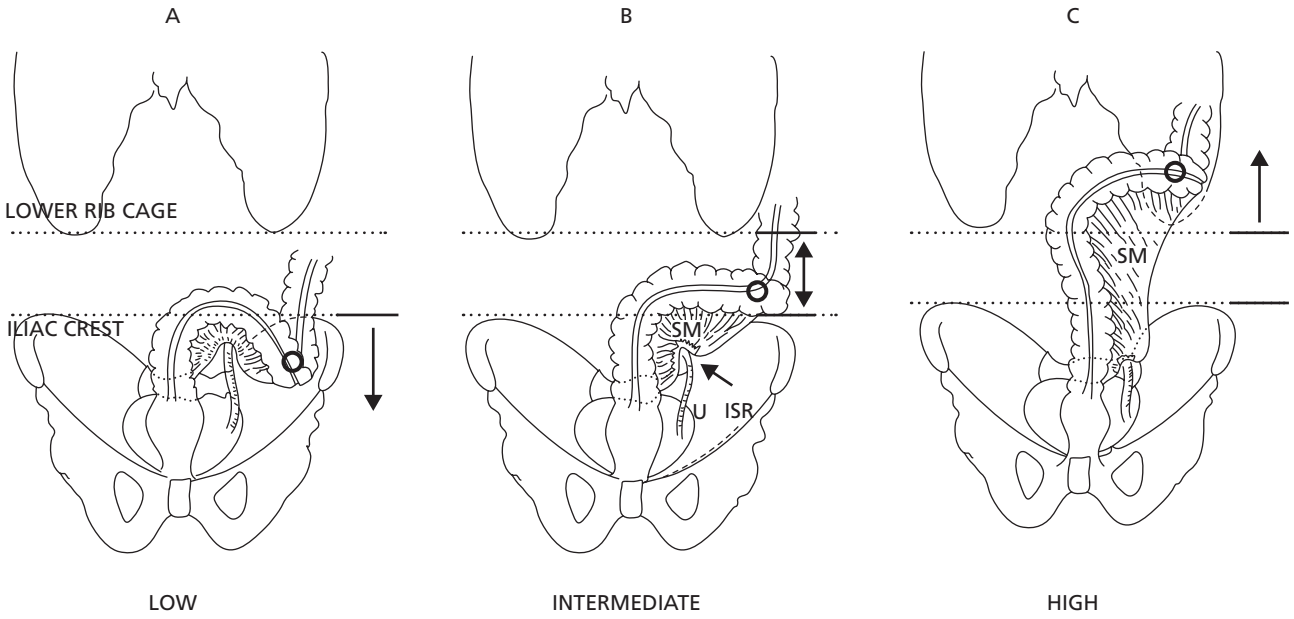

Figure 112.1 Illustrations showing the origin (O) of the sigmoid colon from the descending colon (arrows): (a) normal low-level origin of the sigmoid colon below the iliac crest (bold arrow down); (b) intermediate-level origin between the two levels (bold double arrow); and (c) high-level origin above the rib cage (bold arrow up). The ureter (U) is shown emerging from under the intersigmoid recess (ISR) at the apex of the attachment of the mesocolon (SM).

Source: Madiba and Haffajee (2010). Reproduced with permission from John Wiley & Sons.

intestine, which results in a lack of peristalsis and functional intestinal obstruction (Langer 2013). In most cases, the aganglionosis involves the rectum or rectosigmoid but it can extend for varying lengths; in 5–10% of cases it can involve the entire colon or even a significant amount of the small intestine (Langer 2013). Diagnosis of this condition involves a full thickness biopsy of the rectum to look for the ganglia in the myenteric and submucosal plexuses.

Blood supply

The middle mesenteric artery is rare, occurring in 0.1% of cases (Milnerowicz et al. 2012). It originates directly from the aorta, halfway between the superior and inferior mesenteric arteries, and ascends obliquely in the direction of the hepatic flexure of the colon (Milnerowicz et al. 2012). In malrotation there is transposition of the superior mesenteric artery and the superior mesenteric vein, resulting in changes in the anatomical landmarks for the mesocolon with the origin and course of the ileocolic and right colic vessels being placed to the left of the superior mesenteric artery (Ramachandran et al. 2009). The inferior mesenteric artery has rarely been reported to arise from the superior mesenteric artery (Yi et al. 2008).

Rectum

Additional rectal valves may be present or the valves may be reduced in number.

Anus and anal canal

Anorectal malformations (ARM) remain a significant congenital anomaly, with the reported incidence ranging between 1.2 and 2.5 per 10,000 live births (Moore et al. 2008; Rintala 2009). They include a series of congenital lesions ranging from a slight malposition of the anus to complex anomalies of the hindgut and urogenital organs (Moore et al. 2008; Rintala 2009). In most cases, anorectal malformations present as an absence of an anus in its normal position (Moore et al. 2008; Rintala 2009). In mild forms of anal anomalies, the bowel outlet opens in the perineal region outside the usually well-developed voluntary sphincter complex. In more severe anomalies, bowel outlet opens in an ectopic position in the urogenital tract in males or genital tract in females (Rintala 2009). Recognition of the type of the malformation in neonates is essential for planning the surgical management of anorectal anomalies (Rintala 2009). There can be anorectal atresia.

There is no generally accepted method to classify anorectal malformations (Rintala 2009). A simplified classification has emerged called the Krickenbeck Classification (Holschneider et al. 2005; Rintala 2009), in which ARM are classified according to the presence of a fistula into: (1) those with a fistula; (2) those with no fistula; (3) those with anal stenosis; and (4) complex ones referred to as cloaca (Holschneider et al. 2005; Levitt and Peña 2007; Rintala 2009).

The anal columns may form papillary projections internally.

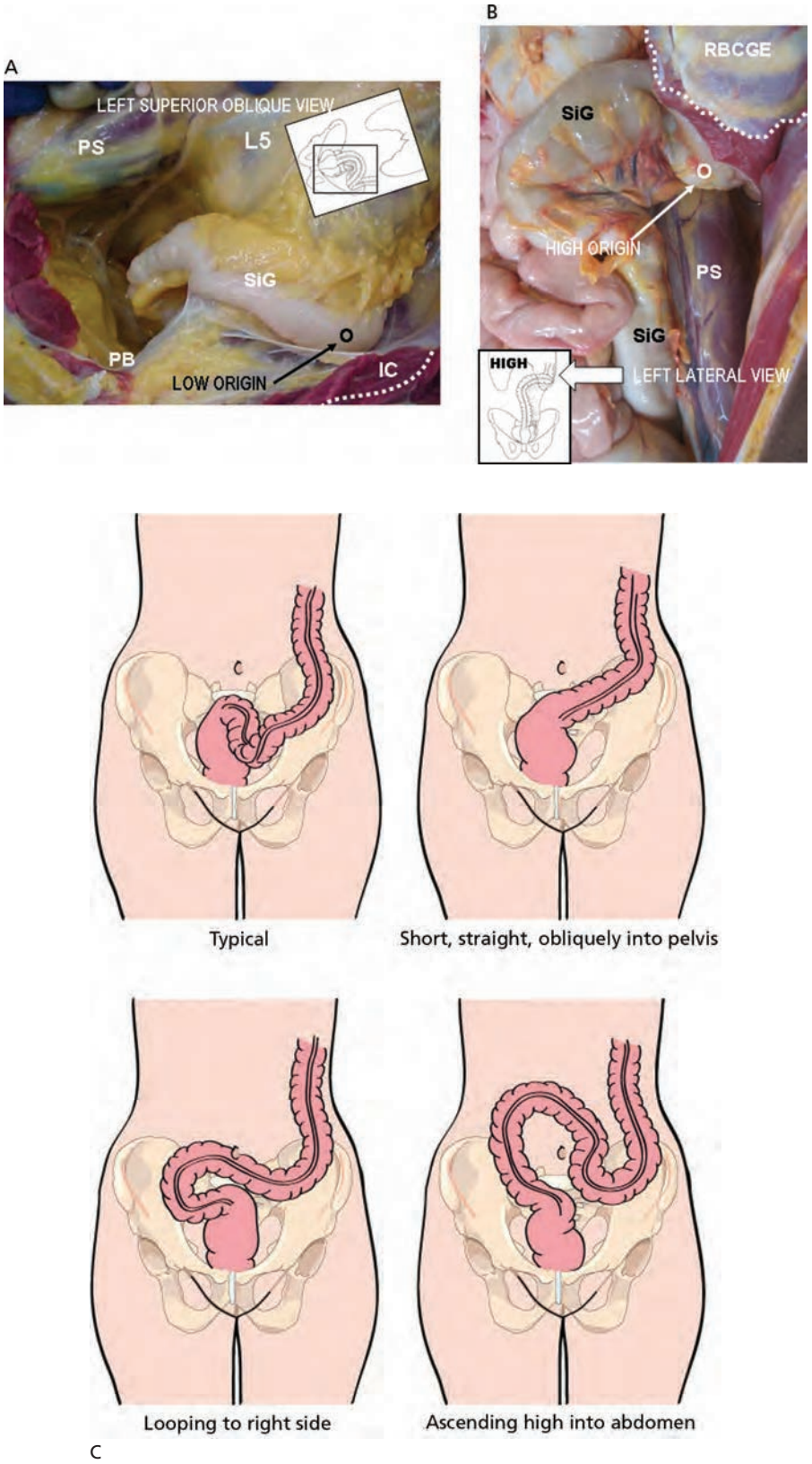

Figure 112.2 (a) A left superior oblique view (inset) of a low-level origin (O) of the sigmoid colon (SiG) *in situ* below the left iliac crest (IC) (dotted white line), passing over the left pelvic brim (PB). The right psoas muscle (PS) is opposite of this. (b) A left lateral view (inset) of an *in situ* picture of a high-level origin of the sigmoid colon. The sigmoid colon (SiG) originates (O) at the level of the rib cage (RBCGE). The costal margin (rib cage) is marked with a white dotted line. The left psoas muscle (PS) is exposed. (c) Other variations of the position of the sigmoid colon, after Netter (2014). (a, b)

Source: Madiba and Haffajee (2010). Reproduced with permission from John Wiley & Sons.

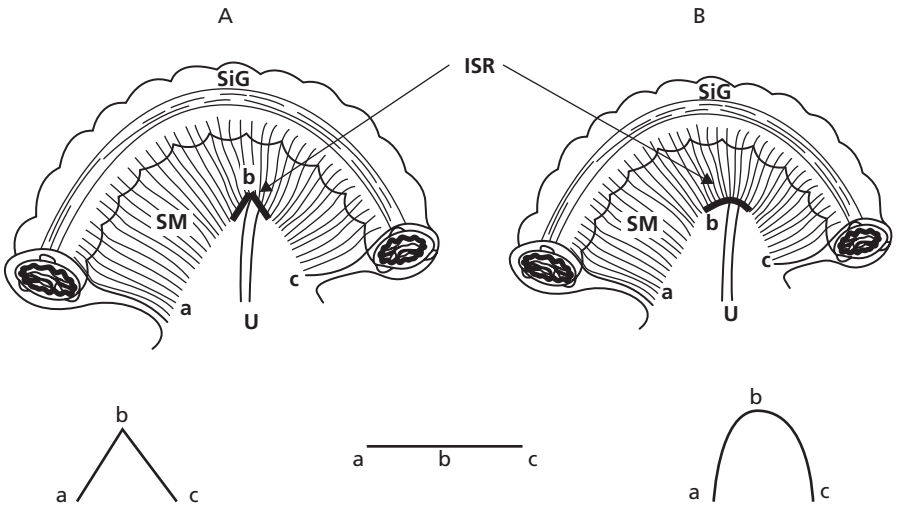

Figure 112.3 Illustrations of the attachment of the sigmoid mesocolon (SM) along the right leaf a–b and left leaf b–c are shown, forming the intersigmoid recess (ISR) at the apex of the attachment (angle b between the leaves a–b and b–c), deep to which is found the ureter (U). (a) The intersigmoid recess has an inverted V-shape, as commonly described in anatomy books. (b) An inverted U-shaped intersigmoid recess. Fully splayed out, the leaves of attachment of the sigmoid colon a–b and b–c form a straight line (a–b–c) as shown in the middle annotation.

Source: Madiba and Haffajee (2010). Reproduced with permission from John Wiley & Sons.

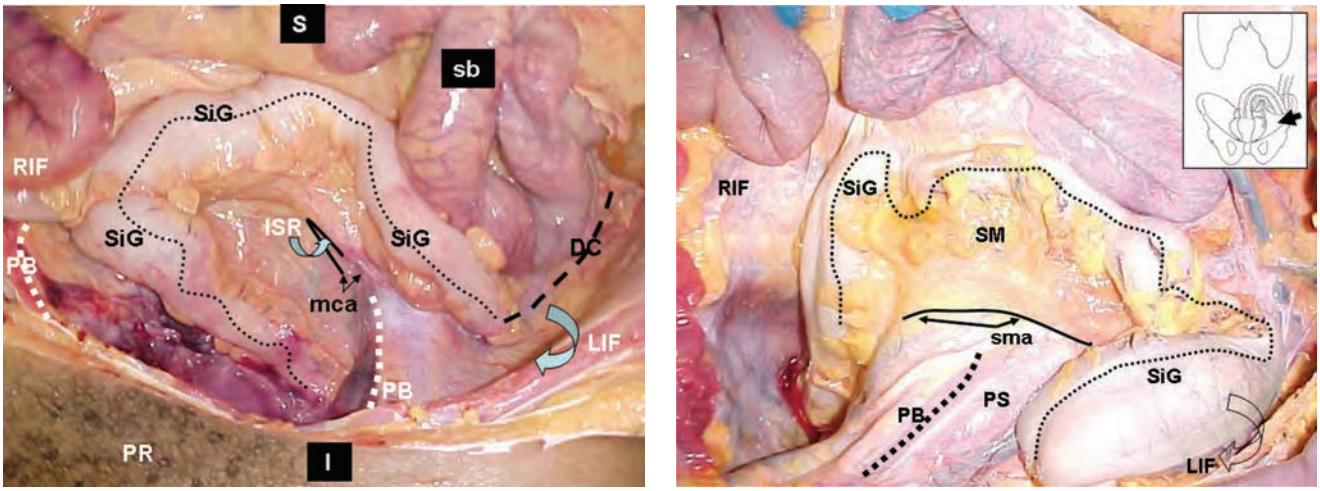

Figure 112.4 *In situ* pictures of the sigmoid colon attachments. (a) The pelvic region (PR), superior (S), and inferior (I) orientation tags, small bowel (sb) above, and V-shaped intersigmoid recess (ISR) of the mesocolon attachment (mca); the left iliac fossa (LIF) (curved arrow) lies below the low origin (O) of the sigmoid colon from the descending colon (DC). SiG denotes the sigmoid colon and PB denotes the pelvic brim (thick-dotted line). (b) An inset picture for orientation, the iliac fossae (RIF, LIF), a "straight" sigmoid mesocolon attachment (sma), of the sigmoid mesocolon (SM), no definite intersigmoid recess and the full extent of the sigmoid colon (SiG).

Source: Madiba and Haffajee (2010). Reproduced with permission from John Wiley & Sons.

Implications

Percutaneous interventions and surgical procedures in the presence of these anatomical variations such as posterolateral position of the colon may lead to complications, such as colonic puncture or perforation, with a mortality of 0.04% and a complication rate of 5% (Faure et al. 2001; Boon et al. 2002; Unal et al. 2004). This should be borne in mind when performing percutaneous interventions, as it necessitates pre-procedure evaluation of the presence of these anatomic variations (Unal et al. 2004). Some of these anatomical variations can lead to difficulty in the interpretation of the imaging investigations such as the finding of small bowel lateral to the interposing colon which can mimic an internal hernia on computed tomography (CT) (Eiref et al. 2010). The elongated sigmoid colon is a predisposing factor for sigmoid volvulus and explains the high incidence of sigmoid volvulus in certain population groups as well as gender differences in these predisposed populations. In malrotation it is crucial for the surgeon to recognize the transposition of the inferior mesenteric artery and inferior mesenteric vein, which results in changes in anatomic landmarks of the mesocolon. Hirschsprung's disease should always be a

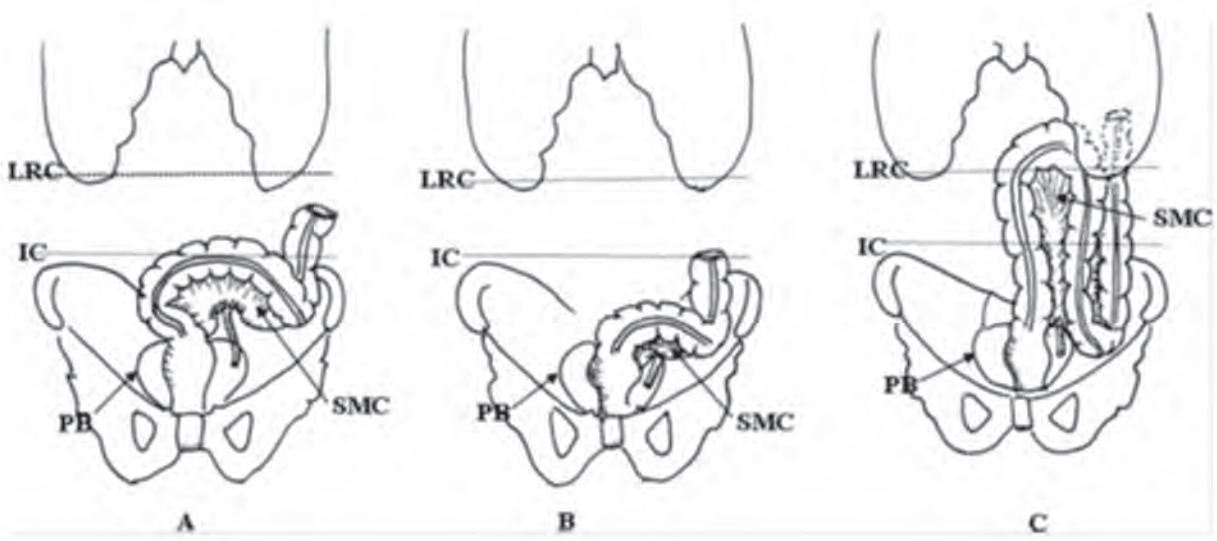

Figure 112.5 Schematic illustration showing the different types of sigmoid colon. (a) A broad suprapelvic sigmoid colon; (b) the classic type, which is closely allied to the brim; and (c) a long-narrow type in a suprapelvic position.

Source: Madiba and Haffajee (2011). Reproduced with permission from John Wiley & Sons.

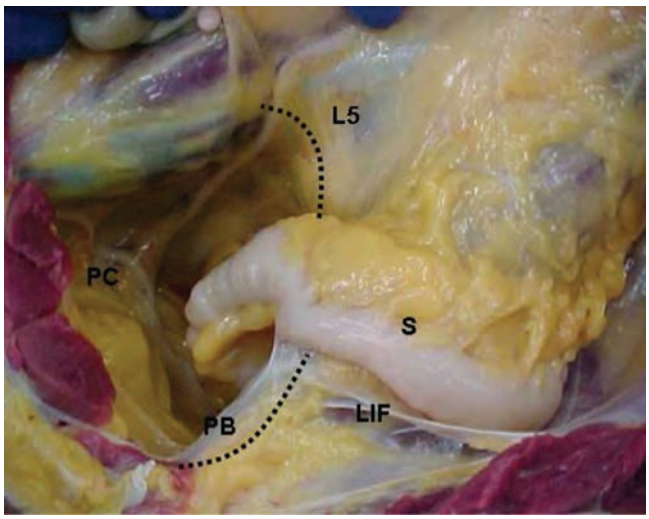

A

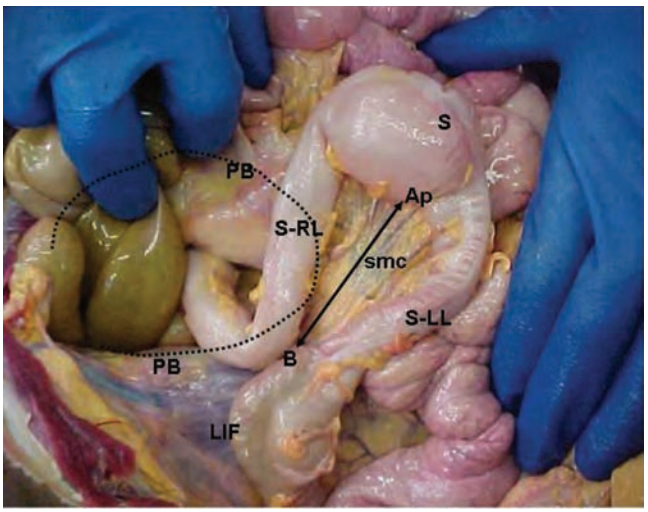

B

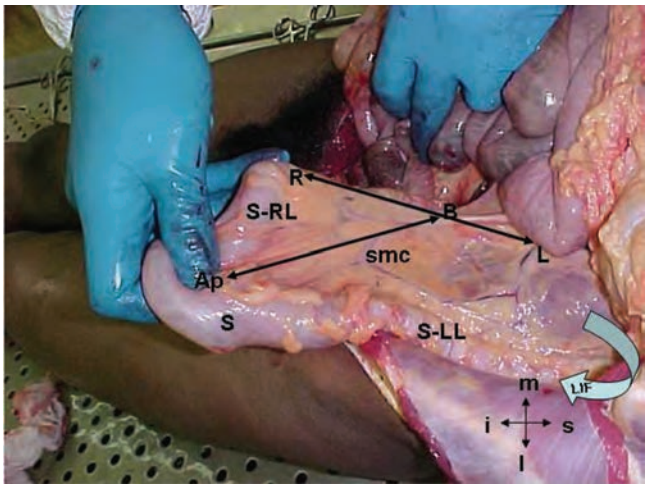

C

Figure 112.6 (a) An *in situ* picture of the classic type of the sigmoid colon. (b) An *in situ* picture of the "long-narrow" type of the sigmoid colon. (c) An *in situ* picture of a broad type. The loop is hovering in front of the pelvic brim. LIF, left iliac fossa; PC, pelvic cavity; PB, pelvic brim; L5, fifth lumbar vertebra; S, sigmoid colon loop; S-RL, right limb of sigmoid; S-LL, left limb of sigmoid; Ap, apex of loop; Ap–B, height of mesocolon; smc, sigmoid mesocolon; R–L, width of base of mesocolon.

Source: Madiba and Haffajee (2011). Reproduced with permission from John Wiley & Sons.

possible consideration in patients with megacolon, and it should be excluded before other diagnoses are entertained. The management of anorectal malformations depend on the site of the anomaly; high anomalies require major surgery such as posterior sagittal anorectoplasty, and low anomalies require a minor procedure to allow the blind-ending rectum to open into the perineum. It is therefore essential that the treating physician accurately defines the anomaly into high or low anomalies prior to embarking on the appropriate operative management.

References

Atar M, Hatipoglu NK, Soylemez H, Pendegul N, Bozkurt Y, Gumus H, Sancaktutar AA, Kuday S, Bodakci MN. 2013. Relationship between colon and kidney: A critical point for percutaneous procedures. *Scand J Urol* 47: 122–125.

Bhatnagar B, Sharma C, Gupta S, Mathur M, Reddy D. 2004. Study on the anatomical dimensions of the human sigmoid colon. *Clin Anat* 17: 236–243.

Boon J, Shinners B, Meiring JH. 2002. Variations of the position of the colon as applied to percutaneous nephrostomy. *Surg Radiol Anat* 23: 421–425.

Eiref SD, Holekamp S, Winestone M, Leitman IM. 2010. Descending colon interposition in a patient presenting with abdominal pain and acute appendicitis. *Int J Anat Var* 3: 146–148.

Faure JP, Richer JP, Chansigaud JP, Scepi M, Irani J, Ferrie JC, Kamina P. 2001. A prospective radiological anatomical study of the variations of the position of the colon in the left pararenal space. *Surg Radiol Anat* 23: 335–339.

Holschneider A, Hutson J, Peña A, Beket E, Chatterjee S, Coran A, Davies M, Georgeson K, Grosfeld J, Gupta D, Iwai N, Kluth D, Martucciello G, Moore S, Rintala R, Smith ED, Sripathi DV, Stephens D, Sen S, Ure B, Grasshoff S, Boemers T, Murphy F, Söylet Y, Dübbers M, Kunst M. 2005. Preliminary report on the international conference for the development of standards for the treatment of anorectal malformations. *J Pediatr Surg* 40: 1521–1526.

Indrajit G, Sudeshna M, Subhra M. 2012. A redundant loop of descending colon and right sided sigmoid colon. *Int J Anat Var* 5: 11–13.

Johnson F. 1981. The digestive system. In: *Cunningham's Textbook of Anatomy*, 12th edition (ed. GJ Romanes). Oxford: Oxford University Press, pp. 411–489.

Langer JC. 2013. Hirschsprung disease. *Curr Opin Pediatr* 25: 368–374.

Last R. 1978. *The Abdomen. Anatomy: Regional and Applied*, sixth edition. Edinburgh: Churchill Livingstone, pp. 255–359.

Levitt MA, Peña A. 2007. Anorectal malformations. *Orphanet J Rare Dis* 2: 33–37.

Madiba TE, Haffajee MR. 2010. Anatomical variations in the level of origin of the sigmoid colon from the descending colon and the attachment of the sigmoid mesocolon. *Clin Anat* 23: 179–185.

Madiba TE, Haffajee MR. 2011. Sigmoid colon morphology in the population groups of Durban, South Africa, with special reference to sigmoid volvulus. *Clin Anat* 24: 441–453.

Milnerowicz S, Milnerowicz A, Taboła R. 2012. A middle mesenteric artery. *Surg Radiol Anat* 34: 973–975.

Moore KL, Dalley AF. 1999. Abdomen. In: *Clinically Orientated Anatomy*, fourth edition (eds KLMoore, AFDalley). Philadelphia: Lippincott, pp. 174–330.

Moore S, Alexander A, Sidler D, Alves J, Hadley GP, Numanoglu A, Banieghbal B, Chitnis M, Birabwa-Male D, Mbuwayesango B, Hesse A, Lakhoo K. 2008. The spectrum of anorectal malformations in Africa. *Pediatr Surg Int* 24: 677–683.

Netter F. 2014. *Netter's Atlas of Human Anatomy*. Philadelphia: Elsevier.

Oldfield A, Wilbur A. 1993. Retrogastric colon: CT demonstration of anatomic variations. *Radiology* 186: 557–561.

Oyar O, Yesildag A, Malas M, Gulsoy U. 2003. Splenodiaphragmatic interposition of the descending colon. *Surg Radiol Anat* 25: 434–438.

Pinto A, Brunese L, Noviello D, Catalano O. 1996. Colonic interposition between kidney and psoas muscle: anatomical variation studied with CT. *Radiol Med* 94: 58–60.

Prassopoulos P, Gourtsoyiannis N, Cavouras D, Pantelidis N. 1994. Interposition of the colon between the kidney and the psoas muscle: A normal anatomic variation studied by CT. *Abdom Imaging* 19: 446–448.

Ramachandran I, Rodgers P, Elabassy M, Sinha R. 2009. Multidetector computed tomography of the mesocolon: Review of anatomy and pathology. *Curr Probl Diagn Radiol* 38: 84–90.

Rintala RJ. 2009. Congenital anorectal malformations: Anything new? *J Pediatr Gastroenterol Nutr* 48: 79–82.

Saunders B, Phillips R, Williams C. 1995. Intraoperative measurement of colonic anatomy and attachments with relevance to colonoscopy. *Br J Surg* 82: 1491–1493.

Skandalakis JE, Gray ST. (eds) 1994. *The peritoneum. Embryology for Surgeons: The Embryological Basis for the Treatment of Congenital Anomalies*, second edition. Baltimore: Williams & Wilkins.

Unal B, Kara S, Aktaş A, Bilgili Y. 2004. Anatomic variations of the colon detected on abdominal CT scans. *Tani Girisim Radyol* 10: 304–308.

Williams PL, Warwick R, Dyson M, Bannister L. (eds) 1989. *The large intestine. Gray's Anatomy*. Edinburgh: Churchill Livingstone, pp. 1365–1376.

Yi SQ, Li J, Terayama H, Naito M, Iimura A, Itoh M. 2008. A rare case of inferior mesenteric artery arising from the superior mesenteric artery, with a review of the review of the literature. *Surg Radiol Anat* 30: 159–165.

113 Kidney, urinary bladder, and ureter

Mohammad Reza Ardalan
Tabriz University of Medical Sciences, Tabriz, Iran

Bilateral anephrogenesis has an incidence of 0.0017%. Heterotopic renal tissue has been reported in the heart and in the suprarenal gland. The kidneys sometimes vary from their normal form, being either longer and narrower or shorter and more rounded. The occurrence of an additional kidney is rare. The characteristic fetal lobulation may persist in the adult (7%). Occasionally, one kidney is very small while the other is proportionally enlarged.

Ectopia or variations in of ascent-pelvic ectopia

Renal ectopia or ectopic kidney is a congenital variant in which at least one kidney is located in an unusual position. It results from the kidney failing to ascend properly from its origin in the true pelvis. Normally, both kidneys are situated posteriorly behind the peritoneum on each side of the vertebral column, at the level of the upper border of the twelfth thoracic vertebra superiorly and the third lumbar vertebra inferiorly (Bergman et al. 2006). Ectopic kidneys, however, can be located anywhere along their path of ascent in the pelvic, iliac, or abdominal areas. The pelvic kidney is opposite the sacrum and below the aortic bifurcation; the lumbar kidney rests near the sacral promontory in the iliac fossa and anterior to the iliac vessels; and the abdominal kidney lies above the iliac crest and adjacent to the second lumbar vertebra (Bauer 2002). There is a slight predominance on the left side and in males. Bilateral pelvic ectopic kidneys can occur with or without fusion. In some cases, one kidney crosses over (crossed renal ectopia) so that both kidneys are on the same side of the body. When a crossover occurs, the two kidneys can grow together and become fused (crossed fused renal ectopia). Since under-ascent is more common than over-ascent, ectopic kidneys are more commonly found in the pelvis or lower abdomen. Over-ascent leads to the kidneys being identified as subdiaphragmatic or intrathoracic (cf. Sfaxi et al. 2002). Factors that can prevent orderly movement of the kidneys include ureteral bud maldevelopment, defective metanephric tissue, genetic abnormalities, maternal illness, and teratogenic causes (Ascher and Rosch 2005). Initially, the kidneys lie close together in the pelvis. They gradually ascend into the abdomen and become separate from each other and inferior to the adrenals by the ninth gestational week. As they ascend they gradually rotate, with the hila starting to be seen anteromedially. Renal ectopia should be differentiated from renal ptosis, in which the kidney is initially located in its proper place with normal vascularity but then moves downward (Bauer 2002). The ureter usually enters the bladder on the ipsilateral side with its orifice situated normally (Bauer 2002).

Incidence of renal ectopia

Ectopic kidneys are thought to occur in approximately 1 in 1000 births, but only about 1 in 10 of these cases is ever diagnosed: it is asymptomatic in most patients, which explains why the incidence in autopsy series (1:1000) is much higher than in clinical presentation (1:10,000) (Moore and Persaud 2008). A radiographic survey of symptom-free potential transplant donors found ectopic kidneys in 2 of 151 individuals (Frick and Goldberg 1980); in earlier reports the incidence was given as 1:2100 and 1:3000 births (Stevens 1937) and 1 in 5000 children (Gleason et al. 1994). A frequency of 1:500 has also been reported by some authors (Bergman et al. 2006). Pelvic ectopic kidney, usually opposite the sacrum and below the aortic bifurcation, has been estimated to occur in 1 of 2100–3000 autopsies without any sex difference (Tsao et al. 2008).

Embryology of renal ectopia

The kidney generally ascends in the developing metanephric blastema in the five- to seven-week embryo. It does not rotate until it reaches its normal lumbar position by the ninth gestational week. The ascent of the kidneys precedes the descent of the gonads into the pelvis. During ascent, each kidney acquires its blood supply from neighboring vessels, initially from the external and internal iliac vessels, but by the eighth week directly from the aorta. An ectopic kidney results from failed ascent of the fetal kidney. If the aortic blood supply is not acquired normally, or if there is an associated abnormality of the spine, cephalad migration of the fetal kidney will not occur (Arnim et al. 2005). During the mesonephros stage, lateral intersegmental arteries (urogenital rete arteriosum), located

Bergman's Comprehensive Encyclopedia of Human Anatomic Variation, First Edition. Edited by R. Shane Tubbs, Mohammadali M. Shoja and Marios Loukas.
© 2016 John Wiley & Sons, Inc. Published 2016 by John Wiley & Sons, Inc.

on both sides of the aorta between the sixth cervical and third lumbar vertebrae, provide vascularization to the adrenal glands, kidneys, and gonads. The kidneys receive branches from vessels close to them during their ascent, first from the common iliac artery, then from the distal end of the aorta; when the highest level is attained they receive new branches from the aorta and the former vessels degenerate. A permanent renal artery develops from one of the persisting branches (Sadler 1990). Malascent can occur because of ureteral or metanephric factors. The urinary tract originates from the mesoblast and has three developmental phases: pronephros, mesonephros, and metanephros. The third phase gives rise to the permanent kidneys. Initially, they localize close to each other at the ventral portion of the sacrum and pelvis. As the abdomen and pelvis grow and the body inclination decreases, they ascend and come into contact with the adrenal gland during the ninth week. The renal hila initially face the ventral aspect during ascent, then after a 90 degree medial turn the hilus of each kidney attains its final permanent position facing the anterolateral aspect. During ascent, the kidneys proceed through a bifurcation formed by the umbilical arteries. If one of the kidneys fails to pass this point, it remains within the pelvis next to the common iliac artery (Sadler 1990; Cocheteux et al. 2001; Cinman et al. 2007).

Signs of pelvic kidney

Most patients with an ectopic kidney are clinically asymptomatic. Signs and symptoms, when they occur, usually develop in the third or fourth decade of life and include vague lower abdominal pain, hematuria, and fever (Kato et al. 2000; Bhatnagar et al. 2004; Boyan et al. 2007). Vague abdominal complaints and pain due to an obstructing stone remain the most frequent symptoms of pelvic ectopic kidney. Acute pyelonephritis can present with the characteristic clinical and laboratory features of a ruptured appendix (Tsao et al. 2008). The prevalence of vesicoureteral reflux (VUR) and pelvic dilatation in renal ectopia is estimated at around 20%, although Calisti et al. (2008) found only a 2% prevalence of VUR. Dilatation of the renal pelvis could result from primary ureteropelvic or ureterovesical obstruction and extrarenal collecting systems with malrotation obstructing the ureteropelvic junction (Gleason et al. 1994). VUR occurs in 30% of children with ectopic kidneys (Guarino et al. 2004). The diagnosis of ectopic kidney in the pelvis can be made by ultrasonography (Lu et al. 2011). Malposition of the colon can suggest the ectopic position of a lumbar or pelvic kidney. The diagnosis is easily made when the excretory urogram or renal ultrasound fails to reveal a kidney in its proper location (Bauer 2002). Ectopic kidneys are more susceptible to the development of hydronephrosis, urinary tract infection, and urinary calculus. The abnormal position of ectopic kidneys results in atypical patterns of direct or referred pain and can be misdiagnosed as acute appendicitis. Pelvic organ inflammatory disease and dystocia could be signs of a pelvic kidney in women. A palpable abdominal mass and renovascular hypertension secondary to an anomalous blood supply could also be signs of pelvic and abdominal kidneys (Kumar et al. 2011). An ectopic kidney is often associated with other abnormalities such as agenesis of the opposite kidney, vascular malformation, and genital anomalies (Kato et al. 2000; Bhatnagar et al. 2004; Boyan et al. 2007).

Abnormalities associated with a pelvic kidney

Many urological abnormalities are associated with the orthotopic kidney, suggesting that renal ectopia is part of a urinary tract malformation complex. This underscores the need for a thorough examination including voiding cystourethrogram (VCUG) and radioisotope studies (Gonzalez et al. 2007). The associated abnormalities most commonly involve the genitourinary, musculoskeletal, and cardiovascular systems. Abnormalities of the uterus are found in 20–66% of women with renal ectopia: unicornuate uterus with or without rudimentary horn, bicornuate or absent uterus, and vaginal atresia or vaginal duplication have been reported (Bauer 2002) and cryptorchidism, hypospadias, or urethral duplications can occur. In most patients with an ectopic kidney, the contralateral kidney is normal. The most common congenital cardiovascular anomalies are septal or valvular defects; pulmonary agenesis and dextrocardia have rarely been reported with an ectopic kidney (Eroglu et al. 2005). Ureteral ectopia can be associated with imperforate anus and tracheoesophageal fistula (Cinman et al. 2007). Prenatal diagnosis of pelvic kidney is available after 24 weeks of gestation (Meizner et al. 1995). In men, associated genital abnormalities are seen in 10–20% of patients, including undescended testes, urethral duplication, and hypospadias (Kocak et al. 2001). The most common arterial variation of an orthotropic kidney is the presence of accessory arteries (28%). Accessory renal arteries vary in size and are usually derived from the aorta (26–30% of all reported kidneys); they can enter the kidneys at any point. The renal veins are less variable than the renal arteries; variations are more common on the right side (28%) (Bergman et al. 2006). Up to 50% of renal units contralateral to pelvic kidneys demonstrate some form of anatomical abnormality, and up to 10% are absent. The ectopic kidney is usually smaller than normal and does not necessarily conform to the usual reniform shape because fetal lobulations are retained. The axis of the kidney is slightly medial or vertical but can be tilted as much as 90° laterally, so that it lies in a true horizontal plane (Someren 1989; Gleason et al. 1994; Benchekroun et al. 2002). The association of pelvic kidney with aorto-iliac aneurysm is rare and has been reported in only 17 cases (Hanif et al. 2005; Marone et al. 2008). An ectopic (pelvic) kidney can be wrongly interpreted as a bulky lymph node, potentially subjecting the patient to operation (Bader et al. 2005). A severe atheromatous involvement of the distal aorta can impair the blood supply to the ectopic kidney (Dretler et al. 1971). Most ectopic kidneys have hydronephrosis of the collecting system. Half of these cases result from obstruction at the ureteropelvic or the ureterovesical junction

(Bauer 2002). An anteriorly placed collecting system of a pelvic kidney and an anomalous vasculature can partially block the major calyces and predispose the ectopic kidney to hydronephrosis. In addition, there is an increased risk of injury from blunt abdominal trauma because the low-lying kidney is not protected by the rib cage (Glodny et al. 2001; Benchekroun et al. 2002; Arnim et al. 2005; Ho et al. 2013). Association of a fused ectopic multicystic dysplastic kidney with ureterocele has been reported (Kiddoo et al. 2005).

Complications of pelvic kidney

Available data suggest no adverse effects on blood pressure or kidney function in children with renal ectopia. Vascular variations associated with an ectopic kidney can predispose to iatrogenic trauma during interventional procedures and emergency operations (Kara et al. 2011). Giant hydronephrosis in an ectopic kidney is an extremely rare disorder that can present as an asymptomatic abdominal mass (Hsieh et al. 2013). The vessels supplying an ectopic kidney usually arise from the nearest large vessels such as the iliac vessels. Trauma to these vessels can cause considerable bleeding and can lead to partial renal infarction or nephrectomy (Aslan et al. 1999). Ectopic kidneys can be associated with a variety of vascular anomalies, including anomalies of the contralateral renal vessels and branches and tributaries of the abdominal aorta and inferior vena cava (Belsare et al. 2002). A pelvic kidney interpreted as a lymph node conglomerate can create some diagnostic confusion (Chao 2012). Ectopic pelvic kidneys have been utilized successfully for kidney transplantation. However, all these donor nephrectomies were performed by open surgery (He and Mitchell 2012). In a woman with breast carcinoma presenting for a follow-up bone scan, initial inspection suggested sacral metastasis; on closer review an absence of renal activity in the left flank was however noted (Pryma and Akhurst 2005). Correlation with a CT scan confirmed a hydronephrotic ectopic kidney overlying the sacrum. Dystocia from a pelvic kidney is a very rare finding, but when it does occur early recognition is mandatory and cesarean section is indicated (Bauer 2002). In acute and elective obstetrical and gynecological operations, the pelvic kidney is susceptible to iatrogenic trauma (Dabiri and Cheung 2006). A pelvic kidney creates potential difficulties in the management of patients requiring aortic surgery (Krahn and Taylor 1993). The renal pelvis is usually anterior to the parenchyma, and surgical operation for acute appendicitis could create complications (Kara et al. 2011). Ectopic kidneys can be associated with autosomal dominant polycystic kidney disease (ADPKD) and a pelvic kidney has been associated with a reverse sigmoid colon (Chen et al. 2010). Renal cell carcinoma (RCC) is a very rare phenomenon in an ectopic kidney; there are only seven reports of RCC in pelvic kidneys (Mahmoudnejad et al. 2009). Surgical approach to ectopic kidneys merits caution because of the uncertain vascular anatomy (Hernández Toriz et al. 2006). In patients with pelvic kidneys, anterior views must be obtained during radionuclide scanning if unnecessary nephrectomy is to be avoided (Allen et al. 2005).

Horseshoe kidney

Horseshoe kidney (HSK) consists of two distinct kidneys lying vertically on either side of the midline and connected at their respective lower poles by a parenchymatous or fibrous isthmus that crosses the midplane of the body. It was first recognized during an autopsy by DeCarpi in 1521 (Weizer et al. 2003). It represents one of the most commonly renal anomalies with a reported incidence of 1/400 to 1/1600 based on autopsy series performed half a century ago. It combines three anatomical abnormalities: sectopia, malrotation, and vascular changes. In rare cases the isthmus connects the upper poles and an inverted HSK is created (Yoshinaga et al. 2002). The kidneys are somewhat low lying and close to the vertebral column, so that a line drawn through the midplane of each kidney bisects the midline inferiorly; this is the characteristic orientation of the collecting system, which is directly posterior to each renal pelvis (Strauss et al. 2000). The failure of normal rotation in HSK cases is responsible for the atypical arrangement of the pelvicalyceal system. The renal hilum lies anteriorly to the calyces, which can point inward toward the spinal column, downward, or both (Gupta et al. 2007).

The presence of HSK can be confirmed by an ultrasound scan or an IVP. When abdominal and retroperitoneal images from 15,320 radiographs, especially from computerized tomography (CT), were evaluated, 23 patients were identified with HSK giving an overall incidence of 1/666. This closely matches past autopsy series in which the reported incidences were 1/400 to 1/1600. The abnormality has been discovered clinically in all age groups ranging from fetal life to 80 years; it is more common in males by a margin slightly greater than 2:1 (Basar et al. 1999; Hobbs et al. 2002; Weizer et al. 2003). No genetic and racial predominance is known, although HSK has been reported in identical twins and in siblings within the same family (Gleason and Kraemer 1995; Yoshinaga et al. 2002). In a study of 1957 potential living kidney donors, solitary or horseshoe or pelvic kidney was found in 0.2% (Lorenz et al. 2010).

HSK is usually asymptomatic and it is revealed incidentally during imaging, but gastrointestinal symptoms such as pain, nausea, and vomiting can occur. In 5% of cases HSK is diagnosed when patients are evaluated for an abdominal mass, a vague abdominal pain possibly radiating to the lower lumbar region. Symptoms, if any, are related to hydronephrosis, infection, or calculus formation. A possible sign is abdominal pain, nausea, and vomiting on hyperextension of the spine. Horseshoe kidneys have been detected after angiography for evaluation of an abdominal aortic aneurysm (Huber et al. 1990; de Brito et al. 1991). An obstruction causing significant hydronephrosis occurs in one-third of patients. Multiple retinal arteries are found in most HSKs and can be an intraoperative hazard for patients due to the risk of unexpected hemorrhage. Precise imaging using modern cross-sectional imaging techniques is therefore very important for preoperative planning (Natsis et al. 2014).

The ureteral bud arises from the Wolffian duct at the end of the fourth week and grows craniad toward the urogenital ridge, acquiring a cap of blastema by the fifth week. The developing metanephric tissue and ureteral bud migrate cephalad, rotating medially on its long axis. The entire process is completed by the eighth week of gestation. The abnormality arises between the fourth and sixth weeks, after the ureteral bud has entered the renal metanephric blastema. Posterior nephrogenic cells migrate abnormally to form an isthmus or connection between the two developing kidneys, creating the horseshoe shape. Because the kidney fails to rotate, the calyces point posteriorly and the axis of each pelvis remains in the vertical or obliquely lateral plane (Weizer et al. 2003).

There are two hypotheses regarding the embryogenesis of HSK. The classical proposal is that during the metanephric stage (fourth week of gestation) while the kidneys are still in the pelvis, their lower poles come into contact and fuse at the midline, forming a HSK with a fibrous isthmus. This fusion can be attributed to abnormal flexion or growth of the developing spine and pelvic organs, causing fusion of the nephrogenic blastemas of the immature kidneys, which lack renal capsules. Normally, the kidneys migrate out of the pelvis during the seventh and eighth weeks and at the same time rotate so that the anteriorly facing renal pelvis turns medially. At the level of the lower lumbar vertebrae, the inferior mesenteric artery (IMA) blocks their upward migration (Cascio et al. 2002; Tijerina et al. 2009). The alternative proposal is that HSK results from a teratogenic event involving the abnormal migration of posterior nephrogenic cells to form a parenchymal isthmus. This could explain the increased incidence of malignancies associated with HSK, such as Wilms' tumor and HSK carcinoid (O'Brien et al. 2008). Prenatal diagnosis is also possible as early as the first trimester of pregnancy, using high-frequency transvaginal sonography (Bronstein et al. 1990).

HSK patients are at risk of reflux, stasis, stone, and infection. Infections complicate up to one-third of HSK patients and are a major cause of death among them (Fernbach and Davis 1986). A variety of benign and malignant tumors are also associated with HSK. The increase in malignancy is attributed to teratogenic factors. Most cases are associated with renal cell carcinoma. Transitional cell carcinoma is related to chronic infections and stone. The incidence of Wilms' tumor is higher than in the general population. Benign tumors that usually accompany HSK include renal angiolipoma and oncocytoma (O'Brien et al. 2008). Horseshoe kidney should not adversely affect pregnancy or delivery. The lower ureter usually enters the bladder normally and is rarely ectopic. Any ureteropelvic junction (UPJ) obstruction probably results from high insertion of the ureters into the renal pelvis. In rare cases, crossing of the ureter over the isthmus can also contribute to a higher prevalence of UPJ. The main complication of HSK is stone formation (16–60% of cases). The orientation of the calyces impairs proper drainage, resulting in stasis and hence stones which are often multiple; there is a significantly increased incidence of staghorn stones (Natsis et al. 2005). HSK predisposes the patient to serious injuries following abdominal trauma (Natsis et al. 2013).

The isthmus is bulky and consists of parenchymatous tissue with its own blood supply. Occasionally it is just a flimsy midline structure composed of fibrous tissue. It usually lies anterior to the aorta and vena cava. Teratogenic factors could be responsible for the abnormal migration of nephrogenic cells to form an isthmus and for the increased potential for carcinoma development in this portion of the kidney (Doménech-Mateu and Gonzalez-Compta 1988; Hohenfellner et al. 1992). The incidence of Wilms' tumor in horseshoe kidneys is more than twice that in the general population. Renal carcinoma has been reported within a horseshoe kidney (Mesrobian et al. 1985; Neville et al. 2002). The isthmus is situated at the level of the third or fifth lumbar vertebra, under the origin of the inferior mesenteric artery (IMA) and anterior to the abdominal aorta (AA) and inferior vena cava (IVC). Rarely, the isthmus is reported to lie posteriorly to the vessels or to run between them. Sometimes it is located at the pelvis or at the sacral promontory (O'Brien et al. 2008).

There is wide variation in the arterial supply to HSKs, considering that the renal arteries (RA) can originate from the AA, the common iliac arteries (CIA), and the IMA. The isthmus can be supplied by a single vessel derived from the AA, or alternatively its blood supply can originate from CIA or IMA (Ferko et al. 1997). The HSK can be supplied by both normal and accessory RAs. With the exception of some of the arteries to the isthmus, no vessel on the dorsal aspect of the kidney has been described. Multiple RAs have been reported in 45 out of 71 reported HSK cases (63%); one or two RAs have been reported in the other 26 (37%). Because of these variations, *en bloc* removal of an HSK with large segments of the AA and IVC is proposed when the HSK is considered as an allograft organ (Stroosma et al. 2000; Goyal et al. 2003). The HSK is frequently accompanied by a retrocaval ureter (Shen et al. 2012) and there are IVC abnormalities such as double, left, and pre-isthmic IVCs in 5.7% of cases (Radermecker et al. 2008; Ichikawa et al. 2012). It is also argued that HSK is associated with cardiovascular malformations (Greenwood et al. 1976) and it is frequently associated with vascular and ureteral abnormalities: ureteral duplication, ureteroceles, UPJ obstruction, vesicoureteral reflux, hydronephrosis, and nephrolithiasis. In 30% of cases there is one RA per kidney. The blood supplies to the isthmus and lower poles are also variable; the isthmus and adjacent parenchymal masses can receive a branch from each main renal artery or have their own arterial supplies originating directly from the aorta or even from branches originating from the inferior mesenteric, common or external iliac, or sacral arteries.

There are many variations in the number and origin of renal-collecting systems in HSK. As a rule, calyces are located in the upper two-thirds of each kidney and an extrarenal calyx or an independent ureter drains the isthmus. The ureters normally end in the bladder, but they can also be ectopic (Cascio et al. 2002). Retrocaval ureter (RCU) is a rare congenital abnormality

associated with HSK, and a pre-isthmic IVC is the direct cause of hydronephrosis and UPJ obstruction. Because the kidney fails to rotate, the calyces point posteriorly and the axis of each pelvis remains in the vertical or obliquely lateral plane.

There are central nervous system problems in 3% of children with HSK. Anorectal abnormalities are frequently encountered in these patients (Salerno et al. 2000). Duplication of the ureter occurs in 10% of patients; vesicoureteral reflux has been noted in more than half of affected individuals (Cascio et al. 2002). DMSA scanning (radionuclide scanning using dimercaptosuccinic acid) of 22 patients with HSK revealed asymmetrical function in 63% (Kao et al. 2003). Metabolic evaluation of 37 patients with HSK revealed altered calcium, oxalate, uric acid, and citrate excretion in 50% of stone formers, suggesting an additional underlying metabolic etiology (Raj et al. 2004). Patau and Gardner syndromes (trisomy 13 and deletion q15q22) have been reported to coexist with HSK. It has also been mentioned that 20% of Down and Edwards syndromes (trisomies 21 and 18, respectively) and 60% of Turner syndromes possess a HSK. The HSK has rarely been related to oral–cranial–digital syndrome or other skeletal abnormalities such as kyphosis, scoliosis, and macrognathia, or to neurological abnormalities. Other associated abnormalities include supernumerary kidneys with horseshoe elements, undescended testis, septate vagina and hypospadias (Mandell et al. 1996; O'Brien et al. 2008).

Sigmoid-shaped kidney

The sigmoid or S-shaped kidney is the second most common anomaly of fusion. The crossed kidney is inferior with the two kidneys fused at their adjacent poles. Each renal pelvis is oriented correctly and they face in opposite directions from one another. An S-shaped kidney is the source of trouble and urogram appearance. The estimated occurrence of a sigmoid-shaped kidney is 1:1000. The lower convex border of one kidney is directly opposite the outer border of its counterpart. The adrenal glands are normally situated. The ureter from the normal kidney courses downward anterior to the outer border of the inferior kidney, and the ectopic kidney's ureter crosses the midline before entering the bladder; at times, the ectopic ureter may pass behind the rectum as it crosses the pelvis.

Intrathoracic kidney

Intrathoracic renal ectopia is a rare congenital malformation. It is often asymptomatic and diagnosed incidentally during the work-up for a possible lung mass near the midline and on the posterior mediastinum along the posterior aspect of the diaphragmatic leaflet on a lateral view (Vázquez et al. 2008). It does not require treatment. Its incidence ranges over 0.5–5% of renal ectopia, with a prevalence of one in 10,000 cases. The condition is rarely bilateral; it occurs mostly on the left side (61%) and in males (1.7:1) (Subramanian and Goldfarb 2008). Four forms of intrathoracic kidney have been documented: a true thoracic ectopia with normally developed diaphragm, congenital diaphragmatic eventration, diaphragmatic hernia, and renal ectopia associated with traumatic rupture of the diaphragm (Pfister-Goedeke and Brunier 1979; Donat and Donat 1988; Hidaka et al. 2012). Wolfromm (1940) reported the first case of intrathoracic kidney, clinically diagnosed by retrograde pyelography in a 43-year-old woman. Intrathoracic ectopia denotes either a partial or a complete protrusion of the kidney above the level of the diaphragm into the posterior mediastinum. A high-positioned kidney can lead to focal eventration of the overlying diaphragm, mimicking a supradiaphragmatic renal position.

Congenital intrathoracic kidney is a rare developmental anomaly; in 13,000 autopsies 27 ectopic kidneys were encountered, and only one of them was intrathoracic (Campbell 1930). This condition is to be differentiated from a congenital or traumatic diaphragmatic hernia, in which other abdominal organs as well as the kidney have advanced into the chest cavity (Drop et al. 2003).

A superior ectopic kidney can appear above, below, or partly through the diaphragm. In the supradiaphragmatic position the kidney lies opposite T7–T9, while in the transdiaphragmatic position it lies opposite T7–11. True thoracic ectopia with a normally developed diaphragm is less common than other types (Kubricht et al. 1999). The kidney usually has a rotation anomaly with the hilus facing anteriorly, a high origin of the renal vessels, a long normal ureter, and medial deviation of the lower pole. Nevertheless, the function of the affected kidney is usually well preserved (Sözübir et al. 2005; Obatake et al. 2006; Dingeldein et al. 2008; Fadaii et al. 2008). A combination of intrathoracic liver and kidney has been reported (Lee et al. 2006). The ureter is elongated to accommodate the excessive distance to the bladder, but it never enters ectopically into the bladder or other pelvic sites.

The adrenal gland is below the kidney, in its normal location, in most of these patients (N'Guessan and Stephens 1983). An abnormally high ascent of the metanephros generates a diaphragmatic defect and subsequently an ectopic kidney in the thorax. An intrathoracic ectopic kidney can be either congenital or acquired. The mechanism by which the kidney migrates to a superior position is not known. It reaches its adult location by the end of the eighth week of gestation when the diaphragmatic leaflets are formed as the pleuroperitoneal membrane, which separates the pleural from the peritoneal cavity. Mesenchymal tissues associated with this membrane eventually form the muscular component of the diaphragm. Delayed closure of the diaphragmatic leaflets allows the kidneys to ascend above the level of the future diaphragm (N'Guessan and Stephens 1983). Delayed involution of mesonephric tissue has also been proposed as a causal factor (Angulo et al. 1992), and intrathoracic kidneys occur in only 0.25% of patients with a diaphragmatic hernia (Donat and Donat 1988). Renal angiography demonstrates either a normal site or a more cranial origin for the renal artery takeoff from the aorta supplying the thoracic kidney.

Plain chest X-ray usually reveals a paravertebral mass in the posterior mediastinum. It should be differentiated from other posterior mediastinal masses. Intravenous urography has been used as a routine method of diagnosis for differentiating other lesions such as mediastinal tumors and hernia (Obatake et al. 2006; Rouanne et al. 2010). The affected hemidiaphragm is usually slightly elevated. The diagnosis should be considered in a patient with a mass at the base of the lung on a chest radiograph (Sidhu et al. 2001). The diagnosis is confirmed by CT or contrast-enhanced CT scan and intravenous urography or magnetic resonance imaging of the kidney (William and Jeans 1996; Clarkson and Potter 2009). Renal cortical scintigraphy could be used to confirm the functional status of the kidney tissue (Louzir et al. 1999; Sözübir et al. 2005). In a reported case of atypical chest pain after myocardial scintigraphy that revealed a large thallium-avid mass in the right hemithorax, subsequent photon emission computed tomography/computed tomography demonstrated the mass to be an ectopic kidney (Du et al. 2010).

Most affected individuals remain asymptomatic. Pulmonary symptoms are exceedingly rare and urinary symptoms are even more infrequent. Most previously reported cases were asymptomatic and were discovered incidentally during investigations for other medical problems. The usual complications such as infection, stone formation, and ureteropelvic junction obstruction that accompany inferior ectopic kidneys such as pelvic kidney are rarely seen in thoracic cases. There are occasional reports of association with nonspecific chest, abdominal, and flank pain (Oon et al. 2005; Fadaii et al. 2008; Subramanian and Goldfarb 2008; Ahmed et al. 2011), urinary stones, or renal carcinoma (Kubricht et al. 1999; Lenz et al. 2003). Spontaneous intracranial hypotension presenting as aggravated headache after sitting and standing was the presenting sign in a young adult with intrathoracic kidney; a focal paraspinal area of increased uptake first supposed to be a site of CSF leakage was then identified by radionuclide cisternography as an intrathoracic renal ectopia (Chiu et al. 2012; Pandey et al. 2012). Left thoracic kidney associated with left Bochdalek hernia has been reported in late adulthood (Karaoglanoglu et al. 2006; Fiaschetti et al. 2010). History of trauma should be considered in patients with intrathoracic kidney (Suárez and de Jesús 1998). Intrathoracic kidney can also be discovered incidentally in the elderly (Sfaxi et al. 2002).

In the neonatal period, sudden breathing difficulties and recurrent attacks of pulmonary infections, cough, wheezing, and vomiting have been reported as the first presenting sign (Karaoglanoglu et al. 2006; Maduekwe et al. 2011). Intrathoracic ectopia with a Bochdalek defect has been reported as a right posterior mediastinal mass and intestinal gas in the right lung field (Obatake et al. 2006). Color Doppler can demonstrate an abnormal course of the renal artery, arising from the aorta and feeding the intrathoracic right kidney; this could provide a diagnosis of thoracic kidney in the prenatal period (Masturzo et al. 2001). Only 13 cases of intrathoracic kidney have been reported in the pediatric age group over the past 25 years. Although the early literature recommended an aggressive surgical approach for all intrathoracic kidneys, surgeons have taken a more selective approach during recent decades. Surgical treatment has been reserved for children with associated bowel herniation or respiratory compromise, as in the case of a child with bilateral intrathoracic kidneys. There is concern about the ongoing growth and development of intrathoracic kidneys due to the potential for vascular or ureteric obstruction. Most symptomatic patients present with respiratory distress (Murphy et al. 2012). A persistent cough for five months with no history of pulmonary infection, and respiratory distress immediately after birth, were the first clues to intrathoracic kidney in a newborn infant and a neonate (Nouri-Merchaoui et al. 2011). It is extremely rare for an intrathoracic kidney to be detected prenatally in a fetus with congenital diaphragmatic hernia (CDH) (Pfister-Goedeke and Brunier 1979; Hidaka et al. 2012). Pneumomediastinum has been reported as the presenting sign of intrathoracic kidney in a neonate (Matsubara et al. 2000).

When the kidneys are not in their normal position but the bladder and amniotic fluid volume are normal, thoracic kidneys should be suspected (Muttarak et al. 2001). Color Doppler ultrasound imaging facilitates identification of the kidneys, as the renal arteries can be seen coursing in a cephalad direction (Suresh et al. 2007). Ureteropelvic junction obstruction in a thoracic kidney causing flank pain has been reported (Hamptom and Borden 2002).

A case of intrathoracic kidney with superimposed renal cell carcinoma has been reported; the patient first presented with hyponatremia and inappropriate antidiuretic hormone secretion (Kubricht et al. 1999). It is usually accompanied by a defect in the hemidiaphragm. Right-sided Bochdalek hernia with dilated colon loops and right kidney within a right hemithorax has been reported (Karaoglanoglu et al. 2006). Rarely, an intrathoracic kidney possesses congenital anomalies such as ureteropelvic junction obstruction, malpositioning, and duplication of the renal pelvis and ureters (Hamptom and Borden 2002). The combination of a duplex system with an intrathoracic renal ectopia is very rare (Beltrán Armada et al. 2004). Association of bilateral intrathoracic kidneys with bilateral diaphragmatic hernias has been reported (Dingeldein et al. 2008).

In the absence of other anomalies or abnormal renal function, an intrathoracic kidney does not interfere with the techniques used during coronary bypass surgery in cases with more than one renal artery. In various studies, a possible association between multiple renal arteries and hypertension has been reported (Glodny et al. 2001; Kem et al. 2005).

An intrathoracic kidney associated with bowel in the chest should undergo standard repair and nephropexy. An isolated intrathoracic kidney without evidence of bowel herniation can safely be ignored (Murphy et al. 2012); in the absence of other renal pathology it requires no surgical intervention (Subramanian and Goldfarb 2008; Murphy et al. 2012). Congenital intrathoracic kidney requires neither medical nor surgical treatment; in cases of posttraumatic diaphragmatic hernia it must be promptly treated surgically (Rouanne et al. 2010),

reducing the intrathoracic kidney into the abdomen (Nouri-Merchaoui et al. 2011).

Ectopic kidneys other than Horseshoe Kidney

Cross-fused ectopic kidney is a congenital displacement of one kidney to the opposite side of the body, and is associated with an increased incidence of congenital and acquired anomalies (Collura et al. 2004; Chung et al. 2009). The causes of a crossed ectopic kidney are unclear; the autopsy incidence is one in 22,000. Crossed renal ectopia usually occurs from left to right, is found more often (3:2) in males than in females (Stimac et al. 2004; Kwon et al. 2004), and can be of various types such as unilateral fused kidney with inferior ectopia, sigmoid or S-shaped kidney, lump or cake-shaped kidney, L-shaped or tandem kidney, disk, shield, or doughnut-shaped kidneys, and unilateral fused kidneys with superior ectopia (Stuart et al. 1992). The ectopic kidney usually functions well unless malrotation affects its excretory capacity. In crossed renal ectopia the kidney is located contralateral to the side where the ureter enters the bladder, usually below the orthotopic organ, and in 90% of cases is fused to the normal kidney (Sood et al. 2005). In this position the wolffian duct (and with it the ureteral bud) crosses over the midline and fuses with the contralateral nephrogenic cord (Cook and Stephens 1977a, b). Crossed renal ectopia, in which one kidney lies on the contralateral side but its ureter passes to the ipsilateral side, is the second most common renal fusion anomaly following horseshoe kidney (Kwon et al. 2004; Boyan et al. 2007).

L-shaped kidney

L-shaped (tandem) crossed renal ectopia is a rare congenital anomaly. It occurs when the crossed kidney assumes a transverse position at the time of its attachment to the inferior pole of the normal kidney. The crossed kidney lies in the midline or in the contralateral paramedian space anterior to the L4 vertebra. Rotation about the long axis of the kidney can produce either an inverted or a reversed pelvic position. The ureter from each kidney enters the bladder on its respective side. Abdominal pain is a major symptom and staghorn calculi in both renal moieties have been reported (Chung et al. 2009; Mishra et al. 2013). Associations of an inverted L-shaped renal ectopia with inverted-Y ureteral duplication, ectopic ureter, and bicornuate uteruses have also been reported (Liu et al. 2010).

Disk kidney

Disk, shield, doughnut, or pancake kidneys are unusual anatomical anomalies that result when both the upper and lower poles of the embryonic kidney become fused at their medial borders to produce a doughnut- or ring-shaped mass. The renal parenchymal mass is located in the pelvis, generally with two pelves and two ureters and with no intervening fibrous septum. The lateral aspect of each kidney retains its normal contour (Heidempergher et al. 2012). This type of fusion differs from the lump or cake kidney in that the reniform shape is better preserved due to the somewhat less extensive degree of fusion. The pelves are anteriorly placed and the ureters remain uncrossed. Renal rhabdomyosarcoma (RMS) is a rare pediatric tumor that was discovered in a 4-year-old boy with metastases to the lung, pelvis, and bone marrow (Walther et al. 2013). This anomaly creates a great technical challenge during aortic reconstruction (Eze et al. 1998).

Lump kidney

A pelvic cake kidney in which there is complete fusion of both kidneys into a single renal parenchymal mass has been described as the rarest of renal fusion anomalies. It can be diagnosed at any age group from childhood to the eighth decade of life and is not necessarily associated with a poor prognosis (Rosenkranz et al. 2010; Schwartz et al. 2010). However, complications potentially associated with anatomical malformations such as urinary stasis, infection, formation of stones, and vascular involvement can cause serious clinical problems. Cake kidneys probably form because the nephrogenic blastemas are compressed between the umbilical arteries at the beginning of the cranial migration of the ureteral buds, and this could lead to their fusion. There has been extensive joining over a wide margin of the maturing renal anlage. The total kidney mass is irregular and lobulated. Ascent usually progresses only as far as the sacral promontory, but in many instances the kidney remains within the true pelvis. Both renal pelves are anterior and they drain separate areas of the parenchyma (Rosenkranz et al. 2010; Schwartz et al. 2010). The ureters do not cross. Most diagnosed cases have been reported to present malformations in other organs or in their blood supply, including abnormal testicular migration, Fallot's tetralogy, vaginal or sacral agenesia, and anal abnormalities. A pelvic cake kidney most commonly drains via two separate ureters; fewer than 10 reports demonstrate a cake kidney drained by a single ureter. In such instances other concomitant abnormalities such as unicornuate uterus or bilateral absence of the vas deferens has been reported (Goren and Eidelman 1987; Martinez-Lazaro and Cortes-Blanco 2000; Calado et al. 2004; Rosenkranz et al. 2010; Schwartz et al. 2010).

Symptoms

Most cases of renal ectopia remain asymptomatic during life and are found incidentally or detected only when complications arise. If manifestations do occur, they usually develop during the third or fourth decade of life and include vague lower abdominal symptoms such as urinary infections, urolithiasis, and abdominal mass (Kwon et al. 2004; Boyan et al. 2007; Ghosh et al. 2008). In different autopsy series it is detected in 1 in 1000–7000 (Hwang et al. 2002), and the number of cases found clinically is estimated to be only 1 in 10,000 patients (Bhatnagar et al. 2004; Guarino et al. 2004). In 0.2% of 12,000 patients investigated for the cause of abdominal pain, renal ectopia was found (Asghar and Wazir 2008), a condition of "pancake kidney"

eventually associated with polycystic disease and abnormal vascular supply. Hypertension and microscopic hematuria were the only clinical signs.

Associated anomalies

There have been reports of uncertain anatomy with multiple renal arteries and veins. Surgeons should be aware of ectopic and fused kidneys to minimize perioperative complications because of this uncertain anatomy. The surgical procedure must be planned according to the anatomical variations of each patient, and the anatomy of the patient's urinary system should be assessed with CT, IVP, and angiography. Crossed ectopia is always combined with abnormally located ureters, which cross the midline at the level of the distal aorta or its bifurcation to enter the bladder at the normal position (Yano et al. 2003; Guarino et al. 2004; Sood et al. 2005). Demonstration of crossed renal ectopia is important because it is a predisposing factor for obstruction, infection, and neoplasia of the urinary system (Boyan et al. 2007). Patients with fusion anomalies have a significantly higher risk of developing certain renal and urothelial tumors possibly related to embryogenic mechanisms, urinary stasis, and infection (Miller and Kropp 1992; Stimac et al. 2004). Rarely, crossed renal ectopia is associated with herniation of the ureter into an inguinal hernia (Rocklin et al. 1989; Hwang et al. 2002). It is usually associated with congenital anomalies of the gut. Development of malignancy in crossed fused ectopic kidney is uncommon. Many other associated syndromes and anomalies have been reported such as Klippel–Feil syndrome, various urogenital anomalies, imperforate anus, TAR syndrome, or cardiovascular septal defects. In cases of familial incidence, autosomal dominant inheritance has been reported (Rinat et al. 2001). There are reported cases of renal cell carcinoma, squamous cell carcinoma of renal pelvis origin, Wilm's tumor, and adenocarcinoma associated with crossed fused renal ectopia (Cook and Stephens 1977a, b; Redman and Beryl 1997; Aquilera Tubet et al. 2005). A lump in the lower abdomen and painless hematuria are signs of malignant involvement of an ectopic kidney (Soni et al. 2012). Associations with the absence of the vas deferens, cryptorchidism, and skeletal abnormalities have been reported. Caudal regression syndrome consists of multiple congenital anomalies, including imperforated anus, rectovesical fistula, sacral agenesis, vertebral anomalies, and club feet. Crossed fused renal ectopia can be associated with fused ureters and urinary obstruction (Duh et al. 2007). Polycystic changes in a pancake kidney have been reported (Heidempergher et al. 2012).

Diagnosis

It has been suggested that crossover and fusion with the opposite kidney could be caused by over-bending and rotation of the caudal end of the embryo. The increased prevalence of crossed renal ectopia in patients with scoliosis supports this hypothesis (Bauer et al. 1992). In most cases the fusion is between the lower pole of the orthotopic kidney and the upper pole of the ectopic kidney. Association with müllerian agenesis has also been reported with a 40% incidence of renal anomalies (Sen and Kapoor 2006). Genitourinary anomalies can present a formidable challenge to the vascular surgeon during abdominal aortic reconstruction. Because of the risk for injury to the kidney during surgery, preoperative evaluation of this anomaly must include computed tomography, angiography, and intravenous pyelography. Preoperative placement of a ureteral catheter can also prevent injury to the anomalous ureter (Yano et al. 2003). Pancake kidney has been associated with bilateral iliac artery aneurysms (Eckes and Lawrence 1997).

Crossed renal ectopia can usually be diagnosed by intravenous urography. Other methods include ultrasonography, intravenous pyelography, computerized tomography, and andrenal scintigraphy (Sharma et al. 2006; Boyan et al. 2007). CT also helps to identify metastatic disease. MRI is another modality for characterizing a focal renal mass. RCC is typically mildly hypointense on T1-weighted and hyperintense on T2-weighted images. Association of squamous cell carcinoma or RCC with crossed fused renal ectopia is relatively rare. CT or MR angiography is a required preoperative study for imaging the supplying vessels; if there are malignant mass lesions a heminephrectomy can be performed (Kraft et al. 2007; Kumar et al. 2008; Liu et al. 2010). Renal cortical scintigraphy is useful for locating the poorly functioning kidney for surgical removal (Gharagozloo and Lebowitz 1995). Diagnosis of renal ectopia can be an accidental finding during scintigraphy performed for other reasons (Cohn and Roach 2003).

Treatment

Treatment of crossed-fused renal ectopia is indicated when complications rather than the anomaly itself require intervention (Ghosh et al. 2008; Liu et al. 2010). Most individuals with crossed renal ectopia have normal longevity and good prognosis. However, some patients are at risk of developing urinary tract infections or renal calculi; Boatman et al. (1972) noted that one-third of their symptomatic patients required a pyelolithotomy. Extracorporeal shock wave lithotripsy therapy and percutaneous nephrolithotomy have rendered most of these unusual patients stone-free (Semerci et al. 1997; Desai and Jasani 2000). If investigations demonstrate an obstruction, surgery to prevent complications can be required (Taslim et al. 2012).

Abnormalities of rotation

Rotational anomalies of kidney are rare (Das and Amar 1984; Nathan and Glezer 1984). During normal development the kidney ascends from its original pelvic position to its final location at the end of the eighth week. It also undergoes rotation so that the hilum, which initially faced its ventral aspect, comes to lie on its medial aspect. This occurs during the ascent of the kidney, between 38 and 49 days of development. When renal rotation takes place before definitive vascularization (Pollack

and McClennan 2000) the hilum is directed anteriorly rather than medially. The true incidence of this condition is underestimated because in many patients it is asympotomatic. Different types of rotation abnormalities have been reported: in unrotated kidneys the renal pelvises face ventrally; in incomplete rotation they face venteromedially; in some cases there is excessive rotation. In the rare reverse and excessive rotation cases, the renal pelvis presents itself in a position depending upon the number of degrees of rotation completed (Das and Amar 1984; Atasever et al. 1992; Pollack and McClennan 2000). Bilateral non-rotation of the kidneys has been reported in an 82-year-old female (Moore et al. 2011).

Renal arteries develop from the lateral splanchnic arteries, which form a network on either side of the aorta. Accessory renal vessels arise as a result of the complicated development and positional anatomy of the kidneys (Bayramoglu et al. 2003). Anomalies associated with rotation of the kidneys, either unilateral or bilateral, are often caused by or related to aberrant vessels and often receive an accessory arterial branch. The accessory arteries usually enter the renal cortex at one of the poles. Accessory renal arteries most commonly pass anterior to the ureter; they are sometimes encountered in patients with hydronephrosis (Malament et al. 1961; Hollinshead 1971; Nathan and Glezer 1984). The accessory vessels can also be located posterior to the ureter, closely related to the ureteropelvic junction (Bayramoglu et al. 2003), creating a clinically important condition.

Although rare, rotational anomalies have important surgical implications because they can be mistaken for a paravertebral mass, and the anterolateral deviation of the urinary system sometimes creates an impression of a lower pole mass. Abnormal rotation creates problems during percutaneous nephrectomy. Anomalies of renal rotation are associated with renal ectopia and fusional abnormalities but can be exhibited with no additional abnormality (Braasch 1931). The possible presence of an accessory renal artery should be considered in abnormally rotated kidney cases (Braasch 1931; Olsson and Wholey 1964). A rare anomaly of the kidneys and its vessels was found in a white adult male cadaver. The anomaly consisted of unrotated kidneys with partially extrarenal calices and pelves. In addition to the normal vessels, each kidney received a branch from a common trunk, originating from the inferior end of the aorta (Nathan and Glezer 1984).

Nephroptosis

Nephroptosis has been defined as renal descent of 5 cm or more (or two vertebral bodies) on changing from the recumbent position to orthostasis. Noted as a common finding, it rarely produces symptoms. It is said to be more common in women and to affect the right kidney more often than the left; it is bilateral in 20% of cases. It has been observed predominantly in slim young women with little supportive perirenal fat. The classical history is of flank pain in the upright position that reduces or is relieved by lying down. It can be associated with intermittent functional excretory obstruction, with forceful traction on the renal artery leading to renal ischemia and with traction on the perirenal nerves. Historically a number of symptoms have at one time or another been linked to this finding. However, it is nephroptotic pain that dominates the picture, although recurrent upper tract urosepsis, hypertension, and renal stone disease have also been linked. Nowadays, a diagnosis based on symptoms can be confirmed by contrast imaging and/or renography, which demonstrate the classical renal descent with significant rotation and decrease in renal blood flow on moving from the supine to the erect state, respectively (Tatevosian et al. 2004). Erect and supine IV urograms or renal scans documenting obstruction are practical diagnostic tests for the condition (see *Campbell's Urology*). New criteria for diagnosing symptomatic nephroptosis and the introduction of imaging and laparoscopic surgical management have replaced the more exotic and unnecessary surgical procedures employed in the past (Moss 1997; Hatzinger et al. 2007).

History

The idea of renal 'ptosis' was described by Matthew Baillie in 1825. Shortly afterwards in 1939, Rayer concluded that this condition was far more common than formerly appreciated; it was frequently overlooked and the patient was often wrongly diagnosed with nervous colic, hypochondria, or lumbosciatic neuralgia. The first nephropexy procedure was performed in 1881 (McWhinnie and Hamilton 1984; O'Reilly and Pollard 1988; Moss 1997; Boccardo 1999). Renal ptosis has a contentious and colorful history. Recently trained physicians are often unfamiliar with it. Over the centuries the condition has received numerous labels including: the moveable kidney, the floating kidney, renmobilis renmigrans, and Wanderniere. Nephropexy, once a routine operation, almost disappeared from American practice more than 40 years ago. Nearly 200 surgical procedures described for this condition were suddenly eclipsed. The label 'an ineffective treatment for an imaginary disease' then stuck to the condition of nephroptosis and its surgical management (Barber and Thompson 2004; Hatzinger et al. 2007).

Floating kidney

Floating kidney and nephroptosis are exactly the same entity; the former term seems to have referred to a self-reducible ptosis. Pierre Rayer discussed the issue extensively in his great monograph on the kidney (published in 1839), noting that the right kidney is more prone to floating than the left. Rayer also recounted the sad tale of a doctor who felt his own kidney floating while taking a bath, and promptly retired from practice to prepare himself for death (Bynum 2001). The first nephropexy was performed in 1881. From that time, surgical treatment of nephroptosis has remained a subject of discussion. By 1936, approximately 170 different surgical methods existed for fixation of the kidney. An accurate diagnosis is imperative before

performing nephropexy. There were times when this operation was carried out much too often, giving it a bad reputation (Moss 1997; Hatzinger et al. 2011). In the past the diagnosis has probably been frequently mistaken, but we should caution against completely rejecting it; it can happen in some special cases. By definition of the 'floating state', the kidneys move at least two vertebral bodies downward in the vertical position, and this movement can be detected by radiography. Also, retrograde pyelography revealed a delay in emptying the renal pelvis in one patient with suspected floating right kidney. Although diagnosis has frequently been wrong in the past and many unnecessary operations have been performed, present imaging techniques make it possible to diagnose the occasional genuine cases of nephroptosis (Newling 2001).

Primary megaureter

Megaureter was first described by Caulk in 1923. Congenital megaureter is a condition usually diagnosed in neonates and children; it is hypothesized to result from failure of the ureterovesical junction (UVJ) to mature or from ureteral wall muscle-fiber abnormalities (Hanna and Wyatt 1975; Gosling and Dixon 1978). Diagnostic criteria include: dilated ureter, absence of vesicoureteral reflux, absence of infravesical obstruction, and absence of distal ureteral obstruction (Domini et al. 1999; Khoury and Bagli 2007). Primary nonrefluxing megaureter is usually a functional and benign congenital malformation that resolves spontaneously. Only a few cases require surgical treatment; this should be reserved for patients who develop ureteral dilation, a decrease in renal function, and/or severe symptoms during follow-up (Areses Trapote et al. 2007). A primary megaureter is an anomaly with a pre-vesical or overall dilated ureter with a diameter of more than 6 mm.

It is important to distinguish between cases of primary nonrefluxing and primary obstructive-refluxing megaureters as they require completely different treatments. The basic diagnostic work-up includes ultrasonography and voiding cystourethrography. Diuretic renography is used to detect the degree of upper urinary tract obstruction. In contrast to most cases of primary non-refluxing megaureter, obstructive refluxing megaureters commonly need to be corrected. Antibiotic prophylaxis can be indicated in infants with a primary obstructive megaureter during the first six months of life because there is a higher risk of complications due to pyelonephritis (Anheuser et al. 2013). Most cases of primary megaureter (PM) resolve spontaneously, but long-term follow-up is recommended because symptoms can develop years later (Di Renzo et al. 2013). A high rate of spontaneous resolution of or decrease in urinary tract dilatation is expected for most cases. Long-term follow-up of children with prenatally diagnosed PM with mild to moderate hydronephrosis confirms a high incidence of resolution and improvement. Ultrasonography should be continued periodically until the child reaches adulthood (Shukla et al. 2005). In adults and adolescents with primary megaureter, large stones can develop in the dilated portion of the ureter due to urinary stasis (Delakas et al. 2002; Hemal et al. 2003; Rosenblatt et al. 2009). Cases of megaureter because of uretropelvic junction obstruction can present with acute flank pain crisis during childhood (Hanna et al. 1976; Anderson et al. 2012). Congenital megaureter is a diagnosis that urologists and radiologists need to consider in the setting of isolated distal ureteral dilation. Although its presentation in adult life is rare it is sometimes identified by point-of-care ultrasound DC, usually during the third or fourth decade, and it is usually unilateral (most often left-sided) (Dorairajan et al. 1975).

Supernumerary kidney

Supernumerary kidney is a rare congenital urinary tract abnormality. The supernumerary kidney is a definitive accessory organ with its own collecting system, blood supply, and distinct encapsulated parenchyma. It is rarely symptomatic but can become symptomatic in early adulthood. It is among the rarest congenital urological anomalies with fewer than 100 cases reported in the English literature. The embryological anomaly results from premature division of the metanephric bud; the number of kidneys probably reflects the number of abnormal divisions of the progenitor cells. It affects males and females equally and usually affects the left side. Bilateral supernumerary kidney is even rarer and only three cases have been reported in the literature. Computed tomography (CT), excretory urography (IVP), and CT angiography (CTA) can be used to confirm the diagnosis of supernumerary kidney (Oto et al. 2002).

Because of the atypical presenting symptomatology, this entity frequently causes a diagnostic as well as a therapeutic dilemma. Back pain has been reported as the presenting sign (Tada et al. 1981). A noncontrast CT scan revealed a left-sided para-aortic mass. An intravenous contrast CT scan revealed an anatomically and functionally supernumerary kidney and no percutaneous biopsy was required (Bernik et al. 2001). The condition is generally discovered when complications arise, for example hydronephrosis (Jira et al. 2002). An acute episode of abdominopelvic pain, secondary to hydronephrosis of a third kidney situated in the pelvis behind the bladder, has been reported (Eberle et al. 2002). A 33-year-old female patient was investigated for right lower quadrant pain. She was treated surgically for a cyst of the right ovary. Finally, excretory urography and a computed tomography examination revealed a normally functioning extra kidney on that side (Koureas et al. 2000). An ectopic supernumerary pelvic kidney is a rare cause of a pelvic mass that can be found incidentally on a computed axial tomographic (CT) examination (Flyer et al. 1994), but most cases are asymptomatic and only an imaging study reveals separate extra kidneys.

Solitary functioning kidney (SFK)

SFK in childhood can be either of primary (congenital) origin (pSFK) or secondary after unilateral nephrectomy (sSFK). These are different anomalies. Unilateral renal agenesis (URA) is defined as congenital absence or a kidney on one side. In a systematic review of 43 cohorts comprising over 2600 patients with URA, the general incidence of URA was 1 in 2000. Because it is difficult to diagnose, the pre-renal incidence of URA is reported around 1 in 8000 (Westland et al. 2013b, 2014). It is suggested that most cases diagnosed as URA are actually cases of renal aplasia, which is not easily detectable on ultrasound (Westland et al. 2013b, 2014). Both agenesis and aplasia are referred to as URA. It should be discriminated from a unilateral nonfunctioning kidney resulting from multicystic renal dysplasia (MCRD); in the latter condition the renal parenchyma exhibits dysplastic and cystic differentiation, with a normally atretic ureter due to abnormal fetal renal development (Schedl 2007; Weber 2012). Its incidence is 1 in 4300 births (Westland et al. 2013b, 2014). Fetal ultrasound now enables individuals with a solitary functioning kidney to be identified prenatally. Congenital solitary kidney affects 1 in 1000 persons, whereas bilateral renal agenesis affects 1 in 5000 and is incompatible with life (McPherson 2007); however, in a meta-analyses of 43 studies (total number of patients 2684, 63% male) the general incidence of URA was 1 in approximately 2000 (Westland et al. 2013b).

Acquired solitary kidneys are frequently due to nephrectomy of a pathological contralateral kidney or to donation of a kidney for renal transplantation. Having a solitary functioning kidney (SFK) entails having an abnormally low number of nephrons, and this leads to adaptive hypertrophy and hyperfiltration in the remaining nephrons with proteinuria, arterial hypertension (AH), and diminished glomerular filtration rate (GFR) as possible sequelae (Gonzalez et al. 2005).

Although hyperfiltration secondary to a 50% reduction of renal mass in humans is considered not to lead to loss of function of the remaining parenchyma, there is an increased risk for proteinuria and progressive renal failure (Fotino 1989; Novick et al. 1991; Gluhovschi et al. 2013). However, other researchers believe that renal function in children with solitary kidney declines gradually over longer periods of follow-up (Abou Jaoudé et al. 2011; Westland et al. 2013a). A recent study demonstrated that 40–50% of adults with URA required dialysis by the age of 30 (Sanna-Cherchi et al. 2009; Westland et al. 2013b). Early presentation can be occult blood in the urine (Anraku et al. 2012). Hydronephrosis combined with ureteral diverticulum has been reported in the solitary kidney because of the blind-ended bifid ureter (Anraku et al. 2012). Offspring and other relatives of individuals with congenital solitary kidney have a significantly increased incidence of renal disease (agenesis, dysplasia, cystic dysplasia) (McPherson 2007). A retrospective study of renal injury markers in children with SFK demonstrated that nearly one-third of the patients had hypertension or albuminuria or used renoprotective medication at a young age (Kaneyama et al. 2004; Dursun et al. 2005). We therefore emphasize that clinical follow-up of all children with an SFK is needed. URA is also associated with extra-renal involvement of systems such as gastrointestinal, cardiovascular, and musculoskeletal (Westland et al. 2013b).

A dromedary hump is a common variant of the left kidney and represents the splenic impression from pressure of the splenic border along the upper lateral half of the renal contour.

Urinary bladder and ureters

Urinary bladders of variable shape (e.g., hourglass bladder) have been reported. The bladder may be doubled. Agenesis has a reported incidence of 1:600,000 (0.00017%).

Variations of the calices, renal pelvis, and ureter include the following.

1. Calices, including absent, aberrant, or unusual number, size or position.
2. Renal pelvis, including absent, rudimentary, double (bifid), multiple (unilateral or bilateral), hydronephrosis (congenital), intrarenal pelvis (unilateral or bilateral), extrarenal pelvis (unilateral or bilateral), or diverticulum of renal pelvis.
3. Ureter, including (a) variations in number, for example single (one ureter absent), double on one side, triple, quadruple, quintuple, or sextuple; (b) complete, incomplete, or branching; or (c) variations in form, size, and position, for example diverticulum of ureter (simple or multiple), inperforate ureter, stricture of ureter (pyo-ureter, hydroureter, megalo-ureter), dilation of ureter (total or partial), "golf hole" type of ureteral orifice, ureter ectopic, misplaced in bladder (at fundus, in diverticulum, near bladder neck, etc.), with extravesical orifice (opening into another ureter, urethra, genital tract, or bowel), ureter twisted or occluded, ureters crossed, or ureter with valve formation.

The calices majores may pass downward for some distance beyond the hilum, and end by joining to form the ureter without undergoing any obvious expansion. In such cases, the pelvis is absent; if the calices dilate, one or two pelves may be present.

The principal variation in the ureter is a more or less complete division into two. As a rule, the two ureters unite a little above the bladder, so that there is only one vesical orifice. When the division is complete there are two separate openings into the bladder. In one study of 26,480 autopsies, 136 double or bifid ureters were found (0.5%).

In rare cases, three or four ureters may be found. Several instances are recorded in which a supernumerary ureter, proceeding from the upper part of the kidney, opened directly into the urethra. Ureters have also been reported to open into the vagina, the seminal vesicle, or the prostatic urethra. The calices minores may vary in number over the range 6–14, the smaller number indicating that some of the calices minores embrace the

apices of several pyramids. Variations in the calices minores and pelvis are more marked. The right ureter has been found passing behind the inferior vena cava (postcaval or retrocaval ureter) between that vessel and the aorta.

References

Abou Jaoudé P, Dubourg L, Bacchetta J, Berthiller J, Ranchin B, Cochat P. 2011. Congenital versus acquired solitary kidney: is the difference relevant? *Nephrol Dial Transplant* 26(7): 2188–2194.

Ahmed AH, Khanam A, Begum S, Khaleque A, Alam MR. 2011. Intrathoracic kidney in adult with an abnormal presentation. *Mymensingh Med J* 20(1): 151–154.

Allen D, Bultitude MF, Nunan T, Glass JM. 2005. Misinterpretation of radioisotope imaging in pelvic kidneys. *Int J Clin Pract Suppl* 147: 111–112.

Anderson CB, Tanaka ST, Pope JC 4th, Adams MC, Brock JW 3rd, Thomas JC. 2012. Acute pain crisis as a presentation of primary megaureter in children. *J Pediatr Urol* 8(3): 254–257.

Angulo JC, Lopez JI, Vilanova JR, Flores N. 1992. Intrathoracic kidney and vertebral fusion: a model of combined misdevelopment. *J Urol* 147(5): 1351–1353.

Anheuser P, Kranz J, Steffens J, Beetz R. 2013. Primary megaureter. *Urologe A* 52(1): 33–38 (in German).

Anraku T, Mizusawa T, Obara K, Sato H, Ajioka Y, Takahashi K. 2012. A case of true ureteral diverticulum on functional solitary kidney. *Nihon Hinyokika Gakkai Zasshi* 103(3): 569–572 (in Japanese).

Aquilera Tubet C, Del Valle Schaan JI, Martin Garcia B, Portillo Martin JA, Gutierrez Banos JL, Ballestero Diego R. 2005. Renal cell carcinoma in crossed fused renal ectopia. *Actas Urol Esp* 29: 993–996.

Areses Trapote R, Urbieta Garagorri MA, Ubetagoyena Arrieta M, Alzueta Beneite MT, Arruebarrena Lizarraga D, Eizaguirre Sexmilo I, Rodríguez Mazorriaga F, Emparanza Knorr JI. 2007. Prenatal detection of primary non–refluxing megaureter. Review of our casuistics. *An Pediatr (Barc)* 67(2): 123–132 (in Spanish).

Arnim AB, Tamussino KF, Winter R. 2005. Ectopic (pelvic) kidney mimicking bulky lymph nodes at npelvic lymphadenectomy. *Gynecol Oncol* 96: 873–875.

Ascher W, Rosch WH. 2005. Congenital abnormalities of the urinary tract. In *Oxford Textbook of Clinical Nephrology*. Oxford: Oxford University Press, Inc. pp. 1402–1412.

Asghar M, Wazir F. 2008. Prevalence of renal ectopia by diagnostic imaging. *Gomal J Med Sci* 6: 2.

Aslan P, Brooks A, Drummond M, Woo H. 1999. Incidence and management of gynecological-related ureter injuries. *Aust N Z J Obstet Gynecol* 39: 178–181.

Atasever A, Ielik HH, Durgun B, Yilmaz E. 1992. Unrotated left kidney associated with an accessory renal artery. *J Anat* 181: 507–508.

Bader AA, Tamussino KF, Winter R. 2005. Ectopic (pelvic) kidney mimicking bulky lymph nodes at pelvic lymphadenectomy. *Gynecologic Oncology* 96: 873–875.

Barber NJ, Thompson PM. 2004. Nephroptosis and nephropexy – hung up on the past? *Eur Urol* 46: 428–433.

Basar H, Basar R, Basar MM, Erbil M. 1999. The comparison of the incidence of horseshoe kidney in autopsy cases versus urologic patient population. *Okajimas Folia Anat Jap* 76(2–3): 137–139.

Bauer SB. 2002. Anomalies of the upper urinary tract. In: *Campbell's Urology*, eighth edition (eds PC Walsh, AB Retik, ED Vaughan Jr, AJ Wein). Philadelphia: WB Saunders, pp. 1885–1924.

Bauer SB, Perlmutter AD, Retik AB. 1992. Anomalies of upper urinary tract. In: *Campbell's Urology*, sixth edition, vol II (eds PC Walsh, AB Retik, TA Stamey, ED Vaughan). Philadelphia: WB Saunders, pp. 1371–1381.

Bayramoglu A, Demiryurek D, Erbil KM. 2003. Bilateral additional renal arteries and an additional right renal vein associated with unrotated kidneys. *Saudi Med J* 24(5): 535–537.

Belsare SM, Chimmalgi M, Vaidya SA, Sant SM. 2002. Ectopic kidney and associated anomalies: a case report. *J Anat Soc India* 51: 236–238.

Beltrán Armada JR, Serrano Durbá A, Coronel Sánchez B, Domínguez Hinarejos C, Estornell Moragues F, García Ibarra F. 2004. Pyeloureteral duplicity and intrathoracic kidney. *Acta Urol Esp* 28(3): 249–251.

Benchekroun A, Kasmaoui EH, Jira H, Iken A, Nouini Y, Benslimane L, Faik M. 2002. Pathological pelvic kidney. Apropos of 11 cases. *Ann Urol (Paris)* 36(4): 231–235.

Bergman RA, Afifi AK, Miyauchi R. 2006. Illustrated Encyclopedia of Human Anatomic Variation, Opus IV. Available at: http://www.anatomyatlases.org/AnatomicVariants/AnatomyHP.shtml (accessed 8 December 2015).

Bernik TR, Ravnic DJ, Bernik SF, Wallack MK. 2001. Ectopic supernumerary kidney, a cause of para-aortic mass: case report and review. *Am Surg* 67(7): 657–659.

Bhatnagar P, Sharma R, Popli M, Sachdev P, Dutta M, Kashyap R. 2004. Crossed renal ectopia with fusion: Presentation on Tc-99m DTPA scan. *Clin Nucl Med* 29: 595–596.

Boatman DL, Culp DA Jr, Flocks RH. 1972. Crossed renal ectopia. *J Urol* 108(1): 30–31.

Boccardo G. 1999. Re: Floating kidneys: a century of nephroptosis and nephropexy. *J Urol* 162: 1705.

Boyan N, Kubat H, Uzum A. 2007. Crossed renal ectopia with fusion: report of two patients. *Clin Anat* 20: 699–702.

Braash WF. 1931. Anomalous renal rotation and associated anomalies. *J Urol* 25: 9–13.

Bronstein M, Kushnir O, Ben-Rafael Z. 1990. Transvaginal sonographic measurement of fetal kidneys in the first trimester of pregnancy. *J Clin Ultrasound* 18: 299–301.

Bynum B. 2001. Discarded diagnosis. *Lancet* 357: 76.

Calado AA, Macedo A Jr, Srougi M. 2004. Cake kidney drained by single ureter. *Int Braz J Urol* 30(4): 321–322.

Calisti A, Perrotta ML, Oriolo L, Ingianna D, Miele V. 2008. The risk of associated urological abnormalities in children with pre and postnatal occasional diagnosis of solitary, small or ectopic kidney: is a complete urological screening always necessary? *World J Urol* 26: 281–284.

Campbell MF. 1930. Renal ectopy. *J Urol* 24: 187–190.

Cascio S, Sweeney B, Granata C, Piaggio G, Jasonni V, Puri P. 2002. Vesicoureteral reflux and ureteropelvic junction obstruction in children with horseshoe kidney: treatment and outcome. *J Urol* 167: 2566–2568.

Chao C-T. 2012. Obstructed solitary ectopic pelvic kidney. *Clin Exp Nephrol* 16(5): 813.

Chen D-P, Ma Y-Y, Mao Z-G, Mei C-L. 2010. Ectopic (pelvic) autosomal dominant polycystic kidney disease. *Intern Med* 49: 2525–2526.

Chiu YL, Tsay DG, Hu C, Wu CS, Du WN, Peng NJ. 2012. Intrathoracic renal ectopia mimicking CSF leakage on radionuclide cisternography demonstrated by SPECT/CT. *Clin Nucl Med* 37: 93–94.

Chung SD, Chueh SC, Chiang HS, Liao CH. 2009. L-shaped cross-fused kidney with stone. *Urology* 73(1): 61–62.

Cinman NM, Okeke Z, Smith AD. 2007. Pelvic kidney: associated diseases and treatment. *J Endourol* 21(8): 836–842.

Clarkson LM, Potter S. 2009. An unusual thoracic mass. *Br J Radiol* 82: e27–e28.

Cocheteux B, Mounier-Vehier C, Gaxotte V, McFadden EP, Francke JP, Beregi JP. 2001. Rare variations in renal anatomy and blood supply: CT appearances and embryological background. *Eur Radiol* 11(5): 779–786.

Cohn DA, Roach P. 2003. Pancake kidney: incidental finding on bone scintigraphy. *Clin Nucl Med* 28(5): 434–436.

Collura G, De Dominicis M, Patricolo M, Caione P. 2004. Hydronephrosis due to malrotation in a pelvic ectopic kidney with vascular anomalies. *Urol Int* 72: 349–351.

Cook WA, Stephens FD. 1977a. Fused kidneys: morphologic study and theory of embryogenesis. In: *Urinary System Malformations in Children* (eds D Bergsma, JW Duckett). New York: Allen R. Liss.

Cook WA, Stephens FD. 1977b. Fused kidneys: morphologic study and theory of embryogenesis. *Birth Defects* 13: 327–340.

Dabiri L, Cheung W. 2006. Unilateral ectopic right kidney, an incidental finding during pelvic sonogram. *J Natl Med Assoc* 98(10): 1710–1712.

Das S, Amar A. 1984. Ureteropelvic junction obstruction with associated renal anomalies. *J Urol* 131: 872–878.

de Brito CJ, Silva LA, Fonseca Filho VL, Fernandes DC. 1991. Abdominal aortic aneurysm in association with horseshoe kidney. *Int Angiol* 10(3): 122–125.

Delakas D, Daskalopoulos G, Karyotis I, Metaxari M, Cranidis A. 2002. Giant ureteral stone in association with primary megaureter presenting as an acute abdomen. *Eur J Rad* 41: 170–172.

Desai MR, Jasani A. 2000. Percutaneous nephrolithotripsy in ectopic kidneys. *J Endourol* 14(3): 289–292.

Di Renzo D, Aguiar L, Cascini V, Di Nicola M, McCarten KM, Ellsworth PI, Chiesa PL, Caldamone AA. 2013. Long-term follow up of primary non-refluxing megaureter. *J Urol* 190(3): 1021–1026.

Dingeldein MW, Kane D, Kim AW, Kabre R, Pescitelli MJ Jr, Holterman MJ. 2008. Bilateral intrathoracic kidneys and adrenal glands associated with posterior congenital diaphragmatic hernias. *Ann Thorac Surg* 86(2): 651–654.

Doménech-Mateu JM, Gonzalez-Compta X. 1988. Horseshoe kidney: a new theory on its embryogenesis based on the study of a 16-mm human embryo. *Anat Rec* 222(4): 408–417.

Domini M, Aquino A, Pappalepore N, Tursini S, Marino N, Strocchi F, Lelli Chiesa P. 1999. Conservative treatment of neonatal primary megaureter. *Eur J Pediatr Surg* 9: 396–399.

Donat SM, Donat PE. 1988. Intrathoracic kidney. A case report with a review of the world literature. *J Urol* 140: 131–133.

Dorairajan LN, Hemal AK, Gupta NP, Wadhwa SN. 1975. Primary obstructive megaureter in adults: need for an aggressive management strategy. *Int Urol Nephrol* 31: 633–641.

Dretler SP, Olsson C, Pfister RC. 1971. The anatomic, radiologic and clinical characteristics of the pelvic kidney: an analysis of 86 cases. *J Urol* 105: 623–627.

Drop A, Czekajska-Chehab E, Maciejewski R, Staśkiewicz GJ, Torres K. 2003. Thoracic ectopic kidney in adults. A report of 2 cases. *Folia Morphol (Warsz)* 62(3): 313–316.

Du WN, Tsay DG, Hu C, Su HM, Lin KH, Peng NJ. 2010. Intrathoracic renal ectopia demonstrated by Tl-201 SPECT/CT. *Clin Nucl Med* 35: 467–468.

Duh YC, Chia ST, Sheu JC, Peng CC. 2007. Crossed fused renal ectopia with segmental fusion of bilateral ureters and abdominal aortic anomalies in a patient with caudal regression syndrome. *Eur J Pediatr Surg* 17(5): 370–372.

Dursun H, Bayazit AK, Büyükçelik M, Soran M, Noyan A, Anarat A. 2005. Associated anomalies in children with congenital solitary functioning kidney. *Pediatr Surg Int* 21: 456–459.

Eberle J, Schwarz E, Abbrederis K. 2002. Kidney calculus episode in a supernumerary 3rd kidney. *Urologe A* 41(4): 362–363 (in German).

Eckes D, Lawrence P. 1997. Bilateral iliac artery aneurysms and pancake kidney: a case report. *J Vasc Surg* 25(5): 927–930.

Eroglu A, Alper F, Turkyilmaz A, Okur A, Karaoglanoglu N. 2005. Pulmonary agenesis associated with dextrocardia, sternal defects, and ectopic kidney. *Pediatr Pulmonol* 40: 547–549.

Eze AR, White JV, Pathak AS, Grabowski MW. 1998. "Pancake kidney": a renal anomaly complicating aortic reconstruction. *Ann Vasc Surg* 12(3): 278–281.

Fadaii A, Rezaian S, Tojari F. 2008. Intrathoracic kidney presented with chest pain. *Ira J Kid Diseases* 2: 160–162.

Ferko A, Krajina A, Jon B, Lesko M, Voboril Z. 1997. Juxtarenal aortic aneurysm associated with a horseshoe kidney. Transfemoral endoluminal repair. *Arch Surg* 132: 316–317.

Fernbach SK, Davis TM. 1986. The abnormal renal axis in children with spina bifida and gibbus deformity – the pseudohorseshoe kidney. *J Urol* 136: 1258–1260.

Fiaschetti V, Velari L, Gaspari E, Mastrangeli R, Simonetti G. 2010. Adult intra-thoracic kidney: a case report of Bochdalek hernia. *Case Rep Med* 2010: 975168.

Flyer MA, Haller JO, Feld M, Kantor A. 1994. Ectopic supernumerary kidney: another cause of a pelvic mass. *Abdom Imaging* 19(4): 374–375.

Fotino S. 1989. The solitary kidney: a model of chronic hyperfiltration in humans. *Am J Kidney Dis* 13(2): 88–98.

Frick MP, Goldberg ME. 1980. Uro- and angiographic findings in a "normal" population: screening of 151 symptom-free potential transplant donors for renal disease. *Am J Roentgenol* 134(3): 503–505.

Gharagozloo AM, Lebowitz RL. 1995. Detection of a poorly functioning malpositioned kidney with single ectopic ureter in girls with urinary dribbling: imaging evaluation in five patients. *Am J Roengenol* 164(4): 957–961.

Ghosh BC, DeSantis M, Kleyner Y, Zak Y. 2008. Crossed fused renal ectopia with calculi. *J Am Coll Surg* 206: 753.

Gleason PE, Kramer SA. 1995. Ectopic kidneys and renal fusion anomalies. *AUA Update Ser* 33: 268–271.

Gleason PE, Kelalis PP, Husmann DA, Kramer SA. 1994. Hydronephrosis in renal ectopia: incidence, etiology and significance. *J Urol* 151: 1660–1661.

Glodny B, Cromme S, Wörtler K, Winde G. 2001. A possible explanation for the frequent concomitance of arterial hypertension and multiple renal arteries. *Med Hypotheses* 56(2): 129–133.

Gluhovschi G, Gadalean F, Gluhovschi C, Petrica L, Velciov S, Gluhovschi A, Timar R. 2013. The solitary kidney – a nephrological perspective. *Rom J Intern Med* 51(2): 80–88.

Gonzalez CC, Bitsori M, Tullus K. 2007. Progression of chronic renal failure in children with dysplastic kidneys. *Pediatr Nephrol* 22: 1014–1020.

Gonzalez E, Gutierrez E, Morales E. 2005. Factors influencing the progression of renal damage in patients with unilateral renal agenesis and remnant kidney. *Kidney Int* 68: 263–270.

Goren E, Eidelman A. 1987. Pelvic cake kidney drained by single ureter. *Urology* 30: 492–493.

Gosling JA, Dixon JS. 1978. Functional obstruction of the ureter and renal pelvis. A histological and electron microscopic study. *Br J Urol* 50: 145–152.

Goyal A, Gaitonde K, Sagade SN, Shah BV, Kamat MH. 2003. Transplantation of horseshoe kidney from living-related donors: report of two cases position. *Transplant Proc* 35: 32–34.

Greenwood RD, Rosenthal A, Nadas A. 1976. Cardiovascular malformation associated with congenital anomalies of the urinary system. Observations in a series of 453 infants and children with urinary system malformations. *Clin Pediatr (Phila)* 15(12): 1101–1104.

Guarino N, Tadini B, Camardi P, Silvestro L, Lace R, Bianchi M. 2004. The incidence of associated urological abnormalities in children with renal ectopia. *J Urol* 172: 1757–1759.

Gupta M, Pandey AK, Goyal N. 2007. Horseshoe kidney – a case report. *Nepal Med Coll J* 9: 63–66.

Hamptom LJ, Borden TA. 2002. Uroteropelvic junction obstruction in a thoracic kidney treated by dismembered pyeloplasty. *Urology* 60: 164.

Hanif MA, Chandrasekar R, Blair SD. 2005. Pelvic kidney and aortoiliac aneurysm – a rare association – case report and literature review. *Eur J Vasc Endovasc Surg* 30(5): 531–533.

Hanna MK, Wyatt JK. 1975. Primary obstructive megaureter in adults. *J Urol* 113: 328–335.

Hanna MK, Jeffs RD, Sturgess JM, Barkin M. 1976. Ureteral structure and ultrastructure. Part II. Congenital ureteropelvic junction obstruction and primary obstructive megaureter. *J Urol* 116: 725–730.

Hatzinger M, Langbein S, de la Rosette J, Sohn, M. Alken P. 2007. Nephropexy in the course of time. Aspects of an historical surgical technique. *Urologe* 46: 166–169.

He B, Mitchell A. 2012. Laparoscopic donor nephrectomy for ectopic kidney. *Transplant Proc* 44: 3051–3054.

Heidempergher M, Landriani N, Airaghi C, Buskermolen M, Barone MT, Scorza D, Cuoccio P, Genderini F, Scandiani L, Genderini A. 2012. Pancake polycystic kidney: case report. *Arch Ital Urol Androl* 84(4): 276–278.

Hemal AK, Ansari MS, Doddamani D, Gupta NP. 2003. Symptomatic and complicated adult and adolescent primary obstructive megaureter – indications for surgery: analysis, outcome, and follow-up. *Urology* 61: 703–707.

Hernández Toriz N, Flores Ojeda R, Ixquiac Pineda G. 2006. Renal tumor in a pelvic kidney. Case report. *Arch Esp Urol* 59(8): 826–829.

Hidaka N, Fujita Y, Satoh Y, Fukushima K, Wake N. 2012. Appearance of intrathoracic kidney in a fetus with left diaphragmatic hernia. *J Clin Ultrasound* 40: 600–602.

Ho S-W, Yeh Y-T, Yeh C-B. 2013. Rupture of ectopic pelvic dysplastic kidney after blunt abdominal trauma presenting as left lower quadrant pain. *J Emergency Med* 44(2): e173–175.

Hobbs CA, Cleves MA, Simmons CJ. 2002. Genetic epidemiology and congenital malformations: from the chromosome to the crib. *Arch Pediatr Adolesc Med* 156(4): 315–320.

Hohenfellner M, Schultz-Lampel D, Lampel A, Steinbach F, Cramer BM, Thüroff JW. 1992. Tumor in the horseshoe kidney: clinical implications and review of embryogenesis. *J Urol* 147(4): 1098–1102.

Hollinshead WH. 1971. *The kidneys, ureter and suprarenal glands*. In *Anatomy for Surgeons*, second edition, volume 2. New York: Harper & Row, pp. 518–573.

Hsieh M-Y, Ku M-S, Tsao TF, Chen S-M, Chao Y-H, Tsai J-D, Lue K-H, Sheu J-N. 2013. Rare case of atrophic ectopic kidney with giant hydronephrosis in a 7-year-old girl. *Urology* 81(3): 655–658.

Huber D, Griffin A, Niesche J, Frawley J, Gray L. 1990. Aortic aneurysm surgery in the presence of a horseshoe kidney. *Aust N Z J Surg* 60(12): 963–966.

Hwang CM, Miller FH, Dalton DP, Hartz WH. 2002. Accidental ureteral ligation during an inguinal hernia repair of patient with crossed fused renal ectopia. *Clin Imaging* 26: 306–308.

Ichikawa T, Sekiguchi T, Kawada S, Koizumi J, Endo J, Yamada Y, Ito C, Sugiyama M, Terachi T, Usui Y, Torigoe K, Imai Y. 2012. Study of the association between an anomalous superior vena cava and horseshoe kidney. *Circ J* 76: 1253–1258.

Jira H, Ghadouane M, Kasmaoui EH, Ameur A, Zannoud M, Abbar M. 2002. A supernumerary kidney. Apropos of a case. *Ann Urol (Paris)* 36(4): 236–239 (in French).

Kaneyama K, Yamataka A, Satake S, Yanai T, Lane GJ, Kaneko K, Yamashiro Y, Miyano T. 2004. Associated urologic anomalies in children with solitary kidney. *J Pediatr Surg* 39: 85–87.

Kao PF, Sheih CP, Tsui KH, Tsai MF, Tzen KY. 2003. The 99mTc-DMSA renal scan and 99mTc-DTPA diuretic renogram in children and adolescents with incidental diagnosis of horseshoe kidney. *Nucl Med Commun* 24(5): 525–530.

Kara E, Öztürk NC, Özgür AA, ÂldÂz AY, Öztürk H. 2011. Ectopic kidney with varied vasculature: demonstrated by CT angiography. *Surg Radiol Anat* 33: 81–84.

Karaoglanoglu N, Turkyilmaz A, Eroglu A, Alici HA. 2006. Right-sided Bochdalek hernia with intrathoracic kidney. *Pediatr Surg Int* 22: 1029–1031.

Kato M, Ioritani N, Aizawa M, Inaba Y, Watanabe R, Orikasa S. 2000. Extracorporeal shock wave lithotripsy for a ureteral stone in crossed fused renalectopia. *Int J Urol* 7: 270–273.

Kem DC, Lyons DF, Wenzl J, Halverstadt D, Yu X. 2005. Renin-dependent hypertension caused by nonfocalstenotic aberrant renal arteries: proof of a new syndrome. *Hypertension* 46(2): 380–385.

Khoury A, Bagli DJ. 2007. Reflux and Megaureter. In: *Campbell–Walsh Urology*, ninth edition (eds AJ Wein, LR Kavoussi, AC Novick, AW Partin, CA Peters). Philadelphia: Elsevier Inc., pp. 3467–3468.

Kiddoo DA, Rellah RD, Carrcross MC. 2005. Fused ectopic multicystic dysplastic kidney with associated ureterocele. *Urology* 66: e3–e5.

Kocak M, Sudakoff GS, Erickson S, Begun F, Datta M. 2001. Using MR angiography for surgical planning in pelvic kidney renal cell carcinoma. *Am J Roentgenol* 177(3): 659–660.

Koureas AP, Panourgias EC, Gouliamos AD, Trakadas SJ, Vlahos LJ. 2000. Imaging of a supernumerary kidney. *Eur Radiol* 10(11): 1722–1723.

Kraft KH, Molitierno JA, Kirsch AJ. 2007. Ten-year-old girl with crossed-fused ectopic kidney and ectopic ureter to vagina. *Urology* 70: 1220–1221.

Krahn CG, Taylor DC. 1993. Aortoiliac occlusive vascular disease in association with congenital pelvic kidney. *Ann Vasc Surg* 7(2): 176–179.

Kubricht WS 3rd, Henderson RJ, Bundrick WS, Venable DD, Eastham JA. 1999. Renal cell carcinoma in an intrathoracic kidney: radiologic findings and surgical considerations. *South Med J* 92: 628–629.

Kumar S, Pandya S, Singh SK, Panigrahy B, Acharya N, Lal A, Mandal AK. 2008. Laparoscopic heminephrectomy in L-shaped crossed fused ectopia. *J Endourol* 22: 979–983.

Kumar S, Bolla SR, Vollala VR. 2011. Unilateral ectopic kidney in the pelvis – a case report. *Chang Gung Med J* 34(6 Suppl): 10–12.

Kwon TW, Sung KB, Kim GE. 2004. Experience of an abdominal aortic aneurysm in a patient having crossed ectopia with fusion anomaly of the kidney. *J Korean Med Sci* 19: 309–310.

Lee C-H, Tsai L-M, Lin L-J, Chen P-C. 2006. Intrathoracic kidney and liver secondary to congenital diaphragmatic hernia recognized by transthoracic echocardiography. *Int J Cardiol* 113: e73–e75.

Lenz DL, Clair DL, Fetzer AE, Wong C. 2003. Percutaneous nephrolithotomy of an intrathoracic kidney. *Urology* 61(2): 462.

Liu L, Yang J, Zhu L, Yi L, Zhu B, Song W, Zhang W, Gong Y. 2010. Crossed-fused renal ectopia associated with inverted-Y ureteral duplication, ectopic ureter, and bicornuate uteruses. *Urology* 75(5): 1175–1177.

Lorenz EC, Vrtiska TJ, Lieske JC, Dillon JJ, Stegall MD, Li X, Bergstralh EJ, Rule AD. 2010. Prevalence of renal artery and kidney abnormalities by computed tomography among healthy adults. *Clin J Am Soc Nephrol* 5(3): 431–438.

Louzir B, Beji M, Chtourou S, Fajraoui N, el-Mekki S, Jouini S, Mnif E, Slim R, Daghfous J. 1999. Diagnosis of an opacity at the lung base: intrathoracic kidney. *Rev Mal Respir* 16(2): 207–209.

Lu C-C, Tain Y-L, Yeung K-W, Tiao M-M. 2011. Ectopic pelvic kidney with urinary tract infection presenting as lower abdominal pain in a child. *Pediatr Neonatol* 52(2): 117–120.

Maduekwe E, Weinberg B, Samaan B, Sheferaw E, Suntharos P. 2011. Right thoracic ectopic kidney in a child with breathing difficulties – sonographic diagnosis. *J Clin Ultrasound* 39: 108–110.

Mahmoudnejad N, Danesh A, Abdi H. 2009. Renal cell carcinoma in presacral pelvic kidney. *J Pak Med Assoc* 59(7): 482–483.

Malament M, Schwartz B, Nagamatsu GR. 1961. Extrarenal calyces: their relationship to renal disease. *Am J Roentgenol* 86: 823–827.

Mandell GA, Maloney K, Sherman NH, Filmer B. 1996. The renal axes in spina bifida: issues of confusion and fusion. *Abdom Imaging* 21: 541–545.

Marone EM, Tshomba Y, Brioschi C, Calliari FM, Chiesa R. 2008. Aorto-iliac aneurysm associated with congenital pelvic kidney: A short series of successful open repairs under hypothermic selective renal perfusion. *J Vasc Surg* 47: 638–644.

Martinez-Lazaro R, Cortes-Blanco AA. 2000. Cake kidney drained by single ureter: MAG3 renogram for diagnosis and function follow-up. *Nephrol Dial Transplant* 15: 1700–1701.

Masturzo B, Kalache KD, Cockell A, Pierro A, Rodeck CH. 2001. Prenatal diagnosis of an ectopic intrathoracic kidney in right-sided congenital diaphragmatic hernia using color Doppler ultrasonography. *Ultrasound Obstet Gynecol* 18: 173–174.

Matsubara K, Sugimoto K, Osaki M, Nigami H, Harigaya H, Baba K. 2000. Intrathoracic kidney combined with pneumomediastinum in an asphyxiated neonate. *Pediat Internat* 42: 715–717.

McPherson E. 2007. Renal anomalies in families of individuals with congenital solitary kidney. *Genet Med* 9(5): 298–302.

McWhinnie DL, Hamilton DNH. 1984. The rise and fall of surgery for the 'floating' kidney. *BMJ* 288: 845–847.

Meizner I, Yitzhak A, Levi A, Barki Y, Barnhard Y, Glezerman M. 1995. Fetal pelvic kidney; a challenge in prenatal diagnosis? *Ultrasound Obst Gynecol* 5: 391–393.

Mesrobian HG, Kelalis PP, Hrabovsky E, Othersen HB Jr, deLorimier A, Nesmith B. 1985. Wilms tumor in horseshoe kidneys: a report from the National Wilms Tumor Study. *J Urol* 133(6): 1002–1003.

Miller DC, Kropp KA. 1992. Transitional cell carcinoma associated with crossed renal ectopia and previous cyclophosphamide therapy. *J Urol* 148: 1244–1246.

Mishra S, Ganesamoni R, Ganpule AP, Sabnis RB, Desai MR. 2013. Supine percutaneous nephrolithotomy for bilateral complete staghorn calculi in an L-shaped cross-fused renal ectopic anomaly. *Urology* 81(1): e3–4.

Moore KL, Persaud TVN. 2008. The urogenital system. In: *The Developing Human: Clinically Oriented Embryology*, eighth edition. Philadelphia: WB Saunders.

Moore KL, Persaud TVN, Torchia MG. 2011. *The Developing Human: Clinically Oriented Embryology*, ninth edition. Philadelphia: Saunders, pp. 288–297.

Moss SW. 1997. Floating kidneys: A century of nephroptosis and nephropexy. *J Urol* 158: 699–702.

Murphy JJ, Altit G, Zerhouni S. 2012. The intrathoracic kidney: should we fix it? *J Pediat Surg* 47: 970–973.

Muttarak M, Peh WCG, Lerttumnongtum P. 2001. Clinics in diagnostic imaging. *Singapore Med J* 42: 139–141.

Nathan H, Glezer I. 1984. Right and left accessory renal arteries arising from a common trunk associated with unrotated kidneys. *J Urol* 132(1): 7–9.

Natsis K, Tsitouridis T, Totlis T, Loutradis Ch, Tarazi L, Pastergiou Ch, Koebke J. 2005. Horseshoe kidney. Anatomical, radiological, embryological approach and clinical importance of eleven cases. *Hellen Nephrol* 17: 311–319.

Natsis K, Piagkou M, Skotsimara A, Protogerou V, Tsitouridis I, Skandalakis P. 2014. Horseshoe kidney: a review of anatomy and pathology. *Surg Radiol Anat* 36(6): 517–526.

Neville H, Ritchey ML, Shamberger RC, Haase G, Perlman S, Yoshioka T. 2002. The occurrence of Wilms tumor in horseshoe kidneys: a report from the National Wilms Tumor Study Group (NWTSG). *J Pediatr Surg* 37(8): 1134–1137.

Newling DWW. 2001. Don't dismiss the floating kidney. *Lancet* 357: 959–960.

N'Guessan G, Stephens FD. 1983. Supernumerary kidney. *J Urol* 130(4): 649–653.

Nouri-Merchaoui S, Mahdhaoui N, Krichène I, Nouri A, Seboui H. 2011. Thoracic congenital ectopic right kidney with diaphragmatic hernia: a rare developmental anomaly. *Arch Pediatr* 18(10): 1103–1106.

Novick AC, Gephardt G, Guz B, Steinmuller D, Tubbs RR. 1991. Long-term follow-up after partial removal of a solitary kidney. *N Engl J Med* 325(15): 1058–1062.

O'Brien J, Buckley O, Doody O, Ward E, Persaud T, Torreggiani W. 2008. Imaging of horseshoe kidneys and their complications. *J Med Imaging Radiat Oncol* 52: 216–226.

O'Reilly PH, Pollard AJ. 1988. Nephroptosis: a cause of renal pain and a potential cause of inaccurate split renal function determination. *BJU* 61: 284–288.

Obatake M, Nakata T, Nomura M, Nanashima A, Inamura Y, Tanaka K, Nagayasu T. 2006. Congenital intrathoracic kidney with right Bochdalek defect. *Pediatr Surg Int* 22: 861–863.

Olsson O, Wholey M. 1964. Vascular abnormalities in gross anomalies of kidneys. *Acta Radiol Diagn (Stockh)* 2: 420–432.

Oon PC, Shen HN, Yang PC. 2005. Intrathoracic kidney. *Formos Med Assoc* 104(2): 120–122.

Oto A, Kerimoğlu U, Eskiçorapçi S, Hazirolan T, Tekgül S. 2002. Bilateral supernumerary kidney: imaging findings. *JBR–BTR*. 85(6): 300–303.

Pandey J, Gujral RB, Kumar A. 2012. Incidentally diagnosed right-sided intrathoracic kidney. BMJ Case Rep 2012, doi: 10.1136/bcr-2012-007117.

Pfister-Goedeke L, Brunier F. 1979. Intrathoracic kidney in childhood with special reference to secondary renal transport in Bochdalek's hernia. *Helv Paediatr Acta* 34: 345–357.

Pollack HM, McClennan BL. 2000. Clinical urography. In: *Congenital Anomalies of the Urinary Tract*, second edition. Philadelphia: WB Saunders Co., pp. 661–911.

Pryma DA, Akhurst T. 2005. Hydronephrotic ectopic pelvic kidney simulates sacral metastasis from breast cancer. *Clin Nucl Med* 30: 244–245.

Radermecker MA, Van Damme H, Kerzmann A. 2008. Association of abdominal aortic aneurysm, horseshoe kidney, and left-sided inferior vena cava: report of two cases. *Vasc Surg* 47: 645–648.

Raj GV, Auge BK, Assimos D, Preminger GM. 2004. Metabolic abnormalities associated with renal calculi in patients with horseshoe kidneys. *J Endourol* 18(2): 157–161.

Redman JF, Beryl DL. 1997. Wilm's tumour in crossed fused renal ectopia. *J Pediatr Surg* 12: 601–603.

Rinat C, Farakas A, Frishberg Y. 2001. Familial inheritance of crossed fused renal ectopia. *Pediatr Nephrol* 16(3): 269–270.

Rocklin MS, Apelgren KN, Slomski CA, Kandzari SJ. 1989. Scrotal incarceration of the ureter with crossed renal ectopia: Case report and literature review. *J Urol* 142: 366–368.

Rosenblatt GS, Takesita K, Fuchs GJ. 2009. Urolithiasis in adults with congenital megaureter. *Can Urol Assoc J* 3(6): E77–80.

Rosenkrantz AB, Kopec M, Laks S. 2010. Pelvic cake kidney drained by a single ureter associated with unicornuate uterus. *Urology* 76(1): 53–54.

Rouanne M, Le Mandat A, Dorgeret S, Philippe-Chomette P, El Ghoneimi A. 2010. A rare case of ectopic intrathoracic kidney in a 1-year-old child. *Urology* 76(1): 57–59.

Sadler TW. 1990. Urogenital system. In *Langman's Medical Embryology*, sixth edition (ed. TWSadler). Baltimore: William and Wilkins, pp. 266–281.

Salerno A, Kohlhase J, Kaplan BS. 2000. Townes-Brocks syndrome and renal dysplasia: a novel mutation in the SALL1 gene. *Pediatr Nephrol* 14(1): 25–28.

Sanna-Cherchi S, Ravani P, Corbani V, Parodi S, Haupt R, Piaggio G, Innocenti ML, Somenzi D, Trivelli A, Caridi G, Izzi C, Scolari F, Mattioli G, Allegri L, Ghiggeri GM. 2009. Renal outcome in patient with congenital anomalies of the kidney and urinary tract. *Kidney Int* 76: 528–533.

Schedl A. 2007. Renal abnormalities and their developmental origin. *Nat Rev Genet* 8(10): 791–802.

Schwartz MJ, Bartolotta R, Brill PW, Kovanlikaya A, Hanna M. 2010. Pelvic cake kidney with a solitary ureter and bilateral congenital absence of the vas deferens. *Urology* 75(1): 170–172.

Semerci B, Verit A, Nazli O, Ilbey O, Ozyurt C, Cikili N. 1997. The role of ESWL in the treatment of calculi with anomalous kidneys. *Eur Urol* 31(3): 302–304.

Sen K, Kapoor A. 2006. Mayer-Rokitansky-Kuster-Hauser syndrome. *Ind J Radiol Imag* 16(4): 805–807.

Sfaxi M, Miladi M, Loussaief H, Mnif A, Chebil M, Ayed M. 2002. Intrathoracic kidney due to diaphragmatic hernia: a case report. *Prog Urol* 12(3): 477–478.

Sharma R, Savita N, Chakravarty KL, Dutta M, Mondal A. 2006. Pancake kidney detected on renal scintigraphy. *Clin Nucl Med* 31(11): 729–730.

Shen HL, Yang PQ, Du LD, Lu WC, Tian Y. 2012. Horseshoe kidney with retrocaval ureter: one case report. *Chin Med J (Engl)* 125: 543–545.

Shukla AR, Cooper J, Patel RP, Carr MC, Canning DA, Zderic SA, Snyder HM 3rd. 2005. Prenatally detected primary megaureter: a role for extended follow up. *J Urol* 173(4): 1353–1356.

Sidhu R, Gupta R, Dabra A, Duseja A. 2001. Intrathoracic kidney in an adult. *Urol Int* 66(3): 174–175.

Someren A. 1989. *Urologic Pathology With Radiologic and Clinical Correlations*. New York: Macmillan.

Soni HC, Jadav VJ, Sumariya B, Venkateshwaran KN, Patel N, Arya A. 2012. Primary malignancy in crossed fused ectopic kidney. *Abdom Imaging* 37: 659–663.

Sood R, Truong MX, Rossleigh MA, Kainer G. 2005. Renal scintigraphy unraveled the diagnostic dilemma of antenatal hydronephrotic solitary kidney – crossed renal ectopia. *Clin Nucl Med* 30(9): 621–622.

Sözübir S, Demir H, Ekingen G, Güvenç BH. 2005. Ectopic thoracic kidney in a child with congenital diaphragmatic hernia. *Eur J Pediatr Surg* 15: 206–209.

Stevens AR. 1937. Pelvic single kidneys. *J Urol* 37: 610–618.

Stimac G, Dimanovski J, Ruzic B, Spajic B, Kraus O. 2004. Tumors in kidney fusion anomalies – report of five cases and review of the literature. *Scand J Urol Nephrol* 38: 485–489.

Strauss S, Dushnitsky T, Peer A, Manor H, Libson E, Lebensart PD. 2000. Sonographic features of horseshoe kidney: review of 34 patients. *J Ultrasound Med* 19(1): 27–31.

Stroosma OB, Scheltinga MRM, Stubenitsky BM, Kootstra G. 2000. Horseshoe kidney transplantation: an overview. *Clin Transplant* 14: 515–519.

Stuart BB, Perlmutter AD, Alan BR. 1992. Anomalies of upper urinary tract In: *Campbell's Urology*, sixth edition (eds C Patrick, AB Retvik, AS Thomas, EDVaughan). Philadelphia: W B Saunders, pp. 1371–1381.

Suárez S, de Jesús Y. 1998. Acquired intrathoracic kidney. *PR Health Sci J* 17(3): 289–291.

Subramanian VS, Goldfarb DA. 2008. Right-sided intrathoracic renal ectopia with Bochdalek's hernia. *Urology* 72: 1016–1017.

Suresh S, Vijayalakshmi R, Indrani S, Lata S. 2007. Antenatal diagnosis of bilateral intrathoracic kidneys. *Ultrasound Obstet Gynecol* 29: 600–603.

Tada Y, Kokado Y, Hashinaka Y, Kadowaki T, Takasugi Y, Shin T, Tsukaguchi I. 1981. Free supernumerary kidney: a case report and review. *J Urol* 126(2): 231–232.

Taslim BB, Abdulwasiu BA, Olusegun S, Oluwatoyin AC, Omolara MM. 2012. Crossed renal ectopia coexisting with nephrolithiasis in a young Nigerian man. *Arab J Nephrol Transplant* 5(2): 107–110.

Tatevosian AS, Tonian AG, Khalafian AA, Opol'skiĭ AB, Shcherbina II, Tatevosian AA, Ul'ianov VA, Sultanov KG. 2004. Pathogenetic criteria of nephroptosis. *Urologiia* 6: 9–15 (in Russian).

Tijerina GO, Uresti J, Urrutia VE, Elizondo-Omana RE, Guzman-Lopez S. 2009. Anatomical study of the horseshoe kidney. *Int J Morphol* 27: 491–494.

Tsao Y-T, Lin SH, Lin YF, Chu P. 2008. Pelvic ectopic kidney with acute pyelonephritis: wolf in sheep's clothing. *Am J Emerg Med* 26: 517.e3–e4.

Vázquez Alonso F, Vicente Prados FJ, Pascual Geler M, Funes Padilla C, Segura Sánchez M, Fernández Sánchez A, Rodríguez Herrera F, Martínez Morcillo A, Cózar Olmo JM, Espejo Maldonado E, Tallada Buñuel M. 2008. Intrathoracic ectopic kidney in an adult: case report and bibliographic review. *Arch Esp Urol* 61(5): 631–633.

Walther A, Cost NG, Garrison AP, Geller JI, Alam S, Tiao GM. 2013. Renal rhabdomyosarcoma in a pancake kidney. *Urology* 82(2): 458–460.

Weber S. 2012. Novel genetic aspects of congenital anomalies of kidney and urinary tract. *Curr Opin Pediatr* 24: 212–218.

Weizer AZ, Silverstein AD, Auge BK, Delvecchio FC, Raj G, Albala DM, Leder R, Preminger GM. 2003. Determining the incidence of horseshoe kidney from radiographic data at a single institution. *J Urol* 170(5): 1722–1726.

Westland R, Kurvers RA, van Wijk JA, Schreuder MF. 2013a. Risk factors for renal injury in children with a solitary functioning kidney. *Pediatrics* 131(2): e478–485.

Westland R, Schreuder MF, Ket JC, van Wijk JA. 2013b. Unilateral renal agenesis: a systematic review on associated anomalies and renal injury. *Nephrol Dial Transplant* 28: 1844–1855.

Westland R, Schreuder MF, van Goudoever JB, Sanna-Cherchi S, van Wijk JA. 2014. Clinical implications of the solitary functioning kidney. *Clin J Am Soc Nephrol* 9(5): 978–986.

William RR, Jeans WD. 1996. Thoracic ectopic kidney in an adult. *Scand J Urol Nephrol* 30: 133–134.

Wolfromm MG. 1940. Situation du rein dans l'kventration a diaphragmatique droite. *Mem Acad Chir* 60: 41–47.

Yano H, Konagai N, Maeda M, Itoh M, Kuwabara A, Kudou T, Ishimaru S. 2003. Abdominal aortic aneurysm associated with crossed renal ectopia without fusion: Case report and literature review. *J Vasc Surg* 37: 1098–1102.

Yoshinaga K, Kodama K, Tanii I, Toshimora K. 2002. Morphological study of a horseshoe kidney with special reference to the vascular system. *Anat Sci Int* 77: 134–139.

114 Adrenal gland

Gülnur Özgüner
Suleyman Demirel University, Isparta, Turkey

The adrenal gland or suprarenal gland is located at the upper pole of the kidney on the posterior abdominal wall (Liwu 1997; Drake et al. 2012). Adrenal glands vary considerably in size and shape. The right gland is quadrilateral (Bergman et al. 1984), triangular (Liwu 1997), or pyramidal (Linos and Van Heerden 2004; Valeria et al. 2013) and is sometimes called the "witch's hat." The left gland is foliate (leaf-like) (Bergman et al. 1984), crescenteric (Liwu 1997), or semilunar (Linos and Van Heerden 2004; Valeria et al. 2013) and is larger and flatter (Linos and Van Heerden 2004). The average weight is 4–6 g (Linos and Van Heerden 2004; Valeria et al. 2013), the left gland usually being heavier than the right. The length ranges over 3.5–7.3 cm, the width 1.5–4.0 cm, and the thickness 0.2–1.8 cm (Bergman et al. 1984; Liwu 1997; Linos and Van Heerden 2004; Valeria et al. 2013).

Variations of these organs can be examined under four main headings: absence, fusion, and malposition of the adrenal glands, and ectopic adrenal glands.

Absence of adrenal glands

Absence of one adrenal gland is quite rare and is usually the result of aplasia or extreme hypoplasia. In such cases there is often a marked hyperplasia of the remaining gland (Valeria et al. 2013). Complete bilateral absence of the adrenal gland was identified during postmortem examination of two stillborn and one pregnancy-termination fetuses and two neoanates (Sethuraman et al. 2011). Bilateral absence of the adrenal glands in a newborn was also observed in another case by Vachharajani et al. (2006).

Fused adrenal glands

A fused adrenal gland is rare; the gland adopts either a horseshoe or a butterfly shape. Six cases of fused adrenal gland were reported in 3537 pediatric-perinatal autopsy cases (Klatt et al. 1998). Fused adrenal glands in association with other anomalies (asplenia, central nervous system defects) have also been reported in infants or abortused feuses (Bell 1979; Strouse et al. 2002). A horseshoe-shaped adrenal gland was incidentally found in a 60-year-old man (Feldmann et al. 2009). A second case of an asymptomatic adult horseshoe-shaped adrenal gland with posterior midline diaphragmatic hernia was also identifed by CT imaging in a 51-year-old woman (Ditkofsky et al. 2013).

Ectopic adrenal gland

Ectopic (also called accessory or aberrant) adrenal gland tissue is a common finding, especially among children. Ectopic adrenal glands are usually round, have their own capsules, and are very small, ranging in size over 1–5 mm (Bergman et al. 1984). Although smaller ectopic glands appear to have no medullary substance, larger ones can have a medulla (Bergman et al. 1984).

The cortex of the adrenal gland develops in close relationship with the urogenital ridge, and most ectopic cortical tissue is associated with either the kidney, the gonads (ovary and testis), the broad ligament of the uterus, or the spermatic cord (Hollinshead 1958; Bergman et al. 1984). Ectopic cortical adrenal gland tissue can occur at any point along the descending path of the gonads including the scrotum, broad ligament, celiac plexus, renal plexus, and various other pelvic regions (Bergman et al. 1984; Piersol 1916). The spermatic cord is its most common location in the male genital region.

Many studies have reported ectopic cortical adrenal gland tissues in the inguinal region (spermatic cord, hernia sac, testis, epididymis, and ovary) with an overall incidence of 1.66–5.14% (Marchetti 1904; Nelson 1939; Gutowski and Gray 1979; Michowitz et al. 1979; Mares et al. 1980; Miersch et al. 1989; Okur et al. 1995; Ventura et al. 1998; Lorenzo Romero et al. 2000; Pérez García et al. 2001; Oguzkurt et al. 2002; Sullivan et al. 2005; Mendez et al. 2006; Vaos et al. 2006; Iyengar and Pittman 2007; Ozel et al. 2007; Ketata et al. 2008; Dobanovacki et al. 2013). The incidence of ectopic (intratesticular) adrenal gland tissue is quite high (42%) among patients with congenital adrenal gland hyperplasia (Avila et al. 1999).

Other studies have reported ectopic cortical adrenal gland tissues in the retrocrural space, the kidney, and the liver (Rolleston 1892). For example, Kirici et al. (2001) reported a case in which the tissue was located on the right retrocrural space with compression symptoms. Ectopic liver tissue has been found in the

Bergman's Comprehensive Encyclopedia of Human Anatomic Variation, First Edition. Edited by R. Shane Tubbs, Mohammadali M. Shoja and Marios Loukas.
© 2016 John Wiley & Sons, Inc. Published 2016 by John Wiley & Sons, Inc.

adrenal gland (Cullen 1925). Ectopic adrenal glands can adhere to the kidney via connective tissue and can be located on or under the capsule of the kidney. Occasionally, they are partially embedded in the substance of the kidney or liver (Hollinshead 1958; Bergman et al. 1984). The adrenal capsules can be supernumerary. Unilateral inclusion of the left adrenal gland in the upper pole of the kidney was found in one specimen in a series of 225 autopsies (Donnellan 1961). Ye et al. (2009) examined nine adult cases and found ectopic adrenal gland cortical tissue in seven and renal-adrenal gland fusion in two. They identified ectopic adrenal gland tissue at the superior pole of the kidney in six cases and in the mid-portion of the kidney in one. Their study also reported that such tissue varied in its growth pattern from plaque-like (n=3), wedge-shaped (n=2), or spherical (n=1) subcapsular lesions to irregular nests deep in the renal parenchyma (n=1). Adrenal gland-renal heterotopia was also previously reported by Weller (1925). An ectopic adrenal gland cortex in the neonatal liver was found by Vestfrid (1980).

Bergman et al. (1984) state that accessory medullary tissue is common and can occur in various places including the heart and along the aorta, and that histological confirmation of an intracranial intradural adrenal gland has been reported. Supradiaphragmatic adrenal gland tissue is extremely rare. Shigematsu et al. (2007) reported a case of ectopic adrenal gland tissue composed of both cortical and medullary cells found incidentally in the paratracheal region in a 99-year-old woman. This tissue was reportedly able to synthesize steroids and catecholamines under the control of adrenocorticotropic hormone (Shigematsu et al. 2007). Fifty-three ectopic adrenal glands (four of them medullary) were found during retroperitoneal dissections (Donnellan 1961).

Malposition of the adrenal glands

One or both glands are sometimes in an unusual position, or are intimately united to surrounding structures even in the normal position (Bergman et al. 1984; Valeria et al. 2013). Malposition of the left adrenal gland was observed by Öztürk et al. (2010) in a 50-year-old male cadaver. In this case, the gland was partly situated over the hilum of the kidney. Its posterior surface was related to the left crus of the diaphram and to the hilum of the left kidney, extending some distance above the medial margin of the kidney. Its anterior surface was totally covered by the body of the pancreas and the splenic artery and vein.

References

Avila NA, Premkumar A, Merke DP. 1999. Testicular adrenal gland rest tissue in congenital adrenal hyperplasia: comparison of MR imaging and sonographic findings. *AJR Am J Roentgenol* 172: 1003–1006.

Bell JE. 1979. Fused adrenal glands in association with central nervous system defects in the first half of foetal life. *J Pathol* 127: 191–194.

Bergman RA, Thompson SA, Afifi AK. 1984. *Catalog of Human Variation*. Baltimore, Munich: Urban & Schwarzenberg.

Cullen TS. 1925. Accessory lobes of the liver and accessory hepatic lobe springing from the surface of the gallbladder. *Arch Surg* 11: 718–764.

Ditkofsky N, Bradley N, Jeon P. 2013. Horseshoe adrenal gland: a rare congenital anomaly. *Surg Radiol Anat* 35: 749–754.

Dobanovacki DS, Maric DM, Maric DL, Vuckovic N, Jokic RR, Slavkovic AR, Miskovic SV. 2013. Ectopic adrenocortical tissue: an incidental finding during inguinal surgery in children. *Fetal Pediatr Pathol* 31: 32–37.

Donnellan WL. 1961. Surgical anatomy of the adrenal glands. *Ann Surg* 154(6): 298–305.

Drake RL, Vogl W, Mitchell AWM. 2012. *Gray's Basic Anatomy*. Philadelphia: Churchill Livingstone, Elsevier.

Feldmann EJ, Berko NS, Jain VR, Haramati LB. 2009. A man with a horseshoe adrenal gland associated with a midline posterior diaphragmatic defect. *J Comput Assist Tomogr* 33: 717–720.

Gutowski WT, Gray GF. 1979. Ectopic adrenal in inguinal hernia sacs. *J Urol* 121: 353–354.

Hollinshead WH. 1958. Anatomy of the endocrine glands. *Surg Clin North Am* 39: 1115–1140.

Iyengar V, Pittman DM. 2007. Ectopic adrenal gland tissue in inguinal hernia sac. *Ann Diagn Pathol* 11: 291–292.

Ketata S, Ketata H, Sahnoun A, Fakh H, Bahloul A, Mhiri MN. 2008. Ectopic adrenal cortex tissue: an incidental finding during inguinoscrotal operations in pediatric patients. *Urol Int* 81: 316–319.

Kirici Y, Mas MR, Saglamkaya U, Oztas E, Ozan H. 2001. Accessory adrenal gland: report of a case. *Surg Radiol Anat* 23: 201–203.

Klatt EC, Pysher TJ, Pavlova Z. 1998. Adrenal fusion. *Pediatr Dev Pathol* 1: 475–479.

Linos D, Van Heerden JA. 2004. *Adrenal Glands Diagnostic Aspects and Surgical Therapy*. Berlin, Heidelberg, New York: Springer–Verlag.

Liwu L. 1997. *Practical Clinical Ultrasonic Diagnosis*. New York: World Scientific Publishing Co. Pte. Ltd.

Lorenzo Romero JG, Segura Martín M, Hernández Millán I, Salinas Sánchez AS, López García S, Ruiz Mondéjar R, Vírseda Rodríguez JA, Martínez Martín M. 2000. Epididymal ectopic adrenal tumor. *Arch Esp Urol* 53: 271–273.

Marchetti G. 1904. Beitrage zur kenntnis der pathologischen anatomie der nebennieren. *Virschows Arch* 177: 227.

Mares AJ, Shkolnik A, Sacks M, Feuchtwanger MM. 1980. Aberrant (ectopic) adrenocortical tissue along the spermatic cord. *J Pediatr Surg* 15: 289–292.

Mendez R, Tellado MG, Somoza I, Liras J, Sanchez-Abuin A, Pais E, Vela D. 2006. Ectopic adrenal tissue in the spermatic cord in pediatric patients: surgical implications. *Int Braz J Urol* 32: 202–207.

Michowitz M, Schujman E, Solowiejczyk M. 1979. Aberrant adrenal tissue in the wall of a hernial sac. *Am Surg* 45: 67–69.

Miersch WD, Vogel J, Molitor D, Winter P. 1989. Ectopic adrenal cortex tissue. *Z Urol Nephrol* 82: 487–490.

Nelson AA. 1939. Accessory adrenal cortical tissue. *Arch Path* 27: 955.

Oguzkurt P, Oz S, Kayaselçuk F. 2002. Ectopic adrenal tissue: an incidental finding during inguinoscrotal operations in children. *Hernia* 6: 62–63.

Okur H, Küçükaydin M, Kazez A, Kontaş O. 1995. Ectopic adrenal tissue in the inguinal region in children. *Pediatr Pathol Lab Med* 15: 763–767.

Ozel SK, Kazez A, Akpolat N. 2007. Presence of ectopic adrenocortical tissues in inguinoscrotal region suggests an association with undescended testis. *Pediatr Surg Int* 23: 171–175.

Öztürk NC, Uzmansel D, Kara A, Öztürk H. 2010. Variation in the position, relation and vasculature of the left adrenal gland: case report. *Surg Radiol Anat* 32: 985–988.

Pérez García FJ, Guate Ortiz JL, Gutierrez García R, Tuero González JS, Lanzas Prieto JM, Gonzalez Naranjo F. 2001. Adrenal ectopy in epididymis. *Arch Esp Urol* 54: 446–448.

Piersol GA. 1916. *Human Anatomy*. Philadelphia: JB Lippincott Company.

Rolleston HD. 1892. Note on the anatomy of the adrenal gland bodies. *J Anat Physiol* 26: 547–553.

Sethuraman C, Parker MJ, Quarrel O, Rutter S, De Krijger RR, Drut R, Cohen MC. 2011. Bilateral absence of adrenal glands: a case series that expands the spectrum of associations and highlights the difficulties in prenatal diagnosis. *Fetal Pediatr Pathol* 30: 137–143.

Shigematsu K, Toriyama K Kawai K, Takahara O. 2007. Ectopic adrenal tissue in the thorax: a case report with in situ hybridization and immunohistochemical studies. *Pathol Res Pract* 203: 543–548.

Strouse PJ, Haller JO, Berdon WE, Rosovsky MA, Bellah RD, Barr M. 2002. Horseshoe adrenal gland in association with asplenia: presentation of six new cases and review of the literature. *Pediatr Radiol* 32: 778–782.

Sullivan JG, Gohel M, Kinder RB. 2005. Ectopic adrenocortical tissue found at groin exploration in children: incidence in relation to diagnosis, age and sex. *BJU Int* 95: 407–410.

Vachharajani A, Bethin K, Mouillet JF, Sadovsky Y, Saunders S. 2006. The rare occurrence of absent adrenals in a term infant: a case report and review of the literature. *Am J Perinatol* 23: 111–114.

Valeria A, Bergamini C, Bellantone R, Lombardi CP. 2013. *Surgery of the Adrenal Gland*. New York: Springer–Verlag.

Vaos G, Zavras N, Boukouvalea I. 2006. Ectopic adrenocortical tissue along the inguinoscrotal path of children. *Int Surg* 91: 125–128.

Ventura L, Leocata P, Hind A, Greco I, Ventura T. 1998. Ectopic adrenal tissue in the spermatic cord. Case report and review of the literature. *Arch Ital Urol Androl* 70: 15–18.

Vestfrid MA. 1980. Ectopic adrenal cortex in neonatal liver. *Histopathology* 4: 669–672.

Weller CV. 1925. Heterotopia of adrenal in liver and kidney. *Am J M Sc* 169: 696.

Ye H, Yoon GS, Epstein JI. 2009. Intrarenal ectopic adrenal tissue and renal-adrenal fusion: a report of nine cases. *Mod Pathol* 22: 175–181.

115 Male genitourinary system

Courtney L. Shepard[1], Dustin T. Gayheart[1] and David B. Joseph[1,2]
[1]University of Alabama at Birmingham, Birmingham, Alabama, USA
[2]Children's of Alabama, Birmingham, Alabama, United States

Penis

Hypospadias

Hypospadias refers to ventral placement of the urethral opening (Hennekam et al. 2013). Hypospadias is a rather common congenital anomaly occurring in 1/250 to 1/300 live births (Baskin 2000). Any description of hypospadias first requires a basic knowledge of penile embryology. The external genitalia are initially neutral and will default to female phenotype unless exposed to androgens during gestational weeks 8–12. Testosterone via the action of 5α-Reductase is converted to dihydrotestosterone, which is primarily responsible for penis formation (Snodgrass 2011). The urethral groove lies on the ventral surface of the phallus between urethral folds. Fusion of the medial edges of the urethral folds in a proximal to distal fashion allows for formation of the penile urethra. Two theories exist for formation of the glanular urethra. The older theory suggests that a solid ectodermal ingrowth of epidermis canalizes the glanular urethra. A newer theory described using immunohistochemical techniques supports the idea that fusion of the urethral folds extends all the way to the tip of the glans. Prepuce formation begins at week 8 of gestation. Preputial folds appear on each side of the penile shaft and join dorsally to form a flat ridge at the proximal coronal edge. Ventral fusion of the prepuce to form the frenulum does not occur until urethral formation is complete (Baskin 2000; Snodgrass 2011).

Etiology

The exact cause of hypospadias is largely unknown; however, there does appear to be a familial link. A large Danish health registry study of 1,201,790 boys with 5,380 hypospadias cases demonstrated similar recurrence risk ratios for twin brothers, brothers, and sons. Transmission in the Danish study was equal through the paternal and maternal sides of the family. These findings were consistent with genetic rather than intrauterine environmental factors as the etiology for familial hypospadias (Shnack et al. 2008).

Evidence supporting an endocrine cause for hypospadias has been limited. The enzymatic defects responsible for the steroidogenic conversion of cholesterol to dihydrotestosterone (DHT) are not common etiologies for hypospadias (Holmes et al. 2004). It has been hypothesized that synthetic compounds with estrogen-like or antiandrogen properties could contribute to hypospadias formation (Snodgrass 2011). This theory is supported by a study showing that pregnant animals exposed to chemicals with estrogen-like or antiandrogen effects produce urogenital anomalies including hypospadias (Gray et al. 2004).

Diagnosis

Hypospadias is diagnosed by physical examination alone. In addition to the proximally placed urethral meatus and ventrally deficient prepuce, other abnormal findings can include downward glans tilt, deviaton of the median penile raphe, ventral curvature, scrotal encroachment onto the penile shaft, midline scrotal cleft, and penoscrotal transposition (Snodgrass 2011). The range of hypospadias varies based on the location of the urethral meatus. Variations from distal to proximal include glanular, coronal, penile, peno-scrotal, scrotal, and perineal (Figs 115.1–115.4). A variant of hypospadias referred to as megameatus intact prepuce includes a normally formed foreskin concealing a glanular to distal shaft hypospadias (Snodgrass 2011).

Treatment

Primary treatment for hypospadias includes surgical correction. Several techniques for hypospadias repair exist with a focus on correction of ventral curvature and urethroplasty. The type of operation often depends on the location of the meatus on the penile shaft. Hypospadias urethroplasty falls into one of three categories including tubularization of urethral plate, substitution of the urethral plate with skin flaps, or urethral plate substitution with grafts (Snodgrass 2011).

Epispadias

Epispadias (Fig. 115.5) covers a wide spectrum of variations but is most often observed as a component of bladder or cloacal exstrophy (Gearhart and Mathews 2011). Epispadias is more common in boys than girls, with reported ratios of 3:1 (Dees 1949) to 5:1 (Kramer and Kelalis 1982). This section will focus on the rare anomaly of isolated male epispadias. Epispadias is characterized by a defect in the dorsal wall of the urethra. The

Bergman's Comprehensive Encyclopedia of Human Anatomic Variation, First Edition. Edited by R. Shane Tubbs, Mohammadali M. Shoja and Marios Loukas.
© 2016 John Wiley & Sons, Inc. Published 2016 by John Wiley & Sons, Inc.

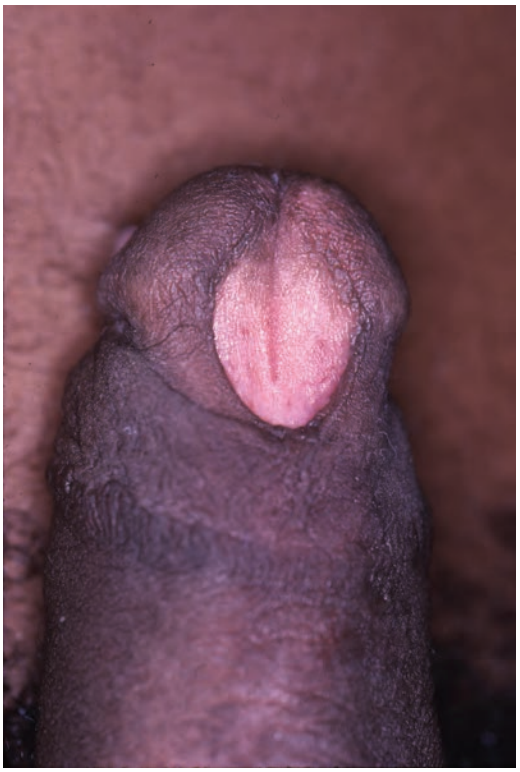

Figure 115.1 Megameatus variant.

Figure 115.3 Midshaft hypospadias.

Figure 115.2 Coronal hypospadias.

Figure 115.4 Scrotal hypospadias.

Figure 115.5 Proximal epispadias with incontinence.

Figure 115.7 Epispadias.

incidence of isolated male epispadias is reported to be 1 in 117,000 males and can range from a mild glanular defect in a covered penis to penopubic displacement of the urethral meatus with complete incontinence (Figs 115.6, 115.7). Approximately 70% of male epispadias patients have complete epispadias with incontinence (Gearhart and Jeffs 1998). In epispadias, a mucosal strip replaces the normal urethra and lines the dorsum of the penis extending toward the bladder. Sphincter incompetence thus incontinence is related to the degree of the dorsally displaced urethral meatus (Gearhart and Jeffs 1998). In the penopubic variant of epispadias, the entire penile urethra is open to the point of the bladder outlet. Epispadias is associated with varying degrees of dorsal chordee. Similar to patients with exstrophy, there is widening of the symphysis pubis caused by outward rotation of the innominate bones which results in divergent penopubic attachments in epispadias (Gearhart and Mathews 2011).

As previously stated, epispadias is most commonly associated with bladder or cloacal exstrophy. Other findings observed in association with isolated epispadias include diastatis of the pubic symphysis, insufficient continence mechanism, and vesicoureteral reflux (Gearhart and Mathews 2011).

Figure 115.6 Glanular epispadias.

Etiology

Epispadias is considered the mildest form of the bladder exstrophy-epispadias complex. The exact cause of the exstrophy-epispadias complex is unknown. From an embryologic standpoint it is thought to be caused by failure of mesoderm ingrowth into the cloacal membrane (Muecke 1964). The cloacal membrane consists of ectodermal and endodermal layers located at the caudal end of the germinal disk that occupies the infraumbilical abdominal wall. Ingrowth of mesoderm between the ectodermal and endodermal layers of the cloacal membrane results in formation of the lower abdominal wall musculature and pelvic bones. Rupture of the defective cloacal membrane results in a variant of the exstrophy-epispadias complex. The timing of the membrane rupture will determine the severity within the exstrophy-epispadias complex (Gearhart and Mathews 2011). If the membrane ruptures before four weeks gestation, then cloacal exstrophy occurs. However, if the membrane ruptures after the urorectal septum has descended at six weeks, epispadias or classic bladder exstrophy occurs (Gearhart and Jeffs 1998).

In a large epidemiological survey of 214 families with bladder exstrophy-epispadias complex, there was no association discovered with parental age, maternal reproductive history, or periconceptional maternal exposure to alcohol, drugs, chemical noxae, radiation, or infection. However, there was an association of periconceptional maternal exposure to smoking in patients with cloacal exstrophy compared to patients with epispadias/classic bladder exstrophy (Gambhir et al. 2008).

Diagnosis

The diagnosis of isolated epispadias is achieved by physical exam. Prenatal diagnosis can be made in cases of bladder exstrophy. A review of 25 prenatal ultrasounds in patients who delivered newborns with classic bladder exstrophy demonstrated five common observations. The observations from most common to

least common included bladder not visualized, lower abdominal bulge representing exstrophied bladder, small penis with anteriorly displaced scrotum, low set umbilical insertion, and abnormal widening of the iliac crests (Gearhart et al. 1995).

Treatment

Much like classic bladder exstrophy, the surgical goals of epispadias repair include achievement of urinary continence, preservation of upper urinary tracts, and reconstruction of cosmetically acceptable genitalia (Gearhart and Mathews 2011). Patients with complete epispadias in good bladder capacity can undergo epispadias repair, and bladder neck reconstruction can be performed in a single stage (Gearhart and Mathews 2011). In those patients with small bladder capacity, urethroplasty and penile elongation should be performed prior to bladder neck reconstruction (Gearhart and Mathews 2011). Multiple techniques for genital reconstruction have been performed. Successful reconstruction requires release of dorsal chordee and division of suspensory ligaments, dissection of the copora from their attachments to the inferior pubic ramus, lengthening of the urethral groove, and lengthening of the corpora (Gearhart and Mathews 2011).

Penile curvature/chordee

Penile curvature, a congenital or acquired condition, can occur in the ventral, dorsal, or lateral directions (Figs 115.8, 115.9). Chordee, a ventral curvature, is the most common form of penile curvature (Palmer 2011). Congenital chordee is most commonly seen in the presence of hypospadias; however, isolated cases of chordee without hypospadias make up 4–10% of congenital chordee cases (Culp 1966; Kramer et al. 1982).

Figure 115.8 Penile curvature.

Figure 115.9 Penile curvature.

Chordee without hypospadias consists of a ventrally tethered penis with a normally positioned penis. Devine and Horton (1973) categorized chordee without hypospadias into three categories. Type I chordee resulted from a deficiency of corpus spongiosum, dartos fascia, and Buck's fascia over the involved urethra. This would cause the urethra to be just beneath the skin and allow the dense fibrous tissue beneath the urethra to produce curvature. In Type II chordee, the spongiosum is normal but dartos and Buck's fascia are deficient. In Type III chordee, dartos fascia is deficient while Buck's fascia and spongiosum are preserved (Devine and Horton 1973). Kramer et al. (1982) added a Type IV chordee without hypospadias to classify those cases caused by corporal disproportion. A more contemporary series by Donnahoo et al. (1998) observed an even distribution of cases based on etiologies including skin tethering, fibrotic dartos and Buck's fascia, and corporal disproportion. A much less common cause was urethral tethering, which was seen in only 6 of 87 patients (Donnahoo et al. 1998).

Diagnosis and treatment

Evaluation of penile curvature should assess the degree of curvature and the presence of associated genital anomalies including hypospadias, urethral hypoplasia, and cryptorchidism. Exam is best performed with compression of the suprapubic fat pad for optimal exposure. Once in the operating room, evaluation should first include inspection for tethering of the glans by the frenulum or a skin bridge which can often be corrected with simple release. Next, if curvature remains then the penis should be degloved and artificial erection created to evaluate for any remaining chordee. Proper degloving should correct curvature due to skin tethering alone. If needed, plication techniques are applied opposite the region of maximum curvature. In cases where plication will cause significant penile shortening, grafting can be performed (Montag and Palmer 2011).

Penile torsion

Penile torsion is a rotational deformity of the penile shaft most commonly in the counterclockwise direction. Penile torsion is

Figure 115.10 Penis with approximately 45 degrees of torsion.

often not recognized until circumcision or retraction of foreskin. Normally the median raphe spirals obliquely around the shaft and does not insert at the normal position below the urethral meatus at the base of the glans (Palmer 2011). The degree of rotation can vary over the range 30–180° (Montag and Palmer 2011; Figs 115.10, 115.11). The cause of penile torsion has not been clearly defined, but skin tethering, disproportionate corporal bodies, and abnormal development of the dartos have been suggested as etiologies. Penile torsion is a common anomaly that can be seen with hypospadias and penile curvature (Bar-Yosef et al. 2007).

Diagnosis and treatment

Surgical correction is only necessary if rotation is at least 60–90° from midline. If release of penile torsion is thought to be needed, then neonatal circumcision should not be performed (Palmer 2011). For most mild forms of penile torsion, surgical correction includes degloving the penis to the penoscrotal junction and realignment via rotating the glans opposite the direction of torsion and suturing the glans to penile shaft skin at the correct position (Bar-Yosef et al. 2007)

Duplication of the urethra

Duplication of the urethra is a rare congenital abnormality which can originate anywhere from the bladder neck to the distal urethra (Fig. 115.12). It is predominantly found in males, but a few cases in females have been reported. Duplications can be complete or incomplete with a blind ending urethra and are most commonly oriented in the sagittal plane, consisting of a ventral and dorsal urethra (Salle et al. 2000). Less common duplications occur in the horizontal plane consisting of a right and left urethra. Horizontal duplications often occur in the setting of duplicated phallus or bladder (Casale 2011). In most cases of duplications in the sagittal plane, the ventral urethra serves as the normal urethra with an intact sphincteric mechanism and verumontanum.

Effman et al. (1976) established a classification system that functionally categorizes variations of duplicated urethra. They described three main types, with Types I and II having subcategories for certain variations. Type I classification includes a blind incomplete urethral duplication or an accessory urethra. Type IA distal, the most common variation, opens on the dorsal or ventral surface of the penis but does not communicate with the urethra or bladder. Type IB proximal is a very rare variation that may be difficult to differentiate from urethral diverticula or Cowper's ducts, as it opens from the urethral channel and ends blindly in the periurethral tissue. Type II classification includes complete patent urethral duplications. Type IIA-1 includes two noncommunicating urethras arising

Figure 115.11 Penis with nearly 90 degrees of torsion.

Figure 115.12 Instrument is marking two urethral meatuses.

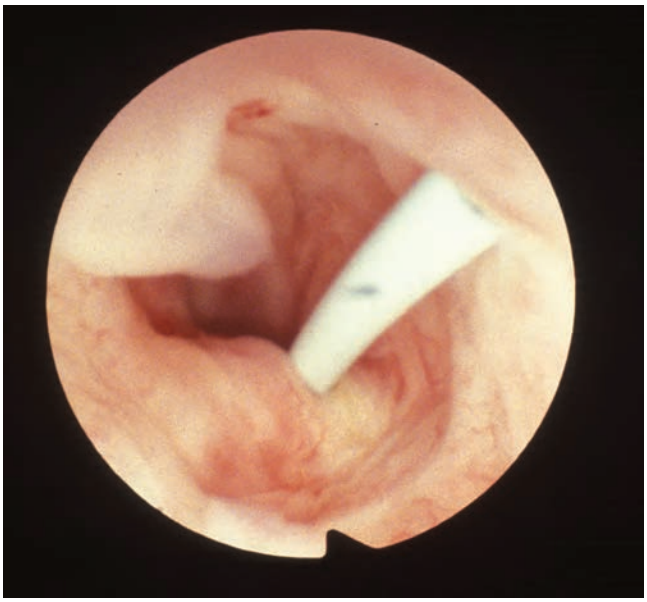

Figure 115.13 Cystoscopic image of the urethra showing a Type IIA-2 urethral duplication. The stent is seen coursing from the accessory urethra into the primary urethra.

independently from the bladder and terminating in two separate meati. Type IIA-2 includes variants in which a second urethral channel arises from the first channel and courses independently into a second meatus (Fig. 115.13). There is a special form of the Type IIA-2 variant which is referred to as the Y-duplication because the second urethra opens in the perineum or rectum. Type IIB consists of two urethras that arise from the bladder or posterior urethra and unite into a common channel distally. Type III classification includes urethral duplications that are a component of partial or complete caudal duplication (Effman et al. 1976).

Etiology

One possible theory for the etiology of duplicated urethra includes misalignment of the termination of the cloacal membrane and genital tubercle (Salle et al. 2000). Duplication of the urethra can include duplication of the bladder and other organs of the caudal end of the body, including the lower vertebral column, colon, rectum, anus, uterus, vagina, and external genitalia (Gray and Skandalakis 1972).

Diagnosis and treatment

The majority of patients are discovered at infancy; however, some will present later with incontinence or infection (Casale 2011). In the series by Salle et al. (2000), 11 of the 16 patients presented with double urethra or urinary stream. Of the remaining cases, 3 were detected at the time of epispadias repair, 1 at the time of hydrocele repair, and 1 at the time of hypospadias repair. Associated findings can include open symphysis pubis, urine dribbling from epispadic meatus, or voiding through the anus (Salle et al. 2000).

Diagnostics vary depending on the type of duplication but should accomplish anatomical delineation of the abnormality, recognition of the functional urethra, and investigation of other anomalies. Most frequently used tests include voiding cystourethrography (VCUG), retrograde urethrography (RUG), cystoscopy, and ultrasound. Salle et al. (2000) considered VCUG alone adequate if both urethras were demonstrated with one clearly larger and continent. Cystoscopy and RUG may be needed to further evaluate the anatomy (Podesto et al. 1998).

Treatment for urethral duplication varies greatly. Asymptomatic patients without incontinence or infection do not require treatment. Interventions include bugbee fulguration of small duplications, excision, and complex urethroplasties for Y-type duplications (Casale 2011).

Aphallia/agenesis of the penis

Aphallia or penile agenesis is a rare anomaly with an estimated incidence of 1 in 10–30 million births (Palmer 2011). Penile agenesis results from a failure of development of the genital tubercle (Roth et al. 1981). This can be due to single gene disorders, teratogenic effects, or malformation sequences. All cases have been sporadic and most have been associated with 46 XY karyotype (Evans et al. 1999). The typical appearance of aphallia is a well-developed scrotum with descended testicles and absent penile shaft. The anus tends to be displaced anteriorly and the urethra opens at the anal verge, next to a skin tag, or into the rectum (Palmer 2011).

Penile agenesis can be an isolated anomaly or, commonly, can be associated with a variety of other malformations. Evans et al. (1999) classified penile agenesis into two categories based on (1) the presence of severe renal aplasia/dysplasia and other caudal anomalies and (2) those with few abnormalities and low mortality. The severe category includes those with likely major disturbances of the caudal mesoderm because of associated anomalies including scrotal hypoplasia, absent raphe, and anal anomalies. The severe category has a much higher mortality due to lethal renal anomalies compared to the second group, which includes those with patent urethra, normal scrotum, raphe, and testes (Evans et al. 1999). Skoog and Belman (1989) classified penile agenesis based on the location of the urethral meatus in relationship to the anal sphincter. Their classification included those that were presphincteric, postsphincteric, and those with urethral atresia. It was observed that the more proximal the urethral meatus, the greater the likelihood of neonatal death and higher incidence of other anomalies. In the Skoog and Belman series, the patients with urethral atresia and vesicorectal fistula for drainage had a 100% mortality rate. Patients with a postsphincteric meatus located on an appendage near the anal verge had an 87% survival rate. Those with presphincteric communcications such as prostatorectal fistula had a 36% neonatal mortality rate (Skoog and Belman 1989).

Diagnosis and treatment

Prompt evaluation by multidisciplinary team should be initiated upon diagnosis of aphallia. Testing includes a karyotype and imaging to evaluate the urinary tract and other organ systems for associated anomalies (Palmer 2011). Gender assignment should be addressed after full evaluation by multidisciplinary team and parental counseling. Historically, these patients underwent gender reassignment surgery; however, this should be performed with caution due to documented cases of male gender identity despite reconstruction as a female (Diamond 1999). There is no ideal technique for penile reconstruction. However, radial forearm flap phalloplasty is a reliable technique for creation of normal appearing penis and scrotum with ability to void standing (Monstrey et al. 2009).

Posterior urethral valves

Urethral anomalies associated with the clinical presentation of bladder neck obstruction include posterior urethral valves (PUVs), hypertrophy of the colliculus seminalis (verumontanum), and Marion's Disease (Gray and Skandalakis 1972). Posterior urethral valves are an obstructive membrane that act as a passive barrier to urine flow. Posterior urethral valves occur in 1 in 8000–25,000 live births (Casale 2011). The incidence is increased in African Americans and children with Down syndrome (Hodges et al. 2009). Posterior urethral valves were first reported by Morgnani in 1717 and Langenbeck in 1802. It was not until 1919 that Hugh Hampton Young named, defined, and classified posterior urethral valves (Young et al. 1919). Young's classification system is still used today.

- Type I valves (Fig. 115.14) arise as a ridge from the verumontanum and pass distally to divide into two membranes, which attach to the lateral walls of the urethra (Gray and Skandalakis 1972). Type I valves make up 95% of all posterior urethral obstructions. Valves vary in thickness and degree of obstruction. The valve consists of a stroma of fibrous tissue covered by transitional epithelium on each side (Casale 2011).
- Type II folds also arise from the verumontanum, but extend along the posterior urethral wall toward the bladder neck. Type II folds are no longer referred to as valves because they are not obstructive. They are likely due to a distal obstruction with resultant hypertrophy of the muscles of the superficial trigone and prostatic urethra from high voiding pressure (Casale 2011).
- Type III valves (Figs 115.15, 115.16) act as a membrane across the urethra with a small perforation near the center. Type III valves make up 5% of posterior urethral valves and are thought to be due to incomplete dissolution of the urogenital portion of the cloacal membrane (Casale 2011).

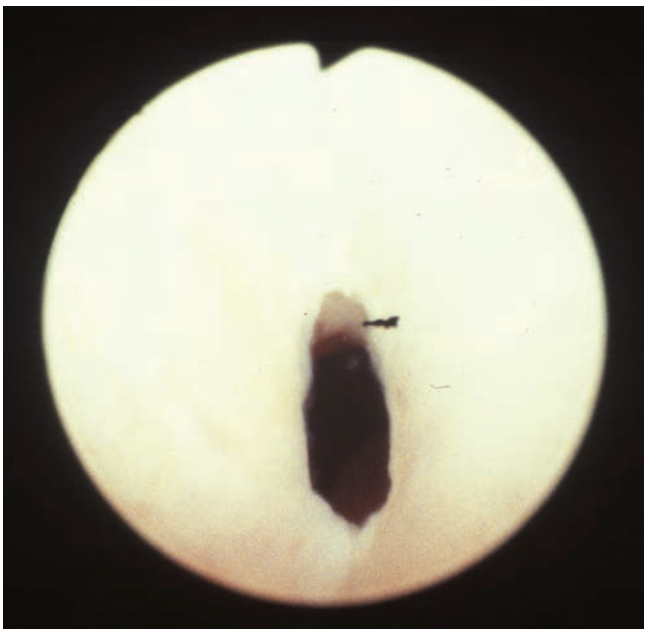

Figure 115.14 Type 1 posterior urethral valves.

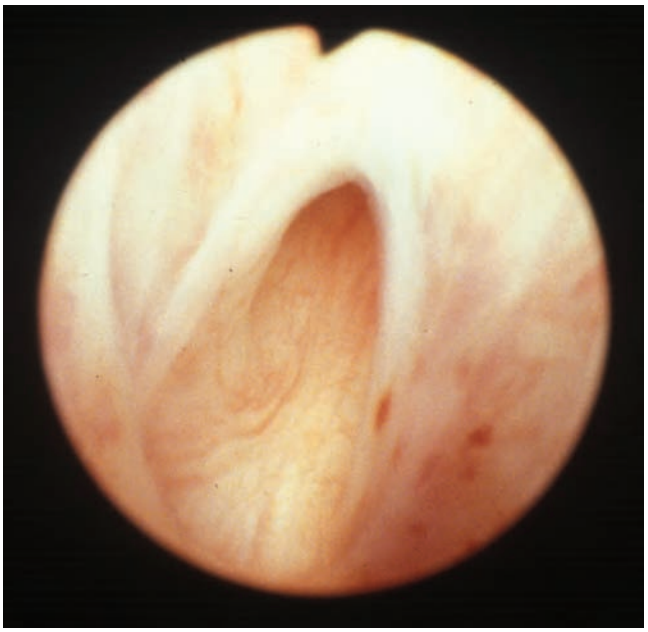

Figure 115.15 Type 3 posterior urethral valves.

Etiology

The embryologic origin of posterior urethral valves remains speculative. Various theories have been considered. Stephens concluded that they were the result of abnormal integration of the wolffian ducts into the urethra. Dewan et al. (1994) created the term COPUM (congenital obstructing posterior urethral membrane) in the 1990s to challenge the traditional nomenclature of posterior urethral valves. Dewan's term more accurately reflected the theory that the obstruction was secondary to a single membrane in the posterior urethra. A detailed anatomical study and software based 3D reconstruction of a noncatheterized stillborn infant with posterior urethral valves,

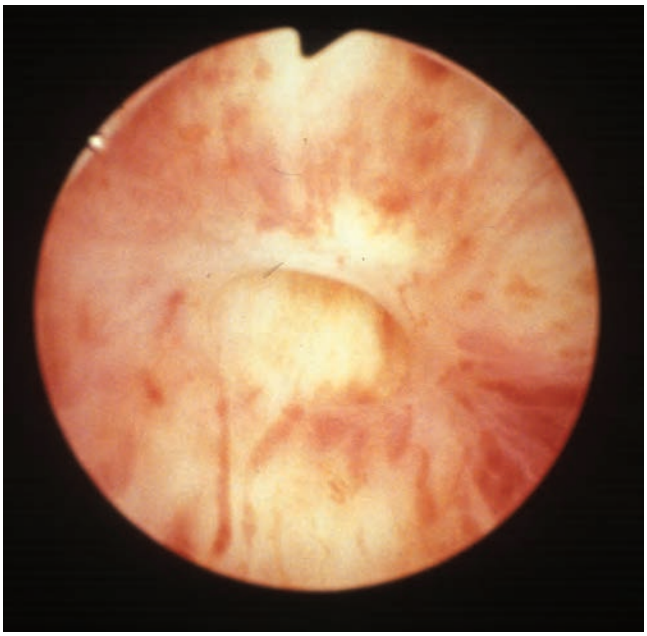

Figure 115.16 Type 3 posterior urethral valves.

published in 1996, demonstrated findings supportive of persistent urogenital membrane as etiology for posterior urethral valves (Krishnan et al. 2006).

Pathophysiology

The effects of posterior urethral valves on the urinary tract are severe and can be seen proximal to the level of the obstruction. Lower and upper urinary tract changes are due to exposure to elevated pressures during development. Histological findings demonstrate hypertrophy and hyperplasia of the detrusor muscle and increases in connective tissue. Clinically this manifests as poor sensation, hypercontractility, and low compliance. The posterior urethra is often distended and bladder neck hypertrophied. Ureteral walls are thickened and the ureteral lumen is dilated (Casale 2011).

Renal injury from posterior urethral valves is due to obstructive uropathy and renal dysplasia. Obstructive uropathy involves tubular and glomerular injury. Tubular injury results in a failure to concentrate or acidify urine. Glomerular injury, which is potentially reversible after treatment, results in decreased perfusion and filtration due to high pressures. Renal dysplasia is characterized as a histologic diagnosis which may be the result of increased pressure during the development of the kidney or abnormal embryologic development. Regardless, the effects of dysplasia are irreversible and play a defining role in long-term renal function (Casale 2011).

Pulmonary hypoplasia is the most life-threatening manifestation of posterior urethral valves in the newborn. Obstruction from valves results in decreased fetal urine output, which leads to oligohydramnios and pulmonary hypoplasia. The most severe cases may be fatal or require respiratory support (Casale 2011).

Diagnosis

Posterior urethral valves normally present as hydronephrosis on prenatal ultrasound now that second trimester ultrasound has become routine obstetrical care. Findings include bilateral hydroureteronephrosis, thick walled bladder, and keyhole sign in the bladder neck of males. Definitive diagnosis is made after birth. Cases not detected prenatally may present as poor urinary stream, UTI, and failure to thrive in the newborn. Older children can present as diurnal enuresis, infections, severe voiding complaints, or hematuria (Hodges et al. 2009). Diagnostic studies after birth include ultrasound, VCUG, and cystoscopy. Neonatal ultrasound findings of posterior urethral valves are identical to fetal ultrasound findings. Voiding cystourethrogram is the primary diagnostic tool for posterior urethral valves (Casale 2011). VCUG findings include dilated posterior urethra, trabeculated bladder, vesicoureteral reflux, and valve leaflets (Hodges et al. 2009).

Treatment

The initial mainstay of treatment of PUV is relieving obstruction and pressure on urinary tract as soon as possible. This is accomplished via catheter drainage of the bladder at birth (Hodges et al. 2009). Blood urea nitrogen (BUN), creatinine, and electrolytes should be monitored closely until plateau. BUN and creatinine will reflect maternal renal function for 48 hours and therefore will not accurately reflect newborn renal function for 48 hours. Following successful bladder drainage and medical stabilization, the valves are permanently destroyed normally by endoscopic ablation. Infants too small for endoscopic treatment should undergo cutaneous vesicostomy until valve ablation can be performed at a later date. A VCUG should be performed some time after the procedure to confirm valve remnants are not obstructive (Casale 2011).

Urethral diverticulum

A congenital diverticulum is a transitional cell epithelium-lined pouch of the urethra. An anterior urethral diverticulum may result from the incomplete development of the urethra, and a congenital diverticulum of the prostatic urethra may be a large remnant of the müllerian duct associated with defects of diminished virilization (Jordan and McCammon 2011). The anterior urethral diverticulum was first reported by Watts and Englander in 1906. Urethral diverticula are often seen in association with anterior urethral valves and have therefore been considered by many to represent the same pathology. Others consider urethral diverticula and anterior urethral valves separate entities (Prakash et al. 2013). In cases of anterior urethral valves and associated diverticula, the valve presents as a mucosal fold that rises during micturition and flattens against the urethral roof. This action creates an obstruction to urinary flow that distends the urethral diverticulum (Prakash et al. 2013).

Diagnosis and treatment

Presentation is associated with a spectrum of symptoms including dribbling, diminished urinary stream, and infection. VCUG is the diagnostic modality of choice for anterior urethral diverticulum

that is associated with anterior valves (Prakash et al. 2013). Posterior diverticula are demonstrated best with cystoscopy or retrograde urethrography (Jordan and McCammon 2011).

Anterior urethral diverticula can be treated with simple endoscopic unroofing (Jordan and McCammon 2011). Large diverticula with minimal supportive tissue may require open excision and primary repair of the urethra (Prakash et al. 2013). Posterior diverticula do not require treatment unless they are very large. Several open approaches have been described for excision of large posterior diverticula (Jordan and McCammon 2011).

Diphallia/supernumerary penises

Diphallia or duplication of the penis is a rare anomaly seen in 1 of 5 million live births (Hollowell et al. 1977). Duplication of the penis is usually associated with other congenital anomalies of the urogenital, musculoskeletal, and gastrointestinal systems (Maruyama et al. 1999; Gyftopoulous et al. 2002). Diphallia can vary from a small accessory penis or duplication of the glans to a complete penile duplication. The duplication can be orthotopic or ectopic. Division of the penises may be sagittal or frontal and be symmetric or asymmetric in shape and size. Diphallia is classified into two categories: true diphallia and bifid phallus. These categories can be furthered divided based on complete or partial duplication. True complete diphallia refers to a duplication in which each penis has two corpora cavernosa and one corpus spongiosum. True partial diphallia refers to duplications in which the duplicate penis is smaller but also has two corpora cavernosa and one corpus spongiosum. Complete bifid phallus indicates the presence of only one corpus cavernosum, but the separation is complete to the base of the shaft. Partial bifid phallus refers to the presence of only one copus cavernosum with separation of the glans only (Gyftopoulous et al. 2002). True diphallia tends to be associated with more severe malformations compared to bifid phallus (Hollowell et al. 1977).

Erectile function in cases of diphallia varies based on anatomy. Typically, one or both penises are capable of erection. Several theories for the embryologic etiology of this rare anomaly exist, but the cause is largely unknown (Gyftopoulous et al. 2002).

Diagnosis and treatment

The initial evaluation and management of patients with diphallia is directed towards defining the entire urinary tract and identifying associated anomalies (Gyftopoulous et al. 2002; Palmer 2011). Initial evaluation should include renal ultrasound and voiding cystourethrogram (Palmer 2011). Lapointe et al. (2001) have described the benefits of MRI in evaluation of congenital anomalies of the external genitalia. Advantages of MRI include excellent anatomic interpretation of complex genital anomalies and associated abnormal pelvic tissues (Lapointe et al. 2001). Surgical correction varies based on case but should focus on separation of the urogenital and gastrointestinal tract, preservation of continence, eradication of infections, and reconstruction of the external genitalia in a functional and aesthetic fashion (Gyftopoulous et al. 2002).

Inconspicuous penis

An inconspicuous penis refers to group of anatomical variants that describe a penis which appears small but has a normal stretched penile length measured from the pubic symphysis to the tip of the glans and has a normal penile shaft diameter (Bergeson et al. 1993). Buried penis, trapped penis, and webbed penis all fall under the category of inconspicuous penis. Inconspicuous penis can be congenital in nature or acquired for instance after neonatal circumcision (Palmer 2011).

Buried penis

Buried penis is a normally developed penis that is hidden by the suprapubic fat pad (Figs 115.17, 115.18). Buried penis is also referred to as concealed penis or hidden penis (Palmer 2011). Buried penis can be caused by poor skin fixation at the base of the penis, cicatricial scarring after penile surgery, and excessive obesity, and potentially results in balanitis, difficult hygiene,

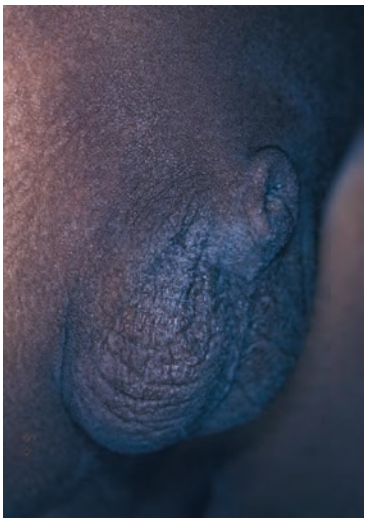

Figure 115.17 Buried penis.

Figure 115.18 Buried penis.

Figure 115.19 Outcome after surgical repair of buried penis.

difficulty holding the penis during voiding, and embarrassment among peers. Casale et al. (1999) classified concealed penis into three different types based on surgical history and physical findings. Type 1 consisted of congenital concealed penis. Type 2 concealed penises are those that are a result of scarring from previous surgery. Types 3 are complex cases involving excessive obesity. Type 1 or congenital concealed penis is thought to be due to poor fixation of the penile skin at the penopubic and penoscrotal angles.

Treatment of buried penis varies based on etiology and presence of symptoms. When concealed penis is thought to be due obesity alone, a period of waiting and treatment of obesity should be initiated. Surgical treatment techniques for buried penis include complete penile degloving with release of tethering bands, release of penoscrotal webbing, excision of suprpubic fat, removal of dense scarring, surgical fixation of the skin at the base of the penis, and penile skin flaps (Casale et al. 1999; Fig. 115.19).

Webbed penis

Webbed penis or penoscrotal fusion is a form of inconspicuous penis that is characterized by scrotal skin extending onto the ventrum of the penis (Figs 115.20–115.21). Like buried penis, it consists of a congenital and acquired forms. The congenital form of webbed penis is an abnormality of the attachment between the penis and scrotum whereas the acquired form is the result of excessive removal of ventral skin during circumcision. This anatomical variant is usually asymptomatic but surgery is often performed for cosmetic reasons (Palmer 2011).

Micropenis

Micropenis is a normally formed penis that is at least 2.5 standard deviations below the mean size in stretched length for age (Aaronson 1994). Stretched penile length correlates well with erectile length and is measured from the attachment to the pubic symphysis to the tip of the glans. The corpora cavernosa can be severely hypoplastic and associated anomalies include small testes, cryptorchidism, and fused scrotum. Micropenis is the result

Figure 115.20 Webbed penis.

Figure 115.21 Outcome after superficial repair of webbed penis.

of a hormonal abnormality occurring after 14 weeks gestation (Palmer 2011). The etiologies for micropenis are numerous but can generally be classified into one of five categories, including: deficient testosterone secretion, defects in testosterone action, developmental anomalies, idiopathic, or associated with other congenital malformations. Those etiologies that fall into the deficient testosterone secretion category can be further differentiated based on whether deficient testosterone secretion is due to hypogonadotropic hypogonadism or primary hypogonadism (Bin-Abbas et al. 1999). The most common cause of micropenis is hypogonadotrophic hypogonadism and can be seen in Kallman's syndrome or Prader-Willi (Palmer 2011).

Diagnosis and treatment

Diagnosis is performed by an accurate measurement of stretched penile length. Evaluation includes karyotype, serum LH and FSH concentrations, testosterone levels before and after hCG stimulation, functional evaluation of the anterior pituitary, and MRI of the head. Initial treatment involves exogenous stimulation with testosterone for penile growth (Palmer 2011).

Ossified penis

Gould and Pyle (1896) have discussed ossification of the penis. These authors quoted earlier desriptions by Velpeaus, Kauffmann, Lenhoseck, and Duploy. The Ephemerides and Paullini also described bony penises.

Foreskin/prepuce

The foreskin/prepuce is a loose fold of skin arising from the penile shaft that normally covers the glans penis in a flaccid state. The frenulum of the foreskin is a band of elastic tissue on the ventral surface of the penis that connects the foreskin to the glans penis (Hennekam et al. 2013). Primary phimosis, the inability to retract the foreskin, is physiologic at birth due to natural adhesions between the glans and preputial skin or a preputial ring. Separation of the prepuce from the glans occurs as epithelial debris known as smegma accumulates under the prepuce and intermittent erections occur (Palmer 2011). Primary phimosis resolves with age. Less than 1% of 17-year-old boys have phimosis (Oster 1968; Kayaba et al. 1996). Paraphimosis is the entrapment of the prepuce behind the glans penis. Severe edema of the foreskin can development and result in gangrene if not promptly treated (Palmer 2011).

Diagnosis and treatment

As previously stated, primary phimosis almost always resolves with age and normally does not require intervention. Reasons to increase retractibility of the prepuce include persistent primary phimosis, secondary phimosis, balanitis, posthitis, balanitis xerotica obliterans, and urinary tract infection. Treatment can be accomplished via topical corticosteroid creams, dorsal slit, or circumcision. Elective neonatal circumcision is controversial (Palmer 2011).

Paraphimosis can normally be treated with manual compression of the glans and distal traction on the edematous foreskin. If reduction of the edematous foreskin cannot be achieved with manipulation, a dorsal slit or circumcision may be required (Palmer 2011).

Scrotum

Bifid scrotum

A bifid scrotum has two completely separate labioscrotal folds. It is associated with proximal hypospadias and is often seen in patients with disorders of sexual development such as 48 XXYY, partial androgen insensitivity syndrome, and 46 XY disorders of sex development (Blanc et al. 2011; Snodgrass 2011; Hughes et al. 2012; Messina et al. 2013). The repair may require scrotal rotation flaps, inguinal based groin flaps, transposition of the penis, or z-plasty (Mokhless et al. 2011; Fig. 115.22).

Penoscrotal transposition

Penoscrotal transposition describes the abnormal location of the scrotum cephalad to the penis. It may be complete, in which

Figure 115.22 Bifid scrotum with pronounced penoscrotal transposition.

Figure 115.23 Bifid scrotum with mild penoscrotal transposition.

the entire scrotum is located above the penis, or, more commonly, partial. The penis may be located in the middle or in a more cephalad position of the scrotum (Mokhless et al. 2011; Figs 115.23, 115.24).

Figure 115.24 Bifid scrotum also with penoscrotal transposition.

Etiology

The cause of penoscrotal transposition is unknown. One hypothesis is that the scrotal and penile tissues have decreased androgen sensitivity, precluding normal migration of the labioscrotal swellings.

Diagnosis and treatment

While the diagnosis is based on of physical exam, obtaining upper tract imaging with renal ultrasound and possibly voiding cystourethrography is encouraged due to the association of penoscrotal transposition with other genitourinary anomalies (Palmer 2012).

Surgical correction is often performed in stages, with correction of the transposition and bifid scrotum if present at least six months prior to performing urethroplasty (Sunay et al. 2009; Mokhless et al. 2011). Many different techniques using flaps have been described (Pinke et al. 2001; Sunay et al. 2009; Mokhless et al. 2011). Surgical transposition of the penis as opposed to the scrotum has also been described (Kolligian et al. 2000).

Associated conditions

Penoscrotal transposition is strongly associated with hypospadias (79% of cases), especially perineal and scrotal hypospadias, chordee (81% of cases), and bifid scrotum (Pinke et al. 2001; Mokhless et al. 2011; Fig. 115.25). Additionally, up to 32% of patients have other anomalies; these most commonly involve the genitourinary tract but also the cardiac, gastrointestinal, musculoskeletal, and central nervous systems. Chromosomal anomalies involving chromosomes 13, 4, and 18 as well as 46 XX/XY and 45 XO/XY mosaicism and Kleinfelter's syndrome have also been associated with penoscrotal transposition (Pinke et al. 2001). Perineal lipoma in conjunction with this condition has also been described (Mohta et al. 2008).

Figure 115.25 Penoscrotal transposition with perineal hypospadias.

Ectopic and accessory scrota

Ectopic and accessory scrota are both extremely rare conditions with just over 20 cases of the former and 30 cases of the latter reported (Park and Hong 2006). An ectopic scrotum is an abnormally placed hemiscrotum which may be suprainguinal (which is most common), infrainguinal, or located on the thigh. The associated testicle may or may not be located within the ectopic scrotum (Chatterjee et al. 2012). Upper tract imaging is indicated in patients with this condition, as it may be associated with anomalies of the ipsilateral upper tract, especially when the ectopic scrotum is suprainguinal. Additional associations include cryptorchidism, inguinal hernia, bladder extrophy, and popliteal ptergium syndrome, although it is also commonly an isolated finding (Palmer 2012). Treatment includes local or pedicle flaps to place the hemiscrotum in an orthotopic location (Park and Hong 2006).

Patients with an accessory scrotum have a normal appearing scrotum with a median raphe, but also have extra scrotal tissue that is most commonly inferior to the scrotum (Fig. 115.26); this has also, but rarely, been reported in other areas such as the penile shaft (Coplen et al. 1995; Park and Hong 2006; Chatterjee et al. 2012). This extra scrotal tissue does not contain a testis (Park and Hong 2006). It is most commonly a solitary finding, but may be associated with other genitourinary or non-genitourinary anomalies such as diphallia, anorectal anomalies, or VACTERL (Chatterjee et al. 2012). Treatment is excision of the accessory tissue (Coplen et al. 1995; Park and Hong 2006).

Figure 115.26 Accessory scrotum inferior to bifid "normal" scrotum.

Accessory and, less commonly, ectopic and other abnormal scrota are associated with perineal lipomas. Reportedly 83% of accessory scrota are associated with perineal lipomas which are usually ipsilateral to the accessory scrota (Sule et al. 1994; Park and Hong 2006). In cases when a perineal lipoma is present, no other genitourinary or non-genitourinary anomalies are evident (Chatterjee et al. 2012; Palmer 2012).

Etiology

In normal embryologic development, labioscrotal swellings appear on each side of the cloacal membrane. These swellings then move inferior and medially before joining in the midline below the penis to form the scrotum by around 12 weeks of gestation (Coplen et al. 1995; Park and Hong 2006). It is thought that an ectopic scrotum may be due to abnormal or early migration of the involved labioscrotal swelling, or alternatively that abnormal gubernacular formation prevents normal migration (Lamm and Kaplan 2006; Redman and Ferguson 2005; Palmer 2012). Two dominant theories also exist regarding cause of accessory scrota. There may be early division of one labioscrotal swelling, which subsequently migrates inferior to the dominant swelling (Park and Hong 2006). Alternatively, mesenchymal tissue (such as a lipoma) may cause discontinuity of the developing labioscrotal swelling.

Scrotal agenesis

Scrotal agenesis is a very rare anomaly, with fewer than five cases reported. The patients have a normal karyotype and normal penis. However, bilateral testes are either cryptorchid or ectopic. Three cases have been associated with other non-genitourinary anomalies and one case with megameatus (Janoff and Skoog 2005). Treatment includes mycocutaneous flaps to construct a scrotum. The use of preputal skin is preferred due to the presence of androgen receptors in this skin as in the scrotum, which could potentially undergo hormonally driven growth with age (Verga and Avdio 1996; Janoff and Skoog 2005).

Testes

Undescended testicle

Undescended testicle, or cryptorchidism, is the most common genital anomaly in males (Barthold and González 2003). The risk of an undescended testicle increases substantially with prematurity and low birth weight (less than 2.5 kg). While the incidence is 1–5% of full-term males, it increases dramatically to 21–45.3% of premature males (Gray and Skandalaskis 1972; Hutson and Clarke 2007; Sijstermans et al. 2008).

Etiology

Testicular descent may be divided into two stages: the transabdominal stage (weeks 8–15) and the inguinoscrotal phase (weeks 25–35). The testicles originate in the abdomen, where they remain and develop even after the lumbar region elon-

gates due to attachment of the cranial ligament. In the transabdominal phase, which is controlled by insulin-like 3 from leydig cells, the gubernaculum develops and the cranial ligament regresses. During the inguinoscrotal phase, the testicle is guided through the inguinal canal into the scrotum by the gubernaculum, which extends from the external ring. This is under the influence of the genito-femoral nerve (Hutson and Hasthorpe 2005). After the testicle exits the external ring, it contracts and the processus vaginalis closes (Gray and Skandalaskis 1972).

The testicle may never initiate its descent or may stop at any point along the course of descent, causing an undescended testicle. The cause of this is thought to be due to androgen insufficiency, anatomic interference (including insufficient spermatic cord or artery length, inguinal canal or ring anomaly, or cremaster muscle or gubernaculum anomaly), or inflammatory adhesions (Gray and Skandalaskis 1972).

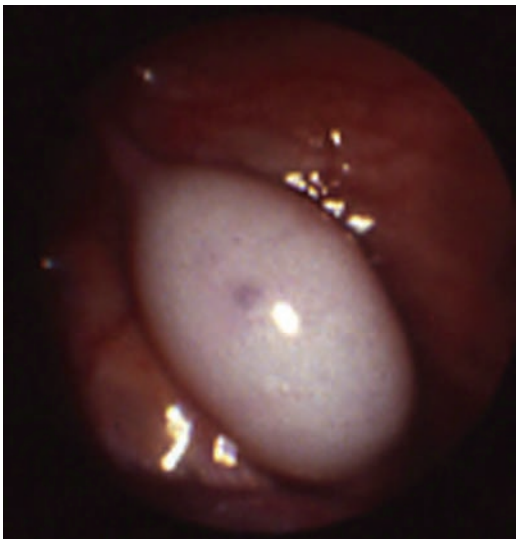

Figure 115.27 Intra abdominal testicle seen on laparoscopy.

Presentation

Undescended testicles are found incidentally on physical exam. In full term males, unilateral cryptorchidism is twice as common as bilateral, which is seen in only 15.5% of cases (Cendron et al. 1993; Barthold and González 2003). However, preterm males have bilateral cryptorchidism in 50–75% of cases (Barthold and González 2003). At birth, right-sided undescended testicles are more common with a 1.8 to 1 right to left ratio; this trend reverses by adulthood with a 0.6 to 1 right to left ratio. However, nonpalpable testicles are more common on the left (Barthold 2012). The testicle may be found in the abdomen (3–34%), near the internal ring (12%), in the inguinal canal (16–75%) or, rarely, may be ectopic or absent (Gray and Skandalaskis 1972; Moul and Belman 1988; Barthold 2012).

Diagnosis

An undescended testicle is a clinical diagnosis, which is somewhat variable and subjective. Experts suggest a testicle should be considered descended when its midpoint lays at the midpoint of the scrotum or lower; any testicle lying above this point is therefore considered undescended. A cryptorchid testicle is nonpalpable. Further classifications include recurrent cryptorchidism, testicles that initially descend spontaneously but then move back to an extrascrotal position, testicular ascent, testicles that were previously scrotal that become cryptorchid without an iatrogenic cause, and secondary testicular cryptorchidism (testicles that move extrascrotal after surgery). Retractile testicles may be brought into a normal scrotal position transiently before they move back out of the scrotum (Barthold 2012).

Treatment

For infants diagnosed with undescended testicles at birth, observation is initially indicated as spontaneous testicular descent may be seen in 56% of premature and 50% of term males by one month of age (Gray and Skandalaskis 1972). By one year of age, the incidence of undescended testicles in premature or low birth rate males falls to 1.9–7.3%, and in term or normal birth rate males it falls to 1–1.5%. However, surgical correction should be performed before age two to help decrease the risk of testicular degeneration and malignancy. Laparoscopy is increasing in popularity for nonpalpable testes, which often require a staged approach Fig. 115.27. Inguinal and scrotal approaches are employed for palpable testicles (Cuda et al. 2011).

Hormonal treatment with hCG to initiate testicular descent has been effective in only a small number of patients, with best results seen in those with testicles in the distal inguinal canal and older children (Palmer 1991). However, treatment with gonadotropin-releasing hormone analogue prior to or after surgical correction as well as treatment with lutinizing hormone-releasing hormone analogue after orchiopexy has been shown to favorably increase fertility potential (Hadziselimović and Herzog 1997; Schwenter et al. 2005).

Associated conditions

Cryptorchidism is associated with increased risk of testicular cancer, subfertility, and testicular atrophy. Patient with undescended testicles have a 2–8 times increased risk of primary testicular cancer with an incidence ration of 2.23 if they undergo orchiopexy before age 13, and an incidence ratio of 5.40 if they undergo orchipexy after age 13 (Pettersson et al. 2007). Contraversy remains as to whether the contralateral testicle is also at a very small increased risk of malignancy (Akre et al. 2009; Wood and Elder 2009). In testicles that do undergo malignant transformation, 74% of persistently cryptorchid testicles will develop seminoma versus 63% of testicles in a scrotal position that develop nonseminomatous tumors.

Cryptorchidism leads to a decrease in the number of spermatogonia and alters spermatogenesis in the undescended testicle, but may also have some deleterious effect on the descended testicle. Early intervention allows for increased preservation of

germ and Sertoli cells, which decreases the risk of subfertility (Elder 1987; Schwentner et al. 2005; Pettersson et al. 2007; Kollin et al. 2012). Of patients whose bilateral cryptorchidism is left untreated, 89% will be azospermic; however, 56% will be infertile despite appropriate intervention (Cortes et al. 2001; Schwentner et al. 2005). Testicular atrophy is also appreciated in the cryptorchid testicle. The degree of atrophy is related to the time the testicle remained cryptorchid and correlates with a depletion of germ and Sertoli cells (Kollin et al. 2012, 2013).

There are more than 250 syndromes and conditions associated with cryptorchidism. The most common is Klinefelter. Others include prune belly syndrome, cerebral palsy, omphalmocele, arthrogyryposis, spina bifida, 46XX male, sex chromosome mosaicisms, Prader-Willi, Beckwith-Widemann, Down syndrome, and Noonan syndrome. There are also familial cases (Foresta et al. 2008; Barthold 2012).

Retractile testicle

The retractile testicle may be considered a subset of the undescended testicle. In one study of 204 retractile testicles, 30% descended spontaneously, 32% became undescended, and 38% remained retractile. Spontaneous descent was seen in 58% of patients over age 7 versus 21% in those younger than 7 (Agarwal et al. 2006). It is more commonly on the right and is bilateral in 36.7–74% of cases (La Scala and Ein 2004; Stec et al. 2007). There has been one report of testicular cancer in a retractile testis (La Scala and Ein 2004).

Ectopic testicle

Approximately 1.6–3.7% of patients who undergo surgery for an undescended testicle will be found to have an ectopic or maldescended testicle (Hutcheson et al. 2000; Ramareddy et al. 2013). The most common location is perineal (Fig. 115.28), but the testicles may also be found to be pubopenile, in the superficial inguinal pouch of Denis Browne, lateral to the scrotum, in or near the contralateral hemiscrotum, or, even more rarely, preperitoneal, femoral, in the thigh, or in the anterior abdominal wall. Bilateral cases are the exception, usually seen only in perineal cases (Gray and Skandalaskis 1972; Hutcheson et al. 2000; Ramareddy et al. 2013). Generally, an ectopic testicle was thought to carry a more favorable prognosis in terms of function, size, and risk of malignancy than an undescended testicle. Reports of malignancy are exceedingly rare (Gray and Skandalaskis 1972). However, more recent studies have demonstrated a decrease in the number of germ cells and size of ectopic testicles, although it may not be as significant as an undescended testicle (Herzog et al. 1992).

Etiology

The etiology remains poorly understood. Theories include abnormal insertion of the gubernaculum or abnormal dominance of a nonscrotal gubernaculum attachment, abnormal functioning of the genitofemoral nerve, endocrine abnormalities or abnormalities of androgen receptors, increased intra-

Figure 115.28 Ectopic testicle seen inferior to the scrotum.

abdominal pressure, or mechanical obstruction (Hutcheson et al. 2000; Koc et al. 2012; Ramareddy et al. 2013). Recent studies have demonstrated that true abnormalities of gubernacular attachments are rare in this condition (Favorito et al. 2003).

Presentation

Patients most commonly present with an undescended testicle. Bilateral cases are rare and there is no significant difference in the incidence on the right versus left (Gray and Skandalaskis 1972; Ramareddy et al. 2013). Some sites of ectopia, such as perineal, pubopenile, or lateral to the scrotum, may be apparent on exam. In cases of transverse or crossed testicular ectopia, defined as both testicles exciting the same inguinal canal, patients may present with an inguinal hernia and contralateral nonpalpable testis. A high level of clinical suspicion should be used in patients with these findings (Aoki et al. 2012; Naji et al. 2012). However, the diagnosis is often not made preoperatively (Malik et al. 2008).

Diagnosis

In the patient presenting with an undescended testicle, the clinician should examine possible ectopic sites for the presence of a testicle. The clinician must consider the possibility of transverse testicular ectopia in the case of a patient with an inguinal hernia and contralateral nonpalpable testicle. In such instances, an ultrasound may be considered to evaluate for the presence of Müllarian structures, especially if the hernia is particularly firm or otherwise unusual. If Müllarian struc-

tures are present on ultrasound, karyotyping and a human chorionic gonadotropin stimulation test should be performed to confirm the patient is 46XY with testicular tissue (Naouar et al. 2008). Commonly, however, an ectopic testicle is diagnosed intraoperatively.

Treatment

Timing of intervention for an ectopic testicle is the same as an undescended testicle. Operative management should take place at six months of age or after, although there is no benefit in delay (Celayir et al. 2001; Nouira et al. 2011). An inguinal incision is commonly utilized for cases other than transverse testicular ectopia. The length of the vas deferens and arteries are usually sufficient (Celayir et al. 2001; Ramareddy et al. 2013). In the case of transverse testicular ectopia, a transseptal orchiopexy or extraperitoneal transposition of the testis can be used. Laparoscopy should be strongly considered for the diagnosis of remnant Müllerian structures (Malik et al. 2008; Naji et al. 2012). However, unless their location interferes with orchiopexy, these do not need to be removed as they are not found to be at risk for malignant degeneration and intervention increases risk of injury to the vas deferens or testicular blood supply (Wuerstle et al. 2007; Naouar et al. 2008). If orchiopexy is not feasible, orchiectomy should be performed (Naouar et al. 2008).

Associated conditions

Although patients with transverse testicular ectopia often have other associated findings, this is rare in patients with other sites of ectopia. Eight percent of patients with an ectopic testicle have a contralateral undescended testicle (Hutcheson et al. 2000). Of patients with transverse testicular ectopia, 40–50% also have an inguinal hernia, 30% have remnant Müllerian structures, and 20% have other anomalies such as hypospadias or disorders of sexual development (Malik et al. 2008; Aoki et al. 2012). Patients may have one common or two separate vas deferens in this condition (Gray and Skandalaskis 1972). It has been reported to be associated with an 18% increased risk of malignant transformation of the testicle (Naouar et al. 2008).

Polyorchidism

Polyorchidism is a rare but well-reported condition with over 100 cases described in the literature. Patients most commonly have three testicles, but may have up to five (Fig. 115.29). The left hemiscrotum is the most common location of the supernumerary testis/testes, occurring in 64.5–75% of cases. It has been seen on the right in up to 30% of cases and bilaterally in 4.3%. A scrotal location is most common (66–75% of cases), although an inguinal location occurs in about 20% and abdominal in less than 10% of patients (Bergholz and Wenke 2009; Nayak and Sreejayan 2011; Kumar et al. 2012). The supernumerary testis is usually found superior to the normal testis, although it may also be seen distal to it or rarely at the same level (Bergholz and Wenke 2009).

Figure 115.29 Patient with triorchidism. Two ipsilateral testes shown.

Etiology

Polyorchidism is caused by abnormal division of the genital ridge with or without abnormal division of the mesonephric duct. The testes develop from the genital ridge at around eight weeks gestation and the epididymis and vas deferens develop from the mesonephric duct (Wolfian duct). The location of the abnormal division or divisions determines whether the supernumerary testicle has its own epididymis or vas deferens. Leung (1988) created a classification system based on the possible divisions. In type 1, there is division at the genital ridge only, and therefore the supernumerary testicle has no epididymis and does not drain into a vas deferens. Types 2 and 3 are incomplete divisions and the most common types. In type 2, the abnormal division occurs in a region where the developing gonad is attatched to the mesonephric duct. The supernumerary testicle drains into the normal testicle and they share a vas deferens. In type 3, there is a longitudinal division of the genital ridge and proximal portion of the mesonephric duct. As a result, the supernumerary testis has its own epididymis but drains into the normal testicle's vas deferens in a parallel fashion. Type 4, the least common type, is due to complete division of the genital ridge and mesonephroci duct. The supernumerary testis therefore has its own epididymis and vas deferens (Nayak and Sreejayan 2011; Kumar et al. 2012).

Presentation

Patients most commonly present with complaints such as a scrotal or inguinal mass, scrotal pain, hernia/hydrocele, undescended testicle, or varicocele (Spranger et al. 2002; Bergholz and Wenke 2009).

Diagnosis

Polyorchidism is often found incidentally during surgery for hernia/hydrocele, undescended testicle, or torsion (Thyoka et al. 2013). However, it may be diagnosed with sonogram or, if sonogram is not clear, MRI. The supernumerary testicle will have

the same characteristics as the normal testicle on both imaging modalities (Bergholz and Wenke 2009; Arslanoglu et al. 2013).

Three primary classification systems have been proposed based on embryologic origin by Leung (1988; Table 115.1), reproductive potential of the supernumerary testicle by Singer et al. (1992; Table 115.2), and more recently Bergholz and Wenke (2009; Table 115.3); see also Nayak and Sreejayan (2011) and Kumar et al. (2012).

Table 115.1 Classification of supernumerary testicle based on embryology. Data from Leung (1988).

Type	Description
1	Supernumerary testicle has no epididymis or vas deferens
2	Supernumerary testicle drains into epididymis of normal testicle; they share a vas deferens
3	Supernumerary testicle has its own epididymis and shares a vas deferens with the normal testicle
4	Supernumerary testicle has its own epididymis and vas deferens (complete duplication)

Table 115.2 Classification of supernumerary testicle based on reproductive potential.

Type	Description
1	Supernumerary testicle *is* connected to the vas deferens
1A	Supernumerary testicle is intrascrotal
1B	Supernumerary testicle is ectopic
2	Supernumerary testicle is *not* connected to the vas deferens
2A	Supernumerary testicle is intrascrotal
2B	Supernumerary testicle is ectopic

Source: Singer et al. (1992). Reproduced with permission from Elsevier.

Table 115.3 Classification of supernumerary testicle based on anatomy.

Type A: Supernumerary testicle *is* connected to the vas deferens	Type B: Supernumerary testicle is *not* connected to the vas deferens
A1: with its own epididymis and vas deferens	B1: with its own epididymis
A2: with its own epididymis but common vas deferens	B2: without its own epididymis
A3: with a common epididymis and a common vas deferents	BX: unknown
A4: with a common epididymis but its own vas deferens	
AX: Unknown	

Source: Bergholtz et al. (2007). Reproduced with permission from Elsevier.

Treatment

Treatment for this rare condition remains controversial. Some propose removing all supernumerary testicles due to the risk of malignancy, while others propose removing all testicles without reproductive potential (not connected to a vas deferens) and any abnormal-appearing testicle (Nayak and Sreejayan 2011). Bergholz and Wenke (2009) propose removing all nonscrotal supernumerary testicles. If a type A testicle is diagnosed on exam or imaging (not intraoperatively), they propose it may be regularly observed and removed if it causes bothersome symptoms or signs of malignancy. All type B testicles and any type A testicle that develops symptoms or findings suspicious of malignancy should undergo biopsy and orhiopexy (if biopsy negative) versus orchiectomy (if biopsy suspicious for malignancy) (Bergholz and Wenke 2009).

Associated conditions

Polyorchidism is associated with an increased risk of testicular neoplasm and decreased fertility. There have been nine reported cases of neoplasm, although eight were malignant. Three seminomas, two choriocarcinomas, two teratomas, one embroynal carcinoma, and one rete testis adenoma have been reported. Four malignant tumors were found on the left side and four on the right, despite the increased incidence of supernumerary testicles on the right. The median age at diagnosis is 19. Abnormal spermatogenesis has been reported in nearly half of patients with polyorchidism, with 26% of patients having azospermia (Bergholz and Wenke 2009).

Testicular fusion

During embryogenesis the testicle may rarely fuse with other organs, including the contralateral testicle, spleen, and liver. This is best reported in reports of splenogonadal fusion, although there have been just over 150 documented cases of this. Only a handful of reports of testicular fusion and hepatotesticular fusion exist.

There are two forms of splenogonadal fusion: continuous, where the spleen is connected to the gonad through a cord-like structure; or discontinuous, where there is no connection between the spleen and gonad. Continuous fusion is slightly more common, seen in 55% of cases (Karaman and Gonzales 1996). Hepatotesticular fusion may be seen as testicular fusion directly to the testicle, an attachment between the liver and testicle with a cord-like structure, or heterotopic liver tissue within the testicle (Ferro et al. 1996; Lund et al. 2001; Fan et al. 2012). Splenogonadal fusion is nearly always on the left, whereas hepatotesticular fusion is seen on the right. Although splenogonadal fusion is a recognized entity in females, this is exceedingly rare (Karaman and Gonzales 1996; Lopes et al. 2012).

Etiology

Two theories for splenogonadal fusion exist. The first is that the two structures fuse during weeks five–eight of embryogenesis, when the developing spleen and left urogenital fold are in close

proximity. The second is inflammation of the peritoneal surfaces covering the spleen and gonadal ridge, resulting in partial fusion (Karaman and Gonzales 1996; Lopes et al. 2012).

Presentation

There is great variability in presentation. Testicular fusion occurs with crossed testicular ectopia, which may be appreciated on clinical exam (Zhapa et al. 2010; Yanaral and Yildirim 2013). Splenogonadal fusion may be initially misdiagnosed as testicular torsion, a testicular mass, or epididymitis. It is often an incidental finding during inguinal exploration for cryptorchidism or a hernia (Karaman and Gonzales 1996; Lin et al. 2010).

Diagnosis

Although transverse testicular ectopia may be appropriately diagnosed preoperatively in a patient with an inguinal hernia and contralateral nonpalpable testicle, a high index of suspicion is needed to diagnose the fused testicles. Other forms of fusion are usually diagnosed incidentally.

Treatment

Due to the rarity of this condition, optimal management is unknown. However, in cases of asymptomatic fusion in a descended testicle, no surgical intervention is required. If surgery is indicated for splenotesticular fusion, the accessory spleen is well capsulated and can therefore usually be easily resected and testicle preserved (Karaman and Gonzales 1996; Lin et al. 2010).

Associated conditions

Testicular fusion is associated with transverse testicular ectopia and, therefore, may also be associated with anomalies such as persistent Müllerian remnants and other known entities associated with this form of ectopia.

Continuous splenogonadal fusion is associated with anomalies in 50% of cases, while associated anomalies are rare in the discontinuous form. The most common anomalies include cryptorchidism, limb defects, and micrognathia. Others include cardiac defects, cleft palate, imperforate anus, spina bifida, and persistent Müllarian duct syndrome (Kameoka et al. 1993; Lin et al. 2010; Lopes et al. 2012).

Testis-epididymal nonfusion

Testis-epididymal nonfusion most commonly occurs in patients with a patent processus vaginalis, especially in those with an undescended testicle, but also in patients with a hernia/hydrocele (Elder 1992; Favorito et al. 2006). It is seen at an increasingly less frequent rate in patients with an undescended testicle or hernia/hydrocele with a partially (36%) or fully closed processus (10–16%; Elder 1992; Barthold and Redman 1996; Han and Kang 2002; Fig. 115.30). While one large case study reported this anomaly in only 7% of patients with undescended testis, most report significantly higher rates of up to 79% (Kraft et al. 2011; Rachmani et al. 2012). The higher the location of the testicle, the greater the likelihood of nonfusion; a high incidence of nonfusion anomalies has been seen in patients with intraabdominal testicles (Sharma and Sen 2013). It has also been reported in 13.3–50% of patients with hernia/hydrocele (Elder 1992; Na et al. 2012). The degree of nonfusion varies from epididymal head nonfusion, epididymal tail nonfusion, and complete nonfusion, with incomplete nonfusion being most common (Barthold and Redman 1996). The higher the position of the undescended testicle, the greater the degree of nonfusion (Kraft et al. 2011).

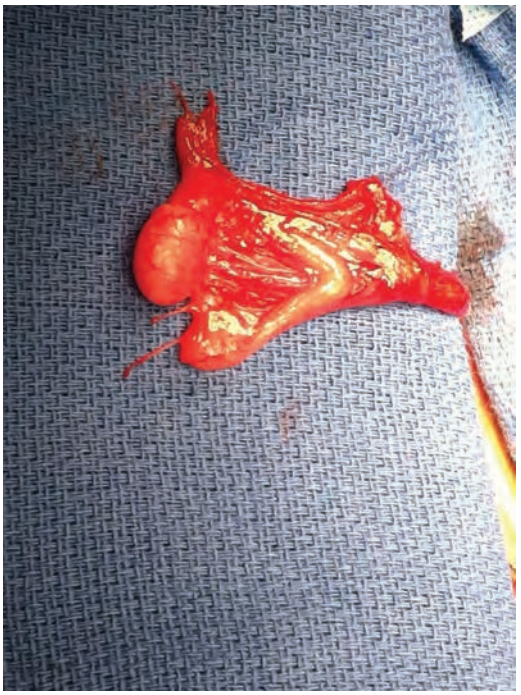

Figure 115.30 Testis-epididymal nonfusion seen in patient undergoing orchiopexy.

Etiology

The fusion of the epididymis and testis as well as the closure of the processus vaginalis is considered to be androgen driven. It is therefore most commonly thought that fusion anomalies occur secondary to insufficient androgen production or decreased sensitivity (Barthold and Redman 1996; Merksz 1998; Kraft et al. 2011).

Presentation

Patients present with an undescended testicle or hernia/hydrocele. Fusion anomalies alone are asymptomatic.

Diagnosis and treatment

Testis-epididymal nonfusion is incidentally noted during surgery for undescended testicle or hernia/hydrocele.

No specific treatment is indicated for nonfusion anomalies. The surgeon should note the finding and proceed with correction of the undescended testicle or hernia/hydrocele as usual.

Associated conditions

Testis-epididymal nonfusion is strongly associated with cryptorchidism, hernia/hydroceles, and patent processus vaginalis. It is also thought to be either the primary or a significantly contributing cause of decreased fertility in these patients. In one series of patients found to have anomalies in fusion during surgery for undescended testicles, 36% were later found to have decreased fertility (De Grazia et al. 1982; Merksz 1998).

Anorchia/monorchia

Anorchia, or the congenital absence of both testicles in an otherwise phenotypically normal male, and monorchia, the congenital absence of one testicle, is also known as vanishing testes and testicular regression syndrome (TRS). This condition was initially discovered by Cabrol in 1564 during an autopsy of a man hanged for rape. It was next reported by Amelar in 1956 (Gray and Skandalaskis 1972). Vanishing testes are seen in less than 5% of cases of cryptorchidism, but in 35–60% of cases when the testes is nonpalpable (Kirsch et al. 1998; Pirgonand Dündar 2012). The incidence is thought to be less than 0.04% (Gray and Skandalaskis 1972). It is more common on the left, as high as 72% incidence on the left versus 28% on the right (Renzulli et al. 2005). Vanishing testes are associated with variable associated structures. In 40 patients with vanishing testes, Lou et al. (1994) found 22% had complete absence of associated structures such as a vas deferens or epididymis, 15% had a blind ending vas deferens, and 67.5% had blind-ending vas deferens and blood vessels. Others have confirmed that residual elements of the vas deferens, spermatic artery, and venous plexus are usually present (Kirsch et al. 1998; Smith et al. 2007). Remnant tissue, often referred to as a testicular "nubbin," most commonly contains only fibrovascular tissue with calcification and hemosiderin deposition. However, it may contain seminiferous tubules in 5–13% and viable germ cells in 3–14% (Rozanski et al. 1996; De Luna et al. 2003; Renzulli et al. 2005; Hegarty et al. 2007; Smith et al. 2007; Storm et al. 2007; Mizuno et al. 2012; Pirgon and Dündar 2012). There has been one reported case of intratubular germ cell neoplasia (Rozanski et al. 1996). The contralateral descended testicle is often hypertrophied secondary to increased germ cell proliferation, suggesting there may be little effect of monorchia on the patient's fertility (Kraft et al. 2012).

Etiology

Vanishing testes (Fig. 115.31) are most commonly thought to be caused by either a vascular event or torsion late in gestation or early in the antenatal period (Rozanski et al. 1996; Smith et al. 2007; Pirgon and Dündar 2012; Teo et al. 2013). It has also been proposed to be associated with abnormal testicular tubule formation after Sertoli cell differentiation (Mizuno et al. 2012).

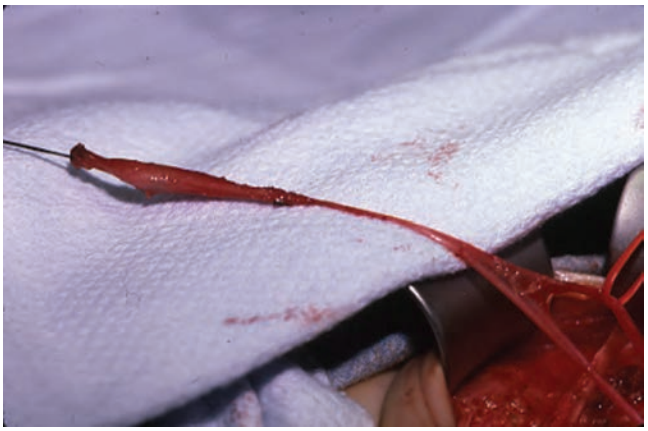

Figure 115.31 Vanishing testis demostrated on inguinal exploration.

While familial occurrences of anorchia have been identified suggesting a genetic factor, these are rare case reports not seen in other larger studies and no genetic factor has been identified (Josso and Briad 1980; de Grouchy et al. 1985; Marcantonio et al. 1994; Parigi et al. 1999; Zenaty et al. 2006). Some propose that TRS could be a part of 46XY gonadal dysgenesis (Marcantonio et al. 1994; Zenaty et al. 2006). Although mutations in the gene for testicular descent (INSL3) and its receptor (LGR8) have been associated with cryptorchidism, no mutation has been found to be associated with testicular regression syndrome (Vinci et al. 2004; Ferlin et al. 2006; Feng et al. 2009). Additionally, mutations in the Y-chromosome-linked testis-determining-factor gene SRY have not been associated with TRS (Lobaccaro et al. 1993; Vinci et al. 2004).

Presentation

The initial presentation is usually a unilateral or bilateral nonpalpable testis. Patients predominantly have a male phenotype, although they may rarely have a micropenis or even more rarely be phenotypically female. The phenotype is thought to be timing of the vascular insult to the testicle and whether one or both testicles are compromised (Josso and Briad 1980; Zenaty et al. 2006; Pirgon and Dündar 2012).

Diagnosis

The criteria for diagnosis of monorchia and anorchia is traditionally a nonpalpable testis and the visualization of blind-ending spermatic vessels in the retroperitoneum or the spermatic vessels and vas deferens exiting a closed internal ring (Pirgon and Dündar 2012). However, some propose that in the presence of bilaterally nonpalpable testes, the absence or low levels of serum anti-Müllerian hormone and inhibin B is adequate for diagnosis of anorchia. Low testosterone levels before and after hCG stimulation are also appreciated, but not considered necessary for diagnosis (Lee et al. 1997; Brauner et al. 2011; Teo et al. 2013).

Treatment

Some controversy exists regarding treatment. Often, especially in the case of monorchia, laparoscopy is performed for diagnosis. If a testicular nubbin is present, it may be removed. If spermatic vessels and a vas deferens are seen exiting a closed internal inguinal ring, some recommend inguinal exploration. If no testicle is seen, the orchiopexy may be performed on the opposite side. Others wait until a patient elects to undergo implantation of a prosthesis to perform inguinal exploration (Van Savage 2001; Pirgon and Dündar 2012). However, as intratubular germ cell neoplasia is extraordinarily rare in anorchia, Teo et al. (2013) suggest that no surgical exploration is necessary if serum AMH levels are low or undetectable.

Associated conditions

Anorchia and monorchia is rarely associated with other abnormalities, but can be seen associated with phenotypic males with micropenis, phenotypic females, mental retardation, and 46XY gonadal dysgenesis (de Grouchy et al. 1985; Marcantonio et al. 1994; Zenaty et al. 2006).

Hernia/hydrocele

Indirect inguinal hernias and communicating hydroceles are common in childhood with an incidence of up to 5% of children born full term, but up to 30% of premature infants. It is most common on the right (about 60%) and most commonly unilateral (75–90%) (Ein et al. 2006; Brandt 2008). While they are associated with a patent processus vaginalis, the vast majority of males with a patent processus vaginalis (88–92%) will never develop a hernia or hydrocele (van Wessem et al. 2003; Brandt 2008).

Etiology

The underlying cause of the indirect inguinal hernia and communicating hydrocele is a failure of the processus vaginalis to obliterate before or after birth (Fig. 115.32). During gestation, the testes descend through the internal ring during weeks 28–30. As they descend through the ring, they bring with them an outpouching of the peritoneum that proceeds and surrounds the testicle. The distal aspect of this outpouching of peritoneum that descends from the abdomen through the inguinal canal closes during gestation weeks 36–40, leaving behind only a portion that directly surrounds the testicle and becomes the tunica vaginalis. This is the reason why hernias/hydroceles are so common in premature boys. Commonly, the processus does not completely close before birth but instead continues to close after birth. Complete closure most commonly occurs in the first few months of life, but in many it is not completed until 2 years of age. It may still close leading into young adulthood. Closure occurs on the left prior to the right as the left testicle descends first, explaining the increased incidence of right-sided pathology. An open processus vaginalis allows for fluid, bowel, and/or testicles to pass between the abdominal cavity and the scrotum (van Wessem et al. 2003; Brandt 2008).

Figure 115.32 Infant with large bilateral hydroceles.

Presentation

Boys typically present with intermittent usually unilateral painless testicular swelling. Swelling is usually most prominent at the end of the day or after activity, during a febrile illness, or after any abdominal straining. Rarely will patients present with an acute scrotum. There are case reports of torsion of an indirect hernia sac within a hydrocele (Tillet et al. 2006).

Diagnosis

History and physical exam is usually sufficient for the diagnosis. The "silk glove sign," which refers to the sensation of the layers of the sac sliding over each other when palpating the spermatic cords over the pubis, is the pathognomonic finding. The inguinal region will also be larger on the involved side. Scrotal ultrasound is usually not required, but may be helpful if the testicle is nonpalpable in order to rule out the presence of a testicular tumor prior to surgery. It should also be used in patients with an acute scrotum to look for more emergent causes of pain.

Treatment

Infants with ipsilateral cryptorchidism and hernia should undergo immediate repair. Otherwise, the infant may be observed for spontaneous closure. If this does not occur, surgical repair may be performed either through traditional and commonly preferred inguinal approach with high ligation of the sac, laparoscopically, or, less commonly, through a scrotal approach. There is a 1% or less chance of recurrence with the inguinal approach. This increases to 4% in the laparoscopic approach. Other complications include testicular atrophy or decreased testicular size, iatrogenic cryptorchidism, or injury to the vas deferens (Brandt 2008). Controversy exists over whether to laparoscopically evaluate the contralateral inguinal canal

for the presence of a patent processus. The risk of developing a metachronous hernia is 3.6–11.6%, usually within the first five years after surgery (Lym et al. 1999; Ein et al. 2006; Brandt 2008; Kim et al. 2012). Those who argue against contralateral exploration argue it is difficult to distinguish between a patent processus and true hernia and leads to many unnecessary procedures with risks of complications. Those who argue for exploration argue there is a substantial risk for developing a contralateral hernia, and exploring at time of the initial procedure avoids a second surgery. However, it is agreed that open exploration is not indicated (Brandt 2008).

Associated conditions

Hernia/hydroceles may be associated with testicular anomalies such as abnormal epididymo-testicular fusion, incomplete testicular descent, and other more rare conditions.

Other hydroceles

Noncommunicating hydrocele

While communicating hydroceles are most common in younger children, noncommunicating hydroceles are most common in older children over 10 years of age and adults. These hydroceles are stable in size instead of fluctuating throughout the day. They are thought to be due to a delayed closure of the processus vaginalis. They are commonly bilateral and commonly resolve spontaneously over time (Osifo and Osaigbovo 2008; Wilson et al. 2008).

Abdominoscrotal hydrocele

The abdominoscrotal hydrocele is a noncommunicating hydrocele that extends from the scrotum, through the inguinal canal, and to the retroperitoneal space in a dumbbell configuration. It is theorized that this form of hydrocele is caused by elevated scrotal pressure caused by a noncommunicating hydrocele that leads to extension of the hydrocele through the inguinal canal (Belman 2001; Bayne et al. 2008). This rare type of hydrocele is bilateral in 30% of cases and can usually be diagnosed on physical exam or even prenatal ultrasound, although scrotal ultrasound can confirm the diagnosis. Surgical treatment is traditionally through an inguinal approach, but there is a movement towards scrotal approach due to concern for potential cord damage with the former approach (Belman 2001; Cozzi et al. 2008). Testicular and epididymal anomalies are common with these hydroceles, although many resolve after hydrocelectomy (Bayne et al. 2008; Cozzi et al. 2008).

Vas deferens

Congenital absence of the vas deferens

Congenital absence of the vas deferens (CAVD) may be unilateral (CUAVD) or bilateral (CBAVD) and may be associated with cystic fibrosis transmembrane conductance regulator (CFTR) gene mutations, other genitourinary anomalies, or have no other associations. While CBAVD is most commonly associated with CFTR gene mutations (55–90%) and uncommonly associated with renal agenesis (10–11.8%), CUABD is more commonly associated with renal agenesis (19–91%) and less commonly associated with CFTR mutations (Schlegel et al. 1996; Stuhrmann and Dörk 2000; McCallum et al. 2001; Kolettis and Sandlow 2002; Mo et al. 2013). CUAVD is also strongly associated with contralateral genitourinary anomalies such as vesicoureteral reflux, varicocele, cryptorchidism, and ureteropelvic junction obstruction (Schlegel et al. 1996; Mo et al. 2013). Patients with CUAVD may have a patent (67%) or obstructed (33%) contralateral vas deferens. Patients with a patent contralateral vas deferens are more likely to have ipsilateral renal agenesis, but never to rarely to have a CFTR gene mutation. Conversely, patients with an obstructed vas deferens are more likely to have a CFTR gene mutation (75–91%), but rarely have renal agenesis (Mickle et al. 1995; Kolettis and Sandlow 2002). Men with CAVD may have absent or abnormal seminal vesicles. Most men with CUAVD have no ipsilateral seminal vesicle, while there is an increased rate of anomalies in patients with CFTR gene mutations (Schlegel et al. 1996).

Etiology

There are two different etiologies of CAVD, and the timing of their embryologic insult explains the associated findings. The mesonephric (Wolffian) duct is the derivative of the ipsilateral kidney, ureter, vas deferens, seminal vesical, and distal two-thirds of the epididymis. The mesonephric duct splits around seven weeks of gestation. The precursors to the kidney and ureter are in one resulting limb, and the genital tract components are in the other limb. An insult to the mesonephric duct prior to this spit or an intrinsic deficit of the duct can therefore lead to anomalies of all components of the ipsilateral genitourinary system. Such an event is thought to be the cause of CAVD in patients without a CFTR gene mutation (McCallum et al. 2001).

However, in patients with CFTR gene mutations, it has been shown that the bilateral vas deferens initially develop normally (Gaillard et al. 1997). It is thought that a secretory defect later leads to atresia of the vas deferens (Schlegel et al. 1996).

Ipsilateral renal and vassal agenesis is thought to be an autosomal dominant with variable penetrance condition (Kolettis and Sandlow 2002). CFTR gene mutations are considered to be autosomal recessive with incomplete penetrance (Shin et al. 1997).

Presentation

As patients with CBAVD and CFTR mutations have no other signs of cystic fibrosis in 70% of cases, patients often initially present for evaluation of infertility (Kim and Cromie 1996). CAVD is seen in approximately 1–2% of men undergoing infertility evaluation and 10% of men with azoospermia (Kim and Cromie 1996; Schlegel et al. 1996; Radpour et al. 2008).

Patients with CBAVD will have low semen volume with low pH and azoospermia (Weiske et al. 2000). Men with CUAVD may present for evaluation for vasectomy or for other genitourinary complaints (Kolettis and Sandlow 2002). CUAVD is up to twice as common on the left (Weiske et al. 2000; Mo et al. 2013).

Diagnosis

The diagnosis of CAVD may be based on a physical exam, although vasography or transrectal ultrasound may confirm the diagnosis (Mo et al. 2013). All patients with CAVD desiring to have children should undergo CFTR mutation testing, understanding that there are more uncommon mutations not covered by routine testing and novel mutations continue to be discovered (Mak et al. 1999; Sharma et al. 2009). CBAVD and CUAVD caused by a CFTR gene mutation are phenotypically identical to those unassociated with a CFTR gene mutation (McCallum et al. 2001; Radpour et al. 2008). It is therefore important for all men with CAVD to undergo abdominal ultrasonography to evaluate for renal agenesis or other renal anomalies. To confirm renal agenesis, if indicated, a technetium 99m-dimercaptosuccinic acid scan may be performed. A VCUG may be considered in the younger population due to the increased risk of contralateral vesicoureteral reflux (Shapiro et al. 2003).

Treatment

No treatment is required for CAVD, but may be required for associated genitourinary findings. Notably, it has been shown that men with CAVD have normal vasal vessels and can therefore undergo varicocelectomy if indicated (Raman and Goldstein 2004). For men desiring children, genetic counseling is advised. Success has been reported obtaining sperm with testicular sperm extraction and performing intracytoplasmic sperm injection (Okada et al. 1999).

Associated conditions

CUAVD not associated with CFTR mutations are associated with ipsilateral renal agenesis as well as other renal anomalies including multicystic kidney, ectopic kidney, and horseshoe kidney. Anomalies of the seminal vesicles and ejaculatory ducts, cryptorchidism, and inguinal hernias are also seen. More rarely, vesicoureteral reflux or ureterovesical obstruction in the contralateral kidney may occur. Ipsilateral agenesis of the adrenal is possible (Mo et al. 2013).

CAVD may also be associated with seminal vesicle anomalies, absence of the body or tail of the epididymis, and ejaculatory duct absence (Schlegel et al. 1996). Spermatogenesis is commonly normal, but may be mildly reduced (Okada et al. 1999).

Duplication of the vas deferens

Duplication of the vas deferens is an uncommon anomaly with 22 known case reports in the literature and an incidence of less than 0.05% in the general male population. It occurs on the left, right, and bilaterally with equal frequency. Complete and partial duplication also occur with near equal frequency (Sirasanagandla et al. 2013). Duplication of the vas deferens in which two vas deferens are present in the spermatic cord should not be confused with double vas deferens, in which an ectopic ureter drains into the ejaculatory system. The latter is associated with ipsilateral renal agenesis and other genitourinary anomalies. The ectopic ureter may be mistaken for a second vas deferens, but there is no actual duplication of the vas (Liang et al. 2012).

Etiology

The embryologic etiology of the duplication of the vas deferens is not completely understood. There are two primary hypotheses. The vas deferens and seminal vesicle derive from the central portion of the mesonephric duct known as the "proximal vas precursor." Duplication of the proximal vas precursor is thought to lead to duplication of the vas. It is also thought that transverse division of the Wolffian duct during organogenesis leads to this condition (Khoudary and Morgentaler 1998; Karaman et al. 2010).

Presentation

Duplication is asymptomatic; it is therefore most commonly found incidentally during inguinal or scrotal procedures such as orchiopexy, inguinal hernia repair, vasectomy, varicocelectomy, or prostatectomy (Sirasanagandla et al. 2013).

Diagnosis and treatment

The diagnosis can be made intraoperatively by identifying the two vas deferens and tracing their course. A doplar may be utilized or vasography may also be performed for confirmation (Khoudary and Morgentaler 1998; Sirasanagandla et al. 2013).

No treatment is indicated for duplication of the vas deferens. However, it is important to recognize this condition during inguinal surgeries to avoid iatrogenic injury to the vas deferens.

Associated conditions

While ipsilateral renal agenesis and other genitourinary anomalies may be associated with a double vas, there are no known cases of non-testicular anomalies associated with duplication of the vas deferens (Liang et al. 2012).

Seminal vesicles

Seminal vesicle cyst

Seminal vesicle cysts are a rare entity affecting less than 0.005% of the male population (Basillote et al. 2004). This form of cyst may be congential or acquired secondary to inflammation or obstruction (Kuo et al. 2011). The congenital form is associated with ipsilateral renal agenesis in as many as 80% of cases, although this entity has been described in less than 100 case reports (Cherullo et al. 2002; Kuo et al. 2011). As this entity is

often asymptomatic, it is thought that the increasing use of CT and MRI has also increased the detection of these cysts (Pereira et al. 2009).

Etiology

A seminal vesicle cyst is thought to be due to a congenital anomaly or absence of the ejaculatory ducts. The associated dysplastic or absent kidney is due growth of the ureteral bud too early or too cranially so that it does not fuse with the metogephrogenic blastema, which is integral for normal renal development. Alternatively, there may be an intrinsic anomaly of the ureter that prevents it from normal interaction with the metanephrogenic blastema (Cherullo et al. 2002; Kuo et al. 2011). A study of infants with seminal vesicle cysts showed that these were most commonly associated with a multicystic dysplastic kidney and less commonly with a dysplastic kidney. They propose that the ipsilateral renal agenesis seen in adults with congenital seminal vesicle cysts may actually be a formerly multicystic dysplastic kidney that has subsequently involuted, as opposed to a congenitally absent kidney (Schukfeh et al. 2009).

Presentation

While most seminal vesicle cysts remain asymptomatic and are found incidentally, when they do cause symptoms, patients usually present in the third–fifth decade of life or when the patient becomes sexually active (Cherullo et al. 2002; Basillote et al. 2004; Kuo et al. 2011). Most commonly they may cause perineal or suprapubic pain or irritative voiding symptoms such as frequency, urgency, dysuria, and hematuria. They may also cause infertility, epididymitis, prostatitis, hematospermia, or even urinary retention (Bernstein et al. 2004; Cherullo et al. 2002; Basillote et al. 2004; Kuo et al. 2011).

Diagnosis

While abdominopelvic and transrectal ultrasound, CT, or IVP may detect a cyst, MRI is considered the imaging modality of choice. Cysts have high-intensity signal on T1-weighted images (Murphy et al. 2003; Pereira et al. 2009). Vasovesiculography is the gold standard, but rarely used except intraoperatively due to its invasiveness (Cherullo et al. 2002; Kuo et al. 2011). The differential diagnosis of a seminal vesicle cyst includes enlarged prostatic utricle, Müllerian duct cyst, intraprostatic cyst, ejaculatory duct cyst, hydronephrotic pelvic kidney or ureters, bladder diverticula, or ureterocele. However, a seminal vesicle cyst is nearly always unilateral with a few documented cases of bilateral cysts reported, lateral to the midline, and unilocular (Sheih et al. 1998; Razi and Imani 2000; Hong et al. 2011).

Treatment

If the patient is asymptomatic, no treatment is indicated. However, if the patient elects to undergo intervention due to symptoms, several approaches have been described. Transrectal aspiration, cystoscopy with transurethral resection of the ipsilateral ejaculatory duct, and intravesical cyst unroofing have been described, but with limited durable success (Cherullo et al. 2002). Surgical excision may be approached open from a retropubic approach or laparoscopic, or robotically from a transperitoneal approach (Hong et al. 2011; Zhang et al. 2012).

Associated conditions

Zinner's syndrome refers to the combination of a seminal vesical cyst and ipsilateral renal agenesis. Other associated conditions include an absent ureter or trigone, testicular ectopia or agenesis, and ureteral bud remnant (Cherullo et al. 2002; Kuo et al. 2011).

Other anomalies of the seminal vesicles

Other documented anomalies of the seminal vesicles include absence and duplication. The incidence of these entities is largely unknown, but considered to be very rare. While duplication of the seminal vesicles is asymptomatic and may only be discovered incidentally on imaging, absence of the seminal vesicles may lead a patient to seek medical attention if it is bilateral and therefore causes infertility (Gray and Skandalaki 1972). Of patients with bilateral absence of the vas deferens, about 45% have also been shown to have aplastic seminal vesicles. These patients usually do not have an identified CFTR mutation (Schlegel et al. 1996).

Prostate

Variations and anomalies of the prostate

Except for size, the prostate is subject to few variations. The normal prostate, which is traversed by the prostatic urethra, weighs 18 g, measures 3 cm in length, 4 cm in width, and 2 cm in depth (Chung et al. 2011). Midway through the prostate the urethra angles anteriorly. This angulation can vary over the range 0–90°. The verumontanum protrudes from the posterior porton of the prostate. The prostatic utricle is a Müllerian remnant that is found at the apex of the verumontanum. The utricle is a small sac that projects backward into the prostate. In cases of males with ambiguous genitalia, the utricle can form large diverticula. The ejaculatory ducts form from the union of the vas deferens and seminal vesicles and open on either side of the prostatic utricle (Chung et al. 2011).

The shape of the prostate apex can vary substantially regarding the overlap of the urethral sphincter. The variation in the degree of overlap has significant clinical implications during radical prostatectomy (Walz et al. 2010). A study by Lee et al. (2006) demonstrated circumferential overlap in 38% of cases, anterior overlap in 25%, posterior overlap in 22%, and no overlap in 15%.

Other reported variations include persistence of the original independence of the lateral lobes, absence of the middle lobe, and presence of fourth lobe. Variations in the termina-

tion of the ejaculatory ducts exist, such as fusion into a single canal, termination in the prostatic utricle, or special canal below the urethral crest (Bergman et al. 1984). An accessory prostate gland can be found between the urethra and the verumontanum.

Bulbourethral glands

Cowper's syringocele

Cowper's syringocele refers to the cystic dilatation of one of the main ducts of the bulbourethral glands. While it is usually congenital, it may be acquired in rare cases due to inflammation or trauma. The true incidence of this usually asymptomatic condition is unknown but is estimated to be around 1.5–3% of the male population (Yaffe and Zissin 1991; Richter et al. 1996; Bevers et al. 2000).

Etiology

The exact etiology of Cowper's syringocele is unknown. With appropriate signaling by dihydrotestosterne, the paired bulbourethral glands arise from the membranous urethra in the urogenital diaphragm around the tenth week of development. The purpose of these glands is to produce alkalinic secretions that are released prior to ejaculation to neutralize the urethra and provide lubricant (Chughtai et al. 2005). It is thought that the Cowper's syringocele is a congenital retention cyst of the ductal portion of the gland that lies within the urethra (Yaffe and Zissin 1991; Richter et al. 1996).

Presentation

Most commonly, Cowper's syringocele causes no symptoms. However, patients may develop recurrent UTIs, bloody urethral discharge or hematuria, dysuria, post void dribbling, a painful perineal mass, or urinary retention (Bevers et al. 2000; Fangbai et al. 2013).

Diagnosis

Diagnosis is performed using retrograde or voiding cystourethrogram, which will show a mass below the bulbomembranous urethra, or through visualization on cystourethroscopy (Colodny and Lebowitz 1978; Richter et al. 1996; Chughtai et al. 2005). Transperineal ultrasound may also be utilized (Chughtai et al. 2005). The differential diagnosis includes partial urethral duplications, urethral diverticulum, or ectopic ureter (Colodny and Lebowitz 1978).

Maizels et al. (1983) recognized four forms of Cowper's syringoceles. Type 1, a simple syringocele, involves a minimally dilated duct. Type 2, a perforated syringocele, is a wide opening that communicates with the urethra. Type 3, an imperforate syringocele, is an intact cyst that does not communicate with the urethra. Type 4, a ruptured syringocele, refers to a thin membrane that remains in the urethra after rupture of the duct (Maizels et al. 1983). Simple syringoceles are most common (Yaffe and Zissin 1991). It has been recently proposed to modify the classification system into "open" syringoceles (types 1, 2, and 4) and "closed" (type 3). Open syringoceles are more likely to cause symptoms such as post void dribbling, whereas closed syringoceles are more likely to cause obstructive voiding symptoms (Fangbai et al. 2013).

Treatment

Treatment is indicated only if the patient is symptomatic. It is usually managed cystoscopically with unroofing, but can be approached transperineally in the case of a large perineal mass (Richter et al. 1996; Bevers et al. 2000; Chughtai et al. 2005; Fangbai et al. 2013).

Associated conditions

There are no strong associations of Cowper's syringocele with other anomalies, although there has been one reported case of association with urethral narrowing and another patient with an acontractile bladder (Chughtai et al. 2005).

References

Aaronson IA. 1994. Micropenis: medical and surgical implications. *J Urol* 152:4–14.

Agarwal PK, Diaz M, Elder JS. 2006. Retractile testis: is it really a normal variant? *J Urol* 175(4): 1496–1499.

Akre O, Pettersson A, Richiardi L. 2009. Risk of contralateral testicular cancer among men with unilaterally descended testis: a meta analysis. *Int J Cancer* 124: 687–689.

Aoki K, Kuwada M, Fujimoto K, Hirao Y. 2012. Transverse testicular ectopia with disorders of sex development. *Indian J Urol* 28(1): 92–93.

Arslanoglu A, Tuncel SA, Hamarat M. 2013. Polyorchidism: color Doppler ultrasonography and magnetic resonance imaging findings. *Clin Imag* 37(1): 189–191.

Barthold JS. 2012. Abnormalities of the testis and scrotum and their surgical management. In: *Campbell's Urology*, 10th edition (ed. PC Walsh). Philadelphia: WB Saunders.

Barthold JS, Redman JF. 1996. Association of epididymal anomalies with patent proccessus vaginalis in hernia, hydrocele and cryptorchidism. *J Urol* 156(6): 2054–2056.

Barthold JS, González R. 2003. The epidemiology of congenital cryptorchidism, testicular ascent and orchiopexy. *J Urol* 170(6): 2396–2401.

Bar-Yosef Y, Binyamini J, Matzkin H, Ben-Chaim J. 2007. Degloving and realignment: simple repair of isolated penile torsion. *Urology* 69: 369–371.

Basillote JB, Shanberg AN, Woo D, Perer E, Rajpoot D, Clayman RV. 2004. Laparoscopic excision of a seminal vesicle cyst in a child. *J Urol* 171(1): 369–371.

Baskin, LS. 2000. Hypospadias and urethral development. *J Urol* 163: 951–956.

Bayne A, Paduch D, Skoog SJ. 2008. Pressure, fluid and anatomical characteristics of abdominoscrotal hydroceles in infants. *J Urol* 180(4): 170–723.

Belman AB. 2001. Abdominoscrotal hydrocele in infancy: a review and presentation of the scrotal approach for correction. *J Urol* 165(1): 225–227.

Bergeson PS, Hopkin RL, Bailey RB, McGill LC, Piatt JP. 1993. The inconspicuous penis. *Pediatrics* 92: 794–799.

Bergholz R, Wenke K. 2009. Polyorchidism: a meta-analysis. *J Urol* 182: 2422–2427.

Bergholz R, Koch B, Spieker T, Lohse K. 2007. Polyorchidism: a case report and classification. *J Pediatr Surg* 42(11): 1933–1935.

Bergman RA, Thompson SA, Afifi AK. 1984. Male Genital System. In *Catalog of Human Variation*. Baltimore, MD: Urban and Schwarzenberg.

Bernstein G, Kehren J, Kaplan K, Kang P, McLeod D. 2004. Aquired seminal vesicle cyst causing acute urinary retention and hydronephrosis. *J Urol* 172(3): 1010–1011.

Bevers FM, Abbekerk EM, Boon TA. 2000. Cowper's syringocele: symptoms, classification and treatment of an unappreciated problem. *J Urol* 163(3): 782–784.

Bin-Abbas B, Conte FA, Grumbach MM, Kaplan SL. 1999. Congenital hypogonadotropic hypogonadism and micropenis: effect of testosterone treatment on adult penile size: why sex reversal is not indicated. *J Pediatr* 134: 579–583.

Blanc T, Ayedi A, El-Ghoneimi A, Abdoul H, Aigrain Y, Paris F, Sultan C, Carel JC, Léger J. 2011. Testicular function and physical outcome in young adult males diagnosed with idiopathic 46XY disorders of sex development during childhood. *Eur J Endocrinol* 165: 907–915.

Brandt ML. 2008. Pediatric hernias. *Surg Clin North Am* 88(1): 27–43.

Brauner R, Neve M, Allali S, Trivin C, Lottmann H, Bashamboo A, McElreavey K. 2011. Clinical, biological and genetic analysis of anorchia in 26 boys. *PLoS One* 6(8): e23292.

Casale AJ. 2011. Posterior Urethral Valves. In *Campbell–Walsh Urology* (eds AJ Wein, LR Kavoussi, AC Novick, AW Partin, CA Peters). Philadelphia, PA: Saunders.

Casale AJ, Beck SD, Cain MP, Adams MC, Rink RC. 1999. Concealed penis in childhood: a spectrum of etiology and treatment. *J Urol* 162: 1165–1168.

Celayir AC, Sanders S, Eliçevik M. 2001. Timing of surgery in perineal ectopic testes: analysis of 16 cases. *Pediatr Surg Int* 17(2): 167–168.

Cendron M, Huff DS, Keating MA, Snyder HM III, Duckett JW. 1993. Anatomical, morphological and volumetric analysis: a review of 759 cases of testicular maldescent. *J Urol* 149(3): 570–573.

Chatterjee S, Gajbhive V, Nath S, Ghosh D, Chattopadhyay S, Das SK. 2012. Perineal accessory scrotum with congenital lipoma: a rare case report. *Case Rep Pediatr* 2012: 757120.

Cherullo EE, Meraney AM, Bernstein LH, Einstein DM, Thomas AJ, Gill IS. 2002. Laparoscopic management of congenital seminal vesicle cysts associated with ipsilateral renal agenesis. *J Urol* 167(3): 1263–1267.

Chughtai B, Sawas A, O-Malley RL, Naik RR, Ali Khan S, Pentyala S. 2005. A neglected gland: a review of cowper's gland. *Int J Androl* 28(2): 74–77.

Chung BI, Sommer G, Brooks JD. 2011. Anatomoy of the lower urinary tract and male genitalia. In *Campbell–Walsh Urology* (eds AJ Wein, LR Kavoussi, AC Novick, AW Partin, CA Peter). Philadelphia, PA: Saunders.

Colodny AH, Lebowitz RL. 1978. Lesions of cowper's ducts and glands in infants and children. *Urology* 11(4): 321–325.

Coplen DE, Mikkelsen D, Manley CB. 1995. Accessory scrotum located on the distal penile shaft. *J Urol* 154(5): 1908.

Cortes D, Thorup JM, Visfeldt J. 2001. Cryptorchidism: aspects of fertility and neoplasms. A study including data of 1335 consecutive boys who underwent testicular biopsy simultaneously with surgery for cryptorchidism. *Horm Res* 55(1): 21–27.

Cozzi DA, Mele E, Ceccanti S, Pepino D, d'Ambrosio G, Cozzi F. 2008. Infantile abdominoscrotal hydrocele: a not so benign condition. *J Urol* 180(6): 2611–2615.

Cuda SP, Srinivasan AK, Kalisvaart J, Kirsch AJ. 2011. Evolution of single practice trends in the surgical approach to the undescended testicle. *J Urol* 185(6): 2451–2454.

Culp OS. 1966. Struggles and triumphs with hypospadias and associated anomalies: review of 400 cases. *J Urol* 96: 339.

De Grazia E, Guttaccio F, Fatta G, Cigna RM, Agosta E. 1982. Epididymo-testicular anomalies in the undescended testis. How important is their effect on fertility? *Acta Eur Fertil* 13(1): 1–17.

De Grouchy J, Gompel A, Salamon-Bernard Y, Kutten F, Yaneva H, Paniel JB, Me Merrer M, Roubin M, Doussau de Bazignan M, Turleav C. 1985. Embryonic testicular regression syndrome and severe mental retardation in sibs. *Ann Genet* 28(3): 154–160.

De Luna AM, Ortenberg J, Craver RD. 2003. Exploration for testicular remnants: implications of residual seminiferous tubules and crossed testicular ectopia. *J Urol* 169(4): 1486–1489.

Dees JE. 1949. Congenital epispadias with incontinence. *J Urol* 62: 513.

Devine CJ, Horton CE. 1973. Chordee without hypospadias. *J Urol* 110: 264.

Dewan PA, Keenan RJ, Morris LL, Le Quesne GW. 1994. Congenital urethral obstruction: Cobb's collar or prolapsed congenital obstructive posterior urethral membrane (COPUM) *Br J Urol* 73(1): 91–95.

Diamond M. 1999. Pediatric management of ambiguous and traumatized genitalia. *J Urol* 162: 1021–1028.

Donnahoo KK, Cain MP, Pope JC, Casale AJ, Keating MA, Adams MC, Rink RC. 1998. Etiology, management and surgical complication of congenital chordee without hypospadias. *J Urol* 160: 1120–1122.

Effman EL, Lebowitz RL, Colodny AH. 1976. Duplication of the urethra. *Radiology* 119: 179–185.

Ein SH, Njere I, Ein A. 2006. Six thousand three hundred sixty-one pediatric inguinal hernias: a 35-year review. *J Pediatr Surg* 41(5): 980–986.

Elder JS. 1987. Cryptorchidism: isolated and associated with other genitourinary defects. *Pediatr Clin North Am* 34(4): 1033–1053.

Elder JS. 1992. Epididymal anomalies associated with hydrocele/hernia and cryptorchidism: implications regarding testicular descent. *J Urol* 148(2): 624–626.

Evans JA, Erdile LB, Greenberg CR, Chudley AE. 1999. Agenesis of the penis: patterns of associated malformations. *Am J Med Genet* 84:47–55.

Fan R, Faught PR, Sun J, Meldrum KK. 2012. Hepatogonadal fusion. *J Pediatr Surg* 47(2): e5–e6.

Fangbai WV, Park E, Udayasankar U. 2013. Cowper gland syringocele. *J Urol* 190(2): 713–714.

Favorito LA, Klojda CA, Costa WS, Sampaio FJ. 2003. Is there a relationship with anomalous insertions of the distal gubernaculum testis and testicular ectopia? Analysis in human fetuses and patients with cryptorchidism. *J Urol* 170(2): 554–557.

Favorito LA, Costa WS, Sampaio FJ. 2006. Analysis of anomalies of the epididymis and processus vaginalis in human fetuses and in patients with cryptorchidism treated and untreated with human chorionic gonadotrophin. *BJU Int* 98(4): 854–857.

Feng S, Alberto F, Truong A, Bathgate R, Wade JD, Corbett S, Han S, Tannour-Louet L, Delores J, Foresta C, Agoulnik A. 2009. INSL3/RXFP2 Signaling in testicular descent. *Ann N Y Acad Sci* 1160: 197–204.

Ferlin A, Bogatcheva NV, Giansello L, Pepe A, Vinanzi C, Agoulnik AI, Foresta C. 2006. Insulin-like factor 3 gene mutations in testicular dysgenesis syndrome: clinical and functional characterization. *Mol Hum Reprod* 12(6): 401–406.

Ferro F, Lais A, Boldrini R, De Peppo F, Federici G, Bosman C. 1996. Hepatogonadal fusion. *J Pediatr Surg* 31(3): 435–436.

Foresta C, Zuccarello D, Garolla A, Ferlin A. 2008. Role of hormones, genes, and environment in human cryptorchidism. *Endocr Rev* 29(5): 560–580.

Gaillard DA, Carre-Pigeon F, Lallemand A. 1997. Normal vas deferens in fetuses with cystic fibrosis. *J Urol* 158(4): 1549–1552.

Gambhir L, Holler T, Muller M, Schott G, Vogt H, Detlefsen B, Ebert AK, Fisch M, Beaudoin S, Stein R, Boyadjiev SA, Gearhart JP, Rosch W, Utsch B, Boemers TM, Reutter H, Ludwig M. 2008. Epidemiological survey of 214 families with bladder exstrophy–epispadias complex. *J Urol* 179: 1539–1543.

Gearhart JP, Jeffs RD. 1998. The bladder exstrophy-epispadias complex. In: *Campbell's Urology*, seventh edition (eds PC Walsh, AB Retick, ED Vaughan, AJ Wein). Philadelphia: WB Saunders.

Gearhart JP, Mathews RI. 2011. Exstrophy-epispadias complex. In *Campbell–Walsh Urology* (eds AJ Wein, LR Kavoussi, AC Novick, AW Partin, CA Peter). Philadelphia, PA: Saunders.

Gearhart JP, Ben-Chaim J, Jeffs RD, Sanders RC. 1995. Criteria for the prenatal diagnosis of classic bladder exstrophy. *Obstet Gynecol* 85: 961.

Gould GM, Pyle WL. 1896. *Anomalies and Curiositites of Medicine*. New York: Bell Publishing.

Gray LE, Ostby J, Furr J, Wolf C, Lambright C, Wilson V, Noriega N. 2004. Toxicant-induced hypospadias in the male rat. *Adv Exp Med Biol* 545:217–241.

Gray SW, Skandalakis JE. 1972. Embryology for Surgeons: The Embryological Basis for the Treatment of Congenital Defects. Philadelphia: WB Saunders Company.

Gyftopoulos K, Wolffenbuttel KP, Nijman RJM. 2002. Clinical and embryologic aspects of penile duplication and associated anomalies. *Urology* 60: 675–679.

Hadziselimović F, Herzog B. 1997. Treatment with luteinizing hormone–releasing hormone analogue after successful orchiopexy markedly improves chance of fertility later in life. *J Urol* 158(3): 1193–1195.

Han CH, Kang SH. 2002. Epididymal anomalies associated with patent processus vaginalis in hydrocele and cryptorchidism. *J Korean Med Sci* 17(5): 660–662.

Hegarty PK, Mushtaq I, Sebire NJ. 2007. Natural history of testicular regression syndrome and consequences for clinical management. *J Pediatr Urol* 3(3): 206–208.

Hennekam RCM, Allanson JE, Biesecker LG, Carey JC, Opitz JM, Vilain E. 2013. Elements of morphology: standard terminology for the external genitalia. *Am J Med Genet Part A* 9999: 1–26.

Herzog B, Steigert M, Hadziselimovic F. 1992. Is a testis located at the superficial inguinal pouch (Denis Browne pouch) comparable to a true cryptorchid testis? *J Urol* 148: 622–623.

Hodges SJ, Patel B, McLorie G, Atala A. 2009. Posterior urethral valves. *TSW Urology* 9: 1119–1126.

Hollowell JG Jr, Witherington R, Ballagas AJ, Burt JN. 1977. Embryologic considerations of diphallus and associated anomalies. *J Urol* 6: 728–732.

Holmes NM, Miller WL, Baskin LS. 2004. Lack of defects in androgen production in children with hypospadias. *J Clin Endocrinol Metab* 89: 2811–2816.

Hong YK, Onal B, Diamond DA, Retik AB, Cendron M, Nguyen HT. 2011. Robot-assisted laparoscopic excision of symptomatic retrovesical cysts in boys and young adults. *J Urol* 186(6): 2372–2378.

Hughes IA, Werner R, Bunch T, Hiort O. 2012. Androgen insensitivity syndrome. *Semin Reprod Med* 30(5): 432–442.

Hutcheson JC, Snyder HM III, Zuñiga, Zderic SA, Schultz DJ, Canning DA. 2000. Ectopic and undescended testes: 2 variants of a single congenital anomaly? *J Urol* 163(3): 961–963.

Hutson JM, Hasthorpe S. 2005. Abnormalities of testicular descent. *Cell Tissue Res* 322(1): 155–158.

Hutson JM, Clarke ML. 2007. Current management of the undescended testicle. *Semin Pediatr Surg* 16(1): 64–70.

Janoff DM, Skoog SJ. 2005. Congenital scrotal agenesis: description of a rare anomaly and management strategies. *J Urol* 173(2): 598–591.

Jordan GH, McCammon KA. 2011. Surgery of the penis and urethra. In *Campbell–Walsh Urology* (eds AJ Wein, LR Kavoussi, AC Novick, AW Partin, CA Peter). Philadelphia, PA: Saunders.

Josso N, Briad ML. 1980. Embryonic testicular regression syndrome: variable phenotypic expression in sibblings. *J Pediatr* 97(2): 200–204.

Kameoka H, Yamada R, Sonoda T, Okuyama A. 1993. Splenic gonadal fusion with persistent müllerian duct syndrome. *Urol Int* 50(3): 170–173.

Karaman A, Karaman I, Yağiz B, Cavuşoğlu YH. 2010. Partial duplication of the vas deferens: how important is it? *J Indian Assoc Pediatr Surg* 15(4): 135–136.

Karaman MI, Gonzales ET Jr. 1996. Splenogonadal fusion: report of 2 cases and review of the literature. *J Urol* 155(1): 309–311.

Kayaba H, Tamura H, Kitajima S, Fujiwara Y, Kato T. 1996. Analysis of shape and retractibility of the prepuce of 603 Japanese boys. *J Urol* 156: 1813–1815.

Khoudary KP, Morgentaler A. 1998. Partial duplication of the vas deferens. *J Urol* 159(3): 988–989.

Kim HG, Jun KK, Choo GY, Park HK, Paick SH, Lho YS. 2012. 1621 incidence of contralateral metachronous hydrocele or inguinal hernia. *J Urol* 187(4): e655.

Kim JH, Cromie WJ. 1996. Congenital bilateral absence of the vas deferens and cryptorchidism without cystic fibrosis. *J Urol* 155(6): 2060.

Kirsch AJ, Escala J, Duckett JW, Smith GHH, Zderic SA, Canning DA, Snyder HM. 1998. Surgical management of the nonpalpable testis: the Children's Hospital of Philadelphia experience. *J Urol* 159(4): 1340–1343.

Koc G, Sural YS, Filiz ND, Yilmaz Y. 2012. Perineal ectopic testis. *Urol J* 9(1): 433–435.

Kolettis PN, Sandlow JI. 2002. Clinical and genetic features of patients with congenital unilateral absence of the vas deferens. *Urology* 60(6): 1073–1076.

Kolligian ME, Franco I, Reda EF. 2000. Correction of penoscrotal transposition: a novel approach. *J Urol* 164(2): 994–996.

Kollin C, Stukenborg JB, Nurmio M, Sundqvist E, Gustafsson T, Söder O, Toppari J, Nordenskjöld A, Ritzén EM. 2012. Boys with undescended testes: endocrine, volumetric and morphometric studies on testicular function before and after orchiopexy at nine months or three years of age. *J Clin Endocrinol Metab* 97(12): 4588–4595.

Kollin C, Granholm T, Nordenskjöld A, Ritzén EM. 2013. Growth of spontaneously descended and surgically treated testes during early childhood. *Pediatrics* 13(4): e1174–e1180.

Kraft KH, Mucksavage P, Canning DA, Snyder H, Kolon TF. 2011. Histological findings in patients with cryptorchidism and testis-epididymis nonfusion. *J Urol* 186(5): 2045–2049.

Kraft KH, Bhargava N, Schast AW, Canning DA, Kolon TF. 2012. Histological examination of solitary contralateral descended testis in congenital absence of testis. *J Urol* 187(2): 676–678.

Kramer SA, Kelalis P. 1982. Assessment of urinary incontinence in epispadias: review of 94 patients. *J Urol* 128:290.

Kramer SA, Aydin G, Kelalis PP. 1982. Chordee without hypospadias in children. *J Urol* 128: 559.

Krishnan A, Souza D, Konijetic R, Baskin LS. 2006. The anatomy and embryology of posterior urethral valves. *J Urol* 175: 1214–1220.

Kumar K, Das D, Shivaraj. 2012. Triorchidism with torsion. *Ann Med Health Sci Res* 2(2): 199–201.

Kuo J, Foster C, Shelton DK. 2011. Zinner's syndrome. *World J Nucl Med* 10(1): 20–22.

La Scala GC, Ein SH. 2004. Retractile testes: an outcome analysis on 150 patients. *J Pediatr Surg* 39(7): 1014–1017.

Lamm DL, Kaplan GW. 1997. Accessory and ectopic scrota. *Urology* 9(2): 149–153.

Lapointe SP, Wei DC, Hricak H, Varghese SL, Kogan BA, Baskin LS. 2001. Magnetic resonance imaging in the evaluation of congenital anomalies of the external genitalia. *Urology* 58: 452–456.

Lee MM, Donahoe PK, Silverman BL, Hasegawa T, Hasegawa Y, Gustafson ML, Chang YC, MacLaughlin DT. 1997. Measurements of serum müllerian inhibiting substance in the evaluation of children with nonpalpable gonads. *NEJM* 336(21): 1480–1486.

Lee SE, Byun SS, Lee HJ, Song SH, Chang IH, Kim YJ, Gill MC, Hong SK. 2006. Impact of variations in prostatic apex shape on early recovery of urinary continence after radical retropubic prostatectomy. *Urology* 68: 137–141.

Leung AK. 1988. Polyorchidism. *American Fam Physician* 38(3): 153–156.

Liang MK, Subramanian A, Weedin J, Griffith DP, Award SS. 2012. True duplication of the vas deferens: a case report and review of the literature. *Int Urol Nephrol* 44(2): 385–391.

Lin CS, Lazarowicz JL, Allan RW, MacLennan GT. 2010. Splenogonadal fusion. *J Urol* 184(1): 332–333.

Lobaccaro JM, Medlej R, Berta P, Belon C, Galifer RB, Guthmann JP, Chevalier C, Czernichow P, Dumas R, Sultan C. 1993. *Clin Endocrinol* 38(2): 197–201.

Lopes RI, de Medeiros MT, Arap MA, Cocuzza M, Srougi M, Hallak J. 2012. Splenogonadal fusion and testicular cancer: case report and review of the literature. *Einstein (São Paulo)* 10(1): 92–95.

Lou CC, Lin JN, Tung TC, Wang KL. 1994. Anatomical findings of the vanishing testis. *Changgeng Yi Xue Za Zhi* 17(2): 121–124.

Lund JM, Bouhadiba N, Sams V, Tsang T. 2001. Hepato-testicular fusion: an unusual case of undescended testes. *BJU Int* 88: 439–440.

Lym L, Ross JH, Alexander F, Kay R. 1999. Risk of contralateral hydrocele or hernia after unilateral hydrocele repair in children. *J Urol* 162(3): 1169–1170.

Maizels M, Stephens FD, King LR, Firlit CF. 1983. Cowper's syringocele: a classification of dilitations of cowper's gland duct based on clinical characteristics of 8 boys. *J Urol* 129(1): 111–114.

Mak V, Zielenski J, Tsui LC, Durie P, Zini A, Martin S, Longley TB, Jarvi KA. 1999. Proportion of cystic fibrosis gene mutations not detected by routine testing in men with obstructive azoospermia. *JAMA* 281(23): 2217–2224.

Malik MA, Iqbal Z, Chaudri KM, Malik NA, Ahmed AJ. 2008. Crossed testicular ectopia. *Urology* 71(5): 984.e5–984.e6.

Marcantonio SM, Fechner PY, Migeon CJ, Perlman EJ, Berkovitz GD. 1994. Embryonic testicular regression sequence: a part of the clinical spectrum of 46,XY gonadal dysgenesis. *Am J Med Genet A* 49(1): 1–5.

Maruyama K, Takahashi A, Kobayashi T, Hatakeyama S, Matsuo Y. 1999. Diphallia and the VATER Association. *J Urol* 162: 2144.

McCallum TJ, Milunsky JM, Munarriz R, Carson R, Sadeghi-Nejad H, Oates RD. 2001. Unilateral renal agenesis associated with congenital bilateral absence of the vas deferens: phenotypic findings and genetic considerations. *Hum Reprod* 16(2): 282–288.

Merksz M. 1998. Fusion anomalies of the testis and epididymis. *Acta Chir Hung* 37(3): 153–170.

Messina MF, Aversa T, Mami C, Briuglia S, Panasiti I, De Luca F, Lombardo F. 2013. Ambiguous genitalia in a 48 XXYY newborn: a casual relationship or a coincidence? *J Pediatr Endocrinol Metab* 26(9–10): 921–923.

Mickle J, Milunsky A, Amos JA, Oates RD. 1995. Congenital unilateral absence of the vas deferens: a heterogenous disorder with two distinct subpopulations based on aetiology and mutational status of the cystic fibrosis gene. *Hum Reprod* 10(7): 1728–1735.

Mizuno K, Kojima Y, Kamisawa H, Kurokawa S, Moritoki Y, Nishio H, Hayashi Y, Kohri K. 2012. Feasible etiology of vanishing testis regarding disturbance of testicular development: histopathological and immunohistochemical evaluation of testicular nubbins. *International J Urol* 19(5): 450–456.

Mo B, Garla V, Wyner LM. 2013. A case of congenital unilateral absence of the vas deferens. *Int Med Case Rep* 6: 21–23.

Mohta A, Das S, Sengar M. 2008. Perineal lipoma associated with penoscrotal transposition in a neonate. *J Indian Assoc Pediatr Surg* 13(4): 155–156.

Mokhless I, Youssif M, Eltayeb M, Hanna M. 2011. Z-plasty for sculpturing of the bifid scrotum in severe hypospadias associated with penoscrotal transposition. *J Ped Urol* 7(3): 305–309.

Monstrey S, Hoebeke P, Selvaggi G, Ceulemans P, Van Landuyt K, Blondeel P, Roche N, Weyers S, De Cuypere G. 2009. Penile reconstruction: is radial forearm flap really the standard technique? *Plast Reconstr Surg* 124: 510–518.

Montag S, Palmer LS. 2011. Abnormalities of penile curvature: chordee and penile torsion. *TSW Urology* 11: 1470–1478.

Moul JW, Belman AB. 1988. A review of surgical treatment of undescended testes with emphasis on anatomical position. *J Urol* 140(1): 125–128.

Muecke EC. 1964. The role of cloacal membrane in exstrophy: the first successful experimental studay. *J Urol* 92: 659.

Murphy JO, Power RE, Akhtar M, Torreggiani WC, McDermott TED, Thornhill JA. 2003. Magnetic resonance imaging in the diagnosis of seminal vesicle cysts and associated anomalies. *J Urol* 170(6): 2386.

Na SW, Kim SO, Yoo DH, Hwang I, Hwang EC, Oh KJ, Jung SI, Kang TW, Kwon DD, Park K, Ryo SB. 2012. 1367 epididymal anomalies in children with cryptorchidism or hydrocele. *J Urol* 187(4): e554–e555.

Naji H, Peristeris A, Stenman J, Svensson JF, Wester T. 2012. Transverse testicular ectopia: three additional cases and a review of the literature. *Pediatr Surg Int* 28(7): 703–706.

Naouar S, Maazoun K, Sahnoun L, Jouini R, Ksia A, Elezzi O, Krichene I, Mekki M, Belghith M, Nouri A. 2008. Transverse testicular ectopia: a three-case report and review of the literature. *Urology* 71(6): 1070–1073.

Nayak SP, Sreejayan MP. 2011. Management of supernumerary testis in an adult: case report and review. *Andrologia* 43(2): 149–152.

Nouira F, Ben Ahmed Y, Jlidi S, Sarrai N, Chariag A, Ghorbel S, Khemakhem R, Chaovachi B. 2011. Management of perineal ectopic testes. *Tunis Med* 89(1): 47–49.

Okada H, Yoshimura K, Fujioka H, Tatsumi N, Gotoh A, Fujisawa M, Gohji K, Arakawa S, Kato H, Kobayashi SI, Isojima S, Koshida M, Kamidono S. 1999. Assisted reproduction technology for patients with CBAVD. *J Urol* 161(4): 1157–1162.

Osifo OD, Osaigbovo EO. 2008. Congenital hydrocele: prevalence and outcome among male children who underwent neonatal circumcision In Benn City, Nigeria. *J Ped Urol* 4(3): 178–182.

Oster J. 1968. Further fate of the foreskin: incidene of preputial adhesions, phimosis, and smegma among Danish schoolboys. *Arch Dis Child* 400: 200–203.

Palmer JM. 1991. The undescended testicle. *Endocrinol Metab Clin North Am* 20(1): 231–240.

Palmer JS. 2011. Abnormalities of the external genitalia in boys. In *Campbell–Walsh Urology* (eds AJ Wein, LR Kavoussi, AC Novick, AW Partin, CA Peters). Philadelphia, PA: Saunders.

Parigi GB, Bardoni B, Avoltini V, Caputo MA, Bragheri R. 1999. Is bilateral congenital anorchia genetically determined? *Eur J Pediatr Surg* 9(5): 312–315.

Park KH, Hong JH. 2006. Perineal lipoma in association with scrotal anomalies in children. *BJU Int* 98(2): 409–412.

Pereira BJ, Sousa L, Azinhais P, Conceição P, Borges R, Leão R, Brandão A, Temido P, Retroz E, Sobral F. 2009. Zinner's syndrome: an up-to-date review of the literature based on a clinical case. *Andrologia* 41(5): 3222–330.

Pettersson A, Richiardi L, Nordenskjold A, Kaijser M, Akre O. 2007. Age at surgery for undescended testis and risk of testicular torsion. *NEJM* 356: 1835–1841.

Pinke LA, Rathbun SR, Husmann DA, Kramer SA. 2001. Penoscrotal transposition: a review of 53 patients. *J Urol* 166(5): 1865–1868.

Pirgon Ö, Dündar BN. 2012. Vanishing testes: a literature review. *J Clin Res Pediatr Endocrinol.* 4(3): 116–120.

Podesto ML, Medel R, Castero R, Ruarte AC. 1998. Urethral duplication in children: surgical treatment and results. *J Urol* 160: 1830–1833.

Prakash J, Dalela D, Goel A, Singh V, Kumar M, Garg M, Mandal S, Sankhwar SN, Paul S, Singh BP. 2013. Congenital anterior urethral valve with or without diverticulum: A single-centre experience. *J Pediatr Urol* 9(6): 1183–1187.

Rachmani E, Zachariou Z, Snyder H, Hadziselimovic F. 2012. Complete testis-epididymis nonfusion anomaly: a typical association with cryptorchid testis. *Urol Int* 89: 355–357.

Radpour R, Gourabi H, Gilani MA, Dizaj AV. 2008. Correlation between CFTR gene mutations in Iranian men with congenital absence of the vas deferens and anatomical genital phenotype. *J Androl* 29(1): 35–40.

Raman JD, Goldstein M. 2004. The presence of vassal vessels in men with congenital bilateral absence of the vas deferens. *J Urol* 172(5): 1941–1943.

Ramareddy RS, Alladi A, Siddappa OS. 2013. Ectopic testis in children: experience with seven cases. *J Pediatr Surg* 48(3): 538–541.

Razi A, Imani B. 2000. Seminal vesicle cyst presenting with lower urinary tract symptoms and huge abdominal mass. *J Urol* 164(4): 1309–1310.

Redman JF, Ferguson SF. 2005. Unilateral perineal ectopic scrotum resulting in debilitating orchalgia: diagnosis and management. *J Urol* 173(1): 104–105.

Renzulli JF II, Shetty R, Mangray S, Anderson KR, Weiss RM, Caldamone AA. 2005. Clinical and histological significance of the testicular remnant found on inguinal exploration after diagnostic laparoscopy in the absence of a patent processus vaginalis. *J Urol* 174(4): 1584–1586.

Richter S, Shalev M, Nissenkorn I. 1996. Late appearance of cowper's syringocele. *J Urol* 160: 128–129.

Roth JK, Marshall RH, Angel JR, Daftary M, Lewis RW. 1981. Congenital absence of the penis. *Urology* 17: 579–583.

Rozanski TA, Wonjo KJ, Bloom DA. 1996. The remnant orchiectomy. *J Urol* 155(2): 712–715.

Salle JLP, Sibai H, Rosenstein D, Brzezinski AE, Corcos J. 2000. Urethral duplication in the male: review of 16 cases. *J Urol* 163: 1936–1940.

Schlegel PN, Shin D, Goldstein M. 1996. Urogenital anomalies in men with congenital absence of the vas deferens. *J Urol* 155(5): 1644–1648.

Schukfeh N, Kuebler JF, Schirg E, Peterson C, Ure BM, Glüer S. 2009. Dysplastic kidney and not renal agenesis is the commonly associated anomaly in infants with seminal vesicle cyst. *BJU Int* 103(6): 816–819.

Schwentner C, Oswald J, Kreczy A, Lunacek A, Bartsch G, Deibl M, Radmayar C. 2005. Neoadjuvant gonadotropin-releasing hormone therapy before surgery may improve the fertility index in undescended testes: a prospective randomized trial. *J Urol* 173(3): 974–977.

Shapiro E, Goldfarb DA, Ritchey ML. 2003. The congenital and acquired solitary kidney. *Rev Urol* 5(1): 2–8.

Sharma N, Acharya N, Singh SK, Singh M, Sharma U, Prasad R. 2009. Heterogenous spectrum of CFTR gene mutations in Indian patients with congenital absence of the vas deferens. *Hum Reprod* 24(5): 1229–1236.

Sharma S, Sen A. 2013. Complete testicular epididymal dissociation in the abdominal cryptorchid testis. *J Pediatr Urol* 9(6): 1023–1027.

Sheih CP, Li YW, Liao YJ, Hung CS. 1998. Bilateral congenital cysts of the seminal vesicle with bilateral duplex kidneys. *J Urol* 160(1): 184–185.

Shin D, Gilbert F, Goldstein M, Schlegel PN. 1997. Congenital absence of the vas deferens: incomplete penetrance of cystic fibrosis gene mutations. *J Urol* 158(5): 1794–1799.

Shnack TH, Zdravkovic S, Myrup C, Westergaard T, Christensen K, Wohlfahrt J, Melbye M. 2008. Familial aggregation of hypospadias: a cohort study. *Am J Epidemiol* 167: 251–256.

Sijstermans K, Hack WW, Meijer RW, van der Voort-Doedens LM. 2008. The frequency of undescended testis from birth to adulthood: a review. *Int J Androl* 31(1): 1–11.

Singer BR, Donaldson JG, Jackson DS. 1992. Polyorchidism: functional classification and management strategy. *Urology* 39 (40): 384–388.

Sirasanagandla SR, Nayak SB, Jetti R, Bhat KM. 2013. Unilateral duplication of vas deferens: a cadaveric case report. *Anat Cell Biol* 46(1): 79–81.

Skoog SJ, Belman AB. 1989. Aphallia: its classification and management. *J Urol* 144: 589–592.

Smith NM, Byard RW, Bourne AJ. 2007. Testicular regression syndrome: a pathological study of 77 cases. *Histopathology* 19(3): 269–272.

Snodgrass WT. 2011. Hypospadias. In *Campbell–Walsh Urology* (eds AJ Wein, LR Kavoussi, AC Novick, AW Partin, CA Peters). Philadelphia, PA: Saunders.

Spranger R, Gunst M, Kühn M. 2002. Polyorchidism: a strange anomaly with unsuspected properties. *J Urol* 168(1): 198.

Stec AA, Thomas JC, DeMarco RT, Pope JC IV, Brock JW, Adams MC. 2007. Incidence of testicular ascent in boys with retractile testes. *J Urol* 178(4): 1722–1724.

Storm D, Redden T, Aqular M, Wilkerson M, Jordan G, Sumfest J. 2007. Histologic evaluation of the testicular remnant associated with the vanishing testes syndrome: is surgical management necessary? *Urology* 70(6): 1204–1206.

Stuhrmann M, Dörk T. 2000. CFTR gene mutations and male infertility. *Andrologia* 32(2): 71–83.

Sule JD, Skoog SJ, Tank ES. 1994. Perineal lipoma and the accessory labioscrotal fold: an etiological relationship. *J Urol* 151(2): 455–457.

Sunay M, Emir L, Karabulut A, Erol D. 2009. Our 21-year experience with the Thiersch-Duplay technique following surgical correction of penoscrotal transposition. *Urol Int* 82(1): 28–31.

Teo AQA, Khan AR, Willimas MPL, Carroll, Hughes IA. 2013. Is surgical exploration necessary in bilateral anorchia? *J Pediatr Urol* 9(1): e78–e81.

Thyoka M, Lall A, Godse A. 2013. Polyorchidism: a torted right-sided supernumerary testis. *BJM Case Rep*, 2013, doi: 10.1136/bcr-2013-008600.

Tillett JW, Elmore J, Smith EA. 2006. Torsion of an indirect hernia sac within a hydrocele causing acute scrotum: case report and review of the literature. *Pediatr Surg Int* 22(12): 1025–1027.

Van Savage JG. 2001. Avoidance of inguinal incision in laparoscopically confirmed vanishing testis syndrome. *J Urol* 166(4): 142–144.

van Wessem KJ, Simons MP, Plaisier PW, Lange JF. 2003. The etiology of indirect inguinal hernias: congenital and/or acquired? *Hernia* 7(2): 76–79.

Verga G, Avdio L. 1996. Agenesis of the scrotum: an extremely rare anomaly. *J Urol* 156(4): 1467.

Vinci G, Anjot MN, Trivin C, Lottmann H, Brauner R, et al. 2004. An analysis of the genetic factors involved in testicular descent in a cohort of 14 male patients with anorchia. *J Clin Endocrinol Metab* 89: 6282–6285.

Walz J, Burnett AL, Costellow AJ, Eastham JA, Graefen M, Guilloneau B, Menon M, Montorsi F, Myers RP, Rocco B, Villers A. 2010. A Critical analysis of the current knowledge of surgical anatomy related to optimization of cancer control and preservation of continence and erection for radiacl prostatectomy. *Eur Urol* 2: 179–192.

Weiske WH, Salzer N, Schroeder-Printzen I, Weidner W. 2000. Clinical findings in congenital absence of the vas deferentia. *Andrologia* 32(1): 13–18.

Wilson JM, Aaronson DS, Schrader R, Baskin LS. 2008. Hydrocele in the pediatric patient: inguinal or scrotal approach? *J Urol* 180(4): 1724–1728.

Wood HM, Elder JS. 2009. Cryptorchidism and testicular cancer: separating fact from fiction. *J Urol* 181(2): 452–461.

Wuerstle M, Lesser T, Hurwitz R, Applebaum H, Lee SL. 2007. Persistent müllerian duct syndrome and transverse testicular ectopia: embryology, presentation, and management. *J Pediatr Surg* 42(12): 2116–2119.

Yaffe D, Zissin R. 1991. Cowper's gland duct: radiographic findings. *Urol Radiol* 13(2): 123–125.

Yanaral F, Yildirim ME. 2013. Testicular fusion in a patient with crossed testicular ectopia: a rare entity. *Urol Int* 90(1): 123–124.

Young HH, Frontz WA, Baldwin JC. 1919. Congenital obstruction of the posterior urethra. *J Urol* 3: 289.

Zenaty D, Dijoud F, Morel Y, Cabrol S, Mouriquand P, Nicolino M, Bouvatier C, Pinto G, Lecointre C, Pienkowski C, Soskin S, Bost M, Bertrand AM, El-Ghoneimi A, Nihoul-Fekete C, Léger J. 2006. Bilateral anorchia in infancy: occurrence of micropenis and the effect of testosterone treatment. *J Pediatr* 149(5): 687–691.

Zhang DX, Li XG, Gao Y, Wang JK, Chen J, Chen L, Wang K, Cui XG, Xu DF. 2012. Transperitoneal laparoscopic excision of seminal vesicle cyst: a single-center experience. *J Endourol* 26(9): 1153–1158.

Zhapa E, Castagnetti M, Alaggio R, Talent E, Rigamonti W. 2010. Testicular fusion with transverse testicular ectopia and persistent müllerian duct syndrome. *Urology* 76(1): 62–64.

116 Female genital system

Sedat Develi
Gulhane Military Medical Academy, Ankara, Turkey

Ovary

Location of the ovary

In the human embryo, the ovaries are located at the posterior wall of the body near the kidneys and develop from the cortex of the initially undifferentiated gonads (Berek and Novak 2007; Standring and Gray 2008). During development the ovaries descend to the true pelvis and in an adult female are located in the ovarian fossa on each side of the uterus, close to the lateral pelvic wall (Standring and Gray 2008).

Disruption of this descent can result in undescended ovaries. The prevalence of maldescended ovaries has been reported as 0.3–2% (Dietrich et al. 2007). The condition is unilateral in many cases (Nichols and Postoloff 1951; Seoud et al. 1987; McCullough et al. 1992; Ombelet et al. 2003a, b) but bilaterality has also been reported (Verkauf and Bernhisel 1996; Rock et al. 1986; Van Voorhis et al. 2000; Gorgen et al. 2002; Bazi et al. 2006). No clear mechanisms have been suggested but coexistence with congenital syndromes such as Mayer-Rokitansky-Küster-Hauser (MRKH) syndrome has been reported. Twenty percent of patients with undescended ovaries and fallopian tubes have MRKH syndrome; the most commonly reported accompanying Müllerian anomaly is a unicornuate uterus (Verkauf and Bernhisel 1996).

Undescended ovaries are usually found during evaluation of infertility (Dietrich et al. 2007). Ectopic pregnancy, cyclic abdominal pain, and inguinal masses have also been reported (Seoud et al. 1987; Bazi et al. 2006).

Number of ovaries

Ectopic ovary is a rare gynecological anomaly in which the ectopic tissue can be adjacent to the normal ovary or in the pelvis, peritoneum, or retroperitoneum. The terms "accessory" and "supernumerary" ovary have sometimes been used instead of ectopic ovary. A prevalence of 1:29,000 to 1:700,000 has been reported (Wharton 1959; Lachman and Berman 1991; Vendeland and Shehadeh 2000; Lim et al. 2004). The condition can be related to embryological anomalies, or secondary to inflammation or surgical operation on the normal ovaries located in the ovarian fossa in the lesser pelvis (Lachman and Berman 1991). Ectopic ovaries are diagnosed incidentally or secondary to clinical conditions such as congenital anomalies, tumors, or hormonal changes.

The prevalence of congenital anomalies has been reported as 23–36%; commonly associated congenital anomalies are accessory fallopian tube, bifid fallopian tubes, accessory tubal ostium, bicornuate or unicornuate uterus, septate uterus, agenesis of kidney or ureter, bladder diverticulum, accessory adrenal gland, and lobulated liver (Vendeland and Shehadeh 2000; Lim et al. 2004). Dermoid cysts, sclerosing stromal tumor, steroid cell tumor, osseous metaplasia, and cystic teratomas are tumors that have been diagnosed on ectopic ovarian masses (Besser and Posey 1992; Badawy et al. 1995; Roth et al. 1996; Andrade et al. 2001; Lim et al. 2004).

Unfortunately, ectopic ovarian tissue can cause pathological hormonal changes by acting as a normal ovary. The coexistence of endometriosis and inconsistency with clomiphen citrate treatment in primary infertility with ectopic ovaries has been reported in the literature (Navarro et al. 1990; Ombelet et al. 2003b).

Rarely, due to retardation of development of the Müllerian duct on one side, ovarian agenesis can occur. The exact prevalence of ovarian agenesis is unknown since the lesion is usually asymptomatic (Dueck et al. 2001), but a prevalence of 1:11241 has been reported (Sivanesaratnam 1986).

Agenesis of the ipsilateral fallopian tube commonly accompanies ovarian agenesis. The etiopathogenesis is debated, but two main mechanisms have been suggested. According to the mechanical hypothesis, adnexal torsion with vascular ischemia is the reason for agenesis (Sivanesaratnam 1986; Silva et al. 1995; Dueck et al. 2001; Krissi et al. 2001). According to the embryological hypothesis, the cause is incomplete development of the Müllerian and Wolffian ducts (Zaitoon and Florentin 1982; Muppala et al. 2008). Patients with ovarian and tubal agenesis present with cystic masses, abdominal pain, infertility, torsion of the pedicles, menorrhagia, and contralateral ovarian cysts (Mylonas et al. 2003).

Arterial supply to ovaries

The blood supply to the ovaries comes from the ovarian arteries, which are lateral branches of the abdominal aorta, and from the uterine artery. The ovarian arteries emerge from the aorta

Bergman's Comprehensive Encyclopedia of Human Anatomic Variation, First Edition. Edited by R. Shane Tubbs, Mohammadali M. Shoja and Marios Loukas.
© 2016 John Wiley & Sons, Inc. Published 2016 by John Wiley & Sons, Inc.

below the renal arteries and descend laterally to the pelvis. They cross the external iliac artery and veins at the pelvic brim and reach the ovaries through the ovarian suspensory ligament. They supply the ovary and uterine tubes, and one branch anastomoses with the uterine artery (Standring and Gray 2008).

Distribution of main arterial supply to ovaries

The ovaries are supplied mainly by the ovarian arteries in 40% of the population, by the uterine artery in 4%, and by both the ovarian and uterine arteries in 56% (Lippert and Pabst 1985).

Four subtypes have been described. In type I, the ovarian and uterine arteries anastomose with each other and their branches supply the ovary equally. In type II, both arteries supply the ovarian gland and also anastomose with each other. In type III, the main source of arterial supply is the uterine artery but there is a small anastomosis with the ovarian artery. In type IV, the ovarian artery supplies the ovarian gland. There is a small anastomosis with the uterine artery or with its tubal branch. Types I and II are more frequent than the other types (Bergman 1988).

Level of aortic origin of the ovarian arteries

The level of aortic origin of the ovarian arteries is classified into three types in the literature. In type 1, the right and left ovarian arteries originate from the anterolateral aspect of the abdominal aorta, below the renal veins, and course inferiorly. The right ovarian artery passes from anterior of the inferior vena cava.

In type 2, the right ovarian artery originates from the anterolateral aspect of the abdominal aorta above the renal vein and travels inferiorly, passing behind the inferior vena cava and anterior to the right renal vein. The left ovarian artery originates from the anterolateral aspect of the abdominal aorta, above the left renal vein, and descends inferiorly and anteriorly to the left renal vein.

In type 3, the right ovarian artery emerges from the anterolateral aspect of the abdominal aorta, below the left renal vein, and arches over the right renal vein. The left ovarian artery originates from the anterolateral aspect of the abdominal aorta, below the left renal vein, and travels inferiorly by arching over the left renal vein (Notkovich 1956).

According to this classification, type 1 is the most common variation and type 3 the least (Notkovich 1956; Terayama et al. 2008). In another variant reported in the literature the ovarian arteries emerge below the renal veins and course posteriorly to the inferior vena cava (Terayama et al. 2008), and the left ovarian artery originates above the renal vein and courses along the posterolateral aspect of left kidney (Rahman et al. 1993).

Origin of the ovarian arteries

The ovarian arteries usually originate from the abdominal aorta but can also originate from the renal, accessory renal, segmental renal, middle suprarenal, lumbar, internal iliac, common iliac, and external iliac arteries (Merklin and Michels 1958; Bergman 1988; Ravery et al. 1993; Machnicki and Grzybiak 1997; Singh et al. 1998; Bergman et al. 2000; Asala et al. 2001; Shoja et al. 2007; Bakheit 2012; Kim et al. 2013; Kwon et al. 2013). They can emerge separately or arise from a common stem (Bergman et al. 1984).

It has been suggested that persistence of the lateral mesonephric arteries is an aspect of the etiopathology of abnormal ovarian arteries (Felix 1912).

The prevalence of ovarian arteries originating from the renal artery, one of its branches, or the accessory renal artery is in the range 4.7–18% (Notkovich 1956; Figley and Muller 1957; Conroy and Molen 1976; Bergman 1988; Bergman et al. 1984, 1992; Asala et al. 2001; Cicekcibasi et al. 2002; Petru et al. 2007; Shoja et al. 2007).

Interestingly, bilateral absence of the ovarian arteries was found in a Tanzanian female cadaver. The ovarian branch of the uterine artery supplied the ovaries in this case (Kasindye et al. 2012).

Other variations accompanying aberrant ovarian arteries have also been reported; in a Japanese female cadaver an aberrant left ovarian artery was found to give rise to the suprarenal and inferior phrenic arteries (Rahman et al. 1993).

Venous drainage of the ovaries

In normal venous anatomy the left ovarian venous plexus drains into the left ovarian veins, which drain into the left renal vein. The right ovarian venous plexus drains into the right ovarian veins, which usually drain directly into the inferior vena cava (Standring and Gray 2008).

Variations of the ovarian veins are rarer than variations of the ovarian arteries. The most commonly reported variation, with a prevalence of 8.8%, is the right ovarian vein draining into the right renal vein (Stones 2003). The suggested cause of the variation is disruption of the embryological development of the venous shift and altered anastomoses between cardinal veins (Phalgunan et al. 2012). Reflux into the ovarian veins due to this abnormal drainage has been described and could be related to abnormal venous flow, dilated or tortuous ovarian and pelvic veins, pelvic pain, and pelvic congestion syndrome (Cura and Cura 2009).

Uterine tubes

Appearance

The uterine tubes develop bilaterally from the cranial parts of the paramesonephric (Müllerian) ducts. During development, while the abdominal ostium (ostium abdominal tubae uterinae, morsus diaboli) develops with the cranial ends remaining, the caudal ends communicating with the uterus become the uterine ostium (ostium uterinum tubae).

Reports of variations of the uterine tubes in the literature are based on congenital anomalies rather than isolated abnormalities. Since the uterine tubes originate from the Müllerian ducts, it has been suggested that the main etiopathological factors are disorders of embryo development. Disturbances of Müllerian

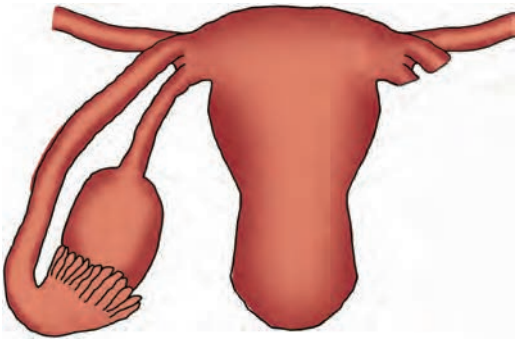

Figure 116.1 Complete absence of uterine tube, usually accompanied by absence of ipsilateral ovary.

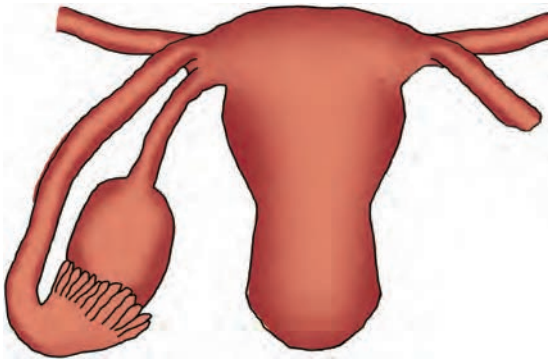

Figure 116.3 Distal segmental absence of uterine tube, usually accompanied by absence of ipsilateral ovary.

duct development such as fusion and resorption failure, disturbance of gonadal development, abnormal sex chromosomes, and asymptomatic torsions have been suggested as mechanisms leading to abnormalities (Nawroth et al. 2006; Falcone and Hurd 2007; Cunningham and Williams 2010; Yazawa et al. 2010; Crum et al. 2011; Stephenson 2012).

Congenital anomalies of the uterine tube are quite rare. The real prevalence is unknown since many cases are asymptomatic and are discovered incidentally. A prevalence of 1:11241 was reported on the basis of 17 years of experience of laparoscopy or laparotomy by Sivanesaratnam (1986).

Agenesis of the uterine tubes is one reported developmental variation (Sirisena 1978; Sivanesaratnam 1986; Gold et al. 1997; Rapisarda et al. 2009; Liu et al. 2013). Absence of the uterus can be total (Fig. 116.1) or segmental (Figs 116.2, 116.3). Segmental absence of the uterine tube can be proximal (Kozlowski and Luciano 1995), mid-segmental (Nishiyama et al. 2010; Yazawa et al. 2010) or distal (Farber and Mitchell 1979; Gold et al. 1997; Rapisarda et al. 2009). Bilateral agenesis of the uterine tubes is very rare (Kriplani et al. 1995; Gold et al. 1997); most reported cases are unilateral. Ovarian agenesis, ectopic kidney, renal agenesis, and pelvic adhesions have been reported to accompany this clinical abnormality. Hysterosalpingography, diagnostic laparoscopy or laparotomy are the methods used to diagnose tubal variations. Interestingly, in most cases with tubal agenesis, the uterus has been reported to be normal (Liu et al. 2013).

Other rare reported anomalies of the uterine tubes are accessory ostium (Fig. 116.4) (Zolcinski et al. 1964; Isherwood et al. 1990), supernumerary uterine tubes (Fig. 116.5) (Rowley 1948; Zolcinski and Robaczynski 1964; Daw 1973; Beyth and Kopolovic 1982; Coddington et al. 1990; Thonell et al. 1993; Venyo 1993; Bugmann et al. 2001; Narayanan and Rajeev 2008; Gandhi et al. 2012), and atresic (Fig. 116.6) (Farber and Mitchell 1979; Kozlowski and Luciano 1995; Dahan et al. 2006; Nawroth et al. 2006; Suh and Kalan 2008) or congenitally torsioned (Fig. 116.7) uterine tubes (Hibbard 1985; Thonell et al. 1993; Paternoster et al. 1998; Lineberry and Rodriguez 2000; Krissi et al. 2001; Casey et al. 2013).

Arterial supply to the uterine tubes

There are conflicting data in the literature about the arterial supply to the uterine tubes. Tubal branches of the uterine and ovarian arteries have been suggested. According to Lippert and Pabst (1985), in 60% of cases, the tubal branch of the uterine

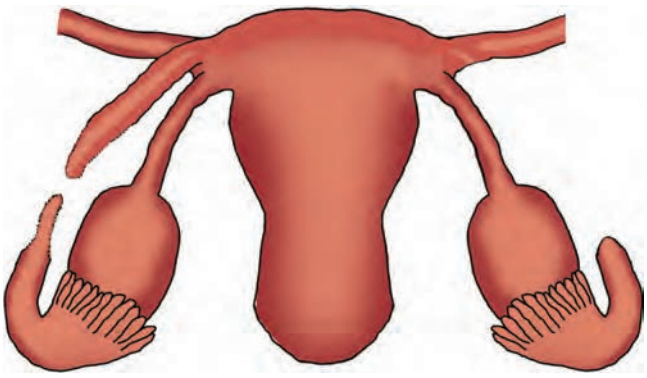

Figure 116.2 Segmental absence of uterine tube. Proximal segmental absence is depicted on the left side and mid-segmental absence on the right.

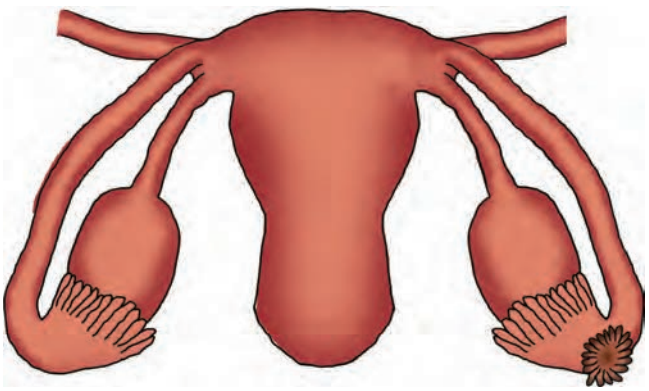

Figure 116.4 Accessory ostium of uterine tube. Ampullar accessory ostium is schematized.

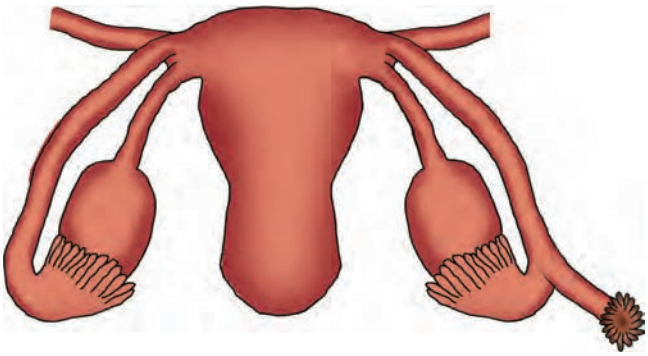

Figure 116.5 Supernumerary uterine tube. Duplication of the tube may be partial or complete; partial duplication is depicted here.

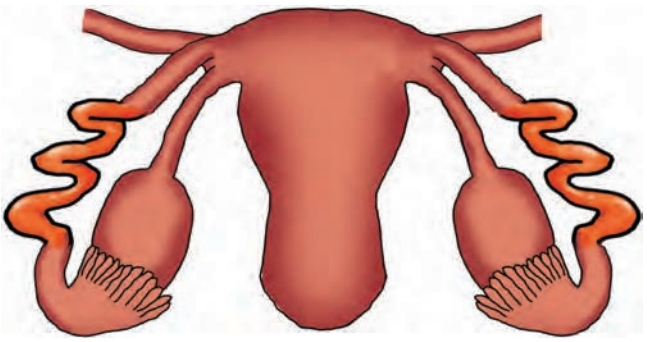

Figure 116.7 Congenital torsion of the uterine tubes.

artery supplies the tubes. The arterial supply to the tubes is derived from the tubal branch of the ovarian artery in 30% of cases and from both tubal branches of the uterine and ovarian arteries in 10% (Lippert and Pabst 1985). On the other hand, it has been suggested that the proximal two-thirds of the uterine tubes are supplied by the uterine artery and the distal one-third by the ovarian artery (Standring and Gray 2008).

Uterus

Appearance

The female genital tract develops from the Müllerian ducts (paramesonephric ducts) during embryogenesis. Disruption of Müllerian duct development can lead to abnormalities (Behr et al. 2012). While the ovaries originate from the dorsal endoderm of the primitive yolk sac, the external genitalia derive from the urogenital sinus (Lin et al. 2002; Behr et al. 2012). Müllerian duct anomalies therefore basically affect the uterus, uterine tubes, and vagina. Normally functioning ovaries and normal external genitalia are usually seen in these anomalies (Falcone and Hurd 2007; Behr et al. 2012). On the other hand, Müllerian-derived structures are usually found to be normal when the ovaries and external genitalia are affected by congenital anomalies (Falcone and Hurd 2007).

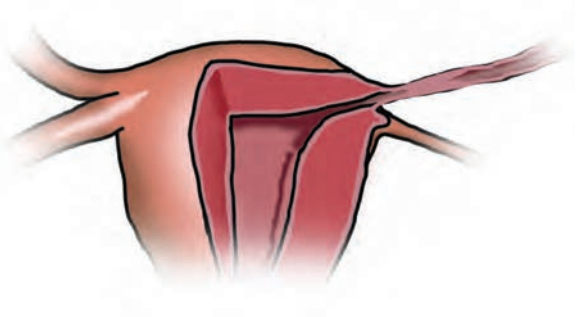

Figure 116.6 Atresia of the uterine tube, which may be partial or complete; partial atresia of the left uterine tube is depicted here.

Alterations in embryonic development have been implicated in the etiology of Müllerian anomalies. Organogenesis errors such as abnormal formation of the Müllerian ducts, abnormal migration, vertical or lateral fusion failures, resorption failures, steroidogenesis, and receptor defects and genetic problems such as chromosomal abnormalities and pharmacological issues are the mechanisms proposed in the literature (Falcone and Hurd 2007; Crum et al. 2011; Stephenson 2012).

It is difficult to establish the real prevalence of the Müllerian anomalies since not all cases are diagnosed. Most are diagnosed during adolescence due to abnormal bleeding or in adulthood because of infertility, recurrent miscarriage, and preterm delivery treatments. It is also known that Müllerian anomalies do not cause infertility in all cases; asymptomatic or subclinical cases have been reported. The reported prevalence of these anomalies therefore varies.

The reported prevalence of female genital tract malformations is 0.17–10% in the normal population (Ashton et al. 1988; Stampe Sorensen 1988; Jurkovic et al. 1997; Raga et al. 1997; Nahum 1998; Byrne et al. 2000; Marten et al. 2003; Chan et al. 2011a). Female genital tract anomalies are more frequent in women with histories of infertility or recurrent miscarriages; a prevalence of 3.5–30% has been reported (Stillman and Asarkof 1985; Acien 1993; Raga et al. 1997; Nahum 1998; Weiss et al. 2005; Devi Wold et al. 2006; Godinjak and Idrizbegovic 2008; Ghi et al. 2009; Chan et al. 2011a).

Renal, skeletal, neurological, and cardiac anomalies are the clinical conditions reported to be associated with female genital tract abnormalities. The most commonly associated anomalies are renal. A prevalence of 30–50% anomalies such as renal agenesis, ectopia, hypoplasia, malrotation, duplication, and horseshoe kidney has been reported in women with Müllerian abnormalities (Li et al. 2000; Troiano and McCarthy 2004; Pittock et al. 2005; Oppelt et al. 2006; Behr et al. 2012). Other associated anomalies are skeletal anomalies such as wedged or fused vertebral bodies, spina bifida, neurological problems such as hearing loss, and cardiological problems (Oppelt et al. 2005; Behr et al. 2012).

Hysteroscopy, hysterosalpingography, two-dimensional or three-dimensional transvaginal ultrasonography, laparoscopy, laparotomy, magnetic resonance imaging, and saline sonohysterography are the diagnostic methods reported in the literature for diagnosing female genital tract abnormalities (Scarsbrook and Moore 2003; Saravelos et al. 2008; Olpin and Heilbrun 2010; Chan et al. 2011b).

Depending on the level of impairment of embryo development, symptoms of developmental female genital tract abnormalities can range from menstrual or obstetric to nongynecological problems. In order to standardize diagnosis, prognosis and treatment, many classification systems have therefore been proposed. Although there is no universal consensus on these classifications, the system of the American Fertility Society (1988) is most widely accepted and used in the literature and textbooks (Grimbizis and Campo 2010; Marcal et al. 2011).

AFS classification

According to the AFS classification, Müllerian anomalies are divided into seven classes (American Fertility Society 1988; Troiano and McCarthy 2004; Marcal et al. 2011) as described in the following sections.

Class 1

This class includes agenesis or various spectra of hypoplasia of the uterus, cervix uteri, and vagina (Fig. 116.8); 5–10% of Müllerian anomalies are reported to be in Class 1 (Heinonen 1997; Troiano and McCarthy 2004). Five subtypes have been described: A, vaginal agenesis or hypoplasia; B, cervical agenesis or hypoplasia; C, fundal agenesis or hypoplasia; D, tubal agenesis or hypoplasia; and E, combined agenesis or hypoplasia (two or more organs) (American Fertility Society 1988; Troiano and McCarthy 2004).

In vaginal agenesis (type A), the vagina is either totally absent or consists of a short distal pouch. A prevalence of 1/4000 to 1/10,000 female births has been reported (American College of Obstetricians and Gynecologists 2006). The uterus and fallopian tubes can also be absent or rudimentary. Patients usually present with primary amenorrhea. The external genital appearance is normal but the urethra can be patulous (Petrozza et al. 1997; Amesse et al. 1999). Ultrasonography and magnetic resonance imaging (MRI) are the diagnostic imaging modalities.

Figure 116.8 Complete absence of uterus, uterine tubes, and vagina.

Source: Netter (2014).

Cervical agenesis (type B) is extremely rare and usually presents with primary amenorrhea and cyclic abdominal pain. Tubal agenesis (type D) is also extremely rare and usually presents with infertility.

The most common and also the most severe form in Class 1 is the combined form (type E), known as Mayer-Rokitansky-Kuster-Hauser (MRKH) syndrome. MRKH syndrome is characterized by agenesis of the uterus, cervix, and proximal portion of the vagina (Pizzo et al. 2013). It is also known as congenital absence of the uterus and vagina (CAUV) or Müllerian aplasia (MA) (Morcel et al. 2007). There are two subtypes of this syndrome. Type 1 is the isolated form, also known as the Rokitansky sequence or simple form. This type comprises agenesis of the uterus, cervix, and vagina and it is the less frequent type of MRKH syndrome. Type 2 includes incomplete Müllerian agenesis and other associated system anomalies such as renal (agenesis or ectopia of the kidney, horseshoe kidney), skeletal (Klippel-Feil anomaly, vertebral deformities), neurological (hearing loss), cardiac or digital (polydactyly, syndactyly) (Troiano and McCarthy 2004; Morcel et al. 2007; Pizzo et al. 2013). Type 2 is also known as the MURCS association (Müllerian duct aplasia, renal dysplasia, cervical somite anomalies), complex form, or GRES (genital renal ear syndrome) (Duncan et al. 1979; Morcel et al. 2007; Pizzo et al. 2013).

Most cases with MRKH syndrome are considered sporadic (Carson et al. 1983) but familial cases have also been reported and an autosomal dominant trait has been proposed (Jones and Mermut 1972; Guerrier et al. 2006; Morcel et al. 2007). A wide spectrum of genes has been implicated in the etiology. Type 1 MRKH syndrome is referred as OMIM 277000 and Type 2 as OMIM 601076 in the Online Mendelian Inheritance in Man database (Morcel et al. 2007).

The prevalence of MRKH syndrome has been reported to be 1 in 4500 female births (Pizzo et al. 2013). Patients have normal karyotype and are 46,XX. In most cases the ovaries are normal, so secondary sexual characteristics are present and the phenotype is normal (Troiano and McCarthy 2004; Pizzo et al. 2013). Patients with MRKH syndrome are usually admitted to hospital for primary amenorrhea (Troiano and McCarthy 2004).

Transvaginal ultrasonography (bidimensional) is a cost-effective and noninvasive diagnostic method. It has been recommended as the first method for diagnosing MRKH syndrome (Blask et al. 1991; Rosenberg et al. 1986; Strubbe et al. 1993; Troiano and McCarthy 2004). Magnetic resonance imaging (MRI) is also a noninvasive diagnostic method for MRKH syndrome and is reported to be more sensitive and specific than bidimensional ultrasonography for diagnosing uterine absence

or Müllerian rudiments. It is recommended that MRI be performed when ultrasonography findings are uncertain (Morcel et al. 2007). On the other hand, 3D ultrasonography, a recent development, has greater sensitivity and specificity than bidimensional ultrasonography and MRI in this context (Deutch and Abuhamad 2008; Pizzo et al. 2013). Hysterosalpingography is not used in diagnosing Müllerian agenesis (Troiano and McCarthy 2004) and laparoscopy is used when noninvasive methods give unreliable results (Pizzo et al. 2013).

Class 2

This class is referred to as unicornuate uterus and has four subtypes: A, a fully developed uterine horn on one side and a rudimentary horn with communicating endometrial cavity on the other; B, a fully developed uterine horn on one side and a rudimentary horn with noncommunicating endometrial cavity on the other; C, a fully developed uterine horn on one side and a rudimentary horn with no endometrial cavity on the other; and D, a fully developed uterine horn on one side and no rudimentary horn on the other (American Fertility Society 1988; Troiano and McCarthy 2004).

Between 10 and 20% of Müllerian anomalies have been reported to be unicornuate uterus (Heinonen 1997; Troiano and McCarthy 2004). Type A is seen in 10% of cases, type B in 22%, type C in 33%, and type D (Fig. 116.9) in 35% (Brody et al. 1998; Buttram and Gibbons 1979; Carrington et al. 1990; Troiano and McCarthy 2004).

The presentation of patients with unicornuate uterus depends on the anatomical structure of the genital tract. Most patients are diagnosed incidentally. Pelvic pain, pelvic mass, dysmenorrhea, retrograde menstruation or hematometra (if the uterine tube is atresic), especially in type B patients, are the main complaints (Acien et al. 2004; Troiano and McCarthy 2004). On the other hand, pregnancy outcomes of patients with unicornuate uterus are lower due to obstetric complications, most commonly preterm deliveries, malpresentations (especially breech presentation), and miscarriages (late first trimester or early second trimester). Ectopic pregnancy rates are also reported to be higher than normal (Brody et al. 1998; Heinonen 1997; Lin et al. 2002; Acien et al. 2004; Lin 2004; Raga et al. 1997).

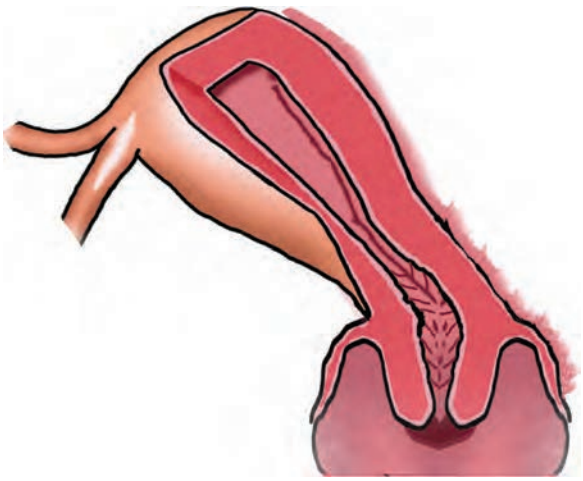

Figure 116.9 Class 2 type D unicornuate uterus; one of the Müllerian ducts is totally absent.

The most commonly associated anomalies are urinary. Approximately 40% of patients with unicornuate uterus have been reported to have urinary tract anomalies, most often renal agenesis, either ipsilateral or contralateral. Other reported urinary anomalies are ectopic kidney, ipsilateral pelvic kidney, and horseshoe kidney (Heinonen 1997; Brody et al. 1998; Lin et al. 2002).

The most commonly used imaging modalities for diagnosing unicornuate uterus are: ultrasonography and MRI as non-invasive methods; and hysterosalpingography as an invasive method (especially for communicating rudimentary horn) (Brody et al. 1998; Troiano and McCarthy 2004).

Class 3

This class of uterine anomalies includes uterus didelphys, which is the fusion failure of the Müllerian ducts at various levels (American Fertility Society 1988; Heinonen 1997; Troiano and McCarthy 2004; Marcal et al. 2011). Fusion failure can be complete or incomplete. In the complete form, the uterus and cervix uteri are totally separated. Between 5 and 10% of Müllerian duct anomalies are reported to be uterus didelphys (Heinonen 1997; Troiano and McCarthy 2004).

Fusion failure of the vagina is also commonly seen in conjunction with uterus didelphys (Fig. 116.10; Troiano and McCarthy 2004; Marcal et al. 2011). A longitudinal vaginal septum has been reported in 75% of the patients (Sarto and Simpson 1978). A transverse vaginal septum can also occur (Lin 2004).

If there is no obstruction in the genital tract, uterus didelphys patients are usually asymptomatic. In cases of obstruction there is cyclic pain and dyspareunia. There is also endometriosis due to retrograde menstruation, especially in obstructive hemivagina (Lin 2004; Troiano and McCarthy 2004; Marcal et al. 2011).

Preterm deliveries, ectopic pregnancy, spontaneous abortions and malpresentations occur in uterus didelphys, but reproductive outcomes are better than for unicornuate uterus cases. On the other hand, the prevalence of cesarean section in uterus didelphys is highest among Müllerian anomalies (Heinonen et al. 1982; Lin 2004).

Ipsilateral renal agenesis has been reported to accompany uterus didelphys (Stassart et al. 1992).

Ultrasonography, magnetic resonance imaging and hysterosalpingography are commonly used imaging modalities for diagnosing uterus didelphys (Scarsbrook and Moore 2003; Troiano and McCarthy 2004; Olpin and Heilbrun 2010; Marcal et al. 2011).

Class 4

This class encompasses bicornuate uterus (American Fertility Society 1988). Bicornuate uterus is defined as incomplete fusion of Müllerian ducts at the level of the uterine fundus (Fig. 116.11).

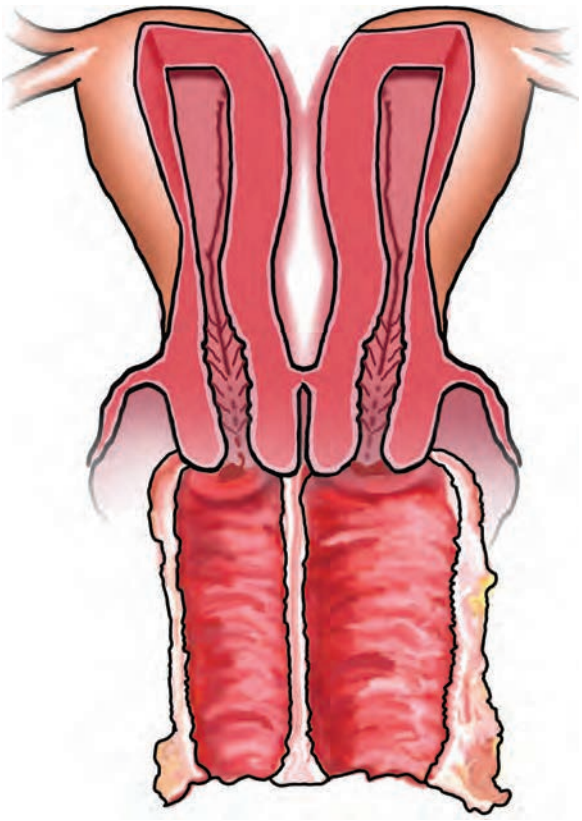

Figure 116.10 Uterus didelphys with longitudinal vaginal septum.

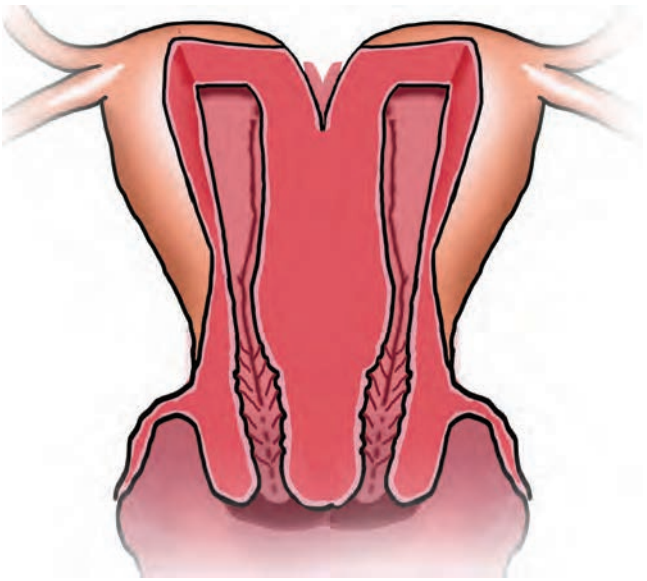

Figure 116.11 Complete bicornuate uterus. Muscular septum reaches internal os.

The lower parts of the genital tract are completely fused. There are two separate uterine cornua and noncommunicating endometrial cavities in the cornua. These uterine cavities communicate with each other in the lower segments of the uterus. In addition, a muscular septum is seen; bicornuate uterus cases are subdivided into complete or partial according to the length of this muscular septum. If the septum reaches the internal os (ostiumanatomicum uteri internum), the bicornuate uterus is complete or type A. If the muscular septum is shorter and limited to the fundal region, the bicornuate uterus is partial or type B (Troiano and McCarthy 2004; Marcal et al. 2011). Between 10 and 17% of Müllerian anomalies are reported to be bicornuate uterus (Heinonen 1997; Troiano and McCarthy 2004).

Reproductive outcomes of bicornuate uterus depend on the length of the muscular septum. Late miscarriages and preterm deliveries are more common in the complete (type A) form (Troiano and McCarthy 2004; Marcal et al. 2011).

It is reported that 25% of cases coexist with longitudinal vaginal septum (Troiano and McCarthy 2004).

Ultrasonography is the first choice for diagnosing bicornuate uterus, but magnetic resonance imaging and hysterosalpingography are more effective in differential diagnosis (Troiano and McCarthy 2004; Marcal et al. 2011).

Class 5

This class is referred to as septate uterus (American Fertility Society 1988), defined as failure of resorption of the median septum after fusion of the Müllerian ducts. If the remaining median septum reaches the external os (ostium uteri) from the uterine fundus, it is called a complete or type A septate uterus (Fig. 116.12). If failure of resorption of the median septum is

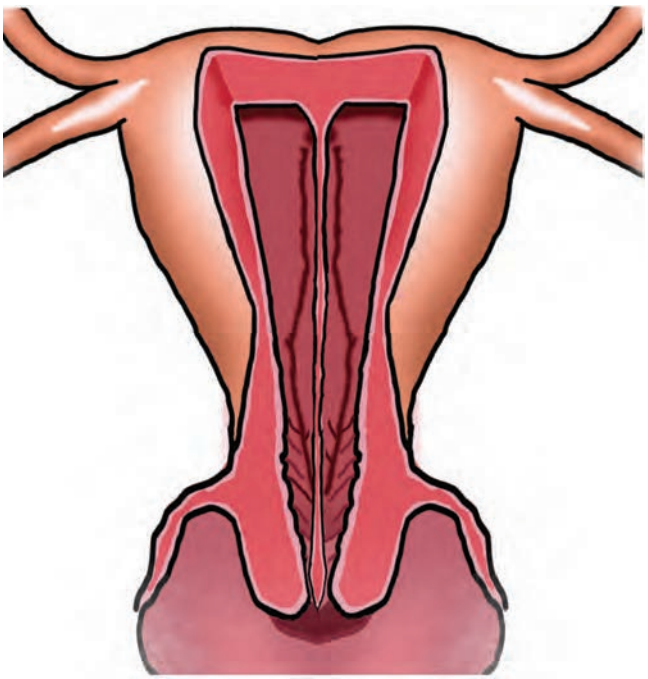

Figure 116.12 Complete septate uterus.

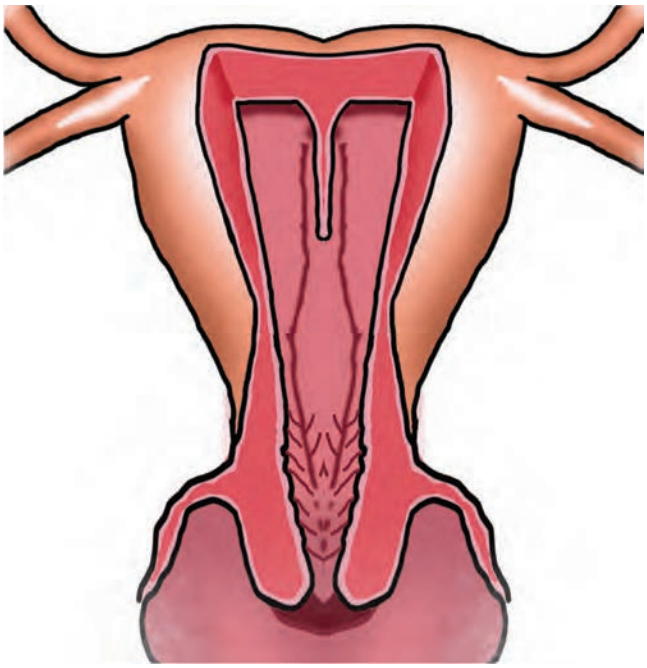

Figure 116.13 Partial septate uterus.

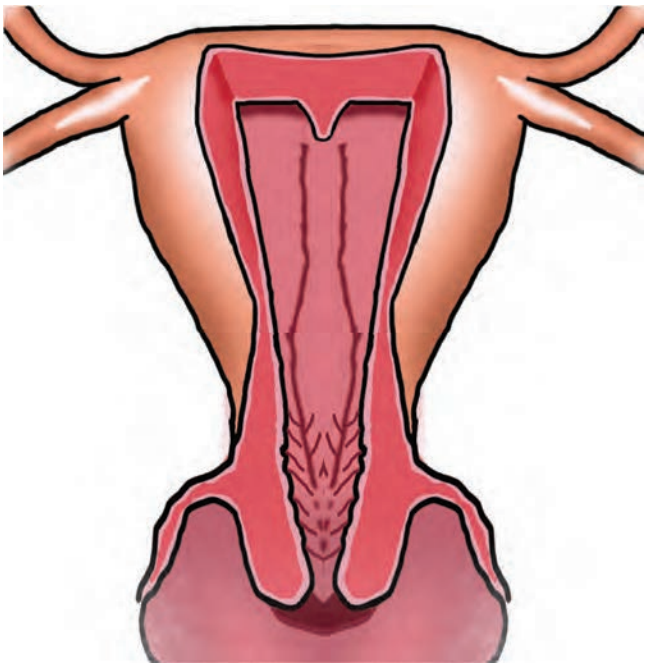

Figure 116.14 Arcuate uterus.

limited to its cranial part, it is called a partial or type B septate uterus (Fig. 116.13) (Lin et al. 2002; Troiano and McCarthy 2004; Marcal et al. 2011).

Septate uterus is the most common type of Müllerian anomaly, accounting for 48–55% of the total (Heinonen 1997; Troiano and McCarthy 2004).

It is reported to be associated with the lowest reproductive outcome among Müllerian anomalies, with the highest rates of spontaneous abortion and preterm delivery (Troiano and McCarthy 2004; Chan et al. 2011a; Marcal et al. 2011). The live birth rate has been reported as 5% (Homer et al. 2000).

Hysterosalpingography is quite useful for diagnosis of septate uterus since it provides data for planning surgery. The sensitivity and specificity of ultrasonography and magnetic resonance imaging are higher (Scarsbrook and Moore 2003; Troiano and McCarthy 2004; Olpin and Heilbrun 2010; Marcal et al. 2011).

Differential diagnosis of septate and bicornuate uterus is important. If the apex of the outer contour of the uterine fundus is up to 5 mm superior to the intertubal line, the uterus is defined as bicornuate. If the apex is more than 5 mm above the intertubal line, it is however defined as septate (Troiano and McCarthy 2004; Marcal et al. 2011).

Class 6

This class includes arcuate uterus (American Fertility Society 1988). It is defined as septal indentation in the caudal portion of the uterine cavity (Troiano and McCarthy 2004). Complete unification of the uterine fundus distinguishes arcuate from bicornuate uterus (Fig. 116.14) (American Fertility Society 1988). A prevalence of 5% has been reported (Heinonen 1997); knowledge about reproductive outcomes is limited.

Ultrasonography, magnetic resonance imaging and hysterosalpingography are commonly used for diagnosing arcuate uterus (Scarsbrook and Moore 2003; Olpin and Heilbrun 2010; Marcal et al. 2011).

Class 7

This class includes diethylstilbestrol (DES) -affected uterus (American Fertility Society 1988). DES is a synthetic estrogen that was previously used for recurrent miscarriages and preterm deliveries (Herbst et al. 1981). Since DES use ceased in 1971, the frequency of in utero DES exposure has decreased. Uterine abnormalities accompanying DES exposure are a uterus with T-shaped cavity, hypoplastic uterus, constriction rings, or intrauterine adhesions (Fig. 116.15). It has also been reported that cervical hypoplasia, cervical collars, vaginal adenosis, vaginal transverse septum, and vaginal clear cell carcinoma are associated with DES exposure (Herbst et al. 1981; Troiano and McCarthy 2004; Rackow and Arici 2007). The most common anomaly (70%) seen in DES exposure is a T-shaped uterine cavity with or without dilated uterine horns (American Fertility Society 1988; Rackow and Arici 2007).

The spontaneous abortion and ectopic pregnancy risk is higher in DES-related uterine anomalies (Goldberg and Falcone 1999).

Other classification systems

As described in detail, the AFS classification depends on the uterine anatomy. Separate anomalies of the female genital tract

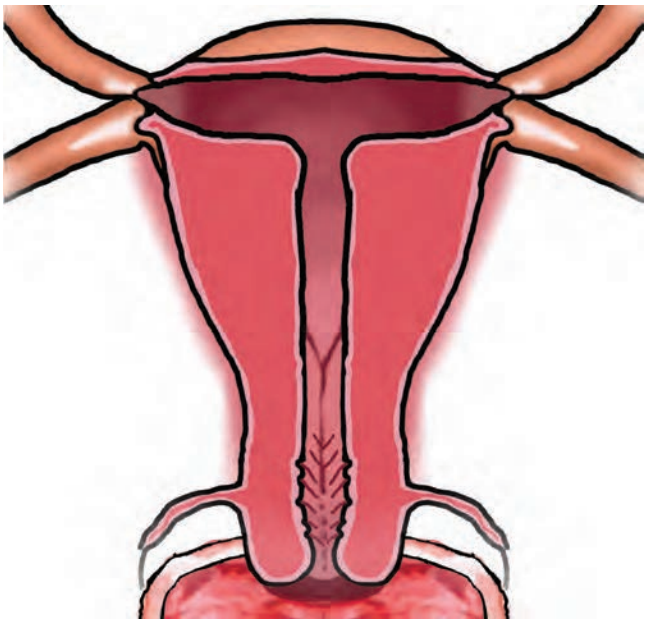

Figure 116.15 DES related uterus. Uterine cavity is T-shaped.

such as imperforate hymen, transverse vaginal septum, or complex combinations of congenital developmental disorders such as bicervical uterus with or without septate vagina (Acien et al. 2009) are not described in this classification. Other classifications have therefore been proposed for female genital tract anomalies.

The VCUAM (vagina cervix uterus adnex-associated malformation) classification was proposed in 2005 and is similar to the TNM (tumor, lymph node, metastasis) classification of malignant tumors (Oppelt et al. 2005). Each abnormality of each organ is described separately:

- V (vagina): 0, normal; 1, hymenal atresia; 2, septate vagina; 3, stenosis of introitus; 4, hypoplasia; 5, atresia; S, sinus urogenitalis; C, cloacae; +, other; #, unknown.
- C (cervix): 0, normal; 1, duplex cervix; 2, atresia/aplasia; +, other; #, unknown.
- U (uterus): 0, normal; 1, arcuate/septate; 2, bicornuate; 3, hypoplastic; 4, rudimentary/aplastic; +, other; #, unknown.
- A (adnexa): 0, normal; 1, tubal malformation; 2, hypoplasia/gonadal streak; 3, aplasia; +, other; #, unknown.
- M (associated malformations): 0, none; R, renal; S, skeleton; C, cardiac; N, neurological; +, other; #, unknown (Oppelt et al. 2005).

For example; isolated bicornuate uterus (Class 4 in the AFS classification) is defined as V0C0U2A0M0 according to the VCUAM classification.

The embryological and clinical classification of female genitourinary malformations (Acien and Acien 2011) was proposed in 2011 (revised and updated from Acien 1992; Acien et al. 2004). According to this classification, genital abnormalities are divided into six groups: 1, unilateral genitourinary agenesis or hypoplasia; 2, uterine duplicity with a blind hemivagina and ipsilateral agenesis; 3, isolated or common uterine or uterovaginal anomalies; 4, accessory uterine masses with an otherwise normal uterus and other possible gubernacula dysfunctions; 5, anomalies of urogenital sinus; and 6, malformative combinations (Acien and Acien 2011).

For example; isolated bicornuate uterus (Class 4 in AFS classification) is classed in group 3 according to the embryological and clinical classification of female genitourinary malformations.

The European Society of Human Reproduction and Embryology (ESHRE) and European Society for Gynecological Endoscopy (ESGE) established the CONUTA (CONgenitalUTerine-Anomalies) working group for a new classification, and in 2013 the ESHRE/ESGE system was proposed (Grimbizis et al. 2013). Female genital tract anomalies are classified as uterine and coexisting cervical/vaginal. Uterine anomalies are classified as: U0, normal uterus; U1, dysmorphic uterus; U2, septate uterus; U3, bicorporeal uterus; U4, hemi-uterus; U5, aplastic; and U6, unclassified malformations. Coexisting cervical anomalies are classified as: C0, normal; C1, septate; C2, double "normal"; and C3, unilateral cervical aplasia; and coexistent vaginal anomalies are classified as: V0, normal; V1, longitudinal non-obstructing vaginal septum; V2, longitudinal obstructing vaginal septum; V3, transverse vaginal septum and/or imperforate hymen; and V4, vaginal aplasia (Grimbizis et al. 2013).

For example, isolated bicornuate uterus (Class 4 in AFS classification) is class U3 and coexistent class CO and VO according to the ESHRE/ESGE system.

Position

In normal anatomy the uterus is located between the bladder and rectum, and in most women it lies in an anteflexed and anteverted position (Fig. 116.16).

Figure 116.16 Anteverted and anteflexed uterus.

Source: Netter (2014).

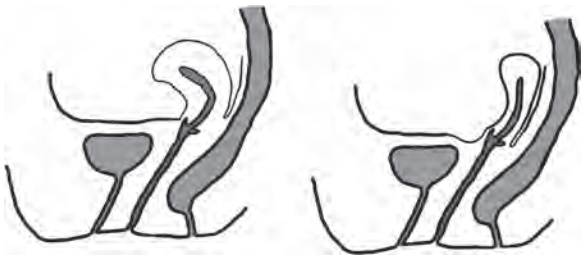

Figure 116.17 Degrees of retroverted uterus.

Source: Netter (2014).

Flexion is described as tilting of the uterus on itself at the level of the ostium uteri internum (internal os). If the uterus bends over forward on itself, this position is called anteflexion. If it bends over backward on itself, this position is called retroflexion.

On the other hand, version refers to the angle between the long axes of the uterus and the vagina. If the long axis of the uterus bends over forward to that of the vagina, this is called an anteverted uterus. If the long axis of the uterus bends over backward to that of the vagina, this is called a retroverted uterus (Fig. 116.17).

The uterus is retroverted in 19–20% (range 10–38%) of the general population (Chi et al. 1990; Smalbraak et al. 1991; Silver et al. 1994; Weinberger and Julian 1995; Hoenigl 1999; Bongers et al. 2002; Henne and Milki 2004; Haylen 2006); retroflexion is extremely rare (Fig. 116.18).

Although retroversion and retroflexion are normal variants of uterine position, these conditions can be associated with relaxation of the pelvic ligaments after delivery, pelvic adhesions due to surgery, or inflammatory conditions such as endometriosis. Transvaginal ultrasonography is effective for diagnosing uterine position (Haylen et al. 2007; Cagnacci et al. 2013).

Figure 116.18 Retroflexed uterus.

Source: Netter (2014).

In general, retroverted and retroflexed positions of the uterus are asymptomatic but pelvic pain due to dyspareunia, dysmenorrhoea, and low backache has been reported (Theron 1963). In addition, the fundus of a retroverted uterus can be entrapped below the sacrum during pregnancy. This condition is called incarceration of the retroverted uterus and can lead to cesarean delivery, urinary retention, or uterine rupture (Love and Howell 2000; Barton-Smith and Kent 2007).

Arterial supply to the uterus

The blood supply to the uterus comes from the uterine artery. In general, this is one of the branches of the anterior division of the internal iliac artery. A common stem with the vaginal, middle rectal, or inferior gluteal artery from the anterior division of the internal iliac artery has been reported (Bergman et al. 1984, 2000; Bergman 1988; Gomez-Jorge et al. 2003). The uterine artery can arise as more than one branch from the anterior division (Pelage et al. 1999) or as an aberrant branch from the abdominal aorta (Ambekar and Vogelzang 2001).

A classification of the branching pattern of the uterine artery from the internal iliac into four types has been proposed: type 1, uterine artery as first branch of inferior gluteal artery (45%); type 2, uterine artery as second or third branch of the inferior gluteal artery (6%); type 3, uterine, inferior gluteal and superior gluteal arteries arise as a trifurcation from the internal iliac artery (43%); and type 4, uterine artery as first branch of the internal iliac artery (6%) (Gomez-Jorge et al. 2003).

The uterine fundus is supplied by the uterine artery in 90% of the population; in 10% the arterial blood supply to the fundus comes from the ovarian artery (Bergman et al. 1984, 2000; Bergman 1988). Anastomoses between the uterine and ovarian arteries have been reported, especially in the cornual region of the uterine corpus, and these have clinical importance in uterine arterial embolization performed for uterine fibroids or postpartum hemorrhage (Matson et al. 2000; Binkert et al. 2001; Razavi et al. 2002; Cicinelli et al. 2004a; Ouyang et al. 2012).

A case of absence of the uterine artery has also been reported. The left uterine artery was absent and the left half of the uterus was supplied by an artery of the round ligament, branching from the inferior epigastric artery (Saraiya et al. 2002).

Venous system of the uterus

The veins of the uterus parallel the arteries, but those of the lower parts of the uterus can drain into the vaginal veins and those of the upper parts into the ovarian veins (Kauppila 1970; Kamina and Chansigaud 1989; Cicinelli et al. 2004b).

There can be arteriovenous malformations in the uterus, either congenital or acquired. The real prevalence is unknown since it is a rare condition and difficult to diagnose. Acquired malformations are related to uterine trauma such as cesarean

delivery or curettage, hormonal disturbances such as those which occur during pregnancy or contraception, infection, and tumors such as trophoblastic disease. It is proposed that disturbance of angiogenesis is associated with congenital malformations (Manolitsas et al. 1994; Hickey and Fraser 2000; Clarke and Mitchell 2003; Timmerman et al. 2003; Grivell et al. 2005).

Vagina

Appearance

Embryonic development of the vagina is controversial and several different origins have been described. Frequently, paramesonephric tissue (Müllerian ducts) is proposed as the origin of the upper vagina and the urogenital sinus (sinovaginalbulbs) of the lower vagina (Koff 1933; Sadler and Langman 2010). On the other hand, molecular findings (bone morphogenic protein 4 or BMP4) in recent studies indicate that the vagina is totally derived from Müllerian ducts under the guidance of BMP4 expressed in the urogenital sinus wall (Cai 2009). Eventually, the development of the vagina is closely related to the upper female genital tract and urogenital sinus. Abnormalities of the vagina are therefore usually evaluated as uterovaginal anomalies and classified as a part of complex malformations (American Fertility Society 1988; Tolete-Velcek et al. 1989; Oppelt et al. 2005; Acien and Acien 2011). In the literature, only a few studies have focused on vaginal abnormalities (Powell et al. 1995; Ruggeri et al. 2012).

In the classification of vaginal anomalies (Powell et al. 1995), vaginal malformations are classified as: type 1, labial fusion; type 2, urogenital sinus and distal vaginal fistula; type 3, distal vaginal atresia and proximal urethrovaginal fistula; and type 4, complete vaginal atresia. According to the classifications of vaginal malformations (Ruggeri et al. 2012) there are six types of vaginal abnormality. Type 1 consists of vaginal agenesis. Subtype 1A refers to vaginal agenesis associated with uterine agenesis (Mayer-Rokitansky-Kuster-Hauser syndrome). Subtype 1B refers to isolated vaginal agenesis. Type 2 consists of vaginal atresia in which the lumen of the vagina is absent. Subtype 2A refers to proximal atresia and subtype 2B to distal atresia. Type 3 consists of atresia with urogenital sinus fistula. Subtype 3A means a proximal fistula (above the external urethral sphincter); subtype 3B means a distal fistula (below the sphincter). Type 4 consists of atresia as diaphragm, indicating a transverse atresia in the vaginal lumen in which a transverse vaginal septum is classed as subtype 4A and an imperforate hymen as subtype 4B. Type 5 consists of duplication of the vagina: subtype 5A means complete duplication, subtype 5B a longitudinal vaginal septum. Type 6 consists of cloaca and urinary tract, internal genitalia and rectum communicating into the urethra.

As described in the different classifications, clinical presentations of vaginal malformations can be related to: obstructions in the genital tract such as vaginal agenesis/atresia, transverse vaginal septum, and imperforate hymen; or abnormal fusion of the urinary, genital, and distal gastrointestinal tracts such as a longitudinal vaginal septum, persistent urogenital sinus, or cloaca.

Agenesis of vagina

Agenesis of the vagina can present as a part of an embryological developmental disorder, or can be related to endocrinopathies leading to sex disorders such as androgen insensitivity syndrome or 17α-hydroxylase syndrome (American College of Obstetricians and Gynecologists 2006).

In Mayer-Rokitansky-Kuster-Hauser syndrome (MRKH), various uterine abnormalities accompany vaginal agenesis (Fig. 116.8). Either the vagina is completely absent or there is a distal pouch (American College of Obstetricians and Gynecologists 2006; Laufer 2012). A prevalence of 1/4000 to 1/10,000 females births has been reported (American College of Obstetricians and Gynecologists 2006). These patients have a normal karyotype (46,XX) and normal secondary sex characteristics. Primary amenorrhea is the typical presentation of these patients, and labial adhesions, imperforate hymen, transverse vaginal septum located by the vestibulum vagina (introitus), and endocrinopathies such as androgen insensitivity syndrome or 17α-hydroxylase syndrome are in the differential diagnosis of vaginal agenesis (Folch et al. 2000; American College of Obstetricians and Gynecologists 2006; Laufer 2012). Renal anomalies such as agenesis, horseshoe kidney, and ectopia, neurological anomalies such as hearing loss, and skeletal anomalies such as MURCS (Müllerian duct aplasia, renal dysplasia, cervical somite anomalies) or TAR (thrombocytopenia-absent radius) syndrome have been observed in MRKH patients (Fore et al. 1975; Griffin et al. 1976; Strubbe et al. 1987, 1994; Patankar et al. 2004; Behera et al. 2005; Griesinger et al. 2005; Pittock et al. 2005; Laufer 2012). Physical examination, pelvic ultrasonography and magnetic resonance imaging are sufficient for diagnosing vaginal agenesis and accompanying anomalies (Reinhold et al. 1997; Laufer 2012).

Androgen insensitivity syndrome and congenital adrenal hyperplasia are endocrinopathies affecting sex development. In 46,XY patients with androgen insensitivity syndrome there are female external genitalia due to androgen unresponsiveness (although the gonads are testes). Internal genital structures (uterus, cervix, and proximal vagina) are absent and secondary sex characteristics are underdeveloped. There is sometimes a distal vaginal pouch.

17α-hydroxylase syndrome is an uncommon form of congenital adrenal hyperplasia. In male patients (46,XY) affected by undervirilization, there are various levels of female external genitalia with distal vaginal pouch. The uterus, fallopian tubes, and proximal parts of the vagina are absent (New 1970; American College of Obstetricians and Gynecologists 2006; Laufer 2012; Wunsch et al. 2012).

On the other hand, distal vaginal agenesis with existing proximal vagina, cervix uteri, and uterus is also seen, albeit rarely (Laufer 2012; Jessel and Laufer 2013).

Transverse vaginal septum

Transverse vaginal septum is a congenital partition within the vagina. It is usually a result of failure of the distal Müllerian ducts to be absorbed (Joki-Erkkila and Heinonen 2003). The prevalence of transverse vaginal septum has been reported as 1/30,000 to 1/84,000 females (Lodi 1951; Brenner et al. 1965; Wenof et al. 1979; Rock et al. 1982). A transverse vaginal septum can be located at any level in the vaginal lumen; 46% have been identified in the proximal part, 14% in the distal part, and 40% in the middle of the lumen (Lodi 1951; Laufer 2012).

A transverse vaginal septum can be complete (Fig. 116.19), partial, or perforated (Polasek et al. 1995; Laufer 2012; Ventolini 2013). Its thickness is usually less than 1 cm and upper transverse vaginal septa have been reported to be thicker (Polasek et al. 1995; Ventolini 2013).

The most common presentations of patients with complete transverse vaginal septum are primary amenorrhea, low abdominal or pelvic pain, and hematocolpos, hematometra, and hematosalpinx due to retrograde menstruation. Patients with partial septa usually present with dysmenorrhea and dyspareunia (Polasek et al. 1995; Caloia et al. 1998; Grant et al. 2010; Ventolini 2013). Ultrasonography and magnetic resonance imaging are the diagnostic modalities.

Transverse vaginal septum is associated with genitourinary anomalies such as ectopic ureter or kidney, agenesis or hypoplasia of the kidney, vesicovaginal fistula, hydronephrosis, gastrointestinal anomalies such as imperforate anus, malrotation of the gut, colonic duplication, cardiovascular anomalies such as atrial septal defect, coarctation of the aorta, and musculoskeletal anomalies such as sacral hypoplasia and polydactyly (Reed and Griscom 1973; Rock et al. 1982; Polasek et al. 1995; Nazir et al. 2006). McKusick-Kaufman syndrome is an autosomal recessive syndrome characterized by hydrometrocolpos, postaxial polydactyly, and cardiopathy (OMIM number 236700), and is reported to be associated with transverse vaginal septum (McKusick et al. 1964; Dungy et al. 1971).

Longitudinal vaginal septum

A longitudinal vaginal septum is a result of resorption failure during fusion of the lateral Müllerian ducts (Haddad et al. 1997; Joki-Erkkila and Heinonen 2003; Heinonen 2006). It can be complete or partial. The complete form is described as a septum extending from the cervix uteri to the vestibulum vagina (introitus) (Figs 116.10, 116.20). The partial form is classified as high, medium, and low partial vaginal septa. The high partial form extends from the cervix uteri to any level of the vaginal lumen. The medium partial form occurs in the vaginal lumen, but in this type the septum does not reach the cervix uteri and vestibulum vagina. The low partial form extends from the hymen to any level of the vaginal lumen but does not reach the cervix uteri (Fig. 116.21; Haddad et al. 1997).

Longitudinal vaginal septum accounts for 12% of vaginal anomalies (Lodi 1951). The complete form accounts for 45.6% of all cases, the high partial form for 36.1% and the medium and

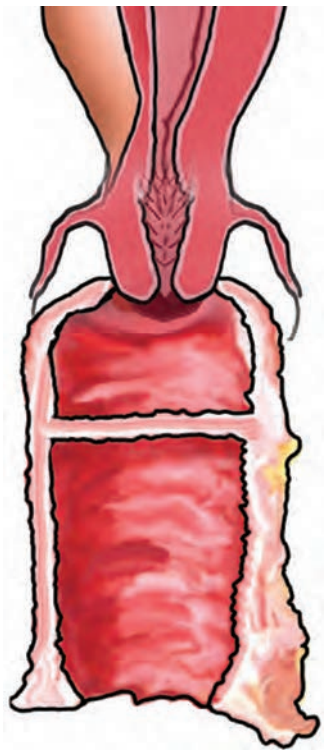

Figure 116.19 Complete transverse vaginal septum.

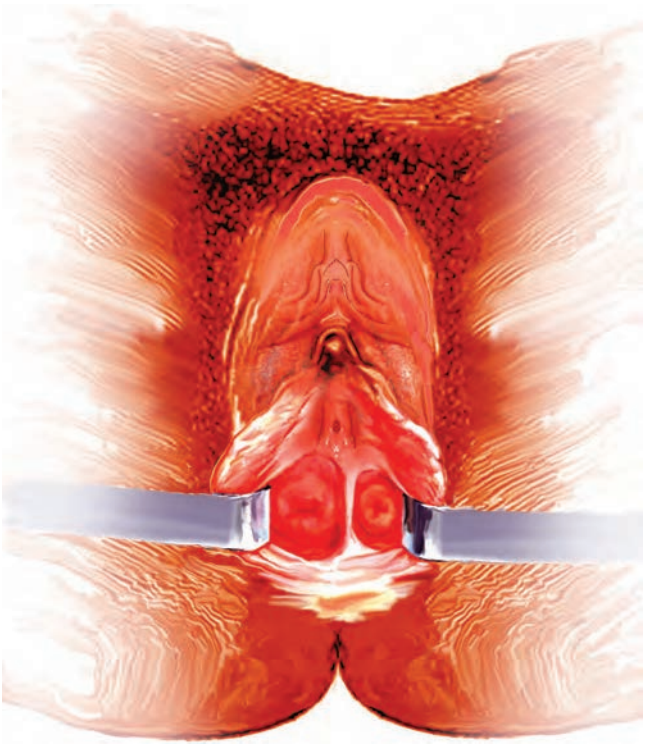

Figure 116.20 Longitudinal vaginal septum.

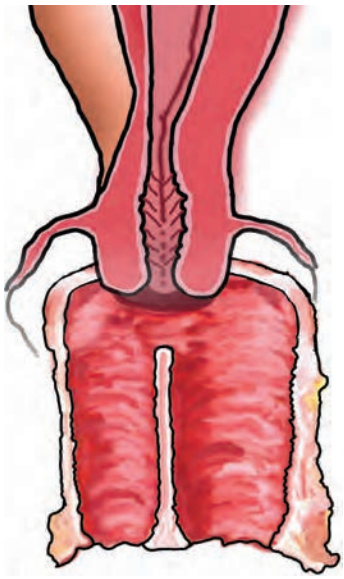

Figure 116.21 Low, partial longitudinal vaginal septum.

low partial forms for 18.3% (Haddad et al. 1997). In another review, the longitudinal vaginal septa was longer than half of the vaginal lumen in 94% of cases (Heinonen 2006).

Uterine malformations are reported to coexist with longitudinal vaginal septa in 87.8% of cases; this frequency increases to 99.4% in complete and partial high septa (Haddad et al. 1997). The most common (34–75%) uterine abnormality is septate uterus (Haddad et al. 1997; Heinonen 2006). The second most common (24%) is uterus didelphys (Haddad et al. 1997). Longitudinal vaginal septum is seen in 75% of patients with uterus didelphys (Grant et al. 2010). Patients with longitudinal vaginal septum are usually asymptomatic but dyspareunia is the most common complaint. Other main symptoms are dysmenorrhea, difficulty with tampon use or coitus, and dystocia (Haddad et al. 1997; Heinonen 2006; Ribeiro et al. 2010).

In some cases of longitudinal vaginal septum, one hemivagina is obstructed (the other is patent). The uterus is didelphic and there are usually accompanying renal anomalies in these cases. Uterus didelphys with blind hemivagina and ipsilateral renal agenesis is known as Herlyn-Werner-Wunderlich (HWW) syndrome or as obstructed hemivagina, ipsilateral renal anomaly (OHVIRA) syndrome (Smith and Laufer 2007; Takagi et al. 2010; Del Vescovo et al. 2012; Mandava et al. 2012; Morino et al. 2013). The reported prevalence of uterus didelphys with HWW syndrome is 1/2000 to 1/28,000 (Del Vescovo et al. 2012). In a retrospective study, a blind hemivagina was found in 6% of patients with longitudinal vaginal septum (Heinonen 2006). These patients usually present with pelvic pain, palpable mass, urinary symptoms, irregular bleeding, hematocolpos, hematometra, and hematosalpinx (Smith and Laufer 2007; Takagi et al. 2010; Del Vescovo et al. 2012; Mandava et al. 2012; Morino et al. 2013).

Ultrasonography, magnetic resonance imaging and hysterosalpingography are commonly used to diagnose longitudinal vaginal septum, but an intravenous pyelogram should be considered if there are accompanying urinary abnormalities.

Hand-foot-genital or hand-foot-uterus syndrome is a rare genetic disorder characterized with extremity abnormalities such as short thumbs and toes, short feet, clinodactyly, and urogenital tract abnormalities such as ectopic ureteral orifices, hypospadias, duplication of the uterus, and longitudinal vaginal septum (Poznanski et al. 1970; Stern et al. 1970; Goodman et al. 2000). The OMIM number is 140000.

Persistent urogenital sinus

A persistent urogenital sinus is a common channel into which both the urinary and genital tracts open and drain through one common orifice. Failure of urethrovaginal septation during gestation is proposed as a cause of this developmental variation. A prevalence of 0.6/10,000 has been reported (Singh et al. 2010). Persistent urogenital sinus can be part of ambiguous genitalia (more common and associated with endocrinopathies such as congenital adrenal hyperplasia) or a pure disorder (Laufer 2012; Wein et al. 2012). It is classified into subgroups:

- High confluence: in this subgroup the urethral opening is in the proximal part of the vaginal lumen, close to the urinary sphincter (or the contrary: the vaginal lumen opens into the proximal urethra). Since a high orifice indicates early arrest during gestation, an anteriorly displaced anus can accompany this situation due to arrested development of the urorectal septum.
- Middle confluence: the urethrovaginal opening is in the middle portion of the vaginal lumen (or the vaginal lumen opens into the middle portion of the urethral lumen).
- Low confluence: the urethral opening is in the distal portion of the vaginal lumen, close to the introitus (or the vaginal lumen opens into the distal part of the urethra). Low confluence indicates a defect later in development (Currarino 1986; Podesta and Urcullo 2008; Park et al. 2011; Laufer 2012; Wein et al. 2012).

In persistent urogenital sinus there are two openings in the perineum, one for the urinary and genital tracts developed anteriorly and one for the gastrointestinal tract developed posteriorly.

Persistent cloaca

A persistent cloaca is a developmental disorder in which distal parts of the urinary, genital, and gastrointestinal tracts fuse. It is associated with failure of the urorectal septum to descend. A prevalence of 1/40,000–50,000 to 1/250,000 is reported (Karlin et al. 1989; Geifman-Holtzman et al. 1997; Wein et al. 2012). There is a single orifice in the perineum. Subtypes of persistent cloaca have been described according to the length of the common channel (Levitt and Pena 2010; Wein et al. 2012).

Arterial supply to the vagina

The vagina is supplied by the uterine and vaginal arteries, which are branches of the anterior trunk of the internal iliac artery. Instead of the anterior trunk, the vaginal artery can originate from the uterine, middle rectal, or superior vesical arteries, or from the anterior trunk as a common stem with the uterine artery (Bergman 1988; Standring and Gray 2008).

Hymen

The hymen is a thin fold of mucous membrane that partly or completely closes the external vaginal orifice.

During gestation, while vaginal canalization is completed at the fifth month, proliferation of the sinovaginal bulbs forms the hymen. Initially the hymen is a complete barrier that separates the vaginal lumen from the urogenital sinus. In the perinatal period this barrier degenerates and becomes perforated (Sadler and Langman 2010; Stewart 2011).

Depending on this degeneration, some hymenal configurations are variants of the norm. Age-related changes have also been described. In the prepubertal period the hymen is thin and friable; this is associated with a lack of estrogen. During adolescence its thickness and elasticity increase, but at menopause its remnants become thin due to loss of estrogen (Mahran and Saleh 1964; Berenson et al. 1992; Pokorny et al. 1998; Berek and Novak 2007; Stukus and Zuckerbraun 2009; Van Eyk et al. 2009; Myhre et al. 2010).

- Annular hymen: this is defined as a circumferential ring with a central opening (Fig. 116.22). It is most common in newborns and its reported prevalence is 10% of examined individuals at 9 years of age (Berenson et al. 1991; Stewart 2011).
- Crescentic hymen: this is described as attachment to the vaginal lumen, usually at the 11 and 1 o'clock positions (Fig. 116.23; Stewart 2011). It is the most common variant of the hymen (Berenson and Grady 2002; Myhre et al. 2010).
- Imperforate hymen: since there is no opening, this condition is an obstructive anomaly. It closes the vaginal introitus completely and patients usually present with obstruction (Fig. 116.24). Common findings are hydrocolpos, hydrometrocolpos, primary amenorrhea, urinary retention, or tenesmus (Botash and Jean-Louis 2001; Bursac et al. 2012; Domany et al. 2013; Mwenda 2013; Vitale et al. 2013). A prevalence of 0.1% has been reported (Mwenda 2013).
- Septate hymen: a thin band splits the orifice (Fig. 116.25; Watrowski et al. 2013).
- Cribriform hymen: This type has multiple small openings (Fig. 116.26; Stewart 2011).
- Microperforated hymen: there is a tiny orifice on the hymen, which can be misdiagnosed as imperforate hymen (Fig. 116.27; Watrowski et al. 2013).
- Redundant or fimbriated hymen: this is described as abundant hymenal tissue folding over on itself or protruding outward (Fig. 116.28; Stewart 2011).

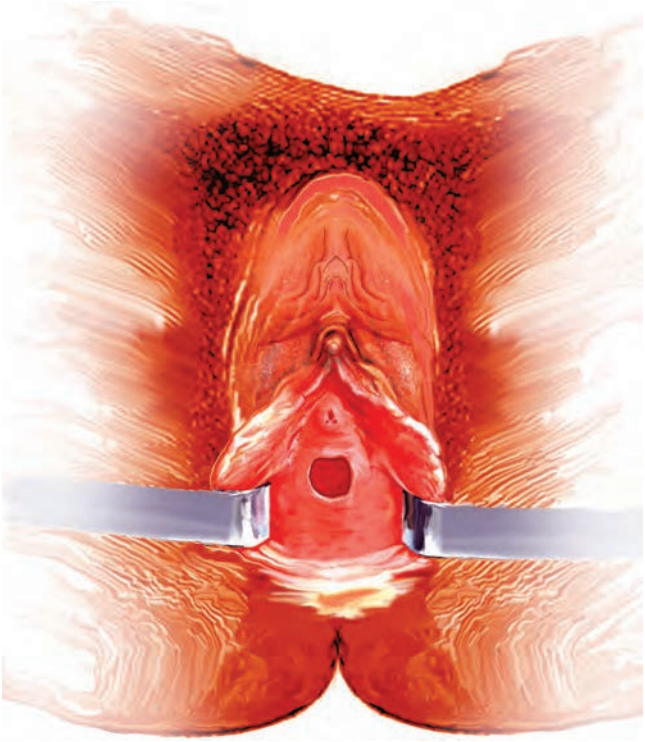

Figure 116.22 Annuler hymen.

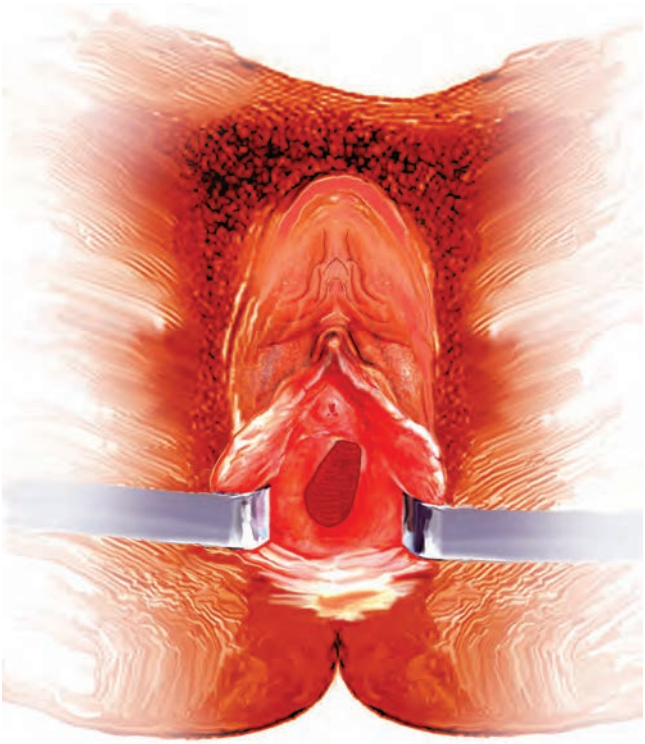

Figure 116.23 Crescentic hymen.

Figure 116.24 Imperforate hymen.

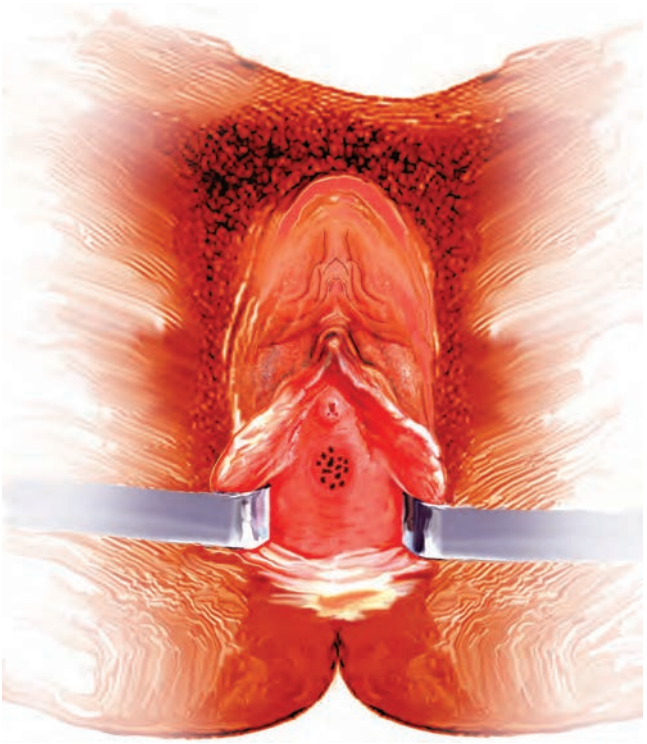

Figure 116.26 Cribriform hymen.

Figure 116.25 Septate hymen.

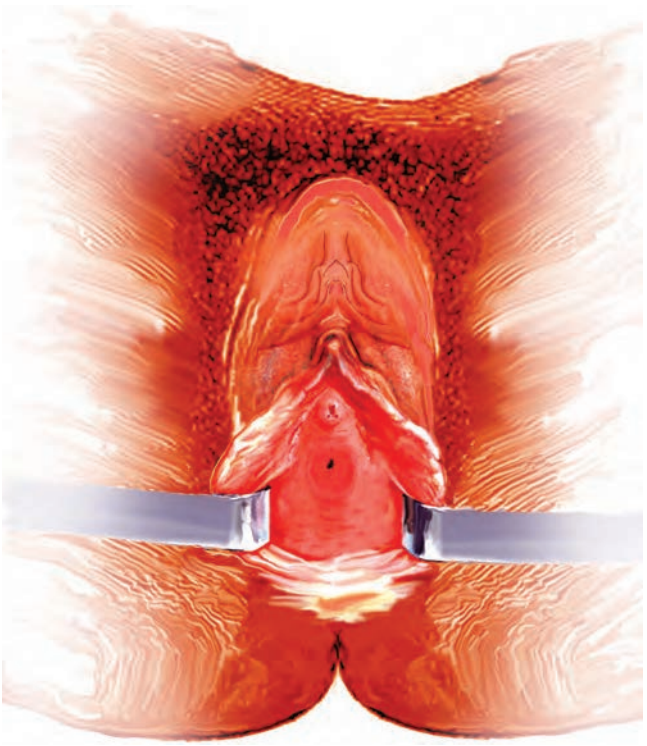

Figure 116.27 Microperforated hymen.

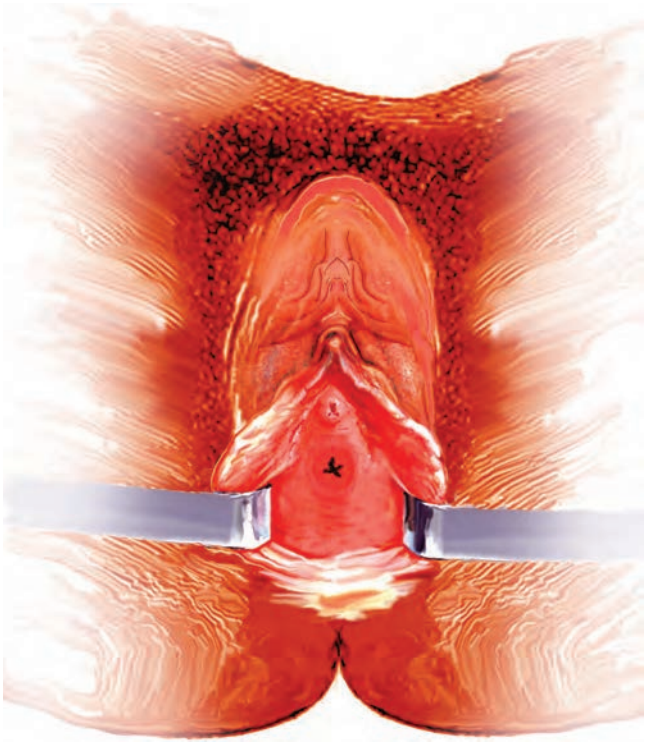

Figure 116.28 Fimbriated or redundant hymen.

In addition, there can be tags, notches, mounds and ridges on the edge of hymen as variants of the normal appearance (Stewart 2011). The hymen may be congenitally absent.

Clitoris

The clitoris comprises erectile tissue and lies at the anterior junction of the labia minora (Standring and Gray 2008).

Abnormalities of the clitoris generally include agenesis, double or bifid clitoris, and clitoromegaly (hypertrophy). Agenesis is usually related to ambiguous genitalia attributable to endocrinopathies, leading to genital development such as congenital adrenal hyperplasia (Martinon-Torres et al. 2000). Bifid or double clitoris is associated with bladder exstrophy (epispadias). It is seen in 1/150,000 to 1/300,000 females. It is suggested that failure of tubularization of the urethral plate is associated with this anomaly (Frimberger 2011; Grady and Mitchell 2002). Clitoromegaly is a pathological condition associated with fetal exposure to androgens. It is also known as macroclitoris. On the other hand, clitoral tumors can mimic clitoromegaly, such as arteriovenous malformations or epidermoid cyts (O'Connell et al. 2005; Geramizadeh et al. 2012; Johnson et al. 2013; Masson et al. 2014). The clitoris can be ossified.

Labia majora

The labia majora are longitudinal, cutaneous folds extending from the mons pubis to the perineum (Standring and Gray 2008).

Agenesis or hypoplasia of the labia majora occurs in genetic disorders (Gorlin et al. 1960; Rudoni et al. 1999). Other morphological variants of the labia majora are related to pathological processes such as hypertrophy or lipodystrophy. Both situations cause asymmetric hypertrophy of the labia majora (Mottura 2009; Lapalorcia et al. 2013).

Labia minora

The labia minora are bilateral cutaneous folds lying between the labia majora. They extend from the clitoris to the perineum (Standring and Gray 2008).

As a variant of normal anatomy, there can be an extra labial fold called the labium tertium on one side (Gottlicher 1994; Standring and Gray 2008). Hypertrophy of the labia minora is another variant of normal anatomy. This can be unilateral or bilateral and is often asymmetric (Kruk-Jeromin and Zielinski 2010; Reddy and Laufer 2010; Zimmer et al. 2012). Agenesis of the labia minora has been reported as a rare morphological variation (Martinon-Torres et al. 2000).

Adhesion of the labia minora is another morphological variation, considered pathological. It is usually associated with chronic vulvar irritation. This condition can mimic agenesis of the vagina (Nevarez Bernal and Meraz Avila 2009; Tahirovic and Toromanovic 2012).

Bulbs of vestibule and greater vestibular glands

The vestibular bulbs are erectile tissue on either side of the vaginal orifice. The greater vestibular glands are located at the posterior ends of the vestibular bulbs; they are a pair of tubuloacinar glands that secrete mucus into the vestibulum vagina (introitus) (Standring and Gray 2008).

Morphological variants of these structures depend on pathological processes. The most common abnormality of the greater vestibular gland is Bartholin's cyst. Infection or abscess formation or cysts and tumors of these anatomical structures make the appearance of this region abnormal (Finan and Barre 2003; Omole et al. 2003; Pundir and Auld 2008; Bora and Condous 2009; Ouldamer et al. 2013).

References

Acien P. 1992. Embryological observations on the female genital tract. *Hum Reprod* 7: 437–445.

Acien P. 1993. Reproductive performance of women with uterine malformations. *Hum Reprod* 8: 122–126.

Acien P, Acien MI. 2011. The history of female genital tract malformation classifications and proposal of an updated system. *Hum Reprod Update* 17: 693–705.

Acien P, Acien M, Sanchez-Ferrer M. 2004. Complex malformations of the female genital tract. New types and revision of classification. *Hum Reprod* 19: 2377–2384.

Acien P, Acien M, Sanchez-Ferrer ML. 2009. Müllerian anomalies "without a classification": from the didelphys-unicollis uterus to the bicervical uterus with or without septate vagina. *Fertil Steril* 91: 2369–2375.

Ambekar A, Vogelzang RL. 2001. Aberrant uterine artery as a cause of uterine artery embolization treatment failure. *Int J Gynaecol Obstet* 74: 59–60.

American College of Obstetricians and Gynecologists. 2006. ACOG Committee Opinion No. 355: Vaginal agenesis: diagnosis, management, and routine care. *Obstet Gynecol* 108: 1605–1609.

American Fertility Society. 1988. The American Fertility Society classifications of adnexal adhesions, distal tubal occlusion, tubal occlusion secondary to tubal ligation, tubal pregnancies, müllerian anomalies and intrauterine adhesions. *Fertil Steril* 49: 944–955.

Amesse L, Yen FF, Weisskopf B, Hertweck SP. 1999. Vaginal uterine agenesis associated with amastia in a phenotypic female with a de novo 46,XX,t(8;13)(q22.1;q32.1) translocation. *Clin Genet* 55: 493–495.

Andrade LA, Gentilli AL, Polli G. 2001. Sclerosing stromal tumor in an accessory ovary. *Gynecol Oncol* 81: 318–319.

Asala S, Chaudhary SC, Masumbuko-Kahamba N, Bidmos M. 2001. Anatomical variations in the human testicular blood vessels. *Ann Anat* 183: 545–549.

Ashton D, Amin HK, Richart RM, Neuwirth RS. 1988. The prevalence of asymptomatic uterine anomalies in women undergoing transcervical tubal sterilization. *Obstet Gynecol* 72: 28–30.

Badawy SZ, Kasello DJ, Powers C, Elia G, Wojtowycz AR. 1995. Supernumerary ovary with an endometrioma and osseous metaplasia: a case report. *Am J Obstet Gynecol* 173: 1623–1624.

Bakheit MA. 2012. Bilateral origin of ovarian arteries from accessory renal arteries. *Saudi Med J* 33: 1122–1124.

Barton-Smith P, Kent A. 2007. Asymptomatic incarcerated retroverted uterus with anterior sacculation at term. *Int J Gynaecol Obstet* 96: 128.

Bazi T, Berjawi G, Seoud M. 2006. Inguinal ovaries associated with Müllerian agenesis: case report and review. *Fertil Steril* 85: 1510 e1515–1518.

Behera M, Couchman G, Walmer D, Price TM. 2005. Müllerian agenesis and thrombocytopenia absent radius syndrome: a case report and review of syndromes associated with Müllerian agenesis. *Obstet Gynecol Surv* 60: 453–461.

Behr SC, Courtier JL, Qayyum A. 2012. Imaging of müllerian duct anomalies. *Radiographics* 32: E233–250.

Berek JS, Novak E. 2007. *Berek & Novak's Gynecology*, 14th edition. Philadelphia, PA: Lippincott Williams & Wilkins.

Berenson AB, Grady JJ. 2002. A longitudinal study of hymenal development from 3 to 9 years of age. *J Pediatr* 140: 600–607.

Berenson A, Heger A, Andrews S. 1991. Appearance of the hymen in newborns. *Pediatrics* 87: 458–465.

Berenson AB, Heger AH, Hayes JM, Bailey RK, Emans SJ. 1992. Appearance of the hymen in prepubertal girls. *Pediatrics* 89: 387–394.

Bergman RA. 1988. *Compendium of Human Anatomic Variation: Text, Atlas, and world Literature*. Baltimore, Md.: Urban & Schwarzenberg.

Bergman RA, Thompson SA, Afifi AK. 1984. *Catalog of Human Variation*. Baltimore: Urban & Schwarzenberg.

Bergman RA, Cassell MD, Sahinoglu K, Heidger PM, Jr. 1992. Human doubled renal and testicular arteries. *Ann Anat* 174: 313–315.

Bergman RA, Afifi AK, Miyauchi R, Virtual Hospital. 2000. *Illustrated Encyclopedia of Human Anatomic Variation*. Iowa City, Iowa: University of Iowa.

Besser MJ, Posey DM. 1992. Cystic teratoma in a supernumerary ovary of the greater omentum. A case report. *J Reprod Med* 37: 189–193.

Beyth Y, Kopolovic J. 1982. Accessory tubes: a possible contributing factor in infertility. *Fertil Steril* 38: 382–383.

Binkert CA, Andrews RT, Kaufman JA. 2001. Utility of nonselective abdominal aortography in demonstrating ovarian artery collaterals in patients undergoing uterine artery embolization for fibroids. *J Vasc Interv Radiol* 12: 841–845.

Blask AR, Sanders RC, Rock JA. 1991. Obstructed uterovaginal anomalies: demonstration with sonography. Part II. Teenagers. *Radiology* 179: 84–88.

Bongers MY, Mol BW, Brolmann HA. 2002. Prognostic factors for the success of thermal balloon ablation in the treatment of menorrhagia. *Obstet Gynecol* 99: 1060–1066.

Bora SA, Condous G. 2009. Bartholin's, vulval and perineal abscesses. *Best Pract Res Clin Obstet Gynaecol* 23: 661–666.

Botash AS, Jean-Louis F. 2001. Imperforate hymen: congenital or acquired from sexual abuse? *Pediatrics* 108: E53.

Brenner P, Sedlis A, Cooperman H. 1965. Complete imperforate transverse vaginal septum: report of a case. *Obstet Gynecol* 25: 135–138.

Brody JM, Koelliker SL, Frishman GN. 1998. Unicornuate uterus: imaging appearance, associated anomalies, and clinical implications. *AJR Am J Roentgenol* 171: 1341–1347.

Bugmann P, Hanquinet S, Brundler MA, Birraux J, Genin B, Le Coultre C. 2001. Intestinal obstruction caused by an ectopic fallopian tube in a child: case report and literature review. *J Pediatr Surg* 36: 508–510.

Bursac D, Duic Z, Partl JZ, Valetic J, Stasenko S. 2012. Hematocolpos resulting from an imperforated hymen diagnosed by ultrasound in a patient with recurrent urinary tract infections. *J Pediatr Adolesc Gynecol* 25: 340–341.

Buttram VC Jr, Gibbons WE. 1979. Müllerian anomalies: a proposed classification (an analysis of 144 cases). *Fertil Steril* 32: 40–46.

Byrne J, Nussbaum-Blask A, Taylor WS, Rubin A, Hill M, O'Donnell R, Shulman S. 2000. Prevalence of Müllerian duct anomalies detected at ultrasound. *Am J Med Genet* 94: 9–12.

Cagnacci A, Grandi G, Cannoletta M, Xholli A, Piacenti I, Volpe A. 2013. Intensity of menstrual pain and estimated angle of uterine flexion. *Acta Obstet Gynecol Scand* 93(1): 58–63.

Cai Y. 2009. Revisiting old vaginal topics: conversion of the Müllerian vagina and origin of the "sinus" vagina. *Int J Dev Biol* 53: 925–934.

Caloia DV, Morris H, Rahmani MR. 1998. Congenital transverse vaginal septum: vaginal hydrosonographic diagnosis. *J Ultrasound Med* 17: 261–264.

Carrington BM, Hricak H, Nuruddin RN, Secaf E, Laros RK, Jr., Hill EC. 1990. Müllerian duct anomalies: MR imaging evaluation. *Radiology* 176: 715–720.

Carson SA, Simpson JL, Malinak LR, Elias S, Gerbie AB, Buttram VC, Jr., Sarto GE. 1983. Heritable aspects of uterine anomalies. II. Genetic analysis of Müllerian aplasia. *Fertil Steril* 40: 86–90.

Casey RK, Damle LF, Gomez-Lobo V. 2013. Isolated fallopian tube torsion in pediatric and adolescent females: a retrospective review of 15 cases at a single institution. *J Pediatr Adolesc Gynecol* 26: 189–192.

Chan YY, Jayaprakasan K, Tan A, Thornton JG, Coomarasamy A, Raine-Fenning NJ. 2011a. Reproductive outcomes in women with

congenital uterine anomalies: a systematic review. *Ultrasound Obstet Gynecol* 38: 371–382.

Chan YY, Jayaprakasan K, Zamora J, Thornton JG, Raine-Fenning N, Coomarasamy A. 2011b. The prevalence of congenital uterine anomalies in unselected and high-risk populations: a systematic review. *Hum Reprod Update* 17: 761–771.

Chi IC, Farr G, Dominik R, Robinson N. 1990. Do retroverted uteri adversely affect insertions and performance of IUDs? *Contraception* 41: 495–506.

Cicekcibasi AE, Salbacak A, Seker M, Ziylan T, Buyukmumcu M, Uysal, II. 2002. The origin of gonadal arteries in human fetuses: anatomical variations. *Ann Anat* 184: 275–279.

Cicinelli E, Einer-Jensen N, Barba B, Luisi D, Alfonso R, Tartagni M. 2004a. Blood to the cornual area of the uterus is mainly supplied from the ovarian artery in the follicular phase and from the uterine artery in the luteal phase. *Hum Reprod* 19: 1003–1008.

Cicinelli E, Einer-Jensen N, Galantino P, Alfonso R, Nicoletti R. 2004b. The vascular cast of the human uterus: from anatomy to physiology. *Ann N Y Acad Sci* 1034: 19–26.

Clarke MJ, Mitchell PJ. 2003. Uterine arteriovenous malformation: a rare cause of uterine bleeding. Diagnosis and treatment. *Australas Radiol* 47: 302–305.

Coddington CC, Chandler PE, Smith GW. 1990. Accessory fallopian tube. A case report. *J Reprod Med* 35: 420–421.

Conroy RM, Molen RL. 1976. Scrotal "arteriocele" from iliac artery occlusion. *AJR Am J Roentgenol* 127: 670–672.

Crum CP, Nucci MR, Lee KR. 2011. *Diagnostic Gynecologic and Obstetric Pathology*, 2nd edition. Philadelphia: Elsevier/Saunders.

Cunningham FG, Williams JW. 2010. *Williams Obstetrics*, 23rd edition. New York: McGraw-Hill Medical.

Cura M, Cura A. 2009. What is the significance of ovarian vein reflux detected by computed tomography in patients with pelvic pain? *Clin Imaging* 33: 306–310.

Currarino G. 1986. Large prostatic utricles and related structures, urogenital sinus and other forms of urethrovaginal confluence. *J Urol* 136: 1270–1279.

Dahan MH, Burney R, Lathi R. 2006. Congenital interruption of the ampullary portion of the fallopian tube. *Fertil Steril* 85: 1820–1821.

Daw E. 1973. Duplication of the uterine tube. *Obstet Gynecol* 42: 137–138.

Del Vescovo R, Battisti S, Di Paola V, Piccolo CL, Cazzato RL, Sansoni I, Grasso RF, Zobel BB. 2012. Herlyn-Werner-Wunderlich syndrome: MRI findings, radiological guide (two cases and literature review), and differential diagnosis. *BMC Med Imaging* 12: 4.

Deutch TD, Abuhamad AZ. 2008. The role of 3-dimensional ultrasonography and magnetic resonance imaging in the diagnosis of müllerian duct anomalies: a review of the literature. *J Ultrasound Med* 27: 413–423.

Devi Wold AS, Pham N, Arici A. 2006. Anatomic factors in recurrent pregnancy loss. *Semin Reprod Med* 24: 25–32.

Dietrich JE, Hertweck SP, Bond S. 2007. Undescended ovaries: a clinical review. *J Pediatr Adolesc Gynecol* 20: 57–60.

Domany E, Gilad O, Shwarz M, Vulfsons S, Garty BZ. 2013. Imperforate hymen presenting as chronic low back pain. *Pediatrics* 132: e768–770.

Dueck A, Poenaru D, Jamieson MA, Kamal IK. 2001. Unilateral ovarian agenesis and fallopian tube maldescent. *Pediatr Surg Int* 17: 228–229.

Duncan PA, Shapiro LR, Stangel JJ, Klein RM, Addonizio JC. 1979. The MURCS association: Müllerian duct aplasia, renal aplasia, and cervicothoracic somite dysplasia. *J Pediatr* 95: 399–402.

Dungy CI, Aptekar RG, Cann HM. 1971. Hereditary hydrometrocolpos with polydactyly in infancy. *Pediatrics* 47: 138–141.

Falcone T, Hurd WW. 2007. *Clinical reproductive medicine and surgery*. Philadelphia: Mosby/Elsevier.

Farber M, Mitchell GW, Jr. 1979. Bicornuate uterus and partial atresia of the fallopian tube. *Am J Obstet Gynecol* 134: 881–884.

Felix W. 1912. Mesonephric arteries. *Man Human Embryol* 2: 820–825.

Figley MM, Muller RF. 1957. The arteries of the abdomen, pelvis, and thigh. I. Normal roentgenographic anatomy. II. Collateral circulation in obstructive arterial disease. *Am J Roentgenol Radium Ther Nucl Med* 77: 296–311.

Finan MA, Barre G. 2003. Bartholin's gland carcinoma, malignant melanoma and other rare tumours of the vulva. *Best Pract Res Clin Obstet Gynaecol* 17: 609–633.

Folch M, Pigem I, Konje JC. 2000. Müllerian agenesis: etiology, diagnosis, and management. *Obstet Gynecol Surv* 55: 644–649.

Fore SR, Hammond CB, Parker RT, Anderson EE. 1975. Urologic and genital anomalies in patients with congenital absence of the vagina. *Obstet Gynecol* 46: 410–416.

Frimberger D. 2011. Diagnosis and management of epispadias. *Semin Pediatr Surg* 20: 85–90.

Gandhi KR, Siddiqui AU, Wabale RN, Daimi SR. 2012. The accessory fallopian tube: A rare anomaly. *J Hum Reprod Sci* 5: 293–294.

Geifman-Holtzman O, Crane SS, Winderl L, Holmes M. 1997. Persistent urogenital sinus: prenatal diagnosis and pregnancy complications. *Am J Obstet Gynecol* 176: 709–711.

Geramizadeh B, Anbardar MH, Shakeri S. 2012. Clitoromegaly caused by cavernous hemangioma: A rare case report and review of the literature. *Urol Ann* 4: 175–177.

Ghi T, Casadio P, Kuleva M, Perrone AM, Savelli L, Giunchi S, Meriggiola MC, Gubbini G, Pilu G, Pelusi C, Pelusi G. 2009. Accuracy of three-dimensional ultrasound in diagnosis and classification of congenital uterine anomalies. *Fertil Steril* 92: 808–813.

Godinjak Z, Idrizbegovic E. 2008. Should diagnostic hysteroscopy be a routine procedure during diagnostic laparoscopy in infertile women? *Bosn J Basic Med Sci* 8: 44–47.

Gold MA, Schmidt RR, Parks N, Traum RE. 1997. Bilateral absence of the ovaries and distal fallopian tubes. A case report. *J Reprod Med* 42: 375–377.

Goldberg JM, Falcone T. 1999. Effect of diethylstilbestrol on reproductive function. *Fertil Steril* 72: 1–7.

Gomez-Jorge J, Keyoung A, Levy EB, Spies JB. 2003. Uterine artery anatomy relevant to uterine leiomyomata embolization. *Cardiovasc Intervent Radiol* 26: 522–527.

Goodman FR, Bacchelli C, Brady AF, Brueton LA, Fryns JP, Mortlock DP, Innis JW, Holmes LB, Donnenfeld AE, Feingold M, Beemer FA, Hennekam RC, Scambler PJ. 2000. Novel HOXA13 mutations and the phenotypic spectrum of hand-foot-genital syndrome. *Am J Hum Genet* 67: 197–202.

Gorgen H, Api M, Delikara N. 2002. Undescended fallopian tubes and ovaries: a rare incidental finding during an infertility investigation work up. *Acta Obstet Gynecol Scand* 81: 371–374.

Gorlin RJ, Chaudhry AP, Moss ML. 1960. Craniofacial dysostosis, patent ductus arteriosus, hypertrichosis, hypoplasia of labia majora, dental and eye anomalies: a new syndrome? *J Pediatr* 56: 778–785.

Gottlicher S. 1994. The labium tertium pudendi feminae. A prospective study of 1,180 patients. *Zentralbl Gynakol* 116: 419–421.

Grady RW, Mitchell ME. 2002. Management of epispadias. *Urol Clin North Am* 29: 349–360, vi.

Grant LA, Sala E, Griffin N. 2010. Congenital and acquired conditions of the vulva and vagina on magnetic resonance imaging: a pictorial review. *Semin Ultrasound CT MR* 31: 347–362.

Griesinger G, Dafopoulos K, Schultze-Mosgau A, Schroder A, Felberbaum R, Diedrich K. 2005. Mayer-Rokitansky-Kuster-Hauser syndrome associated with thrombocytopenia-absent radius syndrome. *Fertil Steril* 83: 452–454.

Griffin JE, Edwards C, Madden JD, Harrod MJ, Wilson JD. 1976. Congenital absence of the vagina. The Mayer-Rokitansky-Kuster-Hauser syndrome. *Ann Intern Med* 85: 224–236.

Grimbizis GF, Campo R. 2010. Congenital malformations of the female genital tract: the need for a new classification system. *Fertil Steril* 94: 401–407.

Grimbizis GF, Gordts S, Di Spiezio Sardo A, Brucker S, De Angelis C, Gergolet M, Li TC, Tanos V, Brolmann H, Gianaroli L, Campo R. 2013. The ESHRE/ESGE consensus on the classification of female genital tract congenital anomalies. *Hum Reprod* 28: 2032–2044.

Grivell RM, Reid KM, Mellor A. 2005. Uterine arteriovenous malformations: a review of the current literature. *Obstet Gynecol Surv* 60: 761–767.

Guerrier D, Mouchel T, Pasquier L, Pellerin I. 2006. The Mayer-Rokitansky-Kuster-Hauser syndrome (congenital absence of uterus and vagina): phenotypic manifestations and genetic approaches. *J Negat Results Biomed* 5: 1.

Haddad B, Louis-Sylvestre C, Poitout P, Paniel BJ. 1997. Longitudinal vaginal septum: a retrospective study of 202 cases. *Eur J Obstet Gynecol Reprod Biol* 74: 197–199.

Haylen BT. 2006. The retroverted uterus: ignored to date but core to prolapse. *Int Urogynecol J Pelvic Floor Dysfunct* 17: 555–558.

Haylen BT, McNally G, Ramsay P, Birrell W, Logan V. 2007. A standardised ultrasonic diagnosis and an accurate prevalence for the retroverted uterus in general gynaecology patients. *Aust N Z J Obstet Gynaecol* 47: 326–328.

Heinonen PK. 1997. Unicornuate uterus and rudimentary horn. *Fertil Steril* 68: 224–230.

Heinonen PK. 2006. Complete septate uterus with longitudinal vaginal septum. *Fertil Steril* 85: 700–705.

Heinonen PK, Saarikoski S, Pystynen P. 1982. Reproductive performance of women with uterine anomalies. An evaluation of 182 cases. *Acta Obstet Gynecol Scand* 61: 157–162.

Henne MB, Milki AA. 2004. Uterine position at real embryo transfer compared with mock embryo transfer. *Hum Reprod* 19: 570–572.

Herbst AL, Hubby MM, Azizi F, Makii MM. 1981. Reproductive and gynecologic surgical experience in diethylstilbestrol-exposed daughters. *Am J Obstet Gynecol* 141: 1019–1028.

Hibbard LT. 1985. Adnexal torsion. *Am J Obstet Gynecol* 152: 456–461.

Hickey M, Fraser IS. 2000. Clinical implications of disturbances of uterine vascular morphology and function. *Baillieres Best Pract Res Clin Obstet Gynaecol* 14: 937–951.

Hoenigl W. 1999. Asymptomatic uterine retroversion at 32 weeks' gestation: sonographic features. *J Ultrasound Med* 18: 795–798.

Homer HA, Li TC, Cooke ID. 2000. The septate uterus: a review of management and reproductive outcome. *Fertil Steril* 73: 1–14.

Isherwood PJ, Ibrahim ZH, Lieberman BA. 1990. Gamete intrafallopian transfer in women with accessory tubal ostia. *Br J Obstet Gynaecol* 97: 542–548.

Jessel RH, Laufer MR. 2013. Management of lower vaginal agenesis in a patient with unicornuate uterus. *J Pediatr Adolesc Gynecol* 26: e21–23.

Johnson LT, Lara-Torre E, Murchison A, Garcia EM. 2013. Large epidermal cyst of the clitoris: a novel diagnostic approach to assist in surgical removal. *J Pediatr Adolesc Gynecol* 26: e33–35.

Joki-Erkkila MM, Heinonen PK. 2003. Presenting and long-term clinical implications and fecundity in females with obstructing vaginal malformations. *J Pediatr Adolesc Gynecol* 16: 307–312.

Jones HW Jr, Mermut S. 1972. Familial occurrence of congenital absence of the vagina. *Am J Obstet Gynecol* 114: 1100–1101.

Jurkovic D, Gruboeck K, Tailor A, Nicolaides KH. 1997. Ultrasound screening for congenital uterine anomalies. *Br J Obstet Gynaecol* 104: 1320–1321.

Kamina P, Chansigaud JP. 1989. Functional anatomy of the pelvic veins in women. *Phlebologie* 42: 363–364.

Karlin G, Brock W, Rich M, Pena A. 1989. Persistent cloaca and phallic urethra. *J Urol* 142: 1056–1059.

Kasindye GU, Mwasunga AS, Fabian FM. 2012. Bilateral absence of ovarian artery in a Tanzanian female cadaver: a rare variation. *International Journal of Anatomical Variations* 5: 73–75.

Kauppila A. 1970. Uterine phlebography with venous compression. A clinical and roentgenological study. *Acta Obstet Gynecol Scand* 3: 1–66.

Kim WK, Yang SB, Goo DE, Kim YJ, Chang YW, Lee JM. 2013. Aberrant ovarian artery arising from the common iliac artery: case report. *Korean J Radiol* 14: 91–93.

Koff AK. 1933. Development of the vagina in the human fetus. *Contrib Embryol* 24: 59–91.

Kozlowski D, Luciano AA. 1995. Bilateral atresia of the proximal ampullary segment of the fallopian tubes. *J Am Assoc Gynecol Laparosc* 3: 99–101.

Kriplani A, Takkar D, Karak AK, Ammini AC. 1995. Unexplained absence of both fallopian tubes with ovary in the omentum. *Arch Gynecol Obstet* 256: 111–113.

Krissi H, Shalev J, Bar-Hava I, Langer R, Herman A, Kaplan B. 2001. Fallopian tube torsion: laparoscopic evaluation and treatment of a rare gynecological entity. *J Am Board Fam Pract* 14: 274–277.

Kruk-Jeromin J, Zielinski T. 2010. Hypertrophy of labia minora: pathomorphology and surgical treatment. *Ginekol Pol* 81: 298–302.

Kwon JH, Kim MD, Lee KH, Lee M, Lee MS, Won JY, Park SI, Lee do Y. 2013. Aberrant ovarian collateral originating from external iliac artery during uterine artery embolization. *Cardiovasc Intervent Radiol* 36: 269–271.

Lachman MF, Berman MM. 1991. The ectopic ovary. A case report and review of the literature. *Arch Pathol Lab Med* 115: 233–235.

Lapalorcia LM, Podda S, Campiglio G, Cordellini M. 2013. Labia majora labioplasty in HIV-related vaginal lipodystrophy: technique description and literature review. *Aesthetic Plast Surg* 37: 711–714.

Laufer MR. 2012. Abnormalities of the female genital tract. In: *Pediatric Surgery*, seventh edition (eds Coran AG, Adzick NS). Philadelphia, PA: Elsevier Mosby.

Levitt MA, Pena A. 2010. Cloacal malformations: lessons learned from 490 cases. *Semin Pediatr Surg* 19: 128–138.

Li S, Qayyum A, Coakley FV, Hricak H. 2000. Association of renal agenesis and Müllerian duct anomalies. *J Comput Assist Tomogr* 24: 829–834.

Lim MC, Park SJ, Kim SW, Lee BY, Lim JW, Lee JH, Huh CY. 2004. Two dermoid cysts developing in an accessory ovary and an eutopic ovary. *J Korean Med Sci* 19: 474–476.

Lin PC. 2004. Reproductive outcomes in women with uterine anomalies. *J Womens Health (Larchmt)* 13: 33–39.

Lin PC, Bhatnagar KP, Nettleton GS, Nakajima ST. 2002. Female genital anomalies affecting reproduction. *Fertil Steril* 78: 899–915.

Lineberry TD, Rodriguez H. 2000. Isolated torsion of the fallopian tube in an adolescent: a case report. *J Pediatr Adolesc Gynecol* 13: 135–137.

Lippert H, Pabst R. 1985. Arterial Variations In Man: Classification and Frequency. München: JF Bergmann.

Liu Q, Liu HQ, Jiang YY, Sun XB. 2013. Is unilateral uterine adnexa absence a congenital developmental abnormality or posteriority? Summary of 39 cases and literature review. *Arch Gynecol Obstet* 288: 555–561.

Lodi A. 1951. Clinical and statistical study on vaginal malformations at the Obstetrical and Gynecological Clinic in Milano 1906–50. *Ann Ostet Ginecol* 73: 1246–1285.

Love JN, Howell JM. 2000. Urinary retention resulting from incarceration of a retroverted, gravid uterus. *J Emerg Med* 19: 351–354.

Machnicki A, Grzybiak M. 1997. Selected cases of atypical course of renal and gonadal arteries and veins. *Folia Morphol (Warsz)* 56: 229–236.

Mahran M, Saleh AM. 1964. The microscopic anatomy of the hymen. *Anat Rec* 149: 313–318.

Mandava A, Prabhakar RR, Smitha S. 2012. OHVIRA syndrome (obstructed hemivagina and ipsilateral renal anomaly) with uterus didelphys, an unusual presentation. *J Pediatr Adolesc Gynecol* 25: e23–25.

Manolitsas T, Hurley V, Gilford E. 1994. Uterine arteriovenous malformation: a rare cause of uterine haemorrhage. *Aust N Z J Obstet Gynaecol* 34: 197–199.

Marcal L, Nothaft MA, Coelho F, Volpato R, Iyer R. 2011. Müllerian duct anomalies: MR imaging. *Abdom Imaging* 36: 756–764.

Marten K, Vosshenrich R, Funke M, Obenauer S, Baum F, Grabbe E. 2003. MRI in the evaluation of müllerian duct anomalies. *Clin Imaging* 27: 346–350.

Martinon-Torres F, Martinon-Sanchez JM, Martinon-Sanchez F. 2000. Clitoris and labia minora agenesis: an undescribed malformation. *Clin Genet* 58: 336–338.

Masson V, Fiquet Francois C, Rausky J, Mazouz Dorval S, Revol M. 2014. Clitoral epidermoid cyst causing clitoromegaly. A rare case report. *Ann Chir Plast Esthet* 59(2): 140–143.

Matson M, Nicholson A, Belli AM. 2000. Anastomoses of the ovarian and uterine arteries: a potential pitfall and cause of failure of uterine embolization. *Cardiovasc Intervent Radiol* 23: 393–396.

McCullough JB, Evans AT, Holley MP. 1992. Supernumerary or ectopic ovary: a case report. *Histopathology* 21: 582–583.

McKusick VA, Bauer RL, Koop CE, Scott RB. 1964. Hydrometrocolpos as a simply inherited malformation. *JAMA* 189: 813–816.

Merklin RJ, Michels NA. 1958. The variant renal and suprarenal blood supply with data on the inferior phrenic, ureteral and gonadal arteries: a statistical analysis based on 185 dissections and review of the literature. *J Int Coll Surg* 29: 41–76.

Morcel K, Camborieux L, Guerrier D. 2007. Mayer-Rokitansky-Kuster-Hauser (MRKH) syndrome. *Orphanet J Rare Dis* 2: 13.

Morino M, Hoshino M, Musha I. 2013. Obstructed hemivagina and ipsilateral renal agenesis with intestinal malrotation. *Pediatr Int* 55: e90–92.

Mottura AA. 2009. Labia majora hypertrophy. *Aesthetic Plast Surg* 33: 859–863.

Muppala H, Sengupta S, Martin JE. 2008. Unilateral absence of tube and ovary with renal agenesis and associated pyloric stenosis: communication. *Eur J Obstet Gynecol Reprod Biol* 137: 123.

Mwenda AS. 2013. Imperforate hymen: a rare cause of acute abdominal pain and tenesmus: case report and review of the literature. *Pan Afr Med J* 15: 28.

Myhre AK, Myklestad K, Adams JA. 2010. Changes in genital anatomy and microbiology in girls between age 6 and age 12 years: a longitudinal study. *J Pediatr Adolesc Gynecol* 23: 77–85.

Mylonas I, Hansch S, Markmann S, Bolz M, Friese K. 2003. Unilateral ovarian agenesis: report of three cases and review of the literature. *Arch Gynecol Obstet* 268: 57–60.

Nahum GG. 1998. Uterine anomalies. How common are they, and what is their distribution among subtypes? *J Reprod Med* 43: 877–887.

Narayanan R, Rajeev M. 2008. Duplication of the fallopian tube. *J Hum Reprod Sci* 1: 35–36.

Navarro C, Franklin RR, Valdes CT. 1990. Supernumerary ovary in association with endometriosis. *Fertil Steril* 54: 164–165.

Nawroth F, Nugent W, Ludwig M. 2006. Congenital partial atresia of the Fallopian tube. *Reprod Biomed Online* 12: 205–208.

Nazir Z, Rizvi RM, Qureshi RN, Khan ZS, Khan Z. 2006. Congenital vaginal obstructions: varied presentation and outcome. *Pediatr Surg Int* 22: 749–753.

Nevarez Bernal RA, Meraz Avila D. 2009. Fusion of the labia minora as a cause of urinary incontinence in a postmenopausal woman. A case report and literature review. *Ginecol Obstet Mex* 77: 287–290.

New MI. 1970. Male pseudohermaphroditism due to 17 alpha-hydroxylase deficiency. *J Clin Invest* 49: 1930–1941.

Nichols DH, Postoloff AV. 1951. Congenital ectopic ovary. *Am J Obstet Gynecol* 62: 195–198.

Nishiyama S, Hirota Y, Nishizawa H, Tada S, Udagawa Y. 2010. Bilateral interruption of mid-fallopian tubes and ovarian anomalies including ectopic ovary and cystic teratoma, a previously unreported combination. *J Minim Invasive Gynecol* 17: 534–537.

Notkovich H. 1956. Variations of the testicular and ovarian arteries in relation to the renal pedicle. *Surg Gynecol Obstet* 103: 487–495.

O'Connell HE, Sanjeevan KV, Hutson JM. 2005. Anatomy of the clitoris. *J Urol* 174: 1189–1195.

Olpin JD, Heilbrun M. 2010. Imaging of Müllerian duct anomalies. *Top Magn Reson Imaging* 21: 225–235.

Ombelet W, Grieten M, DeNeubourg P, Verswijvel G, Buekenhout L, Hinoul P, deJonge E. 2003a. Undescended ovary and unicornuate uterus: simplified diagnosis by the use of clomiphene citrate ovarian stimulation and magnetic resonance imaging (MRI). *Hum Reprod* 18: 858–862.

Ombelet W, Verswijvel G, de Jonge E. 2003b. Ectopic ovary and unicornuate uterus. *N Engl J Med* 348: 667–668.

Omole F, Simmons BJ, Hacker Y. 2003. Management of Bartholin's duct cyst and gland abscess. *Am Fam Physician* 68: 135–140.

Oppelt P, Renner SP, Brucker S, Strissel PL, Strick R, Oppelt PG, Doerr HG, Schott GE, Hucke J, Wallwiener D, Beckmann MW. 2005. The VCUAM (Vagina Cervix Uterus Adnex-associated Malformation) classification: a new classification for genital malformations. *Fertil Steril* 84: 1493–1497.

Oppelt P, Renner SP, Kellermann A, Brucker S, Hauser GA, Ludwig KS, Strissel PL, Strick R, Wallwiener D, Beckmann MW. 2006. Clinical

aspects of Mayer-Rokitansky-Kuester-Hauser syndrome: recommendations for clinical diagnosis and staging. *Hum Reprod* 21: 792–797.

Ouldamer L, Chraibi Z, Arbion F, Barillot I, Body G. 2013. Bartholin's gland carcinoma: epidemiology and therapeutic management. *Surg Oncol* 22: 117–122.

Ouyang Z, Liu P, Yu Y, Chen C, Song X, Liang B, Zhong G, Liu C, Li Z. 2012. Role of ovarian artery-to-uterine artery anastomoses in uterine artery embolization: initial anatomic and radiologic studies. *Surg Radiol Anat* 34: 737–741.

Park S, Ha SH, Kim KS. 2011. Long-term follow-up after feminizing genital reconstruction in patients with ambiguous genitalia and high vaginal confluence. *J Korean Med Sci* 26: 399–403.

Patankar SP, Kalrao V, Patankar SS. 2004. Mayer-Rokitansky syndrome and anorectal malformation. *Indian J Pediatr* 71: 1133–1135.

Paternoster DM, Costantini W, Uglietti A, Vasile C, Bocconi L. 1998. Congenital or torsion–induced absence of Fallopian tubes. Two case reports. *Minerva Ginecol* 50: 191–194.

Pelage JP, Le Dref O, Soyer P, Jacob D, Kardache M, Dahan H, Lassau JP, Rymer R. 1999. Arterial anatomy of the female genital tract: variations and relevance to transcatheter embolization of the uterus. *AJR Am J Roentgenol* 172: 989–994.

Petrozza JC, Gray MR, Davis AJ, Reindollar RH. 1997. Congenital absence of the uterus and vagina is not commonly transmitted as a dominant genetic trait: outcomes of surrogate pregnancies. *Fertil Steril* 67: 387–389.

Petru B, Elena S, Dan I, Constantin D. 2007. The morphology and the surgical importance of the gonadal arteries originating from the renal artery. *Surg Radiol Anat* 29: 367–371.

Phalgunan V, Mugunthan N, Rani DR, Anbalagan J. 2012. A study of renal and gonadal vein variations. *National Journal of Clinical Anatomy* 1: 125–128.

Pittock ST, Babovic-Vuksanovic D, Lteif A. 2005. Mayer-Rokitansky-Kuster-Hauser anomaly and its associated malformations. *Am J Med Genet A* 135: 314–316.

Pizzo A, Lagana AS, Sturlese E, Retto G, Retto A, De Dominici R, Puzzolo D. 2013. Mayer-Rokitansky-Kuster-Hauser syndrome: embryology, genetics and clinical and surgical treatment. *ISRN Obstet Gynecol* 2013: 628717.

Podesta M, Urcullo J. 2008. Perineal mobilization of the common urogenital sinus for surgical correction of high urethrovaginal confluence in patients with intersex disorders. *J Pediatr Urol* 4: 352–358.

Pokorny SF, Murphy JG, Preminger MK. 1998. Circumferential hymen elasticity. A marker of physiologic maturity. *J Reprod Med* 43: 943–948.

Polasek PM, Erickson LD, Stanhope CR. 1995. Transverse vaginal septum associated with tubal atresia. *Mayo Clin Proc* 70: 965–968.

Powell DM, Newman KD, Randolph J. 1995. A proposed classification of vaginal anomalies and their surgical correction. *J Pediatr Surg* 30: 271–276.

Poznanski AK, Stern AM, Gall JC, Jr. 1970. Radiographic findings in the hand-foot-uterus syndrome (HFUS). *Radiology* 95: 129–134.

Pundir J, Auld BJ. 2008. A review of the management of diseases of the Bartholin's gland. *J Obstet Gynaecol* 28: 161–165.

Rackow BW, Arici A. 2007. Reproductive performance of women with müllerian anomalies. *Curr Opin Obstet Gynecol* 19: 229–237.

Raga F, Bauset C, Remohi J, Bonilla-Musoles F, Simon C, Pellicer A. 1997. Reproductive impact of congenital Müllerian anomalies. *Hum Reprod* 12: 2277–2281.

Rahman HA, Dong K, Yamadori T. 1993. Unique course of the ovarian artery associated with other variations. *J Anat* 182(2): 287–290.

Rapisarda G, Pappalardo EM, Arancio A, La Greca M. 2009. Unilateral ovarian and fallopian tube agenesis. *Arch Gynecol Obstet* 280: 849–850.

Ravery V, Cussenot O, Desgrandchamps F, Teillac P, Martin-Bouyer Y, Lassau JP, Le Duc A. 1993. Variations in arterial blood supply and the risk of hemorrhage during percutaneous treatment of lesions of the pelviureteral junction obstruction: report of a case of testicular artery arising from an inferior polar renal artery. *Surg Radiol Anat* 15: 355–359.

Razavi MK, Wolanske KA, Hwang GL, Sze DY, Kee ST, Dake MD. 2002. Angiographic classification of ovarian artery-to-uterine artery anastomoses: initial observations in uterine fibroid embolization. *Radiology* 224: 707–712.

Reddy J, Laufer MR. 2010. Hypertrophic labia minora. *J Pediatr Adolesc Gynecol* 23: 3–6.

Reed MH, Griscom NT. 1973. Hydrometrocolpos in infancy. *Am J Roentgenol Radium Ther Nucl Med* 118: 1–13.

Reinhold C, Hricak H, Forstner R, Ascher SM, Bret PM, Meyer WR, Semelka RC. 1997. Primary amenorrhea: evaluation with MR imaging. *Radiology* 203: 383–390.

Ribeiro SC, Yamakami LY, Tormena RA, Pinheiro Wda S, Almeida JA, Baracat EC. 2010. Septate uterus with cervical duplication and longitudinal vaginal septum. *Rev Assoc Med Bras* 56: 254–256.

Rock JA, Zacur HA, Dlugi AM, Jones HW Jr, TeLinde RW. 1982. Pregnancy success following surgical correction of imperforate hymen and complete transverse vaginal septum. *Obstet Gynecol* 59: 448–451.

Rock JA, Parmley T, Murphy AA, Jones HW, Jr. 1986. Malposition of the ovary associated with uterine anomalies. *Fertil Steril* 45: 561–563.

Rosenberg HK, Sherman NH, Tarry WF, Duckett JW, Snyder HM. 1986. Mayer-Rokitansky-Kuster-Hauser syndrome: US aid to diagnosis. *Radiology* 161: 815–819.

Roth LM, Davis MM, Sutton GP. 1996. Steroid cell tumor of the broad ligament arising in an accessory ovary. *Arch Pathol Lab Med* 120: 405–409.

Rowley WN. 1948. Uterine anomaly; duplication of uterus, three tubes and three ovaries; report of a case. *Ann Surg* 127: 676–680.

Rudoni S, Petit JM, Damatte-Fauchery C, Vaillant G, Verges B, Brun JM. 1999. Breast agenesis and hypoplasia of the homolateral labia majora in a girl with trisomy: a fortuitous association? *Arch Pediatr* 6: 1130–1131.

Ruggeri G, Gargano T, Antonellini C, Carlini V, Randi B, Destro F, Lima M. 2012. Vaginal malformations: a proposed classification based on embryological, anatomical and clinical criteria and their surgical management (an analysis of 167 cases). *Pediatr Surg Int* 28: 797–803.

Sadler TW, Langman J. 2010. *Langman's Medical Embryology*, 11th ed. Philadelphia: Lippincott William & Wilkins.

Saraiya PV, Chang TC, Pelage JP, Spies JB. 2002. Uterine artery replacement by the round ligament artery: an anatomic variant discovered during uterine artery embolization for leiomyomata. *J Vasc Interv Radiol* 13: 939–941.

Saravelos SH, Cocksedge KA, Li TC. 2008. Prevalence and diagnosis of congenital uterine anomalies in women with reproductive failure: a critical appraisal. *Hum Reprod Update* 14: 415–429.

Sarto GE, Simpson JL. 1978. Abnormalities of the Müllerian and Wolffian duct systems. *Birth Defects Orig Artic Ser* 14: 37–54.

Scarsbrook AF, Moore NR. 2003. MRI appearances of müllerian duct abnormalities. *Clin Radiol* 58: 747–754.

Seoud MA, Khayyat H, Mufarrij IK. 1987. Ectopic pregnancy in an undescended fallopian tube: an unusual presentation. *Obstet Gynecol* 69: 455–457.

Shoja MM, Tubbs RS, Shakeri AB, Oakes WJ. 2007. Origins of the gonadal artery: embryologic implications. *Clin Anat* 20: 428–432.

Silva PD, Glasser KE, Virata RL. 1995. Spontaneously acquired, unilateral absence of the adnexa. A case report. *J Reprod Med* 40: 63–64.

Silver RK, MacGregor SN, Muhlbach LH, Kambich MP, Ragin A. 1994. A comparison of pregnancy loss between transcervical and transabdominal chorionic villus sampling. *Obstet Gynecol* 83: 657–660.

Singh G, Ng YK, Bay BH. 1998. Bilateral accessory renal arteries associated with some anomalies of the ovarian arteries: a case study. *Clin Anat* 11: 417–420.

Singh S, Singh P, Singh RJ. 2010. Persistent urogenital sinus. *J Anat Soc India* 59: 242–244.

Sirisena LA. 1978. Unexplained absence of an ovary and uterine tube. *Postgrad Med J* 54: 423–424.

Sivanesaratnam V. 1986. Unexplained unilateral absence of ovary and fallopian tube. *Eur J Obstet Gynecol Reprod Biol* 22: 103–105.

Smalbraak I, Bleker OP, Schutte MF, Treffers PE. 1991. Incarceration of the retroverted gravid uterus: a report of four cases. *Eur J Obstet Gynecol Reprod Biol* 39: 151–155.

Smith NA, Laufer MR. 2007. Obstructed hemivagina and ipsilateral renal anomaly (OHVIRA) syndrome: management and follow-up. *Fertil Steril* 87: 918–922.

Stampe Sorensen S. 1988. Estimated prevalence of müllerian anomalies. *Acta Obstet Gynecol Scand* 67: 441–445.

Standring S, Gray H. 2008. *Gray's Anatomy: The Anatomical Basis of Clinical Practice*, 40th ed. Edinburgh: Churchill Livingstone/Elsevier.

Stassart JP, Nagel TC, Prem KA, Phipps WR. 1992. Uterus didelphys, obstructed hemivagina, and ipsilateral renal agenesis: the University of Minnesota experience. *Fertil Steril* 57: 756–761.

Stephenson SR. 2012. *Diagnostic Medical Sonography: Obstetrics and Gynecology*, 3rd edition. Philadelphia: Wolters Kluwer Health/Lippincott Williams & Wilkins.

Stern AM, Gall JC Jr, Perry BL, Stimson CW, Weitkamp LR, Poznanski AK. 1970. The hand-food-uterus syndrome: a new hereditary disorder characterized by hand and foot dysplasia, dermatoglyphic abnormalities, and partial duplication of the female genital tract. *J Pediatr* 77: 109–116.

Stewart ST. 2011. Hymenal characteristics in girls with and without a history of sexual abuse. *J Child Sex Abus* 20: 521–536.

Stillman RJ, Asarkof N. 1985. Association between müllerian duct malformations and Asherman syndrome in infertile women. *Obstet Gynecol* 65: 673–677.

Stones RW. 2003. Pelvic vascular congestion: half a century later. *Clin Obstet Gynecol* 46: 831–836.

Strubbe EH, Thijn CJ, Willemsen WN, Lappohn R. 1987. Evaluation of radiographic abnormalities of the hand in patients with the Mayer-Rokitansky-Kuster-Hauser syndrome. *Skeletal Radiol* 16: 227–231.

Strubbe EH, Willemsen WN, Lemmens JA, Thijn CJ, Rolland R. 1993. Maye-Rokitansky-Kuster-Hauser syndrome: distinction between two forms based on excretory urographic, sonographic, and laparoscopic findings. *AJR Am J Roentgenol* 160: 331–334.

Strubbe EH, Cremers CW, Dikkers FG, Willemsen WN. 1994. Hearing loss and the Mayer-Rokitansky-Kuster-Hauser syndrome. *Am J Otol* 15: 431–436.

Stukus KS, Zuckerbraun NS. 2009. Review of the prepubertal gynecologic examination: techniques and anatomic variation. *Clin Ped Emerg Med.* 10: 3–9

Suh BY, Kalan MJ. 2008. Septate uterus with left fallopian tube hypoplasia and ipsilateral ovarian agenesis. *J Assist Reprod Genet* 25: 567–569.

Tahirovic H, Toromanovic A. 2012. Adhesion of the labia minora in girls: a common disorder that is rarely considered. *J Pediatr Endocrinol Metab* 25: 631–632.

Takagi H, Matsunami K, Imai A. 2010. Uterovaginal duplication with blind hemivagina and ipsilateral renal agenesis: review of unusual presentation. *J Obstet Gynaecol* 30: 350–353.

Terayama H, Yi SQ, Naito M, Qu N, Hirai S, Kitaoka M, Iimura A, Moriyama H, Steinke H, Itoh M. 2008. Right gonadal arteries passing dorsally to the inferior vena cava: embryological hypotheses. *Surg Radiol Anat* 30: 657–661.

Theron JP. 1963. The retroverted uterus. An evaluation of the Moschcowitz operation. *S Afr Med J* 37: 910–914.

Thonell SH, Kam A, Resnick G. 1993. Torsion of accessory fallopian tube: ultrasound findings in two premenarchal girls. *Australas Radiol* 37: 393–395.

Timmerman D, Wauters J, Van Calenbergh S, Van Schoubroeck D, Maleux G, Van Den Bosch T, Spitz B. 2003. Color Doppler imaging is a valuable tool for the diagnosis and management of uterine vascular malformations. *Ultrasound Obstet Gynecol* 21: 570–577.

Tolete-Velcek F, Hansbrough F, Kugaczewski J, Coren CV, Klotz DH, Price AF, Laungani G, Kottmeier PK. 1989. Utero vaginal malformations: a trap for the unsuspecting surgeon. *J Pediatr Surg* 24: 736–740.

Troiano RN, McCarthy SM. 2004. Müllerian duct anomalies: imaging and clinical issues. *Radiology* 233: 19–34.

Van Eyk N, Allen L, Giesbrecht E, Jamieson MA, Kives S, Morris M, Ornstein M, Fleming N. 2009. Pediatric vulvovaginal disorders: a diagnostic approach and review of the literature. *J Obstet Gynaecol Can* 31: 850–862.

Van Voorhis BJ, Dokras A, Syrop CH. 2000. Bilateral undescended ovaries: association with infertility and treatment with IVF. *Fertil Steril* 74: 1041–1043.

Vendeland LL, Shehadeh L. 2000. Incidental finding of an accessory ovary in a 16-year-old at laparoscopy. A case report. *J Reprod Med* 45: 435–438.

Ventolini G. 2013. Vaginal septum in adolescents: clinical implications. J Genit Syst Disor S1, doi: 10.4172/2325-9728.S1-e002.

Venyo AK. 1993. Supernumerary fallopian tubes. *Br J Obstet Gynaecol* 100: 183.

Verkauf BS, Bernhisel MA. 1996. Ovarian maldescent. *Fertil Steril* 65: 189–192.

Vitale V, Cigliano B, Vallone G. 2013. Imperforate hymen causing congenital hydrometrocolpos. *J Ultrasound* 16: 37–39.

Watrowski R, Jager C, Gerber M, Klein C. 2013. Hymenal anomalies in twins: review of the literature and case report. *Eur J Pediatr* 173(11): 1407–1412.

Wein AJ, Kavoussi LR, Campbell MF. 2012. *Campbell–Walsh Urology*, tenth edition. Philadelphia, PA: Elsevier Saunders.

Weinberger MW, Julian TM. 1995. Voiding dysfunction and incontinence caused by uterine retroversion. A case report. *J Reprod Med* 40: 387–390.

Weiss A, Shalev E, Romano S. 2005. Hysteroscopy may be justified after two miscarriages. *Hum Reprod* 20: 2628–2631.

Wenof M, Reyniak JV, Novendstern J, Castadot MJ. 1979. Transverse vaginal septum. *Obstet Gynecol* 54: 60–64.

Wharton LR. 1959. Two cases of supernumerary ovary and one of accessory ovary, with an analysis of previously reported cases. *Am J Obstet Gynecol* 78: 1101–1119.

Wunsch L, Holterhus PM, Wessel L, Hiort O. 2012. Patients with disorders of sex development (DSD) at risk of gonadal tumour development: management based on laparoscopic biopsy and molecular diagnosis. *BJU Int* 110: E958–965.

Yazawa H, Yabe M, Endo S, Hayashi S. 2010. A case of congenital unilateral partial absence of fallopian tube. *Fukushima J Med Sci* 56: 44–49.

Zaitoon MM, Florentin H. 1982. Crossed renal ectopia with unilateral agenesis of fallopian tube and ovary. *J Urol* 128: 111.

Zimmer EZ, Blazer S, Blumenfeld Z, Bronshtein M. 2012. Fetal transient clitoromegaly and transient hypertrophy of the labia minora in early and mid pregnancy. *J Ultrasound Med* 31: 409–415.

Zolcinski A, Robaczynski J. 1964. Endometriosis in a supernumerary oviduct. *Ginekol Pol* 35: 135–140.

Zolcinski A, Robaczynski J, Ziolkowski M. 1964. On accessory tubes and accessory tubal ostia. *Zentralbl Gynakol* 86: 548–559.

117 Placenta and umbilical cord

Sedat Develi
Gulhane Military Medical Academy, Ankara, Turkey

Placenta

The placenta is a discoid organ that connects the fetus with the maternal uterine wall in order to carry out metabolic functions such as taking in oxygen and nutrients or elimination of metabolic wastes.

Size and weight

The mean diameter of the full-term placenta is 22 cm, the mean thickness is 2.5 cm, and the mean weight is 470 g (Baergen and Benirschke 2005).

In some individuals, the placenta may be smaller than normal (e.g., due to maternal chronic hypertension) or excessively larger than normal (e.g., due to hydrops fetalis; Garcia-Diaz et al. 2012; Taweevisit and Thorner 2012; Nahar et al. 2013; Salge et al. 2013).

Appearance

In 90% of individuals a discoid or oval-shaped placenta is seen (Baergen and Benirschke 2005). Abnormal shapes are seen in 10% of women and include notched or lobed placentas, membranous placentas, and other rare variants.

- Notched placenta: there is a notch within the placenta dividing it into connected lobes. This type is called placenta bipartita (Drechsler 1959; Kao and Sun 1962).
- Lobed placenta: placental membranes separate the placenta into approximately equal lobes. If the placenta is separated into two lobes, this type is called placenta bilobata or bilobed placenta (Kleine 1956; Kikuchi et al. 2011). A prevalence of 2–8% has been reported (Baergen and Benirschke 2005). More than two lobes is called a multilobed placenta (Morales-Rosello and Peralta Llorens 2012). Implantation on areas of poorly perfused uterine cavity (such as leiomyomas, previous operational scars) is thought to be associated with the pathogenesis of abnormal lobulation. Insufficient perfusion leads to atrophy and therefore multilobulation of the placenta (Baergen and Benirschke 2005).
- In addition, in some cases undeveloped areas without lobulation may be found on the placenta. Only fetal membranes cover these deficient areas. This type of placenta is called placenta fenestrata (Kleine 1956; Linhart et al. 2004).
- Placenta membranecea: this term is also known as placenta diffusa. The placental tissue is very thin (approximately 1 cm) and lies almost along the uterine cavity. It is a rare condition and its etiology is unknown (Greenberg et al. 1991; Dinh et al. 1992; Ekoukou et al. 1995; Baergen and Benirschke 2005; Pereira et al. 2013; Ravangard et al. 2013).
- Zonary or ring-shaped placenta: a placenta with a ring shape is thought to be derived from placenta previa with focal atrophy (Steemers et al. 1995; Baergen and Benirschke 2005).
- Placenta circumvallate and circummarginate: normally fetal membranes insert on the edges of the placenta; in some individuals however, the fetal membranes insert on the inner parts from the margin of the placenta. If there is a peripheral ridge or plication on the membranes, this is referred to as placenta circumvallate. If there is no peripheric ridge on the membranes, this is called placenta circummarginate. The two types may combine; placenta circumvallate is seen in 1–6.5% of placentas and placenta circummarginate is seen in 25% of placentas (Wentworth 1968; Benson and Fujikura 1969; Takeda et al. 1990; Baergen and Benirschke 2005; Keski-Nisula et al. 2011; Arlicot et al. 2012).

Number of placentas

Occasionally, more than one placenta may be found. This condition is called placenta succenturiata or accessory placenta (Ross 1953; Brodzinski 1966; Jongkolsiri and Manotaya 2009). Accessory placentas may be single or multiple and attached to the main placenta by membranes and vessels. An incidence of 5–6% has been reported. The umbilical cord commonly connects to the main placenta (Baergen and Benirschke 2005).

Umbilical cord attachment

In general, the umbilical cord attaches to the center of the placenta. In 7% of placentas the umbilical cord is found to be attached to the edge of the placenta; this type is called battledore or eccentric placenta (Jennings 1955; Averback and Wiglesworth 1977; Baergen and Benirschke 2005). In 1% of placentas, the umbilical cord is inserted onto membranes and vessels run on the membranes for some distance before entering the placenta. This type is called placenta velamentosa (Sepulveda et al. 2003; Baergen and Benirschke 2005).

Bergman's Comprehensive Encyclopedia of Human Anatomic Variation, First Edition. Edited by R. Shane Tubbs, Mohammadali M. Shoja and Marios Loukas.
© 2016 John Wiley & Sons, Inc. Published 2016 by John Wiley & Sons, Inc.

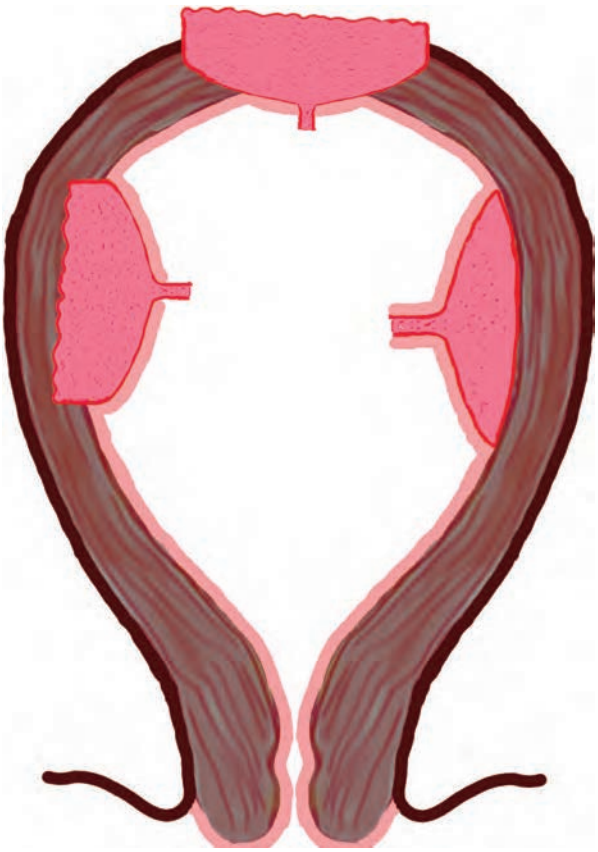

Figure 117.1 Variants of placental attachment to uterine wall. Placenta accreta is depicted on the right side, placenta increta on the left side, and placenta percreta in the middle. (Adapted from Kim et al. Prenatal diagnosis of placenta accreta with pathologic correlation. RadioGraphics 1998;18:237-242 with permission).

Placental attachment to the uterine wall

In normal implantation, chorionic villi invade the decidua. If chorionic villi invade deeper and implant on the myometrium, this variant is called placenta accrete; if chorionic villi implant into the myometrium this variant is called placenta increta; and if choroinic villi invade the whole uterine wall, this is called placenta percreta (Fig. 117.1). A prevalence of 1 in 2500 deliveries has been reported and 75% of these cases are placenta accreta (American College of Obstetricians and Gynecologists 2002; Warshak et al. 2006; Elsayes et al. 2009).

Umbilical cord

The umbilical cord connects the developing fetus to the placenta. Its mean length and diameter is 55 cm and 1–1.5 cm, respectively. Normally, two umbilical arteries and one umbilical vein are seen within the cord (Baergen and Benirschke 2005).

A single umbilical artery or a second umbilical vein are rare conditions. An incidence of 0.2% for a single umbilical artery has been reported (Ogino et al. 1985). A single umbilical artery is seen more often in twins. In some genetic disorders such as trisomy 16, a single umbilical artery also is noted. Supernumerary umbilical veins may accompany the single umbilical artery and a classification has been proposed. Four subtypes of a single umbilical artery are described (Persutte and Hobbins 1995).

- Type 1 is the most common variant and one umbilical artey (allontoic origin) and one vein (derived from left umbilical vein) are noted (98% of the cases).
- In type 2 (1.5% of the cases), there is one umbilical artery (vitelline origin) and one vein (derived from left umbilical vein).
- In type 3, one artery (allantoic origin) and two veins (one from left and one from the right umbilical vein) are noted.
- In type 4, one artery and one vein are found. The vein is derived from the right umbilical vein (Persutte and Hobbins 1995).

In addition, supernumerary umbilical vessels (four vessel cords) are rare conditions (Paize and Yoxall 2006; Karatza et al. 2011).

References

American College of Obstetricians and Gynecologists A. 2002. ACOG committee opinion. Placenta accreta. Number 266, January 2002. *Int J Gynaecol Obstet* 77: 77–78.

Arlicot C, Herve P, Simon E, Perrotin F. 2012. Three-dimensional surface rendering of the chorionic placental plate: the "tire" sign for the diagnosis of a circumvallate placenta. *J Ultrasound Med* 31: 340–341.

Averback P, Wiglesworth FW. 1977. Monochorionic, monoamniotic, double-battledore placenta with stillbirth and postpartum cerebellar syndrome. *Am J Obstet Gynecol* 128: 697–699.

Baergen RN, Benirschke K. 2005. *Manual of Benirschke and Kaufmann's Pathology of the Human Placenta*. New York: Springer.

Benson RC, Fujikura T. 1969. Circumvallate and circummarginate placenta. Unimportant clinical entities. *Obstet Gynecol* 34: 799–804.

Brodzinski W. 1966. Rare case of placenta with multiple accessory placentae. *Wiad Lek* 19: 501–502.

Dinh TV, Bedi DG, Salinas J. 1992. Placenta membranacea, previa and accreta. A case report. *J Reprod Med* 37: 97–99.

Drechsler W. 1959. A rare shape of the placenta; placenta bipartita, bilobata, dimidiata, duplex. *Dtsch Gesundheitsw* 14: 108–111.

Ekoukou D, Ng Wing Tin L, Nere MB, Bourdet O, Elalaoui Y, Bazin C. 1995. Placenta membranacea. Review of the literature, a case report. *J Gynecol Obstet Biol Reprod (Paris)* 24: 189–193.

Elsayes KM, Trout AT, Friedkin AM, Liu PS, Bude RO, Platt JF, Menias CO. 2009. Imaging of the placenta: a multimodality pictorial review. *Radiographics* 29: 1371–1391.

Garcia-Diaz L, Carreto P, Costa-Pereira S, Antinolo G. 2012. Prenatal management and perinatal outcome in giant placental chorioangioma complicated with hydrops fetalis, fetal anemia and maternal mirror syndrome. *BMC Pregnancy Childbirth* 12: 72.

Greenberg JA, Sorem KA, Shifren JL, Riley LE. 1991. Placenta membranacea with placenta increta: a case report and literature review. *Obstet Gynecol* 78: 512–514.

Jennings DR. 1955. The battledore placenta; a comparison of treatment with ergot after and before its delivery. *N Z Med J* 54: 709–710.

Jongkolsiri P, Manotaya S. 2009. Placental cord drainage and the effect on the duration of third stage labour, a randomized controlled trial. *J Med Assoc Thai* 92: 457–460.

Kao MM, Sun CS. 1962. Case report of placenta bipartita associated with velamentous insertion of the cord. *Tsa Chih Gaoxiong Yi Xue Yuan Tong Xue Hui* 61: 1153–1156.

Karatza A, Tsamandas A, Varvarigou A, Davlouros P, Pavlou V, Mantagos S. 2011. Supernumerary umbilical vein in a hydropic neonate with hypertrophic cardiomyopathy. *Fetal Pediatr Pathol* 30: 173–176.

Keski-Nisula L, Heiskanen P, Heinonen S. 2011. Extra-membranous pregnancy, prolonged ruptured membranes and circumvallate placenta. *Acta Obstet Gynecol Scand* 90: 1170–1171.

Kikuchi A, Uemura R, Serikawa T, Takakuwa K, Tanaka K. 2011. Clinical significances of magnetic resonance imaging in prenatal diagnosis of vasa previa in a woman with bilobed placentas. *J Obstet Gynaecol Res* 37: 75–78.

Kim H, Hill MC, Winick AB, et al. 1998. Prenatal diagnosis of placenta accreta with pathologic correlation. *Radiographics* 18: 237–242.

Kleine HO. 1956. Unusual placenta forms; annular placenta, bilobed placenta and placenta fenestrata. *Zentralbl Gynakol* 78: 2029–2032.

Linhart JM, Grafe MR, Saade GR, Velagaleti GV. 2004. Sonographic, pathologic and karyotypic findings in a rare case of placenta fenestrata. *Fetal Diagn Ther* 19: 479–482.

Morales-Rosello J, Peralta Llorens N. 2012. Doppler impedance changes at the fetal brain vessels in a pregnancy affected with a multiple combination of uteroplacental anomalies. *Case Rep Med* 2012: 293156.

Nahar L, Nahar K, Hossain MI, Jahan S, Rahman MM. 2013. Placental changes in pregnancy induced hypertension. *Mymensingh Med J* 22: 684–693.

Ogino M, Jimbo T, Mizuno M, Sakamoto S. 1985. Study on the histopathological abnormalities of the umbilical cord. *Nihon Sanka Fujinka Gakkai Zasshi* 37: 329–335.

Paize F, Yoxall CW. 2006. Supernumerary umbilical vein demonstrated by radiography of a 27-week-gestation neonate. *Pediatr Radiol* 36: 570.

Pereira N, Yao R, Guilfoil DS, Richard SD, Plante LA. 2013. Placenta membranacea with placenta accreta: radiologic diagnosis and clinical implications. *Prenat Diagn* 33: 1293–1296.

Persutte WH, Hobbins J. 1995. Single umbilical artery: a clinical enigma in modern prenatal diagnosis. *Ultrasound Obstet Gynecol* 6: 216–229.

Ravangard SF, Henderson K, Fuller K. 2013. Placenta membranacea. *Arch Gynecol Obstet* 288: 709–712.

Ross WF. 1953. Placenta succenturiata as a cause of ante-partum haemorrhage. *S Afr Med J* 27: 773–774.

Salge AK, Xavier RM, Ramalho WS, Rocha EL, Coelho AS, Guimaraes JV, Siqueira KM, Abdalla DR, Michelin MA, Murta EF. 2013. Placental and umbilical cord macroscopic changes associated with fetal and maternal events in the hypertensive disorders of pregnancy. *Clin Exp Obstet Gynecol* 40: 198–202.

Sepulveda W, Rojas I, Robert JA, Schnapp C, Alcalde JL. 2003. Prenatal detection of velamentous insertion of the umbilical cord: a prospective color Doppler ultrasound study. *Ultrasound Obstet Gynecol* 21: 564–569.

Steemers NY, De Rop C, Van Assche A. 1995. Zonary placenta. *Int J Gynaecol Obstet* 51: 251–253.

Takeda S, Baba K, Kojima T, Kinoshita K, Satoh K, Sakamoto S. 1990. Ultrasonographic monitoring of the placenta in patients with bleeding during the first and second trimesters. *Asia Oceania J Obstet Gynaecol* 16: 211–218.

Taweevisit M, Thorner PS. 2012. Peripheral villous stromal hyperplasia: a distinctive placental lesion in hemoglobin bart hydrops fetalis. *Pediatr Dev Pathol* 15: 345–351.

Warshak CR, Eskander R, Hull AD, Scioscia AL, Mattrey RF, Benirschke K, Resnik R. 2006. Accuracy of ultrasonography and magnetic resonance imaging in the diagnosis of placenta accreta. *Obstet Gynecol* 108: 573–581.

Wentworth P. 1968. Circumvallate and circummarginate placentas. Their incidence and clinical significance. *Am J Obstet Gynecol* 102: 44–47.

118 Breast

Matthew Rubacha
St George's University, School of Medicine, St Georges, Grenada

The development of mammary glands is a hallmark that separates mammals from all other living creatures and is believed to have evolved over 300 million years ago (Oftedal 2002). This defining feature is often referred to as modified sweat glands, which function as secondary reproductive glands. Breasts are organized secretory organs formed from the complex arrangement of epithelial, adipose, vascular, fibroblast, and immune cells which are most commonly found as a single pair on the anterior chest wall in humans. They function in lactation in postpartum females; however, they remain functionless and undeveloped in males (DeCherney et al. 2007).

Development

Early in embryological development, the beginning of breast tissue develops from two ventral ectodermal streaks referred to as the "mammary ridges" or "milk lines". First seen at the fifth or sixth week of development, the ectodermal ridges extend from the axilla to inguinal regions and begin to grow into the underlying mesoderm to form a tissue bud (Bland et al. 1998). In other mammals paired breasts will develop form this growth; in humans, however, most of the ridge will disappear with the exception of a small portion of precursor in the pectoral region, which will form the definitive breast. Failure of involution of part of the milk line can lead to the development of accessory breast tissue (polymastia) or accessory nipples (polythelia) (Hunt et al. 2010).

Once the development of the primary bud has been initiated, 15–20 secondary buds begin to form and chords of epithelium extend into the underlying mesoderm. Next, the major lactiferous ducts develop and open into a shallow mammary pit. Proliferation of the underlying mesenchyme during infancy transforms this pit into a nipple. Failure to complete this process can result in an inverted nipple, seen in approximately 4% of infants (Moore et al. 1998). It is the epithelial–mesenchyme interaction that directs the development of breast tissue and ultimately determines the final positioning of the mammary glands at birth (Macias and Hinck 2012).

Both male and female infants undergo a similar process in early breast development and at birth the mammary glands will contain only the major ducts. Breast enlargement and the secretion of so-called "witch's milk" may occur as an early symptom of the effect of maternal hormones that have crossed the placenta into fetal circulation. Ultimately, this growth will regress shortly after birth and the female breast tissue will remain undeveloped until adolescence (Seltzer 1994).

Anatomy

The adult female breast extends from sternum to anterior axillary line in the lateral dimension and from approximately from the second rib superiorly to the sixth rib inferiorly. The deep border is formed by the facia of pectoralis major, serratus anterior, and the external oblique (Hunt et al. 2010). In response to estrogen and progesterone released from the ovaries at puberty, the epithelial and connective tissue begin to proliferate causing the breast to enlarge; they remain functionally undeveloped until pregnancy, however (Moore et al. 1998). Generally, the breast is composed of 15–20 lobes each divided into several lobules. The intervening connective tissue, known as Cooper's ligaments, provides suspensory support by inserting into the dermis (Hunt et al. 2010). The tail of Spence is generally a triangular section of breast tissue that extends superolaterally into the axilla where it enters the axillary fascia, ultimately terminating in the region of the axillary lymphatics, vessels, and nerves (DeCherney et al. 2007).

The nipple is most commonly found at the tip of the breast as a 2–6 cm diameter circular, pigmented area. The tone varies from pale pink to dark brown depending on various factors including age, parity, and general skin pigmentation (Pandya and Moore 2011). The skin of the areola surrounding the nipple contains the sebaceous glands of Montgomery, which hypertrophy in the third trimester of pregnancy and lubricate the nipple during breast feeding (DeCherney et al. 2007).

Blood supply, lymphatics, innervation

The vascular supply to the breast principally comes from three sources, namely: perforating branches of the internal thoracic artery, lateral branches of the internal intercostal arteries, and

Bergman's Comprehensive Encyclopedia of Human Anatomic Variation, First Edition. Edited by R. Shane Tubbs, Mohammadali M. Shoja and Marios Loukas.
© 2016 John Wiley & Sons, Inc. Published 2016 by John Wiley & Sons, Inc.

Table 118.1 Axillary node anatomy. Data from Pandya and Moore (2011) and Hunt et al. (2010).

Classification	Description
(1) Axillary vein group	4–6 nodes that are positioned medial or posterior to the axillary vein, and receive lymphatic drainage from the upper extremity
(2) External mammary/ anterior/pectoral	5–6 nodes stretching along the lower border of pectoralis minor which track with the lateral thoracic vessels to drain most of the lateral breast
(3) Scapular/posterior/ subscapular	5–7 nodes on the posterior axilla which follow the course of the subscapular vessels to drain the inferior aspect of the posterior neck as well as the posterior trunk and shoulder
(4) Interpectoral/Rotter's nodes	1–4 nodes that lie between pectoralis minor and major, receiving drainage directly from the breast
(5) Central	3–4 groups of nodes found in axillary fat deep to the perctoralis minor muscle, where they drain groups (1)–(4) listed above as well as directly draining the breast
(6) Subclavicular/apical	A variable number of nodes, often 6–12 groups, that lie posterior and superior to the superior pectoralis minor where they receive drainage from groups (1)–(5) as listed above.

branches of the axillary artery (Pandya and Moore 2011). Similarly, the breast drains through three main groups of veins: perforating branches of the internal thoracic vein, posterior intercostal veins, and the axillary vein. Sensory innervation comes from the lateral cutaneous branches of the third–sixth intercostal nerves which transverse through the serratus anterior muscle to their destination (Hunt et al. 2010).

Lymphatic drainage of the breast is variable between individuals, and the drainage borders are not well defined. In general, it is accepted that there are six groups of axillary lymph nodes that will receive more that 75% of drainage (Table 118.1); the remainder, principally from the more medial aspect of the breast, will drain through lymph vessels that track along with the branches of the internal thoracic artery and into the parasternal group lymph nodes (Pandya and Moore 2011).

Asymmetry

Humans display bilateral symmetry in paired morphological traits such as ear size, finger length, and, to a certain extent, breast volume. This observation of symmetry in breast tissue can be influenced by a number of internal and external factors such as the sex hormone estrogen, which plays an important role in breast growth and development (Scutt et al. 2006). Small, random variations that are the result of these factors has been termed "fluctuating asymmetry" and refers to the concept that asymmetry between left and right is random and independent. In embryological studies, this variation has been used as a measure of developmental precision often overlooked in clinical medicine (Thornhill and Moller 1997; Derman and Gold 2004; Scutt et al. 2006).

The development of breast tissue at puberty is considered an important marker of normal development and transition into sexual maturity. When development is somehow misdirected, adolescent females are left feeling self-conscious with the potential to develop self-esteem issues, withdrawal from social contact, and even fulminant depression (Greydanus et al. 1989; De Silva and Brandt 2006). Often at the age of telarche, breast tissue does not grow at an equal rate bilaterally leading to some degree of asymmetry in many variables including volume, position, shape, or nipple location. Fortunately, most asymmetries seen at adolescence will abate to a large degree by adulthood (Greydanus et al. 1989; Dixon and Mansel 1994).

Breast asymmetry is commonly found in association with premature telarche, a condition that can affect breast size unilaterally or bilaterally in the absence of estrogenic stimulation or genital development. Breast development in this situation is rarely progressive and has no effect on the initiation of menarche (Eidlitz-Markus et al. 2010). Interestingly, there have been several reports recently of telarche observed at the early age of 6–7 years, possibly related to high body mass index (Sadove and van Aalst 2005). Clinicians should approach a breast mass in obese children with caution, as the developing breast bud may be the first indicator of oncoming puberty. Removal of fluid or tissue for evaluation of a suspicious mass can result in breast distortion and hypoplasia as an early finding, and ultimately iatrogenic breast asymmetry (Bleiziffer et al. 2004; Eidlitz-Markus et al. 2010).

There have been multiple reports of iatrogenic injury causing asymmetry in breast development. Although there is minimal breast growth and development in early life, prior to puberty, injury to the breast bud/mammary gland precursor tissue in the vicinity of the fourth intercostal space can cause significant growth defects later in life (Singletary et al. 2004). There have been a large number of breast bud injuries secondary to anterolateral or posterolateral thoracotomy, especially if the incision is made in the third or fourth intercostal space (Cherup et al. 1986). As a result, the current surgical recommendations to avoid iatrogenic injury are to position thoracotomy incisions, or even chest tube placement anteriorly in the seventh or eighth intercostal space to avoid division of the pectoralis muscle. If injury is unavoidable, patients should ultimately be referred for surgical reconstruction; the procedure is typically delayed until development of the contralateral breast tissue is complete, however (Singletary et al. 2004).

Congenital causes of breast asymmetry are an important cause of abnormal breast development that may be a superficial clue to an underlying disorder. Poland syndrome, first described in cadaveric dissection in 1841 but not formally classified until 1862 (Singletary et al. 2004), is a rare, non-genetic, congenital anomaly which includes the finding of breast asymmetry

(Neinstein 1999). Poland syndrome includes breast and nipple hypoplasia, diminished subcutaneous tissue, absence of the costosternal portion of the pectoralis major muscle, absence of pectoralis minor, a spectrum of aplasia to deformity of the costal cartilage or ribs two–five, absence of hair growth in the axillary and mammary region, and unilateral brachysyndactyly. All of the findings associated with Poland syndrome listed above are not usually found in the same individual, and the phenotypic presentation will vary between patients with no correlation between the extent of hand, breast, and thoracic abnormalities (Fokin and Robicsek 2002). Diagnosis is three times more common in males than females and is right-sided in 75% of patients. Overall the incidence ranges from 1 in 20,000 to 1 in 50,000 live births. Fortunately, the risk of multiple children in the same family being affected is relatively low (Singletary et al. 2004).

From a pathophysiological perspective, those with Poland syndrome were found to have a decrease in the diameter (approximately 50% reduction) of the subclavian artery with the degree of flow impairment being correlated directly to the extent of the abnormalities observed. A diminished internal thoracic artery is thought to lead to isolated loss of the sternocostal portion of the pectoralis major muscle; however, an isolated reduction in the brachial artery can lead to isolated hand abnormalities. These observations have lead researchers to postulate that Poland syndrome results from interruption of the embryonic blood flow to the upper limb bud and chest wall during the sixth week of development; the etiology remains unclear, however (Perez Aznar et al. 1996; Fokin and Robicsek 2002; Eidlitz-Markus et al. 2010).

In a recent case study, a report of juvenile localized scleroderma was found to be the underlying etiology of breast asymmetry (Eidlitz-Markus et al. 2010). Juvenile localized scleroderma is a relatively uncommon autoimmune disorder that predominantly affects Caucasian females. It is believed that changes in connective tissue and immune cell infiltrates contribute to alterations in breast shape and size leading to asymmetry. Mechanistically, the underlying cause of the pathology is related to mechanical sheer (67%), infection (25%), drugs (5%), and stress (Zulian et al. 2006). Fortunately, there are few cases of breast asymmetry secondary to scleroderma in the literature to date (Treiber et al. 1994; Granel et al. 2001; Shetty et al. 2007). Other causes of breast asymmetry have been described such as fibroadenoma, cystadenoma phyllodes, lipoma, and abscess; these disease processes are however rare, often reversible, and of little clinical significance (Greydanus et al. 1989; Neinstein 1999; Eidlitz-Markus et al. 2010).

At times it can be difficult to interpret physical findings of breast asymmetry. Many clinicians believe that girls with scoliosis have a higher rate of breast asymmetry than the general population. This statement should be interpreted with caution as it is often simply due to progressive spinal curvature or an underlying ribcage defect (psuedoasymmetry). This concept is further complicated by the fact that in girls with progressive right-convex thoracic scoliosis, breast asymmetry may be a true finding resulting from a developmental abnormality in the vascular supply to the chest wall. In addition, iatrogenic injury to the developing breast tissue from corrective scoliosis braces may create some degree of asymmetry that is unrelated to the underlying condition (Eidlitz-Markus et al. 2010).

Figure 118.1 Complete amastia.

Source: Williams (1891). Reproduced with permission from John Wiley & Sons.

An extreme case of breast developmental asymmetry is termed "amastia," the congenital absence of one or both breasts (Fig. 118.1). First described in 1839, the absence of breast tissue results from a failure to form during the fifth–sixth weeks of embryonic development (Singletary et al. 2004; Macias and Hinck 2012). Since the first reports, there have been multiple descriptions of the presentation that are divided into three categories: (1) bilateral absence of breast tissue with congenital ectodermal defects; (2) unilateral absence of breast tissue; and (3) bilateral absence of breast tissue with associated anomalies. Unilateral amastia is the most common of these variants and is usually found in females (Trier 1965). Unfortunately, the precise etiology of amastia is unclear. It has been postulated that insufficient estrogen, a diminished vascular supply during development, environmental exposure, or intrinsic and extrinsic signaling pathways may play a role in interfering with normal breast development. Because of the psychosocial impact of this condition on young females, patients with this condition should be referred for surgical reconstruction which has enjoyed excellent results (Singletary et al. 2004).

Supernumerary

Accessory breast tissue is a relatively common finding often overlooked in clinical medicine (Fig. 118.2). Affecting 0.22–6% of the population, it is usually not identified at a young age (Scanlan and Propeck 1996; Schmidt 1998). In contrast, the

Figure 118.2 An extra breast in a female cadaver seen over the lower left quadrant of the anterior abdominal wall. Note that the normally positioned breasts have been dissected away.

finding usually presents itself during menarche, pregnancy, and/or lactation when patients complain of unusual pain, discomfort during menstruation, discharge, or even restriction in arm movement. This tissue can undergo all the physiological changes seen in normal breast tissue in response to circulating hormonal changes (Sadove and van Aalst 2005). As with breast asymmetry, ectopic breast tissue can also lead to a host of self-esteem and psychological health issues if not addressed appropriately (De Silva and Brandt 2006). Physicians should also be aware in their clinical practice to investigate further any suspected accessory breast tissue as it has equal potential to develop all the pathological and malignant changes associated with normal breast tissue or may be a clue to an underlying congenital abnormality (Scutt et al. 2006).

The development of accessory breast tissue is thought to be multifactorial, that is, dependent on gender, ethnicity, geography, and genetics. Ectopic breast tissue is much more common in females and has been rarely observed in men (Scanlan and Propeck 1996; Schmidt 1998). Likewise, it is a more common finding in Americans of African and Caucasian descent, Native Americans, Japanese, Israeli Jews, and Arabs, with a relative paucity of European children being affected (Velanovich 1995; Gilmore et al. 1996). Generally, the incidence is believed to be the result of a sporadic or idiopathic event; however, in approximately 10% of those found to have ectopic breast tissue, familial associations have been found. Further investigation of this 10% lead to the observation of two common modes of inheritance, namely autosomal dominant with incomplete penetrance and X-linked dominant; however, the pedigree is complicated by variability in phenotypic expression between generations (Urbani and Betti 1995; Tsukahara et al. 1997; Galli-Tsinopoulou et al. 2001).

The term "accessory breast tissue" refers to a host of abnormal tissue ranging from a small nipple or areola only, to a complete nipple, areola, and glandular tissue. Typically, this ectopic tissue is found along the embryonic milk line traveling from the axilla to the groin; however, there have been reports of findings in the face, posterior neck, chest, buttock, vulva, shoulder, thigh, perineum, and even midback (Loukas et al. 2007). There are two postulated theories behind the variability in position, which include displacement of the milk line during embryonic development or the idiopathic differentiation of apocrine sweat glands into breast tissue anywhere these glands are found (Leung et al. 1997). A classification system for accessory breast tissue was created by Kajava (1915) and is still in clinical practice today, 100 years later (Loukas et al. 2007). Generally there are eight categories as described in Table 118.2, with polythelia being the most common presentation seen in 60–70% of those affected (Patel et al. 2012).

Over the years, researchers have proposed that the development of accessory breast tissue can be associated with other congenital abnormalities. Although somewhat controversial, it has been observed that there is an increased incidence of kidney/urinary tract abnormalities in patients with accessory breast tissue over the general population (14.5% v. 1–2%, respectively). This observation merits the postulation that there may, at some level, be a common pathway between the development of accessory breast tissue and kidney/urinary tract anomalies (Meggyessy and Mehes 1987; Grotto et al. 2001; Brown and Schwartz 2004).

Not limited to disorders of the urinary system, accessory breast tissue has also been found to have an association with underlying disorders in the cardiovascular system; however, the precise relationship is yet to be elucidated. There have been two main associations to date, namely: (1) congenital heart anomalies with pulmonary hypertension and cardiomyopathy secondary to myocardial infarction or hypertension are related to the finding of polythelia (Rajaratnam et al. 2000); (2) ectopic breast tissue can indicate disorders in the cardiac conduction system, principally bundle branch blocks and third-degree heart block (Urbani 2004).

Table 118.2 Classification of accessory breast tissue. Data from Kajava (1915).

Class	Description
I	Complete breast including nipple, areola, and glandular breast tissue (also known as polymastia)
II	Nipple and glandular tissue without areola
III	Areola and glandular tissue without nipple
IV	Restricted aberrant glandular tissue
V	Nipple, areola, and pseudomamma (ectopic fat replacing glandular tissue)
VI	Nipple only (also known as polythelia)
VII	Areola only (also known as polythelia areolaris)
VIII	Restricted patch of hair (also known as polythelia pilosa)

Finally there is a genetic syndrome found to be associated with accessory breast tissue. Simpson-Golabi-Behmel syndrome is a rare X-linked recessive disorder characterized by pre- or postnatal overgrowth, facial dysmorphic features, heart malformations, cleft palate, postaxial polydactyly, and polythelia (Urbani and Betti 1995; Loukas et al. 2007).

Shape variation

The tuberous breast deformity is a parenchymal malformation of the mammary gland that was first described in 1976 (Rees and Aston 1976). The name is originally derived from the resemblance of the developed breast to a tuberous plant root (Rees and Aston 1976). There have been multiple synonyms that have been used to describe this condition since then, including "Snoopy" breasts (Grolleau et al. 1999), herniated areolar complexes, and constricted breasts (von Heimburg et al. 1996), leading to confusion in understanding among clinicians (Klinger et al. 2011). This condition presents at a time of breast growth, commonly involves both breasts, and leads to a high degree of asymmetry (Grolleau et al. 1999). Unfortunately, during adolescence, this asymmetry can lead to a high degree of psychosocial distress among suffers and therefore appropriate diagnosis and management becomes essential (Singletary et al. 2004).

The etiology of tuberous breast deformities remains largely unclear; however, it is thought that alterations in collagen fiber orientation and quantity in the absence of amyloid accumulation contributes to its formation. Interestingly, the disruption in connective tissue formation is not limited to the structural fascia of the breast; rather, it is found throughout the breast stroma implying that the disease process is a complex malformation. In addition, the finding of tuberous breast deformities in homozygous twins suggests that there is an underlying genetic or familial transmission pattern (Klinger et al. 2011). This developmental abnormality, although rare, can be a disfiguring asymmetry leading to significant psychosocial complications. It is therefore important that patients are diagnosed and managed appropriately; multiple avenues of corrective treatment options are available (Singletary et al. 2004).

Physiological changes (pregnancy, lactation, involution)

During pregnancy, there is a large increase in circulating ovarian placental estrogens and progestins. These hormones act on the breast tissue to induce structural changes in preparation for lactation. In general, the ductal and lobular epithelium proliferates while the skin overlying the areola becomes darker. The accessory areolar glands, or Montgomery's glands, also grow and become more prominent. Early on in pregnancy, during the first and second trimester, the minor ducts of the breast begin to branch and develop. It is in the third trimester that fat begins to deposit within the breast tissue while colostrum, the first secretions of the breast after birth, begins to accumulate in the ducts and sinuses (Hunt et al. 2010; Macias and Hinck 2012).

Following delivery, circulating estrogen and progesterone levels fall allowing for unopposed action of oxytocin on the breast tissue to promote lactation. Oxytocin acts mainly on the myoepithelial cells of the breast to induce contraction in order to propel milk into the lactiferous sinuses. The induction and maintenance of lactation is by a combination of a neural reflex pathway in the superficial nerves of the nipple areolar complex and the continued production of oxytocin in response to the auditory, visual, and olfactory stimuli of nursing. In the absence of oxytocin, milk remains dormant in the conduction system; this leads to increased pressure and atrophy of the epithelium, and ultimately regression of the breast due to pregnancy (Hunt et al. 2010; Macias and Hinck 2012).

During menopause, there is a decrease in the production of estrogen and progesterone from the ovaries. Without these hormones available to maintain the breast tissue, there is an involution of both the ducts and alveoli. Ultimately, the surrounding fibrous connective tissue becomes less dense and is eventually replaced with fatty infiltrates (Hunt et al. 2010).

Gynecomastia

Gynecomastia is a common, benign finding characterized by unilateral or bilateral enlargement of the male breast that is seen in up to one-third of adult males. Higher incidences have been cited in the adolescent population where it varies over the range 30–60% with highest prevalence being found in the elderly population, reaching 65% in some studies (Niewoehner and Nuttal 1984; Georgiadis et al. 1994). Gynecomastia is caused by proliferation of the underlying glandular tissue and local fat deposition, which can have a distressing impact on emotional well-being and body image. Of note, "psuedogynecomastia," which is common in obese men and secondary to lipoid proliferation and deposition alone without glandular growth, is not considered a true gynecomastia; it is therefore treated differently by the consulting physician, if at all (Johnson and Murad 2009).

The pathophysiology of gynecomastia is thought to lie in a disruption of the balance between circulating estrogens and androgens. Estrogen is known to stimulate the growth and development of breast tissue, whereas androgens inhibit the process (Dimitrakakis et al. 2003). At three times during a male's life he will experience physiological gynecomastia, which is considered a normal part of male development. First, in the neonatal period, placental estrogens act on neonatal breast tissue, temporarily inducing growth. Neonatal gynecomastia typically resolves within four months after birth, and symptoms that persist after one year require further investigation (Hunt et al. 2010; Dickinson 2012). Second, at puberty, up to half of

adolescents will experience gynecomastia, most commonly somewhere between Tanner stages 3–4. At this age, adolescents are particularly self-conscious and vulnerable to self-esteem issues; this condition may therefore warrant a lower threshold for intervention than at other stages. It is believed that at this phase of development, gynecomastia is caused by an excess in the concentration of estradiol relative to testosterone, which lags in production in combination with an increased sensitivity to circulating estrogen. Generally, it is recommended that if symptoms at this stage persist for more than 2 years or beyond 17 years of age, further investigation should be undertaken as it may be a sign of underlying pathology or substance experimentation/abuse (Biro et al. 1990). Third, in the elderly male population, circulating testosterone is decreased, creating a situation of relative hyperestrinism. Typically, physiological gynecomastia is bilateral and symmetrical; during puberty however, the effect of the hormone imbalance can be bilateral, unilateral, or asymmetrical. Irregular masses or densities, especially in the older population, should raise suspicion of malignant growth; however, in general, gynecomastia does not increase the risk of breast cancer above background. The notable exception to this guideline is the hypoandrogenic state found in Klienfelter's syndrome (characterized by 47 XXY genotype) where gynecomastia is a common finding and associated with an increased risk of developing breast cancer (Hunt et al. 2010; Dickinson 2012).

In the setting of pathological gynecomastia, the underlying reason for developing an imbalance between the aforementioned groups of hormones can be the result of a number of disease or physiologic processes (Table 118.3); however, many causes are still not well understood. With approximately 20 clinical conditions and at least 30 medications being implicated as contributing to gynecomastia, up to 50% of cases still have no known underlying pathology (Braunstein 2007). Of note, because a majority of estrogen hormones in males (approximately 80%) are produced by peripheral conversion of two main precursors, namely androstenedione and testosterone by the enzyme aromatase found in adipose tissue, obese patients may show physiological characteristics that are a combination of gynecomastia and psuedogynecomastia (Thompson and Carter 1993; Braunstein 2007).

Table 118.3 Causes of gynecomastia. Data from Braunstein (2007) and Thompson and Carter (1993).

Cause	Description
Physiologic	Maternal hormones in infancy, puberty, old age
Endocrine tumors	Estrogen, steroid, or hCG producing tumors including those of the hypothalamus-pituitary-axis
Endocrine dysfunction	Hypogonad, hyperthyroid, obesity
Non-endocrine disease	Liver disease, renal failure
Drug induced	Medication, performance-enhancing drugs, illicit substances, environmental contaminants
Idiopathic	–

Table 118.4 Classification of gynecomasia. Data from Cordova and Moschella (2008) and Johnson and Murad (2009).

Grade	Description
I	Areola demonstrates increased diameter and slight protrusion
II	Moderate hypertrophy of all breast tissue; nipple-areolar complex remains above the inframammary fold
III	Major hypertrophy of all breast tissue and glandular ptosis; nipple-areolar complex is no more than 1 cm below the inframammary fold
IV	Major hypertrophy of all breast tissue with skin redundancy and glandular ptosis; nipple-areolar complex is more than 1 cm below the inframammary fold.

Clinicians have observed that gynecomastia presents on a scale of severity ranging from simple areolar protrusion all the way to breasts with female resemblance. The hallmarks that are used in classification are breast swelling, areolar diameter, presence of anomalous inframammary fold, glandular ptosis, and skin redundancy. The classification system for gynecomastia defines four grades of increasing severity (Table 118.4), each with a multitude of potential interventions based on individual patient concerns and desired outcomes (Cordova and Moschella 2008; Johnson and Murad 2009).

Gynecomastia is a common condition potentially affecting men over a wide range of ages. Although there are thought to be many different etiological factors that can lead to its development, it is believed that they all act through a common pathway of disrupting the circulating estrogen and androgen concentration balance. There are four grades of gynecomastia according to severity, with many treatment options available ranging from simply watchful waiting or ceasing the offending agent to medical or surgical intervention. Importantly, patients should be reassured of the benign, self-limiting nature of their condition and treatment should be personalized to achieve individual cosmetic goals (Johnson and Murad 2009).

References

Biro FM, Lucky AW, Huster GA, Morrison JA. 1990. Hormonal studies and physical maturation in adolescent gynecomastia. *J Pediatr* 116: 450–455.

Bland K, Howard JH, Romrell L. 1998. Congenital and acquired disturbances of breast development and growth. In: *The Breast: Comprehensive Management of Benign and Malignant Diseases* (eds KI Bland, EM Copeland III). Philadelphia: WB Saunders, pp. 214–232.

Bleiziffer S, Schreiber C, Burgkart R, Regenfelder F, Kostolny M, Libera P, Lange R. 2004. The influence of right anterolateral thoracotomy

in prepubescent female patients on late breast development and on the incidence of scoliosis. *J Thorac Cardiovasc Surg* 127: 1474–1480.
Braunstein GD. 2007. Clinical practice. Gynecomastia. *N Engl J Med* 357: 1229–1237.
Brown J, Schwartz RA. 2004. Supernumerary nipples and renal malformations: A family study. *J Cutan Med Surg* 8: 170–172.
Cherup LL, Siewers RD, Futrell JW. 1986. Breast and pectoral muscle maldevelopment after anterolateral and posterolateral thoracotomies in children. *Ann Thorac Surg* 41: 492–497.
Cordova A, Moschella F. 2008. Algorithm for clinical evaluation and surgical treatment of gynaecomastia. *J Plast Reconstr Aesthet Surg* 61: 41–49.
De Silva NK, Brandt ML. 2006. Disorders of the breast in children and adolescents. Part 1: Disorders of growth and infections of the breast. *J Pediatr Adolesc Gynecol* 19: 345–349.
DeCherney AH, Nathan L, Goodwin TM, Laufer N. 2007. *Current Diagnosis and Treatment Obstetrics and Gynecology*, tenth edition. New York: McGraw-Hill.
Derman O, Gold MA. 2004. Poland's syndrome and premature ovarian failure. *J Pediatr Adolesc Gynecol* 17: 389–392.
Dickson G. 2012. Gynecomastia. *Am Fam Physician* 85: 716–722.
Dimitrakakis C, Zhou J, Wang J, Belanger A, LaBrie F, Cheng C, Powell D, Bondy C. 2003. A physiologic role for testosterone in limiting estrogenic stimulation of the breast. *Menopause* 10: 292–298.
Dixon JM, Mansel RE. 1994. ABC of breast diseases. Congenital problems and aberrations of normal breast development and involution. *BMJ* 309: 797–800.
Eidlitz-Markus T, Mukamel M, Haimi-Cohen Y, Amir J, Zeharia A. 2010. Breast asymmetry during adolescence: Physiologic and nonphysiologic causes. *Isr Med Assoc J* 12: 203–206.
Fokin AA, Robicsek F. 2002. Poland's syndrome revisited. *Ann Thorac Surg* 74: 2218–2225.
Galli-Tsinopoulou A, Krohn C, Schmidt H. 2001. Familial polythelia over three generations with polymastia in the youngest girl. *Eur J Pediatr* 160: 375–377.
Georgiadis E, Papandreou L, Evangelopoulou C, Aliferis C, Lymberis C, Panitsa C, Batrinos M. 1994. Incidence of gynaecomastia in 954 young males and its relationship to somatometric parameters. *Ann Hum Biol* 21: 579–587.
Gilmore HT, Milroy M, Mello BJ. 1996. Supernumerary nipples and accessory breast tissue. *S D J Med* 49: 149–151.
Granel B, Serratrice J, Gaudy C, Weiller-Merli C, Bonerandi JJ, Lepidi H, Coulomb-Marchetti B, Disdier P, Weiller PJ. 2001. Localized morphea after silicone-gel-filled breast implant. *Dermatology* 202: 143–144.
Greydanus DE, Parks DS, Farrell EG. 1989. Breast disorders in children and adolescents. *Pediatr Clin North Am* 36: 601–638.
Grolleau JL, Lanfrey E, Lavigne B, Chavoin JP, Costagliola M. 1999. Breast base anomalies: Treatment strategy for tuberous breasts, minor deformities, and asymmetry. *Plast Reconstr Surg* 104: 2040–2048.
Grotto I, Browner-Elhanan K, Mimouni D, Varsano I, Cohen HA, Mimouni M. 2001. Occurrence of supernumerary nipples in children with kidney and urinary tract malformations. *Pediatr Dermatol* 18: 291–294.
Hunt K, Newman LA, Copeland E, Bland K. 2010. The breast. In: *Schwartz's Principals of Surgery*, ninth edition (eds FCBrunicardi, DK Andersen, TR Billar, DL Dunn, JG Hunter, FB Matthews, RE Pollock). New York: The McGraw-Hill Medical Publishing Division.
Johnson RE, Murad MH. 2009. Gynecomastia: Pathophysiology, evaluation, and management. *Mayo Clin Proc* 84: 1010–1015.
Kajava Y. 1915. The proportions of supernumerary nipples in the Finnish population. *Duodecim* 31: 70.
Klinger M, Caviggioli F, Klinger F, Villani F, Arra E, Di Tommaso L. 2011. Tuberous breast: Morphological study and overview of a borderline entity. *Can J Plast Surg* 19: 42–44.
Leung W, Heaton JP, Morales A. 1997. An uncommon urologic presentation of a supernumerary breast. *Urology* 50: 122–124.
Loukas M, Clarke P, Tubbs R S. 2007. Accessory breasts: A historical and current perspective. *Am Surg* 73: 525–528.
Macias H, Hinck L. 2012. *Mammary gland development*. Wiley Interdiscip Rev Dev Biol 1: 533–557.
Meggyessy V, Mehes K. 1987. Association of supernumerary nipples with renal anomalies. *J Pediatr* 111: 412–413.
Moore KL, Persaud TVN, Torchia MG, Eisenstat DD. 1998. *The Developing Human: Clinically Oriented Embryology*. Philadelphia: Saunders.
Neinstein LS. 1999. Breast disease in adolescents and young women. *Pediatr Clin North Am* 46: 607–629.
Niewoehner CB, Nuttal FQ. 1984. Gynecomastia in a hospitalized male population. *Am J Med* 77: 633–638.
Oftedal OT. 2002. The mammary gland and its origin during synapsid evolution. *J Mammary Gland Biol Neoplasia* 7: 225–252.
Pandya S, Moore RG. 2011. Breast development and anatomy. *Clin Obstet Gynecol* 54: 91–95.
Patel PP, Ibrahim AM, Zhang J, Nguyen JT, Lin SJ, Lee BT. 2012. Accessory breast tissue. *Eplasty* 12: 5.
Perez Aznar JM, Urbano J, Garcia Laborda E, Quevedo Moreno P, Ferrer Vergara L. 1996. Breast and pectoralis muscle hypoplasia. A mild degree of Poland's syndrome. *Acta Radiol* 37: 759–762.
Rajaratnam K, Kumar PD, Sahasranam K. 2000. Supernumerary nipple as a cutaneous marker of mitral valve prolapse in Asian Indians. *Am J Cardiol* 86: 695–697.
Rees TD, Aston SJ. 1976. The tuberous breast. *Clin Plast Surg* 3: 339–347.
Sadove AM, van Aalst JA. 2005. Congenital and acquired pediatric breast anomalies: A review of 20 years' experience. *Plast Reconstr Surg* 115: 1039–1050.
Scanlan KA, Propeck PA. 1996. Accessory breast tissue in an unusual location. *AJR Am J Roentgenol* 166: 339–340.
Schmidt H. 1998. Supernumerary nipples: Prevalence, size, sex and side predilection — a prospective clinical study. *Eur J Pediatr* 157: 821–823.
Scutt D, Lancaster GA, Manning JT. 2006. Breast asymmetry and predisposition to breast cancer. *Breast Cancer* Res 8: 14.
Seltzer V. 1994. The breast: Embryology, development, and anatomy. *Clin Obstet Gynecol* 37: 879–880.
Shetty G, Lewis F, Thrush S. 2007. Morphea of the breast: case reports and review of literature. *Breast J* 13: 302–304.
Singletary SE, Robb GL, Hortobagyi GN. (eds) 2004. *Advanced Therapy of Breast Disease*, second edition. Ontario: BC Decker Inc.
Thompson DF, Carter JR. 1993. Drug-induced gynecomastia. *Pharmacotherapy* 13: 37–45.
Thornhill R, Moller AP. 1997. Developmental stability, disease and medicine. *Biol Rev Camb Philos Soc* 72: 497–548.
Treiber ES, Goldberg NS, Levy H. 1994. Breast deformity produced by morphea in a young girl. *Cutis* 54: 267–268.
Trier WC. 1965. Complete breast absence. Case report and review of the literature. *Plast Reconstr Surg* 36: 431–439.
Tsukahara M, Uchida M, Uchino S, Fujisawa R, Kamei T, Itoh T. 1997. Male to male transmission of supernumerary nipples. *Am J Med Genet* 69: 194–195.

Urbani CE. 2004. Supernumerary nipple and cardiocutaneous associations. *J Am Acad Dermatol* 50: 9.

Urbani CE, Betti R. 1995. The significance of familial polythelia. *J Am Acad Dermatol* 32: 687–688.

Velanovich V. 1995. Ectopic breast tissue, supernumerary breasts, and supernumerary nipples. *South Med J* 88: 903–906.

von Heimburg D, Exner K, Kruft S, Lemperle G. 1996. The tuberous breast deformity: Classification and treatment. *Br J Plast Surg* 49: 339–345.

Williams WR. 1891. Polymastism, with special reference to mammae erraticae and the development of neoplasms from supernumerary mammary structures. *J Anat Physiol* 25(2): 225–256.

Zulian F, Athreya BH, Laxer R, Nelson AM, Feitosa de Oliveira S K, Punaro, MG, Harper J. 2006. Juvenile localized scleroderma: Clinical and epidemiological features in 750 children. An international study. *Rheumatology (Oxford)* 45: 614–620.

Index

Page numbers in *italics* refer to figures, those in **bold** to tables; note that figures and tables are only indicated when there is no text reference on the same page.

abdominal aorta 619–670
abdominal wall muscles 369–378
  anterior 369–371
  lateral 371–374
  posterior 374–378
abdominoscrotal hydrocele 1355
abducent nerve (VI) 1001
  foramen of Luschka relations 951
abductor accessories digiti minimi muscle 444
abductor digiti minimi muscle 318–320
  accessory *see* accessory abductor digiti minimi muscle
  mass appearance 333
  nerve entrapments 328–329, *330*
  vascular effects 332
abductor digiti minimi muscle of foot 443–444
abductor hallucis muscle 440–441, *442*
abductor osis metatarsi digit minimi (abductor os metatarsi digiti minimi) 444
abductor pollicis brevis muscle 315–316, 328, 332
abductor pollicis longus muscle 306–307
abductor pollicis tertius muscle 306
ablepharon 1134
ablepharon-macrostomia syndrome 1134
ACAOS (abnormal coronary artery from the opposite sinus) 505, 540–541
accessorium tricipitis muscle 296
accessorius ad flexorem profundus of Gantzer 302
accessorius profundus digitorum of Gantzer 300
accessory abductor digiti minimi (ADM) muscle *319,* 320
  nerve entrapments 328–329, *330,* 1091, *1092*
accessory appendicular arteries 649
accessory axillary vein 826
accessory cephalic (radial) vein 828, *829, 830*
accessory deep fibular nerve 1124
accessory fibular nerves 1124
accessory hemiazygos vein 833–834, 836, 892
  continuation of IVC 838, 878
  spinal cord drainage 912
  SVC anomalies and 838, 842
accessory hepatic artery 627
accessory hepatic grooves 1272
accessory hepatic lobes 1273–1275
accessory hepatic veins 884, *885*
accessory hypophyseal arteries 463
accessory iliacus muscle 376
accessory iliopsoas muscle 376
accessory inferior thyroid artery 578, *579*
accessory lacrimal glands (of Krause) 1153, 1155, *1156*
accessory lateral collateral ligament, elbow 152, 153, *154,* 155
accessory left colic artery 652–653
accessory left gastric artery 626–627
accessory left hepatic artery (aLHA) *624,* 630
accessory ligament of Malgaigne 125
accessory maxillary sinus ostia 13, 1162
accessory meningeal artery (AMA) 480, 482, 998, *999*
accessory middle colic artery 646, 647
accessory middle genicular artery 744
accessory muscle of Calori 299
accessory nerve (CN XI)
  cervical nerve anastomoses 1047, 1057–1058
  cervical plexus connections 1065–1066
  glossopharyngeal nerve relations 1037
  vagus nerve anastomoses 1043
accessory nerve of Jamieson 1118
accessory obturator nerve 1118
accessory occipital nerve 1058
accessory pancreatic duct 1279–1280
accessory parotid duct 1184
accessory parotid gland 1182, *1183*
accessory phrenic nerve 1063–1064, *1076,* 1077–1078
accessory plantaris muscle 429
accessory popliteus muscle (of Fabrice) 194, 429–430
accessory process, lumbar vertebrae 35
accessory psoas major muscle 376
accessory pudendal artery (APA) 382, 731–733
accessory pudendal nerve 1127
accessory rectal nerve 382
accessory renal arteries 659, 660, *661,* 689–690
  ectopic kidneys 690, 1316, 1318
  literature review **688**
  rotational kidney anomalies 1323
accessory right colic arteries 647–648
accessory right hepatic artery (aRHA) 627, 629, 630, 644, 650
accessory right inferior hepatic vein 884, *885*
accessory sacroiliac joints (ASIJ) 166–168, 172
accessory sinus of Kelch 792
accessory sinus of Verga 792
accessory soleus muscle of Cruveilhier 427, *428*
accessory splanchnic nerve 1053
accessory subscapularis muscle 289, 1096, 1098
accessory subscapularis-teres-latissimus dorsi muscle 268, 289, 1096, 1097
accessory sub-superior bronchus 1229, 1230
accessory superficial fibular nerve 1124
accessory suprascapular artery 579–580
accessory thoracodorsal artery 593
accessory tibialis posterior muscle 430
accessory transverse colic artery 650

Bergman's Comprehensive Encyclopedia of Human Anatomic Variation, First Edition. Edited by R. Shane Tubbs, Mohammadali M. Shoja and Marios Loukas.

© 2016 John Wiley & Sons, Inc. Published 2016 by John Wiley & Sons, Inc.

accessory vertebral vein 823, 842
acetabular dysplasia 176
acetabular labrum 176, 177–178
  limbus 177
  plica 177
  tears 177–178
acetabulum 176–178
  anteversion 177
  notches 85
  ossicles 85, 178
  protrusion 86–87
  retroversion 176–177
achromachia (arachnodactyly) 70, 159
acrocephalosyndactyly type III 1138–1139
acrofacial dysostosis 122
acromial angle 54, 59
acromioclavicularis muscle 291
acromioclavicular joint (ACJ) 51, 126–127
acromion
  separation (os acromiale) 47–48
  shape 45–46, *47*
acute marginal vein of right ventricle (RMV) 860, *861–864,* **868**
ACxPA (abnormal circumflex branch from pulmonary artery) 539
adductor brevis muscle 415–416
adductor hallucis muscle 445–447
adductor longus muscle 415
adductor magnus muscle 416
adductor minimus (quartus) muscle 416
adductor pollicis muscle 317–318
adductor tubercle 92
adrenal (suprarenal) arteries 657–659
adrenal glands 1332–1333
  absence 1332
  ectopic 1332–1333
  fused 1332
  malposition 1333
adrenal veins 890–891
Agger Nasi air cells 1163
aglossia 242
ALADPA (abnormal left anterior descending from pulmonary artery) 539
albinism, oculocutaneous 1141
albumin, diploic veins 773, *774*
ALCAPA (abnormal left coronary artery from pulmonary artery) 505, 537–539
all-median hand 1089, 1092
alopecia universalis congenita 1141
amastia 1392
ambient cistern 962, *963*
amniotic band syndrome 1136
ampulloglomerular organ 1058
amygdaloglossal muscle of Broca 242
amyloidosis macroglossia, systemic 242
anal canal 1310
anastomosis of Valentin 1046
anconeus epitrochlearis muscle *see* epitrochleoanconeus muscle
anconeus muscle 296
anconeus quintus muscle 296
androgen insensitivity syndrome 1374
android pelvis 82
angular artery 457
ankle
  arteries 745–749
  joint 204
  ligaments 205
  perforating veins 907–908
ankyloblepharon 1135
ankyloglossia 243
annular ligament (AL), elbow 148–149, 152, 153, *154*
annular pancreas 1278–1279
annulus fibrosus of Zinn 207
anococcygeal nerves 383, 1127
anodontia 16
anorchia 1353–1354
anorectal malformations 1310, 1314
anotia 1167, 1168
ansa cervicalis 1044–1045, 1046–1047, 1062
ansa hypoglossi *see* ansa cervicalis
ansa of Galen 1043
ansa of von Haller 1028–1029
ansa pectoralis 1079
ansa subclavia 1052
anteater sign 102
anterior abdominal muscles 369–371
anterior accessory saphenous vein 900, 901, 902–903
anterior ascending (pulmonary) artery 571
anterior auricular muscle 221
anterior basal segmental bronchus 1229, 1230
anterior cardiac veins (ACV) 860, *861–864,* **868**
anterior caudate nucleus vein **803,** 804
anterior cecal artery (ACA) 648
anterior cerebral artery (ACA) 454–456
  accessory 454–455
  azygos 455
  bihemispheric 455
anterior cerebral circulation 449–458
anterior chamber of eye 1149
anterior choroidal artery 452–453, 454
anterior circumflex humeral artery 583–584, *585, 587,* 592
anterior communicating (AC) artery 454, 455
anterior condylar vein 819
anterior cruciate ligament (ACL) 186–187
  congenital absence 186, 188
  injuries 181–182
anterior deep temporal artery 480
anterior deep temporal nerve 121
anterior ethmoidal artery 452
anterior ethmoidal nerve 995
anterior facial vein 821
anterior fibular tubercle 95–96
anterior fibulocalcaneus muscle *423,* 424
anterior fontanelle, persistent 6
anterior frenular ligament 425
anterior inferior cerebellar artery (AICA) 462
  facial nerve relations 1006–1007, *1008,* 1009
  foramen of Luschka relations 951
  glossopharyngeal nerve relations 1036
  vestibulocochlear nerve relations 1034
anterior inferior pancreaticoduodenal artery (AIPDA) 642–645
anterior inferior tibiofibular ligament 205
anterior intercavernous sinus 793–794
anterior interosseous artery 609, *610, 612–613*
anterior interosseous nerve 1085, 1088
  communications with other nerves 1088, 1093, 1102
anterior intertrochanteric ridge 91
anterior interventricular coronary artery *see* left anterior descending coronary artery
anterior interventricular vein (AIV) 855, **868**
anterior jugular vein 821
anterior lateral malleolar artery 747
anterior malleolar ligament 121
anterior medial malleolar artery 747
anterior (ventral) median veins 911
anterior meningeal artery 496, *497*
anterior neck muscles 228–232
anterior oblique ligament (AOL), elbow 150–151
anterior parietal artery 457
anterior perimesencephalic membrane 962, *963,* 969
anterior radicular arteries 753–754, **760**
  see also great anterior radicular artery

anterior radiculomedullary arteries 496, *752,* 753
cervicothoracic segment 756, **760**
midthoracic segment 760
summary of variations 767
thoracolumbar segment 761, 762
anterior septal vein (ASV) 803–804
anterior sesamoid cartilages 1211
anterior spinal artery 524, 752–753
anastomoses in lower cord 764–765, 768
area of cord supplied 753
bulbar branches 756, **760**
cervicothoracic segment 754–756, 760
duplicate 754, 755, 766
interrupted 760, 761, 766
midthoracic segment *760,* 761
origin 462, 496, *497,* 754–756, *757–759,* 766
summary of variations 766
thoracolumbar segment 761–762, *763*
anterior superior alveolar nerve 998
anterior superior pancreaticoduodenal artery (ASPDA) 634–635
anterior talofibular ligament 205
anterior temporal artery 456, 457–458
anterior tibial artery (AT; ATA) 744, 745, 746
anterior tibial lymph node 936
anterior tibial recurrent artery (ATRA) 743–744
anterior tibial recurrent nerve (ATRN) 1122–1123
anterior tibial tubercle 95
anterior tibial vein 907
anterior tibiofascialis muscle 421
anterior tibiotalus muscle 421
anterior trunk of left pulmonary artery 572
anterior trunk of right pulmonary artery 569–570
anterior vertebral muscles 245, 250–252
anthropoid pelvis 82
Antonelli's ganglion 1053
antral diaphragm, gastric 1254
antral web, gastric 1254
anus 1310
AOCAP (abnormal origin of both coronary arteries from pulmonary trunk) 540
aorta
abdominal 619–670
ascending *see* ascending aorta
descending *see* descending aorta
embryology 501–502
thoracic 501–526
tortuous 619, *620, 621*
aortic arch(es) 506–521
bovine 507
branching variations 506–510
cervical *512,* 519
coronary artery origin from 534
double 510, *511–512*
embryology 501–502
interrupted 518–519
normal branching 506, *508*
right 510–513, *514–515,* 575, 576, *577*
variant right subclavian artery 507–509
vertebral artery origin 487
aortic bifurcation 619–620, 694, 697
aortic coarctation 513, *516–517*
aortic pseudocoarctation 518
aortic sinuses
anomalous location of coronary ostium 532–534, *536*
coronary origin from improper (opposite) 540–541
coronary origin from non-facing 534, *536, 537*
nomenclature 530, **532**
aortic spindle 519, *520*
aortic valve 502, 1241
bicuspid 502, *503*
quadricuspid 502, 542, *547*
unicuspid 502
aorto-iliac arterial system 694–703
embryology 699–702
variability 697–699
aphallia 1340–1341
apical accessory pudendal artery 731–733
apical segmental renal artery 685–686
APOC (abnormal pulmonary origin of the coronaries) 537–540
appendicular artery 648–649
appendix, vermiform 1297–1299
agenesis 1298
atresia 1298–1299
diverticulum 1298
duplication 1298, *1299*
position 1297–1298
umbilical 1299
apple-peel deformity, small bowel 1292, *1293*
aqueduct of Sylvius 949–950
aqueous humor flow rate 1150
arachnodactyly 70, 159
arachnoid cuff 971–972
arachnoid envelope over pineal region (AEPG) 971–972
arachnoid granulations (AG) 977–978
arachnoid mater 977–978, 984–985
arachnoid membranes 963–972
arachnoid protrusions (APs) 770, 771–773
arachnoid trabeculae (trabeculations) 963, 984–985
arcade of Struthers 1091
ARCAPA (abnormal right coronary artery from pulmonary artery) 505, 540
arch of azygos vein 832
arc of Buhler 650
arc of Riolan *654,* 655
arcuate arteries of kidney 685
arcuate artery of foot 746–747
arcuate foramen 26
arcuate ligament, knee 189, 190, 191
arcuate line 370
arcuate tendinous cord, pharynx 237
arm muscles 293–296
arm veins 829–830
Arnold's nerve (auricular branch of vagus) 1029, 1043
artecularis cubiti anterior 294
arteria lumbalis ima (small lumbar artery) 666, 669
arteria lusoria 576
arteriovenous fistulas
ascending pharyngeal artery 483
coronary 557–558
dural 819
lower limb 900, *901*
arteriovenous malformations, uterus 1373–1374
artery of Adamkiewicz *see* great anterior radicular artery
artery of Casali 581
artery of conus medullaris 761, 763, 764
artery of Cruveilhier 578
artery of Desproges-Gotteron 768
artery of Percheron 462
artery of pterygoid canal 482
articularis cubiti muscle 296
articularis genus muscle 414
articular process agenesis, lumbar spine 35
arymembranous muscle *258, 259,* 260
arytenoepiglottic muscle *258,* 259
arytenoid cartilages 1210, 1211
arytenoid muscle 259–260
arythyrocricoid muscle *256, 258,* 259–260
ascendant vein of hand 827, *828*

ascending aorta
anomalous coronary artery origins 534, *537, 538*
hypoplastic 506, *507*
ascending artery of superior lobe of Appleton 572
ascending cervical artery 579
ascending colic artery 648
ascending colon, mesocolon 1301
ascending lumbar veins 891–892, 912
ascending pharyngeal artery (APA) 117, 120, 482–483
asplenia 1283
microgastria 1253
right bronchial isomerism 1227–1228
total anomalous pulmonary venous connection 846
assimilation joints, lumbosacral 36
astragalus secondarius 99
atelomyelia 988
atlanticomastoideus muscle 252
atlantoaxial instability 27
atlantobasilaris internus muscle 252
atlantomastoid muscle 281, *282*
atlanto-occipital fusion 3–4, *25,* 26
atlanto-occipital membrane
ossification, vertebral artery 488, *494*
paired ossicles 26
atlas (C1) 24–26
assimilation/occipitalization 3–4, *25,* 26
bipartite 25
epitransverse process 26, *27*
ossification 24–25
ATO-Cx (acute take-off of circumflex coronary branch) 547, *548*
atrial appendages 1234
atrial vein 803
atrioventricular node 862, 1244
auditory ossicles 17–18
aural atresia 1173–1175
auricular branch of vagus nerve (Arnold's nerve) 1029, 1043
auriculo-condylar syndrome (ACS) 1171
auriculotemporal nerve 117, 999–1000, 1027–1028
autonomic anastomoses, lower cranial nerves 1047
autonomic nervous system 1050–1055
Axenfeld (intrascleral) nerve loops 1149
axial artery *see* sciatic artery
axillary arch muscle 266–268
chondroepitrochlearis with 343, *344*
innervation 268, 1098
median nerve entrapment 1086
pectoralis quartus with 341, *342*
axillary artery 583–593
brachial plexus relations 1070
classic branching pattern 583, *584*
double 592–593
median nerve relations 1085, 1086
suprascapular artery origination 579, *580,* 584, *591*
variant branching patterns 583–593
axillary cavity veins 829–830
axillary lymph nodes 1391
axillary nerve **1095,** *1096,* 1098–1099
origins 1075, 1098
radial nerve communications 1098
axillary vein 826
axillopectoral muscle *see* axillary arch muscle
axiobasilaris 252
axis (C2) 27
ossification 24
azygos anterior cerebral artery 455
azygos artery of Hyrtl *see* middle genicular artery
azygos fissure 833, *835, 836*
azygos lobe (fissure) of lung 833, *834, 835,* 892, 1222
SVC position 842–844
azygos-pharyngeus muscle 238
azygos vein 832–840, 892
absent 836
arch of 832
caval junction 836
continuation of IVC 836–838, 878–880
course and termination 833, *834, 835–836*
origin 832–833
pseudonodule 833, *836*
spinal cord drainage 912
SVC anomalies and 838, *839,* 842
tributaries 833–836
valves 838–840
azygos venous system 832–840
caval variations and 836–838
embryology 840
valves 838–840

back muscles 262–283
Bardinet's ligament 149–150
Barraya's gland 1199
Bartholin's cyst 1379
Bart syndrome 1254
basal segmental pulmonary arteries 572, 573
basal tentorial artery 450
basal vein of Rosenthal (BVR) 800–802
drainage into torcular 779, *780*
origin 800, 810–811
pineal region 806, 807–809
superior petrosal sinus drainage 784
basilar artery (BA) 461–462, 961–962
basilar artery bifurcation membrane 961–962
basilar venous plexus 791
basilic antebrachial vein *828,* 829, *830*
basilic vein *828,* 829, *830*
basio-deltoideus muscle 291
basioglossus muscle 241
basiotic bone of Albrecht 6
basi-sphenoid 9
basithyrohyoid muscle 230
Bassett's ligament 205
Batson's venous plexus 912
Beckwith–Wiedeman syndrome 242, 1173
Bernard's duct 1280
Berrettini branch (ramus communicans) 1089, *1090,* 1094–1095
biceps brachii muscle 293–295
innervation 1081
tendon of long head 125–126, 294
biceps femoris muscle 193, 416
digastric muscle variant 400, *401,* **402**
biceps femoris tendon (BFT) 188–189, 195
common origin of hamstrings 418, *419*
tibial insertion 193
Bichat-Froment-Rauber anastomosis 1068
bicipital groove 63, 125–126
bicipital plantaris muscle of Hall 429
bile ducts, extrahepatic 1261, 1265–1268
cystic artery relations 631
development 1261
gastroduodenal artery relations 633
intrahepatic duct variants involving 1267, **1268**
biventer cervicis muscle 280
bladder, urinary 1325–1326
bladder exstrophy 86, 1337–1338
Blend White Garland syndrome 505
blepharophimosis 1138
blepharophimosis-ptosis-epicanthus inversus syndrome (BPES) 1133, 1138
blepharoptosis 1138–1139
block vertebrae, congenital 34
Bochdalek's canal 1190
Bochdalek's hernia 349, 1320
bone islands
os coxa 84
wrist 160

Bonthier D'Andernach's ossicle 6
brachial artery 593–597
  median nerve relations 593–597, 1085, 1086
  pronator teres relations 298
brachialis muscle 294
  innervation 1081, 1103
brachial plexus 1068–1103
  cord variations 1075
  division variations 1074
  lateral cord-derived nerves 1078–1081
  medial cord-derived nerves 1081–1095
  morphology and target variations 1073–1075
  origins 1072–1073
  overview 1069
  posterior cord-derived nerves 1095–1103
  postfixed 1072, 1073
  prefixed 1072–1073
  regional relationships 1070
  regional relationship variations 1071–1072
  scalene muscle relations 247–248, 1071–1072
  subclavian artery variation and 1068, *1069*
  supraclavicular-derived nerves 1076–1078
  trunk pseudo-variation 1074, *1075*
  trunk variations 1073–1074
  typical 1069–1070
brachiocephalic artery 475
  aortic arch variations 507, 509, 512
  left coronary artery origin 534
brachiocephalic veins 840–841
brachiofascialis muscle 294
brachioradialis brevis minor muscle 303
brachioradialis muscle 303
brachymesophalangia 69, 158
brachymetacarpia 158
brachyphalangia 69, 158
braided bronchus 1227
brainstem 954–956
brain tissue, ectopic 940
breast 1390–1395
  anatomy 1390
  asymmetry 1391–1392
  blood supply 1390–1391
  congenital absence 1392
  development 1390
  innervation 1391
  lymphatic drainage 1391
  physiological changes 1394
  shape variation 1394
  supernumerary 1392–1394
bregmatic accessory bone 6
bridging bronchus 1226–1227
bridging veins (BVs) 776–777
bronchial arteries 522–524, *525–526*
  coronary artery anastomoses 562
  coronary artery origin 534
bronchial isomerism 1227–1228
bronchial tree 1226–1230
bronchoesophageal muscle 1247
bronchus/bronchi 1226–1230
  braided 1227
  branching patterns 1228–1230
  bridging 1226–1227
  numbering 1226
  tracheal 1214–1215
  X 1226, 1228
buccal branch of facial nerve 1023–1024, 1028
buccal nerve, sensory 1028
Buford complex 45, 124
bulbospongiosus muscle 384
bulbourethral glands 1358
Burn-McKeown syndrome 1136
bursae
  foot 205
  knee joint 183–184
  shoulder joint complex 126
bursae of Poirier 127
bursa of Trolard 27
butterfly vertebra 28, 31, 34

Cabrol, Barthelemy 350
calcaneal tuberosity 96
calcaneocuboid coalition 102
calcaneofibular ligament 205
calcaneonavicular coalition 101, 102
calcaneus 96–98
  bone spurs 97
  talar articular facets 204
calcaneus accessorius 98
calcaneus secondarius 97, 98
calcarine artery 463
calcarine fissure 942
Caldwell–Maloy classification, pelvis 82
callosomarginal artery 456
CALM (congenital absence of left main coronary artery) 549
Calot's triangle 631, 1268
camptodactyly 70, 159, 333
canaliculus, lacrimal 1154
canaliculus sphenoidalis 8
canalis sinuosus 12
canal of Schlemm 1149–1150
canals of Walther 1186
Cantlie line 882
capitate, bipartite 161
capitohamate coalition 72, 161
capitulum humerus 130, 131
capsular arteries of McConnell 451
capsularis subbrachialis 294
caput tertium muscle 427
cardiac lobe of lung 1220
cardiac plexus 1052
cardiac resynchronization therapy (CRT) 856, 867
cardiac veins 854–869
  anastomoses 862–864
  valves 864–866
Carmi syndrome 1254
caroticoclinoid foramen 7
caroticotympanic artery 450, 471
carotid canal 9
carotid-chiasmatic walls 965–966, *967*
carotid cistern 960
carotid sinus nerve (proper) (CSNP) 1037–1038, 1041–1043
carpal bones 71–73, 160–162
  accessory ossicles 71–72, 160
  bipartite 72, 161
  coalitions 72, 160–161
  imaging 160
  specific variations 72–73, 162
carpal boss 71, 160
carpal tunnel syndrome 1087
  anomalous lumbricals 330–331, *1087*
  median artery involvement 597
carpometacarpal (CMC) joint 70, 159
caudal pancreatic arteries 638–639
caudal regression syndrome 37
cavernous sinus 789
cavernous spaces, dural sinuses 794
cavum septum pellucidum 939–940
cavum velum interpositum 939
cavum vergae 940
cecal arteries 648
cecum 1300–1301
  agenesis 1298
  hyperdescent 1288
  mobility 1301
celiac ganglion 1053
celiac trunk (CT) 621–641
  agenesis 625
  branches 625–641
  branching pattern 621–625
  superior mesenteric anastomosis 650
celico-bimesenteric trunk 625, 642, 651

celicomesenteric trunk (CMT) 625, 641, 651
central (Rolandic) artery 457
central ossicle of Perna 85
central retinal artery 451
central sulcus 941
cephalic antebrachial vein 827–828, *829, 830*
cephalic vein of forearm *828,* 829–830
  musculocutaneous nerve relations 1081
ceratoarytenoid muscle *255,* 256
ceratocricoid muscle *255,* 256
ceratoglossus muscle 241
ceratohyoid muscle 261
cerebellar hypoplasia 956
cerebellar precentral membrane (CPM) 971
cerebellar tentorium *see* tentorium cerebelli
cerebellomedullary cistern 963
cerebellopontine angle (CPA), nerve–artery relations 1006–1008
cerebellum 956–958
  hemispheres 956–957
  nuclei 957–958
  tonsils 957
  vermis 957
cerebral aneurysms 468, 470, 471
cerebral circulation
  anterior 449–458
  posterior 461–463
cerebral fissures 940–942
cerebral sulci 941–942
cerebral veins 800–814
  deep 800–809
  superficial 809–814
cerebral ventricles 943–951
cerebrospinal fluid (CSF)
  diploid veins 774
  spinal subarachnoid space 984
cervical accessory thymic tissue 916
cervical agenesis 1368
cervical branch of facial nerve 1024–1025
cervical lymph nodes, thoracic duct termination 926, *929*
cervical lymph trunks 931–932
cervical nerves 1057–1060
  accessory nerve anastomoses 1047, 1057–1058
  communications between dorsal rami 1059–1060
  dorsal rootlet connections 1058–1059
  scalene muscle relations 247–248, 1071–1072
  vagus nerve anastomoses 1044–1045
  see also first cervical nerve; second cervical nerve, etc.
cervical plexus 1062–1066
cervical rami communicantes 1052, 1065
cervical ribs 28, 77–78, 1071
cervical thymic cysts, congenital 916, *917*
cervical vertebrae 24–28
  congenital absence 28
  congenital fusion 28
  eight 28
  spinous processes 28
  transverse foramina 27–28
  uncinate processes 27
  vertebral artery 488, *489–492*
cervicocostohumeralis muscle 229
cervicohumeralis muscle 289
cervicomedullary angle (CMA) 955
cervicovaginal artery 725–726
CHANDS syndrome 1135
Chaput's tubercle 95
CHARGE syndrome 1178
Chassaignac's muscle 338
cheiralgia paresthetica 1101
Chiari I malformation 957
Chiari network 865, 1237
chiasmatic cistern 960
chiasmatic membrane 972
chicken breast 78
cholecystohepatic duct 1267
chondrocoracoid muscle (of Wood) 269, 345
chondroepitrochlearis muscle *267,* 341–345
chondrofascialis muscle 341, *343*
chondrogladiolar breast 78
chondroglossus muscle 241
chondromanubrial deformity 78
chordae tendinae 1237–1238
  false 1241, *1242–1244*
chordae Willisii 794–795
chorda tympani 1016–1017, 1027
chordee 1338
Christmas-tree deformity, small bowel 1292, *1293*
ciliary arteries 451
ciliary ganglion 995–996, 1053–1054
cingulate sulcus 941–942
circle of Willis 454
circular sinus 793–794
circumflex branch of left coronary (Cx) artery 530, **531,** *532*
  abnormal origin from pulmonary artery (ACxPA) 539
  absent 542, *547,* 548
  acute take-off (ATO-Cx) 547, *548*
  muscular bridging/intramural 549, *551*
  origin from aortic sinus #1 541, *544*
  origin from right coronary artery 541, *544*
  twin 554–556, *557*
  typology and dominance 560–562
circumflex scapular artery 592
  origin 584, *585–591,* 592
  scapular sulcus 41
circumolivary bundles (fascicles) 955–956
cisterna chyli 921–923
cisterna magna 963
clavicle 51–59
  anatomic variation 57–58
  aplasia/hypoplasia 57
  bifurcate/duplicate 57
  congenital pseudoarthrosis (CPC) 57
  deltoid process 58
  depths and angles 54, 59
  fractures 51–52
  geometric variation 53–56, 58–59, *60*
  length 53–54, 58–59
  morphological groups 53, 59, *60*
  thickness **54,** 55–56, 59
  width **54,** 55, 59
cleft sternum 78, *79*
cleidoatlanticus muscle 231
cleidocervicalis (levator claviculae) muscle 231, 232, 264, *265, 266*
cleidocranial dysostosis (CCD) 57
cleidoepistrophicus muscle (cleidoaxial muscle of Gruber) 231
cleidofascialis muscle 229
cleidohyoideus muscle 229
cleidomastoideus muscle 231, *265*
cleido-occipitalis cervicalis muscle 263–264, *265*
cleido-occipital platysma muscle 229
clinodactyly 70, 159
clinoid processes, bony bridge between 7
clitoris 1379
clivus
  bony canal in 4, *5*
  emissary veins 819
cloaca, persistent 1376
Cloquet's nodes 935
cluneal nerves 1060–1061
coarctation of aorta 513, *516–517*
coat-hook exostosis 92
coccygeal ganglion 1051–1052
coccygeal gland (Luschka's gland) 669

coccygeal nerves 1060, 1118–1119
coccygeal plexus 1127
coccygeal ribs 38, 78
coccygeofemoral muscle 387
coccygeus (ischiococcygeus) muscle 382
coccyx 37, 38
cochlea 1177–1178
cochlear aqueduct, enlarged 1179
cochlear nerve
  communication with other nerves 1034
  facial nerve relations 1008, *1009*
cochleovestibular hypoplasia 1178
cochleovestibular malformations 1177–1178
Cocket perforators 908
collateral fissure 942
collodion babies 1139
colobomas, eyelid 1135–1137
colon 1301–1302, 1308–1314
  atresia 1302
  blood supply 654–655, 1310
  descending *see* descending colon
  diverticulum 1302
  duplication 1301–1302
  implications of variations 1312–1314
  left colic flexure *see* splenic flexure of colon
  mesocolon of ascending 1301
  normal anatomy 1308
  sigmoid *see* sigmoid colon
  variations 1309–1310
common bile duct 1268
  absence 1267–1268
  development 1261
  double 1268
  ectopic termination 1268
  pancreatic duct junction 1268, 1280
common carotid artery (CCA) 449, 475
  bifurcation 475, 477
common cavity malformation of inner ear **1177,** 1178
common facial vein 821
common fibular (peroneal) nerve 1121, 1122–1123
  origin **1119,** 1121, 1122
  piriformis relations **394,** 396, *399,* 1121–1122
common hepatic artery (CHA) 627–629
  absent 627
  branching pattern 627–629
  origin *622,* 623, *624,* 625, 627, 650
  replaced 627
common hepatomesenteric trunk (CHMT) 651
common iliac arteries (CIA) 669–670
  bifurcation 695
  bilateral absence 620, 669, 697
  branches 670
  dimensions 669, 695
  embryonic development 699–700
  unilateral absence 697
common iliac vein 894–897
  agenesis 895
  continuation into double IVC 878, *880*
  duplication 894, *895*
  high junction 895, *896*
  internal iliac vein drainage patterns and 896
common inferior phrenic artery (CIPA) *622,* 623
common interosseous artery 600, *603,* 604, 606
common palmar digital arteries 606, 609
common palmar digital nerves 1086, 1091
common peroneal nerve *see* common fibular nerve
common plantar digital nerves 1125
common sigmoid trunk *652,* 653, *654*
communicating branch to glossopharyngeal nerve 1017
communicating vein of neck 822
complexus muscle 280
compressor bulbi muscle 384
compressor hemisphericum bulbi muscle 384
compressor venae dorsalis muscle 384
concha bullosa 1161
conductor sonorous 956
condylus tertius 3
cone artery (of Desproges-Gotteron) 768
cone-shaped epiphyses
  foot 106
  hand 69, 158
congenital adrenal hyperplasia 1374
congenital fibrosis of extraocular muscles (CFEOM) 1139
congenital pseudoarthrosis of clavicle (CPC) 57
conjoined gemellus–obturator tendon 403, *404*
conjoint piriformis-obturator internus tendon 400, 403
conjoint tendon of knee 188
conjunctiva 1148–1149
conus artery (third coronary artery) 562, *563*
conus ligament (tendon of infundibulum) 1241
conus medullaris, anastomotic loop (cruciate anastomosis) 753, *754,* 765, 768
Cooper's ligament 149–150
coracoacromial ligament 46, *47*
coracobrachialis accessorius muscle 293
coracobrachialis inferior (longus) muscle 293
coracobrachialis minor (secundus) muscle (of Gruber) 293
coracobrachialis muscle 293
  musculocutaneous nerve relations 1080
  nerve to *1078,* 1080
coracobrachialis superior (brevis) muscle 293
coracocapsularis muscle 293
coracoclavicular joint 43, *44,* 127
coracoclavicular ligaments 43, 44
coracoclavicular syndesmosis 58
coracohumeral ligament 125, 337
coracoid process, scapula 43–44, 127
coracoscapular ligament 44
cornea 1146–1148
corneal thickness
  corneal hydration and 1148
  diurnal variations 1146–1148
  ethnic variations 1146
  female reproductive cycle and 1148
Cornelia de Lange syndrome 64, 1141–1142
corniculate cartilages (Santorini) 1210
corona mortis 720–721
coronary arteries 502–505, 530–562
  absent 548–549
  crossing 553
  ectasia and aneurysm (CAn) 548
  extracardiac circulation 562
  hypoplasia 549
  inadequate arteriolar/capillary ramifications 557
  meandering/tortuous 559
  mixed trunks 541–542, *546–547*
  muscular bridging/intramural 549–552
  normal anatomical features **531**
  preferential pathways 530, *533*
  single 505, 541–542, *544–547*
  subendocardial course (SEC) 552–553
  three elementary trunks 530, **531,** *532*
  typology and dominance 559–562, *563*
  woven 556
coronary arteriovenous fistulae (CAVF) 557–558

coronary artery anomalies (CAAs) 530–559
anastomotic vessels 558–559
classification 530, **532**
intrinsic anatomy 547–557
multiple concomitant (and atypical) 559
origin and course 502–505, 532–547
termination 557–558
coronary ligament, knee 190–191
coronary ostium
anomalous location within/near proper aortic sinus *504,* 505, 532–534, *536*
congenital stenosis or atresia (COSA) 547–548
dimple 548
location outside normal facing aortic sinus 505, 534–540
number 505, *506*
coronary sinus (CS) 855, *856, 857,* **868**
enlargement 842, *843–844,* 866
pathological persistence of valves 865–866
tributaries 855–860
valves 865, 1237, *1238*
variations and anomalies 866–867
coronoid fossa, distal humerus 130
coronoid process of mandible
elongation 15, 120
hyperplasia 120
union with maxilla 120
coronoid process of ulna 140
cartilage thickness 143
height (CH) 141–143
length and width 142
morphological variations 143–144
corrugator supercilii muscle 221
corticospinal tract 988
cor triatriatum dexter 865–866
cor triatriatum sinister 872
costal articulations 30
costocervical trunk 581
costoclavicularis muscle 346
costoclavicular ligament, radiographically visible 58
costocoracoideus (chondrocoracoideus) muscle 269, 345
costocoracoid ligament 76
costo-deltoideus muscle (of Calori) 291
Cowper's syringocele 1358
coxa valga 176
coxa vara 176
cranial nerves 989–1047
cranial sutures, accessory 6
craniocervical junction
bone anomalies, vertebral artery effects 488, *493*
muscles 245–252
cremaster muscle 374
cricocorniculate muscle 260
cricoepiglottic muscle 257, *258*
cricohyoid muscle 254
cricoid cartilage 1210, 1211
cricomembranous muscle 257
cricopharyngeal diverticulum 1248, *1249*
cricothyrohyoid muscle 256, *257*
cricothyroid muscle 237, 254–256, *255*
cricotracheal muscle 254
crista galli, pneumatization 12
crista interosseous fibularis 95–96
crista interosseous tibiae 94
crista terminalis 1235–1236
cruciate anastomosis, conus medullaris 753, *754,* 765, 768
crural cistern 963
Cruveilhier's cervical plexus 1058, 1059
cryptophthalmos 1133–1134
cryptorchidism 1347–1349
cryptotia 1169–1170
cubital fossa
median nerve entrapment 1087
superficial veins 829
cubital tunnel syndrome 1091
cuboid 100–101, 204
cuboid accessorium 100–101
cuboidal sesamoid 425
cuboid ossicle, secondary 101
cubonavicular coalition 102
cuneiform bones 102–104
accessory ossicles 103–104
coalitions 103
cuneiform cartilages (Wrisberg) 1210
cuneocuboid coalitions 102
cup ears 1173
Cupid's bow contour, vertebral endplate 34
cutis laxa, congenital 1139
cyamella (popliteal fabella) 93, 94
cystic artery (CA) 630–631, 1268–1269
bile duct relations 631
hepatobiliary (Calot's) triangle 631, 1268
multiple 630–631, 1269
origin *624,* 631, 635, 1268–1269
cystic cochleovestibular malformation 1178
cystic duct 1265–1266
cystic fibrosis transmembrane conductance regulator (CFTR) gene mutations 1355, 1356
cystoduodenal ligament 1262
cystohepatic duct 1267

Darwin's tubercle 1173
deep auricular artery 117
deep brachial artery 597
median nerve relations *596*
origins 584, *588–589,* 593, 597
types 597, *598–600*
deep cerebral veins 800–809
deep cervical arteries 581
deep femoral artery (profunda femoris) 742, *743*
deep fibular (peroneal) nerve 1123
deep infrapatella bursa 183
deep levator muscle of thyroid gland 255
deep lymph vessels, lower limb 936
deep palmar arterial arch 606–609, *610, 611*
deep petrosal nerve 1027, 1047
deep plantar arterial arch 748–749
deep transverse perineus muscle 384
deep vein of thigh (profunda femoris vein) 904, *905*
deep veins of leg and foot 906–907
deep veins of lower limb 903–907
deep veins of upper limb 826
deep vein thrombosis (DVT) 880–881, 903
Delachapelle's tubercle 15
deltoid muscle 290–291, 1099
deltoid process, clavicle 58
dens, retroverted 27
dens bicornis 27
dentate nucleus 957
denticulate (dentate) ligaments 978, 985
depressor anguli oris muscle 219
depressor labii inferioris muscle 219
depressor septi nasi muscle 220
dermal back flow (DBF), lymph 937
dermomyotome 33
descendens hypoglossi (or cervicalis) 1045–1046, 1062
descending aorta
coronary artery origin 534
double 521
descending colon
normal anatomy 1308
variations 1309
descending genicular artery (DGA) 743–744
dextrocardia 1234

diaphragm 348–349
diaphragma sellae 976
  arachnoid membrane 969–970
  subarachnoid cisterns 960
diaphragma sellae foramen 976
diaphragmatic hernias 349
  intrathoracic ectopic kidney 1319, 1320–1321
diaphyseal cuff, pedal phalanges 106
diencephalic leaf (DL), Liliequist membrane 964, 966, 968–969, 970, 971
diencephalic-mesencephalic membrane (DML) 969–970
diethylstilbestrol (DES) 1371, *1372*
digastric muscle 228, 1017
DiGeorge syndrome 914–915
diphallia 1343
diploic veins (DVs) 770–774
  arachnoid protrusions (APs) 771–773
  cadaveric dissection 770, 773
  laboratory investigation 770, 773, *774*
  magnetic resonance imaging 770–773
  major pathways 770–771, 773
distal femoral epiphyses 91–92
distal fibular epiphysis 95
distal humerus 130–134
distal tibial physis 95
distichia 1141
diverticulum of Kommerell 507–509, 512, *515,* 576, *577*
dorsal arterial system of foot 746–748
dorsal astragaloscaphoid 100
dorsal carpal arterial arch 606, 609, *612–613*
dorsal (posterior) cutaneous branch of ulnar nerve 1090, 1093
dorsal cutaneous nerves of foot 1124
dorsal digital nerves of foot 1123
dorsal digital nerves of hand 1090, 1100
dorsal digital veins, hand 827, *828*
dorsal fissural artery of Cordier and Cabral 572
dorsal interossei muscles of foot 447
dorsal interossei muscles of hand 324–325, 326, *327*
dorsalis pedis artery (DPA) 746
dorsalis pedis veins 907
dorsal lobe (superior accessory fissure) of lung 1217–1220
dorsal median veins 911
dorsal meningeal artery 450
dorsal metacarpal arteries 609
dorsal metacarpal veins 827, *828*
dorsal metatarsal arteries
  first (FDMA) 747
  II, III and IV 748
dorsal metatarsal veins 907
dorsal pancreatic artery (DPA) 636–638, 644, 650
dorsal scapular artery 581, 1072
dorsal scapular nerve 248, 1076
dorsal sulcal veins 910
dorsal talonavicular ossicle 100
dorsal tarsometatarsal ligaments 205
dorsal venous arch of hand 827, *828*
dorsoepitrochlearis muscle 268, *269,* 296
dorsofascialis muscle 263
dorsolateral calcaneocuboid ligament 205
dorsomedial/dorsotibial hallucal artery 748
Down syndrome
  ocular anomalies 1137
  pelvic bone anomalies 86
  radial artery patterns 604
dromedary hump, left kidney 1325
drunken waiter sign 102
Dua's layer 1148
ductus arteriosus 501, *502,* 520, 569
  patent 520, *521,* 569
ductus diverticulum 519–520
duodenum 1289–1291
  diverticulum 1289–1290
  duplication 1290
  ptosis 1289
  stenosis or atresia 1289, 1292
  suspensory ligament 1290–1291
dural folds 974–976
dural sac (DS) 976–977
dural venous sinuses 775–795
  cavernous spaces 794
  chordae Willisii 794–795
  confluences of 778–780
  diploic vein connections 770–771
dura mater 974–977
  duplication 977
  spinal 985
dysphagia lusoria 509, 576, 577
dystopia canthorum 1133

ear 1167–1179
  external 1167–1173
  extrinsic muscles 221
  inner 1177–1179
  middle *see* middle ear
  protruding 1169
ear lobe indentations/pits 1173
ectodermal dysplasia syndromes 1135
ectropion 1139–1140
eighth cervical nerve (C8)
  brachial plexus 1069, *1070,* 1074, 1075
  scalenus anterior relations 248
elbow, veins 827–829, *830*
elbow joint 130–155
  capsule 147–149
  distal humerus 130–134
  ligaments 147, 149–155
  proximal radius 135–139
  proximal ulna 140–147
Ellis–van Crefeld chondroectodermal dysplasia 162
eminentia mandibularis 116
eminentia orbitalis 14
emissary veins 817–819
empty sella syndrome 948
entropion 1140
epiblepharon 1140–1141
epicanthus (epicanthal folds) 1137
epicardial veins 854, 855–860, **868**
epiglottis 1210
epiphrenic diverticulum 1248, *1249*
epipteric bone 6
episcleral melanosis 1148–1149
epispadias 1335–1338
episternal ossicles 78–79
epistropheobasilaris muscle 252
epitarsus 1137
epitransverse process, atlas 26, *27*
epitrochleoanconeus (anconeus epitrochlearis) muscle 296, 300
  innervation 1092
  ulnar nerve entrapment 1091
epitrochleo-olecranonis muscle 296
erector spinae muscle 279–280
esophageal arteries 524–526
esophagotracheal cleft 1250
esophagus 1247–1251
  atresia 1248–1250, *1251*
  congenital stenosis 1251
  diverticulum 1247–1248, *1249*
  duplication cyst 1248, *1250*
  failure of separation from trachea 1250
estrogen
  breast development and 1394–1395
  corneal thickness and 1148
ethmoidal arteries 452
ethmoidal foramina, accessory 12
ethmoid bone 12, 1162–1164
  air cells 12, 1162–1163
  uncinate process 1164
ethmomaxillary sinus 1163
euryblepharon 1137
Eustachian tube 1177

Eustachian valve 865, 1237
exomphalos 1285
extensor carpi radialis accessorius muscle 304
extensor carpi radialis brevis muscle 304, 1103
extensor carpi radialis intermedius muscle 304
extensor carpi radialis longus muscle 304
extensor carpi ulnaris muscle 306
extensor digiti III muscle 307
extensor digiti IV muscle 307
extensor digiti medii muscle 307
extensor digiti minimi accessorius muscle 305
extensor digiti minimi (proprius) (manus) muscle 305–306
extensor digitorum brevis manus muscle 308, 327, 332, 333
extensor digitorum brevis muscle 438–440
extensor digitorum communis muscle 304–305
extensor digitorum longus muscle 422–423
extensor hallucis brevis muscle 438
extensor hallucis capsularis muscle 422
extensor hallucis longus muscle 422
extensor indicis et medii communis muscle 308
extensor indicis muscle 307–308
extensor pollicis brevis muscle 307
extensor pollicis longus muscle 307
extensor tricaudatus of Gruber 422
external abdominal oblique muscle 371–373
external anal sphincter (EAS) 382–383, *385*
  nerve supply 383, 1127
external acoustic meatus 1173–1175
external carotid artery (ECA) 477–483
  branches 477–483
  hypoglossal nerve relations 1045
  origin 475, 477
external carotid plexus 1053
external ear 1167–1173
external iliac artery 697
  absence 697–699
  obturator artery origin 711–721
external iliac vein 898
external jugular vein 821–822
extraocular muscles 207–209
  congenital fibrosis of (CFEOM) 1139
  supernumerary 208, 210
eye(s) 1145–1151
  color 1150–1151, *1152*
  drainage apparatus 1149–1150
  extrinsic muscles 207–210
  facial muscles around 220–221
  globe protrusion 1145
  increased distance between 1133
  refractive error 1145–1146
eyebrows 1141–1142
  absent 1141
  thick 1141–1142
  white 1141
eyelashes 1141–1142
  absent 1141
  ectopic 1141
  thick 1141
  white 1141
eyelids 1133–1141
  abnormal position 1138–1141
  congenital retraction 1140
  major malformations 1133–1137

fabella
  common 93–94
  popliteal (cyamella) 93, 94
fabellofibular ligament 189–190, 191
facet joints, vertebral 31, 35
facial artery 478–479
facial asymmetry 1130–1131
facial (Fallopian) canal
  aberrant course 1010
  dehiscence 1009–1010, 1011–1012, 1014, 1175
  facial nerve 1005
  hump anomaly 1013
  subarachnoid space 972, 1011
facial colliculi 954–955
facial muscles 217–226
  around eyes 220–221
  around mouth 217–219
  around nose 219–220
facial nerve (CN VII) 1005–1029
  aberrant endotemporal course 1010, 1012–1016
  anastomoses among terminal branches 1025–1026
  anastomoses with other nerves 1027–1029
  arterial contacts in cerebellopontine angle 1006–1008
  branching 1016–1029
  buccal branch 1023–1024, 1028
  canalicular segment 1008–1009
  cervical branch 1024–1025
  cisternal segment 1006–1008
  duplication or fenestration 1010, 1014
  endotemporal division 1010, 1012
  endotemporal variations 1009–1016
  extratemporal branches 1017–1018
  foramen of Luschka relations 951
  geniculate segment 1011
  hump anomaly 1013
  labyrinthine segment 1011
  middle ear 1175, **1176**
  parotid gland relations 1017–1018
  parotid region veins and 1026–1027
  pre-parotid branches 1017
  prolapse or displacement 1009–1010, 1011–1012, 1014, 1175
  segments 1005
  sensory auricular branch 1017
  sensory ganglia 1009
  temporal branch 1023
  terminal branching and anastomoses 1018–1029
  tympanic and mastoid segments *1010,* 1011–1016
  vagus nerve anastomoses 1029, 1043
  zygomatic branch 1023
facial vein 821
facies externa accessoria corporis tali 204
falcine sinus 783, 786
falcine venous plexus 786
Fallopian canal *see* facial canal
Fallopian tubes *see* uterine tubes
false tendons, ventricular 1241, *1242–1244*
falx cerebelli 975–976
falx cerebri 974, *975*
fat pad, infrapatellar 185
female genital tract 1364–1379
  arterial supply 725–729
  see also Müllerian duct anomalies
femoral acetabular impingement (FAI) 178
femoral artery 741–742
  deep branches 742–743
  obturator artery origin 712
  persistent sciatic artery and 700, *701,* 741
  proximal branches 742
femoral branch of genitofemoral nerve 1115–1116
femoral condyles 92
  arterial supply 744
  orientation 181–182
femoral head
  developmental spur 90
  ligamental plicae 177
  ossification center 90
femoral intercondylar notch 181–182
femoral intercondylar space 92, 744

femoral neck 176
angle 176
herniation pit 90
notch 90
plicae 177
white line 90
femoral neck/shaft angles 90–91
femoral nerve 1114, 1117
iliacus muscle relations 375, 376, 377
femoral vein 903–904
femur 90–92
anteversion 108
distal 91–92, 181–182
proximal 90–91, 178
shaft 91
fetal alcohol syndrome 1138
fibrous dysplasia, temporomandibular joint 122
fibula 94–96
distal 95–96
proximal 94–95
shaft 95
fibular collateral ligament (FCL) 188–189, 424
fibularis (peroneus) brevis muscle 425
fibularis (peroneus) digiti minimi (quinti) muscle of Huxley 426
fibularis (peroneus) longus muscle 424–425
fibularis (peroneus) quartus muscle 425–426
fibularis (peroneus) quinti digiti muscle 424
fibularis (peroneus) tertius muscle 423–424
fibular lymph node 936
fibular ossicle (os retinaculi) 96
fibulocalcaneocuboideus muscle 426
fibulocalcaneus internus muscle of Macalister 432
fibulocuboideus muscle of Chudzinski 426
fifth cervical nerve (C5)
brachial plexus 1069, *1070,* 1073–1074
phrenic nerve origin 1064
scalene muscle relations 247, 248
serratus anterior innervation 276
fifth lumbar vertebra (L5), sacralization of 36, 37
fifth metatarsal tuberosity, persistent apophysis of 105
fifth metatarsophalangeal (mtp) sesamoids 105
filum terminale (FT) 979, 987
first arch syndrome 122
first cervical nerve (C1) 1057–1058, 1062
dorsal ramus 1057, 1058
dorsal root ganglion 1057, 1058
dorsal roots 1057–1058
first dorsal interosseous muscle 324, 1089
first dorsal metatarsal artery (FDMA) 747
first jejunal artery 644, 649
first lumbrical muscle of foot 445
first lumbrical muscle of hand 321, *322,* 324
first palmar interosseous muscle 325
first sacral vertebra (S1), lumbarization of 36, 37
first septal artery, ectopic origination 557
first thoracic nerve (T1) 77, 1060
brachial plexus 1069, *1070,* 1073, 1074
fissura sterni 78
fissured tongue syndrome 243
flexor carpi radialis brevis muscle 299, 303
flexor carpi radialis muscle 299, 1088
flexor carpi radialis profundus muscle 299
flexor carpi ulnaris muscle 300, 1090, 1092
flexor digiti minimi brevis muscle 447
flexor digiti minimi muscle 320, 329, 333
flexor digitorum accessorius longus (FDAL) muscle 431–432, 445
flexor digitorum brevis muscle 442–443
flexor digitorum longus muscle 430–431
flexor digitorum profundus muscle 301–302
innervation 1088, 1090, 1092
flexor digitorum superficialis (FDS) muscle 300–301
innervation 301, 1088
median nerve compression *1087*
flexor hallucis brevis muscle 445, *446*
flexor hallucis longus (FHL) muscle 431
flexor pollicis brevis muscle 316–317, 332
innervation 317, 1089
flexor pollicis longus muscle 302–303, 1088
Flood's ligament 125
Flower's bone 6
fontanelle of Hamy 5
foot
anomalies 107
arteries 745–749
bursae 205
coalitions 101–102
deep veins 906–907
intrinsic muscles 438–448
joints 204–205
ligaments 205
perforating veins 907–908
sesamoid bones 105–107
skeletal variations 96–107
foramen cecum 1189–1190
emissary vein 819
foramen lacerum
accessory ossicles 11
emissary veins 819
foramen magnum
keyhole 5
shape 4–5
foramen of Civinini 7
foramen of Hüschke 10–11
foramen of Hyrtl 7, 8
foramen of Luschka 950–951
foramen of Magendie 950
foramen of Monro 947
foramen of Vesalius 8
foramen ovale (of heart), patent 1234–1235
foramen ovale (of skull) 8
accessory 998
emissary veins 818
middle meningeal artery 480
foramen rotundum 7–8
foramen spinosum 8
absent 8, 468, 480
foramen thyroideum 1209
foramen tympanicum 11
foramen venosum (of Vesalius) 8
forearm
bones 68
muscles 298–308
sesamoid bones 68
veins 827–829, *830*
forebrain 939–942
foreskin 1345
fossa ovalis 1234–1235
fourth cervical nerve (C4)
brachial plexus 1069, *1070,* 1072–1073
phrenic nerve origin 1064
fourth dorsal interosseous muscle 325
fourth lumbrical muscle of foot 445
fourth lumbrical muscle of hand *322,* 323, 324
fourth palmar interosseous muscle 326
fourth thyroid vein (of Kocher) 823
fourth ventricle 950
fovea capitis 90
foveae articulares craniales atlantis 26
fovea radialis 135, 137, 139
Fraser's syndrome 1134
Froment-Rauber anastomosis 1102
frontal bone 1–3
frontal nerve 995

frontal sinus
absent ostium 1
agenesis 1
pneumatization 1164
septation 1
frontobasal bridging vein (FBBV) 811
frontopolar artery 455
Froriep's ganglion 1058
furcal nerve 1114

Galenic venous system 806–807
see also vein of Galen
Galen's anastomosis 1043
gallbladder 1261–1265
accessory (double) 1263, *1264–1265*
agenesis 1263, *1264*
attachments 1261–1262
bilobed 1263
development 1261
diverticulum 1263
ectopic 1265
floating/hanging 1262
intrahepatic 1262
left-sided 1264–1265
malposition, portal vein anomaly with 882
Phrygian cap 1262
retrohepatic 1265
septate 1262–1263
triple 1263
volume 1261
wall, ectopic tissue 1265
ganglia of Takeda 1054
ganglion impar 1051–1052
ganglion of Svitzer 1053
Gantzer's muscle 301, 302
gastrocnemius bursa 183
gastrocnemius muscle 194, 426–427
venous plexus 906–907
gastrocnemius tertius muscle of Kelch 427
gastroduodenal artery (GDA) 632–635
absent 632
bile duct relations 633
branches 633–635
course 633
origin *624,* 627–629, 632–633, 650
gastrointestinal tract
duplication 1292–1293, 1301–1302
segmental aplasia 1254
gastrosplenic trunk 635
gemelli muscles 401–403
gemellus inferior muscle 402–403
femoral attachment 403, *404*
innervation 1119
gemellus superior muscle 401–402
association with piriformis 400
femoral attachment 403, *404*
innervation 1119–1120
Genee-Wiedemann syndrome 1136, 1140
geniculate ganglion 1005, 1009, 1011
genioepiglottic muscle 261
genioglossus muscle 241
geniohyoid muscle 229
geniopharyngeus muscle (of Winslow) 241
genital branch of genitofemoral nerve 1115–1116
genitofemoral nerve 1114, 1115–1116
genu recurvatum 182
genu valgum 109, 182
genu varum 109, 182
geometric morphometrics, clavicle 53–56, 58–59, *60*
glands of Manz 1155
glands of Stöhr 1186
glaucoma, primary angle-closure (PACG) 1149
glenohumeral joint 124–126
capsule 125
ligaments 125
tendons 125–126
glenoid fossa 124
positions 124
shape 44–45
glenoid hypoplasia 126
glenoid labrum 45, 124
glossoepiglottic muscle 261
glossopalatine ankylosis 243
glossopharyngeal nerve (GN) 1036–1039
anastomotic branches 1039
carotid branch 1037–1038
communicating branch to 1017
extracranial course 1037
facial nerve anastomoses 1027, 1028–1029
intracranial course 1036–1037
lingual division and branches 1038–1039
muscular branches 1038
origin from brainstem 1036
pharyngeal branches 1038
tympanic branch 1037
vagus nerve anastomoses 1039, 1041–1043
gluteal muscles 386–394
gluteal ridge, enlarged 91
gluteoperinealis muscle 387
gluteus maximus muscle 386–387
gluteus medius accessorius muscle 388–389
gluteus medius muscle 387–389, **390**
fusion with gluteus minimus 388, *391,* 393
fusion with piriformis 388, *391, 392,* 400
gluteus minimus muscle 389–394
accessory muscles 394
fusion with gluteus medius 388, *391,* 393
fusion with piriformis 400
gluteus quartus muscle **394**
Goethe's ossicles 6
Goldenhar's syndrome 122, 1135–1136
gonadal arteries 662–665
gonadal veins 892
gorilla ribs 35, 78
gracilis muscle 414–415
great anterior radicular artery (of Adamkiewicz) 524, 761, 762–764
anterior spinal artery junction 761–762
summary of variations 767–768
two or more 763, 764, 767–768
great anterior radiculomedullary vein (GARV) 911
great auricular nerve 1027, 1062–1063
great cardiac vein (GCV) 855, *856, 857,* **868**
great cerebral vein *see* vein of Galen
greater occipital nerve 1059
greater pancreatic artery 638
greater petrosal nerve 1011, 1027
greater sigmoid notch (GSN) 140, 146–147
greater splanchnic nerve 1052–1053
greater trochanteric epiphysis 90
greater vestibular glands 1379
great knob of Keats 104
great saphenous lymph vessels 936–937
great saphenous vein 901–903
Griffiths's point 654–655
growth recovery (arrest) lines 91
Guyon's canal 1091
ulnar nerve compression 328–329, *330,* 331, 1091, *1092*
ulnar nerve trifurcation 1093
gynecoid pelvis 82
gynecomastia 1394–1395

Haglund's exostosis 97
Haglund's groove 93
Haglund's heel/syndrome 97
Hahn's clefts 34

Haller cells 1163
Hallermann–Streiff syndrome 122
Hallopeau's nerve 1125
hallucal sesamoid bones 105–106
  congenital absence 106
  multipartite 105–106
hallux
  interphalangeal sesamoid 106–107
  phalanges 106
hallux valgus deformity 106
hamate 72, 162
hamstring muscles 195, 416–418, *419*
hamulus, bipartite 161
hand
  accessory ossicles 71–72
  all-median 1089, 1092
  arteries 606–609, *610–613*
  intrinsic muscles 315–333
  joints 158–163
  ligaments and cartilaginous structures 162–163
  nerve entrapments 328–331
  sesamoid bones 71, 160
  skeletal variations 68–72
  veins 827
handcuff palsy 1101
handedness, ventricular asymmetry and 944–945
hand-foot-genital (uterus) syndrome 1376
hard palate, duplication 13
harlequin fetus 1139
Harris lines 91
Hartmann's pouch 1262
Hay-Wells syndrome 1135
hearing loss, conductive 469
heart 1234–1245
  dimensions 1234
hemiazygos vein 832, 833–836, 892
  IVC anomalies 878
  spinal cord drainage 912
hemifacial microsomia 122
hemilumbarization 37
hemisacralization 37
hemivertebrae 31, 34
hemorrhoidal nerve *see* inferior rectal nerve
hepatic arteries 627–630
  accessory 627
  double 627
  replaced 627
hepatic (bile) ducts 1266–1268
hepaticocystic duct 1267–1268
hepatic veins 881, 884–885
  extrahepatic course 885
hepatobiliary (Calot's) triangle 631, 1268
hepatogastrophrenic trunk 625
hepatopancreatic duct 1280
hepatosplenic trunk 635
hepatosplenomesenteric trunk 625, 636, 641–642
hepatotesticular fusion 1351
Hering's nerve *see* carotid sinus nerve
Herlyn-Werner-Wunderlich (HWW) syndrome 1376
heterotaxy syndrome 1234
hilar arteries of kidney 690–691
Hilfsmuskel 1290
hindbrain 954–958
hip bone *see* os coxa
hip joint 176–179
  capsule 176
  labrum *see* acetabular labrum
  muscles 178–179
hip muscles
  lateral rotator 394–404
  see also thigh muscles
hippus 1151
Hirschsprung disease 1309–1310, 1312–1314
hitchhiker's thumb 71
Hoffa's fat pad 185
hook angle, proximal ulna 145
horseshoe kidney (HSK) 1317–1319
horseshoe lung 1223
hourglass stomach 1254–1255
Hox genes 30, 78, 954
humeral head 124
  retroversion 63, 124
humerus 63–66
  distal 130–134
hyalinosis cutis et mucosae 242
hydrocele 1354–1355
  abdominoscrotal 1355
  communicating 1354–1355
  noncommunicating 1355
hydronephrosis, pelvic kidneys 1316–1317
17α-hydroxylase syndrome 1374
hymen 1377–1379
hyoangularis muscle 228
hyoepiglottic muscle 261
hyofascialis muscle 229
hyoglossus muscle 241
hyoid bone 22–23
hyoido-stapedial artery 468–469
hyperdense lines, iliac and ischial 84
hyperopia 1145–1146
hyperostosis frontalis interna (HFI) 1–3
hypogastric trunk 710
hypoglossal artery, persistent primitive 469–470
hypoglossal canal 4
hypoglossal nerve 1045–1047
  anastomoses 1043–1044, 1045–1047
  carotid artery relations 1045
hypoglossal transverse arch 1045
hypoglossia 242
hypophyseal arteries, accessory 463
hypoplastic coronary artery disease 549
hypospadias 1335, *1336,* 1346
hypothalamic membrane (HL) 970–971
hypothenar muscles 318–321
  duplications simulating tumors 333
  nerve entrapments 328–329
  vascular problems 332
hypothyroid accessory muscle 230
Hyrtl's ansa suprahyoidea hypoglossi 1045

ileal artery 649
ileocecal valve 1299–1300
ileocolic artery (ICoA) 647, 648–649
ileum 1291–1297
  duplication 1292–1293
  Meckel's diverticulum 1293–1297
  non-Meckelian diverticula 1293
  stenosis or atresia 1292, *1293*
iliacus minimum muscle 377
iliacus minor muscle (Winslow) 375, *376*
iliacus muscle 375–377
iliac veins 894–898
iliocapsularis (Harrison) muscle 375, *376*
iliococcygeus muscle 381, 382
iliocostalis muscles 279
iliofemoral ligament 176
iliohypogastric nerve 1114–1115
ilioinguinal nerve 1113–1114, 1115
iliolumbar artery 734–735
  collateral anastomoses 703
  origin **712, 714,** 734, *735*
iliopsoas muscle 375–378
iliopsoas tendon 178–179, 375
iliopubic anastomoses 720–721
iliosacral complex (ILC) 168
ilium
  articular cartilage 165, 166, 170–171, 172
  horns 83
  hyperdense lines 84
  nutrient foramen 83
Inca bone 6
incisurae mediae obliquus bicaudatus 255
incisura fibularis tibiae 95

incomplete partition of cochlea **1177,** 1178
incus 18
inferior alveolar nerve 1000–1001
inferior anastomotic vein *see* vein of Labbé
inferior cervical ganglion 1051
inferior cervical ganglion of Arnold (Luschka or Rüdinger) 1051
inferior concha bullosa 1158
inferior epigastric artery
  obturator artery anastomoses 721, **722–723**
  obturator artery origin 712, **716,** *717*
  origin 724–725
inferior frontal sulcus 941
inferior glenohumeral ligament (IGHL) 125
inferior gluteal artery
  collaterals 703
  origin 703–705, **712, 713**
inferior gluteal nerve **1119,** 1120
inferior gluteal vein 396
inferior hypophyseal artery 450
inferior intercavernous sinus 794
inferior interventricular coronary artery branch *see* posterior interventricular coronary artery branch
inferior interventricular (middle cardiac) vein (IIV) 855, 856, *857, 858–859,* **868**
inferior lateral genicular artery (ILGA) 743–744
inferior left colic artery (descending branch) *651, 652,* 653
inferior medial genicular artery (IMGA) 743–744
inferior medial trochlear notch, ulnar 142, *143*
inferior mesenteric artery (IMA) 651–656, 1310
  absence 651
  branches 652–656
  duplication 651
  origin 642, 651–652
  superior mesenteric communications 650, 655
inferior nasal concha 12
inferior nasal turbinate 1158
  agenesis 1158
  bifid 1158
  paradoxical 1158
  pneumatization 1158
inferior oblique muscle 208–209
inferior orbital fissure 9
inferior pancreaticoduodenal artery (IPDA) 642–645
inferior pectoral nerve 1079
inferior petrosal sinus 784–785, 1037
inferior pharyngeal constrictor muscle 237
inferior phrenic artery (IPA) 656–658, 660, *661*
  branches 657–658
  origin *622,* 623, 627, 656–657
inferior phrenic vein 891
inferior polar renal arteries 660, *661,* 690–691
inferior polar splenic arteries 640
inferior pulmonary veins 871
inferior rectal artery 383, 703
inferior rectal nerve 382, 383, 1127
inferior rectus muscle 207–208, 209
inferior sagittal sinus *775,* 778
inferior suprarenal arteries (ISRA) 661–662
inferior thyroid artery (InTA)
  targets 524, 1189, 1205
  variations 578–579, 1199–1200
inferior thyroid muscle 260
inferior thyroid vein 823, *824,* 1189
inferior tibiofibular joint 205
inferior transverse scapular ligament 45
inferior vena cava (IVC) 877–881
  accessory hemiazygos continuation 838, 878
  azygos continuation 836–838, 878–880
  double 878, *879*
  embryogenesis 877
  gonadal artery relations 665
  intrahepatic course 881
  left 877–878
  partial or total absence 880–881
  renal artery relations *660,* 661
  tributary variation 881
inferior vesical artery **713,** 730–731
inferior vestibular nerve, facial nerve relations 1008, *1009*
infracardiac lobe of lung 1220
infraclavicularis muscle 345
infrahyoid muscles 229–230
  innervation 1044–1045, 1046–1047, 1062
infraorbital canal, small branch 12
infraorbital foramina, accessory 12
infraorbital nerve 996–997, *998,* 1028
infrapatellar plica 184
infrapatellar space 185
infrascapular bone 40, *41*
infraspinatohumeralis muscle 291
infraspinatus minor muscle 290
infraspinatus muscle 290
infratemporal fossa, muscles 224–226
infratrochlear nerve 995, 1028
inguinal hernia, indirect 1354–1355
inguinal lymph nodes 935
inner ear 1177–1179
innominate canal of Arnold 8
innominate foramen, absent 8
insular veins 810, 811
interarytenoid cartilage 1210
interazygos vein 834–836, *837*
intercalary bone 6
intercarotid nerve of De Castro *see* carotid sinus nerve
intercarotid plexus 1041–1043
intercarpal ligaments 162–163
intercavernous sinuses 793–794
interclavicularis anticus digastricus muscle 346
interclinoid tenia/bony bridge 7
intercostal nerve of Kuntz 1073
intercostal nerves, sternalis muscle 357, 358–361
intercostobrachial nerve 1060, *1084*
  medial antebrachial cutaneous nerve communications 1083
  medial brachial cutaneous nerve communications 1082, 1083
intercuneiform coalitions 103
interfoveolar muscle 372
interlobar pulmonary artery 570, *571, 573*
intermalleolar ligament 205
intermamillary distance (IMD) 949
intermediate (second) cuneiform 103
intermediate cutaneous nerve of thigh 1117
intermediate dorsal cutaneous nerve of foot 1124
intermediate nerve of Wrisberg 1006, 1034
intermetatarsophalangeal bursa of Gruber 205
internal abdominal oblique muscle 371, 373–374
internal acoustic meatus (IAM) 1175
  duplication 1175
  facial and vestibulocochlear nerve relations 1008–1009
  facial nerve 1005, 1008–1009
  narrowing 1175
  vestibular–cochlear nerve anastomosis 1034

internal auditory canal *see* internal acoustic meatus
internal brachial ligament 1089, 1091
internal carotid artery (ICA) 449–454
  aberrant 450, 1176
  agenesis (complete absence) 449, 461, 475–476
  carotid sinus nerve relations 1038, 1042
  cavernous segment (C4) 450–451
  cervical segment (C1) 449, 475–476
  clinoidal segment (C5) 451
  communicating segment (C7) 452–454
  hypoglossal nerve relations 1045
  hypoplasia 449
  kissing intrasellar 451
  lacerum segment (C3) 450
  ophthalmic segment (C6) 451–452
  origin 449, 475, 477
  persistent stapedial artery with aberrant 469
  petrous segment (C2) 449–450
internal carotid artery plexus of Rektorzik 449–450
internal carotid venous plexus 819
internal cerebral vein (ICV)
  arachnoid envelope relations 972
  pineal region 805, 806, **808,** 809
  subependymal vein drainage 803–804
internal cricoid muscle 254
internal frontal arteries 456
internal iliac arteries 694–735
  absence 697–699
  Adachi classification 704–706, **707**
  alternative classification systems 706–708, *709–711, 713*
  branches 708–735
  branching patterns 703–708
  collateral connections 702–703
  length and location 695–697
  level of origin 695
  obturator artery origin 711–718
  sex differences 706, **708**
internal iliac vein 897
  drainage into common iliac vein 896
  duplication 897, *898*
internal jugular vein 823
  inferior petrosal sinus junction 785
  small, with contracted jugular foramen 782
internal lateral cricothyroid muscle 257, *258*
internal nasal nerve 995
internal occipital vein **806, 808,** 809
internal pudendal artery 731
  collaterals 703
  origin 703–705, **712, 713,** 731, *732*
internal thoracic artery (ITA) 577–578
  coronary artery origin 534
  sternalis muscle *358,* 361
  suprascapular artery origin 579, *580*
internal thoracic vein 840
internasal sutures *16*
interosseous artery 745
interosseous muscles of foot 447–448
interosseous muscles of hand 324–326, *327*
  biomechanical dysfunction 332
  camptodactyly 333
  innervation 331
interosseous talocalcaneal ligament 205
interparietal bone 6
interpeduncular cistern 961–962
interscalene block 1064
intersigmoid recess 1309, *1312*
interspinales cervicalis longus muscle *see* spinalis cervicis muscle
interspinales muscles 283
intertaloscaphoid 100
intertransversarii muscles 282–283
intertransversarius lateralis longus muscle 247
intertrochanteric trabeculation, femoral 91
intertubercular sulcus, humerus 63
interventricular septum, venous circulation 862
intervertebral discs
  development 33
  variations 34, 36
intervertebral veins 912
intestinal atresia/stenosis 1292, *1293*
intestines 1285–1302
intracranial aneurysms 468, 470, 471
intracranial arteries, persistent fetal 465–472
intraocular pressure (IOP) 1146, 1147–1148
intraparietal sulcus 941
intraparietal sutures, accessory 6
intrascleral nerve loops (Axenfeld) 1149
intrathecal ligaments (ITL) 978
intrathoracic kidney 1319–1321
intrathoracic veins 832–848
iris 1150–1151, *1152*
ischial spine projections 84
ischiobulbosi muscle 384
ischiocavernosus muscle 384
ischiococcygeus (coccygeus) muscle 382
ischiofemoral ligament 176
ischiopubic synchondrosis 83
ischiopubicus muscle 384
ischio-trochanteric ligament 176
ischium
  absence/hypoplasia/duplication 86
  hyperdense lines 84
IVC *see* inferior vena cava
Ivemark syndrome 1227–1228, 1283
  see also asplenia

Jackson's veil 1301
jejunal arteries 649–650
jejunum 1291–1297
  duplication 1292–1293
  non-Meckelian diverticula 1293
  stenosis or atresia 1292, *1293*
jugular bulb 1176
jugular foramen
  glossopharyngeal nerve 1037
  septation and narrowing 4, *5,* 782
jugular nerve 1047
jugulocephalic anastomosis 829–830
junctura tendinae 305

Kabuki syndrome 1139
Kaplan's anomalous branch of ulnar nerve 1093
keratothyrohyoid muscle 230
Kerckring ossicle 5
kidney 1315–1325
  disk (shield, doughnut, pancake) 1321, 1322
  dromedary hump 1325
  ectopia *see* renal ectopia
  embryonic development 689
  floating 1323–1324
  horseshoe (HSK) 1317–1319
  intrathoracic 1319–1321
  L-shaped 1321
  lump (cake) 1321
  pelvic 1315, 1316–1317
  ptosis 1315, 1323
  rotational abnormalities 1322–1323
  sigmoid- (S)-shaped 1319
  solitary functioning (SFK) 1325
  supernumerary 1324
  vascular segments 685
Kirk's arcade 650
Kirner deformity 70, 159
Klinefelter's syndrome 1349, 1395
Klippel–Feil syndrome 28, 1177

Klippel-Trenaunay syndrome 894
knee
  accessory ossicles 93–94
  arterial supply 743–745
  perforating veins *908,* 909
knee joint 181–195
  bursae 183–184
  capsule 182–183
  fat pad 185
  ligaments 186–193
  menisci 185
  musculotendinous variations 193–195
  retinaculum 185–186
  synovial plicae 184–185
knife clasp deformity 35
Kommerell's diverticulum 507–509, 512, *515,* 576, *577*
Krause (accessory lacrimal) glands 1153, 1155, *1156*

Labbé, Charles 812
labia majora 1379
labia minora 1379
labyrinthine aplasia, complete 1178
labyrinthine artery 463
labyrinthitis ossificans 469
lacrimal apparatus 1153–1155
lacrimal artery 451
lacrimal bone 12
lacrimal canaliculus 1154
lacrimal ducts 1153
lacrimal glands
  bilayered 1153–1154
  dimensions 1153
  macrovariant 1154
  subencapsulated 1153
lacrimal nerve 995
lacrimal tissue, ectopic 1155
lactation, breast changes 1394
Ladd's bands 1286, *1287*
lamellar ichthyoses 1139
laminae, thoracic vertebrae 32
lamina terminalis (LT) cistern 960
Langer's muscle *see* axillary arch muscle
large intestine 1301–1302, 1308–1314
laryngeal cartilages 1209–1211
  major 1209–1210
  ossification 1211
  supernumerary 1210–1211
laryngeal muscles 254–261
  supernumerary fascicles 260–261
laryngotracheoesophageal clefts 1250
lateral abdominal muscles 371–374
lateral accessory pudendal artery 731–733
lateral antebrachial cutaneous nerve *1078,* 1080, 1081
  radial nerve communications 1102
lateral basal segmental bronchus 1229, 1230
lateral brachial cutaneous nerve 1103
lateral carotid membrane 969
lateral circumflex femoral artery (LCFA) 743
lateral circumflex femoral vein 904, *905*
lateral collateral ligament (LCL) of elbow 152–155
lateral collateral ligament (LCL) of knee 188–189
lateral condylar groove, distal femur 92
lateral craniopharyngeal canal 9
lateral cricoarytenoid muscle 257, *258*
lateral (third) cuneiform 103
lateral cutaneous nerve of calf 1123
lateral femoral condyle 92
lateral femoral cutaneous nerve 1114, 1116–1117
lateral internal thoracic artery 578
lateral lacunae (of Trolard) 777
lateral ligaments of ankle 205
lateral ligaments of temporomandibular joint 116–117, 121
lateral malleolus 95
lateral meniscocapsular ligament 185
lateral meniscus of knee 185
  discoid 185
lateral nasal wall 1158–1161
lateral occipital sinus 788
lateral patellar plica 184–185
lateral pectoral nerve *1078,* 1079, 1080
lateral plantar artery 745, 748–749
lateral plantar nerve 1125
lateral plantar veins 906
lateral pontomedullary membrane 970
lateral pontomesencephalic membrane (LPMM) 970
lateral posterior choroidal artery 463
lateral pterygoid muscle 224, 226
  maxillary artery relations 121, 480
  TMJ disc detachment 118
lateral rectus muscle 207–208
lateral sacral arteries 669, 733–734
  numerical variations 733–734
  origin **712, 714,** 733
lateral sinus 778, 781
lateral spinal arteries 753
lateral sural communicating nerve (LSCN) 1125–1126
lateral sural nerve 1123
lateral talocalcaneal ligament 205
lateral tarsal arteries (LTAs) 746
lateral thoracic artery
  branches 592
  double *589*
  origins 583–584, *586, 587,* 592
lateral tibial condyle, arterial supply 744
lateral ulnar collateral ligament (LUCL) 152, 153, 155
lateral (cerebral) venous complex 813
lateral ventricles 943–947
  asymmetry 944–945
  body 946–947
  frontal horn (FH) 946
  occipital horn (OH) 945–946
  shape 945
  size 943–944
  temporal horn (TH) 946
laterocavernous sinus 794
latissimocondyloideus muscle 268, *269,* 296
latissimus dorsi muscle 266–269
  attachment variations 266, *267*
  innervation 1098
  variant muscular slips 266–269
laxator tympani major muscle 212
laxator tympani minor muscle 212
least splanchnic nerve 1053
left accessory colic artery 652–653
left anterior descending (LAD) coronary artery 530, **531,** *532*
  abnormal origin from pulmonary artery (ALADPA) 539
  abnormal origin in pulmonary non-facing sinus 540
  absence of septal branches 557
  absent 549, *550*
  muscular bridging/intramural 549, *551,* 552
  origin from opposite sinus 541, *543*
  split/dual 554, *555–556,* **556**
  typology and dominance 560–562
left atrial appendage 1234
left atrium (LA), veins draining walls *855,* 860, **864,** *864*
left brachiocephalic vein (BV) 840–841, 842
left bronchial isomerism 1227–1228
left colic artery (LCA) 652–653
  branches 653, *654*
  origin 650, *651,* 652–653
  supply to splenic flexure 654–655
left colic flexure of colon *see* splenic flexure of colon

left coronary artery *see* left main coronary artery
left gastric artery (LGA) 625–627
accessory 626–627
course and branching 626
double *624,* 626
inconstant branches 627
origin *622,* 623, *624,* 625–626
left gastroepiploic artery (LGEA) 639–640
left hepatic artery (LHA) 629–630
accessory (aLHA) *624,* 630
combined variations 630
origin *622,* 623, *624,* 627–629
replaced (rLHA) 630
left hepatic vein (LHV) 885
left horizontal fissure of lung 1220–1222
left inferior phrenic artery (LIPA) 656–657
left lower bronchus 1230
left main coronary artery (LMCA; LCA)
absent 532, *534*
anomalous location of ostium 505, 534, *536*
common variations 532, *535*
congenital absence (CALM) 549
origin from ascending aorta 534, *537, 538*
origin from brachiocephalic trunk 534
origin from left ventricular outflow tract 534
origin from non-facing sinus 534, *536*
origin from opposite sinus *503,* 505, 541, *542–543*
origin from pulmonary artery (ALCAPA) 505, 537–539
left marginal vein (LMV) of left ventricle 855, 856, *857,* **868**
left middle colic artery 653
left middle lobe of lung 1220–1222
left posterior (posterolateral) vein (LPV) of left ventricle 855, 856, *857,* **868**
left pulmonary artery 569
lobar branches 572–573
sling 1226, *1227*
left subclavian artery
isolation, right aortic arch with 512–513
right aortic arch with aberrant 512, *513, 515,* 575, 576
left upper bronchus 1229–1230
left ventricle (LV)
false tendons 1241, *1242–1244*
papillary muscles 1238
veins draining 855–860
left ventricular outflow tract (LVOT), coronary artery origin 534–537
leg length inequality 108
leg muscles 421–432
anterior compartment 421–424
deep posterior compartment 429–432
lateral compartment 424–426
superficial posterior compartment 426–429
leg perforating veins 908
lens 1151
lenticulostriate arteries 456
lesser internal cutaneous nerve *see* medial brachial cutaneous nerve
lesser knob of Keats 104
lesser occipital nerve 1059, 1063
lesser palatine canal 13
lesser petrosal nerve 1054
lesser splanchnic nerve 1053
lesser trochanteric epiphysis 90
levator ani muscle 381–382
blood supply 382
nerve supply 382, 1127
levator ani nerve 382
levator claviculae muscle *see* cleidocervicalis muscle
levator costae primae muscle 348
levatores costarum brevis and longus muscle 283
levator glandulae thyroidea (of von Sömmerring) 230–231, 1192–1194, **1195**
levator labii superioris alaeque nasi muscle 219
levator labii superioris muscle 219
levator palpebrae superioris muscle 209–210, 1138
levator scapulae muscle 269–272
aberrant slips and splits 269–272, *273*
attachment variations 269
levator tendinis latissimus dorsi muscle (of Gruber) 269
levator veli palatini muscle 240
levoatriocardinal vein 846–847
ligament of Bessel–Hagen 205
ligament of Humphrey 189, 192
ligament of Struthers 64, *65,* 1086–1087
ligament of Wrisberg 189, 192
ligamentum costo-pleuro-vertebralis (of Zuckerkandl) 250, 1071
ligamentum mucosum 184
ligamentum teres 176
Liliequist membrane (LM), arachnoid 962, 964–971
absence 972
classification 964, 969
diencephalic leaf (DL) 964, 966, 968–969, 970, 971
double (types A and B) 966, *968*
Froelich et al. (2008) study 966–968
hypothalamic leaf (HL) 970–971
mesencephalic leaf (ML) 964, 966, 969, 970–971
posterior communicating artery relations 968–969
presence 964
single (type C) 964–966
triple 969–971
limb deficiencies 108
limbus vertebra 30, 34
linea aspera 91
linea aspera-pilaster complex 91
linea quadrati 91
lingual artery 479
lingual branch of facial nerve 1017
lingual branch of glossopharyngeal nerve (LBGN) 1038–1039
lingual branch of vagus nerve 1043–1044
lingual frenulum, absence 242
lingual nerve 1000, 1017
lingual thyroid 1198
lingua plicata 243
lingular artery *572,* 573
lipomyelomeningocele (LMMC), caudal 986
Lisfranc's ligament 205
liver 1272–1275
accessory grooves 1272
accessory lobes 1273–1275
ectopic tissue 1275
left lobe agenesis/hypoplasia 881–882, 1273
right lobe agenesis/hypoplasia 881, 1272–1273
Lobstein's anastomoses 1043
Lockwood's tendon 207
locus coeruleus 955
long buccal nerve 999
long ciliary nerve 995
longissimus muscles 279
longitudinalis linguae inferior medius 241
long subscapular nerve *see* thoracodorsal nerve
long thoracic nerve 248, 276, *1070,* 1076–1077
longus capitis muscle *249,* 252

longus colli muscle *249,* 250–252
  nerve to 1077–1078
lop ears 1171–1173
lower lateral brachial cutaneous nerve 1099
lower limb arteries 741–749
  embryogenesis 741
  femoral artery and branches 741–743
  foot and ankle 745–749
  knee 743–745
lower limb bones 89–109
  deficiencies 108
  imaging and normal variations 89–90
  length inequality 108
  rotational variation 108, 182
lower limb lymphatics 935–937
lower limb nerves 1113–1127
lower limb veins 900–909
  deep 903–907
  developmental anomalies 900
  perforating 907–909
lower subscapular nerves 1095–1097
lowest splanchnic nerve 1053
lumbar arteries 665–667, 703
lumbarization of S1 36, 37
lumbar multifidus muscles 280
lumbar nerves/nerve roots 1060, 1113–1114
lumbar plexus 1113–1118
lumbar ribs 35, 78
lumbar segment veins 912
lumbar sympathetic ganglia 1051
lumbar veins 891
lumbar vertebrae 33–36
  anatomic variations 34–36
  embryology 33–34
lumbosacral plexus 1113–1127
  postfixed 1114
  prefixed 1114
lumbosacral transitional vertebrae (LSTV) 36, 37, 169
lumbosacral trunk 1114, **1119**
lumbrical muscles of foot 445
lumbrical muscles of hand 321–324
  camptodactyly 333
  median nerve compression 330–331, *1087*
  radial palmar swelling 333
  trigger finger 332
lunar tubercle (of Mouchet and Jeanne) 68
lunate
  accessory ossicles 72, 160
  coalitions 161
  morphology 72, 162
lung fissures 1217–1222
  horizontal (minor) 1217, *1218*
  oblique (major) 1217, *1219–1220*
  supernumerary 1217–1222
lungs 1217–1230
  agenesis/aplasia 1222–1223
  horseshoe 1223
  hypoplasia 1222–1223, 1342
  sequestration *see* pulmonary sequestration
lunotriquetral coalitions 72, 161
lunotriquetral ligaments 162–163
lunula 71
Luschka's duct 1267
Luschka's gland 669
lymphatic vessels
  large trunks/ducts 921–932
  lower limb 936–937
lymphedema, lower limb 937
lymphedema-distichiasis syndrome 1139, 1141
lymph nodes, lower limb 935–936

macroglossia 242
macrotia 1169
Madelung deformity 161
magistral splenic artery 641
malaris muscle 220–221
male genitourinary system 729, 1335–1358
malleolus
  accessory (third) 95
  ossification centers 95
malleus 17
malrotation of midgut 1285–1288
  hyper-rotation 1288
  mixed/partial/incomplete rotation 1286, *1287*
  nonrotation 1285–1286
  reverse rotation 1286–1288
  vascular changes 1310, 1312
mamillary bodies
  distance between 949
  Liliequist membrane relations 964, 965, 966
mandible 14–15
  dysplasia 120
  hyperplasia 15, 120
  hypoplasia 120
  synostosis with maxilla 120
  temporomandibular joint 120
mandibular condyle 116, 119–120
  aplasia and agenesis 119
  hyperplasia 119
  hypoplasia 119
  multilobular 119
  posterior surface concavity 120
  TMJ disc adhesions 118
mandibular-malleolar ligament 121
mandibular nerve (V_3) 117, 998–1001
mandibular rami, absence 120
mandibular symphysis, accessory foramen (of Dubreuil–Chambardel) 15
mandibulofacial dysostosis 122
Manitoba-oculo-trichoanal (MOTA) syndrome 1134, 1136
mannosidosis 242
manubriosternal fusions 80
manubrium 79
Marcus–Gunn jaw-winking syndrome 991, 992
marginal artery 655
marginal mandibular nerve 1024, 1025–1026, 1028
marginal sinus 776, 789
marginal tentorial artery (of Bernasconi and Cassinari) 450
marginal tubercle (of Whitnall) 14
Marinacci communication 1093–1094
Martin–Gruber anastomoses 324, 1093–1094
massa intermedia (MI) 939, 949
masseteric artery 117
masseteric nerve 117, 121
masseter muscle 224
mastication, muscles of 224–226
mastoid emissary vein 817–818
mastoidopharyngeus muscle 238
mastoid process 11
maxilla 12–13
  synostosis with mandible 120
  temporomandibular joint 120
maxillary artery (MA) 117, 480, *481*
  accessory meningeal artery origin 482
  inferior alveolar nerve relations 1000
  lateral pterygoid relations 121, 480
maxillary nerve (V_2) 996–998
maxillary sinus 1162
  accessory ostia 13, 1162
  atelectasis 1162
  hypoplasia/aplasia 12–13, 1162
  septation 13, 1162
maxillary vein 117
Mayer-Rokitansky-Küster-Hauser (MRKH) syndrome 1364, 1368–1369, 1374
McKusick-Kaufman syndrome 1375

Meckel's diverticulum 1293–1297
with fibrous cord *1294,* 1296
heterotopic tissues 1296–1297
variations 1294–1295
Meckel's vein *see* sphenoidal emissary vein
medial antebrachial cutaneous nerve **1082,** *1082,* 1083–1084, 1092
radial nerve communications 1102
medial anterior thoracic nerve *see* medial pectoral nerve
medial basal fissure of lung 1220
medial basal segmental bronchi 1229
medial brachial cutaneous nerve 1082–1083, *1084*
medial circumflex femoral artery (MCFA) 742–743
medial circumflex femoral vein 904, *905*
medial collateral ligament (MCL) of elbow 149–151, *152*
medial collateral ligament (MCL) of knee 188
medial condylar groove, distal femur 92
median craniopharyngeal canal 9
medial cuneiform 102–103
bipartite 102–103
medial cutaneous nerve of thigh 1117
medial dorsal cutaneous nerve of foot 1124
medial femoral condyle 92, 744
medial ligament of talocrural joint 205
medial malleolus 95
medial meniscus of knee 185
medial mesencephalic membrane 969
medial patellofemoral ligament (MPFL) 192
medial pectoral nerve 1079, 1080, 1082
medial plantar artery 748
medial plantar nerve 1125
medial plantar veins 906
medial pontomedullary membrane 970
medial pontomesencephalic membrane (MPMM) 970
medial pterygoid muscle 224
medial rectus muscle 207–208
medial sural communicating nerve (MSCN) 1125–1126
medial tarsal arteries 747
median antebrachial vein *828,* 829
median artery 597, *600, 601–602*
hand 606, *607–609*
median nerve relations 1086
median cubital vein 828, 829
median nerve *1078,* 1084–1089
all-median hand 1089, 1092
brachial artery relations 593–597, 1085, 1086
lateral head 1075, 1088
medial head (root) 1073, 1075, 1081–1082, 1088
musculocutaneous nerve communications *1078,* 1081, 1088
origins 1088
pronator teres relations 298, 1085, 1086
radial nerve communications 1102
regional relationships 1086
targets and branching patterns 1088–1089
thenar motor branch 1086
thenar muscles 316, 317, 318
ulnar nerve communications 1088, *1090,* 1091–1092, 1093–1095
median nerve entrapment 1086–1087
abductor digiti minimi 328, *329*
above elbow 64, 1086–1087
lumbrical muscles 330–331, *1087*
thenar muscles 328, *329*
see also carpal tunnel syndrome
median rhomboid glossitis 243
median sacral artery (MSA) 667–669
mediopatellar plica 184
medulla oblongata 955–956
megacolon 1309–1310
megameatus intact prepuce 1335
megaureter, primary 1324
Meibomian glands 1141
melorheostosis 160
meninges 974–979
spinal 984–985
meningohypophyseal artery 450, 467
meniscal ossicles, knee 94, 185
menisci of knee 185
discoid 185
meniscofemoral ligaments 185, 187, 191–192
meniscofibular ligament 191
mental foramen
absent 15
accessory 14–15
mentalis muscle 219
mental nerve 1001, 1028
double 14
mentohyoid muscle 228
mesencephalic leaf (ML), Liliequist membrane 964, 966, 969, 970–971
mesentericoparietal recess of Broesire 1289
mesiodens 16, 17
mesoappendix 1297–1298
mesocardia 1234
mesocolon
ascending colon 1301
sigmoid 1308, 1309, *1313*
metacarpals
base variations 70, 159
epiphyses 69, 158
pseudoepiphyses 69, 158
radial artery relations 604, *605*
metaphyseal flames 89
metaphyseal stripe 89
metatarsals 104–105
metopic sutures
fusion 1
persistent 1
Michel anomaly 1178
microblepharon 1134
microgastria 1253
microglossia 242
micropenis 1344–1345
microtia 1167–1168
middle cardiac (inferior interventricular) vein 855, 856, *857, 858–859,* **868**
middle cerebral artery (MCA) 456–458
accessory 456–457
duplication 456
middle cervical ganglion 1051
middle cervical ganglion of Arnold (or Luschka) 1051
middle cervical ganglion of Swan (or Krause) 1051
middle cluneal nerves 1061
middle colic artery (MCA) 645–647
absent 645
accessory/double 646, 647
origin *622,* 623, 635, 646
middle deep temporal artery 480
middle ear 1175–1177
bones 17–18
facial nerve 1175, **1176**
muscles 212–215
vascular variations 1176
middle frontal sulcus 941
middle genicular artery (MGA) 743–744
middle glenohumeral ligament (MGHL) 45, 124, 125
middle hemorrhoidal artery 703–705
middle hepatic vein (MHV) 885
middle laryngeal nerve 1038
middle lobe (pulmonary) artery *570,* 571

middle meningeal artery (MMA) 480–482
absent foramen spinosum 8, 480
auriculotemporal nerve relations 117, 999–1000
hyperostosis frontalis interna 1, *2*
ophthalmic artery arising from 452, 480
origin from stapedial artery 468, 480–481
temporomandibular joint 117, 121
middle mesenteric artery 646, 1310
middle nasal turbinate 1158–1161
aberrant 1161
paradoxical 1161
pneumatization 1161
secondary and accessory 1159–1161
trifurcate and triple 1161
middle pectoral nerve 1079
middle petrosal sinus 784
middle pharyngeal constrictor muscle 237
middle rectal artery 721–724
origin **712, 713,** 721–723
route and morphology 724
variability of presence 721, 724
middle subscapular nerve *see* thoracodorsal nerve
middle superior alveolar nerve 997–998
middle suprarenal arteries (MSRA) 658–659
middle temporal artery 457
middle thymothyroid artery 578
middle thyroid vein 823, *824,* 1189
middle vesical artery 730–731
midesophageal diverticulum 1248
midgut rotation 1285–1288
midline intracranial cysts 939–940
Miller syndrome 1136, 1140
minor salivary glands 1187
mirror ear 1171, *1172*
mitral valve 1240–1241
moderator band 1239, *1240*
Mondini malformation 1178
monorchia 1353–1354
Morgagni hernias 349
Mouchet's tubercle 90
Mozart ear 1171, *1172*
mucopolysaccharidosis 242
Müllerian duct anomalies 1367–1372
AFS classification 1368–1371
other classifications 1371–1372
uterine tubes 1365–1366
Müllerian ducts 1367, 1374
multifidus muscles 280
MURCS association 1368
muscle of Knott 290
muscle of Merkel (ceratocricoid) *255,* 256
muscle of Otto 252
muscle of von Sömmerring 230
muscle of Tyrie *see* saphenous muscle
musculocutaneous nerve *1078,* 1080–1081
median nerve communications *1078,* 1081, 1088
targets 293, 294, 324, 325, 1081
musculus accessories (accessory soleus muscle) 427, *428*
musculus coracocervicalis (of Krause) 229
musculus extensor atque abductor pollicis accessory (of Mingazzini) 304
musculus extensor primi internodii hallucis of Wood 422
musculus extensor primi metatarsal of Gruber 422
musculus gracillimus 208
musculus incisurae cartilaginis thyroideae mediae transversus 255
musculus obliquus abdominis externus profundus 372, *373*
musculus saphenous *see* saphenous muscle
musculus singularis 283
musculus tibioastralagus anticus of Gruber 421
musculus tibiofascialis anticus of Macalister 421
musculus uvulae 240–241
myloglossus muscle 241
mylohyoid muscle 228, 1186
mylohyoid nerve 1000, 1038
myocardial bridging, coronary arteries 549–552
myopia 1145–1146
myositis ossificans 84

Nager(–Raynier) syndrome 122, 1136
nail-patella syndrome 83, 93
nasal bones 15, *16*
nasal conchae, inferior 12
nasal glioma 940
nasalis muscle 219–220
nasal turbinates 1158–1161
nasociliary nerve 995
nasolacrimal duct 1154–1155
nasolacrimal sac 1154–1155
nasopalpebral lipoma-coloboma syndrome 1136–1137
navicular 99–100, 204
accessory 99–100
bipartite/supernumerary 99
cornuate (gorilloid) 100
naviculocuneiform coalition 102
neck muscles, anterior 228–232
neck veins 821–824
neonatal asymmetric crying facies 219
nephroptosis (renal ptosis) 1315, 1323
nerve of Henle 1090, 1092–1093
nerve of Jacobson 1037
nerve of Kuntz 1073
nerve of Lejars 1088, 1089, *1095*
nerve of Wrisberg *see* medial brachial cutaneous nerve
nervi erigentes 1054–1055
nervus intermedius *see* intermediate nerve of Wrisberg
Neu-Laxova syndrome 1134, 1139
nipples 1390
supernumerary 1393
noggin (NOG) gene 69
nonrotation of intestine 1285–1286
Noonan syndrome 1138, 1178
notochord
embryology 30, 33
remnants 4
nucleus emboliformis 957
nucleus globosus 957
nutcracker syndrome 878
nutrient foramina
calcaneal tuberosity 96
femur 91–92
ilium 83
metatarsals 105
navicular 99
tibia and fibula 95

oblique arycorniculate muscle 259
oblique arytenoid muscle 259–260
oblique meniscomeniscal ligament 191
oblique muscle of thyroid cartilage prominence 254–255
oblique occipital sinus 787, 788
oblique pectoralis anterior muscle 361
oblique popliteal ligament (OPL) 193
oblique sinus, unusual 794
oblique vein of hand 827, *828*
oblique vein (OV) of left atrium (Marshall) 855, 856, *857,* **868**
obliquus abdominis externus profundus muscle 372, *373*
obliquus capitis inferior (minimus) muscle 280–281

obliquus capitis superior (major) muscle 280–281
obliquus inferior muscle 208–209
obliquus superior muscle 208
obturator artery 710–721
  anastomoses 703, 720–721, **722–723**
  branches 710–711, *714*
  location and course 721
  morphology 711
  origin from common arterial trunks 718–720
  origin from external/internal iliac 711–718
  origin from internal iliac branches 718, *719*
  sex differences 714–715, **717**
  single and multiple rooted 715–717
obturator externus muscle 416
obturator foramen 83
obturator internus muscle 401, *402*
  femoral attachments 403, *404*
  nerve to 1119–1120
obturator nerve 1114, 1117–1118
occipital artery 483
occipital bone 3–6
occipital condyles 3, 25–26
occipital emissary vein 818
occipitalis minor (of Santorini) (transverse nuchae) muscle 222, 282
occipitalization of atlas 3–4
occipital sinus 786–788
  lateral 788
  oblique 787, 788
  termination 788–789
occipital spur 5–6
occipital teres muscle 229
occipital vein 818
occipital vertebrae 3–4
occipitofrontalis muscle 222
occipitojugular air cells of Mouret 6
occipitopharyngeus muscle 238
occipitoscapularis muscle *265*
occipitotemporal vein **806, 808**
ocular drainage apparatus 1149–1150
oculoauriculovertebral spectrum 1177
oculomandibulodyscephaly 122
oculomotor membrane 965, 969
oculomotor nerve (III) 991–992
  Liliequist membrane relations 964–965, 966
  third ventricle relations 949
oculo-oto-facial dysplasia (OOFD) 1136
odontoid process 24, 27
OHVIRA (obstructed hemivagina, ipsilateral renal anomaly) syndrome 1376
olecranon 140
  anterior-posterior diameter (OAPD) 142
  hook angle 145
  width (OW) 140–142
olecranon–coronoid angle 142, 143
olecranon fossa 130
olfactory artery, persistent primitive 454, 471–472
olfactory bulb 989
olfactory cistern 960
olfactory nerve (I) 989
olfactory veins 960
omoclavicularis muscle 266
omohyoid muscle 229–230
omovertebral bone 42
omphalomesenteric duct (umbilical)
  cyst 1294, *1295*
  patent (omphaloileal fistula) 1294, *1295*
  sinus (and polyp) 1294–1295
Onodi cells 1163
ophthalmic artery 451–452, 480
  persistent primitive 470
ophthalmic meningeal artery 482
ophthalmic nerve 995–996
ophthalmic veins 818
ophthalmo-petrosal sinus of Hyrtl 791
  foramen of 784
Oppenheimer's ossicle 35
opponens digiti minimi muscle 320–321
  nerve entrapment 329, *330*
  simulating tumors 333
opponens digiti minimi muscle of foot 447
opponens pollicis muscle 317, *318*
optic canal 9–10, 991
optic chiasm 976, 990
optic disc 990
optic nerve (II) 989–991
optic tract 990
oral-facial-digital syndrome 242
orbicularis oculi muscle 220
orbicularis oris muscle 217
orbital eminence (zygomatic bone) 14
orbital muscles 207–210
orbitofrontal artery 455, 457
orbitozygomatic muscle 220
os accessorium supracalcaneum 97, 99
os acetabuli 178
os acetabuli centrale 178
os acetabuli marginalis superior (anterius) 85, 178
os acromiale 47–48
os Ainoicum 13
os aponeurosis plantaris 97
os bregmaticum 6
os calcanei secundii 97
os calcis, secondary 98
os central 71
os coracosternale vestigale 44
os coxa 82–87
  accessory ossicles 85
  bony islands 84
  individual variations 83–85
  ligament ossification 85
  malformations 85–87
  sexual dimorphism 82
os cuboideum secondarium 101
os cuneiforme I bipartitum 102–103
os cuneiforme I dorsale 102–103
os cuneiforme I plantare 102, 103
os cuneo-I metatarsale-II dorsal 103
os cuneo-I metatarsale-I plantare 103
os epilunatum 72, 160
os Goethei 13
os hamuli proprium 71
os hypolunatum 72, 160
os incisivum 13
os infranaviculare 100
os intercuneiforme 100, 103
os intermaxillare 13
os intermedium antebrachii 71
os intermedium tarsi 99
os intermetatarseum 103–104
os Japonicum 13
os lunatotriquetrum 72
os odontoideum 27
os paracuneiforme 103
os peroneum 100–101
os retinaculi (fibular ossicle) 96
ossicle of Gruber (lacrimal canal) 12
ossicles of Cortese and Riolan 11
ossiculum of Gruber (carpus) 160
ossiculum terminale 27
os styloideum 71, 160
os subcalcis 97
os subfibulare 96
os subtibiale 96, 99
os supranaviculare 100
os supratalare (os supertalare) 99
os supratrochleare dorsale 134, *135*
os sustentaculi 97–98
os talocalcaneale laterale 98
os talocalcaneale posterius 99
os talotibiale 98
osteopoikilosis 160

os tibiale externum 99–100
os triangulare 71
os trigonum 99, 204
os triquetrum secundarium 71
os trochleare calcanei 96, 97
os tuberis calcanei 97
os unci 100
os vesalianum 71
os vesalianum pedis 105
otic artery, persistent 470, 471
otic ganglion 998, 1054
oval window 1176
  aberrant facial nerve course 1013–1014
ovarian arteries 1364–1365
  absence 1365
  course 665
  level of aortic origin 663, 1365
  origin 663, 721, 1365
  uterine artery anastomoses 726–728, 1365, 1373
ovarian veins 892, 1365
ovary 1364–1365
  agenesis 1364
  arterial supply 726, 727, *728,* 1364–1365
  ectopic/supernumerary 1364
  location 1364

palatal tori 13
palatine bone 13
palatine tonsil 919, 1039
palatoglossus muscle 241–242
palatopharyngeal sphincter 236, 238
palatopharyngeus muscle 238–239, 240
palatovaginal canal 9
palmar cutaneous branch of median nerve 1085–1086, 1088–1089, 1102
palmar cutaneous branch of ulnar nerve 1090, 1092–1093
palmar digital branches of median nerve *1085,* 1086
palmar digital branches of ulnar nerve 1091
palmar flexor digitorum superficialis accessorius muscle 300
palmar interossei muscles 325–326, *327*
palmaris brevis muscle 326–327, *328*
  clinical effects of variations 331, 332, 333
palmaris brevis profundus muscle 327, 331
palmaris longus bicaudatus of Gruber 299
palmaris longus inversus 299
palmaris longus (PL) muscle 299
  nerve entrapments *1087,* 1091, *1092*
palmaris profundus muscle 299, *1087*
palmar metacarpal arteries 606, *608,* 609, *610–611*
palpebral artery 452
palpebral fissures 1137–1138
  congenital absence 1133–1134
  orientation and length 1137–1138
palpebral folds 1137–1138
pancreas 1278–1280
  agenesis/hypogenesis 1278
  annular 1278–1279
  bifid tail 1279
  heterotopic 1258, 1279
  portal annular 1279
pancreatic arcades 645
pancreatic ducts 1268, 1279–1280
pancreaticobiliary junction 1268, 1280
panniculus carnosus 363
papillary muscle complex (PMC) 1238, *1239*
papillary muscles 1237–1238, *1239*
paracentral artery 456
paraglenoid sulci 83–84
paranasal sinuses 1162–1164
paraphimosis 1345
parasympathetic ganglia 1053–1054
parathyroid glands 1205–1207
  anatomy 1205
  ectopic 917, 1206–1207
  embryology 1205
  number 1205–1206
paratoepiglossticus muscle 261
paravertebral bronchi 1229
parietal arteries 456, 457
parietal bone 6
parietal emissary vein 818
parieto-occipital artery 463
parieto-occipital fissure 942
Park's lines 91
parotid duct 1182–1184
  accessory 1184
  buccal branch of facial nerve relations 1023
  duplication 1183–1184
parotid gland 1182
  accessory 1182, *1183*
  facial nerve branching 1018–1021, *1022*
  facial nerve relations 1017–1018
parotid region superficial veins, facial nerve relations 1026–1027
partial anomalous pulmonary venous connection (PAPVC) 844, 845–846
Passavant's muscle 236
patella 92–93, 182
  congenital absence 93
  dorsal defect 93
  double 93
  emarginata 93
  multipartite 93
patella cubiti 134, *135,* 296
patellar rete 743–744
patellar retinaculum 185–186
patellar tendon 194, 414
patellar tibial ligament 185
patellofemoral malalignment 182
patellomeniscal ligament 185
patent ductus arteriosus 520, *521,* 569
patent foramen ovale 1234–1235
patent processus vaginalis 1354–1355
pectinate muscles (PM) 1235–1236, *1237*
pectineal ligament, ossified 85
pectineus muscle 412
pectinofoveal fold 177
pectoralis intermedius muscle 341
pectoralis major muscle 335–337
  absence 335–336, *337,* 339
  innervation 1079, 1080, 1082
  sternalis muscle origin 363–364
pectoralis minimus muscle 339, *340*
pectoralis minor muscle 337–339
  innervation 1079, 1080, 1082
pectoralis minor syndrome 338
pectoralis quartus muscle *267,* 341, *342*
pectoralis tertius muscle 341
pectoral nerves 1079–1080, 1082
  sternalis muscle 357, 358, 360
pectus carinatum 78
pectus excavatum 78
pelvic bones 82–87
  Caldwell–Maloy classification 82
pelvic diaphragm 381–382
pelvic digit 84
pelvic ears 84–85
pelvic kidney 1315, 1316–1317
  associated abnormalities 1316–1317
  clinical signs 1316
  complications 1317
pelvic splanchnic nerves 1054–1055, 1127
penis 1335–1345
  agenesis 1340–1341
  buried 1343–1344
  curvature/chordee 1338
  embryology 1335
  inconspicuous 1343–1345
  ossified 1345
  supernumerary/bifid 1343
  torsion 1338–1339
  webbed 1344
penoscrotal transposition 1345–1346

perforans tarsi artery 745
perforating artery of sinus tarsi 747
perforating cutaneous nerve 1120
perforating veins of lower limb 907–909
pericallosal artery 456
pericallosal cistern 961
pericardium 1234
peri-hilar renal arteries 685–687
perimesencephalic membrane 962, *963*
perineal lipomas 1347
perineal muscles 384, *385*
perineal nerve 382, 383
periostitis, physiological, in newborn 91
peristaphylinus muscle 241
peroneal artery (PR)
  foot and ankle 746
  perforating or anterior branch 747
  posterior knee 744, 745
peroneal communicating nerve 1123
peroneal trochlea 96
peroneal veins 906, 907
peronea magna artery 745
peroneocalcaneocuboideus muscle 426
peroneocalcaneus externum muscle of Otto *see* fibularis quartus muscle
peroneocalcaneus internus muscle of Macalister 432
peroneocuboideus muscle of Chudzinski 426
peroneoperoneolongus muscle of Hecker 426
peroneotalocalcaneus muscle of Tubbs 426
peroneotibialis muscle of Gruber 428
peroneus accessorius muscle of Hecker 426
peroneus (fibularis) brevis muscle 425
peroneus (fibularis) digiti minimi (quinti) muscle of Huxley 426
peroneus (fibularis) longus muscle 424–425
peroneus (fibularis) quartus muscle 425–426
peroneus (fibularis) quinti digiti muscle 424
peroneus (fibularis) tertius muscle 423–424
perpendicular plate 12
persistent fetal intracranial arteries 465–472
petrolingual ligament 450
petro-occipital sinus/vein 792–793
petropharyngeus muscle 238, 239
petrosphenoid ligament, ossified 11
petrosquamous sinus 791–792, 818
Peyer's patches 1291–1292
PHACE syndrome 468
phalanges of foot 106
  epiphyses 106
  sesamoid bones 106–107
phalanges of hand
  axial deviations 70, 159
  epiphyses 69, 158
  skeletal variations 69–70, 158–159
pharyngeal muscles 236–239
pharyngeal plexus 1038, 1041–1043
pharyngeal raphe 236–237
pharyngeal tonsil 919
pharyngo-hypo-stapedial artery 469
pharyngo-stapedial artery 469
phimosis, primary 1345
phrenic nerve 1046, 1051, 1063–1064, 1077–1078
phrenic plexus 1053
Phrygian cap appearance, gallbladder 1262
pia mater 978–979, 984
  radicular arterial branches 754
  venous networks 910–911
Pick's bundles 955
Pierre–Robin syndrome 122
pigeon breast 78
pineal gland 939
pineal region
  arachnoid membranes 971–972
  veins 804–809
pineal vein 804–805, 806, **808**
Pirie's bone 99, 100
piriformis muscle 394–400
  association with nearby muscles 388, *391, 392,* 400, 402
  attachments 396
  digastric muscle variant 400, *401,* **402**
  morphology 396–400
  nerve to **1119,** 1120
  numerical variations 400
  sciatic nerve relations 394–396, **397–399,** *399,* 400, 1121–1122
piriformis-obturator internus tendon, conjoint 400, 403
piriformis syndrome 394
Pirogoff's nodes 935
pisiform 73, 162
  coalitions 161
pisimetacarpeus muscle 320
pisiulnaris muscle 320
pisiuncinatus (pisohamatus) muscle 320
pisotriquetral lipping 73, 162
pistol-grip deformity 178
pituitary gland 939
pituitary infundibulum 965, 969–970
placenta 1387–1388
  battledore (eccentric) 1387
  circumvallate/circummarginate 1387
  lobed 1387
placenta accreta 1388
placenta bipartita 1387
placenta fenestrata 1387
placenta increta 1388
placenta membranecea (diffusa) 1387
placenta percreta 1388
placenta succenturiata 1387
placenta velamentosa 1387
plantar arterial network 748–749
plantar digital nerves 1125
plantar digital veins 906
plantar interosseous muscles 447
plantaris muscle 193, 428–429
plantar metatarsal arteries 749
plantar metatarsal veins 906
plantar muscles of foot 440–448
platypelloid pelvis 82
platysma muscle 222–224, 229
pleural fascia, fibrous bands 1071
pleuroesophageal muscle 1247
plicae, synovial
  hip 177
  knee 184–185
pneumatization
  ethmoid bone 12, 1162–1163
  frontal and sphenoid sinuses 1164
  inferior turbinate (PIT) 1158
  middle turbinate 1161
  superior nasal conchae 12
  superior turbinate 1161
Poland syndrome 335, 339, 1391–1392
polar arteries of kidney 690–691
poliosis 1141
polydactyly
  foot 107
  hand 70, 159
polyorchidism 1350–1351
polyotia 1171, *1172*
polyphalangia 70, 159
polysplenia syndrome 1283
  left bronchial isomerism 1227–1228
  situs ambiguous 1234
polysyndactyly 107
polythelia 1393
pons 954–955
popliteal artery *743,* 744–745

popliteal entrapment syndrome 194
popliteal fabella (cyamella) 93, 94
popliteal fossa 92
  arterial supply 744–745
popliteal hiatus 189, 190
popliteal lymph nodes 935–936
popliteal pterygium syndrome (PPS) 1135
popliteal sulcus 189
popliteal vein 904–906, *907*
popliteofibular ligament (PFL) 189, 190–191
popliteomeniscal ligaments 189, 190
popliteus biceps (accessory popliteus) muscle 194, 429–430
popliteus muscle 193–194, 429–430
popliteus tendon 189
  bifurcation 193–194, 430
portal annular pancreas 1279
portal vein 881–884
  branching pattern 882–883
  clinical application 884
  formation 883
postcentral sulcus 941
post-eparterial bronchus 1228
posterior abdominal muscles 374–378
posterior accessory saphenous vein 901, 903
posterior arterial branches of left pulmonary artery 572, 573
posterior ascending pulmonary artery 570
posterior auricular artery 483
posterior auricular muscle 221
posterior auricular nerve 1017, 1027
posterior basal segmental bronchus 1229, 1230
posterior brachial cutaneous nerve 1099
posterior cardinal vein, persistent 881
posterior cecal artery (PCA) 648
posterior cerebral artery (PCA) 462–463
posterior cerebral circulation 461–463
posterior circumflex humeral artery 583–584, *585, 587–589,* 592
posterior communicating artery (PCA) 452, 453–454, 463
  Liliequist membrane relations 968–969
posterior communicating membrane (PCM) 972
posterior condylar emissary vein 817, 819
posterior cricoarytenoid muscle *255,* 256, *258*
posterior cruciate ligament (PCL) 187–188
posterior (dorsal) cutaneous branch of ulnar nerve 1090, 1093
posterior cutaneous nerve of thigh *see* posterior femoral cutaneous nerve
posterior deep temporal nerve 121
posterior descending coronary branch *see* posterior interventricular coronary artery branch
posterior ethmoidal artery 452
posterior femoral cutaneous nerve **1119,** 1120–1121
posterior fibular tubercle 96
posterior frenular ligament 425
posterior gastric artery (PGA) 639
posterior horn vein 803
posterior inferior cerebellar artery (PICA) 462, 496, *497*
  facial nerve relations 1006, 1008
  foramen of Luschka relations 951
  glossopharyngeal nerve relations 1036
  vertebral artery termination 488, *494*
  vestibulocochlear nerve relations 1034
posterior inferior pancreaticoduodenal artery (PIPDA) 642–645
posterior intercavernous sinus 793–794
posterior intercostal veins 834
posterior interosseous nerve of forearm 1100, 1101
  targets 325, 1103
  ulnar nerve communications 1102
posterior intertrochanteric ridge 91
posterior interventricular (or descending) coronary artery branch (PDA)
  absent 549, *551*
  anomalous origin 553
posterior jugular vein of Walther 823
posterior lateral ligament of knee 192
posterior medial choroidal artery 463
posterior median veins 911
posterior meningeal artery 496
posterior oblique ligament (POL) of elbow 151
posterior oblique ligament (POL) of knee 188, 192–193
posterior parietal artery 457
posterior pericallosal artery 463
posterior pericallosal vein **806, 808**
posterior perimesencephalic membrane 962, *963*
posterior radicular arteries 753–754, **760**
posterior radiculomedullary arteries *753,* 767
  cervicothoracic segment 759–760
  midthoracic segment 760–761
  thoracolumbar segment 761, 762
posterior sesamoid cartilages 1210
posterior spinal arteries 524, 752–753
  anastomoses in lower cord 764–765, 768
  area of cord supplied 753
  cervicothoracic segment 756–760
  midthoracic segment 761
  origin 756, 767
  summary of variations 766–767
posterior superior alveolar artery 482
posterior superior alveolar nerve 997
posterior superior pancreaticoduodenal artery (PSPDA) 633–634
posterior talocalcaneal ligament 205
posterior talofibular ligament 205
posterior temporal artery 457
posterior thalamic vein 805
posterior thyroid vein 823
posterior tibial artery (PT; PTA)
  ankle and foot 746, 748
  knee 744, 745
posterior tibial lymph node 936
posterior tibial tubercle 95
posterior tibial veins 906, 907
posterior urethral valves 1341–1342
posterolateral spinal artery 462, 524
posterolateral spinal veins 911
posterolateral structure ligament (PLS) complex of knee 190
prececocolic fascia 1301
precentral cerebellar vein **806, 808**
precentral sulcus 941
pre-eparterial bronchus 1228
prefrontal artery 457
pregnancy
  breast changes 1394
  sacroiliac joint changes 172–173
premaxilla 13
prepatellar bursae 183–184
prepontine cistern 963
prepuce 1345
pre-pyloric diaphragm 1254
presegmental arteries of kidney 685, 686
pretracheal venous plexus 1189
prevertebral muscles 245, 250–252
princeps pollicis artery 609, *611*
principal component analysis (PCA) 52–53
  clavicle shape 59, *60*
proatlantal intersegmental artery 465, 470–471, 495–496
procerus muscle 219
process of Weber 8
processus vaginalis, patent 1354–1355
Procrustes superimposition 52

proeminentia lateralis of Rasche 15
profunda femoris artery 742, *743*
profunda femoris vein 904, *905*
progesterone 1394
pronator quadratus muscle 303
pronator syndrome 1087
pronator teres muscle 298
  innervation 1088
  median nerve entrapment 1087
  median nerve relations 298, 1085, 1086
proper hepatic artery (PHA) 627
prostate 1357–1358
prostatic artery **713,** 729
prostatovesical artery 729
protrusio acetabuli 86–87
proximal femoral physis 90
proximal symphalangism 69
proximal tibial physis 94
proximal ulna dorsal angulation (PUDA angle) 145–146
proximal ulna width (PWD) 142
pseudoepiphyses, hand 69, 158
psoas major muscle 377–378
psoas minor muscle 378
psoas quartus muscle 375, *377*
psoas tertius muscle 375
pterion ossicle 6
pterygoalar foramen 7
pterygofascialis muscle 225
pterygoid canal 9
pterygoideus proprius muscle 224–225
pterygoid muscle 121
pterygomandibular raphe 236
pterygopalatine ganglion 996, 1054
pterygopharyngeus externus muscle 238
pterygospinous foramen 7
pterygospinous muscle 225
ptosis of eyelids (blepharoptosis) 1138–1139
pubic rami, congenital absence 85–86
puboanalis muscle 381
pubococcygeus (pubovisceralis) muscle 381, 382
pubofemoral ligament 176
puboperinealis muscle 381
puboperitonealis muscle 374
puborectalis muscle 381, 382
pubotransverse muscle of Luschka 374
pubovaginalis muscle 381
pubovisceralis (pubococcygeus) muscle 381, 382
PUDA angle (proximal ulna dorsal angulation) 145–146
pudendal nerve 382, **1119,** 1126–1127
pudendal plexus 1126–1127
pulmonary arteries 569–573
  coronary artery origination 537–540
  lobar branches 569–573
pulmonary artery, main (pulmonary trunk) 569
  coronary artery origination 505, 537–540
pulmonary artery sling 1214
pulmonary embolism, recurrent, after IVC filter 878
pulmonary infundibulum
  tendon of 1241
  veins of 862
pulmonary sequestration 1217, 1224–1226
  arterial supply 526, *527,* 1224, *1225,* 1226
  extralobar 1224–1226
  intralobar 1224
pulmonary sinuses, nomenclature 530, **532**
pulmonary valve 1241
pulmonary veins 844–848, 871–876
  anomalous drainage 844–848, 872–876
  development 871, *872*
  meandering 848
pupils 1151
pyloric atresia 1254
pyloric stenosis, congenital (infantile) hypertrophic 1255, *1256*
pylorus, double or triple 1258
pyramidalis muscle 369, 370–371
pyramidal tracts 955–956, 988
pyramids, decussation 956

quadrangular space 1098
quadrate line 91
quadratus femoris muscle 403–404, *405*
  nerve to 1119
quadratus lumborum muscle 283, 375
quadratus plantae muscle 444–445
quadriceps femoris muscle 412–414
quadriceps tendon 194, 414
quadrilateral space syndrome 1098
question mark ear 1170–1171

rachischisis 31, 34–35
radial accessory vein 828, *829, 830*
radial artery 600–604
  branching patterns 600–602, *603*
  dorsum of hand 609, *612–613*
  metacarpal relations 604, *605*
  origins 597, 602
  palm of hand 606–609, *610–611*
radial collateral ligament (RCL) 152, 153
radial head 135–138
  parameterization *140*
  safe zone 138–139
radialis indicis artery 606, *608,* 609, *611*
radialis internus brevis biceps muscle 303
radial neck 135, 138–139
radial nerve 296, 1099–1103
  axillary nerve communications 1098
  entrapment 1101
  lateral antebrachial cutaneous nerve communications 1102
  medial antebrachial cutaneous nerve communications 1102
  median nerve communications 1088, 1102
  origins 1075, **1095,** 1101–1102
  regional relationships 1100–1101
  targets 324, 1102–1103
  ulnar nerve communications 1092, 1102
radial notch, ulnar 141–142
radial recurrent artery 600, 604
radial tunnel syndrome 1101
radial–ulnar synthesis 68
radial veins (of spinal cord) 910
radicular arteries 753–754
radicular veins 911–912
radiculomedullary arteries 753, 754
  cervicothoracic segment 756, 759–760
  midthoracic segment 760–761
  summary of variations 767
  thoracolumbar segment 761, 762
radiculomedullary veins 911–912
radiocarpeus muscle 303
radiocubitocarpien muscle 303
radiopalmaris muscle 300
radius 68
  dysplasia 68
  hypoplasia/absent 68
  proximal 135–139
  short 68
rami communicantes, cervical 1052, 1065
ramus communicans (Berrettini branch) (nerve) 1089, *1090,* 1094–1095

ramus communicans inferius artery 745
ramus communicans medius artery 745
ramus communicans superius artery 745
ramus descendens cervicalis 1062
ramus descendens hypoglossi 1062
ramus intermedius (RI) 532, *535*
ramus perforans cruris 745
ramus saphenous 745
rectal branches of median sacral artery 669
rectococcygeus muscle of Treitz 382
rectosigmoid junction 1308
rectum 1308, 1310
rectus abdominis lateralis muscle 369, 370
rectus abdominis muscle 363, 369–370
rectus capitis anterior muscle 245, 252
rectus capitis lateralis longus muscle 252
rectus capitis lateralis muscle 245, 252
rectus capitis minimus muscle 252
rectus capitis posterior major muscle 280–281
rectus capitis posterior minor muscle 280–281
rectus femoris muscle 412
  femoral head 412, *413, 414*
  quadriceps tendon formation 194
  short 412, *415*
rectus lateralis accessorius muscle 252
rectus muscles of orbit 207–208
rectus sheath 369, *370*
rectus thoracis bifurcalis muscle 361
recurrent artery of foramen lacerum 450
recurrent artery of Heubner 454, 455, 471
recurrent articular nerve 1122–1123
recurrent laryngeal nerve, anastomoses 1043, 1050
recurrent meningeal artery 451
recurrent tibial artery 745
recurvatum proximal ulna 146
refractive error 1145–1146
renal agenesis
  bilateral 1325
  unilateral 1325, 1356–1357
renal arteries (RA) 659–662, 682–691
  accessory *see* accessory renal arteries
  additional (ARAs) 688–690
  branches 661–662
  branching pattern 685–687
  course 660–661, 684–685
  dimensions 659, 684
  embryonic development 689
  historical background 682
  horseshoe kidney 1318
  multiple 659–660, 687–691
  normal anatomy 682
  numerical variations 659–660
  origin by vertebral level 659, 682–683
  ostium locations 659, 683
  peri-hilar branching 685–687
  primary branches 686
  right and left vertical relations 684
  rotational kidney anomalies 1323
  single origin 682–687
  termination 690–691
renal ectopia 1315–1322
  accessory renal arteries 690, 1316, 1318
  crossed 1315, 1321–1322
  crossed fused 1315, 1321–1322
  embryology 1315–1316
  incidence 1315
  intrathoracic 1319–1321
  see also pelvic kidney
renal pelvis 1325
  orientation 1323
  renal artery relations 661, 685
  segmental artery relations 687
renal ptosis 1315
renal veins 891
  gonadal artery relations 665
  renal artery relations 661, 682, 684–685
resegmentation, vertebral column 24, 30
rete vertebralis 488
retinaculum, knee 185–186
retinoic acid embryopathy 1171
retractor bulbi muscle 207–208
retractor glandulae lacrimalis 210
retractor scroti muscle 384
retrobronchial artery (of Hovelacque) 572
retroclavicularis proprius muscle 263
retroclavicular supernumerary muscles 335, *336*
retroduodenal arteries (RDA) 633
retromandibular vein 117, 121, 822
  facial nerve relations 1026–1027
  marginal mandibular nerve relations 1024, *1025*
rhombencephalon 954
rhombencephalosynapsis 957
rhombo-atloid muscle 279
rhomboid major muscle *272,* 273–275
rhomboid minimus (minus) muscle *262, 272,* 274
rhomboid minor muscle *272,* 273–275
rhomboid occipitalis muscle *272,* 274–275
ribs 76–78
  absent 76
  bicipital 76
  bifurcated 77
  cervical 28, 77–78, 1071
  fusion 76
  intrathoracic 77
  lumbar (gorilla) 35, 78
  sacrococcygeal 38, 78
  scapular articulations 41
Riche–Cannieu anastomosis 324, 1094–1095
Riedel's lobe 1274–1275
right aortic arch 510–513, *514–515*
  with aberrant left subclavian artery (II) 512, *513, 515*
  with isolated left subclavian artery (III) 512–513
  with mirror image branching (I) 511–512, *513, 514*
right atrial appendage 1234
right atrium (RA)
  pathological persistence of sinus valves 865–866
  pectinate muscles 1235–1236, *1237*
  tendon of Todaro 1237
  veins draining walls *855,* 860–862, **864**
right brachiocephalic vein 833, 841
right bronchial isomerism 1227–1228
right (anterior) cardiac venous system 860, *861–864*
right carotid artery, coronary artery origin from 534
right colic artery (RCA) 647–648
right coronary artery (RCA) **531,** *532*
  abnormal origin from pulmonary artery 505, 540
  absent 549, *551*
  anomalous location of ostium 505, 534, *536*
  circumflex artery arising from 541, *544*
  muscular bridging/intramural 549
  origin from ascending aorta 534, *537, 538*
  origin from left ventricular outflow tract 534–537
  origin from non-facing sinus 534, *537*
  origin from opposite sinus *504,* 505, 540–541
  split (double) 553, *554*
  typology and dominance 560–562

right coronary (small cardiac) vein (SCV) 855, 860, *862–864,* **868**
right gastric artery (RGA) 631–632
right gastroepiploic artery (RGEA) 635
right hepatic artery (RHA) 629
  accessory (aRHA) 627, 629, 630, 644, 650
  combined variations 630
  origin *622,* 623, 627–629, 635, 650
  replaced (rRHA) 629, 630, 650
right hepatic vein (RHV) 885
right inferior hepatic vein (IRHV) 884, 885
right inferior phrenic artery (RIPA) 656–657
right lower bronchus 1229
right lymphatic duct 932
right marginal (acute marginal) vein (RMV) 860, *861–864,* **868**
right middle bronchus 1228–1229
right pulmonary artery 569
  lobar branches 569–572
right subclavian artery 575–577
  retroesophageal (RRSA) 930
  retrotracheal 575–576
  variant 507–509, 576–577
right top pulmonary vein 873–874, *875*
right upper lobe bronchus 1228
right ventricle (RV)
  coronary artery origin from 534
  false tendons 1241, *1244*
  papillary muscles 1237–1238
  venous drainage *855,* 860, *861–864*
Riolan arcade *654,* 655
risorius muscle 219
Robin anomaly 122
Rokitansky's diverticulum 1248
Rolandic (central) artery 457
Roos bands/muscles 350
Rosenmüller lymph nodes 935
rotator cuff muscles 126, 289–290
rotatores longus and brevis muscles 280
rotator interval 125
round window 1176
Rubinstein-Taybi syndrome 1139, 1141

sacral articular cartilage 165, 166, 170–171
sacralization
  of coccyx 38
  of L5 36, 37
sacral plexus 1118–1126
  lumbar plexus relations 1114
  sacroiliac joint innervation 171
sacral ribs 38, 78
sacral spinal nerves 1118–1119
  muscular branches 382, 1127
  visceral branches 1054–1055, 1127
sacral sympathetic ganglia 1051
sacral veins 912
sacrococcygeal nerves/roots 1060
sacrococcygeal sympathetic ganglia 1051–1052
sacrococcygeal vertebrae 37–38
sacrococcygeus ventralis muscle 382
sacroiliac joints (SIJ) 165–173
  accessory *see* accessory sacroiliac joints
  age-related changes 171–172
  ankylosis 168, 169
  articular cartilage 170–171
  bipartite complex 168
  crescenteric defect 169
  iliosacral complex (ILC) 168
  innervation 171
  mobility-related variations 172–173
  number of articulating surfaces 166–168
  ossification centers 169
  pregnancy-related variations 172–173
  racial and gender differences 172
  sacral articular surface 169–170
  semicircular defect 169
  shape 168–169
  type of joint 165–166
  width and uniformity 169
sacrum 37–38
  articular surfaces 169–170
Saethre-Chotzen syndrome 1138–1139
safe zone, radial head 138–139
sagittal cleft vertebrae 34
salivary ducts 1182–1187
salivary glands 1182–1187
  heterotopic 1186–1187
  minor 1187
salpingopharyngeus muscle 238, 241
salpingo-staphylinus muscle 240
Sandifort's muscle 283
Santorini's duct 1280
saphenous muscle 372–373, 410, *411*
saphenous nerve 1117
sartorius muscle 195, 410–412
Say-Barber syndrome 1140
scalene artery of Stahel 581
scalene muscles 245–250
  brachial plexus relations 247–248, 1071–1072
  nerves to 1077–1078
scalenus anterior muscle 245–246
scalenus medius muscle 246–248
scalenus minimus muscle 245, 250, 1071
scalenus pleuralis muscle 250
scalenus posterior muscle 249
scalp muscles 221–222
scansorius muscle **394,** 410
scaphoid 72–73, 162
  bipartite 161
  coalitions 161
  hypoplasia/aplasia 162
scapholunate ligaments 162–163
scapula 40–48
  articulations with ribs 41
  coracoid process 43–44
  glenoid fossa shape 44–45
  lateral border 41
  medial border 41–42
  snapping 41
  superior border 42
scapular body 40
  curvature 41
  dysplasia 40, *41*
scapular notch 43
scapuloclavicularis muscle *336*
scapulocostalis muscle 348
scapulohumeralis digastricus of Gruber 290
scapulohumeral muscles 289–291
Schlemm's canal 1149–1150
Schmorl's node 34
sciatic (axial) artery
  embryonic development 700, 741, 745
  persistent 700–702, 741
sciatic nerve 1121–1122
  piriformis relations 394–396, **397–399,** *399,* 400, 1121–1122
sciatic veins, persistent 900
scimitar syndrome 847–848, 1223
sclera 1151
scleroderma, juvenile localized 1392
sclerotome 33
scoliosis 984, 1392
scrotum 1345–1347
  agenesis 1347
  bifid 1345, *1346*
  ectopic and accessory 1347
second cervical nerve (C2) 1062
second cuneiform 103
second dorsal interosseous muscle 324–325
second jejunal artery 644
second lumbrical muscle of foot 445

second lumbrical muscle of hand 321–323, 324
second palmar interosseous muscle 326
second thoracic nerve
brachial plexus 1072, 1073, 1074
lateral branch *see* intercostobrachial nerve
segmental aplasia of gastrointestinal tract 1254
segmental renal arteries 685–686, 687
segmental spinal arteries 753–754
segmentation, developing spine 24, 30, 33
segmentation failure
cervical spine 28
lumbar spine 34
occipitalization of atlas 4
thoracic spine 30–31
sella bridge 7
sella turcica 7
semicircular canal aplasia 1178
semimembranosus muscle 195, 418, *419*
semimembranosus muscle-tendon-unit (SMTU) 193
semimembranous tendon, distal 193
seminal vesicles 1356–1357
absence/duplication 1357
cysts 1356–1357
semispinalis capitis muscle 279, 280
semispinalis thoracis muscle 280
semitendinosus muscle 417–418, *419*
septal aperture (supratrochlear foramen), humerus 64–66
septal arteries of heart, ectopic origination 557
septal papillary muscle of conus 1238, *1239*
septal (cerebral) vein (SV) 804
septal veins of heart 862
septum pellucidum
absent 939
cavum 939–940
serratus anterior muscle 275–276
serratus posterior inferior muscle 276–278, **277**
serratus posterior superior muscle 276, **277**
sesamoid bones
foot 105–107, 204
forearm 68
hand 71, 160
Setleis' syndrome 1141
seventh cervical nerve (C7)
brachial plexus 1069, *1070*
scalenus anterior relations 248
serratus anterior innervation 276
shape analysis, statistical 52
shell ear 1170
Shone's syndrome 513
short bowel syndrome 1291
short ciliary nerves 996
short gastric arteries 639
shoulder joint 124–127
bursae and recesses 126
innervation 1099
Sibson's fascia 250, 1071
sigmoid arteries *652,* 653, *654*
sigmoid colon 1308–1314
anatomic variations 1309, *1310–1313*
implications of variations 1312–1314
normal anatomy 1308
sigmoidea ima artery 653
sigmoid mesocolon 1308, 1309, *1313*
sigmoid sinus 781–782
sigmoid volvulus 1312
Simpson-Golabi-Behmel syndrome 1394
sinu-atrial (SA) node 1244
sinuses of Valsalva *see* aortic sinuses
sinus pericranii 819
sinus rectus *see* straight sinus
sinus venosus syndrome 846
sinutubular junction 1245
situs ambiguous 1234
situs inversus 1234
sixth cervical nerve (C6)
brachial plexus 1069, *1070,* 1073–1074
scalenus anterior relations 247, 248
serratus anterior innervation 276
skull 1–18
sling left pulmonary artery 1226, *1227*
small cardiac (right coronary) vein (SCV) 855, 860, *862–864,* **868**
small intestine 1285–1297
atresia and stenosis 1289, 1292, *1293*
duplication 1292–1293
encapsulated 1288–1289
length 1291
malrotation *see* malrotation of midgut
Meckel's diverticulum 1293–1297
non-Meckelian diverticula 1293
small lumbar artery (arteria lumbalis ima) 666, 669
small muscle of Theile and Müller 349
small saphenous lymph vessels 936–937
small saphenous vein 903
snapping hip syndrome 179, 375
snapping scapula 41
socia thyme cervicalis 917
soft palate muscles 240–241
soleal venous plexus 906
soleus muscle 427–428
somatoschisis, anterior 31
somites 33
sphenobasal sinus 790
sphenoethmoid (Onodi) cells 1163
sphenoidal artery 452
sphenoidal emissary foramen 8
sphenoidal emissary vein (vein of Vesalius) 8, 818
sphenoid bone 7–10
sphenoid sinus 7
pneumatization 1164
sphenomandibular ligament 117
sphenopalatine foramen 13
sphenoparietal sinus 789–791
sphenopetrosal sinus 790
sphenopharyngeus muscle 238
sphenotemporalis muscle 226
sphincter colli profundus muscle 229
spina bifida 25, 34–35
spina bifida occulta 32, 34–35
spinal accessory nerve
cervical nerve anastomoses 1047, 1057–1058
cervical plexus connections 1065–1066
see also accessory nerve
spinal accessory nerve plexus 1047
spinal cord 984–988
caudal end 987
cross-sectional asymmetry 988
curvature 984
L1–coccygeal segment lengths 985–986
L1–S1 segment diameters 986
meninges 984–985
subarachnoid space 959, 984
vertebral levels of segments 985, 986
volume 986–987
spinal cord arterial supply 524, 752–768
anastomoses 764–765, 768
cervicothoracic segment 754–760
dorsal component 753
midthoracic segment 760–761
segmented longitudinal trunks 752–753
summary of variations 766–768
thoracolumbar segment 761–764
ventral component 753
spinal cord venous system 910–912
extradural 912
extrinsic 910–912
intrinsic 910

spinalis capitis muscle 279–280, 281
spinalis cervicis muscle 279–280, 283
spinalis thoracis muscle 279
spinal nerves 1057–1061
  dorsal rootlet connections 1058–1059
  see also cervical nerves; sacral spinal nerves
spine
  curvature 984
  embryology 33–34
  see also vertebrae
spine of Broca 3
spinoglenoid ligament 45
spinous processes
  cervical vertebrae 28
  thoracic vertebrae 32
splanchnic nerves 1052–1053
spleen 1282–1283
  accessory 1282–1283
  congenital absence *see* asplenia
  lobulations and clefts (notches) 1282
  wandering 1283
splenial artery 463
splenic artery (SA) 635–641
  branches 636–641
  course 636
  double 636
  origin *622,* 623, *624,* 625, 635–636, 650
  terminal branches 641
  tortuosity 636
splenic (left colic) flexure of colon 1308
  blood supply 654–655
  variations 1309
splenius capitis muscle 278–279
splenius cervicis muscle 278–279
splenogonadal fusion 1351–1352
splenomesenteric trunk 641
splenosis 1283
split cord malformation 35
spondylolisthesis 35
spondylolysis 35
Sprengel's deformity 42, 126
Stahl ear 1170
stapedial artery, persistent 450, 468–469, 1176
  with aberrant internal carotid artery 469
  facial nerve courses 1013
  middle meningeal artery arising from 468, 480–481
stapedius muscle 212, 213–215
stapes 17
  aberrant facial nerve courses 1013–1014
statistical shape analysis 52
Steinberg sign 70
stellate ganglion 1051
Stensen's duct *see* parotid duct
sternal angle 54, 59
sternal clefts 80
sternal foramina 78, 80
sternalis muscle 350–364
  blood supply *358,* 361
  classification 361, *362, 363*
  historical background 350–351
  homology 361–364
  morphology 353–357
  nerve supply 350–351, 357–360
  prevalence 351–353
sternal pseudoforamen 79–80
sternal sclerotic bands 80
sternochondroclavicularis muscle *336*
sternochondroscapularis muscle 335, *336*
sternoclavicularis (anticus) muscle 263, *265,* 346–347
sternoclavicular (SCJ) joint 126
sternocleidomastoid muscle 231–232, 363
sternocostalis muscle *see* transversus thoracis muscle
sternohumeralis muscle *340,* 347
sternohyoideus azygos muscle 229
sternohyoid muscle 230
sternomastalis muscle 361
sternopetrosopharyngeus muscle 230
sternoscapularis (sternoacromialis) muscle *265,* 346–347
sternothyroid muscle 230
sternoxiphoidal fusion 79–80
sternum 78–80
Stieda process 98
stomach 1253–1258
  atresia 1254
  congenital muscular defect 1257
  diverticula 1255–1257
  duplication 1255
  heterotopic pancreatic mucosa 1258
  hourglass 1254–1255
straight arycorniculate muscle *258,* 259
straight sinus 782–783
  absence 783, 786
  confluence of sinuses 778–779
  drainage patterns 780
  termination 788–789
striae medullares 955
styloauricularis muscle 241
stylochondrohyoideus muscle 229
stylodepressor auriculae muscle 241
styloglossus muscle 241
stylohyoid chain, asymmetrical ossification 10, *11*
stylohyoid muscle 228–229
  nerve to 1017
styloid processes
  lumbar vertebrae 35
  temporal bone, elongated 10, *11*
stylomandibular ligament 117
stylomastoid artery, stapedial branch 469
stylopharyngeus muscle 237–238
subacromial bursa 126
subanconeus muscle 296
subarachnoid cisterns 960–963
subarachnoid space 959–972
  cerebral 959
  within facial canal 972, 1011
  size 959–960
  spinal 959, 984
subarachnoid space to ventricular width ratio (SAS:VW) 959
subcallosal arteries 960
subclavian artery (SA) 575–581
  brachial plexus variation and 1068, *1069*
  branches 577–581
  coronary artery origin from 534
  isolated 510, 512–513
  origins 575–577
  scalenus anterior relations 246
  trunk formation 577
  see also left subclavian artery; right subclavian artery
subclavian steal phenomenon 510
subclavian vein 826, *827*
subclavius muscle *265,* 347–348
  nerve to 1077–1078
subclavius posticus muscle 348
subcostal nerve 1113–1114
subcutaneous infrapatella bursa 183
subdiaphragmatic cistern 960
subendocardial coronary course (SEC) 552–553
subependymal veins 802–804
sublabral foramen, glenoid fossa 45, 124
sublabral sulcus (foramen, groove), acetabulum 177
sublingual glands and ducts 1186
submandibular duct of Bartholin 1186
submandibular ducts 1184–1185, *1186*
submandibular ganglion 998, 1054
submandibular glands 1184
  accessory 1184, *1185*
  heterotopic 1186–1187

submandibular venous arch 821
suboccipital muscles 280–281
suboccipital nerve (dorsal ramus of C1) 1057, 1058
subpulmonary infundibulum, veins of 862
subsagittal sutures, accessory 6
subscapular artery
  absence 592
  branching 592, 593, *599*
  origin 583–584, *585–591,* 592
subscapular bursa 126
subscapularis minor (secundus) muscle 289
subscapularis muscle 289–290, 1096
  innervation 1095–1096, 1097
subscapularis-teres-latissimus dorsi muscle, accessory 268, 289, 1096, 1097
subscapular nerves 1095–1097
subscapulo-capsular muscle 289
sub-superior bronchus 1229, 1230
subtalar (talocalcaneal) coalitions 101
subtalar joint 204–205
subtalar sinus 98
Sudeck's point 654
sulci, cerebral 941–942
sulcus arteriae vertebralis 26
superficial brachial artery 584, 593, 594–597
superficial brachial artery superior 593
superficial carotid ansa 1042
superficial cerebral veins 809–814
superficial circumflex iliac artery (SCIA) 742
superficial circumflex iliac vein 901, 902–903
superficial epigastric vein 901, 902, 903
superficial external pudendal artery (SEPA) 742
superficial external pudendal vein 902
superficial fibular nerve 1123–1124
superficial inferior epigastric artery (SIEA) 742
superficial lymph vessels, lower limb 936
superficial middle cerebral (Sylvian) vein 809–812
superficial palmar arterial arch 606, *607*
  incomplete 606, *608–609*
  relations with deep palmar arch 609, *611*
superficial palmar artery 604
superficial peroneal nerve 1123–1124
superficial petrosal emissary vein 819
superficial popliteal artery 745
superficial posterior artery 745
superficial posterior peroneal artery 745
superficial radial artery 600–602, 604
superficial Sylvian (middle cerebral) vein 809–812
superficial temporal artery 117, 480
superficial transverse perineus muscle 384, *385*
superficial ulnar artery 593, 604–606
superficial veins of lower limb 901–903
superficial veins of upper limb 827–830
superior accessory fissure (lobe) of lung 1217–1220, *1221*
superior anastomotic vein *see* vein of Trolard
superior anterior communicating artery 456
superior auricular muscle 221
superior cardiac nerve 1052
superior cerebellar artery (SCA) 462, 487–488
superior cerebellar vein **806, 808**
superior cervical ganglion 1050–1051
superior cluneal nerves 1060–1061
superior cricoarytenoid muscle 257
superior cricothyroid muscle 254
superior geniohyoid muscle of Ferrein 229
superior glenohumeral ligament (SGHL) 125
superior gluteal artery
  collateral connections 703
  origin 703–705, **712, 713, 714**
superior gluteal nerve 396, **1119,** 1120
superior hypophyseal artery 452
superior intercostal vein 840
superior laryngeal artery (SLA) 478, *479*
superior lateral genicular artery (SLGA) 743–744
superior left colic artery (ascending branch) *651, 652,* 653
superior medial genicular artery (SMGA) 743–744
superior mesenteric artery (SMA) 641–650
  aberrant branches 650
  anastomoses 650, 655
  branches 642–650
  course 642, 1310
  origin 625, 641–642
superior mesenteric vein 1310
superior muscle of vocal fold (ventricular muscle) *259,* 260
superior nasal conchae, pneumatization 12
superior nasal turbinate, pneumatization 1161
superior oblique muscle 208
superior orbital fissure 8–9
superior pectoral nerve 1079
superior petrosal sinus 783–784
superior pharyngeal constrictor muscle 236–237
superior phrenic arteries 526
superior polar (splenic) artery (SPoA) 640
superior polar renal arteries 660, *661,* 690–691
superior pulmonary veins 871
superior rectal artery 653–654
superior rectus muscle 207–208
superior sagittal sinus (SSS) 775–777
  arachnoid granulations 978
  bridging veins and lateral lacunae 776–777
  cavernous spaces 794
  confluence of sinuses 778–779, 780
  diploic vein connections 770–771
  duplication 776
  termination 788–789
  unilateral hypoplastic rostral 775–776
superior segmental bronchus 1229, 1230
superior segmental pulmonary arteries *570,* 571–572, 573
superior suprarenal artery (SSRA) 657–658
superior temporal artery 120
superior temporal sulcus 941
superior thoracic artery 584, *591,* 592
superior thyroarytenoid muscle *258,* 260
superior thyroid artery (STA) 1189
  variations 477–478, 1199
superior thyroid vein 823, *824,* 1189
superior transverse scapular ligament 43, 1077
superior vena cava (SVC) 841–844
  atrial junction 842
  azygos lobe and position 842–844
  azygos system anomalies 838, *839,* 842
  azygos vein junction 836
  double 841, 842, *843–844*
  length 842
  persistent left (PLSVC) 842, 866, 867
  solitary left 842, *845*
  unusual tributaries of right 842
superior vermian vein 802, **806, 808**
superior vesical artery **712,** 730

superior vestibular nerve, facial nerve relations 1008, *1009*
supinator brevis accessorius muscle 304
supinator longus accessorius muscle 303
supinator muscle 304
supracalcaneal bursa of Poirier 205
supraclavicular block 1064
supraclavicularis proprius muscle 263, 345, *346*
supraclavicularis proprius posterior muscle *336*
supraclavicular nerve canal 58
supracondylar foramen, humerus 64, *65*
supracondylar process, humerus 64, *65,* 1086–1087
supracostalis anterior muscle 276, *277,* **278,** 347
supracostalis muscles (of Wood) 276–278
supracostalis posterior muscle 276–278, 347
supraduodenal artery (SDA) 633
supraorbital nerve 995, 1028
suprapatellar bursa 183
suprapatellar plica 184
suprapleural membranes 250, 1071
suprapubic ligament, ossified 85
suprarenal arteries 657–659
suprarenal glands *see* adrenal glands
suprascapular artery 579–580, 584, *591*
suprascapular foramen 43
suprascapular nerve 1065, *1076,* 1077
  entrapment 1065
supraspinatus muscle 290
suprasternal bones 79–80
supratrochlear foramen, humerus 64–66, 134
supratrochlear nerve 995, 1028
supratrochlear septum 130
supreme intercostal artery 581
supreme intercostal vein 840
supreme splanchnic nerve 1053
sural communicating nerves 1123, 1125–1126
sural nerve 1123, 1125–1126
suspensory ligament of duodenum 1290–1291
suspensory ligament of greater trochanter (of Gunther) 388
suspensory ligament of thyroid gland 230, 1193
sustentaculum tali, prominent 97
sutura incisiva 13
sutural bones 6, *7,* 13, *16*
sutura mendosa 6
SVC *see* superior vena cava
Sylvian aqueduct 949–950
Sylvian cistern 960–961
Sylvian fissure 940
symblepharon, congenital 1134
sympathetic ganglia 1050–1052
sympathetic nerves, upper arm 1073
sympathetic trunk 1050
symphalangia 69, 159
syndactyly 69–70, 107, 159
syndesmoarytenoid muscle 257, *258*
syndesmopharyngeus 237
syndesmothyroid muscle 261
synophrys 1141
synostosis, congenital 34

TACRAD association 1212
talar beaking 98
talar neck, squatting facet 204
talar nose 98
talocalcaneal (subtalar) coalitions 101–102
talocrural joint 204, 205
talocrural ligament, lateral 205
talonavicular coalition 102
talus 98–99
  articular surfaces 204
  bipartite 98
talus accessorius 99
talus secondarius 99
tarsal bones 96–101
tarsal coalitions 101–102
tarsal kink, congenital 1140
tectal veins **806, 808**
teeth 16–17
tegmental nucleus 957
telarche, premature 1391
telecanthus 1133
telecanthus–hypospadias syndrome 1133
temporal bone 10–12, 120
temporal branch of facial nerve 1023
temporal emissary vein 819
temporalis minor muscle 224
temporalis muscle 224
temporal membrane 965, 968–969
temporal nerves 121
temporobuccal trunk 480
temporobuccinator band 224
temporomandibular joint (TMJ) 116–122
  absence 121, 122
  arterial blood supply 117, 120–121
  articular surface variations 120
  capsule 116, 120
  congenital anomalies 121–122
  dysplasias 122
  hemiplasia 121
  hyperplasia 122
  hypoplasia 122
  intra-articular disc 116, 117–118
  ligaments 116–117, 121
  lymphatics 117, 121
  muscles 121
  nerve supply 117, 121
  synovial membrane 116
  variations 117–121
  venous drainage 117, 121
temporomasseteric trunk 480
temporo-occipital artery 457
tendinous ring of Zinn 207
tendon of infundibulum (heart) 1241
tendon of Todaro 1237
tenia sagittalis 1235–1236
tensor capsulae radiocubitalis (inferioris) muscle 303
tensor fascia colli muscle *see* supraclavicularis proprius muscle
tensor fasciae dorsalis pedis muscle of Wood 421
tensor fasciae plantaris muscle of Wood 429
tensor fascia lata muscle 410
tensor fascia suralis muscle 416, 418
tensor laminae posterioris vaginae musculi rectus 374
tensor laminae profundus fasciale colli muscle 263
tensor laminae superficialis fasciale colli muscle 263
tensor semivaginae articulationis humeroscapularis muscle *see* sternohumeralis muscle
tensor tympani muscle 212, *213*
tensor veli palatini muscle (TVP) 212, *213,* 240
tentorial artery 450
tentorial notch 975
tentorium cerebelli (cerebellar tentorium) 975–976
  arachnoid membranes 966, *967,* 971
  calcification 975
  venous sinuses 785–786
teres major muscle 41, 290, 1097
teres minimus muscle 290
teres minor muscle 290, 1099
terminal nerve (NT) 989

testes 1347–1355
absence 1353–1354
ectopic 1349–1350
fusion 1351–1352
retractile 1349
supernumerary 1350–1351
undescended 1347–1349
vanishing 1353
testicular arteries 662–665
testicular cancer 1348, 1351
testicular regression syndrome 1353
testicular veins 892
testis-epididymal nonfusion 1352–1353
tethered cord syndrome (TCS) 984, 986, 987
thalamostriate vein (TSV) 803, 804
Thebesian valve 865, 1237, *1238*
thenar ansa (loop) *see* Riche–Cannieu anastomosis
thenar muscles 315–318
biomechanical dysfunction 332
mass appearance 332
nerve entrapments 328, *329*
thigh muscles 410–418
anterior compartment 410–414
medial compartment 414–416
posterior compartment 416–418, *419*
thigh perforating veins *908,* 909
third coronary artery 562, *563*
third (lateral) cuneiform 103
third dorsal interosseous muscle 325
third lumbrical muscle of foot 445
third lumbrical muscle of hand *322,* 323, 324, 1089
third malleolus of Destot 95
third mesenteric artery 646
third palmar interosseous muscle 326
third ventricle 939, 947–949
floor 948–949
recesses 948
thoracic aorta 501–526
embryology 501–502
see also aortic arch; ascending aorta; descending aorta
thoracic duct 923–932
abdominal part 923
caliber and diameter 932
cervical part 924–932
duplication 930–931
right-sided termination 927–930
termination 925–930
thoracic part 923–924
tributaries 931–932
valves 932
thoracic nerves/roots 1060
thoracic outlet 1070
thoracic spine
embryology 30
failure of segmentation 30–31
thoracic sympathetic ganglia 1051
thoracic vertebrae 30–32
thoracic wall muscles 335–364
thoracoacromial artery/trunk 584, *585–587,* 592
thoracodorsal artery 584, *590,* 592
thoracodorsal nerve **1095,** *1096,* 1097–1098
thoracoepigastric vein 901
thumb 71, 159–160
extrinsic muscles 302–303, 306–307
hypoplasia 71
index pollicization for absent 332
intrinsic muscles 315–318
triphalangeal 71, 159
thymic artery 578
thymic cysts, congenital cervical 916, *917*
thymoparathyroid aplasia 914–915
thymopharyngeal duct cyst 916
thymus 914–917
accessory tissue 914, **915,** 916
aplasia 914–915
cystic accessory tissue 916, *917*
ectopic 914, 915–916
ectopic parathyroid gland 917, 1206
number of lobes 914
thymus cervicalis 914
thyreotrachealis muscle 231
thyroarytenoid muscle 260
thyrocervical trunk 577
thyroconoid muscle *259,* 260
thyrocorniculate muscle 260
thyrocuneiform muscle 260
thyroepiglottic muscle *258, 259,* 260
thyroglossal duct 1190
thyroglossal duct cyst 1190, 1195–1196
thyrohyoid muscle 230
thyroid cartilage 1209–1210
ossification 1211
thyroidea ima artery 522, 578–579, 1200
thyroideus marginalis inferior 255
thyroideus transversus anomalus 255
thyroid ganglion of Krause 1051
thyroid gland 1189–1200
agenesis/hemiagenesis 1196–1197
anatomy 1189
arterial variations 1199–1200
ectopic/accessory 1198–1199
embryology 1189–1190
innervation 1189
isthmus agenesis 1197, **1198**
lymphatics 1189
pyramidal lobe 1190–1192
suspensory ligament of 230, 1193
variations 1190–1199
thyrolingual trunk 477, 478, 1199
thyrolinguofacial trunk 478, 1199
thyromembranous muscle *258,* 260
thyrotracheal muscle 255–256
thyrotriticeal muscle 261
tibia 94–96
distal 95–96
platycnemic 95
proximal 94–95
shaft 95
torsion 108
tibial collateral ligament (TCL or MCL) 188
tibial eminence 181–182
tibial–fibular syndesmosis 94, 95–96
tibial intercondylar spines 94
tibialis anterior muscle 421
tibialis posterior muscle 430
tibialis secundus muscle of Bahnsen 430
tibial nerve 1121, 1124–1125
origin **1119,** 1121–1122
piriformis relations **394,** 396, *399,* 1122
tibial plafond, articular notching 204
tibial plantar hallucal artery 747–748
tibial slope, knee 182
tibial tuberosity ossification center 94
tibiocalcaneus internus muscle of Testut 427–428
tibiofascialis anticus (anterior) muscle (of Macalister) 421
tibiotarsalis muscle 429
Tillaux spiral 207
tilted sternum 80
tinnitus 819, 1176
TMJ *see* temporomandibular joint
tongue 241–243
bifid 242
fissured and scrotal 243
geographic 243
malformations 242
muscles 241–242
smooth and hairy 242–243
tongue-tie 243
tonsils 919
torcular Herophili 778–780
torus mandibularis 14
torus occipitalis 5–6

torus occipitalis transversus 6
torus palatinus 13
total anomalous pulmonary venous connection 846
trachea 1212–1215
  agenesis 1212, *1213*
  congenital stenosis 1212–1214
  diverticulum 1214
  failure of separation from esophagus 1250
tracheal bronchus 1214–1215
tracheoesophageal fistula 1212, *1213,* 1248–1250, *1251*
trachleoclavicularis muscle 266
track sign 91
transitional vertebrae, lumbosacral (LSTV) 36, 37, 169
transjugular intrahepatic portosystemic shunt (TIPS) 881, 884
transmylohyoid anastomosis of Sappey 1000
transpleuralis subclavius muscle 347
transversalis cervicis anticus muscle (of Retzius) 251, 283
transversalis cervicis medius 247
transversalis cervicis posterior minor muscle 279
transversalis thoracis muscle 279
transverse acetabular ligament 176
transverse arytenoid muscle *259,* 260
transverse cervical artery 580–581
transverse cervical nerve 1064–1065
transverse colic artery, accessory 650
transverse foramina
  cervical vertebrae 27–28
  lumbar vertebrae 35
  thoracic vertebrae 31
  vertebral artery 27, 487, 488, *489–492*
transverse genicular ligament 192
transverse menti muscle 224
transverse nuchae muscle 222, 282
transverse pancreatic artery (TPA) 638
transverse processes
  elongated 1071
  lumbar vertebrae 35, 36
  thoracic vertebrae 31–32
transverse sinus (TS) 780–781
  aplasia/hypoplasia 780, 781
  arachnoid granulations 978
  confluence of sinuses 778–779, 780
  termination 788–789
transverse thyroid muscle 255
transversospinalis muscles 280
transversus abdominis muscle 374
transversus manus muscle 318
transversus thoracis (sternocostalis) muscle *265,* 347, *348*
trapezius muscle 262–266
  absence 262
  attachments 262, *263,* **264,** *264*
  innervation 1065–1066
  supernumerary muscles 263–266
trapezoid
  bipartite 161
  coalitions 161
Trautmann's triangle 782
Treacher Collins syndrome 122, 1136, 1137
triangular fibrocartilage complex (TFCC) 162–163
triangularis sternae muscle *see* transversus thoracis muscle
triceps brachii muscle 295–296
  innervation 296, 1092, 1099, 1102–1103
  long head tendon 126, 296
trichomegaly 1141
tricuspid valve 1240
trigeminal artery, persistent fetal 462, 465–468
trigeminal ganglion 995–996
trigeminal nerve (V) 995–1001
  facial nerve anastomoses 1027–1028
  roots 995–996
trigger finger 332
trigonal process 98, 204
trigoncalcaneal ligament 205
triphalangial thumb (TPT) 71, 159
triquetrum 73, 162
trisomy 21 *see* Down syndrome
triticeal cartilages 1210
trochanter, third 91
trochlea, distal humerus 130, 131–133
trochlear dysplasia, distal femur 182
trochlear groove, distal femur 92
trochlear nerve (IV) 992–995
Trolard, Jean Baptiste Paulin 814
truncus arteriosus 501
tubal tonsil 919
tubercle of Luschka 41
tubercle of Ossaki 124
tubercle of Staurenghi 35
tubercle of Waldeyer 12
tuberculum ligamenti calcaneofibularis 204
tuberculum ligamenti talicalcanei 204
tug lesions
  calcaneus 97
  distal femur 92
  proximal fibula and tibia 94
tympanic nerve 1037
tympanopharyngeal muscle 239

ulna 68
  dysplasia 68
  hypoplasia/aplasia 68
  notch length (NL) 140–142
  proximal 140–147
ulnar artery 604–606
  abductor digiti minimi variants and 332
  branching patterns 600, *602, 603,* 604
  dorsum of hand 609, *612–613*
  origins 594, 597
  palm of hand 606–609, *610–611*
ulnar collateral branch of radial nerve (Krause) 1092, 1099, 1102
ulnar collateral ligament (medial collateral ligament; MCL) 149–151, *152*
ulnaris quinti muscle 306
ulnar nerve 1089–1095
  intrinsic muscles of hand 317, 1090–1091
  median nerve communications 1088, *1090,* 1091–1092, 1093–1095
  origins 1091–1092
  radial nerve communications 1092, 1102
  regional relationships 1091
  targets 1092–1093
ulnar nerve compression 1091, *1092*
  abductor digiti minimi 328–329, *330*
  flexor digiti minimi 329
  opponens digiti minimi 329, *330*
  palmaris brevis 331
ulnocarpeus brevis muscle 303
umbilical appendix 1299
umbilical arteries 699
  internal iliac branching **703,** 706, *709, 711, 713*
  persistent right-sided single aberrant 699
  single 1388
umbilical cord 1388
  placental attachment 1387
umbilical sinus and polyp 1294–1295
umbilical veins
  persistent right 882
  supernumerary 1388
umbilicoileal (omphaloileal) fistula 1294, *1295*
uncal vein 809, 810
uncinate processes of cervical vertebrae 27
uncinate process of ethmoid bone 1164

uncipisiformis muscle 303
upper auricular detachment 1173
upper limb
  arteries 583–609
  muscles 293–296, 298–308
  nerves 1068–1104
upper limb veins 826–831
  anastomoses 830–831
  deep 826
  superficial 827–830
upper subscapular nerves 1095–1097
ureteral arteries 670
ureters 1325–1326
  crossed (fused) renal ectopia 1322
  horseshoe kidney 1318–1319
  retrocaval 1318–1319
urethra
  diverticulum 1342–1343
  duplication 1339–1340
  posterior valves 1341–1342
urinary tract anomalies 1315–1326
  accessory breast tissue and 1393
  Müllerian duct anomalies and 1369
urogenital sinus 1374
  persistent 1376
uterine artery 725–728, 1373
  absence 1373
  anastomoses 726–728, 1365, 1373
  course and branching 725–726
  origin 703–705, **712, 713, 725,** 726
  ovarian supply 1365
uterine (Fallopian) tubes 1365–1367
  agenesis 1364, 1366, 1368
  arterial supply 726, 1366–1367
  other anomalies 1366, *1367*
uterus 1367–1374
  agenesis/hypoplasia 1368–1369
  arcuate 1371
  arterial supply 726, 727–728, 1373
  bicornuate 1369–1370, 1372
  didelphys 1369, *1370,* 1376
  diethylstilbestrol (DES)-affected 1371, *1372*
  incarceration of retroverted 1373
  position 1372–1373
  retroflexion 1373
  retroversion 1373
  septate 1370–1371, 1376
  unicornuate 1369
  venous system 1373–1374
  see also Müllerian duct anomalies

VACTERL association 1212
vagina 1374–1377
  agenesis 1368, 1374
  arterial supply 1377
  longitudinal septum 1369, *1370,* 1375–1376
  transverse septum 1375
vaginal artery 728–729, 1377
  origin **713,** 728
  uterine artery anastomoses 727
vagocervical complex 1044–1045, 1046–1047
vagovagal anastomoses 1043
vagus nerve (CN X) 1041–1045
  accessory nerve anastomoses 1043
  auricular branch 1029, 1043
  carotid sinus nerve proper (CSNP) anastomoses 1038
  cervical nerve anastomoses 1044–1045
  facial nerve anastomoses 1029, 1043
  glossopharyngeal nerve anastomoses 1039, 1041–1043
  glossopharyngeal nerve relations 1037
  hypoglossal nerve anastomoses 1043–1044
  lingual branch 1043–1044
varus angulation, proximal ulna 145, 146
vas aberrans 597
vasa recta 649–650
vas deferens 1355–1356
  congenital absence (CAVD) 1355–1356
  duplication 1356
vasti muscles 412–414
vastus intermedius muscle 194, 413
vastus lateralis muscle 194, 412–413, 414, *416*
vastus medialis muscle 194, 413–414, *417*
VATER association 1226–1227
vein of filum terminale 911
vein of Galen (great cerebral vein) 805, 806–807, **808,** *808,* 809
  arachnoid membranes 971
vein of Kocher 822
vein of Labbé 783, 811, 812–814
vein of Trolard 811, 814
vein of Vesalius (sphenoidal emissary vein) 8, 818
vena anonyma 834
venous angle of brain 803, 804
ventral (anterior) median veins 911
ventral sulcal veins 910
ventricular muscle *259,* 260
ventricular system of brain 943–951
Verga's ventricle 940
Vernet's syndrome 4
vertebrae
  cervical 24–28
  lumbar 33–36
  sacrococcygeal 37–38
  thoracic 30–32
vertebral arch defects 34–35
vertebral artery (VA) 461–462, 487–496
  anastomoses 483, 495–496
  anterior spinal artery origin 462, 496, *497,* 754–756, 766
  bony canal in atlas 26
  branches 496
  duplication 488, *492*
  fenestrations 488, *492, 494*
  foramen of Luschka relations 951
  intradural segment (V4) 487, 488
  origin 487–488, 521–522
  ostial segment (V1) 487
  size, hypoplasia, atresia 491, *495*
  suboccipital segment (V3) 487, 488
  transverse segment (V2) 27, 487, 488, *489–492*
  vestibulocochlear nerve relations 1034
vertebral bodies
  development 33
  lumbar 34
  thoracic 30–31
vertebral endplate, nuclear impressions 34
vertebral pedicles 31, 35
vertebral veins 823–824, 912
vertebral venous plexus 912
vertebra prominens 28
vertebrobasilar arteries 461–463
vertex notch, proximal femur 90
vesical arteries 730–731
vesicodeferential artery **713,** 729
vestibular aqueduct, enlargement 1179
vestibular bulbs 1379
vestibular nerves
  communication with other nerves 1034
  facial nerve relations 1008, *1009*
vestibulocochlear nerve (CN VIII) 1034
  arterial contacts in cerebellopontine angle 1006–1008
  facial nerve anastomoses 1009
  facial nerve relations 1006, 1008, *1009*
  foramen of Luschka relations 951
Vidian artery 450
Vidian canal 9
Vidian nerve 1027, 1047
Villemin arcade 655
vomer 12

vomerobasilar canal 9
vomerovaginal canal 9
von Ebner ducts 1187
von Oort's anastomosis 1034

Waardenburg's syndrome 1133
Wagstaffe–Le Fort tubercle 96
Wartenberg's syndrome 1101
Wilms' tumor 1318
Wirsung's duct 1280
Wolfring's glands 1153
Wormian bones *see* sutural bones
wrist
  accessory ossicles 71–72, 160
  bipartite carpals 161
  carpal coalitions 72, 160–161
  joints 158–163
  ligaments and cartilaginous structures 162–163
  specific bone variations 72–73, 162

xiphihumeralis muscle 341
xiphoid foramen 79
xiphoid process 79, 80

Zenker's diverticulum 1248, *1249*
Zinner's syndrome 1357
Zuckerkandl tubercle 1199
zygomatic bone 13–14
zygomatic branch of facial nerve 1023
zygomaticofacial arteries 451
zygomaticofacial (ZF) canals, multiple 13–14
zygomaticofacial (ZF) nerve 14, 996, 1028
zygomatico-orbital (ZO) foramina, multiple 14
zygomaticotemporal (ZT) canals, multiple 13–14
zygomaticotemporal (ZT) nerve 14, 996, 1027, 1028
zygomatic process, accessory spine 3
zygomaticus major muscle 217–218
zygomaticus minor muscle 218–219
zygosyndactyly 107